Morgan J. Hurley
Editor-in-Chief

SFPE Handbook of Fire Protection Engineering

Fifth Edition

SFPE
Engineering A Fire Safe World

Springer

SFPE Handbook of Fire Protection Engineering

Morgan J. Hurley
Editor-in-Chief

SFPE Handbook of Fire Protection Engineering

Fifth Edition

Springer

Editor-in-Chief
Morgan J. Hurley, P.E., FSFPE
Aon Fire Protection Engineering
Greenbelt, MD, USA

Editors
Daniel Gottuk, Ph.D., P.E.
Hughes Associates

John R. Hall Jr., Ph.D.
National Fire Protection Association

Kazunori Harada, Dr. Eng.
Kyoto University

Erica Kuligowski, Ph.D.
National Institute of Standards and Technology

Milosh Puchovsky, P.E., FSFPE
Worcester Polytechnic Institute

José Torero, Ph.D.
The University of Queensland

John M. Watts Jr., Ph.D., FSFPE
The Fire Safety Institute

Christopher Wieczorek, Ph.D.
FM Global

ISBN 978-1-4939-2564-3 ISBN 978-1-4939-2565-0 (eBook)
DOI 10.1007/978-1-4939-2565-0

Library of Congress Control Number: 2015953225

Springer New York Heidelberg Dordrecht London
© Society of Fire Protection Engineers 2016
This work is subject to copyright. All rights are reserved by the Publisher, whether the whole or part of the material is concerned, specifically the rights of translation, reprinting, reuse of illustrations, recitation, broadcasting, reproduction on microfilms or in any other physical way, and transmission or information storage and retrieval, electronic adaptation, computer software, or by similar or dissimilar methodology now known or hereafter developed.
The use of general descriptive names, registered names, trademarks, service marks, etc. in this publication does not imply, even in the absence of a specific statement, that such names are exempt from the relevant protective laws and regulations and therefore free for general use.
The publisher, the authors and the editors are safe to assume that the advice and information in this book are believed to be true and accurate at the date of publication. Neither the publisher nor the authors or the editors give a warranty, express or implied, with respect to the material contained herein or for any errors or omissions that may have been made.

Printed on acid-free paper

Springer Science+Business Media LLC New York is part of Springer Science+Business Media (www.springer.com)

This edition of the SFPE Handbook of Fire Protection Engineering is dedicated to Philip DiNenno, who was the editor in chief for the first four editions of this handbook. In the mid-1980s, Phil DiNenno, Jack Watts, Doug Walton, Craig Beyler, and Dick Custer had an idea to create a collection of calculation methods for fire protection engineering. From this idea emerged the SFPE Handbook of Fire Protection Engineering, which was first published in 1988.

No other single event had as significant an impact on establishing the profession of fire protection engineering as the publication of this handbook. As Vyto Babrauskas said: "The field [of fire protection engineering] has made very gratifying progress in these last four decades. . .. The most remarkable positive achievement I think has been the SFPE Handbook, published first in 1988. . . . [W]ith the publication of the first edition of the SFPE Handbook in 1988, all of a sudden we could properly describe this as a science-based profession." [Babrauskas, V. "Some Neglected Areas in Fire Safety Engineering," Fire Science and Technology Vol. 32 No. 1 (2013) pp. 35–48.]

When they began creating the first edition, Phil and his colleagues had no model other than handbooks used in other professions. Phil contributed the leadership, vision, and motivation necessary to develop the handbook, and he did so using entirely volunteer resources. This would be an incredible accomplishment for anyone. Phil did it before he turned 35.

Foreword

This edition marks a passing of the torch for the *SFPE Handbook of Fire Protection Engineering*. All of the editors of the prior editions except for two (Jack Watts and John Hall) have retired, and a new editorial team has taken their place. Additionally, Springer has assumed the role of publisher beginning with this edition.

For the first four editions, the *SFPE Handbook of Fire Protection Engineering* was published by the National Fire Protection Association. The Society of Fire Protection Engineers owes a debt of gratitude to NFPA. Without their encouragement and confidence, this handbook might never have existed.

With a new editorial team emerge many changes. The chapters relevant to human behavior in fire have been significantly refocused and augmented. The fundamental engineering chapters have been revised to provide a better foundation for the chapters that follow. Many new chapters related to fire protection system selection and design have been added. The chapters associated with fire resistance design have been modified to reflect advances over the last decade. And, this edition includes several new chapters pertinent to industrial fire protection.

The editors owe a debt of gratitude to those whom they follow. Continuing a successful endeavor is much easier than launching it.

Acknowledgment of Past Authors

Name	1st edition	2nd edition	3rd edition	4th edition
Ahrens, Martha J.			✓	✓
Alpert, Ronald L.			✓	✓
Atreya, Arvind	✓	✓	✓	✓
Babrauskas, Vytenis	✓	✓	✓	✓
Back III, Gerard G.			✓	✓
Barry, Thomas F.		✓	✓	✓
Beck, Vaughan R.		✓		
Beever, Paula F.	✓	✓		
Beller, Douglas K.			✓	✓
Berlin, Geoffrey N.	✓			

(continued)

(continued)

Name	1st edition	2nd edition	3rd edition	4th edition
Beyler, Craig	✓	✓	✓	✓
Bowen, Jr., Jacob Van	✓			
Bryan, John L.	✓	✓	✓	✓
Buchanan, Andy			✓	✓
Bukowski, Richard W.			✓	
Carpenter, Douglas				✓
Chang, Jeremy				✓
Chapman, Robert E.			✓	✓
Charters, David				✓
Cooper, Leonard Y.	✓	✓	✓	
Cox, Geoff			✓	
Croce, Paul A.	✓	✓		
Custer, Richard L. P.		✓	✓	✓
Delichatsios, M. A.	✓	✓		
DiNenno, Philip J.		✓	✓	✓
Dodd, F. J.		✓		
Donegan, H. A.		✓	✓	✓
Drysdale, D. D.	✓	✓	✓	✓
Emmons, Howard W.	✓	✓	✓	✓
Evans, David D.	✓	✓		
Fahy, Rita F.			✓	✓
Fitzgerald, Robert W.	✓	✓	✓	✓
Fleischmann, Charles	✓	✓	✓	✓
Fleming, Russell P.	✓	✓	✓	✓
Franssen, Jean-Marc				✓
Frantzich, Håkan				✓
Friedman, Raymond	✓	✓	✓	✓
Gottuk, Daniel T.		✓	✓	✓
Grant, Casey C.	✓	✓	✓	✓
Gray, Brian			✓	✓
Griffiths, John				✓
Gwynne, Steven				✓
Hadjisophocleous, George				✓
Hall, Jr., John R.	✓	✓	✓	✓
Harmathy, Tibor Z.	✓	✓	✓	✓
Hasemi, Yuji				✓
Heskestad, Gunnar	✓	✓	✓	✓
Hickey, Harry E.	✓	✓	✓	✓
Hinkley, Peter L.	✓	✓		
Hirschler, Marcelo M.		✓	✓	✓
Hu, Yu-Shu		✓		
Hurley, Morgan				✓
Hyslop, J. S.				✓
Iwankiw, Nestor				✓
Jaluria, Yogesh	✓	✓		
Janssens, M.		✓	✓	✓
Jin, Tadahisa			✓	✓
Joglar, Francisco			✓	✓
Johnson, Peter				✓

(continued)

(continued)

Name	1st edition	2nd edition	3rd edition	4th edition
Kandola, B. S.	✓	✓	✓	✓
Kanury, A. Murty	✓	✓	✓	
Kersken-Bradley, Marita	✓			
Klote, John H.	✓	✓	✓	✓
Kodur, V. K. R.			✓	✓
Kuligowski, Erica				✓
Kumar, Suresh			✓	
Lattimer, Brian Y.			✓	✓
Lee, K. Y.	✓	✓	✓	✓
Lie, T. T.	✓	✓	✓	
MacLennan, Hamish A.	✓	✓		
Mawhinney, Jack R.			✓	✓
McCaffrey, Bernard	✓	✓		
McGrattan, Kevin				✓
Meacham, Brian J.		✓	✓	✓
Mehaffey, Jim				✓
Miles, Stewart				✓
Milke, James A.	✓	✓	✓	✓
Modarres, Mohammad		✓	✓	
Morgan, Alexander				✓
Mowrer, Frederick W.			✓	✓
Mudan, Krishna S.	✓	✓		
Mulholland, George W.	✓	✓	✓	✓
Nelson, Harold E.	✓	✓	✓	
Notarianni, Kathy A.			✓	✓
Nowlen, Steven				✓
Ohlemiller, T. J.	✓	✓	✓	✓
Parry, Gareth				✓
Pauls, Jake	✓	✓		
Phillips, William G. B.		✓	✓	✓
Proulx, Guylène			✓	✓
Purser, David A.	✓	✓	✓	✓
Quintiere, James G.	✓	✓	✓	✓
Ramachandran, G.	✓	✓	✓	✓
Roby, R. J.		✓		
Rockett, John A.	✓		✓	✓
Rosenbaum, Eric				✓
Salisbury, Matthew				✓
Scheffey, Joseph L.		✓	✓	✓
Schifiliti, Robert P.	✓	✓	✓	✓
Simmons, Robert F.		✓	✓	✓
Siu, Nathan			✓	✓
Stretton, A. J.	✓	✓	✓	✓
Stroup, David W.		✓		
Tanaka, Takeyoshi				✓
Tewarson, Archibald	✓	✓	✓	✓
Thomas, Ian				✓
Thomas, Philip H.	✓	✓	✓	✓

(continued)

(continued)

Name	1st edition	2nd edition	3rd edition	4th edition
Tien, C. L.	✓	✓	✓	✓
Titus, John J.	✓	✓	✓	✓
Torero, José				✓
Walton, William D.	✓	✓	✓	✓
Watts, Jr., John M.	✓	✓	✓	✓
White, Derek A.			✓	✓
White, Robert H.	✓	✓	✓	✓
Wickström, Ulf				✓
Wolski, Armin				✓
Wood, Christopher				✓
Yung, David		✓		
Zalosh, Robert G.	✓	✓	✓	✓

Metrication

The editors of the *SFPE Handbook of Fire Protection Engineering* have worked toward the expanded use of SI units for this fifth edition. In some instances, however, US customary units have been retained. For example, when equations, correlations, or design methodologies have input variables or constants that have been developed from data originally in US customary units, those units are retained. This is also the case for certain tables, charts, and nomographs. Where equations employing US customary units are used in worked examples, the results are presented as SI units as well.

Contents

Volume I

Introduction to Fluid Mechanics

1

Bart Merci

Fluid Properties

In this section, a number of fluid properties are defined. An implicit assumption in the classical fluid mechanics is the 'continuum hypothesis', implying that we treat fluids as continuous media, not as an ensemble of individual molecules [1]. This is justified in 'normal' circumstances. This way, the fluid and flow quantities are continuous and local quantities to be interpreted as averages over a volume V^* which is very small (but still very large when compared to distances between molecules). This assumption allows to define local fluid and flow properties (e.g. velocity vectors). The continuum hypothesis is adopted here.

A fluid can be a liquid or a gas (vapour).

Density

The mass density is the amount of fluid mass inside a volume:

$$\rho = \frac{m}{V}. \tag{1.1}$$

Its unit is kg/m^3.

In a variable density flow, the density can vary in space and time and the local density at a certain time is defined as in Equation 1.1, taking the local limit for a small volume.

In an incompressible flow, the density does not vary. In general, liquids can be considered 'incompressible'. In gases, the density can vary due to variations in pressure or temperature (see below: ideal gas law).

The reciprocal of density is the 'specific volume' (m^3/kg).

Viscosity

Fluids can flow. The viscosity is the fluid property that indicates how easily molecules can move with respect to each other. Fluid particles with different velocity have the tendency to evolve to the same common velocity, through exchange of momentum. In other words, fluid layers with different velocities exert a shear stress τ onto each other. Most technically relevant fluids are 'Newtonian': the shear stress increases linearly with the strain rate (or velocity gradient):

$$\tau = \mu \frac{dv}{dy}. \tag{1.2}$$

The unit of τ is Pa (= N/m^2).

The proportionality factor, relating the velocity gradient to the shear stress, is the dynamic viscosity μ (unit: Pa.s).

In gases, μ typically increases with temperature, whereas in liquids it decreases with increasing temperature.

B. Merci (✉)
Department of Flow, Heat and Combustion Mechanics, Ghent University, Ghent, Belgium

M.J. Hurley (ed.), *SFPE Handbook of Fire Protection Engineering*,
DOI 10.1007/978-1-4939-2565-0_1, © Society of Fire Protection Engineers 2016

Sometimes, the kinematic viscosity is used:

$$\nu = \frac{\mu}{\rho}. \tag{1.3}$$

Its unit is m^2/s.

The shear stress, Equation 1.2, causes friction losses in case of flow. The higher the viscosity, the larger the flow losses become for the same velocity gradient. In other words, the resistance of the fluid against (imposed) flow increases with increasing viscosity.

The viscosity of a fluid is never zero. The important implication is that, whenever there is a solid boundary, this boundary always exerts an influence on the flow field (e.g. causing the development of a boundary layer).

Specific Heat

The specific heat or thermal capacity, c, is the amount of energy required to cause a temperature rise of 1 K (or 1 °C) in 1 kg of the fluid. Its unit is J/(kg.K).

In gases the value of the specific heat depends on the circumstances under which the energy is supplied. If the pressure is kept constant, the notation is c_p. If the volume is kept constant, the notation is c_v. The difference between the two values is called the gas constant R (also in J/(kg.K)):

$$c_p = c_V + R. \tag{1.4}$$

For liquids and solids, $c_p \approx c_v$.

Conduction Coefficient

The conduction coefficient expresses how easily heat flows inside a material. Its value indicates the heat flux per unit area (W/m^2) related to a spatial temperature gradient (K/m):

$$\vec{\dot{q}} = -k\nabla T = -\lambda\nabla T. \tag{1.5}$$

This is Fourier's law. The minus sign indicates that the heat flux is always from high temperature to low temperature.

The unit of the conduction coefficient (k or λ) is W/(m.K).

The conduction coefficient, specific heat and density can be combined to obtain the thermal diffusivity:

$$\alpha = \frac{k}{\rho c} \tag{1.6}$$

The unit of α is m^2/s.

Diffusion Coefficient

In a mixture of fluids (see below), one species can diffuse in the mixture due to concentration gradients of that species in the mixture. It is common practice to apply Fick's law for many flows:

$$\vec{J}_k = -\rho D_k \nabla Y. \tag{1.7}$$

The diffusion coefficient D thus provides the relation between the diffusion flux J_k ($kg/(m^2s)$) of species k and the spatial gradient of the local mass fraction Y_k (i.e. the amount of mass of species k per kg mixture) of that species. The minus sign expresses that the diffusion flux is always from higher concentration to lower concentration.

The unit of D is m^2/s.

Dimensionless Groups of Fluid Properties

By combining the fluid properties, dimensionless groups can be constructed. Indeed, the units of ν, α and D are the same (m^2/s). Physically, the interpretation is that ν tries to make the velocity field uniform inside a fluid

(through exchange of momentum), α tries to make the temperature field uniform (through heat exchange by conduction) and D tries to make the concentration field in a mixture homogeneous (through concentration gradient driven diffusion).

The resulting dimensionless groups read:

– The Prandtl number:

$$\mathrm{Pr} = \frac{\nu}{\alpha} = \frac{\mu c_p}{\lambda} = \frac{\mu c_p}{k}. \tag{1.8}$$

– The Schmidt number:

$$Sc = \frac{\nu}{D}. \tag{1.9}$$

– The Lewis number:

$$Le = \frac{\alpha}{D}. \tag{1.10}$$

Clearly, these numbers are connected: $Le = Sc.\mathrm{Pr}^{-1}$.

It is important to note that the dimensionless numbers Equations 1.8, 1.9, and 1.10 are still fluid properties, not flow properties.

As long as no mixtures are considered, the Prandtl number is the most relevant dimensionless fluid property, when heat transfer is an issue.

State Properties

State properties describe the state of the fluid, not the material properties of the fluid.

Pressure

The pressure (p) can be defined as the normal force per unit area at a certain point. The unit is Pa. Pressure differences are the driving force for fluid flows.

Temperature

The unit of temperature (T) is Kelvin (K). The temperature must not be confused with heat (the unit of which is Joule, J).

Internal Energy

The local motion of molecules in a fluid is related to the internal energy (e or u, with unit J/kg). This is a measure for the thermal energy.

Enthalpy

The quantity (static) enthalpy (h, with unit J/kg) is related to the internal energy through addition of pressure, divided by mass density:

$$h = u + \frac{p}{\rho} = e + \frac{p}{\rho}. \tag{1.11}$$

Entropy

The entropy is a measure for the disorder in the fluid. It is related to the second law of thermodynamics. This quantity is typically not particularly relevant for fire related issues.

Equation of State

Liquids

In liquids, the density is essentially constant, relatively very weakly dependent on pressure and temperature. Yet, the general expression that provides the equation of state defines the relation between density, temperature and pressure:

$$\rho = f(p, T) \tag{1.12}$$

Gases: Ideal Gas Law

In gases, it is common practice to specify Equation 1.12 as the 'ideal gas law':

$$p = \rho RT \tag{1.13}$$

For fire related flows, this is justified. Most gases behave as air would do and air behaves as an ideal gas (with the exception of extremely low or

high pressure or temperature, but this is not relevant for real-life fire applications). The gas constant R (J/(kg.K)) has been introduced in Equation 1.4 and the temperature T is expressed in Kelvin (K).

Mixtures

In fire related flows, the fluid can be a mixture. Obvious examples are smoke or flames. A distinction must be made between chemical and physical issues. If toxicity is an issue, chemical aspects are important. As long as the flow itself is concerned, the physical behaviour of many gaseous mixtures resembles very much the behaviour of hot air. One reason is that the species most often encountered, have comparable diffusivities (with the important exception of hydrogen, which has a much higher diffusivity). Another reason is that typically by far mixtures in fire related flows consist mainly of air.

As a consequence, the simplification is made very commonly to treat a mixture of hot gases as hot air, applying the ideal gas law (Equation 1.13) with the gas constant for air and using the (temperature dependent) viscosity for hot air. Therefore, mixtures of gases do not receive much attention when fluid mechanics aspects are considered in case of fire.

Yet, a few definitions are introduced here. The mass fraction Y_i of species i is the ratio of the local amount of mass of species i to the local amount of mass of mixture. It is therefore a non-dimensional quantity. Conservation of mass leads to the statement that, everywhere in physical space, the sum of all mass fractions of all species equals unity: $\sum_{i=1}^{N} Y_i = 1$.

Using the notion of mass fractions, the fluid properties of mixtures can be determined from the fluid properties of their constituent species. E.g. the specific heat becomes $c = \sum_{i=1}^{N} Y_i c_i$.

Also state properties can be defined as such. E.g. static enthalpy becomes: $h = \sum_{i=1}^{N} Y_i h_i$.

Conservation Equations

Figure 1.1 visualises a streamline through a surface of a (control) volume. This concept will be used to develop the conservation equations in the integral formulation. A streamline is defined such that locally the velocity vector is tangent to the streamline. A collection of streamlines is called a stream tube.

Conservation of Mass—Continuity Equation

Conservation of mass expresses the following principle:

The amount of mass that flows into a stationary volume per unit time, equals the outflow of mass per unit time out of that same volume plus the amount of mass accumulation per unit time in that same volume.

Mathematically, this is formulated as follows:

- The net outflow per unit time is given by a closed surface integral over the entire area of the manifold ∂V, enclosing the volume V: $\iint_{\partial V} \rho \vec{v}.\vec{n} dA$; in this expression, $\vec{v}$ is the local velocity vector at a certain position on ∂V, $\vec{n}$ the local normal vector on the surface (i.e. the vector with length equal to 1, locally perpendicular to the surface and pointed outward) and dA the area of an infinitesimal element

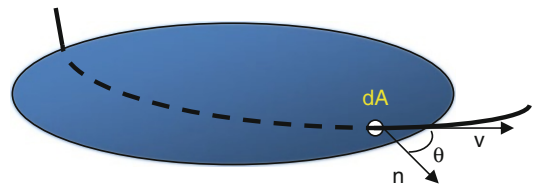

Fig. 1.1 Streamline through a surface. Notation: dA is the area of an infinitesimal part of the surface; n is the normal vector, with length equal to unity, perpendicular to dA and pointing 'outward' of the control volume, spanned by the surface; v is the local flow velocity vector at position dA; θ is the angle between vectors n and v

on the surface; note that the inner product $\vec{v}.\vec{n} > 0$ for outflow, while $\vec{v}.\vec{n} < 0$ for inflow;
- The accumulation of mass per unit time is obtained from a derivation with respect to time of the integral of the mass density over the entire volume: $\frac{\partial}{\partial t}\iiint_V \rho dV$.

The conservation of mass thus reads:

$$\frac{\partial}{\partial t}\iiint_V \rho dV + \iint_{\partial V} \rho \vec{v}.\vec{n} dA = 0. \tag{1.14}$$

This equation is also called the *continuity equation*.

An important simplification is found in the case of *permanent* (or '*steady*') *motion*. In that case, the time derivative disappears in Equation 1.14:

$$\iint_{\partial V} \rho \vec{v}.\vec{n} dA = 0. \tag{1.15}$$

A further simplification concerns *incompressible fluids* (e.g. water in a pipe under normal conditions). In that case, density does not change, so that not only Equation 1.15 applies, but it further simplifies to read:

$$\iint_{\partial V} \vec{v}.\vec{n} dA = 0. \tag{1.16}$$

A very simple illustration of Equation 1.15 is provided on the basis of Fig. 1.2. There is no flow through the solid boundaries (solid lines in Fig. 1.2), so the only contributions to $\iint_{\partial V} \rho \vec{v}.\vec{n} dA$ stem from surfaces 1 and 2. In surface 1, the velocity vector is pointing inward, while the normal vector is by definition pointing outward, so the contribution (under the simplified assumption of uniform flow through the cross-section) becomes: $-\rho_1 v_1 A_1$. On surface 2, the velocity and the normal vectors are pointing outward, leading to: $+\rho_2 v_2 A_2$. Equation 1.15 thus provides: $-\rho_1 v_1 A_1 + \rho_2 v_2 A_2 = 0 \rightarrow \rho_1 v_1 A_1 = \rho_2 v_2 A_2$. In case of incompressible flow (Equation 1.16) this further simplifies to: $v_1 A_1 = v_2 A_2$.

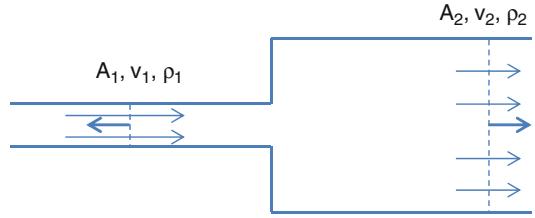

Fig. 1.2 Illustration of conservation of mass for steady flow (Equation 1.15) through a pipe expansion. *Dashed lines*: boundary of control volume. *Bold vectors*: normal vectors (unity length, perpendicular to surface and pointing outward). The other vectors indicate velocity vectors

The integral in Equation 1.14 in fact refers to the total net mass flow rate (kg/s) through a surface with area A:

$$\dot{m} = \iint_A \rho \vec{v}.\vec{n} dA \tag{1.17}$$

If the mass density is not included, the total net volume flow rate (m^3/s) through a surface with area A is found:

$$\dot{V} = \iint_A \vec{v}.\vec{n} dA. \tag{1.18}$$

Expression (1.14) can also be formulated in differential form, applying Green's theorem:

$$\frac{\partial \rho}{\partial t} + \nabla.\left(\rho \vec{v}\right) = 0. \tag{1.19}$$

The symbol ∇ is the divergence operator:

$$\nabla.\vec{v} = \left(\frac{\partial}{\partial x}\vec{1}_x + \frac{\partial}{\partial y}\vec{1}_y + \frac{\partial}{\partial z}\vec{1}_z\right).\left(v_x\vec{1}_x + v_y\vec{1}_y + v_z\vec{1}_z\right) = \frac{\partial v_x}{\partial x} + \frac{\partial v_y}{\partial y} + \frac{\partial v_z}{\partial z}. \tag{1.20}$$

In Equation 1.20, $\vec{1}_x$ is the notation for the unity vector, i.e. a vector with length equal to unity, in the x-direction.

Expression (1.15), for steady flow, reads in differential form:

$$\nabla.\left(\rho\vec{v}\right) = 0, \tag{1.21}$$

while expression (1.16), for incompressible fluids, becomes:

$$\nabla.\vec{v} = 0. \tag{1.22}$$

This shows that the velocity field for any flow of an incompressible fluid is 'divergence free', or 'solenoidal'.

Total Momentum

Now the integral formulation for the conservation of total momentum is discussed. Figure 1.1 again serves as the basic sketch.

Conservation of total momentum refers to the expression of Newton's second law, applied to flows. The net change in momentum of a system per unit time in a certain sense and direction equals the net force on that system in that sense and direction.

Expressed for a stationary volume, this becomes:

The total force onto a stationary volume equals the sum of the net outflow of momentum per unit time out of that same volume plus the accumulation of momentum per unit time in that same volume.

The local amount of momentum per unit volume is $\rho\vec{v}$ (kg/(m^{2}s)). Newton's second law thus reads:

$$\frac{\partial}{\partial t}\iiint_V \rho\vec{v}dV + \iint_{\partial V}\rho\vec{v}\left(\vec{v}.\vec{n}\right)dA = \vec{F}_{tot}. \tag{1.23}$$

Note that Equation 1.19 is a vector equation, i.e. the equation is valid for each component/direction individually.

For a permanent (or 'steady') motion, expression (1.19) simplifies to:

$$\iint_{\partial V}\rho\vec{v}\left(\vec{v}.\vec{n}\right)dA = \vec{F}_{tot}. \tag{1.24}$$

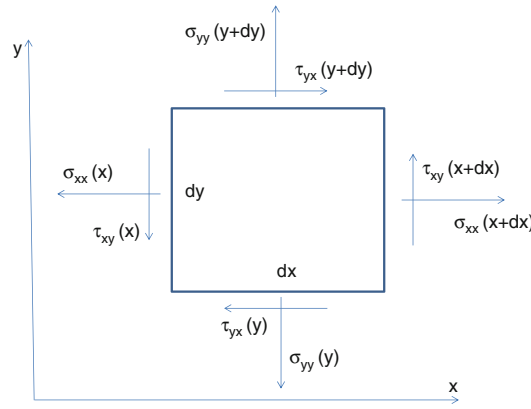

Fig. 1.3 Definition of normal stresses and shear stresses (2D)

The total force consists of:

- Surface forces:
  - Pressure (Pa);
  - Viscous stresses (Pa);
- Body forces:
  - Gravity (N);
  - Others (not relevant for fire related flows).

These forces are discussed now, in differential formulation:

$$\begin{cases} F_{tot,x} = \dfrac{\partial\sigma_{xx}}{\partial x} + \dfrac{\partial\tau_{xy}}{\partial y} + \dfrac{\partial\tau_{xz}}{\partial z} + \rho g_x \\ F_{tot,y} = \dfrac{\partial\tau_{yx}}{\partial x} + \dfrac{\partial\sigma_{yy}}{\partial y} + \dfrac{\partial\tau_{yz}}{\partial z} + \rho g_y \\ F_{tot,z} = \dfrac{\partial\tau_{zx}}{\partial x} + \dfrac{\partial\tau_{zy}}{\partial y} + \dfrac{\partial\sigma_{zz}}{\partial z} + \rho g_z \end{cases} \tag{1.25}$$

The final terms in Equation 1.25 refer to the gravity acceleration vector, multiplied with the local mass density. Figure 1.3 shows how the normal stresses and shear stresses are defined.

The shear stresses are found from Stokes' law:

$$\begin{aligned} \tau_{xy} &= \tau_{yx} = \mu\left(\frac{\partial v_x}{\partial y} + \frac{\partial v_y}{\partial x}\right) \\ \tau_{xz} &= \tau_{zx} = \mu\left(\frac{\partial v_x}{\partial z} + \frac{\partial v_z}{\partial x}\right) \\ \tau_{yz} &= \tau_{zy} = \mu\left(\frac{\partial v_z}{\partial y} + \frac{\partial v_y}{\partial z}\right). \end{aligned} \tag{1.26}$$

The shear stresses are thus proportional to the dynamic viscosity and the local velocity gradients.

The normal stresses contain contributions from stresses due to fluid dilatation (for variable density flows only) and pressure:

$$\begin{aligned}\sigma_{xx} &= -p + \frac{2}{3}\mu\left(\frac{\partial v_x}{\partial x} - \frac{1}{3}\nabla.\vec{v}\right)\\ \sigma_{yy} &= -p + \frac{2}{3}\mu\left(\frac{\partial v_y}{\partial y} - \frac{1}{3}\nabla.\vec{v}\right)\\ \sigma_{zz} &= -p + \frac{2}{3}\mu\left(\frac{\partial v_z}{\partial z} - \frac{1}{3}\nabla.\vec{v}\right).\end{aligned} \tag{1.27}$$

The above results in the *Navier–Stokes equations*:

$$\begin{cases}\frac{\partial}{\partial t}(\rho v_x) + \rho v_x\frac{\partial v_x}{\partial x} + \rho v_y\frac{\partial v_x}{\partial y} + \rho v_z\frac{\partial v_x}{\partial z} = -\frac{\partial p}{\partial x} + \frac{2}{3}\frac{\partial}{\partial x}\left(\mu\left(\frac{\partial v_x}{\partial x} - \frac{1}{3}\nabla.\vec{v}\right)\right) + \frac{\partial \tau_{xy}}{\partial y} + \frac{\partial \tau_{xz}}{\partial z} + \rho g_x\\ \frac{\partial}{\partial t}(\rho v_y) + \rho v_x\frac{\partial v_y}{\partial x} + \rho v_y\frac{\partial v_y}{\partial y} + \rho v_z\frac{\partial v_y}{\partial z} = -\frac{\partial p}{\partial y} + \frac{2}{3}\frac{\partial}{\partial y}\left(\mu\left(\frac{\partial v_y}{\partial y} - \frac{1}{3}\nabla.\vec{v}\right)\right) + \frac{\partial \tau_{xy}}{\partial x} + \frac{\partial \tau_{yz}}{\partial z} + \rho g_y\\ \frac{\partial}{\partial t}(\rho v_z) + \rho v_x\frac{\partial v_z}{\partial x} + \rho v_y\frac{\partial v_z}{\partial y} + \rho v_z\frac{\partial v_z}{\partial z} = -\frac{\partial p}{\partial z} + \frac{2}{3}\frac{\partial}{\partial z}\left(\mu\left(\frac{\partial v_z}{\partial z} - \frac{1}{3}\nabla.\vec{v}\right)\right) + \frac{\partial \tau_{xz}}{\partial x} + \frac{\partial \tau_{yz}}{\partial y} + \rho g_z\end{cases} \tag{1.28}$$

Note that the presence of the gravity force is essential in order to account for the Archimedes force. This is essential for buoyancy-driven forces, which is important in the context of fire.

Also note that pressure gradients (or pressure differences) are the driving force for flows, not the absolute pressure level.

Energy

Conservation of energy refers to the first law of thermodynamics:

The change (*per unit time*) *of the total internal energy of a system equals the sum of the heat added* (*per unit time*) *to the system and the work* (*per unit time*) *exerted onto that system.*

The total internal energy consists of:

- Static internal energy e (J/kg) or ρe (J/m^3);
- Kinetic energy $\rho v^2/2$ (J/m^3).

The mathematical formulation of the first law of thermodynamics for a stationary open system can be found in many textbooks (e.g. [2–9]). It reads:

$$\begin{aligned}\frac{\partial}{\partial t}\int_V\left(\rho e + \frac{1}{2}\rho v^2\right)dV = &-\oint_{\partial V}\left(\rho e + \frac{1}{2}\rho v^2\right)\vec{v}.\vec{n}dS - \oint_{\partial V} p\vec{v}.\vec{n}dS + \oint_{\partial V}\left(\vec{\vec{\tau}}.\vec{v}\right).\vec{n}dS\\ &+\int_V \rho\vec{g}.\vec{v}dV + \int_V \rho S_h dV - \oint_{\partial V}\vec{q}.\vec{n}dS\end{aligned} \tag{1.29}$$

The terms on the right hand side are:

- First term: Net inflow of total internal energy into the control volume ('convection'); the minus sign is necessary to comply with the sign convection (see previous sections: the normal vector is pointing outward).
- Second term: Work of the flow against pressure. This is work from a force (pressure),

exerted onto the surface. The work by the pressure onto the flow is positive for inflow and negative for outflow, which explains the minus sign.
- Third term: Work by the viscous stresses. This is work from a force (viscous stresses, Equations 1.26 and 1.27, exerted onto the surface. With the sign conventions used (Fig. 1.3 and outward pointing normal vector), this is a term with a plus sign.
- Fourth term: Work by gravity. This is work by a volume force, exerted inside the volume. This work is positive for a downward flow, so that with $\vec{g} = -g\vec{1}_y$ no minus sign is required in this term (if the y-direction is positive vertically upward).
- Fifth term: Volumetric source term of heat / internal energy (e.g. radiation). This term can be positive or negative.
- Final term: Net incoming flux of heat/internal energy (e.g. conduction). The flux with the flow cannot be added to this term (as it is already included in the convection term).

The energy equation can also be formulated, using enthalpy Equation 1.11:

$$\frac{\partial}{\partial t}\int_{CV}\left(\rho h+\frac{1}{2}\rho v^2\right)dV=\frac{\partial}{\partial t}\int_{CV}pdV-\oint_{\partial CV}\left(\rho h+\frac{1}{2}\rho v^2\right)\vec{v}.\vec{n}dS+\oint_{\partial CV}\left(\vec{\vec{\tau}}.\vec{v}\right).\vec{n}dS$$
$$+\int_{CV}\rho\vec{g}.\vec{v}dV+\int_{CV}\rho S_h dV-\oint_{\partial CV}\vec{q}.\vec{n}dS. \tag{1.30}$$

In differential formulation, this reads:

$$\frac{\partial}{\partial t}\left(\rho h+\frac{1}{2}\rho v^2\right)+\nabla.\left(\rho\left(h+\frac{1}{2}v^2\right)\vec{v}\right)=\frac{\partial p}{\partial t}+\nabla.\left(\vec{\vec{\tau}}.\vec{v}\right)+\rho S_h+\rho\sum_{i=1}^{N}Y_i\vec{g}.\vec{v}_i-\nabla.\vec{q} \tag{1.31}$$

The (static) enthalpy is the mass-weighted sum of the enthalpies of species i:

$$h=\sum_{i=1}^{N}Y_i h_i. \tag{1.32}$$

The enthalpy h_i is the sum of a reference enthalpy (the chemical standard formation enthalpy of species i) and a 'sensible' (thermal) enthalpy [5–9]. For ideal gases this reads:

$$h_i(T)=h_{ref,i}+\int_{T_{ref}}^{T}c_{p,i}(T)dT, \tag{1.33}$$

with $c_{p,i}$ the specific heat of species i, defined above.

Note that in Equation 1.31, expressed in terms of enthalpy, the source term ρS_h contains e.g. radiation, but not a heat release rate due to combustion. Combustion reactions transform chemically bound enthalpy into sensible enthalpy and as such cause a temperature rise, but the sum of sensible and chemical enthalpy does not change locally. If the energy equation is expressed in terms of temperature (or sensible enthalpy), a source term due to the combustion heat release rate does appear.

The final term in Equation 1.31 reads:

$$\nabla.\vec{q}=-\nabla.(\lambda\nabla T)-\nabla.\left(\rho\sum_{i=1}^{N}h_i D_i\nabla Y_i\right)+D.E. \tag{1.34}$$

The abbreviation 'D.E.' stands for the 'Dufour effect', i.e. and additional enthalpy flux due to species concentration differences. This effect is

ignored in fire related flows. The first terms in Equation 1.34 refer to Fourier's law for heat conduction, Equation 1.5. The middle terms refer to an enthalpy flux due to diffusion, using Fick's law, Equation 1.7.

The general expression, Equation 1.31, can often be simplified. Many fire-induced flows are low-Mach number flows (note: this is not true for explosions). The time derivative of pressure can often be ignored. Also the work done by gravity, by the viscous shear stresses and by the normal stresses becomes very small and the kinetic energy is negligible. Using Equations 1.8 and 1.9, the energy equation becomes:

$$\frac{\partial}{\partial t}(\rho h) + \nabla.\left(\rho h \vec{v}\right) = \nabla.\left(\frac{\mu}{\mathrm{Pr}}\nabla h + \mu\sum_{i=1}^{N}\left(\frac{1}{Sc_i} - \frac{1}{\mathrm{Pr}}\right)h_i \nabla Y_i\right) + \rho S_h \tag{1.35}$$

For unity Lewis number ($Le_i = 1$ for all i, Equation 1.10) fluids, this further simplifies to:

$$\frac{\partial}{\partial t}(\rho h) + \nabla.\left(\rho h \vec{v}\right) = \nabla.\left(\frac{\mu}{\mathrm{Pr}}\nabla h\right) + \rho S_h. \tag{1.36}$$

Hydrostatics

Hydrostatics

From the general Navier–Stokes equations (1.28), the basic law for hydrostatics is immediately recovered. Indeed, setting all velocities in a certain environment equal to zero, the only terms remaining are:

$$\nabla p = \rho_{amb}\vec{g}. \tag{1.37}$$

Equation 1.37 is valid at any time (in the absence of motion). For the special case where $\vec{g} = -g\vec{1}_y$, with g = 9.81 m/s^2, Equation 1.37 reads (in the y-direction):

$$\frac{dp}{dy} = -\rho_{amb} g \tag{1.38}$$

Note that Equation 1.37 in such circumstances also implies that pressure does not vary in the horizontal directions.

Equation 1.38 can be integrated:

$$p = p_{ref} - \rho_{amb} g\left(y - y_{ref}\right). \tag{1.39}$$

Buoyancy

The main relevance of the fundamental law of hydrostatics, Equation 1.37, lies in the fact that in many fire related flows, buoyancy plays a dominant role. This can be learnt from the Navier–Stokes equations, Equation 1.28, combining the forces due to pressure gradients and gravity. In the vertical direction (still with $\vec{g} = -g\vec{1}_y$), using Equation 1.38, the resulting force per unit area reads:

$$-\frac{dp}{dy} - \rho g = (\rho_{amb} - \rho)g. \tag{1.40}$$

In the process of getting to expression (1.40), the implicit assumption is made that pressure differences in the horizontal directions are small.

Equation 1.40 reveals that the driving force in situations where buoyancy dominates, stems from density differences, in the presence of a gravity field. This is known as Archimedes' law. Note that, since gravity acts in the vertical direction only, buoyancy forces by definition also act in the vertical direction only.

For small density differences, the approximation $\rho \approx \rho_{amb}$ is typically made in the Navier–Stokes equations, except that the difference $(\rho_{amb} - \rho)$ is accounted for in combination with gravity (Equation 1.40). This is called Boussinesq's approximation. In the context of small density differences, expression (1.40) can be developed further, using a Taylor series

expansion: $\rho = \rho(T, p) \Rightarrow \rho \approx \rho_{amb} + \left(\frac{\partial \rho}{\partial T}\right)_p (T - T_{amb}) + \left(\frac{\partial \rho}{\partial p}\right)_T (p - p_{amb})$. Typically the pressure correction is much smaller than the temperature correction. Using the thermal volumetric expansion coefficient:

$$\beta = -\frac{1}{\rho}\left(\frac{\partial \rho}{\partial T}\right)_p, \tag{1.41}$$

the Archimedes force becomes:

$$(\rho_{amb} - \rho)g = \rho_{amb}\beta(T - T_{amb})g \quad , \quad if \quad \beta(T - T_\infty) \ll 1. \tag{1.42}$$

The basic expression is thus Equation 1.40, based on density differences, while Equation 1.42 is only valid for small enough temperature differences.

Scaling Laws—Dimensionless Flow Numbers

In this section, starting from the governing equations, some scaling laws and non-dimensional flow numbers are introduced. The characteristic length scale is L, the characteristic velocity is u.

Dimensionless Flow Numbers

Examination of the terms in the Navier–Stokes equations, Equations 1.28 and 1.26, leads to the following proportionalities: $\frac{\rho u}{t} \sim \frac{\rho u^2}{L} \sim \frac{\Delta p}{L} \sim \Delta \rho g \sim \mu \frac{u}{L^2}$. Several non-dimensional flow numbers can be derived now, as follows. The importance of each of the numbers mentioned, depends on the importance of the corresponding terms in the Navier–Stokes equations. The convection term/inertia term is always important, as it characterizes the flow. Depending on the flow configuration, one or more terms are in competition with (or determine) the inertia term (or thus the flow). This is explained next.

When the viscous stresses prevail, the proportionality $\frac{\rho u^2}{L} \sim \mu \frac{u}{L^2}$ leads to the Reynolds number, which is the ratio of inertial forces to viscous forces:

$$\mathrm{Re} = \frac{\rho u L}{\mu} = \frac{uL}{\nu}. \tag{1.43}$$

The viscous forces tend to damp the inherent instabilities in the non-linear convection terms in the Navier–Stokes equations, while these instabilities can evolve towards fully-developed turbulence for large enough Reynolds number. This is addressed in the next section.

When buoyancy is dominant, the proportionality $\frac{\rho u^2}{L} \sim \Delta \rho g$ leads to the Froude number, which is the ratio of inertial forces to the Archimedes force:

$$\mathrm{Fr} = \frac{\rho u^2}{\Delta \rho g L}. \tag{1.44}$$

In the fire community, this is often simplified to:

$$\mathrm{Fr} = \frac{u^2}{gL}. \tag{1.45}$$

Expression (1.44) resembles the underlying physics more than Equation 1.45. On the other hand, the difference between expressions (1.44) and (1.45) is no more than a numerical factor, depending on the densities at hand. Moreover, in many experiments it is much more straightforward to measure velocities than mass densities, so that it is easier to characterize the experimental set-up through formulation (1.45). This explains why the use of Equation 1.45 is popular in diagrams and correlations.

If large (imposed) pressure differences occur, sometimes the Euler number comes into play, through $\frac{\rho u^2}{L} \sim \frac{\Delta p}{L}$:

$$Eu = \frac{\Delta p}{u^2}. \tag{1.46}$$

In fire related flows, this is often not relevant.

In buoyancy driven flows, applying Boussinesq's hypothesis, the driving force (Equation 1.42) can also be made dimensionless as:

$$Ra = \frac{L^3 g\beta\Delta T}{\alpha\nu}. \tag{1.47}$$

This is the Rayleigh number. Alternatively, the Grashof number can be used:

$$Gr = \frac{L^3 g\beta\Delta T}{\nu^2}. \tag{1.48}$$

The relation between the two is: $Ra = Gr.\mathrm{Pr}$, with the Prandtl number as defined in Equation 1.8. The Grashof number can be interpreted as a ratio of buoyancy forces (with Boussinesq's approximation) to the viscous forces. This is relevant in boundary layers (see below).

Scaling

In this section, scaling is briefly discussed in the context of fluid mechanics. As such, only the momentum equation is considered, albeit that at the end of this section, some remarks are formulated on the fire heat release rate (using the energy equation) and the study of unsteady phenomena (using the mass conservation equation). As a consequence, no comments are formulated on e.g. convective heat transfer or conduction through solids, nor on radiation. For an extensive discussion on scaling, the reader is referred to [10, 11].

The main non-dimensional numbers in low-Mach number flows are the Reynolds number Equation 1.43 and the Froude number Equation 1.44 (or Equation 1.45). Firstly, it is mentioned that the only way to preserve both numbers when scaling (up or down) a flow in a certain configuration, is through the use of different fluids. Indeed, assume that the fluid does not change (and that the densities do not change). Then preservation of Re reveals that: $\mathrm{Re}_1 = \mathrm{Re}_2 \Rightarrow \frac{u_1 L_1}{\nu} = \frac{u_2 L_2}{\nu} \Rightarrow u_2 = \frac{u_1 L_1}{L_2}$. Preservation of the Froude number (still with the assumption that densities do not change) leads to: $Fr_1 = Fr_2 \Rightarrow \frac{u_1^2}{gL_1} = \frac{u_2^2}{gL_2} \Rightarrow u_2 = u_1\sqrt{\frac{L_2}{L_1}}$. Clearly, this is inconsistent with the requirement, stemming from the preservation of the Reynolds number. Both numbers can be preserved if, starting from the requirement for preservation of the Froude number, the fluid's viscosity is modified such that also the Reynolds number is preserved. This is not straightforward.

Fortunately, both the Reynolds number and the Froude number have the property that, as soon as they are large enough, their actual value becomes irrelevant. In other words, as soon as they are sufficiently high, the qualification 'high' is sufficient, not the exact number. This is due to turbulence, overwhelming molecular phenomena (see next section). This can also be understood intuitively. The Reynolds number is the ratio of inertia to viscous damping forces. Either the damping force is strong enough to overcome the inherent instabilities in the non-linear convection terms in the Navier–Stokes equations (laminar flow), almost strong enough (transitional flow) or not strong enough (turbulent flow). When turbulence is fully developed, the strength of the viscous stress becomes irrelevant, i.e. the true value of the Reynolds number becomes irrelevant. For the Froude number, it is most instructive to examine expression (1.44). The driving force for buoyancy is in the denominator. If density differences become small, buoyancy becomes irrelevant and the Froude number is high. As such, high values of the Froude number implies that buoyancy is not important and thus that the error is small when the Froude number is not preserved (as long as it stays sufficiently high).

Knowing this, it is instructive to examine the order or magnitude of Reynolds number and Froude number in fire related flows. Indeed, if one of the numbers can be expected to be high,

that number need not be preserved in scaling. Typical dimensions are in the order of 1 m: $L = \mathrm{O}(m)$. Typical velocities are in the order of 1 m/s: $u = \mathrm{O}(m/s)$. Densities are in the order of 1 kg/m^3: $\rho = \mathrm{O}(kg/m^3)$. The dynamic viscosity in gases is in the order of 10^{-6} Pa.s: $\mu = \mathrm{O}\left(10^{-6} Pa.s\right)$. Using these numbers, the Reynolds number Equation 1.43 is: $\mathrm{Re} = \mathrm{O}\left(\frac{1.1.1}{10^{-6}}\right) = \mathrm{O}\left(10^6\right)$, while the Froude number Equation 1.44 is: $\mathrm{Fr} = \mathrm{O}\left(\frac{1.1}{1.10.1}\right) = \mathrm{O}(0.1)$. Obviously, these are rough order of magnitude analyses, but it is clear that in fire related flows, the choice will be made to preserve the Froude number, not the Reynolds number, when scaling is applied.

The energy equation also provides information regarding scaling laws. The simplified formulation (1.36) can be used for fire-related flows. Yet, temperatures are very important in fire related flows, so the energy equation should be interpreted in terms of sensible enthalpy, in which case the fire heat release rate ($\dot{Q}$, in W) comes into play. Knowing that, in terms of dimensions, (sensible) enthalpy differences can be re-written as the product of specific heat and temperature differences, Equation 1.36 leads to the following proportionalities: $\frac{\rho c_p \Delta T}{t} \sim \frac{\rho c_p \Delta T u}{L} \sim \frac{\dot{Q}}{L^3} \sim \frac{k \Delta T}{L^2}$.

This reveals that:

$$\dot{Q} \sim u \rho c_p \Delta T L^2. \tag{1.49}$$

It is common practice to scale configurations such that the temperatures remain the same. This also implies that densities do not change (if the same fluid is applied). As has just been explained, the Froude number Equation 1.44 is preserved, so that the velocity scales as $\sim \sqrt{L}$. As a consequence, the fire heat release rate scales as:

$$\frac{\dot{Q}_1}{\dot{Q}_2} = \frac{\sqrt{L_1} L_1^2}{\sqrt{L_2} L_2^2} \Rightarrow \dot{Q} \sim L^{5/2}. \tag{1.50}$$

Finally, it is noteworthy that the conservation of mass, Equation 1.19, reveals that:

$$t \sim L/u. \tag{1.51}$$

Applying Froude scaling, the velocity scales as $\sim \sqrt{L}$, so that expression (1.51) reveals that the temporal evolution of quantities (e.g. temperature) depends on the dimensions of the configuration as $t \sim \sqrt{L}$. This is relevant when unsteady phenomena are studied.

Turbulence

There are numerous text books on turbulence and turbulent flows, e.g. [12, 13]. Only some introductory comments are presented here.

Reynolds Number

In the previous section it has been mentioned that the Reynolds number Equation 1.43 is the ratio on inertia to viscous forces. It is well-known that the convection term in the Navier–Stokes equations (1.28) is inherently unstable and that the flow becomes turbulent when the viscous forces are not strong enough to damp the instabilities, i.e. when the Reynolds number becomes sufficiently high. Below a certain threshold number, the flow remains 'laminar'. There is no sudden change from 'laminar' to 'turbulent': there is a 'transition' zone in between.

Care must be taken in the definition of this 'critical' Reynolds number, in the sense that the length scale must be defined. In flows over flat plates, it is common practice to use the distance from the leading edge and Re_c is in the order of 500.000. In pipe flows, it is common practice to use the pipe diameter as characteristic length scale and Re_c is in the order of 2.000.

It is important to stress that the Reynolds number is a flow property, not a fluid property.

Turbulence is typically defined on the basis of a number of properties [13]:

- Randomness: there are fluctuations in the flow;
- Three-dimensionality: even if the mean flow is 2D or axisymmetric, the vortices or 'eddies' are always three-dimensional;
- There is a wide range of length scales and time scales in the flow. The largest scales are determined by the configuration at hand,

while the smallest scales are determined by the Reynolds number. The smallest scales can easily be 10,000 times smaller than the largest scales.
- Turbulent mixing is very effective.
- There is a lot of diffusion and dissipation. Turbulence dies out quickly if not sustained by velocity gradients in the mean flow.
- There is vortex stretching, transferring energy from the mean flow to turbulent fluctuations.

It is instructive to briefly explain the randomness in the flow. Indeed, knowing that the Navier–Stokes equations (Equation 1.28) are deterministic, one may pose the question how it is possible that randomness occurs when applying deterministic boundary and initial conditions. The reason is that there are always small fluctuations, i.e. the boundary and initial conditions are never known with infinite precision. Due to the unstable convection terms in the Navier–Stokes equations, turbulent flows are extremely sensitive to details and this creates randomness in the instantaneous flow fields. This makes it impossible to make long-term predictions of instantaneous turbulent flow fields and explains why turbulent flows are tackled in simulation through statistical approaches (see below). Obviously, the mean flow can still be deterministic (see below).

Reynolds Averaging

As mentioned in the previous section, the fluctuations in a turbulent flow make a direct analysis through the Navier–Stokes equations (Equation 1.28) impossible. Therefore, a statistical approach is adopted. The primary interest is often the mean flow. To that purpose, the Navier–Stokes equations are averaged. The concept of Reynolds averaging is explained first.

Consider a turbulent flow. Measuring a velocity component (or e.g. a temperature) at a certain location will then yield a fluctuating signal, as explained. One can now determine the 'average' of that signal. The true definition of a Reynolds average [12, 13] is that many realizations of the 'same' turbulent flow are made, repetitive measurements of the quantity are made at the same location, and the average value of the measurements is determined. In a simplified manner, though, one can think of this procedure as a time averaging, where the averaging period Δt is sufficiently long, compared to the largest turbulent time scales, but sufficiently short compared to time scales associated with possible variations in the mean flow:

$$\overline{v}_x(t) = \frac{1}{\Delta t}\int_{t-\Delta t}^{t} v_x(t)dt; \overline{T}(t) = \frac{1}{\Delta t}\int_{t-\Delta t}^{t} T(t)dt. \tag{1.52}$$

It is clear that this is only possible if the turbulent time scales are short, compared to time scales in the mean flow. The 'integral' turbulent time scale is typically less than 1 s, so in many fire related flows this concept of Reynolds averaging is possible.

Using Equation 1.52, the instantaneous value can be expressed as the sum of the (Reynolds) averaged value and the instantaneous fluctuation around that value:

$$v_x(t) = \overline{v}_x(t) + v_x'(t); T(t) = \overline{T}(t) + T'(t). \tag{1.53}$$

Note that:

$$\overline{v_x'(t)} = 0; \overline{T'(t)} = 0; \overline{\overline{v_x(t)}} = \overline{v_x(t)}; \overline{\overline{T(t)}} = \overline{T(t)}. \tag{1.54}$$

Applying this averaging technique to the conservation equations (1.19), (1.28) and (1.36), the equations are obtained for the Reynolds-averaged quantities. They are very similar to the instantaneous equations, but some additional terms appear:
- Reynolds stresses in the momentum equations;
- Turbulent heat fluxes in the energy equation.

This is explained next. For the sake of ease, the energy equation is simplified here: it is expressed in terms of temperature and no chemical reactions, nor radiation, are considered. The

averaging of the chemical and radiative source terms is a separate problem, not addressed here.

The additional terms appear as a consequence of the presence of products in the instantaneous Equations 1.28 and 1.36. The mean value of the product is not equal to the product of the mean values:

$$\begin{aligned}\overline{v_x v_y} &= \overline{\left(\overline{v}_x + v_x'\right)\left(\overline{v}_y + v_y'\right)} = \overline{\overline{v}_x}\,\overline{\overline{v}_y} + \overline{\overline{v}_x v_y'} + \overline{v_x' \overline{v}_y} + \overline{v_x' v_y'} = \overline{v}_x \overline{v}_y + \overline{v_x' v_y'} \\ \overline{v_x T} &= \overline{\left(\overline{v}_x + v_x'\right)\left(\overline{T} + T'\right)} = \overline{\overline{v}_x}\,\overline{\overline{T}} + \overline{\overline{v}_x T'} + \overline{v_x' \overline{T}} + \overline{v_x' T'} = \overline{v}_x \overline{T} + \overline{v_x' T'}.\end{aligned} \tag{1.55}$$

Simplifying further to a steady boundary layer flow of an incompressible fluid over a flat plate without external pressure gradient, the main remaining dominant terms are:

$$\begin{aligned}&\frac{\partial \overline{v}_x}{\partial x} + \frac{\partial \overline{v}_y}{\partial y} = 0 \\ &\overline{v}_x \frac{\partial \overline{v}_x}{\partial x} + \overline{v}_y \frac{\partial \overline{v}_x}{\partial y} = \frac{\partial}{\partial y}\left(\nu \frac{\partial \overline{v}_x}{\partial y}\right) - \frac{\partial}{\partial y}\left(\overline{v_x' v_y'}\right) \\ &\overline{v}_x \frac{\partial \overline{T}}{\partial x} + \overline{v}_y \frac{\partial \overline{T}}{\partial y} = \frac{\partial}{\partial y}\left(\alpha \frac{\partial \overline{T}}{\partial y}\right) - \frac{\partial}{\partial y}\left(\overline{v_y' T'}\right)\end{aligned} \tag{1.56}$$

Clearly, the final terms, stemming from turbulence, are similar in nature to the molecular viscous stresses and the molecular thermal diffusion terms. The main question is now what the turbulent correlations look like. Indeed, terms like $\overline{v_x' v_y'}$ are only non-zero if the velocity fluctuations in the difference directions are statistically correlated. This is the case, explained from Fig. 1.4, showing a situation in a flow with a mean velocity gradient. The discussion is given here for the top left eddy, but it prevails for all eddies. At the left side of the top left eddy, the instantaneous motion is downward, as indicated by the arrow. Knowing that the mean velocity in the vertical direction equals zero, this implies that $v' < 0$. In its downward motion, the eddy brings along fluid with a higher (mean) velocity in the horizontal direction into a region with lower (mean) velocity. Thus, the impact is a local increase in horizontal velocity, in other words $u' > 0$. Clearly, from a statistical point of view the velocity fluctuations in both directions are correlated, in such a manner that $\overline{u'v'} < 0$. At the right side of the top left eddy, the instantaneous motion is upward ($v' > 0$) and (in the mean) lower horizontal velocity is brought into a region with (in the mean) higher

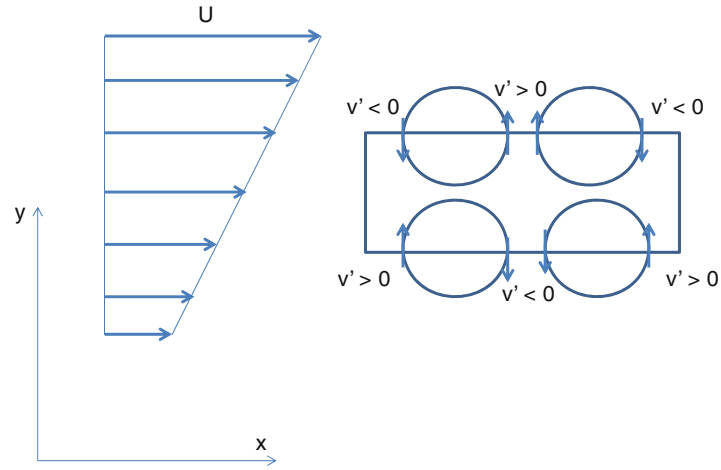

Fig. 1.4 Sketch of turbulent fluctuations (eddies) in a flow with a mean velocity gradient

horizontal velocity, causing u' < 0. Thus, again $\overline{u'v'} < 0$. A similar reasoning can be built up for the temperature fluxes.

Additionally, it is clear that the fluctuations, caused by the turbulent eddy motion, will be larger as the mean velocity (or temperature) gradients are larger.

The above led to the following 'eddy viscosity' modeling concept, introduced by Boussinesq:

$$-\overline{v_x' v_y'} = \nu_t \frac{\partial \overline{v}_x}{\partial y} \tag{1.57}$$

In other words, a 'turbulent' or 'eddy' viscosity is simply added to the molecular viscosity in Equation 1.56. This reflects the physical observation that momentum transfer increases in turbulent flows through the turbulent motion of eddies. These cause 'large scale' momentum transfer.

Similarly, this concept can be applied to the heat fluxes:

$$-\overline{v_y' T'} = \alpha_t \frac{\partial \overline{T}}{\partial y} \tag{1.58}$$

In other words, the addition of the turbulent thermal diffusivity to the molecular thermal diffusivity reflects the physical observation that heat transfer increases in turbulent flows through the turbulent motion of eddies. These cause 'large scale' heat transfer.

Turbulence Modeling

As mentioned above, there is always a wide range of length scales and time scales in turbulent flows. The higher the Reynolds number, the wider this range, because the smallest scales become smaller and smaller.

The largest turbulence scales are called the 'integral' scales. The smallest scales are called the 'Kolmogorov' scales. A detailed discussion of the spectrum is considered beyond the scope of this section, but it is important to appreciate that most of the turbulent kinetic energy is in the integral scale range ('energy containing range'), while turbulence is dissipated at scales around the Kolmogorov scales. Indeed, at those scales, viscous damping 'kills' turbulence, i.e. dissipates the turbulent kinetic energy into heat.

The notion of energy cascade, introduced by Richardson, is worth mentioning. The basic mechanism is as follows:

- Energy is taken from the mean flow and transferred to kinetic energy of turbulent eddies; this occurs around the integral scales;
- The turbulent eddies break up, transferring their energy to the eddies of smaller scale; only little energy is dissipated in this break-up process;
- The break-up process of eddies continues ('cascade process') until the eddies become so small that they cannot survive the damping action of viscosity anymore;
- The dissipation takes place at the smallest turbulence scales.

It is important to appreciate that, whereas the dissipation takes place at the smallest scales, the dissipation rate is determined by the production rate of turbulence from the mean flow in the energy containing range (in equilibrium conditions).

This phenomenology is reflected in the choice for turbulence modeling in CFD (Computational Fluid Dynamics). One extreme approach is not to model turbulence, i.e. to completely resolve all turbulent motions, down to the smallest scales. Knowing that these small scales can easily be in the order of 0.1 mm or less, and realizing that the computational mesh needs to be sufficiently fine to resolve the smallest eddies, it is immediately clear that this approach is not feasible in typical fire related flow simulations, where dimensions are in the order of 1 m. Worse than that, in addition to unacceptable computing time and memory requirements, most of the time and memory would be devoted to simulating the smallest scales [13], whereas the primary interest is typically in the large scale flow phenomena (or in the mean flow).

The other extreme is RANS (Reynolds-Averaged Navier–Stokes) turbulence modeling. In this approach, Reynolds averaging (see previous section) is applied and all turbulent motions, i.e. the entire turbulent spectrum, are modeled. Only the mean flow is resolved. The k-ε model

belongs to this class of models. The advantages of the RANS approach are clear: the computational mesh only needs to be fine enough to resolve the mean flows; the time step (in transient calculations) can be chosen on the basis of mean flow phenomena; one immediately gets a solution for the mean flow. There are major disadvantages, though. Firstly, all turbulence is modeled. Knowing that the largest turbulent scales are configuration dependent, it cannot be expected that a single RANS model can deal with arbitrary configurations in a reliable manner. Second, in fire related flows large scale flow unsteadiness often plays an important role, e.g. in the entrainment process of air into flames or smoke. Such unsteadiness is not captured in (unsteady) RANS and must be modeled. Again, being configuration dependent, RANS models cannot be expected to be as accurate as approaches where this unsteadiness is resolved.

This explains the popularity of the LES (Large-Eddy Simulations) technique in CFD for fire related flows. In this technique, the large scale eddies are resolved and only the effect of the small scale eddies is modeled. This technique offers the advantage of resolving the large-scale flow unsteadiness (and buoyancy effects). Also, the unacceptable fineness of the computational mesh as required in DNS is avoided. Yet, there is a very important caveat. Indeed, in order to guarantee the quality of LES results, 80 % of the turbulent kinetic energy must be resolved [13]. It is common practice to use the computational mesh as filter in the LES approach, i.e. the size of the computational mesh cells determines the size of the eddies still resolved. In many CFD simulations performed on today's computers, the mesh size is in the order of 10 cm or more. Very often, it cannot be guaranteed that 80 % of the turbulent kinetic energy is effectively resolved, so that care must be taken in the interpretation of the CFD results. In other words, blind belief in the exactness of under-resolved LES must be avoided. Also, it must be understood that if the computational mesh is used as filter for the instantaneous Navier–Stokes equations, as is common practice in the fire safety science community, no grid independent results can be expected from LES. Indeed, as the filter of the equations itself is modified, the results inevitably change. This is not the case in RANS simulations, where the results become independent of the mesh applied, provided it is fine enough.

For more discussion on turbulence modeling, in the context of reacting flows, the reader is also referred to [14].

Boundary Layers—External Flows

In section "Scaling", it was mentioned that the absolute value of the Reynolds number Equation 1.43 becomes irrelevant as Re becomes high. In other words, the flow can be considered 'inviscid', i.e. $\mu = 0$. Stated in another manner: viscosity becomes irrelevant in the Navier–Stokes equations. This, however, is only true in the absence of solid boundaries. Indeed, since viscosity is never really equal to zero, there is a 'no-slip' boundary condition at any solid boundary: due to the viscous forces, the fluid locally takes the velocity of the solid boundary, at the solid boundary. In fire-related flows, the solid boundaries typically stand still, so that the no-slip boundary condition implies that the fluid velocity equals zero.

In fire related flows, boundary layers appear as 'external' flows or in 'internal flows'. 'Internal' flows are discussed in the next section.

Examples of fire related boundary layers in external flows are: the flow over surfaces (horizontal or vertical) with e.g. flame spread, flow of smoke underneath a ceiling, atmospheric boundary layers in forest fires, etc. An 'external flow' is a flow where a 'free stream velocity' can be defined, i.e. a velocity that is not affected by the presence of the solid boundary.

Both the boundary layer flow itself and the corresponding (convective) heat transfer can be of importance in the context of fire.

Consider first the situation of a flow with free stream velocity U_∞ over a smooth flat plate, without external pressure gradient, schematically shown in Fig. 1.5. At the flat plate, $U = 0$ (no slip boundary condition), whereas 'sufficiently far away' from the plate $U = U\infty$. The notion

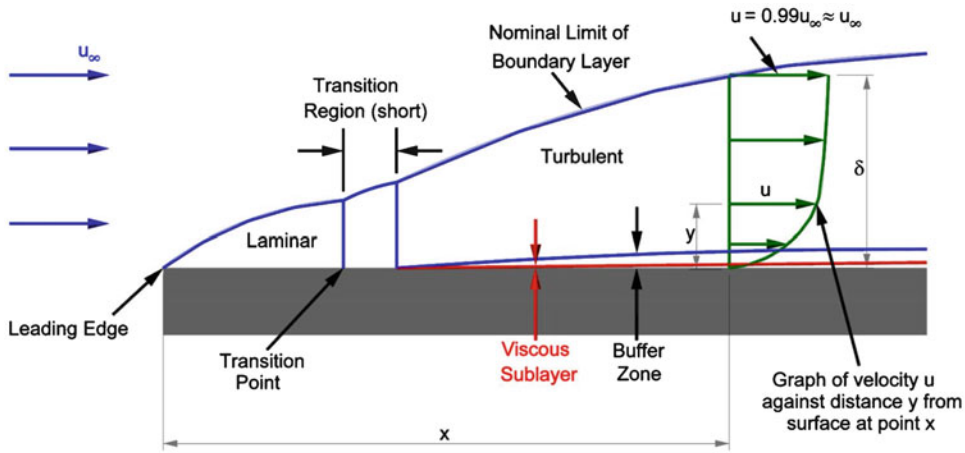

Fig. 1.5 Schematic representation of flow over a flat plate (Source: http://www.cortana.com)

'sufficiently far away' is related to the thickness of the boundary layer, which can be defined as:

$$y = \delta : v_x = 0.99U_\infty. \tag{1.59}$$

In words: the boundary layer thickness δ is the distance from the plate where the velocity equals 99 % of the free stream velocity. Other measures, such as displacement thickness and momentum thickness, can also be used to characterize the boundary layer thickness, but this is not essential for the present discussion.

Two flow regions can be defined:

- $y < \delta$: Strong velocity gradients and viscous shear stresses;
- $y > \delta$: Negligible velocity gradients and viscous shear stresses.

From an order of magnitude analysis, in the assumption that $\delta \ll x$, with x the distance from the leading edge of the flat plate, and in the assumption of laminar flow in the boundary layer, it can be shown that the boundary layer thickness grows as:

$$\delta_{lam} \sim \left(\frac{\mu x}{\rho U_\infty}\right)^{1/2}. \tag{1.60}$$

In words: the laminar boundary layer thickness grows with the square root of the distance from the leading edge. It is thicker as the kinematic viscosity is higher. The latter shows that the influence region of the flat plate is larger for fluids with higher viscosity.

Using x as characteristic distance, the following Reynolds number can be defined:

$$\mathrm{Re}_x = \frac{U_\infty x}{\nu}. \tag{1.61}$$

The viscous shear stress at the plate then becomes:

$$\tau_s = \mu\left(\frac{\partial v_x}{\partial y}\right)\Big|_{y=0} \sim \rho\nu\frac{U_\infty}{\delta} \sim \rho U_\infty^2\left(\frac{U_\infty x}{\nu}\right)^{-1/2}. \tag{1.62}$$

This can be expressed in a non-dimensional manner, by introducing the friction coefficient:

$$C_{f,x} = \frac{\tau_{s,x}}{\frac{1}{2}\rho U_\infty^2} \sim \left(\frac{U_\infty x}{\nu}\right)^{-1/2} = \mathrm{Re}_x^{-1/2}. \tag{1.63}$$

The 'Blasius' solution for laminar boundary layers over smooth flat plates indeed yields:

$$\delta_{lam} = 4.92x\mathrm{Re}_x^{-1/2}; C_{f,x.lam} = 0.664\mathrm{Re}_x^{-1/2} \tag{1.64}$$

However, as mentioned, there are inherent instabilities in the convection terms in the Navier–Stokes equations. These instabilities are damped near the flat plate, primarily due to the blocking effect and the viscous forces, so that turbulent vortices (eddies) cannot develop.

However, as the laminar boundary layer thickness grows with the distance from the leading edge (Equation 1.60), turbulence can start to develop. There is a critical Reynolds number $Re_{x,crit}$ (Equation 1.61) beyond which there is transition from laminar to turbulent flow. For a smooth flat plate, $Re_{x,crit}$ is in the order of 500.000.

As mentioned in the previous section, the momentum (and heat) transfer strongly increase in turbulent motions, as compared to the aligned laminar flow, since momentum (and heat) are transferred on a larger scale through the turbulent eddies. As a result, the surface friction (and heat transfer) increase and the boundary layer becomes thicker. It can be shown that:

$$\delta_{turb} = 0.37 x \mathrm{Re}_x^{-1/5}; C_{f,x,turb} = \frac{\tau_s}{\frac{1}{2}\rho U_\infty^2} = 0.0592 \mathrm{Re}_x^{-1/5}. \quad (1.65)$$

Thus, a turbulent boundary layer grows more rapidly than a laminar boundary layer.

Before discussing the turbulent boundary layer in more detail, it is worth mentioning that, very similar to boundary layers at the level of velocities, thermal boundary layers can be defined. Indeed, the thermal diffusivity α plays the same role for heat transfer as the kinematic viscosity ν does for momentum transfer, as mentioned before. The thermal boundary layer thickness is defined as:

$$y = \delta_T : T - T_s = 0.99(T_\infty - T_s), \quad (1.66)$$

with T_s the surface temperature at the flat plate.

The Prandtl number (Equation 1.8) then determines whether the thermal boundary layer is thicker or not than the flow boundary layer:

- $Pr = 1$: $\delta = \delta_T$;
- $Pr < 1$: $\delta < \delta_T$; example: air;
- $Pr > 1$: $\delta > \delta_T$; example: water.

Now the turbulent layer is discussed in more detail. Figure 1.6 presents a profile as measured in a pipe (which is in fact an internal flow, see next section), but the boundary layer near the solid boundary is very similar.

The results are expressed in a nondimensional manner, introducing the friction velocity:

$$u_* = \sqrt{\frac{\tau_s}{\rho}}, \quad (1.67)$$

and the non-dimensional distance from the solid boundary, expressed in 'viscous' units:

$$y^+ = \frac{y u_*}{\nu}. \quad (1.68)$$

Three regions can be distinguished inside the boundary layer:

- Laminar (or 'viscous') sub-layer, $y^+ < 5$: very close to the solid boundary, all turbulence is damped (due to blocking effect and viscous forces) and the flow is essentially laminar. The velocity increases linearly with the distance from the solid boundary.
- Logarithmic layer, $30 < y^+ < 300$: the motion is turbulent and there is a logarithmic relation between the mean velocity and the distance from the solid boundary.
- Buffer layer: $5 < y^+ < 30$: transitional region between the laminar sub-layer and the logarithmic layer.

It must be stressed that the discussion above refers to smooth surfaces. Roughness on a surface will affect the transition to turbulence and the turbulent boundary layer structures. This can be important, e.g. when the wind load on buildings is considered in built environment or when wind effects are considered in the context of e.g. forest fires. This, however, is considered beyond the scope of the present chapter.

Internal Flows—Flows in Pipes—Pressure Losses

A major difference from the previous section on external flows, is that in internal flows the notion 'free stream velocity' does not exist. In fully developed flow conditions, the flow is entirely affected by the presence of the solid boundary and, consequently, by the fluid's viscosity. The discussion is based here on flows through pipes, since pipes are a common configuration (e.g. water through pipes for sprinklers or water hoses in fire service intervention). Some comments are formulated for flows through ducts in the end.

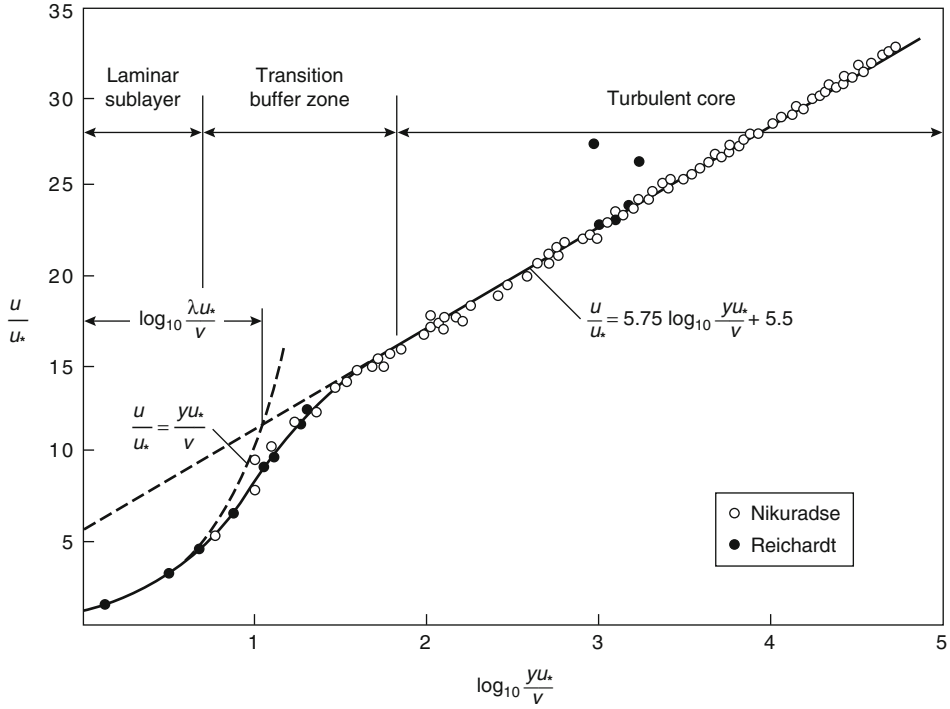

Fig. 1.6 Turbulent velocity profiles as measured in a pipe: different regions in boundary layer

When the entrance region of a smooth pipe is considered, a boundary layer develops from the solid boundary, very similar to what has been described in the previous section. However, since this boundary layer grows on the entire surface, there is a point where the entire cross-section is covered by a 'boundary layer'. This point determines the 'entrance length'. From that point onward, the boundary layers do not evolve and the flow becomes fully developed.

Depending on the Reynolds number, the flow is again laminar or turbulent. It is clear that the distance from the entrance is not a useful characteristic length, since in fully developed flow conditions, the velocity profiles are independent of that distance. Clearly, the pipe diameter is a useful quantity. At the same time, there is no free stream velocity. A mean velocity U_m can be computed from the volume flow rate and the cross-sectional area. Thus, the Reynolds number is now defined as:

$$\mathrm{Re} = \frac{U_m D}{\nu}. \tag{1.69}$$

The critical Reynolds number beyond which the flow becomes turbulent is around $\mathrm{Re}_{crit} = 2300$.

When the cross-section is not round, the diameter D is replaced by the hydraulic diameter D_h, defines as four times the cross-sectional area divided by the cross-section perimeter:

$$D_h = \frac{4A}{P}. \tag{1.70}$$

It is straightforward to show that for fully developed laminar flows, the following expressions hold (with R = D/2 the radius of the pipe and r the radial distance from the pipe symmetry axis):

- Parabolic velocity profile:

$$\frac{u}{U_m} = 2\left(1 - \frac{r}{R}\right)^2; \tag{1.71}$$

- Wall shear stress (friction):

$$\tau_{s,lam} = -\mu \frac{\partial u}{\partial r}\bigg|_{r=R} = 4\mu \frac{U_m}{R}; \tag{1.72}$$

- Friction factor:

$$f_{lam} = \frac{\tau_{s,lam}}{\frac{1}{2}\rho U_m^2} = \frac{16}{\mathrm{Re}_D}; \tag{1.73}$$

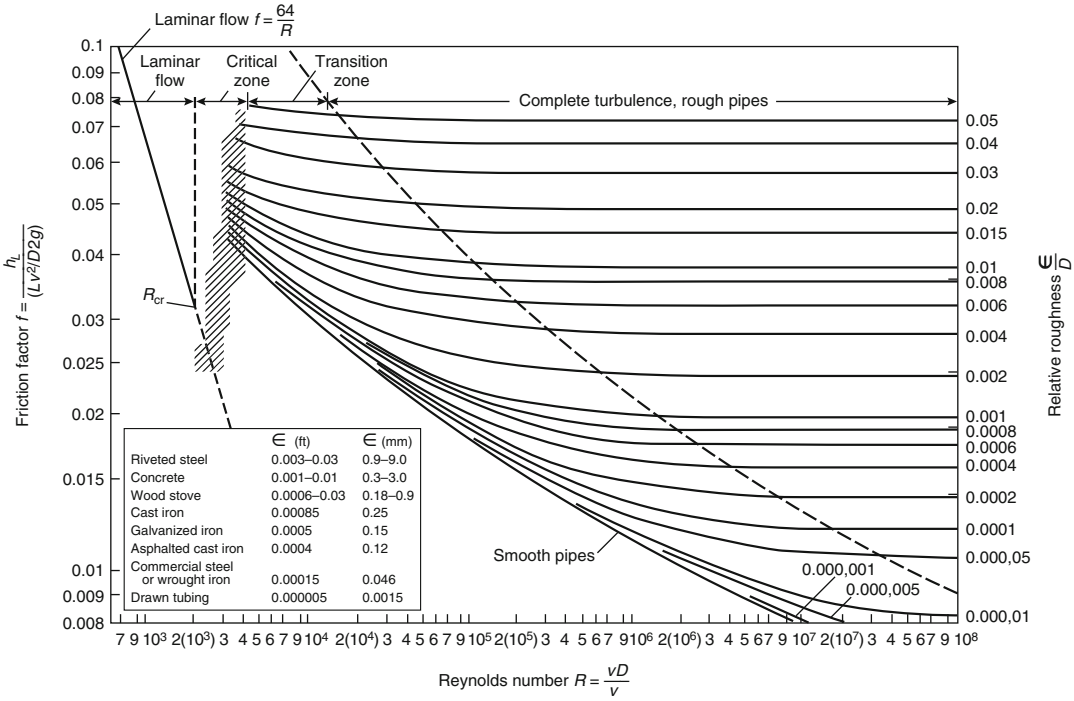

	∈ (ft)	∈ (mm)
Riveted steel	0.003–0.03	0.9–9.0
Concrete	0.001–0.01	0.3–3.0
Wood stove	0.0006–0.03	0.18–0.9
Cast iron	0.00085	0.25
Galvanized iron	0.0005	0.15
Asphalted cast iron	0.0004	0.12
Commercial steel or wrought iron	0.00015	0.046
Drawn tubing	0.000005	0.0015

Fig. 1.7 Moody diagram

- Pressure loss over a distance L in the pipe:

$$\Delta p_{lam} = f_{lam} \frac{1}{2} \rho U_m^2 \frac{4L}{D}. \qquad (1.74)$$

Note that the pressure loss is linear with the length of the pipe and, with Equation 1.73, linear with the mean velocity and inversely proportional with the square of the pipe's diameter. Recall that this is only true for laminar flows.

For turbulent flows, the expressions become more complex. The velocity profile can be approximated as:

$$\frac{u}{U_{\max}} = \left(1 - \frac{r}{R}\right)^{1/7}, U_{\max} = \frac{U_m}{0.817}. \qquad (1.75)$$

Expression (1.74) still holds for the pressure losses, but the friction factor is no longer obtained from Equation 1.73. The Moody diagram [14] (Fig. 1.7) reveals that, for large enough Reynolds number, the friction factor is determined by the relative roughness of the pipe, independent of the Reynolds number. As a consequence, for turbulent flows, the pressure loss is still linear with the length of the pipe, but proportional to the mean velocity squared and inversely proportional with the pipe diameter.

In duct flows, essentially the same reasoning holds. The major difference is in the values for the friction factor f, important to estimate pressure losses. Secondary flows appear in the corners of duct, transporting momentum from the center to the corners and leading to a relative increase in velocity near the corners.

It is instructive to quantify pressure losses for internal flows as:

$$\Delta p_L = C_L \frac{1}{2} \rho U_m^2. \qquad (1.76)$$

The loss coefficient C_L must be defined, depending on the situation (geometry and flow type—laminar/turbulent). All pressure losses must be accounted for in the design. This holds for e.g. the design of the piping system for sprinklers (i.e. what pump must be chosen) or the design of a smoke extraction system

(i.e. what extraction fans are required to overcome all pressure losses, including the ones in the exhaust system).

Some examples are briefly mentioned here:

- Straight sections: Moody diagram, see above.
- Curves/bends: C_L is determined by the total angle and the radius of the bend (e.g. $C_L = 0.14$ for an angle of 90° with radius $2D$, but it is about 1.2 for the same angle of 90° but with radius = 0, i.e. a sharp bend). Curves and bends are always important to consider in calculations of pressure losses.
- Sudden pipe expansion: $C_L = \left(1 - \frac{A_1}{A_2}\right)^2$. A special case concerns the flow into a large space, i.e. $A_2 \to \infty$. Then $C_L = 1$.
- Sudden pipe constriction: the flow is constricted and then widens again behind the constriction. A good estimate for a sudden constriction is $C_L = 0.5$, while C_L goes down to 0 for a very gentle constriction.
- Flows through openings: C_L primarily depends on the edges of the opening. The most typical situation is that the edges are Sharp. In that case C_L typically varies between the values $C_L = 0.4$ and $C_L = 0.7$.

Bernoulli Equation

The Bernoulli equation is of fundamental importance. The equation, valid on any streamline, has been developed for incompressible flows (liquids). Yet, it can also be applied to low-Mach number flows where the density hardly changes (gas flows in fire related flows, as long as the density along the streamline does not vary strongly).

With the notation now that z is the height (i.e. the z-direction is vertically upward), Bernoulli's equation reads:

$$p + \frac{1}{2}\rho v^2 + \rho g z = const. \tag{1.77}$$

A few application examples are briefly mentioned.

Application Example 1: Velocity Measurement with a Pitot Tube Figure 1.8 shows the basic principle of a Pitot tube. The flow is stagnated. By measuring the pressure increase cause by this stagnation, the velocity can be computed. Indeed, applying Bernoulli's Equation 1.77 at constant height z yields:

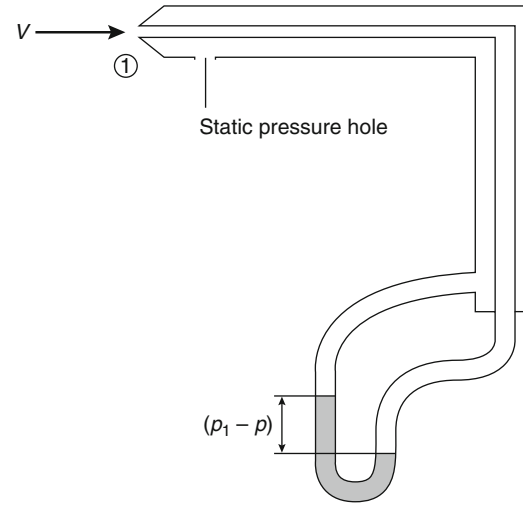

Fig. 1.8 Sketch of Pitot tube

$$p_{tot} + \frac{1}{2}\rho 0^2 = p_{stat} + \frac{1}{2}\rho v^2 \Rightarrow v = \sqrt{\frac{2(p_{tot} - p_{stat})}{\rho}}. \tag{1.78}$$

Application Example 2: Venturi Flowrate Meter Figure 1.9 shows the basic principle of a Venturi meter. It is essentially a converging cone, from which the flowrate through a pipe can be calculated. Indeed, applying Bernoulli's Equation 1.77 at constant height z yields:

$$p_1 + \frac{1}{2}\rho v_1^2 = p_2 + \frac{1}{2}\rho v_2^2. \tag{1.79}$$

Conservation of mass allows elimination of v1: $v_1 = v_2 \frac{A_2}{A_1}$. Insertion in Equation 1.80 and introducing $\dot{V} = v_2 A_2$ yields:

$$\dot{V} = A_2 \sqrt{\frac{2A_1^2(p_1 - p_2)}{\rho(A_1^2 - A_2^2)}}. \tag{1.80}$$

Application Example 3: Flow Out of a Large Tank Figure 1.10 sketches the situation. A large tank is considered, so that the liquid surface can be approximated as standing still, i.e. $v_1 = 0$.

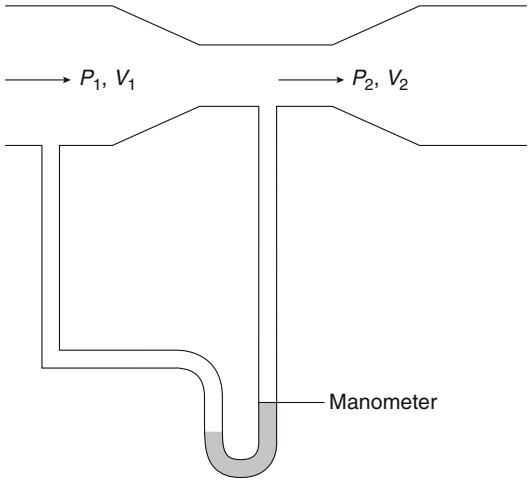

Fig. 1.9 Sketch of Venturi meter

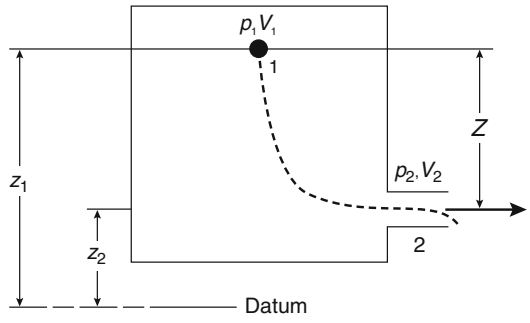

Fig. 1.10 Outflow out of a large tank

Approximating $p_1 = p_2 = p_{atm}$, the flow is generated by the gravity force:

$$\frac{1}{2}\rho v_2^2 = \rho g z \Rightarrow v_2 = \sqrt{2gz}. \tag{1.81}$$

The assumption $p_1 = p_2 = p_{atm}$ is a reasonable assumption if the tank is open and if the liquid density is much higher than the density of air (the latter is practically always fulfilled).

Application Example 4: Flow Through an Orifice In the previous example, the pressure driving the fluid out of the tank stems from gravity. In general, the pressure difference (Δp) over an opening determines the flow through the opening. From the (mean) velocity and the cross-sectional area (A) of the opening, the volume flow rate through that opening can be computed. A discharge coefficient C_d is introduced, though:

$$\dot{V} = C_d A \sqrt{\frac{2\Delta p}{\rho}}. \tag{1.82}$$

This can be interpreted as a 'correction' to the cross-section area that is effectively used for outflow (or inflow). For an orifice, the value of C_d is around 0.6 for e.g. open doors or windows, going up to about 0.7 for flows through small gaps [10].

Finally, it is mentioned that, when pressure losses are considered (see previous section), Bernoulli's equation can be extended to:

$$p_1 + \frac{1}{2}\rho v_1^2 + \rho g z_1 = p_2 + \frac{1}{2}\rho v_2^2 + \rho g z_2 + \Delta p_{L,1-2}. \tag{1.83}$$

In Equation 1.84, the final term reflects the pressure loss between points 1 and 2 on the streamline.

Wind

Wind is an important factor in fire protection engineering. An obvious example is the effect of wind on the development of forest fires, where convection strongly affects the direction and speed of fire spread. Another examples concerns smoke and heat control (SHC) in case of fire inside a building, where wind will exert a pressure load onto the building. The distribution of the load (positive and negative) affects the performance of the SHC system. The wind can also induce internal flows into the building, depending on leakages or open windows or doors.

It is common practice to consider steady wind conditions. Clearly, wind gusts can have an impact in the course of the fire. This is not considered in the discussion below.

Natural Wind Characteristics

A classical method to characterize the boundary layer, when there is no detailed information of surface roughness, is the use of a power law:

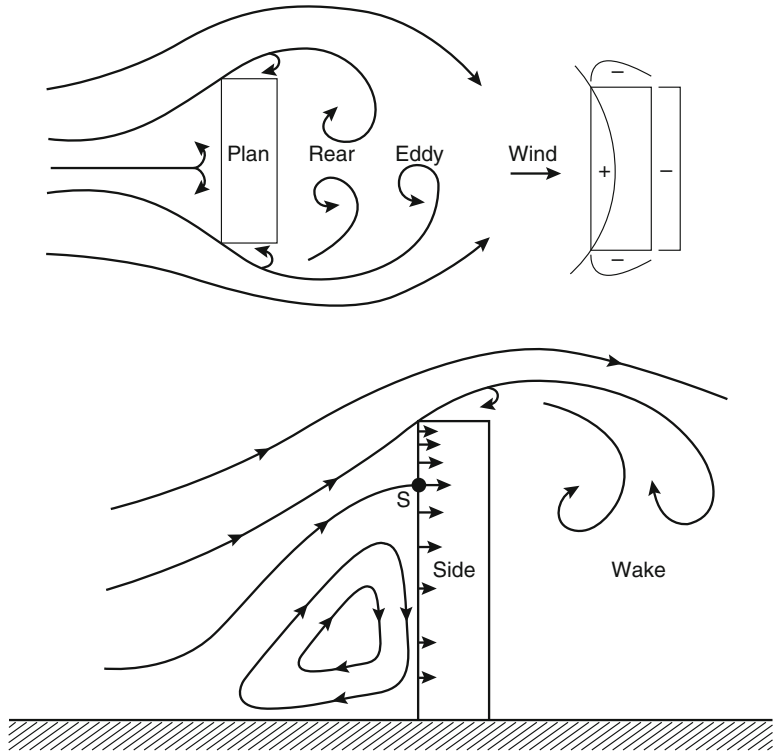

Fig. 1.11 Schematic representation of wind flow, interacting with a tall building

$$v(z) = v(z_{ref})\left(\frac{z}{z_{ref}}\right)^{\alpha}. \qquad (1.84)$$

The exponent α is given the value α = 1/7 for 'smooth' surfaces. This is related to turbulent boundary layer velocity profiles. Other values apply for 'rough' surfaces, i.e. when 'obstacles' such as trees or buildings disturb the boundary layer. An alternative option is then the use of a log law expression:

$$v(z) = \frac{v_*}{\kappa}\ln\left(\frac{z}{z_o}\right). \qquad (1.85)$$

In expression (1.86), v_* is the friction velocity Equation 1.67, κ is the von Karman coefficient ($\kappa = 0.4$) and z_o is the aerodynamic roughness length. The reader is referred to specialized literature for more details (e.g. [15]).

Interaction of Wind with Buildings

It is well-known that wind, impinging in a perpendicular direction onto a rectangular building, causes over-pressure on the windward side and under-pressure on all other sides (including the roof). This is illustrated in Fig. 1.11. This pressure load distribution affects the performance of SHC systems and can cause internal flows (e.g. through open windows or doors), as mentioned. However, it must be stressed that Fig. 1.11 is a strong simplification of reality. Not only is the wind assumed steady and perpendicular to one side of the building, it is also not supposed to be affected by the environment. In reality, tall buildings are situated in a built environment, so the oncoming wind profile need not obey expressions like (1.85) or (1.86) and need not be unidirectional. For obvious reasons, the direction of the oncoming wind, even if not disturbed by the environment, varies in time, depending on atmospheric pressure distributions. Finally, modern buildings are not necessarily rectangular in shape. All these factors indicate the need for either small-scale wind tunnel experiments or extensive CFD studies. For the time being, since it is necessary to consider many wind directions and velocities and the (built) environment can be complex and hard to characterize as boundary conditions in CFD simulations, wind tunnel experiments seem

preferable. The model scale can then be built on a table that can be turned around in the wind tunnel to examine various angles of oncoming wind.

To finalize this section, it is recalled that wind-induced over-pressure and under-pressure are proportional to the wind velocity squared. This is to be expected from Bernoulli's equation 1.77. Clearly, the flow does not stagnate entirely over the entire surface and thus pressure coefficients are introduced:

$$\Delta p_w = \frac{1}{2} C_w \rho_{amb} v_w^2. \tag{1.86}$$

The wind coefficient can be positive (over-pressure at the windward side) or negative (under-pressure). In e.g. [16] more info is found on this topic.

Nomenclature

A_v	Vent area (m^2)
C_p	Specific heat at constant pressure (kJ.kg^{-1}.K^{-1})
C_v	Specific heat at constant volume (kJ.kg^{-1}.K^{-1})
D	Fireball diameter (m)
E_{av}	Total expansion energy (kJ)
L	Latent heat of vaporization (kJ.kg^{-1})
m	Flammable mass (kg)
M_{liq}	Liquid mass (kg)
P	Pressure (Pa)
R	Distance from explosive material (m)
s	Specific entropy (kJ.kg^{-1}.K^{-1})
T	Temperature (K)
t_d	Duration of the fireball (s)
u	Internal energy (kJ.kg^{-1})
V	Vessel volume (m^3)
W_{TNT}	Equivalent mass of TNT (kg)
X_f	Mass fraction of the initial liquid mass that flashes to vapor
X_g	Mass fraction of the initial vapor mass that does not condense during expansion

Greek Symbols

β	Fraction of energy released converted into the blast wave.
γ	Ratio of specific heats $\left(\gamma = \frac{C_p}{C_v}\right)$
ν	Specific volume (m^3.kg^{-1})
ρ	Density (kg.m^{-3})

Subscripts

atm	Atmospheric
gas	Gas
liq	Liquid

References

1. G.K. Batchelor (1967) *An introduction to fluid dynamics*, Cambridge University Press.
2. H.D. Baehr (1978) *Thermodynamik*, Springer Verlag.
3. A. Bejan (1993) *Heat transfer*, John Wiley and Sons.
4. W.M. Rohsenhow, J.P. Hartnett and E.N. Ganić (1985), *Handbook of Heat Transfer Fundamentals* (2nd ed.), McGraw–Hill Book Company.
5. K.K. Kuo (1986) *Principles of combustion*, John Wiley and Sons.
6. T. Poinsot and D. Veynante (2001) *Theoretical and numerical combustion*, Edwards.
7. P.A. Libby and F.A. Williams (1980) *Turbulent reacting flows*, Springer Verlag.
8. N. Peters (2000) *Turbulent combustion*, Cambridge University Press.
9. G. Cox (1995) *Combustion fundamentals of fire*, Academic Press.
10. B. Karlsson and J.G. Quintiere (2000) *Enclosure fire dynamics*, CRC Press.
11. J.G. Quintiere (2006) *Fundamentals of fire phenomena*, John Wiley and Sons.
12. H. Tennekes and J.L. Lumley (1972) *A first course in turbulence*, MIT Press
13. S.B. Pope (2000) *Turbulent flows*, Cambridge University Press.
14. L.F. Moody (1944), "Friction factors for pipe flow", *Transactions of the ASME* 66 (8): 671–684.
15. B. Blocken and J. Carmeliet (2004) "Pedestrian wind environment around buildings: Literature review and practical examples." *Journal of Thermal Envelope and Building Science* 28(2): 107-159.
16. J.H. Klote and J.A. Milke (2002) *Principles of smoke management*, American Society of Heating, Refrigerating & Air-Conditioning Engineers, Inc.

Bart Merci is a Professor at Ghent University (Belgium). He is Head of the research unit "Combustion, Fire and Fire Safety". Having completed a PhD (Ghent University, 2000) on turbulence modeling in CFD simulations of non-premixed combustion, he is an expert in fluid mechanics aspects in reacting flows, more particularly related to fire and smoke dynamics.

Conduction of Heat in Solids

2

Ofodike A. Ezekoye

Introduction

Heat transfer is an area of thermal engineering that focuses on the transport, exchange, and redistribution of thermal energy. The three modes or ways that heat can be transferred have been termed conduction, convection, and radiation. In this chapter, the basic physics associated with conduction heat transfer will be presented, and it will be shown through examples how the tools and analysis typically used for conduction problems can be applied to design and analysis when fire occurs.

Conduction heat transfer only occurs in a medium. This is a distinction between conduction and radiation, which does not require a medium. The medium or state of matter in which conduction takes place can be a gas, liquid, or solid. The distinction between conduction and convection heat transfer is associated with whether the medium has some ordered flow or bulk motion. Heat transfer, when there is a mass averaged velocity, is termed convection. Heat transfer that takes place in a stationary frame of reference is called conduction. More details will be presented on the mechanisms that allow heat transfer to occur in a stationary medium as we proceed through this discussion. Solutions will be provided for selected configurations and scenarios. The treatise of Carslaw and Jaeger [1] covers most solutions for conduction phenomena. Other useful texts that discuss conduction phenomena are readily available [2, 3]. It is useful to build up this discussion by first identifying where conduction heat transfer ties into overall energy conservation and energy transfer.

O.A. Ezekoye (✉)
Department of Mechanical Engineering, University of Texas at Austin, ETC 7.130, MS C2200, TX 78712, Austin

Energy Conservation

The fundamental laws that allow us to analyze and predict fire phenomena are often termed conservation laws. Conservation laws are essentially balance equations that allow us to model how variables that describe the physical world dynamically evolve. In fire systems, we typically model the physical world using mass conservation, momentum conservation, energy conservation, and chemical species conservation. For this chapter, we are interested in describing how heat is transferred in media that are not deforming (i.e., are in rigid body motion with no unbalanced forces) or reacting (fixed chemical species and mass). We do assume, however, that the medium can possibly have heat transferred to it either through interactions with its surrounding or through some other energy input into it. Also, we assume that the medium may have different amounts of thermal energy stored within it at different locations. To more precisely describe energy transfer processes, we rely on the first law of thermodynamics. The energy conservation principle is the basis for heat transfer.

M.J. Hurley (ed.), *SFPE Handbook of Fire Protection Engineering*,
DOI 10.1007/978-1-4939-2565-0_2, © Society of Fire Protection Engineers 2016

Thermodynamic Properties

The first law of thermodynamics is a statement of energy conservation [4, 5]. It states that the change in energy for an identifiable set of matter can only result from heat transferred across the material's boundary or work done either by or on the material. The thermodynamic property or energy function that best describes the molecular, atomic, electronic, and nuclear energy of a material is the internal energy. In terms of the internal energy, U, the first law is

$$\frac{dU}{dt} = \dot{Q}_{net,in} + \dot{W}_{net,in}$$

U is the internal energy, Q is heat added to the system and W is work done on the system.

The total internal energy U is a system integrated value that represents the total thermal energy of the material system of interest. We can describe the local internal energy in terms of a mass specific internal energy, u, that is simply the total internal energy, U, for a region of matter divided by the mass of that region. The internal energy, like any other thermodynamic variable can be defined in terms of other thermodynamic variables. There is an approximation used in thermodynamics that states that the internal energy for an incompressible material can be specified in terms of the temperature. The thermodynamic property specific heat capacity at constant volume, c_v, relates differential changes in the mass specific internal energy to differential changes in temperature.

$$c_v = \frac{du}{dT} \text{ and } mc_v\, dT = dU$$

The mass is defined as the product of density and volume. The control-mass statement of the first law for a case with no net work done becomes:

$$\rho V c \frac{dT}{dt} = \dot{Q}_{net,in}$$

This form of the first law neither provides information about spatial variations in energy within the medium nor describes how energy is transferred. Experience tells us that the heat transfer into some identifiable mass element likely depends on temperature differences. It will be necessary to define the heat transfer rate in terms of temperature differences. The empirical law defining the heat transfer rate to a body immersed in a fluid is called Newton's law of cooling. When Newton's law of cooling is used, the heat transfer rate to the body is $\dot{Q}_{net,in} = hA(T - T_\infty)$ If we apply Newton's law of cooling to the first law, we arrive at a result called the lumped thermal approximation in conduction analysis.

Lumped Thermal Analysis

Briefly, the lumped thermal approximation allows one to model the overall transient thermal response of a body at some initial temperature subjected to either a change to the external fluid temperature or as a result of some local heating within the object. The validity of this approximation will be discussed in more detail in later sections. For the purposes of this discussion, we will say that the approximation is valid when the time scales for internal energy transfer and subsequent homogenization of the temperature field within an object are much smaller than the time scales for energy transfer from the surface of the body to an external thermal reservoir. In short, the lumped thermal approximation is reasonable when temperature differences within a body are relatively small when compared to temperature differences between the surface of the body and a characteristic temperature of the exterior fluid. It can be shown that a nondimensional heat transfer parameter called the Biot number (Bi) which represents the ratio of the internal conductive resistance to the external convective resistance should be small for the lumped thermal approximation to be valid. A mathematical statement of the energy equation in the lumped approximation is (Fig. 2.1):

$$\frac{dT}{dt} = -\frac{h_c A}{\rho V c}(T - T_\infty)$$

This first order ordinary differential equation can be integrated and one form of the solution is:

$$\frac{T - T_e}{T_0 - T_e} = e^{-(h_c A/\rho V c)t} = e^{-t/t_c}$$

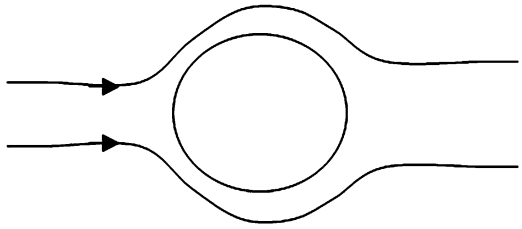

Fig. 2.1 Schematic showing convective flow over an object that will be analyzed using a lumped thermal approximation

In the above, T_0 is the initial temperature of the body and T_e is the external fluid temperature surrounding the object. There is a characteristic time in the problem defined as:

$$t_c = \frac{\rho V c}{hA}$$

The characteristic time provides an estimate of the time required for the nondimensional temperature to relax to its steady value. This relatively simple solution is useful in characterizing a large number of important problems in fire systems [6].

Example 1 The lumped thermal approximation is frequently used to analyze the response of a sprinkler head as it activates due to a change in the environment temperature because of a fire. A sprinkler head fuse can be modeled as a cylinder of diameter 4 mm and length 12 mm. The density can be approximated as being 1000 kg/m^3. The specific heat capacity is approximately 1 kJ/kgK. The heat transfer coefficient of the smoke gases is 20 W/m^{2}K. If the smoke gases are 200 °C and the fuse is initially at 20 °C, how long will it take for the fuse to open if the activation temperature is 80 °C?

The solution is arrived at from inverting:

$$\frac{T - T_e}{T_0 - T_e} = e^{-\left(\overline{h}_c A/\rho V c\right)t} = e^{-t/t_c}$$

$$t_{ACT} = \frac{\rho L c}{\overline{h}_c} \ln \frac{T_0 - T_e}{T_{ACT} - T_e}$$

For the values that we specified, we find that the fuse opens in 243 s. Chapter 3, shows that the heat transfer coefficient is proportional to the fluid velocity $h = Cu^{1/2}$. This results in:

$$\frac{t_{ACT} u^{1/2}}{\ln \dfrac{T_0 - T_e}{T_{ACT} - T_e}} = \frac{\rho L c}{C} = RTI$$

This combination of parameters is the well known response time index for sprinklers.

Fourier's Law of Conduction

As previously noted, the lumped approximation does not allow one to predict the spatial variation of temperature within a body. In some sense, it provides an average or lumped temperature response. To be able to predict the spatial variation of temperature, it is necessary to introduce another physical law that models how heat is transported when temperatures differences exist within a body. We expect heat to flow across a body in proportion to the temperature difference across the body, and perhaps inversely related to the distance across the body. Fourier's law states that the heat flux is proportional to the temperature gradient (the spatial derivative of the temperature). For a one dimensional homogeneous and isotropic object this reduces to the simple expression:

$$q'' = -k \frac{dT}{dx}$$

We use the notation q″ to indicate a heat transfer rate per unit area. The proportionality between the heat flux and the spatial derivative of temperature is the thermal conductivity.

Thermal Conductivity

For materials like air, water, glass, and copper, the thermal conductivity is isotropic (i.e., does not depend on orientation), but it has a temperature dependence. Under conditions in which the overall thermal conductivity difference across the body is small relative to the any particular value of the thermal conductivity in the body, we

can consider k to be essentially a constant. In fire applications, this is often not the case, but for the sake of analysis we will often use this approximation when generating analytical solutions.

There are materials for which the thermal conductivity depends both on the local temperature and also on the orientation. In contrast to isotropic materials for which there is no directional effect, anisotropic materials have this directional dependence. The most commonly encountered anisotropic material in fire applications is wood. The grain structure of wood is the source of the anisotropy. Practically, we would find that for the same temperature difference across a given thickness of wood, the heat transfer rate depends on whether this temperature difference is aligned with the grains or aligned perpendicular to the grains. Of course, as one heats wood, there are also chemical changes to the wood. So, the thermal conductivity depends on the temperature, composition, and orientation. For a simple analysis, the effects of decomposition are often neglected for the initial ignition process.

Again, Fourier's law states that the heat flux vector, $\vec{q}''$, is proportional to the temperature gradient, where the proportionality constant is the thermal conductivity, k. In general, k is a second order tensor and has different values depending on the face and orientation of a differential volume [1–3]. For a general anisotropic material

$$\vec{q}'' = -\begin{bmatrix} k_{xx} & k_{xy} & k_{xz} \\ k_{yx} & k_{yy} & k_{yz} \\ k_{zx} & k_{zy} & k_{zz} \end{bmatrix} \nabla T$$

This suggests that the component of the heat flux vector in the x-direction depends on all components of the temperature gradient.

$$q_x = -\left(k_{xx}\frac{\partial T}{\partial x} + k_{xy}\frac{\partial T}{\partial x} + k_{xz}\frac{\partial T}{\partial x} \right)$$

For some materials that are frequently dealt with in fire analyses, such as wood, there is some simplification in the dependence of thermal conductivity on orientation. Laminates like wood are said to be orthotropic. For an orthotropic material, the off-diagonal elements of the thermal conductivity tensor are zero and the diagonal elements are not equal to each other.

$$k = \begin{bmatrix} k_{xx} & 0 & 0 \\ 0 & k_{yy} & 0 \\ 0 & 0 & k_{zz} \end{bmatrix}$$

For metals, many crystalline solids, many amorphous solids, liquids, and gases, the conduction process is considered to take place in an isotropic medium. For such materials, the thermal conductivity can vary spatially and with temperature, but does not have an orientation effect.

$$k = k(T(x,y)) \begin{bmatrix} 1 & 0 & 0 \\ 0 & 1 & 0 \\ 0 & 0 & 1 \end{bmatrix}$$

Homogeneous Systems

Most obvious in gases, it is known that random molecular motion transfers heat from hot molecules to cooler ones. For solids other wave like effects are important. There is a relatively simple theory that describes the physics of thermal conductivity. Conduction heat transfer can be thought of in terms of a carrier particle with a characteristic velocity and characteristic length scale over which it acts. The development of this perspective of thermal conductivity, based on the properties of notional particles is described by Kaviany [7, 8]. In some sense, this description is a simple generalization of the kinetic theory description of thermal conductivity for gases. For gases, we understand that the kinetic theory of gases describes how k varies in terms of a characteristic gas velocity, u, the number density of molecules, n, the mean free path, l, and the molecular internal energy described by the molecular mass and heat capacity (mc).

$$k \cong \frac{1}{3} mc_v nul$$

In the following table adapted from Kaviany [7, 8], the characteristic parameters for various types of conduction systems are provided (Table 2.1).

Examples of Homogenous Materials

In fire analysis, most solid materials are approximated as being homogeneous. Examples of homogeneous systems in fire applications are

Table 2.1 Characteristic quantities used in microscale carrier model of conduction

Microscale carrier	Fluid particle (random motion)	Phonon (quantal lattice vibration)	Electron
Regimes	Dilute gases	Acoustic phonon and optical phonon	Free electrons and valence electrons
Mean free path	Interparticle spacing	Lattice dimension	Lattice dimension
Carrier concentration	Fluid density	Solid density	Free electron density
Carrier speed	Thermal speed	Speed of sound	Electron drift velocity

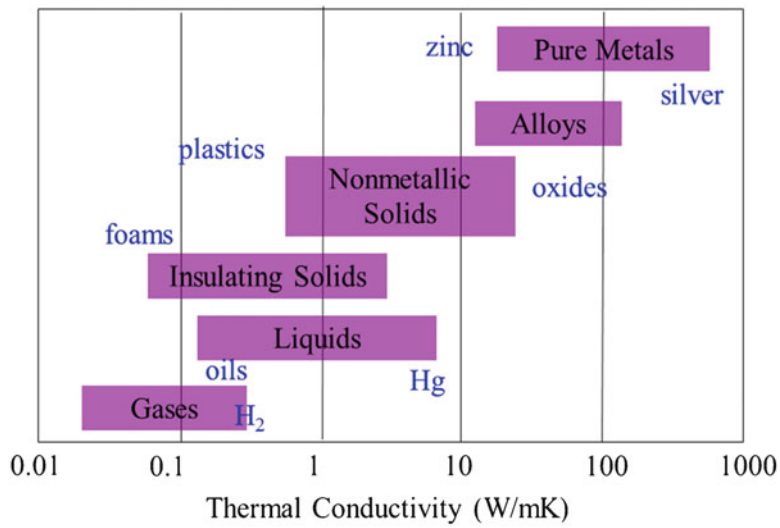

Fig. 2.2 Range of thermal conductivities for different materials (Adapted from [2])

simple polymeric materials, metals, and various types of insulating materials (Fig. 2.2).

Composite Systems

Treatment of composite material thermal conductivity is somewhat more complicated than the treatment for homogeneous materials. With increased use of composite materials like polymer impregnated concrete as structural components, it is useful to discuss how to construct an effective thermal conductivity for such materials. The key to constructing an effective thermal conductivity is to develop a meaningful way to average the thermal properties for the system. A representative averaging volume is the term used to describe the volume over which one can meaningfully average the properties of the composite in order to properly thermally characterize the material. The simplest treatments of composite media thermal conductivity use either series or parallel resistance models. For a mixed medium that is comprised of several different conducting elements, the parallel approximation provides an upper bound on an effective thermal conductivity, while the series approximation provides a lower bound.

Examples of Composite Materials

Examples of composite materials include many types of insulating materials in which at least two types of materials are mixed in various mass fractions. The mass or volume fractions of the constituents can then be used along with their individual conductivities to define an effective conductivity for the system. Various mixing rules have been developed for the effective thermal conductivity. Gebhart [9] discusses a general way of classifying the effective thermal conductivity of a binary system comprised of a matrix material a and added material b as:

$$\frac{k_e}{k_a} = f\left(\frac{k_b}{k_a}, \Phi_b, \frac{L_i}{L}, Bi\right).$$

Depending on the ratio of the thermal conductivities, the ratios of the characteristic lengths of the a and b segments within the medium, and the relative volumetric ratios, different correlations exist for the effective conductivity.

Kaviany [7] presents a correlation for the effective conductivity for random porous solids (e.g., continuous solid and fluid phases) as might occur for a wound insulation material,

$$\frac{\langle k \rangle}{k_f} = \left(\frac{k_s}{k_f}\right)^{0.280 - 0.757 \log(\varepsilon) - 0.057 \log\left(k_s/k_f\right)}$$

which is valid for fluid porosity (volume fraction) in the range of $0.2 < \varepsilon < 0.6$.

Heat Equation Formulations

The heat equation is the name given to the differential equation that models heat conduction in materials. The heat equation is most generally developed in a three dimensional, unsteady form. Depending on the scenario of interest, it is not always necessary to solve the full formulation of the heat equation. By formulating an appropriate reduced form of the heat equation, one can generally compute an accurate representation of the temperature profile and heat flux distribution in the material. In the following sections, several reduced model forms for the heat equation will be discussed.

Steady One Dimensional Models

Under conditions in which there is a primary heat transfer direction, it is appropriate to formulate a one-dimensional form of the heat equation. Further, when the time scale for changes in boundary conditions and sources are large relative to the time scale over which the thermal system equilibrates, the analysis can be treated as being steady. A discussion of how to define the time to equilibrate in conduction systems will follow in a later section.

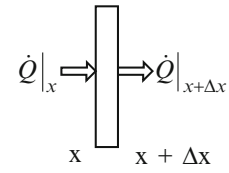

Fig. 2.3 Schematic of differential volume in which steady one dimensional heat equation is developed

To develop the one dimensional conduction model, we consider an elemental volume, ΔV, located between spatial locations x and x + Δx for a heat transfer process that is in steady state. We can apply the first law of thermodynamics to the elemental volume and consider a case in which there is no internal generation (Fig. 2.3).

$$\dot{Q}\big|_x = \dot{Q}\big|_{x+\Delta x} = \text{Constant}$$

$$\dot{Q} = q''A = -kA\frac{dT}{dx}$$

$$\frac{d}{dx}\left(kA\frac{dT}{dx}\right) = 0$$

Application of Fourier's law leads to an energy equation specified in terms of temperature gradients defined within the solid. The solution can be found by simple integration.

If the thermal conductivity, k, is nearly constant over the temperature range of interest to the problem, then we see that a very simple relationship holds between the temperature difference across the solid, the thermal conductivity, and the thickness of the solid. It is apparent that an analogy holds between this form and Ohm's law, where the heat transfer rate is identified as a current, the temperature difference, ΔT is identified as a potential change, and L/kA is identified as a generalized resistance.

Cylindrical Shells

This same type of analysis can be formulated for cylindrical shells. The difference in the analysis is that the cylindrical shell has variable surface area (Fig. 2.4).

Applying Fourier's law over concentric cylindrical elements yields

$$\dot{Q} = Aq = 2\pi rL\left(-k\frac{dT}{dr}\right)$$

Similar to the development for the planar slab geometry, an effective resistance can be defined for the cylindrical system. Integrating the equation twice yields:

$$\dot{Q} = \frac{2\pi kL(T_1 - T_2)}{\ln(r_2/r_1)}$$

We can extract a resistance from this expression to be:

$$R = \frac{\ln(r_2/r_1)}{2\pi kL}$$

Fin Approximation

The fin approximation refers to one dimensional conduction analysis where heat transfer has a predominant direction, there is no transverse temperature gradient, and the heat transfer in the transverse direction is simply defined through Newton's law of cooling. The simplest example of use of the fin approximation is in the development of the pin fin model. A pin fin is slender rod of length L and diameter D with convective heat transfer taking place over most of the rod's surface. At least one end of the rod is assumed to be fixed at a temperature different from the environmental fluid temperature. For one dimensional heat transfer to be valid, the length of the fin divided by the diameter should be large and a Biot number Bi = hD/k for the fin should be small. In a fire scenario, a fully exposed beam might be modeled as being a fin [10]. Development of the pin fin equation begins with a power balance on a differential section of the fin, as shown below (Fig. 2.5).

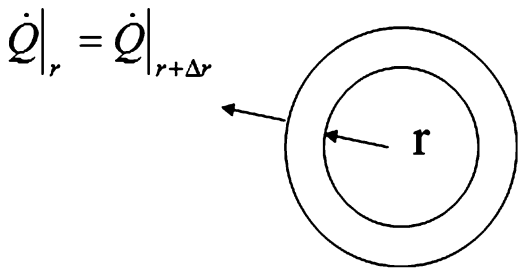

Fig. 2.4 Schematic of cylindrical shell in which one dimensional, steady cylindrical formulation of heat equation is developed

One dimensional analysis (radially lumped) is valid when d/L<<1 and Bi<<1.

The power balance on the differential element coupled with performing a limiting process as Δx approaches zero results in the pin fin equation shown below.

$$kA_c\frac{d^2T}{dx^2} - h_cP(T - T_\infty) = 0$$

This second order ordinary differential equation requires two boundary conditions (BCs). The base temperature is often specified as known (i.e., $T(x = 0)$). Typical BCs at $x = L$ are:

(a) Known tip temperature or Dirichlet condition (e.g., $T(L) = 20\ ^\circ\text{C}$)
(b) Known tip heat flux or Neumann condition (e.g., $q''(x = L) = 0$)
(c) Convection tip or Robin's condition (e.g., $-k\frac{dT}{dx}\big|_{x=L} = h(T(x = L) - T_\infty)$

Solutions and examples of use of the fin approximation will be provided in a later section. It is, however, useful to discuss one limiting case solution for the pin fin. A pin fin is said to be semi-infinite if the effect of the imposed temperature at the fin base does not affect the temperature distribution over the entire length of the fin.

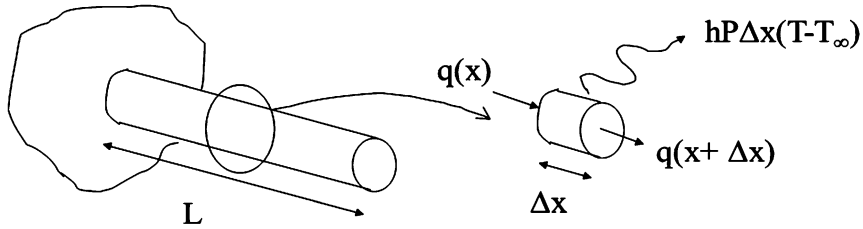

Fig. 2.5 Development of pin fin equation for cylindrical rod

Simple 1D Composite Systems

The simplest composite systems can be thought of in two limiting cases. One might imagine configurations with two different conductors either in a series or in a parallel configuration. For the simpler case, in which the conductors are in series, it is useful to discuss the nature of the interface between the two conductors. The idealized interface between surfaces is considered to be perfect contact in which the interface temperatures are the same on both surfaces. In contrast, an imperfect contact is said to have a contact resistance and there is a temperature discontinuity at the interface between the two surfaces (Fig. 2.6). In the equation shown below h_i is known as the interface conductance with the same units as the heat transfer coefficient (W/m^{2}K)

$$-k_A \left.\frac{dT}{dx}\right|_u = h_i(T_u - T_s) = -k_B \left.\frac{dT}{dx}\right|_s$$

Example 2 A composite wall for a furnace is made of two materials, an insulating material with thermal conductivity k_A and an exterior skin with thermal conductivity k_B. Within the furnace there is an internal heat transfer coefficient $h_{c,i}$ and internal temperature T_i. Outside of this wall there is a heat transfer coefficient hc,o and external temperature T_o. We can calculate the total heat flux (heat transfer rate per unit area) and also the intermediate temperatures (e.g., the interface temperature between the two materials) using a simple resistance analogy (Fig. 2.7).

By identifying a simple conductive resistance for the slabs we see that the heat transfer rate can be specified as

$$\dot{Q} = \frac{T_i - T_1}{1/h_{c,i}A} = \frac{T_1 - T_2}{L_A/k_A A} = \frac{T_2 - T_3}{L_B/k_B A} = \frac{T_3 - T_0}{1/h_{C,o}A}$$

The heat transfer rate can be thought of as being proportional to a potential difference (i.e., the

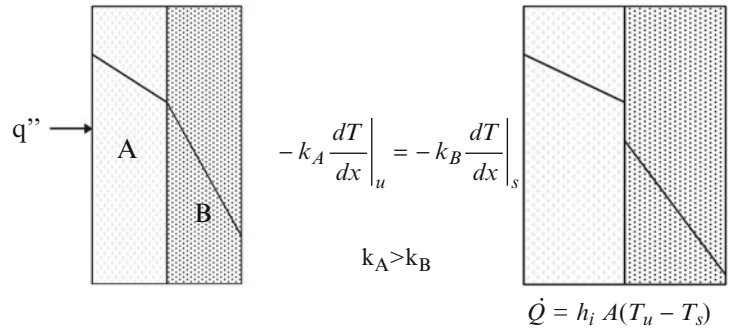

Fig. 2.6 Comparison of perfect and imperfect thermal contact showing contact resistance temperature jump for imperfect contact

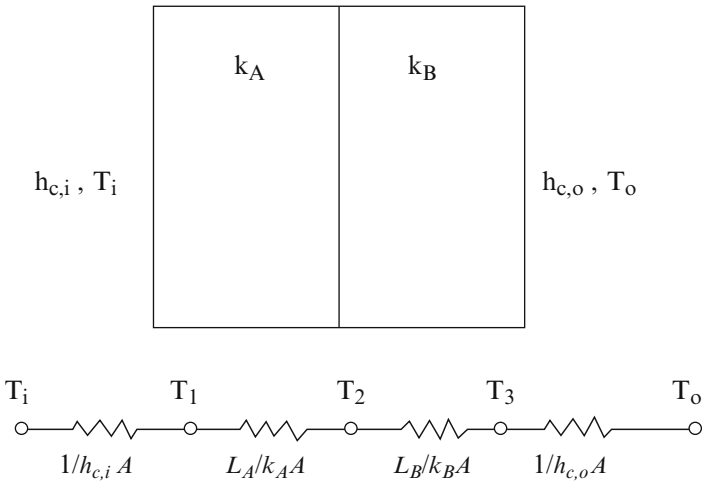

Fig. 2.7 Circuit analogy for conduction in two slabs

temperature drop) and inversely proportional to a resistance. We can use:

$$\dot{Q}R_i = \Delta T_i$$
$$\dot{Q}\sum R_i = \sum \Delta T_i$$

The sum of the individual potential drops equals the total potential difference across the system. Dividing by the sum of the resistances, we get:

$\dot{Q} = \frac{T_i - T_o}{\sum R_i}$ which on a per unit area basis becomes

$q'' = \frac{T_i - T_o}{\sum R_i''}$

For a case with $T_i = 1000\ ^\circ C$, $T_o = 300\ ^\circ C$, $h_{ci} = 30\ W/(m^2K)$, $h_{co} = 10\ W/(m^2K)$, $L_A = 2\ cm$, $L_B = 0.2\ cm$, $k_A = 1\ W/(mK)$, $k_B = 20\ W/(mK)$ we find that the equivalent resistance

$$R_{EQ}'' = \sum R_i'' = 0.153\frac{Km^2}{W}$$

The heat flux is $q'' = \frac{1000-300}{0.153} = 4.56 kW/m^2$. Check the magnitudes of all the resistance elements. If any of these is particularly small compared to the others, we can sometimes neglect that effect in our analysis.

Steady-Multidimensional Models

For problems in which the heat transfer processes internally equilibrate on time scales that are shorter than the times over which external time dependent processes and/or thermal forcing occur, the problem can be formulated as being steady. There are conditions in which there is not a dominant or preferred direction for heat flow for which a one dimensional formulation is inappropriate. For such problems a multidimensional model is required. The governing equation in this formulation is simply:

$$\nabla^2 T = \dot{Q}_v''' \Big/ k$$

Where $\dot{Q}_v'''$ is a volumetric source term. Problems can be set up in Cartesian or cylindrical or spherical coordinate systems depending on the particular type of problem of interest.

Boundary Condition Approximations and Assumptions

Boundary conditions are one of the three types that were previously identified in the fin discussion: prescribed temperature also known as Dirichlet conditions, prescribed flux also known as Neumann conditions, or mixed flux and temperature also known as Robins conditions. For Neumann type conditions, a so-called compatibility condition must hold for a steady formulation to be valid. In practice, this means that the next heat flux into the object must be zero to ensure that a steady solution exists. The three boundary conditions are stated mathematically below.

$$T|_{x=L} = T_s$$
$$-k\left.\frac{\partial T}{\partial x}\right|_{x=L} = q_s$$
$$-k\left.\frac{\partial T}{\partial x}\right|_{x=L} = h_c\left(T|_{x=L} - T_e\right)$$

Transient One Dimensional Models

For formulations in which transient effects must be included, there are conditions in which there is a predominant heat transfer direction. When there is a preferred direction for heat flow, the thermal forcing can either be from one of the boundaries or from an internal source. For most fire problems, the forcing will occur from a boundary or face. While all physical problems have some finite characteristic length, we will discuss an approximation that specifies the extent of the domain to be semi-infinite.

Thermally Thick and Thin Approximations

We can summarize studies of one dimensional unsteady conduction using a map of solution approximations in a Fourier number (Fo) and Biot number (Bi) space. The Fourier number

physically represents the thermal penetration thickness, δ, divided by the geometric dimension of the system, L.

$$Fo = \frac{\alpha t}{L^2} = \left(\frac{\delta}{L}\right)^2$$

As previously noted, the Biot number can be interpreted as a ratio of the conductive resistance to the convective resistance or as the ratio of the temperature differences in the solid to the driving convective temperature difference. Recall that a lumped thermal approximation is valid when Bi<<1.

The Biot number defined in terms of the true length scale of the object can be considered to be the global Biot number for the scenario. A local Biot number can be constructed using the thermal diffusion length as the characteristic length. In the following equation, it can be shown that the local Biot number is specified as the product of the global Biot number and the square root of the Fourier number [11].

$$Bi = \frac{hR}{k} = \frac{h\delta}{k}\frac{R}{\delta} = \frac{h\delta}{k} Fo^{-1/2}$$

$$\frac{h\delta}{k} = Bi\ \ Fo^{1/2} = \frac{T_w - T_o}{T_\infty - T_w}$$

This local Biot number can then be interpreted as an estimate of the temperature difference between the wall and interior temperatures relative to difference between the wall and fluid reservoir temperatures. Because it is a local Biot number and defined in terms of the thermal penetration depth, it also provides insight into what might be considered to be a semi-infinite domain. For small Fourier numbers, the thermal diffusion distance δ is smaller than the global or geometric length of the object. The map below can be used to characterize the various domains for which different types of approximations are valid. The diagonal line in the upper left hand quadrant represents the demarcation between a convective boundary condition and fixed surface temperature on a semi-infinite body (Fig. 2.8).

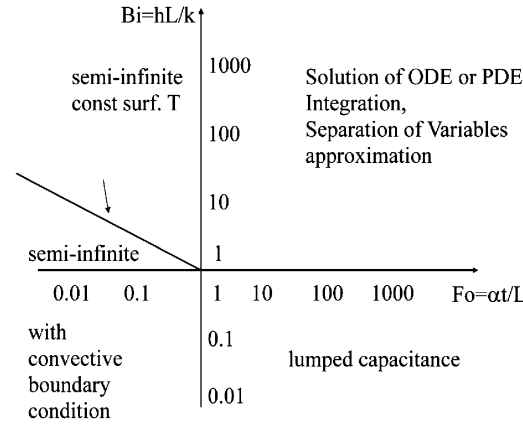

Fig. 2.8 Map identifying different conduction solution regimes as described by Biot and Fourier numbers (Adapted from [12])

Transient Multidimensional Models

For transient multidimensional cases, we rely on the full solution of the heat equation. For simple geometries, we can use analytical methods to construct the solutions. With increased geometrical complexity, computational methods are required. In later sections, both analytical and computational techniques for solving these problems will be detailed.

$$\rho c \frac{\partial T}{\partial t} = \frac{\partial}{\partial x}\left(k\frac{\partial T}{\partial x}\right) + \frac{\partial}{\partial y}\left(k\frac{\partial T}{\partial y}\right) + \frac{\partial}{\partial z}\left(k\frac{\partial T}{\partial z}\right) + \dot{Q}_v'''$$

Analytical Solutions and Examples

Despite the increased accessibility and power of computing devices, analytical models continue to be important in analyzing and characterizing conduction phenomena in fire systems. Analytical solutions are essential in the verification of computational models and are often used to provide back-of-the-envelope engineering guidance. In this section, solutions will be provided for some of conduction formulations that have been discussed.

Steady-One Dimensional Examples

Critical Thickness of Insulation

For the cylindrical system, we noted that the one dimensional steady form of the heat equation is:

$$\frac{d}{dr}\left(rk\frac{dT}{dr}\right)=0$$

Integrating twice, we derive the temperature solution.

$$\frac{T_1-T}{T_1-T_2}=\frac{\ln(r/r_1)}{\ln(r_2/r_1)}$$

The heat transfer rate is given by:

$$\dot{Q}=\frac{2\pi kL(T_1-T_2)}{\ln(r_2/r_1)}$$

A resistance can be defined as:

$$R=\frac{\ln(r_2/r_1)}{2\pi kL}$$

Often in fire scenarios there is a desire to minimize heat transfer to a pipe or rod from the high temperature environment. Insulating the pipe or rod is one approach to minimize the heat transfer rate. The effect of insulating a pipe is explored in this discussion. A schematic of the system is shown below:

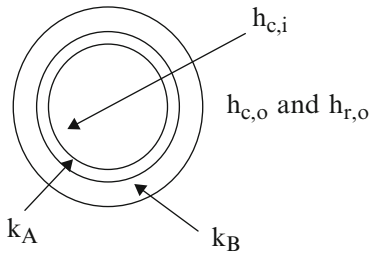

Consider that an internal heat transfer coefficient exists because of the fluid flow within a pipe. The pipe is made of material A and has a thermal conductivity, k_A. Insulation wrapped around the pipe has thermal conductivity, k_B. The fluid flowing in the pipe is at a temperature T_i. External to the insulated pipe is an environment at temperature T_o that interacts with the insulated pipe through convection and radiation. There is a convective heat transfer coefficient $h_{c,o}$ and the radiative transfer process is approximated using a radiation heat transfer coefficient. We can define an overall conductance for the system using the convective resistances and also the conductive resistance that we just developed for cylindrical systems.

$$\dot{Q}=UA(T_i-T_o)=\frac{T_i-T_o}{1/UA}$$

The overall conductance is modeled as $\frac{1}{UA}=\frac{1}{2\pi r_1 L h_{c,i}}+\frac{\ln(r_2/r_1)}{2\pi k_A L}+\frac{\ln(r_3/r_2)}{2\pi k_B L}+\frac{1}{2\pi r_3 L\left(h_{c,o}+h_{r,o}\right)}$ where r_1 is the inner radius of the pipe, r_2 is the outer radius of the pipe, and r_3 is the outer radius of the insulation. We can neglect the internal convection resistance and the conduction resistance of the pipe relative to the external convection resistance and the conduction resistance of the insulation when:

$$\frac{h_{c,o}r_3}{h_{c,i}r_1}<<1 \quad \text{and} \quad \frac{h_{c,o}r_3\ln(r_2/r_1)}{k_A}<<\frac{h_{c,o}r_3\ln(r_3/r_2)}{k_B}$$

For such a case, we find that the heat transfer rate is related to the driving temperature difference as:

$$\dot{Q}=\frac{T_i-T_o}{R}=\frac{T_i-T_o}{\ln(r_o/r_i)/2\pi Lk+1/2\pi Lr_o h_o}$$

While we might assume that the addition of an insulating layer will always result in a decrease in the heat transfer rate, we can easily see that the denominator has a minimum value when there has been addition of insulation. This minimum value of resistance means that the heat transfer rate increases with the addition of some insulation. Taking the derivative of the denominator and identifying the extremum shows that when the insulating layer has a radius of

$$r_0=r_{cr}=\frac{k}{h_o}$$

the heat transfer has a maximum value.

Example 3 An exposed water sprinkler line is within a compartment on fire. The fire products are at a temperature of 1000 °C. We can assume that the heat transfer coefficient between the fire products and the pipe is 30 W/(m^{2}K). The pipe has a diameter of 5 cm, a thickness of 5 mm, and a thermal conductivity of 30 W/(mK). At one section of the pipe, the water has a mean temperature of 30 °C and an internal heat transfer coefficient of 100 W/(m^{2}K). We can calculate the heat flux at this section of pipe using a thermal resistance circuit.

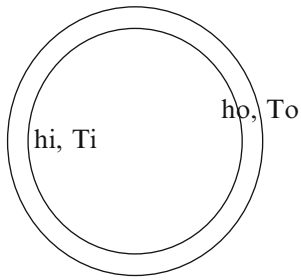

$$q_i'' A_i = \frac{(T_i - T_o)A_i}{\sum R_i''} = \frac{T_i - T_o}{\frac{1}{h_i A_i} + \frac{\ln\left(\frac{r_o}{r_i}\right)}{2\pi k L} + \frac{1}{h_o A_o}}$$

Note that the radial location of the heat flux must be specified as the heat flux is different at the outer edge of the pipe from its value at the inner edge. The total heat transfer rate is 2.7 kW/m of pipe. The heat flux at the inner wall is 9.7 kW/m^2.

For an insulator with thermal conductivity of 1 W/(mK) and the same external heat transfer coefficient of 30 W/(m^{2}K), the critical radius $r_{cr} = \frac{k}{h_o}$ is 0.03 m or 3 cm. Thus, adding 1 cm of an insulator with a thermal conductivity of 1 W/(mK) to the pipe increases the heat transfer rate. We would have:

$$q_i'' A_i = \frac{(T_i - T_o)A_i}{\sum R_i''} = \frac{T_i - T_o}{\frac{1}{h_i A_i} + \frac{\ln\left(\frac{r_p}{r_i}\right)}{2\pi k L} + \frac{\ln\left(\frac{r_o}{r_p}\right)}{2\pi k L} + \frac{1}{h_o A_o}}$$

The total heat transfer rate increases to 2.9 kW/m. As previously noted, while we increased the conductive resistance by the insulation, we decreased the external convective resistance by increasing the area. The total resistance has decreased from 0.354 Km/W to 0.33 Km/W. The choice of insulator matters. The same thickness insulation, but with a thermal conductivity of 0.1 W/(mK) increases the equivalent resistance to 0.59 Km/W and decreases the total heat transfer rate to 1.6 kW/m.

Fin Model of a Beam Extending Between Two Walls

Frequently, engineers must evaluate the thermal response of beams and columns that are affected by high temperature gases associated with a fire [10]. Imagine that two walls of a compartment are at temperatures T_w and a high temperature gas flows around a fully exposed beam. We can evaluate the thermal response of the beam using a fin model (Fig. 2.9).

Earlier, we derived the constant cross-sectional area fin equation:

$$kA_c \frac{d^2T}{dx^2} - h_c P(T - T_\infty) = 0$$

Solutions to this equation are either in terms of exponential functions or hyperbolic sine and cosine. It is convenient to define an excess temperature in terms of the difference between the fin temperature and the fluid temperature (Fig. 2.10).

$$\frac{d^2\theta}{dx^2} - m^2\theta = 0$$
$$\theta = T - T_\infty$$
$$m^2 = h_c P / kA_c$$

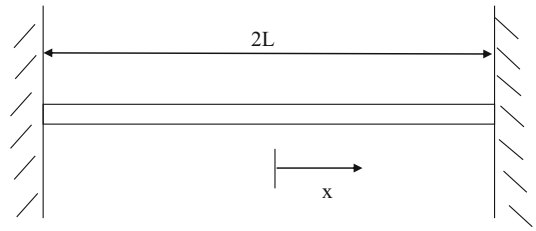

Fig. 2.9 Schematic of beam convectively heated between two walls

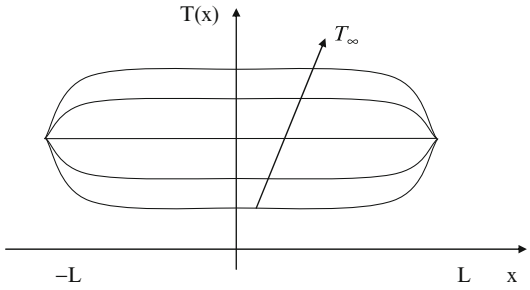

Fig. 2.10 Temperature profiles for suspended beam example showing effect of the gas to wall temperature difference on the temperature profile

For this case in which the walls are at the same temperature we arrive at a solution:

$$T = T_\infty + (T_w - T_\infty)\frac{\cosh(mx)}{\cosh(mL)}$$

If we had defined the origin for the x coordinate as being one of the walls, and if the parameter mL>>1, the exponential solution is appropriate and decays to zero at large x values.

$$\frac{\theta}{\theta_b} = e^{-mx}$$

Example 4 An unprotected round steel bar extends across two compartments. The bar has a diameter of 5 cm. One compartment is fully involved in fire with gas temperatures of 600 °C around the bar. The heat transfer coefficient is 30 W/(m^{2}K). The compartment temperature of the room that the bar extends into is at 20 °C. For convenience, we assume that the void space also has a air temperature of 20 °C and that the heat transfer coefficients are also 30 W/(m^{2}K) in the void space and in the nonfire compartment. We can estimate the temperature of the bar within the void space to see if it might pose an ignition hazard using fin analysis.

For a sufficiently long bar we can use the semi-infinite assumption which states that the temperature distribution in the fin has an exponential variation (Fig. 2.11).

$$\frac{\theta_C(x)}{\theta_{C,B}} = \frac{T(x^+) - T_{C,\infty}}{T_I - T_{C,\infty}} = e^{-mx^+} \text{ and } \frac{\theta_F(x)}{\theta_{F,B}} = \frac{T(x^-) - T_{F,\infty}}{T_I - T_{F,\infty}} = e^{-mx^+}$$

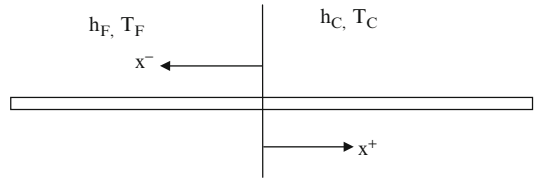

Fig. 2.11 Schematic diagram of a bar extending between two domains with different temperatures and different heat transfer coefficients

At the interface of the fire flow and the cold flow, the bar temperature is continuous and can be specified to be an interface temperature T_I. Also, the heat flux is continuous at the interface. Since the thermal conductivity does not change, we simply write this as:

$$\frac{\partial T}{\partial x^+} = -\frac{\partial T}{\partial x^-}$$

$$-(T_I - T_{C,\infty})\left(\frac{h_A P}{kA_c}\right)^{1/2} = (T_I - T_{F,\infty})\left(\frac{h_F P}{kA_c}\right)^{1/2}$$

$$T_I = \frac{m_F T_{F,\infty} + m_A T_{C,\infty}}{m_F + m_A}$$

For a case in which the heat transfer coefficient is the same on both sides of the interface, the interface temperature is 310 °C and is a simple average of the fire side gas temperature and the cold compartment air temperature. If the heat transfer coefficients had been different, the interface temperature is the weighted average of the two temperatures as shown above.

Flame Temperature Thermocouple Measurement

Consider a thermocouple that is modeled as a rod of diameter D, thermal conductivity k, and length L with half of the thermocouple length in air and the other half inserted into a pool fire flame. It is useful to determine if there is a conduction error in the thermocouple. There are several possible fin models that can be used to illustrate this effect. Here, we take an idealized scenario in which the thermocouple wire is modeled as being a fin with insulated ends in the hot fluid and also in the cold fluid. In reality, there is a convective end condition in the hot region (i.e., at the thermocouple junction) and the termination point in the cold region is often very far away

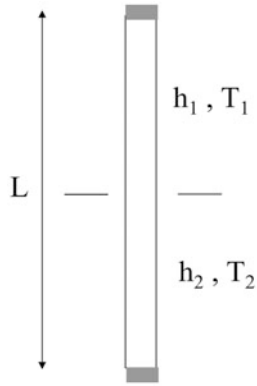

Fig. 2.12 Fin suspended across free surface in fluids with different temperatures and heat transfer coefficients

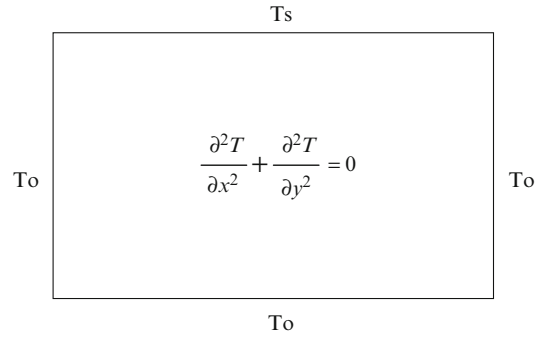

Fig. 2.13 Plate in which Laplace equation is to be solved to determine 2D temperature profile

from the point where the thermocouple is inserted into the flame. The question posed here is whether the temperature at the end placed into the hot fluid (i.e., the flame) reaches the hot fluid temperature (in which case, the thermocouple is measuring the correct temperature) or whether the conduction losses to the cold side are affecting the measurement. The insulated end solution for a rod of diameter D, thermal conductivity k, and length L suspended between two fluids/flows is

$$\frac{\theta_A}{\theta_{A0}}=\frac{T_A-T_{A\infty}}{T_{A0}-T_{A\infty}}=\frac{\cosh[m_A(L_A-x_A)]}{\cosh(m_A L_A)}$$

If the fin is not semi-infinite (i.e., mL is not large relative to unity), we need to use the full solution to get the interface temperature. The interface temperature (Fig. 2.12) is

$$T_{A0}=\frac{T_{A\infty}m_A\tanh(m_A L_A)+T_{B\infty}m_B\tanh(m_B L_B)}{[m_A\tanh(m_A L_A)+m_B\tanh(m_B L_B)]}$$

As we saw earlier, if the heat transfer coefficient is the same on the hot and cold sides, we get an interface temperature that is the simple mean value of the hot and cold temperatures. The error in the measured end temperature

$$\frac{T_A(L)-T_{A\infty}}{T_{A\infty}}=\frac{1}{2}\left(\frac{T_{B\infty}}{T_{A\infty}}-1\right)\left(\frac{1}{\cosh(m_A L_A)}\right)$$

For a case with an air temperature of 300 K and a flame temperature of 2000 K, if the thermocouple has a diameter of 2 mm, a heat transfer coefficient of 30 W/m^{2}K, thermal conductivity of 60 W/(mK), and a length of 6 cm equally split between the hot and cold fluids, we find that the interface temperature is 1150 K and that the tip temperature is 1751 K. This represents an approximately 12 % error in the predicted freestream temperature.

Steady Multidimensional Example

There are many heat transfer systems for which there is a need to generate multidimensional solutions. Often it is appropriate to model a two dimensional temperature variation for geometries in which two characteristic lengths are of comparable magnitude and the third characteristic length is significantly longer. For such geometries, if one is interested in specifying the temperature variation at a cross-section of the geometry at lengths far from the boundaries of the long direction, a two dimensional approximation often proves to be valid. In this section, we discuss the separation of variables approach to solving such problems.

Separation of Variables Applied to Two Dimensional Fin

Example 5 A very long rectangular bar has three sides maintained at temperature 20 °C and one side at temperature 120 °C (Fig. 2.13). Because the bar is very long, we can neglect the axial heat transfer problem and focus our attention on the heat transfer processes at some intermediate slice

within the bar. We are simplifying this three dimensional problem into a two dimensional problem. Further, we can define a new temperature, sometimes called the excess temperature, defined as the temperature subtracting off some reference value. For this problem, it is convenient to think of the 20 °C temperature as a reference value.

We define an excess temperature to be $\theta(x, y) = T(x, y) - 20$. In terms of the excess temperature, we have the following boundary conditions:

$$\begin{aligned} x &= 0, \;\; 0 < y < b; \;\; \theta = 0 \\ y &= 0, \;\; 0 < x < a; \;\; \theta = 0 \\ x &= a, \;\; 0 < y < b; \;\; \theta = 0 \\ y &= b, \;\; 0 < x < a; \;\; \theta = 100 \end{aligned}$$

We use a standard technique for the solution of finite domain partial differential equations called separation of variables to solve for the temperature distribution in the plate section. Separation of variables relies on expanding the dependent function θ(x,y) in terms of an appropriate set of basis functions. For this Cartesian coordinates example, the basis functions turn out to be sine and cosine functions. The members of the family of functions that constitute the set of basis functions are said to be orthogonal to each other in a weighted integral sense. There is a deep relationship between the process in separation of variables and the theory of Fourier series as well as many computational techniques for solving differential equations. One simple starting point for separation of variables solution is to assume a solution form of

$$\theta(x, y) = X(x)Y(y)$$

Upon substituting this solution form into the partial differential equation, one obtains two separable ordinary differential equations: $-\frac{1}{X}\frac{d^2X}{dx^2} = \frac{1}{Y}\frac{d^2Y}{dy^2} = \lambda^2$

The solution of the X(x) equation yields the trigonometric functions, while the solution of the Y(y) equation yields hyperbolic trigonometric functions sinh and cosh. Substitution of this form of solution into the PDE results in unique choices for the parameters λ and also presents an opportunity to define the so-called Fourier coefficients for the problem (Fig. 2.14).

$$\theta(x, y) = 100 \sum_{n=1}^{\infty} \frac{2[1 - (-1)^n]}{n\pi \sinh(n\pi b/a)} \times \sin\frac{n\pi x}{a} \sinh\frac{n\pi y}{a}$$

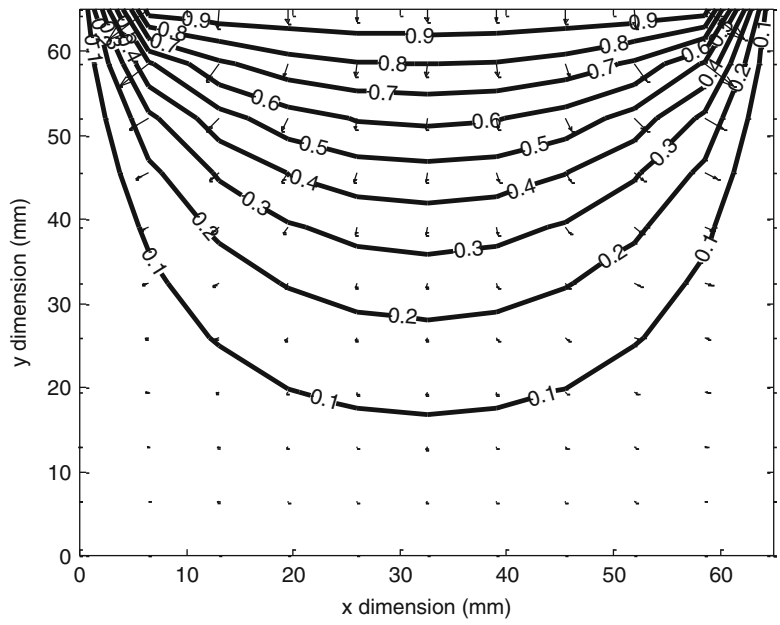

Fig. 2.14 Separation of variables solution ($\theta(x, y)$/100) for 2D plate conduction problem

Transient Lumped Examples with Time Dependent Forcing

Often the transient response of a thermal system must be evaluated. The lumped thermal approximation is valid when the internal conduction resistance is small relative to the external convective resistance.

$$\frac{\text{Internal conduction resistance}}{\text{External convection resistance}} \cong \frac{L/k_s A}{1/\overline{h}_c A} = \frac{\overline{h}_c L}{k_s}$$

Imagine a cold spherical heat sensor emersed in an initially cold gas for which the gas temperature is a linearly increasing function of time. It is useful to understand how the heat sensor's temperature will vary with time. Assume that Bi = 0.1 and Fo ~ 10. T(r,t = 0) = To.

The model used to characterize the temperature variation of the sphere is the same lumped thermal model previously discussed. The difference is that because the reservoir temperature is time varying, the temperature solution is no longer a simple exponential function (Fig. 2.15).

$$\rho V c \frac{dT}{dt} = -\overline{h}_c A (T - T_\infty)$$

$$\frac{dT}{dt} = -\frac{\overline{h}_c A}{\rho V c}(T - T_\infty) \quad \text{with} \quad T_\infty(t) = T_o + at$$

The solution (Fig. 2.16) with $\theta(t) = T - T_o$ is

$$\theta(t) = a\tau\left[\exp\left(\frac{-t}{\tau}\right) - 1\right] + at$$

$$= a\left[t - \tau\left(1 - \exp\left(\frac{-t}{\tau}\right)\right)\right]$$

We see in Fig. 2.16 that there is a time lag between the increasing temperature of the fluid and the increasing temperature of the detector. Additionally, we see that the detector temperature at any given time is always lower than the fluid temperature.

Laplace Transform Methods

The Laplace transform is one of several integral transform methods that can be used in conduction analysis [12]. For time dependent functions, the Laplace transform maps the time dependent derivative terms into algebraic terms that are

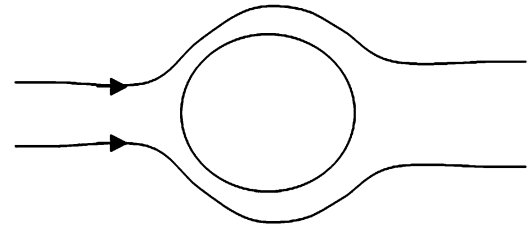

Fig. 2.15 Schematic showing convective flow over an object that will be analyzed using a lumped thermal approximation

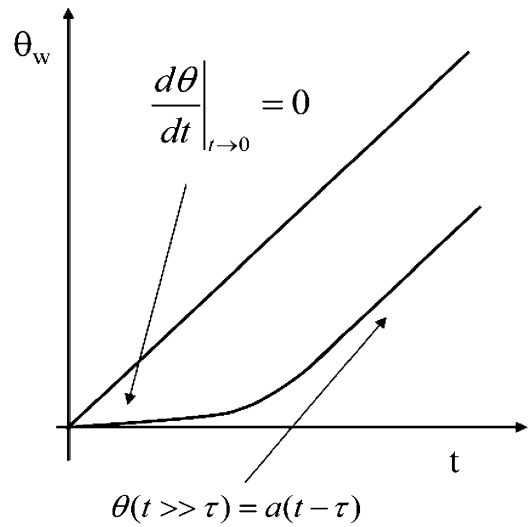

Fig. 2.16 Solution for lumped approximation problem in which fluid temperature is a linearly increasing function of time

parameterized by a new independent variable. For an ordinary differential equation (e.g., a thermally lumped system analysis), application of the Laplace transform yields an algebraic equation that can be solved for the transformed dependent variable. The time dependent form is retrieved using an inversion integral called the Bromwich integral. In the equation below, the Laplace transform integral operator is applied to a general temperature function that depends on time and spatial location. The definition of the Laplace transform is shown below.

$$\mathcal{L}(T) = \hat{T}(x,s) = \int_0^\infty T(x,t) e^{-st} dt$$

An example of the use of the Laplace transform is provided below. Consider the lumped analysis system that we have been using

$$\frac{dT}{dt} = -\frac{\overline{h}_c A}{\rho V c}(T - T_\infty)$$

Straightforward application of the transform yields:

$$s\hat{T}(s) - T(0) = -\frac{\overline{h}_c A}{\rho V c}\left(\hat{T}(s) - \frac{T_\infty}{s}\right)$$

Because the initial condition shows up in this transformation, it is often convenient to use superposition to force the initial condition to be zero. For such a case we have,

$$s\hat{\theta}(s) = -\frac{\overline{h}_c A}{\rho V c}\left(\hat{\theta}(s) - \frac{\theta_\infty}{s}\right)$$

Solving for the transformed temperature variable yields:

$$\hat{\theta}(s) = \frac{\theta_\infty}{\tau_c s\left(s + \tau_c^{-1}\right)}$$

Using any one of a number of inversion tables or online calculators, we retrieve the inverse of this function.

$$\theta(t) = \theta_\infty\left(1 - \exp\left(\frac{-t}{\tau_c}\right)\right)$$

The result above is equivalent to the result shown earlier. The power of the Laplace transform method is that it can be applied to arbitrarily complex differential equations. The challenge of the method has typically been generating the inverse transform. With increasing accessibility of symbolic mathematical software tools, with some freely available online such as Wolfram Alpha, this particular challenge is no longer quite as severe.

Duhamel Integral Methods

The Duhamel integral is a method for generating a solution for an arbitrarily complex time dependent forcing of a conduction system using the solution for a step change. A simple case to present the ideas of this concept is the problem in which there is a step change in the external temperature of a reservoir in contact with a lumped thermal system. We know the solution from earlier sections.

$$\frac{dT}{dt} = -\frac{\overline{h}_c A}{\rho V c}(T - T_\infty)$$

Graphically, a series of external temperature step changes can be looked at as follows:

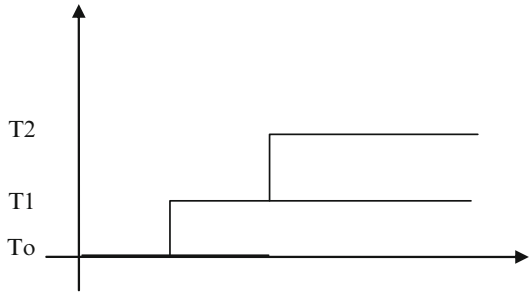

If we focus on the initial step change, this is no different from the original problem that we considered. The offset in time can be addressed using an offset in time. Simply by creating a new time variable, e.g., $s = t - t_1$, we create an offset time variable. To explore what is meant by a step change in the external temperature, we formally formulate the mathematical equation using the Heaviside step function.

$$\frac{dT}{dt} = -\frac{\overline{h}_c A}{\rho V c}(T - T_0 - (T_1 - T_0)H_s(t - t_1) - (T_2 - T_1)H_s(t - t_2))$$

If we now define a relative temperature $T - T_0$, we arrive at the equation

$$\frac{d\theta}{dt} = -\frac{\overline{h}_c A}{\rho V c}(\theta - \Delta\theta_1 H_s(t - t_1) - \Delta\theta_2 H_s(t - t_2))$$

To solve this equation, it is convenient to define a series of linear transformations and use superposition to solve this individual equations.

$$\theta = F + G$$

$$\frac{dF}{dt} + \frac{dG}{dt} = -\frac{\overline{h}_c A}{\rho V c}(F + G - \Delta\theta_1 H_s(t - t_1) - \Delta\theta_2 H_s(t - t_2))$$

$$\frac{dF}{dt} = -\frac{\overline{h}_c A}{\rho V c}(F - \Delta\theta_1 H_s(t - t_1))$$

$$\frac{dG}{dt} = -\frac{\overline{h}_c A}{\rho V c}(G - \Delta\theta_2 H_s(t - t_2))$$

Because $\theta(0) = 0$, we can enforce that both F and G are also equal to zero and have solutions of form:

$$F(t) = \Delta\theta_1\left(1 - e^{-(t-t_1)/t_c}\right)$$

The solution for the excess temperature is then:

$$\theta(t) = \Delta\theta_1\left(1 - e^{-(t-t_1)/t_c}\right) + \Delta\theta_2\left(1 - e^{-(t-t_2)/t_c}\right)$$

For a series of step changes, we can generalize this superposition of solutions to generate:

$$\theta(t) = \sum \frac{\Delta\theta_i}{\Delta\tau_i}\left(1 - e^{-(t-\tau_i)/t_c}\right)\Delta\tau_i = \int_0^t \frac{d\theta}{d\tau}\left(1 - e^{-(t-\tau)/t_c}\right)d\tau$$

We immediately see that for the case in which the freestream temperature is changing as a linear function of time $T_\infty(t) \quad = T_o + at$

We get

$$\theta(t) = \int_0^t a\left(1 - e^{-(t-\tau)/t_c}\right)d\tau$$

$$= at - ae^{-t/t_c}t_c\left(e^{t/t_c} - 1\right)$$

$$= at - at_c\left(1 - e^{-t/t_c}\right) = a\left[t - t_c\left(1 - e^{-t/t_c}\right)\right]$$

which is the same result that we arrived at using a much simpler analysis in an earlier section. The power of the Duhamel formulation is evident in problems like the semi-infinite slab problem for which the solution is expressed in terms of the error function. One interesting application of the Duhamel method that we will use in the section on inverse analysis is the determination of the heat flux from a temperature measurement. The generalization of the Duhamel form states that the time dependent variation of temperature can be defined in terms of an integral of the product of the step response solution, which is time dependent, and the time derivative of the unsteady effect.

Transient Semi-infinite (Thermally Thick) One-Dimensional Examples

For thermally thick problems in which the thermal penetration wave never reaches the back side, analytical solutions are available for a range of boundary conditions. These solutions are generally specified in terms of tabulated functions [13]. Useful approximate solutions can also be developed for these problems using integral approximations and the scaling properties of diffusive transport (Fig. 2.17).

For the thermally thick conduction problem, the solution is often described as being for a semi-infinite domain (Fo<<1). Using either a Laplace transform solution approach or any number of other approaches, one can arrive at the temperature variation for a constant surface temperature boundary condition.

$$\theta = \frac{T - T_0}{T_s - T_0} = 1 - \frac{2}{\pi^{1/2}}\int_0^\eta e^{-u^2}du = \operatorname{erfc}\left(\frac{x}{(4\alpha t)^{1/2}}\right)$$

We see that the solution is defined using the complementary error function (erfc). The surface heat flux variation with time is:

$$q_s = -k(T_s - T_0)\left[-\frac{2}{\pi^{1/2}}e^{-\eta^2}\frac{1}{(4\alpha t)^{1/2}}\right]_{\eta=0} = \frac{k(T_s - T_0)}{(\pi\alpha t)^{1/2}}$$

Interestingly, an approximation for the heat flux that depends on the thermal penetration depth does a reasonable job of predicting the overall trends.

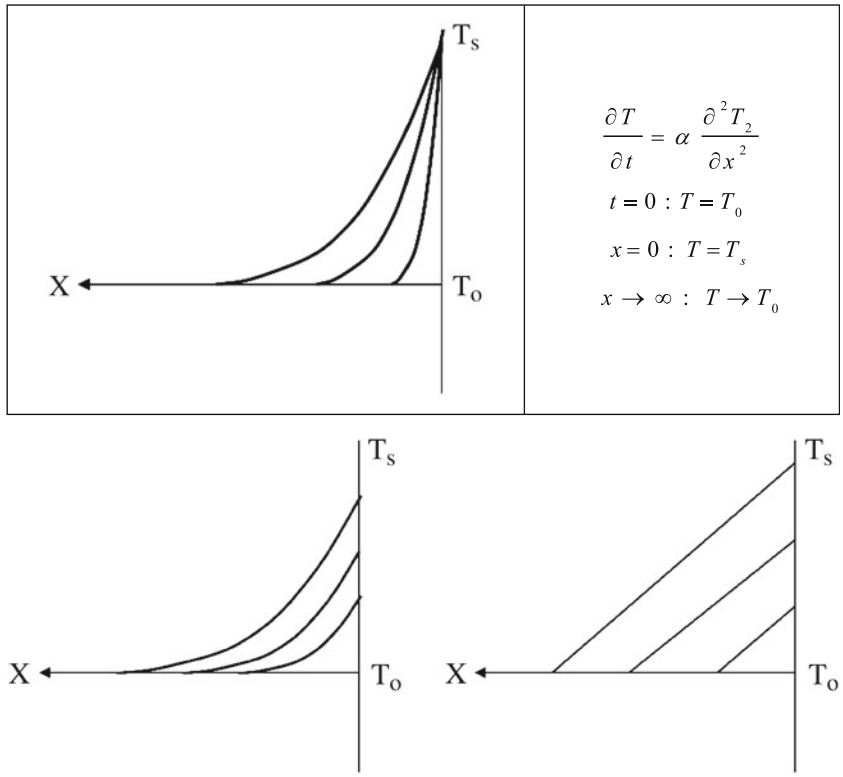

Fig. 2.17 Governing equation for semi-infinite model of conduction in a slab and associated temperature profiles

$$q_s \cong \frac{k(T_s - T_0)}{\delta(t)} = \frac{k(T_s - T_0)}{\sqrt{\alpha t}}$$

In the approximation, we have used the sing the simplified scaling law $\delta \approx \sqrt{\alpha t}$

A similar approximation can be used for the constant surface heat flux boundary condition. We recognize that the approximate variation is as follows:

$$T_s = T_0 + \frac{q_s\sqrt{\alpha t}}{k} = T_0 + \frac{q_s\sqrt{t}}{\sqrt{k\rho c}}$$

The surface temperature has $t^{1/2}$ dependence which we can compare to exact analytical result

$$T(x,t) = T_0 + \frac{q_s}{k}\left[\left(\frac{4\alpha t}{\pi}\right)^{1/2} e^{-x^2/4\alpha t} - x\,\mathrm{erfc}\frac{x}{(4\alpha t)^{1/2}}\right]$$

which at

$$\mathrm{x} = 0 \text{ is } T_s = T_0 + \frac{q_s}{k}\left[\left(\frac{4\alpha t}{\pi}\right)^{1/2}\right]$$

The Newton's law of cooling convective boundary condition case is analytically quite challenging, but can be reduced to a very simple form using the type of scaling previously described (Fig. 2.18).

We note that the internal heat flux can be approximated using a diffusion model and must be balanced by the Newton's law of cooling convection term.

$$q_s \cong \frac{k(T_s(t) - T_0)}{\delta} = h(T_e - T_s)$$

In solving for the wall temperature we arrive at:

$$\frac{T_s(t) - T_0}{(T_e - T_0)} = \frac{\frac{h\sqrt{\alpha t}}{k}}{\left(1 + \frac{h\sqrt{\alpha t}}{k}\right)}$$

At long time, we get constant surface temperature. We can compare this to the exact solution (Fig. 2.19):

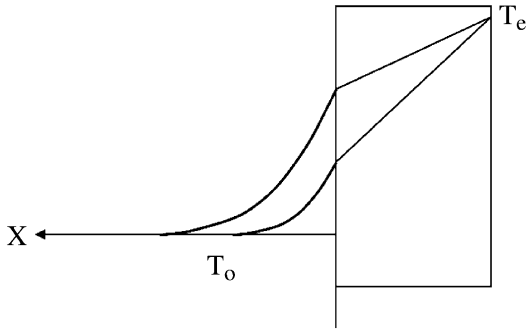

Fig. 2.18 Schematic of semi-infinite model of conduction in a slab with convective boundary conditions

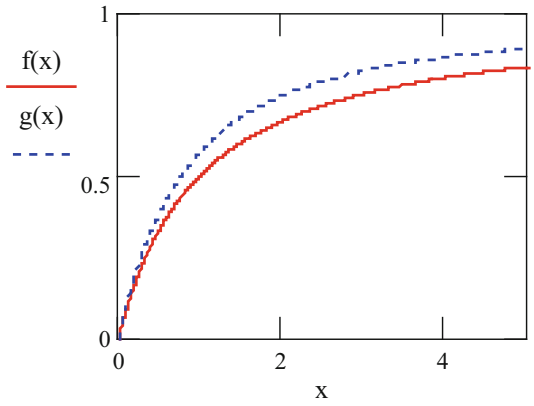

Fig. 2.19 Comparison of approximate and exact solution of semi-infinite model of conduction in a slab with convective boundary conditions

$$\frac{T_s - T_0}{T_e - T_0} = 1 - e^{(h_c/k)^2 \alpha t} \text{erfc}\left[\frac{h_c}{k}(\alpha t)^{1/2}\right]$$

Transient Multidimensional Examples

Multidimensional transient problems represent a class of problems that pose sufficient analytical complexity that we often revert to computational solutions for these systems. For some simple geometries, however, there are tabulated results that are useful for determining the overall

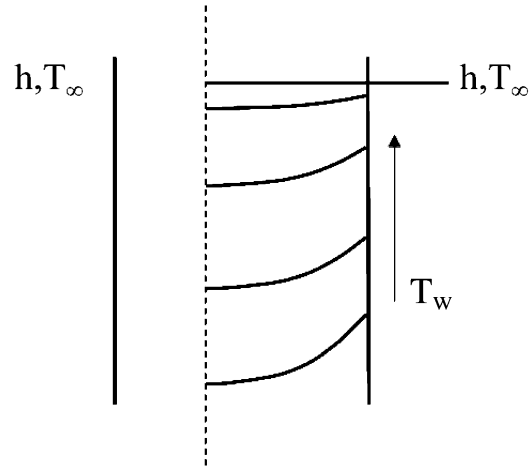

Fig. 2.20 Schematic of one dimensional conduction in a slab with convective boundary conditions

thermal behavior of such systems. The starting point for constructing such solutions is a one dimensional transient problem. As an example, for the slab/wall geometry for which there is convective heating on two sides, there is a separation of variables series solution for the problem. For relatively long times as is defined by the Fourier number (Fo>1), the series solution converges with a small number of terms. Physically, the temperature profile (i.e., the solution) becomes smoother with increasing time. Because so few terms are required to represent the temperature field evolution, it is possible to define the solution in terms of a simple product of a time dependent function and a spatially varying function (Fig. 2.20). The governing equation, initial condition and boundary conditions for the one dimensional problem are:

$$\frac{\partial T}{\partial t} = \alpha \frac{\partial^2 T}{\partial x^2}$$

$$t = 0: \quad T = T_0$$

$$x = 0: \quad \frac{\partial T}{\partial x} = 0$$

$$x = L: \quad -k\frac{\partial T}{\partial x} = h(T - T_\infty)$$

The solution of the one dimensional problem is:

$$\frac{T-T_\infty}{T_0-T_\infty}=\frac{\theta}{\theta_0}=\sum_{n=0}^{\infty} \times \frac{\sin(\lambda_n L)}{\lambda_n L+\sin(\lambda_n L)\cos(\lambda_n L)} \times e^{-\lambda_n{}^2 \alpha t}\cos(\lambda_n x)$$

The eigenvalues of the problem can be written as: $\lambda_n L = \mathrm{Bi}\cot(\lambda_n L)$. Also, the argument of the exponential function can be written as:$\lambda_n^2 \alpha t = (\lambda_n L)^2\left(\frac{\alpha t}{L^2}\right) = (\lambda_n L)^2\,\mathrm{Fo}$. This suggests that the solution is defined by the following parameters:

$$\mathrm{Bi},\ \mathrm{Fo},\ \frac{x}{L}$$

For long enough times, the one term expansion generates [2]:

$$\frac{T-T_\infty}{T_0-T_\infty}=\frac{\theta}{\theta_0}=\frac{\theta}{\theta_{CL}}\times\frac{\theta_{CL}}{\theta_0} = C(\mathrm{Bi})\ \ f(t)g(x)$$

The centerline temperature varies only with time, while the temperature at any location normalized by the centerline temperature is essentially a function of the spatial location.

It can be easily shown that the temperature within a block can be found as the product of the temperatures found from three separate one dimensional solutions (Fig. 2.21):

$$\theta(t,x,y,x)=P(x,t)P(y,t)P(z,t)$$

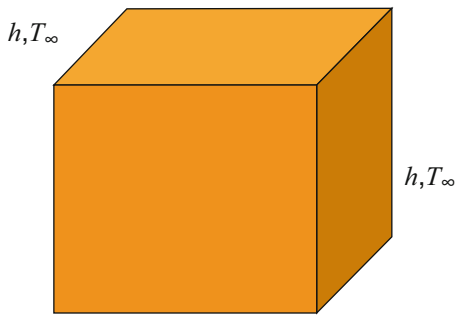

Fig. 2.21 Schematic diagram of cube with external convective heating

Overview of Computational Issues in Conduction

For complex geometries or for problems with nonlinear effects and multiple physical processes, analytical solutions are usually not easily found. For the majority of practical heat transfer processes in fire, a fire engineer will resort to the use of computational tools to characterize the system. Olenick and Carpenter [14] summarize the key features of a number of computational tools available for simulating thermal response associated with fire endurance testing. These tools use a variety of numerical discretization techniques. In the following section, we discuss the types of computational techniques most often used for fire problems and present simple examples for some of these cases to help clarify what underlying steps are taken in some of the tools and codes described in [14]. Useful reference texts for numerical solution of the differential equations associated with conduction are Shih [15] and Ferziger [16].

To start, we define a very simple conduction/diffusion problem with a source (S).

$$\Gamma\frac{d^2\phi}{dx^2}+S=0$$

The analytical solution can be easily found by integrating this equation twice. For the case of a constant source we get:

$$\phi = C_2 + C_1 x - \frac{S}{2\Gamma}x^2$$

Consider the case with boundary conditions:

$$\left.\frac{d\phi}{dx}\right|_{x=0} = 0 \text{ and } \phi(L)=0$$

C_1 is zero by the adiabatic condition, and $C_2 = \frac{S}{2\Gamma}$ such that;

$$\phi=\frac{S}{2\Gamma}(L-x^2)$$

We will compare this solution to those generated by the numerical solutions.

Finite Difference Approximations

The finite difference technique is used to solve differential equations by expanding the dependent variable, at specified positions in the computational space into a Taylor series, appropriately adding and subtracting terms from other series terms together to generate approximations for the derivative terms in the underlying differential equation. As an example, the dependent variable is expanded below in a Taylor expansion at locations 1 and 3 (Fig. 2.22).

$$\phi_1 = \phi_2 - \left.\frac{\partial \phi}{\partial x}\right|_2 \Delta x + \frac{1}{2}\left.\frac{\partial^2 \phi}{\partial x^2}\right|_2 \Delta x^2 + O\left(\Delta x^3\right)$$

$$\phi_3 = \phi_2 + \left.\frac{\partial \phi}{\partial x}\right|_2 \Delta x + \frac{1}{2}\left.\frac{\partial^2 \phi}{\partial x^2}\right|_2 \Delta x^2 + O\left(\Delta x^3\right)$$

By subtracting the two series from each other, we arrive at one representation for the derivatives at location 2.

$$\left.\frac{\partial \phi}{\partial x}\right|_2 = \frac{\phi_3 - \phi_1}{2\Delta x} + O\left(\Delta x^2\right)$$

$$\left.\frac{\partial^2 \phi}{\partial x^2}\right|_2 = \frac{\phi_3 - 2\phi_2 + \phi_1}{\Delta x^2} + O\left(\Delta x^2\right)$$

Substituting the approximations into the original differential equation then provides an algebraic rule by which to evaluate the values of the dependent variable at the prespecified (grid) points.

$$\Gamma \left.\frac{\partial^2 \phi}{\partial x^2}\right|_2 = \Gamma\left(\frac{\phi_3 - 2\phi_2 + \phi_1}{\Delta x^2}\right)$$

And the source term can be approximated as $S_2 = S(\phi_2)$

We see that the final form of the algebraic system of equations is

$$\Gamma\left(\frac{\phi_3 - 2\phi_2 + \phi_1}{\Delta x^2}\right) = -S(\phi_2)$$

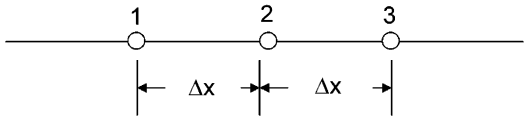

Fig. 2.22 Schematic of finite difference stencil

Symbolically, we can arrange the system of algebraic equations into a form shown below.

$$a_{i-1}\phi_{i-1} - a_i\phi_i + a_{i+1}\phi_{i+1} = b$$

$$a_{i-1} = \frac{\Gamma}{\Delta x}, a_{i+1} = \frac{\Gamma}{\Delta x}, a_i = \frac{-2\Gamma}{\Delta x}, b = -\overline{S}\ \Delta x$$

For the case in which $\Gamma = 0.2$, $0 < x < L$, and $S = 4$

We will use $N = 5$ grid points, $\Delta x = 0.25L$ for $L = 1$

$$a_{i-1} = 1, a_{i+1} = 1, a_i = -2, \quad b = 1$$

$$\begin{bmatrix} -2 & 2 & & & \\ 1 & -2 & 1 & & \\ & 1 & -2 & 1 & \\ & & 1 & -2 & 1 \\ & & & & 1 \end{bmatrix} \begin{bmatrix} \phi_1 \\ \phi_2 \\ \phi_3 \\ \phi_4 \\ \phi_5 \end{bmatrix} = \begin{bmatrix} -1 \\ -1 \\ -1 \\ -1 \\ 0 \end{bmatrix} \text{ with solution } \begin{bmatrix} \phi_1 \\ \phi_2 \\ \phi_3 \\ \phi_4 \\ \phi_5 \end{bmatrix} = \begin{bmatrix} 8 \\ 7.5 \\ 6 \\ 3.5 \\ 0 \end{bmatrix}$$

Which is exactly the same as the answer provided by the exact solution.

Finite Volume Approximation

An alternative way of generating algebraic equations representing the differential equation is the finite volume technique. The finite volume technique is closely related to Galerkin finite element techniques. Both are members of a family of solution techniques called method of weighted residuals. For both types of solution techniques, an integrated form of the underlying differential equation is used to develop the algebraic equations. In both types of techniques, one weights the equation before integrating. Because the weight in the control volume method is just equal to unity, the process to developing the algebraic equations has a simple physical interpretation. The finite volume technique is sometimes called the control volume technique or the subdomain method [17] (Fig. 2.23).

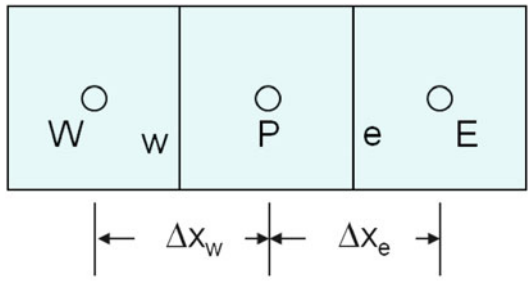

Fig. 2.23 Schematic of finite volume cells

Consider the diffusion equation in conservative form.

$$\frac{d}{dx}\left(\Gamma\frac{d\phi}{dx}\right)+S=0$$

The equation is integrated over the control volume

$\int_w^e \frac{d}{dx}\left(\Gamma\frac{d\phi}{dx}\right)+S\ dx=0$ to become

$$\left(\Gamma\frac{d\phi}{dx}\right)_e-\left(\Gamma\frac{d\phi}{dx}\right)_w+\int_w^e S\ dx=0$$

A linear profile assumption is made between cell centroids for ϕ. Assume S varies linearly over the control volume

$$\frac{\Gamma_e(\phi_E-\phi_P)}{\Delta x_e}-\frac{\Gamma_w(\phi_P-\phi_W)}{\Delta x_w}+\overline{S}\ \Delta x=0$$

Collecting terms and casting into an algebraic equation yields:

$$a_E\phi_E+a_P\phi_P+a_W\phi_W=b$$

$$a_E=\frac{\Gamma_e}{\Delta x_e}, a_W=\frac{\Gamma_w}{\Delta x_w}, a_P=\frac{-2\Gamma_w}{\Delta x_w},\quad b=-\overline{S}\ \Delta x$$

Again, for the case in which $\Gamma=0.25,\quad 0<x<L,$ and $\quad S=4$

We will use $N=5$ grid points, $\Delta x=0.25L$ for $L=1$

$$a_{i-1}=1, a_{i+1}=1, a_i=-2,\quad b=1$$

$$\begin{bmatrix}-2 & 2 & & & \\ 1 & -2 & 1 & & \\ & 1 & -2 & 1 & \\ & & 1 & -2 & 1\\ & & & & 1\end{bmatrix}\begin{bmatrix}\phi_1\\ \phi_2\\ \phi_3\\ \phi_4\\ \phi_5\end{bmatrix}=\begin{bmatrix}-1\\ -1\\ -1\\ -1\\ 0\end{bmatrix}$$

This system of linear equations, written in matrix form has a banded structure and can be solved using a number of linear algebraic solution strategies. For tridiagonal matrices, an efficient algorithm exists (Thomas algorithm) for solving the system [18]. The solution is:

$$\begin{bmatrix}\phi_1\\ \phi_2\\ \phi_3\\ \phi_4\\ \phi_5\end{bmatrix}=\begin{bmatrix}8\\ 7.5\\ 6\\ 3.5\\ 0\end{bmatrix}$$

The solution is exactly the same as the answer provided by the exact solution.

Finite Element Approximations

This discussion is on Galerkin finite element techniques which are a subclass of the method of weighted residuals (MWR) [15, 17]. The method explicitly identifies an approximate solution to the governing equation, for which the approximate solution is generated from a broader class of functions than the true solution resides in. There is an approximation, $\widetilde{\phi}$, to ϕ that produces a residual in the solution of the diffusion equation when the approximation is used.

$$\Gamma\frac{d^2\widetilde{\phi}}{dx^2}+S=R$$

In MWR, the weighted average of the residual is zero, rather than the residual. The weight function is called W(x).

$$\int_{domain} R(x)W(x)dx=0$$

The approximating function is assumed to be expandable in a set of linearly independent "basis functions" $N_j(x)$.

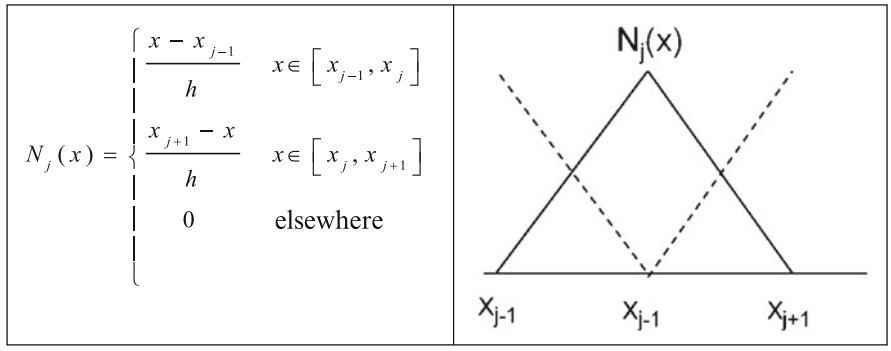

Fig. 2.24 Triangular basis functions and schematic of overlapping functions

$$\widetilde{\phi} = \sum \phi_j N_j(x)$$

In Galerkin FEM the weight function is specified to be the same as the basis function. $W_j(x) = N_j(x)$.

$$\int_{domain} R(x)W(x)dx = 0$$

Effectively, we are forcing the residual to be orthogonal to the basis functions. Properties of the basis function in terms of ease of evaluation, accuracy etc. suggest the use of polynomials.

An example of basis functions is shown below (Fig. 2.24).

The weighted residual becomes:

$$\int_a^b \left(\Gamma \frac{d^2\widetilde{\phi}}{dx^2} + S \right) N_j(x)dx = 0$$

While ϕ should be twice differentiable, the "weak form" allows a wider class of functions to be used. We integrate by parts. We get an equation in terms of integrals of basis functions and coefficients of the unknown function at nodal points.

$$A\phi_{j+1} + B\phi_j + C\phi_{j-1} + D_j = 0$$

Inverse Conduction Heat Transfer Approximations and Examples

Inverse analysis refers to a variety of approaches used to determine model parameters, boundary conditions, initial conditions, etc. The use of the term inverse relates to the idea that the analysis inverts the normal rules of causality in order to find an answer that best agrees with observations. In conduction problems, typical examples of use of inverse analysis are determining the heat flux on a slab given a limited number of interior temperature measurement or identifying material properties that allow a model to best match measured temperature data. There are many approaches to generating an inverse solution, and some of these techniques are essentially optimization methods. One might summarize optimization based analysis as the search for parameters that when used in a forward formulation of the problem of interest generate solutions whose deviation from experimental data is quantified., There are, however, specialized techniques that have been developed for inverse analysis that have not been specifically developed from an optimization perspective. These techniques generally require that the problem be formulated in an inverse sense. For problems formulated in an inverse sense, there ultimately becomes an ill posed mathematical problem. Ill posed problems [19] are those for which the solution is not unique or does not smoothly change relative to small changes in an input parameter. For such problems, there is a need to regularize the underlying system of equations.

If one considers the simple diffusion equation that has been presented in earlier sections and considers the need to specify the source in the medium given some number of temperature

measurements in the slab, the process to determine the source is an inverse analysis. An important fundamental consideration in inverse analysis is the notion that experimental noise exists in the measured data and that such noise corrupts the inversion process.

Given the ODE, we can formulate an integral equation for the temperatures using a delta function source [19, 20]. This is simply a Greens' function solution for the problem. In a forward analysis, we would simply integrate the source distribution in such a way as to generate a temperature at every point given the source distribution. The inversion requires an estimate of the source, given some measurements of temperature. Further, it is assumed that the temperature data are noisy. We see that for each temperature measurement, there is a corresponding quadrature rule that maps the integral equation to an algebraic equation. We see that this process results in a matrix equation in which the source description explicitly shows up as an unknown. Using typical linear algebra techniques, we find that the results for the source are quite noisy and not representative of the input source that was used to drive the forward solution. Note that for this exercise, synthetic measured data are sampled from the forward solution.

The Greens' function solution is constructed using a delta function source:

$$\Gamma\frac{d^2\phi}{dx^2} = -S'''(x) \text{ which for the Green's function is } \frac{\Gamma}{S_o''}\frac{d^2G}{dx^2} = -\delta(x-x_0)$$

Integrating the delta function yields:

$$\begin{aligned} G &= ax+b && x<x_0 \\ \Gamma\frac{dG}{dx}\Big|_{x_0-\varepsilon}^{x_0+\varepsilon} &= S_o'' H_s(x-x_0) \\ G &= Ax+B && x>x_0 \end{aligned}$$

For a case in which ϕ is zero at −L and L, we get the Green's function solutions to be:

$$G(x,x_0) = \frac{-S_o''L}{2\Gamma}(1-x_0/L)(1+x/L) \qquad x<x_0$$

$$G(x,x_0) = \frac{-S_o''L}{2\Gamma}(1+x_0/L)(1-x/L) \qquad x>x_0$$

The final solution for the dependent variable is

$$\phi(x_0) = \frac{L}{2\Gamma}(1-x_0/L)\int_{-L}^{x_0}(1+x/L)S_o''S'(x)dx + \frac{L}{2\Gamma}(1+x_0/L)\int_{x_0}^{L}(1-x/L)S_o''S'(x)dx$$

For the case of a constant source we can show that we retrieve the exact solution. For an inverse formulation, we can imagine that several experimental values of ϕ are assumed to be available through measurements. The linear algebraic system is then:

$$\vec{\phi}(x_i) = \frac{L}{2\Gamma}(1-x_i/L)\sum_{j=1}^{1+(x_i+L)/\Delta x}(1+x_j/L)S'''(x_j)\Delta x + \frac{L}{2\Gamma}(1+x_i/L)\sum_{j=1+(x_i+L)/\Delta x}^{N}(1-x_j/L)S'''(x_j)\Delta x$$

$$x_j = -L + \frac{2L}{N-1}(j-1)$$

$$\vec{\phi}_i = A_{i,j}\vec{S}_j$$

We see that the m×n matrix operator $A_{i,j}$ is not square when there are a limited number (m) of measurements $\vec{\phi}_i$ that require many more evaluations (n) of the source term. To overcome the sensitivity to the data noise and the limited number of available measurements, regularization methods are used to generate smooth approximations to inversely formulated problems. Examples of regularization methods include truncated singular value decomposition (TSVD), Tikhonov regularization, and conjugate gradient based approaches. More details can be found in Hansen [19] and Press et al. [18], on details of these methods. When applied to the example problem, TSVD regularization allows us to easily invert for the source profile.

For the case in which $\Gamma = 0.25$, $-L < x < L$, and $S = 4$, we assume that measurements are made at x = (−.67 L, −0.33 L, 0.33 L, 0.67 L). We will use N = 7 grid points to evaluate the integral in the Greens function solution. This results in a grid spacing of $\Delta x = 0.33L$. For this problem we add random noise to the measured $\vec{\phi}_i$ values to simulate measurement error.

The matrix operations are then

$$\begin{bmatrix} 0 & 0.37 & 0.296 & 0.222 & 0.148 & 0.074 & 0 \\ 0 & 0.296 & 0.593 & 0.444 & 296 & 0.148 & 0 \\ 0 & 0.148 & 0.296 & 0.444 & 0.593 & 0.296 & 0 \\ 0 & 0.074 & 0.148 & 0.222 & 0.296 & 0.37 & 0 \end{bmatrix} \begin{bmatrix} S_1 \\ S_2 \\ \vdots \\ S_6 \\ S_7 \end{bmatrix} = \begin{bmatrix} 4.94 \\ 7.13 \\ 7.61 \\ 4.47 \end{bmatrix}$$

The singular value decomposition of the matrix A results in $A = U\Sigma V^T$. The matrix Σ is a diagonal matrix with the singular values ordered from largest to smallest as the diagonal elements. The number of singular values provides an indication of the number of independent equations in the system of equations. Also the ratio of the largest singular value to the smallest singular value, called the condition number of the matrix, reflects how singular the matrix is and how much amplification of error might be associated with small perturbations propagated through the inversion. For this problem, the singular value decomposition is:

$$\begin{pmatrix} -0.357 & 0.5 & -0.61 & -0.5 \\ -0.61 & 0.5 & 0.357 & 0.5 \\ -0.61 & -0.5 & 0.357 & -0.5 \\ -0.357 & -0.5 & -0.61 & 0.5 \end{pmatrix} \begin{pmatrix} 1.358 & 0 & 0 & 0 \\ 0 & 0.444 & 0 & 0 \\ 0 & 0 & 0.178 & 0 \\ 0 & 0 & 0 & 0.148 \end{pmatrix} \begin{pmatrix} 0 & 0 & 0 & 0 \\ -0.317 & 0.5 & -0.632 & -0.5 \\ -0.516 & 0.5 & 0.258 & 0.5 \\ -0.516 & 0 & 0.258 & 0 \\ -0.516 & -0.5 & 0.258 & -0.5 \\ -0.317 & -0.5 & -0.632 & 0.5 \\ 0 & 0 & 0 & 0 \end{pmatrix}$$

The system of equations is inverted using the numerically accurate inversion (SVD pseudo-inverse) and also using a so-called truncated SVD (TSVD) pseudo-inverse. In the TSVD inversion, the smallest singular value (0.148) is not used in the inversion. The inversion is given by

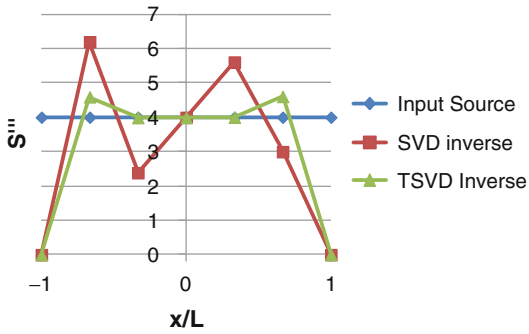

Fig. 2.25 Comparison of SVD inverse and TSVD inverse of noisy input data

$$\vec{S} = \sum_{i=1}^{k} \frac{\vec{u}_i \cdot \vec{\phi}}{\sigma_i} \vec{v}_i$$

In this expression the $\vec{u}_i$ and $\vec{v}_i$ are the column vectors of the U and V matrices in the SVD decomposition. The summation is over the total number of retained singular values. Figure 2.25 shows a comparison of the SVD and TSVD inversions of the noisy measurements. We see that there is considerably more variation and deviation from the exact source values for the SVD inversion relative to the TSVD inversion. The process of truncating the representation of the A matrix acts to smooth or regularize the solution.

This problem is only one example of the many types of techniques that can be applied in inverse heat transfer analysis. Many other types of inversion processes might be used for fire problems. There are many examples of time dependent inversion, as might be done to determine a surface heat flux when measuring internal temperatures that present many different solution approaches for inversion [21, 22]. An interesting analogy exists between the steady example using TSVD based inversion and some types of temporally evolving inverse problems. For linear time dependent problems, analytical solution forms exist for time dependent heating using the Duhamel integral formulation. A simple example from Beck et al. [21] shows the process for determining the heat flux when a single temperature measurement is made using a modification of the Duhamel integral. The Duhamel integral representation looks very much like the Greens function formulation that was detailed. In both cases, one is solving a Fredholm integral equation for some underlying system forcing.

References

1. Carslaw, H. S. and Jaeger, J. C. *Conduction of Heat in Solids*. Oxford University, Oxford, UK (1959).
2. Bergman, T. L., Lavine, A. S., Incropera, F. P., & DeWitt, D. P. *Fundamentals of heat and mass transfer*. Wiley. (2011).
3. Mills, A. F. *Basic heat and mass transfer* (Vol. 2, pp. 745–833). Upper Saddler River, NJ: Prentice hall. (1999).
4. Moran, M. J., Shapiro, H. N., Boettner, D. D., & Bailey, M. *Fundamentals of engineering thermodynamics*. Wiley. (2010).
5. Schmidt, P. S., Ezekoye, O. A., Howell, J. R., & Baker, D. K. *Thermodynamics: an integrated learning system*. Wiley. (2006).
6. Heskestad, G., & Bill, R. G. Quantification of thermal responsiveness of automatic sprinklers including conduction effects. *Fire Safety Journal*, *14*(1), 113–125. (1988).
7. Kaviany, M. *Principles of heat transfer* New York, USA, John Wiley Publishers (2002).
8. Kaviany, M. *Heat transfer physics* Cambridge, UK: Cambridge University Press. (2008).
9. Gebhart, Benjamin. *Heat conduction and mass diffusion*. New York: McGraw-Hill, (1993).
10. Wald, F., Simões da Silva, L., Moore, D. B., Lennon, T., Chladná, M., Santiago, A., and Borges, L. Experimental behaviour of a steel structure under natural fire. *Fire Safety Journal*, *41*(7), 509–522. (2006).
11. Bejan, A, *Heat Transfer*, New York, John Wiley Publishers, (1993).
12. Arpaci, V.S., *Conduction Heat Transfer*, Addison Wesley, (1966).
13. Ozisik, M.N., *Heat Conduction*, New York, John Wiley Publishers, (1993).
14. Olenick, Stephen M., and Douglas J. Carpenter. "An updated international survey of computer models for fire and smoke." *Journal of Fire Protection Engineering* 13.2 87–110. (2003).
15. Shih, T.M., *Numerical Heat Transfer*, Hemisphere publishing Corp, (1984).
16. Ferziger, J.H. *Numerical Methods for Engineering Applications*, New York, John Wiley, (1981).
17. Fletcher, C.A.J., Computational Galerkin Methods, Springer (1984).

18. Press, William H., Brian P. Flannery, Saul A. Teukolsky, and William T. Vetterling. *Numerical Recipes in FORTRAN 77: Volume 1, Volume 1 of Fortran Numerical Recipes: The Art of Scientific Computing*. Vol. 1. Cambridge university press, (1992).
19. Hansen, Per Christian. *Rank-deficient and discrete ill-posed problems: numerical aspects of linear inversion*. Vol. 4. Society for Industrial Mathematics, (1987).
20. Mathews, J., and Walker, R.L., Mathematical Methods of Physics, Addison-Wesley, (1970).
21. Beck, J. V., St Clair, C. R., & Blackwell, B. *Inverse heat conduction*, John Wiley, (1985).
22. Ozisik, M. N. *Inverse heat transfer: fundamentals and applications*, Taylor & Francis, (2000).

Ofodike A. Ezekoye is a professor in the Department of Mechanical Engineering at the University of Texas at Austin.

Convection Heat Transfer

3

Arvind Atreya

This chapter is respectfully dedicated to the author's father, Dr. Dharam Dev Atreya.

Introduction

There are only two fundamental physical modes of energy transfer, conduction and radiation. In conduction, energy slowly diffuses through a *medium* from a point of higher temperature to a point of lower temperature, whereas in radiation, energy is transmitted with the speed of light by electromagnetic waves (or photons), and a transmitting medium is not required. Thus from a conceptual viewpoint, convection is not a basic mode of heat transfer. Instead, it occurs by a combined effect of conduction (and/or radiation) and the motion of the transmitting medium.

Nevertheless, convection plays a very important role in fires. It transports the enormous amount of chemical energy released during a fire to the surrounding environment by the motion of hot gases. This motion may be induced naturally by the fire itself (hot gases rise and cold air rushes to replace them) or by a source external to the fire, such as a prevailing wind. Based on this distinction, the subject of convective heat transfer is usually subdivided into *natural* (free) and *forced* convection. Obviously, both natural and forced convection may occur simultaneously, resulting in a mixed mode of convective heat transfer. A further subdivision based on whether the flow occurs inside (e.g., in a pipe) or outside the body under consideration is also often made. For application of convective heat transfer to fire science, natural convection around objects is clearly far more important than forced convection inside a pipe. Thus greater attention is devoted here to natural convective heat transfer and external flows.

The objective of this chapter is to provide a firm understanding of the physical mechanisms that underlie convective heat transfer, as well as to develop the means to perform convection heat transfer calculations. In the first section of the chapter, basic concepts and relations are developed; calculation methods are illustrated with the help of examples in the second section. Tables of empirical and theoretical results (including their range of applicability) are also provided for quick reference.

Concepts and Basic Relations

A simple, everyday problem of drying a wet body in a stream of warm dry air is shown in Fig. 3.1. From our knowledge of fluid mechanics, we expect the flow of air to slow down next to the surface of the wet body, thus transferring some of its momentum to the body. Conversely, the body will experience a drag force if it moves through stationary air. In addition to this exchange of momentum, the body also losses some of its moisture; that is, transfer of mass takes place

A. Atreya (✉)
University of Michigan

M.J. Hurley (ed.), *SFPE Handbook of Fire Protection Engineering*,
DOI 10.1007/978-1-4939-2565-0_3, © Society of Fire Protection Engineers 2016

from the wet surface to the warm air. Furthermore, for moisture to evaporate at the wet surface the necessary heat must also be transferred from the warm air to the wet body. Hence, the body experiences a simultaneous transfer of momentum, mass, and energy.

To obtain a quantitative description of the above process, note first that all the quantities (mass, momentum, and energy) being transported in the example are conserved, so conservation laws govern their rate of transfer.

These conservation laws need to be supplemented by basic or constitutive relations that relate the rate of transfer to the driving forces and fluid properties. These basic laws are: (1) Newton's law of viscosity, which relates the rate of change of momentum to velocity gradients; (2) Fourier's law of heat conduction, which relates the rate of heat transfer to temperature gradients; and (3) Fick's law of mass diffusion, which relates the rate of mass transfer to concentration gradients. With this framework of conservation and basic laws a majority of laminar convective heat transfer problems can be analyzed, at least in principle. For the turbulent case this framework provides guidance for developing useful empirical correlations.

This section covers the basic laws in the context of laminar flows and their relationships to the more familiar heat transfer coefficients. Later, we see how these heat transfer coefficients can be determined by the application of conservation laws. The effect of turbulence is also discussed and empirical correlations presented.

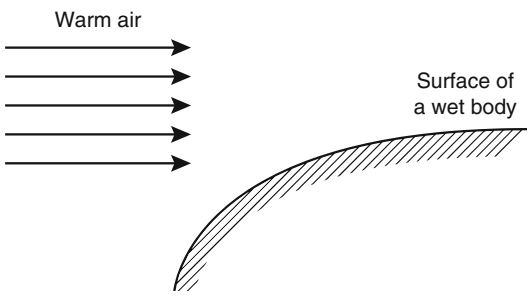

Fig. 3.1 Drying of a wet body in a stream of warm air

Basic Laws of Molecular Transfer

Newton's Law of Viscosity An isothermal system is shown in Fig. 3.2. It consists of a fluid trapped between two impervious flat plates that are infinite in extent and separated by a distance, δ. Experiments show that if the lower plate is fixed and the upper plate is moved at a constant velocity, u_∞, then the velocity of the fluid between the two plates varies from u_∞ near the top plate to zero at the fixed plate. Under steady laminar conditions, a linear velocity profile is established as shown in Fig. 3.2. The fluid thus exerts a shear force on the stationary plate. Experiments also show that τ, the shear force exerted on the bottom plate per unit area, is directly proportional to u_∞ and inversely proportional to the separation distance, δ; that is,

$$\tau \alpha \frac{u_\infty}{\delta} \quad \text{or} \quad \tau = \mu \frac{u_\infty}{\delta}$$

The constant of proportionality, μ, is called the dynamic viscosity of the fluid (units: N·s/m^2) and the force per unit area, τ, is called the shear stress. (In some texts a negative sign is introduced to emphasize the direction of net momentum transfer, i.e., from the fluid at higher velocity to the fluid at lower velocity.) Note that the shear stress τ exerted by the fluid on the fixed plate is in the positive x-direction and that exerted by the fixed plate on the fluid is equal and opposite in direction.) In differential form

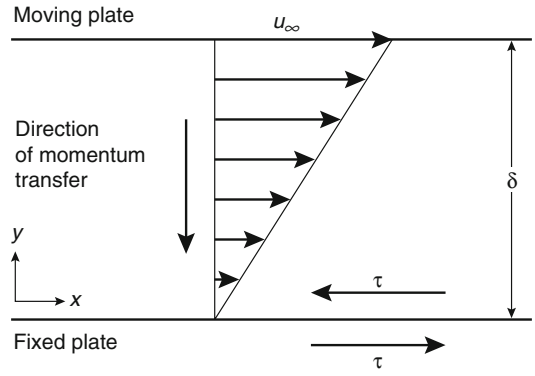

Fig. 3.2 Steady-state velocity distribution in a Newtonian fluid

this relationship expresses the shear stress at any location, y, in the fluid as

$$\tau = \mu \frac{du}{dy} \tag{3.1}$$

This is Newton's law of viscosity. Equation 3.1 states that the shear stress experienced by a fluid layer is directly proportional to the velocity gradient inside the fluid at that location.

Fluids that behave according to Equation 3.1 (i.e., τ is linearly related to the velocity gradient, du/dy, and μ is not a function of the velocity gradient) are called Newtonian fluids. Fortunately, all gases and most simple liquids such as water obey this simple law. For gases, μ roughly increases as the square root of temperature as predicted by the kinetic theory of dilute gases. Liquids, on the other hand, become "thinner" (less viscous), that is, μ decreases with increase in temperature. For non-Newtonian fluids (e.g., pastes, slurries, blood, etc.) the dynamic viscosity also depends on the velocity gradient or the rate of shear.

Fourier's Law of Heat Conduction Two stationary parallel plates separated by a distance, δ_t, are shown in Fig. 3.3. Let the temperature of the upper plate be T_∞ and that of the lower plate be T_s. Under steady conditions and for temperature independent properties of the trapped fluid, a linear temperature distribution as shown in Fig. 3.3 is obtained. Thus, as expected, heat is transferred by the stationary fluid from the hot to the cold plate. The heat flow per unit area per unit time through the fluid ($\dot{q}''$ J/m^{2}s) is found to be directly proportional to the temperature difference, $T_\infty - T_s$, and inversely proportional to the separation distance, δ_t; that is,

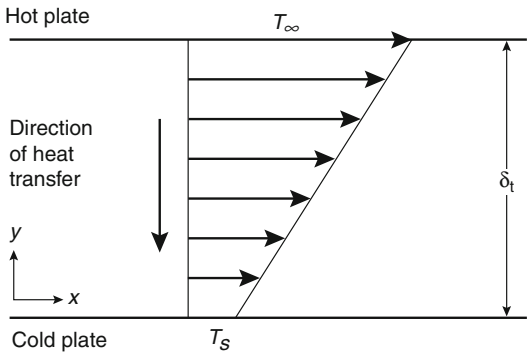

Fig. 3.3 Steady-state temperature distribution

$$\dot{q}'' \alpha \frac{T_\infty - T_s}{\delta_t} = -k \frac{T_\infty - T_s}{\delta_t}$$

The constant of proportionality, k, is called the thermal conductivity (units: J/mKs). The minus sign is a consequence of the second law of thermodynamics, which requires the heat to flow in the direction of decreasing temperature. In differential form the heat across any fluid layer is given by

$$\dot{q}'' = -k \frac{dT}{dy} \tag{3.2}$$

This is known as Fourier's law of heat conduction, which states that the heat flux is directly proportional to the temperature gradient and the heat flux vector is oriented in the direction of decreasing temperature. The thermal conductivity, k, like viscosity, μ, is a physical property of the fluid. The thermal conductivity of gases at low densities increases with increasing temperature (roughly as $\sqrt{T}$ according to the kinetic theory of dilute gases) whereas the thermal conductivity of most liquids decreases with increasing temperature.

Fick's Law of Mass Diffusion Once again, consider the parallel plate example. This time, there are no temperature gradients and no directed motion of the plates. Instead, the top plate is maintained at a higher concentration of species A ($C_{A\infty}$, kg of species A/m^3), assuming that it is wet, and the bottom plate is maintained at a fixed but lower concentration of species A (C_{AW}, kg of A/m^3). Then, under steady conditions a concentration profile, as shown in Fig. 3.4, is established. This nonuniform concentration field is the driving force for species A to diffuse from the top to the bottom plate. The mass flux of species A, $\dot{m}''$ (units: kg/m^{2}s), leaving the top plate and arriving at the bottom plate through the fluid, B, is found to be directly proportional to the concentration difference and

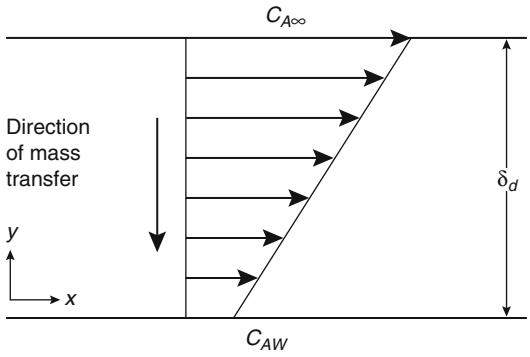

Fig. 3.4 Steady-state concentration distribution

inversely proportional to the separation distance δ_d, that is,

$$\dot{m}_A'' \alpha \frac{C_{A\infty} - C_{AW}}{\delta_d} = -D_{AB} \frac{C_{A\infty} - C_{AW}}{\delta_d}$$

The constant of proportionality, D_{AB}, is called diffusivity of species A through species B and has units of m^2/s. The negative sign once again indicates that the net mass transfer of species A occurs in the direction of decreasing concentration. In the differential form, the mass flux of species A across any layer of fluid B is given by

$$\dot{m}'' = -D_{AB} \frac{dC_A}{dy} \tag{3.3}$$

This is known as Fick's law of mass diffusion, which states that the mass flux across a fluid layer is directly proportional to the local concentration gradient. For binary gas mixtures, D_{AB} increases with increasing temperature roughly as three-halves power, as predicted by the kinetic theory of dilute gases.

Discussion Equations 3.1, 3.2, and 3.3 look very similar—they all relate the flux of the transported quantity to their respective local gradients. Actually, these equations may be considered definitions of the three macroscopic physical properties, μ, k, and D_{AB} of the fluid. In general, these properties are functions of temperature, pressure, and composition. As noted earlier, for low pressure binary gas mixtures (<10 atm) the pressure, temperature, and composition dependence of these properties can be approximately predicted by the kinetic theory of gases. In fact, the physical mechanism of all three transport processes is easily understood by considering the random motion of molecules in an ideal gas.

Molecules of a gas, even in the absence of bulk fluid motion, move around randomly at high speeds and bump into each other. Thus, a given molecule may be found anywhere between the two parallel plates. The problem, however, is how to distinguish one molecule from another. When the upper plate is moving relative to the bottom plate, the molecules adjacent to the upper plate attain a directed velocity over and above their random motion. Consequently, as the molecules near the upper plate find themselves in lower fluid layers (and vice versa) they exchange directed motion (or momentum) by bumping into each other. Similarly, the gas molecules near the hot upper plate are distinguished from those adjacent to the cold lower plate because they possess a higher kinetic energy. Once again, by virtue of random motion, these higher kinetic energy molecules find themselves near the cold plate and collide with low kinetic energy molecules (or vice versa), thus transporting energy. In the case of mass diffusion, the molecules are chemically labeled and their random motion results in mass transfer. Since increasing the gas temperature increases the random molecular motion, the transport processes become more efficient at higher gas temperatures. For gases, the macroscopic physical properties (viscosity, thermal conductivity, and diffusivity) that characterize momentum, heat, and mass transport must also increase with temperature.

Assuming constant properties, Equations 3.1 and 3.2 can be rewritten in the following forms:

$$\tau = \left(\frac{\mu}{\rho}\right) \frac{d(\rho u)}{dy} \tag{3.1a}$$

$$\dot{q}'' = -\left(\frac{k}{\rho c_p}\right) \frac{d(\rho c_p T)}{dy} \tag{3.2a}$$

Here, μ/ρ is known as the kinematic viscosity, ν, and has units of m^2/s. The product, ρu, has units of (kg m/s)/m^3; that is, momentum per unit volume. The quantity, $k/\rho c_p$, is known as the thermal

diffusivity, α, and it too has units of m^2/s. The product, $\rho c_p T$, then becomes enthalpy per unit volume and has units of J/m^3. Comparing these with Equation 3.3, where the mass diffusivity, D_{AB}, also has units of m^2/s and C_A is expressed in kg of species A/m^3, we find that the fluxes are related to their corresponding gradients of volumetric concentration. Furthermore, the ratios of various physical constants yield the familiar nondimensional numbers. These are

$$\text{Prandtl number, Pr} = \nu/\alpha$$
$$\text{Schmidt number, Sc} = \nu/D_{AB}$$
$$\text{Lewis number, Le} = \alpha/D_{AB}$$

Here, the Prandtl number compares the relative magnitude of momentum transfer to heat transfer, the Schmidt number compares momentum transfer to mass transfer, and the Lewis number compares heat transfer to mass transfer. The significance of these nondimensional numbers will become obvious when we discuss boundary layer transfer processes. The balance of this section will discuss primarily heat transfer. The treatment of mass transfer is similar and will not be discussed. However, since fluid motion is central to convective heat transfer, it is necessary to understand momentum transport to solve convective heat transfer problems.

Relationship of Basic Laws to Transfer Coefficients

A flow condition is shown in Fig. 3.5. A fluid of velocity, u_∞, and temperature, T_∞, flows over an arbitrarily shaped stationary surface of area, A_s.

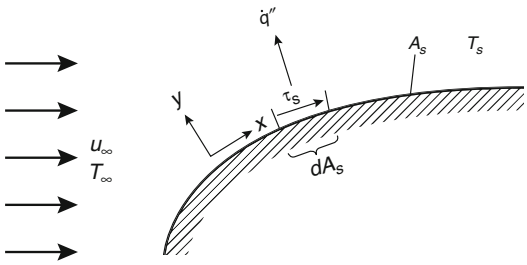

Fig. 3.5 Example of the convection heat transfer problem

If the surface conditions are such that $T_s \neq T_\infty$, we know that convection heat transfer will occur. The convection heat transfer problem is to relate the local heat flux, $\dot{q}''$, to its driving force, $T_s - T_\infty$. By expressing the heat flux as

$$\dot{q}'' = h(T_s - T_\infty) \tag{3.4}$$

the problem is reduced to determining h, which is called the heat transfer coefficient. From Equation 3.2 it is clear that the heat transfer coefficient may be expressed as

$$h = \frac{-k(\partial T/\partial y)\big|_{y=0}}{(Ts - T\infty)} \left(\frac{J}{m^2 s\ \text{K}}\right) \tag{3.5}$$

In Equation 3.5 the partial derivative is used because, in general, temperature is a function of x, y, z, and time. Thus, if the thermal conductivity of the fluid is known, the problem of determining the local heat transfer coefficient is reduced to that of determining the local temperature gradient in the fluid adjacent to the surface. This local temperature gradient can be experimentally measured or obtained theoretically from the solution of the conservation laws. Obviously, the temperature gradient will vary from point to point along the surface of the body. Often, such detail is not required and it may only be necessary to determine an average heat transfer coefficient, $\overline{h}$. This is obtained by integrating over the entire surface area, A_s. The total rate of heat transfer from the body to the fluid is given by

$$\dot{q}(\text{J/s}) = \int_{A_s} \dot{q}''\left(\text{J/m}^2\text{s}\right) \cdot dA_s\left(\text{m}^2\right) \tag{3.6}$$

Defining an average heat transfer coefficient, $\overline{h}$, as

$$\dot{q} = \overline{h} A_s (T_s - T_\infty) \tag{3.7}$$

The following is obtained from the use of Equations 3.4, 3.6, and 3.7

$$\overline{h} = \frac{1}{A_s(T_s - T_\infty)} \int_{A_s} h(T_s - T_\infty) dA_s \tag{3.8}$$

If the surface temperature, T_s, is held constant, then

$$\overline{h} = \frac{1}{A_s}\int_{A_s} h dA_s \left(\frac{\text{J}}{\text{m}^2\text{s K}}\right) \tag{3.9}$$

Similarly, the local shear stress at the surface, τ_s, can be related to its cause, the fluid velocity, u_∞. This relation is derived by defining a local nondimensional friction coefficient, C_f, according to the equation

$$\tau_s \equiv C_f\left(\frac{1}{2}\rho u_\infty^2\right) \tag{3.10}$$

Once again, the problem is reduced to the determination of C_f. Using Equation 3.1 we obtain

$$C_f = \frac{\mu(\partial u/\partial y)\big|_{y=0}}{(1/2)\rho u_\infty^2} \tag{3.11}$$

Thus, the local friction coefficient can be evaluated from the knowledge of the local velocity gradient in the fluid adjacent to the surface. The average friction coefficient can easily be obtained by integrating the local shear stress, τ_s, over the entire surface area, A_s. The total drag force, D, experienced by the body is given by the product of average shear stress, $\overline{\tau}_s$, and the surface area, A_s. In other words,

$$D \equiv \overline{\tau}_s A_s = \int_{A_s} \tau_s dA_s \tag{3.12}$$

Assuming u_∞ to be the same at all locations

$$\overline{\tau}_s = \frac{\left(1/2\rho u_\infty^2\right)}{A_s}\int_{A_s} C_f A_s \tag{3.13}$$

Defining the average friction coefficient, $\overline{C}_f$, as

$$\overline{C}_f \equiv \frac{\overline{\tau}_s}{\left(1/2\rho u_\infty^2\right)} \tag{3.14}$$

we get

$$\overline{C}_f = \frac{1}{A_s}\int_{A_s} C_f dA_s \tag{3.15}$$

To obtain h, $\overline{h}$, C_f, and $\overline{C}_f$ a knowledge of fluid properties and temperature and velocity gradients in the fluid adjacent to the surface is required. To obtain these gradients it is necessary to be more specific about the surface geometry and the flow conditions. The governing conservation equations for an arbitrary surface geometry will be first derived and then applied to a flat plate to illustrate the methodology.

Conservation Equations for Convection Heat Transfer

It has been shown that to determine the heat transfer and friction coefficients, the temperature and velocity distributions in the flow are needed. In principle, these may be obtained from the solution of the conservation equations with appropriate boundary conditions. Although in practice it is difficult, the very knowledge of conservation equations and their solutions for simple cases (such as a flat plate) provide considerable insight about the parameters influencing the heat transfer and friction coefficients. Thus, the necessary equations will be first developed and then applied to a flat plate.

Consider the flow over the surface shown in Fig. 3.6. To simplify the development assume two-dimensional flow conditions, for which x is the direction along the surface and y is normal to the surface. Extension of this to three-dimensional flows is available in the literature [1–5].

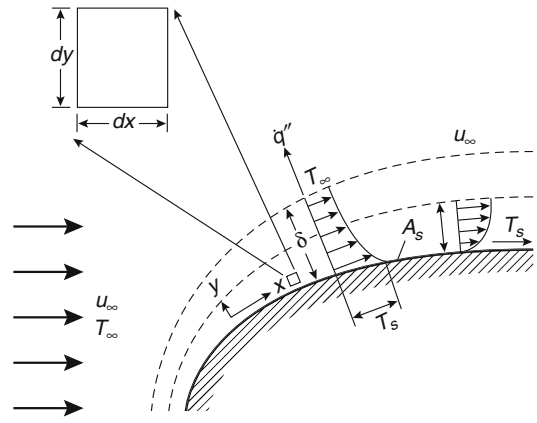

Fig. 3.6 Velocity and temperature distributions inside the fluid for flow over a hot surface

Conservation of Mass (Continuity Equation) The first conservation law that is pertinent to the problem is that matter is neither created nor destroyed. When applied to the differential control volume shown in Figs. 3.6 and 3.7 it states that the net rate of mass flow entering the elemental control volume in the x-direction, plus the net rate of mass flow entering the elemental control volume in the y-direction equals the net rate of increase of mass stored in the control volume. Mass enters and leaves the control volume exclusively through gross fluid motions. Such a transport is often referred to as convective transport.

For a control volume of unit depth in the z-direction, mass entering the left face per unit time, $\dot{M}_x$, is given by

$$\dot{M}_x = \rho\left(\mathrm{kg/m^3}\right) u(\mathrm{m/\ sec})\, dy(\mathrm{m}) \cdot 1(\mathrm{m})$$

Similarly, mass entering the bottom face per unit time, $\dot{M}_y$, is given by

$$\dot{M}_y = \rho \cdot v \cdot dx \cdot 1$$

where v is the fluid velocity in the y-direction.

Since ρu and ρv are continuous functions of x, y, and time, in general they will be different at different locations. To determine ρu at $(x + dx)$, expand ρu about the point x in the Taylor series as

$$\rho u(x + dx, y) = \rho u(x, y) + \left[\frac{\partial(\rho u)}{\partial x}\right]_{x,y} dx \tag{3.16}$$

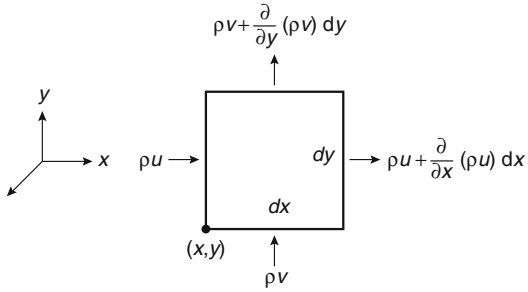

Fig. 3.7 Differential control volume for mass conservation in a two-dimensional flow

Similarly,

$$\rho v(x, y + dy) = \rho v(x, y) + \left[\frac{\partial(\rho v)}{\partial y}\right]_{x,y} dy$$

Thus, mass leaving the right face per unit time, $\dot{M}_{x+dx}$, is given by

$$\dot{M}_{x+dx} = \left[\rho u + \frac{\partial(\rho u)}{\partial x} dx\right] \cdot dy \cdot 1 \tag{3.17}$$

and mass leaving the top face per unit time, $\dot{M}_{y+dy}$, is

$$\dot{M}_{y+dy} = \left[\rho v + \frac{\partial(\rho v)}{\partial y} dy\right] \cdot dx \cdot 1 \tag{3.18}$$

Finally, the rate of increase (or decrease) of mass stored in the control volume, $\dot{M}_s$, is of the form

$$\dot{M}_s = \frac{\partial}{\partial t}(\rho \cdot dx \cdot dy \cdot 1) = \frac{\partial \rho}{\partial t} dxdy \tag{3.19}$$

Thus, conservation of mass requirement may now be expressed as

$$(\rho u)dy + (\rho v)dx - \left[\rho u + \frac{\partial(\rho u)}{\partial x} dx\right] dy - \left[\rho v + \frac{\partial(\rho v)}{\partial y} dy\right] dx = \frac{\partial \rho}{\partial t} dxdy \tag{3.20}$$

After canceling terms and dividing by $dx\, dy$

$$\frac{\partial \rho}{\partial t} + \frac{\partial(\rho u)}{\partial x} + \frac{\partial(\rho v)}{\partial y} = 0 \tag{3.21}$$

This is the *continuity equation*, which is an expression of the overall mass conservation requirement and must be satisfied at every point in the flow. This equation applies for a single species fluid, as well as for mixtures in which species diffusion and chemical reactions may be occurring.

Conservation of Momentum The second conservation law pertinent to the convection heat

transfer problem is Newton's second law of motion. For a differential control volume in a flow field, this requirement states that the sum of all forces acting on the control volume must equal the rate of increase of the fluid momentum within the control volume, plus the net rate at which momentum leaves the control volume (outflow-inflow).

The forces acting on the fluid may be categorized into *body forces* that are proportional to the volume, and *surface forces*, which are proportional to the area. Gravitational, centrifugal, magnetic, and electric fields are familiar examples of body forces. Of these, gravitational body force is the most important from the fire science point of view. The x- and y-components of this body force per unit volume of the fluid will be designated as F_{Bx} and F_{By}, respectively.

The surface forces, F_s, acting on the fluid are called stresses (force/area). These are due to fluid static pressure, p, and viscous stresses. Since pressure is always normal to the surface, the viscous stresses are also resolved into normal stresses, σ_{ii}, which act normal to the surface, and shear stresses, τ_{ij}, which act along or parallel to the surface. Figure 3.8 shows the various viscous stresses acting on the surface of a differential control volume. A double subscript notation is used to specify the stress components. The first subscript indicates the direction of the outward normal to the surface, and the second subscript indicates the direction of the force component. Accordingly, the stress τ_{xy}, acting on the left face, corresponds to the viscous shear force per unit area in the negative y-direction on a face whose normal is in the negative x-direction—resulting in a positive shear stress. All the viscous stresses shown in Fig. 3.8 are positive according to the adopted convention. It should be noted that these forces act on the fluid inside the control volume and are caused by its interaction with the surrounding fluid. Thus, these viscous stresses will vanish if the fluid velocity, or more specifically the velocity gradient in the fluid, becomes zero. The normal viscous stresses shown in Fig. 3.8 must not be confused with static pressure, p, which does not vanish for zero velocity. Since these stresses are continuous functions of x, y, and time, the customary Taylor's expansion is used to express the stresses on the top and right faces of the control volume shown in Fig. 3.8. Thus, the net surface force in the x- and y-directions may be expressed as

$$F_{sx} = \left(\frac{\partial \sigma_{xx}}{\partial x} - \frac{\partial p}{\partial x} + \frac{\partial \tau_{yx}}{\partial y}\right) dxdy \qquad (3.22)$$

$$F_{sy} = \left(\frac{\partial \sigma_{yy}}{\partial y} - \frac{\partial p}{\partial y} + \frac{\partial \tau_{xy}}{\partial x}\right) dxdy \qquad (3.23)$$

To use Newton's second law, the time rate of change of momentum and the momentum influx and outflux must also be evaluated. To focus on the x-direction, the relevant momentum fluxes are shown in Fig. 3.9. The mass flux through the left face is ρu and hence the corresponding

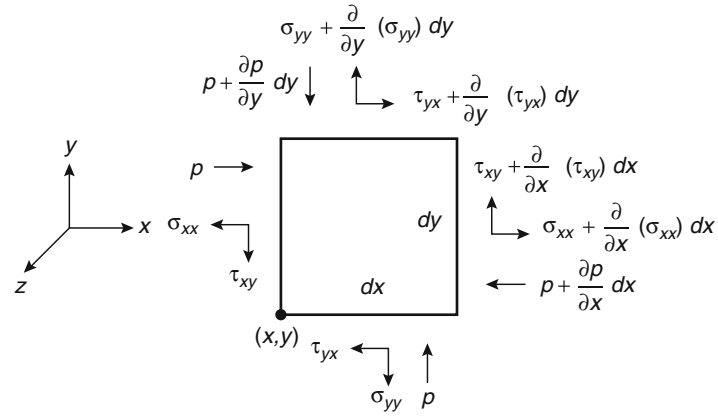

Fig. 3.8 Static pressure, p, and normal and shear viscous stresses acting on a differential control volume in a two-dimensional flow

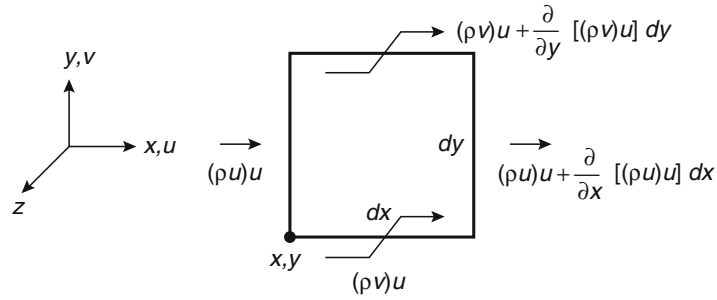

Fig. 3.9 Influx and outflux of x-momentum in the control volume

momentum flux is $(\rho u)u$. Similarly, the x-momentum flux due to mass flow in the y-direction through the bottom face is $(\rho v)u$. Thus the net rate at which momentum leaves the control volume is given by (x-momentum outflow − inflow)

$$\frac{\partial}{\partial x}[(\rho u)u]dx\,dy + \frac{\partial[(\rho v)u]}{\partial y}dy\,dx$$

In addition, the time rate of change of x-momentum of the fluid within the control volume is given by

$$\frac{\partial}{\partial t}(\rho u)dx\,dy$$

Equating the total rate of change in the x-direction to the sum of forces in the x-direction, we obtain

$$\frac{\partial(\rho u)}{\partial t} + \frac{\partial[(\rho u)u]}{\partial x} + \frac{\partial[(\rho v)u]}{\partial y} = \frac{\partial \sigma_{xx}}{\partial x} - \frac{\partial p}{\partial x} + \frac{\partial \tau_{yx}}{\partial y} + F_{Bx} \qquad (3.24)$$

By using Equation 3.21, Equation 3.24 may be expressed in a more convenient form as

$$\rho\left(\frac{\partial u}{\partial t} + u\frac{\partial u}{\partial x} + v\frac{\partial u}{\partial y}\right) = \frac{\partial}{\partial x}(\sigma_{xx} - p) + \frac{\partial \tau_{yx}}{\partial y} + F_{Bx} \qquad (3.25)$$

A similar expression is obtained for the y-direction. This is

$$\rho\left(\frac{\partial v}{\partial t} + u\frac{\partial v}{\partial x} + v\frac{\partial v}{\partial y}\right) = \frac{\partial}{\partial y}(\sigma_{yy} - p) + \frac{\partial \tau_{xy}}{\partial x} + F_{By} \qquad (3.26)$$

In Equations 3.25 and 3.26, the first term on the left side represents the increase in momentum of the fluid inside the control volume, and the remaining terms represent the net rate of momentum efflux from the control volume. The terms on the right side of the equations account for the net viscous, pressure, and body forces acting on the control volume. These equations must be satisfied at every point in the fluid. A solution of Equations 3.21, 3.25, and 3.26 along with appropriate boundary conditions yields the velocity field needed to determine the friction coefficient.

Before a solution to the above equations can be obtained, it is necessary to relate the viscous stresses to the velocity gradients. For a one-dimensional flow of a Newtonian fluid, Equation 3.1 relates the shear stress to the velocity gradient in the fluid. For a two-dimensional flow of Newtonian fluid [2], the required stress-velocity gradient expressions are

$$\sigma_{xx} = 2\mu\frac{\partial u}{\partial x} - \frac{2}{3}\mu\left(\frac{\partial u}{\partial x} + \frac{\partial v}{\partial y}\right) \qquad (3.27)$$

$$\sigma_{yy} = 2\mu\frac{\partial v}{\partial y} - \frac{2}{3}\mu\left(\frac{\partial u}{\partial x} + \frac{\partial v}{\partial y}\right) \qquad (3.28)$$

$$\tau_{xy} = \tau_{yx} = \mu\left(\frac{\partial u}{\partial y} + \frac{\partial v}{\partial x}\right) \qquad (3.29)$$

On substituting Equations 3.27, 3.28, and 3.29 into Equations 3.25 and 3.26, the desired form of the x- and y-momentum equations is obtained. These are

x-momentum equation

$$\rho\left(\frac{\partial u}{\partial t}+u\frac{\partial u}{\partial x}+v\frac{\partial u}{\partial y}\right)=-\frac{\partial p}{\partial x}+\mu\left(\frac{\partial^2 u}{\partial x^2}+\frac{\partial^2 u}{\partial y^2}\right)+\frac{1}{3}\mu\frac{\partial}{\partial x}\left(\frac{\partial u}{\partial x}+\frac{\partial v}{\partial y}\right)+F_{Bx} \tag{3.30}$$

y-momentum equation

$$\rho\left(\frac{\partial v}{\partial t}+u\frac{\partial v}{\partial x}+v\frac{\partial v}{\partial y}\right)=-\frac{\partial p}{\partial x}+\mu\left(\frac{\partial^2 v}{\partial x^2}+\frac{\partial^2 v}{\partial y^2}\right)+\frac{1}{3}\mu\frac{\partial}{\partial y}\left(\frac{\partial u}{\partial x}+\frac{\partial v}{\partial y}\right)+F_{By} \tag{3.31}$$

For an isothermal system, Equations 3.21, 3.30, and 3.31 along with the equation of state ($p = \rho RT$ for an ideal gas) provide a complete set for determining the four dependent variables (u, v, p, and ρ) as a function of the three independent variables x, y, and t. However, for a nonisothermal system such as a fire, energy balance must also be considered.

Conservation of Energy The temperature field inside the fluid, $T(x, y, t)$, needed to determine the heat transfer coefficient is obtained by applying the first law of thermodynamics to the differential control volume shown in Fig. 3.6. Before writing the energy balance for this control volume, it is necessary to identify the items that must be included in the energy budget. These are:

1. The stored energy. This includes the specific internal or thermal energy, e; J/kg, and the kinetic energy of the fluid per unit mass, $V^2/2 = (u^2 + v^2)/2$. Potential energy is neglected because for most problems in convective heat transfer it is substantially smaller than thermal and kinetic energy. Hence, the total energy content per unit volume is given by: $\rho(e + V^2/2)$.
2. Conduction of thermal energy across the surfaces of the control volume. Here, the rate of energy transported per unit area per unit time across the control surface is given by Equation 3.2 as $\dot{q}''_x = -k\partial T/\partial x$ for the x-direction, and $\dot{q}''_y = -k\partial T/\partial y$ for the y-direction.
3. Energy generated per unit volume per unit time inside the control volume (Q watts/m^3). This may be due to chemical reactions (endothermic or exothermic) or may be caused by the radiative loss of heat. Although the specific form of Q will depend on the nature of the physical process, here we will treat it only as a rate of heat loss or gain per unit volume.
4. The rate of work done by surface or body forces. For surface forces, $\mathbf{F_S}$, it is given by: [$\mathbf{F_S}$ · (velocity vector)] (surface area); and for the body forces, $\mathbf{F_B}$, it is given by: [$\mathbf{F_B}$ · (velocity vector)] (volume). Both these expressions have units of watts or work done per unit time.

With these definitions, consider the control volume shown in Figs. 3.6 and 3.10. The conservation of energy for this control volume can be simply stated as

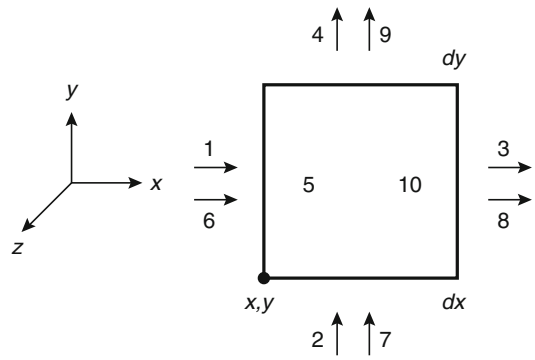

Fig. 3.10 A control volume showing the energy conducted and convected through its control surfaces

$$\begin{pmatrix}\text{Rate of increase}\\ \text{of energy inside}\\ \text{the control volume}\end{pmatrix} = \begin{pmatrix}\text{Net rate of energy flow}\\ \text{into the control volume}\\ \text{by bulk and fluid motion}\end{pmatrix} + \begin{pmatrix}\text{Flow of heat through}\\ \text{the control surface}\\ \text{by conduction}\end{pmatrix} + \begin{pmatrix}\text{Rate of work done by body}\\ \text{and surface forces}\end{pmatrix} + \begin{pmatrix}\text{Energy generated inside}\\ \text{the control volume}\end{pmatrix} \tag{3.32}$$

In Equation 3.32 the rate of increase of energy inside the control volume is given by

$$\frac{\partial}{\partial t}\left[\rho\left(e+\frac{V^2}{2}\right)\right]dxdy$$

The net rate at which the energy enters the control volume by convection or bulk fluid motion is obtained by subtracting the energy going out from that coming in, to yield

$$-\frac{\partial}{\partial x}\left[\rho u\left(e+\frac{V^2}{2}\right)\right]dxdy-\frac{\partial}{\partial y}\left[\rho v\left(e+\frac{V^2}{2}\right)\right]dxdy$$

Similarly, the heat flowing into the control volume by conduction is given by

$$-\left(\frac{\partial \dot{q}_x''}{\partial x}+\frac{\partial \dot{q}_y''}{\partial y}\right)dxdy=\left[\frac{\partial}{\partial x}\left(k\frac{\partial T}{\partial x}\right)+\frac{\partial}{\partial y}\left(k\frac{\partial T}{\partial y}\right)\right]dxdy$$

Finally, the net rate at which work is done on the fluid inside the control volume (Fig. 3.11) is given by the expression

$$\left(uF_{Bx}+vF_{By}\right)dxdy-\left[\frac{\partial(pu)}{\partial x}+\frac{\partial(pv)}{\partial y}\right]dxdy+\left[\frac{\partial}{\partial x}\left(u\sigma_{xx}\right)+\frac{\partial}{\partial y}\left(v\sigma_{yy}\right)+\frac{\partial}{\partial y}\left(u\tau_{yx}\right)+\frac{\partial}{\partial x}\left(v\tau_{xy}\right)\right]dxdy$$

On substituting these expressions into Equation 3.32, simplifying and using Equations 3.27 through 3.31, we obtain

$$\rho C_p\frac{\partial T}{\partial t}+\rho uC_p\frac{\partial T}{\partial x}+\rho vC_p\frac{\partial T}{\partial y}=\frac{\partial}{\partial x}\left(k\frac{\partial T}{\partial x}\right)+\frac{\partial}{\partial y}\left(k\frac{\partial T}{\partial y}\right)+\left(\frac{\partial p}{\partial t}+u\frac{\partial p}{\partial x}+v\frac{\partial p}{\partial y}\right)+\mu\Phi \tag{3.33}$$

In Equation 3.33, the thermodynamic definition of enthalpy ($i = e + p/\rho$ and $di = C_p dT$) has been used. Also, the term $\mu\Phi$ is called the viscous dissipation and is given by

$$\mu\Phi=2\mu\left[\left(\frac{\partial u}{\partial x}\right)^2+\left(\frac{\partial v}{\partial y}\right)^2\right]+\left(\frac{\partial u}{\partial y}+\frac{\partial v}{\partial x}\right)^2-\frac{2}{3}\left(\frac{\partial u}{\partial x}+\frac{\partial v}{\partial y}\right)^2 \tag{3.34}$$

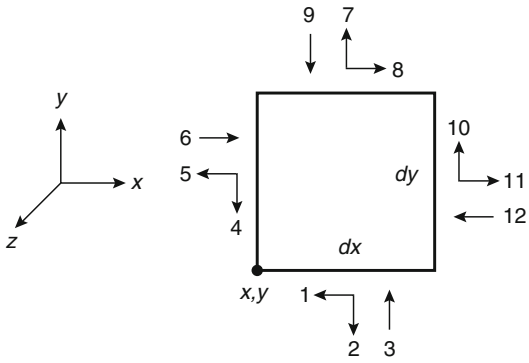

Fig. 3.11 Control volume showing the rate of work done by various surface forces. All units are in watts

Equations 3.21, 3.30, 3.31, and 3.33, along with the equation of state ($p = \rho RT$, for an ideal gas), provide a complete set for determining the temperature and velocity field [$T(x, y, t)$, $u(x, y, t)$, $v(x, y, t)$] inside the fluid. However, it is not possible to solve the above set of coupled nonlinear partial differential equations. Therefore, several simplifying approximations are made. These are discussed below.

Simplifications

1. *Low velocity*. For most problems encountered in convective heat transfer, the flow velocity is low enough (Mach number $< {}^1/_3$) to ignore the contribution of viscous work in the energy equation. This allows the term $\mu\phi$ in Equation 3.33 to be dropped.
2. *Incompressible flow*. Fluid density is assumed to be constant except in the buoyancy terms (F_{Bx}, F_{By}) of Equations 3.30 and 3.31. This is called the Boussinesq approximation and will be discussed later in greater detail.
3. *Steady flow*. This approximation allows all the time derivative terms in the above equations to be dropped.
4. *Constant properties*. Specific heat, thermal conductivity, and viscosity are all assumed to be constant; that is, independent of temperature and pressure.

With these simplifications and assuming that the body force is only due to gravity (i.e., $F_{Bx} = -\rho g_x$ and $F_{By} = -\rho g_y$), Equations 3.21, 3.30, 3.31, and 3.33 become

Continuity

$$\frac{\partial u}{\partial x} + \frac{\partial v}{\partial y} = 0 \tag{3.35}$$

x-momentum

$$u\frac{\partial u}{\partial x} + v\frac{\partial u}{\partial y} = -\frac{1}{\rho}\frac{\partial p}{\partial x} + \nu\left(\frac{\partial^2 u}{\partial x^2} + \frac{\partial^2 u}{\partial y^2}\right) - g_x \tag{3.36}$$

y-momentum

$$u\frac{\partial v}{\partial x} + v\frac{\partial v}{\partial y} = -\frac{1}{\rho}\frac{\partial p}{\partial y} + \nu\left(\frac{\partial^2 v}{\partial x^2} + \frac{\partial^2 v}{\partial y^2}\right) - g_y \tag{3.37}$$

Energy equation

$$u\frac{\partial T}{\partial x} + v\frac{\partial T}{\partial y} = \alpha\left(\frac{\partial^2 T}{\partial x^2} + \frac{\partial^2 T}{\partial y^2}\right) + \frac{1}{\rho C_p}\left(u\frac{\partial p}{\partial x} + v\frac{\partial p}{\partial y}\right) \tag{3.38}$$

Often, the energy equation is further simplified by assuming that the terms ($u\ \partial p/\partial x$) and ($v\ \partial p/\partial y$) are negligible. This assumption is justified since most processes of interest are nearly isobaric. Thus the energy equation becomes

$$u\frac{\partial T}{\partial x} + v\frac{\partial T}{\partial y} = \alpha\left(\frac{\partial^2 T}{\partial x^2} + \frac{\partial^2 T}{\partial y^2}\right) \tag{3.39}$$

Equations 3.35, 3.36, 3.37, and 3.39, along with the equation of state ($p = \rho RT$, for an ideal gas), provide a complete set for determining $u(x, y)$, $v(x, y)$, $T(x, y)$, $\rho(x, y)$, and $p(x, y)$. Once these dependent variables are known, the desired heat transfer coefficient and friction factor are obtained from Equations 3.5 and 3.11, respectively. However, the above equations are still too difficult to solve and a further simplification, known as the boundary layer approximation, is often made.

The Boundary Layer Concept

In 1904, Prandtl proposed that all the viscous effects are concentrated in a thin layer near the boundary and that outside this layer the fluid behaves as though it is inviscid. Thus, the flow over a body, such as the one shown in Fig. 3.6, can be divided into two zones: (1) a thin viscous layer near the surface, called the boundary layer, and (2) inviscid external flow, which can be closely approximated by the potential flow theory. As will be seen later, the fact that the boundary layer is thin compared to the characteristic dimensions of the object is exploited to simplify the governing equations and obtain a useful solution. This boundary layer approximation plays an important role in convective heat transfer, since the gradients of velocity and temperature at the surface of the body are required to determine the heat transfer coefficient and the friction factor.

To illustrate these ideas, consider fluid flow over a flat plate as shown in Fig. 3.12. The fluid particles in contact with the plate surface must assume zero velocity because of no slip at the wall, whereas the fluid particles far away from the wall continue to move at the free stream velocity, u_∞. The transition of fluid velocity from zero to u_∞ takes place in a small distance, δ, which is known as the boundary layer thickness and is defined as the value of y for which $u = 0.99u_\infty$. As is intuitively obvious, the thickness of the boundary layer increases with fluid viscosity and decreases with increasing free-stream velocity. By defining the Reynolds number, Re, as $\mathrm{Re} = u_\infty L/\nu$, where L is the characteristic length of the plate, the boundary layer thickness decreases with increasing Re. For most flows of practical interest, the Reynolds number is large enough such that δ is much less than the characteristic length, L ($\delta \ll L$).

Just as a velocity boundary layer develops because of viscous effects near the surface, a thermal boundary layer develops due to heat transfer between the free stream and the surface if their temperatures are different. The fluid particles that come into contact with the plate surface achieve thermal equilibrium at the plate's surface temperature. In turn, these particles exchange energy with those in the adjoining fluid layer, and temperature gradients develop in the fluid. As shown in Fig. 3.12, the region of the fluid in which these temperature gradients exist is the thermal boundary layer, and its thickness, δ_t, is defined as the value of y for which the ratio $[(T - T_S)/(T_\infty - T_S)] = 0.99$. The thermal boundary layer thickness increases with the thermal diffusivity, α, of the fluid and decreases with increasing free stream velocity. In other words, δ_t is inversely proportional to the product of the Reynolds number and Prandtl number ($\mathrm{Re}\ \mathrm{Pr} = (u_\infty L/\nu)(\nu/\alpha) = u_\infty L/\alpha$). For air, $\mathrm{Pr} \approx 0.7$ and the Reynolds number is sufficiently large for flows of practical interest, consequently $\delta_t \ll L$.

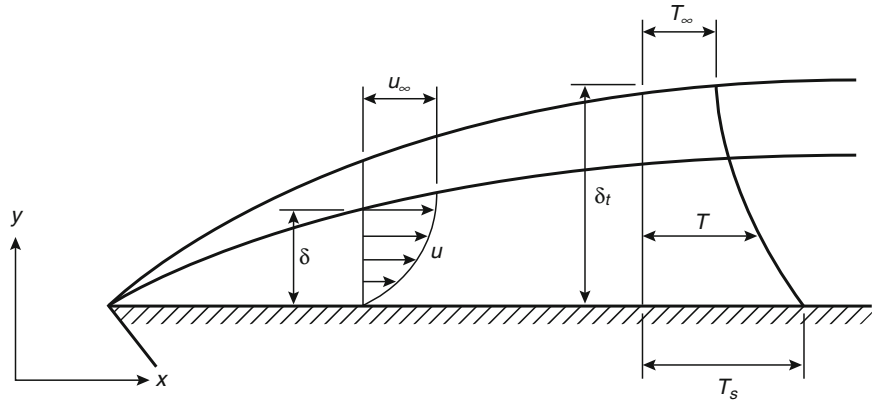

Fig. 3.12 Velocity and thermal boundary layers on a flat plate

Boundary Layer Approximation The governing Equations 3.35 through 3.37 and 3.39 can be further simplified for the case when the Reynolds number is reasonably large ($\mathrm{Re} \sim (L/\delta)^2$; that is, Re is of the order $(L/\delta)^2$) such that $\delta \ll L$. To compare the various terms in the governing equations, first normalize all the variables so that they are of the order of magnitude unity. By defining

$$x^* = \frac{x}{L} \qquad y^* = \frac{y}{\delta} \qquad u^* = \frac{u}{u_\infty}$$

and

$$T^* = \frac{T - T_s}{T_\infty - T_s} \tag{3.40}$$

variables that change from 0 to 1 inside the boundary layer are obtained. Substituting these into Equation 3.35 we find that

$$-\frac{\partial u^*}{\partial x^*} = \left(\frac{L}{\delta u_\infty}\right)\frac{\partial v}{\partial y^*}$$

This suggests that

$$v^* = \frac{Lv}{\delta u_\infty}$$

so that

$$\frac{\partial u^*}{\partial x^*} + \frac{\partial v^*}{\partial y^*} = 0 \tag{3.41}$$

Substituting x^*, y^*, u^*, and v^* into Equation 3.36 and simplifying

$$u^*\frac{\partial u^*}{\partial x^*} + v^*\frac{\partial u^*}{\partial y^*} = -\frac{\partial p^*}{\partial x^*} - g_x^* + \left(\frac{\nu}{Lu_\infty}\right) \times \left[\frac{\partial^2 u^*}{\partial x^{*2}} + \left(\frac{L}{\delta}\right)^2 \frac{\partial^2 u^*}{\partial y^{*2}}\right] \tag{3.42}$$

where $p^* \equiv p/\rho u_\infty^2$ and $g_x^* \equiv g_x L/u_\infty^2$.

In Equation 3.42, the quantity ν/Lu_∞ is recognized as 1/Re which is of the order $(\delta/L)^2$. Thus all terms in Equation 3.42 are of order of magnitude unity except the term $[(\nu/Lu_\infty)\partial^2 u^*/\partial x^{*2}]$, which is much less than 1 and can be ignored. Thus, Equation 3.36 is simplified to

$$u\frac{\partial u}{\partial x} + v\frac{\partial u}{\partial y} = -\frac{1}{\rho}\frac{dp}{dx} - g_x + \nu\frac{\partial^2 u}{\partial y^2} \tag{3.43}$$

Similarly, Equations 3.37 and 3.39 reduce to

$$\frac{\partial p}{\partial y} \approx 0 \tag{3.44}$$

and

$$u\frac{\partial T}{\partial x} + v\frac{\partial T}{\partial y} = \alpha\frac{\partial^2 T}{\partial y^2} \tag{3.45}$$

Equation 3.44 simply implies that $p = p(x)$, that is, the pressure at any plane where $x =$ constant does not vary with y inside the boundary layer and hence is equal to the free stream pressure. To summarize, the boundary layer approximation yields a simpler set of governing equations that are valid inside the boundary layer. These equations for steady flow of an incompressible fluid with constant properties are

Continuity

$$\frac{\partial u}{\partial x} + \frac{\partial v}{\partial y} = 0 \tag{3.35}$$

x-momentum

$$u\frac{\partial u}{\partial x} + v\frac{\partial u}{\partial y} = -\frac{1}{\rho}\frac{\partial p}{\partial x} - g_x + \nu\frac{\partial^2 u}{\partial y^2} \tag{3.43}$$

Energy

$$u\frac{\partial T}{\partial x} + v\frac{\partial T}{\partial y} = \alpha\frac{\partial^2 T}{\partial y^2} \tag{3.45}$$

To illustrate the use of these equations in determining the heat transfer coefficient, consider two classical examples: (1) laminar forced convection over a flat surface, and (2) laminar free convection on a vertical flat surface. Forced convection is chosen as a precursor to free convection because

it is simpler and also allows us to illustrate the difference between them. A flat geometry is also chosen in both cases for simplicity.

Laminar Forced Convection Over a Flat Surface A schematic of this problem is presented in Fig. 3.12, and the objective here is to obtain the gradients of temperature and velocity profile at $y = 0$. By applying the Bernoulli Equation in the potential flow region outside the boundary layer we obtain

$$\frac{u_\infty^2}{2} + \frac{p}{\rho} + gh = \text{constant} \tag{3.46}$$

Since the free stream velocity, u_∞, is constant, for a given height $y = h$ above the flat surface we obtain that $p =$ constant, that is, $p \neq p(x)$ outside the boundary layer in the potential flow region. From Equation 3.44 note that $p \neq p(y)$ inside the boundary layer. Hence, $p =$ constant both inside and outside the boundary layer over a flat surface. This implies that the term $\partial p/\partial x$ equals zero in Equation 3.43. Also, since the flow is forced (i.e., generated by an external agent such as a fan, rather than by buoyancy) the gravitational force, g_x, in Equation 3.43 does not contribute to the increase in momentum represented by the left side of the equation, and $g_x = 0$. Thus Equation 3.43 becomes

$$u\frac{\partial u}{\partial x} + v\frac{\partial u}{\partial y} = \nu\frac{\partial^2 u}{\partial y^2} \tag{3.47}$$

Equations 3.35, 3.45, and 3.47 govern the temperature and velocity distributions inside the boundary layer shown in Fig. 3.12. The associated boundary conditions areno-slip

$$u = v = 0 \qquad \text{at} \qquad y = 0$$

and

$$T = T_s \qquad \text{at} \qquad y = 0 \tag{3.48}$$

also

$$u = u_\infty \text{ and } T = T_\infty \text{ as } y \to \infty$$

Nondimensionalizing Equations 3.35, 3.45, 3.47, and 3.48 according to Equation 3.40[1] we obtain

$$\frac{\partial u^*}{\partial x^*} + \frac{\partial v^*}{\partial y^*} = 0 \tag{3.49}$$

$$u^*\frac{\partial u^*}{\partial x^*} + v^*\frac{\partial u^*}{\partial y^*} = \frac{1}{\text{Re}_L}\frac{\partial^2 u^*}{\partial y^{*2}} \tag{3.50}$$

$$u^*\frac{\partial T^*}{\partial x^*} + v^*\frac{\partial T^*}{\partial y^*} = \frac{1}{\text{Re}_L\text{Pr}}\frac{\partial^2 T^*}{\partial y^{*2}} \tag{3.51}$$

along with the boundary conditions

$$u^* = v^* = T^* = 0 \text{ at } y^* = 0$$

and

$$u^* = T^* = 1 \text{ at } y^* \to \infty \tag{3.52}$$

where

$$\text{Re}_L \equiv \frac{u_\infty L}{\nu}$$

is the Reynolds number based on length, L, and $\text{Pr} \equiv \nu/\alpha$ is the Prandtl number. Note that Equations 3.49 and 3.50 are sufficient for determining u^* (x^*, y^*) and v^* (x^*, y^*) and that once these are known, Equation 3.51 can be independently solved for T^* (x^*, y^*) Also note that for $\text{Pr} = 1$, Equations 3.50 and 3.51 as well as their corresponding boundary conditions are identical. Thus for $\text{Pr} = 1$ only Equations 3.49 and 3.50 need to be solved.

A similarity solution of Equations 3.49 and 3.50 along with the boundary conditions (Equation 3.52) was obtained by Blasius [2]. Blasius observed that since the system under consideration has no preferred length, it is reasonable to suppose that the velocity profiles at different

[1] A more convenient definition of $y^* = y/L$ and $v^* = v/u_\infty$ has been used since we are no longer interested in quantities of order of magnitude unity; instead we are simply interested in eliminating units.

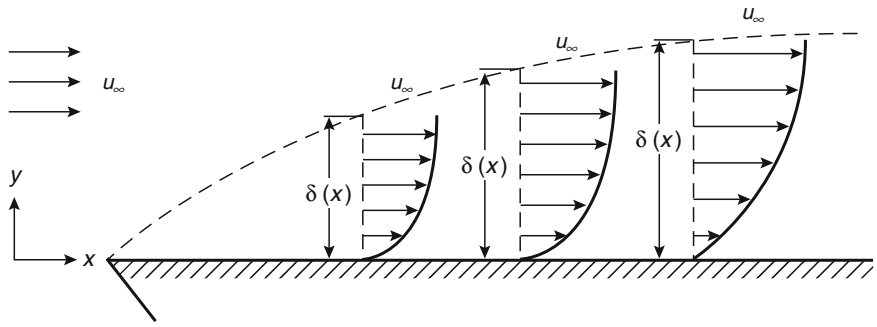

Fig. 3.13 Observed velocity profiles at different values of x

values of x have similar shapes; that is, if u and y are suitably scaled then the velocity profile may be expressed by a single function for all values of x (Fig. 3.13). An obvious choice is

$$\frac{u}{u_\infty} = \phi\left[\frac{y}{\delta(x)}\right]\phi \tag{3.53}$$

This choice, as it stands, is not very useful because $\delta(x)$ is not known. However, in accordance with the boundary layer approximation, $\mathrm{Re}_x \equiv u_\infty x/\nu \sim (x/\delta)^2$. Therefore,

$$\delta \sim \sqrt{\frac{\nu x}{u_\infty}}$$

can be expected. Substituting into Equation 3.53 we obtain

$$u^* = \frac{u}{u_\infty} = \phi\left[\frac{y}{x}\sqrt{\mathrm{Re}_x}\right] = \phi(\eta) \tag{3.54}$$

where

$$\eta \equiv \frac{y}{x}\sqrt{\mathrm{Re}_x} = \left[\left(\frac{y^*}{\sqrt{x^*}}\right)\sqrt{\mathrm{Re}_L}\right]$$

is the similarity variable. By introducing a stream function, ψ, such that

$$u^* = \frac{\partial\psi}{\partial y^*} \quad \text{and} \quad v^* = -\frac{\partial\psi}{\partial x^*} \tag{3.55}$$

Equation 3.49 is identically satisfied. Substituting Equation 3.54 into Equation 3.55 and integrating, we get

$$\psi = \int \phi(\eta)dy^* + f_1(x^*)$$
$$= \frac{\sqrt{x^*}}{\sqrt{\mathrm{Re}_L}}\int \phi(\eta)d\eta + f_1(x^*)$$

Since $v^* = 0$ at $y^* = 0, f_1(x^*)$ is at best an arbitrary constant which is taken as zero. Also, defining a new function $f(\eta) \equiv \int \phi(\eta)d\eta$, we obtain

$$\psi = \sqrt{x^*}\frac{f(\eta)}{\sqrt{\mathrm{Re}_L}} \tag{3.56}$$

therefore,

$$u^* = \left(\frac{\partial\psi}{\partial y^*}\right)_{x^*} = \left(\frac{\partial\psi}{\partial\eta}\right)_{x^*}\left(\frac{\partial\eta}{\partial y^*}\right)_{x^*}$$
$$= f'(\eta) = \frac{df}{d\eta} \tag{3.57}$$

and

$$-v^* = \left(\frac{\partial\psi}{\partial x^*}\right)_{y^*} = \left(\frac{\partial\psi}{\partial x^*}\right)_{\eta} + \left(\frac{\partial\psi}{\partial\eta}\right)_{x^*}\left(\frac{\partial\eta}{\partial x^*}\right)_{y^*}$$
$$= \frac{1}{2}\left(f - \eta f'\right)\sqrt{x^*\mathrm{Re}_L} \tag{3.58}$$

On substituting u^*, v^* into Equation 3.50 and simplifying we obtain

$$2f''' + ff'' = 0 \tag{3.59}$$

where primes represent differentiation with respect to η. Equation 3.59 is a third-order

nonlinear ordinary differential equation. Recall that η was a combination of two independent variables, x^* and y^*, and it was assumed that $u^* = \phi(\eta)$. If this similarity assumption was incorrect, then the partial differential Equation 3.50 would not have reduced to an ordinary differential Equation 3.59—that is, x^* would not have completely disappeared from the governing equation. Note also that even though Equation 3.59 is nonlinear and has to be solved numerically, there are no parameters and therefore it needs to be solved only once. Boundary conditions corresponding to Equation 3.59 become

$$f = f' = 0 \text{ at } \eta = 0, \text{ and } f' = 1 \text{ as } \eta \to \infty \tag{3.60}$$

A numerical solution of Equation 3.59 along with the boundary conditions, Equation 3.60 is shown in Fig. 3.14. Note that for Pr = 1, the solution for T^* is the same as that for u^*. Also, once T^* (x^*, y^*) and u^* (x^*, y^*) are known the heat transfer coefficient and friction factor can easily be obtained from Equations 3.5 and 3.11. Furthermore, from the definition of thermal and velocity boundary layer thickness ($T^* = u^* = 0.99$), we find that η = 5.

Therefore,

$$\eta = \frac{y}{x}\sqrt{\frac{u_\infty x}{\nu}} = 5 \quad \text{for} \quad y = \delta = \delta_t$$

or for Pr = 1,

$$\delta = \delta_t = \frac{5x}{\sqrt{\text{Re}_x}} \tag{3.61}$$

From Equation 3.61 it is clear that δ and δ_t increase with x but decrease with increasing u_∞ (the larger the free stream velocity, the thinner the boundary layer). Now, to determine the heat transfer coefficient and the friction factor we need $\partial T/\partial y\big|_{y=0}$ and $\partial u/\partial y\big|_{y=0}$. From Fig. 3.14, we have

$$\left.\frac{\partial T^*}{\partial \eta}\right|_{\eta=0} = \left.\frac{\partial u^*}{\partial \eta}\right|_{\eta=0} = 0.332$$

Thus,

$$\tau_s = \mu\left.\frac{\partial u}{\partial y}\right|_{y=0} = 0.332 u_\infty \sqrt{\rho\mu u_\infty / x} \tag{3.62}$$

and

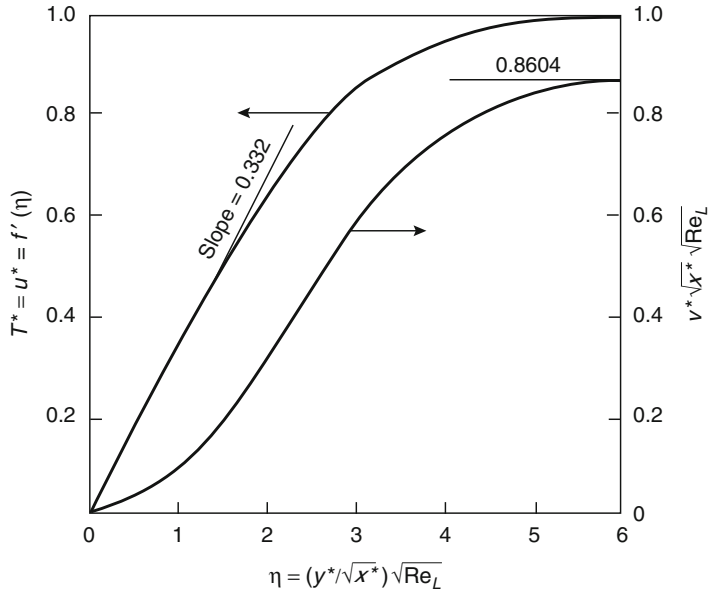

Fig. 3.14 Nondimensional velocity profiles in laminar boundary layer over a flat plate

$$\dot{q}_s'' = -k\frac{\partial T}{\partial y}\bigg|_{y=0} = 0.332(T_s - T_\infty)k\sqrt{\rho u_\infty/\mu x} \tag{3.63}$$

Hence the *local* friction and heat transfer coefficients are

$$C_f = \frac{0.664}{\sqrt{\mathrm{Re}_x}} \tag{3.64}$$

and

$$h = 0.332\frac{k}{x}\sqrt{\mathrm{Re}_x} \tag{3.65}$$

Equation 3.65 is often rewritten in terms of a nondimensional heat transfer coefficient called the Nusselt number, Nu, as

$$\mathrm{Nu} = \frac{hx}{k} = 0.332\sqrt{\mathrm{Re}_x} \tag{3.66}$$

All the above results are for the case when Pr = 1. When Pr ≠ 1, Equation 3.51 must also be solved with the help of the solution just obtained for Equations 3.49 and 3.50. Equation 3.51 becomes

$$\frac{d^2T^*}{d\eta^2} + \frac{\mathrm{Pr}}{2}f\frac{dT^*}{d\eta} = 0$$

with $T^*(0) = 0$ and $T^*(\infty) = 1$. This solution does not change the expressions for δ and C_f given by Equations 3.61 and 3.64. However δ_t and Nu become [2]

$$\delta_t = \frac{5x}{\sqrt{\mathrm{Re}_x}}\mathrm{Pr}^{-1/3} = \delta\mathrm{Pr}^{-1/3} \tag{3.67}$$

and

$$\mathrm{Nu} = 0.332\sqrt{\mathrm{Re}_x}\mathrm{Pr}^{1/3}(\mathrm{Pr}\gtrsim 0.6) \tag{3.68}$$

Note that for Pr < 1 (usually true for gases), δ_t is greater than δ; that is, the thermal boundary layer is thicker than the momentum boundary layer. This is to be expected since Pr < 1 implies that ν is less than α.

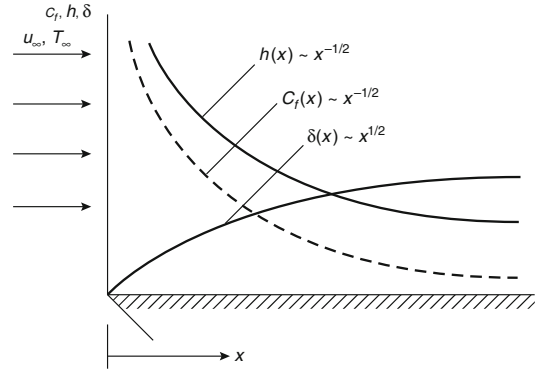

Fig. 3.15 Variation of C_f, h, and δ with x for flow over a flat plate

The results for the friction factor, C_f, and the Nusselt number, Nu, given by Equations 3.64 and 3.68 are for local values; that is, C_f and Nu change with x. This variation is shown in Fig. 3.15. At $x = 0$, both C_f and h tend to infinity. This is physically incorrect and happens because near $x = 0$ the boundary layer approximation breaks down since δ is no longer much less than x.

For many applications, only average values of the heat transfer coefficient, $\overline{h}$, and friction factor, $\overline{C}_f$, are required. These are obtained by using Equations 3.9 and 3.15. In these equations $dA_s = dx \cdot$ (the unit width of the flat plate), and the average can be obtained from $x = 0$ to any length, L (which may be the total length of the plate). Simple integration leads to the following results:

$$\overline{C}_{fL} = 1.328\,\mathrm{Re}_L{}^{-1/2} = 2C_f(\text{Evaluated at } x = L) \tag{3.69}$$

and

$$\overline{\mathrm{Nu}}_L \equiv \frac{\overline{h}_L L}{k} = 0.664\,\mathrm{Re}_L{}^{1/2}\,\mathrm{Pr}^{1/3} = 2\,\mathrm{Nu}(\text{Evaluated at } x = L) \tag{3.70}$$

It is interesting to note that C_f and Nu are closely related. For example, from Equations 3.69 and 3.70 one can easily obtain

$$\overline{\mathrm{Nu}}_L = \frac{C_{fL}\mathrm{Re}_L\mathrm{Pr}^{1/3}}{2}$$

or

$$\mathrm{St} \equiv \frac{\overline{\mathrm{Nu}}_L}{\mathrm{Re}_L \mathrm{Pr}} = \frac{\overline{C}_{fL}}{2} \mathrm{Pr}^{-2/3} \tag{3.71}$$

where St is known as the Stanton number.

This analogy between heat and momentum transfer is called the *Reynolds analogy* which is significant because the heat transfer coefficient can be determined from the knowledge of the friction factor. This analogy is especially useful for cases where mathematical solutions are not available.

Laminar Free Convection In contrast with forced convection, where the fluid motion is externally imposed, for free convection the fluid motion is caused by the buoyancy forces. Buoyancy is due to the combined effect of *density gradients* within the fluid and a *body force* that is proportional to the fluid density. In practice the relevant body force is usually gravitational, although it may be centrifugal, magnetic, or electric. Of the several ways in which a density gradient may arise in a fluid, the two most common situations are due to (1) the presence of temperature gradients, and (2) the presence of concentration gradients in a multicomponent system such as a fire. Here, the focus will be on free convection problems in which the density gradient is due to temperature and the body force is gravitational. Note, however, that the presence of density gradients in a gravitational field does not ensure the existence of free convection currents. For example, the high temperature, lighter fluid may be on top of a low temperature, denser fluid, resulting in a stable situation. It is only when the condition is unstable that convection currents are generated. An example of an unstable situation would be a denser fluid on top of a lighter fluid. In a stable situation there is no fluid motion and, therefore, heat transfer occurs purely by conduction. Here we will only consider the unstable situation that results in convection currents.

Free convection flow may be further classified according to whether or not the flow is bounded by a surface. In the absence of an adjoining surface, free boundary flows may occur in the form of a plume or a buoyant jet. A buoyant plume above a fire is a familiar example. However, here we will focus on free convection flows that are bounded by a surface. A classical example of boundary layer development on a heated vertical flat plate is discussed below.

Heated, Vertical Flat Plate Consider the flat plate shown in Fig. 3.16. The plate is immersed in an extensive, quiescent fluid, with $T_s > T_\infty$. The density of the fluid close to the plate is less than that of the fluid that is farther from the plate. Buoyancy forces therefore induce a free convection boundary layer in which the heated fluid rises vertically, entraining fluid from the quiescent region.

Under steady-state laminar flow conditions, Equations 3.35, 3.43, and 3.45 describe the mass, momentum, and energy balances for the two-dimensional boundary layer shown in Fig. 3.16. Assume that the temperature

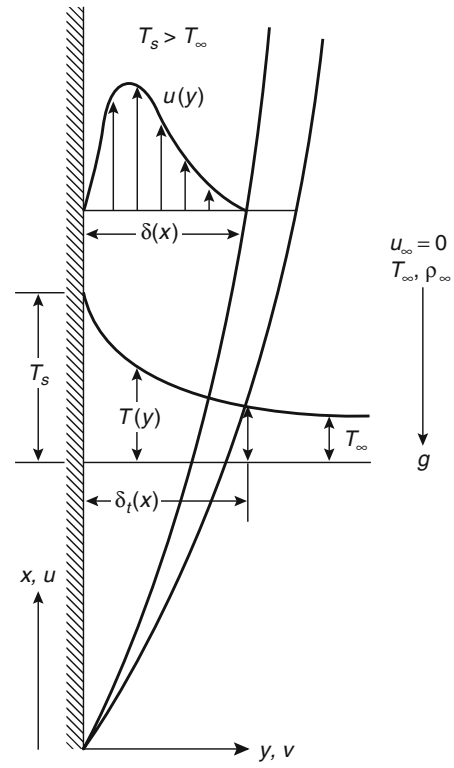

Fig. 3.16 Boundary layer development on a heated vertical plate

differences are moderate, such that the fluid may be treated as having constant properties. Also, with the exception of the buoyancy force term (g_x in Equation 3.43), the fluid can be assumed to be incompressible. Outside the boundary layer, Equation 3.36 is valid, and since $u = v = 0$ outside the boundary layer we obtain: $dp/dx = -\rho_\infty g_x$. Since $\partial p/\partial x = 0$ because of the boundary layer approximation (i.e., $p \neq p(y)$ inside the boundary layer; Equation 3.44), dp/dx inside the boundary layer must be equal to its corresponding value outside, that is, $dp/dx = -\rho_\infty g_x$.

Substituting this into Equation 3.43

$$u\frac{\partial u}{\partial x} + v\frac{\partial u}{\partial y} = g_x\frac{(\rho_\infty - \rho)}{\rho} + \nu\frac{\partial^2 u}{\partial y^2} \tag{3.72}$$

The first term on the right side of Equation 3.72 is the buoyancy force, and the flow originates because the density ρ is variable. By introducing the coefficient of volumetric thermal expansion, β,

$$\beta = -\frac{1}{\rho}\left(\frac{\partial \rho}{\partial T}\right)_\rho \approx -\frac{1}{\rho}\frac{(\rho_\infty - \rho)}{(T_\infty - T)} \tag{3.73}$$

it follows that

$$\frac{(\rho_\infty - \rho)}{\rho} = \beta(T - T_\infty) \tag{3.74}$$

Substituting Equation 3.74 into Equation 3.72 a useful form of the x-momentum is obtained as

$$u\frac{\partial u}{\partial x} + v\frac{\partial u}{\partial y} = g_x\beta(T - T_\infty) + \nu\frac{\partial^2 u}{\partial y^2} \tag{3.75}$$

From Equation 3.75 it is now apparent how buoyancy force is related to temperature difference. Note that the appearance of the buoyancy term in the momentum equation mathematically complicates the situation. The decoupling between the hydrodynamic and the thermal problems achieved in forced convection is no longer possible, since T appears in both Equations 3.45 and 3.75. The boundary conditions associated with the governing equations, Equations 3.35, 3.45, and 3.75, are

$$u = v = 0 \quad T = T_\infty \quad as\ y \to \infty \tag{3.76}$$

Nondimensionalizing Equations 3.35, 3.45, 3.75, and 3.76 with $x^* = x/L$, $y^* \equiv y/L$, $u = u/u0$, $v^* \equiv v/u0$, and $T^* \equiv (T - T_\infty)/(T_s - T_\infty)$, we obtain

$$\frac{\partial u^*}{\partial x^*} + \frac{\partial v^*}{\partial y^*} = 0 \tag{3.77}$$

$$u^*\frac{\partial u^*}{\partial x^*} + v^*\frac{\partial u^*}{\partial y^*} = \frac{g\beta T^*(T_s - T_\infty)L}{u_0^2} + \frac{1}{\mathrm{Re}_L}\frac{\partial^2 u^*}{\partial y^{*2}} \tag{3.78}$$

and

$$u^*\frac{\partial T^*}{\partial x^*} + v^*\frac{\partial T^*}{\partial y^*} = \frac{1}{\mathrm{Re}_L\mathrm{Pr}}\frac{\partial^2 T^*}{\partial y^{*2}} \tag{3.79}$$

Note that u_0 in Equation 3.78 is an unknown reference velocity and not the free stream velocity as in the case of forced convection. Also, the dimensionless parameter

$$\frac{g\beta(T_s - T_\infty)L}{u_0^2}$$

is a direct result of buoyancy forces. To eliminate the unknown reference velocity, u_0 from the dimensionless parameter, we define

$$\text{Grashof number, } \mathrm{Gr}_L \equiv \frac{g\beta(T_s - T_\infty)L}{u_0^2}\left(\frac{Lu_0}{\nu}\right)^2 = \frac{g\beta(T_s - T_\infty)L^3}{\nu^2}$$

Thus, the first term on the right side of Equation 3.78 becomes $\mathrm{Gr}_L/(\mathrm{Re}_L)^2$. The Grashof number plays the same role in free convection as the Reynolds number does in forced convection. Gr is the ratio of buoyancy and viscous forces. The governing equations now contain three parameters—the Grashof number, Reynolds number, and Prandtl number. For the forced convection case it is seen (Equation 3.68) that Nu = Nu (Re, Pr); thus for the free convection case, we expect Nu = Nu (Re, Gr, Pr). If the

buoyancy term in Equation 3.79 is $Gr/(Re)^2 \gg 1$, then we primarily have free convection; that is, $Nu = Nu(Gr, Pr)$. For $Gr/(Re)^2 \ll 1$, the forced convective case exists, where as has already been seen, $Nu = Nu\ (Re, Pr)$. However, when $Gr/(Re)^2 \sim 1$ a mixed (free and forced) convection case is obtained. For the present problem we will assume that $Gr \gg (Re)^2$, thus, Nu must be a function of only Gr and Pr.

Since $Gr \gg Re^2$, it follows that buoyancy forces are much larger than inertia forces; in other words, the primary balance is between the buoyancy and viscous forces. Since the left side of Equation 3.78 represents the inertia forces, the primary balance is between the two terms on the right side, that is,

$$-\frac{g\beta T^*(T_s - T_\infty)L}{u_0^2} \approx \left(\frac{\nu}{u_0 L}\right)\frac{\partial^2 u^*}{\partial y^{*2}}$$

Crudely approximating the various terms, we have in dimensional variables

$$g\beta(T_\infty - T) \approx \nu\frac{u}{\delta^2} \tag{3.a}$$

Similarly approximating Equations 3.77 and 3.79 and expressing the result in dimensional form (it is more convenient to use Equations 3.35 and 3.45), we get from Equation 3.35 or 3.77

$$\frac{u}{x} \approx \frac{v}{\delta} \quad \text{or} \quad v \approx \frac{\delta u}{x} \tag{3.b}$$

and from Equation 3.79 or 3.45 along with relation (3.b)

$$u\frac{(T_\infty - T)}{x} \approx \alpha\frac{(T_\infty - T)}{\delta^2} \quad \text{or} \quad u \approx \frac{\alpha x}{\delta^2} \tag{3.c}$$

Combining (3.a) and (3.c) we obtain an expression for the boundary layer thickness, δ,

$$\delta \approx \left(\frac{\nu\alpha x}{g\beta(T_\infty - T)}\right)^{1/4}$$

Thus, we expect δ to scale with $x^{1/4}$ and u to scale with $x^{1/2}$. (Note that in the forced convective case we found that $\delta \sim x^{1/2}$; Fig. 3.15). Following a reasoning similar to the forced convective case, a similarity variable $\xi \approx y/\delta(x)$ or $\xi = Ay/x^{1/4}$ may be found, where A is an arbitrary constant. Also, motivated by Equation 3.57 for forced convection, it is hoped that $u = Bx^{1/2}f'(\xi)$ where B is an arbitrary constant. Expressing these in nondimensional variables, we get

$$\zeta = Ay^*/x^{*1/4} \tag{3.80}$$

and

$$u^* = Bx^{*1/2}f'(\xi)$$

where $f'(\xi) = df/d\xi$. Note that the definitions of the arbitrary constants A and B have been changed during nondimensionalization. By introducing a stream function, ψ, as in Equation 3.55, Equation 3.77 is identically satisfied.

Thus,

$$\begin{aligned}\psi &= \int Bx^{*1/2}f'(\xi)dy^* + f_1(x^*)\\ &= \int \frac{B}{A}x^{*3/4}f'(\xi)d\xi + f_1(x^*)\\ &= \frac{B}{A}x^{*3/4}f(\xi) + f_1(x^*)\end{aligned} \tag{3.81}$$

Since $v^* = 0$ at $y^* = 0$ (or $\xi = 0$), $f_1(x^*)$ is at best an arbitrary constant which is taken to be zero without any loss of generality. From Equations 3.55 and 3.81 we get

$$v^* = -\frac{B}{4Ax^{*1/4}}\left[3f(\xi) - \xi f'(\xi)\right] \tag{3.82}$$

By using Equations 3.80 and 3.82, Equations 3.78 and 3.79 can be reduced to

$$f''' + 3ff'' - 2\left(f'\right)^2 + T^* = 0 \tag{3.83}$$

and

$$T^{*''} + 3\mathrm{Pr}fT^{*'} = 0 \tag{3.84}$$

where the following definitions of the arbitrary constants A and B have been used:

$$B = \left[\frac{4g\beta(T_s - T_\infty)L}{u_0^2}\right]^{1/2}$$
$$A = \left[\frac{g\beta(T_s - T_\infty)L^3}{4\nu^2}\right]^{1/4} \quad (3.85)$$

Note that in Equation 3.84 it has been assumed that T^* is a function of ξ only. From Equation 3.85 it follows that

$$\xi = \frac{y^*}{x^{*1/4}}\left[\frac{g\beta(T_s - T_\infty)L^3}{4\nu^2}\right]^{1/4}$$
$$= \frac{y^*}{x^{*1/4}}\left(\frac{\mathrm{Gr}_L}{4}\right)^{1/4} \quad (3.86)$$

The associated boundary conditions given by Equation 3.76 become

$$f = f' = 0 \text{ and } T^* = 1 \text{ when } \xi = 0$$

and

$$f' = 0\, T^* = 0 \text{ at } \xi = \infty \quad (3.87)$$

A numerical solution of Equations 3.83 and 3.84 along with the boundary conditions given by Equation 3.87 are shown in Fig. 3.17. Note that the nondimensional x-velocity component, u, may be readily obtained from Fig. 3.17 part (a) through the use of Equations 3.80 and 3.85. Note also that, through the definition of the similarity variable, ξ, Fig. 3.17 may be used to obtain values of u^* and T^* for any value of x^* and y^*. Once $u^*(x^*, y^*)$ and $T^*(x^*, y^*)$ are known, the heat transfer coefficient can easily be obtained from Equation 3.5. Thus, the temperature gradient at $y = 0$ after using Equation 3.86, becomes

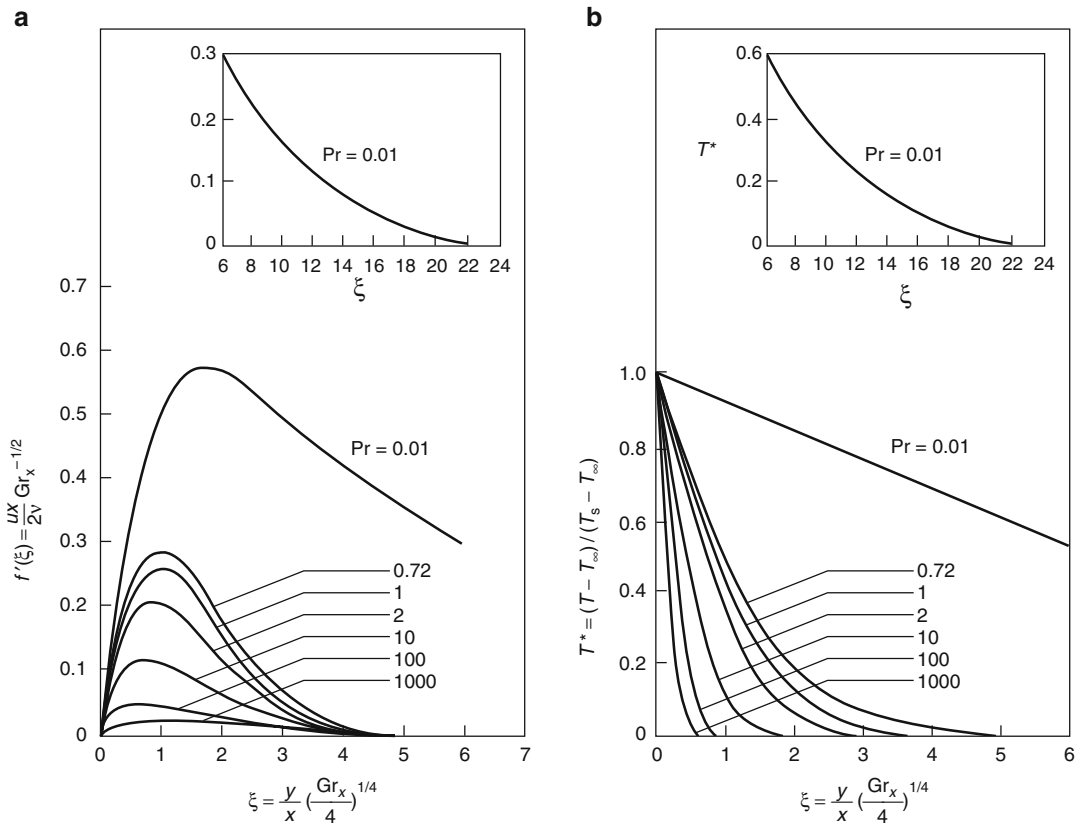

Fig. 3.17 Laminar free convection boundary layer on an isothermal, vertical surface

Table 3.1 Dimensionless temperature gradient for free convection on a vertical flat plate

Pr	0.01	0.72	1	2	10	100	1000
$g(Pr)$	0.081	0.505	0.567	0.716	1.169	2.191	3.966

$$\left.\frac{\partial T}{\partial y}\right|_{y=0} = \frac{(T_s - T_\infty)}{L}\left.\frac{\partial T^*}{\partial y^*}\right|_{y^*=0} = \frac{(T_s - T_\infty)}{Lx^{*1/4}}\left(\frac{\mathrm{Gr}_L}{4}\right)^{1/4}\left.\frac{dT^*}{d\xi}\right|_{\xi=0}$$

The *local* heat transfer coefficient is

$$h = \frac{-k}{Lx^{*1/4}}\left(\frac{\mathrm{Gr}_L}{4}\right)^{1/4}\left.\frac{dT^*}{d\xi}\right|_{\xi=0} \tag{3.88}$$

or

$$\mathrm{Nu} = \frac{hx}{k} = -x^{*3/4}\left(\frac{\mathrm{Gr}_L}{4}\right)^{1/4}\left.\frac{dT^*}{d\xi}\right|_{\xi=0} = \left(\frac{\mathrm{Gr}_x}{4}\right)^{1/4} g(\mathrm{Pr}) \tag{3.89}$$

As is evident from Fig. 3.17, the dimensionless temperature gradient at $\xi = 0$ is a function of the Prandtl number. In Equation 3.89 this function is expressed as $-g(\mathrm{Pr})$. Values of $g(\mathrm{Pr})$ obtained from the numerical solution are listed in Table 3.1.

From Equation 3.88 for the local heat transfer coefficient, the average heat transfer coefficient for a surface of length L is obtained by using Equation 3.9 as follows:

$$\bar{h}_L = \frac{1}{L}\int_0^L h(dx \cdot 1) = \frac{k}{L^{7/4}}\left(\frac{\mathrm{Gr}_L}{4}\right)^{1/4} g(\mathrm{Pr}) \times \int_0^L \frac{dx}{x^{1/4}} = \frac{4k}{3L}\left(\frac{\mathrm{Gr}_L}{4}\right)^{1/4} g(\mathrm{Pr}) \tag{3.90}$$

Thus,

$$\overline{\mathrm{Nu}}_L = \frac{\bar{h}_L L}{k} = \frac{4}{3}\left(\frac{\mathrm{Gr}_L}{4}\right)^{1/4} g(\mathrm{Pr}) \tag{3.91}$$

or from Equation 3.89, with $x = L$ we get

$$\overline{\mathrm{Nu}}_L = \frac{4}{3}\,\mathrm{Nu}\begin{pmatrix}\text{Evaluated}\\ \text{at } x = L\end{pmatrix} \tag{3.92}$$

It should be noted that the foregoing results apply irrespective of whether $T_s > T_\infty$ or $T_s < T_\infty$. If $T_s < T_\infty$, the conditions are inverted from those shown in Fig. 3.16. The loading edge is on the top of the plate, and positive x is defined in the direction of the gravity force.

Integral Solution Methods

For many problems an exact similarity solution is not possible. An alternate approach is to use approximate integral methods originally proposed by von Kárman in 1921 [6]. Intelligent use of integral methods gives good result and it can be very useful for solving difficult fire problems. This method is also very useful for conduction problems.

Forced Flow Laminar Boundary Layer on a Flat Plate

Referring to Fig. 3.12, one can essentially integrate the equations in the y direction across the boundary layer. This eliminates one variable—resulting in ODEs. Integrating the continuity equation:

$$\int_0^\delta \frac{\partial u}{\partial x}dy + \int_0^\delta \frac{\partial V}{\partial y}dy = 0;\ \textit{Since},\ V = 0\ \textit{at}\ \ y = 0,\ V(y = \delta) = -\int_0^\delta \frac{\partial u}{\partial x}dy$$

Integrating the momentum equation:

$$\int_0^\delta u\frac{\partial u}{\partial x}dy + uV|_0^\delta - \int_0^\delta u\frac{\partial V}{\partial y}dy = v\left(\left.\frac{\partial u}{\partial y}\right|_\delta - \left.\frac{\partial u}{\partial y}\right|_0\right)$$

Eliminating V by using continuity and rearranging, the integral form of the boundary layer momentum equation results. It basically states that the decrease in kinetic energy of the fluid in the B.L. occurs because of the wall friction at $y = 0$.

$$\frac{d}{dx}\left[\int_0^\delta (u_\infty - u)u\,dy\right] = v\left.\frac{\partial u}{\partial y}\right|_{y=0}$$

In a similar fashion, the integral form of the boundary layer energy equations may be obtained as:

$$\frac{d}{dx}\left[\int_0^{\delta t} (T_\infty - T)u\,dy\right] = \alpha\left.\frac{\partial T}{\partial y}\right|_{y=0}$$

These equations satisfy the x-momentum and energy conservation requirements in an integral (or average) fashion over the entire boundary layer. In contrast, the original conservation equations satisfy the conservation requirements locally at each point in the boundary layer.

The solution procedure involves:

1. Assuming reasonable functional forms for the unknowns u *and* T in terms of the corresponding (unknown) boundary layer thicknesses.
2. These functional forms must satisfy appropriate boundary conditions.
3. Substituting these forms into the integral equations, expressions for the boundary layer thicknesses are determined and the assumed functional forms are then completely specified.
4. While this method is approximate, it frequently leads to accurate results for the surface parameters that are usually of interest in fire problems.

Now consider the hydrodynamic boundary layer, for which the appropriate boundary conditions are: $u(y=0) = 0;\ u(y=\delta) = u_\infty; (\partial u/\partial y)_{y=\delta} = 0$ Since $u = v = 0\ ; at\ y = 0$, $\partial^2 u/\partial y^2|_{y=0} = 0$.

With these conditions, we could approximate the velocity profile as a third degree polynomial of the form:

$$\frac{u}{u_\infty} = a_1 + a_2\left(\frac{y}{\delta}\right) + a_3\left(\frac{y}{\delta}\right)^2 + a_4\left(\frac{y}{\delta}\right)^3$$

Applying the boundary conditions to determine the coefficients a_1 *to* a_4. It is easily verified that $a_1 = a_3 = 0, a_2 = 3/2$ *and* $a_4 = -1/2$, in which case:

$$\frac{u}{u_\infty} = \frac{3}{2}\left(\frac{y}{\delta}\right) - \frac{1}{2}\left(\frac{y}{\delta}\right)^3$$

This velocity profile is specified in terms of the unknown boundary layer thickness δ which is determined by substituting into the momentum equation and integrating over y to obtain:

$$\frac{13\,u_\infty}{140\,\nu}\frac{d\delta}{dx} = \frac{1}{\delta};\ or\ \ \delta d\delta = \frac{140\,\nu}{13\,u_\infty}dx\ i.e.\ \ \frac{\delta^2}{2} = \frac{140}{13}\frac{\nu x}{u_\infty} + const.$$

Since $\delta = 0$ at the leading edge $(x = 0)$, the integration constant $= 0$. Thus:

$$\delta = 4.641\sqrt{\frac{\nu x}{u_\infty}} = 4.641\,x\,\mathrm{Re}_x^{-1/2}\ ;\ \text{This completely specifies the above velocity profile.}$$

$$\text{Thus } \tau_s = \mu\left.\frac{\partial u}{\partial y}\right|_{y=0};\ \text{differenciating the velocity profile, we get :}\ C_{f,x} \equiv \frac{\tau_s}{\rho u_\infty^2/2} = \frac{0.646}{\mathrm{Re}_x^{1/2}}.$$

The exact solution gave us 0.664 instead of 0.646 as the constant—a minor difference.

Integral Solution for the Thermal Laminar Boundary Layer

Similar to the momentum boundary layer, the temperature profile of the following form is assumed:

$$T^* = \frac{T - T_s}{T_\infty - T_s} = b_1 + b_2\left(\frac{y}{\delta_t}\right) + b_3\left(\frac{y}{\delta_t}\right)^2 + b_4\left(\frac{y}{\delta_t}\right)^3$$

Boundary conditions are:

$$T^*(y=0) = 0; T^*(y=\delta_t) = 1; \left(\partial T^*/\partial y\right)_{y=\delta_t} = 0; \;\&\; \partial^2 T^*/\partial y^2\big|_{y=0} = 0.$$

Applying these conditions: $T^* = \frac{3}{2}\left(\frac{y}{\delta_t}\right) - \frac{1}{2}\left(\frac{y}{\delta_t}\right)^3$.

Substituting both velocity and temperature profiles into the integral energy equation and manipulating for $\mathrm{Pr} \geq 1$:

$\frac{\delta}{\delta_t} = \frac{\mathrm{Pr}^{-1/3}}{1.026}$; This result is in good agreement with the exact solution of 1.0 instead of 1.026. Thus, the heat transfer coefficient may be then computed from:

$$h \equiv \frac{-k_f \partial T/\partial y\big|_{y=0}}{T_s - T_\infty} = \frac{3}{2}\frac{k_f}{\delta_t}\;;$$
$$Nu_x \equiv \frac{hx}{k_f} = 0.332\mathrm{Re}^{1/2}\mathrm{Pr}^{1/3}$$

Same as before within 3 decimal. This analysis proves that good solutions may be obtained using approximate integral methods. These could be very useful in fire problems.

Integral Solution for a Heated Vertical Plate (Laminar Free Convection)

The problem shown in Fig. 3.16, for which the similarity solution was obtained above, can now be solved using integral methods.

Integral Conservation Equations

The integral form of the momentum conservation equation with buoyancy force is derived by using the Archimedes' principle. The buoyancy force per unit volume acting on an element of the warmer fluid in the boundary layer is $g(\rho_\infty - \rho)$ directed vertically upward, where g is the gravitational acceleration, ρ_∞ is the constant fluid density outside the boundary layer, and ρ is the density of the fluid element that varies across the boundary layer. In Fig. 3.18, Newton's second law of motion is applied to the elemental control volume of unit depth Δx and extending to $y = Y$, where Y is greater than the boundary layer thickness. The net momentum outflow from the volume is equal to the buoyancy force minus the viscous drag force exerted by the wall:

$$\int_0^Y \rho u^2 dy\big|_{x+\Delta x} - \int_0^Y \rho u^2 dy\big|_x = \int_0^Y g(\rho_\infty - \rho) dy \Delta x - \mu \frac{\partial u}{\partial y}\Big|_{y=0} \Delta x$$

Notice that there is no momentum flow across the boundary at $y = Y$ since $u(Y) = 0$.

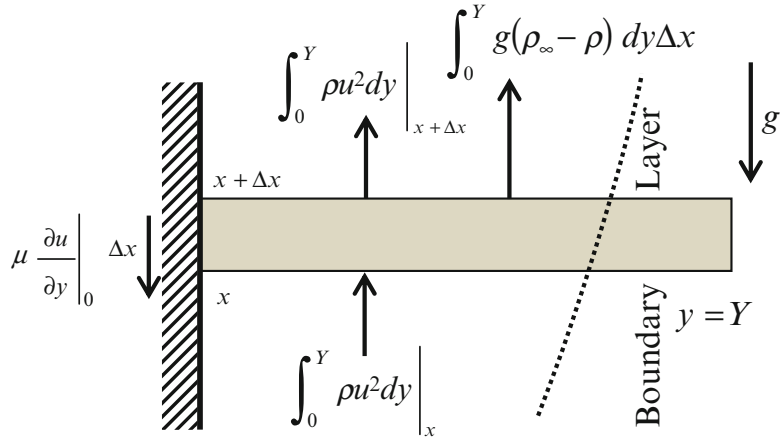

Fig. 3.18 Force balances on an elemental control volume in the boundary layer of a heated vertical plate

Dividing by Δx and letting $\Delta x \to 0$

$$\frac{d}{dx}\int_0^Y \rho u^2 dy = \int_0^Y g(\rho_\infty - \rho)dy - \mu\frac{\partial u}{\partial y}\bigg|_{y=0}$$

The Boussinesq approximation is introduced by taking the density to be constant except in the buoyancy term; dividing by ρ then gives:

$$\frac{d}{dx}\int_0^Y u^2 dy = \int_0^Y g\left(\frac{\rho_\infty - \rho}{\rho}\right)dy - \nu\frac{\partial u}{\partial y}\bigg|_{y=0}$$

Since $\rho = \rho(P, T)$ a Taylor expansion can be written as: $(\rho_\infty - \rho) = (\partial\rho/\partial T)_p(T_\infty - T) + (\partial\rho/\partial T)_T(P_\infty - P) +$ higher order terms. The pressure variation across the boundary layer is negligible; thus, $P = P_\infty$ to obtain:

$$\left(\frac{\rho_\infty - \rho}{\rho}\right) = -\frac{1}{\rho}\left(\frac{\partial\rho}{\partial T}\right)_P (T - T_\infty) = \beta(T - T_\infty),$$

where β is the volumetric coefficient of thermal expansion, as before. For an ideal gas, $\beta = 1/T$. Substituting and letting $Y \to \infty$, since there is no contribution to the integrals for y > Y,

$$\frac{d}{dx}\int_0^\infty u^2 dy = \int_0^\infty g\beta(T - T_\infty)dy - \nu\frac{\partial u}{\partial y}\bigg|_{y=0} \tag{3.93}$$

The integral form of the energy conservation equation is identical to that for forced flow:

$$\frac{d}{dx}\left[\int_0^\infty (T_\infty - T)u\,dy\right] = \alpha\frac{\partial T}{\partial y}\bigg|_{y=0} \tag{3.94}$$

Simultaneous Solution of the Equations

The two ordinary differential equations above, Equations (3.93) and (3.94) are coupled since the variable T appears in both; hence, they must be solved simultaneously. Boundary conditions for the velocity and temperature profiles are:

$$y = 0: \; u = 0, \; T = T_s,$$

a constant for an isothermal wall, and as

$$y \to \infty \; (or \; \delta): \; u = 0, \; T = T_\infty$$

Assuming that the hydrodynamic and thermal boundary layers have the same thickness, *i.e.* $\delta = \delta_t$, which seems reasonable because the momentum is driven by thermal differences. Also assuming the following forms for the velocity and temperature profiles that satisfy the boundary conditions:

$$\frac{u}{u_0} = \frac{y}{\delta}\left(1 - \frac{y}{\delta}\right)^2, \text{ and } \frac{(T - T_\infty)}{T_S - T_\infty} = \left(1 - \frac{y}{\delta}\right)^2$$

Here u_0 is a scaling velocity, which is a function of x only and is yet to be determined. Figure 3.19 shows these profiles; the maximum velocity is $0.148u_0$ at y = δ/3. In the forced-convection problem, the known free-stream velocity was used to scale the velocity profile; here the scaling velocity u_0, as well as the boundary layer - thickness δ, are unknowns. The chosen boundary layer profiles give $\frac{\partial u}{\partial y} = 0$ and $\frac{\partial T}{\partial y} = 0$ at y = δ (i.e., they are smooth at the edge of the boundary layer). However, the velocity profile does not have the correct limiting value of $\frac{\partial^2 u}{\partial y^2}$ at the wall; also, the assumption of $\delta = \delta_t$ is not valid for high-Prandtl-number fluids. But the use of these profiles gives surprisingly good results. Substituting the profiles and performing the indicated operations gives:

$$\frac{d}{dx}\left(\frac{u_0^2\delta}{105}\right) = -\frac{\nu u_0}{\delta} + \frac{g\beta(T_S - T_\infty)\delta}{3}$$

$$\frac{d}{dx}\left(\frac{u_0\delta}{30}\right) = \frac{2\alpha}{\delta}$$

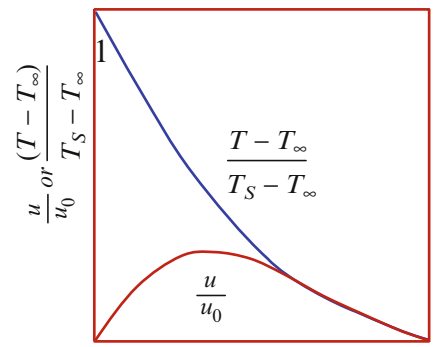

Fig. 3.19 Shape of chosen velocity and temperature profiles

These are two ordinary differential equations for two unknowns: u_0 and δ. Assuming power law variations for δ and U of the form: $\delta = D_1 x^m; u_0 = D_2 x^n$, which give $\delta = 0$ and $u_0 = 0$ at x = 0. Substituting in the above equation gives:

$$\frac{d}{dx}\left(\frac{D_2^2 D_1 x^{2n+m}}{105}\right) = -\frac{\nu D_2^2 x^{n-m}}{D_1} + \frac{g\beta(T_S - T_\infty)D_1 x^m}{3}$$

The x dependence cancels if 2n + m − 1 = n − m = m, which requires m = 1/4, and n = 1/2. The differential equations then reduce to two algebraic equations for D_2 and D_1:

$$\frac{5}{4}\left(\frac{D_2^2 D_1}{105}\right) = -\frac{\nu D_2^2}{D_1} + \frac{g\beta(T_S - T_\infty)D_1}{3}$$

$$\frac{3}{4}\left(\frac{D_2^2 D_1}{30}\right) = \frac{2\alpha}{D_1}$$

Solving gives:

$$D_2 = \frac{80\alpha}{D_1^2}$$

$$D_1 = 3.94\left[\frac{(20/21)\alpha^2 + \nu\alpha}{g\beta(T_S - T_\infty)}\right]^{1/4}$$

The wall heat flux is obtained from the temperature profile as:

$$q_S = -k\left.\frac{\partial T}{\partial y}\right|_{y=0} = \frac{2k}{\delta}(T_S - T_\infty) = h_x(T_S - T_\infty)$$

$$\frac{h_x}{k} = \frac{2}{\delta} = \frac{2}{D_1 x^{1/4}};\ Thus,\ Nu_x = \frac{h_x x}{k} = \frac{2x^{3/4}}{D_1}$$

Substituting for D_1 and rearranging gives:

$$Nu_x = 0.508\left[\frac{\Pr}{0.952 + \Pr}\right]^{1/4} Ra_x^{1/4};\ \text{where } Ra_x = \frac{\beta(T_S - T_\infty)g x^3}{\nu\alpha} \text{ is the Rayleigh number}$$

This result agrees very well with the exact numerical solutions of the differential conservation equations and has been widely used.

Example: Laminar Natural-Convection Boundary Layer on a Vertical Flat Plate A vertical plate at 320 K is immersed in water at 300 K. At a location 10 cm from the bottom of the plate, determine δ, u_0, Nu_x, h_x, and q_s . Also plot the velocity [u(y)] and temperature [T(y)] profiles.

Solution Properties are evaluated at the mean film temperature of 310 K; k = 0.628 W/m K, ρ = 993 kg/m^3, ν = 0. 70 x 10^{-6} m^2/s, Pr = 4.6. Also, $\boldsymbol{\alpha} = \nu/\Pr = 1.52\times10^{-7}$ m^2/s, $\beta = 3.62 \times 10^{-4}$ K^{-1}. The Rayleigh number is checked to see if the flow is laminar:

$$Ra_x = \frac{\beta(T_S - T_\infty)g x^3}{\nu\alpha} = 6.68 \times 10^8 < 10^9 \text{ (laminar)}$$

The boundary layer thickness is $\delta = Dx^{1/4}$, where D is given by the equation above:

$$\delta = D_1 x^{1/4};\ and\ D_1 = 3.94\left[\frac{(20/21)\alpha^2 + \nu\alpha}{g\beta(T_S - T_\infty)}\right]^{1/4} \text{ or, } \delta = \left(4.57 \cdot 10^{-3}\ m^{\frac{3}{4}}\right)(0.1\ m)^{\frac{1}{4}}$$
$$= 2.57 \cdot 10^{-3} m = 2.57\ mm$$

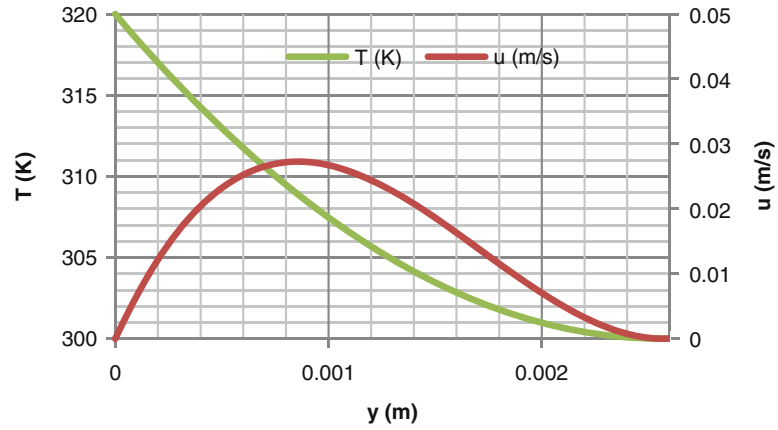

The scaling velocity is: $u_0 = D_2 x^{1/2}$, where $D_2 = \dfrac{80\alpha}{D_1^2} = 0.582\ m^{1/2}/s$;

Thus, $u_0 = (0.582)(0.1)^{1/2} = 0.184$ m/s.

The local Nusselt number:

$$Nu_x = 0.508\left[\frac{\Pr}{0.952 + \Pr}\right]^{1/4} Ra_x^{1/4} = 77.9;$$

At x = 0.1 m. Hence, the local heat transfer coefficient and heat flux are:

$$h_x = (k/x)Nu_x = (0.628/0.1)(77.9)$$
$$= 489\ W/m^2K$$
$$q_s = h_x(T_S - T_\infty)$$
$$= 489(320 - 300)$$
$$= 9790\ W/m^2$$

The velocity and temperature profiles are obtained from:

$$\frac{u}{u_0} = \frac{y}{\delta}\left(1 - \frac{y}{\delta}\right)^2, \text{ and } \frac{(T - T_\infty)}{T_S - T_\infty} = \left(1 - \frac{y}{\delta}\right)^2; \textit{Substituting}: \ \delta = D_1 x^{1/4};\ u_0 = D_2 x^{1/2}$$

$$u = \frac{y x^{1/4} D_2}{D_1}\left(1 - \frac{y}{D_1 x^{1/4}}\right)^2, \text{ and } T = T_\infty + (T_S - T_\infty)\left(1 - \frac{y}{D_1 x^{1/4}}\right)^2$$

From above : $D_1 = 4.57 \times 10^{-3}\ \mathrm{m}^{3/4}$, $D_2 = 0.582 \mathrm{m}^{1/2}/\mathrm{s}$, and $x = 0.1m$

The plot is shown above.

Complications in Practical Problems

In the previous section, two relatively simple problems of laminar forced and free convection on a flat surface were solved. These solutions illustrate the methodology for determining the heat transfer coefficient and provide the necessary insight regarding the relationship between the various dimensionless parameters. Most practical situations are often more complex, and mathematical solutions, such as those presented in the previous section, are not always possible. Complexities arise due to more complex geometry, onset of turbulence, changes in fluid properties with temperature, and because of simultaneous mass transfer from the surface as illustrated in Fig. 3.17. For such cases, empirical correlations are obtained. These correlations are discussed in the next section and the various complications are individually discussed below.

Effect of Turbulence In both forced and free convective flows, small disturbances may be amplified downstream, leading to transition from laminar to turbulent flow conditions. These disturbances may originate from the free

stream or be induced by surface roughness. Whether these disturbances are amplified or attenuated depends on the ratio of inertia to viscous forces for forced flows (the Reynolds number) and the ratio of buoyancy to viscous forces for free convective flows (the Grashof number). Note that in both Reynolds and Grashof numbers, viscosity appears in the denominator. Thus for relatively large viscous forces or small Reynolds and Grashof numbers, the naturally occurring disturbances are dissipated, and the flow remains laminar. However, for sufficiently large Reynolds and Grashof numbers ($Re > 5 \times 10^5$ and $Gr > 4 \times 10^8$, for flow over a flat plate) disturbances are amplified, and a transition to turbulence occurs.

The onset of turbulence is associated with the existence of *random fluctuations* in the fluid, and on a small scale the flow is *unsteady*. As shown in Fig. 3.20, there are sharp differences between laminar and turbulent flows. In the laminar boundary layer, fluid motion is highly ordered and it is possible to identify streamlines along which fluid particles move. In contrast, fluid motion in the turbulent boundary layer is highly irregular and is characterized by velocity fluctuations. These fluctuations enhance the momentum and energy transfers and hence increase the surface friction and convection heat transfer rate. Also, due to the mixing of fluid resulting from the turbulent fluctuations, the turbulent boundary layer is thicker and the boundary layer profiles (of velocity, temperature, and concentration) are flatter than in laminar flow.

In a fully turbulent flow, the primary mechanism of momentum and heat transfer involves macroscopic lumps of fluid randomly moving about in the flow. Turbulent flow contrasts with the random molecular motion resulting in molecular properties discussed at the beginning of this chapter. In the turbulent region, *eddy viscosity* and *eddy thermal conductivity* are important. These eddy properties may be ten times as large as their molecular counterparts.

If one measures the variation of an arbitrary flow variable, P, as a function of time at some location in a turbulent boundary layer, then the typical behavior observed is shown in Fig. 3.21. The variable P, which may be a velocity component, fluid temperature, pressure, or species concentration, can be represented as the sum of a time-mean value, $\overline{P}$, and a fluctuating

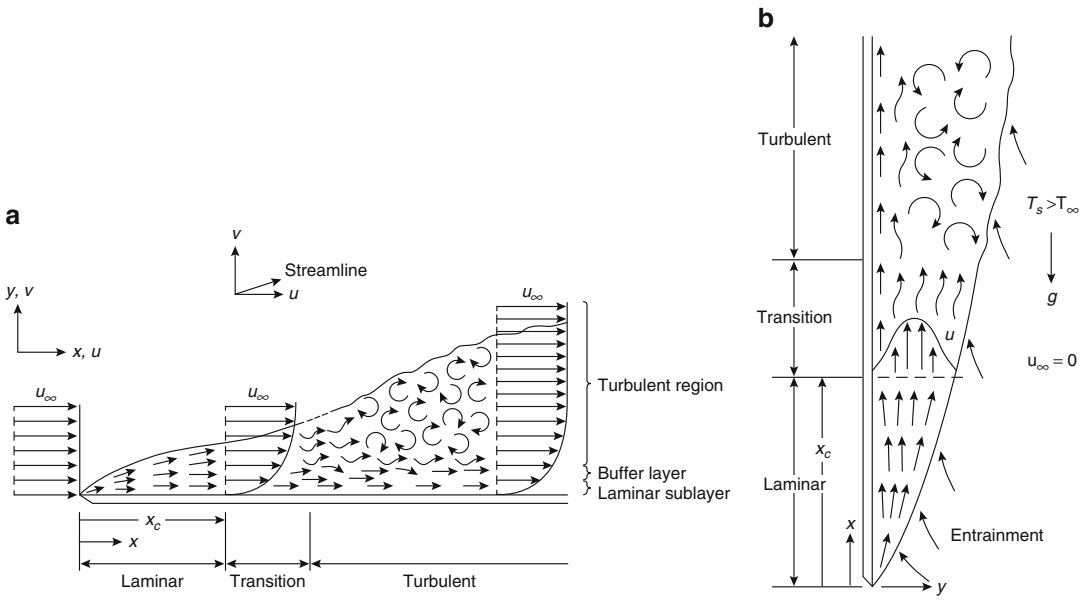

Fig. 3.20 (**a**) Velocity boundary layer development on a flat plate for forced flow; (**b**) velocity boundary layer development on a vertical flat plate for free convective flow

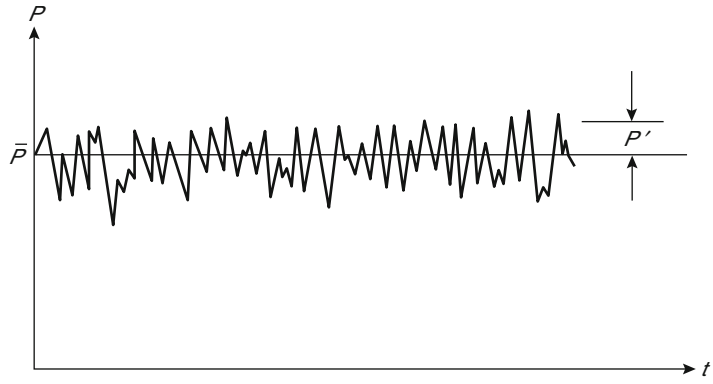

Fig. 3.21 Variation in the variable P with time at some point in a turbulent boundary layer

component, P'. The average is taken over a time interval that is large compared with the period of a typical fluctuation, and if $\overline{P}$ is time independent then the mean flow is steady. Thus, the instantaneous values of each of the velocity components, pressure, and temperature are given by

$$u = \overline{u} + u', \quad v = \overline{v} + v', \quad p = \overline{p} + p'$$
$$T = \overline{T} + T', \quad \text{and} \quad \rho = \overline{\rho} + \rho' \tag{3.95}$$

Substituting these expressions for each of the flow variables into the boundary layer equations (Equations 3.35, 3.43, and 3.45) and assuming the mean flow to be steady, incompressible (ρ = constant) with constant properties, and using the well-established time averaging procedures [1–4], the following governing equations are obtained:

Continuity

$$\frac{\partial \overline{u}}{\partial x} + \frac{\partial \overline{v}}{\partial y} = 0 \tag{3.96}$$

x-momentum

$$\rho\left(\overline{u}\frac{\partial \overline{u}}{\partial z} + \overline{v}\frac{\partial \overline{u}}{\partial y}\right) = \frac{\partial}{\partial y}\left(\mu\frac{\partial \overline{u}}{\partial y} - \rho\overline{u}'\overline{v}'\right) - \frac{\partial \overline{p}}{\partial x} - \rho g_x \tag{3.97}$$

Energy

$$\rho C_p\left(\overline{u}\frac{\partial \overline{T}}{\partial x} + \overline{v}\frac{\partial \overline{T}}{\partial y}\right) = \frac{\partial \overline{T}}{\partial y}\left(k\frac{\partial \overline{T}}{\partial y} - \rho C_p\overline{v}'\overline{T}'\right) \tag{3.98}$$

Equations 3.96 through 3.98 are similar to the laminar boundary layer equations expressed in mean flow variables, except for the presence of additional terms $\rho\overline{u}'\overline{v}'$ and $\rho C_p\overline{v}'\overline{T}'$. Physical arguments [2] show that these terms result from the motion of macroscopic fluid lumps and account for the effect of the turbulent fluctuations on momentum and energy transport.

On the basis of the foregoing result it is customary to speak of total shear stress and total heat flux, which are defined as

$$\tau_{\text{tot}} \equiv \left(\mu\frac{\partial \overline{u}}{\partial y} - \rho\overline{u}'\overline{v}'\right)$$

and

$$\dot{q}_{\text{tot}} \equiv -\left(k\frac{\partial \overline{T}}{\partial y} - \rho C_p\overline{v}'\overline{T}'\right) \tag{3.99}$$

The terms $\rho\overline{u}'\overline{v}'$ and $\rho C_p\overline{v}'\overline{T}'$ are always negative and so result in a positive contribution to total shear stress and heat flux. The term $\rho\overline{u}'\overline{v}'$ represents the transport of momentum flux due to turbulent fluctuations (or eddies), and it is known as the Reynolds stress. The notion of transport of heat and momentum by turbulent eddies has prompted the introduction of transport coefficients, which are defined as the eddy diffusivity for momentum transfer, ε_M, and eddy diffusivity for heat transfer, ε_H, and have the form

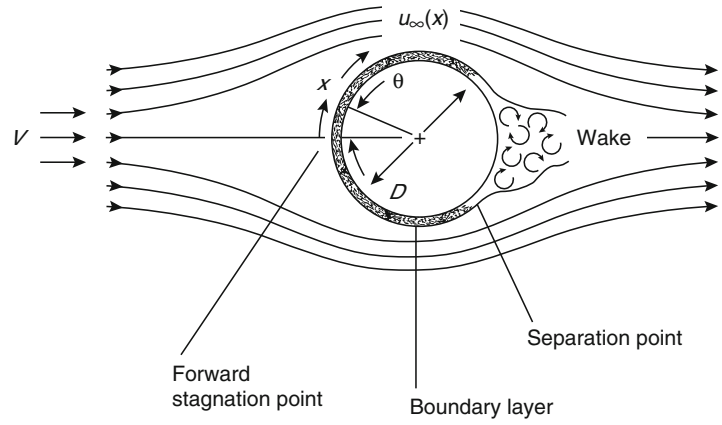

Fig. 3.22 Boundary layer formation and separation on a circular cylinder in cross flow

$$\varepsilon_M \frac{\partial \overline{u}}{\partial y} \equiv -\overline{u}'\overline{v}'$$
$$\varepsilon_H \frac{\partial \overline{T}}{\partial y} \equiv -\overline{v}'\overline{T}' \tag{3.100}$$

Thus Equation 3.99 becomes

$$\tau_{\text{tot}} \equiv \rho(\nu + \varepsilon_M)\frac{\partial \overline{u}}{\partial y}$$

and

$$\dot{q}''_{\text{tot}} \equiv -\rho C_p(\alpha + \varepsilon_H)\frac{\partial \overline{T}}{\partial y} \tag{3.101}$$

As noted earlier, eddy diffusivities are much larger than molecular diffusivities, therefore the heat and momentum transfer rates are much larger for turbulent flow than for laminar flow. A fundamental problem in performing turbulent boundary layer analysis involves determining the eddy diffusivities as a function of the mean properties of the flow. Unlike the molecular diffusivities, which are strictly fluid properties, the eddy diffusivities depend strongly on the nature of the flow. They vary across the boundary layer and the variation can only be determined from experimental data. This is an important point, because all analyses of turbulent flow must eventually rely on experimental data. To date, there is no adequate theory for predicting turbulent flow behavior.

Complex Geometry In a previous section on the boundary layer concept, analysis was limited to the simplest possible geometry, that is, a flat plate. This provided considerable simplification because $dp/dx = 0$ in Equation 3.43 for the forced flow case. However, the situation is not as simple for fluid flow over bodies with a finite radius of curvature.

Consider a common example of flow across a circular cylinder shown in Fig. 3.22. Boundary layer formation is initiated at the forward stagnation point, where the fluid is brought to rest with an accompanying rise in pressure. The pressure is a maximum at this point and decreases with increasing x, the streamline coordinate, and θ, the angular coordinate. (Note: In the boundary layer approximation, the pressure is the same inside and outside the boundary layer. This can be seen from Equation 3.44.) The boundary layer then develops under the influence of a favorable pressure gradient ($dp/dx < 0$). At the top of the cylinder (i.e., at $\theta = 90°$) the pressure eventually reaches a minimum and then begins to increase toward the rear of the cylinder. Thus, for $90° < \theta < 180°$, the boundary layer development occurs in the presence of an adverse pressure gradient ($dp/dx > 0$).

Unlike parallel flow over a flat plate, for curved surfaces the free stream velocity, u_∞, varies with x. (Note that in Fig. 3.22 a distinction has been made between the fluid velocity upstream of the cylinder, V, and the velocity

outside the boundary layer, $u_\infty(x)$.) At the stagnation point, $\theta = 0°$, $u_\infty = 0$. As the pressure decreases for $\theta > 0°$, u_∞ increases according to the Bernoulli equation, Equation 3.46, and becomes maximum at $\theta = 90°$. For $\theta > 90°$, the adverse pressure gradient decelerates the fluid, and conversion of kinetic energy to pressure occurs in accordance with Equation 3.46, which applies only to the inviscid flow outside the boundary layer. The fluid inside the boundary layer has considerably slowed down because of viscous friction and does not have enough momentum to overcome the adverse pressure gradient, eventually leading to boundary layer separation, which is illustrated more clearly in Fig. 3.23. At some location in the fluid, the velocity gradient at the surface becomes zero and the boundary layer detaches or separates from the surface. Farther downstream of the separation point, flow reversal occurs and a wake is formed behind the solid. Flow in this region is characterized by vortex formation and is highly irregular. The separation point is defined as the location at which $(\partial u/\partial y)_{y=0} = 0$. If the boundary layer transition to turbulence occurs prior to separation, the separation is delayed and the separation point moves farther downstream. This happens because the turbulent boundary layer has more momentum than the laminar boundary layer to overcome the adverse pressure gradient.

The foregoing processes strongly influence both the rate of heat transfer from the cylinder surface and the drag force acting on the cylinder. Because of the complexities associated with flow over a cylinder, experimental methods are used to determine the heat transfer coefficient. Such experimental results for the variation of the local Nusselt number with θ are shown in Fig. 3.24 for a cylinder in a cross flow of air. Consider the results for $Re_D \leq 10^5$ (note: Re_D is defined as VD/ν). Starting at the stagnation point, Nu_θ decreases with increasing θ due to the development of the laminar boundary layer. However, a minimum is reached at $\theta \approx 80°$. At this point separation occurs, and Nu_θ increases with θ due to the mixing associated with vortex formation in the wake. For $Re_D \geq 10^5$, the variation of Nu_θ with θ is characterized by two minima. The decline in Nu_θ from the value at the stagnation point is again due to laminar boundary layer development, but the sharp increase that occurs

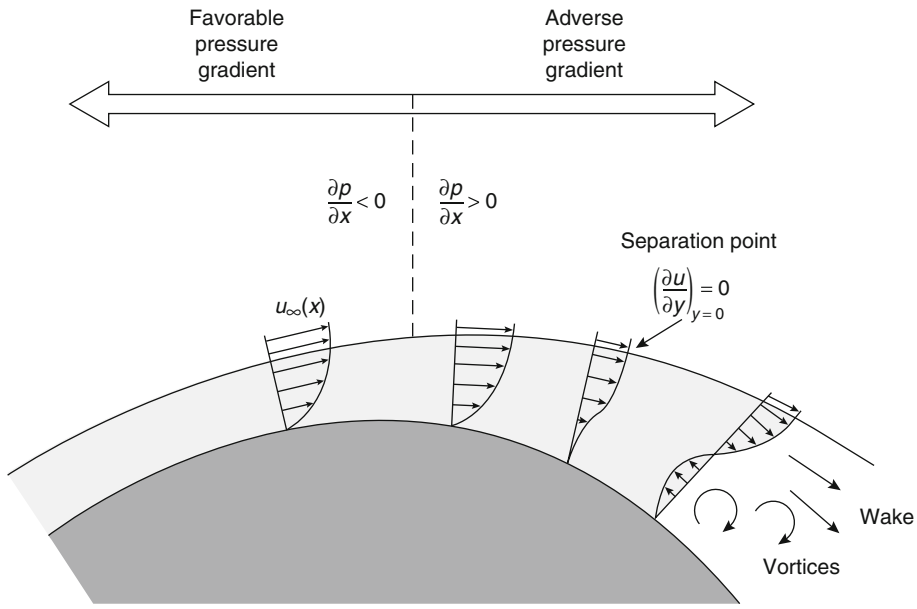

Fig. 3.23 Velocity profiles associated with separation on a circular cylinder in cross flow

between 80° and 100° is now due to boundary layer transition to turbulence. With further development of the turbulent boundary layer, Nu_θ must again begin to decline. However, separation eventually occurs ($\theta \approx 140°$), and Nu_θ increases due to considerable mixing associated with the wake region.

The foregoing example clearly illustrates the complications introduced by nonplanar geometry. Heat transfer correlations for these cases are often based on experimental data. Fortunately, for most engineering calculations the local variation in the heat transfer coefficient such as that presented in Fig. 3.24 is not required; only the overall average conditions are needed. Empirical correlations for average heat transfer coefficients will be presented in the next section.

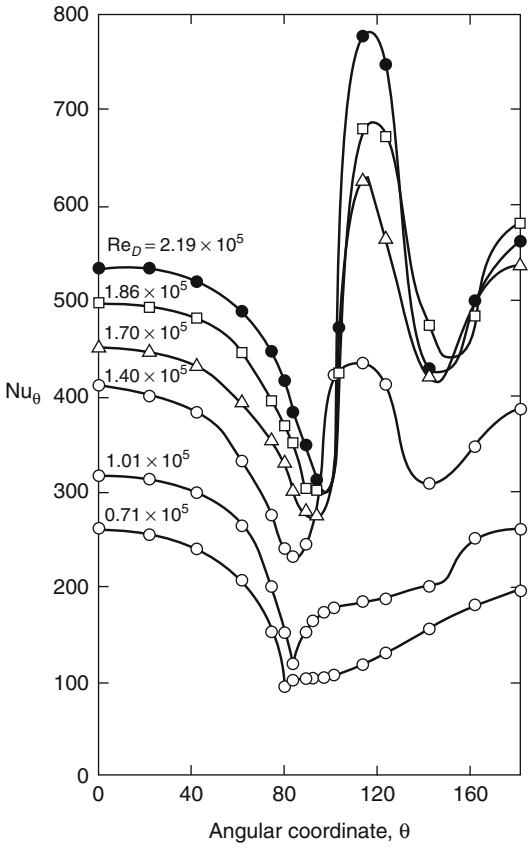

Fig. 3.24 Local Nusselt number for airflow normal to a circular cylinder

Changes in Fluid Properties In the analysis and discussion presented thus far, fluid properties were assumed to be constant. However, fluid properties vary with temperature across the boundary layer and this variation will have a significant impact on the heat transfer rate. In the empirical heat transfer correlations this influence is accounted for in one of two ways: (1) in correlating the experimental data, all properties are evaluated at the mean boundary layer temperature, $T_f = (T_s + T_\infty)/2$, called the film temperature, and (2) alternatively, all properties are evaluated at T_∞ and an additional parameter is used to account for the property variation. This parameter is commonly of the form $(Pr_\infty/Pr_s)^r$ or $(\mu_\infty/\mu_s)^r$, where the subscripts ∞ and s designate evaluation of properties at the free stream and surface temperatures, respectively, and r is an empirically determined constant.

It is important to note that in the empirical correlations to be presented in the next section, the same method that is employed in deriving the correlation should be used when applying the correlation.

Effect of Mass Transfer Special attention needs to be given to the effect that species mass transfer from the surface of the solid has on the velocity and thermal boundary layers. Recall that the velocity boundary layer development is generally characterized by the existence of zero fluid velocity at the surface. This condition applies to the velocity component v normal to the surface, as well as to the velocity component u parallel to the surface. However, if there is simultaneous mass transfer to or from the surface, it is evident that v can no longer be zero at the surface. Nevertheless, for the problems discussed in this chapter, mass transfer is assumed to have a negligible effect, that is, $v \approx 0$. This assumption is reasonable for problems involving some evaporation from gas-liquid or sublimation from gas-solid interfaces. For larger surface mass transfer rates a correction factor (often called the blowing correction) is utilized. This correction factor is simply stated here, and discussed in greater detail by Bird et al. [1]. The correction factor is defined as

$E(\phi) \equiv h^*/h$, where h^* is the corrected heat transfer coefficient and h is the heat transfer coefficient in the absence of mass transfer. According to film theory, $E(\phi)$ is given by

$$E(\phi) = \frac{\phi}{(e^{\phi} - 1)} \tag{3.102}$$

where

$$\phi = \frac{\dot{m}'' C_{pg}}{h}$$

$\dot{m}'' = \rho_s v_s$ is the mass flux coming out of the surface and C_{pg} is the specific heat of the gas.

Empirical Relations of Convection Heat Transfer

The analysis and discussion presented in the section on the boundary layer concept have shown that for simple cases the convection heat transfer coefficient may be determined directly from the conservation equations. In the previous section it was noted that the complications inherent to most practical problems do not always permit analytical solutions, and that it is necessary to resort to experimental methods. Experimental results are usually expressed in the form of either empirical formulas or graphical charts so that they may be utilized with maximum generality. Difficulties are encountered in the process of trying to generalize the experimental results in the form of empirical correlations. The availability of an analytical solution for a simpler but similar problem greatly assists in guessing the functional form of the results. Experimental data is then used to obtain values of constants or exponents for certain significant parameters, such as the Reynolds or Prandtl numbers. If an analytical solution for a similar problem is not available, it is necessary to rely on the physical understanding of the problem and on dimensional or order-of-magnitude analysis. In this section the experimental methods, the dimensionless groups, and the functional form of the relationships expected between them will be discussed; in addition the empirical formulas that will be used in the "Applications" section of this chapter will be summarized.

Functional Form of Solutions The nondimensional Equations 3.49, 3.50, 3.51, and 3.78 are extremely useful from the standpoint of suggesting how important boundary layer results can be generalized. For example, the momentum equation, Equation 3.50, suggests that although conditions in the velocity boundary layer depend on the fluid properties, ρ and μ, the velocity, μ_∞, and the length scale, L, this dependence may be simplified by grouping these variables in a nondimensional form called the Reynolds number. We therefore anticipate that the solution of Equation 3.50 will be of the form

$$u^* = f_1\left(x^*, y^*, \mathrm{Re}_L, \frac{dp^*}{dx^*}\right) \tag{3.103}$$

Note that the pressure distribution, $p^*(x^*)$, depends on the surface geometry and may be obtained independently by considering flow conditions outside the boundary layer in the free stream. Hence, as discussed in the section on complex geometry, the appearance of dp^*/dx^* in Equation 3.103 represents the influence of geometry on the velocity distribution. Note also that in Equation 3.50 the term dp^*/dx^* did not appear because it was equal to zero for a flat plate.

Similarly we anticipate that the solution of Equation 3.78 will be of the form

$$u^* = f_2(x^*, y^*, \mathrm{Gr}_L, \mathrm{Pr}) \tag{3.104}$$

Here, the Prandtl number is included because of the coupling between Equations 3.78 and 3.79. If the flow is mixed, that is, buoyant as well as forced, then the Reynolds number must also be included in the functional relationship expressed by Equation 3.104.

From Equation 3.1, the shear stress at the surface, $y^* = 0$, may be expressed as

$$\tau_s = \mu \left.\frac{\partial u}{\partial y}\right|_{y=0} = \left(\frac{\mu u_\infty}{L}\right) \left.\frac{\partial u^*}{\partial y^*}\right|_{y^*=0}$$

and from Equation 3.10 it follows that the friction coefficient is

$$C_f = \frac{\tau_s}{1/2\rho u_\infty^2} = \frac{2}{\mathrm{Re}_L}\frac{\partial u^*}{\partial y^*}\Big|_{y^*=0} \tag{3.105}$$

From Equation 3.103 it is clear that

$$\left.\frac{\partial u^*}{\partial y^*}\right|_{y^*=0} = f_3\left(x^*, \mathrm{Re}_L, \frac{dp^*}{dx^*}\right) \tag{3.106}$$

Hence, for a prescribed geometry (i.e., dp^*/dx^* is known from the free stream conditions) we have

$$C_f = \frac{2}{\mathrm{Re}_L} f_3(x^*, \mathrm{Re}_L) \tag{3.107}$$

Equation 3.107 is very significant because it states that the friction coefficient may be expressed exclusively in terms of a dimensionless space coordinate and the Reynolds number. For a prescribed geometry, the function that relates C_f to x^* and Re_L can be expected to be *universally* applicable. That is, it can be expected to apply to different fluids and over a wide range of values for u_∞ and L.

Similar results may be obtained for the heat transfer coefficient. Equation 3.51 suggests that the solution may be expressed in the form

$$T^* = f_4\left(x^*, y^*, \mathrm{Re}_L, \frac{dp^*}{dx^*}\right) \tag{3.108}$$

for forced flow, and

$$T^* = f_5(x^*, y^*, \mathrm{Gr}_L, \mathrm{Pr}) \tag{3.109}$$

for free convective flow. Here Re_L, Gr_L, and dp^*/dx^* originate from the influence of fluid motion (u^* and v^*) on Equation 3.51.

From the definition of the convection heat transfer coefficient, Equation 3.5, and Equation 3.40 with $y^* = y/L$ we obtain

$$h = -\frac{k(\partial T/\partial y)\big|_{y=0}}{(T_s - T_\infty)} = +\frac{k}{L}\left.\frac{\partial T^*}{\partial y^*}\right|_{y^*=0} \tag{3.110}$$

Thus

$$\mathrm{Nu} \equiv \frac{hL}{k} = \frac{\partial T^*}{\partial y^*}\Big|_{y^*=0}$$

Note that the Nusselt number, Nu, is equal to the dimensionless temperature gradient at the surface. From Equation 3.108 or Equation 3.107 it follows that for a prescribed geometry, i.e., known dp^*/dx^*

$$\mathrm{Nu} = f_6(x^*, \mathrm{Re}_L, \mathrm{Pr}) \tag{3.111}$$

for forced flow, and

$$\mathrm{Nu} = f_7(x^*, \mathrm{Gr}_L, \mathrm{Pr}) \tag{3.112}$$

for free convective flow. The Nusselt number is to the thermal boundary layer what the friction factor is to the velocity boundary layer. Equations 3.111 and 3.112 imply that for a given geometry, the Nusselt number must be some *universal* function of x^*, Re_L, and Pr. If this function were known, it could be used to compute the value of Nu for different fluids and different values of u_∞, T_∞, and L. Furthermore, since the average heat transfer coefficient is obtained by integrating over the surface of the body, it must be independent of the spatial variable, x^*. Hence, the functional dependence of the average Nusselt number is

$$\overline{\mathrm{Nu}} = \frac{\overline{h}L}{k} = f_8(\mathrm{Re}_L, \mathrm{Pr}) \tag{3.113}$$

for forced flow, and

$$\overline{\mathrm{Nu}} = f_9(\mathrm{Gr}_L, \mathrm{Pr}) \tag{3.114}$$

for free convective flows.

Although it is very helpful to know the functional dependence of Nu, the task is far from complete, because the function may be any of millions of possibilities. It may be a sine, exponential, or a logarithmic function. The exact form of this function can only be determined by an analytical solution of the governing equations, such as Equations 3.70 and 3.91.

Experimental Determination of Heat Transfer Coefficient The manner in which a convection heat transfer correlation may be obtained experimentally is illustrated in Fig. 3.25. If a prescribed geometry, such as the flat plate in parallel flow, is heated electrically to maintain $T_s > T_\infty$, convection heat transfer occurs from the surface to the fluid. It would be a simple matter to measure T_s and T_∞ as well as the electrical power, $E \cdot I$, which is equal to the total heat transfer rate, $\dot{q}$. The average convection coefficient, $\overline{h}_L$, can now easily be computed from Equation 3.7. Also, from the knowledge of the characteristic length, L, and the fluid properties, the values of the various nondimensional numbers—such as the Nusselt, Reynolds, Grashof, and Prandtl numbers—can be easily computed from their definitions.

The foregoing procedure is repeated for a variety of test conditions. We could vary the velocity, u_∞, the plate length, L, and the temperature difference $(T_s - T_\infty)$, as well as the fluid properties, using, for example, fluids such as air, water, and engine oil, which have substantially different Prandtl numbers. Many different values of the Nusselt number would result, corresponding to a wide range of Reynolds and Prandtl numbers. At this stage, an analytical solution to a similar but simpler problem proves very useful in guiding how the various nondimensional numbers should be correlated. For laminar flow over a flat plate it has been seen that in Equation 3.70 the relationship is of the form

$$\overline{\mathrm{Nu}} = C\mathrm{Re}_L^m \mathrm{Pr}^n$$

Thus, we plot the results on a log-log graph as shown in Fig. 3.26 and determine the values of C, m, and n. Because such a relationship is inferred from experimental measurements, it is called an empirical correlation. Along with this empirical correlation it is specified how the temperature-dependent properties were determined for calculating the various nondimensional numbers. When such a correlation is used, it is important that the properties must be calculated in exactly the manner specified. If they are not specified,

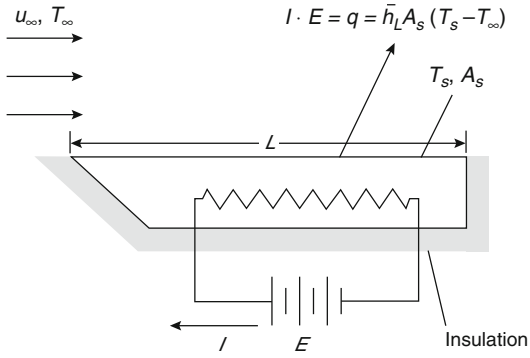

Fig. 3.25 Experiment for measuring the average convection heat transfer coefficient, $\overline{h}_L$

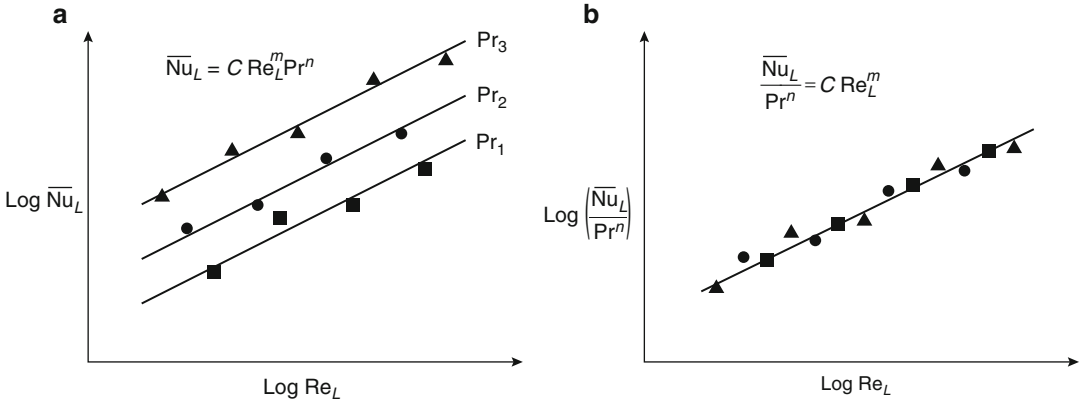

Fig. 3.26 Dimensionless representation of convection heat transfer measurements

then the mean boundary layer temperature, T_f, called the film temperature, must be used.

$$T_f \equiv \frac{T_s + T_\infty}{2} \tag{3.115}$$

A Summary of Empirical and Practical Formulas In this section, selected dimensionless groups (Table 3.2) and a variety of convection correlations (Tables 3.3 and 3.4) for external flow conditions are tabulated. Correlations for both forced and free convection are presented along with their range of applicability. The contents of this section are more or less a collection of "recipes." Proper use of these recipes is essential to solving practical problems. The reader should not view these correlations as sacrosanct; each correlation is reasonable over the range of conditions specified, but for most engineering calculations one should not expect the accuracy to be much better than 20%.

For proper use of the foregoing correlations it is important to note that the flow may not be laminar or turbulent over the entire length of the plate under consideration. Instead, transition to turbulence may occur at a distance x_c ($x_c < L$, where L is the plate length) from the leading edge of the plate. In this mixed boundary layer situation, the average convection heat transfer coefficient for the entire plate is obtained by integrating first over the laminar region ($0 \leq x \leq x_c$) and then over the turbulent region ($x_c < x \leq L$) as follows:

$$\overline{h}_L = \frac{1}{L}\left(\int_0^{x_c} h_{\text{lam}}\,dx + \int_{x_c}^{L} h_{\text{turb}}\,dx\right) \tag{3.116}$$

Table 3.2 Selected dimensionless groups

Group		Definition	Interpretation
Friction coefficient	Local	$C_f = \frac{\tau_2}{\rho u^2 \infty/2}$	Dimensionless surface shear stress
	Average	$\overline{C}_f = \frac{\overline{\tau}_2}{\rho u^2 \infty/2}$	
Reynolds number	Location x	$\text{Re}_x = \frac{u_\infty x}{\nu}$	Ratio of inertia and viscous forces
	Length L	$\text{Re}_L = \frac{u_\infty L}{\nu}$	
	Diameter D	$\text{Re}_D = \frac{u_\infty D}{\nu}$	
Prandtl number		$\text{Pr} = \frac{C p \mu}{k} = \frac{\nu}{\alpha}$	Ratio or molecular momentum and thermal diffusivities
Grashof number	Location x	$\text{Gr}_x = \frac{g\beta(T_s - T_\infty)x^3}{\nu^2}$	Ratio of buoyancy to viscous forces
	Length L	$\text{Gr}_L = \frac{g\beta(T_s - T_\infty)L^3}{\nu^2}$	
	Diameter D	$\text{Gr}_D = \frac{g\beta(T_s - T_\infty)D^3}{\nu^2}$	
Rayleigh number	Location x	$\text{Ra}_x = \text{Gr}_x\text{Pr} = \frac{g\beta(T_s - T_\infty)x^3}{\nu\alpha}$	Product of Grashof and Prandtl numbers
		Replace x by $L$and D to get Ra_L and Ra_D	
Nusselt number	Location x	$\text{Nu}_x = \frac{hx}{k}$	Ratio of convection heat transfer to conduction in a fluid slab of thickness x
		Replace x by L and D to get Nu_L and Nu_D	
Modified Grashof number	Location x	$\text{Gr}_x^* = \text{Gr}_x\text{Nu}_x = \frac{g\beta\dot{q}_s'' x^4}{k\nu^2}$	Product of Grashof and Nusselt numbers
Stanton number		$\text{St} = \frac{h}{\rho u_\infty C_p} = \frac{\text{Nu}}{\text{RePr}}$	Dimensionless heat transfer coefficient

Table 3.3 Summary of forced convection correlations for external flow geometries

Geometry/flow	Type	Equation	Restrictions	Comments
Flat plate/laminar (Ts = constant)	Local	$\mathrm{Nu}_x = 0.332\,\mathrm{Re}_x^{1/2}\,\mathrm{Pr}^{1/3}$	$\mathrm{Re}_x < 5 \times 10^5$	Properties evaluated at $T_t = (T_s + T_\infty)/2$
	Average	$\overline{\mathrm{Nu}}_L = 0.664\,\mathrm{Re}_L^{1/2}\,\mathrm{Pr}^{1/3}$	$0.6 \le \mathrm{Pr} \le 50$	
	Boundary layer thickness	$\frac{\delta}{x} = 5\mathrm{Re}_x^{-1/2}$		
Flat plate/laminar ($\dot{q}_s'' =$ constant)	Local	$\mathrm{Nu}_x = 0.453\,\mathrm{Re}_x^{1/2}\,\mathrm{Pr}^{1/3}$	$\mathrm{Re}_x < 5 \times 10^5$	Properties evaluated at T_f. However, T_s is not known. Instead, q_s'' is known. Thus, $T_f = T_\infty + \left(\overline{T}_s - \overline{T}_\infty\right)/2$ where $\left(\overline{T}_s - \overline{T}_\infty\right) = \frac{q_s L/K}{0.6795\mathrm{Re}_L^{1/2}\mathrm{Pr}^{1/3}}$
			$0.6 \le \mathrm{Pr} \le 50$	
Flat plate/turbulent (Ts = constant)	Local	$\mathrm{Nu}_x = 0.0296\,\mathrm{Re}_x^{4/5}\,\mathrm{Pr}^{1/3}$	$\mathrm{Re}_x < 10^8$	Properties evaluated at T_f
	Boundary layer thickness	$\frac{\delta}{x} = 0.37\mathrm{Re}_x^{-1/5}$	$0.6 \le \mathrm{Pr} \le 60$	
	Mixed average (laminar turbulent)	$\overline{\mathrm{Nu}}_L = \left(0.037\,\mathrm{Re}_L^{4/5} - 871\right)\mathrm{Pr}^{1/3}$	Transition to turbulence at $\mathrm{Re}_{\mathrm{crit}} = 5 \times 10^5$	
Flow across cylinders circular cylinder	Average	$\overline{\mathrm{Nu}}_D = C\mathrm{Re}_D^m\mathrm{Pr}^{1/3}$	$0.4 < \mathrm{Re}_D < 4 \times 10^5$	Properties evaluated at T_f
		Re_D	C	m
		0.4–4	0.989	0.330
		4–40	0.911	0.385
		40–4000	0.683	0.466
		4×10^3–4×10^4	0.193	0.618

Other geometries square		4×10^4–4×10^5	0.027	0.805		
		5×10^3–10^5	0.246	0.588		
		5×10^3–10^5	0.102	0.675		
Hexagon						
						
		5×10^3–1.95×10^4	0.160	0.638		
		$1.95 \cdot 10^4$–10^5	0.0385	0.782		
Vertical plate						
		5×10^3–10^5	0.153	0.638		
		4×10^3–1.5×10^4	0.228	0.731		
Flow across spheres	Average	$\overline{\mathrm{Nu}}_D = 2 + \left(0.4\mathrm{Re}_D^{1/2} + 0.06\mathrm{Re}_D^{2/3}\right)\mathrm{Pr}^{0.4(\mu_\infty/\mu_s)^{1/4}}$			$3.5 < \mathrm{Re}_D < 7.6 \times 10^4$	Properties evaluated at T_∞
					$0.71 < \mathrm{Pr} < 380$	
					$1.0 < \left(\frac{\mu_\infty}{\mu_s}\right) < 3.2$	
Falling drop	Average	$\overline{\mathrm{Nu}}_D = 2 + 0.6\mathrm{Re}_D^{1/2}\mathrm{Pr}^{1/3} \cdot \left[25\left(\frac{x}{D}\right)^{-.07}\right]$			where x is the falling distance measured from rest	Properties evaluated at T_∞

Table 3.4 Summary of free convection correlations for external flow geometries

Vertical plates	Local: (T_s = const)	$\mathrm{Nu}_x g(\mathrm{Pr})$ from Table 3.1 $= \left(\frac{\mathrm{Gr}_x}{4}\right)^{1/4} g(\mathrm{Pr})$	$\mathrm{Gr}_x \leq 4 \times 10^8$ (laminar)	Properties evaluated at $(T_f = T_s + T_\infty)/2$
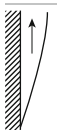	Average: (T_s = const)	$\overline{\mathrm{Nu}}_L = \frac{4}{3}\left(\frac{\mathrm{Gr}_L}{4}\right)^{1/4} g(\mathrm{Pr})$	$\mathrm{Gr}_x \leq 4 \times 10^8$ (laminar)	Properties at T_f
	Average: (T_s = const)	$\overline{\mathrm{Nu}}_L = \left\{0.825 + \frac{0.387\mathrm{Ra}_L^{1/6}}{\left[1 + (0.492/\mathrm{Pr})^{9/16}\right]^{8/27}}\right\}^2$	None	Properties at T_f This correlation may be applied to vertical cylinders if $\left(\frac{D}{L}\right) \geq \left(35/\mathrm{Gr}_L^{1/4}\right)$
or				
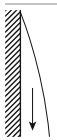	Local: $\left(\dot{q}_s'' = \text{const}\right)$	$\mathrm{Nu}_x = 0.6\left(\mathrm{Gr}_x^* \mathrm{Pr}\right)^{1/5}$	$10^5 < \mathrm{Gr}_x{}^* < 10^{11}$ (laminar)	Properties at T_f
	Local: $\left(\dot{q}_s'' = \text{const}\right)$	$\mathrm{Nu}_x = 0.17\left(\mathrm{Gr}_x^* \mathrm{Pr}\right)^{1/4}$	$2 \times 10^{13} < \mathrm{Gr}_x{}^*\mathrm{Pr} < 10^{16}$	Properties at T_f
	Average: $\left(\dot{q}_s'' = \text{const}\right)$	$\overline{\mathrm{Nu}}_L = 0.75\left(Gr_L^* \mathrm{Pr}\right)^{1/5}$	$10^5 < \mathrm{Gr}_x{}^* < 10^{11}$ (laminar)	Properties at T_f
Horizontal plates (hot surface up or cold surface down) 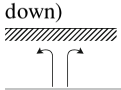	Average: (T_s = const)	$\overline{\mathrm{Nu}}_L = 0.54\ \mathrm{Ra}_L^{1/4}$	$10^5 \lesssim \mathrm{Ra}_L \lesssim 10^7$	Properties at T_f characteristic length L is defined as $L = A_s/P$ where A_s = plate surface area F = perimeter of the plate (1) All properties except β are evaluated at $T_e = T_s - \frac{1}{4}(T_s - T_\infty)$ β is evaluated at T_f
		$\overline{\mathrm{Nu}}_L = 0.15\ \mathrm{Ra}_L^{1/3}$	$10^7 \lesssim \mathrm{Ra}_L \lesssim 10^{10}$	
	Average: $\left(\dot{q}_s'' = \text{const}\right)$	$\overline{\mathrm{Nu}}_L^{(1)} = 0.16\ \mathrm{Ra}_L^{1/3}$	$\mathrm{Ra}_L \leq 2 \times 10^8$	
Horizontal plates (cold surface up or hot surface down) 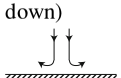	Average: (T_s = const)	$\overline{\mathrm{Nu}}_L = 0.27\ \mathrm{Ra}_L^{1/4}$	$10^5 \leq \mathrm{Ra}_L \leq 10^{10}$	
	Average: $\left(\dot{q}_s'' = \text{const}\right)$	$\overline{\mathrm{Nu}}_L^{(1)} = 0.16\ \mathrm{Ra}_L^{1/3}$	$2 \times 10^8 \leq \mathrm{Ra}_L \leq 10^{11}$	

Inclined plates 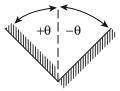 Hot surface	Average: $\left(\dot{q}_s'' = \text{const}\right)$	$\overline{\text{Nu}}_L = 0.56\ (\text{Ra}_L \cos\theta)^{1/4}$ (hot surface facing down) For hot surface facing up $\overline{\text{Nu}}_L = 0.14\left[(\text{Gr}_L\text{Pr})^{1/3} - (\text{Gr}_c\text{Pr})^{1/3}\right] + 0.56(\text{Ra}_L \cos\theta)^{1/4}$ θ = –15*; $\text{Gr}_c = 5 \times 10^9$ –30*; 2×10^9 –60*; 10^8 –75*; 10^5	$\theta < 88''$ $10^5 < \text{Ra}_L \cos\theta < 10^{11}$ –15* > θ > –75* $10^5 < \text{Ra}_L \cos\theta < 10^{11}$	Properties evaluated at $T_e = T_s - 1/4\ (T_s - T_\infty)$ Grashof number
Horizontal cylinders 	Average: (T_s = const)	$\text{Nu}_D = \left\{0.6 + \frac{0.387\ Ra_D^{1/6}}{\left[1 + (0.559/\text{Pr})^{9/16}\right]^{8/27}}\right\}^2$	$10^{-5} < \text{Ra}_D < 10^{12}$	Properties evaluated at T_f
Spheres 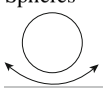	Average: (T_s = const)	$\overline{\text{Nu}}_D = 2 + 0.43\ \text{Ra}_D^{1/4}$ $\overline{\text{Nu}}_D = 2 + 0.5\ \text{Ra}_D^{1/4}$	$1 < \text{Ra}_D < 10^5$ Pr ≈ 1 $3 \times 10^5 < \text{Ra} < 8 \times 10^8$	Properties evaluated at T_f

where x_c may be obtained from the critical Reynolds or Grashof numbers.

Also, several correlations given in Tables 3.3 and 3.4 are for the constant heat flux $\left(\dot{q}_s'' = \text{constant}\right)$ boundary condition. Thus, the surface temperature of the object is unknown and yet the fluid properties are to be determined at $T_f = (T_s + T_\infty)/2$. For such cases an iterative procedure is employed and the average surface temperature can be determined as follows:

$$\dot{q}_s''(\text{Known}) = \overline{h}(T_s - T_\infty) = \frac{\overline{\text{Nu}}_L}{(L/k)}(T_s - T_\infty)$$

thus

$$T_s(\text{Average}) = T_\infty + \frac{\dot{q}_s''(L/k)}{\overline{\text{Nu}}_L} \qquad (3.117)$$

The use of correlations given in Tables 3.3 and 3.4 is illustrated via examples in the next section.

Applications

This section briefly summarizes the methodology for convection calculations and then presents examples to illustrate the use of various correlations.

Methodology for Convection Calculations The application of a convection correlation for any flow situation is facilitated by following a few simple rules:

1. Become immediately cognizant of the flow geometry. Does the problem involve flow over a flat plate, a sphere, a cylinder, and so forth? The specific form of the convection correlation depends, of course, on the geometry.
2. Specify the appropriate reference temperature and then evaluate the pertinent fluid properties at that temperature. For moderate boundary layer temperature differences, it has been found that the film temperature may be used for this purpose. However, there are correlations that require property evaluation at the free stream temperature and include a property ratio to account for the nonconstant property effect.
3. Determine whether the flow is laminar or turbulent. This determination is made by calculating the Reynolds number and comparing the value with the appropriate transition criterion. For example, if a problem involves parallel flow over a flat plate for which the Reynolds number is $\text{Re}_L = 10^6$ and the transition criterion is $\text{Re}_{\text{crit}} = 5 \times 10^5$, it is obvious that a mixed boundary layer condition exists.
4. Decide whether a local or surface average coefficient is required. Recall that the local coefficient is used to determine the flux at a particular point on the surface, whereas the average coefficient determines the transfer rate for the entire surface.

Having complied with the foregoing rules, sufficient information will be available to select the appropriate correlation for the problem.

Example 1 Electrical strip heaters are assembled to construct a flat radiant heater 1 m wide for conducting fire experiments in a wind tunnel. The heater strips are 5 cm wide and are independently controlled to maintain the surface temperature at 500 °C. Construction details are shown in Fig. 3.27. If air at 25 °C and 60 m/s flows over the plate, at which strip is the electrical input maximum? What is the value of this input? The radiative heat loss is ignored.

Solution Assumptions
Steady-state conditions, neglect radiation losses, and no heat loss through the bottom surface.

Properties
$T_f = 535$ K: $\rho = 1$ atm. From air property Table 3.5, $k = 42.9 \times 10^{-3}$ W/m·K; $\nu = 43.5 \times 10^{-6}$ m^2/s; Pr = 0.683.

Analysis
The strip heater requiring the maximum electrical power is that for which the average convection coefficient is the largest. From the knowledge of variation of the local convection

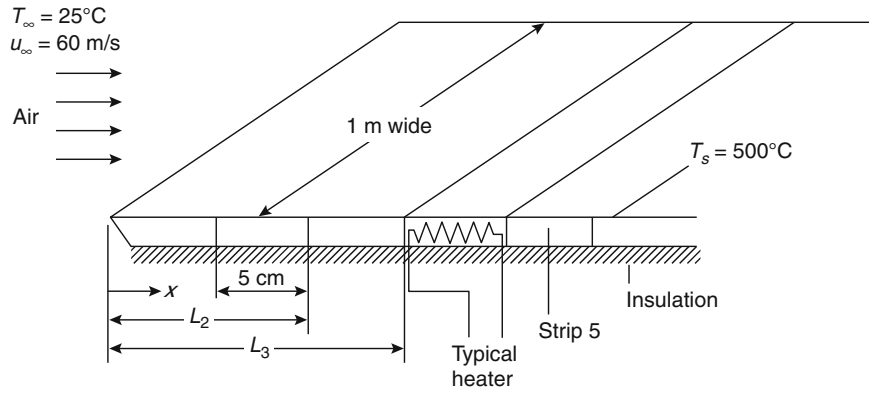

Fig. 3.27 Construction details for wind tunnel experiments

Table 3.5 Thermophysical properties of air at atmospheric pressure

T K	ρ kg/m^3	c_p kJ/kg·K	μ 10^7 N s/m^2	$\nu \cdot 10^6$ m^2/s	k · 10^3 W/m K	α · 106 m^2/s	Pr
100	3.5562	1.032	71.1	2.00	9.34	2.54	0.786
150	2.3364	1.012	103.4	4.426	13.8	5.84	0.758
200	1.7458	1.007	132.5	7.590	18.1	10.3	0.737
250	1.3947	1.006	159.6	11.44	22.3	15.9	0.720
300	1.1614	1.007	184.6	15.89	26.3	22.5	0.707
350	0.9950	1.009	208.2	20.92	30.0	29.9	0.700
400	0.8711	1.014	230.1	26.41	33.8	38.3	0.690
450	0.7740	1.021	250.7	32.39	37.3	47.2	0.686
500	0.6964	1.030	270.1	38.79	40.7	56.7	0.684
550	0.6329	1.040	288.4	45.57	43.9	66.7	0.683
600	0.5804	1.051	305.8	52.69	46.9	76.9	0.685
650	0.5356	1.063	322.5	60.21	49.7	87.3	0.690
700	0.4975	1.075	338.8	68.10	52.4	98.0	0.695
750	0.4643	1.087	354.6	76.37	54.9	109	0.702
800	0.4354	1.099	369.8	84.93	57.3	120	0.709
850	0.4097	1.110	384.3	93.80	59.6	131	0.716
900	0.3868	1.121	398.1	102.9	62.0	143	0.720
950	0.3666	1.131	411.3	112.2	64.3	155	0.723
1000	0.3482	1.141	424.4	121.9	66.7	168	0.726
1100	0.3166	1.159	449.0	141.8	71.5	195	0.728
1200	0.2902	1.175	473.0	162.9	76.3	224	0.728
1300	0.2679	1.189	496.0	185.1	82	238	0.719
1400	0.2488	1.207	530	213	91	303	0.703
1500	0.2322	1.230	557	240	100	350	0.685
1600	0.2177	1.248	584	268	106	390	0.688
1700	0.2049	1.267	611	298	113	435	0.685
1800	0.1935	1.286	637	329	120	482	0.683
1900	0.1833	1.307	663	362	128	534	0.677
2000	0.1741	1.337	689	396	137	589	0.672
2100	0.1658	1.372	715	431	147	646	0.667
2200	0.1582	1.417	740	468	160	714	0.655
2300	0.1513	1.478	766	506	175	783	0.647
2400	0.1448	1.558	792	547	196	869	0.630
2500	0.1389	1.665	818	589	222	960	0.613
3000	0.1135	2.726	955	841	486	1570	0.536

coefficient with distance from the leading edge, the local maximum can be found. Figure 3.15 shows that a possible location is the leading edge on the first plate. A second likely location is where the flow becomes turbulent. To determine the point of boundary layer transition to turbulence assume that the critical Reynolds number is 5×10^5. It follows that transition will occur at x_c, where

$$x_c = \frac{\nu \mathrm{Re}_{crit}}{u_\infty} = \frac{43.5 \times 10^{-6} \times 5 \times 10^5}{60} \mathrm{m}$$
$$= 0.36 \text{ m or on the eighth strip}$$

Thus there are three possibilities:

1. Heater strip 1, since it corresponds to the largest local, laminar convection coefficient
2. Heater strip 8, since it corresponds to the largest local turbulent convection coefficient
3. Heater strip 9, since turbulent conditions exist over the entire heater

For the first heater strip

$$q_{\mathrm{conv},1} = \overline{h}_1 L_1 W (T_s - T_\infty)$$

where $\overline{h}_1$ is determined from the equation below (see also Table 3.3).

$$\overline{\mathrm{Nu}}_1 = 0.664 \mathrm{Re}_1{}^{1/2} \mathrm{Pr}^{1/3}$$
$$= 0.664 \left(\frac{60 \times 0.05}{43.5 \times 10^{-6}} \right)^{1/2} (0.683)^{1/3}$$
$$= 153.6$$

hence,

$$\overline{h}_1 = \frac{\overline{\mathrm{Nu}}_1 k}{L_1} = \frac{153.6 \times 42.9 \times 10^{-3}}{0.05}$$
$$= 131.8 \mathrm{W/m^2 \cdot K}$$

hence,

$$q_{\mathrm{conv},1} = (131.8)(0.05)(1 \text{ m})(500 \ \ 25)$$
$$= 3129 \text{ W}$$

The power requirement for the eighth strip may be obtained by subtracting the total heat loss associated with the first seven heaters from that associated with the first eight heaters. Thus

$$q_{conv,8} = \overline{h}_{1-8} L_8 W (T_s - T_\infty) - \overline{h}_{1-7} L_7 W (T_s - T_\infty)$$

The value of $\overline{h}_{1-7}$ is obtained from the equation applicable to laminar conditions (Table 3.3). Thus

$$\overline{\mathrm{Nu}}_{1-7} = 0.664 \mathrm{Re}_7{}^{1/2} \mathrm{Pr}^{1/3}$$
$$= 0.664 \left(\frac{60 \times 7 \times 0.05}{43.5 \times 10^{-6}} \right)^{1/2} (0.683)^{1/3}$$
$$= 406.3$$
$$\overline{h}_{1-7} = \frac{\overline{\mathrm{Nu}}_{1-7} k}{L_7} = \frac{406.3 \times 42.9 \times 10^{-3}}{7 \times 0.05}$$
$$= 49.8 \mathrm{W/m^2 \cdot K}$$

By contrast, the eighth heater is characterized by mixed boundary layer conditions. Thus use the formula (Table 3.3).

$$\overline{\mathrm{Nu}}_{1-8} = \left(0.037 \mathrm{Re}_8^{4/5} - 871 \right) \mathrm{Pr}^{1/3}$$
$$\mathrm{Re}_8 = 8 \times \mathrm{Re}_1 = 5.52 \times 10^5$$
$$\overline{\mathrm{Nu}}_{1-8} = 510.5$$
$$\overline{h}_{1-8} = \frac{\overline{\mathrm{Nu}}_{1-8} k}{L_8} = 54.7 \mathrm{W/m^2 \cdot K}$$

The rate of heat transfer from the eighth strip is then

$$q_{\mathrm{conv},8} = (54.7 \times 8 \times 0.05 - 49.8 \times 7 \times 0.05) \times (500 - 25) = 2113.8 \text{ W}$$

The power requirement for the ninth heater strip may be obtained by either subtracting the total heat loss associated with the first eight from that associated with the first nine, or by integrating over the local turbulent expression, since the flow is completely turbulent over the entire width of the strip. The latter approach produces

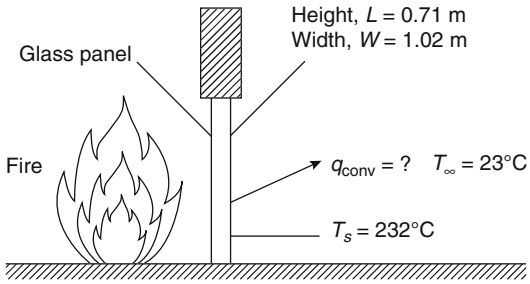

Fig. 3.28 Glass panel fire screen

$$\overline{h}_9 = \left(\frac{k}{L_9 - L_8}\right) 0.0296 \left(\frac{u_\infty}{\nu}\right)^{4/5} \mathrm{Pr}^{1/3} \int_{L_8}^{L_9} \frac{dx}{x^{1/5}}$$

$$\overline{h}_9 = \left(\frac{42.9 \times 10^{-3}}{0.05}\right) 0.0296 \left(\frac{60}{43.5 \times 10^{-6}}\right)^{4/5} \times (0.683)^{1/3} \int_{L_8}^{L_9} \frac{dx}{x^{1/5}}$$

$$= 1825.22\left[(0.45)^{0.8} - (0.4)^{0.8}\right] = 86.7$$

$$q_{conv,9} = 86.7 \times 0.05 \times 1 \times (500 - 25)$$

$$= 2059 \text{ W}$$

hence

$$q_{\mathrm{conv},1} > q_{\mathrm{conv},8} > q_{\mathrm{conv},9}$$

and the first heater strip has the largest power requirement.

Example 2 A glass-door fire screen, shown in Fig. 3.28, is used to reduce exfiltration of room air through a chimney. It has a height of 0.71 m, a width of 1.02 m, and reaches a temperature of 232 °C. If the room temperature is 23 °C, estimate the convection heat transfer rate from the fireplace to the room.

Solution Assumptions
The screen is at a uniform temperature, T_s, and room air is quiescent.

Properties
$T_f = 400$ K, $P = 1$ atm. From air property table (Table 3.5):

$k = 33.8 \times 10^{-3}$ W/m·K; $\nu = 26.41 \times 10^6$ m^2/s;
$\alpha = 38.3 \times 10^{-6}$ m^2/s; Pr = 0.69; $\beta = 1/T_f = 0.0025$ K^{-1}

Analysis
The rate of heat transfer by free convection from the panel to the room is given by

$$q = \overline{h} A_s (T_s - T_\infty)$$

where $\overline{h}$ is obtained from the following equation from Table 3.4.

$$\overline{\mathrm{Nu}}_L = \left\{ 0.825 + \frac{0.387 \mathrm{Ra}_L^{1/6}}{\left[1 + (0.492/\mathrm{Pr})^{9/16}\right]^{8/27}} \right\}^2$$

here

$$\mathrm{Ra}_L = \frac{g\beta(T_s - T_\infty)L^3}{\alpha\nu}$$

$$= \frac{9.8 \times 0.0025 \times (232 - 23) \times (0.71)^3}{38.3 \times 10^{-6} \times 26.4 \times 10^{-6}}$$

$$= 1.813 \times 10^9$$

Since $\mathrm{Ra}_L > 10^9$, transition to turbulence will occur on the glass panel and the appropriate correlation from Table 3.4 has been chosen

$$\overline{\mathrm{Nu}}_L = \left\{ 0.825 + \frac{0.387\left(1.813 \times 10^9\right)^{1/6}}{\left[1 + (0.492/0.69)^{9/16}\right]^{8/27}} \right\}^2$$

$$= 147$$

Hence

$$\overline{h} = \frac{\overline{\mathrm{Nu}}_L \times k}{L} = \frac{147 \times 33.8 \times 10^{-3}}{0.71}$$

$$= 7 \text{ W/m}^2 \cdot \text{K}$$

and

$$q = 7 \frac{W}{\text{m}^2\text{K}} (1.02\text{m} \times 0.71\text{m}) \times (232 - 23)^\circ\text{C}$$

$$= 1060 \text{ W}$$

Note: in this case radiation heat transfer calculations would show that radiant heat transfer is greater than free convection heat transfer.

Example 3 A fire door is constructed as shown in Fig. 3.29. Two thin (but rigid) stainless steel walls are separated by an argon-filled gap of thickness $2b$. The door height, approximately equal to the door width, is much greater than $2b$. All other sides of the door with one dimension $2b$ seal the argon-filled gap and are assumed to be insulated. In the event of a fire, the two vertical walls will be at different temperatures, designated as "hot" and "cold." Assuming that the wall temperatures T_1 and T_2 remain constant and using the *Boussinesq approximation*, derive expressions for velocity and temperature profiles in argon under steady-state conditions. Also determine the heat flux through argon. Does it provide adequate insulation? Note that the gas motion in the y direction is expected to be small; thus it may be neglected along with any edge effects. Viscous dissipation may also be neglected.

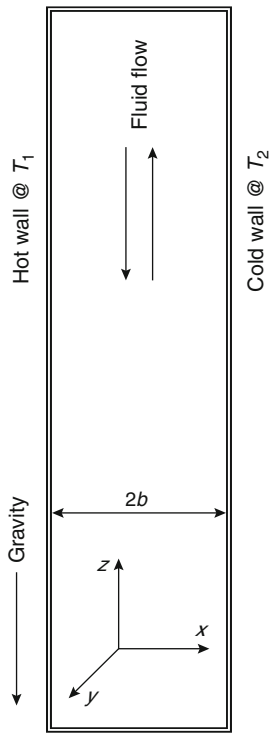

Fig. 3.29 Example 3

Solution We expect the argon near the heated wall to rise, and that near the cold wall to descend. Also, for all practical purposes, the two parallel steel plates are infinite in extent compared with the gap $2b$. Since the gap is sealed, under steady-state conditions any mass going up must be equal to the mass coming down to conserve the total mass of the gas inside the gap.

The velocity vector has three components: V_X, V_Y, and V_Z. Of these, only V_Z is nonzero. Also, based on the assumption made, V_Z varies only with x. The continuity and momentum equations thus become

Continuity

$$\frac{\partial V_Z}{\partial Z} = 0$$

The Z-component of the momentum equation becomes

$$\mu \frac{d^2 V_Z}{dx^2} + \rho_m g \beta (T_m - T) = 0$$

Here T_m is the mean temperature, yet to be defined. The constant value of density ρ_m is also taken at this mean temperature. Any variation above or below this mean temperature will provide the buoyancy force to drive the fluid. Other than in the buoyancy term, throughout the equations ρ_m is taken as constant—this is the *Boussinesq approximation*. Note that with the increase in the mean temperature, the pressure will rise given the rigid walls of the door. Thus, the mean density will remain constant regardless of the temperature. However, the density will vary with temperature.

The boundary conditions are

$$\text{BC1}: x = \pm b,\ V_Z = 0$$

$$\text{BC2}: x = 0,\ V_Z = \text{by symmetry}$$

Temperature can depend on at most three space variables and time. For this problem $T = T(x)$ because T_1 and T_2 are constant and conditions are steady. Thus, the energy equation reduces to

$$k\frac{d^2T}{dx^2} = 0$$

With the boundary conditions

$$\begin{aligned} \text{BC1}: x &= b, T = T_1 \\ \text{BC2}: x &= b, T = T_2 \end{aligned}$$

The energy equation can be integrated directly to give

$$T = \frac{T_1 + T_2}{2} - \frac{x}{2b}(T_1 - T_2)$$

Thus, T_m can be conveniently defined as

$$T_m = \frac{T_1 + T_2}{2}$$

In terms of the mean temperature, the temperature profile becomes

$$\frac{T - T_m}{T_1 - T_2} = -\frac{x}{2b}$$

Thus,

$$q_x'' = -k\frac{dT}{dx} = k\frac{(T_1 - T_2)}{2b}$$

With mean temperature defined, we can now rewrite the momentum equation as

$$\frac{d^2V_Z}{dx^2} = \frac{\rho_m g\beta}{\mu}(T - T_m) = \frac{\rho_m g\beta x(T_2 - T_1)}{2b\mu}$$

This can also be directly integrated as

$$V_Z = \frac{\rho_m g\beta x^3}{12b\mu}(T_2 - T_1) + C_3 x + C_4$$

Applying the boundary conditions, we obtain the velocity distribution as

$$\begin{aligned} V_Z &= \frac{\rho_m g\beta x^3}{12b\mu}(T_2 - T_1) - \frac{\rho_m g\beta bx}{12\mu}(T_2 - T_1) \\ &= \frac{\rho_m g\beta b^2}{12\mu}(T_2 - T_1)\left(\frac{x}{b} - \frac{x^3}{b^3}\right) \end{aligned}$$

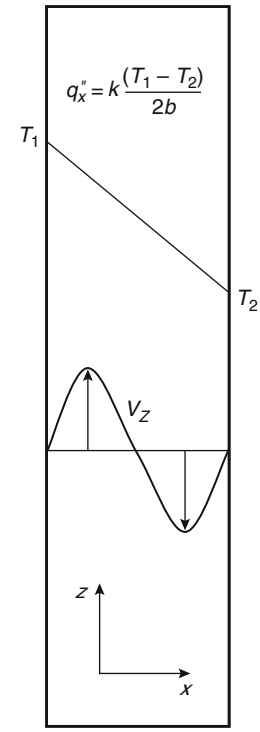

Fig. 3.30 Example 3 solution

As shown in Fig. 3.30, despite the fluid motion inside the door, the temperature profile is linear and effectively heat is conducted through low thermal conductivity argon gas providing excellent insulation. For this condition to hold, door height must be much greater than $2b$.

Nomenclature

$\boldsymbol{A}$	Area (m^2)
$\boldsymbol{A_s}$	Surface area (m^2)
Bi	Biot number
$\boldsymbol{C}$	Molar concentration ($kmol/m^3$)
$\boldsymbol{C_f}$	Friction coefficient
$\boldsymbol{c_p}$	Specific heat at constant pressure (J/kg·K)
$\boldsymbol{c_v}$	Specific heat at constant volume (J/kg·K)
$\boldsymbol{D}$	Diameter (m)
$\boldsymbol{D_{AB}}$	Binary mass diffusion coefficient (m^2/s)

D_h	Hydraulic diameter (m)
E	Specific internal or thermal (sensible) energy (J/kg)
F_{BX}, F_{BY}, F_{BZ}	Components of the body force per unit volume (N/m^3)
F_{SX}, F_{SY}, F_{SZ}	Components of the surface force
F	Friction factor
Gr	Grashof number
G	Gravitational acceleration (m/s^2)
H	Convection heat transfer coefficient (W/m^2 ·K)
$\overline{h}$	Average convection heat transfer coefficient (W/m^2 ·K)
h_m	Convection mass transfer coefficient (m/s)
h_{rad}	Radiation heat transfer coefficient (W/m^2 ·K)
K	Thermal conductivity (W/m·K)
L	Characteristic length (m)
Le	Lewis number
M	Mass (kg)
$\dot{M}$	Mass flow rate (kg/s)
$\dot{m}''$	Mass flux (kg/m^2 · s)
$\dot{m}_i''$	Mass flux of species i (kg/m^2 · s)
Nu	Nusselt number
P	Perimeter (m)
Pe	Peclet number (RePr)
Pr	Prandtl number
P	Pressure (N/m^2)
Q	Energy generation rate per unit volume (W/m^3)
$\dot{q}'$	Heat transfer rate per unit length (W/m)
$\dot{q}''$	Heat flux (W/m^2)
R	Universal gas constant
Ra	Rayleigh number
Re	Reynolds number
r, ϕ, z	Cylindrical coordinates
r, θ, ϕ	Spherical coordinates
Sc	Schmidt number
Sh	Sherwood number
St	Stanton number
T	Temperature (K)
T	Time (s)
U	Overall heat transfer coefficient (W/m^2 ·K)
u, v, w	Mass average fluid velocity components (m/s)
x, y, z	Rectangular coordinates (m)
$x_{fd,h}$	Hydrodynamic entry length (m)
$x_{rd,t}$	Thermal entry length (m)

Greek Letters

α	Thermal diffusivity (m^2/s)
β	Volumetric thermal expansion coefficient (K^{-1})
δ	Hydrodynamic boundary layer thickness (m)
δ_t	Thermal boundary layer thickness (m)
δ_d	Mass transfer boundary layer thickness (m)
η	Similarity variable
θ	Zenith angle (rad)
ϕ	Azimuthal angle (rad)
μ	Viscosity (kg/s·m)
ν	Kinematic viscosity (m^2/s)
ρ	Mass density (kg/m^3)
σ_{ij}	Components of the stress tensor (N/m^2)
ψ	Stream function (m^2/s)
τ	Shear stress (N/m^2)

Subscripts

A,B	Species in a binary mixture
Conv	Convection
D	Diameter; drag
F	Fluid properties
Fd	Fully developed conditions
H	Heat transfer conditions
H	Hydrodynamic; hot fluid
L	Based on characteristic length
Max	Maximum fluid velocity
S	Surface conditions
Sur	Surroundings
T	Thermal
X	Local conditions on a surface
∞	Free stream conditions

References

1. R.B. Bird, W.E. Stewart, and E.N. Lightfoot, *Transport Phenomena,* Wiley, New York (1966).

2. H. Schlichting, *Boundary Layer Theory,* McGraw-Hill, New York (1979).
3. V.S. Arpaci and P.S. Larsen, *Convection Heat Transfer,* Prentice Hall, Englewood Cliffs, NJ (1984).
4. E.R.G. Eckert and R.M. Drake, *Analysis of Heat and Mass Transfer,* McGraw-Hill, New York (1973).
5. F.P. Incropera and D.P. Dewitt, *Fundamentals of Heat Transfer,* Wiley, New York (1981).
6. T. von Karman, Uber laminare und turbulente reibung, ZAMM,1(4), pp. 233–235, 1921

Arvind Atreya is a professor of mechanical engineering at the University of Michigan. He has been actively involved in fire research since 1979.

Radiation Heat Transfer

4

Revised by C. Lautenberger
Original chapter authored by C.L. Tien, K.Y. Lee, and A.J. Stretton

Introduction

Thermal radiation is the dominant mode of heat transfer in flames with characteristic lengths exceeding approximately 0.2 m. It is for this reason that quantitative analysis of fire dynamics requires a working knowledge of thermal radiation. This chapter will introduce the fundamentals of thermal radiation and offer several methods for calculating radiant heat transfer in fires. Basic thermal radiation concepts are presented with an emphasis on application to fire phenomena; the reader is referred the literature for specialized topics [1–4].

Basic Concepts

The Nature of Thermal Radiation

Whereas conduction and convection require direct contact for objects at different temperatures to exchange heat, thermal radiation is a distinct mechanism of heat transfer that allows spatially separated objects at different temperatures to transfer heat. Although the Earth is separated from its Sun by 1.5×10^{11} m of near perfect vacuum, we have all enjoyed its radiative heat transfer on cool days, and cursed it on hot ones.

All objects with a finite temperature emit thermal radiation through a physical mechanism related to electron oscillations and transitions. As an object's absolute temperature increases, these electron oscillations and transitions become more rapid, resulting in increased radiant emission. Since all objects emit radiation, all objects also have a certain amount of thermal radiation impinging upon them (originating from other emitting objects). It is the net difference between incoming and outgoing thermal radiation that leads to a net rate of radiant heat transfer between objects at different temperatures, and quantification of this rate is usually the ultimate goal of a radiation heat transfer analysis.

The nature of thermal radiation transport can be explained on the basis of quantum mechanics or electromagnetic wave theory. In the general quantum mechanical consideration, electromagnetic radiation is viewed as the propagation of an ensemble of particles (usually called photons or quanta). These particles, being generated by sub-molecular processes that are fed by an object's internal energy, carry different energies. The energy of a photon (e, J) is proportional to its frequency (ν, s^{-1}):

$$e = h\nu \tag{4.1}$$

The constant of proportionality in Equation 4.1 is Planck's constant, $h = 6.6256 \times 10^{-34}$ J · s. It is seen that the higher the frequency, the higher

Revised by C. Lautenberger (✉)
Reax Engineering Inc., 1921 University Ave., Berkeley, CA 94704, USA

Original chapter authored by C.L. Tien, K.Y. Lee, and A.J. Stretton

M.J. Hurley (ed.), *SFPE Handbook of Fire Protection Engineering*,
DOI 10.1007/978-1-4939-2565-0_4, © Society of Fire Protection Engineers 2016

the photon energy. Thus, a radiation field is fully described when the flux of photons (or energy) is known for all points in the field for all directions and for all frequencies.

Due to its wave-particle duality, electromagnetic radiation exhibits properties of both particles and waves. Therefore, thermal radiation can also be explained as the propagation of electromagnetic waves. In this context, wavelength (λ) is related to frequency (ν) and the speed of light (c) as:

$$\lambda = \frac{c}{\nu} \tag{4.2}$$

The speed of light in a particular medium is denoted c, and in a vacuum it is denoted c_0 where $c_0 = 2.998 \times 10^8$ m/s. Wavelength has units of length, and for convenience it is usually given in microns (μm, or micrometers) where 1 μm $= 10^{-6}$ m. Substituting Equation 4.2 into Equation 4.1 shows that a photon's energy increases as wavelength decreases:

$$e = \frac{hc}{\lambda} \tag{4.3}$$

Electromagnetic waves of practical significance have wavelengths ranging from 10^{-5} to 10^4 μm. Figure 4.1 shows the electromagnetic spectrum spanning this range. *Thermal radiation* usually refers to electromagnetic waves with wavelengths between 10^{-1} and 10^2 μm. For comparison, visible light has wavelengths between 0.4 and 0.7 μm. Thermal radiation with wavelengths between 0.7 and 100 μm is *infrared* thermal radiation, whereas *ultraviolet* thermal radiation has wavelengths between 0.1 and 0.4 μm.

Example 1 Calculate the energy of photons (in a vacuum) with a wavelength of 10^{-1} μm (ultraviolet limit of thermal radiation) and 10^2 μm (infrared limit of thermal radiation).

Solution Equation 4.3 can be used to calculate photon energies. For the photon at the ultraviolet limit:

$$\begin{aligned} e &= \frac{hc_0}{\lambda} \\ &= \frac{\left(6.6256 \times 10^{-34}\ \text{J}\cdot\text{s}\right)\left(2.998 \times 10^{8}\ \text{m/s}\right)}{10^{-1}\mu\text{m} \times \left(10^{-6}\text{m}/\mu\text{m}\right)} \\ &= 1.99 \times 10^{-18}\ \text{J} \end{aligned}$$

And for the photon at the infrared limit:

$$\begin{aligned} e &= \frac{hc_0}{\lambda} \\ &= \frac{\left(6.6256 \times 10^{-34}\ \text{J}\cdot\text{s}\right)\left(2.998 \times 10^{8}\ \text{m/s}\right)}{10^{2}\mu\text{m} \times \left(10^{-6}\text{m}/\mu\text{m}\right)} \\ &= 1.99 \times 10^{-21}\ \text{J} \end{aligned}$$

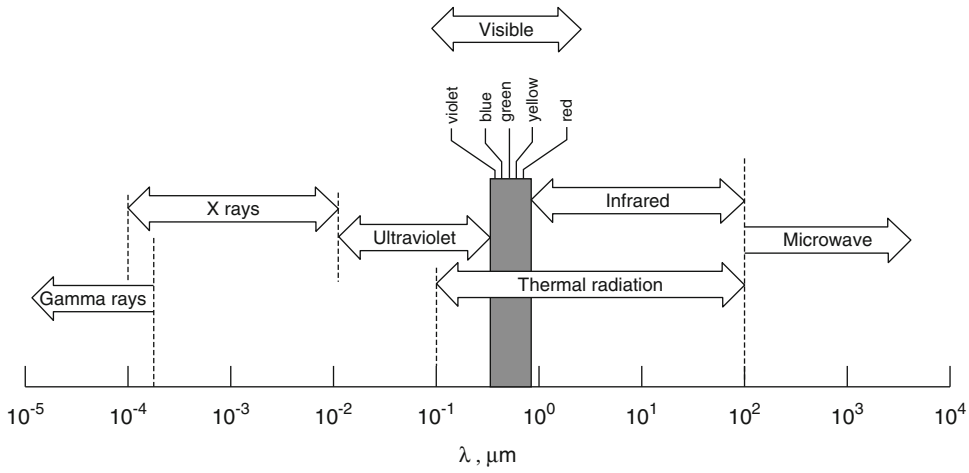

Fig. 4.1 Electromagnetic spectrum. Adapted from Incropera and DeWitt [4]

Spectral Distribution of Radiation from a Perfect Emitter

A *diffuse* surface is an idealized surface that emits thermal radiation equally in all directions, i.e. its emission exhibits no directional dependency. A *perfect emitter* is an idealized surface that emits the maximum possible thermal radiation at every wavelength. A *blackbody* is a diffuse perfect emitter that also absorbs all incident radiation.

The energy spectrum of radiation emitted by a diffuse perfect emitter, or blackbody, can be calculated from Planck's quantum theory. In particular, the spectral (or monochromatic) blackbody emissive power ($E_{\lambda,b}$, W/m^2 · μm) is given by the Planck distribution:

$$E_{\lambda,b}(\lambda,T) = \frac{C_1}{\lambda^5(\exp(C_2/\lambda T)-1)} \qquad (4.4)$$

where $C_1 = 2\pi hc_0^2 = 3.742 \times 10^8$ W · μm^4/m^2 is Planck's first constant (often called the first radiation constant) and $C_2 = hc_0/k = 1.439 \times 10^4$ μm · K is Planck's second constant (or the second radiation constant). Note that k is the Boltzmann constant ($k = 1.3805 \times 10^{-23}$ J/K). In Equation 4.4 and throughout this chapter, a subscript "b" indicates "blackbody" and a subscript λ indicates "wavelength", e.g. $E_{\lambda,b}$ is the blackbody emissive power at a particular wavelength λ.

Spectral emissive power is plotted in Fig. 4.2 as a function of wavelength for several different blackbody temperatures. Also shown in Fig. 4.2 is a line labeled $\lambda_{max} = C_3/T$ (where the third radiation constant is $C_3 = 2897.8$ μm · K) that relates the wavelength corresponding to the peak spectral emissive power (λ_{max}) to the blackbody temperature T. This is Wien's displacement law, which is obtained by differentiating Equation 4.4 with respect to T, setting that result equal to zero, and solving for λT. Wien's displacement law shows that the maximum monochromatic emissive power of a blackbody shifts to shorter wavelengths as its temperature increases. From Equation 4.3, it is also seen that the photons emitted from blackbodies high temperature (shorter wavelengths) carry more energy than photons emitted from blackbodies at lower

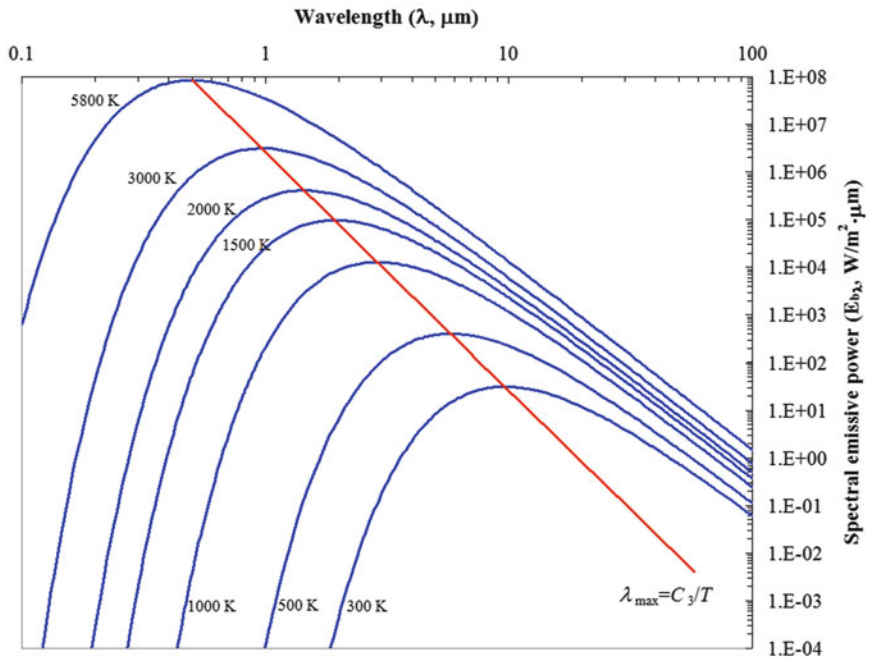

Fig. 4.2 The Planck distribution: blackbody emissive power and Wien's displacement law

temperatures (longer wavelengths), a result that one intuitively expects.

The Stefan-Boltzman Law is obtained by integrating the spectral blackbody emissive power over all wavelengths:

$$E_b = \int_0^\infty E_{\lambda,b}(\lambda)d\lambda = \int_0^\infty \frac{C_1}{\lambda^5(\exp(C_2/\lambda T)-1)}d\lambda = \sigma T^4 \quad (4.5)$$

where σ is the Stefan-Boltzman constant ($\sigma = 5.67 \times 10^{-8}$ W/m$^2 \cdot$ K^4) and E_b is the total (integrated over all wavelengths) blackbody emissive power. It is seen that the oft-cited "fourth power dependency" of thermal radiation on temperature is a direct consequence of integrating the Planck spectral distribution over all wavelengths.

Equations 4.4 and 4.5 can be used to calculate the fraction of a blackbody's radiant emission in a particular wavelength band, i.e. between two wavelengths. Denote $F_{\lambda_1\to\lambda_2}$ as the fraction of a blackbody's radiant emission between wavelengths λ_1 and λ_2. It is then calculated as:

$$F_{\lambda_1\to\lambda_2} = \frac{\int_0^{\lambda_2} E_{\lambda,b}d\lambda - \int_0^{\lambda_1} E_{\lambda,b}d\lambda}{E_b} = F_{0\to\lambda_2} - F_{0\to\lambda_1} \quad (4.6)$$

Thus, $F_{\lambda_1\to\lambda_2}$ can be calculated from two values of $F_{0\to\lambda}$, which is readily tabulated from Equation 4.4 as a function of λT (Table 4.1). This then makes it possible to calculate the fraction of emission between two wavelengths.

Table 4.1 Blackbody radiation fractions

λT (μm · K)	$F_{0\to\lambda}$ (−)	λT (μm · K)	$F_{0\to\lambda}$ (−)
200	0.000000	6200	0.754140
400	0.000000	6400	0.769234
600	0.000000	6600	0.783199
800	0.000016	6800	0.796129
1000	0.000321	7000	0.808109
1200	0.002134	7200	0.819217
1400	0.007790	7400	0.829527
1600	0.019718	7600	0.839102
1800	0.039341	7800	0.848005
2000	0.066728	8000	0.856288
2200	0.100888	8500	0.874608
2400	0.140256	9000	0.890029
2600	0.183120	9500	0.903085
2800	0.227897	10,000	0.914199
3000	0.273232	10,500	0.923710
3200	0.318102	11,000	0.931890
3400	0.361735	11,500	0.939959
3600	0.403607	12,000	0.945098
3800	0.443382	13,000	0.955139
4000	0.480877	14,000	0.962898
4200	0.516014	15,000	0.969981
4400	0.548796	16,000	0.973814
4600	0.579820	18,000	0.980860
4800	0.607559	20,000	0.985602
5000	0.633747	25,000	0.992215
5200	0.658970	30,000	0.995340
5400	0.680360	40,000	0.997967
5600	0.701046	50,000	0.998953
5800	0.720158	75,000	0.999713
6000	0.737818	100,000	0.999905

Example 2 Consider an electrically heated surface used as a heater in a flammability test. What fraction of thermal radiation does this surface emit in the visible range at temperatures of 800 and 1429 K?

Solution The visible range is from 0.4 to 0.7 μm. Thus for the 800 K emitter:

$$(\lambda T)_1 = 0.4\,\mu\text{m} \times 800\,\text{K} = 320\,\mu\text{m}\cdot\text{K and } F_{0\to\lambda_1} = 0.000000$$

$$(\lambda T)_2 = 0.7\,\mu\text{m} \times 800\,\text{K} = 560\,\mu\text{m}\cdot\text{K and } F_{0\to\lambda_2} = 0.000000$$

$$F_{\lambda_1\to\lambda_2} = F_{0\to\lambda_2} - F_{0\to\lambda_1} = 0.000000 - 0.000000 = 0.000000$$

Since the fraction of radiant between 0.4 and 0.7 μm is 0 (to six decimal places), the heater would not appear to be "glowing" at 800 K.

For the 1429 K emitter:

$$(\lambda T)_1 = 0.4\,\mu\text{m} \times 1429\,\text{K} = 572\,\mu\text{m}\cdot\text{K} \text{ and } F_{0\to\lambda_1} = 0.000000$$

$$(\lambda T)_2 = 0.7\,\mu\text{m} \times 1429\,\text{K} = 1000\,\mu\text{m}\cdot\text{K} \text{ and } F_{0\to\lambda_2} = 0.000321$$

$$F_{\lambda_1\to\lambda_2} = F_{0\to\lambda_2} - F_{0\to\lambda_1} = 0.000321 - 0.000000 = 0.000321$$

Since the emission fraction in the visible range is nonzero (albeit very small) the heater would appear to be glowing (if it didn't melt first).

Radiant Intensity and Heat Flux

When analyzing fire phenomena, we usually speak in terms of heat fluxes. For example, a radiant heat flux ($\dot{q}''_r$) of 20 kW/m^2 to the floor is often quoted as a rule of thumb for determining the onset of flashover in a compartment. Consider a target located on the floor of a compartment as it approaches flashover: the radiant heat flux "felt" by this target is the sum of all thermal radiation incident on this target, regardless of where the radiation originated. Some of the radiation incident to the target may have been emitted by flames, another part may have been emitted by the ceiling or walls, and another part may have been emitted by soot particles located in the hot gas layer. Thus, incident radiation comes in from all directions and the radiation felt by the target passes through an imaginary hemisphere surrounding the target. The radiant intensity passing through different parts of this hemisphere will, in general, vary spatially. The radiant intensity passing through part of the hemisphere facing the flames is likely greater than the radiant intensity passing through part of the hemisphere facing away from the flames. It is seen that in order properly analyze a radiant heat transfer problem, it is necessary to take into account the directional nature of radiation. The concept of *radiant intensity* is introduced as a tool to analyze the directional nature of thermal radiation.

Radiant intensity is defined on a per unit solid angle (Ω, sr or steradians) basis. The surface area of a sphere having radius r is $4\pi r^2$ and a unit sphere, i.e. a sphere with a radius of 1, has a surface area of 4π. The solid angle subtended by a surface is the area of a unit sphere covered by the surface's projection onto that unit sphere. For example, a hemisphere subtends a solid angle of 2π steradians, and all space subtends a solid angle of 4π steradians. Referring to the spherical coordinate system in Fig. 4.3, the differential solid angle $d\Omega$ is defined as:

$$d\Omega = \frac{dA}{\left|\vec{R}\right|^2} = \sin(\theta) d\theta d\phi \qquad (4.7)$$

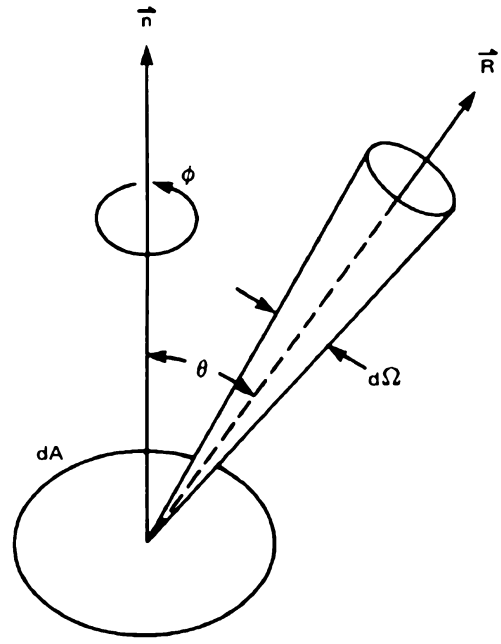

Fig. 4.3 Coordinate system for radiation intensity

where ϕ is azimuthal angle (radians), θ is polar angle (radians), and dA is the differential area normal to the θ and ϕ directions. In simple terms, ϕ can be thought of as degrees longitude and θ can be thought of as degrees latitude on a globe.

Spectral radiant intensity ($W/m^2 \cdot sr \cdot \mu m$) is an inherently directional quantity defined as radiant power per unit area normal to the emitting surface per unit solid angle per unit wavelength:

$$I_\lambda(\lambda, \theta, \phi) = \frac{d\dot{q}}{dA \cdot d\Omega \cdot d\lambda} \tag{4.8}$$

The radiant heat flux at a single wavelength across a surface of an arbitrary orientation is the spectral radiant heat flux [5, 6]:

$$\begin{aligned} \dot{q}''_\lambda(\lambda) &= \int_0^{4\pi} I_\lambda(\lambda, \theta, \phi) \cos(\theta) d\Omega \\ &= \int_0^{2\pi} \int_0^{\pi/2} I_\lambda(\lambda, \theta, \phi) \cos(\theta) \sin(\theta) d\theta d\phi \end{aligned} \tag{4.9}$$

where I_λ is the radiation intensity at wavelength λ per unit solid angle (Fig. 4.3). Intensity is a useful measure for thermal radiation because the intensity of a radiant beam remains constant if it is traveling through a nonparticipating medium. The total radiant heat flux is obtained by integrating Equation 4.9 over all wavelengths:

$$\dot{q}''_r = \int_0^\infty \dot{q}''_\lambda(\lambda) d\lambda \tag{4.10}$$

The salient point here is that radiant intensity is not the same as radiant heat flux. Radiant intensity is a directional (and possibly spectral) quantity. Radiant heat flux is obtained by summing (or integrating) individual contributions over all directions (Equation 4.9) and usually wavelengths (Equation 4.10).

Emission, Irradiation, and Radiosity

Emission

Now define $I_{\lambda,e}(\lambda, \theta, \phi)$ as the spectral intensity of radiation emitted by a surface (subscript "e" means emission or emitted). The emissive power of that surface at wavelength λ is defined in an analogous manner to Equation 4.9, but with $\dot{q}''_\lambda$ replaced by E_λ and I_λ replaced by $I_{\lambda,e}$:

$$\begin{aligned} E_\lambda(\lambda) &= \int_0^{4\pi} I_{\lambda,e}(\lambda, \theta, \phi) \cos(\theta) d\Omega \\ &= \int_0^{2\pi} \int_0^{\pi/2} I_{\lambda,e}(\lambda, \theta, \phi) \cos(\theta) \sin(\theta) d\theta d\phi \end{aligned} \tag{4.11}$$

It is seen that for a surface at a given temperature, the intensity of emitted radiation depends on wavelength and direction. For engineering applications, this directional dependency of surface emission is usually neglected and we instead (implicitly or explicitly) work with *hemispherical* radiation emission. Hemispherical emission can be envisioned by picturing a small (differential) element located at the center of an imaginary hemispherical enclosure (see Fig. 4.4). Due to the directional dependency of surface emission, the intensity of radiation emitted

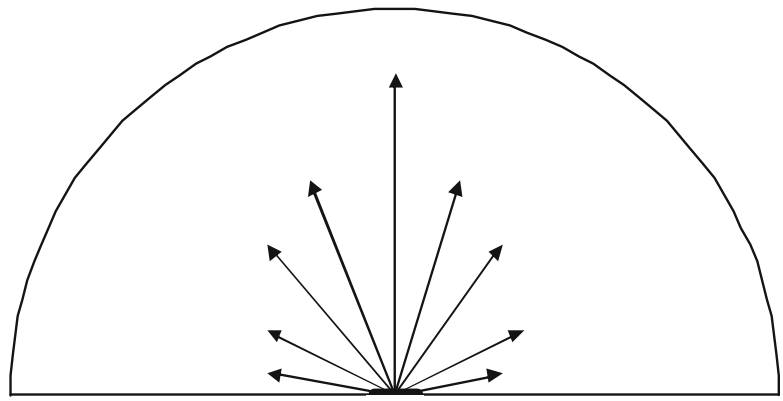

Fig. 4.4 Directional emission from a differential surface. Length of arrows represents spectral directional intensity of emitted thermal radiation

by this surface that impinges on the imaginary hemispherical enclosure may vary with location. However, for engineering purposes, it is usually adequate to neglect the potentially directional character of surface emission and consider only hemispherical emission, meaning the radiant emission that impinges on some part of the imaginary hemispherical enclosure. In practice, this is equivalent to assuming that a surface is a diffuse emitter, meaning the intensity of emitted radiation is independent of direction.

For the reasons described above, in most engineering applications surfaces are approximated as diffuse, which means that $I_{\lambda,e}$ is a constant that does not vary with θ and ϕ, even though emission of thermal radiation from all real surfaces exhibits some directional dependency. Under this diffuse approximation $I_{\lambda,e}$ can be removed from the integrand in Equation 4.11:

$$\begin{aligned} E_\lambda(\lambda) &= \int_0^{2\pi}\int_0^{\pi/2} I_{\lambda,e}(\lambda,\theta,\phi)\cos(\theta)\sin(\theta)d\theta d\phi \\ &= I_{\lambda,e}(\lambda)\int_0^{2\pi}\int_0^{\pi/2}\cos(\theta)\sin(\theta)d\theta d\phi \\ &= \pi I_{\lambda,e}(\lambda) \end{aligned} \tag{4.12}$$

and it is seen that the emissive power of a diffuse surface equals its spectral intensity multiplied by π steradians (for diffuse surfaces $E = \pi I$ and for this reason Equation 4.4 can also be written as $E_{\lambda,b}(\lambda,T) = \pi I_{\lambda,b}(\lambda,T)$). The total emissive power is obtained by integrating over all wavelengths:

$$E = \int_0^\infty E_\lambda(\lambda)d\lambda = \pi I_e \tag{4.13}$$

An important result that is obtained from Equation 4.4 after performing the integration in Equation 4.13 is the Stefan-Boltzman Law, already presented as Equation 4.5.

For a diffuse surface, the fraction of radiation emitted in angle range $\phi_1 \le \phi \le \phi_2$ and $\theta_1 \le \theta \le \theta_2$ can be calculated as:

$$F(\theta_1,\theta_2,\phi_1,\phi_2) = \frac{1}{\pi}\int_{\phi_1}^{\phi_2}\int_{\theta_1}^{\theta_2}\cos(\theta)\sin(\theta)d\theta d\phi \tag{4.14}$$

Example 3 What is the emissive power of a blackbody at 1000 K? What is its emissive power between 1 and 5 μm for all emission angles? What is its emissive power between 1 and 5 μm for $0 \le \phi \le 2\pi$ and $0 \le \theta \le \pi/4$?

Solution Blackbody emissive power is calculated from Equation 4.5:

$$\begin{aligned} E_b &= \sigma T^4 = 5.67\times10^{-8}\times1000^4 \\ &= 56.7\,\mathrm{kW/m^2} \end{aligned}$$

The fraction of this radiation emitted at wavelengths between 1 and 5 μm can be calculated with Equation 4.6 and Table 4.1 as follows:

$$(\lambda T)_1 = 1\,\mu\mathrm{m}\times1000\,\mathrm{K} = 1000\,\mu\mathrm{m}\cdot\mathrm{K} \text{ and } F_{0\to\lambda_1} = 0.000321$$

$$(\lambda T)_2 = 5\,\mu\mathrm{m}\times1000\,\mathrm{K} = 5000\,\mu\mathrm{m}\cdot\mathrm{K} \text{ and } F_{0\to\lambda_2} = 0.633747$$

$$F_{\lambda_1\to\lambda_2} = F_{0\to\lambda_2} - F_{0\to\lambda_1} = 0.633747 - 0.000321 = 0.633426$$

The emissive power between 1 and 5 μm, for all emission angles, is 56.7 $\mathrm{kW/m^2}\times0.633 = 35.9\,\mathrm{kW/m^2}$.

The fraction of radiation emitted in the direction $0 \le \phi \le 2\pi$ and $0 \le \theta \le \pi/4$ can be calculated from Equation 4.14 as:

$$F(\theta_1,\theta_2,\phi_1,\phi_2)=\frac{1}{\pi}\int_0^{2\pi}\int_0^{\pi/4}\cos(\theta)\sin(\theta)d\theta d\phi$$

$$F(\theta_1,\theta_2,\phi_1,\phi_2)=\frac{1}{\pi}\int_0^{2\pi}\left(-\frac{1}{2}\cos^2(\theta)\Big|_{\theta=0}^{\theta=\pi/4}\right)d\phi$$
$$=\frac{1}{4\pi}\int_0^{2\pi}d\phi=\frac{2\pi}{4\pi}=0.5$$

The emissive power between 1 and 5 μm for this angle range is 35.9 kW/m^2 × 0.5 = 18 kW/m^2.

Irradiation

Spectral irradiation $G_\lambda(\lambda)$ (W/m^2 · μm) is the radiant heat flux at wavelength λ to a surface incident from all directions. It is obtained by integrating the incident spectral radiation intensity over all angles in a manner directly analogous to the way that spectral emissive power was defined in Equation 4.11:

$$G_\lambda(\lambda)=\int_0^{2\pi}\int_0^{\pi/2}I_{\lambda,i}(\lambda,\theta,\phi)\cos(\theta)\sin(\theta)d\theta d\phi \tag{4.15}$$

Total irradiation (G, W/m^2) is obtained by integrating G_λ over all wavelengths:

$$G=\int_0^{\infty}G_\lambda(\lambda)d\lambda \tag{4.16}$$

Note that G_λ has no subscript i (for incident) because by definition irradiation is incident on a surface so the "i" would be redundant. G is the total radiant heat flux incident to a target.

Example 4 A surface is uniformly irradiated with a source having the following characteristics:

$G_\lambda = 0\ \text{kW/m}^2\cdot\mu\text{m}$ for $\lambda \le 2\ \mu\text{m}$
$G_\lambda = 5\ \text{kW/m}^2\cdot\mu\text{m}$ for $2 < \lambda \le 8\ \mu\text{m}$
$G_\lambda = 10\ \text{kW/m}^2\cdot\mu\text{m}$ for $8 < \lambda \le 20\ \mu\text{m}$
$G_\lambda = 0\ \text{kW/m}^2\cdot\mu\text{m}$ for $\lambda > 20\ \mu\text{m}$

What is its total irradiation?

Solution Total irradiation can be calculated from Equation 4.16 as:

$$G=\int_0^{\infty}G_\lambda(\lambda)d\lambda=\int_2^8 5d\lambda+\int_8^{20}10d\lambda$$
$$=5\times(8-2)+10\times(20-8)$$
$$=150\ \text{kW/m}^2$$

Radiosity

As will be discussed later, a certain fraction of radiation impinging on a surface may be reflected by that surface. Thus, the total amount of radiation leaving a surface is the sum of the radiation emitted by that surface plus the radiation reflected by that surface. The total radiation leaving a surface, whether emitted or reflected, is called radiosity, J.

Spectral radiosity J_λ is:

$$J_\lambda(\lambda)=\int_0^{2\pi}\int_0^{\pi/2}I_{\lambda,e,r}(\lambda,\theta,\phi)\cos(\theta)\sin(\theta)d\theta d\phi \tag{4.17}$$

Total radiosity (J, W/m^2) is obtained by integrating J_λ over all wavelengths:

$$J=\int_0^{\infty}J_\lambda(\lambda)d\lambda \tag{4.18}$$

Surface Properties

Thermal radiation may be absorbed at, reflected by, or transmitted through a surface. Imprecisely, absorptivity (α) is the fraction absorbed at the surface, reflectivity (ρ) is the fraction reflected by the surface, and transmissivity (τ) is the fraction transmitted through the surface. It follows from a radiation balance:

$$\alpha+\rho+\tau=1 \tag{4.19}$$

where each property in Equation 4.29 may exhibit spectral and directional characteristics

(but such dependency is not explicitly shown). Additionally, emissivity (ε) is the ratio of the actual amount of radiation emitted by a surface to the maximum possible amount of radiation that could be emitted by that surface if it was a blackbody. These properties are defined more precisely in the sections that follow.

Emissivity

Since no surface can emit more thermal radiation than a blackbody, a logical tool for normalizing thermal emission from real surfaces is the blackbody. Spectral surface emissivity is defined as the ratio of the actual spectral intensity of radiation emitted by a surface to the blackbody spectral intensity:

$$\varepsilon_\lambda(\lambda,\theta,\phi,T) = \frac{I_{\lambda,e}(\lambda,\theta,\phi,T)}{I_{\lambda,b}(T)} \tag{4.20}$$

As described earlier, hemispherical radiation quantities are usually applied in engineering applications. The spectral hemispherical emissivity is defined in terms of the blackbody emissive power at wavelength λ and is obtained by integrating Equation 4.20 over all directions with the result:

$$\varepsilon_\lambda(\lambda,T) = \frac{E_\lambda(\lambda,T)}{E_{\lambda,b}(\lambda,T)} \tag{4.21}$$

Spectral normal emissivity (very close to hemispherical emissivity) is shown for several materials in Fig. 4.5 [4].

Total emissivity is obtained by integrating Equation 4.21 over all wavelengths:

$$\varepsilon(T) = \frac{E(T)}{E_b(T)} \tag{4.22}$$

By definition, the emissivity of a blackbody (whether $\varepsilon_\lambda(\lambda, \theta, \phi, T)$, $\varepsilon_\lambda(\lambda, T)$, or $\varepsilon(T)$) is unity. Total normal emissivity (very close to hemispherical emissivity) is shown graphically in Fig. 4.6 for several materials [4]. Representative values of total hemispherical emissivity are tabulated for several materials in Table 4.2 [7] (metals) and Table 4.3 [7] (non-metals).

Absorptivity

In a fire, one of the most important radiative characteristics of a material or surface is its absorptivity, defined loosely as the fraction of the incident radiation that is absorbed by the material. The absorptivity is strongly

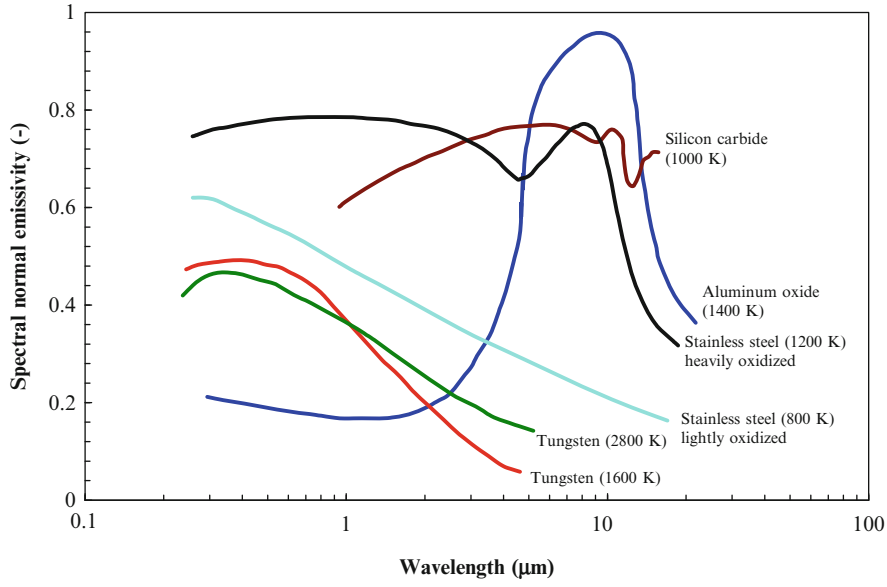

Fig. 4.5 Spectral normal emissivity of several materials [4]

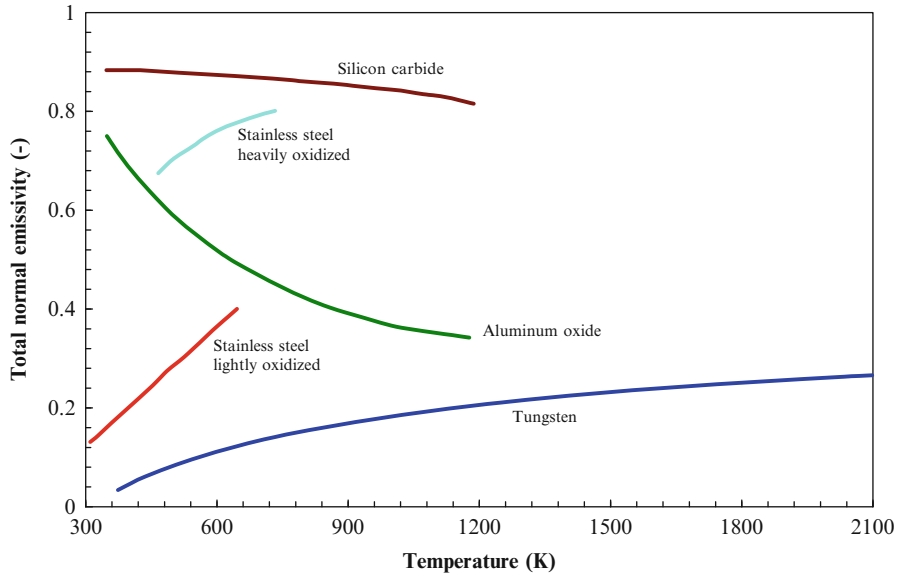

Fig. 4.6 Total normal emissivity of several materials [4].

Table 4.2 Representative total hemispherical emissivity of several metals [7]

Material	Description	Emissivity
Aluminum	Crude	0.07–0.08 (0–200 °C)
	Foil, bright	0.01 (−9 °C), 0.04 (1 °C), 0.087 (200 °C)
	Highly polished	0.04–0.05 (1 °C)
	Ordinarily rolled	0.035 (100 °C), 0.05 (500 °C)
	Oxidized	0.11 (200 °C), 0.19 (600 °C)
	Roughed	0.044–0.066 (40 °C)
	Unoxidized	0.022 (25 °C), 0.06 (500 °C)
Bismuth	Unoxidized	0.048 (25 °C), 0.061 (100 °C)
Brass	After rolling	0.06 (30 °C)
	Browned	0.5 (20–300 °C)
	Polished	0.03 (300 °C)
Chromium	Polished	0.07 (150 °C)
	Unoxidized	0.08 (100 °C)
Cobalt	Unoxidized	0.13 (500 °C), 0.23 (1000 °C)
Copper	Black oxidized	0.78 (40 °C)
	Highly polished	0.03 (1 °C)
	Molten	0.15
	Matte	0.22 (40 °C)
	New	0.07 (40–100 °C)
	Oxidized	0.56 (40–200 °C), 0.61 (200 °C), 0.88 (540 °C)
	Polished	0.04 (40 °C), 0.05 (260 °C), 0.17 (1100 °C)
	Rolled	0.64 (40 °C)
Gold	Polished	0.02 (40 °C), 0.03 (1100 °C)
	Electroytically deposited	0.02 (40 °C), 0.03 (1100 °C)

(continued)

Table 4.2 (continued)

Material	Description	Emissivity
Inconel	Sandblasted	0.79 (800 °C), 0.91 (1150 °C)
	Stably oxidized	0.69 (300 °C), 0.82 (1000 °C)
	Untreated	0.3 (40–260 °C)
	Rolled	0.69 (300 °C), 0.88 (1150 °C)
Inconel X	Stably oxidized	0.89 (300 °C), 0.93 (1100 °C)
Iron	Cast	0.21 (40 °C)
	Cast, freshly turned	0.44 (40 °C), 0.7 (1100 °C)
	Galvanized	0.22–0.28 (0–200 °C)
	Molten	0.02–0.05 (1100 °C)
	Plate, rusted red	0.61 (40 °C)
	Pure polished	0.06 (40 °C), 0.13 (540 °C)
	Red iron oxide	0.96 (40 °C), 0.67 (540 °C)
	Rough ingot	0.95 (1100 °C)
	Smooth sheet	0.6 (1100 °C)
	Wrought, polished	0.28 (40–260 °C)
Lead	Oxidized	0.28 (00–200 °C)
	Unoxidized	0.05 (100 °C)
Magnesium		0.13 (260 °C), 0.18 (310 °C)
Mercury		0.09 (0 °C), 0.12 (100 °C)
Molybdenum	Oxidized	0.78–0.81 (300–540 °C)
Monel	Oxidized	0.43 (20 °C)
	Polished	0.09 (20 °C)
Nichrome	Rolled	0.36 (800 °C), 0.8 (1150 °C)
	Sandblasted	0.81 (800 °C), 0.87 (1150 °C)
Nickel	Electrolytic	0.04 (40 °C), 0.1 (540 °C)
	Oxidized	0.31–0.39 (40 °C), 0.67 (540 °C)
	Wire	0.1 (260 °C), 0.19 (1100 °C)
Platinum	Oxidized	0.07 (260 °C), 0.11 (540 °C)
	Unoxidized	0.04 (25 °C), 0.05 (100 °C), 0.15 (1000 °C)
Silver	Polished	0.01 (40 °C), 0.02 (260 °C), 0.03 (540 °C)
Steel	Calorized	0.5–0.56 (40–540 °C)
	Cold rolled	0.08 (100 °C)
	Ground sheet	0.61 (1100 °C)
	Oxidized	0.79 (260–540 °C)
	Plate, rough	0.94–0.97 (40–540 °C)
	Polished	0.07 (40 °C), 0.1 (260 °C), 0.14 (540 °C), 0.23 (1100 °C)
	Rolled sheet	0.66 (40 °C)
	Type 347, oxidized	0.87–0.91 (300–1100 °C)
	Type AISI 303, oxidized	0.74–0.87 (300–1100 °C)
	Type 310, oxidized & rolled	0.56 (800 °C), 0.81 (1150 °C)
	Sandblasted	0.82 (800 °C), 0.93 (1150 °C)
Stellite		0.18 (20 °C)
Tantalum		0.19 (1300 °C)
Tin	Unoxidized	0.04–0.05 (25–100 °C)
Tungsten	Filament	0.18 (40 °C), 0.11 (540 °C), 0.39 (2800 °C)
Zinc	Oxidized	0.11 (260 °C)
	Polished	0.02 (40 °C), 0.03 (260 °C)

Table 4.3 Representative total hemispherical emissivity of several non-metals [7]

Material	Description	Emissivity
Bricks	Chrome refractory	0.94 (540 °C), 0.98 (1100 °C)
	Fire clay	0.75 (1400 °C)
	Light buff	0.8 (540 °C)
	Magnesite refractory	0.38 (1000 °C)
	Sand lime red	0.59 (1400 °C)
	Silica	0.84 (1400 °C)
	Various refractories	0.71–0.88 (1100 °C)
	White refractory	0.89 (260 °C), 0.68 (540 °C)
Building materials	Asbestos, board	0.96 (40 °C)
	Asphalt pavement	0.85–0.93 (40 °C)
	Clay	0.39 (20 °C)
	Concrete, rough	0.94 (0–100 °C)
	Granite	0.44 (40 °C)
	Gravel	0.28 (40 °C)
	Gypsum	0.9 (40 °C)
	Marble, polished	0.93 (40 °C)
	Mica	0.75 (40 °C)
	Plaster	0.89 (40 °C), 0.48 (540 °C)
	Quartz	0.76 (40 °C)
	Sand	0.83 (40 °C)
	Sandstone	0.83 (40 °C)
	Slate	0.67 (40–260 °C)
Carbon	Baked	0.52–0.79 (1000–2400 °C)
	Filament	0.95 (260 °C)
	Graphitized	0.76–0.71 (100–500 °C)
	Rough	0.77 (100–320 °C)
	Soot (candle)	0.95 (120 °C)
	Soot (coal)	0.95 (20 °C)
	Unoxidized	0.8 (25–500 °C)
Ceramics	Alumina coating on inconel	0.65 (430 °C), 0.45 (1100 °C)
	Zirconia coating on inconel	0.62 (430 °C), 0.45 (1100 °C)
	Earthenware, glazed	0.9 (1 °C)
	Earthenware, matte	0.93 (1 °C)
	Procelain	0.92 (40 °C)
	Refractory, black	0.94 (100 °C)
	Refractory, light buff	0.92 (100 °C)
	Refractory, white Al_2O_3	0.9 (100 °C)
Cloth	Cotton	0.77 (20 °C)
	Silk	0.78 (20 °C)
Glass	Convex D	0.8–0.76 (100–500 °C)
	Fused quartz	0.75–0.8 (100–500 °C)
	Nonex	0.82–0.78 (100–500 °C)
	Pyrex	0.8–0.9 (40 °C)
	Smooth	0.92–0.95 (0–200 °C)
	Waterglass	0.96 (20 °C)
Ice	Smooth	0.92 (0 °C)
Oxides	Al_2O_3	0.35–0.54 (850–1300 °C)
	C_2O	0.27 (850–1300 °C)
	Cr_2O_3	0.73–0.95 (850–1300 °C)
	Fe_2O_3	0.57–0.78 (850–1300 °C)
	MgO	0.29–0.5 (850–1300 °C)
	NiO	0.52–0.86 (500–1200 °C)
	ZnO	0.3–0.65 (850–1300 °C)
Paints	Aluminum	0.27–0.7 (1–100 °C)
	Enamel, snow white	0.91 (40 °C)
	Lacquer	0.85–0.93 (40 °C)
	Lampblack	0.94–0.97 (40 °C)
	Oil	0.89–0.97 (0–200 °C)
	White	0.89–0.97 (40 °C)
Paper	White	0.95 (40 °C), 0.82 (540 °C)
Roofing materials	Aluminum surfaces	0.22 (40 °C)
	Asbestos cement	0.65 (1400 °C)
	Bituminous felt	0.89 (1400 °C)
	Enameled steel, white	0.65 (1400 °C)
	Galvanized iron, dirty	0.90 (1400 °C)
	Galvanized iron, new	0.42 (1400 °C)
	Roofing sheet, brown	0.8 (1400 °C)
	Roofing sheet, green	0.87 (1400 °C)
	Tiles, uncolored	0.63 (1400 °C)
	Tiles, brown	0.87 (1400 °C)
	Tiles, black	0.94 (1400 °C)
	Tiles, asbestos cement	0.66 (1400 °C)
	Weathered asphalt	0.88 (1400 °C)

(continued)

Table 4.3 (continued)

Material	Description	Emissivity
Rubber	Hard, black, glossy	0.95 (40 °C)
	Soft, gray	0.86 (40 °C)
Snow	Fine	0.82 (−10 °C)
	Frost	0.98 (0 °C)
	Granular	0.89 (−10 °C)
Soils	Black loam	0.66 (20 °C)
	Plowed field	0.38 (20 °C)
Water		0.92–0.96 (0–40 °C)
Wood	Beech	0.91 (70 °C)
	Oak, planed	0.91 (40 °C)
	Sawdust	0.75 (40 °C)
	Spruce, sanded	0.82 (100 °C)

wavelength–dependent. For example, at wavelengths below 1 μm the absorptivity of clear Polymethylmethacrylate is close to zero, but at wavelengths above 3 μm it approaches unity.

A blackbody absorbs all incident radiation with no spectral or directional dependency. As with emissivity, the idealized blackbody behavior is used as a normalization tool to quantify the amount of radiation absorbed by a surface relative to the maximum possible amount the surface may absorb (i.e., if it was a blackbody).

Spectral radiant intensity incident on a surface is denoted $I_{\lambda,i}$; it is, in general, a function of λ, θ, and ϕ. Spectral, directional absorptivity is the ratio if the spectral directional radiant intensity absorbed by a surface $I_{\lambda,i,abs}(\lambda, \theta, \phi)$ to the spectral directional radiant intensity incident on that surface $I_{\lambda,i}(\lambda, \theta, \phi)$ (because the latter is the maximum possible radiation that could be absorbed by that surface, i.e. if it was a blackbody):

$$\alpha_\lambda(\lambda,\theta,\phi) = \frac{I_{\lambda,i,abs}(\lambda,\theta,\phi)}{I_{\lambda,i}(\lambda,\theta,\phi)} \tag{4.23}$$

Spectral hemispherical absorptivity, a directionally-averaged property that is obtained by integrating over all incident angles, is the ratio of the spectral irradiation absorbed by the surface ($G_{\lambda,abs}$) to the spectral irradiation of the surface G_λ:

$$\begin{aligned}\alpha_\lambda(\lambda) &= \frac{\int_0^{2\pi}\int_0^{\pi/2} I_{\lambda,i,abs}(\lambda,\theta,\phi)\cos(\theta)\sin(\theta)d\theta d\phi}{\int_0^{2\pi}\int_0^{\pi/2} I_{\lambda,i}(\lambda,\theta,\phi)\cos(\theta)\sin(\theta)d\theta d\phi} \\ &= \frac{G_{\lambda,abs}(\lambda)}{G_\lambda(\lambda)}\end{aligned} \tag{4.24}$$

Finally, total hemispherical absorptivity is obtained by integrating spectral hemispherical absorptivity over all wavelengths:

$$\begin{aligned}\alpha &= \frac{\int_0^\infty G_{\lambda,abs}(\lambda)d\lambda}{\int_0^\infty G_\lambda(\lambda)d\lambda} = \frac{\int_0^\infty \alpha_\lambda(\lambda)G_\lambda(\lambda)d\lambda}{\int_0^\infty G_\lambda(\lambda)d\lambda} \\ &= \frac{G_{abs}}{G}\end{aligned} \tag{4.25}$$

Example 5 A particular diffuse material is idealized as having a spectral absorptivity of zero for wavelengths less than 3 μm and unity for wavelengths greater than 3 μm. Calculate its total hemispherical absorptivity for a blackbody at 800, 1200, and 2000 K.

Solution Assume $G_\lambda(\lambda) = E_{\lambda,b}(\lambda,\mathrm{T}_e)$ where T_e is the temperature of the emitter (800, 1200, and 2000 K) and use Equation 4.25:

$$\alpha(T_e) = \frac{\int_0^\infty \alpha_\lambda(\lambda)E_{\lambda,b}(\lambda,T_e)d\lambda}{\int_0^\infty E_{\lambda,b}(\lambda,T_e)d\lambda} = \frac{\int_0^3 0\times E_{\lambda,b}(\lambda,T_e)d\lambda + \int_3^\infty 1\times E_{\lambda,b}(\lambda,T_e)d\lambda}{\sigma T_e^4} = \frac{\int_3^\infty E_{\lambda,b}(\lambda,T_e)d\lambda}{\sigma T_e^4}$$

It is possible to put this in a form that allows use of the radiation fraction tabulated in Table 4.1:

$$\alpha = \frac{\int_0^\infty E_{\lambda,b}(\lambda, T_e)d\lambda - \int_0^3 E_{\lambda,b}(\lambda, T_e)d\lambda}{\sigma T_e^4}$$

$$= \frac{\sigma T_e^4 - \int_0^3 E_{\lambda,b}(\lambda, T_e)d\lambda}{\sigma T_e^4}$$

$$= 1 - \frac{\int_0^3 E_{\lambda,b}(\lambda, T_e)d\lambda}{\sigma T_e^4} = 1 - F_{0\to 3}(3T_e)$$

For $T_e = 800$ K, $\lambda T_e = 2400\ \mu$m · K and from Table 4.1 $F_{0\to 3} = 0.14$ so $\alpha = 0.86$.
For $T_e = 1200$ K, $\lambda T_e = 3600\ \mu$m · K and from Table 4.1 $F_{0\to 3} = 0.40$ so $\alpha = 0.60$.
For $T_e = 2000$ K, $\lambda T_e = 6000\ \mu$m · K and from Table 4.1 $F_{0\to 3} = 0.76$ so $\alpha = 0.24$.

It is seen that, for this idealized material, the effective absorptivity is a strong function of emitter temperature.

In a fire we are usually interested in the total hemispherical absorptivity defined in Equation 4.25. However, as demonstrated above, the total hemispherical absorptivity depends on the spectral energy distribution of the radiation source. Therefore, a material technically cannot be assigned a single absorptivity value because the spectral distribution of the incoming radiation depends on the temperature of the emitter. Due to Wien's displacement law and the Planck distribution, this is true even if the emitter behaves as a blackbody. In fires, the temperature of radiation sources ranges from approximately ~600 K (smoke layer, hot surfaces) to ~2000 K (flames). Additionally, certain bench–scale fire tests use tungsten–filament heaters that operate at temperatures near 3000 K. Thus, the effect of source temperature on the integrated (or effective) absorptivity has relevance for both real fires and bench-scale fire testing.

Hallman's 1971 Ph.D. dissertation [8] and subsequent publications [9, 10] remain some of the most comprehensive sources of information on the change of polymers' total hemispherical absorptivity with the temperature of the emitter. Hallman measured the spectral absorptivity of several solids and then determined the integrated surface absorptivity of different solids irradiated by hexane flames, blackbodies between 1000 and 3500 K, and solar energy. His absorptivity data are reproduced in Table 4.4. Note that the total hemispherical absorptivity of some materials is relatively insensitive to the temperature of the radiation source (black PMMA) but others are quite sensitive. For example, the absorptivity of clear PMMA decreases from 0.85 for a 1000 K blackbody to 0.25 for a 3500 K blackbody.

Similar measurements were made by Wesson et al. [11] for undegraded wood. Their results are reproduced in Table 4.5. More recently, Försth and Roos [12] conducted similar measurements for wood products (Table 4.6), carpet (Table 4.7), painted plywood (Table 4.8), and plastics (Table 4.9).

During a fire, a material's radiative characteristics may change. Although the integrated absorptivities from Wesson et al. [11] (reproduced in Table 4.5) are relatively low, the absorptivity of charred wood is generally not the same as that of virgin wood. Janssens [13] suggested that blackening causes the absorptivity of wood to increase from ~0.76 (based on Reference [11]) to approximately unity as the surface temperature approaches the ignition temperature. He therefore used an average value of 0.88 in his ignition analyses, and recommends using an integrated absorptivity of 1.0 during flaming combustion [14]. Interestingly, Försth and Roos [12] noted the opposite trend, i.e. a reduction in effective absorptivity as wood darkens. More research is needed in this area.

Wood is not the only class of materials that exhibits a change in radiative characteristics during a fire. Under nonflaming conditions, low density polyethylene has been observed to change from visually opaque to transparent, eventually followed by a darkening of the surface [15]. This indicates that a change in the material's radiative characteristics occurred (at least in the visible range). Modak and Croce [16] reported that for clear PMMA, 39 % of flame radiation is transmitted through the surface, but for "charred" PMMA (previously exposed to a fire environment and then cooled) no radiation penetrates in depth. Bubbling

Table 4.4 Integrated surface absorptivities for polymers from Hallman [9]

		Blackbody emitter temperature (K)						
Generic name	Trade name	1000	1500	2000	2500	3000	3500	Flame
Acrylonitrile butadiene styrene	Cycolac®	0.91	0.86	0.77	0.71	0.65	0.61	0.92
Cellulose acetate butyrate	Uvex®	0.84	0.71	0.56	0.43	0.34	0.27	0.88
Cork		0.64	0.56	0.49	0.46	0.44	0.44	0.60
Melamine/formaldehyde	Formica®	0.91	0.88	0.85	0.82	0.80	0.79	0.91
Nylon 6/6		0.93	0.90	0.86	0.82	0.75	0.71	0.93
Phenolic	Bakelite	0.90	0.86	0.81	0.77	0.75	0.75	0.91
Polycarbonate (rough surface)	Lexan®	0.87	0.83	0.78	0.75	0.72	0.71	0.88
Polyethylene (low density)		0.92	0.88	0.82	0.77	0.72	0.68	0.93
Polymethylmethacrylate (black)	Plexiglas®	0.94	0.94	0.95	0.95	0.95	0.95	0.94
Polymethylmethacrylate (clear)	Plexiglas®	0.85	0.69	0.54	0.41	0.31	0.25	0.89
Polymethylmethacrylate (white)	Plexiglas®	0.91	0.86	0.78	0.70	0.62	0.56	0.92
Polyoxymethylene	Delrin®	0.92	0.86	0.78	0.71	0.64	0.59	0.93
Polyphenylene oxide		0.86	0.78	0.70	0.63	0.57	0.53	0.88
Polypropylene		0.87	0.83	0.78	0.74	0.70	0.68	0.86
Polystyrene (clear)	Styrolux®	0.75	0.60	0.46	0.35	0.28	0.22	0.78
Polystyrene (white)		0.86	0.75	0.63	0.53	0.45	0.40	0.88
Polyurethane thermoplastic	Texin®	0.92	0.89	0.83	0.77	0.72	0.68	0.93
Polyvinyl chloride (clear)		0.81	0.65	0.49	0.38	0.30	0.24	0.85
Polyvinyl chloride (gray)		0.90	0.90	0.89	0.89	0.89	0.89	0.91
PVC/acrylic (gray, rolled)	Kydex®	0.88	0.87	0.86	0.85	0.84	0.83	0.88
PVC/acrylic (red cast)	Kydex®	0.91	0.90	0.89	0.88	0.87	0.86	0.92
Rubber (Buna–N)		0.92	0.93	0.93	0.93	0.93	0.93	0.92
Rubber (Butyl IIR)		0.92	0.93	0.94	0.94	0.95	0.95	0.92
Rubber (natural, gum)		0.88	0.82	0.76	0.72	0.69	0.68	0.89
Rubber (neoprene)		0.91	0.92	0.93	0.93	0.93	0.93	0.91
Rubber (silicone)		0.79	0.66	0.58	0.54	0.52	0.53	0.79

Table 4.5 Integrated surface absorptivity for wood from different emitters (From Wesson et al. [11])

Wood	Flame radiation	Tungsten lamp radiation	Solar radiation
Alaskan cedar	0.76	0.44	0.36
Ash	0.76	0.46	0.36
Balsa	0.75	0.41	0.35
Birch	0.77	0.47	0.39
Cottonwood	0.76	0.48	0.40
Mahogany	0.76	0.49	0.52
Mansonia	0.76	0.47	0.51
Maple	0.76	0.49	0.44
Oak	0.77	0.56	0.49
Redgum	0.77	0.52	0.56
Redwood	0.77	0.51	0.55
Spruce	0.76	0.45	0.35
White pine	0.76	0.49	0.43
Masonite	0.75	0.52	0.61

occurring near the surface of polymers can change their radiative characteristics, but this effect is has not yet been reliably quantified. In a real fire, materials may become coated in soot from flames or a smoke layer, causing their absorptivities to approach unity.

Reflectivity

A fraction of radiation incident on a surface may be reflected. One complicating factor is that reflection may be diffuse, specular, or (most likely) some combination of these two idealizations. A diffuse reflector is a surface for which, analogous to a diffuse emitter, the intensity of reflected radiation is equal in all directions and does not depend on the angle of incoming

Table 4.6 Effective absorptivities for different grey body temperatures for various wood products (From Försth and Roos [12])

Grey body emitter T (K)	674	852	1025	1153	1300	5777
Cone calorimeter irradiation (kWm^{-2})	10	25	50	75	100	Sun
Product	α_{eff}					
Plywood	0.86	0.84	0.81	0.79	0.76	0.40
Dark heat-treated lacquered ash tree floor	0.89	0.88	0.85	0.83	0.80	0.63
Dark heat-treated non-lacquered ash tree floor	0.83	0.81	0.79	0.77	0.74	0.62
Light lacquered ash tree flooring	0.90	0.88	0.86	0.84	0.82	0.40
Light non-lacquered oak flooring	0.86	0.84	0.81	0.80	0.77	0.37
Medium dark lacquered oak flooring	0.91	0.89	0.87	0.85	0.83	0.56
Medium dark non-lacquered oak flooring	0.86	0.84	0.82	0.80	0.77	0.50

Table 4.7 Effective absorptivities for different grey body temperatures for various carpets (From Försth and Roos [12])

Grey body emitter T (K)	674	852	1025	1153	1300	5777
Cone calorimeter irradiation (kWm^{-2})	10	25	50	75	100	Sun
Product	α_{eff}					
Beige PVC carpet	0.92	0.91	0.90	0.89	0.87	0.60
Pink PVC carpet	0.90	0.88	0.86	0.84	0.81	0.39
Red PVC carpet	0.92	0.92	0.91	0.90	0.89	0.80
Blue PVC carpet	0.89	0.87	0.85	0.83	0.80	0.43
Grey PVC carpet	0.90	0.88	0.86	0.84	0.82	0.43
Black PVC carpet	0.93	0.93	0.93	0.93	0.93	0.92
Grey rubber mat	0.91	0.91	0.91	0.91	0.91	0.82
Black rubber mat	0.90	0.90	0.91	0.91	0.91	0.95
White vinyl carpet	0.88	0.86	0.83	0.81	0.79	0.44
Beige vinyl carpet	0.91	0.90	0.89	0.87	0.85	0.51
Brown vinyl carpet	0.90	0.89	0.88	0.88	0.87	0.77
Grey vinyl carpet	0.92	0.91	0.89	0.88	0.87	0.57
Black vinyl carpet	0.93	0.93	0.93	0.93	0.93	0.94
Beige linoleum carpet	0.92	0.91	0.89	0.88	0.86	0.55

radiation. This contrasts to a specular emitter which is an idealized surface where the angle of reflected radiation is equal to the angle of incident radiation, like a billiard ball bouncing off the rail. Rough surfaces approximate diffuse emitters, and polished surfaces are close to specular surfaces. It is seen that, in its most general form, surface reflection is a bidirectional process meaning the intensity of reflected radiation depends not only on the angle of incident radiation, but also on the angle of reflected radiation. As a simplification, we look only at hemispherically-integrated reflection. Then the spectral directional reflectivity is defined as the ratio of the reflected spectral radiant intensity to the incident spectral radiant intensity:

$$\rho_\lambda(\lambda,\theta,\phi) = \frac{I_{\lambda,i,ref}(\lambda,\theta,\phi)}{I_{\lambda,i}(\lambda,\theta,\phi)} \tag{4.26}$$

note that in Equation 4.26, θ and ϕ refer to the direction of the incident radiation, not the reflected radiation (since, for simplification, no consideration is given to the direction of reflected radiation). Spectral hemispherical reflectivity is obtained by integrating over all incident angles:

Table 4.8 Effective absorptivities for different grey body temperatures for various paints painted on plywood (From Försth and Roos [12])

Grey body emitter T (K)	674	852	1025	1153	1300	5777
Cone calorimeter irradiation (kWm^{-2})	10	25	50	75	100	Sun
Product	α_{eff}					
White ceiling water paint	0.86	0.83	0.81	0.78	0.75	0.30
White floor water paint	0.86	0.84	0.81	0.78	0.75	0.24
Mid gray floor water paint	0.90	0.89	0.89	0.89	0.88	0.76
White priming water paint	0.86	0.83	0.81	0.78	0.75	0.27
Red priming water paint	0.90	0.89	0.87	0.86	0.83	0.71
Red priming water paint	0.89	0.87	0.85	0.83	0.80	0.70
White top water paint	0.87	0.84	0.81	0.78	0.75	0.25
Yellow top water paint	0.90	0.88	0.86	0.84	0.82	0.44
Red top water paint	0.89	0.88	0.86	0.84	0.81	0.55
Blue top water paint	0.89	0.87	0.85	0.83	0.81	0.73
White wall water paint	0.84	0.81	0.77	0.74	0.71	0.23
Black wall water paint	0.93	0.93	0.93	0.93	0.93	0.95
Blue wall water paint	0.92	0.91	0.91	0.90	0.90	0.75
White lacquer paint	0.86	0.84	0.81	0.79	0.76	0.26
Blue lacquer paint	0.90	0.89	0.88	0.88	0.87	0.74
Black lacquer paint	0.92	0.92	0.92	0.92	0.93	0.95
Red ceiling lacquer paint	0.87	0.84	0.82	0.79	0.77	0.70
Black ceiling lacquer paint	0.92	0.93	0.93	0.93	0.93	0.95

Table 4.9 Effective absorptivities for different grey body temperatures for various plastics and other materials (From Försth and Roos [12])

Grey body emitter T (K)	674	852	1025	1153	1300	5777
Cone calorimeter irradiation (kWm^{-2})	10	25	50	75	100	Sun
Product	α_{eff}					
White ABS	0.91	0.90	0.88	0.86	0.84	0.31
Black ABS	0.92	0.92	0.92	0.92	0.92	0.94
Nature acetal	0.93	0.93	0.93	0.92	0.91	0.46
Nature PA-6	0.93	0.93	0.94	0.94	0.94	0.74
Clear PC	0.92	0.91	0.89	0.87	0.85	0.24
Clear PC Ultra UV	0.92	0.91	0.90	0.88	0.85	0.46
Brown PC	0.93	0.93	0.93	0.93	0.93	0.93
Nature PE	0.93	0.93	0.93	0.93	0.93	0.62
Yellow PE	0.93	0.92	0.92	0.91	0.90	0.53
Black PE	0.93	0.93	0.93	0.93	0.93	0.95
Clear PMMA G	0.93	0.92	0.91	0.89	0.87	0.23
Yellow PMMA G	0.94	0.93	0.93	0.93	0.92	0.62
Brown PMMA G	0.94	0.94	0.94	0.94	0.94	0.94
Clear PMMA XT	0.93	0.92	0.91	0.89	0.87	0.21
Grey PP	0.92	0.92	0.91	0.91	0.90	0.66
Nature PTFE	0.84	0.78	0.73	0.70	0.66	0.10
Clear PVC	0.91	0.90	0.88	0.86	0.84	0.27
White PVC	0.91	0.89	0.87	0.85	0.82	0.31
White PVC expostandard (foamed)	0.82	0.80	0.78	0.76	0.73	0.31
Grey PVC	0.91	0.90	0.90	0.90	0.90	0.88
Black PVC	0.93	0.93	0.93	0.93	0.93	0.95
Nature PVDF	0.94	0.94	0.94	0.94	0.94	0.78

$$\rho_\lambda(\lambda) = \frac{\int_0^{2\pi}\int_0^{\pi/2} I_{\lambda,i,ref}(\lambda,\theta,\phi)\cos(\theta)\sin(\theta)d\theta d\phi}{\int_0^{2\pi}\int_0^{\pi/2} I_{\lambda,i}(\lambda,\theta,\phi)\cos(\theta)\sin(\theta)d\theta d\phi} = \frac{G_{\lambda,ref}(\lambda)}{G_\lambda(\lambda)} \tag{4.27}$$

Final, total hemispherical reflectivity is obtained by integrating over all wavelengths:

$$\rho = \frac{\int_0^\infty G_{\lambda,ref}(\lambda)}{\int_0^\infty G_\lambda(\lambda)} = \frac{G_{ref}}{G} \tag{4.28}$$

Transmissivity

Directional spectral transmissivity is defined in an analogous manner to the other radiation properties discussed here:

$$\tau_\lambda(\lambda,\theta,\phi) = \frac{I_{\lambda,i,trans}(\lambda,\theta,\phi)}{I_{\lambda,i}(\lambda,\theta,\phi)} \tag{4.29}$$

Hemispherical spectral transmissivity is:

$$\tau_\lambda(\lambda) = \frac{\int_0^{2\pi}\int_0^{\pi/2} I_{\lambda,i,trans}(\lambda,\theta,\phi)\cos(\theta)\sin(\theta)d\theta d\phi}{\int_0^{2\pi}\int_0^{\pi/2} I_{\lambda,i}(\lambda,\theta,\phi)\cos(\theta)\sin(\theta)d\theta d\phi} = \frac{G_{\lambda,trans}(\lambda)}{G_\lambda(\lambda)} \tag{4.30}$$

And total transmissivity is then obtained by integrating over all wavelengths:

$$\tau = \frac{\int_0^\infty G_{\lambda,trans}(\lambda)}{\int_0^\infty G_\lambda(\lambda)} = \frac{G_{trans}}{G} \tag{4.31}$$

Kirchhoff's Law: Relation Between Emissivity and Absorptivity

Kirchoff's law is used extensively in radiation heat transfer calculations. In its most general form, Kirchoff's law states that in order to maintain thermal equilibrium, the spectral directional absorptivity must be equal to the spectral directional emissivity:

$$\alpha_\lambda(\lambda,\theta,\phi) = \varepsilon_\lambda(\lambda,\theta,\phi,T) \tag{4.32}$$

Using the relations presented earlier in the chapter, it can be shown that if the irradiation is diffuse *or* the surface is diffuse, then Kirchoff's law has no directional dependency, i.e.:

$$\alpha_\lambda(\lambda) = \varepsilon_\lambda(\lambda,T) \tag{4.33}$$

If Equation 4.33 applies (i.e., the irradiation is diffuse or the surface is diffuse), then if the surface is also *gray* (meaning α_λ and ε_λ are invariant with λ) *or* the surface is irradiated only by radiation emitted from a blackbody at the same temperature as the surface, its total absorptivity is equal to its total emissivity:

$$\alpha = \varepsilon \tag{4.34}$$

For engineering calculations, Equation 4.34 is most commonly applied for the special case of diffuse and gray surfaces. Fortunately, this is a reasonable approximation for many radiation heat transfer engineering models for participating media in fire applications.

Although real surfaces may exhibit an emissivity that varies with wavelength (see Fig. 4.7), an effective emissivity can be selected so that the integrated emissive power of the gray surface matches the integrated emissive power of the real surface at a particular temperature.

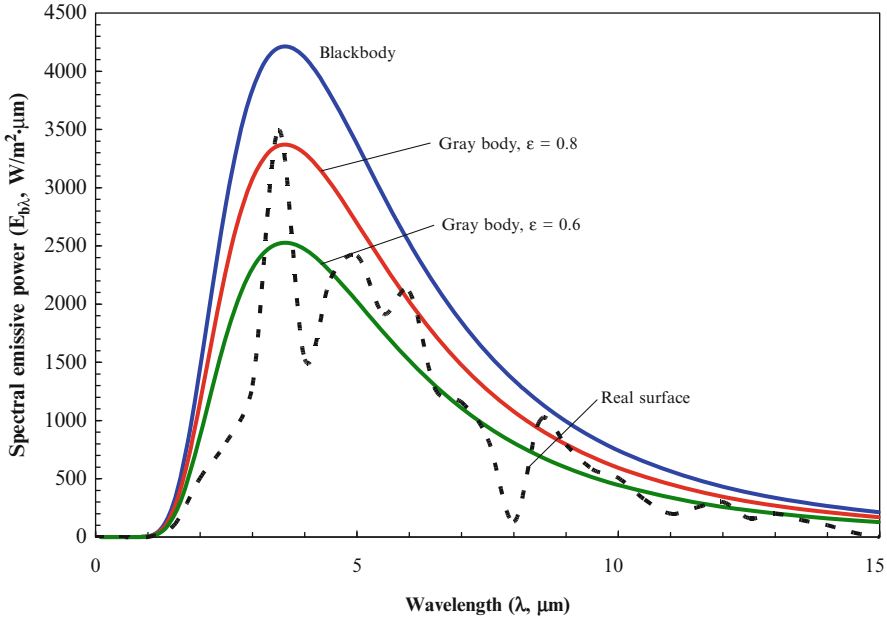

Fig. 4.7 Monochromatic emissive power for black body, two gray bodies, and real surface

Radiant Heat Transfer in Nonparticipating Media

In this section, cases are examined where the surfaces are separated by a medium that does not emit, absorb, or scatter radiation. A vacuum meets this requirement exactly, and common diatomic gases of symmetric molecular structure such as N_2, O_2, and H_2 are very nearly nonparticipating media within the thermal radiation spectrum. The radiative energy transfer between the surfaces depends on the geometry, orientation, temperature, and radiation properties of the surfaces. In practice, surfaces are usually idealized as isothermal, diffuse, and gray to make engineering calculations tractable. The geometry and orientation of each surface is commonly accounted for in calculations by one or more configuration factors, also known as view factors, shape factors, angle factors, and geometric factors [1–7, 17–19].

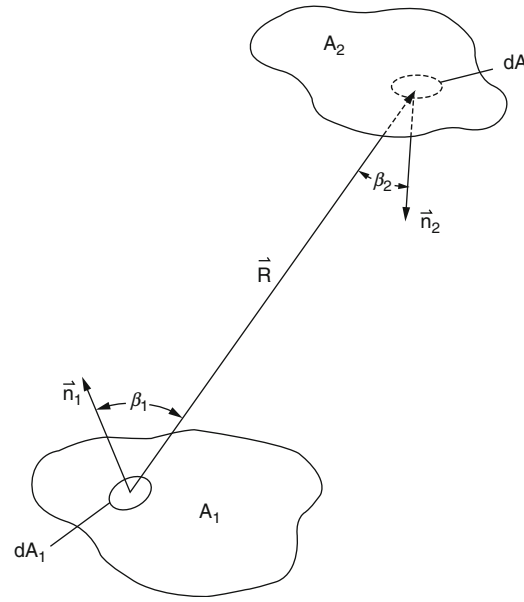

Fig. 4.8 Coordinate system for shape factors

View Factors

A view factor, or configuration factor, is a purely geometrical relation between two surfaces. It is defined as the fraction of radiation leaving one surface which is intercepted by the other surface.

Consider the two arbitrarily oriented surfaces A_1 and A_2 in Fig. 4.8. Assuming that the radiosity from differential area dA_1 is diffuse, the

configuration factor from dA_1 to the finite area A_2, $F_{d1\,-\,2}$, is given by

$$F_{d1-2} = \int_{A_2} \frac{\cos(\beta_1)\cos(\beta_2)}{\pi\left|\vec{R}\right|^2} dA_2 \qquad (4.35)$$

where the separation distance between the two surfaces is $\left|\vec{R}\right|$, β is the angle between the line of sight $\vec{R}$ and the surface normal $\vec{n}$, and A_2 is the area of surface 2. If the radiosity from all of surface A_1 (not just differential are dA_1) is diffuse, then the configuration factor for the finite area A_1 to A_2, $F_{1\,-\,2}$, is calculated as:

$$F_{1-2} = \frac{1}{A_1}\int_{A_1}\int_{A_2} \frac{\cos(\beta_1)\cos(\beta_2)}{\pi\left|\vec{R}\right|^2} dA_1 dA_2 \qquad (4.36)$$

All configuration factors can be derived using the multiple integration of Equations 4.35 and 4.36, but this is generally very tedious except for simple geometries. Several cases have been tabulated with the numerical results or algebraic formulas available in various references [1–7, 17, 18]. Several configuration factors are provided in Appendix D.

The configuration factors in Appendix D can be extended to other geometries by using configuration factor algebra and the method of surface decomposition. In surface decomposition, unknown factors can be determined from known factors for convenient areas or for imaginary surfaces which can extend real surfaces or form an enclosure [1, 6].

When the radiant fluxes from both surfaces are uniformly and diffusely distributed (a common engineering assumption), a reciprocity relation for any given pair of configuration factors in a group of exchanging surfaces is:

$$A_i F_{i-j} = A_j F_{j-i} \qquad (4.37)$$

The summation rule is another useful relation for calculating unknown configuration factors

$$\sum_j F_{i-j} = 1 \qquad (4.38)$$

where F_{i-j} relate to surfaces that subtend a closed system. It is possible for a concave surface to "see" itself, which can make F_{i-i} important in certain situations.

In many cases, it is advantageous to define a single surface (j) as a composite surface consisting of multiple (real or imaginary) surfaces (k), i.e.:

$$A_j = \sum A_k \qquad (4.39)$$

For a composite surface j, made up of multiple surfaces k, since view factors are additive:

$$F_{ij} = \sum A_{ik} \qquad (4.40)$$

Example 6 For the geometry shown below, use shape factor algebra to develop an expression for the view factor between surface 1 and surface 4 that could be evaluated from the shape factor relations provided in Appendix D.

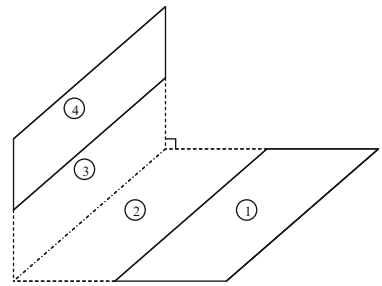

Solution The desired view factor is F_{14}. For simplicity of nomenclature, denote surface A as a composite surface made up of surfaces 1 and 2. Similarly, denote surface B as a composite surface made up of surfaces 3 and 4. Then, from the additive property of shape factors:

$$A_A F_{AB} = A_1 F_{1B} + A_2 F_{2B}$$

Both F_{AB} and F_{2B} can be calculated from the appropriate shape factor in Appendix D. Note that

$$F_{1B} = F_{13} + F_{14}$$

$$F_{13} = F_{A3} - F_{23}$$

Combining these two equations gives an expression for F_{1B}:

$$F_{1B} = F_{A3} - F_{23} + F_{14}$$

Substituting this expression into the first equation above:

$$\begin{aligned} A_A F_{AB} &= A_1(F_{A3} - F_{23} + F_{14}) + A_2 F_{2B} \\ &= A_1 F_{A3} - A_1 F_{23} + A_1 F_{14} + A_2 F_{2B} \end{aligned}$$

Solving for F_{14}:

$$\begin{aligned} F_{14} &= \frac{1}{A_1}(A_A F_{AB} - A_2 F_{2B} - A_1 F_{A3} + A_1 F_{23}) \\ &= \frac{1}{A_1}(A_A F_{AB} - A_2 F_{2B}) + F_{23} - F_{A3} \end{aligned}$$

Note that all of the view factors in the above example can be evaluated from the shape factor relations provided in Appendix D.

Gray Diffuse Surfaces

For engineering applications, thermal emission from most surfaces is treated as having diffuse directional characteristics independent of wavelength and temperature. Real surfaces exhibit radiation properties that are so complex that information about these property measurements for many common materials is not available. The gray diffuse surface is a useful model that alleviates many of the complexities associated with a detailed radiation analysis, while providing reasonably accurate results in many practical situations. The advantage of diffuse surface analysis is that radiation leaving the surface is independent of the direction of the incoming radiation, which greatly reduces the amount of computation required to solve the governing equations. Discussions for specularly reflecting surfaces and nongray surfaces can be found in the literature [1, 6].

A convenient method to analyze radiative energy exchange in a diffuse gray enclosure relies on the concepts of radiosity and irradiation introduced earlier. The irradiation of surface i (G_i) is the radiative flux reaching the i^{th} surface regardless of its origin:

$$G_i = \sum_j F_{i-j} J_j \tag{4.41}$$

where J_j is the surface radiosity, defined as the total radiative flux leaving the j^{th} surface including both emitted and reflected radiation:

$$J_i = E_i + \rho_i G_i = \varepsilon_i E_{bi} + \rho_i G_i \tag{4.42}$$

The net rate at which radiation leaves surface i is given by

$$\begin{aligned} Q_i &= A_i(J_i - G_i) = A_i(E_i + \rho_i G_i - G_i) \\ &= A_i(E_i - G_i(1 - \rho_i)) \\ &= A_i(E_i - \alpha_i G_i) \end{aligned} \tag{4.43}$$

since, for a diffuse gray opaque surface $\rho_i = 1 - \alpha_i$. It must be emphasized that the radiosity-irradiation formulation is based on the assumption that each surface has uniform radiosity and irradiation (or equivalently, uniform temperature and uniform heat flux). Physically unrealistic calculations can result if each surface does not approximately satisfy this condition. Larger surfaces should be subdivided into smaller surfaces if necessary.

The radiosity-irradiation formulation allows a more physical and graphic interpretation using the resistance network analogy. Eliminating the irradiation G_i from Equations 4.41, 4.42 and 4.43, and substituting $\rho_i = 1 - \varepsilon_i$ gives

$$Q_i = \frac{E_{bi} - J_i}{(1 - \varepsilon_i)/(\varepsilon_i A_i)} = \sum_j \frac{J_i - J_j}{\left(A_i F_{i-j}\right)^{-1}} \tag{4.44}$$

Note that the second equality in Equation 4.44 can be written as:

$$Q_i = \sum_j A_i F_{i-j}\left(J_i - J_j\right) = \sum_j Q_{ij} \tag{4.45}$$

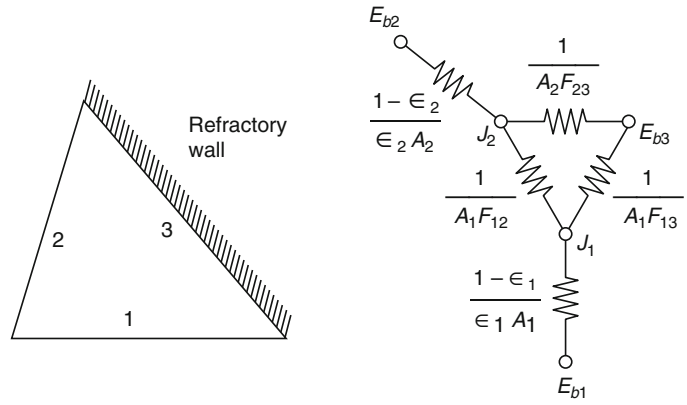

Fig. 4.9 Network analogy for radiative exchange

The denominator in the rightmost term of Equation 4.44 corresponds to resistance in electric circuits. This electrical resistance analogy was first proposed by Oppenheim [20]. As illustrated in Fig. 4.9, the diffuse-gray surface has a radiation potential difference $(E_{bi} - J_i)$ and a resistance $(1 - \varepsilon_i)/\varepsilon_i A_i$. This example also illustrates that an adiabatic surface, such as a reradiating or refractory wall, exhibits a surface temperature that is independent of the surface emissivity or reflectivity.

Thermal Radiation in Participating Media

The Equation of Transfer

The equation of transfer describes the variation in intensity of a radiant beam at any position along its path in an absorbing-emitting-scattering medium. This equation is the foundation upon which detailed radiation analyses are based, and the source of approximate solutions when simplifying assumptions are made. For a given direction line in the medium, the equation of transfer is

$$\frac{1}{\kappa_\lambda(T,S)}\frac{dI_\lambda(S)}{dS} + I_\lambda(S) = I_{\lambda,b}(T) \qquad (4.46)$$

where S represents the physical pathlength and κ_λ represents the spectral extinction coefficient, which includes the effects of both absorption and scattering within the medium. The intensity, $I_\lambda(S)$, is coupled with the spatial distribution of the extinction coefficient and with temperature through conservation of energy in the medium. The contributions of intensity passing through an area must be integrated over all directions to calculate a net radiative energy flux. The integral nature of radiation makes analysis difficult and simplifications necessary for engineering practice.

Spectral Emissivity and Absorptivity

From a microscopic viewpoint, emission and absorption of radiation is attributed to changes in energy levels of atoms and molecules caused by interactions with photons. Tien [21] discusses these effects in gases from an engineering perspective.

Consider a monochromatic beam of radiation passing through a radiating medium of thickness L. For the special case where the temperature and properties of the medium are uniform along this path, the intensity of radiant beam at point x is obtained by integrating Equation 4.46:

$$I_\lambda(x) = I_\lambda(0)\exp(-\kappa_\lambda x) + I_{\lambda,b}(1 - \exp(-\kappa_\lambda x)) \qquad (4.47)$$

which accounts for the loss of intensity by absorption and the gain by emission, and where κ_λ denotes the extinction coefficient. The extinction coefficient is generally the sum of two parts:

the absorption coefficient and the scattering coefficient. In many engineering applications, the effects of scattering are negligible and the extinction coefficient represents only absorption. The spectral emissivity for pathlength S in a uniform gas volume can be readily expressed by considering the case of no incident radiation (or $I_\lambda(0) = 0$):

$$\varepsilon_\lambda = \frac{I_\lambda}{I_{\lambda,b}} = 1 - \exp(-\kappa_\lambda S) \tag{4.48}$$

which compares the fraction of energy emitted to the maximum (blackbody) emission at the same temperature for the pathlength S through the material.

The term $\kappa_\lambda S$ in Equation 4.48 is called optical pathlength or opacity and is denoted τ_λ (not to be confused with transmissivity). It can be defined more generally for nonhomogeneous media as:

$$\tau_\lambda = \int_0^S \kappa_\lambda(x)dx \tag{4.49}$$

If $\tau_\lambda << 1$, the medium is optically thin at wavelength λ and the properties of the participating medium can generally approximated as $\varepsilon_\lambda \approx \tau_\lambda$. The medium is considered optically thick when $\tau_\lambda >> 1$, which implies that the mean penetration distance is much less than the characteristic length of the medium. In optically thick media, as will be described below, the local radiant intensity results only from local emission and the equation of transfer can be approximated by a diffusion equation.

Planck and Rosseland Mean Absorption Coefficients

The mean absorption coefficient is often useful when radiative energy transport theory must be used to describe the local state of a gas at various locations. The mathematical complexity involved in the calculations often dictates a solution based on the gray-gas assumption, where all radiation parameters are considered to be wavelength independent. Thus solutions are given in terms of mean (gray-gas) absorption coefficients representing average properties over the whole spectrum of wavelengths. The appropriate mean absorption coefficients are the Planck mean, κ_P, for optically thin media, and the Rosseland mean, κ_R, for optically thick media [5, 6, 21].

The Planck mean absorption coefficient is defined as

$$\kappa_P \equiv \frac{\int_0^\infty I_{\lambda,b}\kappa_\lambda d\lambda}{\int_0^\infty I_{\lambda,b}d\lambda} = \frac{\pi}{\sigma T^4}\int_0^\infty I_{b\lambda}\kappa_\lambda d\lambda \tag{4.50}$$

This form of the absorption coefficient is a function of temperature alone and is independent of pressure. The effect of the beam source temperature (e.g., a hot or cold wall) in the gas absorptivity is approximated by a ratio correction [21, 22]

$$\kappa_m = \kappa_P(T_s)\frac{T_s}{T_g} \tag{4.51}$$

where T_s is the source temperature and T_g is the gas temperature. When the Planck mean absorption coefficient is used to estimate the emissivity of a gas, the source temperature is set equal to the gas temperature.

The formulation of radiative transfer is simplified when the medium is optically thick. In this case, the radiative transfer can be regarded as a diffusion process (the Rosseland or diffusion approximation), and the governing equation is approximated by:

$$\begin{aligned} q_r'' &\approx -\frac{4}{3}\frac{1}{\kappa_R}\frac{\partial E_{\lambda,b}}{\partial x} = -\frac{4}{3}\frac{1}{\kappa_R}\frac{\partial\left(\sigma T^4\right)}{\partial x} \\ &= -\frac{16\sigma}{3}T^3\frac{1}{\kappa_R}\frac{\partial T}{\partial x} \end{aligned} \tag{4.52}$$

Evaluation of the total heat flux in an optically thick medium is simplified by defining the Rosseland mean absorption coefficient which is independent of wavelength:

$$\frac{1}{\kappa_R} \equiv \int_0^\infty \frac{1}{\kappa_\lambda}\frac{\partial E_{\lambda,b}}{\partial E_b}d\lambda \tag{4.53}$$

In Equation 4.53, $\partial E_{\lambda,b}/\partial E_b$ is evaluated from the Planck distribution after setting $T = (E_b/\sigma)^{1/4}$. The Rosseland mean absorption coefficient is not well defined for gases under ordinary conditions because astronomically long pathlengths are required to make the windows between the bands optically thick. However, the Rosseland limit is useful when dealing with gases in the presence of soot particles, which are characterized by a continuous spectrum. The source temperature effect is accounted for by using Equation 4.51 in the same manner as for the Planck mean absorption coefficient.

The radiating gas in many actual fire systems is neither optically thin nor optically thick, so it may be necessary to use band theory to rigorously calculate a mean absorption coefficient, κ_m. However, with a reasonable estimate of the mean absorption coefficient, radiative transport calculations are much more convenient.

Mean Beam Length for Homogeneous Gas Bodies

The concept of mean beam length is a powerful and convenient tool to calculate the energy flux from a radiating homogeneous gas volume to its boundary surface. It may also be used to approximate radiative energy flux for a nonhomogeneous gas, especially when more elaborate calculations are not feasible. Consider the coordinate system given in Fig. 4.3, where dA is a differential area on the boundary surface of the gas body. The radiative heat flux from the gas body to dA is

$$\dot{q}_r'' = \int_0^\infty \int_\Omega \varepsilon_\lambda(X) I_{\lambda,b} \cos(\theta) d\lambda d\Omega \qquad (4.54)$$

where the spectral emissivity, ε_λ, is a function of pressure pathlength:

$$X \equiv \int_0^S P_a x(\xi) d\xi \qquad (4.55)$$

which in turn varies with solid angle Ω according to the gas body geometry. In practical situations, the calculation of $\dot{q}_r''$ is more convenient in terms of total emissivity, which is often available in chart form. From the definition of total emissivity, Equation 4.54 can be expressed as:

$$\dot{q}_r'' = \frac{\sigma T^4}{\pi} \int_\Omega \varepsilon(X) \cos(\theta) d\Omega \equiv \sigma T^4 \varepsilon(L) \qquad (4.56)$$

which gives the definition of mean beam length, L, for a gas body, where $\varepsilon(L)$ has the same functional form as $\varepsilon(X)$. Physically, the mean beam length represents the equivalent radius of a hemispherical gas body such that it radiates a flux to the center of its base equal to the average flux radiated to the boundary surface by the actual volume of gas. The determination of the mean beam length is simplified when the gas is optically thin and only the geometry of the gas body enters the calculation. In the optically thin limit, it is convenient to define

$$L = L_0 \equiv \frac{1}{\pi} \int_\Omega X \cos(\theta) d\Omega \qquad (4.57)$$

where L_0 is called the geometric mean beam length. In the optically thick limit, a correction factor (C) can be used to obtain reasonable radiative heat flux estimates:

$$L \approx C L_0 \qquad (4.58)$$

In Table 4.10, L_0 and C have been provided for a variety of gas body shapes. For an arbitrarily shaped gas volume, the geometric beam length from the gas volume to the entire boundary surface can be estimated by:

$$L_0 = \frac{4V}{A} \qquad (4.59)$$

where V and A are the volume and the area of the boundary surface of the gas body, respectively. The correction factor C is approximately 0.9.

Table 4.10 Mean beam lengths for various gas body shapes

Geometry of gas body		Radiating to	Geometric mean beam length L_0	Correction factor C
Sphere		Entire surface	0.66 D	0.97
Cylinder H = 0.5 D		Plane and surface	0.48 D	0.90
		Concave surface	0.52 D	0.88
		Entire surface	0.50 D	0.90
Cylinder H = D		Center of base	0.77 D	0.92
		Entire surface	0.66 D	0.90
Cylinder H = 2 D		Plane end surface	0.73 D	0.82
		Concave surface	0.82 D	0.93
		Entire surface	0.80 D	0.91
Semi-infinite cylinder H → ∞		Center of base	1.00 D	0.90
		Entire base	0.81 D	0.80
Infinite slab	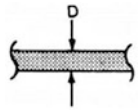	Surface element	2.00 D	0.90
		Both bounding planes	2.00 D	0.90
Cube D × D × 4D	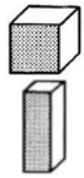	1 × 4 face	0.90 D	0.91
		1 × 1 face	0.86 D	0.83
		Entire surface	0.89 D	0.91

Thermal Radiation Properties of Combustion Products

Radiation Properties of Gases

The emissivity of any gas is a strong function of wavelength, varying by as much as several orders of magnitude over small changes in wavelength. However, the level of accuracy required in engineering calculations, where many of the parameters are difficult to measure or estimate, seldom requires high resolution emissivity spectra. Where wavelength dependence of radiative heat flux is a concern, gas properties may be calculated using the exponential wide-band model [23]. The uncertainties involved in estimating parameters to calculate radiative heat flux make average properties such as total emissivity a useful tool. The first comprehensive total emissivity charts were formulated by Hottel and coworkers to summarize work performed up to about 1945. Modern formulations for the emissivity of gases have been summarized by Edwards [22].

Total emissivity charts for water vapor and carbon dioxide [22] are provided in Figs. 4.10 and 4.11, respectively. Gas emissivity can be

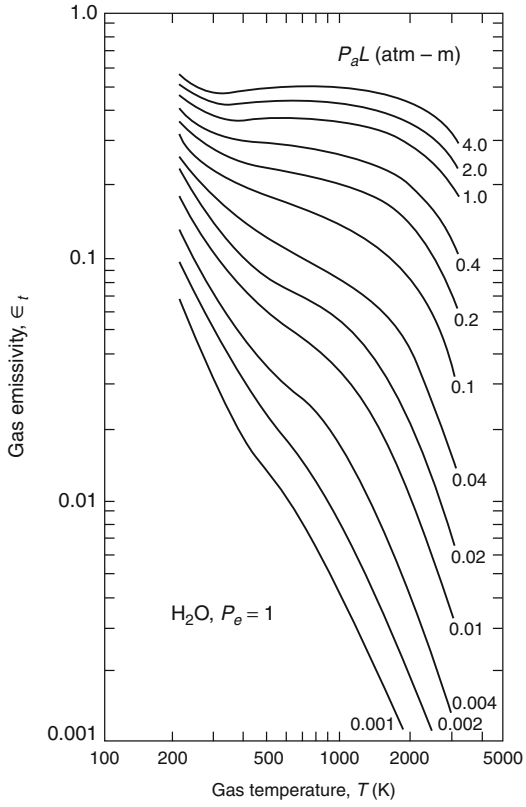

Fig. 4.10 Total emissivity of water vapor

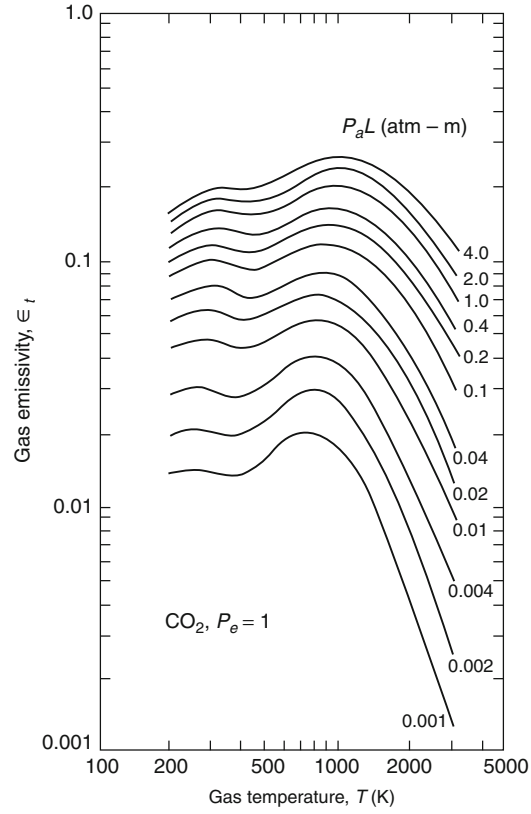

Fig. 4.11 Total emissivity of carbon dioxide

read off these charts from the partial pressure and temperature of each gas and the mean beam length for the gas volume geometry. Correction factors for the chart emissivities are available in the literature for the pressure effect on water vapor emissivity [24], the pressure effect on carbon dioxide emissivity [5, 6], and the band overlap for mixtures of the two gases [25]. For most fire protection engineering applications, the pressure correction factors are 1.0 and the band overlap correction is approximately $\Delta\varepsilon \approx \frac{1}{2}\varepsilon_{CO_2}$ for medium to large fires. Assuming the carrier gas is transparent (e.g., air), the emissivity is:

$$\varepsilon_g = C_{H_2O}\varepsilon_{H_2O} + C_{CO_2}\varepsilon_{CO_2} - \Delta\varepsilon \approx \varepsilon_{H_2O} + \frac{1}{2}\varepsilon_{CO_2} \tag{4.60}$$

At temperatures below 400 K, the older charts by Hottel [5, 6] may be more reliable than the charts in Figs. 4.10 and 4.11, and the use of wide-band models is advised to estimate the band overlap correction instead of using the correction charts at these lower temperatures [26]. For crucial engineering decisions, wide-band model block calculations as detailed by Edwards [22] are recommended over the graphical chart method to determine total emissivity.

Other gases such as sulfur dioxide, ammonia, hydrogen chloride, nitric oxide, and methane have been summarized in chart form [5]. The carbon monoxide chart by Hottel is not recommended for use [27] due to uncertainties most likely introduced by traces of carbon dioxide in the original experiments. Spectral and total properties have been published for some of the important hydrocarbon gases, e.g., methane, acetylene, and propylene [28–30]. Mixtures of several hydrocarbon gases are subject to band

overlapping, and appropriate corrections must be made to avoid overestimating total emissivity of a mixture of fuels.

The total emissivity for a gas in the optically thin limit can be calculated from the Planck mean absorption coefficient. Graphs of the Planck mean absorption coefficient for various gases that are important in fires are shown in Fig. 4.12, which can be used with Equation 4.48 to estimate the total emissivity (by assuming that total properties represent a spectral average value).

Radiation Properties of Soot

In a nonhomogeneous (e.g., with soot) medium, scattering becomes an important radiative mechanism in addition to absorption and emission. The absorption and scattering behavior of a single particle can be described by solving the electromagnetic field equations; however, many physical idealizations and mathematical approximations are necessary. The most common assumptions include perfectly spherical particles, uniformly or randomly distributed particles, and interparticle spacing so large that the radiation for each particle can be treated independently.

Soot particles are produced as a result of incomplete combustion and are usually observed to be in the form of spheres, agglomerated chunks, and long chains. They are generally very small (50–1000 Å where 1 Å $= 10^{-10}$ m $= 10^{-4}$ μm) compared to infrared wavelengths, so that the Rayleigh limit is applicable to the calculation of radiation properties [31, 32]. Soot particles are normally characterized by their optical properties, size, shape, and chemical composition (hydrogen-carbon ratio). From a heat transfer viewpoint, radiation from a soot cloud is predominantly affected by the particle size distribution and can be considered independent of the chemical composition [31]. Soot optical properties are relatively insensitive to temperature changes at elevated temperatures, but as shown in Fig. 4.13, room temperature values representative of soot in smoke do show appreciable deviations.

By choosing appropriate values of optical constants for soot, the solution for the electromagnetic field equations gives [33]

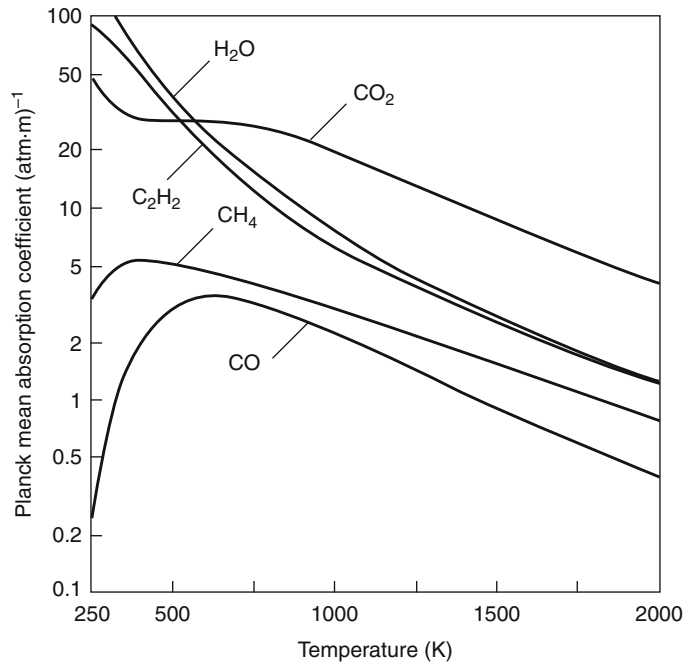

Fig. 4.12 Planck mean absorption coefficient for various gases

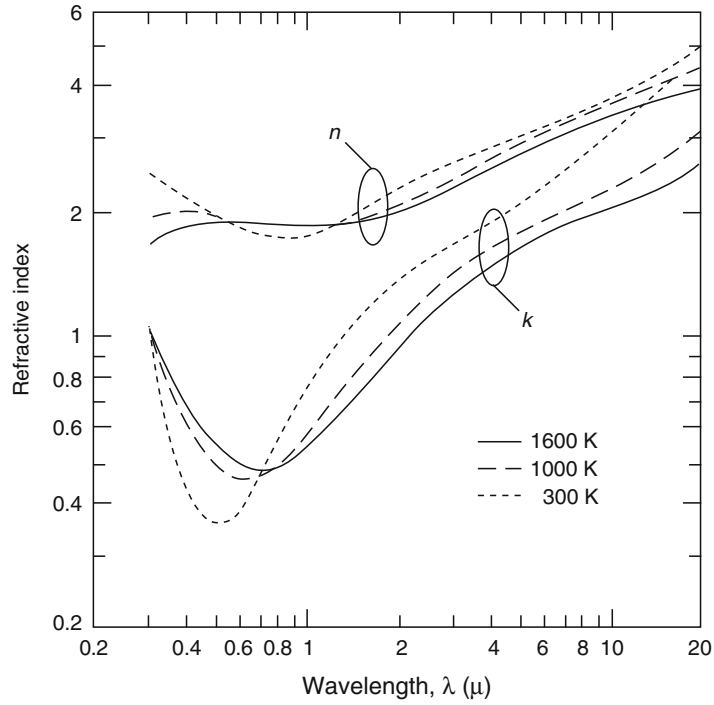

Fig. 4.13 Optical constants for soot

$$k_\lambda = \frac{C_0}{\lambda} f_v \tag{4.61}$$

where f_v is the soot volume fraction (generally about 10^{-6} in flames) and C_0, a constant between 2 and 6 dependent on the complex index of refraction $m = n - ik$, is given by

$$C_0 = \frac{36\pi nk}{\left(n^2 - k^2 + 2\right)^2 + 4n^2k^2} \tag{4.62}$$

Equations 4.61 and 4.62 can be used to evaluate the Planck mean absorption coefficient in the optically thin limit [34], giving:

$$\kappa_P = 3.83 \frac{C_0}{C_2} f_v T \tag{4.63}$$

where C_2 is Planck's second constant (1.4388×10^{-2} m-K). The Rosseland mean absorption coefficient in the optically thick limit is

$$\kappa_R = 3.6 \frac{C_0}{C_2} f_v T \tag{4.64}$$

A mean coefficient that may be used for the entire range of optical thickness is suggested as

$$\kappa_R = 3.72 \frac{C_0}{C_2} f_v T \tag{4.65}$$

to be used in Equation 4.66 for the soot radiation calculations. Typical temperatures, volume fractions, and mean absorption coefficients for soot particles in the luminous flames of various fuels are tabulated in Table 4.11.

Radiation Properties of Gas-Soot Mixtures

The calculation of the total emissivity of a gas-soot mixture requires information on basic flame parameters such as soot volume fraction, soot absorption coefficient, temperature and geometric length of the flame, and partial pressure of the participating gas components [35]. These parameters can be estimated for various types of

Table 4.11 Radiative properties for soot particles

	Fuel, composition	κ_S (m^{-1})	$f_v \times 10^6$	$T_s(K)$
Gas fuels	Methane, CH_4	6.45	4.49	1289
	Ethane, C_2H_6	6.39	3.30	1590
	Propane, C_2H_8	13.32	7.09	1561
	Isobutane, $(CH_3)_3CH$	16.81	9.17	1554
	Ethylene, C_2H_4	11.92	5.55	1722
	Propylene, C_3H_6	24.07	13.6	1490
	n-butane, $(CH_3)(CH_2)_2(CH_3)$	12.59	6.41	1612
	Isobutylene, $(CH_3)_2CCH_2$	30.72	18.7	1409
	1,3-butadiene, $CH_2CHCHCH_2$	45.42	29.5	1348
Solid Fuels	Wood, $\approx (CH_2O)_n$	0.8	0.362	1732
	Plexiglas, $(C_5H_8O_2)_n$	0.5	0.272	1538
	Polystyrene, $(C_8H_8)_n$	1.2	0.674	1486

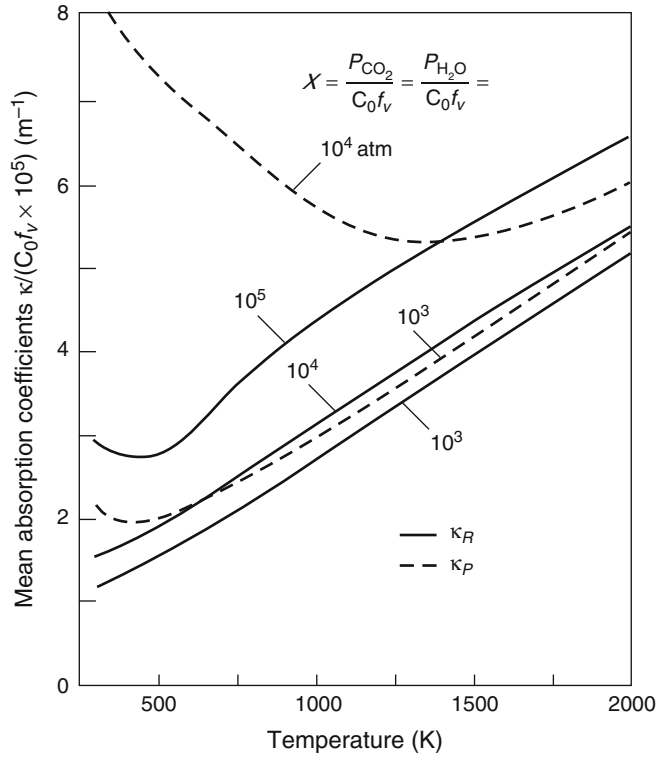

Fig. 4.14 Mean absorption coefficients for luminous flames and smoke

fuel when actual measurements are unavailable for a particular situation. The following equation is a good approximation [36] for total emissivity of homogeneous gas-soot mixtures:

$$\varepsilon_t = (1 - \exp(-\kappa S)) + \varepsilon_g \exp(-\kappa_s S) \quad (4.66)$$

where S is the physical pathlength, ε_g is the total emissivity of the gas alone, and κ_s is the effective absorption coefficient of the soot. The Planck mean absorption coefficients for gas-soot mixtures in luminous flames and smoke are shown in Fig. 4.14.

Application to Flame and Fire

Heat Flux Calculation from a Flame

Prediction of the radiative heat flux from a flame is important in determining ignition and fire spread hazard, and in the development of fire detection devices. The shape of flames under actual conditions is transient, which makes detailed radiation analysis cumbersome. In most calculations, flames are idealized as simple geometric shapes such as plane layers or axisymmetric cylinders and cones. A cylindrical geometry, shown in Fig. 4.15, will be analyzed here and used in a sample calculation.

Assuming κ_λ is independent of pathlength, integration of the transport equation (Equation 4.48) yields [37]

$$I_\lambda = I_{b\lambda}\left(1 - \exp\left(\frac{-2\kappa_\lambda}{\sin(\theta)}\sqrt{r^2 - L^2\cos^2(\phi)}\right)\right) \tag{4.67}$$

where θ, ϕ. r, and L are geometric variables defined in Fig. 4.15. The monochromatic radiative heat flux on the target element is given by

$$\frac{d\dot{q}_r''}{d\lambda} = \int_\Omega \frac{I_\lambda}{\left|\vec{R}\right|}\left(\vec{n}\cdot\vec{R}\right)d\Omega \tag{4.68}$$

Where $\vec{n}$ is a unit vector normal to the target element dA and $\vec{R}$ is the line-of-sight vector extending between dA and the far side of the flame cylinder. Evaluation of Equation 4.68 is quite lengthy, but under the condition of $L/r \geq 3$, it can be simplified to [37]

$$\frac{d\dot{q}_r''}{d\lambda} = \pi I_{\lambda,b}\varepsilon_\lambda(F_1 + F_2 + F_3) \tag{4.69}$$

where the shape factor constants and emittance are defined as

$$F_1 = \frac{u}{4\pi}\left(\frac{r}{L}\right)^2(\pi - 2\theta_0 + \sin(2\theta_0)) \tag{4.70a}$$

$$F_2 = \frac{v}{4\pi}\left(\frac{r}{L}\right)(\pi - 2\theta_0 + \sin(2\theta_0)) \tag{4.70b}$$

$$F_3 = \frac{w}{\pi}\left(\frac{r}{L}\right)\cos^2(\theta_0) \tag{4.70c}$$

$$\varepsilon_\lambda = 1 - \exp(-0.7\mu_\lambda) \tag{4.71}$$

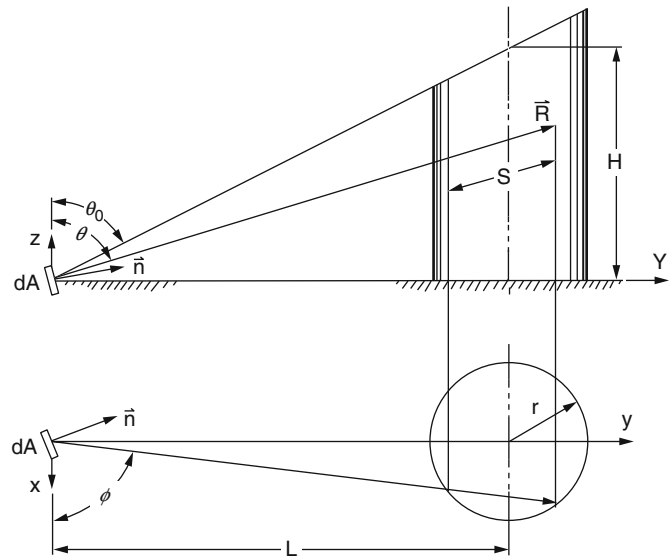

Fig. 4.15 Schematic of a cylindrical flame

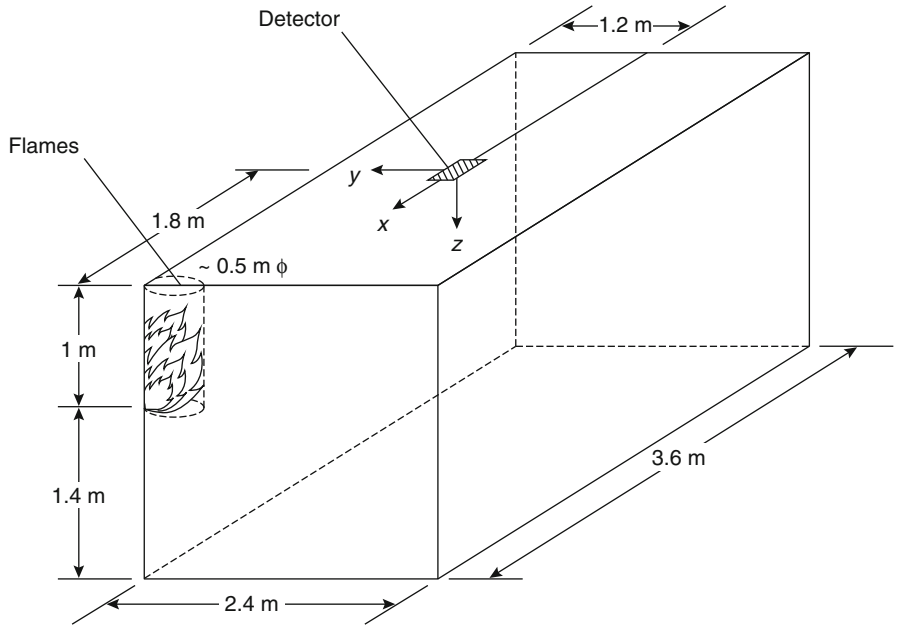

Fig. 4.16 Example calculation for flux to target element from flame

The parameters in the definitions are given by

$$\theta_0 = \tan^{-1}(L/H) \tag{4.72a}$$

$$\mu_\lambda = 2r\frac{\kappa_\lambda}{\sin\left(\frac{\theta_0}{2}+\frac{\pi}{4}\right)} \tag{4.72b}$$

$$\vec{n} = u\vec{i} + v\vec{j} + w\vec{k} \tag{4.72c}$$

If the flame is considered to be homogeneous and Equation 4.69 is integrated over all wavelengths, the total heat flux is:

$$\dot{q}_r'' = \varepsilon_m E_b \sum_{j=1}^{3} F_j \tag{4.73}$$

Example 7 As shown in Fig. 4.16, a fire detector is located at the center of the ceiling in a room (2.4 × 3.6 × 2.4 m) with wood wall linings. The sprinkler system is capable of extinguishing fires smaller than 0.5 m in diameter × 1.0 m high. For this example, determine the appropriate heat flux setting for the detector, using a worst case scenario of ignition in one of the upper ceiling corners.

Solution First, the condition of $L/r \geq 3$ should be checked to verify that the previous analysis is applicable.

$$\frac{L}{r} \approx \frac{\sqrt{1.2^2 + 1.8^2}}{0.25} = 8.65 > 3 \tag{4.74}$$

The unit normal vector to the detector is given by $\vec{n} = \vec{k}$, the polar angle $\theta_0 = \tan^{-1}(1.818) = 1.068$ is determined from Equation 4.72a, and the shape factors are evaluated from Equations 4.70a, 4.70b, and 4.70c:

$$F_1 = 0 \tag{4.75a}$$

$$F_2 = 0 \tag{4.75b}$$

$$F_3 = \frac{1}{\pi}\left(\frac{0.25}{1.818}\right)\cos^2(1.068) = 0.0102 \tag{4.75c}$$

From Equation 4.73, the radiant heat flux can be calculated as:

$$\begin{aligned}\dot{q}_r'' &= (1-\exp(-\kappa_m S))\sigma T_f^4 F_3 \\ &= (1-\exp(-0.8\times 0.5))\times 5.67\times 10^{-8}\times 1732^4\times 0.0102 \\ &= 1.7\ \mathrm{kW/m^2}\end{aligned} \tag{4.76}$$

where wood flame properties were taken from Table 4.11. If the geometry of the example had been $L/r < 3$, it would have been necessary to interpolate between the $L/r = 3$ case and the $L/r = 0$ case, which has been obtained accurately [6, 37]. If the detector is pointed directly at the burning corner in this example (i.e., $\vec{n} = 0.55\vec{i} + 0.83\vec{j}$), the calculated heat flux jumps to 9.0 kW/m^2, showing the strong influence of direction in calculations of radiation heat transfer.

Heat Flux Calculation from a Smoke Layer

Consider the situation shown below in Fig. 4.17 involving radiative heat transfer in a compartment fire with a hot gas layer located below the ceiling.

Hot upper gas layers are composed of strongly participating media such as carbon dioxide, water vapor, and soot particles. Heat flux from the smoke layer is directly related to ignition of remote surface locations such as furniture or floor carpets. The schematic in Fig. 4.17 will be considered in a radiative transport analysis and example calculation. The calculation is based on a considerably simplified formulation which provides reasonable results with only a small penalty in accuracy.

Integration of Equation 4.46 over the pathlength S through the smoke layer yields

$$I(S) = \frac{\sigma T^4}{\pi}\left(1-\left(\frac{T_w}{T}\right)^4\right)\exp(-\kappa S) \tag{4.77}$$

The monochromatic radiative heat flux on a differential target element is again given by Equation 4.68. However, for the present geometry of

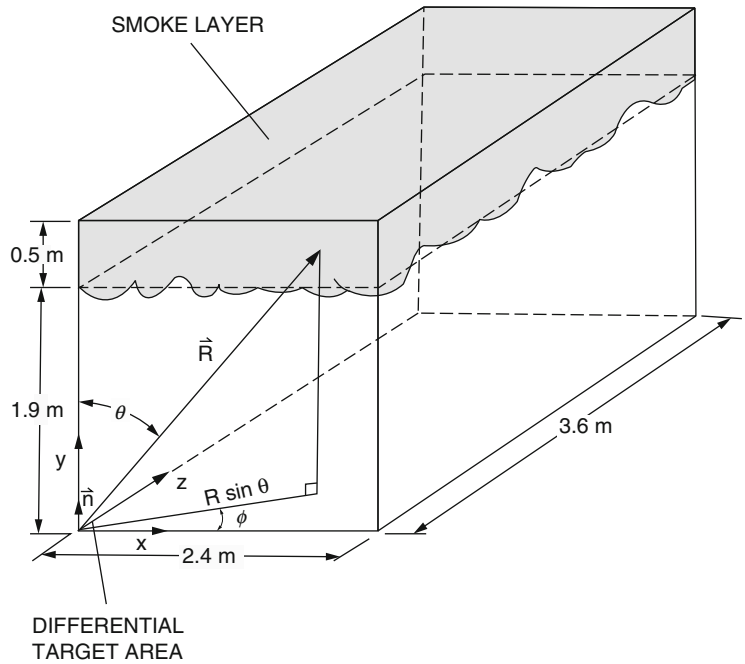

Fig. 4.17 Example calculation for flux to target element from smoke layer

the ceiling layer and enclosure surface, integration of Equation 4.68 is quite time-consuming since the upper and lower bounds of the integral vary with the angle of the pathlength. The calculation can be simplified by assuming as a first order approximation that the lower face of the smoke layer is an isothermal surface. Using this assumption, the problem can be handled using the simple relations of radiative exchange in a nonparticipating medium between gray surfaces (the absorption of the clear air below the smoke layer is negligible). The radiosity and irradiation of each surface in the enclosure is:

$$J_i = \varepsilon_i \sigma T_i^4 + (1 - \varepsilon_i) G_i \tag{4.78a}$$

$$G_i = \sum_j F_{i-j} J_j \tag{4.78b}$$

After solving the simultaneous equations for all J_i and G_i, the net heat flux on any of the surfaces can be calculated from

$$\dot{q}''_{r,i} = J_i - G_i \tag{4.79}$$

This situation is considered in Example 8 below.

Example 8 A smoke layer 0.5 m thick is floating near the ceiling of a room with dimensions of 3.6 × 2.4 × 2.4 m. (See Fig. 4.17.) The floor is made from wood (emissivity = 0.9), and the four side walls are painted concrete (emissivity = 0.94). The calculation will determine the heat flux in a bottom corner of the room, assuming that each surface in the enclosure is kept at constant temperature: the smoke layer at 1400 K, the side walls at 800 K, and the floor at 300 K. Assume there is a differential target area 0.01 m^2 in one of the corners of the floor, and also at the floor temperature of 300 K.

Solution The bottom of the smoke layer will be designated surface 1, the floor will be surface 2, and the differential target area in the bottom corner will be surface 3. Only four surfaces are required since the four side walls can be treated as a single surface 4. Shape factors F_{12} and F_{31} can be found in Appendix D, and from these two factors, the remaining shape factors are determined by shape factor algebra:

$$F_{12} = 0.3242$$

$$F_{31} = 0.1831$$

$$F_{13} = \frac{A_3}{A_1} F_{31} = 0.0002$$

$$F_{14} = 1 - F_{12} - F_{13} = 0.6756$$

Continuing in a similar fashion, the other shape factors are obtained as:

$$\begin{array}{lll} F_{21} = 0.3242 & F_{31} = 0.1831 & F_{41} = 0.2560 \\ F_{22} = 0.0000 & F_{32} = 0.0000 & F_{42} = 0.2561 \\ F_{23} = 0.0000 & F_{33} = 0.0000 & F_{43} = 0.0003 \\ F_{24} = 0.6758 & F_{34} = 0.8169 & F_{44} = 0.4876 \end{array}$$

The emissivity for the smoke layer can be estimated from the mean absorption coefficient for a wood flame (Table 4.11) as:

$$\begin{aligned} \varepsilon_1 &= 1 - \exp(-\kappa_m S) = 1 - \exp(-0.8 \times 0.5) \\ &= 0.33 \end{aligned}$$

The blackbody emissive power of each surface is calculated as σT^4, for example:

$$\begin{aligned} \left(\sigma T^4\right)_1 &= 5.6696 \times 10^{-8} \times 1400^4 \\ &= 217.8 \text{ kW/m}^2 \end{aligned}$$

From Equations 4.78a and 4.78b, the radiative fluxes to and from each surface are determined by solving the eight simultaneous equations:

$$\begin{array}{ll} J_1 = 88.7 \text{ kW/m}^2 & G_1 = 17.7 \text{ kW/m}^2 \\ J_2 = 4.7 \text{ kW/m}^2 & G_2 = 43.3 \text{ kW/m}^2 \\ J_3 = 3.9 \text{ kW/m}^2 & G_3 = 34.8 \text{ kW/m}^2 \\ J_4 = 23.9 \text{ kW/m}^2 & G_4 = 34.3 \text{ kW/m}^2 \end{array}$$

The net radiative heat flux on the target element from Equation 4.79 is

$$\dot{q}''_{r,3} = J_3 - G_3 = -30.9 \text{ kW/m}^2$$

where the negative sign indicates that heat must be removed from the target element so it remains

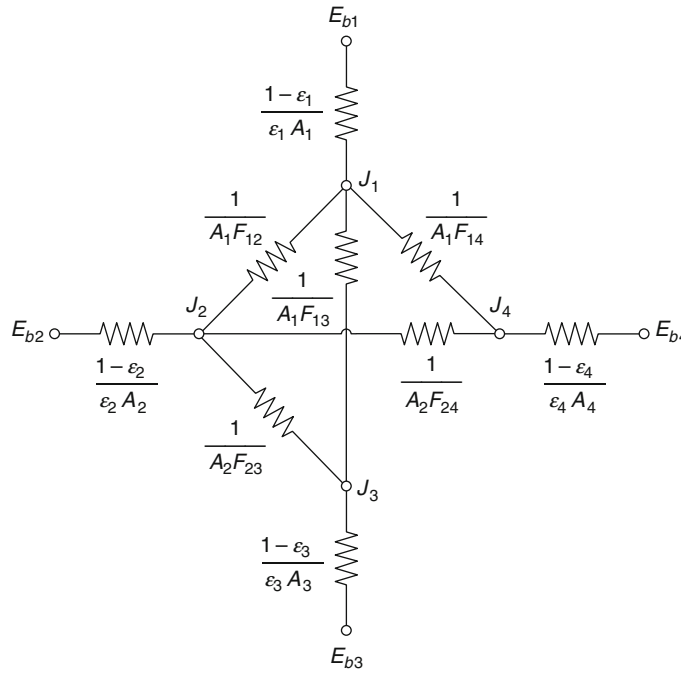

Fig. 4.18 Equivalent resistance network for an enclosure

in equilibrium. This example also could have been solved by the resistance network method shown in Fig. 4.18)

Nomenclature

A	Area (m^2)
C	Correction factor for mean beam length
C_0	Soot concentration parameter
C_2	Planck's second constant (1.4388×10^{-2} m · K)
c	Speed of light in the medium (m/s)
c_0	Speed of light in a vacuum (2.998×10^8 m/s)
E	Radiative emissive power (W/m^2)
F_{i-j}	Configuration factor from surface i to surface j
f_v	Soot volume fraction
G	Irradiation or radiative heat flux received by surface (W/m2)
H	Height (m)
h	Planck's constant (6.6256×10^{-34} J s)
I	Radiation intensity (W/m^2)
$\vec{i}, \vec{j}, \vec{k}$	Cartesian coordinate direction vectors
J	Radiosity or radiative heat flux leaving surface (W/m^2)
k	Boltzmann constant (1.3806×10^{-23} J/K), or infrared optical constant of soot (imaginary component), or thermal conductivity (W/m K)
L	Mean beam length or distance (m)
L_0	Geometrical mean beam length (m)
n	Index of refraction (c_0/c) or infrared optical constant of soot (real component)
$\vec{n}$	Unit normal vector
P_a	Partial pressure of absorbing gas (Pa)
P_e	Effective pressure (Pa)
Q	Energy rate (W)
q''	Heat flux (W/m^2)
$\vec{R}$	Line of sight vector
r	Radius of cylinder (m)
S	Pathlength (m)
T	Temperature (K)
t	Time (s)
u, v, w	Cartesian components of unit vector $\vec{n}$
V	Volume (m^3)

X Pressure pathlength, $\int_0^s P_a x(\xi) d(\xi)$ (atm-m)
x Spatial coordinate (m)

Greek Symbols

α Absorptivity or thermal diffusivity k/pc_p (m^2/s)
β Angle from normal (radians)
ε Emissivity
θ Polar angle (radians)
κ Extinction coefficient or absorption coefficient ($m - l$)
λ Wavelength (m)
μ Micron (10^{-6} m)
μ_λ Defined parameter, Equation 4.73
ν Frequency (s^{-t})
ξ Integration dummy variable
ρ Reflectivity or density (kg/m^3)
Ω Solid angle (steradians)
σ Stefan-Boltzmann constant (5.6696×10^{-B} W/m^2K^4)
τ Transmissivity or optical pathlength
ϕ Azimuthal angle (radians)
χ Fractional measure

Subscripts

a Actual
b Blackbody or base
e External
f Flame
g Gas
i Initial or i^{th} surface
j Summation variable or j^{th} surface
m Mean value
0 Original
P Planck mean
R Rosseland mean
s Surface or soot
t Total
w Wall
λ Spectral wavelength
ν Spectral frequency
∞ Ambient

References

1. J. deRis, *17th Symposium (International) on Combustion*, 1003, Combustion Institute, Pittsburgh, PA (1979).
2. S.C. Lee and C.L. Tien, *Progress in Energy and Combustion Science*, 8, 41 (1982).
3. G.M. Faeth, S.M. Jeng, and J. Gore, in *Heat Transfer in Fire and Combustion Systems*, American Society of Mechanical Engineers, New York (1985).
4. Incropera, F.P. and DeWitt, D.P., *Fundamentals of Heat and Mass Transfer*, John Wiley & Sons, New York, 2002.
5. H.C. Hottel and A.F. Sarofim, *Radiative Heat Transfer*, McGraw-Hill, New York (1967).
6. R. Siegel and H.R. Howell, *Thermal Radiation Heat Transfer*, McGraw-Hill, New York (1981).
7. Bejan, A., *Heat Transfer*, John Wiley & Sons, New York, 1993.
8. Hallman, J.R., "Ignition characteristics of plastics and rubber," Ph.D. Dissertation, University of Oklahoma, 1971.
9. Hallman, J.R., Welker, J.R., and Sliepcevich, C.M., "Polymer surface reflectance–absorptance characteristics," *Polymer Engineering and Science* **14**: 717–723 (1974).
10. Hallman, J.R., Sliepcevich, C.M., and Walker, J.R., "Radiation absorption for polymers: The radiant panel and carbon arcs as radiant heat sources," *Journal of Fire & Flammability* **9**: 353–366 (1978).
11. Wesson, H.R., Welker, J.R., and Sliepcevich, C.M., "The piloted ignition of wood by thermal radiation," *Combustion and Flame* **16**: 303–310 (1971).
12. Försth, M. and Roos, A., "Absorptivity and its Dependence on Heat Source Temperature and Degree of Thermal Breakdown," Fire and Materials 35: 285–301 (2011).
13. Janssens, M., "Piloted ignition of wood: a review," *Fire and Materials* **15**: 151–167 (1991).
14. Janssens, M. and Douglas, B., "Wood and wood products," in *Handbook of Building Materials for Fire Protection*, Ed. Harper, C.A., pp. 7.1–7.58, McGraw–Hill, New York, 2004.
15. Kashiwagi, T. and Ohlemiller, T.J., "A study of oxygen effects on nonflaming transient gasification of PMMA and PE during thermal irradiation," *Proceedings of the Combustion Institute* **19**: 815–823 (1982).
16. Modak, A.T. and Croce, P.A., "Plastic pool fires," *Combustion and Flame* **30**: 251–265 (1977).
17. E.M. Sparrow and R.D. Cess, *Radiation Heat Transfer*, McGraw-Hill, New York (1978).
18. J.R. Howell, *A Catalog of Radiation Configuration Factors*, McGraw-Hill, New York (1982).
19. C.L. Tien, in *Handbook of Heat Transfer Fundamentals*, McGraw-Hill, pp 14.36, New York (1985).

20. Oppenheim, A.K, *Trans. ASME*, **65**, 725, 1956.
21. C.L. Tien, *Advances in Heat Transfer*, 5, 253 (1968).
22. D.K. Edwards, in *Handbook of Heat Transfer Fundamentals*, McGraw-Hill, pp 14.53, New York (1985).
23. D.K. Edwards, *Advances in Heat Transfer*, 12, 115 (1976).
24. G.B. Ludwig, W. Malkmus, J.E. Reardon, and J.A.L. Thompson, *Handbook of Radiation from Combustion Gases*, NASA SP- 3080, Washington (1973).
25. T.F. Smith, Z.F. Shen, and J.N. Friedman, *Journal of Heat Transfer*, 104, 602 (1982).
26. J.D. Felske and C.L. Tien, *Combustion Science and Technology*, 11, 111 (1975).
27. M.M. Abu-Romia and C.L. Tien,, *Journal of Quantitative Spectroscopy and Radiative Transfer*, 107, 143 (1966).
28. M.A. Brosmer and C.L. Tien, *Journal of Quantitative Spectroscopy and Radiative Transfer*, 33, 521 (1985).
29. M.A. Brosmer and C.L. Tien, *Journal of Heat Transfer*, 107, 943 (1985).
30. M.A. Brosmer and C.L. Tien, *Combustion Science and Technology*, 48, 163 (1986).
31. S.C. Lee and C.L. Tien, 18th Symposium (International) on Combustion, Combustion Institute, 1159, Pittsburgh (1981).
32. C.L. Tien, in *Handbook of Heat Transfer Fundamentals*, McGraw-Hill, pp 14.83, New York (1985).
33. G.L. Hubbard and C.L. Tien, *Journal of Heat Transfer*, 100, 235 (1978).
34. J.D. Felske and C.L. Tien, *Journal of Heat Transfer*, 99, 458 (1977).
35. J.D. Felske and C.L. Tien, *Combustion Science and Technology*, 7, 25 (1977).
36. W.W. Yuen and C.L. Tien, *16th Symposium (International) on Combustion*, Combustion Institute, 1481, Pittsburgh (1977).
37. A. Dayan and C.L. Tien, *Combustion Science and Technology*, 9, 41 (1974).

Chris Lautenberger is a fire protection engineer at Reax Engineering Inc. in Berkeley, CA. He is also an Instructor in Cal Poly's Fire Protection Engineering program where he co-teaches courses on Fire Modeling and Fire Dynamics.

Thermochemistry

5

D.D. Drysdale

Introduction

Thermochemistry is the branch of physical chemistry that is concerned with the amounts of energy released or absorbed when a chemical change (reaction) takes place [1–3]. Inasmuch as fire is fundamentally a manifestation of a particular type of chemical reaction, viz., combustion, thermochemistry provides methods by which the energy released during fire processes can be calculated from data available in the scientific and technical literature.

To place it in context, thermochemistry is a major derivative of the first law of thermodynamics, which is a statement of the principle of conservation of energy. However, while concerned with chemical change, thermodynamics does not indicate anything about the rate at which such a change takes place or about the mechanism of conversion; this falls within the topic of chemical kinetics [4]. Consequently, the information it provides is normally used in association with other data, for example, to enable the rate of heat release to be calculated from the rate of burning.

The First Law of Thermodynamics

It is convenient to limit the present discussion to chemical and physical changes involving gases; this is not unreasonable, as flaming combustion takes place in the gas phase. It may also be assumed that the ideal gas law applies, that is,

$$PV = n \cdot RT \tag{5.1}$$

where P and V are the pressure and volume of n moles of gas at a temperature, T (in degrees Kelvin); values of the universal gas constant (R) in various sets of units are summarized in Table 5.1. At ambient temperatures, deviations from "ideal behavior" can be detected with most gases and vapors, while at elevated temperatures such deviations become less significant. In this context, it should be noted that whereas the terms *gas* and *vapor* are sometimes used interchangeably, it is best to make a distinction. Both are in the gaseous state, but as a general rule a vapor at normal temperatures can be made to liquefy if the pressure of the vapor is increased sufficiently. Thus, propane can be stored as a liquid under a relatively low pressure (approximately 8.4 bar at 293 Kelvin) whereas the permanent gases (particularly hydrogen, helium, oxygen, and nitrogen) can only be stored as gases at ambient temperatures, typically in pressure cylinders at 2000 psi (c. 138 bar). Again, as a general rule, vapors tend to deviate more strongly from ideal gas behavior than do the permanent gases.

Internal Energy

As a statement of the principle of conservation of energy, the first law of thermodynamics deals

D.D. Drysdale (✉)
BRE Centre for Fire Safety Engineering, University of Edinburgh, Scotland, UK

M.J. Hurley (ed.), *SFPE Handbook of Fire Protection Engineering*,
DOI 10.1007/978-1-4939-2565-0_5, © Society of Fire Protection Engineers 2016

Table 5.1 Values of the ideal gas constant, R

Units of pressure	Units of volume	Units of R	Value of R
Pa (N/m^2)	m^3	J/K·mol	8.31431
atm	cm^3	cm^3·atm/K·mol	82.0575
atm	*l*	*l*·atm/K·mol	0.0820575
atm	m^3	m^3·atm/K·mol	8.20575×10^{-5}

with the relationship between work and heat. Confining our attention to a "closed system"—for which there is no exchange of matter with the surroundings—it is known that there will be a change if heat is added or taken away, or if work is done on or by "the system" (e.g., by compression). This change is usually accompanied by an increase or decrease in temperature and can be quantified if we first define a function of state known as the internal energy of the system, E. Any change in the internal energy of the system (ΔE) is then given by

$$\Delta E = q - w \tag{5.2}$$

where q is the heat transferred to the system, and w is the work done by the system. This can be expressed in differential form

$$dE = dq - dw \tag{5.3}$$

Being a function of state, E varies with temperature and pressure, that is, $E = E(T, P)$.

According to the standard definition, work, w, is done when a force, F, moves its point of application through a distance, x, thus, in the limit

$$dw = F \cdot dx \tag{5.4}$$

The work done during the expansion of a gas can be derived by considering a cylinder/piston assembly (Fig. 5.1); thus

$$dw = P \cdot A \cdot dx = P\,dV \tag{5.5}$$

where
P = Pressure of the gas
A = Area of the piston
dx = Distance through which the piston is moved; the increment in volume is therefore $dV = A \cdot dx$

The total work done is obtained by integrating Equation 5.5 from the initial to the final state; that is,

$$w = \int_{\text{initial}}^{\text{final}} P \cdot dV \tag{5.6}$$

Combining Equations 5.3 and 5.5, the differential change in internal energy can be written

$$dE = dq - P \cdot dV \tag{5.7}$$

This shows that if the volume remains constant, as $P \cdot dV = 0$, then $dE = dq$; if this is integrated, we obtain

$$\Delta E = q_v \tag{5.8}$$

where q_v is the heat transferred to the constant volume system; that is, the change in internal energy is equal to the heat absorbed (or lost) at constant volume.

Enthalpy

With the exception of explosions in closed vessels, fires occur under conditions of constant pressure. Consequently, the work done as a result of expansion of the fire gases must be taken into account. At constant pressure, Equation 5.5 may be integrated to give

$$w = P \cdot (V_2 - V_1) \tag{5.9}$$

where V_1 and V_2 are the initial and final volumes, respectively. Equation 5.2 then becomes

$$\Delta E = E_2 - E_1 = q_p + PV_1 - PV_2 \tag{5.10}$$

or, rearranging,

$$\begin{aligned} q_p &= (E_2 + PV_2) - (E_1 + PV_1) \\ &= H_2 - H_1 \end{aligned} \tag{5.11}$$

where q_p is the heat transferred at constant pressure, and H is known as the enthalpy ($H \equiv E + PV$). The change in enthalpy is therefore the heat

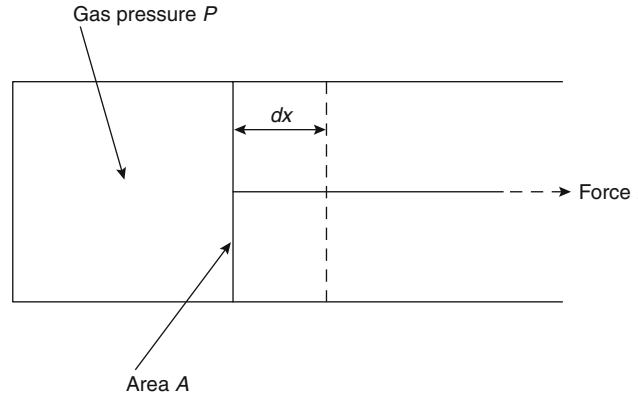

Fig. 5.1 Cylinder/piston assembly

absorbed (or lost) at constant pressure (provided that only $P - V$ work is done), and consequently it is the change in enthalpy that must be considered in fire-related problems.

Specific Heat

Specific heat, or heat capacity, of a body or "system" is defined as the amount of heat required to raise the temperature of unit mass by 1°C; the units are J/kg K, although for most thermochemical problems the units J/mol K are more convenient. The formal definition of the "mole" is the amount of a substance (solid, liquid, or gas) that contains as many elementary units (atoms or molecules) as there are carbon atoms in exactly 0.012 kg of carbon-12 (C^{12}). This number—known as Avogadro's number—is actually 6.023×10^{23}; in its original form, Avogadro's hypothesis was applied to gases and stated that equal numbers of molecules of different gases at the same temperature and pressure occupy the same volume. Thus, the quantity of a substance that corresponds to a mole is simply the gram-molecular weight, but expressed in kilograms to conform with SI units. For example, the following quantities of the gases N_2, O_2, CO_2, and CO represent 1 mole of the respective gas and, according to Avogadro's hypothesis, will each occupy 0.022414 m^3 at 273 K and 760 mmHg (101.1 kPa):

0.028 kg nitrogen (N_2)
0.032 kg oxygen (O_2)
0.044 kg carbon dioxide (CO_2)
0.028 kg carbon monoxide (CO)
0.016 kg methane (CH_4)
0.044 kg propane (C_3H_8)

The concept of specific heat is normally associated with solids and liquids, but it is equally applicable to gases. Such specific heats are required for calculating flame temperatures, as described below. Values for a number of important gases at constant pressure and a range of temperatures are given in Table 5.2.

It is important to note that there are two distinct heat capacities; at constant pressure, C_p, and at constant volume, C_v. Thus, at constant pressure

$$dq_p = dH = C_p \cdot dT \tag{5.12}$$

while at constant volume

$$dq_v = dE = C_v \cdot dT \tag{5.13}$$

For an ideal gas, $C_p = C_v + \mathrm{R}$.

Heats of Combustion

Chemical Reactions and Stoichiometry

When chemical reactions occur, they are normally accompanied by the release or absorption of heat. Thermochemistry deals with the

Table 5.2 Heat capacities of selected gases at constant pressure (101.1 kN/m^2) [5]

Cp (J/mol K)					
Temperature (K)	298	500	1000	1500	2000
Species					
CO	29.14	29.79	33.18	35.22	36.25
CO_2	37.129	44.626	54.308	58.379	60.350
H_2O(g)	33.577	35.208	41.217	46.999	51.103
N_2	29.125	29.577	32.698	34.852	35.987
O_2	29.372	31.091	34.878	36.560	37.777
He	20.786	20.786	20.786	20.786	20.786
CH_4	35.639	46.342	71.797	86.559	94.399

quantification of the associated energy changes. This requires a definition of the initial and final states, normally expressed in terms of an appropriate chemical equation, for example,

$$C_3H_8 + 5O_2 \rightarrow 3CO_2 + 4H_2O \qquad (5.R1)$$

in which the reactants (propane and oxygen) and products (carbon dioxide and water) are specified. This balanced chemical equation defines the *stoichiometry* of the reaction, that is, the exact proportions of the two reactants (propane and oxygen) for complete conversion to products (no reactants remaining). Note that the physical states of the reactants and products should also be specified. In most cases, the initial conditions correspond to ambient (i.e., 25 °C and atmospheric pressure) so that there should be no doubt about the state of the reactants. In this case both are gaseous, but it is more common in fires for the "fuel" to be in a condensed state, either liquid or solid. As an example, the oxidation of *n*-hexane can be written

$$C_6H_{14} + 9.5O_2 \rightarrow 6CO_2 + 7H_2O \qquad (5.R2)$$

but the fuel may be in either the liquid or the vapor state. The consequences of this will be discussed below.

Reaction 5.R1 may be used to calculate the mass of oxygen or air required for the complete oxidation of a given mass of propane. Thus, we deduce that 1 mole of propane (44 g) reacts completely with 5 moles of oxygen ($5 \times 32 = 160$ g); that is, 1 g propane requires 3.64 g oxygen. If the propane is burning in air, then the presence of nitrogen needs to be taken into account, although it does not participate to any significant extent in the chemical change. As the ratio of oxygen to nitrogen in air is approximately 21:79 (or 1:3.76), Reaction 5.R1 can be rewritten

$$C_3H_8 + 5O_2 + 18.8N_2 \rightarrow 3CO_2 + 4H_2O + 18.8N_2 \qquad (5.R3)$$

(where $18.8 = 5 \times 3.76$), showing that 44 g propane requires ($160 + 18.8 \times 28$), or 686.4 g of "air" for complete combustion, that is, 15.6 g air/g propane. Calculations of this type are valuable in assessing the air requirements of fires.

Thus, on the assumption that wood has the empirical formula [5] $CH_{1.5}O_{0.75}$, it can be shown that its stoichiometric air requirement is 5.38 g air for each gram of fuel, assuming complete combustion of wood to CO_2 and H_2O. The relevant stoichiometric equation is

$$CH_{1.5}O_{0.75} + O_2 + 3.76N_2 = CO_2 + 0.75H_2O + 3.76N_2 \qquad (5.R4)$$

In this calculation no distinction is made of the fact that flaming combustion of wood involves oxidation of the volatile gases and vapors produced by the pyrolysis of wood, while the residual char burns much more slowly by surface oxidation.

Measurement of Heats of Combustion

The heat of combustion of a fuel is defined as the amount of heat released when unit quantity is oxidized completely to yield stable end products.

In the present context, the relevant combustion processes occur at constant pressure so that we are concerned with an enthalpy change, ΔH_c. By convention, for exothermic reactions such as oxidation, values of ΔH_c are negative; that is, the reaction produces energy that can then be lost from the system. (By contrast, an endothermic reaction such as the conversion of water to hydrogen and oxygen will take place only if energy is provided in a suitable form.)

Heats of combustion are measured in the combustion bomb calorimeter in which a precise amount of fuel is burned in pure oxygen inside a pressure vessel whose temperature is strictly monitored. The apparatus is designed to reduce heat losses from the calorimeter to a minimum so that the amount of heat released can be calculated from the rise in temperature and the total thermal capacity of the system; corrections can be made for any heat loss. In the past, combustion bomb calorimetry received a great deal of attention within physical chemistry [1, 6] as the technique was able to provide a wealth of data of relevance to thermochemistry. However, the experiment gives the heat released at constant volume; that is, the change in internal energy, ΔE (Equation 5.8). The change in enthalpy is given by

$$\Delta H = \Delta E + \Delta(PV) \tag{5.14}$$

where $\Delta(PV)$ is calculated using the ideal gas law

$$\Delta(PV) = \Delta(nRT) \tag{5.15}$$

The method gives the gross heat of combustion—that is, in which the reactants and products are in their standard states. The net heat of combustion, on the other hand, refers to the situation in which the products are in the sate in which they are formed. For Reaction 5.R1, for example, water is formed in the gaseous phase so that the amount of energy released is less than the gross heat of combustion by an amount equivalent to the latent heat of evaporation of water (2.26 kJ/g). The net heat of combustion is the value that should be used in fire calculations. This is illustrated in the next section: see Reactions 5.R5a and 5.R5b. It should also be remembered that there is a heat of gasification associated with any condensed fuel (liquid or solid); a correction must be made for this if the heat of combustion of the fuel vapor is required.

Table 5.3 contains the heats of combustion (ΔH_c) of a number of combustible gases, liquids, and solids, expressed in various ways, viz., kJ/mole (fuel), kJ/g (fuel), kJ/g (oxygen), and kJ/g (air). The first of these is the form normally encountered in chemistry texts and reference books, whereas the second is more commonly found in sources relating to chemical engineering and fuel technology and is more useful to the fire protection engineer. However, the third and, particularly, the fourth have very specific uses in relation to fire problems. It is immediately apparent from Table 5.3 that ΔH_c (O_2) and ΔH_c (air) are approximately constant for most of the fuels listed, having average values of 13.1 kJ/g and 3 kJ/g, respectively. (See the section on "Rate of Heat Release in Fires".)

The data quoted in Table 5.3 refer to heats of combustion measured at ambient temperature, normally 25 °C. These data will be satisfactory for virtually all relevant fire problems, but occasionally it may be necessary to consider the heat released when combustion takes place at higher temperatures. This requires a simple application of the first law of thermodynamics. If the reaction involves reactants at temperature T_0 reacting to give products at the final temperature T_F, the process can be regarded in two ways:

1. The products are formed at T_0, absorb the heat of combustion, and are heated to the final temperature T_F.
2. The heat of combustion is imagined first to heat the reactants to T_F, then the reaction proceeds to completion, with no further temperature rise.

   By the first law, we can write

$$(\Delta H_c)^{T_0} + C_p^{\mathrm{Pr}} \cdot (T_F - T_0) = (\Delta H_c)^{T_F} + C_p^{\mathrm{R}} \cdot (T_F - T_0) \tag{5.16}$$

where C_p^{Pr} and C_p^{R} are the total heat capacities of the products and reactants, respectively. This may be rearranged to give

Table 5.3 Heats of combustion of selected fuels at 25 °C (298 K) [7]

Fuel	ΔH_c (kJ/mol)	ΔH_c (kJ/g)	ΔH_c[b] (kJ/g[O_2])	ΔH_c (kJ/g[air])
Carbon monoxide (CO)	283	10.10	17.69	4.10
Methane (CH_4)	800	50.00	12.54	2.91
Ethane (C_2H_6)	1423	47.45	11.21	2.96
Ethene (C_2H_4)	1411	50.53	14.74	3.42
Ethyne (C_2H_2)	1253	48.20	15.73	3.65
Propane (C_3H_8)	2044	46.45	12.80	2.97
n-Butane (n-C_4H_{10})	2650	45.69	12.80	2.97
n-Pentane (n-C_5H_{12})	3259	45.27	12.80	2.97
n-Hexane	3861	44.90		
c-Hexane (c-C_6H_{12})	3680	43.81	12.80	2.97
n-Octane (n-C_8H_{18})	5104	44.77	12.80	2.97
Benzene (C_6H_6)	3120	40.00	13.06	3.03
Methanol (CH_3OH)	635	19.83	13.22	3.07
Ethanol (C_2H_5OH)	1232	26.78	12.88	2.99
Acetone (CH_3COCH_3)	1786	30.79	14.00	3.25
D-glucose ($C_6H_{12}O_6$)	2772	15.40	13.27	3.08
Cellulose[c]	—	16.09	13.59	3.15
Polyethylene	—	43.28	12.65	2.93
Polypropylene	—	43.31	12.66	2.94
Polystyrene	—	39.85	12.97	3.01
Polyvinylchloride	—	16.43	12.84	2.98
Polymethylmethacrylate	—	24.89	12.98	3.01
Polyacrylonitrile	—	30.80	13.61	3.16
Polyoxymethylene	—	15.46	14.50	3.36
Polyethyleneterephthalate	—	22.00	13.21	3.06
Polycarbonate	—	29.72	13.12	3.04
Nylon 6,6	—	29.58	12.67	2.94
Polyester	—	23.8	—	—
Wool	—	20.5	—	—
Wood (European beech)	—	19.5	—	—
Wood volatiles (European beech)	—	16.6	—	—
Wood char (European beech)	—	34.3	—	—
Wood (Ponderosa pine)	—	19.4	—	—

[a]Apart from the solids (D-glucose, et seq.), the initial state of the fuel and of all the products is taken to be gaseous
[b]$\Delta H_c(O_2) = 13.1$ kJ/g is used in the oxygen consumption method for calculating rate of heat release
[c]Cotton and rayon are virtually pure cellulose and can be assumed to have the same heat of combustion

$$\frac{(\Delta H_c)^{T_F} - (\Delta H_c)^{T_0}}{T_F - T_0} = \Delta C_p \qquad (5.17)$$

or, in differential form, we have Kirchoff's equation

$$\frac{d(\Delta H_c)}{dT} = \Delta C_p \qquad (5.18)$$

where $\Delta C_p = C_p^{\mathrm{Pr}} - C_p^{\mathrm{R}}$. This may be used in integrated form to calculate the heat of combustion at temperature T_2 if ΔH_c is known at temperature T_1 and information is available on the heat capacities of the reactants and products, thus

$$(\Delta H_c)^{T_2} = (\Delta H_c)^{T_1} + \int_{T_1}^{T_2} \Delta C_p \cdot dT \qquad (5.19)$$

Where

$$\Delta C_p = \sum C_p(\text{products}) - \sum C_p(\text{reactants}) \tag{5.20}$$

and C_p is a function of temperature, which can normally be expressed as a power series in T, for example,

$$C_p = a + bT + cT^2 + \ldots \tag{5.21}$$

Information on heat capacities of a number of species and their variation with temperature may be found in Stull and Prophet [7] and Strehlow [8]. Some data are summarized in Table 5.2.

Heats of Formation

The first law of thermodynamics implies that the change in internal energy (or enthalpy) of a system depends only on the initial and final states of the system and is thus independent of the intermediate stages. This is embodied in thermochemistry as Hess's law, which applies directly to chemical reactions. From this, we can develop the concept of heat of formation, which provides a means of comparing the relative stabilities of different chemical compounds and may be used to calculate heats of chemical reactions that cannot be measured directly.

The heat of formation of a compound is defined as the enthalpy change when 1 mole of that compound is formed from its constituent elements in their standard state (at 1 atm pressure and 298 K). Thus, the heat of formation of liquid water is the enthalpy change of the reaction (at 298 K)

$$H_2(\text{g}) + 0.5\text{O}_2(\text{g}) \rightarrow \text{H}_2\text{O}(\text{l})\Delta H_f = -285.8\text{kJ/mol} \tag{5.R5a}$$

so that ΔH_f (H_2O) (l) = −285.8 kJ/mole at 25 °C. This differs from the heat released by the reaction if the product is water vapor rather than liquid ("The heat of formation of water vapor" kJ/mol [ΔH_f {H_2O(g)} = –241.84 kJ/mol]) by the latent heat of evaporation of water at 25 °C (43.96 kJ/mol). Thus

$$H_2(\text{g}) + 0.5\text{O}_2(\text{g}) \rightarrow \text{H}_2\text{O}(\text{g})\Delta H_f[\text{H}_2\text{O}(\text{g})] = -241.84\ \text{kJ/mol} \tag{5.R5b}$$

By definition, the heats of formation of all the elements are set arbitrarily to zero at all temperatures. This then allows the heats of reaction to be calculated from the heats of formation of the reactants and products, thus

$$\Delta H = \Delta H_f(\text{products}) - \Delta H_f(\text{reactants}) \tag{5.22}$$

where ΔH is the heat (enthalpy) of the relevant reaction. However, most heats of formation cannot be obtained as easily as heats of combustion. The example given in Reaction (5.R5a) is unusual in that the heat of formation of water also happens to be the heat of combustion of hydrogen. Similarly, the heat of combustion of carbon in its most stable form under ambient conditions (graphite) is the heat of formation of carbon dioxide.

Combustion calorimetry can be used indirectly to calculate heats of formation. The heat of formation of ethyne (acetylene), which is the enthalpy change of the reaction

$$2\text{C}(\text{graphite}) + \text{H}_2 \rightarrow \text{C}_2\text{H}_2 \tag{5.R6}$$

can be deduced in the following way: the heat of combustion of ethyne has been determined by bomb calorimetry as −1255.5 kJ/mol at 25 °C (298 K). This is the heat of the reaction

$$\text{C}_2\text{H}_2 + 2.5\text{O}_2 \rightarrow 2\text{CO}_2 + \text{H}_2\text{O} \tag{5.R7}$$

which, by Hess's law (see Equation 5.22), can be equated to

$$(\Delta H_c)^{298}(\text{C}_2\text{H}_2) = 2\left(\Delta H_f\right)^{298}(\text{CO}_2) + \left(\Delta H_f\right)^{298}(\text{H}_2\text{O}) - \left(\Delta H_f\right)^{298}(\text{C}_2\text{H}_2) - 2.5\left(\Delta H_f\right)^{298}(\text{O}_2) \tag{5.23}$$

We know that

$$(\Delta H_c)^{298}(\text{C}_2\text{H}_2) = -1255.5\ \text{kJ/mol}$$
$$(\Delta H_f)^{298}(\text{CO}_2) = -393.5\ \text{kJ/mol}$$

$$(\Delta H_f)^{298}\,(H_2O) = -241.8\ \text{kJ/mol}$$

$$(\Delta H_f)^{298}\,(O_2) = 0.0\ \text{kJ/mol (by definition)}$$

so that by rearrangement, Equation 5.23 yields

$$(\Delta H_f)^{298}\,(C_2H_2) = +226.7\ \text{kJ/mol}$$

This compound has a positive heat of formation, unlike CO_2 and H_2O. This indicates that it is an endothermic compound and is therefore less stable than the parent elements. Under appropriate conditions, ethyne can decompose violently to give more stable species.

The heats of formation of a number of compounds are given in Table 5.4. The most stable compounds (CO_2 and H_2O) have the largest negative values, while positive values tend to indicate an instability with respect to the parent elements. This can indicate a high chemical reactivity, and indeed heats of formation have been used in preliminary hazard assessment to provide an indication of the risks associated with new processes in the chemical industry. It should be noted that the heats of combustion of endothermic compounds do not give any indication of any associated reactivity (compare ethane, ethene, and ethyne in Tables 5.3 and 5.4).

Table 5.4 Heats of formation at 25 °C (298 K)

Compound	$(\Delta H_f)298$ (kJ/mol)
Hydrogen (atomic)	+218.00
Oxygen (atomic)	+249.17
Hydroxyl (OH)	+38.99
Chlorine (atomic)	+121.29
Carbon monoxide	–110.53
Carbon dioxide	–393.52
Water (liquid)	–285.8
Water (vapor)	–241.83
Hydrogen chloride	–92.31
Hydrogen cyanide (gas)	+135.14
Nitric oxide	+90.29
Nitrogen dioxide	+33.85
Ammonia	–45.90
Methane	–74.87
Ethane	–84.5
Ethene	+52.6
Ethyne (acetylene)	+226.9
Propane	–103.6
n-Butane	–124.3
Iso-butane[a]	–131.2
Methanol	–242.1

[a]Heats of formation of other hydrocarbons are tabulated in Weast [9]

Rate of Heat Release in Fires

Although thermochemistry can give information relating to the total amount of energy that can be released when a fuel is burned to completion, it is rarely (if ever) possible to use heats of combustion directly to calculate the heat released in "real" fires. Indeed, it can be argued that the *rate* of heat release is more important than the total available [10]. When a single item is burning in isolation, the rate of burning and the rate of heat release in the flame are coupled. It has been common to express the rate of heat release as the product of the burning rate (i.e., the rate of mass loss $\dot{m}$ [kg/s]) and the net heat of combustion of the fuel (ΔH_c kJ/kg).

$$\dot{Q}_c = \dot{m} \cdot \Delta H_c \qquad (5.24)$$

However, this assumes that combustion is complete, although it is known that this is never so in natural fires, which involve diffusion flames rather than premixed flames. Air and fuel have to mix by the process of diffusion (laminar or turbulent, depending on the size of the fire) before combustion can occur. The mixing process is relatively inefficient, and despite the fact that excess air is drawn (or *entrained*) into the flame, the products of combustion will contain some species that are only partially oxidized, such as carbon monoxide, aldehydes, ketones, and particulate matter in the form of soot or smoke. Their presence indicates that not all the available combustion energy has been released. The "combustion efficiency" is likely to vary from around 0.3–0.4 for heavily fire-retarded materials to 0.9 or higher in the case of oxygen-containing products (e.g., polyoxymethylene) [10, 11]. This is discussed in detail by Tewarson [12].

Fires burning in compartments present a completely different problem. In the first place, there is likely to be a range of different fuels present, each with a different stoichiometric air

requirement. These will burn at different rates, dictated not just by the nature of the fuel but also by the levels of radiant heat existing within the compartment during the fire. The rate of heat release during the fully developed stage of a compartment fire is required for calculating postflashover temperature-time histories for estimating fire exposure of elements of structure, as in the method developed by Pettersson et al. [13]. To calculate the rate of heat release within the compartment, it is assumed that the fire is ventilation controlled and that all combustion takes place within the compartment. The rate of heat release ($\dot{Q}_c$) can be obtained from the expression

$$\dot{Q}_c = \dot{m}_{\text{air}} \cdot \Delta H_c(\text{air}) \tag{5.25}$$

where ΔH_c (air) is the heat of combustion per unit mass of air consumed (3 kJ/g; see Table 5.3), and $\dot{m}_{\text{air}}$ is the mass flow rate of air into the compartment, given approximately by the expression

$$\dot{m}_{\text{air}} = 0.52 A_0 H_0^{1/2} \tag{5.26}$$

where A_0 is the effective area of ventilation (m^2) and H_0 is the height of the ventilation opening (m) [14]. The compartment temperature (as a function of time) is then obtained from heat balance calculations, as described in Drysdale [3], Tewarson [12], and Walton and Thomas [14].

The assumption behind Equation 5.25 is that the burning process is stoichiometric and that all the fuel vapors are burned within the compartment—air is supplied at exactly the rate required to consume the fuel vapors, that is,

$$\frac{\text{Rate of supply of air}}{\text{Rate of supply of fuel}} = r$$

where r is the stoichiometric air-fuel ratio and the maximum possible temperatures will be achieved. However, it is worth noting that this does not take into account the fact that the rate of heat release is not instantaneous. Although (in principle) the ideal stoichiometric mixture is created within the compartment, burning gases will emerge from the opening(s) simply because the reaction takes time to reach completion. Burning gases (i.e., flames) are carried outside the compartment, indicating that not all of the heat of combustion is released within the compartment. For a fully developed (postflashover) fire, it is perhaps more likely that the ratio $\dot{m}_{\text{air}}/\dot{m}_{\text{fuel}}$ (the "equivalence ratio") is less than the stoichiometric ratio r—that is, insufficient air is entering the compartment to burn all the fuel vapors. Under these circumstances, excess fuel vapors will escape from the compartment and burn outside as they mix with external air. The external flame length will depend *inter alia* on the equivalence ratio [15].

Regardless of whether the equivalence ratio is equal to or greater than the stoichiometric ratio, fuel vapor will burn outside the compartment and temperatures based on Equation 5.25 will be high. The method will also overestimate the temperatures achieved if the equivalence ratio is much greater than the stoichiometric ratio. Under these conditions, excess air is drawn into the compartment and will act as a diluent and reduce the average temperatures—if the ventilation is high enough, the rate of heat release will be controlled by the area of the burning surface [3, 16].

Note that the concept of equivalence ratio is used elsewhere in this handbook, specifically by Tewarson [12] and by Gottuk and Lattimer [17] in discussing the yields of products generated in the upper layer during the preflashover fire.

Much useful data on the fire behavior of combustible materials can be obtained by using the technique of "oxygen consumption calorimetry." This is the basis of the "cone calorimeter," in which the rate of heat release from a small sample of material burning under an imposed radiant heat flux is determined by measuring the rate of oxygen consumption [18]. The latter can be converted into a rate of heat release using the conversion factor 13.1 kJ/g of oxygen consumed. (A small correction is required for incomplete combustion, based on the yield of CO.) This technique can be used on a larger scale to measure the rate of heat release from items of furniture, wall lining materials, and so on [19, 20] and is now used routinely in both fire research and fire testing facilities.

Calculation of Adiabatic Flame Temperatures

In the previous sections, no consideration has been given to the fate of the energy released by the combustion reactions. Initially it will be absorbed within the reaction system itself by (1) unreacted reactants, (2) combustion products, and (3) diluents, although it will ultimately be lost from the system by various heat transfer processes. This is particularly true for natural fires in enclosed spaces. However, if we consider a premixed reaction system, such as a flammable vapor-air mixture, and assume it to be adiabatic, that is, there is no transfer of heat (or mass) to or from the system, then we can calculate the maximum theoretical temperature, the adiabatic flame temperature.

Consider a flame propagating through a stoichiometric propane-air mixture of infinite extent (i.e., there are no surfaces to which heat may be transferred) and that is initially at 25 °C. The appropriate equation is given by Reaction 5.R8:

$$C_3H_8 + 5O_2 + 18.8N_2 \rightarrow 3CO_2 + 4H_2O + 18.8N_2 \quad (5.R8)$$

This reaction releases 2044 kJ for every mole of propane consumed. This quantity of energy goes toward heating the reaction products, that is, 3 moles of carbon dioxide, 4 moles of water (vapor), and 18.8 moles of nitrogen for every mole of propane burned. The thermal capacity of this mixture can be calculated from the thermal capacities of the individual gases, which are available in the literature (e.g., JANAF) [7]. The procedure is straightforward, provided that an average value of C_p is taken for each gas in the temperature range involved, giving 942.5 kJ/K as the total thermal capacity of the products per mole of propane consumed (see Table 5.5).

As 2044 kJ are released at the same time as these species are formed, the maximum temperature rise will be

Table 5.5 Thermal capacity of the products of combustion of a stoichiometric propane/air mixture

	No. of moles	Thermal capacity at 1000 K	
		(J/mol·K)	(J/K)
CO_2	3	54.3	162.9
H_2O	4	41.2	164.8
N_2	18.8	32.7	614.8
		Total thermal capacity (per mole of propane)	= 942.5 J/K

$$\Delta T = \frac{2044000}{942.5} = 2169 \text{ K}$$

giving the final (adiabatic) temperature as 2169 + 298 = 2467 K. In fact, this figure is approximate for the following reasons:

1. Thermal capacities change with temperature, and average values over the range of temperatures appropriate to the problem have been used.
2. The system cannot be adiabatic as there will be heat loss by radiation from the hot gases (CO_2 and H_2O).
3. At high temperatures, dissociation of the products will occur; as these are endothermic processes, there will be a reduction in the final temperature.

Of these, (2) and (3) determine that the actual flame temperature will be much lower than predicted. These effects can be taken into account. Thus, with propane burning in air, the final temperature may not exceed 2000 K.

If the propane were burning as a stoichiometric mixture in pure oxygen, then in the absence of nitrogen as a "heat sink," much higher temperatures would be achieved. The total thermal capacity would be (942.5 − 614.8) = 327.7 J/K. However, the amount of heat released remains unchanged (2044 kJ) so that the maximum temperature rise would be

$$\Delta T = \frac{2044000}{327.7} = 6238\text{K}$$

predicting a final temperature of 6263 °C. Because dissociation will be a dominant factor,

this cannot be achieved and the temperature of the flame will not exceed approximately 3500 K.

The occurrence of dissociation at temperatures in the region of 2000 K and above makes it necessary to take dissociation into account. Dissociation is discussed in Chap. 6. However, the simple calculation outlined above can be used to estimate the temperatures of near-limit flames, when the temperature is significantly lower and dissociation can be neglected.

It is known that the lower flammability limit of propane is 2.2 %. The oxidation reaction taking place in this mixture can be described by the following equation:

$$0.022C_3H_8 + 0.978(0.21O_2 + 0.79N_2) \rightarrow \text{products}$$

Dividing through by 0.022 allows this to be written

$$C_3H_8 + 9.34O_2 + 35.12N_2 \rightarrow 3CO_2 + 4H_2O + 4.34O_2 + 35.12N_2 \quad (5.R9)$$

showing that the heat released by the oxidation of 1 mole of propane is now absorbed by excess oxygen (4.34 moles) and an increased amount of nitrogen as well as the combustion products. Carrying out the same calculation as before, it can be shown that the total thermal capacity of the products per mole of propane consumed is 1627.6 kJ/K, which gives the adiabatic flame temperature for this limiting mixture is 1281 °C (1554 K). If the same calculation is carried out for the other hydrocarbon gases, it is found that the adiabatic limiting flame temperature lies in a fairly narrow band, 1600 ± 100 K (Table 5.6). This can be interpreted by assuming that the limit exists because heat losses (by radiation from the flame) exceed the rate of heat production (within the flame). As a consequence, flame cannot sustain itself. This concept can be applied to certain practical problems relating to the lower flammability limit.

Example 1 It is recognized that the leak of propane into a test cell could lead to a flammable atmosphere, and it is decided to keep the atmosphere inert by the addition of nitrogen. Calculate the percentage of nitrogen necessary to prevent ignition of a mixture in which the propane and air are in stoichiometric proportions.

Table 5.6 Adiabatic flame temperature of lower-limiting hydrocarbon/air mixtures

Gas	Adiabatic flame temperature at lower flammability limit (K)
Methane	1446
Ethane	1502
Propane	1554
n-Butane	1612
n-Pentane	1564
n-Heptane	1692
n-Octane	1632

Solution The stoichiometric reaction for propane in air is

$$C_3H_8 + 5O_2 + 18.8N_2 \rightarrow 3CO_2 + 4H_2O + 18.8N_2 \quad (5.R10)$$

and the heat of combustion of propane is 2044 kJ/mole. It is assumed that the heat of combustion is absorbed by the products $3CO_2 + 4H_2O + 18.8\ N_2$. It was shown above that the adiabatic flame temperature (i.e., the temperature of the product gases, assuming no heat losses) will be 2169 K. If the flame temperature can be held below 1600 K (or 1554 K, according to Table 5.6), then flame propagation will not be possible and the introduction of an ignition source will not lead to an explosion. Suppose that the extra quantity of nitrogen required to form an "inert atmosphere" corresponds to X moles per mole of propane. Then

$$C_3H_8 + 5O_2 + 18.8N_2 + XN_2 \rightarrow 3CO_2 + 4H_2O + (18.8 + X)N_2 \quad (5.R11)$$

Following the procedure illustrated in Table 5.5, the thermal capacity of the product gases—$3CO_2 + 4H_2O + (18.8 + X)N_2$—will be $3 \times 54.3 + 4 \times 41.2 + (18.8 + X) \times 32.7 = \Sigma C_p$. If sufficient nitrogen has been added to reduce the adiabatic flame temperature to 1554 K, then the

thermal capacity of the product gases will be given by

$$\sum C_p = \frac{2044000}{1554 - 298} = 1627.4\,\text{kJ/mole of propane}$$

Thus

$$3 \times 54.3 + 4 \times 41.2 + (18.8 + X) \times 32.7 = 1627.4$$

$$X = 20.9$$

Consequently, the amount of nitrogen added to the air in the test cell to render the atmosphere "inert" with respect to a leak of propane corresponds to 20.9 moles of N_2 for every (5 + 18.8) = 23.8 moles of air, that is, the mixture in the cell must be 47 % nitrogen, the balance being air. (Experimentally, a significantly lower figure is obtained—c. 40 %. It should be remembered that in the above calculation it is assumed that the adiabatic temperature assumption is valid and that the reaction will go to completion.)

Example 2 A mechanical engineering research laboratory contains a six-cylinder internal combustion engine that is being used for research into the performance of spark plugs. The fuel being used is methane, CH_4, and the fuel-air mixture can be adjusted at will. The combustion products are extracted from the exhaust manifold through a 30 cm square duct, 20 m long. It is found that the engine will continue to operate with a stoichiometric mixture when only three of the cylinders are firing. If under these conditions the average temperature of the gases entering the duct from the manifold is 700 K, is there a risk of an explosion in the duct?

Solution The stoichiometric reaction for methane in air is

$$CH_4 + 2O_2 + 7.52N_2 \rightarrow CO_2 + 2H_2O + 7.52N_2 \quad (5.R12)$$

If we consider that 1 mole of fuel passes through each of the six cylinders, but of the 6 moles only three are burned, we have overall

$$6CH_4 + 12O_2 + 45.12N_2 \rightarrow 3CH_4 + 3CO_2 + 6H_2O + 6O_2 + 45.12N_2 \quad (5.R13)$$

Dividing through by 3 gives

$$2CH_4 + 4O_2 + 15.04N_2 \rightarrow CH_4 + 2O_2 + CO_2 + 2H_2O + 15.04N_2 \quad (5.R14)$$

The mixture discharged into the exhaust manifold has the composition given by the right-hand side of Reaction 5.R14. If this "burns" at 700 K, the final abiabatic flame temperature may be calculated on the basis of the reaction

$$CH_4 + 2O_2 + CO_2 + 2H_2O + 15.04N_2 \rightarrow 2CO_2 + 4H_2O + 15.04N_2 \quad (5.R15)$$

The total thermal capacity of the product gases ($2CO_2$ + $4H_2O$ + 15.04 N_2) (at 1000 K) can be shown to be 765.3 J per mole of methane burned. Using Kirchoff's equation (Equation 5.19), $\Delta H_c(CH_4)$ at 700 K is calculated as 802.8 kJ/mol, giving $\Delta T = 802800/765.3 =$ 1049 K. This gives a final temperature of 1749 K, which is significantly higher than the limiting flame temperature (1600 K) discussed above. This indicates that there is a risk of explosion, and measures should be applied to prevent this mixture being discharged into the duct.

It should be noted that at 700 K there will be a "slow" reaction between methane and the oxygen present, which could invalidate the tacit assumption that the duct becomes completely filled with the mixture described by the right-hand side of Reaction 5.R13. However, slow oxidation of the methane will tend to make the mixture less flammable, and so the calculation gives a conservative answer.

Nomenclature

A	Area (Equation 5.5)
A_w	Area of ventilation opening
C_p	Specific heat
E	Internal energy
F	Force (Equation 5.4)
H	Height of ventilation opening
H	Enthalpy
ΔH_c	Heat of combustion
ΔH_f	Heat of formation
$\dot{m}$	Mass rate of burning
$\dot{m}_{\text{air}}$	Mass flow rate of air
n	Number of moles
p	Pressure
q	Energy
Q_c	Rate of heat release
R	Universal gas constant
T	Temperature
V	Volume
w	Work

Subscripts

c	Combustion
F	Final
f	Formation
o	Initial
p	Constant pressure
v	Constant volume

Superscripts

Pr	Products
R	Reactants

References

1. W.J. Moore, *Physical Chemistry,* 5th ed., Longman, London (1974).
2. P Atkins and J de Paula, "Atkins' Physical Chemistry" 9th Edition (Oxford University Press, 2009)
3. D.D. Drysdale, *Introduction to Fire Dynamics,* 3rd ed., John Wiley and Sons, Chichester, UK (2011).
4. J.F. Griffiths, "Combustion Kinetics," in *SFPE Handbook of Fire Protection Engineering,* 4th ed. (P.J. DiNenno et al., eds.), National Fire Protection Association, Quincy, MA, pp. 1-220–1-230 (2008).
5. A.F. Roberts, *Combustion and Flame,* 8, p. 245 (1964).
6. G M Barrow, "*Physical Chemistry*" 4th Edition, McGraw-Hill Book Co. (New York, 1961)
7. NIST-JANAF *Thermochemical Tables*: see http://kinetics.nist.gov/janaf/
8. R.A. Strehlow, *Combustion Fundamentals,* McGraw-Hill, New York (1984).
9. R.C. Weast, *Handbook of Chemistry and Physics,* Chemical Rubber Co., Cleveland, OH (1973).
10. V. Babrauskas and R. Peacock, "Heat Release Rate: The Single Most Important Variable in Fire Hazard," in *Fire Safety Journal,* 18, pp. 255–272 (1992).
11. A. Tewarson, in *Flame Retardant Polymeric Materials* (M. Lewin, ed.), Plenum, New York (1982).
12. M. Khan, A. Tewarson, and M. Chaos, "Combustion Characteristics of Materials and Generation of Fire Products," in *SFPE Handbook of Fire Protection Engineering,* 5th ed. Springer, New York, 2015.
13. O. Pettersson, S.E. Magnusson, and J. Thor, *Fire Engineering Design of Structures,* Swedish Institute of Steel Construction, Publication, 50 (1976).
14. W.D. Walton and P.H. Thomas, "Estimating Temperatures in Compartment Fires," in *SFPE Handbook of Fire Protection Engineering,* 4th ed. (P.J. DiNenno et al., eds.), Society of Fire Protection Engineers, Bethesda, MD, pp. 3-204–3-221 (2008).
15. M.L. Bullen and P.H. Thomas, *Seventeenth Symposium (International) on Combustion,* Combustion Institute, Pittsburgh, PA (1979).
16. P.H. Thomas and A.J.M. Heselden, "Fully Developed Fires in Compartments," *CIB Report No. 20; Fire Research Note No. 923,* Conseil International du Batiment, France (1972).
17. D.T. Gottuk and B.Y. Lattimer, "Effect of Combustion Conditions on Species Production," in *SFPE Handbook of Fire Protection Engineering,* 4th ed. (P.J. DiNenno et al., eds.), National Fire Protection Association, Quincy, MA, pp. 2-67–2-95 (2008).
18. V. Babrauskas, "The Cone Calorimeter," in *SFPE Handbook of Fire Protection Engineering,* 4th ed. (P.J. DiNenno et al., eds.), National Fire Protection Association, Quincy, MA, pp. 3-90–3-108 (2008).
19. V. Babrauskas and S.J. Grayson (eds.), *Heat Release in Fires,* Elsevier Applied Science, London (1992).
20. M.L. Janssens, "Calorimetry," in *SFPE Handbook of Fire Protection Engineering,* 5th ed. Springer, 2015.

D.D. Drysdale is professor emeritus in the BRE Centre for Fire Safety Engineering, School of Engineering, at the University of Edinburgh, Scotland. His research interests lie in fire science, fire dynamics, and the fire behavior of combustible materials.

Chemical Equilibrium

6

Raymond Friedman

Introduction

The temperature of a flame must be known in order to calculate convective and radiative heat transfer rates, which control pool-fire burning rates, flame spread rates, remote ignitions, damage to exposed items (e.g., structural steel, wiring), and response of thermal fire detectors or automatic sprinklers.

Chapter 5 provides a simple technique for calculating flame temperature, based on ignoring the dissociations that occur at high temperature. Although the error is small for near-limit flames, this technique gives answers that are too high. For example, if propane (C_3H_8) burns in stoichiometric proportions with air at 300 K, and it is assumed that the only products are CO_2, H_2O, and N_2, then the simple thermochemical calculation yields a flame temperature of 2394 K. On the other hand, if chemical equilibrium is considered, so that the species CO, O_2, H_2, OH, H, O, and NO are assumed present in the products, then the flame temperature, calculated by methods described in this section, comes out to be 2268 K. Flame temperature measurements in laminar premixed propane-air flames agree with the latter value. (The discrepancy in flame temperature caused by neglecting dissociation would be even greater for fires in oxygen-enriched atmospheres.)

The chemical equilibrium calculation yields not only the temperature but the equilibrium composition of the products. Thus, the generation rate of certain toxic or corrosive products such as carbon monoxide, nitric oxide, or hydrogen chloride may be calculated, insofar as the assumption of equilibrium is valid.

For a fire in a closed volume, the final pressure as well as the temperature will depend on the dissociations and therefore require a calculation taking chemical equilibrium into account.

From a fire research viewpoint, there is interest in correlating flammability limits, extinguishment, soot formation, toxicity, flame radiation, or other phenomena; and chemical equilibrium calculations in some cases will be a useful tool in such correlations.

In a later part of this chapter, departure of actual fires from chemical equilibrium will be discussed.

The Chemical Equilibrium Constant

Consider a chemical transformation, such as

$$2CO + O_2 \rightarrow 2CO_2 \qquad (6.1)$$

If this process can occur, presumably the reverse process can also occur (principle of microscopic reversibility, or principle of detailed balancing):

$$2CO_2 \rightarrow 2CO + O_2 \qquad (6.2)$$

R. Friedman (✉)
Retired from FM Global

M.J. Hurley (ed.), *SFPE Handbook of Fire Protection Engineering*,
DOI 10.1007/978-1-4939-2565-0_6, © Society of Fire Protection Engineers 2016

If both processes occur at finite rates in a closed system, then, after a sufficient time, a condition of *chemical equilibrium* will be reached, after which no further change occurs as long as the temperature and pressure remain constant and no additional reactants are introduced. This condition of equilibrium can be expressed as a *mathematical constraint* on the system, which, for the gaseous reaction $2CO + O_2 \rightleftarrows 2CO_2$, can be written

$$K_3 = \frac{p^2_{CO_2}}{p^2_{CO}\, p_{O_2}} \tag{6.3}$$

where the p_i are partial pressures (atm)[1] and K_3 is the equilibrium constant. This expression can be rationalized by the following argument.

According to the chemical "law of mass action," first stated a century ago, the rate of the forward reaction (Equation 6.1) at a given temperature is given by $k_f p^2_{CO} p_{O_2}$ while the rate of the reverse reaction (Equation 6.2) is given by $k_r p^2_{CO_2}$. At equilibrium, the forward rate must be equal to the reverse rate:

$$k_f p^2_{CO} p_{O_2} = k_r p^2_{CO_2} \tag{6.4}$$

which may be rearranged to

$$\frac{p^2_{CO_2}}{p^2_{CO}\, p_{O_2}} = \frac{k_f}{k_r} = K_3 \tag{6.5}$$

Although this appears to be a satisfactory explanation, research over the past hundred years has shown that chemical reactions in fact rarely proceed as suggested by the stoichiometric equation. (This is discussed more fully in Chap. 13.) For example, the three-body collision of two CO molecules and an O_2 molecule, resulting in the formation of two CO_2 molecules, simply does not happen. Rather, the reaction would occur as follows:

$$O_2 + M \rightarrow 2O + M \tag{6.6}$$

(where M is any molecule) followed by

$$O + CO + M \rightarrow CO_2 + M \tag{6.7}$$

Now, observe how Equation 6.3 can be obtained from this reaction sequence.

The reverse of $O_2 + M \rightarrow 2O + M$, namely $2O + M \rightarrow O_2 + M$, can also occur, and the equilibrium constant for this pair of reactions, which actually do occur, is $K6 = p_O{}^2 p_M / p_{O_2} p_M = p_O{}^2 / p_{O_2}$. (The p_M term cancels.)

Similarly the reverse reaction $CO_2 + M \rightarrow O + CO + M$ can occur, and the equilibrium constant is $K_7 = p_{CO_2} / p_{CO}\, p_O$. If we now multiply $K_7{}^2$ by K_6, we obtain

$$K_7^2 K_6 = \left(\frac{p_{CO_2}}{p_{CO}\, p_O}\right)^2 \frac{p_O{}^2}{p_{O_2}} = \frac{p^2_{CO_2}}{p^2_{CO}\, p_{O_2}} = K_3 \tag{6.8}$$

Thus, Equation 6.3 is perfectly valid, even if the "law of mass action" does not correctly describe the reaction process involving CO and O_2.

To get a further understanding of the validity of the equilibrium constant concept, consider the following facts: CO will not react with O_2—even by the above mechanism involving O atoms—unless first heated to quite high temperatures. However, at least a trace of moisture is usually present, and in such cases the reaction occurs by the following process, which can occur at lower temperatures. First, H and OH are formed by dissociation of H_2O. Then, the CO is converted by

$$CO + OH \rightleftarrows CO_2 + H \quad K_9 = \frac{p_{CO_2} p_H}{p_{CO}\, p_{OH}} \tag{6.9}$$

while the O_2 reacts with H:

$$O_2 + H \rightleftarrows OH + O \quad K_{10} = \frac{p_{OH} p_O}{p_{O_2} p_H} \tag{6.10}$$

If the quantity $K_9{}^2 K_{10}$ is now calculated,

$$K_9^2 K_{10} = \frac{p^2_{CO_2}}{p^2_{CO}\, p_{O_2}} \frac{p_H p_O}{p_{OH}} \tag{6.11}$$

[1] In place of partial pressures, the concentrations of the species in moles/liter can be used in these formulae instead (see Chap. 13).

But, the reaction $H + O + M \rightarrow OH + M$ can occur, as well as its reverse, $OH + M \rightarrow H + O + M$. It does not matter if these reactions are actually important in the rate of oxidation of CO in the presence of H_2O. As long as these reactions can occur, then at equilibrium

$$k_f p_H p_O p_M = k_r p_{OH} p_M$$

and

$$\frac{k_f}{k_r} = K_{12} = \frac{p_{OH}}{p_H p_O} \tag{6.12}$$

Substituting this into Equation 6.11

$$\frac{p^2_{CO_2}}{p^2_{CO} p_{O_2}} = K_9^2 K_{10} K_{12} = K_3 \tag{6.13}$$

Thus, the ratio $p^2_{CO_2}/p^2_{CO} p_{O2}$ is a constant at equilibrium (at a given temperature) regardless of the reaction mechanism, even if other (hydrogen-containing) species are involved, because by the principle of microscopic reversibility, these other species (catalysts) affect the reverse reaction as well as the forward reaction.

Let us now consider the mathematical specification of the CO–CO_2–O_2 system at equilibrium. The system, at a given temperature and pressure, may be described by three variables, namely the partial pressures of the three species: p_{CO}, p_{O_2}, and p_{CO_2}. There are already two well-known constraints on the system: (1) The sum of the partial pressures must equal the total pressure, p

$$p_{CO} + p_{O_2} + p_{CO_2} = p \tag{6.14}$$

and (2) the ratio of carbon atoms to oxygen atoms in the system must remain at the original, presumably known, value of C/O:

$$\frac{C}{O} = \frac{p_{CO} + p_{CO_2}}{p_{CO} + 2p_{O_2} + 2p_{CO_2}} \tag{6.15}$$

A third constraint, that of chemical equilibrium, provides a third equation involving p_{CO}, p_{O_2}, and p_{CO_2}:

$$\frac{p^2_{CO_2}}{p^2_{CO} p_{O_2}} = K_3 \tag{6.3}$$

Now the system is completely defined by the simultaneous solution of these three equations. The equilibrium constant varies with temperature but is independent of pressure (except at rather high pressures). It is also independent of the presence of other reactive chemical species.

Generalized Definition of Equilibrium Constant

For a generalized reaction

$$aX_1 + bX_2 \rightleftarrows cY_1 + dY_2$$

K would be given by

$$K = \frac{(pY_1)^c (pY_2)^d}{(pX_1)^a (pX_2)^b}$$

Attention should be paid to the manner in which a chemical reaction is written. For example, instead of writing $2CO + O_2 \rightleftarrows 2CO_2$ one could equally well have written $CO + 1/2O_2 \rightleftarrows CO_2$. The equilibrium constant for the latter formulation is

$$K_{16} = \frac{p_{CO_2}}{p_{CO} p_{O_2}^{1/2}} \tag{6.16}$$

By comparison of Equation 6.16 with Equation 6.3, it is clear that $K_{16} = \sqrt{K_3}$. If the reaction was written as $2CO_2 \rightleftarrows 2CO + O_2$ the equilibrium constant would be equal to $1/K_3$.

Simultaneous Equilibria

In most real chemical systems, one must deal with a number of simultaneous chemical equilibria. For example, air at 2500 K will contain the species N_2, O_2, NO, and O. The following simultaneous equilibria may be considered

$$O_2 = 2O \quad K_{17} = \frac{p_O{}^2}{p_{O_2}} \tag{6.17}$$

$$N_2 + O_2 = 2NO \quad K_{18} = \frac{p^2 NO}{p_{N_2} p_{O_2}} \tag{6.18}$$

$$N_2 + 2O = 2NO \quad K_{19} = \frac{p^2NO}{p_{N_2} {p_O}^2} \tag{6.19}$$

It is easily seen from the above relations that $K_{19} = K_{18}/K_{17}$. Hence, Equations 6.17, 6.18, and 6.19 are not three independent equations, and any *two* of these equations may be used to describe the equilibrium condition; the third would be redundant. To determine the four unknowns, p_{N_2}, p_{O_2}, p_{NO}, and p_O, one would solve the selected two equilibrium relations plus the following two relations:

$$p_{NO} + p_{N_2} + p_{O_2} + p_O = p \tag{6.20}$$

And

$$\frac{p_{NO} + 2p_{N_2}}{p_{NO} + 2p_{O_2} + p_O} = 3.76 \tag{6.21}$$

where 3.76 is the ratio of nitrogen atoms to oxygen atoms in air.

If one knows the temperature, the equilibrium constants may be calculated from the thermodynamic properties of the reactants and products, as discussed in the next section. However, since the various equilibrium reactions release or absorb energy, and accordingly raise or lower the temperature of an adiabatic system respectively, the determination of equilibrium composition of an adiabatic system must proceed simultaneously with the calculation of its temperature; that is, an energy balance must be satisfied as well as the equilibrium equations, the atom-ratio equations, and the $p = \sum p_i$ equation.

As a general rule, a gaseous chemical system *at a given temperature,* containing s kinds of chemical species involving e chemical elements, requires s-e equilibrium relations, e-1 atom-ratio relations, and a $p = \sum p_i$ equation, in order to specify it. If the temperature is unknown, an energy balance equation is also needed. (If the pressure is unknown but the volume is known, then the equation of state must be used in the pressure equation.)

In order to solve an actual problem, one must select the species to be considered. The more species one includes, the more difficult is the calculation. There is no need to include any species that will be present in very small quantity at equilibrium. Some guidelines can be provided.

For combustion of a C–H–O compound in air, it is usually sufficient to include the species CO_2, H_2O, N_2, O_2, CO, H_2, OH, H, O, and NO. These species are adequate if the air-fuel ratio is sufficiently large so that the O/C atomic ratio is greater than one. If the O/C atomic ratio is less than one, then solid carbon must be considered, as well as many additional gaseous species. If chlorine is present, then HCl, Cl_2, and Cl must be added. If sulfur is present, then SO_2 and SO_3 are the primary species, unless there is a deficiency of oxygen.

The Quantification of Equilibrium Constants

While a chemist might establish the numerical value of an equilibrium constant for $A \rightleftarrows B$ by direct measurement of the partial pressures of A and B in a system at equilibrium, this is rarely done because it is difficult to make such measurements in a high-temperature system, and it takes a long time to establish equilibrium in a low-temperature system. Instead, the equilibrium constant is generally determined from the thermodynamic relation first deduced by van't Hoff in 1886 [1]

$$\Delta F^o = -RT \ln K \tag{6.22}$$

If this equation is applied to $A \rightleftarrows 2B$ at absolute temperature T, then $K = p_B^2/p_A$, and ΔF^o is the free energy of two moles (mol) of B at 1 atm and temperature T, minus the free energy of 1 mol of A at 1 atm and temperature T. (The superscript o designates that each substance is in its "standard state," that is, an ideal gas at 1 atm.) By definition

$$\begin{aligned} \Delta F^o &= \Delta H^o - T\Delta S^o \\ &= \Delta E^o + (pV^o) - T\Delta S^o \end{aligned} \tag{6.23}$$

Accordingly, if ΔS^o, the entropy difference, and either ΔH^o, the enthalpy difference, or ΔE^o, the

energy difference, are known for the substances involved in an equilibrium at temperature T, then the equilibrium constant, K, may be calculated. It happens that ΔS^o, ΔH^o, and ΔE^o are well known for almost all substances expected to be present at equilibrium in combustion gases at any temperature up to 4000 K, so the calculation of equilibrium constants is straightforward.

The variation of the equilibrium constant with temperature was shown by van't Hoff [1] to be given by

$$\frac{d \ln K}{dT} = \frac{\Delta H^o}{RT^2} \left(= \frac{\Delta H}{RT^2} \text{ for ideal gases} \right) \tag{6.24}$$

Thus, for an exothermic reaction occurring at temperature T, ΔH is negative and K decreases as T increases. The converse is true for endothermic reactions.

It is appropriate to inquire about the underlying physical reason for the value of K to be governed by ΔF^o (actually ΔH^o and ΔS^o). An explanation is as follows: any chemical system being held at constant temperature will seek to reduce its energy, E, and to increase its entropy, S. The reduction of energy is analogous to a ball rolling downhill. The increase of entropy is analogous to shuffling a sequentially arranged deck of cards, yielding a random arrangement. These two tendencies will often affect the equilibrium constant in opposite directions.

Consider the equation

$$\ln K = \frac{\Delta S^o}{R} - \frac{\Delta E^o}{RT} - \Delta n \tag{6.25}$$

where Δn is the increase in the number of moles of product relative to reactant. Equation 6.25 is obtained by combining Equations 6.22 and 6.23 with the ideal gas law at constant temperature $\Delta(pV^o) = \Delta nRT$. Inspection of Equation 6.25 shows that, if ΔS^o is a large positive quantity and $\Delta S^o/R$ dominates the other terms, K will be large, that is, the reaction is driven by the "urge" to increase entropy. Again, if the reaction is highly endothermic, then $-\Delta E^o/RT$ will be a large negative number and can dominate the other terms to cause K to be small, that is, the reaction prefers to go in the reverse, or exothermic, direction and reduces the energy of the system. (Most spontaneous reactions are exothermic.) The Δn term is generally small compared with the other terms and represents the work done by the expanding system on the surroundings, or the work done on the contracting system by the surroundings.

In summary, Equation 6.25 represents the balance of these various tendencies and determines the relative proportions of reactants and products at equilibrium. Notice that the term $\Delta E^o/RT$ becomes small at sufficiently high temperature, and the entropy term then dominates. In other words, all molecules break down into atoms at sufficiently high temperature, to maximize entropy. The important conclusion from this discussion is that there is no need to consider rates of forward and reverse processes to determine equilibrium.

Table 6.1 provides values of equilibrium constants for 13 reactions involving most species found in fire products at equilibrium, over a temperature range from 600 K to 4000 K. Equilibrium constants for other reactions involving the same species may be obtained by combining these constants, as in Equation 6.13, or as illustrated in the examples below.

Table 6.1 does not include the $\frac{1}{2}\ N_2 = N$ equilibrium, because fire temperatures are generally not high enough for significant N to form. Tables 6.2 and 6.3 present information on the degree to which various gases are dissociated at various temperatures.

In performing calculations, remember that even if a relatively small fraction of dissociation occurs, a rather large amount of energy may be absorbed in the dissociation, with a corresponding large increase in the energy of the system. For example, if water vapor initially at 2800 K is allowed to dissociate adiabatically at 1 atm, only 5.7 % of the H_2O molecules will dissociate, but the temperature will drop from 2800 K to 2491 K; that is, the temperature relative to a 300 K baseline is lower by 12.4 %.

Table 6.1 Values of $\log_{10}$ K for selected reactions

	K_A	K_B	K_C	K_D	K_E	K_F	K_G	K_H	K_I	K_J	K_K	K_L	K_M
600	–18.574	–16.336	18.633	–2.568	34.405	14.318	–7.210	–3.814	–7.710	–5.641	24.077	8.530	5.036
700	–15.449	–13.599	15.583	–2.085	29.506	12.946	–6.086	–2.810	–6.182	–4.431	20.677	7.368	4.374
800	–13.101	–11.539	13.289	–1.724	25.830	11.914	–5.243	–2.053	–5.031	–3.522	18.125	6.494	3.876
900	–11.272	–9.934	11.498	–1.444	22.970	11.108	–4.587	–1.462	–4.133	–2.814	16.137	5.812	3.486
1000	–9.807	–8.646	10.062	–1.222	20.680	10.459	–4.062	–0.988	–3.413	–2.245	14.544	5.265	3.173
1100	–8.606	–7.589	8.883	–1.041	18.806	9.926	–3.633	–0.599	–2.822	–1.799	13.240	4.816	2.917
1200	–7.604	–6.707	7.899	–0.890	17.243	9.479	–3.275	–0.273	–2.328	–1.389	12.152	4.442	2.702
1300	–6.755	–5.958	7.064	–0.764	15.920	9.099	–2.972	0.003	–1.909	–1.059	11.230	4.124	2.520
1400	–6.027	–5.315	6.347	–0.656	14.785	8.771	–2.712	0.240	–1.549	–0.775	10.438	3.852	2.364
1500	–5.395	–4.756	5.725	–0.563	13.801	8.485	–2.487	0.447	–1.236	–0.527	9.752	3.615	2.229
1600	–4.842	–4.266	5.180	–0.482	12.940	8.234	–2.290	0.627	–0.962	–0.311	9.191	3.408	2.110
1700	–4.353	–3.833	4.699	–0.410	12.180	8.011	–2.116	0.788	–0.720	–0.119	8.420	3.225	2.006
1800	–3.918	–3.448	4.270	–0.347	11.504	7.811	–1.962	0.930	–0.504	0.053	8.147	3.062	1.913
1900	–3.529	–3.102	3.886	–0.291	10.898	7.631	–1.823	1.058	–0.310	0.207	7.724	2.916	1.829
2000	–3.178	–2.790	3.540	–0.240	10.353	7.469	–1.699	1.173	–0.136	0.346	7.343	2.785	1.754
2100	–2.860	–2.508	3.227	–0.195	9.860	7.321	–1.586	1.277	0.022	0.472	6.998	2.666	1.686
2200	–2.571	–2.251	2.942	–0.153	9.411	7.185	–1.484	1.372	0.166	0.587	6.684	2.558	1.625
2300	–2.307	–2.016	2.682	–0.116	9.001	7.061	–1.391	1.459	0.298	0.692	6.396	2.459	1.568
2400	–2.065	–1.800	2.443	–0.082	8.625	6.946	–1.305	1.539	0.419	0.789	6.134	2.368	1.517
2500	–1.842	–1.601	2.224	–0.050	8.280	6.840	–1.227	1.613	0.530	0.879	5.892	2.285	1.469
2600	–1.636	–1.417	2.021	–0.021	7.960	6.741	–1.154	1.681	0.633	0.962	5.668	2.208	1.425
2700	–1.446	–1.247	1.833	0.005	7.664	6.649	–1.087	1.744	0.729	1.039	5.460	2.136	1.384
2800	–1.268	–1.089	1.658	0.030	7.388	6.563	–1.025	1.802	0.818	1.110	5.268	2.070	1.347
2900	–1.103	–0.941	1.495	0.053	7.132	6.483	–0.967	1.857	0.900	1.178	5.088	2.008	1.311
3000	–0.949	–0.803	1.343	0.074	6.892	6.407	–0.913	1.908	0.978	1.240	4.920	1.950	1.278
3100	–0.805	–0.674	1.201	0.094	6.668	6.336	–0.863	1.956	1.050	1.299	4.763	1.896	1.248
3200	–0.670	–0.553	1.067	0.112	6.458	6.269	–0.815	2.001	1.118	1.355	4.616	1.845	1.219
3300	–0.543	–0.439	0.942	0.129	6.260	6.206	–0.771	2.043	1.182	1.407	4.478	1.798	1.192
3400	–0.423	–0.332	0.824	0.145	6.074	6.145	–0.729	2.082	1.242	1.459	4.347	1.753	1.166
3500	–0.310	–0.231	0.712	0.160	5.898	6.088	–0.690	2.120	1.299	1.503	4.224	1.710	1.142
3600	–0.204	–0.135	0.607	0.174	5.732	6.034	–0.653	2.155	1.353	1.547	4.108	1.670	1.119
3700	–0.103	–0.044	0.507	0.188	5.574	5.982	–0.618	2.189	1.404	1.589	3.998	1.632	1.098
3800	–0.007	0.042	0.413	0.200	5.425	5.933	–0.585	2.220	1.452	1.629	3.894	1.596	1.077
3900	0.084	0.123	0.323	0.212	5.283	5.886	–0.554	2.251	1.498	1.666	3.795	1.562	1.058
4000	0.170	0.201	0.238	0.223	5.149	5.841	–0.524	2.280	1.541	1.703	3.700	1.529	1.039

Partial pressures of all gases are expressed in atmospheres (Pascals/101,325). Graphite, C(S), is assigned a value of unity in the equilibrium expressions for *KE* and *KF*

Table 6.2 Temperature (K) at Which a given fraction of a pure gas at 1 atm is dissociated

Fraction	CO_2	H_2O	H_2	O_2	N_2
0.001	1600	1700	2050	2200	4000
0.004	1800	1900	2300	2400	—
0.01	1950	2100	2450	2600	—
0.04	2200	2400	2700	2900	—
0.1	2450	2700	2900	3200	—
0.4	2950	3200	3350	3700	—

Table 6.3 Temperature at which air at equilibrium contains a given fraction of nitric oxide, at 1 atm

Fraction	Temperature (K)
0.001	1450
0.004	1750
0.01	2100
0.04	2800

Carbon Formation in Oxygen-Deficient Systems

Solid carbon (soot) may be expected to form in oxygen-deficient combustion products, under some conditions. Since solid carbon does not melt or boil until extremely high temperatures (~4000 K), we only need concern ourselves with solid carbon $C_{(s)}$, not liquid $C_{(l)}$ or gaseous carbon $C_{(g)}$.

Consider pure carbon monoxide at 2000 K. There are three conceivable ways in which it might form solid carbon:

$$\alpha: \mathrm{CO} \rightleftarrows \frac{1}{2}\mathrm{C_{(s)}} + \frac{1}{2}\mathrm{CO_2} \qquad K_\alpha = \frac{\left(p_{\mathrm{CO_2}}\right)^{1/2}}{p_{\mathrm{CO}}}$$

$$\beta: \mathrm{CO} \rightleftarrows \mathrm{C_{(s)}} + \frac{1}{2}\mathrm{O_2} \qquad K_\beta = \frac{\left(p_{\mathrm{O_2}}\right)^{1/2}}{p_{\mathrm{CO}}}$$

$$\gamma: \mathrm{CO} \rightleftarrows \mathrm{C_{(s)}} + \mathrm{O} \qquad K_\gamma = \frac{p_{\mathrm{O}}}{p_{\mathrm{CO}}}$$

Note that solid carbon does not appear in any of the equilibrium expressions. (By convention, a solid in equilibrium with gases is assigned a value of unity.)

From Table 6.1, we see that, at 2000 K,

$$K_\alpha = \frac{K_E^{1/2}}{K_F} = \mathrm{antilog}_{10}\left[\left(\frac{10.353}{2}\right) - 7.469\right] = 5.1 \times 10^{-3}$$

$$K_\beta = \frac{1}{K_F} = \mathrm{antilog}_{10}[0 - 7.469] = 3.4 \times 10^{-8}$$

$$K_\gamma = \frac{K_A}{K_F} = \mathrm{antilog}_{10}[-3.178 - 7.469] = 2.2 \times 10^{-11}$$

We see that K_α, K_β, and K_γ are all small compared with unity, so very little of the CO would decompose by any of these modes. However, K_α is much larger than either K_β or K_γ, so it is the dominant mode for whatever decomposition may occur.

Thus, from the expression $p_{\mathrm{CO_2}} = (\mathrm{K_a}\, p_{\mathrm{CO}})^2$, and taking p_{CO} as 1 atm, we calculate $p_{\mathrm{CO_2}} = \left(5.1 \times 10^{-3}\right)^2 = 2.6 \times 10^{-5}$atm. Since, by process α, 2 mol of CO must decompose for each mole of CO_2 formed, we conclude that $2 \times 2.6 \times 10^{-5}$ or 5.2×10^{-5} mol of CO will decompose to $C_{(s)}$ plus CO_2, per mole of CO originally present, after which we will have reached an equilibrium state. In other words, about 1/20,000 of the CO will decompose.

If the original mixture had consisted of CO at 1 atm plus CO_2 at any pressure greater than 2.6×10^{-5} atm, at 2000 K, then we could conclude that no carbon whatsoever would form.

It can also be shown that addition of a trace of O_2 or H_2O to CO at 2000 K would completely suppress carbon formation. As a general statement, for a chemical system containing fewer carbon atoms than oxygen atoms, the equilibrium condition will favor CO formation rather than that of solid carbon.

For a carbon-containing system with little or no oxygen, carbon may or may not form, depending on the hydrogen partial pressure. For example, carbon may form according to $C_2H_2 \rightleftarrows C_{(s)} + H_2$. The equilibrium expression for this reaction is written

$$\frac{p_{\mathrm{H_2}}}{p_{\mathrm{C_2H_2}}} = K(= 13.9\,\mathrm{at}\,3000\mathrm{K})$$

Again, note that solid carbon does not appear in the expression. If we rewrite the expression in the form $p_{\mathrm{H_2}} > 13.9\, p_{C_2H_2}$, it becomes the criterion for suppression of carbon formation at 3000 K. In other words, as long as $p_{\mathrm{H_2}}$ is more than 13.9 times as large as $p_{\mathrm{C_2H_2}}$, no carbon will form at 3000 K and any carbon present will be converted to C_2H_2. On the other hand, pure C_2H_2 will decompose to $C_{(s)}$ plus H_2 until the H_2/C_2H_2 ratio reaches 13.9, after which no further decomposition will occur at 3000 K.

Another way to view this is to say that H_2, C_2H_2, and solid carbon at 3000 K will be in a state of equilibrium if and only if the ratio $p_{\mathrm{H_2}}/p_{\mathrm{C_2H_2}} = 13.9$, and this is true regardless of the quantity of solid carbon present, and also regardless of the presence of other gases.

For a C–H–O–N system, the threshold conditions for equilibrium carbon formation are

Table 6.4 Threshold atomic C/O ratios for carbon formation (equilibrium at 1 atm, N/O = 3.76)

	Temperature (K)			
Atomic H/C ratio	1600	2000	2400	2800
0	1.00	1.00	1.00	1.00
2	1.00	1.02	1.09	1.30
4	1.00	1.05	1.16	1.56

somewhat more complicated, but the trends are illustrated by the calculated values shown in Table 6.4 for carbon formation thresholds in carbon-hydrogen-air systems at 1 atm.

It must be noted that carbon forms more readily in actual flames than Table 6.4 indicates, because of nonequilibrium effects. In premixed laminar flames, incipient carbon formation occurs at a C/O ratio roughly 60 % of the values shown in Table 6.4. See the next section for further comments on nonequilibrium.

Departure from Equilibrium

This procedure of specifying chemical systems by equilibrium equations will only yield correct results if the system is truly in equilibrium. If one prepares a mixture of H_2 and O_2 at room temperature and then ages the mixture for a year, it will be found that essentially nothing has happened and the system will still be very far from equilibrium. On the other hand, such a system at a high temperature characteristic of combustion will reach equilibrium in a small fraction of a second. For example, a hydrogen atom, H, in the presence of O_2 at partial pressure 0.1 atm will react so fast at 1400 K that its half-life is only about 2 μs. (At room temperature, the half-life of this reaction is about 300 days.)

Since peak flame temperatures are almost always above 1400 K, and sometimes as high as 2400 K, it would appear that equilibrium would always be reached in flames. However, luminous (yellow) flames rapidly lose heat by radiation, turbulent flames may be partially quenched by the action of steep velocity gradients, and flames burning very close to a cold wall may be partially quenched by heat transfer to the wall. Thus, the equilibrium condition is only a limiting case that real flames may approach. The products of a nonluminous laminar flame more than a few millimeters from any cold surface will always be very nearly in equilibrium.

Sample Problems

Example 1 Given a mixture of an equal number of moles of steam and carbon monoxide, what will the equilibrium composition be at 1700 K and 1 atm?

Solution We would expect the species CO, H_2O, CO_2, and H_2 to be present. From Table 6.2, we see that the equilibria $H_2 \rightleftarrows 2H$, $O_2 \rightleftarrows 2O$, and $H_2O \rightleftarrows 1/2H_2 + OH$ can all be neglected at 1700 K, so the species H, O, and OH will not be present in significant quantities.

Since we have four species involving three chemical elements, we will require 4—3 or 1, equilibrium relationship, for the equilibrium $H_2O + CO \rightleftarrows H_2 + CO_2$.

The relationship is

$$\frac{p_{H_2} \cdot p_{CO_2}}{p_{H_2O} \cdot p_{CO}} = K \tag{6.26}$$

In addition, we need 3—1, or 2, atom-ratio relations, which are

$$\frac{H}{C} : \frac{2p_{H_2} + 2p_{H_2O}}{p_{CO} + p_{CO_2}} = 2 \tag{6.27}$$

(because the original mixture of H_2O + CO contains two H atoms per C atom) and

$$\frac{O}{C} : \frac{p_{H_2O} + p_{CO} + 2p_{CO_2}}{p_{CO} + p_{CO_2}} = 2 \tag{6.28}$$

(because the original mixture of H_2O + CO contains two O atoms per C atom). Finally, the sum of the partial pressures equals 1 atm:

$$p_{H_2O} + p_{CO} + p_{H_2} + p_{CO_2} = 1 \tag{6.29}$$

We now have a well-set problem, four equations and four unknowns, which may be solved as soon as K is quantified.

We do not find the equilibrium $H_2O + CO \rightleftarrows H_2 + CO_2$ in Table 6.1. However, if we calculate (K_E/K_FK_C) from Table 6.1, we see that

$$\frac{K_E}{K_FK_C} = \frac{p_{CO_2}}{(1)\cdot p_{O_2}} \cdot \frac{(1)\cdot \left(p_{O_2}\right)^{1/2}}{p_{CO}} \cdot \frac{p_{H_2}\cdot \left(p_{O_2}\right)^{1/2}}{p_{H_2O}} = \frac{p_{CO_2}\cdot p_{H_2}}{p_{CO}\cdot p_{H_2O}} = K$$

From Table 6.1, $\log_{10}(K_EI/K_FK_C)$ at 1700 K = 12.180 – 8.011 – 4.699 = –0.51, and K = antilog$_{10}$ (–0.51) = 0.309.

Upon substituting $K = 0.309$ into Equation 6.26, and then simultaneously solving Equations 6.26, 6.27, 6.28, and 6.29, we obtain

$$p_{CO_2} = p_{H_2} = 0.179 \text{ atm}$$

and

$$p_{H_2O} = p_{CO} = 0.321 \text{ atm}$$

Example 2 One mole of hydrogen is introduced into a 50-L vessel that is maintained at 2500 K. How much dissociation will occur, and what will the pressure be?

Solution Let α be the degree of dissociation of the hydrogen defined by $\left(\alpha = (p_H/2)/\left[p_{H_2} + (p_H/2)\right]\right)$. Thus, α ranges from zero to one. One mole of H_2 partially dissociates to produce 2 α mol of H, leaving 1—α mol of H_2. The total number of moles is then 2 α + 1 – α, or α + 1. In view of the definition of α, the total number of moles present is $\left(\left(p_H + p_{H_2}\right)/\left[p_{H_2} + (p_H/2)\right]\right)$.

By the ideal gas law, $PV = nRT$.

$$\left(p_H + p_{H_2}\right)(50) = \frac{p_H + p_{H_2}}{p_{H_2} + (p_H/2)}(0.08206)(2500) \tag{6.30}$$

which reduces to

$$p_{H_2} + \frac{p_H}{2} = 4.103 \tag{6.31}$$

The equilibrium equation is

$$\frac{p_H}{\left(p_{H_2}\right)^{1/2}} = K_B \tag{6.32}$$

From Table 6.1, $\log_{10}K_B = -1.601$ at 2500 K, and therefore $K_B = 0.0251$. Upon substitution into Equation 6.32 and elimination of p_{H_2} between Equations 6.31 and 6.32, one obtains

$$p_H{}^2 + 0.000316\,p_H - 0.00258 = 0 \tag{6.33}$$

This equation yields a positive and a negative root. The negative root has no physical significance. The positive root is $p_H = 0.0506$ atm. Then, Equation 6.32 yields $p_{H_2} = 4.08$ atm, and the total final pressure is 4.08 + 0.0506 = 4.13 atm. The degree of dissociation, α, comes out to be 0.0062. (This is less dissociation than indicated by Table 6.2 because the pressure is well above 1 atm.)

Example 3 Propane is burned adiabatically at 1 atm with a stoichiometric proportion of air. Calculate the final temperature and composition. The initial temperature is 300 K.

Solution The problem must be solved by a series of iterations. The first step is to assume a final temperature, either based on experience or by selecting a temperature substantially below the value calculated by assuming that CO_2 and H_2O are the only products of combustion. The second step is to solve the set of equations that specify the equilibrium composition at the assumed final temperature. The third step is to consult an overall enthalpy balance equation, which will show that the assumed final temperature was either too high or too low. The fourth step is to assume an appropriate new final temperature. The fifth and sixth steps are repeats of the second and third steps. If the correct final temperature is now found to be bracketed between these two assumed temperatures, then an interpolation should give a fairly accurate value of the true final temperature. Additional iterations may be made to improve the accuracy of the results to the degree desired. As a guess, the final temperature is assumed to be 2300 K.

Now the equilibrium equations at 2300 K are set up. The species to be considered are three principal species: CO_2, H_2O, and N_2, and seven minor species: H_2, O_2, OH, H, O, CO, and NO.

(Based on chemical experience, the following possible species may be neglected at 2300 K when stoichiometric oxygen is present: N, $C_{(g)}$, NH, CN, CH, C_2, HO_2, HCN, O_3, C_3, NO_2, HNO, C_2H, CH_2, C_2O, CHO, and NH_2.) Thus, we consider ten species involving four elements, so 10—4 or 6, equilibrium equations are needed. Any six *independent* equilibria may be selected. We can assure independence by requiring that each successive equilibrium expression we write will introduce at least one new chemical species. Observe that this requirement is met in the following list:

$$CO + \frac{1}{2}O_2 = CO_2 \qquad \frac{p_{CO_2}}{p_{CO} \cdot (p_{O_2})^{1/2}} = K = \frac{K_E}{K_F} \tag{6.34}$$

$$\frac{1}{2}O_2 = O \qquad \frac{p_O}{(p_{O_2})^{1/2}} = K_A \tag{6.35}$$

$$\frac{1}{2}O_2 + \frac{1}{2}N_2 = NO \qquad \frac{p_{NO}}{(p_{O_2} \cdot p_{N_2})^{1/2}} = K_G \tag{6.36}$$

$$H_2 + \frac{1}{2}O_2 = H_2O \qquad \frac{p_{H_2O}}{p_{H_2}(p_{O_2})^{1/2}} = K_C \tag{6.37}$$

$$H_2 + \frac{1}{2}O_2 = H_2O \qquad \frac{p_{OH}}{(p_{H_2} \cdot p_{O_2})^{1/2}} = K_D \tag{6.38}$$

$$\frac{1}{2}H_2 = H \qquad \frac{\overline{p}_H}{(p_{H_2})^{1/2}} = K_B \tag{6.39}$$

Four additional equations are needed to determine the ten unknown partial pressures. These are three atom-ratio equations and a summation of the partial pressures to equal the total pressure. To obtain the atom ratios, we take air to consist of 3.76 parts of N_2 (by volume) per part of O_2, neglecting argon, and other species. Then, from stoichiometry, $C_3H_8 + 5O_2 + (5 \cdot 3.76)N_2 \rightarrow 3CO_2 + 4H_2O + 18.8\ N_2$.

$$\frac{H}{C} : \frac{8}{3} = \frac{p_H + p_{OH} + 2p_{H_2O} + 2p_{H_2}}{p_{CO_2} + p_{CO}} \tag{6.40}$$

$$\frac{H}{N} : \frac{8}{37.6} = \frac{p_H + p_{OH} + 2p_{H_2O} + p_{H_2}}{2p_{N_2} + p_{NO}} \tag{6.41}$$

$$\frac{O}{C} : \frac{10}{3} = \frac{p_O + p_{OH} + p_{NO} + p_{CO} + p_{H_2O} + 2p_{O_2} + 2p_{CO_2}}{p_{CO_2} + p_{CO}} \tag{6.42}$$

Finally,

$$p_{CO_2} + p_{H_2O} + p_{N_2} + p_{H_2} + p_{O_2} + p_{OH} + p_H + p_O + p_{CO} + p_{NO} = 1 \tag{6.43}$$

From Table 6.1 at 2300 K:

	$\log_{10} x$	x
K_E	9.001	–
K_F	7.061	–
K_E/K_F	9.001–7.061	87.1
K_A	–2.307	0.00493
K_G	–1.391	0.0406
K_C	2.682	481
K_D	–0.116	0.766
K_B	–2.016	0.00964

We insert these K values into Equations 6.34, 6.35, 6.36, 6.37, 6.38, and 6.39, and then solve the set of ten equations, Equations 6.34, 6.35, 6.36, 6.37, 6.38, 6.39, 6.40, 6.41, 6.42, and 6.43, for the equilibrium values of the ten partial pressures at 2300 K. This solution may be obtained by a tedious set of successive approximations. The first approximation is obtained by solving for the three principal species N_2, CO_2, and H_2O, assuming the partial pressures of the remaining species are zero. Then, using this trial value of p_{CO_2}, solve for p_{CO} and p_{O_2}, using Equation 6.34 and assuming that $p_{CO} = 2p_{O_2}$. Next, using p_{H_2O} and p_{O_2} as determined, use Equation 6.37 to determine a trial value of p_{H_2}. Then, using all the foregoing partial pressures, determine p_O from Equation 6.35, p_{NO} from Equation 6.36, p_{OH} from Equation 6.38, and p_H from Equation 6.39. Thus, ten trial values of the partial pressures are found. However, upon substitution into Equations 6.40, 6.41, 6.42, and 6.43, none of these equations will be quite satisfied. The partial

pressures of the principal species must then be adjusted so as to satisfy Equations 6.40, 6.41, 6.42, and 6.43, and then a second iteration with the equilibrium equations must be carried out to establish new values for the minor species. After four or five such iterations, the results should converge to a set of partial pressures satisfying all equations.

A faster method is to use a computer program to solve the equations. (See the following section.)

The equilibrium partial pressures at 2300 K will come out to be:

P_{N_2}	0.7195 atm
P_{H_2O}	0.1474 atm
P_{CO_2}	0.1006 atm
P_{CO}	0.0143 atm
P_{O_2}	0.0066 atm
P_{H_2}	0.0038 atm
P_{OH}	0.0037 atm
P_{NO}	0.0028 atm
P_{H}	0.0006 atm
P_{O}	0.0004 atm

Now, we must determine if 2300 K was too high or too low a guess, by writing the enthalpy balance equation (see Chap. 5).

As a basis for the enthalpy balance, we assume that we have exactly 1 mol of products, at 1 atm. Then, if $P_{CO_2} = 0.1006$ atm (see above), we must have 0.1006 mol of CO_2. Similarly, we have 0.0143 mol of CO. Since these are the only two carbon compounds in the products, and since 3 mol of CO_2 + CO must form from each mole of C_3H_8 burned, it follows that $(0.1006 + 0.0143)/3 = 0.0383$ mol of C_3H_8 must have burned. Since the original C_3H_8-air mixture was stoichiometric, it follows that the reactants also consisted of $5 \times 0.0383 = 0.1915$ mol of O_2 and $3.76 \times 0.1915 = 0.7200$ mol of N_2. (Thus, a total of 0.9498 mol of reactant form 1 mol of product, if the product is indeed at equilibrium at 2300 K.)

The enthalpy balance equation is

$$\sum n_i H_{i,T_r} = \sum n_j H_{j,T_p} \qquad (6.44)$$

where n_i and H_i are the number of moles and the enthalpy per mol of each reactant species at reactant temperature T_r, and n_j and H_j are the number of moles and the enthalpy per mol of each product species at product temperature T_p.

The enthalpy of each reactant or product species x at temperature T is given by

$$H_{x,T} = \left(\Delta H_f^\circ\right)_{298.15} + H^\circ - H_{298}^\circ \qquad (6.45)$$

where $(\Delta H_f^\circ,\ _{298.15})_x$ is the enthalpy of formation of a mol of species x from its constituent elements in their standard states at 298 K (see Chap. 5). These constituent elements are H_2, O_2, N_2, and $C_{(s)}$, so $\Delta H_f^\circ,\ _{298.15}$ for each of these four species is zero, by definition.

Values of $(\Delta H_f^\circ)_{298.15}$ and $H^\circ - H_{298}^\circ$ [2] for various species are contained in Table 6.5 on page 1–109. Substitution of numerical values into Equation 6.44 yields:

Reactant species	$(\Delta H_f^\circ)_{298.15}$ (kJ/mol)	$H_{2300}^\circ - H_{298}^\circ$ (kJ/mol)	H_{2300}° (kJ/mol)	n_i (mol)	$n_i H_{i,2300}^\circ$ (kJ)
C_3H_8	–103.85	0.16	–103.69	0.0383	–3.971
O_2	0	0.05	0.05	0.1915	+0.010
N_2	0	0.05	0.05	0.7200	+0.036
				Total =	–3.925

and

Product species	$(H_f^\circ)_{298.15}$ (kJ/mol)	$H_{2300}^\circ - H_{298}^\circ$ (kJ/mol)	H_{2300}° (kJ/mol)	n_i (mol)	$n_i H_{i,2300}^\circ$ (kJ)
N_2	0	66.99	66.99	0.7195	+48.199
H_2O	–241.83	88.29	–153.54	0.1474	–22.632
CO_2	–393.52	109.67	–283.85	0.1006	–28.555
CO	–110.53	67.68	–42.85	0.0143	–0.613
O_2	0	70.60	70.60	0.0066	+0.466
H_2	0	63.39	63.39	0.0038	+0.241
OH	38.99	64.28	103.27	0.0037	+0.382
NO	90.29	68.91	159.20	0.0028	+0.446
H	218.00	41.61	259.61	0.0006	+0.156
O	249.17	41.96	291.13	0.0004	0.116
				Total =	–1.794

The enthalpy of the products (–1.794 kJ) is seen to be 2.131 kJ larger than the enthalpy of the reactants (–3.925 kJ). To put this 2.131 kJ

[2] If $H^\circ - H_{298}^\circ$ is not available from a table, it may be evaluated from the equation $H^\circ - H_{298}^\circ = \int_{298}^{T} C_p\, dT$. For C_3H_8, $Cp = 0.09$ kJ/mol·K at 298 K.

Table 6.5 Enthalpies of selected combustion products[a]

Species	N_2	O_2	O	NO	H_2	H	H_2O (g)	OH	CO_2	CO
$(\Delta H_f^o)_{298.15}$	0.00 kJ/mol	0.00 kJ/mol	249.17 kJ/mol	90.29 kJ/mol	0.00 kJ/mol	218.00 kJ/mol	–241.83 kJ/mol	38.99 kJ/mol	–393.52 kJ/mol	–110.53 kJ/mol
Temp(K)	$H^o - H^o_{298}$, kJ/mol	$H^o - H^o_{298}$, kJ/mol	$H^o - H^o_{298}$, kJ/mol	$H^o - H^o_{298}$, kJ/mol	$H^o - H^o_{298}$, kJ/mol	$H^o - H^o_{298}$, kJ/mol	$H^o - H^o_{298}$, kJ/mol	$H^o - H^o_{298}$, kJ/mol	$H^o - H^o_{298}$, kJ/mol	$H^o - H^o_{298}$, kJ/mol
100	–5.77	–5.78	–4.52	–6.07	–5.47	–4.12	–6.61	–6.14	–6.46	–5.77
200	–2.86	–2.87	–2.19	–2.95	–2.77	–2.04	–3.28	–2.97	–3.41	–2.87
298	0.00	0.00	0.00	0.00	0.00	0.00	0.00	0.00	0.00	0.00
300	0.05	0.05	0.04	0.05	0.05	0.04	0.06	0.05	0.07	0.05
400	2.97	3.03	2.21	3.04	2.96	2.12	3.45	3.03	4.01	2.97
500	5.91	6.08	4.34	6.06	5.88	4.20	6.92	5.99	8.31	5.93
600	8.90	9.24	6.46	9.15	8.81	6.28	10.50	8.94	12.92	8.94
700	11.94	12.50	8.57	12.31	11.75	8.35	14.18	11.90	17.76	12.02
800	15.05	15.84	10.67	15.55	14.70	10.43	17.99	14.88	22.82	15.18
900	18.22	19.24	12.77	18.86	17.68	12.51	21.92	17.89	28.04	18.40
1000	21.46	22.70	14.86	22.23	20.68	14.59	25.98	20.94	33.41	21.69
1100	24.76	26.21	16.95	25.65	23.72	16.67	30.17	24.02	38.89	25.03
1200	28.11	29.76	19.04	29.12	26.80	18.74	34.48	27.16	44.48	28.43
1300	31.50	33.34	21.13	32.63	29.92	20.82	38.90	30.34	50.16	31.87
1400	34.94	36.96	23.21	36.17	33.08	22.90	43.45	33.57	55.91	35.34
1500	38.40	40.60	25.30	39.73	36.29	24.98	48.10	36.84	61.71	38.85
1600	41.90	44.27	27.38	43.32	39.54	27.06	52.84	40.15	67.58	42.38
1700	45.43	47.96	29.46	46.93	42.84	29.14	57.68	43.50	73.49	45.94
1800	48.98	51.67	31.55	50.56	46.17	31.22	62.61	46.89	79.44	49.52
1900	52.55	55.41	33.63	54.20	49.54	33.30	67.61	50.31	85.43	53.12
2000	56.14	59.17	35.71	57.86	52.95	35.38	72.69	53.76	91.45	56.74
2100	59.74	62.96	37.79	61.53	56.40	37.46	77.83	57.25	97.50	60.38
2200	63.36	66.77	39.88	65.22	59.88	39.53	83.04	60.75	103.57	64.02
2300	66.99	70.60	41.96	68.91	63.39	41.61	88.29	64.28	109.67	67.68
2400	70.64	74.45	44.04	72.61	66.93	43.69	93.60	67.84	115.79	71.35
2500	74.30	78.33	46.13	76.32	70.50	45.77	98.96	71.42	121.93	75.02
2600	77.96	82.22	48.22	80.04	74.09	47.85	104.37	75.01	128.08	78.71

2700	81.64	86.14	50.30	83.76	77.72	49.92	109.81	78.63	134.26	82.41
2800	85.32	90.08	52.39	87.49	81.37	52.00	115.29	82.27	140.44	86.12
2900	89.01	94.04	54.48	91.23	85.04	54.08	120.81	85.92	146.65	89.83
3000	92.71	98.01	56.58	94.98	88.74	56.16	126.36	89.58	152.86	93.54
3100	96.42	102.01	58.67	98.73	92.46	58.24	131.94	93.27	159.09	97.27
3200	100.14	106.02	60.77	102.48	96.20	60.32	137.55	96.96	165.33	101.00
3300	103.85	110.05	62.87	106.24	99.96	62.40	143.19	100.67	171.59	104.73
3400	107.57	114.10	64.97	110.00	103.75	64.48	148.85	104.39	177.85	108.48
3500	111.31	118.16	67.08	113.77	107.55	66.55	154.54	108.12	184.12	112.22

$C_{(s)}$	F_2	F	HF	Cl_2	Cl	HCl	Br_{r_2}	Br	HBr
0.00 kJ/mol	0.00 kJ/mol	78.91 kJ/mol	–272.55 kJ/mol	0.00 kJ/mol	121.29 kJ/mol	–92.31 kJ/mol	0.00 kJ/mol	111.86 kJ/mol	–36.44 kJ/mol
$H^o - H^o_{298}$, kJ/mol	$H^o - H^o_{298}$, kJ/mol	$H^o - H^o_{298}$, kJ/mol	$H^o - H^o_{298}$, kJ/mol	$H^o - H^o_{298}$, kJ/mol	$H^o - H^o_{298}$, kJ/mol	$H^o - H^o_{298}$, kJ/mol	$H^o - H^o_{298}$, kJ/mol	$H^o - H^o_{298}$, kJ/mol	$H^o - H^o_{298}$, kJ/mol
–0.99	–5.92	–4.43	–5.77	–6.27	–4.19	–5.77	–21.72	–4.12	–5.77
–0.67	–2.99	–2.23	–2.86	–3.23	–2.10	–2.86	–16.82	–2.04	–2.86
0.00	0.00	0.00	0.00	0.00	0.00	0.00	0.00	0.00	0.00
0.02	0.06	0.04	0.05	0.06	0.04	0.05	0.14	0.04	0.05
1.04	3.28	2.30	2.97	3.54	2.26	2.97	34.61	2.12	2.97
2.36	6.64	4.53	5.88	7.10	4.52	5.89	38.31	4.20	5.90
3.94	10.11	6.72	8.80	10.74	6.80	8.84	42.02	6.28	8.87
5.72	13.66	8.90	11.73	14.41	9.08	11.81	45.76	8.36	11.88
7.64	17.27	11.05	14.68	18.12	11.34	14.84	49.51	10.46	14.96
9.67	20.91	13.19	17.64	21.84	13.59	17.91	53.27	12.57	18.10
11.79	24.59	15.33	20.64	25.59	15.82	21.05	57.03	14.70	21.30
13.99	28.30	17.45	23.68	29.34	18.03	24.24	60.81	16.84	24.56
16.24	32.03	19.56	26.76	33.10	20.23	27.48	64.58	19.01	27.87
18.54	35.77	21.67	29.87	36.88	22.41	30.78	68.37	21.20	31.24
20.88	39.54	23.78	33.04	40.66	24.60	34.12	72.16	23.40	34.65
23.25	43.32	25.89	36.24	44.45	26.77	37.51	75.96	25.61	38.10
25.66	47.11	27.99	39.48	48.25	28.93	40.93	79.76	27.85	41.59
28.09	50.91	30.09	42.76	52.05	31.09	44.39	83.57	30.09	45.11

(continued)

Table 6.5 (continued)

$C_{(s)}$	F_2	F	HF	Cl_2	Cl	HCl	B_{r_2}	Br	HBr
0.00 kJ/mol	0.00 kJ/mol	78.91 kJ/mol	–272.55 kJ/mol	0.00 kJ/mol	121.29 kJ/mol	–92.31 kJ/mol	0.00 kJ/mol	111.86 kJ/mol	–36.44 kJ/mol
$H^o - H^o_{298}$, kJ/mol	$H^o - H^o_{298}$, kJ/mol	$H^o - H^o_{298}$, kJ/mol	$H^o - H^o_{298}$, kJ/mol	$H^o - H^o_{298}$, kJ/mol	$H^o - H^o_{298}$, kJ/mol	$H^o - H^o_{298}$, kJ/mol	$H^o - H^o_{298}$, kJ/mol	$H^o - H^o_{298}$, kJ/mol	$H^o - H^o_{298}$, kJ/mol
30.55	54.72	32.18	46.09	55.86	33.23	47.89	87.38	32.35	48.66
33.02	58.54	34.28	49.44	59.68	35.38	51.41	91.20	34.61	52.24
35.53	62.38	36.37	52.83	63.51	37.51	54.96	95.02	36.88	55.84
38.05	66.22	38.46	56.25	67.34	39.64	58.53	98.85	39.15	59.46
40.58	70.07	40.55	59.69	71.18	41.77	62.12	102.68	41.43	63.10
43.13	73.93	42.64	63.17	75.02	43.89	65.73	106.52	43.70	66.76
45.71	77.80	44.73	66.66	78.88	46.02	69.37	110.36	45.98	70.44
48.29	81.67	46.82	70.18	82.74	48.13	73.01	114.20	48.26	74.13
50.89	85.55	48.91	73.73	86.61	50.25	76.68	118.05	50.54	77.83
53.50	89.45	50.99	77.29	90.50	52.36	80.36	121.91	52.81	81.55
56.13	93.35	53.08	80.87	94.39	54.48	84.06	125.77	55.09	85.28
58.77	97.25	55.17	84.47	98.29	56.58	87.76	129.63	57.36	89.02
61.43	101.16	57.25	88.09	102.21	58.69	91.48	133.49	59.63	92.77
64.09	105.08	59.34	91.72	106.14	60.79	95.21	137.37	61.89	96.53
66.78	109.01	61.42	95.37	110.08	62.90	98.95	141.24	64.15	100.31
69.47	112.94	63.50	99.03	114.03	65.00	102.70	145.13	66.41	104.09
72.17	116.88	65.59	102.71	118.00	67.10	106.46	149.01	68.67	107.88
74.89	120.83	67.67	106.39	121.98	69.20	110.23	152.90	70.92	111.68

[a]These data are taken from the JANNAF thermochemical tables [2]

difference in perspective, note that the heat of combustion of 0.0383 mol of propane at 298 K, to form 3 mol of CO_2 and 4 mol of H_2O per mole of propane, is 0.0383 (3 × 393.52 + 4 × 241.83 – 103.85) = 78.29 kJ. Thus, the 2.131 kJ discrepancy when compared with 78.29 kJ is rather small, showing that the 2300 K "first guess" was very close. Since the products, at 2300 K, are seen to have a slightly higher enthalpy than the reactants, the correct temperature must be slightly less than 2300 K.

To continue the calculation, the next step is to assume that the final temperature is 2200 K instead of 2300 K. The details will not be presented, but this will yield a new and slightly different set of values of the ten partial pressures of the products. Thus, a new enthalpy balance may be attempted, in the same manner as before. When this is done, the result will be that this time the enthalpy of the reactants will come out to be slightly higher than the enthalpy of the products, showing that the correct temperature is above 2200 K.

An interpolation may be made between the 2200 K enthalpy discrepancy and the 2300 K enthalpy discrepancy, which will show that the correct final temperature is 2268 K. Furthermore, the partial pressures of each product species may be obtained by interpolating between the 2200 K partial pressures and the 2300 K partial pressures, with results as follows:

$T = 2268$ K	P_{N_2}	0.7207 atm
	P_{H_2O}	0.1484 atm
	P_{CO_2}	0.1026 atm
	P_{CO}	0.0125 atm
	P_{O_2}	0.0059 atm
	P_{H_2}	0.0034 atm
	P_{OH}	0.0032 atm
	P_{NO}	0.0025 atm
	P_{H}	0.0005 atm
	P_{O}	0.0003 atm

Computer Programs for Chemical Equilibrium Calculations

In view of the extremely tedious calculations needed for determination of the equilibrium temperature and composition in a combustion process, a computer program for executing these calculations would be desirable. Fortunately, such programs have been developed.

However, the user of a computer program should be warned that thorough understanding of the material in this chapter is needed to avoid misinterpreting the computer output. Further, given such understanding, simple manual calculations can be performed to obtain independent checks of the computer output.

One program, entitled GASEQ, can be used with any computer using Windows. It can be downloaded from http://www.gaseq.co.uk. Alternatively, a program may be obtained from Reaction Design, 6440 Lusk Blvd, Suite D209, San Diego, CA 92121. Their e-mail address is <chemkin@ReactionDesign.com>.

These programs will calculate the final equilibrium conditions for adiabatic combustion at either constant pressure or constant volume, given the initial conditions. For the constant-pressure calculations, one specifies the initial temperature, the pressure, and the identities and relative proportions of the reactants. The computer programs contain the properties of selected reactants including: air, oxygen, nitrogen, hydrogen, graphite, methane, acetylene, ethylene, ethane, propane, butane, 1-butene, heptane, octane, benzene, toluene, JP-4, JP-5, methanol, ethanol, and polyethylene. If the fire only involves reactants from this list, no further input is necessary. If the fire involves a reactant not on this list, the input data must include the elemental composition and the enthalpy of formation of the reactant at 298 K, as well as enthalpy versus temperature data for the reactant over the temperature range from 298 K to the initial temperature. (If the initial temperature is 298 K, the last item is not needed.)

The computer programs can handle reactants containing any of the following elements: A, Al, B, Br, C, Cl, F, Fe, H, He, K, Li, Mg, N, Na, Ne, O, P, S, Si, and Xe. Data are included in the program on all known compounds, including liquids and solids, that can form at elevated temperatures from combinations of these elements. It is not necessary for the user to

specify which product species to consider. The program can consider them all, and will print out all equilibrium species present with mole fractions greater than 5×10^{-6}, unless instructed to print out trace values down to some lower specified level.

The program can calculate Chapman-Jouguet detonation products as well as constant-pressure or constant-volume combustion products, if desired.

An addition to the program permits calculation of viscosity and thermal conductivity of gaseous mixtures, selected from 154 gaseous species, at temperatures from 300 K to 5000 K.

Nomenclature

C_p	Heat capacity at constant pressure (kJ/mol·K)
ΔE^o	Energy of products relative to energy of reactants, all at temperature T and 1 atm (kJ/mol)
ΔF^o	Free energy of products relative to free energy of reactants, all at temperature T and 1 atm (kJ/mol)
ΔH^o	Enthalpy of products relative to enthalpy of reactants, all at temperature T and 1 atm (kJ/mol)
K	Equilibrium constant (based on partial pressures expressed in atmospheres)
K	Degrees Kelvin
n	Number of moles (e.g., a mole of oxygen is 32 g)
p_i	Partial pressure of ith species (atm)
p	Total pressure (atm)
R	Gas constant (kJ/mol · K)
ΔS^o	Entropy of products relative to entropy of reactants, all at temperature T and 1 atm (kJ/mol)
T	Absolute temperature (K)

References

1. J. van't Hoff, cf. G. Lewis, M. Randall, K. Pitzer, and L. Brewer, *Thermodynamics,* McGraw-Hill, New York (1961).
2. D.R. Stull and H. Prophet, *JANNAF Thermochemical Tables,* 2nd ed., NDRS-NBS 37, National Bureau of Standards, Washington, DC (1971).

Raymond Friedman was with Factory Mutual Research from 1969 through 1993. During most of this time he was vice president and manager of their Research Division. Currently he is an independent consultant. He has past experience at Westinghouse Research Laboratories and Atlantic Research Corporation. He is a past president of The Combustion Institute, past vice chairman and past secretary of the International Association for Fire Safety Science, and an expert in fire research and combustion.

Thermal Decomposition of Polymeric Materials

7

Artur Witkowski, Anna A. Stec, and T. Richard Hull

Introduction

Polymers are composed of large numbers of repeat units forming very long chain molecules. Most polymers are based on carbon, and hence known as organic polymers. The long-chain structure means that polymers can exist in solid or liquid form, but are too large to be volatile. Polymers fuel the vast majority of unwanted fires, as wood, paper, fabrics, foams and plastics. Flaming combustion is a gas phase process, and it is necessary to understand the stages in the conversion of long molecular chains into volatile fragments. This is often referred to as "pyrolysis" or "gasification", but these terms encompass a complex set of chemical and physical processes, leading to the production of volatile flammable molecules.

Polymeric Materials

A *polymer* is a large molecule constructed from many smaller structural units called *monomers*, covalently bonded together in any conceivable pattern (but often, and most simply in long chains).

If the material is composed of only one type of repeating structural unit, it is known as a *homopolymer*. If the material is composed of more than one type of repeat unit it is known as a *copolymer*.

Thermal decomposition is "a process of extensive chemical species change caused by heat". *Thermal degradation* is "a process whereby the action of heat or elevated temperature on a material, product, or assembly causes a loss of physical, mechanical, or electrical properties" [1]. Used correctly, thermal degradation may describe processes occurring before around 1 % of the mass is lost, while thermal decomposition includes the entire mass loss process.

Polymer Classification

Polymers represent the largest class of combustible materials fuelling unwanted fires. The different ways they can be subdivided provides a useful introduction to this wide and important class of materials.

Natural, Synthetic, Semi-natural and Biobased

Before the widespread use of synthetic polymers in the second half of the twentieth century almost all unwanted fires were fuelled by *natural polymers* such as wood, paper, cotton, wool etc. *Synthetic polymers* are generally derived from oil or coal, and share the flammability of those raw materials. The ease of manufacture and processing of synthetic polymers has driven the increase in their use. As most of the common

A. Witkowski (✉) • A.A. Stec • T.R. Hull
Centre for Fire and Hazards Science, University of Central Lancashire (UCLan), Preston, Lancashire PR1 2HE, UK

M.J. Hurley (ed.), *SFPE Handbook of Fire Protection Engineering*,
DOI 10.1007/978-1-4939-2565-0_7, © Society of Fire Protection Engineers 2016

synthetic polymers are more flammable then their natural counterparts, this has also increased the number and severity of unwanted fires, despite significant advances in fire prevention, detection and control.

Semi-natural polymers are typically purified, and chemically modified natural polymers, such as cellulose acetate, cellophane or rayon. Drivers towards greater environmental sustainability have led to increased developments in *biobased polymers*, which includes the semi-natural polymers and a new polymeric materials, using raw materials derived from living, rather than the fossilised carbon sources. It seems likely that these materials, such as polylactic acid (PLA) and styrene-soya oil-divinyl benzene (SSD), will increase their market share in the next decade.

Chemical Composition of the Repeat Units

Most natural polymeric materials involved in fires are cellulose based. Cellulose is a polymer with alternating repeat units of glucose (Fig. 7.1).

Several of the common synthetic polymers, the so-called vinyl polymers made from vinyl monomers ($-CH_2 = CHX-$), have a repeat units of ($-CH_2-CHX-$), such as polyethylene (X is $-H$); polypropylene (X is $-CH_3$); polyvinyl chloride (X is $-Cl$); polystyrene (X is $-C_6H_5$); polyacrylonitrile (X is $-C \equiv N$); polyvinyl acetate (X is $-OCOCH_3$); polyvinyl alcohol (X is $-OH$). Other "polymers" such as polyamides, polyesters, epoxy resins and polyurethanes are actually classes of materials with similar bonding between the repeat units, but different structures within each repeat unit.

Chemistry of Polymerisation

Synthetic polymers are made by chemical reaction of monomers to form long polymer chains. Since the reverse process, the decomposition of polymers into smaller volatile fuel molecules, is often related to their synthesis, this can also provide insight into their decomposition behaviour. Broadly the process occurs either by step-growth, or chain-growth polymerisation. *Step-growth polymerisation* occurs by chemical reaction of two functional groups to form the linkage, with the release of a small molecule (such as water). This is known as step-growth polymerization as it takes place one molecule at a time. Figure 7.2 shows the familiar esterification reaction, in this case used to produce a polyester.

As water is often the molecule released, this process is also known as *condensation* polymerization. The synthetic process is slow, and the lack of water or other secondary product in the polymer prevents decomposition being simply the reverse of polymerisation. The second process, *chain-growth polymerisation*, involves opening of double bonds to form consecutive links in the polymer chain. For example, styrene

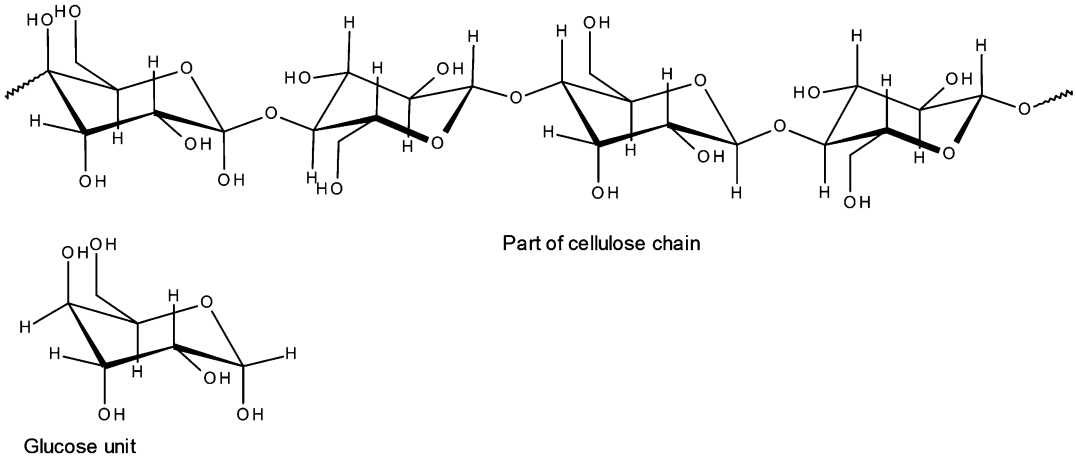

Fig. 7.1 Part of a cellulose polymer chain, and a single glucose unit (monomer)

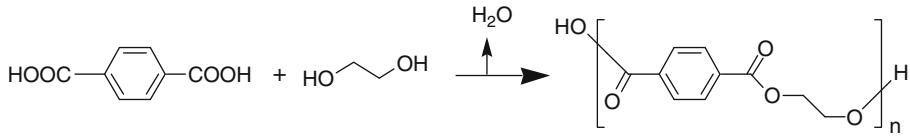

Fig. 7.2 Step-growth polymerisation of polyethylene terephthalate (PET)

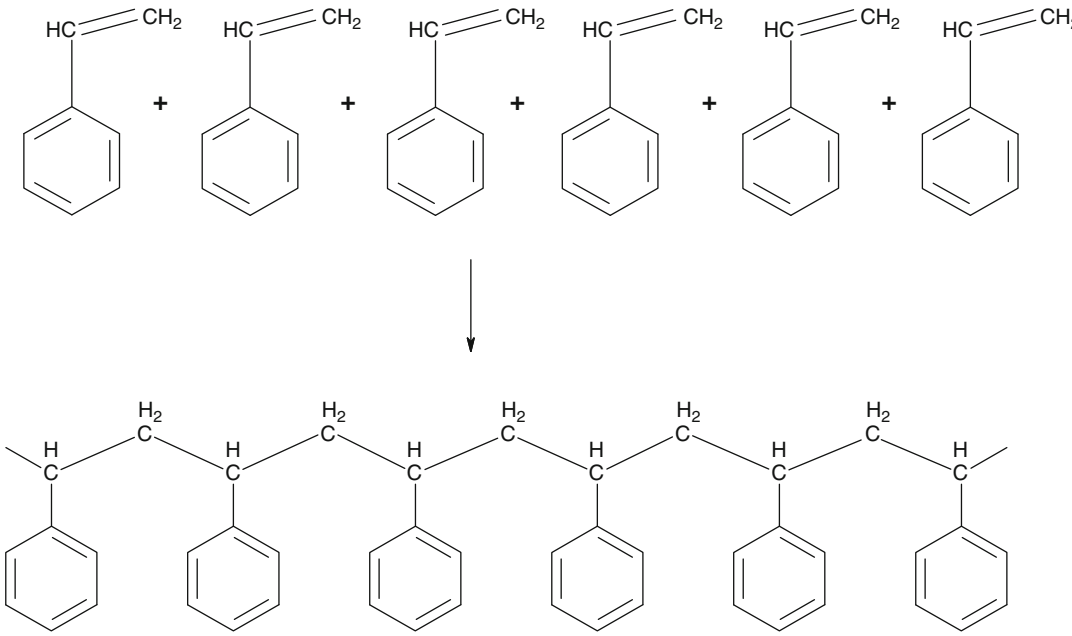

Fig. 7.3 Chain-growth polymerisation of poly(styrene) (PS)

monomers combine to form polystyrene, without release of a secondary product (Fig. 7.3).

The polymerisation reaction is known as *chain-growth* or *addition polymerisation*. Typically, once the monomer becomes activated, the chain grows extremely quickly (less than 1 s), so, during the polymerisation process, only long polymer chains and volatile monomer units will be present. It is highly likely that some monomer will remain at the end of the polymerisation process, since the final material will have very long chains and a high viscosity. During the decomposition of polystyrene, the reverse process occurs, resulting in monomer, dimer and trimer predominating in the vapour phase.

Addition polymerization involves three distinct stages—initiation, propagation and termination. To start the process, an initiator is added to the monomer. The initiator splits to form two free radicals, which attach themselves to a carbon atom of the monomer. When this occurs, the reactive site is transferred to another carbon atom in the monomer, and the chain begins to propagate (Fig. 7.4). Finally the reactivity of the propagating chain end is lost by combination of two reactive sites, or rearrangement, collectively known as termination. In order to maximise the degree of polymerization, the remaining monomers must diffuse towards the reactive chain end, before termination reactions occur.

Addition polymerisation can involve free radical, cationic, anionic, catalytic, or ring opening processes. The means of polymerisation will affect the degree of branching, and the molecular weight and dispersity of the polymer (section "Molecular Mass or Polymer Chain Length"),

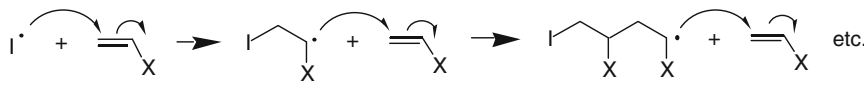

Fig. 7.4 Free radical polymerisation of an alkene ($CH_2 = CHX$)

which will in turn affect its decomposition (section "Decomposition Mechanisms").

Thermoplastics and Thermosets

Synthetic polymers (often referred to as plastics, because of their mouldability) can be subdivided into those which can be repeatedly deformed by heating (*thermoplastics*), so they are melt-processable; and those which once the polymerisation process is complete, cannot be melted or have their shape changed by heating, and decompose directly from solid to vapour (*thermosets* or *thermosetting polymers*). Most thermosets have additional covalent bonds forming crosslinkages between the polymer chains.

Common thermoplastics include polyethylene (PE), polypropylene (PP), polystyrene (PS), polymethylmethacrylate (PMMA), polyvinyl chloride (PVC), polyamides (PA) and some polyesters and polyurethanes.

Thermosets are generally stronger, but more brittle than thermoplastics, have higher thermal stability, higher dimensional stability, higher rigidity, and resistance to creep and deformation under load. Epoxies, vulcanized rubbers, phenolics, unsaturated polyester resins, rigid polyurethanes, urea-formaldehyde and melamine-formaldehyde are examples of thermosets.

Molecular Mass or Polymer Chain Length

The number of repeating units in a synthetic polymer exerts a significant influence on its physical properties. The high molecular weights of polymers increase their viscosity when molten and in solution, decrease their solubility, and of course prevent their volatilisation. Chain length can also be a controlling factor in determining the solubility, elasticity, fibre-forming capacity, tear strength, and impact strength in many polymers. The chain length of commercial polymers is optimised during synthesis for the intended application. For example, PMMA, with an average molecular weight less than 500,000 (around 5000 repeat units) has sufficiently low viscosity to be melt-processable, whereas PMMA with molecular weight of 5,000,000 does not soften sufficiently to allow its shape to be changed on heating, hence it is known as cast PMMA.

The number of repeating units will usually vary as a statistical distribution of chain lengths. This may be classified as a number-average molecular mass $\left(\overline{M}_n\right)$, or a weight-average molecular mass $\left(\overline{M}_w\right)$. Within most synthetic polymers, the most common unit is actually the monomer, although this only represents a tiny proportion by mass. Natural polymers often have narrower molecular mass ranges, or even identical molar masses. The ratio $\overline{M}_n/\overline{M}_w$ is known as the dispersity (or *heterogeneity index*), providing a simple index of the range of chain lengths present. An enzyme, where all the molecules have the same molecular mass is described as monodisperse, a polymer produced by anionic polymerisation will typically have a dispersity around 1.1, a step growth polymer will have a dispersity around 2, while one produced by free radical polymerisation will usually lie between 1.5 and 10.

Consequences of High Molar Mass

Increasing the interaction between polymer molecules leads to increasing cohesive energy per molecule. In polymeric materials this gives rise to certain properties characteristically associated with high molar mass, regardless of their chemical structure:

(i) High crystal melting point (if the polymer is crystalline)
(ii) High viscosity in the melt and in solution
(iii) High mechanical strength
(iv) High flexibility and ductility (unless highly cross-linked)
(v) High resistance to dissolution (especially crystalline polymers)

The average *degree of polymerization*, or D_P, is usually defined as the number of monomeric units in a polymer [2]. For a homopolymer, there is only one type of monomeric unit and the number-average degree of polymerization is given by

$$D_{P_n} = \frac{Number\ average\ molecular\ mass\ of\ polymer}{molecular\ weight\ of\ the\ monomer\ unit} = \frac{\overline{M}_n}{M} \tag{7.1}$$

For most industrial purposes, degrees of polymerization in the thousands or tens of thousands are desired.

Low molecular weight polymeric materials (having short chains) are generally weaker. Although sections may be crystalline, only weak Van der Waals forces hold the crystallites together. This allows the crystalline layers to slip past one another causing a break in the material. Amorphous polymers, with high D_P (such as cast PMMA) have greater strength because the molecules become tangled between layers.

Physical Properties

Polymers can be readily processed by forming or moulding into shapes, either once (thermosets) or repeatedly (thermoplastics). Many are important engineering materials with a wide range of properties, some of which are unattainable from any other material types, and they are generally low in cost. The desirable properties of polymer products include light weight, availability in a wide range of colours, low thermal and electrical conductivity, toughness, and good resistance to acids, bases and moisture.

The applications of a polymer depend most strongly on its mechanical behaviour. The "deformability" of a polymer can be expressed as the ratio of the deformation (strain) resulting from a constant applied stress. The ratio of stress to strain is the elastic modulus.

A large number of synthetic polymers now exist covering a wide range of properties. These can be grouped into three major classes:

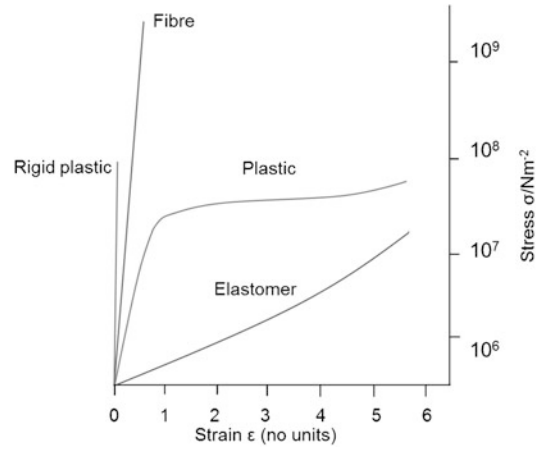

Fig. 7.5 Typical stress—strain plots for a fibre, a flexible plastic, and an elastomer

plastics, fibres, and elastomers. Although there is no firm dividing line between the groups, some distinction between these categories can be obtained from a typical stress—strain plot (Fig. 7.5). Rigid plastics and fibres are resistant to deformation and are characterized by a high elastic modulus and low percentage elongation. Elastomers readily undergo deformation and exhibit large reversible elongations under small applied stresses, i.e., they exhibit elasticity. The flexible plastics are intermediate in behaviour, during the elastic stage of their deformation, and then yield inelastically with typical plastic deformation.

During the final stages of processing, fibres are stretched to three or more times their original length ("drawing") when in a semi-crystalline state, to produce increased chain alignment, crystallinity and strength.

For amorphous materials, the temperature at which the molecules move relative to one another, known as the glass transition temperature (T_g—described in more detail in section "Glass Transition Temperature") exerts a profound influence on the physical properties. In general, elastomers have values of T_g well below room temperature, while rigid, structural polymers have T_g values above room temperature.

Structural Physical and Decomposition Property Data

In order to better understand the range of common polymers, their names, abbreviations, and molecular structures have been listed in Table 7.1. Where available, measurements of their crystallinity, glass transition temperature (T_g) and melting point have also been provided, in order to give the reader an instant guide to the main properties of interest. More detailed tabulations providing citable data have been published [2]. In addition, Lyon et al. [3] have tabulated the decomposition temperatures and Arrhenius parameters E_a and A (section "Kinetics of Polymer Decomposition") for a number of common polymers from literature and the data is reproduced here. Individual polymeric materials will differ according to their method of preparation, thermal history and the definition and method of measurement of the decomposition properties. Therefore individual literature values have been provided to give an indication of the uncertainties in the reported data.

Polymers and Fire

The flammable components of our built and natural environments are almost all based on organic polymers, and the vast majority of unwanted fires are fuelled by these polymers. Smouldering combustion typically occurs by reaction of atmospheric oxygen with a porous, combustible solid matrix, with a reaction zone moving through the solid, releasing gaseous products. Flaming combustion requires the fuel to be present in molecular form in the vapour phase, where it can undergo much more rapid reaction with atmospheric oxygen. Since polymers are much too large to exist in the vapour phase (because the bonding forces holding them in the condensed phase is proportional to their large surface area) they must first break down into volatile fragments. The pyrolysis of a polymer, turning molecular chains of 10,000–100,000 carbon atoms into species small enough to be volatilised, often involves breaking the polymer chain. In some cases, the chain releases groups from its ends most easily, known as *end-chain scission* or unzipping. In others, the chain breaks at random points along its length, known as *random chain scission*. A third process, where groups attached to the backbone as side chains can leave as stable molecules, is known as *chain-stripping*. If the polymer, or the chain resulting from chain stripping, does not undergo chain scission to form volatiles or lose further substituents, it may undergo carbonisation, resulting in *char formation*. Thus the conversion of an organic polymer to volatile organic molecules, and/or a char, may follow one or more of the four general mechanisms. While some polymers fall exclusively into one category, others exhibit mixed behaviour, often dependent on the decomposition conditions.

The temperature of a material is a measure of the kinetic energy of its molecules. At very low temperatures (close to 0 K), molecules are almost stationary, but at all normal temperatures in the solid phase, molecules are in a state of constant vibration. As the temperature increases, the vibrations become stronger, while the strength of the chemical bonds remains constant. For a particular polymer, a critical temperature is reached where there is sufficient kinetic energy to rupture one of the bonds holding the repeat units, or the side chains, of the polymer together. If the resultant molecules are small enough to be volatile, they may escape from the surface of the polymer, or in the case of a thermoplastic, form bubbles within it. When sufficient fuel is present in the vapour phase mixed with air, it can react with oxygen, releasing heat and increasing the free radical concentration. In the presence of a pilot flame or spark, additional free radicals accelerate the ignition process. Ignition and flaming combustion occurs when there is sufficient heat from the flame to replace the gas phase fuel by further pyrolysis. As molecules are released from the decomposing polymer, particularly by chain stripping, this leaves active sites for further reaction. In many cases, such as cellulosic materials, this can result in cross-linking reactions to other polymer chains, leading to char formation. In bulk cellulosic materials such as wood, this can result in the build-up of

Table 7.1 Common properties and some of their physical/decomposition properties

Chemical name	Structure	Common or trade name	Abbreviation	Crystallinity	T_g/K	Melting point/K	Decomposition temperature/K	Kinetic parameters [3]	
								E_a/J mol^{-1}	A/s^{-1}
Polyethylene	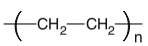	Polythene	PE	40–80 %	175–260	473–508	687	3.00×10^5	6.5×10^{20}
							677	2.64×10^5	2.3×10^{18}
							679	2.77×10^5	2.0×10^{19}
							644	3.01×10^5	2.6×10^{22}
							649	2.64×10^5	1.8×10^{19}
Polypropylene	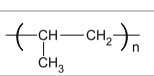		PP	65 %	253	443	660	2.43×10^5	1.7×10^{17}
							624	2.43×10^5	2.2×10^{18}
Polyisobutylene	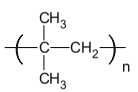		PIB	–	200	229	621	2.05×10^5	1.8×10^{15}
							589	2.05×10^5	1.5×10^{16}
Polyisoprene	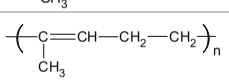	Natural Rubber		Low	203	303	596	2.50×10^5	8.2×10^{19}
							574	2.49×10^5	2.3×10^{19}
Polybutadiene		Butyl rubber					680	2.60×10^5	9.4×10^{17}
								2.60×10^5	3.5×10^{18}
Polystyrene	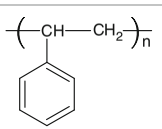		PS	Low	363–378	503	637	2.30×10^5	7.3×10^{16}
							549	2.01×10^5	1.3×10^{17}
							606	2.30×10^5	6.7×10^{17}
Polyacrylonitrile	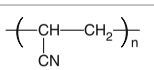	"Acrylic" (wool or textile)	PAN	Low	413	590	512	1.30×10^5	1.8×10^{11}
Poly(vinyl alcohol)	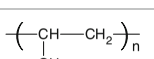		PVAL or PVA		343–373	503–533	na	–	–
Poly(vinyl chloride)	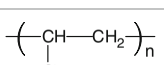		PVC	Low 5 % (plasticised)	353–358	348–378 (485)	563–733	1.34×10^5	7.8×10^{20}
				Med 15 % unplasticised				1.38×10^5	3.0×10^{12}
Poly(vinyl acetate)	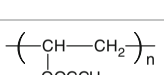	Acetate	PVAc				526	2.24×10^5	1.8×10^{20}
Poly(vinylidene fluoride)	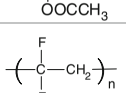	Kynar, Hylar	PVDF	High	313	443–448	738–758	2.01×10^5	4.9×10^{13}

(continued)

Table 7.1 (continued)

Chemical name	Structure	Common or trade name	Abbreviation	Crystallinity	T_g/K	Melting point/K	Decomposition temperature/K	Kinetic parameters [3] E_a/J mol^{-1}	A/s^{-1}
Poly(methyl acrylate)	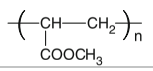								
Poly(methyl methacrylate)	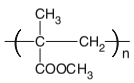	Perspex, Plexiglass	PMMA	Low	388 (synd); 378 (atact); 318 (isotac)	363–378	633–663	2.18×10^5	4.7×10^{16}
							591	2.18×10^5	1.9×10^{17}
							577	2.18×10^5	5.4×10^{17}
							514	1.26×10^5	6.4×10^{10}
Polyformaldehyde, polyoxymethylene	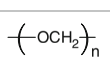	Acetal	POM	High	364–383	448–454	501	1.09×10^5	2.3×10^9
Poly(ethylene oxide) or Polyethylene glycol	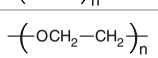		PEG and PEO				618	1.93×10^5	2.1×10^{14}
							601	1.92×10^5	4.9×10^{14}
Poly(tetrafluoro ethylene)	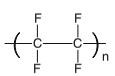	Teflon	PTFE	High	398	600	782	3.39×10^5	4.4×10^{20}
							773	3.14×10^5	1.7×10^{19}
							742	3.37×10^5	5.3×10^{21}
Engineering thermoplastics									
Poly(ethylene terephthalate)	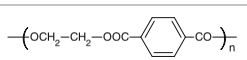	Polyester	PET	High	343–353	523–533	698–713	1.59×10^5	2.6×10^{11}
Poly(butylene terephthalate)	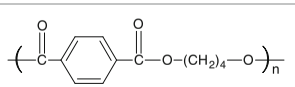	Polyester	PBT	High	318–333	493–503	681	–	–
Poly(hexamethylene adipamide)	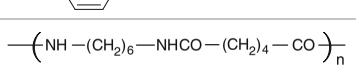	Nylon 6.6, Polyamide 6.6	PA 6.6	Medium	343–363	498–538	703–746	–	–
Polycaprolactam	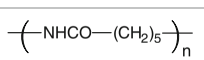	Nylon 6, Polyamide 6	PA 6	Medium	323–353	498–508	708	–	–
Polycarbonate	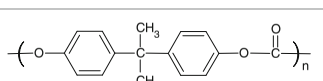	Lexan	PC	Low	418–423	488–503	753–758	–	–
High Thermal Stability Polymers									
Poly(phenylene oxide)	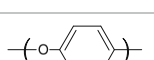	With PS as Noryl	PPO					–	–

Poly(ether ether ketone)	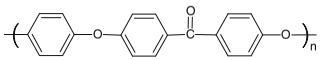		PEEK	High 32 %	416	607	843	–	–
Polyether sulphone	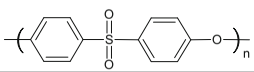		PES	Low			853	–	–
Polyphenylene Sulphide	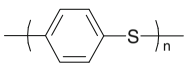		PPS				777		
Polyether imide	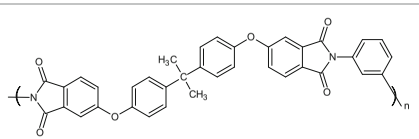		PEI	Low	490		800	–	–
Thermosets									
Epoxy resin	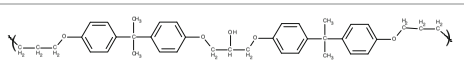		EP	Cross-linked	273–453		673–723	–	–
Urea Formaldehyde resin	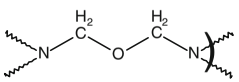		UF	Cross-linked			>473		
Melamine formaldehyde resin	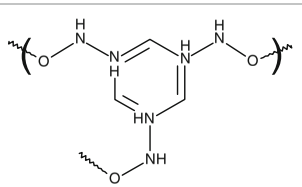	Melaware	MF	Cross-linked	293–333			–	–
Phenol formaldehyde resin	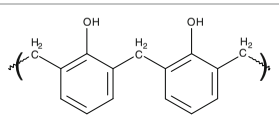	Bakelite	PF	Cross-linked	353–393		723–753	–	–
Polyurethane	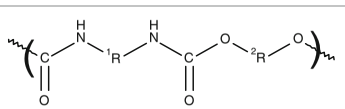		PUR and PUF	Cross-linked	283–493			–	–

(continued)

Table 7.1 (continued)

Chemical name	Structure	Common or trade name	Abbreviation	Crystallinity	T_g/K	Melting point/K	Decomposition temperature/K	Kinetic parameters [3] E_a/J mol^{-1}	A/s^{-1}
Copolymers									
Poly(ethylene co-vinyl acetate)	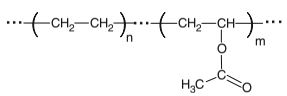		EVA	Medium	233–293	303–383	753	3.45×10^5	1.27×10^{22}
							573	1.66×10^5	6.11×10^{11}
Acrylonitrile-butadiene-styrene copolymer	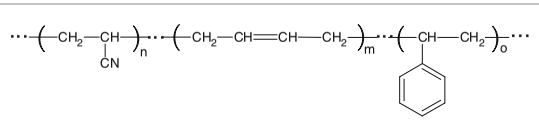		ABS	Low	188–378	383–398	693–701	–	–
Styrene acrylonitrile copolymer	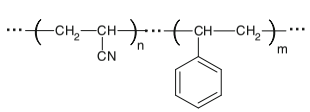		SAN	Low	373– 393	393	693	–	–
Natural and biopolymers									
Cellulose	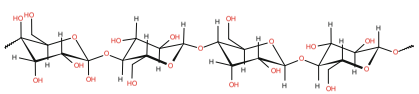			High		Decomposes		–	–
Keratin	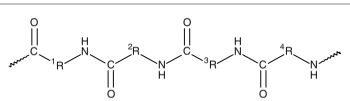	Wool		H-bonded				–	–
Polylactic acid	$(-OCH(CH_3)CO-)_n$		PLA		318–338	423–433	623–643	–	–

the protective layer, shielding the wood from external radiation, slowing the rate of further fuel pyrolysis, and hence the rate of burning.

The burning process can be viewed on either the molecular scale or the macro scale.

The molecular scale

Stage I	Heating	An external source supplies heat causing the temperature of the substance to increase. The extent of temperature change depends on the specific heat of the material. Physical, mechanical, and thermal properties change in the case of polymers. This may include softening, melting and volatilsation
Stage II	Decomposition	At higher temperatures the majority of the bonds reach failure point, causing the release of gaseous molecules which differ depending on the material burning. This can be accelerated by attack of oxygen on the surface of the polymer, producing carbon dioxide and carbon monoxide
Stage III	Oxidation	In the presence of oxygen at high temperatures, oxidation of the gaseous fragments proceeds rapidly, releasing heat, and combustion products (mostly carbon dioxide and water)

The macro scale

Stage I	Heating	Heat causes a temperature rise which will depend on the thermal inertia (kρC) of the material
Stage II	Pyrolysis	Heat causes decomposition of the fuel, followed by pyrolysis of fuel to the gas phase
Stage III	Ignition	Fuel accumulates above the surface, and reacts with oxygen. Once the critical concentration of free radicals is reached, flashing will occur. When the total heat flux to the surface from fuel oxidation is sufficient to pyrolyse enough fuel to replace it, ignition will occur, the rate of reaction will increase and produce carbon dioxide and water
Stage IV	Flame spread	As the radiant heat flux increases it will pyrolyse adjacent materials, leading to a repeated series of ignitions, resulting in fire growth
Stage V	Fire development	As the flame gets larger, it will no longer be able to been entrain sufficient oxygen, and products of incomplete combustion such as carbon monoxide and soot will be produced, increasing the radiative component of heat transfer

Polymer Crystallinity

Although most polymers are solids at room temperature they have more properties in common with glass than with crystalline solids, such as sugar or salt. Glass has an amorphous morphology with properties different to crystalline solids. When heated, it gradually changes, from a brittle solid-like material, softening, and eventually becoming a viscous liquid. In contrast, the application of heat to a crystalline solid turns it sharply to a low viscosity liquid at a particular temperature. The difference lies mainly in the structure of each phase. Crystalline materials have their molecules arranged in repeating patterns. Salt, sugar, ice and most metals are crystalline materials. As such, they all tend to have highly ordered and regular structures. Amorphous materials, by contrast, have their molecules arranged randomly and in long chains which wrap around each other, without any long range order. Both crystalline and amorphous phases exist in polymers.

Polymers can form crystallites either by straightening out the molecules and packing as rods (*extended-chain* crystals), or each chain folds back and forth, so that crystallisation occurs by short segments of the same chain packing together (*folded-chain* crystals) (Fig. 7.6).

Chain-folding is kinetically favoured, as it is a unimolecular process, but orientation of a polymer (such as the "drawing" of a fibre) leads to chain-extension crystal structures. A complete polymer chain is likely pass through many small crystals, tying them together into a strong, coherent mass, surrounded by amorphous sections of polymer. If individual polymer molecules were

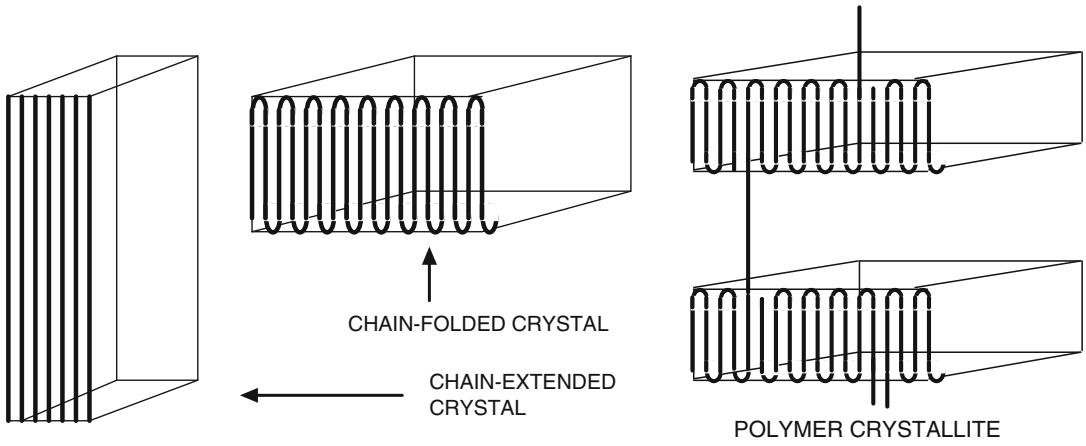

Fig. 7.6 Schematic of chain-folded crystal, chain extended crystal, and polymer crystallite

confined to individual crystals, they would be extremely brittle. The mixtures of small crystals and amorphous material in polymers cause them to melt over a range of temperatures without a sharp melting point. In most polymers, the combination of crystalline and amorphous structures forms a material with advantageous properties of toughness and rigidity.

Some polymers, such as polystyrene and PMMA, are completely amorphous, others have a combination of disordered regions and small crystallites. An amorphous polymer results from polymer chains that lack regular order. If parts of two chains do not pack well together, crystallites do not form. Shorter chains organize themselves into crystalline structures more readily than longer molecules, as those with a high degree of polymerization (D_P) tend to become tangled. The D_P is an important factor in determining the degree of crystallinity of a polymer. The cooling rate also influences the degree of crystallinity (section "Differential Thermal Analysis and Differential Scanning Calorimetry"). Slow cooling provides time for crystallization to occur. Fast cooling yields highly amorphous materials. When characterising the flammability of a material, in order, for example to predict its large scale fire behaviour, it is essential to ensure that all the material has the same thermal history. For example, cone calorimeter plaques prepared from the same semicrystalline polymer may have different decomposition and burning behaviour if they were formed into plaques under different thermal conditions. This can be compensated for by subsequent annealing (heating and holding each specimen at an appropriate temperature below the crystalline melting point, followed by controlled cooling). If the polymer is cooled slowly, this will produce a significant increase in crystallinity, and relieve internal stresses.

The size and shape of the side chains of monomer also influence the polymer morphology. If the monomers are large or irregular, relative to the polymer backbone, as in polystyrene, it is difficult for the polymer chains to arrange themselves in an ordered manner, resulting in a more amorphous material. Likewise, smaller monomers, such as polypropylene, and polymers that have a very regular structure, such as the rod-like structure of PTFE, will form highly crystalline polymers.

Thermal Response Characteristics of Polymers

Physical Transitions

The physical processes occurring during thermal decomposition depend on the material. Thermoplastics can be softened and melted by heating; once polymerisation is complete,

thermosetting polymers are infusible and phase changes such as melting cannot occur. The melting/softening behaviour of thermoplastics on heating depends on the degree of crystallinity. For crystalline materials the intermolecular forces are usually identical, so melting occurs at a well-defined temperature; for amorphous materials a range of intermolecular forces hold the polymer chains to each other, so the polymer will soften over a wider temperature range.

However, many materials cannot undergo the transition to a viscous state without undergoing thermal decomposition. Neither thermosets nor cellulosic materials have a fluid state, so they neither melt or soften. In thermosets, the 3-dimensional network of cross-linking covalent bonds prevents the polymer chains from moving relative to each other. In cellulosic polymers, the extensive hydrogen bonding between the hydroxyl groups and oxygen atoms keeps the polymer chains in place.

Glass Transition Temperature

As the temperature of a polymer rises above a certain critical point, its glass transition temperature, T_g, it becomes more rubber-like. Conversely, as the temperature drops below T_g, it behaves in an increasingly brittle manner. The glass-transition temperature is the point at which the polymer chains in a non-crystalline (amorphous) material acquire sufficient thermal energy to undergo significant translational motion, characteristic of the liquid-like or rubbery state. Below T_g the chains are frozen into a glassy state, where only very localised atomic movement, such as vibration, is possible. If a molten polymer is cooled so quickly that the T_g is reached before the polymer can fully crystallise, then the polymer will remain frozen in its glassy (amorphous) state until its temperature is raised above T_g. The T_g is a transition which is characteristic of non-crystalline phases; it is an important parameter in the selection of materials for particular applications, such as whether rigid or elastomeric properties are required. Above T_g, but well below its melting point, an incompletely crystallised polymer can undergo further crystallisation (section "Differential Thermal Analysis and Differential Scanning Calorimetry").

Melting

The backbone of a typical $(-CH_2CHX-)_n$ polymer is composed of a chain of tetrahedrally bonded carbon atoms covalently bonded to each other so that the molecule can be represented as an extended zigzag chain. The repeating units in a polymer chain are often free to rotate relative to one another. If they are all in a particular position, the polymer molecule will have a linear zigzag shape. If they rotate, this will result in bends in the polymer molecule. While the linear zigzags can stack together easily, each bend will be an obstacle to crystallinity. For polyethylene $(–CH_2CHX–)_n$, a typical value of the molecular weight is 1.6×10^5 g mol^{-1}, so the chain contains 10,000 carbon atoms; thus in the extended zigzag state, the chain would be about 1260 nm long and 0.3 nm diameter. As every group of four atoms in the chain can have three possible stable rotational positions (linear, zigzag or kinking to left or right), a total of $3^{10,000}$ shapes (or additional degrees of freedom) are available to this particular chain, only one of which is the fully extended zigzag. Even though this has the lowest energy, the most probable conformation will be some kind of randomly angled amorphous shape (Fig. 7.7).

The number of different possible states which can exist when leaving the crystalline state (or extended zigzag conformation), known as the entropy change, ΔS, exerts the greatest influence on the melting temperature of a polymer. A large part of this entropy is due to the additional freedom that allows the chain conformational changes to occur in the melt; i.e., the restrictions of the crystalline lattice no longer apply.

In any phase transition, the free energy change involved, ΔG, is zero, since the two phases must be in equilibrium. The free energy is the sum of the chemical bonding forces, or enthalpy ΔH, and the disorder, or number of possible ways the molecule can be arranged. This is the product of the temperature and the entropy change, $-T\Delta S$.

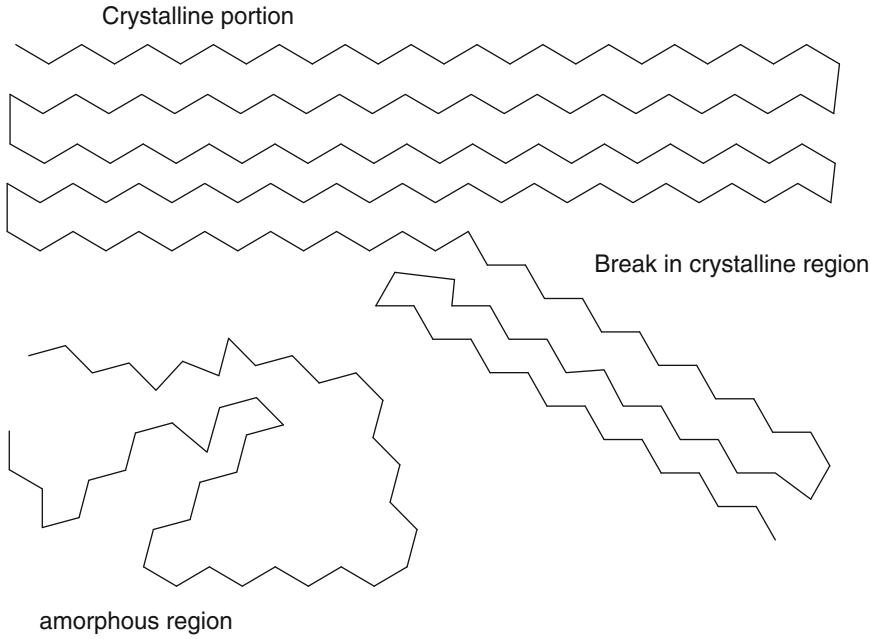

Fig. 7.7 Crystalline and amorphous regions of a polymer

$$\Delta G = \Delta H - T\Delta S = 0 \qquad (7.2)$$

so that during the polymer melting process; the melting temperature T_m is given by

$$T_{\mathrm{m}} = \Delta H_{fusion}/\Delta S_{fusion} \qquad (7.3)$$

The enthalpy of fusion (ΔH_{fusion}) reflects the strength of attractive forces between the molecules. For chemically similar materials (e.g. hydrocarbon polymers) these will not vary greatly. Thus ΔS_{fusion}, the *entropy change on melting*, is the only significant variable.

For polymers, entropy is related to the number of degrees of freedom each polymer molecule has. A molecule in the liquid state has more potential degrees of freedom (bond rotations, bond angle flexions and inversions, translational and rotational motions) than if it is frozen in a crystal. Clearly, the more flexible the polymer chain, the more degrees of freedom it acquires on melting, and the greater is ΔS_{fusion}. A high ΔS_{fusion} leads to a low T_m.

Conversely, the stiffer the polymer chain, the fewer degrees of freedom it acquires on melting, the lower is ΔS_{fusion} and the higher is T_{m}. For completely rigid polymer chains, *only* translational and rotational degrees of freedom are acquired on melting, leading to extremely high values of T_{m}, often well above the decomposition temperature of the polymer.

Table 7.2 Structures and melting temperatures of four polymers

Polymer	T_{m}(°C)
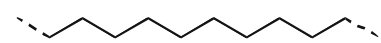	135
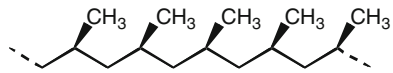	165
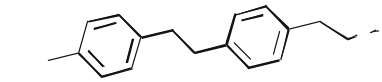	380
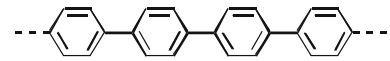	> 600

Table 7.2 shows the variation in melting point for four polymers. In PE every bond is free to rotate; PP is constrained to a small extent by the coiling of the chain to accommodate the methyl groups in a regular manner. Aromatic rings do not allow any rotation so poly-1,4-phenylene

ethylene $(-Ph-CH_2-CH_2-Ph-)_n$ can only rotate between the two $-CH_2-CH_2-$ carbon atoms. In poly-1,4-phenylene $(-Ph-Ph-)_n$ no rotation is possible (as the conjugated aromatic rings must all lie in the same plane, so the polymer molecule exists as a rigid rod), there is no "entropy advantage" to the polymer on melting. Poly-1,4-phenylene decomposes before melting, so it is not melt-processable, so there is no way of forming it into shapes, and so its practical applications are limited to heat resistant fabrics, electrical insulation etc [4].

Bubble Formation

As a consequence of the chemical processes of polymer decomposition, leading to volatile formation, volatile molecules will start to accumulate within the decomposing polymer. If the polymer is molten when decomposition commences, bubbles will form and migrate upwards, eventually erupting from the surface. This causes physical swelling, reducing the thermal inertia of the material, accelerating the rate of surface heating and the onset of ignition.

Chemical Transformations

In the case of thermosets and cellulosic materials, the polymer molecule starts to decompose before the chains have acquired sufficient energy to overcome the forces holding them in place. These materials tend to produce carbonaceous chars on thermal decomposition. The physical structure of these chars will profoundly affect the heat transfer, volatile release, and access of oxygen, all of which will impact on the thermal decomposition processes. The char can undergo glowing combustion in the presence of oxygen. However, it is unlikely that both glowing combustion of the char and significant flaming can occur simultaneously in the same zone above the surface, since the flame will consume all the available oxygen, and the flow of volatiles through the char will tend to drive oxygen away from the char surface. Therefore, in general, char oxidation will only occur after flaming has subsided.

Influence of Oxygen

The thermal decomposition of polymers may proceed by heat alone, or by the combined action of heat and oxygen. In many polymers, the thermal decomposition processes are accelerated by oxygen, lowering the minimum decomposition temperatures. Prior to ignition, thermo-oxidative decomposition results in pyrolysis of fuel and other species. After ignition, during steady flaming, even in well-ventilated conditions, pyrolysis of the condensed phase (pyrolysis zone) is essentially anaerobic, with all the oxidation taking place in the gas phase (flame zone) [5]. Thus, the mass loss, resulting from pyrolysis, the residue formation etc., of a flaming sample corresponds to a decomposition of the material under an inert atmosphere [6]. Unfortunately, there are several published studies of the development of fire retarded materials which appear oblivious to this fundamental principle of fire science. Only for ignition, non-intense flaming, samples near and after extinction, and non-igniting samples will thermo-oxidative decomposition be relevant to the behaviour in a fire. Indeed the observation of bubbles of volatile fuel in decomposing polymers, around the time to ignition (which have been characterised by immersing the test specimen in liquid nitrogen), showed that for many thermoplastics, even prior to ignition, most volatile formation comes from the bulk of the polymer, not its surface, and hence the critical decomposition condition remains anaerobic [7].

The thermal decomposition of polymers has been broken into for general chemical mechanisms. The first three essentially describe the conversion of an involatile polymer molecule into fragments small enough to be volatile. In many cases the decomposition follows more than one of the mechanisms.

(i) Random-chain scission, in which chain scissions occur at apparently random locations in the polymer chain.
(ii) End-chain scission, in which individual monomer units are successively removed at the chain end.
(iii) Chain-stripping, in which atoms or groups not part of the polymer chain (or backbone) are cleaved.

(iv) Cross-linking, in which bonds are created between polymer chains.

These are discussed further in section "Decomposition Mechanisms".

Influence of Chemical Structure on Thermal Stability

The combustion behaviour of a polymeric material can be interpreted in terms of the properties of the volatiles, particularly their composition, reactivity and rate of formation. Thermal stability can be quantified from the temperature dependence of decomposition.

Detailed studies by Madorsky [8] in the 1960s of the effects of chemical structure on the thermal stability of polymeric materials underpin our understanding of the factors controlling the thermal decomposition of polymers. These experiments investigated the thermal stability by determining the temperature, T_h, at which 50 % of a small polymer sample will volatilise in 30 min in an inert atmosphere. Table 7.3 summarises the effects of chemical structure on the thermal stability of polymers, and provides examples of that behaviour. The individual effects are discussed below.

Chain Branching

With two chain branches on every other carbon atom in the chain, polyisobutylene $(-CH_2-C(CH_3)_2-)_n$ has the lowest thermal stability, followed by polypropylene $(-CH_2-CH(CH_3)-)_n$ with one branching point on every other carbon atom. Commercial polyethylene is not composed only of straight polymer chains. It actually contains a number of branches of its linear chains, either of small groups such as CH_3- or longer side chains, which occur randomly during the polymerisation process. These are the most reactive parts of otherwise unreactive structures. Polymethylene $(-CH_2-)_n$ is the name given to the special, unbranched form of polyethylene. The number of branching points in normal polyethylene also affects its crystallinity. Low density polyethylene (LDPE) has around 60 branching points per 1000 carbon atoms. An intermediate density, linear low density polyethylene (LLDPE) is actually a copolymer of ethane and an alkene such as oct-1-ene, so the regularity of the polymer chain is deliberately disrupted by the presence of side chains, 6 carbon atoms in length. High density polyethylene (HDPE) is closer to the idealised polymethylene with around 7 branching points per 1000 carbon atoms. During thermal decomposition, the

Table 7.3 Factors affecting the thermal stability of polymers (From Madorsky [8])

Factor	Effect on thermal stability	Examples	T_h/K
Chain branching	Weakens	Polymethylene	688
		Polyethylene	679
		Polypropylene	660
		Polyisobutylene	621
Double bonds in polymer backbone	Weakens	Polypropylene	660
		Polyisoprene	596
Aromatic ring in polymer backbone	Strengthens	Poly-1,4-phenylene methylene	703
		Polystyrene	637
High molecular weight	Strengthens	PMMA B (MW = 5.1×10^6)	600
		PMMA A (MW = 1.5×10^5)	556
Cross-linking	Strengthens	Polydivinyl benzene	672
		Polystyrene	637
Oxygen in the polymer backbone	Weakens	Polymethylene	688
		Polyethylene oxide	618
		Polyoxymethylene	<473

branching points are the first to break, initiating chain decomposition reactions.

Double Bonds

In a similar way, the double bonds in the polymer chain of polyisoprene $(-CH_2-CH_2-CH=C(CH_3)-)_n$ also provide reactive sites for the initiation of chain decomposition reactions, reducing its thermal stability compared to polypropylene.

Aromatics in Backbone

Conversely, the presence of an aromatic ring, in the polymer backbone, such as poly-1,4-phenylene methylene $(-CH_2-C_6H_4-)_n$, compared to polystyrene $(-CH_2-CH(C_6H_4)-)_n$, where the aromatic ring is a side chain, increases the rigidity of the chain, lowering the entropy of the liquid state, thus raising the melting point. The higher melting point reduces the rate of pyrolysis, since most of the material is protected by the surface layers.

Molecular Weight

In end-chain scission the reaction starts at the end of a polymer chain, since the end molecule is only held by one bond. PMMA A with 1500 repeat units decomposes 55 K lower than PMMA B with 50,000 repeat units. The rate of the decomposition reaction will then depend on the number of end groups available. The higher the molecular weight, the smaller that number will be.

Cross-Linking

Cross-linking will also prevent melting, inhibiting the transport of molecules to the sample surface for pyrolysis as gas phase fuel. Polydivinylbenzene has two reactive groups per monomer unit, and therefore each monomer can be attached to two chains.

Oxygen in Backbone

Oxygen in a polymer chain, such as in polyoxymethylene $(-CH_2-O-)_n$, will also provide a reactive site for polymer decomposition to start, lowering the thermal stability.

In general, the T_h data indicates the ease of conversion to volatiles, which are likely to act predominantly as fuel. However, the fire behaviour will depend on combustibility of the volatiles as they are produced.

Interaction of Chemical and Physical Processes

The chemical composition of the gas phase fuel, and its production rate, depend both on the chemical structure of the polymer as it breaks down to release fuel, and the physical properties of the material. In particular, the transfer of heat through the solid/liquid and its rheological properties (affecting both heat and gas transport), will influence the decomposition and burning behaviour, under a defined set of external conditions. On the microscale (such as that in TGA, section "Thermogravimetric Analysis", or MCC, section "Microscale Combustion Calorimetry"), a single piece of sample of mass 5 mg, heated at 10 K per minute may be in thermal equilibrium to within a few degrees K, but an escaping monomer would still have to pass over a million repeat units, even if following the shortest straight line trajectory from the centre of the sample to the edge, in order to escape. In actuality, a much more tortuous path around the polymer crystallites would need to be followed in order for fuel to escape. Along this path, the monomer or other volatile fragment could recombine with the polymer; only when bubbles form is the reverse process of repolymerization effectively prevented.

Thermoplastics can melt without chemical reaction to form a viscous state (polymer melt), but they may decompose thermally by random chain scission, reducing their molecular mass, increasing the proportion of short chain polymer molecules in the liquid phase, before melting. In the absence of a flame the fluidity of the polymer will accelerate the access of oxygen, and its release of volatile decomposition products.

Thermal Analysis: Methods for Quantifying the Thermal Response of Polymers

Thermal analysis describes a family of techniques which measure changes in physical and chemical properties during controlled heating. The programme may take many forms:

(i) The sample may be subjected to a constant heating (or cooling) rate ($dT/dt = \beta$), for example 10 K min^{-1}.
(ii) The sample may be held isothermally ($\beta = 0$).
(iii) A "modulated temperature programme" may be used where a sinusoidal or other alteration is superimposed onto the underlying heating rate (section "Differential Thermal Analysis and Differential Scanning Calorimetry").
(iv) To simulate special industrial or other processes, a stepwise or complex programme may be used. For example, the sample might be heated at l0 K min^{-1} to 373 K, and held for 10 min, to drive off any absorbed water, then heated at l0 K min^{-1} to 673 K, then held there for 30 min. In addition, the atmosphere can be changed during a particular part of the heating regime, such as switching from nitrogen to oxygen above 1000 K, to quantify the presence, by oxidation, of carbonaceous residues.
(v) The heating may be controlled by the response of the sample itself (e.g. high resolution TGA).

In order to understand, and alter, the behaviour of a material in a fire, it is necessary to know as much as possible about the processes of decomposition. These processes are often highly dependent on the conditions, particularly the heating rate and atmosphere. Moreover, sensitivity to these parameters can give the vital clues needed to interpret the fire behaviour. Thermal analysis tends to be far more sensitive to instrumental parameters than other branches of chemical analysis. The following summarises the key parameters needed to ensure the validity and reproducibility of results obtained by thermal analysis, conveniently summarised by the acronym SCRAM.

The **Sample**: the chemical composition, the source and pre-treatments, together with the history of the sample, impurities and dilution with inert material can all affect results.

The **Crucible**: the material and shape of the crucible or sample holder is important. Deep crucibles may restrict gas flow more than flat, wide ones, and platinum crucibles catalyse some reactions more than alumina ones. The type of holder or clamping used for thermomechanical methods is equally important. The results are also unlikely to be entirely independent of the make and type of instrument used.

The **Rate of heating**: this has most important effects. A very slow heating rate will allow the reactions to come closer to equilibrium and there will be less thermal lag in the apparatus. Conversely, high heating rates will give a faster experiment, may be more representative of the heating rates in fires (section "Choice of Atmosphere and Heating Rate in Thermal Analysis"), but deviate more from equilibrium and result in greater thermal lag. The parameters of special heating programmes, such as modulated temperature or sample control, will also affect the results.

The **Atmosphere**: both the transfer of heat, the supply and removal of gaseous reactants, and the nature of the reactions which occur, or are prevented, depend on the chemical composition of the atmosphere and its flow. Oxidations will occur quickly in oxygen, more slowly in air, and not at all in nitrogen or other inert gas; product removal by a fairly rapid gas flow may prevent reverse reactions occurring.

The **Mass of the sample**: a large mass of sample will require more energy, and heat transfer will be determined by sample mass and dimensions. These include the volume, packing, and particle size of the sample. Fine powders react rapidly, lumps more slowly. Large samples may allow the detection of small effects. Comparison of runs should preferably be made using similar sample masses, sizes and shapes.

Thermogravimetric Analysis

"Thermogravimetry is a technique in which the mass of a test specimen is measured as a function of temperature or time, while the test specimen is subjected to a controlled temperature program." [9] Thermogravimetric analysis (TGA) is the

most commonly used method for investigating the complex thermal decomposition processes of polymers. In TGA experiments, at heating rates around 10 K min^{-1}, a sample size around 5–10 mg is small enough to ensure that it is in thermal equilibrium with the apparatus.

In isothermal TGA, the sample is brought quickly up to the desired temperature, usually by rapid insertion into a preheated furnace, and the weight of the sample is monitored during the course of thermal decomposition. In practice, the sample does not heat instantaneously, so errors arise where the selected temperature is high enough for significant decomposition to occur within the first few minutes.

In dynamic TGA, the sample is subjected to temperature programmed heating. This varies from a fixed rate, such as 10 K min^{-1}, to a variable rate, designed to highlight particular features (such as 10 K min^{-1} up to 650 K followed by 1 K min^{-1} up to 660 K, in order to focus on a particular step. A further modification is high resolution TGA, in which the changes in sample mass are used to slow the heating programme, to get better resolution of particular thermal events. As isothermal TGA is falling into disuse, it is common to refer to "dynamic TGA" simply as TGA.

The cylindrical furnace is designed to have a long constant temperature zone in its centre. TGA experiments rarely use static air, because of the uncertainty of its composition during a run, and the possibility of reverse reactions occurring with the vapour phase effluent. A flowing purge gas is almost always used, although operation under a vacuum is sometimes possible, and useful for techniques involving evolved gas analysis (although the typically boiling points and gasification temperatures are lowered by 150–250 K). The best crucibles are made of platinum, which is inert, does not melt below 2042 K and may be cleaned in strong acid. To reduce their thermal inertia, they are thin, and hence delicate. They can chemisorb hydrogen, giving rise to a spurious weight gain, although this is unlikely in routine polymer decomposition studies. The alternative, ceramic crucibles, can suffer from fusion with molten samples and be very difficult to clean.

A sample is suspended on a highly sensitive balance over a precisely controlled furnace. Usually heating rates of 5–20 K min^{-1} are used to look for broad decomposition stages, while slower heating rates, around 1 K min^{-1} are better for isolating individual events. Sample sizes are usually kept as small as possible, within the limits of sensitivity of the apparatus this is usually around 5 mg per run. This reduces bulk effects, and at higher heating rates, avoids thermal gradients being set up within the sample.

A typical microbalance has a rotating pivot, and is controlled electronically using a zero detection device, as used in a galvanometer, usually a light and photocell and a magnet and moving coil system to restore balance. The control system varies the current passed through the coil to keep the beam of the balance in the zero position. This is known as a null deflection system and has the advantage that it keeps the sample in the same position in the furnace throughout the run.

The results of TGA experiments may be presented as mass losses, usually as a percentage of total mass as a function of temperature, (or time, for isothermal TGA), or may be presented as the differential, showing the peaks of mass loss (DTG). Both formats have their advantages—the mass *vs* temperature plot gives direct information about sample composition, the percentage of non-volatiles etc., while DTG is much easier to see small differences in peak decomposition temperatures, and allows easy quantification of the maximum rate of mass loss (or fuel production in fire science). Figure 7.8 shows the TGA and DTG curves for polyacrylonitrile (PAN) in nitrogen at a heating rate of 10 K min^{-1}, showing three distinct decomposition stages at 550, 700 and 1100 K.

There are three common designs of TGA instrument, each having advantages and disadvantages (Fig. 7.9). The hangdown thermobalance is probably the simplest and most robust design, and dominated in the early instruments. The top-loading thermobalance has the advantages that, for evolved gas analysis the volatiles may be sampled more directly, and the surrounding atmosphere moves more naturally around the crucible (though this will give different results, for example

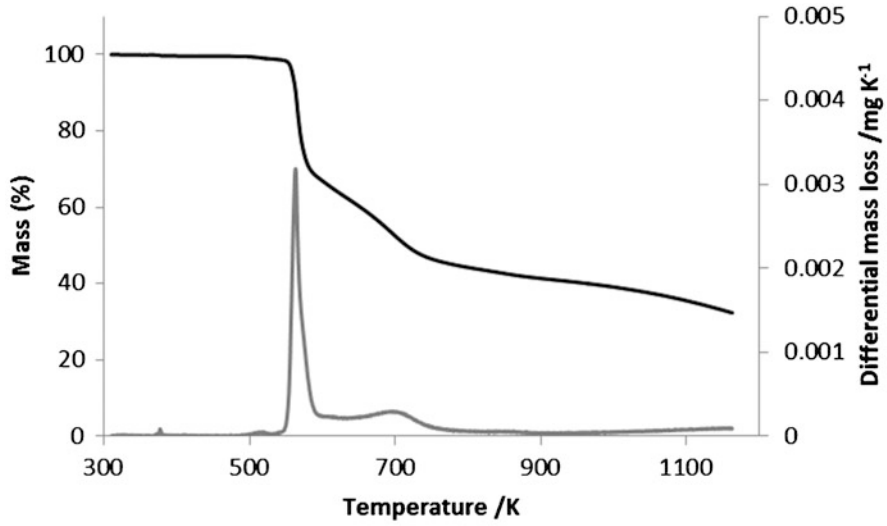

Fig. 7.8 TGA and DTG curves for polyacrylonitrile decomposition in nitrogen at 10 K min^{-1}

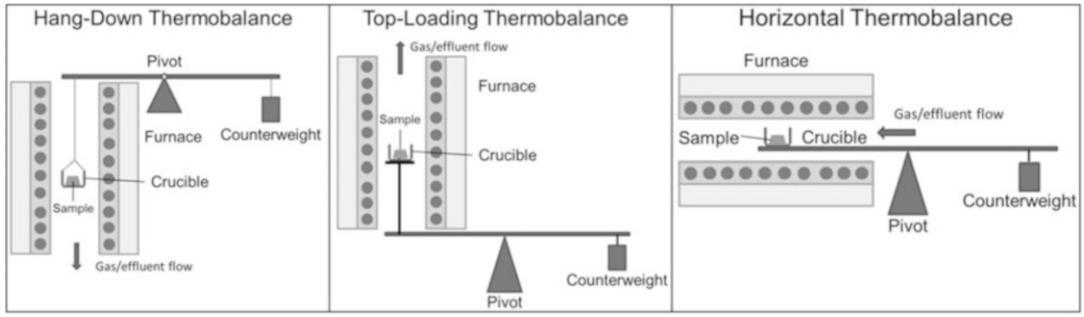

Fig. 7.9 Three common TGA instrument designs

in studies of char oxidation, where the rate is dependent on collisions of oxygen gas with the sample surface). The horizontal thermobalance minimises the effect of gas flow on the recorded mass. In the other two instrument designs this is compensated for by subtracting a blank run from the baseline, with an empty crucible with the same gas and flow rate over the entire temperature range.

Data from thermogravimetric analysis (TGA) is commonly used in the following determinations.

(i) Identification of polymers/materials present in composite materials
(ii) Studies of polymer decomposition
(iii) Generation of evolved products
(iv) Determination of kinetic data
(v) Quantifying thermal stability
(vi) Determination of the content of low volatiles (plasticizer, solvents)
(vii) Quantitative determination of single polymer components
(viii) Filler content (e.g. carbon black, chalk, glass fibre)
(ix) Oxidative stability

Differential Thermal Analysis and Differential Scanning Calorimetry

These two techniques allow quantification of the energy required, or released, during temperature programmed heating. Originally, differential

scanning calorimetry (DSC), invented by Perkin-Elmer, was deemed by the International Conference on Thermal Analysis (ICTA) to describe only the technique where a quantifiable amount of energy, as an electric current, was supplied to the sample (or reference) to maintain the sample and reference temperatures equal, now known as *power compensation DSC*.

In differential thermal analysis (DTA), the temperature of the sample is compared to the temperature of a reference (usually a matching empty crucible) during programmed heating (or cooling). Raw DTA data is a recorded as temperature difference (between the sample and reference pans) as a function of temperature. Prior calibration using materials of known heat capacity, such as sapphire discs, together with software converts the temperature difference into energy units, to make the results comparable to power compensation DSC. Thus, calibrated DTA became known as *heat flux DSC*. Now it is recognized that both techniques provide the same information and are both classed as DSC [10]. Data is reported as a differential, showing endothermic (heat to sample) or exothermic (heat from sample) processes. Unfortunately some manufacturers have the exo-peaks going upward, while others show them going down. Thus there is an established convention to label all DSC plots with an arrow labelled "exo" to show how the results have been reported. DSC provides useful information about polymeric materials and their decomposition. As the most commonly used thermal analysis technique, DSC also provides the following quantitative measurements of physical processes and characteristics.

Thermophysical Properties
- Specific heat capacity

Product Identification and Characterization
- Melting temperatures
- Transition enthalpies
- Phase transformations, phase diagrams
- Crystallization temperatures
- Degree of crystallinity
- Glass transition temperatures

Advanced Material Analysis
- Decomposition and oxidative susceptibility
- Reaction kinetics
- Purity determinations

The basis for obtaining kinetic parameters from DSC is to identify the rate of reaction with the DSC signal, and the extent of reaction with the fractional area of the peak plotted against time. It is possible to obtain the three variables, rate of reaction, extent of reaction and temperature by carrying out a series of isothermal experiments at different temperatures in much the same way as in classic kinetic investigation. The set-up of the experimental procedure is not without difficulty, but the interpretation of the result is less contentious than with the alternative dynamic procedures [10].

Standard protocols have been published covering most of the common DSC measurements [11]. Some of these, such as chemical kinetic parameters, and the enthalpies of these transitions, are of direct value in prediction of thermal decomposition, where others, such as the heat capacity and thermal conductivity, are required when modelling the heat transfer through the condensed phase (such as a $6 \times 100 \times 100$ mm cone calorimeter sample) from microscale thermal analysis data.

Excellent thermal contact is essential between the sample and reference pans and the instrument. Such contact is vulnerable to attack from acids such as hydrogen chloride and carbon rich vapours from the decomposition products of polymers. For these reasons, and the importance of the DSC for characterising the properties of polymers and other materials, DSC is used with some reluctance in polymer decomposition studies.

Prior to thermal decomposition, the enthalpy change of processes occurring in the condensed phase may be quantified using DSC or DTA. The glass transition, T_g is manifested by a *step* rather than a peak in the trace, resulting from an increase in *specific heat capacity* of the sample. On a molecular level, below the T_g, the polymer chains are held in place relative to one another. Above the T_g, movement is possible, as there are

more ways for the polymer to absorb energy, hence the increase in specific heat. For non-crystalline polymers T_g is in fact the *only* observable thermal transition prior to decomposition. For a crystalline polymer, a defined melting point will also be observable. If the polymer has been cooled more quickly than the time required for crystallization, then an exothermic peak known as the cold-crystallization temperature may be observed, when the polymer chains are free to move and become more closely aligned. In some polymers, crystallization is almost instantaneous, for others it can take hours or days. Crystallization can only occur above T_g.

The DSC heating-trace for a crystallisable polymer, which has been cooled so rapidly from the melt that the glassy state was reached before crystallisation occurred, is shown on in Fig. 7.10.

Therefore, when detailed studies are performed on polymeric materials, it is essential to ensure that all samples have the same thermal history (e.g. the same degree of crystallinity) if consistent results are to be obtained.

Crucibles for DSC and DTA

Most commonly, single-use aluminium pans are used for measurements from 120 to 870 K. Although aluminium does not melt until 933 K, there is a risk of irreversible and expensive alloying of the pan and temperature sensors above 870 K. The use of a lid on the pan typically gives an order of magnitude improvement in sensitivity. Crimp-on lids can be used which maintain pressures up to three atmospheres. For measurements in oxidising atmospheres, such as air, of boiling temperatures, or heats of vaporisation, a small hole may be pierced in the lid. Polymer samples which do not decompose, may be pre-melted and pressed onto the base of the pan to optimise thermal conductivity, and enhance the signal. For higher temperatures, platinum, silver, gold, quartz, alumina, or graphite may be suitable.

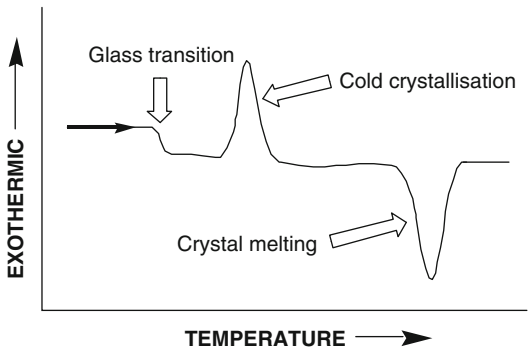

Fig. 7.10 Typical DSC curve obtained during heating of a crystalline polymer that has been subject to fairly rapid cooling

Modulated Temperature DSC (MTDSC)

A minor revolution in thermal analysis occurred with the development by Reading [12] of MTDSC. This allows the two components of enthalpy, such as the heat capacity and a process occurring at a particular temperature, such as T_g or melting, to be separated.

$$\frac{dq}{dt} = C_s\beta + f(t,T) \tag{7.4}$$

Equation 7.4 above separates the two components of the DSC signal, $C_s\beta$, the heat capacity component, and $f(t,T)$ which describes thermal events such as an endothermic transition. The heat capacity of the product of the thermal event will usually differ from that of the reactant, but will be masked by the thermal event. Using a sinusoidally varying heating rate, the reversing (heat capacity), and non-reversing (thermal event) components can be separated. Ideally 4–6 oscillations should occur over the duration of the thermal event.

Simultaneous Thermal Analysis

Simultaneous Thermal Analysis (STA) combines the benefits of TGA and DTA/DSC into a single experiment. The combination has two distinct advantages. It allows unambiguous separation of, or unification of, particular thermal events, such as whether an endothermic process preceded the mass loss stage, or whether the mass loss itself was the endothermic process. The subtle differences in instrumental design of the separate TGA and DSC instruments can make such differentiation problematic. More importantly, during

thermal decomposition mass is often lost. In order to obtain a mass-specific data for a thermal transition (or, for example, the heat capacity of a polymer char), it is necessary to know what mass of material is giving rise to the signal. This can be obtained directly from STA data, since the mass is known across the temperature range.

Thermomechanical Analysis and Dynamic Mechanical Analysis

In thermomechanical analysis (TMA) a probe applies a force to a sample during heating, and the movement of the probe is recorded as a function of temperature. It involves measurement of a specimen's dimensions (length or volume) as a function of temperature whilst it is subjected to a constant mechanical stress. In this way thermal expansion coefficients can be determined and changes in this property with temperature (and/or time) can be monitored. Many materials will deform under the applied stress at a particular temperature which is often connected with the material melting or undergoing a glass transition. Alternatively, the specimen may possess residual stresses which have been "frozen-in" during preparation. On heating, dimensional changes will occur as a consequence of the relaxation of these stresses. Usually the force is static, though modern instruments can offer the facility of an oscillating force. Useful physical data, such as compressive and tensile strength, softening, shrinking, thermal expansion, glass transition, and melting can all be obtained using TMA.

In dynamic mechanical analysis (DMA) a solid sample is held between two moveable clamps and subject to oscillatory forces, and the response measured during temperature programmed heating (or cooling). This allows the measurement of the mechanical properties, such as mechanical modulus or stiffness and damping of a specimen as a function of temperature. DMA is a sensitive probe of molecular mobility within materials and is most commonly used to measure the glass transition temperature and other transitions in macromolecules, or to follow changes in mechanical properties brought about by chemical reactions. For this type of measurement the specimen is subjected to an oscillating stress, usually following a sinusoidal waveform. The applied stress produces a corresponding deformation or strain.

Although TMA and DMA are rarely used for studying the thermal decomposition of polymers, DMA is an essential tool for the development of fire-safe composite materials, such as the carbon-fibre construction of the Airbus A380 or Boeing 787, where maintenance of structural integrity in a fire is at least as important as the suppression of flammability.

Rheology

A decomposing thermoplastic changes from a fluid-like or gel-like solid, to a gel-like or viscous liquid often with no distinct transition from one phase to the other. TMA and DMA are designed for measurement of the fluid or gel-like behaviour of a solid, where rheology is designed to quantify the gel-like or viscous behaviour of a polymer in the liquid state. There is considerable overlap, and many material states can be investigated by both techniques. The term rheology (from *rheo* meaning "to flow") refers to both physical deformation and flow of material under an applied force. Thus, the rheological behaviour of polymers encompasses a wide range of macroscopic phenomena including the flow of viscous liquids, the mechanical properties of elastic solids, and viscoelasticity (the time dependent mechanical properties of a polymer).

The mechanical properties of elastic solids show a region where an applied stress is proportional to the resultant strain (Hooke's law). For liquids, Newton's law describes a region where the applied stress is proportional to the rate of strain. Both are valid only for small strains or rates of strain. In many cases, a polymer will show the characteristics of both a liquid and a solid, and neither of these limiting laws will adequately describe its behaviour. The system is then said to be in a viscoelastic state, where it will respond like an elastic solid to a sudden force, but like a viscous liquid to a slow force.

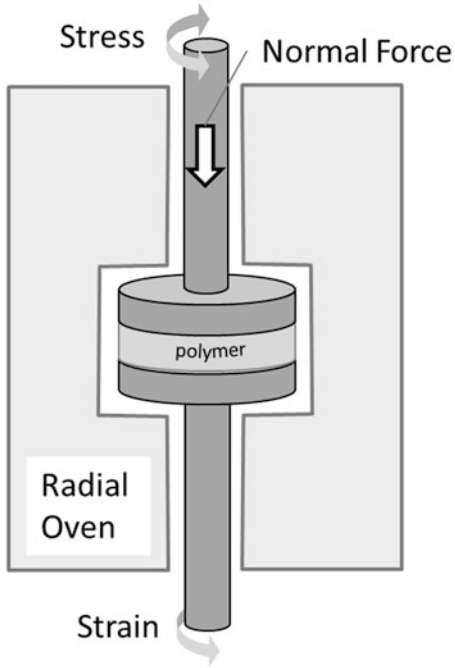

Fig. 7.11 Schematic diagram of a parallel plate rheometer with environmental chamber (oven)

Rheometry provides an essential tool kit for adjusting the conditions in polymer processing. The use of rheometry for studying aspects of the thermal decomposition of polymers is less common. Probably the parallel plate rheometer, with environmental chamber (Fig. 7.11) is most suited to investigating the changing properties of a decomposing polymer. The polymer sample is mounted between two parallel circular metal plates. One plate is driven mechanically with an oscillating motion of fixed angle or torque, and the resistance to the motion is recorded. Various parameters including the elastic and relaxation modulus and the viscosity can be determined. The complex dynamic modulus G* can be separated into two components, the storage modulus G' (representing the solid or gel like behaviour) and the loss modulus G" (representing the viscous or liquid like behaviour).

$$G^* = G' + iG'' \tag{7.5}$$

These are related to the corresponding dynamic viscosities η*.

$$\eta^* = \eta' - i\eta'' \tag{7.6}$$

The release of fuel from a decomposing polymer, as volatiles or bubbles migrating through a viscoelastic medium is a function of its rheological properties.

The Five Regions of Viscoelastic Behaviour

The physical properties of an amorphous polymer are related to its molecular motion, which is governed by the flexibility of the polymer chains and their temperature. For a linear, amorphous polymer, five distinguishable states can be observed if the elastic modulus is measured over a range of temperature. The relaxation modulus E_r (the time dependent change in stress under a constant strain), for polystyrene, plotted as log E_r against temperature, shows these five distinct regions, Fig. 7.12.

(i) **The glassy state**: Below 360 K, even short range motion of one polymer molecule relative to another is frozen, giving the material high rigidity, but with corresponding brittleness.

(ii) **Retarded elastic state**: The glass transition temperature T_g is in this region, and the sharp decrease in modulus with temperature reflects the increase in molecular motion as the temperature rises from T_g to 30 K above T_g. Just above T_g the movement of the chain segments is still rather slow, giving leathery properties to the material.

(iii) **The rubbery state**: At approximately 30 K above T_g the modulus curve begins to flatten out into the plateau region, giving a softer elastic material, since the polymer chains can move relative to each other over a short range, but liquid flow (or long range movement) is still inhibited.

(iv) **Rubbery flow**: After the rubbery plateau, the modulus again decreases as liquid-like flow becomes possible.

(v) **Viscous state**: Above 450 K, there is little evidence of any elastic recovery in the polymer, and all the characteristics of a viscous liquid become evident. Here, there is a steady decrease of the modulus as the temperature increases.

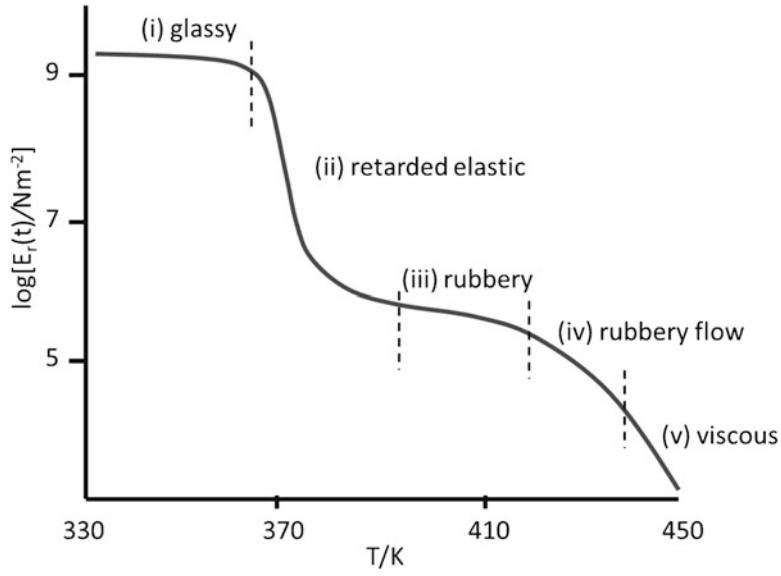

Fig. 7.12 The five regions of viscoelasticity for an amorphous polymer (i) glassy state; (ii) retarded elastic state; (iii) rubbery state; (iv) rubbery flow state; and (v) viscous state

In the glassy, elastic and rubbery states movement of bubbles through the polymer matrix will be inhibited. Sufficient fuel release to support ignition is unlikely in the rubbery flow state. As the polymer moves through the viscous state fuel release will become increasingly easy, allowing a critical concentration to accumulate above the sample to support ignition.

Techniques Involving Chemical Analysis of Decomposition Products

Evolved Gas Analysis (EGA)

Thermogravimetric Analysis (TGA) provides the crucial data with which to interpret the complexities of burning behaviour. For example, ignition can only occur when there is sufficient fuel being released into the gas phase. The temperature at which the first sharp mass loss occurs normally corresponds to the critical surface temperature for ignition, and if, for example, the addition of fire retardants delays this onset, they may also delay ignition. However, if this mass loss is non-combustible (such as the loss of HCl from PVC), it will clearly not result in ignition; it is, therefore, important to know the chemical nature of the products released during mass loss in TGA, as well as the temperature at which they were released. The most widely used fire retardant, aluminium hydroxide releases water vapour as it decomposes; surface oxidation can result in carbon dioxide (CO_2) formation, which tends to delay ignition; evolution of hydrocarbons is indicative of the fuel release step leading to ignition.

In the simplest form of evolved gas analysis (EGA) a non-dispersive infrared analyser (NDIR) may be attached to the exhaust line of a TGA, DSC or STA, in order to provide a time resolved profile of CO_2, carbon monoxide (CO), hydrocarbons and oxygen concentrations as a function of time, during the TGA run [13]. This technique allows the major decomposition products to be distinguished during thermal decomposition, particularly in relation to fuel gases and non-combustible products. The evolution of CO_2 formed on the surface of the decomposing polymer is indicative of the consumption of oxygen and fuel, but accompanied by self-heating. CO_2 is not formed in the gas phase below 500 °C.

Thermal Analysis with Fourier Transform Infrared Analysis

Fourier Transform Infrared (FTIR) has revolutionised infrared analysis, producing spectra of higher resolution in a much shorter time. For polymer decomposition studies this allows the

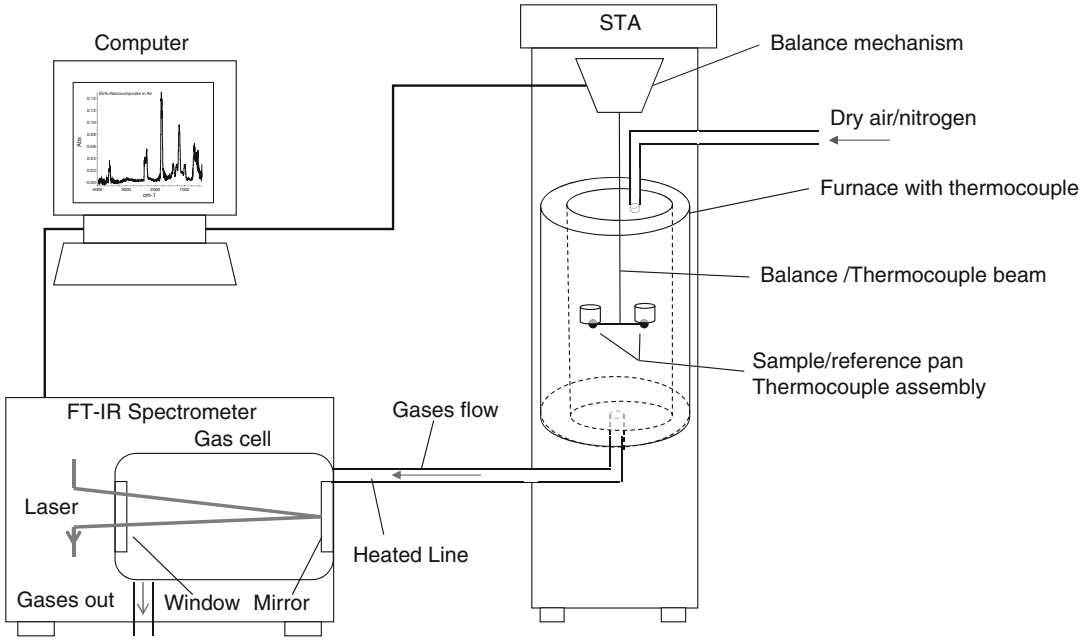

Fig. 7.13 Schematic of a typical STA-FTIR instrument set-up

spectra of gas phase products to be collected continuously as a function of temperature. Gas phase infrared spectra are much sharper than condensed phase spectra, and generally identification of individual molecules is possible in the gas phase, whereas only the presence of functional groups may be obtained from condensed phase spectra. However, when a large number of similar molecules are present, each with their distinctive spectra superimposed, deconvolution software may be necessary in order to identify and quantify the individual components. Figure 7.13 shows a schematic of a typical STA FTIR set up [14].

TGA, DSC or STA, combined with FTIR analysis of the vapour phase provides a very rich profile of polymer decomposition through the spectra of the evolved products. This is shown in Fig. 7.14 for ethylene-vinyl acetate copolymer in nitrogen, and can be deconvoluted to provide profiles with respect to temperature of the evolution of individual species. The technique is gaining popularity amongst the fire retardant community, but the deconvolution of spectra, particularly where compounds are present for which no calibration data has been recorded, limits the applications of the technique.

Pyrolysis-Gas Chromatography Mass Spectrometry

Pyrolysis-gas chromatography–mass spectrometry (py-GCMS) is a three stage process consisting of pyrolysing about 1 mg of sample, separating the mixture of volatile products by gas chromatography, and analysing each of the components by mass spectrometry. From its esoteric origins, gas chromatography–mass spectrometry instruments are now standard, low cost and do not depend on specialist technical support (Fig. 7.15).

Given the large numbers of different products that can result from a single stage in the decomposition of a polymer, separation of the products is often required, before they can be identified. Controlled temperature and heating rate pyrolysis may be followed first by sample collection on a sorption tube, or for rapid pyrolysis, direct injection into a gas chromatography column (py-GC). In its simplest form, a gas chromatograph consists of several metres of capillary tube with a well-controlled flow of a carrier gas through it. The tube or "column" is lined with an absorbent solid coated with an involatile liquid that will adsorb and desorb constituents in the

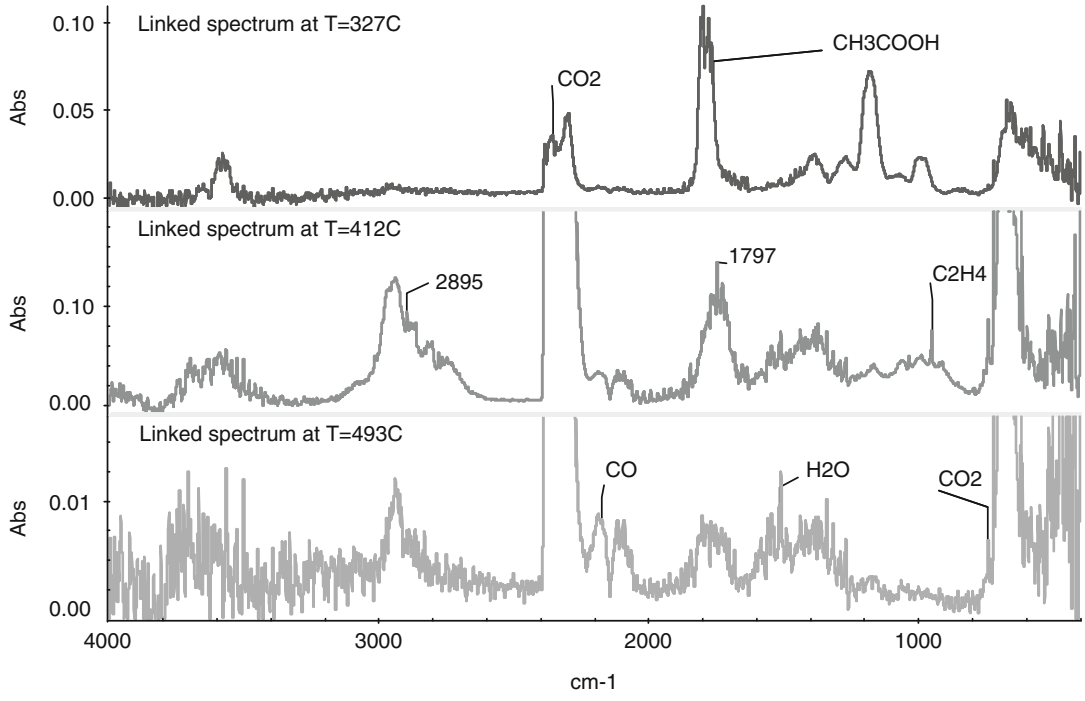

Fig. 7.14 FTIR spectra recorded during decomposition of ethylene vinyl acetate at a heating rate of 10 K min^{-1}

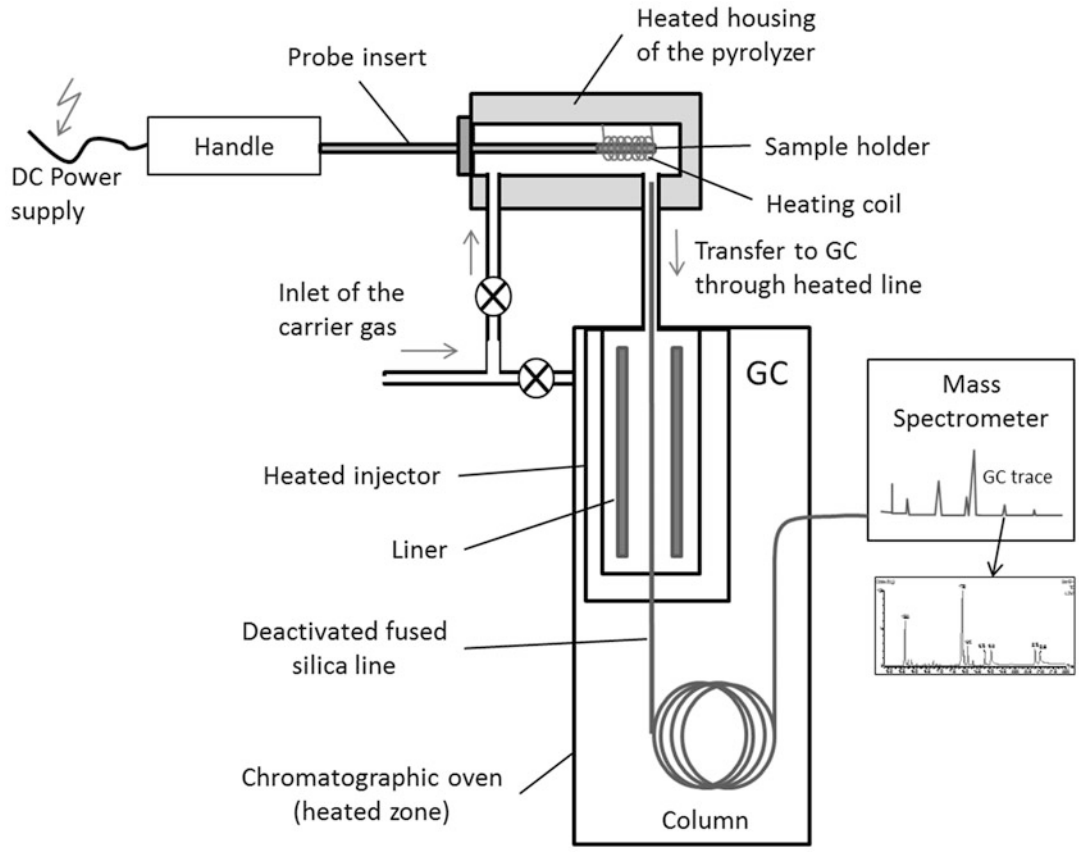

Fig. 7.15 Typical pyrolysis GC-MS apparatus

sample, depending on their affinity for the liquid, and their volatility. The column is located in a temperature programmable oven. Molecules with different adsorption properties relative to the column packing will reach the end of the column at different times, and hundreds of compounds may be separated in a single run. A detector placed at the exit of the gas chromatograph will respond to the concentration of molecules, other than the carrier gas, giving a series of peaks. For a single peak, the time from injection is characteristic of the molecule, and the area under the peak is proportional to its concentration. Column lining, column temperature programming, carrier gas flow rate, sample size, and detector type can be adjusted to achieve optimal separation of the decomposition products.

Simple detectors include the flame ionization detector (FID) which gives a signal roughly proportional to the carbon content of the molecule, and hence its calorific potential. They have a dynamic range spanning several orders of magnitude. However the reduction in cost of the mass spectral analysers, which provide a chemical fingerprint for each separated molecule, which can then be compared to databases such as the NIST mass spectral library, provide the rapid and powerful tool for investigating the true complexity of polymer decomposition. Figure 7.16 shows py-GC/MS chromatograph of the decomposition products of soy-styrene-divinyl benzene (SSD) polymer [15] collected from 323–873 K at 10 K min^{-1}.

Pyrolysis GC-MS complements TGA-FTIR as it provides snapshot identifying all evolved species over a particular temperature range. TGA FTIR shows the variation of the spectrum as a function of temperature, once identified, the temperature evolution profile of a species may be monitored.

Thermal Volatilization Analysis

Another useful method for quantitatively collecting and separating polymer decomposition products is thermal volatilization analysis (TVA) based upon the apparatus and techniques described by McNeill et al. [16]. The apparatus consists of a sample chamber (heated by a programmable tube furnace) connected in series to a primary liquid nitrogen-cooled sub-ambient trap and a set of four secondary liquid nitrogen-cooled cold traps. The whole system is continuously pumped to a vacuum of 1×10^{-7} atm. Volatile condensable products from a ~25 mg sample are initially trapped at two stages: the 'cold-ring' ($T \sim 285$ K) immediately above the heated area of sample tube (for high boiling point materials) and the primary liquid nitrogen cooled sub-ambient trap ($T \sim 77$ K) for lower boiling point species. The pressure increase is proportional to the evolution of both condensable and non-condensable volatiles from the sample [17]. These separated fractions may be subsequently analysed by gas-phase FTIR (section "Thermal Analysis with Fourier Transform Infrared Analysis") and GC–MS (section "Pyrolysis-Gas Chromatography Mass Spectrometry").

Microscale Combustion Calorimetry

A relatively recent innovation in fire calorimetry has been the development of the microscale combustion calorimeter (MCC) [18]. The apparatus was developed by Lyon and Walters at the U.S. Federal Aviation Administration (FAA) [19]. A schematic of the apparatus is shown in Fig. 7.17. It thermally decomposes 1–3 mg of

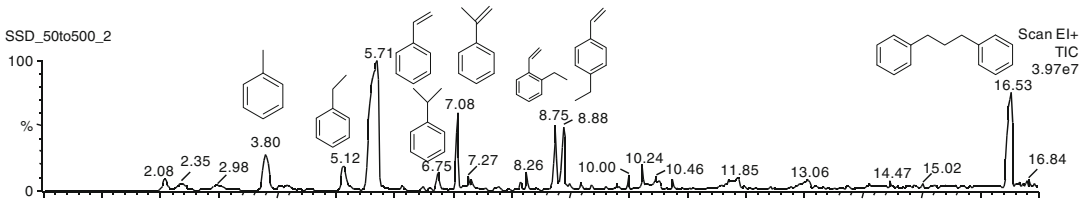

Fig. 7.16 Py-GC/MS chromatographs of the decomposition products of soy-styrene-divinyl benzene (SSD) polymer collected from 323 K to 873 K at 10 K min^{-1}

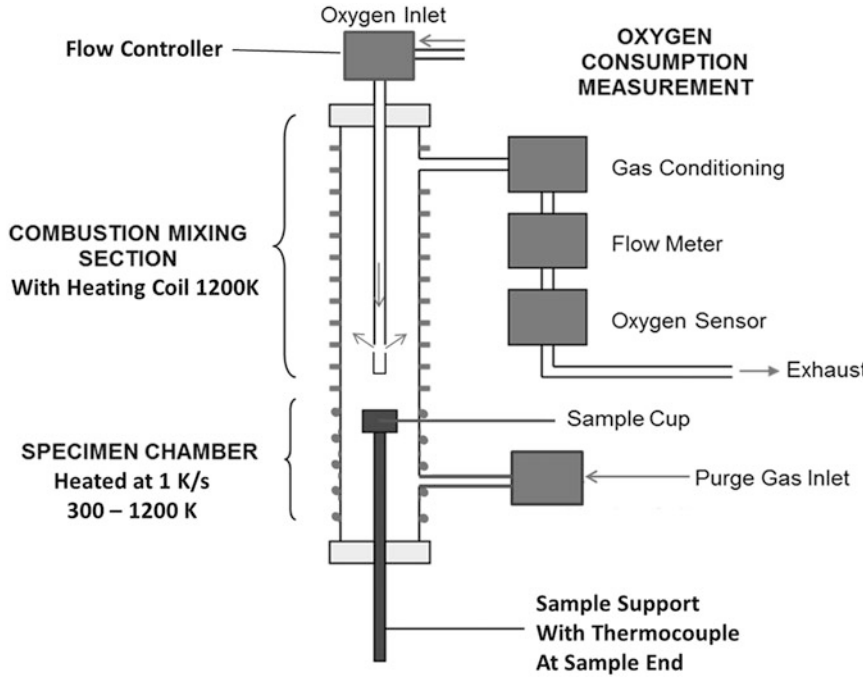

Fig. 7.17 Schematic diagram of MCC

sample in an alumina crucible at a heating rate of 1 K s^{-1} in an atmosphere of nitrogen (or synthetic air). The pyrolysis gases are then passed into the combustor at 1173 K and mixed with oxygen. The oxygen depletion of the dry gas is measured, and a computer algorithm converts the oxygen depletion and mass flow rate data into specific heat release rate (W/g), as a function of temperature. For polymers that decompose to release only fuel, the information obtained is similar to that for DTG in nitrogen. For materials showing gas phase inhibition, the severe oxidising condition of 1173 K will usually suppress any reduction in oxidation. For materials producing char in nitrogen, the mass of residue will increase, though if the experiment is repeated using synthetic air as the pyrolysis gas, the char yield can be separated from the formation of an inorganic residue.

The apparatus has grown in popularity due to its excellent design, relatively low cost and ease of use. It is particularly popular with the aircraft manufacturer, Boeing, who uses it for both materials screening and quality control. However, its popularity has led, for example, to a number of fire retardant development laboratories publishing articles describing their latest fire retardant formulations, based solely on MCC data, paying less regard to what that data actually means.

Figure 7.18 shows the heat release curves for five common polymers measured using the microscale combustion calorimeter. In particular, the pyrolysis temperature and the peak of specific heat release rate of the most useful indicators of fire performance.

Choice of Atmosphere and Heating Rate in Thermal Analysis

Thermal analysis is generally conducted in nitrogen or in dry air. Studies of thermal stability (for example to ensure that a material does not degrade at its normal operating temperature) would normally be carried out in air, or for accelerated ageing, in elevated oxygen atmospheres. The decomposition of a polymer is known to be dependent on the atmosphere in

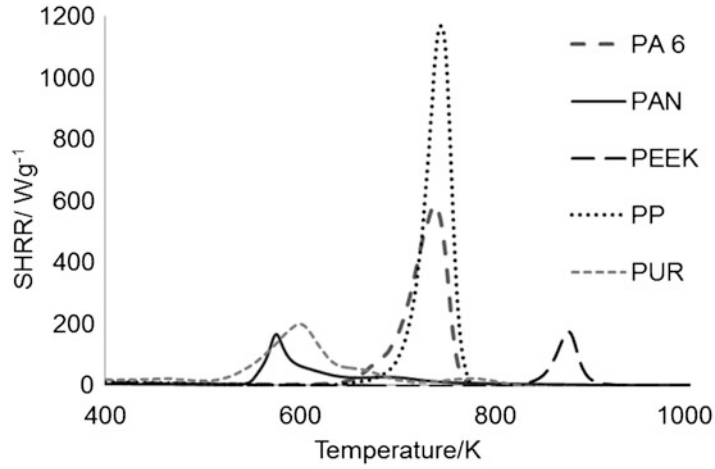

Fig. 7.18 MCC heat release rate curves for common polymers

which the decomposition occurs. For some polymers the decomposition occurs 200 K lower in air than in nitrogen, while for a few others it makes little difference. In other cases, certain decomposition stages are delayed by the presence of oxygen, perhaps through the formation of a more thermally stable char. The decomposition of polypropylene has been widely studied (section "Polypropylene") and it has been shown that the process is accelerated by oxygen, and that the oxygen permeates the decomposing polymer, not only affecting the surface layers.

In contrast, in order to understand the reaction-to-fire behaviour of a material, it should be recognized that

(i) Heating rates in fires are probably closer to 100 K min^{-1} than the 10 K min^{-1} typical of thermal analysis, causing faster fuel production flows and preventing the diffusion of oxygen into the polymer.
(ii) The atmosphere under a flame is practically free of oxygen.
(iii) Fuel is generally released from a decomposing polymer as bubbles of vapour, forcing their way out through a molten or porous condensed phase, and released from the polymer under anaerobic conditions.

These factors all indicate that fire behaviour, both before and after ignition, is better represented by decomposition in nitrogen, than by decomposition in air. However, given the ease with which TGA can be run in flowing air, and the potential for added insight (such as the formation of a more stable char in an oxidising atmosphere) it is often also worthwhile obtaining the TGA in air.

The choice of heating rate during thermal decomposition of polymers has been the subject of much controversy. Low heating rates (around 1 K min^{-1}) produce better quality data and better defined and separated chemical events. High heating rates (around 100 K min^{-1}) are more representative of those found in a fire. However, when analysing the products during the thermal decomposition of a polymer, for example in TGA-FTIR, it is often necessary to use larger amounts of sample (~15 mg) in order to obtain representative spectra. With such larger samples, it is more difficult to maintain thermal equilibrium across the sample bulk, and therefore lower heating rates (around 10 K min^{-1}) are preferable. Conversely, a faster heating rate will produce a higher concentration of volatiles in a shorter time, although these may become mixed in the sampling line before analysis.

Char and Residue Analysis

The complexities of the thermal decomposition of polymeric materials can be investigated by a combination of analysing the volatile components as described above, and by analysing the

chemical composition of the char or residue. In terms of improved fire retardancy, enhancement of the char layer normally provides the best route for improving the fire safety. Chars may show the chemistry of the solid phase processes prior to carbonisation. For example, polyacrylonitrile fibre decomposes to produce materials which ultimately become carbon fibre (a modern, heterocyclic material composed of graphite layers with nitrogen heterocycles along their perimeters).

Unfortunately, chars are predominantly carbon, and can be difficult to analyse. In addition to the chemical composition of chars, the three dimensional and microscopic structure is also important. If the char provides a coherent, uninterrupted layer which seals the underlying polymer from the attack of radiant heat and oxygen, while preventing the escape of fuel, it will be much more effective in reducing the attack of fire. Scanning electron microscopy (SEM) is the most effective tool surveying the permeability of the char or residue layer. With the addition of elemental analysis, more information about the chemistry of the formation of the protective layer can be obtained. For example, some inorganic materials migrate to the surface of the decomposing polymer and form low melting inorganic glasses.

Analysis of the chemical composition of char and residue layers is complicated by the high absorptivity of carbonaceous carbon. If spectroscopic techniques such as Fourier transform infrared (FTIR) are used for the analysis of the carbonaceous layer, very low signals are often found because the infrared radiation is generally absorbed by the black solid, rather than specifically by the organic functional groups of interest. In addition, a high proportion of carbon-carbon bonds will be non-polar, and so will have no dipole moment, and therefore no ability to absorb infrared radiation, so that relatively little useful information can be obtained. Surface analysis techniques such as diamond-attenuated total reflectance FTIR (d-ATR FTIR) can identify the presence of functional groups within the surface layers of the char. Sample preparation is trivial and results can be obtained rapidly. In addition Raman spectroscopy, which uses visible frequency laser light of high intensity and detects scattered wavelengths of lower energy infrared radiation emitted from the sample can be used very effectively to quantify the presence of carbon-carbon single bonds, carbon-carbon double bonds and carbon-carbon aromatic bonds in a carbonaceous char layer, although care must be taken to avoid using a laser wavelength that causes fluorescence. More sophisticated analysis has been undertaken using nuclear magnetic resonance (nmr) with a solids probe (magic angle spinning) to examine the chemical environment of any atomic nuclei with uneven numbers of nucleons, such as C-13, F-19, P-31 etc. [20].

Decomposition of Polymers

Different polymers decompose in different ways. When a polymer is heated its chains will start to break down, which eventually results in the formation of volatile fuel molecules. The pyrolysis of a polymer, which turns polymer chains of 10,000–500,000 carbon atoms into species small enough to be volatilized, often involves breaking the polymer chain. In some cases, the chain releases groups from its ends most easily, known as *end-chain scission* or unzipping. In others, the chain breaks at random points along its length, known as *random chain scission*. A third process, in which groups attached to the backbone as side chains are released, is known as *chain stripping*. If the resulting chain may be prevented from undergoing chain scission to form volatiles or lose further substituents, it may instead undergo carbonization that results in *char formation*. Thus, the conversion of organic polymer into volatile organic molecules may follow four general mechanisms. While some polymers fall exclusively into one category, others exhibit mixed behaviour (Table 7.4).

Decomposition Mechanisms

Random chain scission usually takes place when the bonding energies are similar along the chain. The distinction between random chain and end

Table 7.4 Generalised mechanisms of polymer decomposition

Mechanism	Examples of polymer	Typical products
Random chain scission	Polyethylene	Alkanes, alkenes, very little monomer
	Polypropylene	Alkanes, alkenes, very little monomer
	Polystyrene	Styrene monomer, dimer and trimer
	. . .more generally	Monomers and oligomers
End chain scission	Polymethylmethacrylate	90–100 % monomer
	Polytetrafluoroethylene	90–100 % monomer
	. . ..more generally	monomer
Chain stripping	Polyvinyl chloride	Hydrogen chloride, aromatic hydrocarbons and char
	Polyvinyl alcohol	Water and char
	Generally	Small molecules and char
Cross-linking	Polyacrylonitrile	Hydrogen cyanide and char
	Polyetheretherketone	Volatile aromatics and char
	Generally	Char and volatile products

chain scission is generally based on the extent of monomer evolution, and on the measurement of the polymer's average molecular mass when heating the polymer below its typical pyrolysis temperature. The slow evolution of monomer and rapid decrease of the molecular mass is an indication of random chain scission.

Both end and random chain scission are dominated by free radical processes. The decomposition of a polymer by a free radical mechanism can be divided into three processes.

Initiation—the time taken and for the first bond to rupture, generating two free radicals. In random chain scission each radical will be at the end of a polymer chain, in end chain scission the $H\cdot$ or $\cdot CH_3$ radical released will attach itself to another polymer chain. This is likely to occur at the weakest link in the polymer chain, such as a C–C single bond one bond away from a double bond, triple bond or an aromatic ring $\left(-C^{\gamma}-C^{\beta}-C^{\alpha}=C-\right)$, the β-carbon shown here. These bonds are generally weaker than other C–C or C–H bonds, and significantly weaker than aromatic, double, or triple bonds. Bond breaking can take place as a random or end chain scission. Since larger free radicals are more stable than those on small molecules, the fragmentation in the middle of the polymeric chain is favoured thermodynamically compared to the formation of smaller molecules. However, kinetic factors may also play a role in determining the abundance of a specific compound. The formation of small radicals from the end of a polymeric chain can be kinetically favoured, and, as a result, formation of small radicals in the initiation step is more common than predicted by thermodynamic criteria. In polystyrene, end chain scission produces styrene monomer in competition with random chain scission, which ultimately produces the dimer, trimer, tetramer etc.

Propagation—once a polymer chain has a free radical, the reactivity will propagate along the polymer macromolecule very quickly, releasing monomers or other small volatile molecules.

Termination—at some point the rapid propagation step must end. This may be at the end of the polymer chain, at the branching point, or some other structural irregularity where two radicals can combine.

Thermodynamics of Polymer Decomposition

At every propagation step in the depolymerisation of a vinyl polymer $-(CH_2-CHX)_n-$ a C–C σ-bond is broken, and a $C=C$ π-bond is formed (Fig. 7.19).

The enthalpy on breaking a σ-bond is around 320 kJ mol^{-1}, and that of forming the π-bond in the volatile fragment is around 260 kJ mol^{-1}.

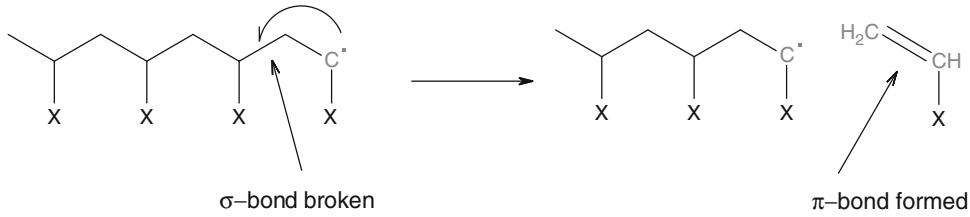

Fig. 7.19 Generalised mechanism for free radical depolymerisation of a vinyl polymer

Thus, in purely enthalpic terms, depolymerisation requires about 60 kJ per mole of volatile alkene formed, i.e. $\Delta H = +60$ kJ mol^{-1}. However, a reaction can only proceed when the *free energy change* ΔG is negative, and since:

$$\Delta G = \Delta H - T\Delta S \tag{7.7}$$

the entropy change involved must also be considered. The entropy (or disorder) of a decomposing polymer is obviously *increasing*, since the number gas molecules is increasing. Thus ΔS is positive, and is typically around +120 J mol^{-1} K^{-1}. At room temperature, 300 K, the free energy change on depolymerisation is thus:

$$\Delta G = +60\,000 - (+300 \times 120)\,\mathrm{J\,mol^{-1}}$$
$$\Delta G = +24\,000\,\mathrm{J\,mol^{-1}} = +24\,\mathrm{kJ\,mol^{-1}}$$

This demonstrates the obvious fact that at room temperature depolymerisation is unfavourable, and hence polymers are thermodynamically stable. However, at a much higher temperature of 570 K, the $T\Delta S$ term is greatly increased:

$$\Delta G = +60\,000 - (+570 \times 120)\,\mathrm{J\,mol^{-1}}$$
$$\Delta G = +8\,400\,\mathrm{J\,mol^{-1}} = -8.4\,\mathrm{kJ\,mol^{-1}}$$

From this it can be concluded that, above a certain temperature, sometimes known as the *ceiling temperature*, depolymerisation will prevail, as polymer chains (formed at lower temperatures) "unzip" to regenerate monomers. The ceiling temperature for polymethylmethacrylate is about 500 K, and for polystyrene 580 K.

In addition to this simplified view of depolymerisation, a burning polymer is a complex situation, where chemical reactions can take place in the condensed phase, between the condensed phase and the gas phase and, for sustained burning, in the gas phase. The applied heat and exothermic release of energy by chemical reactions such as combustion must exceed the energy required for endothermic process such as heating, melting, depolymerisation and volatilisation.

Kinetics of Polymer Decomposition

Chemical kinetics is the study of reaction rates. Theoretically, the rate of a chemical reaction, as a function of state variables such as temperature, pressure, and concentration, can be predicted for any set of conditions. However, since many chemical reactions are the sum of a number of competing processes, such predictions do not often agree with the experimental data. The most common reason for carrying out kinetic studies is to investigate reaction mechanisms, although empirical estimates of gasification rates provide essential data for fire models that include condensed phase fuel. Kinetic data provides insight into the mechanism, although this generally needs to be corroborated with chemical evidence. The simplest media for investigating the kinetics of chemical reactions are gas and solution phases, which are described briefly below.

Gas and Solution Phase Kinetics

For a reaction of A → Products, simple gas or solution phase kinetics classifies reactions in terms of order (Table 7.5).

In gas and solution phases, most reaction rates lie between zero and second order—genuine third order reactions, where three molecules collide simultaneously, and possess sufficient

Table 7.5 Orders of chemical reactions, and their corresponding rate equations

Reaction order	Description	Differential rate equation	Integrated rate equation	Examples
Zero	Reactant concentration does not affect rate	$-\frac{\mathrm{d[A]}}{\mathrm{d}t} = \mathrm{k}$	$\mathrm{k}t = [\mathrm{A}]$	e.g. vaporisation, where the reactants have to pass through a narrow orifice, or when heat is supplied at a fixed rate.
First	Rate of reaction depends on amount of reactant	$-\frac{\mathrm{d[A]}}{\mathrm{dt}} = \mathrm{k}\,[\mathrm{A}]$	$\ln\left(\frac{[\mathrm{A}]_0}{[\mathrm{A}]}\right) = \mathrm{k}t$	Typical of a simple decomposition reaction, or radioactive decay.
Second	Rate of reaction depends on amount present of two reactants (which may both be A)	$-\frac{d[\mathrm{A}]}{dt} = \mathrm{k}[\mathrm{A}]^2$	$\frac{1}{[\mathrm{A}]} - \frac{1}{[\mathrm{A}]_0} = \mathrm{k}\,t$	Common for gas phase processes such as 2A → Products. Kinetics more complex for A + B → Products
nth	Rate is not a simple function of reactant concentration	$\mathrm{Rate} = -\frac{\mathrm{d[A]}}{\mathrm{d}t} = \mathrm{k}\,[\mathrm{A}]^n$	$\mathrm{k}t = \frac{1}{n-1}\left(\frac{1}{[\mathrm{A}]^{n-1}} - \frac{1}{[\mathrm{A}]_0^{n-1}}\right)$	May be a simple fraction (based on kinetic analysis) or an experimental value (for a complex processes)

energy to react, are very unlikely. Where complex reaction pathways occur, particularly with multiple competing processes, precise fractional order processes are also observed.

Solid Phase Kinetics

In the solid phase the reacting molecules do not move freely and collide at a rate controlled by the thermal energy of the system in contrast to gases and liquids. The reacting species cannot move through the solid and so the rate will not depend on concentration within the solid. If a diffusion process controls the mechanism, the rate will be dependent on concentration gradients within the solid. Alternatively, a reaction interface may move through the bulk with pure reactant ahead of it and pure product behind. Here concentration is meaningless and is replaced by fraction reacted, α.

Experimentally, the rate constant (k) has been found to vary as a function of two variables, A and E_a, defined by the Arrhenius equation.

$$k = A\,e^{\frac{-E_a}{\mathrm{RT}}}. \tag{7.8}$$

This is a very flexible mathematical function, allowing the influence of the underlying rate to be described by the pre-exponential factor A, (including the number of collisions, the molecular orientation, and factors intrinsic to the reaction mechanism) and the temperature dependence of the reaction, E_a (the proportion of molecules with sufficient energy to overcome the barriers to reaction, E_a) to be quantified. Unfortunately, even in the gas and solution phases, all theoretical attempts to make general predictions of the value of the pre-exponential factor have been unsuccessful.

The thermal decomposition of a polymer involves many competing chemical processes. The goal of chemical kinetics is to parameterise all the competing processes, so they switch in or out under different conditions. The reality is that such universal mechanisms have so far only been applied to simple gas phase systems such as the combustion methane (which itself involves over 50 reactions) [21].

Generally, solid-phase pyrolysis is assumed to follow the Arrhenius equation with three parameters defining the reaction kinetics. These kinetic parameters are reaction order, activation energy (E_a) and pre-exponential factor (A). Figure 7.20 shows how the pairs of values of A and E_a affect the mass loss rate, for a particular peak pyrolysis temperature (T_p), based on the analysis of Lyon [22]. Rearranging the Arrhenius equation gives

$$T_p = \frac{E_a}{R\ln\left(\frac{A}{k_p}\right)} \tag{7.9}$$

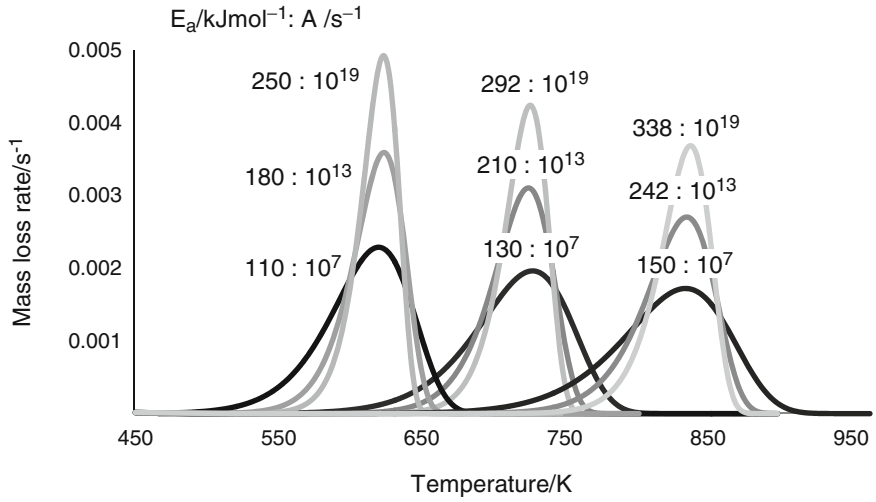

Fig. 7.20 Relationship of Arrhenius parameters A and E_a, shown as E_a in kJmol^{-1}: A in s^{-1} by the peak (T_p) of each mass loss curve, to the pyrolysis temperature and mass loss rate

Polymer decompositions are frequently free radical process, where first a bond is broken resulting in two free radicals (initiation), then the reactive free radical causes a rapid sequence of similar reactions (propagation), until a process occurs which removes the activity of the free radical (termination).

The initiation mechanism in decomposition kinetics can be considered as random- or end-chain initiation with propagation by unzipping or random chain scission, without termination reactions other than exhaustion of the polymer chain by unzipping. The rate of mass loss, $\frac{dm}{dt}$, for random-chain initiation can be considered as

$$\frac{dm}{dt} = D_p k_{ri} m \tag{7.10}$$

Where D_p is the degree of polymerisation, (or number of monomer units per polymer chain); and k_{ri} is the rate constant for the random-chain initiation reaction. Here, the rate constant of the propagation reaction is ignored in the expression because it is very rapid relative to the initiation step. The degree of polymerisation is included in the equation because, for each initiation, D_p monomer units will be released; the remaining mass, m, corresponds to the reactant concentration; and the process is assumed to follow first order kinetics. The polymer unzips completely so the molecular weight of all remaining polymer chains is the same as the initial average molecular weight.

For end-chain initiation, the rate of mass loss, $\frac{dm}{dt}$, is described by

$$\frac{dm}{dt} = D_p k_{ei} 2n \tag{7.11}$$

n the number of the polymer chains, so $2n$ is the number of chain ends, and k_{ei} is the rate constant for end-chain initiation. The number of polymer chains is simply the mass of the sample divided by the molecular weight of each chain, or

$$n = \frac{m}{D_p W_m} \tag{7.12}$$

where W_m is the molecular weight of the monomer, which allows the expression to be rearranged, to give

$$\frac{dm}{dt} = \frac{2k_{ei} m}{W_m} \tag{7.13}$$

It is apparent that for random initiation the rate is dependent on the chain length of the polymer, or "dispersity" of the sample; whereas for end-chain initiation the rate is dependent on the number of chain ends, or initiation sites. However, in both cases, the rate is assumed first order with respect to the mass of the sample and it is assumed that the average value used for D_p

adequately represents the effect of chain length on the kinetic process.

In the random-chain initiation expression, the longer chains are more likely to decompose first because they have more initiation sites, and therefore the longer chains would decompose more quickly than the shorter chains. If the initial sample had a range of molecular weights, the distribution of the molecular weight would change with time. In this case, the rate equation would be,

$$\frac{dm}{dt} = \frac{2k_{ei}m^n}{W_m} \tag{7.14}$$

with $1 < n < 2$.

Depending on the molecular weight distribution the reaction order normally lies between one and two for random-chain initiation leading to complete unzipping of a polydisperse system [23].

This comparison shows how the decomposition process can be influenced by the polymerisation process, and its influence on the molecular weight distribution. The same polymer may be polymerised using free radical, cationic, anionic or catalytic reactions, which result in different molecular weight distribution curves for polymers of the same average molecular weight. For a particular polymer sample, both end and random chain initiation reactions may be important. The activation energies for the different initiation steps may be quite different, leading to large variations in the relative rates with temperature. For instance, in PMMA, at low temperatures (around 570 K), end-chain initiation predominates. At higher temperatures (around 770 K), the random-chain initiation step dominates.

Modelling Polymer Decomposition and Pyrolysis

Historically (from 1950–1990), determination of kinetic parameters for polymer decomposition involved analysis of paper traces from thermal analysis output and numerical calculation, without the aid of computers. Only in the last 25 years has thermal analysis data been readily available in digital form. A great deal of painstaking experimental work and analysis relied on these manual techniques, and the parameters obtained are still valid, and in use today. A compilation of kinetic parameters for several common polymers, prepared by Lyon et al. [3], is included in Table 7.1. In order to set the different methods into context the brief description of the approaches is provided below.

Kinetics describing condensed phase decomposition processes often involves physical and chemical mechanisms. In pyrolysis modelling, the overall kinetic expressions are highly simplified, if considered at all. The most common assumption is that the reaction rate is described by first order or sometimes zero order kinetics.

Since the kinetic parameters cannot be measured directly, they have to be extracted by estimation methods based on microscale data. Generally there are two approaches to property estimation: direct, analytical methods [32, 24–26], and curve-fitting sometimes with the use of evolutionary algorithms [27–32]. Recently, methods based on optimisation algorithms and curve fitting have gained popularity. These methods use specific software for performing the simulation, and can analyse complicated, overlapping reactions and noisy data but still may require significant computational time for the iteration process to converge. Due to the kinetic compensation effect (where a change in the activation energy (E_a) can be partially or completely compensated for by a change in the frequency factor (A) [33], described in section "Solid Phase Kinetics" and Fig. 7.20), and other factors, the solution is not unique. Furthermore, the process is stochastic, so if it is repeated, it may not produce exactly the same parameters. Much simpler and faster are analytic methods, which give unique solutions based on reference points (such as the peak reaction rate) without requiring lengthy iterations, but often have more restrictions and limited accuracy. They only operate well on simple, non-noisy and

non-overlapping, well-separated reactions, and are often limited to a specific reaction path.

If the reaction chemistry is known it can be used to identify the reaction path. For an engineering solution of polymer pyrolysis rates, this is usually too complicated and ambitious. In polymer pyrolysis, several competing reactions occur simultaneously, which may overlap in time and temperature. This leaves pyrolysis and fire modellers with the choice of describing each reaction, with the resultant complex computations, or to mathematically mimic the mass loss rate data in its simplest form, and establish model-specific kinetics that can reproduce the experimental curve. It has been established that the model parameters can compensate for other shortcomings and simplifications [34, 35]. As approximations are inherent in a simplified reaction mechanism, and the "components" included in the mechanism may have no fundamental physical significance, choosing their values freely provides the best possible approximation to fit the experimental data. Within the two broad categories of curve-fitting and analytical methods, a number of different approaches have been developed for estimating the kinetic parameters for the thermal decomposition of polymers.

Experimental Determination of Kinetic Parameters

Solid state kinetic data are of practical interest for both thermal decomposition and combustion of polymeric materials [36]. The most popular experimental techniques used to study kinetics of thermally stimulated reactions are thermogravimetric analysis (TGA) and differential scanning calorimetry (DSC) (sections "Thermogravimetric Analysis and "Differential Thermal Analysis and Differential Scanning Calorimetry"). These techniques are capable of measuring the global kinetics of many types of thermally activated reactions but are not themselves able to give any evidence about the nature of these reactions. Techniques that can provide additional information on the mechanisms of solid state reactions are based on evolved gas analysis (section "Techniques Involving Chemical Analysis of Decomposition Products"). The most detailed detection methods for volatiles produced by thermal analysis techniques are Fourier transform infrared (FTIR) spectroscopy, and mass-spectrometry (MS), particularly when gas chromatography (GC) is used for prior separation of the individual components.

The kinetics of thermal decomposition reactions were traditionally determined under isothermal conditions. Dynamic, linear heating rates are now more common as computers are able to tackle the greater mathematical complexity of the data analyses. Various approaches to kinetic data analysis aim to provide consistent, predictive methods of reaction rate parameterisation, and contribute to a better understanding of the physical and chemical characteristics of solid state decomposition.

Mathematical Models of Polymer Decomposition Kinetics

The pyrolysis process of many polymers may be described by a simple reaction scheme:

$$A_{solid} \rightarrow B_{solid} + C_{volatile}$$

In the kinetic analysis of depolymerisation (section "Kinetics of Polymer Decomposition") it was assumed all the products were volatile, so the sample mass represented the amount of reactants. Here, both reactant and product contribute to the mass, so the rate of reaction must be expressed in terms of the degree of conversion. Kinetic models are usually based on a single-step rate Equation 7.15.

$$\frac{d\alpha}{dt} = k(T)f(\alpha) \qquad (7.15)$$

Where t is time, T is temperature, α is the degree of conversion of reactants to products, and $f(\alpha)$ is the reaction model. The rate constant, k, has the usual Arrhenius form. The kinetic parameters can be decoupled by specifying $f(\alpha)$. A reaction model that is widely used in thermal analysis [37–44], but less in pyrolysis models for fire simulation [44, 45], is the n^{th} order reaction model in which the residual conversion $1-\alpha$ is raised to the power n, so $f(\alpha) = (1-\alpha)^n$.

Solid Phase Mechanisms

Historically, several physical mechanisms of solid phase thermal decomposition kinetics were proposed [46], typically for simple inorganic systems, in order to explain experimentally derived thermal analysis data. The mechanisms have a common starting point of nucleation, where initial bond breaking leads to rearrangement, followed by the formation of gaseous and solid products. This may be repeated randomly, putting strain on the bonds around the product nucleus, and may be geometrically spherical, cylindrical or linear, often dependent upon the structure. Alternatively, a two-dimensional interface sweeps through the reactant from one end to the other. A large number of mechanisms based on diffusion of product have been proposed, which assume the rate depends on movement of gaseous reactants or products through the solid. The most commonly used are shown in Table 7.6 [47, 48, 59, 64, 65], but there is no consensus as to which ones are valid. Most of these models were devised in an attempt to interpret the simpler solid-state decompositions of inorganic solids such as calcium oxalate and calcium carbonate, involving transport processes of less complexity than those of a decomposing polymer.

The first difficulty in studying solid-state kinetics is in deciding which of such a large number of equations is being obeyed. Several equations may give very similar curves and thus appear to give equally good fits to some experimental data. The range of tools and approaches for kinetic parameter determination of solid state decomposition reactions are shown in Fig. 7.21.

For many years the different methods of obtaining the kinetic parameters for pyrolysis reactions were surrounded by controversy, as to which method was the most reliable and efficient. Each method had its limitations, frequently ignoring many factors in order to simplify the model. For example, the limitations of nonisothermal methods include the need to choose a particular reaction model, the error associated with predicting rates outside the range of experimentally determined heating rates, and if the reaction order is used as an adjustable parameter the inability to derive

Table 7.6 Reaction models used to describe the diffusional processes of solid state thermal decomposition

Reaction model		$f(\alpha)$	$g(\alpha)$
1	Power law	$\frac{2}{3}\alpha^{-1/2}$	$\alpha^{3/2}$
2	Power law	$2\alpha^{1/2}$	$\alpha^{1/2}$
3	Power law	$3\alpha^{2/3}$	$\alpha^{1/3}$
4	Power law	$4\alpha^{3/4}$	$\alpha^{1/4}$
5	One-dimensional diffusion	$\frac{1}{2}\alpha^{-1}$	α^2
6	Exponential law	α	$\ln(\alpha)$
7	Mampel (first order)	$\alpha - 1$	$-\ln(1-\alpha)$
8	Second order	$(1-\alpha)^2$	$(1-\alpha)^{-1} - 1$
9	Third-order	$(1-\alpha)^3$	$\frac{1}{2}\left[(1-\alpha)^{-2} - 1\right]$
10	Avrami-Erofe'ev[a]	$4(1-\alpha)[-\ln(1-\alpha)]^{3/4}$	$[-\ln(1-\alpha)]^{1/4}$
11	Avrami-Erofe'ev[a]	$3(1-\alpha)[-\ln(1-\alpha)]^{2/3}$	$[-\ln(1-\alpha)]^{1/3}$
12	Avrami-Erofe'ev[a]	$2(1-\alpha)[-\ln(1-\alpha)]^{1/2}$	$[-\ln(1-\alpha)]^{1/2}$
13	Three-dimensional diffusion	$2(1-\alpha)^{2/3}\left(1-(1-\alpha)^{1/3}\right)^{-1}$	$\left[1-(1-\alpha)^{1/3}\right]^2$
14	Two-dimensional diffusion	$[-ln(1-\alpha)]^{-1}$	$[(1-\alpha)ln(1-\alpha)] + \alpha$
15	Contracting sphere	$3(1-\alpha)^{2/3}$	$1-(1-\alpha)^{1/3}$
16	Contracting cylinder	$2(1-\alpha)^{1/2}$	$1-(1-\alpha)^{1/2}$

[a]Representing 3, 2 and 1 dimensional growth of nuclei respectively

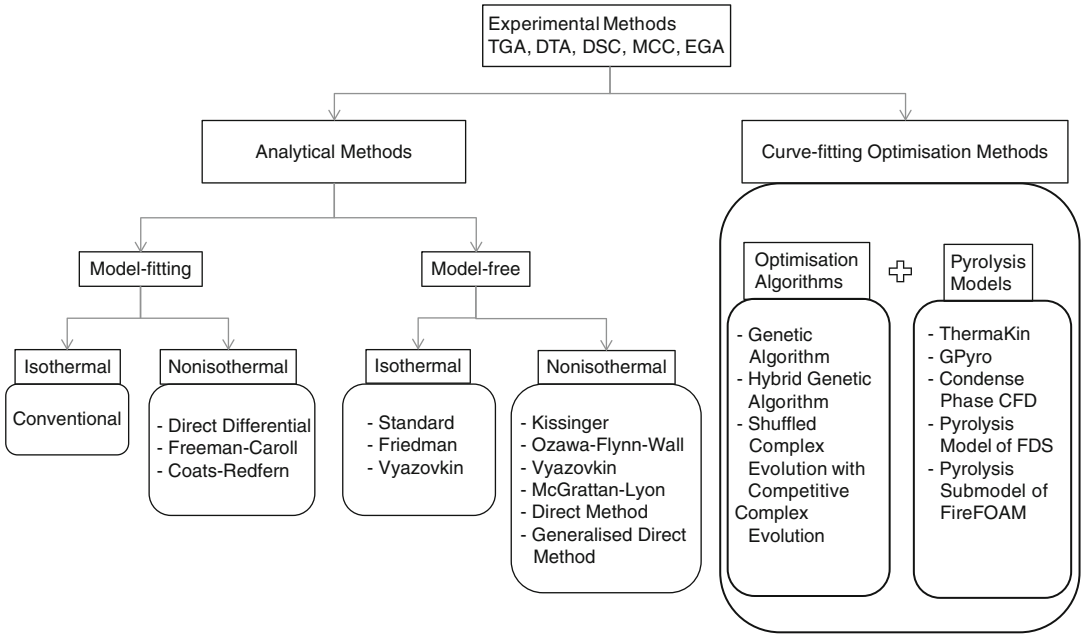

Fig. 7.21 Grouping of methods developed to study solid-phase chemical kinetics

mechanistic information from it. This could be described as curve-fitting where the physical significance of the parameter is (conveniently) ignored. The kinetic parameters that are required to calculate the reaction rates can be obtained from nonisothermal analyses by direct (inspection) and indirect (numerical regression) methods. Direct methods are fast, simple and sufficiently accurate for certain applications. Indirect methods are more flexible but require sophisticated software, and the resulting kinetic parameters may not be unique.

Very often the accuracy of a particular kinetic method and reaction model is not perfect; however such results are sufficient for predicting the time to ignition and surface temperature of a burning solid in fire simulations using a numerical pyrolysis model. Analytical methods can substitute the computationally expensive optimization methods when estimating the parameters of pyrolysis kinetics. The choice of method depends on the accuracy required, and the complexity of the experimental data. Methods with fewer reference values work better in the case of noisy data and overlapping reactions, while more complicated methods yield more accurate results for clean, simple data.

Isothermal Model-Fitting Method (Conventional Method)

This method is identical to that in the kinetics of a simple gas or solution phase reaction. It involves determination of the rate constant (k), for isothermal decomposition at a number of different temperatures.

$$g(\alpha) = kt \tag{7.16}$$

From which specific kinetic parameters such as the activation energy (E_a) and frequency factor (A) of the Arrhenius Equation 7.17 can be determined.

$$k = A\ exp\left(-\frac{E_a}{RT}\right) \tag{7.17}$$

First $g(\alpha)$ is calculated using models, such as zero or first order, or the diffusion models in Table 7.6. Once the best fit model is found, the

slope of $g(\alpha)$ *vs* time provides k for each temperature. Ln k may be plotted against $1/T$ to obtain E_a (slope) and A (intercept).

Non-isothermal Model Fitting Analytical Methods

Direct Differential Method

This method [49, 50] uses the differential form of the non-isothermal rate law

$$\frac{d\alpha}{dT} = \frac{A}{\beta} exp\left(-\frac{E_a}{RT}\right) f(\alpha) \tag{7.18}$$

Taking the logarithm of the non-isothermal rate law, gives:

$$\ln\frac{d\alpha/dT}{f(\alpha)} = \ln\frac{A}{\beta} - \frac{E_a}{RT} \tag{7.19}$$

Plotting the left-hand side versus $1/T$ gives the activation energy E_a and frequency factor A from the slope and intercept, respectively. The model that gives the best linear fit is usually chosen.

Freeman–Carroll Method

The Freeman and Carroll method [51, 52] is a differential method originally developed with a reaction model $f(\alpha) = (1-\alpha)^n$. Taking the natural logarithm of the differential form of the non-isothermal rate law gives,

$$\ln\frac{d\alpha}{dT} = \ln\frac{A}{\beta} - \frac{E_a}{RT} + \ln f(\alpha) \tag{7.20}$$

$$\Delta\ln\frac{d\alpha}{dT} = \Delta\ln f(\alpha) - \frac{E_a}{R}\Delta\frac{1}{T} \tag{7.21}$$

$$\frac{\Delta\ln\frac{d\alpha}{dT}}{\Delta\frac{1}{T}} = \frac{\Delta\ln f(\alpha)}{\Delta\frac{1}{T}} - \frac{E_a}{R} \tag{7.22}$$

$$\frac{\Delta\ln\frac{d\alpha}{dT}}{\Delta\ln f(\alpha)} = -\frac{E_a}{R}\frac{\Delta\frac{1}{T}}{\Delta\ln f(\alpha)} \tag{7.23}$$

The activation energy can be obtained from intercept $-E_a/R$ of Equation 7.22, or from the $-E_a/R$ slope of Equation 7.23.

Coats-Redfern Method

This method [53, 54] uses the integral form of the non-isothermal rate law

$$g(\alpha) = \frac{A}{\beta}\int_0^T exp\left(-\frac{E_a}{RT}\right) dT \tag{7.24}$$

Coats and Redfern utilized the asymptotic series expansion for approximating the temperature integral, producing:

$$\ln\frac{g(\alpha)}{T^2} = \ln\left(\frac{AR}{\beta E_a}\left[1 - \left(\frac{2RT_{exp}}{E_a}\right)\right]\right) - \frac{E_a}{RT} \tag{7.25}$$

Where, T_{exp} is the mean experimental temperature.

Plotting the left-hand side of Equation 7.25 versus $1/T$ gives the activation energy (E_a) and frequency factor (A) from the slope and intercept, respectively. The model with the best linear fit is chosen as the final solution. The Coats-Redfern equation was originally used with a first-order model $g(\alpha) = -\ln(1\text{-}\alpha)$ but later has been generalized to other reaction models as well.

Kissinger Method

Kissinger [41, 42] proposed a kinetic analysis method for reaction-order models ($f(\alpha) = (1-\alpha)^n$) based on taking the derivative of Equation 7.18 giving $d^2\alpha/dT^2$. Accordingly, the maximum reaction rate occurs when the second derivative is zero, from which the following equation can be obtained:

$$\frac{\beta E_a}{RT_{max}^2} = A\left(n(1-\alpha_{max})^{n-1}\right)\exp\left(-\frac{E_a}{RT_{max}}\right) \tag{7.26}$$

Where, T_{max} is the temperature of the maximum rate, β is the heating rate and α_{max} is the conversion value at that maximum rate. The maximum reaction rate represents the peak DTG curve. Taking the natural logarithm of equation above and rearranging gives,

$$\ln\frac{\beta}{T_{max}^2} = \ln\left(\frac{AR\left(n(1-\alpha_{max})^{n-1}\right)}{E_a}\right) - \frac{E_a}{RT_{max}} \tag{7.27}$$

The activation energy (E_a) is obtained by plotting the left-hand side of Equation 7.27 versus $1/T_{max}$ for a series of runs at different heating rates. Equation above has been generalized to any reaction model $f(\alpha)$ [55].

As the Kissinger method is a model-free method it does not require any modelistic assumptions to calculate E_a. However, it is not an isoconversional method because it does not calculate E_a values at progressive values of α but rather assumes a constant E_a [38].

Model-Free/Isoconversional Methods

Isoconversional methods do not rely on mathematical models such as those in Table 7.6, instead they evaluate kinetic parameters at progressive conversion values of α [56]. These methods require several kinetic curves to perform the analysis and have therefore been called, "multi-curve" methods [57, 58]. The term isoconversional derives from the analysis of several curves at different heating rates at the same degree of conversion, α. They determine the activation energy for each conversion point (E_a, α), drawing an isoconversional plot (E_a vs. α). The terms, "isoconversional" and "model-free" are sometimes used interchangeably, but not all model-free methods are isoconversional.

Model-free methods usually only calculate activation energies (E_a) from the slope of a linear equation while terms such as the frequency factor (A) and model are grouped into the intercept, and cannot be determined without assuming a particular model. Isoconversional methodologies can be used to analyse both isothermal and non-isothermal data, as described below.

Standard Isoconversional Method

This method [59, 60] can be derived by taking the logarithm of the isothermal rate law

$$g(\alpha) = Ae^{-\frac{E_a}{RT}}t \tag{7.28}$$

to give:

$$\ln g(\alpha) = \ln A - \frac{E_a}{RT} + \ln t \tag{7.29}$$

This can be rearranged to give:

$$-\ln t = \ln\left(\frac{A}{g(\alpha)}\right) - \frac{E_a}{RT} \tag{7.30}$$

A plot of –ln t versus $1/T$ for each degree of conversion, α, gives E_a from the slope for that α regardless of the model.

Ozawa, Flynn and Wall (OFW) Method

Ozawa [61], and Flynn and Wall [62] independently developed an isoconversional calculation method for nonisothermal data which is commonly referred to as the OFW method. Taking the natural logarithm of the nonisothermal rate law (Equation 7.24) and using Doyle's approximation [63] for the temperature integral gives the following,

$$\ln\beta = \ln\frac{AE_a}{Rg(\alpha)} - 5.331 - 1.052\frac{E_a}{RT} \tag{7.31}$$

For a fixed degree of conversion, α, the plot of ln β vs. $1/T$, obtained from thermograms recorded at several heating rates, should be a straight line whose slope can be used to evaluate the activation energy.

Vyazovkin's Methods

The non-isothermal rate law (Equation 7.24) can be transformed by substituting $x = E_a/RT$ to give

$$g(\alpha) = \frac{AE_a}{\beta R}\int_x^\infty \frac{e^{-x}}{x^2}dx \tag{7.32}$$

or more simply $g(\alpha) = \frac{AE_a}{\beta R}p(x)$ where $p(x) = \int_x^\infty \frac{e^{-x}}{x^2}dx$. The temperature integral $p(x)$ is a function of E_a and temperature, so can also be represented as $p(x) = I(E_a, T)$.

The first Vyazovkin method [64] is based on the assumption that the reaction model is independent of heating rate. Therefore

$$g(\alpha) = \frac{AE_a}{\beta_1 R} I(E_a, T_1) = \frac{AE_a}{\beta_2 R} I(E_a, T_2) = \cdots = \frac{AE_a}{\beta_n R} I(E_a, T_n) \tag{7.33}$$

where β_1, β_2,..., β_n, T_1, T_2, ..., T_n are different heating rates and temperatures respectively, and together with E_a and A they correspond to the same degree of conversion α.

Equation 7.33 can be reduced to:

$$\frac{I(E_a, T_1)}{\beta_1} = \frac{I(E_a, T_2)}{\beta_2} = \cdots = \frac{I(E_a, T_n)}{\beta_n} = \sigma \tag{7.34}$$

where, is a constant.

Therefore:

$$\frac{\beta_1 I(E_a, T_2)}{\beta_2 I(E_a, T_1)} = \frac{\sigma}{\sigma} = 1 \tag{7.35}$$

For n heating rates, the summation of pairs of such inverse ratios can be generalised to:

$$\sum_{i=1}^{n} \sum_{j \neq i}^{n} \frac{\beta_i I(E_a, T_j)}{\beta_j I(E_a, T_i)} = n(n-1) \tag{7.36}$$

or

$$\left(\sum_{i=1}^{n} \sum_{j \neq i}^{n} \frac{\beta_i I(E_a, T_j)}{\beta_j I(E_a, T_i)} \right) - n(n-1) = 0 \tag{7.37}$$

However for experimental data such a difference might not converge to zero, so separate values of E_a could be found for each degree of conversion, α, to find the minimum value of the following equation:

$$\left| \sum_{i=1}^{n} \sum_{j \neq i}^{n} \frac{\beta_i I(E_a, T_j)}{\beta_j I(E_a, T_i)} \right| = \Omega \tag{7.38}$$

where Ω is non-zero constant.

It is known that exponential temperature integral of the non-isothermal rate law, Equation 7.24 has no analytical solution [65, 66] but its approximation can be found in mathematical tables [67].

Later, Vyazovkin [68] modified his isoconversional method to analyse kinetics from isothermal and nonlinear heating rate experiments. In this version, the heating rate β in the nonisothermal rate law (Equation 7.24) represents the heating function with respect to time. Therefore, the temperature integral in Equation 7.24 becomes a time integral, as shown below:

$$g(\alpha) = A \int_0^t exp\left(-\frac{E_a}{RT(t)} \right) dt \tag{7.39}$$

where $T(t)$ is the heating program.

This method allows for use of linear and nonlinear heating rates and also is suitable for isothermal analysis.

Before analogical procedures should be employed as used to get to Equation 7.38 the temperature integral $I(E_a, T)$ needs to be replaced by time integral $J(E_a, T(t))$.

Vyazovkin [69] presented further modification as the advanced isoconversional method (AIC). The principle enhancement in the AIC is the integration over smaller time intervals, to better account for variations in E_a.

Therefore, Equation 7.39 was modified to give:

$$g(\alpha) = A \int_{t-\Delta\alpha}^{t} exp\left(-\frac{E_a}{RT(t)} \right) dt \tag{7.40}$$

where $\Delta\alpha = 1/m$ and m is the number of segments into which the integration is divided, typically m = 10–50.

As in the previous Vyazovkin methods, the activation energy E_a at each α is the value that minimises Ω, as shown in Equation 7.38.

Some other analytical methods for obtaining the kinetic parameters are listed in Table 7.7. These methods are fast and easy to use and they provide relatively unique and efficient solutions for most engineering applications. The direct method (DM) and generalized direct method (GDM) proposed by Matala et al. [70] consider a multiple step of n^{th} order reaction. They both describe reactions being well separated, where the DM, generally, is based on the same approach as Friedman's [26] single-step reaction model

Table 7.7 Analytical methods for obtaining kinetic parameters

Method	Kinetic parameters	
Direct method	E_a	$E_k = N_k R \frac{r_{pk}}{\alpha_k - \alpha_{pk}} T_{pk}^2$
	A	$A_k = r_{pk} \beta \frac{(\alpha_k - \alpha_{k-1})^{N_{k-1}}}{(\alpha_k - \alpha_{pk})^{N_k}} \exp\left(\frac{E_k}{RT_{pk}}\right)$
Generalized direct method	E_a	$E = \frac{-b \pm \sqrt{b^2 - 4ac}}{2a}$
		Where
		$a = \frac{(\alpha_k - \alpha_{pp})^2}{R^2 T_{pp}^4}$
		$b = -\frac{2 r_{pp} N_k (\alpha_k - \alpha_{pp})}{R T_{pp}^2} - \frac{2(\alpha_k - \alpha_{pp})^2}{R T_{pp}^3}$
		$c = r_{pp}^2 (N_k - 1) N_k - r_{T_{pp}} N_k (\alpha_k - \alpha_{pp})$
	A	$A_k = r_{p\,pk} \beta \frac{(\alpha_k - \alpha_{k-1})^{N_{k-1}}}{(\alpha_k - \alpha_{p\,pk})^{N_k}} \exp\left(\frac{E_k}{RT_{pp}}\right)$
Friedman	E_a	$E_k = -R \frac{\ln\left(\frac{r_{2k}}{r_{1k}}\right) + N_k \ln\left(\frac{\alpha_k - \alpha_{1k}}{\alpha_k - \alpha_{2k}}\right)}{\frac{1}{T_{2k}} - \frac{1}{T_{1k}}}$
	A	$A_k = \beta \frac{r_{1k} (\alpha_k - \alpha_{k-1})^{N_{k-1}}}{\exp\left(-\frac{E}{RT_{1k}}\right) (\alpha_k - \alpha_{k-1})^{N_k}}$
McGrattan et al. and Lyon et al.	E_a	$E_k = \frac{e R T_{pk}^2 r_{pk}}{\alpha_k - \alpha_{k-1}}$
	A	$A_k = \frac{e \beta r_{pk}}{\alpha_k - \alpha_{k-1}} \exp\left(\frac{E_k}{RT_{pk}}\right)$

Adapted from Ref. [70]
Note:
Reference points from first derivative of mass data (MLR curve) are: $r_p, r_{1T}, r_{2T}, T_p, T_{pk}, T_{1k}, T_{2k}, \alpha_p, \alpha_k, \alpha_{k-1}, \alpha_{1k}, \alpha_{2k}$
Values to specify from second derivative of mass data are: $r_{pp}, r_{p\,pk}, r_{T_{pp}}, T_{pp}, \alpha_{pp}, \alpha_{p\,pk}$

and the GDM relies on a higher-order derivative of the mass data. McGrattan et al. [24] and Lyon et al. [25] presented equations with slightly different derivations but essentially based on the same idea. They both analysed first-order reaction kinetics. Lyon et al. worked on a single-step reaction path but additionally offered an alternative method for extracting the reaction parameters using the heat release rate from micro-scale combustion calorimeter (MCC) data [71].

Computational Models of Polymer Decomposition

Computer simulation has become an integral part of fire safety engineering and this tendency is expected to increase with the evolution of performance based design. A broad spectrum of options for simulation is currently available, from simple programmes to various high-level packages implementing advanced methods. Despite the continuous development of tools for fire modelling, most of the development has focused on gas phase processes, particularly zone and CFD models. The current state of the art is still not capable of reliable prediction of the time to ignition of a solid polymer exposed to a constant applied heat flux. This leaves predictions of flammability, flame spread, fire growth rate, and fire suppression even further behind. Condensed phase fuel production, which plays a pivotal role in fire growth, has become an increasingly large research area in the last decade, resulting in the development of numerical models of pyrolysis incorporating

complex arrays of physical and chemical processes.

Generally, one of the first modelling tasks is to select the appropriate mechanism to represent the physical phenomena. A computer simulation environment attempts to translate real-world physical laws into their virtual form. How much simplification takes place in the translation process will determine the accuracy of the resulting model. However, this process is often subjective, and detailed justifications of the inclusion or exclusion of the different mechanisms are often lacking.

First, a new multistep decomposition method was proposed by Ohlemiller [72] where the kinetic parameters are calculated by numerical iteration from TGA mass loss (ML) and mass loss rate (MLR) measurements. This method was used by Rein et al. [28] to simulate the decomposition of polyurethane foam and by Matala [73], Lautenberger [74], Lyon and Stoliarov [75, 76] to simulate numerically the decomposition of various materials. A substantial number of studies [29, 32, 77–80] have demonstrated that numerical pyrolysis modelling (using e.g. GPyro [30, 81–83], the general pyrolysis model of FDS [84], pyrolysis submodel of FireFOAM CFD code [85] or ThermaKin [86, 87]) can describe degradation of solid materials exposed to external heat flux, and determine the relationships between the fundamental physical and chemical properties of polymeric materials and their gasification behaviour. Most of the models calculate the ML and MLR of a sample exposed to a heat source in one-dimension. Models with a controlled volume approach combine the transfer of thermal energy with Arrhenius kinetics for the decomposition of the polymer. They can predict the overall behaviour of a pyrolysing polymer by solving a set of mass and energy conservation equations using a fully implicit scheme. In many cases only three species are considered, virgin solid, char (where applicable), and pyrolysis products, and it is assumed that the virgin solid decomposes to char and/or gas phase products through a single heterogeneous *n*th order Arrhenius-type reaction. Material properties for the condensed phase species (i.e. char and/or virgin solid) may also be temperature dependent. Pyrolysis gases are assumed to be in thermal equilibrium with the solid.

Very often it is difficult to establish and quantify the kinetic mechanism of solid phase decomposition with certainty, especially for materials with complex kinetics (multistep decomposition, sequential and parallel reactions etc.) such as most polymers. Usually, condensed and gas phase species in the reactions are not characterised experimentally. However, Bustamante [88] showed that numerical approaches can be used to derive a multiple hypothetical decomposition mechanism for polyurethane foam. Additional parameters, such as chemical analysis of gas and condensed phases support the assignment of the actual decomposition mechanisms better than merely obtaining agreement with the MLR curves. The kinetic parameters in multiple reaction mechanisms, due to their complexity, must be often determined by several curve-fitting algorithms. Evolutionary algorithms are most commonly used, including genetic algorithms (GA) [27–31, 89] or shuffled complex evolution (SCE) [90, 91] algorithms. They operate on a "survival of the fittest" principle. The algorithm uses a mathematical formulation of the experimental pyrolysis data, and the optimisation process starts from a random set of automated trial solutions and tests their fitness against the experimental (TGA) curve. The suitability of the stochastic processes is assessed by its fitness value; the better the fitness value, the greater the probability of the trial solution surviving to the next iteration round. The method has a stochastic component in the mutation (one or more parameters are replaced by a random number), crossover (creating new trial solution by uniting two older solutions) and selection operations to ensure wide exploration and to avoid becoming trapped in local minima or maxima. These algorithms are very efficient for high-dimensional problems with many parameters, resistant to becoming trapped in local optima caused by overlapping reactions or even noisy data. However, they are a bit more complicated to use than the analytical methods; they are heuristic in nature; inefficient for small problems, and they require significant amount of computer resources.

Recently, modelling tools have created a more flexible simulation environment with the possibility of adding any physical effect to the model. All the relevant physical aspects of particular design may be included. Adaptability of modelling platform allows customised solutions to be developed, applicable to unique circumstances. This is very often required for the complicated process of polymer decomposition. Using tools like parameterized geometry, interactive meshing, and custom solver sequences, they can quickly adapt to different, complex requirements. With this kind of all-inclusive modelling environment, increasing the prospect of building models with real-world precision. The growth of complexity in the models has been justified by the implicit assumption that models with a higher number of mechanisms should be more accurate. However, as direct consequence, the number of parameters required to perform a simulation has also increased significantly. It is important to control the accumulation of uncertainty in the input parameters in order to prevent the model's output to extend beyond the limits of reliable prediction [92]. The global error induced by the uncertainty of a large number of parameters may exceed the improvements obtained with the incorporation of complex mechanisms; thus there remains an optimum level of model complexity.

Computational Modelling of Polymer Combustion

The same pyrolysis models may also be used to calculate the mass loss rate of a one-dimensional sample of solid fuel exposed to a uniform heat flux. ThermaKin is an example of such a model, which has been effectively utilised as a practical tool for the prediction and/or extrapolation of the results of fire calorimetry experiments [3, 93–96]. The model, which combines the absorption and transfer of thermal energy with Arrhenius kinetics for the decomposition of the polymer, predicts the overall behaviour of a pyrolysing object through mass and energy conservation equations. These equations are formulated in terms of rectangular finite elements, each element being characterised by component mass and temperature. Additionally, the model describes the transport of gaseous products through the condensed phase and follows changes in the volume of the bulk material.

For thermally thick solids (typically, thicknesses above 15 mm [97]) the thermal inertia, $k\rho c$, the product of thermal conductivity (k), density (ρ), and specific heat (c), of a material governs its ignition and flame spread properties. This determines the rate of rise in surface temperature and consequently, the time to ignition [98]. The time to ignition (t_{ig}) of a thermally thick solid exposed to a constant net heat flux $Q_{\mathrm{R}} = Q_{\mathrm{ext}} - \mathrm{CHF}$, where Q_{ext} is the external heat flux from fire or radiant heater and CHF is the critical heat flux for ignition, has been expressed in Equation 7.41.

$$t_{ig} = \frac{\pi}{4} k\rho c \frac{\left(T_{ig} - T_0\right)^2}{\dot{Q}\dot{R}^2} \tag{7.41}$$

where T_{ig} and T_0 are the ignition and ambient temperatures, respectively. The time to ignition of a thermally thin solid exposed to a constant net heat flux has also been expressed in Equation 7.42.

$$t_{ig} = \rho c \tau \frac{\left(T_{ig} - T_0\right)}{\dot{Q}_{\dot{R}}} \tag{7.42}$$

Where τ refers to material thickness. Equations 7.41 and 7.42 follow from the concept of a constant ignition temperature T_{ign} and temperature-independent thermal inertia. Once ignition has occurred and a flame is established on the surface, the net heat flux becomes $Q_{\mathrm{R}} = Q_{\mathrm{ext}} + Q_{\mathrm{flame}} - \mathrm{CHF_b}$, where Q_{flame} is the additional heat flux supplied by the flame and $\mathrm{CHF_b} \approx \sigma T_b^4$ is the critical heat flux for burning in terms of the surface burning temperature T_{b} and the Boltzmann radiation consant σ. It has been shown that $T_{\mathrm{b}} \approx T_{\mathrm{p}}$ where T_{p} is the pyrolysis temperature measured in laboratory thermal analysis experiments using small samples and constant heating rates [22]. Thus, polymers with high pyrolysis temperatures reradiate more of the incident heat flux from the heater and flame back to the surroundings, and the net heat flux that drives the burning process is reduced accordingly.

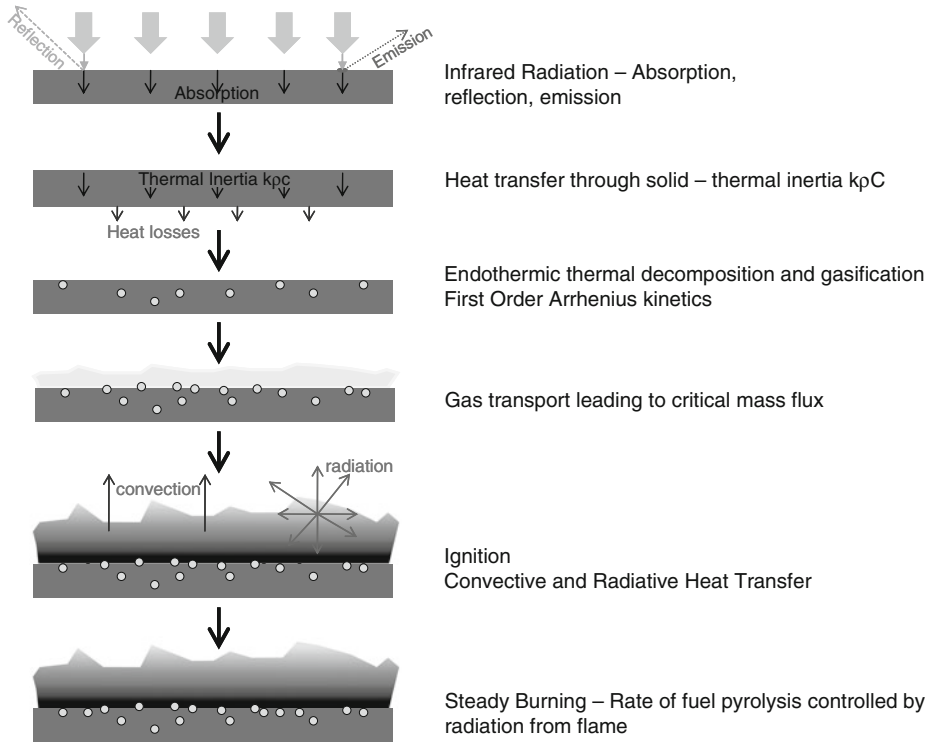

Fig. 7.22 Schematic of processes occurring in the cone calorimeter, as modelled by ThermaKin

The processes modelled by ThermaKin have been summarised in Fig. 7.22. For this study, radiant heat from above the sample is absorbed, emitted or reflected, and the condensed phase heat transfer process is modelled through the solid. The resulting temperature increases drives endothermic decomposition processes, leading to the gasification of volatile fuel components. When a critical mass flux for ignition is reached, ignition will occur, and the incident radiant flux is augmented by radiation from the flame. Thereafter, quasi-steady state conditions pertain, until the sample is so thin that it has no more capacity to absorb heat, and the rate of pyrolysis increases.

Behaviour of Individual Polymers

In general, each polymer decomposes in an individual way, and most generalisations are of limited value. A brief description of the distinctive features of selected individual polymers, their applications and thermal decomposition is provided below.

Thermoplastics

Polyethylene

Three types of polyethylene are generally available, high density polyethylene (HDPE), linear low density polyethylene (LLDPE), and low density polyethylene (LDPE). HDPE is composed of structurally regular chains with very few branch points (less than 1 % of carbon atoms) which pack efficiently, resulting in a highly crystalline material with a correspondingly higher density. The polymer is used to manufacture bottles, crates and pipes. LDPE is approximately 6 % branched with a much lower crystallinity and lower density, with good film forming properties, so that its largest application is as film for packaging, and cable coverings. LLDPE fills the gap between the two materials and is generally prepared as a

copolymer of ethylene with 8–10 % of an α-olefin such as but-1-ene, or oct-1-ene. This produces a chain with a controlled number of similar short chain branches, with densities intermediate between HDPE and LDPE. Initiation of decomposition of each of the different types of polyethylene occurs at the branching points, as observed by Madorsky (section "Chain Branching"). Thus LDPE, having a greater number of branching points and other abnormalities in its structure, decomposes at a slightly lower temperature than HDPE, although the general mechanism is the same for each type of PE. The mechanism of thermal decomposition of polyethylene follows random chain scission, resulting in a mixture of alkanes, alkenes, and dienes. The elimination of ethylene (the monomer) is not favoured energetically and pyrolysis of polyethylene does not occur by end chain scission.

The kinetics of polyethylene pyrolysis has been studied frequently [99]. It has been shown that random chain scission decomposition of polyethylene does not rigorously follow first order kinetics. The reaction order, in both dynamic and isothermal decomposition of a high density polyethylene, was determined [100] to be 0.55. The thermal decomposition of polyethylene with different characteristics, such as density or melt flow index, showed no significant differences, except in the presence of an added catalyst [101].

The thermal decomposition of polyethylene comprises several steps, presented schematically in Fig. 7.23. The temperature increase causes random scission of the polymer backbone resulting in the formation and release of a large amount of small molecules and radicals. Formation of cyclic hydrocarbons and aromatic

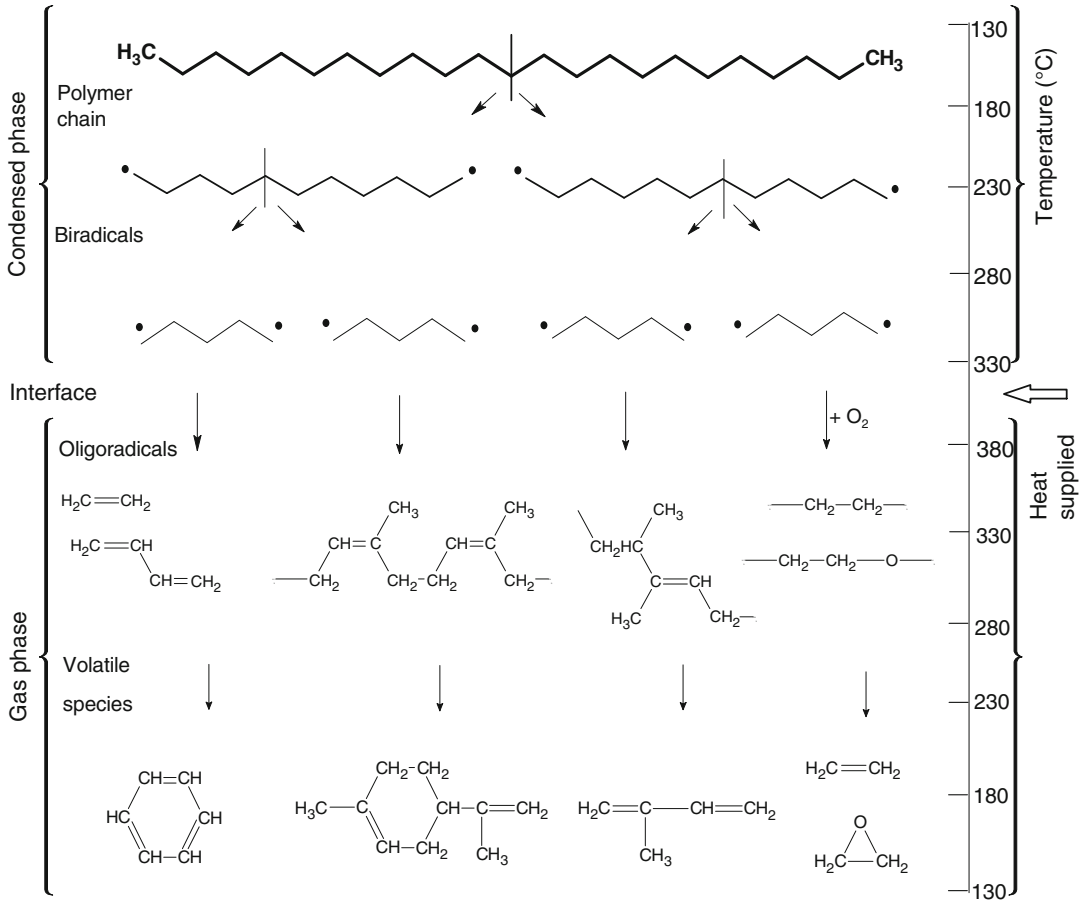

Fig. 7.23 LDPE decomposition processes [103]

rings occurs at higher temperature by Diels-Alder cyclisation reactions of alkenes. The aromatic content of the pyrolysate increases with temperature. The thermal decomposition in air (shown on the right hand side of Fig. 7.23) also produces partially oxygenated products such as aldehydes, ketones and major combustion products such as carbon monoxide, carbon dioxide, water etc.) [102].

Polypropylene

Three types of polypropylene (PP) can be synthesised; isotactic, syndiotactic and atactic, although only the isotactic form is used commercially (the difference lies in the stereochemical positioning of the methyl group relative to the main chain). Isotactic PP is highly crystalline, with a sharp melting point at 443 K. The thermal decomposition of polypropylene in an inert atmosphere also proceeds via random chain scission, to generate between 10 % and 25 % propene, in addition to other fragments, typically containing multiples of three carbon atoms (e.g. 6, 9, 12 up to 18 carbon atoms). The thermal decomposition of PP is particularly sensitive to the presence of even small (<1 %) quantities of oxygen, causing earlier fuel release, and this aspect has been studied extensively. In a detailed study [104] using a set of three isotactic polypropylene samples that had been individually labelled with carbon-13 at each of the three positions in the monomer unit (Fig. 7.24), experiments were conducted to determine the original position of the carbon forming carbon monoxide and carbon dioxide during thermal decomposition. By GC-MS analysis, it was found that 2/3 of the CO_2 was derived from the C(1) [methylene] carbon, while the remaining 1/3 comes from the C(2) [tertiary] carbon, with none coming from the C(3) [methyl group] carbon. The CO also comes mainly from the C (1) [methylene] carbon (~80 %). This is in contrast to the solid-phase oxidation products, which have been found (by C-13 NMR on these same labelled PP materials) to originate predominantly (80–85 %) from oxidation at the C(2) [tertiary] carbon. Thus oxygen preferentially attacks the main carbon backbone, resulting in release of volatile fuel at lower temperatures than from anaerobic decomposition.

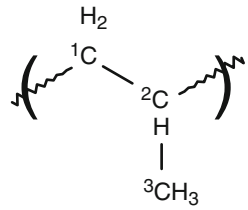

Fig. 7.24 Polypropylene repeat unit showing C (1) methylene, C(2) tertiary and C(3) methyl group carbon positions

A further investigation [105] of the volatile products provided a detailed description of the organic carbon compounds found in the vapour phase above the decomposing polypropylene. Approximately half of the volatile products identified have a methyl ketone at one end of the molecule. In all of the methyl ketones, the carbonyl carbon originates from the C(2) [tertiary] position within the PP molecule, and the terminal methyl group originates from the C (3) [methyl] position. This demonstrates the susceptibility to thermal decomposition of the C (2) branching point (c.f. LDPE and HDPE).

Polystyrene PS

Polystyrene and has good physical properties allowing for easy processing by injection moulding, transparency, good electrical insulating characteristics etc. It is typically found in atactic and amorphous forms, for example in a CD or DVD "jewel case", as well as in expanded form as EPS packaging, or EPS and extruded PS (XPS), for thermal insulation. It is entirely amorphous, with no defined melting point, above T_g it shows the classic five regions of viscoelastic behaviour. The rate of decomposition is influenced by the method of synthesis of polystyrene—anionically initiated polystyrene is more thermally stable than that produced by thermal initiation or with free radical initiators [106], presumably because it has less structural irregularities in its backbone.

Thermal analysis shows that polystyrene degrades thermally in a single step, and that monomeric styrene (~40 %) is the principal volatile, together with a much smaller amount of benzene and toluene. However there is also a significant amount of dimer, trimer, tetramer and

pentamer. These oligomers are formed in intramolecular transfer reactions, in direct competition with the monomer-producing depolymerisation process. A significant feature of the thermal degradation of polystyrene is the rapid initial decrease in molecular weight, which is followed by a more gradual fall as volatilisation exceeds 10 % [107].

Oxygen plays a very important role in the degradation of PS. The degradation mechanism involves depropagation, thermo-oxidative products include benzaldehyde, benzoic acid, phenol, and benzyl alcohol.

Polymethylmethacrylate (PMMA)

PMMA is probably the polymer with most widely studied the thermal decomposition, and the clear favourite amongst fire scientists as a model fuel. Like polystyrene, PMMA is an amorphous polymer with no defined crystalline melting point. Low molecular mass "extrudable" PMMA softens on heating to form a viscous liquid, while higher molecular mass "cast" PMMA decomposes prior to softening. Almost uniquely amongst the common polymers, lower molecular weight PMMA decomposes by end chain scission (Fig. 7.25), while higher molecular weight PMMA decomposes by a combination of end and random chain scission (Fig. 7.26) [108].

In both cases, the decomposition follows a free radical mechanism, stabilised by the four substituents on the α-carbon atom. This allows the unpaired electron to reside on the α-carbon atom long enough for the double bond to reform, releasing methyl methacrylate monomer. The monomer the yield has been quantified as 59–95 % depending on the decomposition conditions [4]. During the decomposition of high molecular weight PMMA, the monomer is evolved from the decomposing solid, avoiding the complexity of sample dripping. The combination of a single gas phase fuel molecule, and avoiding dripping, are possible reasons for this polymer's popularity in fire science. Its atypical decomposition may be one of the reasons fire scientists have not made the necessary progress on condensed phase decomposition and pyrolysis of polymers.

Polycarbonates

Polycarbonates are a class of polymers with good mechanical properties, containing the repeat group $(-O-C(O)-O-)_n$ in their backbone. They are crystal clear, highly impact resistant, amorphous engineering plastics. In addition to CD and DVD discs, they are used in the construction industry and car headlights for tough plastic

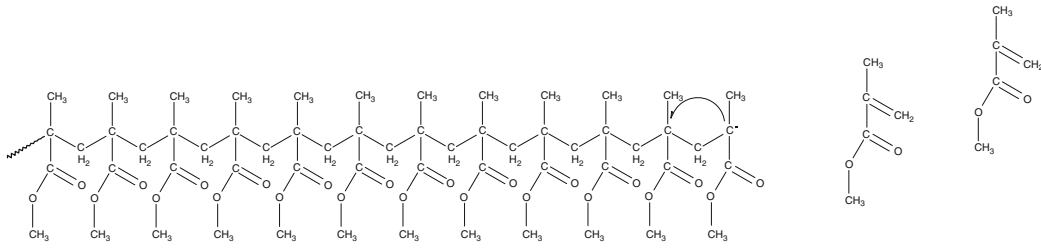

Fig. 7.25 End chain scission of PMMA

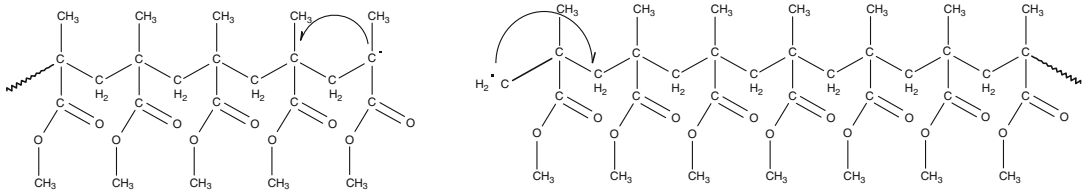

Fig. 7.26 Random chain scission of PMMA

glazing. Polycarbonates are relatively resistant to thermal decomposition, which may take place either by an anionic ester interchange route, or by free radical chain scission [109]. In either case, carbon dioxide is the main decomposition product (~35 %) and the resultant organic material forms a char. Below 675 K the decomposition products also include cyclic dimers and cross-linked species. The decomposition mechanism depends on the temperature and heating rate. Above 775 K most functionality of the original polymer is lost with the formation of aromatic compounds, leading to extensive char formation above 800 K. The maximum rate of decomposition of polycarbonate in nitrogen is around 745 K. The formation of carbon dioxide in the thermal decomposition of polycarbonate [110] can be explained by reactions of the type shown in Fig. 7.27.

The ether typically continues the decomposition process and for this reason there are similarities between the pyrolysis products of aromatic ethers and aromatic carbonates (see section "Polyetheretherketone (PEEK)")

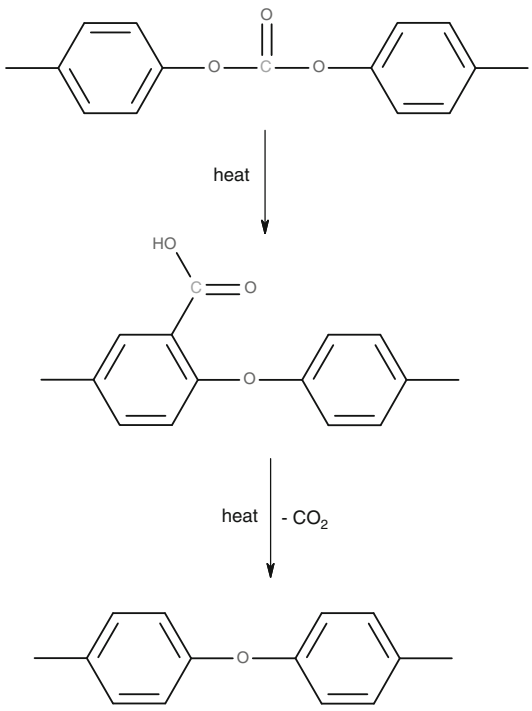

Fig. 7.27 Loss of CO_2 and ether formation in polycarbonate decomposition

Aliphatic Polyamides

Polyamides are the most widely used engineering plastics. In addition to fabrics and fibres, polyamides are widely used in motor vehicles. They are semicrystalline polymers with reasonable thermal stability but high water absorption, frequently used with glass fibre reinforcement for increased stiffness at elevated temperatures. The C—N bonds are the weakest in any polyamide, and these tend to break first, followed by the C(O)—CH_2 bonds. In an inert atmosphere, the decomposition products of polyamide 6 (−NH$(CH_2)_5$CO−)$_n$ at 875 K is predominantly the cyclic monomer (caprolactam) 73 %, with small amounts of CO_2, water and other minor decomposition products. The decomposition products from polyamides made from a diamine and a dicarboxylic acid, such as polyamide 6.6, the most widely used polyamide, include a mixture of hydrocarbons, nitriles, amides and acids [111]. Decomposition at 875 K in an inert atmosphere produced cyclopentane, 39 %, carbon dioxide, 26 %, water, 6 %, and surprisingly caprolactam, 6 % (believed to be formed by the radical bite-back mechanism [112]) and hexane dinitrile 2 %.

Polyesters, Polyethylene Terephthalate and Polybutylene Terephthalate

Polyesters are commonly used both as thermoplastics in various high volume automotive, electrical, and other engineering applications and as textile fibres. They are widely used as structural composites in glass reinforced polyesters (GRP) or "fibreglass". Commercially the most important are polyethylene terephthalate (PET) and polybutylene terephthalate (PBT), although recent demands for sustainability have favoured the development of polylactic acid (PLA), derived from biologically sourced lactic acid.

Thermal decomposition of polyesters usually starts with the scission of the polymer chain through a six-membered ring transition stage [113] (Fig. 7.28). It is believed that this scission is mostly heterolytic and not a free-radical process, although this is still under discussion in the literature. Secondary reactions mostly involve

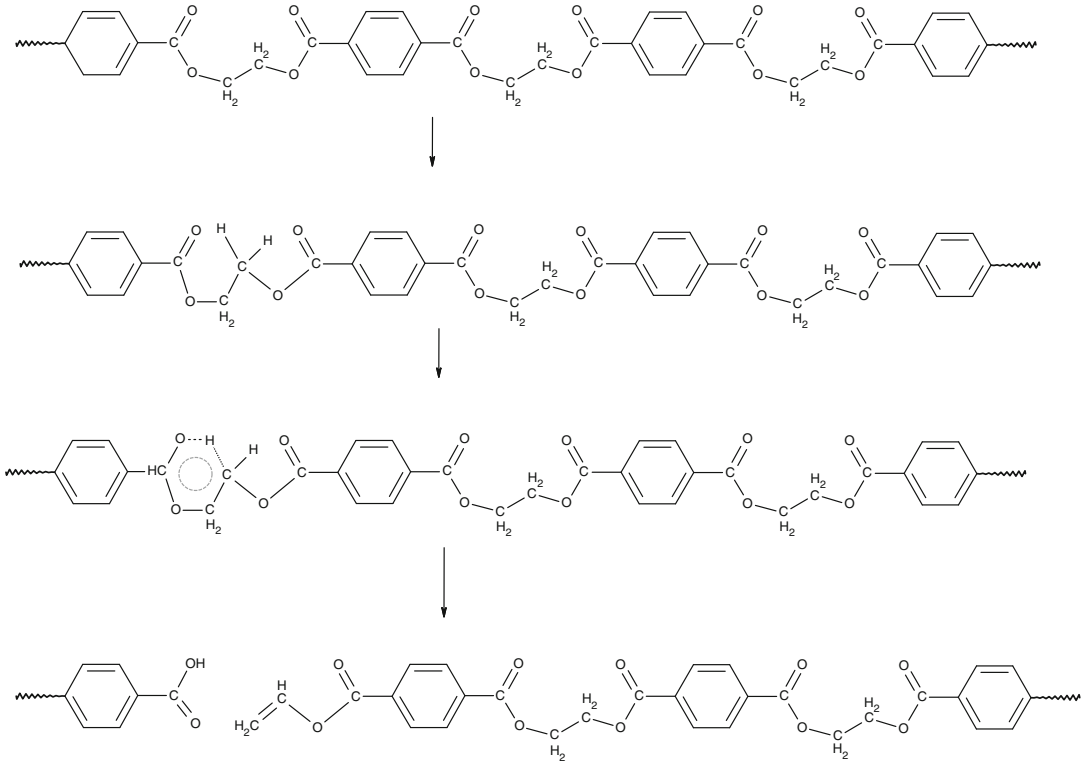

Fig. 7.28 Ring formation in the decomposition of PET

the formation of vinyl ester chain ends (CH_2 = CH-O-C(O)-Ar-) which lead to polyene structures, and crosslinking, but also evolution of light volatile products. In air, polyesters undergo crosslinking, a relatively minor process in an inert atmosphere.

Pyrolysis of PET showed evolution of benzoic acid (43 %), acetaldehyde (16 %), CO_2 (10 %), and the vinyl and divinyl esters of benzoic acid (7 and 4 % respectively). Rapid volatilization of light fragments makes polyesters easily ignitable polymers. Despite the presence of benzene groups in the main polymer chain, thermoplastic polyesters show very limited tendency to char, but instead, aromatic-containing polymer fragments volatilize and feed the flame [114].

Polyacrylonitrile (PAN)

Polacrylonitrile (PAN) is a significant bulk polymer, extensively employed in the textile industry in fibre form, which is significantly more flammable than its natural counterparts, such as wool or cotton. It is also used extensively as a copolymer, for example in acrylonitrile-butadiene-styrene (ABS) formulations. Depending on conditions, polyacrylonitrile either decomposes by cyclisation, or chain scission resulting in volatile formation, or chain stripping with the release of hydrogen cyanide [115]. The resulting structure may either decompose further producing volatiles, such as ethyne by random chain scission, and rearrangements such as cyclisation, resulting in ethyne, ethane, benzene and higher aromatics, or, under different (usually slower) conditions undergo rearrangements such that the polyene may cross-link, ultimately resulting in the formation of a protective char. This may shield the remaining polymer from radiative heating, while acting as a barrier to fuel and oxygen. Indeed, under controlled conditions of slow heating this process is used to manufacture carbon fibre from polyacrylonitrile fibre, and has been studied extensively [116].

Horrocks [117] identified three pairs of competing volatilisation and cyclisation/carbonisation decomposition reactions in pure PAN which depended on atmosphere and heating rate. At the slowest heating rates in air, cyclisation (~625 K) was followed by the first carbonisation processes, around 725 K, followed by volatilisation at around 825 K. At higher heating rates, chain scission leading to volatilisation, at around 625 K competes with cyclisation or carbonisation processes. The residue then undergoes the first carbonisation stage, and the final volatilisation stage. It is this volatilisation stage which is responsible for the high flammability of acrylonitrile polymers in general.

In the production of carbon fibres from PAN, the initial stabilisation stage is conducted under carefully controlled conditions in the presence of oxygen, where a strongly exothermic process occurs around 473 K. In DSC studies, a sharp, narrow exothermic peak is observed under inert conditions in contrast to a broad exotherm, some 50 K higher, associated with oxidising atmospheres [118, 119]. The atmosphere is then changed for nitrogen in the subsequent thermal decomposition stages, in order not to oxidise the carbon fibres.

During the stabilisation stage, the following processes, shown in Fig. 7.29 are believed to occur [120]. Polyacrylonitrile (A), particularly as a result of nucleophilic attack (X), undergoes cyclisation of nitrile groups leading to the formation of hydronaphthiridine rings [121] (B). The hydronaphthiridine rings may undergo oxidative dehydrogenation leading to acridone and other structures [122] (C) increasing the aromaticity [123].

The result is a ladder polymer containing a mixture of acridone, pyridine, hydronaphiridine and other structures. In the early stages of decomposition this ladder polymer alternates with unchanged PAN [124]. Figure 7.30 shows typical ratios of these different components obtained under certain conditions, which started to form the ladder polymer at 180 °C, as shown by FTIR [121].

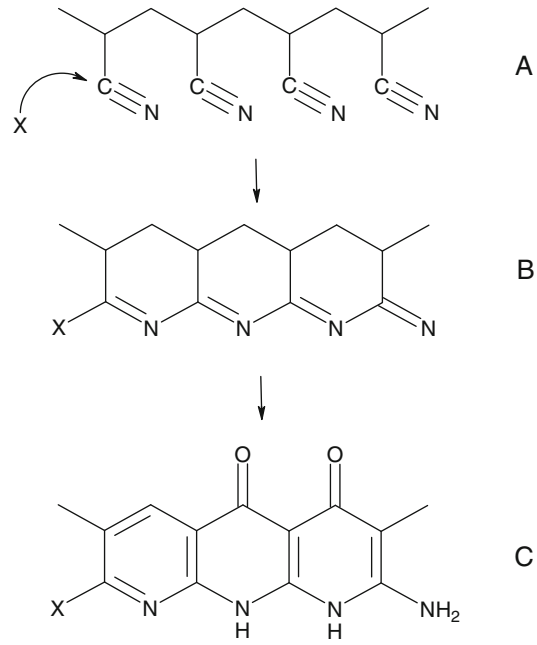

Fig. 7.29 Stages in the decomposition of PAN

Halogenated Polymers

Polyvinyl Chloride (PVC)

PVC is ranked third behind polyethylene and polypropylene in terms of worldwide polymer consumption because it has a good chemical resistance and can be used in many different applications, such as cables, pipes, furniture, etc. As the pure polymer is rather brittle it does not enjoy widespread use. The popularity of PVC lies in its unmatched ability to form a stable, dry, flexible and easily processed material when plasticized. However, this involves adding a significant amount, typically 30 %, of flammable organic liquid such as di-iso-octyl phthalate as a plasticiser, to an otherwise low flammability polymer.

At elevated temperatures PVC undergoes a dehydrochlorination reaction to release hydrogen chloride by β-elimination to form a conjugated polyene [125]. β-elimination is catalysed by acids, such as HCl, and hence the decomposition is auto catalytic and very rapid. As a consequence PVC materials usually contain stabilisers which absorb hydrogen chloride to allow the

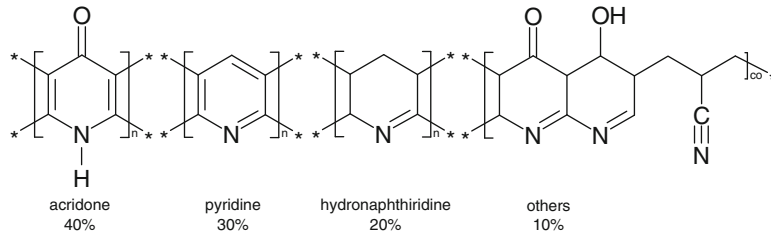

Fig. 7.30 Typical ladder polymer structure [116]

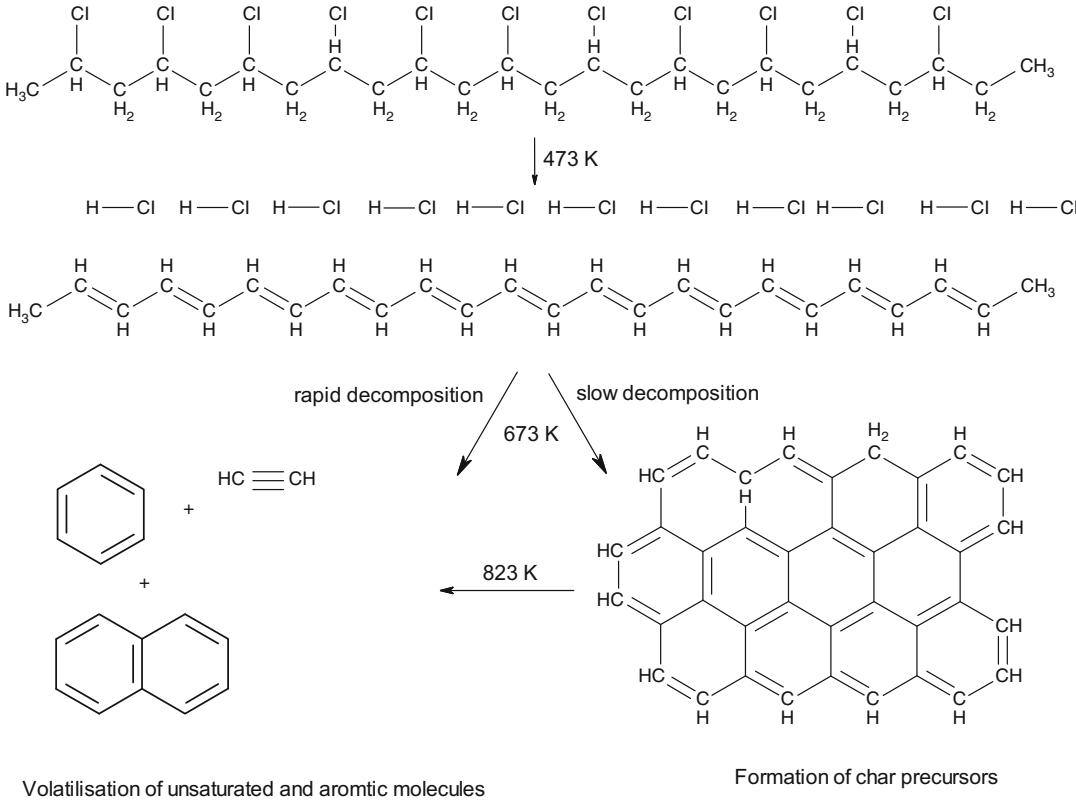

Fig. 7.31 PVC decomposition

extrusion and processing without decomposition. At higher temperatures the polyene undergoes further rearrangements and product elimination to produce a complex pattern of hydrocarbons with aromatic materials predominating (Fig. 7.31). At temperatures between 475 and 575 K, 80–95 % of the chlorine content of rigid PVC is released as HCl, 70 % within one minute at 575 K [126]. Under combustion conditions at 925 K, 75–90 % of chlorine has been recovered as HCl. As HCl is a reasonably efficient free radical trap, it removes high energy H·, ·O · and · OH radicals from the flame zone, which can quench gas phase flaming. In some formulations, some chlorine may remain in the residue. For example calcium carbonate, a common filler in PVC, will react with HCl to produce non-volatile calcium chloride, while releasing non-fuel CO_2

from the carbonate. The chorine content of the residue depends on the decomposition conditions. When a plasticised PVC containing calcium carbonate was decomposed under non-flaming conditions 58 % of chlorine was released as HCl. Under combustion conditions at 925 K, the recovery decreased to 34 %, but at 1275 K, calcium carbonate decomposes to calcium oxide and gas phase chloride recovery increased to 43 % [127].

A small proportion of the chlorine is released as other chorine containing gas or vapour species and a number of chlorine containing species have been identified from large-scale PVC fires, including mono- and dichlorobenzenes and other chloro-aromatic and chloro-aliphatic hydrocarbons [128]. Evidence exists to show that, depending on the fire situation, as much as 20 % of the chlorine may exist in an organic form [129].

PVC has a low heat of combustion, and burns with a low heat release rate, because the halogen atoms in the structure release HCl, almost 60 % of its mass, which then inhibits the conversion of CO to CO_2. This is the major heat release step in polymer combustion. When hydrogen chloride gas (HCl) comes off on heating, this causes a double bond to form between alternate carbons, strengthening the chain. As this residue gets hotter, the chain either cross-links, as double bonds open and attachments to neighbouring chains occur, eventually leading to char formation, or they break down and cyclise to form volatile aromatic hydrocarbons. If the aromatic hydrocarbons only contain a few rings, they may form into soot particles, if they are large or cross-linked the residue may form a stable protective char layer [130].

Polytetrafluoroethylene (PTFE)

PTFE has many applications due to its excellent resistant to thermal decomposition, electrical insulation and mechanical toughness. Despite being polymerised by a free radical process, the polymer has very little chain branching, and is highly crystalline. The thermal decomposition, by end chain scission, starts at 713 K, reaching a maximum at 813 K [131]. The predominant species in the vapour phase is the monomer ($CF_2 = CF_2$) at 800 K, although at 873–973 K larger fragments predominate (C_2F_4, 16 %; C_3F_6, 26 %; C_4H_8 58 %) [132]. In fires PTFE can evolve carbonyl fluoride (COF_2), which hydrolyses to produce toxic carbon monoxide and hydrogen fluoride. Under certain conditions, PTFE was found to produce supertoxic particulates on thermal decomposition [133].

Elastomers

Silicone Polymers

Silicone polymers are typically heat resistant elastomers, used as sealants, adhesives, lubricants, and for electrical insulation. Somewhat surprisingly, in North America and in aircraft, silicone foams have also been used, with some controversy, as firestops [134]. Polysiloxanes are inorganic–organic polymers that have a backbone formed from alternating oxygen and silicon atoms of the form $(-O-Si(R_2)-)_n$. Various substituents (as R) are added to the silicon atom. Polydimethyl siloxane, for example, has two methyl groups attached to the silicon atom. In addition to the linear backbone, polysiloxanes can undergo crosslinking of the macromolecular chains through oxygen bridges, giving them rubber-like properties. Low molecular weight polysiloxanes are sold as silicone fluids with many practical applications. Higher molecular weight siloxanes are cross-linked to make silicone rubbers.

The pyrolysate of polydimethyl siloxane consists of various cyclic siloxanes, such as hexamethylcyclotrisiloxane, octamethylcyclotrisiloxane, decamethylcyclotrisiloxane etc. The formation of these compounds is exemplified below in Fig. 7.32 for the formation of hexamethylcyclotrisiloxane [4].

Polyisoprenes and Other Rubbers

An elastomer is a polymer with elastic properties (section "Physical Properties") whereas a rubber generally refers to a cross-linked compound comprising elastomer and additives (Fig. 7.33).

Polyisoprene was the world's first commercially produced elastomer, originally derived from the latex of the rubber tree *Hevea*

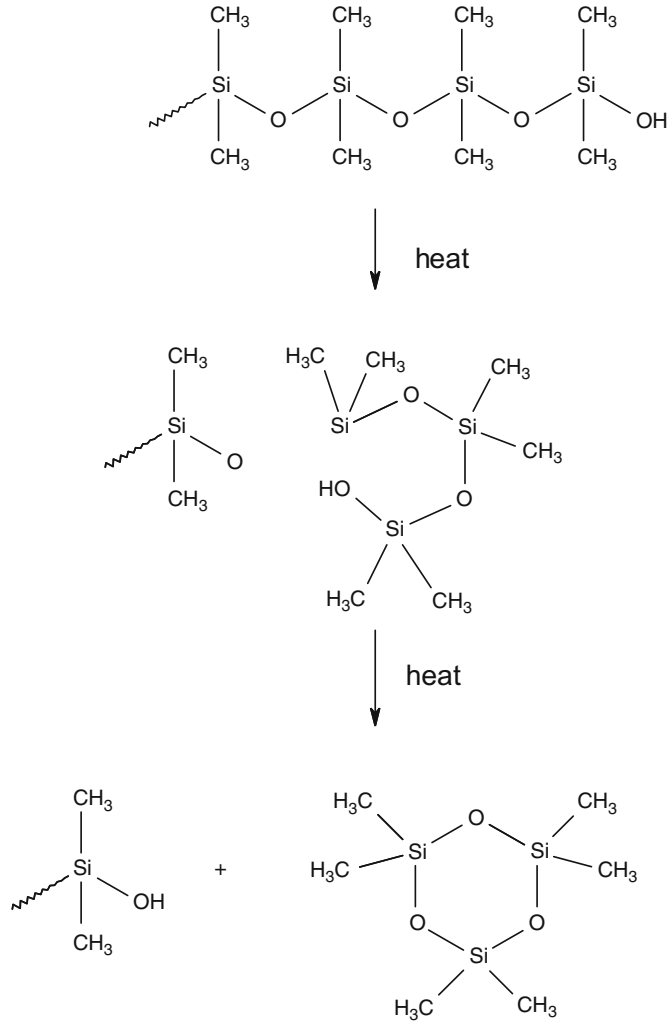

Fig. 7.32 Example decomposition of polydimethyl siloxane to hexamethylcyclotrisiloxane

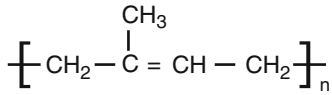

Fig. 7.33 Repeat unit polyisoprene

Brasilienis, although a synthetic equivalent was developed on an industrial scale during World War 2. The main disadvantages of natural (NR) and synthetic isoprene (IR) rubbers are their limited resistance to high temperatures and oils, which has led to the use of other elastomers such as chloroprene (CR), acrylonitrile butadiene rubber (NBR) and ethylene propylene diene modified rubber (EPDM). Nearly all of these alternative polymers have higher damping and dynamic stiffness [135], typically leading to higher noise and greater transmission of vibration.

The thermal decomposition of polyisoprenes has been reviewed elsewhere [136]. NR and IR raw polymer have identical TGA curves with a single large maximum mass loss peak [137] at 646 K in N_2 with less than 0.5 % residue at 773 K. When compounded with carbon black and sulphur into a typical commercial formulation a difference is noted; the NR mix retains a single peak temperature for mass loss, but the IR compound gains a second mass loss peak [138] at around 700 K. It is believed that IR polymer may undergo cyclisation, catalysed by small

quantities of residual titanium tetrachloride used in polymerisation.

Polyisoprene decomposes predominantly by random chain scission, initiated at a 'weak link' due to a chain defect. This defect may be due to residues from polymerisation such as initiator, or some head to head linkages. Common chemical species detected from decomposition include isoprene (2-methylbutadiene) and dipentene (1-methyl-4-(1-methylethenyl)cyclohexene), for which the yield quantities vary considerably, depending on the temperature and conditions of thermal decomposition. Typically, at temperatures below 573 K, the yields of isoprene and dipentene may be in the region of 5 and 15 % [139]. At higher temperatures, however, the isoprene yield may be significantly higher. A simplified process of depolymerisation at lower temperatures has been summarised by Cataldo [140], although at higher temperatures more species are generated, including 2,4-dimethyl-2-ethenylcyclohexene (Fig. 7.34).

Overall, polyisoprene decomposes dramatically to low molecular weight fragments which vaporise into fuel for combustion, with almost no char to slow down decomposition. This is consistent with the observation that polyisoprenes burn readily with high heat release and with high yields of small aromatic species that will create high levels of smoke.

Thermosetting Polymers

Epoxy Resins

Epoxy resins are tough, thermally stable and an important class of thermosetting polymeric material. They are widely used in electronic applications, binding carbon fibres together in metal replacement composites enjoying wide use in aerospace, automotive and even bicycle engineering applications, and find use as excellent adhesives. Typically synthesised from epichlorohydrin and *bis*-phenol A, the pre-polymer contains reactive epoxide groups as part of a polymeric diglycidylether (Fig. 7.35), terminated with epoxy groups. On the addition of an initiator or hardener, the epoxy groups react by crosslinking, resulting in a three dimensional network of polymer chains.

The thermal stability of epoxy resins, as well as their flammability, depends on the structure of the monomer, the structure of the curing agent and the crosslink density [141]. In general, the thermal stabilities of aromatic epoxy resins are higher than those of aliphatic ones, even though the crosslink densities of the aromatic networks may be lower. Usually, thermal decomposition of any epoxy resin starts from the dehydration of the secondary alcohol ($R^1C(R^2)$–OH), leading to the formation of vinylene ethers (the first step in Fig. 7.36). Upon further decomposition, aliphatic

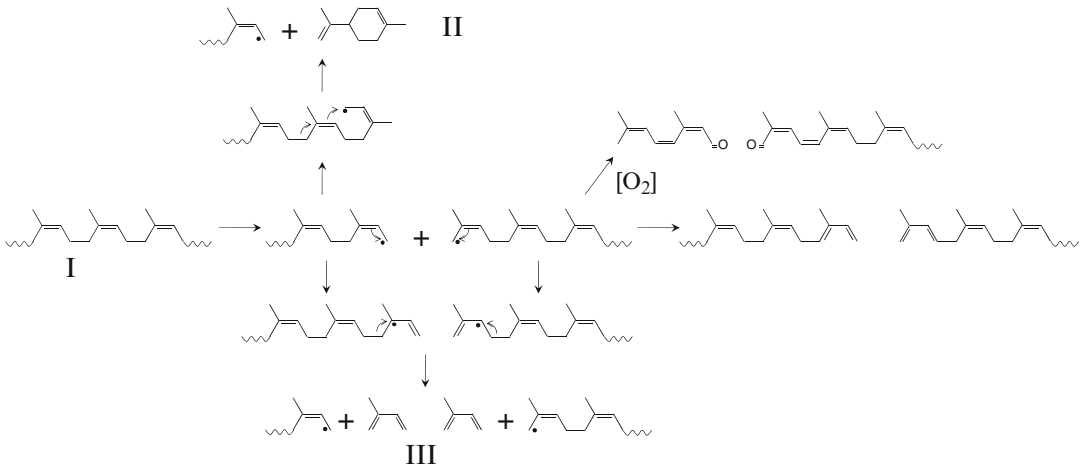

Fig. 7.34 Decomposition scheme for polyisoprene (I—polyisoprene; II—dipentene; III—isoprene) (After Ref. [142])

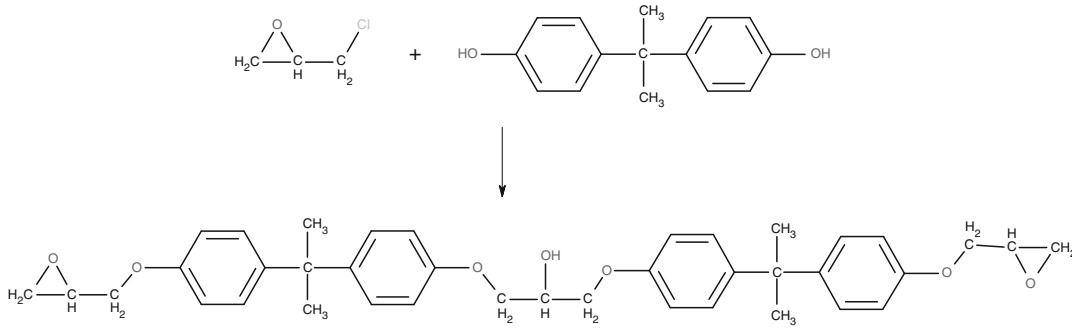

Fig. 7.35 Synthesis of an epoxy resin, showing basic repeat unit, before reaction of terminal epoxy groups

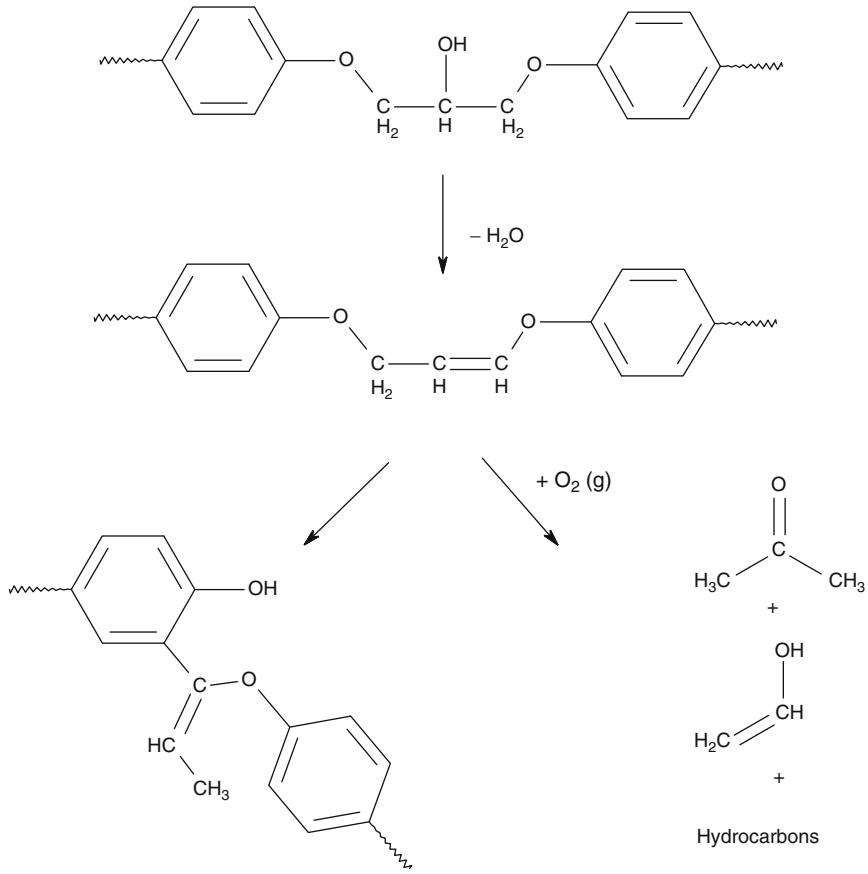

Fig. 7.36 Decomposition of epoxy resins, showing loss of water, to form a vinylene ether, followed by Claisen rearrangement to form a tri-substituted benzene char precursor

chain ends produce light combustible gases, allyl alcohol, acetone and various hydrocarbons. Alternatively, the allylic ethers or amides, formed after losing water, can undergo the Claisen rearrangement (the second step in Fig. 7.36) which changes the paraphenylene group to a 1,2,4-trisubstituted benzene with increased thermal stability [142]. This structure is partially responsible for further crosslinking and charring of epoxy resins.

Polyurethanes

Polyurethanes (PU) represent an important class of polymers and elastomers with a wide variety of structures and properties. As solids, they are used for elastomeric wheels (revolutionising skateboards and rollerblades in the 1980s), suspension components, electrical potting compounds, hoses, high performance adhesives, surface coatings and sealants. As flexible foams (PUF) they are very widely used in upholstered furnishing and carpet underlay. As rigid foams (PUR), they are widely used in thermal insulation products in buildings etc. Although included in the section on thermosets, a class of thermoplastic polyurethanes (TPU) also exist.

Polyurethanes are formed by reaction of an isocyanate ($O = C = N{-}R^1{-}N = C = O$) with a polyol ($HO{-}R^2{-}OH$) to form a polyurethane $(-C(O){-}NH{-}R^1{-}NH{-}C(O){-}R^2{-}O-)_n$. However use of isocyantes or polyols with more than two functional groups, such as $R^1(-N = C = O)_3$ or $R^2(-OH)_3$ will lead to a complex cross-linked structure. For example, in such formulations, the presence of traces of water is one way to promote cross-linking between two unreacted isocyanate groups.

$$2R - N = C = O + H_2O \rightarrow R - NH - C(O) - NH - R + CO_2$$

The reaction can continue between further isocyanate groups, and -NH groups by the formation of biuret linkages (Fig. 7.37).

The decomposition of polyurethanes is dependent on the chemistry of both the polyol and the isocyanate and the polymerisation process. Variation of R1, R2 and the number of functional groups in the polyol and isocyante leads to a large variety of PU polymers. In flexible PU foams, the polymer decomposes to form a pool, isocyanate tends to be released first from the pool, followed by the polyol. In rigid PU foams the greater cross-linking can lead to charring of the foam.

During combustion, particularly in under ventilated conditions, polyurethanes produce toxicologically significant quantities of hydrogen cyanide [143]. This is believed to be a major contributor to fire deaths [144]. The low thermal inertia of PU foams, their resultant flammability and their widespread use, means that that they make a particularly important contribution to fire risk and hazard.

Phenolic Resins

Some of the oldest synthetic polymers were phenolic resins, originally sold as Bakelite. Today their applications include low flammability rigid components of railway seats, snooker balls, circuit boards, adhesives (particularly for plywood and other wood-based composites) and as foam thermal insulation of lower flammability than XPS, EPS or PUR. Phenolic resins are formed by reaction of a phenol with formaldehyde. They contain both aromatic rings and aliphatic carbon in the polymer backbone, and are fully cross-linked thermosetting polymers.

Ten percent of mass loss is observed between 373 and 423 K, and a further 30 % between 673 K and 1173 K in nitrogen (Fig. 7.38), through loss of water. The main volatile products of the thermal decomposition of phenolic resins found in a study using thermogravimetric

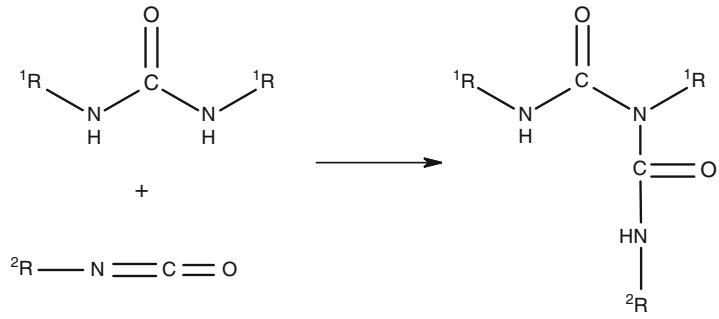

Fig. 7.37 Formation of a biuret linkage in polyurethanes

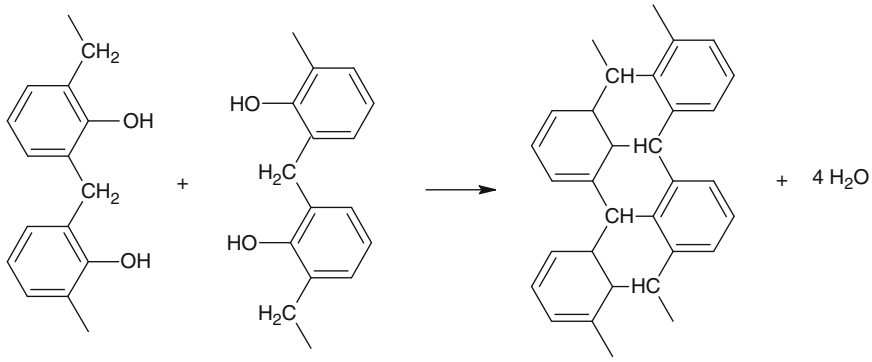

Fig. 7.38 Cross linking of phenolic resins between 373 K and 423 K accounting for 10 % mass loss

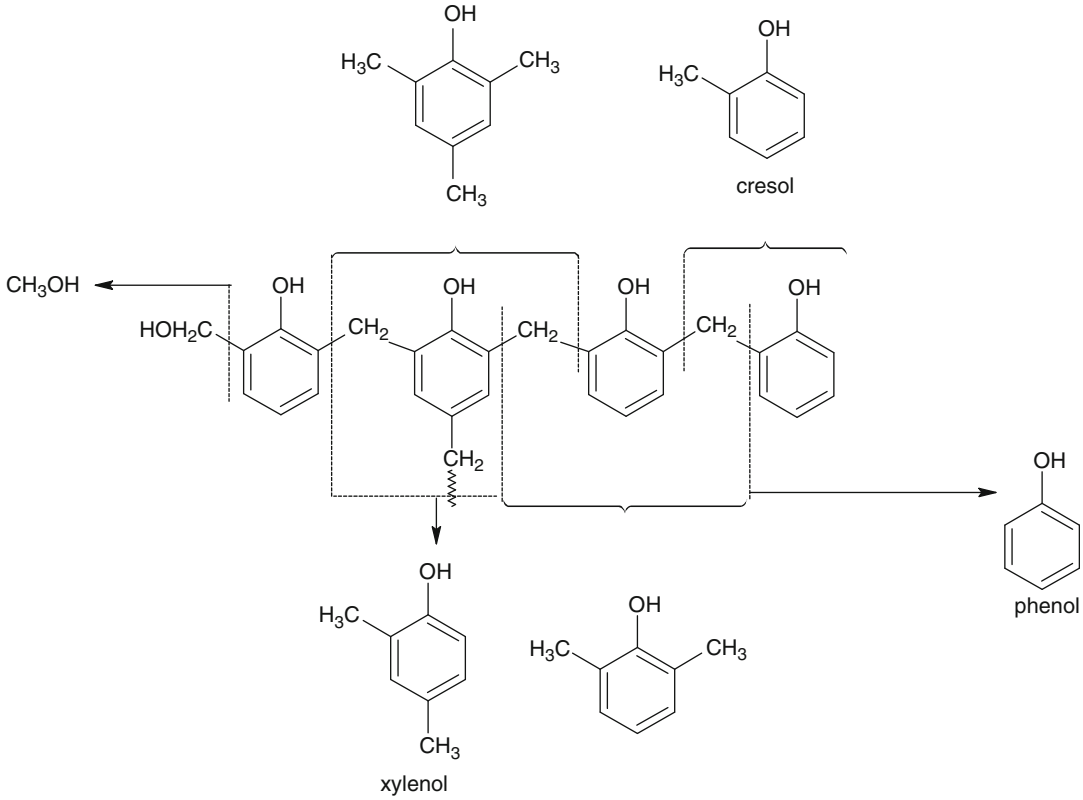

Fig. 7.39 Formation of phenol and its methyl derivatives

analysis and Fourier transform infrared spectroscopy (TGA-FTIR) at 30 K per minute include tars, various phenols and cresols, water, carbon dioxide, methane and carbon monoxide [145] (Fig. 7.39). The char residue was measured as 63 % at 975 K and 60 % at 1275 K.

Polymers with High Thermal Stability

Polyetheretherketone (PEEK)

Poly(oxy-1,4-phenyleneoxy-1,4-phenylenecarbonyl-1,4-phenylene), (PEEK), is a semi-crystalline polymer with excellent mechanical,

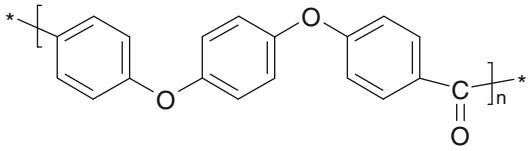

Fig. 7.40 Repeat unit of polyetheretherketone

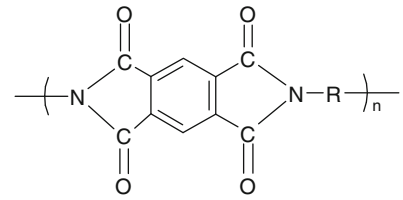

Fig. 7.41 Structure of a repeat unit of polyimide (PI)

chemical and thermal properties which permits for its use in a variety of industries and particularly as an ideal metal replacement with exceptionally high thermal stability [146].

The structure of PEEK is shown in Fig. 7.40. The stable aromatic backbone, which makes up the bulk of the monomer unit, is attributed to giving the polymer its excellent thermal properties [147, 148]. PEEK has a continuous use temperature of 533 K and a melting point of 616 K [149]. The onset of thermal decomposition occurs between 848 and 853 K. The thermal decomposition of PEEK is different in both oxygen and nitrogen environments, however, both show a two step decomposition process. In the first step around 50 % of the mass is lost, (~873 K in nitrogen and ~823 K in air), random chain scission of the ketone and to a lesser extent, the ether bonds is believed to be the main mechanism [150]. The second step is slower, with over 35 % of the residue remaining at 1273 K in nitrogen; in air mass loss is complete at 1000 K.

The main decomposition products contain lower molecular weight volatiles as well as benzene and methylbenzene. As the randomness of the main chain scission increases, other volatile products are formed such as diphenylether and CO and CO_2 at 923 K and dibenzofuran, biphenyl and naphthalene at and above 1023 K [151].

The high char yield suggests that random chain scission is accompanied by carbonisation and pyGC/MS data indicates that carbonisation might be the dominant pyrolysis pathway at temperatures above 1023 K [153].

Polyimide (PI)

Polyimide (PI) is a high-temperature, linear thermoplastic. Similar to PEEK, PI is used in high performance applications as a replacement for glass and metal products. PI contains the sequence CO – NR – CO as part of a ring structure along the backbone, shown in Fig. 7.41, the presence of which gives the polymer its high temperature properties [152].

PI has high oxidative stability and therefore can withstand temperatures of up to 533 K [154]. They are resistant to weak acids and organic solvents but not bases. PI also resists ionising radiation and has good electrical properties, however, exposure to water or steam above 100 °C may cause parts to crack rendering poor hydrolysis resistance [154]. Common uses for PI are appliance bearings, seals and electronic components and products.

Polyetherimide (PEI)

Polyetherimide (PEI) is an amorphous thermoplastic with high temperature resistance, rigidity and impact strength. PEI has similar properties to PI and although it will burn, both have self-extinguishing properties [154]. PEI also has aromatic rings in its backbone (Fig. 7.42)

PEI has low smoke emission and is resistant to alcohols, acids and hydrocarbon solvents however, dissolves in partially halogenated solvents. PEI is sold under the trade name of Ultem™ and similar to PI, the polymer is used widely thorough out the electronics industry. PEI is also used in the automotive industry for temperature sensors and lamp sockets and due to its dimensional stability is used for large, flat parts such as computer hard disks [154].

Polyphenylene Sulphide (PPS)

Polyphenylene Sulphide (PPS) is a high temperature, high strength and highly chemically resistant thermoplastic. This is indicated by the presence of an aromatic benzene ring on the

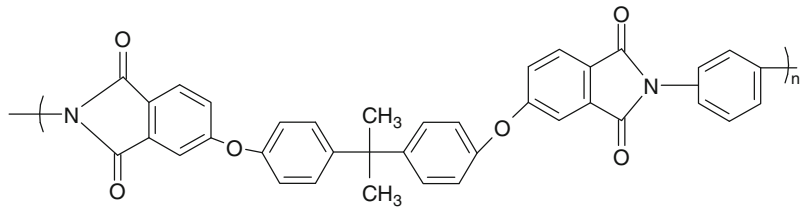

Fig. 7.42 Structure of a repeat unit of polyether imide (PEI)

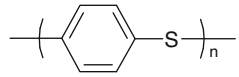

Fig. 7.43 Structure of a repeat unit of Polyphenylene Sulphide (PPS)

Table 7.8 Onset decomposition (T_d), peak mass loss temperature (T_p), and ignition (T_{ig}) temperatures of PEEK, PEI and PPS [155]

Polymer	T_d/K	T_p/K	T_{ig}/K
PEEK	843	873	843
PEI	800	828	801
PPS	777	818	848

backbone of the structure linked with an electronegative sulphur atom [154] shown in Fig. 7.43.

Due to its highly crystalline nature, PPS is brittle and is often reinforced with glass fibre. PPS has similar mechanical properties to other engineering thermoplastics and its intrinsic flame resistance allows for applications in the electronic industry and instances where the material's mechanical properties need to remain constant at elevated temperatures. As such, PPS is used for impellers and pump housings [154].

The onset of decomposition (T_d) in PEEK occurs at a higher temperature (843 K) than in PEI and PPS as is shown in Table 7.8 [153]. In both PEEK and PEI, the peak mass loss temperature (T_p) occurs after ignition, in PPS this occurs before. PPS also ignites at a higher temperature than PEI and PEEK.

Natural Polymers

Polysaccharides

Cellulosic materials contain both bound and unbound water. Unbound water is lost below its normal boiling point of 373 K. Bound water is released above 373 K in a reversible process. At higher temperatures irreversible water loss is also observed, through chemical dehydration leading to crosslinking and char formation (Fig. 7.44).

Wood based products are primarily composed of three components; hemicellulose, cellulose and lignin. Breakdown of these components, however, is not entirely simultaneous. The hemicellulose, particularly its pentosans, decompose first, largely between 473 and 533 K, followed by cellulose at 513 K to 623 K, and finally by the lignin at 653–773 K.

Cellulose evolves water in the first stage of thermal decomposition, before any other significant changes are observable. Early in the pyrolysis of cellulose some of the carbon-oxygen bonds in the links between the glucose units may be expected to undergo random chain scission (Fig. 7.44). During pyrolysis the water present from the first decomposition stage, and if hemicellulose is also present, the acids resulting from its decomposition will also be present; both serve to promote hydrolysis. The decomposition continues until molecules are small enough to be volatile are produced. These include formaldehyde, acetone, glyoxal, glycolic aldehyde, glycolic acid, lactic and dilactic acid, formic and acetic acid, as well as water, carbon monoxide and carbon dioxide.

Proteins

Proteins (poly α-amino acids) $(-NHCHRC(O)-)_n$ are linked in the same way as polyamides, but as the R substituent is different for each of over 20 amino acids, these affect their decomposition. Thermal decomposition of proteins has probably been more extensively studied than the sum of all other polymers, and is more usually described as cooking. The most important protein polymers from a fire safety perspective are silk and wool and others associated with textiles. When heated,

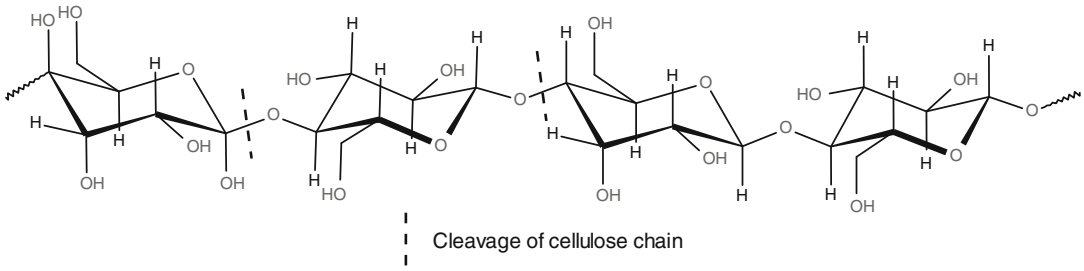

Fig. 7.44 Part of a cellulose chain showing cleavage between two glucose units

silk starts to decompose above 250 °C and forms a char. This charring characteristic is probably largely influenced by the dehydrating and cross-linking tendency of the hydroxyl group within the serine-CH_2OH substituent. Wool fibres and fabrics have significantly greater commercial applications in products such as protective clothing and contract upholstery, where high levels of fire-resistant performance are required. Wool comprises 18 α-amino acids, including nearly 10 % by mass cysteine, (−NHCH(CH_2SH)C(O)−) which dimerises forming cystine linkages (two R groups from different parts of the chain form linkages −CH_2−S−S−CH_2−) providing cross-links between adjacent chains. The high sulphur content (3–4 wt%) coupled with the high nitrogen content (15–16 wt%) contributes to the inherently low flammability of wool. The fibre also contains about 15 wt% of adsorbed moisture under normal atmospheric conditions. When wool is heated, it starts to give off its adsorbed moisture at 100 °C and above, and then starts to thermally degrade rapidly above 200 °C, with the notable evolution of hydrogen sulphide (H_2S) from cleavage of cysteine linkages above 230 °C alongside char formation. The low flammability of the volatiles, coupled with char formation, from cross-linking and dehydration of many α-substituents gives a relatively high ignition temperature of 840–870 K.

Biopolymers

Cellulose Based

Cellulose derived from wood pulp has an average of 3000 repeat units, while cellulose derived from cotton has around 15,000 repeat units. The large

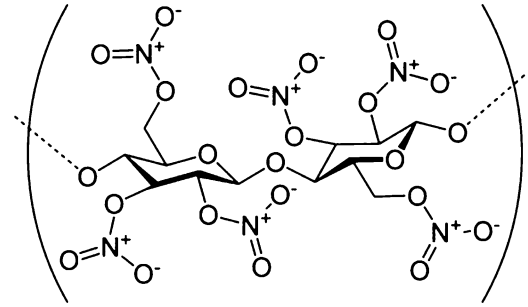

Fig. 7.45 Structure of cellulose nitrate

number of hydroxyl groups on the sugar molecule, which leave the polymer as water molecules during decomposition, result in char formation. Numerous derivates of cellulose have been prepared, including cellulose acetate ("acetate") and cellulose nitrate (once used as a medium for photographic films, now presenting a problem for safe storage of archive film), which is also used as a paint. Cellulose nitrate (or nitrocellulose) deserves special mention as it contains enough oxygen to fuel its own decomposition, and therefore can burn under water, and its heat release is not measurable by oxygen depletion calorimetry. Fortunately, its only other common use is for table-tennis balls (Fig. 7.45).

Polyesters Polylactic Acid (PLA), Polyhydroxybutyrate (PHB)

These materials have an aliphatic backbone, and are therefore more flammable than their aromatic counterparts. As the monomer may be derived from living sources, rather than fossilised material, they are favoured as being part of a cycle which does not contribute to the global increase

in carbon dioxide. They are, however, flammable and this is one of the limitations on their wider use. They are used for packaging, films etc.

Polylactic acid decomposes to produce water, carbon dioxide, acetaldehyde, acetone, acrylic acid, acetic acid and cyclic oligomers [154]. Polyhydroxybutyrate decomposes to give dimer (41 %) crotonic acid (35 %) trimer (12 %) and tetramer (3 %) below 611 K, with crotonic acid predominating at higher temperatures [155].

Fire Retardants

In general, fire retardants are more expensive than their host polymers, and are only added in order to meet regulatory requirements. If a particular polymer is used in a high risk situation (mass transport, electrical and electronic, upholstered furniture, or certain construction applications) and it is too flammable, fire retardants may be incorporated to ensure that it meets regulatory criteria. Understandably, manufacturers will optimise their materials in order to pass regulatory tests, and it is incumbent on the regulators to ensure that their tests continue to be appropriate to the types of fire retardant technologies being deployed.

Drivers in Fire Retardant Development

The history of fire retardants goes back to Egyptian times when solutions of alum (hydrated potassium aluminium sulphate ($KAl(SO_4)_2 .12H_2O$)) were used to treat timber. Gay-Lussac protected theatre fabrics from fire by treatment with mixtures of ammonium phosphate, ammonium chloride and borax which formed a glassy layer on heating [156]. However, the main driver for development came with the growth of the plastics industries and the resultant widespread use of synthetic polymers. During the 1960s and 1970s fires became more common and more severe. Anecdotally, fire fighters reported a change from fires with limited visibility, to those with almost no visibility due to dense smoke, primarily resulting from newly available low-cost polyurethane foam furniture. The increasing severity of the fire problem led to the development from empirical tests for flammability to engineering models capable of providing data on burning behaviour. This was accompanied by a shift in emphasis from ignitability to peak heat release rate. The cone calorimeter provided a reproducible means of quantifying penetrative burning into a sample, but not surface spread of flame. The main drivers in fire retardant development have been summarised in Table 7.9.

According to a survey carried out by SRI Consulting [157], the total market for flame retardants in the United States, Europe and Asia in 2007 amounted to about 1.8 million metric tons (Fig. 7.46). This market was expected to grow at an average annual rate of about 3.7 % per year on a volume basis over the period 2007–2012. It is split roughly equally between Europe, America and Asia, with halogenated flame retardants and antimony oxide comprising around 37.5 %.

Fire Retardant Strategies

The wealth of different fire retardant strategies is a testament to the ingenuity of the chemists who developed them. Fire retardant agents have been

Table 7.9 The main drivers in fire retardant development

Decade	Event	Demand
1960s	Widespread availability of cheap polymer products—more serious fires	Reduced ignitability
1970s	Smoke much worse	Reduced smoke
1980–1990s	Development of Cone Calorimeter (and emphasis on peak heat release rate, rather than ignitability)	Reduced Peak Heat Release
	Increase in deaths from smoke inhalation	Reduced Fire Toxicity
2000s	Halogen FRs found across the ecosystem	Halogen-free FRs
2010s	Climate change and other environmental concerns become mainstream	Sustainable FRs

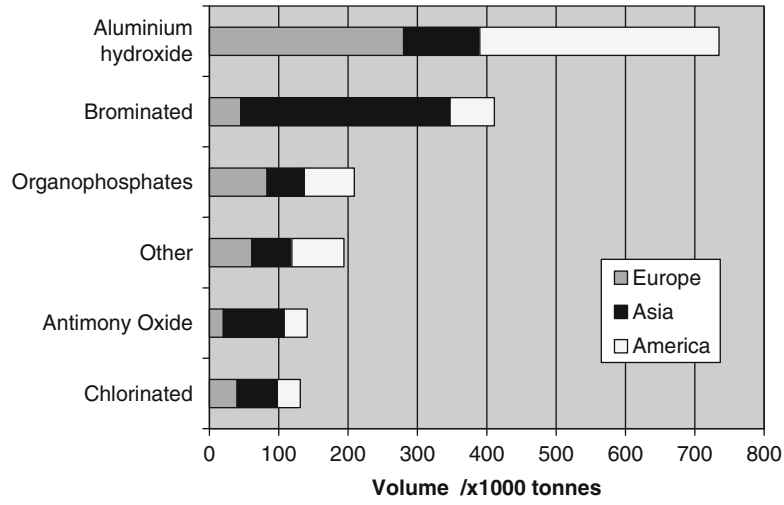

Fig. 7.46 Volume consumption of flame retardants in the USA, Europe and Asia [159]

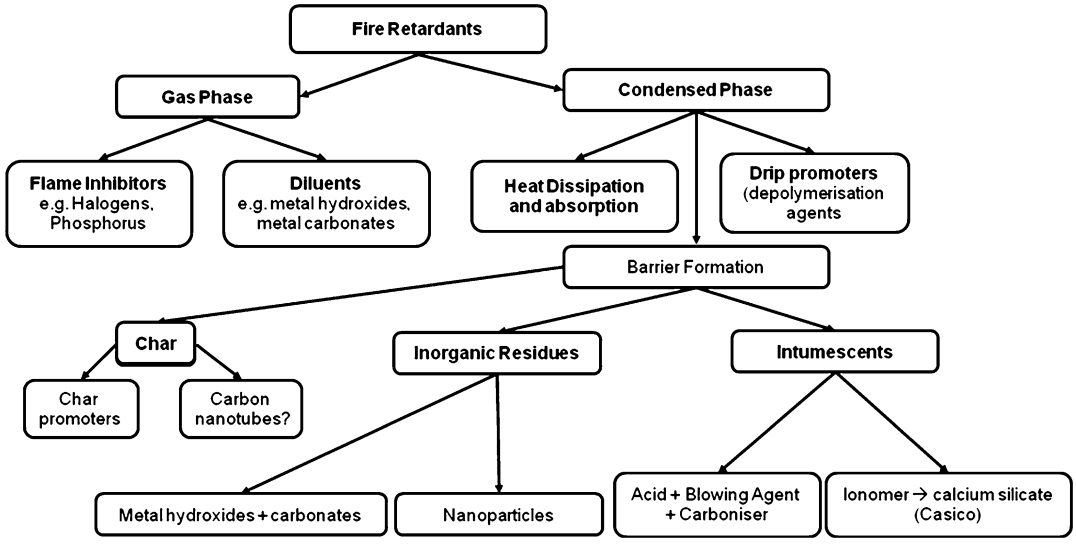

Fig. 7.47 Classification of fire retardant strategies

classified in many ways: place of action—gas or condensed phase; mode of action—physical or chemical; chemical nature of agent—halogen, phosphorus, metal hydroxide or carbonate, etc.; means of incorporation of agent—additive or reactive (i.e. bound onto the polymer chain etc.). Unfortunately, these classifications cannot be unambiguously applied to particular fire retardants—for example, the most widely used fire retardant, aluminium hydroxide releases water, so acting in the gas phase, but in doing so absorbs heat and leaves a protective residue in the condensed phase [158]. It is useful to distinguish within the broadest category: *fire* retardants include any material which reduces the flammability of the polymer; *flame* retardants inhibit the gas phase free radical reactions responsible for flaming combustion. Figure 7.47 illustrates how the major fire retardant strategies could be subdivided. Fire retardants have evolved over the last four decades in order to meet the demands of industry and regulators, from halogen based flame inhibitors to cleaner, char promoters, resulting in less smoke and toxic gas emissions.

While halogenated flame retardants continue to be used in a wide range of existing products, very little new work has been published on them. Instead, research has been heavily focussed on finding suitable halogen-free replacement fire retardants, indicating that the industry has indeed recognised the need for change, in the face of increasing pressure, predominantly resulting from environmental concerns.

A fire retardant should inhibit ignition, and may also suppress the combustion process. Most fire retardants interfere with a particular stage of combustion, e.g. during heating, decomposition, pyrolysis, ignition or sustained burning.

Physical Action

There are several ways in which the combustion process can be retarded by physical action:

- ***By cooling:*** Endothermic processes such as decomposition of additives, cool the substrate to a temperature below that required for sustaining the combustion process.
- ***By formation of a protective layer:*** The combustible components of the condensed phase can be shielded from the gaseous phase with a protective solid layer. The condensed phase is thus protected from radiation, and oxidative attack, while pyrolysis gas evolved is inhibited.
- ***By dilution:*** The incorporation of inert substances (e.g. fillers) and additives which evolve inert gases on decomposition dilutes the fuel in the condensed and gaseous phases so that the lower ignition limit of the gas mixture is not exceeded, and heat to the condensed phase is dissipated.

Chemical Action

Chemical reactions in the condensed and gas phases may interfere with the combustion process.

- ***Reaction in the gas phase:*** The radical mechanism of the combustion process which takes place in the gas phase is interrupted by the flame retardant. The radical concentration falls below a critical value, and flaming cannot occur. The exothermic processes are thus stopped, the thermal feedback to the condensed phase is reduced, so the supply of flammable volatiles is reduced.
- ***Reaction in the solid phase:*** Here two types of reaction can take place. Firstly, breakdown of the polymer can be accelerated by the fire retardant, causing pronounced flow of the polymer allowing it to recede from the flame, usually by dripping. Secondly, the fire retardant can promote the formation of a layer of carbonaceous char on the polymer surface. This can occur, for example, through the dehydrating action of the fire retardant generating double bonds in the polymer. Ultimately, these form the carbonaceous layer by cyclizing and cross-linking.

Additive vs Reactive Fire Retardants

Additive fire retardants are incorporated in the plastic either prior to, during, or, more frequently, following polymerisation. They are used especially in thermoplastics. If they are compatible with the plastic they may act as plasticisers, otherwise they are considered as fillers. They are sometimes volatile or tend to leach out of the polymer, so fire retardance may be gradually lost. The development of high molecular weight products (oligomeric and polymeric fire retardants) can eliminate this problem.

Reactive fire retardants are built into the polymer molecule, for example by attaching a fire retarding group to a monomer group. This prevents them from bleeding out of the polymer and volatilising and their fire retardance is thus retained. In addition, they have no plasticising effect and do not affect the thermal stability of the polymer. They are used mainly in thermosets (especially polyesters, epoxy resins and polyurethanes) in which they can be easily incorporated. They are, however, normally a more expensive solution than additive fire retardants. In crystalline polymers, where the structural integrity, strength and other physical properties depends on the microcrystalline structure, the presence of foreign groups on the polymer

chain is likely to have a detrimental effect on the physical properties.

Combinations of additive or reactive fire retardants with further additives can produce an *additive*, *synergistic* or *antagonistic* effect. While the *additive* effect is the sum of the individual actions, *synergism* is a greater than additive effect, and *antagonism* a less than additive effect. When used alone, some additives show no or only negligible effectiveness. The synergistic effect occurs when they are used together with other specific fire retardants. Such synergists have achieved great importance in practical use because they are often more effective or less expensive than the single fire retardants.

Halogenated Flame Retardants

There are more than 40 brominated flame retardants in current use and an additional number of chlorinated FRs [159]. These are used by simple melt blending with the polymer (additive FRs) or by incorporation into the polymer chain during polymerisation, (reactive FRs). Some additive FRs are small molecules while others are oligomers or polymers. From a health and environmental perspective, small molecules will be easiest to release from the polymer matrix (by evaporation, leaching, end-of-life processing etc.) Oligomeric or polymeric additives may be released during end-of-life processes, while reactive FRs, which have been successfully incorporated into the polymer are only likely to be problematic during burning or incineration or other end-of-life processes.

Mode of Action of Halogenated Flame Retardants

Halogenated flame retardants act by releasing hydrogen halides (HX) during thermal decomposition. If the hydrogen halide release coincides with fuel gasification, then HX can interfere with the gas phase combustion processes. Flaming combustion involves a very small number of highly reactive free radicals to propagate the gas phase oxidation processes. For ignition to occur, the number of radicals must increase. This occurs in reaction 1 and 2 where each "·"represents an unpaired electron.

$$H\cdot + O_2 \rightarrow OH\cdot + \cdot O\cdot \tag{7.43}$$

$$\cdot O\cdot + H_2 \rightarrow OH\cdot + H\cdot \tag{7.44}$$

Halogen-containing flame retardants act by interfering with the radical chain mechanism taking place in the gas phase. The high-energy OH · and H · radicals formed by chain branching are removed by the halogen-containing flame retardant.

At first the flame retardant breaks down to

$$RX \rightarrow R\cdot + X\cdot \tag{7.45}$$

where X · is either Cl · or Br · .

The halogen radical reacts to form the hydrogen halide:

$$X\cdot + RH \rightarrow R\cdot + HX \tag{7.46}$$

which in turn interferes with the radical chain mechanism:

$$HX + H\cdot \rightarrow H_2 + X\cdot \tag{7.47}$$

The removal of H · is key to elimination of the main chain branching step (when 1 unpaired electron becomes 3).

$$HX + OH\cdot \rightarrow H_2O + X\cdot \tag{7.48}$$

The removal of OH · blocks the main heat release step of hydrocarbon combustion, the conversion of CO to CO_2, by replacement with less reactive halogen free radicals in the gas phase [160]. The H· and OH· radicals are essential for many flame reactions and are involved in the main heat release in reaction 7.49.

$$CO + OH\cdot \rightarrow CO_2 + H\cdot \tag{7.49}$$

Loss of H· and OH· will increase the yield of toxic carbon monoxide and other products of incomplete combustion (hydrogen cyanide (HCN), organoirritants and soot).

The high-energy H · and OH · radicals are removed by reaction with HX and replaced with lower-energy X · radicals. The actual flame retardant effect is thus produced by HX. Kinetic reaction

schemes predict that HBr is recycled around seven times in order to account for the observed flame inhibition [161], while the HCl is not recycled.

In the condensed phase, the resulting unsaturated polyenes may act as char precursors, forming products with a tendency to cyclize and condense to yield carbonaceous products, which protect the condensed phase below the flame zone against attack by oxygen and radiant heat. In PVC, after loss of 60 % mass as hydrogen chloride from the surface layers, char formation is a significant fire retardant mechanism protecting the underlying polymer.

The halogen content in the polymer compound, and its chemical binding, will dictate the flame retardant behaviour. In the presence of antimony oxide (Sb_2O_3), the efficiency of halogenated flame retardants is improved, although antimony has no flame retardant effect on its own. This is believed to result from the formation of volatile SbX_3 and other species which are more effective halogen carriers than HX.

Metal Hydroxide and Carbonate Fillers

These involve incorporation of a material that evolves an inert gas on heating. This is often achieved with a filler material such as a metal hydroxide. For example, aluminium hydroxide not only evolves water vapour, but also absorbs a vast amount of heat as it is dehydrated.

$$2\,Al(OH)_3(s) \overset{180-200^\circ C}{\rightarrow} Al_2O_3(s) + 3\,H_2O(g)$$
$$\Delta H = +1.3\,kJ\,g^{-1}$$

This is about the same amount of energy that would heat 1.6 g of polythene to 673 K (its decomposition temperature).

In addition, aluminium hydroxide is a good conductor of heat, reducing the local hot spots, which are responsible for starting fires. Aluminium hydroxide (incorrectly referred to in industry as alumina trihydrate or ATH), accounts for half of all the fire retardant additives used by weight. However, this is partly due to its low price and the requirement for it to be present in a polymer at a 50–70 % loading to be effective.

Alternatives to aluminium hydroxide have also been investigated (Table 7.10).

The absolute contributions of these fillers to fire retardancy have been estimated [160] as shown in Table 7.11 and Fig. 7.48.

Table 7.10 Mineral filler fire retardants

Filler	Formula	T_{decomp}/°C	ΔH_{decomp}/kJ g^{-1}
Aluminium hydroxide	$Al(OH)_3$	180–200	1300
Magnesium hydroxide	$Mg(OH)_2$	300–320	1450
Calcium hydroxide	$Ca(OH)_2$	430–450	1150
Nesquehonite	$MgCO_3.3H_2O$	70–100	1750
Hydromagnesite	$Mg_5(CO_3)_4(OH)_2.4H_2O$	220–240	1300
Huntite	$Mg_3Ca(CO_3)_4$	400	980
Ultracarb	Hydromagnesite/Huntite	220–400	1172
Boehmite	AlO(OH)	340–350	560

Table 7.11 Assumptions for quantification of the magnitude of physical fire retardant effects of mineral fillers

Effect	How quantified
Diluting polymer in condensed phase	Heat capacity of the filler prior to decomposition
Endothermic decomposition of filler	Heat of decomposition
Presence of inert residue	Heat capacity of the residue after decomposition
Presence of diluent gases	Heat capacity of the diluent gases

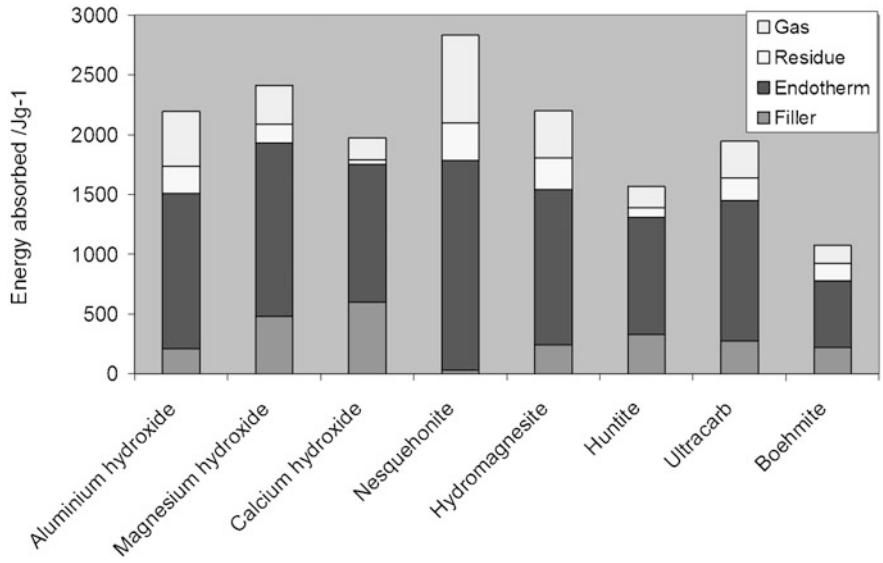

Fig. 7.48 Absolute estimation of the contributions of individual effects to the overall fire retardancy of mineral fillers [160]

Burning Behaviour of Polymeric Materials

Quantifying Fire Behaviour

Polymer flammability has no specific meaning; the flammability of a polymer is often defined by the method used to measure it [162]; flammability has been described as the ease at which a substance will ignite [163] but is also used to indicate the rate of fire growth after ignition: flammability is a function of both gas and solid phase chemistry [164]. Fire tests are crucial to the development, screening and evaluation of materials with improved fire safety. Techniques employed to measure the ignition and burning behaviour of a polymer are numerous. Some examples of fire tests are shown in

Table 7.12 together with the individual fire properties they can quantify [165].

It can be seen from Table 7.12 that no one test covers all the parameters describing fire safety behaviour, but many address more than one parameter. When selecting a test method, it is necessary to determine the end use of the product, and the likely fire scenarios. Aside from materials' development, in fire testing, there are generally two end purposes:

- To meet a regulatory requirement; and
- To demonstrate that the material being tested will perform adequately in a specific fire scenario [166].

A wide range of industry standard tests are used to demonstrate a product's suitability for a particular application, and ultimately all products with specified fire performance must meet these criteria. However, the specification of materials, or the design of fire retardant materials requires simple quantifications of a material's fire behaviour. A relatively small number of fire tests are employed in order to quantify the fire behaviour of a material. The most common of these are the limiting oxygen index (LOI) and the Underwriters' Laboratory UL 94 test, both ease of extinction tests, and the cone calorimeter, which measures time to ignition and rate of heat release.

Ignitability

Ignition is a very important parameter controlling flame spread and fire growth. However, the source of ignition necessarily impacts on the result, and therefore ignition temperature is found to depend on the design of the test used to measure it. The characteristics of several common ignition sources have been reported [167] and are shown in Table 7.13. Tests which use

Table 7.12 Common fire tests and parameters assessed

	Radiant ignition test (ISO 5657)	Glow wire test (IEC 60695-2-10–13)	Small-flame ignitability test (ISO 11925)	UL-94 (IEC 60695-11-10)	Cone calorimeter (ISO 5660)	Laterally induced flame test (ISO 5658)	Limiting oxygen index (ISO 4589-2)	Smoke density chamber (ISO 5659)	Steady state tube furnace (ISO 19700)
Ignitability	x	x	x	x	x	x			
Rate of flame spread			x	x		x			
Rate of heat release					x				
Ease of extinction							x		
Smoke production								x	x
Effluent toxicity									x

Table 7.13 Characteristics of some common ignition sources

Source of ignition	Duration of source/s	Total heat/kJ	Maximum heat flux/kW m^{-2}
Match flames	2–35	6	18–20
Cigarette lighter	30	24	16–24
Diffusion flame, small	30	8	18–32
Diffusion flame, large	30	15	6–37
Premixed flame, small	30	50	58
Premixed flame, large	30		120
Electric spark		<100 mJ	
Electric arc	1	0.4	
Electric arc	5	15	
Electric bulb, 60 W	30	3	
Electric bulb, 100 W	30	8	
Electric hot plate, 1 kW	30	30	
Electric radiator	30	90	20–25
Crumpled paper			
1/2 sheet	85	175	7–10
1 sheet	152	340	7–22
2 sheets	223	680	7–21
3 sheets	333	1020	5–22
4 sheets	335	1600	6–23
Folded paper			
5 sheets	380	1680	14
10 sheets	420	3500	15
Wastepaper basket	360	3400	10–40
	1600	5000	10–40
Small stuffed toy	330	9500	20–39
Scatter cushion	513	11,000	17–28
Bedding	1200	130,000	26

sparks, electric arcs, hot surfaces or open flames for less than 30 s will not deliver more than 100 kJ, and represent low severity tests. Crumpled or folded paper can deliver between 200 and 4000 kJ in 1–8 min, representing a medium severity exposure, while burning bedding can deliver 130,000 kJ in 20 min, representing a high severity exposure. Many standard tests use a gas or liquid fuel ignition source, of specified energy or power, corresponding to one of the "unwanted fire" ignition sources.

Ignition is a complex subject, which has been addressed by several authors [168–172] and comprehensively described and summarized elsewhere [173]. Ignition occurs when the oxidising volatiles feed enough heat back to the polymer to volatilise a similar concentration under the conditions of the test. Thus, the fraction of the heat of combustion passed back to the polymer for a given mass of fuel must be greater than its heat of gasification. This critical condition can be described by the mass loss rate at ignition. For the cone calorimeter the critical mass loss rate is around 1–6 g s^{-1} m^{-2}, and the resulting heat release rate at ignition (HRR_{ig}) is around 20–100 kW m^{-2} [174–176]. Ignition does not directly or necessarily correspond to "flammability" measured by LOI or UL 94, since both of these are ease of extinction tests, and correspond better to the minimum mass loss rate needed for sustained burning or fire propagation [177]. Ignitability can be determined by measurement of the ignition delay time, an important fire parameter, for example using a cone calorimeter.

Ease of Extinction Tests

UL-94 'Bunsen Burner' Test IEC 60695-11-10

This is a small-scale laboratory screening procedure for comparing the relative burning behaviour of vertically or horizontally oriented specimens made from plastic and other non-metallic materials, exposed to a small-flame ignition source of nominal 50 W power [178].

The method determines the linear burning rate and the afterflame/afterglow times, as well as the damaged length of specimens, and is applicable to solid and cellular materials with density of at least 0.25 g cm^{-3}, provided they do not shrink away from the applied flame without igniting. The test method described provides a classification system, which may be used for quality assurance, or the pre-selection of component materials of products, provided that the test sample thickness is the thinnest to be used in the application. The Underwriter's Laboratory designed this standard to indicate a plastic's flammability for use as part of an electrical appliance, rather than the hazards of a material under actual fire conditions. UL 94 flammability testing is the first step toward obtaining a plastic recognition and subsequent listing in the "Plastics Recognized Component Directory" (formerly known as "Yellow Cards").

The 94 V test describes the Vertical Burn test (Fig. 7.10), which is a more stringent test than the Horizontal Burn method 94HB. The set up uses a very small Bunsen flame with a manometer and needle valve to control the gas flow. The criteria for each classification are shown below (Table 7.3). While the test is crude, it is a realistic ignition scenario, and lets the user see what is happening during the test. It is easy to set up a small test burner with a 15 mm blue flame in order to provide an instant simulation of the test (Table 7.14).

For the UL-94 vertical burning test, the conditions and measures are depicted in Fig. 7.49.

Table 7.14 UL94 classifications

V-0 Vertical burn	Burning stops within 10 s after two applications of ten seconds each of a flame to a test bar. NO flaming drips are allowed
V-1 Vertical burn	Burning stops within 60 s after two applications of ten seconds each of a flame to a test bar. NO flaming drips are allowed
V-2 Vertical burn	Burning stops within 60 s after two applications of ten seconds each of a flame to a test bar. Flaming drips ARE allowed
H-B Horizontal burn	Slow horizontal burning on a 3 mm thick specimen, with a burning rate less than 3" per minute or stops burning before the 5" mark. H-B rated materials are considered "self-extinguishing"
	This is the lowest (least flame retardant) UL94 rating

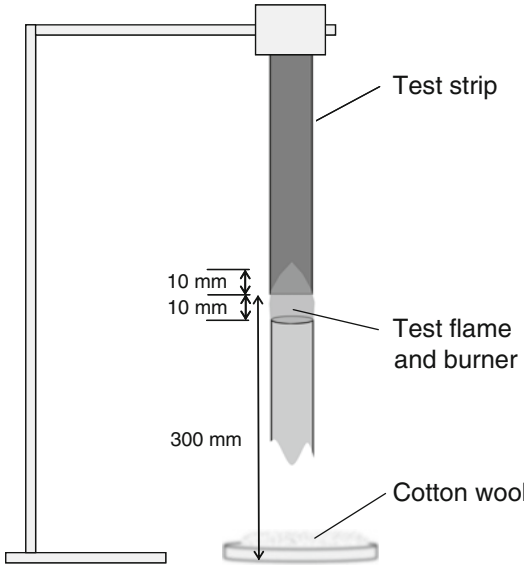

Fig. 7.49 The UL-94 vertical test arrangement

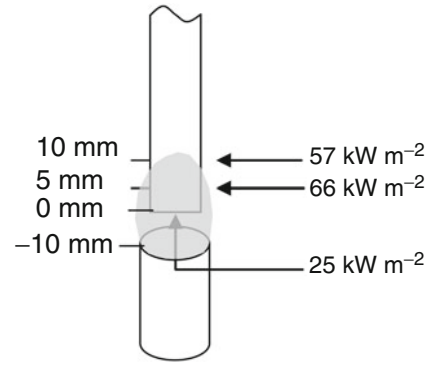

Fig. 7.50 The time-average incident burner flux in the UL-94 V test showing the heat flux at the top of the flame, 5 mm below the top, and at the base of the sample strip [189]

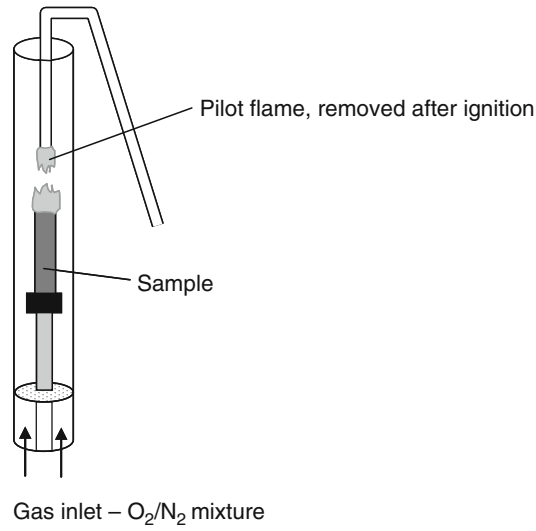

Fig. 7.51 Limiting oxygen index test

Attempts at explaining the phenomena occurring during the test have been made, however understanding the relationship between ignition and small flames has been described as 'poor or lacking' [179]. Several studies have endeavoured to correlate the results of the UL-94 test to other flammability measures, most commonly the cone calorimeter (ISO 5660 [180–185] although correlation to data, where little consensus exists on its interpretation, is ambiguous [96, 186]. The heat flux generated by the Bunsen burner, due to its partially premixed, blue diffusion flame is responsible for the ignition of the polymer and as a result, research has been conducted on determining the values for this parameter [187]. The time-average incident heat flux at height of 0.5 cm and 1 cm for the burner are shown in Fig. 7.50.

Limiting Oxygen Index

This test relates to the minimum concentration of oxygen that will just support flaming combustion in a flowing mixture of oxygen and nitrogen (Fig. 7.51) [188]. A specimen is positioned vertically in a transparent borosilicate glass test column and a mixture of oxygen and nitrogen is forced upwards through the column. The specimen is ignited at the top. If the flame remains for 3 min, or propagates down the length of the sample, the test is repeated at lower oxygen concentrations. If it self-extinguishes the test is repeated at higher oxygen concentration. The oxygen concentration is adjusted in this manner until the specimen just supports combustion. The oxygen concentration reported is the volume percent, with repeatability often as good as $\pm$ 0.1 % O_2.

Downward flame spread may be regarded as a best case scenario, and while a material with limiting oxygen index (LOI) $<$ 21 % should be considered to support downward flame spread,

materials with LOI $>>$ 21 % should still be considered flammable. Particular problems arise with materials with a high dripping propensity, since ignition will only occur under extreme circumstances. Very thin materials often have insufficient heat release per unit area to support combustion, while thicker materials conduct too much heat away from the flame zone. Thus there is a "most flammable thickness" for many materials around 1.6 mm. For non-charring materials, the criteria for ignition (heat transfer from the flame > heat of gasification per unit mass) are replicated in the criteria for extinction. However, while ignition requires a source (whose energy input will affect the result), extinction has no such dependence. The dilution of the flame by nitrogen causes the flame to swell, reducing the amount of heat fed back to the sample below the flame. As a rule of thumb, there is generally some correlation between the time to ignition in the cone calorimeter and the LOI, but none between LOI and heat release rate.

Bench-Scale Measurement of Heat Release

The Cone Calorimeter

The Cone Calorimeter [180, 189] (Fig. 7.52) was developed specifically to determine the rate of heat release and effective heat of combustion of building materials (ISO 5660–1). It was subsequently modified to determine smoke generation (ISO 5660–2) and later applied to furniture.

A horizontal specimen, 100 mm square, typically 3–6 mm, but up to 50 mm, thick is mounted under a steel frame, such that only the surfaces, but not the edges are exposed to a conical radiator pre-set to between 10 and 100 kW m^{-2} mounted beneath an instrumented hood and duct. A spark ignition is used and the specimen is mounted on a load cell. Heat release is quantified by oxygen depletion calorimetry. Measurement of heat release from real fires by oxygen depletion calorimetry is well established, and gives sensible values which relate to the

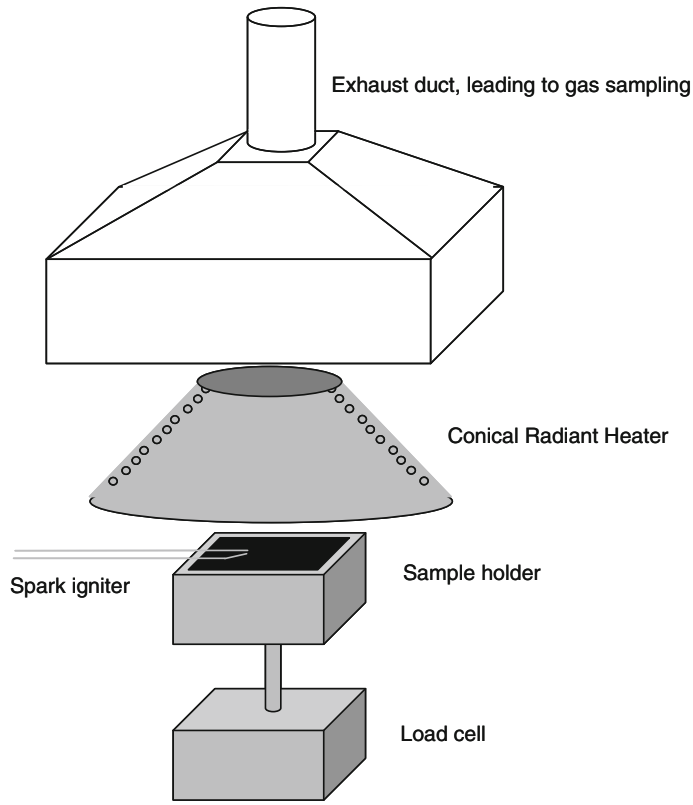

Fig. 7.52 Diagram of cone calorimeter

extent of burning. Provided the effluent flow through the exhaust is carefully controlled, the heat release will be proportional to the oxygen depletion. A sample of the effluent is cooled to remove water and analysed using a paramagnetic analyser and non-dispersive infrared CO and CO_2 analysers. It will not take into account the reduction in heat release due to the endothermic decomposition of metal hydroxide fire retardants, such as aluminium hydroxide (ATH), although this can be compensated for separately. (For PMMA containing 60 % ATH this would result in an overestimation of total heat release by ~8 %). A detailed description of the use and interpretation of data from the cone calorimeter for fire retardant materials development has been published [193]. The cone calorimeter monitors a comprehensive set of fire properties in a well defined fire scenario. The results can be used to evaluate material specific properties, setting it apart from many of the established fire tests which are designed to monitor the fire response of a certain specimen.

The cone calorimeter covers ignition followed by essentially penetrative flaming combustion, where the flame front moves through the bulk of the sample. The ignition parameter measured in the cone calorimeter is the time to ignition, which depends on the thermal inertia, critical heat flux and critical mass loss for ignition, or alternatively the critical surface temperature for ignition. Fire response parameters measured in the cone calorimeter include mass loss, heat release rate (HRR), total heat release (THR), smoke production and CO production. Fire response properties more typical of fully developed or post flashover fire scenarios are not replicated in the cone calorimeter.

There are three distinct uses of cone calorimeter data:

- To compare the fire response of materials: to assess their fire performance; to perform screening for materials development; or to develop pyrolysis and burning models.
- To determine data for input to simulations or predictions of full-scale fire behaviour.
- To determine characteristic parameters such as the maximum HRR (peak heat release rate, pHRR), fire growth rate index (FIGRA), THR etc., for regulatory purposes.

These applications of the cone calorimeter define different techniques and data evaluation. For regulatory purposes, its strengths are its well-defined conditions, reproducibility and unambiguous data evaluation of one or two characteristic values. The use of defined, and in some way ideal, burning behaviour is suitable for developing pyrolysis and burning models and for obtaining reasonable input values for the simulation of fires. However, as a fire scenario, it is not representative of most real fires. Small fires are not usually initiated with radiation from above, piloted by a spark ignition source, and surrounded by a frame which acts as a large heat sink, producing an unusual gas flow field around the flame zone, and where the effects of sample dripping are negligible.

Heat Release Curves from Cone Calorimetry

The heat release rate (HRR) during the cone calorimeter experiment gives rise to a characteristic heat release rate curves versus the time (Fig. 7.53) [174, 190].

Microscale Measurement of Heat Release

Microscale Combustion Calorimetry [192] (MCC) (section "Microscale Combustion Calorimetry") evaluates the combustibility of milligram samples by separately reproducing the solid state and gas phase processes of flaming combustion by controlled pyrolysis of the sample in an inert gas stream, followed by high temperature oxidation of the volatile pyrolysis products. Oxygen consumption calorimetry is used to measure the heat of combustion of the pyrolysis products. The maximum amount of heat released per unit mass per degree of temperature ($J\ g^{-1}\ K^{-1}$) is a material property that appears to be a good predictor of "flammability". The heat release capacity (HRC) and total heat release (THR), obtained by MCC, are related to the char yield and the heat of complete combustion of the volatiles. It takes no account of physical effects, such as dripping, wicking, and sample thickness; or chemical effects such as flame inhibition, because the conditions force

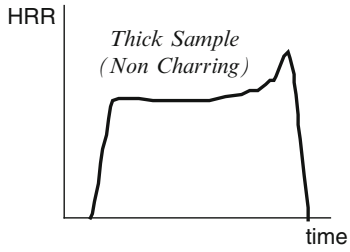	Thermally thick non-charring (or non-residue forming) samples show a strong initial increase after ignition up to a steady HRR[191]. This plateau remains until near the end of the test, when an additional pHRR occurs. This peak is caused by reduction in heat transfer by conductivity through the increasingly thin sample, since the glass wool supporting the sample prevents heat transfer to the sample holder as the pyrolysis zone approaches it.
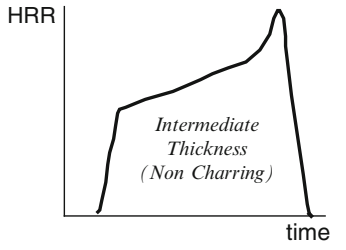	For intermediate thermally-thick, non-charring samples the plateau vanishes. The averaged or steady HRR is only marked by a shoulder. The pHRR increases in comparison with thermally thick non-charring samples since its origin is half way between the thermally-thick non-charring and thermally-thin behaviour.
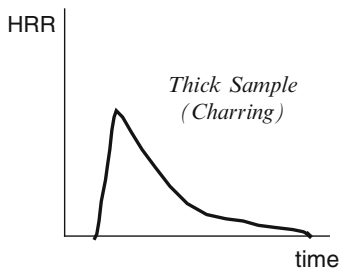	Thermally-thick charring (residue forming) samples show an initial increase in HRR until an effective char layer is formed. As the char layer thickens, this results in a decrease in HRR. The maximum reached at the beginning is the steady HRR and the pHRR. Some thermally thick charring materials, such as wood, show a pHRR at the beginning, typical for charring, and a second pHRR at the end. The second peak may be caused by cracking char or increase in effective pyrolysis temperature, as observed with the thick non-charring materials.
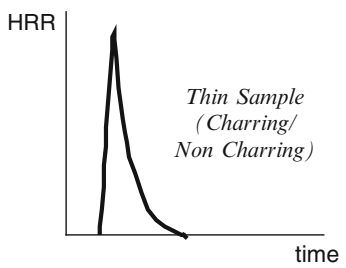	Thermally-thin samples are characterized by a sharp peak in HRR, since the whole sample is pyrolysed at the same time. In this case, the pHRR is determined by their total fire load.

Fig. 7.53 Types of heat release curves from cone calorimetry [191]

pyrolysis and combustion to completion [193]. However, varying the combustion temperature or oxygen concentration results in incomplete combustion as occurring in real fires. The THR results have been correlated to LOI; HRC and char residue to LOI; and HRC and THR with peak heat release rate (pHRR) in the cone calorimeter. It has been used as a screening test for efficacy of flame retardant additives [194].

Influence of Physical Properties on Flammability

The following factors affect polymer combustion in real fires, and should therefore influence the outcome of a suitably designed test.

Fuel production—when the fuel in the gas phase reaches a critical concentration, ignition and flaming can occur. While the fuel production rate during heating is essentially a

material property, the air flow around the sample may profoundly alter the ignition temperature.

Presence of inhibitors or diluents—Cl · or Br · or PO · are stable radicals which will reduce the critical concentration of active radicals such as H · and OH·, in the flame zone. The effect is most pronounced at ignition, and least evident under developed fire conditions.

Rheology of decomposing polymer—Some polymers depolymerise during decomposition reducing their viscosity. This allows better dispersion of heat, and material flow away from the source of heat. This can result in harmless dripping away from the flame zone, or flaming drips allowing flaming to spread downwards. Some additives (e.g. high surface area fillers, such as nanofillers) will increase the viscosity reducing dripping resulting in a more rapid increase in the surface temperature. This will reduce the time to ignition. In some cases free radical initiators are added purely to promote dripping to remove the fuel from the source of heat.

Char formation—the formation of a char on the surface of the polymer will reduce the flow of heat to and fuel from the sample. Intumescent chars bubble up and provide a more effective barrier. However, in a typical fire test, the direction of swelling is often towards the heat source, increasing the radiant flux to the sample.

Orientation of sample—as flames rise, flame spread is easiest from below (going upwards) and hardest from above (going downwards). Because of flow of molten material and ultimately dripping, it is very difficult to correlate vertical burning behaviour with horizontal burning behaviour.

Absorption of radiation—radiation from flames or a radiant panel must be absorbed by the polymer. The presence of absorbing centres (conjugated double bonds, or black pigments) can increase the localisation of the heating. Conversely, a highly reflective surface can significantly lengthen the time to ignition in certain tests.

Smoke Formation—Smoke can act as both the source of radiation (a sooty yellow diffusion flame radiates much more than a blue premixed flame) or block radiation from the flame back to the polymer.

Char Formation

Classifying polymers by the structural units they contain has been used to calculate various flammability parameters and predict burning behaviour [195, 196]. The char-forming tendency (C_{FT}) of polymers may be estimated from the contributions from each structural group, referred to as "molar group contributions". Van Krevelen has taken the char-forming tendency of the individual structural units of polymers as an additive quantity, and based on this, the following relationship has been created:

$$\mathrm{CR} \approx \frac{\sum (C_{FT})_i}{\mathrm{M}} \times 1200 \qquad (7.50)$$

Where

$$\mathrm{CR} = \mathrm{Char\,Residue}\,(\%)$$
$$\mathrm{C_{FT}} = \mathrm{Char-Forming\,Tendency\,(no\,units)}$$
$$\mathrm{M} = \mathrm{Molecular\,Weight\,of\,repeat\,unit}\left(\mathrm{g\,mol^{-1}}\right)$$

Each structural group is assigned a value. This is known as the char-forming tendency (C_{FT}) shown in Table 7.15. Aliphatic groups are generally assigned a value of zero, although if they are connected to aromatic nuclei they can have negative values (Table 7.16). Char forming tendency cannot be calculated for polymers which contain halogenated species as their soot-forming tendencies would significantly affect the char formation.

The char-forming tendency is a statistical concept. For example the phenyl group has a C_{FT} value of 1 C equivalent, which means that on average only 1 in 6 phenyl groups in the polymer forms a char, where the other 5 contribute to tar and gas formation. If the benzene ring contains 4 non-hydrogen, non-aliphatic substituents, all the rings will contribute to the char.

Table 7.15 Molar group contributions for char formation

Group	Contribution to residue per structural unit C_{FT}	Contribution to residue in C-equiv.	Group	Contribution to residue per structural unit C_{FT}	Contribution to residue in C-equiv.
"All" aliphatic groups[a]	0	0	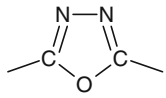	12	1
-CHOH-(exception)	4	1/3	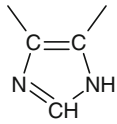	36	3.5
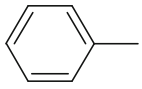	12	1	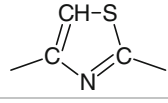	42	3.5
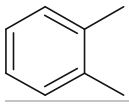	24	2	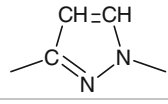	42	3.5
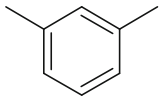	36	3	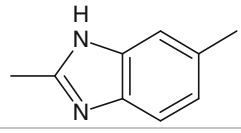	84	7
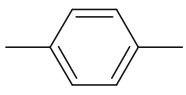	48	4	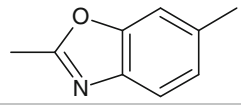	84	7
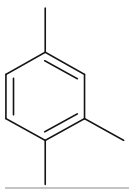	60	5	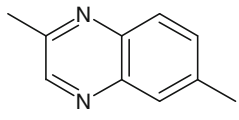	108	9
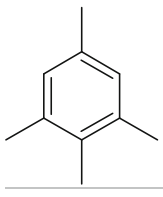	72	6	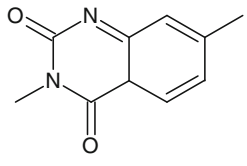	132	11
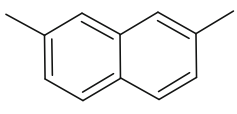	60	5	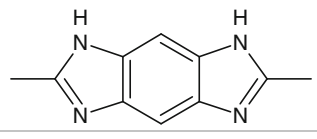	120	10
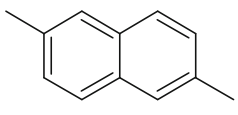	96	8	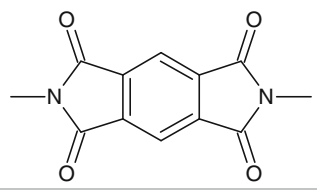	144	12

(continued)

Table 7.15 (continued)

Group	Contribution to residue per structural unit C_{FT}	Contribution to residue in C-equiv.	Group	Contribution to residue per structural unit C_{FT}	Contribution to residue in C-equiv.
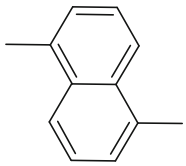	72	6	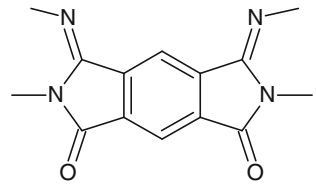	120	10
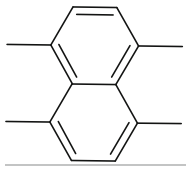	120	10	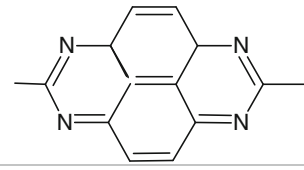	180	15
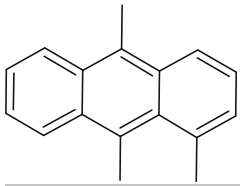	168	14			

[a]Without halogen groups

Table 7.16 Molar group contributions for char formation of aliphatic groups, connected to aromatic nuclei supplying hydrogen for the disproportionation reaction (H shift)

Group	Contribution to residue per structural unit C_{FT}	in C-equivalent
$>CH_2$ and $>CH\text{-}CH_2\text{-}$	−12	−1
$\text{-}CH_3$	−18	−3/2
$\text{-}C(CH_3)_2$	−36	−3
$\text{-}CH(CH_3)_2$	−48	−4

Example: Calculation of Char Forming Tendency (C_{FT})

Figure 7.54 shows the values assigned to the structural groups which make up the monomer unit in polyetheretherketone (PEEK) [197]:

These values are summarised in Table 7.17.

The C_{FT} of PEEK has been determined as 12 and therefore the char residue will amount to 144 g per structural unit of PEEK. The molecular weight of the PEEK monomer unit is 288.3 g mol^{-1}. These can be used to estimate the mass of the char residue (CR) to give:

$$CR \approx \frac{12}{288} \times 1200 = 50\%$$

The calculated char residue (CR) is 50 %. This is slightly greater than char yields determined by experimental methods which give values ranging from 41 % [198] to 47 % [199, 200].

Calculating Polymer Flammability from Molar Group Contributions

Recently, another useful method has been developed to calculate the heat release capacity (HRC) from additive molar group contributions. As a material flammability parameter [201–203] the

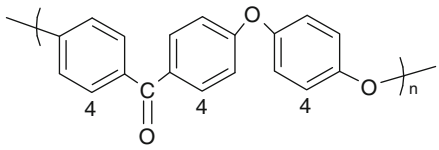

Fig. 7.54 PEEK assigned with structural group contributions for char

Table 7.17 Summary of structural group contributions and their char-forming tendencies

Chemical group	Value	N	C_{FT}
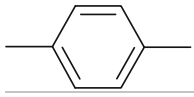	4	3	12
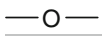	0	2	0
	0	1	0
		Total	12

HRC has been recognized as a tool for analysing fire response and flammability of polymers. A quantitative laboratory pyrolysis-combustion method for directly measuring the heat release capacity has been established [204–206], and experimental data are presented which indicate that HRC can be used to correlate polymer structure with fire behaviour.

The contribution of over 40 M groups has been correlated to HRC [207, 208] as shown in Table 7.18. The measured and estimated heat release capacities for over 80 polymers agree to within ±15 %, demonstrating a capability for prediction of polymer flammability from chemical structure.

Specific heat release rate is a molecular-level fire response parameter of a burning polymer. Lyon et al. determined the specific heat release rate using the MCC (section "Microscale Combustion Calorimetry"). Dividing the specific heat release rate (W g^{-1}) by the rate of temperature rise (K s^{-1}) gives a material fire parameter with the units (J g^{-1} K^{-1}) representing the HRC. They argue that the HRC is a true material property that is rooted in the chemical structure of the polymer, and is calculable from additive molar group contributions [199].

Example: Calculating Heat Release Capacity (HRC)

The calculation of heat release capacity is illustrated by example of molar group contributions for a diglycidylether of bisphenol-A (BPA epoxy) cured by anionic ring opening polymerization. The chemical structure of the repeat unit of the polymer is shown in Fig. 7.55.

The polymer repeat unit is comprised of six basic chemical groups, and the heat release capacity is calculated from the associated N_i, M_i, and ψ_i for these groups, which are listed in Table 7.19.

The molar heat release capacity (η_c) is obtained by summing the group contributions according to their mole fraction in the repeat unit, then dividing by the molar mass of the repeat unit to give the heat release capacity on a mass basis in units of J g^{-1} K^{-1}.

$$\eta_c = \frac{\Psi}{M} = \frac{\sum_i n_i \Psi_i}{\sum_i n_i M_i} = \frac{\sum_i N_i \Psi_i}{\sum_i N_i M_i}$$

$$= \frac{204.5\ kJ/mole - K}{340 g/mole} = 601\,\mathrm{J\,g^{-1}\,K^{-1}}$$

The predicted value of 601 J g^{-1} K^{-1} compares favourably with the measured value of 657 J g^{-1} K^{-1} for this polymer.

Conclusions

Polymeric materials fuel nearly all unwanted fires. All polymeric materials contain large molecular chains, giving them greater strength and resilience, than either small molecules or metallic structures. However, as almost all contain carbon and hydrogen they are easily oxidised and burn readily.

The diversity in the range of polymeric materials is huge and polymers may be classified in several ways: natural, biobased or synthetic; means of polymerization; thermoplastics or thermosets; molecular mass distribution; or physical properties. Each has impacts on their burning behaviour. Some polymers, such as polyamide 6, polyvinyl chloride and polyacrylonitrile differ

Table 7.18 Structural groups and their molar contribution to the heat release capacity (molar group contributions derived from a single polymer are marked*)

Structural group	Contribution/ kJ mol^{-1} K^{-1}	Structural group	Contribution/ kJ mol^{-1} K^{-1}	Structural group	Contribution/ kJ mol^{-1} K^{-1}
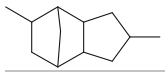	118*	—H	8.1	HO —	−19.8
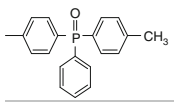	77.0		7.6	Br —	−22.0
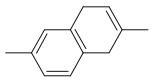	69.5	—CH_2—O—	4.18	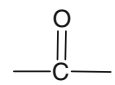	−22.0
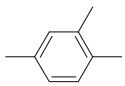	30.6		1.8	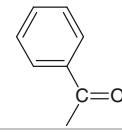	−23.2*
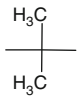	29.5	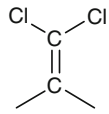	0.1	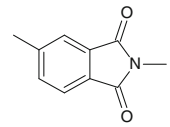	−25.5
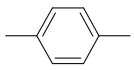	28.8	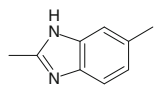	−8.8	Cl—	−34.7
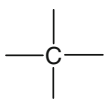	28.3	—S—	−10.9*	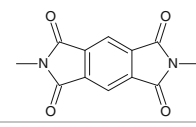	−36.4*
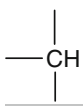	26.6	—O—	−11.6	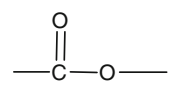	Pendant: −39.5 Backbone: −13.7
H_3C—	22.5	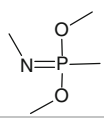	−13.8		−43.0*
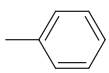	19.0	H_2N—	−13.9*	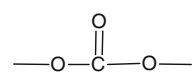	−49.0
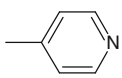	18.7	F_3C—	−14.8	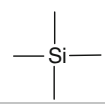	−53.5*
	16.7	—C≡N	−17.6	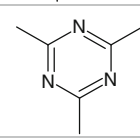	−66.7
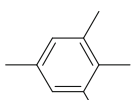	15.1	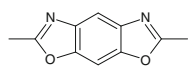	−18.9*	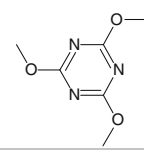	−74.5
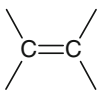	9.7	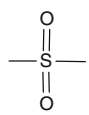	−19.2	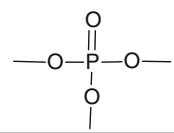	−76.7

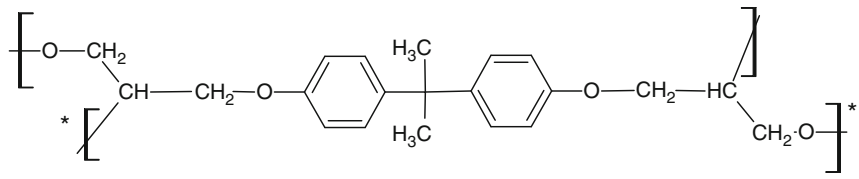

Fig. 7.55 Repeat unit of diglycidylether bisphenol A

Table 7.19 Group contributions used in the calculation of the heat release capacity of bisphenol-A epoxy

Chemical group, i	Number of moles N	Molar mass M_i/g mol^{-1}	Molar heat release capacity Ψ/kJ mol^{-1} K^{-1}	N_iM_i/g mol^{-1}	N_i ψ/kJ mol^{-1} K^{-1}
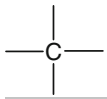	1	12	28.3	12	28.3
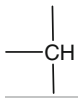	2	13	26.6	26	53.2
	2	15	22.5	30	45.0
	2	76	28.8	152	57.6
	4	14	16.7	56	66.8
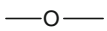	4	16	−11.6	64	−46.4
		Total:		340	204.5

only in their average molecular mass, its distribution and any impurities arising from manufacture. Others such as polyethylene, differ as a result of the polymerization process, so free radical polymerised low-density polyethylene (LDPE) has the most branching points (or starting points for decomposition), catalytically polymerised linear low-density polyethylene (LLDPE) has a smaller number of identical branching points, and high density polyethylene (HDPE) has the least of branching points and hence the highest decomposition temperature. Many polymers, such as polyamides, polyesters, polyurethanes and epoxies represent diverse classes, having only the chemistry of the linkages (e.g. esters or urethanes) between repeat units in common.

Both the physics and chemistry of polymers affect their thermal decomposition and burning behaviour. Depending on their thermal history, most polymers exert a degree of crystallinity, increasing with the duration of cooling, giving a sharper transition between solid and liquid phases. The chemical composition of the molecular chains exerts a profound influence on the thermal decomposition of the polymers, with chain branching, double bonds, or oxygen in the polymer backbone reducing the thermal stability, and aromatic rings and crosslinking of the polymer backbone increasing the thermal stability.

Polymer decomposition can best be studied on a microscale by thermogravimetric analysis, which provides fundamental information about gaseous fuel production rates, quantified by the Arrhenius parameters A and E_a. Other techniques, such as DSC, DTA, DMTA, and rheology provide additional information on the physical transformations occurring, while evolved gas analysis, using FTIR or GCMS, or

oxygen depletion calorimetry, and char analysis, illuminate the chemical processes.

The thermal decomposition of polymers is thermodynamically driven, as higher temperatures favour the formation of gaseous molecules, and is controlled by a frequently complex array of competing kinetic processes. Attempts to identify individual reactions have generally failed, and there is a broad consensus that predicting the rate of fuel gasification will suffice as input to pyrolysis models, and fire models that include condensed phase processes.

The breakdown of individual polymers can follow up to four competing pathways: end chain scission (PMMA, PTFE, PS); random chain scission (PE, PP, PS, PA, polyisoprene etc.); chain-stripping (PVC, PAN, PVA, cellulose etc.); and char formation (PAN, PEEK, cellulose etc.), with a significant variation from individual polymers.

Fire retardants are added to our around a third of plastic materials in order to meet regulatory requirements. In general, these apply to high risk applications, such as construction products, upholstered furnishings, electrical and electronic goods, and materials for mass transport applications. There is considerable diversity in the different fire retardant mechanisms, from the gas phase flame inhibitors, using halogens or organophosphorus compounds, to condensed phase processes ranging from intumescents and char formation, to endothermic dehydration and formation of a refractory shield.

Fire behaviour may be quantified on a bench scale using ease of ignition tests such as the UL 94, or the much criticised limiting oxygen index, or using more sophisticated apparatus such as the cone calorimeter or microscale combustion calorimeter. The physical properties of polymers exert an influence on this process, with perhaps the greatest benefit being conferred by char formation, reducing the rate of thermal attack.

References

1. ASTM E176, "Standard Terminology of Fire Standards", in *Annual Book of ASTM Standards*, 4.07, American Society for Testing Materials, West Conshohocken.
2. J.M.G. Cowie and V. Arrighi, *Polymers: Chemistry and Physics of Modern Materials*, 3rd Edition, CRC Press, Boca Raton (2008).
3. S.I. Stoliarov, N. Safronava, and R.E. Lyon, "The effect of variation in polymer properties on the rate of burning", *Fire and Materials*, 33, pp. 257–271 (2009).
4. S.C. Moldoveanu, *Analytical Pyrolysis of Synthetic Organic Polymers, Techniques and Instrumentation in Analytical Chemistry,* Volume 25, 1st Edition, Elsevier B.V (2005).
5. R.E. Lyon, "Plastics and Rubber", In *Handbook of Building Materials for Fire Protection*, Harper CA (ed), McGraw-Hill, Chap 3:3.1–3.51 (2004).
6. B. Schartel and T.R. Hull, "Development of fire-retarded materials - Interpretation of cone calorimeter data", *Fire and Materials*, 31 (5), pp. 327–354 (2007).
7. A. Fina and G. Camino, Ignition mechanisms in polymers and polymer nanocomposites, *Polym. Adv. Technol*., 22, 1147–1155, (2011)
8. S. L. Madorsky, *Thermal Degradation of Organic Polymers,* Interscience, John Wiley, New York (1964).
9. "Plastics – Thermogravimetry (TG) of polymers – General Principles", *ISO 11358* (1997).
10. P.G. Laye, *Differential Thermal Analysis and Differential Scanning Calorimetry,* in *Principles of Thermal Analysis and Calorimetry*, Edited by P.J. Haines, Royal Society of Chemistry, Cambridge, UK (2002).
11. ISO 11357–1 to 6:2005–2011 "Plastics - Differential scanning calorimetry (DSC) - Parts 1–6.
12. M. Reading, A. Luget, and R. Wilson, *"Modulated differential scanning calorimetry", Thermochimica Acta*, 238, pp. 295–307 (1994).
13. S. Zhang, T.R. Hull, A.R. Horrocks, G. Smart, B.K. Kandola, J. Ebdon, P. Joseph and B. Hunt: *Thermal degradation analysis and XRD characterisation of fibre-forming synthetic polypropylene containing nanoclay: Polym.Degrad.Stab*., 92, 727–732, (2007).
14. A. Witkowski, A.A. Stec and T.R. Hull, *The influence of metal hydroxide fire retardants and nanoclay on the thermal decomposition of EVA, Polym. Degrad. Stab*., 97, 2231–2240, (2012).
15. M. Sacristan, T.R. Hull, A.A. Stec, J.C. Ronda, M. Galia, and V. Cadiz, "Cone calorimetry studies of fire retardant soybean-oil-based copolymers containing silicon or boron: Comparison of additive and reactive approaches," *Polymer Degradation and Stability*, 95, pp. 1269–1274 (2010).
16. I.C. McNeill, L. Ackerman, S.N. Gupta, M. Zulfiquar, and S. Zulfiquar, "Part A: Polymer Chemistry", *Journal of Polymer Science*, 15, p. 2381 (1977).
17. J.P. Lewicki, K. Pielichowski, P.T. De La Croix, B. Janowski, D. Todd, and J.J. Liggat, "Thermal degradation studies of polyurethane/POSS

nanohybrid elastomers", *Polymer Degradation and Stability*, 95, pp. 1099–105 (2010).
18. ASTM D7309-11, "Standard test method for determining flammability characteristics of plastics and other solid materials using microscale combustion calorimetry" (2011).
19. R.E. Lyon and R.N. Walters, "Pyrolysis combustion flow calorimetry", *Journal of Analytical and Applied Pyrolysis*, 71, pp. 27–46 (2004).
20. S. Bourbigot, M.L. Bras, F. Dabrowski, J.W. Gilman and T. Kashiwagi, "PA-6 clay nanocomposite hybrid as char forming agent in intumescent formulations", *Fire Mater*., 24, 201–208, (2000).
21. M.V. Petrova, F.A. Williams, A small detailed chemical-kinetic mechanism for hydrocarbon combustion, *Combustion and Flame*, 144, 526–544, (2006).
22. R. E. Lyon, N. Safronava, and S. I. Stoliarov, *The Role of Thermal Decomposition Kinetics in the Burning of Polymers*. Proceedings of the 12th International Conference on Fire Science and Engineering (INTERFLAM), 2010.
23. L. Reich and S.S. Stivala, *Elements of Polymer Degradation*, McGraw-Hill, New York (1971).
24. K. McGrattan, R. McDermott, and W. Mell, et al., "Modeling the burning of complicated objects using Lagrangian particles", in *Conference proceedings of the twelfth international interflame conference*, pp. 743–753 (2010).
25. R.E. Lyon, N. Safronava, and E. Oztekin, "A simple method for determining kinetic parameters for materials in fire models", *Fire Safety Science*, 10, pp. 765–777 (2011).
26. H. L. Friedman, "New methods for evaluating kinetic parameters from thermal analysis data", *Journal of Polymer Science*, Polymer Letter 7(1), pp. 41–46 (1969).
27. C. Lautenberger, G. Rein, and C. Fernandez-Pello, "The application of a genetic algorithm to estimate material properties for fire modeling from bench-scale fire test data", *Fire Safety Journal*, 41, pp. 204–214 (2006).
28. G. Rein, C. Lautenberger, and C. Fernandez-Pello, "Application of genetic algorithms and thermogravimetry to determine the kinetics of polyurethane foam in smoldering combustion", *Combustion and Flame*, 146, pp. 95–108 (2006).
29. A. Matala, S. Hostikka and J. Mangs, "Estimation of pyrolysis model parameters for solid materials using thermogravimetric data", *Fire Safety Science*, 9, pp. 1213–1223 (2009).
30. C. Lautenberger and C. Fernandez-Pello, "Generalized pyrolysis model for combustible solids", *Fire Safety Journal*, 44, pp. 819–839 (2009).
31. C. Lautenberger and C. Fernandez-Pello, "Optimization algorithms for material pyrolysis property estimation", *Fire Safety Science*, 10, pp. 751–764 (2011).
32. M. Chaos, M. M. Khan, and N. Krishnamoorthy, et al., "Evaluation of optimization schemes and determination of solid fuel properties for CFD fire models using bench-scale pyrolysis tests", *Proceedings of the Combustion Institute*, 33(2), pp. 2599–2606 (2011).
33. A.K. Galwey and M.E. Brown, "Arrhenius parameters and compensation behaviour in solid-state decompositions", *Thermochimica Acta*, 300, pp. 107–115 (1997).
34. A.V. Nikolaev, V.A. Logvinenko, and V.M. Gorbatchev, "Special features of the compensation effect in nonisothermal kinetics of solid-phase reactions", *Journal of Thermal Analysis*, 6, pp. 473–577 (1974).
35. A. Matala and S. Hostikka, "Pyrolysis modeling of PVC cable materials", *Fire Safety Science*, 10, pp. 917–930 (2011).
36. J.H. Flynn, in *Encyclopedia of Polymer Science and Engineering*, ed. H.F. Mark, N.M. Bikales, C.G. Overberger, and G. Menges, pp. 690–723 (Suppl.), New York, Wiley (1989).
37. S. Vyazovkin and C.A. Wight, "Kinetics in Solids", *Annual Review of Physical Chemistry*, 48,125-149 (1997).
38. S. Vyazovkin, and C.A. Wight, "Model-free and Model-Fitting Approaches to Kinetic Analysis of Isothermal and Nonisothermal Data", *Thermochimica Acta*, 340/341, pp. 53–68 (1999).
39. J.H. Flynn and L.A. Wall, "General Treatment of the Thermogravimetry of Polymers", *Journal of Research of the National Bureau of Standards-A, Physics and Chemistry*, 70A(6), pp. 487–523 (1966).
40. A.K. Galwey and M.E. Brown, "Kinetic Background to Thermal Analysis and Calorimetry", in *Handbook of Thermal Analysis and Calorimetry*, Volume 1, *Principles and Practice* (M.E. Brown, ed.), Elsevier, New York, pp. 147–224 (1998).
41. H.E. Kissinger, "Variation of Peak Temperature with Heating Rate in Differential Thermal Analysis", *Journal of Research of the National Bureau of Standards*, 57(4), pp. 217–221 (1956).
42. H.E. Kissinger, "Reaction Kinetics in Differential Thermal Analysis", *Analytical Chemistry*, 29(11), pp. 1702–1706 (1957).
43. J.H. Flynn, "Temperature Dependence of the Rate of Reaction in Thermal Analysis", *Journal of Thermal Analysis*, 36, pp. 1579–1573 (1990).
44. T. Ozawa, "Kinetic Analysis of Derivative Curves in Thermal Analysis", *Journal of Thermal Analysis*, 2, pp. 301–324 (1970).
45. K.B. McGrattan, B. Klein, S. Hostikka, and J. Floyd, "Fire dynamics simulator (version 5) user's guide", *NIST Special Publication 1019–5*, National Institute of Standards and Technology, Gaithersburg, MD (2007).
46. G.R. Heal, "Thermogravimetry and Derivative Thermogravimetry in Principles of Thermal Analysis and Calorimetry", (P. J. Haines, ed.), *Royal Society of Chemistry*, Cambridge, UK (2002).

47. J. Criado, M. Gonzalez, A. Ortega and C. Real, "Some considerations regarding the determination of the activation energy of solid-state reactions from a series of isothermal data", *Journal of Thermal Analysis*, 29, pp. 243–250 (1984).
48. F. Rogers and T. Ohlemiller, "Pyrolysis kinetics of a polyurethane foam by thermogravimetry; a general kinetic method", *Journal of Macromolecular Science*, 1, pp. 169–185 (1981).
49. J.H. Sharp and S.A. Wentworth, "Kinetic analysis of thermogravimetric data," *Analytical Chemistry,* 41, pp. 2060–2062 (1969).
50. B.N.N. Achar, G.W. Brindley and J.H. Sharp, "Kinetics and mechanism of dehydroxylation processes," *Proceedings of the International Clay Conference*, p. 67, Jerusalem (1966).
51. E.S. Freeman and B. Carroll, "The Application of Thermoanalytical Decomposition of Calcium Oxalate Monohydrate," *Journal of Physical Chemistry,* 62, pp. 394–397 (1958).
52. E.S. Freeman and B. Carroll, "Interpretation of the kinetics of thermogravimetric analysis," *Journal of Physical Chemistry,* 73, pp. 751–752 (1969).
53. A.W. Coats and J.P. Redfern, "Kinetic Parameters from Thermogravimetric Data," *Nature,* 201, pp. 68–69 (1964).
54. A.W. Coats and J.P. Redfern, "Kinetic parameters from thermogravimetric data. II.," *Journal of Polymer Science, Part B: Polymer Letter* 3, pp. 917–920 (1965).
55. J.P. Elder, "The general applicability of the Kissinger equation in thermal analysis," *Journal of Thermal Analysis,* 30, pp. 657–669 (1985).
56. P. Simon, "Isoconversional methods: Fundamentals, meaning and application," *Journal of Thermal Analysis and Calorimetry,* 76, pp. 123–132 (2004).
57. J. Zsako, "Kinetic Analysis of Thermogravimetric Data, VI, Some Problems of Deriving Kinetic Parameters from TG Curves," *Journal of Thermal Analysis,* 5, pp. 239–251 (1973).
58. J. Zsako, "Kinetic analysis of thermogravimetric data XXIX. Remarks on the 'many curves' method," *Journal of Thermal Analysis,* 46, pp. 1845–1864 (1996).
59. S. Vyazovkin, "Computational aspects of kinetic analysis.: Part C. The ICTAC Kinetics Project — the light at the end of the tunnel?," *Thermochimica Acta,* 355, pp. 155–163 (2000).
60. A. Khawam and D.R. Flanagan, "Role of isoconversional methods in varying activation energies of solid-state kinetics. I. Isothermal kinetic studies," *Thermochimica Acta,* 429, pp. 93–102 (2005).
61. T. Ozawa, "A new method of analyzing thermogravimetric data," *Bulletin of the Chemical Society of Japan,* 38, pp. 1881–1886 (1965).
62. J.H. Flynn and L.A. Wall, "A quick, direct method for the determination of activation energy from thermogravimetric data," *Journal of Polymer Science, Part B: Polymer Letter,* 4, pp. 323–328 (1966).
63. C. Doyle, "Kinetic analysis of thermogravimetric data", *Journal of Applied Polymer Science*, Vol. 5, No. 15, pp. 285–292 (1961).
64. S. Vyazovkin and D. Dollimore, "Linear and Nonlinear Procedures in Isoconversional Computations of the Activation Energy of Nonisothermal Reactions in Solids," *Journal of Chemical Information and Computer Sciences,* 36, pp. 42–45 (1996).
65. M.E. Brown, *Introduction to thermal analysis: Techniques and applications*, Chapter 10, 2nd ed, Kluwer, Amsterdam (2001).
66. A.K. Galwey and M.E. Brown, "Thermal decomposition of ionic solids: Chemical properties and reactivities of ionic crystalline phases", *Elsevier*, Amsterdam, pp. 139–171 (1999).
67. W. Gautschi and W.F. Cahill, "Exponential integral and related functions", in *Handbook of mathematical functions with formulas, graphs, and mathematical tables* (M. Abramowitz and I. Stegun, eds.), National Bureau of Standards, Washington, DC, pp. 227–237 (1964).
68. S. Vyazovkin, "Evaluation of activation energy of thermally stimulated solid-state reactions under arbitrary variation of temperature," *Journal of Computational Chemistry,* 18, pp. 393–402 (1997).
69. S. Vyazovkin, "Modification of the integral isoconversional method to account for variation in the activation energy," *Journal of Computational Chemistry,* 22, pp. 178–183 (2001).
70. A. Matala, C. Lautenberger and S. Hostikka, "Generalized direct method for pyrolysis kinetic parameter estimation and comparison to existing methods", *Journal of Fire Sciences*, 30(4), pp. 339–356 (2012).
71. R.E. Lyon and R.N. Walters, "Pyrolysis combustion flow calorimetry", *Journal of Analytical and Applied Pyrolysis*, 71, pp. 27–46 (2004).
72. T. Ohlemiller, "Modeling of smoldering combustion propagation", *Progress in Energy and Combustion Science,* 11, 277–310 (1985).
73. A. Matala, "Estimation of Solid Phase Reaction Parameters for Fire Simulation", Master's thesis, Helsinki University of Technology, Finland (2008).
74. C. Lautenberger, "A Generalized Pyrolysis Model for Combustible Solids", Users' guide (2009).
75. S.I. Stoliarov, S. Crowley, R.E. Lyon, and G.T. Linteris, "Prediction of the burning rates of non-charring polymers", *Combustion and Flame*, 156, pp. 1068–1083 (2009).
76. S.I. Stoliarov, N. Safronava, R.E. Lyon, "The effect of variation in polymer properties on the rate of burning," *Fire and Materials*, 33, pp. 257–271 (2009).
77. C. Lautenberger, E. Kim, N. Dembsey, and C. -Fernandez-Pello, "The Role of Decomposition Kinetics in Pyrolysis Modeling – Application to a Fire Retardant Polyester Composite", *Fire Safety Science*, 9, pp. 1201–1212 (2008).
78. J.E.J. Staggs, "A theory for quasi-steady single-step thermal degradation of polymers", *Fire and Materials*, 22, 1998, pp. 109–118 (1998).

79. J. Zhang, M.A. Delichatsios, and S. Bourbigot, "Experimental and numerical study of the effects of nanoparticles on pyrolysis of polyamide 6 (PA6) nanocomposite in the cone calorimeter", *Combustion and Flame*, 156, pp. 2056–2062 (2009).
80. F. Jia, E.R. Galea, and M.K. Patel, "The numerical simulation of the non-charring pyrolysis process and fire development within a compartment", *Applied Mathematical Modelling*, 23, pp. 587–607 (1999).
81. C. Lautenberger, Ph.D. Thesis, University of California, Berkeley, CA, USA (2007) available at <http://repositories.cdlib.org/cpl/fs/>
82. C. Lautenberger, "Gpyro – A Generalized Pyrolysis Model for Combustible Solids" – Users' Guide Version 0.700 (February 19, 2009).
83. GPyro, available at <http://code.google.com/p/gpyro/>
84. K.B. Mc Grattan, S. Hostikka, J.E. Floyd, H.R. Baum, and R.G. Rehm, "Fire Dynamics Simulator (Version 5). Technical Reference Guide", Volume 1: Mathematical Model, NIST Special Publication 1018–5, Gaithersburg, MD, (October 2007).
85. FireFOAM Code, available at <http://code.google.com/p/firefoam-dev/>.
86. S.I. Stoliarov and R.E. Lyon, "Thermo-Kinetic Model of Burning", Federal Aviation Administration Technical Note, DOT/FAA/AR-TN08/17 (2008), <www.fire.tc.faa.gov/reports/reports.asp>
87. S.I. Stoliarov and R.E. Lyon, "Thermo-kinetic model of burning for pyrolyzing materials", in *Proceedings of the Ninth International Symposium on Fire Safety Science*, pp. 1141–1152 (2009).
88. L. Bustamante Valencia, *Experimental and Numerical Investigation of the Thermal Decomposition of Materials at Three Scales: Application to Polyether Polyurethane Foam used in Upholstered Furniture*, Ph.D. Thesis, ENSMA, Poitiers, France (2009).
89. C.R. Houck, J.A. Joines, and M.G. Kay, "GAOT: A Genetic Algorithm for Function Optimization: A Matlab Implementation", Report NCSU-IE TR 95–09 (1995), available at <http://www.ise.ncsu.edu/kay/>
90. Q. Duan, V.K. Gupta and S. Sorooshian, "A shuffled complex evolution approach for effective and efficient global minimization," *Journal of Optimization Theory and Applications*, 76, pp. 501–521 (1993).
91. Q. Duan, S. Sorooshian and V.K. Gupta, "Optimal Use of the SCEUA Global Optimization Method for Calibrating Watershed Models," *Journal of Hydrology*, 158, pp. 265–284 (1994).
92. N. Bal, *Uncertainty and complexity in pyrolysis modelling*, PhD Thesis, University of Edinburgh, UK (2012), available at http://www.era.lib.ed.ac.uk/handle/1842/6511
93. S.I. Stoliarov and R.E. Lyon, "Thermo-Kinetic Model of Burning", Federal Aviation Administration Technical Note DOT/FAA/AR-TN-08/17 (2008).
94. S.I. Stoliarov, S. Crowley, R.E. Lyon, and G.T. Linteris, "Prediction of the Burning Rates of Non-Charring Polymers", *Combustion and Flame*, 156, pp. 1068–1083 (2009).
95. S.S. Rahatekar, M. Zammarano, S. Matko, K.K. Koziol, M.H. Windle, T. Kashiwagi, and J.W. Gilman, "Effect of Carbon Nanotubes and Montmorillonite on the Flammability of Epoxy Nanocomposites", *Polymer Degradation and Stability*, 98, pp. 870–879 (2010).
96. P. Patel, T.R. Hull, A.A. Stec, and R. E. Lyon, "Influence of physical properties on polymer flammability in the cone calorimeter," *Polymers for Advanced Technologies*, 22, pp. 1100–1107 (2011).
97. J.G. Quintiere, *Principles of Fire Behaviour*, Delmar, Albany, NY (1997).
98. D. Drysdale, *An Introduction to Fire Dynamics*, 2nd Edition, John Wiley & Sons, Chichester (1999).
99. T. Faravelli, G. Bozzano, M. Colombo, E. Ranzi, M. Dente, *Kinetic modeling of the thermal degradation of polyethylene and polystyrene mixtures*, Journal of Analytical and Applied Pyrolysis, 70, 761–777, 2003.
100. Z. Gao, I. Amasaki, and M. Nakada, "A thermogravimetric study on thermal degradation of polyethylene," *Journal of Analytical and Applied Pyrolysis*, 67 (1), pp. 1–9 (2003).
101. A. Marcilla, A. Gomez, A.N. Garcia, and M.M. Olaya, "Kinetic study of the catalytic decomposition of different commercial polyethylenes over an MCM-41 catalyst", *Journal of Analytical and Applied Pyrolysis,* 64, pp. 85-101(2002).
102. C.F Cullis and M.M Hirschler, *The combustion of organic polymers*, New York, NY: Oxford University Press (1981).
103. S.L. Madorsky, "Thermal degradation of organic polymers", *Interscience Publishers*, A Division of John Wiley & Sons Inc. (1964).
104. S.M. Thornberg, R. Bernstein, D.K. Derzon, A.N. Irwin, S.B. Klamo, and R.L. Clough, "The genesis of CO_2 and CO in the thermooxidative degradation of polypropylene", *Polymer Degradation and Stability*, 92, pp. 94–102 (2007).
105. R. Bernstein, S.M. Thornberg, R.A. Assink, A.N. Irwin, J.M. Hochrein, J.R. Brown, D.K. Derzon, S.B. Klamo, and R.L. Clough, "The origins of volatile oxidation products in the thermal degradation of polypropylene, identified by selective isotopic labelling," *Polymer Degradation and Stability*, 92, pp. 2076–2094 (2007).
106. G.G. Cameron, W.A.J. Bryce, I.T. McWalter, "Thermal degradation of polystyrene-5. Effects of initiator residues," European Polymer Journal, 20, pp. 563–569 (1984).
107. N. Grassie and G. Scott, *Polymer Degradation and Stabilisation*, Cambridge University Press, Cambridge, UK (1985).
108. W.R. Zeng, S.F Li, and W.K. Chow, "PMMA Review on Chemical Reactions of Burning Poly

(methylmethacrylate)", *Journal of Fire Sciences,* 20, p. 401 (2002).
109. I.C. McNeill and A. Rincon, "Thermal degradation of polycarbonates: Reaction conditions and reaction mechanisms," *Polymer Degradation and Stability*, 39, pp. 13–19 (1993).
110. . A. Davis and J.H. Golden, J. Macromol. Scie. Rev. Macromol. Chem. C, 3, p. 49 (1969).
111. S.C. Moldoveanu, "Analytical Pyrolysis of Synthetic Organic Polymers", *Techniques and Instrumentation in Analytical Chemistry*, Volume 25, 1st Edition, Elsevier (2005).
112. S. Smith, "The re-equilibration of polycaproamide," *Journal of Polymer Science*, 30, pp. 459–478 (1958).
113. L.H. Buxbaum, "The degradation of poly(ethylene terephthalate)," Angewandte Chemie International Edition, 7, pp. 182–190 (1968).
114. S.V. Levchik and E.D. Weil, "A review on thermal decomposition and combustion of thermoplastic polyesters", *Polymers for Advanced Technologies,* 15, pp. 691–700 (2004).
115. T.R. Hull, A.A. Stec, and S. Nazare, "TGA-FTIR Investigation of The Fire Retardant Mechanism of Acrylonitrile Copolymers Containing Nanofillers," in *235th American Chemical Society National Meeting*, APR 06–10, New Orleans, LA (2008).
116. Z. Bashir, "A critical review of the stabilisation of polyacrylonitrile," *Carbon*, 29, pp. 1081–1090 (1991).
117. A.R. Horrocks, J. Zhang and M.E. Hall, "Flammability of polyacrylonitrile and its copolymers II. Thermal behaviour and mechanism of degradation," *Polymer International*, 33, pp. 303–314 (1994).
118. N. Grassie, *Developments in polymer degradation*, Applied Science, Vol. 1, p. 137, London (1977).
119. E. Fitzer and D. Muller, "The influence of oxygen on the chemical reactions during stabilization of PAN as carbon fiber precursor," *Carbon*, 13, p. 63–69 (1975).
120. L.T. Memetea, N.C. Billingham, and E.T.H. Then, "Hydroperoxides in polyacrylonitrile and their role in carbon-fibre formation," *Polymer Degradation and Stability*, 47, pp. 189–201 (1995).
121. N. Grassie, J.N. Hay and I.C. McNeill, "Coloration in acrylonitrile and methacrylonitrile polymers," *Journal of Polymer Science,* 31, p. 205 (1958).
122. J. Brandrup and L.H. Peebles, "On the chromophore of polyacrylonitrile. IV. Thermal oxidation of polyacrylonitrile and other nitrile-containing compounds", *Macromolecules,* 1, 64–72, (1968).
123. M.A. Geiderikh, B.E. Davydov, B.A. Krentsel, I.M. Kustanovich, L.S. Polak, A.V. Topchiev, and R.M. Voitenko, "Preparation of polymeric materials with semiconductor properties," *Journal of Polymer Science*, 54, pp. 621–626 (1961).
124. S.C. Martin, J.J. Liggat and C.E. Snape, "In situ NMR investigation into the thermal degradation and stabilisation of PAN," *Polymer Degradation and Stability*, 74, pp. 407–412 (2001).
125. W.D. Woolley, "Decomposition Products of PVC for Studies of Fires", *British Polymer Journal*, 3(4), pp. 186–193 (1971).
126. . W.D. Wolley, "Studies of the dehydrochlorination of PVC in nitrogen and air", *Building Research Establishment,* Current Paper CP 9/74 (1974).
127. Purser, D.A., Fardell, P.J., Rowley, J., Vollam, S. and Bridgeman, B. An improved tube furnace method for the generation and measurement of toxic combustion products under a wide range of fire conditions. *Proceedings of the 6th International Conference Flame Retardants '94, London, UK* (26–27 Jan 1994). Interscience Communications.
128. K.T. Paul, "Feasibility Study to Demonstrate the Potential of Smoke Hoods in Simulated Aircraft Fire Atmospheres: Development of the fire model", *Fire and Materials*, 14, pp. 43–58, (1989).
129. K. Lebek, T.R. Hull, and D. Price, "Products of burning rigid PVC burning under different fire conditions Fire and Polymers", *Materials and Concepts for Hazard Prevention*, ACS Symposium Series No. 922, Oxford University Press, p. 334–347 (2005).
130. T.R. Hull, A.A. Stec, and K.T. Paul, *Proceedings of the 9th International Symposium on Fire Safety Science*, 665–676 (2008).
131. H.F. Mark, N. Bikales, C.G. Overberger, and J.I. Kroschwitz, eds., *Encyclopedia of Polymer Science and Engineering*, Wiley Europe, vol 1–4 (1989).
132. E.E. Lewis and M.A. Naylor, "*Pyrolysis of Polytetrafluoroethylene*". *Journal of the American Chemical Society,* 69, p. 1968–70 (1947).
133. A. Stec and R. Hull, *Fire Toxicity*, Woodhead Publishing, Cambridge, 2010.
134. E. Ackerman, *Firestopping Through-Penetrations*, in *Science and Technology of Building Seals, Sealants, Glazing, and Waterproofing: Seventh Volume* (J.M. Klosowski, ed.), ASTM STP 1334, American Society for Testing and Materials, West Conshohocken, PA (1998).
135. J. Harris, A. Stevenson, "On the role of nonlinearity in the dynamic behavior of rubber components", *Rubber Chemistry and Technology*, 59 (5), pp. 740-764 (2011).
136. D.J. Kind and T.R. Hull, "A review of candidate fire retardants for polyisoprene," *Polymer Degradation and Stability*, 97, pp. 201–213 (2012).
137. D.W. Brazier and G.H. Nickel, "Thermoanalytical methods in vulcanizate analysis. Derivative thermogravimetric analysis", *Rubber Chemistry and Technology*, *48* (4), pp. 661–677 (1975).
138. A.K. Sircar, "Identification of natural and synthetic polyisoprene vulcanizates by thermal analysis", *Rubber Chemistry and Technology*., *50* (1), pp. 71–82 (1977).
139. S. Straus and S.L. Madorsky, "Thermal Degradation of Unvulcanized and Vulcanized Rubber in a

Vacuum", *Industrial and engineering chemistry*, *48* (7), pp. 1212–1219 (1956).
140. F. Cataldo, "Thermal depolymerization and pyrolysis of cis-1,4-polyisoprene: preparation of liquid polyisoprene and terpene resin", *Journal of Analytical and Applied Pyrolysis*, *44*(2), pp. 121–130 (1998).
141. S.V. Levchik and E.D. Weil, "Thermal decomposition, combustion and flame-retardancy of epoxy resins: a review of the recent literature," *Polymer International*, 53, pp. 1901–1929 (2004).
142. S.C. Lin, B.J. Bulkin and E.M. Pearce, "Thermal Degradation Study Of Phenolphthalein Polycarbonate", *Journal of polymer science, Part A-1, Polymer chemistry*, 19, 2773–2797, (1981).
143. B.C. Levin, M. Paabo, J.L. Gurman and S.E. Harris, "Effects of exposure to single or multiple combinations of the predominant toxic gases and low oxygen atmospheres produced in fires" *Toxicological Sciences*, 9, 236–250 (1987).
144. D.A. Purser, *Asphyxiant components of the fire effluents*, in *Fire Toxicity*, (A.A Stec and T.R. Hull, eds.), Woodhead Publishing, Cambridge (2010).
145. J. Wang, H. Jiang and N. Jiang, Study on the pyrolysis of phenol-formaldehyde (PF) resin and modified PF resin. *Thermochimica Acta,* 2009, **496**, 136–142
146. A. Murari and A. Barzon, "Comparison of New PEEK Seals with Traditional Helicoflex for Ultra High Vacuum Applications", *Vacuum*, Volume 72, Issue 3, pp. 327–334 (2003).
147. S.K. Yesodha, C.K.S. Pillai, and N. Tsutsuni, "Stable Polymeric Materials for Non-Linear Optics: A Review Based on Azobenzene Systems", *Progress in Polymer Science*, Volume 29, Issue 1, pp. 45–74 (2004).
148. M.P. Stevens, *Polymer Chemistry: An Introduction*, Third Edition. Oxford University Press, New York, USA (1999).
149. M.C. Kuo, C.M. Tsai, J.C. Huang, and M. Chen, "PEEK Composites Reinforced by Nano-Sized SiO_2 and Al_2O_3 Particulates", *Materials Chemistry and Physics*, Volume 90, pp. 185–195 (2005).
150. L.H. Perng, C.J. Tsai, and Y.C. Ling, "Mechanism and Kinetic Modelling of PEEK Pyrolysis by TG/MS", *Polymer,* Volume 40, pp. 731–732 (1999).
151. P. Patel, T. R. Hull, R. W. McCabe, D. Flath, J. Grasmeder, and M. Percy, Mechanism of thermal decomposition of poly(ether ether ketone) (PEEK) from a review of decomposition studies, *Polymer Degradation and Stability*, 95, pp. 709–718 (2010).
152. A.-M.M. Baker and J. Mead, *Thermoplastics,* Chapter 1, In C.A. Harper, Modern Plastics Handbook, McGraw-Hill Professional Publishing, Ohio, USA (2000).
153. R.E. Lyon and M.L. Janssens, *Polymer Flammability*, US Department of Transport, Report Number: DOT/FAA/AR-05/14 (2005).
154. F. D. Kopinke, M. Remmler, K. Mackenzie, Thermal decomposition of biodegradable polyesters-I: Poly (hydroxybutyric acid). *Polym. Degrad. Stab.*, 52, 25–38, 1996.
155. H. Morikawa, R.H. Marchessault, Pyrolysis of bacterial polyalkanoates, *Canadian Journal of Chemistry* 59, 2306,1981
156. J.L. Gay-Lussac, *Ann. Chim. Phys.*, 18, p. 211 (1821).
157. SRI Consulting, *Report on Flame Retardants*, Published December 2008
158. T.R. Hull, A. Witkowski, L.A. Hollingbery, "Fire retardant action of mineral fillers", *Polymer Degradation and Stability,* 96, pp. 1462–1469 (2011).
159. A. Bergman, A. Ryden, R.J. Law, J. de Boer, A. Covaci, M. Alaee, L. Birnbaum, M. Petreas, M. Rose, S. Sakai, N. Van den Eede and I. van der Veen, "A novel abbreviation standard for organobromine, organochlorine and organophosphorus flame retardants and some characteristics of the chemicals" Environment International, 49, 57–82, (2012).
160. A. Schnipper, L. Smith-Hansen, and S.E. Thomsen, "Reduced Combustion Efficiency of Chlorinated Compounds Resulting In Higher Yields of Carbon Monoxide", *Fire and Materials,* 19, pp. 61–64, (1995).
161. V. Babushok, W. Tsang, G.T. Linteris, and D. Reinelt, "Chemical Limits to Flame Inhibition", *Combustion and Flame*, 115, pp. 551–560 (1998).
162. M.I. Nelson and J. Brindley, "Polymer combustion: Effects of flame emissivity" *Philosophical Transactions of the Royal Society A: Mathematical, Physical and Engineering Sciences*, 358, 3655–3673 (2000).
163. J.G. Quintiere, *Principles of Fire Behaviour,* Delmar Publishers, New York, USA, (1997).
164. . H. Zhang, *Fire-Safe Polymers and Polymer Composites,* US Department of Transport. Report Number: DOT/FAA/AR-04/11 (2004).
165. P. Patel, T.R Hull, and Colin Moffatt, "PEEK polymer flammability and the inadequacy of the UL-94 classification," *Fire and Materials*, 36, pp. 185–201 (2012).
166. V. Babrauskas, "Fire Test Methods for Evaluation of Fire-Retardant Efficacy in Polymeric Materials", Chapter 3, in *Fire Retardancy of Polymeric Materials* (A.F. Grand and C.A. Wilkie, eds.), CRC Press, New York, USA (2000).
167. K.T. Paul and S.D. Christian, "Standard flaming ignition sources for upholstered composites, furniture and bed assembly," *Journal of Fire Sciences*, 5 (3), pp. 178–211 (1987).
168. D. Hopkins Jr and J.G. Quintiere, "Materials fire properties and predictions for thermoplastics", *Fire Safety Journal,* 26, pp. 241–268 (1996).
169. D.J. Rasbash, D.D. Drysdale, and D. Deepak, "Critical heat and mass transfer at pilot ignition and extinction of a material", *Fire Safety Journal*, 10, pp. 1–10 (1986).
170. H.E. Thomson, D.D. Drysdale, and C.L. Beyler, "An experimental evaluation of critical surface

temperatures as a criterion for piloted ignition of solid fuels", *Fire Safety Journal*, 13, pp. 185–196 (1988).
171. E. Mikkola and I.S. Wichman, "On the thermal ignition of combustible materials", *Fire and Materials*, 14, pp. 87–96 (1989).
172. T. Kashiwagi, "Radiative ignition mechanism of solid fuels", *Fire Safety Journal*, 3, pp. 185–200 (1981).
173. V. Babrauskas, *Ignition Handbook*, Fire Science Publishers, Issaquah WA, USA and SFPE, USA (2003).
174. R.E. Lyon, "Plastics and Rubber", in *Handbook of Building Materials for Fire Protection*, (C.A. Harper, ed), McGraw-Hill, chap 3, 3.1-3.51 (2004).
175. R.E. Lyon, R.N. Walters, and S.I. Stoliarov, "Thermal Analysis of Polymer Flammability", Presented at *228th ACS Meeting Philadelphia* (2004).
176. A. Tewarson, "Generation of Heat and Chemical Compounds in Fires", in *The SFPE Handbook of Fire Protection Engineering*, 3rd edition (P.J. DiNenno, D.D. Drysdale, C.L. Beyler, W.D. Walton, R.L.P Custer, J.R. Hall Jr and J.M. Watts Jr, eds), National Fire Protection Association, Inc., chap 3.4,3-82-3-161 (2002).
177. M. Sibulkin and M.W. Little, "Propagation and extinction of downward burning fires", *Combustion Flame*, 31, pp. 197–208 (1978).
178. IEC 60695-11-10 "Fire hazard testing - Part 11–10: Test flames - 50 W horizontal and vertical flame test methods," (1999).
179. V. Babrauskas, "Ignition: A Century of Research and an Assessment of our Current Status", *Journal of Fire Protection Engineering*, 17(3), pp. 165–183 (2007).
180. ISO 5660–1 "Fire tests – Reaction to fire – Part 1: Rate of heat release from building products (cone calorimeter method)", (1993).
181. A.B. Morgan and M. Bundy, "Cone Calorimeter Analysis of UL-94 V-Rated Plastics", *Fire and Materials*, 31, pp. 257–283 (2007).
182. Y. Wang, F. Zhang, X. Chen, Y. Jin, and J. Zhang, "Burning and Dripping Behaviours of Polymers under the UL-94 Vertical Burn Test Conditions", *Fire and Materials*, 34, pp. 203–215 (2009).
183. M. Bundy and T. Ohlemiller, "Bench-Scale Flammability Measures for Electronic Equipment", *National Institute of Standards and Technology*, NISTIR 7031 (2003).
184. S. Hong, J. Yang, S. Ahn, Y. Mun, and G. Lee, "Flame Retardant Performance of Various UL-94 Classified Materials Exposed to External Ignition Sources", *Fire and Materials*, 28, pp. 25–31 (2004).
185. B. Schartel and U. Braun, "Comprehensive Fire Behaviour Assessment of Polymeric Materials Based on Cone Calorimeter Investigations", *e-Polymers*, Article 13, pp. 1–14 (2003).
186. B. Schartel and T.R. Hull, "Application of Cone Calorimetry to the Development of Materials with Improved Fire Performance", *Fire and Materials*, 31, pp. 327–354 (2007).
187. J.G. Quintiere, B.P. Downey, and R.E. Lyon, "An Investigation of the Vertical Bunsen Burner Test for Flammability of Plastics", *US Department of Transport*, Report Number: DOT/FAA/AR-TN (2010).
188. ISO 4589–2 "Plastics – Determination of burning behaviour by oxygen index – Part-2: Ambient temperature test", (1996).
189. ISO 5660–2 "Reaction-to-fire tests – Heat release, smoke production and mass loss rate – Part 2: Smoke production rate (dynamic measurement)", (2002).
190. B. Schartel and T.R. Hull, *"Application of cone calorimetry to the development of materials with improved fire performance", Fire and Materials*, 31, pp. 327–354 (2007).
191. R.E. Lyon, in *Recent Advances in Flame Retardancy of Polymers*, vol. 13, (M. Lewin, ed.), BCC, Inc., pp. 14-25 (2002)
192. R.E. Lyon and R.N. Walters, "Pyrolysis combustion flow calorimetry", *Journal of Analytical and Applied Pyrolysis*, 71, pp. 27–46 (2004).
193. B. Schartel, K.H. Pawlowski, and R.E. Lyon, "Pyrolysis combustion flow calorimeter: A tool to assess flame retarded PC/ABS materials?", *Thermochimica Acta*, 462, pp. 1–14 (2007).
194. R.E. Lyon, R.N. Walters, M. Beach, and F.P. Schall, "Flammability Screening of Plastics Containing Flame Retardant Additives", ADDITIVES 2007, 16th International Conference, San Antonio, TX (2007).
195. D.W. Van Krevelen, *Properties of Polymers*. Chapter 21 – Thermal Decomposition, 4th Edition, *Elsevier Science Publishers*, Amsterdam (2009).
196. R. Walters and R.E. Lyon, *Calculating Polymer Flammability from Molar Group Contributions*, DOT/FAA/AR-01/31 (2001).
197. P. Patel, Doctoral Thesis, *University of Central Lancashire*, UK (2011).
198. H. Zhang, Fire-Safe Polymers, and Polymer Composites, US Department Of Transport, Report Number: DOT/FAA/AR-04/11, Federal Aviation Administration (2004).
199. R.E. Lyon and M.L. Janssens, *Polymer Flammability*, US Department of Transport, Report Number: DOT/FAA/AR-05/14 (2005).
200. P. Patel, T.R. Hull, R.E. Lyon, S.I. Stoliarov, R.N. Walters, S. Crowley, and N. Safronava, "Investigation of the Thermal Decomposition and Flammability of PEEK and its Carbon and Glass-Fibre Composites", *Polymer Degradation and Stability*, In Press (2011).
201. R.E. Lyon, "Solid-State Thermochemistry of Flaming Combustion," in *Fire Retardancy of*

Polymeric Materials (C.A. Wilkie and A.F Grand, eds.), Marcel Dekker, Inc., NY (2000).
202. R.E. Lyon, "Heat Release Capacity," *Proceedings of the 7th International Conference on Fire and Materials,* San Francisco, CA, pp. 285–300 (2001).
203. R.E. Lyon, "Heat Release Kinetics," *Fire and Materials,* 24, pp. 179–186 (2000).
204. R.N. Walters and R.E. Lyon, "A Microscale Combustion Calorimeter for Determining Flammability Parameters of Materials," *Proceedings 42nd International SAMPE Symposium and Exhibition,* 42(2), pp. 1335–1344 (1997).
205. R.N. Walters and R.E. Lyon, "A Microscale Combustion Calorimeter for Determining Flammability Parameters of Materials," NISTIR 5904 (K. Beall, ed.), pp. 89–90 (1996).
206. R.E. Lyon and R.N. Walters, U.S. Patent 5981290, *Microscale Combustion Calorimeter*, 11/09/1999.
207. R.N. Walters and R.E. Lyon, "Molar Group Contributions to Polymer Flammability," *PMSE Preprints,* 83, 86, ACS National Meeting, Washington, D.C. (August 2000).
208. R.N. Walters and R.E. Lyon, "Calculating Polymer Flammability from Molar Group Contributions," *Proceedings of the BCC Conference on Flame Retardancy of Polymeric Materials,* Stamford, CT (May 22–24, 2000).

Dr Witkowski is a Lecturer at the University of Central Lancashire (UCLan), UK. His work focuses on thermal decomposition of solids and pyrolysis mechanisms, and numerical modelling.

Dr Stec is an Associate Professor in Fire Chemistry and Toxicity at UCLan. Her work focuses on quantification of combustion products and the factors affecting fire toxicity from bench- and largescale tests.

Prof Hull is a Professor of Chemistry and Fire Science at the University of Central Lancashire (UCLan). He obtained his PhD in 1987 in Fire Retardant Mechanisms from the University of Salford, UK. His current research interests include the development of fire retardant materials and the assessment of fire toxicity.

Structural Mechanics

8

Luke A. Bisby

Introduction

Structural mechanics, sometimes called 'solid mechanics' or 'mechanics of materials' is concerned with describing the behavior of structural members under loading, as occurs in all buildings and other structures due to the effects of gravity and other forces (e.g. wind, earthquake, etc.). A detailed understanding of structural mechanics is essential for anyone seeking to perform structural fire engineering analysis or design.

It is not possible within this brief chapter to provide a complete treatment of the topic; however when reviewed in conjunction with Chap. 9 of this handbook, the current chapter provides a basic description of structural mechanics as is required for an initial understanding of the means by which structural stability, and to a certain extent integrity, against fire spread and insulation during fire, are engineered through careful selection and design of building materials.

Philosophy of Structural Design

Structural design is both a creative art and a science, and structural engineers may use considerable creativity in determining the load bearing system for a particular building. In general, the process of structural design under normal (ambient) temperature conditions takes little (if any) explicit account of the possible effects of fire; it typically consists of the following steps:

1. The architect and the engineer establish the aesthetic, general structural layout, and functional requirements for the building.
2. The overall structural framing system and building materials are selected and a structural concept is proposed, based on the competing interests of architectural, functional, economic, and sustainability considerations. At this stage only approximate sizes of structural elements are known.
3. The likely loads which will act on the structure are estimated in accordance with structural engineering principles (discussed below), with due consideration given to all possible loads and their likelihood of acting (on their own or in combination with other loads).
4. A structural analysis is performed to determine the *load path* by which all loads are transferred through the structure from the location where they act and into the structure's foundations. The internal forces and stresses acting within the various structural elements are subsequently determined.
5. The likely *stresses* and *forces* acting in each structural element (the design *loads*) are checked against the capacities of the respective structural elements (the design *resistances*) to ensure that the structural elements have sufficient strength and stiffness to (a) resist the applied loads without collapse

L.A. Bisby (✉)
School of Engineering, University of Edinburgh, UK, The King's Buildings, Mayfield Road, Edinburgh, UK EH93JL

M.J. Hurley (ed.), *SFPE Handbook of Fire Protection Engineering*,
DOI 10.1007/978-1-4939-2565-0_8, © Society of Fire Protection Engineers 2016

(called *ultimate design* considerations), and (b) provide a suitable level of in-service performance of the structure (called *serviceability* considerations; for instance deflections, vibrations, durability, etc.).

6. Steps 3–5 are repeated as necessary, until the structural elements satisfy both ultimate and serviceability design requirements and the building is deemed to satisfactorily achieve the functional requirements set out in the early stages of the design process.

It is clear from the above steps that the structural design process fundamentally involves a comparison between the *loads* acting on and within the structure, and the *resistances* or capacities of the structural elements from which the structure is made. This chapter focuses on how a structural element's resistance to load can be determined using basic structural mechanics; however a description of the means by which the loads acting on a structure are typically estimated by structural engineers is instructive and is briefly treated first.

Structural Design at Ambient Temperature

To understand the goals of structural fire engineering and the means by which these goals are met during design it is first necessary to understand the general framework through which structures are designed to resist the full suite of potential loads to which they might be subjected during their lifetime, as well as the probabilistic basis of this framework which is intended to provide a suitably low probability of failure.

Loads and Load Combinations

Throughout a structure's lifetime it will be subjected to a wide variety of loads. During the structural design process it is essential that all credible loading scenarios be considered and addressed. Loads to be used in structural design are typically specified in design *codes*, which provide empirically determined and statistically characterized worst case credible loads to be assumed in the particular jurisdiction in which the design code is in force. The most common loads for which typical structures are designed are given below.

1. *Dead Loads*: These are loads which are always present, and include the self weight of the structure as well as loads arising from permanent fixtures and equipment. Dead loads may include the weight of floor coverings, walls, doors, suspended ceilings, etc., and are usually estimated based on the dimensions and construction materials of the trial structure under analysis.
2. *Live Loads*: Sometimes called *Imposed Loads*, these are typically specified by design codes on the basis of data obtained from surveys of real buildings and account for the weight of people and moveable fixtures and equipment. It is important to recognize that live loads are likely to be variable throughout the life of a structure, and thus the specified values of live loads given in codes may be considerably higher than those which are actually experienced on a day-to-day basis.
3. *Snow Loads*: As the name implies, these are loads due to the weight of snow and ice which can accumulate on structures in cold climates. Snow loads are estimated based on geographic and climatic data which has been collected and calibrated over many decades. In some design codes loads due to snow may be treated as live loads.
4. *Wind Loads*: Wind loads may cause lateral forces which act on the vertical surfaces of a building, but may also cause uplift on horizontal surfaces such as roofs and slabs. Wind loads are highly variable and again are treated in design codes using empirical correlations based on geography, topography, and the form of the building. Wind loads are particularly important during the design of tall buildings, for which lateral load resistance often governs the design of the overall structural system. Modern tall building design typically includes complex wind tunnel tests to determine the possible distributions of wind pressures over the building's surface given its

geometry and the surrounding climate and topography.

5. *Seismic Loads*: In many parts of the world, loads arising form both vertical and horizontal ground acceleration during earthquake must be considered during design. Design earthquake loads are given in design codes and account for geography, probability and magnitude of possible earthquakes, soil conditions, etc. It is worth noting that the statistical likelihood of a fire and earthquake occurring simultaneously is very low.

It is clear that there is uncertainty associated with the likely magnitude of each of the different loads, and also with the likelihood that each of the loads might be acting at its full (or some lesser) value at any given point in time during the life of a structure. For instance, the self weight of a structure, once designed, is reasonably well known and can be assumed to always be acting, whereas the weight of the people in a structure has large variability and may not ever be known with any degree of certainty either spatially or temporally. Furthermore, it is highly unlikely that all of the noted loads will be acting at their full value at any given time (i.e. the chances are low that a building will be completely full of people, in the middle of winter, with the wind blowing a gale, and during an earthquake).

Most modern building codes deal with the uncertainty around loading using a series of *load combinations* which seek to statistically account for the variability in magnitude and occurrence of the respective loads when acting in combination. These load combinations help engineers to decide which combinations of loads they must consider in designing a structure; any given structure may need to be checked under a variety of potential load combinations to determine the worst possible case which must be used in designing the individual structural elements.

As an illustrative example, some of the loading combinations required by The American Society of Civil Engineers' *Minimum Design Loads for Buildings and Other Structures* (ASCE-7-05) [1], assuming that only those loads noted previously might be acting, include:

$$\begin{gathered} 1.4D \\ 1.2D + 1.6L + 0.5S \\ 1.2D + 1.6S + (L \text{ or } 0.8W) \\ 1.2D + 1.6W + L + 0.5S \\ 1.2D + E + L + 0.2S \end{gathered} \tag{8.1}$$

and so on, where:
D = dead load;
L = live load;
S = snow load;
W = wind load; and
E = earthquake load.

The various load combinations are based on the philosophy that, under any given set of circumstances, the worst case loads on a structure will be described by one of these combinations of loads—with a selected level of statistical confidence as described in the following sections.

Working Stress Design

Once the worst case load acting on a structural element at any given instant is determined using the procedures described above, the structural engineer must assess whether or not the performance of the candidate structural element design is satisfactory under that load. There are a number of means by which this can be accomplished so as to ensure a reasonable level of confidence that the design will not fail. Most modern structural design codes use a procedure which is called *Load and Resistance Factor Design (LRFD)*, or in some codes *Limit States Design* (described in detail in the next section). However, some older codes still use an approach called *Working Stress* or *Allowable Stress Design*.

It is important to recognize that all building materials have their own distinct response under loading (refer to Chap. 9), and that this specific response under loading profoundly influences

their ability to resist deformation and eventual failure. The key parameters of interest are a material's strength (usually described in terms of its failure *stress*) and its resistance to deformation (usually referred to as its *stiffness*). Strength and stiffness are described in the following sections, but it should be noted that there are differing amounts of uncertainty associated with both of these properties—for all building materials. For instance, timber, which is a naturally occurring material with associated defects, has a relatively high level uncertainty associated with its mechanical properties, since these depend on numerous factors including the species of tree, the climate in which the tree was grown, the grade of lumber, the in-service humidity condition, etc., whereas structural steel has relatively little uncertainty since it is manufactured under well controlled factory conditions and is relatively insensitive to humidity, etc. LRFD and Working Stress design provide alternative means by which this variability and uncertainty in material response to loading can be accounted for during design.

In Working Stress Design, the loads expected to be acting on the structure during service are compared against the permissible stress levels which are considered safe for the structural elements under long term loads. The loads to be considered in Working Stress design are determined based on guidance given in building codes, and are intended to represent a conservative estimate of the most likely in-service loading on the structure. The analysis of the structure is subsequently performed under these loads, and the stresses in the structural elements are calculated (using principles presented later). The resulting stresses are compared against the allowable stresses for the materials in question; these are also specified in building codes.

Working stress design loads and allowable stresses have been calibrated over time to provide safe designs by implicitly building a relatively large safety factor into the allowable stress values specified in codes. These methods have now fallen out of favour in most jurisdictions, and all modern building codes are moving towards a Limit States design approach.

Limit States Design

Limit States Design is now the preferred method of design in most national building codes, largely because it (1) removes some of the unnecessary conservatism which is inherent in Working Stress Design and (2) attempts to rationally assess and account for the statistical variability of both the loads acting on a structure and the resistance of the structural elements, including variability associated with material response. Limit States Design accomplishes this by applying reliability concepts to both loads and resistances such that a consistent level of safety or *safety index* is achieved for all designs.

As the name implies, Limit States Design uses a variety of so-called 'limit states' which represent the functional requirements for a structure. *Ultimate Limit States* (ULS) are those associated with structural failure or collapse, and are addressed by checking the capacity of the structural element, with material and member strengths artificially (statistically) *reduced* to account for known variability in material properties, errors and uncertainties in construction, etc., against the credible worst case loads which might act on the structure. The most likely (mean) loads are artificially *increased* to account for their spatial and temporal variability. *Serviceability Limit States* (SLS) are those associated with the in-service performance of the structure and are checked against the loads assumed to be acting in service. Since serviceability limit states are not associated with life safety, the service loads need not be unduly increased during design.

The design checks which are made in Limit States Design can be expressed in general as:

$$\alpha E \leq \phi R \tag{8.2}$$

where:

E = the specified effect of loads acting on the structure;

α = load factors applied to the specified loads which take into account the variability of the load and load patterns and, to some extent, inaccuracy in the structural analysis;

R = the calculated resistance of a member based on specified material properties and cross-sectional dimensions; and

ϕ = the resistance factor applied to the calculated resistance or to specified properties and dimensions, workmanship, type of failure (e.g. brittle versus ductile) and uncertainty in the prediction of resistance.

Serviceability Limit States

For the serviceability limit states, the factored resistance on the right side of Equation 8.1 is replaced with a serviceability criterion such as an allowable deflection, acceleration, etc. The load factors, α, are assigned different values, as described for example in ASCE-7-05 (ASCE 2005); typically close to or less than 1.0.

Material or Member Resistance Factors

As indicated in the definitions of ϕ and R, for ultimate strength design the resistance, R, is scaled by a resistance factor, ϕ, which is typically less than 1.0 to reflect the probability that the full theoretical value of R may not be achieved at all times (i.e., in some cases the structural members and materials may not be as strong as we calculate them to be based on nominal material properties, dimensions, tolerances, and construction qualities). This results from a statistical consideration of the likely ability of a structural member to resist load. In some jurisdictions these resistance factors are applied to structural elements of different types based on the member type (e.g. beam, column, wall, etc.) and materials of construction (e.g. steel, concrete, timber, etc.). Values may vary between about 0.60 and about 0.95. In other jurisdictions resistance factors may be applied to materials rather than to structural elements. Values of resistance factors for structural materials also vary depending on the particular building code and jurisdiction. For structural steel, the value of ϕ is typically in the range of 0.85–0.95. Interestingly, for connections (i.e., bolts, welds, etc.) build from steel, the resistance factor is typically reduced somewhat to ensure that member failure occurs before connection failure; this is preferred because connection failures can occur with little warning whereas member failures generally give some warning prior to failure. Concrete tends to have lower specified material resistance factors in the range of 0.60–0.65 to reflect its higher variability; designers and codes are statistically less confident of its nominal strength.

Safety Index

In Limit States Design, the values of both the load factors, α, and the material or member resistance factors, ϕ, in a given building code have been calibrated to provide the desired level of safety (or rather to give an acceptable probability of failure). This is generally accomplished using the concept of a *safety index, β*.

In reality, both E and R in Equation 8.1 are random statistical variables with an associated probability distribution about a mean value. This is shown schematically in Fig. 8.1, where the probability that either the load, E, or the resistance, R, take on given values is plotted. Clearly, the mean resistance must be greater than the mean load effect to prevent failure; however, because both load and resistance are probabilistic in nature there is always a small chance of failure (occurring when then resistance is less than the applied load). The probability of failure is represented by the shaded overlapping area in Fig. 8.1.

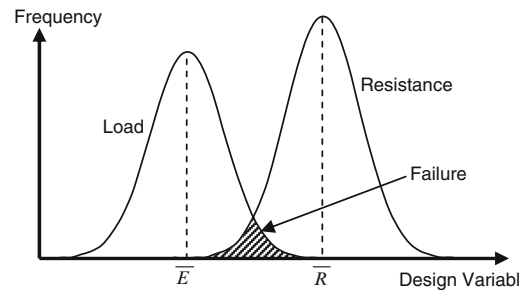

Fig. 8.1 Probabilistic nature of load effect, E, and structural resistance, R

It is clear that the probability of failure can be reduced by artificially increasing the true (nominal) resistance, R, of a structure by imposing smaller values of ϕ (i.e. by shifting the R-curve to the right in Fig. 8.1) or by artificially decreasing the true loads by imposing larger values of α (i.e. by shifting the E-curve to the left). The target *safety index*, β, allows building code developers to determine what these values should be based on known (or approximated) probability distributions for both the loads and the material or member resistances.

Since failure will occur if $R < E$, the probability of failure can be represented by the distribution of $Z = R - E$. This is shown schematically in Fig. 8.2, where failure is again represented by the shaded region. This failure probability distribution also has a mean value and an associated standard deviation. The goal of Limit States Design is to ensure that the mean value is sufficiently above zero.

As shown in Fig. 8.2, the Safety Index is simply the number of standard deviations that the mean value of the Z curve is greater than zero. In most international codes this value is set between 2 and 3. The safety Index can be quantified, provided that the mean and standard deviations of the load and resistance distributions are known, using:

$$\beta = \frac{\overline{Z}}{\sigma_z} = \frac{\overline{R} - \overline{E}}{\sqrt{\sigma_R{}^2 + \sigma_E{}^2}} \tag{8.3}$$

Clearly, to be able to quantify the safety index, it is necessary to have good statistical data for both the applied loads on a structural member and its resistance; in many cases these data are not very well known—particularly during fire.

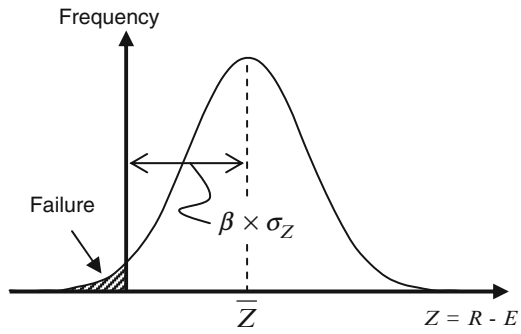

Fig. 8.2 Probabilistic nature of $Z = R–E$, and definition of the Safety Index, β

Structural Design Under Fire Conditions

Structural design for fire conditions generally follows the same approach as for structural design under ambient conditions, however because a severe fire in most buildings is a statistically 'rare' event, the load and resistance factors specified in building codes for the fire limit state change to reflect this fact.

Philosophy and Goals

The design equation during fire is similar to Equation 8.2, and can be expressed in general as:

$$\alpha_\theta E_\theta \leq \phi_\theta R_\theta \tag{8.4}$$

where the subscript θ is added to denote the effects of elevated temperature. Elevated temperature may have an effect on each of the terms in Equation 8.4. For instance:

E_θ = the specified effect of loads acting on the structure at elevated temperature. It should be noted that thermal expansion of structural elements may introduce new loads into the structure due to restraint to thermal expansion, and these should be considered;

α_θ = load factors applied to the specified loads for the elevated temperature condition. These are typically reduced as compared with the ambient temperature values to reflect the most likely load condition at the time of a fire (service loading condition). Typical load combinations for fire are given later in this chapter;

R_θ = the calculated resistance of a member at elevated temperature, based on material properties (and in some cases reduced cross-sectional dimensions) which have been reduced due to the damaging effects of heating. The resistance of a structural element will reduce during the course of a fire as it heats up; and

ϕ_θ = the resistance factor applied to the calculated resistance or to specified properties and dimensions, workmanship, type of failure, and uncertainty in the prediction of resistance at high temperature. These factors are typically set to 1.0 such that the nominal member or material strength at elevated temperature is used in calculations.

It is also important to recognize that structural design for fire typically considers three distinct modes of failure which must be prevented when satisfying Equation 8.4. Recognizing that ensuring that fire does not spread beyond the compartment of origin for the requisite period of time is a fundamental goal of fire safety engineering, these failure modes are:

1. loss of load bearing capacity (i.e. structural collapse);
2. passage of flame or hot gas through a building element (e.g. wall or floor), which would represent a breach of fire compartmentation; and
3. excessive temperature rise at the exposed face of the structural element, which may also represent a breach of fire compartmentation.

Structural Fire Design Loads and Load Combinations

Load combinations for use in Limit States Design for ultimate capacity at ambient conditions were given previously. In the case of structural fire analysis, the load combinations are altered to reflect the statistical unlikelihood of a severe fire occurring in the first place, as well as the fact that the actual likely loads acting on a structure on a day-to-day basis are typically much less than those used for ultimate strength design. Various countries apply slightly different load combinations for fire. As one example, ASCE-7-05 [1] suggests the following load combination for fire:

$$1.2D + A_k + (0.5L \text{ or } 0.25) \tag{8.5}$$

It should be noted that other codes may also include the effects of snow and wind loads during fire, however again at reduced levels as compared with ambient temperature design. The most important outcome of assuming these reduced loads during fire is the realization that, und er day-to-day conditions which are typically used to assess structural performance in fire, most structures are subjected to loads of 50 % or less of their ultimate design capacities [2].

It should be noted that the value of the load or load effect resulting from the extraordinary event (fire) should be included and is denoted by A_k in Equation 8.5.

Structural Mechanics

Thus far, this chapter has concerned itself with the method that structural engineers use to quantify the likelihood of failure of, and hence design, structural members under the influence of the various combinations of loads to which they might be subjected. Structural mechanics is the branch of physics which allows structural engineers to determine the strength, or load bearing capacity, and deformation of structural elements of various types (e.g. beams, columns, slabs) under load. To provide a basic overview of the procedures used, the following sections give a brief summary of the necessary concepts; the steps in any analysis typically include:

1. Calculation of external reaction (support) forces;
2. Determination of internal forces (axial, bending, shear, and torsion); and
3. Prediction of failure modes depending on the materials of construction, the geometry, the support conditions, and the loads.

Statics

With the previous issues in mind, we now move to a discussion of the physics which are used to evaluate the capacities of various types of structural elements. The first of these topics is *statics*. Statics provides the means by which both the *external reactions* and *internal forces* within a structural element can be determined. If a structure is in *equilibrium* (i.e. it is not moving but 'static') then the algebraic sum of all of the *forces*

and *moments* acting on that structure is equal to zero. Otherwise the structure would be accelerating.

Static Equilibrium and Reaction Forces

The first step in the analysis of structural element under load is the determination of its support reactions. For simple two-dimensional (i.e. planar) structures, static equilibrium can be applied using an orthogonal coordinate system, such that the algebraic sum of the forces in the x (horizontal) and y (vertical) directions must be zero, and also the sum of the moments acting on the structure must be zero. These equations can be expressed as follows:

$$\sum F_x = 0, \quad \sum F_y = 0, \quad \sum M_z = 0 \qquad (8.6)$$

In reality structures are three-dimensional, and in this case there would be six equations governing static equilibrium; three translations along x, y and z-axes and moments about all three axes. As is typical in elementary structural mechanics this chapter considers only planar structures for simplicity.

To illustrate the use of these equations consider the planar beam structure shown in Fig. 8.3; this is similar to the example structure used in the previous edition of this handbook [3, 4]. The structure is a solid beam of constant cross-sectional area and materials of construction along its length. The beam is supported on an idealized pin support at Location B and an idealized roller support at Location C. It is loaded by a diagonal tension force at Location A, as well as a distributed load of varying magnitude along its length.

Figure 8.3b shows a free body diagram of the beam, where the supports have been replaced by the unknown reaction forces which they would generate (in the directions in which they *prevent* motion). Note that there are three unknown reaction forces in this case, and since three equations of equilibrium are available in two dimensions, the unknowns can be determined. Such structures are referred to as *statically determinate*. The equations are applied as follows (with units of kN and m):

$$\sum F_y = 0: \quad -6 + R_{By} + R_{Cy} - 1(24) - 2(18)/2 = 0$$

$$\sum M_z = 0: \quad -6(6) + 1(24)(6) - R_{Cy}(18) + 2(18)(9)/2 = 0$$

$$\therefore R_{Cy} = 18, \; R_{By} = 30$$

Note that if this structure had one or more additional supports there would not have been sufficient equilibrium equations to solve for all of the unknown reactions, and the structure would have been referred to as *statically indeterminate*. Unknown support reactions for statically indeterminate structures can only be obtained by considering compatibility of their deformation under load in addition to equilibrium; such methods are beyond the scope of this introductory discussion.

Internal Forces

Once the support reactions for a statically determinate structure are known the internal forces can be determined at any desired location. Again, for a two-dimensional planar structure there are three internal forces which must be considered: Axial force, $N(x)$, shear force, $V(x)$, and moment, $M(x)$. The internal forces are found by taking a section through the structure, which leads to the development of three unknown internal forces. Again the three equations of equilibrium can be applied to solve for the unknowns.

As an example, for the two-dimensional planar structure shown in Fig. 8.3c, the internal forces at any location between B and C can be determined from the following equilibrium equations (again with units of kN and m):

$$\sum F_x = 0: \quad -8 + 8 + N = 0 \rightarrow \quad N = 0$$

$$\sum F_y = 0: \quad -6 - 1(6 + x) + 30 - (2x/18)(x)/2 + V = 0$$
$$\therefore V(x) = -x^2/18 - x + 18$$

$$\sum M_z = 0: \quad M + 6(6 + x) + 1(6 + x)(6 + x)/2 - 30(x) + (2x/18)(x)(x/3)/2 = 0$$
$$\therefore M(x) = -x^3/3 - x^2/2 + 18x - 54$$

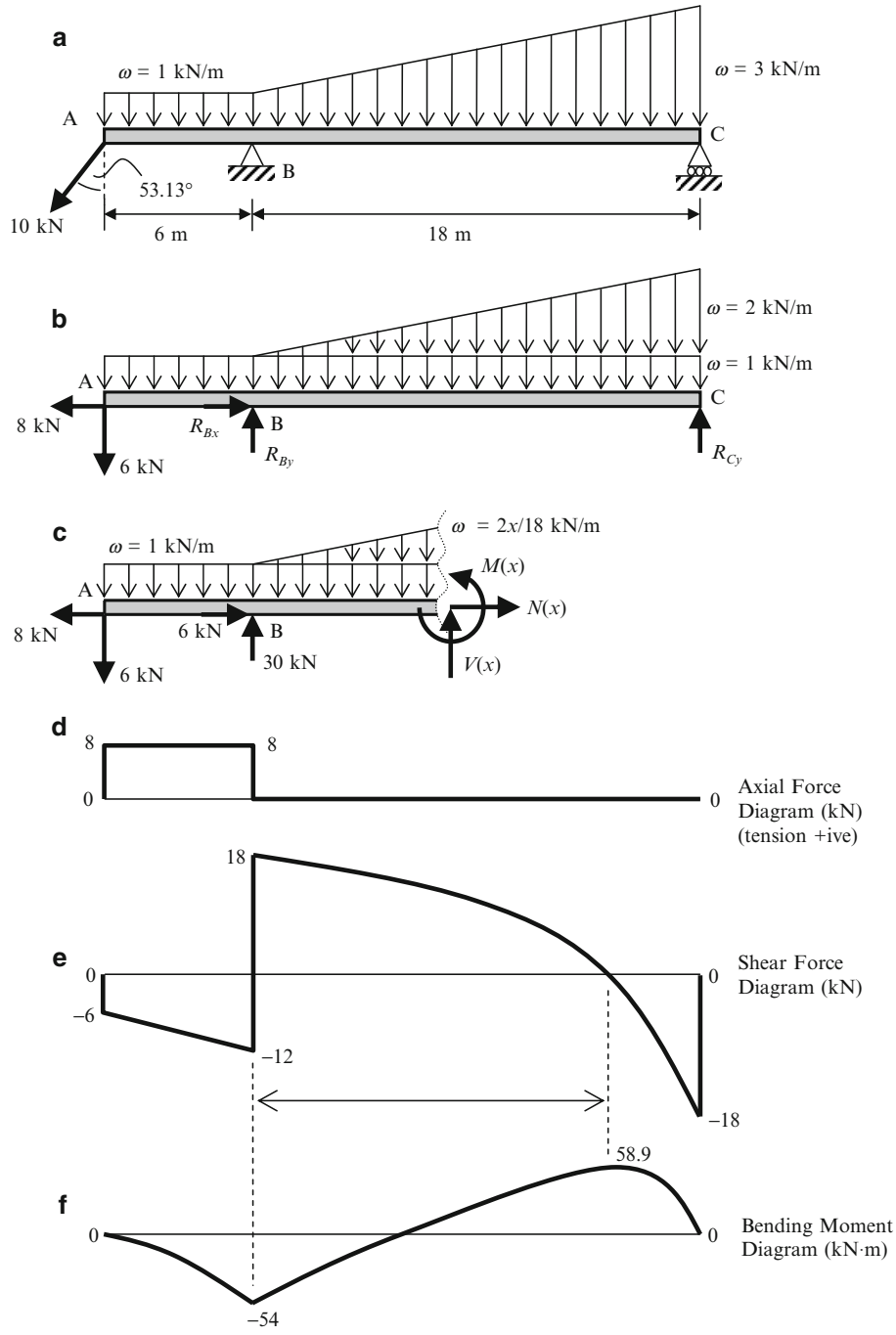

Fig. 8.3 (**a**) Example structure, (**b**) free body diagram, (**c**) section to the left of location x, (**d**) axial force diagram, (**e**) shear force diagram, and (**f**) bending moment diagram

By taking sections at successive locations along the length of the beam and calculating the internal forces it is possible to develop diagrams which plot the variation of the respective internal forces along the length of the structure; these are called the axial force, shear force, and bending moment diagrams, respectively, and are shown in Fig. 8.3d–f for the structure in question.

Strength of Simple Structural Elements

Once the internal forces within a structural element are known using the principles briefly presented above (or using more advanced techniques for statically indeterminate structures) the effects of these forces must be determined so as to check the capacity of the structural element in question against the loading demand. To do this the likely failure mode for the structural element must be determined.

There are a variety of failure modes which must be considered, depending on the type of structural element (i.e. beam, column, etc.) and the material from which it is constructed (some materials are more prone to certain types of failures than other materials). The most important failure modes in buildings are typically tension failure, compression failure, and bending failure. For some structures or structural elements under certain conditions shear failure may also be important; however shear is not treated in this introductory discussion.

Tension Members (Cables and Ties)

Tension members are much less common in buildings that compression elements (columns) or flexural (bending) elements (beams and slabs), however tension members are the simplest structural element because their failure mode can be described in relatively simple terms. Tension elements in real buildings include diagonal bracing, cable-supports and ties, and hangar bars.

Consider a cylindrical steel bar of a given material and length L and cross-sectional area A which is subjected to a tensile axial load, P, in the direction of its longitudinal axis (Fig. 8.4). Using the principles of the preceding section, if the bar is sectioned at any internal location, a tension force, P, will be acting internally (Fig. 8.5).

The force is tensile as it acts to elongate the bar. The average tensile *stress* in the bar, which is a measure of the intensity of force in a material, can be determined from:

$$\sigma = \frac{P}{A} \tag{8.7}$$

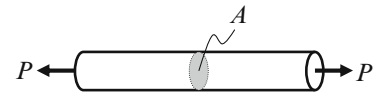

Fig. 8.4 Tensile loading of cylindrical bar of cross-sectional area, A

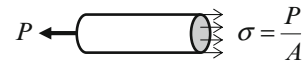

Fig. 8.5 Determination of average axial stress, σ, of cylindrical bar of cross-sectional area, A, under tensile load, P

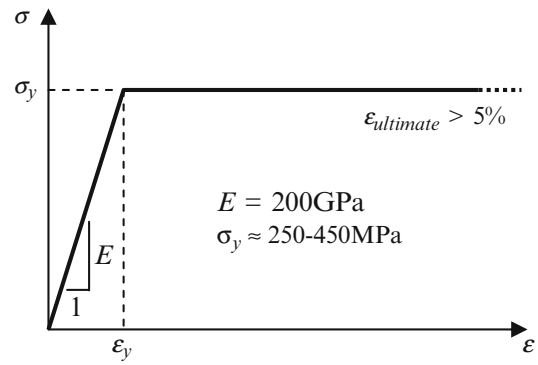

Fig. 8.6 Idealized axial stress, σ, versus axial strain, ε, for typical structural steel

This shows that stress in the bar is proportional to the internal force and is given in units of force per unit area (in this case N/mm^2 or MPa). Using *Hooke's Law* the strain, ε, and hence elongation, δ, of the bar can be determined from the following expressions (within the *linear-elastic* range of material response) from:

$$\begin{aligned} \sigma &= \varepsilon E \\ \varepsilon &= \frac{\delta}{L} \end{aligned} \tag{8.8}$$

In the above expressions, E is the modulus of elasticity of the material from which the bar is made (a material characteristic, see below and Fig. 8.6), and the strain, ε, represents the intensity of deformation.

To determine if the bar will fail under this load (and hence stress) the stress versus strain response of the material from which the bar is

made must be known. As an example, for structural steel a typical idealized plot of stress versus strain is given in Fig. 8.6. Note that in practice this curve would be determined experimentally.

Figure 8.6 shows that the loading response of steel is characterized by a linear increase in stress with increasing strain, with slope E providing the definition of Hooke's Law used previously, up to a given stress, σ_y, which is called the *yield stress*. Beyond the yield stress the strain increases linearly with no further increase in stress. Hence, the steel can be assumed to fail in tension when it reaches its yield stress, and its load carrying capacity (resistance), R, can be easily determined under this condition from:

$$R = \sigma_y A \tag{8.9}$$

Calculation of tensile strength at elevated temperature can be performed in a similar manner provided that the temperature of the structural element and the effect of this temperature on the stress versus strain response of the material are known. Chapter 9 provides information on the probable reductions in mechanical properties of various structural materials at elevated temperature.

For the purposes of illustration, if it is assumed that the yield strength of steel is reduced from σ_y at ambient temperature to $\sigma_{y\theta}$ at elevated temperature, then the tensile strength at elevated temperature, R_θ, can be determined from:

$$R_\theta = \sigma_{y\theta} A_\theta \tag{8.10}$$

It should be noted that the cross-sectional area at elevated temperature, A_θ, may also be reduced in applying Equation 8.10 to reflect a reduction in cross-sectional area due to heating, as would occur for example due to charring of wood for timber elements in fire.

It must be recognized that all structural materials display distinct differences in mechanical response to loading and widely varying strength and stiffness. For example, a typical stress versus strain response for 'normal' strength concrete is shown in Fig. 8.7, where drastic differences in both the qualitative and quantitative aspects as compared with steel are obvious.

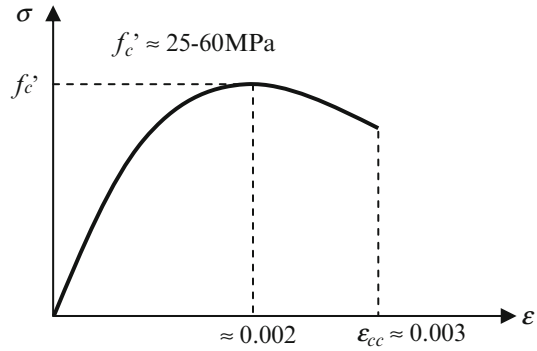

Fig. 8.7 Idealized axial stress, σ, versus axial strain, ε, for typical 'normal' strength concrete

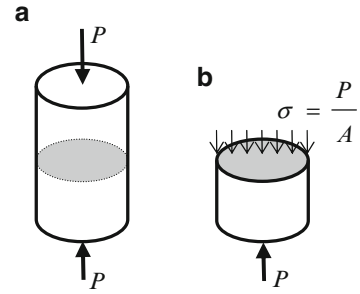

Fig. 8.8 (**a**) Compressive loading of short (stocky) cylindrical bar of cross-sectional area, A, and (**b**) determination of average axial stress, σ

Compression Members (Columns and Struts)

Compression elements are common in buildings and include columns and struts. The strength of these elements can be determined in a similar manner as for tension elements, with the exception that compression elements may also be susceptible to *buckling* failure.

Consider the short, stocky compression element shown in Fig. 8.8. As for the tension element discussed previously, the column has height L, cross-sectional area A, and is subjected to an axial load P (in this case compressive).

Provided that the element is not prone to buckling failure, its compressive (crushing) strength at ambient or elevated temperature can be approximated using Equations 8.9 and 8.10, respectively. However, in reality all compression elements in buildings are susceptible to buckling

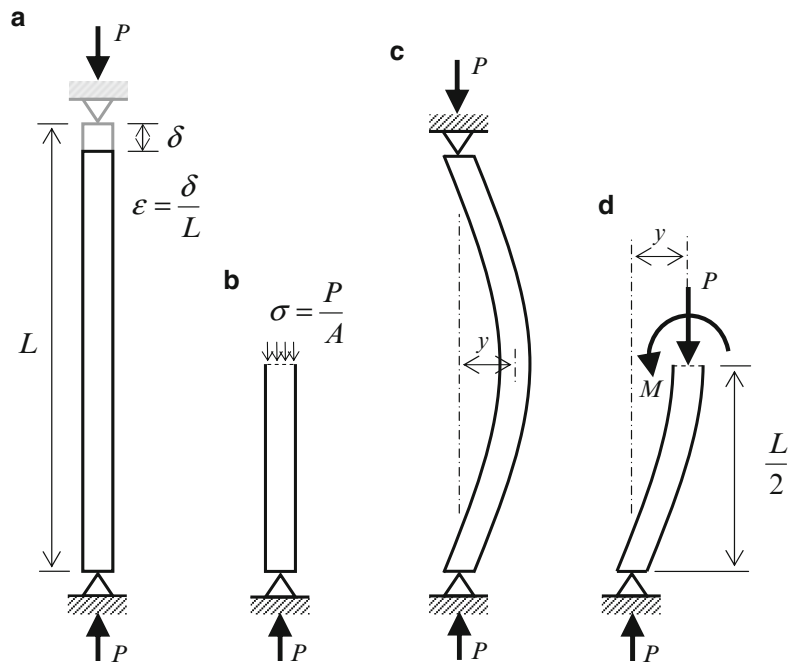

Fig. 8.9 (**a**) Compressive loading of long (slender) bar of cross-sectional area, A, (**b**) determination of average axial stress, σ, of the bar under compressive load, P, (**c**) buckling failure of the bar under load, P, and (**d**) equilibrium of half the bar under buckling failure

failure and to the combined effect of axial load and the inevitable bending which also occurs; failure by buckling must therefore also be checked.

To illustrate the alternative compressive failure mode by buckling, Fig. 8.9 shows a vertical column of height L, cross-sectional area A, and applied load P. The column is assumed to be pin-supported at both ends, such that there is no rotational restraint of its extremities (note that this is not the case for most real columns in buildings). When the load is applied to the column (Fig. 8.9a) the column experiences an axial compressive stress of σ (Fig. 8.9b), and the column's length will reduce by an amount δ (Fig. 8.9a). However, because in reality it is impossible to apply a perfectly concentric compressive load, and because all structural elements contain small imperfections and irregularities, the column will inevitably also experience a small amount of bending (Fig. 8.9c); the result is a lateral deflection, y.

Figure 8.9d shows the bottom half of the column when it is sectioned at its mid-height. If we consider the section's equilibrium under this condition, taking moments at the section the following moment equilibrium equation is obtained:

$$\sum M_z = 0: \quad M - Py = 0 \rightarrow \quad M = Py \tag{8.11}$$

The elastic deformation of an element in bending can be described by the following equation:

$$\frac{M}{EI} = \frac{d^2y}{dx^2} \tag{8.12}$$

where y is the displacement perpendicular to the axis of the element, x is the distance along the element, and M is the internal moment which is acting at the section. I is the *moment of inertia* of the element and is a measure of its resistance to flexural deformation. The moment of inertia it is a function of the element's cross-sectional geometry and can be considered as a flexural analogue of area, A, for calculating tensile strength.

Substituting Equation 8.12 into Equation 8.11 and rearranging gives:

$$\frac{d^2y}{dx^2} - \frac{P}{EI}y = 0 \tag{8.13}$$

This is a second order differential equation which has the following solution:

$$v = C_1 \sin\left(\sqrt{\frac{P}{EI}}x\right) + C_2 \cos\left(\sqrt{\frac{P}{EI}}x\right) \tag{8.14}$$

If the ends of the column are pinned (as in this case), then Equation 8.14 is only satisfied when:

$$\sin\left(\sqrt{\frac{P}{EI}}L\right) = 0 \quad \text{or} \quad \sqrt{\frac{P}{EI}}L = n\pi \tag{8.15}$$

Rearranging for P, the critical buckling load, $P_{critical}$, is obtained; this is the theoretical load which will cause global buckling failure:

$$R = P_{critical} = \frac{n^2\pi^2 EI}{L^2} \quad \text{where :} \quad n = 1, 2, 3\ldots \tag{8.16}$$

It is clear that the lowest value of $P_{critical}$ will govern and that this occurs for $n = 1$. Whilst this equation is only valid for linear elastic materials, as it depends on the assumptions of elastic beam theory (i.e. Equation 8.12), it is instructive for studying the propensity of elements to buckling failure under compressive loads.

An interesting feature of Equation 8.16 is that it shows buckling strength to be proportional to the inverse of the square of the buckling length. Thus, if the length of a column is doubled then its buckling strength decreases by a factor of four, and so on. This can be important for the response of columns in fire in cases where lateral support from beams and slabs is removed by heating of the floorplate.

The preceding section has given two means of calculating the strength of a structural element subjected to compressive axial load. Figure 8.10 plots these two methods versus column length. For very short columns, the crushing strength given by Equation 8.9 will govern, whereas for slender columns buckling (Equation 8.16) will govern. In reality, the transition between the two failure modes is more gradual due to column imperfections and inadvertent load eccentricities, and for intermediate column lengths a combined buckling crushing failure mode will be observed in reality. Building codes contain structural

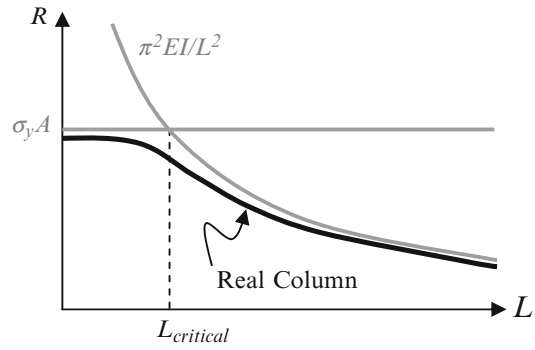

Fig. 8.10 Column compressive strength versus buckling length

design procedures which have been calibrated to take account of the necessary factors.

Calculation of compressive strength at elevated temperature is similar to at ambient temperature, however several additional important considerations are required; these are that:

1. the strength of materials is reduced at elevated temperature, such that the crushing strength will be less than at ambient temperature (see Chap. 9), according to Equation 8.10;
2. the stiffness (i.e. elastic modulus, E) is reduced at elevated temperature (possibly more or less severely than the material's strength), thus reducing the critical buckling load, $P_{critical}$ to:

$$R_\theta = P_{critical,\ \theta} = \frac{n^2\pi^2 E_\theta I_\theta}{{L_\theta}^2} \quad \text{where :} \quad n = 1, 2, 3; \tag{8.17}$$

3. the effective size of the column's cross section may be reduced, thus reducing the moment of inertia of the section from I to I_θ;
4. local increases in temperature may result in additional loads and moments due to interactions with the rest of the structure during fire; for instance thermal restraint to expansion of columns by the cool surrounding structure can increase the compressive loads on a column by 20–30 % in some cases; and
5. thermal expansion of the floorplate may result in lateral forces and displacements being imposed on columns, resulting in unexpected shear forces and so-called second-order bending moments.

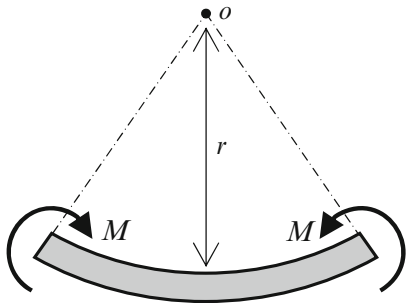

Fig. 8.11 Segment of a beam in bending

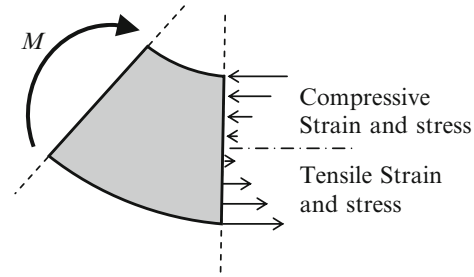

Fig. 8.12 Segment of a beam in bending

Flexural Elements (Joists, Beams and Girders)

Flexural elements in buildings are those which resist the applied loads primarily by bending; these include joists, beams, girders, and slabs. The variation of internal moment in a structural element under a set of loads, E, can be determined using the techniques discussed previously with reference to Fig. 8.3. The resistance of an element to bending, R, must be determined using structural mechanics.

When a structural element is subjected to bending it experiences *curvature*. This is shown in Fig. 8.11, where a short segment of beam is subjected to a moment couple (i.e. an internal bending moment) which causes the segment to bend in a concave-up direction. Lines which were previously vertical drawn on the side of the beam would now both point towards a distant origin called the *center of curvature* (denoted by O in Fig. 8.11). The distance to the center of curvature is called the *radius of curvature*, r.

This concave up condition is typically referred to as a positive or sagging moment. When an internal moment causes bending in a concave down direction it is referred to as a negative or hogging moment.

When the segment is subjected to a sagging moment, material at the top of the beam's cross section is compressed whereas material at the bottom of the beam is elongated, as shown in Fig. 8.12.

At one specific location on the beam's cross section it is neither being compressed nor stretched; this location is called the *neutral plane*, and occurs at the mid-height for sections which are symmetric about a horizontal axis of bending (such as the I-shaped cross section shown in Fig. 8.13).

If it is assumed that the beam is homogenous and fabricated from a linear elastic material (a helpful simplification for illustrative purposes), the distribution of strains over the cross section is linear as shown in Fig. 8.13. Applying Hooke's Law the stress distribution over the cross section is therefore also linear, with maximum compressive stress at the top fibre of the cross section and maximum tensile stress at the bottom fibre. These assumptions can be expressed as:

$$\varepsilon_y = \frac{\varepsilon_{top}}{y_{top}} y = \frac{\varepsilon_{bottom}}{y_{bottom}} y \tag{8.18}$$

$$\sigma_y = \frac{\sigma_{top}}{y_{top}} y = \frac{\varepsilon_{top} E}{y_{top}} y \tag{8.19}$$

If the beam is in equilibrium, then at any section to the total compressive forces must be equal to the total tensile forces. For any small area, dA, located anywhere on the cross section, the resultant force is determined as the stress multiplied by its area:

$$dF = \sigma dA \tag{8.20}$$

Applying equilibrium in the horizontal direction and integrating over the cross section:

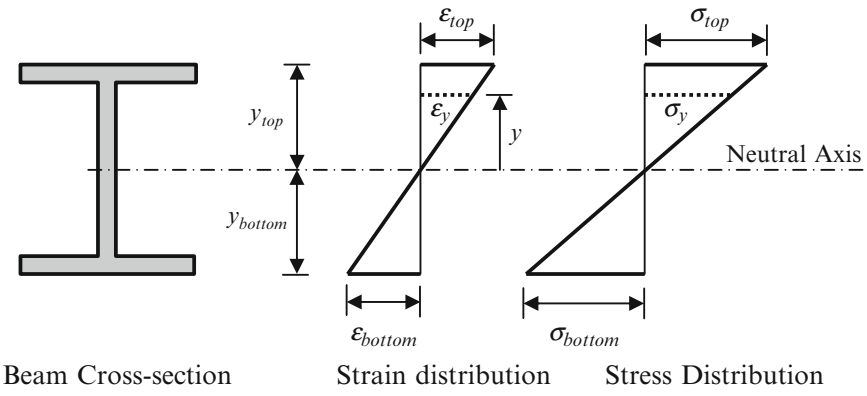

Fig. 8.13 Beam cross-section, strain distribution, and stress distribution for a homogenous, linear elastic beam in bending

$$\sum F_x = 0: \; 0 = \int_A dF = \int_A \sigma dA = \int_A \frac{y}{y_{top}} \sigma_{top} dA = \frac{\sigma_{top}}{y_{top}} \int_A y dA \tag{8.21}$$

Since the term in front of the integrand is non-zero, then for equilibrium it is required that:

$$0 = \int_A y dA \tag{8.22}$$

This is equivalent to stating that the axis of zero strain, called the *neutral axis*, must pass through the *centroid* of the cross section.

Stresses in the beam can also be determined using equilibrium, which requires that the internal moment, M, be equal to the moment produced by integrating the moment contributions of the individual areas over the cross section. This can be expressed as:

$$\sum M = M: \; M = \int_A y dF = \int_A y(\sigma dA) = \int_A y\left(\frac{y}{y_{top}}\sigma_{top}\right) dA = \frac{\sigma_{top}}{y_{top}} \int_A y^2 \, dA \tag{8.23}$$

The term inside the integrand represents the *moment of inertia* (or second moment of area), I, of the cross section, and can be found using simple techniques or tables given in solid mechanics textbooks. Rearranging and incorporating Equation 8.19, an equation for the stress at any location in a cross section is obtained:

$$\sigma_y = \frac{My}{I} \tag{8.24}$$

This is referred to as *The Flexure Formula*, and can be used (for linear elastic materials) to check that the stress in a cross section is less than the failure stress for the material from which a beam is made; and hence to define the resistance of an element, R, with respect to bending failure. This approach works for most statically determinate structures, because for these types of structures the formation of a single flexural failure point (called a *plastic hinge*) is sufficient to cause failure. Statically indeterminate structures are more complicated as they require the formation of more than one location of flexural failure, as discussed below.

The above approach to flexural analysis can also be used for elevated temperature analysis provided that the likely reductions in mechanical properties of a structural member's constituent materials are known, and also provided that reductions in cross sectional area are accounted for.

Similar mechanics can be used to develop equations for stress in sections made from

inelastic or non-linear materials, however these are considerably more involved and are not discussed here. For beams made from steel, which is often considered to be elastic-plastic, as previously shown in Fig. 8.6, or for reinforced concrete which is built up from a combination of steel and concrete (refer to Fig. 8.7), specialist texts should be consulted for information in this area.

Lateral Instability of Beams

The above equations assume failure of a beam by excessive bending stresses. This is analogous to crushing failure of a column in compression. However, in certain cases beams may fail due to instability failures which are akin to buckling failures in compressively loaded columns. Lateral instability failures result when a beam's compression fibre has insufficient lateral support, allowing it to buckle in a direction perpendicular to its longitudinal axis. Obviously, this is more of a problem for slender beams or beams built up from thin plates. In design the propensity of an element to lateral instability is accounted for by limiting the maximum stresses which are permitted in the cross section; this is particularly an issue for structural steel beams (and columns).

In structural fire design it is important to recognize that any members which provide lateral bracing to beams must have sufficient fire resistance to be able to continue to provide this bracing in the event of a fire. This is an important consideration for both beams and, as already noted, for columns. Specialist texts should be consulted for additional information on lateral instability of beams in bending.

Continuity and Full Structure Response

As already noted, most real structures are too complicated to use equilibrium alone to determine all of the external and internal forces which may be acting. In these case more advanced methods of analysis must be used which generally account also for the deformations of structures under loading (in addition to static equilibrium). Such methods are beyond the scope of the current chapter, however the implications of static indeterminacy for real structural response, both at ambient and at elevated temperature, are worthy of brief discussion.

Continuous Beams

Continuous beams are statically indeterminate due to their being, as the name implies, continuous over multiple supports. An example of a relatively simple continuous beam is given in Fig. 8.14. This figure shows that unlike simply-supported beams, which require only a single location of flexural failure for collapse to occur, continuous beams require multiple failure locations before a failure mechanism can form; three failure locations in the case of the beam shown. Continuous beams are therefore *redundant* structures, and they can benefit from beneficial structural actions such as *moment redistribution*, both at ambient temperature and during fire. Techniques to account for moment redistribution during fire are described in detail elsewhere (e.g. [2]).

Frames

The structural response of building frames, for instance the idealized two-dimensional portal frame and moment resisting frame shown in Figs. 8.15 and 8.16, respectively, under gravity loads is complex, and for most real structures requires the use of detailed computer analysis techniques to determine the internal forces and moments. In fire the response of frames is even further complicated; for instance by the effects of thermal expansion and thermal restraint at elevated temperature.

To illustrate some of the important behaviors which may occur in statically indeterminate frame structures during fire, Fig. 8.15 shows a possible sequence of deformation that is likely to occur in a simple planar portal frame structure subjected to a fire in its interior.

The initial geometry of the structure is shown in Fig. 8.15a, where the well-known shape of an industrial building such as a warehouse is evident. Under ambient conditions the stability of the structure is assured by moment

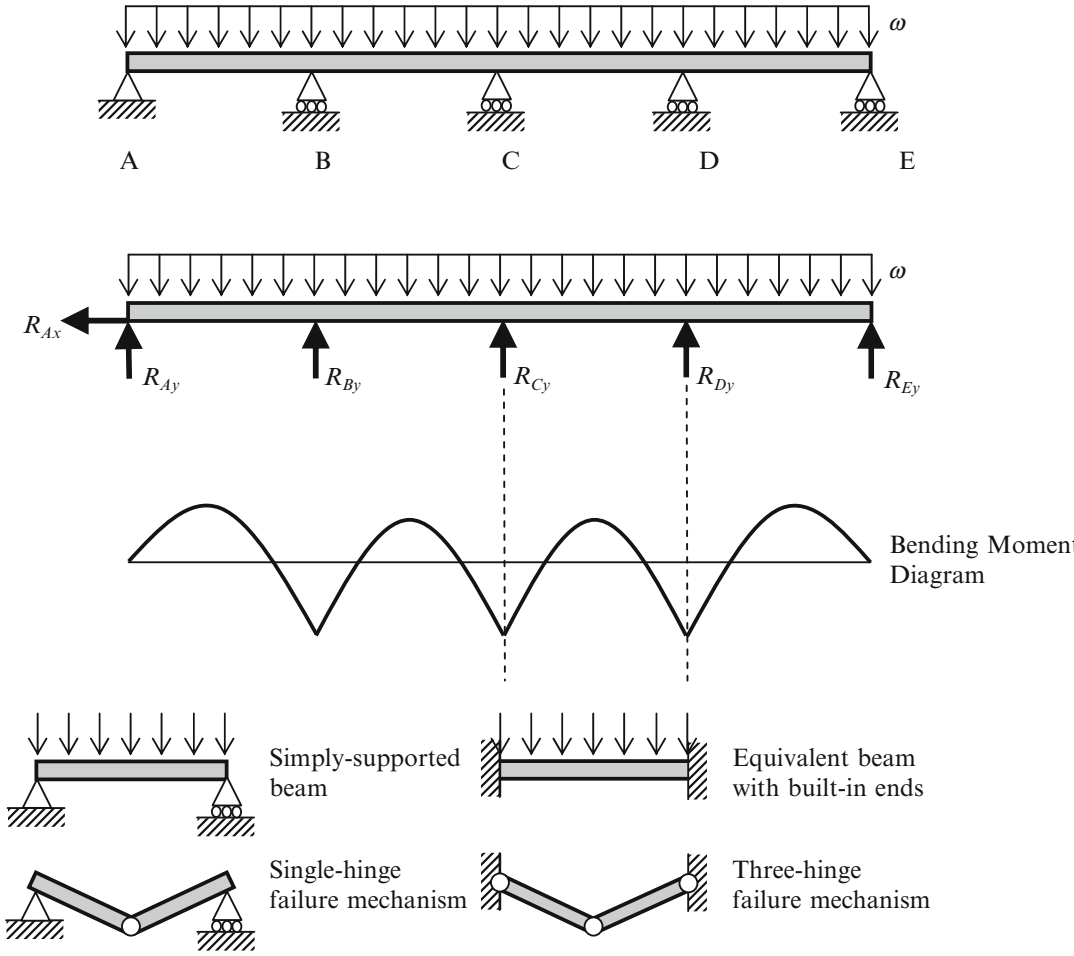

Fig. 8.14 Bending moment diagram and failure mechanism for a continuous beam as compared with a simply-supported beam under a uniformly distributed load

resisting connections at locations B, C, and D (i.e. these connections resist relative rotational displacements between the structural elements framing into the joints). Without moment resisting connections at these locations the structure would be a mechanism and would immediately collapse. The connections to the foundations at A and E are not strictly required to be moment resisting for stability under ambient conditions. Under ambient conditions this structure resists loads by a combination of bending and axial compression in its structural elements.

Figure 8.15b shows how this portal frame might react during the early stages of a fire. The roof elements (B-C and C-D) would initially be heated by the fire, and two important actions would occur:

1. The beams would experience an overall longitudinal thermal expansion, which would tend to increase the length of the beams under heating by amount ΔT, as a function of the constituent materials' coefficient of thermal expansion, α_T. This thermal expansion, if occurring without any axial restraint, would be described by the following expressions:

$$\varepsilon_T = \alpha_T \Delta T \quad \text{or} \quad \Delta L_T = \alpha_T \Delta T L \tag{8.25}$$

The result of this thermal expansion would be to push the columns outwards, and hence to

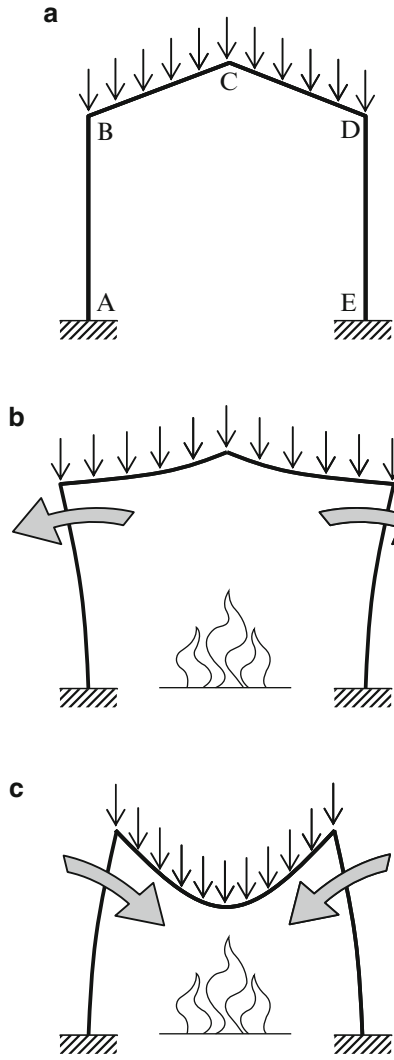

Fig. 8.15 Schematic showing complexities of structural response and possible failure mode of a statically indeterminate portal frame in fire

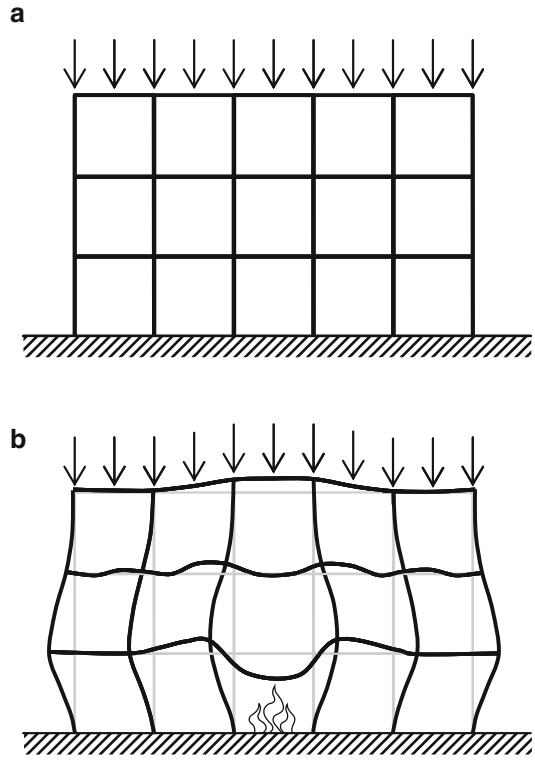

Fig. 8.16 Schematic showing complexities of structural response of a statically indeterminate multi-floor moment resisting frame in fire (Reproduced after Buchanan [2])

increase the moments in the columns and in the connections to the foundation. In reality there would be some restraint to axial thermal expansion, which would also tend to increase the mechanical compressive loads in the beams on heating.

2. The beams, which when heated from below would experience greater heating at their bottom fibre than at their top, would undergo thermal curvature and thermal bowing, to various degrees depending on the materials of construction, the roofing system, etc. The result of this is that the roof beams would bow toward the fire and begin to sag purely as a consequence of the thermal gradient.

As a consequence of the thermal elongation and thermal bowing, combined with reductions in the mechanical properties of the beam on further heating, the peak in the roof would gradually displace downwards under the influence of gravity loads. At some point the peak of the roof, Point C, may displace below the height of points B and D, and the roof would snap-through forming a *catenary*.

Figure 8.15c shows the structure once the roof has snapped through. Under this condition the roof acts in tension (rather than bending and compression) to support the load under a severely deformed geometry. In addition, the moments on the column bases would be reversed and stability of the structure would be assured

only by the moment capacity of the columns and their base connections to the foundations. Eventual failure of the structure would occur with the columns pulled inward leading to collapse.

This relatively simple example clearly illustrates that thermal expansion, thermal bowing, large deflections, and alternative load carrying mechanisms can all be expected to play pivotal roles in the structural mechanics of a real, however simplified, structure during fire.

A more complicated, yet still highly idealized structure is shown in Fig. 8.16; this is a two-dimensional moment resisting frame. Again, Fig. 8.16a shows the frame supporting gravity loads under ambient conditions. Again, the structure resists both vertical (e.g. gravity) and possibly lateral (e.g. wind) loads through a combination of bending and compressive loading.

Figure 8.16b shows a highly exaggerated idealization of the possible deformation of this moment resisting frame under exposure to a fire which is localized to a single internal bay at the ground floor level. This suggests that the response of the structure is far more complex than the response of a single isolated beam presented earlier, and that the effects of continuity, axial restraint, thermal elongations and rotations, and reductions in mechanical properties of the constituent materials will all profoundly affect the forces, stresses, deformations, and ultimately the failure mode of the structure during fire. As a result of the heating during a fire, elements are subjected to loads which may never have been considered during ambient design (for example shearing or unexpected bending of the perimeter columns due to being pushed laterally by the expanding floor plate). Such factors must be considered during design in order for structures to be rationally engineered to resist the effects of fire. Such analysis is extremely complex and requires the use of specialized computer analysis software.

Slabs and Shells (Membrane Actions)

An additional structural action which often plays an important role in the response of real structures during fire is *membrane* action.

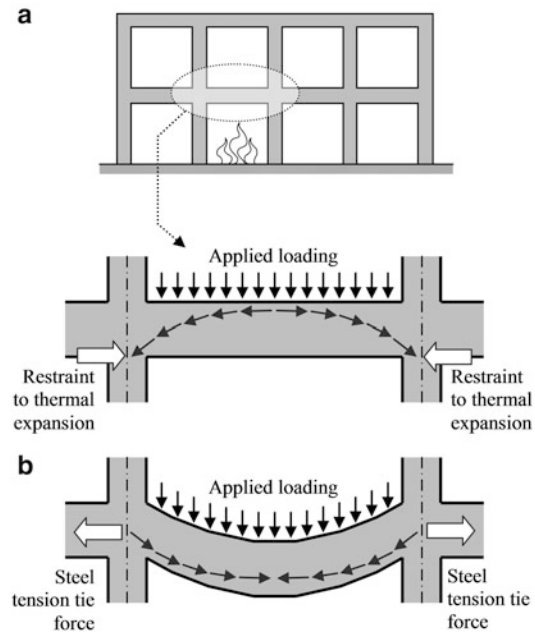

Fig. 8.17 Schematic representation of compressive and tensile membrane actions in a reinforced concrete slab

Membrane action, which can be either compressive or tensile, manifests itself in planar structures such as reinforced concrete floor slabs or steel-concrete composite deck slabs.

Figure 8.17 shows two-dimensional idealizations of both tensile and compressive membrane actions, where compressive membrane action can be though of as *arching* action, and tensile membrane action can be thought of as *catenary* action. In reality these actions normally manifest themselves in three dimensions; think of a dome (compressive membrane) or a net (tensile membrane).

Compressive membrane action is particularly important in continuous reinforced concrete structures during the early stages of a fire, where restrained thermal expansion of concrete slabs can lead to the development significant lateral restraint forces resulting in arching action during fire (provided of course that the thrust forces have a line of action *below* the neutral axis of bending of the slabs).

Tensile membrane action is particularly important during the late stages of fires for structures with relatively thin concrete or

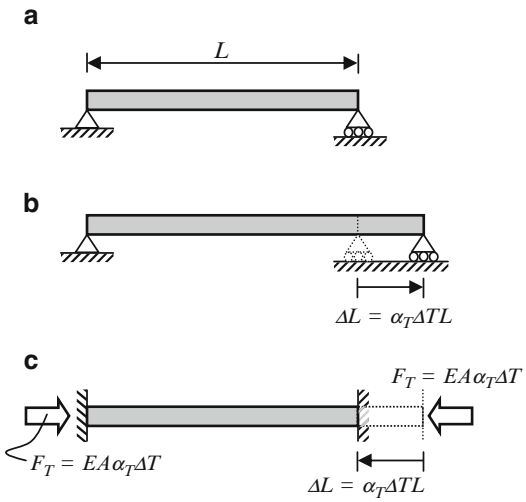

Fig. 8.18 Schematic representation of the possible effects of restraint to thermal expansion of a cylindrical steel bar

steel-concrete composite slabs. In these cases tensile membrane action can prevent structural collapse (however under large vertical deflections) for durations of fire exposure much greater than would be expected on the basis of single element analysis.

Membrane actions are discussed in considerable detail in specialized structural fire engineering references (e.g. [2, 5, 6]).

Thermally-Induced Loading

As discussed previously, thermal expansion (and more importantly restraint to thermal expansion) may significantly affect the deformation and eventual failure of real structures in real fires. To illustrate the possible importance of thermal expansion, consider a simple cylindrical steel bar of length L which is uniformly heated an amount ΔT (Fig. 8.18).

If the bar is free to expand as in Fig. 8.18a then the change in length during heating is described by Equation 8.25 given previously. If however, the bar is rigidly supported between two immovable walls (i.e. a case of perfect axial restraint as in Fig. 8.18b) then the bar is prevented from expanding and as a result it experiences zero thermal strain (i.e. zero elongation) but an increase of thermal stress. By invoking Hooke's Law (Equation 8.8 presented previously) the thermal stress, σ_T (or thermal force F_T), in the bar will be:

$$\begin{aligned} \sigma_T &= E\varepsilon_T = E\alpha_T\Delta T \\ F_T &= \sigma_T A = EA\alpha_T\Delta T \end{aligned} \tag{8.26}$$

If it is assumed that the bar is made from structural steel, with a typical yield strength, σ_y, of 350 MPa and modulus of elasticity E of 200,000 MPa (refer to Fig. 8.6), and if it is further assumed that the coefficient of thermal expansion of steel, α_T, is 13×10^{-6}/K then the increase of temperature required to cause the bar to yield can be determined as follows:

$$\begin{aligned} \varepsilon &= -\varepsilon_T = \alpha_T\Delta T \\ \sigma_y &= -E\varepsilon_T = E\alpha_T\Delta T \\ \therefore \Delta T &= \frac{\sigma_y}{E\alpha_T} = \frac{350}{200{,}000 \cdot 13 \times 10^{-6}} = 134^{\circ}\text{C} \end{aligned} \tag{8.27}$$

In other words, a change in temperature of the perfectly restrained steel bar of +134 °C can cause the bar to reach its failure stress. This simple example, whilst clearly not representative of a real structure, shows that a relatively mild increase of temperature can have a profound influence on the forces and deformations within a structure during heating. Only recently has the significance of thermal interaction within a structure been widely acknowledged within the structural fire engineering community in terms of its possible influences on the overall stability, and likely failure modes, of a building during fire (e.g. [6]).

Other Considerations

There are a host of other important structural mechanics issues which must be considered in the analysis and design of structures to resist the

damaging effects of fire and elevated temperature; it is not possible to discuss all of these here. There are many failure modes and structural interactions which could occur in any given structure, and hence structural fire analysis and design should only be undertaken by individuals with specialist knowledge in this area.

Connections

One area which has not traditionally been explicitly considered within mainstream structural design for fire is the specific performance of connections at elevated temperature. Under ambient conditions structures are generally designed under the assumption that structural members will fail before their connections. Indeed, as already noted more onerous strength reduction factors are typically applied during connection design to ensure that this is the case. The performance in fire of connections of various types is currently a topic of considerable research interest; however a detailed discussion of this topic is avoided here. It is sufficient for the reader to be aware that connection performance in fire should be considered during the fire safe structural design of a building.

Disproportionate Collapse

Disproportionate collapse refers to a situation where localized failure of a single structural element can lead to major or global collapse of a large, or disproportionate, portion of a structure [2]. There have been numerous real examples of disproportionate structural failure due to extreme loading events such as blast, earthquake, and even fire. The most notable case of a disproportionate structural collapse resulting from fire is probably the collapse of Building 7 of the World Trade Center complex in New York on September 11th, 2001.

Design to avoid disproportionate collapse, termed design for redundancy or *resilient design*, requires the provision of structural redundancy and alternative load paths. Again, this topic is beyond the scope of this introductory discussion; additional guidance is available elsewhere (e.g. [7]).

Summary

This chapter has provided a brief, introductory summary of basic structural mechanics, as is relevant to a surface level understanding of the response of structural elements and structures to fire. In conjunction with Chap. 9 of this handbook, it provides a basic understanding of the means by which structural stability, and to a certain extent integrity and insulation during fire, can be engineered through careful selection and design of building materials.

Acknowledgements The overall structure and format of this chapter of the SFPE Handbook has been based on the previous (4/e) version, which was authored by Robert W. Fitzgerald. The significant contribution of Prof. Fitzgerald to the development of this handbook must therefore be gratefully acknowledged.

Nomenclature

A	Area (nm^2)
A_k	Load or load effect resulting from an extraordinary event (e.g. fire)
C_1	Integration constant
C_2	Integration constant
c	Distance from the extreme compression fiber to the neutral axis of bending (mm)
$\mathbf{D}$	Dead load
$\mathbf{E}$	Earthquake load
E	Load effect, or modulus of elasticity (Young's modulus) (GPa)
F	Force (kN)
f_c'	Compressive strength of concrete (MPa)
I	Moment of inertia (mm^4)
$\mathbf{L}$	Live load
L	Length (mm)
M	Moment (kN·m)
n	0, 1, 2. . .
O	Center of curvature
P	Load (kN)
R	Member resistance, or reaction force (kN)

r Radius of gyration (mm)
$\mathbf{S}$ Snow load
V Shear force (kN)
$\mathbf{W}$ Wind load
x Coordinate parallel to the axis of the structural element (mm)
y Coordinate normal to the axis of the structural element (mm), or lateral deflection (mm)
Z Difference between resistance and load demand
α Load factor
α_T Coefficient of thermal expansion (K^{-1})
β Safety index
ε Strain (no units)
ε_{cc} Compressive failure strain of concrete (no units)
ε_y Yield strain (no units)
ΔL Change in length (mm)
ΔT Change in temperature (K)
δ Deformation (mm)
σ Stress (MPa)
σ_y Yield stress (MPa)
ϕ Resistance factor
π Pi
θ Subscript denoting elevated temperature
ω Uniformly distributed loading (kN/m)

References

1. ASCE, *Minimum Design Loads for Buildings and Other Structures (ASCE-7-05)*, American Society of Civil Engineers (2005).
2. A.H. Buchanan, *Structural Design for Fire Safety*, Wiley, New York, NY (2001).
3. R.W. Fitzgerald, *Mechanics of Materials*, Addison-Wesley, Reading, MA (1982).
4. Fitzgerald, R. "Structural Mechanics," *SFPE Handbook of Fire Protection of Engineering*, National Fire Protection Association, Quincy, MA (2008).
5. J.A. Purkiss, *Fire Safety Engineering Design of Structures*, Butterworth-Heinemann, New York, NY (2007).
6. Y. Wang, I. Burgess, F. Wald, M. Gillie, *Performance-Based Fire Engineering of Structures*, Spon Press (2012).
7. Scott et al., 2002 Prevention of Progressive Collapse, Multihazard Mitigation Council Of the National Institute of Building Sciences, Washington, D.C., July.

Professor Luke Bisby is Arup Chair of Fire and Structures, and Royal Academy of Engineering Research Chair, within the BRE Centre for Fire Safety Engineering at the University of Edinburgh. Educated in Canada as a structural engineer, his research and teaching are focused predominantly in the area of Fire Safety Engineering. His reasearch is broadly in the areas of structural engineering and the provision of fire safety across the built environment, with an emphasis on the mechanical response of buildings and construction materials during fire. He has published widely in areas related to the fire behaviour of reinforced concrete structures, and on fibre-reinforced polymers in structural engineering applications. His current reasearch is interested in the response of novel structural materials to heating, including high performance and high strength concretes, polymers and polymer composites for construction, fire protection materials (including reactive fire protection coatings), and structural cross-laminated timber. He is also involved in research projects seeking to better understand and unpick sociological and psychological issues in fire safety engineering and regulation.

Properties of Building Materials

9

V.K.R. Kodur and T.Z. Harmathy

Introduction

Building components are to be designed to satisfy the requirements of serviceability and safety limit states. One of the major safety requirements in building design is the provision of appropriate fire resistance to various building components. The basis for this requirement can be attributed to the fact that, when other measures of containing the fire fail, structural integrity is the last line of defense. In this chapter, the term *structural member* is used to refer to both load-bearing (e.g., columns, beams, slabs) and non-load-bearing (e.g., partition walls, floors) building components.

Fire resistance is the duration during which a structural member exhibits resistance with respect to structural integrity, stability, and temperature transmission. Typical fire resistance rating requirements for different building components are specified in building codes.

In the past, the fire resistance of structural members could be determined only by testing. In recent years however, the use of numerical methods for the calculation of the fire resistance of various structural members is gaining acceptance because these calculation methods are far less costly and time consuming. The fire performance of a structural member depends, in part, on the properties of the materials the building component is composed of. The availability of material properties at high temperature and temperature distributions permits a mathematical approach to predicting the performance of building components exposed to fire. When a structural member is subjected to a defined temperature-time exposure during a fire, this exposure will cause a predictable temperature distribution in the member. Increased temperatures cause deformations and property changes in the materials. With knowledge of the deformations and property changes, the usual methods of structural mechanics can be applied to predict fire resistance performance.

In recent years, significant effort has been undertaken to develop material properties of various construction materials at elevated temperatures. In this chapter, the characteristics of materials are outlined. The various properties that influence fire resistance performance, together with the methods used to develop these properties, is discussed. The trends on the variation of thermal, mechanical, and other material-specific properties with temperature of commonly used construction materials are presented.

Material Characteristics

Classification

Materials, based on composition, can be classified as either a homogeneous or heterogeneous type.

V.K.R. Kodur (✉)
Civil and Environmental Engineering, Michigan State University, East Lansing, Michigan, USA

T.Z. Harmathy

M.J. Hurley (ed.), *SFPE Handbook of Fire Protection Engineering*,
DOI 10.1007/978-1-4939-2565-0_9, © Society of Fire Protection Engineers 2016

Homogeneous materials have the same composition and properties throughout their volume and are rarely found in nature. *Heterogeneous* materials have different composition and properties. Most construction materials are heterogeneous, yet their heterogeneity is often glossed over when dealing with practical problems.

The heterogeneity of concrete is easily noticeable. Other heterogeneities related to the microstructure of materials, that is, their grain and pore structures, are rarely detectable by the naked eye. The microstructure depends greatly on the way the materials are formed. In general, materials formed by solidification from a melt show the highest degree of homogeneity. The result of the solidification is normally a *polycrystalline* material, comprising polyhedral grains of crystals, which, in general, are equiaxial and randomly oriented. Severe cold working in metals may produce an elongated grain structure and crystals with preferred orientations.

Noncrystalline solids are called *amorphous* materials. Gels and glasses are amorphous materials. Gels are formed by the coagulation of a colloidal solution. Glasses (vitreous materials) are solids with a liquid-like, grainless submicroscopic structure with low crystalline order. On heating, they will go through a series of phases of decreasing viscosity.

Synthetic polymers (plastics) are made up of long macromolecules created by polymerization from smaller repeating units (monomers). In the case of *thermoplastic* materials, the mobility of the molecular chains increases on heating. Such materials soften, much like glass. In some other types of plastics, called *thermosetting* materials, polymerization also produces cross-bonds between the molecular chains. These cross-bonds prevent the loosening of the molecular structure and the transition of the material into a liquid-like state.

Some building materials (e.g., gypsum, brick) are formed from a wet, plastic mass or from compacted powders by firing. The resulting product is a polycrystalline solid with a well-developed pore structure. Two important building materials, concrete and gypsum, are formed by mixing finely ground powders (and aggregates) with water. The mixture solidifies by hydration. The cement paste in a concrete has a highly complex microstructure, interspersed with very fine, elaborate pores.

Most building materials can be treated as *isotropic* materials, that is, as though they possessed the same properties in all directions. An exception to this is some of the advanced composite materials, such as fiber-reinforced polymers (FRP), which might possess varying properties in different directions and are classified as *anisotropic* materials.

Among the material properties, those that are unambiguously defined by the current composition and phase are referred to as *structure-insensitive*. Some others depend on the microstructure of the solid or on its previous history. These properties are *structure-sensitive*.

Porosity and Moisture Sorption

The fire performance of a material is dependent on the chemical composition and molecular structure of the material. The presence of water in the material composition influences the properties of materials at elevated temperatures. The two commonly associated terms to describe the composition and the extent of water present in a material are porosity and moisture sorption.

What is commonly referred to as a solid object is actually all the material within its visible boundaries. Clearly, if the solid is porous—and most building materials are—the so-called solid consists of at least two phases: (1) a solid-phase matrix and (2) a gaseous phase (namely, air) in the pores within the matrix. Usually, however, there is also a liquid or liquid-like phase present: moisture either absorbed from the atmosphere to the pore surfaces or held in the pores by capillary condensation. This third phase is always present if the pore structure is continuous; discontinuous pores (like the pores of some foamed plastics) are not readily accessible to atmospheric moisture.

The pore structure of materials is characterized by two properties: *porosity, P* ($m^3 \cdot m^{-3}$), the volume fraction of pores within the visible boundaries of the solid; and *specific surface, S* ($m^2 \cdot m^{-3}$), the surface area of the pores per unit volume of the material. For a solid with

continuous pore structure, the porosity is a measure of the maximum amount of water the solid can hold when saturated. The specific surface and (to a lesser degree) porosity together determine the moisture content the solid holds in equilibrium with given atmospheric conditions.

The *sorption isotherm* shows the relationship at constant temperature between the equilibrium moisture content of a porous material and the relative humidity of the atmosphere. A sorption isotherm usually has two branches: (1) an *adsorption branch,* obtained by monotonically increasing the relative humidity of the atmosphere from 0 to 100 % through very small equilibrium steps; and (2) a *desorption branch,* obtained by monotonically lowering the relative humidity from 100 to 0 %. Derived experimentally, the sorption isotherms offer some insight into the nature of the material's pore structure [1, 2].

For heterogeneous materials consisting of solids of different sorption characteristics (e.g., concrete, consisting of cement paste and aggregates), the sorption isotherms can be estimated using the simple mixture rule (with $m = 1$; see Equation 9.1).

Building materials, such as concrete (or more accurately, the cement paste in the concrete) and wood, because of their large specific surfaces, can hold water in amounts substantial enough to be taken into consideration in fire performance assessments.

Mixture Rules

Some properties of materials of mixed composition or mixed phase can be calculated by simple rules if the material properties for the constituents are known. The simplest mixture rule is [3]

$$\pi^m = \sum_i v_i \pi_i^m \tag{9.1}$$

where

π = Material property for the composite

π_i = Material property for the composite's ith constituent

v_i ($m^3 \cdot m^{-3}$) = Volume fraction of the ith constituent

m (dimensionless) = Constant that has a value between −1 and +1

Hamilton and Crosser recommended the following rather versatile formula for two-phase solids [4]:

$$\pi = \frac{v_1 \pi_1 + \gamma v_2 \pi_2}{v_1 + \gamma v_2} \tag{9.2}$$

where

$$\gamma = \frac{n \pi_1}{(n-1)\pi_1 + \pi_2} \tag{9.3}$$

Here phase 1 must always be the principal continuous phase. n (dimensionless) is a function of the geometry of phase distribution. With $n \to \infty$ and $n = 1$, Equations 9.2 and 9.3 convert into Equation 9.1 with $m = 1$ and $m = -1$, respectively. With $n = 3$, a relation is obtained for a two-phase system where the discontinuous phase consists of spherical inclusions [5].

By repeated application, Equations 9.2 and 9.3 can be extended to a three-phase system [6], for example, to a moist, porous solid that consists of three essentially continuous phases (the solid matrix, with moisture and air in its pores).

Survey of Building Materials

There are burnable (combustible) and nonburnable (noncombustible) building materials. The reason for preferring the use of the words *burnable* and *nonburnable* has been discussed by Harmathy [2]. To a designer concerned with the structural performance of a building during a fire, the mechanical and thermal properties of these materials are of principal interest. Yet burnable building materials may become ignited, and thereby the positive role assigned to these materials by design (i.e., functioning as structural elements of the building) may change into a negative role—that is, becoming fuel and adding to the severity of fire. Those properties of burnable building materials that are related to the latter role are discussed in other chapters of this handbook.

From the point of view of their performance in fire, building materials can be divided into the following groups:

1. *Group L (load-bearing) materials*. Materials capable of carrying high stresses, usually in tension or compression. With these materials, the mechanical properties related to behavior in tension and/or compression are of principal interest.
2. *Group L/I (load-bearing/insulating) materials*. Materials capable of carrying moderate stresses and, in fire, providing thermal protection to Group L materials. With Group L/I materials, the mechanical properties (related mainly to behavior in compression) and the thermal properties are of equal interest.
3. *Group I (insulating) materials*. Materials not designed to carry load. Their role in fire is to resist the transmission of heat through building elements and/or to provide insulation to Group L or Group L/I materials. With Group I materials, only the thermal properties are of interest.
4. *Group L/I/F (load-bearing/insulating/fuel) materials*. Group L/I materials that may become fuel in fire.
5. *Group I/F (insulating/fuel) materials*. Group I materials that may become fuel in fire.

The number of building materials has been increasing dramatically during the past few decades. In the last decade or so, a number of high-performing materials, such as FRP and high-strength concrete (HSC), have been developed to achieve cost-effectiveness in construction. Although many of these high-performing materials possess superior properties at ambient temperatures, the same cannot be said of their performance at elevated temperatures. In materials such as HSC, additional complexities such as spalling arise, which may severely impact the fire performance of a structural member.

By necessity, only a few of those materials that are commonly used will be discussed in this chapter in some detail. These materials are as follows: in Group L—structural steel, light-gauge steel, and reinforcing/prestressing steel; Group L/I—concrete and brick (including fiber-reinforced concrete); Group L/I/F (or Group I/F and L/F)—wood and FRP; and Group I—gypsum and insulation.

Material Properties at Elevated Temperatures

The behavior of a structural member exposed to fire is dependent, in part, on the thermal and mechanical properties of the material of which the member is composed. While calculation techniques for predicting the process of deterioration of building components in fire have developed rapidly in recent years, research related to supplying input information into these calculations has not kept pace. The designer of the fire safety features of buildings will find that information on the properties of building materials in the temperature range of interest, 20–800 °C is not easy to come by. Most building materials are not stable throughout this temperature range. On heating, they undergo physicochemical changes ("reactions" in a generalized sense), accompanied by transformations in their microstructure and changes in their properties. For example, concrete at 500 °C is completely different from the material at room temperature.

The thermophysical and mechanical properties of most materials change substantially within the temperature range associated with building fires. In the field of fire science, applied materials research faces numerous difficulties. At elevated temperatures, many building materials undergo physicochemical changes. Most of the properties are temperature dependent and sensitive to testing method parameters such as heating rate, strain rate, temperature gradient, and so on. Harmathy [7] cited the lack of adequate knowledge of the behavior of building materials at elevated temperatures as the most disturbing trend in fire safety engineering. There has been a tendency to use "notional" (also called "typical," "proprietary," "empirical," etc.) values for material properties in numerical computations—in other words, values that ensure agreement between experimental and analytical results. Harmathy warned that this practice might lead

to a proliferation of theories that lack general validity.

Clearly, the generic information available on the properties of building materials at room temperature is seldom applicable in fire safety design. It is imperative, therefore, that the fire safety practitioner knows how to extend, based on a priori considerations, the utility of the scanty data that can be gathered from the technical literature. Also, knowledge of unique material-specific characteristics at elevated temperatures, such as spalling in concrete or charring in wood, is critical to determine the fire performance of a structural member. These properties are discussed in the following sections.

Reference Condition

Most building materials are porous and therefore capable of holding moisture, the amount of which depends on the atmospheric conditions. Because the presence of moisture may have a significant and often unpredictable effect on the properties of materials at any temperature below 100 °C, it is imperative to conduct all property tests on specimens brought into a moistureless "reference condition" by some drying technique prior to the test. The reference condition is normally interpreted as that attained by heating the test specimen in an oven at 105 °C until its weight shows no change. A few building materials however, among them all gypsum products, may undergo irreversible physicochemical changes when held at that temperature for an extended period. To bring them to a reference condition, specimens of these materials should be heated in a vacuum oven at some lower temperature level (e.g., at 40 °C in the case of gypsum products).

Mechanical Properties

The mechanical properties that determine the fire performance of structural members are strength, modulus of elasticity, and creep of the component materials at elevated temperatures.

Stress-Strain Relationships

The mechanical properties of solids are usually derived from conventional tensile or compressive tests. The strength properties are usually expressed in stress-strain relations, which are often used as input data in mathematical models calculating the fire resistance. Figure 9.1 shows, for a metallic material, the variation of stress, σ (Pa), with increasing strain (deformation), ε ($m \cdot m^{-1}$), while the material is strained (deformed) in a tensile test at a more or less constant rate (i.e., constant crosshead speed), usually of the order of 1 $mm \cdot min^{-1}$. Generally, because of a decrease in the strength and ductility of the material, the slope of the stress-strain curve decreases with increasing temperature.

Modulus of Elasticity, Yield Strength, Ultimate Strength

The modulus of elasticity is a measure of the ability of the material to resist deformation and is expressed as the ratio of the deforming stress to the strain in the material. Generally, the modulus of elasticity of a material decreases gradually with increasing temperature.

The tensile or compressive strength of the material is generally expressed by means of yield strength and ultimate strength. Often the

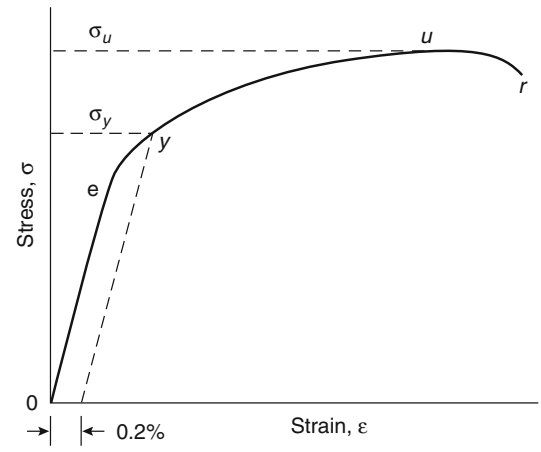

Fig. 9.1 Stress-strain curve (strain rate is roughly constant)

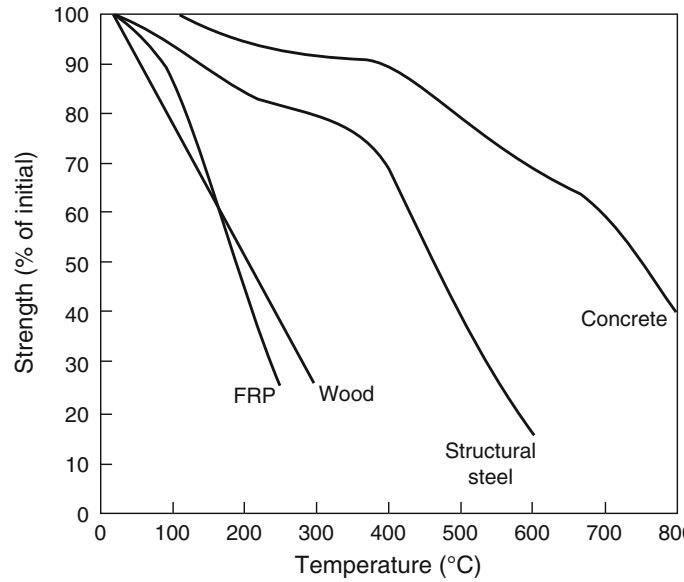

Fig. 9.2 Variation of strength with temperature for different materials

strength at elevated temperature is expressed as a percentage of the compressive (tensile) strength at room temperature. Figure 9.2 shows the variation of strength with temperature (ratio of strength at elevated temperature to that at room temperature) for concrete, steel, wood, and FRP. For all four materials, the strength decreases with increasing temperature; however, the rate of strength loss is different.

For materials such as concrete, compressive strength is of main interest because it has very limited tensile strength at higher temperatures. However, for materials such as steel, both compressive and tensile strengths are of equal interest.

Section 0-*e* of the curve in Fig. 9.1 represents the elastic deformation of the material, which is instantaneous and reversible. The modulus of elasticity, E (Pa), is the slope of that section. Between points *e* and *u* the deformation is plastic, nonrecoverable, and quasi-instantaneous. The plastic behavior of the material is characterized by the yield strength at 0.2 % offset, σ_y (Pa), and the ultimate strength, σ_u (Pa). After some localized necking (i.e., reduction of cross-sectional area), the test specimen ruptures at point *r*. The modulus of elasticity is more or less a structure-insensitive property.

For metals of similar metallurgical characteristics, the stress-strain curve can be reproduced at room temperature at a reasonable tolerance, and the shape of the curve does not depend significantly on the crosshead speed. At sufficiently high temperatures, however, the material undergoes plastic deformation even at constant stress, and the *e*-*r* section of the stress-strain curve will depend markedly on the crosshead speed.

Creep

Creep, often referred to as creep strain, is defined as the time-dependent plastic deformation of the material and is denoted by ε_t ($\mathrm{m \cdot m^{-1}}$). At normal stresses and ambient temperatures, the deformation due to creep is not significant. At higher stress levels and at elevated temperatures, however, the rate of deformation caused by creep can be substantial [8]. Hence, the main factors that influence creep are the temperatures, the stress level, and their duration.

In a creep test the variation of ε_t is recorded against time, t (h), at constant stress (more accurately, at constant load) and at constant (elevated) temperature T (K). A typical strain-time

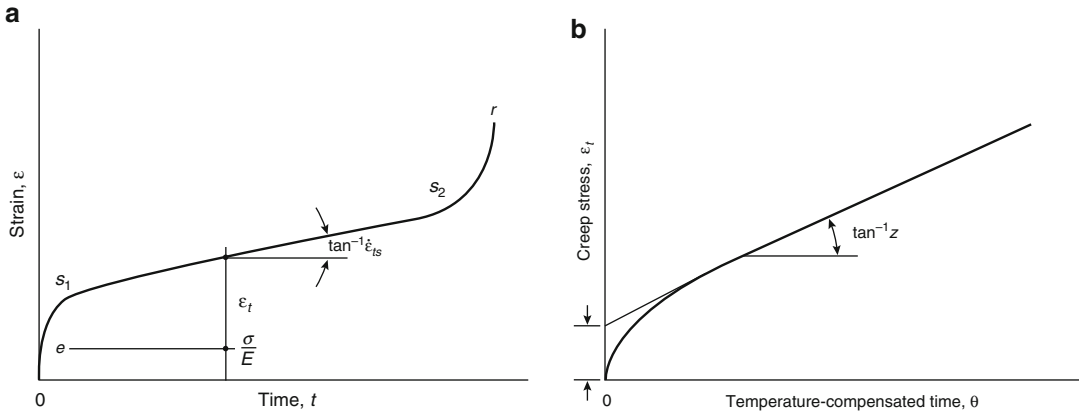

Fig. 9.3 (**a**) Creep strain vs. time curve (T = constant; σ ≈ constant); (**b**) creep strain vs. temperature-compensated time curve (σ ≈ constant)

curve is shown in Fig. 9.3a. The total strain, ε (m·m^{-1}), is

$$\varepsilon = \frac{\sigma}{E} + \varepsilon_t \tag{9.4}$$

The 0-*e* section of the strain-time curve represents the instantaneous elastic (and reversible) part of the curve; the rest is creep, which is essentially nonrecoverable. The creep is fast at first (primary creep, section *e*-s_1 in Fig. 9.3a, then proceeds for a long time at an approximately constant rate (secondary creep, section s_1-s_2), and finally accelerates until rupture occurs (tertiary creep, section s_2-*r*). The curve becomes steeper if the test is conducted either at a higher load (stress) or at a higher temperature.

Dorn's concept is particularly suitable for dealing with deformation processes developing at varying temperatures [9]. Dorn eliminated the temperature as a separate variable by the introduction of a new variable: the "temperature-compensated time," θ (h), defined as

$$\theta = \int_0^t e^{-\Delta H_c/RT} dt \tag{9.5}$$

where ΔHc (J·kmol^{-1}) is the activation energy of creep, and R (J·kmol^1·K^{-1}) is the gas constant.

From a practical point of view, only the primary and the secondary creeps are of importance. It has been shown that the creep strain in these two regimes can be satisfactorily described by the following equation [10]

$$\varepsilon_t = \frac{\varepsilon_{t0}}{\ln 2} \cosh^{-1}\left(2^{Z\theta/\varepsilon_{t0}}\right) \quad (\sigma \simeq \text{constant}) \tag{9.6}$$

or approximated by the simple formula [11]

$$\varepsilon_t \approx \varepsilon_{t0} + Z\theta \quad (\sigma \simeq \text{constant}) \tag{9.7}$$

where Z (h^{-1}) is the Zener-Hollomon parameter, and ε_{t0} (mm^{-1}) is another creep parameter, the meaning of which is explained in Fig. 9.3b. The Zener-Hollomon parameter is defined as [12]

$$Z = \dot{\varepsilon}_{ts} e^{\Delta H/RT} \tag{9.8}$$

where $\dot{\varepsilon}_{ts}$ (mm^{-1}·h^{-1}) is the rate of secondary creep at a temperature, T. The two creep parameters, Z and ε_{t0}, are functions of the applied stress only (i.e., they are independent of the temperature).

For most materials, creep becomes noticeable only if the temperature is higher than about one-third of the melting temperature (on the absolute scale).

The creep of concrete is due to the presence of water in its microstructure [13]. There is no satisfactory explanation for the creep of concrete at elevated temperatures. Anderberg and Thelandersson [14], and Schneider [15] suggested techniques for the calculation of the deformation of concrete under conditions characteristic of fire exposure.

Thermal Properties

The material properties that influence the temperature rise and distribution in a member are its thermal conductivity, thermal expansion, specific heat, thermal diffusivity, and mass loss. These properties depend on the composition and characteristics of the constituent materials.

Thermal Expansion

The thermal expansion characterizes the expansion (or shrinkage) of a material caused by heating and is defined as the expansion (shrinkage) of unit length of a material when it is raised 1° in temperature. The expansion is considered to be positive when the material elongates and is considered negative when it shortens. In general, the thermal expansion of a material is dependent on the temperature. The dilatometric curve is a record of the fractional change of a linear dimension of a solid at a steadily increasing or decreasing temperature. With mathematical symbolism, the dilatometric curve is a plot of

$$\frac{\Delta \ell}{\ell_0} \text{ against T}$$

where $\Delta \ell = \ell - \ell_0$ and ℓ_0 (m) and ℓ (m) are the changed and original dimensions of the solid, respectively, the latter usually taken at room temperature. $\Delta \ell$ reflects not only the linear expansion or shrinkage of the material, but also the dimensional effects brought on by possible physicochemical changes (i.e., "reactions").

The heating of the solid usually takes place at a predetermined rate, 5 °C·min^{-1} as a rule. Because the physicochemical changes proceed at a finite rate and some of them are irreversible, a dilatometric curve obtained by heating rarely coincides with that obtained during the cooling cycle. Sluggish reactions may bring about a steady rise or decline in the slope of the dilatometric curve. Discontinuities in the slope indicate very fast reactions. Heating the material at a rate higher than 5 °C·min^{-1} usually causes the reactions to shift to higher temperatures and to develop faster.

The coefficient of linear thermal expansion, β (m·m^{-1}·K^{-1}), is defined as

$$\beta = \frac{1}{\ell} \frac{d\ell}{dT} \tag{9.9}$$

Since $\ell = \ell_0$ the coefficient of linear thermal expansion is, for all intents, the tangent to the dilatometric curve. For solids that are isotropic in a macroscopic sense, the coefficient of volume expansion is approximately equal to 3β.

The thermal expansion is measured with a dilatometric apparatus, capable of producing curves that show the expansion of the materials with temperature in the range from 20 to 1000 °C. Harmathy [7, 16], using a horizontal dilatometric apparatus, recorded dilametric curves for various types of concrete and brick, some of which are presented in later sections. The sample was 76.2 mm long and about 13 by 13 mm in cross section. It was subjected to a small spring load that varied during the test. Unfortunately, even this small load caused creep shrinkage with those materials that tended to soften at higher temperatures. Furthermore, because the apparatus did not provide a means for placing the sample in a nitrogen atmosphere, in certain cases oxidation may also have had some effect on the shape of the curves.

Mass Loss

The mass loss is often used to express the loss of mass at elevated temperatures. The thermogravimetric curve is a record of the fractional variation of the mass of a solid at steadily increasing or decreasing temperature. Again, with mathematical symbolism, a thermogravimetric curve is a plot of

$$\frac{M}{M_0} \text{ against } T$$

where M and M_0 (kg) are the changed and original masses of the solid, respectively, the latter usually taken at room temperature.

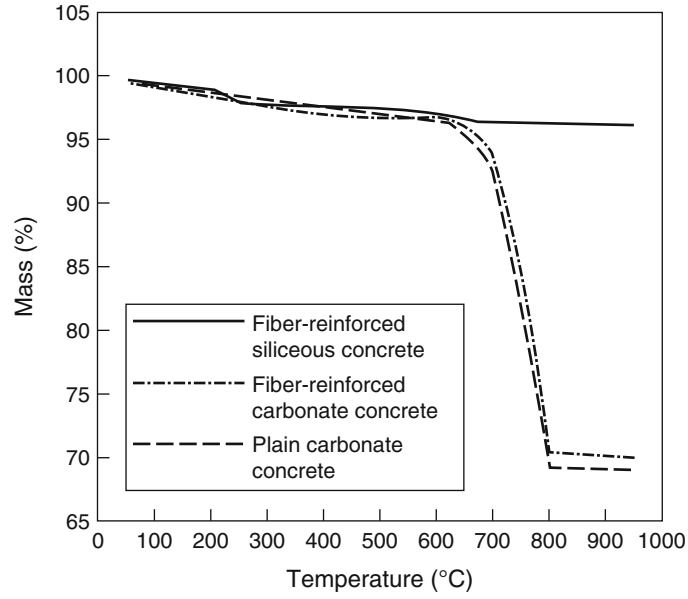

Fig. 9.4 Mass loss of various concrete types as a function of temperature [18]

Generally a heating rate of 5 °C·min^{-1} is used in the measurements.

A thermogravimetric curve reflects reactions accompanied by loss or gain of mass but, naturally, it does not reflect changes in the materials' microstructure or crystalline order. $M/M_0 = 1$ is the thermogravimetric curve for a chemically inert material. Again, an increase in the rate of heating usually causes those features of the curve that are related to chemical reactions to shift to higher temperatures and to develop faster.

The thermogravimetric curves to be shown were obtained by a DuPont 951 thermogravimetric analyzer [17], using specimens of 10–30 mg in mass, placed in a nitrogen atmosphere [7]. The rate of temperature rise was 5 °C·min^{-1}. Figure 9.4 shows the variation of mass loss for concrete in the temperature range from 20 to 1000 °C.

Density, Porosity

The density, ρ (kg·m^{-3}), in an oven-dry condition, is the mass of a unit volume of the material, comprising the solid itself and the air-filled pores. Assuming that the material is isotropic with respect to its dilatometric behavior, its density at any temperature can be calculated from the thermogravimetric and dilatometric curves.

$$\rho = \rho_0 \frac{(M/M_0)_T}{\left[1 + ((\Delta \ell)/(\ell_0))_T\right]} \tag{9.10}$$

where ρ_0 (kg·m^{-3}) is the density of the solid at the reference temperature (usually room temperature), and the T subscript indicates values pertaining to temperature T in the thermogravimetric and dilatometric records.

The density of composite solids at room temperature can be calculated by means of the mixture rule in its simplest form (Equation 9.1 with $m = 1$).

$$p = \sum_i v_i p_i \tag{9.11}$$

where the i subscript relates to information on the ith component. At elevated temperatures, the expansion of the components is subject to constraints, and therefore the mixture rule can yield only a crude approximation.

If, as usual, the composition is given in mass fractions rather than in volume fractions, the volume fractions can be obtained as

$$v_i = \frac{w_i / p_i}{\sum_i w_i / p_i} \tag{9.12}$$

where w_i is the mass fraction of the ith component (kg·kg^{-1}).

True density, ρ_t (kg·m^{-3}), is the density of the solid in a poreless condition. Such a condition is nonexistent for many building materials and, therefore, may be a theoretical value derived on crystallographic considerations, or determined by some standard technique, for example, ASTM C135 [19]. The relationship between the porosity and density is

$$P = \frac{\rho_t - \rho}{\rho_t} \tag{9.13}$$

The overall porosity of a composite material consisting of porous components is

$$P = \sum_i v_i P_i \tag{9.14}$$

where, again, the i subscript relates to the ith component of the material.

Specific Heat

The specific heat of a material is the characteristic that describes the amount of heat required to raise a unit mass of the material at unit temperature. A calorimetric curve describes the variation with temperature of the apparent specific heat of a material at constant pressure, cp (J·kg^{-1}·K^{-1}). The apparent specific heat is defined as

$$c_p = \frac{\delta h}{\delta T_p} \tag{9.15}$$

where h is enthalpy (J·kg^{-1}), and the p subscripts indicate the constancy of pressure. If the heating of the solid is accompanied by physicochemical changes (i.e., "reactions"), the enthalpy becomes a function of the reaction progress variable, ξ (dimensionless), that is, the degree of conversion at a particular temperature from reactant(s) into product(s). For any temperature interval where physicochemical change takes place [2, 6, 20], $0 \leq \xi \leq 1$, and

$$c_p = \overline{c}_p + \Delta h \frac{d\xi}{dT} \tag{9.16}$$

where cp (J·kg^{-1}·K^{-1}) is the specific heat for that mixture of reactants and (solid) products that the material consists of at a given stage of the conversion (as characterized by ξ), and $\Delta\, hp$ (J·kg^{-1}) is the latent heat associated with the physicochemical change.

As Equation 9.16 and Fig. 9.5 show, in temperature intervals of physicochemical instability, the apparent specific heat consists of sensible heat and latent heat contributions. The latter contribution will result in extremities in the calorimetric curve: a maximum if the reaction is endothermic, a minimum if it is exothermic.

In heat flow studies, it is usually the ρcp product (J·m^{-3}·K^{-1}) rather than cp that is needed as input information. This product is referred to as volume specific heat.

Until the 1980s, adiabatic calorimetry was the principal method to study the shape of the cp versus T relationship. Since the 1980s, differential scanning calorimetry (DSC) has been the most commonly used technique for mapping the curve in a single temperature sweep at a desired rate of heating. Unfortunately, the accuracy of the DSC technique in determining the sensible heat contribution to the apparent specific heat may not be particularly good (sometimes it may be as low as ±20 %). The rate of temperature rise was usually 5 °C·min^{-1}. At higher heating rates, the peaks in the DSC curves tend to shift to higher

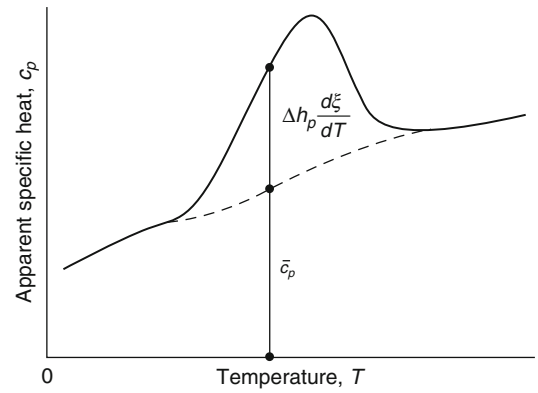

Fig. 9.5 The apparent specific heat

temperatures and become sharper. For temperatures above 600 °C, a high-temperature differential thermal analyzer (DTA) is also used. Harmathy, with the aid of a DuPont 910 differential scanning calorimeter, developed calorimetric curves for a number of materials by placing the samples, 10–30 mg in mass, in a nitrogen atmosphere [7, 21].

Materials that undergo exothermic reactions may yield negative values in the calorimetric curve. A negative value for *cp* indicates that, at the applied (and enforced) rate of heating, the rate of evolution of reaction heat exceeds the rate of absorption of sensible heat by the material. In natural processes, the apparent specific heat can never be negative, because the heat evolving from the reaction is either scattered to the surroundings or, if absorbed by the material, causes a very fast temperature rise. If the heat of reaction is not very high, obtaining nonnegative values for *cp* can be achieved by suitably raising the scanning rate. For this reason, some materials undergoing exothermic reactions must be tested at rates of heating higher than 5 °C·min^{-1}, often as high as 50 °C·min^{-1}.

If experimental information is not available, the *cp* versus *T* relationship can be calculated from data on heat capacity and heat of formation for all the components of the material (including reactants and products), tabulated in a number of handbooks [22, 23]. Examples of calculations are presented in Harmathy [2, 6], where information is developed for the apparent specific heat versus temperature relation for a cement paste and four kinds of concrete.

Thermal Conductivity

The temperature rise in a member, as a result of heat flow, is a function of the thermal conductivity of the material. Heat transmission solely by conduction can occur only in poreless, nontransparent solids. In porous solids (most building materials), the mechanism of heat transmission is a combination of conduction, radiation, and convection. (If pore size is less than that about 5 mm, the contribution of pores to convective heat transmission is negligible.) The thermal conductivity of porous materials is, in a strict sense, merely a convenient empirical factor that makes it possible to describe the heat transmission process with the aid of the Fourier law. That empirical factor will depend not only on the conductivity of the solid matrix but also on the porosity of the solid and the size and shape of the pores. At elevated temperatures, because of the increasing importance of radiant heat transmission through the pores, conductivity becomes sensitive to the temperature gradient.

Because measured values of the thermal conductivity depend to some extent on the temperature gradient employed in the test, great discrepancies may be found in thermal conductivity data reported by various laboratories. A thermal conductivity value yielded by a particular technique is, in a strict sense, applicable only to heat flow patterns similar to that characteristic of the technique employed.

Experimental data indicate that porosity is not a greatly complicating factor as long as it is not larger than about 0.1. With insulating materials, however, the porosity may be 0.8 or higher. Conduction through the solid matrix may be an insignificant part of the overall heat transmission process; therefore, using the Fourier law of heat conduction in analyzing heat transmission may lead to deceptive conclusions. If the solid is not oven-dry, a temperature gradient will induce migration of moisture, mainly by an evaporation condensation mechanism [24]. The migration of moisture is usually, but not necessarily, in the direction of heat flow and manifests itself as an increase in the apparent thermal conductivity of the solid. Furthermore, even oven-dry solids may undergo decomposition (mainly dehydration) reactions at elevated temperatures. The sensible heat carried by the gaseous decomposition products as they move in the pores adds to the complexity of the heat flow process. At present there is no way of satisfactorily accounting for the effect of simultaneous mass transfer on heat flow processes occurring under fire conditions.

The thermal conductivity of layered, multiphase solid mixtures depends on whether the phases lie in the direction of, or normal to, the direction of heat flow and is determined

using the simple mixture rule [4, 25]. At higher temperatures, because of radiative heat transfer through the pores, the contribution of the pores to the thermal conductivity of the solid must not be disregarded [26].

The thermal conductivity of solids is a structure-sensitive property. For crystalline solids, the thermal conductivity is relatively high at room temperature and gradually decreases as the temperature rises. For predominantly amorphous solids, on the other hand, the conductivity is low at room temperature and increases slightly with the rise of temperature. The conductivity of porous crystalline materials may also increase at very high temperatures because of the radiant conductivity of the pores.

The thermal conductivity of materials such as concrete or brick can be measured, in the temperature range between 20 and 800 °C, using a non-steady-state hot wire method [27, 28]. The thermal conductivity values at discrete temperature levels can be plotted to obtain a curve. Unfortunately, no scanning technique exists for acquiring a continuous thermal conductivity versus temperature curve from a single temperature sweep. Special problems arise with the estimation of the thermal conductivity for temperature intervals of physicochemical instability. Both the steady-state and variable-state techniques of measuring thermal conductivity require the stabilization of a pattern of temperature distribution (and thereby a certain microstructural pattern) in the test sample prior to the test. The test results can be viewed as points on a continuous thermal conductivity versus temperature curve obtained by an imaginary scanning technique performed at an extremely slow scanning rate. Because each point pertains to a more or less stabilized microstructural pattern, there is no way of knowing how the thermal conductivity would vary in the course of a physicochemical process developing at a finite rate and varying microstructure.

On account of the nonreversible microstructural changes brought about by heating, the thermal conductivity of building materials (and perhaps most other materials) is usually different in the heating and cooling cycles. Open and solid circles are used in the figures to identify thermal conductivity values obtained by stepwise increasing and stepwise decreasing the temperature of the sample, respectively. Also, often the thermal conductivity of a material is taken as invariant with respect to the direction of heat flow.

Thermal Diffusivity

The thermal diffusivity of a material is defined as the ratio of thermal conductivity to the volumetric specific heat of the material. It measures the rate of heat transfer from an exposed surface of a material to the inside. The larger the diffusivity, the faster the temperature rise at a certain depth in the material. Similar to thermal conductivity and specific heat, thermal diffusivity varies with temperature rise in the material. Thermal diffusivity, α, can be calculated using the relation

$$\alpha = \frac{k}{\rho c_p} \tag{9.17}$$

where
k = Thermal conductivity
ρ = Density
c_p = Specific heat of the material

Special (Material-Specific) Properties

In addition to thermal and mechanical properties, certain other properties, such as spalling in concrete and charring in wood, influence the performance of a material at elevated temperature. These properties are unique to specific materials and are critical for predicting the fire performance of a structural member.

Critical Temperature

In building materials, such as steel and FRP, the determination of failure in a structural member exposed to fire is simplified to the calculation of critical temperature. The critical temperature is defined as the temperature at which the material

loses much of its strength and can no longer support the applied load. When this temperature is reached, the safety factor against failure becomes less than 1.

North American standards (ASTM E119) assume a critical or failure temperature of 538 °C (1000 °F) for structural steel. It is a typical failure temperature for columns under full design load. This temperature is also regarded as the failure temperature in the calculation of fire resistance of steel members. If a load is applied to the member, the test is continued until the member actually fails, which, depending on the load intensity, may occur at a higher or lower steel temperature.

This concept of critical temperature is also used for reinforced and prestressed steel in concrete structural members for evaluating the fire resistance ratings. These ratings are generally obtained through the provision of minimum member dimensions and minimum thickness of concrete cover. The minimum concrete cover thickness requirements are intended to ensure that the temperature in the reinforcement does not reach its critical temperature for the required duration. For reinforcing steel, the critical temperature is 593 °C, whereas for prestressing steel the critical temperature is 426 °C [29].

Spalling

Spalling is defined as the breaking of layers (pieces) of concrete from the surface of the concrete elements when the concrete elements are exposed to high and rapidly rising temperatures, such as those experienced in fires. Spalling can occur soon after exposure to heat and can be accompanied by violent explosions, or it may happen when concrete has become so weak after heating that, when cracking develops, pieces fall off the surface. The consequences may be limited as long as the extent of the damage is small, but extensive spalling may lead to early loss of stability and integrity due to exposed reinforcement and penetration of partitions.

Although spalling might occur in all concretes, high-strength concrete (HSC) is believed to be more susceptible than normal-strength concrete (NSC) because of its low permeability and low water-cement ratio. In a number of test observations on HSC specimens, it has been found that spalling is often of an explosive nature [30, 31]. Hence, spalling is one of the major concerns in the use of HSC and should be properly accounted for in evaluating fire performance. Spalling in NSC and HSC columns is compared in Fig. 9.6 using the data

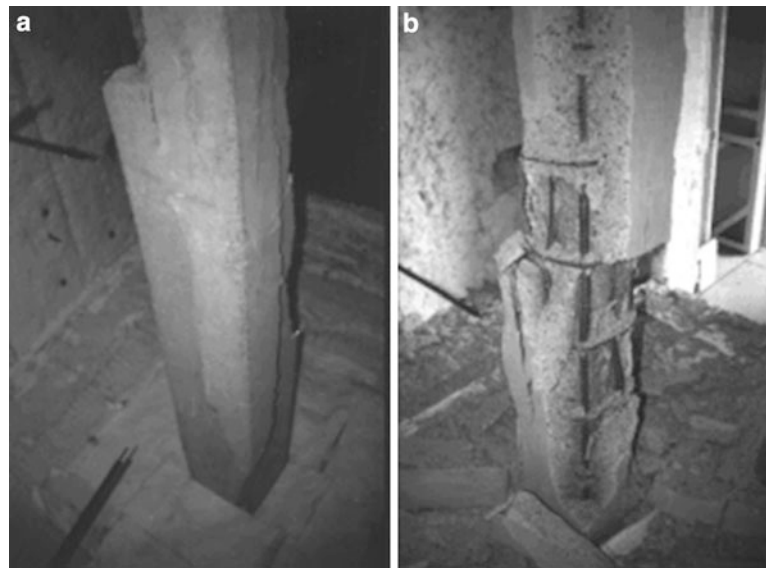

Fig. 9.6 Spalling in NSC and HSC columns after exposure to fire [32]: (**a**) normal-strength concrete column and (**b**) high-strength concrete column

obtained from full-scale fire tests on loaded columns [32]. It can be seen that the spalling is quite significant in the HSC column.

Spalling is believed to be caused by the buildup of pore pressure during heating. The extremely high water vapor pressure, generated during exposure to fire, cannot escape due to the high density (and low permeability) of HSC, and this pressure buildup often reaches the saturation vapor pressure. At 300 °C, the pressure reaches approximately 8 MPa; such internal pressures are often too high to be resisted by the HSC mix having a tensile strength of approximately 5 MPa [33]. The drained conditions at the heated surface, and the low permeability of concrete, lead to strong pressure gradients close to the surface in the form of the so-called "moisture clog." [2, 34] When the vapor pressure exceeds the tensile strength of concrete, chunks of concrete fall off from the structural member. The pore pressure is considered to drive progressive failure; that is, the lower the permeability of concrete, the greater the spalling. This falling off can often be explosive in nature, depending on the fire and concrete characteristics.

However, other researchers explain the occurrence of spalling on the basis of fracture mechanics and state that the spalling results from restrained thermal dilatation close to the heated surface [35]. This leads to compressive stresses parallel to the heated surface, which are released by brittle fractures of concrete, in other words, spalling.

Spalling, which often results in the rapid loss of concrete during a fire, exposes deeper layers of concrete to fire temperatures, thereby increasing the rate of transmission of heat to the inner layers of the member, including the reinforcement. When the reinforcement is directly exposed to fire, the temperatures in the reinforcement rise at a very high rate, leading to a faster decrease in strength of the structural member. The loss of strength in the reinforcement, added to the loss of concrete due to spalling, significantly decreases the fire resistance of a structural member.

In addition to strength and porosity of concrete mix, density, load intensity, fire intensity, aggregate type, and relative humidity are the primary parameters that influence spalling in HSC. The variation of porosity with temperature is an important property needed for predicting spalling performance of HSC. Noumowe et al. carried out porosity measurements on NSC and HSC specimens, using a mercury porosimeter, at various temperatures [36].

Charring

Charring is the process of formation of a layer of char at the exposed surface of wood members during exposure to fire. The charring process also occurs in other members, such as FRP and some types of plastics. When exposed to heat, wood undergoes thermal degradation (pyrolysis), the conversion of wood to char and gas, resulting in a reduction of the density of the wood. Studies have shown that the charring temperature for wood lies in the range of 280–300 °C [29].

The charred layer is considered to have practically no strength. The fire resistance of the member depends on the extent of charring and the remaining strength of the uncharred portion.

The charring rate, a critical parameter in determining the fire resistance of a structural wood member, is defined as the rate at which wood is converted to char. In the standard fire resistance test, it has been noted that the average rate of charring transverse to the grain is approximately 0.6 mm/min [29]. The charring rate parallel to the grain of wood is approximately twice the rate when it is transverse to the grain. Detailed studies on the charring rates for several specimen and timber types are reported by various researchers [37–39] and are summarized in a report [40]. These charring rates were constant (in each study) and ranged from 0.137 to 0.85 mm/min. The assumption of a constant rate of charring is reasonable for thick wood members.

Charring is influenced by a number of parameters, the most important ones being density, moisture content, and contraction of wood. The influence of the moisture content and density of the wood on the charring rate is illustrated in Fig. 9.7 for Douglas fir exposed to the standard

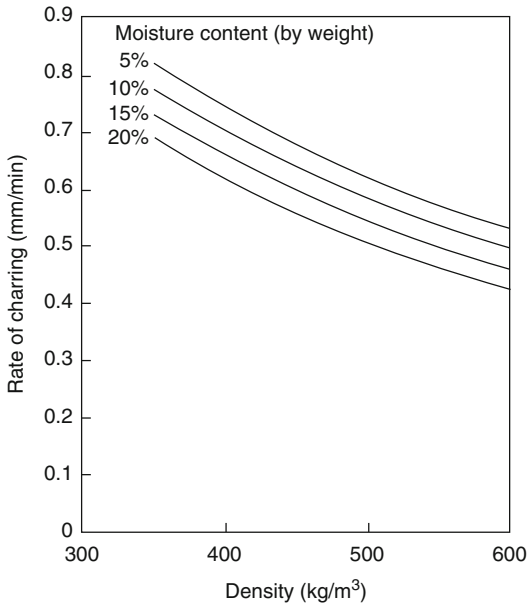

Fig. 9.7 Rate of charring in Douglas fir as a function of its density (dry condition) for various moisture contents when exposed to ASTM standard fire [29]

fire [29]. It can be seen that the charring rate decreases with increasing density of the wood and also with increasing moisture content.

It is important to recognize that the charring rate in real fires depends on the severity of fire to which the wood is exposed. It should be noted that the charring rate is a function of the imposed radiant heat flux. This depends on the fuel load and the ventilation factor of the compartment (for full details see Chap. 30, in this book). Detailed information on the charring of untreated wood—with expressions for charring rate in terms of the influencing factors of density, moisture content, external heat flux, and oxygen concentration—when exposed to real fires is given by Hadvig [41] and Mikkola [42].

Sources of Information

Information on the properties of building materials at elevated temperatures is scattered throughout the literature. There are a few publications, however, that may be particularly valuable for fire safety practitioners. A book by Harmathy [2] and the ASCE manual on structural fire protection [29] present a wealth of information on concrete, steel, wood, brick, gypsum, and various plastics. The thermal properties of 31 building materials are surveyed in an NRCC report [7]. The mechanical and thermal properties of concrete are discussed in an ACI guide [43], and in reports by Bennetts [44] and Schneider [45]. Those of steel are surveyed in the ACI guide, in Bennetts's report, and in a report by Anderberg [46]. Information on the thermal conductivity of more than 50 rocks (potential concrete aggregates) is presented in a paper by Birch and Clark [47]. The relationships for thermal and mechanical properties, at elevated temperatures, for some building materials are listed in the ASCE structural fire protection manual [29]. In most cases these properties are expressed, in the temperature range of 0–1000 °C, as a function of temperature and other properties at ambient temperature. These values can be used as input data in mathematical models for predicting cross sectional temperatures and fire performance of structural members.

Steel

Steel is a Group L material. The steels most often used in the building industry are either hot-rolled or cold-drawn. The structural steels and concrete reinforcing bars are hot-rolled, low-carbon, ferrite-pearlite steels. They have a randomly oriented grain structure, and their strength depends mainly on their carbon content. The prestressing steel wires and strands for concrete are usually made from cold-drawn, high-carbon, pearlitic steels with an elongated grain structure, oriented in the direction of the cold work. In addition, light-gauge steel, made from cold-formed steel, finds wide applications in lightweight framing, such as walls and floors.

Information on the mechanical properties of two typical steels (a structural steel [ASTM A36] and a prestressing wire [ASTM A421]) is presented in Figs. 9.8, 9.9, and 9.10 and in Table 9.1 [48]. Figures 9.8 and 9.9 are stress-strain curves at room temperature (24 °C and

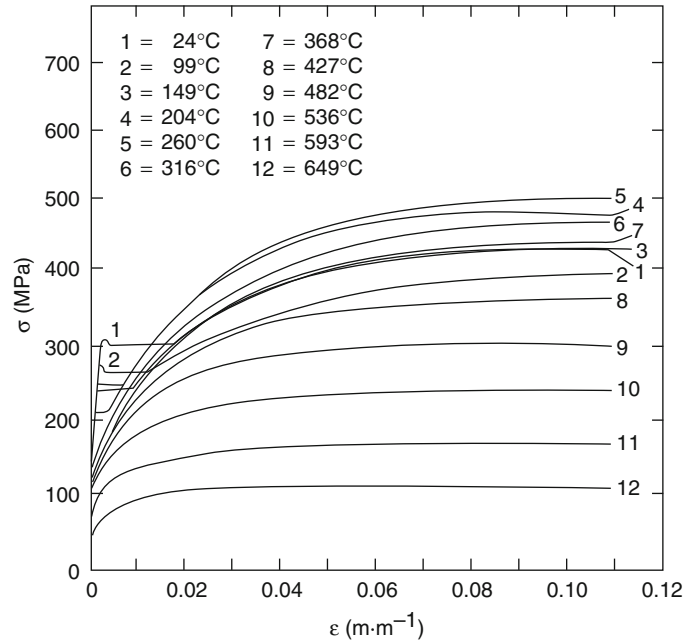

Fig. 9.8 Stress-strain curves for a structural steel (ASTM A36) at room temperature and elevated temperatures [48]

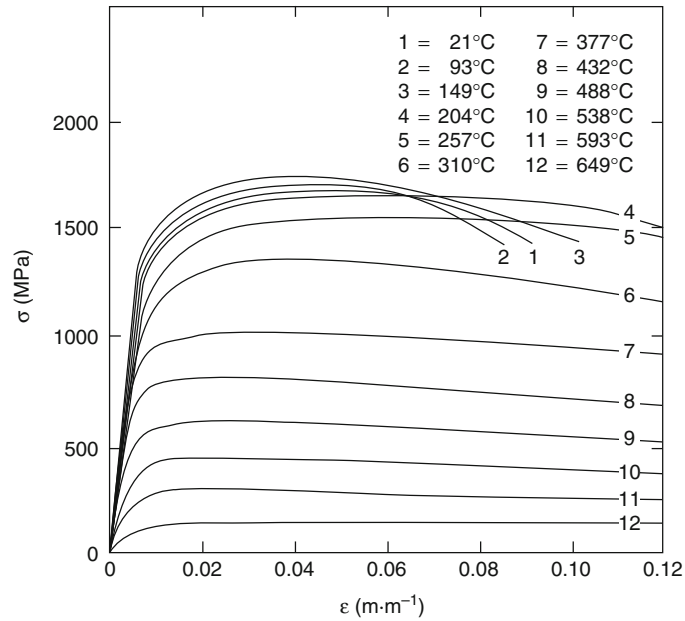

Fig. 9.9 Stress-strain curves for prestressing steel (ASTM A421) at room temperature and elevated temperatures [48]

21 °C, respectively) and at a number of elevated temperature levels. Figure 9.10 shows the effect of temperature on the yield and ultimate strengths of the two steels.

Table 9.1 presents information on the effect of stress on the two creep parameters, Z and ε_{t0} (see Equation 9.7). Because creep is a very structure-sensitive property, the creep parameters may show a substantial spread, even for steels with similar characteristics at room temperature. The application of the creep parameters to the calculation of the time of structural failure in fire is discussed in Hamilton and Crosser [4, 8].

The modulus of elasticity (E) is about 210×10^3 MPa for a variety of common steels at room temperature. Figure 9.11 shows its variation with temperature for structural steels [50] and steel reinforcing bars [49]. (E_0 in Fig. 9.11 is the modulus of elasticity at room temperature.)

The density (ρ) of steel is about 7850 kg·m^{-3}. Its coefficient of thermal expansion (β) is a structure-insensitive property. For an average carbon steel, β is 11.4×10^{-6} m·m^{-1}·K^{-1} at room temperature. The dilatometric curve shown in Fig. 9.12 is applicable to most of the common steels. The curve reveals substantial contraction of the material at about 700 °C, which is associated with the transformation (phase change of steel) of the ferrite-pearlite structure into austenite.

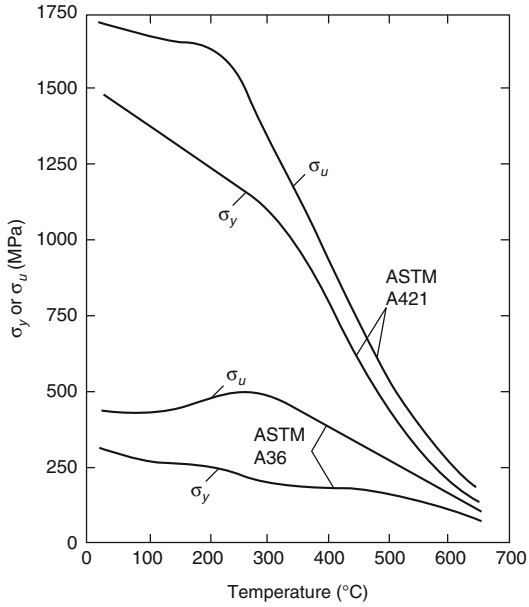

Fig. 9.10 The ultimate and yield strengths for a structural steel (ASTM A36) and a prestressing steel (ASTM A421) at elevated temperatures [48]

Being a structure-sensitive property, the thermal conductivity of steel is not easy to define. For carbon steels it usually varies within the range of 46–65 W·m^{-1}·K^{-1}.

Equations for various properties of steel, as functions of temperature, are available in the ASCE structural fire protection manual [29] and in Eurocode 3 [51, 52]. In the ASCE manual, the same set of relationships is applicable for thermal properties of both structural and reinforcing steel. However, separate relationships for stress-strain and elasticity are given for the two steels with slightly conservative values for structural steel. Recently, Poh proposed a general stress-strain equation that expresses stress explicitly in terms of strain in a single continuous curve [53, 54].

The critical temperature of steel is often used as a benchmark for determining the failure of structural members exposed to fire. This ensures that the yield strength is not reduced to less than that of 50 % of ambient value. The critical temperature for various types of steels is given in Table 9.2.

The above discussed high temperature properties are generally applicable to conventional carbon (mild) steel whose chemical composition consist of iron, carbon, manganese, sulfur and phosphorous. In recent years, a number of new steels are available and these steel are made by adding alloys, such as nickel, titanium, boron and chromium. These alloys influence durability characteristics, as well mechanical properties of steel. For example, molybdenum, chromium and niobium can increase the fire resistance property of steel, while chrome and nickel can enhance the corrosion resistance of steel [56]. Current design rules on fire resistance of steel structures (EC3 2005b [51], BS:5950

Table 9.1 Creep parameters for a structural steel and a prestressing steel [48]

Steel	$\Delta H_c/R$ (k)	$\varepsilon_{t0}(\sigma)$ (m · m^{-1})	$Z(\sigma)$ (h^{-1})
ASTM A36	38,890	$3.258 \times 10^{-17\sigma 1.75}$	$2.365 \times 10^{-20\sigma 4.7}$ if $\sigma \leq 103.4 \times 106$
			$1.23 \times 10^{16} \exp(4.35 \times 10^{-8\sigma})$ if $103.4 \times 10^6 \leq \sigma \leq 310 \times 10^6$
ASTM A421	30,560	$8.845 \times 10^{-9\sigma 0.67}$	$1.952 \times 10^{-10\sigma 3}$ if $\sigma \leq 172.4 \times 10^6$
			$8.21 \times 10^{13} \exp(1.45 \times 10^{-8\sigma})$ if $172.4 \times 10^6 \leq \sigma \leq 690 \times 10^6$

σ is measured in Pa

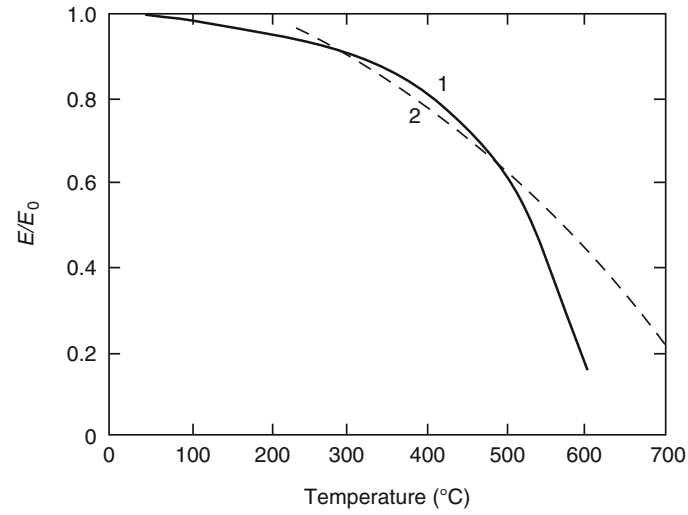

Fig. 9.11 The effect of temperature on the modulus of elasticity of (1) structural steels and (2) steel reinforcing bars [49]

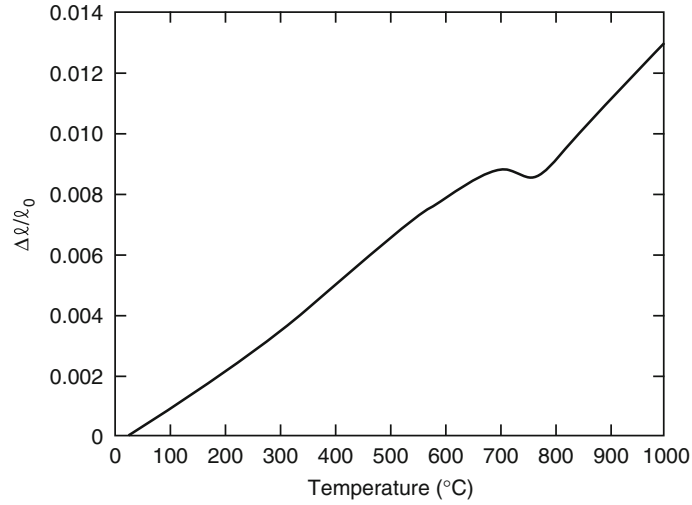

Fig. 9.12 Dilatometric curve for steel

Table 9.2 Critical temperature for various types of steel

Steel	Standard/reference	Temperature (°C)
Structural steel	ASTM	538
Reinforcing steel	ASTM	593
Prestressing steel	ASTM	426
Light-gauge steel	EC 3 [51]	350
	Gerlich et al. [55]	400

2003 [57]) are mainly based on experimental data on mild steel and do not account for specific property variations in new types of alloy steels.

Recent research by Wang et al. [58] clearly show that high strength (Q460) steel exhibits slower loss of strength and modulus throughout 20–800 °C temperature range as compared to mild steel. This is mainly due to the presence of chromium and niobium, which improves fire resistance properties of steel.

Furthermore, tests by Kodur et al. [59] have shown that type of heat treatment has significant influence on strength properties of steel e.g. annealing and normalizing produces normal strength steel, whereas quenching and tempering produces high strength steel. High strength steel, produced using quenching and tempering process, and that is used in bolts (A490 bolts) possesses slightly lower thermal conductivity than that of conventional mild steel.

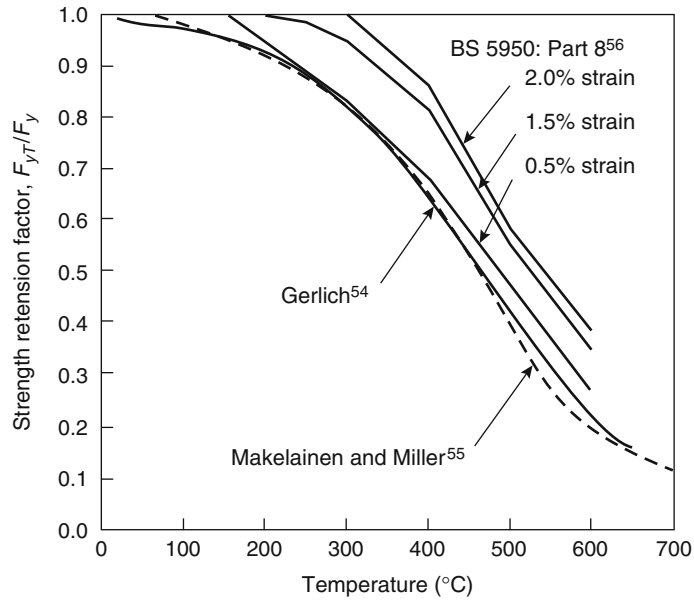

Fig. 9.13 Reduction of the yield strength of cold-formed light-gauge steel at elevated temperatures [57–61]

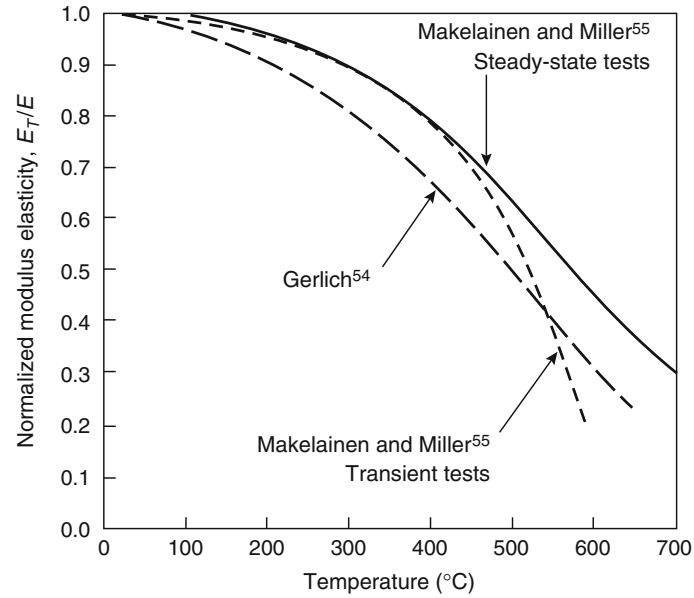

Fig. 9.14 Modulus of elasticity of cold-formed light-gauge steel at elevated temperatures [57–61]

The properties of cold-formed light-gauge steel are slightly different from those of hot-rolled structural steel. Gerlich [60] and Makelainen and Miller [61], based on steady-state and transient tests on cold-formed steel tension coupons (cut from studs) and galvanized sheets, proposed relationships for yield strength and modulus of elasticity. Figure 9.13 shows the variation of yield strength of light-gauge steel at elevated temperatures, corresponding to 0.5 %, 1.5 %, and 2 % strains based on the proposed relationships and on the relationship in BS 5950 [57]. The BS 5950 curves represent a conservative 95 % confidence limit (i.e., a 5 % chance that strength would fall below the curve), whereas the other two curves are representative of mean test data. Figure 9.14 shows the variation of modulus of elasticity of light-gauge steel at elevated

temperatures. The modulus E_T represents the tangent modulus at low stress levels (or initial tangent modulus), because steel stress-strain relationships become increasingly nonlinear at elevated temperatures. The effect of zinc coating on the mechanical properties of steel is of little significance.

The light-gauge steel has somewhat lower thermal expansion when compared to similar expressions for other steels [61]. The other thermal properties of steel, such as specific heat and thermal conductivity, are of little importance for the thermal modeling of light-gauge steel because steel framing plays a minor role in the heat transfer mechanism. A review of some of these properties is presented in a review paper [62].

The critical temperature of light-gauge steel is much lower than for other types of steels. Although Eurocode 3 limits this to a conservative value of 350 °C, in other cases a critical temperature of 400 °C is used (see Table 9.2).

Concrete

Concrete is a Group L/I material. The word *concrete* covers a large number of different materials, with the single common feature that they are formed by the hydration of cement. Because the hydrated cement paste amounts to only 24–43 volume percent of the materials present, the properties of concrete may vary widely with the aggregates used.

Traditionally, the compressive strength of concrete used to be around 20–50 MPa, which is referred to as normal-strength concrete (NSC). In recent years, concrete with a compressive strength in the range 50–100 MPa has become widely used and is referred to as high-strength concrete (HSC). Depending on the density, concretes are usually subdivided into two major groups: (1) normal-weight concretes with densities in the 2150- to 2450-kg·m^{-3} range and (2) lightweight concretes with densities between 1350 and 1850 kg·m^{-3}. Fire safety practitioners again subdivide the normal-weight concretes into silicate (siliceous) and carbonate aggregate concrete, according to the composition of the principal aggregate. Also, a small amount of discontinuous fibers (steel or polypropylene fibers) is often added to the concrete mix to achieve superior performance; this concrete is referred to as fiber-reinforced concrete (FRC). In this section, the properties of concrete are discussed under three groups: namely, NSC, FRC, and HSC.

Normal-Strength Concrete

A great deal of information is available in the literature on the mechanical properties of various types of normal-strength concrete. This information is summarized in reports by Bennetts [44] and Schneider [45], the ACI guide [43], the ASCE fire protection manual [29], and in Harmathy's book [2]. Figure 9.15 shows the stress-strain curves for a lightweight concrete with expanded shale aggregate at room temperature (24 °C) and a few elevated temperature levels [63]. The shape of the curves may depend on the time of holding the test specimen at the target temperature level before the compression test.

The modulus of elasticity (E) of various concretes at room temperature may fall within a very wide range, 5.0×10^3–35.0×10^3 MPa,

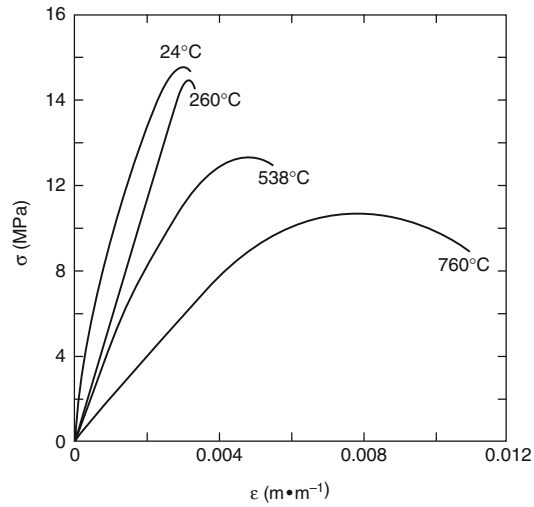

Fig. 9.15 Stress-strain curves for a lightweight masonry concrete at room and elevated temperatures [63]

dependent mainly on the water-cement ratio in the mixture, the age of concrete, the method of conditioning, and the amount and nature of the aggregates. Cruz found that the modulus of elasticity decreases rapidly with the rise of temperature, and the fractional decline does not depend significantly on the type of aggregate [64] (in Fig. 9.16, E_0 is the modulus of elasticity at room temperature). From other surveys [2, 44], it appears, however, that the modulus of elasticity of normal-weight concretes decreases faster with the rise of temperature than that of lightweight concretes.

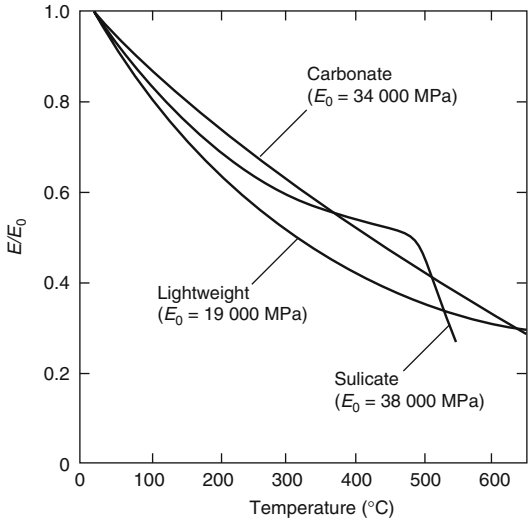

Fig. 9.16 The effect of temperature on the modulus of elasticity of concretes with various aggregates [61]

The compressive strength (σ_u) of NSC may also vary within a wide range. Compressive strength is influenced by the same factors as the modulus of elasticity. For conventionally produced normal-weight concretes, the strength at room temperature is usually between 20 and 50 MPa. For lightweight concretes, the strength is usually between 20 and 40 MPa.

Information on the variation of the compressive strength with temperature is presented in Fig. 9.17 (for a silicate aggregate concrete), Fig. 9.18 (for a carbonate aggregate concrete), and Fig. 9.19 (for two lightweight aggregate concretes, one made with the addition of natural sand) [65]. ($[\sigma_u]_0$ in the figures stands for the compressive strengths of concrete at room temperature.) In some experiments, the specimens were heated to the test temperature without load (see curves labeled "unstressed"). In others they were heated under a load amounting to 40 % of the ultimate strength (see curves labeled "stressed"). Again, in others they were heated to the target temperature without load, then cooled to room temperature and stored at 75 % relative humidity for six days, and finally tested at room temperature (see curves labeled "unstressed residual").

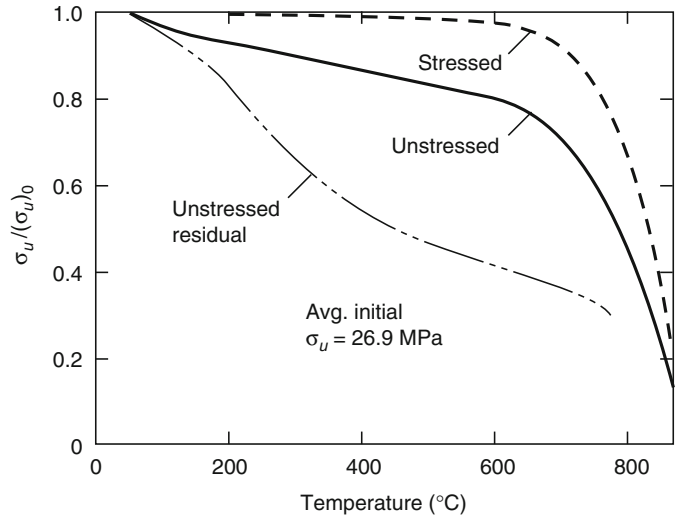

Fig. 9.17 The effect of temperature on the compressive strength of a normal-weight concrete with silicate aggregate [65]

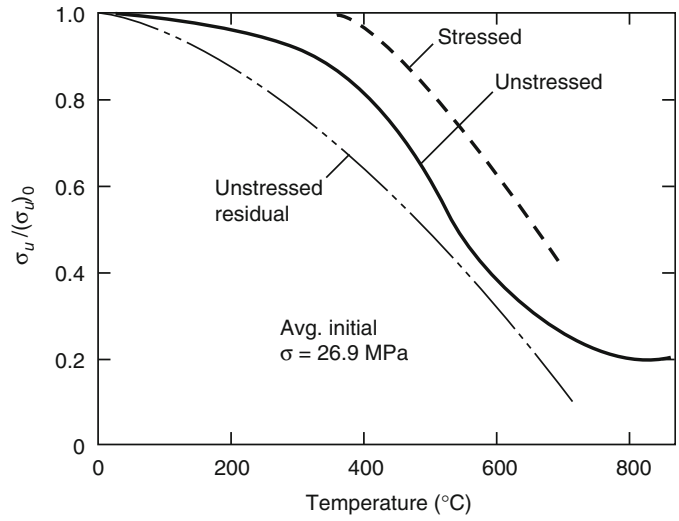

Fig. 9.18 The effect of temperature on the compressive strength of a normal-weight concrete with carbonate aggregate [65]

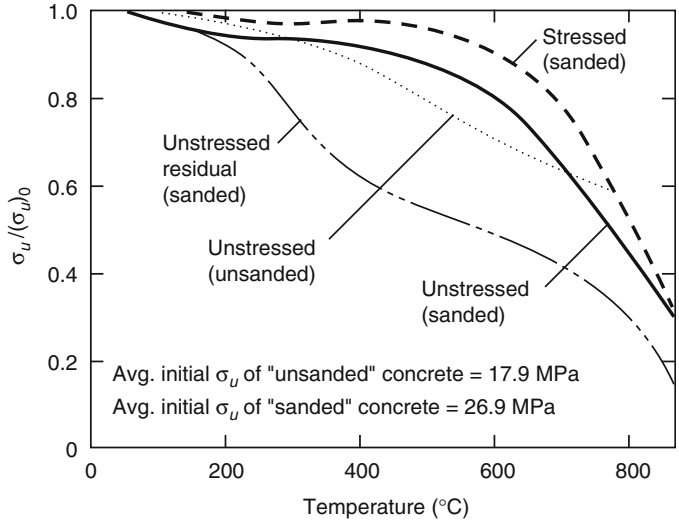

Fig 9.19 The effect of temperature on the compressive strength of two lightweight concretes (one with natural sand) [65]

Some information on the creep of concrete at elevated temperatures is available from the work of Cruz [66], MareÂchal [67], Gross [68], and Schneider et al. [69] The creep curves shown in Fig. 9.20 are those recorded by Cruz for a normal-weight concrete with carbonate aggregates.

Because the aggregates amount to 60–75 % of the volume of concrete, the dilatometric curve usually resembles that of the principal aggregate. However, some lightweight aggregates, for example, pearlite and vermiculite, are unable to resist the almost continuous shrinkage of the cement paste on heating, and therefore their dilatometric curves bear the characteristic features of the curve for the paste.

The dilatometric curves of two normal-weight concretes (with silicate and carbonate aggregates) and two lightweight concretes (with expanded shale and pumice aggregates) are shown in Fig. 9.21 [20]. These curves were obtained in the course of a comprehensive study performed on 16 concretes.

The results of dilatometric and thermogravimetric tests were combined to calculate the volumetric heat capacity (ρcp) versus temperature relation for these four concretes, as shown in

Fig. 9.22. The partial decomposition of the aggregate is responsible for a substantial drop (above 700 °C) in the density of concretes made with carbonate aggregate.

The aggregate type and moisture content have significant influence on the specific heat of concrete. The usual ranges of variation of the volume-specific heat (i.e., the product ρcp) for normal-weight and lightweight concretes are shown in Fig. 9.23. This information, derived by combining thermodynamic data with thermogravimetric observations [2, 6], has since been confirmed by differential scanning calorimetry [7]. Experimental data are also available on a few concretes and some of their constituents [2, 7].

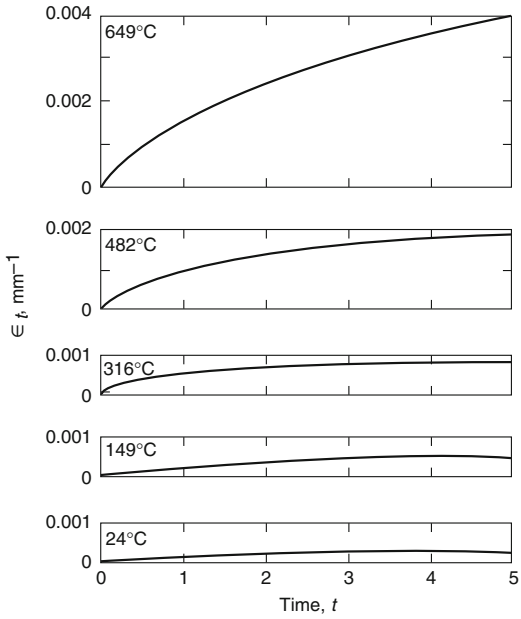

Fig. 9.20 Creep of a carbonate aggregate concrete at various temperature levels (applied stress: 12.4 MPa; compressive strength of the material at room temperature: 27.6 MPa) [66]

The thermal conductivity (k) of concrete depends mainly on the nature of its aggregates. In general, concretes made with dense, crystalline aggregates show higher conductivities than those made with amorphous or porous aggregates. Among common aggregates, quartz has the highest conductivity; therefore, concretes made with siliceous aggregates are on the whole more conductive than those made with other silicate and carbonate aggregates.

Derived from theoretical considerations [6], the solid curves in Fig. 9.24 describe the variation with temperature of the thermal conductivity of four concretes. In deriving these curves, two concretes (see curves 1 and 2) were visualized to represent limiting cases among normal-weight concretes, and the other two (see curves 3 and 4), limiting cases among lightweight concretes. The points in Fig. 9.24 stand for experimental data. They reveal that the upper limiting case is probably never reached with aggregates in common use and that the thermal conductivity of lightweight concretes may be somewhat higher than predicted on theoretical considerations.

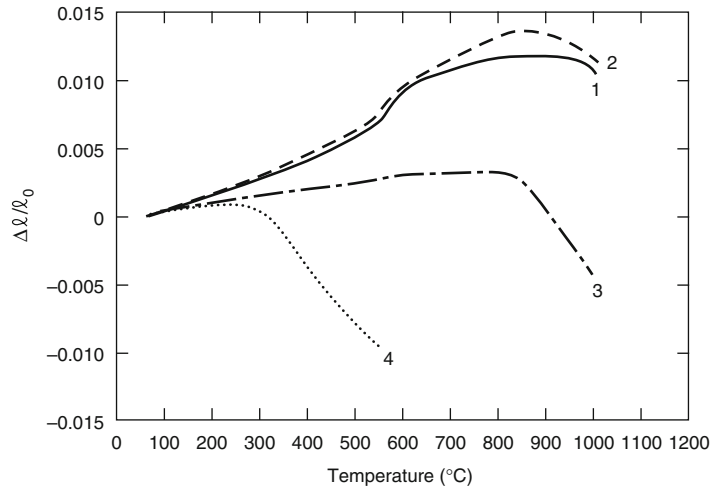

Fig. 9.21 Dilatometric curves for two normal-weight and two lightweight concretes [20]. (1) normal-weight concrete with silicate aggregate, (2) normal-weight concrete with carbonate aggregate, (3) lightweight concrete with expanded shale aggregate, (4) lightweight concrete with pumice aggregate

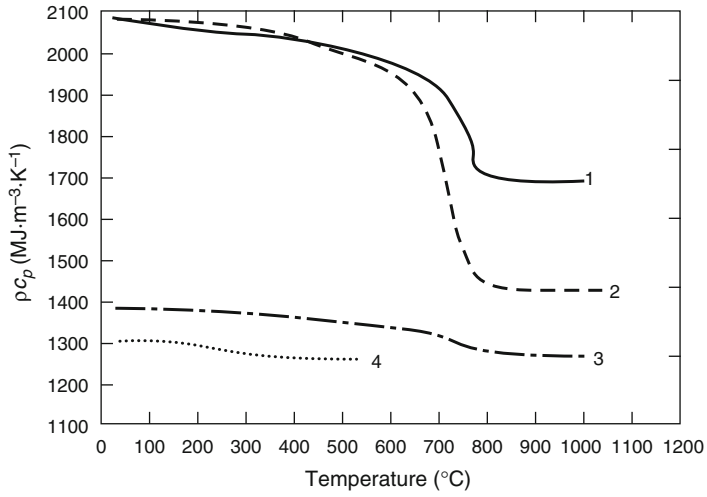

Fig. 9.22 Volumetric heat capacity of two normal-weight and two lightweight concretes [20]. (1) normal-weight concrete with silicate aggregate, (2) normal-weight concrete with carbonate aggregate, (3) lightweight concrete with expanded shale aggregate, (4) lightweight concrete with pumice aggregate

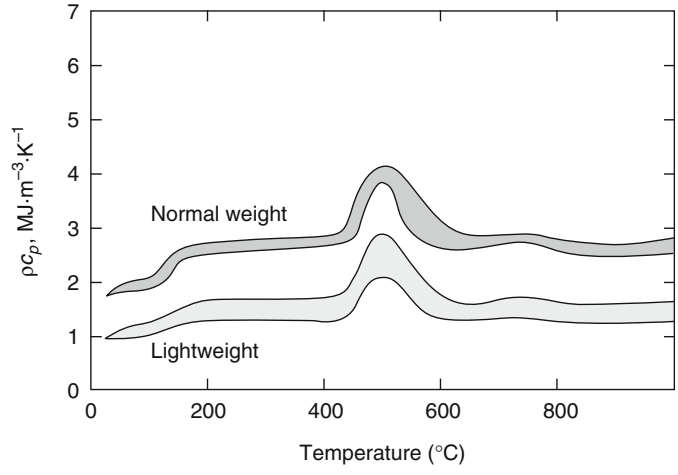

Fig. 9.23 Usual ranges of variation for the volume-specific heat of normal-weight and lightweight concretes [6]

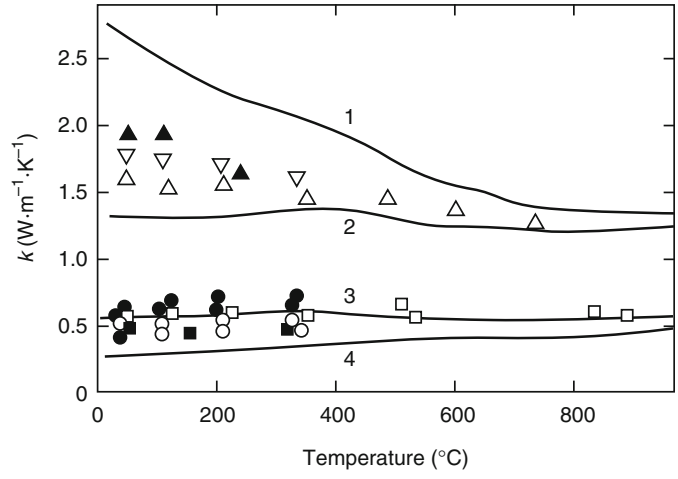

Fig. 9.24 Thermal conductivity of four "limiting" concretes and some experimental thermal conductivity data. 6,19 Symbols: ▼, ▽—various gravel concretes; ●—expanded slag concretes; ■, □—expanded shale concretes; ○—pumice concrete

Further experimental information on the thermal conductivity of some normal-weight and many lightweight concretes is available from the literature [6, 7, 20].

In reinforced concrete structures, the bond between rebars and concrete (at elevated temperatures) plays a major role in determining the fire endurance of structural members. Diederichs and Schneider investigated the variation of bond strength between deformed and plain rebars and concrete as a function of temperature [70]. They found that the bond strength reduction follows the same pattern as compressive strength for deformed and rusted plain bars. However, higher reduction in bond strength was observed for new plain bars. They also found that the bond strength at elevated temperature increases with decreasing coefficient of thermal expansion of concrete, which is significantly influenced by the type of aggregate. Diederichs and Schneider also concluded that the water-cement ratio and the bar diameter have a minor effect on the bond strength between steel and concrete [70]. Figure 9.25 illustrates the variation of bond strength as a function of temperature for reinforced and prestressed concrete.

Fiber-Reinforced Concrete

Steel and polypropylene discontinuous fibers are the two most common fibers used in the concrete mix to improve structural properties of concrete. Studies have shown that polypropylene fibers in a concrete mix are quite effective in minimizing spalling in concrete under fire conditions [71, 72]. The polypropylene fibers melt at a relatively low temperature of about 170 °C and create channels for the steam pressure in concrete to escape. This prevents the small explosions that cause the spalling of the concrete. Based on these studies, the amount of polypropylene fibers needed to minimize spalling is about 0.1–0.25 % (by volume). The polypropylene fibers were found to be most effective for HSC made with normal-weight aggregate.

The addition of fibers improves certain mechanical properties, such as tensile strength, ductility, and ultimate strain, at room temperature. However, there is very little information on the high-temperature properties of this type of concrete [73].

Steel fiber–reinforced concrete (SFRC) exhibits, at elevated temperatures, mechanical properties that are more beneficial to fire resistance than those of plain concrete. There is some information available on SFRC's material properties at elevated temperatures. The effect of temperature on the compressive strength for two types of SFRC is shown in Fig. 9.26. The strength of both types of SFRC exceeds the initial strength of the concretes up to about 400 °C. This is in contrast to the strength of plain concrete, which decreases slightly with temperatures up to 400 °C. Above approximately

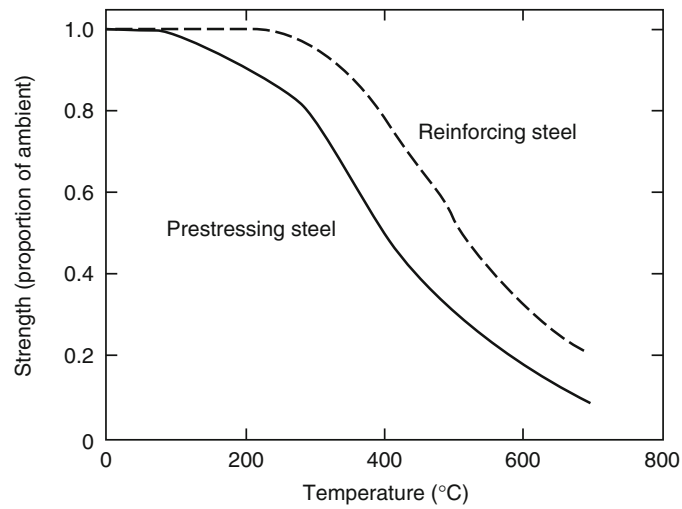

Fig. 9.25 Variation of bond strength as a function of temperature for reinforced and prestressed concrete [70]

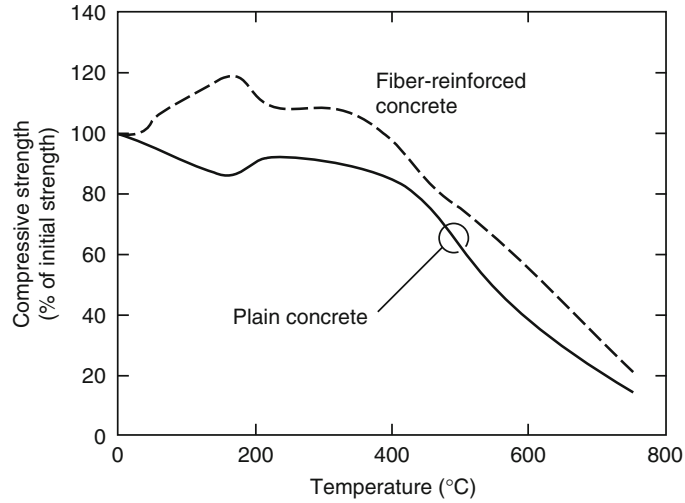

Fig. 9.26 Effect of temperature on compressive strength of steel fiber–reinforced concrete

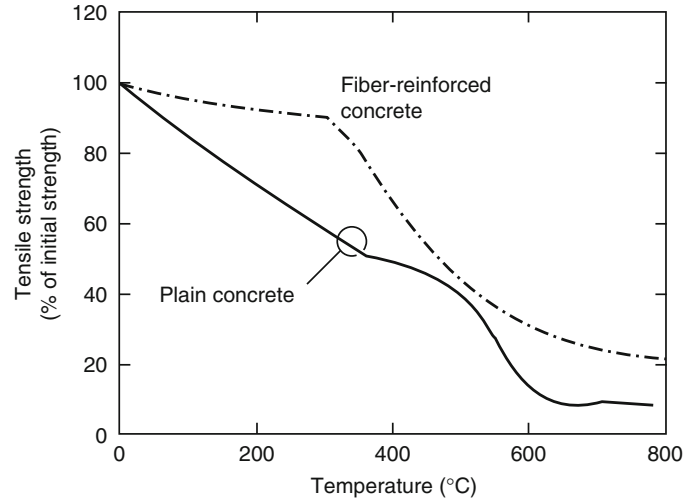

Fig. 9.27 Effect of temperature on tensile strength of steel fiber–reinforced concrete

400 °C, the strength of SFRC decreases at an accelerated rate [74].

The effect of temperature on the tensile strength of steel fiber–reinforced carbonate concretes is compared to that of plain concrete in Fig. 9.27 [75]. The strength of SFRC decreases at a lower rate than that of plain concrete throughout the temperature range, with the strength being significantly higher than that of plain concrete up to about 350 °C. The increased tensile strength delays the propagation of cracks in fiber-reinforced concrete structural members and is highly beneficial when the member is subjected to bending stresses.

The type of aggregate has a significant influence on the tensile strength of steel fiber–reinforced concrete. The decrease in tensile strength for carbonate aggregate concrete is higher than that for siliceous aggregate concrete [75].

The thermal properties of SFRC, at elevated temperatures, are similar to those of plain concrete. Kodur and Lie [27, 73] have carried out detailed experimental studies and developed dilatometric and thermogravimetric curves for various types of SFRC. Based on these studies, they have also developed expressions for thermal and mechanical properties of steel fiber–reinforced concrete in the temperature range 0–1000 °C [18, 76].

High-Strength Concrete

The strength of concrete has significant influence on the properties of HSC. The material properties of HSC vary differently with temperature than those of NSC. This variation is more pronounced for mechanical properties, which are affected by these factors: compressive strength, moisture content, density, heating rate, percentage of silica fume, and porosity [77]. The available information on the mechanical properties of HSC at elevated temperatures is presented in a review report by Phan [30].

The loss in compressive strength with temperature is higher for HSC than that for NSC up to about 450 °C. Figure 9.28 shows the comparison of strengths for NSC and HSC types, together with CEB and European design curves for NSC. The difference between compressive strength versus temperature relationships of normal-weight and lightweight aggregate concrete is not significant. However, HSC mixture with silica fume have higher compressive strength loss with increasing temperature than HSC mixture without silica fume. Based on a series of high-temperature material property tests, Kodur et al. have proposed a set of stress-strain relationships for HSC as a function of temperature [78, 79]. The variation, with temperature, of modulus of elasticity and tensile strength of HSC is similar to that of NSC.

Kodur and Sultan have presented detailed experimental data on the thermal properties of HSC (for both plain and steel fiber–reinforced concrete types) [80]. The type of aggregate has significant influence on the thermal properties of HSC at elevated temperatures. Figure 9.29 shows the thermal conductivity and specific heat of HSC, with siliceous and carbonate aggregates, as a function of temperature. Based on the test data, Kodur and Sultan have proposed relationships for thermal conductivity, specific heat, thermal expansion, and mass loss of HSC as a function of temperature [81].

The variation of thermal expansion with concrete temperature for siliceous and carbonate aggregate HSC is similar to that of NSC, with the aggregate having a strong influence. Overall, the thermal properties of HSC, at elevated temperatures, are similar to those of NSC [82].

HSC, due to low porosity, is more susceptible to spalling than NSC, and explosive spalling may occur when HSC is exposed to severe fire conditions. Hence, one of the major concerns for the use of HSC is regarding its behavior in fire, in particular, the occurrence of spalling at elevated temperatures. For predicting spalling performance, knowledge of the variation of porosity with temperature is essential. Figure 9.30 shows the variation of porosity with temperature for NSC and HSC. The data in this figure are taken from the measurements

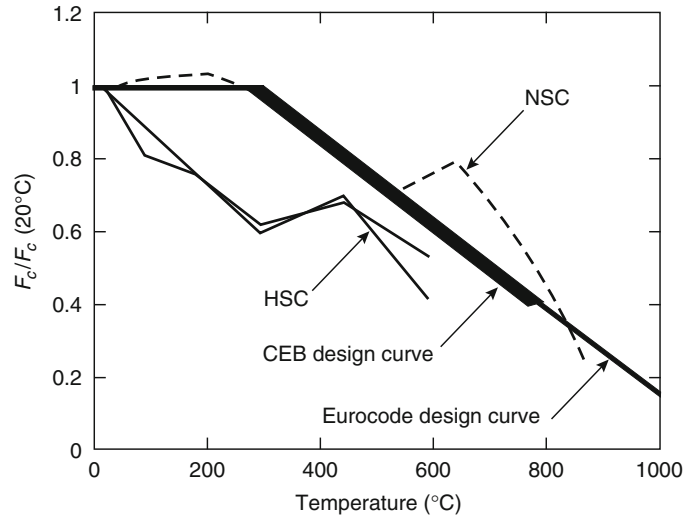

Fig. 9.28 Comparison of design compressive strength and results of unstressed tests of lightweight aggregate concrete [30]

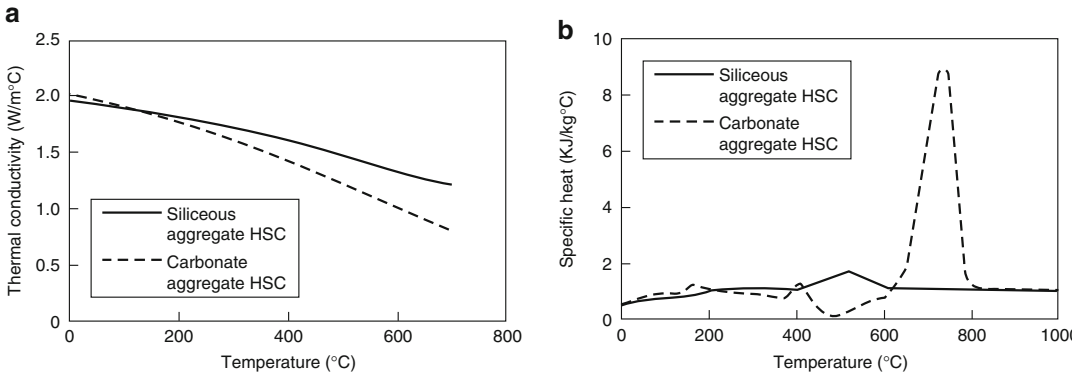

Fig. 9.29 Thermal conductivity and specific heat capacity of HSC as a function of temperature: [80] (**a**) thermal conductivity of high-strength concrete and (**b**) specific heat of high-strength concrete

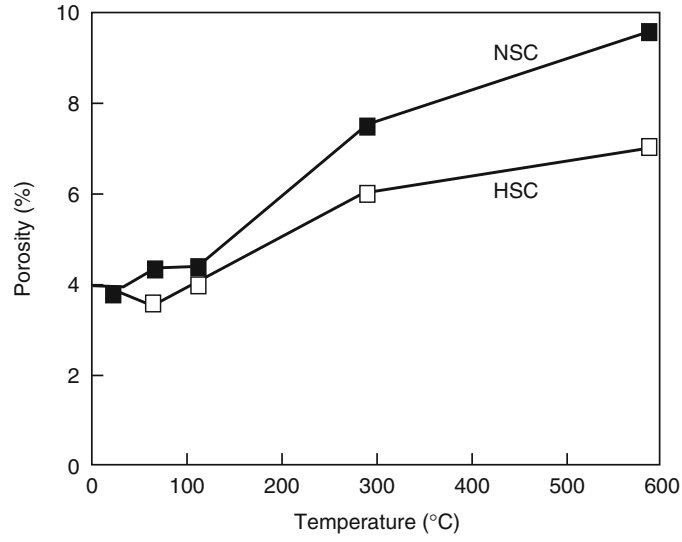

Fig. 9.30 Porosity of HSC and NSC as a function of temperature [36]

of porosity after exposure to different temperatures [36].

The spalling in HSC can be minimized by creating pores through which water vapor can be relieved before vapor pressure reaches critical values. This is usually done by adding polypropylene fibers to the HSC [71, 72, 83]. Also, Kodur et al. have reported that spalling in HSC columns can be minimized to a significant extent by providing bent ties as lateral confinement [77, 84]. Figure 9.31 illustrates conventional and improved tie configuration for minimizing spalling in HSC columns [84].

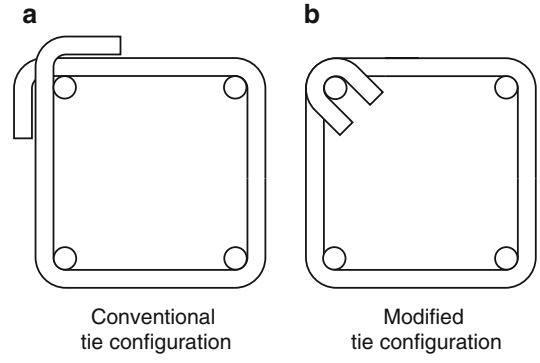

Fig. 9.31 Tie configuration for achieving higher fire resistance in concrete structures [79]

Brick

Building brick belongs in the L/I group of materials. The density (ρ) of bricks ranges from 1660 to 2270 kg·m^{-3}, depending on the raw materials used in the manufacture, and on the molding and firing technique. The true density of the material (ρt) is somewhere between 2600 and 2800 kg·m^{-3}.

The modulus of elasticity of brick (E) is usually between 10×10^3 and 20×10^3 MPa. Its compressive strength (σ_u) varies in a very wide range, from 9 to 110 MPa—50 MPa may be regarded as average [85]. This value is an order of magnitude greater than the stresses allowed in the design of grouted brickwork. Because brick is rarely considered for important load-bearing roles in buildings, there has been little interest in the mechanical properties of bricks at elevated temperatures.

At room temperature, the coefficient of thermal expansion (α) for clay bricks is about 5.5×10^{-6} m·m^{-1} K^{-1}. The dilatometric and thermogravimetric curves for a clay brick of 2180 kg·m^{-3} density are shown in Fig. 9.32 [7]. The variation with temperature of the specific heat and the thermal conductivity of this brick is shown in Figs 9.33 and 9.34, respectively [7].

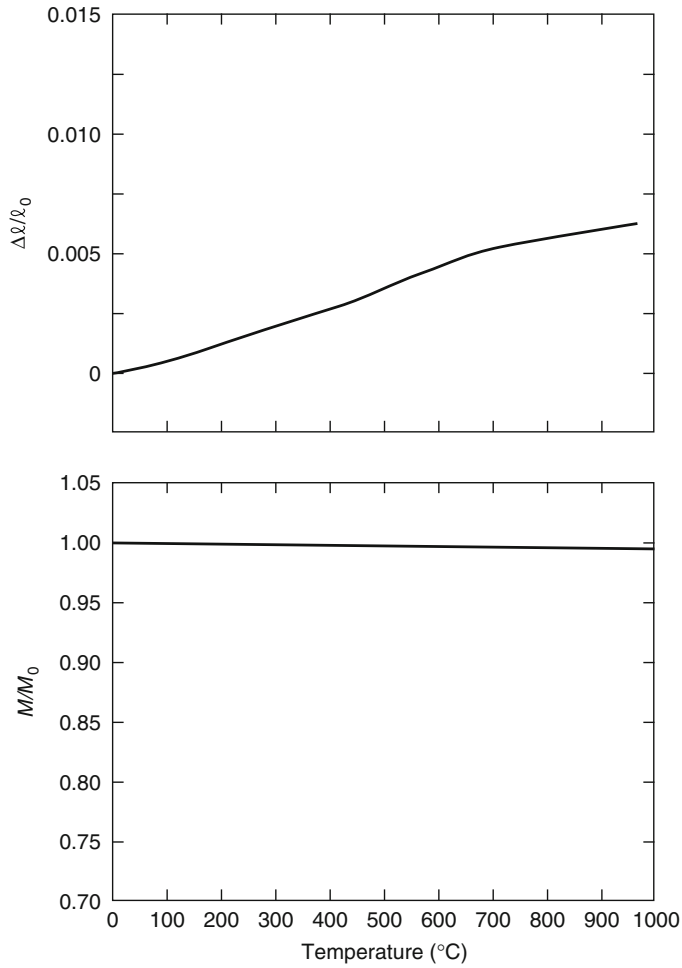

Fig. 9.32 Dilatometric and thermogravimetric curves for a clay brick [7]

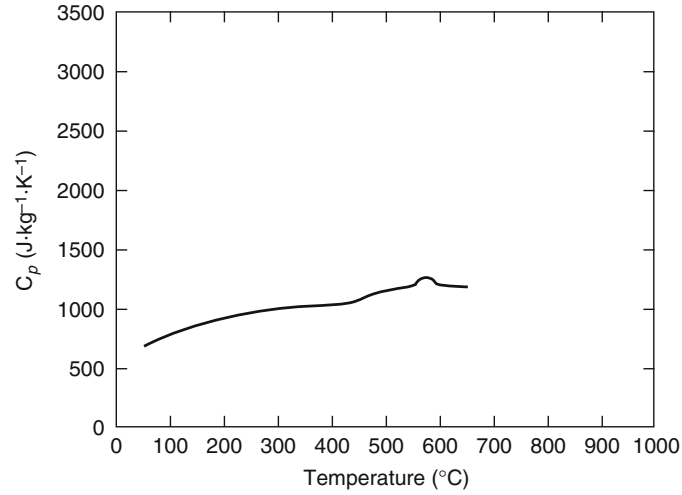

Fig. 9.33 Apparent specific heat of a clay brick [7]

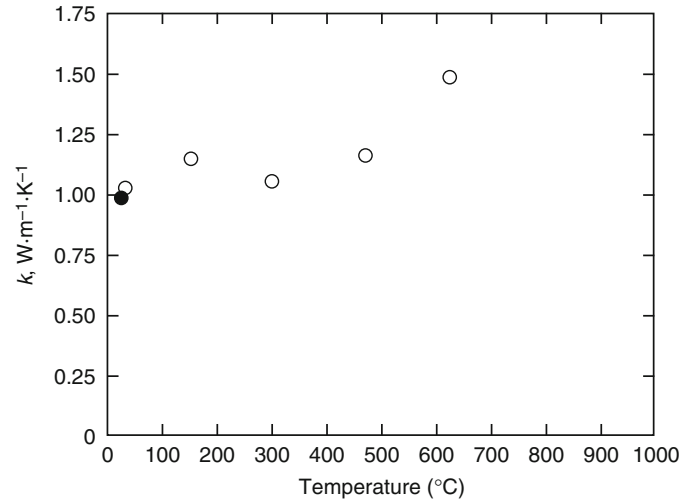

Fig. 9.34 Thermal conductivity of a clay brick. Symbols: ○—heating cycle, ●—after cooling [7]

Wood

Wood is a Group L/I/F or I/F material. As structural members, wood is widely used in residential and low-rise constructions. Although about 180 wood species are commercially grown in the United States, only about 25 species have been assigned working stresses. The two groups most extensively used as structural lumber are the Douglas firs and the southern pines.

The oven-dry density (ρ) of commercially important woods ranges from 300 kg·m^{-3} (white cedar) to 700 kg·m^{-3} (hickory, black locust). The density of Douglas firs varies from 430 to 480 kg·m^{-3} and that of southern pines from 510 to 580 kg·m^{-3}. The true density of the solid material that forms the walls of wood cells (αt) is about 1500 kg·m^{-3} for all kinds of wood. The density of wood decreases with temperature; the density ratio (ratio of density at elevated temperature to that at room temperature) drops to about 0.9 at 200 °C and then declines sharply to about 0.2 at about 350 °C [40].

Wood is an orthotropic material, so the strength and stiffness in longitudinal and transverse directions are influenced by grain orientation. The mechanical properties of wood are

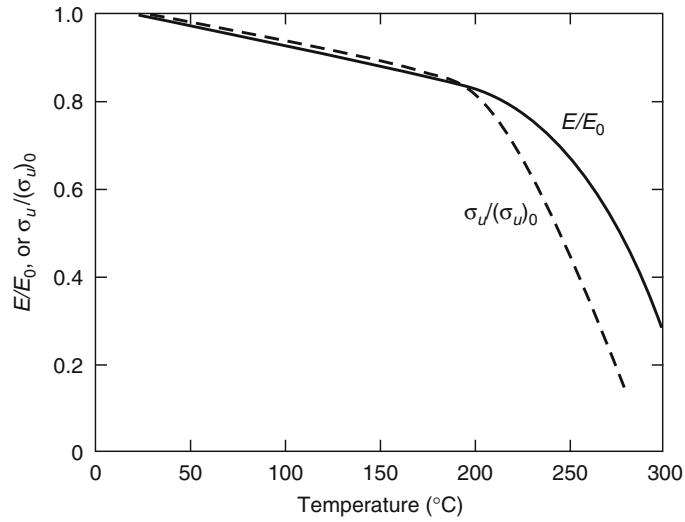

Fig. 9.35 The effect of temperature on the modulus of elasticity and compressive strength of wood [87–89]

affected by temperature and are influenced by moisture content, rate of charring, and grain orientation. The modulus of elasticity (E) of air-dry, clear wood along the grain varies from 5.5×10^3 to 15.0×10^3 MPa, and its crushing strength (σ_u) varies from 13 to 70 MPa. These properties are related and roughly proportional to the density, regardless of the species [86].

Figure 9.35 shows the variation of the modulus of elasticity and compressive strength of oven-dry, clear wood with temperature [87–89]. (E_0 and $[\sigma_u]_0$ in the figure are modulus of elasticity and compressive strength at room temperature, respectively.) The modulus of elasticity decreases slowly with temperature up to about 200 °C, when it reaches about 80 %, and then the decline is more rapid. The compressive strength also drops linearly to about 80 % at about 200 °C, and then the drop is more rapid—to about 20 % around 280 °C.

The tensile strength exhibits behavior similar to that of compressive strength, but the decline in tensile strength with temperature is less rapid. The moisture content plays a significant role in determining the strength and stiffness, with increased moisture content leading to higher reduction. There is very little information on stress-strain relationships for wood. The formulas for reduced stiffness and design strength can be found in Eurocode 5 [90] (Part 1.2).

The coefficient of linear thermal expansion (β) ranges from 3.2×10^{-6} to 4.6×10^{-6} $m \cdot m^{-1} \cdot K^{-1}$ along the grain and from 21.6×10^{-6} to 39.4×10^{-6} $m \cdot m^{-1} \cdot K^{-1}$ across the grain [91]. Wood shrinks at temperatures above 100 °C, because of the reduction in moisture content. Lie [29] reported that the amount of shrinkage can be estimated as 8 % in the radial direction, 12 % in the tangential direction, and an average of 0.1–0.2 % in the longitudinal direction. The dilatometric and thermogravimetric curves of a pine with a 400 $kg \cdot m^{-3}$ oven-dry density are shown in Fig. 9.36 [7].

The thermal conductivity (k) across the grain of this pine was measured as 0.86–1.07 $W \cdot m^{-1} \cdot K^{-1}$ between room temperature and 140 °C [14]. The thermal conductivity increases initially up to a temperature range of 150–200 °C, then decreases linearly up to 350 °C, and finally increases again beyond 350 °C.

Figure 9.37 shows the apparent specific heat for the same pine, as a function of temperature [7]. The accuracy of the curve (developed by differential scanning calorimeter [DSC]) is somewhat questionable. However, it provides useful information on the nature of decomposition reactions that take place between 150 and 370 °C.

Charring is one of the main high-temperature properties associated with wood and should be considered in predicting performance under fire

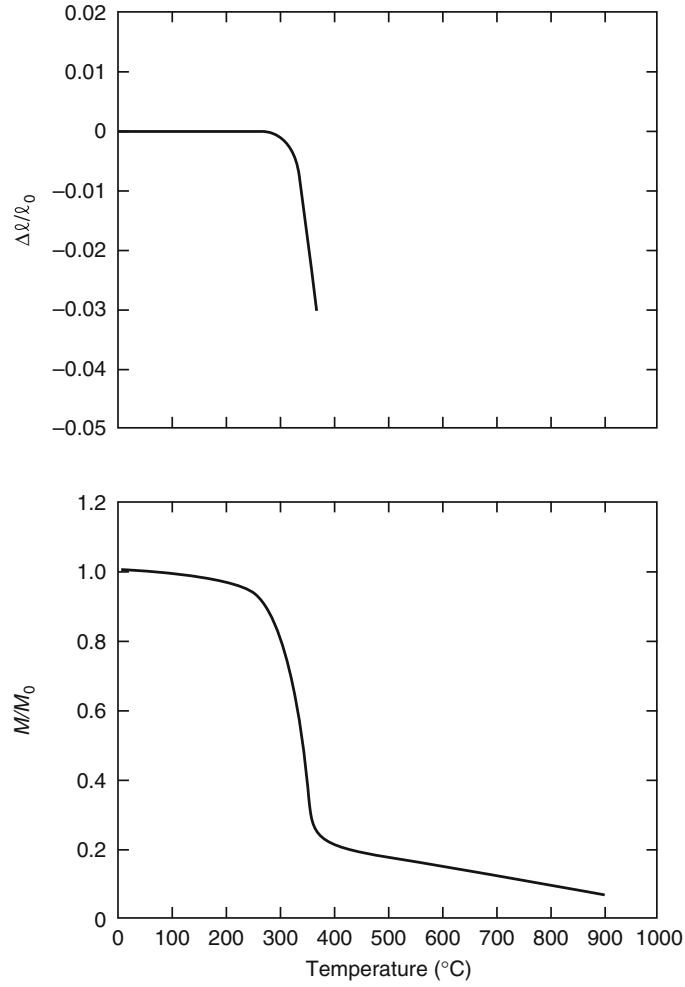

Fig. 9.36 Dilatometric and thermogravimetric curves for a pine of 400 kg·m^{-3} density [7]

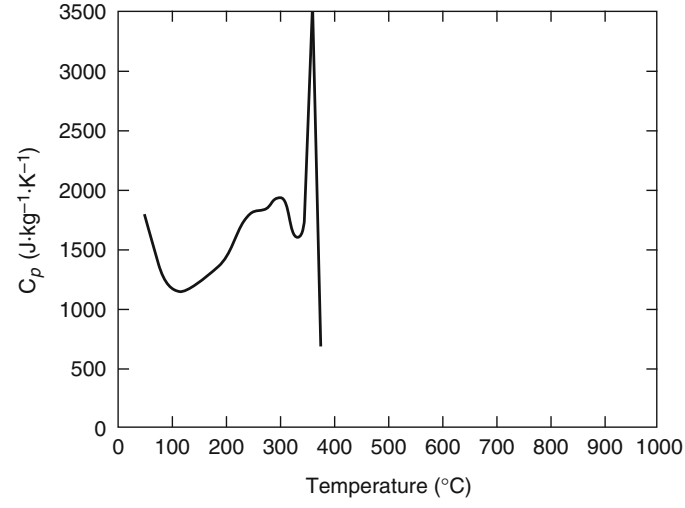

Fig. 9.37 Apparent specific heat for a pine of 400 °C density [7]

conditions. The rate of charring is influenced by the radiant heat flux or, alternatively, the fire severity. Generally, a constant transverse-to-grain char rate of 0.6 mm/min can be used for woods subjected to standard fire exposure [29]. The charring rate parallel to the grain of wood is approximately twice the rate when it is transverse to the grain. These charring rates should be used only when attempting to model the performance of wood sections in the fire resistance furnace.

Charring is influenced by a number of parameters, the most important ones being density, moisture content, and contraction of wood. It is reasonable to modify the 0.6 mm/min to approximately 0.4 mm/min for moist dense wood or to 0.8 mm/min for dry and light wood. The fire retardants often used to reduce flame spread in wood may only slightly increase the time until ignition of wood.

Specific charring rates for different types of wood can be found in "Structural Fire Protection" [29] and Bénichou and Sultan [40]. Eurocode [90] gives an expression for charring depth in a wood member exposed to standard fire. The dependence of charring rate on the radiant heat flux is discussed in *Wood Handbook* [87].

In recent years different types of engineered wood is widely used in residential construction. These engineered wood products (ex: joists and studs) capitalize on the strength of wood and the efficiency of the sectional shapes (ex: I-shaped joists) to enhance load bearing capacity at ambient conditions, while at the same time reducing the mass and cost of the structural member. However, there is very limited data on high temperature thermo-mechanical properties of engineered lumber and fire resistance of engineered joists and studs. Limited research has clearly shown that fire resistance of engineered joists to be significantly lower than that of conventional wood joists [92]. This was mainly attributed to poor thermal, mechanical and charring properties of engineered lumber as compared to conventional wood products. Typically, room temperature thermal conductivity and modulus of elasticity of engineered lumber is higher than other types of wood due to the presence of compressed plies [92]. Comparison of charring rates indicate that engineered lumber has higher rate of charring rate as compared to conventional wood [92].

Fiber-Reinforced Polymers

In recent years, there has been a growing interest in the use of fiber-reinforced polymers (FRPs) in civil engineering applications due to the advantages, such as high strength and durability (resistance to corrosion), that FRP offers over traditional materials. FRP composites consist of two key elements, namely the fibers (glass, carbon, or aramid) and a thermosetting polymer matrix such as epoxy, vinyl ester, phenolic, or polyester resin. The commonly used types of FRP composite materials are glass fiber–reinforced plastic (GFRP), carbon fiber–reinforced plastic (CFRP), and aramid fiber–reinforced plastic (AFRP) composites. FRPs are similar to wood in that they will burn when exposed to fire and can be classified as an L/I/F type material.

FRP is used as an internal reinforcement (reinforcing bars as an alternative to traditional steel reinforcement) and as external reinforcement in forms, such as wrapping and sheeting for the rehabilitation and strengthening of concrete members. One of the main impediments to using FRPs in buildings is the lack of knowledge about the fire resistance of FRP [93, 94].

There are some major differences associated with FRP as a material. The properties depend on the type and composition of FRP, and the availability of various types of FRP makes it difficult to establish the properties at elevated temperatures. The material properties are controlled by the fibers in the longitudinal direction and by the matrix in the transverse direction. In addition to thermal and mechanical properties, factors such as burning, charring, evolution of smoke, and toxicity in fire also play a significant role in determining the fire performance. A summary of typical mechanical properties for various types of FRPs, in comparison to other commonly used construction materials, at room temperature, is presented in Table 9.3.

Table 9.3 Properties of various FRP composites and other materials

Material	Modulus of elasticity E_1 (MPa)	Modulus of elasticity E_2 (MPa)	Tensile strength σ_{t1} (MPa)	Comp. strength σ_{c1} (MPa)	Shear modulus G (MPa)	Shear strength S (MPa)	Poisson's ratio ν	Tensile strength σ_2 (MPa)	Comp. strength σ_{c2} (MPa)
GFRP (glass/epoxy)	55,000	18,000	1050	1050	9000	42	0.25	28	140
GFRP (glass/epoxy) unidirectional	42,000	12,000	700	—	5000	72	0.30	30	—
CFRP (carbon/epoxy) unidirectional	180,000	10,000	1500	—	7000	68	0.28	40	—
CFRP (graphite/epoxy)	207,000	5200	1050	700	2600	70	0.25	40	120
Boron/epoxy	207,000	21,000	1400	2800	7000	126	0.30	84	280
ARP (aramid/epoxy) unidirectional	76,000	8000	1400	—	3000	34	0.34	12	—
Mild steel	200,000	—	550	240	—	380	—	—	—
Concrete (normal strength)	31,000	—	~4	40	—	~7	0.15–0.20	—	—
Wood (Douglas fir)	9800	—	69	—	—	—	—	—	—

E_1 = modulus of elasticity in longitudinal direction
E_2 = modulus of elasticity in transverse direction

There is very little information on the material properties of FRPs at elevated temperatures [93]. The impact of high temperatures on the behavior of FRP composites is severe degradation of their properties: reduction of strength and stiffness, and increase in deformability, thermal expansion, and creep. Above 100 °C temperature, the degradation can be quite rapid as the glass transition temperature of the matrix is reached.

The glass transition temperature, which is often considered the upper use temperature, varies with the type of resin used and was found to be as low as 100 °C in some resins and as high as 220 °C in others. From the limited studies, it appears that as much as 75 % of the GFRP strength and stiffness is lost by the time the temperature reaches 250 °C [93, 95].

The stress-strain relationships, from the studies conducted by Gates [95], for a CFRP composite (IM7/5260) are shown in Fig. 9.38 for various temperatures. It can be seen that the tensile strength of IM7/5260 composite reduces to approximately 50 % at about 125 °C and to about 75 % at a temperature of 200 °C. The strain level, for a given stress, is also higher with the increase in temperature. Recently, Wang and Kodur reported high temperature strength and stiffness properties of glass and carbon FRP rebars; full details of the tests are reported in Wang and Kodur [96].

The variation of strength with temperature (ratio of strength at elevated temperature to that at room temperature) for FRP along with that of other traditional construction materials is shown in Fig. 9.2. The curve showing the strength degradation of FRP is based on the limited information reported in the literature [93, 95]. The rate of strength loss is much greater for FRP than for concrete and steel, resulting in a 50 % strength loss by about 200 °C.

The bond between FRPs and concrete (or between FRP layers or lap splices in multiply layup applications) is essential to transfer loads. This load transfer occurs through the polymer resin matrix and thus relies heavily on the mechanical properties of the polymer.

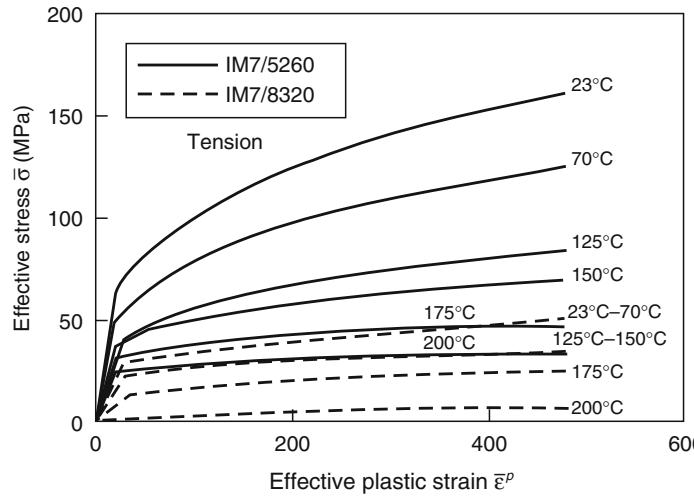

Fig. 9.38 Tensile stress-strain curves for CFRP at various temperatures [95]

Deterioration of the mechanical properties of the matrix material at temperatures above the specific polymer's glass transition temperature, T_g, have the potential to cause loss of bond at only modestly increased temperatures, resulting in loss of interaction between FRP and concrete. The glass transition temperature of commonly used polymer matrix materials is typically in the range of 65–140 °C.

No specific research has yet been reported on the bond between concrete and externally bonded FRP strengthening systems at high temperature, although limited data on the high-temperature residual performance of the FRP concrete bond has recently been presented [97].

Research on the bond properties of FRP bars for concrete reinforcement applications (internal reinforcement) at elevated temperature has been reported in the literature [98–101]. This work has indicated that dramatic decreases in bond strength can be expected, to values of about 10 % of room temperature strength, at temperatures between 100 and 200 °C (i.e., at temperatures close to or above T_g). The observed bond strength reductions have been attributed to changes in the properties of the polymer matrix at the surface of the FRP bars.

It seems clear that temperature effects on the FRP–FRP and FRP–concrete bond are critical, both in FRP internal reinforcement and in externally bonded FRP applications, and a great deal of additional research is required in this area. Thus, bond degradation at elevated temperature is a critical factor to be considered in the design of FRP-reinforced or -strengthened concrete members. This was observed in full-scale fire tests on FRP-strengthened reinforced concrete columns [102].

The critical temperature of FRP is much lower than that for steel and depends on the composition of fibers and matrix. Kodur and Baingo have assumed a critical temperature of 250 °C in modeling the behavior of FRP-reinforced concrete slabs [93]. Recently, Wang and Kodur have developed critical temperature information for glass and carbon FRP reinforcing rebars [103, 104].

They carried out a series of tensile strength tests at high temperatures on two types of commercially available FRP rebars. This included both carbon FRP and glass FRP bars of different diameters. Conventional steel rebars were also tested for comparison. The data were used to determine the variation of average failure strength and elastic modulus for each type of reinforcement with increasing temperature. Full details of experimental studies, including specimen preparation, test setup, test procedure, and observations as well as test data, are described elsewhere [96, 104].

A summary of the results of these studies are shown in Fig. 9.39. For the GFRP and CFRP bars, observed failure strengths were used, whereas for the steel bars, the 0.2 % proof stress was used. The elastic modulus was taken as the

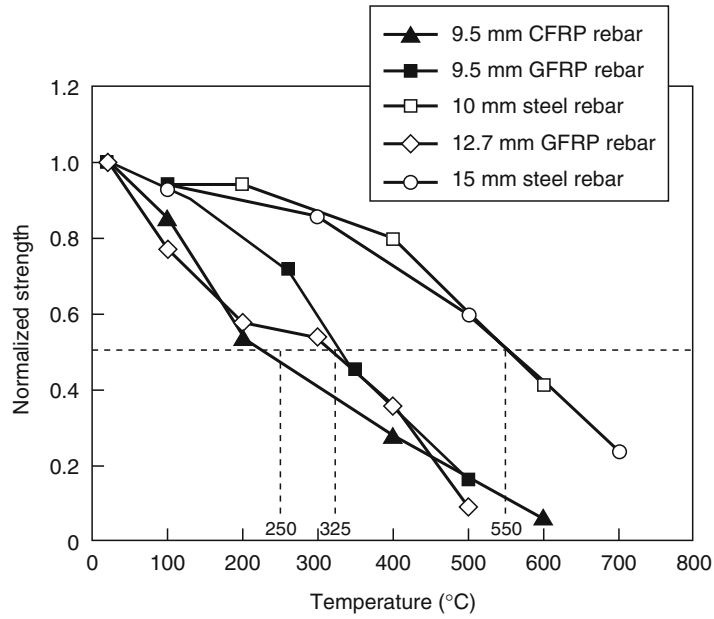

Fig. 9.39 Effect of strength degradation as a function of temperature for FRP [96]

Table 9.4 Thermal properties of various FRPs and other materials at room temperature

	Coefficient of thermal expansion (unidirectional) (β: 10^{-6} m · m^{-1}·°C)		Thermal conductivity k (W · m^{-1} ° C^{-1})	
Material	Longitudinal α_L	Transverse α_T	Longitudinal k_L	Transverse k_T
Glass/epoxy (S-glass)	6.3	19.8	3.46	0.35
Glass/epoxy (E-glass: 63 % fiber)	7.13	—	—	—
Carbon/epoxy (high modulus)	–0.9	27	48.4–60.6	0.865
Carbon/epoxy (ultra-high modulus)	–1.44	30.6	121.1–129.8	1.04
Boron/epoxy	4.5	14.4	1.73	1.04
Aramid/epoxy (Kevlar 49)	–3.6	54	1.73	0.73
Concrete	6.16		1.36–1.90	
Steel	10.8–18		15.6–46.7	
Epoxy	—	54–90	—	0.346

slope of a straight line fitted to the initial linear portion of the recorded stress-strain relationship for each specimen. The critical temperature for the FRP reinforcement was derived based on a 50 % tensile strength reduction, as is the case for steel reinforcement. This resulted in critical temperatures of about 325 °C and 250 °C for GFRP and CFRP reinforcing bars, respectively. These critical temperatures are significantly less than 593 °C, the critical temperature for steel reinforcement, thus highlighting the presumed susceptibility of FRP reinforcement to fire. Figure 9.39 also shows that the steel reinforcing bars in these tests lost about 50 % of their room-temperature yield strength at about 550 °C, a result that agrees well with published data available in the literature.

The variation of elastic moduli of FRP with temperature is different in each direction. Typical values for various types of FRP are given in Table 9.3 [93]. The three values represent the longitudinal, transverse, and shear moduli, respectively, of different unidirectional FRPs. At high temperature, the elastic moduli of FRPs decreases at a faster rate than that for concrete or steel.

Similar to mechanical properties, the thermal properties of FRP are also dependent on direction, fiber type, fiber orientation, fiber volume fraction, and laminate configuration. Table 9.4 shows thermal properties for various types of

FRP at room temperature. In the longitudinal direction, the thermal expansion of FRPs is lower than that of steel. However, in the transverse direction, it is much higher than that of steel. Some of the information available in the literature can be found in a review report by Kodur and Baingo [93]. At room temperatures, FRPs in general have low thermal conductivity, which makes them useful as insulation materials. With the exception of carbon fibers, FRPs have a low thermal conductivity.

Information on the thermal properties of FRP at elevated temperatures is very scarce, which is likely due to the fact that such information is proprietary to the composite materials' manufacturers. Also, there is not much information on evolution of smoke and toxins in FRP composites exposed to fire.

Thermal expansion of FRP reinforcement varies in longitudinal and transverse directions, and the coefficient of thermal expansion highly depends on type of fiber, resin, and volume fraction of fiber. The longitudinal coefficient of thermal expansion is dominated by properties of the fiber, while the transverse coefficient is dominated by properties of the resin. Figure 9.40

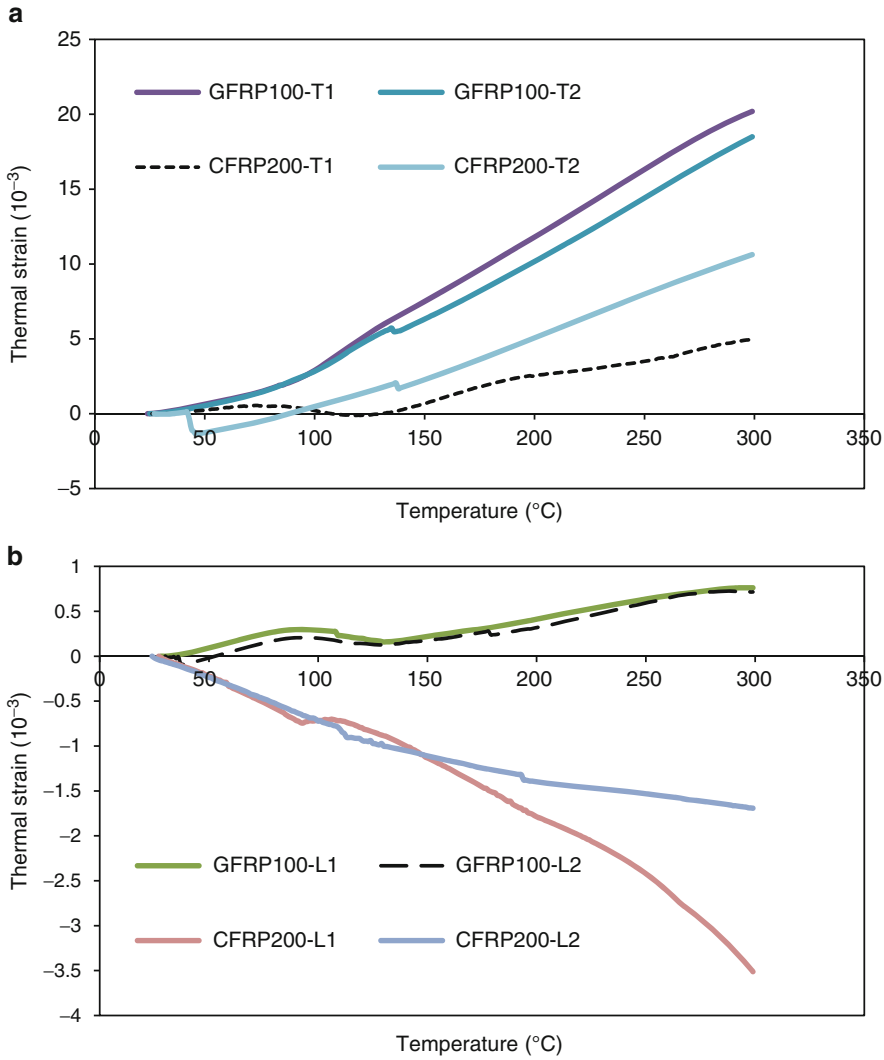

Fig. 9.40 Variation of thermal strain in GFRP and CFRP in (**a**) longitudinal and (**b**) transverse directions as a function of temperature

(a and b) shows longitudinal and transverse coefficients of thermal expansion for typical GFRP and CFRP bars. It can be noted that usually there is a change in expansion rate at around glass transition temperature (Tg), indicating FRP reinforcement experiences different coefficients of thermal expansion before and after phase change (Tg). In transverse direction, the dimension of GFRP and CFRP rebars increase with temperature, and GFRP undergoes higher thermal expansion than that of CFRP. However, in longitudinal direction, GFRP rebar slightly expands with temperature, but CFRP rebar contracts with increase in temperature. The coefficients of thermal expansion in transverse direction for GFRP and CFRP rebars can be taken to be 64.5 and 7.79 $\times$ 10^{-6}/°C, respectively, while the corresponding coefficients of thermal expansion in longitudinal direction are 2.48 and -7.6×10^{-6}/°C, respectively [105]

Gypsum

Gypsum (calcium sulfate dihydrate: $CaSO_4 \cdot 2H_2O$) is a Group I material. Gypsum board is produced by mixing water with plaster of paris (calcium sulfate hemihydrate: $CaSO_4 \cdot {}^1/_2H_2O$) or with Keene's cement (calcium sulfate anhydrite: $CaSO_4$). The interlocking crystals of $CaSO_4 \cdot 2H_2O$ are responsible for the hardening of the material.

Gypsum products are used extensively in the building industry in the form of boards, including wallboard, formboard, and sheathing. The core of the boards is fabricated with plaster of paris, into which weight- and set-controlling additives are mixed. Furthermore, plaster of paris, with the addition of aggregates (such as sand, pearlite, vermiculite, or wood fiber) is used in wall plaster as base coat, and Keene's cement (neat or mixed with lime putty) is used as finishing coat.

Gypsum board, based on composition and performance, is classified into various types, such as regular gypsum board, type X gypsum board, and improved type X gypsum board. A gypsum board with naturally occurring fire resistance from the gypsum in the core is defined as regular gypsum. When the core of the gypsum board is modified with special core additives or with enhanced additional properties, to improve the natural fire resistance from regular gypsum board, it is classified as type X or improved type X gypsum board. There might be significant variation in fire performance of the gypsum board based on the type and the formulation of the core, which varies from one manufacturer to another.

Gypsum is an ideal fire protection material. The water inside the gypsum plays a major role in defining its thermal properties and response to fire. On heating, it will lose the two H_2O molecules at temperatures between 125 and 200 °C. The heat of complete dehydration is 0.61×10^6 J/kg gypsum. Due to the substantial absorption of energy in the dehydration process, a gypsum layer applied to the surface of a building element is capable of markedly delaying the penetration of heat into the underlying load-bearing construction.

The thermal properties of the gypsum board vary depending on the composition of the core. The variation with temperature of the volume specific heat (ρcp) of pure gypsum has been illustrated in Harmathy [106], based on information reported in the literature [107, 108]. The thermal conductivity of gypsum products is difficult to assess, owing to large variations in their porosities and the nature of the aggregates. A typical value for plaster boards of about 700 $kg \cdot m^{-3}$ density is 0.25 $W \cdot m^{-1} \cdot K^{-1}$. Figures 9.41 and 9.42 illustrate the typical variation of the thermal conductivity and the specific heat, respectively, of the gypsum board core with temperature. The plots reflect the expressions proposed recently by Sultan [109], based on tests conducted on type X gypsum board specimens. The specific heat measurements were carried out at a heating rate of 2 °C/min. The dehydration of gypsum resulted in the two peaks that appear in the specific heat curve at temperatures around 100 °C and 650 °C. The peak values are slightly variant to those reported earlier by Harmathy [16]; this may be due to the differences in gypsum composition.

The coefficient of thermal expansion (β) of gypsum products may vary between

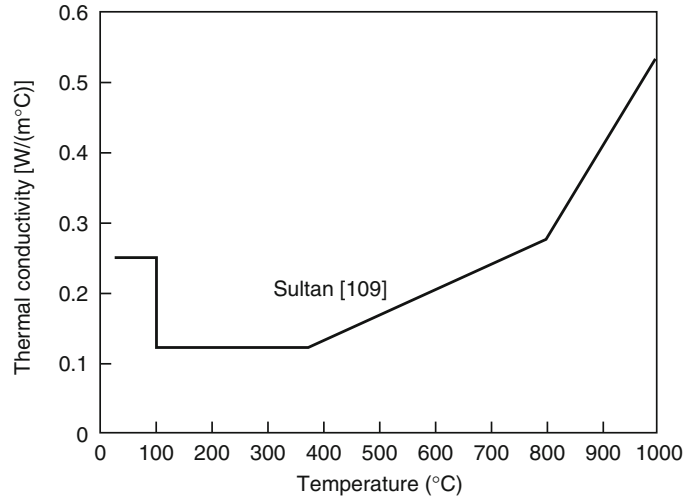

Fig. 9.41 Thermal conductivity of type X gypsum board core as a function of temperature [109]

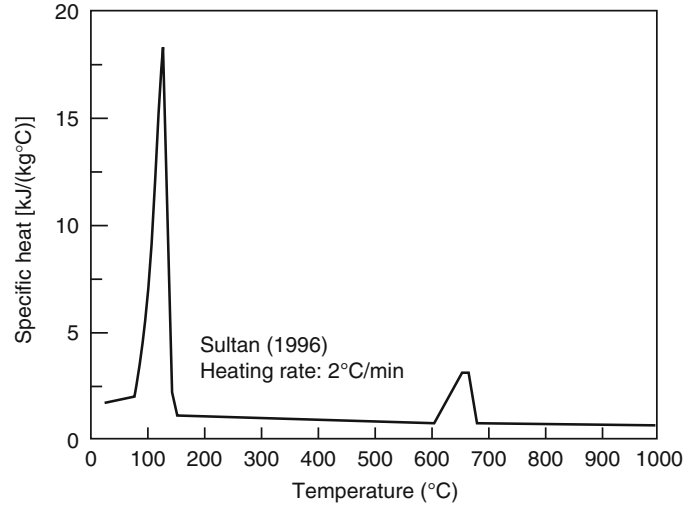

Fig. 9.42 Specific heat of type X gypsum board core as a function of temperature [109]

11.0×10^{-6} and 17×10^{-6} $m \cdot m^{-1} \cdot K^{-1}$ at room temperature, depending on the nature and amount of aggregates used. The dilatometric and thermogravimetric curves of a so-called fire-resistant gypsum board of 678 $kg \cdot m^{-3}$ density are shown in Fig. 9.43.

There is not much information about the mechanical properties of the gypsum board at elevated temperatures because these properties are difficult to obtain experimentally. The strength of gypsum board at an elevated temperature is very small and can be neglected. The Gypsum Association [110] lists typical mechanical properties, at room temperature, for some North American gypsum board products. The attachment details (screw spacing, orientation of gypsum board joints, stud spacing, etc.) may have a noticeable effect on the fire performance of the gypsum board.

Insulation

Insulation is a Group I material and is often used as a fire protection material both for heavy structural members such as columns and beams and for lightweight framing assemblies such as floors and walls. The insulation helps delay the

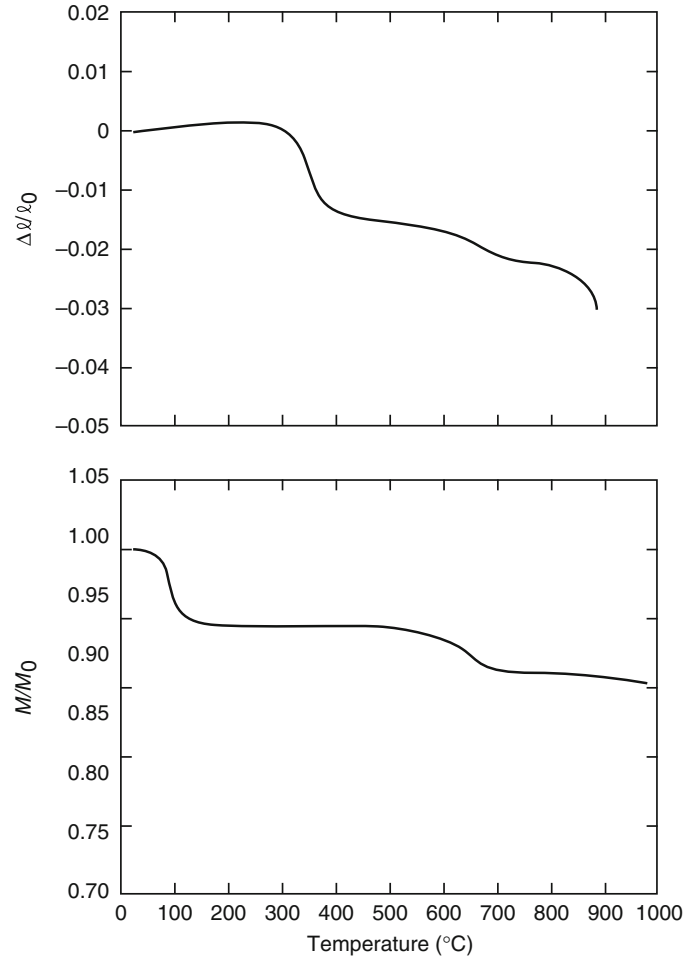

Fig. 9.43 Dilatometric and thermogravimetric curves for a gypsum board of 678 kgm^{-3} density [7]

temperature rise of structural members, thereby enhancing fire resistance. There are a number of insulation materials available in the market. Mineral wool and glass fiber are the two most widely used insulation materials in walls and floors. Other insulation materials used for fire protection include intumescent paints, spray mineral fibers, insulation boards, and compressed fiber board.

The thermal properties of insulation play an important role in determining the fire resistance. However, there is not much information available on the thermal properties of various types of insulation. Figure 9.44 shows the variation of thermal conductivity with temperature for glass and rock fiber insulation types. The differences in thermal conductivity values at higher temperatures are mainly due to variation in the chemical composition of fiber.

Full-scale fire resistance tests on walls and floors have shown that the mineral fiber insulation performs better than glass fiber insulation. This is mainly because glass fiber melts in the temperature range of 700–800 °C and cannot withstand direct fire exposure. The melting point for mineral fiber insulation is higher. The density of glass fiber is about 10 kg/m^3 and is much lower than that of rock fiber, which is about 33 kg/m^3.

The mineral wool insulation, when installed tightly between the studs, can be beneficial for the fire resistance of non-load-bearing steel stud walls because it acts as an additional fire barrier

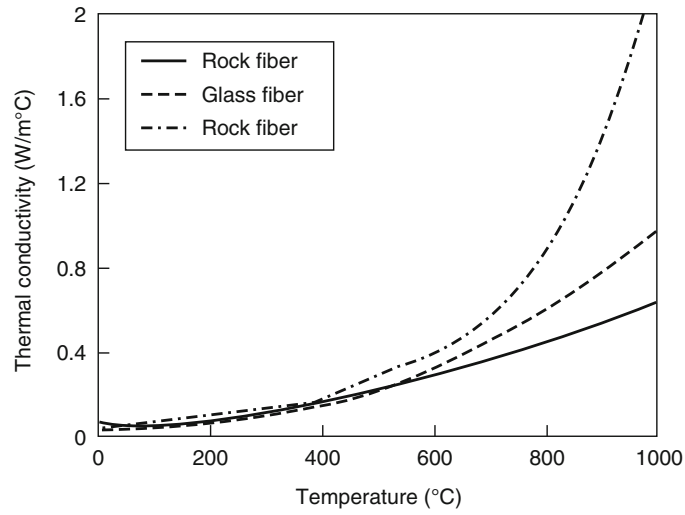

Fig. 9.44 Thermal conductivity of insulation as a function of temperature [40]

Table 9.5 Properties of some commonly used insulation materials [105]

Material	Density ρ (kg/m3)	Thermal conductivity k (W/m·K)	Specific heat c (J/kg·K)	Equilibrium moisture content %
Spray				
Sprayed mineral fibers	300	0.12	1200	1
Perlite or vermiculite plaster	350	0.12	1200	15
High-density perlite or vermiculite plaster	550	0.12	1200	15
Boards				
Fiber silicate or fiber calcium silicate	600	0.15	1200	3
Gypsum plaster	800	0.2	1700	20
Compressed fiber boards				
Mineral wool, fiber silicate	150	0.2	1200	2

after the fire-exposed gypsum board falls off [111]. On the other hand, cavity insulation slows down the flow of heat through the wall assembly and can cause an accelerated temperature rise in the fire-exposed gypsum board.

Another common form of fire insulation applied on steel structural members to achieve required fire resistance is spray applied fire resistive materials (SFRM), which work by delaying temperature rise in steel. SFRM, available under different trade names, offers several advantages over other types of fire insulation such as cost effectiveness, ease of application, and light weight, and therefore is widely used as fire proofing material for steel structures. SFRM is mainly composed of base materials such as gypsum, cementitious and mineral fiber and other additives such as vermiculite.

The thermal properties of some of the commonly used insulation systems are given in Table 9.5 [112]. It should be noted that these values are average property values and can vary depending on the manufacturer and on the proportions of different constituent materials. Also the moisture content of the insulation material has an effect on the thermal properties.

The above listed thermal properties for fire insulation are at room temperature and they can vary significantly with temperature and also with insulation composition, which can vary for different trade names (from different commercial manufactures) among the same type of insulation

(ex: SFRM). However, in practice fire resistance of insulated structural (steel) members is evaluated by considering only room temperature thermal properties of fire insulation [113]. This is mainly due to lack of reliable data on the effect of temperature on thermal properties of fire insulation. Further, there is no data on relative thermal performance of similar fire insulation products (ex: SFRM) produced from different commercial manufactures.

Figure 9.45a shows variation of thermal conductivity with temperature for three types of commercially available SFRM (A, B, and C) generated in a recent research study [114]. The thermal conductivity of three SFRM types at room temperature is in the range of 0.07 and 0.2 W/m.K. This variation of thermal conductivity among three types of SFRM well pertains to the variation in their densities and also to composition of ingredients in each type. The trends in the figure further indicate that temperature has significant effect on thermal conductivity of SFRM. This variation in thermal conductivity at higher temperatures is primarily governed by changes in moisture content and density of different SFRM types.

Insulation materials such as SFRM experience shrinkage at higher temperatures, as opposed to expansion phenomenon in materials such as steel, concrete and wood. The variation of thermal strain for three types of SFRM is plotted as a function of temperature in Fig. 9.45b [114]. This variation of thermal strain with temperature is also linked to changes in moisture content.

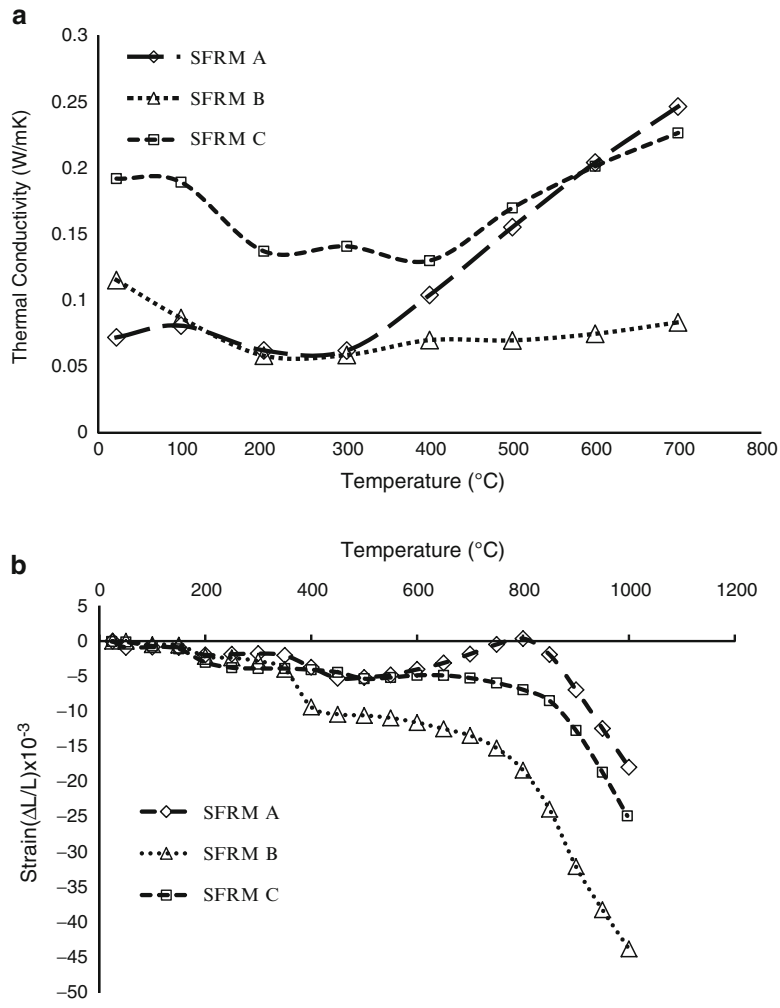

Fig. 9.45 Effect of temperature on (**a**) thermal conductivity and (**b**) thermal contraction, of different SFRMs

Table 9.6 Density of SFRM at room temperature and after exposure to 700 °C

Insulation type	Density (Kg/m^3)		Decrease in density (%)
	Room temp. (20 °C)	700 °C	
SFRM A	298	241.3	19.0
SFRM B	423.2	349.8	17.3
SFRM C	451.8	381.2	15.6

However, the loss of moisture content only account for the shrinkage phenomenon that occurs in 100–400 °C range. The intermediate expansion resulting in increase in thermal strains in 400–800 °C range is dictated by the expansion of intumescent material, such as, vermulite, which is added to SFRM to counteract shrinkage and the percentage of Vermiculite in SFRM has major influence on the level of contraction.

The change in density for three types of SFRM at ambient conditions and after exposure to 700 °C is presented in Table 9.6 [114]. There is a decrease in density in all three types of SFRM at 700 °C, which is predominantly due to the loss of moisture. This decrease in density in SFRM is comparable to that in gypsum, and attributed to dehydration reactions, which takes place with increase in temperature [115].

Other Miscellaneous Materials

Further information is available from the literature on the dilatometric and thermogravimetric behavior, apparent specific heat, and thermal conductivity of a number of materials in Group I, including asbestos cement board, expanded plastic insulating boards, mineral fiber fireproofing, arborite, and glass-reinforced cement board [7]. The properties of plastics and their behavior in fire are discussed in other chapters of this handbook and in Harmathy [2].

Summary

The use of numerical methods for the calculation of the fire resistance of various structural members is gaining acceptance. One of the main inputs needed in these models is the material properties at elevated temperatures. The thermal and mechanical properties of most materials change substantially within the temperature range associated with building fires.

Even to date, there is lack of adequate knowledge of the behavior of many building materials at elevated temperatures. Although there is sufficient information available for some materials, such as normal-strength concrete and steel, there is a complete lack of information on certain properties for widely used materials, such as wood, insulation, and so on. Often, traditional materials are being modified (e.g., high-strength concrete) to enhance their properties at room temperatures without giving due consideration to elevated temperatures. In many cases, these modifications will cause the properties to deteriorate at elevated temperatures and introduce additional complexities, such as spalling in HSC.

In the field of fire science, applied materials research faces numerous difficulties. At elevated temperatures, many building materials undergo physicochemical changes. Most of the properties are temperature dependent and sensitive to testing method parameters such as heating rate, strain rate, temperature gradient, and so on. One positive note is that in the last two decades, there has been significant progress in developing measurement techniques and commercial instruments for measuring the properties. This will likely lead to further research in establishing material properties.

The review on material properties provided in this chapter is a broad outline of the available information. Additional details related to specific conditions on which these properties are developed can be found in cited references. Also, when using the material properties presented in this chapter, due consideration should be given to the material composition and other characteristics, such as fire and loading, because the properties at elevated temperatures depend on a number of factors.

Disclaimer Certain commercial products are identified in this paper in order to adequately specify the experimental procedure. In no case does such identification imply

recommendations or endorsement by the authors, nor does it imply that the product or material identified is the best available for the purpose.

Nomenclature

a	Material constant, dimensionless
b	Constant, characteristic of pore geometry, dimensionless
c	Specific heat ($J \cdot kg^{-1} \cdot K^{-1}$)
$\overline{c}$	Specific heat for a mixture of reactants and solid products ($J \cdot kg^{-1} \cdot K^{-1}$)
E	Modulus of elasticity (Pa)
h	Enthalpy ($J \cdot kg^{-1}$)
Δh	Latent heat associated with a "reaction" ($J \cdot kg^{-1}$)
ΔH_c	Activation energy for creep ($J \cdot kmol^{-1}$)
k	Thermal conductivity ($W \cdot m^{-1} \cdot K^{-1}$)
L_v	Heat of gasification of wood
ℓ	Dimension (m)
$\Delta \ell$	$\ell - \ell_0$
m	Exponent, dimensionless
M	Mass (kg)
n	Material constant, dimensionless
P	Porosity ($m^3 \cdot m^{-3}$)
q_n	Net heat flux to char front
R	Gas constant (8315 $J \cdot kmol^{-1} \cdot K^{-1}$)
S	Specific surface area ($m^2.m^{-3}$)
t	Time (h)
T	Temperature (K or °C)
v	Volume fraction ($m^{-3}.m^3$)
w	Mass fraction ($kg \cdot kg^{-1}$)
Z	Zener-Hollomon parameter (h^{-1})

Greek Letters

α	Thermal diffusivity
β	Coefficient of linear thermal expansion ($m \cdot m^{-1}$)
γ	Expression defined by Equation 9.3, dimensionless
β_0	Charring rate (mm/min)
δ	Characteristic pore size (m)
ε	Emissivity of pores, dimensionless
ε	Strain (deformation) ($m \cdot m^{-1}$)
ε_{t0}	Creep parameter ($m \cdot m^{-1}$)
$\dot{\varepsilon}_{ts}$	Rate of secondary creep ($m.m^{-1} \cdot h^{-1}$)
θ	Temperature-compensated time (h)
ξ	Reaction progress variable, dimensionless
π	Material property (any)
ρ	Density ($kg \cdot m^{-3}$)
σ	Stress; strength (Pa)
σ	Stefan-Boltzmann constant (5.67×10^{-8} $W \cdot m^{-2} \cdot K^{-4}$)

Subscripts

g	Glass transient (temperature)
a	Of air
I	Of the ith constituent
p	At constant pressure
s	Of the solid matrix
t	True
t	Time-dependent (creep)
T	At temperature T
u	Ultimate
y	Yield
0	Original value, at reference temperature

References

1. T.Z. Harmathy, *Technical Paper No. 242,* National Research Council of Canada, Ottawa (1967).
2. T.Z. Harmathy, *Fire Safety Design and Concrete,* Longman Scientific and Technical, Harlow, UK (1993).
3. D.A.G. Bruggeman, *Physik. Zeitschr.,* 37, p. 906 (1936).
4. R.L. Hamilton and O.K. Crosser, *Industrial & Engineering Chemistry Fundamentals,* 7, p. 187 (1962).
5. J.C. Maxwell, *A Treatise on Electricity and Magnetism,* 3rd ed., 1, Clarendon Press, Oxford, UK (1904).
6. T.Z. Harmathy, *Journal of Materials,* 5, p. 47 (1970).
7. T.Z. Harmathy, *DBR Paper No. 1080, NRCC 20956,* National Research Council of Canada, Ottawa (1983).
8. V.K.R. Kodur and M.M.S. Dwaikat, "Effect of high temperature creep on fire response of restrained steel beams", J. of Materials and Structures, 43, 10, pp. 1327–1341 (2010)
9. J.E. Dorn, *Journal of the Mechanics and Physics of Solids,* 3, p. 85 (1954).
10. T.Z. Harmathy, in *ASTM STP422,* American Society for Testing and Materials, Philadelphia (1967).
11. T.Z. Harmathy, "Trans. Am. Soc. Mech. Eng.," *Journal of Basic Engineering,* 89, p. 496 (1967).

12. C. Zener and J.H. Hollomon, *Journal of Applied Physics,* 15, p. 22 (1944).
13. F.H. Wittmann (ed.), *Fundamental Research on Creep and Shrinkage of Concrete,* Martinus Nijhoff, The Hague, Netherlands (1982).
14. Y. Anderberg and S. Thelandersson, *Bulletin 54,* Lund Institute of Technology, Lund, Sweden (1976).
15. U. Schneider, *Fire and Materials,* 1, p. 103 (1976).
16. T.Z. Harmathy, *Journal of the American Concrete Institute,* 65, 959 (1968).
17. *951 Thermogravimetric Analyzer (TGA),* DuPont Instruments, Wilmington, DE (1977).
18. T.T. Lie and V.K.R. Kodur, "Thermal and Mechanical Properties of Steel Fibre-Reinforced Concrete at Elevated Temperatures," *Canadian Journal of Civil Engineering,* 23, p. 4 (1996).
19. ASTM Test Method C135 ± 86, *2007 Annual Book of ASTM Standards,* 15.01, American Society for Testing and Materials, Philadelphia (2007).
20. T.Z. Harmathy and L.W. Allen, *Journal of the American Concrete Institute,* 70, p. 132 (1973).
21. *910 Differential Scanning Calorimeter (DSC),* DuPont Instruments, Wilmington, DE (1977).
22. J.H. Perry (ed.), *Chemical Engineers' Handbook,* 3rd ed., McGraw-Hill, New York (1950).
23. W. Eitel, *Thermochemical Methods in Silicate Investigation,* Rutgers University, New Brunswick, Canada (1952).
24. T.Z. Harmathy, *Industrial & Engineering Chemistry Fundamentals,* 8, p. 92 (1969).
25. D.A. DeVries, in *Problems Relating to Thermal Conductivity,* Bulletin de l'Institut International du Froid, Annexe 1952–1, Louvain, Belgique, p. 115 (1952).
26. W.D. Kingery, *Introduction to Ceramics,* John Wiley and Sons, New York (1960).
27. T.T. Lie and V.K.R. Kodur, "Thermal Properties of Fibre-Reinforced Concrete at Elevated Temperatures," *IR 683,* IRC, National Research Council of Canada, Ottawa (1995).
28. *Thermal Conductivity Meter (TC-31), Instruction Manual,* Kyoto Electronics Manufacturing Co. Ltd., Tokyo, Japan (1993).
29. ASCE, "Structural Fire Protection: Manual of Practice," No. 78, American Society of Civil Engineers, New York (1993).
30. L.T. Phan, "Fire Performance of High-Strength Concrete: A Report of the State-of-the-Art," National Institute of Standards and Technology, Gaithersburg, MD (1996).
31. U. Danielsen, "Marine Concrete Structures Exposed to Hydrocarbon Fires," Report, SINTEF—The Norwegian Fire Research Institute, Trondheim, Norway (1997).
32. V.K.R. Kodur and M.A. Sultan, "Structural Behaviour of High Strength Concrete Columns Exposed to Fire," *Proceedings, International Symposium on High Performance and Reactive Powder Concrete,* Concrete Canada, Sherbrooke, Canada (1998).
33. U. Diederichs, U.M. Jumppanen, and U. Schneider, "High Temperature Properties and Spalling Behaviour of High Strength Concrete," in *Proceedings of Fourth Weimar Workshop on High Performance Concrete,* HAB, Weimar, Germany (1995).
34. Y. Anderberg, "Spalling Phenomenon of HPC and OC," in *International Workshop on Fire Performance of High Strength Concrete, NIST SP 919,* NIST, Gaithersburg, MD (1997).
35. Z.P. Bazant, "Analysis of Pore Pressure, Thermal Stress and Fracture in Rapidly Heated Concrete," in *International Workshop on Fire Performance of High Strength Concrete, NIST SP 919,* NIST, Gaithersburg, MD (1997).
36. A.N. Noumowe, P. Clastres, G. Debicki, and J.-L. Costaz, "Thermal Stresses and Water Vapor Pressure of High Performance Concrete at High Temperature," *Proceedings, Fourth International Symposium on Utilization of High-Strength/High-Performance Concrete,* Paris, France (1996).
37. J.A. Purkiss, *Fire Safety Engineering Design of Structures,* Butterworth Heinemann, Bodmin, Cornwall, UK (1996).
38. E.L. Schaffer, "Charring Rate of Selected Woods—Transverse to Grain," *FPL 69,* U.S. Department of Agriculture, Forest Service, Forest Products Laboratory, Madison, WI (1967).
39. B.F.W. Rogowski, "Charring of Timber in Fire Tests," in *Symposium No. 3 Fire and Structural Use of Timber in Buildings,* HMSO, London (1969).
40. N. Bénichou and M.A. Sultan, "Fire Resistance of Lightweight Wood Frame Assemblies: State-of-the-Art Report," *IR 776,* IRC, National Research Council of Canada, Ottawa (1999).
41. S. Hadvig, *Charring of Wood in Building Fires—Practice, Theory, Instrumentation, Measurements,* Laboratory of Heating and Air-Conditioning, Technical University of Denmark, Lyngby, Denmark (1981).
42. E. Mikkola, "Charring of Wood," *Report 689,* Fire Technology Laboratory, Technical Research Centre of Finland, Espoo (1990).
43. *Guide for Determining the Fire Endurance of Concrete Elements, ACI-216–89,* American Concrete Institute, Detroit, MI (1989).
44. I.D. Bennetts, *Report No. MRL/PS23/81/001,* BHP Melbourne Research Laboratories, Clayton, Australia (1981).
45. U. Schneider (ed.), *Properties of Materials at High Temperatures—Concrete,* Kassel University, Kassel, Germany (1985).
46. Y. Anderberg (ed.), *Properties of Materials at High Temperatures—Steel,* Lund University, Lund, Sweden (1983).
47. F. Birch and H. Clark, *American Journal of Science,* 238, p. 542 (1940).
48. T.Z. Harmathy and W.W. Stanzak, in *ASTM STP464,* American Society for Testing and Materials, Philadelphia (1970).

49. Y. Anderberg, "Mechanical Properties of Reinforcing Steel at Elevated Temperatures," *Tekniska Meddelande,* 36, Sweden (1978).
50. "European Recommendations for the Fire Safety of Steel Structures," *European Convention for Construction Steelwork, Tech. Comm. 3,* Elsevier, New York (1983).
51. Eurocode 3, Design of steel structures, Part 1-2: General rules-structural fire design, Document CEN, European Committee for Standardization, UK (2005).
52. T. Twilt, "Stress-Strain Relationships of Reinforcing Structural Steel at Elevated Temperatures, Analysis of Various Options and European Proposal," *TNO-Rep. BI-91-015,* TNO Build. and Constr. Res., Delft, Netherlands (1991).
53. K.W. Poh, "General Stress-Strain Equation," *ASCE Journal of Materials in Civil Engineering,* Dec. (1997).
54. K.W. Poh, "Stress-Strain-Temperature Relationship for Structural Steel," *ASCE Journal of Materials in Civil Engineering*, Oct. (2001).
55. J.T. Gerlich, P.C.R. Collier, and A.H. Buchanan, "Design of Light Steel-Framed Walls for Fire Resistance," *Fire and Materials,* 20, 2 (1996).
56. G.Q. Li, S.C. Jiang, and Y.Z. Yin, "Experimental studies on the properties of constructional steel at elevated temperatures." J. Struct. Eng., 129, 12, pp. 1717–1721 (2003).
57. BS 5950, "Structural Use of Steelwork in Building," Part 8, in *Code of Practice for Fire Resistant Design,* British Standards Institution, London (2003).
58. W. Wang, L. Bing and V.K.R. Kodur, "Effect of temperature on strength and elastic modulus of high strength steel", in Press: ASCE Journal of Materials in Civil Engineering, pp. 1–24 (2012).
59. V.K.R. Kodur and W. Khaliq, "Effect of temperature on thermal and mechanical properties of steel bolts", ASCE Journal of Materials in Civil Engineering, 24, 6, pp. 765–774 (2012).
60. J.T. Gerlich, "Design of Loadbearing Light Steel Frame Walls for Fire Resistance," Fire Engineering Research Report 95/3, University of Canterbury, New Zealand (1995).
61. P. Makelainen and K. Miller, *Mechanical Properties of Cold-Formed Galvanized Sheet Steel Z32 at Elevated Temperatures,* Helsinki University of Technology, Finland (1983).
62. F. Alfawakhiri, M.A. Sultan, and D.H. MacKinnon, "Fire Resistance of Loadbearing Steel-Stud Walls Protected with Gypsum Board: A Review," *Fire Technology,* 35, 4 (1999).
63. T.Z. Harmathy and J.E. Berndt, *Journal of the American Concrete Institute,* 63, p. 93 (1966).
64. C.R. Cruz, *Journal, PCA Research and Development Laboratories,* 8, p. 37 (1966).
65. M.S. Abrams, in *ACI SP 25,* American Concrete Institute, Detroit, MI (1971).
66. C.R. Cruz, *Journal, PCA Research and Development Laboratories,* 10, p. 36 (1968).
67. J.C. MareÂchal, in *ACI SP 34,* American Concrete Institute, Detroit, MI (1972).
68. H. Gross, *Nuclear Engineering and Design,* 32, p. 129 (1975).
69. U. Schneider, U. Diedrichs, W. Rosenberger, and R. Weiss, *Sonderforschungsbereich 148,* Arbeitsbericht 1978–1980, Teil II, B 3, Technical University of Braunschweig, Germany (1980).
70. U. Diederichs and U. Schneider, "Bond Strength at High Temperatures," *Magazine of Concrete Research,* 33, 115, pp. 75–84 (1981).
71. V.K.R. Kodur, "Fibre-Reinforced Concrete for Enhancing the Structural Fire Resistance of Columns," ACI-SP (2000).
72. A. Bilodeau, V.M. Malhotra, and G.C. Hoff, "Hydrocarbon Fire Resistance of High Strength Normal Weight and Light Weight Concrete Incorporating Polypropylene Fibres," in *Proceedings, International Symposium on High Performance and Reactive Powder Concrete,* Sherbrooke, Canada (1998).
73. V.K.R. Kodur and T.T. Lie, "Fire Resistance of Fibre-Reinforced Concrete," in *Fibre Reinforced Concrete: Present and the Future,* Canadian Society of Civil Engineers, Montreal (1997).
74. U.-M. Jumppanen, U. Diederichs, and K. Heinrichsmeyer, "Materials Properties of F-Concrete at High Temperatures," *VTT Research Report No. 452,* Technical Research Centre of Finland, Espoo (1986).
75. J.A. Purkiss, "Steel Fibre-Reinforced Concrete at Elevated Temperatures," *International Journal of Cement Composites and Light Weight Concrete,* 6, 3 (1984).
76. T.T. Lie and V.K.R. Kodur, "Effect of Temperature on Thermal and Mechanical Properties of Steel Fibre-Reinforced Concrete," *IR 695, IRC,* National Research Council of Canada, Ottawa (1995).
77. V.K.R. Kodur and R. McGrath, "Effect of Silica Fume and Confinement on Fire Performance of High Strength Concrete Columns," *Canadian Journal of Civil Engineering*, p. 24 (2006).
78. F.P. Cheng, V.K.R. Kodur, and T.C. Wang, "Stress-Strain Curves for High Strength Concrete at Elevated Temperatures," *ASCE Journal of Materials Engineering*, 16, 1, pp. 84–90 (2004).
79. V.K.R. Kodur, T.C. Wang, and F.P. Cheng, "Predicting the Fire Resistance Behaviour of High Strength Concrete Columns," *Cements and Concrete Composites Journal*, 26, 2, pp. 141–153 (2003).
80. V.K.R. Kodur and M.A. Sultan, "Thermal Properties of High Strength Concrete at Elevated Temperatures," *CANMET-ACI-JCI International Conference, ACI SP-170,* Tokushima, Japan, American Concrete Institute, Detroit, MI (1998).
81. V.K.R. Kodur and M.A. Sultan, "Effect of Temperature on Thermal Properties of High Strength

Concrete," *ASCE Journal of Materials in Civil Engineering*, 15, 8, pp. 101–108 (2003).
82. V.K.R. Kodur and W. Khaliq, "Effect of temperature on thermal properties of different types of high strength concrete", ASCE Journal of Materials in Civil Engineering, 23, 6, pp. 793–801 (2011).
83. V.K.R. Kodur, "Spalling in High Strength Concrete Exposed to Fire—Concerns, Causes, Critical Parameters and Cures," in *Proceedings: ASCE Structures Congress,* Philadelphia (2000).
84. V.K.R. Kodur, "Guidelines for Fire Resistance Design of High Strength Concrete Columns," *Journal of Fire Protection Engineering*, 15, 2, pp. 93–106 (2005).
85. J.W. McBurney and C.E. Lovewell, *ASTM—Proceedings of the Thirty-Sixth Annual Meeting,* Vol. 33 (II), American Society for Testing and Materials, Detroit, MI, p. 636 (1933).
86. *Wood Handbook: Wood as an Engineering Material,* Agriculture Handbook No. 72, Forest Products Laboratory, U.S. Government Printing Office, Washington, DC (1974).
87. C.C. Gerhards, *Wood & Fiber,* 14, p. 4 (1981).
88. E.L. Schaffer, *Wood & Fiber,* 9, p. 145 (1977).
89. E.L. Schaffer, *Research Paper FPL 450,* U.S. Department of Agriculture, Forest Products Lab., Madison, WI (1984).
90. "Structural Fire Design," Part 1.2, in *Eurocode 5,* CEN, Brussels, Belgium (1995).
91. F.F. Wangaard, Section 29, in *Engineering Materials Handbook (*C.L. Mantell, ed.), McGraw-Hill, New York (1958).
92. V.K.R. Kodur, J. Fike, R. Fike, and M. Tabaddoor, "Factors governing fire resistance of engineered wood I-joists", Proceedings of the Seventh International Conference on Structures in Fire, Zurich, Switzerland, pp. 417–426 (2012).
93. V.K.R. Kodur and D. Baingo, "Fire Resistance of FRP Reinforced Concrete Slabs," *IR 758,* IRC, National Research Council of Canada, Ottawa (1998).
94. V.K.R. Kodur, "Fire Resistance Requirements for FRP Structural Members," *Proceedings—Vol I, 1999 CSCE Annual Conference,* Canadian Society of Civil Engineers, Regina, Saskatchewan (1999).
95. T.S. Gates, "Effects of Elevated Temperature on the Viscoelastic Modeling of Graphite/Polymeric Composites," *NASA Technical Memorandum 104160,* NASA, Langley Research Center, Hampton, VA (1991).
96. Y.C. Wang and V.K.R. Kodur, "Variation of Strength and Stiffness of Fibre Reinforced Polymer Reinforcing Bars with Temperature," *Cement and Concrete Composites*, 27, pp. 864–874 (2005).
97. SK. Foster, "High Temperature Residual Performance of Externally-Bonded FRP Systems for Concrete," *MSc Thesis*, Kingston, Canada, Department of Civil Engineering, Queen's University (2006).
98. A. Katz and N. Berman, "Modeling the Effect of High Temperature on the Bond of FRP Reinforcing Bars to Concrete," *Cement and Concrete Composites Journal*, 22, pp. 433–443 (2000).
99. A. Katz, N. Berman, and L.C. Bank, "Effect of High Temperature on the Bond Strength of FRP Rebars," *Journal of Composites for Construction,* 3, 2, pp. 73–81 (1999).
100. A. Sumida, T. Fujisaki, K. Watanabe, and T. Kato, "Heat Resistance of Continuous Fiber Reinforced Plastic Rods," *Proceedings, Fifth Annual Symposium on Fibre-Reinforced-Plastic Reinforcement for Concrete Structures*, Thomas Telford, London, pp. 557–565 (2001).
101. N. Galati, B. Vollintine, A. Nanni, L.R. Dharani, and M.A. Aiello, "Thermal Effects on Bond Between FRP Rebars and Concrete," *Proceedings, Advanced Polymer Composites for Structural Applications in Construction,* Woodhead Publishing Ltd., Cambridge, UK, pp. 501–508 (2004).
102. V.R. Kodur, L.A. Bisby, and M.F. Green, "Experimental Evaluation of the Fire Behavior of Fibre-Reinforced-Polymer-Strengthened Reinforced Concrete Columns," *Fire Safety Journal, 41, 7, pp. 547–557* (2005).
103. V.R. Kodur and L.A. Bisby, "Evaluation of Fire Endurance of Concrete Slabs Reinforced with FRP Bars," *ASCE Journal of Structural Engineering*, 131, 1, pp. 34–43 (2005).
104. Y.C. Wang, P.M.H. Wong, and V.K.R. Kodur, "An Experimental Study of Mechanical Properties of FRP and Steel Reinforcing Bars at Elevated Temperatures," *Composite Structures*, 80, 1, pp. 131–140 (2007).
105. B. Yu, and V.K.R. Kodur, "Effect of Temperature on Strength and Stiffness Properties of Near-Surface Mounted FRP Reinforcement," *Journal of Composites*, Part B: Engineering, 58, pp. 510–517 (2014).
106. T.Z. Harmathy, in *ASTM STP301,* American Society for Testing and Materials, Philadelphia (1961).
107. R.R. West and W.J. Sutton, *Journal of the American Ceramic Society,* 37, p. 221 (1954).
108. P. Ljunggren, *Journal of the American Ceramic Society,* 43, p. 227 (1960).
109. M.A. Sultan, "A Model for Predicting Heat Transfer Through Noninsulated Unloaded Steel-Stud Gypsum Board Wall Assemblies Exposed to Fire," *Fire Technology,* 32, 3 (1996).
110. "Gypsum Board: Typical Mechanical and Physical Properties," *GA-235–98,* Gypsum Association, Washington, DC (1998).

111. M.A. Sultan, "Effect of Insulation in the Wall Cavity on the Fire Resistance Rating of Full-Scale Asymmetrical (1 × 2) Gypsum Board Protected Wall Assemblies," in *Proceedings of the International Conference on Fire Research and Engineering, Orlando, FL,* SFPE, Boston (1995).
112. A.H. Buchanan, *Structural Design for Fire Safety*, John Wiley & Sons Ltd., Chichester, UK (2002).
113. V.K.R. Kodur, M. Dwaikat and R. Fike, "High-temperature properties of steel for fire resistance modeling of structures," Journal of Materials in Civil Engineering, 22, 5, pp. 423–434 (2010).
114. V.K.R. Kodur and A. Shakya, "Effect of temperature on thermal properties of fire insulation", *Fire Safety Journal*, 61, pp. 314–323 (2013).
115. S. Park, S.L. Manzello, D.P. Bentz, and T. Mizukami, "Determining thermal properties of gypsum board at elevated temperatures", Fire and Materials (2009).

V.K.R. Kodur is a Professor in the department of Civil and Environmental Engineering and also serves as Director of the Center on Structural Fire Safety and Diagnostics at the Michigan State University (MSU). Dr. Kodur's research has focused on the evaluation of fire resistance of structural systems through large scale fire experiments and numerical modelling; characterization of materials under high temperature; and non-linear design and analysis of structural systems. He is a Fellow of the Canadian Academy of Engineering, a Foreign Fellow of Indian National Academy of Engineering and Fellow of ASCE, ACI and SEI. He is an Associate Editor of Journal of Structural Engineering, Chairman of ACI Fire Protection Committee, and Chairman of ASCE-29 (Fire) Standards Committee.

T.Z. Harmathy was head of the Fire Research Section, Institute of Research in Construction, National Research Council of Canada, until his retirement in 1988. His research centered on materials science and the spread potential of compartment fires.

Chemical Kinetics and Fire

10

Gregory T. Linteris and John F. Griffiths

Introduction

The purpose of this chapter is to set out the principles of chemical kinetics as they apply to combustion in flames and fires. Chemical equilibrium, which was discussed in a previous chapter, deals with the final preferred state of a given set of reactants after an infinite time has passed. In contrast, chemical kinetics deals with the rate at which the system proceeds to the equilibrium state, i.e., the specific participating chemical reactions and their rates. Chemical equilibrium and chemical kinetics are related in that the thermodynamic, equilibrium state provides the driving force for chemical reaction. The material in this chapter is covered briefly; more detailed descriptions can be found in chemistry [1] and combustion [2–4] text books, upon which much of the material is based.

The foundations of chemical kinetics have validity in gas, liquid or solid phases, but for fires, the gas phase has the greatest relevance because the main heat release normally occurs during flaming combustion. The role of solid- and liquid-phase chemical kinetics in fires is discussed in Chap. 7. Similarly, smoldering combustion is a surface combustion process and the chemical kinetic description is closely related to that of pyrolyzing materials. The specialized fields of propellants, explosives, and material synthesis also require solid-phase chemical kinetic descriptions, but these are beyond the scope of the present chapter. Nonetheless, many of the fundamental principles of chemical kinetics discussed here are relevant regardless of the phase of the reacting system.

Gas-phase chemical kinetics is of interest in fires for many reasons. The heat release in a fire typically occurs in the gas phase, and is responsible for the gas-phase temperature field, and hence the heat flux to the burning materials (a feedback loop which controls the fuel supply rate in the fire, and hence the geometric growth in fire size with time). Some fundamental fire phenomena, such as ignition and extinction, are clearly controlled by the gas-phase chemical kinetics. Fire suppression is controlled by the rates of chemical reaction, both for the relatively inert agents (e.g., CO_2, water) which reduce the temperature (and hence overall reaction rate) to the point of extinction, and for chemically acting agents (e.g., CF_3Br and hydrofluorocarbons) which interfere with the normal chemistry of the fuels with air. Similarly, the action of the most commonly used fire retardants in polymers is controlled by their gas-phase chemical behavior. In general, chemical reaction rates must be fast enough to match the local residence time for transport (either convective or diffusive); if not, the flame will extinguish.

The formation of soot, the major radiating species from fire plumes, is controlled by gas-phase chemical kinetics, as is the formation

G.T. Linteris (✉)
National Institute of Standards and Technology,
100 Bureau Dr. Stop 8665; Gaithersburg, MD, 20899

J.F. Griffiths
University of Leeds, School of Chemistry, Leeds,
LS2 9JT UK

M.J. Hurley (ed.), *SFPE Handbook of Fire Protection Engineering*,
DOI 10.1007/978-1-4939-2565-0_10, © Society of Fire Protection Engineers 2016

of CO, which is the major toxic compound responsible for fire deaths. In fires, the formation of other toxic compounds, for example of HCN, as well as environmental pollutants (polycyclic aromatic hydrocarbons, dioxins, etc.) is controlled by the chemical kinetics of reactions occurring in the gas-phase. Clearly, understanding chemical kinetics is central to controlling unwanted fires and their deleterious effects. It is of great value if the Fire Scientist can answer the question: "Is the process at hand controlled by the rate of chemical reactions or by some other physical process?" The goal of the present chapter is to provide some fundament materials for approaching such a question.

The reaction of a fuel (for example methane) with air to products can be represented by an expression such as:

$$CH_4 + 2O_2 \rightarrow CO_2 + H_2O \qquad (10.1)$$

which is an example of a global (or overall) reaction. While reaction (10.1) shows the reactants and products, it does not represent the detailed chemical interactions which actually occur. Rather, the conversion of CH_4 to CO_2 and H_2O is a multi-step process involving many species and many reactions. A more complete representation might include some intermediate species along the path:

$$CH_4 \rightarrow \bullet CH_3 \rightarrow CH_2O \rightarrow \bullet CHO \rightarrow CO \rightarrow CO_2, \qquad (10.2)$$

but again, the details are missing.

Figure 10.1 shows reaction pathways for a premixed methane-air flame (initial pressure P_0 and temperature T_0 of 1 bar and 298 K). The

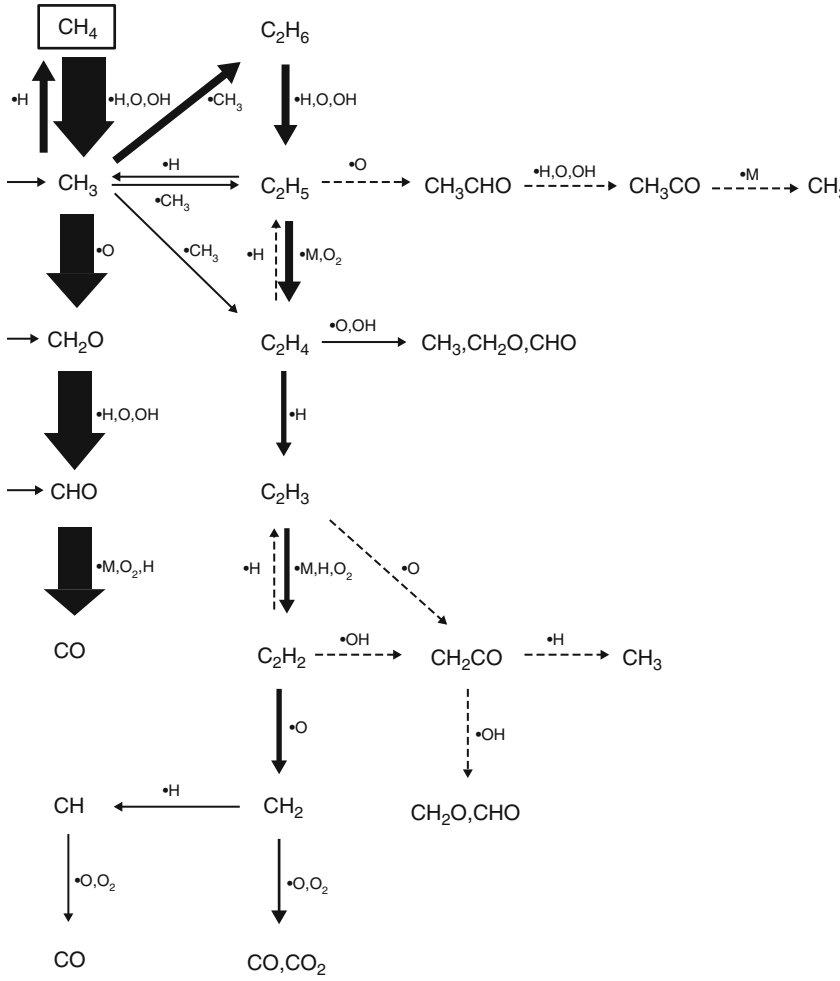

Fig. 10.1 Reaction pathway analysis for premixed stoichiometric methane-air flame (From [5])

arrows connect the initial, intermediate, and product species for the major reaction steps involved in the consumption of methane. For each species in the figure, the major reactants and products are at the ends of the arrows, while participating reaction partners are listed next to the arrow. The thickness of the arrows indicates the fraction of the total reaction flux which proceeds through that particular reaction path (normalized, in this case, by the total reaction rate of CH_4.) The purpose of such a figure is to provide not only detailed knowledge of the important steps in the consumption of a reactant, but also to provide a heuristic understanding of the general features of the chemical system. For example, Fig. 10.2 shows the chemical reaction pathways for methane in the same configuration (a premixed laminar flame), but at a different fuel-air ratio, in this case, fuel rich. In Fig. 10.1, the decomposition of methane proceeds mostly through the sequence shown in Equation 10.2, with the molecule oxidized to smaller and smaller fragments. In contrast, Fig. 10.2 shows that under rich conditions, reaction of CH_3 proceeds largely through its reaction with other CH_3 molecules, in pyrolysis reactions which tend to form larger molecules, and finally, acetylene C_2H_2, which is a precursor for soot.

Pictures such as those in Figs. 10.1 and 10.2 are very useful tools for understanding the role of chemistry in the physical behavior of combustion systems. Indeed, the widespread availability of numerical codes for performing the simulations, chemical databases for the mechanisms, and fast computers have made such simulations integral design tools in many chemical and engineering fields. These include the design of propulsion devices (gas turbines, diesel and spark ignition

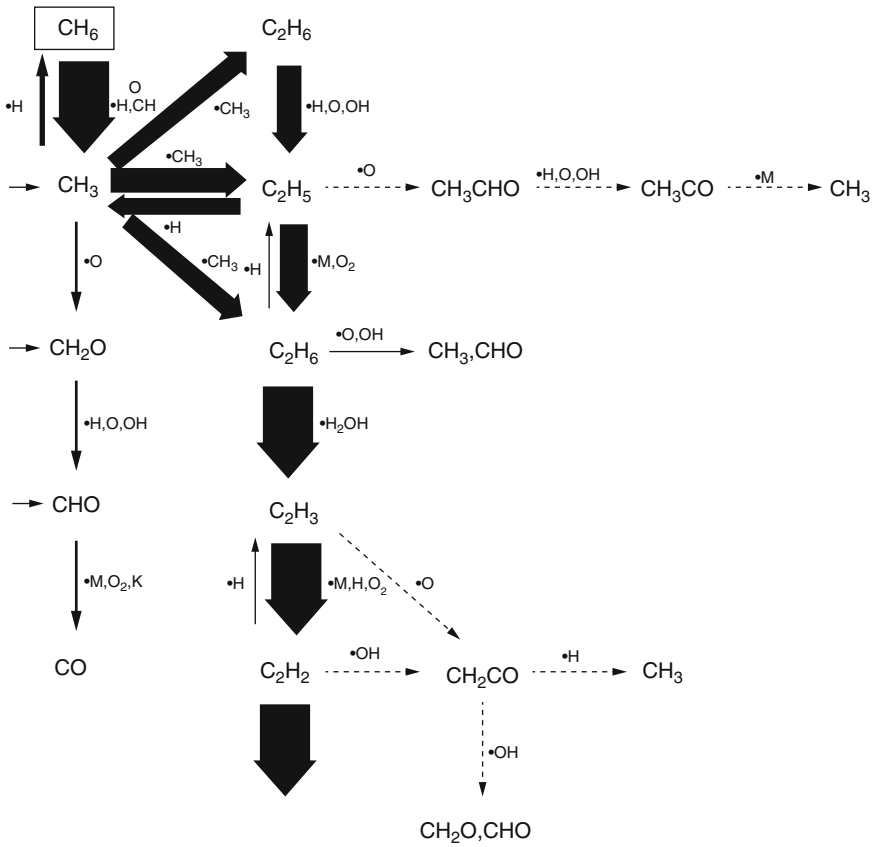

Fig. 10.2 Reaction pathway analysis for premixed fuel-rich methane-air flame (From [5])

engines, etc.) and new power plants and incinerators, particularly in regard to understanding the efficiency and pollutant formation. In fire safety, detailed chemical kinetic descriptions are primarily used in research. As computer models, kinetic mechanisms, and computer speed all improve, however, the contributions of chemical kinetics to the understanding of fire safety will increase, as it has in other fields.

A reaction mechanism (such as that used to produce the reaction pathway analyses in Figs. 10.1 and 10.2) starts with a list of species believed to be participating in chemical reactions for the physical system and conditions of interest. Thermodynamic properties of the species are required, as are the rates of the reaction of each species with all others in the list, and the temperature and pressure dependence on the rates of reaction. The development of such mechanism, and validation of the mechanisms, is a time-consuming and arduous task. Fortunately, there are many combustion and chemical kinetics researchers worldwide working in this area [6–9]. The databases are constantly in development, and versions are freely available, as discussed below. The remainder of this chapter describes the fundamental concepts used in developing chemical mechanisms, and some examples of their application.

Fundamentals

Radical Reactions

In a combustion system, the consumption of a fuel molecule (and its decomposition products) is driven largely by attack from radicals. A radical (or free radical) is an atom, molecule, or ion with one or more unpaired electron or an open shell configuration. A radical can be formed by breaking the bond of a stable molecule, for example due to a high-energy collision: $CH_4 + M => \cdot CH_3 + \cdot H + M$. In this reaction, M (discussed further below) represents any other molecule in the system which can act as a collision partner with CH_4, and thereby supply the energy to break the C-H bond. In this case, the fragments, ·H and $\cdot CH_3$, are radicals. The unpaired electron is typically shown by "·". Radicals tend to be highly reactive, and are responsible for promoting the chemistry occurring in combustion systems. The unpaired electron in a radical attacks bonds in stable molecules, leading to their decomposition. The energy barrier in radical reactions tends to be very low, which is why their reactions are so fast.

In high-temperature gaseous combustion systems, the equilibrium concentration of radicals increases with temperature, and peak radical concentrations can be quite high, with a volume fraction on the order of 1 % in the primary reaction zone of premixed flames. While this number may appear low, recall that radicals are highly reactive: their concentrations do not build up higher because they are consumed so fast.

Typical radicals in combustion are: ·H, ·O·, ·OH, ·CH, $\cdot C_2$, $\cdot CH_2$, ·CHO, $\cdot CH_3$, ·R, etc. Here, ·R denotes any hydrocarbon molecule with an unpaired electron at one site. For example, ·R can be $\cdot CH_3$, $\cdot C_2H_5$, $\cdot C_3H_7$, for the methyl, ethyl, and propyl radicals, formed by the abstraction (removal) of H atom from CH_4, C_2H_6, and C_3H_8. In these cases, the stable molecules can also be represented generically as RH; for example: $C_2H_6 + OH \rightarrow C_2H_5\cdot + H_2O$, which can be written as $RH + OH \rightarrow R\cdot + H_2O$.

In the context of combustion kinetics, explosive behavior corresponds to extremely rapid reaction. There are two types of explosive behavior: thermal explosions, and chain branched explosions. The former is due to temperature rise, while the latter is due to an exponential build-up in radical concentrations. In combustion, the radical pool refers to the chain-carrying radicals which are involved in the branching reactions, for example H, OH, O, and HO_2. It often takes time for this pool to develop, which leads to an induction time for ignition (also called the ignition delay). The buildup, maintenance, and decay of the radical pool in combustion is determined by the relative rates of the production and destruction of radicals, and relies upon certain key branching steps in the reactions scheme, as described below.

The typical steps of radical chain reactions, *initiation*, *propagation*, *branching*, and *termination*, are described here in the context of ignition of H_2/O_2 systems (following Ref. [2]). The initial radicals required to start the process come from the breaking of a bond of a stable molecule (either thermally through collisional energy transfer, or through photolytic interactions, for example in the presence of UV light). Since the bond strengths of most stable molecules relevant to combustion systems tend to be high, the process is slow (photolytic bond breaking is typically unimportant in combustion).

Initiation steps, for example reaction 10.3 in Table 10.1, are those in which two reactive radicals are formed from stable species. *Propagation steps* (reaction 10.4) involve radicals, changing the type, but not the total number of radicals. These reactions tend to have very low activation energies, and hence are very fast. Propagation steps are mostly responsible for the consumption of the fuel and its decomposition products in combustion system. Chain *branching* steps (e.g., reaction 10.6) increase the number of radicals, and hence are responsible for the explosive growth in the radical concentration, which leads to rapid reaction in the system as a whole. *Termination* steps reduce the number of radicals, and thereby shut down the overall combustion. Reaction 10.7, while it technically is a propagation step, is usually thought of as a termination step because at low temperatures the radical HO_2• is relatively unreactive, and its fate is often to be destroyed at walls (as in the reconciling of the explosion limits of the H_2–O_2 system [2–4]). In reaction 10.7, a non-reacting third body (M) takes away energy from the radical-radical combination. In this example, after the reaction of H• + O_2, HO_2• would have too much energy stay together (since it is a relatively small molecule and cannot absorb the energy in vibrational or rotational modes of energy storage). Another example of such a three-body termination reaction is: H + H + M → H_2 + M, which is important in flames. Reaction 10.8 represents the destruction of a radical without another interacting gas molecule (for example through radical quenching at a wall), which can be very important in many situations where solid surfaces are available to the gas-phase reactants. Although it looks as if reaction 10.5 is a propagation step (because there is no increase in the number of unpaired electrons) this is classified as a chain branching reaction since the number of active reaction chains has been multiplied.

There is another class of overall termination steps: the gas-phase catalytic cycles involving flame inhibitors such as FeO, HBr, and HOPO. These catalytic cycles serve to reduce radical concentrations in flames, and are discussed in more detail below.

Table 10.1 Radical reactions important in H_2/O_2 ignition

Initiation	$H_2 + O_2 \rightarrow 2OH\bullet$	(10.3)
Propagation	$OH\bullet + H_2 \rightarrow H_2O + H\bullet$	(10.4)
Branching	$\bullet O\bullet + H_2 \rightarrow OH\bullet + H\bullet$	(10.5)
	$H\bullet + O_2 \rightarrow OH\bullet + O\bullet$	(10.6)
Termination	$H\bullet + O_2 + M \rightarrow \bullet HO_2 + M$	(10.7)
	$H\bullet \rightarrow \frac{1}{2}H_2$	(10.8)

Law of Mass Action

The rate of disappearance of a reactant is generally proportional to the concentrations of participating reactants. For an arbitrary chemical reaction:

$$A + B \rightarrow \text{products}, \tag{10.9}$$

the proportionality is represented by the Law of Mass Action:

$$\frac{d[A]}{dt} = \dot{\omega}_A = -k[A]^1[B]^1 \tag{10.10}$$

Here, the brackets denote concentration (for example with units of mol cm^{-3}), $d[A]/dt$ is the rate of change in the concentration of A with time (t), and k is a proportionality constant. This expression was phenomenologically developed, based on empirical results, but there is a theoretical basis for it. Molecules of A and B must collide to react. Their collision rate depends upon their concentrations (which depend upon the total concentration via the ideal gas law and their volume fraction). Today, k is known as the

specific reaction rate constant (or often just the rate constant). The magnitude of k is usually a function only of temperature, and that dependence is often significant.

Note that the concentration C of species i, C_i, or $[i]$ can be expressed as $C_i = X_i \cdot C_T$, where the total concentration is given by the ideal gas law

$$C_T = \frac{N_T}{V} = \frac{P}{RT} \tag{10.11}$$

in which N_T is the total number of moles in the volume, V, at the given pressure P and temperature T, and R is the universal gas constant (8.314 J mol^{-1} K^{-1}) The mole fraction X_i (known also as the volume fraction), is

$$X_i = \frac{N_i}{N_T} = \frac{N_i}{\sum_i N_i} \tag{10.12}$$

in which N_i is the number of moles of species i, and the summation is over all species in the system.

Global vs. Elementary Rates

The Law of Mass Action can be written for either *global* or *elementary* reactions. An example of a *global reaction* (also called a *net reaction* or *overall reaction*) is

$$2H_2 + O_2 \rightarrow 2H_2O \tag{10.13}$$

in which 2 moles of hydrogen reacts with 1 mole of oxygen to form 2 moles of water; the Law of Mass Action would be:

$$-\frac{d[O_2]}{dt} = -\frac{\frac{1}{2}d[H_2]}{dt} = \frac{d[H_2O]}{dt} = k_G[H_2]^n[O_2]^m \tag{10.14}$$

where k_G is the global rate coefficient, n is the reaction order with respect to H_2, m is the order with respect to O_2, and $m + n$ is the overall order. Note that a distinction is made on the left hand side of the equation between reactant removal and product formation. Reaction 10.13 with 10.14 describe what happens to the reactants globally. Relations such as these are typically obtained experimentally, and are valid only for that experiment and the range of conditions from which it was developed. The expressions are usually complex; the empirical reactions orders are typically not integers, can be negative, and depend upon time and the reaction conditions. Extrapolation to other experimental conditions can be unreliable or incorrect.

Note that reaction 10.13 is not believed to actually occur; detailed experiments have shown that on the molecular level, two molecules of hydrogen do not collide with one molecule of oxygen to form two molecules of water. In contrast, elementary reactions, such as

$$OH + H_2 \rightarrow H_2O + H \tag{10.15}$$

are believed to represent an actual interaction between molecules: an OH molecule collides with an H_2 molecule, and (if there is sufficient energy involved in the collision) they react to form one H_2O molecule and an H atom. The Law of Mass Action for this elementary reaction would be:

$$\frac{d[H_2]}{dt} = -k_{15}[OH]^1[H_2]^1 \tag{10.16}$$

and the specific reaction rate constant k_{15} describes the probability of reaction. The dependence (i.e. reaction order) on the concentrations of H and OH (1 in this example) are the molecularity with respect to that reactant, and the overall molecularity is the sum of individual molecularities of the reactants. Generally, for elementary reactions, the determination of reaction orders is easy: they correspond to the molecularities.

An overall reaction such as reaction 10.13 is the result of a large number of elementary reactions. For example the reaction of hydrogen and oxygen, in a simple but satisfactory form, can be described through a sequence of reactions involving about 8 species and 40 reactions; that for methane 30 species and 400 reactions, and hexane, 450 species 1500 reactions.

Comprehensive representations of mechanisms for the combustion of hydrocarbon fuels run into many hundreds of species involved in many

thousands of reactions, the complexity increasing with their size or the number of compounds in the fuel mixture [6]. Describing a chemical system in terms of elementary reactions is a difficult and time consuming task, but has many advantages. The reaction order of elementary reactions is constant (does not change with system or conditions, as the global orders might), and the specific reaction rate constant varies only with temperature; hence, the rate expressions should be valid over a wider range of conditions than those of one-step global reactions.

Type of Reactions

There are three types of elementary reactions actually observed in gaseous combustion systems: *unimolecular*, *bimolecular*, and *termolecular* (depending upon the number of species involved).

Bimolecular Reactions

Bimolecular reactions are those given by

$$A + B \rightarrow C \tag{10.17}$$

or

$$A + B \rightarrow C + D \tag{10.18}$$

with

$$\frac{d[A]}{dt} = \dot{\omega}_A = -k[A]^1[B]^1 \tag{10.19}$$

These are the most common types of reactions; the molecularity is one for each reactant and two overall (a so-called *second-order reaction*). Common examples would be $H + H_2O \rightarrow OH + H_2$, $CO + OH \rightarrow CO_2 + H$, or $C_4H_{10} + \cdot OH \rightarrow \cdot C_4H_9 + H_2O$. This last reaction is called an *abstraction reaction* because the ·OH radical abstracts a hydrogen atom from the butane molecule.

Unimolecular Reactions

Unimolecular reactions are given by

$$A \rightarrow B \text{ or } A \rightarrow B + C \tag{10.20}$$

with

$$\frac{d[A]}{dt} = -k_{uni}[A]^1 \tag{10.21}$$

Some bimolecular reactions behave as though they were unimolecular. For example, in the bimolecular reaction 10.17 above, $A + B \rightarrow$ products, if the concentration of B is present in large excess as compared to A, its concentration will not change appreciably, so the rate expression Equation 10.19 would be:

$$\frac{d[A]}{dt} = -k_{eff}[A]^1 \tag{10.22}$$

in which the effective rate constant is determined by $k_{eff} = k[B]^1$. Hence, this second-order reaction is pseudo-first order in A.

A special example of a pseudo first-order reaction is the decomposition of the butyl radical $\cdot C_4H_9$ (formed after abstraction of a hydrogen atom from C_4H_{10}) after a collision with another molecule M:

$$\cdot C_4H_9 + M \rightarrow C_3H_6 + CH_3 + M \tag{10.23}$$

The collision partner M, represents any other molecule in the system. It is called a chaperone molecule or a third body (as in reaction 10.7). Conceptually, its role is to provide the energy needed (via a collision) to break the necessary bonds in reactions 10.23, but it does not otherwise participate in the reaction. In reaction 10.7, it serves the opposite role: to carry away the excess energy resulting from the joining of two free radicals.

The role of M can be recognized in the following way. Reaction 10.23 constitutes the breaking of a C–C bond. In order for this to happen it is necessary for sufficient energy to be accumulated at the appropriate part of the $C_4H_9\cdot$ radical. The energy required is approximately equal to the bond dissociation energy (see Chap. 5). $C_4H_9\cdot$ is able to gain the necessary thermal energy via kinetic energy transfer from another species during a collision. So M can be any molecule in the system and the concentration [M] represents the total concentration of species in the system.

As a result of this special function of "M" the order of reaction 10.23 can vary, with k_{eff} showing a complex experimental dependence

on concentration. The reaction is second order overall at low concentrations of species in the system (signifying low pressures), which arises from a first order dependence with respect to both the reactant, $C_4H_9\cdot$ and M, e.g.

$$\frac{d[C_4H_9\cdot]}{dt} = -k_0[C_4H_9\cdot][M] \qquad (10.24)$$

where the subscript o signifies the rate constant at the low pressure limit, and represents the second order case. However, as the concentration (or pressure) of the system is raised the reaction changes to eventually achieve a first order dependence on the principal reactant and with no dependence on M, e.g.

$$\frac{d[C_4H_9\cdot]}{dt} = -k_\infty[C_4H_9\cdot], \qquad (10.25)$$

where the subscript ∞ signifies the rate constant at the high (infinite) pressure limit, and is strictly a first order rate constant. There is a complex dependence of the rate constant on concentration between the two limits, and the overall reaction order varies between 2 and 1. There are sophisticated theories applied in combustion chemistry to interpret these data, but the two limiting conditions can be derived on the basis of simple algebraic analysis as is found in chemical kinetic texts (e.g. [1]).

Termolecular Reactions

Termolecular reactions are described by

$$A + B + M \rightarrow C + M \qquad (10.26)$$

with

$$\frac{d[A]}{dt} = -k_{ter}[A]\,[B]^1[M]^1 \qquad (10.27)$$

Examples of such reactions are the radical recombination reactions $OH + H + M \rightarrow H_2O + M$ and $H + H + M \rightarrow H_2 + M$. (Note that for the latter of these reactions, a factor of two would have to be added to Equation 10.27 for the change in [H] with time, since both A and B (i.e. H) are the same. The rates of these third-order reactions are pressure dependent (each concentration in Equation 10.27 is proportional to P via Equation 10.11). Also, via Le Châtelier's principle, the equilibrium is affect by pressure since there is a change in the number of moles in reaction 10.26. Finally, the efficiency of different species as third bodies can vary substantially. For example, in the reaction $OH + H + M \rightarrow H_2O + M$, the efficiency of N_2, CO, H_2, CO_2, and H_2O, as a third body is enhanced by a factor or 1, 1.8, 2, 3.6, and 6.3 relative to N_2. These different third-body efficiencies are usually accounted for in detailed reaction mechanisms.

Units of Reaction Rate Constant

Since the derivative of the concentration with time d[A]/dt always has the units (concentration/time), but since the number of terms on the right hand side of a rate equation varies with the reaction order n (c.f. Equations 10.19, 10.21, 10.27), the units of the specific reaction rate constant k must change accordingly. The units of k are: $(\text{concentration})^{-(n-1)}\cdot s^{-1}$ (or, for example, $(\text{mol cm}^{-3})^{-(n-1)}\ s^{-1}$) which yields the units shown in Table 10.2 for reaction orders of 0 to 3.

Arrhenius Rate Expression

Specific reaction rate constants can be a strong function of temperature (and show no pressure dependence, except in the situations described above). In the late 1800s, Svante Arrhenius discovered empirically that the rate of chemical reactions is described well by an exponential

Table 10.2 Units of the rate constant for various reaction orders

Reaction order	Rate expression, single component, A	Units of k	(in cgs)
0	$d[A]/dt = k_o$	conc time^{-1}	mol cm^{-3} s^{-1}
1	$d[A]/dt = k_1[A]$	time^{-1}	s^{-1}
2	$d[A]/dt = k_2[A]^2$	conc^{-1} time^{-1}	cm^3 mol^{-1} s^{-1}
3	$d[A]/dt = k_3[A]^2[M]$	conc^{-2} time^{-1}	cm^6 mol^{-2} s^{-1}

function of temperature. The equation which bears his name is

$$k(T) = A' e^{(-E_a/RT)} \tag{10.28}$$

in which A' is the pre-exponential factor and E_a is the activation energy. Later, the pre-exponential factor A' was found, for many reactions, to have some temperature dependence, and today, a modified version of the Arrhenius equation is more commonly used:

$$k(T) = AT^b e^{(-E_a/RT)} \tag{10.29}$$

In combustion, E_a is typically given in units of kcal mol^{-1} or kJ mol^{-1}; alternatively, E_a is divided by R to give an activation temperature T_a ($= E_a/R$), with units of K.

The kinetic theory of gases has provided a theoretical basis for the modified Arrhenius equation. For a bimolecular reaction (10.18, 10.19), the reaction rate is proportional to the concentrations of reactants present. The rate constant k represents the probability of reaction, which in turn depends upon the rate of molecular collisions (embodied in the pre-exponential term AT^b). Not all collisions will have sufficient energy for reaction, however, and the exponential term describes the fraction of molecules in the gas with sufficient energy to overcome a barrier to reaction. Figure 10.3 shows the chemical potential energy diagram for a hypothetical reaction. For the forward reaction, the activation energy is $E_{a,f}$, while for the reverse reaction, it is $E_{a,r}$. For this exothermic reaction, the products have less chemical energy than the reactants (and for an adiabatic system, this difference is typically manifested as an increase in temperature of the products). The reverse reaction has a higher activation energy by an amount corresponding to the exothermicity of the forward reaction. Note that potential energy curves are shown for un-catalyzed (solid line) and catalyzed (dashed line) reactions. A catalyst does not change the energy states of the products or reactants, but lowers the effective activation energy (for both forward and reverse reaction), so the system can more rapidly achieve the equilibrium state.

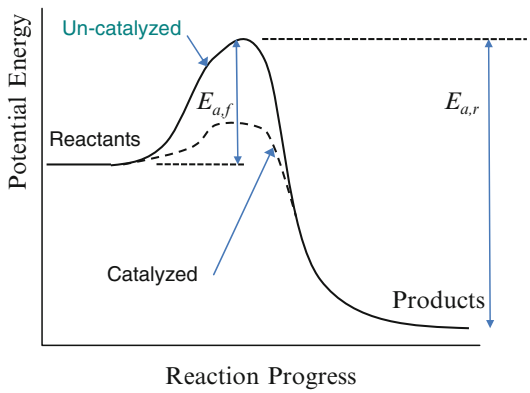

Fig. 10.3 Energy diagram for a chemical reaction

The collision term AT^b in the modified Arrhenius expression represents the frequency of collisions, times the probability of collision—the so-called steric factor, with a typical upper limit of 10^{13}–10^{14} cm^3 mol^{-1} s^{-1}. (Note that the units of AT^b are the same as those of k). Nonetheless, steric factors are often quite low, representing the need for the molecules to have the correct orientation, and have the energy in the molecule (vibrational, rotational, translational) to be distributed optimally for reaction to occur. For unimolecular reactions, A represents the vibrational energy in the molecule which leads to its decomposition. Termolecular reactions are actually two bimolecular reactions in rapid sequence; grouping them together can lead to unusual values for the A and E_a.

Effect of Temperature on Reaction Rates

The parameters for the reaction rate expression are mostly determined through, or validated in, experimental measurements in devices such as shock-tubes, static reactors, flow reactors, premixed and diffusion flames, rapid combustion machines, and combustion bombs. In determining the Arrhenius parameters experimentally, one approach, adopted very early, is to measure the reaction progress for a given set of initial reactant concentrations. By performing experiments over a range of temperatures, it is possible to construct the plot of as ln(k) vs. 1/T as in Fig. 10.4. The activation energy E_a is obtained from the negative slope of the line, while the pre-exponential (as ln (A')) is obtained from the intercept. The results

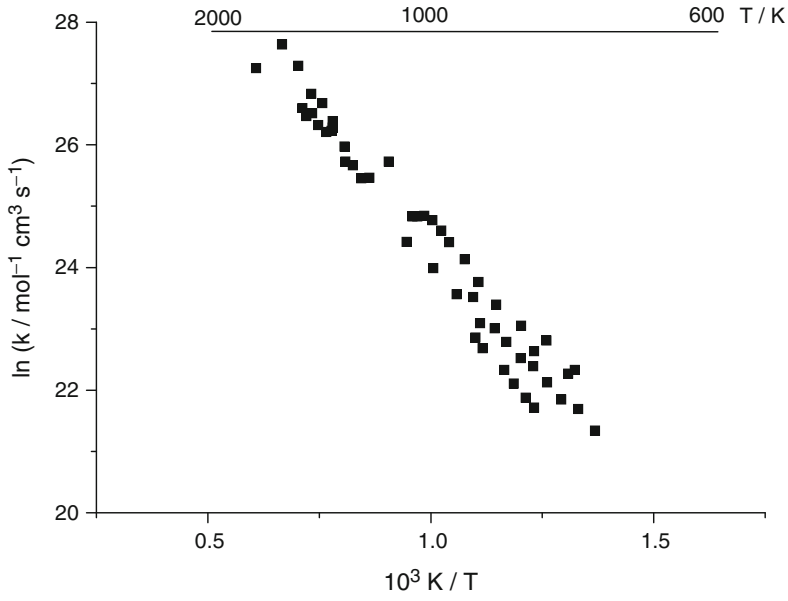

Fig. 10.4 Arrhenius plot from the experimentally determined rate constant for the reaction H + O_2

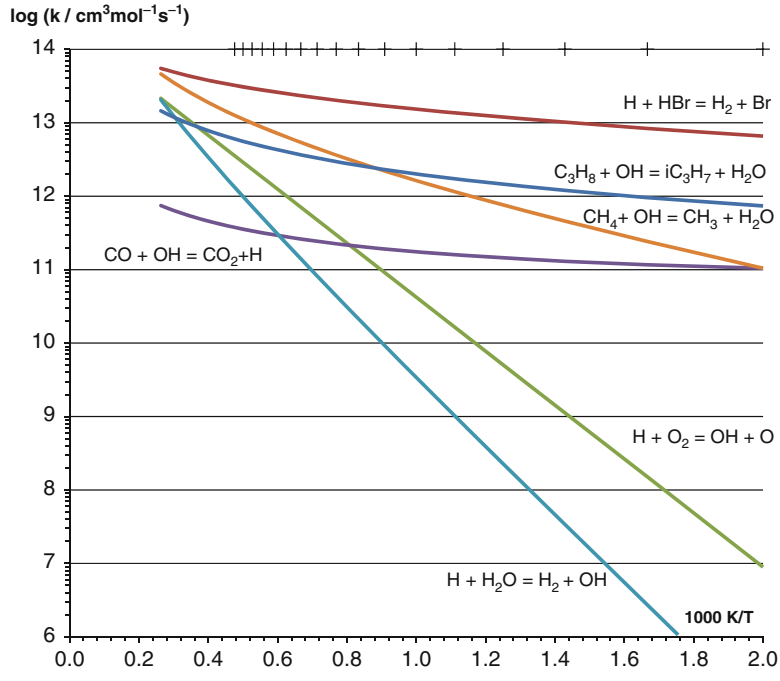

Fig. 10.5 Dependence of reaction rate constant *k* on temperature for various reactions important in combustion

presented in the figure were obtained over a very wide temperature range by many different research groups using a number of different experimental techniques.

Figure 10.5 shows the rate constant for various important reactions in combustion with data from Ref. [10]. As indicated, the reactions CO + OH → CO_2 + H and H + HBr = H_2 + Br have

very low activation energies (E/R =120 K and 290 K respectively), and show very little temperature sensitivity, typical of a radical propagation reactions. The chain-branching reaction $H + O_2 = OH + O$ has a somewhat higher temperature sensitivity (E_a/R = 9,860 K) as does the propagation reaction $H + H_2O \rightarrow H_2 + OH$ (for which the activation energy, $E_a = 82$ kJ mol^{-1}), both of which are endothermic. The lines in Fig. 10.5 that exhibit curvature require the rate constant to be interpreted over the full temperature range using the three parameter representation (Equation 10.29). Otherwise, a different activation energy would have to be applied within more restricted sections of the temperature range, as is reflected in the varying gradient.

Effect of Pressure on Reaction Rates

Pressure manifests itself primarily through its effect on concentration via the Law of Mass Action (Equation 10.10) with the ideal gas law (Equation. 10.11), and in three-body reactions (Equations. 10.26 and 10.27) which are very pressure dependent. In the context of fire, these considerations are most important with regard to the laboratory experiments used to: measure elementary rates, understand a phenomenon, or validate a chemical mechanism. For example, many reaction rates for three-body reactions are in the fall-off regime at ambient pressure. Hence, in specifying the relevant rate, pressure plays a role.

Nonetheless, in actual fires, while small pressure differences have a major effect on the flow of gases, the magnitude of pressure changes typically has little effect on combustion kinetics. Some effect of pressure may be relevant at high altitude, or in aircraft fire safety considerations. Of course, pressure rise in explosions can influence the kinetics. For typical atmospheric pressure fires, however, the limited changes in pressure have little effect on the combustion kinetics.

Important Concepts in Hydrocarbon Combustion Kinetics

Applications of combustion kinetics to fire will be illustrated in examples below.

Ignition

Ignition is defined as the initiation of combustion. Generally, this involves bringing the gas-phase reactants to the point of rapid, exothermic reaction (i.e., explosive behavior). As described above, this high rate of reaction can be induced via thermal or radical chain branching mechanisms. And these, in turn, can be induced by a spark, a local hot spot (due to a hot wire or surface), or a pilot flame. Alternatively, *spontaneous (or auto-)* ignition occurs when a fuel and air mixture, for example in a uniformly heated chamber or next to a hot surface, by itself reaches the explosive reaction conditions. Gas-phase reactions lead to increasing radical concentrations (either due to thermal or chain branching mechanisms), which eventually are high enough for sustained gas-phase flame propagation. A special category of spontaneous ignition takes place when a uniformly mixed gas mixture, at constant initial temperature, is raised instantaneously to a uniformly high temperature after passage of a shock wave, as in a shock tube experiment. This configuration, while not experienced often in fire research, is of significance since most of the experimental and calculated data on ignition delay are obtained using this technique.

In fire research however, the term "ignition" is often used in the context of the initiation of flaming combustion over a solid or liquid material. This process, while also dependent upon the behavior of the gas-phase reactants, largely involves the thermodynamic behavior of the solid material as it heats and decomposes (typically when exposed to an external infrared heat flux, for example from the hot upper layer in a

room fire). Of course, gas-phase reaction and solid material ignition are related in that the solid material ignites when: (1) it is producing gas-phase reactants fast enough, (2) the fuel molecules mix with the oxidizer gas in proportions which are within the flammability limits, and (3) the radical concentrations build up sufficiently, due to heat release, chain-branching, etc. Nonetheless, this last part of the process (ignition, by an externally imposed source, of the gas-phase reactants which are within the flammability limits) is distinctly different from the spontaneous ignition of gas-phase reactants described in the previous paragraph. For the purposes of the discussion below, when discussing "ignition", it is gas-phase spontaneous ignition (not material ignition) with which we are concerned.

Spontaneous ignition is a gas-phase chemical process well described by the detailed kinetic models described above (and below)—provided that the reaction mechanism embraces processes that are relevant to an appropriately wide range of temperatures. For example, if a reactive gas mixture is exposed to a hot surface (or container), and (for the purposes of discussion) uniformly heated, it will reach an explosive condition (i.e., rapid reaction) after some length of exposure time to the heated condition. The parameter of interest is the ignition time or ignition delay τ_{ign}, which is the time it takes for a mixture at a given temperature, to reach the state of rapid reaction. To define the ignition delay, a criterion for the condition of rapid reaction is required. Often, a characteristic temperature rise, the maximum rate of temperature (or pressure) rise, or some minimum radical concentration is used (e.g., $X_{OH} >= 10^{-4}$) is used. Figure 10.6 shows the calculated ignition delay of a stoichiometric H_2/air mixture. As indicated, the ignition delay is a strong function of the initial temperature: it drops by about three orders of magnitude as the initial temperature rises from 925 to 1025 K.

Given a comprehensive kinetic mechanism, ignition delay is readily calculated. The chemistry of homogeneous ignition is often different from that in a flame. Ignition delays are a strong function of the reactants, stoichiometry, initial

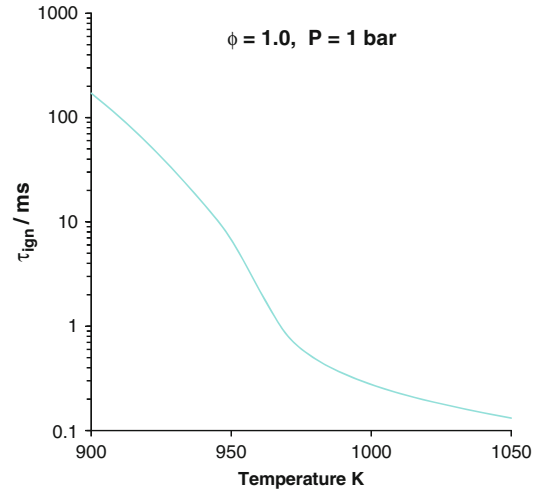

Fig. 10.6 Ignition delay of a stoichiometric H_2/air mixture as a function of initial gas temperature

temperature and pressure, and the presence of trace species. Figure 10.7 shows the H-atom volume fraction and temperature as a function of time for an H_2.air system at an initial temperature of 1000 K. As indicated, the ignition delay is about 1.6×10^{-4} s. The build-up in H radical concentration is exponential in time, and increases drastically for times greater than about 10^{-5} s. Hence, the explosive behavior is predominantly due to a chain-branching mechanism rather than thermal initiation. Some fuels decompose forming H-atoms more readily, and these promote a short ignition delay. Additives which consume H-atoms retard ignition, while those that create H-atoms accelerate ignition.

Competition Between Reactions

The macroscopic behavior in combustion systems is often determined by which of two (or more) possible reaction paths dominate. Reactions proceed in parallel, and which reaction dominates depends upon the temperature and the concentrations of reactants (which can change with time and location in the system), and the pressure. Some examples of combustion reactions in which the competition between alternate reactions are given below.

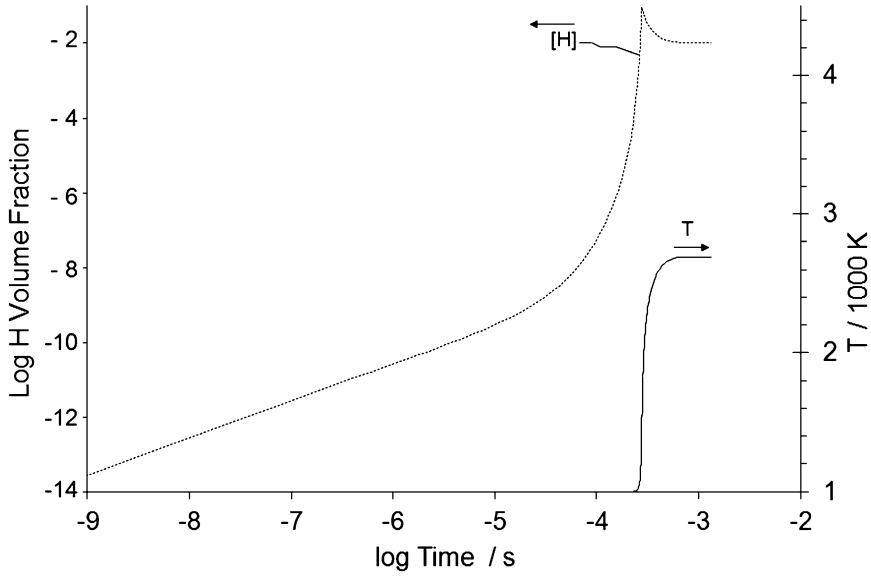

Fig. 10.7 H-atom and temperature increase with time for stoichiometric H_2/air mixture at 1000 K

Initiation Reactions: Thermal Decomposition vs. Oxidation

The homogeneous ignition above requires the buildup in radical concentrations. To get this process started, there must be radical initiation reactions. Two possible initiation routes are the dissociation reaction of H_2, reaction (10.30) and the molecular reaction between H_2 and O_2. reaction (10.31). Figure 10.8 shows the rate constants and the ratio of the rate constants for these two competing reactions. As indicated, reaction (10.31) is 4 and 9 orders of magnitude higher at 2000 K and 1000 K, respectively. Hence, for any reasonable concentration of O_2, the *rate* of the molecular reaction (10.31) (i.e., the rate constant times the relevant concentrations as in Equation 10.19) will be much higher, making it the favored initiation route.

$$H_2 + M \rightarrow H\cdot + H\cdot + M \qquad k = 6.7 \times 10^{14} e^{(-51000/T)} s^{-1} \qquad (10.30)$$

$$H_2 + O_2 \rightarrow HO_2\cdot + H\cdot \qquad k = 1.5 \times 10^{14} e^{(-28{,}500/T)} s^{-1} \qquad (10.31)$$

Relative Rates of Oxidation and Degradation of the Primary Fuel Radical

As described above, the propagation reactions are the principal means of reactant consumption through, for example,

$$RH + \cdot OH \rightarrow R\cdot + H_2O \qquad (10.32)$$

where R· represents an alkyl radical generated from an alkane (e.g. an ethyl radical (C_2H_5) from ethane (C_2H_6)). Whether or not the alkyl radical then decomposes or oxidizes depends upon the temperature and the concentration of oxygen. Consider normal undecane (n-$C_{11}H_{24}$), a component of kerosene. The undecyl radical formed from it in a reaction such as (10.32) may undergo the competitive reactions

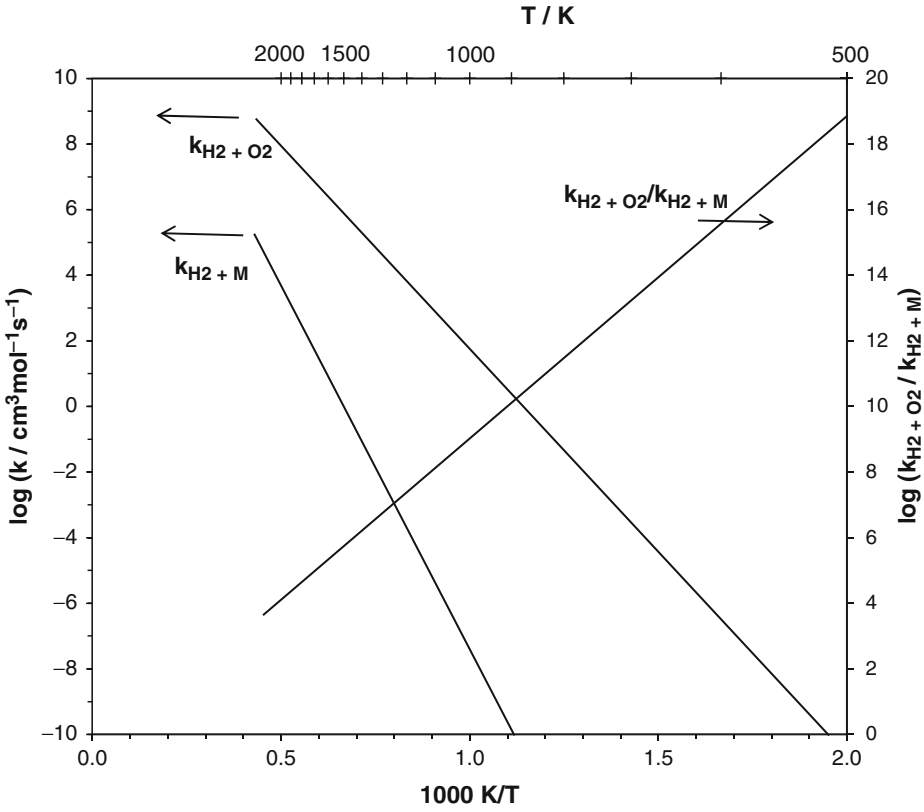

Fig. 10.8 Rate constant (*left scale*) and ratio of the rate constants (*right scale*) for $H_2 + O_2$ abstraction reaction and H_2 + M dissociation reaction, as a function of temperature (*top scale*) and inverse temperature (*bottom scale*)

$$\underset{\text{alkyl radical}}{n-C_{11}H_{23}\cdot} \rightarrow \underset{\text{alkene}}{n-C_6H_{12}} + \underset{\text{lower alkyl radical}}{n-C_5H_{11}\cdot} \qquad k = 2.5\times10^{13}e^{(-14433/T)}s^{-1} \tag{10.33}$$

$$\underset{\text{alkyl radical}}{n-C_{11}H_{23}\cdot} + O_2 \rightarrow \underset{\text{alkene}}{n-C_{11}H_{22}} + \underset{\text{hydroperoxy radical}}{HO_2\cdot} \qquad k = 1.0\times10^{12}e^{(-1000/T)}mol^{-1}cm^3s^{-1} \tag{10.34}$$

Examining the activation energy for the two competing reactions reveals that the first, the thermal decomposition route (E_a/R = 14,443 K), is very temperature sensitive, whereas the second route (E_a/R = 1,000 K), H-atom abstraction by O_2 (a radical propagation reaction), is less temperature sensitive. Figure 10.9 shows the ratio of the rate constant for the two reactions. As indicated, the relative importance of the decomposition reaction to the consumption of n-$C_{11}H_{23}$· increases at higher temperature by many orders of magnitude. To compare the rates of disappearance of the fuel radical d[n-$C_{11}H_{23}$·]/dt by the two routes, it is necessary to use Equation 10.21 and Equation 10.19 for unimolecular and bimolecular reactions, so that the ratio of rates is $\omega_{dec}/\omega_{+O2} = k_{dec}/(k_{+O2}[O_2])$ in which the concentration of [O_2] is determined

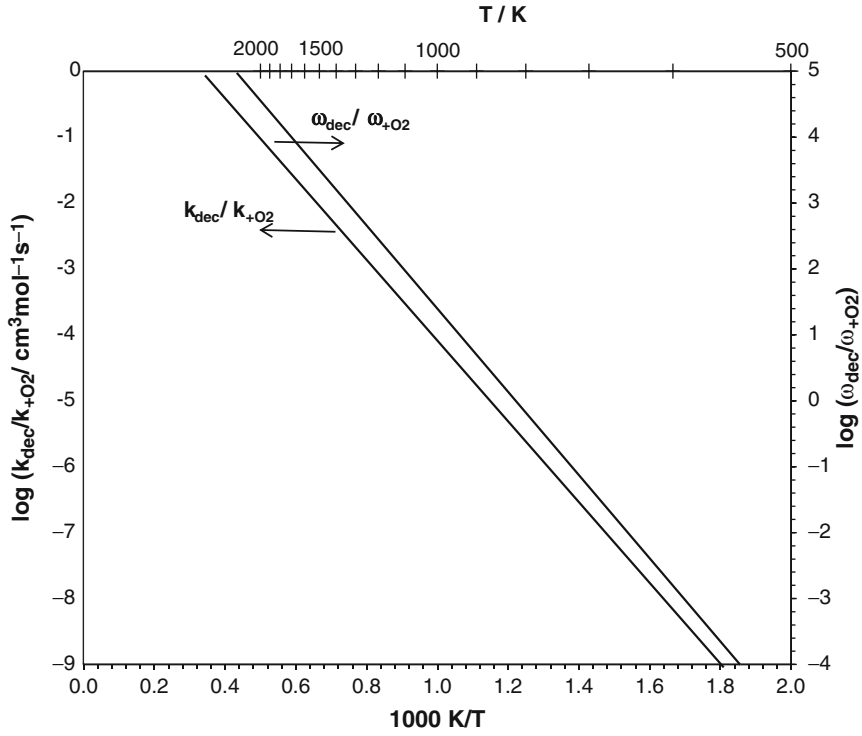

Fig. 10.9 Ratio of the rate constant (*left scale*) and reaction rate (*right scale*) for decomposition (dec) vs. H abstraction by O_2 ($+O_2$) reactions for n-$C_{11}H_{23}{}^{\circ}$, as a function of temperature (*top scale*) and inverse temperature (*bottom scale*)

at each temperature via Equations 10.11 and 10.12, with $X_{O2} = 0.21$ in air. As shown in the figure, the reaction rates are about equal at 850 K; whereas the decomposition rate is 1000 times slower at 600 K, and 1000 times faster at 1500 K, then the abstraction route.

The competition between radical abstraction and thermal decomposition reactions has several consequences. The relative rate of reaction is dependent upon the oxygen concentration, so in fuel rich conditions, thermal decomposition will be favored, leading to the build-up of small fuel radicals, and ultimately acetylene, which is a precursor for soot. Also, at temperatures below 1000 K, the combustion chemistry tends to be specific to the primary fuel structure; whereas at higher temperatures the large fuels will tend to decompose to smaller hydrocarbon fragments, so that ultimately, the important reactions for heat release all involve combustion of the same, much smaller (e.g., one- and two-carbon) hydrocarbon species. This explains why the macroscopic combustion behavior of different hydrocarbons can be very similar in flames.

Relative Rates of Reaction of OH with CO vs. Hydrocarbon

The reaction of carbon monoxide, an intermediate species in hydrocarbon-air flames, controls two of the most important features of fires. (1) Most of the heat release in a flame occurs via conversion of CO to CO_2, and (2) residual CO, the most important toxic by-product of flames (and the species responsible for most fire deaths) is often controlled by its reaction rate. As described below, the consumption of CO in flames occurs almost entirely by its reaction with OH. Hence, it is of interest to compare the rate of OH reaction with CO to that of OH reaction with other hydrocarbon species (for example, the fuel itself).

Figure 10.10 shows the reaction rate constant for OH reaction with n-C_4H_{10} or CO. As the figure indicates, the reaction of OH with n-C_4H_{10} is on the order of 140 times faster than

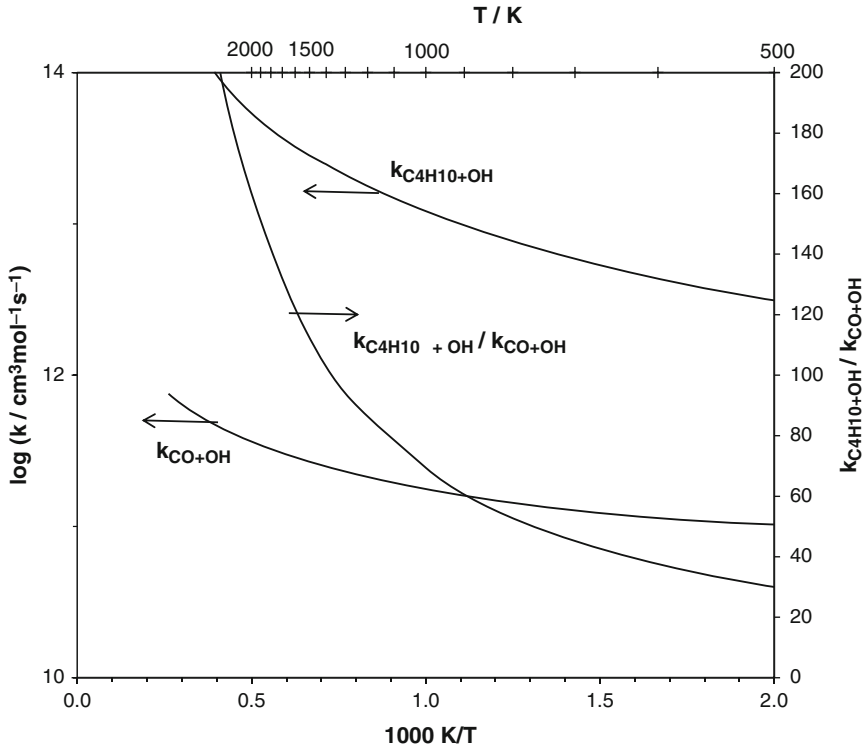

Fig. 10.10 Rate constant k (*left scale*) and ratio of rate constants (*right scale*) for reaction of OH with CO or n-C_4H_{10}, as a function of temperature (*top scale*) and inverse temperature (*bottom scale*)

its reaction with CO at 1800 K. This illustrates that in many flames, the burnout of CO will be kinetically limited until the hydrocarbon content is much lower than the CO concentration; i.e., for n-C_4H_{10} (and many other hydrocarbons) concentrations of 1/140 that of CO, the rate of consumption will be about equal. The burnout of the CO is typically the last stage of reaction sequence and occurs after the hydrocarbon is essentially gone.

H-Atom Reaction with O_2 vs. Reaction with Fuel

The reaction of $H + O_2 \rightarrow OH + O$ (reaction 10.6) is the most important chain branching reaction in combustion, and greatly increases radical concentrations in the flame. Nonetheless, as described above, reactions of hydrocarbon species with radicals (chain propagation processes such as reaction 10.32) are largely responsible for the consumption of the fuel species and its decomposition products. Hence, it is of interest to compare the rates of these two processes.

Figure 10.11 shows the rate constant (left scale) for the H-atom abstraction reaction n-$C_4H_{10} + H \rightarrow C_4H_9 + H_2$ and for the reaction the $H + O_2 \rightarrow OH + O$ (using the rate expressions: $k = 3.1 \times 10^{14}\, exp^{(-4320/T)}$ / mol^{-1}-$cm^3\ s^{-1}$; and $k = 1.99 \times 10^{14}\ exp^{(-8460/T)}$/ $mol^{-1}\ cm^3\ s^{-1}$, respectively). The ratio of the rate constants is also shown (right scale). As indicated, both reactions have a comparatively high temperature sensitivity, so they become increasingly important at high temperatures. Furthermore, the abstraction reaction is roughly 20 times faster at typical flame temperatures (1200–2000 K) and in the range of 50–1000 times faster at temperatures between 650 and 1000 K. Hence, the chain branching reaction is most influential after the hydrocarbon is consumed. This property of the kinetics has a large influence on flame structure. The regime of the

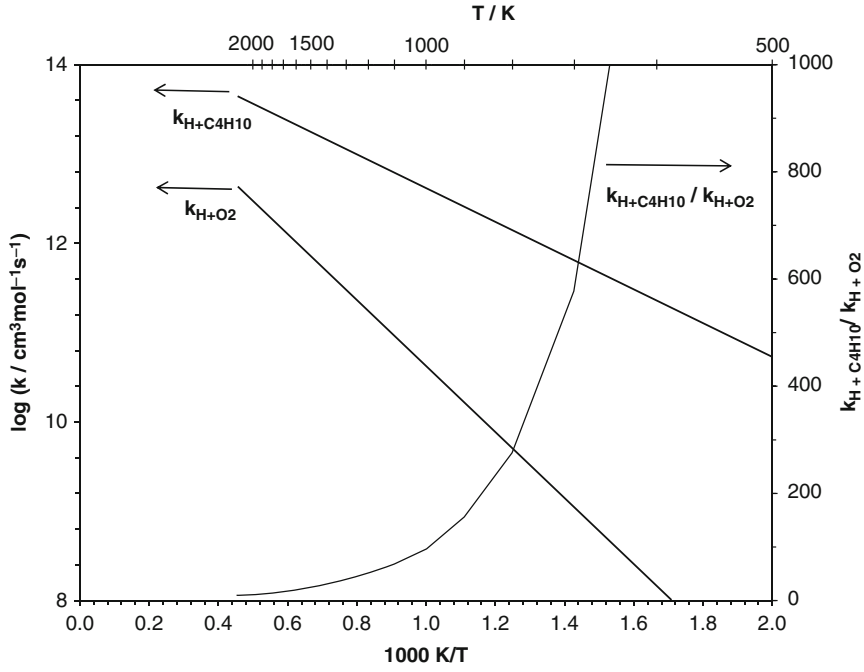

Fig. 10.11 Rate constant k (*left scale*) and ratio of rate constants (*right scale*) for reaction of H with O_2 or n-C_4H_{10}, as a function of temperature (*top scale*) and inverse temperature (*bottom scale*)

chain-branching reactions is separated, either physically or temporally, from the regime of fuel consumption, and one cannot have a large build-up in radical concentrations until the fuel species are significantly depleted. Nonetheless, in the context of spatial structure of a flame, the effect is mitigated somewhat by the diffusion of radicals (especially H atoms) which are transported to regions where they are needed for propagation reactions.

Flame Configuration/Structure Effects on Chemistry

As described above, there often exists competition between possible reaction paths in combustion systems, controlled largely by the temperature and chemical environment. The chemical environment can vary due to different initial conditions, changes with time, or the structure of the flame itself. ("Flame structure" constitutes the profile of concentrations of species, temperature, and flow velocities over space and time.) For example, in a co-flow laminar diffusion flame burner, the high-temperature reaction zone (i.e., the flame sheet) forms a conical shape around the fuel stream above the exit jet of the burner. Figure 10.12 shows of the volume fraction profiles for some of the species as a function of radial position across the high-temperature reaction zone in a cup-burner flame. The peak temperature occurs at $r = 8.5$ mm, and the concentration of O_2 and CH_4 decrease near that location. On the fuel side of the reaction zone (i.e., $r < 8.5$ mm), the species consist mostly of the fuel (CH_4) and its decomposition products (e.g., CH_3); while on the oxidizer side, the major species present are O_2 and the products of combustion (e.g., H_2O, CO_2) which are diffusing radially out from the flame. Due to diffusion, there is some mixing of species from each side. One notable feature is that the peak of the radical pool occurs on the oxidant side of the reaction zone, nearly coincident with the peak temperature.

These results can be explained as follows. First, the major chain branching reaction $H + O_2 \rightarrow OH + O$ (reaction 10.6) has a relatively high

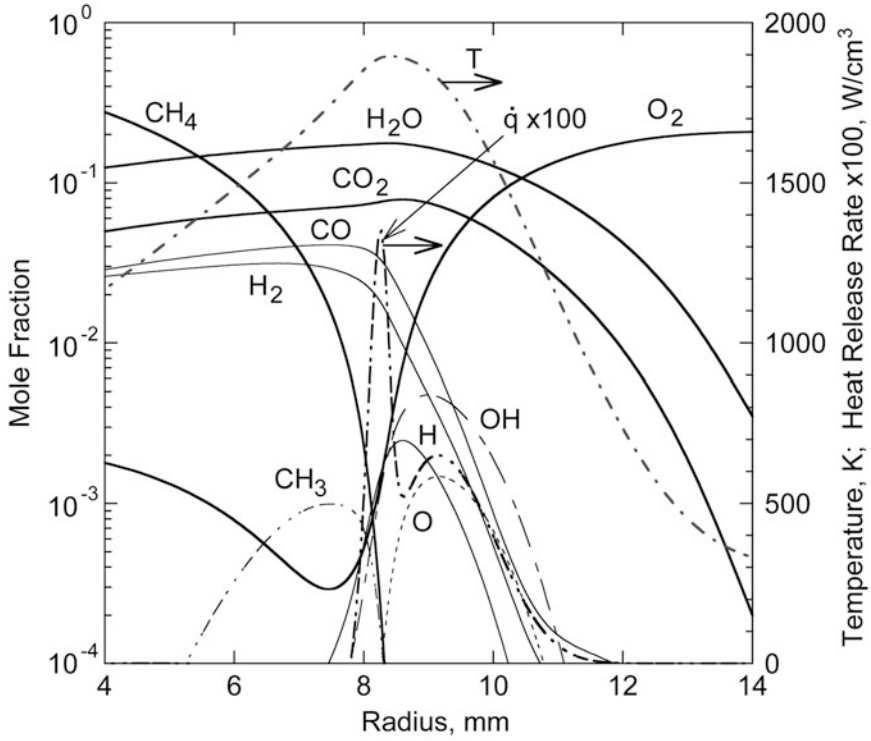

Fig. 10.12 Calculated species volume fraction, temperature, and heat release rate at a height of 11 mm above a cup-burner flame of CH_4 and air

activation energy ($E \sim 70$ kJ mol^{-1}), so its occurrence requires high temperature; but more importantly, it requires O_2, so that reaction must occur primarily on the air side of the flame. Secondly, the rate of reaction of H with CH_4 is much faster than with O_2, so reaction 10.6 cannot dominate on the fuel side. Similarly, the reaction CO + OH $\rightarrow$ CO_2 + H, which is responsible for CO consumption (as discussed above), must also be on the oxidant (air) side of the reaction zone: it needs OH, which would be consumed preferentially by the hydrocarbons on the fuel side. Since the CO + OH reaction, forming CO_2, is also responsible for a large fraction of the heat release, its location also dominates the location of the heat release and peak temperature.

The structure of a premixed flame (Fig. 10.13) also results from the hydrocarbon kinetics described above. As illustrated, the CO consumption and the peak of the chain-branching reaction 10.6 are both retarded until the CH_4 is nearly gone (since, as described above, the radicals required in both reactions react faster with CH_4). The consumption flux of CH_4 creates a dilemma: it needs both CH_4 and H, but they cannot both co-exist at high concentration because the chain-branching reactions producing H will not occur until hydrocarbons are considerably depleted. This is solved by species transport: H atoms are produced at a high rate near the peak temperature, but diffuse rapidly upstream where they are consumed by reaction with CH_4.

Super Equilibrium

Chemical equilibrium is an idealized state, which is sometimes achieved for select conditions in fires, but often is not realized in practice. In premixed and diffusion flames of hydrocarbons with air, for example, the radical pool species H, OH, and O, can achieve concentrations several orders of magnitude higher than those calculated at thermodynamic equilibrium. For example,

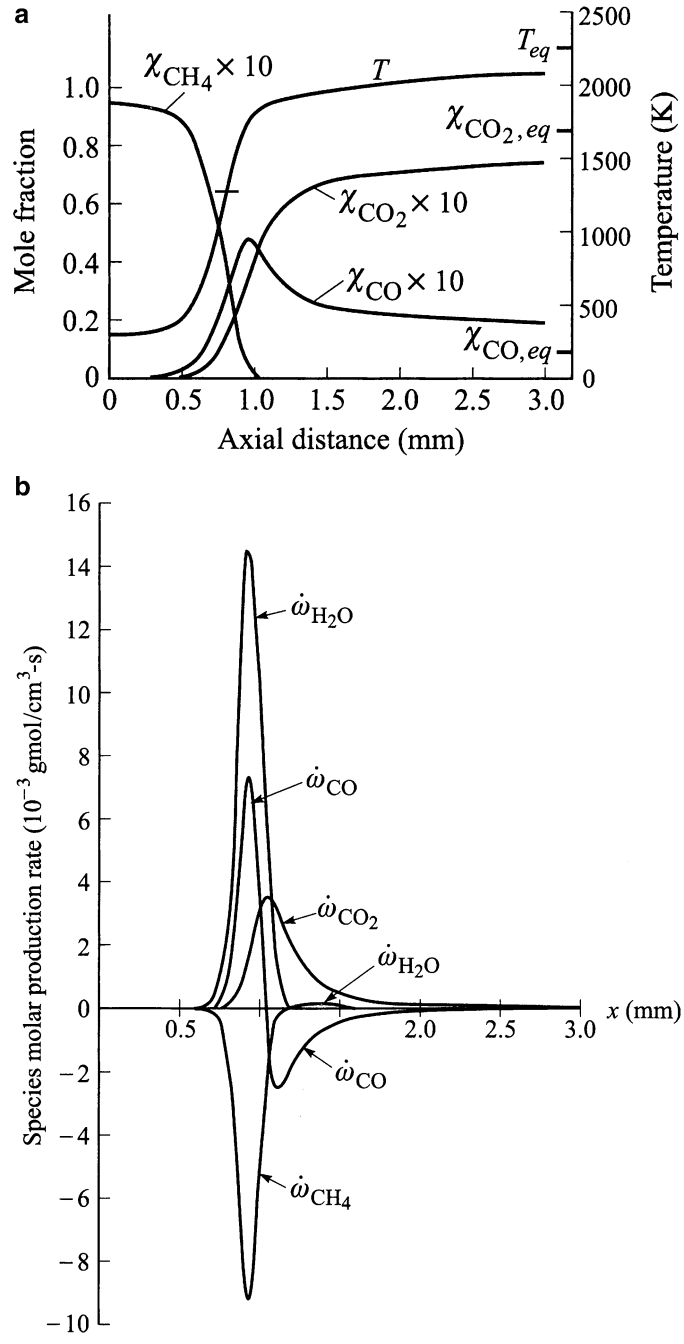

Fig. 10.13 Major species profiles and reaction fluxes for laminar premixed methane-air flame (From [3])

Fig. 10.14 shows the ratio of peak to equilibrium H-atom volume fraction in a methane-air counterflow diffusion flame; the results are plotted as a function of strain rate, which is proportional to the jet velocities of the methane and air streams forming the opposing flows in the burner. As indicated, super-equilibrium ratios range from 1 at zero strain, to 400 at a strain rate of 190 s^{-1}. The super-equilibrium concentrations occur because the reactions which form the radicals

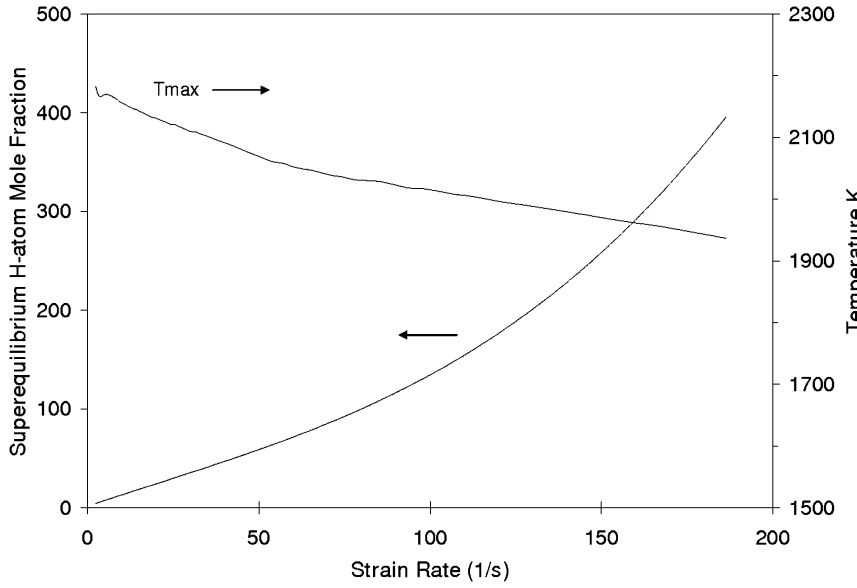

Fig. 10.14 Ratio of peak to final equilibrium H-atom volume fraction as a function of strain rate in a methane-air counterflow diffusion flame

(typically, the chain-branching reactions such as $H + O_2$ and $O + H_2$) are much faster than the reactions which recombine radicals (typically, the three-body recombination reactions such as H + OH + M). The species do not reside long enough in the main reaction zone for the recombination reaction to establish thermodynamic equilibrium at the prevailing temperature. The result is that radical pool species are present in very high concentration, leading to the rapid attack on the fuel species, and fast overall reaction. If the radicals are controlled to be closer to equilibrium levels (even at the elevated temperatures of the flames), the overall reaction rate is greatly reduced.

Premixed flames also have large superequilibrium of radicals. For example, in a stoichiometric methane-air flame, the peak volume fraction of H, O, and OH (which occur near the location of the peak of the $H + O_2$ reaction flux) are 17, 14, and 2.6 times the final equilibrium value, respectively. Note that it is generally accepted that the chemical action of fire suppressants is to decrease the peak radical concentration towards the final equilibrium level.

Role of Trace Species

There are several classic examples in combustion in which very low concentrations of reactants completely change both the route for fuel decomposition, as well as the overall rate of reaction. While they are sometime esoteric, they demonstrate the principles which are important for more practical situations.

Moisture in CO Oxidation

In early research, it was found that the oxidation rate of CO to CO_2 is highly dependent on the presence of trace quantities of water in the system. In fact, many hydrogen containing compounds (e.g., H_2, or a hydrocarbon) can supply the trace hydrogen atom necessary for the faster reaction. In the bone-dry system, the reaction of CO proceeds as follows. The initiation step

$$CO + O_2 \rightarrow CO_2 + \bullet O \bullet \qquad (10.35)$$

is slow. It is believed to be followed by

$$\bullet O \bullet + O_2 + M \rightarrow O_3 + M$$

$$O_3 + CO \rightarrow CO_2 + 2 \bullet O \bullet \quad (10.36)$$

$$CO + \bullet O \bullet + M \rightarrow CO_2 + M \quad (10.37)$$

which are all slow at combustion temperatures.

In contrast, in the presence of water, the reaction proceeds via:

$$CO + O_2 \rightarrow CO_2 + \bullet O \bullet \quad (10.38)$$

$$\bullet O \bullet + H_2O \rightarrow 2OH \bullet$$

$$CO + OH \bullet \rightarrow CO_2 + H \bullet \quad (10.39)$$

$$H \bullet + O_2 \rightarrow OH + \bullet O \bullet \quad (10.40)$$

with the subsequent build-up of the radical pool, followed by fast reaction in the system. A similar mechanism exists if H_2 is present rather than H_2O. At an H_2 content of 0.1 %, the moist reaction route accounts for about 70 % of the CO reaction. Indeed, for a premixed CO-air flame, the presence of only 2000 μL/L (ppmv) of H_2 can increase the burning velocity by factor of two.

Flame Inhibition by Iron-Containing Compounds

In early work with premixed CO-air flames, it was also found that trace contamination of the CO with iron pentacarbonyl strongly affected the reaction mechanism. It was found that iron in the high-pressure steel bottle containing the CO reacted with the CO to form $Fe(CO)_5$, which had high enough vapor pressure to enter the reactant stream (at trace quantities) with the CO. Later work showed that the iron enters into catalytic gas-phase reactions which have a very strong inhibiting effect on the build-up in the radical pool. The inhibiting effect acts similarly for all hydrocarbon flames. Indeed, it has been found that iron compound concentrations as low as 1 μL/L can reduce the burning velocity of premixed hydrocarbon-air flames by 1 %. The mechanism is as follows. The $Fe(CO)_5$ readily decomposes, via a sequence of steps, to form Fe and 5 CO:

$$Fe(CO)_5 \rightarrow Fe + 5CO. \quad (10.41)$$

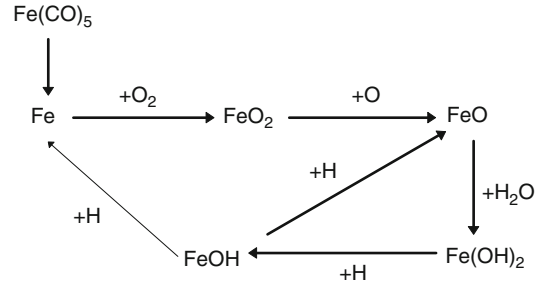

Fig. 10.15 Schematic diagram of reaction pathways of $Fe(CO)_5$ in premixed methane-air flames

This is followed by the formation of the inhibiting species FeO, $Fe(OH)_2$, and FeOH via the sequence shown in Fig. 10.15:

Once formed, the three reactions (forming a triangle on the right side of Fig. 10.15) enter into a gas-phase catalytic cycle:

$$FeO + H_2O \rightarrow Fe(OH)_2 \quad (10.42)$$
$$Fe(OH)_2 + H \bullet \rightarrow FeOH + H_2O \quad (10.43)$$
$$FeOH + H \bullet \rightarrow FeO + H_2 \quad (10.44)$$
$$\text{Net: } H \bullet + H \bullet \rightarrow H_2$$

which effectively recombines H atoms into H_2, thereby greatly reducing the radical concentrations and essentially suppressing the flame propagation chemistry. (Recall that the radicals are typically present at super-equilibrium quantities, so the effect of reactions 10.42 to 10.44 is to drive the system to equilibrium more rapidly.) In the rate constant expression Equation 10.28, the activation energy (E_a/R) for these reactions is low (0 K, 302 K, and 604) K, and the pre-exponential factor A' is high ($10^{13.2}$ s^{-1}, $10^{14.3}$ s^{-1}, and $10^{12.1}$ s^{-1}), so these reactions proceed at nearly gas-kinetic rates: that is, as fast as the molecules can collide, they react. In fact, further analysis has shown that these reactions of iron in flames approach the ideal gas-phase catalytic radical recombination rate [11].

Flame Inhibition by Bromine-Containing Compounds

Similar catalytic cycles are present for bromine added to hydrocarbon flames. For example, the

catalytic cycle of HBr in a methane-air flame can be represented by:

$$H\bullet + HBr = H_2 + Br\bullet \quad (10.45)$$
$$H\bullet + Br_2 = HBr + Br\bullet \quad (10.46)$$
$$Br\bullet + Br\bullet + M = Br_2 + M \quad (10.47)$$
$$\text{Net}: H\bullet + H\bullet \rightarrow H_2$$

The net effect of adding HBr to a flame typically is to recombine H atoms into H_2 (as in the iron mechanism above), and thereby reduce the overall reaction rate. It should be noted that in actual methane-flames, several regeneration steps for the inhibiting molecule HBr are also important, such as $CH_2O + Br\cdot = \cdot HCO + HBr$, and $CH_4 + Br\cdot = \cdot CH_3 + HBr$. These reactions contribute to cycles like reactions 10.45 to 10.47; however, they are not so easy to outline in a concise list because there are many reactions involved in the consumption of other radicals, such as $\cdot CH_3$ and ·HCO. This basic mechanism is believed to occur also during the action of other bromine-containing additives such as CF_3Br (halon 1301).

Chemical Kinetic Models

Overview

A chemical kinetic model starts with a list of species and the reactions between them. The thermodynamic data for the species are required, as are the parameters for the specific reaction rate constants of all reactions. Either the forward or reverse reaction data are required, with the equilibrium relationship usually then providing the rate parameters for the counterpart reaction.

The relevant reactions necessary for inclusion depend upon the environment, and the desired information. For example, a mixture of hydrocarbons and air would have a different chemical mechanism for understanding the atmospheric chemistry at 298 K as opposed to flame chemistry at 2000 K. In the former, only reactions prevalent at low temperature are important, whereas in the latter, high-temperature process are considered; the participating species can be different. Of course, since the reactions are elementary, they should apply to both situations, and the two mechanisms could be combined into a larger, comprehensive unit. Nonetheless, the run time of a simulation depends on the size of the chemical mechanism, so it is usually desirable to minimize the number of species (i.e., the number of variables) and reactions in a model. Selecting the right chemical model, and its complexity, are an essential first step for understanding the chemical behavior of a system. Often, one will eliminate chemistry that is not important for the present problem. For example, while the chemistry for the formation of NO_x is always occurring in high-temperature flames of hydrocarbons with air, the NO_x species are relatively trace compounds, and have a minor effect on the development and overall energetics of flames. Hence, those reactions can be eliminated if the goal of a study is to understand a feature such as the rate of heat release, rather than pollutant (i.e., NO_x) formation.

In combustion, detailed chemical kinetic models are hierarchical: a mechanism for a larger reactant will contain the entire kinetic model of each of the smaller species which are present in the larger model. The simplest kinetic model is that of the H_2/O_2 system, and this is contained in all larger mechanisms; the H_2/O_2 kinetic model is followed in complexity by those for CO, CH_2O, CH_4, and C_2H_6. As a result, a mechanism for cetane ($C_{16}H_{34}$) can have 1200 species and more than 7000 reactions [6]. Usually, each of the smaller, simpler mechanisms is experimentally validated prior to development of the next most complex model, so the reaction sets are internally consistent. Because all the mechanisms are based on elementary rates, the mechanisms should be widely applicable. Unlike the example of NO_x chemistry, the chemistry of smaller hydrocarbon species cannot be eliminated from kinetic models of larger species; rather, they are essential.

Even for a kinetic model based on elementary rates, one still needs to exercise caution in its application. The species and reaction set of a mechanism are developed for a specific range of conditions (e.g., reactant composition and

stoichiometry, flame type, temperature range, etc.). It is incumbent upon the user to understand the conditions for which the mechanism was developed, and interpret if those conditions are close enough to the condition of interest for the mechanism to be useful. An example of this is the NIST chemical kinetic mechanism for hydrofluorocarbon (HFC) inhibition of hydrocarbon flames. The mechanism was developed based on the assumption that the flame inhibitors (for example C_2HF_5) would be added in small amounts (a few percent) to hydrocarbon-air flames. Recently, it has become of interest to understand the flammability of pure refrigerants with air, as well as the reaction of flame inhibitors at very high loading. For these conditions, additional species are likely to participate, and the mechanism will need to be extended.

The important reaction pathways can sometimes be very similar for different fuels. As outlined by Warnatz [12], in combustion at high temperatures (i.e., near 2000 K), larger fuel molecules quickly break down to C_1 and C_2 species, and once these form, their decomposition pathways are similar for all hydrocarbon flames. Similarly, as outlined by Babushok and Tsang [13], the burning velocity of hydrocarbons tends to be controlled by a small set of reactions involving small decomposition products of the larger fuel molecules (and other common species such as O_2). Also, the mechanism of flame inhibition of halogenated compounds also tends to be very similar for different hydrocarbon fuels [13]. The reactions which form and destroy the radical pool are similar, so the effect of the flame inhibitors (which act to reduce radical concentrations) are also related.

Databases

There are many sources, both in publications and online, for thermodynamic data, elementary reaction rates, and comprehensive kinetic models. Some thermodynamic data can be found in [14] and [15], and reaction rate (and other) data in [6–8, 10].

Role of Gas-Phase Kinetics in Some Fire Problems

Understanding Standard Fire Tests Through Kinetic Modeling: The Cup Burner Test

The cup burner method is a standard test [16] used for specifying the amount of fire suppressant to be used in full-scale applications. In this test, a small cup (28 mm dia) holds the liquid fuel, which is supplied to the burner so as to maintain the level of the fuel to the top edge of the cup. For gaseous fuels, a fine screen distributes the low velocity gas evenly over the exit nozzle of the burner. A chimney (10 cm diameter) holds the gaseous oxidizer, which is usually air mixed with fire suppressant. By increasing the volume fraction of the fire suppressant, its extinguishing concentration is determined as the volume fraction in air at which the flame is extinguished.

As with any standard test method, there is always the question as to how the results obtained in small laboratory experiments corresponds to full-scale fires. Insight into this question can be gained by numerically modeling the test method, interpreting the controlling physics, and then comparing those with the parameters believed to be controlling at full scale. Since flame extinction is intimately connected with flame chemistry (and overall reaction rate) a good chemical kinetic description of the flame is necessary. It is possible to model cup-burner flames using direct numerical simulation, in which the momentum, energy, and species conservation equations are solved directly. Using available chemical kinetic mechanisms, the numerical calculation (2-D axi-symmetric) produces detailed information on the flame structure: i.e., the species concentrations, gas velocity and temperature, at all locations in the calculation domain, as a function of time. Using post-processing techniques on the data to generate the reactive and diffusive flux of species, and heat transfer properties of the flame, great insight can be gained (for example, Ref. [17]).

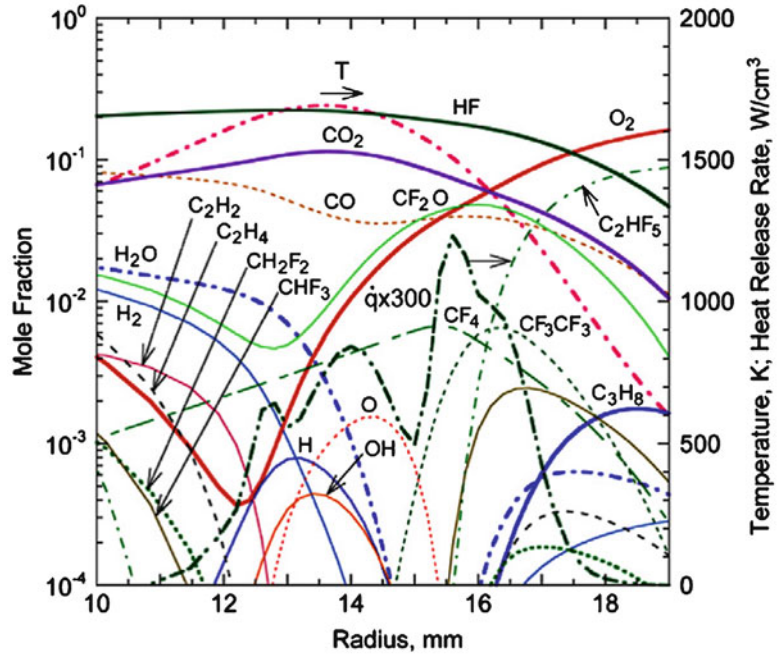

Fig. 10.16 Calculated species profiles at a height of 16 mm above a cup-burner flame of CH_4 and air, with C_2HF_5 added to the air stream at a volume fraction of 9.3 % (From [17])

Figure 10.16 show the calculated flame structure for a cup-burner flame of methane, with C_2HF_5 added to the air stream at a volume fraction just below extinguishment (0.093). Results such as these have been used to answer such questions as:

1. Why do cup-burner flames always extinguish due to flame lift-off, rather than extinction elsewhere?
2. Does a particular fires suppressant work by thermal or chemical kinetic mechanisms?
3. Does a fire suppressant in the air stream add to the heat release in cup-burner flame?
4. Why are cup-burner flames in low gravity harder to extinguish than those in normal gravity?

Analysis of cup-burner flames has shown that:

1. The flame is stabilized at the base, by a partially-premixed region which has a much higher reactivity than the rest of the flame. Addition of the fire suppressant to the air stream lowers the reactivity (either thermally or kinetically) at the flame base. The base can find a new stabilization point if it lifts off further: higher lift-off allows more time for mixing of the fuel and air streams, which leads to more premixed character and a higher reactivity. At the extinguishment agent volume fraction, further lift-off does not sufficiently increase the reactivity to overcome the loss of reactivity caused by agent addition, and the premixed flame base cannot stabilize in the flow field.
2. Simulations have shown that essentially inert agents (such as CO_2, N_2, Ar, He, etc.) act by lowering the temperature at the flame base, reduce reaction rates there, and cause lift off (as described above). For other agents (such as CF_3Br, Br_2, CF_3H, C_2HF_5, etc.) the peak temperature (as well as the temperature in the stabilization region) is actually increased with agent addition; hence, the mechanism cannot be thermal in origin. Further analysis has shown that chemical reactions at the flame base reduce radical concentrations more there than further up in the flame, causing flame extinguishment preferentially at the base.
3. By integrating the heat of reaction for all reactions over the entire calculation domain, it has been demonstrated that, for agent volume fractions just above that for extinguishment, CF_3Br reduces the total heat release, whereas C_2HF_5 increases (i.e. nearly doubles) it.

4. Fire safety in spacecraft requires an understanding of the behavior of flames in zero gravity (0-g_n). Experiments and simulations have shown that despite 0-g_n flames being much weaker, they require more fire suppressant for extinguishment. Simulations have explained this unexpected behavior. The normal-gravity (1-g_n) flames have buoyancy-induced flicker, which causes the flame base to oscillate strongly. This creates a more difficult flow field for flame base stabilization, and causes the flame to blow off earlier than it would without the flame flicker. Hence, the better-stabilized 0-g_n flames require more suppressant to lower the reaction rate at the base and cause blow-off.

The significance of the work to understand the chemical kinetic behavior of laboratory flames goes beyond the goal of understanding standard test methods. Twenty years ago, such 2-D time-dependent simulations with full chemistry were not possible, even for cup-burner flames; but today they are common. As computer speed, numerical methods, and chemical kinetic models all improve, it will not be long before such simulations with detailed chemistry are possible for the larger domains typical of fires. When that happens, the full potential of chemical kinetics for understanding fire problems will start to be realized—as has occurred in other areas of combustion.

References

1. S. Benson, The Foundations of Chemical Kinetics, McGraw-Hill, New York, 1960.
2. J. Warnatz, U. Maas, R.W. Dibble, Combustion, Springer-Verlag, Berlin, 2010.
3. S.R. Turns, An Introduction to Combustion, McGraw-Hill, Boston, 2000.
4. I. Glassman, Combustion, Academic Press, San Diego, CA, 1996.
5. J. Warnatz, in: W.C. Gardiner (Ed.), Combustion Chemistry, Springer-Verlag, New York, 1984.
6. C.K. Westbrook, Pitts, LLNL Chemical Kinetic Mechanisms for Combustion, https://www-pls.llnl.gov/?url = science_and_technology-chemistry-combustion-mechanisms, Lawrence Livermore National Laboratory, 2012.
7. C.K. Law, Law Combustion Group: Chemical Kinetic Database, Princeton University, Princeton, NJ, http://www.princeton.edu/~cklaw/kinetics/, 2012.
8. H. Wang, Available Reaction Models, University of Southern California, Los Angeles, CA; http://ignis.usc.edu/Mechanisms/Model%20release.html, 2012.
9. F.L. Dryer, Kinetic Models, Princeton University, Princeton, NJ; http://www.princeton.edu/mae/people/faculty/dryer/homepage/kinetic_models/, 2012.
10. J.A. Manion, R.E.L.R.D. Huie, D.R. Burgess, V.L. Orkin, Tsang, W.S. McGivern, V.S. Hudgens, V.D. Knyazev, D.B. Atkinson, E. Chai, A.M. Tereza, C.-Y. Lin, T.C. Allison, W.G. Mallard, F. Westley, J.T. Herron, R.F. Hampson, D.H. Frizzell, NIST Chemical Kinetics Database, NIST Standard Reference Database 17, Version 7.0 (Web Version), Release 1.4.3, Data Version 2008.12, National Institute of Standards and Technology, 2012.
11. V.I. Babushok, W. Tsang, G.T. Linteris, D. Reinelt, Combust. Flame 115 (1998) 551–560.
12. J. Warnatz, Pure and Applied Chemistry 72 (2000) 2101–2110.
13. V.I. Babushok, W. Tsang, Combust. Flame 123 (2000) 488–506.
14. A. Burcat, B. Ruscic, Third Millennium Ideal Gas and Condensed Phase Thermochemical Database for Combustion With Updates From Active Thermochemical Tables, ANL-05/20 and TAE 960 Technion-IIT; ftp://ftp.technion.ac.il/pub/supported/aetdd/thermodynamics/BURCAT.THR, Argonne National Laboratory, 2012.
15. in: P.J. Linstrom, W.G. Mallard (Eds.), NIST Chemistry WebBook, NIST Standard Reference Database Number 69, National Institute of Standards and Technology, Gaithersburg MD, 20899 (http://webbook.nist.gov), 2001.
16. NFPA 2001 Standard on Clean Agent Fire Extinguishing Systems 2008 Edition, NFPA, 2007.
17. F. Takahashi, G.T. Linteris, V.R. Katta, O. Meier, Proc. Combust. Inst. 34 (2012) 2707–2717.

Gregory T. Linteris is a mechanical engineer in the Flammability Reduction Group of the Fire Research Division of the Engineering Laboratory at the National Institute of Standards and Technology. Dr. Linteris is a project leader for research on material flammability in the Flammability Reduction Group. He also conducts research to understand the detailed mechanisms of chemically acting fire suppressants. In 1997, Dr. Linteris served as a payload specialist astronaut on two NASA space shuttle missions, conducting microgravity combustion, fluid mechanics and material science experiments while in earth orbit for 20 days.

John F. Griffiths is emeritus professor of combustion chemistry at the University of Leeds in the United Kingdom. His main research interest is the gas-phase combustion of hydrocarbons, which is related both to combustion hazards which may arise from spontaneous ignition processes in the chemical industry and to the efficiency of reciprocating engines.

Diffusion Flames

11

Ali S. Rangwala

Fires involve reactants, usually fuel and air, not intimately mixed at a molecular level before combustion. Usually, the fuel is in the solid or liquid state so transfer of material across a phase boundary (phase change) must also occur. The vaporized fuel must combine with oxygen from air to form a flammable mixture, which when ignited forms the flame zone. In most fire problems, this mixing of fuel vapor and oxygen takes place mostly by diffusion and takes orders of magnitude longer time compared with that of a chemical reaction. Therefore, diffusion of species is the primary controlling process during such burning behavior. A fundamental understanding of diffusion flames then involves exploring the *mechanisms* associated with the transport of the reactants and the resulting flame structure.

In Fire Protection Engineering, diffusion flame theory is used in calculating flame-length, flame-location, and rates of burning. The flame-length, is used for hazard analysis as it provides information to estimate the heat transfer to surrounding surfaces. Knowledge of flame location is necessary for suppression, and finally, the rate of burning provides an estimate of the "size" of the fire and in combination with the heat of combustion is used to calculate the heat release rate.

A.S. Rangwala (✉)
Associate Professor, Department of Fire Protection Engineering, Worcester Polytechnic Institute, 100 Institute Road, Worcester, MA 01609-2280

The Diffusion Coefficient

Diffusion is the phenomena of migration of mass. The mass can be in the form of atoms, molecules, ions, or other particles because of spatial gradient of some quantity (concentration, temperature, pressure etc.). Similar to conduction heat transfer (Fourier's law) and momentum transfer (Newton's law), mass transfer is governed by a law called as Fick's law of diffusion. In a simplified context, Fick's law of diffusion describes the movement of one chemical species A through a binary mixture of A and B because of concentration gradient of A. In most fire problems A is usually fuel vapor, oxidizer or products of combustion, while B represents air. To explain this further, let us consider the example of a candle flame shown in Fig. 11.1. The paraffin of the candle melts because of heat from the flame; it travels by capillary forces through the wick where it then evaporates to become paraffin vapor, a gaseous fuel.

Let F represent fuel vapor, O represent oxygen and P represent products. Fuel vapor will issue out of the wick because of the heat received from the flame. If one traverses along the path X-X' (shown by dashed red line in Fig. 11.1) the concentration of fuel vapor is highest at the wick and reduces until it reaches a concentration most suitable for chemical reaction with oxygen at X'. The concentrations of the various species involved, can be given by the mass fractions, Y_F, Y_O and Y_P, where Y_F denotes the mass of fuel vapor divided by the total mass of

M.J. Hurley (ed.), *SFPE Handbook of Fire Protection Engineering*,
DOI 10.1007/978-1-4939-2565-0_11, © Society of Fire Protection Engineers 2016

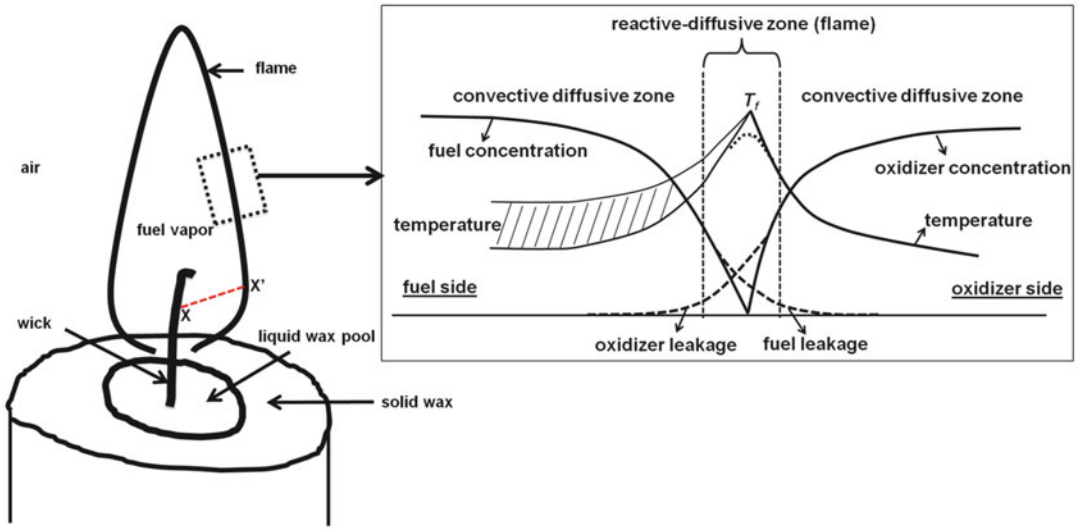

Fig. 11.1 The candle flame

gas-mixture in a given volume and the subscripts O and P denote oxidizer and products, respectively. Initially the mass fraction of F at the wick is 1 at the wick and zero just outside the wick, and this gradient drives the fuel vapor out of the wick. On approaching the flame zone, the mass fractions of the fuel and oxidizer should be such that a stoichiometric mixture should be formed. Now, Fick's law states that the mass transport of fuel vapor along XX' due to mass diffusion can be described by:

$$J_F = \rho D_{FA} \frac{Y_{F,X} - Y_{F,X'}}{XX'}. \tag{11.1}$$

J_F is the mass flow rate of fuel vapor per unit area (or mass flux) and is proportional to the mass fraction difference divided by the distance from the wick to the flame (*XX'*). ρ is the density of the gas-mixture system and D_{FA} is a proportionality factor called as the binary mass diffusivity of fuel vapor with respect to air. In differential form, Equation 11.1 can be written as:

$$J_F = -\rho D_{FA} \frac{dY_F}{dx}. \tag{11.2}$$

The negative sign denotes that the mass fraction of fuel vapor will decrease as one moves along XX', represented as x-direction. This is logical because the fuel vapor originates at the wick (location X). Equation 11.2 is also called the *Ficks law of diffusion* and forms the starting point of our discussion on diffusion flames. Note that similar relationships can be written for oxygen (diffusing towards the flame) and products of combustion (diffusing on either side of the flame).

Table 11.1 gives the binary diffusion coefficients *D* for many common gases. Values refer to atmospheric pressure. The first part of the table gives data for several gases in the presence of a large excess of air. The mass diffusivity *D*, is an important transport property such as thermal diffusivity α and momentum diffusivity (kinematic viscosity) υ, and all three have dimensions of $(\text{length})^2/\text{time}$. The ratios of these quantities, taken as a pair, form three important nondimensional numbers that play a prominent role in analyzing most fire problems. They are Prandtl number, $\text{Pr} = \upsilon/\alpha$, Schmidt number, $\text{Sc} = \upsilon/\text{D}$ and Lewis number, $\text{Le} = \alpha/\text{D}$. Equation 11.2 assumes that the driving force for diffusion is concentration gradient. However, it has been observed, as well as predicted by the kinetic theory of gases, that mass diffusion can occur in the presence of a temperature gradient and pressure gradient. Further, the value of the binary

Table 11.1 Diffusion coefficients of common gases at 0 °C, 760 mmHg. Assuming ideal gas behavior, D can be calculated for other pressures and temperatures using the relation $D \propto P^{-1}T^{3/2}$

Gas-pair	D (cm^2/s)
O_2—air	0.178
CO_2—air	0.138
H_2—air	0.611
H_2O—air	0.220
Methane (CH_4)—air	0.196
Ethane (C_2H_6)—air	0.108
Propane (C_4H_{10})—air	0.0878
Butane (C_3H_8)—air	0.0750
Pentane (C_5H_{12})—air	0.0671
n-Octane (C_8H_{18})—air	0.0505
Benzene (C_6H_6)—air	0.077
Toluene (C_7H_8)—air	0.051
Napthalene ($C_{10}H_8$)—air	0.0513
Anthracen ($C_{14}H_{10}$)—air	0.0421
Methyl alcohol (CH_3OH)—air	0.1325
Ethyl alcohol (C_2H_5OH)—air	0.102

mass diffusivity itself depends on temperature and pressure ($D \sim P^{-1}T^{3/2}$). The diffusion coefficient of common gas-mixtures at various temperatures and pressures can be obtained using this equation in combination with values listed in Table 11.1. However, this effect is usually neglected in fire problems. Further details on the subject can be found in Ref. [1].

Structure of Diffusion Flame

The zoomed inset of the part of the flame zone in Fig. 11.1 shows an illustrative sketch of the structure of a diffusion flame. It consists of a flame separating a fuel-rich zone and an oxidizer-rich zone. The flame or reaction zone incorporates the location of the maximum temperature. For example, for a methane-air flame, this temperature is experimentally observed to be around 1950 K [2]. As shown in Fig. 11.1, fuel and oxidizer both almost disappear in the flame zone, although there is some fuel and oxidizer leakage outside the designated flame zone as shown by the dashed lines. Products of combustion and heat diffuse outwards from the flame zone to both the sides. One of the characteristics of typical hydrocarbon diffusion flames is their yellowness, especially when the fuel can emit soot, and it's appearance can be explained using Fig. 11.2 [3].

The reaction zone usually has a blue emission, especially when the fuel and oxidizer have been mixed in proper proportions. This is mainly due to radiation due to excited CH radicals. The reddish glow arises from radiation from CO_2 and water vapor radiation. Most importantly, the intense yellow radiation which is a characteristic of most fires is due to the presence of carbon particles or soot. Figure 11.2a illustrates a simplified illustrative sketch of three prominent zones in a diffusion flame. Note that emphasis is given to the fuel side. The cracking zone is a region on the fuel side of the reaction zone before the soot formation zone. This where the molecules crack and polymerize forming lighter fuel molecules which chemically react with the oxygen in the reaction zone and rest convert to carbonaceous and tarry substances in a soot formation zone that exists just before the reaction zone. Soot generally forms as particles with diameters of the order of several nanometers by a process called as inception or nucleation. These particles then undergo surface growth. One mechanisms attributed to the surface growth is called as the Hydrogen Abstraction by C2H2 Addition (HACA) mechanism [6] where H-atoms impacting on the soot surface activate acetylene addition thereby increasing the mass of soot particles. The process of nucleation occurs concurrently with coagulation, where small particles coalesce to form larger primary particles, and agglomerations where multiple primary particles line up end-to-end to form larger structures resembling a string of pearls as shown in Fig. 11.2b [5]. When the soot particles pass through the flame front they oxidize whereby the mass of soot is decreased by heterogeneous surface reactions between soot particles and oxidizing species. Incandescent soot results in the

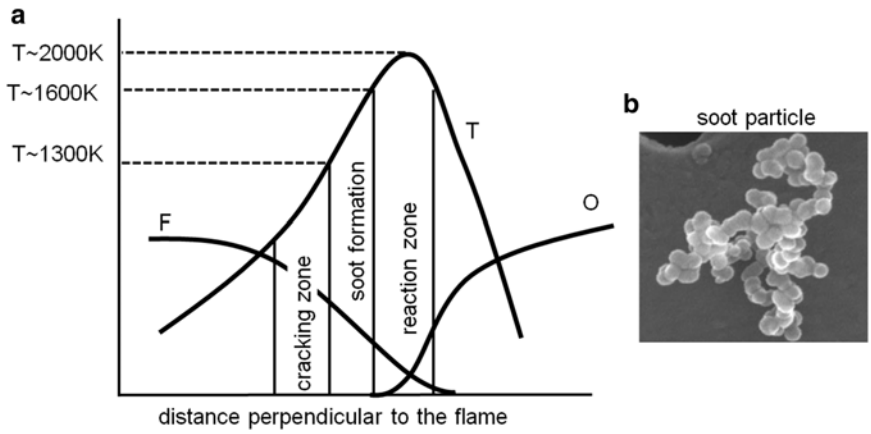

Fig. 11.2 (**a**) Zones in a diffusion flame [4] (**b**) soot particle observed under a scanning electron microscope—resemblance to string of pearls [5]

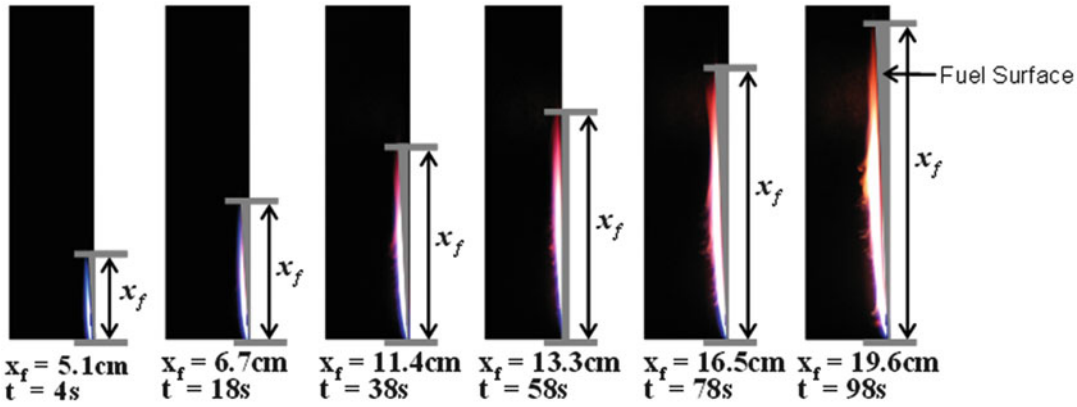

Fig. 11.3 Upward propagating flame on a PMMA surface

characteristic yellow-color of most hydrocarbon diffusion flames. The processes leading to cracking and soot formation are dependent on fuel type and ambient conditions and form an important research topic in fire safety [7–9]. This is mainly because most of the flame radiation from fires originates from soot particles. The luminous radiation from soot often makes it difficult to observe the blue emission from the reaction zone. The blue radiation is observable for small flames (less than 15 cm) as shown in Fig. 11.3 where the initial stages of a wall fire (PMMA, 1.2 cm thick, 5 cm wide, 50 cm long) are shown. The size of the soot particles depends on the time allowed for their growth, the fuel composition and temperature of the flame zone. Since time increases with linear dimensions longer flames are usually yellower, smokier than shorter flames, indicating the escaping of the soot particles out of the flame zone. Large carbon particles will radiate more heat as shown in Fig. 11.3 [10]. A laminar natural convection flame is blue at the base, yellow in the center and red/orange at the tip. The latter condition means that so much heat has been lost by radiation from the carbon particles, that when it does cross the reaction zone into a region where oxygen is available for combustion, it is too cold to burn. The result is emission of smoke.

A useful material-property called **smoke-point** of a fuel can be defined based on this radiative heat loss mechanism by soot. A fuels smoke point is the maximum height of its laminar flame (or fuel mass flow rate) burning in air at which soot is just released from the flame tip. Another definition (and more applicable to fire safety) is the heat release rate at which smoke just begins to be released from the flame tip. Smoke point is a simplified ranking scheme for soot production and was first introduced by Kent and Wagner [11]. Smoke-point can be easily determined for gases and vapors by adjusting the flow rate of the fuel from a simple burner. For liquid fuels a wick-fed lamp (ASTM D1322) is used. Determining the smoke point for solid fuels is difficult, although some progress has been made in this direction by de Ris and Cheng [12]. It has been shown [12–14] that smoke point can provide a convenient measure of the flame radiant fraction. A comprehensive review on the development of an engineering model capable of predicting the release of soot and radiation given the smoke point of the fuel, stoichiometric mass ratio of the reactants and the adiabatic stoichiometric flame temperature is discussed by Lautenberger [15].

Diffusion Flame Theory

The theory of diffusion flames consists of an analysis of factors controlling the mixing of fuel and oxidizer. Main factors controlling the mixing are mass diffusivity (D), gradient of species mass fraction (dY/dn) normal to the condensed fuel surface and the flow field. Unlike premixed flame analysis, the rates of the reaction mechanisms do not dominate the burning behavior in diffusion flames. As discussed earlier, in diffusion flames, fuel and oxidizer come together in a reaction zone through diffusion. This diffusion can be just molecular transport (candle flame, laboratory flames) or be enhanced several times by convection, which may be even turbulent (most large-scale fires such as pool, building, forest etc.) The theoretical solution of the diffusion flame is best approached by considering a candle flame once again. Focus on a control volume in the gas phase as shown by the dashed boxed. The fuel vapor and oxidizer diffuse from opposite directions and approach the flame in a normal direction (Fig. 11.1, LHS). The concentrations of fuel and oxidizer at the flame are in stoichiometric proportion. In other words, the diffusion flame surface is defined as the locus of all points in space where the fuel and oxygen meet at stoichiometric proportions. **A one-step** chemical reaction given by Equation 11.3 can be used to represent the overall chemical process.

$$1\ \mathrm{g}[FUEL] + s\ \mathrm{g}[OXIDIZER] \rightarrow (1+s)\ \mathrm{g}[PRODUCTS] + Heat \quad (11.3)$$

The assumption made here is that the net disappearance rate of the reactants (fuel and oxidizer) is infinitely fast. This is represented by the zoomed inset in Fig. 11.1, where solid lines are used to indicate the profiles of temperature and mass fractions of the reactants. The flame zone is infinitesimally thin, and both fuel and oxygen are consumed at this "zero-thickness" flame sheet. However, in the actual scenario, the assumption of infinitely fast reaction is not true as indicated by the profiles in dashed lines in the flame structure inset in Fig. 11.1, where the flame zone has finite thickness and both the oxygen and the fuel leak through this flame zone. The details of flame broadening are beyond the scope of this chapter. However, an interested reader may refer to a book related to the topic [16]. For our purposes, the infinite rate chemistry assumption is sufficient in predicting parameters such as the mean flame zone location and mass burning rate.

The **one-step** and **infinitely fast** reaction assumptions also imply that $\dot{\omega}_F''' = \frac{\dot{\omega}_O'''}{s} = \frac{-\dot{\omega}_P'''}{1+s}$, where $\dot{\omega}'''$ denotes the nonlinear rate term representing the rate of formation or destruction of a species per unit volume. Subscripts F, O and P, denote fuel, oxidizer and products, respectively. The conservation equations for the control volume are given by:

Species Conservation

Assumption: binary diffusion coefficients are equal for all species.

$$\rho\frac{\partial Y_O}{\partial t}+\rho u_i\frac{\partial Y_O}{\partial x_i}=\frac{\partial}{\partial x_i}\rho D\frac{\partial Y_O}{\partial x_i}-\dot{\omega}_O''', \quad (11.4)$$

$$\rho\frac{\partial Y_F}{\partial t}+\rho u_i\frac{\partial Y_F}{\partial x_i}=\frac{\partial}{\partial x_i}\rho D\frac{\partial Y_F}{\partial x_i}-\dot{\omega}_F''', \quad (11.5)$$

$$\rho\frac{\partial Y_P}{\partial t}+\rho u_i\frac{\partial Y_P}{\partial x_i}=\frac{\partial}{\partial x_i}\rho D\frac{\partial Y_P}{\partial x_i}+\dot{\omega}_P'''. \quad (11.6)$$

Energy Conservation

$$\rho c_p\frac{\partial T}{\partial t}+\rho u_i c_p\frac{\partial T}{\partial x_i}=\frac{\partial}{\partial x_i}\lambda\frac{\partial T}{\partial x_i}+\dot{\omega}_F'''\Delta H_c\left[\text{or }\frac{\dot{\omega}_O'''\Delta H_c}{s}\text{ or }\frac{\dot{\omega}_P'''\Delta H_c}{1+s}\right]. \quad (11.7)$$

In the above equations, ρ represents the gas phase density, c_p represents the specific heat and λ equals the thermal conductivity. ΔH_c represents the heat of combustion of the fuel and D equals the diffusion coefficient which is assumed to be the same for oxygen—air, fuel—air and product—air The nonlinear rate terms ($\dot{\omega}'''$) can be eliminated from the equations by suitable subtractions and assuming that the Lewis number is unity $\left(Le=\frac{\lambda}{\rho c_p D}=1\right)$. Multiply Equation 11.4 by $\frac{1}{s}$, Equation 11.6 by $\frac{1}{1+s}$ and Equation 11.7 by $\frac{c_p}{\Delta H_c}$ to get the modified conservation equations.

Modified Species Conservation Equations

$$\rho\frac{\partial(Y_O/s)}{\partial t}+\rho u_i\frac{\partial(Y_O/s)}{\partial x_i}=\frac{\partial}{\partial x_i}\rho D\frac{\partial(Y_O/s)}{\partial x_i}-\frac{\dot{\omega}_O'''}{s}, \quad (11.8)$$

$$\rho\frac{\partial Y_F}{\partial t}+\rho u_i\frac{\partial Y_F}{\partial x_i}=\frac{\partial}{\partial x_i}\rho D\frac{\partial Y_F}{\partial x_i}-\dot{\omega}_F''', \quad (11.9)$$

$$\rho\frac{\partial[Y_P/(1+s)]}{\partial t}+\rho u_i\frac{\partial[Y_P/(1+s)]}{\partial x_i}=\frac{\partial}{\partial x_i}\rho D\frac{\partial[Y_P/(1+s)]}{\partial x_i}+\frac{\dot{\omega}_P'''}{1+s}. \quad (11.10)$$

Modified Energy Conservation Equation

$$\rho\frac{\partial\left(Tc_p/\Delta H_c\right)}{\partial t}+\rho u_i\frac{\partial\left(Tc_p/\Delta H_c\right)}{\partial x_i}=\frac{\partial}{\partial x_i}\frac{\lambda}{c_p}\frac{\partial\left(Tc_p/\Delta H_c\right)}{\partial x_i}+\dot{\omega}_F'''. \quad (11.11)$$

Equations 11.8, 11.9, 11.10, and 11.11 can be combined into a single equation given by

$$L(\beta)=0, \quad (11.12)$$

where β can take several values as shown in Table 11.2 and the operator L is expressed as,

$$L(\beta)\equiv\rho\frac{\partial\beta}{\partial t}+\rho u_i\frac{\partial\beta}{\partial x_i}-\frac{\partial}{\partial x_i}\rho D\frac{\partial\beta}{\partial x_i}. \quad (11.13)$$

In the operator L, the first term represents the accumulation of thermal energy or chemical species, the second term represents the convection efflux thorough the control surfaces and the third represents the diffusion efflux. The non-linear volumetric reactive effects are eliminated using

Table 11.2 Different forms of the coupling function β introduced in Equation 11.12

β	Value
β_{FO}	$Y_F-\frac{Y_O}{s}$
β_{FP}	$Y_F+\frac{Y_P}{1+s}$
β_{FT}	$Y_F+\frac{Tc_p}{\Delta H_c}$
β_{OP}	$Y_O+\frac{Y_P}{1+s}$
β_{OT}	$Y_O+\frac{Tc_p}{\Delta H_c}$
β_{PT}	$Y_P+\frac{Tc_p}{\Delta H_c}$

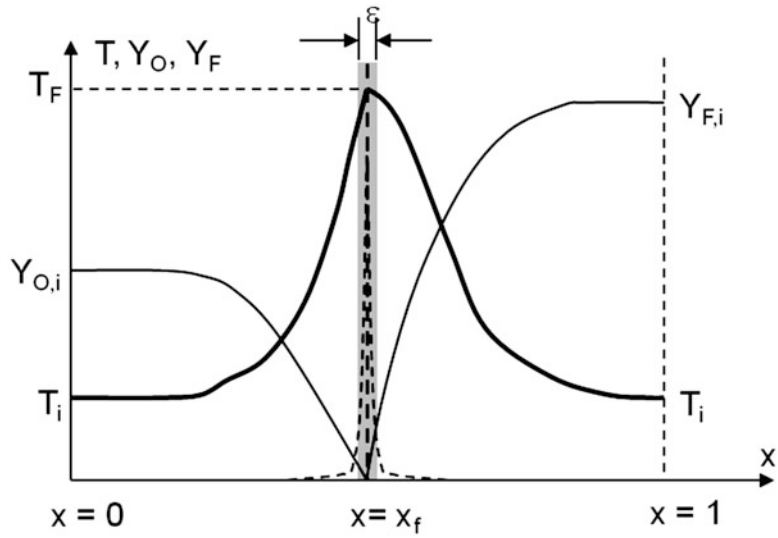

Fig. 11.4 The onedimensional diffusion flame mathematical model

the coupling function β, which can take 6 forms as shown in Table 11.2. This methodology is referred to as the Shvab-Zeldovich transformation after two classical papers by Shvab [17] and Zeldovich [18] that first used the coupling function. Note that although Shvab-Zeldovich proposed a general solution, the original idea was first proposed by Burke-Schumann [19] in 1928.

Equation 11.12 can be solved with knowledge of initial and boundary conditions. However, this is not an easy task! For example, the convective term is also non-linear unless the velocity is constant. Further, many added assumptions such as constant, ρD, steady state ($\frac{\partial \beta}{\partial t} = 0$), one-dimensional system, constant pressure and low speed flow are required before analytical solutions to some problems can be obtained. Nevertheless the coupling function β is a powerful tool that is used extensively in diffusion flame problems. One example is considered below.

Diffusion Flame Location

The diffusion flame surface is defined as the locus of all points in space where the fuel and oxygen meet at stoichiometric proportions. The position of the flame front of a diffusion flame is dependent on the surrounding geometry and the flow rates of the various gas streams. It is apparent, then, that each accidental flame is dependent on the details of the environment in which it burns. Thus the possible variations in behavior are endless. The one-dimensional flame structure discussed earlier will be used once again to describe the problem. A further set of assumptions will be imposed to simplify the math and facilitate physical understanding.

Assumptions

1. The oxidizer enters the system at $x = 0$ with a temperature T_i, a concentration of $Y_{O,i}$ and a velocity of $u = U$ which is a constant.
2. The fuel enters the system at $x = 1$ with a temperature T_i, a concentration of $Y_{F,i}$ and a velocity of $u = U$ Fig. 11.4.
3. The reaction occurs at $x = x_f$ in a zone with thickness, $\varepsilon \to 0$.
4. All reactants are consumed at the reaction zone so for: $\begin{matrix} x < x_f & Y_F = 0 \\ x > x_f & Y_O = 0 \end{matrix}$

Conservation Equations

Since the flow field is assumed to be known and constant ($u = U$), there is no need to solve the overall mass and momentum conservation equations. Thus,

Species Conservation

$$\left(U\frac{d(Y_O/s)}{dx}\right)=-\frac{\dot{\omega}_F'''}{s\rho}+D\left(\frac{d^2(Y_O/s)}{dx^2}\right) \quad (11.14)$$

$$\left(U\frac{dY_F}{dx}\right)=-\frac{\dot{\omega}_F'''}{\rho}+D\left(\frac{d^2Y_F}{dx^2}\right) \quad (11.15)$$

Energy conservation

$$\left(u\frac{d\left(T/\left(\Delta H_c/c_p\right)\right)}{dx}\right)=\frac{\dot{\omega}_F'''}{\rho}+\alpha\left(\frac{d^2\left(T/\left(\Delta H_c/c_p\right)\right)}{dx^2}\right), \quad (11.16)$$

where $\alpha=\frac{\lambda}{\rho c_p}$ represents the thermal diffusivity.

Boundary Conditions

$$\begin{array}{llll} x=0 & T=T_i & Y_O=Y_{O,i} & Y_F=0 \\ x=1 & T=T_i & Y_O=0 & Y_F=Y_{F,i} \end{array} \quad (11.17)$$

The conservation equations are coupled using Equation 11.12. Note that with the steady, 1-D system discussed in the example, the L operator reduces to $L(\beta)\equiv\rho U\frac{d\beta}{dx}-\rho D\frac{d^2\beta}{dx^2}$. This gives,

$$\left(U\frac{d\beta}{dx}\right)=\alpha\left(\frac{d^2\beta}{dx^2}\right). \quad (11.18)$$

Three β-variables will be selected such that the values of temperature and mass fractions of fuel and oxygen (three variables obtained by solving three equations) can be evaluated later. The choices are β_{OF}, β_{OT} and β_{FT}. The variables and the boundary conditions are listed below:

$$\begin{array}{lll} \beta_{OF}=\dfrac{Y_O}{s}-Y_F & and & \begin{array}{ll} x=0, & \beta_{OF}=\dfrac{Y_{O,i}}{s} \\ x=1, & \beta_{OF}=-Y_{F,i} \end{array} \\ \beta_{OT}=\dfrac{Y_O}{s}+\dfrac{Tc_p}{\Delta H_c} & and & \begin{array}{ll} x=0, & \beta_{OT}=\dfrac{Y_{O,i}}{s}+\dfrac{Tc_p}{\Delta H_c} \\ x=1, & \beta_{OT}=\dfrac{Tc_p}{\Delta H_c} \end{array} \\ \beta_{FT}=Y_F+\dfrac{Tc_p}{\Delta H_c} & and & \begin{array}{ll} x=0, & \beta_{FT}=\dfrac{Tc_p}{\Delta H_c} \\ x=1, & \beta_{FT}=Y_{F,i}+\dfrac{Tc_p}{\Delta H_c} \end{array} \end{array} \quad (11.19)$$

As shown above, the coupling function or the Shvab-Zedovich transformation eliminates the nonlinear reaction rate terms from the conservation equations. We are still left with 6 boundary conditions for the three linear equations that can be obtained with β_{OF}, β_{OT} and β_{FT}. We can further decrease the difficulty in the solution procedure without altering the nature of the solution by replacing β with a new normalized variable, $Z=\frac{\beta(x)-\beta(0)}{\beta(1)-\beta(0)}$, which is called as a mixture fraction. Note that β (0) and β (1) are constants obtained from the boundary conditions. Since the boundary conditions for the variable Z at the boundaries $x=0$ and $x=1$ are $Z=0$ and $Z=1$, respectively, irrespective of the β-variable that defines Z, the solution is unique and we need to obtain the solution to one mixture fraction equation only. This simple algebraic manipulation allows us to obtain a single differential equation with normalized boundary conditions given by:

$$\left(U\frac{dZ}{dx}\right)=\alpha\left(\frac{d^2Z}{dx^2}\right) \quad where \quad \begin{array}{l} x=0\rightarrow Z=0 \\ x=1\rightarrow Z=1 \end{array} \quad (11.20)$$

The solution to this differential equation is

$$Z=\frac{\left(e^{x/\delta}-1\right)}{\left(e^{1/\delta}-1\right)} \qquad where \qquad \delta=\frac{\alpha}{U} \quad (11.21)$$

Going back to the dimensional values (oxygen concentration, fuel concentration and temperature) requires the determination of the flame location. Based on the assumption that the flame will place itself where fuel and oxidizer arrive in stoichiometric proportions, the flame location can be expressed by: $\beta\left(x_f\right)=\frac{Y_O}{s}-Y_F=0$. Substituting the appropriate expression for Z(x) in terms of β and evaluating

$$\beta_{OF}(x)=\frac{Y_{O,i}}{s}-\left(\frac{Y_{O,i}}{s}+Y_{F,i}\right)\left[\frac{e^{x/\delta}-1}{e^{1/\delta}-1}\right], \quad (11.22)$$

the flame location, x_f, is obtained as

$$x_f = \delta \; Ln\left[\frac{Y_{O,i}}{s}\frac{\left(e^{1/\delta}-1\right)}{\left(\frac{Y_{O,i}}{s}+Y_{F,i}\right)}+1\right]. \quad (11.23)$$

Finally, assuming there is no oxidizer in the fuel zone and no fuel in the oxidizer zone the fuel and oxygen concentrations can be defined as:

$$\begin{array}{llll} x<x_f & Y_O = s\beta_{OF}(x) & and & Y_F = 0 \\ x>x_f & Y_O = 0 & and & Y_F = -\beta_{OF}(x) \end{array} \quad (11.24)$$

A similar method can be followed when determining the temperature distribution, from f_2 for $x < x_f$ and f_3 for $x > x_f$. This is explained in the worked example.

There are several advantages in introducing the mixture fraction. The mixture fraction (Z) should satisfy the balance equation

$$L(Z) \equiv \rho\frac{\partial Z}{\partial t} + \rho u_i \frac{\partial Z}{\partial x_i} - \frac{\partial}{\partial x_i}\rho D\frac{\partial Z}{\partial x_i} = 0, \quad (11.25)$$

based on the definition of the operator L of Equation 11.10. The boundary condition equation is $Z = 1$ in the fuel stream and $Z = 0$ in the oxidizer stream. This equation converts all the Shvab-Zeldovich variables (β) into a single parameter. Equation 11.25 greatly simplifies the modeling of diffusion flames. Note that there is no source term in Equation 11.25.

Comments on the Formulation and Analysis

It is important to reiterate the assumptions used in working out the solution discussed earlier. 1. **One-step** and **infinitely fast** reaction, 2. Lewis number = 1, 3. Binary diffusion coefficients are equal for all species, 4. ρD = constant, 5. Velocity (U) is constant, 6. Steady state, 7. One-dimensional, and 8. Constant specific heat, thermal diffusivity and density. Assumptions 1, 2 and 3 are necessary for implementing the Shvab-Zeldovich transformation. This is because Z couples the transport of heat and species into a single variable. In some cases, heat and different species may have different diffusivities and therefore can be transported at different rates. Consequently, β and Z are no longer conserved. However, by making the equal diffusivity and Le = 1 assumption, we are requiring that these diffusive fluxes are transported at the same rate and hence preserving the conserved nature of Z. Assumption 4 is used in most fire problems, however, can be relaxed. Assumptions 5–8 were used to solve our specific example of a one-dimensional flame. Of these 5 can be most questionable. This is because the flow-field plays a significant role in diffusion problems. An exact representation of the flow-field can be obtained by solving the overall mass and momentum conservation or the Navier–Stokes equations, which require proper pressure–velocity coupling since most fires are incompressible in nature. Assumption 6 is reasonable mainly because of the slow regression rates observed for most condensed fuels. Assumption 7 facilitated an analytical solution. Assumption 8 is reasonable so long as the properties are chosen correctly. The correct choice of properties is hugely important in all problems of this nature. This is further discussed below.

Property Estimation

Most theoretical and empirical expressions to solve fire problems usually rely on the assumption of constant thermophysical properties. An important issue in using these expressions in practice therefore necessitates a proper method to evaluate the thermophysical properties such that results obtained through them match with experimental data. A first step in property estimation is obtaining certain average temperature.

For a diffusion flame, the temperature can vary from a few hundred degrees at the fuel side to around 1500–2000 K at the flame zone. Surrounding temperature can also be of the order of a few tens to a few hundred degrees based on the problem. Composition of the gas mixture within this range varies from a pure fuel vapor near the interface to pure air in the far field.

Within this range, there exists many gas species formed because of thermal cracking of the fuel vapor as well as combustion products such as CO_2, CO and H_2O. Therefore the process of arriving at an "average" mixture property based on specific mixture composition and average temperature is a nontrivial issue.

This problem of an average gas-composition at an average temperature whose properties can be used for correlations with constant property assumptions has been investigated by several researchers (c.f. Rangwala et al. [20] for a list of references related to the topic). The main method reported in most combustion textbooks is by Law and Williams [21] and employs flame, ambient (or surrounding) and interface temperature to arrive at an average temperature. The average mixture composition is calculated using some proportions of fuel and air. The disadvantage of using the Law and Williams [21] scheme in fire problems is the need to know the fuel-vapor composition which is difficult to evaluate for complex materials usually involved. A much simpler scheme using only properties of air was recently developed by Rangwala et al. [20]. The scheme has been tested in several diffusion controlled problems involving burning behavior of both gaseous liquid and solid fuels. The scheme considers forced convection and variable oxygen concentration. This scheme is simpler to use and recommended for fire problems. In this scheme, the average thermal conductivity is estimated as the thermal conductivity of air calculated at a temperature given as one third the sum of ambient and the adiabatic flame temperature. The gas phase specific heat is estimated as the specific heat of air at adiabatic flame temperature. Adiabatic flame temperatures for several fuels are tabulated in standard fire dynamics textbooks [22, 23].

Solved Example

On a geometrical configuration identical to that of the one-dimensional non-viscous problem presented earlier, a mixture of 22 % oxygen and 78 % nitrogen as oxidizer and a mixture 80 % Ethane and 20 % nitrogen as fuel (all percentages are in volume) do the following: (1) Plot the mixture fraction as a function of "x". (2) Find the flame location (x_F). (3) Plot the fuel and oxygen concentrations as a function of "x". (4) Plot the temperature as a function of "x". Solve for two situations of U = 1 mm/s and U = 0.1 mm/s and U = 1 mm/s. Comment on what is the meaning of the "characteristic length scale δ" and what is the effect of U on δ, the flame location and the flame temperature. Assume thermal properties as those of air at 1000 K.

Part 1: Mixture Fraction

A plot of $Z(x) = \frac{e^{\frac{x}{\delta}}-1}{e^{\frac{1}{\delta}}-1}$ is shown in Fig. 11.5. The value for delta ($\delta = \frac{\alpha}{U}$) based on U of 1 mm/s equals 0.168 m. It is assumed that the thermal diffusivity is that of air at 1000 K ($\alpha = 168 \times 10^{-6}\, m^2/s$).

Part 2: Flame Location

The flame is located at the position where $\beta_{OF} = \frac{Y_O}{s} - Y_F = 0$. This corresponds to a stoichiometric mixture. The flame location can be found using Equation 11.23. Based on the problem statement, $Y_{O,i} = \frac{0.22\times30}{0.22\times32+0.78\times28} = 0.244$ and $Y_{F,i} = \frac{0.8\times30}{0.8\times30+0.2\times28} = 0.811$, where, the molecular weight of ethane is 30 g/mol. $s = \left(\frac{Y_o}{Y_F}\right)_{stoic}$ is

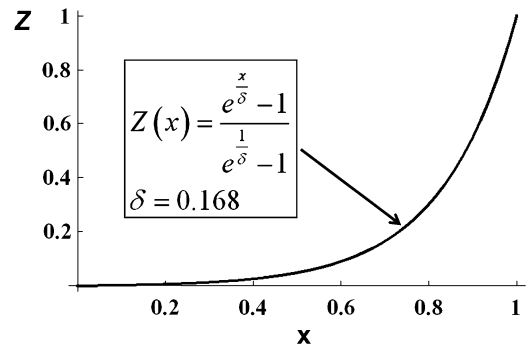

Fig. 11.5 Mixture fraction (Z) vs. x

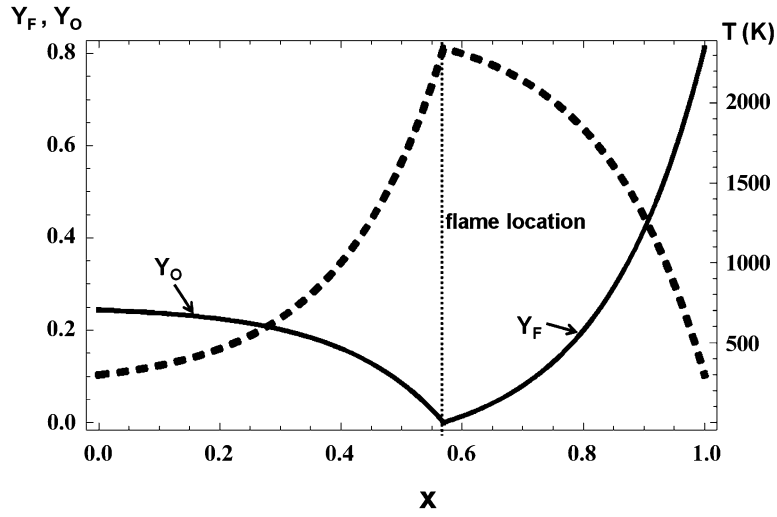

Fig. 11.6 Profiles of oxygen, fuel and temperature

obtained assuming a one step overall reaction of ethane reacting with oxygen $C_2H_6 + \frac{7}{2}O_2 \rightarrow 2CO_2 + 3H_2O$ and equals $s = \frac{112}{30} = 3.73$. Substituting these values in Equation 11.23 gives,

$$x_f = 0.168 \ln\left(\frac{\left(\frac{0.244}{3.73}\right)\left(e^{\frac{1}{0.168}} - 1\right)}{\left(0.811 + \frac{0.244}{3.73}\right)} + 1\right) = 0.57.$$

The location of the flame is shown in Fig. 11.6. It occurs at a location where the concentration of fuel (Y_F) and oxidizer (Y_O) are zero. Note that since the chemical reaction is assumed to be infinitely fast, there is no fuel or oxidizer leakage on either side of the flame. Further, the flame location occurs at the location of maximum temperature. Profiles of fuel, oxidizer and temperature are evaluated in Part 3 and 4 discussed next.

Part 3 and 4: Profiles of Oxygen, Fuel and Temperature

First assume that there is no oxygen in the fuel zone and no fuel in the oxidizer zone. Use f_1 to find the fuel and oxygen mass fractions.

$$\begin{aligned} x < x_f \quad & Y_o = \phi f_1(x) \ \ and \ Y_f = 0 \\ x > x_f \quad & Y_o = 0 \quad\ \ and \ Y_f = -f_1(x) \end{aligned}$$

Since the oxygen and fuel mass fractions are known, the temperature can be plotted using f_2 or f_3.

$$f_3(x) = \Psi(x)(f_3(1) - f_3(0)) + f_3(0) = \left(\frac{e^{\frac{x}{\delta}} - 1}{e^{\frac{1}{\delta}} - 1}\right)\left(Y_{f,i} + \frac{T_i}{(\Delta H_c/c_p)} - \frac{T_i}{(\Delta H_c/c_p)}\right) + \frac{T_i}{(\Delta H_c/c_p)}$$

$$T(x) = (\Delta H_c/c_p)\left(\left(\frac{e^{\frac{x}{\delta}} - 1}{e^{\frac{1}{\delta}} - 1}\right)\left(Y_{f,i} + \frac{T_i}{(\Delta H_c/c_p)} - \frac{T_i}{(\Delta H_c/c_p)}\right) + \frac{T_i}{(\Delta H_c/c_p)} - Y_f(x)\right)$$

The specific heat, $c_p = 1.14\frac{J}{g}$ @ $1000K$ and the heat of combustion is equal to $\Delta H_c = 47500\frac{J}{g}$. The temperature profile is shown in Fig. 11.6.

The characteristic length scale δ represents the ratio of the mass diffusion to the velocity of the gas stream. This characteristic distance

represents the extent that heat mass is diffusing against the gas flow into the gas stream.

Final Note

The example discussed uses constant surface boundary conditions at fuel and oxidizer side. For the case of condensed fuels at the interface between fuel and air, specifying a constant mass fraction for the species as the boundary condition at the interface provides great simplicity in formulating an analytical solution. However, determining an approximate value of $Y_{F,x\,=\,\text{surface}}$, the fuel mass fraction at the interface, is complicated as it involves solving a heat and mass balance at the fuel surface [24]. Further complication is that typically the species concentrations are discontinuous at the interface between two materials, whereas temperature is continuous. To take an example, consider a heptane pool fire. If we are interested in determining the rate at which heptane vapor is transferred to the gas-phase, we would need to specify the vapor concentration of heptane in the gas-phase side of the heptane-air interface. The mass fraction of heptane inside the pool is unity (neglecting the small amount of oxygen or nitrogen dissolved in heptane). However, it would be incorrect to assume $Y_{F,x\,=\,\text{surface}} = 1$ for the gas-phase mass fraction of heptane vapor at the interface. This value primarily depends on the interface temperature besides the pressure. Interface temperature is determined by the heat balance analysis between gas-phase to interface. The conditions at the interface are based on relationships that are theory-based or deduced from experiments. An additional nondimensional number called as B-number arises during the solution of establishing the mass fraction of fuel vapor at the interface. The B-number is an important derived property, which is dependent on the thermo-physical properties of the system, that provides an expression for the mass burning rate eventually. This leads us to the next section which discusses an important parameter usually used to quantifying the fire-hazard associated with a given material—its mass burning rate as a function of time.

Mass Burning Rate

The mass burning rate per unit area ($\dot{m}''$) or mass burning flux is an important parameter to quantify the hazard associated with fire. As mentioned earlier, this mass flux varies with B-number [3], which accounts for the thermodynamic effects, and the Nusselt number to account for the gas-phase convective effects. A general relationship will be derived in this section to account for a variety of physical flow conditions. In fire problems, the fuel is usually a solid or liquid burning in free convective conditions. The fuel vaporizes first, then diffuses toward the oxygen from the ambient. To solve such problems one needs to have information on the velocity, temperature and mass fraction profiles. The solution can be initiated by writing down a heat balance at the surface of the burning fuel,

$$\dot{m}'' L = \dot{q}'', \tag{11.26}$$

where L represents the latent heat of vaporization (for a liquid) or the heat of gasification (for a solid). $\dot{q}''$ is the net heat flux to the surface and depends on the nature of the flow field and boundary conditions (free stream temperature, ambient oxygen concentration etc.). It also depends on $\dot{m}''$, an effect called as the "blocking effect [22]." If the net heat flux to the surface increases, then logically mass flux or mass loss rate per unit area will also increase. This causes the boundary layer to thicken causing reduction in gradients. The burning rate therefore does not increase linearly with external heat flux and to develop a general solution requires generalization of the heat flux to the fuel. It can be assumed that the heat flux to the surface is a product of the heat transfer coefficient (h) and temperature difference between the flame and the surface. If the flame temperature is denoted by T_f and surface temperature by T_s the mass loss rate per unit area can be represented as:

$$\dot{m}'' = \frac{\dot{q}''}{L} = \frac{h\left(T_f - T_s\right)}{L} = B\frac{h}{c_p}, \tag{11.27}$$

Table 11.3 B-number values for different fuels [25]

Solids	Formula	B-number	Liquids	Formula	B-number
Polypropylene	C_3H_6	1.29	Methanol	CH_3OH	2.53
Polyethylene	C_2H_4	1.16	Ethanol	C_2H_5OH	2.89
Polystyrene	C_8H_8	1.55	Propanol	C_3H_7OH	3.29
Nylon 6/6	$C_{12}H_{22}N_2O_2$	1.27	Butanol	C_4H_8OH	3.35
Polycarbonate	$C_6H_{14}O_3$	1.41	n-pentane	C_5H_{12}	7.63
PMMA	$C_5H_8O_2$	1.78	n-hexane	C_6H_{14}	6.67
PVC	C_2H_3Cl	1.15	n-heptane	C_7H_{16}	5.92
Fir wood	$C_{4.8}H_8O_4$	1.75	n-octane (gasoline)	C_8H_{18}	5.42
α-cellulose	$C_6H_{10}O_5$	6.96	iso octane	C_8H_{18}	6.59
Polyoxymethylene	CH_2O	1.47	n-nonane	C_9H_{20}	4.89
			n-decane	$C_{10}H_{22}$	4.61
			n-undecane	$C_{11}H_{24}$	4.43
			n-dodecane (kerosene)	$C_{12}H_{26}$	4.13
			Acetone	C_3H_2O	7.28

where $B = \frac{c_p(T_f - T_s)}{L}$ is nondimensional and represents the mass transfer number. L in Equation 11.27 denotes the latent heat of gasification, h represents the convective heat transfer coefficient, T_f and T_s denote an average flame temperature and temperature of the fuel surface and c_p denotes the specific heat of the gas. The B-number (also called the Spalding mass transfer number) was first introduced by Spalding [3] in 1950 to characterize liquid fuel droplet burning and physically relates the heat release related to combustion (the numerator) to the losses associated with combustion (the denominator). The heat transfer coefficient (h) is expressed in terms of a nondimensional Nusselt number, defined as $Nu = \frac{hx}{\lambda}$, where λ denotes the thermal conductivity of the gas-mixture at the interface between the condensed fuel and air and x is a characteristic length scale. In case of a flat fuel surface x can be defined as the distance from the leading edge and in the case of a sphere or cylinder refers to the diameter. The earlier expression is now equal to:

$$\dot{m}'' = B\frac{\lambda}{xc_p}Nu \tag{11.28}$$

In order to account for the blocking effect, the Nusselt number is first evaluated without the blocking effect and then corrected for this effect through the ratio Nu/Nu_o

$$\dot{m}'' = B\frac{\lambda}{xc_p}\frac{Nu}{Nu_o}Nu_o \tag{11.29}$$

Nondimensionalizing both sides by ρU_∞, where U_∞ is a characteristic velocity representing the flow-field subjected to or induced by the diffusion flame, the above expression can be re-written as:

$$\frac{\dot{m}''}{\rho U_\infty} = B\frac{\lambda}{c_p\mu}\frac{\mu}{\rho U_\infty x}Nu_o\frac{Nu}{Nu_o} \tag{11.30}$$

$$= B(\mathrm{PrRe})^{-1}Nu_o\frac{Nu}{Nu_o} \tag{11.31}$$

The quantity $\frac{\lambda}{c_p\mu}$ equals $1/Pr$ where Pr = Prandtl number. The ratio $\frac{Nu}{Nu_o}$, the blocking effect can be calculated for several laminar flows and equals $\frac{\ln(1+B)}{B}$ for small B. For turbulent flows it can be calculated empirically only. Typical values of B for many fuels are listed in Table 11.3.

Expressions for Nu_o for many geometrical configurations are available in standard heat and mass transfer textbooks and shown in Table 11.4. For example, using Table 11.4, an expression for

Table 11.4 Nu_o values for some standard geometries and flow conditions. $\mathrm{Re} = \frac{U_\infty X}{\upsilon}$, and $Gr = \frac{gX^3\left(T_f - T_o\right)}{T_o \upsilon^2}$

Flow field type	Illustration	Nu_o
Free convective flow		
Vertical plate (laminar, $Gr < 10^9$)	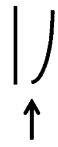	$0.59\ (GrPr)^{1/4}$
Vertical plate (turbulent, $Gr > 10^9$)		
Horizontal plate burning face up (laminar, $Gr < 10^7$)	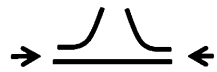	$0.54\ (GrPr)^{1/4}$
Horizontal plate burning face up (turbulent, $Gr > 10^7$)		$0.14(GrPr)^{1/3}$
Horizontal plate burning face down (turbulent)		$0.27(GrPr)^{1/4}$
Horizontal cylinder		$0.525(GrPr)^{1/4}$
Sphere		$2 + 0.6\ Gr^{1/4}Pr^{1/3}$
Forced flow		
Horizontal flat plate (laminar)		$0.332Re^{1/2}\ Pr^{1/3}$
Horizontal flat plate (turbulent $Re > 10^5$)		$0.036Re^{0.8}\ Pr^{0.3}$
Pool fire (laminar and axisymmetric)		$0.11\ Re^{1/2}\ Pr^{2/3}$

(continued)

Table 11.4 (continued)

Flow field type	Illustration	Nu_o
Droplet (laminar)		$0.37Re_d^{0.6}$
Cylinder (laminar)		$0.891Re^{1/2}$
Cylinder (turbulent, $Re > 40{,}000$)	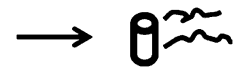	$0.27\ (GrPr)^{1/4}$

mass loss rate of a vertical plate in a laminar free convective flow can be calculated as:

$$\dot{m}'' = C_o B^m \frac{\lambda}{c_p x}(Gr\,\mathrm{Pr})^{1/4} \tag{11.32}$$

A mass burning rate for the same plate in a turbulent natural convective flow-field is:

$$\dot{m}'' = C_o B^m \frac{\lambda}{c_p x}(Gr\,\mathrm{Pr})^{1/3} \tag{11.33}$$

The constant C_o can take different values and usually lies between 0.5 and 1.5. The value of the exponent m on B is ~ 0.5. Recently Ali et al. [26] have extended the correlation (laminar case) to include several orientation angles. The mass burning rate of a plate oriented at an angle θ with respect to the vertical for a plate in a free convective flow-field is given by [26]:

$$\dot{m}'' = 0.737(Gr_x\,\mathrm{Pr}_x)^{0.25}\frac{\ln(1+B)}{B^{0.15}}, \tag{11.34}$$

where $Gr_x = \frac{g_{\mathrm{eff}}\beta\Delta T x^3}{\upsilon^2}$ and $g_{\mathrm{eff}} = g\cos\theta$ for $0 < \theta < 90°$ and $g_{\mathrm{eff}} = g(\cos\theta - \sin\theta)$ for $-90° < \theta \leq 0°$. Note that 0° represents the vertical case, −90° denotes a pool fire and 90° denotes a ceiling configuration. The mass loss rate per unit area $\dot{m}''$ can also be expressed as a regression rate $\dot{m}''/\rho_s$ where ρ_s is the density of the fuel (condensed phase). Typical regression rates of most fuels (solids/liquids shown in Table 11.3) vary between 0.02 and 0.4 mm/s. The regression rates are very small and are essentially due to the diffusion controlled nature of the problem.

Diffusion Flame Height

When gaseous fuel issues out of a tube into ambient atmosphere of air and the gas is ignited a flame is established as shown in Fig. 11.7. The question we will try to answer is how high is the resulting diffusion flame? The problem can be solved using conservation equations with certain approximations as was first shown by Burke and Schuman [19]. However, for practical purposes a simple physical reasoning exercise will be adopted here. It will be shown later that the relationship obtained is similar to that obtained using the more rigorous approach.

Imagine a fuel molecule, shown in Fig. 11.7 by the red circle, initially located at the center of the burner tube. The molecule can traverse two extreme paths (depicted by o-x and o-y) to meet with oxygen at the flame surface. The time taken to traverse horizontally along o-x is given by $d^2/4D$, where D is the diffusion coefficient between methane and air. The relationship is obtained by a dimensional analysis of the two parameters: distance over which diffusion must occur (m) and diffusion coefficient (m^2/s).

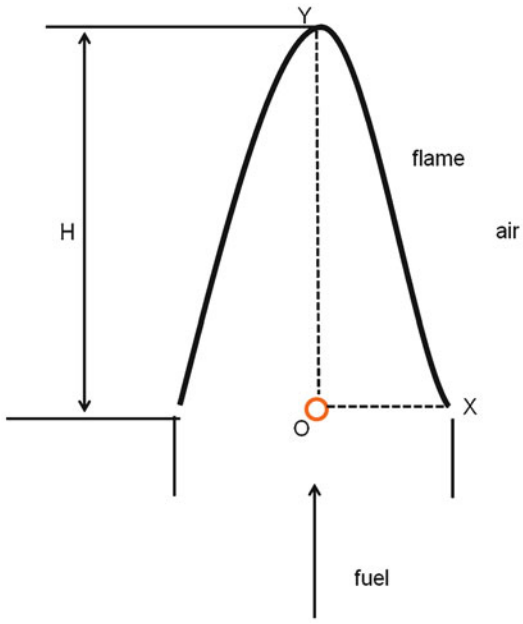

Fig. 11.7 The diffusion jet-flame

The only way of obtaining a time scale from these two quantities is to divide the square of the distance by the diffusion coefficient. The length of the flame will correspond to the condition that a point on the stream axis where combustion is complete, the average depth of penetration of air into gas must equal to the radius of the burner tube.

Similarly, the time taken to traverse vertically along O-Y is given by H_f/V, where H_f is the flame height and V is the velocity of the gas issuing of the burner. Equating the two times gives, $H_f/V \sim d^2/4D$ or $H_f \sim d^2V/4D$. This simple result is reflected in all the correlations (developed by Roper [27, 28]) related to diffusion flame height shown in Table 11.5. An important element in the expression developed is the influence of fuel properties, geometry (of the duct). The influence of fuel properties is usually incorporated in the flame temperature and stoichiometric coefficient (s) shown in Table 11.5.

The inverse error function is generated in the same way as inverse trigonometric functions and is tabulated in standard textbooks (For example see Table 9.4 in Turns [29]). The parameter, I typically takes values between 1 and 1.5. $I = 1$ for uniform flow and $I = 1.5$ for fully developed parabolic exit velocity profile. The subscript "m" denotes that the flow-field is momentum controlled and subscript "b" denotes buoyancy controlled. To determine if the flame is momentum or buoyancy controlled the flame Froude number Fr must be calculated as

Table 11.5 Flame height correlations (all quantities in SI m, m^3/s etc.)

Geometry	Flame height (H_f)
Circular	$H_f = \frac{Q_F(T_\infty/T_F)}{4\pi D \ln\left(1+\frac{1}{s}\right)}\left(\frac{T_\infty}{T_f}\right)^{0.67}$
Square	$H_f = \frac{Q_F(T_\infty/T_F)}{16D\left[\text{inverf}(1+s)^{-0.5}\right]^2}\left(\frac{T_\infty}{T_f}\right)^{0.67}$
Slot	$H_{f_m} = \frac{b\beta^2 Q_F}{hlDY_{F_{stoic}}}\left(\frac{T_\infty}{T_F}\right)^2\left(\frac{T_f}{T_\infty}\right)^{0.33}$ $H_{f_B} = \left[\frac{9\beta^4 Q_F{}^4 T_\infty{}^4}{8D^2 ah^4 T_F{}^4}\right]^{1/3}\left[\frac{T_f}{T_\infty}\right]^{2/9}$ $\beta = \frac{1}{4\text{inverf}\left(1+\frac{1}{s}\right)}$

Q_F volumetric fuel flow rate (m^3/s), D diffusivity (m^2/s), T_∞ ambient temperature (K), T_f mean flame temperature (K), T_F fuel temperature (K), s molar stoichiometric oxidizer-fuel ratio, *inverf* inverse error function, $\omega = inverf[erf(\omega)]$, a = mean buoyant acceleration $\approx 0.6g\left(\frac{T_f}{T_\infty} - 1\right)$ (m^2/s)

$$Fr_f = \frac{(V_e I Y_{F,stoic})^2}{aH_f}. \tag{11.35}$$

If $Fr_f \gg 1$ then flame is momentum controlled and if $Fr_f \ll 1$ then the flame is buoyancy controlled. If $Fr_f \approx 1$, then the flame lies in a transitional zone which is both momentum and buoyancy controlled. In this case,

$$H_{f_T} = \frac{4}{9}H_{f_m}\left(\frac{H_{f_B}}{H_{f_m}}\right)^3\left\{\left[1 + 3.38\left(\frac{H_{f_B}}{H_{f_m}}\right)^3\right]^{2/3} - 1\right\}, \tag{11.36}$$

where H_{f_m} and H_{f_B} represent the momentum and buoyancy controlled flame heights and can be obtained using the correlation presented in Table 11.3. Note that for a circular and square port geometry the equations are applicable for both momentum and buoyancy controlled.

The equations shown in Table 11.5 demonstrate that some of the primary controlling parameters influencing the flame height of a diffusion flame are flow rate, geometry, and stoichiometry. The

flow rate and geometry influence can be characterized by the nondimensional Froude number. The molar stoichiometric ratio (s) is mainly a function of fuel type. For a generic hydrocarbon C_xH_y burning in air the chemical balance equation assuming complete combustion can be written as:

$$C_xH_y + \grave{a}(O_2 + 3.76N_2) \rightarrow xCO_2 + \frac{y}{2}H_2O + 3.76aN_2, \qquad (11.37)$$

where, $a = x + \frac{y}{4}$ and $s = \left(\frac{\text{moles air}}{\text{moles fuel}}\right)_{stoic} = \frac{\left(x+\frac{y}{4}\right)}{X_{O_2}}$. X_{O_2} is the mole fraction of oxygen in air and equals 1/4.76. As the carbon content in the fuel increases (y/x increases) the flame length increases. For example a propane flame (C_3H_8) is nearly 2.5 times longer than a methane flame (CH_4). Fuels which have oxygen in their molecule (e.g. CO) show an even smaller flame length. If the fuel is diluted with an inert gas, the flame height reduces. The molar stoichiometric ratio in this case, is $s = \frac{x+y/4}{\left(\frac{1}{1-X_{dil}}\right)X_{O_2}}$, where X_{dil} is the mole fraction of the inert in the fuel stream.

The discussion so far pertains to gaseous jet flames. Roper's correlations can be extended to predicting flame height of condensed fuels as well. For example, an approximate fuel flow velocity in a candle flame can be obtained by assuming the candle wick to be a vertical cylinder. Using Roper's correlation for a circular burner (Table 11.3) and substituting $Q_F = \frac{\dot{m}_F}{\rho_F}$ and using heat transfer coefficients for a finite vertical cylinder (represents candle wick) and a hot surface facing up (which represents the top face of candle wick) it can be shown that [30]

$$H_f \sim 0.5D\left(\frac{L}{D}Ra^{1/4} - 2\right)^n, \qquad (11.38)$$

where, D equals the diameter of the wick, L is equal to the length of the wick from the base, Ra is the Rayleigh number defined using the wick diameter, and n is a constant approximately equal to 0.7. Sunderland et al. [30] have shown the above relationship to provide a good match with experimental data using candle wicks of different thicknesses.

Turbulent Diffusion Flames

Most fires can be classified as turbulent diffusion flames, and extensive studies related to the basic understanding of the problem can be found in literature [31–38]. Besides the important aspects of height of a diffusion flame and rate of burning, which were discussed in the previous sections, an important fire safety concern with the advent of turbulence is the enhancement in the transport processes, changes in the flame structure, extent and shape, and the radiant energy flux emitted by the flame [39, 40]. In large fires, a solid fuel is normally gasified by radiative heat flux from the fire (and hot zones) and the evolved gases mix with surrounding air. The mixing process is determined by buoyancy induced flow rather than by the forced convection as in jets and sprays usually studied in the field of combustion in engines and furnaces, for example. The advent of turbulence, which is a random process, necessitates the use of statistical methods, thus making the solution probabilistic in nature. Thus an exact solution is seldom possible. Given our current state of understanding a solution that falls in a reasonable range is acceptable. The coupling function described as the mixture fraction (Equation 11.25) plays a central role in reducing problems in the analysis of turbulent diffusion flames to problems associated with non-reacting turbulent flows.

The turbulent flow field can be visualized as being comprised of eddies having wide range of length scales, the larger of which extract energy from the mean flow. The large eddies break up into smaller eddies, which in turn break up into even smaller ones, until the smallest eddies, called Kolmogorov eddies form, and dissipate the energy back to the main flow as viscous dissipation. This concept was first proposed by Kolmogorov is described as the eddy/energy cascade hypothesis in turbulent literature [33]. Note that the size of the smallest eddies are several orders of magnitude larger than the mean free path of the molecules of the gas or fluid. Due to this reason, the turbulent flow field can be considered as continuum and the conservation equations of mass (species), momentum

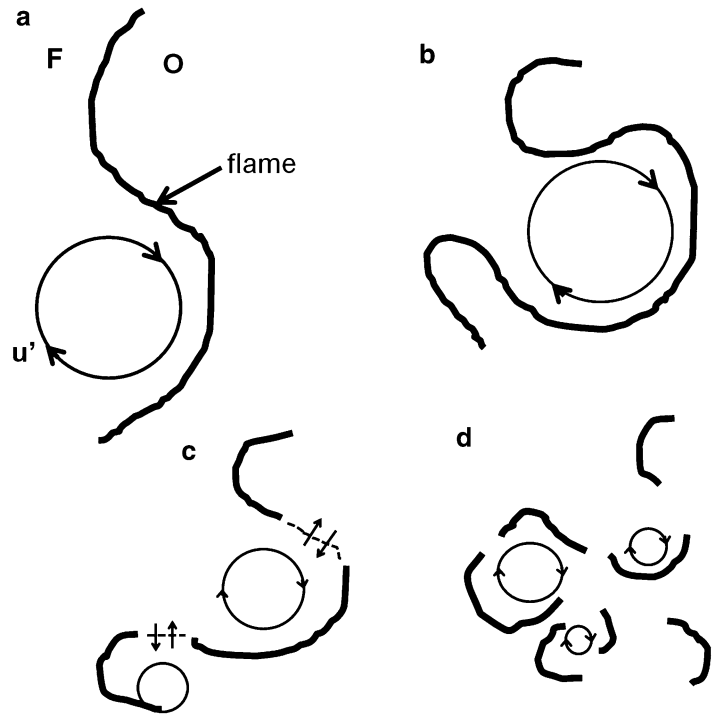

Fig. 11.8 Illustrative sketch of laminar flamelet concept of turbulent diffusion flames. The turbulent intensity increases from (**a**) to (**d**). Local extinction is observed in (**c**) due to flame stretching

and energy are still applicable. The question then arises that how does this flow pattern influence a diffusion flame? For this, the general theory proposed by Williams [41] and models by Peters [38] and Kuznetsov [42] will be discussed. The general model is named as the flamelet model mainly because of the tendency of turbulence to break the flame into several tiny flames or flamelets. Both strain and shear at the interface of eddies increase the concentration gradient between the reactants thereby enhancing the mixing. Going back to Equation 11.1 (Ficks law) as the *gradient* $\frac{\partial Y}{\partial x_i}$, increases, the rate of mixing should also increase eventually. However, this increase is not due to a change in the molecular diffusivity D_{AB}. Thus, in order to model this increase in the overall mixing process, an improvised *turbulent diffusivity* is defined. Note that the turbulent diffusivity is an empirical concept and incorporates both the molecular diffusivity as well as some function which can represent the influence of intensity and scale of turbulence on the mixing at the flamelet level. The flamelets are considered as thin reactive-diffusive layers, considered in general as laminar, embedded within an otherwise non-reacting turbulent flow field. This allows us to use the mixture fraction to describe turbulent flames as well.

If we assume that the turbulent transport of momentum, species and thermal energy are all equal (Sc = Pr = Le) we can substitute existing correlations from the fluid mechanics literature related to turbulent momentum diffusivity (eddy viscosity) to apply for turbulent mass diffusivity and thermal diffusivity as well.

Figure 11.8 shows the influence of increased turbulent intensity on a turbulent flame. As we move from Fig. 11.8a to d, eddies are capable of corrugating a flame and eventually breaking the corrugations and distributing the flame sheet into smaller flamelets. Thus at sufficiently high strain, there is also local extinction achieved. Another aspect, and most important from an aspect of fire safety is an understanding of flame radiation due to large turbulent hydrocarbon diffusion flames. For example flame radiation is an important parameter in design of safe separation distances. The primary factors influencing the problem are the

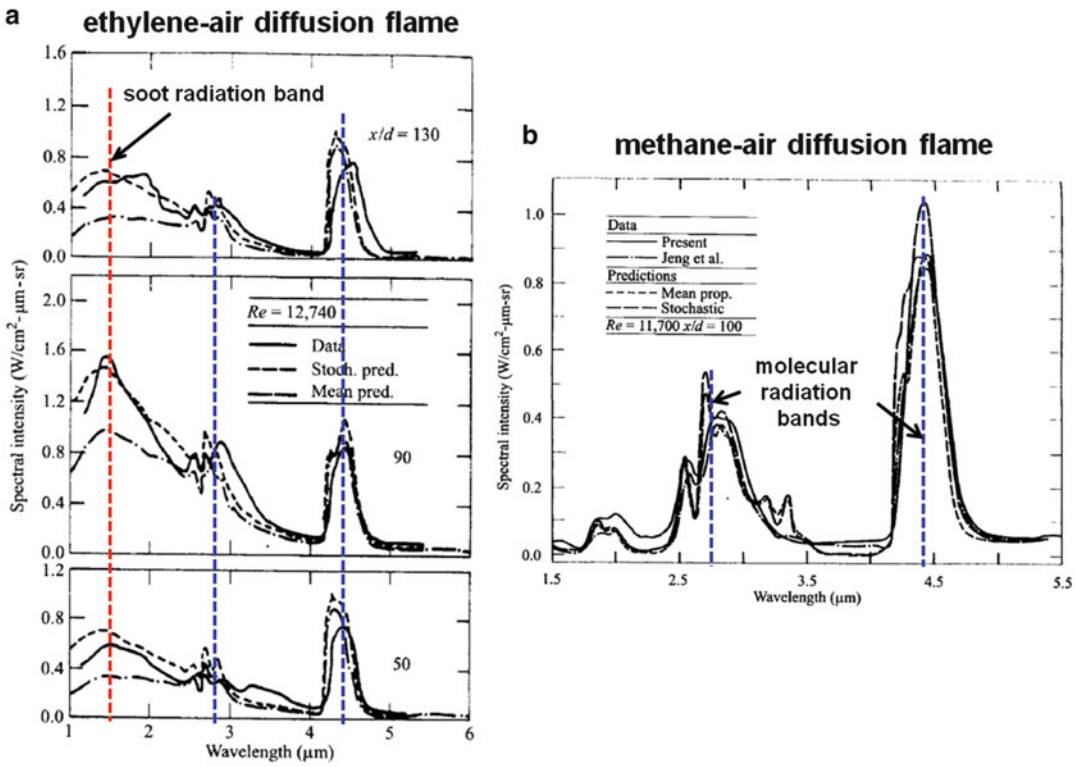

Fig. 11.9 Spectral measurements of thermal radiation from a turbulent (**a**) ethylene-air flame [43] and (**b**) methane-air flame [44]

concentration of soot, CO_2, H_2O, temperature profiles (at different locations in the flame) and geometry of the problem. Incandescent soot formed within the flame is the primary source of flame radiation in large-scale fires, although gaseous products of combustion (CO_2, H_2O) can also emit heat. The radiation emitted from CO_2 and H_2O is usually called molecular radiation. The easiest way to understand (and explore) the difference between the radiation from soot and gaseous products (CO_2, H_2O) is by comparing two diffusion flames.

Figure 11.9a [43] and Fig. 11.9b [44] depict spectral radiation intensities for an ethylene-air and methane-air diffusion flame respectively. The ethylene-air flame produces more soot when compared with the methane-air flame. Correspondingly, it exhibits intensity peaks at 1.5 μm corresponding to the in-flame soot. In comparison, the methane-air flame shows significant intensity peaks at 2.5–3 μm and 4–5 μm corresponding to the molecular radiation from CO_2 and H_2O.

Prediction of flame radiation necessitates knowledge of formation and oxidation of soot in the flame, its concentration profiles, as well as concentration and temperature of sources of molecular radiation such as CO_2 and H_2O, besides the type of fuel and the residence time available. A common approach used in fire problems, is identifying a radiant fraction which represents the ratio of radiant heat transfer rate from the flame to the surroundings to the total heat released by the flame. The radiant fraction is denoted as χ_R, and is expressed as:

$$\chi_R = \frac{\dot{Q}_{rad}}{\dot{m}_F \Delta H_c}, \tag{11.39}$$

where $\dot{Q}_{rad}$ denotes the radiant energy transferred from the flame in the form of radiation. Based on

our current understanding and knowledge-base, χ_R is estimated using empirical correlations. χ_R depends on both flame size and heat release rate and the general trend is for χ_R to increase with flame size. Depending on the fuel type and flow conditions, the radiant fraction can range from a few percent to more than 50 % [45–47].

Flame Extinction

General strategies for extinguishing diffusion flames are cooling, reactant removal, chemical inhibition, and flame removal. These strategies are achieved for example, by adding sufficiently large quantities of a material (such as water) that cools the condensed fuel thereby slowing combustion, removing an essential reactant from the system, adding a chemical suppressant (such as Halon) that inhibits the reactions taking place in the flame zone, or physically removing the flame from the reactant mixture by inducing high gas velocities (for example by explosives in large production-well fires).

The rate of gas-phase chemical reaction that was denoted by $\dot{\omega}_i'''$ in Equations 11.4, 11.5, and 11.6 was thus far ignored. However, it plays an important role in flame extinction (as well as ignition). It is therefore necessary to formulate an expression to quantify $\dot{\omega}_i'''$ in order to establish critical extinction criteria. This is usually done by employing a one-step Arhenius approximations to the rates. The analysis can be generalized using a non-dimensional Damkohler number [48]. To better understand the concept, let us perform an exercise of nondimensionalizing the energy conservation equation (gas-phase) using nondimensional variables: $\widehat{u} = u/u_c$, $\widehat{v} = v/u_c$, $\widehat{x} = x/L_c$, $\widehat{y} = y/L_c$, $\widehat{T} = T/T_c$, where $u_c =$ some characteristic velocity, which we will denote as u_∞ and $L_c =$ L is some characteristic length scale. The definition of u_∞ and L, depends on the nature of the problem. For example, if the flowfield is natural convective mostly (large open pool fires, wall fire etc.) $u_\infty \sim \sqrt{gL}$ where L is for example the diameter of the pool fire or the length of the wall in the case of a wall fire. T_c which is a characteristic temperature can be represented as $\Delta H_c/c_p$. Substituting the nondimensional variables in the energy equation gives,

$$\rho c_p u_\infty \left(\widehat{u}\frac{\partial \widehat{T}}{\partial \widehat{x}} + \widehat{v}\frac{\partial \widehat{T}}{\partial \widehat{y}}\right) = \Delta H_c \frac{A Y_o^{n-j} Y_f^{j} e^{-E/RT}}{s} + \lambda \frac{\Delta H_c}{L^2 c_p}\left(\frac{\partial^2 \widehat{T}}{\partial \widehat{x}^2} + \frac{\partial^2 \widehat{T}}{\partial \widehat{y}^2}\right). \tag{11.40}$$

The term $\frac{\dot{\omega}_O''' \Delta H_c}{s}$, representing the energy released due to the chemical reaction between fuel and oxidizer is expressed using an *empirical* Arhenius expression $\Delta H_c \frac{A Y_o^{n-j} Y_f^{j} e^{-E/RT}}{s}$, or specifically, the rate at which fuel is lost per unit volume is given by $A Y_o^{n-j} Y_f^{j} e^{-E/RT}$. In the expression, A is a constant called as the pre-exponential constant or the frequency factor. The terms, $Y_o^{n-j} Y_f^{j}$ represent the mass fraction of oxidizer and fuel (n and j are empirical constants) to emphasize the fact that the rate of loss of fuel is dependent on the initial concentration of fuel and oxidizer. To simplify the mathematical analysis and gain physical insight into the problem, we will assume a simpler expression of the form $K e^{-E/RT}$, where K is a constant. Note that so far we have been able to neglect this term by assuming the infinitely fast reaction assumption and the resulting Shvab-Zeldovich transformation. We therefore never worried about defining this term. However, for both ignition and extinction analysis, the nonlinear source term cannot be ignored. Rearranging terms gives

$$\left(\widehat{u}\frac{\partial \widehat{T}}{\partial \widehat{x}} + \widehat{v}\frac{\partial \widehat{T}}{\partial \widehat{y}}\right) = \Delta H_c \frac{K e^{-E/RT}}{s} \times \frac{L c_p}{\rho c_p u_\infty \Delta H_c} + \lambda \frac{\Delta H_c}{L^2 c_p} \times \frac{L c_p}{\Delta H_c \rho c_p u_\infty}\left(\frac{\partial^2 \widehat{T}}{\partial \widehat{x}^2} + \frac{\partial^2 \widehat{T}}{\partial \widehat{y}^2}\right) \tag{11.41}$$

or

$$\left(\widehat{u}\frac{\partial\widehat{T}}{\partial\widehat{x}}+\widehat{v}\frac{\partial\widehat{T}}{\partial\widehat{y}}\right)=\frac{e^{-E/RT}}{s}\left[\frac{L/u_\infty}{\rho/K}\right]+\left[\frac{L/u_\infty}{L^2/\alpha}\right]\left(\frac{\partial^2\widehat{T}}{\partial\widehat{x}^2}+\frac{\partial^2\widehat{T}}{\partial\widehat{y}^2}\right) \quad (11.42)$$

The rearrangement of the terms as shown in Equation 11.42 provides some interesting nondimensional numbers. Firstly, we can define some time scales such that:

$\tau_{residence}=\frac{L}{u_\infty}=$ Time the reactants are present in the CV

$\tau_{chemical}=\frac{\rho}{K}=$ Time it take s for a chemical reaction to occur.

$\tau_{conduction}=\frac{L^2}{\alpha},\quad \alpha=\frac{\rho c_p}{\lambda}=$ Pre-heat time

We can now express, the terms on the right hand side of Equation 11.42, in square brackets as two nondimensional numbers which are denoted as:

$$\mathrm{Da}_1=\frac{\tau_{residence}}{\tau_{chemical}}=\frac{L/u_\infty}{\rho/K}, \quad (11.43)$$

and

$$\mathrm{Da}_2=\frac{\tau_{residence}}{\tau_{conduction}}=\frac{L/u_\infty}{L^2/\alpha}. \quad (11.44)$$

"Da" stands for Damkohler number, after Damkohler [49]. As Da_1 (or Da_2) decrease, suppression is obtained. This is explained using the residence and chemical times defined. $\tau_{residence}$ is the residence time which refers to the length of time the fuel vapors remain in the reaction zone. The residence time will depend on the fluid dynamics of the flame. A diffusion flame can be extinguished by the mechanism of blowout, familiar with the small flames of matches and candles. The mechanism involves the distortion of the reaction zone, within the flame in such a way as to reduce the time that the fuel vapors have to react. Blowout can occur if sufficient airflow can be achieved to reduce $\tau_{residence}$ and consequently T_f, thus reducing the Da_1 number below a critical value. This behavior is also observed in turbulent flames where with sufficiently high intensity, the laminar flamelets are distorted to an extent such that the fuel vapor does not have sufficient time to react with the oxygen. This results in further distortion of the corrugated flame illustratively shown in the transition from Fig. 11.8c, d. $\tau_{chemical}$ is the chemical reaction time, i.e. the time taken for the chemical reaction of combustion to occur. $\tau_{chemical}$ can be reduced by influencing the chemical reaction taking place at the flame. For example chemical suppressants such as Halon are effective reduce the rate of gas phase reaction.

If the conduction losses are increased (denominator of Da_2) extinction can be achieved by quenching due to heat losses (in-depth conduction, re-radiation, and radiative feedback from the flame). For example, if the fuel supply can be decreased by say lowering the vaporization rate of a condensed fuel by adding water, the flame approaches the surface and thus looses more heat which may ultimately result in quenching due to increase in heat losses. The quenching due to lack of fuel supply has not been studied extensively with condensed fuels and works by Roberts and Quince [50] and Torero et al. [51] represent the few studies that define a minimum fuel supply stability limit for diffusion flames established over a condensed fuel. Torero et al. [51] show that for diffusion flames spreading on condensed fuel surfaces, such as upward spread along walls, or horizontal spread or lateral spread on floors, the mechanism of gas-phase flame quenching is dependent on blow-out mechanisms (reduction of Da_1) for the leading edge (location of flame anchored to the surface) and quenching (reduction of Da_2) for the trailing edge (location of the flame tip).

Extinction of diffusion flames can also be physically explained using a critical flame temperature concept. The "S-curve" first studied by Fendell [52] and Linan [53] is usually used to represent the response of temperature to the system Damkohler number. For most fire problems the critical flame temperature at which a diffusion flame ceases to exist is approximately 1300 °C [54, 55]. However, this value should be used with caution. A recent study by Tien and Endo [56] show that there is no unique critical extinction temperature for different materials and the flame temperature at extinction is a strong function of flow parameters.

Final Comments and Conclusions

This chapter discussed the problem of diffusion flames also called as non-premixed flames. The discussion illustrates two important aspects. Analysis of diffusion flames involves knowledge of transport properties such as diffusivity, specific heat of species involved in the process and a thorough understanding of the flow system. Both are limited by the postulates that are made in setting up the simple examples discussed in this chapter. It is therefore absolutely necessary to do experiments in order to establish the flow regime and quantify material and gas-phase properties. The inherent non-linear nature of the governing equations makes the subject difficult and solution to simplified geometries is only possible at this stage. Other aspects such as onset of instabilities and turbulent transport are not clearly understood. This leaves the topic with several fascinating areas of research that need further work.

References

1. Arias-Zugasti, M. and Rosner, D.E., *Soret transport, unequal diffusivity, and dilution effects on laminar diffusion flame temperatures and positions*. Combustion and flame, 2008. **153**(1): p. 33–44.
2. Smyth, K.C., Miller, J.H., Dorfman, R.C., Mallard, W.G., and Santoro, R.J., *Soot inception in a methane/air diffusion flame as characterized by detailed species profiles*. Combustion and flame, 1985. **62**(2): p. 157–181.
3. Spalding, D.B., *Combustion of liquid fuel in gas stream*. Fuel, 1950. **29**: p. 2–7.
4. Spalding, D.B., *Some fundamentals of combustion*. Gas turbine series vol. 2. 1955, London: Academic Press, Butterworths Scientific Publications.
5. Chakrabarty, R.K., Moosmüller, H., Arnott, W.P., Garro, M.A., Tian, G., Slowik, J.G., Cross, E.S., Han, J.-H., Davidovits, P., and Onasch, T.B., *Low fractal dimension cluster-dilute soot aggregates from a premixed flame*. Physical review letters, 2009. **102**(23): p. 235504.
6. Frenklach, M. and Wang, H. *Detailed modeling of soot particle nucleation and growth*. in *Symposium (International) on Combustion*. 1991. Elsevier.
7. Sunderland, P. and Faeth, G., *Soot formation in hydrocarbon/air laminar jet diffusion flames*. Combustion and flame, 1996. **105**(1): p. 132–146.
8. Lautenberger, C.W., De Ris, J.L., Dembsey, N.A., Barnett, J.R., and Baum, H.R., *A simplified model for soot formation and oxidation in cfd simulation of non-premixed hydrocarbon flames*. Fire Safety Journal, 2005. **40**(2): p. 141–176.
9. Vander Wal, R.L. and Tomasek, A.J., *Soot oxidation: Dependence upon initial nanostructure*. Combustion and flame, 2003. **134**(1): p. 1–9.
10. Rangwala, A.S. *Flame spread analysis using a variable b-number*. in *Proc. Fire Safety Sci.* 2008. Karlsruhe, Germany.
11. Kent, J. and Wagner, H.G., *Who do diffusion flames emit smoke*. Combustion Science and Technology, 1984. **41**(5–6): p. 245–269.
12. De Ris, J. and Cheng, X.F., *The role of smoke point in material flammability testing*. Proc. Fire Safety Sci., 1994. **4**: p. 301–312.
13. Markstein, G.H. *Correlations for smoke points and radiant emission of laminar hydrocarbon diffusion flames*. in *Symposium (International) on Combustion*. 1989. Elsevier.
14. Delichatsios, M., *Smoke yields from turbulent buoyant jet flames*. Fire Safety Journal, 1993. **20**(4): p. 299–311.
15. Lautenberger, C.W., *Cfd simulation of soot formation and flame radiation*, 2002, WORCESTER POLYTECHNIC INSTITUTE.
16. Zeldovich, I., Barenblatt, G.I., Librovich, V., and Makhviladze, G., *Mathematical theory of combustion and explosions*. Moscow: Nauka, 1985.
17. Shvab, V.A., Goz. Energ. izd. Moscow-Leningrad, 1948.
18. Zel'dovich, Y.B., Zhur. Tekhn. Fiz. English translation: NACA Tech. Memo No. 1296 (1950), 1949. **19**: p. 1199.
19. Burke, S.P.a.S., T. E. W.,, *Diffusion flames*. Industrial & Engineering Chemistry, 1928. **20**(10): p. 998–1004.
20. Rangwala, A.S., Raghavan, V., Sipe, J.E., and Okano, T., *A new property evaluation scheme for mass transfer analysis in fire problems*. Fire Safety Journal, 2009. **44**(4): p. 652–658.
21. Law, C.K. and Williams, F.A., *Kinetics and convection in the combustion of alkane droplets*. Comb. Flame, 1972. **19**: p. 393–405.
22. Quintiere, J.G., *Fundamentals of fire phenomena*. 2006: John Wiley & Sons, New York.
23. Drysdale, D., *An introduction to fire dynamics*. 1998: John Wiley & Sons, New York.
24. Raghavan, V., Rangwala, A., and Torero, J., *Laminar flame propagation on a horizontal fuel surface: Verification of classical emmons solution*. Combustion Theory and Modelling, 2009. **13**(1): p. 121–141.
25. Annamalai, K. and Sibulkin, M., *Flame spread over combustible surfaces for laminar flow systems part i: Excess fuel and heat flux*. Combustion Science and Technology, 1979. **19**(5): p. 167–183.
26. Ali, S.M., Raghavan, V., and Rangwala, A.S., *A numerical study of quasi-steady burning characteristics of a condensed fuel: Effect of angular orientation of fuel surface*. Combustion Theory and Modelling, 2010. **14**(4): p. 495–518.
27. Roper, F., *The prediction of laminar jet diffusion flame sizes: Part i. Theoretical model*. Combustion and flame, 1977. **29**: p. 219–226.

28. Roper, F., *Laminar diffusion flame sizes for curved slot burners giving fan-shaped flames*. Combustion and flame, 1978. **31**: p. 251–258.
29. Turns, S.R., *An introduction to combustion, 2000*, McGraw-Hill, New York.
30. Sunderland, P., Quintiere, J., Tabaka, G., Lian, D., and Chiu, C.-W., *Analysis and measurement of candle flame shapes*. Proceedings of the Combustion Institute, 2011. **33**(2): p. 2489–2496.
31. Bilger, R., *Turbulent diffusion flames*. Annual Review of Fluid Mechanics, 1989. **21**(1): p. 101–135.
32. Bilger, R. *The structure of turbulent nonpremixed flames*. in *Symposium (International) on Combustion*. 1989. Elsevier.
33. Peters, N., *Turbulent combustion*. 2000: Cambridge university press.
34. Libby, P.A. and Williams, F.A., *Turbulent reacting flows*. Turbulent Reacting Flows, 1980. **1**.
35. Dahm, W. and Dimotakis, P., *Measurements of entrainment and mixing in turbulent jets*. AIAA journal, 1987. **25**(9): p. 1216–1223.
36. Takeno, T. and Kotani, Y. *Transition and structure of turbulent jet diffusion flame*. in *AIAA, Aerospace Sciences Meeting*. 1977.
37. Pope, S.B., *Turbulent flows*. 2000: Cambridge university press.
38. Peters, N., *Laminar diffusion flamelet models in non-premixed turbulent combustion*. Progress in Energy and Combustion Science, **10**(3): p. 319–339.
39. Tamanini, F. *A numerical model for the prediction of radiation-controlled turbulent wall fires*. in *Symposium (International) on Combustion*. 1979. Elsevier.
40. Delichatsios, M. and Orloff, L. *Effects of turbulence on flame radiation from diffusion flames*. in *Symposium (International) on Combustion*. 1989. Elsevier.
41. Williams, F., *Recent advances in theoretical descriptions of turbulent diffusion flames*. Turbulent mixing in nonreactive and reactive flows, p. 202–208.
42. Kuznetsov, V., *The effect of turbulence on the formation of large superequilibrium concentrations of atoms and free radicals in diffusion flames*. Akademiia Nauk SSSR, Izvestiia, Mekhanika Zhidkosti i Gaza, p. 3–9.
43. Gore, J. and Faeth, G. *Structure and spectral radiation properties of turbulent ethylene/air diffusion flames*. in *Proc. Combust. Instit.* 1988. Elsevier.
44. Faeth, G., Gore, J., Chuech, S., and Jeng, S.-M., *Radiation from turbulent diffusion flames*. Annual Review of Heat Transfer, 1989. **2**(2).
45. De Ris, J.a.O., L.,, *The role of buoyancy direction and radiation in turbulent diffusion flames on surfaces*. Fifteenth Symposium (International) on Combustion, 1974. **15**: p. 175–182.
46. Orloff, L., De Ris, J., and Delichatsios, M., *Radiation from buoyant turbulent diffusion flames*. Combustion Science and Technology, 1992. **84** (1–6): p. 177–186.
47. Delichatsios, M., De Ris, J., and Orloff, L. *An enhanced flame radiation burner*. in *Symposium (International) on Combustion*. 1992. Elsevier.
48. Williams, F., *A review of flame extinction*. Fire Safety Journal, 1981. **3**(3): p. 163–175.
49. Damköhler, G., *The effect of turbulence on the flame velocity in gas mixtures*. 1947.
50. Roberts, A. and Wuince, B., *A limiting condition for the burning of flammable liquids*. Combustion and flame, 1973. **20**(2): p. 245–251.
51. Torero, J.L., Vietoris, T., Legros, G. And Joulain, P.,, *Estimation of a total mass transfer number from the standoff distance of a spreading flame*. Combustion Science and Technology, 2002. **174**(11): p. 187–203.
52. Fendell, F.E., *Ignition and extinction in combustion of initially unmixed reactants*. J. Fluid Mech, 1965. **21**(2): p. 281–304.
53. Linan, A., *The asymptotic structure of counterflow diffusion flames for large activation energies*. Acta Astronautica, 1974. **1**(7): p. 1007–1039.
54. Rasbash, D.J., *The extinction of fires by water sprays*. Fire Res. Abst. Rev., 1962. **4(1)**(28–53).
55. Quintiere, J. and Rangwala, A., *A theory for flame extinction based on flame temperature*. Fire and Materials, 2004. **28**(5): p. 387–402.
56. T'ien, J.S. and Endo, M., *Material flammability: A combustion science perspective*. Proceedia Eng., 2013. **62**: p. 120–129.

Ali S. Rangwala is an associate professor at the department of Fire Protection Engineering at Worcester Polytechnic Institute (WPI) (2006 – present). He has a BS in Electrical Engineering, from the Government College of Engineering, Pune, India (2000), an MS in Fire Protection Engineering from the University of Maryland, College Park (2002), and a PhD in Mechanical and Aerospace Engineering from the University of California, San Diego (2006).

Professor Rangwala's research interests are in the area of industrial fire and explosion safety, specifically deflagration of combustible dust clouds, ignition behavior of combustible dust layers, in-situ burning of oil, spread of oil slicks, measuring techniques in fire induced flows, and flame propagation and burning rate behavior of condensed fuel surfaces. He teaches three graduate courses: Explosion Protection, Industrial Fire Protection, and Combustion at Worcester Polytechnic Institute, Department of Fire Protection Engineering

Fundamentals of Premixed Flames

12

Grunde Jomaas

Lavoisier, Berthollet and Dalton were pioneers in the understanding of the mixture composition needed for a flame existence, and in the early 1800s, Sir Humphry Davy created a miner's lamp with a fine meshed net that improved the safety for mine workers, as the mesh was finer than the quenching distance and hence reduced the number of accidental explosions. When Bunsen created the burner associated with his name in 1855 [1], the premixed flame was considered to be However, as the following will show, there was, in the words of Richard Feynman, plenty of room at the bottom [126].

There are two main types of flames, namely the non-premixed flame, which is often referred to as a diffusion flame, and the premixed flame. The former is the more common type of flame in fire situations, where the atmospheric oxidizer and the vaporized (liquids) or pyrolyzed (solids) fuel and oxidizer are not mixed until they react in the flame sheet. In the premixed flame, the fuel and the oxidizer are mixed before reaching the reaction zone, where chemical energy is converted to heat and light. This type of flame is seen in petrol (gasoline) engines, gas turbines, some explosions and elsewhere.

In both flame configurations, chemical reactions must convert the fuel and oxidizer into products and they typically release heat in the process. The rate at which the products and concomitant heat are generated is governed by the Arrhenius reaction rate, $\dot{m} \sim Y_F Y_O e^{-E/RT}$, which states that the fuel and oxidizer must have the proper concentrations in order to react and the molecules must have sufficient energy in order to begin to chemically react. In a premixed flame, the fuel and oxidizer are mixed before the heat required to overcome the activation energy, E, and to initiate the chemical chain reactions is added. The added heat is often in the form of a spark, increased temperature or an open flame. The ratio of the fuel and oxidizer must be within the flammability limits (see Chap. 17), which have both lower and upper bounds, and the heat applied must be sufficient to get the chain reactions going, and this is typically referred to as the minimum ignition energy (MIE) (see Chaps. 17 and 69) if it is not a purely thermal explosion (for Auto-Ignition Temperatures, AIT, see Chap. 17). Although premixed flames can be formed directly or indirectly from solids and liquids (e.g. grain elevator explosion), the current discourse will focus on gaseous fuels.

A premixed flame is a wave phenomenon and it will propagate into the unburned mixture if not forced to do otherwise. The wave can either be propagated at subsonic speeds by the heat release from chemical chain reactions (deflagration) or at supersonic speeds with a leading shock initiating combustion (detonation). This contrasts a premixed flame to the non-premixed

G. Jomaas (✉)
Department of Civil Engineering, Brovej, DTU Building 118, Technical University of Denmark (DTU), DK-2800 Kgs. Lyngby, Denmark

M.J. Hurley (ed.), *SFPE Handbook of Fire Protection Engineering*,
DOI 10.1007/978-1-4939-2565-0_12, © Society of Fire Protection Engineers 2016

(diffusion) flame, which will try to situate itself at the stoichiometric location of the incoming streams of fuel and oxidizer.

It is quite common to refer to a premixed flame as an explosion because the reactions and the wave-front created by the expansion of the gases are occurring very quickly. However, the word explosion should technically be reserved for the case of a purely thermal explosion, which is a fast rate of reaction in a premixture without a wave [2–6]. The classic theories by Semenov and Frank-Kamenetskii [7, 8] use different approaches to show that the chemical gain from exothermic reactions has to exceed the conduction losses in the system for a thermal runaway to occur.

As the reaction rate is proportional to the energy release, and the reaction rate is exponential with respect to temperature, the result of increasing the temperature is typically a thermal runaway (explosion). This requires that the number of chain branching reactions is larger than the number of chain terminating reactions. In the classic example with H_2-O_2, the detailed chemical reaction scheme along with the reaction rates of the reaction steps will reveal the chain initiating reactions (creation of the first free radicals), the chain branching reactions (more free radicals in the products than in the reactants), the chain carrying reactions (equal number of free radicals in the reactants and the products) and the chain terminating reactions (fewer free radicals in the products than in the reactants), and thus reveal the bottle necks of the explosive process [9]. As such, a detailed study of the chemistry can help us understand how to prevent such a runaway, for example by introducing competing radicals that will inhibit the chain branching, which is the fundamental operational aspect of several fire extinguishment agents, such as halons and their more environmentally friendly replacements.

The laminar flame speed is a thermo-chemical property embodying information about the diffusive and reactive aspects of a combustible mixture, and is thus a central link to understanding of premixed flames. Furthermore, high fidelity laminar flame speed data enables precise and accurate studies of other premixed flame phenomena. In order to computationally simulate a flame phenomenon such as the laminar flame speed, reliable and accurate data on the chemical, thermodynamic, and transport properties must be available over a wide range of experimental conditions, and as such this presents a major challenge. These modeling obstacles can be circumvented to some degree by optimizing the kinetic mechanisms based on experimental observations of fundamental properties such as ignition delay times in shock tubes, extinction limits, flame structures, and laminar flame speeds. The following will therefore focus on the theoretical, numerical and experimental work that has enabled the current understanding of premixed flames. Most combustion textbooks contain chapters on Premixed Flames that have discourses ranging from more practical applications to advanced mathematical formulations and derivations, and the reader is encouraged to consult these for further information on the topic [10–24].

Rankine-Hugoniot Relations – Infinitely Thin Flames

In order to analyze the propagation of a premixed flame, the one-dimensional equations for a reacting flow have to be discussed. Figure 12.1 shows the configuration and the relevant parameters in the unburned (left) and the burned (right) region of the infinitely thin flame. In this frame of reference, the flame is stationary such that the unburned gas velocity

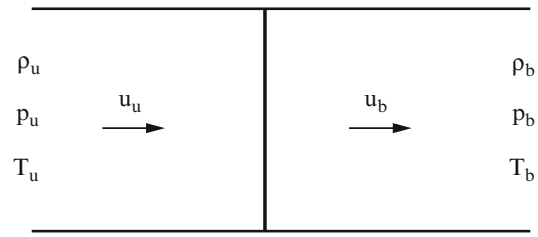

Fig. 12.1 Schematic of the one-dimensional premixed flame, with unburned gases (reactants) to the left and burned gases (products) to the right of the infinitely thin flame

and density match the mass consumption rate of the flame.

The one-dimensional governing equations for conservation of mass, momentum and energy (the energy release, q_c, equals zero for a shock wave) are:

$$\rho_u u_u = \rho_b u_b$$
$$p_u + \rho_u u_u^2 = p_b + \rho_b u_b^2$$
$$h_u + \frac{1}{2}u_u^2 + q = h_b + \frac{1}{2}u_b^2$$

The subscripts refer to the unburned (u) and the burned (b) regions, respectively. The total enthalpy, h, equals the sensible plus the chemical enthalpy (see Chap. 5.)

$$h = c_p T + h^0$$

In addition, we have the equation of state

$$p_u = \rho_u R T_u$$

After some algebraic manipulation of the four equations with five unknowns [13, 15, 16, 19, 24], we can produce the Rankine-Hugoniot [25, 26] diagram, see Fig. 12.2, which enables us to plot the solutions of the underdetermined problem. A key point in this plot is the Chapman-Jouguet point, which is named after Chapman [27] and Jouguet [28].

The diagram offers numerous solutions, but not all the mathematically possible solutions for the burned state are physically possible. The velocity u_u is real and positive in the upper left region. However, it does not exist (imaginary) in the upper right region, as it would require a compression wave to move in the negative direction, which is impossible. The lower left corner is inaccessible because it is impossible to decrease the pressure and the specific volume simultaneously. Similarly, the upper right corner is inaccessible because it is impossible to increase the pressure and the specific volume at the same time.

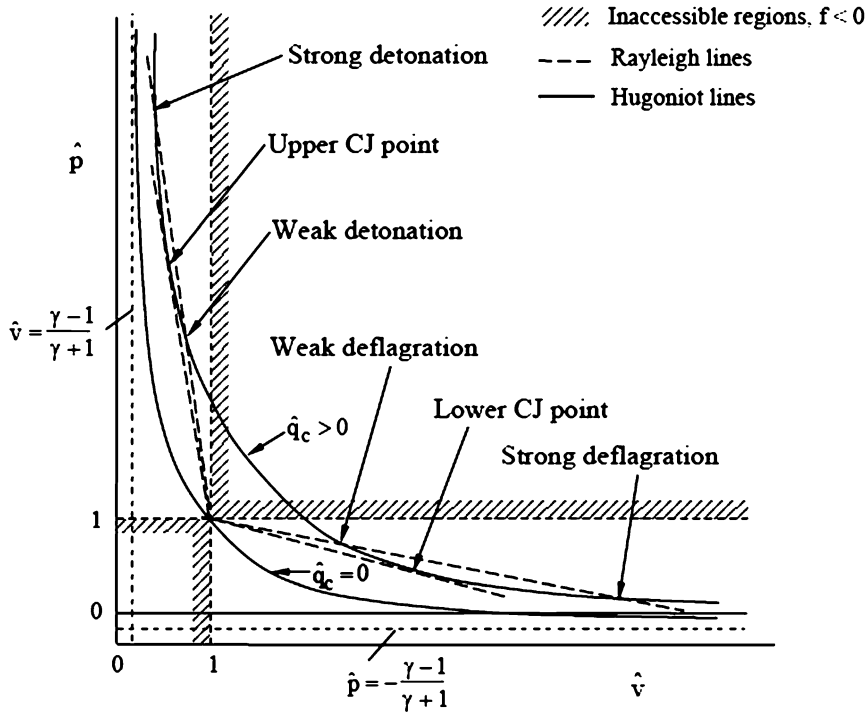

Fig. 12.2 Rankine-Hugoniot plot for the one-dimensional premixed flame. Two lines are shown, one associated with a shockwave ($q = 0$) and one for a wave with a given heat release [13]

The plot is then left with four solution regions, where two are for compression waves and two are for expansion waves [13, 19].

Compression waves (high velocity, the specific volume decreases, the pressure and the density increase when moving from the initial state to the final state)

1. Strong detonation, $p_b > p_{CJ}$, supersonic to subsonic (p_{CJ} is the pressure at the CJ point)
   - Rarefaction waves in the post-combustion gases cause this region to be unstable and waves that occur here will always slow down and end up with a velocity corresponding to that of the upper CJ point. Note that there are theoretical solutions for situations with steady, overdriven detonation waves [127].
2. Weak detonation, $p_b < p_{CJ}$, subsonic to supersonic
   - Does not exist (based on structure analysis)

   Expansion waves (low velocity, the specific volume increases, the pressure and the density decrease when moving from the initial state to the final state)
3. Weak deflagration, $p_b > p_{CJ,\,L}$ ($p_{CJ,\,L}$, pressure at lower CJ point), subsonic to subsonic
   - Deflagration (expansion waves), which requires the structure to be analyzed
4. Strong deflagration, $p_b < p_{jb}$, subsonic to supersonic
   - Does not exist, as it is impossible to have heat addition and proceed past the sonic condition in a constant area duct (Rayleigh flow).

Thus, only region 3 and the upper CJ point exist.

In summary, a Rankine-Hugoniot plot arises from the conservation equations for steady, 1-D flow. The plot shows that combustion waves can either be deflagration or detonation waves, that is, they can, respectively, either be slower or faster than the speed of sound in the medium they traverse. In order to study the deflagration solution, a flame structure is needed, which means that studies of the species concentrations, the flame thickness, diffusion rates, and the temperature become relevant. For the deflagration scenario, one more equation is needed for the underdetermined set of equations, and the flame structure provides this information through the introduction of the heat release rate.

Flame Structure and the Flame Speed

The fact that the flame has a structure is essential, as this means that it has a finite thickness, which is needed in order to move away from the Landau limit (flame sheet, no thickness) in which the flames are intrinsically unstable to all wavelengths [29]. The flame thickness therefore introduces stability.

The detailed structure of a premixed flame contains a preheat zone and a reaction zone, see Fig. 12.3. The laminar flame speed depends on the chemical kinetics and the thermal and mass diffusion.

Although many other methods with more mathematical rigor and more refined physical assumptions [13, 15, 16, 19, 24] exist, the considerations of Mallard and Le Chatelier [30] provide a good starting point for the introductory discussion herein. Also, the main outcome is the same of all the theories, namely that the laminar burning velocity and the flame thickness have a physical dependency on the fuel-air mixture and the ambient conditions. This knowledge can be used for safety design through stabilization and control of the flames.

The following will introduce more details and results associated with the laminar flame speed, which is a steady, self-sustained propagation of an 'exothermic reaction wave' at a low

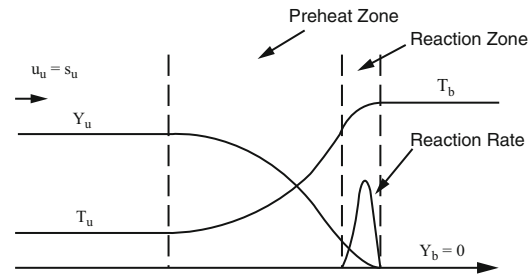

Fig. 12.3 The structure of a premixed flame [13]

subsonic velocity in a direction normal to itself. For the most part, radiative heat transfer and second-order (coupled) transport effects, such as thermal diffusion, are neglected, and the focus is placed on heat conduction, diffusion and the rapid exothermic chemical reactions. Due to the small pressure difference, it can be considered isobaric, and the momentum equation is not needed. As a result, only the mass balance (of each species) and the energy balance are considered.

As the analysis focuses on conservation of mass and energy across the flame (1-D, adiabatic, steady and planar flame propagation into stationary, combustible mixture in a doubly infinite domain), transport and reaction parameters are key. The problem therefore calls for two parameters, which are the laminar flame velocity and the flame thickness.

Mallard and Le Chatelier

The basis for the theoretical development by Mallard and Le Chatelier [30] requires the concept of an ignition temperature, but an actual ignition temperature does not exist in a flame (and hence cannot be determined). The ignition temperature in approach is also not to be confused with the adiabatic flame temperature (See Chaps. 5, 17, and 18). Still, the matching of the timescales and the length scales in a preheat zone and a reaction zone provides useful insight to the physical problem. The governing equations indicate that convection, diffusion and reaction are the relevant transport and reaction processes that should be considered, see Fig. 12.4. The first assumption is that there is no reaction in the far upstream and the far downstream domains, so the reaction timescales go to infinity there. In the preheat zone, the reaction timescale is long due to the low temperature, so convection and diffusion dominate, and have to have matching timescales for the physical problem to be balanced. In the reaction zone, the reaction timescale is small due to the high temperature, so the length scale has to be small so that the thermal and mass gradients, which govern the rate of diffusion, are large. Because convection is a first order differential and diffusion a second order differential, we can deduce that diffusion will be dominating over convection for the small length scales present in the reaction zone. Consequently, we have that diffusion and reaction balance each other in the reaction zone. Finally, at the ignition temperature, all three timescales have to be of approximately the same order.

This approach also allows us to obtain the key parameter for studies on laminar premixed flames, namely the laminar burning velocity, without getting into discussions on the reaction progress variable and details about the reaction rate and the mathematical challenges it causes through its non-linearity.

The assumptions in this approach are that the gases are heated by conduction in the preheat

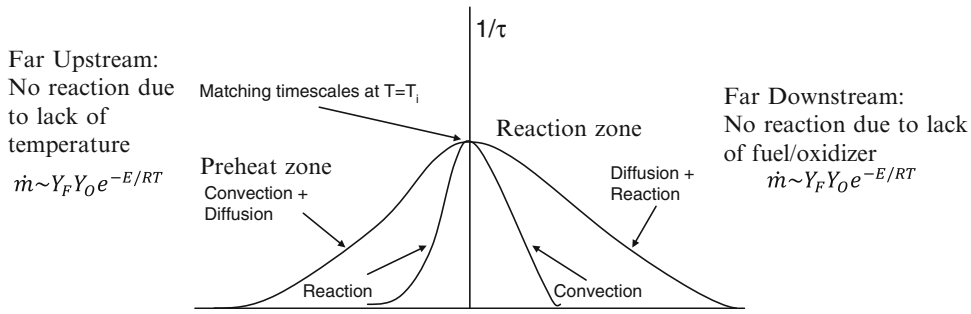

Fig. 12.4 Overview of the laminar premixed flame problem. See also Figs. 12.1 and 12.3

zone and reach ignition at the ignition boundary, that the chemical enthalpy is converted into sensible enthalpy in the chemical reaction zone, and that the temperature curve is linear. The enthalpy balance gives

$$q_{preheat} = q_{conduction}$$
$$\dot{m} c_p (T_i - T_u) = \lambda A \frac{T_b - T_i}{\delta}$$

where $\dot{m}$ is the mass burning rate, c_p is the heat capacity, λ is the thermal conductivity (often estimated to be the average of the unburned and the burned values), A is the surface area, and δ is the flame thickness. The left hand side represents the amount of energy that is absorbed as the unburned mixture flows into the entrance of the preheat zone, raising it to the ignition temperature, T_i. The right hand side represents the heat flux (conduction) to the interface. As such, the heat needed to raise the unburned gas from T_u to T_i equals the heat conducted from the reaction zone.

By using the definition of the mass burning rate, the area cancels out from the equation, and the laminar burning speed is introduced and can be isolated for, as follows.

$$\dot{m} = \rho_u u_u A = \rho_u S_L A$$
$$c_p \rho_u S_L (T_i - T_u) = \lambda \frac{T_b - T_i}{\delta}$$
$$S_L = \frac{\lambda / c_p}{\rho_u \delta} \left(\frac{T_b - T_i}{T_i - T_u} \right)$$

We thereby have that the laminar flame speed depends on the thermal diffusivity of the mixture, $\alpha = \frac{\lambda / c_p}{\rho}$, is inversely proportional to the flame thickness, and is dependent on the reactivity of the mixture, as represented by the ratio of the temperature gradients.

If we then estimate the flame thickness as $\rho_u S_L = \dot{\omega} \delta$, where $\dot{\omega}$ is the volumetric reaction rate, the expression for the flame speed becomes

$$S_L = \sqrt{\frac{\lambda / c_p}{\rho} \left(\frac{T_b - T_i}{T_i - T_u} \right) \frac{\dot{\omega}}{\rho}} \sim \left(\alpha \frac{\dot{\omega}}{\rho} \right)^{1/2}$$

The theoretical results for the laminar flame speed have been compared with experimental results for more than 100 years, with varying success, precision and accuracy. In the following, a series of important experimental findings will be presented.

Flame Speed Measurements

There are numerous methods that enable the measurement of the laminar flame speed. One of the most basic methods is the use of a Bunsen-type burner, see Fig. 12.5, which establishes the flame speed, $S_L = u_u \sin(\alpha)$, based on geometrical considerations. Here, α is the half angle at the top of the flame. Another classic method is the use of flat flame burner and

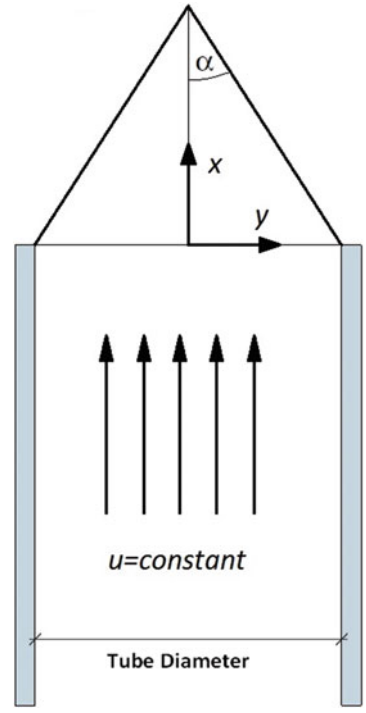

Fig. 12.5 Burner for measuring flame speed

after Spalding [31] introduced the concept of correction for heat losses, see Fig. 12.6, much improved results were obtained. This method is still very relevant today, and substantial research efforts have been undertaken to further develop the fidelity of the measurements [32, 33].

A third method that has been used for more than half a century is the outwardly propagating flame method, which requires that the premixture is contained upon ignition by a spark [10]. This containment can be a soap bubble, a balloon or a chamber. As mentioned, this method requires correction for the expansion that is caused by the hot combustion products, and if the experiments are conducted in a fixed volume chamber, then there is also a need for correction due to the pressure increase in the chamber as the flame propagates.

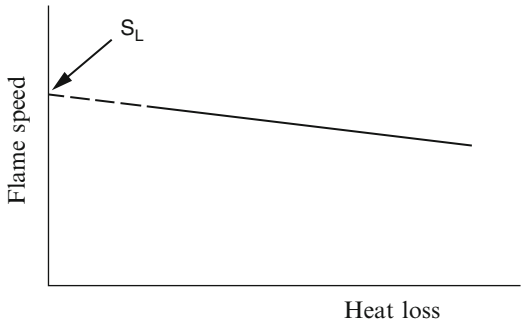

Fig. 12.6 The flame speeds obtained on a flat flame burner have to be corrected for the losses to the burner, as pointed out by Spalding [31]

However, in 1972 Andrews and Bradley [34] pointed out that something was not well understood when it came to the laminar flame speed measurements, despite the fact that more than 100 years had passed since Bunsen's breakthrough experiment for premixed flames and numerous researchers had worked on establishing the flame speed for half a century using all the methods described above. They created a plot of the type shown in Fig. 12.7, which displays the majority of the reported laminar flame speeds for stoichiometric (equivalence ratio, ϕ, equals 1) methane-air flames at normal ambient initial conditions (1 atm, 298 K) as a function of the year the result was published. It can be seen that there was a major discrepancy between the reported results for what should have yielded one data point. It is important to recognize that moderate extents of

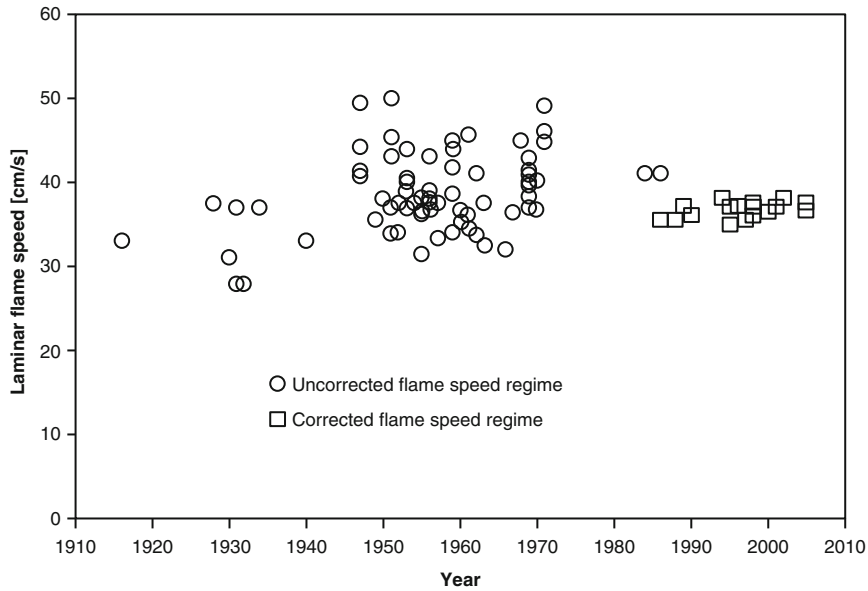

Fig. 12.7 The reported laminar flame speed for stoichiometric methane-air flames at ambient conditions (1 atm, 298 K) versus the year the results were published

error in the laminar flame speed could result in noticeable differences in the chemical mechanisms developed, as the accuracy of the developed mechanism must necessarily depend on the corresponding accuracy of its target points. Such mechanisms, which are developed and validated against incorrect experimental results, will yield poor predictive capabilities and this could lead to dangerous engine designs. Furthermore, it is to be noted that this was for conditions perceived to be simple, as compared to situations with other fuels, fuel mixtures, leaner or richer conditions, higher pressures, other inerts, etc., which will be discussed later.

Wu and Law [35] suggested that the observed scatter in existing experimental methane flame speed data in Fig. 12.7 was caused by the lack of correction for flame stretch (aerodynamic non-uniformity and/or unsteady effects that lead to changes in the flame surface area, which results in a modified reaction rate change, and therefore also in the propagation rate) and diffusion effects, and proposed a methodology to systematically subtract the effects of stretch from flame speed measurements. In particular, they designed a stagnation flow experiment in which flame stretch (aerodynamic non-uniformity and/or unsteady effects) could be measured, and then obtained the unstretched, fundamental flame speed through a linear extrapolation to zero stretch, see Fig. 12.8. Utilizing this technique and applying the stretch correction to other available experimental data, they were able to significantly reduce the discrepancies between measured flame speeds and narrow the discrepancies in the determined fundamental flame speeds of methane and hydrogen, respectively. The impact that this correction method had is obvious from the increased uniformity of the results published thereafter, see 'Corrected flame speed regime' data in Fig. 12.7.

Figure 12.9 is a plot of recent results for the laminar flame speed for methane-air flames at

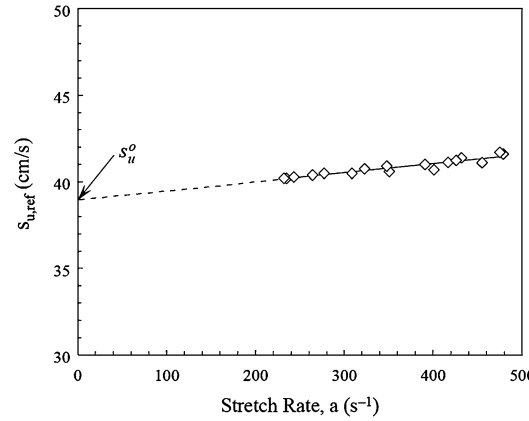

Fig. 12.8 The flame speeds obtained in a burner should be corrected for the stretch rate, as pointed out by Law [35]

atmospheric conditions from various methods that have utilized the abovementioned correction methods [36–39]. The good comparison, also with the numerical results (Wang-mechanism [40]), indicates that the problem of the laminar flame speed is now well-understood. These results have then enabled increased accuracy of the numerical results obtained using detailed chemical reaction schemes, a result that also validates the mechanism due to the fact that the laminar flame speed is the eigenvalue of the initial problem. As such, the theoretical (mathematics, physics and chemistry), numerical and experimental development combined with the utilization of technological developments (computers, cameras, measuring devices) have enabled us to understand the challenging physical problem through a structured effort. Often, the error bars posed in practical, real-life fire problems and in fundamental research problems in the field of fire safety are of the order that the laminar flame speed problem used to have, and the structured effort undertaken to solve the flame speed problem should be of inspiration for other fields of fire and combustion safety [41].

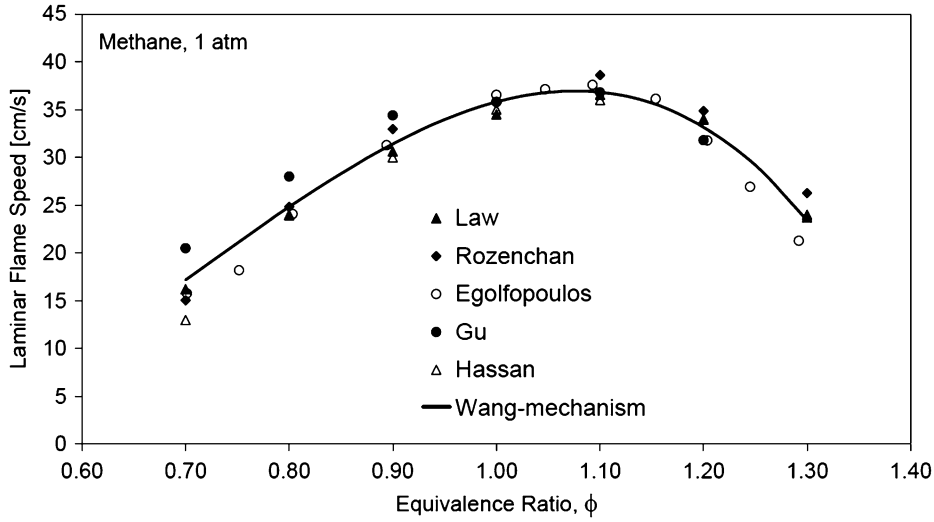

Fig. 12.9 The laminar flame speed as a function of the equivalence ratio for methane-air flames at atmospheric conditions from different experiments [36–39]. The *solid line* represents numerical results from a detailed chemical mechanism [40]

Parameters Affecting the Laminar Flame Speed

The laminar flame speed is a function of a range of practical parameters that will be described in the following.

Fuel Type and Equivalence Ratio

As discussed, the laminar flame speed primarily depends on the thermal diffusivity of the mixture and the reaction rate, and hence on the flame temperature. Given the fact that the flame temperature is dominated by the chemical potential energy stored in the fuel, we therefore expect different fuels to have different laminar flame speeds. The enthalpy of different fuels can be found in Chap. 5. Figure 12.10 shows the calculated adiabatic flame temperatures for a range of hydrocarbon-air mixtures, and the results suggest that acetylene should have the highest flame speed among the hydrocarbons, followed by ethylene. As expected, the reactivity decreases as the mixture is moved from stoichiometric conditions (apart from for acetylene), both towards leaner and richer conditions. As such, most of the fuels have a temperature maximum around stoichiometric conditions, and research has shown that the peak lies slightly on the rich side [42].

The expectations for the flame speed based on the temperature results are confirmed in Fig. 12.11, which shows the experimentally obtained laminar flame speeds of numerous hydrocarbons at standard initial ambient conditions (1 atm, 298 K) using the constant-pressure spherical flame technique [44, 45]. Results from the outwardly propagating spherical flame configuration are chosen, as this configuration is known to yield high accuracy results and has been central in the increased accuracy of the measurements and results that has taken place over the last three decades, as shown in Fig. 12.7 [38, 46–51]. This type of apparatus also easily allows for variations of the initial pressure, for which results will be presented and discussed below. Still, current research is carried out in order to further improve the understanding of the accuracy of various flame speed measurement techniques [137].

Acetylene (C_2H_2) vs. Ethylene (C_2H_4) vs. Ethane (C_2H_6) is one interesting comparison, as the results indicate that the molecular structure

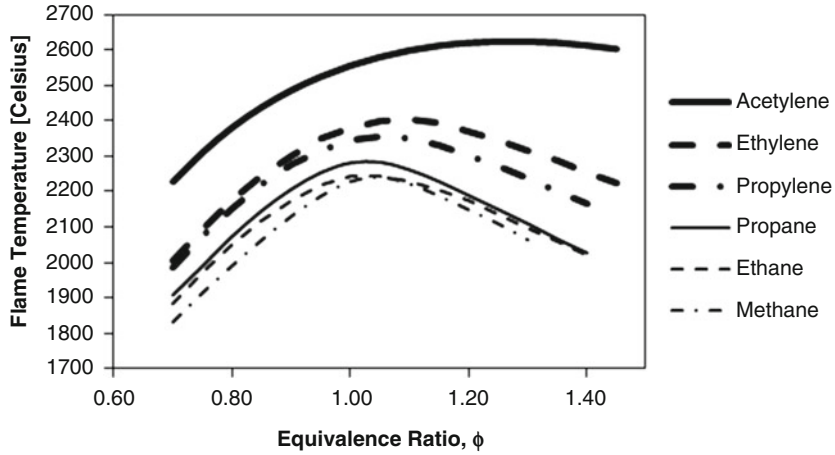

Fig. 12.10 The adiabatic flame temperature as a function of equivalence ratio for a range of hydrocarbons in air. The calculations are based on equilibrium considerations [43]

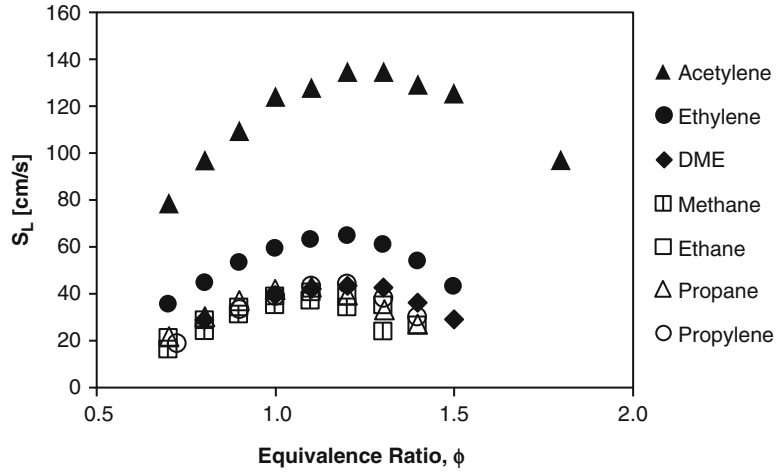

Fig. 12.11 Laminar flame speeds as a function of the equivalence ratio for various hydrocarbons in air at standard conditions

has an effect on the laminar burning velocity. However, as Fig. 12.10 showed that the temperature also was significantly different for the three fuels, further studies were needed to confirm that the molecular structure played a role. Law diluted mixtures of the three fuels with nitrogen so that they all had the same adiabatic flame temperature, and the results were conclusive, in that the ranking from highest to lowest flame speed still was acetylene, ethylene and ethane [13]. Therefore, the flame temperature dominates the laminar flame speed with a second order effect arising from the transport properties of the fuel.

Another point worth noting is that the flame speed for many alkanes is about 40 cm/s for stoichiometric conditions and this has been shown to be the case for numerous fuels in the entire range from methane to octane [52]. However, isomers, alcohols and aromatics display a larger variation in the flame speed at this condition. Just as the flame temperature did, the laminar flame speed decreases as the mixtures move

away from the stoichiometric condition, both towards leaner and richer conditions. Thus, as the flames become leaner/richer, the flame temperature is reduced, the flame speed is reduced and the flame becomes thicker (inversely proportional to the flame speed). The plot for the flame thickness as a function of the equivalence ratio is actually not very unlike the plot for the Minimum Ignition Energy in form (for more on MIE, see Chaps. 17 and 69) and the plot for quenching distance, which also scales with the flame thickness (see Chap. 17). Furthermore, the flammability limits (see Chap. 17) create a sort of asymptote for the characteristic parabolic shape that the flame speed, the flame temperature and the flame thickness have, and estimates on the needed flame temperature for sustained reaction are made in Chap. 5.

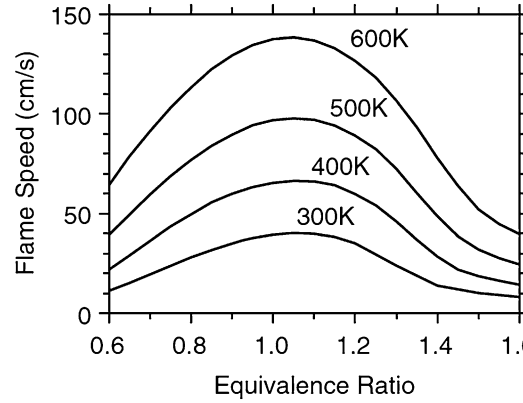

Fig. 12.12 Laminar flame speeds as a function of the upstream mixture temperature for methane at different equivalence ratios at atmospheric pressure [24]

Upstream Temperature

Given the importance that the temperature has on the flame speed, it is also expected that increasing the upstream (unburned) temperature should have an effect on the flame speed. First, it is envisioned that this increase could influence the adiabatic flame temperature. However, as seen in Chap. 5, the adiabatic flame temperature can be estimated as $T_{ad} = T_u + Y_u\, q_c/c_p$, and this effect is therefore small, because T_u is small compared to $Y_u q_c/c_p$. As such, from this perspective, the main effect of the increase in the upstream temperature is to facilitate the reaction by increasing the reaction rate, which has a weak dependence on the temperature for small increases in the upstream temperature. In the more rare cases where the upstream temperature is significantly increased, the effect of the enhanced reaction rate must be given greater attention than in the current string of arguments. Second, there is a small effect due to change in transport properties, because $\left(\lambda/c_p\right) \sim T^{\gamma}$, but this is a mild dependence, as γ is smaller than unity. Finally, there are changes associated with the density change. For a given fixed burning flux, $\dot{m} \sim \rho_u S_L$, the laminar burning speed will increase with an increase in the upstream temperature: $T_u \uparrow \Rightarrow \rho_u \downarrow \Rightarrow S_L \uparrow$. Thus, for an increase in upstream temperature, it is the changes in the density that lead to the only significant increase in the laminar flame speed.

Experimental and numerical results confirm that the laminar flame speed increases as the upstream temperature is increased, as seen in Fig. 12.12. In summary, the reason for this increase is that the laminar flame speed is proportional to the thermal diffusivity, α, which in turn scales as $\alpha \sim T^{3/2} p^{-1}$. Thus, the laminar burning velocity goes up as the temperature is increased.

Inert Type and Oxygen Percentage

As the creation of an inert or partially inert atmosphere is a common fire safety strategy, it is of interest to understand how this influences the flame speed. The type of inert will affect the laminar burning velocity in different ways. Experiments and calculations with detailed chemistry support this, and the most typical comparison is one between nitrogen, argon and helium as inerts for a fuel/oxygen/inert mixture with molar ratio of oxygen to inert equal to 0.21/0.79. In the following, the burning flux, $\dot{m} \sim \rho_u S_L$, is considered, as this parameter is the true eigenvalue of the problem, and thus isolates the

effects of inert addition better than the flame speed does.

The specific heat depends on the degrees of freedom for the respective inert, with increasing c_p for increasing freedom. Monatomic gases have smaller c_p than diatomic gases, so $c_{p,He} = c_{p,Ar} < c_{p,N_2}$. The thermal conductivity is inversely related to the mass of the inert, thus $\lambda_{Ar} \approx \lambda_{N_2} < \lambda_{\mathrm{He}}$ (somewhat larger for N_2 than for Ar). As the burning flux is a function of the ratio of these two parameters, $\dot{m} \sim (\lambda / c_p)$, and as a result, we have that $\dot{m}_{He} > \dot{m}_{Ar} > \dot{m}_{N_2}$, which is shown to hold for methane in Fig. 12.13 and similar results have been reported for other fuels [11, 53].

Figure 12.14 shows that the laminar flame velocity is a strong function of the oxygen concentration in the premixture, which is consistent with the fact that the flame temperature is a strong function of the oxygen concentration. Only a few experimental data points (solid markers) are presented along with the numerical results, as the flames are more and more affected by cellular flame front instabilities (see below) as the flame becomes thinner (flame velocity increases). Also, some of the very rich flames were clearly sooty, and such conditions tend to slow the flame due to increased radiative heat transfer and thus decreased flame temperature. Finally, it is worth noting that the chemical kinetic scheme used to obtain the numerical results is not validated for reduced oxygen concentrations and the results should therefore be used with caution.

It is important to note that these experiments with reduced oxygen concentration reveal that the flames can still propagate in such an environment. This is of interest, as a commonly used safety measure is to reduce the oxygen concentration in a room to around 15 % oxygen in air, as this typically prevents ignition of a non-premixed flame or extinguishes the same type of flame rapidly. However, if a premixture is created in such an environment, ignition and propagation are still possible.

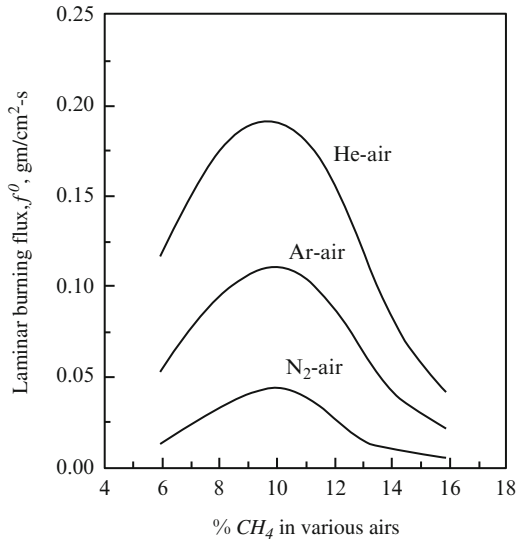

Fig. 12.13 Laminar burning flux for methane-oxygen-inert at different methane concentrations ($\phi = 1$ at 9.5 %) at atmospheric pressure [13]. The molar ratio of oxygen-inert was 0.21–0.79 for all mixtures

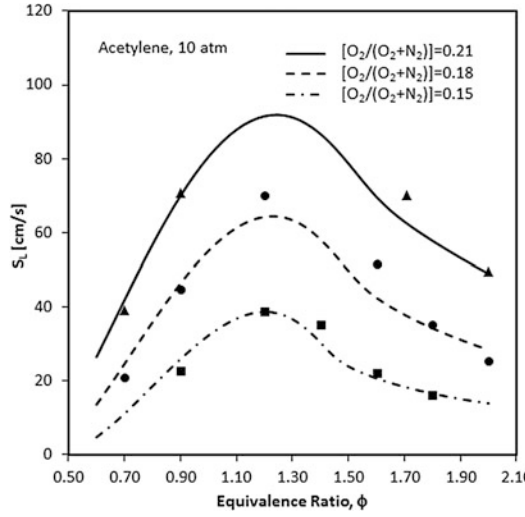

Fig. 12.14 Numerical and experimental laminar flame speeds as a function of the oxygen concentration in the initial environment for acetylene at different equivalence ratios at an initial pressure of 10 atm

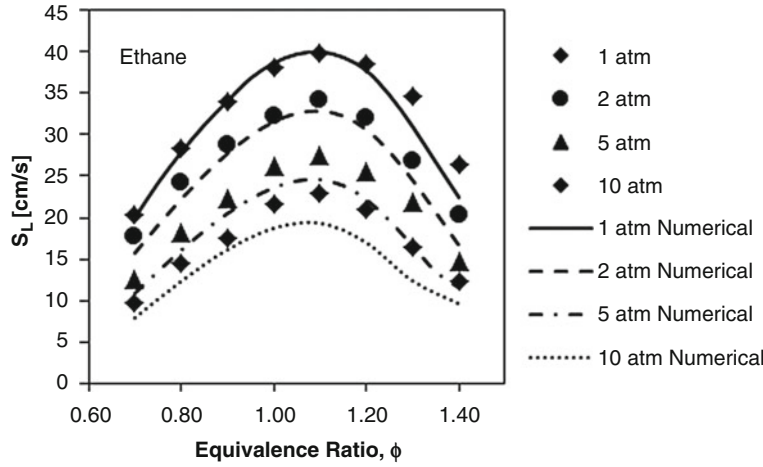

Fig. 12.15 Numerical and experimental laminar flame speeds as a function of pressure for ethane-air at different equivalence ratios

Pressure

The functionality of the laminar flame speed with respect to pressure is $S_L \sim p^{(n/2)-1}$, where n is the reaction order (sometimes referred to as the pressure exponent), which indicates the influence of pressure on the concentrations of the reactants and thus on the reaction rate. For elementary reactions, n can be 1, 2, or 3, and if the reaction order is 2, then it is predicted that the laminar flame velocity should be insensitive to pressure variations [54]. However, the reaction order is smaller than 2 for most hydrocarbons, so the laminar flame speed typically decreases as the pressure is increased. Experiments have validated this, as shown in Fig. 12.15.

However, as mentioned, the true eigenvalue of the problem is the mass burning flux, which is the product of the laminar burning velocity and the density, and this parameter should increase as the pressure is increased. Figure 12.16 shows that the mass burning flux indeed increases as the pressure increases. High-pressure accidents are therefore more severe than low pressure accidents, because the momentum is much higher.

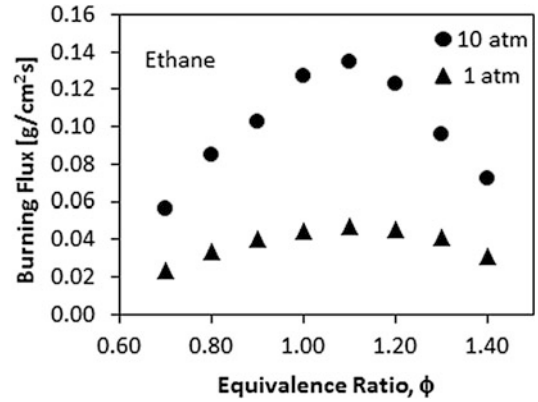

Fig. 12.16 The burning flux of ethane-air (and other fuel-air mixtures) increases as the pressure increases. The results are obtained by multiplying the density obtained from equilibrium calculations with the experimentally obtained flame velocity

Fuel Mixture

Based on the knowledge of the properties of the gases, custom-made compositions can be made to meet the desired design or safety criteria, both for the propagation velocity and for the stability (see below) [55–57]. This becomes very relevant for all the new fuel types, such as syngas and biofuels, as one can either change the burners, or create the mixture (through use of inerts or other fuels) such that it will perform as desired in the existing design. Results for a range of syngas mixtures are shown in Fig. 12.17, and similar results for a range of pressures are shown in the paper by Sun et al. [55].

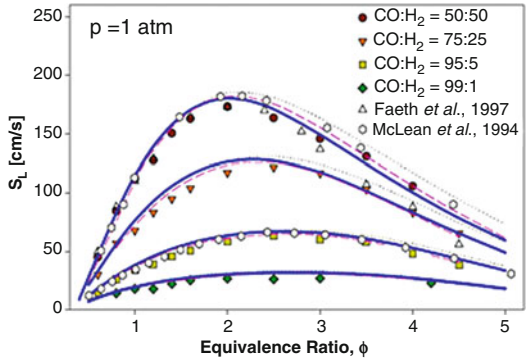

Fig. 12.17 The laminar flame speed of various mixtures of hydrogen and carbon monoxide (syngas) in air at standard conditions [48, 55, 58]. The symbols represents experimental results, whereas the lines represents calculated values

Flame Instabilities and Acceleration

Due to the practical importance of cellular flames in combustion at elevated pressures, and also for safety considerations at atmospheric conditions, the last decade has seen significant experimental efforts pursuing a more thorough understanding of the fundamentals of the phenomenon. An outwardly propagating flame will typically not have instabilities initially, but the flame front will eventually become filled with cellular instabilities, which can either be hydrodynamic or thermal-diffusive in nature, something which has been shown extensively both in experiments and theory [29, 57, 59–68]. Figure 12.18 shows the evolution of a hydrogen flame from a point-source ignition (e.g. accidental explosion) for three different initial conditions. Research has shown that although these cellular instabilities accelerate the propagation velocity [69–74], there is no transition from a laminar to a turbulent flame in an unconfined environment [75]. Bradley has also shown that large scale experiments correlate well with small scale experiments [76, 77]. Under confinement in tubes with or without obstacles [78, 112, 128–131], which is common in places where accidental gas leaks are ignited, initially slow flames may accelerate spontaneously up to supersonic speed, and deflagration to detonation transition (DDT) is possible. These large scale phenomena are challenging to model, given the vast span of the scales, but there are validated models that can handle the problem reasonably well [79].

Flame Structure and Detailed Chemistry of Premixed Flames

Standard tools exist to calculate the flame propagation with detailed chemistry, and one can extract details about all the relevant parameters from such calculations. It is important that such calculations are done in an 'infinite' domain so that boundary conditions do not influence the calculations. This is easily achieved over a small domain, given the fact that premixed flames are very thin. The calculation results presented herein were obtained using the Sandia PREMIX code [80], which simulates the propagation of a planar flame through a premixture under adiabatic conditions. The C_2–C_3 flames were simulated using the detailed reaction mechanism of Qin et al. [40], which includes 70 species and 463 reactions. Other mechanisms exist, either for specific fuels, or for ranges of fuels, with the smallest being that for hydrogen with 9 species and 21 reactions to larger mechanisms with hundreds of species and several thousand reactions [81–89]. As this is a field in rapid development, newer mechanisms and improvements to existing ones are published continuously, and lately there has been a great focus on obtaining results and understanding for biofuels and other alternative fuels [90].

In addition to providing global results such as the propagation velocity of the flames, these detailed mechanisms provide insight into the intermediate steps that take place as reactants are turned into products. For example, calculations with hydrocarbons have shown (in the reaction coordinate, see Fig. 12.19) that the CO is formed before the CO_2 and that temperature goes up as the hydrocarbon is

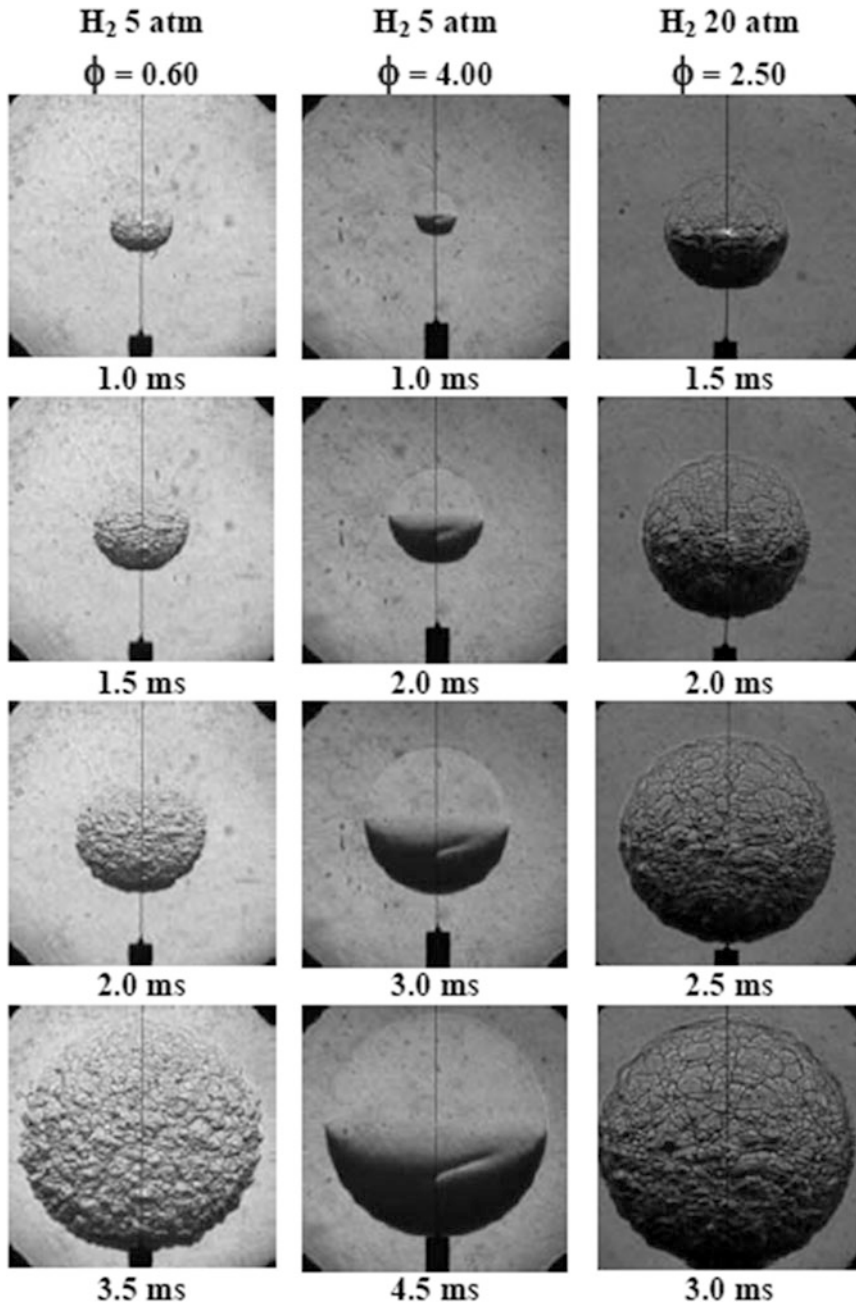

Fig. 12.18 Evolution of an outwardly propagating spherical flame from a point-source ignition in a premixture of hydrogen and air at three different pressures [13]. The lean flame (*left*) has a cellular structure due to thermal-diffusive instabilities, whereas the rich flame at the same pressure (*middle*) is smooth. The rich flame to the right has hydrodynamic cellular instabilities over the flame front as a result of the decrease in flame thickness with the increase in pressure (the flame thickness scales inversely with the laminar flame speed). The increased surface area leads to an increase in the propagation velocity, and the flame no longer traverses into the unburned mixture with the laminar flame velocity

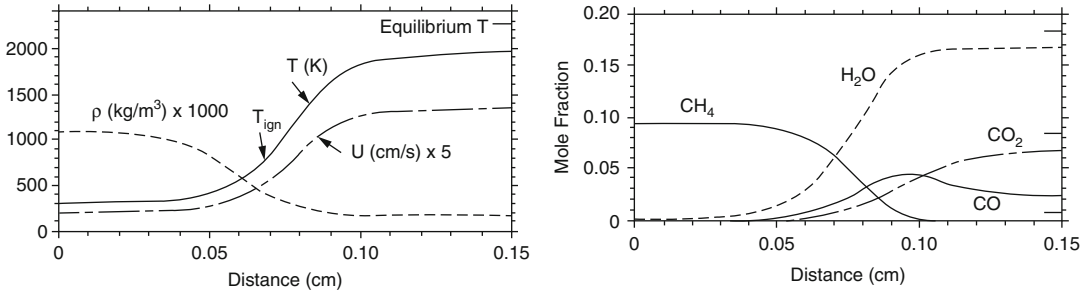

Fig. 12.19 Reaction coordinate view of the physical properties (*left*) and species (*right*) for a methane-air flame [24]

consumed. Further, as the concentration of the hydrocarbon diminishes, the CO concentration is at its max, before decaying as it is converted into CO_2. The intermediate carbon-containing species of the reaction, such as CH_3, CH_2O, HCO and CH exist in a very small zone, whereas HO_2 and H_2O_2 exist over a somewhat broader zone. As such, the reaction zone is very narrow, whereas the equilibrium temperature is reached relatively slowly. The increase in the reaction rate comes with the activation of the reaction, whereas the decrease is caused by depletion of the reactants. The fact that the temperature and fuel depletion profiles are not completely symmetric, indicates that the thermal and the mass diffusion are not equal throughout the flame, which means that the Lewis number (ratio of thermal and mass diffusion) is not equal to unity, as opposed what is typically assumed in a basic flame analysis. Very detailed information and in-depth understanding of flame chemistry and flame structures can be found in numerous classic textbooks [18–22].

Numerical Simulations of Premixed Flames

A proper discussion of Direct Numerical Simulations (DNS), Large Eddy Simulations (LES) and Computational Fluid Dynamics (CFD) modeling requires a book of its own, and excellent ones do exist [89, 90]. In addition, numerous new methods have been developed to deal with the complexity and large computational times that are introduced when detailed chemistry is included in reacting flow scenarios and these methods should be consulted to obtain high fidelity results at reasonable calculation cost [93–96].

Other Aspects Related to Premixed Flames

There are numerous other aspects to the study of premixed flames than the laminar flame speed, but they are all, to some extent, variations or different phases of the main propagation mode. Some of these aspects are briefly mentioned in the following.

Adiabatic Flame Temperature for Constant Pressure Versus Constant Volume Combustion

Another parameter of interest in the study of premixed flames is the adiabatic flame temperature, which is based on thermochemistry (see Chap. 5). The flame temperature of a premixed flame can be estimated as

$$T_b = T_u + \frac{Y_{F,u} q_c}{c_p}$$

where q_c is the chemical heat release.

The adiabatic flame temperature, T_{ad}, is estimated from the total enthalpy, which is the sum of the chemical and the sensible energy (see Chap. 5 for further details). For a constant pressure process, we have that the enthalpy of the reactants should equal the enthalpy of the products, so that

$$H_{react} = H_{prod}$$

$$\sum_{react} N_i h_i = \sum_{prod} N_i h_i = \sum_{prod} N_i \left[h^0_{f,i} + c_{p,i} (T_{ad} - T_u) \right].$$

For a constant volume process, on the other hand, we have the internal energy of the reactants match the internal energy of the products, so that

$$U_{react} = U_{prod}$$

$$H_{react} = H_{prod} + R_u \left(N_{react} T_u - N_{prod} T_{ad} \right).$$

Thus, for the same initial conditions, a constant volume combustion process results in much higher temperatures than a constant pressure combustion process does. This is a consequence of the pressure forces not doing any work when the volume is fixed.

Ignition

In comparison to other premixed phenomena, ignition can be considered a low temperature phenomenon. As for studies of chemical kinetics, both low and high temperature and homogenous and non-homogenous phenomena have to be understood. In the piloted ignition scenario, a local energy is supplied, which will provide situation where the Damköhler number (the ratio of characteristic fluid time and the characteristic chemical time) has to be larger than a critical Damköhler number for ignition to occur. Typical ignition sources for fire scenarios are very large compared to the MIE. Sparks are used for establishing the MIE, and a small spark with short duration is enough. The only requirement is that the duration is long enough compared to the chemical time scale, which typically is so short that it is very unlikely for any spark not to exist for a sufficient time to ignite a premixture within the flammability limits. As such, a non-ignition scenario from a spark means that the energy density (a larger spark will have to heat a larger mass) was not sufficient. Again, several levels of mathematical complexity can be offered for the analysis, which reveals that ignition parameters are a function of the laminar flame speed (and the flame thickness). The critical ignition radius is proportional to the flame thickness (and thus inversely proportional to the laminar burning velocity). Given the fact that the laminar burning velocity is decreasing as the pressure is increased, we have that ignition of most premixtures is facilitated as the pressure is increased.

Turbulence

As reaction is a flame surface phenomenon, it is predicted that the turbulent burning velocity is higher than the laminar burning velocity due to the increased area of a turbulent flame and the increase in the transport at the flame surface, which will lead to increased reaction rate and consequently larger velocity. The reader can consult several resources to learn more on the effect of turbulence on premixed flames [67, 97–110].

Tube Flames

Reacting flow and premixed flames in tubes are of great importance for efficient and safe engine and burner design [11, 111–114]. The pressure dependence in a closed tube creates acoustic excitation (spherical configuration has acoustic decay). The Rayleigh criterion (oscillations) shows that heat must be added in phase with pressure if energy is to be transferred into acoustic waves [115]. The classical demonstration consisted of a hydrogen flame burning

inside an open tube. Pressure variations in the tube cause the flow of gas, and therefore the heat release, volume expansion, and backpressure on the nozzle to vary during the vibration. In Rijke's tube, which is open at both ends, energy from heat is turned into sound from a standing wave [116]. If the product of the fluctuating parts of the heat release and the backpressure, integrated over a cycle of the vibration, is positive, in the absence of damping the vibration will be maintained. In other words, if the fluctuating heat release is more in phase than out of phase with the vibration in the resonator, conditions are right for feeding energy into the vibration.

Experiments [132, 133] and theory [134] have demonstrated a variety of possible outcomes of flame-acoustic interaction, such as flame stabilization by sound waves, a parametric instability and spontaneous turbulization of the flame front. In particular, the spontaneous turbulization may develop as a result of a flame-acoustic resonance with strong increase of pressure and burning rate in the process [135, 136].

Detonation

The main motion of this chapter has been the subsonic propagation of premixed flames, but as shown in Fig. 12.2, the solutions to the equations also predict a regime that is supersonic, and this propagation is referred to as detonation. Whereas the propagation velocity of the laminar premixed flames in the deflagration regime moved with a velocity of the order of 1 m/s, detonation velocities are of the order of 1 km/s. As opposed to what is the case for laminar premixed flames, heat conduction and radical diffusion do not control the velocity for detonations, and the hot gases follow the wave for detonations. The shock wave structure and the developed supersonic wave raise the temperature and pressure substantially and cause explosive reaction and the energy release that sustains the wave propagation. As such, the detonation velocity is the velocity of the unburned gases moving into the wave, and at the Chapman-Jouguet point, the detonation velocity equals the velocity of sound in the gases behind the detonation wave plus the mass velocity of these gases.

From a practical point, it could be of interest to know if the detonation velocity of fuel-oxygen-argon is faster than that of fuel-oxygen-helium. As both have a unity Mach number behind the detonation, and assuming that the flame temperature is not too different (it is different, but not 10 times), the following shows that it all comes down to the molecular weight dependence of the speed of sound, and that the detonation velocity in helium is significantly higher.

$$\frac{u_{He}}{u_{Ar}} = \sqrt{\frac{(\gamma RT)_{He}}{(\gamma RT)_{Ar}}} \approx \sqrt{\frac{R_{He}}{R_{Ar}}} = \sqrt{\frac{R^0/MW_{He}}{R^0/MW_{Ar}}} = \sqrt{\frac{MW_{Ar}}{MW_{He}}} = \sqrt{10}$$

As with the other smaller topics in this subchapter, there is significant knowledge to be found in the literature on detonations [99, 117–125], as well as in Chaps. 69 and 70.

The Role of Premixed Flames in Fire Safety Engineering

As fire safety engineers, our main objective is to avoid ignition. This can be achieved by creating an environment with no or small energy sources, by keeping the atmosphere outside of the flammability limits through design or by use of detection systems, through flame arrestors that will lead to quenching, through creating an overall inert atmosphere (remove oxygen, increase nitrogen). However, if ignition does occur, we want to have appropriately scaled and positioned pressure vents for explosions, or introduce heat losses or energy absorption for flames, which can be

done either chemically or physically. Further information can be found in Chaps. 69 and 70.

Igniting a premixture in a tube that is open at both ends will lead to a combustion wave with transport processes involving heat conduction and diffusion of radicals, which therefore will result in a speed that is lower than the speed of sound in the unburned mixture (deflagration). If, on the other hand, the tube filled with the same premixture is closed at one end, then there is a possibility of a transition from deflagration to detonation (supersonic). This can for example happen in mine explosions. Thus, it is clear that the environment plays a significant role for what happens with the 'explosive' mixture.

The main lesson to be learned for a fire safety engineer from this chapter is that detailed and accurate knowledge of a complex problem like that of premixed burning is achievable, as shown in Fig. 12.7. With structured efforts over time, the field of fire safety can grow into a science in its true form. The challenge lies in scaling up fire [41].

References

1. Bunsen, R, & Roscoe H., 1857 Photochemische Untersuchungen: Maafsbestimmung der Chemische Wirkungen des Lichts, Poggendorff's Annalen der Physik 100, 43–88, http://gallica.bnf.fr/ark:/12148/bpt6k15185v/f55.image.
2. Semenov, N.N. 1927 *Z. Phys.*, **46**, 109; *Chemical Kinetics and Chain Reactions*, Clarendon, London, 1935.
3. Hinshelwood, C.N. and Thompson, H.W. 1928 *Proc. R. Soc. London A*, **118**, 171;
4. Hinshelwood, C.N. 1929 *Kinetics of Chemical Change in Gaseous Systems*, 2nd Edition, Clarendon, Oxford.
5. Houston, P.L. 2001 *Chemical Kinetics and Reaction Dynamics*, McGraw-Hill
6. Laidler, K.J. 1987 *Chemical Kinetics*, Pearson Education.
7. Semenov N. N. 1958 *Some Problems in Chemical Kinetics and Reactivity*. Vol. I. Princeton University Press.
8. Frank-Kameneskii, D. A. 1969 *Diffusion and heat Transfer in Chemical Kinetics*, Plenum Press.
9. Wang, X. & Law, C.K. 2013 "An analysis of the explosion limits of hydrogen-oxygen mixtures," Journal of Chemical Physics **138**, 134305, 1–12.
10. Lewis, B. & von Elbe, G. 1951 *Combustion, Flames and Explosions of Gases*, Academic Press, New York.
11. Lewis, B. & von Elbe, G. 1987 *Combustion, Flames and Explosions of Gases*, 3rd edn. Academic.
12. Strehlow, R.A. 1979 *Fundamentals of Combustion*, Kreiger Publishing Company, New York.
13. Law, C. K. 2006 Combustion Physics, Cambridge University Press.
14. Zel'dovich, Y. B., Barenblatt, G. I., Librovich, V. B. & Makhviladze, G. M. 1985 *The Mathematical Theory of Combustion and Explosions*. Consultants Bureau.
15. Kuo, K. K. 2002 *Principles of Combustion*, 2nd edn. John Wiley.
16. Williams, F. A. 1985 *Combustion Theory*. Addison-Wesley.
17. Turns, S. R. 2000 *An Introduction to Combustion: Concepts and Applications*. McGraw-Hill.
18. Glassman, I. 1996 *Combustion*. Academic.
19. Gaydon, A. G. & Wolfhard, H.G. 1970 *Flames*. Chapman and Hall.
20. Fristrom, R. M. & Westenberg, A. A. 1965 *Flame Structure*. McGraw-Hill.
21. Gardiner, W. C., Jr. 1999 *Combustion Chemistry*, Springer-Verlag.
22. Fenimore, C. P. 1964 *Chemistry in Premixed Flames*. Pergamon.
23. Buckmaster, J. D. & Ludford, G. S. S. 1982 *Theory of Laminar Flames*. Cambridge.
24. McAllister, S. Chen, J-Y & Fernandez-Pello, A.C. 2011 Fundamentals of Combustion Processes, Springer.
25. Rankine, W. J. M. (1870). "On the thermodynamic theory of waves of finite longitudinal disturbances". *Philosophical Transactions of the Royal Society of London* **160**: 277–288, doi:10.1098/rstl.1870.0015.
26. Hugoniot, H. (1887). "Mémoire sur la propagation des mouvements dans les corps et spécialement dans les gaz parfaits (première partie) [Memoir on the propagation of movements in bodies, especially perfect gases (first part)"] (in French). *Journal de l'École Polytechnique* **57**: 3–97. See also: Hugoniot, H. (1889) "Mémoire sur la propagation des mouvements dans les corps et spécialement dans les gaz parfaits (deuxième partie)" [Memoir on the propagation of movements in bodies, especially perfect gases (second part)], *Journal de l'École Polytechnique*, vol. 58, pages 1–125.
27. Chapman, D. L. 1899 "On the rate of explosion in gases", *Philosophical Magazine*, Series 5, **47** (284): 90–104.
28. Jouguet, J.C.E. 1906 "Sur la propagation des réactions chimiques dans les gaz" [On the propagation of chemical reactions in gases], *Journal des Mathématiques Pures et Appliquées*, Series 6, Vol. 1, pp. 347–425 (1905), continued in Vol. 2, pp. 5–85 (1906).

29. Landau, L.D. 1944 On the theory of slow combustion. *Acta Physicochim. U.R.S.S.* **19**, 77–85.
30. Mallard, E. & Le Chatelier, H.L. 1883 *Ann. Mines* **4**, 379.
31. Botha, J. P. & Spalding, D. B. 1954 The laminar flame speed of propane/air mixtures with heat extraction from the flame. *Proc. R. Soc. Lond.*, Series A, *Mathematical and Physical Sciences* 225, 71–96.
32. de Goey, L. P. H., van Maaren, A. & Quax, R. M. 1993 Stabilization of adiabatic premixed laminar flames on a flat flame burner *Combust. Sci. Technol.* 92, 201–207.
33. Bosschaart, K.J. & de Goey, L.P.H. 2004 "Detailed analysis of the heat flux method for measuring burning velocities," Combustion and Flame 132, 170–180.
34. Andrews, G.E. & Bradley, D. 1972 Determination of burning velocities: A critical review. *Combust. Flame* **18**, 133–153.
35. Wu, C.K. & Law, C.K. 1984 On the determination of laminar flame speeds from stretched flames. *Proc. Combust. Instit.* **20**, 1941–1949.
36. Hassan, M.I., Aung, K.T. & Faeth, G.M. 1998 Measured and predicted properties of laminar premixed methane/air flames at various pressures. *Combust. Flame* **115**, 539–550.
37. Vagelopoulos, C.M. & Egolfopoulos, F.N. 1998 Direct experimental determination of laminar flame speeds. *Proc. Combust. Instit.* **27**, 513–519.
38. Rozenchan, G., Zhu, D.L., Law, C.K. & Tse, S.D. 2002 Outward propagation, burning velocities, and chemical effects of methane flames up to 60 atm. *Proc. Combust. Instit.* **29**, 1461–1469.
39. Gu, X.J., Haq, M.Z., Lawes, M. & Woolley, R. 2000 Laminar burning velocity and Markstein lengths of methane-air mixtures. *Combust. Flame* **121**, 41–58.
40. Qin, Z., Lissianski, V., Yang, H., Gardiner, W.C., Davis, S.G. & Wang H. 2000 Combustion Chemistry of Propane: A Case Study of Detailed Reaction Mechanism Optimization. *Proc. Combust. Inst.* **28**, 1663–1669.
41. Torero, J.L., 2013 Scaling-up Fire, *Proc. Combust. Instit.* 34 99–124.
42. Law, C.K., Makino, A. & Lu, T.F. 2006 "On the Off-Stoichiometric Peaking of Adiabatic Flame Temperature with Equivalence Ratio," *Combust. Flame* **145**, 808–819.
43. Reynolds, W. C. 1986 The element potential for chemical equilibrium analysis: implementation in the interactive program STANJAN. *Tech. Rept.* A-3391, Dept. of Mechanical Engineering, Stanford University.
44. Tse, S.D., Zhu, D.L. & Law, C.K. 2004 An optically accessible high-pressure combustion apparatus. *Rev. Sci. Instrum.* **75**, 233–239.
45. Jomaas, G., Zheng, X.L., Zhu, D.L., & Law, C.K. 2005 Experimental determination of counterflow ignition temperatures and laminar flame speeds of C2-C3 hydrocarbons at atmospheric and elevated pressures. *Proc. Combust. Instit.* **30**, 193–200.
46. Dowdy, D.R., Smith, D.B., Taylor, S.C. & Williams, A. 1990 The use of expanding spherical flames to determine burning velocities and stretch effects in hydrogen/air mixtures. *Proc. Combust. Instit.* **23**, 325–332.
47. Bradley, D. & Harper, C.M. 1994 The development of instabilities in laminar explosion flames. *Combust. Flame* **99**, 562–572.
48. Hassan, M.I., Aung, K.T. & Faeth, G.M. 1997 Properties of laminar premixed CO/H_2/air flames at various pressures, *Journal of Propulsion and Power* **13**, 239–245.
49. Hassan, M.I., Aung, K.T. & Faeth, G.M. 1998 Measured and predicted properties of laminar premixed methane/air flames at various pressures. *Combust. Flame* **115**, 539–550.
50. Hassan, M.I. Aung, K.T. Kwon, O.C. & Faeth, G.M. 1998 Properties of laminar premixed hydrocarbon/air flames at various pressures. *J. Prop. Power* **14**, 479–488
51. Tse, S.D., Zhu, D.L. & Law, C.K. 2000 Morphology and burning rates of expanding spherical flames in H_2/O_2/inert mixtures up to 60 atmospheres. *Proc. Combust. Instit.* **28**, 1793–1799.
52. Davis, S.G. & Law, C.K. 1998 Determination of fuel structure effects on laminar flame speeds of C_1 to C_8 hydrocarbons. *Combust. Sci. Tech.* **140**, 427–449.
53. Kwon, O.C. & Faeth, G.M. 2001 Flame/stretch interactions of premixed hydrogen-fueled flames: Measurements and predictions. *Combust. Flame* **124**, 590–610.
54. Law, C.K. 2006 "Propagation, structure, and limit phenomena of laminar flames at elevated pressures," Combustion Science and Technology **178**, 335–360.
55. Sun, H., Yang, S.I., Jomaas, G. & Law, C.K. 2007 High-pressure laminar flame speeds and kinetic modeling of carbon monoxide/hydrogen combustion. *Proc. Combust. Instit.* **31**, 439–446.
56. C.K. Law, G. Jomaas, J.K. Bechtold, Proceedings of the Combustion Institute 30 (2005) 159–167.
57. G. Jomaas, C.K. Law, J.K. Bechtold, Journal of Fluid Mechanics 583 (2007) 1–26.
58. Mclean, I.C., Smith, D.B. & Taylor, S.C. 1994 The use of carbon monoxide/hydrogen burning velocities to examine the rate of the CO + OH reaction. *Proc. Combust. Instit.* **25**,749–757.
59. Darrieus G. 1938 Propagation d'un front de flamme. *La Technique Moderne* **30**, No. 18.
60. Markstein, G.H. 1951 Experimental and theoretical studies of flame-front stability. *J. Aero. Sci.* **18**, 199–209.

61. Groff, E.G. 1982 The cellular nature of confined spherical propane-air flames. *Combust. Flame* **48**, 51–62.
62. Markstein, G. H. 1964 *Nonsteady Flame Propagation*. Pergamon.
63. Frankel, M.L. & Sivashinsky, G.I. 1983 On effects due to thermal expansion and Lewis number in spherical flame propagation. *Combust. Sci. Tech.* **31**, 131–138.
64. Sivashinsky, G.I. 1977 Diffusional-thermal theory of cellular flames. *Combust. Sci. Tech.* **15**, 137–146.
65. Bechtold, J.K. & Matalon, M. 1987 Hydrodynamic and diffusion effects on the stability of spherically expanding flames. *Combust. Flame* **67**, 77–90.
66. Joulin, G. & Clavin, P. 1979 Linear stability analysis of nonadiabatic flames: Diffusional-thermal model. *Combust. Flame* **35**, 139–153.
67. Clavin, P. 1985 Dynamic behavior of premixed flame fronts in laminar and turbulent flows. *Prog. Energy Combust. Sci.* **11**, 1–59.
68. Istratov, A.G. & Librovich, V.B. 1969 On the stability of gasdynamic discontinuities associated with chemical reactions. The case of a spherical flame. *Astronautica Acta* **14**, 453–467.
69. Sivashinsky, G.I. 1979 On self-turbulization of a laminar flame. *Acta Astronautica* **6**, 569–591.
70. Filyand, L., Sivashinsky, G.I. & Frankel, M.L. 1994 On self-acceleration of outward propagating wrinkled flames. *Physica D* **72,** 110–118.
71. Bychkov, V.V. & Liberman, M.A. 1996 Stability and the fractal structure of a spherical flame in a self-similar regime. *Phys. Rev. Lett.* **76,** 2814–2817.
72. Gostintsev, Y.A., Istratov, A.G. & Shulenin, Y.V. 1989 Self-similar propagation of a free turbulent flame in mixed gas mixtures. *Combustion, Explosion and Shock* Waves **24**, 563–569.
73. Gostintsev, Y.A., Istratov, A.G., Kidin, N.I & Fortov, V.E. 1999 Autoturbulization of gas flames: Theoretical treatment. *High Temperature* **37**, 603–607.
74. Sivashinksy, G.I. 1983 Instabilities, pattern formation, and turbulence in flames. *Ann. Rev. Fluid Mech.* **15**, 179–199.
75. F. Wu, G. Jomaas, and C.K. Law, "An Investigation on Self-Acceleration of Cellular Spherical Flames," Proceedings of the Combustion Institute, Vol. 34, 937–945, *2013*.
76. Bradley, D. 1999 Instabilities and flame speeds in large-scale premixed gaseous explosions. *Phil. Trans. R. Soc. Lond. A* **357**, 3567–3581.
77. Bradley, D. Cresswell, T.M. & Puttock, J.S. 2001 Flame acceleration due to flame-induced instabilities in large-scale explosions. *Combust. Flame* **124**, 551–559.
78. Dorofeev, Kuznetsov, Alekseev, Efimenko, and Breitung "Evaluation of limits for effective flame acceleration in hydrogen mixtures," Journal of Loss Prevention in the Process Industries 14, 2001.
79. Skjold, T., Pedersen, H.H., Bernard, L., Ichard, M., Middha, P., Narasimhamurthy, V.D., Landvik, T., Lea, T & Pesch, L. (2013). A matter of life and death: validating, qualifying and documenting models for simulating flow-related accident scenarios in the process industry. Fourteenth International Symposium on Loss Prevention and Safety Promotion in the Process Industries, Florence, 12–15 May 2013, published in Chemical Engineering Transactions, 31: 187–192. ISBN: 978-88-95608-22-8. ISSN: 1974-9791, http://www.aidic.it/cet/13/31/032.pdf.
80. Kee, R.J., Grcar, J.F., Smooke, M.D. & Miller, J.A. 1985 A FORTAN program for modeling steady laminar one-dimensional premixed flames. *Sandia Report* SAND85-8240.
81. Smith, G.P., Golden, D.M., Frenklach, M., Moriarty, N.W., Eiteneer, B., Goldenberg, M., Bowman, C.T., Hanson, R.K., Song, S., Gardiner, W.C., Lissianski, V. & Qin, Z. GRIMech homepage, Gas Research Institute, Chicago, 1999, http://www.me.berkeley.edu/gri-mech/.
82. Li, J., Zhao, Z., Kazakov, A. & Dryer, F.L. 2004 An updated comprehensive kinetic model of hydrogen combustion. *Int. J. Chem. Kinet.* **36**, 566–575.
83. Davis, S.G., Joshi, A.V., Wang, H. & Egolfopoulos, F.N. 2005 An optimized kinetic model of H_2/CO combustion. *Proc. Combust. Instit.* **30**, (2005), 1283–1292.
84. Curran, H.J., Fischer, S.L. & Dryer F.L. 2000 The Reaction Kinetics of Dimethylether. II: Low-Temperature Oxidation in Flow Reactors. *Int. J. Chem. Kinet.* **32**, 741–759.
85. Curran, H. J., Gaffuri, P., Pitz, W. J. & Westbrook, C. K. 2002 A comprehensive modeling study of iso-octane oxidation. Combustion and Flame 129, 253–280.
86. Farrell, J. T., Cernansky, N. P, Dryer, F. L., Friend, D. G., Hergart, C. A., Law, C. K., McDavid, R. M., Mueller, C. J., Patel, A. K. & Pitsch, H. 2007 Development of an experimental database and kinetic models for surrogate diesel fuels. 2007 SAE World Congress 2007-01-0201.
87. Fisher, E. M., Pitz, W. J., Curran, H. J. & Westbrook, C. K. 2000 Detailed chemical kinetic mechanisms for combustion of oxygenated fuels. Proceedings of the Combustion Institute 28, 1579–1586.
88. Pitz, W. J., Cernansky, N. P., Dryer, F. L., Egolfopoulos, F. N., Farrell, J. T., Friend, D. G. & Pitsch, H. 2007 Development of an experimental database and chemical kinetic models for surrogate gasoline fuels. 2007 SAE World Congress 2007-01-0175.
89. Sirjean, B., Dames, E., Sheen, D. A., You, X.-Q., Sung, C., Holley, A. T., Egolfopoulos, F. N., Wang, H., Vasu, S. S., Davidson, D. F., Hanson, R. K., Pitsch, H., Bowman, C. T., Kelley, A. P., Law, C. K., Tsang, W., Cernansky, N. P., Miller, D. L., Violi, A. & Lindstedt, R. P. 2009 A high-temperature

chemical kinetic model of n-alkane oxidation, JetSurF version 1.0. http://melchior.usc.edu/JetSurF/JetSurF1.0/Index.html.
90. Liu W., Sivaramakrishnan R., Davis M.J., Som S., Longman D.E., Lu T.F., 2013 "Development of a Reduced Biodiesel Surrogate Model for Compression Ignition Engine Modeling," Proc. Combust. Inst. 34, 401–409.
91. D. Poinsot, T. & Veynante, D. 2005 *Theoretical and Numerical Combustion*. 2nd Edition R.T. Edwards, Inc., Flourtown.
92. Warnatz, J., Maas, U. & Dibble, R. W. 2001 *Combustion: Physical and Chemical Fundamentals, Modeling and Simulation, Experiments, Pollutant Formation*. Springer-Verlag.
93. Lu T.F., Law C.K., 2006 "On the Applicability of Directed Relation Graph to the Reduction of Reaction Mechanisms," Combust. Flame, 146, 472–483.
94. Lu T. F., Law C.K., 2009 "Toward Accommodating Realistic Fuel Chemistry in Large-Scale Computation," Prog. Energy Combust. Sci., 35, 192–215.
95. Lu T.F., Ju Y., Law C.K., 2001 "Complex CSP for Chemistry Reduction and Analysis," Combust. Flame, 126, 1445–1455.
96. Pope, S. B., 1997 Computationally efficient implementation of combustion chemistry using in situ adaptive tabulation. *Combust. Theory Modeling* 1, 41–63.
97. Bradley, D. 1992 "How fast can we burn?" Proc. Combust. Inst. 24, 247–262.
98. Peters, N. 2000 *Turbulent Combustion*. Cambridge.
99. Clavin, P. 2000 Dynamics of combustion fronts in premixed gases: From flames to detonations. *Proc. Combust. Instit.* **28**, 569–585.
100. Palm-Leis, A. & Strehlow, R.A. 1969 On the propagation of turbulent flames. *Combust. Flame* 13, 111–129.
101. Bray, K. N. C. 1980 Turbulent flows with premixed reactants. *Turbulent Reacting Flows* (ed. Libby, P. A. & Williams, F. A.). pp. 115–183. Springer-Verlag.
102. Bray, K. N. C. 1996 The challenge of turbulent combustion. *Proc. Combust. Inst.* 26, 1–26.
103. Bray, K. N. C., Libby, P. A., Masuya, G. & Moss, J. B. 1981 Turbulence production in premixed turbulent flames. *Combust. Sci. Technol.* 25, 127–140.
104. Borghi, R. 1988 Turbulent combustion modeling. *Prog. Energy Combust. Sci.* 14, 245–292.
105. Libby, P. A. & Williams, F. A. 1980 *Turbulent Reacting Flows*. Springer-Verlag.
106. Libby, P. A. & Williams, F. A. 1994 *Turbulent Reacting Flows*. Academic.
107. Poinsot, T. 1996 Using direct numerical simulation to understand premixed turbulent combustion. *Proc. Combust. Inst.* 26, 219–232.
108. Pope, S. B. 1985 PDF method for turbulent reactive flows. *Prog. Energy Combust. Sci.* 11, 119–192.
109. Pope, S. B. 1990 Computations of turbulent combustion: progress and challenges. *Proc. Combust. Inst.* 23, 591–612.
110. Pope, S. B. 2000 *Turbulent Flows*, Cambridge.
111. Bradley, D. 2000 "Flame Propagation in a Tube: The Legacy of Henri Guénoche," Combustion Science and Technology 158, 15–33.
112. V. Bychkov, A. Petchenko, V. Akkerman, L.-E. Eriksson, 2005 *Theory and Modeling of Accelerating Flames in Tubes*, Phys. Rev. E **72**, 046307.
113. V.V. Bychkov, S.M. Golberg, M.A. Liberman, L.E. Eriksson, 1996 *Propagation of Curved Flames in Tubes*, Phys. Rev. E **54**, 3713.
114. Candel, S. 2002 Combustion dynamics and control. *Proc. Combust. Inst.* 29, 1–28.
115. Rayleigh, Nature 1878 #18 p 379
116. Rijke, P.L. 1859, "Notiz über eine neue Art, die in einer an beiden Enden offenen Röhre enthaltene Luft in Schwingungen zu versetzen" (Note on a new way to create oscillation of the air contained in a tube with both ends open), Annalen der Physik 183, 339–343.
117. Lee, J. H. S. 2001 Detonation waves in gaseous explosives. *Handbook of Shock Waves*, (eds. Ben-Dor, G., Igra, O. & Elperin, T.), Chapter 17, Volume 3. Academic.
118. Döering, W. 1943 On detonation processes in gases. *Ann. Phys.* 43, 421–436.
119. Fickett, W. & Davis, W.C. 1979 *Detonation*, University of California Press.
120. Sharpe, G.J. 2000 The structure of planar and curved detonation waves with reversible reactions. *Phys. Fluids* 12, 3007–3020.
121. Taylor, G. I. 1950 The dynamics of the combustion products behind plane and spherical detonation front in explosives. *Proc. R. Soc. Lond.* A 200, 235–247.
122. Urtiew, P. A. & Oppenheim, A. K. 1966 Experimental observations of the transition to detonation in an explosive gas. *Proc. Roy. Soc.* A 295, 13–28.
123. von Neumann, J. 1942 Theory of detonation waves. *John von Neumann*, *Collected Works* 6, (ed. Taub, A. J.), Macmillan, 1963.
124. Zel'dovich, Y. B. 1940 On the theory of propagation of detonation in gaseous systems. *Zhur. Eksp. Teor. Fiz.* 10: 542–568. (English translation: NACA TM 1261,1950).
125. Zel'dovich, Y. B. & Kompaneets. A.S. 1960 *Theory of Detonation*, Academic.
126. http://metamodern.com/2009/12/29/theres-plenty-of-room-at-the-bottom%E2%80%9D-feynman-1959/
127. Sharpe, G.J. 1999 Linear Stability of pathological-detonations. J. Fluid Mech. 401, 311–338.
128. Bychkov and Akkerman, Phys. Rev. E 73, 066305 (2006).
129. Bychkov, et al Phys. Rev. Lett. 101, 164501 (2008) 1417
130. Valiev, et al Phys. Rev. E 80 036317 (2009).
131. Valiev, et al Combust. Flame 157, 1012 (2010).
132. Searby, Combust. Sci. Techn. 81: 221 (1992).

133. Searby and Rochwerger, J. Fluid. Mech. 231: 529 (1991).
134. Bychkov Phys. Fluids 11: 3168 (1999). 1423
135. Petchenko et al., Phys. Rev. Lett. 97: 164501 (2006).
136. Petchenko et al., Combust. Flame 149: 418 (2007).
137. J. Jayachadran, A. Lefebvre, R. Zhao, F. Halter, Emilien Varea,2 B. Renou, F. N. Egolfopoulos, 2015"Study of Propagation of Spherically Expanding and Counterflow Laminar Flames Using Direct Measurements and Numerical Simulations," Proceedings of the Combustion Institute 35, XXX–XXX.

Grunde Jomaas is an Associate Professor at the Technical University of Denmark.

Fire Plumes, Flame Height, and Air Entrainment

13

Gunnar Heskestad

Introduction

Practically all fires go through an important, initial stage in which a coherent, buoyant gas stream rises above a localized volume undergoing combustion into surrounding space of essentially uncontaminated air. This stage begins at ignition, continues through a possible smoldering interval, into a flaming interval, and may be said to end prior to flashover. The buoyant gas stream is generally turbulent, except when the fire source is very small. The buoyant flow, including any flames, is referred to as a fire plume.

Combustion may be the result of pyrolysis of solid materials or evaporation of liquids because of heat feedback from the combustion volume or of pressurized release of flammable gas. Other combustion situations may involve discharge of liquid sprays and aerosols, both liquid and solid, but these will not be discussed here. In the case of high-pressure releases, the momentum of the release may be important. Flames in these situations are usually referred to as *diffusion flames*, being the result of combustible vapor or gas mixing or diffusing into an ambient oxidant, usually air, as opposed to being premixed with an oxidant.

Properties of fire plumes are important in dealing with problems related to fire detection, fire heating of building structures, smoke filling rates, fire venting, and so forth. They can also be important in fire suppression system design.

This chapter deals primarily with axisymmetric, turbulent fire plumes and reviews a number of relations for predicting the properties of such plumes. It is assumed throughout the chapter that the surrounding air is uncontaminated by fire products and that it is uniform in temperature, except where specifically treated as temperature stratified. Release of gas from a pressurized source is assumed to be vertical unless noted otherwise (subsection on "Jet Flames in Horizontal Discharge"). The relations cease to be valid at elevations where the plume enters a smoke layer.

Main topics are flame heights, plume temperatures and velocities, virtual origin, air entrainment, and effects of ambient temperature stratifications. At the end of the chapter, a few additional aspects of fire plumes are discussed, including flame pulsations, rise times of plume fronts propagating upward from suddenly initiated fires, and nonaxisymmetric plume situations including wall/corner effects, wind effects, and jet diffusion flames from horizontal gas discharge. Knowledge of the behavior of fire plumes presented in this chapter is based mostly on observations and dimensional analysis, complemented by analytical models.

G. Heskestad (✉)
Retired from FM Global in 2004 as a Consulting Research Scientist

M.J. Hurley (ed.), *SFPE Handbook of Fire Protection Engineering*,
DOI 10.1007/978-1-4939-2565-0_13, © Society of Fire Protection Engineers 2016

Note on Numerical Modeling

Methods of numerical analysis are now showing promise in modeling turbulent fires, e.g., the Fire Dynamics Simulator (FDS). FDS is based on large eddy simulation (LES) of the turbulent convective motion [1, 2] and requires a combustion model. Recent FDS contributions for fire plumes incorporate subgrid mixture-fraction based combustion models and include Ma and Quintiere [3], who compared general predictive capabilities to selected literature data characterized as "the best", and Xin et al. (two separate studies) who compared detailed predictions to careful measurements in the base regions up to an estimated one fourth of the flame height of a 7.1-cm diameter methane burner [4] and a 1-m diameter methane fire [5] (measurements by Tieszen et al. [6]). The challenge is to reproduce experimental results to a high degree of accuracy, which was achieved to a considerable extent in the base-region calculations by Xin et al. [4, 5], although the temperature calculations required an assumption about radiant heat loss.

Another approach is the LES solver, FireFOAM [7], which is based on the open source code OpenFOAM [8] and also incorporates a subgrid mixture-fraction based combustion model. The code has been applied by Wang et al. [9] to model fire plumes on a 0.3-m square burner for comparison with existing data. With an assumption of a constant radiant fraction of 20 % (although the code allows for a more fundamental treatment of thermal radiation), results of axial plume temperatures and velocities are in approximate agreement with the experiments. Flame heights and air entrainment compare favorably with experimental values. Fluctuating velocities are comparable to reported experimental values, whereas fluctuating temperatures are excessive. (The long-term goal is stated to be predictive capability for large scale industrial fires and water-based suppression on the OpenFOAM platform, incorporating pyrolysis and soot models, already available capabilities in FireFOAM.)

Earlier methods were based on Reynolds-Averaged Navier Stokes (RANS) models and are included in a survey of fire models prepared by Olenick and Carpenter [10].

The ultimate approach is to solve the governing equations more fundamentally with Direct Numerical Simulation (DNS), which is becoming gradually more feasible for fire problems with the availability of increasing computing power. At this writing, DNS still remains a great challenge and is not likely to become a viable tool in fire applications for some time because of its demand on resources. Numerical modeling may eventually reproduce actual experiments, with a bonus of numerous variables of the mean and turbulent flow fields hardly accessible by physical experiments.

Fire Plume Features

Figure 13.1 shows a schematic representation of a turbulent fire plume originating at a flaming source, which may be solid or liquid. Volatiles driven off from the combustible by heat feedback from the fire mix with the surrounding air and form a diffusion flame. Laboratory simulations often employ controlled release of flammable gas through a horizontal, porous surface. The mean height of the flame is L. Surrounding the flame and extending upward is a boundary (broken lines) that confines the entire buoyant flow of combustion products and entrained air. The air is entrained across this boundary, which instantaneously is very sharp, highly convoluted, and easily discernible in smoky fires. The flow profile could be the time-averaged temperature rise above the ambient temperature, the concentration of a gas (such as CO_2) generated by the fire, or the axial velocity in the fire plume.

Figure 13.1 suggests qualitatively, based on experimental observations [12–16], how the temperature rise on the centerline, ΔT_0, and the velocity on the centerline, u_0, might behave along the plume axis. In this example of a relatively tall flame, the temperatures are

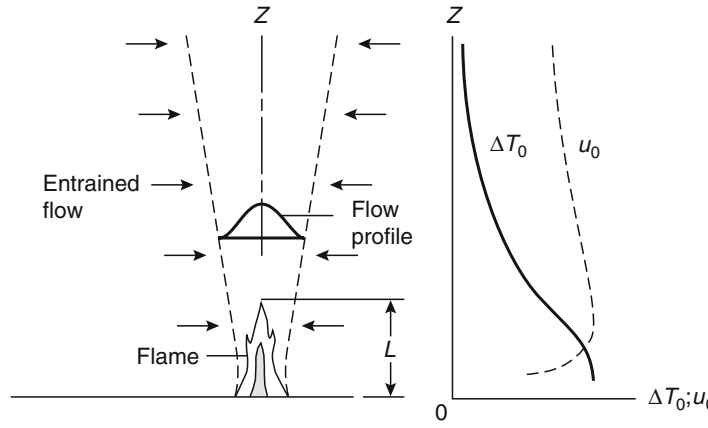

Fig. 13.1 Features of a turbulent fire plume, including axial variations on the centerline of mean excess temperature, ΔT_0, and mean velocity, u_0 [11]

nearly constant in the lower portion of the flame. Temperatures begin to decay in the intermittent, upper portion of the flame as the combustion reactions trail off and air entrained from the surroundings cools the flow. The centerline velocities, u_0, tend to have their maxima slightly below the mean flame height and always decay toward higher elevations. If the combustible is porous and supports internal combustion, there may not be as pronounced a falloff in the gas velocity toward the top of the combustible as suggested in Fig. 13.1 [14].

The total (or chemical) heat release rate of a fire source, $\dot{Q}$, is either convected, $\dot{Q}_c$, or radiated, $\dot{Q}_r$, away from the combustion region. In a fire deep in a porous combustible pile (e.g., a stack of wood pallets), some of the total heat generated is trapped by and stored in the not yet burning material; the rest escapes from the combustible array as either convective or radiative energy flux. If most of the volatiles released undergo combustion above the fuel array, as in pool fires of liquids and other horizontal-surface fires, and even in well-developed porous pile fires, then the convective fraction of the total heat release rate is rarely measured at less than 60–70 % of the total heat release rate [17, 18]. The convective flux, $\dot{Q}_c$, is carried away by the plume above the flames, while the remainder of the total heat liberated, $\dot{Q}_r$, is radiated away in all directions.

For large fires, the radiative fraction tends to decrease with increasing fire size [19] and the convective fraction tends to increase. This result is especially striking in smoky hydrocarbon fires [20] where radiation is increasingly absorbed in the mantle of combustion products surrounding the flames (dashed lines in Fig. 13.1) as the fire increases in size, although the smoke itself will emit some radiation. However, even mantles of combustion products from sufficiently large fires of a clean burning fuel, such as liquefied natural gas (LNG), will absorb significant and increasing amounts of radiation as the fires become larger because of water vapor and carbon dioxide, both major combustion products and radiation-absorbing gases. Another reason for decreasing radiative fraction with increasing size of larger fires is that the flames are optically thick and the radiation-emitting area (flame area) per unit fire power (kW) decreases with increasing fire size (based on Equation 13.8 and constant heat release rate per unit fire area).

The total heat release rate, $\dot{Q}$, is often assumed to be equal to the *theoretical* heat release rate, which is based on complete combustion of the burning material. The theoretical heat release rate in kW is evaluated as the mass burning rate in kg/s multiplied by the lower heat of complete combustion in kJ/kg. The ratio of the total heat release rate to the theoretical heat release rate, which is the combustion efficiency,

is indeed close to unity for some fire sources (e.g., methanol and heptane pools) [17], but may deviate significantly from unity for others (e.g., a polystyrene fire, for which a combustion efficiency of about 45 % [18] has been measured, and a fully involved stack of wood pallets, for which a combustion efficiency has been measured at 63 % [17]).

Calculation Methods

This section presents calculation methods for flame height; plume temperature and velocity; effects of ambient temperature stratification on plume temperature, velocity, and other plume variables; virtual origin of a fire plume, a point source from which the plume appears to originate; and entrainment of air from the surroundings into a fire plume. The calculation methods are illustrated by examples.

Flame Heights

The visible flames above a fire source contain the combustion reactions. Tamanini [21] has investigated the manner in which combustion approaches completion with respect to height in diffusion flames.

Typically, the luminosity of the lower part of the flaming region appears fairly steady, while the upper part appears to be intermittent. Sometimes vortex structures, more or less pronounced, can be observed to form near the base of the flame and shed upward. [22, 23].

Figure 13.2 helps to define the mean flame height, L [23]. It shows schematically the variation of flame intermittency, I, versus distance above the fire source, z, where $I(z)$ is defined as the fraction of time that at least part of the flame lies above the elevation, z. The intermittency decreases from unity deep in the flame to smaller values in the intermittent flame region, eventually reaching zero. The mean flame height, L, is the distance above the fire source where the intermittency has declined to 0.5. Objective determinations of mean flame height according to intermittency measurements are fairly consistent with (although tending to be slightly lower than) flame heights that are averaged by the human eye [23].

The mean flame height is an important quantity that marks the level where the combustion reactions are essentially complete and the inert plume can be considered to begin. Several expressions for mean flame height have been proposed. Figure 13.3, taken from McCaffrey [24], shows normalized flame heights, L/D, as a function of a Froude number, $\dot{Q}^*$ (represented as $\dot{Q}^{*2/5}$ to compress the horizontal scale), from

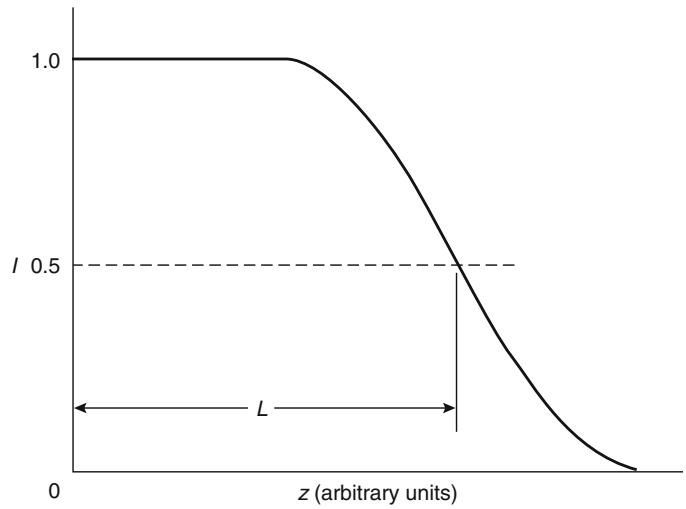

Fig. 13.2 Definition by Zukoski et al. [23] of mean flame height, L, from measurements of intermittency, I

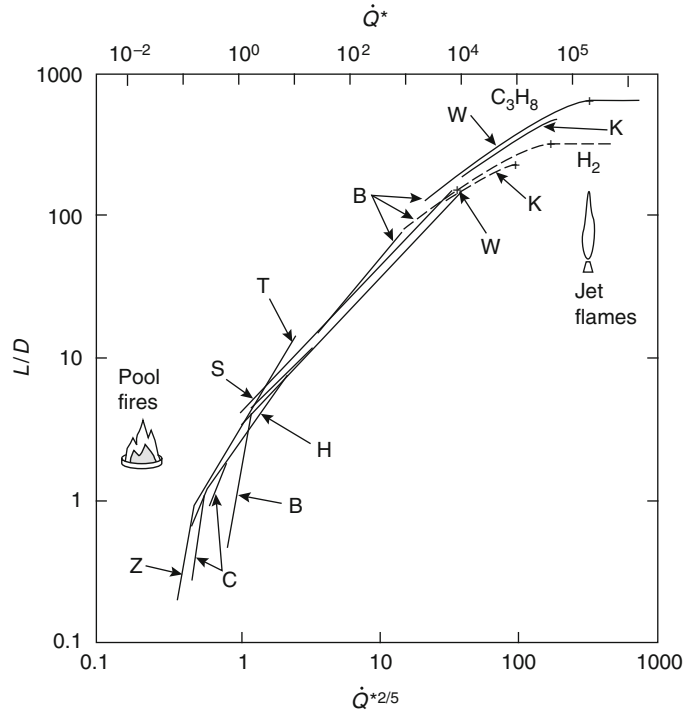

Fig. 13.3 Flame height correlations compiled by McCaffrey [24]. Capital letters without subscripts correspond to various researchers as follows: *B* Becker and Liang [25], *C* Cox and Chitty [26], *H* Heskestad [27], *K* Kalghatgi [28], *S* Steward [29], *T* Thomas [30], *W* Hawthorne et al. [31], and *Z* Zukoski [32]. Capital letters with subscripts represent chemical formulae

data correlations available in the literature. This Froude number is defined as

$$\dot{Q}^* = \frac{\dot{Q}}{\rho_\infty c_p T_\infty \sqrt{gD}D^2} \tag{13.1}$$

where

$\dot{Q}$ = Total heat release rate (given in terms of the mass burning rate, $\dot{m}_f$, as $\dot{m}_f H_c$)
ρ_∞ and T_∞ = Ambient density and temperature, respectively
c_p = Specific heat of air at constant pressure
g = Acceleration of gravity
D = Diameter of the fire source

Quoting McCaffrey with respect to this figure: "On the left are pool-configured fires with flame heights of the same order of magnitude as the base dimension D. In the middle is the intermediate regime where all flames are similar and the $\dot{Q}^{*2/5}$ is seen as a 45 degree line in the figure. Finally, in the upper right is the high Froude number, high-momentum jet flame regime where flame height ceases to vary with fuel flow rate and is several hundred times the size of the source diameter."

Buoyancy Regime The correlation by Heskestad (*H*) represented in Fig. 13.3 covers the entire $\dot{Q}^*$ range except the momentum regime and has the following form given by McCaffrey [24]:

$$\frac{L}{D} = -1.02 + 3.7\dot{Q}^{*2/5} \tag{13.2}$$

Actually, this correlation was originally presented in the form [27]

$$\frac{L}{D} = -1.02 + 15.6N^{1/5} \tag{13.3}$$

As before, D is the diameter of the fire source (or effective diameter for noncircular fire sources such that $\pi D^2/4$ = area of fire source) and N is the nondimensional parameter defined by

$$N = \left[\frac{c_p T_\infty}{g\rho_\infty^2 (H_c/r)^3}\right]\frac{\dot{Q}^2}{D^5} \tag{13.4}$$

where H_c is the actual lower heat of combustion and r is the actual mass stoichiometric ratio of air to volatiles.

It is readily shown that N and $\dot{Q}^*$ are related as follows:

$$N = \left(\frac{c_p T_\infty}{H_c/r}\right)^3 \dot{Q}^{*2} \tag{13.5}$$

This equation, combined with Equation 13.3, leads to Equation 13.2 when typical values are substituted for the environmental and fuel variables.

The parameter N was derived specifically by consideration of the flaming region [27], whereas $\dot{Q}^*$ was originally derived by Zukoski [33] from analysis of the nonreacting turbulent plume. Subsequently, Heskestad [34] presented results of flame height measurements at widely varying ambient temperatures. The parameter $\dot{Q}^*$ did not account correctly for the observed variations in flame height (increasing flame height with increasing ambient temperature), while the parameter N did. For that reason, N is considered the more appropriate scaling parameter.

Equation 13.3 [27] is anchored in the 50 % intermittency flame heights measured by Zukoski et al. [23] for 81 experimental fires of natural gas (essentially methane), burned on circular porous beds of three diameters, 0.10, 0.19, and 0.50 m. The author extended this body of data into the low-N region based on propane fires on a 0.76-m diameter sand bed [35]. Other contributing data [27, 35] were based on time-averaged flame heights, mostly by eye, including (but not limited to) 51 and 102 mm- diameter gas jets of various fuels [36]; 102 and 279 mm-diameter natural-gas sandbox burners [37]; pool fires of gasoline varying from 0.3 to 23 m in diameter [38]; pool fires of JP-4 fuel varying from 1× 1 m to 10× 10 m [39] (treated as circular pools of diameters corresponding to their burn areas); sand filled, 1.52 m-diameter pans initially saturated with acetone or methanol [40]; and pool fires of diameters 1.22, 1.74, and 2.44 m of methanol, heptane, a silicone transformer fluid and a hydrocarbon transformer fluid [15]. Deviations of observed values from values calculated according to Equation 13.3 may be associated with subjective flame-height averaging by eye or photography (including assigning a value for the instantaneous flame height when detached flame fragments appear), departure of fire area from circular, nonuniform volatilization rates across a burning surface (as observed in Wood et al. [40]), density of volatiles, effects of the surrounding topography and wind, and effects of flame Reynolds number (increases with fire size).

Some large scale pool fires of LNG on water as well as on land, reviewed by Mudan [41], appear to have produced flame heights generally a little lower than, but still quite consistent with Equation 13.3 for both water and land sites and from two different investigations. Flame heights from land measurements of a third investigation had great scatter, with a smallest flame height value about one third as large as calculated from Equation 13.3.

Subsequent to its derivation, the Equation 13.3 was found also to represent large, deep storages when the flames extended above the storage and flame heights were measured above the base of the fire (bottom of storage in the experiments) [42]. The storages investigated included 4.5-m-high palletized storage of different commodities, 3- to 6-m-high rack storage of two different commodities, and wood pallets stacked 0.3–3.3 m high. In these cases the fire diameter was calculated as the diameter of a fire area equal to the ratio of heat release rate to heat release rate per unit area.

A convenient form of Equation 13.3 can be developed. Let

$$A = 15.6\left[\frac{c_p T_\infty}{g\rho_\infty^2 (H_c/r)^3}\right]^{1/5} \tag{13.6}$$

Then Equation 13.3 can be written in the dimensional form

$$L = -1.02D + A\dot{Q}^{2/5} \tag{13.7}$$

The coefficient, A, varies over a rather narrow range, associated with the fact that H_c/r, the heat liberated per unit mass of air entering the combustion reactions, does not vary appreciably

among various combustibles. For a large number of gaseous and liquid fuels, H_c/r remains within the range of 2900–3200 kJ/kg, for which the associated range of A under normal atmospheric conditions (293 K, 760 mmHg) is 0.240–0.226 (m $kW^{-2/5}$), with a typical value of $A = 0.235$. Hence, under normal atmospheric conditions

$$L = -1.02D + 0.235\dot{Q}^{2/5} \tag{13.8}$$

(L and D in m; $\dot{Q}$ in kW).

Fairly common fuels that deviate significantly from the cited range 0.240–0.226 for A include acetylene and hydrogen (0.211). In general, the coefficient $A = 0.235$ in Equation 13.8 may be considered adequate unless actual values of H_c and r are known that indicate otherwise and/or atmospheric conditions deviate significantly from normal. While values of H_c/r for complete combustion have been used to calculate the coefficients A, Huggett [43] found a number of years ago that the heat of combustion per unit mass of oxygen consumed, and hence H_c/r for a standard atmospheric composition, was little affected by incompleteness of combustion in a number of test calculations.[1]

Referring to any of the flame-height relations in Equations 13.3, 13.7, and 13.8, it can be seen that negative flame heights are calculated for sufficiently small values of the heat release rate. Of course, this situation is unphysical and the correlation is not valid here. For pool fires, there are indications that a single flaming area breaks down into several zones when heat release rates decrease to the point where negative flame height (L) is calculated [35].

Grove and Quintiere [45] have developed new correlations for flame height, including linear sources (not considered here). They present their results in terms of $\dot{Q}^*$ rather than N.

Newman and Wieczorek [46] have examined "chemical flame heights", defined by the ratio of CO to CO_2 yields decaying to the limit for well-ventilated fires of the combustible material. They found good agreement with determinations of flame height based on flame luminosity. They claim certain attributes for this method, such as the results not being subject to visual bias and available in cases where visual observations are not feasible (presumably as in cases of obscuring smoke, where infrared imaging may also work).

EXAMPLE 1 Consider a 1.5-m-diameter pan fire of methyl alcohol with a heat release intensity of 500 kW/m^2 of surface area. Normal atmospheric conditions prevail (760 mmHg, 293 K). Calculate the mean flame height.

SOLUTION Available values of the lower heat of combustion ($H_c = 21{,}100$ kJ/kg) and stoichiometric ratio ($r = 6.48$) give $H_c/r = 3260$ kJ/kg. With this value for H_c/r substituted in Equation 13.6, together with $c_p = 1.00$ kJ/kg K, $T_\infty = 293$ K, $g = 9.81$ m/s^2, and $\rho_\infty = 1.20$ kg/m^3, the coefficient A is calculated as 0.223 (m $kW^{-2/5}$). The total heat release rate is $\dot{Q} = 500\pi 1.5^2/4 = 884$ kW. Equation 13.7 gives a mean flame height of $L = -1.02 \cdot 1.5 + 0.223 \cdot 884^{2/5} = 1.83$ m.

EXAMPLE 2 This example is similar to Example 1, except for new atmospheric conditions representative of Denver, Colorado, on a hot day: 630 mmHg pressure and 310 K temperature.

SOLUTION Using Equation 13.6, the new coefficient, A, increases from 0.223 to 0.249 [most readily calculated from $(310/293)^{3/5}$ $(760/630)^{2/5}$ $0.223 = 0.249$, where the equation of state for a perfect gas has been used]. Using Equation 13.7, the new flame height is $L = 2.23$ m, increased from 1.83 m for normal atmospheric conditions.

Note Assuming that gas radiation is dominant in heat transfer to the pool surface in the example, that the absorption coefficient varies linearly with atmospheric pressure [47] and using the methanol pool fire data of Burgess et al. [102],

[1] As a further aid in assessing variations in A, Tewarson [44], in his Table 3–4.12, lists values of ΔH_O for complete combustion of many fuels, the lower heat of combustion per unit mass of oxygen consumed. From these values, H_c/r (kJ/kg) can be easily calculated, the lower heat of combustion per unit mass of air (of standard composition) consumed and, hence, the coefficient A.

the burning rate associated with the reduced atmospheric pressure is estimated to decrease by a negligible amount.

EXAMPLE 3 One 1.2-m-high stack of wood pallets (1.07 × 1.07 m) burns at a total heat release rate of 2600 kW under normal atmospheric conditions. Calculate the mean flame height above the base of the pallet stack.

SOLUTION The square flaming area can be converted to an equivalent diameter: $\pi D^2/4 = 1.07^2$, which gives the equivalent diameter, D, of 1.21 m. Since the combustion efficiency of wood is considerably less than 100 %, it is difficult to select reliable and consistent values for H_c and r to form the ratio H_c/r. Instead, it can be assumed that $A = 0.235$, the typical value. Using Equation 13.7, the mean flame height above the base of the pallet stack is calculated as $L = -1.02 \cdot 1.21 + 0.235 \cdot 2600^{2/5} = 4.22$ m.

Momentum Regime In Fig. 13.3 it is seen that at high values of $\dot{Q}^*$ the normalized flame heights begin to level off and eventually attain constant values, but not at the same value of $\dot{Q}^*$ and not at the same normalized flame height.

Flame heights of vertical turbulent jet flames have been studied by a number of investigators reviewed by Blake and McDonald [48, 49], who proposed a new correlation of normalized flame heights versus a "density-weighted Froude number." Although an improvement over previous work, the correlation still exhibits significant scatter. At about the same time, Delichatsios [50] proposed an alternative approach. Previously, other authors had proposed flame height relations, including Becker and coworkers [25, 51], and Peters and Göttgens [52]. Subsequent to these publications, Heskestad [53] also considered the high-momentum regime, especially with respect to defining an unambiguous transition to momentum control and flame heights in this regime.

Heskestad's work [53] was based on an extension of the author's correlation for buoyancy-controlled turbulent diffusion flames. A momentum parameter is defined, which is the ratio of gas release momentum to the momentum generated by a purely buoyant diffusion flame:

$$R_M = 1.36\left[\left(\frac{T_\infty}{T_L}\right)\left(\frac{c_p \Delta T_L}{(H_c/r)}\right)^{4/5}\right]\left(\frac{\rho_\infty/\rho_s}{r^2}\right)N^{2/5} \tag{13.9}$$

Here, T_L and ΔT_L are the plume centerline temperature and excess temperature (above ambient), respectively, at the mean flame height of purely buoyant diffusion flames, and ρ_s is the density of the source gas in the discharge stream. A value of 500 K is assigned [53] to ΔT_L. Note that the first two sets of parentheses are nearly constant for normal ambient temperatures and fuels with comparable values of (H_c/r). Under these circumstances, the momentum parameter is closely linked to the parameter N but is affected quite significantly by the source gas density at the discharge conditions as well as the mass stoichiometric ratio. If the gas discharge is sonic or choked, the density of the source gas can be considerably higher than is the case at atmospheric pressure.

Figure 13.4 presents flame heights of jet diffusion flames in the form L/L_B versus R_M, where L is the flame height reported by various investigators and L_B is the buoyancy-controlled flame height according to Equation 13.3. The data scatter about a value $L/L_B = 1.2$, approximately, for $R_M < 0.1$. At higher values of R_M, the flame height ratio approaches an asymptotic slope of $-1/2$, indicated by a dashed line. The associated values of N are so large that we can take $L_B/D \propto N^{1/5}$ (see Equation 13.3), which together with Equation 13.9 imply that L/D is constant when the slope is equal to $-1/2$ (for constant source gas and discharge density). Constant slope and constant L/D (for a given gas and density) appear to be achieved reasonably quickly above $R_M = 0.1$.

The fact that the low-R_M flame height ratios in Fig. 13.4 tend to scatter about a level higher than

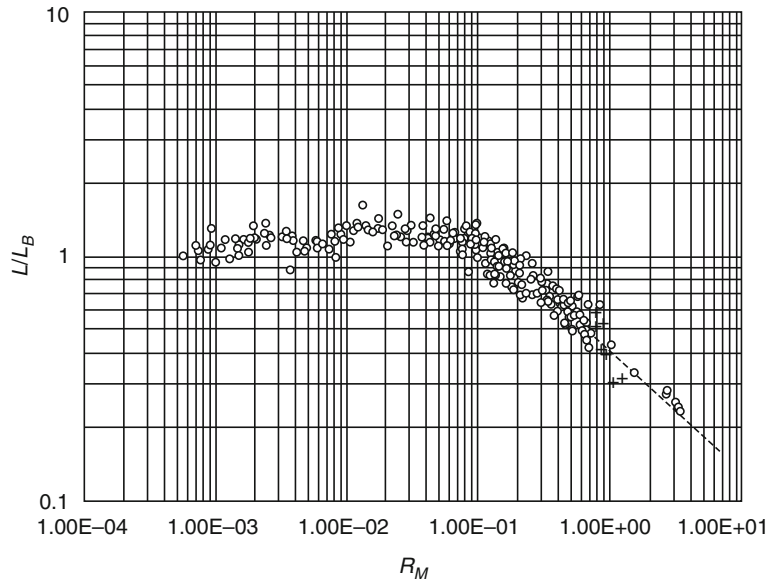

Fig. 13.4 Data on flame heights of turbulent jet diffusion flames in ratio to the corresponding buoyancy-controlled flame heights, plotted versus the ratio of gas release momentum to buoyancy momentum (from Heskestad [53]). Data plotted as + pertain to choked discharge of hydrogen

unity has been attributed to several possible factors [53]. One of the two most important may be the working definition of mean flame height employed by some investigators, producing greater values than the 50 % flame-intermittency height. Another may be retinal retention of flame images in visual averaging of rapidly pulsating flames (typical of the scales of the experiments), tending to make an observer exaggerate the mean flame height.

Above $R_M = 0.1$, adopting the dashed line in Fig. 13.4 as representative of the momentum regime, the normalized flame height is

$$\frac{L_M}{D} = \left[5.42\left(\frac{T_L}{T_\infty}\right)^{1/2}\left(\frac{H_c/r}{c_p \Delta T_L}\right)^{2/5}\right]\left(\frac{\rho_s}{\rho_\infty}\right)^{1/2} r \tag{13.10}$$

where L_M is the flame height in the momentum regime. For $H_c/r = 3100$ kJ/kg (many common gases), $\Delta T_L = 500$ K, and $T_\infty = 293$ K, Equation 13.10 becomes

$$\frac{L_M}{D} = 18.5\left(\frac{\rho_s}{\rho_\infty}\right)^{1/2} r \tag{13.11}$$

In this case the nondimensional flame height in the momentum regime depends in a simple manner on the mass stoichiometric ratio and the source gas density at discharge.

It should be pointed out that the transition to the momentum regime, $R_M = 0.1$, and the flame height in the momentum regime, Equations 13.10 and 13.11, differ significantly from previously proposed relations, as discussed in Heskestad [53].

EXAMPLE 4 Calculate the normalized height of a hydrogen jet flame from a 5-mm-diameter nozzle connected to a reservoir (tank, pipe, etc.) at ambient temperature of 293 K and a pressure of either (a) 150 kPa or (b) 300 kPa.

SOLUTION

(a) The ratio of ambient pressure (101 kPa) to the reservoir pressure (150 kPa) is 0.673, corresponding to subsonic discharge (sonic discharge occurs at a pressure ratio of 0.528, as for air). The mass flow of hydrogen from the nozzle is calculated with the aid of a compressible flow formula (e.g., Shapiro [54]) as 1.74 g/s, using a ratio of specific heats $k = 1.4$ (as for air). Based on a heat of combustion of 120,000 kJ/kg, the heat release rate is $\dot{Q} = 209$ kW. The source

gas density in the discharge stream, ρ_s, is calculated from the source gas density at ambient temperature and pressure, $\rho_{s\infty}$, as follows:
$\rho_s = (\rho_s/\rho_{s\infty})\rho_{s\infty} = (\rho_s/\rho_{s0})(\rho_{s0}/\rho_{s\infty})\rho_{s\infty}$, where ρ_{s0} is the source gas density in the gas reservoir. The density ratios can be expressed in terms of pressure ratios with the result $\rho_s = (p_s/p_{s0})^{1/k}(p_{s0}/p^{\infty})\rho_{s\infty}$, where p_s is the pressure in the discharge stream (ambient pressure for subsonic discharge) and p_{s0} is the pressure of the gas reservoir. Finally, we obtain $\rho_s = (101/150)^{1/1.4}$ (150/101) $\rho_{s\infty} = 1.12\times\ 0.083 = 0.093$ kg/m^3, where 0.083 (kg/m^3) is the density of hydrogen at ambient temperature and pressure. Now the momentum parameter can be calculated from Equation 13.9, taking $\Delta T_L = 500$ K, $H_c = 120{,}000$ kJ/kg, $r = 34.3$, and $\rho_s = 0.093$ kg/m^3, yielding $R_M = 1.16 \times 10^{-3}\ N^{2/5}$. The parameter N is calculated from Equation 13.4 with the result $N = 6.76 \times 10^6$, which results in $R_M = 0.62$ and places the flame in the momentum regime. The normalized flame height is calculated from Equation 13.10 as $L_M/D = 185$. NOTE: The calculated height may include the visual-averaging bias toward somewhat higher than actual values built into the database.

(b) The ratio of ambient pressure (101 kPa) to reservoir pressure (300 kPa) is 0.337, corresponding to sonic, or choked, discharge. The mass flow of hydrogen from the nozzle is calculated with the aid of an appropriate compressible flow formula for choked discharge (e.g., Shapiro [54]) as 3.65 g/s, corresponding to a heat release rate of 436 kW. The source gas density for choked flow is calculated as in (a), except the ratio (p_s/p_{s0}) is set equal to the value for a Mach number of unity, 0.528; that is, $\rho_s = 0.528^{1/k}(\rho_{s0}/\rho_{s\infty}) \times 0.083 = 0.634(300/101) \times 0.083 = 0.156$ kg/m^3. The parameter N is calculated from Equation 13.4 as 294×10^7 and the momentum parameter from Equation 13.9 as $R_M = 6.93 \times 10^{-4}\ N^{2/5} = 0.67$, indicating the flame is in the momentum regime as in (a). The normalized flame height is calculated from Equation 13.10 as $L_M/D = 239$, somewhat higher than for the lower discharge pressure in (a).

Note If the nozzles of cases (a) and (b) are sharp-edged holes or openings instead, it is recommended that the source diameter be multiplied by (discharge coefficient)$^{1/2}$; see, for example, Shapiro [54] for values of the discharge coefficient of sharp-edged orifices in compressible flow (varying from 0.60 near incompressible flow conditions to 0.77 for choked flow).

Plume Temperatures and Velocities

The first plume theories (Schmidt [55], Rouse et al. [56], Morton et al. [57]) assumed the following:

1. Turbulent flow
2. Point source of buoyancy
3. Variations of density in field of motion small compared to ambient density
4. Air entrainment velocity at the edge of the plume proportional to the local vertical plume velocity
5. Profiles of vertical velocity and buoyancy force in horizontal sections of similar form at all heights

Morton et al. [57] developed an integral formulation on the further assumption that the profiles are uniform "top hat" profiles. The mean motion is then governed by the following three conservation equations for continuity, momentum, and buoyancy:

$$\text{Continuity}: \quad \frac{d}{dz}\left(b^2 u\right) = 2\alpha b u \tag{13.12}$$

$$\text{Momentum}: \quad \frac{d}{dz}\left(b^2 u^2\right) = b^2 g \frac{\rho_\infty - \rho}{\rho_\infty} \tag{13.13}$$

$$\text{Buoyancy}: \quad \frac{d}{dz}\left(b^2 u g \frac{\rho_\infty - \rho}{\rho_\infty}\right) = 0 \tag{13.14}$$

In these equations, z is the elevation above the point source of buoyancy; b is the radius to the edge of the plume; u is the vertical velocity in the plume; α is the entrainment coefficient (the proportionality constant relating the inflow velocity due to entrainment at the edge of the plume to u); ρ is the density in the plume; and ρ_∞ is the ambient density. Equation 13.14 can be integrated immediately to

$$b^2 u g \frac{\rho_\infty - \rho}{\rho_\infty} = B = \text{constant} \tag{13.15}$$

Here, B is the buoyancy flux in the plume which remains constant at all heights. The flux can be related to the convective heat in the plume, $\dot{Q}_c$, by noting

$$\begin{aligned} \dot{Q}_c &= \rho u \pi b^2 c_p (T - T_\infty) \\ &= \pi u b^2 c_p (\rho_\infty - \rho) T_\infty \end{aligned} \tag{13.16}$$

where the ideal gas law has been used. In this equation, T is the plume temperature and T_∞ is the ambient temperature. Combining Equations 13.15 and 13.16 gives

$$B = g\left(\pi c_p T_\infty \rho_\infty\right)^{-1} \dot{Q}_c \tag{13.17}$$

Solutions to Equations 13.12, 13.13, and 13.15 can be determined [57] in the form (expressing B in terms of $\dot{Q}_c$ using Equation 13.17)

$$b = \frac{6\alpha}{5} z \tag{13.18}$$

$$u = \frac{5}{6}\left(\frac{9}{10\pi\alpha^2}\right)^{1/3} g^{1/3} \left(c_p \rho_\infty T_\infty\right)^{-1/3} \dot{Q}_c{}^{1/3} z^{-1/3} \tag{13.19}$$

$$\frac{\Delta\rho}{\rho_\infty} = \frac{5}{6}\left(\frac{9\pi^2\alpha^4}{10}\right)^{-1/3} g^{-1/3} \left(c_p \rho_\infty T_\infty\right)^{-2/3} \dot{Q}_c{}^{2/3} z^{-5/3} \tag{13.20}$$

Equations 13.18, 13.19, and 13.20 are the weak plume (small density deficiency) relations for point sources. To account for area sources, a virtual source location or virtual origin, z_0, is introduced [57, 58] and z in Equations 13.18, 13.19, and 13.20 is replaced by $z - z_0$. In addition, to accommodate large density deficiencies as are present in fire plumes, Morton's extension of the weak-plume theory [59] leads to the result that $\Delta\rho/\rho_\infty$ in Equation 13.20 should be replaced by $\Delta\rho/\rho$ ($= \Delta T/T_\infty$ using the ideal gas law). Also, Equation 13.18 for growth in plume radius should incorporate the additional factor $(\rho_\infty/\rho)^{1/2}\left[= (T/T_\infty)^{1/2}\right.$ using the ideal gas law] on the right side of the equation. Relaxing the assumption that the flow profiles are uniform renders the numerical coefficients in the resulting equations in doubt.

Measurements in fire plumes above the flames have to a large extent supported the theory. The plume radius and centerline values of mean excess temperature and mean velocity have been found [11] to obey the following relations:

$$b_{\Delta T} = 0.12\left(\frac{T_0}{T_\infty}\right)^{1/2} (z - z_0) \tag{13.21}$$

$$\Delta T_0 = 9.1\left(\frac{T_\infty}{g c_\rho^2 \rho_\infty^2}\right)^{1/3} \dot{Q}_c^{2/3} (z - z_0)^{-5/3} \tag{13.22}$$

$$u_0 = 3.4\left(\frac{g}{c_p \rho_\infty T_\infty}\right)^{1/3} \dot{Q}_c^{1/3} (z - z_0)^{-1/3} \tag{13.23}$$

Here, $b_{\Delta T}$ is the plume radius to the point where the temperature rise has declined to $0.5\Delta T_0$; T_0 is the centerline temperature, $\dot{Q}_c$ is the convective heat release rate, z is the elevation above the fire source, and z_0 is the elevation of the virtual origin above the fire source.[2] (If z_0 is negative, the virtual origin lies below the top of the fire source).

The virtual origin is the equivalent point source height of a finite area fire. This origin is

[2] For normal atmospheric conditions ($T_\infty = 293$ K, $g = 9.81$ m/s^2, $c_p = 1.00$ kJ/kg K, $\rho_\infty = 1.2$ kg/m^3), the factor $9.1\left[T_\infty/\left(\left(g c_p^2 p_\infty^2\right)\right]^{1/3}\right.$ has the numerical value 25.0 K m$^{5/3}$ kW$^{-2/3}$, and the factor $3.4[g/(c_p \rho_\infty T_\infty)]^{1/3}$ has the numerical value 1.03 m$^{4/3}$ s^{-1} kW$^{-1/3}$.

usually located near the fuel surface for pool fires and may be assumed coincident with the fuel surface when the plume flow is predicted at high elevations. Near the fire source, however, it is important to know the location of the virtual origin for accurate predictions. Calculation of the virtual origin is discussed in the following section for both pool fires and three-dimensional storage arrays.

Equations 13.21, 13.22, and 13.23 are known as the *strong plume relations*. The numerical coefficients for the relations have been determined from data sets for which the locations of the virtual origin, z_0, have been established and the convective heat release rates, $\dot{Q}_c$, are known [15, 60].

We may compare the experimentally derived numerical coefficients in Equations 13.21, 13.22, and 13.23 to the theoretical coefficients indicated in Equations 13.18, 13.19, and 13.20, which are based on the integral theory of Morton et al. [57] for weak plumes, point sources, and top hat profiles. Forcing equality between the predictions of Equations 13.22 and 13.20 (interpreting $\Delta\rho/\rho_\infty$ as $\Delta T/T_\infty$), we obtain a value for the entrainment coefficient of $\alpha = 0.0964$. With this value for α, the theoretical coefficient for centerline velocity in Equation 13.19 becomes 2.61, compared to the experimental value 3.4 in Equation 13.23. The theoretical coefficient for plume radius in Equation 13.18 becomes 0.116, compared to the experimental value 0.12 in Equation 13.21. There is good consistency between the theoretical and experimental coefficients. However, the theoretical expression for mass flow rate in a weak plume, generated from the product $\rho_\infty u(\pi b^2)$ (using Equations 13.18 and 13.19) and the value for α above, produces a numerical coefficient that is only 56 % of the coefficient based on experiments (see discussion of Equation 13.40 later in the chapter).

In addition to the temperature radius of a plume, $b_{\Delta T}$, a velocity radius, b_u, can also be defined. The velocity radius is the plume radius to the point where the gas velocity has declined to 0.5 u_0. The most reliable measurements [60] indicate that b_u is perhaps 10 % larger than $b_{\Delta T}$. Other measurements indicate ratios $b_u/b_{\Delta T}$ of 0.86 [56], 1.00 [61], 1.08 and 1.24 [62], 1.31 [16], 1.05 [12], and 1.5 [13]. The widely differing results can probably be attributed to the difficulty of positioning the measuring probes accurately with respect to the plume centerline and to different, intrinsic errors associated with the diverse types of anemometers used (pitot tube, bidirectional flow probe, hot wire, vane anemometer, cross-correlation techniques, laser Doppler anemometer).

Often profiles of temperature rise and velocity are represented as Gaussian in shape, although there is no theoretical foundation for this distribution.

$$\Delta T = \Delta T_0 \exp\left[-\left(\frac{R}{\sigma_{\Delta T}}\right)^2\right] \tag{13.24}$$

$$u = u_0 \exp\left[-\left(\frac{R}{\sigma_u}\right)^2\right] \tag{13.25}$$

Here, ΔT and u are the local values, at the radius, R, in the plume of temperature rise and gas velocity. The quantities $\sigma_{\Delta T}$ and σ_u are measures of the plume width, corresponding to the radii where local values of temperature rise and velocity are $e^{-1} = 0.368$ multiplied by the centerline values. For Gaussian profiles, the plume radii $\sigma_{\Delta T}$ and σ_u are 1.201 multiplied by the plume radii, $b_{\Delta T}$ and b_u, discussed previously.

Equations 13.21, 13.22, and 13.23 cease to be valid at and below the mean flame height. However, it is possible to represent ΔT_0 such that a general plot of experimental temperature variations is produced throughout the length of the plume, including the flames. The method is based on the observation that $\dot{Q}_c^{2/3}(z - z_0)^{-5/3}$ in Equation 13.22 can be written as $\left[(z - z_0)/\dot{Q}_c^{2/5}\right]^{-5/3}$. This result suggests plotting ΔT_0 versus $(z - z_0)/\dot{Q}_c^{2/5}$. Figure 13.5 shows the result in logarithmic coordinates for normal atmospheric conditions. For values of the abscissa greater than 0.15–0.20 (m/kW$^{2/5}$), the centerline temperature rise falls off with the $-\frac{5}{3}$ power of the abscissa, in accordance with the

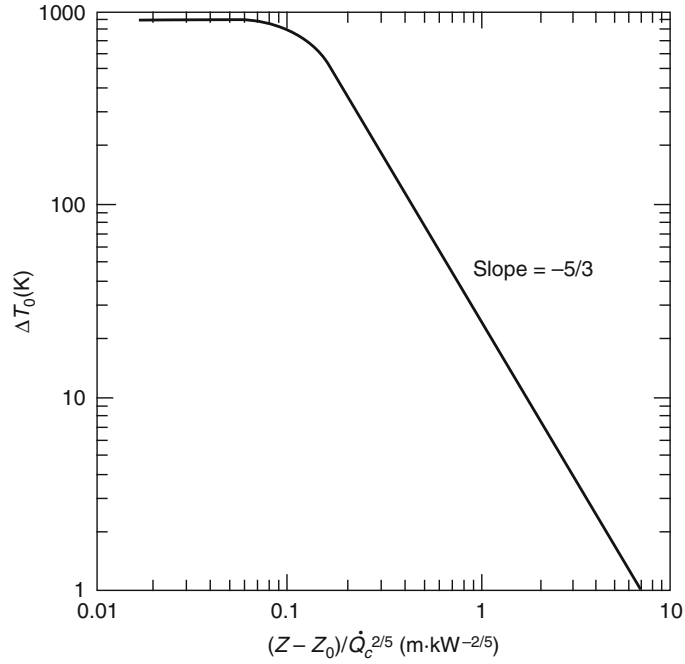

Fig. 13.5 Temperature rise on the plume centerline of pool fires for normal atmospheric conditions [11] in a form attributable to McCaffrey [12], and Kung and Stavrianidis [15]

plume law for temperature (Equation 13.22). Abscissa values in the 0.15–0.20 range correspond to the mean flame height (see Equation 13.37); an associated temperature rise of about 500 K is indicated in Fig. 13.5. At smaller abscissa values, the experimentally observed temperature rise increases more slowly, approaching a value deep in the flame of approximately $\Delta T_0 = 900$ K. When closer to the fuel surface than represented in Fig. 13.5, the temperatures on the plume axis tend to decrease again [12, 13, 16].

Figure 13.5 is based on the pool fire data of Kung and Stavrianidis [15] of methanol, heptane, a silicone transformer fluid, and a hydrocarbon transformer fluid, for the three pool diameters 1.22, 1.74 and 2.44 m and using 1-mm diameter bare bead thermocouples. For the fires that produced the highest values of temperature rise in the deep-flame region, near 900 K, which include all the fluids except the silicone fluid, the data from the various combinations of fluid and pool diameter were in good agreement.

The plume law for velocity, Equation 13.23, may be combined with the plume law for temperature, Equation 13.22, to produce the following useful nondimensional parameter: [14]

$$\xi = \left[\frac{T_\infty^{2/5}\left(c_p\rho_\infty\right)^{1/5}}{g^{2/5}}\right]\frac{u_0}{\left(\Delta T_0\dot{Q}_c\right)^{1/5}} \qquad (13.26)$$

In the plume region where Equations 13.22 and 13.23 are valid, their numerical coefficients correspond to a constant value $\xi = 2.2$. This value has been confirmed for a number of test fires [14], at heights as low as the mean flame height and even somewhat lower. Equation 13.26 with $\xi = 2.2$ is a useful relation for determining the maximum velocity in the plume, which occurs slightly below the mean flame height where the temperature rise may be taken at approximately $\Delta T_0 = 650$ K. For normal atmospheric conditions and the value $\xi = 2.2$, Equation 13.26 becomes

$$\frac{u_0}{\left(\Delta T_0\dot{Q}_c\right)^{1/5}} = 0.54 \qquad (13.27)$$

The maximum velocity just under the mean flame height, u_{0m}, is obtained by setting $\Delta T_0 = 650$ K

$$u_{0m} = 1.97\dot{Q}_c^{1/5} \tag{13.28}$$

Fires with low flame height-to-diameter ratios have not been investigated extensively and may require special consideration. For one particular fire with very low flame height [15] in which a proprietary silicone transformer fluid was burned in a 2.44-m-diameter pool, a flame height ratio of $L/D = 0.14$ was measured[3] at a convective heat release rate of $\dot{Q}_c = 327$ kW. Using the results in the next section, the virtual origin is calculated at $z_0 = -1.5$ m, assuming $\dot{Q}_c/\dot{Q} = 0.7$. With respect to the abscissa in Fig. 13.5, the lowest possible value is $-z_0/\dot{Q}_c^{2/5}$ corresponding to the fuel surface, $z = 0$. For the present case, $-z_0/\dot{Q}_c^{2/5} = 1.5/327^{2/5} = 0.15\left(\text{m kW}^{-2/5}\right)$. At this abscissa value, a centerline temperature rise of 580 K is indicated in Fig. 13.5. From the experiment [15], a near surface ΔT_0 of 440 K can be determined by slight extrapolation, fairly close to the prediction from Fig. 13.5. Fires with very low flame height-to-diameter ratios may generally be expected to produce lower maximum mean temperatures than other fires. However, it is not yet clear whether the type of prediction attempted here for a particular low L/D fire is generally valid.

There is also uncertainty associated with assuming that ξ in Equation 13.26 remains completely constant down to the flame level in low L/D fires. It may be found that ξ still remains approximately constant down to the height where the maximum gas velocity occurs, although this maximum will probably occur above the flames. The associated temperatures at this height cannot as yet be predicted. Consequently, the relation in Equation 13.28 becomes somewhat uncertain as L/D decreases (ΔT_0 is overestimated, resulting in u_{0m} being overestimated, although the effect is probably not very large because of the slow, ⅕th power dependence on ΔT_0).

The turbulence intensities in a fire plume are quite high. On the axis, George et al. [60] report an intensity of temperature fluctuations of approximately $T'/\Delta T_0 = 0.38$, where T' is the root mean square (rms) temperature fluctuation. Centerline values of the intensity of axial velocity fluctuations were measured near $u'/u_0 = 0.27$ by George et al. [60] and near $u'/u_0 = 0.33$ by Gengembre et al. [16], where u' is the rms velocity fluctuation in the axial direction.

EXAMPLE 5 Example *1* concerned a 1.5-m-diameter methyl alcohol fire burning under normal atmospheric conditions, generating $\dot{Q} = 884$ kW with a calculated mean flame height of 1.83 m. For an elevation of 5 m and given a virtual origin $z_0 = -0.3$ m (from Example 8), calculate the temperature radius, $b_{\Delta T}$, as well as the centerline value of temperature rise, ΔT_0, and gas velocity, u_0. Also calculate the maximum gas velocity in the flame.

SOLUTION Assume[4] $\dot{Q}_c = 0.8\ \dot{Q}$ and first calculate the temperature rise, using Equation 13.22 and properties for normal atmospheric conditions ($T_\infty = 293$ K, $g = 9.81$ m/s^2, $c_p = 1.00$ kJ/kg K, $\rho_\infty = 1.20$ kg/m^3)

$$\Delta T_0 = 9.1\left(\frac{293}{9.81 \cdot 1.00^2 \cdot 1.20^2}\right)^{1/3}(0.8 \cdot 884)^{2/3} \times (5+0.3)^{-5/3} = 123\,\text{K}$$

The temperature radius can now be calculated from Equation 13.21 as

$$b_{\Delta T} = 0.12\left(\frac{123+293}{293}\right)^{1/2}(5+0.3) = 0.76\ \text{m}$$

[3] A ratio $L/D = 0.02$ can be calculated from Equation 13.7 assuming $H_c/r = 3470$ kJ/kg, an average for silicone oils from values reported by Tewarson [63] and assuming a convective heat fraction $\dot{Q}_c/\dot{Q} = 0.7$. If a value of H_c/r near the bottom of the reported range [63] is selected, 3230 kJ/kg, the observed value $L/D = 0.14$ is reproduced; slight changes in the assumed convective fraction will also reproduce the measured value.

[4] Without specific knowledge, $\dot{Q}_c/\dot{Q}$ may usually be assumed at 0.7. However, methyl alcohol produces a fire of low luminosity and radiation, for which $\dot{Q}_c/\dot{Q} = 0.8$ is a good estimate.

The velocity is calculated from Equation 13.23 as

$$u_0 = 3.4\left(\frac{9.81}{1.00 \cdot 1.20 \cdot 293}\right)^{1/3}(0.8 \cdot 884)^{1/3} \times (5 + 0.3)^{-1/3} = 5.3 \text{ m/s}$$

Instead of Equation 13.23, the velocity can also be calculated from Equation 13.26 in this case, since ΔT_0 is already known. Actually, because normal ambient conditions prevail, Equation 13.27 can be used as follows:

$$u_0 = 0.54(123 \cdot 0.8 \cdot 884)^{1/5} = 5.3 \text{ m/s}$$

Finally, the maximum velocity in the flame is given by Equation 13.28 as

$$u_{0m} = 1.97(0.8 \cdot 884)^{1/5} = 7.3 \text{ m/s}$$

EXAMPLE 6 Recalculate the quantities called for in Example 5 using ambient conditions representative of Denver, Colorado, on a hot day: 630 mmHg pressure and 310 K temperature. (See Note on heat release rate for EXAMPLE 2.)

SOLUTION Changed ambient variables entering the equations include $T_\infty = 310$ K and $\rho_\infty = 0.78$ kg/m^3. From Equation 13.22, the new temperature rise is

$$\Delta T_0 = 167 \text{ K} (\text{versus } 123 \text{ K in Example 5})$$

The new velocity from Equation 13.23 is

$$u_0 = 6.0 \text{ m/s} (\text{versus } 5.3 \text{ m/s})$$

For the new ambient conditions, the relation analogous to Equation 13.28 is calculated as

$$u_{0m} = 2.10\dot{Q}_c^{1/5}$$

from which the new maximum velocity in the flame is

$$u_{0m} = 7.8 \text{ m/s} \text{ (versus } 7.3 \text{ m/s)}$$

Plumes in Temperature-Stratified Ambients

When a buoyant, turbulent plume rises, it cools by entrainment of ambient air. If the ambient air increases in temperature with height, which is normal in buildings, and the fire source is weak, the temperature difference between the plume and the ambient, which gives the plume buoyancy, may vanish and actually reverse in sign. Eventually the plume ceases to rise.

The maximum height achieved by plumes in temperature-stratified space has been given by Heskestad [64], based on pioneering theoretical and experimental work by Morton et al. [57]

$$z_m = 3.79\left[\frac{T_{a1}}{g\left(\rho_{a1}c_p\right)^2}\right]^{1/8}\dot{Q}_c^{1/4}\left(\frac{dT_a}{dz}\right)^{-3/8} \tag{13.29}$$

Here, dT_a/dz is the ambient temperature gradient, T_{a1} and ρ_{a1} are the ambient temperature and density, respectively, at the level of the fire source, and the constant 3.79 traces to experiments using dyed light liquid injected into a density stratified salt solution [57]. Other results are presented in Fig. 13.6, which shows the ratio on the plume centerline of stratified value versus unstratified value for various plume variables: temperature rise relative to the pre-existing value at each level (curve A), axial velocity (curve B), plume radius (curve C), and volume concentration of a combustion species (curve D). The ratios are plotted against the fraction of maximum elevation achieved by the plume, z/z_m. By definition, the stratified velocity (B) decreases to zero at $z/z_m = 1$. The stratified temperature rise (A) becomes negative below the maximum reach. The stratified plume radius (C) grows rapidly in approach to the maximum plume reach. However, there is little effect of the stratification on the centerline variation of concentration of a combustion species.

Fire experiments in temperature stratified space [66] have largely supported the validity of Fig. 13.6 for temperature rise (A) and volume concentrations (D), except that the experimental values needed an incremental height, roughly equal to 25 % of the theoretical plume reach, to return to zero.

The maximum plume reach can be interpreted in terms of a critical ambient temperature rise

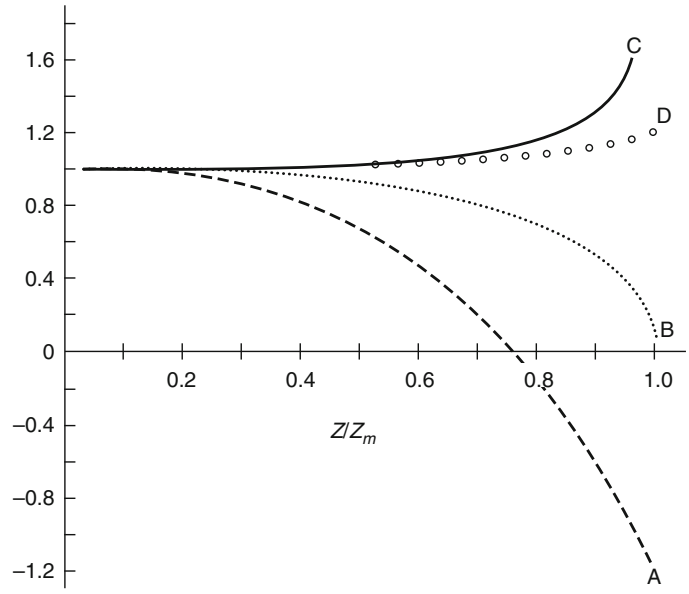

Fig. 13.6 Theoretical behavior of centerline plume variables in linearly temperature-stratified ambients. From Heskestad [64, 65], traceable to Morton et al. [57] *Curve A*: ratio of temperature rises (stratified versus unstratified). *Curve B*: ratio of axial velocities. *Curve C*: ratio of plume radii. *Curve D*: ratio of volumetric species concentrations

from the source level to an elevated observation plane, just strong enough to prevent plume fluid from penetrating the plane. Experiments [66] show that the critical ambient temperature rise for a linear profile is *7.4 times the centerline temperature rise at the level of the observation plane that results from a fire source in a uniform environment*. Furthermore, the critical temperature rise is surprisingly insensitive to the shape of the stratification profile. For a profile where one-half of the ambient temperature rise to the observation plane occurred higher than 75 % of the elevation of the observation plane above the source, the critical ambient temperature rise was only 12 % greater than that for the linear profile.

Effects of ambient temperature stratifications have been considered anew by Watanabe and Tanaka [67]. They developed their own model and tested it against experiments using a smoldering fire source.

EXAMPLE 7 Consider a 20-m-high atrium where the temperature rise, floor to ceiling, is 5 K. What heat release rate is required of a floor-level fire to drive the plume to the ceiling? What would be the effect of doubling the ceiling height?

SOLUTION The temperature rise in unstratified space is required as a reference and is calculated from Equation 13.22, taking $z_0 = 0$ for simplicity since deviations of the virtual origin from the level of the fire can be assumed to be inconsequential in this case. We have

$$\Delta T_0 = 25.0 \dot{Q}_c^{2/3} z^{-5/3} \tag{13.30}$$

The temperature rise of the stratification, 5 K, is 7.4 times the value of ΔT_0 for this associated unstratified-space fire, which will just drive the plume to the ceiling. Solving Equation 13.30 for $\dot{Q}_c$, setting $\Delta T_0 = 5/7.4$ K and $z = 20$ m, we get $\dot{Q}_c = 7.9$ kW. Assuming a ratio of 0.7 for convective in ratio to the total heat release rate, the latter is $\dot{Q} = 11.4$ kW. If the ceiling height is doubled to 40 m, the new result is $\dot{Q} = 64$ kW.

Virtual Origin

Pool Fires As pointed out earlier in this chapter, knowledge of the virtual origin of fire plumes is important for predicting the near-source plume behavior. The virtual origin is a point source

from which the plume above the flames appears to originate.

The virtual origin of a test fire is most conveniently determined from temperature data above the flames along the plume axis. According to Equation 13.22, a plot of $\Delta T_0^{-3/5}$ versus z should produce a straight line that intercepts the z-axis at z_0. Despite this apparent simplicity of obtaining z_0, the task is very difficult in practice. Slight inaccuracies in the determinations of centerline temperatures have large effects on the intercept, z_0; such inaccuracies may be associated with off-axis placement of sensors, radiation-induced errors in the temperature signal, or inadequate averaging of the signal.

Data obtained in this manner on the virtual origin for pool fires varying in diameter from 0.16 to 2.4 m [12, 14, 15], were examined for consistency with a theoretical model by Heskestad [68]. The model relied heavily on the flame-height correlation represented by Equation 13.3 and led to the prediction

$$\frac{z_0}{D} = -1.02 + F\frac{\dot{Q}^{2/5}}{D} \tag{13.31}$$

where F is a rather complex dimensional function of environmental variables c_p, T_∞, ρ_∞, g; H_c/r for the combustible, the fraction of the total heat release carried away by convection, and the mean centerline temperature at the mean flame height, T_L. It appeared that F could be considered a constant for wide variations in ambient temperature and pressure but might be affected by wide swings in the fuel variables, H_c/r, and convective fraction. The available data did not reflect any sensitivity to fuel identity within their scatter and led to the determination $F = 0.083$ m kW$^{-2/5}$, with Equation 13.31 becoming

$$\frac{z_0}{D} = -1.02 + 0.083\frac{\dot{Q}^{2/5}}{D} \quad (\dot{Q} \text{ in kW},\ D \text{ in m}) \tag{13.32}$$

Later, Hasemi and Tokunaga [69] analyzed their temperature measurements in plumes from gas burners of diameters in the 0.2–0.5 m range and established alternative correlations for the virtual origin. In terms of the nondimensional parameter $\dot{Q}^*$ defined in Equation 13.1, their correlations are

$$\begin{aligned} \frac{z_0}{D} &= 2.4\left(\dot{Q}^{*2/5} - 1\right) && \dot{Q}^* \geq 1.0 \\ \frac{z_0}{D} &= 2.4\left(\dot{Q}^{*2/3} - \dot{Q}^{*2/5}\right) && \dot{Q}^* < 1.0 \end{aligned} \tag{13.33}$$

For normal ambient conditions, these correlations can be written in terms of the variable $\dot{Q}^{2/5}/\mathrm{D}$ (cf. Equation 13.32) as

$$\begin{aligned} \frac{z_0}{D} &= -2.4 + 0.145\frac{\dot{Q}^{2/5}}{D} && \frac{\dot{Q}^{2/5}}{D} \geq 16.5 \\ \frac{z_0}{D} &= 0.0224\left(\frac{\dot{Q}^{2/5}}{D}\right)^{5/3} - 0.145\frac{\dot{Q}^{2/5}}{D} && \frac{\dot{Q}^{2/5}}{D} < 16.5 \end{aligned} \tag{13.34}$$

Cetegen et al. [70] have proposed correlations for the virtual origin on the basis of their air entrainment measurements in fire plumes and attempts to apply entrainment theory for a point source to the laboratory fires. Their experiments involved gas burners (natural gas) with diameters of 0.10, 0.19, 0.30, and 0.50 m. The experiments were performed with and without a floor mounted flush with the upper surface of the burners located some distance above the floor of the laboratory. Their correlations for the virtual origin are

$$\begin{aligned} \frac{z_0}{D} &= c + 1.09\dot{Q}^{*2/5} && \dot{Q}^* > 1 \\ \frac{z_0}{D} &= c + 1.09\dot{Q}^{*2/3} && \dot{Q}^* \leq 1 \end{aligned} \tag{13.35}$$

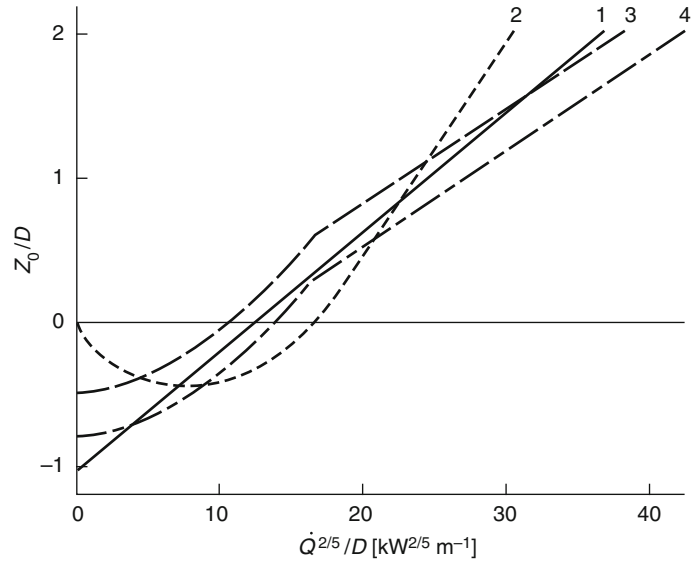

Fig. 13.7 Correlations for the virtual origin of pool fires. *Curve 1*: Equation 13.32; *Curve 2*: Equation 13.34; *Curve 3*: Equation 13.36 with floor; *Curve 4*: Equation 13.36 without floor

where $\dot{Q}^*$ has been defined by Equation 13.1, and where $c = -0.50$ with a flush floor around the burners and $c = -0.80$ without a flush floor. Using Equation 13.1, Equation 13.35 can be written in terms of $\dot{Q}^{2/5}/D$ yielding

$$\begin{aligned} \frac{z_0}{D} &= c + 0.0659\frac{\dot{Q}^{2/5}}{D} \qquad & \frac{\dot{Q}^{2/5}}{D} &> 16.5 \\ \frac{z_0}{D} &= c + 0.01015\left(\frac{\dot{Q}^{2/5}}{D}\right)^{5/3} \qquad & \frac{\dot{Q}^{2/5}}{D} &\le 16.5 \end{aligned} \tag{13.36}$$

where $c = -0.50$ and $c = -0.80$ with and without a flush floor, respectively.

Figure 13.7 is a composite plot of the various correlations for the virtual origin of pool fires, plotted as z_0/D versus $\dot{Q}^{2/5}/D$. Despite the diverse approaches, the overall correlations are surprisingly similar. Precise measurements are not yet available to clearly identify an optimal correlation. In the meantime, curve 1 in Fig. 13.7 (i.e., Equation 13.32) is recommended for its simplicity, clear foundation in theory [68], and central position among the other correlations.

Other Fire Types The original derivation of Equation 13.31 for pool fires [68] includes the following expression:

$$z_0 = L - 0.175\dot{Q}_c^{2/5} \qquad (L \text{ and } z_0 \text{ in m}; \dot{Q}_c \text{ in kW}) \tag{13.37}$$

In addition to representing pool fires, Equation 13.37 has also been verified to represent deep storage fires [42], allowing the location of the virtual origin to be calculated from knowledge of the mean flame height and the convective heat release rate. As discussed earlier, mean flame heights above the base of a fire in storages can be determined from Equation 13.3 when the flames extend above the storage, which implies that values of z_0 calculated refer to the distance above the base of the fire (usually the base of the storage). Equation 13.37 may also be assumed to be valid for turbulent jet fires.

EXAMPLE 8 Example *1* concerned a 1.5-m-diameter methyl alcohol fire generating $\dot{Q} = 884$ kW. Calculate the virtual origin.

SOLUTION In this example, $D = 1.5$ m. Direct substitution into Equation 13.32 gives

$$\frac{z_0}{D} = -1.02 + \frac{0.083(884)^{2/5}}{1.5} = -1.02 + 0.83 = -0.19$$

from which

$$z_0 = -0.19 \cdot 1.5 = -0.29 \text{ m}$$

This is the value for z_0 (rounded off) used in Example 5.

EXAMPLE 9 Negative values for z_0 are often calculated for low heat release fires and sufficiently large fire diameters, as in Example 8. Positive virtual origins are often found for high heat release fires. Substituting heptane for methyl alcohol in Example 8 (2500 kW/m^2 rather than 500 kW/m^2 measured for methyl alcohol) [17], calculate the new virtual origin.

SOLUTION The new heat release rate is

$$\dot{Q} = \frac{\pi 1.5^2}{4} 2500 = 4420 \text{ kW}$$

From Equation 13.32,

$$\frac{z_0}{D} = -1.02 + 0.083 \cdot \frac{4420^{2/5}}{1.5} = 0.57$$

from which

$$z_0 = 0.57 \cdot 1.5 = 0.85 \text{ m}$$

EXAMPLE 10 A 3-m-deep storage is known to produce a heat release rate per unit floor area of 4000 kW/m^2 when fully involved. At a stage of fire development in such a storage, a heat release rate of 1500 kW is reached. What is the location of the virtual origin?

SOLUTION First determine the flame height. Evaluate the effective fire diameter from $\pi D^2/4 = 1500/4000 = 0.375$ m^2, which gives $D = 0.69$ m. From Equation 13.8, calculate the flame height as 3.67 m (above base of storage), which is 0.67 m above the top of the storage. The height of the virtual origin above the base of the storage is calculated from Equation 13.37, assuming $\dot{Q}_c = 0.7\ \dot{Q} = 1050$ kW, yielding $z_0 = 3.67 - 0.175 \times 1050^{2/5} = 0.84$ m.

Entrainment

After ignition, the fire plume carries fire products diluted in entrained air to the ceiling. A layer of diluted fire products, or smoke, forms under the ceiling, which thickens and generally becomes hotter with time. The fire environment is intimately tied to the behavior of this layer, which, in turn, depends to a major extent on the mass flow rate of plume fluid into the layer. Consequently, it is important to be able to predict the mass flow rate that may occur in a fire plume.

The mass flow at a particular elevation in a fire plume is almost completely attributable to air entrained by the plume at lower elevations. The mass flow contributed by the fire source itself is insignificant in comparison.

For a weak plume, the mass flow rate at a cross section can be written

$$\dot{m}_{\text{ent}} = E \rho_\infty u_0 b_u^2 \tag{13.38}$$

where E is a nondimensional constant of proportionality. With the aid of Equation 13.23 and the equivalent of Equation 13.21 written for b_u (setting $T_0/T_\infty = 1$ because of the weak plume assumption), Equation 13.38 becomes

$$\dot{m}_{\text{ent}} = E \left(\frac{g \rho_\infty^2}{c_p T_\infty} \right)^{1/3} \dot{Q}_c^{1/3} (z - z_0)^{5/3} \tag{13.39}$$

Early measurements by Yih [71] indicated a value $E = 0.153$.

Cetegen et al. [70, 72] concluded from theoretical analysis that Equation 13.39 also applies to strongly buoyant plumes. From extensive entrained-flow measurements for natural gas burners of several diameters, these authors proposed a coefficient $E = 0.21$ based on the total

heat release rate, corresponding to $E = 0.24$ based on the convective heat release rate as in Equation 13.39 (assuming a convective fraction of 0.7). However, the plume flow rates at large heights were somewhat overpredicted and those at low heights, approaching the flames, were somewhat underpredicted.

Heskestad [73] reconsidered the entrainment problem for strong plumes, assuming self-preserving density deficiency profiles instead of self-preserving excess temperature profiles as traditionally assumed. This approach led to the following extension of Equation 13.39:

$$\dot{m}_{\text{ent}} = E\left(\frac{g\rho_\infty^2}{c_p T_\infty}\right)^{1/3} \dot{Q}_c^{1/3}(z - z_0)^{5/3} \cdot \left[1 + \frac{G\dot{Q}_c^{2/3}}{\left(g^{1/2} c_p \rho_\infty T_\infty\right)^{2/3}(z - z_o)^{5/3}}\right] \tag{13.40}$$

Equation 13.40, with $E = 0.196$ and $G = 2.9$, was found to represent the data of Cetegen et al. [70, 72] very well over the entire nonreacting plume for all their fire diameters, ranging from 0.10 to 0.50 m [73]. At large heights, the bracketed term involving G approaches unity, and at levels approaching the flame tip (Equation 13.3), this term approaches 1.5, approximately. Equation 13.40, with $E = 0.196$ and $G = 2.9$ is the recommended relation for calculating mass flow rates in plumes, at and above the mean flame height.

The entrained flow at the mean flame height, $\dot{m}_{\text{ent},L}$, follows from setting $z - z_0 = L - z_0$ in Equation 13.40 (with $E = 0.196$ and $G = 2.9$), taking L from Equation 13.3 and z_0 from Equation 13.31 (with substitution of full expression for F), with the result,

$$\dot{m}_{\text{ent},L} = 0.878\left[\left(\frac{T_L}{T_\infty}\right)^{5/6}\left(\frac{T_\infty}{\Delta T_L}\right) + 0.647\right]\frac{\dot{Q}_c}{c_p T_\infty} \tag{13.41}$$

The numerical values are linked to the experimental calibration coefficient for F (based on $F = 0.083$ m kW$^{-2/5}$ at normal atmospheric conditions as indicated under Equation 13.31) and taking $\Delta T_L = 500$ K. Interestingly, $\dot{m}_{\text{ent},L}$ is independent of the acceleration of gravity, g.

Mass flow rates in fire plumes at levels below the flame tip have been found to increase linearly with height for fire diameters of 0.3 m and greater [73], where the flames are substantially turbulent, from zero (essentially) at the fire base to the flame-tip value in Equation 13.41, that is,

$$\dot{m}_{\text{ent}} = \dot{m}_{\text{ent},L} z/L \tag{13.42}$$

Measurements in the flaming region for fire diameters *smaller* than 0.30 m do not show a linear variation of mass flow rate with height, including data by Cetegen et al. [70, 72] (fire diameters of 0.10 and 0.19 m) and Beyler [74] (0.19 and 0.13 m). (It is important to note, however, that all these data are consistent with an approach to the mass flow rate at the mean flame height given by Equation 13.41 [73].) Neither do the mass flow measurements in turbulent jet flames by Delichatsios and Orloff [75] show a linear variation with height (estimated values of N in range 50–6300 and momentum parameter R_M in range 0.0015–0.010); in fact, these measurements indicate a 5/2 power dependence, within the flames, of mass flow rate on height above the nozzle exit. As a guide to entrainment estimates in the flaming region for sources smaller than 0.30 m in diameter, it appears that a second power variation of mass flow rate with height is quite representative of the fire sources referred to above of diameters 0.13 and 0.10 m, in which case Equation 13.42 is replaced by

$$\dot{m}_{\text{ent}} = \dot{m}_{\text{ent},L}\left(\frac{z}{L}\right)^2 \tag{13.43}$$

The 0.19-m-diameter sources generated scattered results between the linear and second power variation [73]. Delichatsios [76] as well as Quintiere and Grove [77] have also analyzed mass flow rates in the flaming region.

We digress briefly on the appropriateness of relating entrainment behavior to the diameter of the fire source. The governing parameters for fire plumes from horizontal, circular sources have been considered so far to be the parameter N and the momentum parameter R_M. However,

for small fire sources it is common to see a laminar flame sheet preceding transition to turbulence around the rim of the fire source, and the degree to which such laminar regions and effects exist will depend on the flame Reynolds number. A flame Reynolds number can be formulated as $u_{0m}b_{um}/v_m$, where u_{0m} is the characteristic gas velocity in the flame, proportional to $\dot{Q}^{1/5}$ according to Equation 13.28; b_{um} is the associated characteristic flame radius, proportional to [78] $\dot{Q}^{2/5}$; and v_m is the kinematic viscosity evaluated at the mean maximum flame temperature, which can be considered constant. Hence, the flame Reynolds number can be considered proportional to $\dot{Q}^{3/5}$. Assuming the discharge momentum is not important (small R_M), the flame entrainment behavior should be a function of N and $\dot{Q}$. When the entrainment behavior is represented on $N, \dot{Q}$ coordinates for the various test fires indicated above, it is found that the fires with linear increase of mass flow rate with height in the flame plot above a line $\dot{Q} \propto N^{1/2}$, with some uncertainty about the precise level. With the aid of Equation 13.4 it becomes clear that this relation implies an equivalent limit line $D =$ *constant,* which justifies relating the entrainment behavior to the source diameter.

For normal atmospheric conditions Equations 13.40, 13.41, and 13.42 can be written as follows for the plume mass flow rate at various heights:

Above the mean flame height, L ($\dot{Q}_c$ in kW, z and z_0 in m)

$$\dot{m}_{\text{ent}}(\text{kg/s}) = 0.071\dot{Q}_c^{1/3}(z - z_0)^{5/3} \cdot \left[1 + 0.027\dot{Q}_c^{2/3}(z - z_0)^{-5/3}\right] \tag{13.44}$$

At the mean flame height, $L(\Delta T_L = 500\ \text{K})$

$$\dot{m}_{\text{ent},L}(\text{kg/s}) = 0.0058\dot{Q}_c(\text{kW}) \tag{13.45}$$

At and below the mean flame height, L, for fire source diameters of 0.3 m and greater

$$\dot{m}_{\text{ent}}(\text{kg/s}) = 0.0058\dot{Q}_c(\text{kW}) \cdot \frac{z}{L} \tag{13.46}$$

Under the prevailing assumptions, and the further assumption $\dot{Q}_c/\dot{Q} = 0.7$ and $H_c/r \approx 3100$ kJ/kg, Equation 13.45 implies that the mass flow at the flame tip is 13 times the mass stoichiometric requirement of the fuel [73].

Fires with very low flame height-to-diameter (L/D) ratios have not been investigated extensively. It is not clear to what L/D limit the entrained-flow relations presented here apply, but this limit is smaller than 0.9, the lowest L/D ratio associated with the data of Cetegen et al. [70, 72] For plume mass flows above the flames, there is no L/D limit for predictions at the higher elevations, but predictions of mass flows at levels just above the flames may begin to deteriorate before $L/D = 0.14$ is reached, as seems to be implied in the observations following Equation 13.28.

Further, mention should be made of a plume mass flow formula often used because of its simplicity, originally developed for the flaming region of large fires by Thomas et al. [79]

$$\dot{m}_{\text{ent}} = 0.096\left(g\rho_\infty\rho_{f\ell}\right)^{1/2}W_f z^{3/2} \tag{13.47}$$

Here $\rho_{f\ell}$ is the gas density in the flames and W_f is the fire perimeter. This formula has also been tested against mass flow data above the flames by Hinkley [80], who claims it is very satisfactory for heights up to 10 times the linear dimension (or diameter) of a fire, although there is little theoretical justification for its use above the flames. The following version of Equation 13.47 is often used [80] (based on normal atmospheric conditions and an assumed flame temperature):

$$\dot{m}_{\text{ent}}(\text{kg/s}) = 0.188W_f(m)z(m)^{3/2} \tag{13.48}$$

It is instructive to compare the predictions of Equations 13.44 and 13.48 for plume regions above the flames. In a number of comparisons for heat release rates in the range 1000–8000 kW, heat release rates per unit area in the range 250–1000 kW/m^2, and heights varying from the flame level to 128 m, the predictions of Equation 13.48 range from 0.64 to 1.38 times the predictions of Equation 13.44.

Cetegen et al. [70, 72], whose data have contributed most to the mass flow recommendations in this text, have carefully pointed out that their fire plumes were produced in as quiet an atmosphere as could be maintained in their laboratory. They report that small ambient disturbances could provide 20–50 % increases in the measured plume mass flows. Clearly, there is need for further research.

Grove and Quintiere [45] have developed new correlations for entrainment, including linear sources (not considered here). They state their near-field entrainment correlations show some differences with others.

EXAMPLE 11 Calculate plume mass flow rates for the methyl alcohol fire of Examples *1*, 5, and 8.

SOLUTION From Example *1*, $\dot{Q} = 884$ kW and $L = 1.83$ m; from Example 5, $\dot{Q}_c = 0.8\ \dot{Q} = 707$ kW; from Example 8, $z_0 = -0.29$ m. At the mean flame height, 1.83 m, the mass flow rate follows from Equation 13.45:

$$\dot{m}_{\text{ent},L} = 0.0058 \cdot 707 = 4.1 \text{ kg/s}$$

Mass flow rates in the flaming region are calculated using Equation 13.46 as

$$\dot{m}_{\text{ent}}(\text{kg/s}) = 4.1 \cdot \frac{z}{1.83} = 2.2\, z \text{ (m)}$$

Mass flow rates above the flames are obtained from Equation 13.44; for example, at a height of 3.66 m (twice the flame height)

$$\begin{aligned}\dot{m}_{\text{ent}} &= 0.071 \cdot 707^{1/3}(3.66 + 0.29)^{5/3} \\ &\quad \cdot \left[1 + 0.027 \cdot 707^{2/3}(3.66 + 0.29)^{-5/3}\right] \\ &= 6.24(1 + 0.22) \\ &= 7.6 \text{ kg/s}\end{aligned}$$

Illustration

In addition to the previous examples, it is instructive to work through a somewhat larger problem to illustrate handling of the equations and their limitations. Units used throughout this section are kW for heat release rate, m for length, s for time, K for temperature, and m/s for velocity.

The example can be used of a large building that will allow clear, uncontaminated air to exist around a particular growing fire for at least 10 min before smoke begins to recirculate into the region. Normal atmospheric conditions prevail. Wood pallets are stored in a large, continuous array on the floor to a height of 1.2 m. This array is ignited locally at an interior point, and the fire spreads in a circular pattern at constant radial speed (as predicted and observed for wood cribs) [81], such that the heat release rate grows with the second power of time as

$$\dot{Q}(kW) = 1000\left(\frac{t}{t_g}\right)^2 \tag{13.49}$$

Here, t is time and t_g is the so-called growth time. When t_g is 60 s, the fire grows through a magnitude of 1000 kW in 60 s. When t_g is 600 s, the fire grows through a magnitude of 1000 kW in 600 s, a much slower growth rate. In this illustration, it is assumed that the growth time is $t_g = 140$ s. It is also assumed that the fully involved pallet storage generates a total heat release rate of 2270 kW/m^2 of floor area. [17] The objective is to determine flame height as a function of time, as well as the variation of plume centerline temperature, plume centerline velocity, and plume width at an elevation of 5 m above the base of the fuel array where a structural member may cross and be heated by the plume.[5]

For the assumed growth time, $t_g = 140$ s, the variation of total heat release rate with time comes from Equation 13.49 as follows:

$$\dot{Q} = 5.10 \times 10^{-2} t^2 \tag{13.50}$$

The convective heat release rate is assumed at 70 % of the total heat release rate as

[5] In addition to convective heating, which depends on gas temperature and velocity, radiative heating would also be important in such cases and might even dominate over convective heating if the structure is immersed in flames.

$$\dot{Q}_c = 3.57 \times 10^{-2} t^2 \tag{13.51}$$

The instantaneous fire diameter, D, is determined as follows. Since the heat release rate per unit floor area is 2270 kW/m^2,

$$\dot{Q} = 2270 \frac{\pi D^2}{4} \tag{13.52}$$

Upon eliminating $\dot{Q}$ between Equations 13.50 and 13.52, the following can be obtained:

$$D = 5.35 \times 10^{-3} t \tag{13.53}$$

First, the behavior of flame height may be calculated using Equation 13.8. Substitution of Equations 13.50 and 13.53 into Equation 13.8 gives the following relation of flame height as a function of time:

$$L = -5.46 \times 10^{-3} t + 7.15 \times 10^{-2} t^{4/5} \tag{13.54}$$

This relation is plotted in Fig. 13.8 for the 10-min (600-s) fire interval and is labeled L.

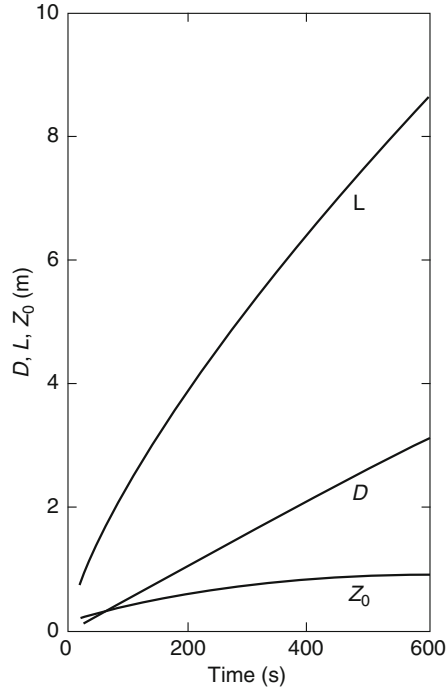

Fig. 13.8 Growing fire illustration: fire diameter, D, flame height, L, and virtual origin, z_0

The fire diameter, D, is also plotted in Fig. 13.8, based on Equation 13.53.

The virtual origin, z_0, is determined from Equation 13.32, with substitutions for $\dot{Q}$ from Equation 13.50 and for D from Equation 13.53

$$z_0 = -5.46 \times 10^{-3} t + 2.52 \times 10^{-2} t^{4/5} \tag{13.55}$$

The curve labeled z_0 in Fig. 13.8 represents the virtual origin according to Equation 13.55. It is seen that z_0 nearly levels off in the time interval plotted in the figure; actually, z_0 begins to decrease again at somewhat larger times.

With this foundation, there is sufficient information to calculate gas temperatures, velocities, and plume widths at the 5 m height above the base of the fuel array.

The temperature rise on the plume centerline at the selected height is determined from Equation 13.22 by substituting $z = 5$ (m); z_0 from Equation 13.55; $\dot{Q}_c$ from Equation 13.51; and values of T_∞, g, c_p, and ρ_∞ for the normal atmosphere, yielding

$$\Delta T_0 = \frac{2.71 t^{4/3}}{\left(5 + 5.46 \times 10^{-3} t - 2.52 \times 10^{-2} t^{4/5}\right)^{5/3}} \tag{13.56}$$

This relation is valid up to the time that a temperature rise associated with the flame tip, $\Delta T_0 = 500$ K, is felt at the selected height, which occurs at $t = 303$ s. The plot of ΔT_0 in Fig. 13.9 is according to Equation 13.56 up to the time $t = 303$ s. At larger times, ΔT_0 is determined from Fig. 13.5 in the following manner: at each selected time, $z - z_0$ is calculated using Equation 13.55; $\dot{Q}_c$ is calculated from Equation 13.51; the quantity $(z - z_0)/\dot{Q}_c^{2/5}$ is determined and ΔT_0 is read from Fig. 13.5. The resulting extension of the ΔT_0 curve is seen in Fig. 13.9.

The centerline gas velocity at the 5 m height above the base of the fuel array can then be considered. Equation 13.23 can be used up to the moment that the flame tip reaches the 5 m height, that is, at $t = 303$ s. After substitution of

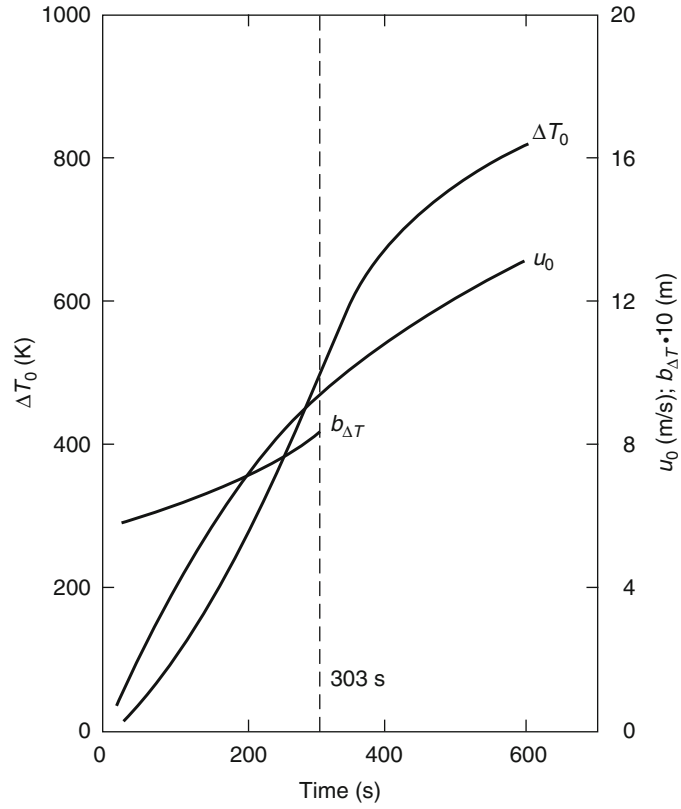

Fig. 13.9 Growing fire illustration: plume width, $b_{\Delta T}$, and centerline values of temperature rise, ΔT_0, and velocity, u_0, at 5 m above the base of the fuel

$z = 5$ (m), z_0 from Equation 13.55, $\dot{Q}_c$ from Equation 13.51, and normal ambient conditions, Equation 13.23 becomes

$$u_0 = \frac{0.339 t^{2/3}}{\left(5 + 5.46 \times 10^{-3} t - 2.52 \times 10^{-2} t^{4/5}\right)^{1/3}} \tag{13.57}$$

The u_0 curve in Fig. 13.9 follows Equation 13.57 to the limit, $t = 303$ s. As stated in conjunction with Equation 13.27, the maximum velocity (for a given size fire) occurs just below the mean flame height where $\Delta T_0 = 650$ K, which corresponds to $(z - z_0)/\dot{Q}_c^{2/5} = 0.135$ according to Fig. 13.5. Using $z = 5$ (m), and z_0 and $\dot{Q}_c$ from Equations 13.55 and 13.51, the 0.135 limit is found to correspond to a time of $t = 385$ s, where Equation 13.28 gives the centerline velocity in terms of $\dot{Q}_c$. In fact, it appears that Equation 13.28 can be used with good accuracy to even larger times, at least to times associated with a lower limit of $(z - z_0)/\dot{Q}_c^{2/5} = 0.08$, according to available measurements [12, 16]. Since the largest time in Fig. 13.9 corresponds to $(z - z_0)/\dot{Q}_c^{2/5} = 0.092$, Equation 13.28 has been used to calculate the entire extension of the u_0 curve in Fig. 13.9.

The temperature radius of the plume at the 5 m height above the fuel array is calculated from Equation 13.21, which can be written

$$b_{\Delta T} = 0.12 \left(1 + \frac{\Delta T_0}{T_\infty}\right)^{1/2} (z - z_0) \tag{13.58}$$

With substitution of $z = 5$ (m), ΔT_0 from Equation 13.56, and z_0 from Equation 13.55, Equation 13.58 becomes

$$b_{\Delta T} = 0.12 \left[\frac{1 + 9.25 \cdot 10^{-3} t^{4/3}}{\left(5 + 5.46 \cdot 10^{-3} t - 2.52 \cdot 10^{-2} t^{4/5}\right)^{5/3}}\right]^{1/2} \cdot \left(5 + 5.46 \cdot 10^{-3} t - 2.52 \cdot 10^{-2} t^{4/5}\right) \tag{13.59}$$

This equation is plotted in Fig. 13.9 up to the time the flames reach the 5 m height at $t = 303$ s. The temperature radius at the 5 m height is seen to vary from 0.59 m early in the fire to 0.83 m at 303 s. Plume fluid will reach a minimum of twice the temperature radius, $b_{\Delta T}$; hence, the total width of the plume in this example will be at least four times $b_{\Delta T}$, growing from a minimum of 2.4 m early in the fire to a minimum of 3.3 m as the flames reach the 5 m height.

Additional Plume and Flame Topics

Other aspects of fire plumes than those already discussed have been studied and may be of interest, including (1) flame intermittency length scale, (2) flame pulsations and (3) the rise of a plume front or cap after ignition into undisturbed air. Both of these aspects are essentially axisymmetric, whereas three others are not: (4) effects on a fire plume of proximity to a wall or corner, (5) effects of wind, and (6) behavior of turbulent jet diffusion flames in horizontal discharge. These topics are discussed briefly here.

Flame Intermittency Length Scale

The flame intermittency has been discussed in connection with the definition of flame height in Fig. 13.2, based on the work of Zukoski et al. [23]. Zukoski and coworkers [82] also defined a flame intermittency length scale, L_I, with the aid of the maximum (negative) slope of the intermittency (I) curve and the intersections of this slope with $I = 0$ and $I = 1$. L_I was defined as the difference in elevations z between these two intersections.

Figure 13.10 presents results [27] from simultaneous measurements of the flame height ratio, L/D, and the flame intermittency length scale to flame height ratio, L_I/L, for the three circular porous bed fires of natural gas investigated by

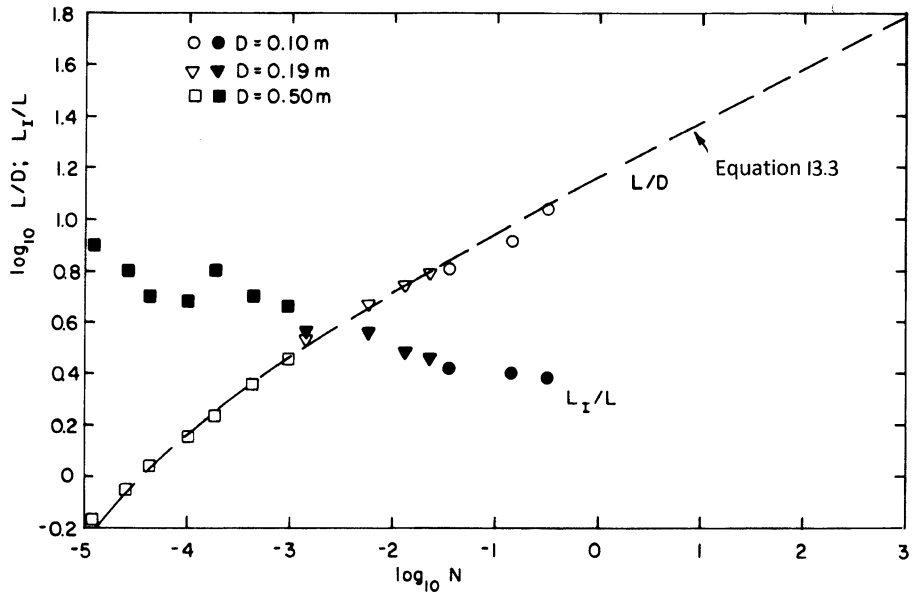

Fig. 13.10 Flame heights and intermittency scales according to flame-intermittency data of Zukoski et al. [82]

Zukoski et al. [23, 82] The open symbols represent the nondimensional flame heights L/D, which compare well with the reference curve according to Equation 13.3. It is seen that L_f/L generally increases as N and the nondimensional flame height decrease, implying an accompanying increase in flame fluctuations. Wood et al. [40] reported that coherent flaming in their pool fires changed to distributed flamelets for L/D values smaller than about 0.5 ($\log_{10} L/D = -0.30$), which occurs near $\log_{10} N = -5$ ($N = 10^{-5}$) in Fig. 13.10. This behavior seems to correlate well with L_f/L near unity.

Flame Pulsations

Flame pulsations have been studied by a number of investigators, tracing at least as far back as Rashbash et al. [83] and reviewed in conjunction with an investigation reported by Cetegen and Ahmed [84]. Byram and Nelson [85] describe the pulsation cycle as starting with the expansion of the flames near the base of the fire, followed by a sudden collapse of these flames toward the center of the fire. A flame bulge then travels upward to the flame tip in an even, wavelike motion. Expansion of the lower part of the flames starts the cycle again.

Cetegen and Ahmed [84] summarize the published data on pulsation frequency in a single plot for burner or pool diameters ranging from 0.03 to 20 m and propose the simple curve fit

$$f(Hz) = 1.5[D(m)]^{-1/2} \tag{13.60}$$

As a measure of the data scatter it is noted that measured frequencies near a given diameter agree within a factor of two.

Flame pulsations are not always easy to detect visually. For example, Wood et al. [40] reported visual pulsations for a flame on their 1.52-m diameter sandfilled pan when initially saturated with methanol, but not when initially saturated with acetone. Other than visually, pulsations have been detected based on temperature and velocity records in the flames, motion picture records, or pressure fluctuations on the surface of the fire source.

Rise of Plume Front

Measurements by Tanaka et al. [86] of the rise times of plume fronts from suddenly initiated fires at steady heat release rate (such as pool fires) have been represented by Heskestad [87] in the following formula:

$$t_R^* = 0.46 \tag{13.61}$$

Here, $t_R{}^*$ is the nondimensional rise time to a given height, z, defined as

$$t_R^* = \left[g/\left(c_p T_\infty \rho_\infty\right)\right]^{1/3} \dot{Q}_c^{1/3} z^{-4/3} t_R \tag{13.62}$$

where t_R is the physical rise time to the elevation z.

As an example, if $\dot{Q} = 100$ kW and assuming $\dot{Q}_c = 0.7 \cdot 100 = 70$ kW, the physical rise time to an elevation of 30 m in a normal atmosphere is calculated as

$$t_R = 0.46 \cdot [9.81/(1.00 \cdot 293 \cdot 1.2)]^{-1/3} \cdot 70^{-1/3} \cdot 30^{4/3}$$
$$t_R = 34\,\text{s}$$

New measurements by Hu et al. [88] have closely reproduced the result in Equation 13.61 (0.43 compared to 0.46). In addition, these investigators measured rise times for plumes near a building wall, giving essentially the same result as the case of a free plume, and near a building corner (interior) where the rise times were about ¾ of the free plume values.

Wall/Corner Effects

McCaffrey [24] has reviewed effects on flame height of placing fire sources next to a wall or in a corner, referring to experiments by Hasemi and Tokunaga [89], Back et al. [90], Mizuno and Kawagoe [91], and Kokkala [92]. The effects are generally reported to be small. In more recent

work, Poreh and Garrad [93] and Lattimer and Sorathia [94] have made further studies.

Windblown Flames

The main effect of wind is to bend or deflect the flames away from the vertical. Another effect, observed in wind tunnel studies by Welker and Sliepcevich [95], is "flame trailing," in which the flames trail off the burner along the floor in the downwind direction for a significant distance. Flame trailing was thought to be associated primarily with fuel vapors of greater density (higher molecular weight) than air, as was the case with all the various liquid fuels used in the experiments.

Wind tunnel measurements of flame deflection angle, involving fire diameters in the range 0.10–0.60 m, and large-scale data for square LNG pools in the effective diameter range 2–28 m, obtained by Attalah and Raj [96], have been found to correlate well against the ratio of wind velocity to the maximum velocity in the flame according to Equation 13.28 [65]. The relationship indicates that a flame deflection angle of approximately 25° can be expected for a velocity ratio of 0.10. Effects of wind on flame length were minor for velocity ratios up to 0.35 (flame deflection angle of approximately 60°). Data by Huffman et al. [97] indicate that at the considerably higher velocity ratio of 1.0, flame lengths are approximately 30 % greater than under quiescent conditions.

For turbulent jet diffusion flames, discussed under the subheading "Momentum Regime" of the section "Flame Heights," Brzustowski et al. [98] found reduced flame length in a range of small wind velocities for a laboratory hydrogen flame. Related to this finding is an observation reported to the author by a staff member of a major supplier of flare equipment that the flames of flares are typically seen to increase in length by some 30 % when winds calm down from about 0.4 m/s. Finally we call attention to measurements by Sönju and Hustad [99], conducted mostly outdoor, which indicate agreement of measured flame lengths with laboratory results in one case (a methane series) and 10–40 % smaller lengths in another case (a propane series) [53]. The smaller lengths may have been associated with a slight wind.

Jet Flames in Horizontal Discharge

Becker et al. [100] have studied flame geometries resulting from horizontal gas discharge and have provided extensive data and correlations. For ease of application, their results have been reformulated by the author as functions of the momentum parameter R_M of Equation 13.9 (and Fig. 13.4), using supporting data from Becker and Liang [25].

The flames were stabilized against blow-off with hydrogen or oxygen, when necessary, and photographed from the side in 1-s exposures. The results are presented in Fig. 13.11, where the inset defines the selected measures of flame geometry with X and Y being the maximum horizontal and vertical flame excursions, respectively. In the figure, maximum excursions (derived from faired curves [100]) have been made nondimensional with flame heights in vertical discharge (from faired curves [24]), L, and plotted as functions of R_M. Seven different gases were employed in the experiments, as indicated. Note that the vertical flame heights, L, were interpreted as the highest points "at which flaming gas was seen to dwell with an appreciable frequency." [25]

Calculation of R_M has been illustrated in Example 4. Note in the figure that as R_M approaches 1, the entire flame practically projects horizontally and has a length nearly the same as in vertical discharge (X/L near 0.9). There is some uncertainty in this comparison since the bases of the X and L measurements are not quite identical.

The inset sketch in Fig. 13.11 is actually the outline of an ethane flame from a photograph [100] at $R_M = 0.14$.

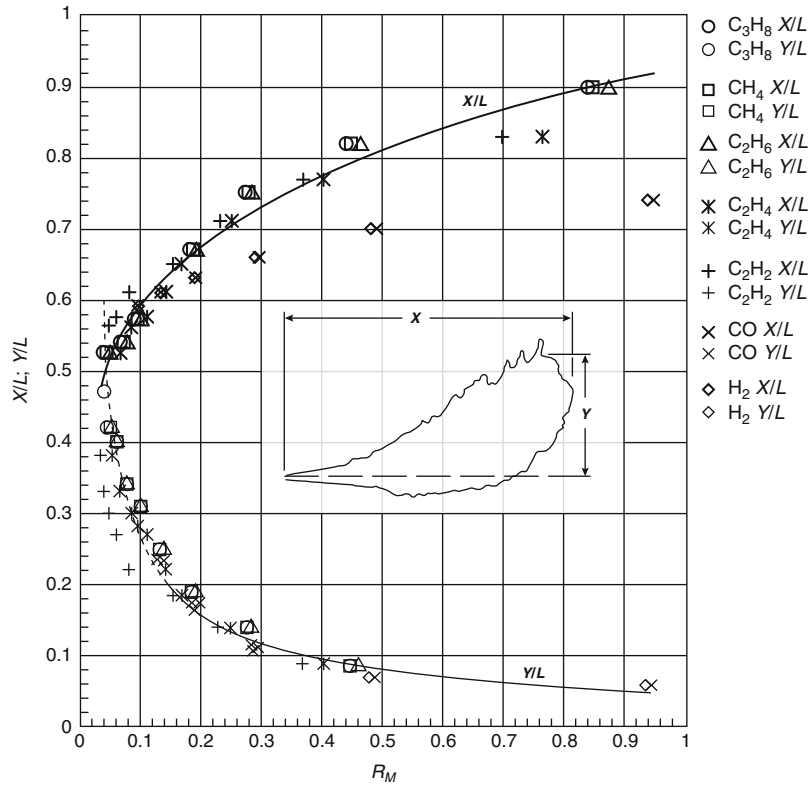

Fig. 13.11 Data from Becker et al. [100] on maximum nondimensional horizontal and vertical flame excursions of turbulent jet diffusion flames in horizontal gas discharge, formulated as functions of the momentum parameter R_M of Equation 13.9 and Fig. 13.4

Research Needs

All of the areas discussed in this chapter will benefit from further study. However, certain needs stand out from the discussion.

Temperature measurements in fire with bare-bead thermocouples usually involve radiation errors and undoubtedly such errors were present in the measurements for Fig. 13.5. Newman and Croce [101] in their study of aspirated thermocouples determined radiation errors for a centerline location close to the flame tip of a 0.230-m diameter acetone pan fire. For a 1-mm diameter bare-bead thermocouple their measurements translate to a thermocouple temperature 170 K less than the actual gas temperature as a result of radiation to the environment. (The aspirated thermocouple design of Newman and Croce nearly eliminated the radiation error.) Careful experiments are needed to establish near error-free temperatures.

Fires with low flame height-to-diameter ratios were discussed following Equation 13.28 and several uncertainties noted. Research on such fires can fill in areas of uncertainty.

There may be secondary effects on flame height (and other flame properties) of variables enumerated in the paragraph before Equation 13.6, which should be investigated, including nonuniform volatilization rate across the fuel bed, departure of fire area from circular, density of volatiles, and effect of flame Reynolds number (which depends on fire diameter and heat release rate).

Attention is directed to the end of subsection "Pool Fires" of the section "Virtual Origin," where more precise measurements of virtual origins for pool fires are recognized as a need.

Near the end of subsection "Entrainment," the observations of Cetegen et al. [68, 70] on the sensitivity of air entrainment in a plume to ambient disturbances were noted. Since air entrainment scenarios (as in room fires) often involve disturbances, it is important to be able to account for these.

Data Sources

NFPA 92B, *Standard for Smoke Management Systems in Malls, Atria, and Large Spaces* [103], was referenced in this chapter for tables of heat release rate per unit floor area, kW/m^2, and growth times, t_g, of a number of fuel arrays. The same information has been incorporated by Alpert and Ward [104], together with additional data.

In Appendix 3 tables are provided to estimate combustion efficiencies as well as total and convective heat release rates per unit exposed area of materials under full-scale burning conditions.

Nomenclature

A	Defined in Equation 13.6 (m·kW$^{-2/5}$)
B	Buoyancy flux defined in Equation 13.15 (m^4·s^{-3})
b	Plume radius (m)
$b_{\Delta T}$	Plume radius to point where $\Delta T/\Delta T_0 = 0.5$ (m)
b_u	Plume radius to point where $u/u_0 = 0.5$ (m)
b_{um}	b_u at level of maximum gas velocity near flame tip (m)
c	Adjustable constant, Equation 13.35
c_p	Specific heat of air at constant pressure (kJ/kg·K)
D	Diameter (m)
F	Function (c_p, T_∞, ρ_∞, g); see Equation 13.31 (m·kW$^{-2/5}$)
f	Frequency (s^{-1})
g	Acceleration due to gravity (m/s^2)
H_c	Actual lower heat of combustion (kJ/kg)
ΔH_O	Tewarson's [44] lower heat of combustion per unit mass of oxygen consumed (kJ/kg)
I	Intermittency
k	Ratio of specific heats, constant-pressure versus constant-volume
L	Mean flame height above base of fire (m)
L_B	Buoyancy controlled flame height (m)
L_I	Intermittency length scale
L_M	Momentum controlled flame height (m)
$\dot{m}_{ent}$	Entrained mass flow rate in plume (kg/s)
$\dot{m}_{ent,L}$	$\dot{m}_{ent}$ at the mean flame height, L(kg/s)
$\dot{m}_f$	Mass burning rate (kg/s)
N	Nondimensional parameter defined in Equation 13.4
p_s	Pressure in source gas discharge stream (Pa)
p_{s0}	Pressure in source gas reservoir (Pa)
$\dot{Q}$	$\dot{m}_f H_c$ total heat release rate (kW)
$\dot{Q}_c$	Convective heat release rate (kW)
$\dot{Q}_r$	Radiative heat release rate (kW)
$\dot{Q}^*$	Nondimensional parameter defined in 13.1
R	Radius (m)
r	Actual mass stoichiometric ratio, air to fuel volatiles
R_M	Momentum parameter defined in Equation 13.8
T	Mean temperature (K)
T_0	Mean centerline temperature in plume (K)
T_∞	Ambient temperature (K)
T'	rms temperature fluctuation (K)
$T_a(z)$	Ambient temperature at level z (K)
T_{a1}	Ambient temperature at source level (K)
T_L	T_0 at mean flame height (K)
ΔT	$T - T_\infty$, mean temperature rise above ambient (K)
ΔT_0	Value of ΔT on plume centerline (K)
ΔT_L	$T_L - T_\infty$(K)
t	Time (s)
t_g	Growth time; see Equation 13.49 (s)
t_R	Rise time of plume front (s)
t_R^*	Nondimensional rise time of plume front, see 13.62
u	Mean axial velocity (m/s)
u_0	Mean axial velocity on centerline (m/s)
u_{0m}	Maximum value of u_0, near flame tip (m/s)
u'	rms velocity fluctuation in axial direction (m/s)

W_f	Fire perimeter (m)
z	Height above base of fire (m)
z_0	Height of virtual origin above base of fire (m)
z_m	Maximum vertical penetration of plume fluid in stratified ambient (m)
α	Entrainment coefficient
ξ	Nondimensional parameter defined in Equation 13.26
ν_m	Kinematic viscosity of flame gases at maximum flame temperature ($m^2 \cdot s^{-1}$)
ρ	Mean density (kg/m^3)
ρ_{a1}	Ambient density at source level (kg/m^3)
ρ_{fe}	Mean density in flames (kg/m^3)
ρ_s	Density of source gas discharge stream (kg/m^3)
ρ_{s0}	Density of source gas in reservoir (kg/m^3)
$\rho_{s\infty}$	Density of source gas at ambient temperature and pressure (kg/m^3)
ρ_∞	Ambient density (kg/m^3)
$\Delta\rho$	$\rho_\infty - \rho$, mean density deficiency (kg/m^3)
$\sigma_{\Delta T}$	Plume radius to point where $\Delta T/\Delta T_0 = e^{-1}$ (m)
σ_u	Plume radius to point where $u/u_0 = e^{-1}$ (m)

References

1. Rehm, R.G, Baum, H.R., "The Equations of Motion for Thermally Driven, Buoyant Flows," *J. Res. Nat. Bur. Stand.* 83, pp. 297–308 (1978).
2. H.R. Baum, K.B. McGrattan, and R.G. Rehm, "Mathematical Modelling and Computer Simulation of Fire Phenomena," *Fire Safety Science-Proceedings Fourth International Symposium,* International Association of Fire Safety Science, London, UK (ed. T. Kashiwagi), pp. 185–193 (1994).
3. T.G. Ma and J.G. Quintiere, "Numerical Simulation of Axi-Symmetric Fire Plumes: Accuracy and Limitations," *Fire Safety Journal,* 38, pp. 467–492 (2003).
4. Y. Xin, J.P. Gore, K.B. McGrattan, R.G. Rehm, and H.R. Baum, "Fire Dynamics Simulation of a Turbulent Buoyant Flame Using Mixture-Fraction-Based Combustion Models," *Combustion and Flame,* 141, pp. 329–335 (2005).
5. Xin, Y., Filatyev, S.A., Biswas, K., Gore, J.P., Rehm, R.G., and Baum, H.R., "Fire Dynamics Simulations of a One-Meter Diameter Methane Fire," *Combustion and Flame,* 153, pp.499–509 (2008).
6. Tieszen, S.R., O'Hern, T.J., Schefer, R.W., Weckman, E.J. and Blanchat, T.K., "Experimental Study of the Flow Field In and Around a One Meter Diameter Methane Fire," *Combustion and Flame,* 129, pp. 378–391 (2002).
7. FireFoam, released by FM Global, available from < http://code.google.com/p/firefoam-dev/>
8. OpenFoam, produced by OpenCFD Ltd, available from < http://www.openfoam.com/>
9. Wang, Y, Chatterjee, P. and de Ris, J.L., "Large Eddy Simulation of Fire Plumes," Proceedings of the Combustion Institute, 33, pp. 2473–2480 (2011).
10. Olenick, S.M. and Carpenter, D. J., "An Updated International Survey of Computer Models for Fire and Smoke," Journal of Fire Protection Engineering, 13, pp. 87–110 (2003).
11. G. Heskestad, "Engineering Relations for Fire Plumes," *Fire Safety Journal,* 7, pp. 25–32 (1984).
12. B.J. McCaffrey, "Purely Buoyant Diffusion Flames: Some Experimental Results," *NBSIR 79–1910,* National Bureau of Standards, Washington, DC (1979).
13. G. Cox and R. Chitty, "A Study of the Deterministic Properties of Unbounded Fire Plumes," *Combustion and Flame,* 39, pp. 191–209 (1980).
14. G. Heskestad, "Peak Gas Velocities and Flame Heights of Buoyancy-Controlled Turbulent Diffusion Flames," *18th Symposium on Combustion,* Combustion Institute, Pittsburgh, PA, pp. 951–960 (1981).
15. H.C. Kung and P. Stavrianidis, "Buoyant Plumes of Large-Scale Pool Fires," *19th Symposium on Combustion,* Combustion Institute, Pittsburgh, PA, pp. 905–912 (1983).
16. E. Gengembre, P. Cambray, D. Karmed, and J.C. Bellet, "Turbulent Diffusion Flames with Large Buoyancy Effects," *Combustion Science and Technology,* 41, pp. 55–67 (1984).
17. G. Heskestad, "A Fire Products Collector for Calorimetry into the MW Range," *Report OC2E1.RA,* Factory Mutual Research Corp., Norwood, MA (1981).
18. A. Tewarson, "Physico-Chemical and Combustion/Pyrolysis Properties of Polymeric Materials," *NBS-GGR-80-295,* National Bureau of Standards, Washington, DC (1982).
19. C.L. Beyler, "Fire Hazard Calculations for Large, Open Hydrocarbon Fires," *The SFPE Handbook of Fire Protection Engineering,* 3rd ed., Society of Fire Protection Engineering and National Fire Protection Association, Quincy, MA (2002).
20. B. Hägglund and L.E. Persson, "The Heat Radiation from Petroleum Fires," Försvarets Forskningsanstalt, Stockholm, FDA Report C20126-D6(A3) (1976).

21. F. Tamanini, "Direct Measurements of the Longitudinal Variation of Burning Rate and Product Yield in Turbulent Diffusion Flames," *Combustion and Flame,* 51, pp. 231–243 (1983).
22. E.E. Zukoski, T. Kubota, and B. Cetegen, "Entrainment in Fire Plumes," *Fire Safety Journal,* 3, pp. 107–121 (1980–81).
23. E.E. Zukoski, B.M. Cetegen, and T. Kubota, "Visible Structure of Buoyant Diffusion Flames," *20th Symposium on Combustion,* Combustion Institute, Pittsburgh, PA, pp. 361–366 (1985).
24. B. McCaffrey, "Flame Height," *The SFPE Handbook of Fire Protection Engineering,* 2nd ed., Society of Fire Protection Engineers and National Fire Protection Association, Quincy, MA, pp. 2-1–2-8 (1995).
25. H.A. Becker and D. Liang, "Visible Length of Vertical Free Turbulent Diffusion Flames," *Combustion and Flame,* 32, pp. 115–137 (1978).
26. G. Cox and R. Chitty, "Some Source-Dependent Effects of Unbounded Fires," *Combustion and Flame,* 60, pp. 219–232 (1985).
27. G. Heskestad, "Luminous Heights of Turbulent Diffusion Flames," *Fire Safety Journal,* 5, pp. 103–108 (1983).
28. G.T. Kalghatgi, "Lift-Off Heights and Visible Lengths of Vertical Turbulent Jet Diffusion Flames in Still Air," *Combustion Science and Technology,* 41, pp. 17–29 (1984).
29. F.R. Steward, "Prediction of the Height of Turbulent Diffusion Buoyant Flames," *Combustion Science and Technology,* 2, pp. 203–212 (1970).
30. P.H. Thomas, "The Size of Flames from Natural Fires," *Ninth Symposium on Combustion,* Combustion Institute, Pittsburgh, PA, pp. 844–859 (1963).
31. W.R. Hawthorne, D.S. Weddel, and H.C. Hottel, "Mixing and Combustion in Turbulent Gas Jets," *Third Symposium on Combustion,* Williams and Wilkins, Baltimore, pp. 288–300 (1949).
32. E.E. Zukoski, "Fluid Dynamic Aspects of Room Fires," *Fire Safety Science—Proceedings of the First International Symposium,* Hemisphere, New York, pp. 1–30 (1984).
33. E.E. Zukoski, "Convective Flows Associated with Room Fires," *Semi-Annual Progress Report to National Science Foundation,* California Institute of Technology, Pasadena (1975).
34. G. Heskestad, "On Q^* and the Dynamics of Turbulent Diffusion Flames," *Fire Safety Journal,* 30, pp. 215–227 (1998).
35. G. Heskestad, "A Reduced-Scale Mass Fire Experiment," *Combustion and Flame,* 83, pp. 293–301 (1991).
36. H. Vienneau, "Mixing Controlled Flame Heights from Circular Jets," *BSc Thesis*, Dept. Chem. Eng., Univ. New Brunswick, Fredericton, N.B., 1964.
37. M.V. D'Souza and J.H. McGuire, "ASTM E-84 and the Flammability of Foamed Thermosetting Plastics," *Fire Technology*, 13, p 85–94 (1977).
38. V.I. Blinov and G.N. Khudiakov, "Certain Laws Governing Diffusive Burning of Liquids," *Dokl. Acad. Nauk SSSR,* 113, p 1094–1098 (1957).
39. B. Hägglund and L.E. Persson, "The Heat Radiation from Petroleum Fires," Försvarets Forskningsanstalt, Stockholm, FDA Rep. C20126-D6 (A3), 1976.
40. B.D. Wood, P.L. Blackshear, Jr. and E.R.G. Eckert, "Mass Fire Model: An Experimental study of the Heat Transfer to Liquid Fuel Burning from a Sand-Filled Pan Burner," *Combust. Sci. Technol.,* 4, p. 113 (1971).
41. K.S. Mudan, "Thermal Radiation Hazards from Hydrocarbon Pool Fires," *Prog. Energy Combust. Sci.,* 10, pp. 59–80 (1984).
42. G. Heskestad, "Flame Heights of Fuel Arrays with Combustion in Depth," *Fire Safety Science—Proceedings of the Fifth International Symposium,* International Association for Fire Safety Science, pp. 427–438 (1998).
43. Huggett, C., "Estimation of Rate of Heat Release by Means of Oxygen Consumption Measurements," *Fire Mater*. 4, pp. 61–65 (1980).
44. Tewarson, A.," Generation of Heat and Gaseous, Liquid, and Solid Products in Fires," *The SFPE Handbook of Fire Protection Engineering,* 4th ed, Society of Fire Protection Engineers and National Fire Protection Association, Quincy, MA, pp. 3-109–3-194 (2008).
45. B.S. Grove and J.G. Quintiere, "Calculating Entrainment and Flame Height in Fire Plumes of Axisymmetric and Infinite Line Geometries," *Journal of Fire Protection Engineering,* 12, pp. 117–137 (2002).
46. Newman, J.S. and Wieczorek, C.J., "Chemical Flame Heights," Fire Safety Journal, 39, pp. 375–382 (2004).
47. de Ris, J, Wu, P. and Heskestad, G., "Radiation Fire Modeling," *Proceedings of the Combustion Institute,* 118, pp. 51–60 (1999).
48. T.R. Blake and M. McDonald, "An Examination of Flame Length Data from Vertical Turbulent Diffusion Flames," *Combustion and Flame,* 94, pp. 426–432 (1993).
49. T.R. Blake and M. McDonald, "Similitude and the Interpretation of Turbulent Diffusion Flames," *Combustion and Flame,* 101, pp. 175–184 (1995).
50. M.A. Delichatsios, "Transition from Momentum to Buoyancy-Controlled Turbulent Jet Diffusion Flames and Flame Height Relationships," *Combustion and Flame,* 33, pp. 349–364 (1993).
51. H.A. Becker and S. Yamazaki, "Entrainment, Momentum Flux and Temperature in Vertical Free Turbulent Diffusion Flames," *Combustion and Flame,* 33, pp. 123–149 (1978).
52. N. Peters and J. Göttgens, "Scaling of Buoyant Turbulent Jet Diffusion Flames," *Combustion and Flame,* 85, pp. 206–214 (1991).
53. G. Heskestad, "Turbulent Jet Diffusion Flames: Consolidation of Flame Height Data," *Combustion and Flame,* 118, pp. 51–60 (1999).

54. A.H. Shapiro, *The Dynamics and Thermodynamics of Compressible Fluid Flow,* Vol. 1, The Ronald Press Company, New York (1953).
55. W. Schmidt, "Turbulente Ausbreitung eines Stromes erhitzer Luft," *Zeitschrift für Angewandte Mathematik und Mechanik,* 21, pp. 265–278 (1941).
56. H. Rouse, C.S. Yih, and H.W. Humphreys, "Gravitational Convection from a Boundary Source," *Tellus,* 4, pp. 201–210 (1952).
57. B.R. Morton, G.I. Taylor, and J.S. Turner, "Turbulent Gravitational Convection from Maintained and Instantaneous Sources," *Proceedings of the Royal Society A,* 234, pp. 1–23 (1956).
58. B.R. Morton, "Forced Plumes," *Journal of Fluid Mechanics,* 5, pp. 151–163 (1959).
59. B.R. Morton, "Modeling of Fire Plumes," *10th Symposium on Combustion,* Combustion Institute, Pittsburgh, PA, pp. 973–982 (1965).
60. W.K. George, R.L. Alpert, and F. Tamanini, "Turbulence Measurements in an Axisymmetric Buoyant Plume," *International Journal of Heat and Mass Transfer,* 20, pp. 1145–1154 (1977).
61. S. Yokoi, "Study on the Prevention of Fire-Spread Caused by Hot Upward Current," *Report No. 34,* Building Research Institute, Japan (1960).
62. G. Heskestad, "Fire Plume Simulator," *Report 18792,* Factory Mutual Research Corp., Norwood, MA (1974).
63. A. Tewarson, "Experimental Evaluation of Flammability Parameters of Polymeric Materials," in *Flame-Retardant Polymeric Materials,* Plenum, New York, pp. 97–153 (1982).
64. G. Heskestad, "Note on Maximum Rise of Fire Plumes in Temperature-Stratified Ambients," *Fire Safety Journal,* 15, pp. 271–276 (1989).
65. G. Heskestad, "Dynamics of the Fire Plume," *Philosophical Transactions of the Royal Society of London A,* 356, pp. 2815–2833 (1998).
66. G. Heskestad, "Fire Plume Behavior in Temperature Stratified Ambients," *Combustion Science and Technology,* 106, pp. 207–228 (1995).
67. J-I. Watanabe and T. Tanaka, "Experimental Investigation into Penetration of a Weak Fire Plume into a Hot Upper Layer," *Journal* of *Fire Sciences,* 22, pp. 405–420 (2004).
68. G. Heskestad, "Virtual Origins of Fire Plumes," *Fire Safety Journal,* 5, pp. 109–114 (1983).
69. Y. Hasemi and T. Tokunaga, "Flame Geometry Effects on the Buoyant Plumes from Turbulent Diffusion Flames," *Fire Science and Technology,* 4, pp. 15–26 (1984).
70. B.M. Cetegen, E.E. Zukoski, and T. Kubota, "Entrainment in the Near and Far Field of Fire Plumes," *Combustion Science and Technology,* 39, pp. 305–331 (1984).
71. C.-S. Yih, "Free Convection Due to a Point Source of Heat," *Proceedings of the U.S. National Congress of Applied Mechanics,* New York, pp. 941–947 (1952).
72. B.M. Cetegen, E.E. Zukoski, and T. Kubota, "Entrainment and Flame Geometry of Fire Plumes," *Report G8-9014,* California Institute of Technology, Daniel and Florence Guggenheim Jet Propulsion Center, Pasadena (1982).
73. G. Heskestad, "Fire Plume Air Entrainment According to Two Competing Assumptions," *21st Symposium on Combustion,* Combustion Institute, Pittsburgh, PA, pp. 111–120 (1986).
74. C.L. Beyler, *Development and Burning of a Layer of Products of Incomplete Combustion Generated by a Buoyant Diffusion Flame,* Ph.D. Thesis, Harvard University, Cambridge, MA (1983).
75. M.A. Delichatsios and L. Orloff, "Entrainment Measurements in Turbulent Buoyant Jet Flames and Implications for Modeling," *20th Symposium on Combustion,* Combustion Institute, Pittsburgh, PA (1985).
76. M.A. Delichatsios, "Air Entrainment into Buoyant Jet Flames and Pool Fires," *The SFPE Handbook of Fire Protection Engineering,* 2nd ed., Society of Fire Protection Engineers and National Fire Protection Association, Quincy, MA, pp. 2-20–2-31 (1995).
77. J.Q. Quintiere and B.S. Grove, "A Unified Analysis for Fire Plumes," *27th Symposium on Combustion,* Combustion Institute, Pittsburgh, PA, pp. 2757–2766 (1998).
78. G. Heskestad and T. Hamada, "Ceiling Jets of Strong Fire Plumes," *Fire Safety Journal,* 21, pp. 69–82 (1993).
79. P.H. Thomas, P.L. Hinkley, C.R. Theobald, and D.L. Sims, "Investigation into the Flow of Hot Gases in Roof Venting," *Fire Technical Paper No. 7,* H. M. Stationery Office, Joint Fire Research Organization, London (1963).
80. P.L. Hinkley, "Rates of 'Production' of Hot Gases in Roof Venting Experiments," *Fire Safety Journal,* 10, pp. 57–65 (1986).
81. M.A. Delichatsios, "Fire Growth Rates in Wood Cribs," *Combustion and Flame,* 27, pp. 267–278 (1976).
82. Zukoski, E.E., Kubota, T. and Cetegen, B., "Entrainment in the Near Field of Fire Plumes," California Institute of Technology, Daniel and Florence Guggenheim Jet Propulsion Center, August 1981
83. D.J. Rasbash, Z.W. Rogowski, and G.W.V. Stark, "Properties of Fires of Liquids," *Fuel,* 35, pp. 94–107 (1956).
84. B.M. Cetegen and T.A. Ahmed, "Experiments on the Periodic instability of Buoyant Plumes and Pool Fires," *Combustion and Flame,* 23, pp. 157–184 (1993).
85. G.M. Byram and R.M. Nelson, Jr., "The Modelling of Pulsating Fires," *Fire Technology,* 6, pp. 102–110 (1970).
86. T. Tanaka, T. Fujita, and J. Yamaguchi, "Investigation into Rise Time of Buoyant Fire Plume Fronts," *International Journal of Engineering Performance-Based Fire Codes,* 2, pp. 14–25 (2000).
87. G. Heskestad, "Rise of Plume Front from Starting Fires," *Fire Safety Journal,* 36, pp. 201–204 (2001).
88. L.H. Hu, Y.Z. Li, R. Huo, L. Yi, and C.L. Shi, "Experimental Studies on the Rise-Time of Buoyant Fire Plume Fronts Induced by Pool Fires," *Journal of Fire Sciences,* 22 pp. 69–84 (2004).

89. Y. Hasemi and T. Tokunaga, "Some Experimental Aspects of Turbulent Diffusion Flames and Buoyant Plumes from Fire Sources Against a Wall and in a Corner of Walls," *Combustion Science and Technology,* 40, pp. 1–17 (1984).
90. J. Back, C. Beyler, and P. DiNenno, "Wall Incident Heat Flux Distributions Resulting from Adjacent Flames," *Proceedings of the Fourth International Symposium on Fire Safety Science,* International Association for Fire Safety Science, London, UK, pp. 241–252 (1994).
91. T. Mizuno and K. Kawagoe, "Burning Rate of Upholstered Chairs in the Center, Alongside a Wall and in a Corner of a Compartment," *Fire Safety Science—Proceedings of the First International Symposium,* Hemisphere, New York, pp. 849–857 (1984).
92. M.A. Kokkala, "Characteristics of a Flame in an Open Corner of Walls," *Interflam 1993,* Interscience Communications Limited, London (1993).
93. M. Poreh and G. Garrad, "A Study of Wall and Corner Fire Plumes," *Fire Safety Journal,* 34, pp. 81–98 (2000).
94. B.Y. Lattimer and U. Sorathia, "Thermal Characteristics of Fires in a Noncombustible Corner," *Fire Safety Journal*, 38 pp. 709–745 (2003).
95. J.R. Welker and C.M. Sliepcevich, "The Effect of Wind on Flames," *Technical Report No. 2,* NBS Contract XST 1142 with University of Oklahoma, Norman (1965).
96. S. Attalah and P.K. Raj, "Radiation from LNG Fires," *Interim Report on Phase II Work,* Project IS-3.1 LNG Safety Program, American Gas Association, Arlington, VA (1974).
97. K.G. Huffman, J.R. Welker, and C.M. Sliepcevich, "Wind and Interaction Effects on Free-Burning Fires," *Technical Report No. 1441–3,* NBS Contract CST 1142 with University of Oklahoma, Norman (1967).
98. T.A. Brzustowski, S.R. Gollahalli, and H.F. Sullivan, "The Turbulent Hydrogen Diffusion Flame in Cross-Wind," *Combustion Science and Technology,* 11, pp. 29–33 (1975).
99. O.K. Sönju and J. Hustad, "An Experimental Study of Turbulent Jet Diffusion Flame," *9th ICODERS,* American Institute of Aeronautics and Astronautics, Poitiers, France (1984).
100. H.A. Becker, D. Liang, and C.I. Downey, "Effect of Burner Orientation and Ambient Airflow on Geometry of Turbulent Free Diffusion Flames," *18th Symposium on Combustion,* Combustion Institute, Pittsburgh, PA, pp. 1061–1071 (1981).
101. Newman, Jeffrey S. and Croce, Paul A., "A Simple Aspirated Thermocouple for Use in Fires," *Journal of Fire and Flammability,* 10, pp. 326–336 (1979).
102. Burgess, D.S., Grumer, J., and Wolfhard, H.G., "Burning Rates of Liquid Fuels in Large and Small Open Trays," International Symposium on the Use of Models in Fire Research, Publication 786, National Academy of Sciences - National Research Council, Washington, DC, 1961, p68.
103. NFPA 92B, *Standard for Smoke Management Systems in Malls, Atria, and Large Spaces,* National Fire Protection Association, Quincy, MA (2005).
104. R.L. Alpert and E.J. Ward, "Evaluation of Unsprinklered Fire Hazards," *Fire Safety Journal,* 7, pp. 127–143 (1984).

Gunnar Heskestad retired from FM Global in 2004 as an assistant vice president and consulting research scientist. He has specialized in fluid mechanics and heat transfer of fire with applications to fire protection issues.

Ceiling Jet Flows

14

Ronald L. Alpert

Introduction

Much of the hardware associated with detection and suppression of fire in commercial, manufacturing, storage, and modern residential buildings is located near the ceiling surfaces. In case of a fire, hot gases in the fire plume rise directly above the burning fuel and impinge on the ceiling. The ceiling surface causes the flow to turn and move horizontally under the ceiling to other areas of the building remote from the fire position. The response of smoke detectors, heat detectors, and sprinklers installed below the ceiling so as to be submerged in this hot flow of combustion products from a fire provides the basis for building fire protection.

Studies quantifying the flow of hot gases under a ceiling resulting from the impingement of a fire plume have been conducted since the 1950s. Studies at the Fire Research Station in Great Britain [1, 2], Factory Mutual Research Corporation [3–7], the National Institute of Standards and Technology (NIST) [8, 9], and at other research laboratories [10, 11] have sought to quantify the gas temperatures and velocities in the hottest portion of the flow produced by steady fires beneath smooth, unconfined horizontal ceilings.

Ceiling jet refers to the relatively rapid gas flow in a shallow layer beneath the ceiling surface that is driven by the buoyancy of the hot combustion products from the plume. Figure 14.1 shows an idealization of an axisymmetric ceiling jet flow at varying radial positions, r, beneath an unconfined ceiling. In actual fires within buildings, the simple conditions pictured—a hot, rapidly moving gas layer sandwiched between the ceiling surface and tranquil, ambient-temperature air—exist only at the beginning of a fire, when the quantity of combustion gases produced is not sufficient to accumulate into a stagnant, heated gas layer in the upper portion of the compartment. Venting the ceiling jet flow through openings in the ceiling surface or edges can retard the accumulation of this heated gas layer.

As shown in Fig. 14.1, the ceiling jet flow emerges from the region of plume impingement on the ceiling, flowing radially away from the fire. As it does, the layer grows thicker by entraining room air at the lower boundary. This entrained air cools the gases in the jet and reduces its velocity. As the hot gases move out across the ceiling, heat transfer cools the portion adjacent to the ceiling surface.

Steady Flow Under Horizontal, Unconfined Ceilings

Weak Plume-Driven Flow Field

A generalized theory to predict gas velocities, gas temperatures, and the thickness (or depth) of a steady fire-driven ceiling jet flow has been developed by Alpert [4] for the case of a weak

R.L. Alpert (✉)
Alpert FireProtection Science

M.J. Hurley (ed.), *SFPE Handbook of Fire Protection Engineering*,
DOI 10.1007/978-1-4939-2565-0_14, © Society of Fire Protection Engineers 2016

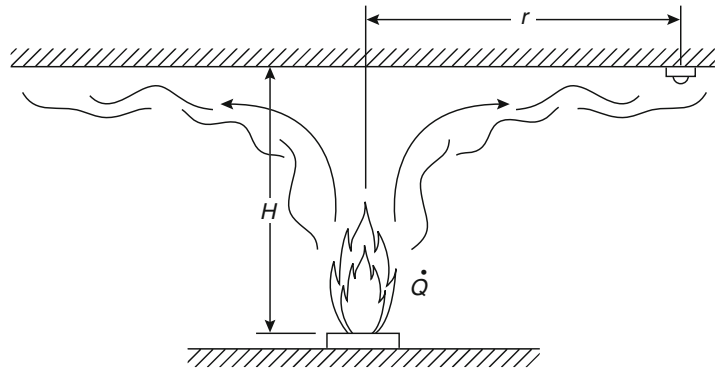

Fig. 14.1 Ceiling jet flow beneath an unconfined ceiling

plume, when flame height is much less than the height, H, of the ceiling above the burning fuel. This work involves the use of several idealizations in the construction of the theoretical model, but results are likely to provide reasonable estimates over radial distances of one or two ceiling heights from the point of fire plume impingement on the ceiling.

Ceiling Jet Thickness Alpert defined the thickness of the ceiling jet, ℓ_T, as the distance below the ceiling where the excess of gas temperature above the ambient value, ΔT, drops to $1/e$ (1/2.718 ...) of the maximum excess temperature. Based on this definition, measurements obtained with a liquid pool fire 8 m beneath a ceiling show that ℓ_T/H is about 0.075 at an r/H of 0.6, increasing to a value of 0.11 for r/H from about 1 to 2. These results are in good agreement with detailed measurements and analysis for the region $r/H < 2$ performed by Motevalli and Marks [12] during their small-scale (0.5- and 1.0-m ceiling heights) experiments. The following correlation for ℓ_T/H developed by Motevalli and Marks from their temperature data confirms the predicted constancy of ceiling jet thickness (at about 10–12 % of H) for r/H from Alpert's theory:

$$\frac{\ell_T}{H} = 0.112\left[1 - \exp\left(-2.24\frac{r}{H}\right)\right] \quad \text{for } 0.26 \le \frac{r}{H} \le 2.0 \tag{14.1}$$

Additional measurements of ceiling jet thickness, for steady flows induced by strong plumes and for transient flows, are discussed later.

Within the ceiling jet flow, the location of maximum excess temperature and velocity are predicted [4] to be highly scale dependent, even after normalization by the ceiling height. Measurements of the distance below the ceiling at which these maxima occur have been made mainly for 1-m scale experiments [12, 13]. Results show distances below the ceiling ranging from about 1 % to 2 % of the ceiling height for r/H from less than 1 to 2, with predicted reductions in the percent of ceiling height at larger scales.

Much of the discussion below deals with predictions and correlations of the maximum excess temperature and velocity in the ceiling jet flow, which occur, as already noted, relatively close to the ceiling surface. Often fire detectors or sprinklers are placed at ceiling standoff distances that are outside of this region and therefore will experience cooler temperatures and lower velocities than predicted. In facilities with very high ceilings, the detectors could be closer to the ceiling than 1 % of the fire source-to-ceiling separation and will fall in the ceiling jet thermal and viscous boundary layers. In low-ceiling facilities, it is possible for sprinklers or detectors to be placed outside of the ceiling jet flow entirely if the standoff is greater than 12 % of the fire source-to-ceiling height. In this case, response time could be drastically increased.

Ceiling Jet Excess Temperature and Velocity Alpert [3] has developed easy-to-use correlations to quantify the maximum excess gas temperature (above the ambient value) and velocity at a given position in a ceiling jet flow

produced by a steady fire. These correlations are widely used in hazard analysis calculations. Evans and Stroup [14] have employed the correlations in the development of a generalized program to predict heat detector response for the case of a detector totally submerged in the ceiling jet flow. The correlations are based on measurements collected during fire tests involving fuel arrays of wood and plastic pallets, empty cardboard boxes, plastic materials in cardboard boxes, and liquid fuels. Heat release rates for these fuels range from 600 kW to 98 MW, total ceiling heights range from 4.6 to 18 m, and radial positions for most measurements range out to a little more than twice the ceiling height. In SI units, Alpert's [3] correlations for maximum ceiling jet excess temperatures and velocities are as follows:

$$T - T_\infty = 16.9 \frac{\dot{Q}^{2/3}}{H^{5/3}} \qquad \text{for } r/H \leq 0.18 \tag{14.2}$$

$$T - T_\infty = 5.38 \frac{\dot{Q}^{2/3}/H^{5/3}}{(r/H)^{2/3}} \quad \text{for } r/H > 0.18 \tag{14.3}$$

$$U = 0.947 \left(\frac{\dot{Q}}{H}\right)^{1/3} \qquad \text{for } r/H \leq 0.15 \tag{14.4}$$

$$U = 0.197 \frac{(\dot{Q}/H)^{1/3}}{(r/H)^{5/6}} \qquad \text{for } r/H > 0.15 \tag{14.5}$$

where temperature, T, is in °C; velocity, U, is in m/s; total heat release rate, $\dot{Q}$ is in kW; and radial position and ceiling height (r and H) are in m.

Data from these fire tests are correlated using the rate at which heat is actually released in the fire, $\dot{Q}$, based on measured fuel mass loss rates and the best estimates for actual heat of combustion that were available in 1970–1971. Even though it is the convective component of this total heat release rate that is directly related to the buoyancy of the fire, accurate estimates for this convective component were not readily available for all the fuels tested when the correlations were first developed. For the liquid alcohol pool fires that constitute the primary basis of the correlation developed by Alpert, the convective heat release rate, $\dot{Q}_c$, is now known to be about 74 % of the actual heat release rate. However, for the remaining solid commodities and pallets, the convective heat release rate varies from about 60 % to 70 % of the actual heat release rate for mixed plastic/cardboard commodities and wood, respectively, with flammable liquids similar to heptane being in the middle of this range. Hence, for general commodities, it would be desirable to use ceiling jet excess temperature and velocity correlations based on convective heat release rate (see such correlations in Equations 14.7 and 14.8).

The preceding correlations for both temperatures and velocities (Equations 14.2, 14.3, 14.4, and 14.5) are broken into two parts. One part applies for the ceiling jet in the area of the impingement point where the upward flow of gas in the buoyant plume turns to flow out beneath the ceiling horizontally, with an assumed unchanged velocity magnitude. The impingement point or turning region correlations (Equations 14.2, 14.3 and 14.4) are independent of radius and represent plume temperatures

and velocities calculated at the ceiling height above the fire source. The other correlations (Equations 14.3 and 14.5) apply outside of this turning region as the flow moves away from the impingement area. It is important to recognize that these correlations implicitly assume that there is a point buoyancy source for the impinging plume located at the top surface of the burning fuel. Hence, there is no dependence on the horizontal dimension (e.g., effective diameter) of the fire source in the correlations, and the height of the fuel array is restricted to being a small fraction of the ceiling height.

In order to remedy deficiencies discussed above in the existing correlations, much of the original data from the 1970s has been reanalyzed by the author. This new analysis ignores a small number of measurements where an accurate estimate of convective heat release rate for the corresponding fire sources (plastic pallets and one cardboard box commodity) would be very difficult to obtain. For the remaining large-scale fire tests, the convective heat release rate is calculated from measurements of fuel mass loss rate and handbook values of the convective heat of combustion. Instead of arbitrarily correlating measurements with the ceiling elevation above the top fuel surface, H, the new analysis uses the ceiling elevation above the location of the virtual plume origin, $z_H - z_v$. The location, z_v, of the virtual plume origin above a reference location is given (see Chap. 13) by a correlation based on the actual heat release rate, $\dot{Q}$, and the effective diameter, D_{eff}, of the fuel array. When height in the plume, z, is measured from the base of the flame zone instead of the top surface of the burning fuel, the following expression for virtual origin height has been found to be applicable even to complex fuel arrays:

$$z_v = 0.083\dot{Q}^{2/5} - 1.02D_{\text{eff}} \tag{14.6}$$

In Equation 14.6, z_v is the distance above the base of a burning fuel array and D_{eff} is the diameter of a circle having the same plan area as for the actual array. The result of correlating excess temperature and velocity measurements from full-scale tests using the same functional relationships as in Equations 14.3 and 14.5 but based on $\dot{Q}_c$ instead of $\dot{Q}$ and $z_H - z_v$ instead of H is shown in Figs. 14.2 and 14.3. Further details of this reanalysis of ceiling jet data from the early 1970s is provided in a recent lecture by the author [15].

In Figs. 14.2 and 14.3, the ordinates are the dimensional quantities

$$\frac{(T - T_\infty)(z_H - z_v)^{5/3}}{\dot{Q}_c^{2/3}} \quad \text{and} \quad \frac{U(z_H - z_v)^{1/3}}{\dot{Q}_c^{1/3}}$$

respectively. Values for these ordinates at the plume axis (see Chap. 13) are shown for comparison with the ceiling jet values. Regression fits based on data only from the ethanol pool fires, for which heat release rates are known most accurately, are also shown in these figures. Based on the data from all of the full-scale fire tests, the following new correlations are obtained for excess gas temperature and velocity in the ceiling jet:

$$T - T_\infty = 7.22\frac{\dot{Q}_c^{2/3}}{(z_H - z_v)^{5/3}}\left(\frac{r}{z_H - z_v}\right)^{-0.678} \tag{14.7}$$

$$\text{for } \frac{r}{z_H - z_v} > 0.16$$

$$U = 0.229\frac{\dot{Q}_c^{1/3}}{(z_H - z_v)^{1/3}}\left(\frac{r}{z_H - z_v}\right)^{-1.017}$$

$$\text{for } \frac{r}{z_H - z_v} > 0.228 \tag{14.8}$$

where the limits on $\frac{r}{z_H - z_v}$ in Equations 14.7 and 14.8 are obtained from the respective intersections of the ceiling jet regression fits with the axis values shown from the plume correlations. Within the turning region (i.e., for $\frac{r}{z_H - z_v} \leq$ the limits shown) existing correlations for maximum temperature and velocity in the plume can be used.

A further improvement to the ceiling jet excess temperature and velocity correlations can be obtained [15] by using just the ethanol pool and heptane spray fire data, not only because these are the best documented fire

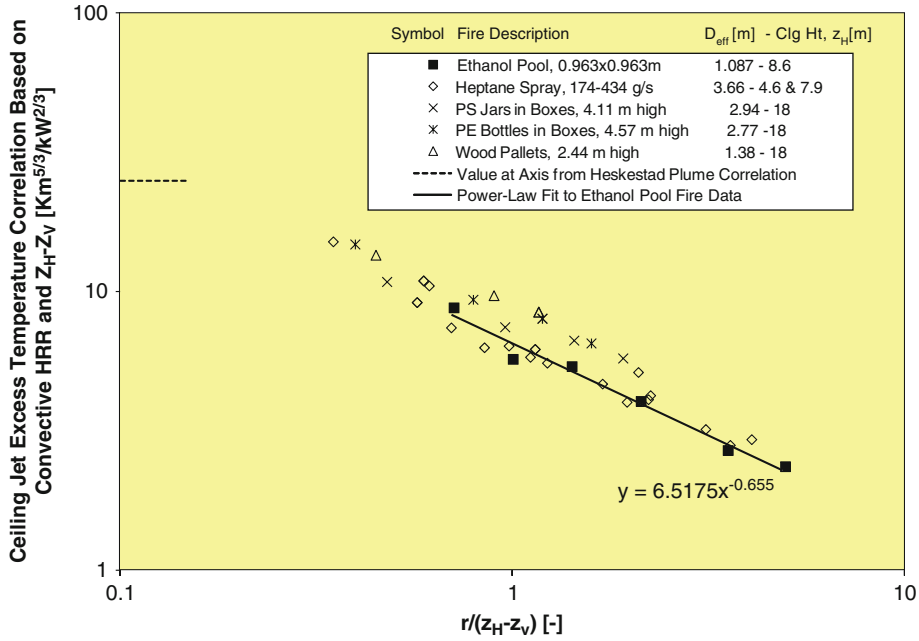

Fig. 14.2 Correlation of maximum ceiling jet excess temperature data from full-scale fire tests (Note that "PE bottles" previously was called "PVC bottles," an error discovered by comparing known test numbers involving the commodity with descriptions in a test report; Also note that previously, data for heptane sprays had not contained the virtual origin correction applied to data for the other commodities, due to a spreadsheet error)

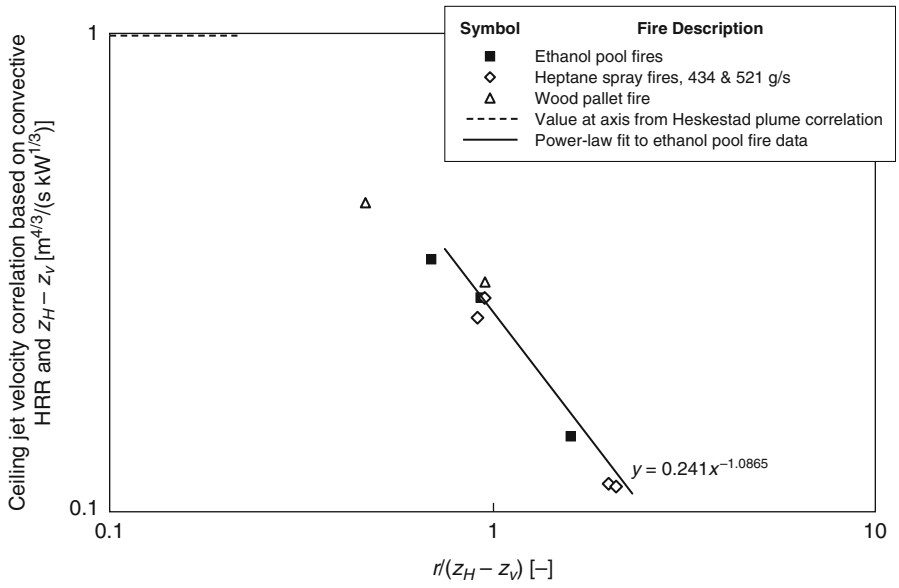

Fig. 14.3 Correlation of maximum ceiling velocity data from full-scale fire tests (See legend from Fig. 14.2)

sources from the original study, in terms of combustion parameters, but also because these are the only near steady-state fire sources. Fires in piles of solid fuels are inherently transient, which makes a data correlation difficult when transient velocity and temperature data are not available.

Modern handbook values [16] for actual and convective heats of combustion for the two fuels selected will now be used instead of what had been assumed (from the knowledge available at time) in the original ceiling-jet study. As a result, the value of $\dot{Q}$ is 13 % greater for ethanol and 8 % less for heptane compared to the values used for the correlations in Equations 14.7 and 14.8. With these new values, virtual source heights and convective heat release rates can be obtained [15]. For both the heptane spray and ethanol pool data taken together, the resulting regression fit equations and regression coefficients (R^2 values) are given below:

$$T - T_\infty = 6.721 \frac{\dot{Q}_c^{2/3}}{(z_H - z_v)^{5/3}} \left(\frac{r}{z_H - z_v} \right)^{-0.6545} \quad R^2 = 0.958 \quad \text{for} \frac{r}{z_H - z_v} > 0.134 \tag{14.7A}$$

$$U = 0.2526 \frac{\dot{Q}_c^{1/3}}{(z_H - z_v)^{1/3}} \left(\frac{r}{z_H - z_v} \right)^{-1.0739} \quad R^2 = 0.972 \quad \text{for} \frac{r}{z_H - z_v} > 0.246 \tag{14.8A}$$

Certain constraints should be understood when applying these correlations in the analysis of fire flows. The correlations apply only during times after fire ignition when the ceiling flow may be considered unconfined; that is, no accumulated warm upper layer is present. Walls close to the fire affect the temperatures and velocity in the ceiling jet independent of any effect on the fire-burning rate due to radiant heat received from the walls. The correlations were developed from test data to apply in cases where the fire source is at least a distance 1.8 times the ceiling height from the enclosure walls. For special cases where burning fuel is located against a flat wall surface or two wall surfaces forming a 90° corner, the correlations are adjusted based on the method of reflection. This method makes use of symmetry to account for the effects of the walls in blocking entrainment of air into the fire plume. For the case of a fire adjacent to a flat wall, $2\dot{Q}$ is substituted for $\dot{Q}$ in the correlations. For a fire in a 90° corner, $4\dot{Q}$ is substituted for $\dot{Q}$ in the correlations [3]. More accurate formulas for ceiling jet gas temperature, as well as ceiling heat flux, in a 90° corner that were obtained from experiments with a propane burner can be found in the section following on "Corner Configuration with Strong Plumes".

Experiments have shown that unless great care is taken to ensure that the fuel perimeter is in contact with the wall surfaces, the method of reflection used to estimate the effects of the walls on ceiling jet temperature will be inaccurate. For example, Zukoski et al. [17] found that a circular burner placed against a wall so that only one point on the perimeter contacted the wall behaved almost identically to a fire far from the wall with plume entrainment only decreasing by 3 %. When using Equations 14.2, 14.3, 14.4, and 14.5, this fire would be represented by replacing $\dot{Q}$ with $1.05\dot{Q}$ and not $2\dot{Q}$ as would be predicted by the method of reflections. The value of $2\dot{Q}$ would be appropriate for a semicircular burner with the entire flat side pushed against the wall surface.

Consider the following calculations, which demonstrate typical uses of the correlations, Equations 14.2, 14.3, 14.4, and 14.5.

(a) The maximum excess temperature under a ceiling 10 m directly above a 1.0-MW heat-release-rate fire is calculated using Equation 14.2 as

$$T - T_\infty = \frac{16.9(1000)^{2/3}}{10^{5/3}}$$
$$= \frac{16.9(100)}{46.42}$$
$$\Delta T = 36.4°\text{C}$$

(b) For a fire that is against noncombustible walls in a corner of a building and 12 m below the ceiling, the minimum heat release rate needed to raise the temperature of the gas below the ceiling 50 °C at a distance 5 m from the corner is calculated using Equation 14.3 and the symmetry substitution of $4\dot{Q}$ for $\dot{Q}$ to account for the effects of the corner as

$$T - T_\infty = 5.38\frac{(4\dot{Q})^{2/3}/H^{5/3}}{(r/H)^{2/3}}$$
$$50 = 5.38\frac{(4\dot{Q})^{2/3}}{12^{5/3}(5/12)^{2/3}}$$
$$\dot{Q} = \frac{5}{4}\left[\frac{50(12)}{5.38}\right]^{3/2}$$
$$\dot{Q} = 1472\ \text{kW} = 1.472\,\text{MW}$$

(c) The maximum velocity at this position is calculated from Equation 14.5, modified to account for the effects of the corner as

$$U = 0.197\frac{(4\dot{Q}/H)^{1/3}}{(r/H)^{5/6}}$$
$$= \frac{0.197(5888)^{1/3}}{(5/12)^{5/6}12^{1/3}}$$
$$U = 3.2\ \text{m/s}$$

Nondimensional Ceiling Jet Relations Heskestad [7] developed correlations[1] for maximum ceiling jet excess temperature and velocity based on alcohol pool-fire tests performed at the U.K. Fire Research Station in the 1950s. These correlations are cast in the following heat release rate, excess temperature, and velocity variables that are nondimensional (indicated by the superscript asterisk) and applicable to steady-state fires under unconfined ceilings (indicated by the subscript 0):

$$\dot{Q}_0^* = \frac{\dot{Q}}{\rho_\infty c_p T_\infty g^{1/2} H^{5/2}} \tag{14.9}$$

$$\Delta T_0^* = \frac{\Delta T/T}{\left(\dot{Q}_0^*\right)^{2/3}} \tag{14.10}$$

$$U_0^* = \frac{U/\sqrt{gH}}{\left(\dot{Q}_0^*\right)^{1/3}} \tag{14.11}$$

Figure 14.4 shows a plot of the Heskestad correlation for excess temperature and velocity data as solid line curves. The correlations developed by Alpert [3] are plotted as broken curves, using the same dimensionless parameters with assumed ambient temperature of 293 K (20 °C), normal atmospheric pressure, and convective heat release rate equal to the total heat release rate, $\dot{Q}_c = \dot{Q}$. Generally, the results of Heskestad [7] predict slightly higher excess temperatures and substantially greater gas velocities than Alpert's [3] results. Another curve shown in Fig. 14.2 is a fit to the mean ceiling jet velocity predicted by the generalized theory of Alpert [4], which also predicts that the turning-region boundary should be at $r/H = 0.17$. This predicted velocity is reasonably close to Heskestad's [7] experimental correlation for velocity. Based on the results shown in Fig. 14.4, the nondimensional excess temperature from the Heskestad [7] correlation and the nondimensional velocity from Alpert's theory [4, 13] are recommended for the prediction of steady ceiling jet flows beneath unobstructed ceilings. The Heskestad correlation and the Alpert theory are adequately fit, respectively, by the following expressions:

[1] Originally developed by G. Heskestad and C. Yao in "A New Approach to Development of Installation Standards for Fired Detectors," *Technical Proposal No. 19574,* prepared for The Fire Detection Institute, by Factory Mutual Research Corporation, Norwood, MA (1971).

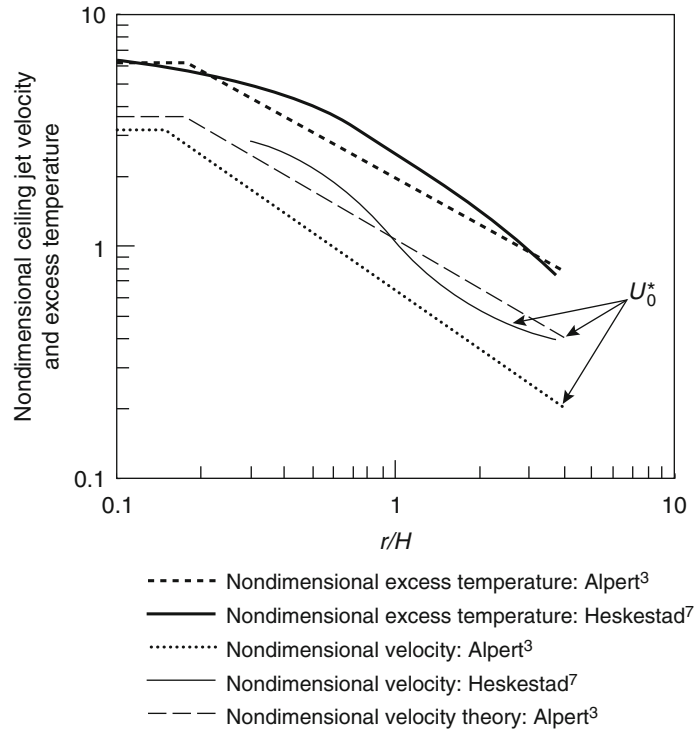

Fig. 14.4 Dimensionless correlations for maximum ceiling jet temperatures and velocities produced by steady fires. *Solid line*: Heskestad [7]; *dotted line*: Alpert [3]

$$\Delta T_0^* = \left(0.225 + 0.27\tfrac{r}{H}\right)^{-4/3} \quad \text{for } 0.2 \le r/H < 4.0 \tag{14.12}$$

$$\Delta T_0^* = 6.3 \quad \text{for } r/H \le 0.2 \tag{14.13}$$

$$U_0^* = 1.06\left(\frac{r}{H}\right)^{-0.69} \quad \text{for } 0.17 \le r/H < 4.0 \tag{14.14}$$

$$U_0^* = 3.61 \quad \text{for } r/H \le 0.17 \tag{14.15}$$

Heskestad and Delichatsios [18] examined the original data from Heskestad [7] and concluded that nondimensional velocity and temperature could be related by the following equation:

$$\frac{U_0^*}{\sqrt{\Delta T_0^*}} = 0.68\left(\frac{r}{H}\right)^{-0.63} \quad \text{for } r/H \ge 0.3 \tag{14.16}$$

The preceding relation has been found applicable to a much wider range of conditions than just steady-state alcohol pool fires having weakly buoyant plumes. For example, this relationship between ceiling jet velocity and excess temperature is consistent with measurements [18] for time-dependent fires having strong plumes.

Other methods used to calculate ceiling jet velocity and maximum possible (when the ceiling is adiabatic) ceiling jet temperatures are reported by Cooper and Woodhouse [9]. A critical review of correlation formulas for excess temperature and velocity in the ceiling jet under

a variety of conditions has been assembled by Beyler [19]. To apply these and the preceding expressions to realistic burning situations, it is recommended that the convective heat release rate should be used.

Strong Plume-Driven Flow Field

When the flame height of a fire plume is comparable to the height of the ceiling above the burning fuel, the resultant ceiling jet is driven by a strong plume. Additional information about this type of flow field is provided in the section on "Sloped Ceilings" (see the special case of zero inclination angle, i.e., a horizontal ceiling).

Ceiling Jet Temperature Heskestad and Hamada [6] measured ceiling jet temperatures for ratios of free flame height (in the absence of a ceiling, obtained from existing knowledge of flame heights) to ceiling height ranging from 0.3 up to 3. A correlation of excess temperatures could be achieved by using the plume radius, b, at the ceiling as a normalizing length scale, rather than the ceiling height used for the case of a weak plume. This correlation takes the form:

$$\frac{\Delta T}{\Delta T_p} = 1.92\left(\frac{r}{b}\right)^{-1} - \exp\left[1.61\left(1-\frac{r}{b}\right)\right] \quad \text{for } 1 \le \frac{r}{b} \le 40 \tag{14.17}$$

where ΔT_p is the excess temperature on the plume centerline at the level of the ceiling (obtained from Equations 14.2 or 14.13 or other fire-plume relations) and b is the radius where the velocity of the impinging plume is one-half the centerline value. The expression for this characteristic plume radius is given by

$$b = 0.42\left[\left(c_p\rho_\infty\right)^{4/5} T_\infty^{3/5} g^{2/5}\right]^{-1/2} \frac{T_p^{1/2}\dot{Q}_c^{2/5}}{\Delta T_p^{3/5}} \tag{14.18}$$

The Heskestad and Hamada [6] correlation is derived from measurements made with propane burner fires having heat release rates from 12 to 764 kW and beneath ceilings up to 2.5 m in height. This correlation is found to be accurate for ratios of free flame height to ceiling height less than or equal to about 2.0. At greater flame-height ratios, significant heat released in the ceiling jet itself appears to be the cause for a lack of agreement with the correlation.

Flame Lengths in the Ceiling Jet It is very interesting to note an often-overlooked finding of Heskestad and Hamada [6]. When there is flame impingement on the ceiling (flame-height ratio >1), the mean flame radius along the ceiling from the plume centerline is observed to be about equal to the difference between the free flame height and the ceiling height. Hence, Heskestad and Hamada find that the total average length of flame from the burning fuel to the flame tip under the ceiling is virtually the same as the free flame height.

In an earlier study involving small (0.36–8 kW) pool fires beneath ceilings up to 0.336 m in height, Yu (You)[2] and Faeth [10] measure the mean flame radius along the ceiling. Their results yield a flame radius about one-half the difference between the free flame height and the ceiling height, or one-half that of Heskestad and Hamada, perhaps due to the smaller scale of their experiment.

Ceiling Jet Thickness For strong plumes, Atkinson and Drysdale [20] demonstrate that much of the plume kinetic energy is lost (possibly 75 % of that in the incident plume) during the process of ceiling impingement. As a result of this kinetic energy loss, the initial ceiling jet thickness after the turning region may be twice that expected for the case of weak plumes, about 11 % of the ceiling height at $r/H = 0.2$. Measurements made by Atkinson and Drysdale and by Yu [5] show that the ceiling jet thickness may reach a minimum of 8 % of ceiling height at $r/H = 0.5$ and then increase up to 12 % of ceiling height at large radial distances, as for weak plumes.

[2] H. Z. Yu formerly published under the spelling *You*.

Convective Heat Transfer to Horizontal Unconfined Ceilings

Convection is the dominant mode of heat transfer for the case of weak plumes impinging on ceilings. This heat-transfer regime is important for the prediction of activation times for detection devices and the prediction of damage for objects, such as cables or pipes, suspended below the ceiling. However, damage to the ceiling structure itself will much more likely be the result of strong plume (flame) impingement, for which heat transfer due to thermal radiation will be just as important or more important than convection [21]. The maximum convective heat flux to a ceiling occurs when the ceiling surface is at or near ambient temperature, T_∞, before there has been any significant heating of the ceiling material. This maximum convective flux is the subject of the following discussion. For additional discussion of ceiling heat loss, see Chap. 25.

Weak Plume Impingement (Turning) Region

Quantification of convective heat transfer from weak fire plumes impinging on ceiling surfaces has been an area of research activity for many years. In the turning region, a widely used correlation is derived by Yu and Faeth [10] from experiments with small pool fires (convective heat release rates, $\dot{Q}_c$, from 0.05 to 3.46 kW; ceiling heights, H, less than 1 m). This correlation gives convective heat flux to the ceiling, $\dot{q}''$, as

$$\frac{\dot{q}'' H^2}{\dot{Q}_c} = \frac{31.2}{\mathrm{Pr}^{3/5}\mathrm{Ra}^{1/6}} = \frac{38.6}{\mathrm{Ra}^{1/6}} \qquad (14.19)$$

where Pr is the Prandtl number, and the plume Rayleigh number, Ra, is given by

$$\mathrm{Ra} = \frac{g\dot{Q}_c H^2}{3.5 p \nu^3} = \frac{0.027\dot{Q}_c H^2}{\nu^3} \qquad (14.20)$$

for gases similar to air, having ambient absolute pressure, p, and kinematic viscosity, ν. It is recommended that when these expressions are applied to actual heat-transfer problems, the ceiling height should be corrected for the location of the virtual point source for the plume.

Note that the heat-flux parameter on the left side of Equation 14.19 is proportional to the classic heat-transfer Stanton number and that the Rayleigh number is proportional to the cube of the plume Reynolds number, Re (defined in terms of centerline velocity, characteristic plume diameter, $2b$, and kinematic viscosity at the plume centerline temperature).

Equation 14.19 has been established for mainly weak plumes with Rayleigh numbers from 10^9 to 10^{15}. Kokkala [22] has verified this impingement zone heat-transfer correlation, using up to 10 kW natural gas flames, for flame heights up to 70 % of the ceiling height. For greater flame height to ceiling height ratios, Kokkala [22] finds that heat-transfer rates are many times higher than predicted, partly due to thermal radiation.

Alpert [23] performed small-scale (0.3 m ceiling height) experiments at elevated air pressures, which allow Rayleigh numbers greater than 2×10^{15} to be achieved while maintaining somewhat better control of ambient disturbances than in 1-atm experiments. Results of these experiments essentially confirm the predictions of the correlation in Equation 14.19, as well as an expression recommended for the plume impingement region by Cooper [8]. The latter expression yields nondimensional ceiling heat transfer, in terms of the plume Reynolds number defined by Alpert [23], as follows:

$$\frac{\dot{q}'' H^2}{\dot{Q}_c} = 49 \times \mathrm{Re}^{-1/2} = 105\left(\frac{\dot{Q}_c^{1/3} H^{2/3}}{\nu}\right)^{-1/2} \qquad (14.21)$$

Although Equations 14.19 and 14.21 have identical dependence of impingement heat flux on fire heat release rate and ceiling height, heat-flux values from Equation 14.21 are about 50 % higher, since this expression is derived from data on turbulent jets.

Ceiling Jet Region

Outside of the turning region, the convective flux to the ceiling is known to drop off sharply with increasing radial distance from the plume axis. The experiments of Yu and Faeth [10] described in the preceding section were also used to determine this radial variation in ceiling jet convective flux. Their own data, as well as data from small-scale experiments (ceiling heights of 0.5 to 0.8 m) by Alpert [13] and by Veldman [11] are all consistent with the following correlation that is given by Yu and Faeth [10][3]:

$$\frac{\dot{q}'' H^2}{\dot{Q}_c} = 0.04\left(\frac{r}{H}\right)^{-1/3} \quad \text{for } 0.2 \le \frac{r}{H} < 2.0 \tag{14.22}$$

An alternate derivation of Equation 14.22 can be obtained by using Alpert's correlation for ceiling jet excess temperature (Equation 14.3) and Alpert's theory for average ceiling jet velocity (Equation 14.14) with the Reynolds/Colburn analogy, as discussed by Yu and Faeth [10] and Veldman [11]. From the Reynolds/Colburn analogy, the heat-transfer coefficient at the ceiling, h, should be related to ceiling jet average velocity and density as follows:

$$\frac{h}{\rho_\infty U c_p} = \mathrm{Pr}^{-2/3}\frac{f}{2} \tag{14.23}$$

where Pr is the Prandtl number and f is the ceiling friction factor. By using Equation 14.14 for average ceiling jet velocity, U, the ceiling heat-transfer coefficient becomes

$$h = 0.246 f \left(\frac{\dot{Q}_c}{H}\right)^{1/3}\left(\frac{r}{H}\right)^{-0.69} \quad \text{for } 0.17 \le \frac{r}{H} < 4.0 \tag{14.24}$$

With $f = 0.03$, Equation 14.24 is identical to the simplified expression listed in Beyler's extensive compilation [19]. The nondimensional heat flux to a ceiling at ambient temperature can then be expressed as follows, since $\dot{q}'' = h\Delta T$, with ΔT given by Equation 14.3:

$$\frac{\dot{q}'' H^2}{\dot{Q}_c} = 1.323 f \left(\frac{r}{H}\right)^{-1.36} \quad \text{for } 0.2 \le \frac{r}{H} < 4.0 \tag{14.25}$$

Equations 14.22 and 14.25 are in good agreement for a friction factor of 0.03, which is comparable with the value of 0.02 deduced from Alpert's [4] theory.

Sloped Ceilings

There have been very few studies of the ceiling jet flow resulting from plume impingement on an inclined, flat ceiling, i.e., where the ceiling is inclined at some angle, θ, to the horizontal. One such study, by Kung et al. [24], obtained measurements showing pronounced effects in the velocity variation along the steepest run from the point of impingement of a strong plume, both in the upward and downward directions. In the upward direction, the rate of velocity decrease with distance, r, from the intersection of the plume vertical axis with the ceiling was reduced significantly as the ceiling slope increased. In the downward direction, the flow separated from the ceiling and turned upward at a location, $-r$, denoted by Kung et al. [24] as the penetration distance. These results were the outcome of experiments with 0.15- and 0.228-m-diameter pan fires located 0.279 to 0.889 m beneath an inclined 2.4-m square ceiling and were limited to convective heat release rates in the range of 3–13 kW.

Following Heskestad and Hamada [6], Kung et al. developed correlations by scaling near-maximum excess temperature and velocity, as well as radial distance along the ceiling, in terms of the quantities in the undeflected plume at the impingement point. These correlations take the following form:

$$\frac{\Delta T}{\Delta T_p} = \exp\left[(0.12\sin\theta - 0.42)\left(\frac{r}{b} - 1\right)^{0.7}\right] \tag{14.26}$$

[3] Note that there is a typographical error in the exponent of r/H in Equation 14.17 of this reference.

$$\frac{U}{V_p} = \exp\left[(0.79\sin\theta - 0.52)\left(\frac{r}{b} - 1\right)^{0.6}\right] \tag{14.27}$$

for $r/b \geq 1$(upward direction from the impingement point, i.e., r = r_{up}) and θ = 0 − 30°;

$$\frac{\Delta T}{\Delta T_p} = (0.15\sin\theta - 0.11)\left(\frac{r}{b}\right) + 0.97 - 0.06\sin\theta \tag{14.28}$$

$$\frac{U}{V_p} = (0.21\sin\theta - 0.10)\left(\frac{r}{b}\right) + 0.99 - 1.17\sin\theta \tag{14.29}$$

for $r/b < 0$ (downward direction from the impingement point), valid only for θ = 0 − 30°, and for ΔT and U ≥ 0.

In Equations 14.26, 14.27, 14.28, and 14.29, the characteristic plume radius is proportional to that defined in Equation 14.18 but with a slightly different magnitude, namely,

$$b = 0.548\left[\left(c_p\rho_\infty\right)^{4/5}T_\infty^{3/5}g^{2/5}\right]^{-1/2}\frac{T_p^{1/2}\dot{Q}_c^{2/5}}{\Delta T_p^{3/5}} \tag{14.30}$$

Equation 14.29 shows that the ceiling jet velocity first becomes zero in the downward direction at values of r/b equal to −5.6, −3.5, and −2.0 for ceiling slopes of 10°, 20°, and 30°, respectively.

About 10 years after the work by Kung et al., additional measurements of gas temperature and velocity under inclined ceilings with thermocouples and bidirectional tubes, respectively, were obtained by Sugawa et al. [25]. These experiments involved nearly full-scale conditions (ceiling clearance, H, on the fuel centerline of 1.25–2.5 m) with a 200 mm diameter propane gas burner fire providing 10–100 kW heat release rates. Formulas for ceiling jet excess temperature and velocity along the "upslope" and perpendicular to the "upslope" directions are provided for slope angles from 0° to 60°. In many of these experiments, there is flame impingement on the ceiling and flame in the ceiling jet.

Very recently (about 10 years after the preceding studies by Sugawa et al.), new correlations have been developed by Y. Oka and colleagues at Yokohama National University from significant additional measurements under ceilings inclined from the horizontal up to a maximum angle, θ, of 40° and having a centerline clearance, H, above the fuel surface of 1 m. In these studies [26, 27], ceiling jet gas velocity is measured not only with bi-directional tubes but also with a Particle Imaging Velocimetry (PIV) system that makes use of smoke particles naturally present in the plume from the 0.285 m square heptane pan fire (heat release rate of 43 kW). By having two methods for measuring velocity, the authors [26] determined that the bidirectional probe generally provided a bulk mean velocity whereas the high resolution PIV system could provide a true maximum velocity. The ratio of the former to the latter is determined to be 0.828 instead of 0.707, as would be expected for the classic half-Gaussian velocity profile. Algebraic expressions for ceiling jet velocity have been obtained [26] both for the case of the flame tip below the inclined ceiling and for flame impingement on the inclined ceiling. In the latter case, gas velocity continues to increase in the flame zone in the steepest upward direction from the impingement point (as occurs in the fire plume itself) before becoming nearly constant and then decreasing with distance in the upward direction. Oka et al. [27] have now developed, from data for $0 < \theta < 40°$, a single algebraic expression for maximum ceiling jet gas velocity, U_{up}, at the steepest upward radial distance, r_{up}, from plume impingement, which covers cases both with and without flame impingement on a ceiling, as follows:

$$\frac{U_{up}}{\sqrt{g\left(H + r_{up}\sin\theta\right)}} = \alpha\left[\frac{r_{up}\cos\theta}{H + r_{up}\sin\theta}\right]^{\beta}\left\{Q_c^*(1 + \sin\theta)\right\}^{1/3} \tag{14.31}$$

where, for

$$\begin{array}{lll} 0.037 < r_{\text{up}} \cos\theta / \left(H + r_{\text{up}} \sin\theta\right) \leq 0.151 & \alpha = 6.051, & \beta = 0.458 \\ 0.151 < r_{\text{up}} \cos\theta / \left(H + r_{\text{up}} \sin\theta\right) \leq 0.350 & \alpha = 2.540, & \beta = 0 \\ 0.350 < r_{\text{up}} \cos\theta / \left(H + r_{\text{up}} \sin\theta\right) \leq 1.80 & \alpha = 0.855, & \beta = -1.040 \end{array}$$

and $Q_c^* =$ the usual definition (see Equation 14.9) with $\dot{Q}$ the convective component of heat release rate

The corresponding algebraic expression for near-maximum excess ceiling jet gas temperature from extensive thermocouple measurements that covers cases both with and without flame impingement on the ceiling is given by the following:

$$\frac{\Delta T}{T_\infty} = 2.778 \left[\frac{r_{up} \cos\theta}{H}\right]^{-0.781} \left\{Q_c^* (1 + \sin\theta)\right\}^{2/3} \quad 0.1 \leq r_{up} \cos\theta / H \leq 2.4 \tag{14.32}$$

The detailed velocity and excess temperature measurements discussed above have allowed Oka et al. [26] also to derive algebraic expressions for Gaussian ceiling jet velocity and excess temperature thickness under sloped ceilings. They determined that ceiling jet thickness was not affected by flame impingement as long as data corresponding to any region of continuous flaming are excluded. The expression for Gaussian thermal thickness under a sloped ceiling is given by:

$$\frac{L_T}{H} = \{0.00254\theta + 0.112\}\left[1 - exp\left(\beta_T \frac{r_{up}}{H}\right)\right] \tag{14.33}$$

where $\beta_T = -2.91 + 2.20[1 - \exp(-0.0662\theta)]$ and valid for $0.4 \leq r_{up}/H \leq 2.4$; $0 \leq \theta \leq 40°$.

Time-Dependent Fires

Quasi-Steady Assumption

For time-dependent fires, all estimates from the previous section may still be used, but with the constant heat release rate, $\dot{Q}$, replaced by an appropriate time-dependent $\dot{Q}(t)$. In making this replacement, a "quasi-steady" flow has been assumed. This assumption implies that when a change in heat release rate occurs at the fire source, full effects of the change are immediately felt everywhere in the flow field. In a room-sized enclosure, under conditions where the fire is growing slowly, this assumption is reasonable. However, in other cases, the time for the heat release rate to change significantly may be comparable to or less than the time, $t_f - t_i$, for gas to travel from the burning fuel to a detector submerged in the ceiling jet. The quasi-steady assumption may not be appropriate in this situation, unless the following condition is satisfied, depending on the accuracy desired:

$$\frac{\dot{Q}}{d\dot{Q}/dt} > t_f - t_i \tag{14.34}$$

where t_i is an ignition reference time.

The quasi-steady assumption, together with the strong plume-driven ceiling jet analysis of Heskestad and Hamada [6], has been used by Kung et al. [28] to correlate ceiling jet velocity and temperature induced by growing rack-storage fires. Although gas travel times for these large-scale experiments may amount to many seconds, Equation 14.34 shows that a sufficiently small fire-growth rate allows a quasi-steady analysis to be used.

Testing has shown that the heat release rate during the growth phase of many fires can often be characterized by simple time-dependent polynomial or exponential functions. The most extensive research and analysis have been performed with heat release rates that vary with the second power of time.

Power-Law Fire Growth

The growth phase of many fires can be characterized by a heat release rate increasing proportionally with a power, p, of time measured from the ignition reference time, t_i, as follows:

$$\dot{Q} = \alpha(t - t_i)^p \tag{14.35}$$

Figure 14.5 shows one case where the heat release rate for a burning foam sofa during the growth phase of the fire, more than 80 s (t_i) after ignition [29], can be represented by the following equation:

$$\dot{Q} = 0.1736(t - 80)^2 \tag{14.36}$$

Heskestad [30] used the general power-law behavior given by Equation 14.35 to propose a set of theoretical modeling relations for the transient ceiling jet flow that would result from such a time-varying heat release rate. These relations were validated in an extensive series of tests conducted by Factory Mutual Research Corporation [18, 31], where measurements were made of maximum ceiling jet temperatures and velocities during the growth of fires in three different sizes of wood crib. Subsequent to this original experimental study, Heskestad and Delichatsios [32] corrected the heat release rate, $\dot{Q}$, computed for the crib tests and also generalized their results to other types of fuels by using the more relevant convective heat release rate, $\dot{Q}_c$. The resulting dimensionless correlations for maximum ceiling jet temperatures and velocities are given by

$$\Delta T_2^* = 0 \quad t_2^* \le \left(t_2^*\right)_f \tag{14.37}$$

$$\Delta T_2^* = \left(\frac{t_2^* - \left(t_2^*\right)_f}{0.126 + 0.210r/H}\right)^{4/3} \quad t_2^* > \left(t_2^*\right)_f \tag{14.38}$$

$$\frac{U_2^*}{\sqrt{\Delta T_2^*}} = 0.59\left(\frac{r}{H}\right)^{-0.63} \tag{14.39}$$

where

$$t_2^* = \frac{t - t_i}{\left(A\alpha_c H^{-4}\right)^{-1/5}} \tag{14.40}$$

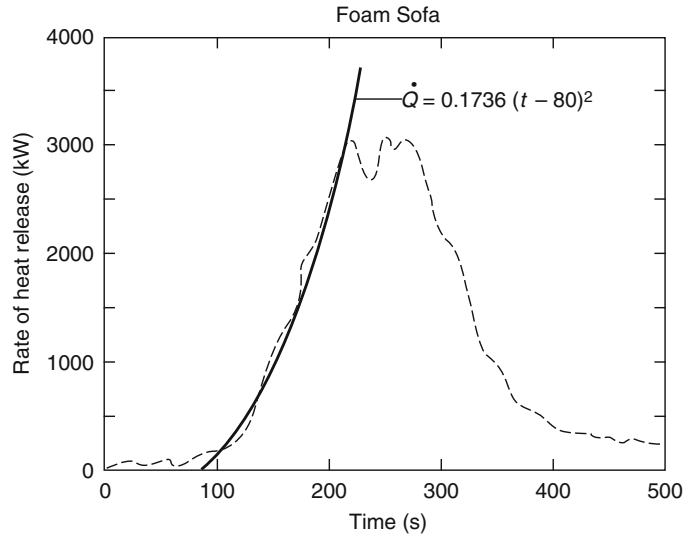

Fig. 14.5 Heat release rate history for a burning foam sofa [29]

$$U_2^* = \frac{U}{(A\alpha_c H)^{1/5}} \tag{14.41}$$

$$\Delta T_2^* = \frac{(T - T_\infty)/T_\infty}{(A\alpha_c)^{2/5} g^{-1} H^{-3/5}} \tag{14.42}$$

$$A = \frac{g}{\rho_\infty c_p T_\infty} \tag{14.43}$$

$$\alpha_c = \frac{\dot{Q}_c}{(t - t_i)^2} \tag{14.44}$$

$$(t_2^*)_f = 0.813\left(1 + \frac{r}{H}\right) \tag{14.45}$$

and where dimensionless variables are indicated with the superscript asterisk.

Notice that in Equation 14.38 the dimensionless time, t_2^* , has been reduced by the time $(t_2^*)_f$. This reduction accounts for the gas travel time, $t_f - t_i$, between the fire source and the location of interest along the ceiling at the specified r/H. For dimensionless times after ignition less than $(t_2^*)_f$, the initial heat front has not yet arrived at r/H so the gas temperature is still at the ambient value, as shown in Equation 14.37. In dimensional terms, the gas travel time is given by the following, after using the definition of t_2^* in Equation 14.45:

$$t_f - t_i = H^{4/5} \frac{0.813(1 + r/H)}{(A\alpha_c)^{1/5}} \tag{14.46}$$

Substitution of Equation 14.35 into Equation 14.34 shows that for power-law fire growth, the quasi-steady assumption will always be valid beginning at a sufficiently long time after ignition. For the specific case of t^2 fire growth, substitution of Equation 14.44 and the expression for the gas travel time, Equation 14.46, into Equation 14.34 results in the following requirement if a quasi-steady analysis is to be appropriate:

$$\frac{t - t_i}{2} > H^{4/5} \frac{0.813(1 + r/H)}{(A\alpha_c)^{1/5}} \tag{14.47}$$

In the limit of very large values of $t - t_i$, Equation 14.47 will always be satisfied and a quasi-steady limit is achieved, as shown by an alternative method by Heskestad [18]. The value of the quasi-steady excess temperature, $(\Delta T_2^*)_{qs}$, in this limit of $t_2^* \gg (t_2^*)_f$ becomes, from Equation 14.38

$$(\Delta T_2^*)_{qs} = \left(\frac{t_2^*}{0.126 + 0.210 r/H}\right)^{4/3} \tag{14.48}$$

The preceding correlations of ceiling jet temperatures and velocities are the basis for the calculated values of fire detector spacing found in *NFPA 72®*, *National Fire Alarm Code®*, Appendix B, "Engineering Guide for Automatic Fire Detector Spacing" [33]. In *NFPA 72,* three or four selected fire heat release rates assumed to increase proportionally with the square of time are used as the basis for the evaluation. These fire heat release rate histories are chosen to be representative of actual fires involving different commodities and geometric storage arrangements. The chosen release rate histories are as follows:

Slow $\dot{Q} = 0.00293 t^2$ (14.49)

Medium $\dot{Q} = 0.01172 t^2$ (14.50)

Fast $\dot{Q} = 0.0469 t^2$ (14.51)

Ultrafast $\dot{Q} = 0.1876 t^2$ (14.52)

where $\dot{Q}$ is in kW and t is in s.

EXAMPLE Sofa fire: Consider how the following calculation demonstrates a use of the correlation (Equations 14.38 and 14.39) for calculating the ceiling jet maximum temperature and velocity produced by a t^2 fire growth.

A foam sofa, of the type analyzed in Fig. 14.5, is burning in a showroom 5 m below a suspended ceiling. The showroom temperature remote from the fire remains at 20 °C at floor level as the fire begins to grow. Determine the gas temperature and velocity at the position of a ceiling-mounted fire detector submerged in the ceiling jet flow 4 m away from the fire axis when the convective heat release rate (assumed to equal the total heat release rate) first reaches 2.5 MW.

Figure 14.5 shows that the heat release rate from the sofa first reaches 2.5 MW (2500 kW) at about 200 s after ignition. Using the analytic formula for the time-dependent heat release rate, Equation 14.36, the time from the virtual ignition of the sofa at 80 s to reach 2500 kW is

$$2500 - 0.1736(t - 80)^2$$
$$(t - 80) = 120 \text{ s}$$

In this problem, the low-level heat release rate up to 80 s after actual ignition of the sofa is ignored. Thus, the sofa fire can be treated as having started at $t = 80$ s and grown to 2.5 MW in the following 120 s. Equations 14.40, 14.41, 14.42, 14.43, 14.44, and 14.45 are used to evaluate parameters of the problem, using the dimensionless correlations for ceiling jet temperature and velocity.

For the sofa fire in the showroom example, $T_\infty = 293$ K, $\rho = 1.204$ kg/m^3, $c_p = 1$ kJ/kg·K, $g = 9.8$ m/s^2, $\alpha_c = 0.1736$ kW/s^2, $A = 0.0278$ m^4/kJ · s^2, $r = 4$ m, $H = 5$ m, $\left(t_2^*\right)_f = 1.46$, $t - t_i = 120$ s, and $t_2^* = 11.40$. For the conditions of interest, $t_2^* > \left(t_2^*\right)_f$, so the correlation (Equation 14.38) is used to evaluate the dimensionless ceiling jet temperature

$$\Delta T_2^* = \left[\frac{11.40 - 1.46}{0.126 + 0.210(4/5)}\right]^{4/3}$$
$$\Delta T_2^* = 109.3$$

Equation 14.39 is used to calculate the dimensionless ceiling jet velocity

$$U_2^* = 0.59(4/5)^{-0.63}\sqrt{109.3} = 7.10$$

The dimensional excess temperature and velocity are calculated using Equations 14.42 and 14.41, respectively, to yield

$$\Delta T = 147\,\text{K}$$
$$T = 147\,\text{K} + 293\,\text{K} = 440\,\text{K} = 167^\circ\text{C}$$
$$U = 3.37\,\text{m/s}$$

The corresponding gas temperature calculated with the quasi-steady analysis of Equation 14.48 instead of the fire analysis is 197 °C.

EXAMPLE Rack storage: Yu and Stavrianidis [34] were interested in predicting activation times of quick-response sprinklers protecting high rack storage of plastics. Since the sprinklers are activated typically in less than 1 min by the ceiling jet flow, information on flow temperature and velocity shortly after ignition is required. The objective was to correlate properties of the ceiling jet induced by fires in 2- to 5-tier-high rack storage, consisting of polystyrene cups packaged in corrugated paper cartons on pallets. When this fuel array is ignited at its base, the initial growth period ($t_f - t_i \approx 25$ s) can be characterized as heat release rates increasing by the third power of time, as follows:

$$\dot{Q}_c = \alpha_c (t - t_i)^3 \tag{14.53}$$

where $\alpha_c = 0.0448$. Because of upward and lateral flame propagation during the transient rack-storage fire, the virtual origin elevation, z_o, of the plume changes during the course of fire growth, as follows:

$$z_o = -2.4 + 0.095\dot{Q}_c^{2/5} \tag{14.54}$$

thereby complicating the effort to correlate ceiling jet properties. Nevertheless, Yu and Stavrianidis were able to develop correlations based on the following dimensional temperature and velocity variables, which are similar to those first proposed by Heskestad [30] for power-law fire growth:

$$\Delta\hat{T}_m = \alpha_c^{-1/3}(H - z_o)^{1/3}\frac{\Delta T_m}{T_\infty} \tag{14.55}$$

$$\hat{U}_m = \alpha_c^{-1/6}(H - z_o)^{-1/3}U_m \tag{14.56}$$

where the maximum ceiling jet excess temperature, $\Delta\hat{T}_m$, and velocity, $\hat{U}_m$, variables depend on the following heat release rate and radial distance parameters, respectively:

$$X = \alpha_c^{-1/6}(H - z_o)^{-2/3}\dot{Q}_c^{1/3} \tag{14.57}$$

$$\hat{R} = \frac{r}{H - z_o} \tag{14.58}$$

The exact form of the preceding correlations, in terms of detailed formulas, is provided by Yu and Stavrianidis [34].

In addition to maximum excess gas temperature and velocity, Yu and Stavrianidis [34] also measured the depth of the ceiling jet, in terms of the distance below the ceiling where the velocity and excess temperature are $1/e$ of the respective maximum values. Results show the ceiling jet depth based on velocity to be very similar to that based on excess temperature and both depths to be fairly insensitive to the transient fire growth process. Typical values for the ratio of ceiling jet temperature depth to effective ceiling height, $\ell_T/(H - z_o)$, for radial positions, $r/(H - z_o)$ of 0.217, 0.365, 1.75, and 4.33 are about 0.07, 0.1, 0.14, and 0.2, respectively.

Confined Ceilings

Channel Configuration

Previous discussions of ceiling jets in this chapter have all dealt with unconfined radial spread of the gas flow away from a ceiling impingement point. In practice this flow may be interrupted by ceiling beams or corridor walls, creating a long channel that partially confines the flow. Knowledge of the resultant ceiling jet flows is important in determining fire detector response times. For the channel configuration, the flow near the impingement point will remain radial (i.e., axisymmetric), but after spreading to the walls or beams that bound the ceiling, the flow will become generally parallel with the confining boundary. Delichatsios [35] has developed correlations for steady-state ceiling jet temperature and velocity, which apply to the channel flow between beams and down corridors. In the case of corridors, the correlations apply when the corridor half-width, ℓ_b, is greater than 0.2 times the ceiling height, H, above the fire source. Note that this value of ℓ_b corresponds approximately to the outer radius of the ceiling jet turning region. In the case of beams, the flow must also be contained fully so that only a flow in a primary channel results, without spillage under the beams to the adjoining secondary channels. For the latter condition to be satisfied, the beam depth, h_b, must be greater than the quantity $(H/10)(\ell_b/H)^{-1/3}$. Downstream of where the ceiling jet flow is parallel to the beams or corridor walls and in the absence of spillage, Delichatsios [35] determined that the average excess ceiling jet temperature and velocity within the primary channel are given by the following:

$$\frac{\Delta T}{\Delta T_p} = \mathrm{a}\left(\frac{H}{\ell_b}\right)^{1/3} \exp\left[-6.67\mathrm{St}\frac{Y}{H}\left(\frac{\ell_b}{H}\right)^{1/3}\right] \tag{14.59}$$

$$U = 1.102\sqrt{H\Delta T}\left(\frac{H}{\ell_b}\right)^{1/6} \tag{14.60}$$

under the conditions

$$Y > \ell_b$$
$$h_b/H > 0.1(\ell_b/H)^{-1/3}$$
$$\ell_b/H > 0.2$$
$$0.5 < \frac{Y}{H}\left(\frac{\ell_b}{H}\right)^{1/3} < 3.0$$

where

ΔT_p = Excess temperature on the plume centerline defined previously in Equation 14.17

Y = Distance along the channel measured from the plume impingement point

St = Stanton number, whose value is recommended to be 0.03

Based on the minimum value of $\ell_b/H = 0.2$, the limit on h_b/H implies that the beam depth to ceiling height ratio must be at least 0.17 for the fire gases to be restricted to the primary channel. The constant a in Equation 14.59 is determined by Delichatsios to be in the range 0.24–0.29. This equation is based on the concept that the channel flow has undergone a hydraulic jump, which results in greatly reduced entrainment of cooler, ambient air from below. Reductions in ceiling jet temperature or velocity are then mainly due to heat losses to the ceiling and would thus be dependent on ceiling composition to some extent.

Additional detailed measurements of the ceiling jet flow in a primary beamed channel have been obtained by Koslowski and Motevalli [36]. Their data generally validate the

Delichatsios beamed ceiling correlation (Equation 14.61) and ceiling jet flow behavior, but additional measurements for a range of beam depth to ceiling height ratios has allowed the correlation to be generalized. Furthermore, Koslowski and Motevalli recast the correlation in terms of the nondimensional heat release rate defined by Heskestad and Delichatsios (Equations 14.9 and 14.10), instead of centerline plume conditions at the ceiling, with the following result:

$$\Delta T_0^* = \mathrm{C}\left(\frac{H}{\ell_b}\right)^{1/3} \exp\left[-6.67\,\mathrm{St}\frac{Y}{H}\left(\frac{\ell_b}{H}\right)^{1/3}\right] \tag{14.61}$$

where the Stanton number is recommended to be 0.04, rather than 0.03, and the constant, C, has the following dependence on the ratio of beam depth, h_b, to ceiling height, H:

$$\mathrm{C} = -25.38\left(\frac{h_b}{H}\right)^2 + 13.58\frac{h_b}{H} + 2.01 \quad \text{for } 0.5 \le \frac{Y}{H} \le 1.6 \tag{14.62}$$

To derive Equation 14.62, Koslowski and Motevalli vary the h_b/H ratio from 0.07 up to 0.28. In so doing, they note that C increases steadily with this ratio until leveling off near $h_b/H = 0.17$, determined by Delichatsios as the condition for the fire gases to be restricted to the primary channel. Between values of h_b/H of 0.07 (or even much less) and 0.17, spillage from the primary channel to adjacent secondary channels is steadily reduced, thereby increasing temperatures in the primary channel. Characteristics of the ceiling jet flow in the secondary channels, as well as the primary channel, have also been studied by Koslowski and Motevalli [37].

Corner Configuration with Strong Plumes

An open configuration of two walls at a 90° angle to form a corner, covered by a ceiling, with a fire source at the base of and in close contact with the corner, is often used as a hazardous environment in which to test the flammability of wall and ceiling linings. This wall-ceiling-corner configuration also occurs naturally in many types of enclosures (see below) where hot gases from the fire source may be partially or completely confined by more than just the ceiling and corner walls themselves, resulting in the formation of a hot gas layer near the ceiling. In this section, the environment of an open corner with inert lining surfaces is discussed, where a ceiling jet develops due to impingement of a fire plume or flames from the source fire at the base of the wall corner onto the ceiling covering the wall-corner. A careful study of this environment based on full-scale tests was conducted by Lattimer and Sorathia [38]. These tests used a ceiling clearance of 2.25 m above the surface of a 0.17–0.50 m^2 or L-shaped line (each leg being 0.17–0.50 m) sand burner having propane heat release rates from 50 to 300 kW.

Thermocouple measurements [38] of excess gas temperature at a radial distance from the corner, r, in the ceiling jet could be correlated (with a regression coefficient of 0.85) by the following formulas:

$$T - T_\infty = 950 \quad \text{for} \quad \frac{r+H}{L_{f,tip}} \le 0.55 \tag{14.63}$$

$$T - T_\infty = C\left[\frac{r+H}{L_{f,tip}}\right]^{-2} \quad \text{for} \quad \frac{r+H}{L_{f,tip}} > 0.55 \tag{14.64}$$

The specific value of 950 for the maximum excess of corner fire gas temperature above ambient in Equation 14.63 may vary for fire sources other than the propane burner or for corner walls having thermal characteristics different from those used in these specific tests. However, it is expected that the functional dependencies for ceiling jet temperature should be preserved. Note that the constant, C, in Equation 14.64 is 288 for the square burner of side, D, and 340 for the L-shaped line burner, each leg of which is length, D and that $L_{f,tip}$ is the flame length from the surface of either type burner to the flame tip, the furthest location where flame

tips are observed visually, as determined from the correlation [38],

$$\frac{L_{f,tip}}{D} = 5.9\sqrt{Q^*} \qquad (14.65)$$

where Q^* is based on actual fire heat release rate and the burner length-scale, D (instead of the usual ceiling clearance, H).

Lattimer and Sorathia [38] also used twenty Schmidt-Boelter gauges to measure heat flux to the bounding surfaces of the corner configuration from the propane sand burner flames. Their measurements of total heat flux, $\dot{q}''$, to the ceiling surface from the ceiling jet flames and/or hot gases could be correlated by the following for either the square or L-shaped line burner:

$$\dot{q}'' = 120 \quad \text{for} \quad \frac{r+H}{L_{f,tip}} \leq 0.58 \qquad (14.66)$$

$$\dot{q}'' = 18\left[\frac{r+H}{L_{f,tip}}\right]^{-3.5} \quad \text{for} \quad \frac{r+H}{L_{f,tip}} > 0.58 \qquad (14.67)$$

where the flame tip total length is given by Equation 14.65, above. This same formula is found also to predict the maximum heat flux to the top portion of the wall from the ceiling jet flow, where now the variable, r, represents distance from the corner along the top of the wall.

Again, the specific maximum heat flux of 120 kW/m^2 that was measured in the corner configuration by Lattimer and Sorathia [38] may vary for fuels with thermal radiation characteristics much different from those of propane or for different burner configurations. For example, it is well known that peak heat fluxes in pool and solid fuel fires can exceed 140–160 kW/m^2, as discussed by Coutts [39].

General Enclosure Configurations

The analyses in preceding sections for unconfined ceiling jet flows may be sufficient for large industrial or commercial storage facilities. In smaller rooms, or for very long times after fire ignition in larger industrial facilities, a quiescent, heated layer of gas will accumulate in the upper portion of the enclosure. This heated layer can be deep enough to totally submerge the ceiling jet flow. In this case, temperatures in the ceiling jet can be expected to be greater than if the ceiling jet were entraining gas from a cooler, ambient-temperature layer. It has been shown by Yu and Faeth [10] that the submerged ceiling jet also results roughly in a 35 % increase in the heat transfer rate to the ceiling.

There are analytical formulas to predict temperature and velocity in such a two-layer environment, in which the ceiling jet is contained in a heated upper layer and the fire is burning in a lower, cool layer. This type of prediction, which has been developed by Evans [40, 41], Cooper [42], and Zukoski and Kubota [43], can best be used to check the proper implementation of readily available numerical models (e.g., zone or field/CFD) of fire-induced flows in enclosures. An example of a zone model to predict activation of thermal detectors by a ceiling jet submerged in a heated layer is the algorithm developed by Davis [44]. This model, which assumes that thermally activated links are always located below the ceiling at the point of maximum ceiling jet temperature and velocity, is based partly on a model and thoroughly documented software developed by Cooper [45].

Formulas to predict the effect of the heated upper layer in an enclosure are based on the assumption that the ceiling jet results from a fire contained in a uniform environment at the heated upper-layer temperature. This substitute fire has a heat release rate, $\dot{Q}_2$, and location below the ceiling, H_2, differing from those of the real fire. Calculation of the substitute quantities $\dot{Q}_2$ and H_2, depends on the heat release rate and location of the real fire, as well as the depths and temperatures of the upper and lower layers within the enclosure.

Following the development by Evans [41], the substitute source heat release rate and distance below the ceiling are calculated from Equations 14.68, 14.69, 14.70, and 14.71. Originally developed for the purpose of sprinkler and heat detector response time calculations, these

equations are applicable during the growth phase of enclosure fires.

$$\dot{Q}^*_{I,2} = \left(\frac{1 + C_T \dot{Q}^{*\,2/3}_{I,1}}{\xi C_T} - \frac{1}{C_T} \right)^{3/2} \tag{14.68}$$

$$Z_{I,2} = \left\{ \frac{\xi \dot{Q}^*_{I,1} C_T}{\dot{Q}^{*\,1/3}_{I,2} \left[(\xi - 1)(\beta^2 + 1) + \xi C_T \dot{Q}^{*\,2/3}_{I,2} \right]} \right\}^{2/5} Z_{I,1} \tag{14.69}$$

$$\dot{Q}_{c,2} = \dot{Q}^*_{I,2} \rho_{\infty,2} c_{p\infty} T_{\infty,2} g^{1/2} Z^{5/2}_{I,2} \tag{14.70}$$

$$H_2 = H_1 - Z_{I,1} + Z_{I,2} \tag{14.71}$$

Further explanation of variables is contained in the nomenclature section.

Cooper [42] has formulated an alternative calculation of substitute source heat release rate and distance below the ceiling that provides for generalization to situations in which portions of the time-averaged plume flow in the lower layer are at temperatures below the upper-layer temperature. In these cases, only part of the plume flow may penetrate the upper layer sufficiently to impact on the ceiling. The remaining portion at low temperature may not penetrate into the hotter upper layer. In the extreme, when the maximum temperature in the lower-layer plume flow is less than the upper-layer temperature, none of the plume flow will penetrate significantly into the upper layer. This could be the case during the decay phases of an enclosure fire, when the heat release rate is small compared to earlier in the fire growth history. In this calculation of substitute fire-source quantities, the first step is to calculate the fraction of the plume mass flow penetrating the upper layer, m^*_2, from Equations 14.72 and 14.73.

$$m^*_2 = \frac{1.04599\sigma + 0.360391\sigma^2}{1 + 1.37748\sigma + 0.360391\sigma^2} \tag{14.72}$$

where

$$\sigma = \left(\frac{\xi}{\xi - 1} \right) \left[\frac{1 + C_T \left(\dot{Q}^*_{I,1} \right)^{2/3}}{\xi} - 1 \right] \tag{14.73}$$

Then, analogous to Equations 14.69, 14.70, and 14.71 of the previous method:

$$Z_{I,2} = Z_{I,1} \xi^{3/5} \left(m^*_2 \right)^{2/5} \left(\frac{1 + \sigma}{\sigma} \right)^{1/3} \tag{14.74}$$

$$\dot{Q}_{c,2} = \dot{Q}_{c,1} \left(\frac{\sigma m^*_2}{1 + \sigma} \right) \tag{14.75}$$

$$H_2 = H_1 - Z_{I,1} + Z_{I,2} \tag{14.76}$$

The last step is to use the substitute source values of heat release rate and distance below the ceiling, as well as heated upper-layer properties for ambient conditions, in the correlations developed for ceiling jet flows in uniform environments.

To demonstrate the use of the techniques, the previous example in which a sofa was imagined to be burning in a showroom may be expanded. Let all the parameters of the problem remain the same except that at 200 s after ignition ($t - t_i$ = 120 s), when the fire heat release rate has reached 2.5 MW, a quiescent heated layer of gas at a temperature of 50 °C is assumed to have accumulated under the ceiling to a depth of 2 m. For this case, the two-layer analysis is needed to determine the ceiling jet maximum temperature at the same position as calculated previously (a radial distance of 4 m from the plume impingement point on the ceiling).

All of the two-layer calculations presented assume quasi-steady conditions. From Equation 14.47 with the values of parameters in the single-layer calculation, it can be shown that the time after sofa ignition must be at least 31 s for a quasi-steady analysis to be acceptable. Since the actual time after ignition is 120 s, such an analysis is appropriate. It will be assumed that this finding will carry over to the two-layer case.

Using Equations 14.68, 14.69, 14.70, and 14.71 from the work of Evans [41], values of the heat release rate and position of the substitute fire source that compensates for the two-layer effects on the plume flow can be calculated. The dimensionless heat release rate of the real fire source evaluated at the position of the interface between the upper and lower layers is as follows:

$$\dot{Q}^*_{I,1} = \frac{\dot{Q}}{\rho_\infty c_{p\infty} T_\infty g^{1/2} Z_{I,1}^{5/2}} \qquad (14.77)$$

For an actual heat release rate of 2500 kW, ambient temperature of 293 K, and distance between the fire source and the interface between the lower and upper layers of 3 m, Equation 14.77 becomes

$$\dot{Q}^*_{I,1} = \frac{2500}{1.204 \times 1 \times 293 \times 9.8^{1/2} \times 3^{5/2}} = 0.1452$$

Using the ratio of upper-layer temperature to lower-layer temperature, $\xi = 323/293 = 1.1024$, and the constant, $C_T = 9.115$, the dimensionless heat release rate for the substitute fire source is

$$\dot{Q}^*_{I,2} = 0.1179$$

Using the value for the constant $\beta^2 = 0.913$, the position of the substitute fire source relative to the two-layer interface is

$$Z_{I,2} = 3.161$$

Now, from Equations 14.76 and 14.77, the dimensional heat release rate and position relative to the ceiling are found to be

$$\dot{Q}_2 = 2313\,\text{kW} \quad H_2 = 5.161\,\text{m}$$

The analogous calculations for substitute fire-source heat release rate and position following the analysis of Cooper [42], Equations 14.72, 14.73, 14.74, 14.75, 14.76, and 14.77, are

$$\sigma = 23.60$$
$$m_2^* = 0.962$$
$$Z_{I,2} = 3.176$$
$$\dot{Q}_2 = 2308\,\text{kW}$$
$$H_2 = 5.176\,\text{m}$$

These two results are essentially identical for this type of analysis.

Since it has been shown that the quasi-steady analysis is appropriate for this example, the dimensionless maximum temperature in the ceiling jet flow, 4 m from the impingement point, can now be calculated from $(\Delta T_2^*)_{qs}$ in Equation 14.48. Using the ceiling height above the substitute source, this equation yields the result

$$(\Delta T_2^*)_{qs} = \left[\frac{11.40}{0.126 + 0.210(4/5.161)}\right]^{4/3} = 134.4$$

For the given time after ignition of 120 s and the assumed fire growth, the calculated $\dot{Q}_2$ value implies that α equals 0.1606, instead of the original sofa fire growth factor of 0.1736. Substitution of this new α in Equation 14.42, along with H_2 and the upper-layer temperature as the new ambient value, yields the following dimensional excess temperature at the 4-m radial position in the ceiling jet:

$$\Delta T = \frac{134.4 \times 323 \times (0.0278 \times .01606)^{2/5}}{9.8 \times 5.161^{3/5}}$$
$$\Delta T = 190\,\text{K}$$
$$T = 190\,\text{K} + 323\,\text{K} = 513\,\text{K} = 240^\circ\text{C}$$

This is 73 °C above the temperature calculated previously using the quasi-steady analysis and a uniform 20 °C ambient, demonstrating the effect of flow confinement on gas temperature.

Ceiling Jet Development

At the beginning of a fire, the initial buoyant flow from the fire must spread across the ceiling, driven by buoyancy, to penetrate the cooler ambient air ahead of the flow. Research studies designed to quantify the temperatures and velocities of this initial spreading flow have been initiated [46]. At a minimum, it is useful to become aware of the many fluid mechanical phenomena embodied in a description of the ceiling jet flow in a corridor up to the time when the ceiling jet is totally submerged in a quiescent, warm upper layer. Borrowing heavily from a description of this flow provided by Zukoski et al. [46], the process is as follows.

A fire starts in a small room with an open door to a long corridor having a small vent near the floor at the end opposite the door. As the fire

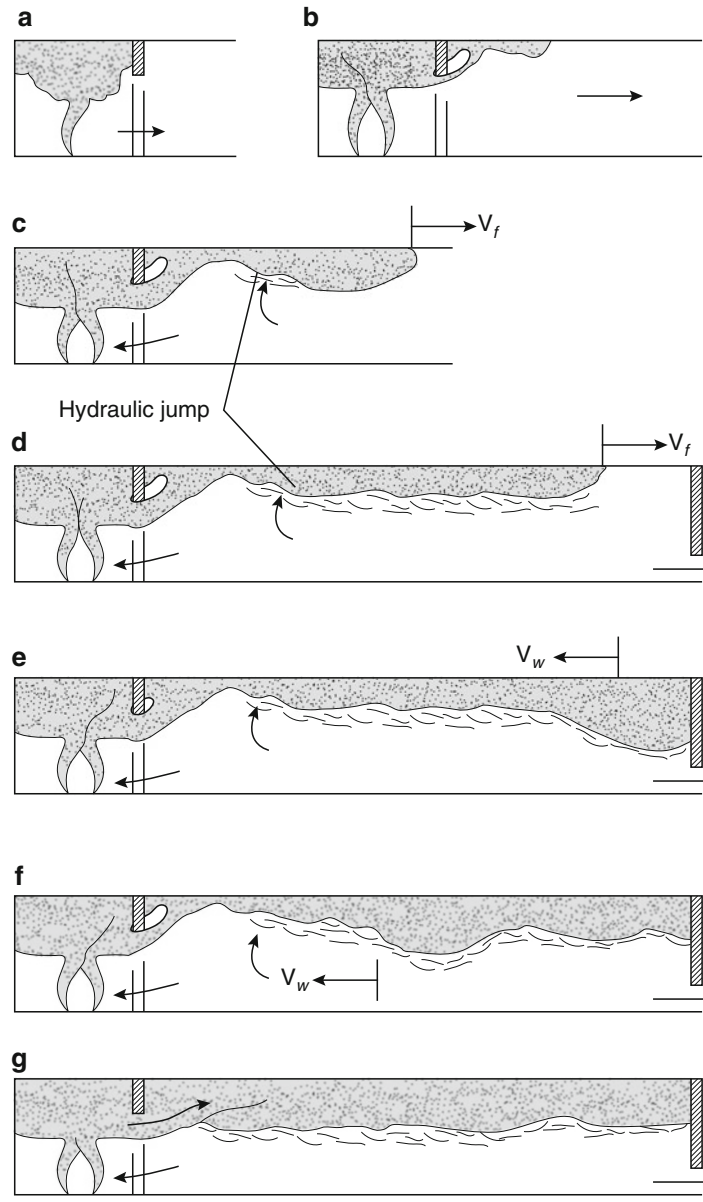

Fig. 14.6 Transient ceiling jet flow in a room and corridor [45]

starts, smoke and hot gases rise to form a layer near the fire room ceiling. The layer is contained in the small room by the door soffit (Fig. 14.6a). As the fire continues, hot gas from the room begins to spill out under the soffit into the hallway. The fire grows to a relatively constant heat release rate.

The outflowing gas forms a short, buoyant plume (Fig. 14.6b) that impinges on the hallway ceiling, producing a thin jet that flows away from the fire room in the same manner that the plume within the room flows over the interior ceiling. The gas flow in this jet is supercritical, analogous to the shooting flow of liquids over a weir. The velocity of the gas in this flow is greater than the speed of gravity waves on the interface between the hot gas and the cooler ambient air. The interaction of the leading edge of this flow with the ambient air ahead of it produces a hydraulic, jumplike condition, as shown in Fig. 14.6c.

A substantial amount of ambient air is entrained at this jump. Downstream of the jump, the velocity of the gas flow is reduced and mass flow is increased due to the entrainment at the jump. A head is formed at the leading edge of the flow. Mixing between this ceiling-layer flow and the ambient cooler air occurs behind this head.

The flow that is formed travels along the hallway ceiling (Fig. 14.6c, d) with constant velocity and depth until it impinges on the end wall (Fig. 14.6e). A group of waves are reflected back toward the jump near the fire room, traveling on the interface. Mixing occurs during the wall impingement process (Fig. 14.6f), but no significant entrainment occurs during the travel of the nonbreaking reflected wave. When these waves reach the jump near the fire room door, the jump is submerged in the warm gas layer, eliminating the entrainment of ambient lower-layer air at this position (Fig. 14.6g).

After several wave reflections up and down the corridor along the interface, the wave motion dies out, and a ceiling layer uniform in depth is produced. This layer slowly grows deeper as the hot gas continues to flow into the hallway from the fire room.

It is clear from the preceding description that quantification of effects during development of a submerged ceiling jet flow is quite complex.

Analyses and experiments have been performed to better understand the major features of a developing ceiling jet flow in a corridor [47, 48]. One such study [49] contains a description somewhat different from that already given.

Summary

Reliable formulas are available to predict maximum gas temperatures and velocities and approximate temperature/velocity profiles in fire-driven ceiling jet flows beneath unobstructed ceilings for both steady and power-law fire growth. These predictive formulas, which also apply to certain situations where the ceiling jet flow is confined by beams or corridor walls, are very useful for verifying that detailed numerical models of fire phenomena (e.g., Hara and Shinsuke [50]) have been implemented properly. The predictive techniques are the basis for acceptable design of fire detection systems, as exemplified by Appendix B of *NFPA 72®, National Fire Alarm Code* [33].

Nomenclature

A	$g/(\rho_\infty c_p T_\infty)$ (m^2/kg)
a	Constant in Equation 14.59, equal to 0.24–0.29
b	Effective plume radius at the intersection with the ceiling elevation (m)
C_T	Constant [17], related to plume flow, equal to 9.115
c_p	heat capacity at constant pressure (J/kg K)
D	Burner dimension (m)
D_{eff}	Effective diameter of the base of the flame zone or the burning fuel
f	Ceiling friction factor
g	Gravitational acceleration (m/s^2)
H	Ceiling height above fire source; for sloped ceiling, on the fire axis (m)
h	Heat transfer coefficient (kW/m^2 K)
h_b	Depth of beams in a primary beam channel (m)
$L_{f,tip}$	Visible flame length from burner to furthest flame tip (m)
ℓ_b	Half-width for corridor or primary beam channel (m)
ℓ_T	Ceiling jet thickness based on $1/e$ depth of excess temperature profile (m)
m_2^*	Fraction of fire-plume mass flux penetrating upper layer
p	Ambient air pressure (Pa); also, as exponent of time for general power-law fire growth
Pr	Prandtl number
$\dot{Q}$	Total heat release rate (kW)
$\dot{Q}_c$	Convective heat release rate (kW)

$Q^*, \dot{Q}_0^*$	$\dot{Q}/\left(\rho_\infty c_p T_\infty \sqrt{g} H^{5/2}\right)$
Q_{fc}^*	$\dot{Q}_c/\left(\rho_\infty c_p T_\infty \sqrt{g} H^{5/2}\right)$
$\dot{q}''$	Rate of heat transfer per unit area (heat flux) to the ceiling surface (kW/m^2)
R	Radial distance to detector (m)
$\hat{R}$	$r/(H - z_o)$
Ra	Rayleigh number
Re	Reynolds number
r	Radial distance from axis of fire plume (m)
r_{up}	Radial distance in steepest upward direction from axis of fire plume (m)
St	Stanton number, $h/(\rho U c_p)$
T	Ceiling jet gas temperature (K)
T_∞	Ambient air temperature (K)
T_p	Peak gas temperature in plume at the intersection with ceiling elevation (K)
ΔT	Excess gas temperature, $T - T_\infty$ (K) or (°C)
t	Time (s)
U	Ceiling jet gas velocity (m/s)
U_{up}	Maximum ceiling jet gas velocity in the steepest upward direction (m/s)
V_p	Maximum plume velocity at the intersection with ceiling elevation (m/s)
Y	Distance along channel or corridor, measured from plume axis (m)
Z_I	Distance of layer interface above the real or substitute fire source (m)
z	Vertical distance above the base of the flame zone
z_H	Distance of ceiling above the base of the flame zone
z_o	Virtual origin elevation in a transient rack storage fire
z_v	Distance of virtual plume origin above the base of the flame zone
$d\dot{Q}/dt$	Rate of change of heat release rate with time (kW/s)

Greek Letters

α	Growth parameter for t^2 fires (kW/s^2)
β^2	Constant [17] related to plume flow, equal to 0.913
ν	Kinematic viscosity (m^2/s)
θ	Angle of inclination of the ceiling with respect to the horizontal (degrees)
ρ	Gas density (kg/m^3)
σ	Parameter defined in Equation 14.73
ξ	Ratio of temperatures, $T_{\infty,2}/T_{\infty,1}$

Subscripts

0	Based on steady-state fire source
1	Associated with lower layer
2	Associated with upper layer; or parameter associated with t^2 fire growth
∞	Ambient, outside ceiling jet or plume flows
c	Convective fraction
f	Associated with gas travel time delay
I	Value at the interface position between the heated upper layer and cool lower layer
i	Reference value at ignition
p	Associated with plume flow
qs	Quasi-steady flow condition

Superscripts

*	Dimensionless quantity
^	Quantity related to transient rack-storage fire

References

1. R.W. Pickard, D. Hird, and P. Nash, "The Thermal Testing of Heat-Sensitive Fire Detectors," *F.R. Note 247,* Building Research Establishment, Borehamwood, UK (1957).
2. P.H. Thomas, "The Distribution of Temperature and Velocity Due to Fires Beneath Ceilings," *F.R. Note 141,* Building Research Establishment, Borehamwood, UK (1955).
3. R.L. Alpert, "Calculation of Response Time of Ceiling-Mounted Fire Detectors," *Fire Technology,* 8, p. 181 (1972)
4. R.L. Alpert, "Turbulent Ceiling Jet Induced by Large-Scale Fires," *Combustion Science and Technology*, 11, 197 (1975)
5. H.Z. Yu (You), "An Investigation of Fire-Plume Impingement on a Horizontal Ceiling: 2-Impingement and Ceiling-Jet Regions," *Fire and Materials,* 9, 46 (1985)
6. G. Heskestad and T. Hamada, "Ceiling Jets of Strong Fire Plumes," *Fire Safety Journal,* 21, 69, (1993)

7. G. Heskestad, "Physical Modeling of Fire," *Journal of Fire & Flammability,* 6, p. 253 (1975).
8. L.Y. Cooper, "Heat Transfer from a Buoyant Plume to an Unconfined Ceiling," *Journal of Heat Transfer,* 104, p. 446 (1982).
9. L.Y. Cooper and A. Woodhouse, "The Buoyant Plume-Driven Adiabatic Ceiling Temperature Revisited," *Journal of Heat Transfer,* 108, p. 822 (1986).
10. H.Z. Yu (You) and G.M. Faeth, "Ceiling Heat Transfer during Fire Plume and Fire Impingement," *Fire and Materials*, 3, 140 (1979)
11. C.C. Veldman, T. Kubota, and E.E. Zukoski, "An Experimental Investigation of the Heat Transfer from a Buoyant Gas Plume to a Horizontal Ceiling—Part 1: Unobstructed Ceiling," *NBS-GCR-77–97,* National Bureau of Standards, Washington, DC (1977).
12. V. Motevalli and C.H. Marks, "Characterizing the Unconfined Ceiling Jet Under Steady-State Conditions: A Reassessment," *Fire Safety Science, Proceedings of the Third International Symposium* (G. Cox and B. Langford, eds.), Elsevier Applied Science, New York, p. 301 (1991).
13. R.L. Alpert, "Fire Induced Turbulent Ceiling-Jet," *Technical Report Serial No. 19722–2,* Factory Mutual Research Corporation, Norwood, MA, p. 35 (1971).
14. D.D. Evans and D.W. Stroup, "Methods to Calculate the Response Time of Heat and Smoke Detectors Installed Below Large Unobstructed Ceilings," *Fire Technology*, 22, 54 (1986).
15. R.L. Alpert, "The Fire Induced Ceiling-Jet Revisited," in The Science of Suppression, Proceedings of Fireseat 2011 at the National Museum of Scotland, 9 November 2011, The University of Edinburgh, Edinburgh, Scotland, pp. 1–21.
16. A. Tewarson, "Generation of Heat and Gaseous, Liquid and Solid Products in Fires," SFPE Handbook of Fire Protection Engineering, this volume, (p. 3–142 in 4th Edition).
17. E.E. Zukoski, T. Kubota, and B. Cetegen, "Entrainment in Fire Plumes," *Fire Safety Journal*, 3, 107 (1981)
18. G. Heskestad and M.A. Delichatsios, "The Initial Convective Flow in Fire," *17th International Symposium on Combustion,* Combustion Institute, Pittsburgh, PA (1978).
19. C.L. Beyler, "Fire Plumes and Ceiling Jets," *Fire Safety Journal,* 11, p. 53 (1986).
20. G.T. Atkinson and D.D. Drysdale, "Convective Heat Transfer from Fire Gases," *Fire Safety Journal,* 19, p. 217 (1992).
21. Y. Hasemi, S. Yokobayashi, T. Wakamatsu, and A. Ptchelintsev, "Fire Safety of Building Components Exposed to a Localized Fire: Scope and Experiments on Ceiling/Beam System Exposed to a Localized Fire," *AsiaFlam 95—1st International Conference,* Interscience Communications, Ltd., London, p. 351 (1995).
22. M.A. Kokkala, "Experimental Study of Heat Transfer to Ceiling from an Impinging Diffusion Flame," *Fire Safety Science, Proceedings of the Third International Symposium* (G. Cox and B. Langford, eds.), Elsevier Applied Science, New York, p. 261 (1991).
23. R.L. Alpert, "Convective Heat Transfer in the Impingement Region of a Buoyant Plume," *ASME Journal of Heat Transfer,* 109, p. 120 (1987).
24. H.C. Kung, R.D. Spaulding, and P. Stavrianidis, "Fire Induced Flow Under a Sloped Ceiling," *Fire Safety Science, Proceedings of the Third International Symposium* (G. Cox and B. Langford, eds.), Elsevier Applied Science, New York, p. 271 (1991).
25. O. Sugawa, T. Hosozawa, N. Nakamura, A. Itoh and Y. Matsubara, "Flow Behavior under Sloped Ceiling," in Fifteenth Meeting of UJNR Panel on Fire Research and Safety, NISTIR 6588, National Institute of Standards and Technology, Gaithersburg, MD USA, March 2000.
26. Y. Oka, M. Ando and K. Kamiya, "Ceiling Jet Flow Properties for Flames Impinging on an Inclined Ceiling," *Fire Safety Science, Proceedings of the Tenth International Symposium,* International Association for Fire Safety Science, London, 2012.
27. Y. Oka and M. Ando, "Temperature and Velocity Properties of a Ceiling Jet Impinging on an Unconfined Inclined Ceiling," accepted for publication in *Fire Safety Journal,* 2012.
28. H.C. Kung, H.Z. Yu (You), and R.D. Spaulding, "Ceiling Flows of Growing Rack Storage Fires," *21st Symposium (International) on Combustion,* Combustion Institute, Pittsburgh, PA, p. 121 (1986).
29. R.P. Schifilliti, *Use of Fire Plume Theory in the Design and Analysis of Fire Detector and Sprinkler Response,* Thesis, Worcester Polytechnic Institute, Worcester, MA (1986).
30. G. Heskestad, "Similarity Relations for the Initial Convective Flow Generated by Fire," *ASME Paper No. 72-WA/HT-17,* American Society of Mechanical Engineers, New York (1972).
31. G. Heskestad and M.A. Delichatsios, "Environments of Fire Detectors," *NBS-GCR-77-86* and *NBSGCR-77-95,* National Bureau of Standards, Washington, DC (1977).
32. G. Heskestad and M.A. Delichatsios, "Update: The Initial Convective Flow in Fire," Short Communication, *Fire Safety Journal,* 15, p. 471 (1989).
33. *NFPA 72®, National Fire Alarm Code®,* National Fire Protection Association, Quincy, MA (1999).
34. H.Z. Yu and P. Stavrianidis, "The Transient Ceiling Flows of Growing Rack Storage Fires," *Fire Safety Science, Proceedings of the Third International Symposium (*G. Cox and B. Langford, eds.), Elsevier Applied Science, New York, p. 281 (1991).
35. M.A. Delichatsios, "The Flow of Fire Gases Under a Beamed Ceiling," *Combustion and Flame,* 43, 1 (1981).
36. C. Koslowski and V. Motevalli, "Behavior of a 2-Dimensional Ceiling Jet Flow: A Beamed Ceiling Configuration," *Fire Safety Science, Proceedings of the Fourth International Symposium* (T. Kashiwagi,

ed.), International Association of Fire Safety Science, Bethesda, MD, p. 469 (1994).
37. C.C. Koslowski and V. Motevalli, "Effects of Beams on Ceiling Jet Behavior and Heat Detector Operation," *Journal of Fire Protection Engineering,* 5, 3, p. 97 (1993).
38. B. Lattimer and U. Sorathia, "Thermal Characteristics of Fires in a Noncombustible Corner," *Fire Safety Journal*, 38, p. 709 (2003).
39. D. Coutts, "An Emissive Power Correlation for Solid Fuel Packages," *Journal of Fire Protection Engineering*, 21, p. 133, 2011.
40. D.D. Evans, "Thermal Actuation of Extinguishing Systems," *Combustion Science and Technology,* 40, p. 79 (1984).
41. D.D. Evans, "Calculating Sprinkler Actuation Time in Compartments," *Fire Safety Journal*, 9, 147 (1985).
42. L.Y. Cooper, "A Buoyant Source in the Lower of Two Homogeneous, Stably Stratified Layers," *20th International Symposium on Combustion,* Combustion Institute, Pittsburgh, PA (1984).
43. E.E. Zukoski and T. Kubota, "An Experimental Investigation of the Heat Transfer from a Buoyant Gas Plume to a Horizontal Ceiling—Part 2: Effects of Ceiling Layer," *NBS-GCR-77-98,* National Bureau of Standards, Washington, DC (1977).
44. W.D. Davis, "The Zone Fire Model Jet: A Model for the Prediction of Detector Activation and Gas Temperature in the Presence of a Smoke Layer," *NISTIR 6324,* National Institute of Standards and Technology, Gaithersburg, MD (1999).
45. L.Y. Cooper, "Estimating the Environment and the Response of Sprinkler Links in Compartment Fires with Draft Curtains and Fusible Link-Actuated Ceiling Vents—Theory," *Fire Safety Journal,* 16, pp. 137–163 (1990).
46. E.E. Zukoski, T. Kubota, and C.S. Lim, "Experimental Study of Environment and Heat Transfer in a Room Fire," *NBS-GCR-85-493,* National Bureau of Standards, Washington, DC (1985).
47. H.W. Emmons, "The Ceiling Jet in Fires," *Fire Safety Science, Proceedings of the Third International Symposium* (G. Cox and B. Langford, eds.), Elsevier Applied Science, New York, p. 249 (1991).
48. W.R. Chan, E.E. Zukowski, and T. Kubota, "Experimental and Numerical Studies on Two-Dimensional Gravity Currents in a Horizontal Channel," *NIST-GCR-93-630,* National Institute of Standards and Technology, Gaithersburg, MD (1993).
49. G. Heskestad, "Propagation of Fire Smoke in a Corridor," *Proceedings of the 1987 ASME/JSME Thermal Engineering Conference,* Vol. 1, American Society of Mechanical Engineers, New York (1987).
50. T. Hara and K. Shinsuke, "Numerical Simulation of Fire Plume-Induced Ceiling Jets Using the Standard $\kappa - \varepsilon$ Model," *Fire Technology,* 42, p. 131 (2006).

Dr. Ronald L. Alpert received his undergraduate and graduate education at the Massachusetts Institute of Technology, where he majored in mechanical engineering. For nearly 35 years, he was with FM Global in various technical and managerial positions, ending his career there as an assistant vice president and manager of the Flammability Technology Research Program. Dr. Alpert was editor in chief of the *Journal of Fire Protection Engineering for 10 years and a section editor of the NFPA Fire Protection Handbook, 20th edition. He has published numerous papers in refereed journals and technical reports.*

Vent Flows

15

Takeyoshi Tanaka

Introduction

Fire releases a great amount of heat that causes the heated gas to expand. The expansion produced by a fire in a room drives some of the gas out of the room. Any opening through which gas can flow out of the fire room is called a *vent*.

The most obvious vents in a fire room are open doors and open or broken windows. Ventilation ducts also provide important routes for gas release. A room in an average building may have all of its doors and windows closed and, if ventilation ducts are also closed, the gas will leak around normally closed doors and windows and through any holes made for pipes or wires. These holes will act as vents. (If a room were hermetically sealed, a relatively small fire would raise the pressure in the room and burst the window, door, or walls.)

Gas will move only if it is pushed. The only forces acting on the gas are the gas pressure and gravity. Since gravity acts vertically, it might seem that gas could only flow through a hole in the floor or ceiling. Gravity, however, can produce horizontal pressure changes, which will be explained in detail below. A gas flow that is caused directly or indirectly by gravity is called a *buoyant flow*.

When a pressure difference exists across a vent, fluid (liquid or gas) will be pushed through. Precise calculation of such flows from the basic laws of nature can only be performed today by the largest computers. For fire purposes, and all engineering purposes, calculations are carried out with sufficient precision using the methods of hydraulics. Since these formulas are only approximate, they are made sufficiently accurate (often to within a few percent) by a flow coefficient. These coefficients are determined by experimental measurements.

Calculation Methods for Nonbuoyant Flows

If a pressure drop, $\Delta p = p_1 - p_2$, exists across a vent of area, A, with a fluid density, ρ, the flow through the vent has (Fig. 15.1) [1]

$$\text{Velocity} \quad u = \sqrt{\frac{2\Delta p}{\rho}} \tag{15.1}$$

$$\text{Volume flow} \quad \dot{V} = CA\sqrt{\frac{2\Delta p}{\rho}} \tag{15.2}$$

and

$$\text{Mass flow} \quad \dot{m} = CA\sqrt{2\rho\Delta p} \tag{15.3}$$

In these formulas C is flow coefficient and the SI units are $\Delta p = (\text{Pa}) = (\text{N/m}^2)$, $A = (\text{m}^2)$, $\rho = (\text{kg/m}^3)$, $u = (\text{m/s})$, $\dot{V} = (\text{m}^3/\text{s})$, $\dot{m} = (\text{kg/s})$.

T. Tanaka (✉)
Fire Science and Technology, Kyoto University

M.J. Hurley (ed.), *SFPE Handbook of Fire Protection Engineering*,
DOI 10.1007/978-1-4939-2565-0_15, © Society of Fire Protection Engineers 2016

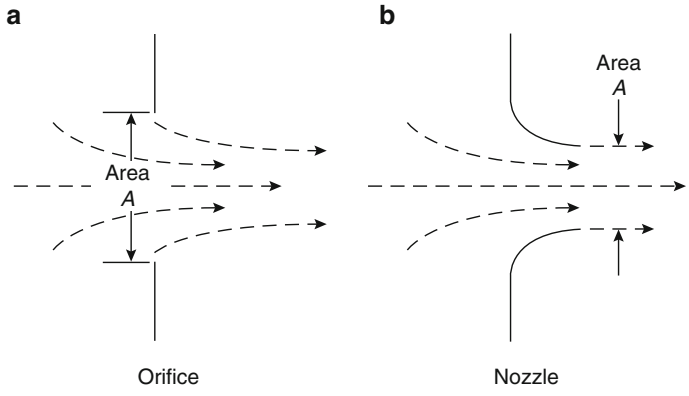

Fig. 15.1 Most fire vents are orifices

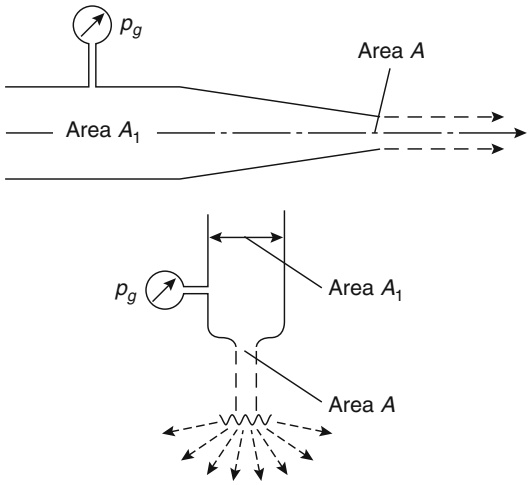

Fig. 15.2 A hose nozzle and a sprinkler nozzle

If the flow of water from a fire hose or sprinkler (Fig. 15.2) is to be calculated and the pressure, p_g, is read on a gauge (in lb/in.^{2}) at the entrance to the nozzle where the area is A_1, the previous formulas provide the velocity, volume flow, and mass flow by using

$$\Delta p = \frac{6895\, p_g}{1 - (A/A_1)^2} \tag{15.4}$$

where A is area of vent and A_1 is area of supply pipe. The factor 6895 converts pressure in lb/in.^{2} to Pascals while the factor $\left[1 - (A/A_1)^2\right]$ corrects Δp for the dynamic effect of the inlet velocity in the supply hose or pipe.

In the atmosphere, the pressure at the ground, p_a, is just sufficient to support the weight of the air above. If the air density is ρ_a, the pressure, p, at height, h, is less than p_a by the weight of the air below height, h. Thus the pressure difference is

$$\Delta p = p_a - p = \rho_a g h \tag{15.5}$$

It is sometimes convenient when considering fire gases to use $h = \Delta p/\rho a\, g$, the pressure head, in meters of ambient air, in the velocity and flow rate formulas given above.

The previous discussion supposes that the flowing fluid is of constant density. For liquids this is true for all practical situations. The density of air or fire gases will not change significantly during the flow through the vent so long as the pressure change is small, so they can also be treated as constant density fluids.

If the pressure drop is large, the equations become more complicated [2]. If the pressure and density upstream of the vent are p_1 and ρ_1 while the pressure after the vent is p_2, the equations for velocity and mass flow become

$$u = \sqrt{\frac{2p_1}{\rho_1}}\left\{\frac{\gamma}{\gamma - 1}\left(\frac{p_2}{p_1}\right)^{2/\gamma}\left[1 - \left(\frac{p_2}{p_1}\right)^{(\gamma-1)/\gamma}\right]\right\}^{1/2} \tag{15.6}$$

$$\dot{m} = CA\sqrt{2\rho_1 p_1}\left\{\frac{\gamma}{\gamma-1}\left(\frac{p_2}{p_1}\right)^{2/\gamma}\left[1-\left(\frac{p_2}{p_1}\right)^{(\gamma-1)/\gamma}\right]\right\}^{1/2} \tag{15.7}$$

where $\gamma = c_p/c_v$.

The value of γ depends on the complexity of the molecules of the flowing gas. For fire gases (which always contain a large amount of air) the value of γ will fall between 1.33 and 1.40. For most fire purposes the diatomic gas value (air) of 1.40 is sufficiently accurate.

The mass flow given by the previous equation has a maximum at

$$\frac{p_2}{p_1} = \left(\frac{2}{\gamma+1}\right)^{\gamma/(\gamma-1)} \tag{15.8}$$

For $\gamma = 1.40$, the maximum flow is reached for a downstream pressure $p_2 = 0.528\,p_1$. For all lower back pressures the flow remains constant at its maximum

$$\dot{m} = CA\sqrt{\rho_1 p_1}\left[\gamma\left(\frac{2}{\gamma+1}\right)^{(\gamma+1)(\gamma-1)}\right]^{1/2} \tag{15.9}$$

With these equations, the mathematical description of the rate of flow of liquids and gases through holes is complete as soon as the appropriate flow coefficients are known. The coefficients, found by experiment, correct the formulas for the effect of the fluid viscosity, the nonuniformity of the velocity over the vent, turbulence and heat transfer effects, the details of nozzle shape, the location of the pressure measurement points, and so forth. The corrections also depend on the properties and velocity of the fluid. The most important coefficient correction for any given vent geometry is the dimensionless combination of variables called the Reynolds number, Re, and

$$\mathrm{Re} = \frac{uD\rho}{\mu} \tag{15.10}$$

where

u = Velocity of the fluid given by the previous equations

D = Diameter of the nozzle or orifice

ρ = Density of the fluid approaching the vent

μ = Viscosity of the fluid approaching the vent

A door or window vent is almost always rectangular, not circular. The D to be used in the Reynolds number should be the hydraulic diameter

$$D = \frac{4A}{P} \tag{15.11}$$

where

A = Area of the vent

P = Perimeter of vent

For a rectangular vent, a wide and b high, $A = ab$, $P = 2(a+b)$.

$$D = \frac{2ab}{(a+b)} \tag{15.12}$$

The experimental values of the flow coefficients for nozzles and orifices, C, are given in Fig. 15.3 [2]. Flow coefficients for nozzles are near unity while for orifices are approximately 0.6, as can be seen in Fig. 15.1, where the flow from an orifice separates from the edge of the orifice and decreases to a much smaller area, in fact about 0.6 of the orifice area.

For most fire applications the Reynolds number will be about 10^6. Sprinklers and fire nozzles are small but the velocity is quite high. Conversely, ventilation systems of buildings are larger but have a lower velocity. Finally, doors and windows in the areas of a building not too near the fire are still larger but the velocity is still smaller. For most purposes the flow coefficient can be set as $C = 0.98$ for a nozzle and $C = 0.60$ for an orifice.

Buoyant Flows Through Vertical Vents

A fire in a room causes gases to flow out through a vent by two processes. The heating of the air in a room causes the air to expand, pushing other air

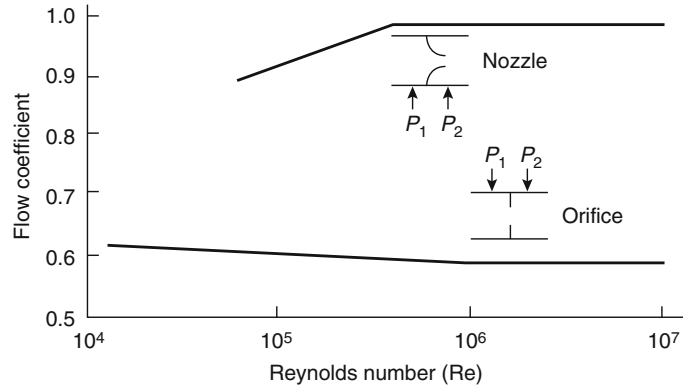

Fig. 15.3 Orifice and nozzle flow coefficients

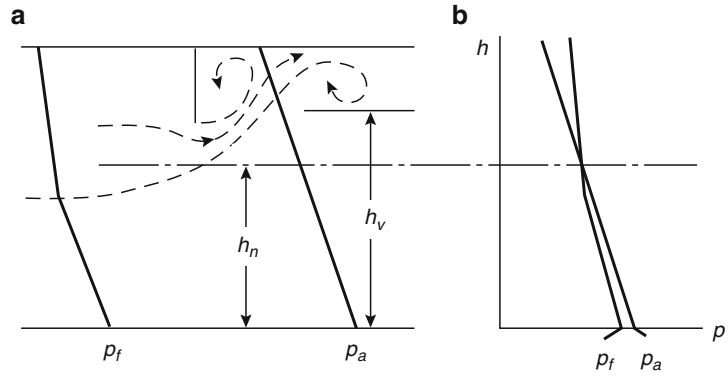

Fig. 15.4 Pressure gradients: (**a**) each side of a door; (**b**) superimposed on a pressure versus height graph

out through all available vents and hence throughout the entire building. At the same time, the heated air, with products of combustion and smoke, rises in a plume to the ceiling. When the hot layer of gas at the ceiling becomes deep enough to fall below the top of a vent, some hot gas will flow out through the vent. As the fire grows, the buoyant flow out will exceed the gas expansion by the fire. Thus the pressure in the fire room at the floor will fall below atmospheric, and outside air will flow in at the bottom. A familiar sight develops, where smoke and perhaps flames issue out the top of a window while fresh air flows in near the bottom. This buoyant flow mechanism allows a fire to draw in new oxygen so essential for its continuation.

For these buoyantly driven flows to occur, there must be a pressure difference across the vent. Figure 15.4 illustrates how these pressure differences are produced. The pressure difference at the floor is

$$\Delta p_f = p_f - p_a \tag{15.13}$$

where

$p_f =$ Pressure at the floor inside the room in front of the vent

$p_a =$ Pressure at the floor level outside of the room just beyond the vent

The pressure at height y is less than the pressure at the floor and can be found by the following hydrostatic equations:

$$\text{Inside} \quad p_1 = p_f - \int_0^y \rho_1 g dy \tag{15.14}$$

$$\text{Outside} \quad p_2 = p_a - \int_0^y \rho_2 g dy \tag{15.15}$$

The pressure difference at height, h, is

$$\Delta p = p_1 - p_2 = \Delta p_f + \int_0^h (\rho_2 - \rho_1) g \, dy \tag{15.16}$$

Since the outside density, ρ_2, is greater than the inside density, ρ_1, the integral is positive so that Δp is often positive (outflow) at the top of the vent and negative (inflow) at the bottom. The flow properties at the elevation, h, are the same as previously given.

$$u = \sqrt{\frac{2\Delta p}{\rho}} \tag{15.17}$$

$$\frac{\dot{V}}{A} = C\sqrt{\frac{2\Delta p}{\rho}} \tag{15.18}$$

$$\frac{\dot{m}}{A} = C\sqrt{2\rho\Delta p} \tag{15.19}$$

Since they are not the same at different heights in the vent, the volume and mass flow are given as flow per unit area.

Measuring Vent Flows in a Fire Experiment

Sufficient measurements must be made to evaluate ρ and Δp to allow use of Equation 15.19. There are four different available methods that differ in simplicity, accuracy, and cost.

Method 1 The dynamic pressure distribution can be measured in the plane of the vent. This measurement requires a sensitive pressure meter. The pressure difference is almost always less than the atmospheric pressure difference between the floor, p_f, and the ceiling, p_c. For a room 2.5 m in height the atmospheric pressure difference is

$$p_f - p_c = \rho_a g H = 1.176 \times 9.81 \times 2.5$$
$$= 28.84 \text{ Pascals} \quad (3.0 \text{ mm } H_2O)$$

This is only

$$\frac{p_f - p_c}{p_a} = \frac{28.84}{101,325}$$
$$= 0.00028 \text{ fraction of atmospheric pressure}$$

Thus the buoyantly driven flow velocities induced by a room fire could be as high as

$$u = \sqrt{\frac{2\Delta p}{\rho}} = \sqrt{\frac{2 \times 28.84}{1.176}} = 7.00 \text{ m/s} \quad (23 \text{ ft/s})$$

Since the pressure varies with height and time, a series of pressure probes is required and each should have its own meter or a rapid activation switch. Although standard pitot tubes are the most accurate dynamic pressure probes, they are sensitive to flow direction and would have to be adjusted at each location for the direction of the local flow, especially for outflow and inflow. The probe orientation would need to be continually changed as the fire progressed.

A single string of fixed-orientation pressure probes arranged vertically down the center of the door increases convenience of the measurement but forces a decrease in accuracy. The out-in flow problem is avoided by use of bidirectional probes in place of pitot tubes [3] (Fig. 15.5). These probes give velocities within 10 % over an angular range of ±50 degrees of the probe axis in any direction.

Determination of the local velocity also requires the measurement of the local gas density. The density of fire gases can be determined from measured gas temperatures with sufficient accuracy by the ideal gas law

$$\rho = \frac{Mp}{RT} \tag{15.20}$$

where

M = Average molecular weight of flowing gas

$R = 8314 \frac{\text{J}}{\text{kg mol K}}$ = Universal gas constant

As noted previously, the pressure changes only by a very small percentage throughout a building so its effect on gas density is negligible.

Fire gases contain large quantities of nitrogen from the air and a variety of other compounds. The average molecular weight of the mixture will be close to but somewhat larger than that of air. Incomplete knowledge of the actual composition of fire gas prevents high-accuracy calculations. For most fire calculations, it is accurate enough

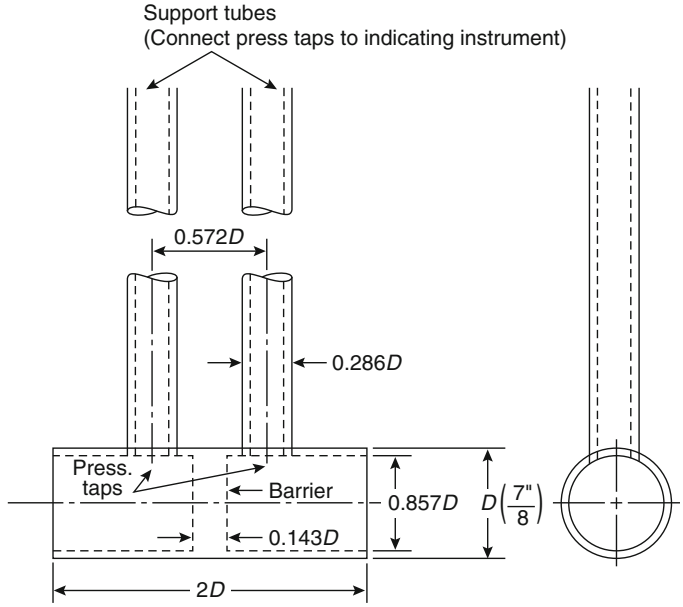

Fig. 15.5 A bidirectional flow probe

to neglect the effect of the change of molecular weight from that of air ($M_a = 28.95$). Density of gas is determined primarily by its temperature (which may vary by a factor of 4 in a fire). Thus

$$\rho = \frac{352.8}{T}\ \frac{\text{kg}}{\text{m}^3} \tag{15.21}$$

where T is temperature in Kelvin (= °C + 273).

A string of thermocouples must be included along with the bidirectional probes to measure vent flows. For higher accuracy, aspirated thermocouples must be used or a correction made for the effect of fire radiation [3]. The temperature and, hence, the gas density will vary over the entire hot vent outflow. To determine the temperature distribution so completely would require an impracticably large number of thermocouples. Fortunately, the temperature in the vent is a reflection of the temperature distribution in the hot layer inside the room, which normally is stratified, and hence varies most strongly with the distance from the ceiling. Thus a string of thermocouples hanging vertically on the centerline of the vent is usually considered to be the best that can be done in a practical fire test. Special care must be exercised to keep the test fire some distance away from the entrance to the vent. Since a fire near a vent has effects at present unknown, fire model calculations of real fire vent flows under such conditions will be of unknown accuracy. The velocity distribution vertically in the vent is given by

$$u = 0.93\sqrt{\frac{2\Delta p}{\rho}} \tag{15.22}$$

where ρ follows from Equation 15.21 using the temperature distribution *in the vent* with a calibration factor of 0.93 for the bidirectional probes [4]. Using ρ from Equation 15.21 gives the directly useful forms

$$u = 0.070\sqrt{T\Delta p} \qquad \Delta p\left(\frac{N}{\text{m}^2}\right)$$
$$u = 5.81\sqrt{T\Delta p} \qquad \Delta p\left(\frac{\text{lb}}{\text{in.}^2}\right) \qquad \text{pressure measured with bidirectional probe} \tag{15.23}$$

where

$$u \text{ is in (m/s)}$$

$$T \text{ is in (K)}$$

Except for very early stages of a room fire, there will be flow out at the top (u, $\Delta p > 0$) and flow in at the bottom (u, $\Delta p > 0$).[1] Thus there is a position in the vent at which $u = 0$, which is the vertical location where the pressure inside is equal to that outside. This elevation, h_n, is called the neutral axis. Defining the elevation of the vent sill as h_b ($h_b = 0$ for a door) and the elevation of the soffit as h_t, the flows are given by

$$\text{Flow out} \quad \dot{m}_u = C\int_{h_n}^{h_t} \rho u b \; dy \tag{15.24}$$

$$\text{Flow in} \quad \dot{m}_d = C\int_{h_b}^{h_n} \rho u b \; dy \tag{15.25}$$

where

b = Width of the vent

C = Experimentally determined flow coefficient (= 0.68) [5]

Using Equations 15.21 and 15.22 and $C = 0.68$ into these equations, the most convenient forms are

$$\text{Flow out} \quad \dot{m}_u = 16.79\int_{h_n}^{h_t} b\sqrt{\frac{\Delta p}{T_v}}dy \quad \text{(kg/s)} \tag{15.26}$$

$$\text{Flow in} \quad \dot{m}_d = 16.79\int_{h_b}^{h_n} b\sqrt{\frac{\Delta p}{T_v}}dy \quad \text{(kg/s)} \tag{15.27}$$

where

Δp = Pressure drop in Pascals measured with bidirectional probe as a function of y

b = Width of the vent in m

T_V = Temperature (K) in the vent measured as a function of y

[1] Equation 15.23 should be written $u = (\text{sign } \Delta p)K\sqrt{\mathrm{T}|\Delta p|}$ since when $\Delta_p < 0$ the absolute value must be used to avoid the square root of a negative number and the sign of the velocity changes since the flow is in and not out.

If the bidirectional probe pressures are measured in psi, the coefficient 16.79 must be replaced by 1394.

Method 2 A somewhat simpler but less accurate procedure to measure vent flows requires the measurement of the pressure difference at the floor (or some other height). One pressure difference measurement together with the vertical temperature distribution measurement, T_1, *inside the room* (about one vent width in from the vent) and T_2, *outside the vent* (well away from the vent flow), provides the density information required to find the pressure drop at all elevations (Equation 15.16).

$$\Delta p = \Delta p_f + 3461\int_0^y \left(\frac{1}{T_2} - \frac{1}{T_1}\right) dy \tag{15.28}$$

For most fires, Δp_f will be negative; that is, the pressure at the floor inside the fire room will be less than the pressure outside. This is only true for a fire room with a normal size vent (door, window). For a completely closed room the inside pressure is well above the outside pressure. Since the temperature inside the fire room is higher than that outside, Equation 15.28 gives a Δp that becomes less negative, passes through zero at the neutral axis, h_n, and becomes positive at higher levels in the fire room. The vertical location of the neutral axis is, therefore, readily found from Equation 15.28.

The calculation of the pressure distribution requires measurement of the temperature distribution both inside, T_1, and outside, T_2, of the vent. However, calculation of the flow requires a knowledge of the density distribution in the vent itself. Thus a third thermocouple string is required to measure the temperature distribution, T_u, in the vent. The desired flow properties [6] are

Velocity

$$u = \sqrt{\frac{2\Delta p}{\rho}} = 4.33\sqrt{T_v\int_{h_n}^{y}\left(\frac{1}{T_2} - \frac{1}{T_1}\right) dy} \quad \text{(m/s)} \tag{15.29}$$

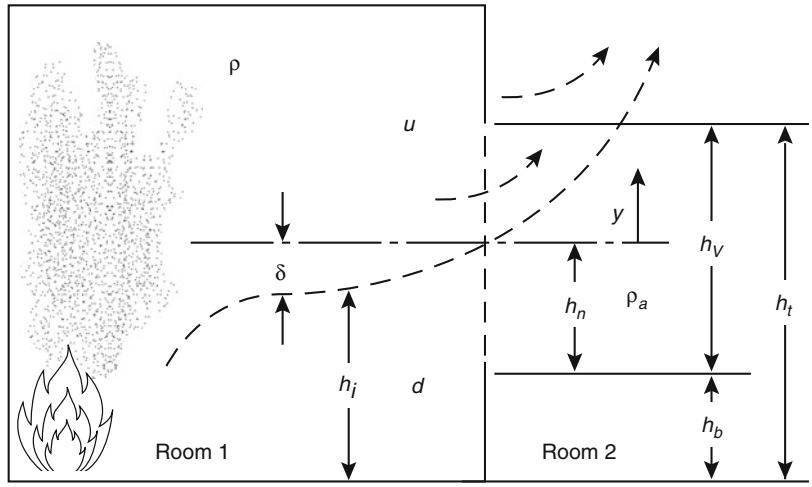

Fig. 15.6 Buoyant flow out of the window of a fire room

Flow out

$$\dot{m}_u = C\int_{h_n}^{h_t} \rho bu \; dy$$

$$= 1063\int_{h_n}^{h_t} b\left[\frac{1}{T_v}\int_{h_n}^{y}\left(\frac{1}{T_2}-\frac{1}{T_1}\right)dy\right]^{1/2} dy \tag{15.30}$$

Flow in

$$\dot{m}_d = C\int_{h_b}^{h_n} \rho bu \; dy$$

$$= 1063\int_{h_n}^{h_t} b\left[\frac{1}{T_v}\int_{h_b}^{y}\left(\frac{1}{T_2}-\frac{1}{T_1}\right)dy\right]^{1/2} dy \tag{15.31}$$

where

b = Width of the vent at height y

Δp = Calculated from Equation 15.16 using the temperatures (and thus densities) *inside and outside of the room*

ρ = Density computed from the temperature *in the vent*

(Note that for inflow Δp is negative. Therefore, the equation takes the square root of the magnitude $|\Delta p|$ while its sign gives the flow direction.)

Method 3 The use of a sensitive pressure meter can be avoided entirely by visually (or better, photographically) locating the bottom of the outflow *in the vent* during the test at the position of the neutral axis, h_n, where $\Delta p = 0$. Method 3 is the same as Method 2 except that the neutral axis location is found directly by experiment rather than being deduced from the pressures. The distribution of pressure drop across the vent is found by integrating Equation 15.16 above ($\Delta p > 0$) and below ($\Delta p < 0$) h_n using the density distribution *inside*, ρ_1, and *outside*, ρ_2, *the room*. The flow properties are computed as before from Equations 15.29, 15.30 and 15.31.

Method 4 A simpler but less accurate method uses the fair assumption that the gas in the fire room soon separates into a nearly uniform hot layer of density, ρ, with a nearly uniform cold layer below of density, ρ_d. This separation with appropriate notation is shown in Fig. 15.6. In this approximation the appropriate flow formulas [5] are

$$\text{Outflow} \quad u_u = \left(2g\frac{\rho_a - \rho}{\rho}y\right)^{1/2} \tag{15.32}$$

where y is distance above the neutral plane

$$\dot{m}_u = \frac{2}{3}Cb\sqrt{2g\rho(\rho_a - \rho)}(h_v - h_n)^{3/2} \tag{15.33}$$

The inflow by this two-layer method depends on δ, which is small and cannot be determined

with sufficient accuracy because of the effect of gas motions in the fire room.

The neutral axis may be found in several ways:

1. It may be located visually or photographically during the test.
2. It may be found from the vent temperature distribution by locating [visually on a plot of $T_V(y)$] the position just below the most rapid temperature rise from bottom to top of the vent.

The lower-layer temperature, T_d, of the two-layer model is taken as the gas temperature just above the vent sill. The upper-layer temperature, T_u, is chosen so that the two-layer model has the same total mass (i.e., the same mean density) in the vent as the real flow.[2]

$$\left(\frac{1}{T}\right) = \frac{1}{h_v}\int_0^{h_v} \frac{dy}{T} = \frac{h_n}{h_v T_d} + \frac{h_v - h_n}{h_v T_u} \qquad (15.34)$$

The densities ρ_a and ρ are found using Equation 15.21 from the temperatures T_a and T_u, respectively.

The outflow velocity and mass flow are found from Equations 15.32 and 15.33.

An estimate of the air inflow rate can be found if the test has included the measurement of the oxygen concentration in the gases leaving the fire room. The gas outflow rate is equal to the inflow rate plus the fuel vaporized, except for the effect of transient variations in the hot layer depth. Thus

$$\dot{m}_d = \dot{m}_u \left(\frac{1 + y_{O_2}\lambda}{1 + 0.23\lambda}\right) \qquad (15.35)$$

where λ is the effective fuel-air ratio.

[2] Sometimes the mean temperatures, $\overline{T}$ of the two-layer model and the real flow are also used and both h_n and T_u are determined (using T_d as above). The requirement of identical $\overline{T}$ is arbitrary, sometimes leads to impractical results, and is not recommended.

The flow coefficient to be used for buoyant flows is 0.68 as determined by specific experiments designed for the purpose. For nonbuoyant flows (nozzles and orifices), the flow coefficients are determined to better than 1 % and presented as a function of the Reynolds number as in Fig. 15.3. This accuracy is possible because the fluid can be collected and measured (by weight or volume).

For buoyant flows the experiments are much more difficult because the hot outflow and cold inflow cannot be collected and weighed. The best fire-gas vent flow coefficient measurements to date [6, 7] have ±10 % accuracy with occasional values as bad as ±100 % (for inflow). The most accurate buoyant flow coefficients were measured not for fire gases but for two nonmiscible liquids (kerosene and water) [7]. In this case the two fluids could be separated and measured, and the value 0.68 was found except for the very low flow rates (near the beginning of a fire). When buoyant flow coefficients can be measured within a few percent accuracy, they will be a function of the Reynolds number, $\mathrm{Re} = uh_v\rho/\mu$; the Froude number, $\mathrm{Fr} = u^2\rho_a/gh_v(\rho - \rho_a)$; and the depth parameter, h_n/h_v.

The best option now available is to use $C = 0.68$ and expect ±10 % errors in flow calculations.

Note that the above four methods require a knowledge of h_n, the dividing line between outflow above and inflow below. It would be useful to have a simple formula by which h_n could be calculated without any special measurements. What determines h_n?

The fire at the start sends a plume of heated gas toward the ceiling and, by gas expansion, pushes some gas out of the vent. The hot plume gases accumulate at the ceiling with little, if any, flowing out the vent. After a time, depending on the size of the room, the hot layer depth becomes so large that its lower surface falls below the top of the vent. Hot gas begins to flow out.

When a fire has progressed to a second room, there is a hot layer on each side of a connecting vent. Thus (with two layers on each side) there

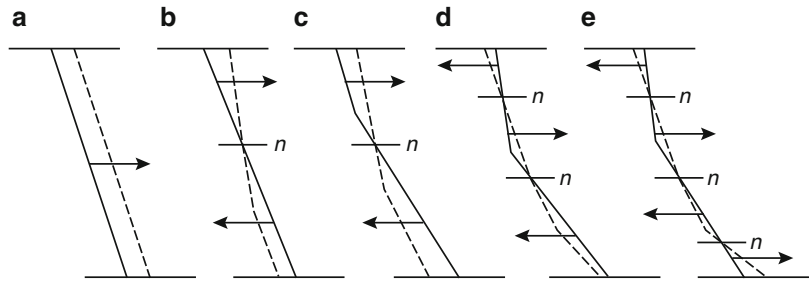

Fig. 15.7 Some selected two-layer vent pressure drop distributions. *Dotted line* is pressure distribution in room 1; *solid line* is pressure distribution in room 2

are as many as four different gas densities: ρ_{d_1} is greater than ρ_1, densities below and above in room 1, and ρ_{d_2} is greater than ρ_2, densities below and above in room 2. There are also four pertinent levels: h_b, sill height (0 if the vent is a door); h_t, soffit height; h_{i_1}, interface height in room 1; h_{i_2}, interface height in room 2. There are many different flow situations possible depending on these eight values.

The pressure variation from floor to ceiling in each room depends on the densities and layer heights in the room. In addition, the pressure difference between the two rooms (at the floor, for example) may have any value depending on the fire in each room, all the room vents, and especially the vent (or vents) connecting the two rooms. Figure 15.7 shows a few of the possible pressure distributions. The pressure distribution in room 1 is shown with a dotted line while that in room 2 is shown as a solid line.

In Fig. 15.7a, there are no hot layers, the pressure in room 1 at every level is higher than that in room 2, and the flow is everywhere out (positive) (room 1 to room 2).

In Fig. 15.7b, a common situation exists. The density in room 2 is uniform (perhaps the outside atmosphere). Room 1 has a hot layer and a floor pressure difference such that there is outflow at the top, inflow at the bottom, and a single neutral axis somewhat above the hot-cold interface in the room.

In Fig. 15.7c, the flow situation is similar to that in Fig. 15.7b, although there are hot layers in both rooms (but with a neutral axis above the interface in room 1 and below the interface in room 2).

In Fig. 15.7d, the densities (slopes of pressure distribution lines) are somewhat different than those in Fig. 15.7c (the hot layer in room 2 is less deep but hotter than that in room 1). Consequently, there are two neutral axes with a new small inflow layer at the top, three flow layers in all—two in and one out.

In Fig. 15.7e, the densities and floor level pressure difference are such that there are four flow layers, two out and two in, with three neutral axes.

These five cases do not exhaust the possible vent flow situations.

Figure 15.7a, b accounts for all cases early in a fire and all cases of vents from inside to outside of a building. They are also the only cases for which experimental data are available. The case illustrated in Fig. 15.7c is common inside a building after a fire has progressed to the point that hot layers exist in the two rooms on each side of a vent. The cases illustrated in Fig. 15.7d, e have not been directly observed but probably account for an occasional confused flow pattern. (In fact, the above discussion assumes two distinct layers in each room.) The layers are seldom sharply defined and in this case there may be many neutral axes, or regions, with a confusing array of in-out flow layers. These confused flow situations are probably not of much importance in a fire since they seldom occur and when they do they don't last very long.

The previous discussion of the possible two-layer flow situation is very important for the zone modeling of a fire. Fire models to date are all two-layer models (a three- or more layer model will present far more complex vent flows than those pictured in Fig. 15.7). In fire computation by a zone model, cases such as (d) and

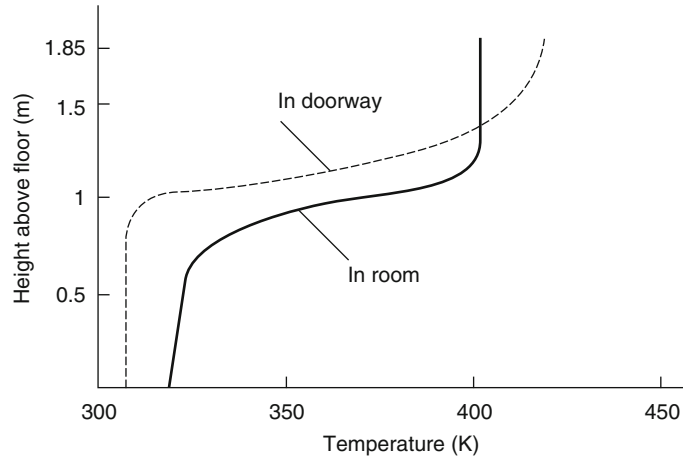

Fig. 15.8 Sample fire room and doorway temperature distributions

(e) in Fig. 15.7 will be unimportant to fire development. However, since these situations can arise, they should be handled via fire computation, that is, by computing the flow layer by layer. Each layer has a linear pressure variation from sill, interface, or neutral axis up to the next interface, neutral axis, or soffit.

By use of the pressure drop at the floor and the room densities on each side of the vent in Equation 15.16, the position, h_i, of all layers and the sill, interfaces, neutral axes, and soffit will be known. Thus, for each layer (defined as j) the pressure drop at the bottom, Δp_j, and at the top, Δp_{j+1}, will be known. Since the room densities are constant in each room for each layer, the vent pressure drop will vary linearly from Δp_j to Δp_{j+1}. The flow in each layer from room 1 to room 2, found by integration [8], is given by

$$\dot{m}_i = (\operatorname{sign}\alpha) C \frac{2}{3} b \left(h_{j+1} - h_j\right) \sqrt{2\rho} \times \left(\frac{|\Delta p_j| + \sqrt{|\Delta p_j \Delta p_{j+1}|} + |\Delta p_{j+1}|}{\sqrt{|\Delta p_j|} + \sqrt{|\Delta p_{j+1}|}} \right) \tag{15.36}$$

where

$\alpha = \left(\dfrac{\Delta p_j + \Delta p_{j+1}}{2} \right)$ whose sign determines the in-out direction of the flow

ρ = Density of the gas flowing in the flow layer i

Thus

$$\rho = \begin{cases} \text{Density in room 1 at height } h_j^+ & \textit{if } \alpha > 0 \\ \text{Density in room 2 at height } h_i^+ & \textit{if } \alpha < 0 \end{cases}$$

This flow calculation appears complex but can be coded quite easily for computer use and then used to calculate all the possible cases.

Although all vent flows can now be calculated, the path of each layer of gas flow when it enters a room is still needed for fire modeling. If the two-layer model is to be preserved, each inflow must mix with the hot layer or the cold layer, or be divided between them. No information is yet available as to the best solution to this problem.

To illustrate these various methods of flow calculation, some test data from a steady burner fire in a room at the U.S. Bureau of Standards [6] are used. Some typical data are shown in Fig. 15.8. Accurate results, even in a steady-state fire, are difficult to obtain and questions about the data in this figure will be noted as appropriate. The vent temperatures were measured by small-diameter bare thermocouples for which there is some unknown radiation correction. This unknown correction may account for the top vent temperature being higher than that in the fire room.

The vent was 1.83 m high, 0.737 m wide, and the outflow measured with bidirectional probes (not corrected for flow angle) was 0.588 kg/s for a fire output of 0.63 kW. The ambient

temperature was 21.3 °C (= 294.3 K). This flow was determined by using Method 1.

Method 2 uses the known location of the neutral axis and requires the integration of Equations 15.30 and 15.31. In this way the data of Fig. 15.8 gives outflow of 0.599 kg/s, 1.8 % higher compared to Method 1 and inflow of 0.652 kg/s. A measured (by bidirectional probes) inflow is not given, but it seems odd that the inflow is greater than the outflow since inflow must be smaller than the outflow by the mass rate of fuel burned at steady state.

Data for use of Method 3 are not available.

Method 4 requires the selection from Fig. 15.8 of a neutral axis location and inlet temperature. In the figure the rapid temperature rise *in the vent* begins at about 1 m. Hence this height is chosen as the neutral axis. The lowest inlet temperature is $T_d = 308$ K. By computing $(1/T_v)$ the average value was found to be $(1/T_v) = 2.875 \times 10^{-3}$. Now by Equation 15.34

$$2.875 \times 10^{-3} = \frac{1.00 - 0}{1.83 \times 308} + \frac{1.83 - 1.00}{1.83 T_u}$$

Thus $T_u = 411.9$ K. The corresponding density is $\rho = 352.8/411.9 = 0.8565$ kg/m^3. From the ambient temperature, T_a, we find $\rho_a = 352.8/294.3 = 1.199$ kg/m^3. Thus the outflow by Equation 15.33 is

$$\dot{m}_u = \frac{2}{3} 0.68 \times 0.737 [2 \times 9.81 \times 0.8565 (1.199 - 0.8565)]^{1/2} \times (1.83 - 1)^{3/2} = 0.607 \ \text{kg/s}$$

This value is 3.2 % higher compared to Method 1.

Buoyant Flows Through Horizontal Vents

Unlike flows through vents in a vertical wall or non-buoyant flows through orifices, not ample quantitative works have been done on buoyant flows through vents in horizontal or slightly sloped surfaces. Such buoyant flows through horizontal vents can become issue in some situations associated with fire, particularly in such a configuration as exemplified in Fig. 15.9, which may arise in fires in basements of buildings, holds in ships and multi-floor building containing rooms closed to the outdoors.

The flow rate through a horizontal opening can be treated, as done in vertical vents, by using Bernoulli's equation if there is no temperature difference between the connecting spaces

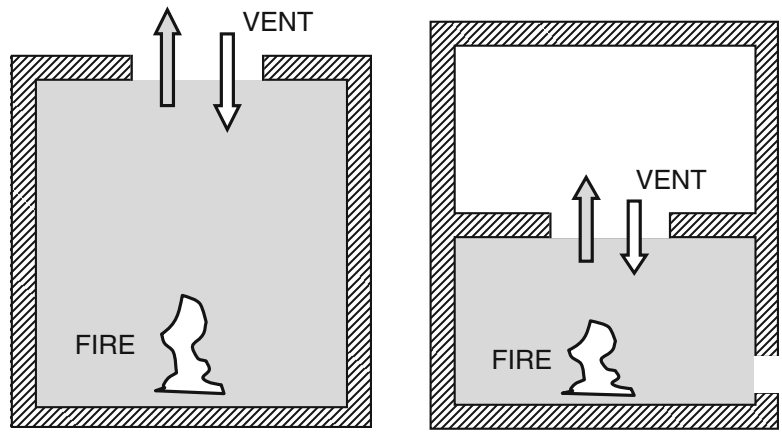

Fig. 15.9 Possible scenarios of horizontal vent flow in fire where the standard Bernoulli's flow equation becomes inadequate

or if there is a large enough pressure difference across the vent. Let Δp be the pressure difference across the vent defined by

$$\Delta p = p_U - p_L \tag{15.37}$$

where

p_U and p_L = Pressures at the vent elevation in the upper and lower spaces, respectively.

The standard vent flow model using Bernoulli's equation would predict the flow rate through a horizontal vent as follows according to the value of Δp, illustrated in Fig. 15.10:

$$\text{(a)} \quad \text{when } \Delta p < 0: \quad \dot{V}_U = CA_V\sqrt{2\Delta p/\rho_L}; \quad \dot{V}_L = 0 \tag{15.38a}$$

$$\text{(b)} \quad \text{when } \Delta p = 0: \quad \dot{V}_U = 0; \quad \dot{V}_L = 0 \tag{15.38b}$$

$$\text{(c)} \quad \text{when } \Delta p > 0: \quad \dot{V}_U = 0; \quad \dot{V}_L = CA_V\sqrt{2|\Delta p|/\rho_U} \tag{15.38c}$$

where

$\dot{V}_U$ and $\dot{V}_L$ = Volume rates of flows to upper and lower spaces through the vent, respectively

A_V = Vent area

C = Vena contracta

ρ_L and ρ_U = Air densities in lower and upper spaces, respectively.

However, this method will fail, over certain ranges of pressure difference, when temperature difference exists between the spaces due to the antagonistic effect of buoyancy to pressure gradient. Consider the situation where the lower space temperature is higher than upper space temperature, for example. There is a flow across the vent due to the air density difference $\Delta\rho(=\rho_U - \rho_L)$ even if the pressure difference, Δp, is basically zero. In such a case as mentioned earlier in Fig. 15.9, where a pace has no other air passage besides the vent between the connecting spaces, a bidirectional flow will occur through the vent in a certain range around $\Delta p = 0$ and the upward and downward flow rates will become equal due to continuity.

The horizontal vent flows under zero pressure difference, $\Delta p = 0$, was investigated by Epstein [9], Tan and Jaluria [10] and others, using brine-water scale models. In these experiments, the effects of vent configuration on the flow characteristics were investigated for a large range of opening size and aspect ratio. Also, Heiselberg [11] conducted the experiments for the same purpose using a single opening test room set in a full-scale thermostatic chamber, where the air in the test room was heated by an electric heating system while the temperature in the thermostatic chamber was controlled by an air conditioning system. While circular orifices were used in the brine-water experiments by Estein and others, square openings were adopted in the Heiselberg's experiments as the vent. The conceptual configuration of the vents in their experimental setup is illustrated in Fig. 15.11.

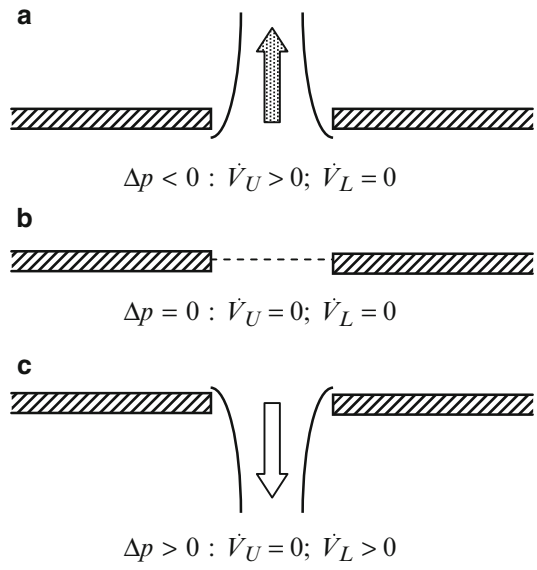

Fig. 15.10 The standard vent flow model for horizontal vents

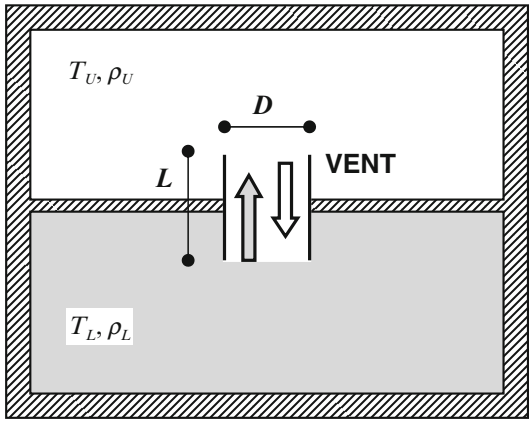

Fig. 15.11 Schematic configuration of vents in the existing experiments for horizontal vent flow

The flow through a horizontal vent under $\Delta p = 0$ condition is often unstable. Epstein [9] identified four regimes of the exchange flow as a function of aspect ratio of the vent as follows:

Regime I ($L/D < 0.15$): Oscillatory exchange flow

Regime II ($0.15 < L/D < 0.4$): Countercurrent orifice flow

Regime III ($0.4 < L/D < 3.25$): Combination of an orifice flow and turbulent diffusion flow

Regime IV ($3.25 < L/D$): Turbulent and slow exchange flow, where counterflow within the tube appears to be mixture of warm and cold fluids with chaotic motion

where

D = Diameter of the vent

L = Length of the vent

Epstein defined the Froude number, Fr, as

$$Fr = \frac{\dot{V}_{EX}}{\sqrt{\frac{g(T_L - T_U)L^5}{T_L}}} \tag{15.39}$$

and developed the formulas for the exchange flow through a horizontal vent according to the above regimes based on his brine-water experiment data as follows:

$$Fr = \begin{cases} 0.055 & \left(\frac{L}{D} < 0.15\right) \\ 0.147\left(\frac{L}{D}\right)^{1/2} & \left(0.15 < \frac{L}{D} < 0.4\right) \\ 0.093\frac{1}{\sqrt{1 + 0.084\left(\frac{L}{D} - 0.4\right)^3}} & \left(0.4 < \frac{L}{D} < 3.25\right) \\ 0.32\left(\frac{L}{D}\right)^{-3/2} & \left(3.25 < \frac{L}{D} < 10\right) \end{cases} \tag{15.40}$$

where

$\dot{V}_{EX}$ = Exchange volume flow rate

T_L = Temperature in lower space

T_U = Temperature in upper space

g = acceleration due to gravity

Heiselberg, adopting the same Fr as Equation 15.39, developed a similar formula based on his experimental data using the airs at different temperature as follows:

$$Fr = \begin{cases} 0.050 & \left(\frac{L}{D} < 0.115\right) \\ 0.147\left(\frac{L}{D}\right)^{1/2} & \left(0.115 < \frac{L}{D} < 0.55\right) \\ 0.077\left(\frac{L}{D}\right)^{-1/2} & \left(0.55 < \frac{L}{D} < 4.455\right) \end{cases} \tag{15.41}$$

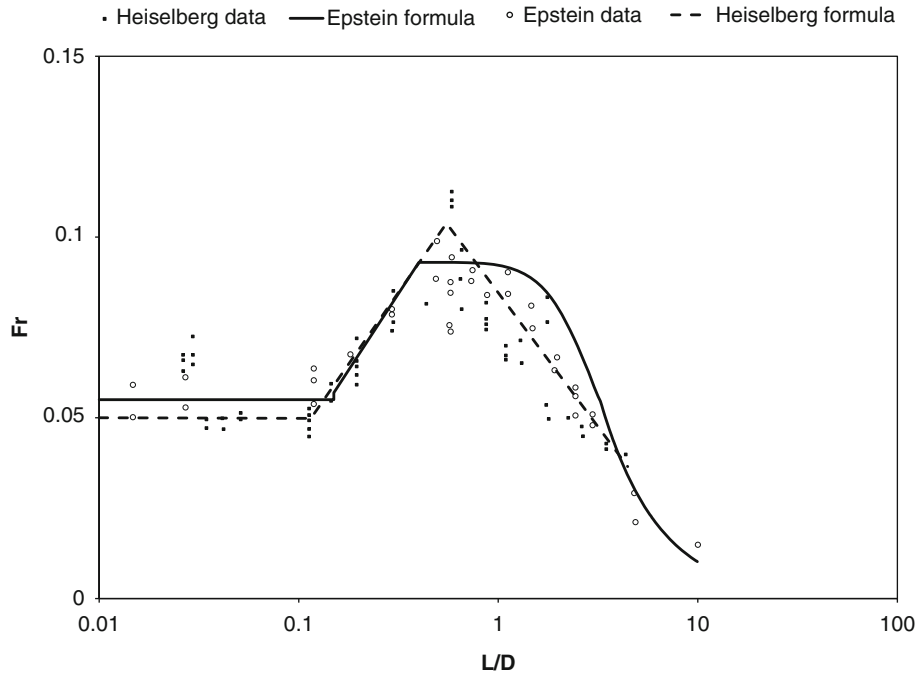

Fig. 15.12 Comparison of Epstein's brine-water scale experiments and Heiselberg's full-scale experiments for horizontal vent flow

Since the vents in Heiselberg's experiments were square, the vent diameter D was converted from the side length of the square vent, A_V, in his experiments as

$$D = \sqrt{\frac{4}{\pi}}S \approx 1.128S \tag{15.42}$$

Figure 15.12 plots the experimental data and the equations from Epstein and Heiselberg together. Albeit the difference of the fluids used in their experiments, the distributions of the measured data seem to show a similar trend when plotted in terms of the Fr.

In such an unstable configuration as where a high density fluid is above and low density fluid is below, a bi-directional flow takes place through the vent in the region of pressure around $\Delta p = 0$. However, as the pressure difference, Δp, is increased the exchange flow in the direction of opposing to the pressure gradient decreases. If Δp exceeds some critical value, Δp_C, then the flow becomes uni-directional. The flows in such ranges of Δp were investigated by Epstein and Kenton [12], Tan and Jaluria [10] and Heskestad and Spaulding [13]. Of these, the pressure difference, Δp, was not directly measured in the experiments by Epstein and Kenton so the critical condition of transition from bi-directional to uni-directional flow was determined by the flow rate. The critical (flooding) condition is dependent on vent condition and buoyancy strength. For analyzing the above existing results, Cooper [14] introduced the following non-dimensional parameters defined as follows:

Grashof number

$$Gr = \frac{2gD^3\overline{\rho}\Delta\rho}{\mu^2} \tag{15.43}$$

Froude number

$$Fr = \frac{\dot{V}_U}{A_V\sqrt{2gD\dfrac{\Delta T}{\overline{T}}}} \tag{15.44}$$

Non-dimensional pressure difference

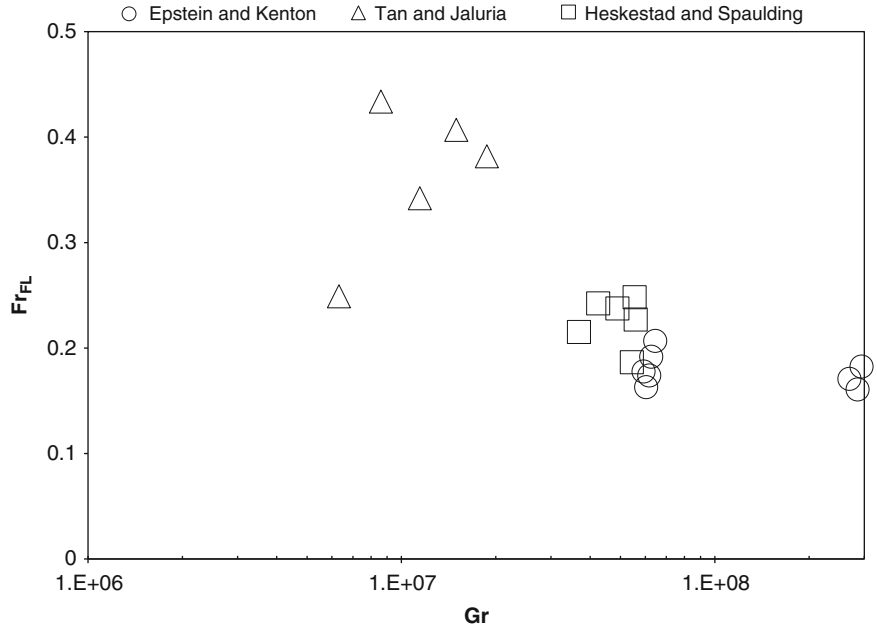

Fig. 15.13 Plot of Fr_{FL} as a function of Gr for small L/D data

$$\Pi = \frac{\Delta p}{4g\Delta\rho D} \tag{15.45}$$

where

A_V = Vent area

$\overline{T} = (T_U + T_L)/2$

$\overline{\rho} = (\rho_U + \rho_L)/2$

$\Delta\rho = \rho_L - \rho_U$

$\Delta T = T_L - T_U$; Temperature difference

$\Delta p = p_U - p_L$

Let the critical volume flow rate and pressure difference where transition from bi-directional flow to uni-directional flow just occur be $\dot{V}_{U,FL}$ and Δp_{FL}, respectively, and let the corresponding Fr and Π be Fr_{FL} and Π_{FL}, respectively. Figure 15.13 plots the critical (flooding) Froude number, Fr_{FL}, vs Grashof number, Gr, which were reduced from the existing experiments. As seen in this figure, Fr_{FL} is relatively insensitive to changes in Gr in the range about $3 \times 10^7 < Gr < 3 \times 10^8$. However, there is a significant increase in Fr_{FL} for $Gr < 1.4 \times 107$, i.e., for the data of Tan and Jaluria [10], which seems to be attributed to the relatively small vent size in their experiments. Similar dependence of Fr_{FL} on Gr is found by Heskestad and Spaulding [13]. The experiments for $Gr < 1.4 \times 10^7$ may be in the range of laminar or transitional flow.

From the viewpoint of practical applications to realistic building fire configurations, the horizontal vent flows of interest are probably in the large Gr range, i.e., turbulent flow regime. The critical Froude number, Fr_{FL}, from the existing data in large Gr range are plotted vs non-dimensional temperature difference, $\Delta T/\overline{T}$, in Fig. 15.14. Note here that when $\Delta T < 0$, Fr_{FL} denotes the critical Froude number to purge the downward flow and attain the upward flooding flow. The critical (flooding) non- dimensional pressure difference, Π_{FL}, is plotted also vs $\Delta T/\overline{T}$ in Fig. 15.15 although the data are only available from Heskestad and Spaulding [13].

The effect of buoyancy will not disappear as soon as the pressure difference exceeds the critical value and the vent flow has changed from bi-directional to uni-directional. Even after uni-directional flow has been established, significant buoyancy effect still remains. For this

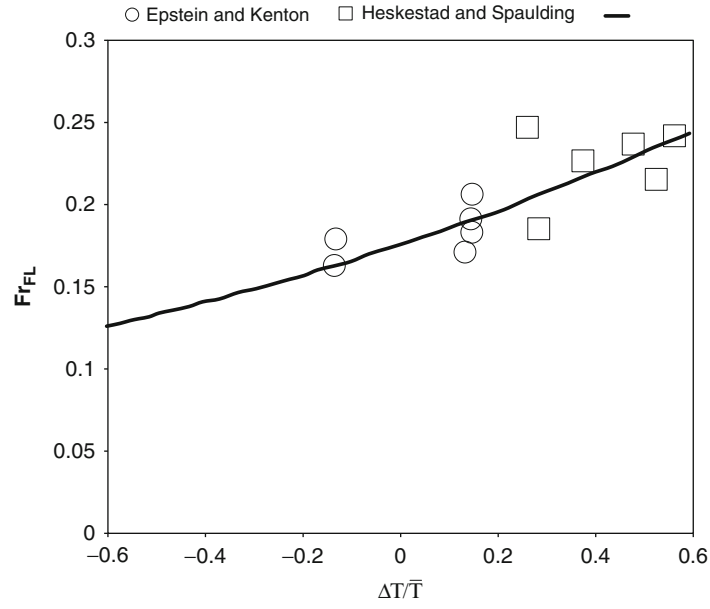

Fig. 15.14 Plot of Fr_{FL} as a function of $\Delta T/\overline{T}$ for small L/D data

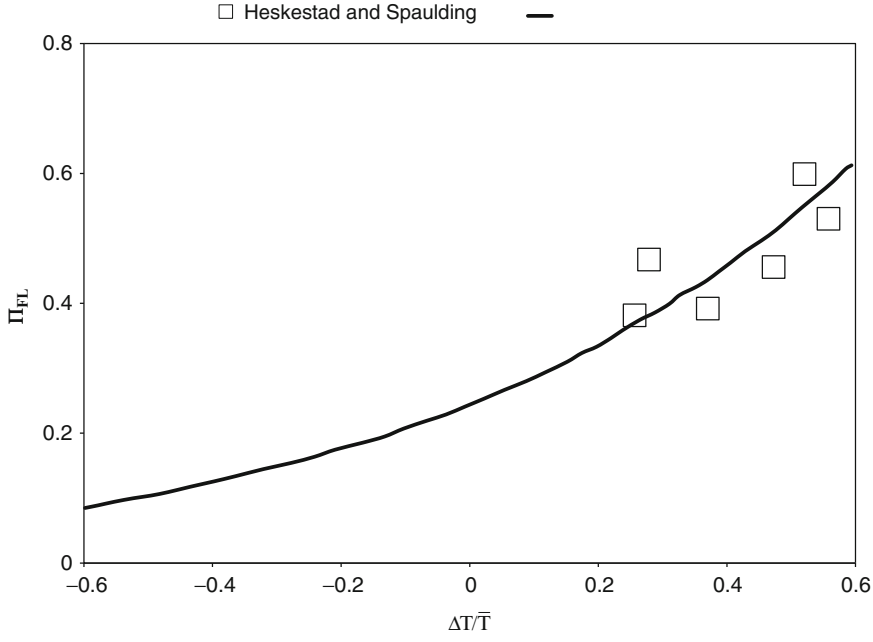

Fig. 15.15 Plot of Π_{FL} as a function of $\Delta T/\overline{T}$ for small L/D data

uni-directional flow regime, Cooper presented a plot of $\dot{V}_U/\dot{V}_{U,FL}$ vs $\Delta p/\Delta p_{FL}$ as seen in Fig. 15.16, where $\dot{V}_{U,FL}$ and Δp_{FL} are critical (flooding) volume flow rate and pressure difference, respectively. From this figure, it can be seen that the standard Bernoulli flow equation, expressed by dashed line, overestimates the expected flow rate by a factor in excess of 3, and that only after $\Delta p/\Delta p_{FL}$ exceeds 3 or 4 the standard model provides flow estimate

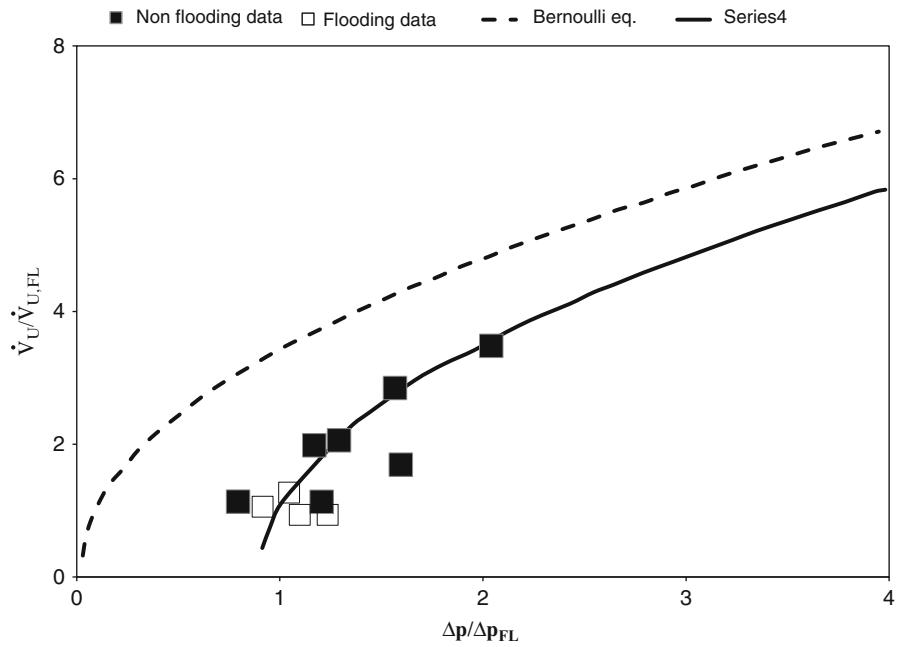

Fig. 15.16 Plot of $\dot{V}_U/\dot{V}_{U,FL}$ as a function of $\Delta p/\Delta p_{FL}$ ($= Fr/Fr_{FL}$ as a function of $\Pi/\Pi p_{FL}$) for uni-directional flow regime

correct to within a few tens of percent. If the values of Fr_{FL} and Π_{FL}, which depend on temperature difference, are determined using Figs. 15.14 and 15.15, respectively, $\dot{V}_{U,FL}$ and Δp_{FL} can be calculated using Equations 15.44 and 15.45, respectively. Then it follows that uni-directional flow rate, $\dot{V}_U$, can be obtained for arbitrary pressure difference, Δp, from Fig. 15.16.

The range of pressure $0 \leq \Delta p \leq \Delta p_{FL}$ is the mixed flow regime where there will be a bi-directional flow through the vent, i.e., a flow from the upper to the lower space, $\dot{V}_U$, and a flow from the lower to the upper space, $\dot{V}_L$. The $\dot{V}_L$ is also called exchange flow, $\dot{V}_{EX}$. At the two extremes of the mixed flow regime, $\dot{V}_U = \dot{V}_L$ at $\Delta p = 0$ and $\dot{V}_U = \dot{V}_{U,FL}$; $\dot{V}_L = 0$ at $\Delta p = \Delta p_{FL}$. Let $\dot{V}_N$ be the net volume flow rate from the upper, or the higher pressure, space to the lower space, i.e., $\dot{V}_U - \dot{V}_L$. Generally, in the intermediate range $0 < \Delta p < \Delta p_{FL}$, $\dot{V}_N = \dot{V}_U - \dot{V}_L = \dot{V}_U - \dot{V}_{EX} \geq 0$. This net volume flow rate, $\dot{V}_N$, can be said pressure-driven part of the flow.

The maximum value of the exchange flow rate, $\dot{V}_{EX,MX}$, is attained at $\Delta p = 0$. For shallow circular vents, this is obtained from Epstein [9] as

$$\dot{V}_{EX,MX} = 0.055\left(\frac{4}{\pi}\right)A_V\sqrt{gD\frac{\Delta T}{\overline{T}}} \qquad (15.46)$$

Cooper [14] presented the relationship of $\dot{V}_L/\dot{V}_{Ex,MX}$ and $\dot{V}_N/\dot{V}_{U,FL}$ as a function of $\Delta p/\Delta p_{FL}$ as shown in Fig. 15.17. Then, it follows that using this figure and Equation 15.46 together with the critical (flooding) pressure and volume flow rate, the exchange flow rate and the net flow rate can be estimated. Cooper also showed that his method well correlated the data of the flow through tube-like vents (i.e., moderate-to-large L/D) rather than shallow vents, as shown in Fig. 15.18.

Accuracy of Vent Flow Calculations

For nonbuoyant flows (using nozzles or orifices in a straight run of pipe made and calibrated with a specific geometry over a known Reynolds

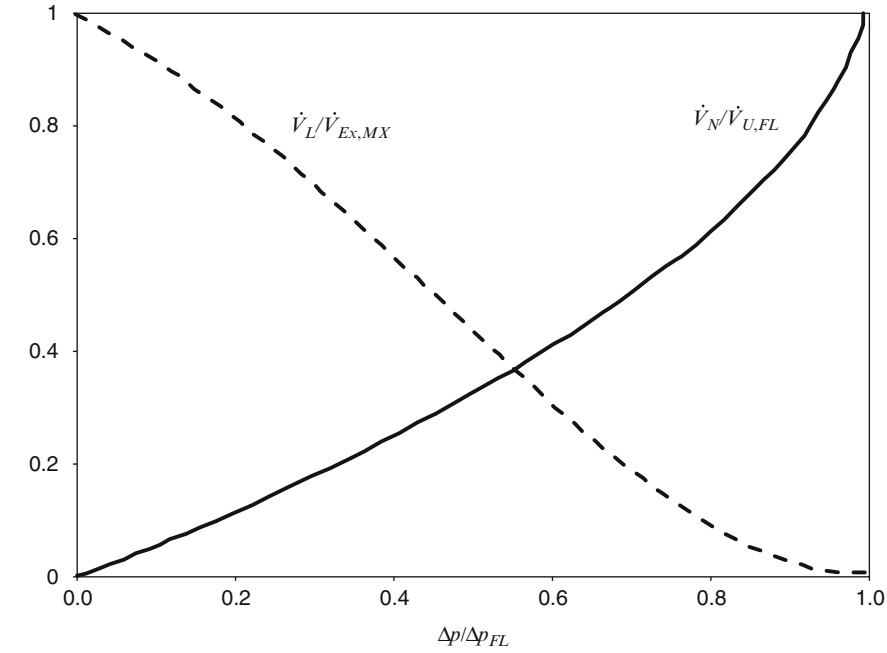

Fig. 15.17 Plots of $\dot{V}_L/\dot{V}_{Ex,MX}$ and $\dot{V}_N/\dot{V}_{U,FL}$ as a function of $\Delta p/\Delta p_{FL}$

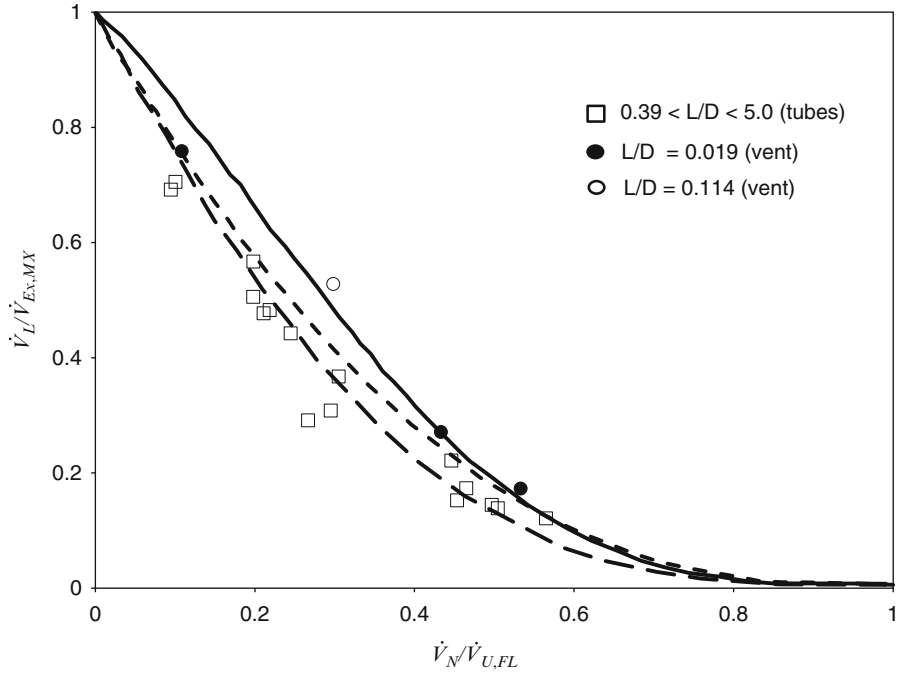

Fig. 15.18 Plots of $\dot{V}_L/\dot{V}_{Ex,MX}$ from Epstein and Kenton [12] as a function of $\dot{V}_N/\dot{V}_{U,FL}$

number range) one easily obtains 2 % accuracy. Thus, Equations 15.1, 15.2, 15.3, 15.4, 15.5, 15.6, 15.7, 15.8, and 15.9 are capable of high accuracy.

For vents in vertical walls with limited internal room fire circulations, the best methods of measurement may get 5 % accuracy. However, in real fires, induced circulations are often severe and unknown. Thus, errors of 10 % or higher must be expected. Even if flow instrumentation is located in the vent itself, there is never enough to really account for variations over the vent surface and time fluctuations originating in the fire phenomena inside the fire room.

For vents in a horizontal surface, the majority of the results presented here are from water-brine experiments in small holes. The experimental accuracy is 10 %. However, for a real fire, the errors are probably much higher. A typical case is a hole in the ceiling burned through by the flames from below. The hole geometry is very irregular and is completely unknown. Furthermore, a fire directly below the hole supplies hot gas with a considerable vertical velocity. Also, the ceiling jet flow often provides considerable cross flow.

Full-scale experimental results determining the effects of fire circulation, large density ratios, and large Reynolds numbers are needed.

Vents as Part of the Building Flow Network

A building is an enclosed space generally with floors and walls that divide the space both vertically and horizontally into rooms, corridors, and stairwells. A fire that starts at any place in the building causes gas expansion, which raises the local pressure and pushes air throughout the building through all pathways leading to the outside. If a window is open in the room of fire origin, and there is little or no wind, little flow moves through the remainder of the building. If there is no open window, the flow will move toward cracks and leaks wherever they may be in the building. All these flows are initially nonbuoyant. The flow through the building is simply flow through a complex system of pipes and orifices. As the fire grows larger, hot gas flows buoyantly out of the place of origin, while cold gas flows in below. Thus, while the net flow (out-in) is just sufficient to accommodate the fire gas expansion, the actual volumetric hot gas outflow may be 2.5 times larger than the inflow. A layer of hot gas moves along the ceiling of connected spaces and at the first opportunity proceeds up a stairwell or other ceiling (roof) opening into regions above [15]. The accumulating hot gas will help spread the fire while the newly created hot fire gases build a new hot layer in the adjacent spaces. The flow and pressure drop across each vent will then progress through a succession of situations as previously discussed. The flow throughout the building is, therefore, determined by the vent and flow friction drops along *all* of the available flow paths from the fire to the outside of the building.

The vent flow calculation procedures described in this section are sufficiently accurate and general to compute the required flow-pressure drop relations for building flow networks (except slow buoyant flows through horizontal vents).

Room Pressure

General Equation to Control Room Pressure

The above vent flow equations give flow rates of air and smoke through a vent as a function of pressure difference between the spaces at both sides of an arbitrary vent. The next question is "How could we know the pressure difference?" It can be obtained from the conservations of mass and heat of the rooms concerned and the ideal gas law. That is, the following equations hold for an arbitrary room, *i:*

Mass conservation

$$\frac{d}{dt}(\rho V_R) = \sum \left(-\dot{m}_{ij} + \dot{m}_{ji}\right) \tag{15.47}$$

Heat conservation

$$c_p \frac{d}{dt}(\rho V_R T) = \dot{Q} - \dot{Q}_h + c_p \sum \left(-\dot{m}_{ij} T + \dot{m}_{ji} T_j\right) \tag{15.48}$$

Ideal gas law

$$\rho T = \frac{M p}{\mathrm{R}} \tag{15.49}$$

where

j = Index of adjacent room connected by vents with the room considered
V, V_R = Volume of the room
$\dot{m}_{ij}$ = Mass outflow rate from room i to an adjacent room j
$\dot{m}_{ji}$ = Mass inflow rate to room i from an adjacent room j
$\dot{Q}$ = Heat release rate of fire source
$\dot{Q}_h$ = Heat loss from the room gas due to heat transfer
$\sum$ = Summation with respect to all the vents between all the adjacent rooms

In these equations subscript i is omitted for ρ, T, $\dot{Q}, \dot{Q}_h$, and V_R of the room considered for simplicity of equation form. Normally, $\dot{Q} = 0$ for rooms other than the fire room. Strictly speaking, the terms for mass fuel input and heat input due to temperature rise of the fuel gasification should be added to Equations 15.47 and 15.48, respectively, if the room being considered is a fire room. Here these terms are disregarded for clarity of the equations and for their relatively small significance.

Since the room volume, V_R, is constant, the left-hand side of Equation 15.48 can be extended as

$$c_p \frac{d}{dt}(\rho V_R T) = c_p \rho V_R \frac{dT}{dt} + c_p T \frac{d}{dt}(\rho V_R) \tag{15.50}$$

Hence, using Equation 15.47 into Equation 15.48 yields the equation for temperature as follows:

$$c_p \rho V_R \frac{dT}{dt} = Q - \dot{Q}_h + c_p \sum \dot{m}_{ji}\left(T_{ji} - T\right) \tag{15.51}$$

Now consider a leaky room condition in which the magnitude of pressure buildup induced by the heat release of the fire is insignificant compared with the absolute atmospheric pressure, which is the case in most building fires. Since ρT is a constant under such conditions, the left-hand side of Equation 15.48 becomes 0; hence,

$$\dot{Q} = \dot{Q}_h + c_p \sum \left(-\dot{m}_{ij} T + \dot{m}_{ji} T\right) = 0 \tag{15.52}$$

The mass flow rates in Equation 15.52, $\dot{m}_{ij}$ and $\dot{m}_{ji}$, are given as a function of the differences of the pressure between room i and adjacent spaces; in other words, this equation can be regarded as the condition that the pressure of room i must satisfy. Incidentally, the same equation can be obtained by using $d\rho/dt = -(\rho/T)dT/dt$, from ρT = constant, and Equation 15.51 into Equation 15.47, the mass conservation.

In case a room contains stratified upper and lower layers, the heat conservation equations for the layers are written as

$$c_p \frac{d}{dt}(\rho_u V_u T_u) = \dot{Q}_{(u)} - \dot{Q}_{h(u)} + c_p \sum_u \left(-\dot{m}_{ij} T + \dot{m}_{ji} T_j\right) \tag{15.53a}$$

$$c_p \frac{d}{dt}(\rho_l V_l T_l) = \dot{Q}_{(l)} - \dot{Q}_{h(l)} + c_p \sum_l \left(-\dot{m}_{ij} T + \dot{m}_{ji} T_j\right) \tag{15.53b}$$

where (u) and (l) denote that only the quantities associated with the upper and lower layers are considered, respectively. It is meant in the above equations that heat transfer by radiation and mass transport through a fire plume and/or entrainment of opening jet that can occur between the upper and lower layers are included as well as those between adjacent rooms.

Now, adding up Equations 15.53a and 15.53b, noting that $\rho_u T_u = \rho_l T_l$ = constant and $V_u + V_l = V_R$ (constant) and that the heat and mass transport between the upper and lower layers in the same room offset each other, yields the same equation as Equation 15.52; that is,

Equation 15.52 holds for the two-layer configuration also. Note also that Equation 15.52 holds universally for transient as well as steady-state conditions.

EXAMPLE 1 For a clearer understanding of the relationship between the conservations of mass and heat and the room pressure, consider the simple example shown in Fig. 15.19. An upper hot layer is developing under the ceiling due to the fire plume flow above a fire source in a room. The room has only one vent at the bottom. The mass conservations in this configuration can be written for the upper and lower air layers, respectively, as

$$\frac{d(\rho_u V_u)}{dt} = \dot{m}_p \tag{15.54a}$$

$$\frac{d(\rho_a V_l)}{dt} = -\dot{m}_p - \dot{m}_d \tag{15.54b}$$

where m_d is the rate of air flow through the bottom vent. Adding up these equations yields the mass conservation of the room as a whole as follows:

$$\frac{d}{dt}(\rho_u V_u + \rho_a V_l) = -\dot{m}_d \tag{15.55}$$

This equation implies that, in the smoke-filling stage, the upper-layer volume with smaller density is increasing while the lower layer with greater density is decreasing; thereby the total mass in the room is decreasing just at the rate of the vent flow.

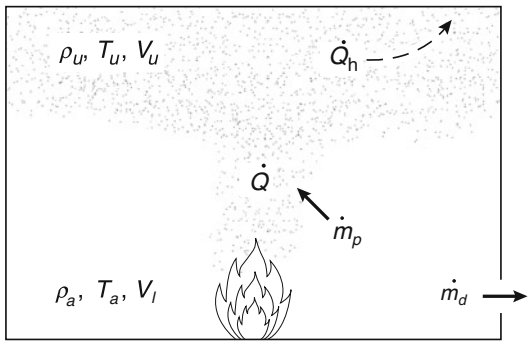

Fig. 15.19 Fire room at the stage of smoke layer filling

The vent flow rate can be obtained by considering the heat conservations for the layers as follows:

$$c_p \frac{d(\rho_u V_u T_u)}{dt} = \dot{Q} - \dot{Q}_h + c_p T_a \dot{m}_p \tag{15.56a}$$

$$c_p \frac{d(\rho_a V_l T_a)}{dt} = -c_p T_a \dot{m}_p + c_p T_a \dot{m}_d \tag{15.56b}$$

Noting that $\rho_u T_u = \rho_a T_a$ and $V_u + V_l = V_R$ (constant) so that

$$c_p \frac{d}{dt}(\rho_u T_u V_u + \rho_a T_a V_l) = c_p \rho_a T_a \frac{d(V_u + V_l)}{dt} = c_p \rho_a T_a \frac{dV_R}{dt} = 0$$

adding up Equations 15.56a and 15.56b yields

$$\dot{Q} - \dot{Q}_h - c_p \dot{m}_d T_a = 0 \tag{15.57}$$

Therefore, the air flow rate through the vent at such a stage of fire is given by

$$\dot{m}_d = \frac{\dot{Q} - \dot{Q}_h}{c_p T_a} \tag{15.58}$$

Invoking Equation 15.3, the vent flow equation, in Equation 15.58 or 15.57, the pressure difference between the room and the outside can be obtained as [16]

$$\Delta p = \frac{1}{2\rho_a (CA)^2} \left(\frac{\dot{Q} - \dot{Q}_h}{c_p T_a} \right)^2 \tag{15.59}$$

That is, the room pressure in this configuration depends on the net heat input (i.e., heat release – heat loss to boundary walls). At the very first stage the upper layer is thin in thickness and low in temperature, so the heat transfer rate, $\dot{Q}_h$, is small but as the upper layer develops the $\dot{Q}_h$ increases. Therefore, if the heat release rate, $\dot{Q}$, is constant, the room pressure will rise very rapidly at first and then will go down gradually.

Although it is not necessary to know the room pressure to calculate the vent flow rate in this particular case, it is required to know the pressure in general cases such as when there is a pressure

difference distribution over the height of a vent and when multiple vents are involved.

Equation to Control Pressure at Steady State

Strictly speaking, there is no steady state in building fire phenomena but there are stages at which fire behavior can be regarded as nearly steady. At steady state $dT/dt = 0$ in Equation 15.51; hence, Equation 15.52 becomes

$$\begin{aligned}\dot{Q} - \dot{Q}_h + c_p \sum \left(-\dot{m}_{ij} T + \dot{m}_{ji} T_j\right) &= \left[\dot{Q} - \dot{Q}_h + c_p \sum \dot{m}_{ji}\left(T_j - T\right)\right] \\ &\quad + c_p T \sum \left(-\dot{m}_{ij} + \dot{m}_{ji}\right) \\ &= 0 + c_p T \sum \left(-\dot{m}_{ij} + \dot{m}_{ji}\right) = 0\end{aligned}$$

Hence, Equation 15.52 is reduced to

$$\sum \left(-\dot{m}_{ij} + \dot{m}_{ji}\right) = 0 \tag{15.60}$$

that is, the mass conservation equation. Of course, this relation can also be obtained by letting $d\rho/dt = 0$ in Equation 15.47.

EXAMPLE 2 Consider a room with only one vent that is at steady state and uniform temperature as shown in Fig. 15.20. Letting Δp be the room pressure difference relative to the outdoor space at the height of the sill of the vent, the neutral plane height, h_n, is

$$h_n = -\frac{\Delta p}{(\rho_a - \rho)g} \tag{15.61}$$

Since Δp and h_n are in one-to-one correspondence, solving the pressure and solving the neutral plane height means the same. Incidentally, Δp in Equation 15.61 is negative in this particular case. The mass inflow and outflow rates through the vent, m_d and m_u, are given as a function of h_n as follows:

$$\dot{m}_d = \frac{\sqrt{2}}{3} Cb \sqrt{2g\rho_a(\rho_a - \rho)}\, h_n^{3/2} \tag{15.62a}$$

$$\dot{m}_u = \frac{\sqrt{2}}{3} Cb \sqrt{2g\rho_a(\rho_a - \rho)}\, (h_v - h_n)^{3/2} \tag{15.62b}$$

The neutral plane height, h_n, can be solved by invoking Equation 15.60, which is simply $\dot{m}_d = \dot{m}_u$ in this case, as follows:

$$h_n = \frac{h_v}{1 + \left(\frac{\rho_a}{\rho}\right)^{1/3}} = \frac{h_v}{1 + \left(\frac{T}{T_a}\right)^{1/3}} \tag{15.63}$$

Using Equation 15.63 into Equations 15.62a and 15.62b, the vent mass flow rates can be concretely obtained. Incidentally, Equation 15.63 is identical to the following pressure difference at the height of the sill of the vent:

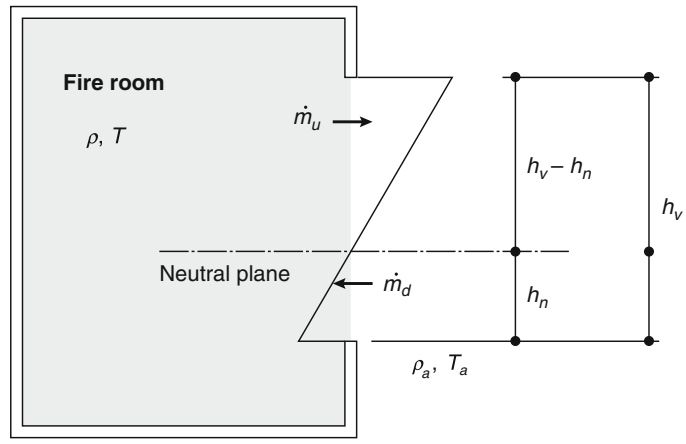

Fig. 15.20 Single room at steady state with uniform temperature

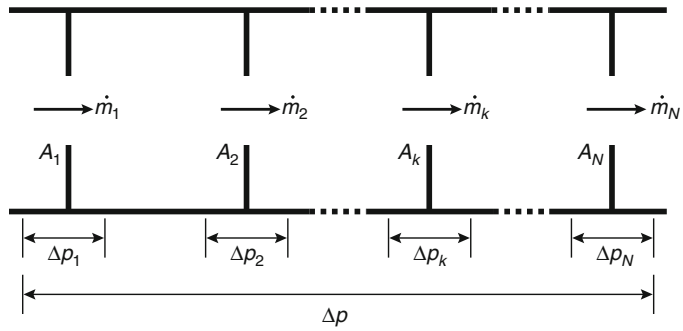

Fig. 15.21 Effective vent area of a series of vents

$$\Delta p = -(\rho_a - \rho)h_n = -\frac{(\rho_a - \rho)h_v}{1 + \left(\frac{T}{T_a}\right)^{1/3}} \quad (15.64)$$

EXAMPLE 3 Equivalent vent area of a series of vents may be a typical example in which steady-state mass conservation law is invoked. Figure 15.21 illustrates a system of spaces connected by N vents with different areas through which vent airflows are induced due to a given pressure difference between both ends, Δp. In this case, from the mass conservation for the $N - 1$ rooms involved in the system of spaces, all the vent flow rates have to be the same; that is,

$$\dot{m}_1 = \dot{m}_2 \cdots = \dot{m}_k \cdots \dot{m}_N (\equiv \dot{m}) \quad (15.65)$$

The pressure difference across an arbitrary vent, Δp_k, is unknown but the following equation holds

$$\Delta p_1 + \Delta p_2 + \cdots + \Delta p_k + \cdots + \Delta p_N = \Delta p \quad (15.66)$$

and the pressure difference across an arbitrary vent, Δp_k, is expressed as

$$\Delta p_k = \frac{\dot{m}^2}{2\rho(CA_k)^2} \quad (15.67)$$

where ρ is the flowing air density.

Substituting Equation 15.67 into Equation 15.66 reveals that the mass flow rate, $\dot{m}$, can be calculated using the given pressure difference, Δp, as

$$\dot{m} = CA_e\sqrt{2\rho\Delta p} \quad (15.68)$$

where A_e is the equivalent vent area, which is given by

$$A_e = \left(\frac{1}{A_1^2} + \frac{1}{A_2^2} + \cdots + \frac{1}{A_k^2} + \cdots + \frac{1}{A_N^2}\right)^{-1/2} \quad (15.69)$$

Incidentally, since the equation

$$\dot{m} = CA_k\sqrt{2\rho\Delta p_k} = CA_e\sqrt{2\rho\Delta p} \quad (15.70)$$

holds for any of the vents, the pressure difference across an arbitrary vent, Δp_k, can be calculated simply by

$$\Delta p_k = \left(\frac{A_e}{A_k}\right)^2 \Delta p \quad (15.71)$$

EXAMPLE 4 Natural smoke venting is a smoke control method that removes smoke from fire in a building space to the outdoor space through a smoke vent arranged in a roof or upper part of a wall of a room. Figure 15.22a illustrates a typical configuration of natural smoke venting at an early stage of fire in a room having a smoke vent at height, h_e, and an inlet above the floor, where we assume a constant heat release rate of fire source, $\dot{Q}$, and steady-state smoke layer properties such as temperature, T, and layer interface height, y. Under such a condition, the pressure difference as shown by Fig. 15.22b develops with height due to the temperature difference between the indoor and the outdoor space. As a result, the pressure difference across the smoke vent, $\Delta p(h_e)$, which is the driving force of the smoke discharge, is induced. If the indoor pressure at the floor level is $-\Delta p(0)$, relative to

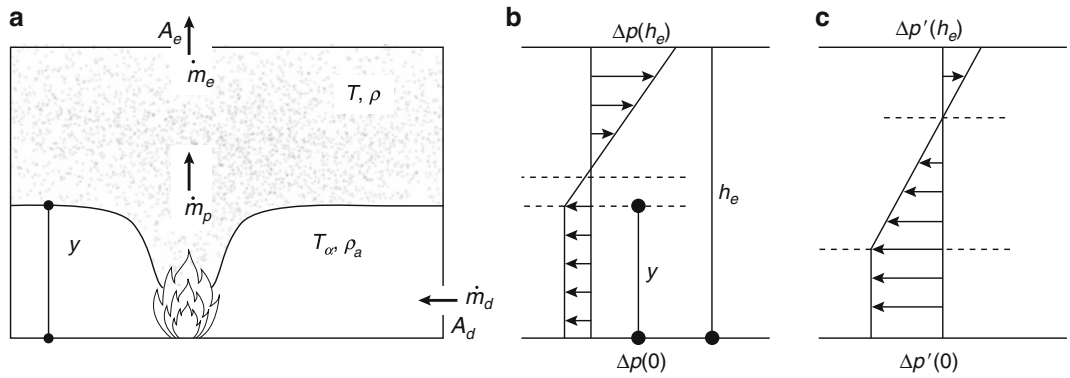

Fig. 15.22 Configuration and pressure profile of natural smoke venting. (**a**) Natural smoke venting configuration. (**b**) Pressure difference profile for large A_d. (**c**) Pressure difference profile for small A_d

the outdoor space, the pressure difference at height, h_e, is

$$\Delta p(h_e) = -\Delta p(0) + (\rho_a - \rho)\, g\,(h_e - y) \qquad (15.72)$$

so that the rate of smoke exhaustion through the vent, m_e, is

$$\dot{m}_e = CA_e\sqrt{2\rho\Delta p(h_e)} = CA_e\sqrt{2\rho[-\Delta p(0) + (\rho_a - \rho)g(h_e - y)]} \qquad (15.73)$$

In Equation 15.73, $-\Delta p(0)$, ρ, and y are unknown so we need to seek additional relationships.

The air inflow rate through the inlet above the floor, $\dot{m}_d$, is expressed as

$$\dot{m}_d = CA_d\sqrt{2\rho_a\Delta p(0)} \qquad (15.74)$$

The plume flow rate at the layer interface height, m_p, can be estimated using some appropriate plume formula such as

$$\dot{m}_p = 0.08\dot{Q}^{1/3}y^{5/3} \qquad (15.75)$$

At steady state, mass conservation holds for the smoke and the air layers so that

$$\dot{m}_e = \dot{m}_p = \dot{m}_d (\equiv \dot{m}) \qquad (15.76)$$

Furthermore, an additional equation to obtain smoke layer density is necessary. It can be provided from some appropriate energy conservation equation for the smoke layer; for example,

$$\dot{Q} = c_p\dot{m}(T - T_a) + \alpha_k A_W(T - T_a) \qquad (15.77)$$

where A_W is the boundary wall area exposed to heat transfer from the smoke layer and α_K is the effective heat transfer coefficient [17–19].

Using the above equations and the equation of gas state, we can obtain the smoke layer temperature and interface height, the vent flow rates, the plume flow rate at the interface height, and the pressure differences, although some trial-and-error method must be invoked because of the nonlinearity of Equation 15.75.

On the other hand, it is more practical to know the necessary smoke vent area to assure a certain level of clear height for evacuation or fire fighting than to predict the behaviors of the smoke layer and vent flows under arbitrary conditions. If the critical layer interface height, y_c, is specified, the required smoke vent area, A_e, can be obtained by simply following the procedure below one by one, without invoking any trial-and-error method [18].

1. Calculate the plume flow rate at height, y_c:

$$\dot{m} = 0.08\dot{Q}^{1/3}y_c^{5/3} \qquad (15.78a)$$

2. Calculate the smoke layer temperature:

$$T = T_a + \frac{\dot{Q}}{c_p m + \alpha_K A_W} \tag{15.78b}$$

3. Calculate the smoke layer density:

$$\rho = \frac{352.8}{T} \tag{15.78c}$$

4. Calculate the pressure at floor level:

$$\Delta p(0) = \frac{\dot{m}^2}{2\rho_a (CA_d)^2} \tag{15.78d}$$

5. Calculate the pressure at the smoke vent:

$$\Delta p(h_e) = -\Delta p(0) + (\rho_a - \rho) g (h_e - y_c) \tag{15.78e}$$

6. Calculate the smoke vent area:

$$A_e = \frac{\dot{m}}{C\sqrt{2\rho \Delta p(h_e)}} \tag{15.78f}$$

Incidentally, Equation 15.73 might suggest that the smoke exhaust rate would increase in proportion to the smoke vent area, but it is not necessarily the case. It is true that the larger the smoke vent area the larger the smoke exhaust rate, but the smoke exhaust rate is affected by the size of the air inlet at the bottom. This is because the mass conservation expressed by Equation 15.76 requires the smoke venting rate, $\dot{m}_e$, be the same as the air inflow rate through the inlet, $\dot{m}_d$. Even though the smoke vent area, A_e, is very large, the indoor pressure at floor height, $-\Delta p(0)$, becomes low when the inlet area is small, which eventually results in a small pressure difference across the smoke vent, $\Delta p(h_e)$, as understood from Equation 15.72 and illustrated by Fig. 15.22c.

Numerical Computation of Room Pressure

Except in particularly simple cases such as the above examples, solving room pressure problems requires using numerical computation. Even in the case of single fire rooms, it is too difficult to solve room pressure problems without using numerical methods if multiple vents, mechanical ventilation, transient condition, and fuel mass input are involved.

When considering the pressures in building rooms, it is convenient to take them relative to the outdoor space rather than to use absolute atmospheric pressure since vent flows in fire are induced by only trivial fractions of the atmospheric pressure. In the case of a single room, if the room pressure, p, is taken as such a relative pressure to the outdoor space at the level of the room floor, any vent flow rate can be given as a function of the only pressure. Therefore, Equation 15.52 can be expressed as

$$\begin{aligned} f(p) \equiv \dot{Q} - \dot{Q}_h &+ c_p \sum (-\dot{m}_u T + \dot{m}_d T_a) \\ &= 0 \end{aligned} \tag{15.79}$$

Because the vent flow terms in Equation 15.79 are a function of p, the problem is reduced to the solution of $f(p) = 0$ for p.

If the room is at uniform temperature, for example, the neutral plane height is given as a function of p as

$$h_n = \frac{-p}{g(\rho_a - \rho)} \tag{15.80}$$

Pressure profile across a vent varies depending on the height of the vent relative to the neutral plane as shown in Fig. 15.23. The vent flow rates are given as a function of the neutral plane height as follows:

1. when $h_n < h_b$

$$\begin{aligned} \dot{m}_u &= \frac{2}{3} C b \sqrt{2\rho g (\rho_a - \rho)} \times \left[(h_t - h_n)^{3/2} - (h_b - h_n)^{3/2} \right] \\ \dot{m}_d &= 0 \end{aligned} \tag{15.81a}$$

2. when $h_b < h_n < h_t$

$$\begin{aligned} \dot{m}_u &= \frac{2}{3} C b \sqrt{2\rho g (\rho_a - \rho)} (h_t - h_n)^{3/2} \\ \dot{m}_d &= \frac{2}{3} C b \sqrt{2\rho g (\rho_a - \rho)} (h_n - h_b)^{3/2} \end{aligned} \tag{15.81b}$$

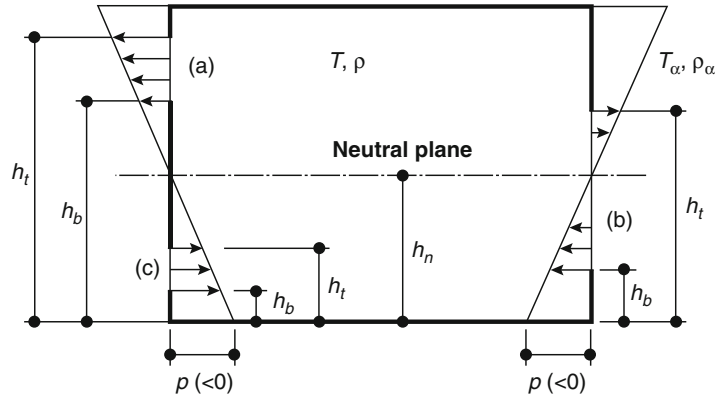

Fig. 15.23 Pressure profile across vents for nonstratified room condition

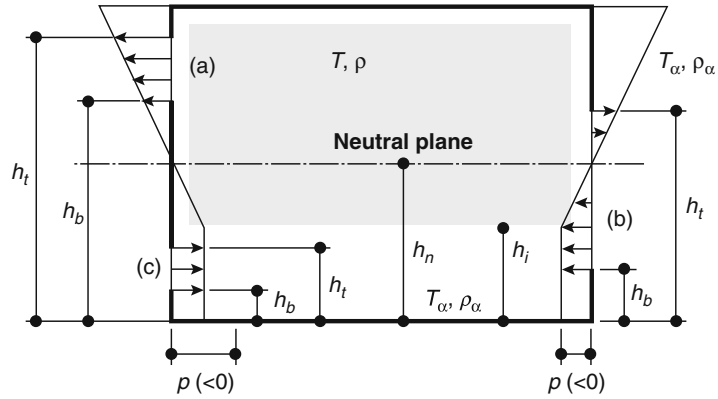

Fig. 15.24 Pressure profile across vents for stratified room condition

3. when $h_t < h_n$

$$\begin{aligned}\dot{m}_u &= 0\\ \dot{m}_d &= \frac{2}{3}Cb\sqrt{2\rho_a g(\rho_a-\rho)}\\ &\quad\times\left[(h_n-h_b)^{3/2}-(h_n-h_t)^{3/2}\right]\end{aligned} \tag{15.81c}$$

From Equations 15.80 and 15.81, it is easily understood that Equation 15.79 is a nonlinear function with respect to p.

If the room is stratified into two uniform layers, a little more complicated situation can emerge; that is, the pressure profile across a vent is affected by the layer interface as well as the neutral plane as exemplified in Fig. 15.24. In this particular example in which the lower layer is at the same temperature as the outdoor space, the neutral plane height is given by

$$h_n = \frac{-p}{g(\rho_a-\rho)} + h_i \tag{15.82}$$

The neutral plane height, h_n, can be lower than the interface height, h_i, under some conditions, such as rapid transient expansion of the upper layer and mechanical air supply to the room, although most often h_i is lower than h_n. In case h_i is lower than h_n, the vent flow rates are calculated as follows: [15, 20, 21]

1. when $h_n < h_b$

$$\begin{aligned}\dot{m}_u &= \frac{2}{3}Cb\sqrt{2\rho g(\rho_a-\rho)}\\ &\quad\times\left[(h_t-h_n)^{3/2}-(h_b-h_n)^{3/2}\right]\\ \dot{m}_d &= 0\end{aligned} \tag{15.83a}$$

2. when $h_b < h_i < h_n < h_t$

$$\begin{aligned}\dot{m}_u &= \frac{2}{3}Cb\sqrt{2\rho g(\rho_a - \rho)}(h_t - h_n)^{3/2} \\ \dot{m}_d &= \frac{2}{3}Cb\sqrt{2\rho g(\rho_a - \rho)}\,(h_t - h_n)^{3/2} \\ &\quad + Cb\sqrt{2\rho_a(-p)}(h_i - h_b)\end{aligned} \tag{15.83b}$$

3. when $h_t < h_i$

$$\begin{aligned}\dot{m}_u &= 0 \\ \dot{m}_d &= Cb\sqrt{2\rho_a(-p)}(h_t - h_b)\end{aligned} \tag{15.83c}$$

Needless to say, Equation 15.79 becomes a nonlinear function with respect to p in this case also.

If the lower temperature is different from the outdoor space, the pressure profiles across the vents are generally more complex. Nevertheless, the vent flow rates can be given as a function of p.

Since Equation 15.79 is nonlinear, it is impossible to obtain an analytical solution except in very limited cases, so usually a numerical method is employed. The idea of the Newton–Raphson method, which is a typical example of iterative numerical solution methods, is illustrated in Fig. 15.25. In this method the pressure is estimated successively starting from the first estimate until the pressure acceptably satisfies $f(p) = 0$ according to the procedure as follows:

$$p^{(k+1)} = p^{(k)} - \left(\frac{df}{dp}\right)^{-1} f\left(p^{(k)}\right) \tag{15.84}$$

where $p^{(k)}$ is the kth estimate of the pressure.

In the case of a structure having multiple rooms, every room has to satisfy Equation 15.52 and the flow through the vents in the boundary of the room is a function of the pressure difference with the adjacent rooms. If a structure consists of N rooms connected arbitrarily to each other, Equation 15.52 for an arbitrary room i may be expressed in the most general form as [20, 21]

$$\begin{aligned}&f_i(p_1, \ldots, p_i, \ldots, p_N) \\ &\equiv \dot{Q} - \dot{Q}_h + c_p \sum \left(-\dot{m}_{ij}T + \dot{m}_{ji}T_j\right) = 0\end{aligned} \tag{15.85}$$

Since every room in the structure must satisfy the identical equation, the problem is reduced to the solution of the coupling equations as follows:

$$\left.\begin{aligned}&f_1(p_1, \ldots, p_i \ldots, p_N) = 0 \\ &\cdots\cdots\cdots\cdots\cdots\cdots\cdots \\ &f_i(p_1, \ldots, p_i \ldots, p_N) = 0 \\ &\cdots\cdots\cdots\cdots\cdots\cdots\cdots \\ &f_N(p_1, \ldots, p_i \ldots, p_N) = 0\end{aligned}\right\} \tag{15.86}$$

A multidimensional Newton–Raphson method may be used for the solution of Equation 15.86. The iteration procedure is expressed by

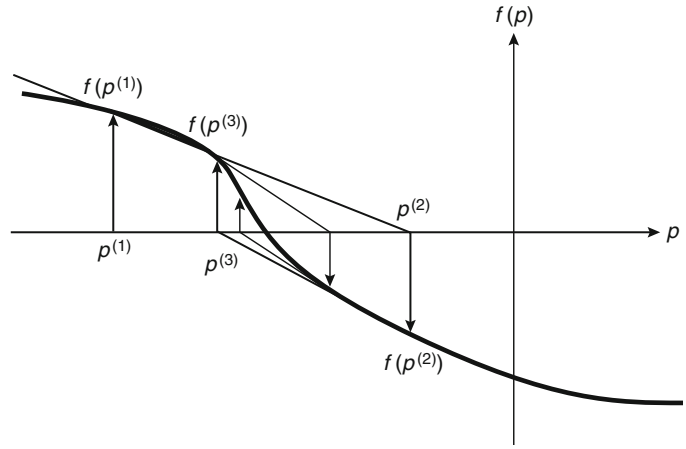

Fig. 15.25 Iterative numerical solution of room pressure by Newton–Raphson method

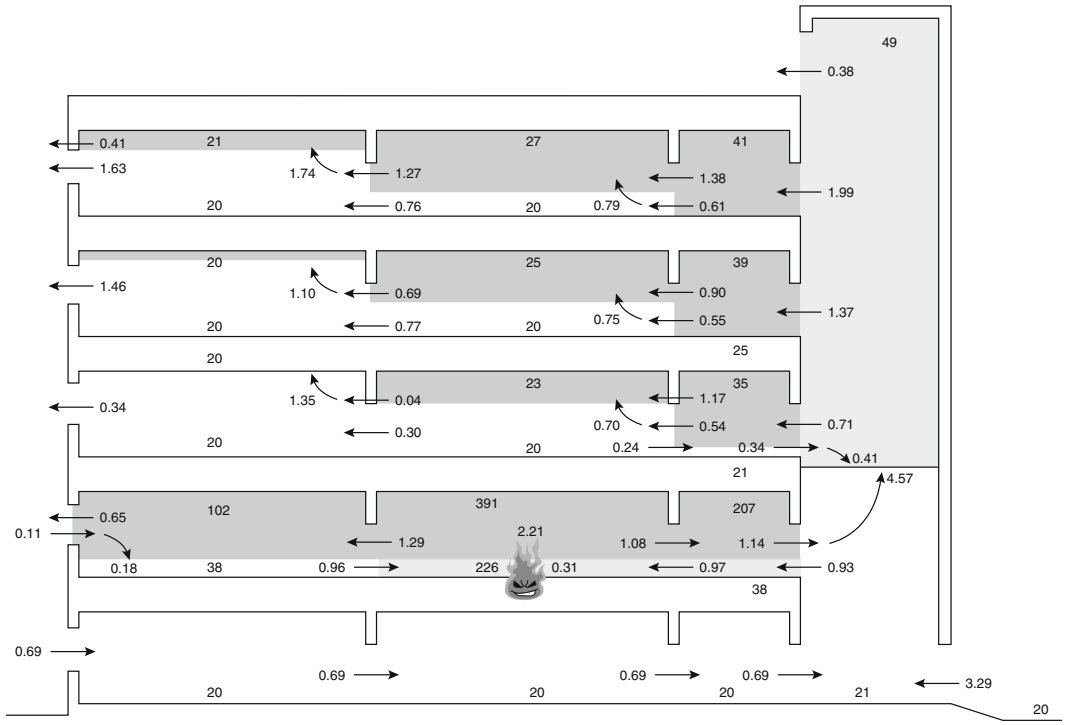

Fig. 15.26 An example of smoke movement prediction by a two-layer zone model (Number: temperature [°C], number →: vent flow rate or plume flow rate [kg/s])

$$\boldsymbol{p}^{(k+1)} = \boldsymbol{p}^{(k)} - \left[\boldsymbol{J}^{(k)}\right]^{-1} \boldsymbol{f}\left[\boldsymbol{p}^{(k)}\right] \tag{15.87}$$

where $\boldsymbol{p} = (p_1, \ldots, p_i, \ldots, p_N)$ and $\boldsymbol{f} = (f_1, \ldots, f_2, \ldots, f_N)$ and $[J]$ is the Jacobian matrix defined by

$$[J] = \begin{bmatrix} \partial f_1/\partial p_1 & \cdots & \partial f_1/\partial p_j & \cdots & \partial f_1/\partial p_N \\ \cdots & \cdots & \cdots & \cdots & \cdots \\ \partial f_i/\partial p_1 & \cdots & \partial f_i/\partial p_j & \cdots & \partial f_j/\partial p_N \\ \cdots & \cdots & \cdots & \cdots & \cdots \\ \partial f_N/\partial p_1 & \cdots & \partial f_N/\partial p_j & \cdots & \partial f_N/\partial p_N \end{bmatrix} \tag{15.88}$$

In actual calculation, the inverse matrix of the Jacobian matrix, $[J^{(k)}]^{-1}$, is not calculated but the coupling linear equations

$$\left[J^{(k)}\right] \Delta \boldsymbol{p} = -\boldsymbol{f}\left[\boldsymbol{p}^{(k)}\right] \tag{15.89}$$

are directly solved using an appropriate method such as Gaussian elimination for correction pressure increments Δp and the new estimate is calculated as

$$\boldsymbol{p}^{(k+1)} = \boldsymbol{p}^{(k)} + \Delta \boldsymbol{p} \tag{15.90}$$

Figure 15.26 shows an example of smoke movement in a building predicted using the two-layer zone model BRI2, in which vent smoke and air flows were calculated using the above multidimensional Newton–Raphson method.

Summary

Most of the equations for vent flows in this chapter are basically derived from Bernoulli's equation for steady flow of ideal and incompressible fluid. The mass and volume vent flows are given as a function of the flowing gas density, area of the vent, and the pressure difference across the vent with a coefficient called flow coefficient or opening coefficient. The value of the flow coefficient, C, varies depending on the size and shape

of a vent. For usual doorway openings and windows in a building, the value of the C is known to be from 0.6 to 0.7 from many experimental measurements.

In a building fire, the heat release and the flows induced by the fire cause temperature distributions in spaces in the building, which then cause vertical pressure difference distribution across a vent. When such a vertical temperature distribution exists across a vent, it is often convenient for calculation of the vent flow rates to first obtain the neutral plane height, which is given as a function of the pressure difference at a reference height and gas density difference in the spaces at both sides of the vent.

The equation to control the space (room) pressures at a reference height in building spaces can be obtained by considering the mass and heat conservations in the spaces and the equation of gas state. In general, the equation is a function of the vent flow rates, the temperatures of the spaces, and the heat addition and loss, but at steady state, it is reduced to be the mass conservations of the spaces. When multiple spaces are involved in a calculation of the flows in fire, analytical solutions are only possible for very limited conditions, so generally some numerical calculation method must be invoked to solve the coupling nonlinear equations for the space pressures.

Nomenclature

A	Area (m^2)
a	Length (m)
b	Width (m)
C	Flow coefficient (−)
c_p	Specific heat at constant pressure (kJ/kg K)
c_v	Specific heat at constant volume (kJ/kg K)
D	Orifice diameter (m)
Fr	Froude number (−)
g	Gravity constant (m/s^2)
Gr	Grashof number (−)
h	Height (m)
$[J]$	Jacobian matrix
L	Orifice length (m)
M	Molecular weight (kg/kg mol)
$\dot{m}$	Mass flow rate (kg/s)
P	Perimeter (m)
p	Pressure (Pa)
$\dot{Q}$	Heat release rate of fire source (kW)
$\dot{Q}_h$	Heat loss by heat transfer (kW)
R	Gas constant (J/kg mol K)
Re	Reynolds number (−)
T	Temperature (K)
u	Velocity (m/s)
V	Volume (m^3)
$\dot{V}$	Volume flow rate (m^3/s)
V_R	Room volume (m^3)
y	Vertical coordinate (m)
α_K	Effective heat transfer coefficient (kW/m^2K)
Δ	Increment of
δ	Depth (see Fig. 15.6) (m)
$\gamma = c_p/c_v$	Isentropic exponent (−)
Π	Non-dimensional pressure (−)
ρ	Density (kg/m^3)
μ	Viscosity (Ns/m^2)

Subscripts

a	Atmosphere
b	Sill of vent
c	Ceiling of room
d	Lower
f	Floor
g	Gauge
i	Hot-cold interface
ij	From room (layer) i to room (layer) j
j	Index of layer
L, l	Lower
n	Neutral axis
O_2	Oxygen
t	Soffit of vent
u, U	Upper
v, V	Vent, in the vent
0	Reference height
1	Upstream of orifice
2	Downstream of orifice

References

1. H. Rouse, *Fluid Mechanics for Hydraulic Engineers,* McGraw-Hill, New York (1938).
2. *Mark's Mechanical Engineers Handbook,* McGraw-Hill, New York (1958).

3. J.S. Newman and P.A. Croce, *Serial No. 21011.4,* Factory Mutual Research Corp., Norwood, MA (1985).
4. D.J. McCaffrey and G. Heskestad, "Robust Bidirectional Low-Velocity Probe for Flame and Fire Application—Brief Communications," *Combustion and Flame,* 26, pp. 125–127 (1976).
5. J. Prahl and H.W. Emmons, "Fire Induced Flow Through an Opening," *Combustion and Flame,* 25, pp. 369–385 (1975).
6. K.D. Steckler, H.R. Baum, and J. Quintiere, *20th Symposium on Combustion,* Pittsburgh, PA (1984).
7. J. Quintiere and K. DenBraven, *NBSIR 78–1512,* National Bureau of Standards, Washington, DC (1978).
8. H.E. Mitler and H.W. Emmons, *NBS-GCR-81-344,* National Bureau of Standards, Washington, DC (1981).
9. M. Epstein, "Buoyancy-driven exchange flow through small openings in horizontal partition, with special reference to flows in multicompartment enclosures", Journal of Heat Transfer, 110, pp.885–893 (1988)
10. Q. Tan and Y. Jaluria, *NIST-G&R-92-607,* National Institute of Standards and Technology, Gaithersburg, MD (1992).
11. Heiselberg, P. and Li, Z., (2007), "Experimental study of buoyancy driven natural ventilation through horizontal openings", Proceedings of Roomvent 2007 : Helsinki 13–15 June 2007..
12. M. Epstein and M.A. Kenton, "Combined Natural Convection and Forced Flow Through Small Openings in a Horizontal Partition, with Special Reference to Flows in Multicompartment Enclosures," *Journal of Heat Transfer,* 111, pp. 980–987 (1989).
13. G. Heskestad and R. D. Spaulding, "Inflow of air required at wall and ceiling apertures to prevent escape of fire smoke", Proceeding of the 3rd International Symposium on Fire Safety Science, pp.919–928 (1991)
14. L. Y. Cooper, "Combined buoyancy- and pressure-driven flow through a shallow, horizontal, circular vent", HTD-Vol. 299, Heat Transfer With Combined Modes, ASME, Chicago (1994).
15. T. Tanaka, "A Model of Multiroom Fire Spread," *Fire Science and Technology,* 3, p. 105 (1983).
16. S. Yamada and T. Tanaka, "Reduced Scale Experiments for Convective Heat Transfer in the Early Stage of Fires," *International Journal on Engineering Performance-Based Codes,* 1, 3, pp. 196–203 (1999).
17. T. Tanaka and T. Yamana, "Smoke Control in Large Scale Spaces (Part 1, Analytic theories for simple smoke control problems)," *Fire Science and Technology,* 5, 1, pp. 31–40 (1985).
18. T. Tanaka, "Performance-Based Fire Safety Design Standards and FSE Tools for Compliance Verification," *International Journal on Engineering Performance-Based Codes,* 1, 3, pp. 104–117 (1999).
19. B.J. McCaffrey, J.G. Quintiere, and M.F. Herkeleroad, "Estimating Room Temperature and Likelihood of Flashover Using Fire Test Data Corrections," *Fire Technology,* 17, 2, pp. 98–119 (1981).
20. T. Tanaka and K. Nakamura, "A Model for Predicting Smoke Transport in Buildings," Report of the Building Research Institute, No. 123, Ministry of Construction, Tsukuba, Japan (1989).
21. T. Tanaka and S. Yamada, "BRI2002: Two Layer Zone Smoke Transport Model," *Fire Science and Technology,* 23, Special Issue (2004).

Takeyoshi Tanaka is a professor emeritus at Kyoto University. His performance–based areas of expertise are fire modeling, smoke control, and fire safety design. His professional experience includes research for the Building Research Institute of Japan's Ministry of Construction.

Effect of Combustion Conditions on Species Production

16

Daniel T. Gottuk and Brian Y. Lattimer

Introduction

A complete compartment fire hazard assessment requires a knowledge of toxic chemical species production. Although combustion products include a vast number of chemical species, in practical circumstances the bulk of the product gas mixture can be characterized by less than 10 species. Of these, carbon monoxide (CO) represents the most common fire toxicant (see Chap. 63). Over half of all fire fatalities have been attributed to CO inhalation [1, 2]. Concentrations as low as 4000 ppm (0.4 % by volume) can be fatal in less than an hour, and carbon monoxide levels of several percent have been observed in full-scale compartment fires. A complete toxicity assessment should not only include the toxicity of CO but also include the synergistic effects of other combustion products, such as elevated CO_2 and deficient O_2 levels.

The transport of combustion products away from the room of the fire's origin is of the utmost importance, because nearly 75 % of the fatalities due to smoke inhalation occur in these remote locations [3]. However, conditions close to the compartment of origin will govern the levels that are transported to remote locations. The research in this area has focused on characterizing species levels produced under a variety of conditions, both inside and nearby the compartment of fire origin.

D.T. Gottuk (✉) • B.Y. Lattimer
Jensen Hughes, 3610 Commerce Drive, Suite 817, Baltimore, MD 21227, USA

Species product formation is affected by the compartment geometry, ventilation, fluid dynamics, thermal environment, chemistry, and mode of burning. The mode of burning and ventilation are two of the key conditions that dictate product formation. These conditions can be used to classify fires into three general categories: (1) smoldering, (2) free- (or open-) burning fires, and (3) ventilation-limited fires. Smoldering is a slow combustion process characterized by low gas temperatures and no flaming. Under these conditions, high levels of CO can be generated. Chapters 63, 19, and 36 discuss this mode of burning in detail; thus, it will not be discussed further here. Free-burning fires are flaming fires that have an excess supply of air. These well-ventilated fires (discussed in Chap. 36) are generally of little concern in terms of generating toxic species. This chapter focuses primarily on the third category, ventilation-limited flaming fires. These fires consist of burning materials inside an enclosure, such as a room, in which airflow to the fire is restricted due to limited ventilation openings in the space. As a fire grows, conditions in the space will transition from overventilated to underventilated (fuel rich). It is normally during underventilated conditions that formation of high levels of combustion products, including CO, creates a major fire hazard.

This chapter discusses the production of species within a compartment fire and the transport of these gases out of the fire compartment to adjacent areas. Engineering correlations are presented along with brief reviews of pertinent work on

M.J. Hurley (ed.), *SFPE Handbook of Fire Protection Engineering*,
DOI 10.1007/978-1-4939-2565-0_16, © Society of Fire Protection Engineers 2016

species production in compartment fires. These sections provide the background and basis for understanding the available engineering correlations and the range of applicability and limitations. An engineering methodology is presented to utilize the information given in this chapter.

This chapter is organized according to the following outline:
Basic Concepts
Species Production Within Fire Compartments
Hood Experiments
Compartment Fire Experiments
Chemical Kinetics
Fire Plume Effects
Transient Conditions
Species Transport to Adjacent Spaces
Engineering Methodology

Basic Concepts

In a typical compartment fire, a two-layer system is created. The upper layer consists of hot products of combustion that collect below the ceiling, and the lower layer consists of primarily ambient air that is entrained into the base of the fire (Fig. 16.1). Initially, the fire plume is totally in the lower layer, and the fire burns in an overventilated mode similar to open burning. Due to excess air and near-complete combustion, little CO formation is expected in this mode. (See Chap. 36, for yields.) As the fire grows, ventilation paths in the room restrict airflow, creating underventilated (fuel-rich) burning conditions. It is generally under these conditions that products of incomplete combustion are created. Typically, the fire plume extends into the upper layer, such that layer gases recirculate through the upper part of the plume.

Depending on both the size of the room and the size of the fire, it is possible to have a fire plume that cannot be contained within the room, resulting in flame extension out of windows or doors. Flame extension can occur when the fire plume impinges on the ceiling and the ceiling jets are longer than the distance from the plume to outside vent openings (Fig. 16.2). Flame extension is different from a second burning phenomenon outside of the fire compartment, called external burning, which is discussed below. The main point to understand is that flame extension outside of the fire compartment is a result of a fire that is too large to be contained in the room. Flame extension can occur during both over- and underventilated burning conditions. To estimate when flame extension may occur, the maximum heat release rate that can be supported by the compartment ventilation needs to be determined. Flame length correlations can then be used to determine whether flames will extend outside of the compartment.

As a fire progresses and the upper layer descends, the layer will spill below the top of doorways or other openings into adjacent areas. The hot, vitiated, fuel-rich gases flowing into adjacent areas can mix with air that has high O_2 concentrations to create a secondary burning zone outside of the compartment (Fig. 16.3). This is referred to as external burning. External

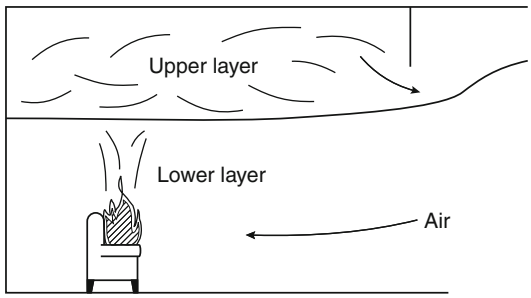

Fig. 16.1 An overventilated compartment fire with the fire plume below the layer interface

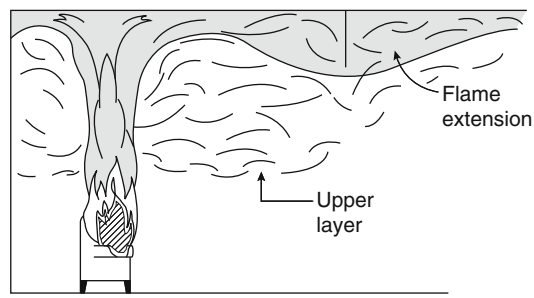

Fig. 16.2 A fire compartment with flame extension out of the doorway

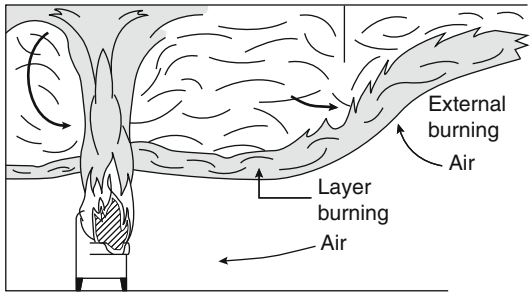

Fig. 16.3 An underventilated compartment fire with external burning of fuel-rich upper layer gases

burning can also be accompanied by layer burning. Layer burning is the ignition of fuel-rich upper-layer gases at the interface between the upper and lower layers. External burning and layer burning occur due to the buildup of sufficient fuel in an atmosphere that is able to mix with available oxygen. These phenomena can only occur during underventilated burning conditions. In some circumstances, external burning can decrease human fire hazard through the oxidation of CO and smoke leaving the fire compartment (see the section in this chapter, "Species Transport to Adjacent Spaces").

The occurrence of external burning has been predicted using a compartment layer ignition model developed by Beyler [4] (see Chap. 17). Beyler derived a relationship called the ignition index to predict the ignition of gases at the interface of the upper and lower layers inside a compartment. The ignition index, I, is defined as

$$I = \sum_j \frac{\left(C_j/100\right)\Delta H_{c,j}}{\int_{T_o}^{T_{SL,j}} n_{\text{prod}} C_p dT} \geq 1.0 \qquad (16.1)$$

where

j = Fuel species of interest

C_j = Volume concentration of fuel j when fuel stream is stoichiometrically mixed with oxidant stream

$\Delta H_{c,j}$ = Heat of combustion of the species j (kJ/g·mol)

$T_{\text{SL},j}$ = Adiabatic flame temperature at the stoichiometric limit for fuel species j (K)

T_o = Temperature of the gas mixture prior to reaction (K)

n_{prod} = Number of moles of products of complete combustion per mole of reactants (stoichiometric mixture of fuel and oxidant streams)

C_p = Heat capacity of products of complete combustion (kJ/g·mol K)

The use of the ignition index is discussed in detail in Chap. 17, of this book. An ignition index greater than 1.0 indicates that ignition is expected if the mixture contains sufficient fuel.

Species Yields

The generation of fire products in compartment fires can be quantified in terms of species yields, Y_i, defined as the mass of species i produced per mass of fuel burned (g/g):

$$Y_i = \frac{m_i}{m_f} \qquad (16.2)$$

Similarly, oxygen is expressed as the depletion of O_2 (i.e., D_{O2}), which is the grams of O_2 consumed per gram of fuel burned:

$$D_{O_2} = \frac{m_{O_2}}{m_f} \qquad (16.3)$$

The normalized yield, f_i, is the yield divided by the theoretical maximum yield of species i for the given fuel, k_i. For the case of oxygen, f_{O_2} is the normalized depletion rate, where k_i is the theoretical maximum depletion of oxygen for the given amount of fuel. As a matter of convenience, the use of the term yield throughout this chapter will also include the concept of oxygen depletion. As in Chap. 36, the normalized yield is also aptly referred to as the "generation efficiency" of compound i. By definition, the normalized yields range from 0 to 1, and are thus good indicators of the completeness of combustion. For example, under complete combustion conditions the normalized yields of CO_2, H_2O, and O_2 are 1. As a fire burns more inefficiently, these yields decrease. The use of normalized yields is also useful for establishing mass balances. The conservation of carbon requires that

$$f_{CO} + f_{CO_2} + F_{THC} + f_{resid.C} = 1 \quad (16.4)$$

where f_{THC} is the normalized yield of gas-phase total hydrocarbons and $f_{resid.C}$ is the normalized yield of residual carbon, such as soot in smoke or high molecular weight hydrocarbons that condense out of the gas sample.

For two-layer systems the yield of all species except oxygen can be calculated as follows:

$$Y_i = \frac{X_{i_{wet}}(\dot{m}_f + \dot{m}_a)M_i}{\dot{m}_f M_{mix}} \quad (16.5)$$

where

$X_{i_{wet}}$ = The wet mole fraction of speciesi
$\dot{m}_a$ = The mass air entrainment rate into the upper layer
$\dot{m}_f$ = The mass loss rate of fuel
M_i = The molecular weight of speciesi
M_{mix} = The molecular weight of the mixture (typically assumed to be that of air)

The depletion rate of oxygen is calculated as

$$D_{O_2} = \frac{0.21\dot{m}_a M_{O_2}/M_a - X_{O_{2wet}}(\dot{m}_f + \dot{m}_a)M_{O_2}/M_{mix}}{\dot{m}_f} \quad (16.6)$$

The normalized yield, f_i, is simply calculated by dividing the yield by the maximum theoretical yield

$$f_i = \frac{Y_i}{k_i} \quad (16.7)$$

Typical operation of common gas analyzers requires that water be removed from the gas sample before entering the instrument. Consequently, the measured gas concentration is considered dry and will be higher than the actual wet concentration. Equation 16.8 can be used to calculate the wet mole fraction of species $X_{i_{wet}}$, from the measured dry mole fraction, $X_{i_{dry}}$. As can be seen from Equation 16.8, the percent difference between $X_{i_{dry}}$ and $X_{i_{wet}}$ is on the order of the actual H_2O concentration which, depending on conditions, is typically 10–20 % by volume.

$$X_{i_{wet}} = (1 - X_{H_2O_{wet}})X_{i_{dry}} \quad (16.8)$$

Reliable water concentration measurements are difficult to obtain. Therefore, investigators have calculated wet species concentrations using the above relationship with the assumption that the molar ratio, C, of H_2O to CO_2 at any equivalence ratio is equal to the calculated molar ratio at stoichiometric conditions [5, 6]. Based on this assumption, Equation 16.9 can be used to calculate wet species concentrations from dry concentration measurements.

$$X_{i_{wet}} = \frac{X_{i_{dry}}}{1 + CX_{CO_{2dry}}} \quad (16.9)$$

Equivalence Ratio

The concept of a global equivalence ratio (GER) can be used to express the overall ventilation of a control volume, such as a fire compartment. However, due to the complex interaction between the plume and the upper and lower layers, as well as the potential extension of the fire beyond the initial compartment, a unique definition for the GER does not exist. Therefore, if one uses the term GER, it must be associated with a defined control volume.

The first efforts in developing the GER concept were based on hood experiments [7–11] (e.g., as in Fig. 16.4) in which the idea of a plume equivalence ratio was introduced. The plume equivalence ratio, ϕ_p, is the ratio of the mass of fuel burning, m_f, to the mass of oxygen entrained, m_a, into the fire plume (below the upper layer) normalized by the stoichiometric fuel-to-oxygen ratio, r_{O_2}.

$$\phi_p = \frac{m_f/m_{O_2}}{r_{O_2}} \quad (16.10a)$$

Since oxygen is typically entrained into a fire plume via air, ϕ_p is commonly defined as

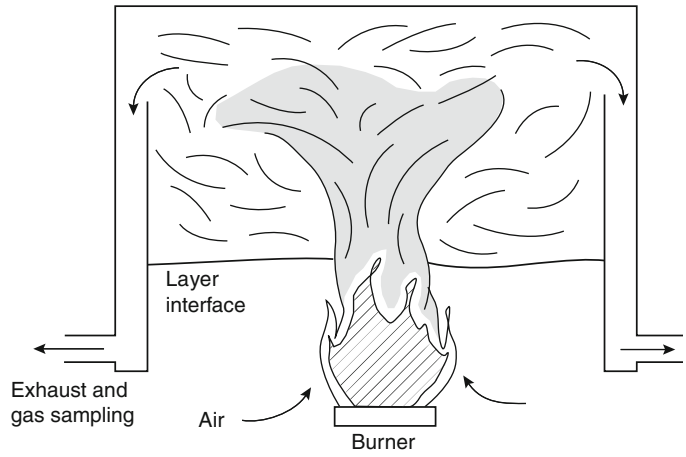

Fig. 16.4 Schematic of the two-layer system created in the hood experiments of Beyler [8, 9]

$$\phi_p = \frac{m_f/m_a}{r} \qquad (16.10b)$$

where m_a is the mass of air entrained into the plume (in the lower layer) and r is the stoichiometric mass fuel-to-air ratio. As discussed in the section on species production within fire compartments, this simple characterization of the equivalence ratio well represented the global conditions that existed in the first hood and compartment fire experimental configurations.

In order to more accurately describe the time integrated conditions within the upper layer, a second equivalence ratio was defined for this control volume [7, 10, 11]. The upper-layer equivalence ratio, ϕ_{ul}, is the ratio of the mass of the upper layer that originates from fuel sources, to the mass of the upper layer that originates from any source of air into the upper layer, divided by the stoichiometric fuel-to-air ratio.

The two equivalence ratios (ϕ_p and ϕ_{ul}) are not necessarily the same. As a fire grows, the upper-layer composition represents a collective time history of products. In an ideal two-layer fire, where all air enters the upper layer through the plume, ϕ_{ul} is the same as ϕ_p only during steady burning conditions. If the burning rate of the fire changes quickly compared to the residence time of the gases in the upper layer, the upper-layer equivalence ratio lags behind the plume equivalence ratio. The residence time, t_R, can be defined as the time required for a unit volume of air to move through the upper-layer volume, and can be characterized according to Equation 16.11.

$$t_R = \frac{V_{ul}\rho_{ul}}{\dot{m}_{\text{exhaust}}} \qquad (16.11)$$

where

$\dot{m}_{\text{exhaust}}$ = Mass flow rate of gases out of the layer (kg/s)
ρ_{ul} = Density of the upper-layer gases (kg/m^3)
V_{ul} = Volume of the upper layer (m^3)

For example, consider a compartment fire burning with a plume equivalence ratio of 0.5 with upper layer gases that have a residence time of 20 s. If the fire grows quickly such that ϕ_p increases to a value of 1.5 in about 5 s, ϕ_{ul} would now lag behind (less than 1.5). The fuel rich ($\phi_p = 1.5$) gas mixture from the plume is effectively diluted by the upper-layer gases since there has not been sufficient time (greater than 20 s) for the layer gases to change over. The result is that ϕ_{ul} will have a value between 0.5 and 1.5. Another instance when ϕ_{ul} can differ from ϕ_p is when additional fuel or air enters the upper layer directly. An example of this would be the burning of wood paneling in the upper layer.

The calculation of ϕ_{ul} can be a complex task. Either a fairly complete knowledge of the gas composition is needed [7] or time histories of ventilation flows and layer residence times are needed to be able to calculate ϕ_{ul}. Toner [7] and Morehart [12] present detailed methodologies

for calculating ϕ_{ul} from gas composition measurements. Equation 16.12 can be used to calculate ϕ_{ul} if the mass flow rates can be expressed as a function of time.

$$\phi_{ul} = \frac{1\int_{t-t_R}^{t} \dot{m}_f(t')dt'}{r\int_{t-t_R}^{t} \dot{m}_a(t')dt'} \tag{16.12}$$

Although termed the upper-layer equivalence ratio, ϕ_{ul} actually represents the temporal aspect of the equivalence ratio no matter what the control volume. For instance, the control volume may be the whole compartment, as shown in Fig. 16.1. In this case, the compartment equivalence ratio, ϕ_c, is defined as the ratio of the mass, m_f, of any fuel entering or burning in the compartment to the mass, m_a, of air entering the compartment normalized by the stoichiometric fuel-to-air ratio.

In a compartment fire, air is typically drawn into the space through a door or window style vent. If all of the air drawn into the compartment is entrained into the lower layer portion of the plume, then the plume equivalence ratio can be an adequate representation of the fire environment. However, if layer burning occurs, or multiple vents cause air to enter the upper layer directly, the use of a compartment equivalence ratio is more appropriate. As a practical note, for fires within a single compartment, the equivalence ratio is calculated (and experimentally measured) based on the instantaneous fuel mass loss rate, $\dot{m}_f$, and air flow rate, $\dot{m}_a$, into the compartment (Equation 16.13a).

$$\phi = \frac{\dot{m}_f \dot{m}_a}{r} \tag{16.13a}$$

As noted previously, r is defined as the stoichiometric fuel-to-air ratio. Unfortunately, the ratio r is sometimes defined as the air-to-fuel ratio, r_a. Therefore, consideration must be given to values obtained from tabulated data. Keeping with the nomenclature of this chapter, the equivalence ratio can also be expressed as

$$\phi = \frac{\dot{m}_f}{\dot{m}_a} \cdot r_a = \frac{\dot{m}_f}{\dot{m}_a} \frac{r_o}{Y_{O_2,\text{air}}} \tag{16.13b}$$

where

r_a = Mass air-to-fuel ratio
r_o = Oxygen-to-fuel mass ratio
$Y_{O_2,\text{air}}$ = Mass fraction of oxygen in air (0.23)

The formulation of Equation 16.13b allows direct use of values tabulated for various fuels in Appendix 3, Table 3.2, of this handbook. Another useful expression for ϕ can be derived from Equation 16.13b by multiplying the numerator and denominator by the fuel heat of combustion, Δh_c, and recognizing that the heat release per mass of oxygen consumed, E, is equal to Δh_c over r_o, yielding

$$\phi = \frac{\dot{Q}}{\dot{m}_a} \cdot \frac{1}{EY_{O_2,\text{air}}} = \frac{\dot{Q}}{\dot{m}_a} \cdot \frac{1}{3030} \tag{16.13c}$$

where

$\dot{Q}$ = Ideal heat release rate of the fire (kW)
$\dot{m}_a$ = Air flow rate (kg/s)
$E \approx 13{,}100$ kJ/kg (Drysdale [13])

Note that Q is the ideal heat release rate, which is determined by multiplying the mass loss rate by the heat of combustion, and is not limited by the amount of air flowing into the compartment or control volume. To date, Equation 16.13c has not been utilized in the literature and therefore has not been well established. However, it offers a convenient means to calculate the equivalence ratio without the need to know the fuel chemistry.

The equivalence ratio is an indicator of two distinct burning regimes, overventilated (fuel lean) and underventilated (fuel rich). Overventilated conditions are represented by equivalence ratios less than one, while underventilated conditions are represented by equivalence ratios greater than one. An equivalence ratio of unity signifies stoichiometric burning, which, in an ideal process, represents complete combustion of the fuel to CO_2 and H_2O with no

excess oxygen. During underventilated conditions there is insufficient oxygen to completely burn the fuel; therefore, products of combustion will also include excess fuel (hydrocarbons), carbon monoxide, and hydrogen. It follows that the highest levels of CO production in flaming fires is expected when underventilated conditions occur in the compartment on fire. This basic chemistry also suggests that species production can be correlated with respect to the equivalence ratio. Although the not-so-ideal behavior of actual fires prevents accurate theoretical prediction of products of combustion, experimental correlations have been established.

A simple model for the most complete combustion of a fuel can be represented by the following expressions: [8]

$$f_{CO_2} = f_{O_2} = f_{H_2O} = 1 \quad \text{for } \phi < 1 \tag{16.14a}$$

$$f_{CO_2} = f_{O_2} = f_{H_2O} = 1/\phi \quad \text{for } \phi > 1 \tag{16.14b}$$

$$f_{CO} = f_{H_2} = 0 \quad \text{for all } \phi \tag{16.14c}$$

$$f_{THC} = 0 \quad \text{for } \phi < 1 \tag{16.14d}$$

$$f_{THC} = 1 - 1/\phi \quad \text{for } \phi < 1 \tag{16.14e}$$

These expressions assume that for ϕ greater than 1, all excess fuel can be characterized as unburned hydrocarbons. Since compartment fire experiments have shown that significant levels of both CO and H_2 are produced at higher equivalence ratios, Expression 16.14c is not always representative, and reveals a shortcoming of assuming this simple ideal behavior. However, for the products of complete combustion (CO_2, O_2, and H_2O), this model serves as a good benchmark for comparison of experimental results.

Example 1 Consider a piece of cushioned furniture to be primarily polyurethane foam. The nominal chemical formula of the foam is $CH_{1.74}O_{0.323}\,N_{0.07}$. Calculate the stoichiometric fuel-to-air ratio, the maximum yields of CO, CO_2, and H_2O, and the maximum depletion of O_2.

Solution For complete combustion of the fuel to CO_2 and H_2O, the following chemical equation can be written

$$CH_{1.74}O_{0.323}N_{0.07} + 1.2735(O_2 + 3.76\,N_2) \rightarrow 1.0CO_2 + 0.87H_2O + 4.823N_2$$

The molecular weight of the fuel, M_f, $= 1(12) + 1.74(1) + 0.323(16) + 0.07(14) = 19.888$.

The stoichiometric fuel-to-air ratio is

$$r = \frac{(1 \text{ mole fuel})\,(M_f)}{(\text{moles of air})\,(M_a)} = \frac{19.888}{1.2735\,(4.76)\,(28.8)}$$

$$r = 0.1139$$

The stoichiometric air-to-fuel ratio is

$$\frac{1}{r} = 8.78$$

The maximum yield of CO (i.e., k_{CO}), is calculated by assuming that all carbon in the fuel is converted to CO. Therefore, the number of moles of CO formed, n_{CO}, equals the number of moles of carbon in one mole of fuel. For the polyurethane foam, $n_{CO} = 1$.

$$k_{CO} = \frac{n_{CO}(M_{CO})}{n_f(M_{fuel})} = \frac{(1)\,(28)}{(1)\,(19.888)} = 1.41$$

Similarly, k_{CO_2} and k_{H_2O} are calculated as

$$k_{CO_2} = \frac{(1)\,(44)}{19.888} = 2.21$$

$$k_{H_2O} = \frac{(0.87)\,(18)}{19.888} = 0.787$$

The maximum depletion of oxygen, k_{O_2}, refers to the mass of oxygen needed to completely combust one mole of fuel to CO_2 and H_2O. This is the same as the stoichiometric requirement of oxygen.

$$k_{O_2} = \frac{n_{O_2}(M_{O_2})}{n_f M_f} \quad \frac{(1.2735)\,(32)}{(1)19.888} = 2.05$$

Example 2
The fuel specified in Example 1 is burning at a rate of 9 g/s and entraining air at a rate of 56 g/s. Measurements of the upper layer gas composition reveal dry concentrations of 3.7 % by volume CO, 14.3 % CO_2, and 0.49 % O_2. Correct the concentrations for the water removed during the gas analysis process (i.e., calculate the wet concentrations).

Solution In order to use Equation 16.9 to calculate the wet mole fractions, the stoichiometric molar ratio of H_2O to CO_2 for C needs to be calculated. This ratio is simply obtained from the stoichiometric chemical equation in Example 1.

$$C = \frac{n_{H_2O}}{n_{CO_2}} = \frac{0.87}{1} = 0.87$$

Once C is obtained, the wet mole fractions can be calculated as

$$X_{CO_{wet}} = \frac{0.037}{1 + 0.87(0.143)} = 0.033$$

$$X_{CO_{2wet}} = \frac{0.143}{1 + 0.87(0.143)} = 0.127$$

$$X_{O_{2wet}} = \frac{0.0049}{1 + 0.87(0.143)} = 0.0044$$

The estimated mole fraction of water is

$$X_{H_2O} = CX_{CO_{2wet}} = 0.87(0.127) = 0.11$$

Therefore, the corrected gas concentrations on a percent volume basis are 3.3 % CO, 12.7 % CO_2, and 0.44 % O_2.

Example 3 Continuing from Example 2, calculate the yields and normalized yields for each species measured. The wet mole fractions are $X_{CO_{wet}} = 0.033$, $X_{CO_{2wet}} = 0.127$, and $X_{O_{2wet}} = 0.0044$.

Solution Using Equations 16.5 and 16.7, the yield and normalized yield of CO, CO_2, and H_2O can be calculated. The maximum yields calculated in Example 1 are $k_{CO} = 1.41$, $k_{CO_2} = 2.21$, $k_{H_2O} = 0.787$, and $k_{O_2} = 2.05$.

$$Y_{CO} = \frac{X_{CO_{wet}}(\dot{m}_f + m_a)M_{CO}}{\dot{m}_f M_a} = \frac{(0.033)(9+56)(28)}{9(28.8)} = 0.23$$

$$f_{CO} = \frac{Y_{CO}}{k_{CO}} = \frac{0.23}{1.41} = 0.16$$

$$Y_{CO_2} = \frac{(0.127)(9+56)(44)}{9(28.8)} = 1.40$$

$$f_{CO_2} = \frac{1.40}{2.21} = 0.63$$

$$Y_{H_2O} = \frac{(0.11)(9+56)(18)}{9(28.8)} = 0.50$$

$$f_{H_2O} = \frac{0.50}{0.787} = 0.63$$

The depletion of oxygen is calculated using Equation 16.6, assuming the molecular weight of the gas mixture, M_{mix}, to be approximately that of air.

$$D_{O_2} = \frac{0.21\dot{m}_a M_{O_2}/M_a - X_{O_{2wet}}(\dot{m}_f + \dot{m}_a)M_{O_2}/M_{mix}}{\dot{m}f}$$

$$D_{O_2} = \frac{0.21(56)32/28.8 - 0.0044(9+56)32/28.8}{9}$$

$$D_{O_2} = 1.42$$

The normalized yield is calculated as

$$f_{O_2} = \frac{D_{O_2}}{k_{O_2}} = \frac{1.42}{2.05} = 0.69$$

Species Production Within Fire Compartments

Hood Experiments

Beyler [8, 9] was the first to publish major species production rates in a small-scale two-layer environment. The experiments performed consisted of situating a burner under a 1-m-diameter, insulated collection hood. The result was the formation of a layer of combustion products in the hood similar to that found in a two-layer compartment fire (see Fig. 16.4). By varying the fuel supply rates and the distance between the burner and layer interface, and, consequently, the air entrainment rate, a range of

equivalence ratios was obtained. Layer gases were exhausted at a constant, metered flow rate from the periphery of the hood at a depth of 15 cm below the ceiling. The general procedure was to allow steady-state burning conditions to develop, so the layer maintained a constant depth below the exhaust flow location. Tests revealed a reasonably well-mixed uniform layer both in temperature and chemical composition during the steady-state conditions. Gas analysis was performed on samples taken from the exhaust stream. Table 16.1 shows the physicochemical properties of the fuels tested.

Beyler's results show that species yields correlate very well with the plume equivalence ratio. Figure 16.5 shows normalized yields of major species for propane fires plotted against the plume equivalence ratio. The trends seen in these plots for propane are fairly representative of the other fuels tested. For overventilated conditions, the yield of CO_2 and H_2O and depletion of O_2 are at a maximum, and there is virtually no production of CO, H_2, or unburned hydrocarbons (*THC*). As underventilated burning conditions ($\phi \geq 1$) are approached, products of incomplete combustion (CO, H_2, and *THC*) are generated.

For comparison, the expressions for ideal complete combustion (Equations 16.14a, 16.14b, 16.14c, 16.14d, and 16.14e) are shown on each plot in Fig. 16.5. The CO_2 yield departs from Equation 16.14b as CO production increases at higher equivalence ratios. This departure, which is fairly independent of ϕ for $\phi > 1$, has been described by the yield coefficient [5]. The ratios of the normalized yield of CO_2, H_2O, or normalized depletion of O_2 to the theoretical maximums expressed by Equations 16.14a, 16.14b, 16.14c, 16.14d, and 16.14e are defined as the yield coefficients, B_{CO_2}, B_{H_2O}, and B_{O_2} respectively [5].

$$B_{CO_2} = \frac{f_{CO_2}}{1} \qquad \text{for } \phi < 1 \qquad (16.15a)$$

$$B_{CO_2} = \frac{f_{CO_2}}{1/\phi} \qquad \text{for } \phi > 1 \qquad (16.15b)$$

$$B_{H_2O} = \frac{f_{H_2O}}{1} \qquad \text{for } \phi < 1 \qquad (16.16a)$$

$$B_{H_2O} = \frac{f_{H_2O}}{1/\phi} \qquad \text{for } \phi > 1 \qquad (16.16b)$$

$$B_{O_2} = \frac{f_{O_2}}{1} \qquad \text{for } \phi < 1 \qquad (16.17a)$$

Table 16.1 Physicochemical data for selected fuels

Fuel	Empirical chemical formula of volatiles	Empirical molecular weight	Maximum theoretical yields				
			k_{CO}	k_{CO_2}	k_{O_2}	k_{H_2O}	$1/r^c$
Acetone	C_3H_6O	58	1.45	2.28	2.21	0.93	9.45
Ethanol	C_2H_5OH	46	1.22	1.91	2.09	1.17	8.94
Hexane	C_6H_{14}	86	1.95	3.07	3.53	1.47	15.1
Isopropanol	C_3H_7OH	60	1.40	2.20	2.40	1.20	10.3
Methane	CH_4	16	1.75	2.75	4.00	2.25	17.2
Methanol	CH_3OH	32	0.88	1.38	1.50	1.13	6.43
Propane	C_3H_8	44	1.91	3.00	3.64	1.64	15.6
Propene	C_3H_6	42	2.00	3.14	3.43	1.29	14.7
Polyurethane foam	$CH_{1.74}O_{0.323}\ N_{0.0698}$	20	1.41	2.21	2.05	0.79	8.78
Polymethylmethacrylate	$C_5H_8O_2$	100	1.40	2.20	1.92	0.72	8.23
Toluene	C_7H_8	92	2.13	3.35	3.13	0.78	13.4
Wood (ponderosa pine[a])	$C_{0.95}H_{2.4}O$	30	0.89	1.40	1.13	0.73	4.83
Wood (spruce[b])	$CH_{3.584}O_{1.55}$	40	0.69	1.09	0.89	0.80	3.87

[a]From Beyler [9] chemical formula estimated from $\phi < 1$ yield data
[b]Gottuk et al. [5]
[c]r = stoichiometric fuel-to-air ratio

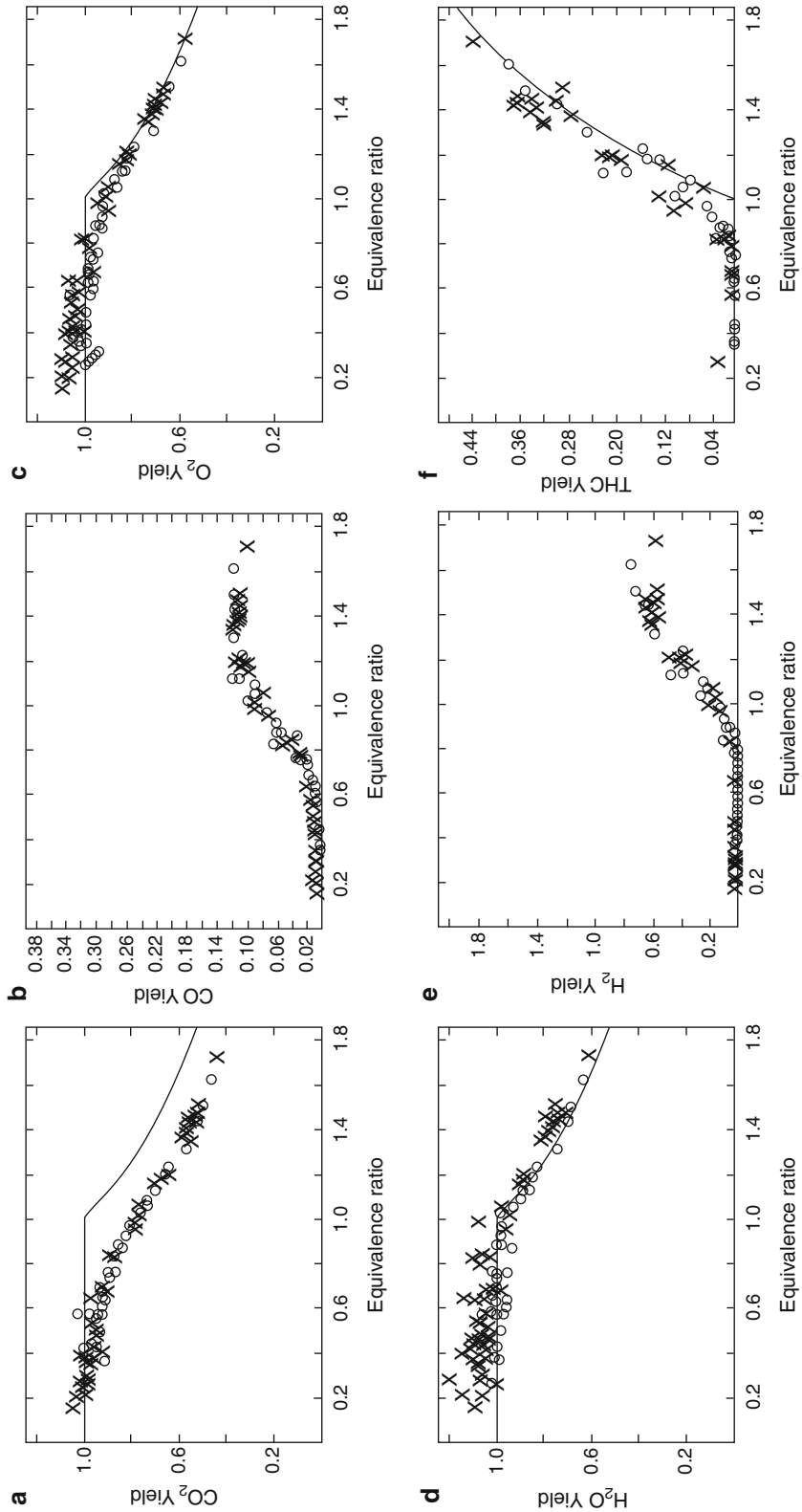

Fig. 16.5 Normalized yields of measured chemical species as a function of the equivalence ratio for propane experiments using a 13 cm (o) or 19 cm (x) burner with supply rates corresponding to 8 to 32 kW theoretical heat release rate [8]

$$B_{O_2} = \frac{f_{O_2}}{1/\phi} \quad \text{for } \phi > 1 \qquad (16.17b)$$

These terms are useful in discussing characteristics of the combustion efficiency. For example, an O_2 yield of 1 indicates complete utilization of available O_2. In the case of CO_2 and H_2O, deviation from the model (as indicated by B_{CO_2} or $B_{H_2O} < 1$) is a measure of the degree of incomplete combustion. It can be seen from Fig. 16.5 that the production of CO is primarily at the expense of CO_2 (i.e., B_{O_2} and B_{H_2O} remain nearly 1, while B_{CO_2} is about 0.8). Table 16.2 shows average yield coefficients for underventilated fires.

Figure 16.6 shows unnormalized CO yields plotted against the plume equivalence ratio for fuels tested by Beyler [8, 9]. The correlations agree quite well for all fuels. Below an equivalence ratio of 0.6, minimal CO production is observed. Above ϕ_p equal to 0.6, carbon monoxide yield increases with ϕ_p and, for most fuels, tends to level out at equivalence ratios greater than 1.2. Toluene, which creates large amounts of soot, is anomalous compared to the other fuels studied. As can be seen in Fig. 16.6, the CO yields from toluene fires remain fairly constant at about 0.09 for both overventilated and underventilated burning conditions.

It should be noted that Beyler originally presented all correlations with normalized yields, f_{CO}. However, better agreement is found between unnormalized CO yield-equivalence ratio correlations for different fuels, Y_{CO} (shown in Fig. 16.6), rather than normalized yields. One point of interest, though, is that when CO production is correlated as normalized yield, a more distinct separation of the data occurs for ϕ_p greater than 1. The degree of carbon monoxide production (represented as f_{CO}) during underventilated conditions can be ranked by chemical structure according to oxygenated hydrocarbons greater than hydrocarbons greater than aromatics. This ranking is not observed for unnormalized yield correlations.

Toner et al. [7] and Zukoski et al. [10, 11] performed similar hood experiments with a different experimental setup. The hood used was a 1.2 m cube, insulated on the inside with ceramic fiber insulation board. The layer in the hood formed to the lower edges where layer gases were allowed to spill out. Gas sampling was done using an

Table 16.2 Average yield coefficients and upper-layer temperatures for underventilated fires[a] (values in parentheses are standard deviations)

Fuel	B_{CO_2}	B_{O_2}	B_{H_2O}	Temperature (K)	Reference
Acetone	0.78 (0.03)	0.92 (0.04)	0.99 (0.04)	529 (76)	Beyler [8]
Ethanol	0.79 (0.01)	0.97 (0.01)	1.00 (0.04)	523 (72)	Beyler [8]
Hexane	0.61 (0.10)	0.82 (0.02)	0.87 (0.03)	529 (25)	Beyler [8]
Hexane	0.83 (0.05)	0.96 (0.06)	NA	1038 (62)	Gottuk et al. [5]
Isopropanol	0.75 (0.01)	0.89 (0.01)	0.96 (0.01)	513 (33)	Beyler [8]
Methane	0.80 (0.05)	1.00 (0.04)	1.01 (0.03)	713 (101)	Toner et al. [7]
Methane	0.69 (0.03)	0.87 (0.07)	0.86 (0.06)	547 (12)	Morehart et al. [12]
Methanol	0.79 (0.03)	0.99 (0.00)	0.94 (0.02)	566 (53)	Beyler [8]
Propane	0.78 (0.05)	0.97 (0.03)	1.05 (0.04)	557 (62)	Beyler [8]
Propene	0.77 (0.08)	0.92 (0.08)	1.02 (0.10)	629 (51)	Beyler [8]
Polyurethane foam	0.87 (0.04)	0.97 (0.02)	NA	910 (122)	Gottuk et al. [5]
Polymethylmethacrylate	0.77 (0.06)	0.92 (0.19)	0.72 (0.04)	525 (37)	Beyler [9]
Polymethylmethacrylate	0.93 (0.04)	0.98 (0.04)	NA	1165 (126)	Gottuk et al. [5]
Toluene	0.57 (0.04)	0.62 (0.05)	0.78 (0.03)	509 (23)	Beyler [8]
Wood (ponderosa pine)	0.85 (0.05)	0.89 (0.03)	0.79 (0.10)	537 (37)	Beyler [9]
Wood (spruce)	0.90 (0.00)	0.95 (0.00)	NA	890 (0)	Gottuk et al. [5]

[a]Values have been calculated from data found in the cited references. Values for Toner et al. [7], Beyler [8], Beyler [9], and Morehart et al. [12] are from hood experiments, and values for Gottuk et al. [5] are for a reduced-scale enclosure

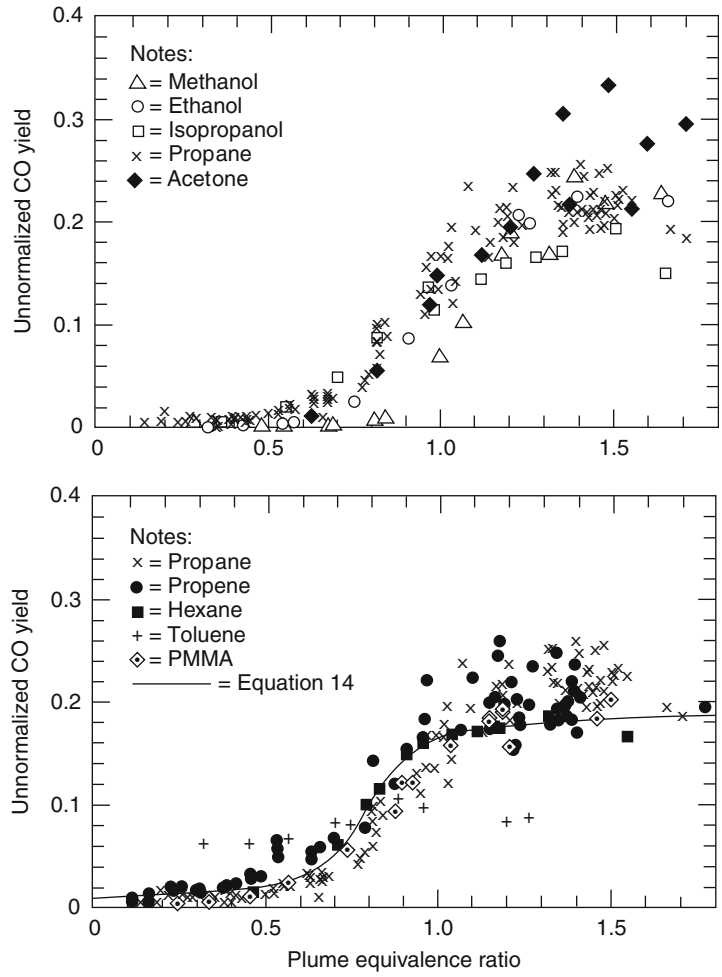

Fig. 16.6 Unnormalized carbon monoxide yields as a function of the plume equivalence ratio for various fuels studied by Beyler in a hood apparatus [8, 9]

uncooled stainless-steel probe inserted into the layer. Detailed gas species measurements were made using a gas chromatograph system. The upper-layer equivalence ratio was determined from conservation of atoms using the chemical species measurements, the measured composition of the fuel, and the metered fuel flow rate. Natural gas flames with heat release rates of 20–200 kW on a 19-cm-diameter burner were studied. The layer in the hood was allowed to form and reach a steady-state condition before gas sampling was performed.

It was concluded that species concentrations were well correlated to the upper-layer equivalence ratio, ϕ_{ul}, and insensitive to temperatures for the range studied (490–870 K). Since these experiments were conducted during steady-state conditions, with mean upper-layer residence times of about 25–180 s, it can be concluded that ϕ_p and ϕ_{ul} were equal.

The data of Toner et al. [7] have been used to plot CO and CH_4 yields versus upper-layer equivalence ratio in Figs. 16.7 and 16.8, respectively. The correlations are qualitatively similar to the correlations obtained by Beyler for different fuels. An analysis of these test results also showed that normalized CO_2 and O_2 yield versus equivalence ratio data is represented reasonably well by Equations 16.15, 16.16, and 16.17. Similar to Beyler's propane results, the average B_{O_2} value is about 1 and B_{CO_2} is 0.8 for underventilated burning conditions (the use of yield coefficients is discussed further in the section on engineering correlations).

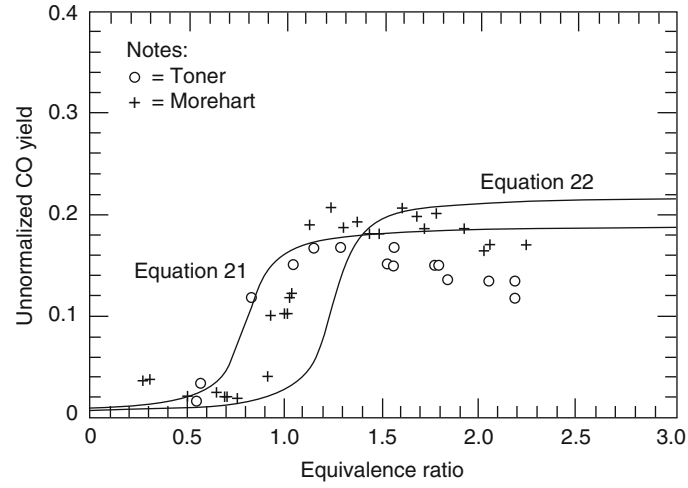

Fig. 16.7 Unnormalized carbon monoxide yields as a function of equivalence ratio for methane fires studied by Toner et al. [7] and Morehart et al. [12] in hood experiments

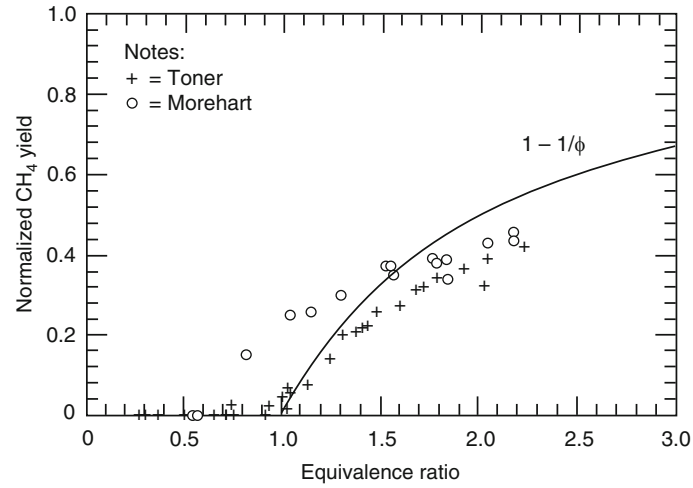

Fig. 16.8 Normalized yields as a function of equivalence ratio for methane fires studied by Toner et al. [7] and Morehart et al. [12] in hood experiments

Toner compared the measured species concentrations to the calculated equilibrium composition of the reactants at constant temperature and pressure. The layer composition was modeled quite well by the chemical equilibrium composition for very overventilated conditions but not for underventilated conditions. His observance of CO production for near-stoichiometric and underventilated fires, at the expense of CO_2 production, led them to suggest that the oxidation of CO was "frozen out" before completion. (At low temperatures, there is insufficient energy for CO to chemically react to CO_2.) [7] Since the results showed that species production was independent of temperature for the range studied (490–870 K), Toner et al. concluded that, if a freeze-out temperature existed, it must be higher than 900 K. Work by Pitts [14] and by Gottuk et al. [15], discussed later, shows that a freeze-out temperature does exist in the range of 800–900 K, depending on other factors.

Zukoski, Morehart, et al. [11] performed a second series of tests similar to that described above for Zukoski et al. [10] and Toner et al. Much of the same apparatus was used except for a different collection hood. The hood, 1.8 m square by 1.2 m high, was larger than that used by Toner et al. and was uninsulated.

Morehart et al. [12] experiments consisted of establishing steady-state burning conditions such

that the burner-to-layer interface height was constant. A constant ϕ_p was maintained based on this constant interface height in conjunction with the fact that the mass burning rate of fuel was metered at a constant rate. Additional air was then injected into the upper layer at a known flow rate until a new steady-state condition was achieved. This procedure established a ϕ_{ul} that was lower than the ϕ_p, since ϕ_p was based on the ratio of the mass burning rate to the mass of air entrained into the plume from room air below the layer interface. By increasing the air supply rate to the upper layer, a range of ϕ_{ul} was established while maintaining a constant ϕ_p.

Although similar, the correlations obtained by Morehart et al. deviated from those obtained by Toner et al. Figs. 16.7 and 16.8 compare the CO and CH_4 yields calculated from the data of Morehart et al. with the yields calculated from the data of Toner et al. For overventilated conditions, Morehart et al. observed higher CO and CH_4 yields, signifying that the fires conducted by Morehart et al. burned less completely. For underventilated methane fires, Morehart et al. observed lower CO, CO_2, and H_2O and higher CH_4 and O_2 concentrations than Toner et al. The only apparent differences between experiments was that Morehart found layer temperatures were 120–200 K lower for fires with the same equivalence ratio as those observed by Toner, that is, they ranged from 488 to 675 K. Due to the similarity in experimental apparatus, except for the hood, Morehart concluded that the temperature difference resulted from having a larger uninsulated hood.

Morehart studied the effect of increasing temperature on layer composition by adding different levels of insulation to the hood. Except for the insulation, the test conditions (e.g., ϕ of 1.45 and layer interface height) were held constant. Residence times of layer gases in the hood were in the range of 200–300 s. For the range of temperatures studied (500–675 K), substantial increases in products of complete combustion (i.e., CO_2 and H_2O) and decreases in fuel and oxygen occurred with increasing layer temperature. Upper-layer oxygen mass fraction was reduced by approximately 70 % and methane was reduced by 25 % [11, 12]. Excluding one outlier data point, CO concentrations increased by 25 %. This is an important result. Although the gas temperatures were well below 800 K, an increase in the layer temperature resulted in more fuel being combusted to products of complete combustion and additional CO (see the section "Chemical Kinetics" later in this chapter).

Compartment Fire Experiments

The hood experiments performed by Beyler and Zukoski et al. differ from actual compartment fires in several ways. The hood setup allowed considerable radiation to the lab space below. Conversely, a real compartment would contain most of the radiation, thus resulting in higher wall and upper-layer temperatures. Consequently, higher fuel mass loss rates for pool fires would be expected for an actual compartment fire. Also, the hood setup results in a lower layer that has an infinite supply of air which is neither vitiated nor heated. In a real compartment fire, the air supply is limited by ventilation openings (doors, windows, etc.) and the depth of the upper layer. The air that is entrained into the lower layer of an actual compartment fire can be convectively heated by hot compartment surfaces prior to fire plume entrainment. The hood experiments did not include any significant ceiling and wall flame jets. These dynamic flame structures enhance mixing of the upper layer in actual compartment fires and extend the flame zone beyond the plume. Lastly, the hood experiment correlations were developed from sustained steady-state burning conditions. Actual fires of interest are usually in a continual growth stage, and, thus, are more transient in nature.

Tewarson reported that CO and CO_2 yields and O_2 depletion were correlated well by the air-to-fuel stoichiometric fraction (i.e., the reciprocal of the equivalence ratio) for wood crib enclosure fires [16]. Enclosure fire data was taken from previous work in the literature for cellulosic-base fiberboard and pine wood cribs burned in various compartment geometries, 0.21–21.8 m^3 in volume, with single and dual

horizontal and vertical openings centered on the end walls. Additional data were obtained for pine wood cribs burned in a small-scale flammability apparatus that exposed the samples to variable external radiant heat fluxes with either natural or forced airflow from below.

The characteristics of the correlations presented by Tewarson are similar to the correlations developed by Beyler. The CO_2 yield and O_2 depletion are relatively constant for low equivalence ratios and decrease sharply as the equivalence ratio increases for underventilated conditions. The CO yield correlates with the equivalence ratio but with a fair amount of scatter in the data.

Due to the lack of measurements, the air entrainment rate used to calculate the mass air-to-fuel ratio was estimated from the ventilation parameter, $Ah^{1/2}$, where A is the cross-sectional area and h is the height of the vent. Although the general shape of the correlations are valid, the use of the ventilation parameter assumption causes the equivalence ratio data to be suspect. In addition, the elemental composition of the fuel volatiles for the wood was not corrected for char yield. A correction of this sort would tend to decrease the calculated equivalence ratio and increase the CO and CO_2 yields.

Gottuk et al. [5, 17] conducted reduced-scale compartment fire tests specifically designed to determine the yield-equivalence ratio correlations that exist for various fuels burning in a compartment fire. A 2.2 m^3 (1.2 m $\times$ 1.5 m $\times$ 1.2 m high) test compartment was used to investigate the burning of hexane, PMMA, spruce, and flexible polyurethane foam. The test compartment was specially designed with a two-ventilation path system that allowed the direct measurement of the air entrainment rate and the fuel volatilization rate. The setup created a two-layer system by establishing a buoyancy-driven flow of air from inlet vents along the floor, up through the plume, and exhausting through a window-style exhaust vent in the upper layer. There was no inflow of air through the exhaust vent. The upper-layer gas mixture was sampled using an uncooled stainless steel probe placed into the compartment through the center of the exhaust vent. This location for the probe was chosen after species concentration and temperature measurements, taken at several locations in the upper layer, showed a well-mixed, uniform layer.

Table 16.1 shows the physicochemical properties used for the four fuels. It should be noted that in determining properties of a fuel, such as maximum yields or the stoichiometric fuel-to-air ratio, the chemical formula must characterize the volatiles, not necessarily the base fuel. For liquid fuels or simple polymers, such as PMMA, the composition of the volatiles is the same as the base fuel. However, more complex fuels can char or contain nonvolatile fillers, as found in polyurethane foams. As a result, the composition of the volatiles differs from that of the base material. As an example, the composition of the wood volatiles used in this study was obtained by adjusting the analyzed wood composition for an observed average of 25 % char [5].

The results of these compartment tests showed similarities to Beyler's hood experiments. However, some significant quantitative differences exist. Figure 16.9 compares the CO yield correlations from Beyler's hood study and that of these compartment tests for hexane fires. This plot illustrates the primary difference observed between the hood and compartment hexane and PMMA fire test results. An offset exists between the rise in CO yield for the two studies. For the hood experiments, higher CO production was observed for overventilated ($\phi_p < 1$) and slightly underventilated burning conditions. For the compartment fire experiments, negligible CO was produced until underventilated conditions were reached. Consistent with the increased CO production and the conservation of carbon, CO_2 yields were lower for the hood experiments compared to the compartment fires. The spruce and polyurethane compartment fires produced similar CO yield-equivalence ratio correlations to those observed by Beyler in hood experiments (i.e., high CO yields were observed for overventilated fires).

The differences in CO formation can be explained in terms of temperature effects. For the region of discrepancy between equivalence

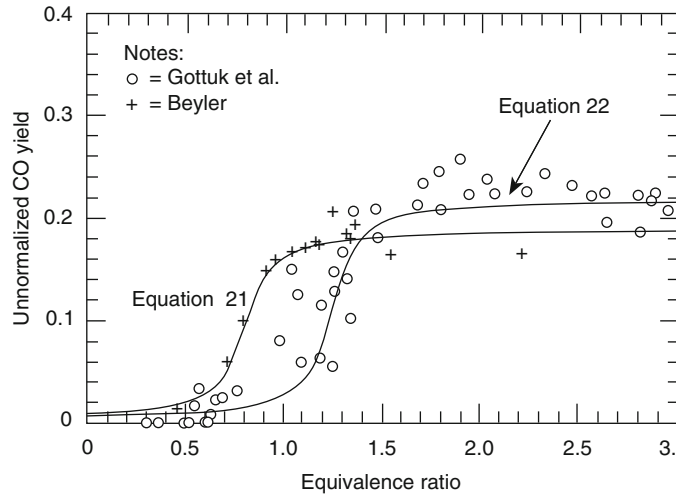

Fig. 16.9 Comparison of unnormalized CO yield correlations for hexane fires in a compartment and under a hood apparatus. (Figure taken from Gottuk et al. [5])

ratios of 0.5 and 1.5, upper-layer temperatures in Beyler's hood experiments and the spruce and polyurethane compartment fire experiments were typically below 850 K, whereas temperatures for the hexane and PMMA fires were above 920 K (temperatures typically associated with postflashover fires) [18].

As is detailed in the section on chemical kinetics, the temperature range between 800 and 900 K is a transition range over which the oxidation of CO to CO_2 changes from a very slow to a fast reaction. That is, for upper-layer temperatures below 800 K, the conversion of CO to CO_2 does not occur at an appreciable rate to affect CO yields. Since the oxidation of a fuel first results in the production of CO, which then further reacts to form CO_2, the low temperatures (<800 K) prevent CO from oxidizing. This results in high CO yields. For temperatures greater than 900 K, the reactions that convert CO to CO_2 occur faster as temperature increases. Therefore, for the overventilated conditions discussed above, the high temperatures associated with the hexane and PMMA compartment fires resulted in virtually all CO being oxidized to CO_2 for $\phi_p < 1$.

Overall, the compartment fire test results revealed that the production of CO is primarily dependent on the compartment flow dynamics (i.e., the equivalence ratio) and the upper-layer temperature.

The National Institute of Standards and Technology (NIST), Building and Fire Research Laboratory, has also performed reduced-scale compartment fire experiments using a natural gas burner for the heat source [6]. The compartment (0.98 m × 1.46 m × 0.98 m high) had a single ventilation opening consisting of a 0.48 m wide by 0.81 m high doorway. A large number of tests were conducted covering a range of heat release rates from 7 to 650 kW. Fires greater than 150 kW resulted in upper-layer temperatures greater than 870 K and flames 0.5–1.5 m out of the door. This single ventilation opening and the large fires (up to 650 kW) produced nonuniform upper-layer conditions. For fires with heat release rates greater than about 250 kW ($\phi > 1.5$), carbon monoxide concentrations in the front of the compartment were approximately 30–60 % higher than in the rear. Temperature gradients of 200–300 °C were observed from the back to the front of the compartment. Due to the nonuniform air entrainment at the base of the fire and possible mixing of additional air near the front, it is difficult to determine the local equivalence ratio for each region. The concentration gradient from front to rear of the compartment may have been due to differences in the local equivalence ratios. Nonetheless, plots of concentration measurements in the rear of the compartment versus equivalence ratio are quite similar to the data of Zukoski

et al. and Toner et al. Yield data for these results have not been reported.

A second set of experiments was performed by NIST to investigate the generation of CO in wood-lined compartments [19]. Douglas fir plywood (6.4 mm thick) was lined on the ceiling and on the top 36 cm of the walls of the compartment described above. Natural gas fires ranging from 40 to 600 kW were burned in the compartment. The results showed that, for tests in which wood pyrolysis occurred, increased levels of CO were observed compared to burning the natural gas alone. Carbon monoxide concentrations (dry) reached levels of 7 % in the front and 14 % in the rear of the compartment. These are extremely high concentrations compared to the peak levels of 2–4 % observed in the unlined compartment fire tests with the methane burner only. Typical peak CO concentrations observed for a range of fuels (including wood) in hood experiments [8–11] and the compartment fire experiments of Gottuk et al. [5] also ranged from 2 % to 4 %. However, concentrations greater than 5 % have also been reported for cellulosic fuels burning in enclosures [16, 20].

Since wood is an oxygenated fuel, it does not require additional oxygen from entrained air to form CO. This enhances the ability of the wood to generate CO in a vitiated atmosphere. Therefore, there are two reasons that high CO concentrations can result in fires with oxygenated fuels in the upper layer. First, the fuel-bound oxygen allows the fuel to generate CO during pyrolysis. Second, due to preferential oxidation of hydrocarbons over CO, the limited oxygen in the upper layer reacts with the pyrolyzing wood to form additional CO. Aspects of this chemistry are discussed in the next section.

These initial test results for fires with wood on the walls and ceiling emphasized the importance of adding additional fuel to the upper layer. The practical implications are significant, as many structures have cellulosic-based wall coverings and other combustible interior finishes. Because of the initial studies by NIST, Lattimer et al. [21] conducted a series of tests to evaluate the effect on species production from the addition of wood in the upper layer of a reduced-scale enclosure fire. The enclosure was the same as used by Gottuk et al. [5], measuring 1.5 m wide, 1.2 m high, and 1.2 m deep. Two primary sets of tests were conducted for cases with and without Douglas fir plywood suspended below the ceiling, with (1) a 0.12 m^2 window vent opening and (2) a 0.375 m^2 doorway opening, both leading to a hallway.

In the compartment with a window opening and wood burning in the upper layer, Lattimer et al. measured CO concentrations of 10 % on average, which is nearly three times greater than the levels measured without the wood. Peak concentrations were as high as 14 %, the same as measured by Pitts et al. [19] CO concentrations were similarly high when the doorway opening was used. In this case, the quasi-steady state average CO concentrations were 8 % with peaks greater than 10.6 % with wood compared to approximately 5.7 % average levels with a doorway vent and no wood. Regardless of the vent opening, these tests showed that wood in the upper layer resulted in CO concentrations increasing dramatically (10.1 %, vs. 3.2 % without wood) with only small increases in the CO_2 concentrations (11.6 %, vs. 10.4 % without wood). These trends are summarized in Table 16.3, which presents the

Table 16.3 Summary of quasi-steady state average species concentrations (percent volume dry) for underventilated reduced-scale compartment fire tests with and without wood in the upper layer [21, 22]

Window vent tests [21]	No wood in upper layer	Wood in upper layer
CO	3.2	10.1
CO_2	10.3	11.6
O_2	0.2	0.04
Doorway vent test [21]		
CO	5.7	8.0
CO_2	8.7	9.6
O_2	0.2	0.1
	NIST results [22]	
Doorway vent		
CO	2.6/1.8[a]	5.5/11.5[a]
CO_2	6.5/7.5[a]	10/15.5[a]
O_2	0.1/0[a]	0/0.5[a]

[a]Front and back, respectively

average upper-layer species concentrations for tests with and without wood for both window and doorway vent conditions. For comparison, the data from the NIST research has also been included.

The compartment equivalence ratio was calculated for both the tests with and without wood in the upper layer when the window vent was used. Figures 16.10, 16.11, and 16.12 show the corresponding calculated yields of CO_2, O_2, and CO plotted as a function of equivalence ratio. Also included in these plots are the data from the compartment fires of Gottuk et al. [5] The results show that the global equivalence ratio concept is capable of predicting the CO_2, O_2, and CO yields, although somewhat fortuitously, in a compartment with wood pyrolyzing in the hot, vitiated upper layer. These tests also indicate that the correlations hold to fairly high equivalence ratios of about 5.5, as observed for the tests with wood. More work is needed to determine whether the global equivalence ratio concept can predict species levels when

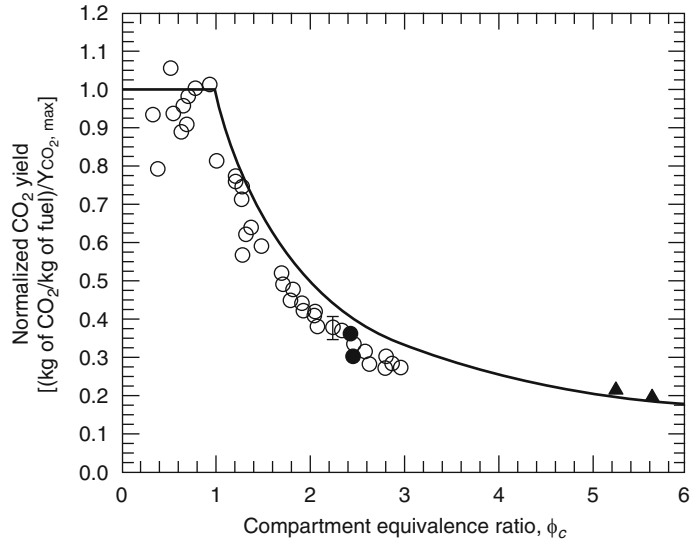

Fig. 16.10 The normalized CO_2 yield data of Gottuk et al. [5] (○), data from Lattimer et al. [21] with no wood in the compartment upper layer (●), and data from Lattimer et al. [21] with wood in the upper layer (▲). Also shown in this plot is the normalized CO_2 yield estimated using the complete combustion model of Equation 16.14 (—)

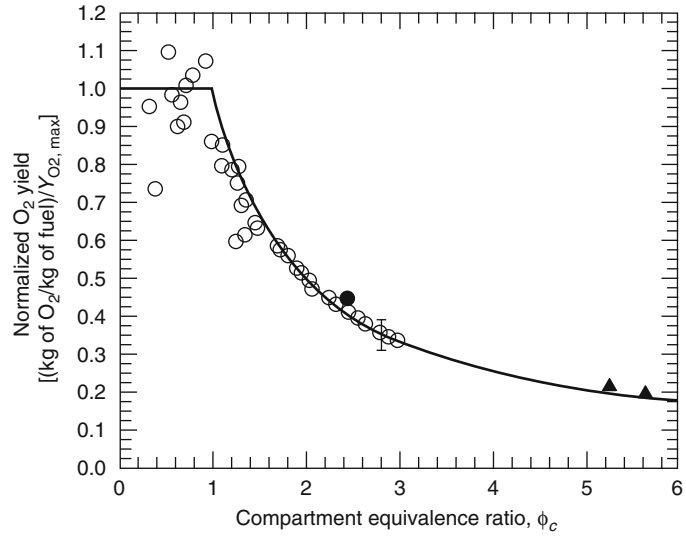

Fig. 16.11 The normalized O_2 yield data of Gottuk et al. [5] (○), data from Lattimer et al. [21] with no wood in the compartment upper layer (●), and data from Lattimer et al. [21] with wood in the upper layer (▲). Also shown in this plot is the normalized O_2 yield estimated using the complete combustion model of Equation 16.14 (—)

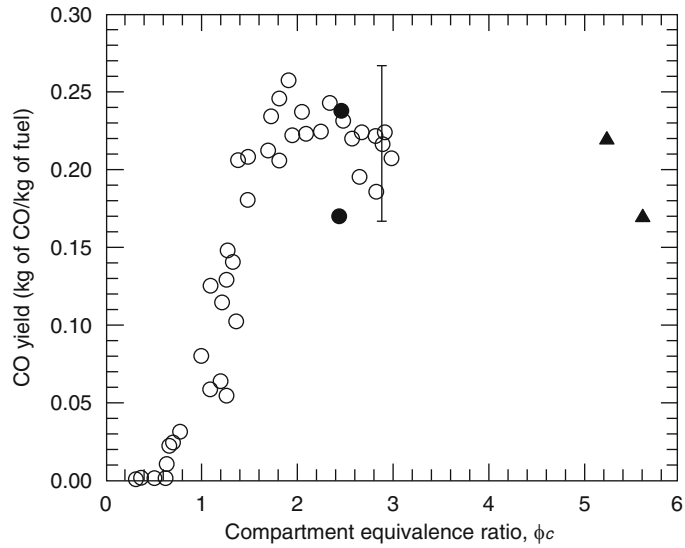

Fig. 16.12 The unnormalized CO yield data of Gottuk et al. [5] (○), data from Lattimer et al. [21] with no wood in the compartment upper layer (●), and data from Lattimer et al. [21] with wood in the upper layer (▲)

nonoxygenated fuels are in the upper layer. It is also unclear whether other oxygenated fuels will follow the correlations as well as the available wood fire data.

The data in Table 16.3 should provide an assessment of the effect of the ventilation opening on species generation. However, it is uncertain whether the differences are due more to differences in sampling locations relative to the flame regions. In the tests with a doorway vent, the larger opening resulted in larger air flow rates and, thus, larger fires in the compartment (approximately 500 kW vs. 220 kW with the window vent). The larger fires increased the flame zone within the compartment. Consequently, the sampling probe was probably within the flame zone at times, which would yield higher CO and lower CO_2 concentrations than measurements from the window vent tests in which the sampling probe was not sampling from a flame zone. With the window vent, the fires were small enough such that there were no ceiling jets at the level of the sampling probe.

The research discussed thus far has concentrated on reduced-scale enclosures. Limited full-scale studies have been reported in the literature to date. One study by NIST systematically examined the production of species in light of the global equivalence ratio concept. NIST conducted a set of tests using a standard enclosure (as defined by ISO 9705) to compare the results from the NIST reduced-scale enclosure tests to fires conducted in a full-scale enclosure [23–26]. The enclosure measured 2.44 m wide, 3.67 m deep, and 2.44 m tall, with a door (0.76 m by 2 m) centered at one end of the compartment. The fires consisted of a 35-cm-diameter natural gas burner centered in the enclosure. The burner was scaled to provide the same exit gas velocities as in the reduced-scale enclosure tests. Twelve tests were conducted, with fires ranging in size from 0.5 to 3.4 MW. In one test, the ceiling and upper portions of the walls were lined with 12.7 mm thick plywood.

In the full-scale enclosure, fires greater than 1250 kW created underventilated conditions. The NIST researchers concluded that although the reduced-scale and full-scale enclosures were geometrically similar, with good agreement between predicted mass flows, the differences in measured gas concentrations indicated that the generation of combustion products is not entirely controlled by the ventilation within the compartment. CO concentrations (upwards of 6 % by volume) were as much as two times higher in the full-scale enclosure than in the reduced-scale tests. These results also coincided with higher upper-layer temperatures, approaching 1400–1500 K. The variation in CO concentrations from front to back in the

enclosure was reversed in the full-scale enclosure compared to the reduced-scale enclosure. In the full-scale enclosure, higher CO concentrations were observed in the back of the compartment. In the reduced-scale enclosure, higher concentrations were measured in the front. Pitts primarily associates the higher CO concentrations with the high layer temperatures that are in the range that strongly favor the formation of CO toward equilibrium concentrations (values can approach 16 % at ϕ of 3) [26].

One full-scale enclosure test was conducted with wood in the upper layer. This test resulted in high CO concentrations of 8 % in the front and 12 % in the rear for a 2 MW fire. The temperatures were lower than those observed in the full-scale tests without wood. These results are similar to those observed in the NIST reduced-scale enclosure.

Chemical Kinetics

The field of chemical kinetics can be used to describe the changes in gas composition with time that result from chemical reactions. The kinetics of actual combusting flows are dependent on the initial species present, temperature, pressure, and the fluid dynamics of the gases. Due to the inability to adequately characterize the complex mixing processes and the significant temperature gradients in turbulent flames, the use of kinetic models is restricted to simplified combusting flow processes. Consequently, the fire plume in a compartment fire is beyond current chemical kinetics models. However, the reactivity of the upper-layer gas composition can be reasonably modeled if one assumes that the layer can be characterized as a perfectly stirred reactor, or that the layer gases flow away from the fire plume in a plug-flow-type process [14, 15]. Pitts has shown that no significant differences between results exist for either modeling approach when applied to these upper layers [14].

Several kinetics studies have been performed to examine aspects of the reactivity of upper-layer gases [12, 14, 15]. Comparisons between different hood experiments and between hood and compartment fire experiments have indicated that upper-layer temperatures have an effect on CO production. The results of these chemical kinetics studies provide insights into CO generation in compartment fires, which also serve to explain the differences in CO yields between experiments with respect to temperature effects. These studies primarily focused on the question "What would the resulting composition be if the upper-layer gases in the hood experiments existed at different isothermal conditions (constant temperature)?" A particular focus was to examine the resulting compositions for cases modeled under the high temperatures characteristic of compartment fires. Chemical kinetics models calculate the change in species concentrations with respect to time. Calculations are dependent on the reaction mechanism (i.e., the set of elementary reactions and associated kinetic data) and the thermodynamic data base used.

Thermodynamic data are fairly well known and introduce little uncertainty into the modeling. However, reaction mechanisms do vary. Pitts presents a comparison of the use of various mechanisms in the literature [14]. The comparison indicates that reaction kinetics for high temperatures (greater than 1100 K) are fairly well understood. However, the elementary reactions for the range of 800–1000 K are not as certain; therefore, quantitative modeling results in this range may be suspect. Nevertheless, the general trends presented below are valid despite any uncertainty associated with the mechanisms used.

Chemical kinetics modeling shows that significantly different trends occur for overventilated and underventilated burning conditions. This can be seen in Figs. 16.13 and 16.14, which present major species concentrations with respect to time for an overventilated and underventilated condition, respectively. Figure 16.13 shows a modeled case for ϕ equal to 0.91 and a temperature of 900 K. The initial composition is taken from Beyler's data for a fire with a layer temperature of 587 K. The temperature of 900 K corresponds to the temperature observed by Gottuk et al. for a

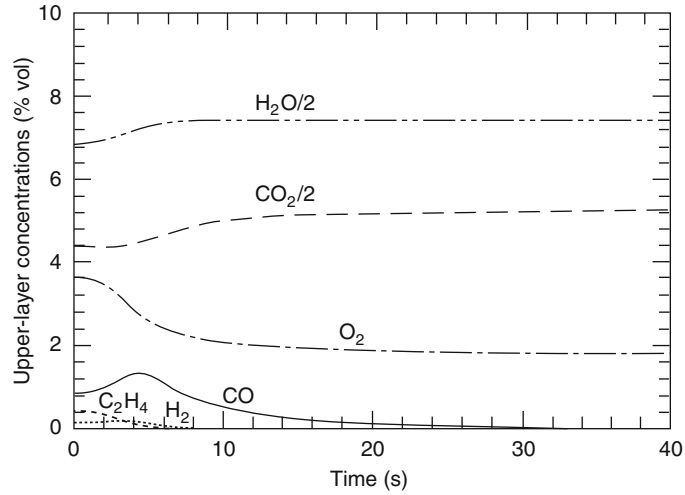

Fig. 16.13 Chemical kinetics model calculated species concentrations versus time for an overventilated ($\phi = 0.91$) burning condition with an upper-layer temperature of 900 K [15]

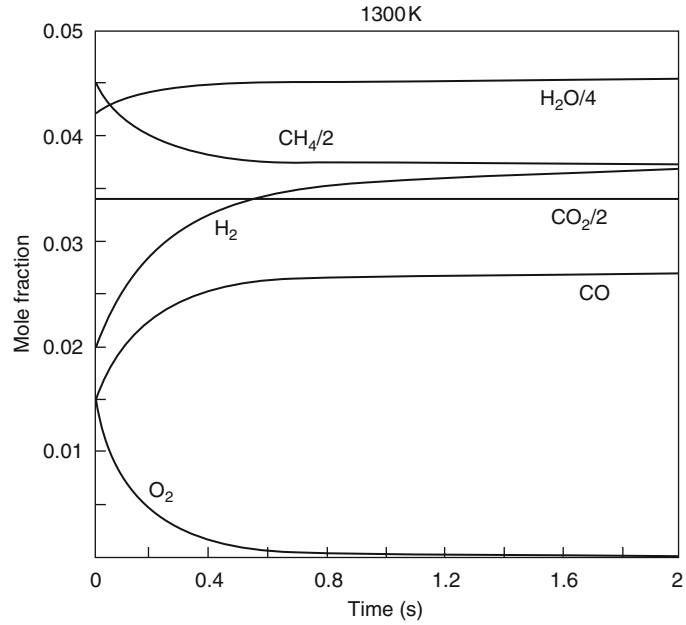

Fig. 16.14 Chemical kinetics model calculated species concentrations versus time for an underventilated ($\phi = 2.17$) burning condition with an upper-layer temperature of 1300 K [14]

hexane compartment fire at the same global equivalence ratio. For overventilated conditions, increased temperatures cause CO concentrations to initially increase. As can be seen in Fig. 16.13, this is due to the incomplete oxidation of hydrocarbons (modeled as C_2H_4). Once the hydrocarbons are consumed, available O_2 is used in the oxidation of CO to CO_2. Since overventilated conditions indicate excess oxygen, CO concentrations are reduced to zero given sufficient time. This is representative of the case of the overventilated hexane and PMMA compartment fires studied by Gottuk et al., in which the higher compartment temperatures, compared to the hood tests of Beyler, resulted in near-zero CO yields for ϕ less than 1.

Figure 16.14 shows an underventilated case for ϕ equal to 2.17 and a temperature of 1300 K. The initial composition is taken from Morehart et al.

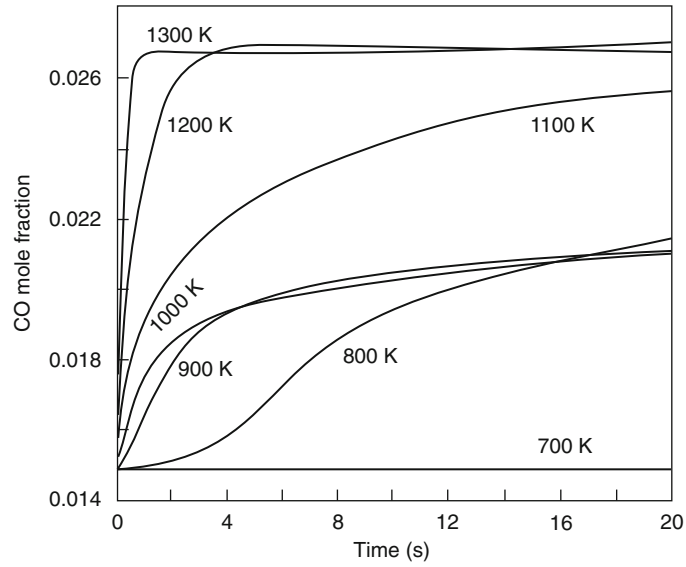

Fig. 16.15 Carbon monoxide concentrations as a function of time for a range of isothermal conditions. Initial concentrations from a methane hood fire at $\phi = 2.17$ [14]

for a methane hood experiment [12]. Similar to the overventilated conditions, CO increases due to the oxidation of hydrocarbons (CH_4). However, the available oxygen is depleted before the hydrocarbons are fully oxidized. The resulting composition consists of higher levels of CO and H_2 and decreased levels of unburned fuel. Carbon dioxide levels remain virtually unchanged. The much higher temperature studied in this case results in much quicker reaction rates, as is reflected in the 2 s time scale for Fig. 16.14 compared to 30 s for Fig. 16.13.

It is clear from Figs. 16.13 and 16.14 that hydrocarbon oxidation to CO and H_2 is much faster than CO and H_2 oxidation to CO_2 and H_2O, respectively. This is a result of the preferential combination of free radicals, such as OH, with hydrocarbons over CO. Carbon monoxide is oxidized almost exclusively by OH to CO_2 [27]. Therefore, it is not until the hydrocarbons are consumed that free radicals are able to oxidize CO to CO_2.

The formation and consumption of CO in a reactive gas mixture is dependent on both the temperature of the mixture and the amount of time over which the mixture reacts. This point is illustrated in Fig. 16.15, which shows the resulting CO concentrations at different isothermal conditions from an initial gas mixture taken from an underventilated fire ($\phi = 2.17$). Pitts noted that there are three distinct temperature regimes. At temperatures under 800 K, the gas mixture is unreactive and the CO to CO_2 reactions are said to be "frozen out." As the temperature increases in the range of 800–1000 K, the mixture becomes more reactive and CO is formed at faster rates, due to the oxidation of unburned hydrocarbons. For the time period shown, it is interesting to note that the ultimate concentration is approximately constant[1] for each case in this temperature range. The third regime of high temperatures above 1100 K is characterized by fast reaction rates and much higher CO production for the 20 s reaction time shown. With sufficient time, the ultimate CO concentration for the 800–1000 K conditions would approach the same value as that seen for the higher temperatures.

Results of Zukoski et al. [10] and Gottuk et al. [15] indicated that layer temperatures of 850–900 K or higher are needed for the layer gases to be reactive. Considering that the

[1] Note that although the ultimate CO concentration is roughly constant, the value of 2.1 % for this illustration is not to be taken as a universal limit for this temperature range. In general, the resulting CO concentration will depend on the initial gas composition and the time over which the mixture is allowed to react.

minimum (freeze out) temperature above which a gas mixture is reactive is dependent on the time scale evaluated. These values are consistent with the results shown in Fig. 16.12. In terms of compartment fires, the time over which the gases react can be taken as the residence time of the gases in the upper layer, which is calculated according to Equation 16.11. In many practical cases of high-temperature compartment fires, it would be reasonable to assume that the residence time of layer gases would be longer than the time needed for the gas mixture to react fully.

Fire Plume Effects

Although a fire plume is too complex to adequately model the chemistry, the hood experiments discussed earlier provide significant insights with respect to the fire plume and species production in compartment fires. Results of Beyler's hood experiments suggest that the production of upper-layer gases is independent of the structure and fluid dynamics of the flame.

Beyler modified a 19 cm propane burner by including a 2.8 cm lip to enhance turbulence and the large-scale structure of the flame [8]. Compared to the no-lip burner, the flame was markedly changed, and air entrainment was increased by 30 %. Yet, the upper-layer species-equivalence ratio correlations were the same for both burners. Additionally, as shown in Fig. 16.5, correlations for different size burners are also identical.

The insensitivity of species yields to the details of the flame structure is also suggested by the compartment fire hexane results of Gottuk et al. [5] The correlations include data from fires utilizing various size burn pans and with a wide range of air entrainment rates. In several cases, nearly equal steady-state equivalence ratio fires were obtained with quite different burning rates and air entrainment rates. Although the conditions varied significantly, the positive correlation between yields and equivalence ratio suggests that the yields are not sensitive to the details of the flame structure.

The temperature of the fire plume has a significant effect on species production from the fire plume. It is reasonable to assume that differences in upper-layer temperature are also reflective of a similar trend in the average temperature of the fire plume gases. An increase in the upper-layer temperature can increase the fire plume temperature in two ways. For plumes that extend into the upper layer, entrainment of hotter upper-layer gases will result in increased plume temperatures compared to plumes in layers with lower temperature gases. Secondly, an increase in the surrounding temperature (both gases and compartment surfaces) reduces the radiant heat loss from the plume, thus resulting in a higher plume temperature.

The effect of temperature on species generation in a fire plume can be found in the methane hood experiments of Morehart et al. [12] and Zukoski et al. [11] Morehart studied the effect of increasing temperature on layer composition by adding different levels of insulation to his hood. Except for the insulation, the test conditions (e.g., ϕ of 1.45 and layer interface height) were held constant. For the range of temperatures studied (500–675 K), substantial increases in products of complete combustion and decreases in fuel and oxygen occurred with increasing layer temperature. Upper-layer oxygen mass fraction was reduced by approximately 70 % and methane was reduced by 25 %. Excluding one outlier data point, CO concentrations increased by 25 %. The temperatures of the Morehart et al. upper layer were well below 700 K. Therefore, based on kinetics modeling, these layers were unreactive at these low temperatures. It follows that the change in layer composition must have been due to changes in the plume chemistry. The more complete combustion can be attributed to an extension of the flammability limits (or reaction zone) in the plume due to raising the flame temperature. The above discussion demonstrates that increasing the plume temperature substantially increases the consumption of O_2 and fuel, and primarily increases the levels of products of complete combustion.

The effect of changing temperature on a compartment fire upper-layer composition is twofold: (1) the generation of species in the fire plume is changed, and (2) oxidation of post-flame gases in the layer is affected. Elevated compartment temperatures correlate with increased fire plume temperatures and more complete oxidation of the fuel to CO_2 and H_2O within the fire plume. The layer temperature dictates post-flame oxidation in the upper layer.

Upper-layer temperatures below about 800 K indicate chemically unreactive layers. As such, combustion within the fire plume controls the final CO levels that would be measured in the upper layer. At these low temperatures significant levels of CO can be generated even for some overventilated conditions ($0.5 < \phi < 1$). The yield of CO is inversely proportional to temperature for overventilated conditions and directly proportional to temperature for underventilated conditions.

Upper-layer temperatures of about 900 K and higher indicate chemically reactive layer gases. As such, reactions in the layer dictate final CO production. Temperatures above 900 K allow nearly complete oxidation of CO to CO_2 for overventilated conditions. For underventilated fires, chemical kinetics modeling indicates that higher temperature environments may result in slightly higher CO yields due to preferentially accelerated hydrocarbon oxidation compared to CO oxidation.

During underventilated conditions, two mechanisms affecting net CO formation compete (i.e., CO and hydrocarbon oxidation). Increasing gas temperatures above 900 K depletes CO by accelerating the CO to CO_2 conversion. However, incomplete oxidation of unburned hydrocarbons increases the CO production. Since hydrocarbon oxidation is much faster than CO oxidation, net CO levels increase until all available oxygen is consumed.

Transient Conditions

Transient conditions cause the upper-layer equivalence ratio to differ from the plume equivalence ratio. A fast-growing fire will tend to have a ϕ_{ul} that is less than ϕ_p. Conversely, a fire that is dying down quickly, such that ϕ_p is decreasing rapidly, will have a ϕ_{ul} that is higher than ϕ_p. These trends result due to the upper layer being a temporary collection reservoir for the gases from the fire plume.

In an effort to characterize transient conditions, Gottuk et al. defined a steady-state time ratio, τ_{SS}, as the ratio of the residence time, t_R, to a characteristic growth time of the fire. Since fire growth is directly related to the fuel volatilization rate, a representative growth time of the fire was defined as the ratio of the fuel mass loss rate, $\dot{m}_f$, to the derivative of the fuel volatilization rate, $\ddot{m}_f$. An increase in τ_{SS} is indicative of more transient conditions.

$$\tau_{SS} = \frac{t_R}{\dot{m}_f / \ddot{m}_f} \tag{16.18}$$

An analysis of the transient nature of the compartment fires studied by Gottuk et al. showed that values well below 1 indicated near steady-state conditions, such that the plume and upper-layer equivalence ratios could be considered equal. Investigation of individual fires showed that the steady-state time ratio decreased below 1.0 at very early times in the fire. Typically, the ratio was 0.1 or less for the quasi-steady-state periods over which data was averaged. For some fires, during the highly transient transition from overventilated to underventilated conditions, the τ_{SS} increased quickly, approaching a value of 1.

The correlations presented in the engineering methodology represent data that have been averaged over steady-state (hood experiments) or quasi-steady-state (compartment fires) periods. For the purpose of modeling fires with respect to time it is of interest to know how the species yields correlate with the equivalence ratio during transient conditions (i.e., as the fire is growing). Determining this correlation was accomplished by plotting the yield to equivalence ratio data for individual fires from the time of ignition to the steady-state period. These transient correlations were compared to the steady-state correlations obtained from steady-state averaged data from all tests (e.g., the CO yield correlation shown in

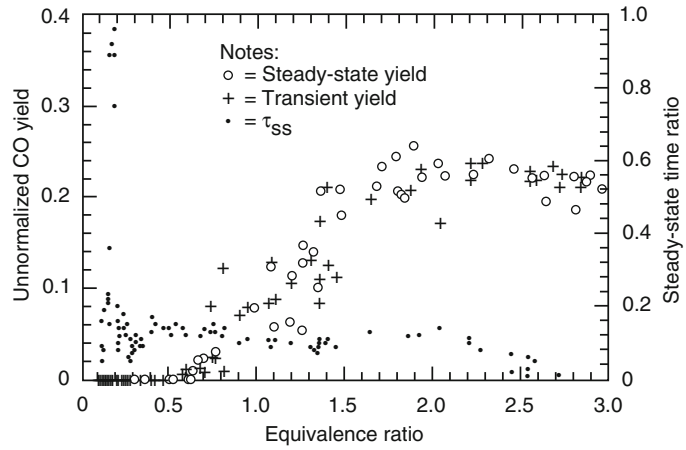

Fig. 16.16 Comparison between a transient, unnormalized CO yield correlation for a hexane fire with an average steady-state ϕ_p of 3 and the steady-state correlation for all hexane fires studied by Gottuk et al. The steady-state time ratio, τ_{SS}, data are shown as solid dots [17]

Fig. 16.9). An example of one comparison is shown in Fig. 16.16. Figure 16.16 shows the steady-state hexane CO yield correlation along with the transient yield vs. equivalence ratio data for a hexane compartment fire that obtained a steady-state average ϕ_p of 3. The solid dots in Fig. 16.16 represent the steady-state time ratio data, τ_{SS}. For this example, τ_{SS} remained fairly constant at about 0.1 for the entire fire. And as can be seen, the agreement between the transient and steady-state correlations is quite good, even for the transition to underventilated conditions. Good agreement between transient and steady-state data was also observed for CO_2 and O_2 yield correlations.

Although more transient in nature than the hood experiments, the compartment fires are characterized as primarily quasi-steady and, therefore, do not differ significantly from Beyler's hood experiments in this respect. This analysis also shows that the species yield correlations developed for steady-state conditions are representative of the transient growth periods of these fires.

In terms of full-scale application, these results suggest that ϕ_p and ϕ_{ul} are approximately equal for compartment fires characterized by relatively slow growth compared to the upper-layer residence time (i.e., $\tau_{SS} \ll 1$). However, the low τ_{SS} values observed in the reduced-scale compartment fires may not always be representative of full-scale fires. The reduced-scale compartment fires had residence times typically between 4 and 20 s. These short residence times were a result of having relatively large fires compared to the compartment volume. Until flashover conditions are approached, a full-scale compartment fire will most likely have smaller fires compared to the volume of the space. As a result, the residence time of gases in the upper layer of a full-scale fire may be much longer. Times on the order of 5–10 min may not be unrealistic in some cases. Therefore, in the case of a fast-growing full-scale fire, values of ϕ_p could increase relative to ϕ_{ul}. The application point is that the control volume used for the equivalence ratio must be considered with respect to the residence time of gases in the upper layer.

Species Transport to Adjacent Spaces

The species levels transported from a compartment depend on a variety of conditions produced during the course of the fire. As compartment fire gases exit the compartment, they entrain the gases present in the adjacent space (Fig. 16.17). If a fuel-rich mixture is produced in the compartment, the gases flowing out may ignite, causing burning in the adjacent space. This burning is an indication that oxidation reactions are taking place, which ultimately affects the species levels transported to remote areas. As the gases continue to flow through the adjacent space, they are cooled by mixing with surrounding gases and heat losses to the boundaries. Eventually, gases are cooled to a temperature below which

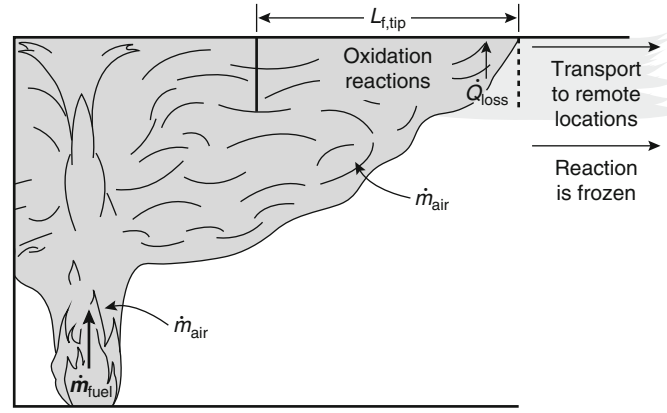

Fig. 16.17 Phenomena controlling species transport to remote locations

oxidation reactions do not readily occur. At this point the reactions are said to be frozen. The amount of combustion products that exist at this point will continue to flow throughout the rest of the structure. As a result, combustion product levels in the overall structure will accumulate as the fire inside the compartment persists and/or additional items in the structure begin to burn.

Conditions inside the fire compartment and in the directly adjacent space will govern the species levels transported to remote locations. The primary consideration is the conditions that develop inside the compartment. If burning outside of the fire compartment occurs due to either flame extension or external burning, gases will continue to react outside of the compartment influencing the species levels transported to remote areas. The degree to which gases react outside the compartment depends on the mixing of oxygen with the fuel-rich gases flowing out of the compartment, and the addition of fuel to the gases flowing along the adjacent space.

General Effects of Burning Outside the Compartment

Species levels transported to remote locations will be equivalent to those formed inside the compartment unless burning occurs outside. Chemical kinetics indicate that oxidation reactions cannot occur efficiently outside the compartment unless gas temperatures are near those produced at the onset of flashover (775–875 K) (see the section "Chemical Kinetics" in this chapter). In the presence of oxygen, hydrocarbons begin to react efficiently when temperatures are above 700 K [14]. Perhaps more importantly, the oxidation of CO to CO_2 does not readily occur until temperatures rise above 800 K. The occurrence of burning outside the compartment, either from flame extension or the onset of flashover, will result in local temperatures in excess of 1300 K [4]. At these temperatures, oxidation reactions for both hydrocarbons and CO occur in the presence of available oxygen.

The occurrence of burning outside the compartment has been shown, in most situations, to reduce the incomplete combustion products (including smoke and CO levels) transported to remote locations [5, 28–30]. The burning in unconfined adjacent areas (e.g., open surroundings) has been measured to decrease incomplete combustion products more efficiently than burning in confined adjacent areas (e.g., a corridor). In addition, the consumption of incomplete combustion products during burning in confined areas was found to be sensitive to the air entrainment into the plume/ceiling jet flow. This entrainment is a function of the mass flow from the compartment, the geometry of the opening between the compartment of fire origin and the adjacent space, and the geometry of the adjacent space itself. Smoke layers that develop in confined adjacent spaces can cause lower oxygen levels to be entrained into the plume/ceiling jet flow in the adjacent space, increasing the incomplete combustion product levels transported to remote areas.

Burning in Unconfined Adjacent Areas

Unconfined adjacent areas are those areas where the flame extending from the compartment of origin is not redirected by the boundaries of the adjacent area, and the gases are allowed to burn as a buoyant plume. Examples of unconfined adjacent areas include outdoor surroundings, atriums, and corridors with high ceilings relative to the door height of the burning compartment. Gottuk et al. [15, 31] investigated the impact of external burning on combustion products downstream of an unconfined jet. The compartment was connected to its surroundings through a window opening. Tests were performed with compartment fires with and without external burning. In these tests, a compartment equivalence ratio of 1.6 was the lowest ϕ_c where external burning was noted to occur. The effects of external burning on the CO levels downstream of the fire are shown in Fig. 16.18. With a compartment equivalence ratio greater than 1.6, CO levels were measured decreasing below the fire compartment levels. The CO yield is shown to decrease to a minimum of 0.02 at ϕ greater than 2.0. The decrease in CO represents a 75–90% reduction of the CO generated in the fire compartment.

Burning in Confined Adjacent Areas

Burning in a confined adjacent area, such as a corridor or room, causes the external flame to impinge on a ceiling, and possibly on walls. Compared with flow in an unconfined area, the ceiling and walls in the confined area will reduce the amount of air entrainment into the gas jet exiting the fire compartment. The effects of burning in confined areas on species transport have been investigated by Ewens et al. [28, 32] and Lattimer et al. [29, 30] using the same fire compartment design in the unconfined external burning study (Figs. 16.19 and 16.20) [17, 31]. The transport of species to remote locations is geometry dependent and can be affected by smoke layers that develop in the confined area. However, species levels transported to remote areas can be predicted by defining an equivalence ratio for a control volume involving both the fire compartment and the burning in the adjacent space.

Species transport has been evaluated for two common compartment-hallway configurations. Ewens [28] and Lattimer et al. [30] evaluated species transport in a configuration with the fire compartment on the end of a hallway (see

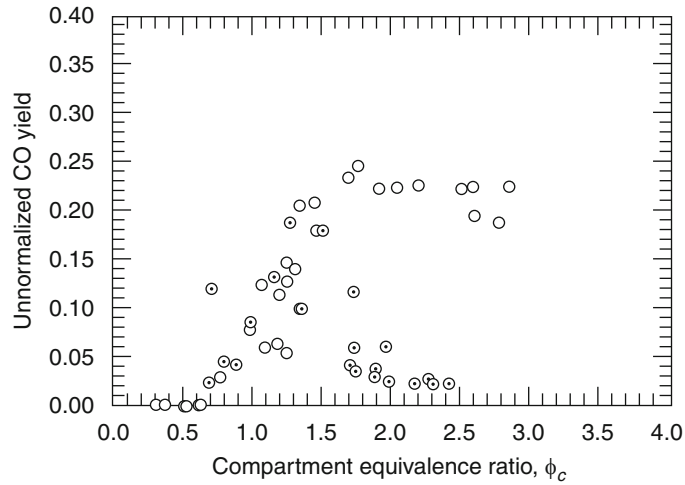

Fig. 16.18 Effect of external burning on CO levels downstream of an unconfined adjacent area. CO yield versus compartment equivalence ratio for hexane compartment fires with an exhaust jet to the open atmosphere through a window opening; (○) compartment levels, (⊙) downstream levels [17, 31]

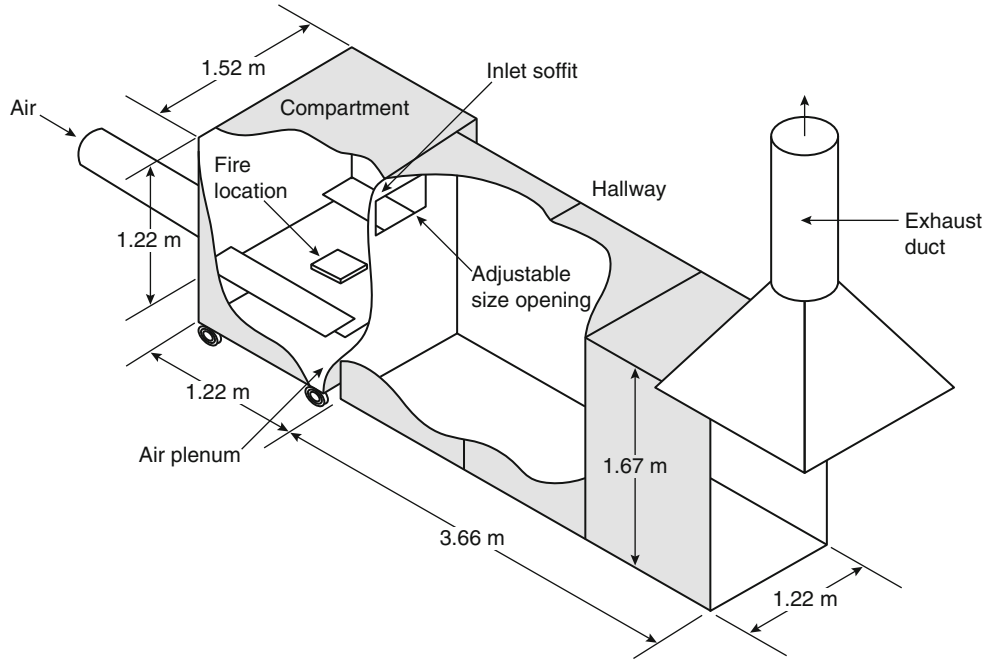

Fig. 16.19 Compartment on the end of a hallway [28, 30, 32]

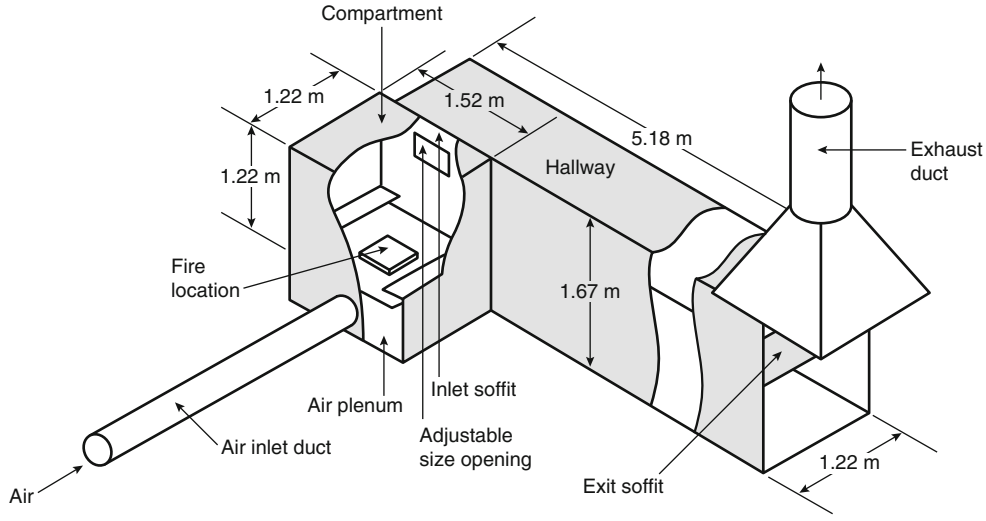

Fig. 16.20 Compartment on the side of a hallway [29, 30]

Fig. 16.19). Lattimer et al. [29, 30] performed a study with the fire compartment on the side of a hallway (see Fig. 16.20). In both studies, most tests were performed with a window connecting the compartment and hallway.

Using the apparatus shown in Fig. 16.19, Ewens [28] evaluated the effects of different geometric variables and compartment stoichiometry on CO levels (in addition to other species) downstream of the external burning where

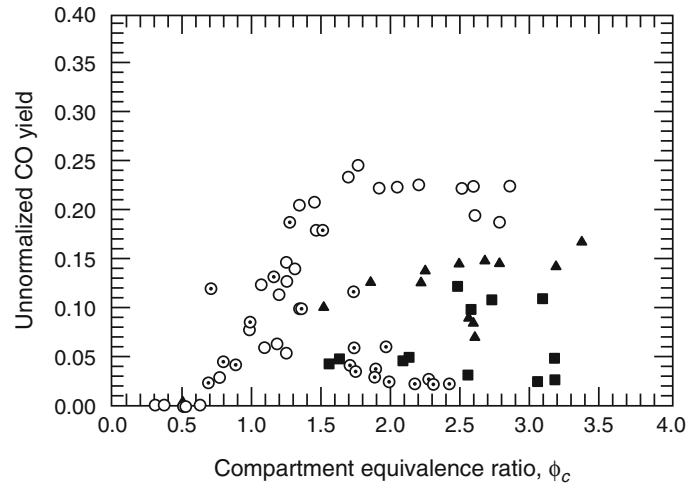

Fig. 16.21 Effect of external burning on CO levels downstream of a postflashover compartment fire. Adjacent hallway with a (▲) 0 m inlet soffit and (■) 0.20 m inlet soffit. (⊙) Unconfined area and (○) inside the compartment [17, 28, 31, 32]

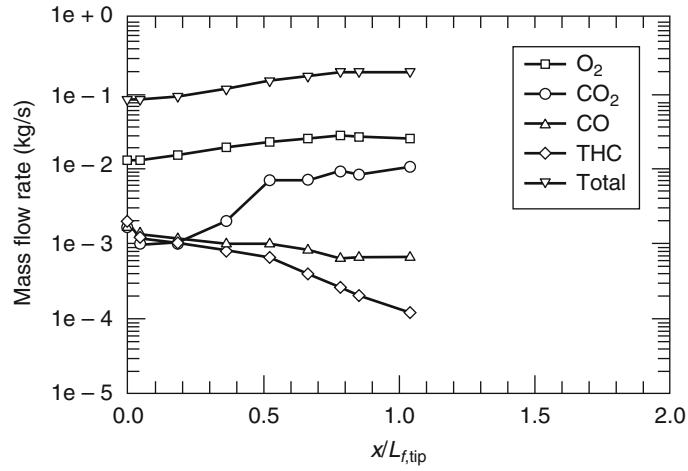

Fig. 16.22 The mass flow rates in a space adjacent to a postflashover fire with external burning plotted versus the ratio of the distance down the hall, x, to the length of the flame to its tip, $L_{f,tip}$. Opening of 0.12 m^2, no inlet soffit above the opening, and an average compartment ϕ = 2.0 [28]

reactions were considered frozen. As shown in Fig. 16.21, Ewens [28] demonstrated that burning in confined areas outside the compartment decreases incomplete combustion product levels, but not always to the same extent as when the fire gases spill into an unconfined space. The degree of oxidation was found to be dependent on both air entrainment into the gases exiting the compartment and the fuel flowing out of the compartment. The data of Ewens show that both fire size and geometric parameters will affect species production. The two important results to understand are that geometries which increase air entrainment in the adjacent space (e.g., an inlet soffit vs. no soffit) or reduce the layer depth in the adjacent space will enhance the oxidation reactions and result in lower levels of incomplete combustion products, such as CO.

Fire gases flowing into and through the adjacent space entrain surrounding gases as they flow away from the fire compartment. These gases can undergo chemical reactions, particularly as they are within the flaming region. A sample plot of the species variation along the flame length in the hallway is shown in Fig. 16.22 [28]. Results shown in Fig. 16.22 are from postflashover hexane fire tests with an average compartment equivalence ratio of ϕ = 2.0, a 0.12 m^2 opening

(0.50 m wide × 0.24 m high) connecting the compartment and adjacent space, and no inlet soffit above the opening in the hallway. These data represent time-averaged conditions 0.025 m below the ceiling along the hallway during the quasi-steady-state period of the fire, when external burning was occurring.

Gases entered the adjacent space as a ceiling jet, but were allowed to expand horizontally until intersecting the walls of the hallway. For this geometry, the largest increase in the total mass flow rate was during the first half of the flame length, which was 2.7 m (on average) from the compartment. By $x/L_{f,\text{tip}} = 0.75$, the total mass flow rate had reached a maximum. This indicated that all of the entrainment into the ceiling jet flow occurred by $x/L_{f,\text{tip}} = 0.75$. The majority of the oxidation reactions had also occurred by $x/L_{f,\text{tip}} = 0.75$. The mass flow rates of CO, CO_2, and O_2 were essentially constant downstream of $x/L_{f,\text{tip}} = 0.75$. This indicates that the oxidation of CO to CO_2 was frozen by an $x/L_{f,\text{tip}} = 0.75$. Small amounts of total hydrocarbons (THC) continued to react from $0.75 < x/L_{f,\text{tip}} < 1.0$; however, this was not measured to significantly increase CO levels.

Analysis of data in Fig. 16.22, as well as other data by Ewens et al. [28, 32] and Lattimer et al. [29, 30], indicates that by the flame tip all of the oxidation reactions have occurred. As a result, the mass flow rates of the major combustion products beyond the flame tip will be transported to remote locations. The mass flow rate levels will be influenced by the oxygen availability in the flaming region. Based on test results from Ewens et al. [28, 32] and Lattimer et al. [29, 30], mixing near the compartment has been shown to have the most significant influence on the combustion products transported to remote areas.

Predicting Species Levels

Lattimer [33] performed additional analysis on Ewens' data to develop a correlation between species transported and ϕ for a control volume consisting of part of the area in the adjacent space where burning occurred. In this set of data, the mixing in the adjacent space (hallway) was varied by using windows with different areas and aspect ratios to connect the compartment to the adjacent space, and by adding a 0.20 m soffit above the window. The equivalence ratio in this analysis was calculated using a control volume that extended to the sampling point located in the adjacent space. Using this control volume, the mass flow rate of air for the ϕ_{cv} calculation in Equation 16.13 was the air flow rate into the compartment plus the air entrainment into the plume/ceiling jet flow in the adjacent space, up to the sampling location. In these experiments, gas sampling was always performed in or just downstream of the flame within the hallway.

In Figs. 16.23, 16.24, 16.25, and 16.26 the species yields are plotted vs. the control volume equivalence ratio, ϕ_{cv}. Note that CO yields are not normalized because for various fuels unnormalized CO yields were found to correlate best with ϕ. The lines in the normalized O_2 depletion and CO_2 and THC yield plots represent the results from the complete combustion model presented in Equation 16.14. Due to limited data near the compartment, there are few data points at high ϕ_{cv}.

The trends in the species data were similar to those observed in the hood experiments by Beyler [8, 9] and in the compartment experiments by Gottuk et al. [5] The normalized O_2 depletion is approximately unity at ϕ_{cv} less than 1.0 and decays at the rate prescribed by the complete combustion model at higher ϕ_{cv}. CO_2 normalized yields are near unity up to a ϕ_{cv} of approximately 0.8. At ϕ_{cv} greater than 0.8, the CO_2 levels begin to decay and are consistently less than the level predicted by the complete combustion model. This behavior is consistent with the rise in incomplete combustion products, such as CO and THC, at ϕ_{cv} ranging from 0.6 to 0.8. These results indicate that species levels in adjacent spaces can be adequately correlated by the same global equivalence ratio correlations obtained for species production in fire compartments as long as ϕ_{cv} is calculated using the appropriately defined control volume. ϕ_{cv} accounts for the effects of external burning on

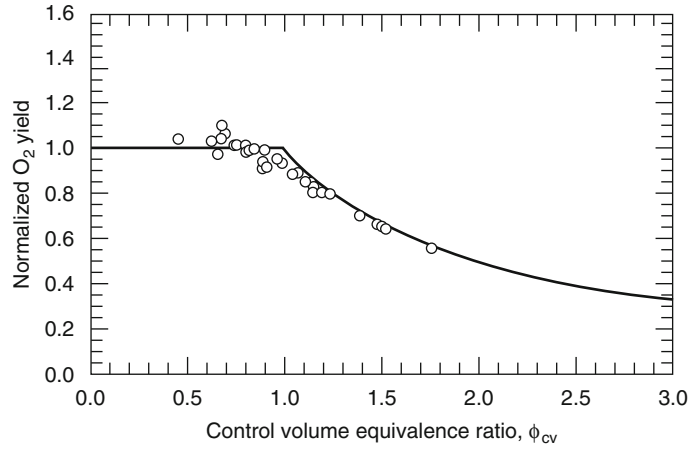

Fig. 16.23 Normalized O_2 depletion of gases in a space adjacent to a postflashover compartment fire. Control volume includes fire compartment and a portion of the adjacent space where burning occurs

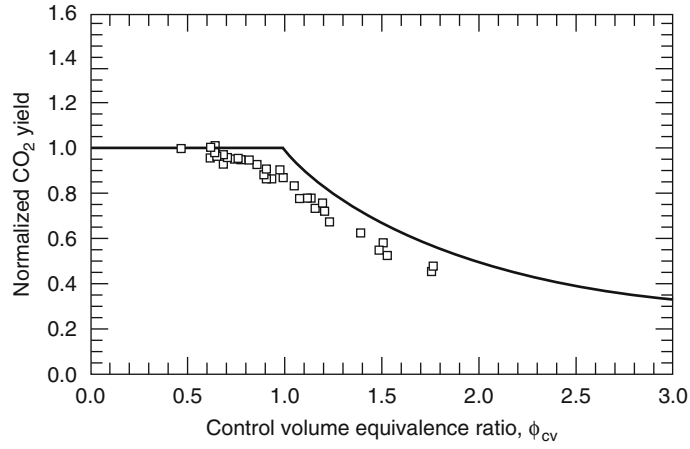

Fig. 16.24 Normalized CO_2 yields of gases in a space adjacent to a postflashover compartment fire

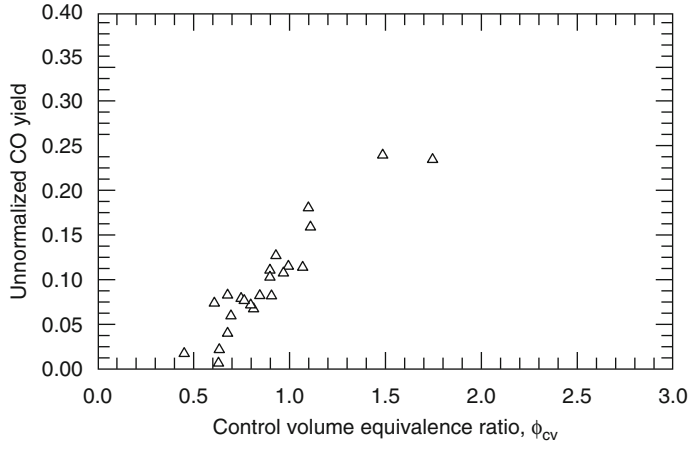

Fig. 16.25 Unnormalized CO yields of gases in a space adjacent to a postflashover compartment fire.

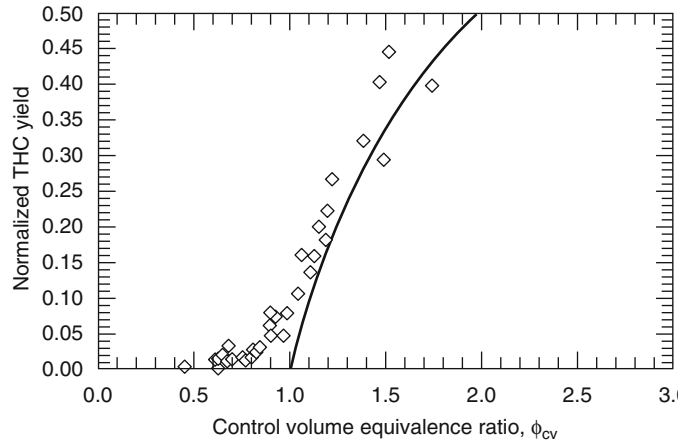

Fig. 16.26 Normalized THC yields of gases in a space adjacent to a postflashover compartment fire

species levels and can be used with Equations 16.19, 16.20, 16.21, 16.22, 16.23, 16.24, and 16.25 to estimate species transported to remote areas.

Effects of Oxygen-Deficient Smoke Layers in Adjacent Spaces

The development of hot, oxygen-deficient smoke layers in the adjacent space affects both the entrainment into the plume/ceiling jet and the amount of oxygen mixing with the fuel-rich gases flowing from the fire compartment.

Ewens et al. [28, 32] demonstrated that layers as thin as 0.20 m may have an impact on incomplete combustion products being transported to adjacent areas. Lattimer et al. [29, 30] performed a series of tests with different oxygen-deficient layer depths in the space directly adjacent to a postflashover fire (see Fig. 16.20). Tests were performed with three different opening sizes connecting the compartment to the adjacent space, but the compartment stoichiometry was approximately the same in all tests. In each test, the layer depth was kept at a constant level by the use of an exit soffit. In order to change the layer depth from test to test, the height of the exit soffit was adjusted for each test.

Except for cases with a deep smoke layer in the adjacent space, external burning occurred in all tests. Figure 16.27 contains a plot of time to ignition for tests with different layer depths. Layer depth is represented as a dimensionless depth, $\gamma = \delta/z$, which relates the distance between the ceiling and the bottom of the visible smoke layer, δ, to the distance between the ceiling and the bottom of the gases flowing out of the compartment, z. (For a window configuration, z is measured to the bottom of the window.) As shown in Fig. 16.27, the smoke layer did not affect the time to ignition until the visible smoke layer was nearly deep enough to prevent ignition altogether (indicated by the infinite time to ignition). At layer depths greater than $\gamma = 1.7$, external burning did not occur since the exiting fire gases were not able to entrain sufficient fresh air to provide the necessary oxygen for combustion. Rather, the gases exiting the fire compartment entrained primarily vitiated gases in the upper layer of the adjacent space.

The CO, CO_2, and THC yields measured at a remote location (in the exhaust duct) for the different window opening sizes are shown plotted in Figs. 16.28, 16.29, and 16.30 with respect to the smoke layer depth. Each data point is the time-averaged yield during the quasi-steady-state part of the fire. For this geometry, combustion product levels were not significantly affected by the smoke layer until it fell below the bottom of the opening ($\gamma > 1.0$). As the layer depth increased from $\gamma = 1.0$–1.8, the burning outside the compartment became increasingly less efficient. This resulted in an increase in CO and

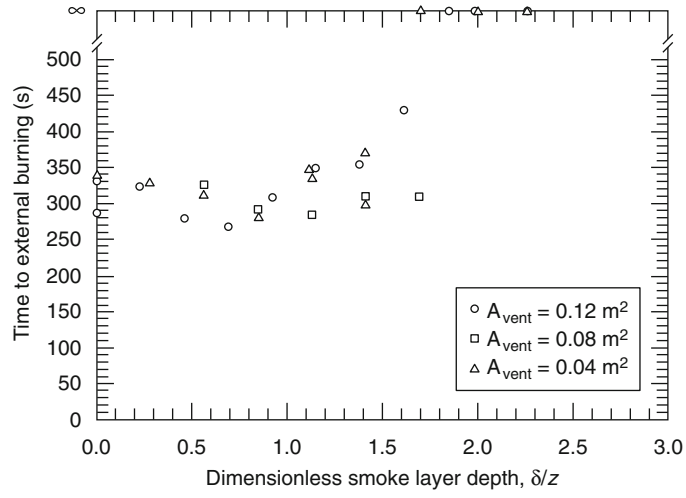

Fig. 16.27 Time for external burning in tests with a range of layer depths in the adjacent space with a 6.32 m^2 floor plan area [30]

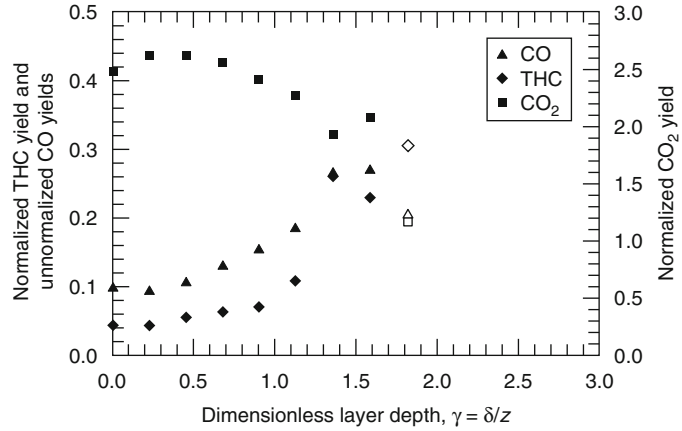

Fig. 16.28 The effect of an oxygen-deficient upper layer on downstream species yields from a postflashover fire extending into a hallway. Opening of 0.12 m^2, 0.20 m soffit above the opening, and an average $\phi_c = 3.1$. Open symbols are tests with no external burning. $\gamma > 1$ indicates layer is below the bottom of the vent [28, 29]

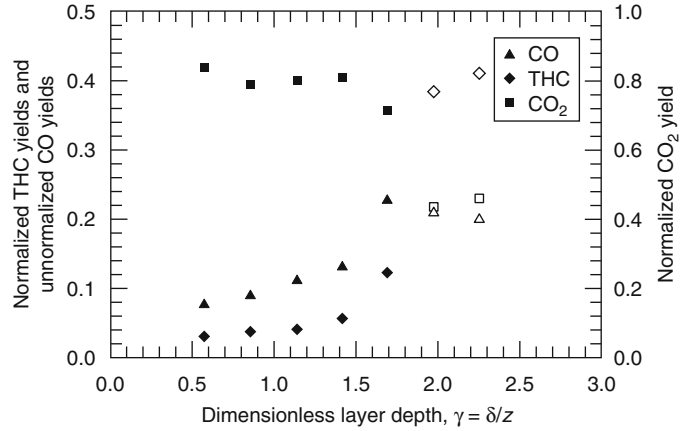

Fig. 16.29 The effect of an oxygen-deficient upper-layer on downstream species yields from a postflashover fire extending into a hallway. Opening of 0.08 m^2, 0.20 m soffit above the opening, and an average $\phi_c = 2.8$. Open symbols are tests with no external burning [30]

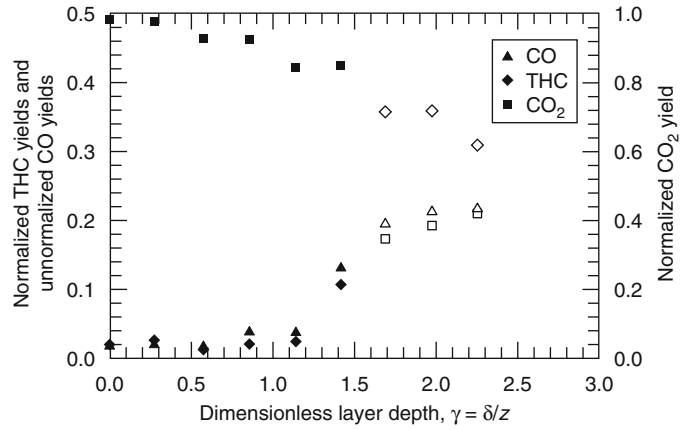

Fig. 16.30 The effect of an oxygen-deficient upper layer on downstream species from a postflashover fire extending into a hallway. Opening of 0.04 m^2, 0.20 m soffit above the opening, and an average $\phi_c = 2.8$. Open symbols are tests with no external burning [29, 30]

THC yields and a decrease in the CO_2 yield. The increase in CO and THC yields was attributed to reducing the oxygen available to oxidize the combustion products. When the smoke layer was increased to a dimensionless layer depth of $\gamma = 1.7–1.8$, external burning was not observed and downstream species yields were consistent with levels inside the fire compartment.

External burning in some tests with deep oxygen deficient upper layers actually caused additional CO formation in the adjacent space. As shown in Fig. 16.28, in tests with the largest opening, 0.12 m^2, and a dimensionless layer depth of $\gamma = 1.3–1.5$, CO yields increased to approximately 0.27 kg/kg, which is approximately 0.05 kg/kg higher than compartment levels. In addition, corresponding normalized THC yields were on average 0.06 kg/kg lower than compartment levels. These results indicate that available oxygen is being used to preferentially oxidize THC instead of CO. This oxidation of THC forms additional CO, causing an increase in CO levels transported to remote locations. The exact conditions in the adjacent space necessary to produce these results have not been fully established.

Other Considerations

There are other variables that may influence the combustion product levels being transported to remote locations that have not been fully explored. These variables include the effects of air addition through forced ventilation, additional fuel decomposition in the adjacent space, and heat losses to the ceiling and walls.

The addition of air to the system through forced ventilation may have an influence on species levels, depending on where the air is added relative to the external burning. Forced ventilation in the region where external burning is occurring will introduce additional oxygen into the flow, and possibly induce additional mixing. This may result in better oxidation of incomplete combustion products, such as CO. Addition of air to the system downstream of the external burning will dilute the gases, but will not reduce the amount (in terms of mass) of incomplete combustion products being transported to remote locations.

Decomposition of fuel in the adjacent space may affect species levels transported to remote locations. This effect may be sensitive to the location of the decomposing fuel, the type of fuel, whether it is flaming or smoldering, and the conditions surrounding the fuel.

Heat losses to the ceiling and walls can cause gas temperatures in the adjacent space to decrease more readily for some materials, compared to well-insulated boundaries. An example of this may be steel decks and bulkheads on ships. A decrease in gas temperature may cause temperatures to reach levels where no reactions can occur sooner than those observed in well-insulated cases. As a result, higher heat loss to

the boundaries may result in higher incomplete combustion products, including CO, to be transported to remote areas.

Species concentrations may not always be transported away from the compartment in a uniform manner. In experiments performed by Lattimer et al. [29, 30] with the compartment located on the side of a hallway, the bulk flow from the compartment was measured to flow across the hallway and down the side of the hallway opposite the fire compartment. This resulted in higher CO, CO_2, and THC levels (and lower O_2) flowing along the side of the hallway opposite the fire compartment. For example, CO levels were measured to be as high as 1.9 % along the side of the hallway opposite the fire compartment, while on the side of the hallway with the fire compartment the maximum CO level was measured to be 1.0 %. As these gases flow farther from the compartment, they are expected to become more uniform across the hallway. However, the distance away from the compartment where mostly uniform flow occurs was not quantified.

Engineering Methodology

In light of the experimental work and chemical kinetics considerations discussed previously, several correlations can be used as guidelines for fire protection engineering. The production of chemical species in compartment fires has been shown to be correlated with the control volume equivalence ratio, ϕ_{cv}. For most purposes, the equivalence ratio can be calculated using instantaneous fuel burning rates and air mass flow rates assuming quasi-steady-state conditions. The following methodology presents a guide to determining bounds on species production as well as comments on the limits of this approach.

The methodology for estimating species transported to remote locations is provided in Fig. 16.31. This approach considers the occurrence of external burning outside the compartment. In general, the primary steps in the analysis are:

1. Determine the compartment equivalence ratio, ϕ_c.
2. If ϕ_c is less than 1, estimate species levels using the global equivalence ratio-yield correlations presented in Equations 16.19, 16.20, 16.21, 16.22, 16.23, 16.24, and 16.25 with the ϕ_c.
3. If ϕ_c is greater than 1, determine whether external burning will occur outside of the compartment. External burning can be assumed to occur at a ϕ_c (plume or compartment) of 1.6, or by calculating the ignition index using Equation 16.1.
4. If there is no external burning, use the ϕ_c and Equations 16.19, 16.20, 16.21, 16.22, 16.23, 16.24, and 16.25 to calculate the species transported.
5. If external burning is occurring, determine the effect of the smoke layer using the dimensionless smoke depth, $\gamma = \delta/z$, where δ is the depth of the layer below the ceiling and z is the lowest elevation of gases exiting the compartment.
6. If γ is greater than 1.0 and external burning is predicted, the smoke layer can be assumed to inhibit oxidation in the adjacent space. CO and other incomplete-combustion products are not reduced. The ϕ_c and Equations 16.19, 16.20, 16.21, 16.22, 16.23, 16.24, and 16.25 can be used to estimate the species transported to remote locations.
7. If γ is less than 1.0 and external burning is predicted, the smoke layer does not inhibit the oxidation in the adjacent space and incomplete-combustion products, such as CO, will be reduced. The species transported can be estimated using Equations 16.19, 16.20, 16.21, and 16.22 and the equivalence ratio for a control volume, ϕ_{cv}, that incorporates the compartment and the adjacent space out to the flame tip (see Fig. 16.17).

It should be noted that this methodology may not provide the maximum levels of incomplete combustion products that can be produced in a fire. Equations presented in this methodology for species yields as a function of equivalence ratio have been shown to provide good correlations

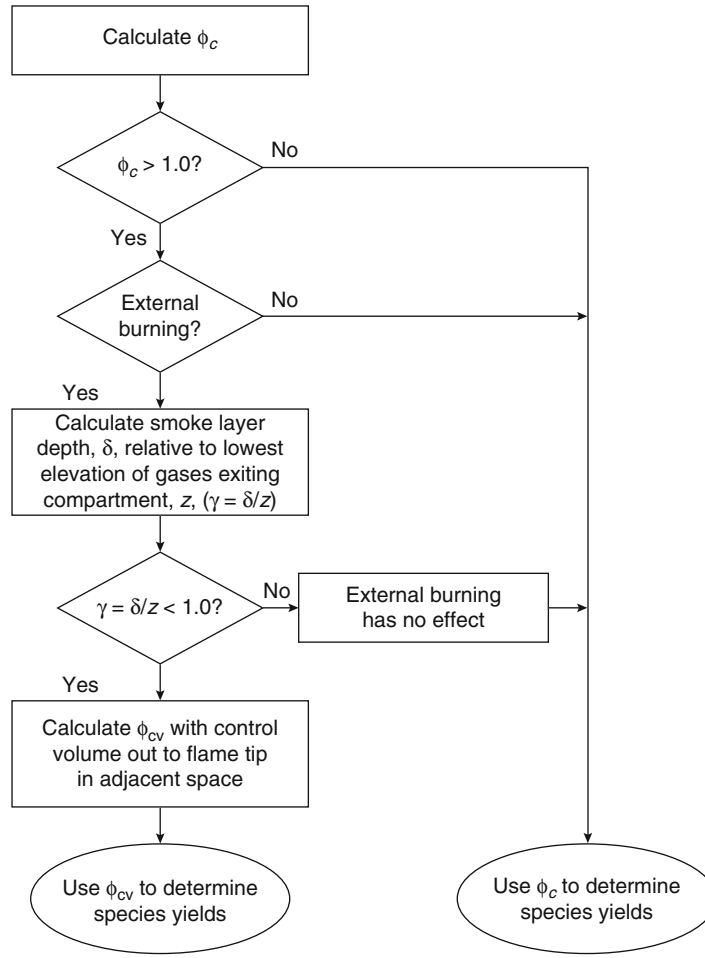

Fig. 16.31 General methodology for predicting species levels transported to remote locations from a fire compartment

even for wood as a secondary fuel pyrolyzing in the hot upper layer. However, it is not clear whether these correlations will hold for nonoxygenated fuels in the upper layer or how well they will represent other oxygenated fuels.

Several empirical correlations have been developed to predict species levels at a range of equivalence ratios. Different correlations are given in the following paragraphs to accommodate analyses of various levels of complexity.

Due to its toxicity, CO production is of primary importance. Four correlations (see Equations 16.19, 16.20, 16.21, and 16.22) are presented, representing varying degrees of complexity. In each case, the correlations basically represent a lower bound for the yield of CO. Equations 16.19a and 16.19b represents a "zeroth order" correlation between CO yield and equivalence ratio. For overventilated burning conditions, there is no CO production and for underventilated conditions CO is produced at a yield of 0.2 g per gram of fuel burned. This correlation applies best to fires with average upper-layer temperatures greater than 900 K.

$$f_{CO} = 0 \quad \text{for } \phi < 1 \tag{16.19a}$$

$$f_{CO} = 0.2 \quad \text{for } \phi > 1 \tag{16.19b}$$

Equations 16.20a, 16.20b, and 16.20c accounts for some of the temperature effect by including a linear rise in CO yield over the transition region from ϕ of 0.5 to 1.5.

$$f_{CO} = 0 \quad \text{for } \phi < 0.5 \tag{16.20a}$$

$$f_{CO} = 0.2\phi - 0.1 \quad \text{for } 0.5 < \phi < 1.5 \tag{16.20b}$$

$$f_{CO} = 0.2 \quad \text{for } \phi > 1.5 \tag{16.20c}$$

The temperature effect on CO production is best represented in the following two correlations. Equation 16.21, which represents a fit to the hexane data of Beyler's hood experiments, is suggested for compartment fires with average upper-layer temperatures below 800 K. Equation 16.22 is used for fires with upper-layer temperatures above 900 K. Equation 16.15 is an approximate fit to the compartment fire hexane data of Gottuk et al. For the most part, CO yields from hexane fires represent lower limits observed for the fuels studied to date [5, 8]. Therefore, these equations provide a *minimum* CO production that can be used for hazard analysis.

$$Y_{CO} = (0.19/180)\tan^{-1}(X) + 0.095 \text{ for } T < 800\text{ K} \tag{16.21}$$

where $X = 10(\phi - 0.8)$ and $\tan^{-1}(X)$ is in degrees

$$Y_{CO} = (0.22/180)\ \tan^{-1}(X) + 0.11 \text{ for } T > 900\text{ K} \tag{16.22}$$

where $X = 10(\phi - 1.25)$ and $\tan^{-1}(X)$ is in degrees

The figures presented earlier of CO yield versus equivalence ratio also show plots of Equations 16.21 and 16.22. Figure 16.7 shows the CO yield data for methane hood experiment fires in which upper-layer temperatures ranged from 490 to 870 K. The CO yield data of Zukoski et al. and Toner et al. lie between the curves of Equations 16.21 and 16.22, particularly for slightly overventilated and stoichiometric conditions. This is consistent with the fact that these fires had temperatures that were higher than those represented by Equation 16.14 and some were within the transition range of 800–900 K.

The simple model presented as Equations 16.14a, 16.14b, 16.14c, 16.14d, and 16.14e with the inclusion of the empirically determined yield coefficients, is fairly adequate for predicting CO_2, O_2, and H_2O normalized yields (see Equations 16.23, 16.24, and 16.25). Suggested average yield coefficients for compartment fires of elevated temperatures ($T > 900$ K) are 0.88 for B_{CO_2} and 0.97 for B_{O_2} [5]. Suggested values for low upper-layer temperatures ($T < 800$ K) are 0.77 for B_{CO_2}, 0.92 for B_{O_2}, and 0.95 for B_{H_2O}. Average yield coefficients for underventilated fires are shown in Table 16.2.

$$f_{CO_2} = 1 \quad \text{for } \phi < 1 \tag{16.23a}$$

$$f_{CO_2} = B_{CO_2}/\phi \quad \text{for } \phi > 1 \tag{16.23b}$$

$$f_{O_2} = 1 \quad \text{for } \phi < 1 \tag{16.24a}$$

$$f_{O_2} = B_{O_2}/\phi \quad \text{for } \phi > 1 \tag{16.24b}$$

$$f_{H_2O} = 1 \quad \text{for } \phi < 1 \tag{16.25a}$$

$$f_{H_2O} = B_{H_2O}/\phi \quad \text{for } \phi > 1 \tag{16.25b}$$

As presented in Equations 16.23, 16.24, and 16.25, normalized chemical species yields, *f*, can be correlated quite well by the global equivalence ratio. This is true for a wide range of fuel types. However, it is worthwhile to point out that for different fuels, the CO_2, O_2, and H_2O yields to equivalence ratio correlations only collapse down to a single curve when the yields are normalized by the maximum possible yield for a given fuel (i.e., presented as *f* rather than *Y*). Although complete combustion does not occur, combustion efficiencies with respect to equivalence ratio are similar enough between fuels that the stoichiometry of a particular fuel will dictate the generation of CO_2 and the depletion of O_2. Therefore, the species associated with complete combustion (CO_2, O_2, and H_2O) are not expected to have equal yields for different fuels, since varying fuel compositions will dictate different limits of CO_2 and H_2O that can be generated and O_2 that can be consumed for a gram of fuel burned. By normalizing the yields, the variability of fuel composition is removed.

On the other hand, carbon monoxide production is best correlated by the equivalence ratio when represented as a simple yield, Y_{CO}, rather than a normalized yield, f_{CO}. This is one indicator that CO production is not strongly dependent on fuel type, as is production of CO_2 and O_2. The reason for this is believed to be due to the fact that CO is effectively an intermediate product that depends more on the elementary chemistry than on fuel composition, which determines products of complete combustion.

Once yields are determined using the above correlations, species gas concentrations can be calculated. Equation 16.26 can be used to calculate the concentration of species i for all species except oxygen. Oxygen concentrations can be calculated from the depletion of oxygen using Equation 16.27.

$$X_{i_{\text{wet}}} = \frac{Y_i \dot{m}_f M_{\text{mix}}}{(\dot{m}_f + \dot{m}_a) M_i} \tag{16.26}$$

$$X_{O_{2\text{wet}}} = \frac{0.21 \dot{m}_a M_{O_2}/M_a - D_{O_2} \dot{m}_f}{(\dot{m}_f + \dot{m}_a) M_{O_2}/M_a} \tag{16.27}$$

The yield-equivalence ratio correlations shown in Fig. 16.9, which are also represented by Equations 16.21 and 16.15, have been replotted as CO concentration vs. equivalence ratio in Fig. 16.32. As indicated previously, the yield correlations in Fig. 16.9 (and thus, the concentrations in Fig. 16.32) represent a reasonable lower bound for a range of typical fuels. Higher concentrations of CO can be created, particularly when additional fuel is added to a vitiated upper layer. Corresponding to Fig. 16.32, CO_2 and O_2 concentrations for hexane compartment fires are shown in Figs. 16.33 and 16.34, respectively. Even though the peak concentrations of CO_2 will be dependent on the fuel type, the oxygen concentration as a function of will be similar for most hydrocarbons [5].

The ratio of CO to CO_2 concentrations can be used as an indicator of the combustion mode. Higher combustion efficiency is obtained as more fuel is burned completely to CO_2 and H_2O and is indicated by a ratio of CO to CO_2 near zero. Since CO is a product of incomplete combustion, the ratio of CO to CO_2 concentrations will increase as fires burn less efficiently. The ratio increases with equivalence ratio even for underventilated conditions, as evidenced by experimental data (e.g., Gottuk et al. [5]) and the engineering correlations presented above.

Example 4 Consider that the piece of furniture described in Example 1 is burning in a room such that a two-layer system develops. The only ventilation to the room is an open doorway through which 217 g/s of air is being entrained. The material is burning at a rate of 37 g/s, and the

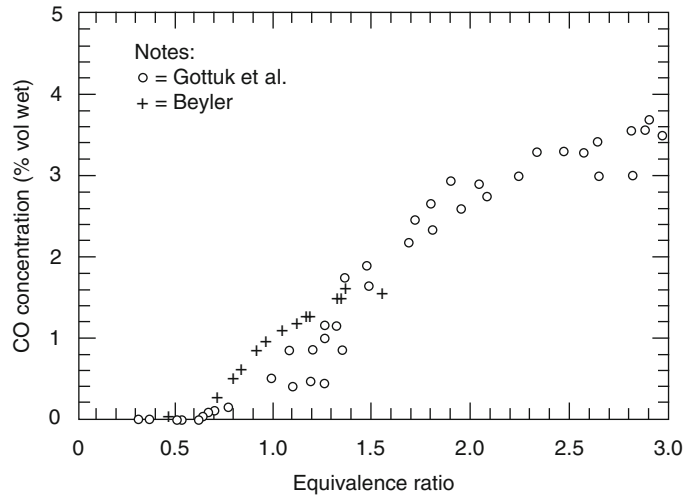

Fig. 16.32 Carbon monoxide concentrations as a function of equivalence ratio for hexane fires in a compartment (o) and under a hood (+). Data represent the same tests shown in Fig. 16.9 as unnormalized yields

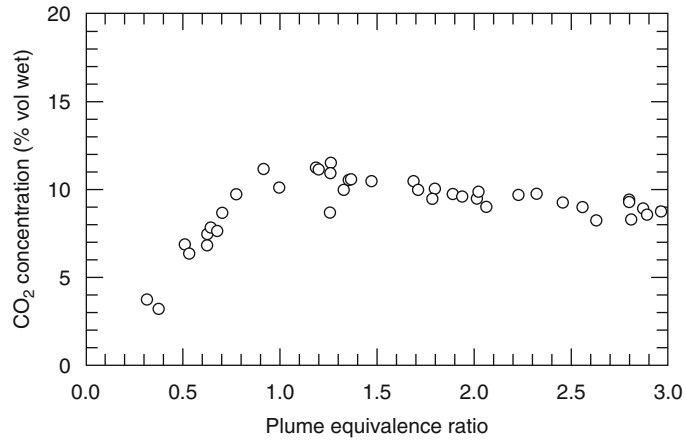

Fig. 16.33 CO_2 concentrations as a function of equivalence ratio for hexane compartment fires [5]

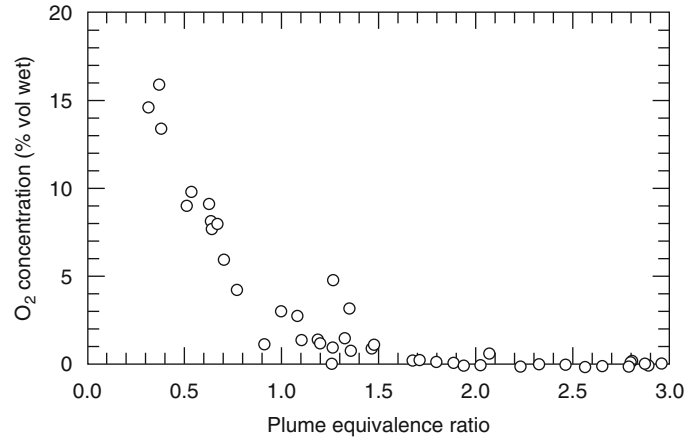

Fig. 16.34 O_2 concentrations as a function of equivalence ratio for hexane compartment fires [5]

average temperature of the upper layer is 700 °C. Calculate the plume equivalence ratio and determine the yield of CO and depletion of O_2.

Solution The plume equivalence ratio is calculated using Equation 16.10b. The stoichiometric fuel-to-air ratio, *r,* has already been calculated in Example 1.

$$\phi_p = \frac{\dot{m}_f/\dot{m}_a}{r} = \frac{37/217}{0.1139} = 1.5$$

Because the average upper-layer temperature $(700°\text{C} + 273 = 973\ \text{K})$ is above 900 K, Equation 16.22 is used to calculate the yield of CO. The argument, *X,* of the inverse tangent is

$$X = 10(\phi_p - 1.25) = 10(1.5 - 1.25) = 2.5$$

$$Y_{\text{CO}} = \left(\frac{0.22}{180}\right)\tan^{-1}(X) + 0.11$$

$$Y_{\text{CO}} = \left(\frac{0.22}{180}\right)\tan^{-1}(2.5) + 0.11$$

$$Y_{\text{CO}} = 0.19$$

Therefore, 0.19 g of CO are produced for every gram of polyurethane foam that burns. The production rate of CO is equal to that yield, Y_{CO}, multiplied by the fuel burning rate (0.19 × 37 g/s = 7.0 g/s).

The normalized yield of oxygen is determined using Equation 16.24, and the recommended yield coefficient, B_{O_2}, of 0.97.

$$f_{O_2} = \frac{B_{O_2}}{\phi} = \frac{0.97}{1.5} = 0.65$$

From Example 1, we obtain the maximum theoretical depletion of oxygen, k_{O2}, and calculate the depletion of oxygen as

$$D_{O_2} = f_{O_2} k_{O_2} = 0.65\,(2.05)$$
$$= 1.33 \text{ g of } O_2 \text{ per gram of fuel burned}$$

The depletion rate of oxygen is 49.2 g/s (1.33 × 37 g/s).

Example 5 For the piece of furniture burning in Example 4, calculate the CO and O_2 concentrations in the upper layer.

Solution Gas concentrations can be calculated from the yields determined in Example 4 using Equation 16.26 for CO and Equation 16.27 for O_2.

$$X_{CO_{wet}} = \frac{Y_{CO}\dot{m}_f M_{mix}}{(\dot{m}_f + \dot{m}_a)M_{CO}} = \frac{0.19(37)\,(28.8)}{(37+217)\,(28)} = 0.028$$

$$X_{O_2} = \frac{0.21\dot{m}_a M_{O2}/M_a - D_{O_2}\dot{m}_f}{(\dot{m}_a + \dot{m}_f)M_{O_2}/M_a}$$
$$= \frac{0.21(217)\,32/28.8 - 1.33(37)}{(32+217)\,32/28.8}$$
$$X_{O_2} = 0.005$$

The resulting concentrations of CO and O_2 are 2.8 and 0.5 % by volume, respectively.

Example 6 A fire is burning in a room that has one door open and no other ventilation. The room is 7 m wide and 4 m deep with a 2.43 m high ceiling. The door measures 0.76 m wide and 2.05 m high (area = 1.56 m^2). The peak heat release rate of the fire has been estimated to be 4.5 MW. Determine how much CO can be transported to other rooms in the building.

Solution The first step is to calculate the compartment equivalence ratio, ϕ_c. Since details of the fire are not provided, the mass burning rate of the fuel is not known. Therefore, ϕ_c is estimated via Equation 16.13c using the heat release rate, Q, of 4.5 MW.

$$\phi_c = \frac{Q}{\dot{m}_a} \cdot \frac{1}{3030} = \frac{4,500 \text{ kW}}{\dot{m}_a \cdot 3030}$$

The mass flow rate of air, $\dot{m}_a$, into the room is estimated using the ventilation parameter [33] as follows:

$$\dot{m}_a = 0.5A\sqrt{h} = 0.5 \cdot 1.56\sqrt{2.05} = 1.12\,\text{kg/s}$$

Substituting $\dot{m}_a$ into the equation above for the compartment equivalence ratio yields a ϕ_c of 1.3. Since ϕ_c is greater than 1, the occurrence of external burning must be considered. However, using the criteria that ϕ_c is less than 1.6, it is assumed that no external burning will occur. Species levels inside the room are calculated by Equations 16.19, 16.20, 16.21, 16.22, 16.23, 16.24, and 16.25 using ϕ_c. The yield of CO is calculated using Equation 16.21 or 16.22, depending on the temperature of the upper layer. The upper-layer temperature can be estimated using the McCaffrey, Quintiere, and Harkleroad (MQH) correlation [34] that is presented in Chap. 30 of this book. According to the MQH correlation, the upper-layer gas temperatures exceed 900 K for fires above 1100 kW. For temperatures above 900 K, Equation 16.22 is used to calculate the CO yield as

$$Y_{CO} = (0.22/180) \cdot \tan^{-1}[10(\phi - 1.25)]$$
$$+ 0.11 = 0.14$$

Since there is no external burning, the CO generated in the compartment (0.14 kg of CO per kg of fuel burned) will flow to other parts of the building. Before dilution occurs away from the fire compartment, the initial concentration of CO in the gases from the fire compartment can be calculated using Equation 16.26:

$$X_{CO_{wet}} = \frac{Y_{CO}\dot{m}_f M_{mix}}{(\dot{m}_f + \dot{m}_a)M_{CO}} = \frac{0.14(\dot{m}_f)28.8}{(\dot{m}_f + 1.12)28}$$

Since there is no information on the contents burning in the room, an accurate assessment of the fuel mass burning rate, $\dot{m}_f$, cannot be obtained. An estimate of $\dot{m}_f$ can be made using Equation 16.13a, with an assumed value of r, the stoichiometric fuel-to-air ratio. Values of r are presented in Table 16.1 for various fuels as $1/r$. In order to bound the possible CO

concentrations, values of $1/r$ of 4–15 are chosen to represent a reasonable range of hydrocarbon fuels that may be burning in the room. The following shows an example of the $\dot{m}_f$ calculation using Equation 16.13a and $1/r = 4$:

$$\dot{m}_f = \frac{\phi \cdot \dot{m}_a}{1/r} = \frac{1.3(1.12\ \text{kg/s})}{4} = 0.36\ \text{kg/s}$$

The corresponding calculation for $1/r$ of 15 yields an $\dot{m}_f$ of 0.097 kg/s. Substituting the values for $\dot{m}_f$ into the above equation for $X_{\text{CO}_{\text{wet}}}$ results in CO concentrations of 3.5 and 1.1 %, respectively.

Nomenclature

B_i	yield coefficients of species i
C	stoichiometric molar ratio of water to carbon dioxide
C_j	volume concentration of fuel j when fuel stream is stoichiometrically mixed with oxidant stream
C_p	heat capacity of products of complete combustion, (kJ/g · mol K)
D_{O_2}	mass depletion of oxygen per gram of fuel burned (g/g)
E	energy released per kg of oxygen consumed
F	normalized yield or generation efficiency
$\Delta H_{c,j}$	heat of combustion of the species j, (kJ/g · mol)
j	fuel species of interest
k	maximum theoretical yield
$L_{f,\text{tip}}$	length of flame tip for flame extending down a corridor ceiling
M	molecular weight
m_a	mass of air
$\dot{m}_a$	mass flow rate of air
m_f	mass of fuel
$\dot{m}_f$	mass loss rate of fuel
$\ddot{m}_f$	derivative of the fuel mass loss rate
$\dot{m}_{\text{exhaust}}$	mass flow rate out of the layer
n	molar quantity
n_{prod}	number of moles of products of complete combustion per mole of reactants (stoichiometric mixture of fuel and oxidant streams)
Q	ideal heat release rate
r	stoichiometric fuel-to-air ratio
r_a	stoichiometric air-to-fuel ratio
r_{O_2}	stoichiometric fuel-to-oxygen ratio
T	temperature
$T_{\text{SL},j}$	adiabatic flame temperature at the stoichiometric limit for fuel species j (K)
T_o	temperature of the gas mixture prior to reaction (K)
t	time
t_r	residence time of gases in the upper layer
τ_{SS}	steady-state time ratio
V_{ul}	volume of the upper layer
X	mole fraction
$X_{i_{\text{dry}}}$	dry mole fraction of species i (H_2O removed from sample)
$X_{i_{\text{wet}}}$	wet mole fraction of species i
Y	yield (g/g) also refers to D_{O_2}
$Y_{O_2,\text{air}}$	mass fraction of oxygen in air
z	distance between the bottom of the compartment outflow and the ceiling in the adjacent space
γ	dimensionless layer depth in adjacent space ($\gamma = \delta/z$)
δ	layer depth in the adjacent space
ϕ	equivalence ratio
ϕ_c	compartment equivalence ratio
ϕ_{cv}	equivalence ratio defined per a specified control volume
ϕ_p	plume equivalence ratio
ϕ_{ul}	upper-layer equivalence ratio
ρ_{ul}	density of the upper layer

Subscripts

A	air
f	fuel
CO	carbon monoxide
O_2	oxygen
CO_2	carbon dioxide
H_2O	water
H_2	hydrogen

THC	total unburned hydrocarbons
resid,C	residual carbon
$X_{i_{\text{wet}}}$	wet gas concentration with water in the mixture
$X_{i_{\text{dry}}}$	dry gas concentration with no water in the mixture

References

1. R.A. Anderson, A.A. Watson, and W.A. Harland, "Fire Deaths in the Glasgow Area: II The Role of Carbon Monoxide," *Medicine, Science, & the Law,* 21, pp. 289–294 (1981).
2. B. Harwood and J.R. Hall, "What Kills in Fires: Smoke Inhalation or Burns?" *Fire Journal,* 83, pp. 29–34 (1989).
3. R.J. Gann, V. Babrauskas, and R.D. Peacock, "Fire Conditions for Smoke Toxicity Measurements," *Fire and Materials,* 18, 3, pp. 193–199 (1994).
4. C.L. Beyler, "Ignition and Burning of a Layer of Incomplete Combustion Products," *Combustion Science and Technology,* 39, pp. 287–303 (1984).
5. D.T. Gottuk, R.J. Roby, M.J. Peatross, and C.L. Beyler, "Carbon Monoxide Production in Compartment Fires," *Journal of Fire Protection Engineering,* 4, pp. 133–150 (1992).
6. N.P. Bryner, E.L. Johnsson, and W.M. Pitts, "Carbon Monoxide Production in Compartment Fires—Reduced-Scale Enclosure Test Facility," *NISTIR 5568,* National Institute of Standards and Technology, Gaithersburg, MD (1995).
7. S.J. Toner, E.E. Zukoski, and T. Kubota, "Entrainment, Chemistry, and Structure of Fire Plumes," *NBS-GCR-87-528,* National Institute of Standards and Technology, Gaithersburg, MD (1987).
8. C.L. Beyler, "Major Species Production by Diffusion Flames in a Two-Layer Compartment Fire Environment," *Fire Safety Journal,* 10, pp. 47–56 (1986).
9. C.L. Beyler, *Fire Safety Science—Proceedings of First International Symposium,* Hemisphere, Washington, DC, pp. 430–431 (1986).
10. E.E. Zukoski, S.J. Toner, J.H. Morehart, and T. Kubota, *Fire Safety Science—Proceedings of the Second International Symposium,* Hemisphere, Washington, DC, pp. 295–304 (1989).
11. E.E. Zukoski, J.H. Morehart, T. Kubota, and S.J. Toner, "Species Production and Heat Release Rates in Two-Layered Natural Gas Fires," *Combustion and Flame,* 83, pp. 324–332 (1991).
12. J.H. Morehart, E.E. Zukoski, and T. Kubota, "Species Produced in Fires Burning in Two-Layered and Homogeneous Vitiated Environments," *NBS-GCR-90-585,* National Institute of Standards and Technology, Gaithersburg, MD (1990).
13. D. Drysdale, *An Introduction to Fire Dynamics,* 2nd ed., John Wiley and Sons, Chichester, UK (1999).
14. W.M. Pitts, *24th Symposium (International) on Combustion,* Combustion Institute, Pittsburgh, PA (1992).
15. D.T. Gottuk, R.J. Roby, and C.L. Beyler, "The Role of Temperature on Carbon Monoxide Production in Compartment Fires," *Fire Safety Journal,* 24, pp. 315–331 (1995).
16. A. Tewarson, "Fully Enveloped Enclosure Fires of Wood Cribs," *20th Symposium (International) on Combustion,* Combustion Institute, Pittsburgh, PA, p. 1555 (1984).
17. D.T. Gottuk, "The Generation of Carbon Monoxide in Compartment Fires," *NBS-GCR-92-619,* National Institute of Standards and Technology, Gaithersburg, MD (1992).
18. W.D. Walton and P.H. Thomas, "Estimating Temperatures in Compartment Fires," *The SPFE Handbook of Fire Protection Engineering,* National Fire Protection Association, Quincy, MA, Ch. 2-2 (1988).
19. W.M. Pitts, E.L. Johnsson, and N.P. Bryner, "Carbon Monoxide Formation in Fires by High-Temperature Anaerobic Wood Pyrolysis," presented at the *25th Symposium (International) on Combustion,* Combustion Institute, Pittsburgh, PA (1994).
20. D. Gross and A.F. Robertson, *10th Symposium (International) on Combustion,* Combustion Institute, Pittsburgh, PA, pp. 931–942 (1965).
21. B.Y. Lattimer, U. Vandsburger, and R.J. Roby, "Carbon Monoxide Levels in Structure Fires: Effects of Wood in the Upper Layer of a Post-Flashover Compartment Fire," *Fire Technology,* 34, 4 (1998).
22. W.M. Pitts, "The Global Equivalence Ratio Concept and the Prediction of Carbon Monoxide Formation in Enclosure Fires," *NIST Monograph 179,* National Institute of Standards and Technology, Gaithersburg, MD (1994).
23. N.P. Bryner, E.L. Johnsson, and W.M. Pitts, "Carbon Monoxide Production in Compartment Fires: Full-Scale Enclosure Burns," in *Proceedings of the Annual Conference on Fire Research, NISTIR 5499,* National Institute of Standards and Technology, Gaithersburg, MD (1994).
24. W.M. Pitts, N.P. Bryner, and E.L. Johnsson, "Combustion Product Formation in Under and Overventilated Full-Scale Enclosure Fires," in *Proceedings of Combustion Fundamentals and Applications, Joint Technical Meeting,* San Antonio, TX (1995).
25. N.P. Bryner, E. L. Johnsson, and W.M. Pitts, "Scaling Compartment Fires—Reduced- and Full-Scale Enclosure Burns," in *Proceedings, International Conference on Fire Research and Engineering* (D.P. Lund and E.A. Angell, eds.), Society of Fire Engineers, Boston (1995).
26. W.M. Pitts, "An Algorithm for Estimating Carbon Monoxide Formation in Enclosure Fires," *Fire Safety*

Science—Proceedings of the Fifth International Symposium, International Association of Fire Safety Science," pp. 535–546 (1997).
27. J. Warnatz, "Rate Coefficients in the C/H/O System," in *Combustion Chemistry,* (W.C. Gardiner, ed.), Springer-Verlag, New York, pp. 224–232 (1984).
28. D.S. Ewens, "The Transport and Remote Oxidation of Compartment Fire Exhaust Gases," M.S. Thesis, Virginia Polytechnic Institute and State University, Department of Mechanical Engineering, Blacksburg, VA (1994).
29. B.Y. Lattimer, U. Vandsburger, and R.J. Roby, "The Transport of Carbon Monoxide from a Burning Compartment Located on the Side of a Hallway," *26th Symposium (International) on Combustion,* Combustion Institute, Naples, Italy, pp. 1541–1547 (1996).
30. B.Y. Lattimer, U. Vandsburger, and R.J. Roby, "The Transport of High Concentrations of Carbon Monoxide to Locations Remote from the Burning Compartment," *NIST-GCR-97-713,* U.S. Department of Commerce (1997).
31. D.T. Gottuk, R.J. Roby, and C.L. Beyler, "A Study of Carbon Monoxide and Smoke Yields from Compartment Fires with External Burning," *24th Symposium (International) on Combustion,* Combustion Institute, Pittsburgh, PA, pp. 1729–1735 (1992).
32. B.Y. Lattimer, D.S. Ewens, U. Vandsburger, and R.J. Roby, "Transport and Oxidation of Compartment Fire Exhaust Gases in Adjacent Corridor," *Journal of Fire Protection Engineering,* 6, 4 (1994).
33. B.Y. Lattimer, unpublished data (2000).
34. B.J. McCaffery, J.G. Quintiere, and M.F. Harkleroad, "Estimating Room Fire Temperatures and the Likelihood of Flashover Using Fire Test Data Correlations," *Fire Technology,* 17, 2, pp. 98–119 (1981).

Dr. Daniel T. Gottuk is VP of Specialty Services and the Technical Director of Jensen Hughes. He is actively involved in fire hazard analyses, fire research and testing, and forensic engineering relative to fire dynamics and fire detection.

Brian Y. Lattimer is a Professor in Mechanical Engineering at Virginia Tech. His research areas include fire dynamics, heat transfer from fires, and material response to fires.

Flammability Limits of Premixed and Diffusion Flames

17

Craig Beyler

Introduction

It is well known that not all fuel/oxidant/diluent mixtures can propagate flame. Normal flame-type combustion cannot be sustained outside certain limits definable in terms of fuel/oxidant/diluent composition. Definition of these limits has received a great deal of attention in premixed combustion conditions, that is, in systems where the fuel and oxidant are mixed prior to combustion. Despite scientific interest in the subject dating back to the nineteenth century, the mechanism responsible for flammable limits is not yet understood. Nonetheless, a great deal has been learned that has practical application.

Much less investigation into the nature and cause of limits in diffusion flames has been undertaken. Empirically, clear parallels exist between diffusion and premixed limits, and these will be explored in the latter portion of this chapter.

Premixed Combustion

Premixed flame fronts can only propagate within a range of compositions of fuel and oxidant. The composition limits within which a flame can propagate are known as the upper and lower flammable limits and are expressed as concentrations of the fuel in a specified oxidant/diluent mixture at a specified temperature and pressure. For instance, the lower flammable limit (LFL) of methane in air at normal temperature and pressure is 5 % by volume, and the upper flammable limit (UFL) is 15 % by volume. As such, only methane/air mixtures with methane concentrations between 5 % and 15 % methane will support propagation of flame. For most simple hydrocarbons, the lower and upper flammable limits in air correspond to an equivalence ratio of approximately 0.5 and 3, respectively. The lower flammable limit concentrations for these fuels is approximately 48 g/m^3 (Fig. 17.1) [1].

The most widely used method of measuring flammable limits was developed by the U.S. Bureau of Mines [2]. The apparatus consists of a 1.5-m-long, 0.05-m-diameter vertical tube which is filled with the fuel/oxidant/diluent mixture to be tested. The top of the tube is closed, and the base of the tube can be closed until the start of the test to prevent diffusion of the mixture from the tube. With the base of the tube open, the mixture is ignited by a spark or small pilot flame at the base of the tube, and the travel of the flame front up the tube is observed. The mixture is deemed to be within the flammable limits if the flame can propagate halfway up the 1.5 m tube. The test is designed to identify the range of mixture compositions capable of flame propagation remote from the ignition source.

C. Beyler (✉)
Jensen Hughes, 3610 Commerce Drive, Suite 817, Baltimore, MD 21227, USA

M.J. Hurley (ed.), *SFPE Handbook of Fire Protection Engineering*,
DOI 10.1007/978-1-4939-2565-0_17, © Society of Fire Protection Engineers 2016

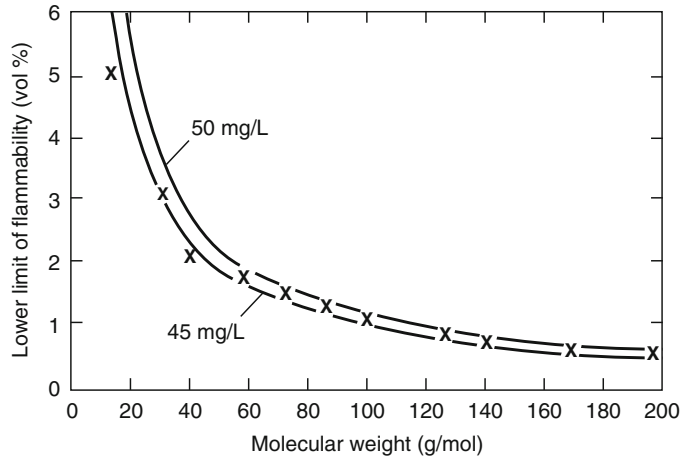

Fig. 17.1 Effect of molecular weight on lower limits of flammability of alkanes at 25 °C [1]

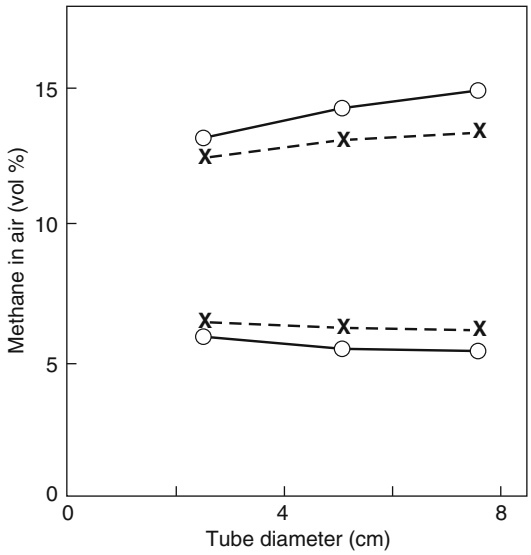

Fig. 17.2 Upper and lower flammable limits of methane as determined in a vertical tube apparatus for upward propagation (*circles*), and for downward propagation (*crosses*) [3]

The apparatus can be used with ignition at the top of the tube, but the flammable limits determined for downward propagation are narrower than for upward propagation. The 0.05 m diameter of the tube was chosen as the smallest diameter at which the heat losses from the flame to the tube wall had minimal effect on the flammable limits determined (Fig. 17.2) [3]. Several other methods for determining flammable limits are available [4–7]. Some methods are designed for use in special conditions, and others simply reflect national differences. Although each method gives substantially similar results, some variations in results do exist (see, for example, Smedt et al. [8] and Goethals et al. [9]).

Mixtures are capable of combustion outside the flammable limits, but external energy must be provided throughout the mixture volume in order to allow propagation of a flame [10]. An example of this behavior is shown in Fig. 17.3. A small hydrogen diffusion flame is used as a pilot source in a lean methane/air mixture. At methane concentrations less than 5 %, combustion occurs only in the wake of the pilot flame. Above 5 %, the flame can propagate away from the pilot flame, regardless of the orientation of the pilot flame.

Flammable limits are a function of the oxygen and inert concentrations, as well as the mixture temperature and pressure. As the concentration of inerts is reduced and the oxygen concentration is increased, the upper flammable limit is increased, whereas the lower limit is relatively unchanged. This result can be understood by observing that at the lower flammable limit there is always more than enough oxygen present for complete combustion, but at the upper limit less than the stoichiometrically required oxygen is present. Hence, at the upper limit the additional oxygen participates in the combustion process, whereas at the lower limit the additional oxygen simply replaces inert gas.

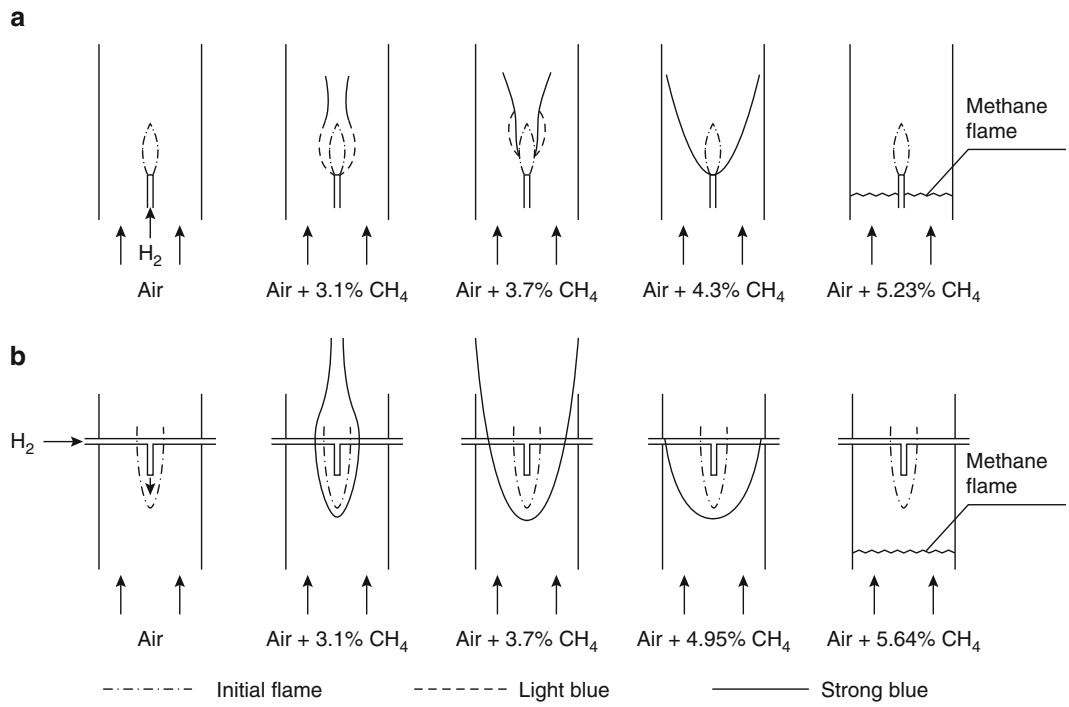

Fig. 17.3 A small jet diffusion flame in a coflowing (**a**) and contraflowing (**b**) stream as the concentration of the fuel in the stream is gradually increased up to ignition. The stream velocity is 0.222 m/s, and the hydrogen jet diameter is 1.52 mm [10]

The lower flammable limit is also insensitive to the pressure, except at pressures well below atmospheric. The upper limit shares this insensitivity at subatmospheric pressures, but the upper limit increases with increasing pressure above atmospheric (Fig. 17.4) [1].

The flammable limits widen with increases in mixture temperature as illustrated in Fig. 17.5; [1] this aspect will be discussed further later in this chapter. Figure 17.5 also relates flammable limits with the saturation vapor curve and the autoignition temperature (AIT). The flashpoint of a liquid is given in the figure as T_L. At that temperature, the vapor pressure at the liquid surface is at the lower flammable limit. The corresponding upper limit temperature is given as T_U. If a liquid is contained within a closed vessel and the vapors are allowed to come into equilibrium at temperatures above the upper limit temperature, the vapors in the vessel will be above the upper flammable limit, for example, as typically occurs in an automobile gas tank. If the liquid is not enclosed fully, there will be a location above the surface of the liquid where the fuel/air mixture will be diluted below the upper flammable limit and will ignite if an ignition source is present.

Predicting Lower Flammable Limits of Mixtures of Flammable Gases (Le Chatelier's Rule)

Based on an empirical rule developed by Le Chatelier in the late nineteenth century, the lower flammable limit of mixtures of multiple flammable gases in air can be determined. A generalization of Le Chatelier's rule was given by Coward et al. [11]

$$\sum_{i=1}^{n} \frac{C_i}{\mathrm{LFL}_i} \geq 1 \qquad (17.1)$$

where C_i is the volume percent of fuel gas, i, in the fuel/air mixture, and LFL_i is the volume

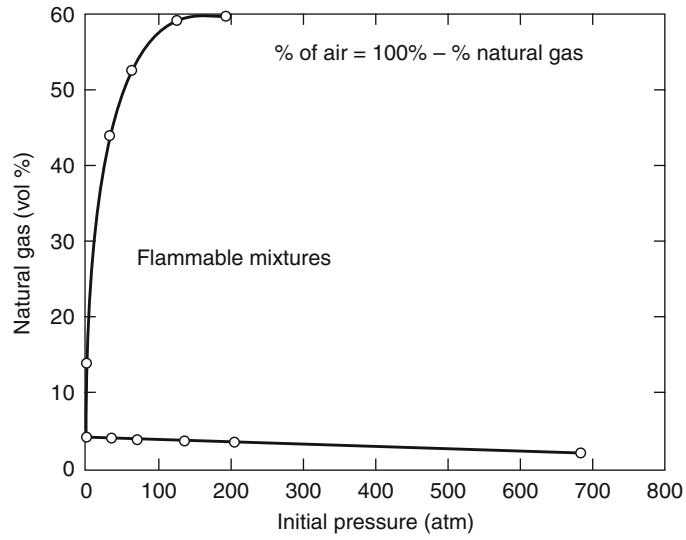

Fig. 17.4 Effect of pressure on the limits of flammability of natural gas in air at 28 °C [1]

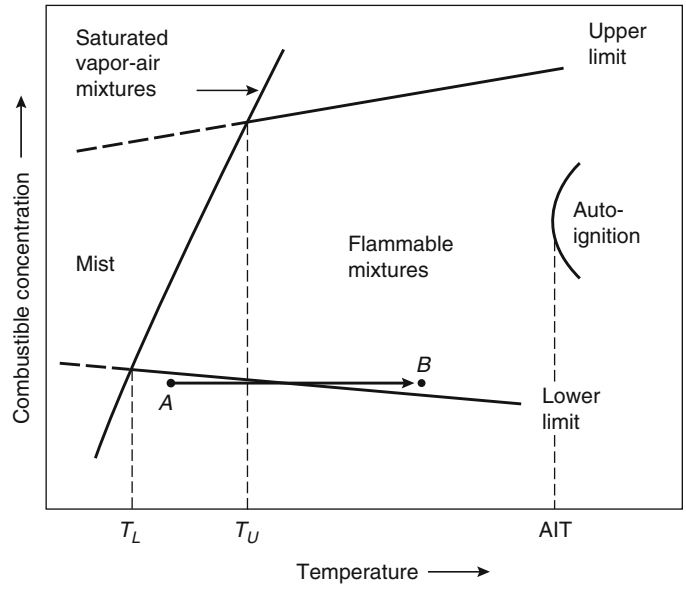

Fig. 17.5 Effect of temperature on limits of flammability of a combustible vapor in air at constant initial pressure [1]

percent of fuel gas, *i,* at its lower flammable limit in air alone. If the indicated sum is greater than unity, the mixture is above the lower flammable limit. This relationship can be restated in terms of the lower flammable limit concentration of the fuel mixture, LFL_m , as follows:

$$\mathrm{LFL}_m = \frac{100}{\sum_{i=1}^{n} \left(C_{f_i}/\mathrm{LFL}_i\right)} \tag{17.2}$$

where C_{f_i} is the volume percent of fuel gas i in the fuel gas mixture.

Example 1 A mixture of 50 % methane, 25 % carbon monoxide, and 25 % hydrogen is mixed with air. Calculate the lower flammmable limit of this fuel gas mixture.

Solution Referring to Table 17.1, LFLs of methane, carbon monoxide, and hydrogen are

Table 17.1 Summary of limits of flammability, Lower Temperature Limits (T_L), and Minimum Autoignition Temperatures (*AIT*) of individual gases and vapors in air at atmospheric pressure [1]

Limits of flammability (vol %)					Limits of flammability (vol %)				
Combustible	LFL[a]	UFL[a]	T_L (°C)	AIT (°C)	Combustible	LFL[a]	UFL[a]	T_L (°C)	AIT (°C)
Acetal	1.6	10	37	230	Cumene	0.88[b]	6.5[b]	–	425
Acetaldehyde	4.0	60	–	175	Cyanogen	6.6	–	–	–
Acetic acid	5.4[b]	–	40	465	Cycloheptane	1.1	6.7	–	–
Acetic anhydride	2.7[c]	10[d]	47	390	Cyclohexane	1.3	7.8	–	245
Acetanilide	1.0[e]	–	–	545	Cyclohexanol	1.2[e]	–	–	300
Acetone	2.6	13	–	465	Cyclohexene	1.2[b]	–	–	–
Acetophenone	1.1[e]	–	–	570	Cyclohexyl acetate	1.0[e]	–	–	335
Acetylacetone	1.7[e]	–	–	340	Cyclopropane	2.4	10.4	–	500
Acetyl chloride	5.0[e]	–	–	390	Cymene	0.85[b]	6.5[b]	–	435
Acetylene	2.5	100	–	305	Decaborane	0.2	–	–	–
Acrolein	2.8	31	–	235	Decalin	0.74[b]	4.9[b]	57	250
Acrylonitrile	3.0	–	−6	–	*n*-Decane	0.75[f]	5.6[g]	46	210
Acetone-cyanohydrin	2.2	12	–	–	Deuterium	4.9	75	–	–
Adipic acid	1.6[e]	–	–	420	Diborane	0.8	88	–	–
Aldol	2.0[e]	–	–	250	Diesel fuel (60 cetane)	–	–	–	225
Allyl alcohol	2.5	18	22	–	Diethyl amine	1.8	10	–	–
Allyl amine	2.2	22	–	375	Diethyl analine	0.8[e]	–	80	630
Allyl bromide	2.7[e]	–	–	295	1,4-Diethyl benzene	0.8[b]	–	–	430
Allyl chloride	2.9	–	−32	485	Diethyl cyclohexene	0.75	–	–	240
o-Aminodiphenyl	0.66	4.1	–	450	Diethyl ether	1.9	36	–	160
Ammonia	15.0	28	–	–	3,3-Diethyl pentane	0.7[b]	–	–	290
n-Amyl acetate	1.0[b]	7.1[b]	25	360	Diethyl ketone	1.6	–	–	450
n-Amyl alcohol	1.4[b]	10[b]	38	300	Diisobutyl carbinol	0.82[b]	6.1[h]	–	–
tert-Amyl alcohol	1.4[e]	–	–	435	Diisobutyl ketone	0.79[b]	6.2[b]	–	–
n-Amyl chloride	1.6[i]	8.6[b]	–	260	2-4,Diisocyanate	–	–	120	–
tert-Amyl chloride	1.5[j]	–	−12	345	Diisopropyl ether	1.4	7.9	–	–
n-Amyl ether	0.7[e]	–	–	170	Dimethyl amine	2.8	–	–	400
Amyl nitrite	1.0[e]	–	–	210	2,2-Dimethyl butane	1.2	7.0	–	–
n-Amyl propionate	1.0[e]	–	–	380	2,3-Dimethyl butane	1.2	7.0	–	–
Amylene	1.4	8.7	–	275	Dimethyl decalin	0.69[b]	5.3[k]	–	235
Aniline	1.2[l]	8.3[l]	–	615	Dimethyl dichlorosilane	3.4	–	–	–
Anthracene	0.65[e]	–	–	540	Dimethyl ether	3.4	27	–	350
n-Amyl nitrate	1.1	–	–	195	*n,n*-Dimethyl formamide	1.8[b]	14[b]	57	435
Benzene	1.3[b]	7.9[b]	–	560	2,3-Dimethyl pentane	1.1	6.8	–	335
Benzyl benzoate	0.7[e]	–	–	480	2,2-Dimethyl propane	1.4	7.5	–	450
Benzyl chloride	1.2[e]	–	–	585	Dimethyl sulfide	2.2	20	–	205
Bicyclohexyl	0.65[b]	5.1[m]	74	245	Dimethyl sulfoxide	–	–	84	–
Biphenyl	0.70[k]	–	110	540	Dioxane	2.0	22	–	265
2-Biphenylamine	0.8[e]	–	–	450	Dipentene	0.75[m]	6.1[m]	45	237
Bromobenzene	1.6[e]	–	–	565	Diphenylamine	0.7[e]	–	–	635

(continued)

Table 17.1 (continued)

Limits of flammability (vol %)					Limits of flammability (vol %)				
Combustible	LFL[a]	UFL[a]	T_L (°C)	AIT (°C)	Combustible	LFL[a]	UFL[a]	T_L (°C)	AIT (°C)
Butadiene (1,3)	2.0	12	–	420	Diphenyl ether	0.8[e]	–	–	620
n-Butane	1.8	8.4	−72	405	Diphenyl methane	0.7[e]	–	–	485
1,3-Butandiol	1.9[e]	–	–	395	Divinyl ether	1.7	27	–	–
Butene-1	1.6	10	–	385	*n*-Dodecane	0.60[e]	–	74	205
Butene-2	1.7	9.7	–	325	Ethane	3.0	12.4	−130	515
n-Butyl acetate	1.4[i]	8.0[b]	–	425	Ethyl acetate	2.2	11	–	–
n-Butyl alcohol	1.7[b]	12[b]	–	–	Ethyl alcohol	3.3	19[n]	–	365
sec-Butyl alcohol	1.7[b]	9.8[b]	21	405	Ethyl amine	3.5	–	–	385
tert-Butyl alcohol	1.9[b]	9.0[b]	11	480	Ethyl benzene	1.0[b]	6.7[b]	–	430
tert-Butyl amine	1.7[b]	8.9[b]	–	380	Ethyl chloride	3.8	–	–	–
n-Butyl benzene	0.82[b]	5.8[b]	–	410	Ethyl cyclobutane	1.2	7.7	–	210
sec-Butyl benzene	0.77[b]	5.8[b]	–	420	Ethyl cyclohexane	2.0[o]	6.6[o]	–	260
tert-Butyl benzene	0.77[b]	5.8[b]	–	450	Ethyl cyclopentane	1.1	6.7	–	260
n-Butyl bromide	2.5[b]	–	–	265	Ethyl formate	2.8	16	–	455
Butyl cellosolve	1.1[m]	11[h]	–	245	Ethyl lactate	1.5	–	–	400
n-Butyl chloride	1.8	10[b]	–	–	Ethyl mercaptan	2.8	18	–	300
n-Butyl formate	1.7	8.2	–	–	Ethyl nitrate	4.0	–	–	–
n-Butyl stearate	0.3[e]	–	–	355	Ethyl nitrite	3.0	50	–	–
Butyric acid	2.1[e]	–	–	450	Ethyl propionate	1.8	11	–	440
α-Butryolactone	2.0[m]	–	–	–	Ethyl propyl ether	1.7	9	–	–
Carbon disulfide	1.3	50	–	90	Ethylene	2.7	36	–	490
Carbon monoxide	12.5	74	–	–	Ethyleneimine	3.6	46	–	320
Chlorobenzene	1.4	–	21	640	Ethylene glycol	3.5[e]	–	–	400
m-Cresol	1.1[m]	–	–	–	Ethylene oxide	3.6	100	–	–
Crotonaldehyde	2.1	16[n]	–	–	Furfural alcohol	1.8[p]	16[q]	72	390
Gasoline					2-Monoisopropyl				
100/130	1.3	7.1	–	440	biphenyl	0.53[h]	3.2[r]	141	435
115/145	1.2	7.1	–	470	Monomethylhydrazine	4	–	–	–
Glycerine	–	–	–	370	Naphthalene	0.88[s]	5.9[t]	–	526
n-Heptane	1.05	6.7	−4	215	Nicotine	0.75[b]	–	–	–
n-Hexadecane	0.43[e]	–	126	205	Nitroethane	3.4	–	30	–
n-Hexane	1.2	7.4	−26	225	Nitromethane	7.3	–	33	–
n-Hexyl alcohol	1.2[b]	–	–	–	1-Nitropropane	2.2	–	34	–
n-Hexyl ether	0.6[e]	–	–	185	2-Nitropropane	2.5	–	27	–
Hydrazine	4.7	100	–	–	*n*-Nonane	0.85[u]	–	31	205
Hydrogen	4.0	75	–	400	*n*-Octane	0.95	–	13	220
Hydrogen cyanide	5.6	40	–	–	Paraldehyde	1.3	–	–	–
Hydrogen sulfide	4.0	44	–	–	Pentaborane	0.42	–	–	–
Isoamyl acetate	1.1	7.0[b]	25	360	*n*-Pentane	1.4	7.8	−48	260
Isoamyl alcohol	1.4	9.0[b]	–	350	Pentamethylene glycol	–	–	–	335
Isobutane	1.8	8.4	−81	460	Phthalic anhydride	1.2[l]	9.2[v]	140	570
Isobutyl alcohol	1.7[b]	11[b]	–	–	3-Picoline	1.4[e]	–	–	500
Isobutyl benzene	0.82[b]	6.0[h]	–	430	Pinane	0.74[w]	7.2[w]	–	–
Isobutyl formate	2.0	8.9	–	–	Propadiene	2.16	–	–	–

(continued)

Table 17.1 (continued)

Limits of flammability (vol %)					Limits of flammability (vol %)				
Combustible	LFL[a]	UFL[a]	T_L (°C)	AIT (°C)	Combustible	LFL[a]	UFL[a]	T_L (°C)	AIT (°C)
Isobutylene	1.8	9.6	–	465	Propane	2.1	9.5	−102	450
Isopentane	1.4	–	–	–	1,2-Propandiol	2.5[e]	–	–	410
Isophorone	0.84	–	–	460	b-Propiolactone	2.9[d]	–	–	–
Isopropylacetate	1.7[e]	–	–	–	Propionaldehyde	2.9	17	–	–
Isopropyl alcohol	2.2	–	–	–	*n*-Propyl acetate	1.8	8	–	–
Isopropyl biphenyl	0.6[e]	–	–	440	*n*-Propyl alcohol	2.2[n]	14[b]	–	440
Jet fuel					Propyl amine	2.0	—	–	–
JP-4	1.3	8	–	240	Propyl chloride	2.4[e]	–	–	–
JP-6	–	–	–	230	*n*-Propyl nitrate	1.8[x]	100[x]	21	175
Kerosene	–	–	–	210	Propylene	2.4	11	–	460
Methane	5.0	15.0	−187	540	Propylene dichloride	3.1[e]	–	–	–
Methyl acetate	3.2	16	–	–	Propylene glycol	2.6[y]	–	–	–
Methyl acetylene	1.7	–	–	–	Propylene oxide	2.8	37	–	–
Methyl alcohol	6.7	36[n]	–	385	Pyridine	1.8[n]	12[a]	–	–
Methyl amine	4.2[e]	–	–	430	Propargyl alcohol	2.4[i]	–	–	–
Methyl bromide	10	15	–	–	Quinoline	1.0[e]	–	–	–
3-Methyl butene-1	1.5	9.1	–	–	Styrene	1.1[z]	–	–	–
Methyl butyl ketone	S51.2	8.0[b]	–	–	Sulfur	2.0[aa]	–	247	–
Methyl cellosolve	2.5[x]	20[l]	–	380	*p*-Terphenyl	0.96[e]	–	–	535
Methyl cellosolve					*n*-Tetradecane	0.5[e]	–	–	200
acetate	1.7[m]	–	46	–	Tetrahydrofurane	2.0	–	–	–
Methyl ethyl ether	2.2[e]	–	–	–	Tetralin	0.84[b]	5.0[m]	71	385
Methyl chloride	7[e]	–	–	–	2,2,3,3-Tetramethyl				
Methyl cyclohexane	1.1	6.7	–	250	pentane	0.8	–	–	430
Methyl					Tetramethylene glycol	–	–	–	390
cyclopentadiene	1.3[b]	7.6[b]	49	445	Toluene	1.2[b]	7.1[b]	–	480
Methyl ethyl ketone	1.9	10	–	–	Trichloroethane	–	–	–	500
Methyl ethyl ketone					Trichloroethylene	12[bb]	40[a]	30	420
peroxide	–	–	40	390	Triethyl amine	1.2	8.0	–	–
Methyl formate	5.0	23	–	465	Triethylene glycol	0.9[l]	9.2[bb]	–	–
Methyl cyclohexanol	1.0[e]	–	–	295	2,2,3-Trimethyl butane	1.0	–	–	420
Methyl isobutyl					Trimethyl amine	2.0	12	–	–
carbinol	1.3[e]	–	40	–	2,2,4-Trimethyl				
Methyl isopropenyl					pentane	0.95	–	–	415
ketone	1.8[i]	9.0e	–	–	Trimethylene glycol	1.7[e]	–	–	400
Methyl lactate	2.2[b]	–	–	–	Trioxane	3.2[e]	–	–	–
α-Methyl naphthalene	0.8[e]	–	–	530	Turpentine	0.7[b]	–	–	–
2,Methyl pentane	1.2[e]	–	–	–	Unsymmetrical				
Methyl propionate	2.4	13	–	–	dimethylhydrazine	2.0	95	–	–
Methyl propyl ketone	1.6	8.2	–	–	Vinyl acetate	2.6	–	–	–
Methyl styrene	1.0[e]	–	49	495	Vinyl chloride	3.6	33	–	–

(continued)

Table 17.1 (continued)

Limits of flammability (vol %)					Limits of flammability (vol %)				
Combustible	LFL[a]	UFL[a]	T_L (°C)	AIT (°C)	Combustible	LFL[a]	UFL[a]	T_L (°C)	AIT (°C)
Methyl vinyl ether	2.6	39	–	–	*m*-Xylene	1.1[b]	6.4[b]	–	530
Methylene chloride	–	–	–	615	*o*-Xylene	1.1[b]	6.4[b]	–	465
Monoisopropyl					*p*-Xylene	1.1[b]	6.6[b]	–	530
bicyclohexyl	0.52	4.1[r]	124	230					

[a]$T = 70$ °C
[b]$T = 100$ °C
[c]$T = 75$ °C
[d]$T = 75$ °C
[e]Calculated
[f]$T = 53$ °C
[g]$T = 86$ °C
[h]$T = 175$ °C
[i]$T = 50$ °C
[j]$T = 85$ °C
[k]$T = 110$ °C
[l]$T = 140$ °C
[m]$T = 150$ °C
[n]$T = 60$ °C
[o]$T = 130$ °C
[p]$T = 72$ °C
[q]$T = 117$ °C
[r]$T = 200$ °C
[s]$T = 78$ °C
[t]$T = 122$ °C
[u]$T = 43$ °C
[v]$T = 195$ °C
[w]$T = 160$ °C
[x]$T = 125$ °C
[y]$T = 96$ °C
[z]$T = 29$ °C
[aa]$T = 247$ °C
[bb]$T = 30$ °C

5.0 %, 12.5 %, and 4.0 % by volume, respectively. Using Equation 17.2 we find

$$\mathrm{LFL}_m = \frac{100}{50/5 + 25/12.5 + 25/4} = 5.48\%$$

The composition of the lower flammable limit fuel/air mixture is 2.74 % methane, 1.37 % carbon monoxide, 1.37 % hydrogen, and 94.5 % air.

Critical Adiabatic Flame Temperature at the Lower Flammable Limit

As early as 1911, Burgess and Wheeler [12] noted the constancy of the potential heat release rate per unit volume of normal alkane/air lower flammable mixtures at room temperature. Since the heat capacity of the products of complete combustion are nearly the same for all hydrocarbons, their observation also implies that the adiabatic flame temperature (AFT) at the lower flammable limit is a constant. Examination of a wide range of C,H,O-containing fuels indicates that the adiabatic flame temperature at the LFL is approximately 1600 K (±150 K) for most C,H,O-containing fuels, with the following notable exceptions: hydrogen, 980 K; carbon monoxide, 1300 K; and acetylene, 1280 K. This result indicates that the adiabatic flame temperature at the lower flammable limit is an indication

of the reactivity of the fuel. The lower the adiabatic flame temperature, the more reactive the fuel.

The utility of the concept of a critical adiabatic flame temperature at the lower flammable limit goes beyond that outlined above. It has been demonstrated that the adiabatic flame temperature at the lower flammable limit is relatively insensitive ($\pm$100 K) to the diluent used and to the initial temperature of the mixture [13–15].

The adiabatic flame temperature at the limit is insensitive to initial temperature only so long as significant preflame combustion reactions do not occur. As such, for a mixture near or above its autoignition temperature (AIT) for a significant length of time, the adiabatic flame temperature at the limit is not expected to be constant. Weinberg [15] has shown that a mixture of 1 % methane (LFL = 5 % at 293 K) in air can burn if it is preheated to 1270 K, even though the flame only increases that temperature by about 250 K, in accordance with the expected adiabatic flame temperature. This result was achieved by mixing the methane and air just before the flame so that preflame reactions were not allowed to proceed significantly.

Due to the constancy of the adiabatic flame temperature at the lower limit, the concept can be utilized to predict the effect of variable mixture temperature and diluents on the flammable limits of a mixture. Coward and Jones [2] have examined variable oxygen/diluent ratios, using nitrogen, carbon dioxide, water, argon, and helium as diluents. Their work shows that the limit temperature is insensitive to the oxygen/diluent ratio. Figure 17.6, adapted from Macek [16], illustrates the change in adiabatic flame temperature at the lower flammable limit as additional nitrogen is added to decrease the oxygen/nitrogen ratio. The figure shows an increase in the adiabatic flame temperature at the lower flammable limit from 1550 K to over 1700 K as we move from normal air to the stoichiometric limit. Beyond the stoichiometric limit, no fuel-lean mixture can burn. The region beyond the stoichiometric limit can be best understood in the context of flammability diagrams and upper flammable limits. We will examine these later in the chapter.

The insensitivity of the limit temperature to the chemical structure of C,H,O-containing fuels contributes significantly to the utility of the concept of a critical adiabatic flame temperature at the lower flammable limit. No systematic evaluation of the limit temperature concept for fuels containing sulfur, nitrogen, or halogens has been undertaken. Existing data indicate that

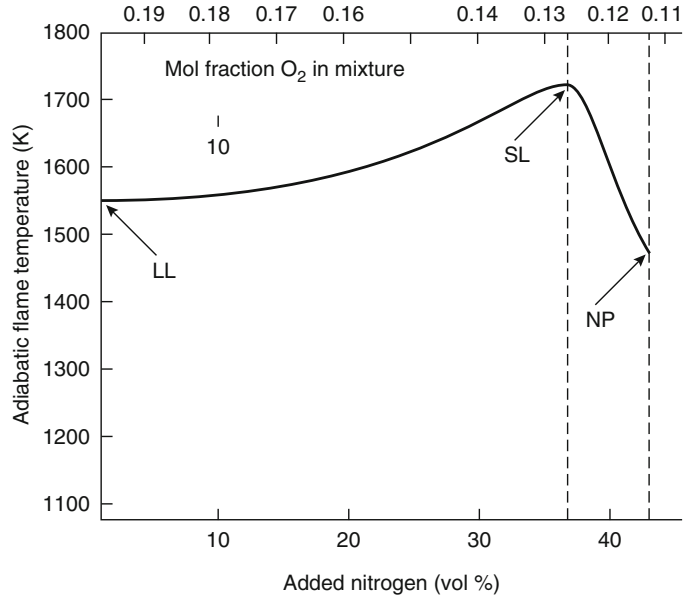

Fig. 17.6 Computed adiabatic flame temperature along the lower branch of the flammability limits of propane (Adapted from Macek) [16]. SL and NP are defined in Fig. 17.9

halogen-containing fuels have limit temperatures several hundred degrees higher than C,H,O fuels. Since halogens are combustion inhibitors, this conclusion is consistent with the idea that the adiabatic flame temperature at the lower flammable limit is indicative of the reactivity of the fuel. Thus, possible exceptions to the generalization that the adiabatic flame temperature at the lower flammable limit is approximately 1600 K may be identifiable by considering the reactivity of the fuel gas.

Egerton and Powling [17] have shown that the limit temperatures at the upper flammable limit for hydrogen and carbon monoxide are equal to their limit temperatures at the lower flammable limit. Stull [18] has reported the same result for methane. However, it is not generally possible to calculate the adiabatic flame temperature for other fuels, since the products of combustion under fuel-rich conditions include a mixture of products of combustion and pyrolysis, which cannot be predicted by assuming chemical equilibrium is achieved or by detailed chemical kinetics calculations. Equilibrium calculations indicate that the only carbon-containing species that should be produced are CO, CO_2, CH_4, and solid carbon. This conclusion is not generally a good approximation under fuel-rich conditions.

Example 2 The lower flammable limit of propane at 20 °C is 2.1 % by volume. Find the lower flammable limit at 200 °C.

Solution For adiabatic combustion, all the heat released is absorbed by the products of combustion:

$$\left(\frac{\text{LFL}}{100}\right)\Delta H_c = \int_{T_0}^{T_{f,\text{LFL}}} nC_p dT \qquad (17.3)$$

where

ΔH_c = Heat of combustion of the fuel
LFL/100 = Mole fraction of fuel
n = Number of moles of products of combustion per mol of fuel/air mixture
C_p = Heat capacity of the products of combustion
T_0 = Initial temperature of the fuel/air mixture
$T_{f,\text{LFL}}$ = Adiabatic flame temperature of a lower flammable limit mixture

This equation uses concepts developed in Chap. 5. For the present purposes, it is suitable to use an average value of the heat capacity. This adjustment reduces Equation 17.3 to

$$\left(\frac{\text{LFL}}{100}\right)\Delta H_c = nC_p\left(T_{f,\text{LFL}} - T_0\right) \qquad (17.4)$$

We know that $T_{f,\text{LFL}} = 1600$ K, and for $T_0 = 20$ °C, we also know that LFL = 2.1 %. Rearranging Equation 17.4 yields

$$\begin{aligned}\frac{\Delta H_c}{nC_p} &= \frac{\left(T_{f,\text{LFL}} - T_0\right)}{\text{LFL}/100} \\ &= \frac{1600\ \text{K} - 293\ \text{K}}{2.1/100} \\ &= 6.22 \times 10^4 \text{K}\end{aligned}$$

Both the heat of combustion and the heat capacity are weak functions of temperature, and these effects will be ignored. As such we can use the above expression to predict the lower flammable limit for an initial temperature of 200 °C.

$$\begin{aligned}\frac{T_{f,\text{LFL}} - T_0}{\text{LFL}/100} &= \frac{1600\ \text{K} - 473\ \text{K}}{\text{LFL}/100} \\ &= 6.22 \times 10^4 \text{K} \\ \text{LFL} &= 1.8\ \text{percent}\end{aligned}$$

Flammability Diagrams

Whereas the flammable limits of a fuel in air can be characterized by the lower and upper flammable limits, it is necessary to represent flammable limits of more general fuel/oxidant/inert mixtures by using flammability diagrams. Examples of flammability diagrams for methane/oxygen/nitrogen mixtures are shown in Figs. 17.7 and 17.8. Based on an extensive series of tests with a range of mixture compositions, a flammability diagram can be constructed indicating the regions of mixture compositions within the flammable limits.

Two types of flammability diagrams are often used. The first type uses three axes in which each of the three constituent gases is explicitly represented, and the second diagram utilizes only two axes in which the third gas concentration is determined by the difference between the sum

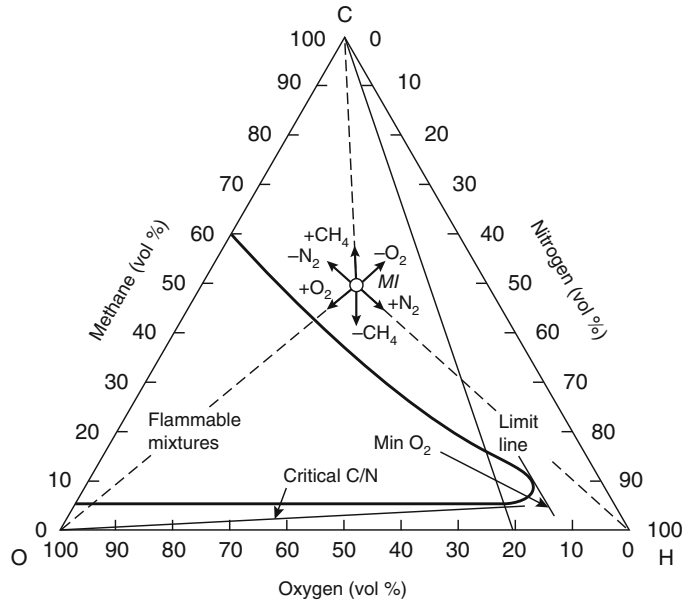

Fig. 17.7 Three-axis flammability diagram for the system methane/oxygen/nitrogen at atmospheric pressure and 26 °C [1]

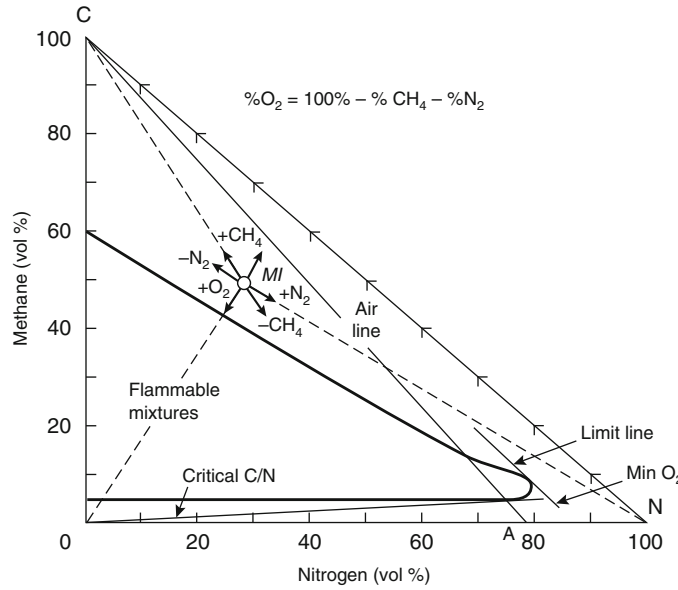

Fig. 17.8 Two-axis flammability diagram for the system methane/oxygen/nitrogen at atmospheric pressure and 26 °C [1]

of the other two gases and 100 %. Both types give the same information.

Shown in Figs. 17.7 and 17.8 are the air and limit lines. Anywhere along the air line the ratio of oxygen to nitrogen is the same as in air. The limit line represents a range of mixtures with a fixed oxygen-to-nitrogen ratio which is tangent to the flammable region. Any oxygen/nitrogen mixture with an oxygen-to-nitrogen ratio less than that of the limit line will not support flame propagation when mixed with any amount of methane. This condition is known as the limiting oxygen concentration (LOC).

The LOC is an important concept in inerting. If the oxygen concentration can be maintained below the LOC, then premixed burning can be

prevented. The LOC is a function of the temperature, pressure, fuel, and inert gas. Table 17.2 shows the LOC [19–23] of a wide range of fuels with nitrogen and carbon dioxide as the inert diluents. The tabulated values apply to diluted air/fuel mixtures at normal temperature and pressure. Like flammable limits, the dynamics of the LOC can generally be understood using the AFT concepts.

As can be seen in Table 17.2 with nitrogen diluent, the LOC is generally in the 10–12 % range. Fuels like carbon monoxide and hydrogen

Table 17.2 Limiting oxygen concentrations at normal temperature and pressure

Gas or vapor	Limiting oxidant concentration N_2/air (volume % O_2 above which deflagration can take place)	Limiting oxidant concentration CO_2/air (volume % O_2 above which deflagration can take place)	Reference
Ethane	11	13.5	Coward and Jones [19]
Propane	11.5	14.5	Coward and Jones [19]
n-Butane	12	14.5	Coward and Jones [19]
Isobutane	12	15	Coward and Jones [19]
n-Pentane	12	14.5	Coward and Jones [19]
Isopentane	12	14.5	Jones et al. [20]
n-Hexane	12	14.5	Coward and Jones [19]
n-Heptane	11.5	14.5	Jones et al. [20]
Ethylene	10	11.5	Coward and Jones [19]
Propylene	11.5	14	Coward and Jones [19]
1-Butene	11.5	14	Coward and Jones [19]
Isobutylene	12	15	Jones et al. [20]
Butadiene	10.5	13	Coward and Jones [19]
3-Methyl-1-butene	11.5	14	Zabetakis [22]
Benzene	11.4	14	Coward and Jones [19]
Gasoline			
(73/100)	12	15	Jones et al. [20]
(100/130)	12	15	Jones et al. [20]
(115/145)	12	14.5	Jones et al. [20]
Kerosene	10 (150 °C)	13 (150 °C)	Zabetakis and Rosen [23]
JP-1 fuel	10.5 (150 °C)	14 (150 °C)	Jones et al. [20]
JP-3 fuel	12	14.5	Jones et al. [20]
JP-4 fuel	11.5	14.5	Jones et al. [20]
Natural gas			
(Pittsburgh)	12	14.5	Coward and Jones [19]
n-Butyl chloride	14	–	Kuchta et al. [21]
	12 (100 °C)	–	Kuchta et al. [21]
Methylene chloride	19 (30 °C)	–	Kuchta et al. [21]
	17 (100 °C)	–	Kuchta et al. [21]
Ethylene dichloride	13	–	Kuchta et al. [21]
	11.5 (100 °C)	–	Kuchta et al. [21]
1,1,1-Trichloroethane	14	–	Kuchta et al. [21]
Trichloroethylene	9 (100 °C)	–	Kuchta et al. [21]
Acetone	11.5	14	Zabetakis [22]
n-Butanol	–	16.5 (150 °C)	Zabetakis [22]
Carbon disulfide	5	7.5	Zabetakis [22]

(continued)

Table 17.2 (continued)

Gas or vapor	Limiting oxidant concentration N_2/air (volume % O_2 above which deflagration can take place)	Limiting oxidant concentration CO_2/air (volume % O_2 above which deflagration can take place)	Reference
Carbon monoxide	5.5	5.5	Zabetakis [22]
Ethanol	10.5	13	Zabetakis [22]
2-Ethyl butanol	9.5 (150 °C)	–	Zabetakis [22]
Ethyl ether	10.5	13	Zabetakis [22]
Hydrogen	5	5.2	Zabetakis [22]
Hydrogen sulfide	7.5	11.5	Zabetakis [22]
Isobutyl formate	12.5	15	Zabetakis [22]
Methanol	10	12	Zabetakis [22]
Methyl acetate	11	13.5	Zabetakis [22]
Methyl ether	10.5	13	Zabetakis [22]
Methyl formate	10	12.5	Zabetakis [22]
Methyl ethyl ketone	11	13.5	Zabetakis [22]

Data were determined by laboratory experiment conducted at atmospheric temperature and pressure. Vapor-air-inert gas samples were placed in explosion tubes and ignited by electric spark or pilot flame
Source: Adapted from Table C-1, NFPA 69, *Standard on Explosion Prevention Systems*

have lower LOCs, and chlorinated fuels have higher values. These trends are expected based on AFT concepts at the LFL. For carbon dioxide as a diluent, the LOCs are generally 2–3 % higher than for nitrogen diluent. Again this is expected based on AFT concepts due to the higher molar heat capacity of carbon dioxide.

Figure 17.9 is yet another representation of the flammable limits of fuel/oxidant/inert mixtures. The dilution of a fuel/air mixture is given by the percent of inert gas in excess of the nitrogen present in air. Figure 17.9 includes only mixtures that lie to the right of the air line, and as such is a magnification of a portion of the region included in Figs. 17.7 and 17.8. Also shown in Fig. 17.9 are several lines and points of specific interest. The highest concentration of nitrogen that will allow propagation of a flame is known as the nitrogen point (NP). Of course, this concept can be generalized to any inert (IP). If the concentration of the inert is greater than that at the inert point, no mixture of fuel and oxidant will propagate a flame remote from the ignition source.

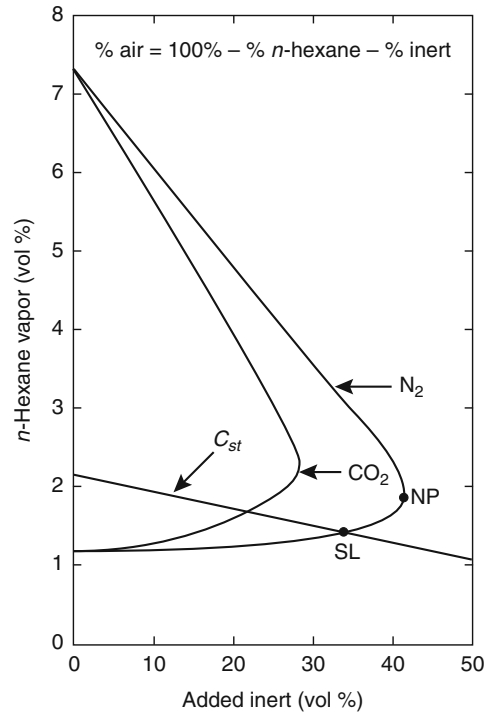

Fig. 17.9 Limits of flammability of various n-hexane/inert gas/air mixtures at 25 °C and atmospheric pressure [1]

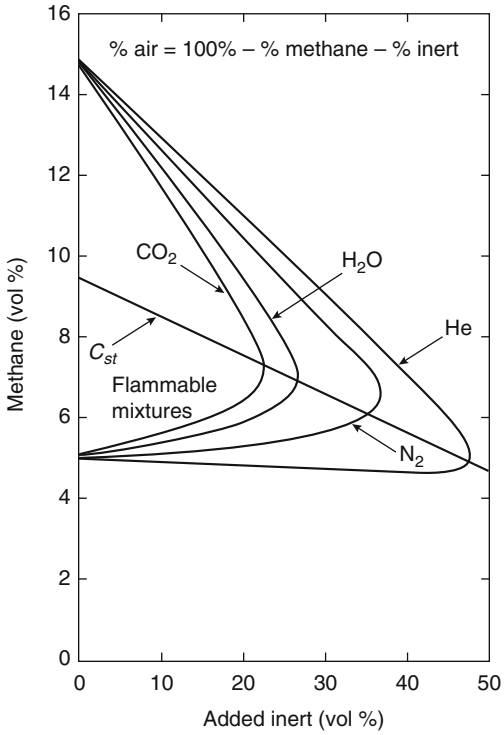

Fig. 17.10 Limits of flammability of various methane/inert gas/air mixtures at 25 °C and atmospheric pressure [1]

As shown in Fig. 17.9, the stoichiometric line passes through the flammable region. The point at which the stoichiometric line intersects the boundary of the flammable region is known as the stoichiometric limit (SL). The SL is the most dilute stoichiometric mixture that will propagate a flame remote from the ignition source. In the case of methane, the peak of the flammable region occurs near the stoichiometric limit (Fig. 17.10). For longer chain alkanes, the peak shifts to the rich side of the stoichiometric line (Fig. 17.9). For C_5 and higher hydrocarbons, the peak of the flammable region is bisected by the stoichiometric line defined by combustion to CO rather than to products of complete combustion. This shift has been attributed to incomplete combustion [16] and to preferential diffusion of reactants [24]. A similar shift of the maximum burning velocity to the rich side of stoichiometry is also observed. In this case, preferential diffusion of reactants has been shown to be the responsible factor.

Flammability diagrams are useful not only in determining the flammability of a given mixture, but also in developing strategies for avoiding flammable mixtures while diluting fuel-rich mixtures. In order to make use of the diagrams in this fashion, we must examine the change in position on the diagram when fuel, oxygen, or inert gas is added to the mixture. Consider a mixture given by point MI in the three-axis diagram (Fig. 17.7). The arrows indicate the change in the mixture composition with the addition or removal of each gas species. In the three-axis diagram, moving toward the vertex corresponding to 100 % of any one of the gases corresponds to the addition of that gas, since adding an infinite amount of a single gas will reduce the concentrations of the other gases to zero. Adding air corresponds to moving toward the point on the air line at which there is no fuel. Clearly, following these examples, the effect of adding any gas or gas mixture can be plotted in the three-axis diagram. In the two-axis diagram in Fig. 17.8, moving toward the vertex with 0 % inert, 0 % fuel corresponds to the addition of oxygen. In Fig. 17.9 moving toward the 0 % inert, 0 % fuel vertex corresponds to adding air.

Figure 17.10 shows the effect of various inert diluents on the flammable region. As indicated by the critical adiabatic flame temperature concept, the lower flammable limit is increased in proportion to the heat capacity of the diluent (see Chap. 5).

Example 3 A methane leak fills a 200 m^3 room until the methane concentration is 30 % by volume. Calculate how much nitrogen must be added to the room before air can be allowed in the space.

Solution The initial mixture in the room is given by the point B in Fig. 17.11. Adding nitrogen moves along the line toward pure nitrogen (the N point). Drawing the line from the air point, A, tangent to the flammable region defines the mixture C: the mixture with the least nitrogen added that, on mixing with air, will not form a flammable mixture. Referring to Fig. 17.11 we see that

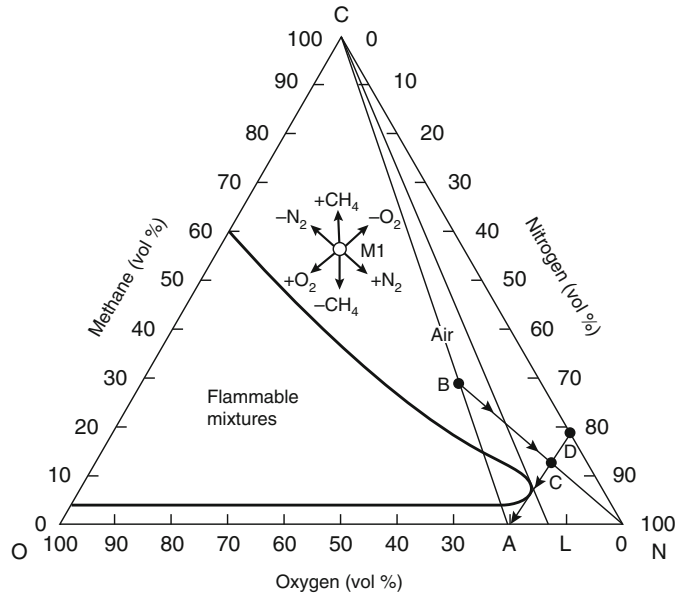

Fig. 17.11 Graphic solution of Example 3 (Adapted from Zubetakis) [1]

point C corresponds to a methane concentration of 13 %. In order to reduce the methane concentration from 30 % to 13 %, an as yet unknown amount of nitrogen must be added. If we could remove only the initial mixture and replace it with nitrogen, the amount of nitrogen would simply be

$$\frac{30-13}{30} \times 200\ \mathrm{m}^3 = 113\ \ \mathrm{m}^3$$

However, there is generally no way to prevent mixing of the initial mixture to be exhausted and the nitrogen being introduced to replace it. As such, inerting nitrogen is also lost. We can model this occurrence by assuming that the room is well mixed during nitrogen injection so that the concentrations are uniform everywhere. Under these conditions the methane concentration, C, is given by

$$C = C_0 \exp\left(\frac{-V_\mathrm{N}}{V}\right)$$

where
C_0 = Initial methane concentration
V_N = Volume of nitrogen added
V = Volume of the room

Rearranging this equation we find

$$V_\mathrm{N} = -V \ln\left(\frac{C}{C_0}\right) = -200\ \ \mathrm{m}^3 \ln\left(\frac{13}{30}\right)$$
$$= 167\ \ \mathrm{m}^3$$

Of course, the flow of gases out of the room contains methane and may burn on mixing with air. Mixing air and the initial gases in the room results in mixtures along the line AB (see Fig. 17.11), some of which are clearly flammable. As such, ignition sources must be excluded near the room exhaust, or the exhaust also needs to be inerted.

Example 4 A 1 kg/s flow of methane is being dumped into the atmosphere. How much nitrogen must be mixed with methane to avoid a flammable mixture in the open?

Solution In order to make the methane nonflammable, it needs to be diluted with enough nitrogen so that on further addition of air the flammable region is missed. Such a mixture of methane and nitrogen is given by extrapolating the line AC back to zero oxygen; that is, point D

on Fig. 17.11, where the mixture is 82 % nitrogen, 18 % methane. The ratio of the flow rates of nitrogen to methane must equal the ratio of the concentrations of nitrogen and methane. Since concentrations expressed as volume percent are directly related to mole fractions, the flow rates of nitrogen and methane must be expressed as molar flow rates, $\dot{n}$,

$$\frac{\dot{n}_{N_2}}{\dot{n}_{CH_4}} = \frac{C_{N_2}}{C_{CH_4}}$$

The molar flow rate of methane is given by

$$\dot{n}_{CH_4} = \frac{\dot{m}_{CH_4}}{MW_{CH_4}}$$

where MW is the molecular weight and $\dot{m}$ is the mass flow rate.

$$\begin{aligned}
\dot{n}_{N_2} &= \left(\frac{\dot{m}_{CH_4}}{MW_{CH_4}}\right)\left(\frac{C_{N_2}}{C_{CH_4}}\right) \\
&= \left(\frac{100\ \text{g/s}}{16\ \text{g/mol}}\right)\left(\frac{82\%}{18\%}\right) \\
&= 285\ \text{mol/s} \\
\dot{m}_{N_2} &= \dot{n}_{N_2} MW_{N_2} \\
&= (285\ \text{mol/s})(28\ \text{g/mol}) \\
&= 7970\ \text{g/s}\ \text{ or }\ 7.97\ \text{kg/s}
\end{aligned}$$

Ignition Energies and Quenching Diameters

The energy required to ignite flammable mixtures is generally quite low, on the order of a few tenths of a millijoule (mJ) for near-stoichiometric mixtures in air and as low as a few thousandths of a millijoule in oxygen. Here again, preferential diffusion causes the minimum to occur for rich mixtures for fuels with molecular weights greater than that of air [24]. As the flammable limits are approached, the ignition energy increases sharply.

Several methods exist for preventing the initiation of an explosion. These include avoiding flammable mixtures, excluding ignition sources whose energy is greater than the minimum ignition energy, and enclosing any ignition sources in an enclosure that will not allow the propagation of the flame to the outside. We have already discussed the first of these. Some low-power electrical equipment can be designed such that the worst fault condition cannot produce the minimum ignition energy for a specified gas. Such equipment is termed "intrinsically safe" and may be used where there is a risk of a flammable atmosphere being formed.

Where this method is not feasible, the electrical equipment may be housed in an "explosionproof" enclosure that will not allow propagation of the flame out of the enclosure, which is accomplished by making the size of the openings small enough that sufficient heat is lost by the flame as it passes through the opening that it is quenched. The quenching distance is most often determined by placing a pair of flanged electrodes in a gas mixture and attempting to ignite the gases. The flanges are parallel plates, and if the mixture can be ignited in the presence of the plates, the separation of the plates is greater than the quenching distance. The quenching distance with parallel plates, $d_{||}$, is 65 % of the quenching diameter in circular tubes. Figure 17.12 [25] shows the relation of the quenching distance to the minimum ignition energy for a number of hydrocarbon/air mixtures. The relation can be expressed as $E_{min} = 0.06 d_{||}^2$, where E_{min} is the minimum ignition energy in air given in mJ and $d_{||}$ is the quenching distance in air given in mm.

Because the hot quenched flame gases in an enclosure will expand through the opening, they may autoignite outside the enclosure. It has been found that the minimum experimental safe gap (MESG) for most hydrocarbons is approximately half the quenching distance [25].

Dusts and Mists

The lower flammable limit of dusts and mists would be expected to be higher than their gaseous counterparts due to the need to volatilize the dust or mist. For very small particles with high surface-area-to-volume ratios, the lower flammable limit is independent of particle diameter, and the limit concentrations are approximately the same as the analogous gaseous fuel for fuels that volatilize completely. Hertzberg et al. [26] have

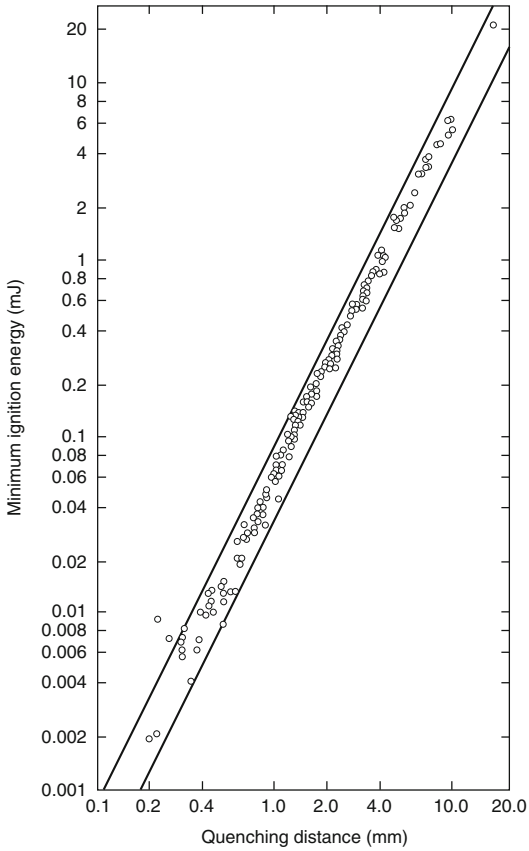

Fig. 17.12 The relation between flat-plate quenching and spark minimum ignition energies for a number of hydrocarbon-air mixtures [25]

shown that bituminous coal dusts with particle diameters of 50 mm or less and polyethylene dusts with particle diameters of 100 μm or less have lower flammable limits in air that are independent of particle diameter. Figure 17.13 shows the measured lower flammable limit concentration for Pittsburgh bituminous coal as a function of average particle diameter and oxygen concentration. Notice that the lower flammable limit in the small-particle limit is a function of the oxygen concentration, unlike gaseous fuels. Also note that the lower flammable limit concentration is much higher than the 48 g/m^3 typical of gaseous hydrocarbons. These effects are due to the fact that not all the coal dust is volatilized. The fraction of dust that is volatilized is a function of the particle diameter and the oxygen concentration. As the oxygen concentration affects the maximum flame temperature and, hence, the heat flux to the particle, both the ability of heat to penetrate the particle and the rate of heating are affected. It is well known that the fraction of the material volatilized increases with the rate of heating. It is not expected that the lower flammable limit can be reduced below 50 g/m^3, even at 100 % oxygen.

As the particle size increases, it would be expected that the lower flammable limit would also increase due to the difficulty of getting the fuel into the gas phase where combustion will take place. This result does in fact occur, but depending on the geometry of the test, the apparent lower flammable limit of mists can actually decrease with increasing particle diameter due to the effects of gravity [27]. If the ignition source is at the bottom of the container and the aerosol is not kept well mixed, the particles can begin to settle out, causing the local concentration in the lower portions of the apparatus to be higher. This laboratory effect can also be expected to operate under actual conditions, depending on the degree of mixing of the aerosol.

Although it is in principle possible for flame propagation to occur as a result of heterogeneous combustion of particles, this appears not to be an important mechanism for organic materials. Lower flammable limits of anthracite coal dusts with only a 20 % volatile yield can be explained solely on the basis of gas-phase combustion [28]. On the other hand, flame propagation by heterogeneous combustion is important for metal and graphite dusts.

Diffusion Flame Limits

The limits of flammability for diffusion flames were first examined by Simmons and Wolfhard [29]. In their experiments, they determined the minimum level of dilution of the oxidant stream necessary to prevent the stabilization of a diffusion flame for a variety of gas and liquid fuels. The oxygen mole fraction, X_{O_2}, of the oxidant stream at the flammability limit is known as the limiting oxygen index (LOI), or simply the oxygen index (OI). Simmons and Wolfhard's results are included in Table 17.3. They observed that the oxygen index of their diffusion flames

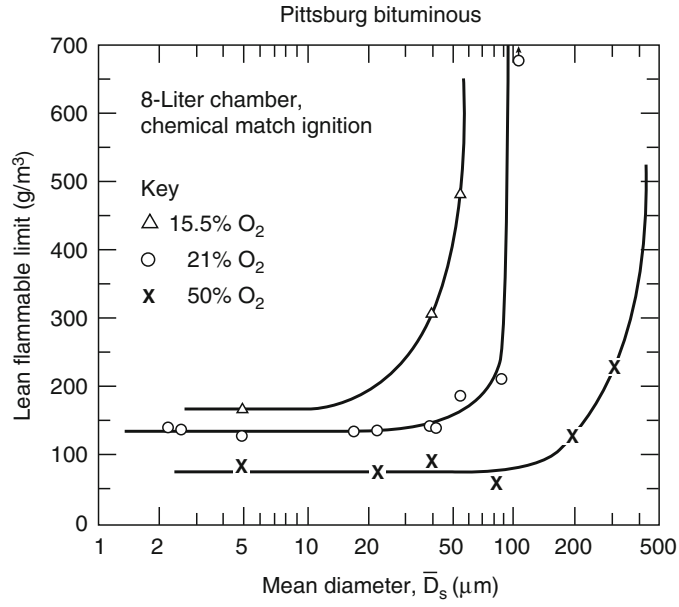

Fig. 17.13 Lean flammability limit data for Pittsburgh bituminous coal as a function of particle size for three oxygen concentrations [26]

Table 17.3 Thermodynamic equilibrium properties at extinction (Adapted from Macek [16] and Strehlow [25])

Fuel	LFL (vol %)	*T(LFL)* (K)	*X(SL)*[a]	*T(SL)* (K)	*X(NP)*[a]	*T(NP)* (K)	OI[a]	*X(OI)*[a]	*T(OI)* (K)
CH_4	5.0	1480	0.123	1720	0.117	1610	0.139	0.130	1780
C_2H_2	2.7						0.085		1540
C_2H_4	2.7						0.105		1610
C_2H_6	3.0	1530	0.114	1620	0.111	1540	0.118	0.114	1630
C_3H_8	2.1	1540	0.125	1730	0.114	1470	0.127	0.124	1720
n-C_4H_{10}	1.8	1640	0.134	1830	0.121	1490	–	–	–
n-C_5H_{12}	1.4	1590	0.135	1810	0.115	1410	0.1325	0.130	1760
n-C_6H_{14}	1.2	1610	0.135	1800	0.117	1420	0.1335	0.132	1770
n-C_7H_{16}	1.05	1620	0.134	1770	0.118	1430	–	–	–
n-C_8H_{18}	0.90	1650	0.134	1770	0.118	1440	0.134	0.133	1780
n-$C_{10}H_{22}$							0.1345	0.133	1780
CH_3COCH_3	2.6						0.1285		1730
CH_3OH	6.7	1550	0.112	1690	0.085	1430	0.111	0.103	1530
C_2H_5OH	3.3	1490	0.118	1700	0.106	1430	0.126	0.121	1670
n-C_3H_7OH	2.2	1490					0.128	0.124	1700
n-C_4H_9OH	1.7	1510					0.129	0.126	1710
n-$C_5H_{11}OH$	1.4	1550					0.130	0.128	1730
n-$C_6H_{13}OH$	1.2	1490					0.1315	0.130	1740
n-$C_8H_{17}OH$							0.1315	0.130	1750
C_6H_6	1.3						0.133		1810
C_6H_{12}	1.2						0.134		1770
H_2	4.0						0.054		1080
CO	12.5						0.076		1450

[a]Expressed as mole fraction of oxygen

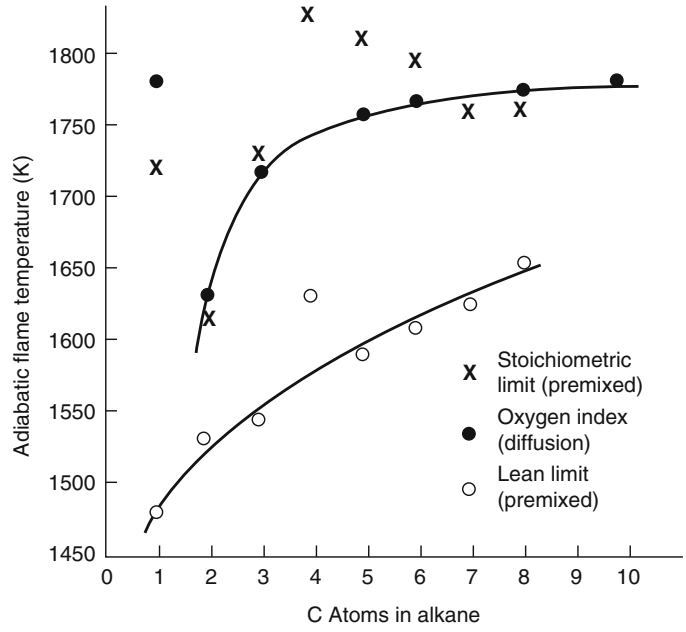

Fig. 17.14 Computed adiabatic flame temperatures at flammability limits for n-alkanes (Adapted from Macek) [16]

equaled the ratio, $X_{O_2}/(X_{O_2} + X_{\text{diluent}})$, found in a premixed stoichiometric-limit mixture involving the same fuel. This result implies that the adiabatic flame temperature for the limit diffusion flame, calculated on the basis of stoichiometric combustion of the fuel and oxidant streams, is equal to the adiabatic flame temperature at the stoichiometric limit of a premixed system involving the same fuel, oxidant, and diluent.

Figure 17.14 graphically illustrates the relationship of the adiabatic flame temperatures at the lean, premixed limit in air, at the stoichiometric limit (premixed), and at the oxygen index (premixed). As the figure shows, the adiabatic flame temperature at the stoichiometric limit and the oxygen index are essentially equal, and the adiabatic flame temperature at the lower flammable limit in air is approximately 150 K less. Ishizuka and Tsuji [30] verified Simmons and Wolfhard's results for methane and hydrogen, and showed that the adiabatic flame temperature at the limit is the same whether dilution is of the fuel or oxidizer stream.

The information in Fig. 17.14 forms the basis of a method for the evaluation of diffusion flame limits for fuel mixtures. In essence, the ability of a fuel and oxidant pair to react in a diffusion flame is evaluated by examining the flammability of a premixed stoichiometric mixture of the fuel and oxidant.

To do this, we assume that Le Chatelier's rule holds at the stoichiometric limit; that is,

$$\sum_{i=1}^{n} \left(\frac{C_i}{\text{SL}_i} \right) \geq 1 \tag{17.5}$$

and that the adiabatic flame temperature at the stoichiometric limit for each fuel is a constant, leading to the expression

$$\sum_{i=1}^{n} \frac{(C_i/100)\Delta H_{c,i}}{\int_{T_0}^{T_{f,\text{SL},i}} n_p C_p dT} \geq 1 \tag{17.6}$$

where

C_i = Volume percent of fuel species, i, when the fuel stream is mixed stoichiometrically with the oxidant stream

$T_{f,\text{SL},I}$ = Adiabatic flame temperature of the stoichiometric limit mixture for fuel species i
- = 1700 K for most hydrocarbons
- = 1450 K for carbon monoxide
- = 1080 K for hydrogen

T_0 = Temperature of the stoichiometric mixture prior to reaction

$\Delta H_{c,I}$ = Heat of combustion of fuel species
=620 kJ/mol for hydrocarbons (per carbon, assuming $H/C = 2$)
=283 kJ/mol for carbon monoxide
=242 kJ/mol for hydrogen

n_p = Number of moles of products of combustion per mole of reactants (stoichiometric mixture of the fuel and oxidant streams)

C_p = Heat capacity of the products of combustion

This approach has been successfully used to predict the flammability of the hot gas layer formed in enclosure fires [31].

Although the hot gas layer formed in enclosure fires can become flammable, under some conditions the oxygen concentration in the hot layer can cause extinction of flames fully immersed in the hot layer. Based on the analogies between premixed and diffusion flames, one would expect the oxygen concentration in the layer at extinction to be approximately equal to the premixed LOC. In fact, comparing the nitrogen diluent in Table 17.2 with Table 17.3, one can see a very close correspondence between the LOC and the LOI.

Morehart, Zukoski, and Kubota [32] examined the oxygen concentration at extinction of flames by dilution of air with combustion products. They found that flames were extinguished at oxygen concentrations of 12.4–14.3 %, with the lower value occurring for a 50-cm-diameter pool burner and the higher value occurring for a 9 cm pool burner. These results are consistent with diesel pan fire tests (0.62 m and 0.84 m diameters) conducted by Peatross and Beyler [33] in which oxygen concentrations below 14 % could not be achieved during pool burning in a compartment. It is also consistent with the results of Back et al. [34], who measured oxygen concentrations at extinction in water mist extinguishment tests in obstructed machinery space fires. They found an average oxygen concentration of 14.5 % for heptane spray fires and 13.5 % for pool fires at extinction. Since the molar heat capacity of water vapor is midway between nitrogen and carbon dioxide, one would expect water mist and combustion product extinction limits to be between nitrogen and carbon dioxide.

All of the above results are for relatively quiescent conditions. It is well known that at higher strain rates, the oxygen concentration at extinction increases. This phenomenon can most easily be seen in counterflow diffusion flame extinction experiments such as Hamins et al. [35]

Example 5 As part of a hazard analysis of a particular room fire, the composition of the hot layer during fire development has been estimated. The results of the analysis indicate that the following composition represents the highest concentration of fuel gases expected:

Hot layer—700 K, 10 % total hydrocarbons (THC), in the form of CH_2, 2 % CO, 1 % H_2, 15 % CO_2, 2 % O_2, 70 % N_2

Cold layer—300 K, 21 % O_2, 79 % N_2

Will the hot layer burn?

Solution The working equation is Equation 17.6. The first step is to write a balanced chemical equation for stoichiometric burning:

$$0.1\,CH_2 + 0.02\,CO + 0.01\,H_2 + 0.02\,O_2 + 0.7\,N_2 + 0.15\,CO_2 + x(O_2 + 3.78\,N_2) \rightarrow 0.27\,CO_2 + 0.11\,H_2O + (0.7 + 3.78X)N_2$$

We can find x by requiring that both sides of this equation have the same amount of oxygen:

$$\underset{\frac{0.02}{2}}{CO} + \underset{0.02}{O_2} + \underset{0.15}{CO_2} + \underset{x}{air} = \underset{0.27}{CO_2} + \underset{\frac{0.11}{2}}{H_2O} \rightarrow x = 0.145$$

The concentrations in the stoichiometric mixture can be determined from the balanced chemical equation:

$$C_i = \left(\frac{n_i}{n_T}\right) \times 100\%$$

$$n_T = 0.1 + 0.02 + 0.01 + 0.02 + 0.7 + 0.15 + 0.145 + 0.145(3.78) = 1.693$$

$$C_{THC} = \left(\frac{0.1}{1.693}\right) \times 100\% = 5.9\%$$

$$C_{CO} = \left(\frac{0.02}{1.693}\right) \times 100\% = 1.2\%$$

$$C_{H_2} = \left(\frac{0.01}{1.693}\right) \times 100\% = 0.6\%$$

Similarly, the number of moles of products per mole of reactants can be determined from the chemical equation

$$n_p = \frac{[0.27 + 0.11 + 0.7 + 0.145(3.78)]}{1.693} = 0.962$$

This result is lower than typical values of 1–1.1, because the unknown hydrocarbon mixture is taken as CH_2 . This choice is not an error, since CH_2 has been consistently used for the heat release and heat capacity as well. For convenience, we will use constant average specific heats taken from Drysdale: [3]

	C_p (J/mol · K)	C (%)[a]
CO_2	54.3	16.2
H_2O	41.2	6.6
N_2	32.7	77.2

Calculated by the same method as the fuel gas concentrations

$$\begin{aligned} n_p C_p &= n_p \sum \left(\frac{C_i}{100}\right) C_{p,i} \\ &= 0.96[(0.162)(54.3) + (0.066) \\ &\quad \times (41.2) + (0.772)(32.7)] \\ &= 35.3 \text{ J/mol K} \end{aligned}$$

Notice that the average specific heat is near that of nitrogen, since it is the major constituent of the mixture. In calculating T_0 , the initial temperature of the mixture, we will ignore variations in C_p between the hot and cold layers.

$$T_0 = \frac{n_h Th + n_c Tc}{n_h + n_c} \quad n_h + n_c = n_T$$
$$= \frac{(1)(700\ K) + (0.69)(300\ \text{K})}{1.69} = 537\ \text{K}$$

where n_h and n_c are the number of moles originating in the hot and cold layers, respectively. Substituting into Equation 17.5,

$$\sum_{i=1}^{n} \frac{(C_i/100)\Delta H_{c,i}}{C_p(T_{f,SL,i} - T_0)} = \frac{(0.059)(620)10^3}{35.3(1700 - 537)} + \frac{(0.012)(283)10^3}{35.3(1450 - 537)} + \frac{(0.006)(242)10^3}{35.3(1080 - 537)} = 1.07 \tag{17.7}$$

Since the result is greater than one, the hot layer *will* ignite and burn.

Although the approach to the onset of layer burning used in Example 5 has a great deal of generality, it requires a very detailed characterization of the upper and lower layers. It has been shown by Beyler [31] that a much simpler method can be used to evaluate the conditions required for layer burning.

The method [31] is based on the very simple chemical model

$$\text{Fuel} + \text{Oxidizer} \rightarrow \begin{cases} \text{Products} + \text{Excess oxidizer for } \phi < 1 \\ \text{Products} + \text{Excess fuel for } \phi > 1 \end{cases} \tag{17.8}$$

where the equivalence ratio, ϕ, is given by

$$\phi = \frac{\dot{m}_f}{\dot{m}_{air} \cdot r} \qquad r = \left(\frac{m_f}{m_{air}}\right)_{\text{Stoichiometric}} \tag{17.9}$$

According to this model, the fuel mass fraction in the upper layer is

$$\begin{aligned} Y_f &= 0 && \text{for } \phi < 1 \\ Y_f &= \frac{1 - 1/\phi}{1 + 1/\phi r} && \text{for } \phi > 1 \end{aligned} \tag{17.10}$$

Equation 17.6 can be expressed on a mass basis for this application as

$$\frac{Y_f \Delta H_c}{m_p C_p (T_{SL} - T_0)} \geq 1 \tag{17.11}$$

where ΔH_c is the heat of combustion of the fuel, and m_p is the mass of products resulting from burning a unit mass of upper layer gases.

Substituting the $\phi > 1$ relationship for Y_f into Equation 17.6, expressing the heat release in terms of oxygen consumed using

$$\Delta H_c = \frac{\Delta H_{O_2} Y_{O_2}}{r} \tag{17.12}$$

and recognizing that

$$m_p = 1 + \frac{Y_f}{r} \tag{17.13}$$

Yields

$$\left(\frac{1 - 1/\phi}{1 + r}\right)\left[\frac{\Delta H_{O_2} Y_{O_2}}{C_p(T_{SL} - T_0)}\right] \geq 1 \tag{17.14}$$

Equation 17.14 can be solved for the equality condition to give the equivalence ratio at which layer burning begins, ϕ_{ig},

$$\phi_{ig} = \frac{k}{k - r - 1} \tag{17.15}$$

where

$$k = \frac{\Delta H_{O_2} Y_{O_2}}{C_p(T_{SL} - T_0)}$$

T_0 is the precombustion temperature resulting from stoichiometric mixing of the air and fuel streams. Here, the upper layer contains the fuel and the lower layer contains the air. T_0 can be expressed as

$$T_0 = \frac{T_u + (Y_f/r)T_l}{1 + Y_f/r} \tag{17.16}$$

Using Equations 17.15 and 17.16, a relationship between the critical ignition equivalence ratio and the layer temperatures can be developed. Using normal values for the semi-universal constants, $\Delta H_{O_2} = 13.4$ MJ/kg, $C_p = 1.1$ kJ/kg K, $T_{SL} = 1700$ K. Using air properties for the lower layer, $Y_{O_2} = 0.233$ and $T_l = 300$ K. Using a typical $r = 0.07$ yields the relationship between ϕ_{ig} and T_u shown in Fig. 17.15. The results shown in Fig. 17.15 are consistent with the measurements of Beyler [31], where ϕ_{ig} was found to be 1.7 for T_u of 500–600 K. Gottuk [36] found that external burning was first observed in flashes at $\phi = 1.4 \pm 0.4$, and sustained external burning was first observed at $f = 1.9 \pm 0.3$ when T_u was in the range 900–1100 K. While in Gottuk's [36] experiments it was difficult to observe burning at the layer interface due to soot deposits on the viewing ports, layer interface burning was

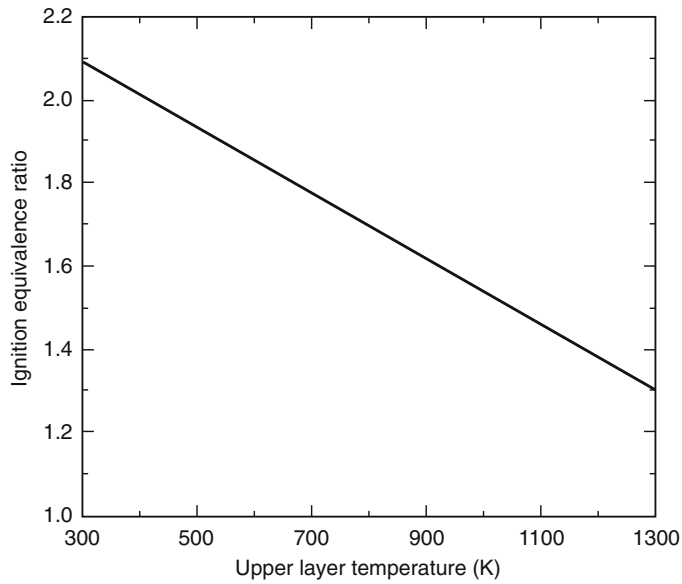

Fig. 17.15 Equivalence ratio required for upper layer ignition as a function of the upper layer temperature determined using Equations 17.15 and 17.16 with typical properties. Using normal values for the semi-universal constants, $\Delta H_{O_2} = 13.4$ MJ/kg, $C_p = 1.1$ kJ/kg K, $T_{SL} = 1700$ K. Using air properties for the lower layer, $Y_{O_2} = 0.233$, $T_l = 300$ K. Using a typical $r = 0.07$ yields the relationship between ϕ_{ig} and T_u

generally observed shortly after the initiation of flashes in the exhaust. Because the exhaust flow was isolated from the inflow in the experiment, there is some issue of the availability of a pilot flame which does not arise in normal two-directional vents found in most fires. Thus, Gottuk's work is generally consistent with Fig. 17.15.

Oxygen Index Test Method

The original oxygen index test method, used to determine the oxygen index of liquid and gas fuels, utilizes a counterflow diffusion flame formed at the stagnation region of a porous cylinder or sphere through which fuel vapors are fed. A low-velocity oxidant stream passes over the porous body. This arrangement yields the most favorable aerodynamic conditions for flame stabilization. As such, fuel and oxidant streams that can burn in the low-velocity counterflow system may not burn under less favorable aerodynamic conditions characterized by higher velocities and shear.

It is also important to point out the difference between the oxygen index as measured for gas and liquid fuels and the oxygen index of solids as measured using a candle-type test [37, 38]. The oxygen indexes of the gas and liquid fuels as tested by Simmons and Wolfhard [29] were governed by gas-phase effects. In the American Society for Testing and Materials test [33] for solids, the extinction can be caused by gas- and solid-phase effects. As such, the oxygen index of a solid fuel is not directly relevant to gas-phase diffusion flame limits and should not be used to calculate adiabatic flame temperature at the limit for use in the expressions presented here.

Nomenclature

AIT	Autoignition temperature (C or K)
C	Concentration (volume percent)
Cp	Heat capacity (J/kg K)
LFL	Lower flammable limit (volume percent)
M	Mass (kg)
n	Moles
NP	Nitrogen point
OI	Oxygen index
r	Stoichiometric fuel/air ratio
SL	Stoichiometric limit (volume percent)
T	Temperature (C or K)
V	Volume (m^3)
X	Mole fraction
Y	Mass fraction
ΔH_c	Heat of combustion (J/kg)
ϕ	Equivalence ratio

Subscripts

C	Combustion
i	Species
ig	Ignition
f	Flame or fuel
l	Lower layer
L	Liquid or lower limit
m	Mixture
N	Nitrogen
O	Initial or ambient
p	Products of combustion
u	Upper layer
U	Upper limit

References

1. M.G. Zabetakis, *Bulletin No. 627,* U.S. Bureau of Mines, Washington, DC (1965).
2. H.F. Coward and G.W. Jones, *Bulletin No. 503,* U.S. Bureau of Mines, Washington, DC (1952).
3. D.D. Drysdale, *An Introduction to Fire Dynamics,* John Wiley and Sons, New York (1999).
4. ASTM E681-94, *Standard Test Method for Concentration Limits of Flammability of Chemicals,* American Society for Testing and Materials, Philadelphia (1994).
5. ASTM E918-83, *Standard Test Method for Concentration Limits of Flammability of Chemicals,* American Society for Testing and Materials, Philadelphia (1993).
6. DIN 51 649 Teil 1, *Bestimmung der Explosionsgrenzen von Gasen and Gasgemischen in*

Luft, Deutsches Institute fur Normung, Berlin, Germany (1986).
7. VDI 2263 Part 1, *Test Methods for the Determination of the Safety Characteristics of Dusts,* Verein Deutscher Ingenieure (1990).
8. G. Smedt, F. Corte, R. Notele, and J. Berghmans, "Comparison of Two Standard Test Methods for Determining Explosion Limits of Gases at Atmospheric Conditions," *Journal of Hazardous Materials,* A70, pp. 105–113 (1999).
9. M. Goethals, B. Vanderstraeten, J. Berghmans, G. Smedt, S. Vliegen, and E. Van't Oost, "Experimental Study of the Flammability Limits of Toluene–Air Mixtures at Elevated Pressure and Temperature," *Journal of Hazardous Materials,* A70, pp. 99–104 (1999).
10. G.A. Karim, I. Wierzba, M. Metwally, and K. Mohon, "Combustion of a Fuel Jet in a Stream of Lean Gaseous Fuel-Air Mixtures," in *18th Symposium (International) on Combustion,* Combustion Institute, Pittsburgh, PA (1981).
11. H.F. Coward, C.W. Carpenter, and W. Payman, "The Dilution Limits of Inflammability of Gaseous Mixtures. Part III. The Lower Limits of Some Mixed Inflammable Gases with Air. Part IV. The Upper Limits of Some Gases, Singly and Mixed, in Air," *Journal of the Chemical Society,* 115, pp. 27–36 (1919).
12. M.J. Burgess and R.V. Wheeler, "The Lower Limit of Inflammation of Mixtures of the Paraffin Hydrocarbons with Air," *Journal of the Chemical Society,* 99, pp. 2013–2030 (1911).
13. A.G. White, "Limits for the Propagation of Flame in Inflammable Gas–Air Mixtures. Part III. The Effects of Temperature on the Limits," *Journal of the Chemical Society,* 127, pp. 672–684 (1925).
14. M.G. Zabetakis, S. Lambiris, and G.S. Scott, "Flame Temperatures of Limit Mixtures," in *7th Symposium (International) on Combustion,* Combustion Institute, Pittsburgh, PA.
15. F.J. Weinberg, "Combustion Temperatures: The Future?" *Nature,* 283, 239 (1971).
16. A. Macek, "Flammability Limits: A Re-Examination," *Combustion Science and Technology,* 21, pp. 43–52 (1979).
17. A. Egerton and J. Powling, "The Limits of Flame Propagation at Atmospheric Pressure. II. The Influence of Changes in the Physical Properties," *Proceedings of the Royal Society A,* 193, London, UK, pp. 190–209 (1948).
18. D.R. Stull, *Fire Research Abstracts and Reviews,* 13, 161 (1971).
19. H.F. Coward and G.W. Jones, "Limits of Flammability of Gases and Vapors," *Bulletin 503,* U.S. Bureau of Mines, Washington, DC (1952).
20. G.W. Jones, M.G. Zabetakis, J.K. Richmond, G.S. Scott, and A.L. Furno, "Research on the Flammability Characteristics of Aircraft Fuels," *Technical Report 52–35, Supplement I,* Wright Air Development Center, Wright-Patterson AFB, OH (1954).
21. J.M. Kuchta, A.L. Furno, A. Bartkowiak, and G.H. Martindill, "Effect of Pressure and Temperature on Flammability Limits of Chlorinated Combustibles in Oxygen-Nitrogen and Nitrogen Tetroxide-Nitrogen Atmospheres," *Journal of Chemical and Engineering Data,* 13, 3, p. 421 (1968).
22. M.G. Zabetakis, "Flammability Characteristics of Combustible Gases and Vapors," *Bulletin 627,* U.S. Bureau of Mines, Washington, DC (1965).
23. M.G. Zabetakis and B.H. Rosen, "Considerations Involved in Handling Kerosene," *Proceedings AP1,* 37, p. 296 (1957).
24. B. Lewis and G. Von Elbe, *Combustion, Flame, and Explosions of Gases,* Academic, New York (1961).
25. R.A. Strehlow, *Combustion Fundamentals,* McGraw-Hill, New York (1984).
26. M. Hertzberg, K. Cashdollar, and R. Conti, "Domains of Flammability and Thermal Ignitability for Pulverized Coals and Other Dusts: Particle Size Dependences and Microscopic Residue Analyses," in the *19th Symposium (International) on Combustion,* Combustion Institute, Pittsburgh, PA, pp. 717–729 (1981).
27. J.H. Burgoyne and L. Cohen, "The Effect of Droplet Size on Flame Propagation of Liquid Aerosols," *Proceedings of the Royal Society A,* 225, 375, pp. 375–392 (1954).
28. M. Hertzberg, K. Cashdollar, and C. Lazzara, "The Limits of Flammability of Coals and Other Dusts," *18th Symposium (International) on Combustion,* Combustion Institute, Pittsburgh, PA, pp. 717–730 (1981).
29. R.F. Simmons and H.G. Wolfhard, "Some Limiting Oxygen Concentrations for Diffusion Flames in Air Diluted with Nitrogen," *Combustion and Flame,* 1, pp. 155–161 (1957).
30. S. Ishizuka and H. Tsuji, "An Experimental Study of Effect of Inert Gas on Extinction of Laminar Diffusion Flames," *18th Symposium (International) on Combustion,* Combustion Institute, Pittsburgh, PA, pp. 695–703 (1981).
31. C.L. Beyler, "Ignition and Burning of a Layer of Incomplete Combustion Products," *Combustion Science and Technology,* 39, pp. 287–303 (1984).
32. J. Morehart, E. Zukoski, and T. Kubota, "Characteristics of Large Diffusion Flames Burning in a Vitiated Atmosphere," in *Third International Symposium on Fire Safety Science,* Elsevier Science Publishers, UK, pp. 575–583 (1991).
33. M. Peatross and C. Beyler, "Ventilation Effects on Compartment Fire Characterization," in *Fifth International Symposium on Fire Safety Science,* Elsevier Science Publishers, UK, pp. 403–414 (1997).
34. G. Back, C. Beyler, R. Hansen, "A Quasi Steady-State Model for Predicting Fire Suppression in Spaces

Protected by Water Mist Systems," *Fire Safety Journal,* 35, pp. 327–362.
35. A. Hamins, D. Trees, K. Seshadri, H. Chelliah, "Extinction of Nonpremixed Flames with Halogenated Fire Suppressants," *Combustion and Flame,* 99, pp. 221–230 (1994).
36. D.T. Gottuk, "The Generation of Carbon Monoxide in Compartment Fires," PhD Dissertation, Virginia Polytechnic and State University, Blacksburg, VA (1992). [Also in NIST-GCR-92-619, National Institute of Standards and Technology, Gaithersburg, MD (1992).]
37. C.P. Fenimore and F.J. Martin, "Flammability of Polymers," *Combustion and Flame,* 10, 135 (1966).
38. ASTM D2863-97, *Standard Test Method for Measuring the Minimum Oxygen Concentration to Support Candle-Like Combustion of Plastics (Oxygen Index),* American Society for Testing and Materials, Philadelphia (1997).

Dr. Craig Beyler earned a Ph.D. in engineering science at Harvard University under the direction of Professor Howard Emmons and served on the faculty of Worcester Polytechnic Institute's Center for Firesafety Studies. Dr. Beyler is currently technical director of Hughes Associates, Inc., Fire Science and Engineering.

Ignition of Liquids

18

D.D. Drysdale

Introduction

The purpose of this chapter is to discuss the ignition characteristics of combustible liquids that are in widespread use as fuels and solvents and are encountered as process fluids in the chemical and process industries. Ignition leads to flaming combustion in which the fuel undergoes a change of state and is converted from liquid to vapor.

Unlike the flaming combustion of solid fuels, this conversion does not involve any chemical change to the fuel molecules that simply evaporate from the exposed surface.[1] The flammable vapors mix with air to burn as a diffusion flame. When combustible solids exhibit flaming combustion, the change of state from solid to vapor involves chemical decomposition (see Chap. 7). Unlike liquids for which the process of evaporation is reversible (the evolved vapors can be converted back to the original liquid by cooling or by compression), the conversion is irreversible, breaking down the large polymeric molecules of which the solid is composed into fragments that are small enough to vaporize and enter the gas phase. Some solids, such as the thermoplastics (e.g., polypropylene and polystyrene), first soften and liquefy before producing molecular fragments that are small enough to vaporize. Others such as wood do not liquefy but release gases and vapors directly leaving behind an involatile carbonaceous char that, if permitted to do so, will undergo surface oxidation (smoldering) at a much slower rate. As a general rule, fires involving combustible liquids are associated only with flaming combustion, but there are exceptions that will be discussed later.

The underlying physics of the vaporization process for liquids provides a relatively simple key to understanding the conditions under which liquids can be ignited. The vapors from combustible liquids are flammable and exhibit exactly the same properties and behavior as the common flammable gases such as methane and propane (see Chap. 17). Thus, we can identify flammability limits, autoignition temperatures, minimum ignition energies, quenching distances, and so on. Of these, the most important are the flammability limits. If the concentration of vapor above a liquid surface is below the lower flammability limit, then the vapors cannot be ignited, flame will not propagate through the vapor-air mixture, and the liquid will not "burn." The limiting condition of the liquid at which the vapors are at the lower flammability limit is known as the flashpoint. Experimentally, this can be measured in a closed cup apparatus in which the vapor-air mixture in the closed volume above the surface (the "headspace") is at equilibrium with the liquid—the vapor will be at a pressure (the

[1] There are exceptions to this generalization. High molecular weight liquids with high flashpoints (e.g., cooking oil, flashpoint 321 °C) will be undergoing some chemical decomposition at temperatures associated with vapor formation.

D.D. Drysdale (✉)

M.J. Hurley (ed.), *SFPE Handbook of Fire Protection Engineering*,
DOI 10.1007/978-1-4939-2565-0_18, © Society of Fire Protection Engineers 2016

saturation vapor pressure) that is defined by the temperature of the liquid. This "closed cup flashpoint" provides us with a relatively simple method of ranking flammable liquids according to the hazard they present in everyday use. In principle, the concept of flashpoint can also be applied to combustible solids, but because the phase change (solid to vapor) is irreversible there is no corresponding simple method for classifying solids according to their ignition hazard. The ignition of solids depends on a large number of factors including the physical form of solid and the mode and intensity of the heat transfer process. Such issues are discussed in Chap. 21.

For combustible liquids, the flashpoint is closely linked to the flammability limits of the vapor. If the liquid is in an unconfined cup or present as a pool, the minimum liquid temperature at which the vapors can be ignited and burn is found to be higher than the "closed cup flashpoint" as defined above and is called the "open cup flashpoint." The reason for this is simply that the vapors will diffuse away from the liquid surface and for successful ignition from a "pilot" (a small flame or a spark) the pilot must be located in a region where the mixture is flammable. In general, a higher liquid temperature is required to ensure that the pilot is in a flammable zone. However, the "flash" of flame that occurs as flame propagates through the flammable mixture is not necessarily followed by sustained burning of the liquid. A criticality must be exceeded before this will occur. It is only then that the liquid can properly be said to have been ignited to flaming combustion. This is known as the firepoint, which will be discussed in a later section entitled "Measurement of Flashpoint and Firepoint."

Vaporization of Liquids

The liquids of general interest to the fire protection engineer are those that are stable at normal atmospheric temperatures and pressures (say, 10–30 °C and 101.3 kPa). These include common liquid fuels (such as gasoline and kerosene), many solvents (e.g., acetone, diethyl ether, etc.), some paints and varnishes, and so on. Most are blends, but for convenience and clarity in the following discussion, a one-component system (such as pure *n*-hexane) will be considered.

The classic phase diagram for a one-component system is shown schematically in Fig. 18.1. The variables are pressure and temperature and the so-called "phase space" is divided into three areas corresponding, respectively, to solid, liquid, and gas (vapor). For a pure compound at constant pressure (illustrated by the horizontal dashed line) we can identify the melting point (T_M) and the boiling point (T_B), which are uniquely defined at any given pressure. The values quoted in the literature refer to normal atmospheric pressure. The upper pair of lines that intersect at the point T in Fig. 18.1 represent equilibrium states between solid and liquid and between liquid and vapor, respectively.[2]

The line (TC) defines how the vapor pressure of the liquid varies with temperature. Thus, for *n*-hexane at normal atmospheric pressure, $T_B = 69$ °C, which corresponds to the temperature at which the (saturated) vapor pressure is 101.3 kPa. The variation of boiling point with pressure is best illustrated using pure water as the example. At sea level (101.3 kPa) it has a boiling point of 100 °C, but, as with all other liquids, this point decreases with elevation. In Banff, Scotland (at sea level), water boils at 100 °C but in Banff, Alberta (elevation 1463 m), it boils at about 95 °C. On the summit of Mount Everest (8848 m) where the pressure is approximately 33 kPa, or one-third of the value at sea level, it boils at about 72 °C. As will be seen, the flashpoints of combustible liquids also change with a change of atmospheric pressure but for a subtly different reason, as will be discussed later.

On the phase diagram, temperature and pressure may be varied independently provided that only one phase is present: there are two degrees

[2] The third line in Fig. 18.1, below the intersection at T, represents the equilibrium states between solid and vapor. Solid converts directly to vapor by the process of sublimation. It will not be considered further here.

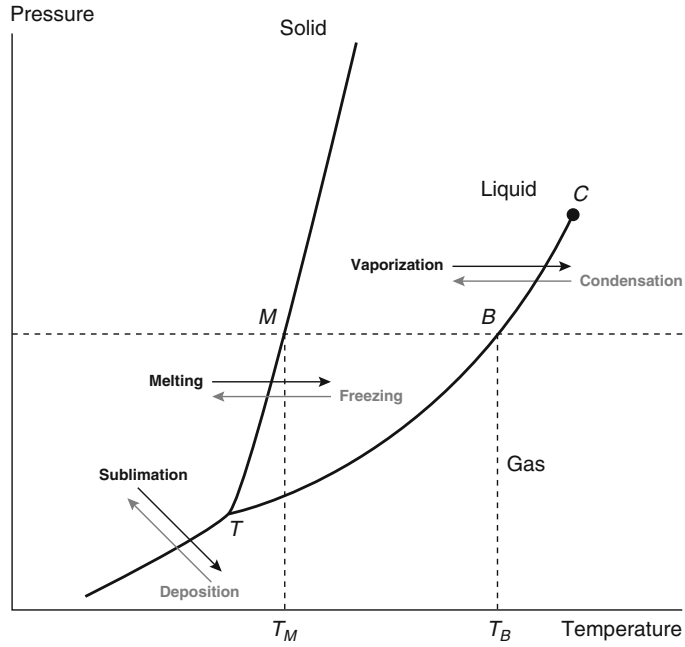

Fig. 18.1 Typical phase diagram for a one-component system. Points on the curve TC correspond to the equilibrium ("saturated") vapor pressure of the liquid, as given in Equation 18.3. T is the "triple point" and C defines the critical temperature and pressure (Table 18.1)

of freedom (i.e., independent variables), which in this case are temperature and pressure. Thus, a gas can be compressed and heated at the same time and still remain a gas (no change in state). The ideal gas law encapsulates this in the equation

$$PV = n\mathrm{R}T \tag{18.1}$$

where
P = Pressure
V = Volume
T = Temperature (K)
n = Number of moles of gas present (mass divided by the molecular weight)
R = Ideal gas constant[3]

However, when two phases are present and in equilibrium, corresponding to a point on one of the lines on the phase diagram, then P and T cannot be varied independently without changing the number of phases present. For example, at point B, liquid and vapor are in equilibrium, with the saturated vapor pressure of n-hexane equal to 101.3 kPa (760 mmHg, or 1 bar) at 69 °C. If we increase the temperature, the resulting vapor pressure is defined by the line BC and (unless atmospheric pressure is increased in step) complete conversion of liquid to vapor will occur, and the number of phases present is reduced from two to one as expressed in Gibbs's phase rule:

$$F = c - p + 2 \tag{18.2}$$

where f is the number of degrees of freedom (independent variables), c is the number of components, and p is the number of phases present (e.g., see Moore [2] and Atkins and de Paula [3]). For the one-component system (e.g., pure n-hexane), $c = 1$, so that when $p = 2$ (liquid *and* vapor present) the number of degrees of freedom $f = 1$. That is, we can change either the temperature or the pressure, but we cannot change them independently without changing the number of phases present. (Note that the intersection of the three lines on the phase diagram marked T is known as the triple point, where the three phases are in equilibrium; that is, $p = 3$. The number of degrees of freedom is, therefore, zero so that this point is uniquely defined.)

In summary, the lines that divide the phases in Fig. 18.1 represent equilibrium states: the line

[3] The numerical value of R depends on the units used for P and V (see Chap. 5).

Table 18.1 Critical temperatures and pressures [1]

	Normal boiling point (°C)	Critical temperature (°C)	Critical pressure (bar)
Hydrogen (H_2)	−252.9	−240	13
Nitrogen (N_2)	−195.8	−146.9	34
Oxygen (O_2)	−183.0	−118.5	50.5
Methane (CH_4)	−164	−82.3	46.5
Ethane (C_2H_6)	−88.6	32.2	48.3
Propane (C_3H_8)	−42.1	96.6	42.5
n-Butane (*n*-C_4H_{10})	−0.5	152.3	37
n-Hexane (*n*-C_6H_{14})	69	234.5	29.9

that separates the liquid and gaseous phases defines how the saturated vapor pressure of the liquid varies with temperature. However, this line does not continue indefinitely but ceases at the critical point marked *C*. At temperatures and pressures above the critical point, only one phase exists—the distinction between the liquid and gas disappears. Some values of critical temperatures and pressures are given in Table 18.1. A gas such as propane (boiling point −42 °C) is below its critical temperature at ambient temperatures and can be liquefied by pressurization. However, the so-called "permanent gases," which include oxygen and nitrogen, are above their respective critical temperatures and cannot exist as liquids at ambient temperature (e.g., 25 °C) regardless of the pressure. They are stored under pressure as gases in cylinders, typically at 140 bar. A single phase then exists within the cylinder. The only way that a permanent gas can be stored as a pressurized liquid is to cool it below its critical temperature. Large quantities of natural gas (mainly methane) can be stored economically as a refrigerated (cryogenic) liquid: its critical temperature is −82.3 °C and its normal boiling point is −164 °C as given in Table 18.1.

If a liquid is in an enclosed space, such as a can, tank, or bottle, the vapor will be contained within the headspace and quickly reach equilibrium (i.e., the saturated vapor pressure will be reached). This value is predicted in the phase diagram and is a function of temperature (see Equations 18.3, 18.4, and 18.5). It represents a dynamic state in which vaporization continues but at a rate that is balanced exactly by condensation of vapor back to the liquid state (see Fig. 18.1). For this reason, if the liquid is unconfined (e.g., forming a pool in the open), the liquid will eventually undergo complete evaporation as vapor continuously diffuses away from the surface of the liquid. Consequently, the vapor pressure at the surface will be less than the saturated vapor pressure and equilibrium cannot be achieved. The rate of mass loss by evaporation will be determined by the temperature of the liquid, the exposed area of the pool, and any air movement over the liquid surface (see, for example, Wade [4] and Clancy [5]). Boiling occurs when the vapor pressure is equal to atmospheric pressure, as discussed above.

However, if the liquid is in a closed (sealed) container capable of withstanding high internal pressures, the two phases (liquid and vapor) will remain in equilibrium at temperatures well above the atmospheric boiling point. Thus, propane and butane (which have normal boiling points of −42.1 °C and −0.5 °C, respectively) can be stored as liquids at 25 °C at 9.6 bar and 2.3 bar (957 and 231 kPa), respectively, in appropriate pressure vessels. These pressures correspond to the saturated vapor pressures of these two hydrocarbons at 25 °C. The reduction in volume associated with condensation is very large, making liquefaction a particularly effective means of storing these and similar gases. They can be liquefied simply by compression, although this is not possible with the so-called permanent gases, as discussed above.

Clearly, methane, propane, and butane cannot exist as stable liquids at normal temperatures and pressures. If liquefied methane (at −163 °C) is

released from a refrigerated tank and spilled on the ground, it will form a pool and boil vigorously until the surface of the ground has cooled to about −163 °C. Thereafter, it will behave as a stable liquid, evaporating at a rate dictated by the rate of heat transfer from the ground (see Thyer [6]).

Although methane is much lighter than air at ambient temperature, the vapor that evolves from the pool will be initially at −163 °C and much denser than the surrounding air. Consequently, it will spread horizontally until it gains sufficient heat from the surroundings to regain its buoyancy. Although propane is sometimes stored as a cryogenic liquid, propane and butane are more commonly stored in pressure vessels. Catastrophic release due to vessel failure gives rise to a BLEVE (boiling liquid expanding vapor explosion), a term originally coined for a pressure burst of a boiler containing superheated water (see Chap. 66). (It is defined by the Centre for Chemical Process Safety as "an explosion resulting from the failure of a vessel containing a liquid at a temperature significantly above its boiling point at normal atmospheric pressure." [7]) The liquid boils throughout its volume once the pressure is released and a substantial quantity will convert to vapor. The heat of vaporization is taken from the remaining liquid so that the BLEVE produces a vapor cloud containing a significant proportion of the original mass as liquid droplets. These may fall to the ground, although if ignition occurs (as it will if the pressure burst has been the result of exposure of the vessel to fire), there will be a fireball that will burn out rapidly (see, for example, Abbassi and Abbassi [8]).

Calculation of Vapor Pressure

If the space above the liquid is enclosed (as in a bottle or other container), evaporation will take place until the vapor pressure reaches its saturation value. This equilibrium is described by a form of the Clapeyron-Clausius equation, which gives the saturated vapor pressure (p°) as a function of the temperature of liquid (T K).

$$\frac{d(\ln p^\circ)}{dT} = \frac{L_v}{RT^2} \tag{18.3}$$

where L_v is the latent heat of evaporation of the liquid (kJ/kg) and R is the ideal gas constant. The derivation of this expression requires a number of approximations and may be found in most texts on physical chemistry [2, 3]. Integration of the equation gives the vapor pressure as a function of temperature; thus,

$$p^o = \text{Cexp}[-L_v/\text{R}T] \tag{18.4}$$

or

$$\ln p^\circ = \ln C - \frac{L_v}{\text{R}T} \tag{18.5}$$

A plot of ln p° versus $1/T$ will be a line of slope $-L_v$/R, although it is not strictly linear over an extended temperature range. However, it may be assumed to be linear within the range of temperatures with which we are concerned (i.e., we can assume that L_v is constant). Values of L_v for a range of liquids are given in Table 18.2.

The expression for vapor pressure is normally given in the form shown in Equation 18.5. The 53rd edition of the CRC *Handbook of Chemistry and Physics* [13] (and perhaps some later editions) gives an extensive table of data on p° (T), but in a modified form as follows:

$$\log_{10} p^o = -0.2185\frac{A}{T} + B \tag{18.6}$$

where p° is given in mmHg. Values of A and B for some typical liquid fuels are given in Table 18.3 (converting the data from $\log_{10}$ to $\log_e$ [i.e., ln] and from mmHg to kPa is a hazardous process that has not been attempted here). Vapor pressures may also be calculated from data in Yaws [12].

Example 1 Using the data in Table 18.3, calculate the pressure in a cylinder containing liquid isobutane at 25 °C. How can you determine how much fuel remains in the cylinder after drawing gas from it for a period of time?

Solution For isobutane, $A = 5416.2$ K and $B = 7.349085$. $T = 25 + 273$ K $= 298$ K. Substituting these values in Equation 18.4 gives

Table 18.2 Selected ignition properties of some fuels in air[a]

Fuel	Formula	Molecular weight	Boiling point (°C)	L_v (kJ/kg)	H (MJ/kg)	Flashpoint (°C)		Flammability limits[b] (% by volume)		AIT (°C)
						Closed	Open	Lower	Upper	
Alkanes										
Methane	CH_4	16	−162	509	50.2	–	–	5.0	15.0	600
Ethane	C_2H_6	30	−89	489	47.6	–	−135	3.0	12.5	515
Propane	C_3H_8	44	−42	426	46.4	–	−104	2.1	9.5	450
n-Butane	C_4H_{10}	58	0	386	45.9	–	−60	1.8	8.5	405
i-Butane	–	–	−10	366	–	−117	–	1.8	8.4	460
n-Pentane	C_5H_{12}	72	36	365	45.5	–	−49	1.4	7.8	260
i-Pentane	–	–	13	371	–	–	−51	1.4	7.6	420
n-Hexane	C_6H_{14}	86	69	365	45.2	−22	–	1.2	7.5	234
i-Hexane	–	–	–	–	–	−29	–	1.2	7.0	–
n-Heptane	C_7H_{16}	100	98	365	45.0	−4	–	1.0	7.0	223
i-Heptane	–	–	–		–	−18	–	1.0	6.0	–
n-Octane	C_8H_{18}	114	125	298	44.9	−13	–	0.8	6.5	220
i-Octane	–	–	–	–	–	−12	–	1.0	5.6	–
n-Nonane	C_8H_{20}	128	151	288	44.8	31	–	0.7	5.6	206
n-Decane	$C_{10}H_{22}$	142	174	360	44.7	44	–	0.75	5.4	208
n-Undecane	$C_{11}H_{24}$	156	196	308	44.6	–	65	0.7	4.8	202
n-Dodecane	$C_{12}H_{26}$	170	216	293	44.6	72	–	0.60	4.7	204
Kerosene[†]	~$C_{14}H_{30}$	~198	~232	~291	~44.0[a]	~49	–	(~0.6)	(~5.6)	~260
Alkenes										
Ethylene	C_2H_4	29	−104	516	47.3	−121	–	2.7	36	450
Propene	C_3H_6	42	−48	437	45.9	−108	–	2.0	11.0	457
1-Butene	C_4H_8	56	−6	398[a]	45.4	−80	–	1.6	9.3	384
1-Pentene	C_5H_{10}	70	30	314	46.9	–	−1.8	1.5	8.7	273
Hexelene	C_6H_{12}	84	67	388	47.5	–	–	–	–	253
Cycloparaffins										
Cyclopropane	C_3H_6	42	−34	588	46.3	−95	–	2.4	10.4	498
Cyclobutane	C_4H_8	56	13	483	44.8	−65	–	1.8	11.1	427
Cyclopentane	C_5H_{10}	70	49	443	44.3	−37	–	1.4	9.4	361
Cyclohexane	C_6H_{12}	84	81	358	43.9	−20	–	1.3	8.0	260
Cycloheptane	C_7H_{14}	98	119	376	43.7	9a	–	1.1	7.1	–
Dimethyl cyclohexane	C_8H_{16}	112	119	300	46.3[a]	11	–	0.9	6.5	304
Aromatics										
Benzene	C_6H_6	78	80	432	40.7	−11	–	1.4	7.1	562
Toluene	C_7H_8	92	110	362	41.0	4	7	1.2	7.1	536
m-Xylene	C_8H_{10}	106	139	343	41.3	25	–	1.1	7.0	528
o-Xylene	–	–	141	347	41.3	17	24	1.0	6.0	464
p-Xylene	–	–	137	339	41.3	25	–	1.1	7.0	529
Styrene	C_8H_8	104	145	–	40.5	32	–	1.1	6.1	490
bi-Phenyl	$C_{12}H_{10}$	154	254	–	40.6	113	124	0.8	6.7	540
Naphthalene	$C_{10}H_8$	128	218	316[c]	40.3	79	88	0.9	5.9	587
Anthracene	$C_{13}H_{10}$	166	340	310[c]	40.0[c]	121	196	0.7	–	540
Ethyl benzene	C_8H_{10}	106	136	320[c]	43.1	15	24	1.0	6.7	432
Butyl benzene	$C_{10}H_{14}$	134	173	277[c]	43.7	49	63	0.8	5.8	412

(continued)

Table 18.2 (continued)

Fuel	Formula	Molecular weight	Boiling point (°C)	L_v (kJ/kg)	H (MJ/kg)	Flashpoint (°C)		Flammability limits[b] (% by volume)		AIT (°C)
						Closed	Open	Lower	Upper	
Alcohols										
Methanol	CH_3OH	32	64	1101	20.8	12	16	7.3	36.0	469
Ethanol	C_2H_5OH	46	78	837	27.8	13	22	4.3	19.0	423
n-Propanol	C_3H_7OH	60	97	686	31.3	15	29	2.0	12.0	371
i-Propanol	–	–	82	667	33.1	12	–	2.0	12.6	399
Allyl alcohol	C_3H_6O	58	95	684	31.9	21	24	2.5	18.0	378
n-Butanol	C_4H_9OH	74	117	621	36.1	29	43	1.4	11.2	343
i-Butanol	–	–	107	578	36.1	28	–	1.7	9.8	406
2-Pentanol	$C_5H_{11}OH$	88	119	575[c]	–	–	41	1.5	9.7	343
i-Amyl alcohol	$C_5H_{11}OH$	88	130	501	35.3	43	46	1.2	9.0	350
3-Pentanol			118	575[c]	–	34	39	1.2	9.0	435
n-Hexanol	$C_6H_{13}OH$	102	159	458	36.4	45	74	1.2[a]	8.2	285
Cyclohexanol	–	–	161	460[c]	36.6	68	–	1.2	9.3	300
n-Heptanol	$C_7H_{15}OH$	116	176	439	39.8	–	71	1.0	7.2	–
1*n*-Octanol	$C_8H_{17}OH$	130	196	408	40.6	81	–	0.9	6.4	282
2*n*-Octanol			180	419	–	74	82	0.8	6.5	–
Nonanol	$C_9H_{19}OH$	144	214	403	40.3	–	–	0.8	6.1	–
i-Decanol	$C_{10}H_{21}OH$	158	235	373	–	–	–	0.7	5.5	–
Carbonyls										
Formaldehyde	CH_2O	30	97	826	18.7	93	–	7.0	73.0	430
37 % in H_2O	–	–	97	826[c]	–	54	93	(7.0[c])	–	424
Acetaldehyde	C_2H_4O	44	21	570	25.1	−38	–	1.6	10.4	185
i-Butyraldehyde	C_4H_8O	72	61	444[c]	33.8	−40	−24	1.6	10.6	254
Crotonaldehyde	C_4H_6O	70	102	490[c]	34.8	13	–	2.1	15.5	232
Diethyl acetaldehyde	$C_4H_{12}O$	76	118	500[c]	–	294	–	–	–	–
Ethyl hexaldehyde	$C_8H_{16}O$	128	163	325[c]	39.4	–	52	–	–	–
Paraldehyde	$C_6H_{12}O_3$	132	124	328	–	17	36	1.3	16.2	238
Salicyl aldehyde	$C_7H_6O_2$	122	196	396	–	78	–	1.4	8.4	–
Benzaldehyde	C_7H_6O	106	179	362	–	64	74	1.4	7.8	192
Ketones										
Acetone	C_3H_6O	58	56	521	29.1	−18	−9	2.6	128	538
2-Butanone	C_4H_8O	72	80	443	33.8	−2	1	1.8	10.0	516
Diethyl ketone	$C_5H_{10}O$	86	101	380	33.7	–	13	1.5	8.0	452
Methyl *i*-butyl ketone	$C_6H_{12}O$	100	116	345[c]	35.2	23	24	1.4	7.5	454
Dipropyl ketone	$C_7H_{14}O$	114	144	317	38.6	–	–	1.1	7.0	–
Methyl *n*-propyl ketone	$C_5H_{10}O$	86	375	376[c]	33.7	7	16	1.5	8.2	452
Methyl vinyl ketone	C_4H_6O	70	81	440[c]	–	−7[c]	–	–	–	–
Acids										
Formic acid	CH_2O_2	46	101	502	5.7	69	–	18.0	57.0	601
Acetic acid	$C_2H_4O_2$	60	118	405	14.6	40	57	5.4	16.0	427
Benzoic acid	$C_7H_6O_2$	122	250 s	270[c]	24.4	121	–	1.4	8.0	574

(continued)

Table 18.2 (continued)

Fuel	Formula	Molecular weight	Boiling point (°C)	L_v (kJ/kg)	H (MJ/kg)	Flashpoint (°C)		Flammability limits[b] (% by volume)		AIT (°C)
						Closed	Open	Lower	Upper	
Miscellany										
Camphor	$C_{10}H_{16}O$	152	204 s	265[c]	38.8	66	93	0.6	3.5	466
Carbon disulfide	CS_2	76	47	–	13.6	30	–	1.3	50.0	90
m-Creosol	C_7H_8O	108	203	–	34.6	86	–	1.1	7.6	559
o-Creosol	–	–	191	–	34.1	81	–	1.4	7.6	599
p-Creosol	–	–	202	–	34.1	86	–	1.1	7.6	559
Furan	C_4H_4O	68	31	399	–	−35	–	2.3	14.3	–
Pyridine	C_5H_5N	79	114	449	35.0	20	–	1.8	12.4	482
Aniline	C_6H_7N	93	183	434	36.5	76	91	1.3	11.0	617
Acetal	$C_6H_{14}O2$	118	103	277	31.8	−21	–	1.6	10.4	230
p-Cymene	$C_{10}H_{14}$	134	176	283	43.9	47	63	0.7	5.6	436
o-Dichloro benzene	$C_6H_4Cl_2$	146	180	–	19.3	66	74	2.2	9.2	647
1,1-Dichloro ethylene	$C_2H_2Cl_2$	96	37	–	–	–	−10	7.3	16.0	582
1,2-Dichloro ethylene	–	–	61	–	–	6	–	5.6	12.8	460
Monochloro benzene	C_6H_5Cl	112	132	–	–	32	38	1.3	7.1	638
Resorcinol	$C_6H_6O_2$	110	276	–	26.0	127	–	1.6	9.8	567
Ethyl formate	$C_3H_6O_2$	74	54	–	22.5	−20	−12	2.7	13.5	455
Ethyl acetate	$C_4H_8O_2$	88	77	–	25.9	−4	−1	2.2	11.4	427
Methyl propionate	$C_4H_8O_3$	104	80	–	22.2	−2	–	(2.4)	(13.0)	469
Acrolein	C_3H_4O	56	53	–	29.1	–	−26	2.8	31.0	234
Acrylonitrile	C_3H_3N	53	77	–	24.5	–	0	2.4	17.3	481
n-Amyl acetate	$C_7H_{14}O_2$	130	149	–	33.5	24	27	1.1	6.8	357
1-Amyl acetate	–	–	153	–	–	25	38	1.0	7.5	360
1, 3-Butadiene	C_4H_6	54	−4	–	–	−76	–	2.0	11.5	429
n-Butyl acetate	$C_6H_{12}O_2$	116	127	–	30.0	22	32	1.7	7.6	421
n-Butyl ether	$C_8H_{18}O$	130	141	–	39.7	25	38	1.5	7.6	–
Dimethyl ether	C_2H_6O	46	−24	–	31.6	−41	–	3.4	18.0	350
Divinyl ether	C_4H_4O	70	39	–	–	−30	–	(1.7)	(27)	360
Diethyl ether	$C_4H_{10}O$	74	35	–	37.4	−45	–	1.9	48	180
Gasoline[†]	–	–	~33	–	~44.1	~45	–	(~1.4)	(~6.8)	~371
Naptha[†]	–	–	~177	–	–	~41	–	(~0.8)	(~5.0)	~246
Petroleum ether[†]	–	–	~78	–	–	~ − 18	–	(~1.4)	(~5.9)	~288

Note: *s* indicates sublimes at normal pressures; L_v is latent heat of evaporation; H is heat of combustion; ~ indicates approximate values; – indicates not available; [†] indicates liquid blend

[a]Adapted from Kanury [9]. The data were originally from references *International Critical Tables of Numerical Data* [10] and *Handbook of Industrial Loss Prevention* [11] but the flammability limits and autoignition temperatures have been taken from Yaws [12]. It is not clear whether the flashpoint measurements quoted in Yaws [12] refer to the closed cup or the open cup tests so these have not been adopted

[b]The figures in brackets are taken from Kanury [9]

[c]Estimated value

Table 18.3 Calculation of saturated vapor pressures

	A (K)	B (−)
Methane (CH_4)	2128.8	7.027729
Propane (C_3H_8)	4811.8	7.392262
n-Butane (*n*-C_4H_{10})	5801.2	7.492753
i-Butane (*i*-C_4H_{10})	5416.2	7.349085
n-Pentane (C_5H_{12})	6595.1	7.489673
n-Hexane (C_6H_{14})	7627.2	7.717119
n-Heptane (C_7H_{16})	8928.8	8.258500
i-Octane (C_8H_{18})	9086.6	8.113870
n-Decane ($C_{10}H_{22}$)	10,912.0	8.248089
n-Dodecane ($C_{12}H_{26}$)	11,857.7	8.150997

Data for Equation 18.5 [13]

$\log_{10}(p^o) = 3.378$, or $p^o = 2386.7$ mmHg, or 3.14 bar. If the temperature remains 25 °C, this pressure will remain unchanged for as long as there is any liquid isobutane left in the container. Pressure is no guide to the amount of isobutane remaining. The only way to determine how much liquid is left is to weigh the container, assuming that you know the tare.

Example 2 Calculate the normal boiling point of *n*-hexane from the data in Table 18.3, assuming the atmospheric pressure is 760 mmHg.

Solution Take $p^o = 760$ mmHg, so that $\log_{10}(760) = 2.881$. For *n*-hexane, $A = 7627.2$ K and $B = 7.717119$, so by substitution and rearrangement:

$$2.881 = -0.2185\frac{7627.2}{T} + 7.717119$$

$$4.836T = 1666.543$$

$$T = 344\,\text{K} = 71.6^\circ\text{C}$$

which is about 2 K higher than the measured value quoted in Table 18.2.

Example 3 Calculate the temperature at which the vapor pressure of *n*-decane corresponds to the lower flammability limit for *n*-decane vapor. Assume that this vapor pressure is 0.75 % by volume (Table 18.3) and that the atmospheric pressure is 760 mmHg.

Solution The vapor pressure corresponding to the lower flammability limit of *n*-hexane is 0.75 % of 760 mmHg, or 5.7 mmHg. The calculation is exactly the same as for the previous example, except that $\log_{10}(p^\circ) = \log_{10}(5.7) = 0.756$. Thus

$$0.756 = -0.2185\frac{10,912.0}{T} + 8.24809$$

$$7.4922T = 2384.272$$

$$T = 318.2\,\text{K} = 45.2^\circ\text{C}$$

The closed cup flashpoint of *n*-decane is given in Table 18.2 as 317 K, or 44 °C. Sources of the difference between the calculated flashpoint and that measured in a standard test will be discussed below.

Vapor Pressure of Liquid Blends

Most commonly encountered fuels are in fact blends of different compounds. Gasoline, for example, contains several hundred individual hydrocarbons including a significant proportion of aromatics. The total vapor pressure is the sum of the partial vapor pressures of the individual components, which in turn depend on the concentration of the individual components in the blend. To illustrate how the vapor pressures of the components may be calculated, consider a mixture of two hydrocarbon liquids, A and B. At a given temperature, the partial vapor pressures of components A and B are given by Raoult's Law [2, 3]:

$$p_A = x_A p_A^o \quad p_B = x_B p_B^o \tag{18.7}$$

where x_A and x_B are the mole fractions of A and B, respectively, given by

$$x_A = \frac{n_A}{n_A + n_B} \quad x_B = \frac{n_B}{n_A + n_B} \tag{18.8}$$

and n_A and n_B are the number of moles of A and B present (i.e., the mass of the component present divided by its molecular weight).

Suppose that A and B are *n*-hexane and *n*-decane, respectively, and the mixture is at a temperature of 25 °C. These hydrocarbons form an "ideal mixture" in that the molecules of A and B are so similar that they do not interact with one another, either physically or chemically

(i.e., the interactions between A and B are no different from the interactions between A and A, or B and B).

As an example, consider a mixture containing 5 % hexane (by mass) in *n*-decane. Would its flashpoint be above or below 25 °C? (The flashpoints of *n*-hexane and *n*-decane are −29 °C and 44 °C, respectively.) This can be ascertained by calculating the partial vapor pressures of the two components at 25 °C and using Le Chatelier's Principle (see Chap. 17) to discover if the total vapor pressure ($p_{\text{total}} = p_{n\text{-hexane}} - p_{n\text{-decane}}$) is above or below the lower flammability limit. The principle states that a mixture of flammable vapors in air will be at the lower flammability limit if

$$\sum_i \frac{l_i}{L_i} = 1 \tag{18.9}$$

where l_i is the percentage composition (molar proportion) of component i in the vapor-air mixture and L_i is the corresponding value for the lower flammability limit of component i. To calculate the equilibrium partial vapor pressures of *n*-hexane and *n*-decane above a 5 % hexane/95 % *n*-decane mixture (*by mass*), the respective mole fractions must be calculated; thus,

$$\begin{aligned} x_{n-\text{hexane}} &= \frac{0.05/MW_A}{0.05/MW_A + 0.95/MW_B} \\ x_{n-\text{decane}} &= \frac{0.95/MW_B}{0.05/MW_A + 0.95/MW_B} \end{aligned} \tag{18.10}$$

where the molecular weights are $MW_A = 86$ and $MW_B = 142$. According to Equation 18.6 and Table 18.3, the partial pressures of *n*-hexane and *n*-decane are 10.66 mmHg and 1.65 mmHg, respectively. Using Equation 18.8 with $L_{n\text{-hexane}} = 1.2$ % and $L_{n\text{-decane}} = 0.75$ % (see Table 18.2),

$$\frac{10.66/760}{0.012} + \frac{1.65/760}{0.0075} = 1.46 \tag{18.11}$$

indicating that the mixture is above the lower flammability limit at 25 °C (i.e., the flashpoint of this mixture is below 25 °C).

Example 4 Determine by calculation whether *n*-decane containing 1 % *n*-pentane (*by volume*) would be classified as a Class 1C or a Class II flammable liquid according to the NFPA Standard. [14] (This is equivalent to posing the question, "Is the flashpoint above or below 37.8 °C?")

Solution This calculation is identical to that discussed previously, but the densities of the two liquids must be taken into account and the calculation carried out at 37.8 °C. The mixture can be taken as 0.01 × 626 kg of *n*-pentane + 0.99 × 730 kg of *n*-decane (where the densities of *n*-pentane and *n*-decane are 626 kg/m^3 and 730 kg/m^3, respectively). The mole fractions are

$$\begin{aligned} x_{n-\text{pentane}} &= \frac{(0.01 \times 626)/MW_A}{(0.01 \times 626)/MW_A + (0.99 \times 730)/MW_B} \\ x_{n-\text{decane}} &= \frac{(0.99 \times 730)/MW_B}{(0.01 \times 626)/MW_A + (0.99 \times 730)/MW_B} \end{aligned} \tag{18.12}$$

where now $MW_A = 72$ (the molecular weight of pentane) and $MW_B = 142$. These give $x_{n\text{-pentane}} = 0.0141$ and $x_{n\text{-decane}} = 0.986$. From Equation 18.6 and Table 18.3, the saturated vapor pressures of *n*-pentane and *n*-decane at 37.8 °C are 713.11 mmHg and 3.773 mmHg, respectively, so that the partial pressures are 10.05 mmHg and 3.72 mmHg. Applying the Le Chatelier Principle (with the lower flammability limit of *n*-pentane vapor as 1.4 %),

$$\sum_i \frac{l_i}{L_i} = \frac{10.05/760}{0.014} + \frac{3.72/760}{0.0075} = 1.6 \tag{18.13}$$

This is above the lower flammability limit and, consequently, the mixture has a flashpoint below 37.8 °C and is definitely not a Class II liquid. (Further calculation could be carried out to ascertain if the mixture is Class IB or IC; see below.)

This calculation reveals that the partial vapor pressure of the more volatile component can be disproportionately high and for this reason it will evaporate from the mixture much more rapidly than the less volatile component. Consequently, care must be taken when determining the flashpoints of such mixtures. The liquid to be tested should be kept in a closed container and a sample transferred to the flashpoint apparatus as quickly as possible to minimize evaporative loss. In some circumstances, it might be wise to refrigerate the liquid and chill the apparatus. The author has experience of assessing the flashpoint of a sample of crude oil that (without refrigeration) gave a flashpoint of 28 °C, but a flashpoint of 15 °C occurred if the liquid (and the apparatus) was cooled to 0 °C before opening the sample container. (The problem of evaporative loss is also encountered in the more extreme example of trying to identify traces of gasoline or other flammable liquids that may have been used in an arson attack.)

In the examples discussed above, the vapor pressure of liquid mixtures was calculated using Raoult's Law (Equation 18.7), which applies only to ideal mixtures such as blends of hydrocarbons. It is important to note that many other liquid mixtures, such as alcohol and water, are not ideal as there is some interaction between the molecules of the different components (*A* and *B*). Instead of Equation 18.7, it is necessary to use Equation 18.14:

$$p_A = \alpha_A p_A^o \qquad p_B = \alpha_B p_B^o \tag{18.14}$$

where α_A is known as the activity of component *A* in the mixture, and $p_A{}^o$ is the saturation vapor pressure of pure *A*, and so on. The activity coefficient α_A is the product of the mole fraction of *A* (Equation 18.15) and the activity coefficient γ_A:

$$\alpha_A = \gamma_A n_A \qquad \alpha_B = \gamma_B n_B \tag{18.15}$$

where γ_A is the activity coefficient of component *A* in the mixture (note that for a pure liquid, $\gamma = 1$). For a two-component mixture of *A* and *B*, the activity coefficients are given by the Van Laar equations:

$$\log_{10}\gamma_A = \frac{C_A}{[1 + (C_A x_A / C_B x_B)]^2}$$
$$\log_{10}\gamma_B = \frac{C_B}{[1 + (C_B x_B / C_A x_A)]^2} \tag{18.16}$$

Table 18.4 Examples of data for the Van Laar equation for binary (two-component) systems [15]

Component A	Component B	C_A	C_B
Ethanol	Water	0.67	0.42
Methanol	Water	0.25	0.20
Acetone	Water	0.89	0.65
n-Heptane	CCl_4	0.2164	0.0618

Essentially the same set of calculations can be carried out to establish the flammability properties of nonideal mixtures, but the activity coefficients (Equations 18.15 and 18.16) must be calculated from Equations 18.16 using data such as those contained in Table 18.4.

Another more general data set than that given in Table 18.4 is given by Babrauskas [16].

Effect of Atmospheric Pressure on Flashpoint

The calculations that are provided above all refer to the standard atmosphere at sea level where the pressure is 101.3 kPa (760 mmHg), conventionally normalized as 1 bar. If the atmospheric pressure changes, this change has no significant effect on the vapor pressure, which is a function of the temperature of the liquid. At a constant temperature but a reduced pressure, the vapor-air ratio in the headspace will be increased (i.e., it will become richer in fuel). This has significant consequences for liquid fuels because it will reduce the flashpoint.

Consider the following argument. In Example 3, the temperature at which the saturated vapor pressure of *n*-decane corresponds to the lower flammability limit was shown by calculation to be 45.2 °C, which compares well with the measured value of the closed cup flashpoint (44 °C). At 45.2 °C, the vapor pressure was

assumed to be 5.7 mmHg, which is 0.75 % of normal atmospheric pressure (760 mmHg). If the temperature remains the same (45.2 °C) but the pressure is reduced—say to the value appropriate to Denver, Colorado (at 1 mile high, 631 mmHg)—then the volumetric concentration of *n*-decane vapor in air becomes 5.7/631 = 0.009, or 0.9 %. It has been shown that the lower flammability limit is remarkably insensitive to a reduction in pressure until it falls below 200–300 mmHg (27–40 kPa) [17, 18]. Clearly, at 45 °C the saturated vapor pressure of *n*-decane is above the lower flammability limit. The effect on the flashpoint can be shown in the following example.

EXAMPLE 5 Calculate the flashpoint of *n*-decane if measured in Denver, Colorado, where the atmospheric pressure is 631 mmHg. Assume that the lower flammability limit of *n*-decane vapor is 0.75 %.

SOLUTION The vapor pressure corresponding to the lower flammability limit of *n*-hexane is 0.75 % of 631 mmHg, or 4.73 mmHg. The calculation is exactly the same as in Example 3, except that $\log_{10}(p^\circ) = \log_{10}(4.73) = 0.675$. Thus,

$$0.075 = -0.2185\frac{10,912.0}{T} + 8.24809$$

$$7.573T = 2384.272$$

$$T = 314.8\,\mathrm{K} = 41.8^\circ\mathrm{C}$$

The value obtained in Example 3 at normal atmospheric pressure was 45.2 °C. The difference is not insignificant and could be very important for liquids close to the boundary between two classifications (see later discussion). The issue becomes more significant at higher altitudes such as Mexico City (2240 m) and Lhasa in Tibet (3650 m). In these cities, the flashpoint of *n*-decane would be approximately 39.4 °C and 35.9 °C, respectively.

An interesting consequence of this relates to the headspace in the fuel tanks of aircraft. The kerosene grades of commercial aviation fuel have closed cup flashpoints in the range of 35–63 °C [19], as measured at sea level. As an aircraft gains altitude after takeoff, the air pressure in the headspace will fall relatively rapidly, while the fuel will cool rather slowly. There is the potential for the vapor-air mixture in the headspace to become flammable. On long-haul flights, of course, the hazard will be relatively short-lived as the fuel loses heat and cools to below the local flashpoint, relevant to the pressure at cruising altitude. This phenomenon is discussed in NFPA's *Fire Protection Handbook* [19].

Measurement of Flashpoint and Firepoint

There are a number of standard tests available for measuring the closed cup [20, 21] and open cup [22, 23] flashpoints (Fig. 18.2). The former measurement is directly related to the lower flammability limit of the fuel vapor and is used to classify liquids according to their ignition hazard [18]. Its relationship to equilibrium vapor pressure of the liquid is discussed in an earlier section.

Closed Cup Flashpoints

In the closed cup test, such as the Pensky-Martens apparatus [20] and the Tag tester [21], the flammability of the saturated (equilibrium) vapor-air mixture in the space above the liquid surface (i.e., the headspace) is tested by introducing a small pilot flame (see Fig. 18.2). The apparatus is designed to allow the miniature explosion within the headspace to vent through an aperture that is opened to admit the pilot ignition source, which also allows the "flash" of flame to be observed. The procedure involves raising the temperature of the liquid slowly from approximately 10–20 K below the anticipated flashpoint at a rate of 5–6 K/min, introducing the ignition source at intervals corresponding to about a 1 °C (1 K) temperature rise. The slow rate of heating is intended to allow enough time for equilibrium conditions to be

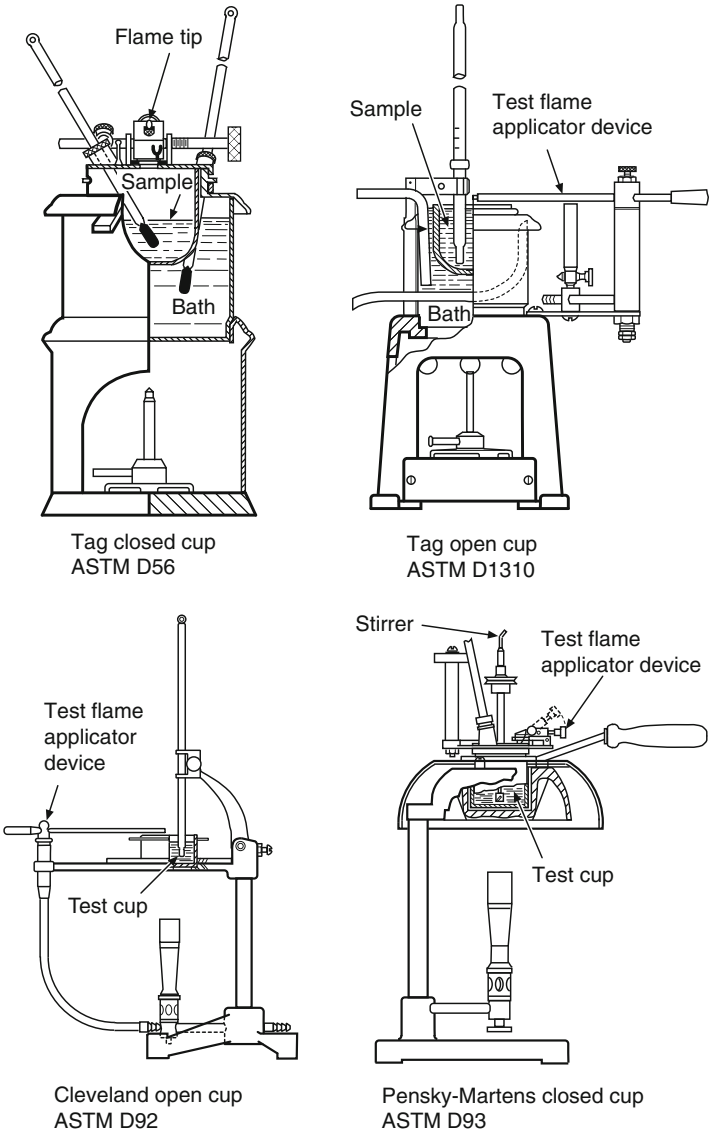

Fig. 18.2 Four of the commonly used apparatuses for determining flashpoints of flammable or combustible liquids [19]

reached within the headspace (see below). The lowest temperature at which a flash of flame is observed is recorded as the closed cup flashpoint. It is expected that it can be determined to an accuracy of better than ±1 °C for liquids with flashpoints below 100 °C. Values of the closed cup flashpoint for a range of liquids are given in Table 18.2. All refer to standard atmospheric pressure (101.3 kPa). If the closed cup flashpoint is measured when the atmospheric pressure differs from 760 mmHg, the value may be corrected using Equation 18.17:

$$\text{Corrected flashpoint} = T - 0.033\,(760\ - P) \tag{18.17}$$

where T is the measured flashpoint (°C) and P is the ambient atmospheric (barometric) pressure (mmHg). This is intended for relatively small excursions that are commonly experienced on a day-to-day basis. No guidance is given that is relevant to high-altitude locations.

In general, there is reasonable but not exact agreement between measured values and those calculated on the basis that the vapor pressure

must correspond to the lower flammability limit. The reason for this may be that the lower flammability limit is based on the ability of a flame to propagate approximately 75 cm inside a vertical tube, 5 cm in diameter [24], whereas the flashpoint is observed as a localized ignition in the vicinity of the ignition source. Similar localized ignition occurs in the flammability limit apparatus but at a concentration of fuel in air that sustains only limited flame propagation. If this explanation is accurate, the "calculated" flashpoint would be expected to be greater than the measured one—as indeed the calculation above shows (Example 3).

Care should be taken when testing liquids of reduced flammability, such as certain chlorinated hydrocarbons. James and Tyler [25] investigated reports of fire and explosions that involved a commercial cleaning fluid, of which the principal component was methyl chloroform (1,1,1 trichloroethane, CCl_3CH_3). This compound does not give a flashpoint in the standard test, but a flashpoint of 12 °C was recorded in vessels of diameter greater than 12.4 cm [26]. Babrauskas [16] draws attention to a problem with blends containing halogenated components. If these are of high volatility, the blend may give a high flashpoint as a consequence of the inhibiting effect of the halogenated component. However, if this halogenated component is lost as a result of preferential evaporation over a period of time, the effective flashpoint can decrease, which is the reverse of the effect of the preferential loss of lighter hydrocarbons from fuel blends as discussed above.

The closed cup flashpoint is sometimes referred to as the "lower flashpoint." Although not widely used, this term does emphasize the link to the lower flammability limit of the vapor and allows the concept of the "upper flashpoint" to be introduced. This term corresponds to the temperature at which the vapor concentration in the headspace is at the upper flammability limit, signifying that the mixture will not ignite when an ignition source is introduced, although a weak diffusion flame may exist briefly at the open aperture. Upper flashpoint is seldom measured, although Hasegawa and Takishi [27] have obtained some results in the Setaflash apparatus [16]. It is useful in identifying the temperature range within which the vapor-air mixture in the headspace is flammable. For example, at ambient temperatures, the vapor-air mixture in the headspace of a gasoline tank is well above the upper flammability limit and cannot be ignited. However, the upper flashpoint of the lower alcohols (in particular methanol and ethanol) appears to be in the mid-20s, only 10–15 K or so above the lower flashpoint. This means that at ambient temperatures (say, 15–20 °C) a partially full can of alcohol contains a flammable vapor-air mixture that can be easily ignited. This is a significant hazard that can give rise to serious consequences. For example, if an attempt is made to top-up a conventional flambé lamp directly from the fuel container before the flame has extinguished and if the temperature of the alcohol in the container is between the lower and upper flashpoints, flame will propagate into the container, perhaps causing it to burst or otherwise expel burning liquid. Such occurrences have led to a number of serious accidents in restaurants [28]. Provision of a flame arrester in the opening of the container would prevent such an occurrence.

Open Cup Flashpoints and Firepoints

Open cup flashpoints are not routinely available in the literature although they are clearly relevant to the ignition of open pools of liquid. They are determined using an open cup, the most common of which is the Cleveland apparatus [22] as shown in Fig. 18.2. Instead of the vapor accumulating immediately above the liquid surface, it is lost to the atmosphere by diffusion. Consequently, the concentration of vapor in air deceases with height above the liquid surface. In the standard test, the ignition source (a small diffusion flame at the end of a swivel arm) is moved across the top of the cup, no more than 2 mm above its rim, in a trajectory that carries the flame over the center. The process of heating the fuel is essentially the same as for the closed cup test, but in this case the result is more strongly apparatus

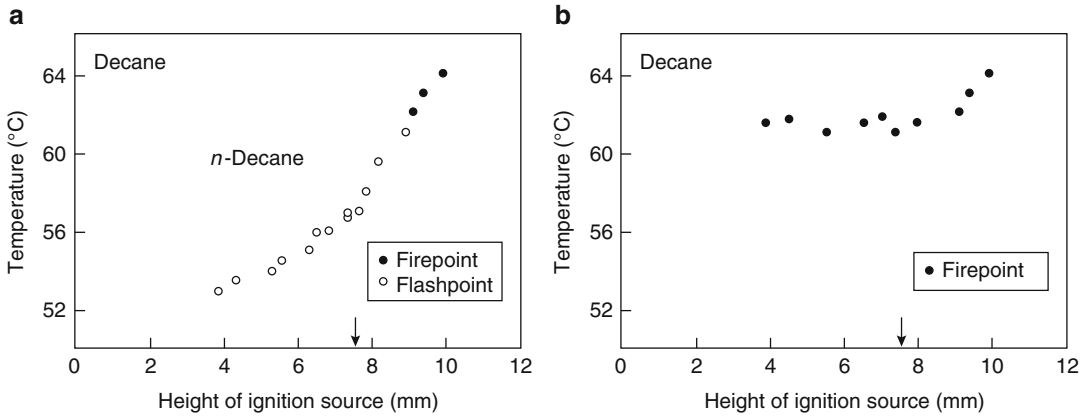

Fig. 18.3 Open cup flashpoint (o) and firepoint (•) of n-decane as a function of the height of the ignition source above the liquid surface. (**a**) Flashpoint, revealing how the onset of sustained burning occurs when the temperature of the liquid is above the firepoint (61.5 °C); (**b**) Firepoint as a function of the height of the ignition source, showing that it is relatively insensitive to heights less than about 9 mm. The arrow shows the height of the ignition source in the standard test [29]

dependent. A flash of flame is observed when the ignition source first encounters a mixture at the lower flammability limit. For this reason, the measured open cup flashpoint is very sensitive to the height of the ignition source above the surface. This was demonstrated very clearly by Glassman and Dryer [29], as shown in Fig. 18.3a. Clearly, this measurement is apparatus-specific and cannot provide information about the ignitability of the liquid that can properly be generalized—the flashpoint of an open pool of liquid will depend on the distance the vapor has to travel before meeting a suitable ignition source. Indeed, instead of observing a flashpoint, the liquid may catch fire and continue to burn (i.e., its temperature is above the firepoint [see Fig. 18.3a]).

This burning will occur when fuel vapors are being released at a high enough rate to support a diffusion flame. At the flashpoint (closed cup and open cup), the mixture is fuel lean and all the fuel vapor is consumed in the premixed flame. However, if the temperature of the liquid is high enough to produce a fuel-rich vapor-air mixture, a self-sustained diffusion flame becomes possible, as illustrated clearly in Fig. 18.3a, which reveals that a minimum fuel temperature must be achieved for this result to occur. This minimum temperature at which a self-sustaining diffusion flame becomes possible is known as the firepoint. Glassman and Dryer [29] found the firepoint to be much less sensitive to the height of the ignition source, as shown in Fig. 18.3b.

In general, firepoints are not routinely measured and there is not a good database. Some values quoted by Babrauskas [16] are given in Table 18.5. A different selection is given by Kanury [9], but these are all blends that are poorly defined. Typically the firepoint is 10–20 K above the closed cup flashpoint, but one cannot rely on this generalization. The difference appears to be erratic and can be much greater and more uncertain for high-flashpoint liquids (see Babrauskas [16]). The lower alcohols seem to behave in a very different manner. Glassman and Dryer [29] found the open cup flashpoints and the firepoints of methanol and ethanol were equal and—even more surprisingly—considerably less than the closed cup flashpoint. This anomaly disappeared if a spark ignition source was used instead of a flame in the open cup measurement: the open cup flashpoint and the firepoint remained equal but were now higher than the closed cup flashpoint (see Table 18.5). This observation has still to be explained satisfactorily, but clearly the behavior of the alcohols is not typical.

Several attempts have been made to define the firepoint of liquids (and indeed solids) in terms of the heat and mass transfer processes involved

Table 18.5 Some values of closed cup flashpoint, open cup flashpoint, and firepoint temperatures

	Closed cup FP (°C)	Open cup FP (°C)	Firepoint (°C)
n-Hexane	−22	[a]	NA
n-Heptane	−4	−1	2
Methanol[b]	12	1.0, 13.5[b]	1.0, 13.5[b]
n-Octane	12	17	18
Ethanol[b]	13	6, 18.0[b]	6, 18.0[b]
s-Butanol	24	NA	29
m-Xylene	25	NA	44
p-Xylene	25	31	44
n-Butanol	29	36	36, 38, 50
n-Nonane	31	37	42
o-Xylene	32	36	42
JP-6	NA	38	43
n-Decane	44	52	61.5, 66
Decalin	NA	57	63
Tetraline	NA	71	74
Bicyclohexyl	NA	74	79
n-Dodecane	74	NA	103
Fuel oil no. 2	124	NA	129
Fuel oil no. 6	146	NA	177
Glycerol	160	176	207
Motor oil	216	NA	224

Unless otherwise stated, these data come from the *Factory Mutual Handbook,* as quoted by Babrauskas [16]
NA Not available
[a]The open cup flashpoint of *n*-hexane is quoted as −26 °C in the original *Factory Mutual Handbook* and repeated in Babrauskas [16]. This is incorrect
[b]Data from Glassman and Dryer [29]. The lower values were obtained with ignition by a pilot flame. The upper values refer to spark ignition

in the combustion of the fuel vapors close to the fuel surface. For a diffusion flame to become established at the surface of the liquid, the rate of evolution of flammable vapor must be greater than a certain critical value. It has been argued that it is determined by the need to establish a self-sustaining process whereby the energy required to maintain (and promote) the evolution of vapors comes from the flame by convective and radiative heat transfer. However, if the flow rate of vapors is too small, the flame will be too close to the surface and self-extinguish as a consequence of heat losses to the surface.

Valuable contributions to the definition of firepoint as a criticality have been made by Roberts and Quince [30], Rasbash [31], and Beyler [32]. In particular, they have used Spalding's *B*-number, first used to describe the rate of burning of fuel droplets [33], to develop the concept of ignition [30, 31] and extinction [31, 32] criticalities. It is a dimensionless transfer number that can be used to express the conservation of heat (B_H) or mass (B_M), the values of which can be used to define the rates of heat and mass transfer, respectively. They can be expressed as follows:

$$B_H = \frac{\left(m_{og}H/r\right) - c\left(T_g - T_{ls}\right)}{Q} \tag{18.18}$$

and

$$B_M = \frac{m_{fs} - \left(m_{og}/r\right)}{1 - m_{fs}} \tag{18.19}$$

where m_{og} is the mass fraction of oxygen in the atmosphere, m_{fs} is the mass fraction of fuel vapor immediately above the liquid surface, H is the heat of combustion of the fuel vapor, r is the stoichiometric ratio (mass of O_2 required to burn unit mass of fuel), c is the specific heat, T_g is the ambient air temperature, and T_{ls} is the temperature of the surface of the liquid. B_H and B_M are assumed equal when the diffusivities of heat and mass are equal (the Lewis number is unity). However, this assumption carries with it the hidden assumption that radiative heat transfer can be ignored and only convection need be considered. For small flames—particularly those associated with the burning of small droplets for which this approach was developed—this approximation is reasonable.

The rate of burning can be expressed as a mass flux ($\dot{m}''$, the rate of mass transfer per unit surface area) in terms of the *B*-number using the following equation:

$$\dot{m}'' = \frac{h}{c}\ln(1 + B) \tag{18.20}$$

where h is the (convective) heat transfer coefficient. Following the argument developed by Roberts and Quince [9], which invokes the concept that there is a critical temperature below

which a flame will extinguish (see Chap. 5), a critical B-number can be formulated as

$$B_{crit} = \frac{m_{og}}{r}\left(\frac{T_{f,\max} - T_{ls}}{T_{f,\max} - T_{f,crit}}\right) \qquad (18.21)$$

where $T_{f,\max}$ is the theoretical flame temperature assuming no heat losses to the surface of the liquid, $T_{f,crit}$ is the critical flame temperature below which the flame will extinguish, and T_{ls} is the surface temperature of the liquid—the firepoint temperature. B_{crit} can be calculated from Equation 18.19 for B_M, substituting for m_{fs} the mass concentration of fuel vapor above the liquid surface at the firepoint (calculated from the saturation vapor pressure derived from data similar to that contained in Table 18.3), allowing the critical temperature hypothesis to be tested. The theoretical temperature $T_{f,\max}$ can be deduced from a heat balance at the surface, assuming that the flame loses no heat to the surface (i.e., it is adiabatic). For a range of fuels (identified in Table 18.2), $T_{f,crit}$ was found to have a mean value of 1350 °C (albeit ±100 K), which is not inconsistent with measured and predicted values for premixed flames close to the lower flammability limit (about 1300 °C) (see Chap. 5).

Observations of the firepoint temperatures of a number of fuels reveal that the saturated vapor pressure at the firepoint is above stoichiometric. Roberts and Quince [9] reported values from 1.33× to 1.92× stoichiometric. Clearly, the mixture immediately above the surface is rich by a significant margin but is still within the flammability range. (Zabetakis [24] has shown that the upper flammability limit is between 2.5× and 4× the stoichiometric concentration.) The firepoint represents a criticality, the rate of evolution of vapors being just sufficient to allow the establishment of a diffusion flame at the surface. It is closely linked to the "quenching distance," a characteristic of premixed flames that are quenched (extinguished) within 1 or 2 mm of the surface due to heat losses and (probably) the loss of free radicals (see Chap. 12). The flow rate of vapors at the firepoint must be sufficient to allow a nascent diffusion flame to form far enough from the surface so that the quenching process does not occur. The critical flow rate of vapors at the firepoint will, therefore, be given by

$$\dot{m}''_{crit} = \frac{h}{c}\ln(1 + B_{crit}) \qquad (18.22)$$

$\dot{m}''_{crit}$ has not been determined for any liquid fuels but values have been reported for a range of solids (see Chap. 36).

Classification of Liquid Fuels

Although this chapter is entitled "Ignition of Liquids," most of the emphasis has been on understanding the flashpoint, the minimum liquid temperature at which the vapor can be ignited. It is clear that it is the firepoint that determines whether or not sustained flaming of the liquid will occur, yet combustible liquids are classified—quite properly—in terms of their flashpoints. Measurement of the closed cup flashpoint provides a method of classifying flammable liquids according to the hazard they represent. Systems of classification have been developed in several countries, but they have as the common basis the need to identify and make provision for those liquids that can be easily ignited at ambient temperatures. Thus, in the United Kingdom under the Highly Flammable Liquids and Liquefied Petroleum Gases (HFL/LP-gas) Regulation 1972 [34], liquids with closed cup flashpoints less than 32 °C were classified as "highly flammable liquids." NFPA 30, *Flammable and Combustible Liquids Code* [14], assigns liquids with flashpoints less than 37.8 °C (100 °F) to a similar category, known as Class I. Figure 18.4 compares the U.K. and U.S. systems and shows how the Class I liquids are subdivided into three subclasses A, B, and C. The boundary between I (A and B) and IC is set at 22.8 °C (73 °F), whereas Class IA liquids are distinguished from Class IB in having normal boiling points less than 37.8 °C (100 °F).

"Flammable liquids" (1972 Regulations, U.K.) and Class II liquids (U.S.) have a common upper bound of 60 °C. These are liquids that must

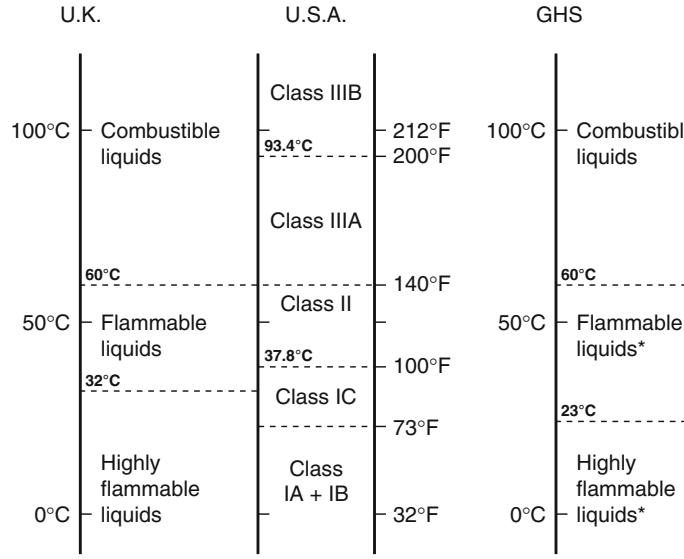

Fig. 18.4 A comparison of the U.K. and U.S. classifications of flammable and combustible liquids with the UN Globally Harmonized System

be heated significantly above ambient temperature before the evolved vapor can be ignited, although it is clear that some caution is required if ambient temperatures above 32–37.8 °C are encountered. For example, strict application of the U.K. Highly Flammable Liquid Regulations or NFPA 30 would be highly inappropriate in Dubai where the average maximum temperature during the summer months is about 40 °C. Liquids with flashpoints above 60 °C are considered to be relatively "safe" in that significant temperature increases are required before they can be ignited. In the United Kingdom these are called "combustible liquids," whereas in the United States they belong to Class III (which is further divided into Class IIIA and Class IIIB, as shown in Fig. 18.4).

Within the European Union (EU), new classification systems have evolved following the introduction of new regulations arising from EU Directives. These relate, rather confusingly, to the three main "endpoints" (i.e., storage, supply, or transport, each slightly different[4]). Over the years, the United Kingdom has modified the HFL/LP-gas regulations to conform to the EU system and as a consequence the 1972 U.K. Regulations have effectively been replaced by the Dangerous Substances and Explosive Atmospheres Regulations (DSEAR 2002) in which the classification system shown in Table 18.6 has been adopted.

Table 18.6 Classification system used in DSEAR 2002 [35]

Classification	Flashpoint	Boiling point
Extremely flammable	<0 °C	<35 °C
Highly flammable	<21 °C	>35 °C
Flammable	≥21 °C and <55 °C	

This is not the place to attempt to describe the finer points of these classification systems (of which there are many), but it is relevant to

[4] Storage: "The Highly Flammable Liquids and Liquefied Petroleum Gases Regulations (HFL/LP-gas)"; Supply: "The Chemical (Hazard Information and Packaging for Supply) Regulations (CHIPS)"; and Transport: "The Carriage of Dangerous Goods and Use of Transportable Pressure Equipment Regulations (CDG)."

Table 18.7 Classification developed by the UN for transport of hazardous chemicals, known as the GHS system [36]

Category	Criteria
1	Flashpoint <23 °C and initial boiling point ≤35 °C
2	Flashpoint <23 °C and initial boiling point >35 °C
3	Flashpoint ≥23 °C and ≤60 °C
4	Flashpoint >60 °C and ≤93 °C

draw the reader's attention to the classification that has recently been adopted for transportation by the United Nations (UN) to facilitate international trade. It defines four categories of liquid, as shown in Table 18.7. This classification is the UN Globally Harmonized System (GHS) and is compared in Fig. 18.4 with the original U.K. (1972 Regulations) and U.S. systems of classification.

Sustained Ignition of Liquids

Provided that the temperature of a liquid is above its firepoint, ignition of the vapors above a pool will be followed by the establishment of a flame at the surface. If the temperature is only slightly above the firepoint, the initial diffusion flame will be weak but will strengthen as it transfers heat to the surface, causing the temperature to rise thus generating an increased rate of supply of fuel vapors. Eventually, a steady-state rate of burning will be achieved, controlled by the heat and mass balance of the surface of the fuel at a temperature close to the normal boiling point. [18] The standard open cup tests are designed to heat the liquid uniformly (bulk heating), but in practice such bulk heating is difficult to achieve unless the liquid is used in some process that requires an elevated temperature. An obvious example is the deep fat fryer and similar devices used in cooking, but oils and other high-flashpoint liquids may be used in heat exchangers and other devices at temperatures above their firepoints. If they are released, then in principle a small ignition source may ignite the vapors and cause a fire. This form of ignition is known as piloted ignition: spontaneous ignition, or "autoignition," is discussed below.

A pool of a high-firepoint liquid at ambient temperature is difficult to ignite by means of a locally applied ignition source, such as a flame. If a flame is applied to the surface (e.g., using a blowtorch), convection currents are established that remove hot liquid from the point of flame application, replacing it with cooler (cold) liquid from below. This process occurs because of a surface tension–driven flow at the surface, first identified by Sirignano and Glassman [37] in their study of flame spread over liquid surfaces. It is a consequence of the fact that surface tension decreases with temperature so that there is a net force at the surface that draws the hotter liquid on the surface at the point of flame impingement toward the cooler regions. The movement at the surface created by this force effectively disperses the heat transferred to the surface and delays ignition. However, if the liquid is absorbed onto a porous substrate—a "wick"—then application of an ignition source in the form of a small flame will quickly raise the temperature of the liquid to its firepoint and burning will be established. There are two factors that contribute to this behavior: first, the liquid is held as a thin film on the material of the wick and surface tension–driven flows are suppressed; and, second, most wick materials have low thermal conductivities and insulate the liquid from heat loss through the wick (by conduction). The best-known example of the effectiveness of a wick in promoting ease of ignition is with the common candle. The wax melts at a relatively low temperature (about 100 °C), but the wick holds the molten wax in place, permitting easy ignition by a match flame. The amount of energy required has never been measured, but in principle it could be calculated assuming the liquid film acts as a thermally thin "solid." However, the heat transfer characteristics of such ignition sources are difficult to quantify and the calculation would be rather academic.

Burgoyne and Roberts [38] studied the ignition of pools of high-flashpoint liquids from flames established on wicks that dipped into the liquid at one end of a 0.4-m-long tank. They

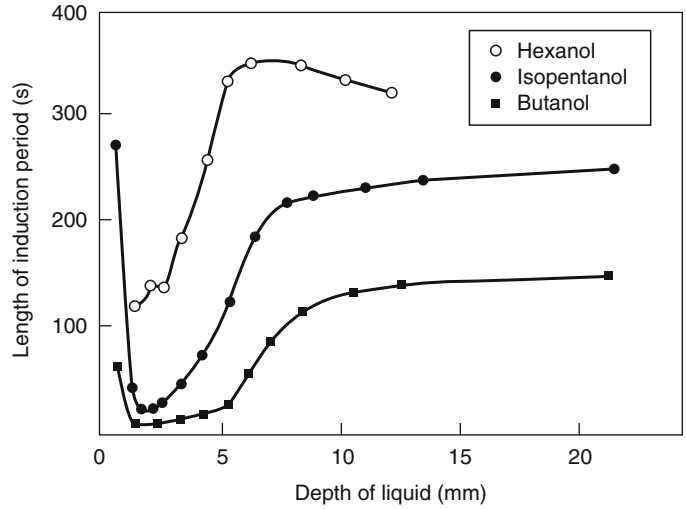

Fig. 18.5 Spread of flame over the surface of a liquid from a flame established on a wick at one end of a pool contained in a long trough [38]. Effect of liquid depth on the duration of the induction period (the time taken for flame to begin to spread over the surface). The open cup flashpoints of hexanol, isopentanol (aka isoamyl alcohol) and butanol, are 74 °C, 46 °C and 43 °C, respectively. (The firepoints are not available)

found that ignition of the pool would occur after a delay (induction period), the length of which was determined by the depth of the pool. In this case, ignition of the pool comprised gradual heating of the surface layers by heat transfer from the flame on the wick until the firepoint temperature was achieved in the vicinity of the wick, after which the flame would spread over the surface of the pool. Minimum induction periods were observed for layers less than 5 mm, increasing by as much as an order of magnitude as the depth was increased to 8–10 mm, depending on the fuel. As an illustration, Fig. 18.5 shows the results obtained by Burgoyne and Roberts for three alcohols [38]. There appears to have been no further systematic studies of this mode of ignition, but it is reasonable to assume that the time to full ignition of a pool of liquid fuel will depend both on the firepoint of the liquid and the depth of the pool.

It is appropriate to note at this point that high-flashpoint liquids (both "flammable" and "combustible" according to the U.K. classification system as shown in Fig. 18.4) can be ignited very easily if dispersed in air as a spray or mist. This behavior is analogous to a dust explosion, which involves dispersion of fine solid particles in air (see Chap. 70). The concept of flammability limits applies and in all other respects a mist of combustible liquid exhibits the same properties as a flammable vapor-air mixture. Spray ignition is discussed in the review by Aggarwal [39].

Autoignition

If the temperature of a flammable vapor-air mixture is increased sufficiently, it can ignite spontaneously without the introduction of a source of ignition—a "pilot"—such as a flame or spark. The concentration of fuel in air at which the autoignition temperature is a minimum corresponds to the stoichiometric vapor-air mixture, which is known to be the most reactive [24]. Values of the (minimum) autoignition temperatures (AIT) of a large number of liquid fuels (gases and liquids) are given in Table 18.2. These have been obtained in a standard test using the Setchkin apparatus [40, 41]. The measurement is made (for liquids) by dropping a small quantity of the liquid (0.1 ml) into a 500 ml spherical flask that has been heated to a carefully controlled temperature [18, 41]. If ignition is not observed within 10 min, the experiment is repeated at higher temperatures. The minimum autoignition temperature (AIT) is determined by repeated experiments, "bracketing" the final value. The values of AIT quoted in Table 18.2 were obtained in this way, but in fact these measurements are highly apparatus dependent. Lower values of AIT are found if the test is carried out in a larger vessel, specifically with a lower surface-to-volume ratio (Table 18.8). This is entirely consistent with the theory of spontaneous combustion (see Chap. 20).

Table 18.8 Comparison of the AIT (°C) of combustible liquids in spherical vessels of different sizes [41]

	Volume of vessel ($m^3 \times 106$)				
	8	35	200	1000	1200
Diethylether	212	197	180	170	160
Kerosene	283	248	233	227	210
Benzene	668	619	579	559	–
Methanol	498	473	441	428	386
n-Pentane	295	273	–	258	–
n-Heptane	255	248	–	223	–

However, the Setchkin test [40] provides data on autoignition under highly idealized conditions in which the liquid vaporizes inside an enclosed volume at a uniform temperature. A relatively uniform fuel/air mixture will be formed that will undergo autoignition if the temperature is high enough. However, this scenario is rarely encountered in practice: more commonly, a liquid fuel may come into contact with a hot surface, such as a bearing assembly or an exhaust manifold, which is exposed to the open atmosphere. The liquid evaporates from the hot surface and the vapor mixes with air at ambient temperature, or at a temperature that is significantly lower than that of the hot surface. Under these circumstances, the minimum AIT derived from the Setchkin test is not relevant as neither the temperature nor the concentration of vapor in air will be uniform. Logically one would expect the autoignition process to take place where the fuel concentration is at or close to stoichiometric (the most reactive mixture) and the local temperature is sufficiently high. To achieve this, the surface temperature will have to be much higher than the quoted literature value of the corresponding AIT.

If the boiling point of the liquid is lower than the AIT (e.g., for *n*-decane, these temperatures are 174 °C and 201 °C, respectively), then spilling the liquid onto a hot, open surface cannot give rise to autoignition because the vapor cannot be at a temperature greater than the boiling point of the liquid. The situation would be different for a combustible liquid with a boiling point much higher than the AIT. Paraffin wax (a solid at room temperature but melting at temperatures less than 100 °C) boils at >370 °C, but the AIT is quoted as 245 °C. In principle, if the conditions are right, the hot vapor produced when paraffin wax is dropped onto a hot surface (>370 °C) may autoignite if a flammable vapor/air mixture is formed near the surface at a sufficiently high temperature (certainly >245 °C). However, the temperature of the surface at which autoignition will occur cannot be defined uniquely. Colwell and Resa [42] studied the autoignition of a range of liquid fuels and engine lubricants when single drops fell on to a flat, heated plate. It was necessary for them to present their results in terms of the probability of ignition, carrying out a large number of tests over a range of plate temperatures. Jet A fuel (similar to kerosene) did not autoignite at temperatures below 510 °C, despite the fact that the AIT (of kerosene) as measured in the Setchkin Test is quoted as 233 °C (see Table 18.8). If the plate temperature was 583 °C, the ignition probability was 50 %, increasing to 100 % above 650 °C. The probability distribution for kerosene and other fuels and lubricants, as determined by Colwell and Resa, is shown in Fig. 18.6. Similar studies, with similar conclusions, have been carried out by Shaw and Weckman [43] for diesel fuels and Davis et al. [44] for high performance fuels used in motorsports. Note that these results are specific to a flat surface, 0.579 m by 0.108 m which is horizontal and unconfined: the distribution will shift to lower temperatures if the surface is confined, or significantly profiled, or to higher temperatures if the surface is vertical or significantly smaller in area.

If a high-boiling point liquid (such as cooking oil) is overheated, autoignition can occur, with flame appearing spontaneously in the plume of hot vapor rising from the surface. As the liquid is already very hot (perhaps close to its boiling point), the fire that follows will immediately be burning at or close to its maximum rate. This type of behavior can be demonstrated using corn oil in a Cleveland open cup and is likely to be the cause of flaming fires in deep fat fryers. This cannot occur with low-boiling liquid fuels such as gasoline (as explained above), which accounts for the fact that if gasoline is spilled

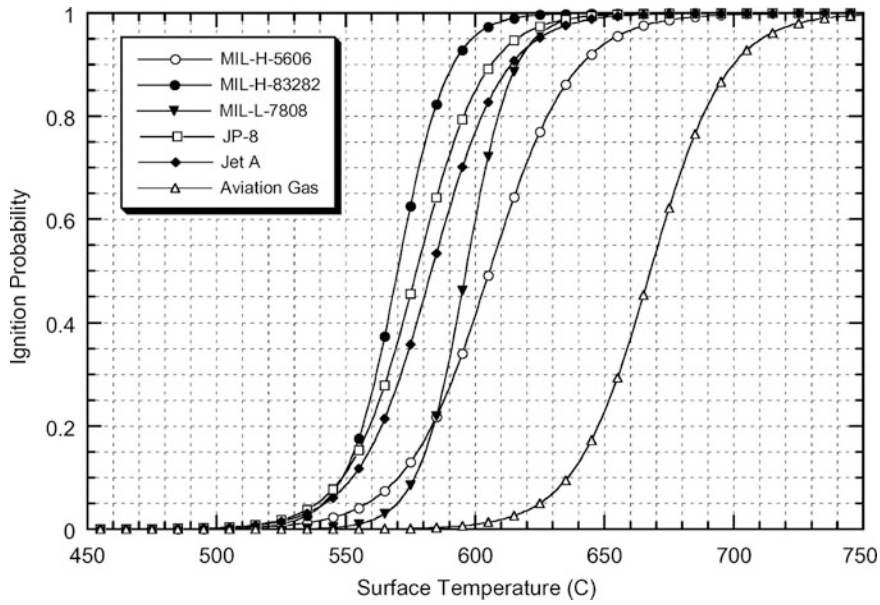

Fig. 18.6 Ignition probability as a function of the surface temperature of a flat plate for aviation fluids [42]. With kind permission from Springer Science+Business Media B.V.

on to a hot exhaust, autoignition will not occur, although ignition will occur if there is a pilot source (e.g. a spark or flame) nearby. On the other hand, heavier fuels and lubricating oils (with high boiling points) may autoignite under these circumstances. There has been much interest in this issue [16].

Ignition of Liquids in Porous Materials

This chapter has so far dealt with the ignition of liquids, leading either to a transient premixed flame or to sustained, flaming combustion. However, under the right conditions, liquid fuels with high boiling points can undergo a form of smoldering combustion, although this form of combustion is normally associated with combustible solids that yield a solid char on heating (see Chap. 19). Clearly, a bulk liquid cannot undergo charring, but if it is dispersed as a thin film within a porous substrate (such as an insulating material) and provided it is of low volatility, it may undergo a slow exothermic reaction that leaves a charlike residue on the fibers of the substrate. The process starts insidiously, by a self-heating process in which the liquid reacts heterogeneously with oxygen from the air. If there is sufficient insulation, the rate of heat released by this process will be greater than the rate at which it can be removed and the temperature will rise. The phenomenon of self-heating in solids is discussed at length in Chap. 20.

The best-known example of self-heating (and spontaneous combustion) of liquids involves the so-called "drying oils," such as linseed oil and tung oil. To quote Bowes [45], "The risk of self-heating and ignition in textile fibres impregnated with readily oxidisable oils has been recognised for a long time," citing a paper by Hapke that refers to such incidents dating back to the eighteenth century. Self-heating of some of the vegetable oils that were used in wool blending in the nineteenth century were known to be the cause of fires and for this reason a test was devised in the United Kingdom to identify the oils that were particularly hazardous (the Mackey Test [45, 46]). The most hazardous are the unsaturated vegetable oils containing a high proportion of carbon–carbon double bonds, which are prone to oxidation. The proportion of these unsaturated linkages can be quantified in terms of the "iodine number,"

which is effectively the percentage of iodine absorption due to the reaction of iodine at the carbon–carbon double bonds. The higher the iodine number, the greater the propensity of the oil to exhibit self-heating when dispersed onto rags, and so on. Typical ranges of values are shown in Table 18.9 (extracted from Bowes [45]).

The most hazardous oils can self-heat when dispersed onto quite small amounts of material—as low as 25 g has been reported. This means that rags used to apply linseed oil or tung oil–based finishes to wood surfaces can self-heat if they are not disposed of properly. The less reactive oils will present problems if dispersed on much larger quantities of porous material, such as bales of wool. Qualitative information on a wide range of liquids may be found in NFPA's *Fire Protection Handbook®* [47], which provides a list of materials that are subject to spontaneous heating. This information has been extracted and is presented in Table 18.10.

Under the right conditions, self-heating of these dispersed liquids will lead to the onset of smoldering combustion. The self-heating process is a slow oxidation involving the carbon–carbon double bonds, resulting in changes to the structure of the absorbed liquid. The chemical mechanism has not been studied in detail, but the consequence appears to be that char is produced on the fibers, which can then oxidize more vigorously, producing a smolder that has the potential to undergo transition to flaming. The smolder will involve the substrate if it is combustible (e.g., cotton rags, wool, etc.), but it is not necessary for the substrate to be combustible, at least for the more reactive oils.

Table 18.9 Ranges of iodine values [45]

Oil	Iodine number	Hazard
Tung, linseed	160–185	Most hazardous
Sunflower seed	127–136	↑
Soya bean	124–133	
Cottonseed	103–111	
Olive oil	80–85	
Coconut oil	8–10	Least hazardous

Another situation in which liquids can initiate self-heating, leading to spontaneous fires, is in the case of oil-soaked lagging [45, 48]. This situation is encountered in industrial plants where thermal insulation is provided around vessels and pipework to conserve heat and maintain process fluids at high temperatures. If the fluid leaks into the insulation, it will be dispersed through the open structure of the insulant. If the leak is too large, then the material will become logged with the fluid and self-heating will not occur. However, if the leak is small, then the fluid will become dispersed onto the fibers of the insulation material, creating a large area of fuel exposed to air within the interstices of the material—an ideal situation to promote self-heating, particularly as both the fluid and the insulation are already hot. The volatility of the fluid is important here: if at the relevant temperature its vapor pressure is too high, then the oxygen concentration in the pores of the insulation may be too low to allow the self-heating process to develop sufficiently.

There have been studies of the propensity of different fluids to undergo self-heating when dispersed on porous insulation materials and an empirical expression has been derived to assess the hazard. This is reported by Lindner and Seibring [49] and developed by Britton [50]. Self-heating may be an issue if

$$\frac{AIT}{AIT - FP} > 1.55 \qquad (18.23)$$

where AIT is the autoignition temperature and FP is the (closed cup) flashpoint. Although it may seem illogical to incorporate AIT (which refers to autoignition in the gas phase) into a correlation that deals with a heterogeneous process, the significance of AIT is that it is a measure of the reactivity of the fuel. FP is also associated with a gas-phase process, but in this expression, it is a surrogate for a measure of the volatility of the fuel as it correlates with the boiling point (see, for example, Babrauskas [16]). A "reactive fuel" (low AIT) of low volatility (high FP) will, therefore, give a high value of AIT/(AIT – FP)—consistent with the above inequality. However, this is at least two steps removed from

Table 18.10 Liquids capable of self-heating when dispersed on fibrous materials [47]

Name	Tendency to spontaneous heating	Usual shipping container or storage method	Precautions	Remarks
Castor oil	Very slight	Metal barrels, metal cans in wooden boxes	[a]	Possible heating of saturated fabrics in badly ventilated piles
Coconut oil	Very slight	Drums, cans, glass	[a]	Only dangerous if fabrics, etc., are impregnated
Cod liver oil	High	Drums, cans, glass	[a]	Impregnated organic materials are extremely dangerous
Corn oil	Moderate	Barrels, tank cars	[a]	Dangerous heating of meals, etc., unlikely unless stored in large piles while hot
Cottonseed oil	Moderate	Barrels, tank cars	[a]	May cause heating of saturated material in badly ventilated piles
Fish oil	High	Barrels, drums	[a]	Impregnated porous or fibrous materials are extremely dangerous. Tendency of various fish oils to heat varies with origin
Lanolin	Negligible	Glass, cans, metal drums, barrels	[a]	Heating possible in contaminated fibrous matter
Lard oil	Slight	Wooden barrels	[a]	Dangerous on fibrous combustible substances
Linseed oil	High	Tank cars, drums, cans, glass	[a]	Rags or fabrics impregnated with oil are extremely dangerous. Avoid piles etc.
				Store in closed containers, preferably metal
Menhaden oil	Moderate to high	Barrels, drums, tank cars	[a]	Dangerous on fibrous product
Mustard oil, black	No	Barrels	[a]	Avoid contamination of fibrous combustible materials
Olive oil	Moderate to low	Tank cars, drums, cans, glass	[a]	Impregnated fibrous materials may heat unless ventilated. Tendency varies with origin of oil
Paint containing drying oil[b]	Moderate	Drums, cans, glass	[a]	Fabrics, rags, etc. impregnated with paints that contain drying oils and dryers and extremely dangerous. Store in closed containers, preferably metal
Palm oil	Low	Wooden barrels	[a]	Impregnated fibrous materials may heat unless ventilated. Tendency varies with origin of oil
Peanut oil	Low	Wooden barrels, tin cans	[a]	Impregnated fibrous materials may heat unless ventilated. Tendency varies with origin of oil
Perilla oil	Moderate to high	Tin cans, barrels	[a]	Impregnated fibrous materials may heat unless ventilated. Tendency varies with origin of oil
Pine oil	Moderate	Glass, drums	[a]	Impregnated fibrous materials may heat unless ventilated. Tendency varies with origin of oil
Red oil	Moderate	Glass bottles, wooden barrels	[a]	Impregnated porous or fibrous materials may heat unless ventilated. Tendency varies with origin of oil
Soybean oil	Moderate	Tin cans, barrels, tank cars	[a]	Impregnated fibrous materials may heat unless well ventilated
Tung oil	Moderate	Tin cans, barrels, tank cars	[a]	Impregnated fibrous materials may heat unless well ventilated. Tendency varies with origin of oil
Whale oil	Moderate	Barrels and tank cars	[a]	Impregnated fibrous materials may heat unless well ventilated. Tendency varies with origin of oil

[a]In every case, the recommended precaution to prevent spontaneous heating is to "avoid contact of leakage from containers with rags, cotton, or other fibrous combustible materials"

[b]This is a well-known hazard in the trade. Impregnated rags are laid out flat to dry. Self-heating will only occur if the rags are left in a crumpled state, providing insulation for the interior

understanding the process involved. The theory of self-heating is described in Chap. 20, but it is only recently that the parameters relevant to understanding lagging fires have been examined in detail [51].

Summary

Flammable and combustible liquids present a range of fire hazards in our everyday lives, whether it be in industry, commerce, or the home. In this chapter, an attempt has been made to outline the fundamental parameters that determine the flammability of liquids, bearing in mind that the hazard may present itself in a number of ways: as an unconfined pool of liquid, as a dispersion of droplets, or as liquid absorbed on a porous substrate. The simplest way of classifying the flammability of a liquid is in terms of its flashpoint, the lowest temperature at which the saturated vapor pressure of the liquid corresponds to the lower flammability limit of the vapor in air at normal atmospheric pressure. The classification schemes used in the United States and the United Kingdom are based simply on the flashpoint, but it is important to recognize that the flashpoint temperature decreases with atmospheric pressure, while the actual flashpoint is not relevant if the liquid is presented to an ignition source as a mist or spray. Indeed, liquids with flashpoints above 300 °C may be ignited by a small flame or a spark if they are dispersed in droplet form.

A distinction must be made between flashpoint, as defined above, and firepoint. The latter refers to the lowest temperature at which a liquid will continue to burn following ignition of the vapors by a pilot ignition source. It is higher than the flashpoint, generally by 10–20 K. Values of autoignition temperature (AIT) are quoted in the literature, but these are not related to either the flashpoint or the firepoint. The AIT represents the lowest temperature at which flame develops spontaneously in a uniformly heated closed vessel into which a small sample of liquid is introduced. This idealized configuration must be taken into account when "autoignition" of liquids in practical situations is considered (e.g., spilling gasoline onto a hot exhaust).

If a combustible liquid is absorbed into a porous medium, such as a rag or the insulation around a hot pipe, then it may undergo a self-heating process leading initially to a smoldering-type reaction. Reactive drying oils such as linseed will undergo this process at ambient temperatures and can lead to flaming combustion under suitable conditions. Similarly, hot process fluid contaminating the insulation around pipework in industrial plants can lead to "lagging fires," which are difficult to control. The hazard associated with liquids under these conditions is poorly understood, which makes awareness of the problem even more important.

References

1. D.R. Lide (ed.), *Handbook of Chemistry and Physics,* 80th ed., CRC, Boca Raton, FL (2001/2002).
2. W.J. Moore, *Physical Chemistry,* 5th ed., Longman, London, UK (1972).
3. P.W. Atkins and de Paula, *Physical Chemistry,* 8th ed., Oxford University Press, Oxford, UK (2006).
4. S.H. Wade, "Evaporation of Liquids in Currents of Air," in *Proceedings of the Institution of Chemical Engineers,* Institution of Chemical Engineers, Rugby, UK (Jan. 1942).
5. V.J. Clancey, "The Evaporation and Dispersion of Flammable Liquid Spillages," in *Proceedings of the Symposium on Chemical Process Hazards,* University of Manchester, Institution of Chemical Engineers, Rugby, UK (1974).
6. A.M. Thyer, "A Review of Data on Spreading and Vaporization of Cryogenic Liquids Spills," *Journal of Hazardous Materials,* 99, pp. 31–40 (2003).
7. Center for Chemical Process Safety, "Guidelines for Evaluating the Characteristics of Vapor Cloud Explosions, Flash Fires and BLEVEs," AIChE, New York (1994).
8. T. Abbassi and S.A. Abbassi, "The Boiling Liquid Expanding Vapor Explosion (BLEVE): Mechanism, Consequence, Assessment, Management," *Journal of Hazardous Materials,* 141, pp. 489–519 (2007).
9. A.M. Kanury, "Ignition of Liquid Fuels," in *SFPE Handbook,* 3rd ed., National Fire Protection Association, Quincy, MA, pp. 2-188–2-199 (2002).
10. E.W. Washburn (ed.), *International Critical Tables of Numerical Data: Physics, Chemistry and Technology,* McGraw-Hill, New York (1927).
11. Factory Mutual System, *Handbook of Industrial Loss Prevention,* Factory Mutual Research Corporation, Norwood, MA (1968).

12. C.L. Yaws (ed.), *Chemical Properties Handbook: Physical, Thermodynamic, Environmental, Transport, Safety and Health Related Properties for Organic and Inorganic Chemicals*. McGraw Hill, New York (1999).
13. R.C. Weast (ed.), *Handbook of Chemistry and Physics*, 53rd ed., CRC, Cleveland, OH (1972/1973).
14. NFPA 30, *Flammable and Combustible Liquids Code,* National Fire Protection Association, Quincy, MA (2008).
15. P.F. Thorne, Fire Research Note 1022, Fire Research Station, Borehamwood, UK; P.F. Thorne, "Flashpoints of Mixtures of Flammable and Non-Flammable Liquids," *Fire and Materials,* 1, pp. 134–140 (1976).
16. V. Babrauskas, *Ignition Handbook,* Fire Science Publishers, Issaquah, WA (2003).
17. B.P. Mullins and S.S. Penner, *Explosions, Detonations, Flammability and Ignition,* Pergamon Press, London, UK (1959).
18. D. Drysdale, *Introduction to Fire Dynamics,* 3rd ed., John Wiley and Sons, New York (2011).
19. NFPA, *Fire Protection Handbook,* 20th ed., National Fire Protection Association, Quincy, MA, pp. 21-135–21-149 (2008).
20. American Society for Testing and Materials, "Standard Test Method for Flashpoint by the Pensky-Martens Closed Tester," ASTM D-93-94, ASTM, West Conshohocken, PA (1994).
21. American Society for Testing and Materials, "Standard Test Method for Flashpoint by the Tag Closed Tester," ASTM D-56-87, ASTM, West Conshohocken, PA (1987).
22. American Society for Testing and Materials, "Standard Test Method for Flashpoint and Firepoint by the Cleveland Open Cup," ASTM D-92-90, ASTM, West Conshohocken, PA (1990).
23. American Society for Testing and Materials, "Standard Test Method for Flashpoint and Firepoint of Liquids by the Tag Open Cup Apparatus," ASTM D-1310-86, ASTM, West Conshohocken, PA (1986).
24. M.G. Zabetakis, "Flammability Characteristics of Combustible Gases and Vapours," *Bulletin 627,* U.S. Bureau of Mines, Washington, DC (1961).
25. J.J. James, "A Method for Flammability Testing of Low Flammability Liquids," MSc Thesis, University of Manchester, Manchester, UK (1991).
26. B.J. Tyler, personal communication.
27. K. Hasegawa and K. Kashuki, "A Method for Measuring the Upper Flashpoint—Practical Method Using the Setaflash Closed Cup Apparatus," Report of the Fire Research Institute No. 71, Fire Research Institute, Tokyo, Japan (1991).
28. H. Mundwiler, "Brand im Hotel International Zürich, 16. Februar 1988"/"Incendie à l'Hôtel International, Zurich, 16 février 1988"; Schweizerische Feuerwehrzeitung/*Journal des Sapeurs-Pompiers Suisses*/*Giornale dei Pompieri Svizzeri,* 116, 3, pp. 144–162 (Mar. 1990).
29. I. Glassman and F.L. Dryer, "Flame Spreading Across Liquid Fuels," *Fire Safety Journal,* 3, pp. 123–138 (1980/1981).
30. A.F. Roberts and B.W. Quince, "A Limiting Condition for the Burning of Flammable Liquids," *Combustion and Flame,* 20, pp. 245–251 (1973).
31. D.J. Rasbash, "Relevance of Firepoint Theory to the Assessment of Fire Behavior of Combustible Materials," *International Symposium on Combustible Materials,* Edinburgh University, Edinburgh, Scotland (1974).
32. C.L. Beyler, "A Unified Model of Fire Suppression," *Journal of Fire Protection Engineering,* 4, pp. 5–16 (1992).
33. D.B. Spalding, "Some Fundamentals of Combustion," Butterworths, London, UK (1957).
34. Highly Flammable Liquids and Liquefied Petroleum Gases Regulations, Her Majesty's Stationery Office, London, UK (1972).
35. Chemicals (Hazard Information and Packaging for Supply): Regulations 2002, HSE Booklet L131, Health and Safety Executive, London, UK (2002).
36. *Globally Harmonised System of Classification and Labelling of Chemicals (GHS),* 1st rev. ed., UN Publication ST/SG/AC. 10/30/Rev.1, United Nations, Geneva, Switzerland (2005).
37. W.A. Sirignano and I. Glassman, "Flame Spreading Above Liquid Fuels: Surface Temperature Driven Flows," *Combustion Science and Technology,* 1, pp. 307–312 (1970).
38. J.H. Burgoyne and A.F. Roberts, "Spread of Flame Across a Liquid Surface Part 2," *Proceedings of the Royal Society,* London, A308, pp. 55–68 (1968).
39. S.K. Aggarwal, "A Review of Spray Ignition Phenomena: Present Status and Future Research," *Progress in Energy and Combustion Science,* 24, pp. 565–600 (1998).
40. American Society for Testing and Materials, "Standard Test Method for Autoignition Temperature of Liquid Chemicals," ASTME, 659–78 (Reapproved 2000) (1978).
41. N.P. Setchkin, "Self-Ignition Temperatures of Combustible Liquids," *Journal of Research National Bureau of Standards,* 53, pp. 49–66 (1954).
42. J.D. Colwell and A. Reza,. "Hot surface ignition of automotive and aviation fluids" *Fire Technology* **41** 105–123. (2005).
43. A Shaw and E Weckman, "Evaluation of the ignition of diesel fuels on hot surfaces" *Fire Technology* **46** 407– (2010).
44. S. Davis, S Kelly and V Somandepalli, "Hot surface ignition of performance fuels" *Fire Technology* **46** 363–374 (2010).
45. P.C. Bowes, "Self-Heating: Evaluating and Controlling the Hazards," HMSO, London (1984).
46. W. McD Mackey, *Journal of the Society of Chemical Industry,* London, 14, p. 940 (1895); 15, p. 90 (1896).
47. National Fire Protection Association, *Fire Protection Handbook,* 20th ed., Table 6.17.11 "Materials Subject

to Spontaneous Heating," National Fire Protection Association, Quincy, MA (2008).
48. P.C. Bowes, "Fires in Oil-Soaked Lagging," BRE Current Paper, CP 35/74, Fire Research Station, Borehamwood, UK (1974).
49. H. Lindner and H. Seibring, "Self-Ignition of Organic Substances in Lagging Material," *Chemie Ingenieur Technik,* 39, p. 667 (1967).
50. L.G. Britton, "Spontaneous Insulation Fires," *AIChE Loss Prevention Symposium,* San Diego, CA (August 19–22, 1990).
51. A.C. McIntosh, M. Bains, W. Crocombe, and J.F. Griffiths, "Autoignition of Combustible Fluids in Porous Insulating Materials," *Combustion and Flame,* 99, pp. 541–550 (1994).

D.D. Drysdale is professor emeritus in the BRE Centre for Fire Safety Engineering, School of Engineering, at the University of Edinburgh, Scotland. His research interests lie in fire science, fire dynamics, and the fire behavior of combustible materials.

Smoldering Combustion

19

Guillermo Rein

Introduction

Smoldering combustion is the slow, low temperature, flameless burning of porous fuels and the most persistent type of combustion phenomena. The heat is released when oxygen directly attacks the surface of a solid fuel [1]. It is especially common in porous fuels which form a char on heating [2], like cellulosic insulation, polyurethane foam or peat. Smoldering combustion is among the leading causes of residential fires [3, 4], and it is a source of safety concerns in industrial premises as well as in commercial and space flights. Smoldering is also the dominant combustion phenomena in wildfires of natural deposits of peat and coal which are the largest and longest burning fires on Earth [5]. These fires contribute considerably to global greenhouse gas emissions, and result in widespread destruction of ecosystems and the waste of natural resources.

Smoldering constitutes a hazard in the built environment, as emphasized in this chapter, for two main reasons. First, it typically yields a higher conversion of the fuel to toxic compounds than flaming, though this occurs more slowly. Second, smoldering provides a path to a flaming fire via heat sources too weak to directly ignite a flame. A burning cigarette or charcoal embers are familiar examples of smoldering combustion. The latter is illustrated in Fig. 19.1 (left). A less familiar case but more common fire threat is the burning of foam in upholstery as seen in Fig. 19.1 (right). The smouldering combustion of polymer foams and other building insulation materials is gaining importance because of their extensive use by the construction industry which is seeking higher energy efficiency.

Despite its broad implications to safety and the environment, our current understanding of smoldering combustion is limited, and considerably less advanced than flaming combustion. This is due to its complexity and coupling of transport and thermochemical processes inside a reactive porous media, The most comprehensive reviews of smouldering combustion in the literature include Ohlemiller [1], T'ien et al. [6], Ohlemiller [7], Babrauskas [8], Rein [9] and Drysdale [2].

Smoldering vs. Flaming Combustion

The core of any combustion process is a global exothermic reaction that results in the release of heat, and both gaseous and solid products. Whether smoldering or flaming will be the dominant mode is dictated by which chemical species is oxidized. If the oxidation takes place in the solid phase, smouldering is dominant; if the oxidation takes place in the gas phase then flaming dominates.

G. Rein (✉)
Department of Mechanical Engineering, Imperial College London, London, SW72AZ, UK

M.J. Hurley (ed.), *SFPE Handbook of Fire Protection Engineering*,
DOI 10.1007/978-1-4939-2565-0_19, © Society of Fire Protection Engineers 2016

In general, the combustion of a solid fuel involves countless elementary chemical reactions, but the global reaction, in its simplest form, can be approximated by two lumped chemical pathways: pyrolysis (Equation 19.1) followed by oxidation (Equations 19.2a or 19.2b).

Pyrolysis:

$$\text{Fuel (solid)} + \text{Heat} \rightarrow \text{Pyrolyzate (gas)} + \text{Char (solid)} + \text{Ash (solid)} \tag{19.1}$$

Heterogeneous oxidation:

$$\text{Char (solid)} + \text{O}_2\text{ (gas)} \rightarrow \text{Heat} + \text{CO}_2 + \text{H}_2\text{O} + \text{other gases} + \text{Ash (solid)} \tag{19.2a}$$

Gas-phase oxidation:

$$\text{Pyrolyzate (gas)} + \text{O}_2\text{ (gas)} \rightarrow \text{Heat} + \text{CO}_2 + \text{H}_2\text{O} + \text{other gases} \tag{19.2b}$$

Pyrolysis[1] results in gaseous and solid products. Of these, both the pyrolysate and the char are susceptible to subsequent oxidation.[2] Char oxidation (Equation 19.2a) is a heterogeneous reaction (involving solid and gaseous species) and takes place on the char produced by the pyrolysis reaction and leads to smoldering combustion. Oxidation of the pyrolysate (Equation 19.2b) is airborne and takes place in the gas phase, which is a homogenous reaction (involving only gaseous species) and leads to flaming combustion.

Char is a carbon-rich porous material, also called charcoal or black carbon, with a high surface-to-volume ratio and a high heat of reaction. The attack of oxygen is facilitated by metal and mineral impurities which can catalyze the oxidation process. The other important solid species is ash, a mineral-rich residue of negligible reactivity that is left after the fire.

[1] Pyrolysis in this context is the chemical decomposition of a solid material solely by heating. It does not involve oxidation reactions and it is endothermic. It involves the irreversible and simultaneous change of chemical composition and physical phase.

[2] Oxidation in this context is the reaction of a species with the oxygen in the air. It is an exothermic reaction.

General Characteristics of Smoldering Combustion

The characteristic temperature, spread rate and power of smoldering combustion are low compared to flaming combustion. Typical peak temperatures for smoldering are in the range from 450 °C to 700 °C, although very energetic and dense fuels such as coal can reach peaks at around 1000 °C. The effective heat of combustion taking into account the combustion efficiency is in the range from 6 to 12 kJ/g. These are much lower compared to typical values of around 1500 °C and 16–30 kJ/g respectively for flaming combustion. The heat release rate per unit area of burning front is low and ranges from 10 to 30 kW/m^2 [10]. Because of these characteristics and despite the considerable variation in the chemical nature of smoldering fuels, smoldering spreads in a creeping fashion, typically around 1 mm/min, which is two orders of magnitude slower than flame spread.

As we will see in the following sections, smoldering combustion can be initiated with weaker ignition sources and is more difficult to suppress than flaming combustion. This makes smoldering the most persistent combustion mode. In the presence of a large quantity of fuel, a smoldering fire can burn for very long periods (days, weeks, months) despite fire-fighting attempts, extensive rain or weather changes. Indeed, the longest-burning urban fire in modern history occurred

Fig. 19.1 (*Left*) Smoldering embers and ash residue (Photo by J. B. Nielsen, Public domain, via Wikimedia Commons). (*Right*) Cross-section of a polyurethane slab 125 mm in diameter smoldered in microgravity conditions (Photo by NASA)

after the collapse of the Word Trade Center towers on Sept. 11, 2001. The immense piles of debris smoldered for 3–5 months in the middle of one of the most heavily populated cities of the world, resisting all suppression attempts until the slow removal of debris cleared the pile [11]. The oldest continuously burning fire on Earth is *The Burning Mountain* in New South Wales, Australia, a large coal seam which has been smoldering for more than 6000 years [12].

Many materials can sustain a smoldering fire. These include synthetic fuels such as charring polymers, polyurethane foam, cellulosic insulation, particleboard and sawdust, and natural fuels like wood, peat, forest litter, and coal. In chemical terms, most smoldering fuels form a char on heating. In physical terms, smoldering fuels consist of a permeable medium formed by grains, fibers or some other porous matrix. This aggregate nature provides a large surface area per unit volume, which facilitates the heterogeneous reaction with oxygen, and permits transport of oxygen through the fuel bed [1]. For example, synthetic foams prone to charring, like polyurethane foam (see Fig. 19.1, right), are highly susceptible to smoldering combustion. Liquid fuels soaked in an inert porous matrix can also sustain smoldering fires, examples include lagging fires (Drysdale [2], Chap. 18) and soil remediation based on the assisted burning of liquid contaminants [13].

For most smoldering fuels under typical conditions, the two mechanisms controlling the rate of spread are the oxygen supply and the heat transfer [1]. Both mechanisms are dictated by heat and mass transfer in porous media. At the micro scale, smoldering takes place on the surface of the pores of a solid fuel, while at the macro scale, it is a bulk phenomenon affecting the fuel bed at large. The fire can penetrate deep into the bed of fuel if oxygen can be transported from a free surface (open atmosphere, crack or channel). Depending on the depth of the fire, the importance of the heat and mass transfer mechanisms vary. The rate of oxygen supply to the reaction zone enhances the spread. But this oxygen supply decreases with depth inside a fuel bed. The rate of heat loss to the environment from the reaction zone hinders the spread. But this heat loss decreases with depth inside a fuel bed. Thus, depending on the fuel bed characteristics and wind conditions, there are minimum and maximum depths between which smoldering can spread, and an optimal depth at which burning is fastest. The concept of an optimal depth is not sufficiently studied yet and could vary for different systems in the scale from cm to m.

Each location of a burning fuel bed sees the successive arrival of four distinct thermal and chemical subfronts that form the structure of a smoldering fire. These are the preheating, drying, pyrolysis and oxidation subfronts [1, 14].

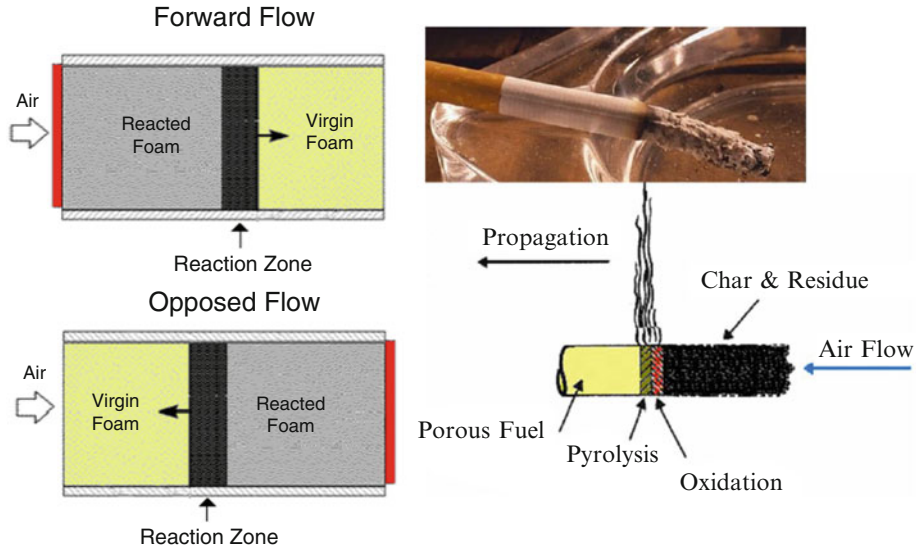

Fig. 19.2 (*Left*) Forward and opposed configurations of one-dimensional smoldering propagation inside a slab of porous fuel. (*Right*) Structure of a one-dimensional front in forward smoldering and approximate correspondence with a burning cigarette (By G. Rein, CC BY license)

The endothermic preheating, drying and pyrolysis subfronts store or consume thermal energy and move ahead of the oxidation subfront The heat that sustains the spread is released at the oxidation subfront, and from there it is transferred via a combination of conduction, convection and radiation to the other subfronts. The preheating subfront does not involve chemical reactions or gas emissions in any significant quantity. The drying subfront follows with evaporation becoming significant above 50 °C, emitting water vapour and leaving behind dry fuel. Drying is most significant for fuels with substantial moisture contents (>10 % in dry weight), so it is negligible in most residential fire scenarios but important in the natural environment (see section "Smoldering Wildland Fires"). The pyrolysis subfront (Equation 19.1) follows the preheating and drying when the fuel temperature increases above a certain threshold. This threshold[3] is approximately at 200 °C for polyurethane, and to 250 °C for cellulose [15]; subsequent heating above this temperature increases the pyrolysis rate and char production. The oxidation subfront consumes char and oxygen, releasing heat. It involves the oxidation of the fuel and the char, but char oxidation (Equation 19.2a) is much more exothermic. The oxidation and pyrolysis subfronts may overlap in space. The extent of this overlap depends on the propagation conditions [16] and is discussed in the section "Smoldering Kinetics".

It is convenient to characterize one-dimensional smoldering by its direction of propagation relative to the direction of the oxygen supply. Two one-dimensional modes exist. Forward propagation occurs when the oxygen supply is moving in the direction of the smolder front. Opposed propagation (also called reverse) occurs when the oxygen supply is moving opposite to the smolder front. These are illustrated in Fig. 19.2. The most familiar example of forward propagation is a cigarette, as seen in Fig. 19.2 (right). Although one-dimensional spread is an idealized situation, it can occasionally be found in fires, but in general, real smoldering fires are multidimensional and cannot be classified into a single mode.

[3] The onset of pyrolysis or oxidation does not occur at one fixed temperature but it is known to be a function of the heating rate and start over a range of temperatures; higher onset temperatures are observed for higher heating rates. See Rein et al. [15] and the section "Smoldering Kinetics" for evidence of this.

In forward propagation, the pyrolysis subfront is located at the leading edge of the front, and the oxidation subfront at the trailing edge, where oxygen is drawn (see Fig. 19.2, right). The oxygen supply flows first through the char where it is consumed. Then the hot, oxygen-depleted gases of combustion flow through the virgin fuel. This convective transport results in enhanced drying and preheating, but it also results in water condensation on the virgin fuel as the combustion gases cool down.

In opposed propagation, the oxygen supply flows first through the virgin fuel, and through the preheating and evaporation subfronts before reaching the char where the oxidation subfront is located. Then the hot, oxygen-depleted gases of combustion flow through the char and ash residues. This means that heat is transferred by convection in the opposite direction to the virgin fuel, reducing the extend of the drying and preheating, which in turn results in a weaker smoldering process. Consequently, forward smolder is faster than opposed under the same fuel and oxidizer supply, and allows for more complete combustion of the fuel [17]. In opposed propagation, the pyrolysis and oxidation subfronts overlap on top of each other from the leading edge to the trailing edge [16].

Ignition

The process of smoldering ignition requires the supply of heat, and is governed by heat transfer and fuel kinetics, with the oxygen supply rate playing a secondary role. Above a critical threshold of heat supply, the temperature increase initiates endothermic pyrolysis, which is followed by the onset of oxidation. When the heat released by oxidation is high enough to balance the heat required for the endothermic processes (heat losses, pyrolysis, drying and preheating of fuel), propagation occurs and the reaction might become self-sustaining (only then oxygen supply rate will play an important role). This section discusses four types of ignition sources: radiant, conductive, ember and self-heating. For all four, it is proven that the critical energy condition needed for smoldering is significantly lesser than that for flaming. The results discussed here are on individual fuel samples. But note that a particularly important smoldering scenario, that of upholstery and bedding fires, is a composite problem with the ignition propensity of both the fabric and the substrate contributing to the overall behavior [18].

Radiant Ignition

The effects of exposing polyurethane foam to an external radiant heat flux of increasing magnitude is illustrated in Fig. 19.3. The heat flux needed to initiate smoldering is significantly lower than that for flaming (see Table 19.1). For instance, the critical radiation heat flux for smolder ignition of polyurethane foam is

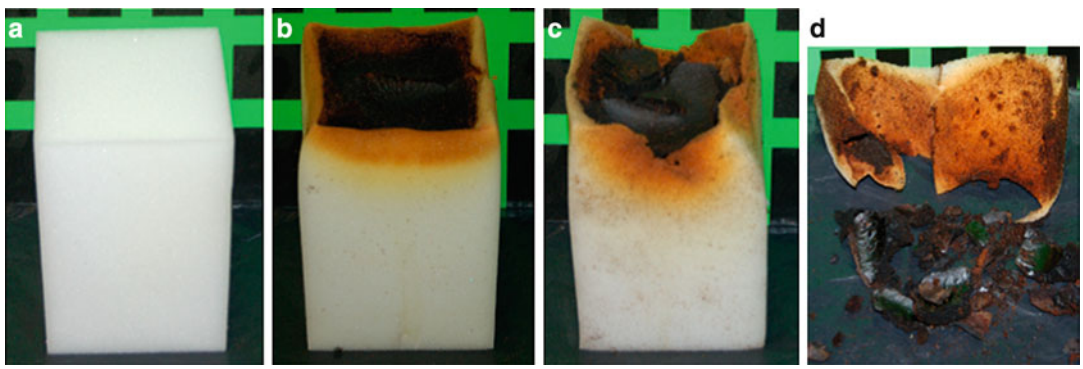

Fig. 19.3 Images of polyurethane foam samples exposed to increasing levels of radiation (from *left* to *right*): (**a**) virgin foam (not exposed to radiation), (**b**) charred foam in which a smoldering front did not propagate, (**c**) sample in which smoldering propagated, and (**d**) sample which underwent flaming ignition (By R. Hadden [19], CC BY license)

7 kW/m^2, while for spontaneous flaming is 30 kW/m^2 [19]. For piloted flaming ignition, the critical level is 13 kW/m^2 (Chap. 36).

It has been shown that the onset of smoldering involves a range of threshold temperatures. A single threshold temperature is not a valid criterion for ignition but it is part of a multi-criteria signature [20]. Several experimental studies have found that the minimum temperature measured during ignition of polyurethane foam is in range from 300 °C to 450 °C [19–21]. This is much lower than the threshold surface temperature of 600 °C required for spontaneous flaming ignition of the same material [19]. Figure 19.4 (left) shows the experimental data on the peak temperature reached inside a slab of polyurethane foam for the cases of no ignition, smoldering or flaming ignition. The same experiments (see Fig. 19.4 (right)) also show that the time to smoldering ignition by radiation depends on the heat flux level and ranges from 1 to 20 min for a heat flux of 45–7 kW/m^2 respectively. Flaming ignition was observed for heat fluxes above 30kW/m^2 and was fast, less than 1 min. The dependence of the time to ignition with radiant heat flux shown in Fig. 19.4 (right) resembles a an inverse square-root law with the incident heat flux. This suggests that smoldering ignition can be explained in terms of heat transfer, in the same way that a an inverse square-root law explains the flaming ignition of a thermally thick fuel (Chap. 21). This law originates from the time it takes for heat conduction to result in a critical temperature at a key location. For flaming, the key location is the free surface of the fuel, but for smoldering the key location is inside the fuel bed, at a sufficient depth such that an insulating layer of char is formed over the oxidation front [21]. The concept of a critical depth for ignition is not sufficiently studied yet but could be expected to vary for different materials and external conditions in the scale from 1 to 10 cm roughly.

Table 19.1 Critical heat fluxes found experimentally for the ignition of smoldering and spontaneous flaming combustion in samples of different sizes (Data from Hadden et al. [19])

Sample size (mm)	Critical heat flux for smoldering ignition (kW × m^{-2})	Critical heat flux for flaming ignition (kW × m^{-2})
50	18–19	32–45
100	8–9	32–37
140	7–8	30–31

Conductive Ignition

The heat source that can start a smoldering fire with the lowest heat flux is the conductive type.

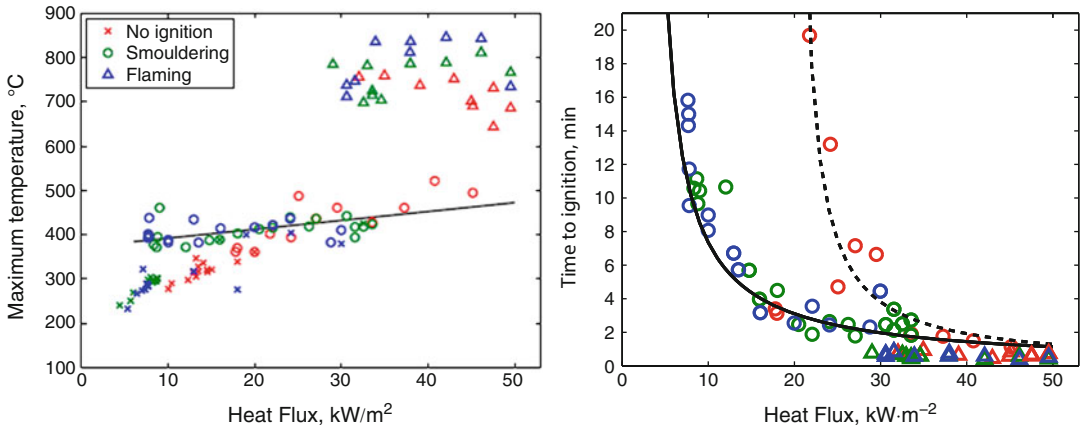

Fig. 19.4 Radiant ignition of smoldering and flaming in polyurethane samples of different sizes in still air. (*Left*) Maximum temperatures observed. (*Right*) Time to ignition. *Red*, *green* and *blue* represent 50, 100 and 140 mm side square samples respectively (Data from Hadden et al. [19])

This scenario occurs when a large and hot object is in direct contact with the fuel bed. Heat is transferred by conduction, but in porous fuels, convection also plays a role. Anthenien and Fernandez-Pello [21] studied the initiation of smoldering using an electric heater in contact with a sample of polyurethane foam under forced airflow. Ignition was reported at heat fluxes as low as 3 kW/m^2 and the relationship between time to ignition and heat flux was shown to follow a an inverse square-root law. Ignition was found to be weakly dependent on the airflow.

Conductive ignition has also been studied on a bed of particles [22]. A series of beds of anthracitic coal particle of uniform diameter ranging from 7 to 45 mm was investigated inside a cubic box (side of 100 mm) with the top side open to the atmosphere and multiple perforations on the other sides. The heat source was an electric wire that delivered 80 W. Figure 19.5 shows that the relationship of the time to ignition with particle diameter has a 'U' shape. It was not possible to ignite a bed which particle diameter was smaller than 7 mm. For very small particle sizes, the bed exhibits poor internal convection which limits the airflow and a long ignition time is required. But as the particle sizes increase, the porosity and the flow permeability of the fuel bed increase and a minimum time to ignition of 130 min (average) is required for a particle diameter of 25 mm. As particles become larger, the inter-particle conduction rate decreases resulting in a longer time to ignition.

Ignition by Embers

In close connection with conductive sources, a fuel bed can also be ignited by hot embers. This is related to ignition by hot works and also to the phenomenon of spotting in wildland fires, when lofted embers land downwind, leading to secondary fires in the wildland or in urban areas remote from the originating flame front. Ignition by embers is a transient phenomenon involving the loss of heat from the ember to the fuel by conduction and convection. Embers can be classified by material (metal or biomass) and thermal state (hot, smoldering or flaming).

Manzello et al. [23] compared the ember ignition of three fuel types and found that a bed of shredded paper was much more prone to smoldering than pine needles or mulch. The experimental study of Hadden et al. [24] found a relationship between ember size and the critical initial temperature required for ignition of a bed of cellulose powder. They used steel spheres with diameters in the range 0.8–19 mm at initial temperatures between 500°C and 1300°C. Smaller embers require higher temperatures to initiate combustion. Their data shows two distinct boundaries as the ember temperature

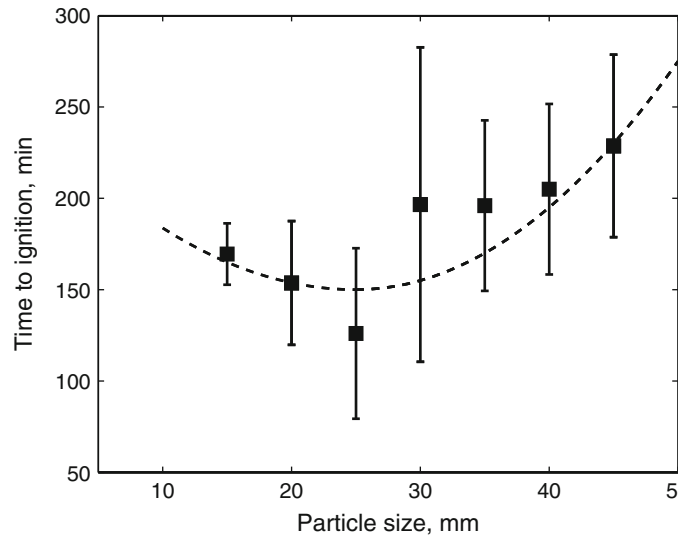

Fig. 19.5 Experimentally observed relationship between time to ignition and particle size in a bed of anthracite coal (Data from Hadden and Rein [22])

increases, one separating no-ignition from smoldering ignition, and the other from smoldering to flaming ignitions. The minimum ember temperature at which smoldering could be initiated was 550 °C, and the minimum temperature for flaming ignition occurred at 650 °C. Krause and Schmidt [25] also observed a decrease of the critical temperature with ember size for a series of organic powder samples (cork, beech and cocoa), and reported a minimum temperatures of 400 °C for smoldering ignition.

Self-Heating Ignition

Self-heating of a solid fuel can initiate smoldering fire deep within a pile of fuel without any external source, even at ambient temperatures. Self-heating refers to the tendency of certain porous solid fuels to undergo spontaneous exothermic reactions in oxidative atmospheres at low temperatures ([2, 26], Chap. 20). It is a well-known problem in the store of large amounts of carbon-rich materials (e.g., waste, coal heaps, organic powders) and in the process industries. The process is as follows: initially, the pile of the material releases small amounts of heat by very slow oxidation at ambient temperature. Somewhere near the center of the pile, where the fuel is most insulated, the heat accumulates in the long term and results in a sustained increase of the local temperature, which in turn accelerates the oxidation rate. Large pile sizes and poor ventilation conditions facilitate the buildup of heat. The process self-accelerates for some time (hours, days or weeks) and above a certain threshold temperature it leads to a thermal runaway. This results in a smoldering fire that can spread from the inside to the outside, and may undergo transition to flaming at a later stage when it reaches the free surface (discussed in section "Transition to Flaming").

Size Effects and Ignition

There is a minimum size below which a fuel sample will not undergo ignition. This is determined by the balance between the rates of heat generation and heat loss from the system. The rate of heat loss scales with the surface area, and the rate of heat generation scales with the volume. Consequently, as the size of a sample decreases, the surface -to-volume ratio[4] of the smoldering front increases. Below a certain size, heat losses overwhelm heat generation and ignition will not occur.

Palmer [27] found experimentally that the minimum thickness for smoldering of horizontal layers of sawdust was around 10 mm. Ohlemiller and Rogers [28] found the minimum thickness for cellulosic insulation to be 35 mm. A more recent experimental investigation of the effect of sample size [19] is reported in Table 19.1 and Fig. 19.4. Both the critical heat fluxes for smoldering and flaming ignition increase with decreasing sample size, with smoldering ignition being significantly more sensitive to the sample size than flaming. Krause and Schmidt [25] studied the ignition of organic dust samples by embers, and found that the larger the samples, the lower the critical ember temperature. The fact that large samples are easier to ignite than small samples has implications for testing standards and the translation of results from small-scale testing to real scale.

The process of ignition is related to self-sustained propagation (as discussed in the section "Smoldering Spread") which allows an approximate analytical treatment. The critical size L_c for self-sustained propagation in a prismatic sample of square cross-section can be estimated by Equation 19.3 provided by Rein [9] based on the energy balance by Torero and Fernandez-Pello [14] and Bar-Ilan et al. [29, 30].

$$L_c = \frac{4\delta U(T_s - T_0)}{Q_s \dot{m}''_{O_2}} \qquad (19.3)$$

where δ is the smolder-front thickness perpendicular to the propagation direction, T_s is the peak temperature, and Q_s is the heat of smoldering, which all depend on the fuel. The overall heat loss coefficient U, the ambient temperature T_0 and

[4] The surface-to-volume ratio of a sample is inversely proportional to its characteristic length (e.g., thickness for a very wide layer, diameter for a cylinder, side length for a prism or diameter for a sphere).

the supply of oxidizer $\dot{m}''_{O_2}$ depend on the geometry and external conditions. For polyurethane foam, Equation 19.3 says the critical size is around 160 mm [19]. If a sample is below the critical size L_c, sustained smoldering will not be achieved. Smoldering will only spread if the heat losses are reduced or the rate of heat generation is increased, or both. The former would involve insulating the reaction front or supplying additional heat from an external source, and the latter would involve increasing the supply of oxidizer.

Smoldering Spread

The spread of smoldering is controlled by the oxygen supply and heat transfer [1]. Conditions sufficient to yield smolder initiation, especially near an external heat source, might not be sufficient for self-sustained spread away from the ignition region. If the external heat supply continues, assisted propagation is possible. Otherwise, once the external heat supply ceases, smoldering reaction will be self-sustained or lead to extinction.

Experimental and modeling work has demonstrated that the smolder spread rate is linearly dependent on the total air supply rate to the smoldering front [1, 29, 30]. Some of these results are presented in Fig. 19.6. Torero and Fernandez-Pello [14] reported than this linear increase breaks down for opposed propagation at high airflows and stars decreasing (at ~3 mm/s for polyurethane foam slabs of 150 mm square cross section). In general, air is transported to the reaction front by convection and diffusion. Convection can be natural (buoyant) or forced. In the absence of forced flow, buoyancy tends to dominate over diffusion in regions of lesser flow resistance, for example near the free surface or in a bed of large particles. The diffusion flux is dominant when deep layers of a pile of fine particles is ignited [27]. Forced convection in smoldering fires usually takes the form of an air current flowing through the fuel bed or over the free surface of the bed. Forced convection directly flowing through the bed of the fuel is often used in laboratory studies (e.g., see Fig. 19.6). The advantage is that it provides controllable conditions to investigate the phenomena also deeper into the bed. These studies have found a critical air supply rate required for self-sustaining propagation (around 0.6 g/m^{2}s of oxygen flow for opposed mode in a 120 mm diameter slab of polyurethane foam [30]). This critical supply

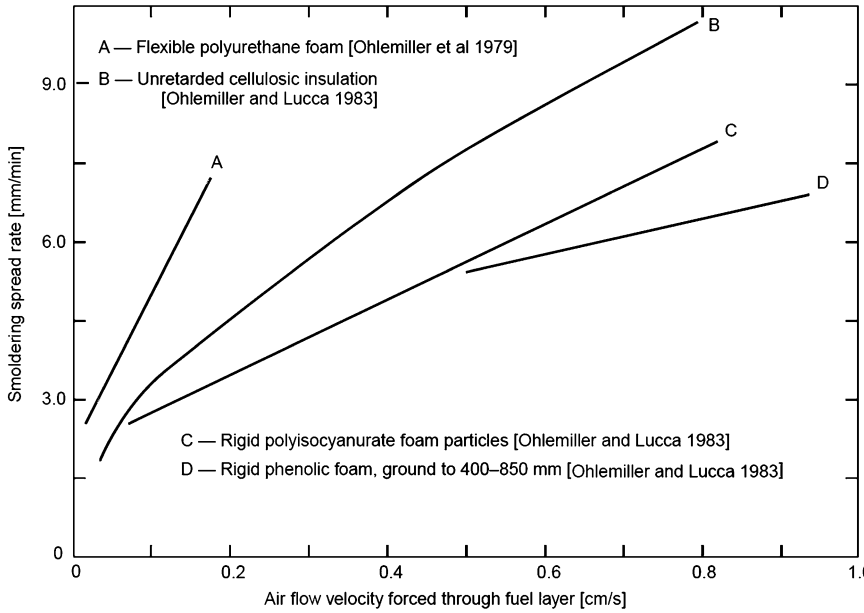

Fig. 19.6 Spread rate of smoldering assisted by airflow forced through the bed in opposed mode for a variety of materials (After Ohlemiller [7])

rate is known to be a function of the heat losses. For example, microgravity experiments on the same polyurethane samples [30] have shown that the removal of lateral heat losses by natural convection allows self-sustained propagation at significantly lower oxygen supplies (0.3 g/m^{2}s).

When a bed of fuel is ignited locally, in general the spread will be multidimensional and include both horizontal and vertical spread. Each front will be dominated by forward or opposed propagation (or a combination) depending on the roles of buoyancy, wind and diffusion. Two important configurations are presented in Fig. 19.7 where the spread is either downwards or upwards though the fuel bed.

If initiation occurs on the top surface of the fuel bed, the fire will spread laterally and downward. It leads to a void or hole in the general shape of a semi-ellipsoid or pan. Downward spread is dominated by forward smoldering (Fig. 19.7, left), and creates a growing layer of ash that only decreases if wind carries the particles away. The horizontal spread is enhanced by a direct supply of atmospheric oxygen, which is readily available, and the rate is significantly greater than downward spread where oxygen transfer is limited by the layer of ash and char. Combustion of the uppermost layer is typically quenched due to large convective and radiant heat losses; this leaves a very thin layer of charred material on top while smoldering continues below. The fact that horizontal spread is faster a few cm below the surface leads to the formation of an overhang pointing inwards at the rim of the void (overhang not shown in figure 19.7). Horizontal spread accelerates in response to an increased wind. Palmer [27] examined this in thin horizontal layers (3–57 mm) of

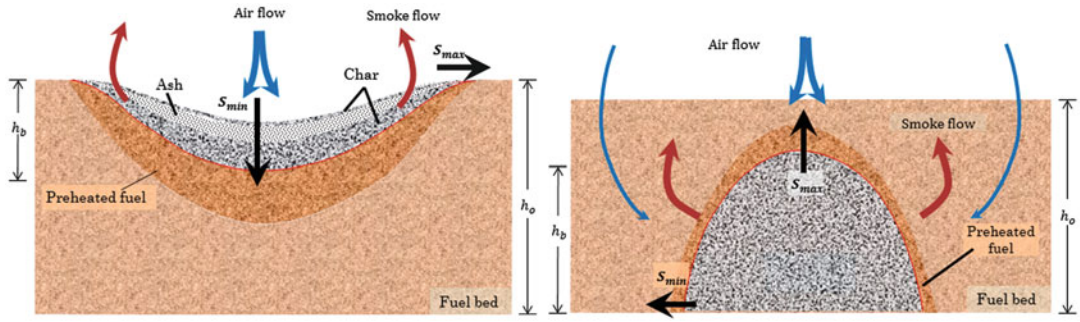

Fig. 19.7 Diagrams of downward (*left*) and upward (*right*) propagation in a porous fuel bed Huand and Rein [31]

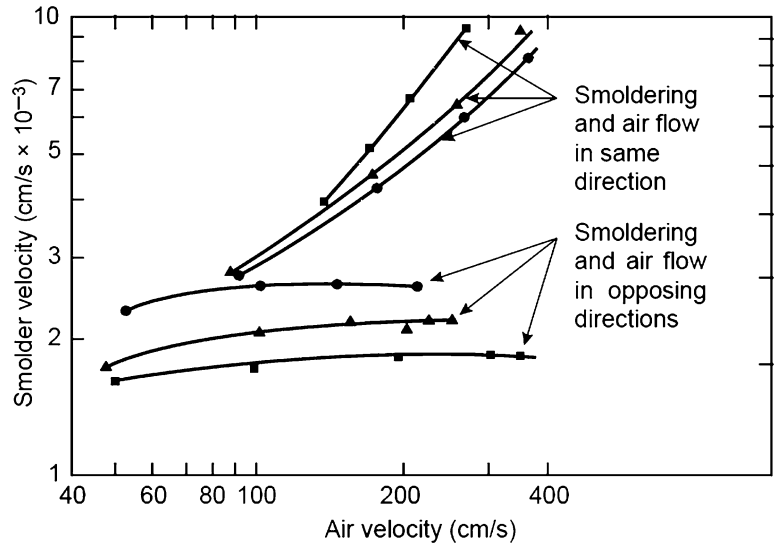

Fig. 19.8 Smoldering spread rate through horizontal layers of sawdust as a function of the horizontal airflow over the topmost layer. *Circles*: 120 mm particle size; *triangles*: 190 μm particle size; *squares*: 480 mm particle size (Data from Palmer [27], after Ohlemiller [7])

various cellulosic particles (cork, pine, beech, grass). The results in Fig. 19.8 show that the horizontal airflow has a greater effect in forward propagation, but that airflow in opposed propagation and the particle size have a weaker effect. In the absence of any forced flow over the fuel layer, the flow induced by the buoyant plume supplies oxygen for the horizontal spread at the topmost fuel layer. Oxygen then penetrates into the layer mostly by diffusion [32].

If initiation occurs deep within a layer of fuel and the nearest free surface is on the top, the fire will slowly spread upwards dominated by opposed smoldering (Fig. 19.7, right). The thick layer of virgin fuel above the reaction front hinders the oxygen supply, but also reduces the rate of heat losses. Ultimately, the spread is faster towards the free surface driven by oxygen diffusion, thus leading to fronts in the shape of an elongated bell. The reaction front usually spreads without fully consuming the char left behind. The upward case was studied in Palmer's work [27], which consists of a collection of observations from simple experiments involving the initiation of a smoldering front at the base of sawdust heaps (cork, elm and mixed wood). Some of the results are shown in Fig. 19.9. Note the scales reported in this data; the time to smolder up through a layer 1 m deep is about 2 weeks, and the process gave little hint of its presence until it was close to the surface of the fuel heap (smoke gets trapped inside the porous bed). The slope of the curve indicates that the time for upward smolder to penetrate a fuel layer is proportional to the square of the layer depth. Palmer showed that such dependence suggests the smolder front spread is proportional to the diffusion rate of oxygen from the free surface, through the unburned fuel, to the reaction front.

Data from other experiments on a variety of fuels and air supply conditions are summarized in Table 19.2.

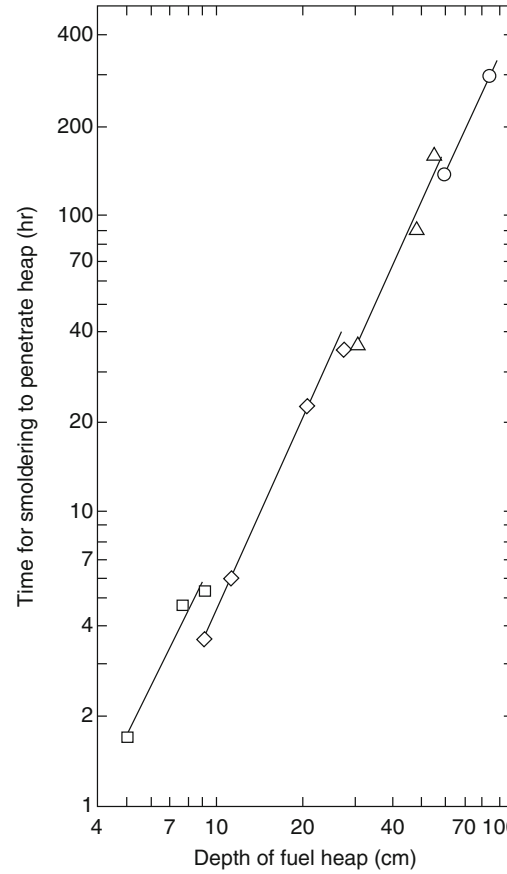

Fig. 19.9 Upward spread of smouldering through a bed driven by air diffusion. Ignition at base of the fuel bed and spread upwards in heaps of wood sawdust. *Squares*: layer 0.025 m deep in 0.3 m square box; *diamonds*: layer 0.052 m deep in 0.3 m square box; *triangles*: layer 0.052 m deep in 0.6 m square box; *circles*: layer 0.052 m deep in 0.9 m square box (Data from Palmer [27], after Ohlemiller [7])

Smoldering Kinetics

The spread rate of self-sustained smoldering is typically controlled by oxygen transport and heat transfer. Yet, heterogeneous chemical kinetics governs the front structure and is ultimately responsible for determining the conditions under which a material ignites and extinguishes.

Smoldering combustion of a solid fuel involves multiple pathways to chemical reactions, and these pathways are not yet fully understood. In spite of the complex kinetic behavior, experimental evidence suggests that mechanisms consisting of only a few global reactions capture the most important characteristics of the chemical process and allow an approximate analysis. Smoldering chemistry in its simplest form can be understood as a two-step process: pyrolysis of fuel (Equation 19.1) produces the char that is then oxidized

Table 19.2 Experimental data on smoldering in various fuels and configurations (After Ohlemiller [7])

Fuel	Configuration	Air supply	Spread rate	Peak temperature	Reference	Comments
Pressed fiber insulation board, 230–290 kg/m^3	13 mm thick horizontal strip, width large compared to thickness	Natural convection	0.8–1.3 mm/min	NA	Palmer [27]	Smolder velocity increased ≈ 50 % for strips with width ≈ thickness
Pressed fiber insulation board, 230–290 kg/m^3	13 × 13 mm strip at varied vertical inclinations	Natural convection	1.6–2.8 mm/min	NA	Palmer [27]	Smolder velocity highest for upward spread; lowest for horizontal spread
Fiber insulation board	13 × 50 mm strip forward smolder	Airflow over 20–1500 cm/s	2.1 mm/min (20 cm/s airflow) 7.8 mm/min (1400 cm/s airflow)	790 °C (900 cm/s airflow)	Palmer [27]	Some samples extinguished due to cooling at airflows >1450 cm/s
Fiber insulation board	13 × 50 mm strip opposed smolder	Airflow over strip, 80–900 cm/s	1.7–2.1 mm/min	NA	Palmer [27]	Extinguishment >900 cm/s
Fiber insulation board (pine or aspen)	13 mm thick sheet, horizontal, forward smolder	Airflow over sheet, 10–18 cm/s	1 mm/min	NA	Brenden and Schaffer [33]	
Cardboard	Vertical rolled cardboard cylinder, downward propagation, diameter 1.9–3.8 mm	Natural convection	3–5 mm/min	NA	Kinbara et al [34]	Small dia. ≈2× faster than large dia.; ambient temp. effect measured
Shredded tobacco	8 mm diameter cigarette, horizontal, in open air	Natural convection	1.8–3 mm/min	820 °C	Egerton et al. [35]	
Cotton upholstery fabric	Double fabric layer, 2 mm thick, horizontal, forward smolder	Airflow over fabric, 10 cm/s	~6 mm/min	770 °C	Donaldson and Yeadon [36]	Smolder behavior dependent on alkali metal content
Cellulosic upholstery fabric on substrates	Various weight fabrics horizontal on fiberglass, PU foam, cotton	Natural convection	1.8–45 mm/min (depends on substrate)	Reported values suspiciously low	Donaldson and Yeadon [36], Stiefel et al. [37]	Smolder fastest on inert fiberglass substrate
Cotton batting, densities 5–100 kg/m^3	15 cm cube, hold together by metal mesh and open to the air on all sides	Natural convection	2–4 mm/min (decrease as density increases)	690 °C	Hagen et al. [38]	Lower densities or repeated heating of sample result in higher ignition temperature
Wood char, densities 290–435 kg/m^3	22 cm tall packed bed of particles, diameter 1–3 mm	Natural convection	Upward ~0.4 mm/min. Downward ~0.05 mm/min	Upward 530 °C. Downward 800 °C	He and Behrendt [39]	Downward peak temperature decreases as the height of ash layer increases
Cork, beech and cocoa powders	Mesh wire baskets with volumes of 0.8–200 l	Natural convection	0.1–1.5 mm/min and decreasing relationship with basket volume	260–375 °C and decreasing relationship with basket volume	Krause and Schmidt [25]	Ignition sources tested include hot body, glowing nest and electric coil

in situ (Equation 19.2a). In this section we explore more comprehensive kinetics.

To begin with, the simple two-step scheme proposed in Equations 19.1 and 19.2a can be extended to include the direct oxidation of the fuel. Char oxidation (Equation 19.2a) is the principal heat source in most self-sustained smolder propagation processes; the potential for smoldering combustion thus exists with any material that forms a significant amount of char during thermal decomposition. The fuel is oxidized as well (Equation 19.4) but the most exothermic reaction is that of char, and therefore the simplest overall mechanisms does not include fuel oxidation. Fuel oxidation is also related to self-heating when it takes place at low temperature close to ambient (see Chap. 20).

Direct heterogeneous oxidation of the fuel:

$$\text{Fuel (solid)} + O_2 \rightarrow \text{Heat} + CO_2 + H_2O + \text{other gases} + \text{Char (solid)} + \text{Ash (solid)} \tag{19.4}$$

The materials for which smoldering kinetics are best known are polyurethane foam and cellulose. Kashiwagi and Nambu [40] provided a quantified three-step mechanism for cellulose, including cellulose pyrolysis, cellulose oxidation and char oxidation and accounting for three solid species; cellulose, char and ash. In flexible polyurethane foam, the presence of oxygen during degradation plays another key role, because without oxygen, many foams do not form char [41]. Rein et al. [15] provided a five-step mechanism for polyurethane consisting of two foam pyrolysis, two foam oxidations and one char oxidation reaction, and accounting for four solid species (foam, β-foam, char and residue). This mechanism was developed and the kinetic constants found from thermogravimetric experiments, as shown in Fig. 19.10. This multi-step mechanism allows explaining the different contributions of the pyrolysis and oxidation reaction to the degradation of the foam in the presence of air, as seen in Fig. 19.11.

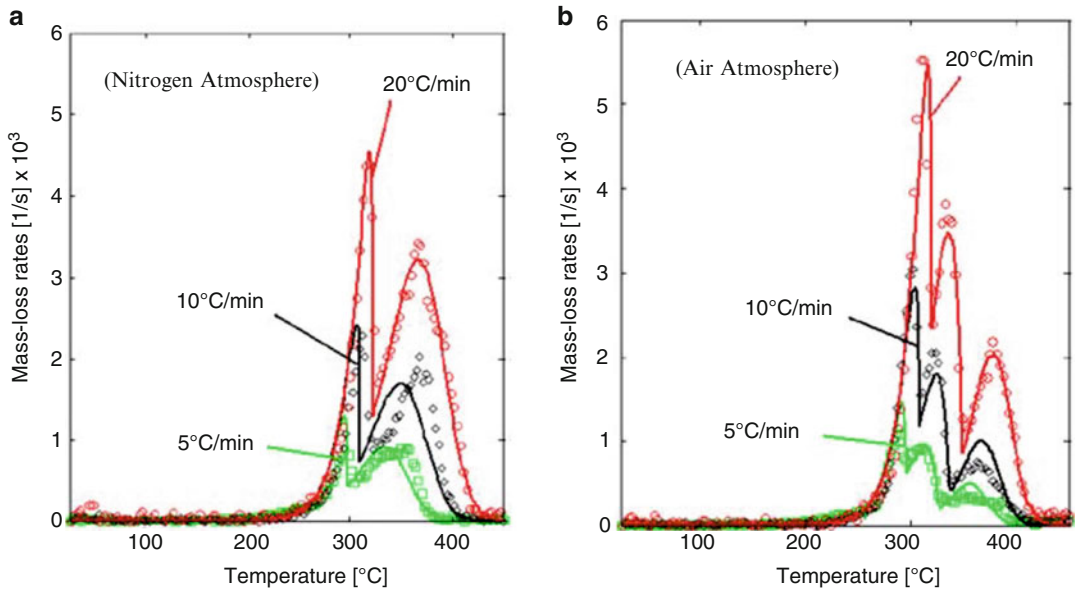

Fig. 19.10 Thermogravimetric mass loss rate of polyurethane foam in; (**a**) nitrogen atmosphere, and (**b**) air atmosphere, as a function of temperature for three heating rates (Symbols are data from experiments of Chao and Wang [42], and lines are data from numerical simulations of Rein et al. [15])

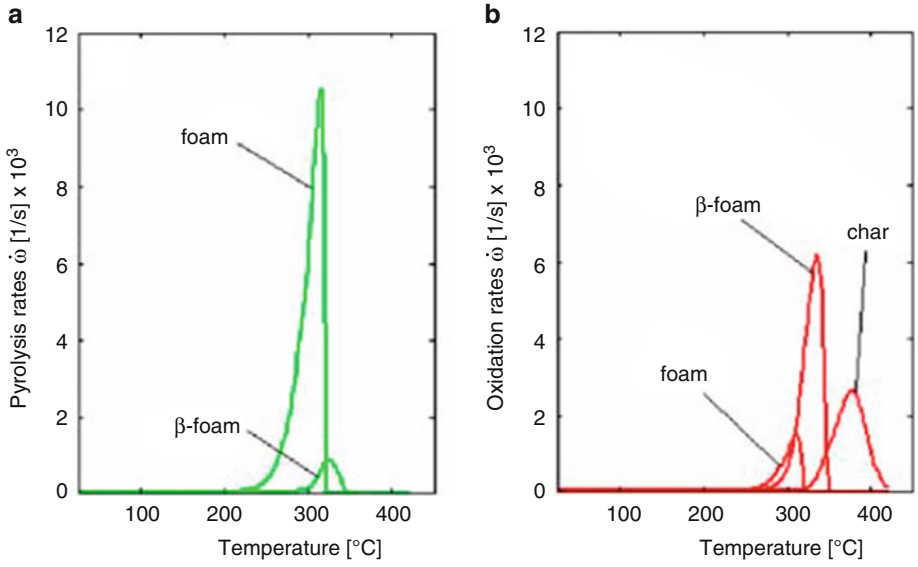

Fig. 19.11 Numerical results for the different reactions rates (pyrolysis on the *left*, oxidation on the *right*) in polyurethane foam decomposition in air atmosphere. This simulates the experimental thermogravimetric data of Fig. 19.10 (*right*) and allows explaining the origin of the three mass-loss peaks (Data from Rein et al. [15])

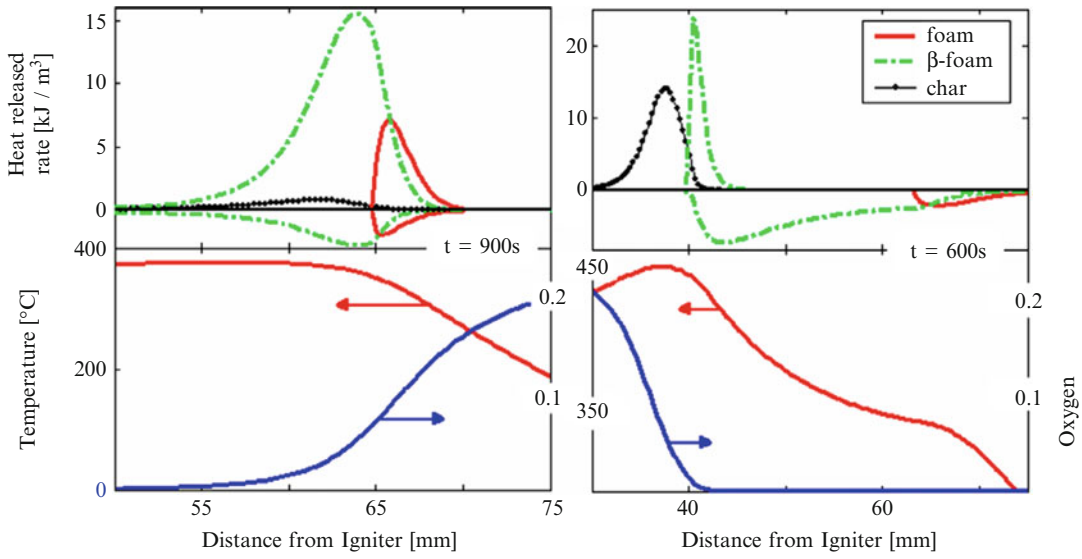

Fig. 19.12 Numerical results for the front structure during self-propagation; (*left*) opposed smoldering; and (*right*) forward smoldering. *Top* figures show the heat-released rate of each reaction (positive for oxidation, negative for pyrolysis). *Bottom* figures show the temperature and oxygen profiles (Data from Rein et al. [16])

The separation of pyrolysis from oxidation is essential in any smouldering kinetics scheme.

It was the work of Rein et al. [16] that proved that the same kinetic mechanism was able to explain both forward and opposed smoldering. In forward smoldering propagation (Fig. 19.12, right), the oxidation and the pyrolysis reactions form two distinct propagating sub fronts. The pyrolysis sub front arrives first to the virgin foam and then followed by the oxidation sub front. In opposed smoldering (Fig. 19.12, right), the oxidation and the pyrolysis reactions overlap

to form a single front. Previously to the work of Rein et al. [16], smoldering chemistry had been described as a function of the propagation mode: forward smoldering with two-step chemistry, and opposed smoldering with one-step chemistry.

Smoldering kinetics is an immature field of solid phase chemistry due to is complexity and secondary role in fire spread. It has been the objective of few studies to date. Despite the recent advances reviewed in this section, the topic remains mostly undeveloped.

Suppression

A smoldering fire can be extraordinarily difficult to suppress. Experiments on heaps of coal show that smoldering requires large amounts of water. For example, the amount of water required to suppress smoldering coal was measured to be in the range from 1 to 2 l of water per kg of burning fuel. Moreover, smoldering requires lower oxygen concentration to be smothered, around 10 % O_2, compared to 16 % O_2 for flaming [43, 44]. Oxygen removal is insufficient unless it is continued until the whole fuel bed is cooled to a point where oxygen readmission will not cause re-ignition. Because volumetric cooling of a fuel bed is a very slow process (long thermal response time), this means that the holding time for smothering are much longer for smoldering than for flaming[5] (months vs. hours) [22].

One practical problem in suppressing a large fuel bed is the tendency of the extinguishing fluid agents to follow higher permeability channels and thereby miss significant in-depth burning zones. Channeling arises when a substantial fraction of the fluid takes the same flow path through the bed, resulting in limited contact surface area between the agent and the burning fuel. This, coupled with the lower residence times in regions of high permeability because of the high flow velocities, requires large quantities of water for suppression.

[5] Avoidance of flaming re-ignition of a non-porous fuel requires cooling of the surface layer only.

Hadden and Rein [22] investigated three water suppression methods (pipe, shower and spray) on a small-scale coal bed. They showed that the most efficient method with respect to total water required is the shower. However, using a spray results in less water runoff and thus offers a higher efficiency. The injection pipe is significantly less efficient, requiring three times more water than a spray, and resulting in >80 % lost as run-off. Tuomisaari et al. [45] tested a number of extinguishing agents (liquids: water, water with additives; gases: N_2, CO_2, Ar and Halon) in series of tests on a small bed of smoldering wood chips. The result was that gaseous CO_2, injected from the bottom, was found to be the most effective.

Gas Emissions

Gas emissions from smoldering fires differ significantly to those from flaming fires. First, the emissions rate per unit area is much lower but also the chemistry is different. Smoldering is characteristically an incomplete combustion, releasing species and quantities that substantially depart from that in stoichiometric and complete combustion. For example, the CO/CO_2 ratio which can be thought of as an index of the incompleteness of combustion is ~0.4 in smoldering but ~0.1 in flaming combustion [46]. The presence of pyrolysate in the products of smouldering, significantly contributes to of a complex gaseous mixture including volatile organic compounds (VOC), polyaromatic hydrocarbons (PAH), other hydrocarbons and particulate matter (PM). While the yield of toxic species is larger in smoldering fires than in flaming fires [47], the production rate, which is proportional to the spread rate, is much lower. This means that inside an enclosure, a smoldering fire of long duration (in the range from 1 or 3 h for a single bedroom size compartment [48]) can lead to a lethal dose of toxicity, especially CO. But there are not as yet sufficient data on the toxicity of smoldering materials to definitively understand the issue of life safety. Some more information is presented in Chap. 62 and in [47].

Limited information is available on the aerosol emitted by a smolder source. The residual char left behind the smolder front and the original porous bed act as filters for aerosol. This finding explains the observation by Palmer [27] that upward smoldering in a thick layer of fuel was not detected until it neared the surface (like in Fig. 19.7 right). The mean particle size of the aerosol in smoldering cellulose was measured to be in the range from 2 to 3 μm [49]; this is about 50–200 times larger than the sooty particulates produced by flaming combustion.

The low heat release rate of smoldering fires means that the buoyant plume is weak, which has implications on the location of smoke detectors in rooms. The morphology of the smoke from smouldering is different to smoke from flaming, and this affects smoke detection. This means smoke is slow to reach the ceiling, or it may never reach it, and often the building mechanical ventilation controls the smoke movement [50] (see also Chap. 13).

In the natural environment, the low buoyant strength of large smoldering fires leads to haze episodes because the plume accumulates near the ground and can slide into populated areas, choking towns and cities for weeks [5]. The composition of haze measured by Bertschi et al. [51] in the tropical savanna shows it contains 130 % more CO and 670 % more hydrocarbons in mass basis, but 15 % less CO_2 and no NO_x when compared to the flaming wildfires.

Smoldering Wildland Fires

In the natural environment, smoldering fires burn two types of biomass: thick fuels, like tree branches or logs, and organic soil, like the duff layer or peat [5]. These are characterized by having a significantly greater thermal time compared to fine fuels like foliage. Thick fuels favor the slow burning of smoldering combustion. The persistent smoldering of thick fuels is typically observed for a few days after a flaming wildfire has passed, and it is often referred to as *residual smoldering combustion*. Overall, smoldering is responsible for up to 50 % or more of the total burned biomass during wildfires [51–53].

But it is the soil rich in organic matter, in particularly that in peatlands, which is most affected ecosystem by smoldering fires, both in frequency and size. Peat soils are made by the natural accumulation of partially decayed biomass and are the largest reserves of terrestrial organic carbon [54]. Because of this vast accumulation of fuel, once ignited, smoldering peat fires burn for very long periods of time (e.g., months, years) despite extensive rains, weather changes or fire-fighting attempts. These are the largest fires on Earth and large contributors of greenhouse gases [5, 54]. Peat fires occur with some frequency worldwide in tropical, temperate and boreal regions (e.g., in Indonesia, Australia, Alaska, Canada, Florida, British Isles, Siberia). Droughts, drainage and changes in land use are thought to be main causes leading to the high flammability conditions of dry peatlands. Possible ignition events can be natural (e.g., lightning, self-heating, volcanic eruption) or anthropogenic (land management, accidental ignition, arson).

The most studied peat megafire took place in Indonesia in 1997 and led to an extreme haze event. The smoke covered large parts of South-East Asia, even reaching Australia and China, and induced a surge of respiratory emergencies in the population and disruption of shipping and aviation routes for weeks. It was estimated that these fires released between 0.81 and 2.57 Gton of carbon gases [55]. This is equivalent to 13–40 % of global man-made emissions of the year 1997. The 1997 megafire was not an isolated case in the region. Analysis of 1960–2006 data shows that smoldering haze episodes have drifted to South East Asian countries once every 3 years on average [56]. Rough figures at the global scale estimate that the average greenhouse gas emissions from peat fire is equivalent to >15 % of man-made emissions. Moreover, because peat is ancient carbon, and smoldering is enhanced under warmer and drier climates, it creates a positive feedback mechanism in the climate system, a self-accelerating global process [5].

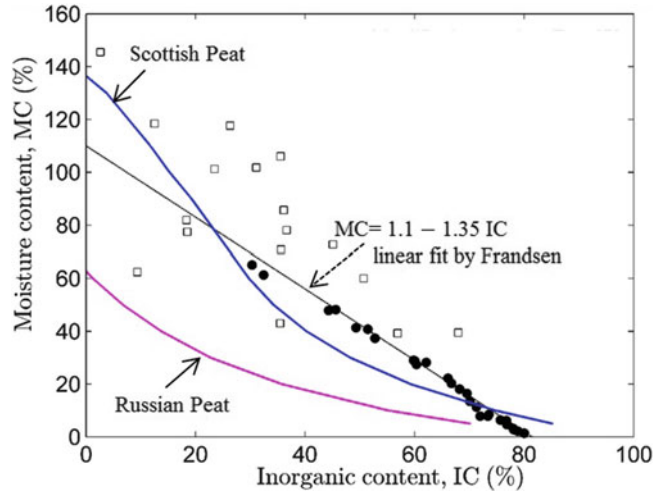

Fig. 19.13 The data separates the ignition (bottom) from the no-ignition (top) limits for a mixture of peat, moisture and mineral contents. Circles and sequre symbols are experimental data by Frandsen [58]. Lines are computational simulations by [59].

Because the water content of wildland fuels like peat can vary naturally over a wide range of values (from dry to flooded in water), and because water represents a significant energy sink, moisture content is the single most important property governing the ignition and spread of smoldering wildfires. The critical moisture content for ignition (related to the moisture of extinction [57]) of boreal peat has been measured in the range 110–120 % in dry basis[6] [16, 58]. Any peat drier than this is susceptible to smoldering. The prominent role of moisture is such that natural or anthropogenic-induced droughts are the leading cause of smoldering megafires.

The second most important property is the mineral content.[7] As found experimentally by Frandsen [58] and computationally by Huang et al [59], there is a decreasing relationship between the mineral content and the critical moisture content: higher mineral loads mean soil can only ignite at lower moistures. This is because the inert content is a heat sink to the fire. The results are shown in Fig. 19.13. This rule can be applied to most organic soils or fuel beds to determine if they are susceptible to smoldering. Any soil which composition is more than 80 % mineral, cannot be ignited [58, 59]. After moisture and mineral contents, other important properties are bulk density, porosity, flow permeability and organic composition.

Because the fuel layers found in the natural environment (soil depths from 0.5 to 30 m) can be much thicker than those in the built environment (~0.1 m), smoldering wildfires can be classified in shallow or deep fronts. Each has significantly different dynamics because of the different role played by the controlling mechanisms of oxygen supply and heat losses.

Organic material located close to the surface of the soil burns in shallow fires (roughly <1 m under the surface). These have a good supply of atmospheric oxygen, but are exposed to large convective heat losses. They propagate laterally and downwards along the organic layers of the ground, leave voids or holes in the soil (see Fig. 19.7 left). This has prompted that fuel consumption can be estimated using the depth of burn to calculate the volume of the void. Depth of burn is the vertical distance between the original soil

[6] The water content in dry basis is the mass of water divided by the mass of a dried sample expressed as a %.

[7] The mineral content is the % of the fuel mass (on dry basis) that will not burn or react at high temperatures. It results in ash.

location and the post-fire soil location. A typical value for the depth of burn reported in several field studies is around 0.5 m, which means that the average fuel consumptions per unit area is around 75 kg/m^2. This value is more than two orders of magnitude larger than that in flaming fires [5]. For this reason and in terms of fuel consumption, these are classed as megafires.

Deep fires take place in organic the subsurface layers fed by oxygen infiltrating the ground via large cracks, piping systems or channels. For example, it is known that peatlands have an in-built natural piping system for water movement; when drained this system becomes the delivery network for oxygen transport to deeper locations and smoke exhaust to the atmosphere. Deep fires have a poorer supply of atmospheric oxygen but are better insulated from heat losses than shallow fires.

Smoldering fires have detrimental effects on the forest soil, its microflora and microfauna. This is because it consumes the soil (>90 % mass loss) and also because the long residence time of smoldering means that heat penetrates deep into the soil layers [5]. On the contrary, flames produce high temperatures above the ground for short periods of time (in the order of 15 min). This results in minimal heating of the soil below depths of a few cm, reaching peak temperatures of 300 °C at superficial layers (<10 mm) and below 80 °C at layers more than 40 mm deep [60]. This superficial heating can leave the soil system relatively unharmed. However, smoldering fires lead to enhanced heat transfer into the soil (see the discussion on the depth of burn above) for much longer durations (i.e. in the order of 1 h) and peak temperatures of 500 °C [61]. As a comparison, these thermal conditions are more severe than medical sterilization treatments, and mean that the soil is exposed to conditions that are lethal to biological agents.

Coal Seam Fires

Coal fires are a smoldering phenomenon that has attracted a larger amount of research, especially from geologists and petrologists [37, 62] and share many similarities with deep smoldering wildfires. Due to the higher density and higher fraction of carbon in coal, the fire spreads slower (~0.1 mm/min) but burns hotter (~1000 °C peak temperature) compared to other smoldering fuels. Because of these characteristics, coal particles smoldering near the free surface are more frequently accompanied by flames than any other fuel.

There is evidence to suggest that burning coal seams are the oldest continuously burning fires on Earth. The best examples is *The Burning Mountain* in New South Wales, Australia is a large coal seam which has been smoldering for more than 6000 years [12]. Thousands of underground coalmine fires have been identified around the world, especially in China, the United States, and India [63]. Elusive, unpredictable and costly, coal fires burn indefinitely while there is fuel, choking the life out of a community and the environment while consuming a valuable energy resource. The associated financial costs run into millions of dollars including the loss of coal, closure of mines, damage to the environment and fire-fighting efforts. There are some well-documented cases. In 1962, an abandoned mine pit in Centralia, Pennsylvania, USA was accidentally lit. Several unsuccessful attempts were made to extinguish it, letting the fire continue to burn after more than 40 years. It is currently being monitored with the front advancing at ~20 m/year [64].

Transition to Flaming

Smoldering and flaming combustion are closely related, and one can lead to the other. Figure 19.14 shows snapshots of an experiment on the transition to flaming in a foam slab. The transition from smoldering to flaming is a severe threat in residential fires, and together with the slow buildup of CO and other incapacitating gases, they pose the largest life hazards of bedding or upholstery fires. The transition to flaming is also a concern in wildfires, since it offers the means for flaming fronts to re-establish in unexpected locations (e.g., across a fire break) and at unexpected times (e.g., long after burn out of the initial flaming front).

Fig. 19.14 Series of photographs of a combustion experiment illustrating the transition to flaming in a smoldering polyurethane slab 40 cm high under external forced flow (Photo by group of Prof. Carlos Fernandez-Pello, University of California at Berkeley). After 1 h of smoldering only half the sample has burned (Photo 1, far *left*). When the rapid transition to flaming takes place (Photos 2 and 3), the whole sample is engulfed in flames in just a few seconds (Photos 4 and 5, far *right*)

However, it has received little attention so the current understanding of this transition is limited. In particular, whether the transition is possible or not or when it will occur cannot be predicted because of a lack of valid models. Babrauskas and Krasny [65] did a literature survey of fire tests on a variety of upholstered furniture items (chairs, sofas and mattresses) where a smoldering fire was ignited and allowed to progress. Out of the 102 fire tests examined, 64 % did transition to flaming. The time to transition observed ranged from 22 to 306 min, with an average of 88 min. Revisiting the data from previous experiments on smoldering of furniture, Quintiere et al. [48] showed that the likelihood of having transition to flaming occur peaks with a 36 % probability at 50–100 min after ignition. They also showed that within the time period from 50 to 200 min, the likelihood of a transition event is comparable with the likelihood of reaching a lethal CO dose inside a single bedroom compartment.

The transition is a spontaneous gas-phase ignition supported by the smoldering reaction, which acts both as the source of gaseous fuel, the pyrolysate produced in Equation 19.1, and the source of the heat required to initiate the flame (Equation 19.2b) [2, 32]. The transition occurs not at the foam/air interface, but rather within the depth of the char left by the smolder front [66, 67]. This is the location where both critical conditions of flammability of the pyrolysate mixture and the net excess of heat released by char oxidation are met. The heat driving the transition is released mostly by the secondary char oxidation [14, 66], which is more exothermic and takes places at higher temperatures (~700 °C for polyurethane [68]) than char oxidation in Equation 19.2a. This temperature range is towards the highest temperatures typical of smoldering combustion and hence secondary char oxidation is only of importance during the transition to flaming [66].

A smoldering fuel responds to an increased oxygen supply (e.g., wind) by becoming faster and hotter until, eventually, flames might erupt. This effect was first studied quantitatively by Palmer [27] for airflows over horizontal layers of wood sawdust. Depending on the material, the transition occurred at airflow velocities from about 0.9 to 1.7 m/s. Ohlemiller [69] did obtain transition to flaming in layers of fibrous insulation materials in forward smolder at air velocities

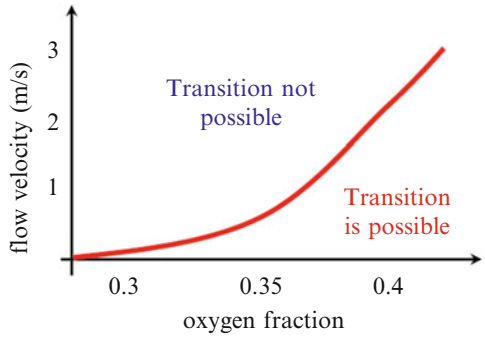

Fig. 19.15 Transition map from smoldering to flaming on polyurethane samples (Data from [70])

of about 2 m/s. Bar-Ilan et al. [70] conducted experiments on small samples of polyurethane foam and showed that the transition can be triggered by a combination of increasing the airflow velocity, the oxygen concentration or the external radiant heat. A map of airflow vs. oxygen fraction is shown in Fig. 19.15. A similar map is presented in Bar-Ilan et al. [70] for airflow vs. external heat. They also provide an analytical expression for the transition boundary.

The transition to flaming has only been observed in forward propagation. Ohlemiller [69] argued that this is because in forward mode, the hot gases of combustion preheat the fuel ahead and thereby enhancing the combustion; while in opposed mode, the cool air reduces preheating. However, upward propagation inside a pile of fuel (Fig. 19.7 right), which is mostly in opposed mode, can lead to the transition to flaming once the reaction breaks through to the free surface and finds a good supply of oxygen.

Concluding Remarks

We have seen that smoldering fires are a source of safety and environmental concerns. It is a type of combustion quite distinct from that in flaming fires, but as diverse and complex. The most studied fuels to date are cellulose and polyurethane foam.

The most important concepts to bear in mind are the following. Smoldering combustion can be initiated with weaker ignition sources (radiant, conductive, embers and self-heating) and is more difficult to suppress than flaming combustion. This makes smoldering the most persistent combustion mode. Large samples are easier to ignite than small samples, which affects the translation of laboratory testing results to the real scale. Smoldering fuels include synthetic materials such as charring polymers or cellulosic insulation, and natural fuels like peat or coal. In chemical terms, most smoldering fuels form a char on heating. In physical terms, smoldering fuels consist of a permeable medium formed by grains, fibers or some other porous matrix. The chemistry involves multiple pathways to chemical reactions, but in its simplest form can be understood as a two-step process: the pyrolysis of fuel and char oxidation. It is characteristically an incomplete combustion reaction, releasing pollutants in greater yields than flaming but at a lower rate. The transition from smoldering to flaming is a severe threat and can be triggered by a combination of increasing airflow, oxygen concentration and external heat.

An emerging topic is smoldering wildland fires of organic soils, like peat, which are megafires in terms of the fuel consumption, and together with coal seam fires are the largest and oldest continuously burning fires on Earth.

Regrettably, the state of the art is incomplete, and accurate calculations on smoldering phenomena are not possible. Current understanding is fragmented in different areas, as suggested by the many different names applied to it: non-flaming combustion, oxidative pyrolysis, glowing combustion, filtering combustion, low oxygen combustion, deep seated fire, hidden fire, lagging fire, smoking material, in-situ combustion, fireflood or underground gasification [9]. More experimental and theoretical studies, and a multidisciplinary research approach to smoldering combustion are needed.

Acknowledgements I am most grateful to Thomas J. Ohlemiller whose pioneering research and reviews on smoldering combustion provided not only the best sources of knowledge and inspiration for my own research and understanding but also contributed to this chapter in the form of material that I reused from his previous version [7]. This chapter is the culmination of 15 years of work on

smoldering combustion that I have conducted at four universities. These are, in chronological order University of Texas at Austin, University of California at Berkeley, University of Edinburgh and Imperial College London. This work would not have been possible without the contributions and encouragements of my mentors, collaborators and PhD students. Of these, I am especially thankful to Carlos Fernandez-Pello, José Torero, Rory Hadden, Claire Belcher, Chris Lautenberger, Matt Davies and Xinyan Huang. A series of institutions have funded this work along the way: Royal Academy of Engineering, Leverhulme Trust, UK Engineering and Physical Science Research Council, IFIC Forensics, Met Office and NASA Space flight Program.

References

1. TJ. Ohlemiller, "Modeling of Smoldering Combustion Propagation," *Progress in Energy and Combustion Science,* 11, p. 277 (1985).
2. D. Drysdale, An Introduction to Fire Dynamics, 3rd ed. Wiley, UK, 2011.
3. M. Ahrens. U.S. Home Structure Fires, National Fire Protection Association Fire Analysis and Research, Quincy, MA April 2013.
4. J.R. Hall, The Smoking-Material Fire Problem, (Fire Analysis and Research Division of The National Fire Protection Association, November 2004, Massachusetts).
5. G Rein, Smouldering Fires and Natural Fuels, Chapter 2 in. Fire Phenomena in the Earth System – An Interdisciplinary Approach to Fire Science, C Belcher (editor). Wiley and Sons, 2013. http://dx.doi.org/10.1002/9781118529539.ch2
6. T'ien, J.S., Shih, H., Jiang, C., Ross, H.D., Miller, F. J., Fernandez-Pello, A.C., Torero, J.L., and Walther, D.C., Mechanisms of Flame Spread and Smolder Wave Propagation, Chapter 5 in. Microgravity Combustion: Fire in Free Fall, H.D. Ross, Editor, Academic Press, 2001, pp. 299–417.
7. T. J. Ohlemiller, Smoldering Combustion, Chapter 9; Section 2; SFPE Handbook of Fire Protection Engineering. 3rd Edition, DiNenno, P. J.; Drysdale, D.; Beyler, C. L.; Walton, W. D., Editor(s), 2/200-210 p., 2002. http://fire.nist.gov/bfrlpubs/fire02/art074.html
8. V. Babrauskas, Ignition Handbook, 2003 Fire Science Publishers, Issaquah WA, USA. ISBN-10: 0-9728111-3-3.
9. G Rein, Smouldering Combustion Phenomena in Science and Technology, International Review of Chemical Engineering, 1, 1, pp. 3–18, 2009.
10. TJ. Ohlemiller and W. Shaub, "Products of Wood Smolder and Their Relation to Wood-Burning Stoves," *NBSIR 88-3767,* National Bureau of Standards, Washington, DC (1988). fire.nist.gov/bfrlpubs/fire88/PDF/f88017.pdf
11. J. Beard, Ground Zero's fires still burning, 3 December 2001, New Scientist, New York. http://www.newscientist.com/article/dn1634-ground-zeros-fires-still-burning.html
12. CD Ellyett, Fleming, A.W. (1974) Thermal infrared imagery of The Burning Mountain coal fire. Remote Sensing of Environment 3: 79–86; doi: 10.1016/0034-4257(74)90040-6.
13. C. Switzer, P Pironi, G Rein, JL Torero, JI Gerhard, Self-Sustaining Smoldering Combustion: A Novel Remediation Process for Non-Aqueous-Phase Liquids in Porous Media, Environmental Science and Technology 43, pp. 5871–5877, 2009. doi: 10.1021/es803483s.
14. J. Torero and C. Fernandez-Pello, Forward Smolder of Polyurethane Foam in a Forced Air Flow, *Combustion and Flame,* 106, pp. 89–109 (1996).
15. G Rein, C Lautenberger, AC Fernandez-Pello, JL Torero, DL. Urban, Application of Genetic Algorithms and Thermogravimetry to Determine the Kinetics of Polyurethane Foam in Smoldering Combustion, Combustion and Flame 146 (1-2), pp 95–108, 2006. doi:10.1016/j.combustflame.2006.04.013.
16. G Rein, AC Fernandez-Pello, DL Urban, Computational Model of Forward and Opposed Smoldering Combustion in Microgravity, Proceedings of the Combustion Institute 31 (2), pp. 2677–2684, 2007. doi:10.1016/j.proci.2006.08.047.
17. TJ. Ohlemiller and D. Lucca, "An Experimental Comparison of Forward and Reverse Smolder Propagation in Permeable Fuel Beds," *Combustion and Flame,* 54, p. 131 (1983).
18. M. Ortiz-Molina, T-Y. Toong, N. Moussa, and G. Tesoro, *17th Symposium (International) on Combustion,* Combustion Institute, Pittsburgh, PA (1979).
19. R Hadden, A Alkatib, G Rein, JL Torero, Radiant Ignition of Polyurethane Foam: the Effect of Sample Size, Fire Technology 50 (3), pp. 673–691 (2014) doi:10.1007/s10694-012-0257-x.
20. M. Anderson, R. Sleight, and J. Torero, "Downward Smolder of Polyurethane Foam: Ignition Signatures," Fire Safety Journal, 35, pp. 131–147 (2000).
21. R. Anthenien and C. Fernandez-Pello, A Study of Forward Smolder Ignition of Polyurethane Foam, Proceedings 27th Symposium (International) on Combustion, Vol. 2, Combustion Institute, Pittsburgh, PA, pp. 2683–2690 (1998).
22. R Hadden, G Rein, Burning and Suppression of Smouldering Coal Fires, Chapter 18 in. Coal and Peat Fires: A Global Perspective, Volume 1, pp. 317–326, Stracher, Prakash and Sokol (editors), Elsevier Geoscience, 2011. ISBN 9780444528582. doi: 10.1016/B978-0-444-52858-2.00018-9.
23. Manzello, S. L.; Cleary, T. G.; Shields, J. R.; Maranghides, A.; Mell, W. E.; Yang, J. C., Experimental Investigation of Firebrands: Generation and Ignition of Fuel Beds, Fire Safety Journal, Vol. 43, No. 3, 226–233, April 2008.
24. R Hadden, S Scott, C Lautenberger and AC Fernandez-Pello, Ignition of Combustible Fuel Beds

by Hot Particles: An Experimental and Theoretical Study, Fire Technology 47 (2), pp. 341–355, 2011, doi:10.1007/s10694-010-0181-x
25. U Krause, Schmidt M (2000) Propagation of smouldering in dust deposits caused by glowing nests or embedded hot bodies. J Loss Prev Process Indus 13 (3-5):319–326. doi:10.1016/S0950-4230(99)00031-5
26. P. Bowes, *Self-Heating: Evaluating and Controlling the Hazards,* Elsevier, New York, Chap. 7 (1984).
27. K. Palmer, "Smoldering Combustion in Dusts and Fibrous Materials," Combustion and Flame, 1, p. 129 (1957).
28. TJ. Ohlemiller and F. Rogers, "Cellulosic Insulation Material II. Effect of Additives on Some Smolder Characteristics," *Combustion Science and Technology,* 24, p. 139 (1980).
29. A. Bar Ilan, Rein G, Fernandez Pello AC, Torero JL, Urban DL (2004a) Forced forward smoldering experiments in microgravity. Exper Thermal and Fluid Science 28 (7):743–751. doi:10.1016/j.expthermflusci.2003.12.012
30. A. Bar Ilan, Rein G, Walther DC, Fernandez Pello AC, Torero JL, Urban DL (2004b) The effect of buoyancy on opposed smoldering. Combust Sci Technol 176(12):2027–2055. doi:10.1080/00102200490514822
31. X Huang, G Rein, "Smouldering Combustion of Peat in Wildfires: Inverse Modelling of the Drying and the Thermal and Oxidative Decomposition Kinetics," *Combustion and Flame* 161 (6), pp. 1633–1644, 2014. doi:10.1016/j.combustflame.2013.12.013.
32. TJ. Ohlemiller, "Smoldering Combustion Propagation Through a Permeable Horizontal Fuel Layer," *Combustion and Flame,* 81, p. 341 (1990a).
33. J. Brenden and E. Schaffer, "Wavefront Velocity in Smoldering Fiberboard," *Research Paper FPL 367,* U.S. Forest Products Laboratory (1980).
34. T. Kinbara, H. Endo, and S. Sega, *Proceedings of the Combustion* Institute, p. 525 (1967).
35. A. Egerton, K. Gugan, and F. Weinberg, "The Mechanism of Smoldering in Cigarettes," *Combustion and Flame,* 7, p. 63 (1963).
36. D. Donaldson and D. Yeadon, "Smoldering Phenomena Associated with Cotton," *Textile Research Journal,* March, p. 160, (1983).
37. W. Stiefel, R. Bukowski, J. Hall, and F. Clarke, "Fire Risk Assessment Method: Case Study 1, Upholstered Furniture in Residences," *NISTIR 90-4243,* National Institute of Standards and Technology, Gaithersburg, MD (1990).
38. Bjarne C. Hagen, Vidar Frette, Gisle Kleppe, Bjørn J. Arntzen, Onset of smoldering in cotton: Effects of density, Fire Safety Journal, Volume 46, Issue 3, 2011, Pages 73–80, http://dx.doi.org/10.1016/j.firesaf.2010.09.001.
39. H Fang, Frank Behrendt, Experimental investigation of natural smoldering of char granules in a packed bed, Fire Safety Journal, Volume 46, Issue 7, 2011, Pages 406–413, ISSN 0379-7112, http://dx.doi.org/10.1016/j.firesaf.2011.06.007.
40. T. Kashiwagi, H. Nambu, Global kinetic constants for thermal oxidative degradation of a cellulosic paper, Combustion and Flame, Volume 88, Issues 3–4, March 1992, Pages 345–368, http://dx.doi.org/10.1016/0010-2180(92)90039-R.
41. F. Rogers and T. Ohlemiller, "Smolder Characteristics of Flexible Polyurethane Foams," *Journal of Fire and Flammability,* 11, p. 32 (1980).
42. C.Y.H. Chao, J.H. Wang, 2001a, Comparison of the Thermal Decomposition Behavior of a Non-Fire Retarded and a Fire Retarded Flexible Polyurethane Foam, Journal of Fire Science 19, pp. 137–155.
43. C Belcher, J Yearsley, R Hadden, J McElwain, G Rein, Baseline intrinsic flammability of Earth's ecosystems estimated from paleoatmospheric oxygen over the past 350 million years, Proceedings of the National Academy of Sciences 107 (52), pp. 22448–22453, 2010. doi:10.1073/pnas.1011974107.
44. R Hadden, G Rein, C Belcher, Study of the competing chemical reactions in the initiation and spread of smouldering combustion in peat, Proceedings of the Combustion Institute 34, pp. 2547–2553, 2013. doi:10.1016/j.proci.2012.05.060.
45. M. Tuomisaari, D. Baroudi, and R. Latva, "Extinguishing Smoldering Fires in Silos," *Publication 339,* VTT Technical Research Centre of Finland, Espoo, Finland (1998).
46. G Rein, S Cohen, A Simeoni, Carbon Emissions from Smouldering Peat in Shallow and Strong Fronts, Proceedings of the Combustion Institute 32, pp. 2489–2496, 2009.
47. A. Stec, T.R Hull, Assessment of the fire toxicity of building insulation materials, Energy and Buildings 43 (2011) 498–506.
48. J. Quintiere, M. Birky, F. McDonald, and G. Smith, An Analysis of Smoldering Fires in a Closed Compartment and Their Hazard due to Carbon Monoxide, Fire and Materials, 6, p. 99, 1982.
49. G. Mulholland and T. Ohlemiller, "Aerosol Characterization of a Smoldering Source," *Aerosol Science and Technology,* 1, p. 59 (1982).
50. H. Hotta, Y. Oka, and O. Sugawa, "Interaction Between Hot Layer and Updraft from a Smoldering Source. Part 1. An Experimental Approach," *Fire Science and Technology,* 7, p. 17 (1987).
51. I Bertschi, Yokelson, R.J., Ward, D.E., et al. (2003) Trace gas and particle emissions from fires in large diameter and belowground biomass fuels. Geophysical Research 108 (D13): 8472; doi: 10.1029/2002JD002100.
52. G. M. Davies, A Gray, G Rein, CJ Legg, Peat consumption and carbon loss due to smouldering wildfire in a temperate peatland, Forest Ecology and Management 308, pp. 169–177, 2013. doi:10.1016/j.foreco.2013.07.051
53. E.R.C. Rabelo, C.A.G. Veras, J.A. Carvalho, E.C. Alvarado, D.V. Sandberg, J.C. Santos, Log

smoldering after an Amazonian deforestation fire, Atmospheric Environment 38 (2004) 203–211.
54. M. Turetsky, B. Benscoter, S. Page, G. Rein, G.R. van der Werf, A. Watts, Global vulnerability of peatlands to fire and carbon loss, (invited progress paper), Nature Geoscience 8 (1), pp. 11–14, 2015. doi:10.1038/NGEO2325.
55. S.E. Page, Siegert, F., Rieley, J.O., Boehm, H.D.V., Jaya, A. & Limin, S. (2002) The amount of carbon released from peat and forest fires in Indonesia during 1997. Nature 420: 61–65.
56. W Field, Shen, Nature Geoscience 2, 185–188 (2009) Human amplification of drought-induced biomass burning in Indonesia since 1960, doi:10.1038/ngeo443
57. X. Huang, G. Rein, Computational Study of Critical Moisture and Depth of Burn in Peat Fires, International Journal of Wildland Fire 24 (in press), (2015). doi:10.1071/WF14178.
58. W Frandsen, Ignition probability of organic soils, Can. J. For. Res. 27(9): 1471–1477 (1997).
59. X. Huang, G. Rein, H. Chen, Computational Smoldering Combustion: Predicting the Roles of Moisture and Inert Contents in Peat Wildfires, Proceedings of the Combustion Institute 35, pp. 2673–2681, (2015). doi:10.1016/j.proci.2014.05.048.
60. RA Hartford, Frandsen W.H. (1992) When it's hot, it's hot. . . or maybe it's not! (surface flaming may not portend extensive soil heating). International Journal of Wildland Fire 2: 139–44. doi: 10.1071/WF9920139.
61. G. Rein, N. Cleaver, C. Ashton, P. Pironi, JL. Torero, The Severity of Smouldering Peat Fires and Damage to the Forest Soil, Catena 74, 304–309, 2008
62. Stracher, Prakash and Sokol, Coal and Peat Fires: A Global Perspective, Elsevier Geoscience, 2010, ISBN 9780444528582
63. G.B. Stracher, T.P. Taylor, Coal fires burning out of control around the world: thermodynamic recipe for environmental catastrophe, International Journal of Coal Geology 59 (2004) 7–17.
64. M.A. Nolter, D.H. Vice, Looking back at the Centralia coal fire: a synopsis of its present status, International Journal of Coal Geology 59 (2004) 99–106.
65. V. Babrauskas and J. Krasny, "Upholstered Furniture Transition from Smoldering to Flaming," *Journal of Forensic Sciences,* Nov., pp. 1029–1031 (1997).
66. O. Putzeys, A. Bar-Ilan, G. Rein, A.C. Fernandez-Pello, D.L. Urban, 2007, The role of the Secondary Char Oxidation in Smoldering and its Transition to Flaming by Ultrasound Probing, Proceedings of the Combustion Institute 31 (2007) 2669–2676 doi:10.1016/j.proci.2006.08.006.
67. S.D. Tse, A.C. Fernandez-Pello, K. Miyasaka, Controlling Mechanisms in the Transition from Smoldering to Flaming of Flexible Polyurethane foam, Proceedings of the Combustion Institute 26 (1996) 1505–1513.
68. TJ. Ohlemiller, 1991. Smoldering Combustion Propagation On Solid Wood. Fire Safety Science 3: 565–574. doi:10.3801/IAFSS.FSS.3-565
69. TJ. Ohlemiller, "Forced Smolder Propagation and the Transition to Flaming in Cellulosic Insulation," *Combustion and Flame,* 81, p. 354 (1990b).
70. A. Bar-Ilan, Putzeys OM, Rein G, et al., 2005, Transition from forward smoldering to flaming in small polyurethane foam samples, Proceedings of the Combustion Institute, 30 (2) pp. 2295–2302, 2005. doi:10.1016/j.proci.2004.08.233.

Guillermois Rein is Reader (Associate Professor) in Mechanical Engineering at Imperial College London, and Editor-in-Chief of *Fire Technology*. His professional activities are centered on research in fire and combustion, and teaching of thermofuild sciences to engineers. He has studied a wide range of fire dynamics topics in the built and the natural environments, including pyrolysis, fire modeling, wildfires, structures and fire, and forecasting techniques. Over the course of the last 15 years he has also specialized in smoldering combustion, conducting both computational and experimental studies on a variety of fuels like polyurethane foam, cellulose, peat and coal.

Spontaneous Combustion and Self-Heating

20

Brian F. Gray

Introduction

The term *spontaneous combustion* will be used here to refer to the general phenomenon of an unstable (usually oxidizable) material reacting and evolving heat, which to a considerable extent is retained inside the material itself by virtue of poor thermal conductivity of either the material or its container. Under some circumstances this process can lead to flaming combustion and overt fire, in which case it is properly called *spontaneous ignition,* which here is regarded as a special case of spontaneous combustion. This has been responsible for significant losses of life and enormous losses of property. Fire loss statistics from many sources show that spontaneous ignition is quoted as the cause in a much greater proportion of cases with multimillion-dollar losses than in smaller fires. Of course, one should also note that the proportion of "cause unknown" results follows a similar trend, probably due to the greater degree of destruction, and hence evidence loss, in larger fires.

In other circumstances, clearly delineated from the former, only relatively mild self-heating occurs. This may be referred to as *self-heating,* spontaneous combustion, or by research scientists as *subcritical* behavior. By the same token, spontaneous ignition would be referred to as *supercritical* behavior. The well-defined boundary between the two types of behavior is referred to as the *critical condition,* and it plays an absolutely central role in the area, both conceptually and pedagogically. It can crudely but pictorially be thought of as a watershed.

The critical condition is actually a whole set of combinations of parameters that affect the behavior. The most important of these are the ambient (surrounding) temperature, and the size and shape of the body of material involved. Thus for a given body of a particular material we would normally talk about the *critical ambient temperature* (CAT). If we were dealing with a situation where the size of the body were always fixed by commercial practice, for instance, this would be the normal statement of the critical condition. However, in the case of storage of a variable amount of material in a constant temperature environment, then one would talk about the critical size or the critical diameter of the body for a given fixed temperature. The CAT is the most commonly used and stated critical condition.

For both fire prevention and fire cause investigation, it is essential to be able to identify the critical condition if spontaneous ignition is a possibility either before or after the event. It is also important to be aware of other possible factors operating in particular cases, such as solar irradiation in outdoor storage and preheating if recently manufactured or processed goods are involved. In such cases as hot laundry; hot new chipboard; hot, oily, porous food products (instant noodles, fried fish scraps);

B.F. Gray (✉)
School of Mathematics and Statistics, University of Sydney, Sydney 2006, Australia

M.J. Hurley (ed.), *SFPE Handbook of Fire Protection Engineering*,
DOI 10.1007/978-1-4939-2565-0_20, © Society of Fire Protection Engineers 2016

bagasse[1]; and the like, the temperature of the material itself is a most important parameter affecting criticality in addition to the usual ones. In such cases we have to deal with and determine a *critical stacking temperature* (CST), which refers to the temperature of the material itself not the ambient temperature. The CST is dependent on the CAT and the size of the body so such cases are a degree more complicated than the traditional ones involving usually agricultural materials stacked at ambient temperature. In addition, in such cases with preheated materials the time to ignition (defined precisely later) is usually very much shorter than it is where the material is stacked at ambient temperature.

Because the basic processes competing with each other in spontaneous combustion are heat generation by chemical reaction and heat loss to the surroundings mainly by conduction, it is easy to see qualitatively why both a larger body and a higher ambient temperature will favor ignition rather than subcritical behavior as they both decrease the rate of heat loss. Generally the temperature profile across the body itself is roughly parabolic in shape with a peak at the center. Most chemical reaction rates increase almost exponentially with temperature, whereas heat loss processes such as conduction increase only linearly. Thus the center of the body where the temperature is highest is the region where ignition, or *thermal runaway*, will commence if it is going to take place at all. Many bodies that have undergone spontaneous ignition show this telltale signature of charring or complete destruction to ash in the center while retaining an almost pristine appearance on the outside, sometimes presenting rather dangerous situations for fire fighters in large-scale examples such as bagasse, woodchip, or peat piles. Similarly, the deep-seated nature of the burning started by spontaneous ignition can be difficult to extinguish completely, often reigniting days after apparent extinction.

[1] Bagasse is the residue from sugar cane after extraction, usually containing 50 % water.

The purpose of this article is to expound the detailed nature of the situations described above in a manner that approaches the principles involved in a way that minimizes mathematical formulation as far as is reasonable. The subject will be approached from the point of view of its relevance to fire cause and fire investigation and as such will refer mainly to solid systems. Many of the basic principles used were actually clarified by experimental work on gaseous systems; such systems still play a central role in current research on this topic, particularly ones where the chemical kinetics are simple and well understood in their own right.

A closely related aspect to be discussed here is the subject of *runaway reaction,* or *thermal runaway*. In the past two decades this topic has developed a literature of its own [1] and threatened to lose contact with the extensive literature on spontaneous combustion. These two terms, which can be taken as synonymous, are applied to supercritical conditions as defined above but only in the context of a chemical reactor. The reactor may be of batch, semibatch, or continuous flow type, but it will almost invariably be well stirred either mechanically or by deliberate turbulent mixing. Therein lies the attraction from a pedagogical point of view of such studies because the main difficulties in mathematical modeling of solid spontaneous combustion arising from spatial temperature variation and gradually decreasing concentration of reacting material are not present. Thus a mathematical theory describing such processes exactly serves as a first approximation, and a tractable one at that, to the more complex topic of solid spontaneous combustion. In addition, the difficult and messy "corrections" to the simplest possible theories due to Semenov [2] and Frank-Kamenetskii [3] are often impossible to apply in practical situations due to the dearth of data and/or their numerical uncertainties.

In addition, in the rare event that precise input data are available and detailed chemical kinetics are known, it is now entirely feasible for particular cases to invoke numerical integration of the relevant equations directly without use of the empirical and semiempirical curve fits involved

in the classical corrections to the simplest theories. At the time of writing, average laptop computers are quite capable of such calculations for all but the most irregularly shaped bodies where finite element methods need to be invoked and custom written.

Accordingly we will spend some time here expounding the simplest possible theory (Semenov), which contains all the essential concepts for the understanding of criticality, the tangency between heat release and heat loss curves, and the existence (or otherwise) of stable and unstable steady states. We then move on briefly to the application of such ideas to more complex chemistry and the idea of thermal runaway in continuous stirred tank reactors (CSTR).

We then discuss the Frank-Kamenetskii version of thermal explosion theory, which considers temperature gradients within the self-heating body (thereby generalizing Semenov) and often gives better agreement with experiment for solid bodies with low thermal conductivity. For this reason it is much used in fire investigations, particularly when it is necessary to predict the CAT for a large-scale industrial body from small-scale laboratory tests. However, this type of extrapolation requires great care in its application to all but the simplest chemistry.

We then present some ways in which corrections can be made to the predictions of the Frank-Kamenetskii theory occurring under conditions where some of its assumptions are not sufficiently accurate. This occurs when the heat of reaction is relatively small and/or when the resistance to heat flow in the boundary of the body (or container wall) is relatively large compared to that inside the body itself (case of small Biot number). Corrections are also necessary when more than one chemical reaction generates heat and when oxygen diffusion into the interior of the body is rate limiting.

All of these factors are difficult to handle quantitatively, but fortunately none of them really alter the *qualitative* conceptual nature of what is going on. It is important in gaining an understanding of spontaneous combustion *not* to be confused by these corrections, although in certain cases they can be quite large.

We will then move on to discuss experimental testing methods, both on a laboratory and a larger scale where possible. A large array of calorimetric methods can be used to obtain relevant information, but not all of them, particularly differential scanning calorimetry (DSC) and differential thermal analysis (DTA), can give other than very general information and therefore can often be misleading. Nevertheless, such methods have their purpose when material of unknown origin and composition is involved. Sometimes one needs to know whether the unknown is capable of exothermic reaction at all as postulation of spontaneous ignition because a fire cause looks rather silly in its absence (this happens!). However, activation energies, in particular those obtained from DSC tests, should be treated with great suspicion.

A characteristic of fires where spontaneous ignition is suspected as the cause is that they often occur on premises that have been closed up or unoccupied for a significant period of time. A question of very great interest in such a context is, What is the time scale expected for a body of a given size in a given ambient temperature to reach ignition, that is, the appearance of overt flame? As one would expect, by application of Murphy's law, this question is very difficult to answer with confidence except in the simplest of cases. The time to ignition is a parameter that is not only extremely sensitive to many factors that are often unknown but is also extremely sensitive to the degree of supercriticality, that is, how far the body is from the watershed. Not only does it depend on how far the body is from the watershed, but it depends sensitively on the direction as well. In other words, the term *degree of supercriticality* needs to be refined before any idea of time to ignition can be properly formulated.

A number of investigations of this problem have been carried out, and it is essential to recognize that most of the earlier ones addressed the question of time to ignition for the initial temperature of the body equal to the ambient temperature—such as would be the case in the building of a haystack. Hot stacked material requires totally different considerations for the evaluation

of times to ignition, and classical formulas cannot be used in such situations. Such bodies can ignite in times that may be an order of magnitude shorter than predicted by uncritically using classical formulas.

In the penultimate section of this article, we move on to discuss the actual fire scene where spontaneous ignition has been the cause, or suspected cause, of the fire. We discuss factors that would be either positive or negative indicators of spontaneous ignition, and also the appropriate examination of the aftermath of the fire for pointers as to whether or not spontaneous ignition was the cause. We then proceed to illustrate all of the above with a number of case histories, some of them common and illustrative of the basic principles expounded here, others of a novel nature involving quite subtle and detailed investigations that nevertheless can give very definite results.

The Literature

There is a large and varied literature on the topic of spontaneous combustion ranging from sophisticated mathematical theory to technical measurements on industrial and agricultural products. It is scattered over a very wide range of journals, magazines, and disciplines. The most comprehensive publication is probably the book written by Bowes [4], *Self-Heating: Evaluating and Controlling the Hazards.* This book was published in 1984 and contains references to work published up to 1981, so at the present time it is in need of updating. However, it is the most useful reference available for those working, or commencing work, in the field from either an academic or a technical viewpoint. The *Ignition Handbook* by Babrauskas [5], published in 2003, contains a very useful chapter on self-heating and has become an indispensable reference for anyone working in the area of ignition.

Although much of the understanding of spontaneous combustion has come from the basic study of gas-phase reactions, where it is generally referred to as *autoignition,* this article will be limited to spontaneous combustion of solid materials generally. Many advances have been made in the field of gaseous autoignition over the last decade or so, stemming from accurate and detailed kinetic measurements and considerable advances in computing power. The critical condition for gaseous systems is a very complex locus in the parameter space characterized by ambient temperature (as for solids), pressure, and composition. Many organic materials, such as hydrocarbons, exhibit more than one autoignition temperature, and many also exhibit the phenomenon of igniting on *decreasing* ambient temperature. Many older tabulations of autoignition temperatures do not recognize these peculiarities and should be used with great caution. A detailed description of the reasons for such complexities and their importance in a hazard context is given by Griffiths and Gray [6] in the twenty-fourth Loss Prevention Symposium of the American Institute of Chemical Engineers (1990). A comprehensive list of references up to 1990 can be found in this article.

Reference to liquid reactions and related spontaneous ignitions and thermal instabilities will be given later in this article in the section on spatially homogeneous or "well-stirred" systems. Otherwise, references will be given at points throughout this text resulting in a reasonably complete bibliography.

Concept of Criticality

Over the last two decades the concept of criticality, which has been present in the thermal context for many years [7], has been recognized as a branch of bifurcation theory [8], an area of nonlinear applied mathematics that has grown rapidly and proven to be extremely powerful in solving nonlinear problems. In our case the nonlinearity comes from the temperature dependence of the chemical reaction (and therefore heat production) rate. The Arrhenius form for this for a single reaction is $Ze^{-E/RT}$, where E is the activation energy and R is the universal gas constant. T is the absolute temperature, of course. At temperatures rather less than E/R (which can typically be 10,000 K or more), the Arrhenius

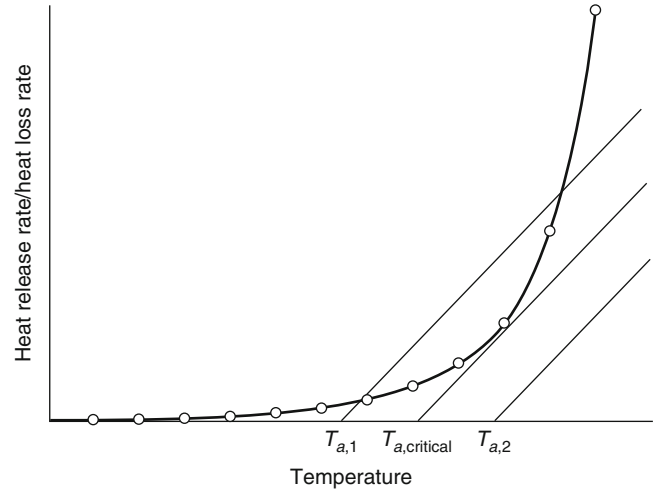

Fig. 20.1 Typical Arrheniusheat release and loss curves

function is very convex; that is, it curves upward rather rapidly with temperature. In contrast, the rate of heat loss from a reacting body is generally only a linear function of temperature, for example, conduction. Although radiation losses are nonlinear functions of temperature, they are much more weakly nonlinear than the Arrhenius function and also generally rather small at the low temperatures involved in solid spontaneous combustion although they are important in flame extinction. Typical heat generation per unit volume and heat loss (proportional to surface volume ratio as plotted) loci are shown in Fig. 20.1.

The low temperature range of the Arrhenius curve is seen here to be rather convex and rapidly increasing with temperature. The three straight lines represent the rate of heat loss from a body of fixed given size at various ambient temperatures $T_{a,1}$, $T_{a,\text{critical}}$, and $T_{a,2}$.

At $T_{a,1}$ it can be seen that the heat production and loss curves intersect at two points. At $T_{a,2}$ they do not intersect at all, and at $T_{a,\text{critical}}$ they intersect at only one point and, in fact, touch tangentially.

Because intersections represent conditions where heat production and loss balance exactly, we expect them to represent some sort of "equilibrium" or stationary point where the temperature of the body remains constant in time. It is important to remember that they do not represent equilibrium in any thermodynamic sense.

In the region of the lower intersection at $T_{a,1}$ it can be seen from the diagram that the temperature of the body will increase up to the balance point from below as heat release is greater than heat loss in this region. On the other hand, just above this balance point the temperature of the body will move down to it because the heat release is lower than the heat loss in this region. Thus the lower balance point occurring at ambient temperature $T_{a,1}$ is recognized as a *stable* balance, or stationary, point. Small perturbations from it will be nullified, and the body in this region will tend to stay at the balance point. Note that the temperature of the balance point is not $T_{a,1}$ but slightly above it, usually by 5–20 °C. It represents subcritical self-heating and can cause loss of the material but not by overt ignition or fire. It can appear as degradation or discoloration of many materials, making them useless for their required purpose. For example, woodchips degraded in this way are not suitable for paper or cardboard production, and dried milk powder when discolored is unacceptable.

The second balance point at the ambient temperature $T_{a,1}$ can be seen by a similar simple analysis to be *unstable* in the sense that, in the temperature region just below it, the heat production is *lower* than the heat loss, so the temperature tends to drop. In the temperature region just above it, the converse is true, so the body temperature tends to rise and leave the balance point.

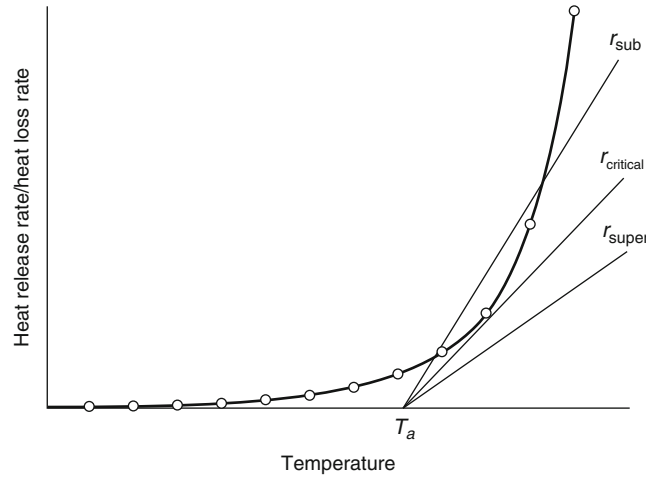

Fig. 20.2 Disappearance of balance points with body size increase

The latter acts as a watershed between two totally distinct types of behavior, that is, the temperature of the body dropping to the lower balance point or running away to the right of the diagram and much higher temperatures, representing ignition.

Here the temperature at the higher balance point would actually be the *critical stacking temperature,* or CST, for this particular body when stored at ambient temperature $T_{a,1}$. We can immediately see that if the ambient temperature is increased, that is, the straight line is moved to the right with fixed slope (which is determined by the size and shape of the body as we shall see later), the CST will *decrease,* a physically reasonable and intuitive result.

Thus this oversimplified but extremely useful model gives a simple understanding of what Bowes refers to as *thermal ignition* of the second kind, that is, what is probably better referred to as the *hot stacking problem,* a much more descriptive term. Not only that, but it also gives us a qualitatively correct picture of the more common or "normal" type of thermal ignition when the body self-heats from ambient to ignition without any preheating. At $T_{a,1}$ if we very slowly increase the ambient temperature after the steady state has been reached, we can see that the now "quasi-steady state" will also slowly increase until at $T_{a,\text{critical}}$ the quasi-steady state and the CST merge at the point of tangency. Beyond this ambient temperature there is no balance point, and in this temperature region the heat release curve is now *always above the loss line* and therefore the temperature can only increase. Subsequent ignition will then occur. It will occur after some delay because the rate of temperature increase in this simple model is proportional to the imbalance between heat production and loss (i.e., the vertical distance between the two curves). This is initially quite small, increasing as the temperature rises. In this observation lie the seeds of the calculation of the *ignition delay* or *time to ignition* (TTI) to be examined later.

Even more insights can be obtained from this simple type of reasoning. As we shall see later, the slope of the heat loss line is dependent on the surface area/volume ratio of the body in question. Thus for a body of given shape the surface/volume ratio increases as the body gets smaller and decreases as the body gets larger. In Fig. 20.2 we can see the effect of increasing the size of a body at a fixed ambient temperature. For this fixed ambient temperature we can speak of subcritical, critical, and supercritical sizes for the body, depending on whether any balance points exist.

Thus for a body with characteristic dimension r_{sub} we see the existence of both a CST and a balance point. For a larger body with dimension r_{super} we see that neither exists and we expect temperature to rise to ignition. The critical condition, in this case expressed as a radius or body dimension, is given again by the tangency condition. This critical condition, of course, is

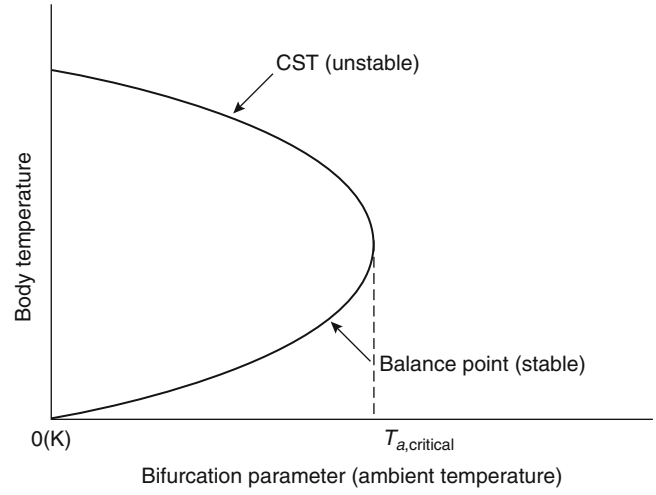

Fig. 20.3 Variation of CST and stable subcritical temperature with ambient temperature and fixed body size

identical with that obtained by thinking of the quasi-static variation of the ambient temperature as well. The critical radius for a given ambient temperature will be identical with the CAT for a body of that same radius. How we describe it is simply a matter of where we are coming from.

Of course, we do not usually continuously vary the size of a body but we *do* often stack bodies together, for example, bales of cotton, bales of hay, and so on, and allow larger than normal quantities to accumulate, for example, coal stockpiles. Even from the point of view of this very rudimentary theory, it is obvious that the CAT of two bales in contact will be considerably less than that for a single bale. Thus tests of the CATs of single bodies that are going to be stacked in groups for either transport or storage are useless unless a theory is available enabling calculation of the dependence of CAT on body size. The theory allowing this is thus extremely useful in relating practical tests on small bodies to be applied to storage of large numbers of them (with certain caveats to be discussed later).

To conclude this section it remains to show a convenient method of representing the behavior of the stable balance point and the unstable CST as a control parameter is varied (i.e., the ambient temperature or size of the body). This method enables a quick and convenient representation of the discussion given above on a single diagram (a bifurcation diagram) and also gives us a useful link to the mathematical developments of bifurcation theory.

Figure 20.3 shows what happens to the balance point temperature and the CST when T_a is varied continuously from below its critical value to above it. This takes place at constant body size. In this case the ambient temperature is known as the bifurcation parameter. We should note that, even at very low ambient temperatures, the CST tends to a finite limit. In fact it becomes very insensitive to the ambient temperature, and no matter how cold the ambient temperature, there is no corresponding *rise* in the CST. Storing hot products in a cold warehouse does not help the problem much!

Conversely Fig. 20.4 shows how the CST rises indefinitely as the size of the body decreases at fixed ambient temperature. Regardless of ambient temperature it does pay to keep hot stored bodies small! Figure 20.4 also shows how, for sizes above the critical radius, there is no alternative but ignition. Of course the critical radius depends on the ambient temperature, and as the latter goes down the critical radius goes up. It is sometimes very useful to draw a critical radius versus critical ambient temperature graph, and we will see how to do this later.

The whole discussion above assumes that we are dealing with a given material so that the thermal and chemical properties do not vary. The effects of varying thermal conductivity, heat transfer coefficients, and density on the

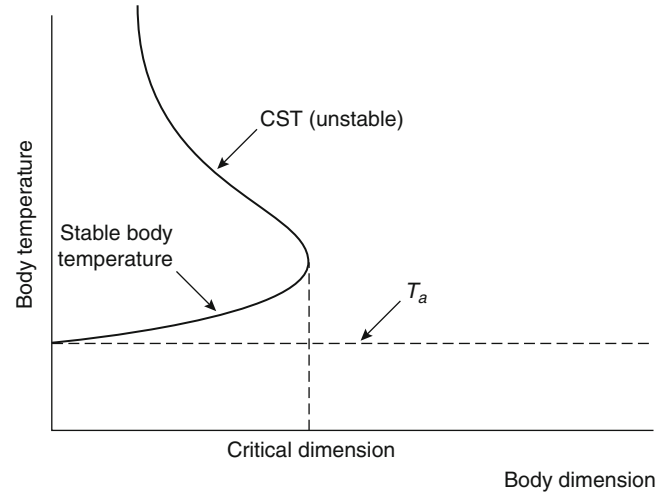

Fig. 20.4 Variation of CST and stable subcritical temperature with body dimension and fixed ambient temperature

critical condition are also important but only when comparing different materials. The dependence of the critical condition on these properties will be enunciated in a later section.

One final point needs to be mentioned here. The Arrhenius function does actually level out to an asymptote at very high temperatures, which are off the scale in Figs. 20.1 and 20.2. Thus theoretically there is another balance point at very high temperatures, but in fact this point is not physically significant as it usually occurs at many thousands of degrees, well beyond the region where the assumptions of the model are valid. It also gives rise to a high temperature branch of the curves in Figs. 20.3 and 20.4, which is disjoint from the curves shown. Again it can be ignored from the point of view of low-temperature spontaneous ignition.

The Semenov (Well-Stirred) Theory of Thermal Ignition

The Semenov theory represents the simplest mathematical formulation of the ideas presented above in qualitative form. As such it is a valuable introduction to quantitative aspects of spontaneous ignition without introducing the technical difficulties associated with more elaborate forms of theory where spatial variations of temperature and reaction rate within the body are considered.

Assumptions of the Semenov Theory

The three assumptions of the Semenov theory are as follows:

1. **The temperature within the reacting body is spatially uniform:** A spacially uniform temperature implies that either the material of the body is well stirred (i.e., it would have to be liquid or gas) or the resistance to heat flow within the body is so low compared to that within the container or boundary that it can all be assumed to be concentrated within the boundary. The latter results in a temperature discontinuity at the boundary of the material and is a good approximation in deliberately stirred fluids [9].

   It is not a good approximation for materials of vegetable origin where thermal conductivities of materials such as cellulose are low and of the order of 0.05 W/mK. Nevertheless, even for such materials semiquantitative conclusions can be drawn from this theory if the spatially averaged temperature of the body is used.
2. **The heat generation is assumed to be due to a single chemical reaction:** This assumption is often a reasonably good approximation, particularly when a "lumped" or empirically determined rate law has been measured independently. It does not mean that the chemical reaction taking place is only a single-step

reaction. In fact this empirical approximation works quite well in many cases that are not single-step reactions.

3. **Both the heat of reaction and activation energy are assumed to be sufficiently large to support ignition behavior:** The reasons for these assumptions will become clearer later, but it is intuitively obvious that if there is zero heat of reaction, ignition cannot occur. Likewise with zero activation energy (acceleration of reaction rate with temperature increase), ignition cannot occur either.

With these assumptions we can write down two equations that determine the temperature and fuel concentration as functions of time (but uniform in space). These are simply the conservation of energy and the kinetic rate law, respectively. They are

$$C_v \rho V \frac{dT}{dt} = VQf(c)e^{\frac{-E}{RT}} - S\chi(T - T_a) \quad (20.1)$$

$$\frac{dc}{dt} = -f(c)e^{\frac{-E}{RT}} \quad (20.2)$$

where

C_v = Heat capacity at constant volume
ρ = Density
V = Volume
T = Temperature of the reacting material (in K)
T_a = Ambient temperature of the surroundings (assumed constant in time)
Q = Heat of reaction per unit concentration of fuel
$f(c)$ = Kinetic rate law
c = Concentration of fuel
E = Activation energy of the reaction
R = Universal gas constant
S = Surface area of the interface across which heat is lost to the surroundings
χ = Heat transfer coefficient

The independent variable is time.

The first term on the right-hand side of Equation 20.1 represents the rate of heat generation by the self-heating reaction. The second term represents the heat lost to the surroundings. The left-hand side represents the difference between these two. Equation 20.2 simply expresses the fact that as the reaction proceeds, the concentration c decreases as the fuel is used up. The commonest and simplest form for $f(c)$ is Zc where Z is known as the pre-exponential factor, a constant. This case is known as a first-order reaction. These two terms are shown graphically in Fig. 20.1 for any particular value of c.

Despite their apparent simplicity these two equations are not soluble by classical methods, so we cannot write down their solution. Nevertheless, we can in fact write down the critical condition exactly (and other important quantities) using bifurcation theory. We will illustrate this for the simplest possible case only, remembering that it can also be done for more realistic and complicated cases as well within the confines of the Semenov theory.

First we write Equations 20.1 and 20.2 in dimensionless form (see nomenclature for details),

$$\frac{du}{d\tau} = \nu e^{\frac{-1}{u}} - \ell(u - u_a) \quad (20.3)$$

$$\frac{d\nu}{d\tau} = -\varepsilon \nu e^{\frac{-1}{u}} \quad (20.4)$$

where

u = Dimensionless temperature
ν = Fuel concentration
ε = A dimensionless version of the ratio C_v/Q (i.e., a measure of the amount of fuel decomposition required to produce a temperature rise of 1 °C)
τ = A dimensionless time
ℓ = A dimensionless heat transfer coefficient

The most frequently used version of this theory, without fuel consumption, corresponds to taking the limit $\varepsilon \to 0$, thus maintaining ν at its initial value ν_0. We have only a single equation to deal with now, that is,

$$\frac{du}{d\tau} = \nu_o e^{\frac{-1}{u}} - \ell(u - u_a) \quad (20.5)$$

Even this much-simplified equation is not analytically soluble. However, it relates exactly to Fig. 20.1 and can be used to calculate the critical condition readily. We first note that the balance points in Fig. 20.1 must satisfy the equation

$$v_0 e^{\frac{-1}{u_s}} - \ell(u_s - u_a) = 0 \qquad (20.6)$$

For subcritical values of the ambient temperature, this equation will have three solutions for a given set of parameter values, v_0, u_a, and ℓ. From Fig. 20.1 it can be seen that at the critical condition ($T_{a,\text{critical}}$ corresponding to $u_{a,\text{critical}}$) not only do the two terms of Equation 20.6 balance, but their *slopes* also balance at this condition. Mathematically this means that their differential coefficients with respect to temperature must also be equal, that is,

$$\left[\frac{\partial\left(v_0 e^{\frac{-1}{u}}\right)}{\partial u}\right]_{u=u_s} = v_0 e^{\frac{-1}{u_s}}/u_s^2 = \ell \qquad (20.7)$$

The critical value of u_s is then obtained by solving Equations 20.6 and 20.7 simultaneously, which interestingly can be done in closed form simply by eliminating the exponential, leaving a quadratic equation:

$$u_{s,\text{ critical}}^2 - u_{s,\text{ critical}} + u_{a,\text{ critical}} = 0 \qquad (20.8)$$

From our definition of $u = RT/E$ and the general knowledge that $R/E \cong 0.0001$ for most combustion reactions, we can see that at normal ambient temperatures for ignition we will have $u_{a,\text{critical}} \cong 0.02$, or in any case $u_{a,\text{critical}} \ll 1$. Using the standard formula for the solution of a quadratic equation and expanding the radical occurring, we can derive

$$u_{s,\text{ critical}} = u_{a,\text{ critical}} + u_{a,\text{ critical}}^2 + \ldots \qquad (20.9)$$

which is the lower of the two roots (the upper one is unphysical).

If we substitute this back into either Equation 20.6 or 20.7 we get a relationship between the parameters of the problem, *that holds at criticality only*. Thus if we use Equation 20.6, we obtain, after some rearrangement,

$$\ell_{\text{critical}} = \frac{-1}{v_0 e^{u_{a,\text{ critical}}\left(1+u_{a,\text{ critical}}\right)}} \Big/ u_{a,\text{ critical}}^2\left(1+u_{a,\text{ critical}}\right)^2 \qquad (20.10)$$

We can interpret this equation in a number of ways. Since ℓ_{critical} involves the size of the body as the only physically variable parameter, and v_0 is proportional to the bulk density of the material, we can take this equation to give us the critical size body for a given ambient temperature and bulk density. $u_{a,\text{critical}}$ is the only parameter here that cannot easily be made the argument of the equation.

Converting Equation 20.9 into dimensional form quickly gives us the relationship:

$$T_{s,\text{critical}} - T_{a,\text{critical}} \equiv \Delta T_{\text{critical}} \cong RT_{a,\text{critical}}^2/E \qquad (20.11)$$

at the critical condition. $\Delta T_{\text{critical}}$ would typically be 20–30 °C for ambient temperatures around 30–40 °C. Not surprisingly, it is independent of the body shape, being dependent only on the total surface area through which heat is lost. Nevertheless, even this oversimplified result can be very useful in an emergency situation. If E is not known, it is a useful rule of thumb (especially for agricultural cellulosic materials) that self-heating of more than 30° above ambient, that is, typically a body temperature of more than 60–70 °C, represents imminent spontaneous ignition, whereas an internal body temperature of 35–40 °C represents subcritical heating unlikely to run away but quite likely to lead to degradation of the material.

Two further points need to be made before leaving this simplified model. First, in order for Equation 20.8 to have real roots, it is necessary to require that

$$E \geq 4RT_{a,\text{critical}} \qquad (20.12)$$

Physically this means that the chemical heat generation rate is sufficiently accelerative to produce the phenomenon of criticality. If it is not satisfied, there is only a single stable balance point for all conditions and no abrupt change in behavior can occur.

Second, if we examine Equation 20.10, the critical condition, we should note that where the concentration v_0 appears, in the case of gases we would normally convert this to pressure. Thus, in this case, Equation 20.10 gives a relationship between ambient temperature and

pressure at the critical condition. This is the familiar explosion limit curve extensively used in the study of gaseous explosions.

Inclusion of Fuel Consumption

If we do not make the assumption $\varepsilon \to 0$ in Equation 20.4, the clear distinction between subcritical and supercritical behavior no longer exists. We can no longer define the critical condition as the disappearance of two balance points. Equations 20.3 and 20.4 possess only a single balance point, $u = u_a$ and $c = 0$ for all possible parameter values; and this refers to the equilibrium state when all fuel has been exhausted and nothing is happening—clearly a condition of no interest. For the definition of criticality in such a case it is helpful to examine the *experimental* or *phenomenological* definition. The experimentalist determines the critical condition by performing various tests at differing ambient temperatures (we will outline the details of test procedure in a later section) and by measuring the temperature-time history at the center of the sample. He or she will plot the maximum temperature attained against ambient temperature and will find there is a very steep increase in slope over a narrow region of ambient temperature. This is illustrated in Fig. 20.5.

The distinction between points 1 and 2 is very clear in terms of both the maximum temperature attained and the physical condition of the material itself after the test is finished. Typically at point 2 the material is hardly different visually from the initial condition, whereas at point 1 there is usually no more than a small amount of ash remaining. The temperature attained at point 1 is often of the order of hundreds of degrees above ambient compared with probably 30° above ambient at point 2.

It is impossible to get points between 1 and 2 experimentally without wasting a great deal of time due to the extreme sensitivity in this region, so the convention is to define the CAT as the arithmetic mean of $T_{a,1}$ and $T_{a,2}$. With good equipment these will be only 3° or 4° apart at the most.

From the point of view of theoretical calculation of the CAT in this case, we note that the points in Fig. 20.5 can be joined by a smooth curve with a very steep region around an inflection point. It has been shown (Gray [10]) that this definition of the CAT, when fuel consumption is significant, leads to a relation between the usual parameters and this relation passes over smoothly to the one derived from the tangency condition as $\varepsilon \to 0$. For $\varepsilon \cong 0.05$ or less, which is the case for most practically important materials, the corrections arising from fuel consumption are not usually significant. This is especially the case in fire investigations where a posteriori numerical knowledge of parameter values is rather limited, and this correction (and others) is not justified.

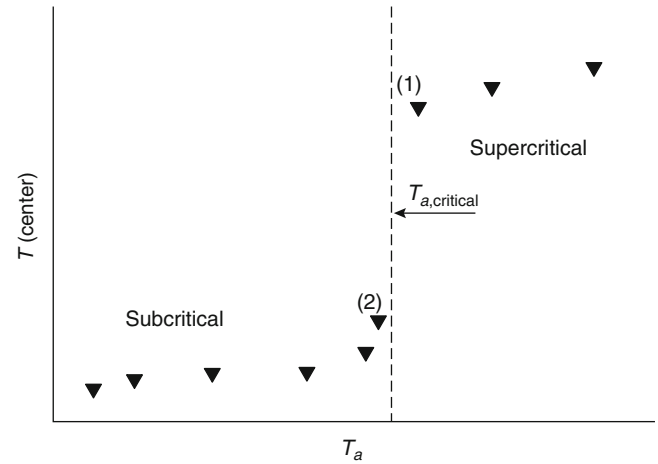

Fig. 20.5 Typical experimental results for criticality tests

Extensive discussion of earlier work on the fuel consumption correction is given in Bowes's book [4]. Many empirical and semiempirical corrections were devised based on approximated integration of Equations 20.3 and 20.4. These corrections will not be discussed here because the advent of powerful PC and laptop computational capabilities has rendered them irrelevant. Equations 20.3 and 20.4 can be integrated with great speed and precision if accurate parameter values are available. Even so, it is necessary to have a definition of criticality when a computed or experimental version of Fig. 20.5 has been obtained. With the definition given in Gray [10] allied with numerical integration, the problem can be regarded as solved for all practical purposes.

Extension to Complex Chemistry and CSTRs

Complex Chemistry

Other than elementary gas-phase reactions, very few examples of chemical change occur via a single step as assumed above. As already remarked, the simple theory is more useful than might be expected because many complex chemical reactions behave as if they were a single step, over limited temperature ranges. This is usually because a single step does dominate the heat production rate, for example, when two reactions occur in parallel. If the activation energies are rather different, they will each in turn dominate the heat generation in two different temperature ranges, and in each of these ranges the simple theory will hold. Of course, it will not hold in the changeover region.

Another case where the simple theory can hold unexpectedly is when a number of reactions are in series and one is particularly slow. The slow reaction will determine the overall heat generation rate and its parameters will dominate the critical condition. If none of the above conditions hold, it is still possible to derive a generalization of the theory that is conceptually very closely related. It is possible to prove (Gray [11]) that if the heat release rate is defined as the sum of the heat release rates of all reactions taking place in the system, then the critical condition can be defined as the tangency of this quantity with the heat loss line. Thus a diagram like Fig. 20.1 can be drawn and the same constructions used, provided the total heat release curve for all the reactions is used.

The heat release curve in this case can have a complex shape, and thus *more than one* critical condition can occur. This state of affairs is extremely important in the ignition of most organic vapors, particularly hydrocarbons [6] where some critical conditions occur on *decreasing* the ambient temperature. Also in the ignition of some commonly occurring solids, particularly when wet, more than one heat-generating reaction can be important, for example, in the spontaneous ignition of moist bagasse [12]. In this case there are two critical conditions, one where a jump from virtually no self-heating to self-heating of ~35 °C occurs, and a second critical condition where this intermediate state jumps to full-fledged ignition. Modelling of such situations is possible but beyond the scope of this chapter; however, similar behavior is likely to occur in other moist cellulosic materials, including hay, chipboard, and so forth.

At this stage it is worth pointing out that for bagasse at least, microbial "heat production" is not a factor in these phenomena. Although natural bagasse contains large numbers of microorganisms, sterilization by various methods *does not affect heat production or self-heating* at all, as measured by Dixon [13] and predicted on the basis of bacterial microcalorimetric data by Gray [14]. Similar work on hay is under way.

CSTRs and Thermal Runaway

Strangely, this topic has become uncoupled from work on spontaneous ignition over recent years even though the basic principles and mathematical methods used are similar. It is a huge problem in the chemical process industry and receives much attention. For example, in 1998 the Joint

Research Centre of the European Commission, Institute for Systems Informatics and Safety, produced a book describing the proceedings of a European Union seminar held in Frankfurt in 1994 that managed to avoid almost completely any reference to the fundamentals of the problem or related material. *Risk analysis* appears to have replaced fundamental scientific understanding in some aspects of this problem.

We will confine ourselves here to writing down the basic equations governing a single exothermic chemical reaction taking place in a CSTR (continuously stirred tank reactor) to exhibit their similarity to the equation describing a spontaneously ignitable material, that is, Equations 20.3 and 20.4.

The appropriate equations for this case are in fact 3 and 4 with terms representing inflow and outflow of reactants and products, that is,

$$V\rho C_v \frac{dT}{dt} = QVf(c)e^{\frac{-E}{RT}} - S\chi(T - T_a) - FC_v\rho\left(T - T_f\right) \tag{20.13}$$

$$V\frac{dc}{dt} = -Vf(c)e^{\frac{-E}{RT}} + F\left(c_f - c\right) \tag{20.14}$$

F is a volumetric flow rate and the subscript f refers to feed values. These equations can be cast in dimensionless form also. Here we simply note that they possess steady-state (balance point) solutions without making any approximations at all (such as neglect of fuel consumption), and Fig. 20.1 can be applied directly in slightly modified form. The critical condition referred to earlier occurs here also, but it can now be stated in terms of the CAT or a critical feed temperature or, indeed, a critical flow rate.

A critical size also occurs and this is particularly prominent in CSTR considerations where "scaleup" from prototype size to commercially viable size has resulted in exceeding the critical condition. Some references to this are given in *Safety and Runaway Reactions* [1], and there are many more in the chemical engineering literature and the study of self-heating in catalyst particles. See Aris [15] for an excellent discussion of this area.

The Frank-Kamenetskii Theory of Criticality

In its original form, the Frank-Kamenetskii theory included a more realistic model of heat transfer within the reacting solid, that is, by incorporating the heat conduction law of Fourier. This law allows a calculation of the variation of temperature within the self-heating body itself and allows comparison of measured and calculated self-heating to take place. However, it sacrifices the simple description of time-dependent behavior given by the Semenov model because such considerations involve the solution of partial differential equations. This is now much faster than even a few years ago, in terms of numerical computation, and improving day by day. Nevertheless, such numerical solutions do not lend themselves to simple interpretation even with the use of rapidly developing visualization techniques. Construction of appropriate meshes for finite element computation, necessary for practically occurring three-dimensional shapes, is also far from trivial.

As a result, the Frank-Kamenetskii theory is still mainly used for interpretation of testing experiments on self-heating and subsequent evaluation of parameters for individual systems. This is a viable proposition for materials with sufficiently large heats of reaction and activation energies. In such cases we shall see that the stationary (in time) conditions assumed in the Frank-Kamenetskii theory are indeed well approximated for the duration of typical tests in practical cases. In its original form this theory also neglects fuel consumption, as does the Semenov theory, with similar consequences. With these assumptions, the equation describing the theory is

$$\kappa\nabla^2 T + Qf(c_0)e^{\frac{-E}{RT}} = 0 \tag{20.15}$$

with the boundary condition $T = T_a$ on the wall(s) of the body. T_a is the ambient temperature of the surroundings. This boundary condition assumes instantaneous transfer of heat from the surface of the body to the surrounding medium (usually air).

When this is not approximately correct, very important consequences follow, as we shall see in a later section on the interaction of self-heating bodies with each other. In this formulation the shape of the body and its size both enter the mathematical formulation through the boundary condition only.

As usual, Equation 20.15 is not analytically soluble. However for a one-dimensional infinite slab of material by using an approximation to the Arrhenius function (Frank-Kamenetskii [3]), the modified equation can be solved analytically. The same approximation was later shown to be analytically soluble for an infinite cylinder by Chambre [16].

With this approximation, Equation 20.15 takes the form

$$\nabla^2\theta + \delta e^{\vartheta} = 0 \tag{20.16}$$

with $\theta = 0$ on the boundary. θ is a dimensionless temperature defined by

$$\theta = \frac{E(T - T_a)}{RT_a^2} \tag{20.17}$$

that is, it is a measure of the temperature excess within the body at various points. The dimensionless parameter δ is defined by Equation 20.18:

$$\delta = \frac{QEr^2 f(c_0) e^{\frac{-E}{RT_a}}}{\kappa RT_a^2} \tag{20.18}$$

where the symbols are already defined apart from r, which is usually one-half of the smallest dimension of the body, that is, the radius of a cylinder, the radius of a sphere, or the half-width of a slab. Mathematical treatment of Equation 20.16, whether it is exactly soluble or not, indicates that a solution satisfying the boundary conditions exists only when δ is less than or equal to δ_{critical} where δ_{critical} is some number depending on the shape of the body only. For an infinite slab of material $\delta_{\text{critical}} = 0.878$, and for an infinite cylinder it has the value 2.000. For other shape bodies, the critical value has to be obtained either numerically or by semiempirical methods outlined in some detail by Bowes [4]. For convenience, a few of the values are listed in Table 20.1.

Table 20.1 Values of δ_{critical} for various geometries

Geometry	Dimensions	δ_{critical}
Infinite plane slab	Width 2_r	0.878
Rectangular box	Sides *2 l, 2r, 2 m;* $r < l, m$	0.873 $(1 + r^{2/12} + r^2/\text{m}^2)$
Cube	Side 2_r	2.52
Infinite cylinder	Radius $_r$	2.00
Equicylinder	Height 2_r, radius $_r$	2.76
Sphere	Radius $_r$	3.32
Infinite square rod	Side 2_r	1.700

The tabulation of figures for infinite slab or infinite square rod is useful insofar as they are often rather good approximations for real bodies, provided one or more of their dimensions are much larger than the others. Thus for the rectangular box, if we take $r = l = 1$, $m = 10$, we get $\delta_{\text{critical}} = 1.75$ compared to 1.700 for the infinite square rod. If we now look at Equation 20.18 for the particular case of a cube as an example, we get

$$\frac{QEf(c_0)r^2 e^{\frac{-E}{RT_{a,\text{critical}}}}}{\kappa RT_{a,\text{critical}}^2} = 2.52 \tag{20.19}$$

at the critical condition. We have a number of choices as to interpretation of this equation depending on which parameter can be made the argument. If r is chosen as the argument, then the equation would be interpreted as giving a critical size for the body at a fixed ambient temperature T_a. Because c_0 depends on the density of the material, Equation 20.19 could be rearranged to give a critical density for that particular size body at ambient temperature T_a. What is not possible is isolation of T_a as the argument of the equation, and this is often the most easily varied parameter in a typical test oven.

This complex dependence of the critical condition on T_a is dealt with by rearranging Equation 20.18 and taking natural logarithms as follows:

$$\ln\left[\frac{\delta_{\text{critical}} T_{a,\text{critical}}^2}{r^2}\right] = \ln\left[\frac{QEf(c_0)}{R\kappa}\right] - E/RT_{a,\text{critical}} \tag{20.20}$$

from which it can be seen that a plot of $\ln[\delta_{\text{critical}} T_{a,\text{critical}}^2/r^2]$ against $1/T_{a,\text{critical}}$ will be a straight line with slope $-E/R$ and intercept $\ln[QEf(c_0)/\kappa R\delta_{\text{critical}}]$. The traditional and recommended test protocol for spontaneous ignitions makes explicit use of this logarithmic form of the critical condition. Not only does it yield the activation energy from the slope, but the occurrence of a straight line plot assures us that the assumption of an Arrhenius temperature dependence for the heat-generating reaction is correct over the temperature range investigated.

Equation 20.20 can also be regarded as a scaling law, in principle enabling the prediction of CATs for large-scale bodies from measured CATs for much smaller laboratory-sized samples. However, as we shall see, it is necessary to ensure that the same chemical kinetics applies over the whole temperature range involved, that is, $f(c_0)$ *does not vary*. Finally, if it becomes necessary to estimate the CAT for a complex shape, not included in Table 20.1, an excellent and comprehensive discussion of approximation methods is given by Boddington, Gray, and Harvey [17].

Experimental Testing Methods

Experimental testing methods are traditionally based on the scaling relationship (Equation 20.20). Appropriate containers (usually stainless steel gauze baskets) of various dimensions are used, being limited only by the size and heating capability of an accurately thermostatted oven, which must also have a spatially homogeneous ambient-temperature distribution (±0.5 °C is recommended). The gauze containers may be any convenient shape, equicylindrical or cubic being preferred due to ease of construction. The gauze does not restrict oxygen ingress through the boundary, nor does it restrict egress of carbon dioxide and other product gases during combustion. If the air inside the oven is sufficiently turbulent, usually the boundary conditions of the Frank-Kamenetskii theory will hold quite well.

The boundary condition is easier to satisfy when the thermal conductivity of the material inside the gauze baskets is relatively low, as it is with many agricultural materials containing cellulose ($\kappa \sim 0.05$ W/mK). The efficacy of the boundary condition is determined by the heat transfer rate from the gauze to the oven air relative to the conduction rate within the material itself. This ratio ($\chi r/\kappa$) is known as the Biot number, and the larger it gets, the more accurate the Frank-Kamenetskii boundary condition ($T = T_a$) becomes. In practice a Biot number greater than 30 is effectively infinite as the CAT becomes extremely insensitive to it. We will return to this topic in a later section where the dependence of the critical condition on the Biot number will be outlined.

The test procedure involves starting with the smallest basket and a trial oven temperature. The sample is equipped with one or more fine thermocouples placed at the center of the sample and, if desired, at various places along a radius if a spatial profile is wanted (this is generally not necessary). The sample is placed in the preheated oven and the center temperature followed as a function of time. If the oven temperature is well below the CAT, the sample will simply approach the oven temperature asymptotically. If it is slightly below, but getting close, it will cross above the oven (ambient) temperature and attain a maximum of the order of 1–30 °C above ambient before declining. This represents the subcritical condition.

The sample is discarded and replaced with a fresh, similar one. If the previous run was subcritical, the oven temperature will be increased by usually 20 °C or less depending on the experience of the operator. The run is then repeated. If it is still subcritical, the procedure is again repeated until a supercritical oven temperature is attained. The arithmetic mean of the lowest supercritical temperature and the highest subcritical temperature is taken as the first estimate of the CAT. The uncertainty may be quite large at this stage so the process is usually continued by testing at the estimated CAT. The process is repeated, halving the difference between highest subcritical and lowest supercritical temperatures each time until the desired errors are obtained. Typical

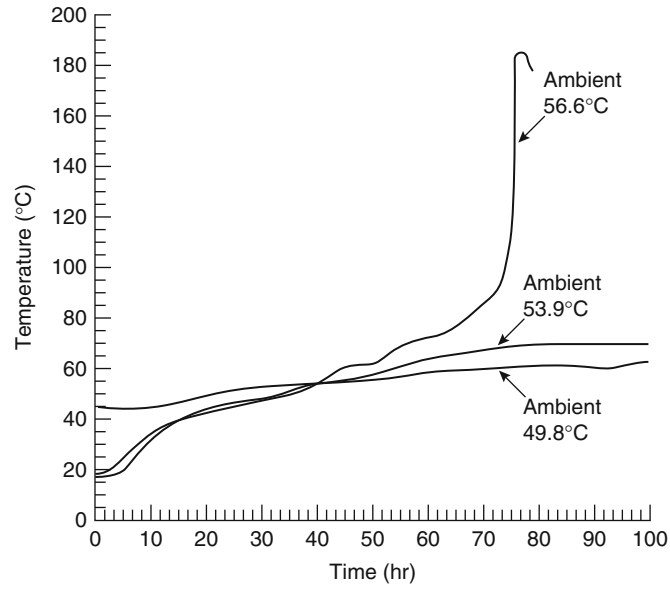

Fig. 20.6 Two subcritical and one supercritical center temperature/time traces for a 0.175-m-radius equicylinder of hydrated calcium hypochlorite [17]

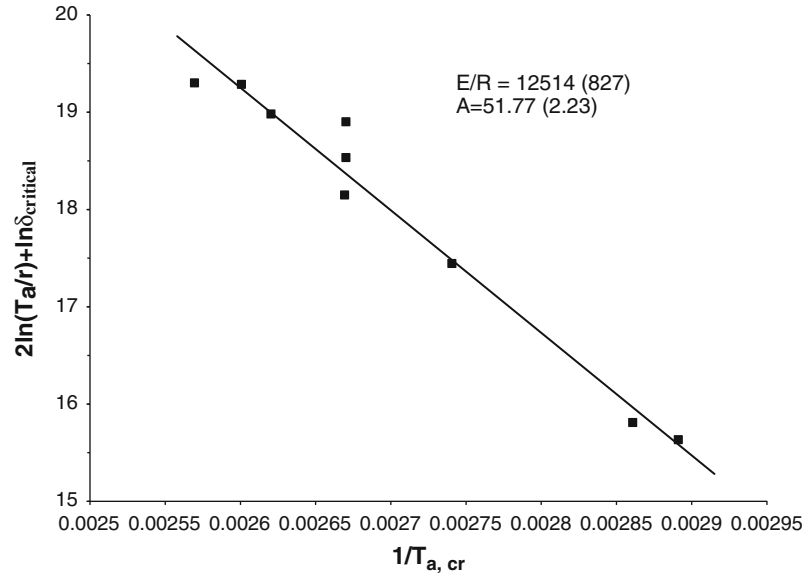

Fig. 20.7 Recalculated Frank-Kamenetskii plot for the data of Uehara et al. on anhydrous calcium hypochlorite [19]

temperature-time plots showing the critical separation are shown in Fig. 20.6.

This reaction is an exothermic decomposition evolving oxygen [18]. From these measurements one would conclude that the CAT was 55.2 ± 1.34 °C. For greater accuracy the next test would be run at an ambient temperature of 55.2 °C. After at least four or five such sets of runs have been carried out in different size containers, giving four or five CATs at various radii, then the next step is to construct the Frank-Kamenetskii plot of the scaling Equation 20.20. A typical plot is shown in Fig. 20.7.

This plot shows a range of CATs for cylinders ranging in radius from 0.191 m down to 0.026 m, the larger radii corresponding to commercial containers. From the slope of this line, E/R can be read off directly, and, from the intercept, so

can the dimensionless group occurring in the scaling equation. Sometimes components of this group may be known from independent measurements, for example, Q from calorimetry, κ from direct measurement, or $f(c_0)$ from kinetic measurements, in which case all the parameters can be obtained.

Special Cases Requiring Correction

Presence of Water

When water is present in spontaneously combustible material, special considerations apply. First it is necessary to note that endothermic evaporation would be expected to partly offset some of the heat generation by the exothermic reactions taking place. Although this is true, it is often the case that at the high oven temperatures used in testing small samples, the low activation energy for evaporation (~40 kJ/mol) leads to rapid evaporation before the exothermic process has got under way fully. Many spontaneous combustion reactions have activation energies around 100 kJ/mol, particularly the group of reactions of cellulosic materials.

As a result, the high-temperature CATs reflect the properties of the dry material, in particular the thermal conductivity. Consequently, extrapolations to temperatures well below 100 °C will be questionable for this reason alone. In the lower temperature range the heat transfer will be significantly affected by the presence of water and its transport from the hotter to the cooler regions of the body by evaporation, diffusion, and condensation.

Many cellulosic materials are known to exhibit a "wet reaction" [20, 21] in addition to the dry exothermic reaction. This reaction involves liquid water as a reactant and further complicates the picture as far as high-temperature testing is concerned. Simultaneous evaporation, diffusion, condensation, and reaction involving water have been modeled recently in connection with bagasse [22, 23], using an experimentally measured rate law for the wet reaction [24] giving results that are in good agreement with measured results for commercial-size piles of this material (minimum dimension 5–10 m).

The detailed nature of the wet reaction with a rate maximum around the 50–60 °C mark has led to false identification with microbial activity. In bagasse at least it has been shown [25] that microbial activity does not contribute to self-heating to any significant degree. Piles sterilized by various methods showed self-heating rates indistinguishable from those of nonsterile piles. Microbial counts were carried out in all cases and large decreases did not affect the self-heating rates. It would be rather surprising if similar results were not obtained from tests on hay and straw where microbiological activity (but not necessarily heating) are known to occur, and it is surprising that such tests have not yet been carried out.

Parallel Reactions

If more than one exothermic reaction can take place in the material, and these reactions have rather different activation energies, then each will dominate in its own temperature range. Thus the higher activation energy reaction will cut in at higher temperatures and be insignificant at lower temperatures when the low activation energy reaction will dominate the heat generation. The wider the divergence in activation energies, the sharper the discontinuity in slope, that is, the narrower the temperature range over which both will contribute. Hydrated calcium hypochlorite shows a clear example of this, and it is reflected in a sharp break in the slope of the Frank-Kamenetskii plot where the changeover occurs. Figure 20.8 shows this plot. The low temperature activation energy for this system is about 48 kJ/mol while that of the higher temperature reaction is around 125 kJ/mol, the transition temperature being around 120 °C [17]. Extrapolation of the high temperature line in this case gives CATs for large commercial-size containers that are seriously in error; that is, they are predicted to be much higher than they actually are. In the general case of two reactions

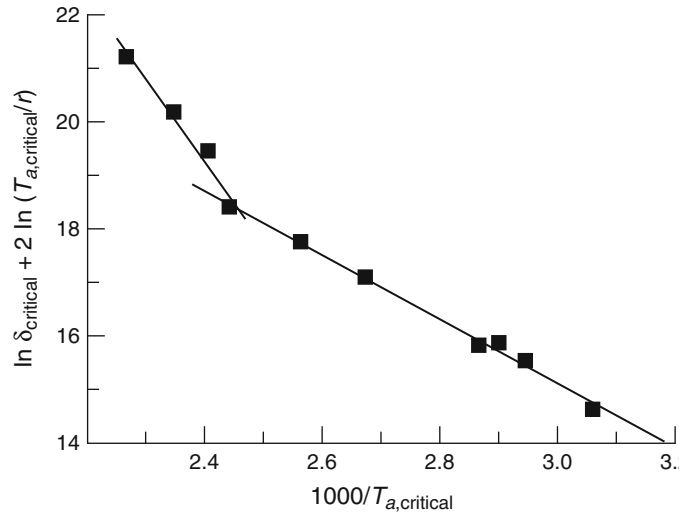

Fig. 20.8 Frank-Kamenetskii plot for hydrated calcium hypochlorite with reaction mechanism change

with different activation energies, this will always be the case as the high activation energy reaction is "frozen out" at low temperatures, and the low activation energy reaction is "swamped" at higher temperatures.

The spontaneous decomposition of calcium hypochlorite has caused extensive container ship losses, particularly in the late nineties. Some due to *hydrated* calcium hypochlorite (UN 2880), defined by the International Maritime Organization [26] to contain not less than 5.5 % moisture and not more than 16 % moisture result from faulty extrapolation as can be seen from Fig. 20.8.

The discontinuity in slope of the F-K plot is undoubtedly due to the effect of moisture mediating chain reactions, the decomposition becoming extremely sensitive to trace metal concentrations.

This is confirmed by the work of Uehara et al. [19] on UN 1748 ("anhydrous") calcium hypochlorite where the lower section of the line is missing. Thus the samples with lower moisture content (<1 %) are much less prone to thermal runaway. So are samples of UN 2880 tested in gauze baskets which allow rapid evaporation of moisture during the tests themselves, behaving in a very similar manner to Fig. 20.7.

Unfortunately the IMO has been inactive in defining moisture content limits for UN 1748 and some manufacturers have taken anything up to 5.5 % to be admissible resulting in large variations in the thermal stability of this product.

On the other hand the P and I (Protection and Indemnity) clubs have taken a proactive stance and largely refused to insure such cargoes unless they are shipped in refrigerated containers (reefers). The resultant increase in cost is probably leading to failure to declare some cargoes of this material as dangerous goods.

Also strategies have yet to be worked out to minimize the possibility of thermal runaway in the event of a power failure on board ship. The heat transfer coefficients of reefers are a fraction of those for normal containers, reducing the effective CATs of reefers without power to very low figures indeed. An obvious emergency strategy would be to open the doors of reefers in such a situation, but this would put serious restrictions on stowage possibilities.

Other examples of mechanism change are known and discussed by Bowes [4]. In such cases accurate predictions of CATs can still be made within each temperature range. This type of example emphasizes the need for tests covering as wide a range of temperatures as possible. Recent methods put forward as viable alternatives to the standard method, for example, Jones [27] and Chen [28], are restricted to either measurement at a single temperature or over a

limited temperature range and can give dangerously flawed results. Empirical tests such as the Mackey test [29] and the crossover test [30] are not reliable and cannot be properly related to the basic principles of spontaneous ignition theory.

Finite Biot Number

The Biot number is defined as

$$\mathrm{Bi} = \frac{\chi r}{\kappa} \tag{20.21}$$

where
χ = Surface heat transfer coefficient
r = Smallest physical dimension of the body
κ = Thermal conductivity of the material

It is the dimensionless measure of the ratio of the resistance to heat transfer within the body to that from the surface to the surroundings. Thus the Semenov theory is often referred to as *zero Biot number* and the Frank-Kamenetskii theory as *infinite Biot number*. They are both special cases of a more general (and more exact) formulation, as was originally pointed out by Thomas [31, 32].

In general the boundary condition at the edge of a self-heating body has the form of a *continuity condition,* which refers to the energy flux across the boundary. It states that the energy flux within the body (given by Fourier's law) and the energy flux from the body surface to the surrounding air must be equal, that is,

$$-\kappa \frac{\partial T}{\partial n} = \chi(T - T_a) \tag{20.22}$$

In dimensionless form this becomes

$$-\frac{\partial T}{\partial n} = Bi(u - u_a) \tag{20.23}$$

This boundary condition does not hold if there exist any heat sources on the boundary of the body itself, as can occur when there is incidence of radiation or when there is heat generated by friction as can occur in pulverization of materials capable of self-heating. Such cases (in the shape of an infinite cylinder) have been treated and the modified critical condition obtained [33, 34]. Similarly modified boundary conditions must be used when surface reactions occur due to catalysis by surface material.

The values of the critical parameter δ quoted for the Frank-Kamenetskii theory are all for the limiting case $Bi \to \infty$, and both Thomas and Barzykin have given semiempirical functions exhibiting the dependence of $\delta_{\mathrm{critical}}$ on Bi, which are detailed in the book by Bowes. As the Biot number decreases so does $\delta_{\mathrm{critical}}$ and hence so does the CAT, all compared with the standard Frank-Kamenetskii theory. For Biot numbers greater than 30, the correction is rather small but is significant for smaller values. Typical heat transfer coefficients from smooth solid surfaces to rapidly stirred air (in a test oven, for example) are of the order of 20 W/m^{2}K, and thermal conductivities of typical cellulosic materials (such as sawdust) are around 0.05 W/mK, giving a ratio of 400/m. Clearly for laboratory-size test bodies ($r \sim 0.1$ m), the Biot number is rather large.

For this reason a significant amount of work has simply *assumed* a sufficiently large Biot number without investigation of its actual numerical value. Sometimes the assumption is not justified, particularly where inorganic materials are involved, as their thermal conductivities can be quite large. For example, typical inorganic salt thermal conductivities lie in the range 0.2–3.0 W/m·K, giving for the ratio (χ/κ) a value of 7–100/m. Clearly for test bodies with $r \sim 0.1$ m, the Biot number will be only 0.7–10. The effect of the small Biot number on $\delta_{\mathrm{critical}}$ is to reduce it by a factor ranging from 0.21 to 0.83, respectively. Clearly for such materials, the more general boundary condition suggested by Thomas must be used, and it is good practice for all but the most strongly insulating materials to estimate the thermal conductivity (particularly in the presence of water) independently of the standard testing regime.

A further important feature of self-heating bodies with a finite Biot number is that their CATs will be sensitive to the heat transfer coefficient from their surface to the surrounding air.

Thus the value of the CAT obtained may well be test-oven sensitive and be strongly influenced by air movement. For example, it has been shown for hydrated calcium hypochlorite [18] that in stirred air in a typical test oven the CAT is 60 °C for a 0.175-m-radius container, but in still air the CAT is 55 °C.

This observation raises serious questions about the value of empirical testing methods such as the SADT test for shipping of self-heating materials [35] that determines criticality-related parameters under vaguely defined conditions of forced airflow in a test oven. The results are then used to determine "safe" conditions for shipping such materials in *still air* inside, for example, a shipping container. Almost invariably many self-heating bodies are stacked inside the same still air inside a container, and they will interact with each other to a very significant extent if the transfer of heat through the container wall is not very rapid. In practice such transfer is rather slow, involving two successive air-metal transfers. As a result the self-heating bodies collectively heat the air inside the container and produce a "cooperative CAT," which can be tens of degrees lower than the CAT of a single body. The Semenov-type theory for this collective ignition has been formulated by Gray [36]. A more accurate version, where the individual bodies are assumed to obey the general boundary condition put forward by Thomas, has also been formulated. The predictions of this theory have been compared to the experimental CAT for eighteen 14 kg equicylinders packed in a rectangular steel box with good agreement [37]. The CAT was reduced from 62.5 °C for a single keg in still air to 54 °C for 18 kegs in still air.

Times to Ignition (Induction Periods)

The terms *time to ignition* and *induction periods* tend to be used synonymously. Here we will abbreviate using TTI. This represents the most difficult area of spontaneous combustion insofar as prediction is concerned. There are three principal reasons for this:

1. The theoretical treatment is much more difficult than that of criticality itself.
2. The actual definition has been greatly confused from case to case.
3. The TTI, however defined, can be extremely sensitive to quantities that have hardly any effect on the position of the critical condition.

Theoretical Treatment

We refer the reader to Bowes [4] and Babrauskas [5] for discussion of earlier treatments. For illustrative purposes we will initially follow Bowes and define TTI from Equation 20.5 by integration from ambient temperature to some value u_1, say

$$\tau_i = \int_{u_a}^{u_1} \left[\nu_0 e^{\frac{-1}{u}} - \ell(u - u_a) \right]^{-1} du \qquad (20.24)$$

This is, of course, in dimensionless form. Our present interest is the implicit use of u_a as the lower limit; that is, it is the time for the sample to go from ambient temperature to some predetermined arbitrary figure, possibly the maximum temperature attained (it turns out that the integral is not sensitive to this limit, provided it is sufficiently high).

Although the maximum temperature attained is a meaningful figure for laboratory tests under some circumstances, it does not always correspond to practical large-scale circumstances. For example, it requires recording the time taken for the center of the sample to heat up in a test oven to ambient temperature and using this as the reference time for TTI. Unfortunately, when the center has reached this point, other parts of the body have often attained rather higher temperatures [38], and the subsequent TTI will be reduced compared to a large-scale body that may well have been built at ambient temperature and be quite uniform initially. Extrapolations of such laboratory tests will not then be reliable since the initial condition will not be appropriate.

The TTI for the hot stacking problem is qualitatively different from that in which the body is

formed uniformly at ambient temperature. Generally this time is *much shorter* than the TTI for the more common case of initially ambient temperature throughout the body. The reasons have been given, with a comparison of the two cases, by Gray and Merkin [39]. Similar considerations apply when part of the body is at a high temperature (hot spot), and this case has been discussed in detail by Thomas [40].

With the ready availability of powerful and fast numerical techniques, it is now feasible to integrate routinely the time-dependent heat conduction equation for this problem, which is probably the best solution. Zinn and Mader [41] were early participants in this effort, and more recently Gray, Little, and Wake [38] have noted that such numerical results can be usefully used to predict a very good lower bound to the TTI. These results are desirable as they err on the side of safety.

Very close to criticality, perturbation treatments have been formulated [42–46], but these are mainly of theoretical interest. At the critical condition the TTI becomes infinite, and close to this condition it is extremely sensitive to the degree of criticality, so unless this is known accurately (hardly ever the case), use of such formulas is not advised.

Other, Largely Chemically Kinetic, Difficulties

In addition to the difficulties discussed above, which apply even when only a single simple reaction is assumed, there are others that are largely chemically kinetic. It has long been known that chain reactions, whether branching or not, can exhibit very long induction periods followed by very rapid onset of (sometimes non-explosive) reaction. Many exothermic spontaneous ignition reactions do possess some chain characteristics even though these do not manifest themselves once the reaction is well underway. Thus it is feasible for complex chain mechanisms to determine the details of the TTI but not be at all important in determining the critical condition where gross heat balance considerations are crucial. In many cases this leads to extremely irreproducible TTIs without similar variation of CATs or other properties. In case this list of difficulties leads to an overly pessimistic view of the topic of TTI, there are some things that can generally be relied on as far as the practical situation of fire investigation is concerned.

Very crudely speaking, notwithstanding the above discussion, the larger the body, the longer the TTI will usually be. Thus a fire thought to have been caused by spontaneous ignition of a pile of linseed oil–contaminated rags contained in a wastepaper basket will usually appear within a few hours of the rags being placed there. On the other hand, a fire resulting from spontaneous ignition of thousands of metric tons of woodchips would occur only after some months of assembly, assuming the pile was assembled at ambient temperature. For such bodies it is generally true that the TTI increases with size in this manner. Accordingly haystacks tend to ignite (if they are supercritical) after a few weeks and coal stockpiles after a few months. However, the TTI can decrease dramatically if the body is very far beyond the CAT.

For hot stacked bodies, on the other hand, times are generally much shorter and not particularly sensitive to the ambient temperature. Thus stacks of freshly manufactured chipboard with a volume of a few cubic meters can ignite much more quickly—that is, hours rather than days—than a similarly sized body self-heating from ambient. Beyond these general comments one has to treat each separate case on its merits with a careful eye for exceptions to any general rules. For example, the presence of any catalytic material, such as rusty metal (a common contaminant of many materials), can dramatically decrease the TTI. This indicates the presence of free-radical or chain reactions and is fairly common, although the CATs and CSTs are only slightly affected.

In summary, in fire cause investigation, where spontaneous ignition is suspected, it is wise to be very circumspect about time factors without very thorough investigation and detailed knowledge of the initial conditions likely to have existed when the body was put in place. Even the

traditional linseed-oil rag example can be thrown out of the normal pattern by the presence of mineral turpentine, a very common diluent for oil-based stains. The evaporation of this from the rags can greatly prolong the TTI by virtue of the consequent cooling effect and also the exclusion of air by the vapor. Depending on the circumstances, these factors could add 2 or 3 days to a TTI that would normally be no more than a few hours.

Investigation of Cause of Possible Spontaneous Ignition Fires

From the investigative point of view, it is helpful to list the practical factors that enhance the possibility of spontaneous ignition as a possible fire cause.

The Size of the Body of Material The larger the size of the body of material, the greater the likelihood of spontaneous ignition. By *size of the body* we mean the parts that are in thermal contact. A large pile of cotton bales with aisles through it would not necessarily be a large body in the thermal sense used here. This classification would be true even if (as often happens), once ignited, fire could spread easily from one section to the next.

High Ambient Temperatures Because the air around the body in question has to act as a heat sink, the higher the ambient temperature, the more inefficient is the air as a coolant. Also direct placement underneath a metal roof or adjacent to a northwest- (southern hemisphere) or southeast- (northern hemisphere) facing wall is a positive factor.

Thermal Insulation Sometimes spontaneously ignitable materials are stored in chemical warehouses or elsewhere packed against inert solids that prevent free airflow over the surface, thus reducing heat losses. This effect is evidenced by the appearance of maximum charring or self-heating that is off center and closer to the insulated side of the body. It also results in a reduced CAT.

Fibrous Nature and Porosity of Material Fibrous or porous materials allow greater access of air than otherwise (solid wood is not subject to spontaneous ignition at normal ambient temperatures, but woodchips and sawdust certainly are!). The concept that packing such porous materials by compression will increase the CAT by oxygen exclusion is badly flawed. This procedure increases the density (thus *lowering* the CAT) and has virtually no effect on the availability of oxygen. During the preflame development, the oxygen requirement is very low; by the time overt flame is observed, there are usually broad channels of destroyed material (chimneys) that will allow ready access.

Pure cotton in a test oven with a nitrogen atmosphere has been shown to undergo spontaneous ignition but with a longer induction period than in the presence of air [47]. This could be due to adsorbed oxygen on the cellulose fibers or due to exothermic decomposition of the cellulose in the absence of air [48].

Otherwise "harmless" materials (i.e., liquids with very high flashpoints) can undergo spontaneous ignition at temperatures more than a hundred degrees below either their flashpoints or their so-called autoignition temperatures. The familiar drying oils (flashpoints around 230 °C) spread on cotton afford such an example, igniting sometimes at room temperature under the appropriate conditions. In bulk such oils pose little threat of fire causation.

Similarly, hydraulic fluids, specifically designed for nonflammability and with extremely high flashpoints, can undergo spontaneous ignition if allowed to leak onto thermal lagging, such as mineral wool, fiberglass, and so forth, which are characterized by having particularly high surface areas. Practical cases of this and experimental tests have been reported by Britton [49], with particular reference to ethylene oxide fires. More recently a modeling project has been carried out [50, 51] based on adaptation of the Semenov theory of ignition to a porous solid that was wetted with combustible liquid.

Temperature of Stacking The factor of temperature of stacking is simple—the hotter the worse! The main question is, How hot? The CST (critical stacking temperature) is only weakly dependent on the ambient temperature at low ambient temperatures, but it is sensitive to the size of the hot body. This situation arises with freshly manufactured products such as foodstuffs (milk powder, flour, instant noodles, fried batter, etc.), synthetic materials such as chipboard, cotton bales straight from the ginning process, bagasse straight from the sugar mill, fresh laundry (usually in commercial quantities), and so on.

To evaluate the CST requires full testing to obtain the parameters for the material (such as E, Q, κ, etc.) and then application of one of the methods in the literature for its calculation. Thomas [40] has given a method for hot spots of material, and Gray and Scott [52] have given a generalization of this, removing the approximation to the Arrhenius function made by Thomas. A simpler method of calculation of the CST has been given by Gray and Wake [53]. It uses a spatially averaged temperature in the Arrhenius function and then obtains exact results for this simplified problem.

Length of Time Undisturbed Material that has been in place for longer than usual is reason to suspect spontaneous ignition as a fire cause. Many industrial procedures involve the temporary storage of materials that are *normally* above their CAT but that are not left undisturbed for a period longer than or equal to their TTI. Thus under normal circumstances fire does not occur even though the TTI is regularly exceeded. If processes are slowed down for some reason, or storage is prolonged due to vacation, fire can occur even though no other parameters have been changed.

The Aftermath

There are very often very characteristic signs of spontaneous ignition even after it has been the cause of a very large fire. Internal charring and ash is very characteristic in cellulose materials. Combustion starts in the well-insulated internal areas of the body, and warm or hot combustion products rise by convection through the path of least resistance (which is not always vertically upward), forming a "chimney" of discolored and partially combusted material. Because large bodies of material are rarely uniform in density or porosity, there can be more than one chimney formed and this is the norm. The occurrence of multiple chimneys and consequent discovery of more than one heavily charred or ashed area inside the body have led to erroneous charges of arson on the basis of the myth that more than one fire seat means the fire was deliberately lit. When a chimney reaches the edge of the body, smoke first becomes visible, then ingress of air causes flame. The latter may engulf more flammable materials in the building, and the whole structure can be destroyed while the spontaneously combusting material may well be chugging away slowly throughout most of its volume. This can even be the case after the fire has been extinguished. The result is then plenty of evidence as to the cause and origin of the fire. The author has measured temperatures as high as 200 °C in buried, spontaneously ignited material more than 2 weeks after the extinction of the fire!

The internal burning of large piles or stacks of material can cause mechanical instability, and often the body collapses inward in the later stages of ignition. This inward collapse can cause some confusion in excavations, which should always be carried out if spontaneous ignition is suspected along with photographic and thermocouple temperature probe records at all stages.

It should be emphasized that the occurrence of significant amounts of unconsumed, spontaneously ignitable material does not mean that spontaneous ignition was not the cause of the fire. Frequently, oily rags are recovered almost intact from the bottom of waste bins that have been the seat of very large fires. The lower rags tend to be protected from incineration by a layer of char and also by lack of oxygen in the lower reaches of the bin.

Case Histories and Examples

Cottonseed Meal: Living Dangerously

A transit warehouse temporarily storing cottonseed meal to a depth of about 3 m burned down and was completely destroyed. The length and breadth of the building were much larger than the depth of the meal, so the relevant physical dimension (for substitution into the formula for $\delta_{critical}$) was 3 m. Spontaneous ignition was suspected because of the known presence of unsaturated fatty acids prone to this. Standard CAT tests for small laboratory samples were carried out, and the extrapolation to life size was expected to be reasonably accurate because only small amounts of water were present and wet reaction was not suspected.

The body of meal in the warehouse turned out to be supercritical for the average ambient temperature in the area. The unusual factor in this particular case was the fact that the meal had been left undisturbed for much longer than usual due to a transport strike. It remained in place for longer than the TTI, although under normal circumstances it would have been moved on to customers well before significant self-heating could take place.

In this case an enlightened management installed underfloor ducting to produce a high-pressure air blast capable of rearranging the meal substantially from time to time. A similar solution has long been practiced for coal stockpiles, although in that case the disturbance is usually caused by a front-end loader.

Flaming Instant Noodles

Some years ago an instant noodle factory burned down soon after new management had taken over. New management was not satisfied with the throughput of the production line and wanted higher productivity. The latter was dependent on the speed of a single conveyer belt that conveyed the raw noodles through a hot oil bath, then under a number of powerful fans to remove excess oil and cool the cooked noodles for packing and palleting. Increasing the speed of the conveyer certainly increased the throughput in proportion, but the smaller length of time the noodles spent in the hot oil resulted in incomplete cooking. Thus the oil-bath temperature was increased substantially to compensate for this and again produce fully cooked noodles. However, the faster moving belt was now conveying cooked noodles to the packing area in a shorter time than before, *and* they were also coming out of the fryer hotter than before. The result was that they were packed and palleted at a significantly higher temperature than under previous management.

Although the scientific and technological literature contained no reference to spontaneous ignition of noodles, their porous and oily nature indicated a possibility that this could occur. This was confirmed by laboratory tests obtaining the CAT for a particular size noodle block. On this basis a full series of tests was carried out, and the parameters for the noodles obtained from the Frank-Kamenetskii plot in the usual way. With these parameters available, it was possible to calculate the CST for a pallet full of noodle packages as these were shrink-wrapped onto the pallets and completely encased in plastic, that is, the whole pallet full of noodles was in fact the body in question. The calculated CSTs (for a range of feasible ambient temperatures) turned out all to lie above the temperatures reached with the old process parameters but well below the temperatures reached with the new high-productivity parameters. The "bean counters" managed to achieve a productivity of zero until the factory was rebuilt.

Bagasse Storage: Some Complex Chemistry

The sugar industry in Australia wished to use bagasse containing the usual 50 % moisture as a biomass for cogeneration of electricity as large excess tonnages are produced biannually. Removal of moisture increases the calorific (and hence monetary) value of the material as a fuel, provided it can be removed at no energy

cost. At the same time it has been known for some time that large piles of bagasse are prone to spontaneous ignition and self-heating with consequent loss of value and also considerable pollution from the combustion products. An obviously desirable aim would be to create piles of bagasse that are not large enough to be supercritical but nevertheless large enough to self-heat significantly and hence drive off some of the moisture at no cost. Thus one would turn a dangerous energy release into a benefit. Clearly the balance would have to be just right. Consequently, a major research project was undertaken, both experimental and theoretical.

Application of the standard laboratory test methods to bagasse [54] results in a prediction of critical radius for a pile at ambient temperature 30 °C, which is an order of magnitude greater than the observed value. This is now known to be due to the fact that laboratory test CATs are above 100 °C and simply drive off the moisture before the self-heating can get under way. The extrapolated results are therefore only good predictors for dry piles of material. In practice the water content of bagasse is close to 50 % on a dry-weight basis, and this has recently been shown to be instrumental in partaking in a heat-producing reaction in addition to the one predominating in the dry material at higher temperatures [20, 21]. This wet reaction has been characterized in isothermal calorimetric measurements over the temperature range 30–90 °C, and in this range the high-activation-energy dry reaction is almost completely shut down by the negative exponential in the Arrhenius function.

The wet reaction does not follow an Arrhenius temperature dependence at all, rather having a maximum rate at about 55–60 °C. It also has a sharp, almost discontinuous dependence on water concentration, cutting out completely below 20 % moisture. These characteristics are probably responsible for its occurrence being mistaken for microbiological activity. Inclusion of such complex chemistry in a generalization of the Frank-Kamenetskii theory for distributed temperatures, as well as the evaporation, condensation, and diffusive movement of water vapor through the pile, results in probably the most complex modeling yet of ignition phenomena.

Nevertheless, this model describes quantitatively the behavior of real bagasse piles and answers the questions that led to its creation, that is, How does one choose a pile size in order to maximize the water removal without losing the pile to spontaneous ignition? The modeling is described in a number of publications (e.g., Gray et al. [12]) and shows that present-day computing power coupled with appropriate knowledge of physical parameters enables quantitative or at worst semiquantitative modeling of spontaneous ignition situations with input of realistic chemistry and transport processes. Such developments have also taken place in the modeling of realistic chemistry in gas-phase ignition of hydrocarbons and related organic materials.

It seems that we are not far from a situation where the simplified theories that have been useful tools for so long (with their empirical corrections) will be superseded by more detailed calculation of the required properties such as CATs and CSTs. Nevertheless, the simplified theories will never lose their pedagogical value and will remain a firm conceptual foundation for more sophisticated models.

Milk Powder: A Numerical Example

This example is due to Beever [55]. In a milk-drying plant, air entering the spray dryer was heated to 200 °C, and it was thought that surfaces in the region of the inlet would also reach this temperature. Any collection of powder on hot surfaces could cause spontaneous ignition, which would not only spoil the product but also act as a source of ignition for a dust explosion. These have occurred in milk-drying plants with devastating consequences. Farther down the dryer, where there was deemed to be a greater likelihood of powder accumulation, surface temperatures of 80 °C occurred. Three laboratory basket sizes were tested with half side-lengths of 0.025, 0.0375, and 0.050 m. The CATs of these were 171 °C, 156 °C, and 141.5 °C, respectively.

For a cube we can substitute the value 2.52 for δ_{critical} in Equation 20.20:

$$\ln\left[\frac{\delta_{\text{critical}} T_{a,\text{critical}}^2}{r^2}\right] = 41.85 - \frac{9497}{T_{a,\text{critical}}}$$

We can make r the argument of this equation and then substitute for $T_{a,\text{critical}}$ as required. If we require the critical temperature for a layer of material, we would use the value for δ_{critical} appropriate to an infinite slab, that is, 0.88. For such a flat layer with ambient temperature on each side of 200 °C, a critical thickness of 0.017 m is obtained. For the cooler regions of the dryer at 80 °C, a critical thickness of 0.4 m is obtained. It was decided that these critical thicknesses were sufficiently realistic to require regular cleaning inside the dryer to remove buildup. This problem is actually more complicated than indicated here because the critical parameters are rather sensitive to moisture content, the critical thickness increasing significantly with moisture content, which can be up to 4 % [56].

Technical and Legal Matters

SADT

Many definitions, particularly those published by the United Nations (UN), the International Maritime Organisation (IMO), and the U.S. Department of Transportation (DOT), are incorporated *in toto* in various regulations and statutes, thus attaining a rigorous legal standing. As a result, they assume a status that scientifically they do not deserve by virtue of being wrong, ambiguous, confusing, or all three and more.

The centerpiece of such consideration is the *self-accelerating decomposition temperature*, or SADT. *Some* of the definitions of SADT (there could be more) are presented here. The UN's *Manual of Tests and Criteria* [35], in its section "Recommendations on the Transport of Dangerous Goods," contains at least four definitions. Some are inconsistent with each other and some are actually defined so as to be *up to 5 °C above the critical ambient temperature*. The materials could therefore blow up well below the SADT!

Definition 1. Test Method H1—U.S. SADT Test

The SADT is defined as the lowest oven temperature at which the sample temperature exceeds the oven temperature by 6 °C or more.

The test is run for 7 days, the time origin being when the sample temperature is 2 °C below the oven temperature, assuming the body is at room temperature when inserted. The occurrence of three completely arbitrary numbers (7 days, 2 °C, and 6 °C) should arouse suspicion in even the most scientifically illiterate person that this SADT definition cannot be a fundamental property of the body tested. Detailed considerations using fundamental thermal ignition theory show that the SADT definition does not indicate that the test body will not blow up below the SADT. Some materials could do so, and similarly some may not do so when placed in an ambient temperature above the SADT.

On the other hand the *critical ambient temperature* (CAT) defined and discussed in this article is a rigorous dividing value between ignition and subcritical self-heating. Why any version of the SADT would have found its way into the scientific fringe literature of regulation and litigation is rather incomprehensible, but things get worse when we consider the UN tests H2 (adiabatic storage test) and H3 (isothermal storage test). We will not go into the experimental details of these tests but go straight to the definitions of SADT arising out of them. Both tests make use of a diagram (plotted from the test results) that is in fact identical to Fig. 20.1. This diagram is given as Figure 28.4.2.2 and again as Figure 28.4.3.2 in the *Manual of Tests and Criteria*. Both of these diagrams show and explicitly refer to the *critical ambient temperature* but unbelievably go on to define the SADT as follows.

Definition 2. Test Methods H2 and H3—The Adiabatic Storage Test and Isothermal Storage Test, Respectively

The SADT is the CAT rounded up to the next higher multiple of 5 °C.

It follows from this that

Every material can blow up below its SADT as defined by UN tests H2 and H3.

The U.S. Department of Transportation uses SADT values *measured by any of these tests* to

impose requirements for temperature-controlled transportation (CFR 49). Clearly it does not err on the side of safety.

ASTM E698-01

ASTM E698-01 is entitled *Standard Test Method for Arrhenius Constants for Thermally Unstable Materials,* and the abstract states [57]:

> The kinetics of exothermic reactions are important in assessing the potential of materials and systems for thermal explosion. This method provides a means for determining Arrhenius activation energies and pre-exponential factors using differential thermal methods.

A paper has recently been published [58] that throws very considerable doubt on the activation energies obtained by this method notwithstanding the caveats in the standard itself. Calcium hypochlorite can be used to illustrate a difficulty arising from the lack of sensitivity of typical differential scanning calorimetry (DSC) results when two reactions are involved and they have widely differing kinetic parameters. The Kissinger plot gives a good straight line but in fact the presence of a low activation energy, low-temperature reaction is not detected. The exotherm obtained relates to the high-temperature, high activation energy reaction, albeit somewhat inaccurately. In the large-scale practical situation the low-temperature reaction is in fact the cause of thermal ignition, and the conclusions drawn from DSC results are dangerously in error.

Modeling experiments in which either reaction is left out show that the *low-temperature reaction* does not show an exotherm until a temperature about 200 °C above the position of the exotherm for the *high-temperature reaction* under the conditions of DSC tests.

The practically dangerous low-temperature reaction does not produce heat at a sufficiently high rate to be detected in a typical DSC until very high temperatures. Before such high temperatures can be reached during a temperature ramp, the material is consumed by the high-temperature reaction, and the low-temperature reaction is missed completely.

Such errors in activation energies are disastrous in the prediction of critical ambient temperatures because these are extremely sensitive to the activation energy. Generally speaking, the very factors that endow a substance with the propensity to ignite spontaneously also tend to increase the "correction factor" for the standard method of data extraction from DSC results. These are well known to be low thermal conductivity, low activation energy, large heat of reaction, and high pre-exponential factor. The fact that necessary corrections to classical DSC results are directly proportional to the Frank-Kamenetskii parameter very clearly illustrates this problem for the use of DSC in estimating self-ignition propensities in self-heating materials.

Nomenclature

C_v	Heat capacity at constant volume per unit mass (J/K·mol)
c	Concentration (mol/m^3)
c_f	Feed concentration in CSTR (mol/m^3)
CAT	Critical ambient temperature (K)
CST	Critical stacking temperature (K)
E	Activation energy (J/mol)
F	Feed rate in CSTR (m^3/s)
$f(c)$	Chemical reaction rate (mol/m^3·s)
Q	Heat of reaction (J/mol)
R	Universal gas constant (J/mol·K)
r	Characteristic radius
S	Surface area (m^2)
T	Temperature (K)
T_a	Ambient temperature (K)
$T_{a,\text{critical}}$	Critical ambient temperature (CAT) (K)
T_f	Feed temperature in CSTR (K)
TTI	Time to ignition (s)
u	Dimensionless temperature (RT/E)
u_a	Dimensionless ambient temperature
V	Volume of self-heating body (m^3)
ν	Dimensionless concentration (c/c_0)
δ	Frank-Kamenetskii parameter
θ	Frank-Kamenetskii dimensionless temperature
ρ	Bulk density (mol/m^3)
κ	Thermal conductivity (W/m·K)
χ	Heat-transfer coefficient (W/m^2·K)
ε	Inverse dimensionless heat of reaction

τ	Dimensionless time
l	Dimensionless heat transfer coefficient
Bi	Biot number ($\chi r/\kappa$)
$\partial()/\partial n$	Differential coefficient in a direction normal to the boundary of the body

References

1. *Safety and Runaway Reactions,* Institute for Systems Informatics and Safety, Joint Research Centre European Commission, EUR 17723 EN (1998).
2. N.N. Semenov, *Zeitschrift für Physikalische Chemie,* 48, p. 571 (1928).
3. D.A. Frank-Kamenetskii, "Diffusion and Heat Transfer" in *Chemical Kinetics,* Plenum Press, New York (1969).
4. P.C. Bowes, *Self-Heating: Evaluating and Controlling the Hazards,* HMSO, London (1984).
5. V. Babrauskas, *Ignition Handbook,* Fire Science Publishers, Issaquah, WA (2003).
6. J.F. Griffiths and B.F. Gray, "Fundamentals of Autoignition of Hydrocarbon and Other Organic Substrates in the Gas Phase," in *24th Loss Prevention Symposium,* American Institute of Chemical Engineers, San Diego, 92b (1990).
7. N.N. Semenov, *Some Problems in Chemical Kinetics and Reactivity* (English translation), Princeton University Press, Princeton, NJ (1959).
8. G.C. Wake, J.B. Burnell, J.G. Graham-Eagle, and B.F. Gray, *Reaction Diffusion Equations* (K.J. Brown and A.A. Lacey, eds.), Oxford, UK, pp. 25–37 (1990).
9. J.F. Griffiths and J.A. Barnard, *Flame and Combustion,* Blackie, Glasgow, Scotland (1994).
10. B.F. Gray, "Critical Behaviour in Chemically Reacting Systems III—An Analytical Criterion for Insensitivity," *Combustion and Flame,* 24, p. 43 (1975).
11. B.F. Gray, "Unified Theory of Explosions, Cool Flames and Two Stage Ignitions," *Transactions of the Faraday Society,* 65, p. 1603 (1969).
12. B.F. Gray, M.J. Sexton, B. Halliburton, and C. Macaskill, "Wetting Induced Ignition in Cellulosic Materials," *Fire Safety Journal,* 37, pp. 465–479 (2002).
13. T. Dixon, "Spontaneous Combustion in Bagasse Stockpiles," in *Proceedings of the Australian Society of Sugar Cane Technologists,* 53 (1988).
14. B.F. Gray, unpublished.
15. R. Aris, *The Mathematical Theory of Diffusion and Reaction in Permeable Catalysts,* Oxford, UK (1975).
16. P.L. Chambre, *Journal of Chemical Physics,* 20, p. 1795 (1952).
17. T. Boddington, P. Gray, and I. Harvey, "Thermal Theory of Spontaneous Ignition," *Philosophical Transactions of the Royal Society,* A270, p. 467 (1971).
18. B.F. Gray and B. Halliburton, "The Thermal Decomposition of Hydrated Calcium Hypochlorite UN 2880," *Fire Safety Science,* 35, pp. 223–239 (2000).
19. Y. Uehara, H. Uematsu, and Y. Saito, "Thermal Ignition of Calcium Hypochlorite," *Combustion and Flame,* 32, p. 85 (1978).
20. I.K. Walker, W.J. Harrison, and F.H. Jackson, *New Zealand Journal of Science,* 21, p. 487 (1978).
21. R.A. Sisson, A. Swift, G.C. Wake, and B.F. Gray, "Critical Conditions for the Exothermic Combustion of Damp Cellulose, Part 1," *IMA Journal of Applied Mathematics,* 50, p. 285 (1993).
22. R.A. Sisson, A. Swift, G.C. Wake, and B.F. Gray, "Critical Conditions for the Exothermic Combustion of Damp Cellulose, Part 2," *IMA Journal of Applied Mathematics,* 49, p. 273 (1992).
23. B.F. Gray and G.C. Wake, "The Ignition of Hygroscopic Combustible Materials by Water," *Combustion and Flame,* 79, p. 2 (1990).
24. B. Halliburton, Ph.D. Dissertation, Macquarie University, Sydney, Australia, p. 2109 (2002).
25. T. Dixon and N. Ashbolt, Private communication, Sugar Research Institute, Mackay, Queensland, Australia (1985).
26. International Maritime Dangerous Goods Code, International Maritime Organization, London, 2010.
27. J.C. Jones, "On the UN test for the Spontaneous Heating of Solids," *Loss Prevention in the Process Industries,* 13, pp. 177–178 (2000).
28. X.D. Chen and L.V. Chong, "Self-Ignition Kinetics of Combustible Solids," *Transactions of Institution of Chemical Engineers,* 76B, p. 90 (1998).
29. W. Mackey, "On a Spontaneous Ignition Test," *Journal of the Society of Chemical Industry,* 15, p. 90 (1896).
30. N. Kirov, "The Crossover Test," *CSIRO Technical Note,* Chatswood, Australia (1954).
31. P.H. Thomas, "On the Thermal Conduction Equation for Self-Heating Materials with Surface Cooling," *Transactions of the Faraday Society,* 54, p. 60 (1958).
32. P.H. Thomas, *Transactions of the Faraday Society,* 56, p. 833 (1960).
33. B.F. Gray and G.C. Wake, "Criticality in the Infinite Slab and Cylinder with Surface Heat Sources," *Combustion and Flame,* 55, p. 23 (1984).
34. B.F. Gray, A. Gomez, and G.C. Wake, "Friction and Localised Heat Initiation of Ignition," *Combustion and Flame,* 61, p. 177 (1985).
35. "Transport of Dangerous Goods," *Manual of Tests and Criteria,* 2nd ed., United Nations, New York and Geneva (1995).
36. B.F. Gray, "On the Critical Conditions for an Assembly of Interacting Thermons, Series B," *Journal of the Australian Mathematical Society,* 43, pp. 1–12 (2001).
37. B.F. Gray, "Interpretation of Small Scale Test Data," *Interflam 2001, 9th International Fire Science and Engineering Conference,* Edinburgh, Scotland, pp. 719–729 (2001).
38. B.F. Gray, S.G. Little, and G.C. Wake, "The Prediction of a Practical Lower Bound for Ignition Delay Times," *24th International Combustion Symposium,* Combustion Institute, Pittsburgh, PA, p. 1785 (1992).

39. B.F. Gray and J.H. Merkin, "Thermal Explosion Escape Times in the Uniform Temperature Approximation," *Mathematical Engineering in Industry,* 4, p. 13 (1993).
40. P.H. Thomas, "An Approximate Theory of Hot Spot Criticality," *Combustion and Flame,* 21, p. 99 (1973)
41. J. Zinn and L. Mader, "Thermal Initiation of Explosives," *Journal of Applied Physics,* 31, p. 323 (1960).
42. T. Boddington, C. Feng, and P. Gray, "Thermal Explosion, Times to Ignition and Near Critical Behaviour in Uniform Temperature Systems, Part 2," *Journal of the Chemical Society, Faraday Transactions,* 2, 79, p. 1299 (1983).
43. T. Boddington, C. Feng, and P. Gray, "Thermal Explosion, Times to Ignition and Near Critical Behaviour in Distributed Temperature Systems, Part 3," *Journal of the Chemical Society, Faraday Transactions,* 2, 80, p. 1155 (1984).
44. T. Boddington, C. Feng, and P. Gray, "Thermal Explosion and Times to Ignition I, Reactant Consumption Ignored," *Proceedings of the Royal Society,* A385, pp. 289–311 (1982).
45. T. Boddington, C. Feng, and P. Gray, "Thermal Explosion and Times to Ignition II, Reactant Consumption Included," *Proceedings of the Royal Society,* A391, p. 269 (1984).
46. B.F. Gray and J.H. Merkin, "Thermal Explosion: Escape Times in the Uniform Temperature Approximation: I Effects of Parameter Perturbations," *Journal of the Chemical Society, Faraday Transactions,* 2, 86, p. 597 (1990).
47. S.G. Little, Master's Thesis, School of Chemistry, Macquarie University, Sydney, Australia, p. 2109 (1991).
48. Y.I. Rubtsov, A.I. Kazakov, L.P. Andrienko, and S.B. Manelis, "High Temperature Pyrolysis of Cellulose," *Combustion, Explosion, and Shock Waves,* 29, p. 710 (1993).
49. L.G. Britton, "Spontaneous Ignition of Liquids on Porous Media," *24th Loss Prevention Symposium,* American Institute of Chemical Engineers, San Diego (1990).
50. A.C. McIntosh and B.F. Gray, "Self Heating of Combustible Vapor in Porous Material When Fibres Are Completely Covered by Fluid," *Combustion Science and Technology,* 113, p. 503 (1996).
51. A.C. McIntosh, B.F. Gray, and G.C. Wake, "Analysis of the Bifurcational Behaviour of a Simple Model of Vapor Ignition in Porous Material," *Proceedings of the Royal Society,* A453, p. 281 (1997).
52. B.F. Gray and S.K. Scott, "The Influence of Initial Temperature Excess on Critical Conditions for Thermal Explosion," *Combustion and Flame,* 61, p. 227 (1985).
53. B.F. Gray and G.C. Wake, "Critical Conditions for Thermal Ignition," *Mathematical and Computer Modelling,* 18, pp. 65–75 (1993).
54. B.F. Gray, J.F. Griffiths, and S.M. Hasko, "Spontaneous Ignition Hazards in Stockpiles of Cellulosic Materials," *Journal of Chemical Technology and Biotechnology,* 34A, p. 453 (1984).
55. P. Beever, "Self Heating and Spontaneous Combustion," in *SFPE Handbook of Fire Protection Engineering,* 2nd ed. (P.J. DiNenno et al., eds.), pp. 2-180–2-189 (1988).
56. C.M. Rivers, Master's Thesis, Massey University, Palmerston North, New Zealand (1994).
57. ASTM E698-01, *Standard Test Method for Arrhenius Constants for Thermally Unstable Materials,* ASTM International.
58. B.F. Gray and C. Macaskill, "The Role of Self-Heating in the Estimation of Kinetic Constants for Unstable Materials Using DSC," *Interflam 2004, 10th International Fire Science and Engineering Conference,* Interscience Communications, London, UK (2004).

Brian Gray has published extensively on spontaneous combustion and ignition of gases and solids, gas ignition, flame propagation, and related topics for many years. He now runs a combustion consulting company in Sydney, Australia, and was professor of chemistry at Macquarie University, Sydney, from 1976 to 1998.

Flaming Ignition of Solid Fuels

21

José Torero

Introduction

This chapter will describe how heating of a solid fuel leads to flaming ignition. The discussion will be centred on flaming ignition of solid fuels but will not address smouldering or spontaneous ignition since these subjects will be covered in Chaps. 19 and 20 respectively. Thus, the presence of a source of heat decoupled from the solid and fuel gasification will be assumed throughout the chapter.

The main focus of this chapter is to assist the reader in understanding the phenomena, assumptions and simplifications embedded in different models and tests that attempt to predict ignition phenomena or to extract the parameters controlling it. The methodology to be followed goes from the general to the specific. Therefore, the problem will be initially formulated in as general a manner as possible. A series of common simplifications will then be made leading to reduced formulations. These simplifications are introduced for many reasons that include:

- Simplifications where the nature of the material studied allows the exclusion of some specific phenomena
- Simplifications where some processes disappear due to the characteristics of the test used to assess the material
- Simplifications where the required precision does not warrant the inclusion of higher levels of complexity
- etc.

To highlight the impact of simplifications, whenever possible, a comparison between the comprehensive description and the reduced formulation will be made to allow the reader to assess potential errors. As this chapter progresses the resulting formulations become simpler and of greater practical use, nevertheless the impact of the assumptions strengthens increasing the potential for error or misuse of the information. The chapter closes with a presentation of the simplest methodologies that correspond to classic treatments and are mainly associated to standard tests.

Most of the existing data on ignition is intimately related to the methodology used to extract it. Therefore, it is always conditioned by the nature of the test procedures, the hardware used and by the data analysis method. Given that the objective of this chapter is to provide a phenomenological description of flaming ignition of solid fuels emphasis will be given to the different processes and not to reviewing available data. Throughout this chapter the reader will be directed to other chapters and references where data will be presented in the context of the testing protocols used to obtain it. As an example, some of the most comprehensive compilations of ignition data can be found in Chap. 36, in textbooks such as Ref. [1] or professional guidelines [2].

J.Torero (✉)
School of Civil Engineering, The University of Queensland, St Lucia, QLD, Australia

M.J. Hurley (ed.), *SFPE Handbook of Fire Protection Engineering*,
DOI 10.1007/978-1-4939-2565-0_21, © Society of Fire Protection Engineers 2016

The Process of Ignition

When a solid material, initially at ambient temperature, is subject to an external source of energy the temperature of the exposed surface starts to increase. This moment will be defined as the onset of the ignition process, $t = 0$. A series of physical and chemical phenomena are initiated as the energy reaches the surface of the material. This chapter will attempt to describe these phenomena.

Without loss of generality and for simplicity, the ignition process will be described in a one-dimensional frame of reference with a single coordinate, x. Only one surface of the material will be heated and the origin of the coordinate system, $x = 0$, will be placed at the exposed surface of the material. This frame of reference will move with a velocity V_R as the fuel consumes and the surface regresses. For some materials regression rates are very small and can be neglected, but this will not be assumed at this stage. A schematic of a generic solid material undergoing heating is presented in Fig. 21.1. Figure 21.1 also shows all the different variables that evolve through the heating process. These variables will be described in detail later.

For simplicity, all processes involved will be divided in two groups, those associated with the solid phase and those with the gas phase. The solid phase treatment will lead to a description of the production of gas phase fuel ($\dot{m}''_P$) and the gas phase analysis will focus on how the ensemble of gaseous fuel and oxidizer lead to a flame. The solid phase will be treated first (section "The Solid Phase"), then the boundary conditions between both phases will be established, to finalize with a description of what happens in the gas phase (section "The Gas Phase").

The Solid Phase

The temperature of the solid, initially at ambient (T_o), increases as the heat reaches the surface of the material. Highest temperatures will be

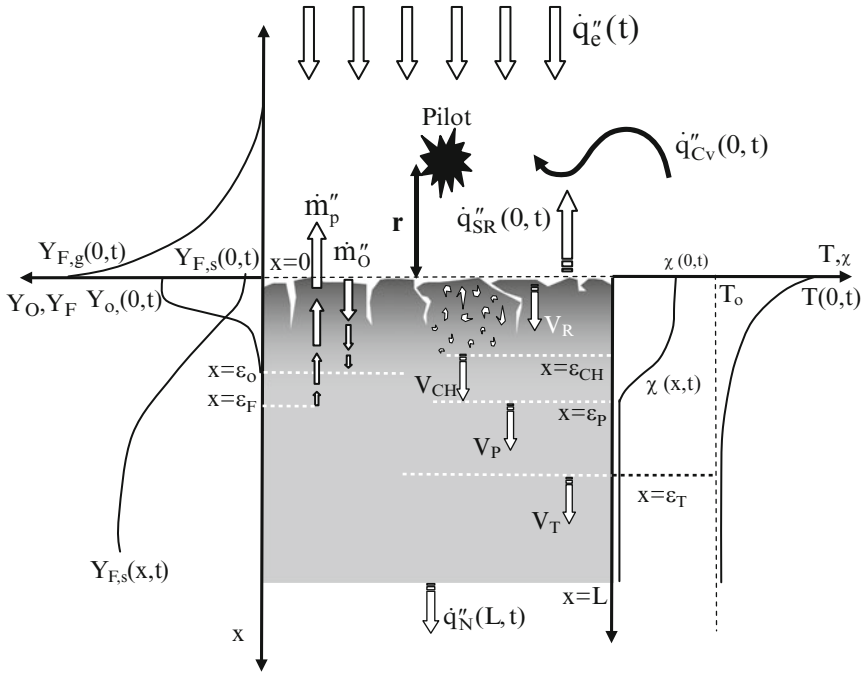

Fig. 21.1 Schematic of the different processes occurring as a material undergoes degradation prior to ignition induced by an external source of heat

achieved close to the surface, but energy transfer in-depth will result in an increase in temperature of a significant part of the solid. Therefore, the temperature will vary in-depth and in time, thus temperature needs to be represented as a function of both variables, T(x,t). Figure 21.1 shows a generic representation of the temperature distribution at a particular instant in time, t. The evolution of the temperature is defined by an energy balance in control volumes between both surfaces of the solid (x = 0 and x = L). The surfaces will define the heat transfer in/out of the solid fuel or mathematically, the boundary conditions. It is important to note, that if other dimensions were to be considered, similar boundary conditions will have to be established at each surface of the material.

Pyrolysis Process

The process by which the solid transforms into gas phase fuel is called pyrolysis and generally implies the breakdown of the molecules into different, most of the time smaller, molecules. This is an important difference between solid and liquid gasification. In the case of liquids a change of phase is not necessarily accompanied by a chemical change (see Chap. 18 for details on ignition of liquids). Pyrolysis tends to be an endothermic process generally controlled by many chemical reactions (some time hundreds) which are a strong function of the temperature. Most pyrolysis reaction rates tend to be described by Arrhenius type functions of the temperature

$$\dot{\omega} = A Y_O{}^m Y_S{}^n e^{-E/RT} \qquad (21.1)$$

But could also be described by other simple expressions like polynomials such as

$$\dot{\omega} = C Y_O{}^m Y_S{}^n (T/T_o)^b \qquad (21.2)$$

The reaction rate is generally defined in units of inverse seconds $(\dot{\omega}[1/s])$ and only when multiplied by the fuel density gives a gasification rate per unit volume ($\dot{\omega}'''$, kg/s.m^3). The constant "A" is also given in inverse seconds (1/s) and generally named the pre-exponential constant. In the case of a polynomial description, "A" will be replaced by another constant that is here defined as "C." These constants are a characteristic of each specific chemical reaction. "E" is the activation energy whose magnitude is also specific to each reaction and "R" has the value of 8.314×10^{-3} kJ mol^{-1} K^{-1}.

The process of pyrolysis can be extremely complex and depending on the fuel and heating characteristics can follow distinctively different paths. These paths can be a compendium of numerous reactions that could be sequential or compete against each other. Furthermore, the chemical pathways followed can be strongly influenced by the presence of oxygen as indicated in Equations 21.1 and 21.2. In both equations Y_O and Y_S are intended to be generic representations of oxygen and solid fuel mass fractions participating in the solid degradation and "m" and "n" are constants.

It is important to note that while degradation of some fuels will show dependency on the oxygen concentration many others will not [3, 4]. In those cases "m" is assumed to be zero.

The chemical pathways leading to the pyrolysis of most solid fuels of interest in fire are fundamentally incomplete as much as the constants associated to the equations that will serve to quantify the rate of each reaction step. Many studies have evaluated reduced chemical mechanisms for the pyrolysis of different solids [5–7] but there is still great uncertainty on the chemical pathways, the number of steps required and the constants associated to them [8, 9]. Figure 21.2 shows an example of chemical kinetic compiled obtained for PMMA by using an expression similar to Equation 21.1.

Thermo-Gravimetric Analysis (TGA) has been used in the past to establish reduced chemical reaction mechanisms as well as the associated constants. The principles behind TGA studies and some applications to materials relevant to fire are presented in Chap. 7. As an example, a reduced kinetic mechanism for polyurethane (PU) can be found in Ref. [6]. The authors propose a four step mechanism of the form:

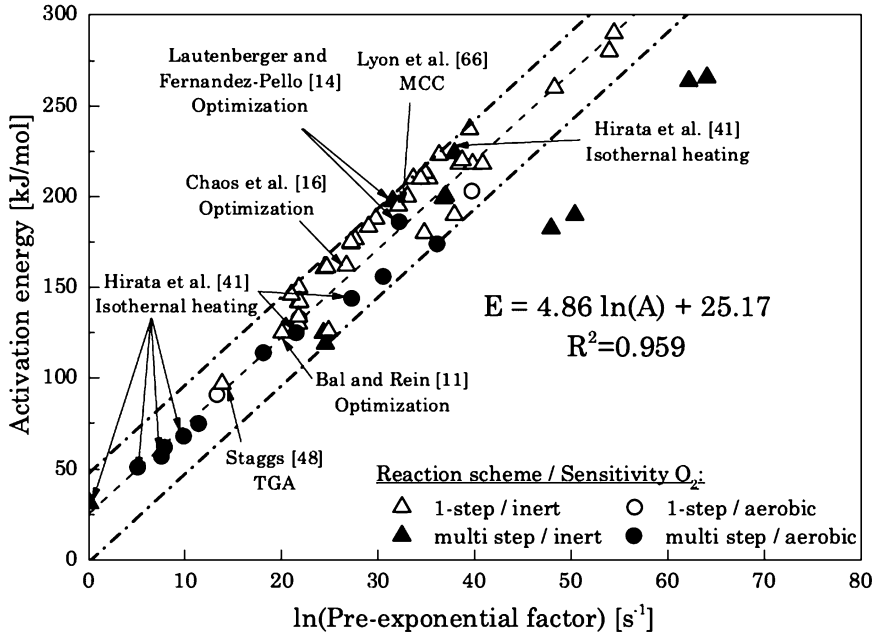

Fig. 21.2 Kinetic parameters of the pyrolysis decomposition of PMMA as reported in the literature [8]

$$
\begin{aligned}
&\text{Step i} = 1 \quad \text{PU} \rightarrow \nu_{\beta,\,p}\ \beta\text{-PU} + \nu_{g,\,p}\ \text{Gas}\\
&\text{Step i} = 2 \quad \beta\text{-PU} \rightarrow \nu_{c,\,p\beta}\ \text{Char} + \nu_{g,\,p\beta}\ \text{Gas}\\
&\text{Step i} = 3 \quad \begin{cases} \text{PU} + \nu_{O2,o}\ O_2 \rightarrow \nu_{c,o}\ \text{Char} + \nu_{g,o}\ \text{Gas} \\ \beta\text{-PU} + \nu_{O2,o}\ O_2 \rightarrow \nu_{c,o}\ \text{Char} + \nu_{g,o}\ \text{Gas} \end{cases}\\
&\text{Step i} = 4 \quad \text{Char} + \nu_{O2,c}\ O_2 \rightarrow \nu_{r,c}\ \text{Residue} + \nu_{g,c}\ \text{Gas}
\end{aligned}
$$

where the reaction rate for each step $(\dot{\omega})$ is presented by an expression of the form of Equation 21.1. The first two steps encompass purely thermal degradation, while the last two steps include oxidation. Two intermediate products are formed from the initial degradation of the polyurethane, β-PU and Char. While the terms Gas and Residue represent the gaseous and solid products of the degradation. It is important to note that there are sequential and competing reactions; while steps 1 and 2 are sequential, step 3 competes with both previous steps. The authors use independent TGA data [10] to obtain all 12 constants thus establishing a complete model for the degradation of polyurethane.

Figure 21.3 shows two curves extracted from Ref. [6] where the model is compared to experimental data for inert and air atmospheres. The figures show the sample mass loss rate as a function of time. The effect of oxygen and the impact of the heating rate are evident from the data. The results show very good agreement with the four step model for all conditions studied.

Despite the generalized use of TGA data, there is increasing recognition that pyrolysis reaction pathways are sensitive to the heating rate. The basic nature of TGA studies requires heating rates of the order of 1–20 °C/min which is generally an order of magnitude slower that heating rates typical of fires. Recent studies have

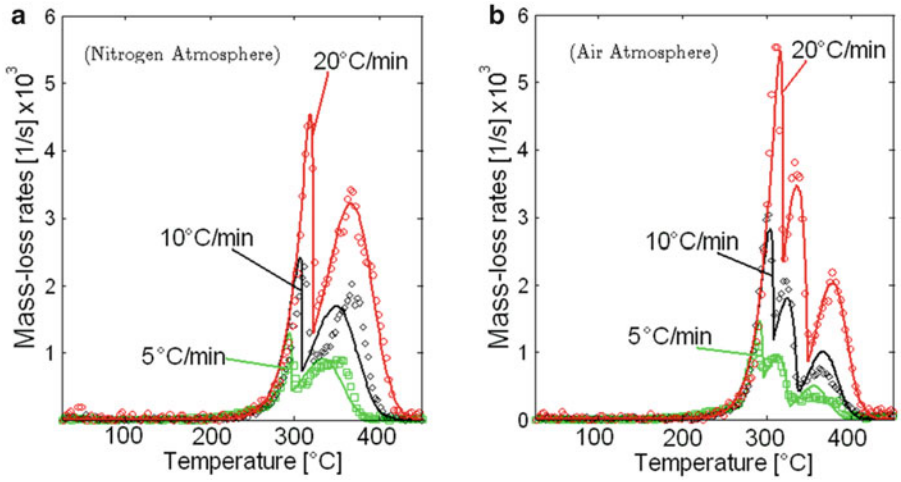

Fig. 21.3 TGA data for polyurethane extracted from reference [10] (*symbols*) superposed to the reduced kinetic model from reference [7] (*lines*) for inert atmosphere (**a**) and air (**b**)

established methodologies that use standard test methods and advanced optimization techniques to establish reduced reaction schemes and their associated constants [7, 11–14]. Although, these procedures allow exposing the materials to heating rates typical of fires and obtaining comprehensive sets of constants they have only been applied to a reduced number of materials. Currently, these methodologies remain fundamentally research tools.

It is important to note that the qualitative and quantitative agreement described in the above example is not usual for materials commonly present in fire and the problem of establishing the chemistry of pyrolysis is far from being solved. Therefore, when studying flaming ignition of solids it is common to make strong simplifications to handle chemical degradation as the solid fuel is heated. Such simplifications will be made later and their impact will be assessed.

The Production of Gaseous Fuel

Before flaming ignition can occur, fuel in the gas phase needs to be produced. Solid materials that are not susceptible to spontaneous ignition will show very little evidence of chemical reactions at ambient temperatures, thus can be deemed as inert. The reaction rates associated to pyrolysis can be considered negligible and therefore the material will not follow any transformation. As the temperature increases the reaction rates increase and the solid fuel starts changing. Given the temperature distribution within the material, the rates of decomposition are a function of "x," with larger production of pyrolyzates close to the surface and lower production in-depth.

Local production of fuel is not the only important variable. The gas phase fuel produced might be the result of a combination of pyrolysis and oxidation reactions, thus its composition might include large quantities of fully oxidized compounds such as carbon dioxide (CO_2), partially oxidized gases such as carbon monoxide (CO) and other molecules that can have all levels of partial oxidation. Therefore, together with the reaction rates, the mass fraction of inert gases needs to be subtracted leaving the remaining reactive gases. As an example, Kashiwagi and Nambu [15] studied the degradation products of cellulosic paper showing that there is a significant presence of inert gases like water vapour, fully oxidized gases like CO_2, partially oxidized products like CO and fuel like CH_4 and H_2.

There is very little data available on the degradation products of most materials relevant to fire, therefore, the mass fraction of flammable gases present in the local products of degradation will be described here by means of a single variable, $Y_{F,s}(x,t)$, which represents a global contribution of all compounds that can be further

oxidized. Figure 21.1 represents $Y_{F,s}(x,t)$ as an increasing function with a minimum at the surface ($Y_{F,s}(0,t)$). This is based on the assumption that where there is a higher presence of oxygen there is higher levels of oxidation.

Oxygen can migrate inside a fuel resulting also in an in-depth distribution ($Y_O(x,t)$) that reaches ambient values at the surface ($Y_O(0,t)$). In-depth oxygen and fuel diffusion is controlled by the structure of the solid. Some materials are highly permeable and allow unrestricted transport of species in and out of the solid. For other materials oxidation will occur only very close to the surface and could be potentially neglected. The permeability of the fuel can be a function of many variables including the degradation and consumption of the material and has deserved very little attention in the fire literature. In the absence of a well defined permeability function, here, a simple variable associated to the fuel permeability ($\chi(x,t)$) will be introduced and assumed to describe in a generic manner the fraction of the fuel produced that can flow through the solid material. It has to be noted that $\chi(x,t)$ is not strictly a permeability function (as per Darcy's law) but a combination of permeability, porosity and any fractures within the material.

Oxygen and fuel concentrations will be controlled by the local permeability and by production/consumption rates, thus indirectly by the temperature distribution ($T(x,t)$). This makes necessary to treat them independently, therefore two independent variables emerge, $\varepsilon_F(t)$ and $\varepsilon_O(t)$. The former represent the region where fuel is being produced while the latter represents the region where oxygen is present in relevant quantities.

If all the reactions occurring can be represented in an Arrhenius form (Equation 21.1) then the local mass production ($\dot{m}'''_P(x,t)$) can be the summarized into a function of the form:

$$\dot{m}'''_P(x,t) = Y_{F,s}(x,t)\sum_{i=1}^{i=N}\left[A_i Y_O^{m_i}(x,t) Y_S^{n_i}(x,t) e^{-E_{i_i}/RT(x,t)}\right] \tag{21.3}$$

where the summation is not truly a sum of all the different "N" reaction steps but just some global combination of them that includes sequential and competitive reactions.

To obtain the total fuel production at the surface per unit area ($\dot{m}''_P(0,t)$) it is necessary to integrate Equation 21.3 across the entire depth including the permeability function described above. It is important to note that fuel produced in-depth does not have to come out, and in many cases pressure increases within the fuel structure can be observed. The effects of permeability and pressure are combined in a complex manner to define the flow within the porous medium. This remains an unresolved problem, thus the use of a simple variable such as $\chi(x,t)$ is justified. Integrating Equation 21.3 we obtain the following expression

$$\dot{m}''_P(0,t) = \int_0^L \chi(x,t)\left(Y_{F,s}(x,t)\sum_{i=1}^{i=N}\left[A_i Y_O^{m_i}(x,t) Y_S^{n_i}(x,t) e^{-E_{i_i}/RT(x,t)}\right]\right)dx$$

Assuming that any production of fuel is negligible for $x > \varepsilon_F$ then the boundaries of integration can be changed to

$$\dot{m}''_P(0,t) = \int_0^{\varepsilon_F} \chi(x,t)\left(Y_{F,s}(x,t)\sum_{i=1}^{i=N}\left[A_i Y_O^{m_i}(x,t) Y_S^{n_i}(x,t) e^{-E_{i_i}/RT(x,t)}\right]\right)dx \tag{21.4}$$

Where the chemical reactions are left in a generic form while recognizing that, due to the absence of oxygen, the reactions occurring between $\varepsilon_O < x < \varepsilon_F$ might differ significantly from those occurring between $0 < x < \varepsilon_F$.

To summarize, the production of fuel is controlled by the following variables:

Temperature	$T(x,t)$
Local fuel concentration	$Y_S(x,t)$
Local oxygen concentration	$Y_O(x,t)$
Residual fuel fraction	$Y_{F,s}(x,t)$
Permeability function	$\chi(x,t)$
Oxygen penetration depth	$\varepsilon_O(t)$
Reactive depth	$\varepsilon_F(t)$
Kinetic constants	A_i, m_i, n_i, E_i

Charring

For the purpose of ignition of a solid fuel the process of charring has an impact on both heat and mass transport therefore needs to be briefly addressed. A general summary of the chemical processes leading to charring can be obtained in Chap. 7, and more details form Cullis and Hirschler [16] for polymers and in the case of wood from Drysdale [17], thus will not be described here. Instead an attempt will be made to explain the role of charring in ignition.

For charring materials pyrolysis leads to the production of gaseous fuel (pyrolyzate) and a residual solid phase char. The char is mainly a carbonaceous solid that could be further decomposed. The secondary decomposition could be complete, leading to an inert ash or to a secondary char that can be further decomposed in a single or multiple steps. Non-charring materials decompose leaving no residue behind.

From the perspective of ignition, the exposed surface represents the boundary between the gas and the solid. This boundary moves as the material is completely removed. The rate at which the surface moves is the regression rate (V_R). For charring and non-charring materials, this will be the boundary where complete consumption of the fuel is achieved. Although, regression rates can be very different between charring and non-charring materials, at the surface, the main difference between the two material types is the temperatures that can be achieved. Carbonaceous chars can reach much higher temperatures, leading in many cases to vigorous oxidation (surface glowing) that can be the catalyser for gas phase ignition. This will be part of the gas phase discussion. In what concerns the production of fuel, the differences appear mostly in-depth where temperature is controlled by heat transfer through the char and fuel production is affected by an overall permeability function. The effects of permeability were described above and temperature effects on fuel production will be discussed in the context of the calculation of the temperature distributions.

The Thermal Depth (ε_T)

When a heat flux is applied to one of the solid surfaces, the heat travels across the solid fuel. Initially only a very small area is affected, but as the thermal wave travels through material a larger and larger fraction of the solid is heated. The velocity of the thermal wave is represented in Fig. 21.1 by $V_T(t)$. $V_T(t)$ is a function of time because it will decrease as the thermal wave moves away from the heating source and towards the cold back surface. The region that has been heated is quantified by the characteristic length $\varepsilon_T(t)$. It is important to note that, given that temperature is a continuous function, $\varepsilon_T(t)$ has to be arbitrarily defined simply as the end of the heated region. There is no exact mathematical definition for this length but physically it means that the temperature is approaching ambient temperature ($T \approx T_0$) or the gradient of the temperature is approaching zero ($dT/dx \approx 0$). The proximity that temperature or the gradient have to achieve when approaching these targets is only a matter of what precision is required by those making the analysis.

The length scale $\varepsilon_T(t)$ is extremely important because it characterizes solids into different groups. This breakdown enables the simplification of the energy equation and the generation of simple analytical expressions for the temperature distribution. For the purpose of ignition, solid fuels are classified in:

Semi-infinite Solid ($L > \varepsilon_T$) If the thermal wave is far from the end of the sample, the heat coming from the exposed surface has still not migrated to the back end. The temperature at the back end is ambient (T_0) and there are no heat losses through this surface. The thickness of the sample is no longer a relevant quantity and therefore the fuel can be treated as a semi-infinite solid ($L \rightarrow \infty$). Materials do not show semi-infinite solid behaviour forever, as time progresses the thermal wave will eventually reach the end of the sample. In many cases materials will behave as semi-infinite solids for the period of interest, in which case the assumption of $L \rightarrow \infty$ is valid. The boundary condition for the energy equation becomes:

$$x = L \rightarrow \infty \tag{21.5}$$

$$\dot{q}''_N(\infty, t) = 0$$
$$T = T_0$$

Thermally-Thick and Thermally-Thin Solid ($\varepsilon_T \geq L$) The thermal wave has reached the end of the sample and therefore heat losses at the back end need to be quantified. The thickness of the sample, L, becomes a relevant dimension of the problem and a boundary condition for $x = L$ needs to be defined. This group can be sub-divided into two different cases, thermally thick and thermally thin. A solid can be defined as thermally thick if a significant thermal gradient exists within the solid through the period of ignition. In contrast, in a thermally thin solid the gradient is negligible for most of the time before ignition. A simple criterion based on the Biot number (Bi) is generally used for the purpose of establishing if a material is thermally thin or thick. The Biot number is defined as $Bi = hL/k$, where "h" is a global heat transfer coefficient (W/m^2K) and "k" is the thermal conductivity (W/mK). If $Bi << 1$ then temperature gradients inside the solid are negligible, while if the Biot number is not much smaller than unity then temperature gradients need to be considered. While this is an important distinction for the energy equation, it does not have an effect on the boundary condition at $x = L$, so if $\varepsilon_T \geq L$ then the boundary condition is defined as:

$$x = L \tag{21.6}$$

$$-k\left.\frac{dT}{dx}\right|_{x=L} = \dot{q}''_N(L, t)$$

where $\dot{q}''_N(L, t)$ will be left as a generic heat loss term at the back end of the solid fuel.

The Pyrolysis (ε_P) and Charring Depths (ε_{CH})

Within the region where the temperature has increased above ambient significant chemical activity can occur. The chemical activity leads to the production of fuel at a rate specified by equations of the type of (21.1) or (21.2). The depth at which the chemistry can be assumed to be significant is commonly defined as a pyrolysis depth (ε_P) which propagates at a velocity V_P. As with the thermal depth, there is no mathematical function that describes the location of the pyrolysis front, $x = \varepsilon_P$ because the reaction equations are also continuous functions. Nevertheless, if the assumption is made that pyrolysis reactions have high activation energy then the transition between the zones of significant and negligible reactivity can be considered as being abrupt [18]. This permits the definition of critical parameters that can be considered to define the onset of pyrolysis. The most common parameter is a pyrolysis temperature, T_P, below which the solid fuel can be considered inert. It is important to note that the pyrolysis temperature is not a true physical parameter but a simple way to track the onset of high activation chemical reactions.

As described above, for $x > \varepsilon_P$ the solid can be considered inert, thus thermal properties can be defined as those of the original solid fuel. The thermal properties relevant to ignition are

Density	$\rho(x,t)$	Kg/m^3
Thermal conductivity	$k(x,t)$	W/m.K
Specific heat	$C(x,t)$	J/kg.K

which are all functions of temperature. Since the temperature varies in-depth they are also functions of "x." The evolution of these properties with temperature for common materials can be found in most heat transfer book [19], nevertheless, for materials typically present in fires (wood, complex plastics, composites, etc.) these properties are in many cases unknown [20, 21].

For $x > \varepsilon_P$ the chemical reactions have initiated the decomposition of the material. The relevant properties remain the same, nevertheless pyrolysis introduces further changes to the properties. The gasification of the fuel and its transport towards the surface will strongly affect the density, while any potential voids will force to redefine thermal conductivity and specific heat to account for the existence of at least two phases.

The process of pyrolysis can lead directly to gasification with no residue (non-charring) or to a carbonaceous residue (charring). Figure 21.1 shows the case of a charring material where a second front for charring ($x = \varepsilon_{CH}$) is formed behind the pyrolysis front. The charring front will propagate at a velocity V_{CH} and will leave behind a residue that will have a new set of properties that are potentially very different to those of the fuel. The properties are still the permeability, the density, thermal conductivity and specific heat but precise values are mostly unknown for most chars issued of materials relevant to fires.

It is common to see in the char region large voids and cracks that compromise the one-dimensional treatment provided here. These have been considered when addressing materials such as wood but will not be described here.

Melting and the Evaporation of Water

Melting or water evaporation have not been considered in the description of the ignition until this point. These two processes are endothermic phase changes that can have a significant effect on the temperature distribution in the solid. Numerous models have been built in the past to describe the heat sinks associated to melting and several studies have attempted to quantify the impact of melting on practical situations such as dripping.

Phase changes are generally incorporated to the energy equation as heat sinks where some rate function is created to describe the conversion from one phase to the other. The simplest procedure is to assign a critical temperature to the phase change (i.e. 100 °C for water) and a heat of melting or evaporation (ΔH_M). Once the fuel or water reaches this temperature it is converted to the high temperature phase. The phase change process is assumed to be infinitely fast and therefore the rate is defined by the available energy reaching the location where the phase change is occurring. All the energy is then used for the phase change and the thermal wave can only proceed once the transition has been completed. This approach is inappropriate if the available energy is very low, in this case thermodynamic equilibrium equations will define the rate of vaporization or melting. Other more complex models that include processes such as re-condensation can be found in the literature but will not be discussed here.

The consequences of melting or water evaporation are various. Phase changes can affect the thermal properties of the fuel significantly and can result in motion of the molten fuel or water vapour. This leads to convective flow of energy or mass transfer.

Understanding the physical processes behind phase change does not represent a great challenge. Furthermore, the potential impact of phase change on ignition is clear. Thus it is evident that any predictive tool for ignition should attempt to quantify the impact of phase change on ignition. Nevertheless, the formulation of a model that can describe these processes in a comprehensive manner is extremely complex and the measurements that could serve for its validation are mostly non-existent.

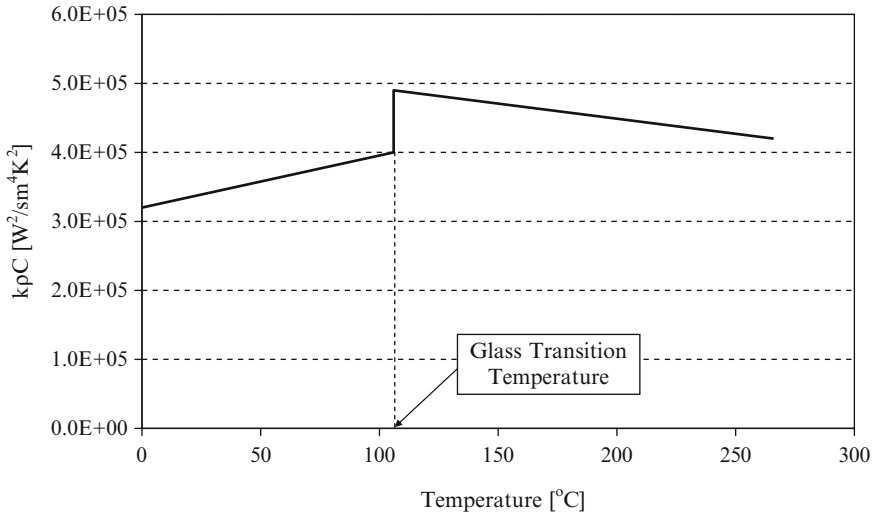

Fig. 21.4 Evolution of the product of the thermal conductivity, density and specific heat (kρC) for PMMA as a function of temperature

Given that, phase change is fundamentally an additional heat sink that will have to be incorporated to the energy equation in an arbitrary manner, it is justifiable to exclude the treatment of this subject from the present analysis. Nevertheless, this is done with the clear warning that its exclusion will have a significant impact on any quantitative assessment of the ignition process.

Other processes that deserve to be addressed are softening or glass transition. Many materials such as thermoplastics will undergo gradual or drastic property changes with temperature. These property changes are not endothermic but will affect the progression of heat through the sample and could lead to dripping. Softening or glass transition will be directly incorporated in the analysis through the variable properties described in section "The Pyrolysis (ε_P) and Charring Depths (ε_{CH})". An example of how these properties change with temperature is shown in Fig. 21.4. Figure 21.4 presents the evolution of the product of all three thermal properties (kρC) for PMMA as a function of temperature, indicating the abrupt change occurring at the glass transition temperature.

The Temperature Distribution

As explained in section "The Production of Gaseous Fuel", to determine the fuel production it is necessary to define the evolution of the temperature inside the solid fuel. This can be achieved by defining a comprehensive energy equation. Figure 21.4 represents a typical control volume for $x < \varepsilon_P$ where all the main heat transfer mechanisms are incorporated.

For the purposes of this description the coordinate system will be anchored to the regressing surface, thus "x" will move with a velocity V_R. A mass flow of fuel will therefore cross the control volume presented in Fig. 21.5 carrying energy in and out ($\dot{q}''_S$). The gaseous products of pyrolysis and oxygen diffusion will also carry energy in and out of the control volume ($\dot{q}''_P$, $\dot{q}''_O$ respectively) and the generic expression for the mass flow of these gases ($\dot{m}''_P$, $\dot{m}''_O$) incorporates the regression rate. Heat is conducted in and out of the control volume ($\dot{q}''_{CND}$) and for generality in-depth radiative absorption is allowed ($\dot{q}'''_{RAD}$). Since for $x < \varepsilon_P$ the temperature is sufficiently high to allow for chemical reactions all heat

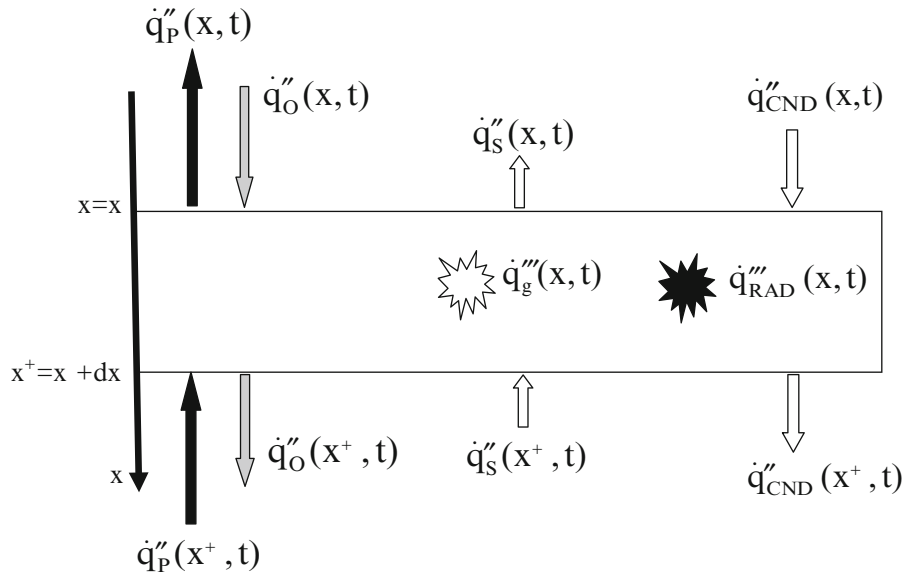

Fig. 21.5 Typical control volume for $x < \varepsilon_P$ showing the main heat transfer mechanisms

Table 21.1 Summary of all energy transport within a generic control volume for $x < \varepsilon_P$. $\Delta H_{P,i}$ is the net heat resulting from each individual chemical reaction. The net heat will be endothermic for most pyrolysis processes and exothermic for oxidative reactions. The summation is not truly a summation, but as explained earlier, is the overall set of chemical reactions where some could be sequential and others competing

Description	In	Out	Formulation
Energy transported by gaseous fuel traversing the control volume	$\dot{q}''_P(x^+,t)$		$\dot{m}''_p(x^+,t)C_{P,P}(x^+,t)T_P(x^+,t)$
		$\dot{q}''_P(x,t)$	$\dot{m}''_p(x,t)C_{P,P}(x,t)T_P(x,t)$
Energy transported by oxygen traversing the control volume		$\dot{q}''_O(x^+,t)$	$\dot{m}''_O(x^+,t)C_{P,O}(x^+,t)T_O(x^+,t)$
	$\dot{q}''_O(x,t)$		$\dot{m}''_O(x,t)C_{P,O}(x,t)T_O(x,t)$
Energy transported by solid fuel traversing the control volume	$\dot{q}''_S(x^+,t)$		$\rho_S(x^+,t)V_R(t)C_S(x^+,t)T(x^+,t)$
		$\dot{q}''_S(x,t)$	$\rho_S(x,t)V_R(t)C_S(x,t)T(x,t)$
Heat conduction	$\dot{q}''_{CND}(x,t)$		$-k_S\frac{dT}{dx}\Big\|_{x=x}$
		$\dot{q}''_{CND}(x^+,t)$	$-k_S\frac{dT}{dx}\Big\|_{x=x^+}$
Radiative absorption	$\dot{q}'''_{RAD}(x,t).dx$		$\dot{q}'''_{RAD}(x,t).dx$
Chemical energy (generation/sink)	$\dot{q}'''_g(x,t).dx$		$\sum_{i=1}^{i=N}\Delta H_{P,i}\rho_S(x,t)\left[A_i Y_O^{m_i}(x,t)Y_F^{n_i}(x,t)e^{-E_i/RT(x,t)}\right]$

sources and sinks associated to all chemistry need to be included. Table 21.1 summarizes all terms incorporated in Fig. 21.5.

Estimation of the net heat transfer will lead to a change in the energy accumulated within the control volume. The following expression summarizes the energy balance:

$$\frac{\partial E_{CV}}{\partial t} = \left[\dot{q}''_S(x^+,t)+\dot{q}''_P(x^+,t)+\dot{q}''_0(x,t)+\dot{q}''_{CND}(x,t)\right] - \left[\dot{q}''_O(x+,t)+\dot{q}''_{CND}(x+,t)+\dot{q}''_S(x,t)+\dot{q}''_P(x,t)\right] + \dot{q}'''_{RAD}(x,t)\,dx + \dot{q}'''_g(x,t)\,dx$$

where $E_{CV} = \rho_S(x,t)C_S(x,t)T(x,t)\ dx$, which after appropriate substitutions results in the general energy equation for the control volume.

$$\frac{\partial[\rho_S C_S T]}{\partial t} = \frac{\partial}{\partial x}\left[k_S \frac{\partial T}{\partial x}\right] + \frac{\partial\left[\dot{m}''_P C_{P,P} T_P\right]}{\partial x} - \frac{\partial\left[\dot{m}''_O C_{P,O} T_O\right]}{\partial x} + \frac{\partial[\rho_S V_R C_S T]}{\partial x} + \dot{q}'''_{RAD} + \sum_{i=1}^{i=N} \Delta H_{P,i} \rho_S \left[A_i Y_O^{m_i} Y_S^{n_i} e^{-E_i/RT}\right] \quad (21.7)$$

Given the differential nature of the equation all variables are assumed to be functions of "x" and "t" so these dependencies are no longer indicated. Many of the terms are left in a generic form and not quantified. Their quantification is complex, thus a more detailed discussion will be provided later in those cases where it is necessary.

The solution to Equation 21.5 will provide the evolution of the temperature distribution along the sample and as a function of time (T(x,t)). This solution can then be incorporated in Equation 21.4 to establish the fuel production rate. It is important to note that thermal equilibrium between phases has not been assumed, thus there are three different temperatures in Equation 21.5, T, T_P and T_O. Expressions similar to Equation 21.5 can be defined for each phase and will have to be solved in a simultaneous manner. The boundary condition will be the exchange of heat between phases, this is generally done using empirical correlations for heat transfer in porous media [22]. The alternative approach is to demonstrate thermal equilibrium between the phases (heat transfer is much faster than mass transfer within the pores), in which case all temperatures will be the same and only Equation 21.5 will have to be solved.

To summarize, and in addition to the variables established in sections "The Production of Gaseous Fuel" and "The Pyrolysis (ε_P) and Charring Depths (ε_{CH})", the temperature distribution is controlled by the following variables:

Thermal conductivity	$k_S(x,t)$
Specific heat	$C_S(x,t)$ $C_{P,P}(x,t)$ $C_{P,O}(x,t)$
Density of the solid	$\rho(x,t)$
Regression rate	$V_R(t)$
Mass flow	$\dot{m}''_P$ $\dot{m}''_O$
Temperature of the gas phase	T_P T_O
Radiative properties of the solid (absorptivity, $\alpha_S(x,t)$)	$\alpha_S(x,t)$
Heat of reaction	$\Delta H_{P,i}$

The Surface Boundary Conditions (x = 0 and x = L)

Figure 21.1 shows all the different modes of heat transfer through the surface control volumes. In theory, control volumes at $x = 0$ and $x = L$ could be represented in a generic manner that makes them identical. In practise this is generally not the case because materials tend to have an exposed face and one that is in contact with some backing. The backing will define a conductive boundary condition while the open face a convective/radiative one. For illustration purposes, this distinction will be made here and the exposed face will be defined as an open boundary, thus $\dot{q}''_N(0,t)$ will include convection and radiation, while the back-face, $\dot{q}''_N(L,t)$, will be attached to a substrate, thus will be defined as an impermeable conductive boundary condition. It needs to be emphasized that this is an arbitrary simplification that is only done to illustrate two different types of boundary conditions because they are mutually exclusive. In many cases a material might be sandwiched between two solids or exposed at both ends. The appropriate choice of boundary conditions needs to be made

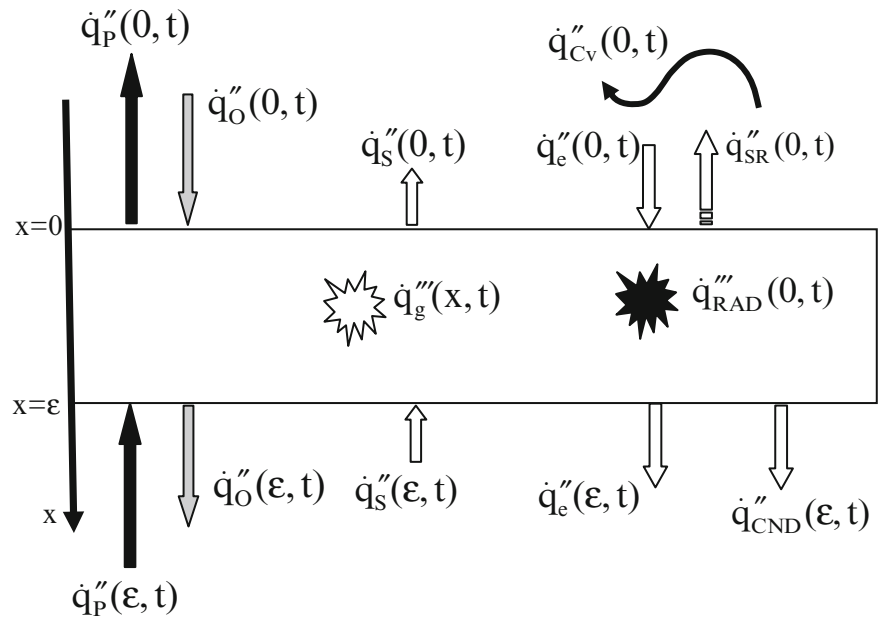

Fig. 21.6 Boundary control volume for x = 0 showing the main heat transfer mechanisms

but the processes to be described will not be different.

Figure 21.6 shows the open boundary condition (x = 0) at a specific point in time. The different components are mainly those described in Table 21.1 leading to a very similar expression for the energy balance as that presented in section "The Temperature Distribution". So at the x = 0 surface

$$\frac{\partial E_{CV}(0,t)}{\partial t} = \left[\dot{q}''_S(\varepsilon,t) + \dot{q}''_P(\varepsilon,t) + \dot{q}''_0(0,t)\right] - \left[\dot{q}''_O(\varepsilon,t) + \dot{q}''_{CND}(\varepsilon,t) + \dot{q}''_S(0,t) + \dot{q}''_P(0,t) + \dot{q}''_{SR}(0,t) + \dot{q}''_{Cv}(0,t)\right] + \dot{q}'''_{RAD}(x,t)\varepsilon + \dot{q}'''_g(x,t)\varepsilon$$

where the terms that remain undefined are described in Table 21.2. Radiation absorption within the surface control volume is represented as $\dot{q}''_{RAD}(0,t)\varepsilon = \dot{q}''_e(0,t) - \dot{q}''_e(\varepsilon,t)$ to remain consistent with the notation of the previous section.

For the boundary control volume the characteristic thickness $\varepsilon \to 0$, which eliminates all energy transported by mass flow, radiation absorption and energy generation. The final expression for the exposed boundary condition is then:

$$0 = k_S \left.\frac{\partial T}{\partial x}\right|_{x=0^+} - \varepsilon_S(0,t)\sigma\left(T^4(0,t) - T_0^4\right) - h_{Cv}(t)\left(T(0,t) - T_0\right) \tag{21.8}$$

Table 21.2 Summary of all energy transport within the surface control volume. Only terms not presented in Table 21.1 are described here. The Stefan-Boltzmann Constant is: $\sigma = 5.670 \times 10^{-8}$ W/m^{2}K^4, $\varepsilon_S(0,t)$ is the surface emissivity and h_{Cv} is the convective heat transfer coefficient. Only for illustration purposes two different approaches are used to describe radiation, absorption is allowed to happen in-depth while emission is treated as a surface process. The spectral emissivity and absorptivity of the material will define the most appropriate treatment for each specific case

Description	In	Out	Formulation
Radiation from the exposed surface to the environment		$\dot{q}''_{SR}(0,t)$	$\varepsilon_S(0,t)\sigma\left(T^4(0,t)\text{-}T_0^4\right)$
Convective losses from the surface		$\dot{q}''_{Cv}(0,t)$	$h_{Cv}(T(0,t)\text{-}T_0)$
External radiative heat-flux	$\dot{q}''_e(0,t)$		$\dot{q}''_e(0,t)$

A similar treatment can be followed with the back end boundary condition (x = L). In this case the back surface is assumed to be in direct contact with another solid. Mass transfer, convection and radiative losses to the environment are therefore precluded. The boundary condition will only include conductive terms and can be described as:

$$0 = -k_S \left.\frac{\partial T}{\partial x}\right|_{x=L^-} + k_B \left.\frac{\partial T_B}{\partial x}\right|_{x=L^+} \tag{21.9}$$

where k_B is a global thermal conductivity of the backing material that could include the thermal resistance between the two solids. In most cases the contact between both solids is not perfect, leaving air gaps or requiring adhesives, in these cases it is important to define the thermal conductivity in a manner that includes the contact resistance. The variable T_B is the temperature of the backing solid, these temperature will come out of a solution to an additional energy balance of the form of Equation 21.5. Note that if k_B is very small the backing can be assumed as an insulator and the boundary condition can be summarized to no losses at the back. This eliminates the need to solve a second energy equation for T_B.

To summarize, and in addition to the variables established in sections "The Production of Gaseous Fuel", "The Pyrolysis (ε_P) and Charring Depths (ε_{CH})" and "The Temperature Distribution", the temperature distribution is controlled by the following variables:

Global thermal conductivity of the backing material	$k_B(x,t)$
Temperature of the backing material	$T_B(x,t)$
Emissivity of the solid	$\varepsilon_S(x,t)$
Convective heat transfer coefficient	$h_{Cv}(t)$
Ambient temperature	T_0

The Gas Phase

The sequence of events leading to the ignition of a gas phase flame will be described in this section. It will be assumed that gaseous fuel emerges from the solid following the description provided in section "The Solid Phase".

After the onset of pyrolysis gas begins to emerge from the fuel surface, initially in very small quantities, but as ε_F and T(x,t) increase Equation 21.4 shows that the fuel mass flux will increase. The emerging fuel will encounter the ambient oxidizer and eventually produce a flammable mixture. Given that fuel is migrating into the oxidizer flow, the definition of a flammable mixture is not a simple one. In standard test methods the ambient flow is well defined, mixed convection generated by a horizontal heated surface and the extraction system in the cone calorimeter [23], natural convection resulting from a vertical heated surface in the LIFT apparatus [24] and forced convection over the fuel surface (horizontal or vertical) in the FM Global Fire Propagation Apparatus [25]. In real fires, flow fields are defined by the flames

themselves and by the geometry of the environment (obstacles, fuel geometry, etc.) with the possibility of complex flow patterns. The only mechanisms to establish the fuel distribution within the gas phase are detailed measurements or modelling [26–28]. Nevertheless, from a phenomenological perspective, to achieve ignition, what is required is to achieve a flammable condition in at least one location in the gas phase.

The definition of a flammable mixture is for the fuel concentration to be found between the Lower or Lean Flammability Limit (LFL) and the Upper or Rich Flammability Limit (UFL). Although the LFL and UFL are apparatus dependent measurements, it is clear that the precision required for flaming ignition of solids does not require a more universal description of flammability. For a more detailed discussion on flammability limits and their limitations the reader is referred to Chap. 12.

Auto-ignition

Once a flammable mixture has been attained, this mixture needs to increase in temperature until a combustion reaction can occur. This process is described in great detail by Torero [29] and by Fernandez-Pello [30, 31], who cites a series of experiments by Niioka [32] where ignition is studied using a stagnation point flow over a solid fuel surface. In these experiments the heat to initiate the combustion reaction is provided by a hot flow impinging on a fuel surface that acts as a heat sink. Niioka [32] identifies an induction time and a pyrolysis time. The pyrolysis time corresponds to the time required to attain a flammable mixture while the induction time is the time for the mixture to reach a temperature at which ignition can occur. Given the specific configuration, the pyrolysis time decreases with the flow velocity (enhanced heat transfer to the fuel surface) while the induction time increases (reduced residence time in the gas phase). Although these observations are not universally applicable, they serve to illustrate the process of auto-ignition. Fernandez-Pello [30, 31] describes Niioka's conclusions graphically by means of the schematic, this schematic is simplified and presented in Fig. 21.7. Figure 21.7 shows how the summation of the pyrolysis and induction times leads to an ignition time.

In auto-ignition there is no hot spot that will serve as an initiation point for the reaction, thus the mixture has to absorb enough energy to reach ignition. The exact amount of energy required for ignition can be associated to a Damköhler number [18]. The Damköhler number corresponds to the ratio between a local residence and chemical time. The chemical time represents the necessary

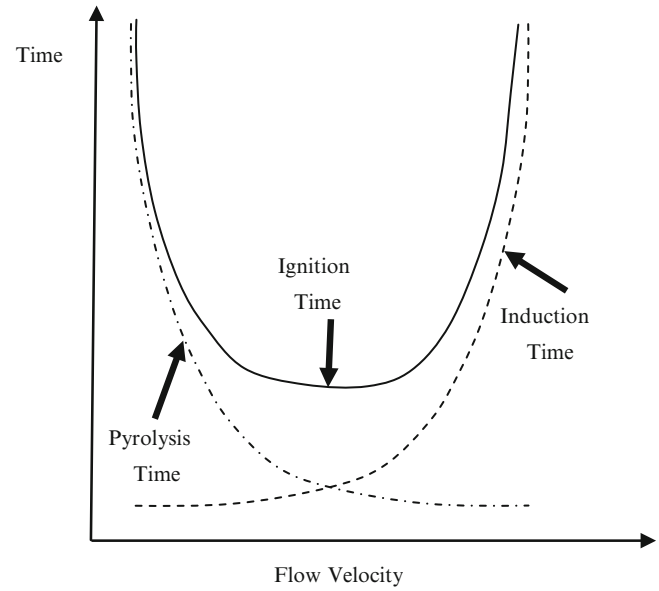

Fig. 21.7 Schematic of the characteristic times involved in the ignition of a flat plate subject to a hot stagnation point flow. This schematic is based on the work by Niioka [32] and adapted from Fernandez-Pello [30, 31]

time for the reaction chemistry to occur and is expressed as the inverse of the reaction rate. Combustion reactions can be described by expressions like that presented in Equation 21.1 thus the chemical time is directly affected by the temperature of the reactants. The higher the temperature, the greater the reaction rates and the shorter the chemical time. The residence time is a measure of the strain (or dissipation rates) or the time the reactants remain together at a specific location thus it is directly related to the velocity field. The faster the flow or the velocity gradients, the shorter the residence time. If the chemical times are shorter than the residence times the reaction has enough time to proceed and a flame can exist. A critical Damköhler number for ignition can then be established, above which a combustion reaction can proceed [18]. In the schematic presented in Fig. 21.7, critical Damköhler numbers will be attained at both sides of the ignition curve preventing ignition. This is probably the most precise way to describe ignition but it requires the full resolution of the flow and temperature fields as well as comprehensive knowledge of the kinetic constants associated to the combustion reaction. While the flow field can be resolved by means of Computational Fluid Dynamics (CFD) the chemistry of most fire related fuels still remains uncertain. Qualitative assessment of the Damköhler number for ignition has only been achieved for a few very well defined experimental conditions such as stagnation flows [6, 32, 33] or boundary layers [34]. Other alternative representations of the ignition conditions that rest on the same fundamental approach have been discussed by Quintiere [35] and by Gray and Lee [36].

An important aspect of the ignition process that remains to some extent unresolved is the origin of the heat that is necessary for the gaseous fuel to reach the critical Damköhler number. If the air flow is hot, like in Niioka's experiments [32], then the energy will come from the oxidizer and the problem is immensely simplified. If the oxidizer is cold and there is an external radiative heat source, then solid and gas will heat at different rates. The solid will absorb heat and its surface temperature will change following Equation 21.5 while the gas will absorb heat based on its absorptivity and dissipate it in a manner governed by the flow field. The absorptivity of the gas is a strong function of the fuel type and concentration, thus also requires detailed knowledge of the flow field. The two possible outcomes are that the gas phase heats faster than the solid phase or the opposite. In the former case ignition will occur away from the fuel surface, since the fuel will act as a heat sink for the gas. In the latter case, ignition will occur closer to the fuel surface since the fuel acts as a heat source. This latter scenario is common with charring materials where oxidation of the char contributes to increase the surface temperature [37].

It is clear that auto-ignition is a complex process that fully involves interactions of the solid and gas phases. Therefore, to characterize auto-ignition of solid fuels it is necessary to established well defined experimental conditions and simplifications to the analysis. Data obtained from different experimental conditions and with a specific analysis will generally not be compatible with other data that was obtained from a different experiment or deduced by means of an alternative analysis. Thus, scatter in the reported data is common for auto ignition.

Data on auto-ignition is generally reported as Auto-Ignition Temperatures (AIT) which corresponds to a recorded temperature at the moment where ignition of a flame is first observed. A summary of much of the data available is presented in Chap. 14 of Ref. [1] together with a series of references to relevant papers and textbooks [38, 39]. Given the complexity of the processes leading to auto-ignition, these values can only be taken as reference values that are a direct function of the specific test conditions. Generally, significant discrepancy is found in the literature where reported Auto-Ignition Temperatures can vary in more than 150 °C for the same material. The greatest discrepancies tend to be found when the orientation of the solid fuel is varied and the fluid mechanics and heat transfer are significantly altered [1]. Auto-Ignition Temperatures are most consistent for

gaseous mixtures (Chap. 12) and liquid fuels (Chap. 18) where tests are conducted in enclosed vessels where the fuel has been fully evaporated.

Piloted Ignition

As discussed in the previous section, the process of auto-ignition is extremely difficult to describe in a quantitative manner, even under simple experimental configurations. Therefore, as an example, it is not practical to rely on auto-ignition to describe the susceptibility of solid materials to ignite. A mechanism to simplify the process is to include a pilot flame or a hot spot. This is a practical experimental simplification that has a basis on reality, since in most ignition scenarios there will be a region of high temperature. The presence of a pilot strongly simplifies the gas phase processes and reduces the influence of environmental variables. While characterization of the flow field is still required to establish the presence of a flammable mixture, it is no longer necessary to resolve heat transfer between phases or to define the absorption of energy by the gas. In the presence of a pilot, ignition can be assumed at the moment where a flammable mixture (LFL) is attained at the location of the pilot.

Currently, all standard test methods that attempt the description of the ignitability of solids use some form of a pilot. In some cases, the pilot is a large flame [24] while in others is either a small pilot flame [25] or a high energy spark [23]. Both methods have their advantages and disadvantages, sparks produce only local heating thus have a weaker tendency to influence the solid phase by acting as a heat source. - Nevertheless, given their small volume, ignition is strongly influenced by the spark location. The flow field has to establish a flammable mixture at exactly the location of the pilot. In contrast, large pilot flames have a tendency to supply heat to the fuel surface, but cover a large volume, therefore are less sensitive to the flow field. Because of its practical relevance, all subsequent discussion will concern piloted ignition.

To attain the LFL at the pilot location it is necessary to resolve the momentum and mass transport equations simultaneously with the surface boundary conditions explained above. Figure 21.1 shows an arbitrary distribution of the fuel concentration external to the sample, $Y_{F,g}$. A similar representation could be made for the oxygen concentration ($Y_{O,g}$). The characteristic equation that describes the flow field is as follows:

$$\rho_0 \frac{D\vec{u}}{Dt} = -\nabla P + \rho_0 \vec{g} + \mu_0 \nabla^2 \vec{u} \qquad (21.10)$$

Where $\vec{u}$ is the velocity field, ρ_0 the density of the air, P the pressure field, $\vec{g}$ the gravity vector and μ_0 the viscosity of the air. Temperature dependencies of the properties have been omitted for simplification assuming that air is the main constituent and it will remain close to ambient temperature. Conservation of fuel and oxygen concentrations can then be defined by:

$$\rho_0 \frac{DY_{F,g}}{Dt} = \rho_0 D_{F,O} \nabla^2 Y_{F,g} \qquad (21.11)$$

$$\rho_0 \frac{DY_{O,g}}{Dt} = \rho_0 D_{F,O} \nabla^2 Y_{O,g} \qquad (21.12)$$

where species transport is assumed to be non-reactive, thus the source/sink has been omitted. This is an adequate assumption for pure mixing. To obtain the solution of Equations 21.8, 21.9 and 21.10 it is necessary to add the following variables to those established in sections "The Production of Gaseous Fuel", "The Pyrolysis (ε_P) and Charring Depths (ε_{CH})", "The Temperature Distribution" and "The Surface Boundary Conditions (x=0 and x=L)":

Density of air	ρ_0
Velocity field	$\vec{u}$
Pressure field	P
Viscosity of air	μ_0
Diffusivity of fuel in air	$D_{F,0}$
Pilot location	$\vec{r}$

At this point, there is no need to specify a critical Damköhler number for ignition because

of the presence of the pilot, although in absolute rigour, this assumes that the flow conditions are such that blow-off of the flame kernel does not occur, thus the pilot will allow the establishment of a flame across the flammable mixture.

"Flash Point" and "Fire Point"

Once ignition has been achieved a flame can propagate through the regions where a flammable mixture is present consuming the reactants. Independent of the flow field, it is most likely that a flammable mixture will be established close to the solid fuel surface. The pyrolysis rates at the moment when the flame is established will determine if a flame can continue to exist or if the combustion reaction will cease after the gas phase mixture is consumed. The feedback from the flame will enhance pyrolysis, but usually, the relatively large thermal inertia of the solid will result in a slow response, therefore it will be necessary for pyrolysis rates to be sufficient even in the absence of the flame heat feedback. If pyrolysis rates are not sufficient, the flame will extinguish and continuous pyrolysis will lead once again to the formation of a flammable mixture and subsequent ignition. This manifests itself as a sequence of flashes that precede the establishment of a flame over the combustible solid. This process is identical to the "flash point" generally associated to liquid fuels (Chap. 18) and for solid fuels has been described in detail by Atreya [37].

The transition between the "flash point" ignition and the established flame, which could also be named the "fire point" in an analogy with liquid fuels, deserves especial attention. The characteristics of the diffusion flame established on a solid fuel surface are defined by the flow field and the supply of fuel. The rate at which both reactants reach the flame zone defines the flame temperature and thus the characteristic chemical time. If the amount of fuel reaching the flame is small, then the flame temperature will be low and the chemical time will be long. As described above, the flow field defines the residence time. A second critical Damköhler number appears, but this time is one of extinction. This concept has been described many times explicitly in the combustion literature [18] but only implicitly in the fire literature. There are only few studies where a critical extinction Damköhler number has been presented to describe the "fire point" but in all cases they concern idealized flow fields that allow establishing a direct correlation between fuel production and flame temperature [33, 34]. In most discussions simplifications have been assumed leading to simpler parameters that can serve as surrogates for the Damköhler number. Williams [40] discusses a critical gas phase temperature below which extinction will occur. If the residence time remains unchanged, then extinction is only associated to the chemical time, thus can be directly linked to a critical gas phase temperature. It can be further argued that extinction is much more sensitive to temperature than to flow, thus only radical changes in the residence time need to be addressed making this criterion a robust one. A more practical surrogate to the Damköhler number is a critical fuel mass flux criterion. Under specific testing conditions the flow field will remain invariable. In this case the attainment of a critical mass flux of fuel will be the single parameter defining the flame temperature and thus the Damköhler number [41, 42]. Furthermore, under more restrictive conditions the critical mass flux can be associated to a critical solid phase temperature [43]. Drysdale [17] and Beyler [44] provide a detail description of the classic approaches to this subject while Quintiere and Rangwala address some of the more current studies [45].

The sequence of events relating "flash" and "fire" points is not trivial because they represent distinctively different processes. For piloted ignition, the "flash point" only requires a flammable mixture while for the "fire point" the rate of fuel supply has to be enough to achieve a chemical time shorter than the residence time. Thus a number of different scenarios can be observed that in many cases can affect the consistency of different ignition studies. A simple example will be used to illustrate this. For example; if the pilot is very close to the fuel surface then a flammable

mixture will be achieved at the pilot location soon after the onset of pyrolysis. In this case fuel supply will be far from that required to sustain a flame. A significant delay will exist between flash and fire points where several flashes will be observed. If the pilot is distanced from the fuel surface it will take longer to attain a flammable mixture and therefore at the moment of the first flash the fuel supply would have increased and a smaller number of flashes will be observed before the flame is fully established. Greater separation of the pilot from the fuel surface might result in the flammable mixture being attained at the pilot location at the same time as the fuel supply is sufficient to sustain a flame. In this case the fire point will correspond with the first flash. A further increase in the distance between pilot and fuel will not change the physical manifestation but will continue to delay ignition. In this case ignition will occur when a flammable mixture is attained at the pilot but will not be related to the flash or fire points. This example has been presented to illustrate the sensitivity of ignition studies to different variables and the importance of detailed observations to the validity of conclusions and comparisons. In this case pilot location was used as the example, but a similar analysis could be made with the heat flux, the oxygen concentration, the flow field [31, 46] or the ambient pressure [47].

The only added variable required to model the "fire point" will be the critical Damköhler number for extinction ($Da_{e,cr}$) or any equivalent way to represent the extinction condition. As mentioned above, other criteria can be used to establish the extinction condition and that are partially equivalent to the critical Damköhler number. Such criteria are a critical mass transfer numbers (B_{cr}) [34, 48], critical mass fluxes [11, 28, 30, 42] or critical temperatures (T_{cr}) [17, 35, 40, 43, 45].

Simplifications and Standardization

To predict flaming ignition of a solid fuel is necessary to solve Equations 21.1, 21.2, 21.3, 21.4, 21.5, 21.6, 21.7, 21.8, 21.9, and 21.10. A number of authors have attempted the solution to these equations for a number of materials. Furthermore, they have in some cases added further complexity by including phenomena such as intumescent behaviour [49] or bubbling [50]. Extensive reviews of these modelling efforts can be found in Refs. [4, 51–54] and some of the more recent modelling exercises have achieved significant success [55–59]. In most cases some simplifications have been necessary and in general the critical limitation of these models is associated to the inadequate definition of many of the relevant variables and parameters listed in the previous sections. As mentioned before, the current trend is to optimise parameters by fitting complex models to specific experimental results by means of sophisticated optimization techniques. The optimization process results in ranges of possible values for all parameters stipulated. The results have then been extrapolated to other experimental conditions. While success has been reported [6, 7], these optimization processes are only as good as the models whose parameters they optimize. It is therefore important to note that even in the most complex models some simplifying assumptions have been made. Currently, the use of such models remains a research subject with increasing applicability to the modelling of flaming ignition of solid fuels.

This section will take the equations presented in previous sections and suggest simplifications that will lead to models commonly used in the analysis of standard test methods evaluating the flaming ignition of solid fuels.

The Inert Solid Assumption

The assumption that the solid remain inert until ignition is probably the most far reaching of all proposed simplifications. As a result of this assumption the energy equation is dramatically simplified. Despite the far reaching implications of assuming that the solid remains inert until ignition there is very limited work that assesses the validity of this assumption.

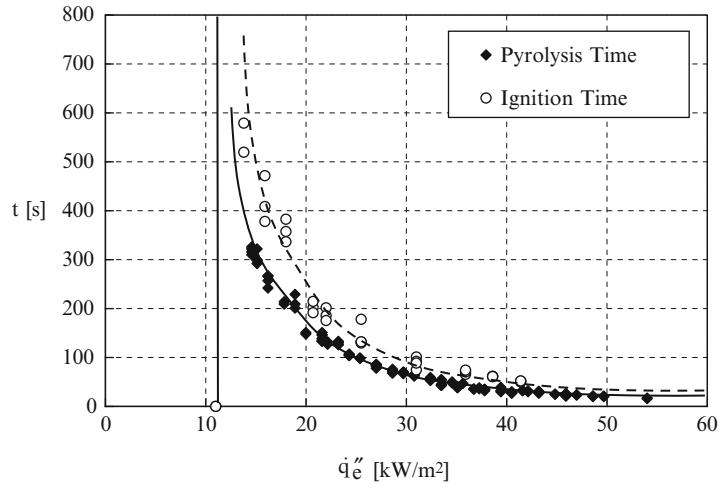

Fig. 21.8 Characteristic ignition delay times (t_{ig}) and times to the onset of pyrolysis (t_P) for PMMA and a wide range of external heat fluxes extracted from Ref. [60]. Onset of pyrolysis or ignition did not occur below 11 kW/m^2

To the knowledge of the author, the only explicit studies that discuss the importance of assuming that the material is inert are those by Fereres et al. [42], Dakka et al. [60] and Beaulieu and Dembsey [61]. In the first two studies transparent Poly(methyl methacrylate) (PMMA) was used while on the latter work the detailed analysis is done with black PMMA but a number of other materials serve to confirm the conclusions. Despite the bias towards PMMA, the discussion is appropriate here to illustrate the potential errors associated to this simplification.

Figure 21.8 presents characteristic ignition delay times (t_{ig}) and pyrolysis delay times (t_P) for PMMA. The ignition delay time was recorded as the first flash while the pyrolysis delay time as the moment when the fuel initiates its endothermic degradation. The onset of pyrolysis was characterized by means of mass loss measurements, flow visualization and IR-Thermography. These results show that for these particular experiments there is a significant difference between the "flash point" and the onset of pyrolysis (could be up to 100 %) therefore the assumption that the fuel remains inert until ignition might not be justified.

The breakdown of the inert solid heating assumption is further discussed by Beaulieu and Dembsey [61] who show that an analysis following this approximation will lead to shorter ignition delay times for realistic heat fluxes. The biggest errors were observed at the higher heat fluxes. Their tests were done for a comprehensive array of materials and with heat fluxes up to 200 kW/m^2.

Despite these experimental results, this assumption still remains the backbone of all standard test method analyses for ignition [23–25]. If this approach is followed and the regression rate is assumed to be negligible, $V_R \approx 0$, Equation 21.5 is reduced to

$$\frac{\partial[\rho_S C_S T]}{\partial t} = -\frac{\partial}{\partial x}\left[-k_S \frac{\partial T}{\partial x}\right] + \dot{q}'''_{RAD} \quad (21.13)$$

And the boundary conditions to

$$x = 0 \quad 0 = k_S \left.\frac{\partial T}{\partial x}\right|_{x=0^+} - \varepsilon_S(0,t)\sigma\left(T^4(0,t) - T_0^4\right) - h_{Cv}(t)(T(0,t) - T_0) \quad (21.14)$$

$$x = L \quad 0 = -k_S \left.\frac{\partial T}{\partial x}\right|_{x=L^-} + k_B \left.\frac{\partial T_B}{\partial x}\right|_{x=L^+} \tag{21.15}$$

Absorption of Radiation and Global Properties

The next major simplifications that are commonly accepted are to assume that most of the incident heat flux is absorbed at the surface ($\alpha(t) \approx 1$) and that the thermal properties of the solid can be considered invariant ($\rho_S(x,t) \approx \overline{\rho}_S$, $C_S(x,t) \approx \overline{C}_S$, and $k_S(x,t) \approx \overline{k}_S$). These assumptions further simplify Equation 21.11 because it allows neglecting in-depth radiative absorption. The thermal properties can then be extracted from the differential terms and external radiation now appears in the exposed boundary condition:

$$\overline{\rho}_S \overline{C}_S \frac{\partial [T]}{\partial t} = \overline{k}_S \left[\frac{\partial^2 T}{\partial x^2}\right] \tag{21.16}$$

$$x = 0 \quad 0 = \overline{k}_S \left.\frac{\partial T}{\partial x}\right|_{x=0^+} + \dot{q}''_e - \sigma\left(T^4(0,t) - T_0^4\right) - h_{Cv}(t)\left(T(0,t) - T_0\right) \tag{21.17}$$

$$x = L \quad 0 = -\overline{k}_S \left.\frac{\partial T}{\partial x}\right|_{x=L^-} + \overline{k}_B \left.\frac{\partial T_B}{\partial x}\right|_{x=L^+} \tag{21.18}$$

There is little true justification in the literature to support these assumptions, nevertheless they are of practical use since for many fire related materials the absorptivity (or emissivity) will approach unity [62], or in the case of testing the material surface can be treated with a coating that has these properties [25].

A series of recent studies have explored the absorptivity [63] of PMMA and the interaction between the heat source and PMMA [64, 65]. Figure 21.9 shows that when using an electrical resistance (cone heater [23]) the transmissivity of PMMA can be neglected and the absorption can be assumed to occur at the surface. Instead, when using tungsten lamps (from the Fire Propagation Apparatus [25]) in-depth absorption cannot be neglected. This information allowed explaining significant differences in the piloted ignition delay times obtained with both tests but mostly emphasize the potential importance of assuming an absorptivity of unity.

Furthermore, thermal properties vary with temperature, but a global set of properties can be established to provide a good fit to ignition data. An example of a comprehensive assessment of the impact of variable thermal properties is provided by Steinhaus [66].

The Boundary Conditions

To standardize the ignition process it is important to provide a controlled environment, so that test results can be consistent between laboratories and different users of the standard. Therefore, standard test methods provide clear definition of the environmental conditions, thermal characteristics of the backing material and pilot location [23–25]. Equations 21.8, 21.9 and 21.10 do not have to be solved to obtain the fuel concentration at the pilot location. Instead the impact of the gas phase on the results is ignored. This is done on the basis that flow conditions are the same between tests thus their impact on the transport of fuel and oxidizer to the pilot is the same.

Standardization of the flow conditions has a deep effect on the meaning of the results. The thermal properties associated to the analysis are no longer true thermal properties of the material but global properties that are a combination of the solid and the standardized gas phase

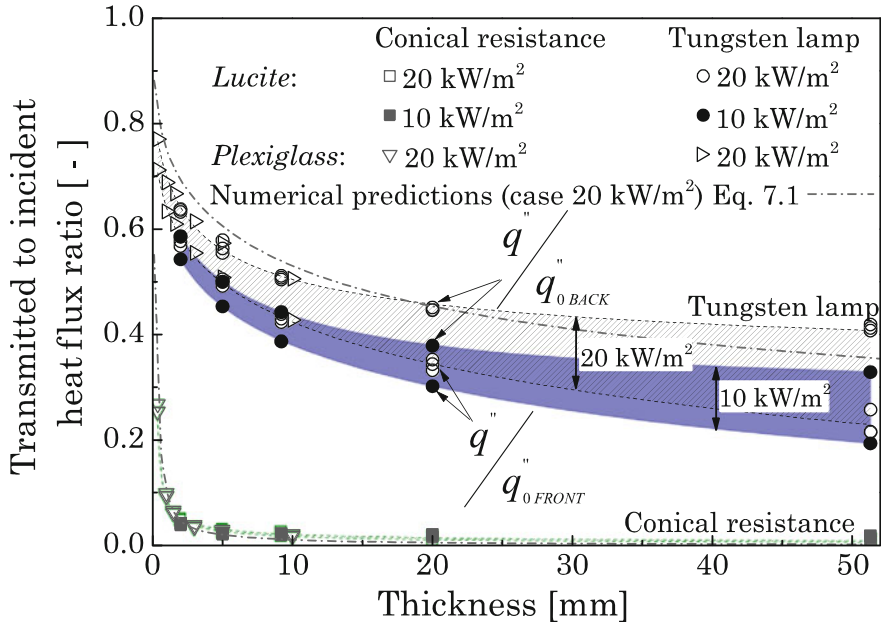

Fig. 21.9 Transmitted to incident heat flux ratio for clear PMMA samples (*Lucite* and *Plexiglass*) exposed to a radiative source (conical resistance and tungsten lamp) providing 10 and 20 kW/m^2 for thicknesses ranging between 0.375 and 51 mm [65]

conditions. This is of critical importance, because, as a product of standardization, test results can be compared among themselves (if the same method is used), nevertheless can not be extrapolated to conditions different to those of the test. This applies to other standard tests or to real fire conditions. Cordova et al. [46] provides a graphical assessment of the effect of varying the flow conditions on the resulting thermal properties showing that small variations in the flow field can result in drastic variations of the resultant thermal properties.

It is common to apply ignition data from standard tests to fire models and is only recently that CFD models such as the Fire Dynamics Simulator (Version 5 and above) allow realistic representations of the solid phase that include true thermal properties [67]. It is important to note that extrapolation is not necessarily incorrect. Nevertheless, it has to be done with great care to guarantee that the effect of the environment on the thermal properties can either be neglected or an appropriate correction is provided.

Different test methods will use different flow fields therefore values for the convective heat transfer coefficient vary with the authors. A commonly cited value is 15 W/m^{2}K. Furthermore, it is common to linearize surface radiation to define a single total heat transfer coefficient ($h_T \approx 45$ W/m^{2}K). More precise values and models are present in the literature [26–28, 31] but they correspond to very specific scenarios and therefore are hard to generalize.

Most test methods define the backing material as a good insulator ($\overline{k}_B \rightarrow 0$) neglecting heat losses through the back end of the sample. Finally, characteristic ignition delay times can be considered much shorter than the time required for the thermal wave to travel through the sample therefore $L > \varepsilon_T$ and the solid is generally assumed as semi-infinite.

These last set of simplifications are truly not necessary because a simple numerical solution can be obtained without linearizing surface radiation or assuming a semi-infinite solid. Many studies have attempted to establish the impact of these simplifications by means of numerical

solutions that relax these assumptions, the most recent of these papers is by Mowrer [68]. If surface radiation is described by means of constant heat transfer coefficient, then a correction is necessary to account for the growth of this coefficient as the surface temperature increases. Mowrer [68] showed that a correction to the global thermal properties could be made to account for this effect. The back end boundary condition is a more difficult problem. For low heat fluxes the thermal wave reaches the end of the sample, $L < \varepsilon_T$, before ignition occurs and heat is exchanged between the sample and the insulating material. Quantification of this heat exchange can be done numerically, as indicated in section "The Surface Boundary Conditions (x=0 and x=L)", but this is not a simple process because it needs to properly describe the different components associated to the way the sample is arranged during tests. The alternative solution of providing a well defined insulating boundary and neglecting back end losses has been preferred and detailed analyses have been conducted to characterize the physical arrangements of sample and insulating material. Among the most comprehensive of these studies is presented in Ref. [69].

If all these assumptions are made, Equations 21.12, 21.17, and 21.18 can be reduced to:

$$\overline{\rho}_S \overline{C}_S \frac{\partial T}{\partial t} = \overline{k}_S \left[\frac{\partial^2 T}{\partial x^2}\right] \tag{21.19}$$

$$x = 0 \quad 0 = \overline{k}_S \left.\frac{\partial T}{\partial x}\right|_{x=0^+} + \dot{q}''_e - h_T(T(0,t) - T_0) \tag{21.20}$$

$$x \to \infty \quad 0 = -\overline{k}_S \left.\frac{\partial T}{\partial x}\right|_{x=L^-} \tag{21.21}$$

The Ignition Condition

If the solid is assumed to be inert until ignition and the gas phase can be summarized into a single total heat transfer coefficient (h_T) this amounts to the assumption that ignition will occur at the onset of pyrolysis and that these process can be simply characterized by the attainment of a characteristic surface temperature that is commonly labelled the ignition temperature, T_{ig}. If the sample is suddenly exposed to an external heat flux, then the time delay between exposure and ignition is named the ignition delay time, t_{ig}. These two parameters represent then the entire process of ignition.

A final link can be made to establish a critical ignition condition. If the ignition delay time is infinitely long, then there will be no gradients of temperature within the solid and surface heat losses will be equivalent to the heat input. This represents the minimum heat flux required to achieve T_{ig}, and thus flaming ignition of the solid fuel. This heat flux is named the minimum heat flux for ignition, $\dot{q}''_{0,ig}$. Since surface temperatures are more difficult to measure than heat fluxes, the minimum heat flux for ignition can be used to establish the ignition temperature. Equation 21.18 can then be re-written to

$$T_{ig} = T_0 + \frac{\dot{q}''_{0,ig}}{h_T} \tag{21.22}$$

Equation 21.14 is an idealized expression that assumes that no temperature gradients exist in the solid, this can lead to errors in the calculation of T_{ig}. To establish a relationship between external heat fluxes and surface temperature that includes in-depth heat transfer a sample can be allowed to reach thermal equilibrium and the surface temperature recorded. The obtained relationship represents a more accurate representation of Equation 21.14 and can be used to extract ignition temperatures from measured heat fluxes. A graphic representation of this relationship can be found in Ref. [34].

Again, both minimum heat flux for ignition and ignition temperature are not material properties but a combination of the material and the specific environmental conditions associated to the test [46]. Extrapolation to realistic scenarios and fire models has to be done with significant care.

The Solution

Imposing a constant external heat flux ($\dot{q}''_e$ = constant) and using all the above assumptions allows for an analytical solution to Equation 21.13. This solution establishes the evolution of the solid temperature as a function of time. This solution can be found in any heat transfer book [19] but was first postulated for the flaming ignition of a solid fuel by Quintiere [70] and incorporated in ASTM E-1321 [24]. Alternate solutions have been postulated for other test methods and will be briefly discussed in Chaps. 28 and 36. More detailed discussion of methodologies and nomenclature can be found in the description of the standard tests [23, 25].

The solution for T(x,t) is given by

$$T(x,t) - T_0 = \frac{\dot{q}''_e}{(h_T)}\left[\operatorname{erfc}\left(\frac{x}{\sqrt{4\overline{\alpha}_D t}}\right) - e^{\frac{(h_T)}{\sqrt{\alpha_D}\sqrt{\overline{k}_S\overline{\rho}_S\overline{C}_S}}x + \frac{(h_T)^2}{\overline{k}_S\overline{\rho}_S\overline{C}_S}t}\operatorname{erfc}\left(\frac{(h_T)}{\sqrt{\overline{k}_S\overline{\rho}_S\overline{C}_S}}t^{\frac{1}{2}} + \frac{x}{\sqrt{4\overline{\alpha}_D t}}\right)\right] \tag{21.23}$$

Where $\overline{\alpha}_D = k_S/\rho_S C_S$ is the global thermal diffusivity and "erfc" is the complement to the error function. To obtain the surface temperature (T_s), x is set equal to 0 and $T = T(0,t) = T_s$. Therefore Equation 21.21 simplifies to:

$$T_s = T_0 + \frac{\dot{q}''_e}{(h_T)}\left[1 - e^{\left(\frac{(h_T)^2}{\overline{k}_S\overline{\rho}_S\overline{C}_S}\right)t}\operatorname{erfc}\left(\frac{(h_T)}{\sqrt{\overline{k}_S\overline{\rho}_S\overline{C}_S}}t^{\frac{1}{2}}\right)\right] \tag{21.24}$$

from Equation 21.15,

$$\overline{T} = \frac{\dot{q}''_e}{(h_T)} \tag{21.25}$$

can be defined as a characteristic temperature and,

$$t_c = \frac{\overline{k}_S\overline{\rho}_S\overline{C}_S}{(h_T)^2} \tag{21.26}$$

is defined as a characteristic time. Equation 21.15 is the general solution to the surface temperature at all levels of incident heat flux. To obtain the ignition delay time (t_{ig}) the surface temperature (T_s) is substituted by T_{ig} and Equation 21.15 can be rewritten as:

$$T_{ig} = T_0 + \overline{T}\left[1 - e^{\frac{t_{ig}}{t_c}}\operatorname{erfc}\left(\left(\frac{t_{ig}}{t_c}\right)^{\frac{1}{2}}\right)\right] \tag{21.27}$$

To avoid the complex form of the error function simplified solutions have been proposed in the literature [70, 71]. In order to solve for the ignition delay time (t_{ig}) a first order Taylor series expansion of Equation 21.18 is conducted. The range of validity of this expansion is limited, thus cannot be used over a large range of incident heat fluxes. Thus, the domain has to be divided at least in two.

The first domain corresponds to high incident heat fluxes where the ignition temperature (T_{ig}) is attained very fast, thus $t_{ig} << t_c$. Application of the first order Taylor Series Expansion to Equation 21.18 around $t_{ig}/t_c \to 0$ yields the following formulation for the ignition delay time (t_{ig}):

$$\frac{1}{\sqrt{t_{ig}}} = \frac{2}{\sqrt{\pi}\sqrt{\overline{k}_S\overline{\rho}_S\overline{C}_S}}\frac{\dot{q}''_e}{(T_{ig} - T_0)} \tag{21.28}$$

As can be seen from Equation 21.19, the short time solution for the ignition delay time (t_{ig}) is independent of the total heat transfer coefficient term (h_T). Thus the ignition delay time (t_{ig}) is

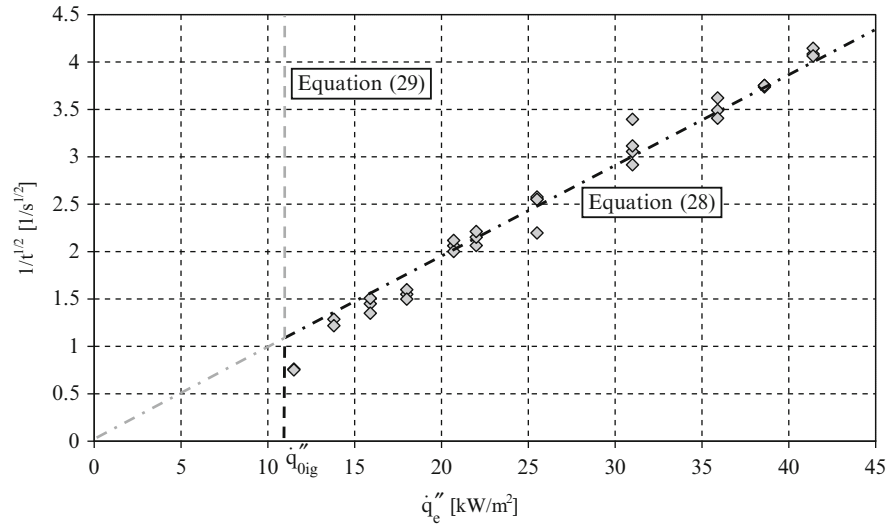

Fig. 21.10 Ignition delay time ($1/t_{ig}^{-0.5}$) for different external heat fluxes using PMMA as a solid fuel (Data extracted from Ref. [60])

only a function of the external heat flux ($\dot{q}''_e$) and the global properties ($\overline{k}_S$, $\overline{\rho}_S$, $\overline{C}_S$) of the solid fuel and the ignition temperature (T_{ig}).

For low incident heat fluxes $t_{ig} \geq t_c$, the Taylor series expansion is made around $t_{ig}/t_c \rightarrow \infty$, where the first order approximation yields:

$$\frac{1}{\sqrt{t_{ig}}} = \frac{\sqrt{\pi} h_T}{\sqrt{\overline{k}_S \overline{\rho}_S \overline{C}_S}} \left[1 - \frac{h_T \left(T_{ig} - T_\infty \right)}{\dot{q}''_e} \right] \quad (21.29)$$

Equations 21.19 and 21.20 establish the relationship between ignition delay time and external heat flux. It is convenient to express the ignition delay time data presented in Fig. 21.7 as $1/\sqrt{t_{ig}}$ where T_{ig} is obtained from the experimental minimum heat flux for ignition and Equation 21.14. Such a plot is presented in Fig. 21.8. Substituting T_{ig} in Equation 21.19 allows extracting the product of the three thermal properties ($\overline{k_S \rho_S C_S}$) as a single experimental parameter representing the global material properties controlling flaming ignition of solid fuels that can be considered semi-infinite. Quintiere terms this product the thermal inertia [70] (Fig. 21.10).

When describing ignition propensity of solid fuels is customary to summarize the description of the materials on the basis of only two parameters, the ignition temperature, T_{ig}, and the thermal inertia, $\overline{k_S \rho_S C_S}$. Several tables have been produced in the past with comprehensive lists of materials typical of fires. As an example, Table 21.3 presents the data as compiled by Quintiere [70]. A comprehensive list is not presented here because a comprehensive compilation of data is provided in Appendix 3 or in Refs. [1] and [2].

Thermally Thin Materials

A very similar analysis can be conducted for thermally thin materials where in the absence of thermal gradients and after all relevant simplifications Equations 21.13, 21.20, and 21.21 can be combined into a single energy equation and a boundary condition

$$\overline{\rho}_S \overline{C}_S L \frac{\partial T}{\partial t} = \dot{q}''_e - h_T (T(t) - T_0) \quad (21.30)$$

Table 21.3 Ignition data from ASTM E-1321 per Quintiere [72]

Material	T_{ig} [°C]	$\overline{k_S \rho_S C_S}$ [(kW/m^{2}K)^2.s]
Wood fiber board	355	0.46
Wood hardboard	365	0.88
Plywood	390	0.54
PMMA	380	1.00
Flexible foam plastic	390	0.32
Rigid foam plastic	435	0.03
Acrylic carpet	300	0.42
Wallpaper on plasterboard	412	0.57
Asphalt shingle	378	0.70
Glass reinforced plastic	390	0.32

$$x = L \quad \dot{q}''_N(L,t) = 0 \tag{21.31}$$

when the external heat flux is much larger than the losses this equation can be integrated to deliver Equation 21.22 [73].

$$t_{ig} = \frac{\overline{\rho}_S \overline{C}_S L\left(T_{ig} - T_0\right)}{\dot{q}''_e} \tag{21.32}$$

This is once again not a necessary assumption but has the practical advantage of leaving the product $\overline{\rho_S C_S}$ as a single experimental parameter that can be extracted from the slope of a simple plot presenting $1/t_{ig}$ vs $\dot{q}''_e$. $\overline{\rho_S C_S}$ represents then the global material properties controlling flaming ignition of thermally thin solid fuels. A comprehensive data review of this product is provided in Refs. [1] and [2].

Summary

A review of flaming ignition of solid fuels has been presented. Emphasis has been given to a comprehensive description of all processes involved. Some minor simplifications have been made to the original formulation leading to approximately 30 variables and parameters controlling flaming ignition of a solid fuel.

A section follows where the common simplifications associated to the methodologies of interpretation of standard test methods are applied. Analytical solutions are obtained showing that the description of the ignition process can be summarized to two material related parameters and two specified environmental conditions (T_0, $\dot{q}''_e$). The material related parameters are as follows:

Thermally thin materials	T_{ig}	$\overline{\rho_S C_S}$
Thermally thick materials	T_{ig}	$\overline{k_S \rho_S C_S}$

It is important to insist that these parameters are a function of the material and the environmental conditions at which they were obtained. They can be directly applied for comparison between materials (flammability assessment) but extrapolation to conditions beyond the tests where they were obtained is not always possible and if performed, has to be done with great care.

References

1. Babrauskas, V., "Ignition Handbook," Fire Science Publishers & Society of Fire Protection Engineers, 2003.
2. Engineering Guide: Piloted Ignition of Solid Materials Under radiant Exposure, Society of Fire Protection Engineers, Bethesda, Maryland, USA, 2002.
3. Hirata, T., Kashiwagi, T. and Brown, J.E., "Thermal and oxidative degradation of Poly (methyl methacrylate): Wight loss," Macromolecules, 18, 1410–1418, 1985.
4. Di Blasi, C., "Modeling and Simulation of Combustion Processes of Charring and Non-Charring Solid Fuels," *Progress in Energy and Combustion Science*, **19**, 71–104, 1993.
5. Ohlemiller, T.J., "Modeling of Smoldering Combustion Propagation," *Progress in Energy and Combustion Science,* **11**, 277–310, 1986.
6. Rein, G., Lautenberger, C., Fernandez-Pello, A.C., Torero, J.L. & Urban, D.L., "Application of Genetic Algorithms and Thermogravimetry to Determine the Kinetics of Polyurethane Foam in Smoldering Combustion," *Combustion and Flame* **146** 95–108 (2006).
7. Lautenberger, C., Rein, G. & Fernandez-Pello, A.C., "The Application of a Genetic Algorithm to Estimate Material Properties for Fire Modeling from Bench-Scale Fire Test Data," *Fire Safety Journal* **41** 204–214 (2006).
8. Bal, N., "Uncertainty and complexity in pyrolysis modelling," PhD Dissertation, University of Edinburgh, 2012.
9. Bal, N. and Rein, G., "Uncertainty and Calibration in Polymer Pyrolysis Modelling," Recent Advances in

Flame Retardancy of Polymeric materials, vol. 23, C. Wilke (Editor), BCC, May 2012.
10. Chao, Y.H. and Wang, J.H., "Comparison of the Thermal Decomposition Behavior of a Non-Fire Retarded and a Fire Retarded Flexible Polyurethane Foam," *Journal of Fire Science*, 19, pp. 137–155, 2001.
11. Lautenberger C. and Fernandez-Pello, A.C., "Optimization algorithms for material pyrolysis property estimation," Fire Safety Science, 10, 751–764, 2011.
12. Chaos, M. Khan, M.M., Krishnamoorthy, N., De Ris, J.L. and Dorofeev, S.B. "Evaluation of optimization schemes and determination of solid fuel properties for CFD fire models using bench-scale pyrolysis tests," Proceedings of the Combustion Institute, 33, 2599–2606, 2011.
13. Bruns, M.C., Koo, J.H. and Ezekoye, O.A., "Population-based models of thermoplastic degradation: Using optimization to determine model parameters," Polymer degradation and stability, 94, 1013–1022, 2009.
14. Lyon, R.E., Safronava, N. and Oztekin, E., "A simple method for determining kinetic parameters for materials in fire models," Fire Safety Science, 10, 765–777, 2011.
15. Kashiwagi, T. and Nambu, H., "Global Kinetics constants for thermal oxidative degradation of a cellulosic paper," *Combustion and Flame*, 88, 345–368, 1992.
16. Cullis, C.F. and Hirschler, M.M., "*The Combustion of Organic Polymers*," International Series of Monographs in Chemistry, Oxford Science Publications, Oxford, United Kingdom, 1981.
17. Drysdale, D., *An Introduction to Fire Dynamics*. Second Edition. John Wiley and Sons, New York, 1999.
18. Williams, F.A., Combustion Theory, 2nd Edition, Addison-Wesley Publishing Company, Inc., 1985.
19. Incropera, F.P., Dewitt, D.P., Bergman, T.L., Lavine, A.S., Fundamentals of Heat and Mass Transfer, 6th Edition, John Wiley and Sons, 2006.
20. Oztekin, E.S., Crowley, S.B., Lyon, R.E., Stoliarov, S. I., Patel, P. and Hull, T.R., Sources of variability in fire test data: a case study on poly(aryl ether ether ketone) (PEEK), Combustion and Flame, 159, 1720–1731, 2012.
21. Stoliarov, S.I., Safronava, N. and Lyon, R.E., "The effect of variation in polymer properties on the rate of burning," Fire and Materials, 33, 257–271, 2009.
22. Nield, D.A. and Bejan, A., "Convection in Porous Media," Springer-Verlag, 1992.
23. ASTM E-1354-03, Standard Test Method for Heat and Visible Smoke Release Rates for Materials and Products Using an Oxygen Consumption Calorimeter, American Society for Testing and Materials, Philadelphia, 2003.
24. ASTM 1321-97a, Standard Test Method for Determining Material Ignition and Flame Spread Properties, American Society for Testing and Materials, Philadelphia, 1997.
25. ASTM E-2058-03, "Standard Method of Test for Measurement of Synthetic Polymer Material Flammability Using the Fire propagation Apparatus (FPA)," American Society for Testing and Materials, Philadelphia, 2003.
26. Staggs, J.E.J., "Convection heat transfer in the cone calorimeter," Fire Safety Journal, 44, 469–474, 2009.
27. Staggs, J.E.J., "A reappraisal of convection heat transfer in the cone calorimeter," Fire Safety Journal, 46, 125–131, 2011.
28. Zhang, J. and Delichatsios, M.A., "Determination of the convective heat transfer coefficient in three-dimensional inverse heat conduction problems," Fire Safety Journal, 44, 681–690, 2009.
29. Torero, J.L. "Scaling-Up Fire," Proceedings of the Combustion Institute, 34 (1), 99–124, 2013.
30. Fernandez-Pello, A.C., "The Solid Phase," In *Combustion Fundamentals of Fire*, Ed. G. Cox, Academic Press, New York, pp. 31–100, 1995.
31. Fernandez-Pello, A.C. "On fire ignition," Fire Safety Science, 10, 25–42, 2011.
32. Niioka, T., Takahashi, M., Izumikawa, M., 1981, "Gas-phase ignition of a solid fuel in a hot stagnation point flow", *18th Symposium on Combustion*, The Combustion Institute, Pittsburgh, PA, pp. 741–747.
33. Delichatsios M A and Delichatsios M M, "Critical Mass Pyrolysis rates for Extinction of Fires over solid Materials" Fifth Symposium on Fire Safety Science, 153–164, 1996.
34. Torero, J.L., Vietoris, T., Legros, G., Joulain, P. "Estimation of a Total Mass Transfer Number from Stand-off Distance of a Spreading Flame," *Combustion Science and Technology*, **174** (11–12), pp. 187-203, 2002.
35. Quintiere, J.G., "Fundamentals of Fire Phenomena," John Wiley and Sons, 2006.
36. Gray, P. and Lee, P. R. "Thermal Explosion Theory," *Oxidation and Combustion Reviews*, **2**, 3–180, 1967.
37. Atreya, A., "Ignition of Fires," *Philosophical Transactions of the Royal Society A: Mathematical, Physical, and Engineering Sciences* **356** 2787–2813 (1998).
38. Horrocks, A.R., Gawande, S., Kandola, B. and Dunn, K. W., "*Recent Advances in Flame Retardancy of Polymeric Materials*," Business Communications Co., Norwalk, Connecticut, USA, 2000.
39. Backer, S., Tesoro, G.C., Toong, T.Y. and Moussa, N. A., "*Textile Fabric Flammability*," The MIT Press, Cambridge, Massachusetts, USA, 1976.
40. Williams, F.A., "A Review of Flame Extinction," *Fire Safety Journal*, **3**, 163–175, 1981.
41. Rasbash D J, Drysdale D D, and Deepak D, "Critical Heat and Mass Transfer at Pilot Ignition and Extinction of a Material," *Fire Safety Journal*, **10**, 1–10, 1986.
42. Fereres, S., Lautenberger, C., Fernandez-Pello, A.C., Urban, D. and Ruff, G., "Mass flux at ignition in reduced pressure environments," Combustion and Flame, 158, 1301–1306, 2011.

43. Thomson H E, Drysdale D D, and Beyler C L, "An Experimental Evaluation of Critical Surface Temperature as a Criterion for Piloted Ignition of Solid Fuels," *Fire Safety Journal*, **13** 185–196, 1988.
44. Beyler, C., "A Unified Model of Fire Suppression," *Journal of Fire Protection Engineering*, **4** (1), 5–16, 1992.
45. Quintiere, J.G. and Rangwala, A.S., "A theory for flame extinction based on flame temperature," *Fire and Materials*, Volume 28, Issue 5, September/ October, Pages: 387–402, 2004.
46. Cordova, J.L., Walther, D.C., Torero, J.L. and Fernandez-Pello, A.C. "Oxidizer Flow Effects on the Flammability of Solid Combustibles," Combustion Science and Technology, 164, No. 1–6, pp. 253–278, 2001.
47. McAllister, S., Fernandez-Pello, A.C., Urban, D. and Ruff, G., "The combined effect of pressure and oxygen concentration on piloted ignition of a solid combustible," Combustion and Flame, 157, 1753–1759, 2010.
48. Roberts, A.F. and Quince, B.W., "A Limiting Condition for Burning of Flammable Liquids," *Combustion and Flame*, 20, 245–251, 1973.
49. Lautenberger, C. and Fernandez-Pello, A.C. "A generalized pyrolysis model for combustible solids," 5th International Seminar on Fire and Explosion Hazards, April, 23–27, Edinburgh, UK.
50. Butler, K. M. Mixed Layer Model for Pyrolysis of Bubbling Thermoplastic Materials, National Institute of Standards and Technology, Gaithersburg, MD, NISTIR 6242; October 1998.
51. Kashiwagi, T., "Polymer Combustion and Flammability-Role of the Condensed Phase," *Proceedings of the Combustion Institute*, **25**, 1423–1437, 1994.
52. Di Blasi C., "The state of the art of transport models for charring solid degradation," *Polymer International* **49** 1133–1146, 2000.
53. Moghtaderi, B., "The State-of-the-Art in Pyrolysis Modeling of Lignocellulosic Solid Fuels," *Fire and Materials* **30** 1–34, 2006.
54. Lautenberger, C. & Fernandez-Pello, A.C., "Pyrolysis Modeling, Thermal Decomposition, and Transport Processes in Combustible Solids," to appear in *Transport Phenomena in Fires*, Ed. M. Faghri & B. Sunden, WIT Press, 2008.
55. Lautenberger, C., Kim, E., Dembsey, N. and Fernandez-Pello, A.C., "The role of decomposition kinetics in pyrolysis modelling – Application to a fire retardant polyester composite," Fire Safety Science, 9, 1201–1212, 2009.
56. Stoliarov, S.I., Crowley, S., Walters, R.N. and Lyon, R. E., "Prediction of the burning rates of charring polymers," Combustion and Flame, 157, 2024–2034, 2010.
57. Stoliarov, S.I., Crowley, S., Lyon, R.E. and Linteris, G.T., "Prediction of the burning rates of non-charring polymers," Combustion and Flame, 156, 1068–1083, 2009.
58. Bal, N. and Rein, G., "Numerical investigation of the ignition delay time of a translucent solid at high radiant heat fluxes," Combustion and Flame, 158, 1109–1116, 2011.
59. Wasan, S.R., Rauwoens,P., Vierendeels, J. and Merci, B., "An enthalpy-based pyrolysis model for charring and non-charring materials in case of fire," Combustion and Flame, 157, 715–734, 2010.
60. Dakka, S.M., Jackson, G. S. and Torero, J.L., "Mechanisms Controlling the Degradation of Poly (methyl methacrylate) Prior to Piloted Ignition" *Proceedings of the Combustion Institute*, **29**, 281–287, 2002.
61. Beaulieu, P.A., and Dembsey, N.A., "Flammability Characteristics at Applied Heat Flux Levels up to 200 kW/m^2", *Fire and Materials*, 2007.
62. Hallman. J., "Ignition Characteristics of Plastics and Rubber," Ph. D. Thesis, University of Oklahoma, Norman, OK, USA, 1971.
63. Jiang, F., deRis J.L. and Khan, M.M. "Absorption of thermal energy in PMMA by in-depth radiation," Fire Safety Journal, 44, 106–112, 2009.
64. Girods, P., Bal, N., Biteau, H., Rein, G. and Torero, J. L., "Comparison of pyrolysis behaviour results between the Cone Calorimeter and the Fire Propagation Apparatus heat sources," Fire Safety Science, 10, 889–901, 2011.
65. Bal, N., Raynard, J., Rein, G., Torero, J.L., Försth, M., Boulet, P., Parent, G., Acem, Z. and Linteris, G., "Experimental study of radiative heat transfer in a translucent fuel sample exposed to different spectral sources," International Journal of Heat and Mass Transfer, (in press), 2013.
66. Steinhaus, T. 1999 "Evaluation of the Thermophysical Properties of Poly(Methyl Methacrylate): A Reference Material for the Development of a Flammability Test for Micro-Gravity Environments," *Masters Thesis*, University of Maryland.
67. McGrattan, K., Klein, B., Hostikka, S., Floyd, J., "Fire Dynamics Simulator (Version 5), User's Guide," NIST Special Publication 1019–5, October 1, 2007.
68. Mowrer, F.W., "An analysis of effective thermal properties of thermally thick materials," *Fire Safety Journal*, Volume 40, Issue 5, Pages 395–410, July 2005.
69. deRis, J. L. and Khan, M. M., "A Sample Holder for Determining Material Properties," *Fire and Materials*, **24**, 219–226, 2000.
70. Quintiere, J.G., "A Simplified Theory for Generalizing Results from a Radiant Panel Rate of Flame Spread Apparatus," *Fire and Materials*, Vol. 5, No. 2, 1981.
71. Wickman, I. S., "Theory of Opposed flame Spread," *Progress in Energy and Combustion Science*, 18, 6, pp. 553–593, 1993.

72. Quintiere, J.G., "Principles of Fire Behavior," Delmar Publishers, 1997.
73. Lautenberger, C. Torero, J.L. and Fernandez-Pello, A.C., "Understanding Materials Flammability," Chapter 1, *Flammability Testing of Materials in Building, Construction, Transport and Mining Sectors*, V. B. Apte Editor, pp. 1-21, CRC Press, 2006.

José Torero is the Head of the School of Civil Engineering at The University of Queensland. He holds a BSc for the Pontificia Universidad Católica del Perú (1989), and an MSc (1991) and PhD (1992) from the University of California, Berkeley. Jose is a Chartered Engineer (UK), a fellow of the Australian Academy of Technological Sciences and Engineering, the Royal Academy of Engineering (UK) and the Royal Society of Edinburgh (UK).

Electrical Fires

22

Vytenis Babrauskas

Introduction

An electrical fire is generally understood to be a fire that is caused by the flow of an electric current or by a discharge of static electricity. It is not defined as a fire involving an electrical device or appliance. For example, a fire on an electric range that occurs due to overheating and ignition of the oil in a deep-fry pan is not classed as an electrical fire, even though it involves an electrical appliance. Conversely, an electrical device or appliance is not always needed for an electrical fire to occur. Lightning-caused fires are a form of electrical fires and these can ignite, for example, a dry bush, which is not an electrical device.

As with other categories of fires, there are three main aspects of electrical fires to be considered: ignition, combustion behavior, and suppression. This chapter deals mostly with the ignition aspects. Combustion behavior of electrically initiated fires is normally dominated by the fuel characteristics of the primary combustibles that are involved. These will most commonly be cellulosic or plastic fuels, although with some sustained electrical faults combustion of aluminum (e.g., busbars) can play a significant role. Copper and steel generally do not burn even in worst-case electrical fires. Sustained burning of aluminum generally does not take place except in installations of at least 480 V and of high current capacity. The traditional segregation of electrical fires as Class C fires has been based primarily on concerns of potential shock hazard to fire-fighting personnel. But research studies [1, 2], show that this would be a realistic concern only for high-voltage installations. Even for these, the hazard is minimal. For example, the most recent study on this topic [3] showed that a fire fighter would have to be holding a straight-stream nozzle 1.0 m from a 45 kV power line for a shock hazard, defined as 10 mA passing through the body, to be created. For a fog nozzle, no hazard could be produced at a 2.0 m distance even with a 200 kV line (smaller distances were not measured) and current with the 200 kV line was only 0.35 mA.

This chapter discusses the differences between electric current and static electricity, outlines the various forms of heating that can take place due to electrical activity, and discusses how ignition of various substances may take place due to electrical activity. The electrical characteristics of lightning are also discussed, since this is a form of electrical discharge. Several reviews of electrical fires have been published by Babrauskas [4–6]; these provide additional details on the status of research and practical applications.

Static Electricity and Electric Current

In the simplest terms, electricity is a form of energy associated with the movement of

V. Babrauskas (✉)
Fire Science and Technology Inc., San Diego, CA, USA

M.J. Hurley (ed.), *SFPE Handbook of Fire Protection Engineering*,
DOI 10.1007/978-1-4939-2565-0_22, © Society of Fire Protection Engineers 2016

electrons. The movement can be sustained (i.e., electric current) or not. Sustained movement requires a conductive path to be established, but the limited movement of electrons possible in insulators can allow charge separation to occur. Once this happens and a certain amount of charge is accumulated, a discharge may be possible and this whole process is known as static electricity. Static electricity, however, does not mean an absence of electric current, since current (flow of electrons) occurs both in charging and in discharging. Instead, static electricity is a somewhat imprecise concept implying that the primary flow of electrons is either in insulators or in conductors that are not connected into the form of a closed circuit.

Electrical Discharges

Breakdown Phenomena

Electrical *breakdown* means that a substance that is normally an insulator suddenly (and possibly just temporarily) breaks down, and becomes a conductor. The process is somewhat different in gases, liquids, and solids. In a gas, the medium is *self-healing*—if the driving force is removed, the medium restores itself essentially to its original condition, although a slight chemical change may occur (e.g., some ozone can be created by an electrical discharge in air). Liquids are also largely self-healing, but the chemical changes entailed may have some long-term implications. The best example of this is oil-filled transformers that can withstand a certain amount of discharges if these are not too energetic. But each discharge causes degradation of the liquid and eventually the transformer may suffer a catastrophic failure due to this degradation. Discharges in solids, on the other hand, are usually highly destructive. With most solid materials, an electrical discharge creates a path that is permanently damaged or destroyed. The majority of insulating solids are organic substances and a discharge through an organic solid has the effect of carbonizing the material, but a portion of the material may also be ablated.

A more detailed explanation [7] of the breakdown process is as follows. Due to cosmic radiation and other factors, a small number of free electrons are always present in air. If an electric field is applied, the electrons move in the direction opposite to the electric field (i.e., to the positive electrode). If the electric field is sufficient, an electron can travel only a short distance before it collides inelastically with an atom/molecule and ionizes it, now leaving two free electrons. Both of these electrons now continue to travel and each one will again collide, and create a new pair of electrons (original electron, plus electron removed from an atom) at this collision. It can be seen that this process leads to exponential growth and one electron, starting at the cathode, will result in n electrons reaching the anode, where $n = e^{\alpha d}$, with d = gap distance and α = Townsend's first ionization coefficient, with has the units of 1/distance. The value $1/\alpha$ then represents the distance between successive ionizing collisions. The generation of electrons is further augmented by the positive ions which are created in the process and which move, much more slowly, towards the cathode. When a positive ion collides with the cathode, it then liberates γ electrons, with γ being known as Townsend's second ionization coefficient. If only electrons that naturally get liberated from the cathode enter into this process, augmented by electrons liberated due to collisions with neutral species along the path, then the discharge (a discharge is the flow of a detectable amount of current) is called a *Townsend discharge*, named after J. S. Townsend, an early researcher of gas discharges. A Townsend discharge is nonluminous and the current flow is small. If the process increases so that a sizable current starts to flow, term *breakdown* is applied, and the two main types of breakdown modes are: electric arc (if sustained) and electric spark (if not). An electric arc requires that a sufficiently high current (more than approximately 0.1 A) be available.

As soon as a conducting path gets established across the gap, the delivery of energy into the arc channel rapidly increases, but the rate of current growth is largely determined by the external circuit parameters. The actual arc channel starts out

small, then grows rapidly in *diameter*. This radial growth is so fast that it is modeled as a shock wave propagation [8]. The shock front, however, does not correspond identically with the channel boundary. The channel expands in two stages. Initially it expands by means of the expanding shock wave until the shock wave detaches from the luminous core. After that point it detaches more slowly until an ultimate value is reached. During the initial expansion phase, the channel conductivity [9] is 1.5×10^4 S m^{-1} and the channel radius r (mm) increases [10] according to:

$$r = 294 \frac{I^{1/3} t^{1/2}}{\rho_o^{1/6}}$$

where I = current (A), t = time (s), and ρ_o = ambient density of air (kg m^{-3}).

Paschen's Law

The kinetic energy W gained by an electron when accelerated by an electric field E over a distance L is:

$$W = EeL$$

where e is the charge of the electron (1.6022×10^{-19} C). The simplest estimate of breakdown would be that a self-sustained avalanche is created when W attains a sufficient value so that a traveling electron can knock off an outer-shell electron from molecules of the gas through which it is traveling. The distance L is the mean free path (average distance between two collisions) for an electron in ambient air, which is experimentally found to be about 0.4 μm. This value is not to be confused with the mean free path of the molecules of air, which is around 0.068 μm, a smaller distance to the fact that air molecules are much larger than electrons. The energy required to ionize an oxygen molecule is 13.5 eV, while for nitrogen it is somewhat higher at 15.8 eV. An electron volt (eV) is a unit of energy equal to 1.6022×10^{-19} J. Thus, the simple estimate would be that breakdown would occur when

$$E = \frac{W}{eL} = \frac{13.5 \times 1.6022 \times 10^{19}}{1.6022 \times 10^{19}\left(0.4 \times 10^{-6}\right)}$$
$$= 34 \times 10^6 \mathrm{Vm}^{-1} = 34 \mathrm{MVm}^{-1}$$

This estimate is about a factor of 10 too high, and this is because this simplest effort at estimating ignored the electron avalanche effect. In actual fact, breakdown in air at 1 atm requires a field of roughly 3 MV m^{-1}, and Paschen's paper of 1889 [11] is credited with defining a relation between breakdown voltage, spacing of electrodes, and gas pressure, which has become known as Paschen's Law. According to Paschen's Law, the pressure × gap distance product is the controlling variable and the breakdown voltage V is given by:

$$V = \frac{c_1 pd}{c_2 + \ln(pd)}$$

where p = pressure, d = gap distance, and c_1 and c_2 are constants. Thus, when the electric field exceeds about 3 MV m^{-1}, breakdown is estimated to occur. Modern measurements [12] of Paschen's Law curves for air and for nitrogen are shown in Fig. 22.1. For gaps greater than about 0.1 mm, it can be seen that the curve is essentially a straight line. For smaller gaps, however, the breakdown voltage does not go to zero and, instead, a minimum breakdown voltage is found. This minimum of the Paschen curve is approximately 340 V, and it occurs at a Pd product of 0.007 atm-mm. In other words, in ambient air, the minimum breakdown voltage occurs for a gap of 0.007 mm (7 μm). This is an exceedingly small distance, and two conductors this far apart would appear to be touching to the naked eye.

For practical applications, it can be more convenient to present results in the form of the *dielectric strength* (MV m^{-1}), which is the breakdown voltage divided by the distance between the electrodes. This is shown in Fig. 22.2 and indicates that for larger distances, the dielectric strength of air is approximately 3.0 MV m^{-1}; the value for nitrogen is quite similar.

Paschen's Law is not absolute but rather depends on experimental conditions. These

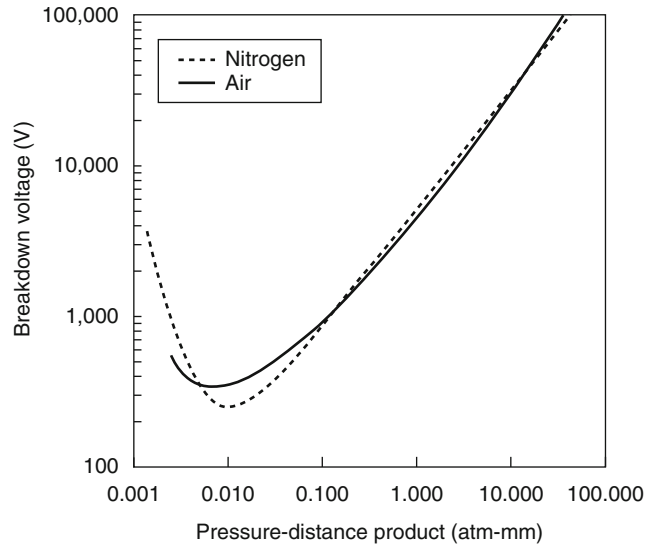

Fig. 22.1 The breakdown voltage (Paschen's Law) between spherical electrodes in air and nitrogen. The voltage refers either to DC voltage or to the peak value, for AC voltage (From Ignition Handbook [7], used by permission)

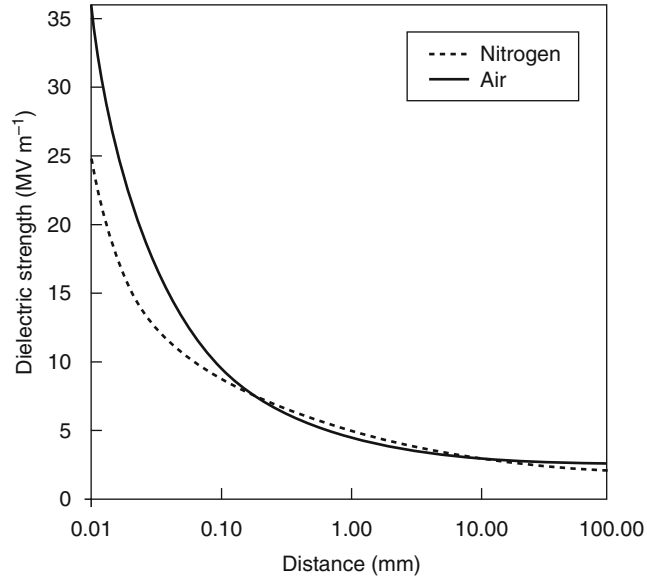

Fig. 22.2 The dielectric strength at 1 atm, as a function of distance (From Ignition Handbook [7], used by permission)

include electrode shape, the material of the electrodes, electrode surface contamination, humidity, and the polarity (if electrodes are not identical). The law also assumes that the impressed electric field is uniform and deviations occur if the field has nonuniformities.

Paschen's Law curves are identical for both AC and DC voltages. But since AC voltages are normally described by their root-mean-square (rms) values and not the peak values, if results are to be applied to AC voltages, then the values indicated in Fig. 22.1 need to be divided by $\sqrt{2}$. Thus, on an rms basis, the minimum AC breakdown voltage is $340/1.414 = 240$ V(rms). It must be emphasized that Paschen's Law is not used in the design of low-voltage equipment. There are many standards worldwide that govern gap sizes (clearances) required for low- or medium-

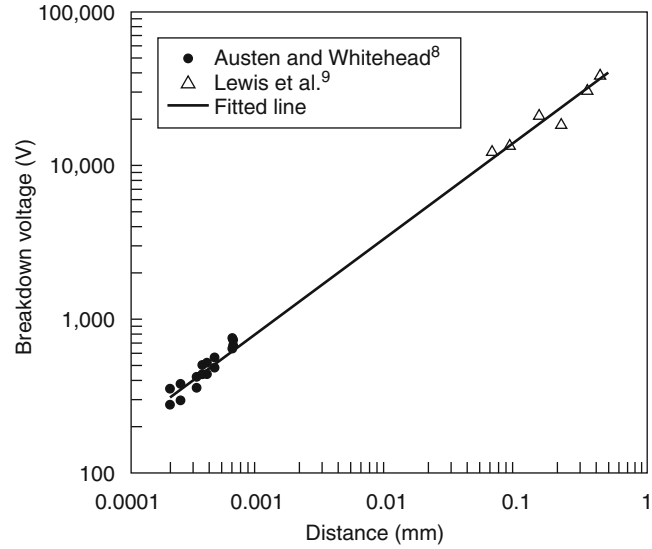

Fig. 22.3 Breakdown voltage for mica as a function of gap distance

voltage equipment, but they all mandate values much larger than the minimum that would suffice to prevent breakdown. This is for serviceability reasons and also takes into account surges.

Dielectric Strength of Solid or Liquid Insulators

The dielectric strength of solids and liquids can also be characterized by similar graphs, but only limited specialized references exist [13]. Most of this literature covers solely the HV regime, and data for voltages below 1 kV are extremely scarce. Mica is one of the rare insulators for which low-voltage data are available, with the results of Austen and Whitehead [14] and Lewis et al. [15] being shown in Fig. 22.3. For polymers, some data obtained by Abed [16] on polystyrene, PVC, and PTFE are shown in Fig. 22.4. Also shown are data on polyethylene obtained by Mason [17] and a single data point given by Austen [18]. The latter indicates that breakdown occurs at 150 V when the insulation thickness is reduced to 0.003 mm. The most common insulator for low-voltage[1] wiring is poly(vinyl chloride), PVC. A more recent review paper [19], however, indicated that no breakdown data for PVC are available below 0.07 mm, at which thickness the breakdown voltage is still in the kV range (approximately 7 kV).

The available data suggest that plastics most likely show a relationship where the breakdown voltage approaches zero as the electrode spacing becomes infinitesimal. But the available data are too few to establish this quantitatively.

Arcs

Definitions of *Arc* and *Spark* Both an electric arc and an electric spark fall under the general definition of a continuous, luminous discharge of electric current crossing a gap or an insulating surface between two conductors [7]. They are distinguished in that an arc is a sustained event while a spark is transient. Matters are clouded by the fact that some researchers refer to a "spark phase" of an arc, but this type of definition is not widely held and is not used in fire safety engineering. *Spark,* however, also has another very different definition: a small incandescent particle. For clarity, the latter can be referred to as a *mechanical spark*.

[1] *Low voltage* is defined by various institutions as being lower than 600, 660, or 1,000 V.

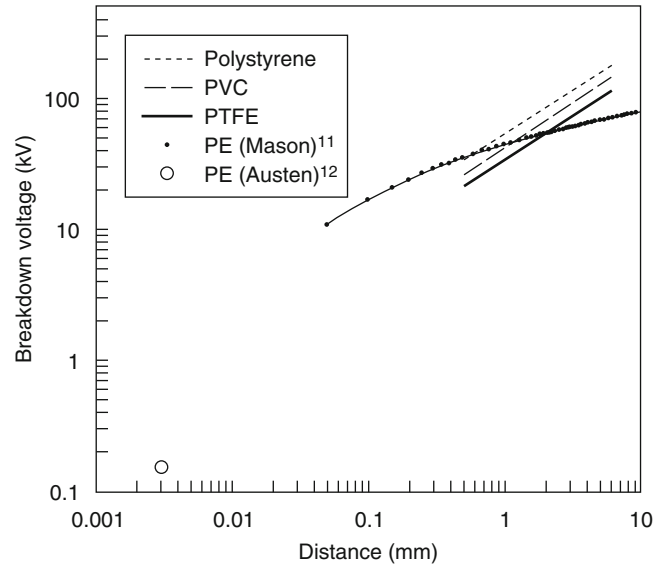

Fig. 22.4 Breakdown voltage for several polymers as a function of gap distance

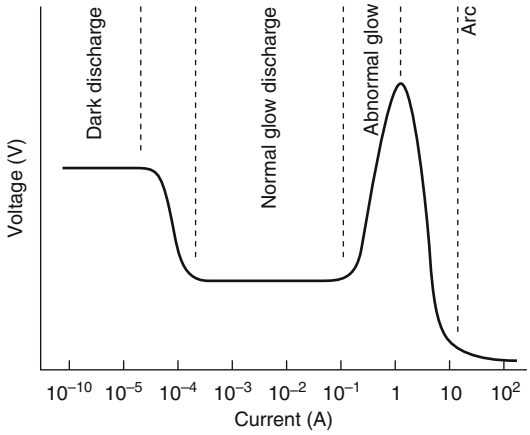

Fig. 22.5 Schematic representation of steady-state voltage and current for several discharge types (From Ignition Handbook, used by permission)

Characteristics of an Arc An arc is actually only one of several types of steady electrical discharges that are possible, as shown in Fig. 22.5. But, of these, only the arc is important from a safety viewpoint, and it corresponds to discharges of the highest current and the lowest voltage.

The temperature of an arc can vary widely. Under ambient pressure conditions, it is commonly 6,500–12,000 K but can reach 50,000 K. The primary factor governing arc temperature is the arc current. Experimental data, along with some theoretical predictions, are shown in Fig. 22.6. Also shown is the following empirical data fit:

$$T = 6,500 I_a \leq 4.5\,\text{A}$$

$$T = 4,010 + 1,658 \ln I_a I_a > 4.5\,\text{A}$$

The theoretical predictions are only loosely obeyed, so the empirical data fit should be sufficient for calculation purposes.

Means of Creating Arcs An arc can be created by a variety of means, primarily the following:

- Raising the voltage across a fixed pair of electrodes until breakdown occurs
- Opening or closing the contacts in a current-carrying circuit
- Transitioning from arcing across a carbonized path (arc tracking)
- Glow-to-arc transition
- Introducing ionized gases in between two electrodes (e.g., from a flame)

Creating an arc by raising the voltage across a fixed pair of electrodes is very common for testing purposes. It also occurs in some accidental circumstances, as discussed below.

Contact arcs regularly occur in electric switches, relays, and similar devices. They also occur inadvertently, when, for example, two bare

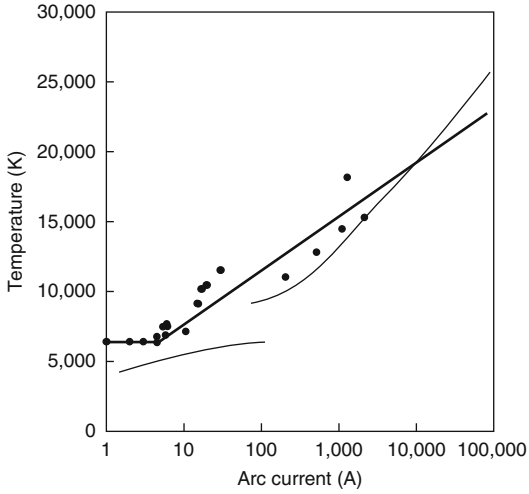

Fig. 22.6 Temperature of arcs in ambient-pressure air, along with predictions from theory (*light lines*) and an experimental data fit (*bold line*) (From Ignition Handbook, used by permission)

current-carrying conductors are accidentally shorted. When considering electric switch contacts, the arc caused by closing the switch is called a make-arc (or closing arc), whereas the arc caused in opening the switch is a break-arc (or opening arc, or parting arc). The process of creating an arc (at voltages that may be much less than Paschen's Law minimum of 340 V) is quite similar for both types of contact arcs. In the case of a break-arc the steps involved are the following:

1. The electrodes that were originally touching at numerous spots start to touch at only a few very small spots.
2. A high current density passes through the small metal diameter of contact area that is available.
3. The metal bridge joining the two contacts starts to melt.
4. The bridge elongates and rises in temperature.
5. The bridge reaches the metal's boiling point, becomes unstable, and ruptures.
6. Voltage rises rapidly across the gap, thermionic emission from the hot cathode starts, and eventually the gap becomes ionized and an arc forms.
7. The diameter of the arc expands from that of the bridge to its eventual free-burning diameter.

The voltage across the gap at the moment of rupture is only approximately 1 V. The reason Paschen's Law does not apply is that it describes the characteristics of room-temperature, nonionized gases, and the space between the contacts is ionized and at high temperature. Even though 10–15 V is needed for the steady-state operation of an arc, the arc is able to initiate with only a 1 V drop due to inductive effects of the wiring.

In closing switch contacts (a make-arc), the sequence of events is very similar. Contact is initially made at only a few high spots. These have limited current-carrying capacity and proceed to melt and rupture, at which point an arc develops. That arc is normally extinguished by heat losses when the contacts close together more tightly.

Arcing across a carbonized path (arc tracking) is arcing that is supported by a carbonized path on a solid, as discussed below, and this is a low-current process. If this process continues and accelerates, one possible outcome is a normal, high-current arc across air. The conditions leading to this have not been explored in detail, however. Glow-to-arc transition is a rare phenomenon not normally encountered in fires [20].

The dielectric strength of a hot, ionized gas is tiny compared to that of normal ambient air. Thus, when the distance between two conductors is such that there would be no possibility of breakdown in normal air, introducing ionized gases in between two electrodes (e.g., from a flame) can lead to arcing. This is why, in many fires, a large number of artifacts are found suggesting that an arc occurred there. It is not because several different places arced simultaneously and each erupted into fire [21]. Instead, a single fire introduced flames into various locales where conductor-to-conductor spacing was such that arcing could not be supported in ambient air but could be supported in an ionized, hot medium.

Arc Flash The thermal radiation from an arc is referred to as *arc flash* and a sustained, high-current arc can lead to severe injury or death of an individual so exposed. IEEE Std 1584 [22] provides a

calculational method for estimating arc flash radiation, whereas ASTM F 1506 [23] and ASTM F 1959 [24] provide procedures for assessing the actual effectiveness of protective clothing.

Arc Extinguishment A DC arc will extinguish only if the power supply is removed or if enough material erodes to make the gap too large. In an AC circuit, an arc will self-extinguish 2 × 60 times (2 × 50 times with 50 Hz power) per second, each time the current goes to zero. But it may reignite thereafter if conditions are right. Whether or not the arc reignites afterwards depends on whether the arc channel can recover so that it will not break down again with the new imposed voltage. Arcs in circuits of less than 150 V tend to extinguish and not reignite when the waveform goes through the zero crossing. Arcs in circuits of over 600 VAC tend to draw very high currents and, consequently, may be relatively safer since a circuit protection device is likely to open. Voltages between 150 and 600 V are considered the most hazardous in regard to fires being ignited from arcing [25]. This is because the arcs tend to not be extinguished, yet the current flows are small enough that circuit protection devices operate slowly. Typical waveforms [26] for arcing in 120 VAC circuits are shown in Fig. 22.7. Note the intermittent nature of the arc as it extinguishes and reignites.

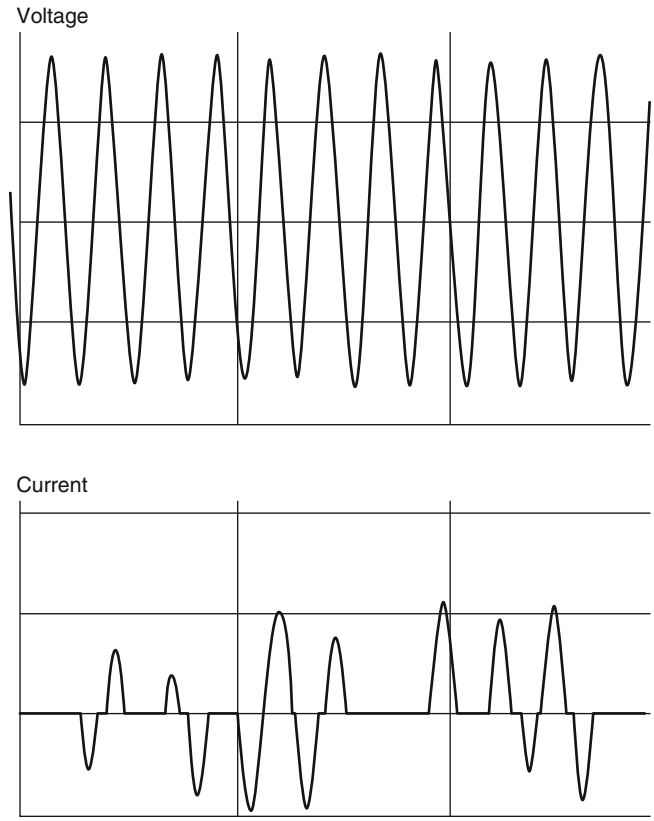

Fig. 22.7 Typical waveforms during a branch-circuit arcing event

Ignition Modes Involving Electric Current

Sparking or Arcing

Electric sparking or arcing can ignite materials in all phases: gases, liquids, solids, liquid aerosols, and dust clouds. Ignition in gaseous and dust cloud media has been studied extensively. Ignition in bulk liquids is rare, apart from oil-filled transformers and other HV devices. Ignition of liquid sprays, fogs, or aerosols is problematic in some industries, however. Ignition of solids from arcing or sparking is common but has not been researched to any satisfactory degree.

Gases If an atmosphere exists where a flammable gas has been dispersed into an oxidant gas (commonly air) and the mixture is within its flammable limits, spark ignition is generally very easy. Arc ignition has normally not been studied. Since a very low-energy transient energy discharge ignites such mixtures, a sustained energy discharge will be much more capable of ignition. For this reason, the phenomenon is referred to as spark ignition rather than arc ignition. Flammability limits for a number of gases are given in Chap. 17. A larger collection of data is provided in the *Ignition Handbook* [7]. Some values for minimum ignition energy (MIE) are given in Table 22.1; more extensive tables are available in the *Ignition Handbook* [7]. It should be observed that these energies are exceedingly small and are tabulated in millijoules. To appreciate the magnitude, one can consider the fact that if a coffee mug is raised by 0.3 m, its potential energy is increased by roughly 1.0 J.

Table 22.1 Minimum ignition energy (MIE) of some common gases and vapors

Substance	Energy (mJ)
Acetone	2.15
Acetylene	0.03
Ammonia	680
Benzene	0.91
Butane	0.26
Carbon disulfide	0.039
Cyclohexane	2.65
Ethane	0.42
Ethylene	0.114
Ethylene oxide	0.105
Furan	0.328
Heptane	1.15
Hexane	0.29
Hydrogen	0.03
Hydrogen sulfide	0.077
Iso-octane	2.9
Methane	0.71
Methanol	0.3
Pentane	0.82
Propane	0.5
Propylene	0.418
Toluene	2.5
Vinyl acetylene	0.095
p-Xylene	0.2

From *Ignition Handbook,* used by permission

Dust Clouds Dust clouds are significantly more difficult to ignite than gases, but explosions due to this cause remain an important concern in manufacturing, mining, and agricultural industries. The lower flammability limit of dust clouds has generally been erroneously reported in most data compilations because apparatuses used to measure the lower flammability limit (LFL) of dust clouds have had gross, systematic errors, leading to reported values for many substances being much lower than their true value [7]. But, as a very rough rule, dust clouds will not reach their LFL unless visibility is down to zero in that location. The upper flammability limit (UFL) for dust clouds is rarely measured, simply because it is generally very difficult to generate a dust cloud that exceeds the UFL.

Minimum ignition energies have been tabulated and it is believed that those are more reliable. Some typical values are shown in Table 22.2. Unlike gases, where MIE values are typically below 1 mJ, MIE values for dust clouds are typically some two orders of magnitude higher. Nonetheless, these are all still low, even though they are higher than for gases.

Solids Ignition of solids from electric sparks or arcs is unfortunately common. The cause can be

Table 22.2 Minimum ignition energy for various dust clouds

Substance	MIE (mJ)
Aluminum	50
Aspirin	25–30
Black powder	320
Coal	250
Cocoa	100–180
Coffee	160
Cornstarch	30–60
Cotton linters	1,920
Dextrin	40
Flour, cake	25–80
Grain dust	30
Magnesium	40
Manganese	305
Nitrostarch	40
Nylon	20–30
Paper dust	20–60
Phenol formaldehyde	10–6,000
Polyethylene	70
Polyethylene terephthalate	35
Polystyrene	40–120
Rice	40–120
Silicon	100
Soap powder	60–120
Sugar, powdered	30
Tantalum	120
Tin	80
Titanium	25
TNT	75
Urea formaldehyde	80–1,280
Wheat starch	25–60
Wood flour	30–40
Zinc	960

From *Ignition Handbook,* used by permission

either static electricity or circuits carrying an electric current. Some of the mechanisms have been studied, and these are discussed later. However, the problem of understanding the response of solid materials to a spark or arc ignition source has been neglected. Apart from metals and some other rare substances, there are no combustible solids with an ignition temperature over 1,000 °C. Figure 22.6 shows that the temperature of an electric arc is at least 6,500 K and may be much higher. Yet, an electric arc impinging onto a combustible solid is not necessarily assured of igniting it. There are two primary factors operating in such cases: (1) The arc impingement may be very brief, many combustible materials can resist enormous heat fluxes if these are sustained only briefly. (2) The material may ablate too rapidly to allow ignition. These mechanisms, however, are understood only qualitatively—there have not been research studies to successfully quantify them.

Arcing Across a Carbonized Path

Many electrical fires are due to arcing across a carbonized path. If a carbonized path is created where current may potentially flow, arcing may then occur along this path, possibly leading to ignition either of the combustible insulator itself, or some other nearby fuel. A carbonized path can be created in at least three ways [27], such as the following:

1. Arc tracking
2. Overheating (by electrical overcurrent, external radiant heating, etc.)
3. Impingement of fire on solid electrical insulation material

Arc Tracking Of these three possibilities, substantive research has been done only on arc tracking. Arc tracking is a progressive creation by electrical means of a carbonized path along the surface of an insulator that separates two current-carrying conductors. Arc tracking is subdivided into two types: dry tracking and wet tracking. Dry tracking can be induced by causing an electric arc to impinge onto the surface of an organic material. Wet tracking can occur if a film of water covers the surface of the insulator and spans between two conductors.

The electric conductivity of pure water is very low, but when ionic contaminants are dissolved in water, its conductivity increases and it becomes possible to create a current flow if the layer of moisture has access to conductors from both sides of the line. The flow of current then has a drying effect on the moisture layer. The drying is nonuniform, and eventually dry patches

start to be formed along the current path. With buildup of carbonization along the path, small electrical discharges, called scintillations, can then occur. Since part of the current flow is through an electrolyte of significant resistance, these scintillations represent a very small current flow and would not trip any overcurrent-protection devices. The ultimate event, if it occurs, is the actual flaming ignition of the material over which tracking is occurring.

If the tracking is dry, the processes that occur along the surface are similar. Although an overcurrent-protection device cannot be expected to protect against arcing across a carbonized path (unless this escalates to a high-current fault), arc fault circuit interruption (AFCI) devices, which have been developed in recent years [28], are intended to respond to this condition; because they are relatively new, however, field-performance data do not yet exist, although it is known that some models of first-generation devices have not been highly successful [29].

Surprisingly, temperatures up to 1,000 °C can be generated by such surface leakage discharges. These elevated temperatures then continue the process of polymer carbonization. Thus, in the tracking process, a carbon track is laid down along the surface, and that track has a low enough resistivity that current can subsequently start to flow along the carbonized track, which, in turn, causes more carbonization and more heating. A runaway situation can then develop. Scintillations can vary widely in their discharge energy, with the low end of the scale being mild events that would not be expected to damage metals (although they might ignite some potential targets). Nakamura et al. [30] measured scintillations on PVC and reported values that ranged from 100 to 3,000 J. But, they did not endeavor to set up their experiments to elicit the lowest possible discharge energy.

To create arc tracking, a vastly lower voltage can suffice than for breakdown in air between two electrodes. For example, with many plastics, Yoshimura et al. [31] found that 600 VAC was sufficient to cause an arc discharge across a 4 mm gap. By contrast, breakdown across a 4 mm gap in air requires about 10,000 VAC. On cables, wet tracking will normally not be initiated unless a conductive moisture film exists that has electrical contact to two conductors that have a voltage difference between them. This may happen if a cable is mechanically damaged so that two current-carrying conductors are exposed. Moisture then collects on the damaged area, and pollutants are present that ionize the layer. But on some materials, arc tracking does not require a direct contact between an electrode and the surface of the insulator; tracking over phenolic and melamine surfaces can be initiated even when the electrodes are separated by gaps of about 0.25 mm from the insulator surface. In general, in low-voltage circuits, a carbonized path is probably most commonly created by a poor connection or other source of locally elevated temperatures, but moisture or pollutants can also be of significant importance.

Oba [32] conducted experiments where he damaged the insulation on Japanese PVC-insulated power cable to expose the conductors and then sprayed electrolyte onto the area to initiate arc tracking. By varying the AC voltage supplied to the cord, he obtained a char length relation as a function of voltage (Fig. 22.8). Below 50 V, progress of charring

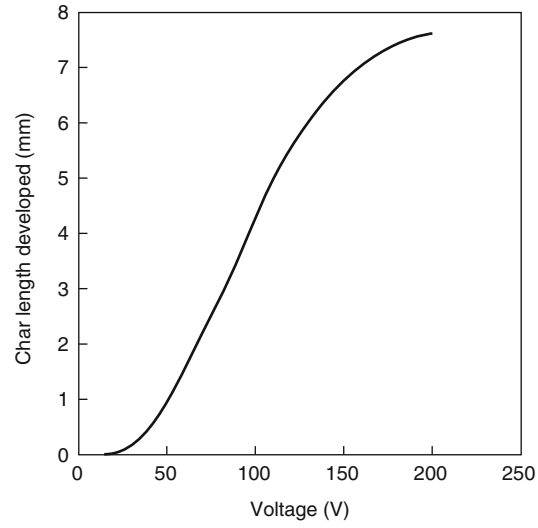

Fig. 22.8 Char length developed after 70 h in the wet arc-tracking experiments of Oba (From Ignition Handbook, used by permission)

was very limited. He repeated the experiments by depositing powdered carbon onto the damaged area and found, in that case, for arc tracking to occur, the applied voltage had to exceed 24 V. Below 50 V, small incandescent spots could be produced but not flaming ignition. Flaming ignition was readily possible for voltages of 100–150 V. Above 200 V, flaming ignition readily occurred, but increased char lengths were not obtained since the events were explosively forceful and blew off the carbonized material and the melted conductor portions. Under other conditions, much less than 24 V is sufficient to cause arc tracking. Bernstein [33] reports that arc tracking can occur in 6 V battery circuits, provided the battery has sufficient current capacity to sustain the arc. Arc-tracking problems have been troublesome in a variety of models and types of motor vehicles in circuits operating at around 14 VDC (nominal 12 V) [7].

For polymers, the molecular structure is the main determinant of arc-tracking propensity [34]. Aliphatic polymers (e.g., polyethylene, PTFE) tend not to undergo arc tracking, whereas aromatic ones or ones containing alternating double bonds (e.g., phenolic, polyethylene terephthalate, polystyrene) do because the latter, when pyrolyzed, leave residues that are electrically conductive or semiconductive. Also tending to exhibit arc tracking are polymers that, although lacking aromatic rings or double bonds originally, form rings or double bonds during thermal degradation; PVC and polyacrylonitrile are examples.

It was also found that oxygen is not a requisite for the formation of arc tracks and that materials can be made to arc-track in a nitrogen atmosphere. Generally, arc tracking can only happen if a polymer can char, since a conductive track can only be established in char. Practical difficulties arise in evaluating this because charring is not an absolute property of polymers but, rather, depends on environmental details. It has also been found [35] that arc tracking is promoted by the presence of halogen atoms in the polymer. Conversely, alumina trihydrate ($Al_2O_3 \cdot 3H_2O$), a common filler for many polymers, is highly effective in reducing the arc-tracking propensity in certain polymers [36, 37].

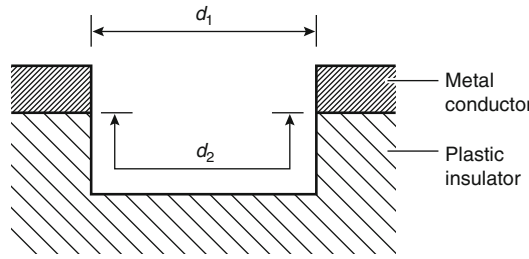

Fig. 22.9 Simplified view illustrating clearance and creepage distances (From Ignition Handbook, used by permission)

Most research studies have not focused on the time element and none have done so in a systematic way. The minimum current needed, however, has been studied. Wilkins and Billings [38] obtained the following minimum values: PVC 0.15–0.20 mA, PVA 0.3 mA, Ebonite (butadiene/methylstyrene rubber) 1.1 mA, phenolic/paper 1.15 mA, polycarbonate 1.2 mA, and PTFE 2.3 mA.

Creepage In design, the resistance to arc tracking is controlled by two means: (1) selection of well-performing insulation materials, and (2) observing adequate creepage distances. The latter concept is illustrated in Fig. 22.9. For arcing in air from metal to metal, the governing distance is called the clearance distance, d_1. But since arc tracking proceeds only along solid surfaces, the distance across which arc tracking must travel, if failure is to occur, is called the creepage distance, d_2. Creepage distances are set down in numerous military and industrial specifications, but the rationale is usually empirical and not much scientific research is available on the topic.

Surface Flashover

Fire protection engineers need to be aware that the term *flashover* is used in a very different way in electrical engineering, where it means "a discharge which occurs over the surface of a solid dielectric in a gaseous or liquid medium." [39]

The dielectric strength of air is lower than that of any commonly used electrical insulators, so if the path through air and the path through a solid insulator are of similar length and breakdown occurs, it will go through air, not through the solid insulator. The surface of an insulator may become polluted so that its breakdown strength becomes low; this problem is common in locales exposed to salty air near the sea. The material with the lowest breakdown strength may be this pollutant film and, if breakdown occurs along this film, it is referred to as "surface flashover." This reaction does not constitute arcing across a carbonized path, since the path, although of low breakdown strength, is not carbonized. The problem is relevant only to high-voltage (HV) circuits and would be a source of ignition only in the vicinity of HV installations.

Overloads and Related Phenomena

Gross Overloads Excessive overload can lead to fires, but this condition is much rarer than is an arcing fault. It can arise if either a circuit breaker is faulty or a cable is used that is of much smaller gauge than is the rating of the circuit breaker. Both of these situations are relatively uncommon. Ampacity ratings of wires and cables are conservative enough that an overload of roughly 2× is not expected to create any significant problems, at least in the short term (long-term thermal degradation of insulation material is a separate issue).

If a sufficiently overloaded condition persists, then cables may be able not just to ignite but also to create a propagating, self-sustained fire. Experimental studies [7] indicate that, for this event to occur, the current carried must be 300–700 % of the rated current (ampacity). However, all existing tests have been short-term. Even a current at 200 % of rated ampacity, if sustained for a protracted period of time, may deteriorate the insulation enough so that carbonization can begin. Eventually, failure may not be the melting and shorting commonly involved in ignitions from short-term overloads but, rather, some form of tracking damage.

Ignition in the excessive-overload mode is unlikely to occur if the cable is in a circuit that is protected by a circuit breaker/fuse correctly matched to the rating of the cable, since tripping would occur rapidly under 3× and greater overloads. But ignitions can readily occur if a much smaller gauge cable is used than corresponds to the rating of the circuit breaker. An overload may not directly ignite an insulated wire but may significantly raise the temperature of both the wire and the insulator. Old-style rubber-insulated wires used to be prone to a sleeving effect, whereby insulation closest to the wire is thermally degraded and shrinks back from the conductor.

For wires insulated with thermoplastic insulation (including the majority of today's common cable types), a somewhat different effect is found. Elevated temperatures cause copper to elongate but the insulation to shrink. As a result, copper wires readily "pop out" of the softened insulation. A direct metallic contact can then occur, with this short circuit being a localized place of ignition [7]. By contrast, if a PVC-insulated cable is externally heated (by fire or otherwise), it usually chars rather than melts. But melting, rather than charring, may occur if the external heating is with a very low heat flux [40], below about 15 kW m^{-2}. Bubbling of thermoplastic insulation has been experimentally found only to occur from overcurrent and not due to external heating [40].

Excessive Thermal Insulation Ampacity ratings for cables are based on a certain amount of convective cooling being available, which can be defeated by thermal insulation. Thus, even if the current passed through a cable is within its rating, embedding it in thermal insulation can cause the temperature to rise to values that are no longer reasonable for the particular class of insulation used. If, in addition, an overload condition is created, the heating can be greatly exacerbated. Bunching of cables together can also lead to overheating, since ampacity ratings envision only a limited aggregation of adjacent conductors. Goodson et al. [41] observed a house

during construction where charring damage was already found on bunched NM cables. Thus, they ran wall-cavity tests using bunched, 90 °C-rated NM cables and obtained charring when the stud cavity was insulated with polyurethane foam insulation.

Prior to World War II, knob-and-tube wiring was common in the United States. This form of wiring uses two separate conductors that are not grouped into a cable but are individually strung on widely spaced porcelain knobs. The current-carrying capacity of this form of wiring is dependent on there being unobstructed air cooling of the wires. Fires have occurred when the wires were buried in thermal insulation. A similar problem can be encountered when extension cords, which are rated for exposed-air use, are buried under thermally insulating objects or else are coiled in multiple layers on a cord reel while carrying a high current but one still within the nominal rating.

Stray Currents and Ground Faults Stray currents occur when circumstances cause current to flow through paths not intended to carry current. Ground faults are a well-known example [42]. They can occur if a conductor is abraded or damaged and contacts metal siding, roofing, and so on. Kinoshita et al. [43] documented that a current of only 5 A was required for ignition when a three-conductor, PVC-insulated cable contacted a galvanized iron roof. The Consumer Product Safety Commission (CPSC) has hypothesized that the Beverly Hills Supper Club fire, one of the deadliest U.S. fires of the twentieth century, was made possible by improper wiring of the neutral conductors and triggered by a ground fault that occurred [44].

If a building has conductive components throughout it, such as metal lath, aluminum siding, an electric fault can result in an electrified house, leading to multiple ignitions [7]. The fault is commonly contact with HV wiring.

An unusual mode of ignition from a ground fault is where current flows through a gas line. The current can cause overheating of the metal and lead to a rupture of the pipe [45].

In recent years, a related problem has been fires or explosions in houses due to use of CSST (lightweight corrugated stainless steel tubing) gas piping instead of black iron [46]. These products proved to be particularly susceptible to puncturing by lightning strikes, which do not need to be direct enough to cause other damage. Gas escapes from the small holes created and a gas explosion or a house fire ensues. In cold climates, it is not rare for individuals to thaw a frozen water pipe by attaching a welding transformer and passing current through it. Fires have resulted due the very large currents that are involved [47].

Overvoltage, Floating Neutrals, and Surges Ignitions from an overvoltage is relatively rare, as concerns branch-circuit wiring. The materials used for wires and wiring devices are well able to withstand the normal surges that are a regular event in a power distribution system. To experience ignitions, one of the following events is generally needed:

1. Lightning strike
2. Accidental delivery of high voltage into low-voltage wiring
3. A floating neutral
4. A large voltage spike (surge)

Lightning strikes can result in massive ignitions, not just of wiring but also of all sorts of combustibles.

Occasional fire reports are encountered in which, due to some malfunction in the power distribution network, high voltage got applied to wiring intended to carry only 120/240 V. A case is documented [48] in which a utility transformer fault caused all the ground-fault circuit interrupter devices in a house to fail, along with igniting a fire due to an explosion of a TV set. In another case, a faulty transformer caused the service entrance wires to ignite and burn inside a house. A systematic study of such fires does not exist, but ignition should be considered very likely any time that such a failure occurs.

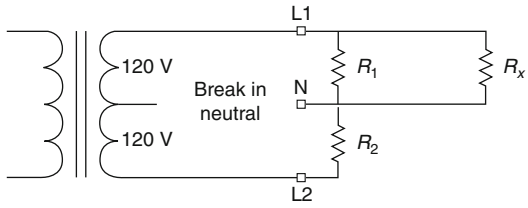

Fig. 22.10 Floating neutral (From Ignition Handbook, used by permission)

A floating neutral (sometimes called *open neutral*) can lead to ignition in 120/240 V wiring circuits due to a special nature of that circuit topology.[2] In a single-phase service entrance, there are three current-carrying wires: two hot wires and one neutral. Figure 22.10 illustrates the normal feed from an outdoor transformer to a building. Inside the building, the system becomes effectively a four-wire system, since a safety grounding wire is also run that is connected to the neutral and terminates at a ground rod.[3]

All 240 V loads are directly connected across L1 and L2 and do not depend on the presence of the neutral. But 120 V loads are connected across N and either L1 or L2. If a neutral is in place, the loads will receive the intended 120 V voltage. However, if a break occurs in the neutral, the voltage delivered to 120 V loads can swing widely, in principle from barely above 0 to almost 240 V, although in practice the range is not quite as large. Figure 22.10 shows the circuit arrangement. The voltage present across a particular load R_x will be determined by the voltage divider action of other loads in the system, designated as R_1 and R_2. The voltage across R_x will be

$$V_x = \frac{240}{1 + \frac{R_2}{R_1} + \frac{R_2}{R_x}}$$

Most electrical or electronic equipment can ignite if a voltage much in excess of the intended one is fed to it. Conversely, most devices will not ignite if the voltage delivered to them is too low. Electric motors, however, are an exception, and flaming fires can result from certain motors running at a sufficiently undervoltage condition.

An ignition due to undervoltage can also occur if one hot leg of a 240 V circuit is disconnected. If the circuit has any 240 V appliances and these are energized, then they can transfer power from the live leg to the disconnected leg. But the delivery will be through a sizeable resistance and much less than 120 V will be delivered.

The preceding discussion ignored the presence of the ground wire. According to The *National Electrical Code* [49], a grounding electrode must be connected from the neutral to an earth ground at the service entrance. But, provided that the neutral is functioning properly, this ground wire serves no observable function. Consequently, there may be little to prevent its deterioration or abuse over the years. If a break in the neutral then occurs, a sizable current can flow through the ground wire. If the ground wire passes near or through combustibles, and an excess current ends up flowing through it, then an ignition might occur at that place. Fires have also been reported [50] in installations using armored cable when a floating neutral occurred and current that would normally flow through the neutral instead flowed through the armor.

Surprisingly large voltage spikes can be found on 120/240 V systems. Without any overt fault conditions, simply the operation of a motor controller can create a 2,000–3,000 V spike [51]. The majority of voltage surges, however, are due to external—not in-premises—factors. The primary causes are lightning, electrical utility switching transients, and failures of components in the high-voltage electrical transmission system [19].

To evaluate the role of voltage surges, it is essential to recognize that there is a fundamental dividing-line voltage. Surges above approximately 6,000 V(peak) lead to a "sparkover of clearances" widely throughout the house. In other words, the householder will typically find the majority of outlets and other electrical devices have suffered calamitous damage, and

[2] The discussion here is based on electrical practice in North America.

[3] Mobile homes normally have a four-wire service from pole to building.

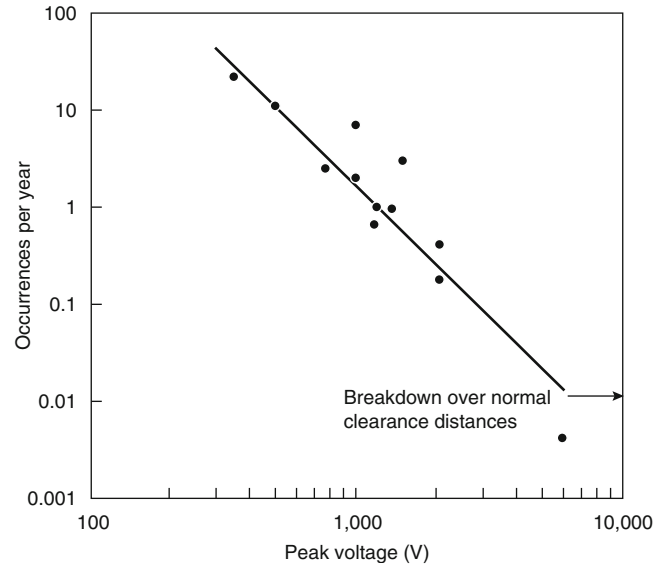

Fig. 22.11 Surge voltages experienced in branch-circuit wiring

possibly multiple fires were ignited. Conversely, surges below about 6,000 V(peak) will generally appear benign. But appearances may be deceiving in the case of surges that are in the kilovolt range but below 6,000 V. The 6,000 V value corresponds to the level at which wiring devices[4] that are properly designed, installed, and operated will typically suffer a breakdown. But devices that have a manufacturing or installation defect may break down at less than 6,000 V. The hazard comes about if that breakdown is not visually obvious (e.g., concealed inside a wall or within plastic).

A breakdown of plastic insulation will lead to the formation of a carbonized path along which the discharge occurred. As explained earlier, once a carbonized path is formed that extends electrode to electrode, arc tracking can start. The process is slow, although an exact time frame has not been established. In one documented case, electrical fires due to this cause occurred after a modest lightning strike struck a house that did not initially lead to fire or widespread visible electrical damage. The fires erupted about 4 months after the lightning strike [19]. In the case of breakdown of insulation due to below-6,000 V surges or spikes, a delayed fire can occur in the following two ways:

1. The initial fault clears itself and the circuit breaker is not tripped (or fuse not blown).
2. The circuit breaker trips, but the householder resets it, and operation seems "normal."

In either case, after a certain period in which arc tracking progresses unnoticed, fire breaks out.

It should be noted that applying Paschen's Law to clearances typically specified by electrical standards, it would be expected that widespread sparkover of clearances would require about 6,500 V(rms) or 9,200 V(peak). The empirical observation that 6,000 V(peak) is typically sufficient evidently reflects the fact that devices in the field do not quite behave as ideally as their laboratory testing would suggest.

The 6,000 V(peak) value is vastly greater than the operating voltage of $120\sqrt{2} = 170$ V(peak). But such peak voltages are not rare, as indicated by several field studies. Figure 22.11 indicates that an individual house would expect to suffer such a surge roughly once every 100 years [19]. Thus, the risk for an individual house is

[4] This refers to outlets, plugs, and similar devices. Electric and electronic appliances are often designed to much less stringent standards and may fail or start burning at significantly smaller surge levels.

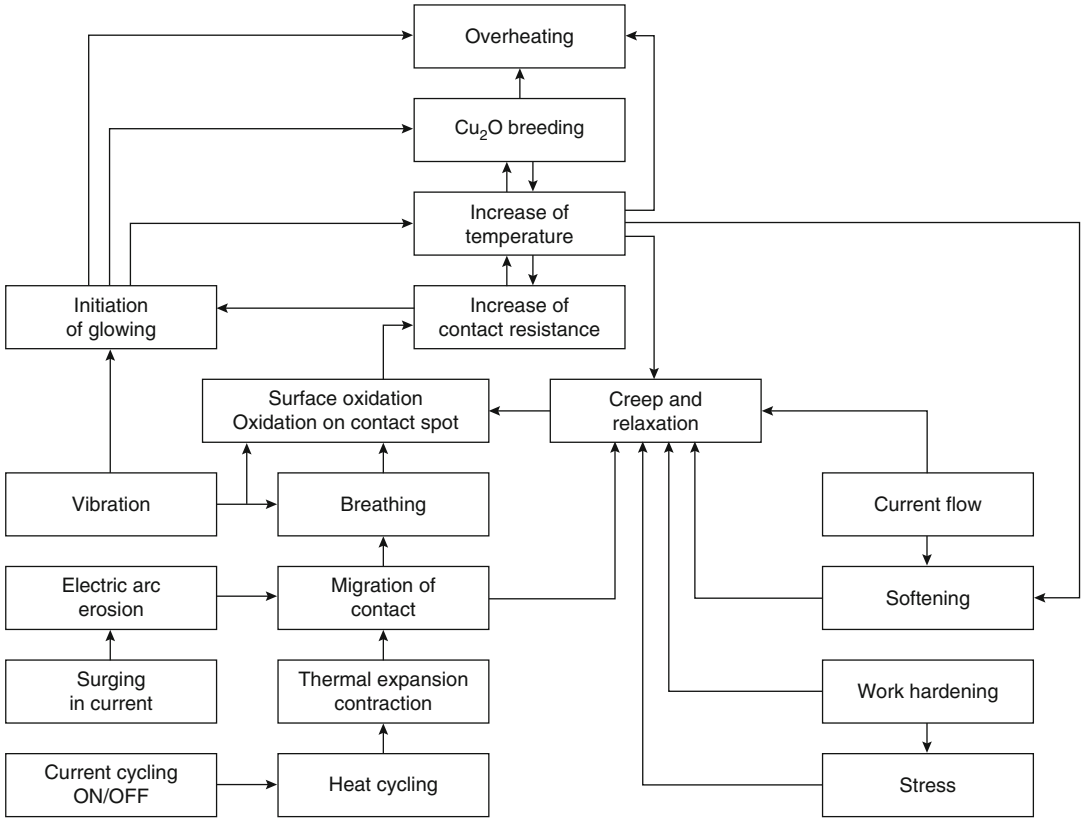

Fig. 22.12 Mechanisms for overheating at electrical connections, as outlined by Kuroyanagi et al [52] (From Ignition Handbook, used by permission)

low, but within a given community there can be a number of such events every year. It must be noted that the field studies were all completed before the current era of widespread use of surge suppressors. Thus, houses where a sizable number of surge-suppression devices are used can be expected to be at lower risk than these statistics indicate.

Overheating Connections

Failures of electrical connections are generally due to manufacturing defects, installation defects, design defects, abuse, damage, or environmental effects. In addition, it can be expected that much like any other mechanical device, an electrical connection will have a finite lifetime, but—apart from the aluminum-wiring problem discussed later—there currently exist no useful studies on this point.[5]

The physics and chemistry of electrical connections are very complex, as illustrated by the phenomenological flowchart put forth by Kuroyanagi and coworkers [52]. From Fig. 22.12 it can be seen that numerous phenomena are involved, but not all have been studied systematically and in detail. In the simplest terms, failure can be understood to involve the following factors:

- Localized heating takes place, due to smaller effective area available for current flow compared to a bulk, undamaged conductor.

[5] The NFPA Research Foundation is currently conducting a study on aging electrical wiring and there may be conclusions obtained from it concerning the potential lifetime of electrical connections.

- Heating accelerates oxidation and promotes creep.
- Creep causes relaxation of the mechanical forces restraining the connection, leading to fewer micro-areas through which effective current flow can take place.
- This relaxation further raises the temperature, which further accelerates oxidation.
- Oxidation diminishes the area through which current can readily flow.
- Expansion and contraction from thermal cycling may cause further loosening. This may cause certain areas of micro-contact to make and break, while a more severe effect entails irrecoverable plastic deformations. Thermal cycling may be due to ambient temperature fluctuations, or due to fluctuations in current, leading to changes in I^2R heating.
- The presence of moisture or corrosive gases in the environment can accelerate failure due to additional chemical degradation. In the case of PVC insulation, once sufficient overheating takes place, HCl gas will get liberated from the plastic, and this is highly corrosive.
- The presence of vibrations also serves to make and break micro-contact areas, resulting in worsening of the connection.

The simplest theoretical model of an overheating connection is obtained by assuming that heat is produced at a constant rate in an infinitesimally thin plane section across the wire. The wire is represented as a cylinder without any change of geometry at the point of connection [53]. The solution for the temperature of that cross section is

$$\Delta T(t) = q'' \sqrt{\frac{r}{2\pi\lambda h}\gamma\left(\frac{1}{2}, t/\tau\right)}$$

where

q'' = Power density at the plane section (W m^{-2})
r = Radius of the wire (m)
λ = Thermal conductivity of the wire (W m^{-1} K^{-1})
h = Effective heat transfer coefficient from the surface of the wire (W m^{-2} K^{-1})
γ = Incomplete gamma function [54]

and the time constant τ (s) is given by

$$\tau = \frac{r}{2}\frac{\rho C}{h}$$

where ρ = density (kg m^{-3}) and C = heat capacity of copper (J kg^{-1} K^{-1}). The equilibrium value of the temperature rise is

$$\lim_{t\to\infty} \Delta T(t) = q'' \sqrt{\frac{r}{2\lambda h}}$$

As an example, for a copper wire of 14 AWG, $r = 1.63/2 = 0.815$ mm, $\rho = 8{,}890$ kg m^{-3}, $C = 385$ J kg^{-1} K^{-1}, and $\lambda = 400$ W m^{-1} K^{-1}. Assuming that $h = 50$ W m^{-2} K^{-1}, and that 10 W is dissipated in the connection, giving $q'' = 10/\text{p}r^2 = 4.8 \times 10^6$ W m^{-2}. Then

$$\Delta T(\infty) = 4.8 \times 10^6 \sqrt{\frac{0.815 \times 10^{-3}}{2 \times 400 \times 50}} = 685$$

If the ambient temperature = 20 °C, then the temperature at the overheating connection will be 20 + 685 = 705 °C, which is much higher than the ignition temperature of most combustibles. This theoretical treatment is highly simplified; nonetheless, it indicates that very high temperatures can be anticipated.

In the early stages of failure, bad connections give little external evidence of their deteriorating condition. It is sometimes considered the infrared (IR) thermal imaging can be used as a preventive maintenance operation, since the technique can graphically show hot spots. However, research studies have shown that this is not possible until very late in the process [55]. In the earlier stages, the cool metalwork surrounding the overheated spot essentially preclude finding and identifying the spot.

Evidence of overheating is clear when mechanical connections between two current-carrying conductors start to show glowing. Normally, good electric connections should not be subject to a temperature rise much in excess of that for the conductors themselves. This depends on the connection having a very low resistance. Most metals that are used for carrying electrical current are subject to oxidation when exposed to

atmosphere. The metal oxide film formed on the surface has a very high resistivity. Thus, a connection where the mating parts are oxidized will be a high resistance connection and will overheat if significant current is passed through it. Temperatures of a glowing connection vary widely, but peak values at the hottest point have been measured from 1,100 °C [56] to 1,500 °C [57, 58], for copper connections. Temperatures up to approximately 300 °C have been measured on metal parts some distance away from the hot point [54]. Even though copper melts at 1,083 °C, much higher temperatures can be found, since the hottest portion is on the metal oxide which is being formed and not on the metallic copper.

One of the earliest studies on glowing connections was published [59] in 1961 (Fig. 22.13) and it was found that the connection acts as a nonlinear circuit element. For currents over 10 A, drops of around 2 V were found. But for small currents, voltage drops in the tens of volts can be found. At a maximum current of 20 A, 50 W is dissipated in a copper/brass connection and around 35 W for copper/iron. The study also noted that the power dissipation depends only on the materials involved and not on the nominal size of the contacts.

The Cu_2O breeding process at a glowing connection has been studied by several Japanese research groups [60, 61], that provided numerous details of this complex process [7]. One of the things learned was that the process is primarily confined to solid conductors; significant currents are hard to sustain at a glowing connection of a stranded wire—the wire tended to break at the point of heating.

Overheating can occur in electrical connections of all types, but historically the most notorious case was that of *aluminum wiring* during the early 1970s. In the late 1960s some U.S. house builders introduced a cost-cutting measure whereby aluminum was substituted for copper conductors in house-wiring branch circuits. This substitution was done without adequate research or field-testing and the outcome was a rash of house fires. The Consumer Products Safety Commission and the National Institute of Standards and Technology (NIST) conducted extensive studies on the phenomenon and found that the problem occurs due to a combination of metallurgical factors including creep, hardness,

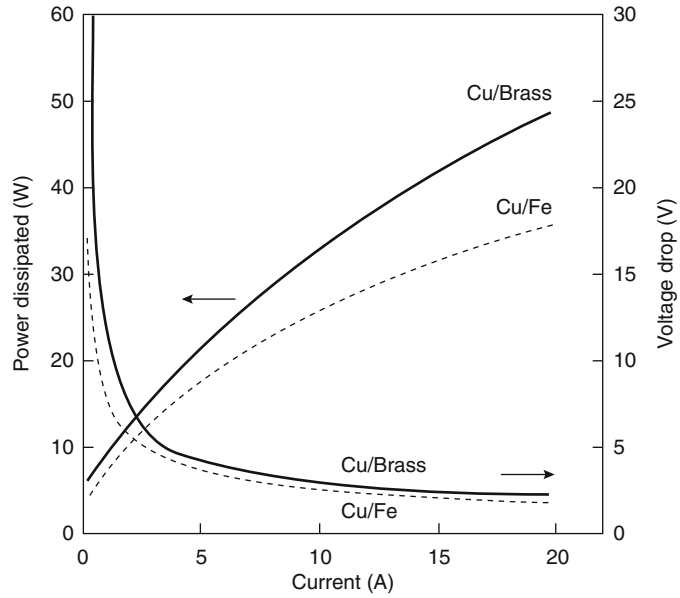

Fig. 22.13 Power dissipation and voltage drop across glowing connections of two types (From Ignition Handbook, used by permission)

and oxide characteristics [7]. The outcome is that small-diameter aluminum wires[6] cannot be reliably terminated by a screw connection and show rapid deterioration and failure. Details concerning the failures of various specific types of electrical connections can be found in the *Ignition Handbook* [7].

Ejection of Hot Particles

Electrical short circuits and arcs sometimes eject incandescent metal particles (i.e., mechanical sparks, sometimes called 'ejecta'). These particles can then ignite nearby combustible materials, especially if the material is low density or smolder-prone. The particles can be propelled a modest distance in a residential wiring situation; for instance, in one study [62] particles were found up to 1.5 m away. It has also been documented [7] that ignition-causing particles can be ejected from openings in a receptacle (which can superficially appear to be undamaged) and from within a metal box with a metal cover (since small holes are invariably contained).

Miscellaneous Phenomena

Some additional phenomena have been documented but are rare. These include harmonic distortion-caused overload, eddy currents, and dendrites [7]. Slightly less rare is the formation of adventitious batteries, which involves a potential difference created by electrochemical action when an electrolyte is present in conjunction with two dissimilar metals. This process sometimes leads to a hydrogen explosion, since the electrolysis process separates water into hydrogen and oxygen [7]. Numerous studies have been published examining the possibility of very strong radio-frequency fields causing sparks and ignition of flammable atmospheres, but it does not appear that any actual incidents have been reported [7].

Time for Fire to Initiate from an Electrical Cause

One area in which research is seriously lacking is for the time frame associated with electrical fires. In some cases, such as a major lightning strike or a high-current arcing fault in a 480 VAC busbar, the ignition may be essentially immediate. But in the case of the most common faults—a bad connection or arcing across a carbonized path—overt ignition usually takes a long time after the initial conditions were established for the fault. These processes are qualitatively known to be of long term, but means for quantification do not currently exist.

Static Electricity

General Principles

Static electricity represents electric charges that are notionally static; that is, they are collected on a surface and are not continuously flowing in an electrical current. The steps involved in a static electricity discharge are schematically illustrated in Fig. 22.14. For significant charge separation (sometimes loosely called *charge generation*) to

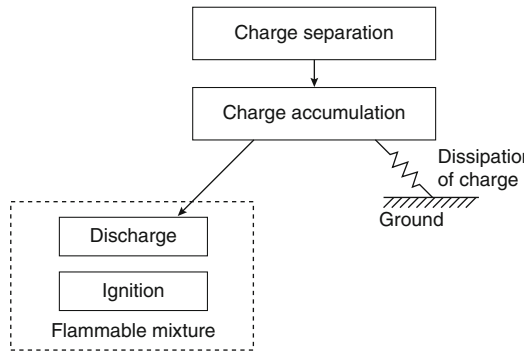

Fig. 22.14 Static electricity fundamentals (From Ignition Handbook, used by permission)

[6] The problem is only pertinent to small-diameter, 10 AWG (2.588 mm) or smaller, conductors; service-entrance cables and other large-diameter aluminum conductors can generally be reliably terminated.

occur, at least one material must be involved that is an electrical insulator. An electrical insulator is considered to be a substance that has a resistivity above about 10^8 Ω-m, which includes most organic substances.

Means by Which Charge Separation Occurs

Electric charge may be separated by the following means [7]:

1. Contact and separation or friction between solids
2. Relative motion at a phase interface (liquid–solid, liquid–gas, or between two liquid phases)
3. Induction (whereby charge is moved due to the presence of an electric field), also sometimes termed *polarization*
4. Ion collection from a discharge process (e.g., from corona discharge)
5. Double-layer charging
6. Fragmentation of solids having nonuniform surface charge densities
7. Mechanical fracture (electron emission due to strained or ruptured bonds within solids), also termed *piezoelectrification*
8. Thermal cycling (e.g., charging by freezing), also sometimes termed *pyroelectrification*

Contact or friction between two dissimilar substances can produce a charge separation if either of the two substances is an insulator. The contact may be solid-solid, solid–liquid, or liquid-liquid. The most common modes pertinent to fire ignitions are the following:

1. Contact and separation between dissimilar solids
2. Flowing powders
3. Flowing liquids

A mild amount of charging can be created simply when two surfaces come into firm contact and are then separated. Friction merely enhances the charging by increasing the effective area of contact. Traditional wisdom is that not only must the materials be dissimilar, but that sizable charging will take place only if they are far apart on the *triboelectric series*, which is a rank-order listing of materials according to how much of a negative or positive charge they tend to collect [63]. The triboelectric series is determined by the material's dielectric constant [64], however, current understanding is that electrification is not precluded in contact between objects made of the same material. Thus, plastic chips falling down a chute made of the same plastic are known to be able to undergo electrostatic charging [65]. It is believed that this may involve both physical factors (e.g., stresses at the surface) and chemical factors (contamination).

Electrification due to ionized gases flowing past surfaces can arise, but if the gas is at normal temperatures (i.e., not a hot plasma) and is not contaminated with solid or liquid particles, then the charging that can be achieved is trivial, amounting to less than a volt [66]. Gases that contain solid–liquid aerosols or gas streams that generate liquid or solid particulates (e.g., the discharge of a CO_2 extinguisher, the rapid evaporation of liquid propane) can pick up a sizable charge, however.

For certain materials, moisture in the air promotes the dissipation of charge since it decreases the electrical resistivity of some materials; it never affects the separation of charge. For many other materials, however, the resistivity is not lowered due to atmospheric moisture. Adding vapor-phase moisture does not actually change the electrical conductivity of the air; adding a mist or spray, however, raises the conductivity [67].

Discharge Types

Discharges of static electricity can involve the following geometries:

- Discharge between two conductive electrodes
- Discharge involving one conductive electrode and a diffuse insulating medium
- Discharge from one mist or cloud to another

Apart from events taking place solely in the atmosphere (which are considered later in the section called "Lightning"), discharges involved in accidental ignitions are classified as the following:

1. Spark
2. Corona discharge
3. Brush discharge
4. Powder heap discharge
5. Propagating brush discharge (Lichtenberg discharge)
6. Lightning-like discharge

Additional details on discharges are given in the *Ignition Handbook* [7] and by Britton [68].

Spark

A normal electric spark discharge occurs through the air separating two electrodes when the electric field reaches a value of approximately 3 MV m^{-1}. Thus, for a gap distance d, the voltage V required is $3d$, where V is in megavolts and d is in meters. For a spark to be incendive, the gap distance normally must be equal to or greater than the quenching distance. Considering 2 mm as a typical quenching distance, the voltage required is on the order of 6 kV. Up to about 1,000 mJ can be delivered in a static-discharge spark. This is a sizeable amount of energy, well beyond the minimum ignition energy (MIE) of most substances. Spark discharges are distinguished from other electrostatic discharges in that breakdown occurs across the *whole* gap separating two electrodes.

Corona Discharge

A corona discharge (sometimes called *point discharge*) is a slow, diffuse discharge that originates at a metallic electrode and branches out in a diffuse manner into space or towards poorly conducting surfaces. A corona discharge requires an electrode that has a needle-like point, typically less than 5 mm diameter. Charging such an electrode results in an electric field which is distorted, being generally low, but much greater near the point. When the electric field exceeds the local dielectric strength, breakdown occurs. Corona discharge has the lowest energy of the electrostatic discharge types. It is visible as a violet glow in a darkened room. A corona discharge can also occur in the presence of second electrode, but is still considered a 'one-electrode' discharge since the discharge does actually reach the second electrode. A minimum voltage of about 2–6 kV is necessary for a corona discharge to occur, with smaller potentials needed for finer-pointed needles. The maximum energy normally realizable from a corona discharge—not much over 0.01 mJ—would even theoretically suffice to ignite only the most ignitable of gases, such as CS_2 or H_2. However, actual ignition requires that the energy be delivered into a small kernel, and the diffuse nature of a corona discharge precludes that. Corona discharges are often used in processes and machinery as a safety measure for lowering charge accumulation.

Brush Discharge

When a grounded conductor is brought into an electric field that is near its dielectric breakdown strength, a gas discharge can occur in the form of a brush discharge. The discharge is able to occur because of electric field distortion introduced by the electrode, which locally raises the field above its breakdown value. The name comes from the brush-like shape of the discharge. It differs from a corona discharge, in that the latter is visually observed to be diffuse. A brush discharge is similar to corona discharge in being a low-energy, one-electrode discharge, but whereas a corona discharge requires a needlelike electrode, a brush discharge occurs when electrodes have a radius of 5–50 mm.

The incendivity of brush discharges is proportional to the radius—larger-radius conductors are more likely to lead to ignition than ones of smaller radius. Commonly, the high electric field will occur due to the presence of a charged insulator. It is estimated that the energy from a brush discharge will not exceed about 4 mJ. In addition, most of the energy released during a brush discharge does not contribute to incendivity, since the energy is not just localized at the place where a flame kernel is formed. The high electric fields necessary for a brush discharge are readily found in many powder operations, in mists, and also with movement of plastic films.

Circumstances leading to a brush discharge can include:

- approaching a highly-charged insulator such as plastic films or plastic pipes with a finger or a metal tool;

- discharging of solids from plastic bags in the vicinity of metal parts;
- filling a tank at a high velocity with an insulating liquid, with the charged liquid surface approaching an internal fitting that can act as an electrode;
- lowering a conductive cup, etc., into a highly charged liquid;
- projection of metal parts into a cloud of highly charged dust or aerosol;
- pouring of insulating powders into silos when the fill surface approaches a conductive fitting;
- projection of ships' masts, flagpoles, or antennas into a powerful atmospheric electric field—this is known as St. Elmo's fire.

Even though about 3.6 mJ can be delivered in a brush discharge [69] and there are dust clouds that have an MIE $\approx$ 1 mJ, most studies have concluded that brush discharges will not ignite dust clouds [70], provided that the cloud is not a hybrid dust/gas mixture.

Powder Heap Discharge

In some cases, when rapidly filling large containers such as silos or flexible intermediate bulk containers (FIBC) with powders, a much higher charge can build up in the settled powder than was present in the air through which the material moved and a discharge can then take place. This occurs because a growing volume of powder is aggregated, plus when the powder is compacted, its charge likewise gets compacted if the powder is insulating and charge cannot get dissipated. The powder heap discharge is also called a *cone discharge* or a *bulking discharge*. It occurs along the exposed surface of the powder. A minimum particle size [71] of ca. 0.1 mm is needed for powder heap discharge to occur, but the majority of the actual incidents have involved polymeric resin particles in the 1–10 mm range.

Early recommendations used to state that up to 10 mJ can be delivered in a single discharge step. Some indirect evidence suggests that discharges as large as 1,000 mJ may be anticipated for large particles flowing into a large silo. A minimum product feed rate is needed for a powder heap discharge to occur. This has been estimated at 3,000–5,000 kg h^{-1} for 3 mm particles, rising to 25,000–30,000 kg h^{-1} for 0.8 mm particles [81]. Powders having a resistivity of less than 10^{10} Ω-m are conservatively judged to not be susceptible to explosions from powder heap discharges [72]; powders which have caused explosions have had resistivities $> 10^{12}$ Ω-m.

Propagating Brush Discharge

A very vigorous discharge can occur when certain conditions are met for the charging of a surface. There is a limit to the amount of surface charging that can be sustained on a surface without discharging by ionizing the air (2.65×10^{-5} C m^{-2}). This limit can be increased if a double layer of charges of opposite polarity is accumulated.

A way for this to occur is when an insulating layer is directly on top of a grounded metallic layer. This allows opposite polarity charges to build on the second side of the insulating layer (Fig. 22.15). Under those conditions, the maximum surface charge is governed by the breakdown strength of the insulator, which may be on the order of 20–40 MV m^{-1}, instead of the 3 MV m^{-1} for air.

In addition, the dielectric constant of many common insulators is 2–4 times that of air. These two factors combine to give maximum surface charges of around 5×10^{-4} C m^{-2}, and

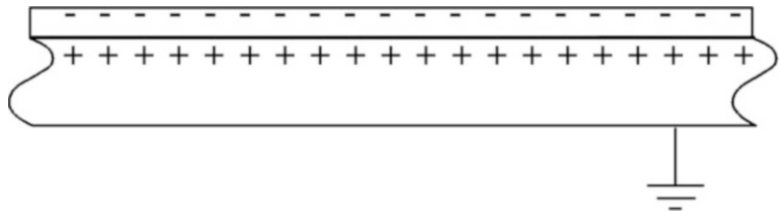

Fig. 22.15 Double-layer charging (charge pairing) occurring when a charged insulator is adjacent to a grounded conductor

it is considered that 2.5×10^{-4} C m^{-2} is the minimum surface charge needed for a propagating brush discharge. With very thin films of certain plastics, surface charge densities up to 8×10^{-3} C m^{-2} have been measured [73].

A propagating brush discharge can ignite most flammable mixtures, including dust clouds. A discharge occurs in one of two ways: (1) a grounded electrode is brought near the charged insulator surface; or n a dielectric breakdown of the insulating layer, resulting in a local puncture. A minimum voltage of ca. 4 kV is needed for a propagating brush discharge to occur with very thin films (10–20 μm) rising to 8 kV for 0.2 mm thick ones. Up to ca. 1,000 mJ can be delivered in a propagating brush discharge.

Circumstances leading to a propagating brush discharge can include:

- conveying an insulating powder at high velocity through plastic pipes or bins that are grounded on their exterior;
- conveying an insulating liquid at high velocity through plastic pipes that are grounded on the outside, or metallic pipes that have an insulating interior coating;
- loading of insulating powders into large, non-conductive silos;
- high velocity operation of conveyor belts that have metallized outer surfaces and an insulating core;
- repeated collisions of dust particles on an insulating surface atop a grounded layer.
- In some cases, a propagating brush discharge can occur without an overt grounded layer, for instance when rain is falling on a plastic pipe conveying an insulating powder [74].

Lightning-Like Discharge

Lightning in the atmosphere can occur when water droplets and ice particles are charged to very high potentials. Since particles in dust clouds will also pick up an electric charge, lightning-like discharges have been observed to occur in the dust clouds formed during volcanic eruptions. What is unanswered is whether such discharges can occur on a smaller scale, to wit, in connection with storage silos. A number of accidents have been blamed on such discharges, but the details of the circumstances have never been clear. Lightning-like discharges would presumably be able to ignite almost any combustible matter, so the conditions—if any—that might lead to such lightning would be important to quantify.

Electrostatic Charging and Discharging of Solids

For simple geometries, the amount of charge that an isolated solid can accumulate and the voltage to which it can be charged can be computed [7]. The maximum charge density, σ_{max} (C m^{-2}), that can be built up on the isolated object is given by:

$$\sigma_{max} = \varepsilon \varepsilon_o E_{max}$$

where ε = dielectric constant (–), ε_o = permittivity of vacuum (8.854×10^{-12} S s m^{-1}), and the abbreviation C denotes coulombs, whereas S denotes Siemens. Since the dielectric constant for air = 1.0 and E_{max}, the breakdown strength of air, is approximately 3 MV m^{-1}, then σ_{max}, the maximum charge density possible for an isolated object in air = 26.5 μC m^{-2}. If the object is spherical, then its area = $4\pi r^2$, where r = radius (m), and the maximum charge that can accumulate on it is

$$Q_{max} = 4\pi r^2 \times 26.5 = 333\, r^2 \mu C$$

Now, since voltage V is, by definition, equal to the field strength E times distance,

$$V = E_{max} r = 3.0 \times 10^6 r$$

which gives the maximum voltage to which the spherical object can be charged in air. But capacitance C is defined as = Q/V,

$$V = \frac{Q}{C} = \frac{Q}{4\pi\varepsilon\varepsilon_o r} = E_{max} r = 3.0 \times 10^6 r$$

Then the capacitance with respect to ground of an isolated sphere can evaluated as

$$C = 4\pi\varepsilon\varepsilon_o r$$

where C = capacitance (farads; F), and the symbol C here must not be confused with the unit C denoting coulombs. Assuming that no losses occur, the energy W (joules) that can be delivered from a spark discharge is

$$W = \frac{1}{2}CV^2$$

Substituting the above gives

$$W = 501r^3$$

For many hydrocarbon vapors, a value of MIE ≈ 0.25 mJ is applicable. Then, to cause an incendive discharge from a charged, isolated body, its radius must be at least

$$r = \left(\frac{0.25 \times 10^{-3}}{501}\right)^{1/3} = 0.008\,\text{m}$$

Since this limit is only 8 mm, it would be very difficult to develop a safety measure on limiting the physical size of bodies that pick up a charge. In practice, somewhat higher minimum sizes will pertain, since ideally efficient conditions will not be present for discharge. For a propane-air mixture (MIE = 0.26 mJ), a minimum radius of 12 mm was found necessary in order to have an incendive discharge [75]. Capacitance values for some common objects are given in Table 22.3.

Electrostatic Charging and Discharging of Persons

A mild shock due to electrostatic discharge is common for human beings. Such discharges can also be incendive. Shoes charge the wearer because each time the foot is raised, the capacitance to ground is decreased and charge accumulates on the person. Charging readily occurs when apparel is worn that is highly insulating and the apparel contacts and separates from external objects. The charge picked up on the apparel then induces a similar charge in the body. Although standard values are sometimes proposed for the capacitance of a human being, the actual capacitance [76] varies with the thickness of the footwear, as shown in Fig. 22.16.

The resistance of the human body [77], measured to a fingertip, is about 1,300–2,000 Ω, but if the person undergoes a discharge via a grasped metallic object, the body's effective resistance may be only 360–700 Ω.

Table 22.3 The estimated capacitance of some objects

Object	Capacitance (pF)
Buckets, small drums	5
55-gal drum	100
Automobile	500
Tank truck	1,000
Large tractor-trailer	3,000

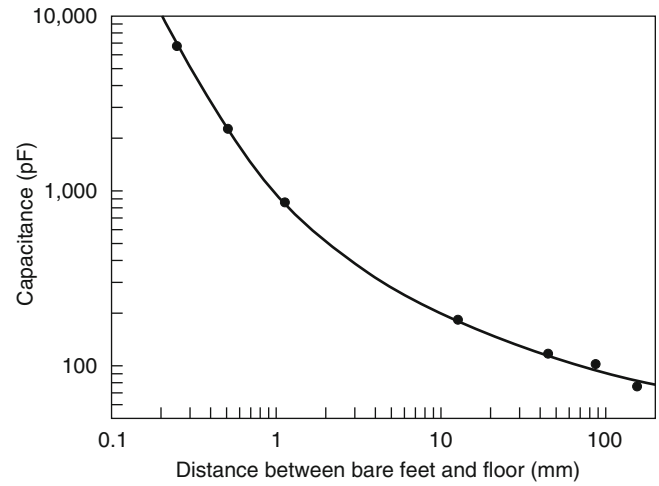

Fig. 22.16 Effect of footwear thickness on the capacitance of a person (assumed standing on a floor of moderate conductivity) (From Ignition Handbook, used by permission)

In dry air, the body can charge up to 5–25 kV, although voltages toward the high end of this range are uncommon and are limited by corona discharge. Thus, under the worst circumstances, the energy that is stored and is available for release in a spark is

$$W = \frac{1}{2}CV^2 = \frac{1}{2} \cdot 300 \times 10^{-12} \cdot \left(25 \times 10^3\right)^2 = 94 \text{ mJ}$$

If this much energy could be effectively applied, it would be enough to ignite all common ignitable vapors and also many dusts. However, more typical values of stored energy due to friction of apparel are 5–20 mJ. A value of 25 mJ has been adopted by a British standard [78] as the maximum practical value needing to be considered. At an RH of 50 %, a person walking on a carpet will generate no more than about 3 kV, and for RH greater than or equal to 60 % it is impossible to create a significant voltage [79]. Thus, the problem is limited to dry atmospheric conditions.

Guidelines are also available (Table 22.4) which relate the energy discharge from a person to the sensation [68, 80]. A perceptible sensation corresponds requires that the person be charged to about 2 kV [64]. In view of the above results, discharges that are perceptible but not severe are likely to lead to ignition if the person is in a space containing a gas in its flammable range. However, since people do not generally walk around in flammable atmospheres, it is found that electrostatic discharge from humans is actually a rare cause of unwanted ignition of gases [81].

Table 22.4 Human responses corresponding to various levels of discharge energy

Energy	Response
1 mJ	Perceptible
10 mJ	Prick
30 mJ	Sharp prick
100 mJ	Slight jerk
250 mJ	Severe shock
> 1 J	Possible unconsciousness
> 10 J	Possible cardiac arrest

Electrostatic Charging and Discharging of Granular Materials

When granular materials—powders, dusts, grains, and so on—are in motion, they can pick up a charge. Insulating powders—those with a resistivity greater than about 10^{12} Ω-m—do not easily dissipate a surface charge they may acquire and, thus, can be prone to spark discharges. This is especially a problem if they are conveyed or stored in insulating pipes or silos. The tendency for powders to pick up a charge is roughly proportional to their surface/mass ratio (or inversely proportional to particle diameter). The resistivity of powders changes drastically with moisture. At conditions of RH greater than 60–65 %, any charge formed is rapidly leaked away and hazardous conditions would not be expected [82].

Discharging of dry chemical (sodium bicarbonate or ammonium phosphate/ammonium sulfate) fire extinguishers can cause static electricity buildup. It was found experimentally that this can result in charging voltages that would correspond to discharge energies of up to 54 mJ [83]. Energies of this magnitude may ignite many dusts, not just gases.

Pneumatic transport systems cause a buildup of charge largely due to bends in the pipeline, but within a few meters of travel distance a steady-state value of charge is reached [84]. For a given air velocity, increasing the product mass flow rate decreases the charging tendency. Charging tendency is also reduced by reducing air velocity and by increasing particle size of the granular material.

Electrostatic discharges commonly occur whenever granular materials are pneumatically conveyed. These are typically nonincendive corona discharges. It is the possibility of spark discharges or other more energetic forms that forms the crux of the fire safety problem in these applications. Silos can build up very high potentials when granular materials are conveyed into them; in one study [84], up to 150 kV was measured.

During loading or conveying of powders, local non-incendive discharges (corona and possibly brush discharges) may occur which are helpful, rather, than deleterious, since they serve to reduce the charge buildup. Based on this observation, to reduce the incendivity of bulking discharges, it is commonly recommended that a grounded wire be strung through the center of a container receiving insulating powders. This causes small corona-like discharges to occur to the grounding wire, instead of large sparks to the container itself. A ground wire is equally effective if the container is insulating, instead of conductive [85]. The ground wire must be thin (around 1 mm) in order to ensure a corona-like discharge.

Electrostatic Charging and Discharging of Liquids

Many liquids are prone to undergo charge separation when they move past either a solid surface or the interface with another liquid. If a sufficiently high charge is accumulated, an electric discharge may occur. This discharge may cause an ignition under appropriate fuel-air ratio conditions. Charge relaxation readily occurs if the liquid has a high electric conductivity and for such liquids a high charge does not build up. Unfortunately, many organic liquids (i.e., aliphatic, aromatic, and cyclic hydrocarbons; ethers; some silicones) are good insulators (Table 22.5). Liquids with conductivities less than 5×10^{-11} S m^{-1} are considered to be of low enough conductivity that electrostatic hazards must be carefully guarded against. However, if the conductivity is extremely low, then ionized species that could cause charge buildup are also largely absent. Liquids with a conductivity of less than 10^{-13} S m^{-1} are considered to be in the latter category. Thus, the peak hazard involves liquids with conductivities from 10^{-13} to 5×10^{-11} S m^{-1}. Pure hydrocarbons do not exhibit electrostatic charging; however, even impurities at the 0.001 ppm level change this

Table 22.5 Electrical conductivity of common liquids [7]

Hazard	Example substances	Typical electrical conductivity (S m^{-1})
	Hexane	10^{-17}
Low:	Carbon disulfide	8×10^{-16}
Conductivity less than 10^{-13}	Benzene	5×10^{-15}
	Heptane	3×10^{-14}
	Xylene	10^{-13}
	Dioxane	10^{-13}
	Toluene	10^{-12}
High:	Cyclohexane	2×10^{-12}
Conductivity of 10^{-13}–5×10^{-11}	Styrene	10^{-11}
	Kerosene	1.5×10^{-11}
	Hexamethyldisilazane	2.9×10^{-11}
	Jet-A fuel	$2–3 \times 10^{-11}$
	Gasoline	10^{-10}
	Turpentine	4×10^{-10}
	Crude oils	10^{-9} to 10^{-7}
	Halogenated hydrocarbons	10^{-8}
Low:	Methyl alcohol	10^{-7}
Conductivity greater than 5×10^{-11}	Ethyl alcohol	1.4×10^{-7}
	Cetones	10^{-5}
	Water: deionized	10^{-5}
	Iso-propanol	10^{-4}
	Water: acid rain	10^{-2}

situation [86]. The presence of a small amount of water in the product can increase the electrostatic charging effect up to 50-fold.

For insulating liquids flowing in conducting pipes, the charge density (C m^{-3}) picked up is linearly proportional to the liquid's flow velocity, and the charge density reaches a steady-state value after a certain distance down the pipe, with the charging voltage being roughly proportional to the flow velocity. However, when liquids flow in insulating pipes, little streaming current occurs because the charge induced in the pipe walls does not get dissipated to ground. Flows that consist of two-phase liquids, liquids with suspended solids, or mixtures of immiscible liquids tend to build up higher charges than single-phase liquids. Charge buildup can especially increase if the liquid flows through a fine-pore filter.

When a low-conductivity liquid is in motion in a conducting pipe, not just separation but also an actual flow of charge occurs. This flow is called a streaming current and it arises because ions in the liquid tend to move with the flow, while the opposite charge on the wall dissipates to earth. For it to occur, the liquid must have a conductivity in the range of about 10^{-13}–10^{-7} S m^{-1}. Experimental studies [87] indicate that, for these liquids, the streaming current I (amperes) can be estimated as

$$I = 9.42 \times 10^{-6}(uD)^2$$

where u = velocity (m s^{-1}) and D = diameter (m). An empirical expression [88] for the charge density is

$$Q''' = 5 \times 10^{-7}\, u/D$$

Moisture and impurities can greatly increase the charge density, but experiments have to be set up carefully to illustrate this. The effect is not found unless the liquid is pumped through filters [89]; charge generation associated with tank-loading in the absence of filtering does not show deleterious effects of impurities. Metallic trash in tanks can act as 'charge collectors' and greatly reduce the charge density necessary to cause an electrostatic discharge [89]. The effect takes place since small metallic objects can be buoyed up by turbulence or by foaming of the product. The combination of filtering and splash loading was found to be highly conducive to discharges; removing either of the two factors greatly diminished the potential for a discharge. In low-viscosity liquids, splash loading by itself produces a charged foam in the tank which can lead to discharges even when the inflowing liquid has little charge on it.

Liquid sprays can cause intense static electrification; this was first observed near waterfalls in the nineteenth century and is called spray electrification [90]. The process occurs due to the presence of a double layer of charge at the liquid surface. Small pieces of material in the form of droplets removed from the surface can then possess an unbalanced charge. By this process, a water stream may ignite a flammable atmosphere, and this concern arises in operations, for example, where a water spray is used to clean equipment that was used to store flammable liquids.

Lightning

Electrical Characteristics

Lightning becomes possible because electric charge can become separated and accumulated in clouds. Clouds are highly complex entities and, even today, the physicochemical environment of clouds is by no means comprehensively understood. One theory by Ermakov and Stozhkov [91] is illustrated in Fig. 22.17.

Thundercloud formation begins when a cold air mass meets a warm one. Ionized, warm, moist air rises but is then progressively cooled at higher elevations and condensation of water vapor on nucleation centers begins. In the initial phase, condensation proceeds faster on negatively charged nuclei than on positive ones, and the upward air flux produces large-scale separation of charge and a resultant electric field. The latent heat released in condensation assists the buoyancy of the upward air current. Cosmic rays produce ionized showers of particles.

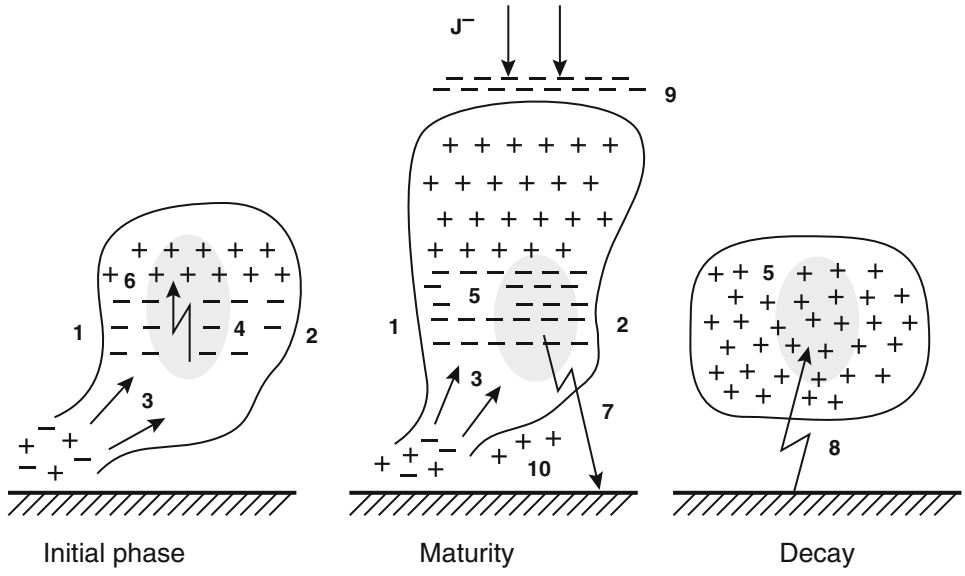

Fig. 22.17 Formation of thunderclouds as described by Ermakov and Stozhkov [91]. 1, warm air front; 2, cold air front; 3, ascending flux of wet ionized air; 4 and 5, extensive air showers produced by primaries with energies over 10^{14} eV or 10^{15} eV, respectively; 6, cloud-to-cloud lightning; 7, cloud-to-ground lightning; 8, ground-to-cloud lightning; 9, negative screen layer; 10, positive charge at cloud base; J^- current of negative ions from the ionosphere to the top of the cloud

When the electric field exceeds 0.2–0.3 MV m^{-1}, electron avalanches occur; ionized tracks link with each other and form a conducting tree structure, which allows cloud-to-cloud discharges to occur. In the mature phase, droplets grow and coagulate. There are ascending and descending airflows and the cloud becomes asymmetric with an excess of negative charge at its base. The electric field between the cloud and earth's surface increases, leading to cloud-to-ground discharges. *Thunder* is an acoustic shock wave that originates in the gas breakdown region and then propagates out through the air.

The origins of a lightning strike are due to a separation of charges in clouds. Lightning becomes possible when a potential of 10–100 MV with respect to the ground has been reached. A lightning flash is composed of several events. The actual discharge begins with the formation of the first stepped leader, which is a localized gas breakdown of about 50 m length. The process continues in a stair-step fashion until a leader gets to within about 50 m of the ground (or an object on the ground). The negative charge of the stepped leader induces a positive charge in the earth below. Protruding grounded objects start to conduct heavier point-discharge currents.

A streamer then arises from one of these objects or from the earth itself, connects to the leader, and starts a return stroke. The return stroke is the brightly visible lightning stroke. After the first return stroke, a dart leader may descend directly to the ground without stair-stepping. This dart leader is ball shaped. It will be followed by a second return stroke. There may be three or four, but occasionally many more, strokes per the total event, comprising the lightning flash. The total lightning flash may last from 0.01 to 2 s, with 0.2 to 0.4 s being typical, but each individual stroke only lasts about 30 μs. The interval between strokes may be around 40 ms.

The current carried by the stepped leader is small, only on the order of 100 A. But each return stroke will typically carry 10–20 kA of current, and peak currents in excess of 100 kA are occasionally recorded. A cloud-to-ground stroke may discharge about 25 C per stroke. The average length of a stroke is 3 km, and the average energy

released is 10^5 J m^{-1}, making an average energy release of 3×10^8 J per stroke [92].

In electrical circuit terms, a lightning stroke can be considered a constant-current source. Therefore, the energy dissipated in the object along its path is

$$\int I^2 R dt$$

where I = current (A), R = resistance (Ω), and t = time (s). This accounts for the much greater damage found for objects of poor conductivity than for metals. Design values for the current of 100–200 kA are commonly used [93] since only about 1 % of lightning strokes give currents in excess of 200 kA [92].

The current from a second or subsequent stroke is typically less than half that of the first one. When a lightning strike occurs, nearby metallic objects can have a current induced in them, including not only electrical wiring but also other metallic objects such as building beams. The electric field induced by a lightning strike of a known current value can be estimated [94] according to:

$$E = 33\frac{I}{r}$$

where E = electric field (V m^{-1}), I = current (kA), and r = distance from strike (km). Thus, for example, a strike with a current of 100 kA is expect to induce a field of 1,100 V m^{-1} at a distance of 3 km.

A *direct strike* to a building or structure is one where the ground-side termination of the lightning bolt attaches to any part of the building. A *side flash* is a strike where the lightning bolt terminates on a nearby object, but a secondary flash occurs from that locale to the building. A side flash is considered to also be a type of direct strike. An *indirect strike* is one where the main bolt terminates elsewhere, but some energy from the bolt is delivered to the building by means of power lines, metallic underground pipes, or other conductive paths.

Ignitions from Lightning

The primary damages [95] to residences from lightning are the following:

- Brick, concrete, and other solid surfaces moved or cracked
- Plumbing pipe punctures
- Holes burned or punctures in roofs
- Arc damage to metal structures such as window frames
- Arcs across wiring

The last three of these, of course, may also be accompanied by ignition of combustible materials. Because the temperature rise in an object is proportional to its resistance, a metallic object (e.g., a lightning rod) may sustain limited temperature rise, whereas a poor conductor such as wood may become ignited.

Multiple ignitions from a single strike are not rare. Whether combustibles will be ignited from a lightning flash or not depends critically on whether there is a flow of continuing current in the channel after the stroke. About 25–50 % of lightning strikes exhibit this characteristic—these are sometimes called hot bolts. Lightning strikes that are positive (i.e., the cloud being positive with respect to the ground) are much rarer than the converse, but these are precisely the ones that are most likely to cause ignitions, since their peak currents and total charge transfer are much larger. Positive flashes do not have the stepped-leader characteristic of the common, negative strikes, and consist of a single stroke, followed by a period of continuing current flow.

The probability [96] of igniting a house fire from a lightning strike is much higher if the house has plastic plumbing pipes as opposed to metallic ones. This is because the lightning current may flow to ground through a metallic pipe network, but if electric wiring is the only substantive metallic path, the current is likely to go through electric wiring, where heating will be much greater due to the smaller area of the conductors.

Safety Measures Against Lightning

The lightning rod was invented by Benjamin Franklin in 1752. This is a metallic rod which is grounded at one end and raised in the air at the other. When the initial streamers from the cloud start to form, there is not a highly specific place along the ground level where the initial return stroke is preferentially located. By providing a ground-potential conductor in the air, a preference is established, and the lightning current flows down the rod (which must be of adequate dimension in order not to overheat).

Franklin recommended that the tip of the rod (*air terminal*, in the jargon of the lightning protection industry) be pointed, because this leads to a point discharge. In earlier times, this point discharge (corona discharge) was considered necessary to 'attract' the lightning stroke. More recently, experiments showed that a smoothly rounded tip is more successful in attracting lightning to itself and avoid strikes to nearby objects [97]. The first comprehensive engineering guide to proper installation of lightning protection systems was published by Anderson [98] in 1879 and, perhaps surprisingly, few of his recommendations have been overturned by more modern research. Müller-Hillebrand [99] reviewed some of the early concepts of lightning protection.

A lightning protection system basically comprises three main components:

- air terminals
- downconductors
- ground terminals.

Franklin recommended that each air terminal provides a downward 'cone of protection,' with the cone's angle from vertical being 58°. The origin of this recommendation is unclear and it was evidently not evolved from experiments. Subsequent experience suggested that this angle is much too large, and during the nineteenth century the recommendations slowly went downward to about 30°. However, even using a 30° angle of protection, failures were documented [100]. In more recent times, Lee [100] synthesized a design method for protecting buildings, evolved from advanced calculations used by electric utilities for protection of power lines. The method is applicable only to structures of 45 m height or less and is described in the following way: Imagine a rolling sphere of 45 m radius (Fig. 22.18). The sphere starts rolling along the ground from a distance far away from the structure in question, then roll up to and over the structure and its protective air terminal(s). If the sphere only ends up touching the air terminal(s) and the ground and cannot come into contact with the structure to be protected, then air terminals of sufficient height and quantity have been erected, otherwise additional protection is needed. This more realistic protection concept is more liberal than the 30° fixed-angle scheme for low structures and more conservative for high structures. The 45 m dimension is used because it corresponds to the typical length of the stepped leader, which is about 50 m.

In view of the enormous currents of around 20,000 A that are involved in a lightning strike, it is perhaps surprising that gigantic-size

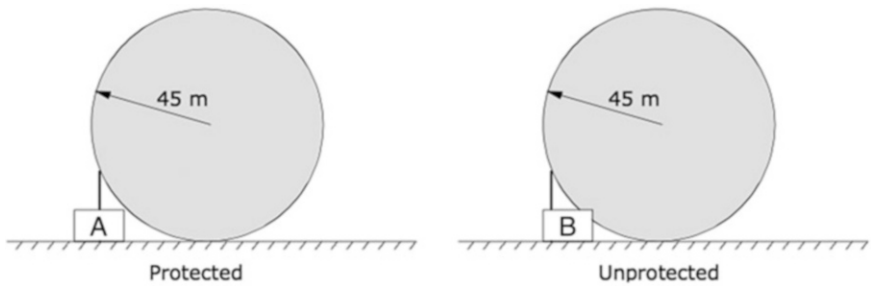

Fig. 22.18 Sphere of protection from an air terminal: structure A is protected, structure B is not

downconductors are not required to safely conduct the electricity. The minimum size of conductor does not need to be huge since the flow of current is so brief—much less than 1 s—and heating is proportional to the time of current flow. The simplest model that can predict this is the adiabatic lumped-capacitance model:

$$W = I^2Rt = \rho C_p V\left(T_f - T_o\right)$$

where W = energy (J) flowing into a piece of metal, I = current (A), R = resistance (Ω), t = time (s), ρ = density (kg m^{-3}), C_p = heat capacity (J kg^{-1} K^{-1}), V = volume (m^3), T_f = final temperature (°C), and T_o = initial temperature (°C). This assumes that the current flow is constant over the time t; if the current flow is varying, then the expression becomes:

$$W = R\int I^2 dt = \rho C_p V\left(T_f - T_o\right)$$

where R is assumed to be time-invariant and has been taken outside the integral. Applying the above relation to copper wire, ρ = 8,890 kg m^{-3}, C_p = 385 J kg^{-1} K^{-1}, $V = A \cdot L$, where A = cross-sectional area (mm) and L = length (m). The resistance of a copper wire can be expressed as:

$$R = \rho_e \frac{L}{A}$$

where ρ_e = electrical resistivity of copper = $1.7241 \times 10^{-8}\ \Omega \cdot \mathrm{m}$. The initial temperature T_o can be taken as 20 °C, while the final (allowable) temperature T_f must be set to some reasonable value below the melting point. Since the downconductor may come into contact with combustibles such as dry leaves, it seems appropriate to limit T_f to 200 °C. Based on studies of lightning discharges, $\int I^2 dt = 5 \times 10^6\ \mathrm{A}^2 \cdot \mathrm{s}$ is commonly used. The equation can then be evaluated as:

$$1.7241 \times 10^{-8}\left(\frac{L}{A}\right) \cdot 5 \times 10^6 = 8890 \times 385\,(A \cdot L)180$$

and it can be noted that the actual length of the wire sensibly cancels out of the equation. This gives $A^2 = 1.4 \times 10^{-10}\,\mathrm{m}^4$, or $A = 1.18 \times 10^{-5}\,\mathrm{m}^2 = 11.8\ \mathrm{mm}^2$. If the temperature criterion were the melting point of copper (1,083 °C), then A = 4.9 mm^2, using the same 'action integral' of $5 \times 10^6\ \mathrm{A}^2 \cdot \mathrm{s}$.

In US practice, however, a more conservative approach is taken, with conductor areas being greater than 11.8 mm^2, in order to allow for mechanical damage, some unusually potent lightning strikes, etc. The most commonly followed guidance is that published by NFPA [101]. NFPA 780 divides structures into two Classes, Class I being those up to 75 ft (22.9 m), with Class II being those higher. For Class I structures, the required downconductor area is 29 mm^2 for copper and 50 mm^2 for aluminum. The cross-sectional area required for copper conductors in Class II service is 2× that for Class I. Generally, stranded or braided conductors are used, to minimize loss of current-carrying capacity due to skin effect (this electromagnetic effect pertains to transient current flows and leads to current flowing disproportionately near the surface). A lead coating is often used to minimize loss of metal due to corrosion from flue gases. Properly-installed and maintained lightning protection systems are highly effective, with one report [102] quoting old US studies giving 99.3 % and 99.9 % effectiveness values.

For configuration of the air terminal, modern studies by Moore et al. [103] concluded that the optimum tip-height to tip-radius ratio is about 680. Thus, a rod erected at 10 m height ought to have a tip of 14.7 mm radius.

Ignition and Values of Voltage, Current, or Power

Are there minimum values of voltage, current, or power that must be exceeded for ignition to be possible? Sometimes the stance is taken that, under certain circumstances, an energized electrical device cannot be the source of a fire.

This stance is usually couched in terms of power but has also been couched in terms of current or voltage. For example, some authors [104] claim that ignition is not possible for devices that cannot consume more than 20 W. Certain UL standards [105] consider the limit to be 15 W. A more conservative view [106] is "several watts." Such a limit would be attractive in that it can simplify such standards, but there does not exist a research basis that would support these notions.

Instead, research findings indicate that minuscule values may suffice, ones that are so low as to not form a useful criterion. For example, some flammable gas mixtures can be ignited by arcing from a resistive circuit having only 4–5 V, whereas in inductive circuits, a 0.5 V power supply may suffice [7]. In terms of power, it has been documented that breaking an 0.95 W incandescent lamp can suffice to cause an explosion of a methane/air mixture, whereas a broken 3 W lamp can cause an explosion of coal dust in air [107].

Although solids are generally harder to ignite than gases or dust clouds, very limited testing indicates that exceedingly low values can also suffice for solids. For example, a Dacron comforter was ignited from a 6 W night-light lamp, bamboo decorations from a 25 W lamp, and cellulose attic insulation from a 50 W lamp [7]. Notebook paper was ignited [7] from a resistor rated at 1/8 W that was dissipating 1.25 W at the time. Power values associated with arc-tracking ignitions have rarely been explored, but in one study it was found that 4.8 W sufficed to ignite PBT plastic [108]. This should be interpreted in the context that PBT is one of the more arc-tracking resistant plastics and plastics more prone to arc-tracking (such as PVC) would presumably require less.

Finally, it must be noted that the values cited above are values that sufficed to cause an ignition or explosion during limited testing. These values are not intended to imply lower-value limits. Ignitions, in fact, may occur under conditions or regimes not encompassed in the research that has been published to date.

Electrical Explosions

Most explosions in which electricity plays a role can be grouped into three categories:

1. Pure arc explosions
2. Pure fuel explosions
3. Mixed mode explosions.

In a pure electrical arc explosion, the main source of explosion energy is the arc itself. Combustion, i.e., oxidation, plays only a modest role, if any. In the case of copper or steel conductors, oxidation is generally negligible, while in the case of aluminum conductors some of the exothermicity comes from oxidation of the aluminum.

For such explosions to be damaging, significant arc power is normally required. Thus pure arc explosions are mostly of interest in high voltage transmission and distribution equipment, in industrial facilities, or in commercial installations where significant short-circuit currents are available.

Pure fuel explosions are ones where the only role of electricity is to provide a spark or a low-energy arc, with the explosion energy corresponding to burning of fuel. The most common example is spark from an electrical switch causing an explosion in a house which filled with natural gas. This category also includes electrically initiated explosions of solid or liquid explosives, for example, by use of an exploding bridgewire. Pure fuel explosions are treated in depth in the *Ignition Handbook* [7] but are outside the scope of this Chapter. In addition, there are numerous monographs which discuss the physical, chemical, or civil engineering aspects of explosions of all types [109–113].

Mixed mode explosions are explosions which are initiated by an electric spark, arc, or hot surface, and where the fuel was delivered due to an electrical fault. The best known mixed mode explosions are explosions of oil-filled transformers and explosions of underground electric distribution cables, including manhole explosions. In these explosions, an electrical fault gasifies the dielectric liquid or solid,

which is then ignited by a localized source of energy. Mixed mode explosions are also experienced when lead-acid batteries explode and in other cases of adventitious generation of hydrogen. In recent years, explosions of residential dishwashers have been identified as an additional example of mixed mode explosions. (Explosions in a purposive hydrogen-production facility initiated by an electric spark are categorized as pure fuel explosions, since an electric fault does not play a role in generating the fuel.)

Basic Phenomena

Electric arc explosions involve complicated phenomena, and none of the standard monographs on explosions cover this specialized topic. The only review of the topic has been by Babrauskas [114], and here some of the main findings will be summarized.

Electric arcing in circuits with sizable maximum short-circuit current capacity can be a highly energetic effect. In fact, buildings have collapsed due to arc pressure, since in an enclosed space some surprisingly large pressures can be built up. For instance, in one test explosion overpressures of 83 atm were obtained. The magnitude of this can best be appreciated by considering that a fuel-air deflagration will typically attain only around 7–8 atm, barring pressure-piling effects or other turbulence enhancements. During normal operation of a circuit breaker, arc pressures of roughly 3 atm magnitude can be expected [115], but these devices are designed to sustain the pressures generated by the normal arcing associated with circuit opening.

Arc explosions are not rare in industry, and in other situations where 480 V, or higher, voltages are utilized, but published case histories are scarce. Neither of the two large electrical accident compilations [116, 117] mentions the subject. Lee [118] published four brief case histories, Crawford et al. [119] documented seven case histories of arc explosions inside motor terminal boxes, including one fatality, while Heberlein et al. [120] described two non-fatal explosions inside motor control centers. The best-known incident was in an Atlanta high-rise building that took place on 30 June 1989. The fumbling of an electrician replacing a fuse caused a 480 VAC bus duct explosion [121] and the explosion and subsequent fire led to five fatalities.

Lightning strikes can lead to arc explosions in any type of premises. In 1773, Lind demonstrated that if a conductor from a lightning arrester is run down through a house, but with a small gap in this conductor, this can form a spark gap and a strike to the arrester can result in an arc explosion capable of destroying the house [122]. Individuals have been bodily knocked over when in proximity both to electrical fault arcs and lightning strikes, although interestingly often there have been negligible injuries to the individual knocked over [123]. But in cases where roofs collapse, the outcome may be traumatic if persons are present underneath.

Eardrum rupture can be expected at explosion overpressures of 19 kPa (10 % probability) or 45 kPa (50 % probability), while death due to lung damage is 120 kPa (10 % probability) or 141 kPa (50 % probability). The above values come from an extensive statistical study by Eisenberg et al. [124]; older data are somewhat different, but not greatly. In any case, they indicate that it does not take large overpressures for injury or death to result from explosion pressures.

An arc explosion arises due a very rapid heating of air or other medium. In the process, electrical energy is converted into other forms of energy: dissociation, ionization, and heating of the gas, including its compression; thermal radiation; and conduction losses into adjacent solids such as electrodes.

In addition, some electrode metal is vaporized and this contributes to the total volume which is being explosively heated, yet, the role of chemical reactions has only recently been explored. When an arc breakdown is initiated, energy gets deposited into the arc channel at a rate much greater than can be removed from the area by the shock wave that is created. This causes a rapid pressure rise and, if the arc energy is sufficiently high, this will be perceived as an explosion.

For a low-energy arc, the perceived sound may simple be a 'snap,' 'crackle,' or 'pop.' But within the scientific community there is not an agreed-upon, quantitative definition of the term 'explosion,' nor are there studies to quantify the fraction of the arc energy that gets delivered as sound energy, i.e., vibrations in the 20–20 kHz range.

In an open environment, arc pressures will rarely be highly destructive. Theoretical modeling suggests that very high pressures may be created, but experimental studies do not bear this out, which only show overpressures below about 10 kPa. However, if arc explosions occur within enclosures which are sealed, or nearly so, then, as mentioned above, huge overpressures may be found.

Electric arc explosions are not combustion phenomena—they are predominantly physical explosions, due to very rapid conversion of electrical energy into heat. Chemical reactions play a role, but only a supporting role, in such explosions. Recent studies suggest that chemical reactions are mainly ones which convert air to species such as O_3 and NO_x. While these may comprise oxidation, they are very different from a fuel-air explosion of a normal sort. Some of the electrode metal is also vaporized in an arc explosion, and arc temperatures are high enough so that presumably much of this metal vapor may get oxidized. However, the electrode oxidation effect is quantitatively only a small part of the heat balance in an arc explosion. Thus, first-order estimates of arc explosions treat the process solely as converting electrical energy to heat and ignore chemical reaction contributions.

Shock Waves from Electric Arcs

If in a gaseous medium there is an abrupt change in pressure, temperature, or volume created at some location, a wave will be generated which will propagate through the medium. The wave can be a sound wave, a shock wave, or both, depending on the characteristics of the source. In the case of an electric arc, while a shock wave will be generated and it is audibly perceived as an explosion (unless of very small scale), the shock wave does not constitute a detonation, which would require that the shock wave be supported by an exothermic reaction occurring behind the shock front. For subsonic sound waves in air, the decay in pressure with distance from the source goes as $1/\sqrt{r}$ for the infinite-cylinder geometry and $1/r$ for the sphere. But for shock waves, these simple wave-equation relationships are not applicable.

A reasonably short arc will be represented by a short cylinder, but this is not a geometry that lends itself to simple theoretical solutions. Baker presented calculated data on a point sources [125], along with experimental data on bursting explosions of short cylindrical vessels and spherical vessels. His results showed that, unless only examined over small intervals, the actual relationship is not even of a power-law type.

In an electric arc, when breakdown is initiated, a narrow conducting filament first bridges the gap, and then grows rapidly in diameter until it reaches an ultimate value and the 'arc channel' is fully established. In the course of this, there are two disturbances that a propagated: a sound wave propagating at the speed of sound and a shock wave propagating at two or three times that.

Flowers [126] made detailed measurements and found velocities of 1,000–2,000 m s^{-1} for the radial expansion of the arc channel; these are well above the 340 m s^{-1} of sound speed, indicating that shock waves are being generated in all cases. The arc channel eventually reaches a steady-state diameter and no longer expands, and Flowers found that a time of 3–35 μs was required for the final diameter to be attained in his experiments, but the actual value is dependent on external circuit parameters which limit the current growth rate.

When the final diameter is achieved, Flowers found that the arc channel cross-sectional area is linearly proportional to the current, with the proportionality being 11 A mm^{-2}. Later Vanyukov et al. showed that the expanding shock front and the channel are initially of the same diameter, but subsequently the channel typically approaches a maximum diameter, while the shock front continues expanding outwards

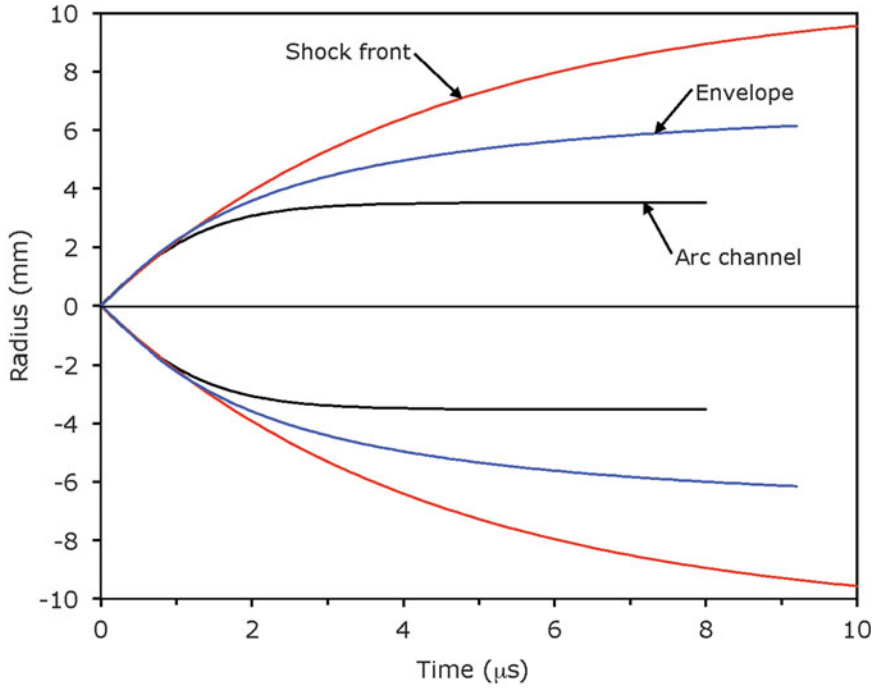

Fig. 22.19 Results of Vanyukov et al. on the expansion of the arc channel and growth of the shock wave

[127] (Fig. 22.19). Intermediate between these is the 'envelope,' which is the boundary between compressed gas (outside the boundary) and rarefied gas (inside). In some cases, however, arc channel diameter growth continues for a protracted period, especially at higher current values [128].

Pressures from Arcs in the Open

Baker [125] treated arc explosions in the open using results from acoustical theory. The pressure rise $\Delta p = (p_1 - p_o)$ is assumed to be due to the arc effectively generating a certain volume V of air at the ambient density ρ_o. Then from acoustical theory, the pressure rise at any particular distance r (m) from the arc is:

$$\Delta p = \frac{\gamma - 1}{\gamma} \frac{\dot{P}}{4\pi r p_o}$$

where $\dot{P}$ = first derivative of electrical power developed in the arc (W s^{-1}), and γ is defined as: $\gamma = c_p/c_v$. Air can assumed to be an ideal diatomic gas, giving $\gamma = 7/5 = 1.4$. This equation predicts that the pressure rise will vary linearly with $\dot{P}$ and decrease with distance proportionally to $1/r$.

The only extensive series of experiments available to examine the relationship between $\dot{P}$ and the pressure rise has been that of Drouet and Nadeau [129]. Unfortunately Fig. 22.20 suggests that there was a systematic error in the measurements. The slightly different than expected slope for long arcs could well be due to a limitation of theory, but the short-arc results are most likely erroneous, not only because they have a dissimilar slope, but mainly because they imply that in excess of 100 % of the power of the arc is realized as compression of air.

Pressures from Arcs in an Enclosure

If an arc discharge occurs within an enclosure which is of modest size, then the whole enclosure will get measurably pressurized. In addition, of course, there will be local shock wave propagation,

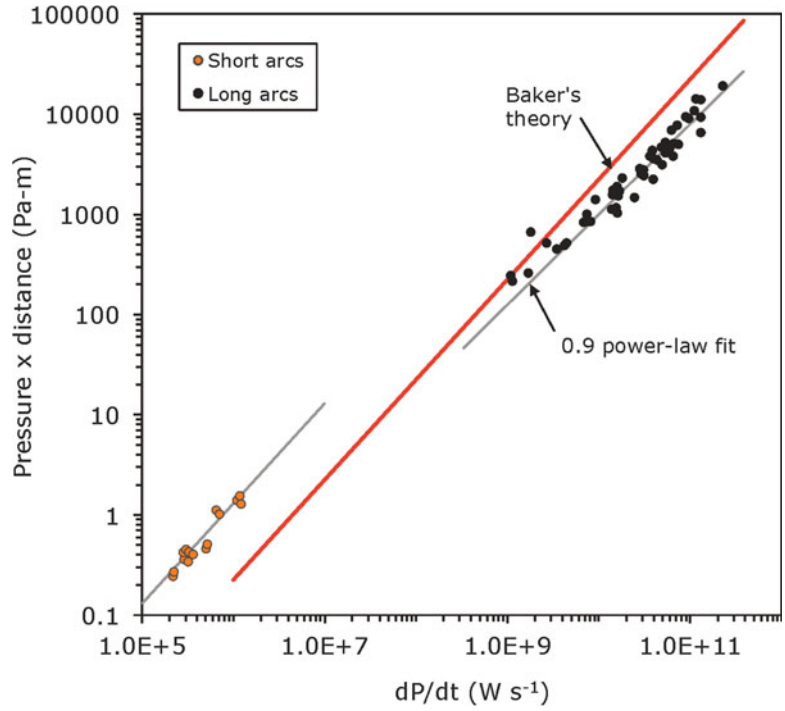

Fig. 22.20 The results of Drouet and Nadeau compared to Baker's theory

and also reflections of shock waves from compartment walls. Modeling such details in the system would require numerical calculations. But, for many practical purposes, what is of most interest is the peak, quasi-steady overpressure that is achieved, and this can be approximated in a simple way. Neglecting all transient and hydrodynamic effects, the discharge of an arc in a single, closed compartment can be treated as an ideal gas within a isolated, isochoric (constant volume) system. If an amount of heat or energy ΔW is injected into the volume, the change in pressure Δp is [130]:

$$\Delta p = \frac{R}{Mc_v}\frac{\Delta W}{V}$$

where M = molar mass, R = universal gas constant = 8.314 J mol^{-1} K^{-1}, and c_v constant-volume heat capacity (J kg^{-1} K^{-1}). Using the relations between c_v, c_p, and γ, the relation is more usefully written as:

$$\Delta p = (\gamma - 1)\frac{\Delta W}{V}$$

This shows that, all else being equal, the overpressure is inversely proportional to the volume. Consistent with the theoretical prediction, when using very small enclosures and large arc currents, some exceedingly large pressures can be obtained. Graneau [122] conducted experiments in a tiny cubical cavity, 12.7 mm on a side (2×10^{-6} m^3), with the electrode gap also being 12.7 mm. For a spark discharge of 40 kV and a peak current of 38 kA, he measured an average pressure of 409 atm in the cavity, with even higher pressures during the peak of the discharge. Baldrey and Hudson [131] conducted tests within a small pressure vessel and got an overpressure of 83 atm in the worst case. Numerous other studies have also been published [114].

The analysis is complicated since not all of the electrical energy delivered actually goes into heating the gas. Conversely, in the case of aluminum electrodes, an additional energy term comes from the combustion of the aluminum. Thus, because of differing experimental conditions, published results tend to lack generality. An additional complication is that many studies were done not on fully sealed enclosures, but on ones with certain small openings. This makes the results highly dependent on the specifics of the geometry.

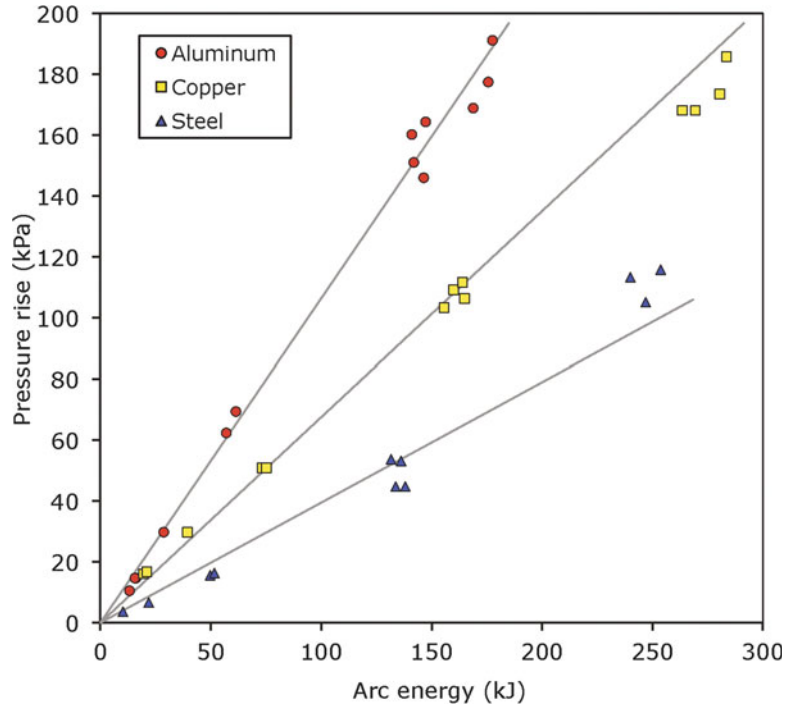

Fig. 22.21 Arc pressure rise, as function of electrode material, measured by Tanaka et al. in an 0.32 m^3 enclosure for 0.1 s duration AC arcs

In addition, many studies were at very low overpressures. Such results are more readily amenable to analysis, but do not necessarily reflect on more damaging explosion incidents. An example of results where at least moderately high overpressures were achieved is the study of Tanaka et al [132]. Figure 22.21 shows their results obtained for AC arcs of fixed 0.1 s duration. The higher values obtained for aluminum electrodes reflect the contribution of the combustion of electrode metal.

Efforts have been made to use commercial CFD codes for computing pressure rises in enclosures, but the validity of such efforts has been problematic. Capelli-Schellpfeffer et al. published two CFD modeling studies intended to simulate an experimental arc fault in 480 VAC switchgear in which an arc energy of 20 kJ was delivered and a peak overpressure of 2.6 atm was measured [133]. In the first study [133], a peak of 0.2 atm was computed, while in the second [134] a peak of 16,000 atm was predicted. Interestingly, the same 20 kJ value of arc energy was used by Caillard et al. [135] but in a capacitive discharge circuit and they predicted a peak overpressure of 1,700 atm while measuring a peak of 0.26 atm. Other researchers [136] obtained reasonable agreement, but only by using a custom-designed CFD code.

Summary

Fires arising due to static electricity or electric current can be difficult to understand for the nonspecialist because, apart from fire science, the separate discipline of electrical science is invoked. Partly because of this discipline-straddling nature of the phenomenon, research has not been as vigorously pursued as in some other aspects of fire science. But at the present time, the fundamentals have been well enough established that general guidance can be given. The ways by which the "heat" leg of the fire triangle is produced in electrical fires has been outlined in this chapter. The most highly specialized of these mechanisms is the electrical arc, and its characteristics have been reviewed in this chapter. Electric arc explosions are a highly specialized phenomenon and are primarily physical explosion, rather than chemical, although some chemical reactions may occur.

Nomenclature

A	Area (m^2)
C	Capacitance (F)
C_p	Heat capacity, constant-pressure ($J\ kg^{-1}\ K^{-1}$)
C_v	Heat capacity, constant-volume ($J\ kg^{-1}\ K^{-1}$)
c_1	Constant (-)
c_2	Constant (-)
D	Diameter (m)
d	Distance (m)
d_1	Clearance distance (m)
d_2	Creepage distance (m)
e	Charge of the electron (C)
E	Electric field ($V\ m^{-1}$)
h	Heat transfer coefficient ($W\ m^{-2}\ K^{-1}$)
I	Current (A)
L	Distance (m)
M	Molar mass (kg/mol)
p	Pressure (Pa)
P	Power (W)
$\dot{P}$	First derivative of electrical power ($W\ s^{-1}$)
q''	Power density ($W\ m^{-2}$)
Q	Charge (C)
Q'''	Charge density ($C\ m^{-3}$)
r	Radius (m)
R	Resistance (W)
R	Universal gas constant (8.314 $J\ mol^{-1}\ K^{-1}$)
t	Time (s)
T	Temperature (K)
u	Velocity ($m\ s^{-1}$)
V	Potential difference ("voltage"; V)
V	Volume (m^3)
W	Energy (J)
α	Townsend's first ionization coefficient, (m^{-1})
ε	Dielectric constant (–)
ε_o	Permittivity of vacuum ($S\ s\ m^{-1}$)
γ	Ratio C_p/C_v (—)
γ	Incomplete gamma function (–)
γ	Townsend's second ionization coefficient (-)
λ	Thermal conductivity ($W\ m^{-1}\ K^{-1}$)
ρ	Density ($kg\ m^{-3}$)
ρ_e	Electrical resistivity of copper ($\Omega \cdot m$)
σ	Charge density ($C\ m^{-2}$)
τ	Time constant (s)

References

1. J.A. Frank, "Characteristics and Hazards of Water and Water Additives for Fire Suppression," in *Fire Protection Handbook,* 19th ed., National Fire Protection Association, Quincy MA, pp. 10-12–10-15 (2003).
2. J.F. Casey, "Handling Utility Fires," in *The Fire Chief's Handbook,* 4th ed., Technical Publishing Co., New York, pp. 264–270 (1978); note that this material does not appear in more recent editions of the handbook.
3. T. Verlo, "The Use of Water as an Extinguishing Agent for Live Electrical Installations" (Report EFI TR A3866), SINTEF EFI, Trondheim, Norway (1991).
4. Babrauskas, V., How Do Electrical Wiring Faults Lead to Structure Ignitions? *Fire and Arson Investigator* **52**:3, 39–45, 49 (Apr. 2002).
5. Babrauskas V., Research on Electrical Fires: The State of the Art (The Emmons Plenary Lecture), pp. 3–18 in *Fire Safety Science—Proc. 9th Intl. Symp.*, Intl. Assn. for Fire Safety Science, London (2009).
6. Babrauskas, V., Electrical Fires: Research Needed to Improve Fire Safety, *Fire Protection Engineering* No. 46, 20–22, 24–26, 28–30 (2nd Q. 2010).
7. V. Babrauskas, *Ignition Handbook,* Fire Science Publishers/Society of Fire Protection Engineers, Issaquah, WA (2003)
8. Somerville, J. M., **The Electric Arc**, Methuen, London (1959).
9. Uman, M. A., **Lightning**, Dover Publications, New York (1984).
10. Braginskii, S. I., Theory of the Development of a Spark Channel, pp. 188–200 in **Electrical Breakdown in Gases**, J. A. Rees, ed., MacMillan, London (1973).
11. Paschen, F., Über die zum Funkenübergang in Luft, Wasserstoff und Kohlensäure bei verschiedenen Drucken erforderliche Potentialdifferenz [On the Required Potential Difference for Spark Discharges in Air, Hydrogen, and Carbon Dioxide at Various Pressures], *Annalen der Physik* **37**, 69–96 (1889).
12. T.W. Dakin et al., "Breakdown of Gases in Uniform Fields—Paschen Curves for Nitrogen, Air, and Sulfur Hexafluoride," *Electra* (CIGRE, Paris), 32, pp. 61–82 (Jan. 1974).
13. T.W. Dakin, "Insulating Materials—General Properties," in *Standard Handbook for Electrical Engineers,* 13th ed. (D.G. Fink and H.W. Beaty, eds.), McGraw-Hill, New York, pp. 4-117–4-160 (1993).

14. A.E.W. Austen and S. Whitehead, "The Electric Strength of Some Solid Dielectrics," in *Proceedings Royal Society A,* 176, pp. 33–49 (1940).
15. A.B. Lewis, E.L. Hall, and F.R. Caldwell, "Some Electrical Properties of Micas," *Journal of Research NBS,* 7, pp. 403–418 (1931).
16. Y. Abed, "Experimental and Digital Determination of Breakdown Voltage of Different Synthetic Insulating Materials," in *Conference Record of the 1982 I.E. International Symposium on Electrical Insulation,* IEEE, New York, pp. 123–126 (1982).
17. J.H. Mason, "Breakdown of Solid Dielectrics in Divergent Fields," *IEE Proceedings,* 102C, pp. 254–263 (1955).
18. A.E.W. Austen and H. Pelzer, "The Electric Strength of Paraffins and Some High Polymers," *Journal of IEE,* 93, pp. 525–532 (1946).
19. V. Babrauskas, "Mechanisms and Modes for Ignition of Low-Voltage, PVC-Insulated Electrotechnical Products," *Fire & Materials* (2005).
20. J.D. Cobine, *Gaseous Conductors: Theory and Engineering Applications,* Dover, New York (1958).
21. L. West and D.A. Reiter, "Full-Scale Arc Mapping Tests," in *Fire & Materials 2005,* Interscience Communications Ltd., London, pp. 325–339 (2005).
22. Guide for Performing Arc-Flash Hazard Calculations (IEEE Std 1584), IEEE, New York, 2002.
23. Standard for Performance Specification for Flame Resistant Textile Materials for Wearing Apparel for Use by Electrical Workers Exposed to Momentary Electric Arc and Related Thermal Hazards (ASTM F 1506), ASTM, West Conshohocken, PA, 2012.
24. Standard Test Method for Determining the Arc Thermal Performance Value of Materials for Clothing (ASTM F 1959), ASTM, West Conshohocken, PA, 2006.
25. T. Bernstein, "Electrical Fires: Causes, Prevention, and Investigation," in *Electrical Hazards and Accidents: Their Cause and Prevention* (E.K. Greenwald, ed.), Van Nostrand Reinhold, New York, pp. 116–134 (1991).
26. J. Engel, M. Walz, and J. McCormick, "Arc Fault Circuit Interrupters," *Third Joint FAA/DoD/NASA Conference on Aging Aircraft,* Albuquerque, NM (1999).
27. T. Bernstein, "Electrocution and Fires Involving 120/240-V Appliances," *IEEE Transactions on Industry Applications,* IA-19, pp. 155–159 (1983).
28. G. Gregory, "AFCIs Target Residential Electrical Fires," *NFPA Journal,* 94, pp. 69–71 (Mar./Apr. 2000).
29. A.C. Eberhardt, "Testing and Performance of Line Interrupters in Structure Fires," presented at Defense Research Institute, Product Liability Conference, New Orleans (2004).
30. S. Nakamura, H. Kaneda, M. Ieda, and G. Sawa, "Correlation between Resistance to Tracking and Energy of Scintillation Discharge for Polyvinylchloride Doped with Aluminium Hydroxide and Aluminium Oxide," in *4th International Conference on Dielectric Materials, Measurements and Applications,* IEEE, New York, pp. 295–298 (1984).
31. N. Yoshimura, M. Nishida, and F. Noto, "Light Emission from Tracking Discharges on Organic Insulation," *IEEE Transactions on Electrical Insulation,* EI-19, pp. 149–155 (1984).
32. K. Oba, "Identification of Melting Marks of Electric Wires" (unpublished report), Yamagata Prefecture Police Headquarters, Criminal Scientific Laboratory, Japan (1980).
33. T. Bernstein, "Electrical Fires: Causes, Prevention, and Investigation," in *Electrical Hazards and Accidents: Their Cause and Prevention* (E.K. Greenwald, ed.), Van Nostrand Reinhold, New York, pp. 116–134 (1991).
34. M.J. Billings, A. Smith, and R. Wilkins, "Tracking in Polymeric Insulation," *IEEE Transactions on Electrical Insulation,* IE-2, pp. 131–137 (Dec. 1967).
35. K.N. Mathes and E.J. McGowan, "Electrical Insulation Tracking—A Design-Engineering Problem," *Electro-Technology (New York),* 69, 4, pp. 146–151 (1962).
36. R.S. Norman and A.A. Kessel, "Internal Oxidation Mechanism for Nontracking Organic Insulation," *AIEE Transactions,* 77, p. 632 (1958).
37. F. Noto and K. Kawamura, "Tracking and Ignition Phenomena of Polyvinyl Chloride Resin under Wet Polluted Conditions," *IEEE Transactions on Electrical Insulation,* EI-13, pp. 418–425 (1978).
38. R. Wilkins and M.J. Billings, "Effect of Discharges between Electrodes on the Surface of Organic Insulation," *Proceedings IEE,* 116, pp. 1777–1784 (1969).
39. *Standard Dictionary of Electrical and Electronics Terms,* IEEE, New York (1998).
40. J.L. Ferrino, "An Investigation of Fire Phenomena in Residential Electrical Wiring and Connections," M.S. thesis, University of Maryland, College Park, MD (2002).
41. M. Goodson, T. Perryman, and K. Colwell, "Effects of Polyurethane Foam Systems on Wiring Ampacity," *Fire & Arson Investigator,* 52, 4, pp. 47–50 (July 2002).
42. B. Béland, "Fires of Electrical Origin," *Fire & Arson Investigator,* 43, pp. 35–41 (Dec. 1992).
43. K. Kinoshita, T. Hagiwara, and J. Kinbara, "Ignitability of VVF Cable in Contact with Grounded Object," *Journal of the Japanese Association of Fire Science and Engineering,* 28, 3, pp. 30–37 (1978).
44. U.S. Consumer Product Safety Commission Staff Report on the Beverly Hills Supper Club Fire of May 28, 1977, CPSC, Washington [n.d.].
45. M. Goodson, D. Sneed, and M. Keller, "Electrically Induced Fuel Gas Fires," *Fire & Arson Investigator,* 49, 4, pp. 10–12 (1999).

46. Rousseau, A., Validation of Installation Methods for CSST Gas Piping to Mitigate Lightning Related Damage - Phase 1, Prepared by SIFTIM, Fire Protection Research Foundation, Quincy MA (2011).
47. B. Béland, "Some Fires of Electrical Origin," *Fire & Arson Investigator,* 37, 2, pp. 37–38 (Dec. 1986).
48. K.F. Davis, "Building Fires Attributed to Be Caused by Electrical Wiring Faults," in *Proceedings of the 27th International Conference on Fire Safety,* Product Safety Corp., Sissonville, WV, pp. 101–110 (1999).
49. NFPA 70, *National Electrical Code,* National Fire Protection Association, Quincy, MA, 2014.
50. P. Cushing, "BX Cable and Fire Cause Determination," *Fire Engineering,* 153, p. 46 (July 2000).
51. S. Turkel, "In Search of Transients," *EC&M,* 99, 16, p. 18 (Oct. 2000).
52. T. Kuroyanagi, S. Inoue, and H. Suzuki, "Glowing Phenomena of Copper and Copper Materials and Their Electrical Characteristics," *Copper Promotion Technical Research Group Journal,* 20, pp. 198–204 (1981).
53. O. Keski-Rahkonen and J. Mangs, "Electrical Ignition Sources in NPPs: Statistical, Modelling, and Experimental Studies," International Atomic Energy Agency, Technical Committee Meeting on "Fire Experience in NPPs and Lessons Learned" (J7-TC-2001.7), Vienna (July 9–13, 2001).
54. M. Abramovitz and I.A. Stegun, *Handbook of Mathematical Functions* (AMS55), NBS, Gaithersburg, MD (1964).
55. Wilson, C., McIntosh, G., and Timsit, R. S., Contact Spot Temperature and the Temperature of External Surfaces in an Electrical Connection, *Proc. ICEC-ICREPEC2012 – Joint Conf. of the 26th Intl. Conf. on Electrical Contacts and 4th Intl. Conf. on Reliability of Electrical Products and Electric Contacts*, Beijing, China (2012).
56. W.J. Meese and R.W. Beausoliel, "Exploratory Study of Glowing Electrical Connections" (NBS BSS 103), NBS, Gaithersburg, MD (1977).
57. D. Newbury and S. Greenwald, "Observations on the Mechanisms of High Resistance Junction Formation in Aluminum Wire Connections," *Journal of Research NBS,* 85, pp. 429–440 (1980).
58. Shea, J. J., Glowing Contact Physics, pp. 48–57 in *52nd IEEE Holm Conference on Electrical Contacts,* IEEE, New York (2006).
59. "Tests of Insulating Materials for Resistance to Heat and Fire," Report of CEE Working Group "Hot Mandrel Test," CEE (031) D126/61, Deutsches Komitee der CEE beim Verband Deutscher Elektrotechniker, Frankfurt am Main (1961).
60. T. Kawase, "The Breeding Process of Cu_2O," *IAEI News,* 47, pp. 24–25 (July/Aug. 1975); Second Report, 49, pp. 45–46 (Nov./Dec. 1977).
61. Y. Hagimoto, K. Kinoshita, and T. Hagiwara, "Phenomenon of Glow at the Electrical Contacts of Copper Wires," *National Research Institute of Police Science Reports—Research on Forensic Science,* 41, pp. 30–37 (Aug. 1988).
62. J. Aronstein, "Fire Due to Overheating Aluminum-Wired Branch Circuit Connections," Wright Malta Corp., Ballston Spa NY (1983).
63. Guest, P. G., Static Electricity in Nature and Industry (Bulletin 368), Bureau of Mines, US Government Printing Office, Washington (1933).
64. Lüttgens, G., and Glor, M., **Understanding and Controlling Static Electricity**, Expert Verlag, Ehningen (1989).
65. Pratt, T. M., Electrostatic Initiation of Explosions in Dusts, *Cereal Foods World* **23**, 601–605 (1978).
66. L.B. Loeb, "Static Electrification-I," in *Progress in Dielectrics,* vol. 4, Academic, New York, pp. 249–309 (1962).
67. E.M. Cohn and P.G. Guest, "Influence of Humidity upon the Resistivity of Solid Dielectrics and upon the Dissipation of Static Electricity" (IC 7286), Bureau of Mines, Pittsburgh (1944).
68. Britton, L. G., **Avoiding Static Ignition Hazards in Chemical Operations**, AIChE (1999).
69. Glor, M., Ignition of Gas/Air Mixtures by Discharges between Electrostatically Charged Plastic Surfaces and Metallic Electrodes, *J. Electrostatics* **10**, 327–333 (1981).
70. Bartknecht, W., **Dust Explosions: Course, Prevention, Protection**, Springer-Verlag, Berlin (1989).
71. Glor, M., Conditions for the Appearance of Discharges during the Gravitational Compaction of Powders, *J. Electrostatics* **15**, 223–235 (1984).
72. Glor, M., Overview of the Occurrence and Incendivity of Cone Discharges with Case Studies from Industrial Practice, *J. Loss Prevention in the Process Industries* **14**, 123–128 (2001).
73. Maurer, B., Glor, M., Lüttgens, G., and Post, L., Hazards Associated with Propagating Brush Discharges on Flexible Intermediate Bulk Containers, Compounds and Coated Materials, pp. 217–222 in *Electrostatics '87—7th Intl. Conf. on Electrostatic Phenomena (Conf. Series No. 85),* Institute of Physics, London (1987).
74. Cross, J. A., **Electrostatics: Principles, Problems and Applications**, Adam Hilger, Bristol, England (1987).
75. Y. Tabata and S. Masuda, "Minimum Potential of Charged Insulator to Cause Incendiary Discharges," *IEEE Transactions on Industry Applications,* IA-20, pp. 1206–1211 (1984).
76. P.G. Guest, V.W. Sikora, and B. Lewis, "Static Electricity in Hospital Operating Suites: Direct and Related Hazards and Pertinent Remedies" (RI 4833), Bureau of Mines, Pittsburgh (1952).
77. Fisher, R. J., A Severe Human ESD Model for Safety and High Reliability System Qualification Testing (SAND89-0194C), Sandia Natl. Labs., Albuquerque NM (1989).

78. Code of Practice for Control of Undesirable Static Electricity (BS 5958 Part 1), British Standards Institution, London (1980).
79. G.W. Brundrett, "A Review of Factors Influencing Electrostatic Shocks in Offices," *Journal of Electrostatics,* 2, pp. 295–315 (1976/77).
80. Klinkenberg, A., and van der Minne, J. L., **Electrostatics in the Petroleum Industry**, Elsevier, Amsterdam (1958).
81. Lüttgens, G., and Wilson, N., **Electrostatic Hazards**, Butterworth-Heinemann, Oxford (1997).
82. P. Boschung and M. Glor, "Methods for Investigating the Electrostatic Behaviour of Powders," *Journal of Electrostatics,* 8, pp. 205–219 (1980).
83. S.J. Collocott, V.T. Morgan, and R. Morrow, "The Electrification of Operating Powder Chemical Fire Extinguishers," *Journal of Electrostatics,* 9, pp. 191–196 (1980).
84. S. Singh, P. Cartwright, and D. Thorpe, "Silo Electrostatic Hazards" (SMS-84-052), National Grain and Feed Association, Washington, DC (1984).
85. Blythe, A. R., and Reddish, W., Charges on Powders and Bulking Effects, pp. 107-114 in *Electrostatics 1979* (Conf. Series No. 48), The Institute of Physics, London (1979).
86. A. Klinkenberg and J.L. van der Minne, *Electrostatics in the Petroleum Industry,* Elsevier, Amsterdam (1958).
87. L.B. Britton and J.A. Smith, "Static Hazards of Drum Filling," Paper 54e, *21st Loss Prevention Symposium,* AIChE (1987).
88. H.L. Walmsley and J.S. Mills, "Electrostatic Ignition Hazards in Road Tanker Loading: Part 1. Review and Experimental Measurements," *Journal of Electrostatics,* 28, pp. 61–87 (1992).
89. Bachman, K. C., Variables Which Influence Spark Production Due to Static Electricity in Tank Truck Loading, *Lightning and Static Electricity Conf.*, Royal Aeronautical Society, London (1975).
90. L.B. Loeb, "Static Electrification-I," in *Progress in Dielectrics,* vol. 4, Academic, New York, pp. 249–309 (1962).
91. V.I. Ermakov and Y.I. Stozhkov, "New Mechanism of Thundercloud Electricity and Lightning Production," in *11th International Conference on Atmospheric Electricity* (NASA/CP-1999-209261) (H.J. Christian, ed.), NASA, Marshall Space Flight Center, AL, pp. 242–245 (1999).
92. W.C. Hart and E.W. Malone, *Lightning and Lightning Protection,* Don White Consultants, Gainesville, VA (1979).
93. M.M. Frydenlund, *Lightning Protection for People and Property,* Van Nostrand Reinhold, New York (1993).
94. Frey, O., The Origin, the Effects and the Simulation of Transients, as Well as Their International Standardization, *Electro 82*, Boston (1982).
95. Recommended Practice for Protecting Residential Structures and Appliances against Surges (Document # PEAC.0545.R), EPRI PEAC Corp., Knoxville, TN (1999).
96. M.M. Frydenlund, *Lightning Protection for People and Property,* Van Nostrand Reinhold, New York (1993).
97. Frydenlund, M. M., **Lightning Protection for People and Property**, Van Nostrand Reinhold, New York (1993).
98. Anderson, R., **Lightning Conductors: Their History, Nature and Mode of Application**, E&FN Spon, London (1879).
99. Müller-Hillebrand, D., The Protection of Houses by Lightning Conductors—An Historical Review, *J. Franklin Institute* **274**, 34–54 (1962).
100. Lee, R. H., Protection Zone for Buildings against Lightning Strikes using Transmission Line Protection Practice, *IEEE Trans. Industry Applications* **IA-14**, 465–470 (1978).
101. Standard for the Installation of Lightning Protection Systems (NFPA 780), NFPA.
102. The Basis of Conventional Lightning Protection Technology: A Review of the Scientific Development of Conventional Lightning Protection Technologies and Standards, Federal Interagency Lightning Protection User Group, [n.p] (2001).
103. Moore, C. B., Rison, W., Mathis, J., and Aulich, G., Lightning Rod Improvement Studies, *J. Applied Meteorology* **39**, 593–609 (2000).
104. T.E. Eaton, *Notes on Electrical Fires,* 3rd ed. and 1990 supplement, Eaton Engineering Co., Nicholasville, KY (1989).
105. Safety of Information Technology Equipment, Including Electrical Business Equipment (UL 1950), Underwriters Laboratories Inc., Northbrook IL, 2006.
106. J. Sletback, R. Kristensen, H. Sundklakk, G. Nåvik, and R. Munde, "Glowing Contact Areas in Loose Copper Wire Connections," in *Proceedings 37th IEEE Holm Conference on Electrical Contacts,* IEEE, New York, pp. 244–248 (1991).
107. E.L. Litchfield, T.A. Kubala, T. Schellinger, F.J. Perzak, and D. Burgess, "Practical Ignition Problems Related to Intrinsic Safety in Mine Equipment: Four Short-Term Studies" (RI 8464), Bureau of Mines, Pittsburgh (1980).
108. M. Saito and W. Sakurai, "An Evaluation Method of Electrical Fire Hazard Caused by Tracking Breakdown," in *Proceedings Electrical/Electronics Insulation Conference,* IEEE, New York, pp. 137–141 (1979).
109. Médard, L. A., **Accidental Explosions**, 2 vols., Ellis Horwood, Chichester, England (1989).
110. Crowl, D. A., **Understanding Explosions**, CCPS/AIChE, New York (2003).
111. Bodurtha, F. T., **Industrial Explosion Prevention and Protection**, McGraw-Hill, New York (1980).

112. Hattwig, M., and Steen, H., eds., **Handbook of Explosion Protection and Prevention**, Wiley-VCH, Weinheim, Germany (2004).
113. Baker, Wilfred E., Cox, P. A., Westine, P. S., Kulesz, J. J., and Strehlow, R. A., **Explosion Hazards and Evaluation**, Elsevier, Amsterdam (1983).
114. Babrauskas, V., Electric Arc Explosions, pp. 1283–1296 in *Interflam 2010—Proc. 12th Intl. Conf.*, Interscience Communications Ltd, London (2010).
115. Lindmayer, M., and Paulke, J., Arc Motion and Pressure Formation in Low Voltage Switchgear, *IEEE Trans. on Components, Packaging, and Manufacturing Technology* **A21**, 33–39 (1998).
116. Nabours, Robert E., Fish, R. M., and Hill, P. F., **Electrical Injuries: Engineering, Medical and Legal Aspects**, 2nd ed., Lawyers & Judges Publishing Co. (2004).
117. Mazer, W. M., **Electrical Accident Investigation Handbook**, 3 vols., Electrodata, Inc., Glen Echo MD (var. dates).
118. Lee, R. H., Pressures Developed by Arcs, *IEEE Trans. on Industry Applications* **IA-23**, 760–764 (1987).
119. Crawford, K. S., Clark, D. G., and Doughty, R. L., Motor Terminal Box Explosions due to Faults, *IEEE Trans. on Industry Applications* **29**, 257–267 (1993).
120. Heberlein, G. E. jr., Higgins, J. A., and Epperly, R. A., Report on Enclosure Internal Arcing Tests, *IEEE Industry Applications Magazine* **2**:3, 35–42 (May/-June 1996).
121. Jennings, C., Fire-Fatality High-Rise Office Building Fire, Atlanta, Georgia (June 30, 1989), US Fire Admin., [Emmitsburg MD], (1989).
122. Graneau, P., The Cause of Thunder, *J. Physics D: Applied Physics* **22**, 1083–1094 (1989).
123. Lee, R. H., The Shattering Effect of Lightning—Pressure from Heating of Air by Stroke Current, *IEEE Transactions on Industry Applications* **22**, 416–419 (1986).
124. Eisenberg, N. A., Lynch, C. J., and Breeding, R. J., Vulnerability Model: Assessing Damage from Maritime Spills by Computer Simulation (CG-D-136-75), US Coast Guard, Washington (1975).
125. Baker, W. E. et al., **Explosion Hazards and Evaluation**, Elsevier, Amsterdam (1983).
126. Flowers, J. W., The Channel of the Spark Discharge, *Physical Review* **64**:7/8, 225–235 (1943).
127. Vanyukov, M. P., Isaenko, V. I., and Khazov, L. D., Investigation of Light Phenomena Related to the Development of the Spark-Discharge Channel, *Zhurnal tekhnicheskoì fiziki* **25**, 1248 (1955).
128. Higham, J. B., and Meek, J. M., The Expansion of Gaseous Spark Channels, *Proc. Physical Society B* **63**, 649–661 (1950).
129. Drouet, M. G., and Nadeau, F., Pressure Waves due to Arcing Faults in a Substation, *IEEE Trans. on Power Apparatus and. Systems* **PAS-98**, 1632–1635 (1979).
130. Dasbach, A., and Pietsch, G., Investigation of the Power Balance of High Current Faults, pp. 15–18 in *Proc. 9th Intl. Conf. on Gas Discharges and Their Applications (GD88)*, Venice (1988).
131. Baldrey, H. W., and Hudson, A. A., Pressures Generated by Fault Arcs in Small Enclosures (Ref. Z/T134), The British Electrical and Allied Industries Research Assn., Leatherhead, Surrey, England (1961).
132. Tanaka, S., Miyagi, T., Ohtaka, T., Iwata, M., Amakawa, T., and Goda, Y., Influence of Electrode Material on Pressure-rise due to Arc in a Closed Chamber, *IEEJ Trans. PE* **128**, 1561–1568 (2008).
133. Capelli-Schellpfeffer, M.,, Miller, G. H., and Humilier, M., Thermoacoustic Energy Effects in Electrical Arcs, pp. 19–32 in *Occupational Electrical Injury: An Intl. Symp., / Annals of the New York Academy of Sciences*, Vol. 888, New York Academy of Sciences, New York (1999).
134. Bowen, J. E., Wactor, M. W., Miller, G. H., and Capelli-Schellpfeffer, M., Catch the Wave: Modeling the Pressure Wave Associated with Arc Fault, *IEEE Industry Applications Magazine* **10**:4, 59–67 (Aug. 2004).
135. Caillard, J., de Izarra C., Brunet, L, Vallée, O., and Gillard, P., Assessment of the Blast Wave Generated by a Low-Energy Plasma Igniter and Spectroscopic Measurements, *IEEE Trans. on Magnetics* **39**, 212–217 (2003).
136. Friberg, G., and Pietsch, G. J., Calculation of Pressure Rise due to Arcing Faults, *IEEE Trans. on Power Delivery* 14, 365–370 (1999)

Surface Flame Spread

23

Yuji Hasemi

Introduction

Surface flame spread is a process of a moving flame in the vicinity of a pyrolyzing region on the surface of a solid or liquid that acts as a fuel source. It is distinct from flame propagation in a premixed fuel and oxygen system in that the surface spread of flame occurs as a result of the heating of the surface due to the direct or remote heating by the flame generated from the burning surface. The surface flame spread is very often critical to the destiny of fires in natural and built environments. This spread applies whether the fire is an urban conflagration or is the first growth after ignition of a room's draperies. This chapter provides fire safety engineers with an overview of surface flame spread during the growth of a fire and the modeling of different modes of flame spread to improve understanding of their effects on the outcomes of fires.

Surface Flame Spread Basics

Flame Spread Process

The surface flame spread is caused as a result of the cycle of the following processes:

1. Vaporization of solid or liquid due to the heating from flame over the fuel's surface
2. Mixing of the pyrolized gas and oxygen in the vicinity of the fuel surface
3. Combustion of the pyrolized gas and formation of the diffusion flame
4. Heating of the unburnt fuel surface to ignition temperature from the diffusion flame

The oxygen and fuel concentrations together with the heat transfer between the flame and the solid phase strongly affect the process. Taking the surface flame spread as a successive ignition front over a combustible object, the speed of spread and its sustainability are controlled by the balance of the flame heating and the rise of surface temperature (see Chap. 21). If the flame ignites the virgin surface of the area larger than that of the burning surface before local extinction, the spread will accelerate. From this point of view, relative configuration of the flame to the surface is critical for the dynamics and the hazard of surface flame spread.

Flame spread in the direction of the mean flow due to wind or buoyancy is called wind-aided or concurrent spread, and, on the contrary, flame spread occurring in a direction opposite to that is called opposed-flow spread.

Difference of the significance of the mode of flame spread for fire safety can be illustrated through the typical process of fire growth in a room with highly combustible lining ignited on the floor, as shown in Fig. 23.1. The spread of fire over the floor is a typical opposed-flow spread because the flame induces unheated air along the

This chapter is based in part on material by Professor J. Quintiere appearing in previous editions of this handbook.

Y. Hasemi (✉)
Wasada University

M.J. Hurley (ed.), *SFPE Handbook of Fire Protection Engineering*,
DOI 10.1007/978-1-4939-2565-0_23, © Society of Fire Protection Engineers 2016

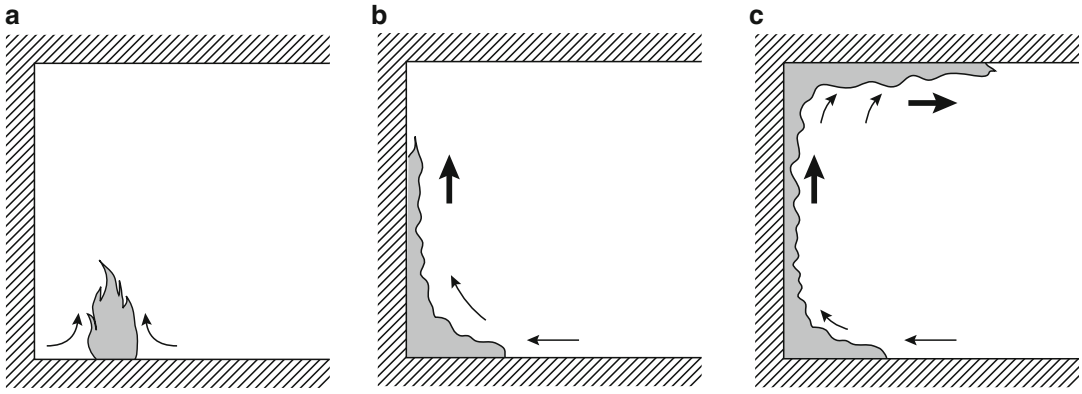

Fig. 23.1 Orientation of combustible surface and the modes of flame spread over (**a**) floor, (**b**) wall, and (**c**) ceiling

carpet surface in the direction against the spread of the flame (Fig. 23.1a). The surface flame spread at the initial stage of a room fire is generally slow and can even be unstable; but once the wall lining is ignited, the buoyancy makes the flame develop along its surface and exposes the lining surface above the burning region to the flame (Fig. 23.1b). This condition generally makes the flame spread much faster than on the floor, even if the floor and the wall are lined with identical material.

If not extinguished at this stage, fire may finally reach and ignite the ceiling. The buoyancy makes the flame spread laterally beneath the ceiling toward the opening, exposing the overall surface of the ceiling to the flame heating (Fig. 23.1c). As widely recognized, flame spread beneath the ceiling is generally fast and could cause flashover by igniting remaining furniture and wall surface far from the ignition source within the room. The Bradford Stadium fire disaster in the United Kingdom (1985) is one of the most significant examples of lateral flame spread beneath a combustible roof or ceiling. During lateral flame spread beneath the ceiling, downward flame spread over the wall lining is often observed within the smoke layer. It is an opposed-flow spread, yet its spread velocity is generally fast due to the additional heating from the smoke layer.

As seen in the growth of room fire, the wind-aided flame spread presents a number of key processes escalating the hazard of building and mass fires. In mass fires such as urban conflagrations and forest fires, fire brands have an additional but sometimes essential role in enhancing fire spread in the wind direction. The importance of opposed-flow flame spread can become significant when the temperature of the fire environment has been raised enough to preheat the wide range of surfaces of combustibles. Although the two modes of flame spread are apparently distinct from each other, there is notable ambiguity in fires on an inclined combustible surface. On an upward inclined surface, the angle between the flame flow and the surface is reduced with an increase of the angle of inclination, and finally the flame begins to crawl over the surface [1] (Fig. 23.2). This change occurs generally at 15–30°, depending on the width, side confinements, and other conditions; inclination of roofs, escalators, and slopes for wheelchairs are generally within the range where wind-aided flame spread is anticipated. The escalator fire at the Kings Cross Subway Station Fire Disaster (1987) is a significant example of wind-aided flame spread along an inclined configuration under the enhancement of buoyancy due to the confinement of air supply by the side walls [2].

Research Background

Large numbers of experiments on and models of surface flame spread with diverse levels of theoretical sophistication and practical relevance

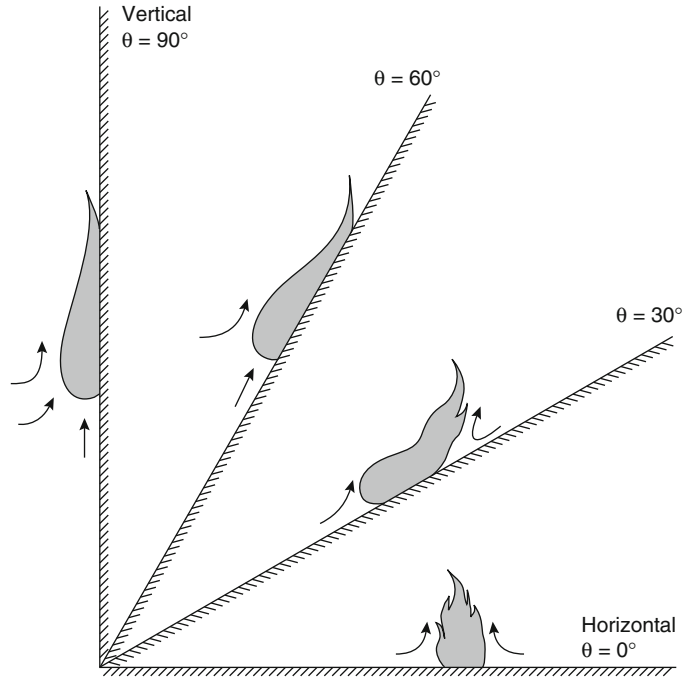

Fig. 23.2 Change of the mode of surface flame spread according to the slope angle

have been conducted, and it is impossible to make a precise review of all the important research on this subject. It is recommended to seek comprehensive reviews such as Drysdale [3], Quintiere [4], Fernandez-Pello and Hirano [5], Hirano [6], and Williams [7]. However, as long as surface flame spread is discussed for the assessment of fire safety of natural or artificial composites, the phenomena are generally modeled as a thermal process causing the successive piloted ignition on the surface due to the heating from the burning of the material itself under the gravity and the atmospheric conditions of the earth.

Active research on thermal modeling of surface flame spread has occurred since the late 1960s, and significant progress was made in the basic understanding of flame spread through theoretical sophistication and laboratory experiments throughout the 1970s. Later, during the 1980s, the approach was extended to turbulent flames for the application to the fire hazard assessment of lining materials. In the 1990s, further studies were conducted to analyze and assess the general behavior of room fires through input from and validation against large-scale tests with around one-story-high wall specimens or with standard and larger-scale room tests. These studies have revealed the importance of the surface configurations on the general behavior of flame spread; examples of acceleration of flame spread on grooved combustible surfaces, in corner walls, and in a vertical, inclined, or downward channel lined with combustible material show the significance of the configuration effect. Together with the substantial progress in the measurement technology of the combustibility of materials through the 1980s and the 1990s, these studies have made it possible to predict surface flame spread in a room to some extent using material properties obtained from bench-scale tests.

Wind-Aided Flame Spread

The wind-aided flame spread is the most important mode of surface flame spread for fire hazard assessment. In this section, modeling and assessment are introduced regarding the two most significant examples of wind-aided flame spread in building fires: upward wall flame spread and

flame spread beneath the ceiling. Upward wall flame spread along a wall has drawn the particular interest of fire safety engineers for its primary importance in the determination of the destiny of a room fire and for the rich variety of configurations of wall surfaces that may influence the general behavior of flame spread. In this section, theories of wind-aided flame spread developed essentially for wall fires are applied to provide technical insight in the assessment of room fires or the combustibility of lining materials in general.

Upward Turbulent Wall Flame Spread

Figure 23.3 is a schematic of upward flame spread typical of wind-aided flame spread. The flame spread is thus perceived in two different manners: first by the advancement of flame front and second by the advancement of the ignition front of the solid surface. The rate of movement of the ignition front is normally defined as the flame spread velocity for modeling purpose. The location of the ignition front of a burning surface, $x_p(t)$, is identified as the location where surface temperature has reached the ignition temperature, T_{ig}.

Flame Heat Transfer For Fig. 23.3, one-dimensional thermal conduction in the direction normal to the wall surface can be reasonably assumed and evolution of the surface temperature at x above the fire origin at time t, $T(x,t)$, is formulated as

$$T(x,t) - T_o = \int_0^t \dot{q}''_f(x,\tau)\phi(t-\tau)d\tau \qquad (23.1)$$

where

T_0 = Initial surface temperature

$\dot{q}''_f$ = Flame heat flux

$\phi(t-\tau)$ = Impulse response of the surface temperature at timet t to the surface heat flux at τ

$\phi(t-\tau) = [\pi k\rho c(t-\tau)]^{-1/2}$ and $\phi(t-\tau) = [\rho c\delta(t-\tau)]^{-1}$ apply for a thermally thick wall and for a thin wall with thickness of δ respectively with k, ρ, and c thermal conductivity, density, and specific heat of the solid. Equation 23.1 can be solved for flame spread velocity, $V_p = dx_p/dt$, for simple conditions by further introducing engineering relations on the flame heat flux, $\dot{q}''_f = F(x,\tau)$.

Flame heat flux is normally represented as relative location to the flame length, x_f; that is, $\dot{q}''_f = F(x/x_f)$, Applying the Froude modeling for the flame height (see Chap. 21) to a line fire along a wall, x_f is generally expressed as function of heat release rate per unit width as

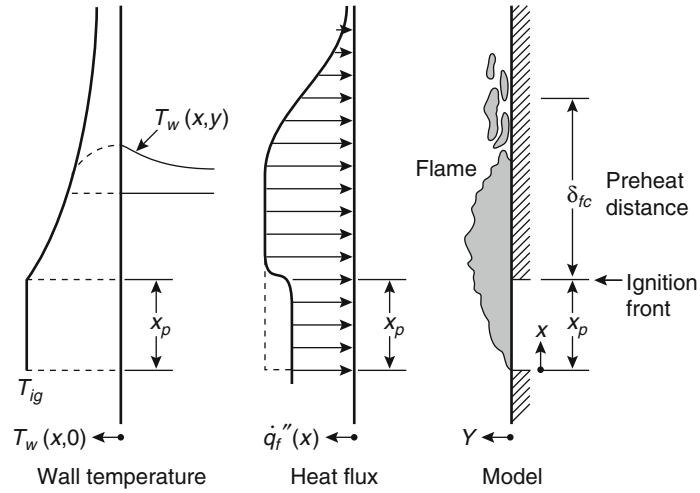

Fig. 23.3 Upward wall flame spread [9]

$$x_f/D = k\dot{Q}_\ell^{*n} \tag{23.2}$$

Where

D = Characteristic lengthof the burning area (normally height or depth), $\dot{Q}_\ell^* = \dot{Q}_\ell/cT_0\rho_\infty g^{1/2}D^{2/3}$.

k = Empirical coefficient

$\dot{Q}_\ell$ = Heat release rate per unit width of fire source

Figure 23.4 illustrates a relation between heat release rate per unit width and flame length for line burners against a constant temperature inert wall. It shows that $k = 6.0$ for intermittent flame and $n \sim 2/3$ for $\dot{Q}_\ell \geq 1.0$, as anticipated for an ideal line source by dimensional analysis [8]. The value of k depends on the definition and measurement of flame length, and experimental k values range from 4.65 to 7.0 [8–11]. Newman and Wieczorek reviewed reported values for k and n [12]. With $n = 2/3$ in Equation 23.2, flame length is found to be independent of the dimension of the burning region and is represented as

$$x_f = \left(k^{3/2}/c_pT_o\rho_\infty g^{1/2}\right)^{2/3}\dot{Q}_\ell^{2/3} = k'\dot{Q}_\ell^{2/3} \tag{23.3}$$

The k' value is roughly 0.01 k; for Fig. 23.3, k' value is found to be $k' = 0.057$ m$^{1/3}$ kW$^{-2/3}$, whereas k' values in literature range from 0.043 m$^{1/3}$ kW$^{-2/3}$ to 0.067 m$^{1/3}$ kW$^{-2/3}$ [8, 9, 12, 13]. For a limited range of $\dot{Q}_\ell$, flame length can be linearized against heat release rate or the characteristic length of burning region for engineering purposes as

$$x_f \approx k_f\dot{Q}_\ell = k_f\dot{Q}_\ell''D = aD \tag{23.4}$$

where $\dot{Q}_\ell''$ is the characteristic heat release rate per unit width, k_f, and $a \equiv k_f\dot{Q}_\ell''$ depends on heat release rate, but $k_f \sim 0.006$–0.01 m^2/kW is suitable for lining materials in practice [14–16].

Figure 23.5 is a general relation between the total incident heat flux from wall flame to wall surface and the distance from the lower edge of the burning surface normalized by x_f. It is a summary of experiments on wall flames

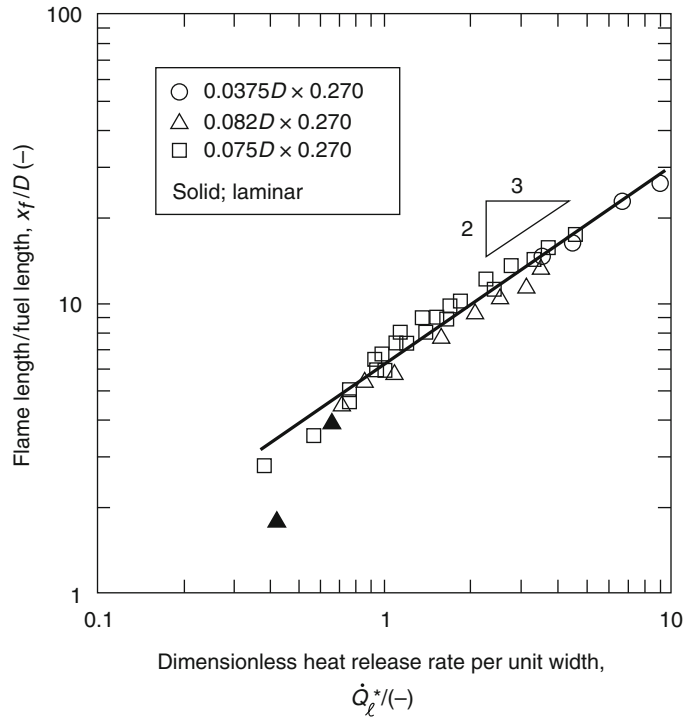

Fig. 23.4 Relation between the length of intermittent wall flame and dimensionless heat release rate per unit width [9]

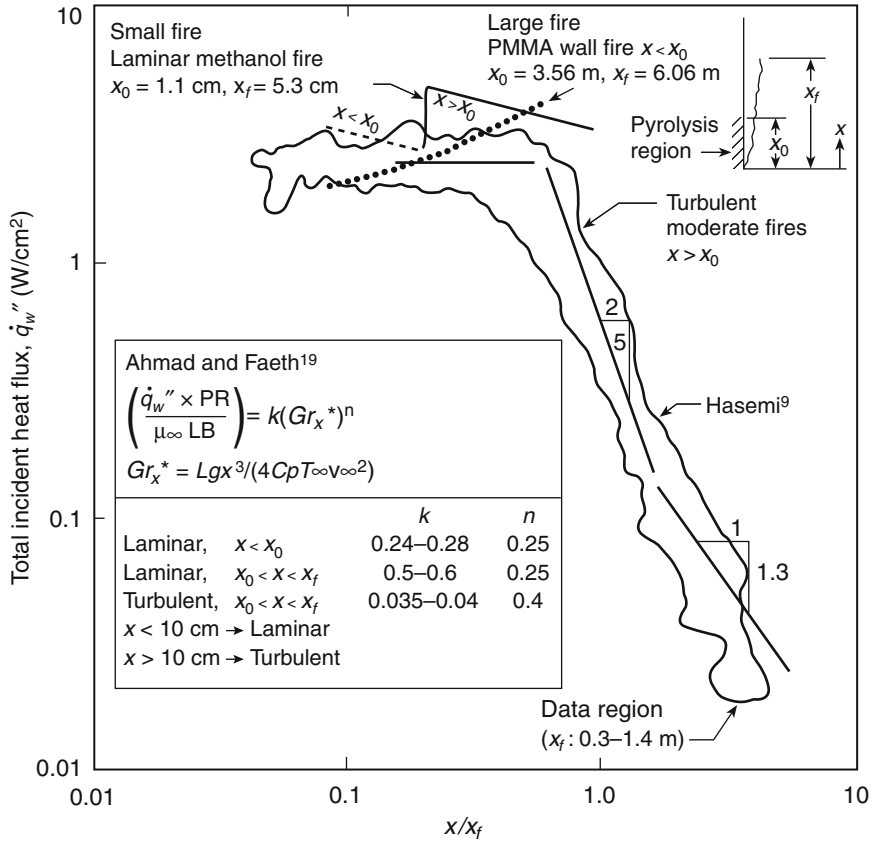

Fig. 23.5 Wall flame incident heat flux for materials [17], for laminar flames [19], and for a large PMMA wall fire [18]

from steady porous burners, vertical wicks, and burning of specimens of finite-surface area of materials in practice [9, 17–19]. For more detailed flame heat flux data and correlations on different configurations, see Chap. 25.

As thermal conduction theories suggest, response of surface temperature to heat input depends significantly on the thickness of the solid; modeling of surface flame spread requires different approaches for thermally thick solid and thin materials. Except for items such as paper, garments, or draperies in a room, in practice most solids should behave as thermally thick under flame spread conditions. Engineering treatment of surface flame spread might appear to regard solids thicker than 1 mm as thermally thick. Up to a thickness of 1–2 cm, flame spread could depend on thickness and on the substrate material adjacent to the solid. Based on these factors, it is apparent that the thermally thick case is more significant.

With the unique dependence of flame heat flux on dimensionless height, x/x_f, Equation 23.1 can be solved to provide a characteristic steady flame spread velocity $V_p = x_p/t$ for a thermally thick solid as

$$V_p = \left[\int_0^\infty \dot{q}_f''(\xi + x_p)/\sqrt{\xi d\xi}\right]^2 / \pi k\rho c\left(T_{ig} - T_o\right)^2 \tag{23.5}$$

The numerator has the dimension of $(\mathrm{kW/m^2})^2$ m, and Equation 23.5 can be represented more simply as $\dot{q}_{fc}'' 2\delta_{fc}$ with characteristic flame heat flux, $\dot{q}_{fc}''$, and characteristic

preheat distance, δ_{fc}. Equation 23.5 is thus expressed as

$$V_p = 4\dot{q}_{fc}^{''2}\delta_{fc} \Big/ \pi k\rho c\left(T_{ig} - T_o\right)^2 = \left(x_{fc} - x_p\right) \Big/ t_{ig}^* \tag{23.6}$$

where

$$x_{fc} = x_p + \delta_{fc}$$
$$t_{ig}^* \equiv \pi k\rho c\left(T_{ig} - T_o\right)^2 / 4\dot{q}_{fc}^{''2}$$

Equation 23.6 is essentially in the same form with the flame spread velocity obtained for flame heat flux decaying exponentially with distance from the ignition front [20]. The preheat distance, δ_{fc}, is essentially the distance between the flame front and the ignition front.

Controlling Parameters of Upward Wall Flame Spread In Equation 23.6, it is important that the characteristic preheat distance, δ_{fc}, is essentially controlled only by the heat release rate in a one-dimensional flame configuration, and $k\rho c(T_{ig} - T_0)^2$ is the central part of material property to control ignitability.

Another important parameter that may control the general behavior of flame spread is the local burnout. Consider local burnout occurring at t_b after the local ignition (Fig. 23.6), $D = V_p t_b$. If the local burnout time is short compared to the characteristic time to ignition, it will become difficult to sustain successive thermal ignition on the surface. Taking the linearized flame length approximation (Equation 23.4), we introduce the following dimensionless flame spread acceleration factor: [14]

$$b = (a - 1) - t_{ig}{}^*/t_b \tag{23.7}$$

where $(a - 1)$ represents the significance of flame heating, and if $t_{ig}{}^*/t_b$ is large, it will become difficult for successive ignition to sustain. Obviously, $b = 0$ stands for Equation 23.6 and is the condition for the achievement of steady-state spread. The sign of b dictates the general behavior of wind-aided flame spread: $b > 0$ will lead to the acceleration of spread, whereas $b < 0$ will result in the deceleration of spread and finally autonomous extinction. There is more sophisticated discussion on the general behavior of wind-aided flame spread [15, 16, 21–24], which may still await future validation. But every kind of thermal model and analysis based on the linearized flame length approximation (Equation 23.4) finally eventuates the recognition of b as the central parameter for the assessment of hazard of flame spread.

Figure 23.7 is a summary of the correlation between the time to flashover in ISO 9705 room-corner tests with combustible linings and b [14]. The elements of b, namely a, $t_{ig}{}^*$, and t_b, are all material properties that can be quantified with bench-scale tests such as the cone calorimeter. Although there is still some discussion on what external heat flux level should be chosen for the quantification, use of 30–50 kW/m^2 external radiant flux seems to lead to reasonable explanation of the growth of room fire from Equation 23.7. For a charring material, heat release rate generally decays with time after the sharp peak just after the ignition and can be more suitably represented by an exponential function of time, namely $\dot{Q}^{''}(t) = \dot{Q}^{''}_{\max}\exp(-t/t_c)$. Analysis of the results of room-corner tests and the cone calorimeter on wood-based materials suggests use of $k_f\dot{Q}_{\max}$ and t_c for a and t_b respectively leads to a result consistent with Fig. 23.7 [15, 22] for such materials.

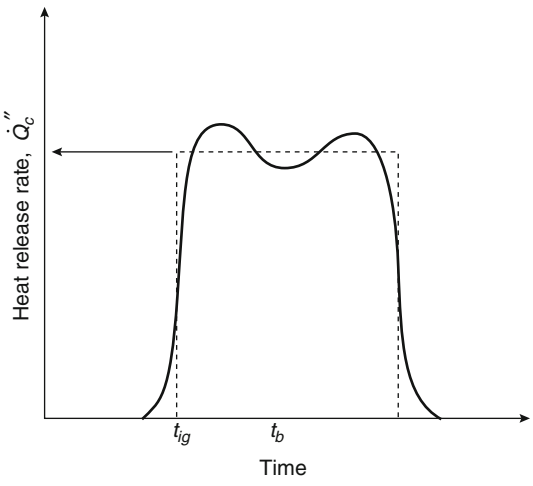

Fig. 23.6 Time history of heat release rate from fixed area burning surface

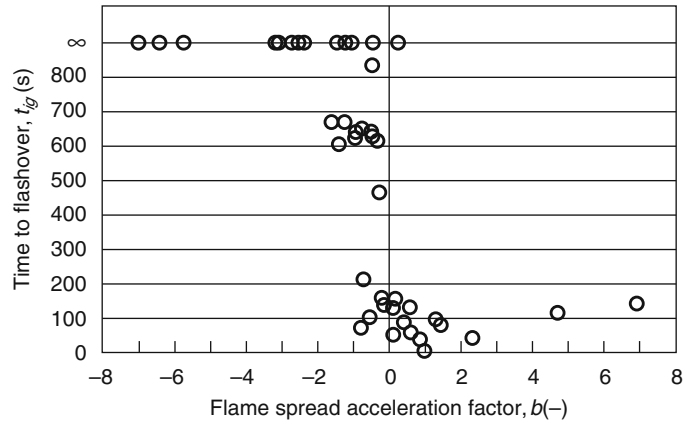

Fig. 23.7 Time to flashover in the ISO 9705 room-corner test versus the flame spread acceleration factor [14]

Equation 23.7 is simple but provides useful insights in the overall understanding of wind-aided flame spread. It is especially noteworthy that material properties are not the single factor to quantify this equation. Time to ignition and time to burnout are dependent on the ambient temperature and external heating; and a, essentially the flame-length to pyrolysis-length ratio, can be augmented not only by external heating through enhancement of vaporization but also by increase of pyrolizing surface area due to any finishing treatment such as roughness and grooves. Existence of the source of external heating has thus two implications for the acceleration of flame spread: first through the increase of the temperature of the unburnt surface and second through the promotion of vaporization of fuel due to additional heating of the burning surface [25]. Grooves or trench-like configurations of the burning surface can reduce air entrainment to the vaporizing region and extend the flame length. Configuration effect is as important as material properties in the fire safety assessment of any assembly with a combustible surface.

Flame spread can be significantly enhanced in parallel wall configuration, where the flame on either wall stimulates pyrolysis and preheating of the other surface and generates mutual acceleration of flame spread. If the wall distance is small compared to the wall width, the air supply to the burning surface will be restricted and further prolong the flame length. Even though parallel-wall configuration is not common in building design, commodities or cargoes piled in warehouses or in mass merchandise outlets often make "valleys with combustible cliffs," which can be considered as parallel walls from the flame spread point of view. A number of fire tests of cargoes and commodities in typical warehouse configuration demonstrate significant acceleration of fire growth in such a configuration [24, 26]. A cavity within a wall or a roof sandwiched by combustible surfaces is another significant example capable of showing the parallel-wall effect. Surface flame spread can be further enhanced in a vertical or inclined cavity by the stack effect due to general temperature rise within the cavity. The fast fire spread throughout whole high-rise building at the Beijing Television Cultural Center fire (2009) is partly attributed to these configuration effects. The vertical long cavity lined with polymer insulation within the facades on both sides of the building should have helped acceleration of fire spread once the fire penetrated into the cavity.

Also, in a corner of walls, flame is generally prolonged due to the restriction of entrainment and the mutual radiation between the walls, which can result in faster flame spread. There are experiments and measurements of upward turbulent flame spread on nearly full-scale specimens of various materials in practice [11, 18, 26–29]. These reports would provide valuable information necessary for consideration in running large-scale flame spread tests with materials in practice.

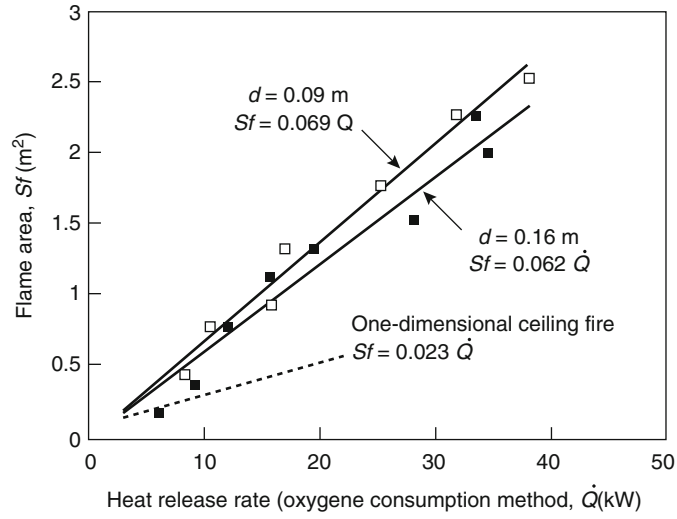

Fig. 23.8 Area covered by ceiling flame versus effective heat release rate [30, 31]

Surface Flame Spread Beneath Ceiling

Although fewer studies have been conducted on the ceiling fires, the mechanism of the surface spread is essentially similar to the upward wall spread. Flame spreading beyond the pyrolysis front is the dominant force for the successive ignition of unburnt ceiling surface. According to the measurements of flame size and flame heat flux for one-dimensional ceiling flames in a corridor-like configuration and for circular ceiling flames from downward porous propane sources [30] (Fig. 23.8), the area covered by a visible ceiling flame is nearly proportional to the heat release rate, and the heat release rate per unit flame area is significantly larger for one-dimensional flames than for circular flames. This situation indicates uniform entrainment of air beneath a ceiling flame, but the rate of entrainment could depend on the configuration. Flame length is thus proportional to heat release rate per unit width in corridor configuration, $x_f = 0.0122\ \dot{Q}_{le}$ with $\dot{Q}_{le}$ as the effective heat release rate per unit width (kW/m) for corridor ceiling configuration [31] and proportional to the half power of heat release rate beneath an unconfined ceiling.

As shown in Chap. 25, total heat flux from the ceiling flame to the ceiling surface can be represented as a unique function of distance from the windward edge of the burning surface divided by the flame length. From these facts, the engineering framework for the assessment of surface flame spread on a wall applies suitably for the flame spread beneath a combustible ceiling, whereas such physical constants as a should be different from the wall fire configuration.

Under an unconfined ceiling, heat flux within the solid ceiling flame is decreased weakly with distance within the range of 20–30 kW/m^2, and is generally weaker than in upward wall flames of similar heat output, because of the buoyancy reducing the thickness of ceiling flame.

Ambient thermal conditions and surface configurations of the ceiling could also affect the general behavior of flame spread beneath the ceiling. One of the important issues to be considered in the understanding and fire hazard assessment of flame spread beneath the ceiling in a room is the effect of preheating due to ceiling jet and smoke layer, which normally come in contact with the ceiling earlier than flame in a likely fire growth scenario in a room. Corridor ceiling flame spread tests lined with medium-density fiberboard (MDF) with uniform external radiation to the ceiling surface demonstrate significant sensitivity of the ultimate burn length to pilot flame length ratio, x_{poff}/x_{po}, to the ceiling

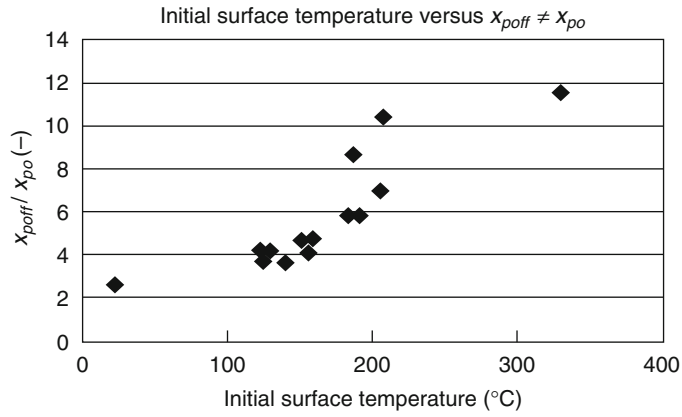

Fig. 23.9 Relation between the surface temperature due to external heating at piloted ignition to ceiling and the ultimate burnt length to pilot flame length ratio for MDF [31]

surface temperature just prior to the ignition by pilot flame, T_o (Fig. 23.9) [31]. T_o was controlled by the upward radiant panel. In the tests resulting in $x_{poff}/x_{po} > 10$, almost the whole ceiling surface was finally pyrolyzed and flame spread itself was strongly accelerated. Flame spread was less sensitive to heat flux within the range of 0–10 kW/m^2. The remarkably fast flame spread beneath a nearly unconfined roof/ceiling observed at the event of the Bradford Stadium fire disaster (1985) is attributed partly to the use of roof material of low ignition temperature. Increase of the effective combustible surface area due to beams, decorations, and so forth can also increase *a* value and accelerate flame spread. Stenstad and Karlsson have demonstrated a significant example of such effect by a large-scale experiment [32].

Opposed-Flow Flame Spread

Mechanism of Opposed-Flow Flame Spread

In the opposed-flow spread, the front of the pyrolyzing region moves in the opposite direction of the flame flow. As seen in Fig. 23.10, the unburnt surface beyond the pyrolysis front is heated by remote flame; the flame spread velocity is less dependent on flame length or heat release rate, and the distance that the flame heating covers should be quite limited. For this reason, in the modeling of opposed-flow flame spread, spread velocity is normally assumed as steady state. Consider that the pyrolysis front traverses Δ within the time interval τ on a combustible solid of the thickness δ small enough to ensure practically uniform temperature across the thickness with no heat loss from the back surface. The flame spread velocity can be given by $V_p = \Delta/\tau$, and the energy conservation for the control volume Δ distance from the pyrolysis front can be described as

$$\rho c \delta V_p \left(T_{ig} - T_o\right) = \dot{q}'' \Delta \tag{23.8}$$

The net flame heat flux due to the gas-phase conduction can be given by

$$\dot{q}'' \approx k_g \left(T_f - T_r\right)/\Delta \tag{23.9}$$

where k_g, T_f, and T_r are gas-phase conductivity, flame temperature, and reference temperature for the control volume. T_r can be correlated with either T_{ig} or T_o. From these equations, the flame spread velocity can be represented as a function of thermal properties and the configuration condition as

$$V_p = k_g \left(T_f - T_r\right)/\rho c \delta \left(T_{ig} - T_s\right) \tag{23.10}$$

The flame temperature, T_f, should ideally be taken as that due to adiabatic stoichiometric combustion but, in general, could be thought of as less due to heat losses and chemical kinetic effects. Under these ideal theoretical considerations, it can be shown that

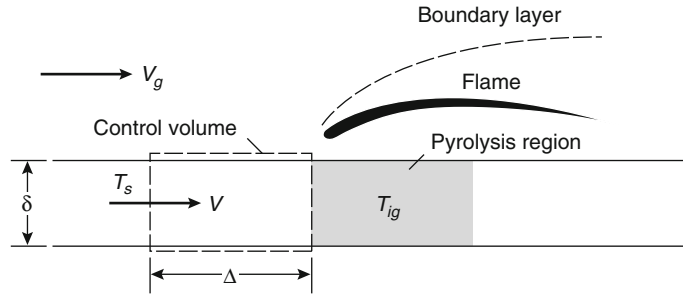

Fig. 23.10 Energy conservation in opposed-flow spread

$$T_f - T_{ig} = \frac{\left(T_\infty - T_{ig}\right) + \left(Y_{ox,\infty}/rc_g\right)\left(\Delta H - L\right)}{1 - Y_{ox,\infty}/r} \tag{23.11}$$

where ΔH and L are heat of combustion and heat of gasification of the solid fuel, respectively. T_∞ and $Y_{\mathrm{ox},\infty}$ are gas-phase ambient temperature and oxygen concentration, respectively, and r and c_g are stoichiometric mass ratio of oxygen to fuel and specific heat of the gas phase, respectively. Because $\Delta H/L$ and $Y_{\mathrm{ox},\infty}/r$ are large, and heat of combustion per unit mass of consumed oxygen, ΔH_{ox}, is nearly constant for most of combustible solids in practice (13 kJ/g), the flame temperature can be approximated as

$$T_f - T_{ig} \approx Y_{ox,\infty}\Delta H_{ox}/c_g \tag{23.12}$$

and we realize that the flame temperature is primarily sensitive to only the ambient oxygen concentration. This suggests that flame spread over a ceiling would be reduced in a room as the oxygen within the smoke layer near it is reduced.

For a thermally thin solid, δ can be taken as constant. Combining Equations 23.8 and 23.9, flame spread velocity is given as

$$V_p = \Delta/\tau = k_g\left(T_f - T_o\right)/\rho c\delta\left(T_{ig} - T_r\right) \tag{23.13}$$

For a thermally thick solid, δ should represent the depth of thermal penetration, which depends on time; that is, from the heat conduction equation for a semi-infinite thick slab as $\delta = \sqrt{k\tau/\rho c}$. Substituting this into Equation 23.8, we have

$$V_p = \dot{q}''^2\Delta/k\rho c\left(T_{ig} - T_o\right)^2 \tag{23.14}$$

In Equations 23.13 and 23.14, the flame spread velocity is apparently independent of the opposed-flow velocity, V_g. However, the independence is only the case as long as chemical effects are unimportant. Chemical kinetic effects become important when the time for chemical reactions to be completed in the flame, t_{chem}, becomes long compared to the fluid flow transit time through the flame, t_{flow} . If the flow is too fast, chemical reaction will be incomplete. Because the flow transit time is proportional to V_g-1 and mixing should be enhanced by the decrease of V_g, the flow transit time to chemical reaction time ratio, normally referred to as the Damköhler number, Da, can be represented as

$$Da = t_{\mathrm{flow}}/t_{\mathrm{chem}} \propto 1/V_g^2 \tag{23.15}$$

The flame spread velocity is reduced with an increase of Da. Taking the flame spread velocity given by Equation 23.10 as $V_{p,\mathrm{ideal}}$, the actual flame spread velocity to $V_{p,\mathrm{ideal}}$ ratio can be illustrated qualitatively as shown in Fig. 23.11.

However, for a thermally thick solid, the relation between flame spread velocity and opposed-flow velocity is more complicated. Figure 23.12 is a significant such example showing either increase or decrease of V with V_g depending on the ambient oxygen concentration [33]. This illustration suggests the dependence of $V_{p,\mathrm{ideal}}$ on V_g in the flame spread over a

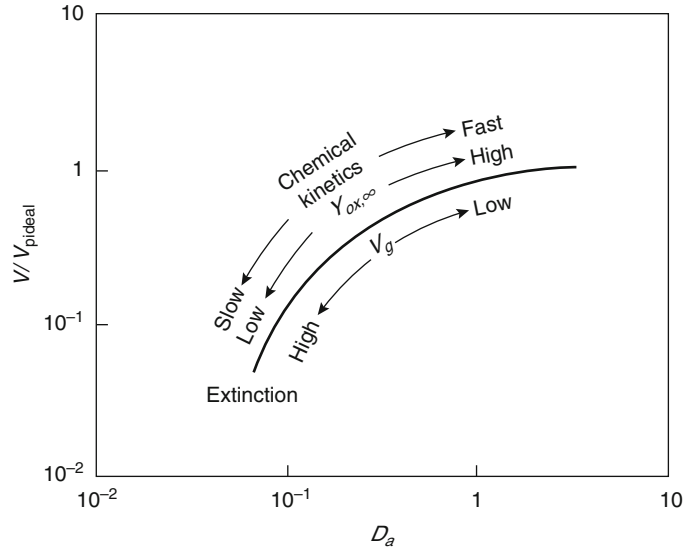

Fig. 23.11 Qualitative dependence of opposed-flow flame spread with Damköhler number, Da

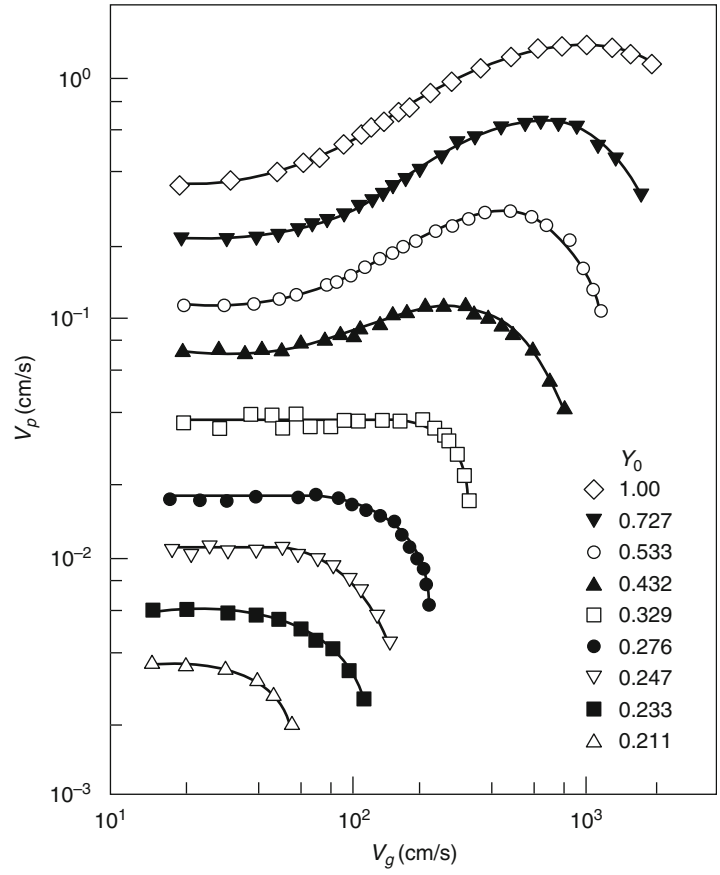

Fig. 23.12 Effect of opposed-flow velocity and oxygen concentration of flame spread speed for thick PMMA (Taken from Fernandez-Pello et al.) [33]

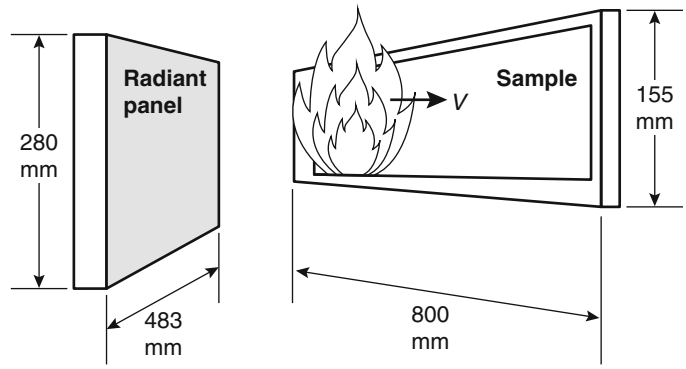

Fig. 23.13 Outline of the heating and flame spread in the LIFT apparatus

thermally thin solid. Attributing this effect to the dependence of the preheat distance, which is the length of the control volume shown in Fig. 23.10, and assuming the balance of gas-phase heat conduction with convection due to the opposed flow has the velocity of V_g, $\rho_g c_g V_g \partial T/\partial x \approx k_g \partial^2 T/\partial x^2$, then the following estimate can be derived:

$$\Delta \approx k_g/\rho_g c_g V_g \tag{23.16}$$

By substituting Equations 23.9 and 23.16, Equation 23.14 yields the expression first derived by de Ris: [34]

$$V_p \approx V_g\left(k_g\rho_g c_g\right)\left(T_f - T_r\right)^2/k\rho c\left(T_{ig} - T_o\right)^2 \tag{23.17}$$

Modeling of Opposed-Flow Flame Spread

Significant progress has been made on the understanding and modeling of opposed-flow flame spread, but most of the research has concentrated on poly(methyl methacrylate) (PMMA) and other rather ideal materials from the viewpoint of combustion and pyrolysis modeling. Few models have been attempted on the opposed-flow turbulent flame spread over charring materials and composites in practice. Because it is the numerator of Equation 23.17 that is hard to quantify for materials in practice, Equation 23.17 can be rewritten as

$$V_p \approx \Phi/k\rho c\left(T_{ig} - T_o\right)^2 \tag{23.18}$$

with Φ, a parameter depending on V_g and $Y_{ox,\infty}$ that could be quantified with a bench-scale test for practical materials. Quintiere and Harkleroad [14] examined this approach using the lateral ignition and flame spread test (LIFT) apparatus (Fig. 23.13) and have quantified the effective opposed-flow flame spread properties as summarized in Table 23.1. See Chap. 21 for more detail on the ignitability parameters. Equation 23.18 also suggests the importance of the ignitability parameter, $k\rho c(T_{ig}–T_o)^2$ for the fire hazard assessment of any material. Existence of a source of external heating, such as exposure to smoke layer, flame sheet spreading beneath the ceiling, and the like, may have a significant influence on the spread velocity.

Mass Fires

Urban fires, wildland fires, and forest fires are serious fire disasters in various districts. The conflagrations at the Great Hanshin earthquake (1995) revealed significant risk of earthquake urban fires in Japan and other districts featuring urban areas densely inhabited with buildings with relatively weak fire protection. Land development of wildland near urban districts in North America and Australia has caused a risk of occurrence of urban–wildland interface fire disasters. Albini reviewed research resources for forest and wildland fires [35]. Recent investigation

Table 23.1 Effective opposed-flow flame spread properties [14]

Material	T_{ig} (°C)	$k\rho c$ (kW^{2}s/m^{4}K^2)	Φ (kW^2/m^3)	$T_{s,\min}$ (°C)	$\Phi/k\rho c$ (mK^2/s)
PMMA polycast (1.59 mm)	278	0.73	5.4	120	8
Polyurethane (S353M)	280	—	—	105	82
Hardboard (6.35 mm)	298	1.87	4.5	170	2
Carpet (acrylic)	300	0.42	9.9	165	24
Fiberboard, low density (S119M)	330	—	—	90	42
Fiber insulation board	355	0.46	2.2	210	5
Hardboard (3.175 mm)	365	0.88	10.9	40	12
Hardboard (S159M)	372	—	—	80	18
PMMA type g (1.27 cm)	378	1.02	14.4	90	14
Asphalt shingle	378	0.70	5.3	140	8
Douglas fir particle board (1.27 cm)	382	0.94	12.7	210	14
Wood panel (S178M)	385	—	—	155	43
Plywood, plain (1.27 cm)	390	0.54	12.9	120	24
Chipboard (S118M)	390	—	—	180	11
Plywood, plain (0.635 cm)	390	0.46	7.4	170	16
Foam, flexible (2.54 cm)	390	0.32	11.7	120	37
GRP (2.24 mm)	390	0.32	9.9	80	31
Mineral wool, textile paper (S160M)	400	—	—	105	34
Hardboard (gloss paint) (3.4 mm)	400	1.22	3.5	320	3
Hardboard (nitrocellulose paint)	400	0.79	9.8	180	12
GRP (1.14 mm)	400	0.72	4.2	365	6
Particle board (1.27 cm stock)	412	0.93	4.2	275	5
Gypsum board, wallpaper (S142M)	412	0.57	0.79	240	1
Carpet (nylon/wool blend)	412	0.68	11.1	265	16
Carpet #2 (wool, untreated)	435	0.25	7.3	335	30
Foam, rigid (2.54 cm)	435	0.03	4.0	215	141
Polyisocyanurate (5.08 cm)	445	0.02	4.9	275	201
Fiberglass shingle	445	0.50	9.0	415	18
Carpet #2 (wool, treated)	455	0.24	0.8	365	4
Carpet #1 (wool, stock)	465	0.11	1.8	450	17
Aircraft panel epoxy Fiberite	505	0.24	*	505	*
Gypsum board, FR (1.27 cm)	510	0.40	9.2	300	23
Polycarbonate (1.52 mm)	528	1.16	14.7	455	13
Gypsum board, (common) (1.27 mm)	565	0.45	14.4	425	32
Plywood, FR (1.27 cm)	620	0.76	*	620	*
Polystyrene (5.08 cm)	630	0.38	*	630	*

Note: Values are only significant to two places
*Flame spread was not measurable

witnesses the increase of the frequency and the hazard of forest fires in polar Russia, Alaska, and Canada since about the 1990s [36].

Flame spread in a forest or in an urban district depends on radiant heat transfer, convective heating, and leeward spread of fire brands due to wind or the slope of the terrain. Figure 23.14 is a summary of the fire spread velocity for urban and wildland fires superimposed on the correlation between fire spread velocity and wind velocity summarized on Japanese urban fires from the 1910s to the 1950s [37, 38]. The significant fire spread velocity recorded in past urban and wildland fires, from the order of 100 m/h to 10 km/h,

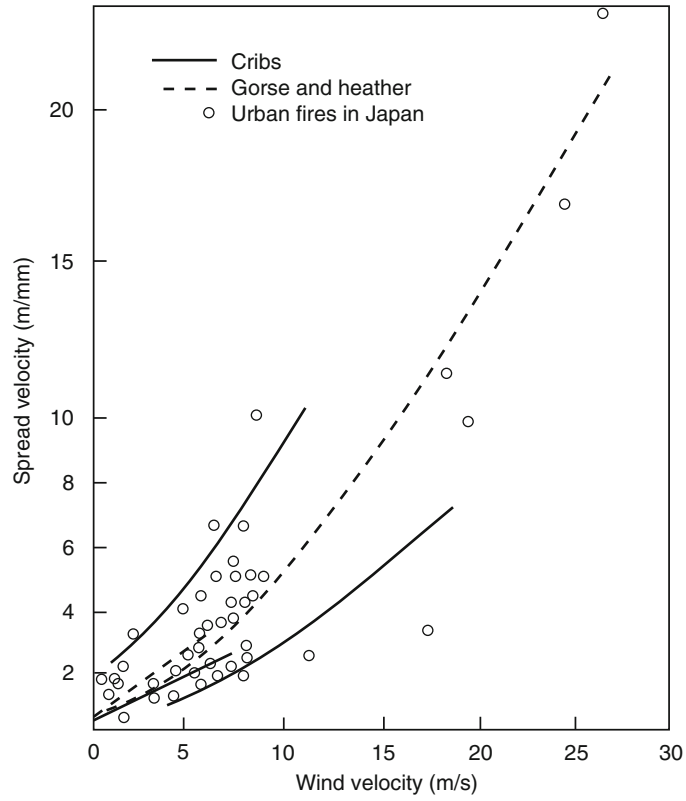

Fig. 23.14 Comparison of rates of fire spread for urban and wildland fires as a function of wind speed (From Kawagoe [38] and Thomas [37])

cannot be explained by convective or radiant heating and suggests the importance of the role of fire brands in the wind-aided spread of mass fires.

In urban fires, collapse of wooden buildings due to fire is the typical and most significant source of fire brands. In wildland and forest fires, the porous bush along the terrain is involved, and dried bush, fallen bark and pine needles, and so forth can be typical sources of fire brands. Even though weight per area of bush, bark, and dried leaves is small and their flaming might not last so long, they are quick to ignite by fire brand due to the large surface area to weight ratio of these materials. In that sense, fire brands should have primary importance in the growth of forest fires. However, in more severe fires, the crowns of the trees may also be involved.

Flame Spread Over Liquids

Flame spread over a horizontal pool of liquid fuels is essentially opposed flow, but its spreading velocity is very often significantly larger than estimated from the thermal theory [39]. The difference is attributed to the convective flow within the liquid moving concurrently with the flame. The convection is due to the surface tension, which is reduced with increase of temperature and pulls the flame toward the unburnt surface of the liquid. This is illustrated in Fig. 23.15 for a thin liquid layer, δ. Under steady conditions, the viscous forces on the control volume are balanced by the surface tension forces. Thus, the shear stress, τ, at the bottom surface equals the surface tension gradient ($d\sigma/dx$) along the free surface:

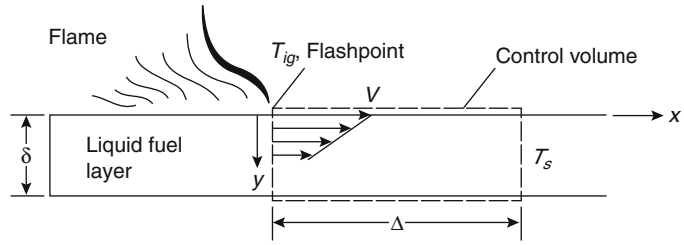

Fig. 23.15 Enhanced flame spread speed in liquids due to surface-tension induced flow

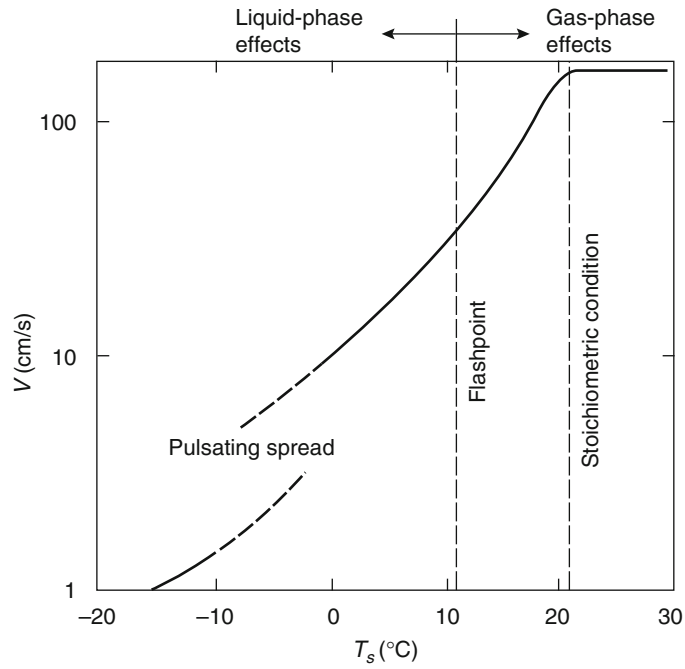

Fig. 23.16 Relationship between the liquid temperature and the rate of plane flame spread of methanol, based on Akita [40]

$$\tau = d\sigma/dx = (d\sigma/dT)(\partial T/\partial x) \qquad (23.19)$$

For a thin liquid layer, the surface tension effect results in nearly a Couette flow (constant shear) over the layer thickness, δ. Hence, it can be approximated that

$$\tau = (\mu \partial u/\partial y)_{y=0} \approx \mu V/\delta \qquad (23.20)$$

where μ is the liquid viscosity. By further approximating the surface tension gradient as a difference over length Δ, the flame speed can be estimated as

$$V = \frac{\left[\sigma(T_s) - \sigma\left(T_{ig}\right)\right]\delta}{\mu\Delta} \qquad (23.21)$$

provided $\sigma(T)$, the surface tension, is known as a function of temperature for the liquid, and Δ can be estimated for the conditions of speed. Also, δ, as in the thermally thick case for solids, is only the physical liquid depth for pools less than about 1 mm and, therefore, must be reinterpreted for pools of larger depth. For example, one might estimate δ as $\sqrt{(\mu/\rho)(\Delta/V)}$ for the deep-pool case.

Typical flame spread characteristics over a liquid fuel are sketched in Fig. 23.16 for liquid methanol from the data of Akita [40]. Below the flashpoint, $T_s < T_{i\ g} \sim 11$ °C, the spread is governed by transport phenomena within the liquid fuel. For initial liquid bulk temperatures above the flashpoint, a flammable mixture

always exists everywhere above the surface so that propagation is governed by gas-phase effects. Above a liquid temperature, which corresponds to stoichiometric conditions above the surface, the flame speed remains constant and usually above the normal premixed laminar flame speed. A study by Ito and Kashiwagi [41] used holographic interferometry to examine the liquid phase for subflashpoint liquid bulk temperatures. They examined the pulsating region depicted in Fig. 23.16, and the adjacent uniform region of spread just below the flame; both appear to contribute to flame spread rate in the uniform region.

Summary

This chapter has provided the practicing engineer with some insight into the nature of fire spread over materials. In general, surface flame spread depends on the heat transfer processes at the flame front. These transport processes depend not only on the fuel but also on the fuel's configuration and orientation and on ambient environmental conditions. Thus, estimates of flame spread require complex analysis and specific material data. The current state of knowledge does provide limited formulas and material data to make some estimates. In this chapter, the full scope of flame spread phenomena has not been addressed. For example, flame spread in mines, ducts, and buildings presents an entirely new and complex array of conditions. Thus, flame spread on materials must be evaluated in the context of their use, and appropriate data must be made available for proper assessments of materials.

Nomenclature

a	$k_f \dot{Q}''_\ell$
b	flame spread acceleration factor $(= (a - 1) - t_{ig}^*/t_b)$
c	specific heat of solid
c_g	specific heat of gas
c_p	specific heat of air
δ	fuel thickness
δ_{fc}	characteristic preheat distance
D	characteristic length of the burning area (height, etc.)
Da	Damköhler number
Δ	distance from the pyrolysis front
ΔH	heat of combustion
ΔH_{ox}	$\Delta H/r$
g	gravitational acceleration
k	$x_f/\dot{Q}_\ell^{*n}$
k'	constant $\left(k^{3/2}/c_p T_o g^{1/2}\right)^{2/3} \dot{Q}_\ell^{2/3}$
k	$x_f/\dot{Q}_\ell$
k_g	gas thermal conductivity
L	heat of gasification
μ	viscosity
q''	heat flux due to gas-phase conduction
q_f''	flame heat flux
q_{fc}''	characteristic flame heat flux
$\dot{Q}_\ell$	heat release rate per unit width
$\dot{Q}_\ell$	dimensionless heat release rate per unit width
$\dot{Q}_{\ell e}^*$	effective heat release rate per unit width
r	stoichiometric mass ratio oxygen/fuel
ρ	density
ϕ	impulse response function
Φ	opposed-flow preheat factor (numerator in n)
σ	surface tension
t	time
t_b	time to local burnout
t_c	characteristic decay time of pyrolysis
t_{ig}^*	characteristic time to ignition
τ	time
T_f	flame temperature
T_{ig}	ignition temperature
T_o	initial surface temperature
T_r	reference temperature
T_s	surface temperature
T_∞	ambient temperature
V_g	gas velocity
V_p	flame spread velocity
x_f	flame length
x_p	pyrolysis front length
x_{po}	pilot flame length
x_{poff}	maximum pyrolysis front length
$Y_{ox,\infty}$	mass fraction of oxygen
x, y	coordinates

Superscripts

$\cdot$	per unit time
$'$	per unit length
$''$	per unit area

References

1. T. Hirano, S. Noreikis, and T. Waterman, "Measured Velocity and Temperature Profiles of Flames Spreading over a Thin Combustible Solid," *Combustion and Flame,* 23, p. 83 (1974).
2. D.D. Drysdale, A.J.R. Macmillan, and D. Shilitto, "King's Cross Fire: Experimental Verification of the "Trench Effect," *Fire Safety Journal,* 18 (1992).
3. D.D. Drysdale, *An Introduction to Fire Dynamics,* 2nd ed., John Wiley and Sons, New York (1999).
4. J.G. Quintiere, *Fundamentals of Fire Phenomena,* John Wiley and Sons, New York (2006).
5. A.C. Fernandez-Pello and T. Hirano, "Controlling Mechanism of Flame Spread," *Combustion Science and Technology,* 32, pp. 1–31 (1983).
6. T. Hirano, "Physical Aspects of Combustion in Fires," in *Proceedings of the 3rd International Symposium on Fire Safety Science,* International Association for Fire Safety Science, Boston, MA, pp. 27–44 (1991).
7. F. Williams, "Mechanism of Fire Spread," in *Proceedings of the 16th Symposium (International) on Combustion,* Combustion Institute, Pittsburgh, PA, pp. 1281–1294 (1976).
8. M.A. Delichatsios, "Modeling of Aircraft Cabin Fires," Technical Report, Factory Mutual Research Corp. (1984).
9. Y. Hasemi, "Thermal Modeling of Upward Wall Flame Spread," in *Proceedings of the First International Symposium on Fire Safety Science,* International Association for Fire Safety Science, Boston, MA, pp. 87–96 (1985).
10. T.I. Eklund, "A Vortex Model for Wall Flame Height," *Journal of Fire Science,* 4, pp. 4–14 (1986).
11. M. Kokkala, D. Baroudi, and W.J. Parker, "Upward Flame Spread on Wooden Surface Products: Experiments and Numerical Modelling," in *Proceedings of the 5th International Symposium on Fire Safety Science,* International Association for Fire Safety Science, Boston, MA, pp. 309–320 (1997).
12. J.S. Newman and C.J. Wieczorek, "Chemical Flame Heights," *Fire Safety Journal,* 39, pp. 375–382 (2004).
13. K.-M. Tu and J.G. Quintiere, "Wall Flame Heights with External Radiation," *Fire Technology,* pp. 195–203 (Aug. 1991).
14. J.G. Quintiere and M. Harkleroad, "New Concepts for Measuring Flame Spread Properties," in *Proceedings of Fire Safety: Science and Engineering,* a symposium sponsored by ASTM Committee E-5 on Fire Standards and the Society of Fire Protection Engineers, ASTM STP 882, ASTM International, W. Conshohocken, PA, pp. 239–267 (1985).
15. B. Karlsson, "Models for Calculating Flame Spread on Wall Lining Materials and the Resulting Heat Release Rate in a Room," *Fire Safety Journal,* 23, pp. 365–386 (1994).
16. D. Baroudi, "A Discrete Dynamical Model for Flame Spread over Combustible Flat Solid Surfaces Subject to Pyrolysis with Charring—An Application Example to Upward Flame Spread," *Fire Safety Journal,* 38, pp. 53–84 (2003).
17. J.G. Quintiere, M. Harkleroad, and Y. Hasemi, "Wall Flames and Implications for Upward Flame Spread," *Combustion Science and Technology,* 48, 3–4, pp. 191–222 (1986).
18. L. Orloff, A.T. Modak, and R.L. Alpert, "Burning of Large-Scale Vertical Surfaces," in *Proceedings of the 16th Symposium (International) on Combustion,* Combustion Institute, Pittsburgh, PA, pp. 1345–1354 (1976).
19. T. Ahmad and G.M. Faeth, "Turbulent Wall Fires," in *Proceedings of the 17th Symposium (International) on Combustion,* Combustion Institute, Pittsburgh, PA, pp. 1149–1160 (1979).
20. M. Sibulkin and J. Kim, "The Dependence of Flame Propagation on Surface Heat Transfer ii. Upward Burning," *Combustion Science and Technology,* 17, pp. 39–49 (1977).
21. K. Saito, J.G. Quintiere, and F.A. Williams, "Upward Turbulent Flame Spread," in *Proceedings of the 1st International Symposium on Fire Safety Science,* International Association for Fire Safety Science, London, pp. 75–86 (1985).
22. D. Baroudi and M. Kokkala, "Analysis of Upward Flame Spread," *VTT Publications,* 89 (1992).
23. Y. Hasemi and N. Yasui, "A Strategy to Develop Engineering Upward Flame Spread Evaluation Methodology Based on the Linearized Flame Height Approximation," *Fire Science and Technology,* 15, 1–2, pp. 17–28 (1995).
24. G. Grant and D.D. Drysdale, "Numerical Modelling of Early Flame Spread in Warehouse Fires," *Fire Safety Journal,* 24, pp. 247–278 (1995).
25. A.C. Fernandez-Pello, "Upward Laminar Flame Spread Under the Influence of Externally Applied Thermal Radiation," *Combustion and Flame,* 17, p. 87 (1977).
26. H. Ingason and J. de Ris, "Flame Heat Transfer in Storage Geometries," *Fire Safety Journal,* 31, pp. 39–60 (1998).
27. Y. Hasemi, M. Yoshida, N. Yasui, and W.J. Parker, "Upward Flame Spread along a Vertical Solid for Transient Local Heat Release Rate," in *Proceedings of the 4th International Symposium on Fire Safety Science,* International Association for Fire Safety Science, Boston, MA, pp. 385–396 (1994).
28. M.M. Delichatsios, P. Wu, M.A. Delichatsios, G.D. Lougheed, G.P. Crampton, C. Qian, H. Ishida, and K. Saito, "Effect of External Radiant Heat Flux on

Upward Fire Spread: Measurements on Plywood and Numerical Predictions," in *Proceedings of the 4th International Symposium on Fire Safety Science,* International Association for Fire Safety Science, Boston, MA, pp. 421–432 (1994).
29. B.Y. Lattimer, S.P. Hunt, M. Wright, and C. Beyler, "Corner Fire Growth in a Room with a Combustible Lining," in *Proceedings of the 7th International Symposium on Fire Safety Science,* International Association for Fire Safety Science, Boston, MA, pp. 419–430 (2002).
30. Y. Hasemi, D. Nam, and M. Yoshida, "Experimental Flame Correlations and Dimensional Relations in Turbulent Ceiling Fires," in *Proceedings of the 5th Asia Oceania Symposium on Fire Science and Technology,* International Association for Fire Safety Science, Boston, MA, pp. 379–390 (2001).
31. Y. Hasemi, M. Yoshida, Y. Yokobayashi, and T. Wakamatsu, "Flame Heat Transfer and Concurrent Flame Spread in a Ceiling Fire," in *Proceedings of the 5th International Symposium on Fire Safety Science,* International Association for Fire Safety Science, Boston, MA, pp. 379–390 (1997).
32. V. Stenstad and B. Karlsson, "Flame Spread on a Solid Wooden Ceiling," *Conference Proceedings of Interflam 2007,* 1, Interscience Communications, London, UK, pp. 45–57 (2007).
33. A.C. Fernandez-Pello, S.R. Ray, and I. Glassman, in *Proceedings of the 18th Symposium (International) on Combustion,* Combustion Institute, Pittsburgh, PA (1981).
34. J. de Ris, "Spread of a Laminar Diffusion Flame," in *Proceedings of the 12th Symposium (International) on Combustion,* Combustion Institute, Pittsburgh, PA, pp. 241–252 (1968).
35. F.A. Albini, "An Overview of Research on Wildland Fire," in *Proceedings of the 5th International Symposium on Fire Safety Science,* International Association for Fire Safety Science, Boston, MA, pp. 59–74 (1997).
36. H. Hayasaka, "Recent Large-Scale Fires in Boreal and Tropical Forests," *Journal of Disaster Research,* 2, 4, pp. 276–283 (2007).
37. P.H. Thomas, "Rates of Spread of Some Wind-Driven Fires," *Forestry,* 44, 2 (1971).
38. K. Kawagoe (ed.), *Fire Safety in Buildings,* Architectural Studies and Engineering Series, 21, Shokokusha (1970) (in Japanese).
39. I. Glassman and F.L. Dryer, "Flame Spreading Across Liquid Fuels," *Fire Safety Journal,* 3, pp. 123–138 (1980).
40. K. Akita, "Some Problems of Flame Spread Along a Liquid Surface," in *Proceedings of the 14th Symposium (International) on Combustion,* Combustion Institute, Pittsburgh, PA, pp. 1075–1083 (1973).
41. A. Ito and K. Kashiwagi, "Characterization of Flame Spread over PMMA Using Holographic Interferometry Sample Orientation Effects," *Combustion and Flame,* 71, pp. 189–204 (1988).

Yuji Hasemi is professor in the Department of Architecture, Faculty of Science and Engineering, Waseda University, Tokyo, Japan.

Smoke Characterization and Damage Potentials

24

Jeffrey S. Newman, Geary G. Yee, and Paul Su

Introduction

Smoke is a mixture of (1) particulates consisting of soot, semi-volatile organic compounds (SVOC), and solid inorganic compounds; and (2) non-particulates consisting of very volatile organic compounds, volatile organic compounds, and liquid and gaseous inorganic compounds. Soot creates bridging between electrical conductors and conveys corrosive products, resulting in damage to electronics and electrical circuits through leakage current and corrosion, while SVOC and non-particulates stain and impart malodor to surfaces. Soot is also a very effective adsorbent and transport mechanism for SVOC, non-particulates and inorganic compounds.

The smoke problem (exclusive of toxicity or escape potential considerations) is ultimately characterized by the quantification of damage due to the deposition of combustion products onto building surfaces and contents (e.g., equipment, furnishings, and commodities). It is instructive to categorize the assessment of smoke damage potentials into two regimes: "far-field" at some distance away from the fire/smoke source and "near-field" close to the source, where it is likely to have simultaneous heat damage (and water damage such as in the case of fire sprinkler protection). In general, fire damage in the "near-field" is dominated by heat/water damage with smoke of a much lesser impact, while smoke can often be the governing damage mechanism in the "far-field" and, due to extent of travel and area coverage, of far greater impact.

Figure 24.1 illustrates, for example, the various components that are necessary to evaluate smoke damage potentials, especially in the "far-field". As shown in the figure, the impact of the smoke deposition profile resulting from smoke release, typically from a fire event, is quantified by the comparison of a defined damage function with its associated damage threshold. As will be subsequently discussed, the damage function can represent a variety of types of smoke damage including leakage current, corrosion and stain/odor. The deposition profile is assessed through the coupling of smoke generation, the characterization of pertinent smoke properties and the transport of smoke resulting in time and spatially resolved concentration profiles. Detection and active response both affect and are affected by these concentration profiles. Knowledge of the smoke deposition velocity is also an important component for the quantification of the resulting smoke deposition profile.

For reference, the solid gray-shaded blocks shown in Fig. 24.1 will be covered in detail in this Chapter while the three unshaded blocks labeled Concentration Profile, Transport and Generation are place holders that are outside of this Chapter's scope. In should be noted that

J.S. Newman (✉)
Retired from FM Global, 1151 Boston Providence Turnpike, Norwood, MA 02062 USA

G.G. Yee • P. Su
FM Global, 1151 Boston Providence Turnpike, Norwood, MA 02062 USA

M.J. Hurley (ed.), *SFPE Handbook of Fire Protection Engineering*,
DOI 10.1007/978-1-4939-2565-0_24, © Society of Fire Protection Engineers 2016

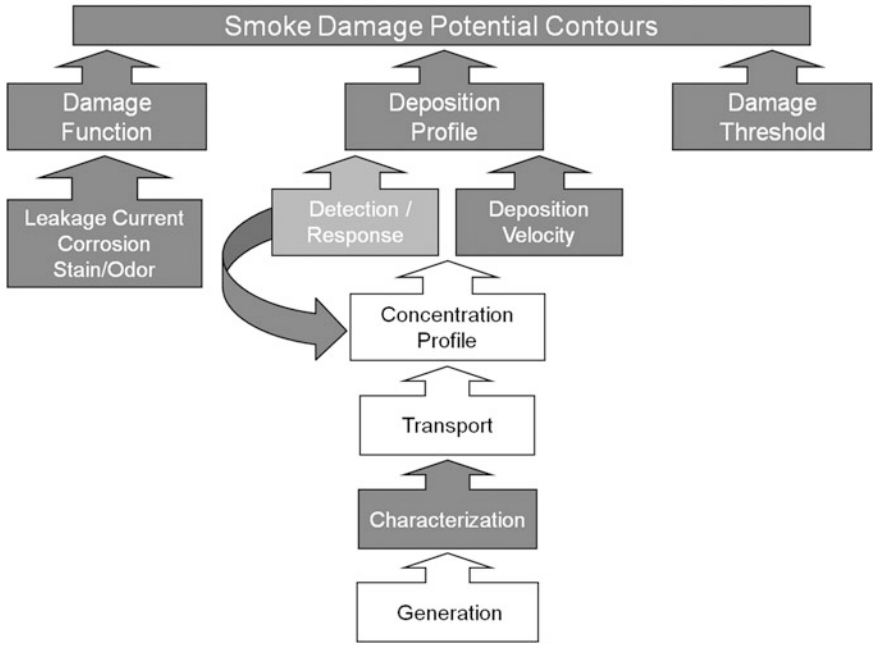

Fig. 24.1 Outline of components to evaluate smoke damage potentials

Generation refers to heat and gas species' production and is a function of the prescribed fire scenario with the content of Chap. 36 of this Handbook providing useful specific smoke and heat generation properties for a variety of materials. Transport and Concentration Profile data can be obtained from any number of physical correlations [1] or computer models [2, 3] coupled with the prescribed Generation information. Finally, Detection/Response is shown in light gray as it is covered only as an overview of important considerations as relating to the smoke Deposition Profile with details on detection given in Chap. 40 of this Handbook.

Deposition Profile

Deposition Velocity

The process by which smoke can deposit on various surfaces is often complex and can result from either a single dominant physical mechanism or a combination of mechanisms including particle inertia, sedimentation or gravitational settling, Brownian diffusion, thermophoresis or thermodiffusion, and electrostatic precipitation [4]. For electrically neutral aerosols, the governing mode of smoke deposition is primarily dependent on whether the transport flow is laminar or turbulent and the particle size.

The flow regime for smoke particle motion can be characterized by the magnitude of the particle Reynolds number, i.e.,

$$\mathrm{Re}_p = \frac{\rho_g d_p V}{\eta} \tag{24.1}$$

where ρ_g is the gas density, d_p the particle diameter, V the particle velocity and η is the gas viscosity.

Laminar Flow ($\mathrm{Re}_p < 1$)

1. For smoke particles >1 μm in diameter, the deposition is primarily due to gravitational settling. Stokes's Law applies to particle motion when inertial forces are negligible compared with viscous forces, and gives the particle terminal settling velocity, V_{TS} as

$$V_{TS} = \frac{\rho_p d_p^2 g}{18\eta} \tag{24.2}$$

where g is gravitational acceleration.

2. For smoke particles <1 μm in diameter, both Brownian diffusion as well as gravitational settling are important deposition mechanisms. An important assumption in Equation 24.2 is that the relative velocity of the gas at the surface of the particle is zero, which is not met for particle sizes that approach the mean free path of the gas. The particles move faster than predicted by Stokes's law and a slip correction factor, C_c, is needed [5]:

$$C_c = 1 + \frac{2.52\Lambda}{d_p} \tag{24.3}$$

where Λ is mean free path, which is 0.066 μm for air at 1 atm and 20 °C. The slip correction factor is a multiplicative factor applied to the right-hand side of Equation 24.2, increasing the terminal settling velocity.

Turbulent Flow ($Re_p > 1$)

1. For smoke particles >1 μm in diameter, the deposition begins to be influenced by both particle inertia as well as viscous effects, which was first shown by Friedlander and Johnstone in 1957 [6]. Inertial deposition occurs when a particle near a wall (surface) in the turbulent region is given sufficient lateral velocity toward the wall to be transported through the laminar layer and deposit on the wall (surface). The particle settling velocity transitions from a d_p^2 dependence in the Stokes regime to a $d_p^{1/2}$ dependence in the Newton drag regime. This transition can be accounted for by the introduction of a drag coefficient, C_D, in the calculation of settling velocity, i.e.,

$$V_{TS} = \left[\frac{4\rho_p d_p g}{3C_D\rho_g}\right]^{1/2} \tag{24.4}$$

Figure 24.2, for example, illustrates the functional relationship between C_D and Re_p for spherical particles. Numerous correlations have been developed to describe the drag coefficient and Reynolds number functional relationship. A particularly useful formulation covers the transition region ($1 < Re_p < 1000$) [4]:

$$C_D = \frac{24}{Re_p}\left(1 + 0.15Re_p^{0.687}\right) \tag{24.5}$$

2. For smoke particles <1 μm in diameter, Brownian diffusion becomes important. The

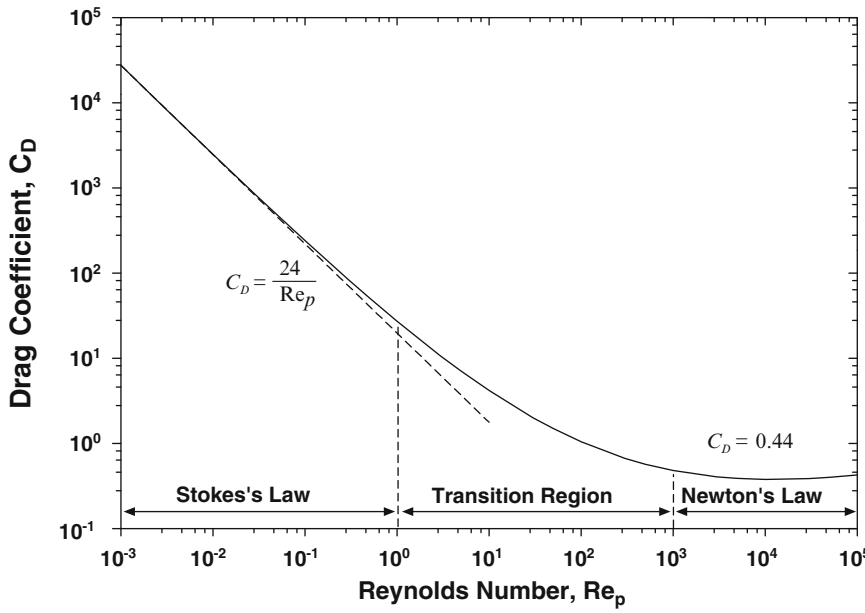

Fig. 24.2 Drag coefficient versus particle Reynolds number

diffusion coefficient of an aerosol/smoke particle can be expressed in terms of particle properties by the Stokes-Einstein derivation [7]. In this derivation, the diffusion force on the particles, which causes the particles' net motion along the concentration gradient, is equated to the force exerted by the gas resisting the particles' motion, i.e.,

$$D = \frac{k_B T C_c}{3\pi\eta d_p} \tag{24.6}$$

where D is the particles' diffusion coefficient, k_B Boltzmann's constant and T is the absolute temperature.

Thermophoresis can be important where large temperature gradients exist, e.g., from a smoke hot layer to a cold surface such as a wall or ceiling in an enclosure. Thermophoresis is the aerosol particle movement that results from the force exerted by a temperature gradient in a gas, resulting in a flow in the direction of decreasing temperature. This would be the dominant mechanism for very small particles <0.1 μm, even at small gradients of 1 °C/cm [4].

In addition, another phenomenon can occur at relatively high smoke concentrations. Cloud settling or mass subsidence occurs when the smoke concentration is sufficient to cause the entire cloud to move as an entity at a velocity significantly greater than the individual particle settling velocity [8]. (An aerosol or smoke cloud is defined as a region of high smoke concentration having a definite boundary in a much larger region of smoke-free air.) The difference in density causes the bulk motion of the smoke particles.

Table 24.1 gives illustrative examples of experimentally measured smoke deposition velocities for "far-field" conditions, i.e., locations away from the combustion/smoke source, where the primary observed deposition mechanism was characterized as gravitational settling [9]. As indicated in the table, the deposition velocities are on the order of 10^{-4} m/s and are quite similar in two different scale enclosures (1 m^3 smoke box and a 1200 m^3 enclosure). For "near-field" conditions, e.g., on the ceiling above a fire or for direct flame impact on an adjacent wall, the primary deposition mechanism is generally accepted as thermophoretic, with the deposition velocity dominated by the local temperature gradient. Thus, the thermophoretic smoke deposition velocity [10–12] is given by:

Table 24.1 Smoke deposition velocities [9]

	Deposition velocity (10^{-4} m/s)	
Material	1.0 m^3 smoke box	1200 m^3 enclosure
Nylon	2.5	–
Polycarbonate	1.9	–
Polyethylene	–	1.2
Polymethylmethacrylate	2.1	1.9
Polypropylene	–	1.3
Polyvinylchloride	1.4	–
Polystyrene	6.9	7.3

$$V_{TH} = \frac{K_{TH}\eta}{\rho_g T}\left(\frac{dT}{dx}\right) \tag{24.7}$$

where the gas properties are evaluated at the film temperature, i.e., the average between the wall and gas temperature at the location of interest. dT/dx is the gas phase temperature gradient at the surface. K_{TH} is the thermophoretic velocity coefficient which approaches a constant value of 0.55 as the Knudsen Number, given by the ratio of the molecular mean free path length Λ to the smoke particle diameter d_p, becomes large (>10) [11]. Examples of the characterization and quantification of fire-induced thermophoretic deposition are given in Refs. [13–16].

Detection Overview

While the detailed design of smoke detection systems is given elsewhere in this Handbook (Chap. 40), it is instructive to present here a brief overview of detection criteria as well as the potential need for specific smoke characteristics. Fire detection is achieved by using various types of detectors: (1) heat detectors (e.g., fixed-temperature, rate-of-rise sensors); (2) chemical compound – smoke detectors (e.g., ionization, photoelectric sensors and gas detectors such as CO or CO_2 sensors);

(3) flame detectors (e.g., ultraviolet and/or infrared sensors), etc. For effective detection of a fire, the most important parameter to evaluate is the total time associated with:

1. the occurrence of a specified hazard to people, buildings and contents created by the fire, t_H;
2. the transit time of the fire product(s) to the detector location, t_t;
3. the fire growth time to reach a detectable level of fire product(s) at the detector location, t_f;
4. the detector response time once t_f has occurred, t_D; and
5. the "effective" response time once the fire has been detected, t_E. The relationship between these times can be expressed as [17, 18]:

$$t_r = t_H - \left(t_t + t_f + t_D + t_E\right) \tag{24.8}$$

where t_r = residual time, which must be greater than or equal to zero. As an example, t_H depends on the defined hazard, which is a function of material properties and configuration and, for the smoke problem, would be the time to reach a specified damage threshold as outlined in Fig. 24.1. Similarly, t_f is identified with the generation step in the figure and t_t with the transport step.

In general, the response of a smoke (or gas species) detector can be treated as a first-order system coupled with a time lag, i.e.,

$$\frac{dC_s}{dt} = \frac{1}{\tau}[C_o(t - t_l) - C_s(t)] \tag{24.9}$$

where C_s is the instantaneous smoke concentration as measured by the detector at time t; C_o, identified with the concentration profile step in Fig. 24.1, is the "true" of reference concentration (outside the detector) at time $t - t_l$; τ is the detector time constant; and t_l is the lag time. Two apparent detector characteristics, τ and t_l, can be noted in Equation 24.9. τ can be thought of as the time constant for the specific sensor used in the detector, while t_l is associated with a delay in smoke (or a specific gas species) transport to the sensor such as through filters, sampling lines, etc. Equation 24.9 can be used to assess the detection time associated with the detection/response step in Fig. 24.1.

Smoke Characterization

The characterization of smoke requires increasingly more specific information concerning instantaneous smoke properties, particularly when assessing fire environments in enclosures. These properties include volume fraction, mass concentration, generation efficiency, particle size and yield. Smoke characteristics and yields of chemical compounds can change dramatically with a change in ventilation conditions, such as in an enclosure environment where the supply of air may be restricted. Quantifying changes in smoke properties have been shown to be useful in addressing the impact of ventilation on fire chemistry, which in turn relates to the smoke damage potential of a given fire scenario.

Optical techniques to characterize smoke are especially attractive since they provide continuous measurements without disturbing the environment. When a monochromatic beam of light passes through smoke, the fraction of light transmitted can be expressed as

$$\frac{I}{I_o} = \exp(-OD_\lambda l) \tag{24.10}$$

where I is the transmitted intensity; I_o is the initial intensity; OD_λ is the optical density (also referred to as the turbidity or extinction coefficient) of the smoke (m^{-1}); and l is the optical path length (m). The optical density is an intricate function of the smoke particle diameter, the smoke size distribution, the incident light wavelength and the complex refractive index of the smoke. It has previously been shown that the smoke volume fraction (i.e., the ratio of the smoke particle volume to the total gas volume) for a variety of materials can be related to the optical density through the following expression [19]:

$$f_v = \frac{OD_\lambda \lambda}{c} \tag{24.11}$$

where λ is the incident wavelength; and c is defined as an average coefficient of smoke extinction. For over-ventilated conditions, the

smoke mass concentration, C_s (kg/m^3) can be related to the smoke volume fraction through the smoke particle density, i.e.,

$$C_s = \rho_s f_v = \frac{\rho_s OD_\lambda \lambda}{c} \tag{24.12}$$

Reported values [19–23] for ρ_s typically range from 800 to 1800 kg/m^3, with 1100 to 1500 kg/m^3 common values. This perceived discrepancy in density is primarily related to the measurement technique, although combustion conditions and the specific material smoke source can influence the "apparent" density. For example, a value of 1100 kg/m^3 has been shown to be the resulting "apparent" density for a wide range of materials during over-ventilated flaming combustion and is recommended when optical methods are used to assess the relationship represented by Equation 24.12 with a value for c of 7.0 [19]. This value for the density has also been shown to derive consistent smoke yields for various materials. However, it is more important to maintain the ratio of ρ_s to c as a constant than to use a specific value for the smoke particle density. Thus, if value of 8.0 is used for c, a value of 1300 kg/m^3 should be used for the corresponding density. It should be noted that the ratio of $c/\rho_s\lambda$ is equivalent to the often referenced mass specific extinction coefficient, which has been extensively tabulated and generally shown to be relatively independent of fuel type [24–27].

Smoke Particle Size

Smoke particle sizes are typically characterized by specifying some representative particle diameter with a corresponding size distribution. Particle size characteristics are often represented by a log-normal particle size distribution function. For this type of distribution, the log of the particle diameter follows a Gaussian distribution. Therefore, the geometric mean diameter, d_g, is given by:

$$\ln d_g = \frac{\sum n_i \ln d_i}{N} \tag{24.13}$$

where n_i is the number of particles with diameter d_i and N is the total number of particles. The geometric standard deviation, σ_g, is given by:

$$\ln \sigma_g = \left[\frac{\sum n_i \left(\ln d_i - \ln d_g\right)^2}{N-1}\right]^{1/2} \tag{24.14}$$

The geometric standard deviation is dimensionless with a value equal to or greater than 1.0. One geometric standard deviation represents the range of particle sizes from (d_g/σ_g) to $(d_g \times \sigma_g)$. A variety of representative diameters can be used based on particle volume or mass. (For example, Refs. [15] and [30] tabulate the geometric particle diameters and distributions for a number of materials under both flaming combustion and pyrolysis.) A particularly useful particle representation uses the concept of an aerodynamic equivalent diameter (d_a), which is the diameter of a unit-density sphere having the same gravitational-settling velocity as the measured particle. The aerodynamic equivalent diameter takes into account the shape, roughness, and aerodynamic drag of the particle [4]. For example, Stokes's law, given in Equation 24.2, rewritten in terms of d_a and a standard particle density, ρ_0 (1000 kg/m^3) gives the following for the terminal settling velocity, V_{TS} in air:

$$V_{TS} = \frac{\rho_0 {d_a}^2 g}{18\eta} \tag{24.15}$$

Table 24.2 presents the aerodynamic equivalent mass mean diameter, d_{ag} for smoke generated from flaming plastic fires in various scale enclosures [9] and ducts/low velocity wind tunnels [28, 29]. The width of the distribution, σ_g is also given for reference. References [15] offers a detailed summary review of aerodynamic diameters from a number of additional materials including gases and liquids under various other configuration and combustion conditions.

Table 24.2 Aerodynamic mass mean diameter of smoke from flaming plastics[a]

Material	d_{ag}, μm	σ_g	Environment
Nylon	0.4	2.0	1.0 m^3 smoke box
Polycarbonate	3.0	3.4	1.0 m^3 smoke box
Polyethylene	1.0	2.5	1200 m^3 enclosure
Polymethylmethacrylate	2.3	4.4	1200 m^3 enclosure
	0.7–1.0	NR	0.37 m^2 duct [28]
Polypropylene	1.2	2.0	1200 m^3 enclosure
Polyurethane	2.0	1.8	0.18 m^2 duct [29]
Polyvinylchloride	1.1	1.8	1.0 m^3 smoke box
Polystyrene	2.0	2.6	1.0 m^3 smoke box
	2.4	2.1	1200 m^3 enclosure
	1.5–2.5	NR	0.37 m^2 duct [28]

NR- Not Reported
[a]Data from Ref. [9] except as noted

Damage Functions

Leakage Current

Leakage current between two conducting elements occurs as a result of circuit bridging due to the presence of a conducting medium between the elements, such as water, conductive ions, soot, or dust. The increase of leakage current on electronic circuit boards can change overall circuit characteristics, e.g., degrade and/or damage circuit properties. This principle has been used to design a leakage current target for the measurement of smoke corrosivity [31–33]. The target, as shown in Fig. 24.3, has a comb-like pattern made of thin strips of copper with 40 insulating spaces between them. The dimensions of the target are shown in the figure. Specifically, for example, with respect to the manufacture of semiconductors, leakage current is uncontrolled ("parasitic") current flowing across region(s) of semiconductor structure/device in which no current should be flowing. Leakage is one of the main factors limiting increased computer processor performance. The presence of ionic compounds and soot in smoke deposited on the surface of a semiconductor is expected to damage the processor's functionality through an increase in leakage current.

An example of leakage current (LC) data for polycarbonate smoke deposition versus relative humidity (RH) is shown in Fig. 24.4 [34]. Values of measured LC somewhat surprisingly remain nearly constant at $1.8 \pm 0.3 \times 10^{-4}$ A over the range of relative humidity from 30 % to 90 %. For reference, measured LC data for targets without exposure are also plotted in the figure, and as expected are much smaller than for targets exposed to polycarbonate smoke. For example, at 90 % RH, the LC of an unexposed target at 1.1×10^{-6} A is much smaller than the LC of 1.8×10^{-4} A for a target exposed to the polycarbonate smoke. This indicates that the effect of soot bridging is the major contributor to the increase of LC for targets exposed to polycarbonate smoke and the contribution due to increase of RH is relatively minor. Reference [34] also gives similar data for nylon and polyvinylchloride. Figure 24.5 presents normalized smoke leakage currents for nylon, polycarbonate and polyvinylchloride. The data in the figure were normalized by dividing the leakage current results as illustrated in Fig. 24.4 by the average smoke deposition (g/m^2) which occurred over the duration of the LC target exposure. As indicated in Fig. 24.5, the average normalized LC ranges from $7.2 \pm 0.5 \times 10^{-5}$ A-m^2/g for nylon to $6.1 \pm 0.9 \times 10^{-4}$ A-m^2/g for polycarbonate. Relative humidity appears to have a limited effect, with a trend to slightly lower normalized LC above 60 % RH. Table 24.3 summaries the average results for the three materials studied.

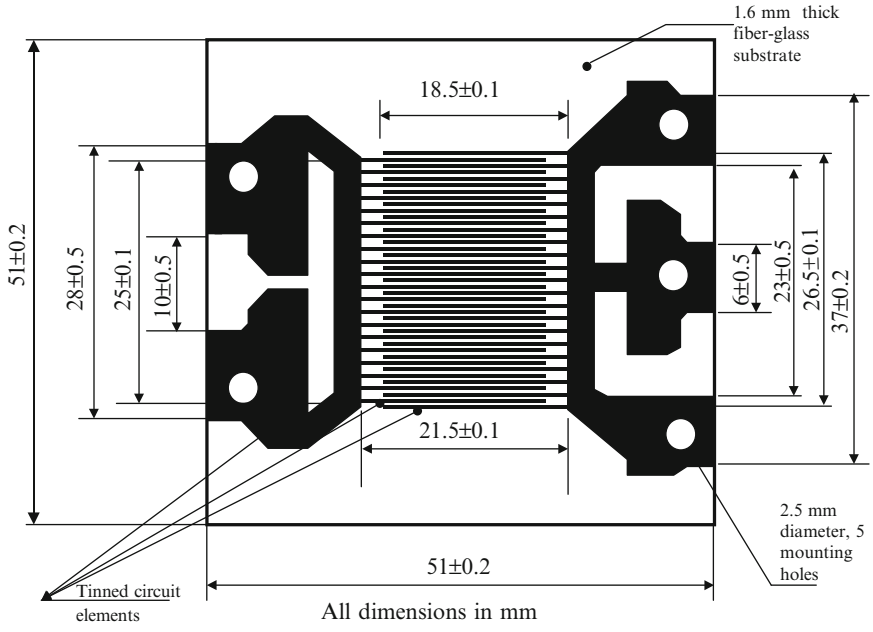

Fig. 24.3 Sketch of leakage current target (Taken from Ref. [32])

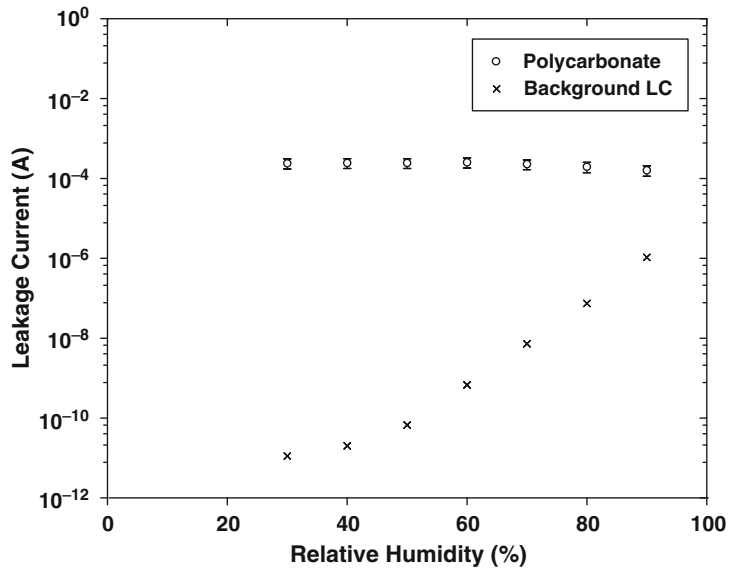

Fig. 24.4 Leakage current versus RH for LC targets exposed to polycarbonate smoke

Corrosion

Corrosion involves the reaction between a metal or alloy and its environment. It is an irreversible interfacial reaction, which causes the gradual deterioration of metal surface by moisture and corrosive chemicals. In aqueous or humid environments, corrosion is an electrochemical reaction in nature; it involves electron (e^-) transfer between anodic and cathodic

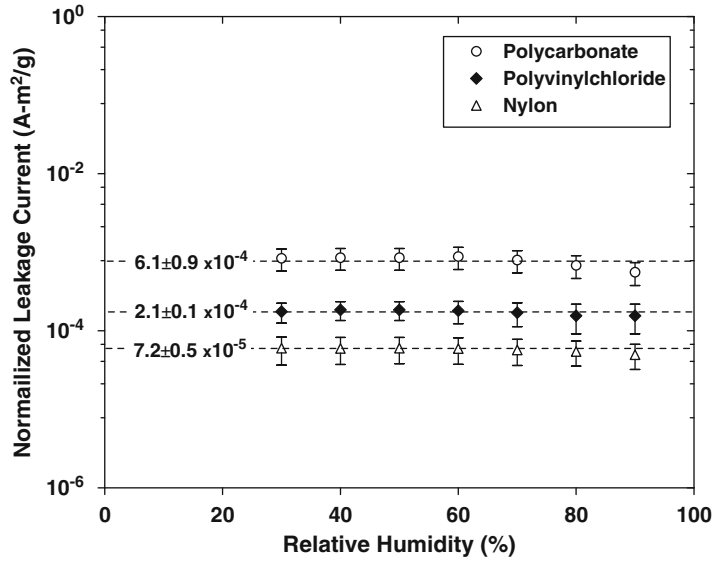

Fig. 24.5 Normalized leakage current versus relative humidity

Table 24.3 Leakage currents [34]

Material	Average leakage current (10^{-5} A)	Average smoke deposition (g/m^2)	Average normalized LC (10^{-4} A-m^2/g)
Nylon	18 ± 3	0.30 ± 0.11	6.1 ± 0.9
Polycarbonate	9.6 ± 0.5	0.45 ± 0.02	2.1 ± 0.1
Polyvinylchloride	0.94 ± 0.07	0.13 ± 0.02	0.72 ± 0.05

reaction sites. For corroding metals, the anodic reaction is the oxidation of a metal to its ionic state:

Anodic reaction:	$M \Rightarrow M^{n+} + ne^-$	[1]
Specific examples of anodic reactions:	$Cu \Rightarrow Cu^{2+} + 2e^-$	[2]
	$Al \Rightarrow Al^{3+} + 3e^-$	[3]
	$Sn \Rightarrow Sn^{2+} + 2e^-$	[4]

The cathodic reaction is a reduction process. For metallic corrosion, cathodic reactions like Reactions [5–7] are frequently encountered. In acid solutions, hydrogen evolution and oxygen reduction reactions (Reactions [5] and [6]) are the main cathodic reactions. In neutral or basic solutions, oxygen reduction reaction (Reaction [7]) is the primary cathodic reaction.

Cathodic reactions:		
Hydrogen evolution	$2H^+ + 2e^- \Rightarrow H_{2(g)}$	[5]
Oxygen reduction (acid solutions)	$O_2 + 4H^+ + 4e^- \Rightarrow 2\,H_2O$	[6]
Oxygen reduction (neutral or basic solutions)	$O_2 + 2H_2O + 4e^- \Rightarrow 4OH^-$	[7]

In general, corrosion caused by smoke is due to the presence of inorganic anions in smoke such as chloride (Cl^-), bromide (Br^-), and fluoride (F^-) plus moisture in the environment. In fires, corrosive combustion products such as HCl, HBr and HF are emitted along with the other combustion products, which are present as gases, liquids and solids. The corrosive combustion products are generally emitted as gases and liquids with inorganic anions in the structure. The non-corrosive combustion gases and liquids are emitted as inorganic and organic compounds and water, whereas solids are emitted as soot and inorganic metals and dust. The solid combustion products are broadly defined as particulates and the gaseous and liquid combustion products are broadly defined as non-particulates. The mixture of particulates and non-particulates that include products with inorganic atoms is defined as smoke. The main hazards regarding the exposure

Table 24.4 Failure mechanisms and causes for electrical/mechanical equipment damage

Failure mechanism	Failure cause
Corrosion	Metal contacts, cause open circuits
Shorts	Circuit bridging between contacts, cause leakage of current and shorts
Contact resistance	Coating of electrical contacts
Binding	Mechanical equipment (timers, hard disk drives, etc., impeded)

of electrical/mechanical equipment to smoke is the damage due to circuit bridging, corrosion, and binding, defined as smoke corrosivity. Circuit bridging occurs in reducing surface insulation and increasing leakage current for digital safety systems, multiplexers and functional circuit boards. In contrast, corrosion damage by acids and anions from smoke can be observed either short term or long after the fire. Smoke contamination also leads to other types of electrochemical corrosion degradation of circuit boards, such as dendrite metal migration between conduction lines, localized corrosion of uncoated metal wires and contacting areas, etc. Failure mechanisms and causes for electrical/mechanical equipment as a result of exposure to smoke are listed in Table 24.4 [35, 36].

The linear polarization resistance (LPR) and electrical resistance techniques based on electrochemistry can be used to evaluate smoke-induced corrosion on metals. The LPR technique enables the corrosion rate of metals in solution to be measured as in milli-inch per year (mpy). For example, the smoke and acid gases produced during material combustion can be captured and passed through a water-based solution. The corrosivity (or corrosion rate) of the solution can then be measured by the LPR technique. Table 24.5 shows LPR data for nylon, polycarbonate and polyvinylchloride from Ref. [34]. The normalized corrosion rate is defined as corrosion rate normalized with the amount of soot deposited on filters prior to acid gas collection in a water-based solution. Solutions from the polyvinylchloride tests demonstrated the highest corrosion rates among these three materials

Table 24.5 Smoke corrosion rates of copper [34]

Material	Corrosion rate (mpy)	Average smoke deposition on filters (10^{-5} g/m^2)	Average normalized corrosion rate (10^5 mpy-m^2/g)
Nylon	0.78 ± 0.17	0.38 ± 0.13	2.40 ± 1.50
Polycarbonate	0.03 ± 0.02	1.24 ± 0.43	0.03 ± 0.03
Polyvinylchloride	13.31 ± 4.3	2.19 ± 0.95	6.25 ± 0.76

averaging 13.31 mpy, while solutions from the polycarbonate tests demonstrated the lowest corrosion rates averaging 0.03 mpy. Similarly, solutions of polyvinylchloride tests demonstrated the highest normalized corrosion rates among these three materials tested averaging 6.25×10^5 mpy-m^2/g; solutions of polycarbonate tests exhibited the lowest normalized rates averaging 0.03×10^5 mpy-m^2/g.

Smoke Stain

In the characterization of staining of a surface from smoke deposition, it is useful to understand the mechanism by which the surface can undergo a discernable change in appearance. When light strikes an opaque object, as shown in Fig. 24.6, the total amount of reflected light is characterized as two distinctly different light reflections from the surface: specular reflection and diffuse reflection. Specular reflection is light that is directed at an angle opposite to the incident light and is perceived by the observer to be glare caused by the shininess or glossiness of the sample. To see the apparent color of the sample, observers must move their eyes away from the glare (specular) and concentrate on examining the diffuse (scattered) reflectance from the sample. Any changes in this diffuse reflectance due to deposition of smoke would be an indication of staining, i.e., potential smoke damage. Brightness is defined as the diffuse reflectivity of an opaque surface to light in the blue portion of the spectrum. Brightness is typically measured at an effective wavelength of 457 nm. Light of this wavelength appears blue to the human eye. In the appearance of paper, for example, brightness is an especially important property not only

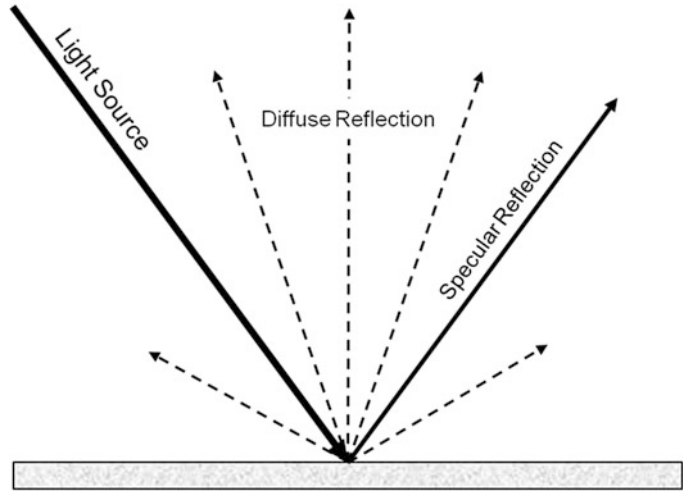

Fig. 24.6 Reflectance of light

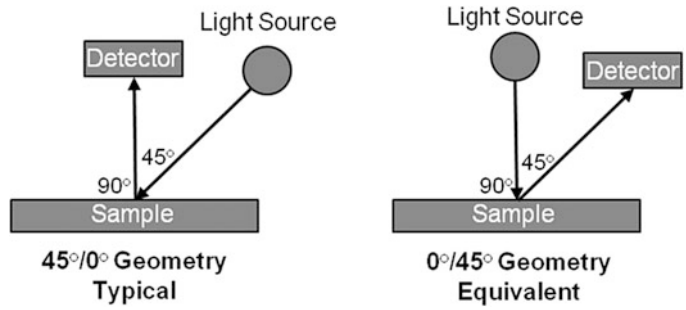

Fig. 24.7 Measurement of brightness

because of its aesthetic value, but also because of its effect on legibility and contrast between print and paper. Brightness should not be confused with "whiteness". The degree of whiteness of a paper conveys information on its color neutrality. It should be noted that the measurement of brightness is also an important tool in the characterization of the appearance of textiles, especially in the effectiveness of detergent cleaning agents.

A widely accepted method of brightness measurement, designated "Brightness 457", is described by TAPPI (Technical Association of the Paper Industry) Standard T 452 [37]. The method evaluates brightness at an effective wavelength of 457 nm and is illustrated by Fig. 24.7. Brightness 457 measures brightness with directional light incident at 45° with respect to the normal to the sample as shown by the illustration on the left in the figure. The detector is mounted on the normal and receives light reflected along the normal-conditions sometimes expressed by the shorthand notation (45° illumination, 0° observation). An equivalent geometry is shown on the right in the figure, where illumination is provided on the normal and the detector is located on the incident at 45° and can be described as (0° illumination, 45° observation). While the difference in optical geometry between the two configurations leads to equivalent brightness readings, the 0°/45° geometry in general provides a somewhat better measurement for surfaces that may be coated non-uniformly.

Figure 24.8 plots data from Ref. [38] for the characterization of smoke deposition from the combustion of polystyrene, polymethylmethacrylate and paper (i.e., liner board used in the manufacture of corrugated boxes) onto 47 mm dia filter targets. In the figure, the brightness change is plotted as a percent difference

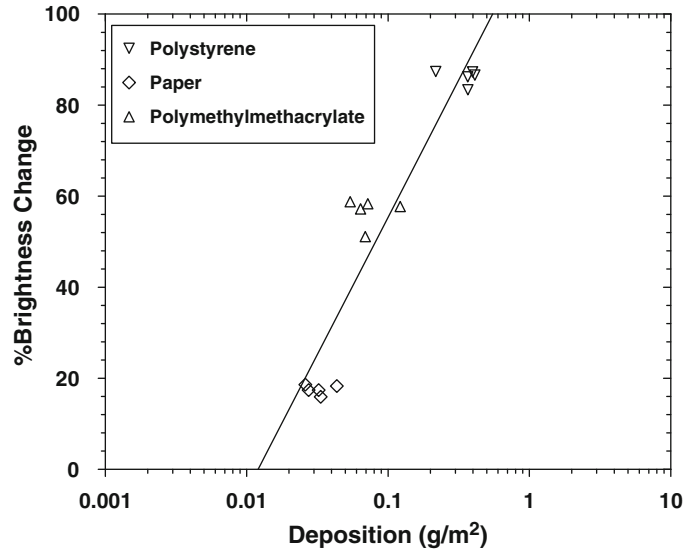

Fig. 24.8 Change in brightness versus deposition

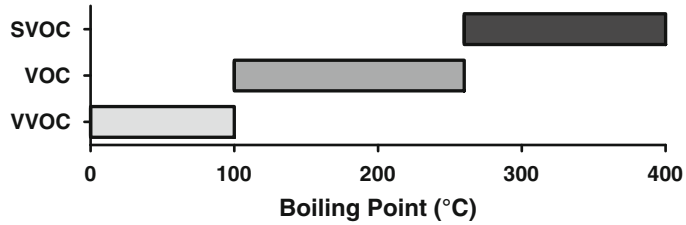

Fig. 24.9 Classification of volatile organic compounds by boiling point

from an uncontaminated reference of the filter substrate (polytetrafluoroethylene) versus smoke deposition for each of the tested materials. The black line through the data in the figure is given by

$$\%\,Brightness\ Change = 116 + 26.2 \times \ln Deposition \tag{24.16}$$

where *Deposition* has units of g/m^2. See Ref. [38] for additional experimental details including a calibration of the brightness measurement technique with carbon black.

Smoke Odor

While the particulate portion of smoke deposition consisting of solid soot particles, semi-volatile organic compounds (SVOC) and solid inorganic compounds is responsible for stain damage, the non-particulates in deposited smoke are the likely source for any potential odor damage. Smoke deposited from fires is highly porous [20] and can contain substantial quantities of adsorbed organic compounds [39, 40]. These non-particulates typically consist of volatile (VOC) and very volatile (VVOC) organic compounds that have boiling points between 0 °C and about 260 °C. Figure 24.9 illustrates the approximate boiling point ranges for each of the three classes of volatile organic compounds. Potential odors derived from smoke deposited after a fire can result from either dislodged smoke particles containing odor causing VOCs and VVOCs or direct desorption of organics from surfaces contaminated by smoke. The quantification of odor is highly complex and can require the quantification of five basic properties: (1) intensity, (2) degree of offensiveness, (3) character, (4) frequency and (5) duration.

Table 24.6 Total adsorbed volatiles onto deposited smoke [38]

Material	Volatile mass fraction (g volatiles/g deposited smoke)
Paper	0.31 ± 0.08
Polystyrene	0.35 ± 0.06
Polymethylmethacrylate	0.11 ± 0.02

The combination of these properties characterizes the perception of odor and ultimately any potential damage or risk contributed by smoke particles [41].

It can be useful to take a global approach to quantify odor from smoke due to the complexity of characterizing the perception of odor. For example, all volatile and semi-volatile organic compounds (VOCs and SVOCs) can be treated as potential odorants and consolidated into a single value associated with the deposition of smoke from the combustion of a given material. A useful technique [38] is to pass a known volume of smoke through quartz filter targets. Any deposited smoke is then analyzed by standard Thermal Desorption-Gas Chromatography-Mass Spectroscopy (TD-GC-MS) methods to assess the quantity and character of any adsorbed volatiles. Table 24.6 summarizes the total measured volatiles using this methodology normalized by the total mass of deposited smoke for paper, polystyrene and polymethylmethacrylate for data presented in Ref. [38].

While little is known about the quantitative adsorption of organics onto smoke particulates, the adsorption capacity of activated carbon has been widely investigated and has been shown to be very close to smoke particulates as well as characterized with similar adsorption mechanisms. [42] Therefore, the following analysis and discussion is directed toward activated carbon as a viable surrogate for the understanding of adsorption of organics onto smoke particulates.

The adsorption process of volatile organics onto activated carbon can be evaluated by assuming that a dynamic equilibrium, as proposed by Langmuir [43], exists between adsorbed gaseous molecules and the free gaseous molecules:

$$A_g + S \overset{adsorption\rightarrow}{\leftarrow desorption} AS \tag{24.17a}$$

where A is a gas molecule and S is a smoke particulate adsorption site. At equilibrium, the overall rate constant K is given by:

$$K = \frac{k_{ad}}{k_d} = \frac{[AS]}{[A_g][S]} \tag{24.17b}$$

where k_{ad} is the adsorption rate constant, k_d is the desorption rate constant and the bracketed quantities are the molecular concentrations. Using benzene as a representative VOC present in typical smoke from polymeric materials, the relative adsorption and desorption rate processes can be assessed. Figure 24.10, for example, plots the *ln* of the rate constant versus the inverse of the absolute temperature (1/K) [44]. As shown in the figure, the desorption rate of benzene gas molecules has a much stronger dependency on temperature than the adsorption rate. For example, desorption rates reduce by a factor of about 100 for a 100 °C drop in temperature, while adsorption rates reduce by less than a factor of 10 for the same temperature drop. The divergence in adsorption/desorption rates is illustrated further in Fig. 24.11, where the *ln* of equilibrium constant is plotted versus 1/K. Therefore, devolatilization rates of organics from deposited smoke particulates are expected to be low at normal ambient temperatures.

Figure 24.12 gives the adsorption capacity of benzene onto activated carbon versus the concentration of benzene relative to the saturation concentration. As shown in the figure, the adsorption capacity reaches a plateau for a mass fraction of about 0.38 (g of benzene adsorbed per g of activated carbon). This is similar to the mass fractions of VOCs found to be adsorbed on smoke deposited from paper and polystyrene, 0.31 and 0.35, respectively. This would suggest that the deposited smoke from these two materials is nearly saturated with volatile organic compounds. An explanation for lower mass

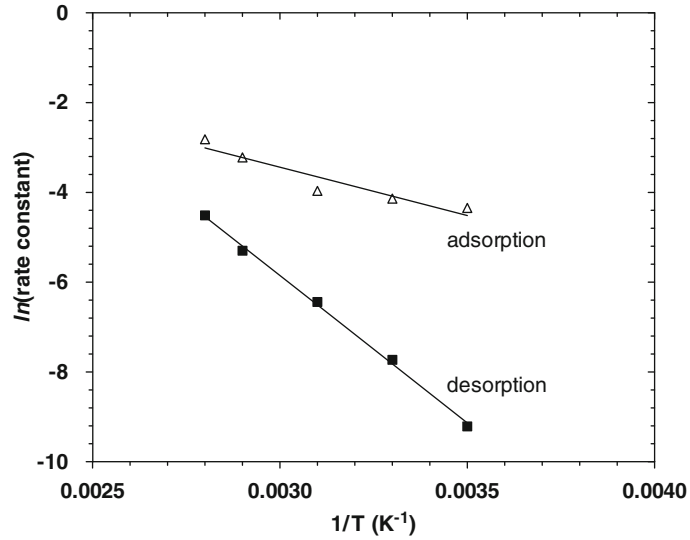

Fig. 24.10 Adsorption-desorption rate constants for benzene onto activated carbon

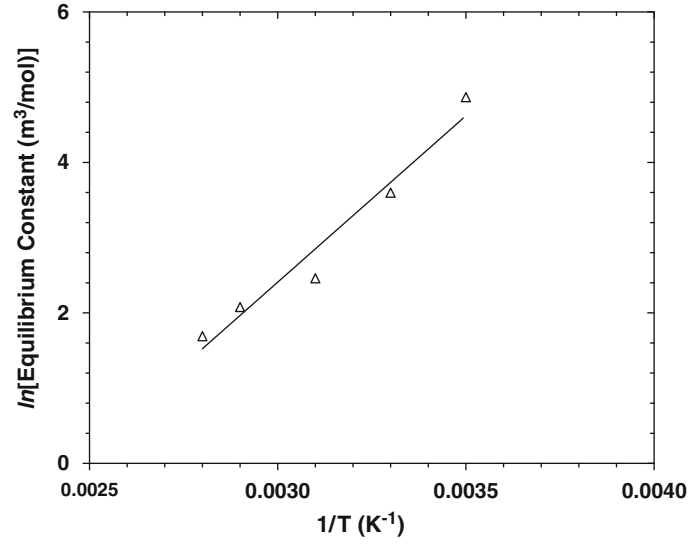

Fig. 24.11 Equilibrium constants for benzene onto activated carbon

fraction of 0.11 found for polymethylmethacrylate may reside in the somewhat unique combustion mechanism for polymethylmethacrylate, which initially decomposes into a monomer leading to the production of small highly combustible molecules [45]. This process could likely result in the production of fewer intermediate stable VOC products. Finally, for comparison purposes, Table 24.7 gives activated carbon adsorption capacities for two other common VOCs found in deposited smoke – acetone and toluene [46]. Similar capacities as previously discussed for benzene are noted and appear to be independent of the moisture condition of the activated carbon.

Damage Thresholds

The specification of damage thresholds can be rather arbitrary depending on the type of anticipated damage. For example, leakage

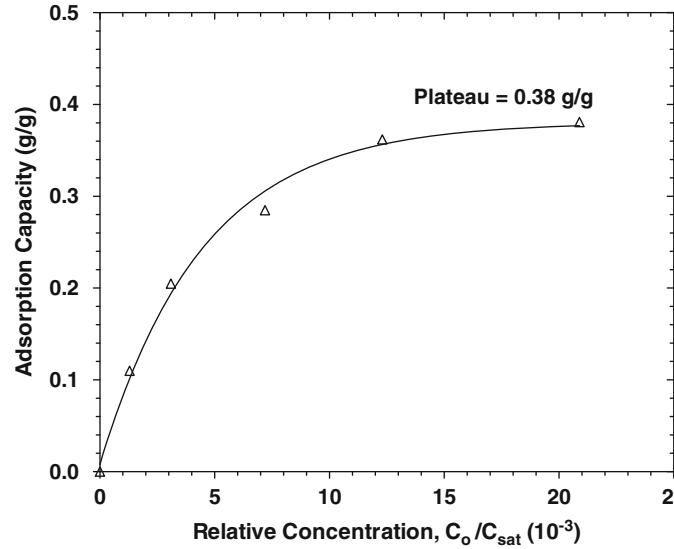

Fig. 24.12 Adsorption capacity of benzene onto activated carbon

Table 24.7 Activated carbon adsorption capacities [46]

	Activated carbon	
VOC	State	Adsorption capacity (g/g)
Acetone	Dry	0.33
	Wet	0.34
Toluene	Dry	0.41
	Wet	0.41

Table 24.8 Leakage current classifications

Leakage current (A)	Class
$LC < 10^{-8}$	Very low
$10^{-6} > LC > 10^{-8}$	Low
$LC > 10^{-6}$	High

current damage thresholds, while defined broadly, are relatively well-specified. Conversely, stain and odor thresholds are primarily driven by perception. Suggested specific thresholds are covered in the following discussion for leakage current and stain. A methodology for setting of odor thresholds is also proposed.

The classification or ranking of leakage current (LC) has been proposed in an ASTM draft, as shown in Table 24.8 [47]. Leakage currents less than 10^{-8} A are classified as very low, currents between 10^{-8} and 10^{-6} A are classified as low, while currents greater than 10^{-6} A are classified as high. This classification system can be used as one of the criteria for evaluating smoke damage of electrical circuits by measuring the value of LC for targets exposed to different materials as given previously in Table 24.3. The specific application would be used to denote the target LC levels, with smoke exposure to highly sensitive electronic components most likely in the very low range (e.g., semiconductor fabrication facilities and data centers) and machine components in the low range (e.g., machine shops and printing facilities).

As noted above, stain and odor damage thresholds are driven by human sensory perception unlike damage thresholds for leakage current. The field of psychophysics [48], for example, attempts to quantitatively study perception through the functional relationships between the physical properties of stimuli and the psychological responses to them. In particular, one important quantifier is the "Difference Threshold" (or "Just Noticeable Difference" often abbreviated as JND). The JND is the minimum amount by which stimulus intensity must be changed in order to produce a noticeable variation in sensory experience. Weber's Law

Table 24.9 Weber fractions for various stimuli

Stimuli	Weber fraction
Brightness	0.079
Loudness	0.048
Finger span	0.022
Heaviness	0.020
Line length	0.029
Taste	0.083
Electric shock	0.013
Odor	0.25

[48] (also known as the Weber–Fechner law) states that the JND depends on a percentage of change in a stimulus rather than on a fixed amount of change:

$$k_W = \Delta S/S \tag{24.18}$$

where ΔS represents the difference threshold (JND), S represents the initial stimulus intensity and k_W signifies that the proportion on the right side of the equation remains constant despite variations in the S term. k_W is typically referred to as the Weber fraction and is given in Table 24.9 for sensory perception response to a number of different stimuli [49, 50].

The Weber fractions for brightness and odor, i.e., 0.079 and 0.25, respectively, are of particular interest for assessing smoke damage thresholds for stain and odor. Applying a brightness threshold of 0.079 [corresponding to a % *Brightness Change* of 7.9 % in Equation 24.16] to the smoke deposition data in Fig. 24.8, results in a smoke damage threshold of ~0.015 g/m^2 for smoke stain.

Odor thresholds for smoke damage are somewhat more difficult to assess than those for stain. A useful approach is first to establish a reasonable odor baseline without smoke deposition for the target surface. If, for example, the target surface is a typical packaging material, then the inherent concentration of volatile organic compounds (VOCs) of the packaging would be relevant. For instance, odor in recycled packaging papers has been related to several VOCs such as phenols and aldehydes [51]. The typical average concentration is about 100 ppm (or 1.0×10^{-4} g VOC per g paper). Similar or higher VOC concentrations have been found for other types of papers and plastic packaging materials [52–54]. The food and pharmaceutical industries are particularly concerned with odor and/or taste transfer from VOCs contained in product packaging. For example, the sources of VOCs in paper packaging can be from the original paper manufacturing process, including the paper itself, inks, binders, adhesives and coatings. Recycled paper, especially from newspaper, can have VOC contents of up to 4000 ppm (or 4.0×10^{-3} g VOC per g paper) [55].

As a further illustration, the baseline odor threshold for a typical paper boxed commodity stored in a warehouse can be determined by a combination of three factors: (1) the packaging VOC content, (2) the paper density (often referred to as basis weight or grammage in g/m^2) and (3) the odor difference threshold or Weber fraction (i.e., 0.25). Typical paper densities for liner board used to construct the paper box range from a low of 125 g/m^2 to a high of over 440 g/m^2. Using 100 ppm as a typical average VOC content with a paper density of, for instance, 200 g/m^2, the baseline volatile organic content of the target paper surface can be estimated as:

$$\left[\frac{100\,x\,10^{-6}\,g\,VOC}{g\,paper}\right] \times \left[\frac{200\,g\,paper}{m^2\,paper}\right] = \left[\frac{0.020\,g\,VOC}{m^2\,paper}\right]$$

The odor threshold corresponding to the JND would be 25 % higher or 0.025 g VOC/m^2.

Example Application to Semiconductor Fabrication Facilities

Semiconductor fabrication facilities are high-value properties that contain very expensive process equipment and related support equipment. During semiconductor fabrication, process liquid heating and other electrical sources present potential ignition hazards. Note that semiconductor fabrication cleanrooms are always provided

with sprinkler protection, and the likely fire scenario involves combustible plastics resulting in complete equipment loss due to heat damage in the vicinity of the fire origin, and partial or complete loss at some distance from the fire origin due to smoke damage. The majority of smoke damage is due to surface contamination, leading to leakage current and long-term corrosion on electronic products and equipment. As previously described, this type of damage can be linked to smoke deposition by the use of damage functions. Therefore, the estimation of smoke damage in semiconductor cleanrooms requires a methodology that connects the fire source and the damage function, and allows for mapping the damage area for a given facility size.

Damage Estimation Model

The general model for estimating smoke damage is described in detail in Ref. [56], and includes the definition of the fire source based on experiments, simulation of smoke transport and deposition using numerical models, and calculation of smoke damage based on measurements. When fire scenarios involve fire growth and sprinkler suppression, current theories and models can not predict either the burning rate or the smoke generation rate and the fire source needs to be defined based on experimental data. Figure 24.13 illustrates the procedures and data sources for this general model. It should be noted that an important assumption and limitation of the transport model is that CO_2 is an adequate surrogate for smoke, with smoke particles transporting as the gas phase. This assumption may not hold for larger smoke particles.

Fire Scenario and Results

The selected fire scenario [56] uses a numerical simulation following the geometry of a typical bay-and-chase cleanroom configuration. Figure 24.14 shows a cleanroom module used in the numerical simulation. This module stands for a section of four pairs of clean bays in the middle of the left half of the cleanroom. The clean bays with wet bench and etch tools (two right bays) were duplicated to create a four-bay long module. The simulated fire source consists of a growing polycarbonate fire within a cleanroom stocker which peaks at a heat release rate of about 300 kW. (Stockers are self-contained units used for the storage of in-process and finished semiconductor wafers, which are commonly stored in plastic boxes in open shelves within the stocker.) Figure 24.15 plots the maximum expected smoke deposition versus radial distance from the stocker fire. The damage functions for polycarbonate (i.e., leakage current from Table 24.3 and corrosion from Table 24.5) can be used to convert the smoke deposition values in the figure into the corresponding expected leakage currents and corrosion rates. These results are given in Fig. 24.16. Finally, applying the proposed leakage current damage thresholds as given in Table 24.8, yields expected smoke damage potentials as illustrated in Fig. 24.17.

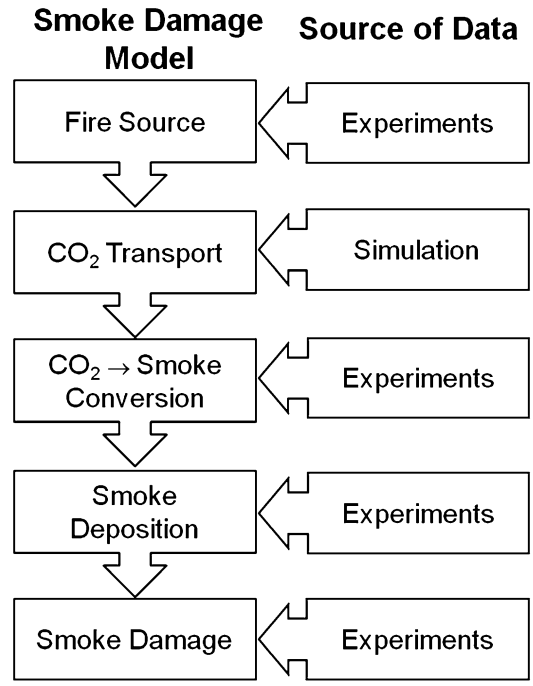

Fig. 24.13 General methodology for modeling smoke damage

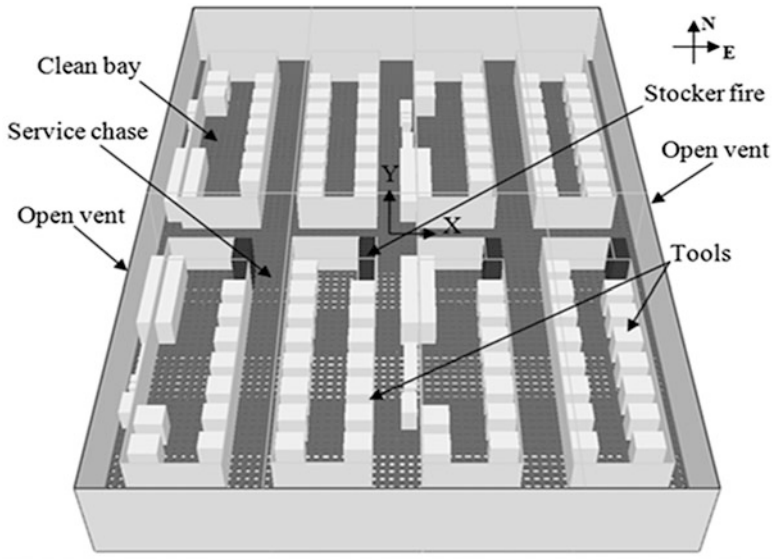

Fig. 24.14 Cleanroom module used in numerical simulation [56]

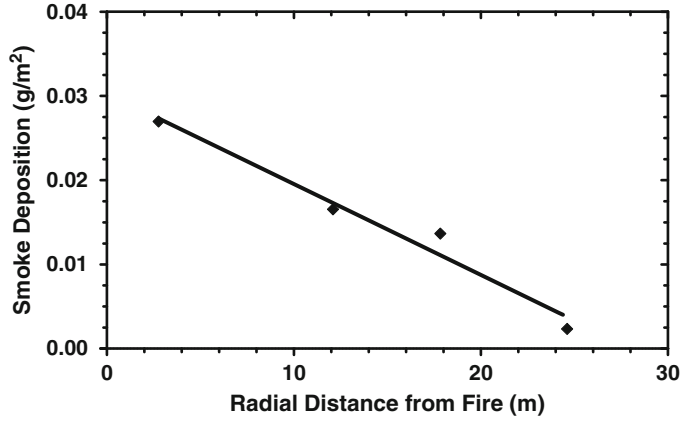

Fig. 24.15 Smoke deposition versus radial distance [56]

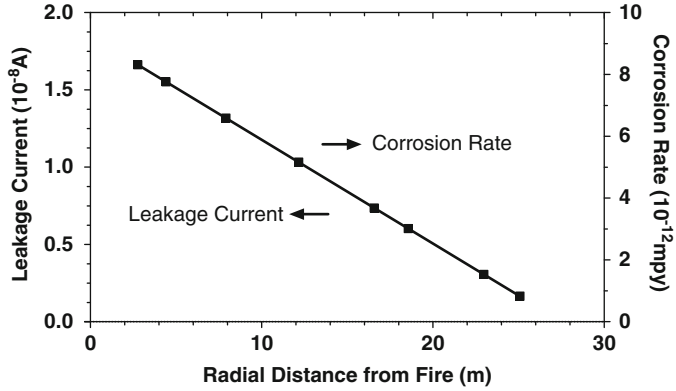

Fig. 24.16 Leakage current and corrosion rate versus radial distance [56]

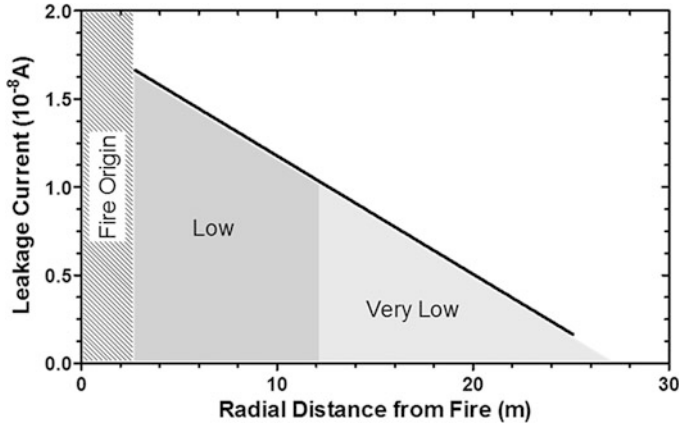

Fig. 24.17 Estimated smoke damage potentials [56]

Nomenclature

c	Average coefficient of smoke extinction
C_c	Slip correction factor
C_o	Reference concentration
C_s	Smoke mass concentration
d_a	Aerodynamic equivalent mass diameter
d_{ag}	Aerodynamic equivalent geometric mean mass diameter
d_g	Geometric mean diameter
d_p	Particle diameter
D	Diffusion coefficient
f_v	Smoke volume fraction
g	Gravitational acceleration
η	Gas viscosity
I	Transmitted light intensity
I_o	Initial light intensity
k_{ad}	Adsorption rate constant
k_B	Boltzmann's constant
k_d	Desorption rate constant
k_W	Weber fraction
K	Overall rate constant
K_{TH}	Thermophoretic velocity coefficient
l	Pathlength
LC	Leakage current
λ	Wavelength of light
Λ	Mean free path
n_i	Number of particles with diameter d_i
N	Total number of particles
ρ_g	Gas density
ρ_o	Standard particle density
ρ_s	Smoke particle density
σ_g	Geometric standard deviation
Re_p	Particle Reynolds number
OD_λ	Optical density at wavelength λ
S	Stimulus
ΔS	Change in stimulus
t	Time
τ	Time constant
T	Temperature
V	Particle velocity
V_{TH}	Thermophoretic deposition velocity
V_{TS}	Terminal settling velocity

References

1. J.S. Newman and Y. Xin, "Characterization of Room Environments in Growing Enclosure Fires," *Fire Safety Journal*, 39, pp. 239–253 (2004).
2. K. McGrattan, S. Hostikka, J. Floyd, H. Baum and R. Rehm, "Fire Dynamics Simulator (Version 5) Technical Reference Guide," National Institute of Standards and Technology, NIST Special Publication 1018–5, October 2007.
3. Y. Wang, P. Chatterjee, and J.L. de Ris, "Large Eddy Simulation of Fire Plumes," *Proceedings of the Combustion Institute*, 33, pp. 2473–2480 (2011).
4. W.C. Hinds, *Aerosol Technology – Properties, Behavior, and Measurement of Airborne Particles*, 2nd edition, John Wiley & Sons, Inc., New York, 1999.
5. E. Cunningham, "On the Velocity of Steady Fall of Spherical Particles through Fluid Medium," *Proceedings of the Royal Society A*, 83, pp. 357–365 (1910).
6. S.K. Friedlander and H.F. Johnstone, "Deposition of Suspended Particles from Turbulent Gas Streams," *Industrial and Engineering Chemistry*, 49, 7, pp. 1151–1156 (1957).

7. A. Einstein, “On the Kinetic Molecular Theory of Thermal Movements of Particles Suspended in a Quiescent Fluid,” *Annalen der Physik*, 17, pp. 549–560 (1905).
8. W.C. Hinds, A. Ashley, N.J. Kennedy, N.J. and P. Bucknam, “Conditions for Cloud Settling and Rayleigh-Taylor Instability,” *Aerosol Science and Technology*, 36, 12, pp. 1128–1138 (2002).
9. J.S. Newman, P. Su. and G.G. Yee, “Smoke Deposition Velocity in Industrial Fire Environments,” *Fire Safety Science: Proceedings of the Tenth International Symposium*, International Association for Fire Safety Science, London, UK, pp. 655–668 (2011).
10. J.R. Brock, "On the Theory of Thermal Forces Acting on Aerosol Particles," *Journal of Colloid Science*, 17, pp.768-780 (1962).
11. L. Waldmann and K.H. Schmitt, "Thermophoresis and Diffusiophoresis of Aerosols," In *Aerosol Science* (C. N. Davies, ed.), Academic Press, London, pp. 137–162 (1966).
12. L. Talbot, R.K. Cheng, R. Schefer, R. and D. Willis, “Thermophoresis of Particles in a Heated Boundary Layer,” *Journal of Fluid Mechanics*, 101, 4, pp. 737–758 (1980).
13. S. Riahi, C.L. Beyler and J. Hartman, “Wall Smoke Deposition from a Hot Smoke Layer,” *Fire Technology*, (2012).
14. S. Suzuki, K. Kuwana and R. Dobashi, “Effect of Particle Morphology on Thermophoretic Velocity of Aggregated Soot Particles,” *International Journal of Heat and Mass Transfer*, 52, pp. 4695–4700 (2009).
15. K.M. Butler and G.W. Mulholland, “Generation and Transport of Smoke Components,” *Fire Technology*, 40, pp. 149–176 (2004).
16. H. Ono, R. Dobashi and T. Sakuraya, “Thermophoretic Velocity Measurements of Soot Particles under a Microgravity Condition,” *Proceedings of the Combustion Institute*, 29, pp. 2375–2382 (2002).
17. J.S. Newman, “Prediction of Fire Detector Response,” Fire Safety Journal, 12, pp. 205–211 (1987).
18. J.S. Newman, “Principles for Fire Detection,” *Fire Technology*, 24, 12, pp. 116–127 (1988).
19. J.S. Newman and J. Steciak, “Characterization of Particulates from Diffusion Flames,” Combustion and Flame, 67, pp. 55–64 (1987).
20. K.J. Rockne, G.L. Taghon and D.S. Kosson, “Pore Structure of Soot Deposits from Several Combustion Sources,” *Chemosphere*, 41, pp. 1125–1135 (2000).
21. P.F. DeCarlo, J.G. Slowik, D.R. Worsnop, P. Davidovits and J.L. Jimenz, “Particle Morphology and Density Characterization by Combined Mobility and Aerodynamic Diameter Measurements. Part 1: Theory,” *Aerosol Science and Technology*, 38, pp. 1185–1205 (2004).
22. J.G. Slowik, K. Stainken, P. Davidovits, L.R. Williams, J.T. Jayne, C.E. Kold, D.R. Worsnop, Y. Rudich, P.F. DeCarlo and J.L. Jimenz, “Particle Morphology and Density Characterization by Combined Mobility and Aerodynamic Diameter Measurements. Part 2: Application to Combustion-Generated Soot Aerosols as a Function of Fuel Equivalence Ratio,” *Aerosol Science and Technology*, 38, pp. 1206–1222 (2004).
23. F-X. Ouf, J. Vendel, A. Coppalle, M. Weill and J. Yon, “Characterization of Soot Particles in the Plumes of Over-Ventilated Diffusion Flames,” *Combustion Science and Technology*, 180, pp. 674–698 (2008).
24. I. Colbeck, B. Atkinson and Y. Johar, “The Morphology and Optical Properties of Soot Produced by Different Fuels,” *Journal of Aerosol Science*, 28, 5, pp. 715–723 (1997).
25. G.W. Mulholland and M.Y. Choi, “Measurement of the Mass Specific Extinction Coefficient for Acetylene and Ethene Smoke Using the Large Agglomerate Optics Facility,” *Proceedings of the 27th International Symposium on Combustion*, pp. 1515–1522 (1998).
26. G.W. Mulholland and C. Croarkin, “Specific Extinction Coefficient of Flame Generated Smoke,” *Fire and Materials*, 24, pp. 227–230 (2000).
27. S. Riahi, “New Tools for Smoke Residue and Deposition Analysis,” PhD Dissertation, George Washington University, Washington D.C., January 2011.
28. R.A. Martin and D.L. Fenton, “Full-Scale Measurements of Smoke Transport and Deposition in Ventilation System Ductwork,” Los Alamos National Laboratory, Los Alamos, NM, NUREG/CR-4321 (LA-10478-MS), 1985.
29. D.W. Weinert, T.G. Cleary, G.W. Mulholland and P.F. Beever, “Light Scattering Characteristics and Size Distribution of Smoke and Nuisance Aerosols,” *Fire Safety Science: Proceedings of the Seventh International Symposium*, International Association for Fire Safety Science, London, UK, pp. 209–220 (2003).
30. G.W. Mulholland, “Smoke Production and Properties,” *SFPE Handbook of Fire Protection Engineering*, 4th edition, National Fire Protection Association, Quincy, MA, pp. 2–291 to 2–302, 2008.
31. T.J. Tanaka, “Measurements of the Effects of Smoke on Active Circuits,” *Fire and Materials*, 23, pp. 103–108 (1999).
32. IEC/TS 60695-5-3 Ed. 1, “Fire Hazard Testing-Part 5.3: Corrosion Damage Effects of Fire Effluent-Leakage Current and Metal Loss Test Method,” 89/545/DTS, 2002.
33. R.P. Frankenthal, D.J. Siconolfi and J.D. Sinclair, "Accelerated Life Testing of Electronic Devices by Atmospheric Particles: Why and How," *Journal of the Electrochemical Society*, 140, 11, pp. 3129–3134 (1993).
34. J.S. Newman, P. Su, G.G. Yee and S. Chivukula, “Development of Smoke Corrosion and Leakage Current Damage Functions,” *Fire Safety Journal*, 61, pp. 92–99 (2013) J.S. Newman, P. Su, G.G. Yee, K.L.T. Jamison and S. Chivukula, “Strategic Smoke

Damage Program: Development of Smoke Damage Functions for the Semiconductor Industry," FM Global Technical Report, Project ID 0003038685, September 2010.
35. T.J. Tanaka and S.P. Nowlen, "Results and Insights on the Impact of Smoke on Digital Instrumentation and Control", Sandia National Laboratories, Albuquerque, NM, NUREG/CR-6597 (SAND99-1320), 2001.
36. R.D. Peacock, T.G. Cleary, P.A. Reneke and D.C. Murphy, "A Literature Review of the Effects of Smoke from a Fire on Electrical Equipment," National Institute of Standards and Technology, Gaithersburg, MD, NUGEG/CR-7123, 2012.
37. TAPPI Technical Association of the Paper Industry Test Method T 452 om-08, "Brightness of Pulp, Paper and Paperboard (Directional Reflectance at 457 nm)," Norcross, GA, 1998.
38. J.S. Newman, G.G. Yee and P. Su, "Development of Smoke Damage Functions for Warehouse Applications," *Fire and Materials*, Proceedings of the 13th International Conference Exhibition, San Francisco, CA (2013); J.S. Newman, G.G. Yee and P. Su, "Strategic Smoke Damage Program: Development of Smoke Damage Functions for Warehouse Applications," FM Global Technical Report, Project ID 0003043053, April 2012.
39. C.C. Austin, D. Wang, D.J. Ecobichon and G. Dussault, "Characterization of Volatile Organic Compounds in Smoke at Experimental Fires," *Journal of Toxicology and Environmental Health, Part A*," 63, pp. 191–206 (2001).
40. B-J. De Vos, M. Froneman, and E.R. Rohwer, "Organic Vapors Emitted from the Plumes of Pool Fires on Carpet Materials," *Journal of Fire Sciences*, 17, pp. 383–420 (1999).
41. P. Dalton, "Odor Perception and Beliefs about Risk," *Chemical Senses*, 21, pp. 447–458 (1996).
42. V.I. Berezkin, I.V. Viktorovsii, L.V. Golubev, V.N. Petrova and L.O. Khoroshko, "A Comparative Study of the Sorption Capacity of Activated Charcoal, Soot, and Fullerenes for Organochlorine Compounds," *Technical Physics Letters*, 28, pp. 885–888 (2002). [Translated from *Pis'ma v Zhurnal Tekhnicheskoi Fiziki*, 28, pp. 11–21 (2002).]
43. I. Langmuir, "The Constitution and Fundamental Properties of Solids and Liquids. Part I. Solids," *Journal of the American Chemical Society*, 38, pp. 2221–2295 (1916).
44. C.L. Chuang, P.C. Chiang, E.E. Chang and C.P. Huang, "Adsorption-Desorption Rate of Nonpolar Volatile Organic Compounds onto Activated Carbon Exemplified by C_6H_6 and CCl_4," *Practice Periodical of Hazardous, Toxic, and Radioactive Waste Management*, 7, pp. 148–155 (2003).
45. W.R. Zeng, S.F. Li and W.K. Chow, "Preliminary Studies on Burning Behavior of Polymethylmethacrylate (PMMA)," *Journal of Fire Sciences*, 20, pp. 297–317 (2002).
46. F. Delage, P. Pre and P. Le Cloirec, "Effects of Moisture on Warming of Activated Carbon Bed during VOC Adsorption," *Journal of Environmental Engineering*, 125, pp. 1160–1167 (1999).
47. BSR/ASTM Z0334Z-200x Draft Standard, "Test Method for Measurement of the Leakage Currents from Smoke Deposited on Electric Circuits," ASTM International, West Conshohocken, PA, 2003.
48. G.A. Gescheider, *Psychophysics: The Fundamentals*, 3rd edition, Psychology Press, London, 1997.
49. R. Teghtsoonian, "On the Exponents in Steven's Law and the Constant in Ekman's Law," *Psychological Review*, 78, pp. 71–80 (1971).
50. H. Stone, "Factors Influencing Behavioral Responses to Odor Discrimination – A Review," *Journal of Food Science*, 31, pp. 784–790 (1966).
51. E. Martinez Martin and D. Ramirez Martin-Corbalan, "Chemical Substances Content in Recycled Packaging Papers," AIDIMA Furniture, Wood and Packaging Technology Institute, Paterna, Spain, 2005.
52. P.A. Tice, and C.P. Offen, "Odors and Taints from Paperboard Food Packaging," *Tappi Journal*, 77, p. 149–154 (1994).
53. H. Kim-Kang, "Volatiles in Packaging Materials," *Critical Reviews in Food Science and Nutrition*, 29, 4, pp. 255–271 (1990).
54. P. Landy, S. Nicklaus, E.Semon, P. Mielle and E. Guichard, "Representativeness of Extracts of Offset Paper Packaging and Analysis of the Main Odor-Active Compounds," *Journal of Agricultural and Food Chemistry*, 58, pp. 2326–2334 (2004).
55. M. Biedermann, Y. Uematsu and K. Grob, "Mineral Oil Contents in Paper and Board Recycled to Paperboard for Food Packaging," *Packaging Technology and Science*, 24, 2, pp. 61–73 (2011).
56. Y. Xin and J.S. Newman, "Numerical Simulation of Smoke Damage in a Semiconductor Cleanroom," *Proceedings of the 9th International Conference on Performance-Based Codes and Fire Safety Design Methods*, the Excelsior, Hong Kong, June 20–22, 2012.

Jeffrey S. Newman, retired, was an assistant vice president and principal engineer for FM Global. He specialized in characterization of fire environments including modeling, flammability of materials, smoke damage, full-scale fire testing, and smoke and fire detection.

Dr. Geary G. Yee is a physical chemist and senior research specialist for FM Global. He has specialized in polymer pyrolysis, microbial corrosion, small lab-scale fire testing, smoke characterization, and material failure analysis.

Dr. Paul Su is a senior research specialist and technical team leader for FM Global. He has specialized in materials and corrosion research including corrosion testing and control, failure analysis, smoke corrosivity, nanomaterials research, and chemical product development.

Heat Transfer from Fires to Surfaces 25

Brian Y. Lattimer

Introduction

The heat transfer from fires to adjacent surfaces is an important consideration in many fire analyses. Some example applications that may require knowledge of the heat transfer from a flame include heating and failure of structural beams, heat transfer through walls and ceilings, and the ignition and flame spread along combustible surfaces.

Flames transfer heat to adjacent surfaces primarily through convection and radiation. Techniques for efficiently modeling the heat transfer from flames are still being developed; however, experimental data and empirical correlations have been generated to predict flame heat transfer for a number of common geometries. This chapter will focus on the data and empirical correlations that have been developed.

Empirical correlations for predicting heat transfer from flames are typically simple to use; however, their use is usually limited to a particular type of fire or the geometry of the surface being heated. The types of fires considered in this chapter include

- Exposure area fires (burning objects)
- Wall and ceiling fires
- Window flames

Exposure area fires are burning objects located adjacent to or near the surface being heated. Wall and ceiling fires are those fires produced by a burning wall or ceiling. Window flames are flames extending outside of a compartment containing a fire.

The heat transfer from fires has been characterized for a range of different surface geometries. The geometries included in this chapter are

- Flat vertical wall
- Flat unconfined and confined ceilings
- Parallel flat vertical walls
- Corner walls at 90°
- Corner walls at 90° with a ceiling
- Horizontal I-beams beneath a ceiling

The majority of the data presented in this chapter is from water-cooled heat flux gauge measurements. Using these data, correlations were developed from tests where important parameters were varied (i.e., heat release rate, fire base dimension, etc.). The range of the data and the correlating parameters need to be taken into consideration before applying the correlations. For example, the heat flux along the length of the flame has historically been correlated with flame length measured in that particular study. Measured flame lengths can vary depending on the measurement technique, definition, and surrounding geometry. For the studies considered in this chapter, the data were nondimensionalized with either the average (50 % intermittent) flame length or the flame tip length. Therefore, heat flux correlations should be applied using either the flame length correlation developed in the study or one that has been demonstrated to predict the flame length in that study.

B.Y. Lattimer (✉)
Virginia Tech, Mechanical Engineering, 635 Prices Fork Road, Goodwin Hall413C, Blacksburg, VA 24060, USA

M.J. Hurley (ed.), *SFPE Handbook of Fire Protection Engineering*,
DOI 10.1007/978-1-4939-2565-0_25, © Society of Fire Protection Engineers 2016

Heat Transfer Boundary Condition

The heat flux boundary condition for a material surface exposed to a fire includes the exposure heat flux from the fire and the reradiation losses from the surface. The exposure heat flux from the fire is composed of a radiative heat flux plus a convective heat flux. The heat flux boundary condition for a fire heating an adjacent surface is

$$-k\frac{dT}{dx} = q_s'' = \varepsilon_s q_{\text{rad}}'' + h\left(T_f - T_s\right) - \varepsilon_s \sigma T_s^4 \tag{25.1}$$

assuming negligible heating from the surroun ding environment.

Heat Flux Gauges

The radiation and convective heat flux terms in Equation 25.1 are difficult to accurately calculate due to the dependence of these terms on geometry and fire properties. As a result, water-cooled total heat flux gauges are commonly used to measure the maximum total exposure heat flux (or cold surface heat flux) from fires in different configurations. The maximum total exposure heat flux measured using the gauge can be used to quantify the heat flux into the material surface.

The total heat flux onto a water-cooled heat flux gauge is described by the following equation:

$$q_{hfg}'' = \varepsilon_{hfg} q_{\text{rad}}'' + h\left(T_f - T_{hfg}\right) - \varepsilon_{hfg}\sigma T_{hfg}^4. \tag{25.2}$$

These gauges are cooled so that their surface temperatures remain near ambient (20–80 °C), and they are coated with a high emissivity paint $(\varepsilon \sim 0.95)$ to maximize the absorbed radiation. Cooling the gauge surface maximizes the convective heat transfer and minimizes the radiative losses; thus, the cooled heat flux gauges measure the maximum total exposure heat flux.

The heat flux measured using the gauge can be used to determine the heat flux to an adjacent surface being heated by a fire. By solving for the radiation from the fire in Equation 25.2, the equation for the boundary condition in Equation 25.1 becomes

$$q_s'' = \frac{\varepsilon_s}{\varepsilon_{hfg}}\left[q_{hfg}'' - h\left(T_f - T_{hfg}\right) + \varepsilon_{hfg}\sigma T_{hfg}^4\right] + h\left(T_f - T_s\right) - \varepsilon_s \sigma T_s^4 \tag{25.3}$$

Assuming the heat transfer coefficient at the heat flux gauge is the same as the heat transfer coefficient at the material surface, Equation 25.3 can be reorganized resulting in

$$q_s'' = \frac{\varepsilon_s}{\varepsilon_{hfg}} q_{hfg}'' + \left(1 - \frac{\varepsilon_s}{\varepsilon_{hfg}}\right) hT_f - h\left(T_s - \frac{\varepsilon_s}{\varepsilon_{hfg}} T_{hfg}\right) - \varepsilon_s \sigma\left(T_s^4 - T_{hfg}^4\right) \tag{25.4}$$

As a result, the need to determine the radiation heat flux from the fire has been removed. However, this expression still requires the gas temperature near the surface to be measured, T_f, and the emissivity of the adjacent surface, ε_s, to be known in order to calculate the net heat flux into the surface. Assuming the emissivity of the adjacent surface is equal to the heat flux gauge emissivity $\left(\varepsilon_s = \varepsilon_{hfg}\right)$, Equation 25.4 reduces to the following:

$$q_s'' = q_{hfg}'' - h\left(T_s - T_{hfg}\right) - \varepsilon_{hfg}\sigma\left(T_s^4 - T_{hfg}^4\right) \tag{25.5}$$

Through Equation 25.5, the net heat flux into an adjacent surface can be determined using the heat flux from a water-cooled gauge, gauge temperature, gauge emissivity, and heat transfer coefficient. The gauge temperature and emissivity are typically known; therefore, the only unknown is the convective heat transfer coefficient.

An estimate of the local heat transfer coefficient, h, is needed to calculate the heat flux into the material. The heat transfer coefficient is dependent on the local velocity, gas temperature, and geometry. For natural convection on

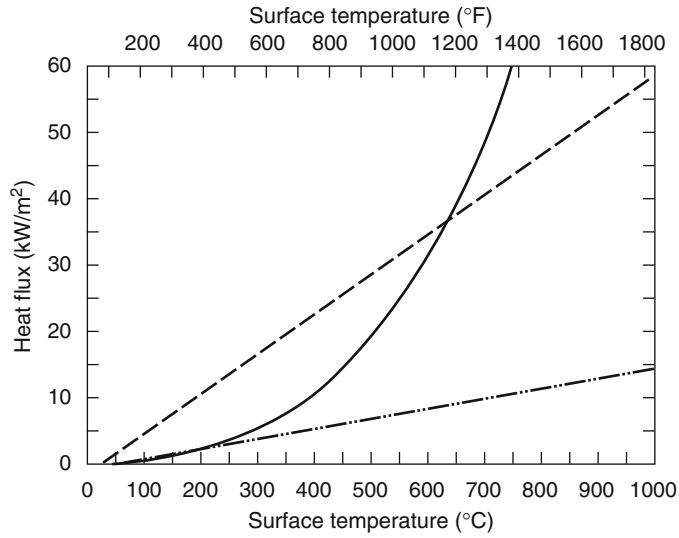

Fig. 25.1 Magnitude of the radiative and convective terms in Equation 25.5: radiation (—); convection with h = 0.015 kW/(m^2-K) (– · · –); and convection with h = 0.050 kW/(m^2-K) (– – –)

horizontal and vertical surfaces, the heat transfer coefficient varies from approximately 0.010 to 0.020 kW/m^2-K. These coefficients apply to fires flowing against walls or along ceilings. Higher heat transfer coefficients are expected in areas where fires impinge on surfaces. Based on data from Kokkala [1, 2] and You and Faeth [3, 4], the local convective heat transfer coefficient where a diffusion flame impinges on a ceiling is on the order of 0.050 kW/(m^2-K).

Figure 25.1 contains a plot of the radiative and convective heat flux terms in Equation 25.5 that are subtracted from the measured heat flux. The convective term is plotted using convective heat transfer coefficients of 0.015 kW/m^2-K and 0.050 kW/m^2-K. The radiative term is larger than the convective term at temperatures higher than 300 °C with a heat transfer coefficient of 0.015 kW/m^2-K and at temperatures greater than 600 °C with a heat transfer coefficient of 0.050 kW/m^2-K. Based on results in this plot, a non-conservative boundary condition will result if the heat transfer coefficient is over estimated.

The following examples are provided to illustrate how the heat flux into the material varies as the material surface temperature increases and how different assumptions (i.e., surface emissivity, heat transfer coefficient) affect the heat flux into the material surface.

Example 1 A water-cooled heat flux-gauge is used to measure the total incident heat flux from a fire against a wall painted black. The measured heat flux is 30 kW/m^2 and the water cooling the gauge is measured to be 350 K. Both the wall emissivity and the heat flux gauge have a surface emissivity of 0.95, and the heat transfer coefficient is 0.01 kW/m^2-K. Determine the net heat flux into the wall when the wall surface temperature is 600 K, 700 K, and 800 K.

Solution Equation 25.5 can be used to determine the heat flux into the wall when the wall is at different temperatures.

$$q_s'' = q_{hfg}'' - h\left(T_s - T_{hfg}\right) - \varepsilon_{hfg}\sigma\left(T_s^4 - T_{hfg}^4\right)$$

$$q_s'' = 30 - 0.01(T_s - 350) - (0.95)\left(5.67 \times 10^{-11}\right) \times \left(T_s^4 - 350^4\right)$$

- Wall surface temperature of 600 K

$$q_s'' = 30 - 0.01(600 - 350) - (0.95)\left(5.67 \times 10^{-11}\right) \times \left(600^4 - 350^4\right)$$

$$q_s'' = 21.3 \text{ kW/m}^2$$

- Wall surface temperature of 700 K

$$q_s'' = 30 - 0.01(700 - 350) - (0.95)\left(5.67 \times 10^{-11}\right) \times \left(600^4 - 350^4\right)$$

$$q_s'' = 14.4 \text{ kW/m}^2$$

- Wall surface temperature of 800 K

$$q_s'' = 30 - 0.01(800 - 350) - (0.95)\left(5.67 \times 10^{-11}\right) \times \left(800^4 - 350^4\right)$$
$$q_s'' = 4.2 \text{ kW/m}^2$$

Example 2 A water-cooled heat flux gauge is used to measure the total incident heat flux from a fire against a wall. The heat flux gauge measured a heat flux of 30 kW/m^2 while the gas temperature was measured to be 1173 K. The water cooling the gauge was measured to be 350 K. The heat flux gauge has a surface emissivity of 0.95, and the heat transfer coefficient is 0.01 kW/m^2-K. With a wall surface temperature of 700 K, determine the net heat flux into the wall if the surface emissivity is 0.94, 0.90, 0.70, and 0.50. In each case, what is the percent error associated with assuming the wall surface emissivity is equal to the heat flux gauge surface emissivity?

Solution Due to the surface emissivity of the wall being different from that of the heat flux gauge, the heat flux into the wall is determined using Equation 25.4:

$$q_s'' = \frac{\varepsilon_s}{\varepsilon_{hfg}} q_{hfg}'' + \left(1 + \frac{\varepsilon_s}{\varepsilon_{hfg}}\right) hT_f - h\left(T_s - \frac{\varepsilon_s}{\varepsilon_{hfg}} T_{hfg}\right) - \varepsilon_s \sigma \left(T_s^4 - T_{hfg}^4\right)$$
$$q_s'' = \frac{\varepsilon_s}{0.95} 30 + \left(1 - \frac{\varepsilon_s}{0.95}\right) 0.01(1173) - 0.01\left(700 - \frac{\varepsilon_s}{0.95} 350\right) - \varepsilon_s 567 \times 10^{-11}\left(700^4 - 350^4\right)$$

The heat flux into the surface where the wall and the gauge have the same emissivity is taken from Example 1b and is $q_s'' = 14.4$ kW/m^2.

- Surface emissivity of 0.94

$$q_s'' = 14.2 \text{ kW/m}^2$$

The assumption of equal surface emissivity results in a heat flux 0.7 % higher.

- Surface emissivity of 0.90

$$q_s'' = 13.9 \text{ kW/m}^2$$

The assumption of equal surface emissivity results in a heat flux 3.8 % higher.

- Surface emissivity of 0.70

$$q_s'' = 11.8 \text{ kW/m}^2$$

The assumption of equal surface emissivity results in a heat flux 17.7 % higher.

- Surface emissivity of 0.50

$$q_s'' = 9.8 \text{ kW/m}^2$$

The assumption of equal surface emissivity results in a heat flux 31.8 % higher.

Example 3 A water-cooled heat flux gauge is used to measure the total incident heat flux from a fire against a wall painted black. The measured heat flux is 30 kW/m^2 and the water cooling the gauge is measured to be 350 K. Both the wall emissivity and the heat flux gauge have a surface emissivity of 0.95. With a wall surface temperature of 700 K, determine the net heat flux into the wall with heat transfer coefficients of 0.01 kW/m^2-K, 0.015 kW/m^2-K, and 0.02 kW/m^2-K.

Solution Equation 25.5 can be used to determine the heat flux into the wall when the wall is at different temperatures.

$$q_s'' = q_{hfg}'' - h\left(T_s - T_{hfg}\right) - \varepsilon_{hfg} \sigma \left(T_s^4 - T_{hfg}^4\right)$$
$$q_s'' = 30 - h(700 - 350) - (0.95)\left(5.67 \times 10^{-11}\right)\left(700^4 - 350^4\right)$$

- Heat transfer coefficient of 0.01 kW/m-K

$$q_s'' = 14.4 \text{ kW/m}^2$$

- Heat transfer coefficient of 0.015 kW/m-K

$$q_s'' = 12.6 \text{ kW/m}^2$$

- Heat transfer coefficient of 0.02 kW/m-K

$$q_s'' = 10.9 \text{ kW/m}^2$$

Adiabatic Surface Temperature

The adiabatic surface temperature has been proposed as a means for quantifying the thermal boundary condition in fire environments [5–8]. The adiabatic surface temperature is the surface temperature that would exist if the surface were perfectly insulated. From Equation 25.1, the adiabatic flame temperature is defined as

$$0 = \varepsilon_s q_{rad}'' + h\left(T_f - T_{ast}\right) - \varepsilon_s \sigma T_{ast}^4 \quad (25.6)$$

Combining with Equation 25.1, a relationship between the heat flux at the surface and the adiabatic surface temperature is

$$q_s'' = \varepsilon_s \sigma \left(T_{ast}^4 - T_s^4\right) + h\left(T_{ast} - T_s\right) \quad (25.7)$$

The expression provides a relationship between the adiabatic surface temperature and the heat flux to the surface. Equation 25.7 has a form similar to Equation 25.1 when the radiation term, q_{rad}'', is taken as the radiation from a blackbody source, σT_{rad}^4. Based on this, adiabatic surface temperature can be thought of as an effective gas temperature that embodies the radiation and convection gas temperatures. The adiabatic surface temperature can then be used as the boundary surface temperature for calculating the thermal response of materials exposed to fire conditions, knowing the heat transfer coefficient and surface emissivity. The adiabatic surface temperature has been successfully used as an effective gas temperature to quantify the thermal boundary condition for thermo-structural analysis [6, 8]. Analysis has not been reported on whether the boundary condition using the adiabatic surface temperature provides the same results as using cold surface heat flux measurement, q_{hfg}'', and Equation 25.5.

Plate thermometers have been used to measure the adiabatic surface temperature in furnace environments [5–8]. Due to the time constant of the devices [5–8], the adiabatic surface temperature measurement provided by plate thermometers need to be carefully considered in applications where the fire environment is transient.

Objects Immersed in Flames

Some of the highest heat fluxes measured from diffusion flames have been measured in tests with objects immersed in large, open hydrocarbon pool fires. In these tests, small and large objects (relative to the fire size) were placed within the pool fires. These tests were performed to evaluate the heat transfer from fires to large objects such as fuel tanks, weapons, and nuclear containers.

The maximum heat fluxes measured in these tests are summarized in Tables 25.1 and 25.2. From data in these tables [9–19], the size of the object relative to the pool fire has a significant impact on the incident heat flux to the object.

Table 25.1 Heat fluxes to objects immersed in large pool fires [9–19]

Test	Pool size	Fuel	Peak heat flux (kW/m^2)
AEA Winfrith [9]	0.5 × 9.45 m	Kerosene	150
US DOT [9]	Not listed	Kerosene	138
USCG [9]	Not listed	Kerosene	110–142
US DOT [9]	Not listed	Kerosene	136–159
Sandia [9]	Not listed	Kerosene	113–150
HSE Buxton [9]	Not listed	Kerosene	130
Shell Research [9]	4.0 × 7.0 m	Kerosene	94–112
Large cylinder [10]	9.1 × 18.3 m	JP-4	100–150
Small cylinder [10]	9.1 × 18.3 m	JP-4	150–200
Russell and Canfield [10]	2.4 × 4.8 m	JP-5	175

Large calorimeters were measured to be exposed to heat fluxes of 100–150 kW/m^2. McLain [17] and Taylor et al. [18] measured slightly lower heat fluxes (75–85 kW/m^2) in their tests with large items that were similar in size to the pool fire. In studies with small calorimeters, peak heat fluxes were measured to range from 150 to 200 kW/m^2. The difference in the heat fluxes measured for small and large items immersed in pool fires has been attributed to the difference in the convective heat transfer coefficient, the flame thickness, and the impact of the object on the flame temperature. Small-scale calorimeter data provide a bound for heat fluxes to an item immersed in a pool fire. Based on the available data, a bounding heat flux of 175 to 200 kW/m^2 is possible.

Table 25.2 Heat fluxes to different size objects immersed in fires [10–19]

Object	Peak heat flux (kW/m^2)
Large calorimeter [10]	100–150
Large calorimeter [12]	85
Large calorimeter [13]	100
Large calorimeter [14]	110
Large calorimeter [15]	100
Large calorimeter [16]	105
Large calorimeter [17]	85[a]
Large calorimeter [18]	75[a]
Large wall (3.0 × 0.6 m) [19]	80–120
Small calorimeter [11]	175
Small calorimeter [10]	150–200

[a]Object size comparable to pool fire size

Exposure Fires

Fires Adjacent to Flat Walls

Heat fluxes from exposure fires adjacent to flat walls have been experimentally studied using propane sand burners and characterized for various burning objects. The experimental study provides a systematic approach of calculating heat fluxes for this geometry.

An extensive experimental study was performed by Back et al. [20] to characterize the heat transfer from a fire to a directly adjacent wall. In this study, fires were generated using square propane sand burners with edge lengths of 0.28, 0.37, 0.48, 0.57, and 0.70 m. Heat flux fields were measured for fires ranging from 50 to 520 kW.

A plot of the peak heat fluxes measured for each type of fire evaluated is shown in Fig. 25.2. Peak heat fluxes for the different fires evaluated were determined to be a function of fire heat release rate. This dependence was attributed to the larger size fires resulting in thicker boundary layers, which is related to the radiation pathlength. Based on gray-gas radiation theory, the authors found the following relation adequately represented the data:

$$q''_{cl} = q''_{\text{peak}} \quad z/L_f \leq 0.4 \tag{25.8}$$

These peak heat fluxes were measured in the lower part of the fire ($z/L_f \leq 0.4$) along the

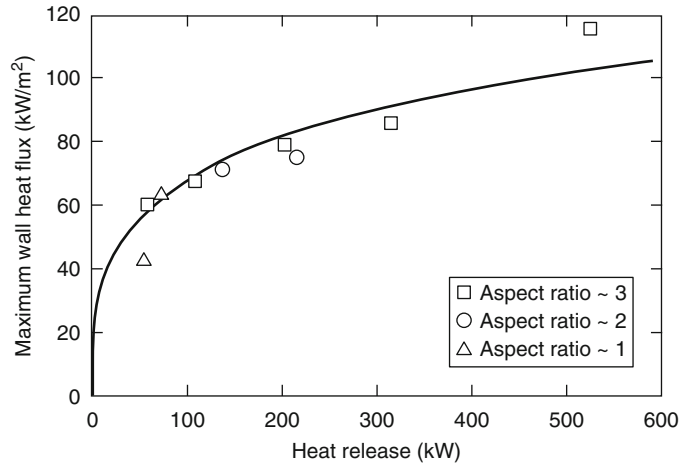

Fig. 25.2 Peak heat release rates measured in square propane burner fires against a flat wall [20]

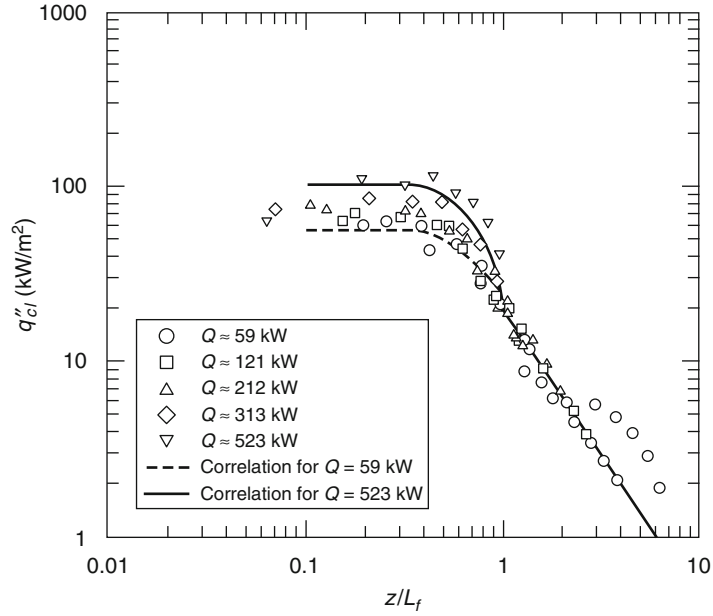

Fig. 25.3 Vertical heat flux distribution along the centerline of a square propane burner fire adjacent to a flat wall [20]

centerline, with the flame length taken from Heskestad [21]:

$$L_f = 0.23Q^{2/5} - 1.02D \tag{25.9}$$

Above this region, the heat fluxes were measured to decrease with distance above the fire. The heat flux data measured along the centerline is shown in Fig. 25.3. Lines in this plot are a general correlation of the centerline data:

$$q''_{cl} = q''_{\text{peak}} \quad z/L_f \le 0.4 \tag{25.10a}$$

$$q''_{cl} = q''_{\text{peak}} - \frac{5}{3}(z/L_f - 2/5)\left(q''_{\text{peak}} - 20\right) \quad 0.4 < z/L_f \le 1.0 \tag{25.10b}$$

$$q''_{cl} = 20\left(z/L_f\right)^{-5/3} \quad z/L_f > 1.0 \tag{25.10c}$$

Heat fluxes were measured to decrease with horizontal distance from the centerline, as shown in Fig. 25.4. The normalized lateral heat flux distribution data shown in Fig. 25.4 was found to be half-Gaussian in shape over the half width of the burner. The line in the plots is a fit to the data in Fig. 25.4a:

$$q'' = q''_{cl}\exp\left[-\left(\frac{x}{0.5D}\right)^2\right] \quad \frac{x}{0.5D} \le 1.0 \tag{25.11a}$$

$$q'' = 0.38q''_{cl}\left(\frac{x}{0.5D}\right)^{-1/7} \quad \frac{x}{0.5D} > 1.0 \tag{25.11b}$$

Heat fluxes from burning objects to an adjacent wall have been measured for a variety of items; however, limited data have been published on this work [22, 23]. Heat fluxes at the rim of wastebasket fires were reported by Gross and Fang [22]. At the rim, heat fluxes as high as 50 kW/m^2 were measured; however, the authors noted that peak heat fluxes for these fires occurred approximately 0.22 m above the rim.

Mizuno and Kawagoe [23] performed experiments with upholstered chair fires against a flat wall. In these tests, Mizuno and Kawagoe measured heat fluxes to the wall of 40–100 kW/m^2 over the continuous flaming region (~$z/L_f < 0.4$). All of these tests were performed using foam-padded chairs.

Fires in a Corner

Fires in a corner of a room lined with a combustible material have been shown to cause more

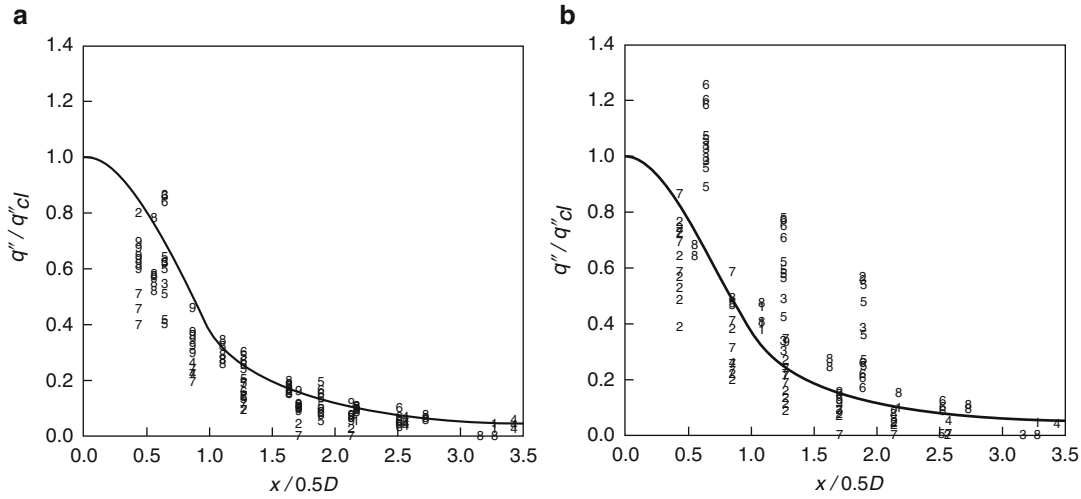

Fig. 25.4 Lateral heat flux distribution with distance from the centerline of square propane burner fires against a flat wall [20] (**a**) in the flaming region and (**b**) in the plume

rapid flame spread and growth to flashover compared to cases with fires in other locations within the room. For these reasons, a significant amount of work has been performed to characterize the heat fluxes produced by corner fires. Heat flux measurements have been performed both in an open environment to quantify the heat flux due to the exposure fire alone and within rooms to measure the heat flux due to the exposure fire and the room environment.

The heat flux from the exposure fire has been quantified in several studies performed in an open laboratory environment [24–29]. All the studies were performed in a noncombustible corner with a ceiling except the study of Kokkala [26], which was performed in a noncombustible corner without a ceiling. A comparison of the heat flux fields measured in the study with a ceiling [29] and the study without a ceiling [26] is shown in Fig. 25.5. Note that the contour plot of Lattimer and Sorathia is relative to the floor, while the plot of Kokkala is relative to the top of the burner. Lattimer et al. used a burner 0.15 m high.

Up to approximately 1.8 m above the floor, the heat flux distributions are similar. In the case with the ceiling, the ceiling jet and the radiation from the fire flowing along the ceiling were heating the top part of the wall. This resulted in higher heat fluxes farther out from the corner along the top part of the wall.

A series of fire tests were performed by Lattimer and Sorathia [29] to develop empirical correlations to estimate heat fluxes from an exposure fire to the walls and ceiling of a corner. Tests were performed using 0.17-, 0.30-, and 0.50-m square propane burners placed directly against the corner. Heat flux fields were measured for fires ranging from 25 to 300 kW.

Correlations were developed for three regions in the corner: along the height of the walls in the corner, along the top of the walls near the ceiling, and along the ceiling. The region containing the walls in the corner extended from the top of the fire to approximately 1.8 m above the floor, which is approximately the ceiling height minus twice the ceiling jet thickness ($\delta = 0.1H$). Correlations for the top part of the walls, which are heated by the ceiling jet, were developed using data at locations greater than 1.8 m above the floor.

Along the height of the walls in the corner, the peak heat fluxes were typically measured near the base of the fire. The peak heat fluxes along the height of the walls in the corner were measured to be a function of the fire diameter, as shown in Fig. 25.6. The curve in Fig. 25.6 is a

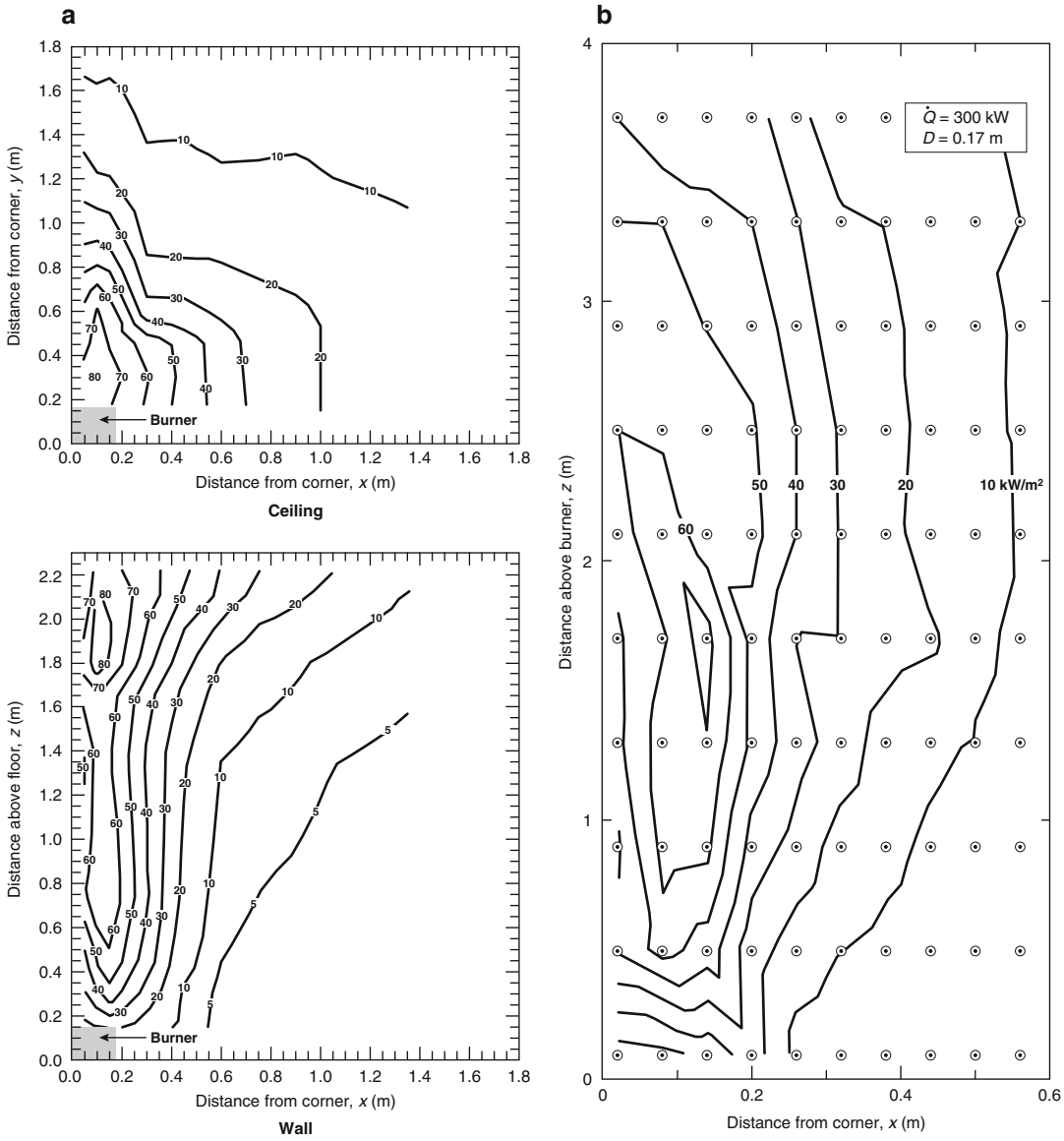

Fig. 25.5 A comparison of the heat flux fields produced in a corner (**a**) with a ceiling [29] and (**b**) without a ceiling [26]. The fire was produced by a 0.17-m-square propane burner with a heat release rate of 300 kW. Note data of Lattimer and Sorathia [29] are plotted relative to the floor, and the data of Kokkala [26] are plotted relative to the top of the burner

correlation to the data and is expressed using the following relation:

$$q''_{\text{peak}} = 120[1 - \exp(-4.0D)] \qquad (25.12)$$

The vertical distribution in the maximum heat flux along the walls near the corner is shown in Fig. 25.7 plotted with the vertical distance normalized with respect to the flame tip,

$$L_{f,\text{tip}}/D = 5.9Q_D^{*1/2} \qquad (25.13)$$

where

$$Q_D^* = \frac{Q}{\rho_\infty C_p T_\infty \sqrt{g} D^{5/2}} \qquad (25.14)$$

Peak heat flux levels were measured in the lower part of the flame ($z/L_{f,\text{tip}} \leq 0.4$) and decreased

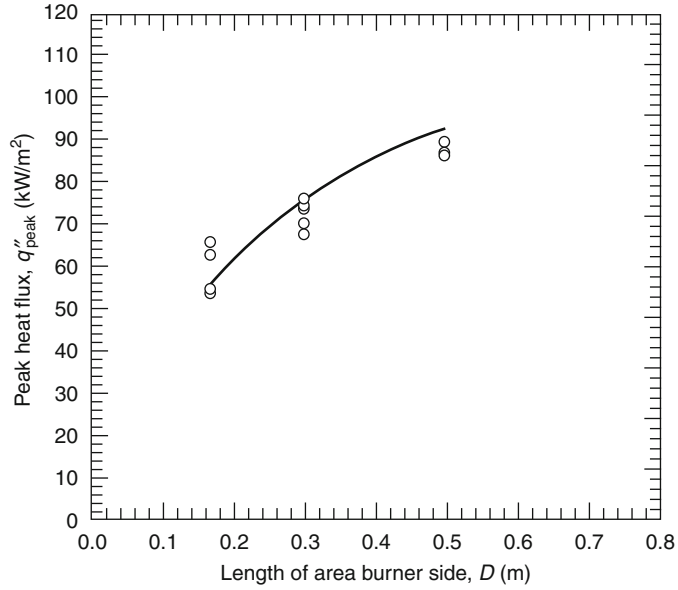

Fig. 25.6 Peak heat flux along the height of the walls in the corner [29]

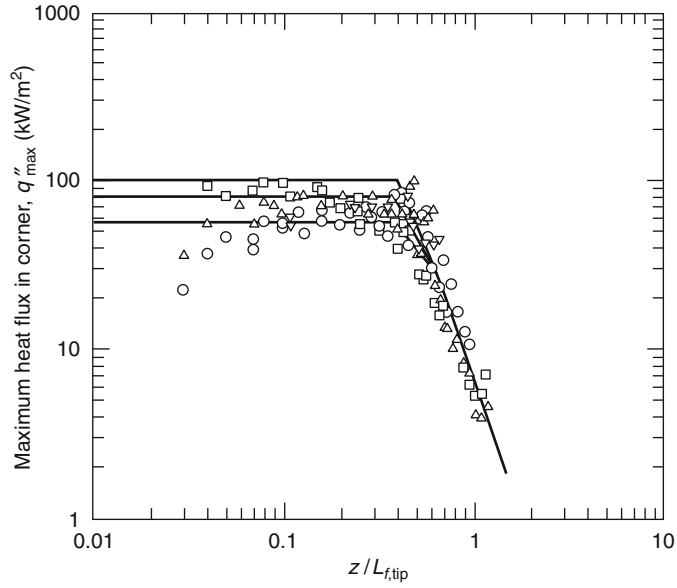

Fig. 25.7 Maximum heat fluxes to the walls near the corner with square burner sides of 0.17 m (○), 0.30 m (Δ), 0.30 m (elevated) (▽), and 0.50 m (□), and fire sizes ranging from 50 to 300 kW [29]

with distance above $z/L_{f,\text{tip}} = 0.4$. A general correlation to represent this behavior is

$$q''_{\max} = q''_{\text{peak}} \quad z/L_{f,\text{tip}} \le 0.4 \tag{25.15a}$$

$$q''_{\max} = q''_{\text{peak}} - 4\left(\frac{z}{L_{f,\text{tip}}} - \frac{2}{5}\right)\left(q''_{\text{peak}} - 30\right) \quad 0.4 < z/L_{f,\text{tip}} \le 0.65 \tag{25.15b}$$

$$q''_{\max} = 7.2\left(\frac{z}{L_{f,\text{tip}}}\right)^{-10/3} \quad z/L_{f,\text{tip}} \ge 0.65 \tag{25.15c}$$

This is similar to the form used by Back et al. [20] to correlate heat fluxes from an exposure fire to a wall (see Equations 25.10a, 25.10b, and 25.10c), except the constants are different.

The horizontal distribution in the heat flux along the wall is shown in Fig. 25.8 to best

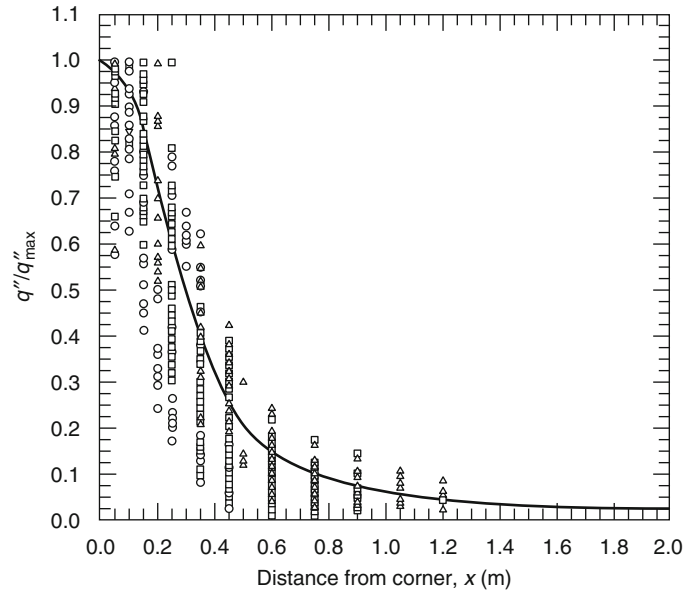

Fig. 25.8 Lateral distribution in the heat flux along the walls with distance from the corner with square burner sides of 0.17 m (○), 0.30 m (Δ), 0.30 m (elevated) (▽), and 0.50 m (□), and fire sizes ranging from 50 to 300 kW [29]

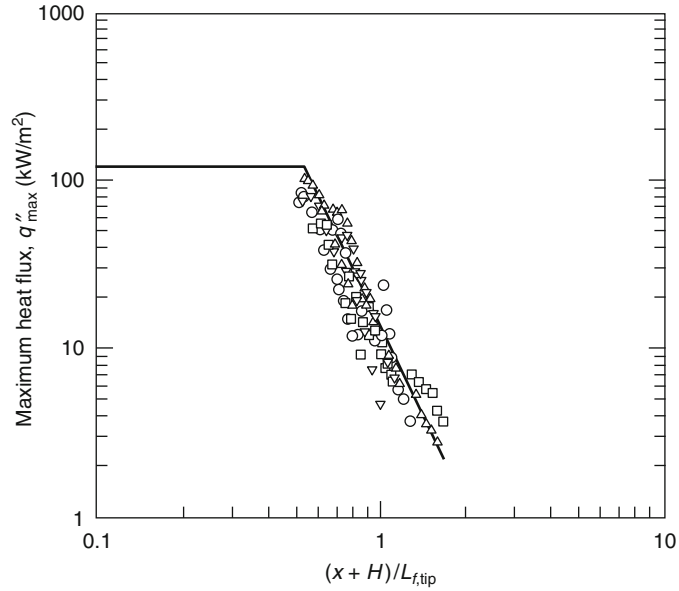

Fig. 25.9 Maximum heat flux along the top of the walls during a corner fire test with square burner sides of 0.17 m (○), 0.30 m (Δ), 0.30 m (elevated) (▽), and 0.50 m (□), and fire sizes ranging from 50 to 300 kW [29]

correlate with actual distance from the corner [29]. This was attributed air being entrained in the corner, pushing the fire into the corner. Near the corner the shape is half-Gaussian; however, heat fluxes outside of this decrease slower. The trend in the data, which is shown as the line in Fig. 25.8, can be represented using the following relations:

$$q'' = q''_{max}\exp[-7.5x^2] \quad x \leq 0.4 \text{ m} \quad (25.16a)$$

$$q'' = 0.058q''_{max}x^{-1.8} \quad x > 0.4 \text{ m} \quad (25.16b)$$

It has not been established whether this correlation holds for fire sources larger than 0.50 m in length on a single side.

Along the top part of the wall the maximum heat fluxes were measured at locations less than 0.15 m below the ceiling. The maximum heat fluxes are shown in Fig. 25.9 plotted against the

normalized distance along the flame $(x + H)/L_{f,\text{tip}}$, where x is the distance from the corner. These heat fluxes can be estimated using the following relations:

$$q''_{\max} = 120 \quad \left(\frac{x+H}{L_{f,\text{tip}}}\right) \leq 0.52 \qquad (25.17a)$$

$$q''_{max} = 13.0\left(\frac{x+H}{L_{f,\text{tip}}}\right)^{-3.5}\left(\frac{x+H}{L_{f,\text{tip}}}\right) > 0.52 \qquad (25.17b)$$

The assumed plateau in the correlation was based on the maximum heat flux expected from a flame, according to Equation 25.12.

The heat fluxes to the ceiling were determined to be a function of normalized distance along the flame length, $(r + H)/L_{f,\text{tip}}$. All of the ceiling heat flux data taken in the study with a square burner in the corner are shown in Fig. 25.10. Heat fluxes along the ceiling due to the exposure fire were similar to those measured along the top of the wall. This resulted in similar correlations to estimate the heat flux to the ceiling:

$$q'' = 120 \quad \left(\frac{r+H}{L_{f,\text{tip}}}\right) \leq 0.52 \qquad (25.18a)$$

$$q'' = 13.0\left(\frac{x+H}{L_{f,\text{tip}}}\right)^{-3.5}\left(\frac{r+H}{L_{f,\text{tip}}}\right) > 0.52 \qquad (25.18b)$$

Again, the assumed plateau in the correlation was based on the maximum heat flux expected from a flame, according to Equation 25.12.

Similar levels were measured by Hasemi et al. [25] with an exposure fire in the corner, simulated burning corner walls, and an exposure fire and simulated burning corner walls in the corner.

Room Environment Effects Corner fires are currently used to evaluate fire growth potential of a combustible lining material. As such, several studies have been conducted to characterize the heat flux from an exposure fire inside a room [30–33]. In these cases, the heat flux to the surface will be due to both the exposure fire and the room environment.

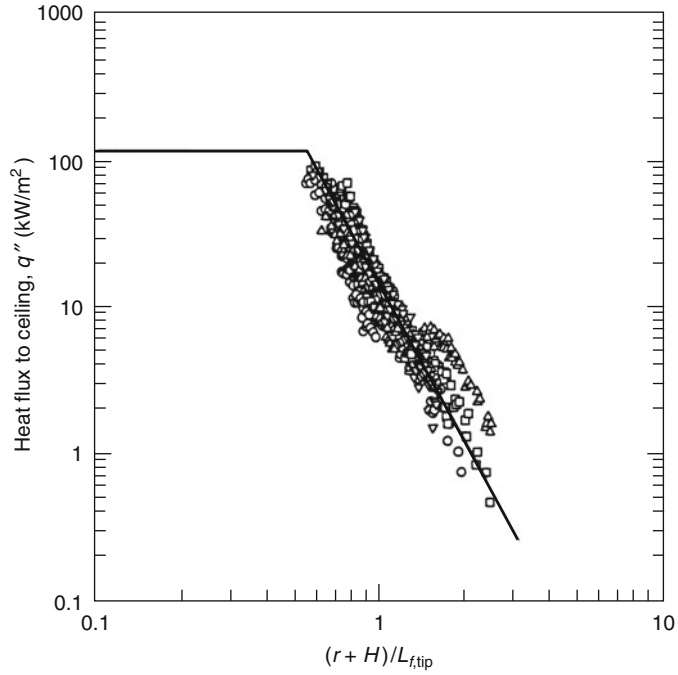

Fig. 25.10 The heat flux along the ceiling above a fire located in a corner for tests with square burner sides of 0.17 m (○), 0.30 m (Δ), 0.30 m (elevated) (▽), and 0.50 m (□), and fire sizes ranging from 50 to 300 kW [29]

The effect of the room environment on the heat fluxes was clearly demonstrated through the work performed by Dillon [33] in an ISO 9705 room [34]. The incident heat fluxes from the fire were determined by measuring the temperature rise at several locations on an insulated steel plate. Heat fluxes were calculated using a two-dimensional heat balance on the plate. Heat fluxes included contributions from both the exposure fire and the room environment. Using the surface temperature measurements and initial heat flux measurements after the burner was ignited, the heat fluxes to the hot steel plate were corrected for both reradiation from surfaces in the room and heating by the hot gas layer.

The effects of the room environment on the heat fluxes to the corner boundaries is discussed here for the case with a 300 kW fire in the corner, produced using a 0.17-m square burner. The heat fluxes shown in Fig. 25.11a represent the heat flux from the fire only, as measured using a heat flux gauge (i.e., cold surface). Note that the top of the burner is 30 cm above the floor. In general, the heat fluxes in Fig. 25.11a compare well with the total heat flux data shown in Fig. 25.5a.

Heat fluxes shown in Fig. 25.11b correspond to heat fluxes due to the fire and the room environment (i.e., hot gas layer and reradiation from walls), as measured using a heat flux gauge. For this room environment, the heat fluxes including the room environment were higher than the heat fluxes from the exposure fire to a cold wall. The magnitude of the increase depends on the elevation inside the room. Measurements in the lower part of the room showed less of an increase compared with those near the ceiling. Heat fluxes in the upper part of the room increased by as much as 20 kW/m^2, an increase largely attributed to the hot gas layer that forms inside the room during the fire. For the 300-kW fire inside the ISO 9705 compartment, average gas temperatures in the upper part of the room were measured to be approximately 680 K. Note that the heat flux due to the room environment is dependent on the gas layer temperature, which is dependent on the fire size, room geometry, ventilation, and thermal properties of the boundaries. A room or fire different from that used to produce the data in Fig. 25.11b may result in a different gas layer temperature, which will result in a different heat flux contribution due to the room environment.

Heat fluxes due to the hot layer environment inside a room were measured by Tanaka et al. [35]. In tests conducted in a 3.3-m-wide, 3.3-m-deep, 2.35-m-high room with the propane fire in the center of the room, heat fluxes were measured at different locations on one of the side walls. The average heat flux measured in the upper layer formed inside of the room is shown in Fig. 25.12 versus the layer temperature for different compartment door widths. The line in the plot represents the blackbody heat flux using the layer gas temperature, $q'' = \sigma T_g^4$. As seen in the Fig. 25.12, the blackbody heat flux using the layer gas temperature provides a reasonable estimate of the incident heat flux to the walls inside a compartment; however, the measured heat fluxes are generally higher than the blackbody heat flux. A more detailed investigation of the heat flux to compartment fire surfaces was performed by Toflio et al. [36] Through this study, it was determined that the higher heat flux was attributed to convection between the hot gas layer and the wall. In addition, as fires became large in size, radiation exchange between the fire and the walls could also increase the heat flux to wall surfaces.

Effects of Fire Standoff Distance Several researchers have investigated the effects of moving the exposure fire away from the corner (i.e., standoff distance) [24, 30, 37]. As one might expect, moving the fire away from the corner decreases the heat fluxes to the room boundaries. Tests were performed by Williamson et al. [30] in a full-scale ISO 9705 room using a 0.30-m-diameter burner. Heat fluxes to the wall were strongly dependent on whether the flame was attached to the corner walls or burned freely near the wall. At a heat release rate of 40 kW, with the burner against the corner walls, the flame was attached to the walls and heat fluxes were measured to be as high as 50 kW/m^2. When

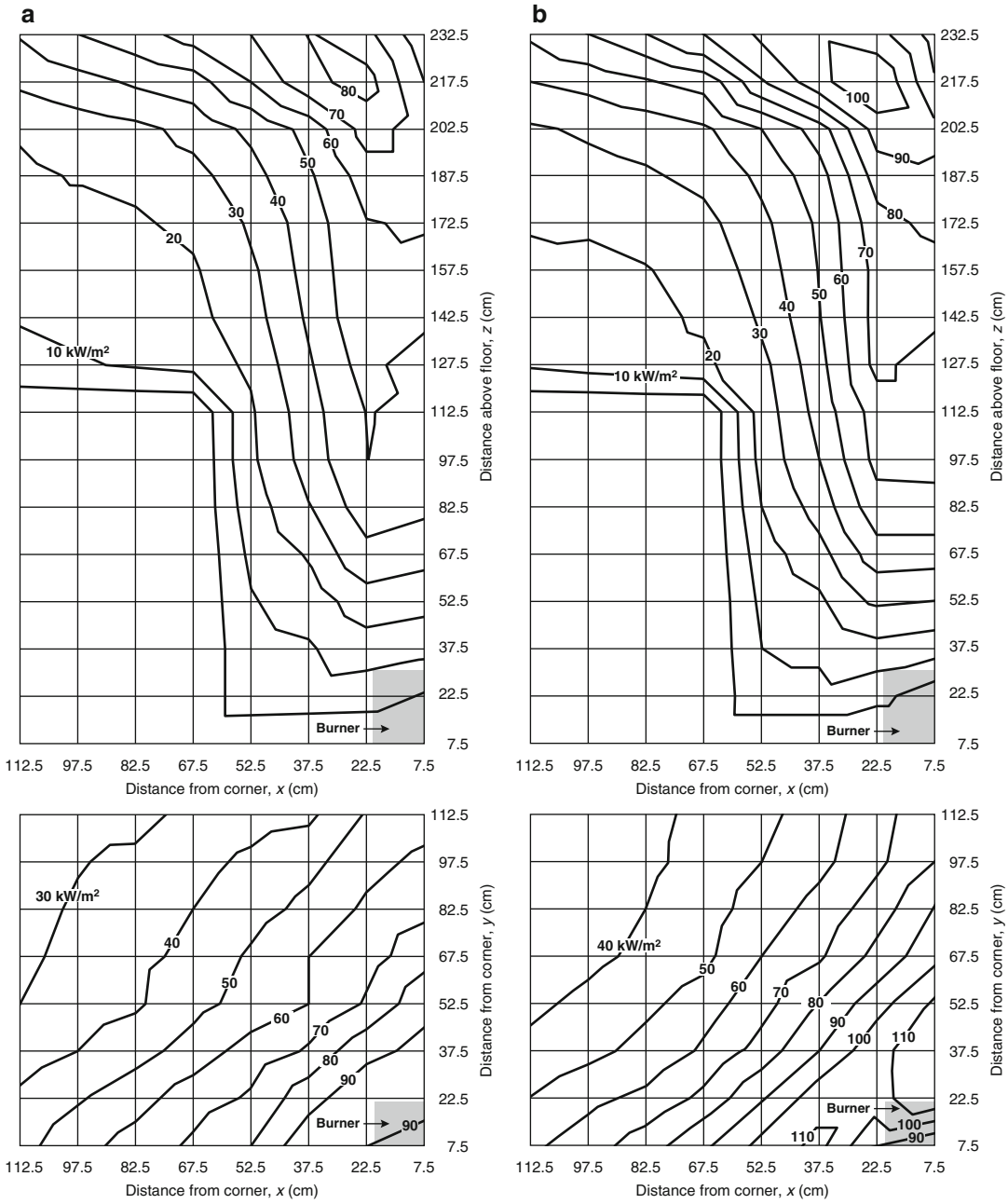

Fig. 25.11 Heat fluxes to corner boundaries from (**a**) 300-kW, 0.17-m square propane sand burner exposure fire alone to a "cold" surface and from (**b**) the 300-kW exposure fire and the room environment [33]

the fire was moved 50 mm from the walls, the flames were observed to be detached from the walls with the highest heat fluxes measured to be approximately 25 kW/m^2. In tests with a heat release rate of 150 kW, the fire was observed to be attached to the walls and heat fluxes of 40–60 kW/m^2 were measured at the walls. Additional work needs to be performed to investigate distances at which fires attach to nearby surfaces, such as a flat wall or walls in a corner.

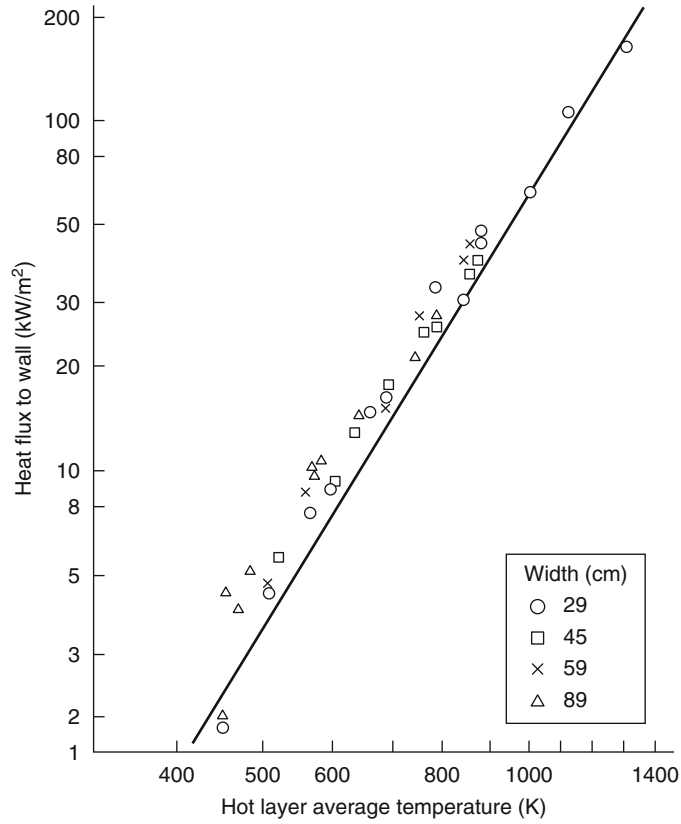

Fig. 25.12 Heat flux to the walls inside a compartment containing a hot gas layer [35]

Fires Beneath Unconfined Ceilings

There have been several experimental and theoretical studies performed on fires impinging on an unbounded ceiling [1–4, 38–41]. Total heat fluxes from fires and fire plumes impinging on the ceiling were measured by Hasemi et al. [38], You and Faeth [3, 4], and Kokkala [1, 2].

Hasemi et al. [38] conducted a series of fire tests using propane gas burners located at different distances beneath a noncombustible ceiling. Fires as large as 400 kW (approximated) were considered in the study. Heat flux gauges were used to measure the incident heat flux along the ceiling at different distances away from the fire centerline, or stagnation point. The measured heat flux at the stagnation point is shown in Fig. 25.13 to plateau at approximately 90 kW/m^2. In order to collapse the data, the flame tip length was normalized with respect to the distance between the ceiling and fire, H, plus the virtual source location, z'. The virtual source location for this geometry was determined using the following relations:

$$z' = 2.4D\left(Q_D^{*2/5} - Q_D^{*2/3}\right) \quad Q^* < 1.0 \tag{25.19a}$$

$$z' = 2.4D\left(1 - Q_D^{*2/5}\right) \quad Q^* \geq 1.0 \tag{25.19b}$$

where Q_D* is defined as in Equation 25.14 with D being the diameter of the exposure fire. The length of the flame, $L_{f,\text{tip}}$, in this geometry is defined as the distance between the fire and the ceiling, H, plus the radial extension of the flame out from the center of the fire, L_H. The location of the flame tip in this geometry was found to correlate with Q_H*, which is defined the same as in Equation 25.14 except D is replaced by H. The flame tip correlation was determined to be

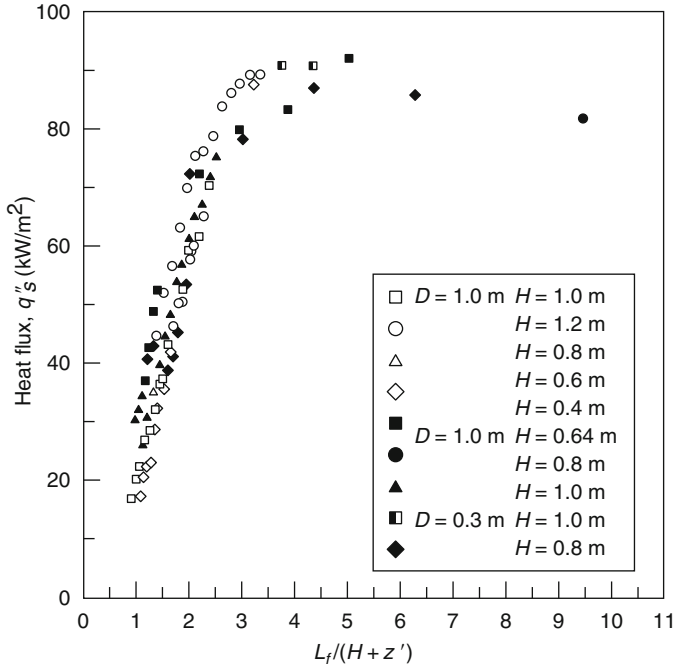

Fig. 25.13 Stagnation point heat fluxes on an unbounded ceiling with a fire impinging on it [38]

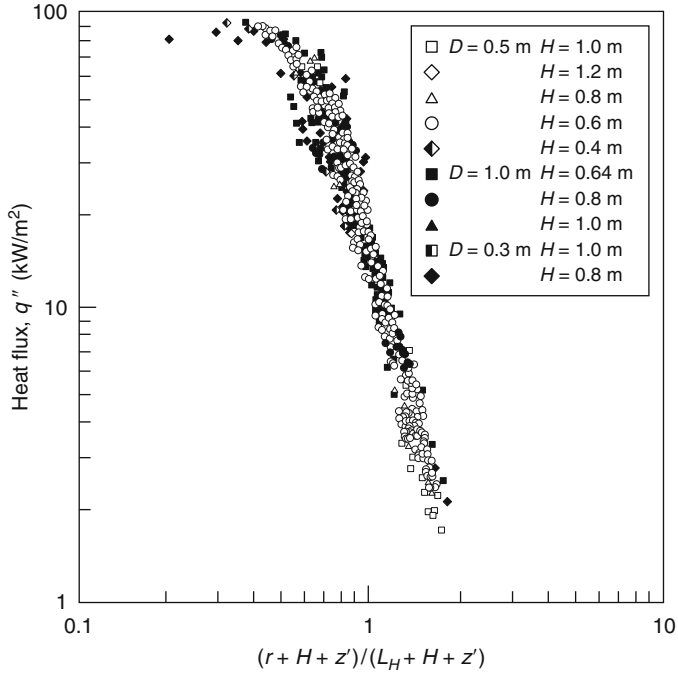

Fig. 25.14 Heat fluxes to a ceiling due to a propane fire impinging on the surface [38]

$$\frac{(L_H + H)}{H} = L_{f,\text{tip}}/H = 2.89 Q_H^{*1/3} \qquad (25.20)$$

The heat flux was measured to decrease with distance from the fire stagnation point. Figure 25.14 contains a plot of the heat flux to the ceiling as a function of location within the flame. The correlation recommended by Wakamatsu [42] can be used to predict the heat fluxes:

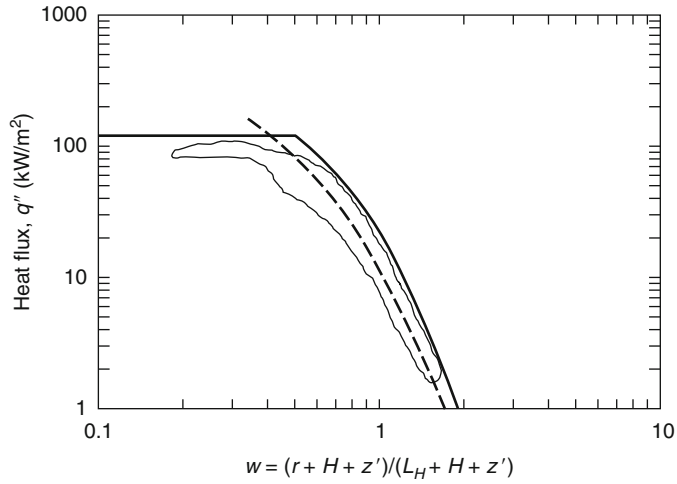

Fig. 25.15 A comparison of the best fit curve proposed by Wakamatsu [42] (– –) and a bounding fit to the data (—). The unbounded ceiling data of Hasemi et al. [38] is represented as the outlined area

$$q'' = 518.8e^{-3.7w} \tag{25.21a}$$

where

$$w = \left(r + H + z'\right)/\left(L_H + H + z'\right) \tag{25.21b}$$

Figure 25.15 contains a plot of Equation 25.21a (dashed line) along with a representation of the data of Hasemi et al. [38] for a flat unbounded ceiling. Equation 25.21a adequately estimates the data when w is greater than 0.45 but significantly overestimates heat flux levels for smaller values of w. Based on the data from Hasemi et al. [38] and other data from fires impinging on I-beams mounted to a ceiling [43], a correlation was developed to predict the bounding heat flux levels to an unconfined ceiling:

$$q'' = 120 \quad w \leq 0.5 \tag{25.22a}$$

$$q'' = 682\exp(-3.4w) \quad w > 0.5 \tag{25.22b}$$

where w is defined in Equation 25.21b. This correlation is shown in Fig. 25.15 as the solid line. The peak heat flux of 120 kW/m^2 at w less than or equal to 0.5 bounds nearly all of the heat flux measurements made in this range for the studies of Hasemi et al. [38] and Myllymaki and Kokkala [43].

Heat flux measurements with smaller fires (<11 kW) beneath a ceiling were made by Kokkala [1, 2] and You and Faeth [4]. Kokkala used natural gas as a fuel and measured heat fluxes to plateau at 60 kW/m^2 at the stagnation point (Fig. 25.16). Due to the small burners used in this study ($D = 0.064$ m), Kokkala's data collapsed without applying a virtual source origin correction. Heat fluxes measured in the natural gas fire tests were lower than those measured by Hasemi et al. [38], an effect that can partly be attributed to the higher radiation levels from the propane flames. The heat fluxes measured by Kokkala [1] at different locations from the stagnation point are plotted in Fig. 25.17. The distribution in the heat flux along the ceiling radially out from the stagnation point was measured to be similar to that measured by Hasemi et al. [38] with larger propane gas fires.

Fires in Corridors

There are few reported studies that have measured heat fluxes to the ceiling or walls of a corridor. Hinkley et al. [44–46] performed experiments with a town gas burner located at the end of a hallway. Tests with a noncombustible ceiling were performed in a 1.2-m-wide hallway using a range of heat release rates (170–600 kW) with the burner at various distances (0.37–1.20 m) below the ceiling. Heat fluxes were determined through temperature

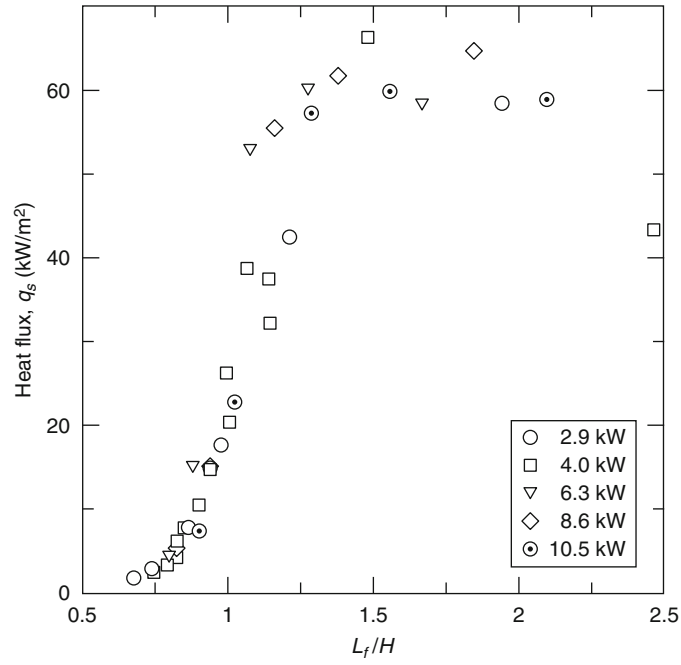

Fig. 25.16 Heat fluxes at the stagnation point on a ceiling for tests with natural gas fires impinging on the ceiling [1]

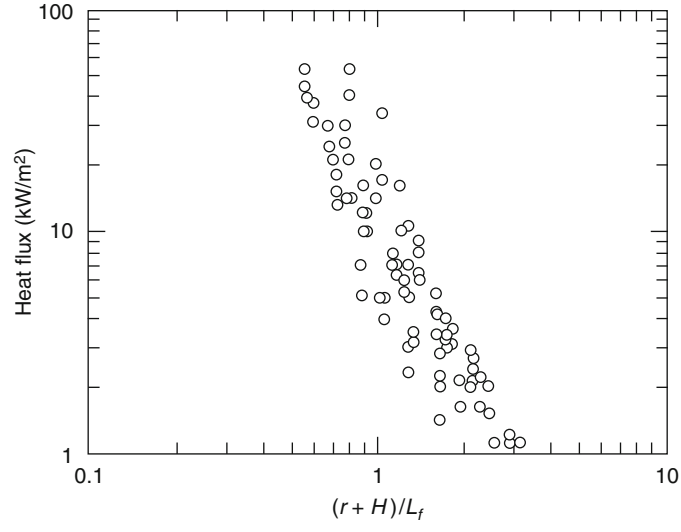

Fig. 25.17 Heat fluxes to a ceiling due to a natural gas fire impinging on the surface [1]

measurements on exposed and unexposed sides of the ceiling material.

The heat fluxes determined in these experiments are provided in Fig. 25.18, plotted as a function of $(x + x')/L$, where x' is the virtual source and L is the flame length from the virtual source. This plot indicates that heat fluxes as high as 160 kW/m^2 can exist in these types of scenarios. The increase in the heat flux over the unconfined ceiling data of Hasemi et al. [38], with peak heat fluxes of approximately 90 kW/m^2, may be due in part to the thicker layer of flames formed in the corridor. However, due to the method used to develop the heat fluxes, the accuracy of the heat flux data reported by Hinkley et al. is uncertain [44, 45].

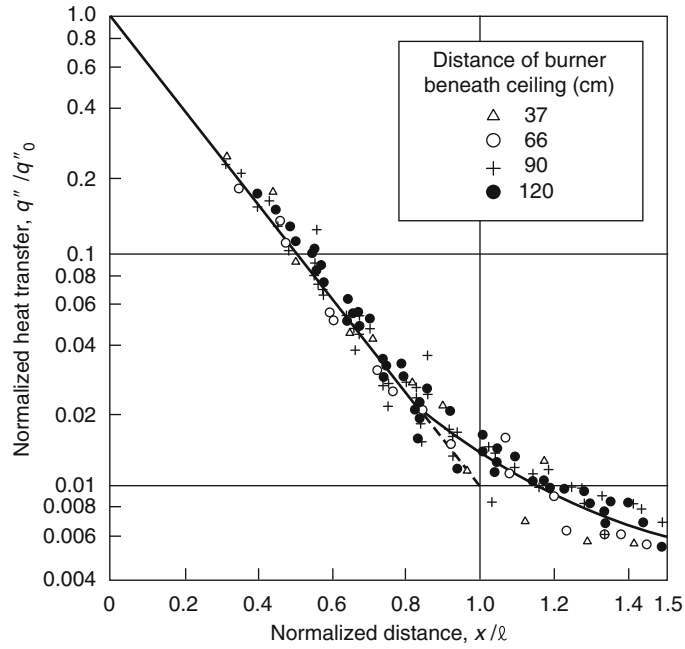

Fig. 25.18 Heat fluxes to the ceiling in a corridor with an exposure fire at the closed end [44]

Lattimer et al. [47] conducted a separate study to measure and correlate heat fluxes from a fire at the closed end of a corridor. The apparatus and burner were similar to that used by Hinkley et al. [45] The corridor was 2.44 m (8 ft) long, 1.22 m (4 ft) wide, and 2.1 m (6.8 ft) high, with one end of the corridor blocked. The bottom portion of the corridor was open to allow air to flow freely into the corridor along its length. Tests were conducted with the interior surface of the corridor apparatus lined with a 25-mm (1.0 in.) thick, 96 kg/m^3 (6 lb/ft^3) Unifrax Durablanket noncombustible ceramic blanket.

A rectangular propane gas sand burner was located at the blocked end of the corridor. The burner had dimensions of 1.15 m (3.8 ft) wide and 0.46 m (1.5 ft) deep. Tests were conducted with the burner located 0.60 m (2.0 ft) and 1.1 m (3.6 ft) below the ceiling and using heat release rates ranging from 100 to 400 kW.

Thermal characterization included the measurement of flame lengths, total heat flux to the ceiling, and gas temperatures just below the ceiling. Total heat flux was measured using water-cooled Schmidt-Boelter-type heat flux gauges. Flame lengths were visually determined during the tests and were reported as total flame lengths, which include the part of the height of the flame below the ceiling and the flame extension along the ceiling.

Figure 25.19 contains a plot of the flame length data from this study along with data from Hinkley et al. [45] in a similar corridor apparatus. The flame length data from these tests agree well with flame lengths reported by Hinkley et al. [45] The correlation in the plot is described using the following relation:

$$L_{f,\text{tip}} = 0.075 Q'^{2/3} \tag{25.23}$$

where $L_{f,\text{tip}}$ is the total flame length determined by adding flame height below a ceiling with flame extension along a ceiling (m) and Q' is the heat release rate of the fire per unit width of a hallway (kW/m). The correlation represents a best fit to the corridor data as well as larger-scale test data from fires in tunnels [48], which is a similar geometry. The correlation with the corridor and tunnel flame length data is shown in Fig. 25.20. The data are a reasonable fit for all the data but do underpredict the higher heat release rate data by Hinkley et al. [45]

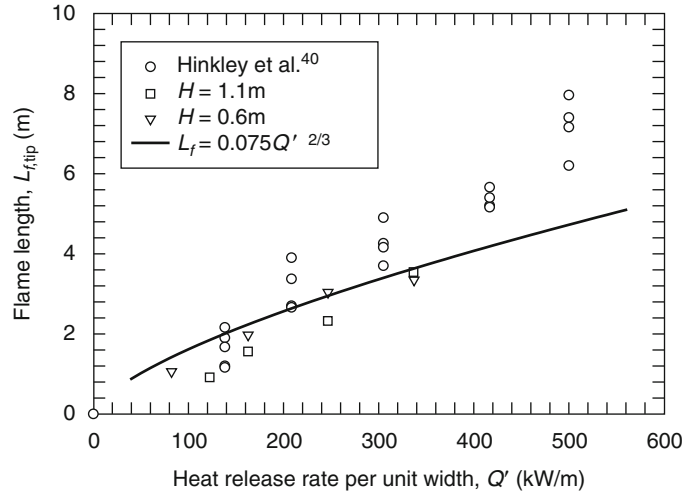

Fig. 25.19 Flame length data from tests in corridor tests by Lattimer et al. [47] and Hinkley et al. [45]

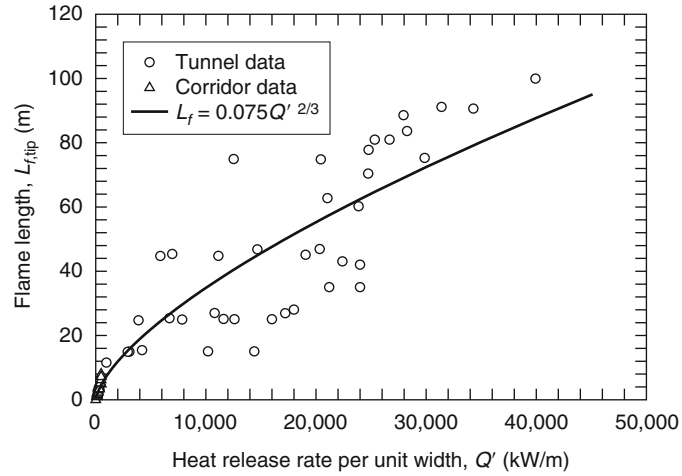

Fig. 25.20 Flame length correlation compared with corridor and tunnel data [48]

A plot of the average heat fluxes to the corridor ceiling is provided in Fig. 25.21 as a function of dimensionless distance along the flame length. Also shown in the plot are some of the data from Hinkley et al. [45] The data from these tests match well with data from the tests by Hinkley et al. [45] A correlation for the heat flux along the ceiling is also shown in the figure and can be predicted through these equations:

$$q'' = 160 \quad \left[(x+H)/L_{f,\text{tip}}\right] < 0.25 \tag{25.24}$$

$$q'' = 26.39\left[(x+h)\right]/L_{f,\text{tip}}\Big]^{-1/3} \quad \left[(x+H)/L_{f,\text{tip}}\right] \geq 0.25 \tag{25.25}$$

where H is the distance between the fire and the corridor ceiling (m), x is the distance along the corridor (m), and $L_{f,\text{tip}}$ is the flame tip length (m). Close to the impingement point of the fire, the heat fluxes were measured to reach 160 kW/m^2. This is 70 kW/m^2 higher than similar fires in an unconfined ceiling geometry.

All of these tests are with the gas burner width being the same as the corridor width. As the width of the fire is decreased relative to the corridor width, heat fluxes are expected to provide results closer to the unconfined ceiling data. Heat release rate and fire location below the ceiling will also affect heat fluxes to the ceiling in these situations.

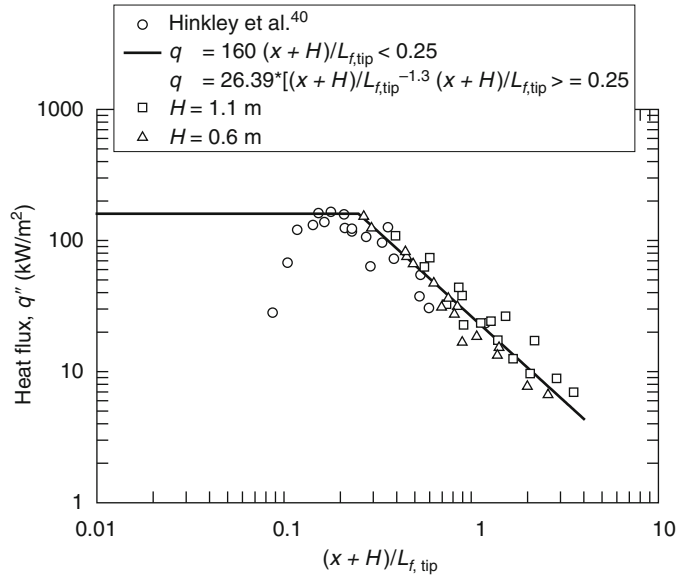

Fig. 25.21 Heat fluxes to a corridor ceiling with dimensionless distance along the flame length

Fires Beneath I-Beams

Three studies have evaluated the heat flux incident onto an I-beam mounted to a ceiling with an exposure fire impinging on the beam [38, 43, 49]. These studies all measured the heat flux to the four surfaces shown in Fig. 25.22 on the I-beam: downward face of the lower flange, upward face of the lower flange, the web, and downward face of the upper flange. For each of these surfaces, heat fluxes were measured from the stagnation point of the fire (centerline of the fire) past the location of the flame tip.

The study by Wakamatsu et al. [49] provides a framework for determining heat fluxes to different parts of the I-beam. The I-beam evaluated in the study was 3.6 m long, a web 150 mm high and 5 mm thick, and flanges 75 mm wide and 6 mm thick. Tests were performed using fires from 0.5- or 1.0-m propane burners with heat release rates ranging from 100 to 900 kW. The distance between the fire source and I-beam was also varied.

When the fire impinges on the I-beam, the flame length is different on the lower flange compared to the flame length on the upper flange (Fig. 25.23). Flame lengths along the lower flange, L_B, were shorter than those observed

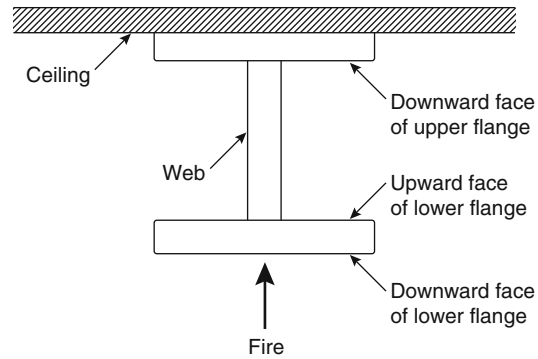

Fig. 25.22 Location of heat flux measurements on I-beams

near the upper flange, L_C. Heat fluxes along the lower flange were taken to be a function L_B while heat fluxes to other surfaces were related to L_C. Flame lengths were related to the dimensionless Q^*, as defined in Equation 25.14, with D being replaced by the appropriate distance between the fire and the flange,

$$Q^*_{H_B} = \frac{Q}{\rho_\infty C_p T_\infty \sqrt{g} H_B^{5/2}} \tag{25.26}$$

$$Q^*_{H_C} = \frac{Q}{\rho_\infty C_p T_\infty \sqrt{g} H_C^{5/2}} \tag{25.27}$$

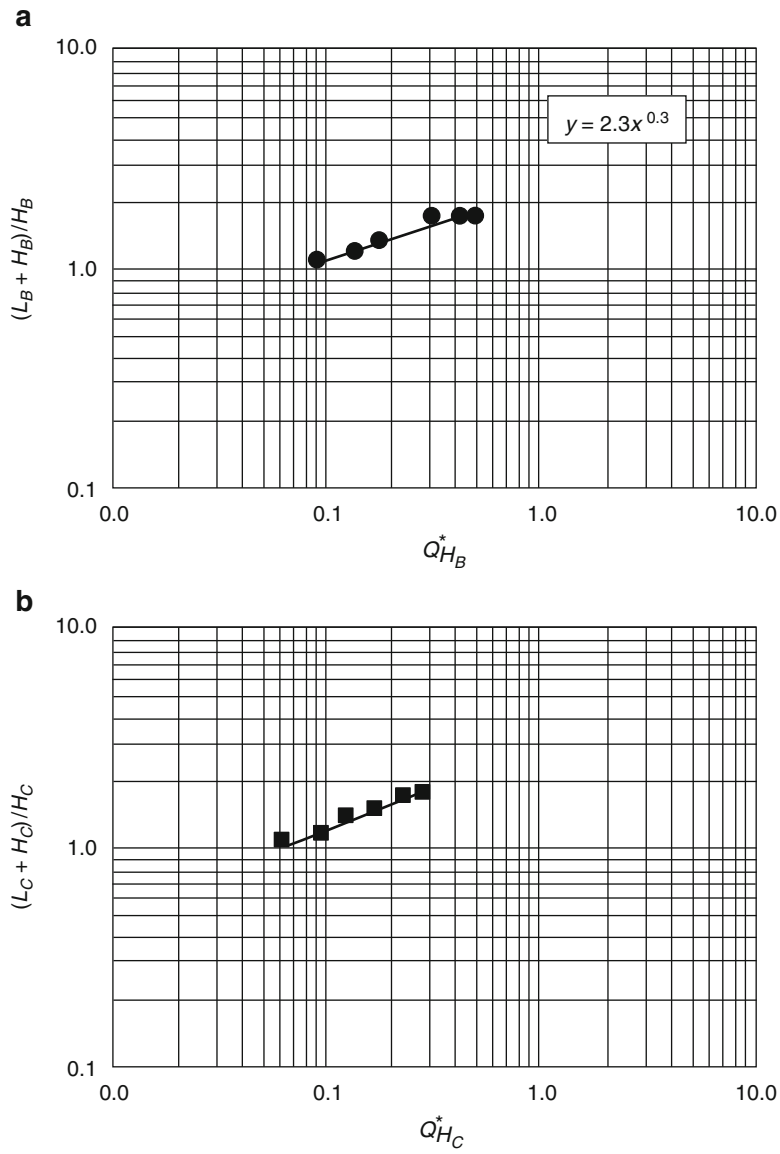

Fig. 25.23 Flame lengths (**a**) along the lower flange (Equation 25.28a) and (**b**) along the upper flange in I-beam tests performed by Wakamatsu et al. [49]

Correlations were developed to predict the flame tip length along the lower and upper flanges:

$$(L_B + H_B)/H_B = 2.3Q^{*0.3}_{H_B} \qquad (25.28a)$$

$$(L_C + H_C)/H_C = 2.9Q^{*0.4}_{H_C} \qquad (25.28b)$$

The heat flux measured at the stagnation point on the downward face of the lower flange was found to be the same as that measured for a fire beneath a ceiling (Fig. 25.24). The location of the virtual origin, z', was determined using Equation 25.19. The variation in the heat flux along the downward face of the lower flange with horizontal distance, r, from the stagnation point is shown in Fig. 25.25. The data appear to fall between the range of the data measured in the unconfined ceiling tests, which are represented by the dashed and solid lines. These heat fluxes were the highest measured on the I-beam assembly and can be estimated using the following correlation:

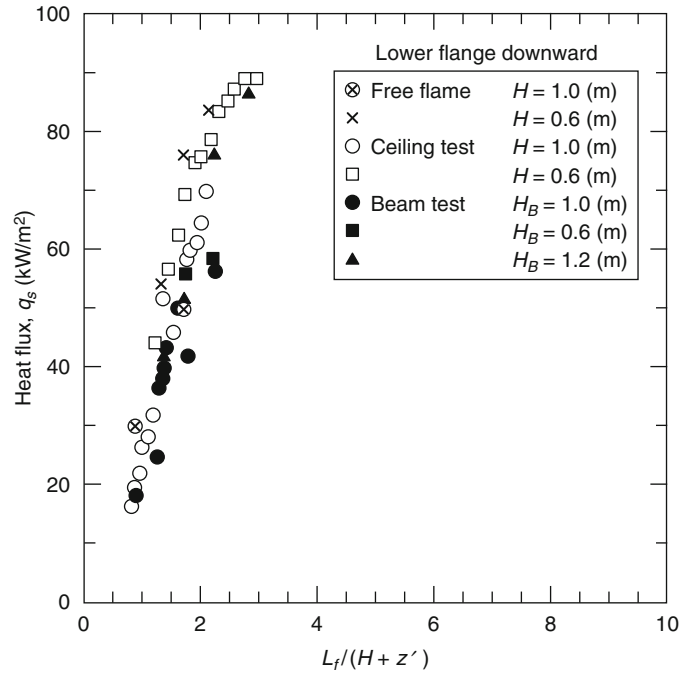

Fig. 25.24 Heat flux at the stagnation point on the downward face of the lower flange [49]

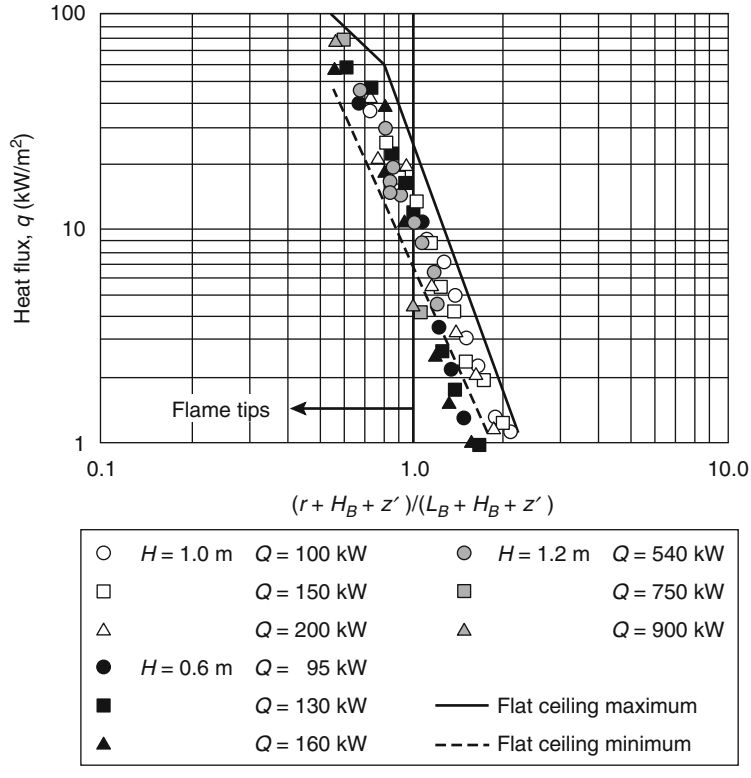

Fig. 25.25 Heat flux along the downward face of the lower flange [49]

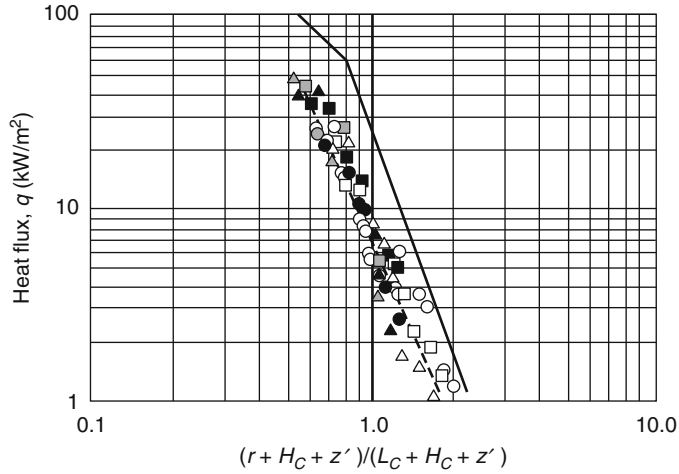

Fig. 25.26 Heat flux along the upward face of the lower flange (key same as in Fig. 25.25) [49]

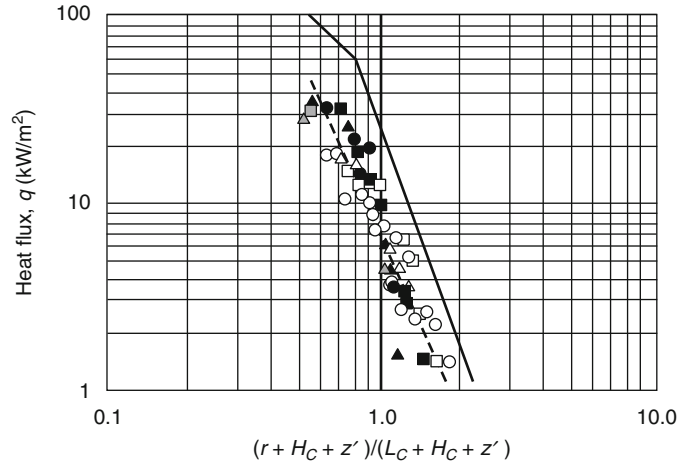

Fig. 25.27 Heat flux along web (key same as in Fig. 25.25) [49]

$$q'' = 518.8e^{-3.7w} \quad (25.29a)$$

where

$$w = \left(r + H_B + z'\right)/\left(L_B + H_B + z'\right) \quad (25.29b)$$

The heat fluxes to the upward face of the lower flange and the web are shown in Figs. 25.26 and 25.27 to be lower than those on the downward face of the lower flange. This was attributed to the lower flange shielding these parts of the I-beam from radiative and convective heat transfer. These data can be represented by the following expression:

$$q'' = 148.1e^{-2.75w} \quad (25.30a)$$

where

$$w = \left(r + H_C + z'\right)/\left(L_C + H_C + z'\right) \quad (25.30b)$$

The lowest heat fluxes on the I-beam were measured on the downward facing part of the upper flange. As seen in Fig. 25.28, heat fluxes to this part of the I-beam are slightly less than those measured on an unconfined ceiling. Heat fluxes to the downward face of the upper flange can be estimated using the following fit to the data:

$$q'' = 100.5e^{-2.85w} \quad (25.31a)$$

where

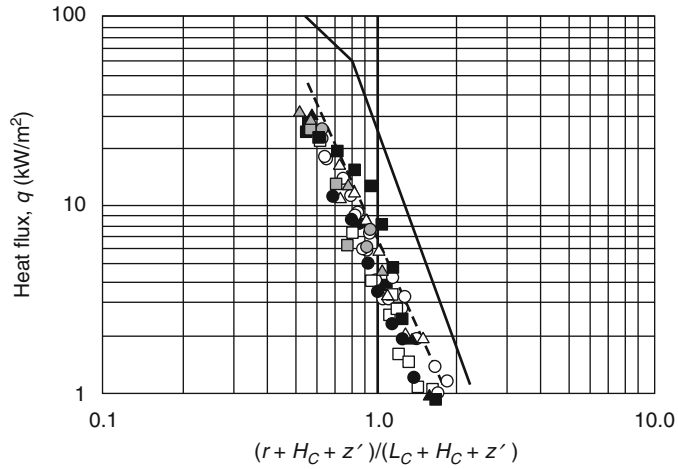

Fig. 25.28 Heat flux along the downward face of the upper flange (key same as in Fig. 25.25) [49]

$$w = \left(r + H_C + z^{'}\right) / \left(L_C + H_C + z^{'}\right) \quad (25.31b)$$

Myllymaki and Kokkala [43] evaluated the use of the approach and data of Wakamatsu et al. [49] to estimate heat fluxes onto I-beams exposed to fires as large as 3.9 MW. They found that for fires over 2.0 MW, the correlations suggested for the upward face of the lower flange, web, and downward face of the upper flange underestimate the heat flux to these areas on the I-beam. For these large fires, the I-beam becomes completely engulfed in fire. As a result, heat fluxes on all parts of the I-beam follow the correlation suggested for the downward face of the lower flange provided in Equation 25.29. Heat fluxes to the downward face of the lower flange, the upper flange, and the web are shown in Fig. 25.29, along with the correlations recommended by Wakamatsu [42]. The highest heat fluxes measured in the tests performed by Myllymaki and Kokkala [43] were approximately 130 kW/m^2 and were along the downward face of the upper flange.

Data from these studies demonstrate that the heat flux to the I-beam can be conservatively estimated using the bounding heat flux correlation in Equation 25.32:

$$q^{''} = 120 \quad w \leq 0.5 \quad (25.32a)$$

$$q^{''} = 682\exp(-3.4w) \quad w > 0.5 \quad (25.32b)$$

using the appropriate expression for w provided in Equations 25.29b, 25.30b, and 25.31b. Figure 25.30 provides a plot of this correlation along with the I-beam data [43].

Burning Walls and Ceilings

Fires from burning boundaries typically produce thinner flames than those generated by exposure fires. As a result, heat fluxes from burning boundary flames are typically lower than those measured for exposure fires in a similar geometry. As was the case with heat fluxes from exposure fires, heat fluxes from burning boundaries are dependent on the geometry of the burning surfaces.

Wall Fires

Heat fluxes from a burning wall flame back to the surface have been studied fairly extensively. Most of the work in this area has been performed with smaller fires. Though the data indicate that these heat fluxes are dependent on both fire size and smoke production, no reported study has fully characterized this behavior.

Much of the detailed heat flux measurements for fires produced by burning flat surfaces have been done with smaller-scale fires (<100 kW). Through this work, the heat fluxes from flames

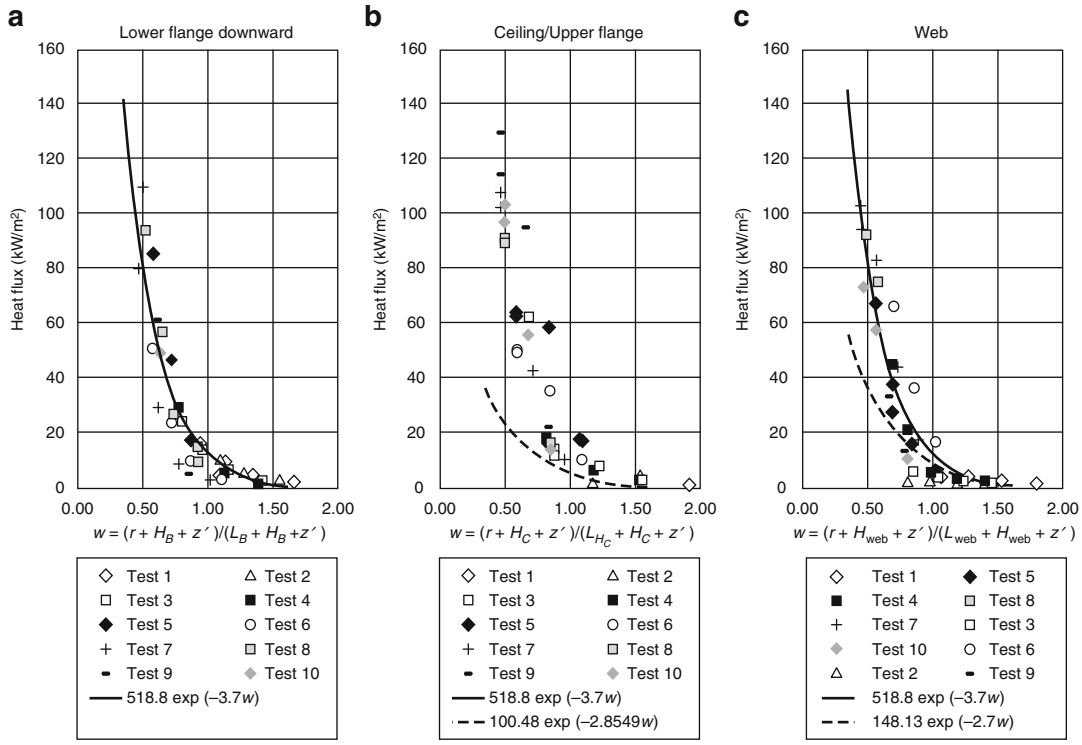

Fig. 25.29 Heat fluxes measured at the (**a**) downward face of the lower flange, (**b**) upper flange, and (**c**) the web on an I-beam in the study by Myllymaki and Kokkala [43], with fires as large as 3.9 MW

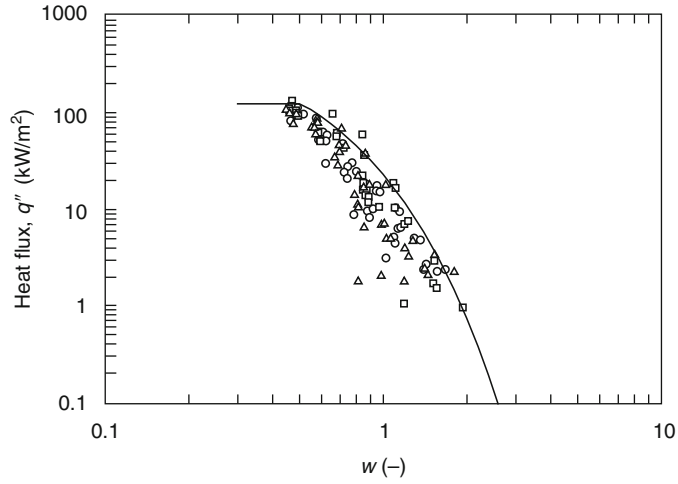

Fig. 25.30 Heat flux measured on the bottom flange (○), web (□), upper flange (Δ) of an I-beam mounted below an unbounded ceiling for fires 565–3870 kW [43]. The line in the plot is the curve given in Equation 25.32

produced by a variety of different burning materials have been characterized [50–53]. All of these studies were conducted with fires over flat, solid surfaces except the study of Ahmad and Faeth [50, 51], which was performed using wicks soaked in different alcohols. Ahmad and Faeth performed flat wall fire experiments using a 0.66-m-wide, 0.81-m-high flat wall test apparatus, with the lower part of the wall being an alcohol-soaked wick. Different wick heights

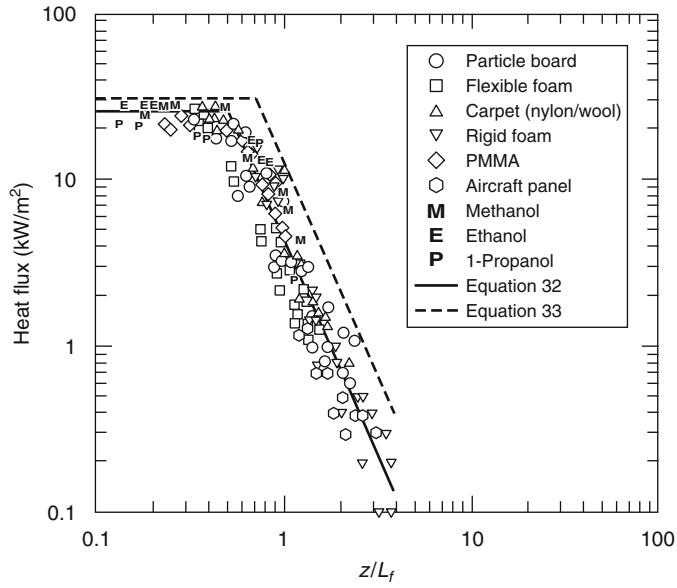

Fig. 25.31 The heat fluxes from burning flat surfaces for fires less than 100 kW [50–52]

and different types of alcohol were included in the study. Data from Quintiere et al. [52] were attained using samples 0.28 m by 0.28 m exposed to different external heat fluxes to generate different heat release rate fires from the same sample. Experiments performed by Orloff et al. [53] were conducted using a 0.41-m-wide, 1.57-m-high sample of PMMA.

Data from the studies of Ahmad and Faeth [50, 51] and Quintiere et al. [52] are shown in Fig. 25.31. Heat fluxes are approximately 20–30 kW/m^2 in the lower part of the flame ($z = 0.5L_f$) for a wide range of fuels. Peak heat fluxes measured by Orloff et al. [53] (22 kW/m^2) were also in this 20–30 kW/m^2 range. The value of L_f can be determined by using a flame height correlation for a line fire, such as that proposed by Delichatsios: [54]

$$L_f = 0.052Q'^{2/3} \tag{25.33}$$

where Q' is the heat release rate per unit length of burning wall.

Several empirical correlations have been proposed in the literature [55–58] to predict heat fluxes to walls. All correlations assume a constant heat flux in the lower part of the fire and a power law decay above this. The difference in these correlations is the peak heat flux over the bottom part of the fire and the empirical constants that govern the decay. Similar to that proposed by Hasemi [55], the line in the plot is an average fit to the data:

$$q'' = 25 \quad (z/L_f) \le 0.5 \tag{25.34a}$$

$$q'' = 4.4(z/L_f)^{-2.5} \quad (z/L_f) > 0.5 \tag{25.34b}$$

A more conservative fit that bounds this data set was developed:

$$q'' = 30 \quad (z/L_f) \le 0.7 \tag{25.35a}$$

$$q'' = 12.3(z/L_f)^{-2.5} \quad (z/L_f) > 0.7 \tag{25.35b}$$

Line burners have been used by some researchers to simulate a fire produced by a burning surface such as a wall. Hasemi [55, 59, 60] measured the heat flux from a methane line burner fire to an incombustible wall. In this study, the fire heat release rate per unit length of burner (0.30 m) was varied from 16.7 to 218.2 kW/m and two different liner burner widths (0.037 m and 0.082 m). For the test conditions considered, the heat fluxes along the flame are seen in Fig. 25.31 to be similar for each test condition. In addition, heat fluxes measured in this study are shown in Fig. 25.32 to be similar

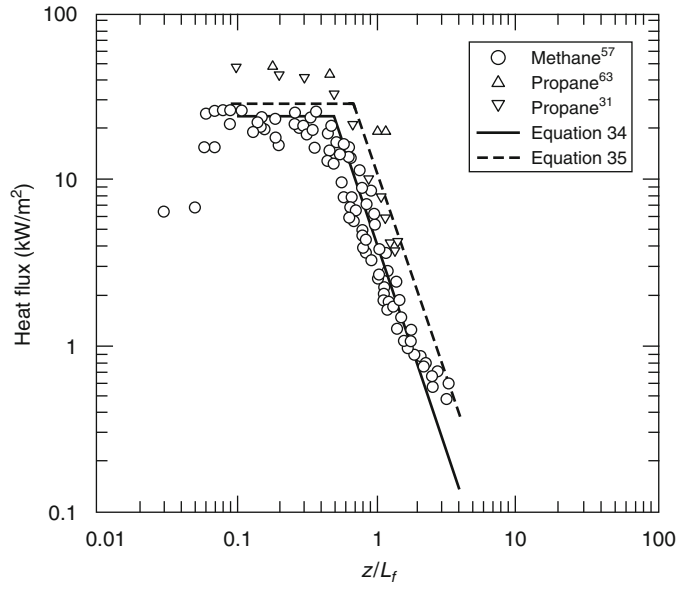

Fig. 25.32 The heat fluxes from methane line burners against a flat wall [29, 55, 61]

to those shown in Fig. 25.31. The correlations presented in Equations 25.34 and 25.35 adequately bound the data. Line burner experiments using propane as fuel have resulted in higher heat fluxes than those measured with methane as the fuel. In tests using propane with $Q' = 83 - 167$ kW/m, Kokkala et al. [61] and Lattimer [29] both measured heat fluxes of approximately 45 kW/m^2 in the lower half of the flame ($z = 0.5\ L_f$). Though not shown on the plot, Foley and Drysdale [62] measured 40–50 kW/m^2 from propane line burners with $Q' = 11.6$ and 20.9 kW/m. These data indicate that the radiation from the fire to the surface is dependent on fuel smoke production.

Slightly larger-scale fire tests were performed by Kulkarni et al. [63, 64] In this study, heat flux measurements were made along the length of different 0.3-m-wide, 1.2-m-high samples of solid combustibles. Fires were initiated using a line burner at the bottom of the sample, and heat fluxes were continuously measured during the test. Heat fluxes and flame lengths were continuously monitored as the fire spread along the combustible material. These transient heat flux and flame length measurements were averaged over particular time periods and plotted to determine the heat flux at different locations along the flame length.

Figure 25.33 provides the heat flux data for the different materials included in the study. Peak heat fluxes measured for the different materials were measured to range from 25 to 60 kW/m^2. Heat fluxes from burning masonite board, cardboard, and white pine board were in the 20 to 30-kW/m^2 range, similar to that measured in experiments by Ahmad and Faeth [50, 51] and Quintiere et al. [52]. However, fires involving PMMA, polyurethane foam, and velour fabric were all measured to produce heat fluxes greater than 30 kW/m^2. The PMMA and polyurethane foam had the highest flame lengths of all the materials (~1.75 m), which is comparable to the flame lengths reported by Quintiere et al. [52] for similar materials (PMMA and flexible foam). This indicates that the heat release rates for the PMMA and polyurethane foam are comparable in the two studies. The reason for the differences in the peak heat fluxes (e.g., 30–60 kW/m^2 in tests by Kulkarni et al. [63, 64] with PMMA, while 20–26 kW/m^2 in tests by Quintiere et al. [52]) is not known.

Less detailed heat flux measurements have been reported in the literature for larger fires. Orloff et al. [65] and Delichatsios [54] reported data on heat fluxes from flames produced by a 3.6-m-high burning PMMA wall. Total heat fluxes incident on the PMMA were calculated

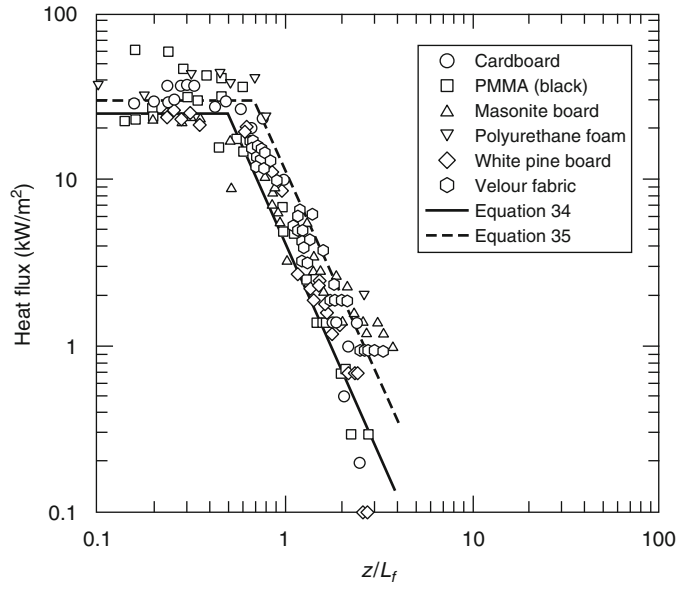

Fig. 25.33 Heat fluxes for different materials [64, 64]

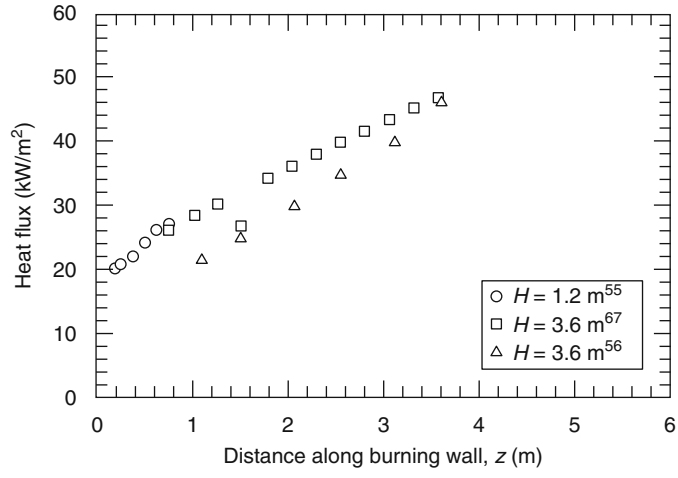

Fig. 25.34 Heat flux from a PMMA wall flame back to the fuel surface [53, 54, 65]

using theory and mass loss rate data. Heat fluxes are shown in Fig. 25.34 to increase with height. All the data in this plot were at positions where z/L_f is less than 0.5. This behavior is different than that observed with smaller fires, where heat flux is relatively constant over this region.

Markstein and de Ris [66] also explored the effects of larger fire size and soot production on the heat flux incident on the burning surface. The apparatus used in the study was 0.38 m wide and 1.98 m high, with the bottom 0.79 m of the wall being a sintered metal gas burner. Heat flux data for methane, ethane, ethylene, and propylene fires were reported. The impact of fire size on the heat flux distribution along the height of the panel is shown in Fig. 25.35. Similar to the PMMA results, the heat fluxes were measured to increase with height in the test with the higher heat release rate (816 kW/m).

The heat flux from the flame is shown in Fig. 25.36 to also be a function of fuel smoke production rate. Methane and ethane have low smoke yields (less than 0.013 g/g) [67] and are measured to produce heat fluxes as high as

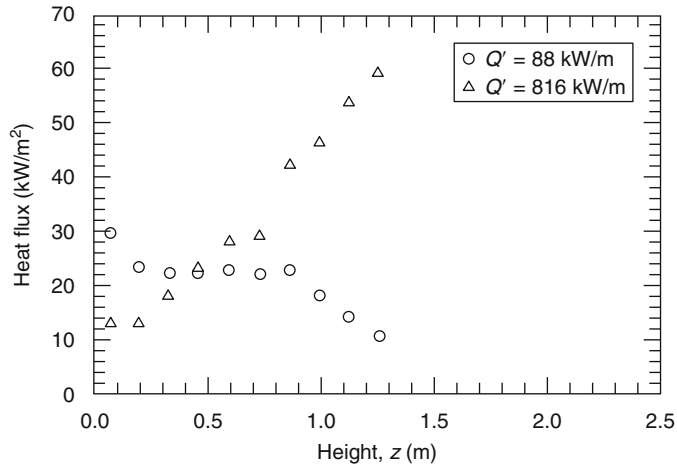

Fig. 25.35 Heat fluxes along a propylene gas wall fire at different heat release rates per unit width [66]. Burning wall height was 0.79 m

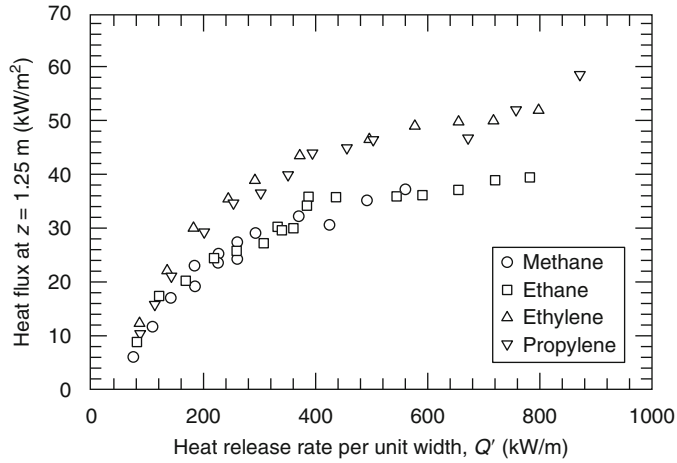

Fig. 25.36 Heat flux at a height of z = 1.25 m for different size fires and different fuels [66]. Burning wall height was 0.79 m

35–38 kW/m^2. The smoke yield of ethylene (0.043) [67] is less than that of propylene (0.095), but similar heat fluxes were measured with height along the apparatus. Peak heat fluxes of 59 kW/m^2 were measured for the largest propylene fire considered in the study.

Heat fluxes were measured in tests on large (2.4-m-high, 0.60-m-wide) plywood walls [68]. The peak heat fluxes measured in these tests are provided in Table 25.3 for various preheat levels. As the heat release rate per unit width increases, the heat flux from the fire to the wall increases. Though heat fluxes are not as high as those measured for a burning PMMA wall, the heat flux is 8–20 kW/m^2 higher than the 30-kW/m^2 peak level measured in the smaller-scale tests.

Table 25.3 Peak heat flux from flames measured in 2.4-m-high, 0.60-m-wide plywood wall experiments [68] (measurements up to 1.8 m above floor)

Fuel	Radiant exposure (kW/m^2)	Heat release rate per unit width Q′ (kW/m)	Peak heat flux (kW/m^2)
Plywood	4.8	175	38
(Finished side exposed)	5.2	197	40
	7	292	45
Plywood	7.5	217	45
(Unfinished side exposed)	11	417	50

Similar experiments were performed by Ohlemiller and Cleary [69] on composite panels. The peak heat fluxes measured in this study are provided in Table 25.4. Similar to

the results of Delichatsios et al. [68], heat fluxes were measured to increase with an increase in heat release rate (i.e., increase in external heat flux).

Data presented in this section demonstrate that both heat release rate and smoke production rate of the fuel can influence the heat flux levels produced by wall flames back onto the burning surface. Larger fires with high smoke production rates can result in heat fluxes to the walls of approximately 60 kW/m^2. Additional research needs to be performed to better quantify the transition between the smaller-fire experiments and the large-fire results.

Table 25.4 Heat fluxes from 1.2-m-High, 0.3-m-wide Composite panel fires [69]

Fuel	Radiant exposure (kW/m^2)	Heat release rate per unit width Q' (kW/m)	Peak heat flux (kW/m^2)
Fire-retarded vinyl ester	2.5	—	35
	7.5	—	48
	11	—	52
Polyester	0	—	35

Corner Wall Fires

Limited work has been performed to quantify the heat fluxes from burning boundaries in a corner. In general, the heat fluxes produced by burning corner walls are higher than those produced by a wall flame.

Qian et al. [70, 71] measured heat fluxes produced in a corner of burning PMMA walls beneath an incombustible ceiling. In these experiments, a 1.6-m-high corner was lined with 12.7-mm-thick PMMA 0.20 m in width. During the tests, the walls were ignited using a torch at the bottom of the corner and were allowed to burn until flames had spread to the top of the walls. The peak heat release rate of the fire was estimated to be 80 kW. The heat fluxes measured during the growing fire are shown in Fig. 25.37. In the lower half of the flame, heat fluxes were measured to be, on average, 33 kW/m^2. Above this, the heat fluxes were measured to decay similarly to heat fluxes measured for wall fires (see Equations 25.35 and 25.36).

A series of experiments were conducted by Hasemi et al. [25] using L-shaped sintered

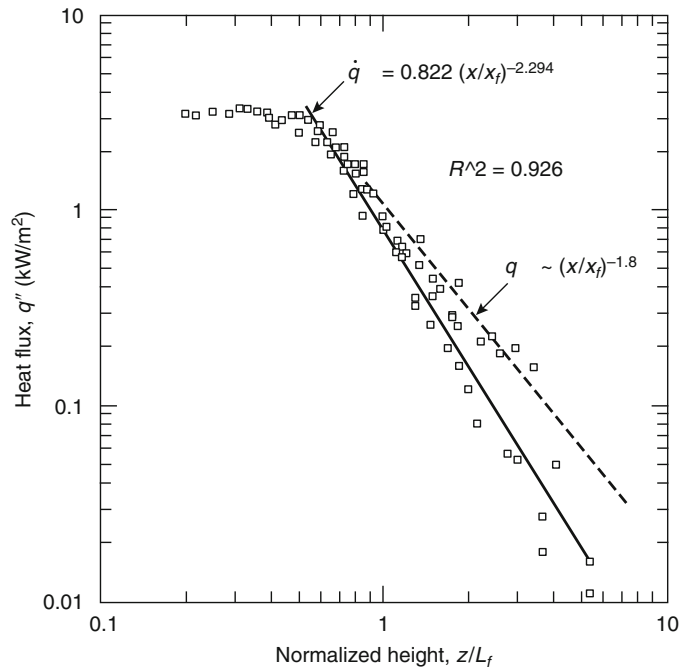

Fig. 25.37 Heat flux from burning PMMA corner walls (1.6 m high and 0.20 m wide) [71]

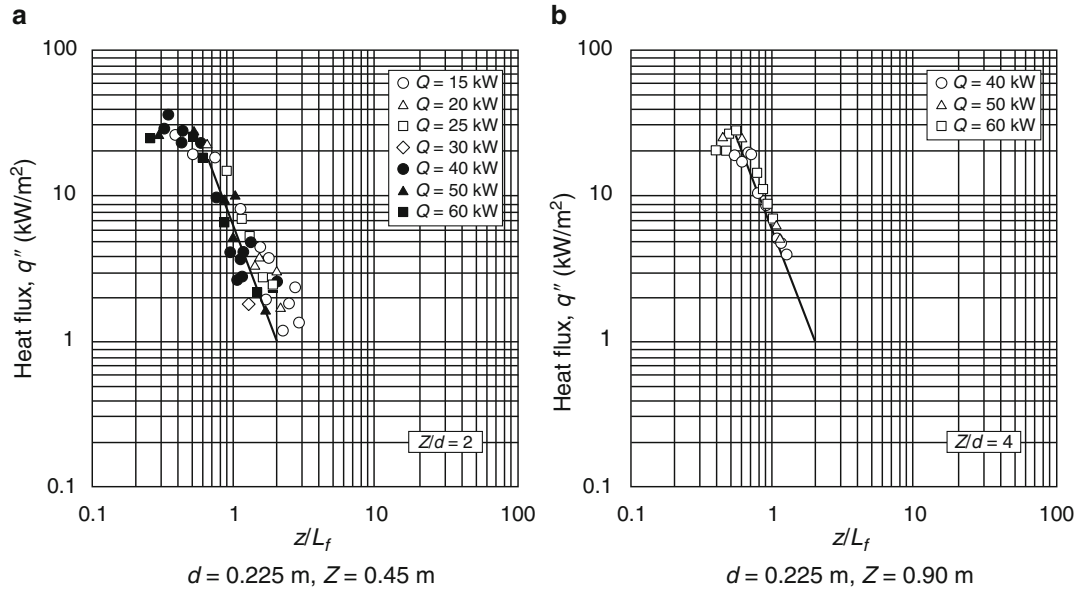

Fig. 25.38 Heat fluxes to a corner from a simulated burning corner fire using propane as fuel [25]

metal burners mounted to the walls of the corner to simulate burning corner walls. Using propane gas as fuel, experiments were conducted using two different burner sizes (0.23 m wide and 0.45 m high, 0.23 m wide and 0.90 m high) mounted to an open corner of walls with no ceiling. The heat fluxes above the burners in these fires are provided in Fig. 25.38 for fire heat release rates of 15–60 kW. The line on the plots represents the decay in the heat flux of a wall fire. Peak heat fluxes in the lower part of the flame were measured to range from 28 to 38 kW/m^2 and were constant up to approximately half the flame length. Above this, heat fluxes were measured to decay in a manner similar to that determined for burning walls.

Hasemi et al. [72] also performed tests in a 1.8-m-high corner with a ceiling. Tests were performed with the top 1.35 m of the corner lined with 0.23-m-wide sintered metal burners and with the top 0.45 m of the corner lined with sintered metal burners. Heat fluxes to the ceiling were measured to be as high as 40 kW/m^2, while heat fluxes as high as 60 kW/m^2 were measured along the top of the walls near the ceiling.

Lattimer et al. [29] performed a detailed study using L-shaped propane line burners in the corner. Burners were placed in a 2.4-m-high corner with a ceiling, with all surfaces constructed of noncombustible materials. In this study, heat fluxes were measured for different size burners (single side length of 0.17 m, 0.30 m, and 0.50 m) and various heat release rates (50–300 kW).

Similar to the approach used to develop the heat flux correlations for area burners, burning boundary correlations were developed for three regions in the corner: along the height of the walls in the corner, along the top of the walls near the ceiling, and along the ceiling. The region containing the walls in the corner extended from the top of the fire to approximately 1.8 m above the fire, which is approximately the ceiling height minus twice the ceiling jet thickness ($\delta = 0.1H$). Above 1.8 m was considered to be the region along the top of the wall, or the wall-ceiling interface region.

Heat flux data for these fires were normalized with respect to the flame tip location. The flame tip was the farthest distance at which flaming was visually observed. In cases where the fire impinged and flowed along the ceiling, the flame tip length was taken to be the corner height plus the flame extension along the ceiling. Lattimer et al. [29] developed the following

correlation to predict the flame tip of a burning boundary fire:

$$L_{f,\text{tip}}/d = 5.9Q_d^{*1/2} \tag{25.36}$$

where dimensionless Q_d* is

$$Q_d^* = \frac{Q}{\rho_\infty C_p T_\infty \sqrt{g} d^{5/2}} \tag{25.37}$$

Equations 25.35b and 25.36 are similar to those used in predicting flame heights from area burners in a corner except the length scale is *d,* which is the width of the burning area on the wall or the side of a single L-shaped burner. In the L-shaped line burner tests, d is the length of a single side; however, in a burning corner d was found to be the average width of the burning on the walls. For fires in a 2.4-m-high corner, the width of the burning 0.90 m above the floor was found to adequately represent the average burning width [29].

The vertical distribution in the maximum heat flux along the walls near the corner is shown in Fig. 25.39 plotted with the vertical distance normalized with respect to the flame tip. Peak heat fluxes were measured over the initial half of the flame length. Above this, heat fluxes decayed in a fashion similar to that observed for wall fires. The line in the plot represents a fit to the data, which can be described by the following expressions:

$$q''_{\max} = 70 \quad (z/L_f) < 0.5 \tag{25.38a}$$

$$q''_{\max} = 10(z/L_f)^{-2.8} \quad (z/L_f) > 0.5 \tag{25.38b}$$

Heat fluxes in the decay region $(z/L_f) > 0.5$ decrease with dimensionless height raised to the -2.8 power, which is a slightly lower power than the decay for wall fires (-2.5).

Peak heat fluxes in the corner are shown in Fig. 25.40 to have some dependence on the heat release rate of the fire. The increase in the peak heat flux with increase in fire size was attributed to an increase in radiative pathlength. Assuming the gases to be gray, the following curve fit was developed:

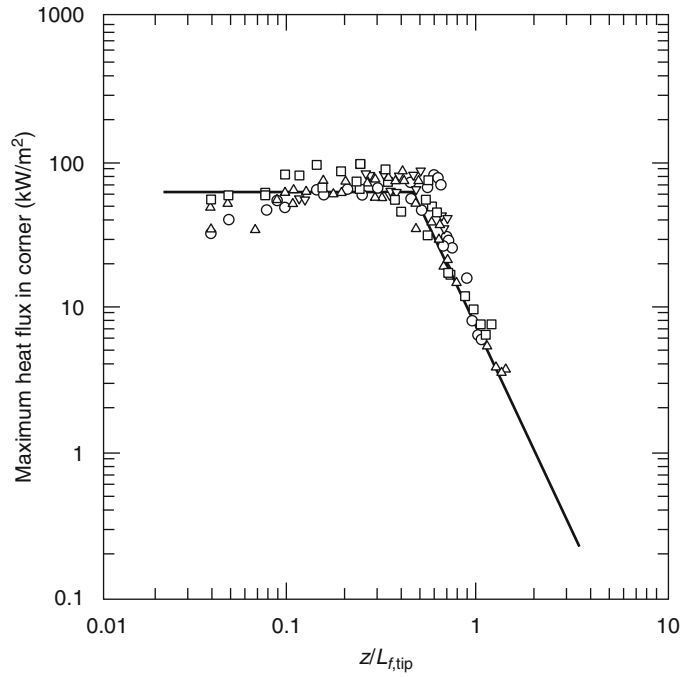

Fig. 25.39 Heat flux from simulated corner wall fires back to the corner walls at a height less than 1.8 m above the floor. L-shaped line burner with single side lengths of 0.17 m (○), 0.30 m (Δ), 0.30 m (elevated) (▽), and 0.50 m (□) and fire sizes ranging from 50 to 300 kW [29]

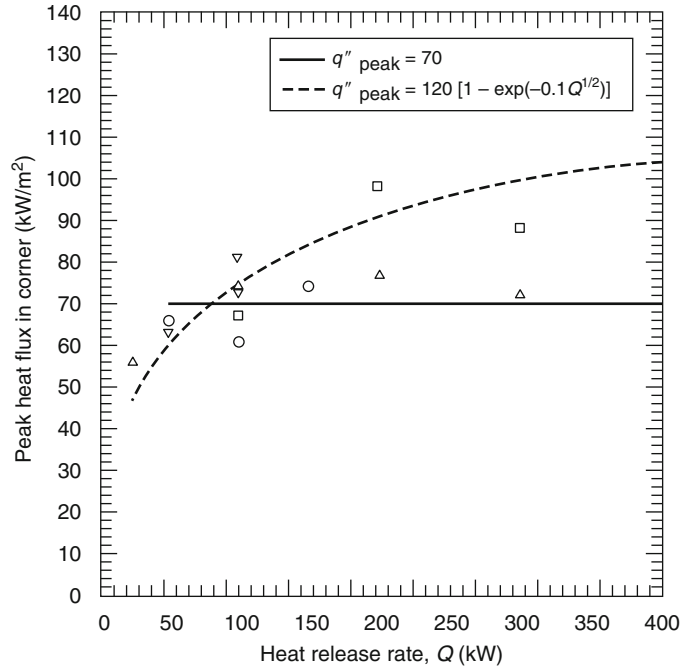

Fig. 25.40 Peak heat flux to the walls in the corner as a function of wall heat release rate less than 1.8 m above the floor. L-shaped line burner with single side lengths of 0.17 m (○), 0.30 m (Δ), 0.30 m (elevated) (▽), and 0.50 m (□) and fire sizes ranging from 50 to 300 kW [29]

$$q''_{\text{peak}} = 120\left[1 - \exp\left(-0.1Q^{1/2}\right)\right] \quad (25.39)$$

Based on Equation 25.38b, a more conservative fit to the data in Fig. 25.39 was developed:

$$q''_{\max} = q''_{\text{peak}} \quad (z/L_f) \le 0.5 \quad (25.40a)$$

$$q''_{\max} = q''_{\text{peak}} - 5(z/L_f - 0.5) \quad \left(q''_{\text{peak}} - 27\right) \quad 0.5 < (z/L_f) \le 0.7 \quad (25.40b)$$

$$q''_{\max} = 10.0(z/L_f)^{-2/8}(z/L_f) > 0.7 \quad (25.40c)$$

The maximum heat fluxes along the height of the corner shown in Figs. 25.39 and 25.40 were measured approximately 0.05–0.10 m outside of the corner. Heat fluxes decrease with horizontal distance from the corner. The horizontal heat flux distributions at heights less than 1.8 m above the floor are shown in Fig. 25.41 to be half-Gaussian in shape over the flame, but decays slower than predicted by a half-Gaussian curve outside of the flaming region. The line in this plot is a fit to the data, which can be represented by the following expressions:

$$\frac{q''}{q''_{\max}} = \exp\left[-1.0(x/d)^2\right] \quad \frac{x}{d} < 1.3 \quad (25.41a)$$

$$\frac{q''}{q''_{\max}} = 0.30\left(\frac{x}{d}\right)^{-1.8} \quad \frac{x}{d} \ge 1.3 \quad (25.41b)$$

Burning boundary beneath a ceiling will form a ceiling jet that will heat the top part of the walls and the ceiling. The maximum heat flux along the top part of the walls is shown in Fig. 25.42. The line in the plot represents a fit to the data, which can be represented by the following expressions:

$$q''_{\max} = 120 \quad \left(\frac{x+H}{L_{f,\text{tip}}}\right) \le 0.52 \quad (25.42a)$$

$$q''_{\max} = 13.0\left(\frac{x+H}{L_{f,\text{tip}}}\right)^{-3.5}\left(\frac{x+H}{L_{f,\text{tip}}}\right) > 0.52 \quad (25.42b)$$

The assumed plateau in the correlation is based on the maximum heat flux expected from a flame in this configuration. This correlation is the same as that determined for area fires in a corner.

The heat flux to the ceiling was correlated to the dimensionless distance away from the burner,

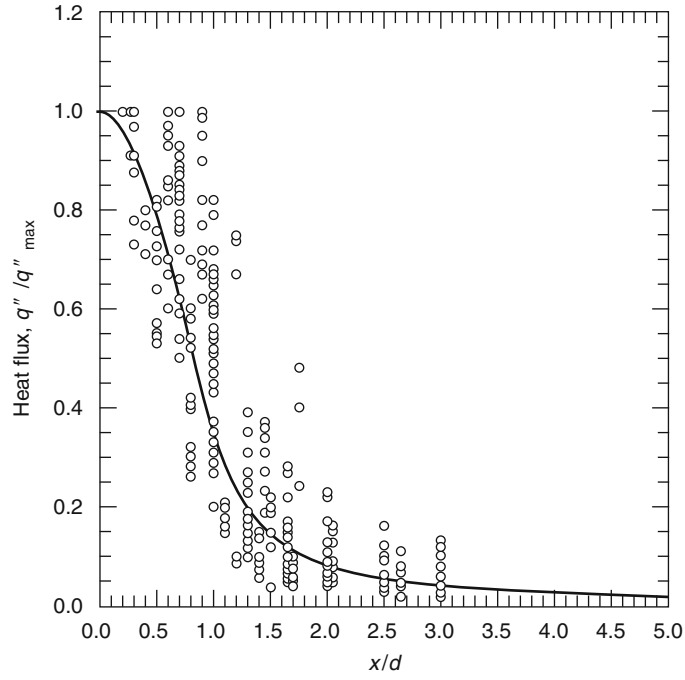

Fig. 25.41 Horizontal heat flux distribution on the walls out from the corner at a height less than 1.8 m above the floor [29]

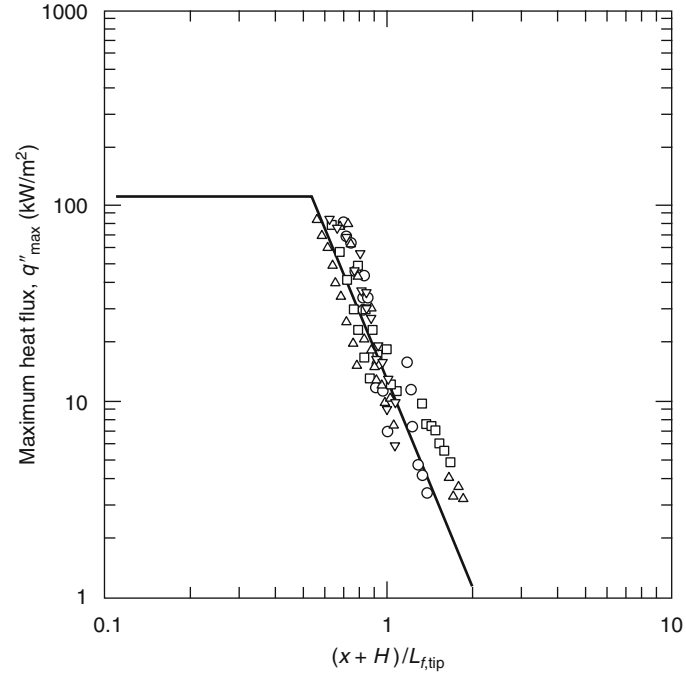

Fig. 25.42 Maximum heat flux along the top of the walls with a simulated burning boundary fire in the corner. L-shaped line burner with single side lengths of 0.17 m (○), 0.30 m (Δ), 0.30 m (elevated) (▽), and 0.50 m (□) and fire sizes ranging from 50 to 300 kW [29]

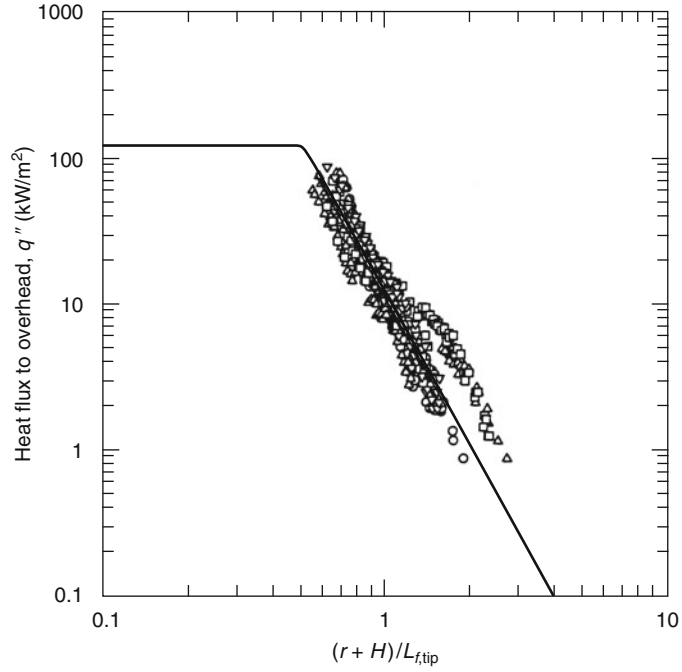

Fig. 25.43 Heat flux along the ceiling with a simulated burning boundary fire in the corner. L-shaped line burner with single side lengths of 0.17 m (○), 0.30 m (Δ), 0.30 m (elevated) (▽), and 0.50 m (□) and fire sizes ranging from 50 to 300 kW [29]

$(r + H)/L_{f,\text{tip}}$. A plot of the heat flux versus this dimensionless parameter is shown in Fig. 25.43. The line in this plot is a fit to the data, which are represented through the following relations:

$$q'' = 120 \quad \left(\frac{r+H}{L_{f,\text{tip}}}\right) \leq 0.52 \qquad (25.43a)$$

$$q'' = 13.0\left(\frac{r+H}{L_{f,\text{tip}}}\right)^{-3.5}\left(\frac{r+H}{L_{f,\text{tip}}}\right) > 0.52 \qquad (25.43b)$$

This is the same relation used for the top of the corner walls, except the length scale in the overhead data is r. In addition, this is the same relation determined using the ceiling heat flux data from tests with an area burner.

Ceiling Fires

Heat fluxes from burning ceilings have been evaluated for both unconfined ceilings and ceilings in a corridor. Due to buoyancy effects, flames from burning ceilings tend to be relatively thin. As a result, peak heat fluxes from burning ceilings range from 20 to 30 kW/m^2, which is similar to those measured for small wall fires.

Unconfined Ceiling Fires Heat fluxes from unconfined ceiling fires were measured by Hasemi et al. [73] using different sizes of sintered metal propane gas burners mounted into a 1.8-m-square incombustible ceiling. Using two different circular burner sizes ($D = 0.09$ and 0.16 m), heat flux to the ceiling was measured for fire heat release rates of 2.5–38 kW.

The radius of the flame (intermittent) measured using the two burners is shown in Fig. 25.44 to be slightly dependent on burner size, with the larger burner having a lower radius. However, as the fires become larger, the dependence on burner diameter becomes small. Flame lengths are proportional to the heat release rate raised to the one-half power.

Hasemi et al. [73] also measured the heat fluxes as a function of distance from the center of the burner. The measured heat fluxes are shown in Fig. 25.45 to be at peak levels in the first $0.4L_f$ and then decay with distance from the burner. Peak heat fluxes were measured to range from

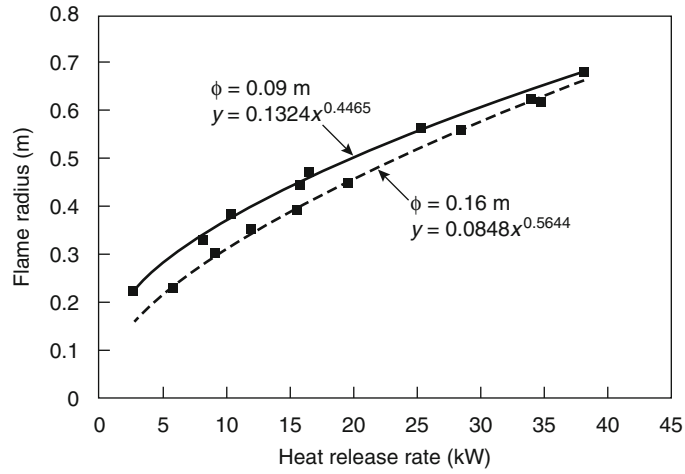

Fig. 25.44 Flame radius produced by a simulated burning ceiling in an unconfined area [73]

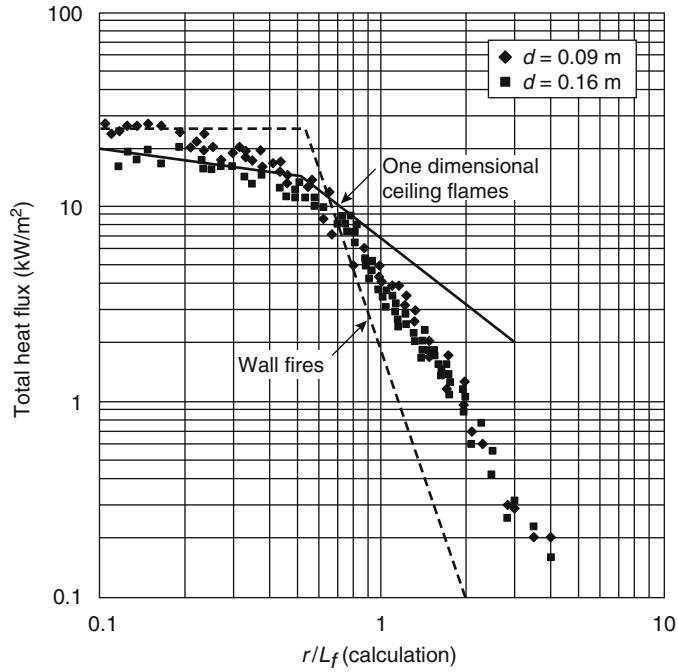

Fig. 25.45 Heat flux from fires beneath an unconfined ceiling [73]

16 to 27 kW/m^2, with the smaller burner producing higher heat fluxes. These peak heat fluxes were similar to those measured for burning ceilings in a corridor (i.e., one-dimensional ceiling flames) and for small wall fires. Heat fluxes from the unconfined ceiling fires were measured to decay at a rate between that measured for wall fires and that observed for a burning ceiling in a corridor.

Ceiling Fires in a Corridor Heat fluxes from flames produced by burning ceilings in a corridor were investigated by Hasemi et al. [72]. Tests were performed beneath a 2.73-m-long ceiling with two 0.10-m-high soffits mounted along the length of the ceiling to form a 0.30-m-wide channel. At the closed end of the channel, a 0.30-m-wide, 0.04-m-long porous propane burner was mounted in the ceiling. Heat flux distributions along the

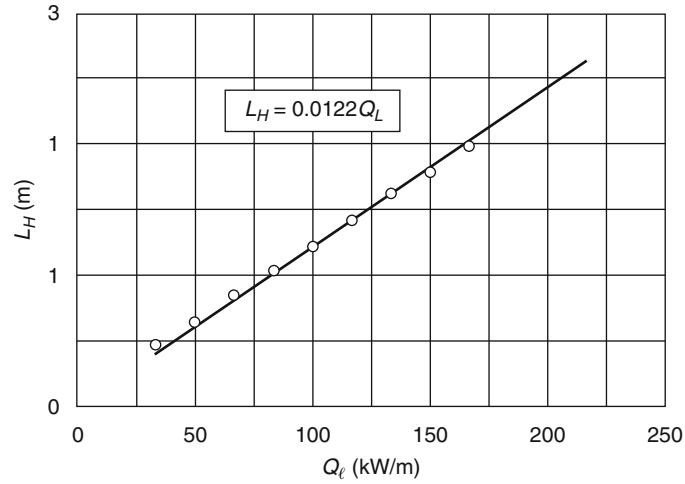

Fig. 25.46 Flame length produced by a burning ceiling in a corridor [72]

corridor were measured for fire heat release rates ranging from 10 to 50 kW (33–166 kW per meter of corridor width).

The intermittent flame lengths from these fires are seen in Fig. 25.46 to increase linearly with heat release rate per unit hallway width. A fit to these data produced the following relation to predict flame length due to a burning ceiling in a corridor:

$$L_f = 0.0122Q^{'} \qquad (25.44)$$

The heat flux distributions along the center of the corridor are shown in Fig. 25.47 for the different fires considered in the study. The line in the plot represents a best fit to the methane line burner data of Hasemi [55]. Heat fluxes were measured to be constant at approximately 20 kW/m^2 up to 0.4 L_f. Above this, heat fluxes were measured to decay at a slower rate than that previously measured for wall fires. Heat fluxes along a flame from a burning ceiling in a corridor (not shown in the figure) can be determined using the following expressions:

$$q^{''} = 20 \quad (x/L_f) \leq 0.4 \qquad (25.45a)$$

$$q^{''} = 6.36(x/L_f)^{-5/4} \quad (x/L_f) > 0.4 \qquad (25.45b)$$

Burning Parallel Vertical Surfaces

A common configuration encountered when commodities are being stored in rooms or warehouses is parallel vertical surfaces. As a result, several studies have focused on both experimentally and analytically characterizing this configuration [62, 74, 75]. Ingason and de Ris [76] also performed experiments in a rack storage configuration with a fire between four equally spaced storage towers.

Part of the work by Tamanini [74, 75] investigated the effects of wall spacing on the fuel mass loss rate of combustible parallel vertical walls. Walls were 0.94 m high and 0.460 m wide with the spacing varied from 0.470 to 0.025 m and no floor at the base of the walls. The average fuel mass loss rate was measured to increase (i.e., the average heat flux to the wall increased) with an increase in spacing until the spacing was less than 0.076 m. At a spacing of 0.038 m or less, the average mass loss rate was less than that measured with no parallel wall. At a spacing of 0.038 m (or wall height divided by spacing of 25 with a fire size of approximately 180 kW), the flames from the two burning surfaces were observed to merge together approximately two-thirds the distance up the walls.

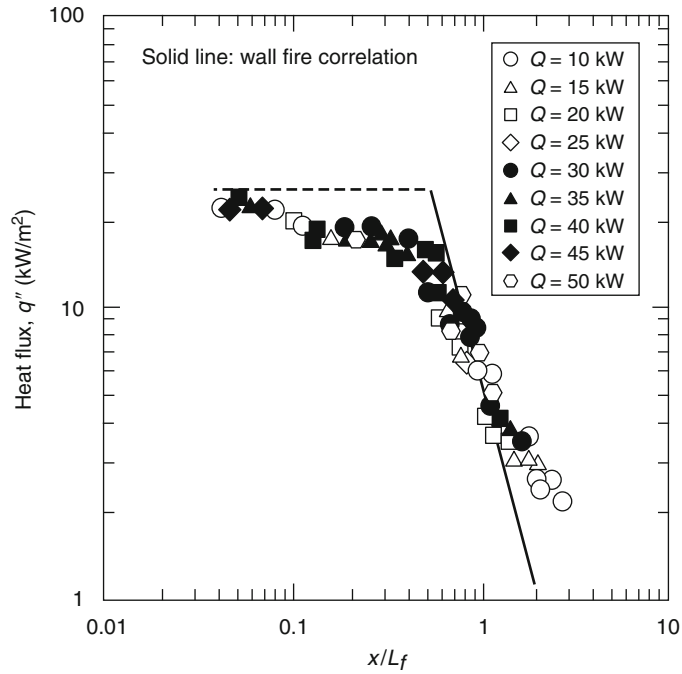

Fig. 25.47 Heat fluxes to the ceiling of a corridor [72]

Though not evaluated in this study, the presence of a floor may cause the flames to merge together at larger spacings.

Heat fluxes due to a fire between two parallel vertical surfaces were measured by Foley and Drysdale [62]. The study was performed using two 0.61-m-wide, 0.81-m-high walls separated by a gap of 0.06, 0.10, or 0.14 m. The fire was a 0.60-m-long propane line burner that had either a 11.6-kW/m or a 20.9-kW/m heat release rate per unit length. One of the walls was instrumented with four heat flux gauges that could be moved to measure the heat flux distribution on the walls. Heat fluxes were measured as far as 0.150 m from the centerline of the wall. For the different gap and heat release rate fires, heat fluxes were measured with the burner against the instrumented wall and with the fire in the center of the gap between the two walls. The effect of air entrainment flow path was also evaluated by performing tests with and without a floor between the panels. Results were correlated using a/d where the spacing between the walls, a, is divided by the burner length, d, and the dimensionless quantity Q_d^*, as defined in Equation 25.14, with d being the burner length.

The heat flux distributions measured with the fire against the instrumented wall are shown in Fig. 25.48. As seen in Fig. 25.48a, heat fluxes reached as high as 80 kW/m^2 with an open base (no floor between the walls). Heat fluxes on the panel can be estimated using the following expression:

$$q'' = 67.38\left\{z(a/d)^{0.36}/\left[Q_d^{*2/3}d\left(y'/d\right)^{0.38}\right]\right\}^{-1.47} \tag{25.46}$$

where $y' = 0.5d - y$ with y being the horizontal distance from the burner centerline.

With the base of the walls closed (a floor between the walls) and the fire against the instrumented wall, the heat flux data in Fig. 25.48b were seen to be as high as 70 kW/m^2. Heat fluxes for this case are slightly lower than the open-base case. A similar expression to that in Equation 25.45b was developed by Foley and Drysdale [62] to predict heat fluxes with the base of the walls closed:

$$q'' = 23.31\left\{z(a/d)^{0.905}/\left[Q_d^{*2/3}d\left(y'/d\right)^{2/3}\right]\right\}^{-1.2} \tag{25.47}$$

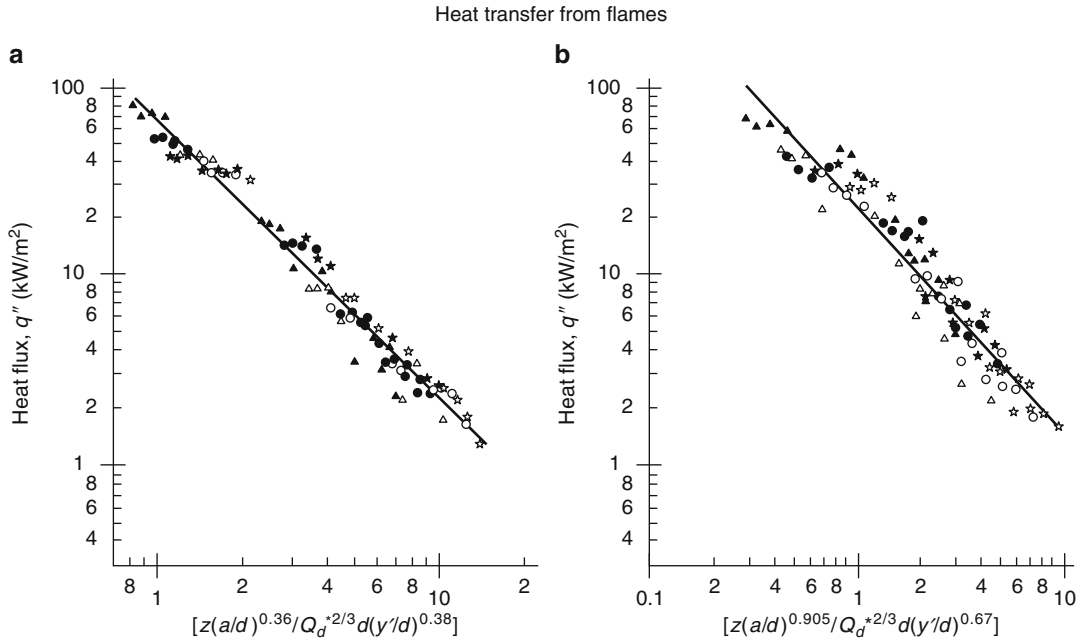

Fig. 25.48 Heat fluxes measured with the fire against the instrumented wall with (**a**) an open base (no floor in the gap) and (**b**) a closed base (a floor in the gap): 0.140-m spacing (⋆), 0.10-m spacing (○), 0.060-m spacing (Δ); open symbols, $Q' = 11.6$ kW/m; closed symbols, $Q' = 20.9$ kW/m [62]

Heat fluxes were also measured with the fire in the center of the gap between the two walls. In the case with an open base (no floor), the heat fluxes were measured to be 50 % lower than those measured with the fire against the instrumented wall. As seen in Fig. 25.49a, the peak heat flux was measured to be approximately 30 kW/m^2. This decrease was attributed to the air being drawn up at the base of the walls, preventing the fire from attaching to the instrumented wall. The line in the figure is the best fit to the data, which are given by the following expression:

$$q'' = 22.71\left\{z(a/d)^{1.04}/\left[Q_d^* d\left(y'/d\right)^{0.806}\right]\right\}^{-0.797} \quad (25.48)$$

The case with the base closed and the fire in the center of the gap resulted in the highest heat fluxes measured in the study. As seen in Fig. 25.49b, heat fluxes greater than 100 kW/m^2 were measured in this case. In the tests with the high heat fluxes, the flames were observed to occupy the width of the gap. This behavior was attributed to only allowing air to be entrained into the fire through the sides of the gap. The following expression can be used to estimate the heat flux to the walls for this case:

$$q'' = 23.94\left\{z(a/d)^{1.7}/\left[Q_D^* d\left(y'/d\right)^{1.34}\right]\right\}^{-1.04} \quad (25.49)$$

Additional research needs to be performed with this configuration to further validate the results. Larger-scale tests need to be conducted to verify the results of Foley and Drysdale [62]. In addition, the transition from wall fire heat fluxes to gap fire heat fluxes needs to be identified. Heat fluxes produced by area fires between parallel walls also need to be quantified.

Exposure Fires and Burning Walls and Ceilings

A series of tests were performed by Lattimer et al. [77] to investigate the use of steady-state heat flux correlations, developed using burners

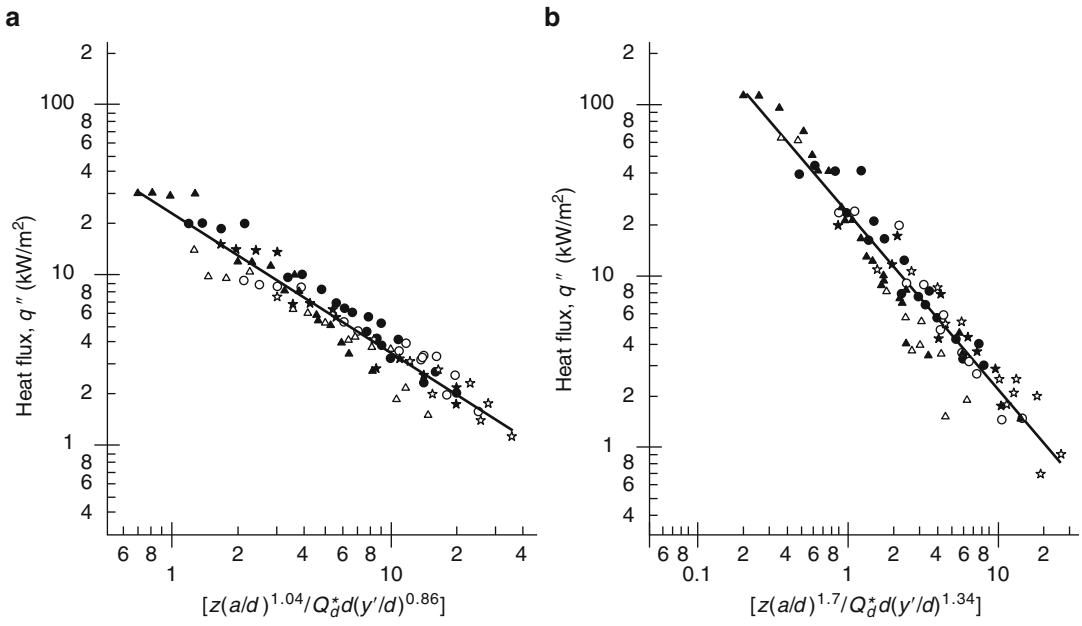

Fig. 25.49 Heat fluxes measured with the fire in the center of the gap with (**a**) an open base (no floor in the gap) and (**b**) a closed base (a floor in the gap): 0.140-m spacing (⋆), 0.10-m spacing (○), 0.060-m spacing (Δ); open symbols, $Q' = 11.6$ kW/m; closed symbols, $Q' = 20.9$ kW/m [62]

and noncombustible boundaries, for estimating the heat fluxes in growing fires. Three tests were performed in an 2.4-m-high, 2.0-m-wide open corner lined with a combustible material. A single test was performed on three different lining materials: 12-mm-thick Douglas fir plywood, 12-mm-thick E-glass fire-retarded vinyl ester, and 88-mm-thick sandwich composite (76-mm-thick balsa wood with 6-mm-thick E-glass fire-retarded vinyl ester facings). The initiating fire in the test was a square propane sand burner with a 0.17 m side length and a heat release rate of 100 kW for 10 min followed by 300 kW for 10 min, total test time of 20 min. Total heat release during the test was measured by performing oxygen calorimetry on the gases collected in an exhaust hood, and flame lengths were measured through visual observation. Heat fluxes were measured 0.075 m from the corner along at eight different elevations, 0.15 m below the ceiling along the top of the wall, and along the ceiling on a 45° diagonal out from the corner. Due to mounting the heat flux gauges along the top of the wall too far below the ceiling, no comparison between predicted and measured heat fluxes was done for the region along the top of the wall.

Transient data were averaged every 30 s to create a reasonable amount of data to compare to the developed correlations. A comparison of the flame length predicted using Equations 25.13 and 25.36 and the measured flame length is shown in Fig. 25.50. The dimensionless length used in this calculation was the width of the burner, D, while the burning had spread laterally less than the width of the burner. When the average lateral flame spread 0.90 m above the floor exceeded the burner width, the dimensionless length was taken to be the horizontal flame front location 0.9 m above the floor. The flame front at 0.9 m above the floor was approximately the average flame front on the wall.

Heat fluxes to the walls near the corner are provided in Fig. 25.51. Measured heat fluxes were slightly higher than values predicted by both the initiating fire correlation and the burning boundary correlation (assuming the heat flux is

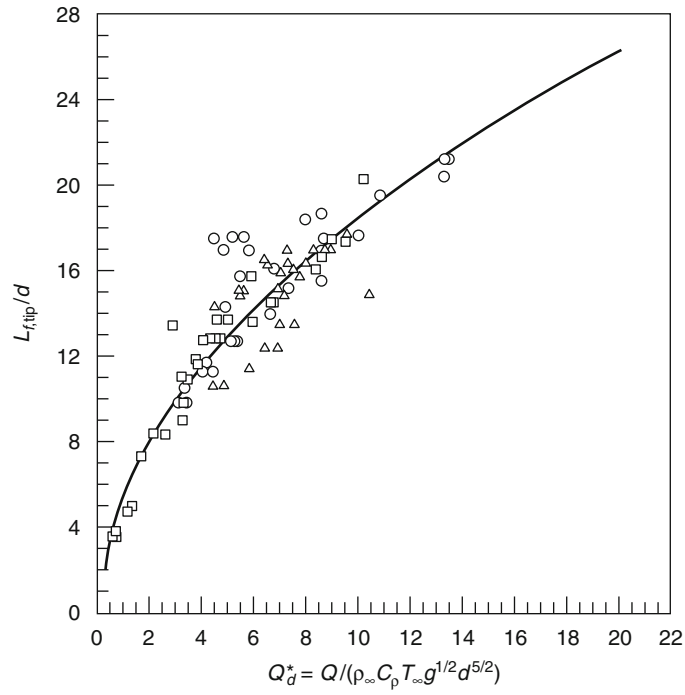

Fig. 25.50 Flame lengths measured in combustible corner fire tests compared with the flame length correlations developed for initiating and burning boundary fires in Equations 25.13 and 25.36: plywood (□), E-glass FR vinyl ester (○), sandwich composite (Δ) [77]

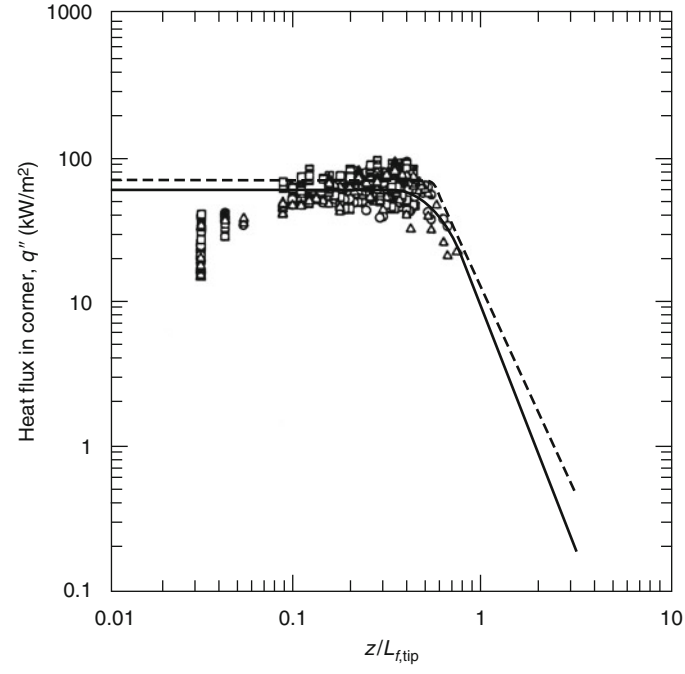

Fig. 25.51 Heat fluxes along the height of the corner in tests with different combustible boundaries compared with the heat flux predicted using Equation 25.38 (—) and Equation 25.15 (– – –): plywood (□), E-glass FR vinyl ester (○), sandwich composite (Δ) [77]

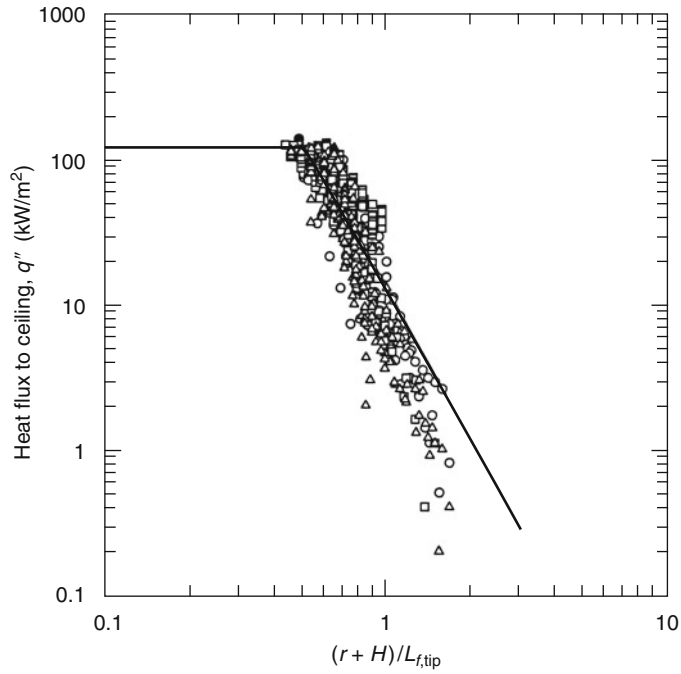

Fig. 25.52 Heat fluxes to the ceiling during open corner tests with the corner lined with a combustible material compared with the heat flux predicted using Equation 25.43: plywood (□), E-glass FR vinyl ester (○), sandwich composite (Δ) [77]

independent of the wall heat release rate). Inspection of the data indicates better agreement between the data and the correlations can be achieved using the initiating fire correlation up to when ignition occurs in the corner. After this, the corner wall heat flux correlations in Equations 25.38b and 25.40 can be used to estimate heat fluxes in the corner.

A comparison of the heat fluxes along the ceiling and the heat fluxes predicted using Equation 25.43 is shown in Fig. 25.52. In general, heat fluxes are adequately predicted by the correlation, with heat fluxes as high as 130 kW/m^2 measured during a test. This indicates that Equation 25.43 can be used to estimate heat fluxes to the ceiling near the corner containing the fire.

Fires from Windows

Fires that have reached flashover conditions typically result in burning outside of the actual burn room. Flames from postflashover fires extending out of a building through a window will buoyantly rise along the exterior of the building. Experiments characterizing the heat fluxes to the wall above the window of a postflashover compartment fire have been performed by Oleszkiewicz [78, 79], Thomas and Bullen [80], and Beitel and Evans [81]. In these studies, heat fluxes as high as 200 kW/m^2 have been measured.

Experiments performed by Oleszkiewicz [78, 79] were conducted using two differently sized full-scale rooms with a wall above the window that extended as much as two stories above the burn room (Fig. 25.53). The effects of window size, window aspect ratio, and fire size inside the compartment were evaluated in the study. Heat fluxes from the flames extending outside the burn room for different door sizes and different fires sizes are shown in Figs. 25.54 and 25.55 for propane gas fires. Note that the heat release rate of the fires stated in Figs. 25.54 and 25.55 is the ideal heat release rate of the compartment fire, which was determined from the gas flow rate and the heat of combustion for propane. Data in Fig. 25.54 show the effect of fire heat release rate and window size on the heat flux 0.5 m above the window. The distribution in the heat flux along the height exterior wall is shown in Fig. 25.55 for the case with a window 2.6 m wide and 1.37 m high.

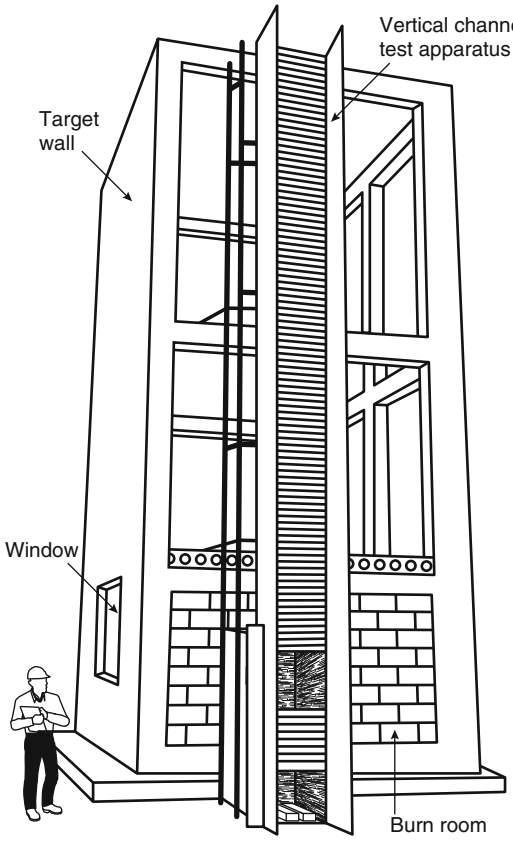

Fig. 25.53 Exterior wall fire test facility used by Oleszkiewicz [79]

Quintiere and Cleary [32] found that flame lengths for this situation can be estimated using the relation developed by Yokoi [82]. With L_f being the distance from the bottom of the opening to the average flame height, the heat release rate outside of the compartment, Q, and the effective diameter of the window, D, can be used to predict the flame length above the window with the following expression:

$$L_f = 0.0321\left(\frac{Q}{D}\right)^{2/3} \tag{25.50a}$$

where

$$D = 2\sqrt{\frac{H_o W_o}{2\pi}} \tag{25.50b}$$

Heat Fluxes in Standard Tests

Heat fluxes in some standard tests are provided in this section to compare with heat fluxes measured in realistic geometries presented in this chapter. Heat fluxes in room-corner tests such as ISO 9705 and NFPA 286, *Standard Methods of Fire Tests for Evaluating Contribution of Wall and Ceiling Interior Finish to Room*

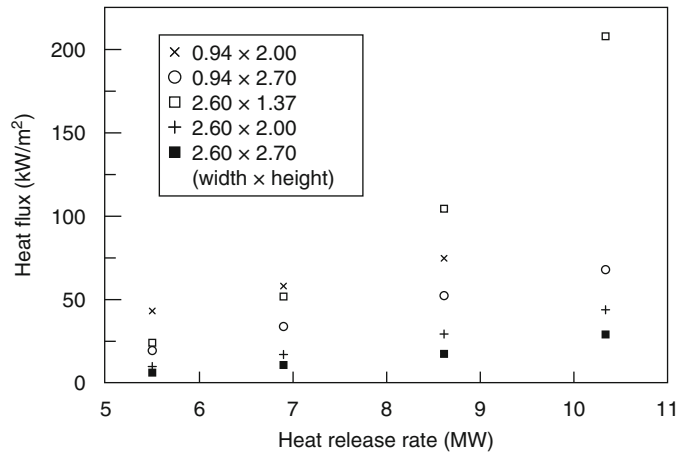

Fig. 25.54 Heat fluxes from a window flame 0.5 m above the top of the window for different size propane fires inside the compartment [79]

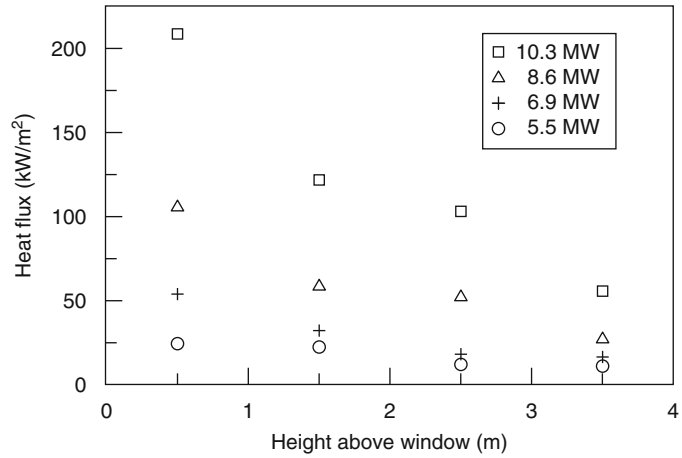

Fig. 25.55 Heat fluxes from window flames along the exterior wall above a 2.6-m-wide, 1.37-m-high window [79]

Fire Growth, can be determined using heat flux data previously presented in the section on heat fluxes from exposure fires in a corner. This section will focus on heat fluxes produced in other tests including fire resistance test furnaces and the ASTM E84 flame spread test. Note that these heat fluxes, along with most data previously presented for room-corner tests, were typically measured with a noncombustible, insulating surface mounted to the test apparatus. The heat flux to actual test specimens could be different depending on specimen thermal properties, the occurrence of sample ignition and burning, as well as other factors.

Fire Resistance Tests

Several furnace fire exposures are used throughout the world to evaluate the fire resistance of products. These fire exposures have peak temperatures ranging from 1050 °C to 1350 °C after a 3-h exposure (Fig. 25.56). The type of exposure used depends on the end-use application of the product. Tunnel and offshore oil rig applications have the highest temperature, most severe fire exposures, whereas less severe exposures are used for different building applications.

The ASTM E119 [83] and ISO 834 [84] time-temperature curves are perhaps the most common furnace exposures used in fire resistance testing. These furnace exposures are utilized to evaluate the fire resistance of structural elements on buildings, on ships, and in some transportation applications (e.g., railcars). ASTM E119 is primarily used in North America whereas ISO 834 is used more internationally (e.g., Europe and Australia). As seen in Fig. 25.56, the two time-temperature curves are similar, with the ISO 834 temperatures being slightly higher at times greater than 1 h. The ASTM E119 furnace exposure is measured using shielded thermocouples, whereas the ISO 834 furnace exposure is measured using sheathed thermocouples.

Though the time-temperature curves in these tests are similar, the actual heat flux exposure early in the ASTM E119 fire exposure is more severe due to the type of thermocouples used to control the furnace [85, 86]. The European standard EN1363-1 [87] uses the ISO 834 time-temperature curve, but the furnace is controlled using plate thermometers, which provide a more severe exposure compared with ISO 834 thermocouples for the test duration [88, 89]. Compared with ASTM E119 shielded thermocouples, Sultan [90] measured that plate thermometers resulted in a slightly less severe exposure during the first 10 min of the test, but thereafter the thermal exposures were the same.

The total heat flux measured in an ASTM E119 furnace test is provided in Fig. 25.57 for a wall and floor furnace. Total heat fluxes were measured using a water-cooled Gardon gauge.

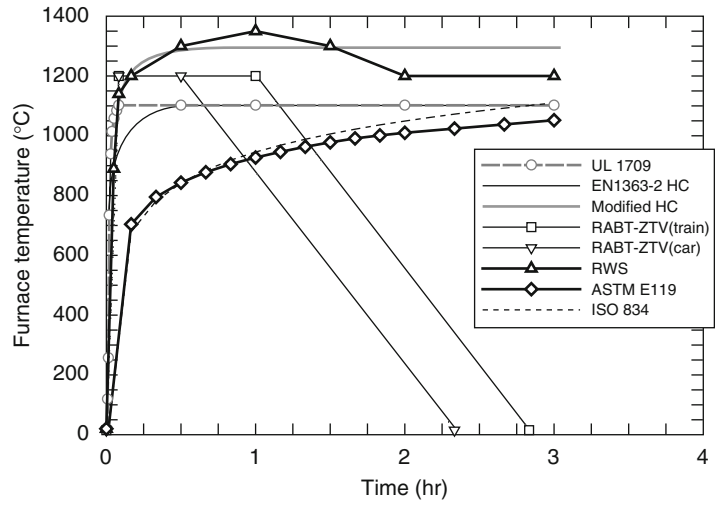

Fig. 25.56 Furnace time-temperature exposure curves

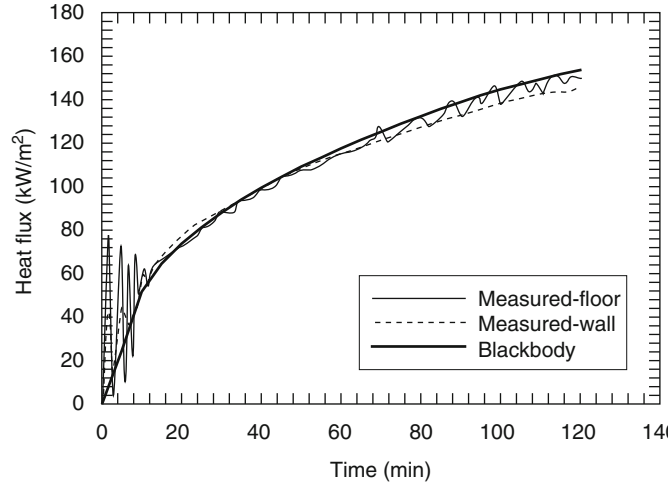

Fig. 25.57 Heat flux measured during ASTM E119 furnace exposure in floor and wall furnaces. Blackbody heat flux was calculated from the ASTM E119 furnace temperature curve

In this test, gaseous fuel was used and the temperature was controlled with ASTM E119 shielded thermocouples [91]. The wall furnace was lined with ceramic fiber while the floor furnace was lined with brick. The same furnace controlled with a plate thermometer provided similar heat flux levels at times after 10 min. Also provided in the plot is the blackbody heat flux based on the furnace temperatures specified in ASTM E119. As seen in the figure, the blackbody heat flux is similar to heat fluxes measured in the furnace except during the initial 10 min.

The higher temperature fire exposure curves in Fig. 25.56 are used to evaluate products used in petrochemical, offshore oil platform, and some tunnel applications. The UL 1709 [92] hydrocarbon pool fire exposure and the EN1363-2 [93] hydrocarbon curve (HC) are typically used for offshore oil platform applications, whereas the other higher-temperature curves are used to represent a large hydrocarbon fire inside a tunnel.

The UL 1709 and EN1363-2 [93] both have a maximum gas temperature of 1100 °C; however, the UL 1709 exposure reaches 1100 °C faster than does the EN1363-2 exposure (in 5 min versus after 25 min, respectively). Unique to this fire exposure curve, the UL 1709 fire exposure also has a heat flux requirement. During a calibration test with a UL 1709 exposure, the heat flux as measured from a water-cooled heat flux gauge mounted to a calibration specimen must be

204 ± 16 kW/m^2 while the furnace temperature is 1093 ± 111 °C. This heat flux is approximately equal to the blackbody heat flux at the furnace temperature (i.e., 1093 °C results in a blackbody flux of 197 kW/m^2).

The curves for tunnel applications have peak temperatures that range from 1200 to 1350 °C. The RABT-ZTV curves were developed in Germany to represent different vehicle fires in tunnels. These curves reach a peak temperature of 1200 °C in 5 min and remain at that temperature for 30–60 min. Thereafter, the temperatures decrease linearly with time to ambient conditions after 2.5–3.0 h. Estimated peak heat fluxes, as the blackbody flux using the peak furnace temperature, in these tests are 267 kW/m^2. A modified version of the EN1363-2 HC curve has been used in France to represent fires in tunnels. The Modified HC curve peaks at 1300 °C instead of 1100 °C. Estimated peak heat flux in this test, based on the blackbody flux using the peak furnace temperature, is 347 kW/m^2. The RWS fire curve was developed by the Rijkswaterstaat, Ministry of Transport, in the Netherlands based on results from testing conducted by TNO in the Netherlands. The RWS curve peaks at a temperature of 1350 °C, which is the highest of all time-temperature curves. Estimated peak heat flux in this test, based on the blackbody flux using the peak furnace temperature, is 393 kW/m^2. The potential for these temperatures in tunnel fires was validated through vehicle testing in the Runehamar test series, where temperatures ranging from 1280 °C to 1365 °C were measured [48].

ASTM E84 Tunnel Test

The ASTM E84 test is a "tunnel" test that provides flame spread and smoke production data from wall and ceiling lining materials. The test chamber is approximately 18 in. (0.46 m) wide, 12 in. (0.30 m) high, and 25 ft (7.63 m) long, with a gas burner located at one end and exhaust ducting located at the other. The test material is oriented on the "ceiling" of the tunnel by attaching a 24-ft (7.32-m) long sample of the test material to the underside of the removable lid of the test chamber. A flow of 240 ft/min (1.22 m/s) is established through the test chamber. The initiating fire is an 88 kW gas burner located at one end of the sample. The flames from the two burner pipes impinge on the sample at two off-center locations, producing a flame that flows 1.2 m down the sample.

Parker [94] measured heat fluxes from the initiating fire with a noncombustible ceiling in the tunnel. The highest heat fluxes were measured where the burner flames impinge on the ceiling. A plot of heat flux, measured using a water-cooled heat flux gauge, at this location is shown in Fig. 25.58. The heat flux during the initial 2 min of the test was 20–30 kW/m^2. By 4 min, the heat flux increased to 50–60 kW/m^2 where it

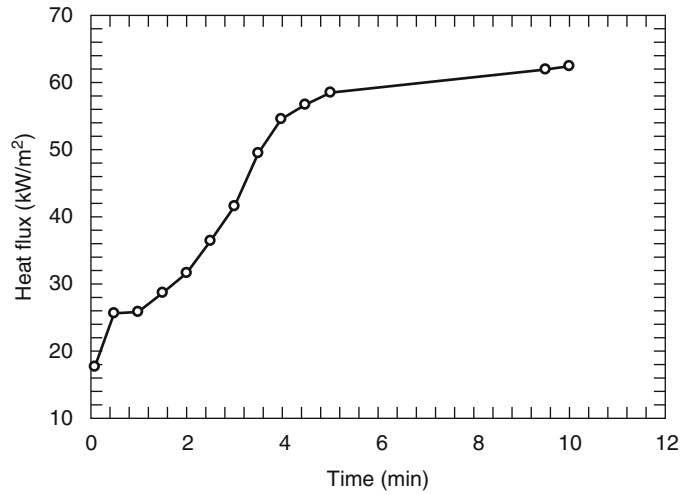

Fig. 25.58 Heat flux at the ASTM E84 burner impingement point

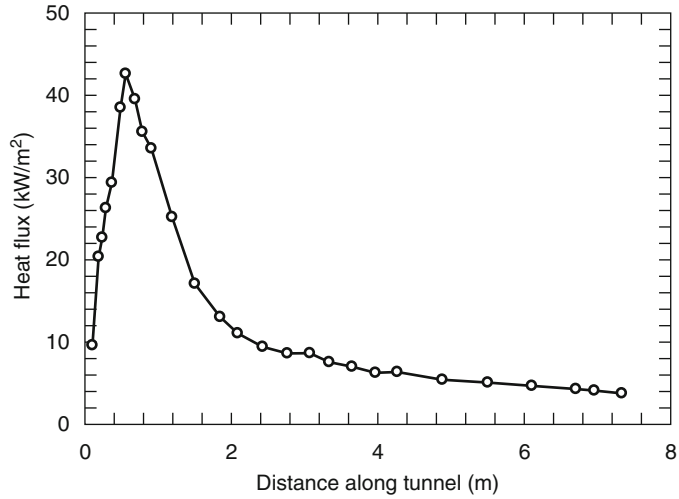

Fig. 25.59 Calculated incident heat flux along the length of the ASTM E84 tunnel

remained for the duration of the test (10 min). The increase in heat flux with time was attributed to reradation from the tunnel surfaces.

Incident heat fluxes along the center of the tunnel length were calculated using surface temperature measurements. Figure 25.59 provides the heat fluxes after a 20-min exposure, which is 10 min longer than the actual test. Heat fluxes near the burner are approximately 40 kW/m^2 and then decrease rapidly with distance along the tunnel. In a test with flames along the entire length of the tunnel, heat fluxes were calculated to be 70 kW/m^2 at 2.0 m from the burner and 30 kW/m^2 at the end of the tunnel 7.3 m from the burner.

Cable Tests

Gandhi et al. [95] measured heat fluxes due to the exposure fire in three different standard cable tests : UL 910, UL 1666, and UL 1685. Heat fluxes were measured using water-cooled Gardon gauges.

The UL 910 test is conducted in the ASTM E84 tunnel apparatus to evaluate low power cables without conduit in air handling spaces. The sample is in a horizontal orientation for this test with the flame impinging on the underside of the cables. Average heat flux measurements along the length of the ASTM E84 tunnel where the cable would be located over the test period are shown in Fig. 25.60. The peak heat flux was measured to be 49 kW/m^2 approximately 1.0 m down the tunnel. The heat fluxes are similar to those determined by Parker [94], except the Gandhi et al. [95] measured the peak heat flux location 0.5 m further down the tunnel. Gandhi et al. [95] stated that this difference may be due to using actual heat flux gauges instead of using an inverse method as well as the sample location differences. Transient heat fluxes measured by Gandhi et al. [95] determined that the heat fluxes increase during the test by approximately 10 kW/m^2 at locations 0.13–1.65 m along the tunnel.

A UL 1666 test is used to evaluate cables used in high rise buildings installed in riser shafts or floor-to-floor installations. The sample is in a vertical orientation in this test adjacent to a diffusion burner. The exposure fire in this test produces a peak heat flux of 43 kW/m^2 0.30 above the burner and decays to 6 kW/m^2 by 1.5 m above the burner.

A UL 1685 test is performed to evaluate cables used in applications other than air handling or floor-to-floor. The sample is located in a vertical orientation during the test with a propane gas-air premix burner impinging on the bottom of the cables. The exposure fire produced peak heat fluxes of 46 kW/m^2 at the burner elevation and decayed to 2 kW/m^2 by 1.5 m above the burner.

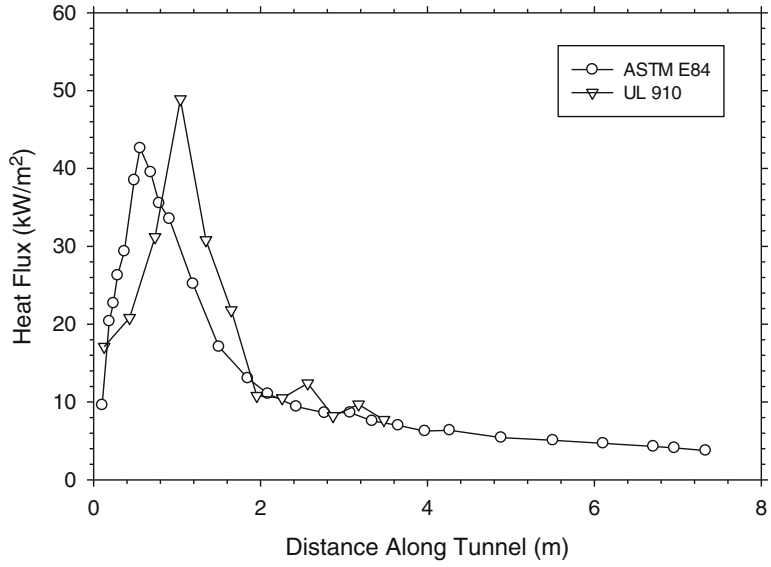

Fig. 25.60 Test average heat fluxes measured in the UL 910 experiment by Gandhi et al. [95] compared with the ASTM E84 measurements made by Parker [94]

Effects of Other Variables

The environment in which a fire is burning can affect the heat flux levels incident on the surface. Studies have been conducted by Atreya and Mekki [96], Santo and Tamanini [97], Mekki et al. [98], and Chao and Fernandez-Pello to evaluate the impact of oxygen concentration on the heat fluxes transferred by flames to surfaces. In tests with methane fires, Atreya and Mekki [96] found that flame radiation (and the total heat flux to the surface) was increased by increasing the oxygen concentration.

More important for most problems in fire is the effect of decreasing the oxygen concentration on heat fluxes from the flame. Santo and Tamanini [97] found that decreasing the surrounding oxygen concentration from 20.9 % to 18.0 % the radiative flux to an external target was decreased to an external target by 40 %. This decrease was attributed to a decrease in lower soot concentrations in flames in lower oxygen environments. Chao and Fernandez-Pello [99] found that this reduction in heat transfer to the surface reduces the flame spread rate along combustible panels.

Nomenclature

a	spacing between parallel walls (m)
C_p	specific heat capacity of air at 300 K (0.998 kJ/[kg-K])
d	length of single side on L-shape burner, length of line burner, width of burning area on corner wall (m)
D	length of single side of square burner, diameter (m)
g	acceleration of gravity (9.81 m/s^2)
H	distance between fire and ceiling (m)
H_B	distance between fire and lower flange of I-beam (m)
H_C	distance between fire and upper flange of I-beam (m)
H_o	height of room window (m)
h	convective heat transfer coefficient (kW/[m^2 -K])
k	thermal conductivity (kW/m-K)
L_B	flame tip length along lower flange of I-beam (m)
L_C	flame tip length along upper flange of I-beam (m)
L_{web}	flame tip length along center of web on I-beam (m)

L_f average flame length (m)
$L_{f,\text{tip}}$ flame tip length (m)
L_H flame extension along ceiling away from stagnation point (m)
Q fire heat release rate (kW)
Q' fire heat release rate per unit width (kW/m)
Q^* dimensionless parameter, $Q_D^* = \frac{Q}{\rho_\infty C_p T_\infty \sqrt{g} D^{5/2}}$, with D being length scale
r distance from corner or stagnation point to measurement location (m)
q'' heat flux (kW/m^2)
T_f local gas temperature (K)
T_g room gas temperature (K)
T_s material surface temperature (K)
T_∞ ambient temperature (300 K)
W_o width of room window (m)
w dimensionless distance along ceiling or I-beam, $w = \left(r + H_B + z^{'}\right)/\left(L_{HB} + H_B + z^{'}\right)$
x horizontal coordinate (m)
y horizontal coordinate (m)
y' distance from center of line burner, $y^{'} = 0.5d - y \ \ (m)$
Z burner height (m)
z vertical coordinate (m)
z' virtual source location (m)

Greek Letters

ε material surface emissivity (−)
ρ_∞ ambient density of air (1.2 kg/m^3)
π constant (3.14159)
σ Stefan-Boltzman constant $\left(5.67 \times 10^{-11} kW/\left[m^2 - K^4\right]\right)$

Subscripts

cl centerline
conv convective
d defined using d as length scale
D defined using D as length scale
H defined using H as length scale
hfg heat flux gauge
B defined using H_B as length scale
C defined using H_C as length scale
web defined using H_{web} as length scale
inc incident
m measured
max max level
net net
peak peak
rad radiative
rr reradiated
s material surface

References

1. M. Kokkala, "Heat Transfer to and Ignition of Ceiling by an Impinging Diffusion Flame," *VTT Research Report 586,* Technical Research Centre of Finland, Escopo, Finland (1989).
2. M. Kokkala, "Experimental Study of Heat Transfer to Ceiling from an Impinging Diffusion Flame," *Fire Safety Science—Proceedings of the 3rd International Symposium,* Elsevier Applied Science, New York, pp. 261–270 (1991).
3. H.Z. You and G.M. Faeth, "Ceiling Heat Transfer During Fire Plume and Fire Impingement," *Fire and Materials,* 3, 3, pp. 140–147 (1979a).
4. H.Z. You and G.M. Faeth, "An Investigation of Fire Impingement on a Horizontal Ceiling," NBS-GCR-79-188, U.S. Department of Commerce, Washington, DC (1979b).
5. Wickstrom, U., "Adiabatic Surface Temperature and the Plate Thermometer for Calculating Heat Transfer and Controlling Fire Resistance Furnaces," *Fire Safety Science -Proceedings of the Ninth Fire Safety Science*, 2008, pp.1227–1238
6. Wickstrom, U. Dathinh, D., and McGrattan, K., "Adiabatic Surface Temperature for Calculating Heat Transfer to Fire Exposed Structures," *Proceedings of the 11th International Conference on Fire Science and Engineering Interflam*, 2007
7. Wickstrom, U., "The Plate Thermometer-A Simple Instrument for Reaching Harmonized Fire Resistance Tests," Fire Technology 2:195–208
8. Duthinh, D., McGrattan, K., and Khaskia, A., (2008) "Recent Advances in Fire-Structural Analysis," Fire Safety Journal 43:161–167
9. L.T. Cowley, "Behaviour of Oil and Gas Fires in the Presence of Confinement and Obstacles," *Miscellaneous Report TNMR.91.006,* Shell Research Limited, Thornton Research Center, Combustion and Fuels Department, Chester, UK (Feb. 1991).
10. J.J. Gregory, R. Mata, and N.R. Keltner, "Thermal Measurements in a Series of Large Pool Fires," *Sandia Report Number SAND85-0196,* Sandia National Laboratories, Albuquerque, NM (1987).
11. L.H. Russell and J.A. Canfield, "Experimental Measurements of Heat Transfer to a Cylinder

Immersed in a Large Aviation Fuel Fire," *Journal of Heat Transfer,* pp. 397–404 (Aug. 1973).
12. G. Wachtell and J. Langhaar, "Fire Test and Thermal Behavior of 150-Ton Lead-Shielded Casks," DP 1070, *Engineering and Equipment, TID-4500,* E.I. DuPont De Nemours and Co., Wilmington, DE (1966).
13. C. Anderson et al., "Effects of a Fire Environment on a Rail Tank Car Filled with LPG," *Report No. FRA-OR&D 75–31,* U.S. Department of Transportation, Federal Railroad Administration, Washington, DC (1974).
14. National Academy of Science, Committee on Hazardous Materials, Division of Chemistry, and Chemical Technology (National Research Council), *Pressure-Relieving Systems for Marine Cargo Bulk Liquid Containers,* National Academy of Sciences, Washington, DC (1973).
15. K. Moodie et al., "Total Pool Fire Engulfment Trials on a 5-Tonne LPG Tank," *HSE Internal Report No. IR/L/FR/87/27,* Health and Safety Executive, London, UK (1987).
16. M. Tunc and J. Venart, "Incident Radiation from an Engulfing Pool Fire to a Horizontal Cylinder, Part I and II," *Fire Safety Journal,* 8, pp. 81–95 (1985).
17. W. McLain, "Investigation of the Fire Safety Characteristics of Portable Polyethylene Tanks Containing Flammable Liquids," *Report No. CG-M-1-88,* U.S. Coast Guard, Washington, DC (1988).
18. A. Taylor et al., "Engulfment Fire Tests on Road Tanker Sections," *Rarde Technical Report 7/75,* Controller HMSO, London (1975).
19. M. Schneider and L. Kent, "Measurement of Gas Velocities and Temperatures in a Large Open Pool Fire," *Fire Technology,* pp. 51–81 (Feb. 1989).
20. G. Back, C.L. Beyler, P. DiNenno, and P. Tatem, "Wall Incident Heat Flux Distributions Resulting from an Adjacent Fire," *Fire Safety Science—Proceedings of the 4th International Symposium,* International Association of Fire Safety Science, Ottawa, Canada, pp. 241–252 (1994).
21. G. Heskestad, "Luminous Heights of Turbulent Diffusion Flames," *Fire Safety Journal,* 5, pp. 103–108 (1983).
22. D. Gross and J.B. Fang, "The Definition of a Low Intensity Fire," in *NBS Special Publication 361, Volume 1: Performance Concept in Buildings, Proceeding of the Joint RILEM-ASTM-CIB Symposium,* National Bureau of Standards, Washington, DC, pp. 677–686 (1972).
23. T. Mizuno and K. Kawagoe, "Burning Behaviour of Upholstered Chairs, Part 2: Burning Rate of Chairs in Fire Tests," *Fire Science and Technology,* 5, 1, pp. 69–78 (1985).
24. M. Daikoku and K. Saito, "A Study of Thermal Characteristics of Vertical Corner Wall in Room Fire," *Proceedings of the ASME/JSME, Thermal Engineering,* Book No. H0933C-1995 (L.S. Fletcher and T. Aihara, eds.), pp. 83–90 (1995).
25. Y. Hasemi, M. Yoshida, S. Takashima, R. Kikuchi, and Y. Yokobayashi, "Flame Length and Flame Heat Transfer Correlations in Corner-Wall and Corner-Wall-Ceiling Configurations," in *Proceedings of Interflam '96* (Franks and Grayson, eds.), Interscience Communications Ltd., London, pp. 179–188 (1996).
26. M. Kokkala, "Characteristics of a Flame in an Open Corner of Walls," in *Proceedings from Interflam '93,* Interscience Communications, Ltd., London, pp. 13–24 (1993).
27. T. Ohlemiller, T. Cleary, and J. Shields, "Effect of Ignition Conditions on Upward Flame Spread on a Composite Material in a Corner Configuration," *Fire Safety Journal,* 31, pp. 331–344 (1998).
28. T.J. Ohlemiller and J.R. Shields, "The Effect of Surface Coatings on Fire Growth Over Composite Materials in a Corner Configuration," *Fire Safety Journal,* 32, 2, pp. 173–193 (1999b).
29. B.Y. Lattimer and U. Sorathia, "Thermal Characteristics of Fires in a Noncombustible Corner," *Fire Safety Journal,* 38, pp. 709–745 (2003).
30. R.B. Williamson, A. Revenaugh, and F.W. Mowrer, "Ignition Sources in Room Fire Tests and Some Implications for Flame Spread Evaluation," *Fire Safety Science—Proceedings of the 3rd International Symposium,* Elsevier Applied Science, New York, pp. 657–666 (1991).
31. H. Tran and M. Janssens, "Modeling the Burner Source Used in the ASTM Room Fire Test," *Journal of Fire Protection Engineering,* 5, 2, pp. 53–66 (1993).
32. J.G. Quintiere and T.G. Cleary, "Heat Flux from Flames to Vertical Surfaces," *Fire Technology,* 30, 2, pp. 209–231 (1994).
33. S.E. Dillon, "Analysis of the ISO 9705 Room/Corner Test: Simulations, Correlations and Heat Flux Measurements," *NIST-GCR-98-756,* U.S. Department of Commerce, National Institute of Standards and Technology, Washington, DC (1998).
34. International Standards Organization, ISO 9705:1993 (E), *International Standard for Fire Tests—Full-Scale Room Test for Surface Products,* International Organization for Standardization (ISO), Geneva, Switzerland (1993).
35. T. Tanaka, I. Nakaya, and M. Yoshida, "Full Scale Experiments for Determining the Burning Conditions to Be Applied to Toxicity Tests," *Fire Safety Science—Proceedings of the 1st International Symposium,* Hemisphere Publishing, Gaithersburg, MD, pp. 129–138 (1985).
36. Tofilo, P., Delicatsios, M.A., and Silcock, G.W.H., (2005), "Effect of Fuel Sootiness on the Heat Fluxes to the Walls in Enclosure Fires," Fire Safety Science-Proceedings of the Eighth International Symposium, Beijing, China, pp. 987–998.
37. W. Takashi et al., "Flame and Plume Behavior in and Near a Corner of Walls," *Fire Safety Science—Proceedings of the 5th International Symposium* (Y. Hasemi, ed.), International Association for Fire Safety Science, Melbourne, Australia, pp. 261–271 (1997).
38. Y. Hasemi, S. Yokobayashi, T. Wakamatsu, and A. Ptchelintsev, "Fire Safety of Building Components Exposed to a Localized Fire—Scope and Experiments

on Ceiling/Beam System Exposed to a Localized Fire," *Proceedings from ASIAFLAM,* Kowloon, Hong Kong, pp. 51–361 (1995).
39. R.L. Alpert, "Convective Heat Transfer in the Impingement Region of a Buoyant Plume," *Transactions of ASME,* 109, pp. 120–124 (1987).
40. H.Z. You, "An Investigation of Fire-Plume Impingement on a Horizontal Ceiling 2—Impingement and Ceiling-Jet Regions," *Fire and Materials,* 9, 1, pp. 46–56 (1985).
41. L.Y. Cooper, "Heat Transfer from a Buoyant Plume to an Unconfined Ceiling," *ASME Journal of Heat Transfer,* 104, pp. 446–452 (1982).
42. T. Wakamatsu, personal communication (Sept. 1999).
43. J. Myllymaki and M. Kokkala, "Thermal Exposure to a High Welded I-Beam Above a Pool Fire," *First International Workshop on Structures in Fires,* Copenhagen, pp. 211–226 (2000).
44. P.L. Hinkley, H.G.H. Wraight, and C.R. Theobald, "The Contribution of Flames under Ceilings to Fire Spread in Compartments," *Fire Safety Journal,* 7, pp. 227–242 (1984).
45. P.L. Hinkley, H.G.H. Wraight, and C.R. Theobald, "The Contribution of Flames under Ceilings to Fire Spread in Compartments, Part I: Incombustible Ceilings," *Fire Research Note No. 712,* Fire Research Stations, Borehamwood, Herts, UK (1968).
46. P.L. Hinkley, H.G.H. Wraight, and C.R. Theobald, "The Contribution of Flames under Ceilings to Fire Spread in Compartments, Part II: Combustible Ceiling Linings," *Fire Research Note No. 743,* Fire Research Stations, Borehamwood, Herts, UK (1969).
47. B. Lattimer, J. Beitel, and C. Mealy, "Heat Fluxes to a Corridor Ceiling," unpublished data (2006).
48. A. Lonnermark and H. Ingason, "Fire Spread and Flame Length in Large-Scale Tunnel Fires," *Fire Technology,* 42, pp. 283–302 (2006).
49. T. Wakamatsu, Y. Hasemi, Y. Yokobayashi, and A.V. Ptchelintsev, "Experimental Study on the Heating Mechanism of a Steel Beam Under Ceiling Exposed to a Localized Fire," in *Proceedings from Interflam '96* (Franks and Grayson, eds.), Interscience Communications, Ltd., London, pp. 509–518 (1996).
50. T. Ahmad and G.M. Faeth, "Fire Induced Plumes Along a Vertical Wall, Part III: The Turbulent Combusting Plume," *NBS Report for Grant No. 5–9020,* U.S. Department of Commerce, Washington, DC (1978).
51. T. Ahmad and G.M. Faeth, "Turbulent Wall Fires," in *17th Symposium (International) on Combustion,* Combustion Institute, Pittsburgh, PA, pp. 1149–1160 (1979).
52. J.G. Quintiere, M. Harkelroad, and Y. Hasemi, "Wall Flames and Implications for Upward Flame Spread," *AIAA-85-0456,* American Institute of Aeronautics and Astronautics, Reno, NV (1985).
53. L. Orloff, J. de Ris, and G.H. Markstein, "Upward Turbulent Fire Spread and Burning of Fuel Surface," in *15th Symposium (International) on Combustion,* Combustion Insititute, Pittsburgh, PA, pp. 183–192 (1975).
54. M.A. Delicatsios, "Flame Heights in Turbulent Wall Fires with Significant Flame Radiation," *Combustion Science and Technology,* 39, pp. 195–214 (1984).
55. Y. Hasemi, "Experimental Wall Flame Heat Transfer Correlations for the Analysis of Upward Wall Flame Spread," *Fire Science and Technology,* 4, 2, pp. 75–90 (1984).
56. H. Mitler, "Predicting the Spread Rates on Vertical Surfaces," in *23rd Symposium (International) on Combustion,* Combustion Institute, Pittsburgh, PA, pp. 1715–1721 (1990).
57. C.L. Beyler, S.P. Hunt, N. Iqbal, and F.W. Williams, "A Computer Model of Upward Flame Spread on Vertical Surfaces," in *Fire Safety Science—Proceedings of the 5th International Symposium* (Y. Hasemi, ed.), International Association for Fire Safety Science, Melbourne, Australia, pp. 297–308 (1997).
58. F.W. Williams, C.L. Beyler, S.P. Hunt, and N. Iqbal, "Upward Flame Spread on Vertical Surfaces," *NRL/MR/6180—97-7908,* Navy Technology for Safety and Survivability, Chemistry Division (1997).
59. Y. Hasemi, "Thermal Modeling of Upward Wall Flame Spread," *Fire Safety Science—Proceedings of the 1st International Symposium,* Hemisphere Publishing, Gaithersburg, MD, pp. 87–96 (1986).
60. Y. Hasemi, "Deterministic Properties of Turbulent Flames and Implications on Fire Growth," *Interflam '88,* John Wiley and Sons, Cambridge, UK, pp. 45–52 (1988).
61. M. Kokkala, D. Baroudi, and W.J. Parker, "Upward Flame Spread on Wooden Surface Products: Experiments and Numerical Modelling," *Fire Safety Science—Proceedings of the Fifth International Symposium,* International Association for Fire Safety Science, Melbourne, Australia, pp. 300–320 (1997).
62. M. Foley and D.D. Drysdale, "Heat Transfer from Flames Between Vertical Parallel Walls," *Fire Safety Journal,* 24, pp. 53–73 (1995).
63. A.K. Kulkarni, C.I. Kim, and C.H. Kuo, "Heat Flux, Mass Loss Rate and Upward Flame Spread for Burning Vertical Walls," *NIST-GCR-90-584,* U.S. Department of Commerce, Washington, DC (1990).
64. A.K. Kulkarni, C.I. Kim, and C.H. Kuo, "Turbulent Upward Flame Spread for Burning Vertical Walls Made of Finite Thickness," *NIST-GCR-91-597,* U.S. Department of Commerce, Washington, DC (1991).
65. L. Orloff, A.T. Modak, and R.L. Alpert, "Burning of Large-Scale Vertical Surfaces," in *16th Symposium (International) on Combustion,* Combustion Institute, Pittsburgh, PA, pp. 1345–1354 (1977).
66. G.H. Markstein and J. de Ris, "Wall-Fire Radiant Emission, Part 2: Radiation and Heat Transfer from Porous-Metal Wall Burner Flames," in *24th Symposium (International) on Combustion,* Combustion Institute, Pittsburgh, PA, pp. 1747–1752 (1992).

67. Kahn, M., et al. "Combustion Characteristics of Materials and Generation of Fire Products" *SFPE Handbook of Fire Protection Engineering,* 5th ed. (M. J. Hurley, ed.), Springer (2015).
68. M.M. Delichatsios, P. Wu, M.A. Delichatsios, G.D. Lougheed, G.P. Crampton, C. Qian, H. Ishida, and K. Saito, "Effect of External Radiant Heat Flux on Upward Flame Spread: Measurements on Plywood and Numerical Predictions," *Fire Safety Science—Proceedings of the 4th International Symposium,* International Association of Fire Safety Science, pp. 421–432 (1994).
69. T.J. Ohlemiller and T.G. Cleary, "Upward Flame Spread on Composite Materials," *Fire Safety Journal,* 32, pp. 159–172 (1999a).
70. C. Qian, H. Ishida, and K. Saito, "Upward Flame Spread Along PMMA Vertical Corner Walls, Part II: Mechanism of *M* Shape Pyrolysis Front Formation," *Combustion and Flame,* 99, pp. 331–338 (1994a).
71. C. Qian and K. Saito, "An Empirical Model for Upward Flame Spread over Vertical Flat and Corner Walls," in *Fire Safety Sceince—Proceedings from the 5th International Symposium* (Y. Hasemi, ed.), Melbourne, Australia, pp. 285–296 (1994b).
72. Y. Hasemi, M. Yoshida, Y. Yokobayashi, and T. Wakamatsu, "Flame Heat Transfer and Concurrent Flame Spread in a Ceiling Fire," in *Fire Safety Science—Proceedings from the 5th International Symposium* (Y. Hasemi, ed.), International Association for Fire Safety Science, Melbourne, Australia, pp. 379–390 (1997).
73. Y. Hasemi, M. Yoshida, and R. Takaike, "Flame Length and Flame Heat Transfer Correlations in Ceiling Fires," poster at Fire Safety Science—*6th International Symposium,* International Association for Fire Safety Science, Poitiers, France (1999).
74. F. Tamanini, "Calculations and Experiments on the Turbulent Burning of Vertical Walls in Single and Parallel Configurations," *FMRC J.I.OAOE7.BU-2,* FMRC Technical Report, Factory Mutual Research Corporation, Norwood, MA (1979).
75. F. Tamanini and A.N. Moussa, "Experiments on the Turbulent Burning of Vertical Parallel Walls," *Combustion Science and Technology,* 23, pp. 143–151 (1980).
76. H. Ingason and J. de Ris, "Flame Heat Transfer in Storage Geometries," *Fire Safety Journal,* 31, pp. 39–60 (1998).
77. B.Y. Lattimer and H. Sorathia, "Thermal Characteristics of Fires in a Combustible Corner," *Fire Safety Journal,* 38, pp. 747–770 (2003).
78. I. Oleszkiewicz, "Heat Transfer from a Window Fire Plume to a Building Façade," *ASME HTD,* 23, pp. 163–170 (1989).
79. I. Oleszkiewicz, "Fire Exposure to Exterior Walls and Flame Spread on Combustible Cladding," *Fire Technology,* 26, 4, pp. 357–375 (1990).
80. P.H. Thomas and M.L. Bullen, "Compartment Fires with Non-Cellulosic Fuels," in *17th Symposium (International) on Combustion,* Combustion Institute, Pittsburgh, PA, pp. 1139–1148 (1979).
81. J.J. Beitel and W.R. Evans, "Multi-Story Fire Evaluation Program," *SwRI Project 01–6112,* Final Report, Volume 1, Southwest Research Institute, San Antonio, TX, and Society of the Plastics Industry, Inc., New York (1980).
82. S. Yokoi, "Study on the Prevention of Fire Spread Caused by Hot Upward Current," *Report No. 34,* Building Research Institute, Tokyo, Japan (1960).
83. ASTM E119, *Standard Test Method for Fire Tests of Building Construction and Materials,* American Society for Testing and Materials, West Conshohocken, PA.
84. ISO, ISO 834, *Fire-Resistance Tests—Elements of Building Construction,* International Organization for Standardization, Geneva, Switzerland (1999).
85. T. Harmathy, M. Sultan, and J. MacLaurin, "Comparison of Severity of Exposure in ASTM E119 and ISO 834 Fire Resistance Tests," *Journal of Testing and Evaluation,* pp. 371–375 (Nov. 1987). In *Handbook of Experimental Mechanics* (A.S. Kobayashi, ed.), Society for Experimental Mechanics, Prentice-Hall, Inc., Englewood Cliffs, NJ (1987).
86. V. Babrauskas and B. Williamson, "Temperature Measurement in Fire Test Furnaces," *Fire Technology,* 13, 3, pp. 226–238 (1978).
87. EN1363-1, *Fire Resistance Tests, Part 1: General Requirements,* European Committee for Standardization (CEN), Brussels, Belgium (1999).
88. P. Fromy and M. Curtat, "Application of a Zone Model to the Simulation of Heat Transfer in Fire Resistance Furnaces Piloted with Thermocouples or Plate Thermometers," in *Fire Safety Science—Proceedings of the 6th International Symposium,* International Association for Fire Safety Science, pp. 531–542 (1999).
89. P.H. van de Leur and L. Twilt, "Thermal Exposure in Fire Resistance Furnaces," *Fire Safety Science—Proceedings of the 6th International Symposium,* International Association for Fire Safety Science, pp. 1087–1098 (1999).
90. M. Sultan, "Fire Resistance Furnace Temperature Measurements: Plate Thermometers vs. Shielded Thermocouples," *Fire Technology,* 42, pp. 253–267 (2006).
91. M. Sultan, N. Benichou, and Y. Byung, "Heat Exposure in Fire Resistance Furnaces: Full-Scale vs. Intermediate-Scale," *Fire and Materials,* 27, pp. 43–54 (2003).
92. UL 1709, "Rapid Rise Fire Tests of Protection Materials for Structural Steel," Underwriters Laboratories, Northbrook, IL (1991).
93. EN1363-2, *Fire Resistance Tests, Part 2: Alternative and Additional Procedures,* European Committee for Standardization (CEN), Brussels, Belgium (1999).
94. W. Parker, "An Investigation of the Fire Environment in the ASTM E84 Tunnel Test," *NBS Technical Note 945,* U.S. Department of Commerce, National Bureau of Standards, Washington, DC (1977).
95. Gandhi, P., Caudill, L., Hoover, J., and Chapin, T., (1996), "Determination of Fire Exposure Heat Flux in

Cable Fire Tests," Fire Safety Science-Proceedings of the Fifth International Symposium, Portier, France, pp. 141–152.
96. A. Atreya and K. Mekki, "Heat Transfer During Wind-Aided Flame Spread on a Ceiling Mounted Sample," in *24th Symposium (International) on Combustion,* Combustion Institute, Pittsburgh, PA, pp. 1677–1684 (1992).
97. G. Santo and F. Tamanini, "Influence of Oxygen Depletion on the Radiative Properties of PMMA Flames," in *18th Symposium (International) on Combustion,* Combustion Institute, Pittsburgh, PA, pp. 619–631 (1981).
98. K. Mekki, A. Atreya, S. Agrawal, and I. Wichman, "Wind-Aided Flame Spread over Charring and Non-Charring Solids: An Experimental Investigation," in *23rd Symposium (International) on Combustion,* Combustion Institute, Pittsburgh, PA, pp. 1701–1707 (1990).
99. Y.H. Chao and A.C. Fernandez-Pello, "Flame Spread in a Vitiated Concurrent Flow," Heat Transfer in Fire and Combustion Systems, *ASME HTD,* 199, pp. 135–142 (1992).

Brian Y. Lattimer is a Professor in Mechanical Engineering at Virginia Tech. His research areas include fire dynamics, heat transfer from fires, and material response to fires.

Heat Release Rates

26

Vytenis Babrauskas

Introduction

Calculations of fire behavior in buildings are not possible unless the heat release rate of the fire is known. This chapter on heat release rates provides both theoretical and empirical information. The chapter is organized so that theory and basic effects are considered first, then a compendium of product data is provided, which is arranged in alphabetic order.

Definitions

The essential characteristic that describes quantitatively *How big is the fire?* is the heat release rate. This is so important that it has been described as the single most important variable in fire hazard [1]. The heat release rate (HRR) of a burning item is measured in kilowatts (kW). It is the rate at which the combustion reactions produce heat. The term "burning rate" is also often found. This is a less specific term, and it may either denote the HRR or the mass loss rate. The latter is measured in units of kg s^{-1}. It is best to reserve 'burning rate' for non-quantitative fire descriptions and to use either HRR or mass loss rate, as appropriate. The relationship of these two quantities can be expressed as:

$$HRR = \Delta h_c \times MLR \qquad (26.1)$$

where h_c is the effective heat of combustion (kJ kg^{-1}) and MLR is the mass loss rate (kg s^{-1}). Such an equation implies that HRR and MLR are simply related by a constant. This is not in general true. Figure 26.1 shows the results obtained from a test on a 17 mm sample of Western red cedar. It is clear that the effective heat of combustion is not a constant; it is roughly 12 MJ kg^{-1} for the first part of the test, but increases to around 30 MJ kg^{-1} during the charring period at the end of the test.

In principle, the effective heat of combustion can be determined by theory or by testing. In practice, if the effective heat of combustion is not a constant, then experimental techniques normally involve directly measuring the HRR, rather than using Equation 26.1.

Measuring the HRR, Full-Scale

The simplest case is when full-scale HRR can be directly measured. This can be grouped into two types of techniques:

- Open-burning HRR calorimeters
- Room fire tests.

Open-burning HRR calorimeters were developed in the early 1980s at NIST by Babrauskas and colleagues [2] and at FMRC by Heskestad [3]. The operating principles of these calorimeters are described in Chap. 27. Based on this work, a large number of different test

V. Babrauskas (✉)
Fire Science and Technology Inc.

M.J. Hurley (ed.), *SFPE Handbook of Fire Protection Engineering*,
DOI 10.1007/978-1-4939-2565-0_26, © Society of Fire Protection Engineers 2016

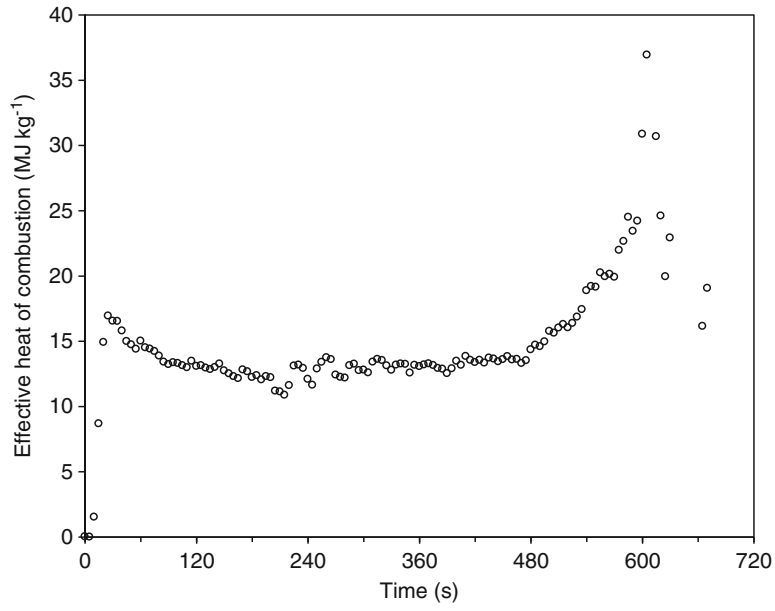

Fig. 26.1 Effective heat of combustion for 17 mm thick Western red cedar, tested at an irradiance of 65 kW m^{-2}

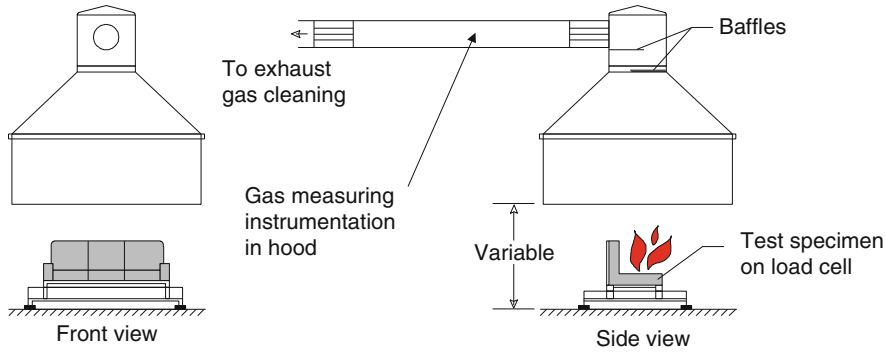

Fig. 26.2 NORDTEST NT FIRE 032 calorimeter

standards have been issued, for example [4–8]. A discussion of a number of other standards can be found [9].

The NORDTEST furniture calorimeter [7] is shown in Fig. 26.2. Open-burning HRR measurements are simpler to make since a test room does not need to be constructed. The HRR within a room and under open conditions are, clearly, identical at very low HRR. What happens at higher values of HRR depends on the situation at hand. If the fire is so large that room flashover can be reached (about 1.5–1.75 MW if ventilation is through a single normal-sized door opening) then actual room HRR values post-flashover can be drastically different from their open-burning rates. This is due primarily to additional radiant heat flux contribution from the hot gas layer and the hot room surfaces, although ventilation effects can also play a role.

For upholstered chairs, extensive studies have shown that room effects are only at the 20 % level up to a 1 MW fire [10]. The same study, however, showed that for mattresses, a room presence effect shows up at much lower HRR values. For liquid pools, the HRR is strongly

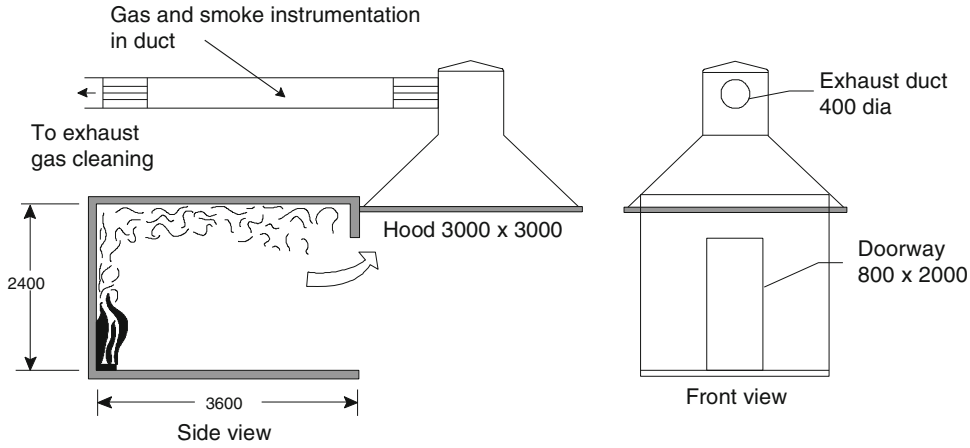

Fig. 26.3 ISO 9705 room HRR test

affected by the surrounding room [11]. For most other commodities, this issue has not been studied.

The degree by which the room affects the HRR is largely determined by how 'open' the fuel package itself is. A liquid pool on the floor has a view factor of 0 to itself and 1.0 to the room. By contrast, the reason that chairs tend to be little-affected by the room is that the chair 'sees' its own surfaces to a significant extent, rather than being fully-exposed to the room. Some useful error analyses of large open calorimeter measurements have been reported [12]; a theoretical discussion of the 'ideal' large scale calorimeter has also been presented [13].

Room fire tests should be commissioned when room effects are anticipated to be strong, or when a more precise estimate is needed. Apart from cost, there is a drawback to room fire testing. This is because the

HRR measured in a room fire cannot be extrapolated to any rooms with larger ventilations. Open-burning HRR data could, by contrast, be applicable to such well-ventilated rooms.

The development of the modern room HRR test took place at several institutions, including Fisher and Williamson at the University of California [14], Lee at NIST [15], and Sundström at the Swedish National Testing and Research Institute [16]. Room test standards include [17, 18] and also [4, 5]. A typical standard room fire test, ISO 9705 is shown in Fig. 26.3; a similar room fire test is ASTM E 2257 [19]. This test equipment is available for commercial testing in North America, Europe, Asia, and other places.

Measuring the HRR, Bench-Scale

To measure the HRR in a bench-scale test is nowadays an easy task. Most commonly, the Cone Calorimeter [20] developed at NIST by Babrauskas will be used (Fig. 26.4). These instruments are available at commercial and research laboratories worldwide. The procedures for conducting Cone Calorimeter tests are described in ASTM E 1354 [21] and ISO 5660 [22]. Other HRR calorimeters, such as the Ohio State University apparatus or the Factory Mutual Research Corp. Flammability Apparatus are also in use at some laboratories. A textbook is available which discusses many of the details of HRR measuring technology [23]. Thus, the modeler can assume that if at least enough material is available to run several small samples (100 mm × 100 mm, in the case of the Cone calorimeter), an empirical HRR curve can be obtained by running bench-scale tests.

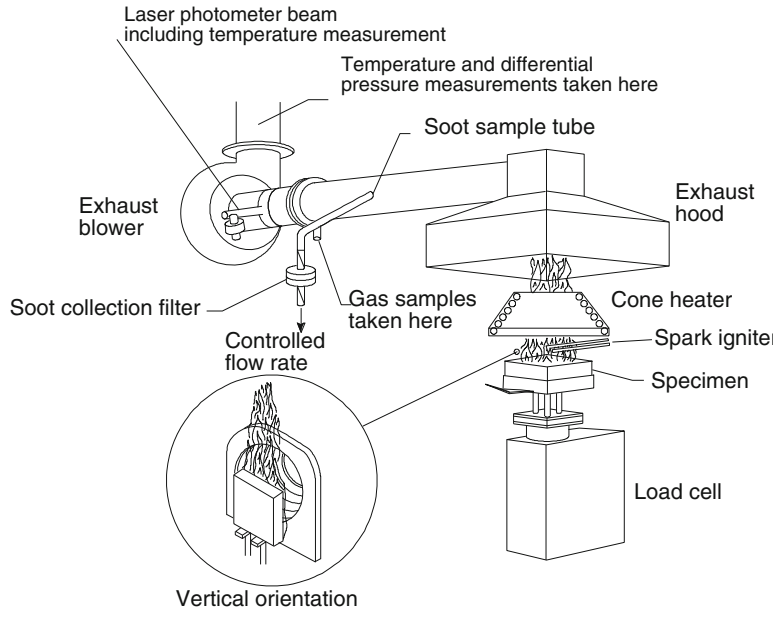

Fig. 26.4 The cone calorimeter

Measuring the HRR, Intermediate-Scale

The newest experimental technology for determining the HRR is intermediate-scale calorimetry. Various earlier efforts have been made, but the first instrument to receive standards support is the ICAL, developed at Weyerhaeuser [24] (Fig. 26.5). It has been standardized as ASTM E 1623 [25]. This test method accommodates 1.0 m by 1.0 m specimens, which allows for complex or highly non-homogenous constructions to be tested. However, since the data are still not of full scale, some additional analysis is needed to be able to utilize the test data in fire modeling.

Modeling Implications for Using Full-Scale HRR Data

If access is available to full-scale HRR data, then the task of defining the fire is on a solid basis. Even here, however, there are a number of problems and caveats. Apart from the obvious issue that the available full-scale data must be known to describe the specific fuel source in question (and not some possibly very differently performing 'similar' item), there are some additional concerns. Supposing one finds full-scale test results on one's exact commodity, can the data simply be used unquestioningly? The answer, of course, is not. There are two main issues:

- The available data may be open-burning calorimetry data. One must then determine if there is an enclosure effect to be accounted.
- The available data may be room fire data, but the test enclosure may not correspond to the room for which modeling is to be done.

The first of these issues was briefly touched on above already. The availability of quantitative guidance is lacking. For upholstered chair fires in a room of about the size of the ISO 9705 room, one can estimate a 20 % augmentation over the open-burn rates when considering fires in the 100–1000 kW range. For mattresses, the effect is large and without adequate guidance. For liquid pools, a pool sub-model must be specifically present in the fire model used, since no simple approximation is adequate. For wood cribs, there are formulas for guidance [26], although of course wood cribs are hardly a feature of most real fires. For other combustibles, neither data nor guidance is available.

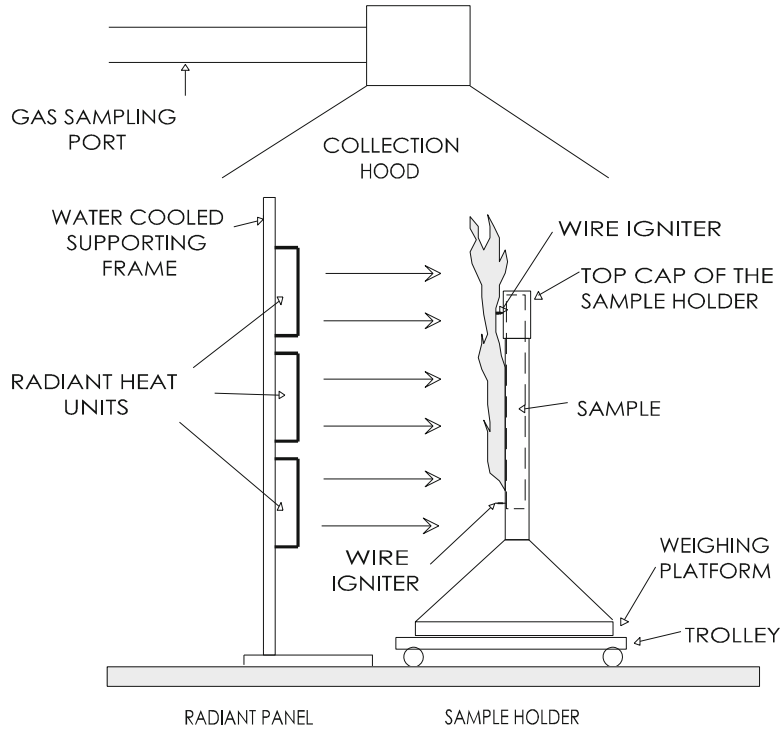

Fig. 26.5 Intermediate scale (ICAL) calorimeter

A very similar problem is faced when the modeler has available full-scale HRR data, but the test was run in a room of rather different size or ventilation conditions than is the intended application. Only two studies on this topic have been published in the literature. Kokkala and colleagues compared [27] some room wall/ceiling linings in a large room to the values obtained in the ISO 9705 room. Also, during the CBUF project some furniture fires were done in rooms of two scales [10]. Neither of these studies looked at this issue comprehensively enough to yield numerical guidance.

Some European designers have proposed that 250 or 500 kW m^{-2} of floor area is an appropriate peak value of HRR according to which to design buildings of almost any kind [28]. It is not clear how these values were obtained, but one must consider whether they are conservative. Figure 26.48 gives HRR data for one pallet and half a pallet loads of some elastomer pellets. While these are 'industrial' materials, nonetheless substances of similar heat of combustion and state of aggregation can readily be found in shops, storage rooms, and various other places in diverse building types. The test data showed that the whole-pallet test had to be extinguished at about 4500 kW m^{-2}; the fire was still growing, and its ultimate HRR would have been higher.

Growth curves for the FM data listed in Table 26.8 are not available; nonetheless the peak values of roughly 2,000–20,000 kW m^{-2} are sobering. Goods of this kind cannot occupy anywhere close to 100 % of the floor area, of course, but even assuming coverage at ¼ to ½, the actual HRR values are enormous. Now, there are clearly occupancies where it is impossible to introduce high fuel loads—swimming facilities may be an example. But other facilities, even if designed to be spartan in actual use (e.g., ceremonial lobbies) may sustain large fuel loads during construction, remodeling, expansion, and similar activities.

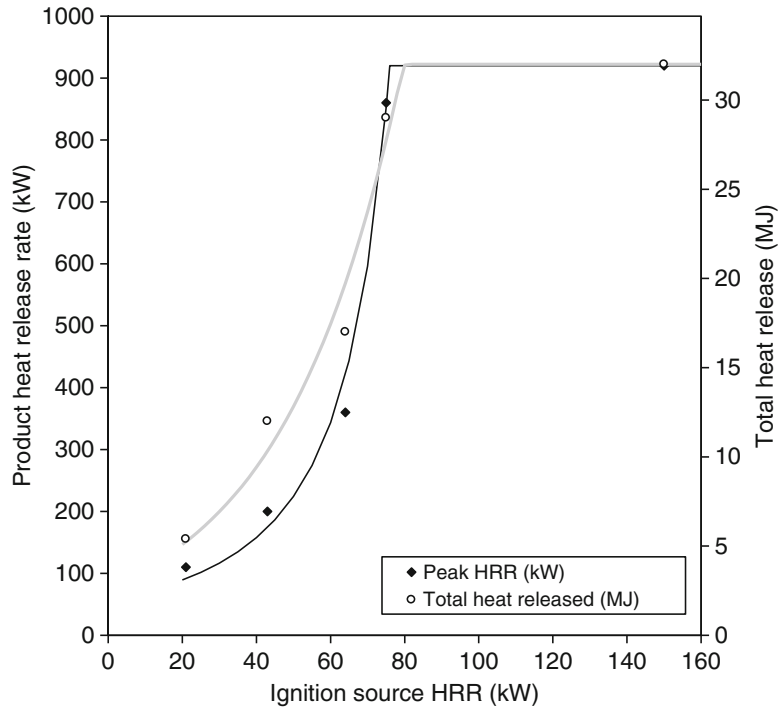

Fig. 26.6 Effect of ignition source on the HRR of PVC foam wall coverings

Effect of Ignition Source on Full-Scale HRR

Full-scale tests for HRR usually do not impose an *overall* radiant heat flux and are ignited with localized flame sources. But locally, the heat fluxes from various ignition sources will differ both in their magnitude and in the size of the area subjected to the heat flux. Most plastic commodities that do not contain fire retardants (and are not made from an intrinsically-FR plastic) can be ignited with very small flame sources, often no bigger than a paper match. FR commodities, however, will resist ignition from small flames, but may be ignited from a large-flame ignition source. Commonly, such products show an all-or-nothing behavior. That is, ignition sources below a certain size will cause essentially no heat release from the test article, while a larger ignition source may cause a large fraction of, if not the total, combustible mass of the article.

For example, it was shown [29] that a television cabinet made from a plastic fire retarded to the extent of obtaining a V-0 classification in the UL 94 [30] test gave no heat release when using a 10 kW burner, but burned well when exposed to a 30 kW burner. Dembsey [31] conducted room tests on rooms partially lined with a PVC-foam wall covering. His results are shown in Fig. 26.6. Note that the curve is very steep and could be represented reasonably by a step-function. Apart from a few examples, this type of data, unfortunately, is very rarely available for practical commodities of engineering interest.

Effects of Other Variables

Some *thermoplastic materials* have a highly pronounced tendency to melt and flow. Consequently, commodities made from these materials, when burning, will often exhibit object burning above the floor and an accompanying pool fire at the floor, formed by the melt material. Sherratt and Drysdale [32] studied the problem in intermediate scale, by burning vertical polypropylene sheets above various floor materials.

Major differences were found both in the peak HRR and in the time-resolved HRR curve, depending on the floor type. The differences were largely attributable to thermal characteristics (thickness, density, thermal conductivity, etc.) of the floor materials. Upholstered furniture using plastic foam padding often burns with a secondary pool fire underneath, however, this behavior occurs only in some cases.

Modeling with Bench-Scale HRR Data

If full-scale data on HRR are available, then these are simply used in the fire model. In many cases, however, such data are not available, often due to cost of testing or unavailability of large size specimens. In such cases, it is desirable to be able to use bench-scale data, denoted as and measured in units of kW m^{-2}. With the bench-scale HRR, there are two main questions: (1) can it be predicted from some more fundamental measurements? and (2) how can the full-scale HRR be predicted from the bench-scale HRR?

Predicting Bench-Scale HRR from Fundamental Considerations

The former question has been of considerable interest to fire researchers, but practical engineering methods are not yet at hand. This task is often described as creating a 'pyrolysis model,' since the degradation of a material when it is exposed to heat is known as pyrolysis. When a material heats up, degrades, ignites, and burns, some very complicated physical and chemical phenomena are taking place. In addition to a change of phase, there is often flow of moisture simultaneously with heat flow.

The material may undergo several different types of phase changes during the decomposition process, each accompanied by changes in density and porosity. Bubbles may be created within the bulk of the material and migrate to the surface. These may be accompanied by molten flow ejection at the surface. Oxygen may or may not directly interact with the surface to create a glowing combustion.

The chemical reactions being undergone are commonly several in number and occurring at different temperature regimes. Finally, the material may undergo large-scale cracking, buckling, or sloughing. Each of these physical phenomena may significantly affect the rate of specimen decomposition. From even this very brief description, it is clear that computing the pyrolysis of a material may be a difficult task. Thus, today for any fire hazard analysis purposes, HRR is invariably measured, rather than being computed from more fundamental theory.

Readers wishing to look more closely at the type of modeling needed to represent the pyrolysis process can refer to the dissertation of Parker [33] as a good example of how charring materials need to be treated. Some half-dozen other dissertations have been written on the same topic. Melting type materials have proven to be even more interesting as a subject of advanced research. Several hundred of papers have been published on various aspects of modeling the pyrolysis behavior of just one common material, poly(methylmethacrylate). References [34–40] can provide an introduction to this research.

Predicting Full-Scale HRR from Bench-Scale Data: Overview

Prediction of full-scale HRR is probably the single most important engineering issue in successful modeling of fires. Schematically, we may write that:

$$\dot{q} = \int \dot{q}'' dA \tag{26.2}$$

This representation does not fully reveal the difficulties involved. More explicitly,

$$\dot{q}(t) = \int \dot{q}''(t, x, y, z) dA(t) \tag{26.3}$$

This makes more clear that the instantaneous per-unit-area HRR is a function of time and also of the location of the burning element. The instantaneous burning area, A(t), is also a function of time. In addition, while we have not written this explicitly, $\dot{q}''(t)$ depends on the heating boundary conditions to the element. This quantity usually identified as the *heat flux* or *irradiance* incident upon the element. The latter term is commonly used since in full-scale fires the heating is dominated by the radiant component.

By examining the nature of dA(t), we can also identify the role of flame spread in characterizing the HRR of full-scale fires. A bench-scale HRR test specimen is usually ignited nearly-instantaneously over its entire surface. Full-scale fire, by contrast, nearly always exhibit finite spread rates. The flame spread velocity in a full-scale fire can be identified with the movement of the boundaries of the flame-covered area dA(t). Flame spread may occur in several directions over walls, ceilings, floors, and over individual surfaces of discrete commodities burning in a space. Consequently, it can be seen that tracking flame spread and dA(t) is a major undertaking. This task, by its nature, is incompatible with zone-type of fire models, since it presumes that a mechanism is in place to track very small surface elements. Such mode line is variable with CFO models [41] the quality of production is dependent on fuel type and the user needs to verify the permanent details.

Our approach will have to be restricted to identifying some of the attempts which have been made to simplify the problem in order to make it tractable for zone modeling. Simplifications are not yet possible for the 'general' case. Instead, we must examine specific combustibles, for which appropriate flame spread representations have been established. This is illustrated in a number of the sections below. Before we do this, however, it is important to examine in more detail some of the variables which influence the HRR.

Predicting Full-Scale HRR from Bench-Scale Data: The Role of Irradiance

Engineering variables such as HRR, ignitability, flame spread, etc. are sometimes viewed as material fire properties. This is a useful view, but it must be kept in mind that such 'properties' are not solely properties defined by the physical/chemical nature of the substance. Instead, they are also determined by the boundary conditions of exposure. The boundary conditions can be divided into two types: (1) intended, and (2) unintended. The intended boundary conditions include irradiance (since the heat fluxes in room fires are dominated by the radiant component, the terms irradiance and imposed heat flux are used interchangeably) and thickness. Unintended boundary conditions, sometimes known as *apparatus-dependencies*, include such factors as edge effects, perturbations due to non-uniform heating, drafts and uncontrolled air velocities, etc. The latter are usually small if a well-designed test apparatus was used for measuring the response of the specimen.

The most significant intended boundary condition is the heat flux imposed on the specimen. This variable is crucial and no reduced-scale HRR results have meaning without knowing the irradiance. A test apparatus can impose a very wide range of specimen irradiances. For example, the Cone Calorimeter is capable of irradiances from zero to 100 kW m^{-2}. For the user of the data, the crucial question becomes what irradiance to select when requesting a test. There are no simple answers to this, but we summarize here the main conclusions of an extensive study [42].

The major consideration in the selection of the test irradiance must come from a knowledge of heat fluxes associated with real fires. In theory, this could range from zero to an upper value which would be $\varepsilon\sigma\left(T_f^4 - T_o^4\right)$, where ε = emissivity (–), σ = Stefan-Boltzmann constant (5.67 10^{-11} kW m^{-2} K^{-4}), T_f = flame temperature (K), and T_o = ambient temperature (K). But the

$\varepsilon \approx 1$ for larger flames, and the ambient temperature contribution is insignificant, since $T_o << T_f$.

The adiabatic flame temperature for most organic fuels [43] is approximately 2300 K. This would give a maximum irradiance limit of some 1500 kW m^{-2}. This limiting value is, of course, nearly 10 times the actual maximum that is found in building fires of normal types. Thus, it is evident that the theoretical bounds to possible heat fluxes do not offer any guidance for testing. Instead, it is necessary to look at experimental data on heat fluxes found in actual building fires. We divide this into several types of building fires to be examined. More detailed data on heat fluxes from various objects and ignition sources is contained in the *Ignition Handbook* [44].

(a) **Heat fluxes in the vicinity of ignition sources**

First, we must be clear by what is meant by 'ignition source.' The innate definition of the term does not have limits—a burning building can be the ignition source to its neighboring building, as can a fire bomb. For discussion here, however, ignition sources can be limited to those that are small with respect to a fully-developed room fire. Since the latter will be in the range of over 1 MW, the range of fires considered to be ignition sources might be taken as $<$ ca. 300 kW.

A NIST study examined various ignition sources, ranging from 5 W to over 300 kW [45]. The sources included both realistic igniting objects (cigarettes, matches, burning paper lunch bags, etc.) and schematic ones (small gas burners and wood cribs). It was found that, as the power output of the ignition source increased, the peak heat flux generally did not increase. Instead, only the area covered by the peak heat flux progressively increased. For flames ranging from a 0.3 kW Bunsen-type burner to a 50 kW wastebasket, the peak fluxes were remarkably constant at 30–40 kW m^{-2}. Thus, for HRR from objects being ignited with a small ignition source, a test irradiance of 35 kW m^{-2} can be selected. There are some unusual sources having a much higher flux, and these are discussed elsewhere [42].

For larger burners, such as used in room fire tests, higher heat fluxes may have to be assumed. For porous square-faced gas burners, the wall heat flux was found to depend on the burner face size [46]. In some cases, fluxes up to 65–80 kW m^{-2} were noted, although for most cases fluxes of 30–50 kW m^{-2} are considered appropriate [47].

At the extreme, ignition can occur due to a high velocity jet, such as from a failure on an oil-drilling rig. There, heat fluxes in the vicinity of 150–300 kW m^{-2} have been observed [48]. Such situations, however, are very specialized. For ignitions from small wood cribs or other solid-fuel ignition sources, it can be estimated that the heat flux to adjacent objects in the same 35 kW m^{-2} range as for small flaming sources. The picture is more complicated, however, for the heat flux from these sources to the object underneath. These heat fluxes may be much higher [42], but they are highly non-uniform and difficult to model.

(b) **Heat fluxes in preflashover room fires**

After ignition, the combustibles in a room can be considered to be exposed to preflashover conditions. Heat fluxes occurring in preflashover room fires will vary widely. Away from the initial source of fire there will be essentially no heating at all. Near a small initial fire source, heat fluxes of the sort described in the preceding section will be seen. With increasing fire spread and involvement, a hot gas layer will build up below the ceiling. The heat fluxes will be significantly hotter within this layer than in lower spaces. Söderbom [49] found values typically $<$ 45 kW m^{-2} at the center of the ceiling during preflashover fires. The value at the floor level is, of course, always $<$ 20 kW m^{-2} prior to flashover, since attaining 20 kW m^{-2} at floor level is one definition of flashover [50]. Since there is surprisingly little general guidance on this point, the user will have to make some assumptions or *ad hoc* calculations.

(c) **Heat fluxes on burning walls**

Heat fluxes from burning items of larger types have, in general, not been studied in enough detail to be systematically known. The notable exception is for upward flame spread on vertical

surfaces. For this configuration, a number of studies have explored the heat fluxes from the flame to the yet-unignited portion of the surface.

Hasemi studied this problem in detail [51] and provided correlations. For his experiments, peak values of ca. 25 kW m^{-2} were seen for the region downstream of the ignited area, but before the tip of the flames; beyond the flame tip, fluxes were no longer constant, but dropped off further downstream. Additional similar data have also been presented in a summary form [52]. Work by Kulkarni and co-workers has enlarged the diversity of material types to have been studied [53]. The value of 25 kW m^{-2} is seen from these more extensive studies to be the lower bound of where data are clustered—most of the data are in the interval from 25 to 45 kW m^{-2}. Thus, a value of 35 kW m^{-2} might better capture the mean behavior.

A 35 kW m^{-2} heat flux, then, can be used to characterize the peak level of heating to a vertical surface element from its own upstream flame, just prior to its ignition. This value will need to be increased if the material is so situated as to be in a hot gas layer that is accumulating in the upper reaches of the room. Apart from the data of Söderbom, discussed above, this additional heating has not been studied in detail.

(d) **Heat fluxes in post-flashover room fires**

The maximum temperatures actually seen in post-flashover room fires are ca. 1100 °C. A perfect black-body radiator at that temperature would produce heat fluxes of approximately 200 kW m^{-2}. Actual heat fluxes measured in post-flashover room fires can come close to this value, but are usually somewhat lower. For instance, examining the extensive room burn data of Fang [54], one finds the following ranges of experimental results shown in Table 26.1.

Table 26.1 Heat fluxes measured in postflashover room fires

	Heat flux (kW m^{-2})		
	Ceiling	Walls	Floor
Maximum	106–176	116–229	119–143
Average	68–147	91–194	–

One might reasonably conclude that a heat flux of ca. 150 kW m^{-2} would be needed to properly represent the environment of the post-flashover room fire. Today's bench-scale HRR apparatuses, however, can only go to about 100 kW m^{-2} or less. Interestingly, the inability to realistically create the heat fluxes of the post-flashover fire has not been seen to be a problem in fire testing. Often, the situation is avoided in its entirety by assuming that the maximum burning rate that will occur within the room is consistent with the available oxygen supply [55]. Nonetheless, if for more detailed fire modeling the HRR of individual items in the post-flashover fire would be required, such high heat flux values would be required.

The Dependence of the HRR on the Heat Flux

In the simplest case, the relationship of the HRR to the irradiance is very simple, as shown in Fig. 26.7. Here, we see that the HRR depends in a linear manner on the irradiance. The curve does not pass through the origin due to the existence of flame flux. The total heat flux seen by the specimen can be viewed as comprised of two components: the external irradiance, and the flux from its own flame. Only if the flame flux were zero would the curve pass through the origin. Otherwise, the x-axis intercept is equal to (minus) the flame flux.

Flame flux is very difficult to measure experimentally, as decomposing materials tend to foul the instrumentation and invalidate the readings. A value of ca. 35 kW m^{-2} has been reported for the flame flux of PMMA burned in the horizontal orientation in the Cone Calorimeter [56]. In another study, estimates of flame flux were made for several plastics burned in a similar manner [57]. These showed 30, 25, and 14 kW m^{-2}, respectively, for nylon, polyethylene, and polypropylene. The furniture research program CBUF [10] determined that the flame fluxes in the Cone Calorimeter associated with fabric/foam composites are in the range 20–25 kW m^{-2}. Finally, some data are

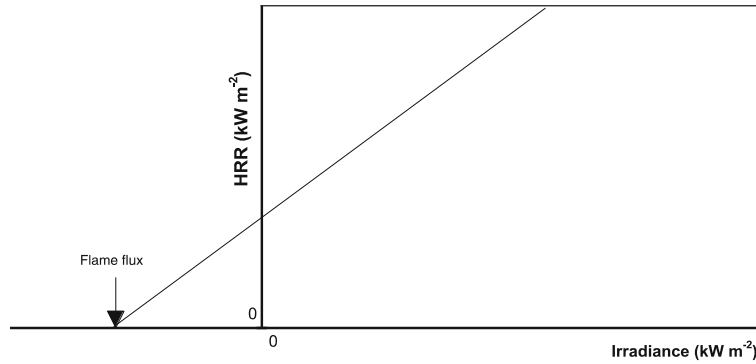

Fig. 26.7 The simplest form of HRR dependence on irradiance

available [58] for liquids in containers of similar size as a Cone Calorimeter specimen holder. Flame fluxes of about 10–15 kW m^{-2} are seen for alcohols and about 15–20 kW m^{-2} for some hydrocarbons (heptane, methylmethacrylate, toluene, styrene).

The value appears to depend only slightly on the chemical nature of the fuel. Gore et al. [58] specifically determined that this value does not increase with increasing fuel sooting tendencies. All of the above data refer specifically to the horizontal specimen orientation. There is very little data for the vertical orientation, although Janssens deduces that for wood products the vertical-orientation flame flux is ca. 10–15 kW m^{-2}, of which only about 1 kW m^{-2} is due to radiation [59].

With regards to linearity, the following very broad generalization can be made: for many products, over a substantial heat flux range, the HRR is linearly proportional to the heat flux. This generalization, however, will be seen to have only limited utility, since it is rarely known *a priori* whether or not it will be obeyed. Furthermore, there is a distinct tendency for most materials and products to deviate from linearity at very high and at very low heat fluxes.

This behavior is best illustrated by an example. Some data obtained by Sorathia and co-workers [60] on advanced composites are shown in Fig. 26.8. It is clear that the results are somewhat linear, but not precisely so. Some old, but still suggestive data were obtained in the 1970s by Parker [61]. His results for a number of fire-retardant grades of polyurethane foam are shown in Fig. 26.9. Of the five formulations shown, three show somewhat linear behavior, whereas two clearly do not. For most categories of specimens, however, substantially linear behavior can be seen.

Predicting Full-Scale HRR from Bench-Scale Data: The Effect of Thickness

The same material may be used in different applications in varying thicknesses. Thickness does affect the HRR response. In general, a thin material will show a spike of HRR, whereas a thick product will commonly (but not always) show some quasi-steady period of burning. This variable has not been extensively explored, and there is not much guidance available. Figure 26.10 shows results from Paul [62] on a thermoplastic, PMMA. This illustrates that near-steady burning behavior can be seen when the thickness approaches ca. 20 mm. Some similar data on polyethylene [63] have been published, but the maximum thickness specimens examined in that study, 10 mm thick, did not reach steady burning.

Data for medium-density wood fiberboard obtained by Tsantaridis [64] are shown in Fig. 26.11. If tested over the standard substrate (lightweight mineral fiber blanket), wood-family materials show a second HRR peak which corresponds to the accelerated burning when the specimen becomes nearly burned through.

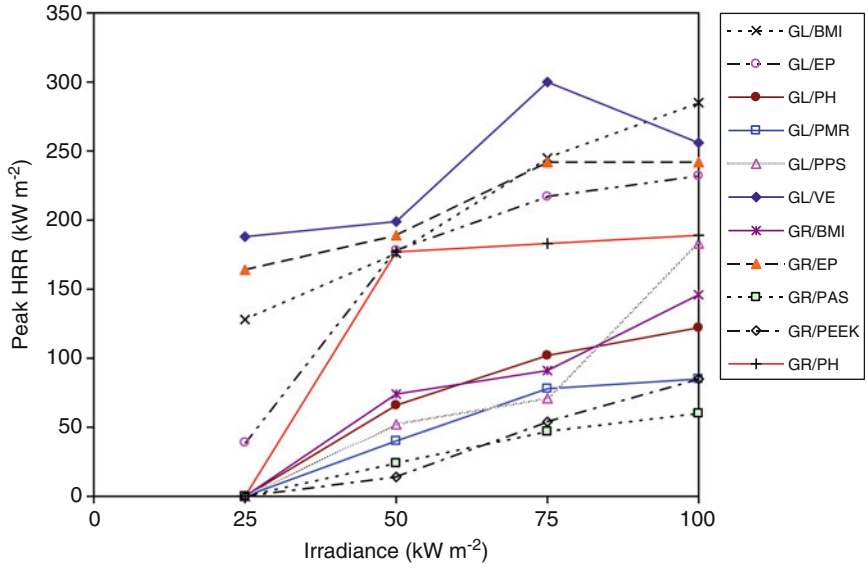

Fig. 26.8 Response to irradiance of some advanced composite materials. Reinforcements: *GL* glass, *GR* graphite. Resins: *BMI* bismaleimide, *EP* epoxy, *PAS* polyaryl sulfone, *PEEK* poly(ether ether ketone), *PH* phenolic, *PMR* monomer-reactant polyimide, *PPS* polyphenylene sulfide, *VE* vinyl ester

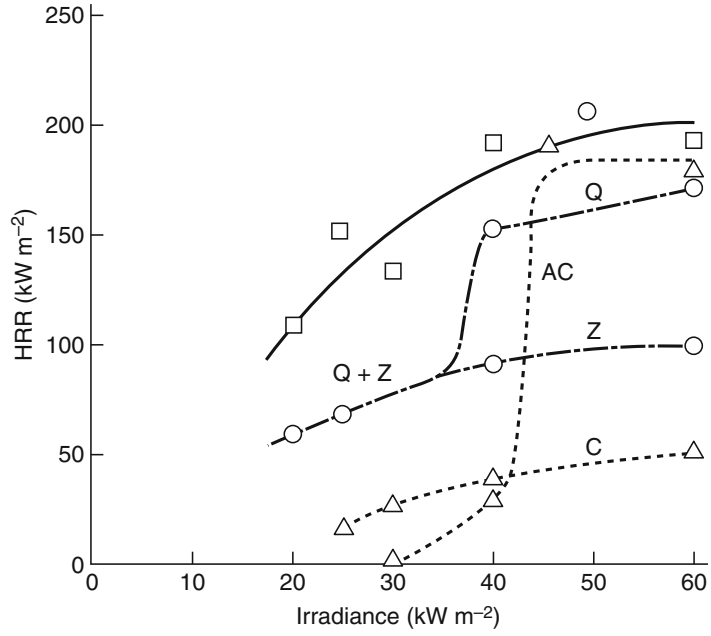

Fig. 26.9 HRR of FR polyurethane foams, as measured in the NBS I calorimeter by Parker

For foams, by contrast, no reasonable amount of thickness will normally show steady-state burning. Of special interest are polystyrene foams. These are normally very low density foams of around 16 kg m^{-3}. When exposed to heat, PS foams tend to collapse their cell structure and become a thin liquid film. This occurs before ignition takes place. Thus, after ignition what is burning is a thin coating on whatever was the substrate. This is the reason why the HRR of PS foams tends to be so apparatus-dependent that it is hard to discern

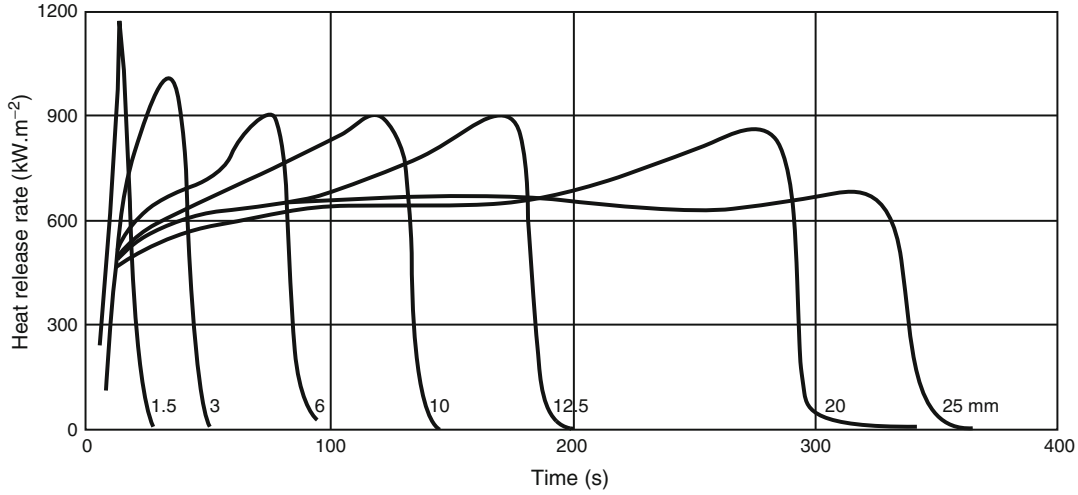

Fig. 26.10 Effect of thickness on the HRR for PMMA (heat flux = 35 kW m^{-2})

Fig. 26.11 Effect of thickness on the HRR for medium-density fiberboard (heat flux = 50 kW m^{-2})

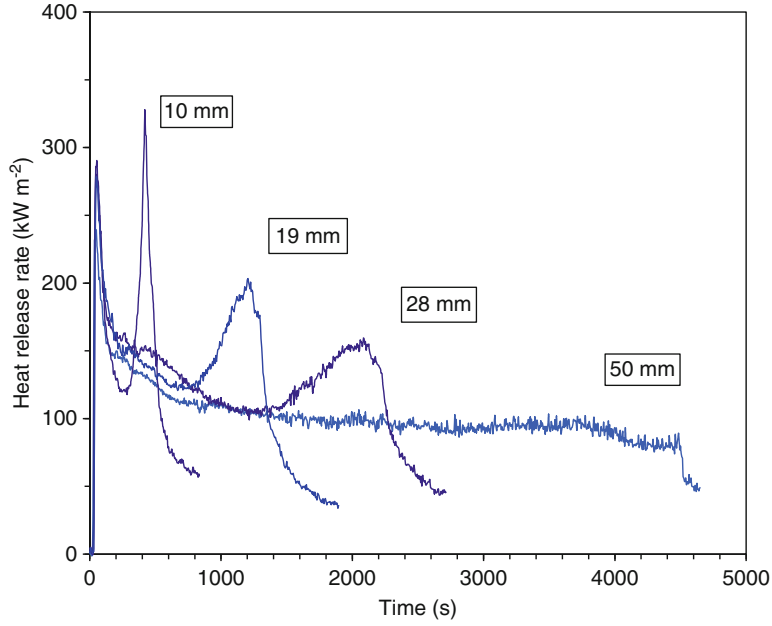

any 'intrinsic' response of the material at all: its performance is totally dominated by the specimen-holder and edge conditions [65].

Predicting Full-Scale HRR from Bench-Scale Data: The Effect of Orientation

Routine testing in the Cone Calorimeter is specified by the ASTM standard to be done only in the horizontal orientation. This is because (1) many products show serious testing difficulties (e.g., melting) when tested in the vertical orientation. (2) Conversely, the vertical orientation does not provide 'a better simulation' of the burning of vertical objects. This is because there is no direct connection between flame fluxes in a bench-scale test and in a real-scale fire. The actual fluxes occurring in a real-scale fire are determined by many factors, including

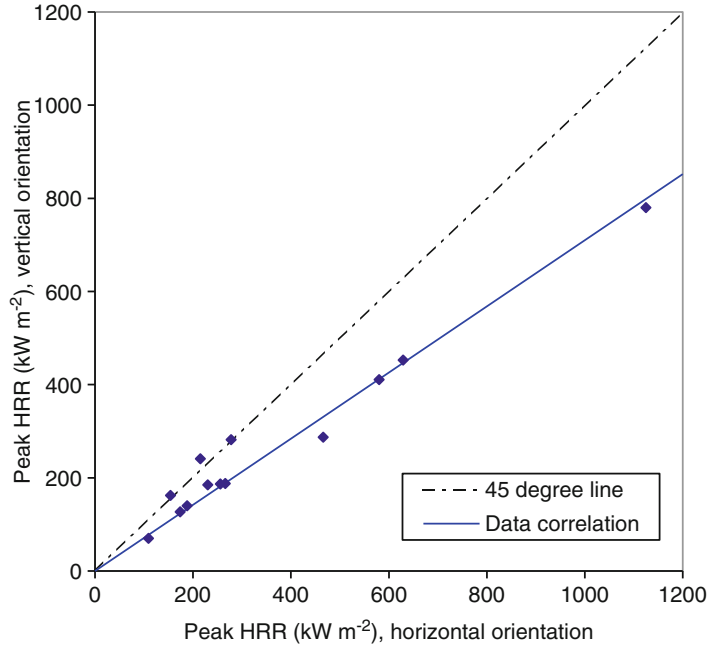

Fig. 26.12 Orientation effect on the peak HRR, as determined from two Cone Calorimeter round robins

size of room, thickness of hot gas layer, flame spread occurring over other surfaces, etc. None of these are subject to the control of the bench-scale apparatus but, rather, must be specifically modeled.

Orientation effects will also make a difference during the bench-scale testing of specimens. Even though routine testing is done only in the horizontal orientation, a small body of work exists where both orientations were explored. This is best illustrated by the results of two round robins which were conducted on the Cone Calorimeter, one under the auspices of ASTM and one under ISO. The data were taken at two irradiances, 25 and 50 kW m^{-2}, and the results are briefly summarized in the Appendix to ASTM E 1354 [20]. Such results are especially valuable since the values tabulated are the 'best estimate' values and are not subject to the specific errors of any one particular laboratory. A comparison for the peak HRR is shown in Fig. 26.12, while the comparison for the 180 s average value of HRR is given in Fig. 26.13. In both cases, the data points plotted represent all of the data analyzed within the two round robins for which horizontal and vertical orientation results were obtained on a product.

For the peak HRR, a least-square regression gives that:

$$\dot{q}''_{pk}\ (V) = 0.71\ \dot{q}''_{pk}\ (H) \qquad (26.4)$$

While for the 180 s average HRR, the corresponding relation is:

$$\dot{q}''_{180}\ (V) = 0.72\ \dot{q}''_{180}\ (H) \qquad (26.5)$$

Both can be adequately approximated by the general relation that:

$$\dot{q}''\ (V) = 0.7\ \dot{q}''\ (H) \qquad (26.6)$$

This clearly verifies that the thin, boundary-layer type flames occurring in the vertical orientation provide a lower heat flux than the pool-like flames in the vertical orientation.

Predicting Full-Scale HRR from Bench-Scale Data: Other Controlling Variables

Numerous other variables can, in principle, affect the HRR of specimens. This can include local velocities, scale and intensity of turbulence, etc. For room fire modeling purposes, such effects

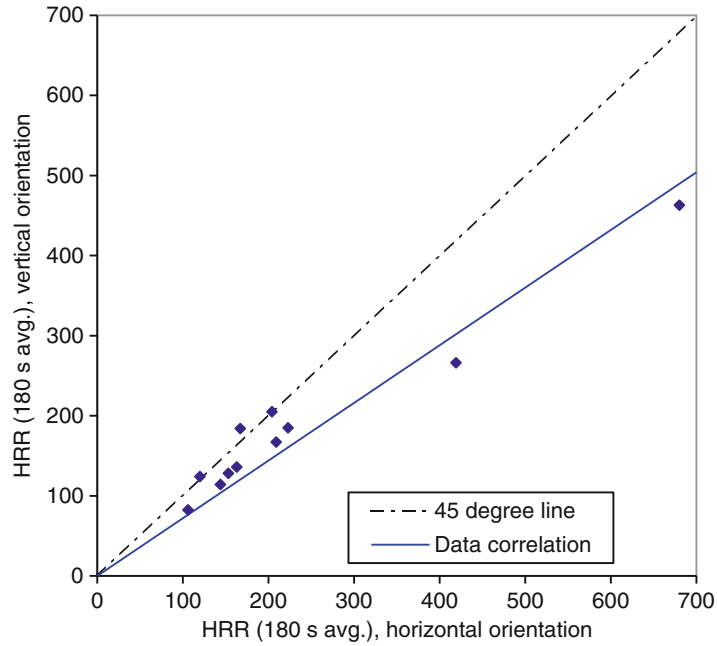

Fig. 26.13 Orientation effect on the 180-s-average HRR, as determined from two Cone Calorimeter round robins

can be assumed to be small. Two effects which are often of specific interest, however, are scale and vitiation effects. Scale effects are, in principle, normalized out when the per-unit area variable is computed. These effects will not be zero, however.

One factor affecting them is the flame flux found in the bench-scale test apparatus. This will have some scale effect. The studies in this area are not extensive. A study using a custom Cone Calorimeter with 200 mm × 200 mm specimen size tested horizontally found only a very small scale effect, when compared to standard Cone data [66]. A comparison between the ICAL and the Cone Calorimeter for a series of wood products showed that systematic differences were surprisingly small, despite the 10× difference in linear dimension of the specimens [67]. Note, however, that in this case the specimens were tested in the vertical orientation. In such orientation, the specimen flames are thin and there is little variations with scale. Of additional guidance is a study by Orloff [68] where a vertical 3.56 m high PMMA slab was burned. The mass loss rate, per unit area was found to be:

$$\dot{m}'' = 5.32 + 3.97x \qquad (26.7)$$

where x is the vertical distance (m). Note that this result implies that there is but little variation for specimens with height < 0.5 m, but significant increases for very large specimens.

In the case of objects burning in the horizontal orientation, large 'pool' flames surmount the specimen. The flux from such flames will vary greatly with scale. Guidance provided for estimating burning rates of pools (addressed later in this chapter) can be directly applied to this case.

HRR for Real Products

For many objects and commodities, published HRR are not available, thus, laboratory tests will have to be run if an answer is needed. For some commodities, however, exemplar data have been published and are available to the public. The tabulated test data can be very useful as generic representatives of items constructed of these materials, and with this general geometry.

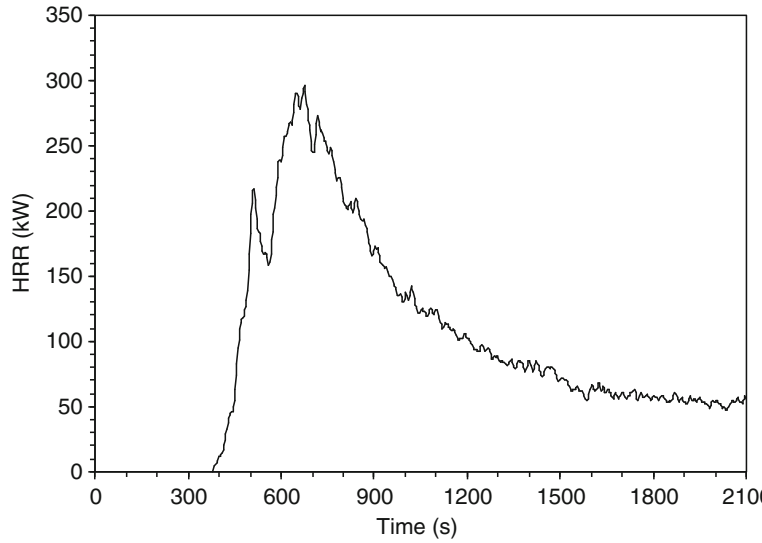

Fig. 26.14 HRR of a small air conditioner with a plastic housing

Where the analysis is intended to evaluate a specific product, that product should be tested in a suitable calorimeter and the data then used in the analysis. It must be strongly emphasized that in no case should generic database information be used when the purpose of the analysis is to seek regulatory approval for a product or to demonstrate the performance of a specific product in a court of law. In all such cases, actual laboratory testing on the item in question must be done.

In the case of a few product categories, methods are available for estimating large-scale HRR on the basis of bench-scale HRR data. The question then becomes: where can bench-scale HRR data be found? For a few product categories, some data are provided in the sections below. For the user interested in a more comprehensive look at bench-scale HRR data, the textbook *Heat Release in Fires* [23] and the Cone Calorimeter Bibliography [69] are good sources. Also, Chap. 36, "Combustion Characteristics of Materials and Generation of Fire Products," provides some data on pure chemicals.

For convenience, the sections below are arranged alphabetically by type of product. However, many of the ideas are an offshoot of pioneering studies on pool fires. Thus, it is recommended that the user first read through the section on "pools" before progressing to other product categories.

Air Conditioners

Beard and Goebeldecker [70] tested a small European in-room air conditioner 466 × 406 × 855 mm high. The unit had an ABS plastic housing, polystyrene foam inside, and a mass of 35 kg, of which 26 kg remained post-test; the total HR was 212 MJ (Fig. 26.14).

Audio Equipment

EFRA [70] tested two bookshelf-size micro-stereo systems, each comprising a receiver and a pair of stereo speakers. The receiver enclosures were made HIPS plastic, but one system had fiberboard speaker cabinets (P), while the other had HIPS cabinets (G). The systems were both very small, with the mass before test being only 4.1 kg (specimen G) and 4.9 kg (specimen P). Figure 26.15 shows the HRR results for the two tests.

Bedding

Ohlemiller et al. [71] tested inert beds (twin-size) with 12 different bedding combinations, with the peak HRR values found ranging from 38 to 200 kW. Detailed HRR curves are shown in Fig. 26.16 for one bedding combination. This

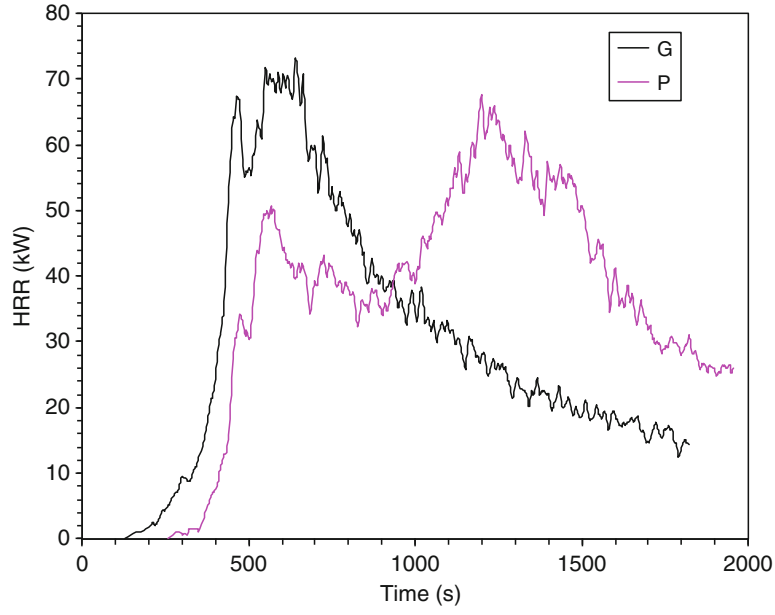

Fig. 26.15 HRR values for two small stereo systems

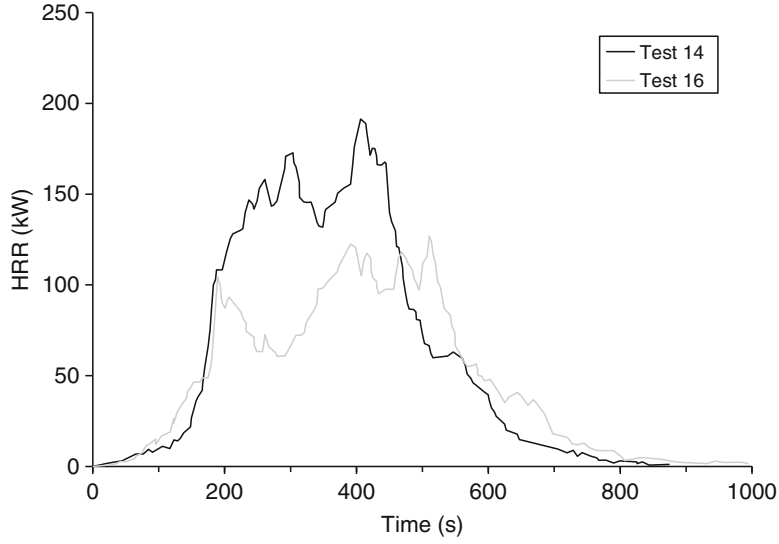

Fig. 26.16 HRR results for two replicate tests for a bedding set on an inert, twin-size bed

combination involved 2 polyester/cotton sheets, a mattress pad, a pillow, an acrylic blanket, and a medium-weight comforter. The HRR (average for the replicates) was exceeded by only one other combination, which gave values about 5–10 kW higher. The latter comprised two polyester/cotton sheets, a mattress pad, a pillow, a polyester blanket and a medium-weight comforter. The pillows were filled with polyester fiber filling in for both combinations and were covered with a polyester/cotton pillow case. Detailed HRR curves were not published for other combinations. The lowest peak HRR values were for a combination with two sheets and a pillow only, which showed 38 and 73 kW for the two replicates.

NRCC [72] conducted four tests on bedding and got peak HRR results up to 388 kW.

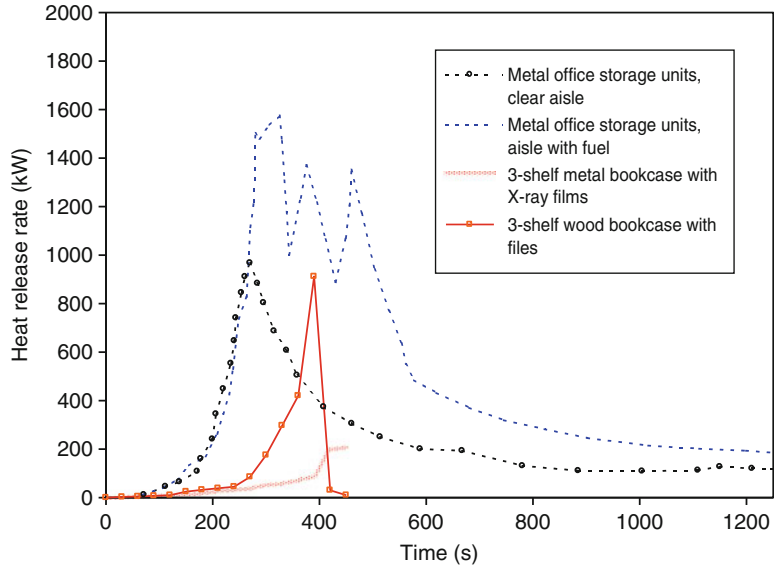

Fig. 26.17 HRR of storage units

Bookcases, Casegoods and Storage Units

In most cases, for storage furniture the fire hazard is created by the contents, not by the furniture item itself. An exception is modular storage units made of thermoplastic materials, which tend to burn very vigorously [73], but quantitative HRR data have not been published. Storage furniture made of wood or wood covered with thin layers of thermosetting plastic tend to resist ignition unless filled with combustible contents. Some data are illustrated in Fig. 26.17. The metal office storage units tests [147] arrangement involved two tiers of shelving with an 0.76 m aisle in between. Each test contained 480 kg of paper fuel load in shelving units totaling 1.67 m^2 of floor area. For the configuration with fuel in the aisle, only 3 kg was placed in the aisle, but this extra fuel provided a major difference in fire severity. The data on X-ray film shelves and wooden bookcase are from Ref. 170. For storage of paper files, it is known that the arrangement is more important than the quantity of fuel. Especially, storing files in cardboard boxes so that they can exfoliate exacerbates burning. Exfoliation occurs when paper folders are placed parallel, rather than perpendicular to the front of the shelf. When fire attacks the front, folders progressively fall out and burn in the aisle. While well-known, this effect has not been documented with HRR testing.

Boxes and Packaging

Full-scale tests were run at Western Fire Center [74] to measure the HRR of fruit/berry baskets (i.e., small plastic containers), packaged in cardboard shipping cartons, and assembled into pallet loads. In each case, no fruit goods were actually included, the boxing material being packaged as would be delivered from the manufacturer. For all tests, only a single pallet was used. Identification of materials is given in Table 26.2, while HRR results are given in Fig. 26.18. Southwest Research Institute [75] tested pallets similar to Sample A, but assembled as a 2 × 2 × 2 array of pallets. This test gave a peak HRR of 8695 kW and the results are shown in Fig. 26.19.

Carpets and Other Floor Coverings

Carpets which are in the room of fire origin are not likely to contribute significantly to fire

Table 26.2 Packaged fruit cartons tested in shipping pallets

Sample	Overall dimensions of pallet load (m)	Mass before test (kg)	Mass after test (kg)	Peak HRR (kW)	Eff. heat of comb. (MJ/kg)
A	0.75 × 1.14 × 1.83	393	307	4923	17.3
B	1.02 × 1.26 × 1.83	308	222	3553	14.0
C	0.99 × 1.19 × 1.87	421	393	3044	12.1
D	1.33 × 0.80 × 1.17	430	344	896	11.9
E	1.18 × 1.07 × 2.29	461	319	3894	11.0
F	1.00 × 1.22 × 2.00	254	192	4280	13.9

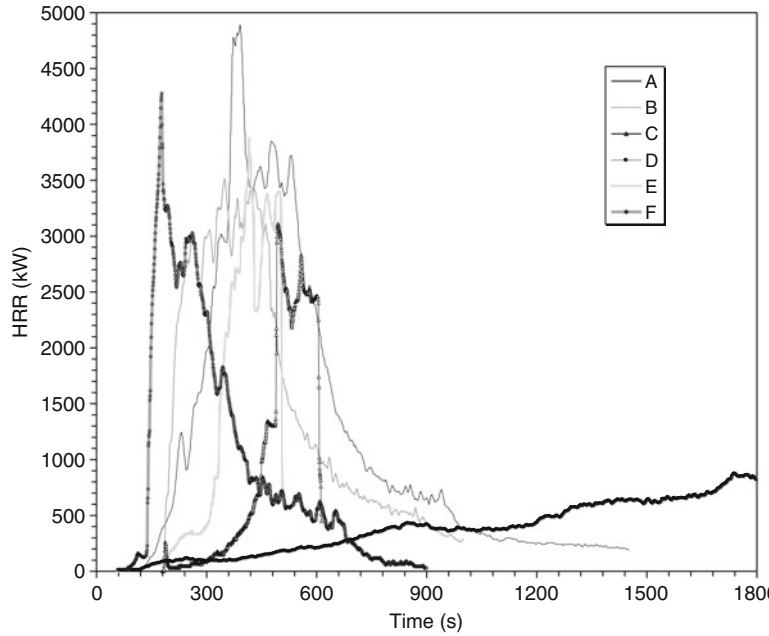

Fig. 26.18 HRR of single pallet-loads of packaged fruit/berry baskets

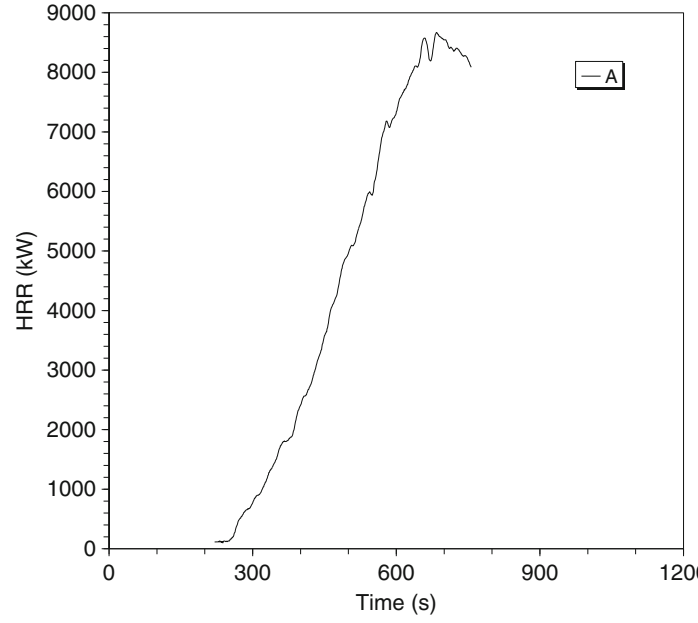

Fig. 26.19 HRR of a 2 × 2 × 2 pallet array of packaged fruit/berry baskets

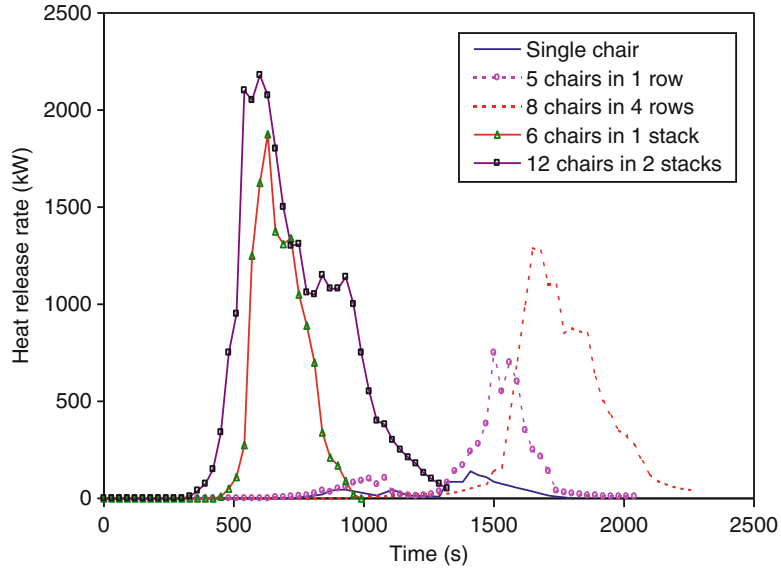

Fig. 26.20 HRR of stackable chairs, polypropylene with steel frame, no padding

growth. This has been demonstrated experimentally [76]. It is also consistent with modeling considerations: the floor area is convectively cooled and has normally the smallest view factor to the hot regions, which tend to be in the upper regions. The same material may be much more hazardous if installed on wall surfaces, although it must be pointed out that commercial textile wall coverings are normally similar, but not identical to carpeting.

The hazard from floor coverings arises when an unsuitable product is used in a corridor, especially if this is an escape path. In such situation, very rapid flame spread and high HRR can result due to the fact that the corridor floor covering becomes involved due to a room fire feeding it. Not only carpeting, but solid materials such as linoleum and wood parquet flooring are also subject to becoming fully involved down the length of a corridor. A recent study has quantified this behavior and has also provided a predictive method [77]. It is shown that floor coverings with a peak HRR of less than 200 kW m^{-2}, measured in the Cone Calorimeter under an irradiance of 25 kW m^{-2} tend not to show accelerating flame spread down a corridor.

Some carpeting materials can present a rapid fire spread hazard when installed on stairs. A residential carpet installed over a stairway has been measured to produce a peak HRR of 3 MW [78]. The test carpet was 80 % acrylic/20 % nylon; no other types of carpeting were explored.

Chairs, Stackable

Stackable chairs are most commonly used in hotels and banqueting facilities. These chairs typically have metal legs and frame and only a small amount of combustible padding or structural material. Thus, a single chair can be expected to represent negligible hazard. However, when not in active use, they are stored in tall piles and many of these piles may be aggregated together. The hazard of even a single pile of modest height can be notable. Figure 26.20 illustrates some typical data on non-upholstered, molded chairs [169]. Figure 26.21 illustrates some data on lightly-upholstered chairs [79]. For the latter, the effect of radiant augmentation from burning in a corner is also illustrated.

Clothing Items

Two men's jackets (anoraks) were tested by SP [10] as potential ignition sources. One was a

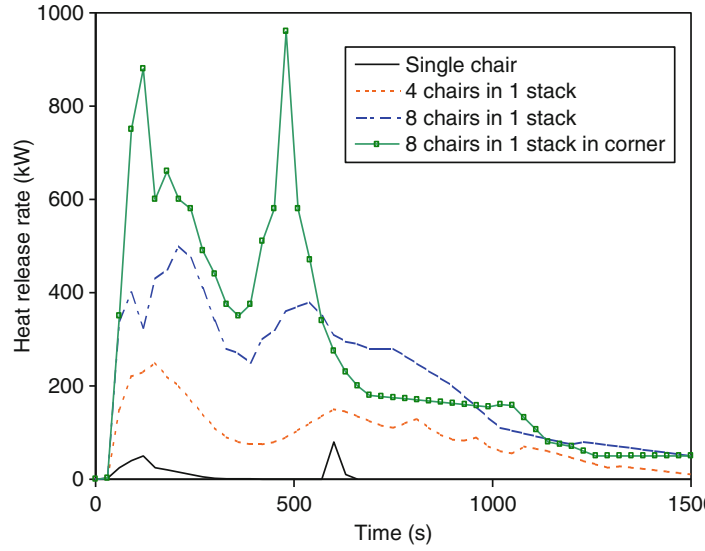

Fig. 26.21 HRR of metal-frame, upholstered stacking chairs

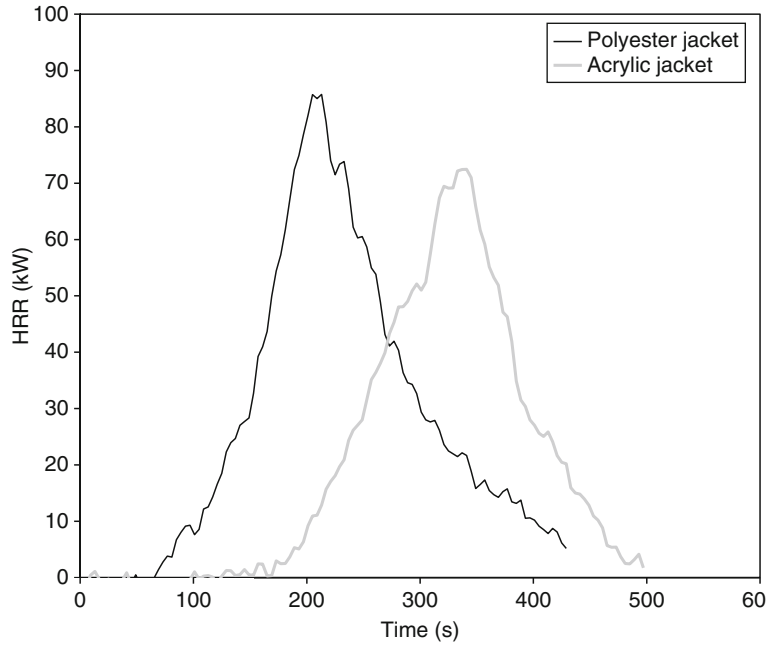

Fig. 26.22 HRR of men's jackets (laid loose)

'polyester' jacket with an outer fabric comprising 65/35 cotton/polyester, an inner fabric of 100 % polyamide, and a filling of 100 % polyester wadding. The total weight was 739 g. The second jacket tested was an 'acrylic' jacket with a fabric of nylon/Taslan and a filling of 100 % acrylic wadding. The total weight was 618 g. The HRR of these jackets are shown in Fig. 26.22. Stroup et al. [80] measured the HRR of racks of men's suits, such as might be found in a retail shop. Each rack held 48 suits, made of polyester and wool and arranged in two rows vertically. The

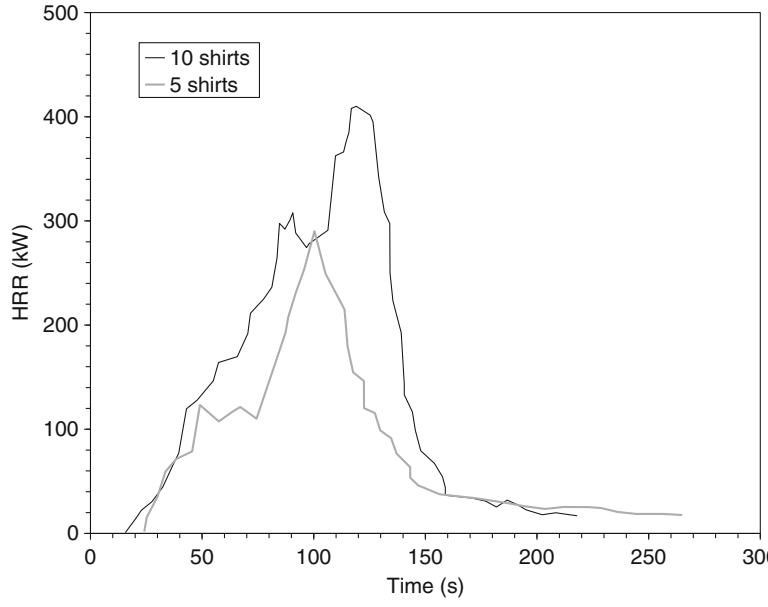

Fig. 26.23 HRR of hanging, cotton shirts

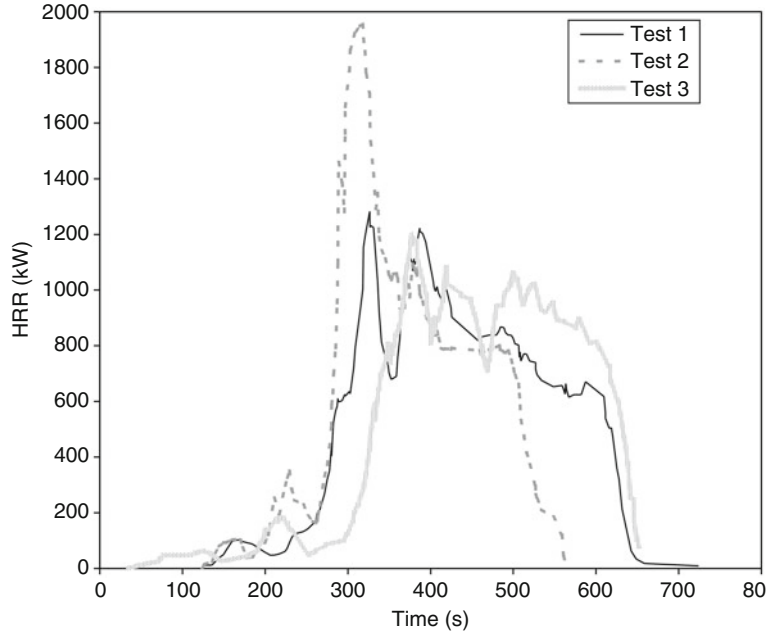

Fig. 26.24 HRR of racks of men's suits; the rack was 1.8 m long (arranged as two rows side-by-side)

results of three replicate tests are shown in Fig. 26.24. There is a lot of scatter, since the suits fall as they are burning. Japanese results [81] were reported for cotton shirts, hanging on a rack. These results are given in Fig. 26.23. The authors also tested a single hanging cotton shirt, which gave a peak HRR of 70 kW, and a pile of 10 folded shirts, which only showed a peak of 35 kW. Additional data are given under "Shop displays" later in this chapter.

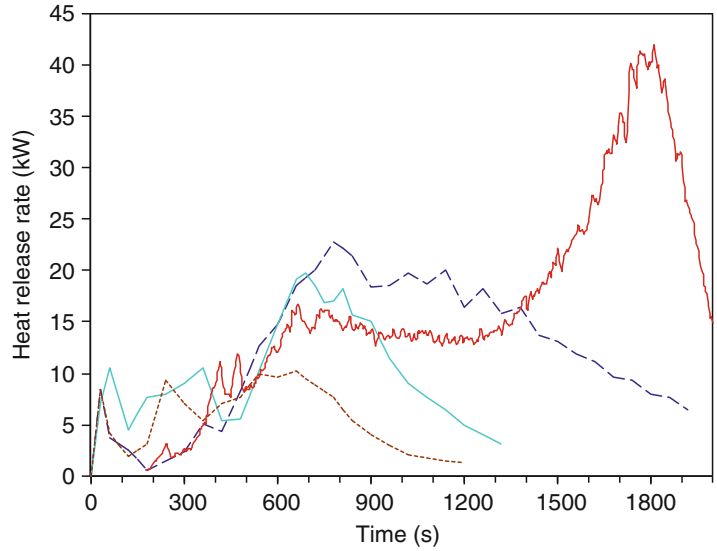

Fig. 26.25 HRR of coffee makers

Coffee Makers

The HRR of several coffee makers weighing 0.8–1.4 kg is shown in Fig. 26.25 [70, 169]. The material for the unit showing the highest HRR was identified as polypropylene [70], the others were not specified.

Computers and Electronic Equipment

Here are given results on HRR testing of computers and electronic equipment, set up as intended to be used. Additional results are given under *Industrial commodities* for packaged goods.

Computer CPUs. Two computer CPUs were tested by SP [82]. One was made by IBM, using a plastic facing rated V0 according to UL 94 [30]. This could not be ignited from a small ignition source. The second unit, of HP manufacture, could be ignited by a small ignition source and its HRR is shown in Fig. 26.26.

Computer keyboards. Bundy and Ohlemiller [83] tested at NIST three polystyrene computer keyboards weighing 580 g. These were ignited with a needle flame and the results are shown in Fig. 26.27.

Computer mice. Edenburn [84] tested two brands of computer mice. Both were ignitable by a needle flame and one brand showed a peak HRR of 3.6 kW and a total heat release of 1.20 MJ. The second brand was tested in the Cone Calorimeter with an applied external heat flux. Using a 25 kW m^{-2} flux, a peak HRR of 5.0 kW was found and a heat release of 1.35 MJ; at a 50 kW m^{-2} heat flux, a peak HRR of 6.1 kW and a heat release of 1.45 MJ were found.

Computer monitors. Bundy and Ohlemiller [83] tested at NIST a series of 480 mm (19 in.) computer monitors of the CRT type. Three ignition sources of progressively greater intensity were used: a needle flame, a burning polystyrene keyboard, and a radiant panel providing a heat flux of 21 kW m^{-2} onto the specimen (Table 26.3). Selected results are shown in Figs. 26.28, 26.29, 26.30, 26.31, and 26.32.

Computer printers. Three computer printers were tested by SP [85]. All were of the personal type, manufactured by Epson, HP, and Lexmark; the results are given in Fig. 26.33. The printers were tested without paper or toner.

Computer tapes. A test was conducted on a set of open steel shelves holding 90 computer

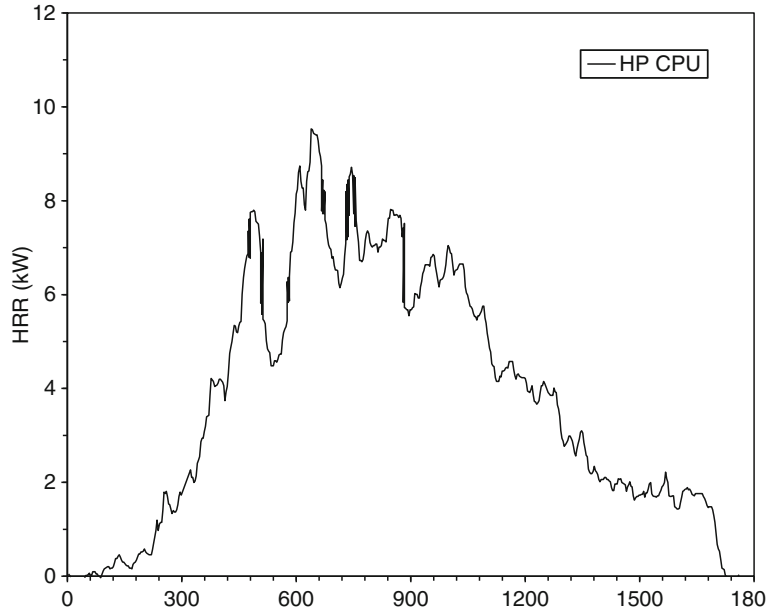

Fig. 26.26 HRR of computer CPU tested by SP

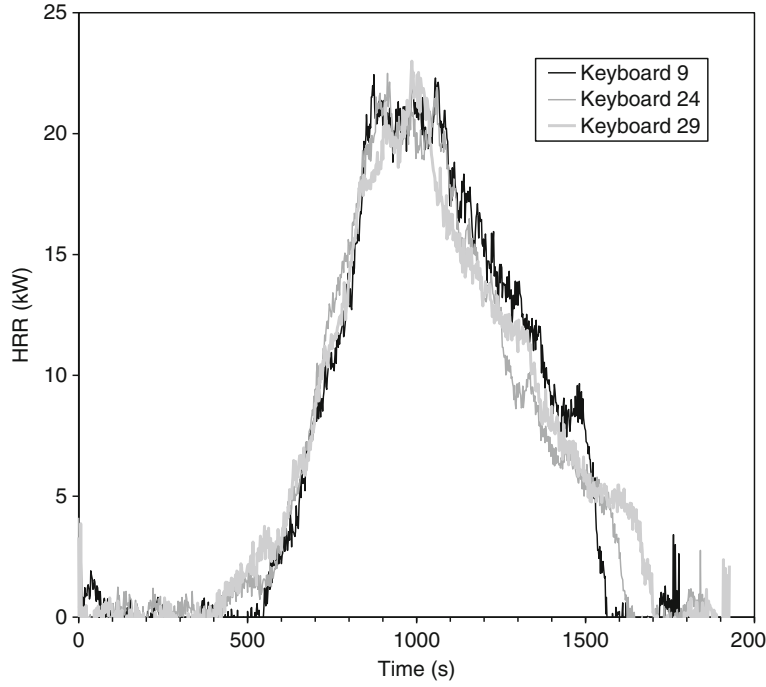

Fig. 26.27 HRR of polystyrene computer keyboards tested at NIST

tapes [86]. The tapes were 300 mm diameter and the total mass of 99 kg was distributed on four shelves, two tiers deep. The results are given in Fig. 26.34.

Racks with computer equipment. Zicherman and Stevanovic [87] tested stainless steel mesh-type racks containing computer and electronic equipment. The rack size was

Table 26.3 Computer monitors tested at NIST

Specimen ID	Material	UL 94 rating	Test #	Ignition source	CRT	Peak HRR (kW)	Total mass loss (g)
7	ABS	V0	6	Needle flame	No	DNI	
7	ABS	V0	11	Needle flame	No	DNI	
7	ABS	V0	6a	Keyboard	No	43.6	797
7	ABS	V0	11a	Keyboard	No	31.3	831
7	ABS	V0	27	Keyboard	Yes	34.5	830
7	ABS	V0	13	Radiant panel	No	0.0	24
7	ABS	V0	15	Radiant panel	No	0.0	23
7	ABS	V0	23	Radiant panel	No	25.2	765
1	PC	V0	7	Needle flame	No	DNI	
1	PC	V0	8	Needle flame	No	DNI	
1	PC	V0	7a	Keyboard	No	45.8	768
1	PC	V0	8a	Keyboard	No	120.2	2048
1	PC	V0	28	Keyboard	Yes	54.7	
1	PC	V0	31	Keyboard	No	54.4	1626
1	PC	V0	18	Radiant panel	No	124.0	1504
1	PC	V0	20	Radiant panel	No	117.2	1441
18	HIPS	V1	2	Needle flame	No	DNI	
18	HIPS	V1	10	Needle flame	No	DNI	
18	HIPS	V1	2a	Keyboard	No	114.5	1483
18	HIPS	V1	10a	Keyboard	No	88.8	1607
18	HIPS	V1	25	Keyboard	Yes	72.4	
18	HIPS	V1	16	Radiant panel	No	87.7	1267
18	HIPS	V1	21	Radiant panel	No	94.2	1329
13	PP	V2	5	Needle flame	No	DNI	
13	PP	V2	12	Needle flame	No	DNI	
13	PP	V2	5a	Keyboard	No	205.1	2469
13	PP	V2	12a	Keyboard	No	198.5	2545
13	PP	V2	30	Keyboard	Yes	180.0	3303
13	PP	V2	17	Radiant panel	No	192.6	1776
13	PP	V2	22	Radiant panel	No	166.2	1849
3	HIPS	HB	1	Needle flame	No	207.2	2401.0
3	HIPS	HB	4	Needle flame	No	199.8	2478.0
3	HIPS	HB	26	Needle flame	Yes	143.8	3309.0
3	HIPS	HB	14	Radiant panel	No	239.2	2475
3	HIPS	HB	19	Radiant panel	No	189.8	2413

1.73 m high, 0.92 m wide, and 0.61 m deep, with each rack having six shelves. The top shelf contained a CRT monitor and a personal computer, the next four shelves each contained two small data acquisition units (each fully metal-cased), while the bottom shelf held a dot-matrix printer and a 75 mm high stack of computer paper. A keyboard and a power strip were hung from the top shelf. Three tests were run on replicate units. A barbeque lighter was used to ignite the computer monitor in Test 1, the stack of paper in Test 2, and likewise the paper in Test 3. Test 3 differed from the others in that each of the top five shelves also contained a 0.60 × 0.90 cardboard sheet, which was treated with an antistatic treatment. The sheets were located directly on top of each shelf and underneath the electronic equipment. The HRR results are shown in Fig. 26.35. They have an important

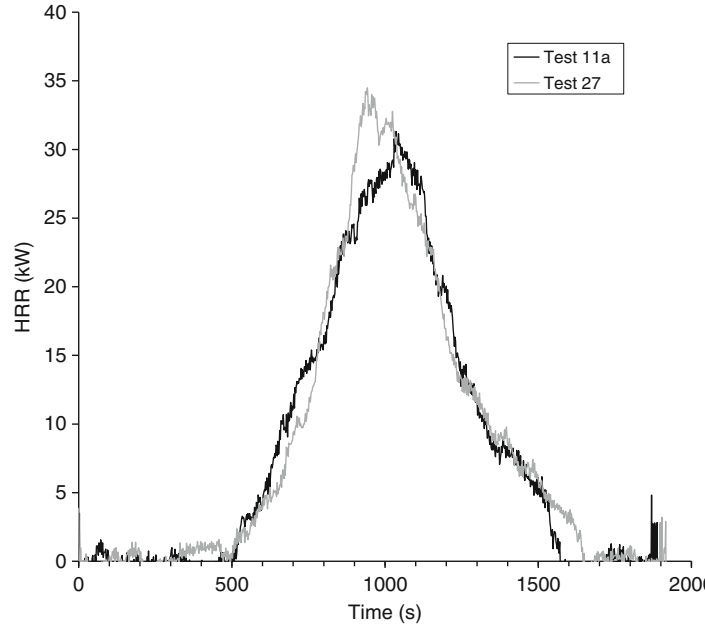

Fig. 26.28 HRR results of ABS monitors, rated UL 94 V0

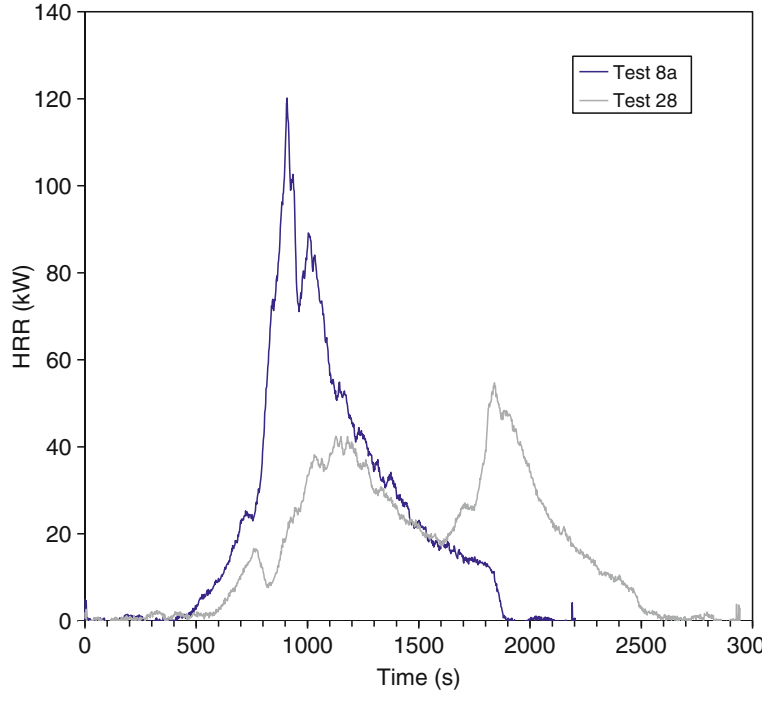

Fig. 26.29 HRR results of polycarbonate monitors, rated UL 94 V0

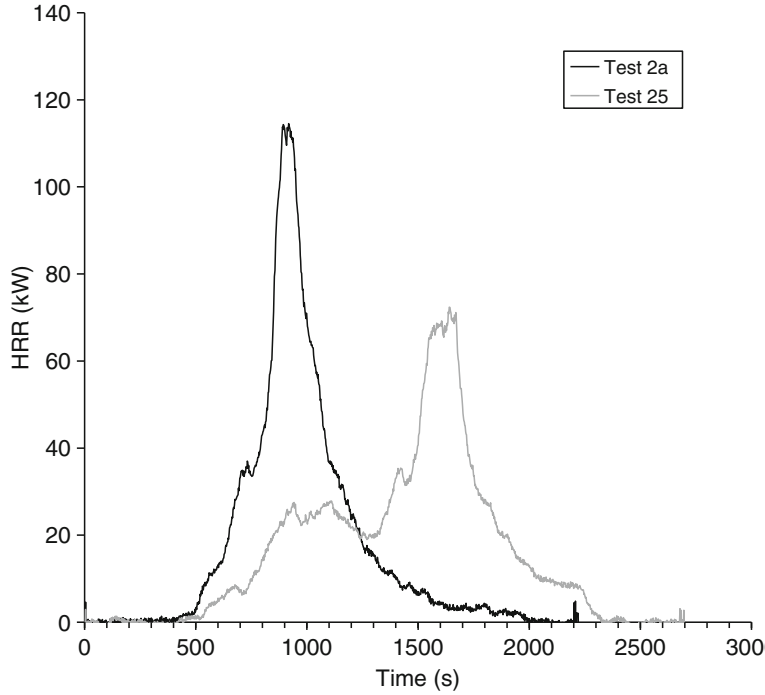

Fig. 26.30 HRR of high-impact polystyrene (HIPS) monitors, rated UL 94 V1

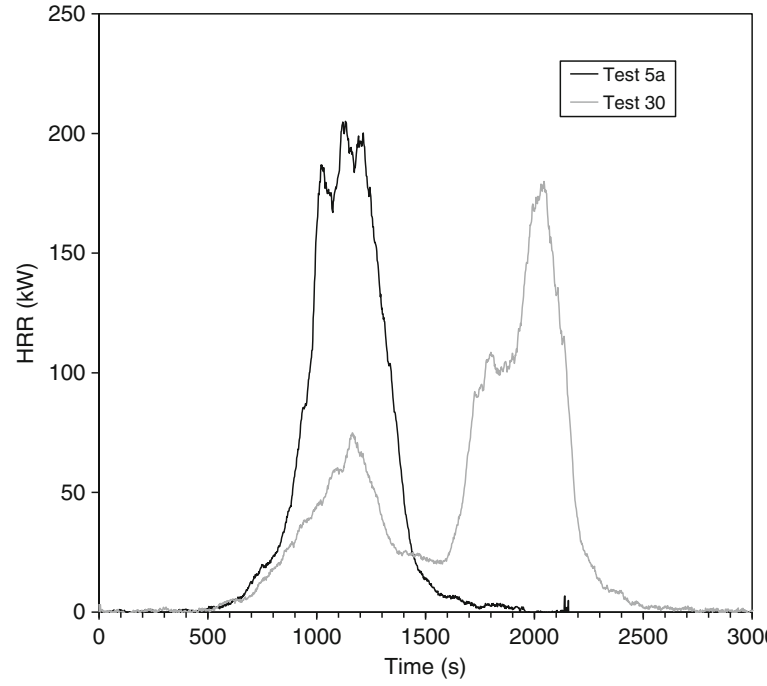

Fig. 26.31 HRR of polypropylene computer monitors, rated UL 94 V2

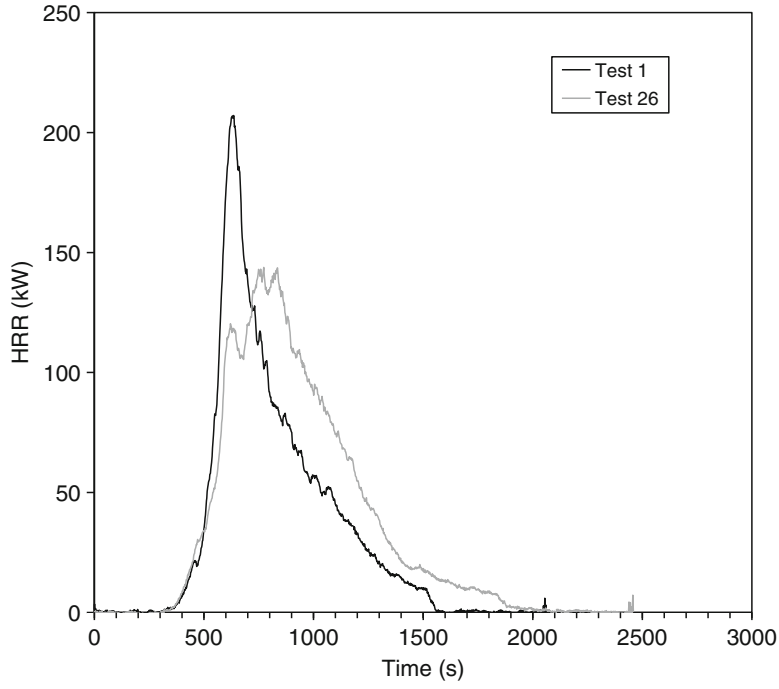

Fig. 26.32 HRR of high-impact polystyrene (HIPS) monitors, rated UL 94 HB

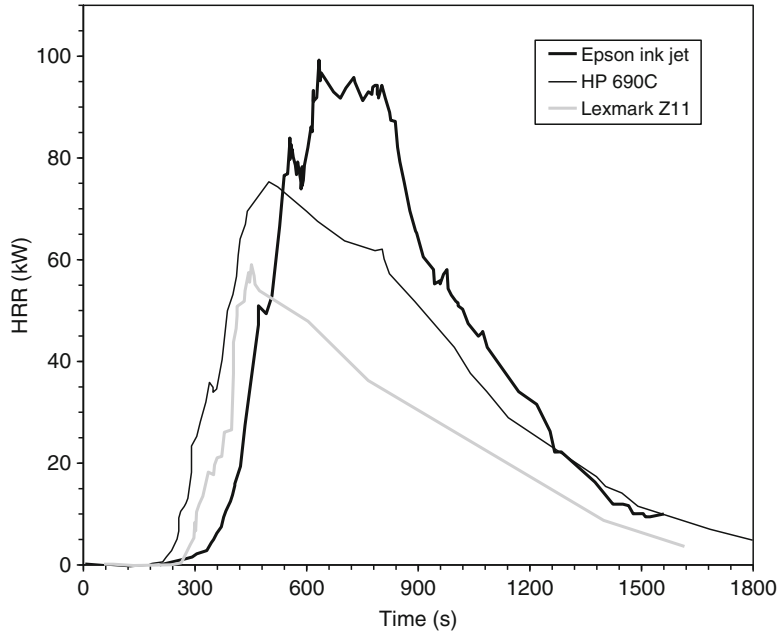

Fig. 26.33 HRR of two, personal-type printers tested at SP

instructive value in demonstrating that minor changes in the fuel loading or fuel arrangement can have drastic influences on the HRR. In this case, introducing the cardboard sheets raised the peak HRR from 155 kW (Test 2) to 528 kW (Test 3). Conversely, changing the ignition location had a major effect on the time of the peak, but essentially no effect on the HRR peak value (146 kW in Test 1, 155 kW in Test 2).

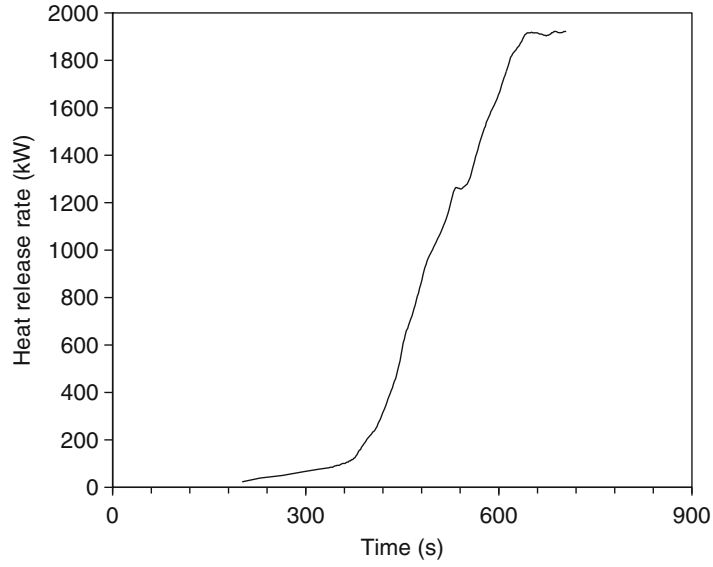

Fig. 26.34 HRR of a rack of computer tapes

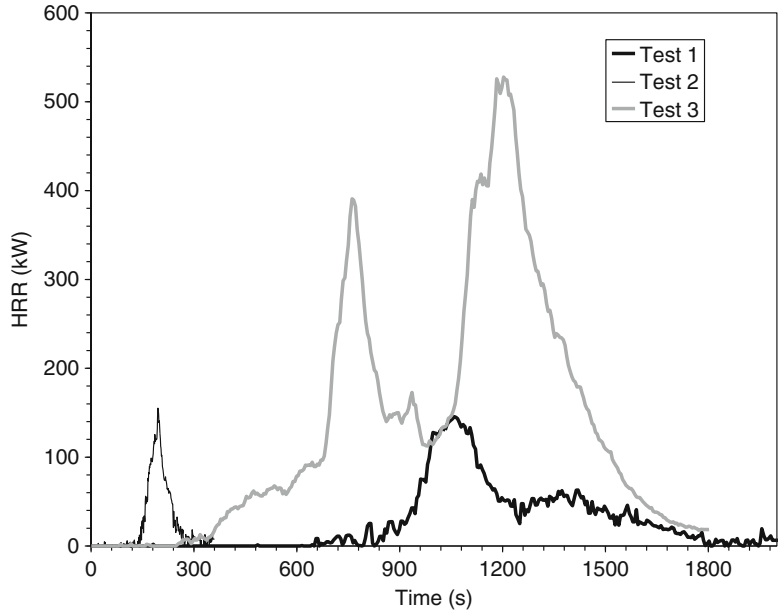

Fig. 26.35 HRR of computer equipment racks

Miscellaneous electronic equipment cabinets. Babrauskas et al. [88] tested two types of plastic business machine cabinets. The cabinets were tested as pairs (two identical units) and ignited with a 50 kW burner. The cabinets had 3 mm wall thickness and each pair of cabinets weighed 3.5 kg. The HRR results are shown in Fig. 26.36.

Two series of tests on steel cabinets used for housing nuclear power-plant control electronics were conducted by VTT [89, 90]. These showed HRR peaks of 100–200 kW. The authors also proposed computation formulas for predicting the HRR level to cause internal cabinet 'flash-over' and for burning to reach a ventilation limit [91]. Such computations are based on the

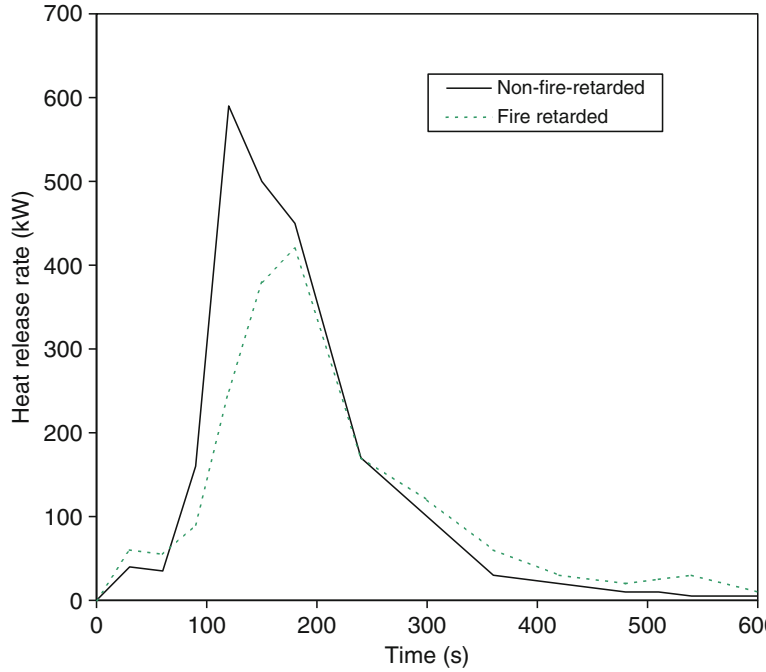

Fig. 26.36 HRR of business-machine cabinets made from polyphenylene oxide

assumption that air flow occurs only through fixed cabinet openings. In such cases, the peak HRR (or, a quasi-steady-state plateau) can be computed and actual testing would not be needed. However, some cabinets may react to fire by effectively increasing their air inflow area, e.g., if doors warp open or fall from the cabinet. Researchers at Institut de Radioprotection et de Sûreté Nucléaire (IRSN) extended the VTT theory and conducted numerous validation experiments [92]. They found that, in most cases, predictions based on ventilation-controlled burning were quite closely borne out by experiments. In a few cases, fires did not develop sufficiently to cause internal flashover, and the theory conservatively over-predicts the HRR for such instances. With an extremely flammable fuel (PMMA), but one which is probably unrealistic for actual industrial electronics cabinets, they did note that actual HRR can exceed the prediction, since some of the pyrolysis gases which lack sufficient oxygen to burn inside the cabinet can leave the cabinet and burn as a fire plume outside. However, since industrial electronics equipment is usually selected with at least some attention being paid to avoidance of excessive flammability behavior, in their tests with actual electronic equipment—as opposed to PMMA—they did not find any instances of such external burning.

Cribs (Regular Arrays of Sticks)

Cribs here are taken to mean regular, three-dimensional arrays of sticks. Each stick is of a square cross-section and of a length much greater than its thickness. The sticks are placed in alternatingly oriented rows, with an air space separating horizontally adjacent sticks. (See Fig. 26.37). Wood crib burning rates have been studied longer than any other product, with early data available from the 1930s [93]. Different analysis formulas have been presented over the years by numerous authors. Here we present a method of analysis [26] based largely on the voluminous experimental data of Nilsson [94] on wood cribs and the functional form suggestions of Yamashika and Kurimoto [95]. The scant available data on plastic cribs are from Harmathy [96] and Quintiere and McCaffrey [97]. The conditions of most interest

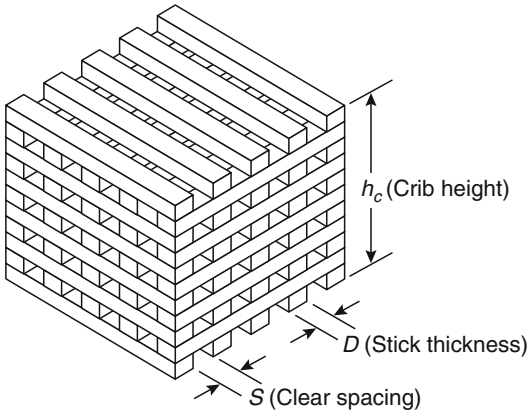

Fig. 26.37 General arrangement of a wood crib

are when cribs are ignited instantaneously, as with the use of a small amount of combustible liquid underneath. The first group of equations below represents this case. There is occasionally an interest in a crib fire where only one end of a crib is ignited, and a slow fire propagation is seen. An analysis for this situation has also been made [98]. A similar analysis is also available for the center-ignited, fire-spreading crib scenario [99].

For cribs ignited uniformly overall, the burning rate can be governed by one of three conditions: (1) the natural limit of stick surfaces burning freely; this limit applies to cribs with wide inter-stick spacings; (2) the maximum flow rate of air and combustion products through the air holes in the crib; this governs for tightly packed cribs; and (3) the maximum oxygen that can be supplied to the room; this effect is discussed separately. The numerical expressions are as follows:

Fuel surface control:

$$\dot{m} = \frac{4}{D} m_o v_p \left(1 - \frac{2 v_p t}{D}\right) \tag{26.8}$$

or

$$\dot{m} = \frac{4}{D} m_o v_p \left(\frac{m}{m_o}\right)^{1/2} \tag{26.8a}$$

with

Table 26.4 Fuel type versus regression velocity v_p for cribs

Material	v_p
Wood	$2.2 \times 10^{-6} D^{-0.6}$
Polymethylmethacrylate	$1.4 \times 10^{-6} D^{-0.6}$
Thermosetting polyester	$3.1 \times 10^{-6} D^{-0.6}$
Rigid polyurethane foam	$3.8 \times 10^{-6} D^{-0.6}$

$$m = m_o - \sum_i^t \dot{m}_i(t_i)\Delta t \tag{26.9}$$

Crib porosity control:

$$\dot{m} = 4.4 \times 10^{-4} \left(\frac{S}{h_c}\right)\left(\frac{m_o}{D}\right) \tag{26.10}$$

Room ventilation control:

$$\dot{m} = 0.12 A_v \sqrt{h_v} \tag{26.11}$$

The *least* of Equations 26.8, 26.10, or 26.11 is to be taken as the governing rate (Equation 26.11 is discussed later in this chapter). Equation 26.8a is necessary instead of the simpler Equation 26.8 when a switch of burning regime occurs during the course of the fire, e.g., the burning changes from porosity control to fuel surface control at some point. This can happen since Equation 26.8 or (26.8a) is a time-dependent expression. Thus, a crib may start burning under porosity or room ventilation-controlled conditions, then later switch to fuel surface control.

In the above equations, D is the stick thickness, m_0 is the crib initial mass, t is the time since ignition, h_c is crib height, S is the clear spacing between sticks, and room ventilation variables are A_v, the ventilation opening area, and h_v, the ventilation opening height. The fuel surface regression velocity, v_p, depends on the stick thickness and on the fuel type, as shown in Table 26.4. The experimental data for the plastic materials are extremely scant, however, so the values should be viewed as indicative rather than quantitative.

For the case of the center-ignited crib, the burning regimes are divided according to whether at a particular time the flame spread has reached the edge of the crib. This time is defined as t_0.

$$t_o = 15.7n \tag{26.12}$$

where n = the number of sticks per row. For time $t < t_o$, the following relation holds [99]:

$$\dot{m} = 0.0254\, m_o \frac{v_p t^2}{n^2 D} \tag{26.13}$$

For $t > t_o$, Equations 26.8 through 26.11 are used. The heat release rate is determined from Equation 26.1. For plastics, the heat of combustion is commonly fairly constant and can be taken from tabulations or from Cone Calorimeter testing. For wood cribs, commonly the heat of combustion is taken to be 12×10^3 kJ kg^{-1}. However, as illustrated in Fig. 26.1, the heat of combustion of wood is a varying function of time. A better procedure would be to either predict the HRR of wood cribs directly, without going through Equation 26.1, or else to be able to have recourse to a realistic value of Δh_c (t). Neither of these possibilities have currently been developed.

Room Fire Effects Experimentally, it has long been observed [94] that, unlike a pool fire, which can burn in a room in a highly fuel-rich manner, a wood crib does not burn more than approximately 30–40 % fuel rich. Conditions more fuel rich than that are not sustained, presumably, because of the highly vitiated air being supplied to the crib under those conditions. The stoichiometric fuel pyrolysis rate can be estimated as [11]

$$\dot{m}_p(st) = \frac{1}{r} \cdot 0.5 A_v \sqrt{h_v} \tag{26.14}$$

where the stoichiometric air/fuel mass ratio, r, for wood can be taken as $r = 5.7$. Comparing, then, the maximum pyrolysis rate given by Equation 26.11 with the stoichiometric rate given by Equation 26.14, it can be seen that a limit of approximately 37 % fuel rich is reached when Equation 26.11 becomes the governing limit to the burning rate. Similar limits may possibly exist for other classes of combustibles, but experimental data are only available for wood cribs.

Curtains

Thermoplastic curtains often do not sustain any appreciable burning when ignited by a flame. Instead, a small piece ignites, but it falls off and the rest of the material still in place does not burn. The dropped-down material will usually continue burning, but its HRR will be trivial. There is no systematic study available that would elucidate under what conditions curtains will burn in place (and release a significant amount of heat), versus burning only to a trivial extent.

Even if curtains ignite and burn in place, the heat content and HRR are generally moderate, but curtains can contribute to the severity of a fire by quickly propagating fire over large surfaces. Moore has done the most extensive study of curtains and draperies [100]. His test specimens were ignited with a match along the bottom. The results are summarized in Table 26.5 and Fig. 26.38. His results show primarily the effect of fabric weight. Lightweight fabrics, of weight around 125 kg m^{-2}, can show heat release rate peaks almost as high as heavy ones (around 300 kg m^{-2}); however, their potential to ignite surrounding objects is much smaller, as demonstrated in Fig. 26.38. These conclusions hold for both thermoplastic and cellulosic materials, but not for constructions using foam backings, for which insufficient data were available. Whether the curtain was in the closed or in the open position seemed to make little difference. The reason for the more severe fire performance of the heavyweight curtains was largely due to their increased burning time, which was typically about twice that for the lightweight curtains. Additional data on the HRR of curtains have been published by VTT [156] and by SP [101].

Yamada et al. [102] conducted full-scale tests on curtains of 0.9–1.2 m width and 2.0 m length. They tried 10, 30 and 50 kW square burners and found that generally at least the 30 kW burner needed to be used if full flame development was to be reached. Polyester curtains, both FR and non-FR, melted and failed to show a sustained

Table 26.5 HRR data for curtains. Nominal curtain size: two curtains each, 2.13 m high by 1.25 m wide. Wall area covered: 2.13 m high by 1.0 m wide (in closed position)

Type of fiber	Weight (g/m^2)	Configuration	Peak HRR (kW)	Number of wall and ceiling panels ignited[a]
Cotton	124	Closed	188	1
Cotton	260	Closed	130	7
Cotton	124	Open	157	0
Cotton	260	Open	152	7
Cotton	313	Closed	600	3
Rayon/cotton	126	Closed	214	0
Rayon/cotton	288	Closed	133	6
Rayon/cotton	126	Open	176	0
Rayon/cotton	288	Open	191	2
Rayon/cotton	310	Closed	177	8
Rayon/acetate	296	Closed	105	4
Acetate	116	Closed	155	0
Cotton/polyester	117	Closed	267	1
Cotton/polyester	328	Closed	338	5
Cotton/polyester	117	Open	303	0
Rayon/polyester	367	Closed	658	2
Rayon/polyester	268	Closed	329	7
Rayon/polyester	53	Closed	219	0
Cotton/polyester	328	Open	236	7
Polyester	108	Closed	202	0
Acrylic	99	Closed	231	0
Acrylic	354	Closed	1177	8
Acrylic	99	Open	360	0
Acrylic	354	Open	NA	7
Cotton/polyester/foam	305	Closed	385	1
Rayon/polyester/foam	284	Closed	326	0
Rayon/fiberglass	371	Closed	129	5
Rayon/fiberglass	371	Closed	106	5

[a]Maximum possible number of panels to ignite = 10

fire, as did FR cotton and FR rayon. Acrylic, modacrylic, non-FR rayon and non-FR cotton showed sustained burning, attaining 100–250 kW peak HRR values when subjected to the 50 kW ignition source.

Decks

The California Office of State Fire Marshal reported some HRR tests [103] done on outdoor decks, comparing wood, wood/plastic composite, and various all-plastic constructions. For samples sized 0.61 × 0.61 m, a redwood deck gave a peak HRR of 12 kW. Wood/plastic composites ranged between 10 and 394 kW, while all-plastic products ranged from 10 to 1055 kW.

Desks

Chow et al. [104] measured the HRR of a small wooden office desk. The desk was 0.6 × 1.2 × 0.8 m high The ignition source

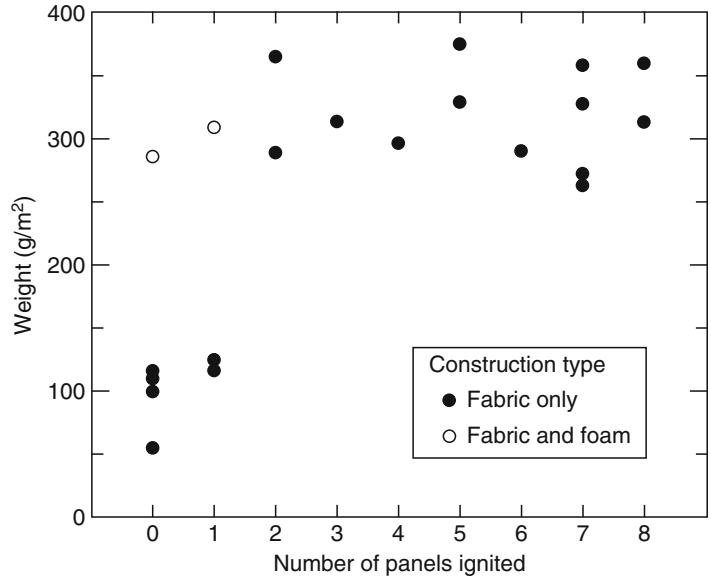

Fig. 26.38 Effect of fabric weight on number of curtain panels ignited

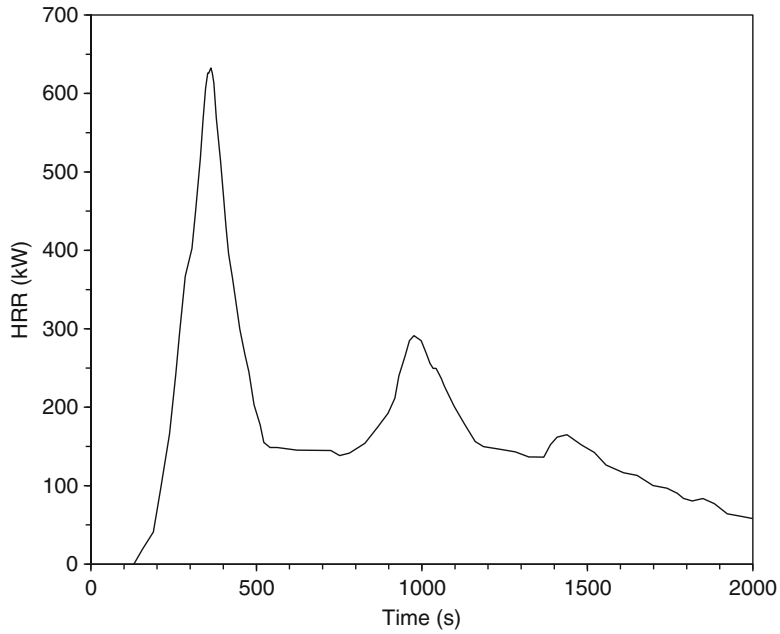

Fig. 26.39 HRR of a wooden desk tested by Chow et al.

was a pool of 0.5 L gasoline which, by itself, produced a peak HRR of 40 kW. These results are shown in Fig. 26.39.

Dishwashers

VTT tested [105] European dishwashers using a propane burner of 1 kW. The specimens are described in Table 26.6, while test results are shown in Fig. 26.40. These results must *not* be applied to appliances used in North America, since European appliance styles are different from North American ones and also because local standards are such as to permit appliances of greater flammability in Europe. HRR data on North American dishwashers are not available.

Dressers

A test of a wooden dresser has been conducted by NIST [106], see Fig. 26.41.

Dryers

Results for a small European clothes dryer (40 kg) have been published [70]. Even though use of plastics in North American clothes dryers has been increasing, nonetheless it would appear that the unit was more typical of the European market than the American one. In the test (Fig. 26.42), 11 kg of mass was lost and 253 MJ of heat was released.

Table 26.6 European dishwashers tested by VTT

Specimen	D1	D2
Initial mass (kg)	35.6	47.5
Mass loss (kg)	6.1	8.4
Peak HRR (kW)	476	347
Total heat (MJ)	165	206

Electric Cable Trays

Cable tray fires present almost an endless plethora of combinations of cable materials, tray construction, stacking, ignition sources, etc. Only a very few of these have been explored. The most systematic studies available are those from Tewarson et al. [107] and Sumitra [108]. A useful engineering analysis of their data has been prepared by Lee [109]. Lee provided a basic correlation of Tewarson's and Sumitra's data (see Fig. 26.43), which shows that the peak full-scale heat release rate $\dot{q}_{fs}$ (kW m^{-2}) can be predicted according to bench-scale heat release rate measurements:

$$\dot{q}_{fs} = 0.45\dot{q}''_{bs} \cdot A$$

where $\dot{q}''_{bs}$ is the peak bench-scale HRR (kW m^{-2}), measured under 60 kW m^{-2} irradiance, and A is the exposed tray area actively pyrolyzing (m^2). The active pyrolysis area, in turn, is estimated from Fig. 26.44, which gives dA/dt as a function of $\dot{q}''_{bs}$. Thus, at any given time, t,

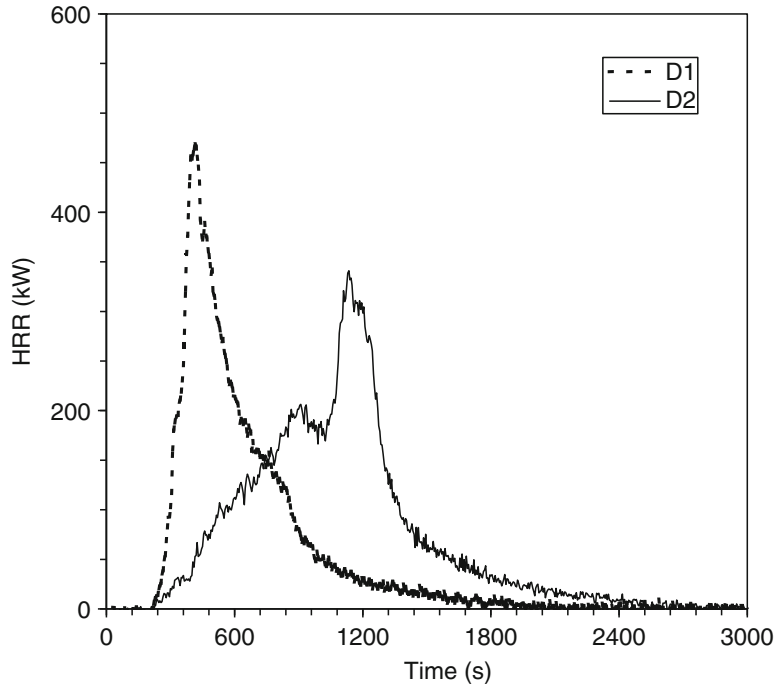

Fig. 26.40 HRR of European dishwashers tested by VTT

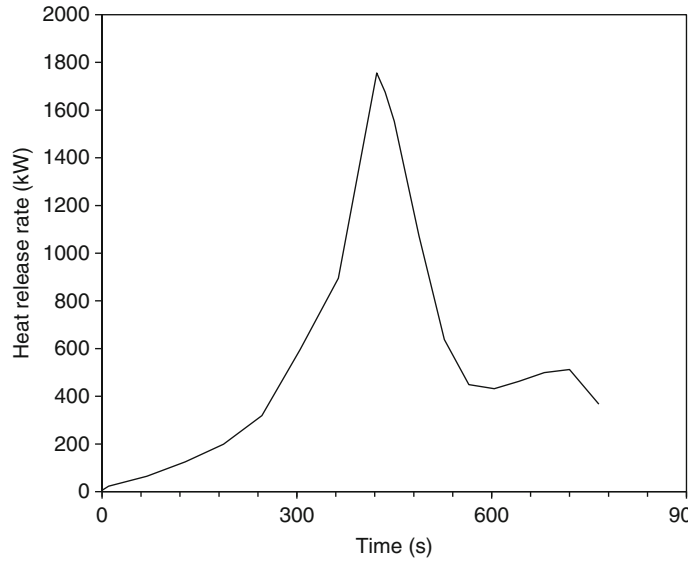

Fig. 26.41 HRR of wooden dresser

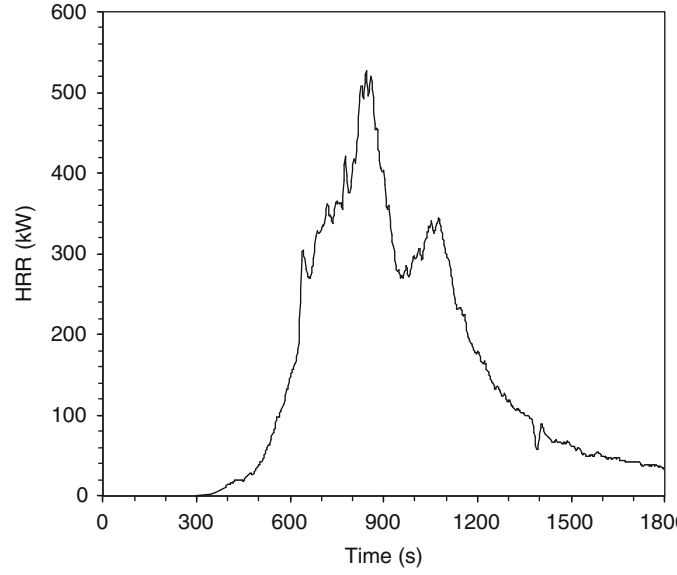

Fig. 26.42 HRR for a small European clothes dryer

$$A(t) = A_o + \frac{dA}{dt} \cdot t$$

Finally, Table 26.7 gives a selection of measured values of $\dot{q}''_{bs}$ for various cable types.

Foodstuffs

SP reported on a test [110] to simulate the burning of snack foods in a shop. Retail bags of two types of snacks were tested in a single test—potato chips and cheese nibbles. A total fuel load of 275 kg was set up in a tightly-packed, three-shelf high shelving unit, 5.4 m long. The HRR results are shown in Fig. 26.45. Visual observations indicated that potato chips burned more vigorously than cheese nibbles.

NIST [111] ran two full-scale tests on bags of potato chips on a rack with open-wire-mesh shelves. Each shelf had 20 bags of potato chips. The bags were arranged five across and four

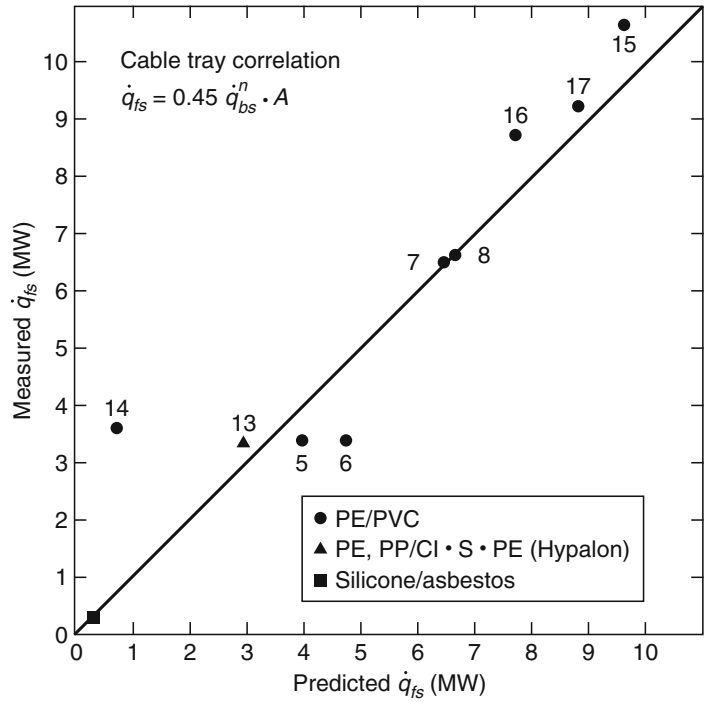

Fig. 26.43 HRR prediction for cable trays (numbers at data points identify full-scale tests)

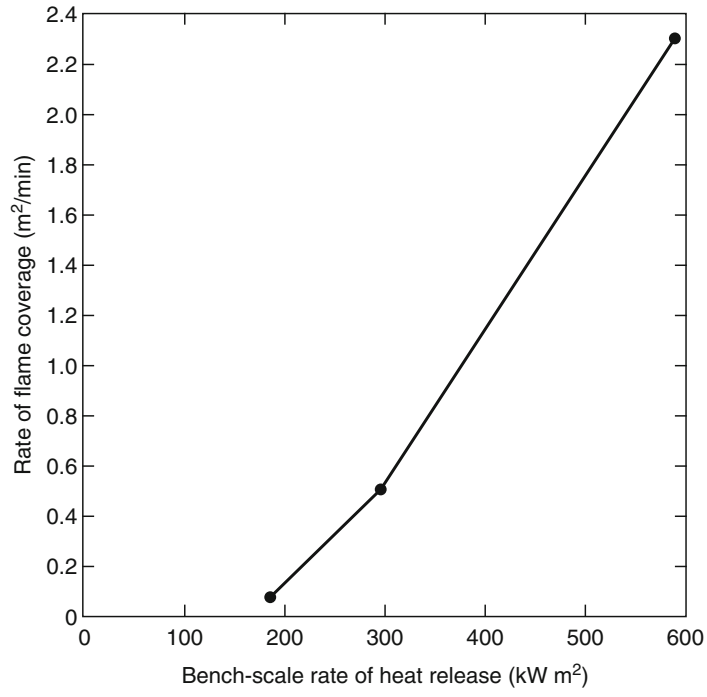

Fig. 26.44 Effect of bench-scale cable heat release rate on full-scale rate of flame coverage

Table 26.7 Heat release rates of typical cables in bench-scale tests

Specimen number	Cable sample	IEEE 383 test	$\dot{q}''_{bs}$ (kW m^{-2})
20	Teflon	Pass	98
21	Silicone, glass braid	Pass	128
10	PE, PP/Cl · S · PE	Pass	177
14	XPE/XPE	Pass	178
22	Silicone, glass braid asbestos	Pass	182
16	XPE/Cl · S · PE	Pass	204
18	PE, nylon/PVC, nylon	[a]	218
19	PE, nylon/PVC, nylon	[a]	231
15	FRXPE/Cl · S · PE	Pass	258
11	PE, PP/Cl · S · PE	Pass	271
8	PE, PP/Cl · S · PE	Pass	299
17	XPE/Neoprene	Pass	302
3	PE/PVC	[a]	312
12	PE, PP/Cl · S · PE	Pass	345
2	XPE/Neoprene	[a]	354
6	PE/PVC	[a]	359
4	PE/PVC	Fail	395
13	XPE/FRXPE	Pass	475
5	PE/PVC	Fail	589
1	LDPE	[a]	1071
20	Teflon	Pass	98

[a]Test not conducted

deep, with a total fuel load of 27.1 kg. Each bag of chips was approximately 200 mm wide by 100 mm (thick) by 360 mm high. Each bag weighed 33.8 g, of which chips accounted for 32.5 g and the plastic bag for the rest. The potato chip ingredients were listed by the manufacturer as: potatoes, sunflower oil and salt. Two replicate heat release rate experiments were conducted (Fig. 26.46). It is interesting to note that the NIST tests showed the same peak HRR (6 MW) as the SP test, albeit with a much shorter duration time due to the fact that the fuel load was 1/10 of SP amount.

Industrial Stored Commodities

Pallet loads of plastic-based commodities are commonly stored in factories, warehouses, and wholesale establishments. Most tests have involved multiple pallets being tested, and most of these have also involved some manner of water application being done during the test. But there have been a few tests reported where single pallet-loads were tested, without water. SP [112] tested single pallet-loads of four kinds:

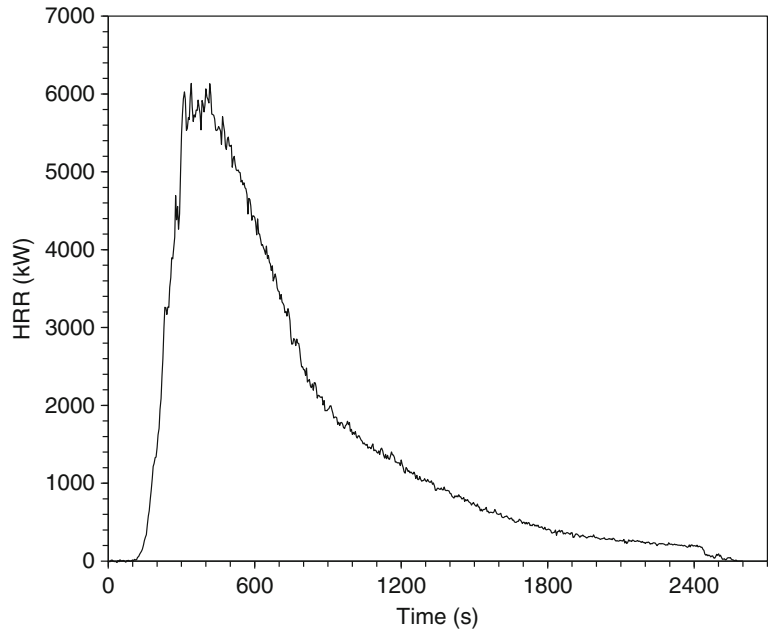

Fig. 26.45 HRR of potato chips and cheese nibbles set up in a shop display unit

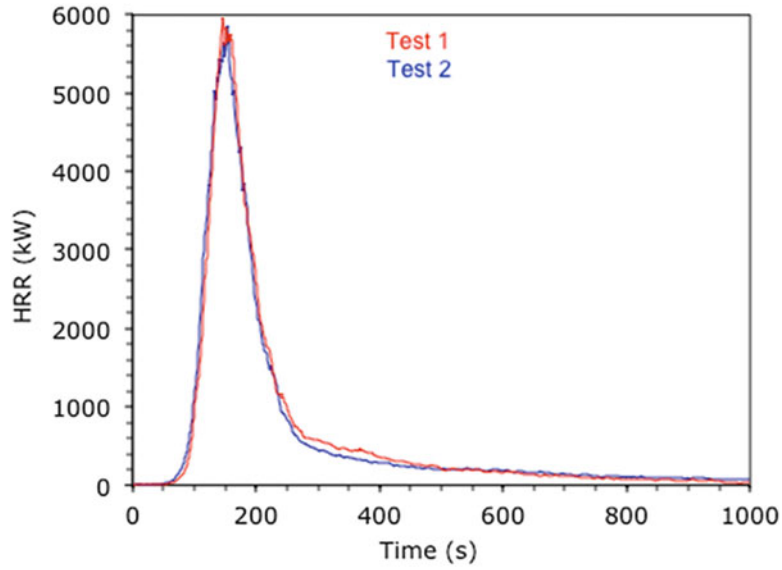

Fig. 26.46 Potato chip bags tested at NIST

- FM Group A plastic standard commodity (see Table 26.10)
- CEA standard commodity. Each corrugated-cardboard box is 450 × 550 × 370 mm and each (wood) pallet holds 12 boxes in a 2 × 2 × 3 array. Each box weighs 805 g and is filled with 340 g of polystyrene chips. The pallet-load is 800 × 1200 mm with a height of 1110 mm, excluding the pallet itself.
- SCEA standard commodity. This is a Swedish version of the CEA, with each box being 380 × 570 × 380 mm. Each box weighs 700 g and holds 420 g of chips. The pallet-load is 800 × 1200 mm with a height of 1140 mm, excluding the pallet itself.
- Large SCEA standard commodity. This is a variant where the box is 800 × 600 × 500 mm. Each box weighs 1470 g and contains 1220 g of chips. Each pallet holds a 1 × 2 × 2 array of boxes.

The HRR results for these tests are shown in Fig. 26.47.

Despite the intention being that Group A plastics represent a severe fire hazard, some plastic commodities produce significantly more HRR. In tests by Babrauskas [113], pellets of SBR (styrene-butadiene rubber) were packed in paper bags and loaded on a wooden pallet, with a total weight of 680 kg of pellets. The pallet was over-wrapped with clear plastic film and spillage did not occur during the test. The full-pallet test was ignited with a propane torch at the bottom. The half-pallet test was ignited with a propane torch at the top. The full-pallet test (Fig. 26.48) showed a HRR of close to 7 MW when conditions required that the commodity be extinguished; peak HRR conditions had not been reached.

Heskestad [114, 115] analyzed a large series of palletized[1] storage tests conducted at FM in 1975 by Dean [116]. These experiments pre-dated the availability of HRR calorimeters, so Heskestad obtained peak HRR values by using mass loss rate data and values of effective heat of combustion. The test arrangement was 2 × 2 × 3 pallets high, with a flue space running in only one direction. Heskestad also analyzed a later series of rack-storage tests by Yu and Kung [117, 118]. The test arrangement was 2 × 2, with heights being two, three, or four pallets, and with flue spaces running in both directions.

[1] 'Palletized' denotes a storage configuration where pallets are stored directly on top of each other, without use of shelving.

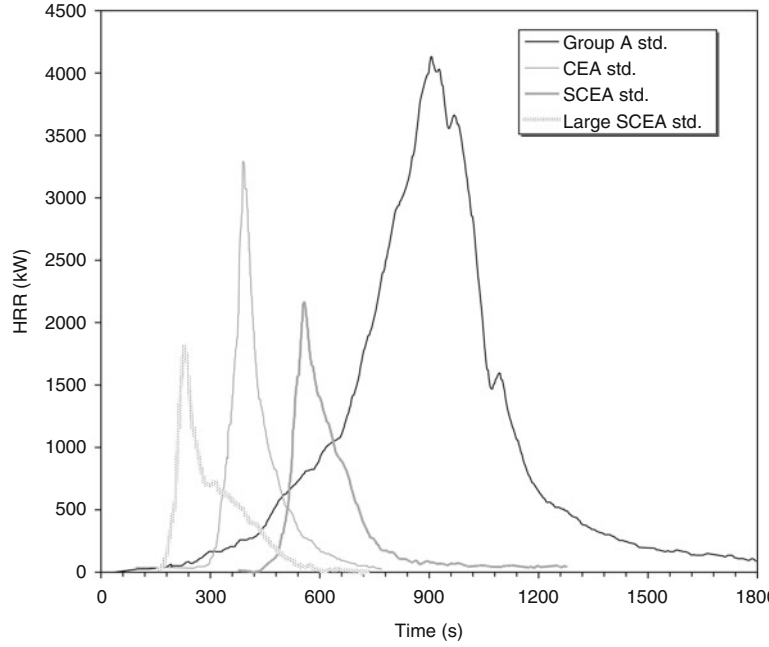

Fig. 26.47 HRR of single pallet-loads of various commodities tested at SP

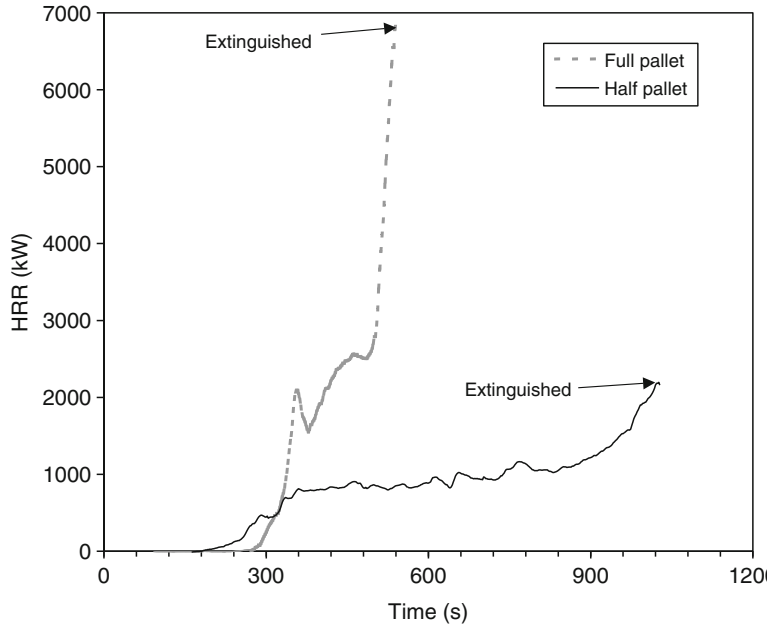

Fig. 26.48 HRR of pallets holding bags of SBR pellets

Heskestad's tabulated peak HRR values are given in Table 26.8. The peak HRR values were obtained by dividing the value in kilowatts by the floor area occupied by the commodity. The palletized test commodities occupied a floor area of 2.44 × 2.59 m, while the rack storage tests were 2.29 × 2.29 m. The cardboard cartons with metal liner are 'FM Standard Class II Commodity' (Table 26.10 [119, 122]) while the PS cups are 'FM Standard Plastic Commodity'

Table 26.8 HRR values of palletized and rack-storage commodities tested at FM

Test	Commodity	Storage ht. (m)	Peak HRR (kW m^{-2})	Time of peak (s)
SP-4	PS jars in compartmented CB cartons	4.11	16,600	439
SP-13	PS foam meat trays, wrapped in PVC film, in CB cartons	4.88	10,900	103
SP-23	PS foam meat trays, wrapped in paper, in CB cartons	4.90	11,700	113
SP-30A	PS toy parts in CB cartons	4.48	5,210	120
SP-35	PS foam insulation	4.21	26,000	373
SP-44	PS tubs in CB cartons	4.17	6,440	447
SP-15	PE bottles in compartmented CB cartons	4.20	5,330	434
SP-22	PE trash barrels in CB cartons	4.51	28,900	578
SP-43	PE bottles in CB cartons	4.41	4,810	190
SP-6	PVC bottles in compartmented CB cartons	4.63	8,510	488
SP-19	PP tubs in compartmented CB cartons	4.26	5,870	314
SP-34	PU rigid foam insulation	4.57	1,320	26
SP-41	Compartmented CB cartons, empty	4.51	2,470	144
RS-1	CB cartons, double tri-wall, metal liner	2.95	1,680	260
RS-2	″ ″	2.95	1,490	89
RS-3	″ ″	2.95	1,680	180
RS-4	″ ″	4.47	2,520	120
RS-5	″ ″	4.47	2,250	240
RS-6	″ ″	5.99	3,260	210
RS-7	PS cups in compartmented CB cartons	2.90	4,420	95
RS-8	″ ″	2.90	4,420	100
RS-9	″ ″	2.90	4,420	120
RS-10	″ ″	4.42	6,580	100
RS-11	″ ″	5.94	8,030	148

CB cardboard, *PE* polyethylene, *PP* polypropylene, *PS* polystyrene, *PU* polyurethane

Table 26.9 Miscellaneous stored commodities tested by FM

Commodity	Storage ht. (m)	Peak HRR (kW m^{-2})
Fiberglass (polyester) shower stalls, in cartons	4.6	1,400
Mail bags, filled	1.52	400
PE letter trays, filled, stacked on cart	1.5	8,500
PE and PP film in rolls	4.1	6,200

(Group A Plastic). Note that there does not exist a scaling rule that would enable HRR values to be computed for stack/rack heights other than those tested. Thus, the reported values could conservatively be applied to shorter heights, but cannot be extrapolated to greater heights. Some older data [120] are listed in Table 26.9. These have not been re-analyzed by Heskestad.

The effect of storage height [121] on the HRR growth curve for Class II commodities is shown in Fig. 26.49. An initial period of limited fire growth has been removed from these curves. These results are from FM testing in the 1980s. Also shown is the HRR curve for a $2 \times 2 \times 2$ array tested in 2005. For much of the time, the HRR exceeded the earlier results. This is because FM identified that the standard Class II commodity supplied in 2005 is somewhat different than that supplied earlier [125]. The early fire growth period [122] for Class I, III, and IV commodities is shown in Fig. 26.50. The early fire growth period for the FM Standard Plastic Commodity is shown in Fig. 26.51. These results are based on early FM studies [123, 124] which were

Table 26.10 FM Commodities and standard test commodities

Class	Products	Examples	Test commodity
Class I	Essentially noncombustible; may be in light cardboard cartons and may be on wood pallets	Glass, minerals, metals, ceramics	Single-wall corrugated cardboard carton measuring 21″ (0.533 m) on side, divided into five horizontal layers by corrugated cardboard sheets. Each layer was divided by interlocking cardboard partitions forming a total of 125 compartments. Each compartment occupied by one 16-oz (0.47 l) glass jar, without lid, open side facing down to prevent collection of water. A pallet load consists of one wood pallet and eight of the above-described cartons.
Class II	Class I products with more or heavier packaging and containers	Class I products in multiwall cartons, boxes, or barrels.	Double triwall (approx. 25 mm thick total) corrugated cardboard carton measuring 42" (1.07 m) on a side containing a 24 ga. (0.56 mm) sheet metal liner box measuring 38″ × 38″ × 36″ (1.07 × 1.07 × 1.02 m) high. A pallet load consisted of one wood pallet and one the above described cartons.
Class III	Combustible products in combustible wrapping or containers on wood pallets. May contain a limited amount of plastic.	Products of wood, paper, leather, and some foods	Single-wall corrugated cardboard carton measuring 21″ (0.533 m) on a side, divided into five horizontal layers by corrugated cardboard sheets. Each layer divided by interlocking corrugated cardboard partitions forming a total of 125 compartments. Each compartment occupied by one 16-oz (0.95 l) paper jar (wide mouth container/ cup), without lid, open side facing down to prevent the collection of water. A pallet load consists of one wood pallet and eight of the above described cartons.
Class IV	Class I, II, or III with considerable plastic content in product, packaging or pallets	Typewriters and cameras of metal and plastic parts	Single-wall corrugated cardboard carton measuring 21″ (0.533 m) on a side, divided into five horizontal layers by corrugated cardboard sheets. Each layer divided by interlocking corrugated cardboard partitions forming a total of 125 compartments. Each compartment occupied by forty 16-oz (0.95 l) polystyrene and eighty-five 16-oz (0.95 l) paper jars (wide mouth container/ cup), without lids, open side facing down to prevent the collection of water. A pallet load consists of one wood pallet and eight of the above described cartons.
Standard plastic (Group A Plastic)	Commodities containing a greater amount of plastic than would be permitted in Class IV commodities		Single-wall corrugated cardboard carton measuring 21″ (0.533 m) on a side, divided into five horizontal layers by corrugated cardboard sheets. Each layer divided by interlocking corrugated cardboard partitions forming a total of 125 compartments. Each compartment occupied by one 16-oz (0.95 l) polystyrene jar, without lids, open side facing down to prevent the collection of water. A pallet load consists of one wood pallet and eight of the above described cartons.

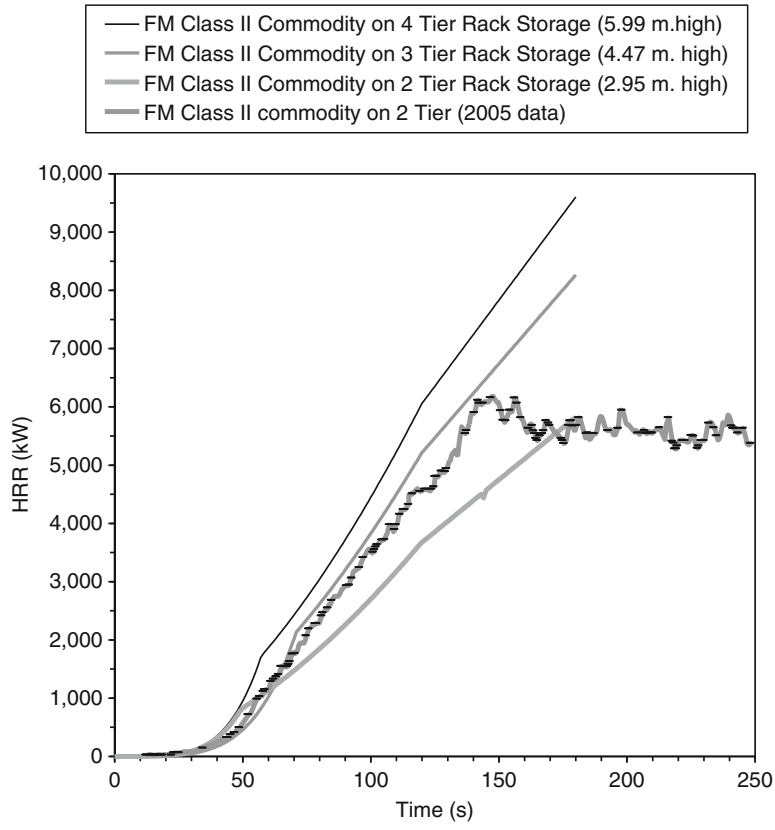

Fig. 26.49 Effect of storage height for Class II commodities

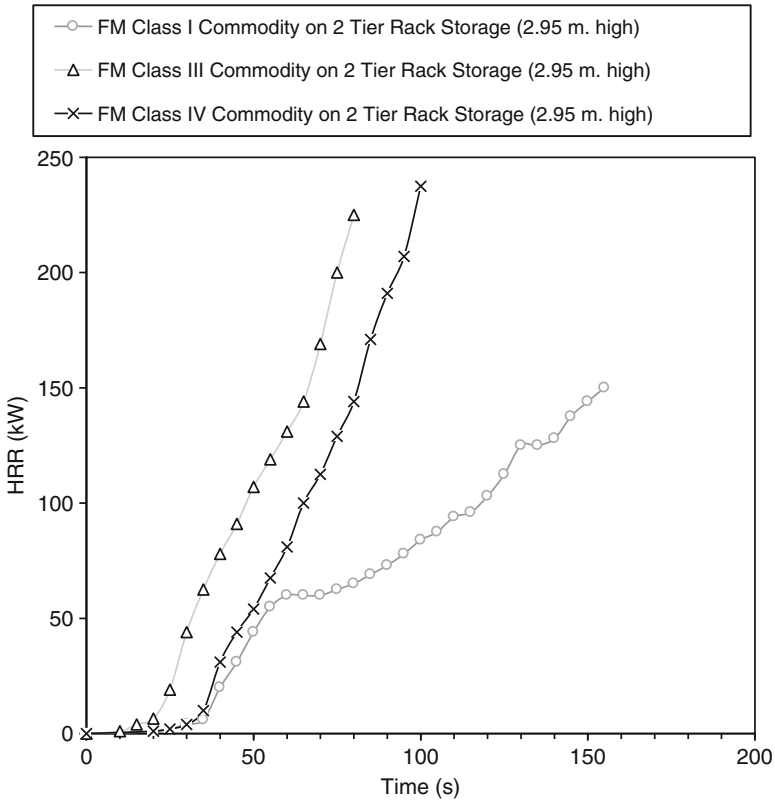

Fig. 26.50 The early fire-growth period for Class I, III, and IV commodities

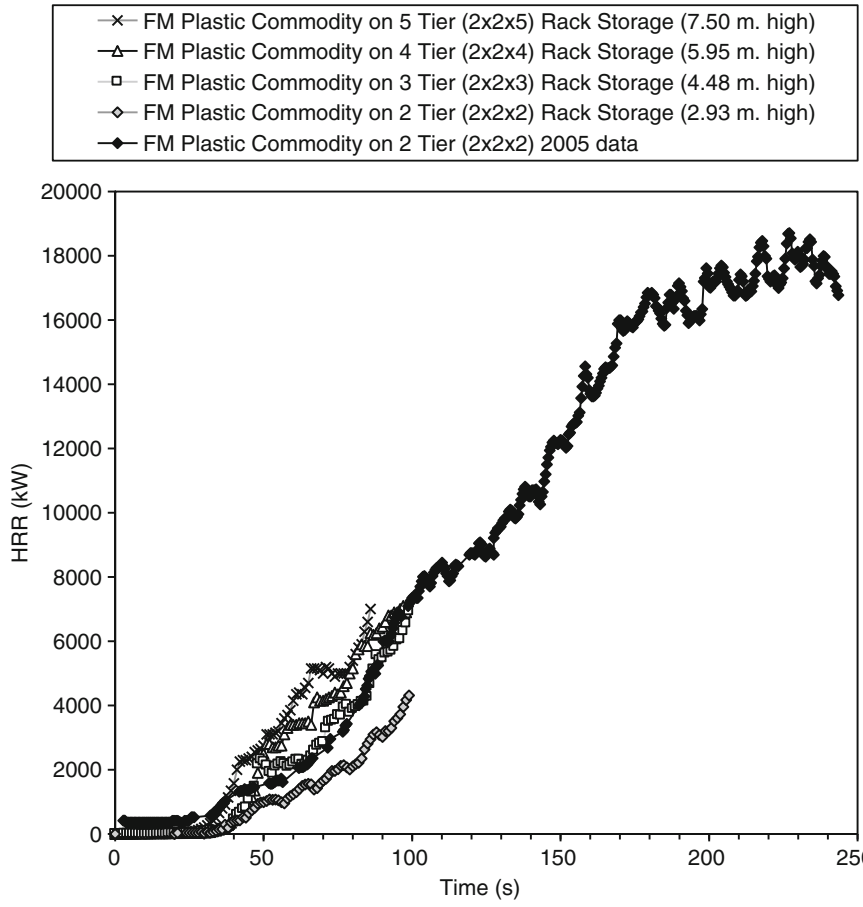

Fig. 26.51 The early fire-growth period for FM Standard Plastic commodity, as a function of storage height

conducted in their Norwood MA facility. Also shown are the results obtained in 2005 at their West Gloucester RI facility for the 2 × 2 × 2 configuration [125].

Additional FMRC data for different commodities loaded onto wooden pallets are shown in Fig. 26.52. The egg carton test [126] used foam-polystyrene egg cartons of 12-egg capacity. Polyethylene bags were used to hold 200–216 of these egg cartons, open and nested into each other. Each pallet held about 20.4 kg of egg cartons. Each pallet contained about 22.7 wood, and the load also contained about 0.4 kg polyethylene. In this test, a low density of water extinguishment was applied, but this did not appear to significantly reduce the HRR of the commodity. Only the convective portion of the HRR was measured. Polystyrene shows a very high radiant heat release fraction, thus, to account for the radiant fraction and for the diminution due to water spraying, the total HRR curve shown in Fig. 26.52 was estimated by multiplying the measured convective portion by a factor of 2. The polyurethane foam results [127] are for a three-tier (4.27 m high) stack of foam in cardboard boxes and used a PUR foam of high HRR; other results (not shown) were also obtained by FM for fire-retardant grades. The PET (polyethylene terephthalate) bottles test [128] used 46 bottles of a 2 L size packed into single-wall corrugated cardboard boxes. Each box contained 2.55 kg of plastic and 1.29 kg of cardboard. Total test arrangement comprised eight pallet loads arranged in a 2 × 2 × 2 arrangement. Each pallet contained eight cartons of the size 0.53 × 0.53 × 0.53 m. The

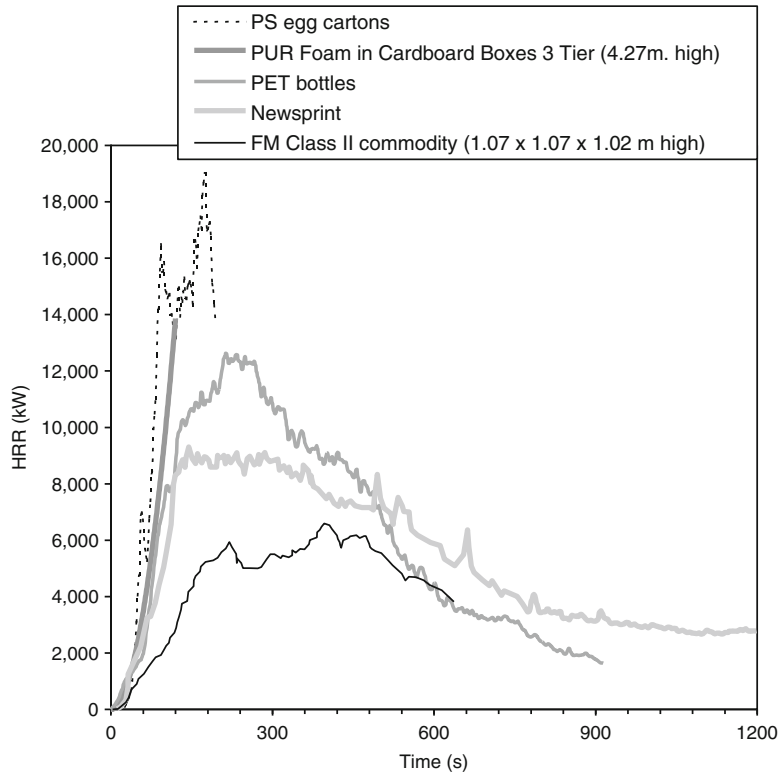

Fig. 26.52 FMRC HRR results for several additional commodities

Table 26.11 Boxed computer items tested by Hasegawa et al.

Code	Items	Peak HRR (kW)
P1	Boxed monitors, one pallet of 12	4700
P8	Boxed monitors, one pallet of 12, point-source ignition	5030
P5	Boxed monitors, one pallet of 12 (stabilized from collapse)	6400
P6	Boxed monitors, two pallets (side-by-side) of 12 each	17,300
P10	Boxed monitors, stack of two pallets high, 10 per pallet	14,100
P3	Boxed desktop computers, one pallet of 16	1400
P7	Boxed desktop computers, pallet of 16 + boxed accessory boxes on top	8190
P9	polystyrene foam in boxes	6730
P11	Monitor boxes, one pallet of 12	4600

newspaper test [129] comprised 8.2 kg of shredded newsprint placed in a $0.53 \times 0.53 \times 0.51$ m single-wall corrugated cardboard box of 2.73 kg. Eight cartons comprised one pallet load. The pallets were arranged in a $2 \times 2 \times 2$ arrangement. The newsprint test [130] used a $2 \times 2 \times 2$ arrangement of pallets, each load being $1.07 \times 1.07 \times 1.02$ m high. The Class II commodity results are from Khan [130].

Packaged computers and computer accessories were tested by Hasegawa et al. [131, 132]. They tested pallet-loads of packaged goods and also individual items, as packaged and boxed in individual cardboard boxes. The items were ignited using a line burner placed near the bottom edge of the package or stack. Ignition sources in the range of 50–200 kW were used. Table 26.11 identifies the specimens tested, while Figs. 26.53 through

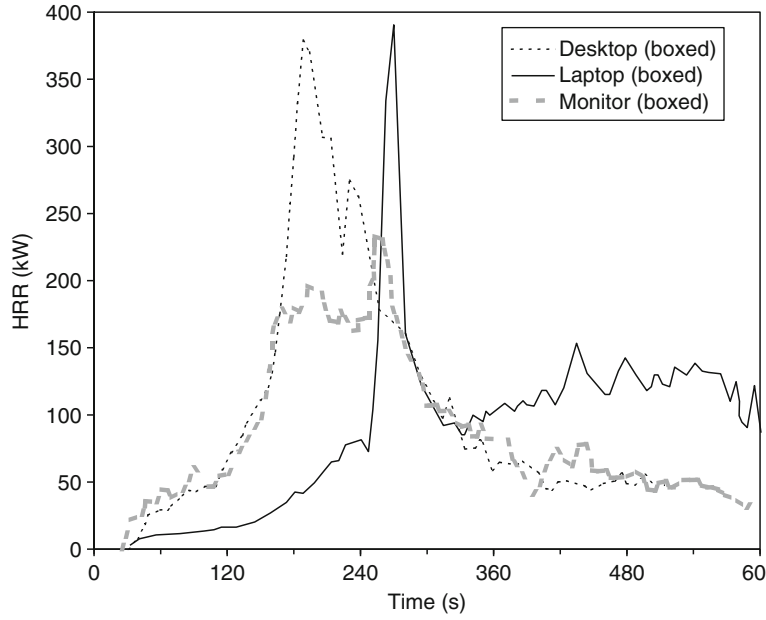

Fig. 26.53 HRR of single, packaged and boxed computers and monitors

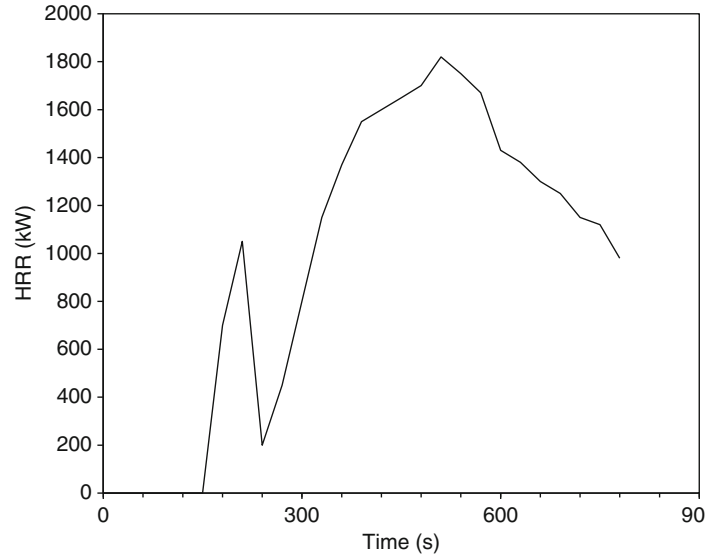

Fig. 26.54 HRR of a stack of polystyrene foam boards

26.57 show the results. The monitors were 16.8 kg each, while the desktop computers were 4.9 kg ea. The pallet load in test P1 collapsed during test and the full HRR was not registered, consequently, it was re-tested with supported sides.

A stack of expanded polystyrene boards was burned by Dahlberg at SP and results are reported by Särdqvist [97]. The total stack size was 1.2 × 1.2 × 1.2 m, with a mass of 1.4 kg. Ignition was with a 1 MW burner at the side of the stack. The HRR curve is shown in Fig. 26.54. Numerous other example data are tabulated by Särdqvist [97].

Dillon et al. [133] tested several commodities in a furniture calorimeter: acrylic yarns in boxes,

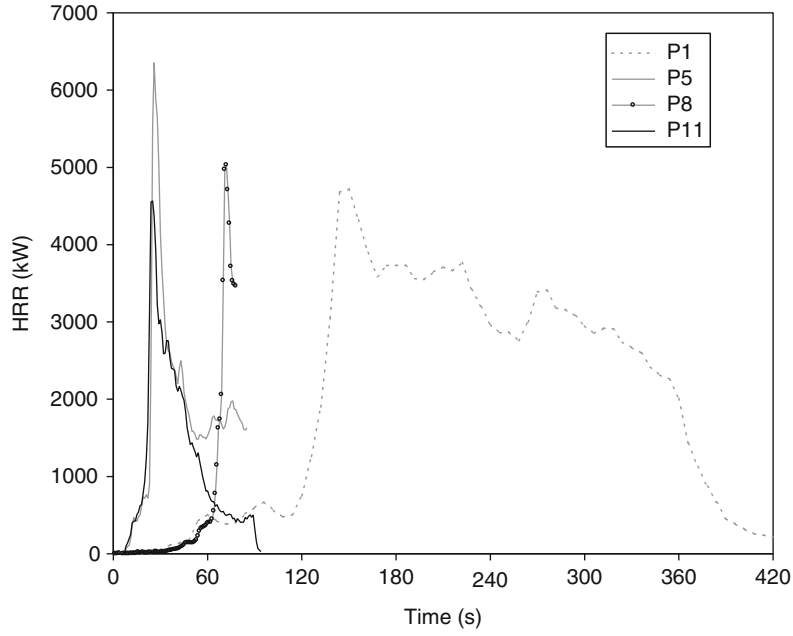

Fig. 26.55 HRR of pallets of packaged, boxed computer monitors

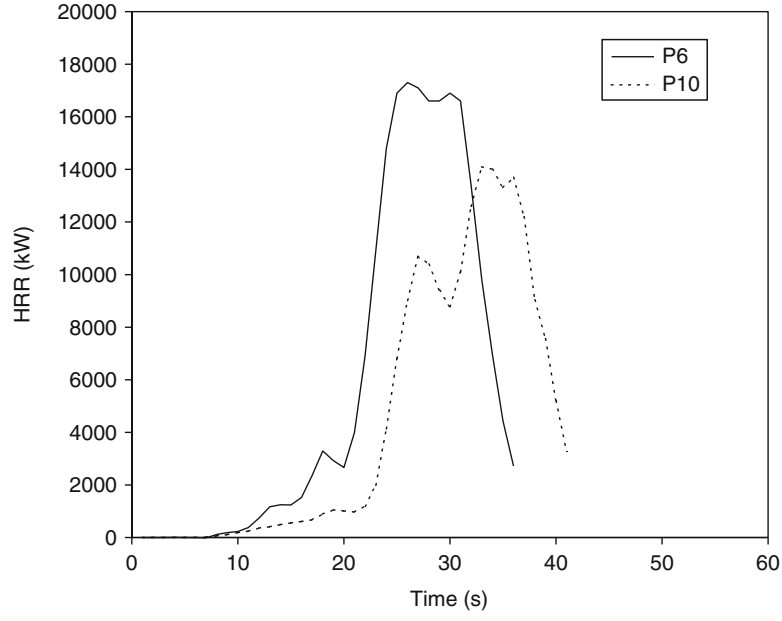

Fig. 26.56 HRR of pallets of packaged, larger arrays of computer monitors

computer monitors (US models, 430 mm [17″] screen) packed in shipping boxes, plastic coolers, and potato chip bags packed in cardboard boxes. The coolers with both insulated with polyurethane foam and had polyethylene outer shells; the #1 sample had a polystyrene liner while the #2 sample had a polypropylene liner. The computer monitors were padded with

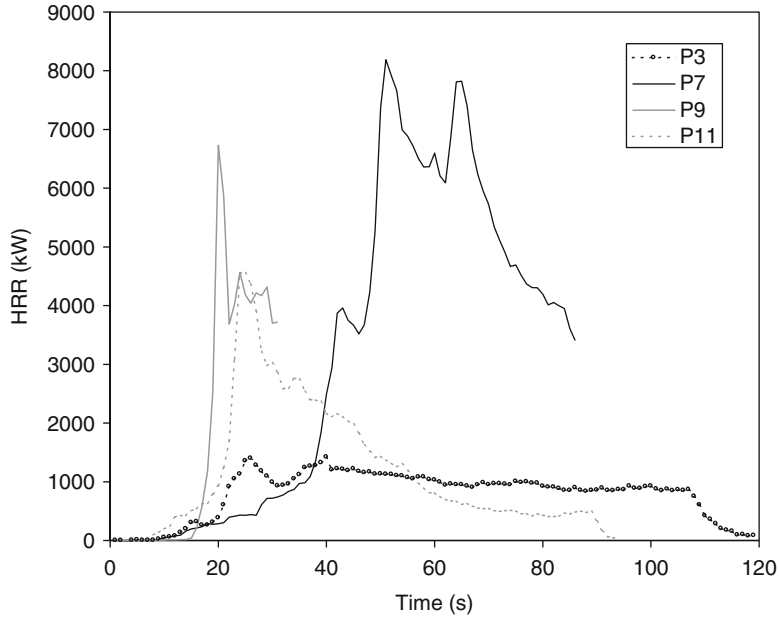

Fig. 26.57 HRR of pallets of miscellaneous computer items

Table 26.12 HRR of packaged household commodities tested by Dillon et al.

Commodity	Mass (kg)	Peak HRR (kW)	Time to peak (s)	Total HR (MJ)
Acrylic yarn skeins	8.7	263	210	127
Computer monitor	24.6	140	398	70
Cooler #1	6.4	400	648	147
Cooler #2	5.2	276	702	128
Potato chips	8.3	322	230	139

expanded polystyrene foam, as is customary for shipping. Their results are summarized in Table 26.12.

A study has been reported on burning pallet loads of organic peroxides [134]. Liquids were packaged in plastic containers within cardboard boxes, while solids were packaged in cardboard drums. The data are given only for a few packaging configurations with sufficient data not being available to generalize HRR predictions to other configurations.

For all rack storage tests, the times are very strongly affected by the ignition source location. Not enough data exist to make general correlations, but Fig. 26.58 illustrates the basic effect. The storeroom test [135] comprised a mocked-up small storeroom in a retail shop, with miscellaneous goods boxed in cardboard boxes, placed on shelving 2.4 m high. A small amount of additional shelving was provided across an aisle 1.4 m wide. The FMRC test involved pallets in a 2 × 2 × 2 arrangement. In the storeroom test, ignition was at the base of the face of the 'main' storage rack. The FMRC test [136] used the standard FMRC procedure whereby an igniter is also placed at the base, but is located internally, at the two-way intersection of flue spaces between piles. The data for the storeroom test are plotted as real time, while the FMRC test data were shifted 470 s to make the steep HRR rise portions coincide. From a comparison of this kind, one can roughly estimate that igniting a rack at the front face causes events to occur 470 s later than would happen if ignition were at the center of the flue spaces.

Kiosks

NIST have reported [137] some HRR results on full-scale tests of kiosks. These are the booths used in shopping malls, exhibitions, and other

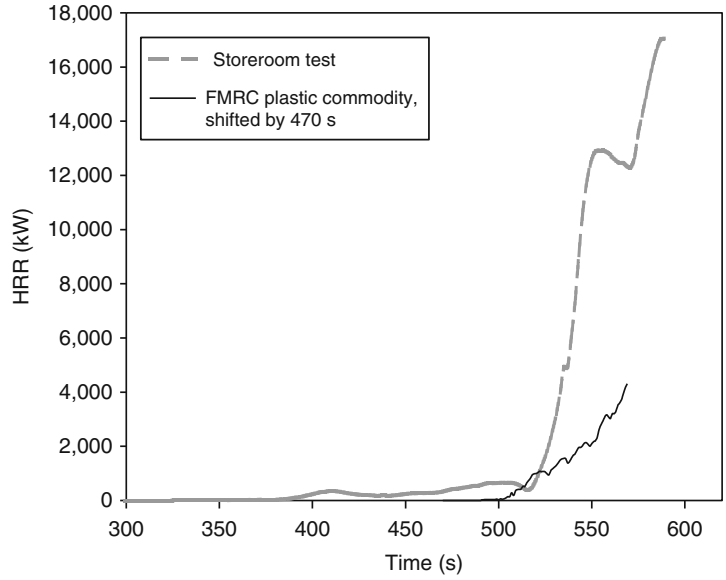

Fig. 26.58 Effect of ignition source location on fire development

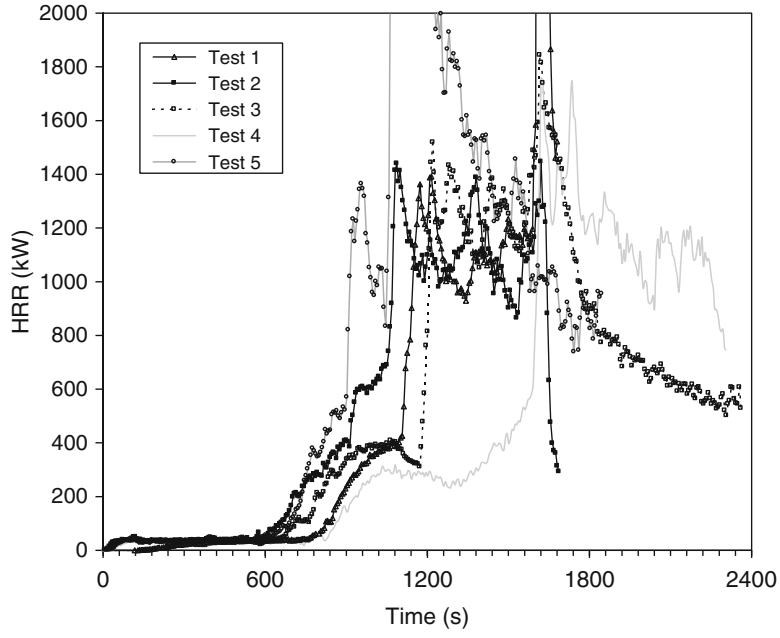

Fig. 26.59 HRR of display kiosks

places wherein a small amount of merchandise display or sales occur. Some HRR curves are illustrated in Fig. 26.59 for a kiosk, built largely of wood, which measured 1.2 m × 1.2 m × 2.1 m high. Tests 2–5 are all of the same sized kiosk, but refer to various configurations of the openable panels. Test 5 appears to have been more severe since all the panels were closed. Test 1 involved the same kiosk placed in a room, rather than in the furniture calorimeter.

Luggage

At the LSF Laboratories, Messa [138] tested the HRR of two suitcases filled with clothes. Ignition was with a square-ring burner applying approximately 5.5 kW. The test articles are described in Table 26.13 and the results are given in Fig. 26.60.

Magazine Racks

Chow et al. [139] conducted full-scale tests on several steel magazine racks, holding magazines, newspapers, and books. Ignition was with a small pool of gasoline. Test details are given in Table 26.14, while HRR results are shown in Fig. 26.61. The larger ignition source used Test 2 led to much greater HRR, despite the fact that the mass of paper goods was smaller than in Test 3. While all tests were conducted in an ISO 9705 room, the large HRR in Test 2 was evidently attributable to room-effect radiant heat flux reinforcement, which was of less significance for the other tests. Thus, for design purposes, only Tests 1 and 3 should be considered, unless the end-use environment is a relatively small room.

Table 26.13 Test description for suitcases tested at LSF

Condition	Soft suitcase	Hard suitcase
Mass empty (kg)	0.98	5.20
Mass filled (kg)	3.06	10.34
Burner HRR (kW)	5.5	5.5
Burner application time (s)	180	240
Total heat released (MJ)	33.4	139.0

Mattresses

Despite the relatively simple shape of mattresses, the prediction of mattress HRR from bench-scale data is difficult. Even the use of full-scale HRR data is problematic, due to a peculiarity of mattress fires. Most other combustibles interact only modestly with their environment, until large HRR values are reached or until room flashover is being approached. Liquid pools on the other hand, as discussed below, interact very strongly with a room, if either the room size or the available ventilation are not very large in comparison to the pool's HRR. The identical phenomenon is

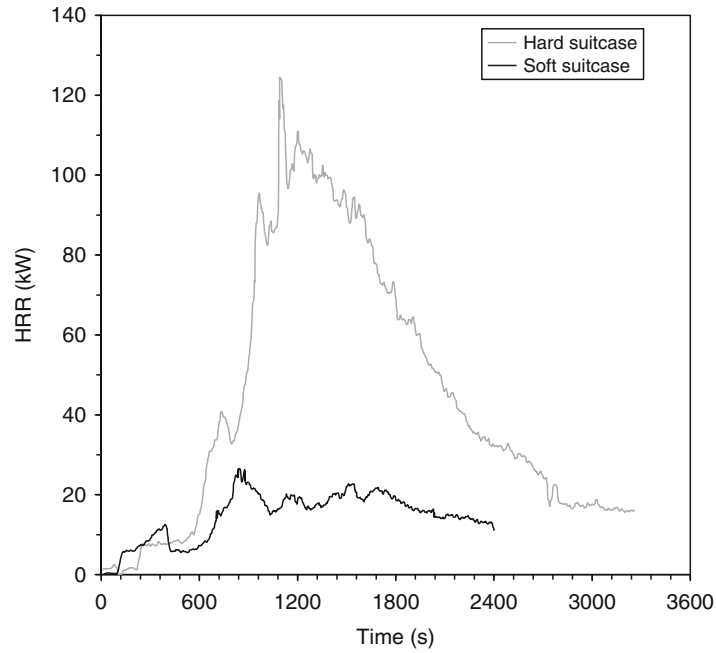

Fig. 26.60 HRR of suitcases

Table 26.14 Details of magazine rack tests

Test no.	Size of each rack (WxH), m	Location of racks in room	Mass of paper goods (kg)	Ignition source, quantity of gasoline (L)
1	1 × 2.2	Left, back	15	2
2	2 × 2.2	Back, right	60	15
3	2 × 2.2	Left, back, right	90[a]	3

[a]Of which 15 kg was placed on floor, in front of racks

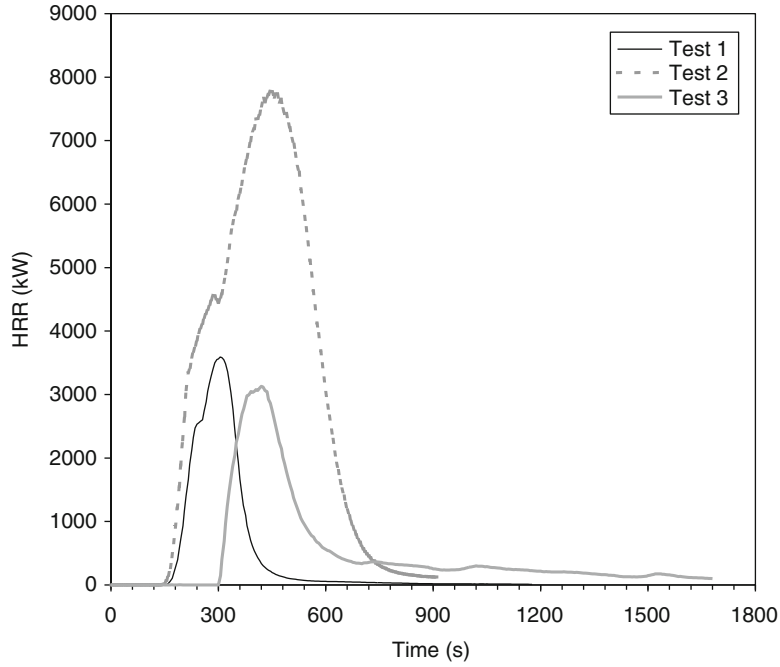

Fig. 26.61 HRR of magazine racks loaded with magazines, newspapers, and books

Table 26.15 Some mattress HRR data; full-scale data are for small or no room effect, bench-scale data are peak values, taken at 25 kW m^{-2} irradiance

Padding material	Ticking material	Combustible mass (kg)	Peak HRR, full-scale (kW)	Bench-scale HRR (kW m^{-2})
Latex foam	PVC	19	2720	479
Polyurethane foam	PVC	14	2630	399
Polyurethane foam	PVC	6	1620	138
Polyurethane foam	Rayon	6	1580	179
Polyurethane foam	Rayon	4	760	NA
Neoprene	FR cotton	18	70	89
Cotton/jute	FR cotton	13	40	43

observed with mattresses. Thus, there may not be a single value of the HRR of a mattress, the HRR having to be considered related to the room itself.

Some example data are compiled in Table 26.15 to illustrate the peak full-scale HRR values that are found for common material combinations [45]. The full-scale test protocol used a complete set of bedding; ignition was achieved with a wastebasket. Figure 26.62 illustrates the relation of bench-scale to full-scale

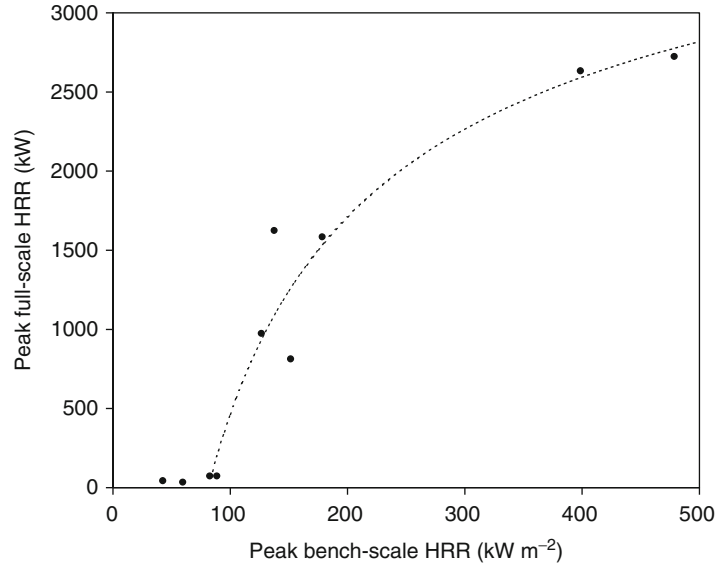

Fig. 26.62 HRR of mattresses predicted from bench-scale results. Full-scale tests under conditions of negligible room effect; bench-scale HRR measured at 25 kW m^{-2} irradiance

Table 26.16 Some mattress HRR data; full-scale data include room effect of small bedroom

Padding material	Ticking material	Combustible mass (kg)	Peak HRR, full-scale (kW)	180 s avg HRR, bench-scale (kW m^{-2})
Polyurethane foam	Unidentified fabric	8.9	1716	220
Melamine-type PUR/cotton batting/polyester fiber pad	Polyester/ polypropylene	NA	547	169
Polyurethane foam/cotton batting/ polyester fiber pad	Unidentified fabric	NA	380	172
Polyurethane foam/polyester fiber pad	PVC	NA	335	195
Melamine-type PUR	FR fabric	15.1	39	228
FR cotton batting	PVC	NA	17	36
FR cotton batting	Polyester	15.7	22	45
Neoprene	PVC	14.9	19	31

data from the same data set, where full-scale testing was done under conditions not leading to significant room fire effect. Not enough specimens were tested to develop a usable correlation, so the results should be taken only as indicative.

King-size mattresses dating from before the Federal HRR regulations can produce very high HRR values, even absent a room effect. NIST [140] tested a king-size bed assembly which contained box springs and an innerspring mattress consisting of polyurethane foam and felted cotton padding. Additional bedding included two pillows, pillowcases, two sheets, and a comforter. Two tests were run in an open calorimeter—in one test, an electric match was used to ignite the bed, while in the other test a newspaper-filled wastebasket was the ignition source. Unlike the typical findings in the case of upholstered furniture, here the ignition source type had a major effect, with the larger ignition source resulting in a peak HRR over 5000 kW, while the smaller only showed about 3500 kW and burner a longer

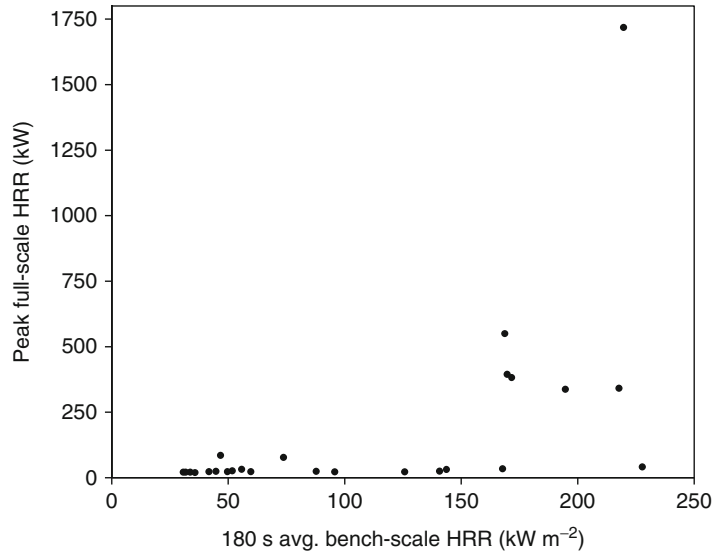

Fig. 26.63 HRR of mattresses predicted from bench-scale results. Full-scale tests under conditions of significant room effect; bench-scale HRR measured at 35 kW m^{-2} irradiance

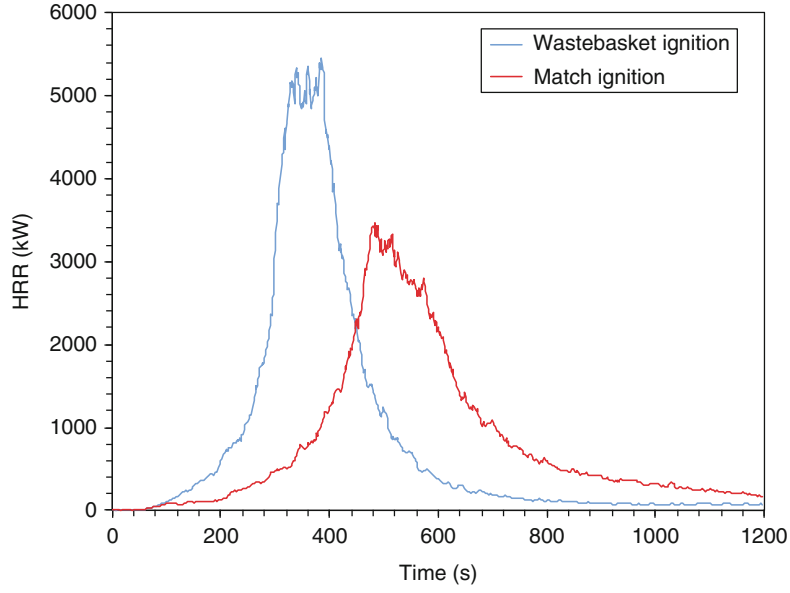

Fig. 26.64 Effect of ignition source on king-size bed assemblies

time at a slower rate (Fig. 26.64). In either case, however, the HRR values would suffice to cause flashover in a bedroom environment, especially in view of the fact that the HRR would be much higher due to room effect augmentation.

Some full-scale data obtained under conditions where a strong room interaction effect was seen are shown in Table 26.16 [141, 142]. The full-scale test setup was different for this data set, in that no bedding was used and ignition was with a burner flame at the edge of the mattress. Thus, some mattresses were able to show essentially zero HRR since bedding was not available to sustain burning, and the ignition source could be 'evaded' by receding specimens. A relation between full-scale and bench-scale

Table 26.17 Results on mattress from the CBUF study

Pk. HRR furn. calor. (kW)	Pk. HRR room (kW)	Springs	Thick. (mm)	Thick. factor	$\dot{q}''_{60}$	$\dot{q}''_{180}$	$\dot{q}''_{180} \times$ th. fac.	q''_{tot}	Prop. fire
26	42	Sofabed	22	0.44	162	135	59	50	N
31	45	N	50	1.00	136	82	82	21	N
47	61	Y	10	0.20	225	227	45	43	N
47	NA	Y	20	0.40	111	118	47	45	N
275	NA	N	90	1.00	111	118	118	45	Y
348	471	Y	20	0.40	327	159	64	30	Y
313	1700	N	100	1.00	256	191	191	62	Y
917	2550	N	140	1.00	232	198	198	37	Y

results from this study is shown in Fig. 26.63. The behavior in that study was found to be:

- Mattresses with a bench-scale HRR (180 s average value) of < 165 kW m^{-2} led to room fires of less than 100 kW.
- Mattresses with a bench-scale HRR (180 s average value) of > 165 kW m^{-2} generally led to room fires on the order of 1–2 MW.
- The transition between those extremes was very abrupt.

The sharp transition between trivial fires and room flashover conditions can be attributed to the details of the test room, but also to the use of an ignition source which specimens of intermediate characteristics could 'evade.'

Additional data on mattress HRR have been published by SP [143], Lund University [144], and in the CBUF project [10]. The CBUF study included full-scale room fire tests, open-burning furniture calorimeter tests, and Cone Calorimeter tests. The mattress results are given in Table 26.17. In both of the full-scale test environments, no bedding was used, but a square-head burner was applied to the top surface of the specimen, precluding complications from any receding-surface behavior. The bench-scale test data presented were obtained at a 35 kW m^{-2} irradiance. The results indicate that, when tested in the standard ISO 9705 room, a very drastic room effect occurs for open-air HRR values over about 300 kW.

The bench-scale data indicated that when widely varying mattress thicknesses exist, a simple relation of bench-scale to full-scale HRR cannot be sought, even if only predictions of open-burning (furniture calorimeter) results would be desired. As a first cut, it was concluded that mattresses can be grouped into two groups—those leading to propagating fires (the mattress being consumed in flaming combustion during a relatively short time), and those that do not. The former can be considered to be of the highest hazard, while the latter present only trivial hazard. Since, for practical reasons, all mattress composites must be tested in the Cone Calorimeter using a 50 mm thickness, to take into account effects due to thin mattresses, a thickness factor is defined:

$$Th.fac. = \min\left(\frac{thickness, mm}{50},\ 1.0\right)$$

For mattresses where the innersprings are used, the thickness is measured from the top of the mattress down to top of the metal springs; it is not the total thickness. To determine whether the mattress fire will propagate or not, the following rules were developed:

If $\dot{q}''_{180} \cdot (Th.fac.) < 100$ kW m^{-2}
and

$$\dot{q}''_{60} < 250 \text{ kW m}^{-2}$$

then,

$\dot{Q} < 80\ kW$ (non-propagating fire)

else,

$\dot{Q} > 80\ kW$ (propagating fire)

The HRR values over 80 kW in fact are flashover values of up to 2.5 MW, but the scheme does not assign a specific HRR number. Qualitatively, this scheme reflects the type of abrupt behavior change found in earlier studies

(Fig. 26.63), but here some more refined rules were developed that avoid non-predictions which would occur from simple correlation. During the same CBUF project, a more sophisticated mattress fire model has been developed by Baroudi et al.; this model is not easy to use, but details are available [10, 145].

In the US, mattresses made after July 1, 2007 have been required by law to conform to the 16 CFR 1633 standard of the Consumer Product Safety Commission. The latter augments the previous standard (16 CFR 1632) for smoldering by a flaming test procedure. The primary requirement for the new standard is that the peak HRR not exceed 200 kW; in addition the total heat release during the first 10 min of test must not exceed 15 MJ. NRCC [72] tested an example of one such mattress and did confirm a peak HRR < 200 kW. However, a room fire test run with this same model of mattress, an equally-conforming mattress foundation, and a set of bedding produced a peak HRR of 1812 kW. This would likely lead to flashover in a room of the ISO 9705 room size and doorway dimensions. Another test run by NRCC showed an extreme radiant feedback effect, since mattresses not made to the Federal standard typically showed HRR values in excess of 3000 kW even for small mattress sizes, while a bunk bed attained > 6000 kW in the room test.

Mining Equipment

Hansen and Ingason [146] tested two pieces of mining equipment, burning them in an underground mine facility. The first item was a Toro 501 DL diesel-powered wheel loader. The machine weighs 36,000 kg and stands 2.85 m tall. The structure is steel, but it also contains rubber tires, hydraulic oil, diesel fuel, and smaller components, including driver's seat, cables, etc., for an estimated fuel content of 76 GJ, the majority of this being the giant tires. The second item was a Rocket Boomer 322 drilling rig. This item weighs 18,400 kg and stands 2.95 m tall. Its fuel content was estimated at 46 GJ, with the fuel comprising hydraulic oil, hoses, tires, diesel fuel, cables, and

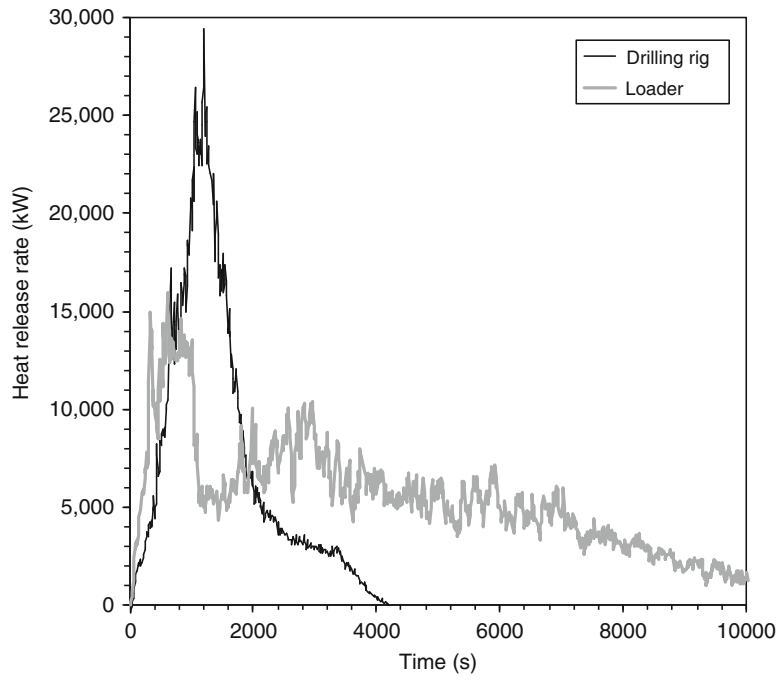

Fig. 26.65 HRR for two types of mining equipment

miscellaneous smaller items. With both items, the fuel tank was partly emptied and poured out to create a pool fire under the specimen, and this pool was ignited to start the fire. Figure 26.65 shows the HRR results, with loader achieving a peak value of 15.9 MW, while the drilling rig showing 29.4 MW.

Office Furniture

Office worker cubicles ('workstations') have been tested in several projects at NIST [147–149]. Figure 26.66 show that severe fire conditions can be generated by these arrangements. In some cases, fires of nearly 7 MW were recorded from the burning of a single person's workstation. The identification of the main conditions in these tests is given in Table 26.18. In one test series [147] replicates were tested in an open furniture calorimeter, then the configuration was tested again in a room test; this is illustrated in Fig. 26.67.

In 2004, NIST [150] reported results of some tests of modern office furniture, i.e., primarily plastics-based. Two full-scale tests were conducted, a single person cubicle, and a four-person cluster of cubicles. The one-person cubicle was tested in an open environment, while the four-person cluster was in a semi-open arrangement: three walls and a ceiling were present, but not the fourth wall. The results (Fig. 26.68) indicate both a radiant augmentation due to the ceiling and an augmentation due to multiple fuel

Table 26.18 Workstations tested by NIST in 1988 and 1992

Code	Combustible mass (kg)	Description	Number of sides w. acoustic panels	Ref.
A	291	Mostly old-style wood furniture	0	146
B	291	Semi-modern furniture	1	146
C	335	Modern furniture	2	148
D	NA	Modern furniture	3	148
E	291	Modern furniture	4	146
F	NA	Modern furniture	4	148

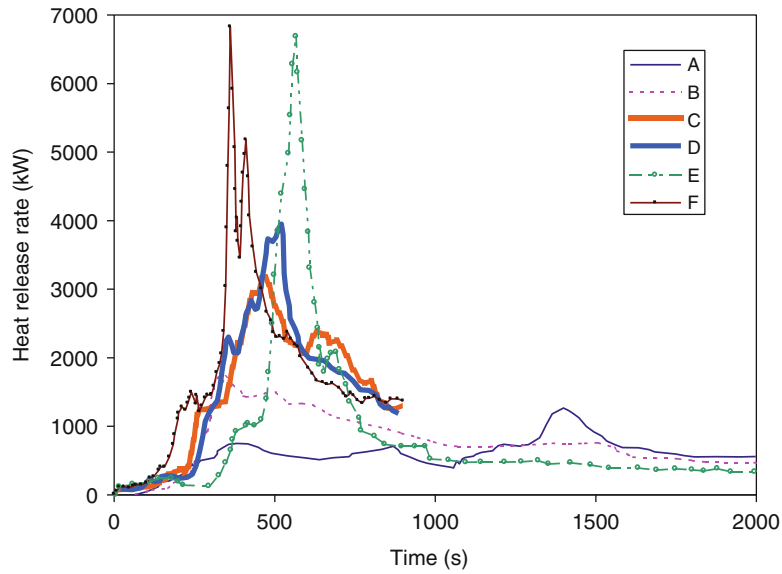

Fig. 26.66 HRR of office workstations tested by NIST in 1988 and 1992

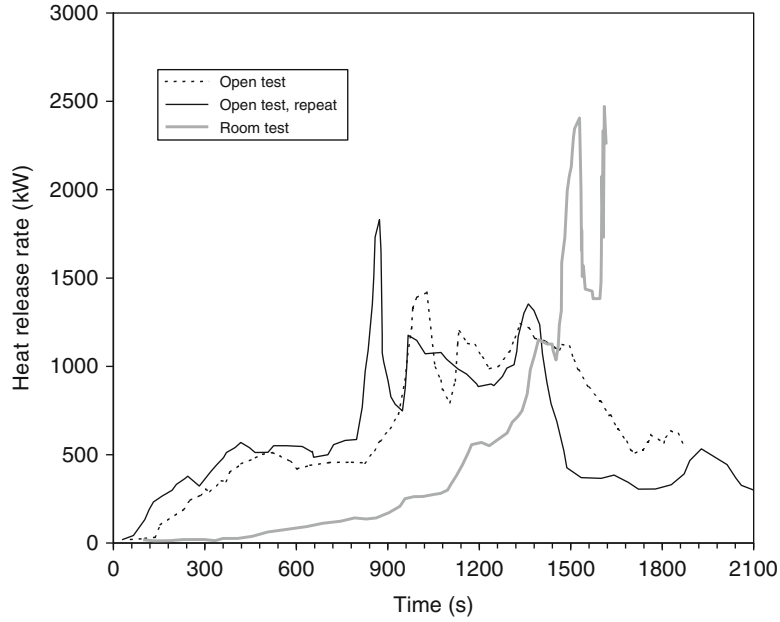

Fig. 26.67 NIST results for workstation tests of 1988 and 1992

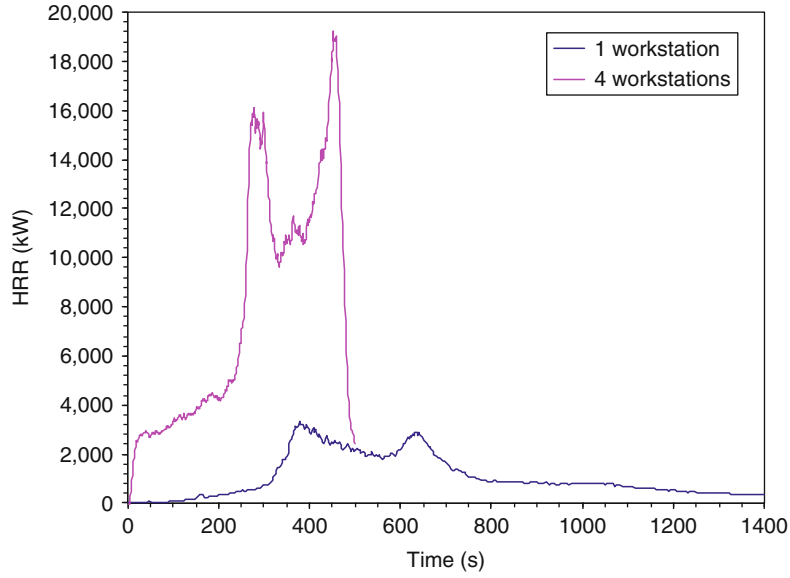

Fig. 26.68 NIST results for workstation tests of 2004

loads being present in direct proximity. In that same study, NIST also ran open calorimeter tests on two office chairs, a swivel chair and a chair with a fixed metal frame (Fig. 26.69). The gross mass for the chairs were 20.5 kg, and 11.8 kg, respectively, but the mass of the combustible portions was not evaluated, although the major fraction of the total mass was the mass of the steel components. The swivel chair had major components comprising hard-plastic shell material, and the fire involvement of these components was the cause of the second HRR peak.

Additional tests were conducted by Kakegawa et al. [151] at Japan's National Research Institute of Fire and Disaster. Each test was started by a

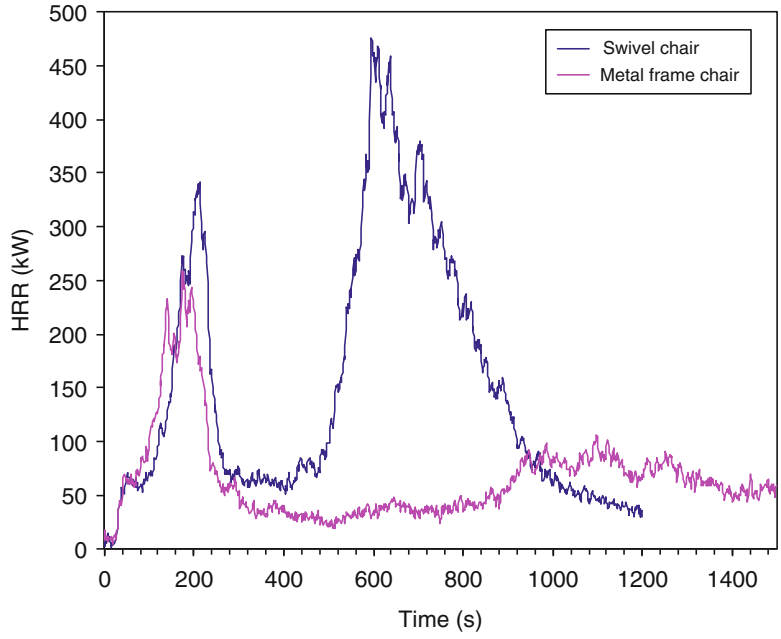

Fig. 26.69 HRR results for the two office chairs tested

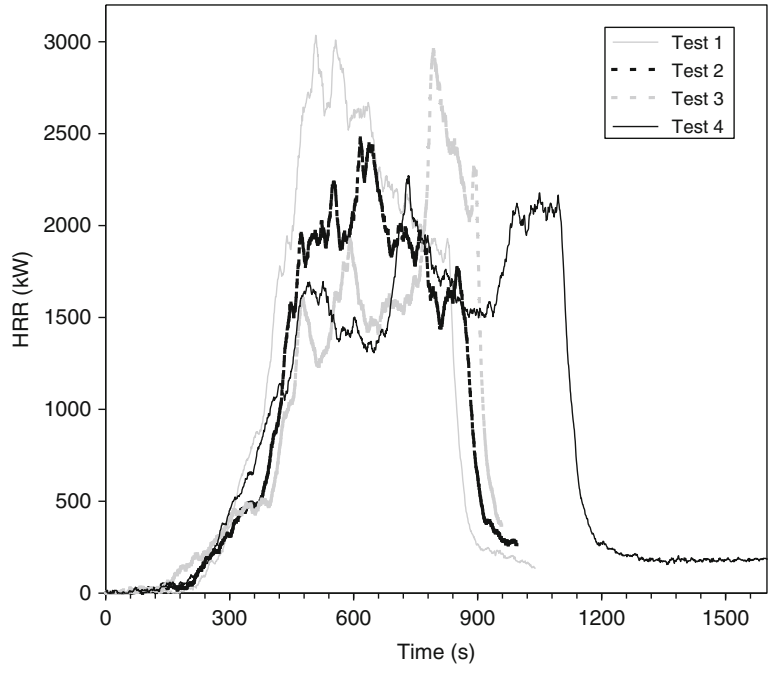

Fig. 26.70 HRR of four-unit workstations tested at NRIFD

polypropylene wastebasket filled with 0.2 kg of paper. The wastebasket, by itself, was found to show a peak HRR of 50–60 kW. The desks were of modern metal-frame construction, with plastic trim parts. In addition, the workstations contained small filing cabinets, telephones, chairs, computers, and a modest amount of office paper. The HRR results for the four-unit

Table 26.19 Workstations tested by NRIFD

Test	Combustible mass (kg)	Type of workstation	No. of desk units	Partition panels	Peak HRR (kW)	Time to peak (s)
1	570	Clerical	4	N	3035	508
2	597	Clerical	4	Y	2476	616
3	1054	Engineering	4	N	2957	793
4	1086	Engineering	4	Y	2271	732
11	272	Engineering	1	Y	1602	441
12	264	Engineering	1	N	1870	412
14	263	Engineering	1	N	1219	601

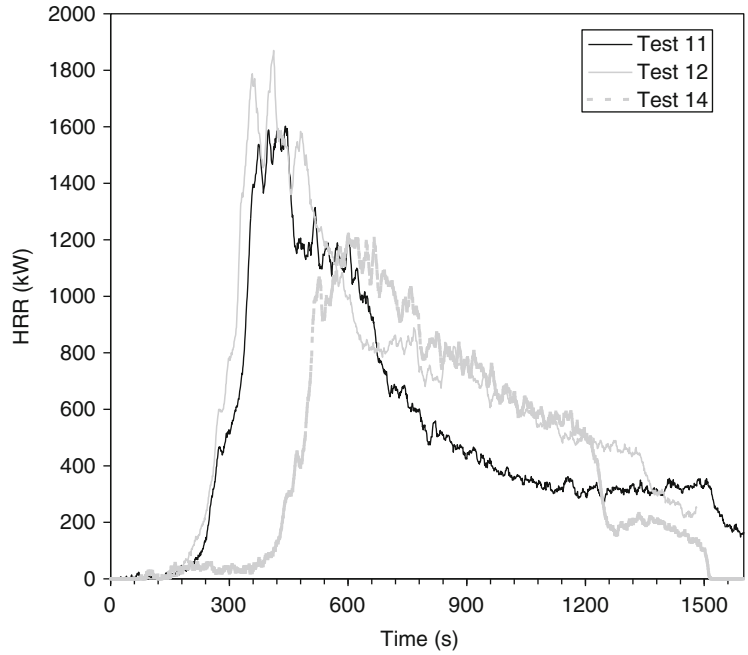

Fig. 26.71 HRR of one-unit workstations tested at NRIFD

workstations are shown in Fig. 26.70, while those for the one-workstation units are shown in Fig. 26.71. Even though the four-unit workstations had a very high fuel load, the HRR values were lower than the American units studied at NIST. This is presumably due to a more protected arrangement of the fuel, plus the fact that only short (0.45 m high) partition panels were used (Table 26.19).

Pallets

Conceptually, a wood pallet is a similar arrangement to a wood crib. The geometry, however, is different. Instead of being composed of identical rows of square-section sticks, pallets are made up of rectangular elements in a traditionally dimensioned configuration as shown in Fig. 26.72. The fire safety concern with pallets arises when they are idle and stacked many units high. Krasner [152] has reported on a number of tests where the burning rate of pallets was measured. A typical experimental heat release rate curve is shown in Fig. 26.73. This curve shows that, much like for a wood crib, a substantially constant plateau burning can be seen if the stack is reasonably high. The results for a standard pallet size of 1.22 × 1.22 m can be given as a general heat release rate expression

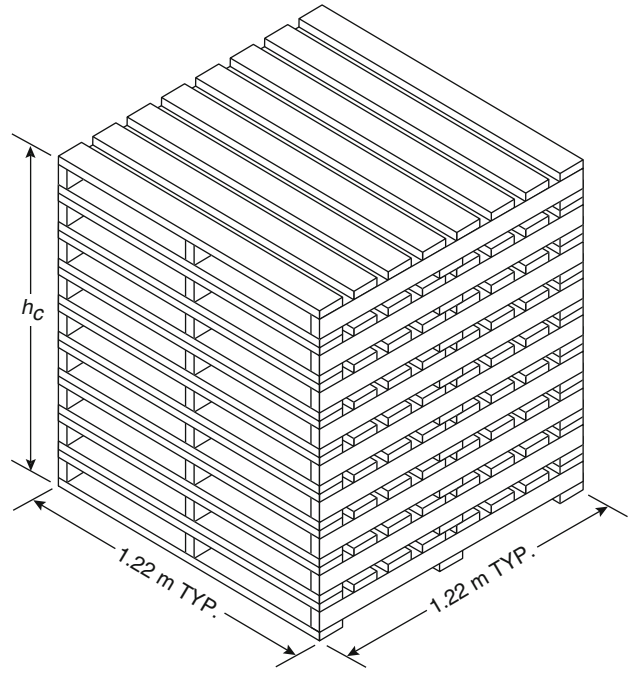

Fig. 26.72 The geometric arrangement of a stack of wood pallets

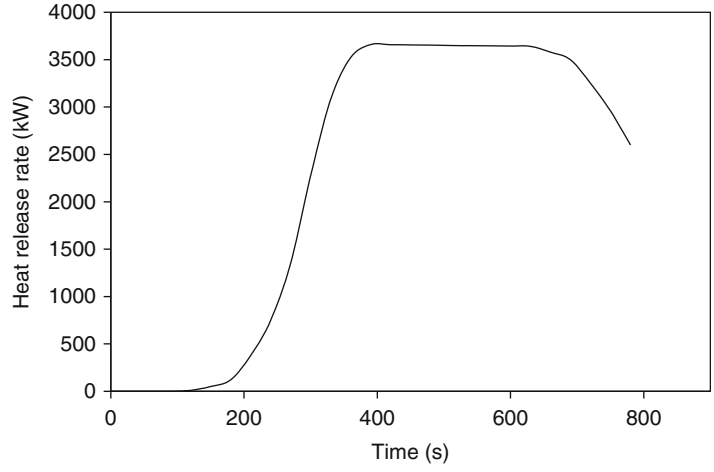

Fig. 26.73 HRR of a typical wood pallet stack (1.22 × 1.22 × 1.22 m high)

$$\dot{q} = 1368\left(1 + 2.14h_p\right)(1 - 0.03M) \qquad \dot{q}'' = 919\left(1 + 2.14h_p\right)(1 - 0.03M)$$

where h_p is stack height (m), M is moisture (%), and a net heat of combustion of 12×10^3 kJ kg^{-1} has been assumed. For convenience in applying to nonstandard pallet sizes, this can be expressed on a per-unit-pallet-floor-area basis as:

The agreement between the above equations and experimental data is seen to be good over a wide range of pallet heights (Fig. 26.74), but the expressions do somewhat overpredict the burning rates if applied to short stacks, with stack height $h_p < 0.5$ m.

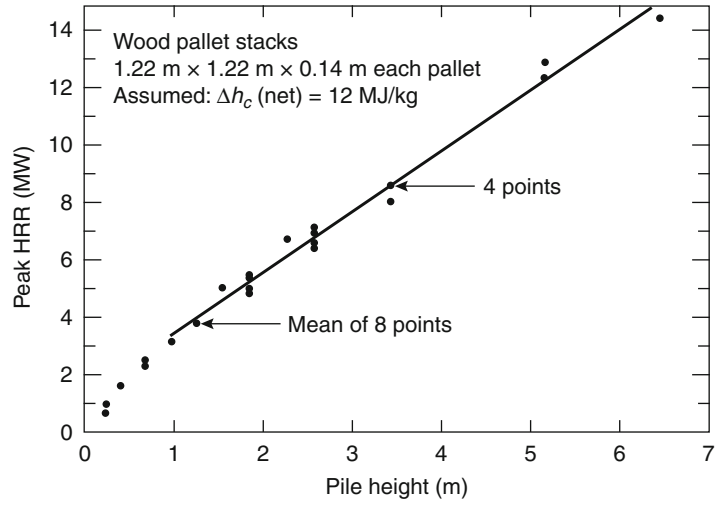

Fig. 26.74 Dependence of pallet HRR on stack height

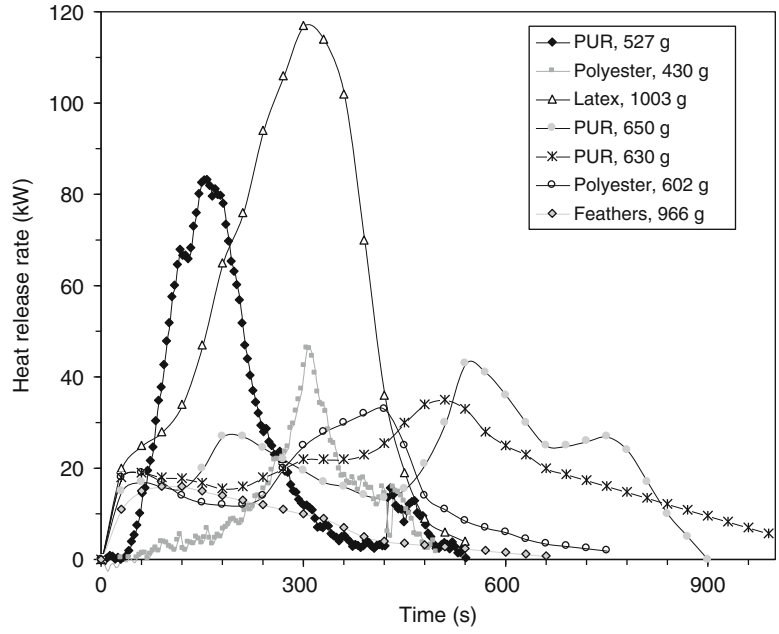

Fig. 26.75 HRR of pillows

Pillows

Pillow tests have been reported by NIST [153] and SP10. The results are given in Fig. 26.75.

Pipe Insulation

The available data are from the configuration where pipe insulation is used to entirely cover the ceiling of a test room. The test method used is a variant of ISO 9705 especially configured for pipe insulation testing [154]. Data on this configuration have been published by Wetterlund and Göransson [155] and by Babrauskas [156].

Plants and Vegetation

Trees, Natural

Some tests on Christmas trees were reported by VTT [157] and by Damant and Nurbakhsh [158].

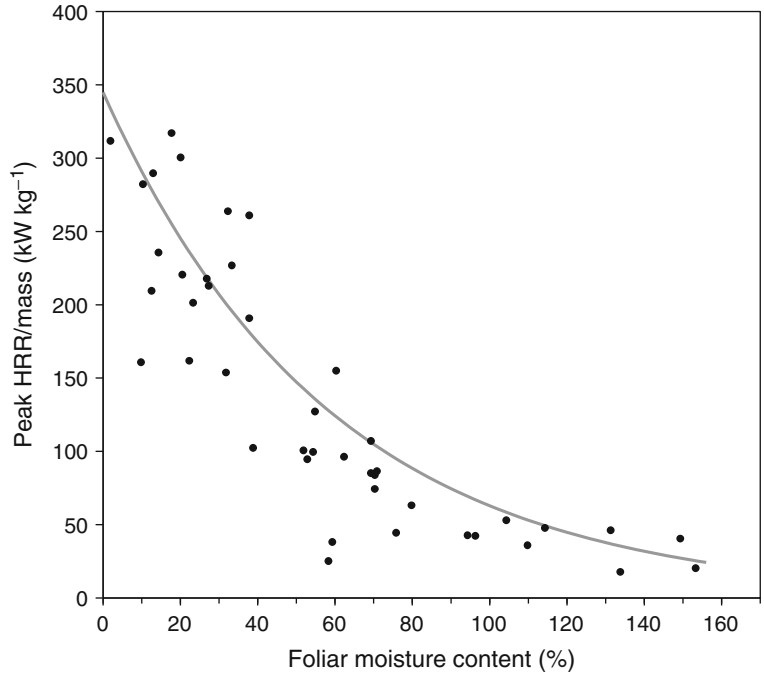

Fig. 26.76 The peak HRR for Douglas-fir Christmas trees, as a function of moisture and mass

Newer studies, however, indicated that these tests, which examined only a few trees, did not capture the full range of HRR values associated with Christmas trees. The main variables that govern the HRR of Christmas trees are the following:

- Moisture content of the needles
- Mass of the tree
- Species
- Ignition source used

Moisture is the dominant variable and this had not been studied previously. The results of an extensive series of fire tests [159] on Douglas-fir (*Pseudotsuga menziesii*) trees are shown in Fig. 26.76, while the HRR of a typical test is illustrated in Fig. 26.77. The trees were about 2.1 m tall, had an average mass of 11 kg. The trees were cut, placed in a watering stand, and watered according to various watering programs. The average tree was kept for 10 days prior to testing. The relation of the curve fit in Fig. 26.76 is:

$$\dot{q}/mass = \frac{400}{1 + 0.0538MC}$$

where MC = foliar moisture (%) and the units of $\dot{q}/mass$ are kW kg^{-1}. Moisture is measured on a dry basis, so values can readily exceed 100 %; also note that it is the needle (foliar) moisture that governs the burning behavior—trunk moisture is not a relevant variable. The mass of the tree used here is the entire mass; Evans et al. [160] suggested that if data are available only for the foliar mass, but not the mass of the entire tree, the approximation be used:

$$mass = 2 \times mass_{foliar}$$

To ignite trees with a small flame requires that the moisture content be below 50–60 %. Otherwise, ignition is still possible if using larger combustible objects. In the work reported, the trees which could not be ignited by a small flame were all ignited by first igniting wrapped gift packages placed under the tree. For design purposes, it should be adequate to assume that the heat release curve is a triangle. This requires knowing only the peak HRR and the total heat released. To estimate the latter, it was found in the tests that the Christmas trees showed an effective heat of combustion of 13.1 MJ kg^{-1}. Thus, from knowing the mass of the tree and the effective heat of combustion, the total heat

release may be estimated. The needle moisture may not be known for design purposes. It is governed both by the watering program and by the innate biology, e.g., the species, of the tree. No model is available at the present time that can predict the moisture. However, the research indicated that Douglas-firs are a notably short-lasting species. The data points shown in Fig. 26.76, with one exception, represent trees that had been on display for less than 16 days; some were watered carefully and regularly, while others were not. Other species of Christmas trees, such as Noble fir or Fraser fir are considered to be longer-lasting, but are less commonly bought.

A smaller test series on Scotch pine trees was tested at NIST by Stroup et al. [161]. They examined trees of 2.3–3.1 m height and mass between 9.5 and 20.0 kg; with one exception, the trees were of mass 12.7 kg or greater. Apart from one tree, which is not considered here since it was not successfully ignited, the trees were left without water for 3 weeks in a room at 50 % RH and 23 °C. Ignition was with an electric match to a lower branch of the tree. The Scotch pines were substantially taller and heavier than the Douglas-firs, so it is not surprising that higher peak HRR values were attained. The peak HRR values ranged from 1620 to 5170 kW. Normalized per mass, the average was 183 kW kg^{-1}, with the range being 103–259 kW kg^{-1}. The moisture of the branches was not recorded, but presumably was <20 % in all cases. Comparing to the above results, Douglas-firs showed about 160–330 kW kg^{-1}. This would suggest that there is a species effect and that Scotch pines show a HRR/mass ratio approximately 0.75 of that found for Douglas-firs. This conclusion is very tentative, however, since the test programs did not use the same test protocol. Part of the difference might also be attributed to a height effect, since this cannot separately be taken into account.

Madrzykowski [162] ran more recent tests at NIST on 2.05–2.54 m tall Fraser fir trees with a moisture content of 6–9 %. The peak HRR values ranged from 3231 to 4344 kW, while the mass of the specimens ranged from 10.97 to 13.81 kg, giving an average peak HRR/mass value of 286 kW kg^{-1}, with a range of 218–348 kW kg^{-1}. The author also ran one interesting test where a tree was burned lying on its side, instead of vertical. This gave a much lower peak HRR value of 1603 kW, indicating a major role of geometry.

Jackman et al. [163] tested Noble fir and Norway spruce specimens. For a relatively dry (26 % MC) Noble fir (16.3 kg, 3.07 m tall) they got a peak HRR of 2880 kW. A similar Norway spruce (20 % MC, 14.9 kg, 3.02 m high) showed only 1590 kW. Because very few tests were run, this should not be taken to indicate an intrinsic species effect.

Bushes, Natural

Stephens et al. [164] tested Tam juniper (*Juniperus savina tamariscifolia*) shrubs of various moisture contents, ignited by a medium gas flame. For MC < 50 %, rapid combustion resulted and samples showed 1800–2100 kW peak HRR. Specimens of 50–80 % MC typically showed 600–800 kW, while specimens of higher MC did not burn significantly. Unfortunately, neither the mass nor the size of the specimens were specified, except that they were denoted as "mature." Shrubs of this species in general reach about 0.45 m height and cover about 1 m of width.

Etlinger [165] conducted more extensive tests on a series of decorative-shrub species: Armstrong juniper (*Juniperus chinensis* 'Armstrongii'), hedge saltbush (*Rhagodia spinescens*), milkflower cotoneaster (*Cotoneaster lacteus*), mountain lilac (*Ceanothus ray* 'Hartman'), oleander (*Nerium oleander*), purple rockrose (*Cistus purpureus*), quail bush (*Atriplex lentiformis*), sageleaf rockrose (*Cistus salvifolius*), Santa Barbaras ceanothus (*Ceanothus impressus* 'Eleanor Taylor'), trailing rosemary (*Rosmarinus officinalis* 'Prostrata'), and vine hill manzanita (*Arctostaphylos densiflora* 'Howard McMinn'). The bushes were typically in the range of 0.5–1.0 m tall and weighed 1–3 kg. He ignited the bushes first with a 40 kW burner, which did not cause the specimens to show a significant HRR output, followed by an exposure to a 150 kW burner. Some typical results upon exposure to a 150 kW burner are shown in Fig. 26.78.

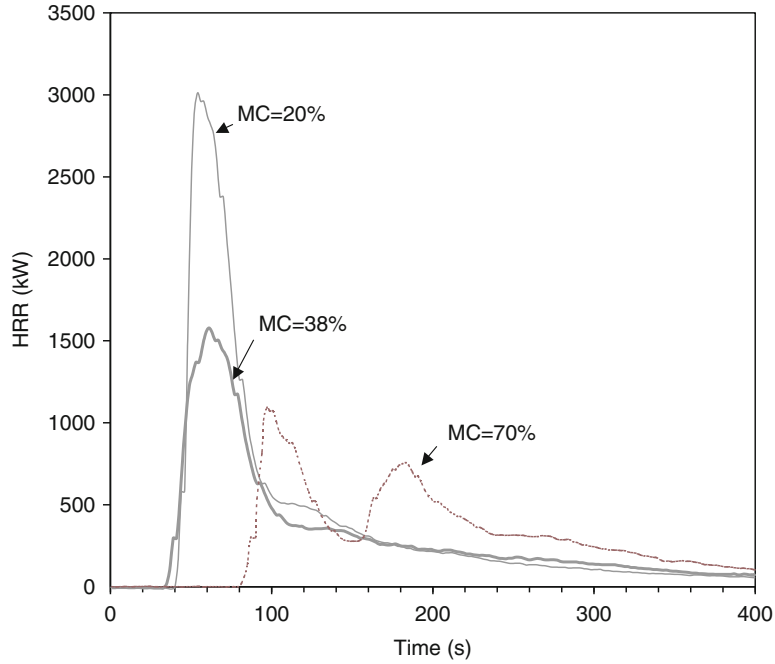

Fig. 26.77 Typical HRR curves of Douglas-fir Christmas trees

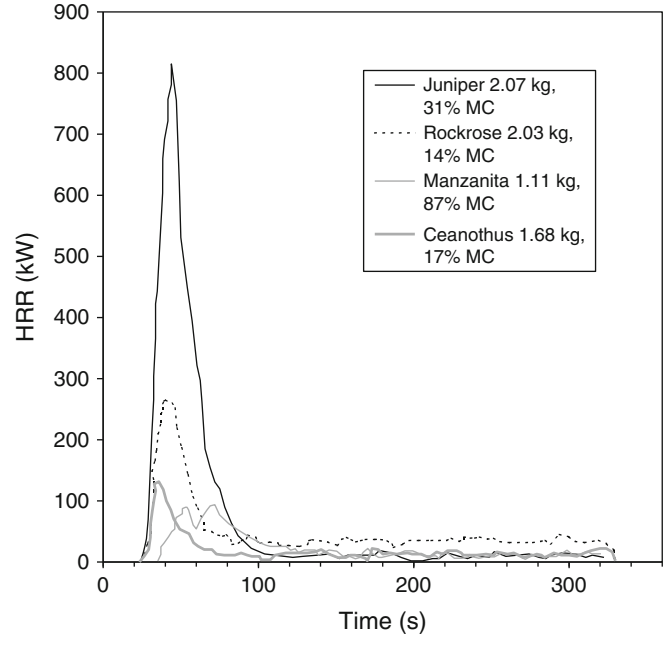

Fig. 26.78 Typical HRR for bushes obtained by Etlinger

A summary of Etlinger's peak HRR values is shown in Fig. 26.79. There is a significant amount of scatter, but the results for the bushes are not systematically different from those for trees, which are also shown on the same plot. Thus, a single expression for the peak HRR can be derived which is suitable for both trees and bushes:

$$\dot{q}/mass = \frac{700}{1 + 0.1295MC}$$

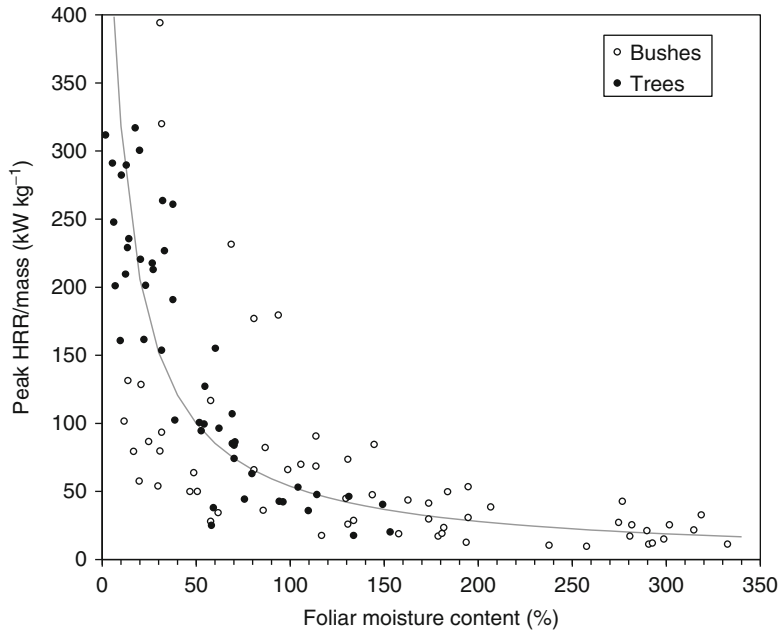

Fig. 26.79 HRR of bushes and trees, plotted on a unified basis

Trees, Plastic

UL had published a procedure for testing artificial Christmas trees. This was identified as Subject 411 [166]. It was eventually withdrawn due to lack of activity in this area, but the basic test procedure is sound. In the UL procedure, the ignition source comprises 454 g of shredded newspaper, conditioned at 35–40 % RH, and dispersed in a 610 mm diameter circle around the base of the tree. The newspaper is ignited at four points around the perimeter of the circle. This ignition source is realistic, since it represents the effect of burning gift packages or decorations at the base of the tree. Babrauskas [167] tested PVC trees of 4.2–4.7 kg mass and 1.96–2.01 m height.

Figure 26.80 shows the results for two replicates using the exact using the UL procedure and a third test where the newspaper was ignited at one point only. The specimens proved impossible to ignite with a small flame, but using the UL procedure they produced rapidly developing fires, with 500 kW being attained 11–20 s after ignition. The peak flame heights of the two specimens ignited in four places was 4.8–5.1 m. Using the Zukoski [168] or McCaffrey [169] flame height/HRR correlations, such flame heights imply peak HRR values of 2800–3100 kW. The values actually measured are systematically low due to two reasons: (1) mixing dilution effects due to use a large, room-sized calorimeter hood; and (2) inability of instrumentation to respond to a fast-growing fire.

Jackman et al. [162] tested three artificial trees (2.0–2.5 m height) and obtained peak HRR values of 100–400 kW. It is not clear whether these low values represent an intrinsically low HRR of these trees (of unspecified plastic) or whether it simply reflects the fact that an ignition source was used which is much less serious than the one in the UL procedure.

Bushes, Plastic

Some HRR data on plastic house plants are shown in Fig. 26.81 [170].

Pools, Liquid or Plastic

Possibly the simplest geometric arrangement of fuel is a liquid (or thermoplastic) pool. Over the last four decades, an enormous number of studies have been conducted where pool burning was

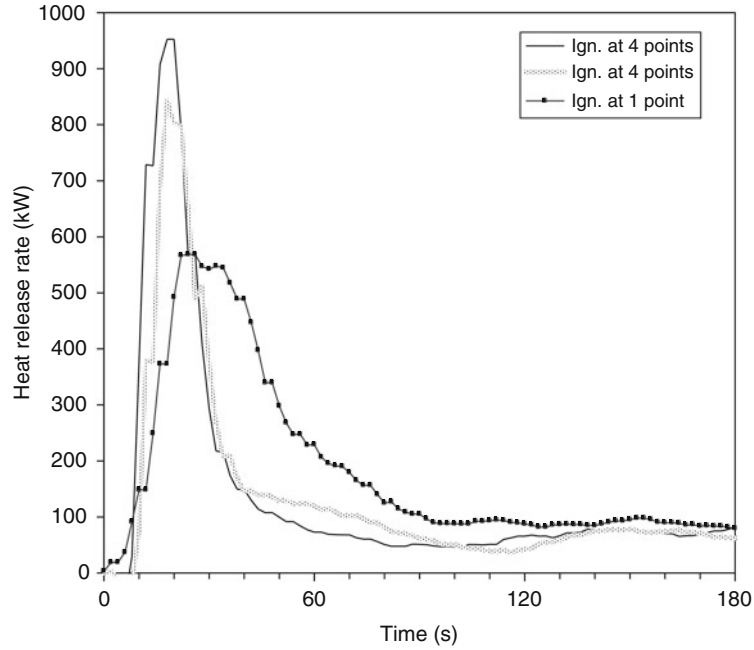

Fig. 26.80 Recorded HRR for PVC Christmas trees (actual HRR was greater, due to very fast rise time)

considered theoretically or measured empirically. The most systematic early study was by two Russian researchers, Blinov and Khudiakov [171]. Their results were analyzed by Hottel [172], who pointed out that conservation of energy can be applied to the pool:

$$\dot{q} = \dot{q}'' \times A = \left(\dot{q}_r'' + \dot{q}_c'' - \dot{q}_{rr}'' - \dot{q}_{loss}''\right) \times \left(\frac{\Delta h_c}{\Delta h_g}\right) \times A$$

where $\dot{q}$ is the heat release rate of the pool; double-prime denotes per unit area; A is the area of the pool (m^2); $\dot{q}_r''$ is the radiant heat flux absorbed by the pool; $\dot{q}_c''$ is the convective heat flux to the pool; $\dot{q}_{rr}''$ is the heat flux re-radiated from the surface of the pool; and into $\dot{q}_{loss}''$ are lumped wall conduction losses and non-steady terms. The heat of gasification is Δh_g (kJ kg^{-1}), while the (lower, or net) heat of combustion is Δh_c. Note that some authors use the symbol L for the heat of gasification. The heat of gasification is defined as the enthalpy required to bring a unit of mass of liquid-phase substance at 25 °C to the gaseous state at the temperature T_b, its boiling point. It should not be confused with the latent heat of evaporation Δh_v, which is the enthalpy required to change a unit mass of liquid to a gas at 25 °C. The relation between these two quantities is:

$$\Delta h_g = \Delta h_v + (T_b - 25) \times C_{pv}$$

where we have taken the simplification that C_{pv}, the heat capacity of the vapor (kJ kg^{-1} K^{-1}) is a constant. An extensive tabulation of these constants is provided by Babrauskas [173].

Table 26.20 The burning regimes for liquid pools

Diameter (m)	Burning mode
< 0.05	Convective, laminar
0.05–0.2	Convective, turbulent
0.2–1.0	Radiative, optically thin
> 1.0	Radiative, optically thick

Hottel's analysis of Blinov and Khudiakov's data showed two basic regimes are possible: radiatively dominated burning for large pool diameters, D, and convectively dominated burning for small D. Furthermore, in the convective regime the flow can be either laminar or turbulent (being always turbulent for radiatively driven pools), while in the radiative regime the flames

can be optically thin or thick. These distinctions can, in the simplest analysis, be made solely on the basis of pool diameter. Such a simple classification is possible if the pool is strictly circular, radiant heating is only from the pool's flames and not augmented by external sources, and there are no interferences to the flow streamlines which could trip the onset of turbulence. In such a simplified case, the regimes can be identified as in Table 26.20.

In the convective limit (small pools), one may make the following approximation:

$$\dot{q} = \dot{q}_c'' \times \left(\frac{\Delta h_c}{\Delta h_g}\right) \times A$$

however, the values of $\dot{q}_c''$ to be taken are not easily determined. Some additional details are given in [174]. For fire hazard analysis purposes, liquid pool fires will rarely be significantly dangerous if they are smaller than about 0.2 m in diameter. Thus, it will often only be necessary to treat pools burning in the radiative regime. In the radiative regime, it is found that data for most organic liquids can be well correlated by:

Table 26.21 Pool burning: thermochemical and empirical constants for a number of common organic fuels

Material	Density (kg m^{-3})	Δh_g (kJ kg^{-1})	Δh_c (MJ kg^{-1})	$\dot{m}_\infty''$ (kg m^{-2} s^{-1})	$k\beta$ (m^{-1})
Cryogenics					
Liquid H_2	70	442	120.0	0.017 (±0.001)	6.1 (±0.4)
LNG (most CH_4)	415	619	50.0	0.078 (±0.018)	1.1 (±0.8)
LPG (mostly C_3H_8)	585	426	46.0	0.099 (±0.009)	1.4 (±0.5)
Alcohols					
Methanol (CH_3OH)	796	1195	20.0	[a]	[a]
Ethanol (C_2H_5OH)	794	891	26.8	[a]	[a]
Simple organic fuels					
Butane (C_4H_{10})	573	362	45.7	0.078 (±0.003)	2.7 (±0.3)
Benzene (C_6H_6)	874	484	40.1	0.085 (±0.002)	2.7 (±0.3)
Hexane (C_6H_{14})	650	433	44.7	0.074 (±0.005)	1.9 (±0.4)
Heptane (C_7H_{16})	675	448	44.6	0.101 (±0.009)	1.1 (±0.3)
Xylenes (C_8H_{10})	870	543	40.8	0.090 (±0.007)	1.4 (±0.3)
Acetone (C_3H_6O)	791	668	25.8	0.041 (±0.003)	1.9 (±0.3)
Dioxane ($C_4H_8O_2$)	1035	552	26.2	0.018	5.4
Diethyl ether ($C_4H_{10}O$)	714	382	34.2	0.085 (±0.018)	0.7 (±0.3)
Petroleum products					
Benzine	740	–	44.7	0.048 (±0.002)	3.6 (±0.4)
Gasoline	740	330	43.7	0.055 (±0.002)	2.1 (±0.3)
Kerosene	820	670	43.2	0.039 (±0.003)	3.5 (±0.8)
JP-4	760	–	43.5	0.051 (±0.002)	3.6 (±0.1)
JP-5	810	700	43.0	0.054 (±0.002)	1.6 (±0.3)
Transformer oil, hydrocarbon	760	–	46.4	0.039	0.7
Fuel oil, heavy	940–1000	–	39.7	0.035 (±0.003)	1.7 (±0.6)
Crude oil	830–880	–	42.5–42.7	0.060	0.62
Solids					
Polymethylmethacrylate	1184	1611	24.9	0.020 (±0.002)	3.3 (±0.8)
Polyoxymethylene $(CH_2O)_n$	1425	2430	15.7		
Polypropylene $(C_3H_6)_n$	905	2030	43.2		
polystyrene $(C_8H_8)_n$	1050	1720	39.7		

[a]See text

$$\dot{q} = \Delta h_c \dot{m}''_\infty \left(1 - e^{-k\beta D}\right) \times A$$

This requires determining two empirical constants: $\dot{m}''_\infty$ and the term $(k\beta)$; the first of these is the asymptotic mass loss rate per unit area as the pool diameter increases towards infinity; the second is the product of the extinction-absorption coefficient k and the beam-length corrector β. These constants are given in Table 26.21 for a number of common fuels.

The net heat of combustion, Δh_c, is also listed in the table. In principle, a slightly lower value, the *effective heat of combustion*, should be used instead of the net heat of combustion that is determined with oxygen bomb calorimetry. Some bench-scale values of a combustion efficiency factor to convert oxygen bomb values into experimentally-measured values are given in Chap. 36, "Combustion Characteristics of Materials and Generation of Fire Products." For most liquids, however, the bench-scale values are not greatly below unity and realistic large-scale measurements are not available, thus the improvement in accuracy by extrapolating from bench-scale results may be nil.

Alcohol fuels show minimal radiative flux, in comparison to other fuel types. Thus, the best recommendation previously had been to use constant values of $\dot{m}''$, independent of diameter. Based on some newer test results [175], it is clear that a diameter effect does exist, although it cannot be expressed in standard form. Thus, it is recommended that for methanol or ethanol the values be used: $\dot{m}'' = 0.015$ (D < 0.6 m); $\dot{m}'' = 0.022$ $(0.6 < \mathrm{D} < 3.0$ m); and $\dot{m}'' = 0.029$ (D > 3.0 m).

The above discussion implicitly assumed that the pool depth is at least several millimeters. If liquids are spilled on a horizontal surface that has no low spots and no diking, then a liquid layer will form that is less than 1 mm thick. *Thin-layer pools* of this nature (which can occur in arson cases) show a lower HRR than do pools of greater depths. Putorti et al. [176] studied gasoline spills on wood parquet, vinyl floor tiles and carpeting. When a specified volume of liquid is spilled, the problem to be solved can be separated into two components: (1) determining the area of the spill, or, equivalently, the spill thickness; and (2) determining the HRR per unit area.

For wood floors, Putorti found the $A = 1.5\ V$, where $A =$ area (m^2) and $V =$ volume (L). For vinyl tile, a similar relation was also found, but the constant being 1.8. Converted into layer thicknesses, the thickness for wood was 0.67 mm

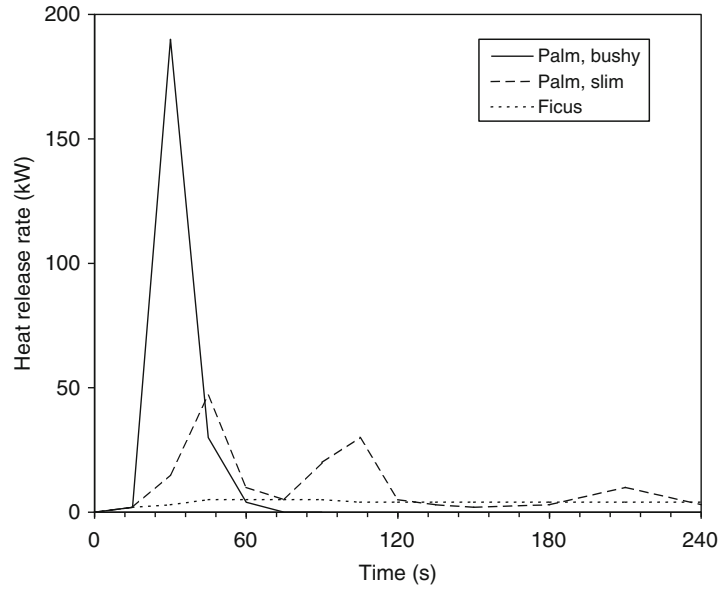

Fig. 26.81 HRR of plastic house plants

and for vinyl tile it was 0.56 mm. Earlier work has indicated that a relation of this kind should only be applied to smooth floor surfaces. For rough, absorptive surfaces a constant thickness is not obtained, and larger spill volumes produce, effectively, greater layer thicknesses [177].

Putorti's study with carpets both indicated large differences between carpet types and also showed that the data could not be represented as a constant layer thickness. The HRR per unit area values are shown in Fig. 26.82. For the solid surface pours, the spill areas were in the range 0.4–1.8 m^2. As presented above, pools of large depths in this size range would show HRR values of 1900–2400 kW m^{-2}. Thus, the carpet-surface values are about 70–80 % of values that would have been computed using the normal pool fire formulas. The smooth-surface values, however, are only about 1/5 of the values that would be found for pools of sizable depths.

A similar study by Gottuk et al. [178] also describes HRR values for spills on hard surfaces that are, very roughly, about 1/5 of those for 'normal' pools. The relationships found by Putorti can only be expected to hold on dead-flat surfaces. If surfaces are crooked, then ponding at low spots will occur and uniform spill depths should never be anticipated.

DeHaan [179] conducted two tests using 1.9 L of Coleman camping fuel. This is a straight-run petroleum distillate containing normal and iso-alkanes ranging from hexane to undecane. When poured on an unpadded carpet, a HRR peak of 1150 was found, with a burning time of roughly 3 min. When poured upon a carpet that had an pad underneath it, a lower HRR peak (890 kW) was found, the peak was slightly delayed (85 s, versus 65 s) and there was a long tail to the HRR curve.

The discussion above pertains only to open-burning fires. Thus, the literature-derived burning rates can be used only in the case of a very large, well-ventilated room (compared to the size of the fire). If calculations show that the 'free-burning' pool would cause a temperature rise of more than, say, 100 °C, then it is clear that radiative feedback will start being important and such an approximation cannot be made. No simple formulas exist for computing the enhanced burning rates when a pool receives significant room radiation. If computations under these conditions are necessary, the theoretical study of Babrauskas and Wickström [11] should be consulted. The computer program COMPF2 [180] can also be used to treat this case.

The problem of pool burning is interesting from a combustion science point of view, and over the years there has been a very large number of studies which attempted to go beyond empirical predictions [181–184]. In addition, work is occurring to provide more detailed experimental measurements for specific fuels [185, 186].

Table 26.22 HRR of European refrigerators

Specimen	R1	R2	R3
Initial mass (kg)	70.0	67.2	43.7
Mass loss (kg)	18.0	14.3	18
Peak HRR (kW)	2125	1816	852
Extinguishment time (s)	925	722	–
Total heat (MJ)	537	404	432

Refrigerators

VTT tested [105] two European refrigerators using a propane burner of 1 kW (designated R1, R2), while EFRA tested a single refrigerator (R3), ignited with a needle-flame burner. The specimens are described in Table 26.22, while test results are shown in Fig. 26.83. The VTT specimens were extinguished before the ultimate peak burning would have occurred, while the EFRA specimen was not. These results must not be applied to appliances used in North America, since European appliance styles are different from North American ones and also because local standards are such as to permit appliances of greater flammability in Europe.

Shop Displays

Chow [187] tested shop displays of three types: clothing display, compact disc (CD) display, and

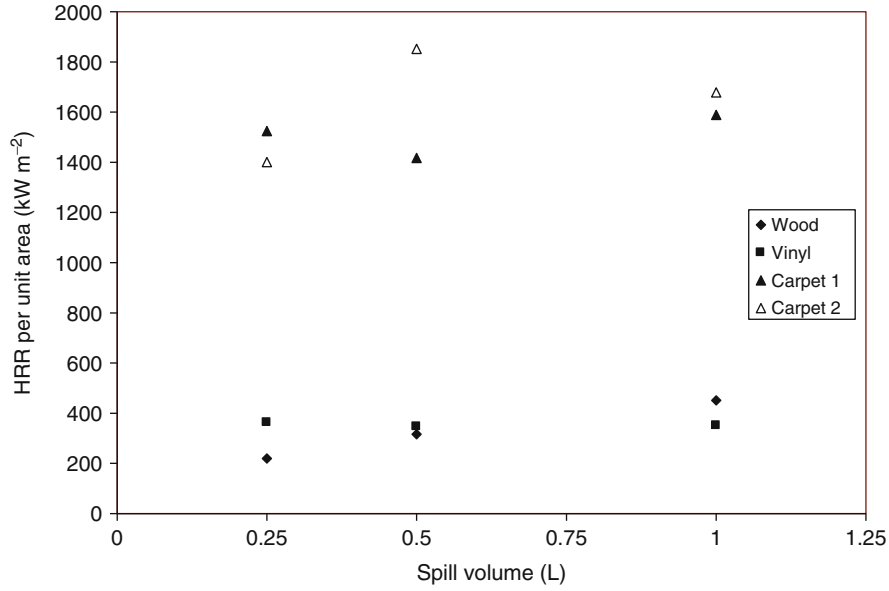

Fig. 26.82 HRR of thin pools of gasoline over various surfaces

Table 26.23 Shop-display commodities tested by Chow

Display type	Combustible mass (kg)	Size (m)	Ignition source (kW)	Peak HRR (kW)
Clothing			470	2400
Compact discs		2 ea, 1.5 m wide × 1.6 m high	1100	
Newsstand	15	2 ea, 1 m wide × 2.2 m high	400	3600

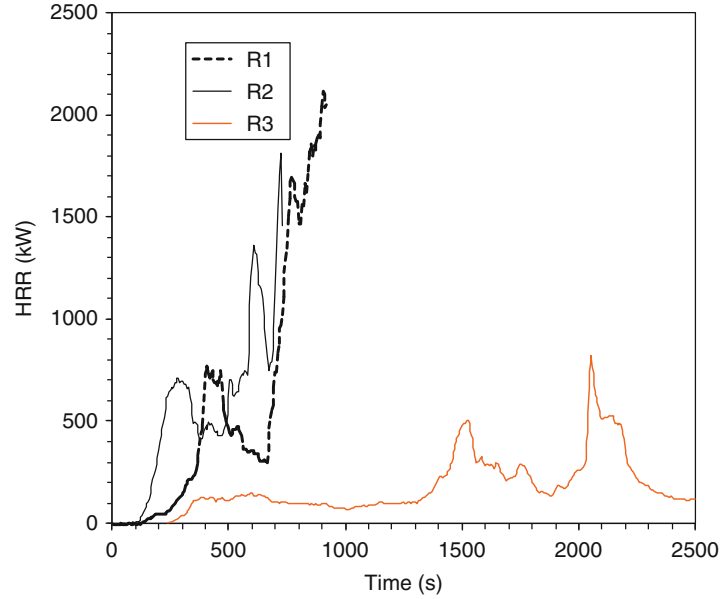

Fig. 26.83 HRR of European refrigerators tested by VTT and EFRA

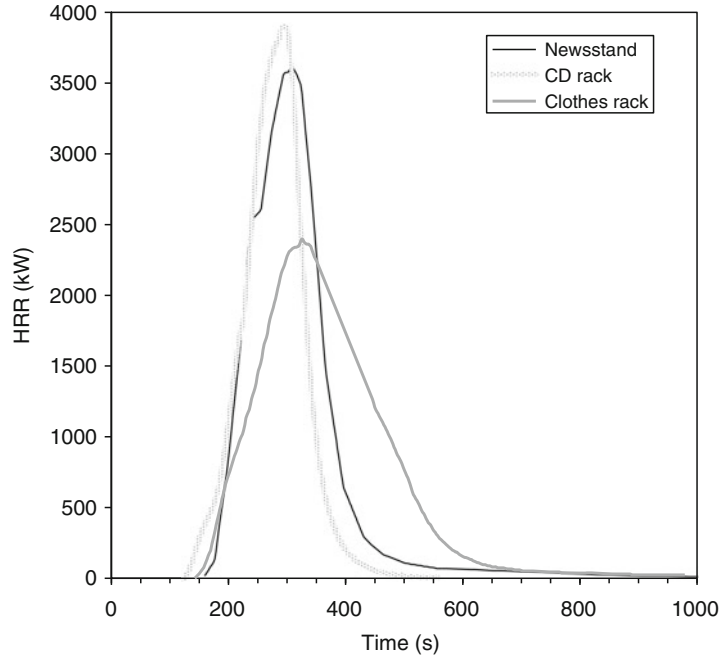

Fig. 26.84 HRR of various shop-display commodities tested by Chow

newsstand. The clothing display comprised all-cotton T-shirts arranged on four small display racks. The CD display contained a total of 240 discs. The ignition source in each case was a small pool of gasoline, to represent an arson fire. The results are shown in Table 26.23 and Fig. 26.84.

Television Sets

The burning characteristics of TV sets depend greatly on whether they have been made for the North American market, following the requirements of UL, or not. In countries where UL standards do not apply, plastic TV cabinets are generally highly flammable, commonly being made of plastics that only have an HB rating according to the UL 94 [30] procedures. These are readily ignitable from small-flame ignition sources and burn vigorously when ignited [44, 188]. By contrast, sets made for the North American market have to obtain a V-0 classification under UL 94 and will resist ignition from small flame sources.

Babrauskas et al. [88] tested at NIST small polystyrene television cabinets of two types, fire-retarded and not. Since the circuit components contribute negligible HRR in comparison to the outer shell, only the cabinets were tested. Two very small ("personal size") units were tested side-by-side in each test. This can represent either two appliances or simply the mass of one larger set.

SP tested two television sets [29], a US-market set with housing having a V-0 rating, and a Swedish set with a housing having an HB rating. The US set was a 690 mm (27 in.) model, while the Swedish one was 710 mm (28 in.). The US set had a total combustible mass of 6.5 kg, with 2.9 kg comprising the enclosure, while the Swedish set had 6.0 and 2.7 kg, respectively. The Swedish set was successfully ignited and burned with a small flame the size of a match flame. The US set resisted ignition from this source and was then subjected to a 10 kW burner. With this challenge, the set burned, but showed little HRR beyond the 10 kW of the source. Finally, the test protocol chosen was a 30 kW burner. The burner HRR was subtracted out from the data shown in Fig. 26.85.

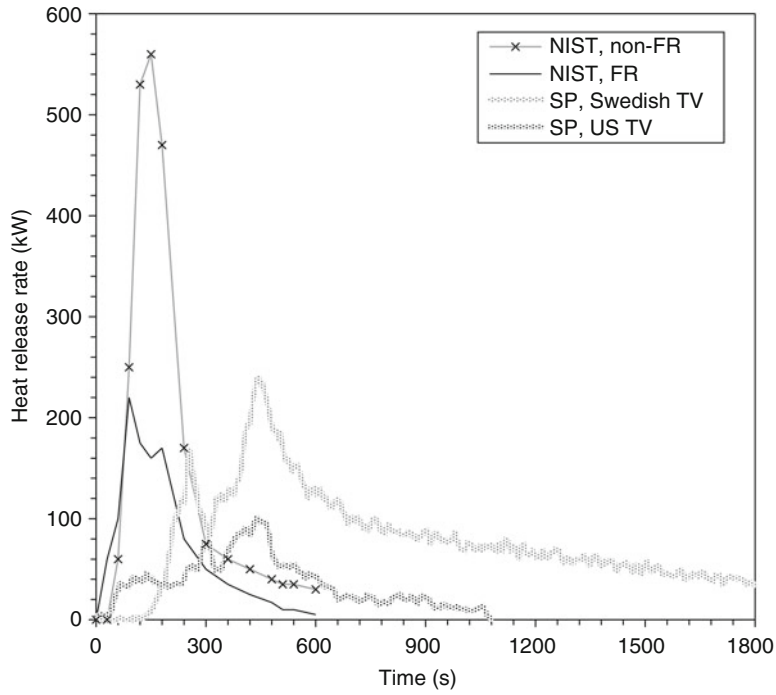

Fig. 26.85 HRR of various television sets tested by NIST and SP

Table 26.24 European televisions tested by VTT

Specimen	TW1	TW3	TP1	TP2	TP3
Type	Wood	Wood	Plastic	Plastic	Plastic
Size (inches)	24	26	28	25	28
Initial mass (kg)	32.7	39.8	31.8	24.4	30.5
Mass loss (kg)	10.2	10.2	5.2	4.6	5.3
Peak HRR (kW)	230	290	274	239	211
Total heat (MJ)	146	150	140	116	137

VTT conducted two projects where TV sets were tested. In the first study [156], they tested two old, 1960s vintage (black-and-white) televisions with large wood cabinets; these were ignited with a small cup of alcohol. In a newer study [105], they tested modern plastic-cabinet televisions using a propane burner of 1 kW. The specimens are described in Table 26.22, while test results are shown in Fig. 26.86. Nam et al. [189] tested a modern TV set (plastic cabinet) together with a wood stand for it. They obtained peak HRR values of 200–300 kW, although the peak took 20–40 min to reach.

The most recent results come from Hoffmann et al. [190] who tested TV sets in a wooden entertainment center. The ignition source was a small amount of alcohol for HB-rated cabinets. For the V-0 rated cabinets, some small consumer goods, HB rated, were first ignited and these were then used to ignite the test TV sets (Tables 26.24 and 26.25). After the initial peak (Fig. 26.87), the burning involved the wood entertainment center, thus the latter portion of these HRR curves is not germane to TV sets per se.

Transport Vehicles and Components

Passenger car HRR was measured at the Fire Research Station [191] and VTT [192]. The FRS laboratory examined a 1982 Austin Maestro and a 1986 Citroën BX, while VTT examined a Ford Taunus, a Datsun 160, and a Datsun 180. The dates of manufacture were only stated as late 1970s. These results are shown in Fig. 26.88. Additional tests were reported by MFPA [193] and SP [194]. MFPA tested a Citroën, a Trabant, and a Renault Espace, while SP tested a Fiat 127 of unspecified vintage. These results are shown in Fig. 26.89. The peak values range

Table 26.25 Characteristics of TV sets tested by Hoffmann et al.

	TV					
Test No.	Screen Size	Rating	Other HB Devices	Ignition Source	Peak HRR (kW)	Time to Peak (s)
1A	510 mm (20 in.)	V0	1 cordless Phone, 1 small radio	5 mL IPA	363	273
2A	510 mm (20 in.)	V0	1 telephone	5 mL IPA adjacent to phone	199	594
3A	480 mm (19 in.)	HB	None	5 mL IPA	>1450	615
1B	510 mm (20 in.)	V0	1 cordless phone, 1 small radio	5 mL IPA	>1000	216
2B	510 mm (20 in.)	V0	1 telephone	5 mL IPA adjacent to phone	299	975

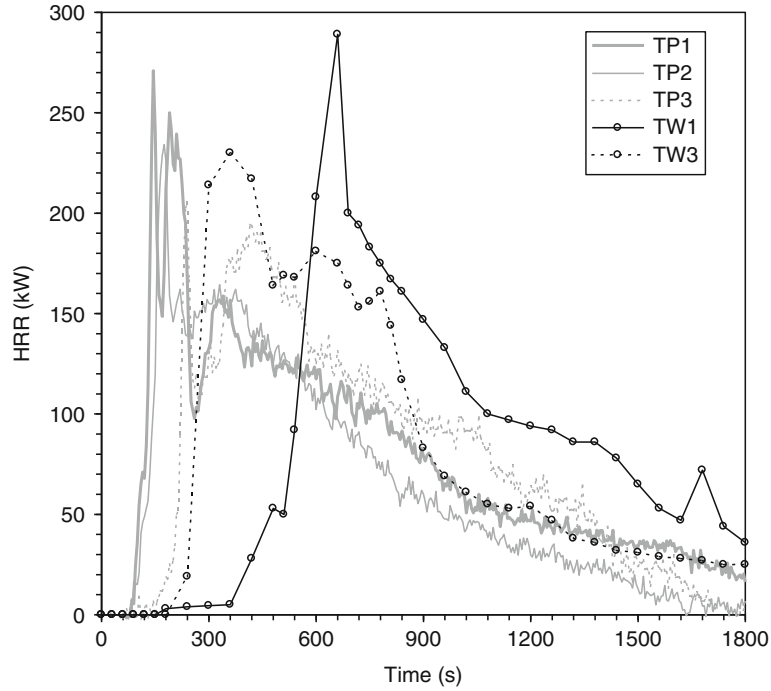

Fig. 26.86 HRR of European television sets tested by VTT

from 1.5 to 8.5 MW. These numbers are rather widely disparate and it is not fully clear why, except that this is not due to the fraction of polymer content onboard.

Some very extensive testing was conducted at CTICM, as shown in Fig. 26.90. Test 2 was a Renault 18 (951 kg), Test 3 a Renault 5 (757 kg), Test 4 another Renault 18 (955 kg), while the specimens for the remaining tests were only identified as a "Large car, 1303 kg" (Test 7), and "Small car, 830 kg" (Test 8). Additional tests were run in a two-car configuration, involving one small car (790 kg) side-by-side to a large car (1306 kg). These results are shown in Fig. 26.91, but test details were not published. The mass loss values are shown in Table 26.26.

Okamoto et al. [195] ran a series of experiments where they tested replicates of the same vehicle (Toyota Cressida, also known as Mark2 GX81) but varied the test conditions (Table 26.27). Figure 26.92 shows the HRR results; spikes judged to be spurious were

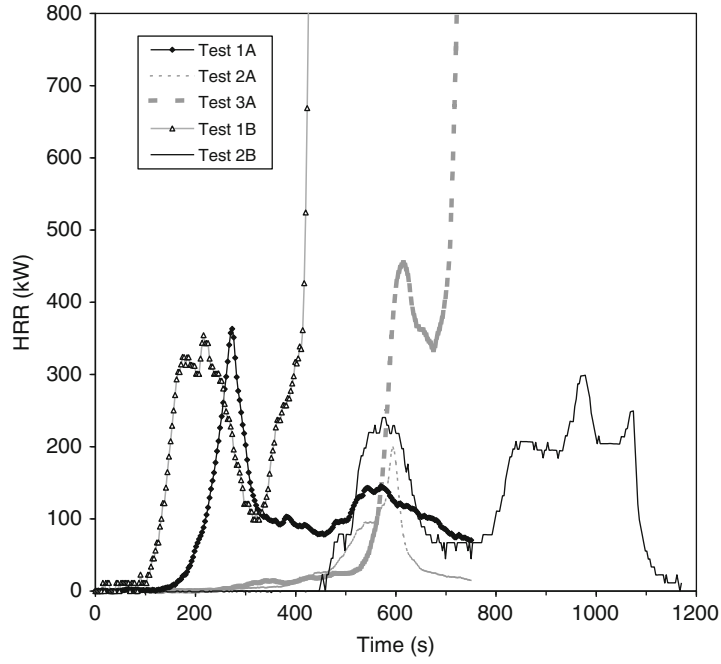

Fig. 26.87 HRR of TV sets tested by Hoffmann et al.

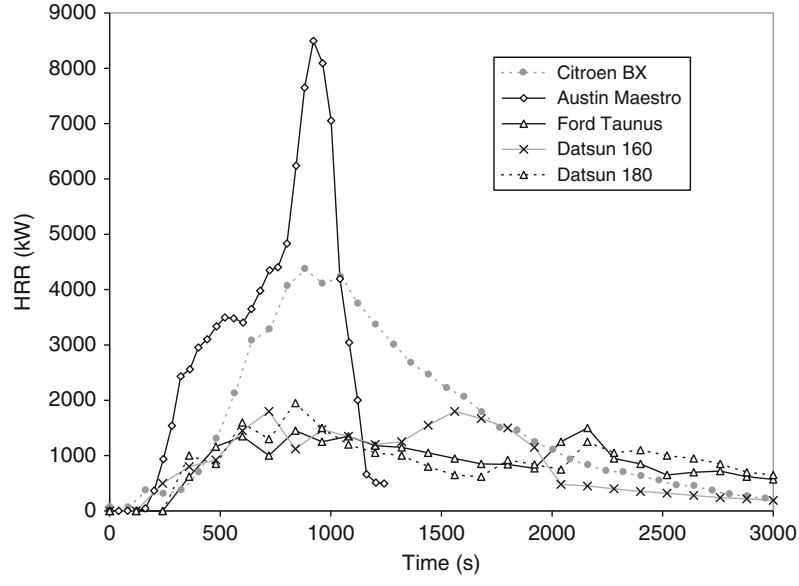

Fig. 26.88 HRR of cars tested at FRS and VTT

removed from these data. In Test B, an explosion occurred at 1517 s, when pyrolysates accumulated in the passenger compartment suddenly ignited. Explosions did not occur with the other tests. The tests are especially valuable since, in their paper, the authors documented many details of fire development in these experiments. The results suggest that small differences in test conditions can affect the time scale of fire development in an automobile quite notably, also that windows should be open if maximum HRR conditions are to be elicited. It

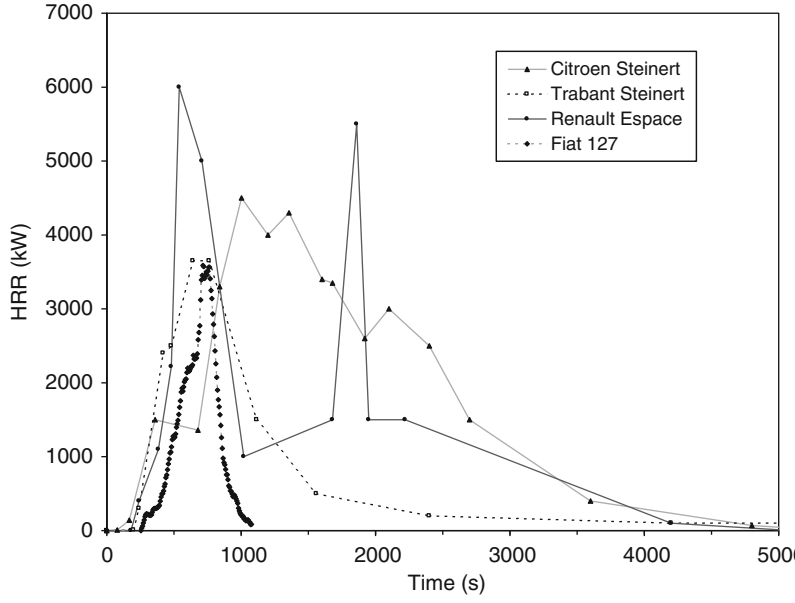

Fig. 26.89 HRR of cars tested at MFPA and SP

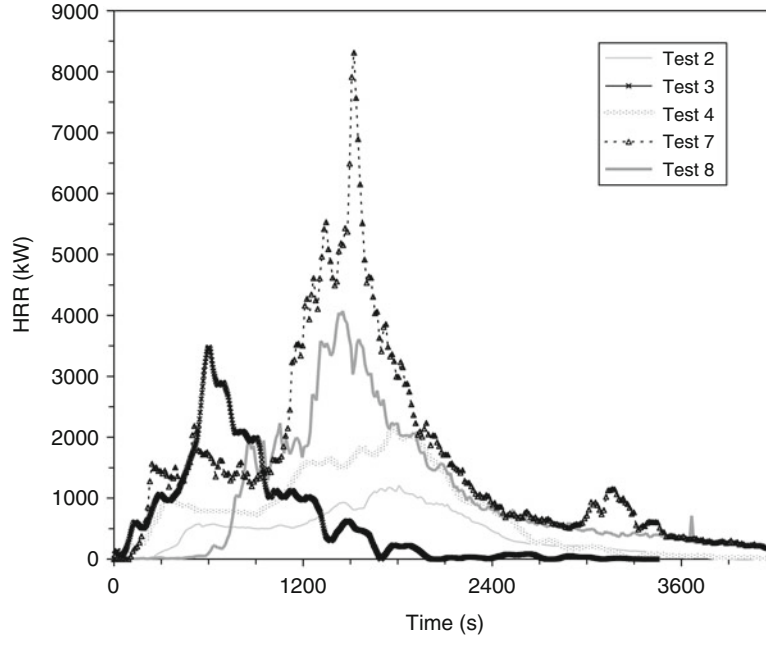

Fig. 26.90 HRR results of CTICM one-car tests

Table 26.26 Results of CTICM car tests

Test	Peak HRR (kW)	Total heat released (MJ)	Mass loss of car #1 (kg)	Mass loss of car #2 (kg)
2	1208	1758	185	–
3	3476	2100	138	–
4	2159	3080	145	–
7	8310	6670	278	–
8	4073	4090	184	–
9	7500	8890	124	172
10	8230	8380	175	166

Table 26.27 Test conditions for sedan vehicles tested by Okamoto et al.

Test	Windows	Amount of fuel in tank (L)	Ignition point	Peak HRR (kW)	Total HR (MJ)
A	Open	10	Rear wheel splashguard	3512	4950
B	Closed	10	″	3034	4860
C	Closed	20	″	1856	4930
D	Closed, exc. part of left-front window	10	Left front seat	2395	5040

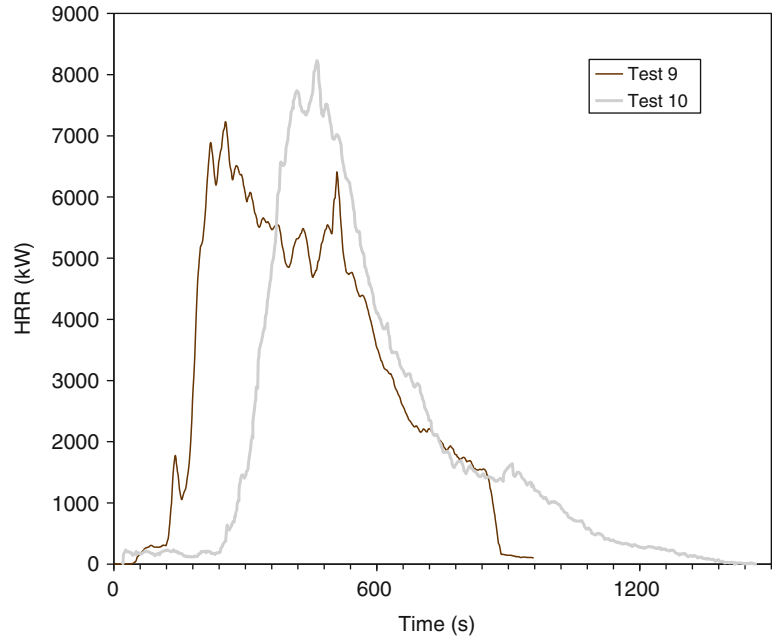

Fig. 26.91 HRR results of CTICM two-car tests

Table 26.28 Test conditions for minivan vehicles tested by Okamoto et al.

Test	Windows	Amount of fuel in tank (L)	Ignition point	Peak HRR (kW)	Total HR (MJ)
A	Closed	10	Rear wheel splashguard	3603	5367
B	Closed	10	Right front bumper	3144	5006
C	Closed	10	Center of the second row seat	–	–
D	Closed, exc. part of left-front window	10	Center of the third row seat	4094	5153

is also noteworthy that the total HR values were nearly identical for all tests.

Okamoto et al. [196] later ran tests on minivan type vehicles, using only one model of vehicle (Nissan Serena), but four different test conditions (Table 26.28). The vehicle weighed 1440 kg and had a 2.0 L gasoline-powered engine. Same as for the sedan vehicles, the HRR development was ragged and not approximately triangular or constant (Fig. 26.93). In Test C, the fire self-extinguished due to dropping oxygen levels since no windows broke.

Ohlemiller and Shields [197] tested a number of individual components from a passenger vehicle (a minivan). The components that has a mass of around 2 kg or less all showed small HRR

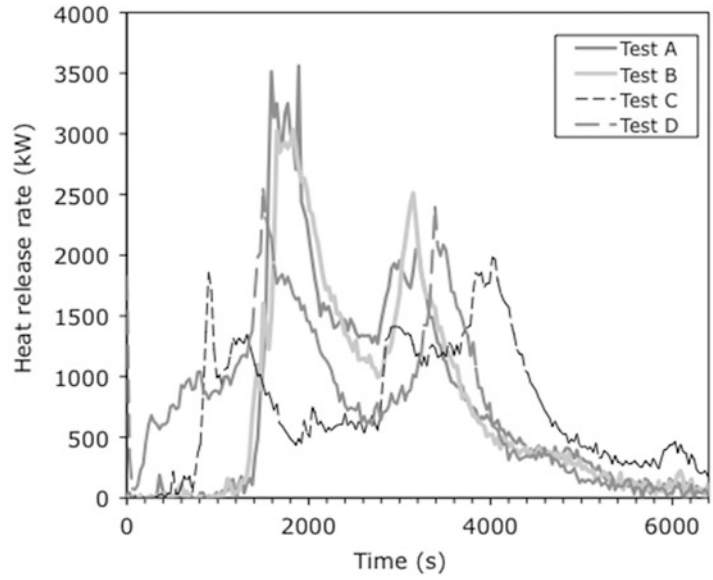

Fig. 26.92 HRR results for automobiles tested by Okamoto et al.

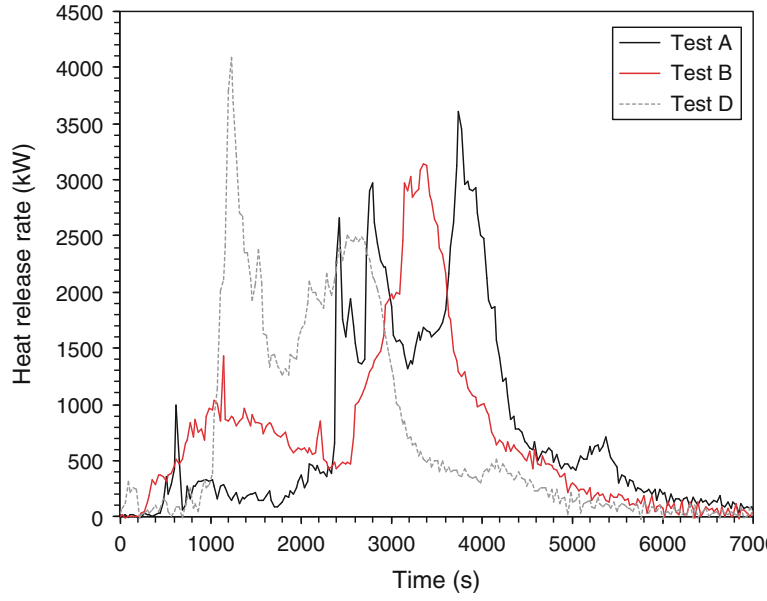

Fig. 26.93 HRR results for minivans tested by Okamoto et al.

values, typically less than 80 kW. Three components, however, showed substantial HRR values—an empty plastic fuel tank (8.5 kg), a passenger seat (8 kg), and an instrument panel (10.6 kg). The HRR curves for these items are shown in Fig. 26.94. In a separate study, Ohlemiller [198] tested one production version of an automotive HVAC unit, along with two experimental versions containing fire-retardant agents. The non-FR version showed HRR in excess of 200 kW, while the FR versions developed only about 5 kW.

Railway car results were reported by SP [197] and by Steinert [198]. Figure 26.95 shows a passenger railway car (European type IC train) reported by SP and an ICE train car by Steinert, who also published the data labeled as "two halves." The latter comprised two half cars, one being aluminum

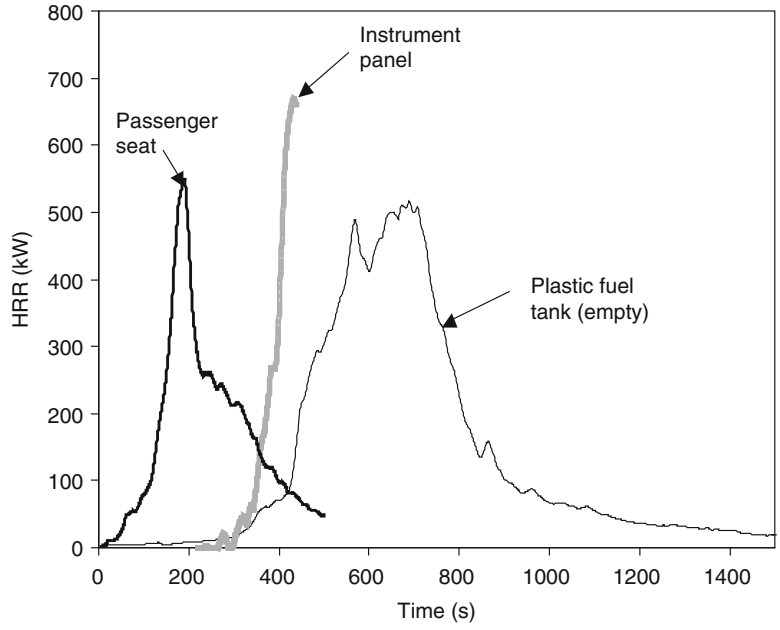

Fig. 26.94 HRR of some larger components from a passenger vehicle

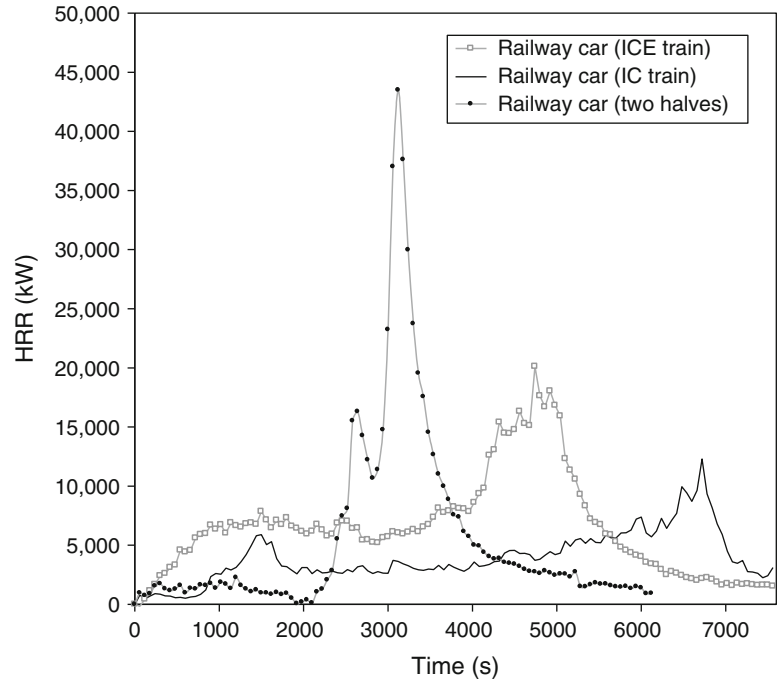

Fig. 26.95 HRR of railway cars

and the other steel. These were abutted to form one test specimen. A fire was ignited in the aluminum car, but did not become rapid until windows failed at around 40 min. SP also reported results on two subway cars [205] and half a tram car [169]; these results are shown in Fig. 26.96. Data on school buses from SP [199] and Steinert [200] are shown in Fig. 26.97.

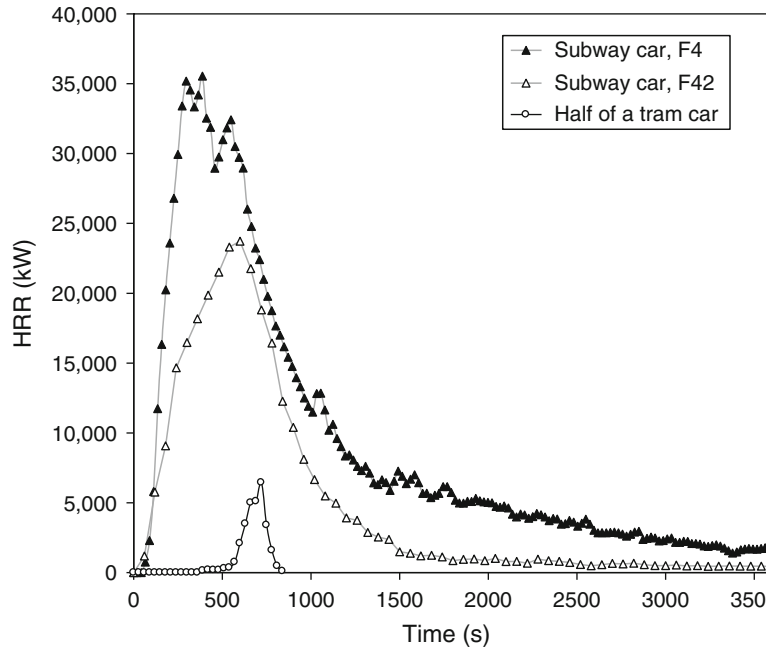

Fig. 26.96 HRR of subway cars and half a tram car

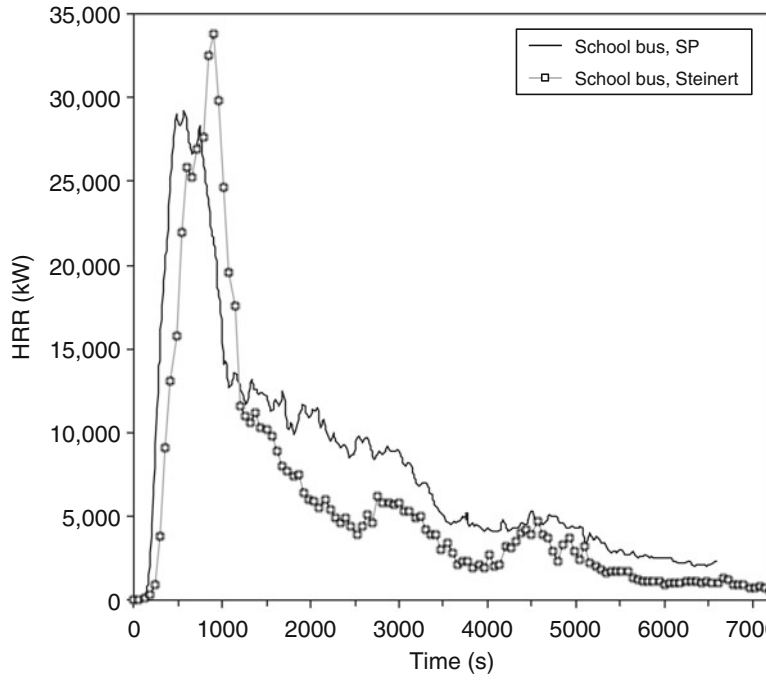

Fig. 26.97 HRR of school buses

A number of researchers have tested portions of various heavy vehicles. Tests on transport seating were done at SP [201]. They measured an array of four double bus seats and a similar arrangement of train seats. The foam was HR polyurethane, while the cover was a viscose/wool/polyester/polyamide blend for the bus seats and 100 % wool fabric for the train seats. These HRR results are shown in Fig. 26.98.

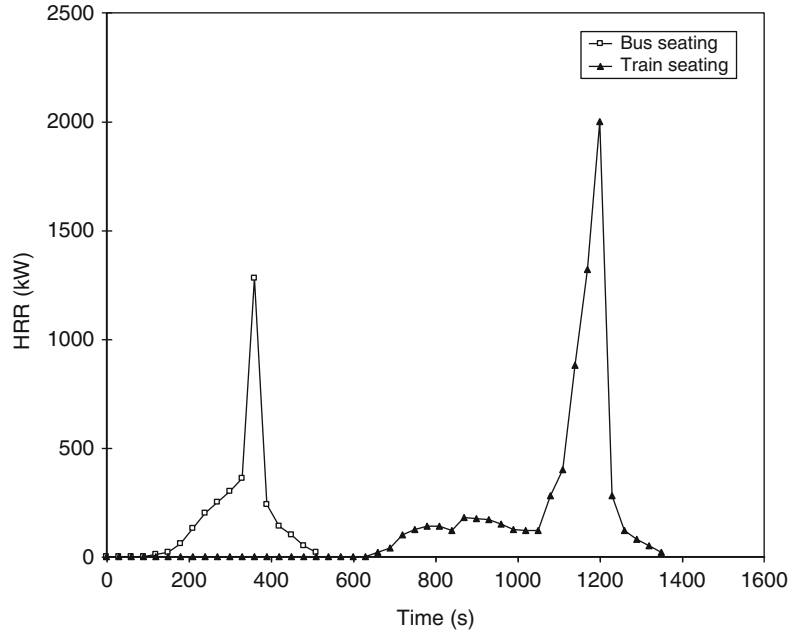

Fig. 26.98 HRR of seating components of heavy vehicles

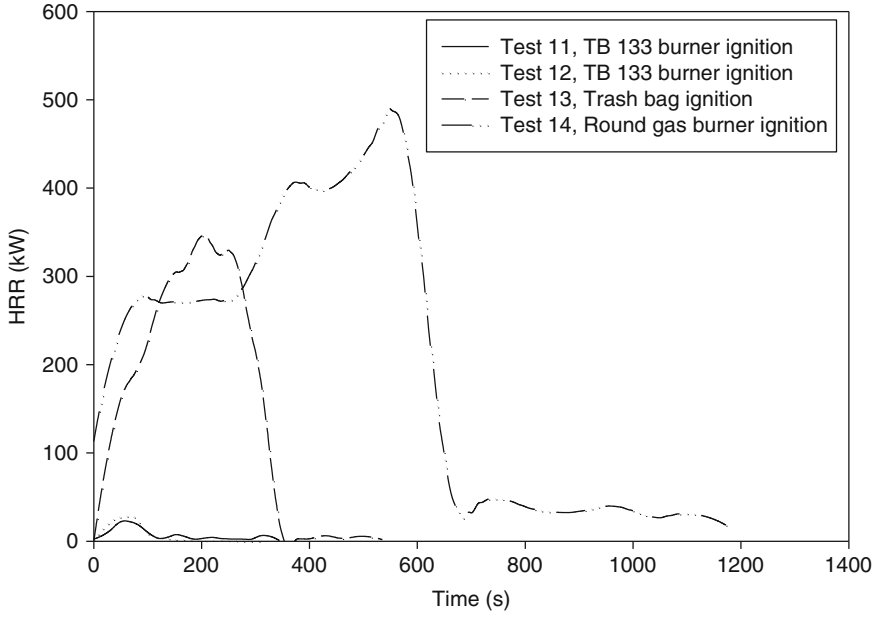

Fig. 26.99 HRR of Amtrak seats (pair), as tested by NIST, exposed to various ignition sources

NIST conducted tests [202] on a pair of Amtrak seats, presented with various ignition sources; these results are shown in Fig. 26.99. In the same research study, NIST also tested sleeping Amtrak berths; these results are shown in Fig. 26.100. Quite high HRR values were seen from Amtrak wall/soffit carpeting tested in the same study (Fig. 26.101). These test specimens were only 1.0 m wide by 1.5 m high for wall carpeting, while the test that also added soffit carpeting had an 0.5 m deep carpeted soffit. Additional test results were obtained for Amtrak

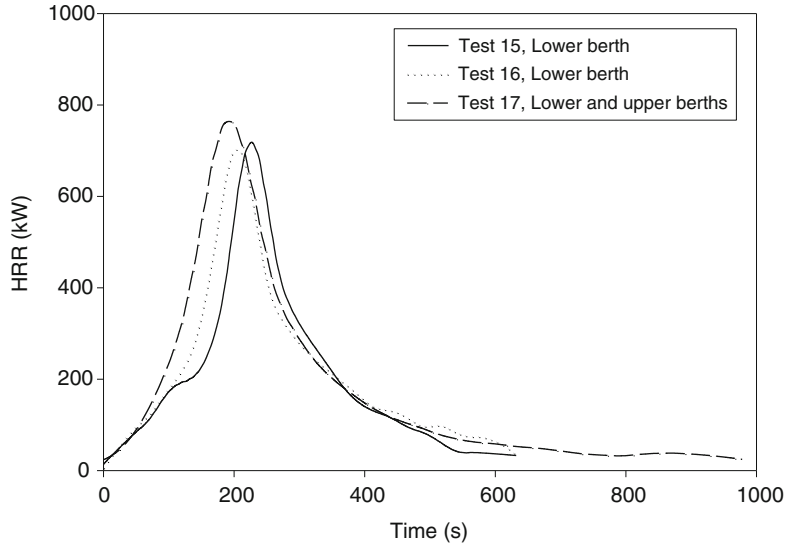

Fig. 26.100 HRR of Amtrak sleeping berths

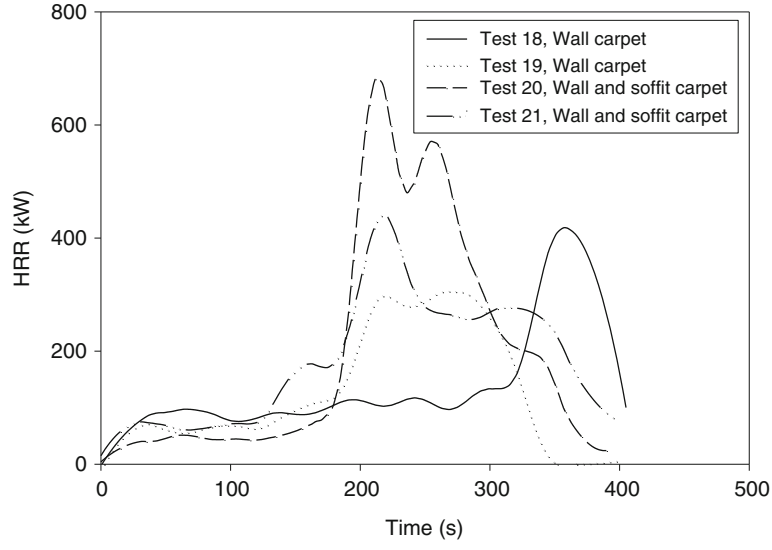

Fig. 26.101 HRR of Amtrak wall carpet and wall/soffit carpet specimens

window drapes (Fig. 26.102) and compartment door privacy curtains (Fig. 26.103). Amtrak window assemblies are made from polycarbonate glazing material and also have polymeric gasketing and trim; these show substantial HRR (Fig. 26.104).

Vehicle tires can ignite from an overheated axle and can release a substantial amount of heat if they burn. There is one study in the literature which documents such a fire. Hansen [203] burned a pair of 285/80 R22.5 truck tires mounted on a tandem wheel arrangement. The HRR curve is given in Fig. 26.105.

Vehicle tires are also prone to be ignited and to burn in tire dumps. The HRR will depend directly on the geometry and on the amount of tires involved. Some quantitative HRR experiments have been reported [204] on experiments done at the Fire Research Station. These experiments were for flaming tires, but most recent tire dump problems have been associated with a smoldering condition and no

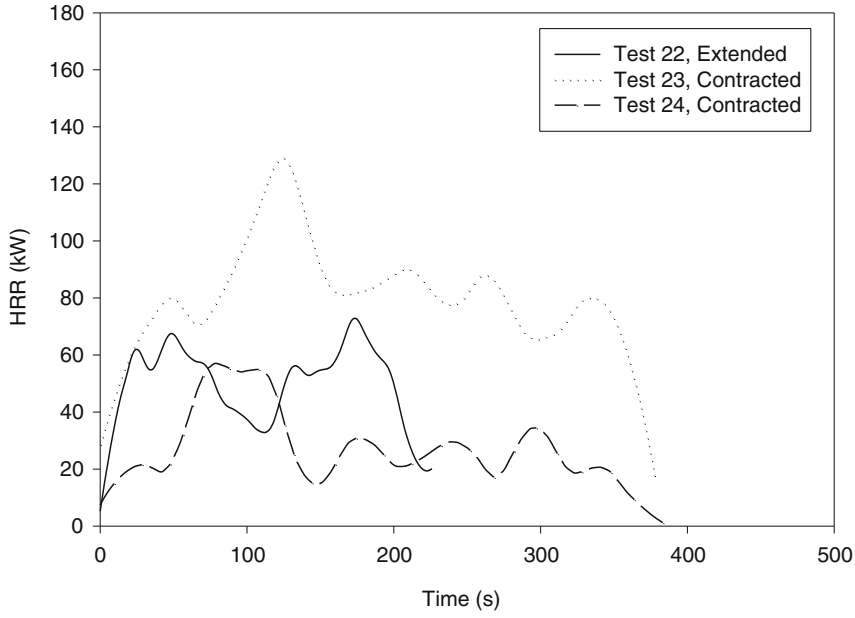

Fig. 26.102 HRR of Amtrak window drapes

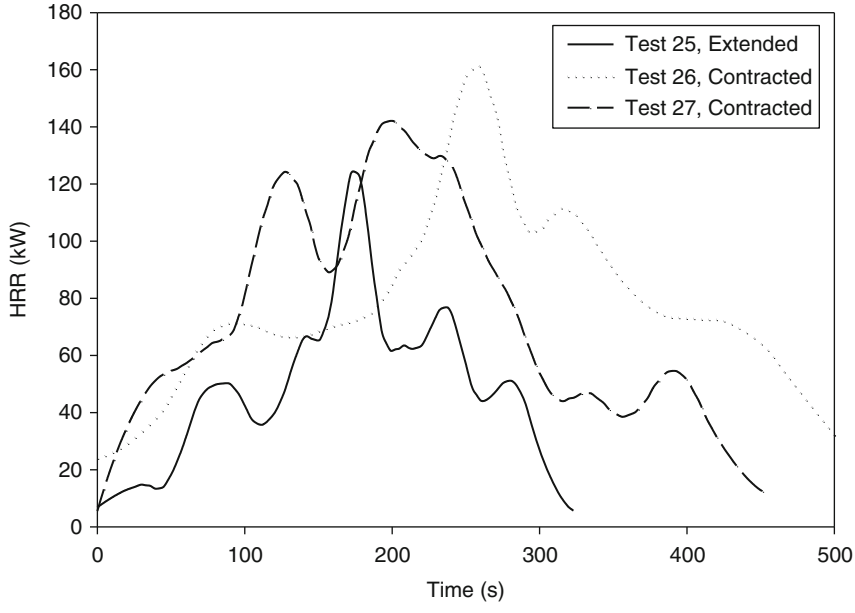

Fig. 26.103 HRR of Amtrak privacy curtains

HRR quantification under these conditions has been reported.

Tests were also reported on two plastic mud guards [205], as used on large tanker trucks. One specimen failed to get ignited from a 100 kW burner, while the HRR for the second specimen is shown in Fig. 26.105. The ignition source was a 100 kW burner, and its HRR has not been subtracted from the results shown.

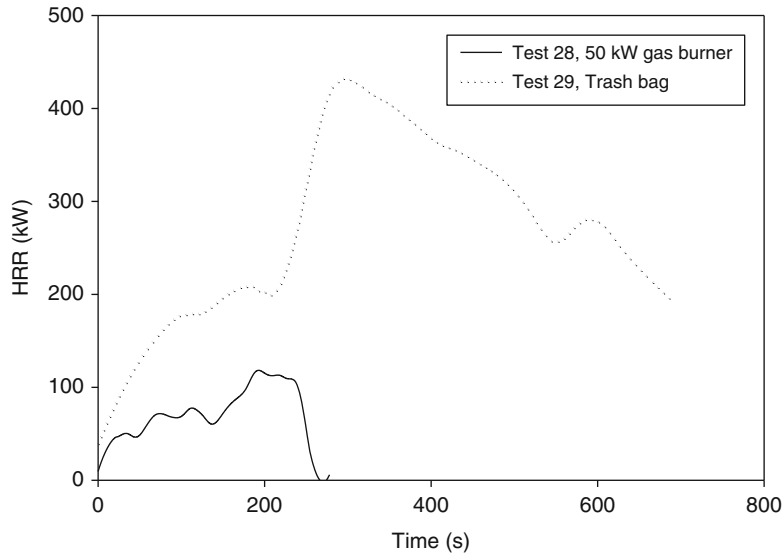

Fig. 26.104 HRR of Amtrak coach window assembly

Table 26.29 Characteristics of the SP Runehamer Tunnel tests

Test	Load	Total mass (kg)	Peak HRR (MW)	Time to peak (s)	Total heat release (MJ)	Fire growth rate during linear-growth period (MW s^{-1})
T1	380 wood pallets, 74 polyethylene pallets	11,010	201.9	1110	242,000	0.335
T2	216 wood pallets, 240 PUR foam mattresses	6,930	156.6	846	141,000	0.438
T3	Mixed goods, comprising plastic and wood furniture, fixtures, and toys; also 10 large tires	8,550	118.6	600	131,000	0.273
T4	600 cardboard cartons with 18,000 polystyrene cups, 40 wood pallets	2,850	66.4	444	57,000	0.282

For heavy-goods vehicles, the heat content of the combustibles being hauled is likely to greatly exceed the heat content of the vehicle itself. Thus, a recent research program at SP conducted by Ingason and Lönnermark [206] ("Runehamer Tunnel tests") characterized the HRR of some typical commodities of this type. Four large-scale tests were conducted (Table 26.29), with the results shown in Fig. 26.106. The commodities were arranged as volume 10.45 m long, 2.9 m wide, and 4.5 m high, but were not enclosed by a trailer body. In many cases, the trailer body is aluminum or tarpaulin, thus nearly-free burning may be expected in such worst-case situations.

For all except T4, the goods themselves were wrapped with polyethylene film. The authors especially noted that the primary period of fire growth in each case, up to ca. 100 MW (66 MW in the case of test T4), was linear and not of a t^2 type. These linear-growth rates are given in Table 26.29. These results are especially noteworthy since they represent the highest HRR fires, of realistic products thus far studied. An earlier European research program [207–209] estimated the HRR of a truck loaded with 2,000 kg of modern upholstered furniture; however, these estimated HRR values, as derived by several investigators, varied widely.

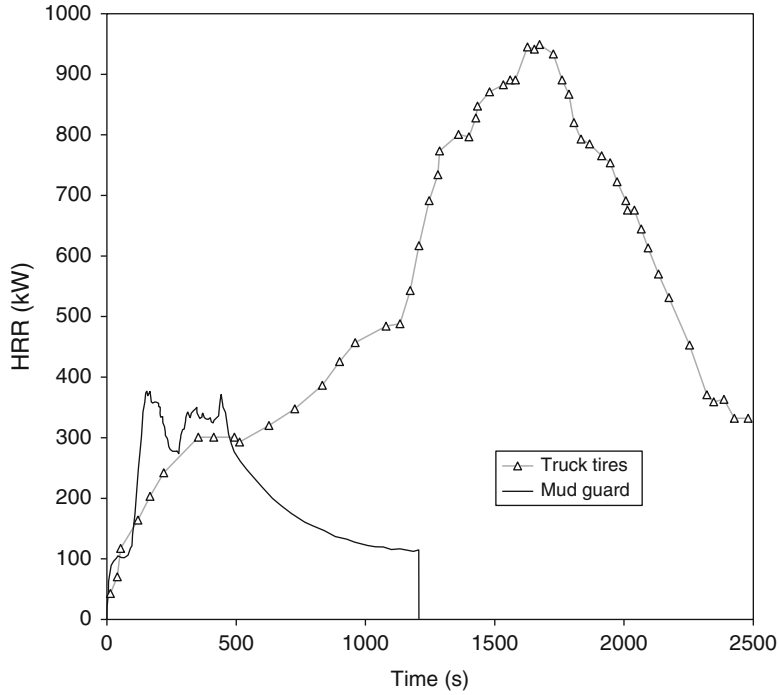

Fig. 26.105 HRR for truck tires and mud guard

Table 26.30 Some data obtained at VTT on 14 L polyethylene wastebaskets showing effect of packing density and basket construction

Basket sides	Basket mass (kg)	Filling type	Filling mass (kg)	Filling density (kg m^{-3})	Peak HRR (kW)	Total heat released (MJ)
Solid	0.63	Shredded paper	0.20	14	4	0.7
Netted	0.63	Milk cartons	0.41	29	13	3.0
Solid	0.53	Shredded paper	0.20	14	18	7.3
Netted	0.53	Milk cartons	0.41	29	15	5.8

Trash Bags and Containers

Bench-scale measurements of trash are not readily feasible, due to the naturally irregular arrangement of these combustibles. There are full-scale test results available, however, that can suggest appropriate values to be used in different circumstances. A small "bathroom size" (6.6 L) plastic wastebasket stuffed with 12 milk cartons used at NIST as an ignition source in early HRR testing [45] was found to show a HRR of about 50 kW, sustained for about 200 s.

This value evidently represents a worst-case condition, since most researchers have measured significantly lower HRR rates. For example, Mehaffey et al. [210] tested a similar wastebasket filled with mixed paper/plastic fuel load and obtain a HRR curve which can be approximated as being 30 kW for 60 s. NIST [140] tested slightly larger, 8.5 L "office style" round polypropylene wastebaskets, filled with sheets of newspaper, totaling about 300 g of newspaper in a 315 g container. These gave peak HRR values of 28–35 kW and an active burning time of ca. 800 s. Table 26.30 shows some additional data [156], where, over a certain range, increasing packing density is seen to increase the heat release rate. Some typical trash-bag fires are shown in Fig. 26.107 [109].

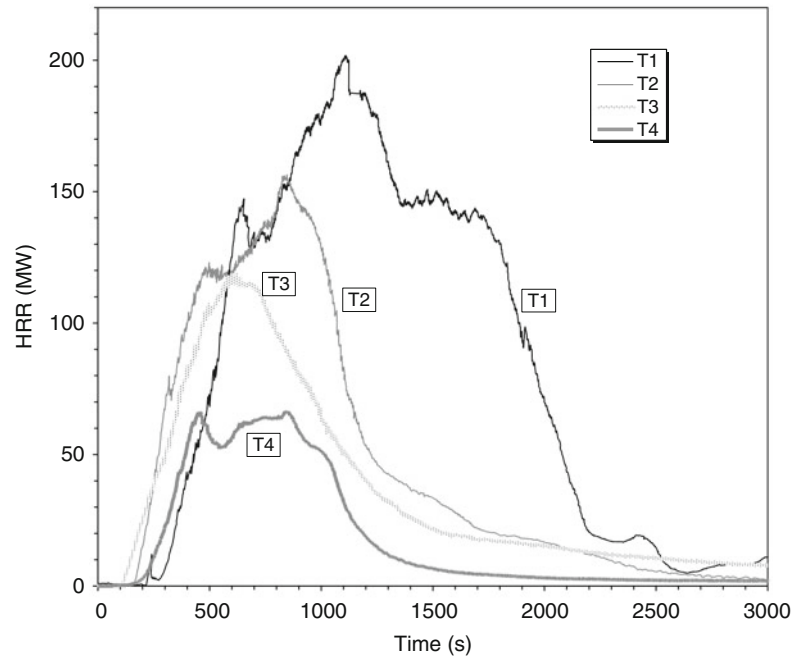

Fig. 26.106 HRR of representative heavy-goods vehicle cargo, as determined in SP's Runehamer Tunnel tests

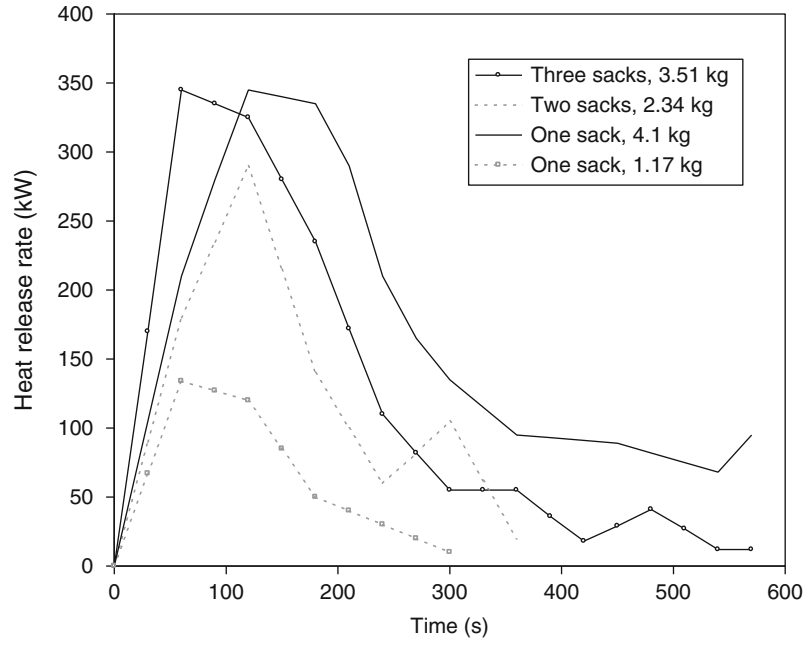

Fig. 26.107 HRR of trash bags

Lee has correlated the peak heat release values according to the effective base diameter and packing density [109]. Figure 26.108 shows that the total burning rate (kW) increases with effective base diameter, but decreases with the tighter packing densities. Figure 26.109, conversely, illustrates that when the results are normalized per unit base area, a downward trend is seen. The correlations according to packing density should only be considered rough observations, and not firm guidelines. For design purposes, the range of 50–300 kW appears to cover the bulk of the expected fires

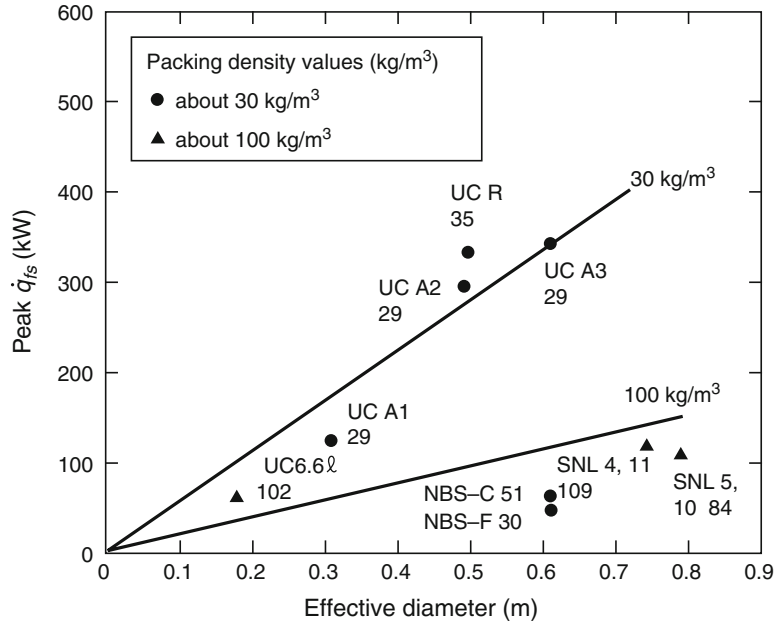

Fig. 26.108 Peak HRR of trash fires

Table 26.31 Peak HRR of small wastebaskets

	Fuel load	
Wastebasket material	PS	paper
Steel	12	8
Polyethylene	50	30
Polypropylene	50	40
Polystyrene	37	22

from normal residential, office, airplane, or similar occupancy trash bags and trash baskets.

Yamada et al. [102] measured the HRR of 6.5–11.8 L wastebaskets made of steel and plastic and filled with paper and polystyrene foam trash. The peak HRR values found are shown in Table 26.31. The authors concluded that the HRR characteristics could be reasonably well represented by one of two paradigms: (1) 30 kW for 600 s; or (2) 50 kW for 300 s.

NIST conducted tests [200] on trash bags collected from Amtrak overnight trains. The bags were about 450 mm diameter and 800 mm high and were ignited with a 25 kW burner. Test results are shown in Fig. 26.110. Based on these results, NIST researchers endeavored to create a 'standard' trash bag by filling the bag with 110 sheets (2.7 kg) of crumpled newspaper; these results are shown in Fig. 26.111.

NIST also tested [211] 30-gal size (136 L) plastic trash containers made from high-density polyethylene (HDPE) and filled with construction-site debris. The debris included cut pieces of lumber, sawdust, cardboard, paper, cups, food wrappers and pager bags. The containers were 515 mm diameter, 700 mm tall and had a mass of 3.6 kg. The debris totaled 10 kg for each test. Figure 26.112 shows the results for two test replicates.

Tests have been reported on some very large (364 L, 96 gal) polyolefin garbage cans (wheeled, household type) [212]. These were tested empty, and they were ignited with the wood crib specified in UL 1975 [213]. That particular crib weighs 340 g and is ignited with 20 g of excelsior. Three tests were conducted; two gave fairly similar peak HRR values (2383 and 1942 kW), while the third one was much lower at 977 kW (Fig. 26.113). Such variability is typical of polyolefin products, when they are tested in an arrangement where the product can melt and recede from the ignition source.

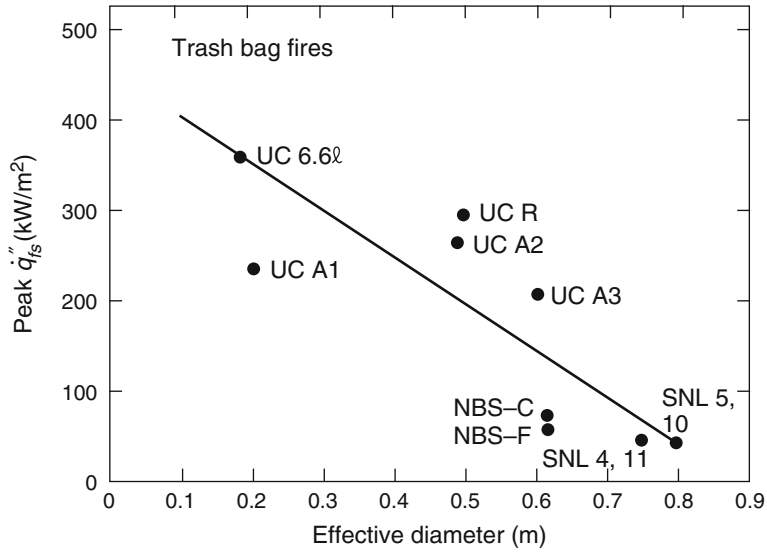

Fig. 26.109 Trash heat release rates, normalized per unit base area

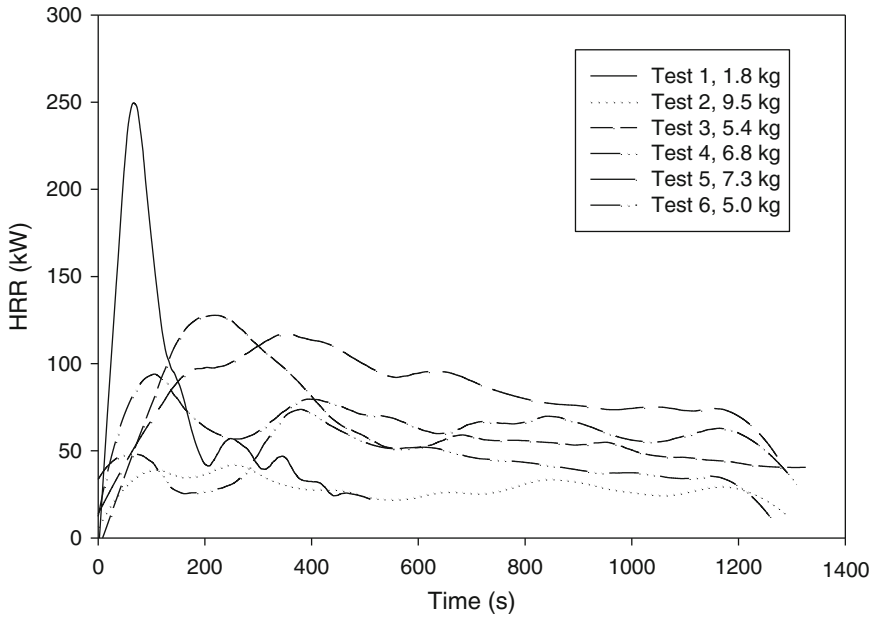

Fig. 26.110 HRR of Amtrak trash bags in NIST tests

Upholstered Furniture

The HRR of upholstered furniture can be determined in three different ways: (1) by room fire testing; (2) by testing in the furniture calorimeter; (3) by conducting bench-scale tests in the Cone Calorimeter and then using a mathematical method to predict the full-scale HRR. Of all the occupant goods that can be found in a normal residence, upholstered furniture normally has the highest HRR, thus knowledge of its performance is essential for many applications.

Until the 1970s, upholstered furniture used to be made from 'traditional' materials. Thus,

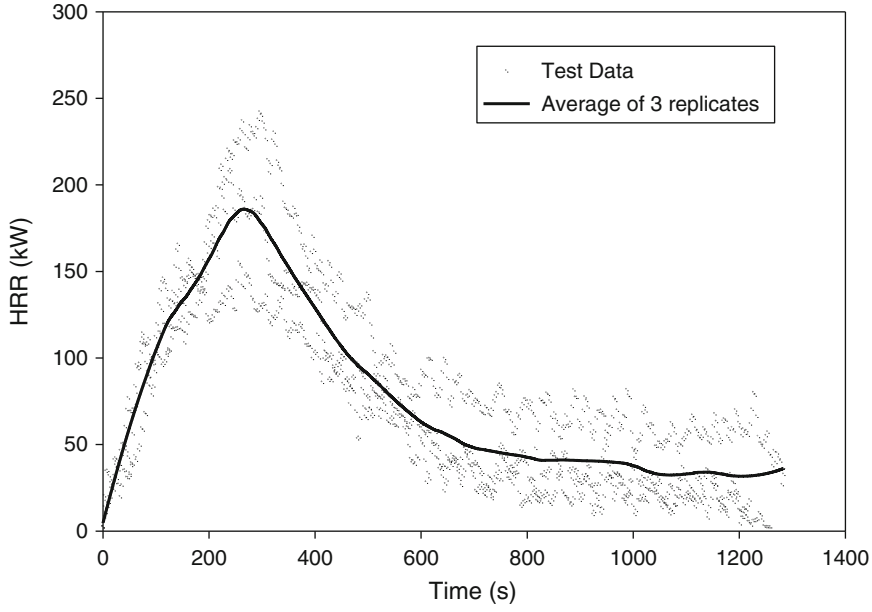

Fig. 26.111 HRR of 'standard' Amtrak trash bag, based on crumpled newspaper

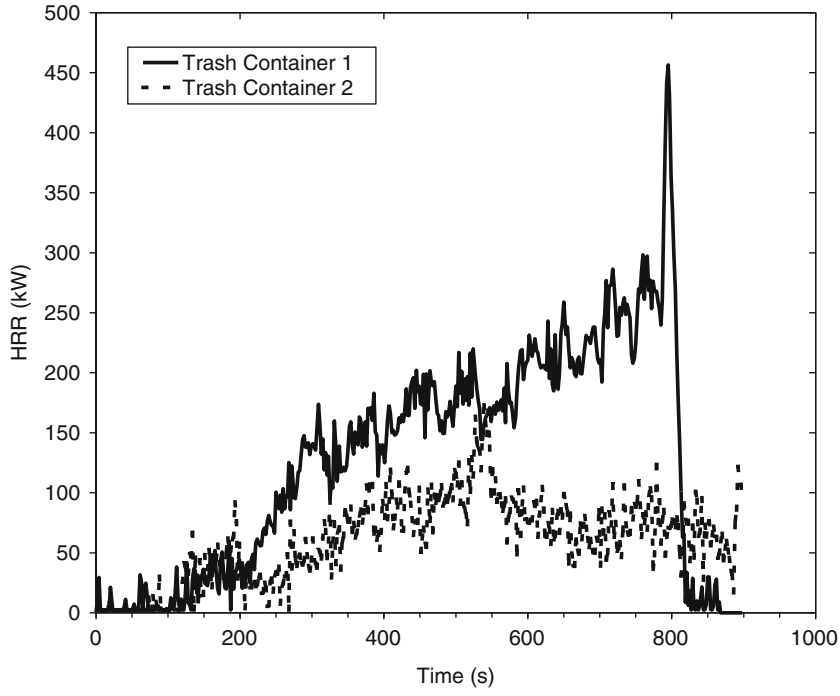

Fig. 26.112 HRR of 136-L HDPE trash containers filled with construction-site debris

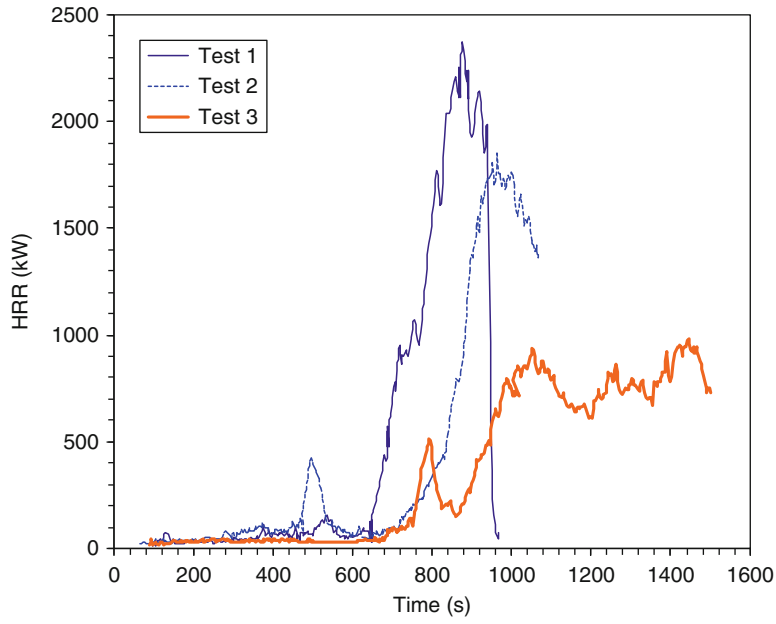

Fig. 26.113 HRR of 364 L (96 gal) PE garbage cans

during the 1950s and 60s, in the US furniture commonly had a wood frame, steel springs, cotton batting padding, and an upholstery fabric which was commonly a natural fiber such as wool, silk, or cotton. A fraction of the furniture used latex foam padding instead of cotton batting. In earlier-yet times, furniture was commonly stuffed with rubberized horse hair. By the 1970s, however, the predominant padding material became polyurethane foam, and fabric selection became very wide, including both thermoplastic synthetics and natural fibers. The HRR of the modern furniture were found to be many times that of traditional types [214], apart from the special case of latex foam. The latter shows HRR values distinctly higher than for polyurethane foam, but the material has a finite life and few specimens would survive to this day.

Figure 26.114 illustrates several furniture items tested at NIST [2]. Chair F21 used polyurethane foam complying with the 1975 California TB 117 standard [215] and polyolefin fabric. A specimen using ordinary polyurethane foam gave essentially identical results. This level of performance represents a very common, but unfortunately worst-performance furniture item widely bought by consumers. Specimen F32 is a sofa made from the same materials. Chair F24 illustrates the large improvement in HRR when cotton fabric is substituted for polyolefin fabric. The peak HRR decreases by about 2/3, from 2 MW to 700 kW. Further improvements, at present, are not readily available on the retail market. Contract furniture can be procured to advanced specifications, however, notably California TB 133 [213]. The latter limits the peak HRR to values less than 80 kW, which will present negligible fire hazard in almost any circumstance.

In the case of the tests discussed above, ignition was from the flame of a 50 kW burner placed at the side of the specimen, representing the burning of a small trash can. Such an ignition source provides the minimum time between ignition and peak HRR. The effect of ignition source on the HRR curve has been found to be almost exclusively that of time shifting—use of smaller flames, non-flaming sources, or placing of ignition sources in less vulnerable locations results in an increase of time to peak HRR (Fig. 26.115), but otherwise does not have a statistically significant effect on the HRR curve [216–218].

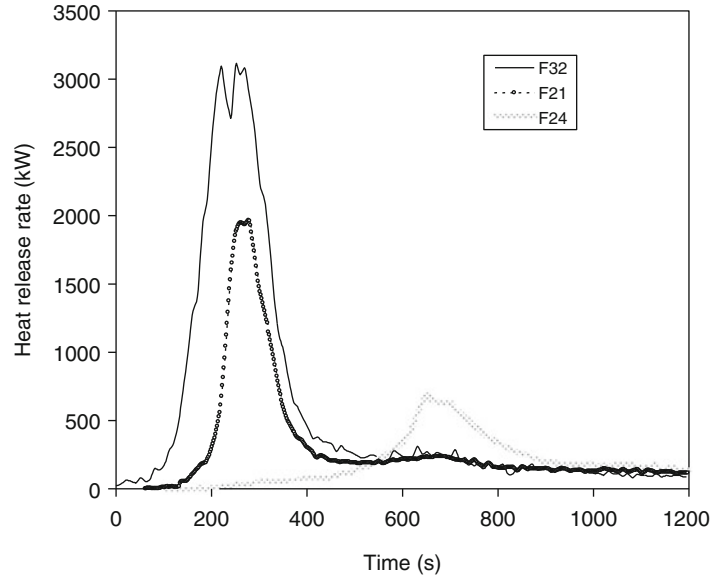

Fig. 26.114 HRR of several upholstered furniture items tested at NIST

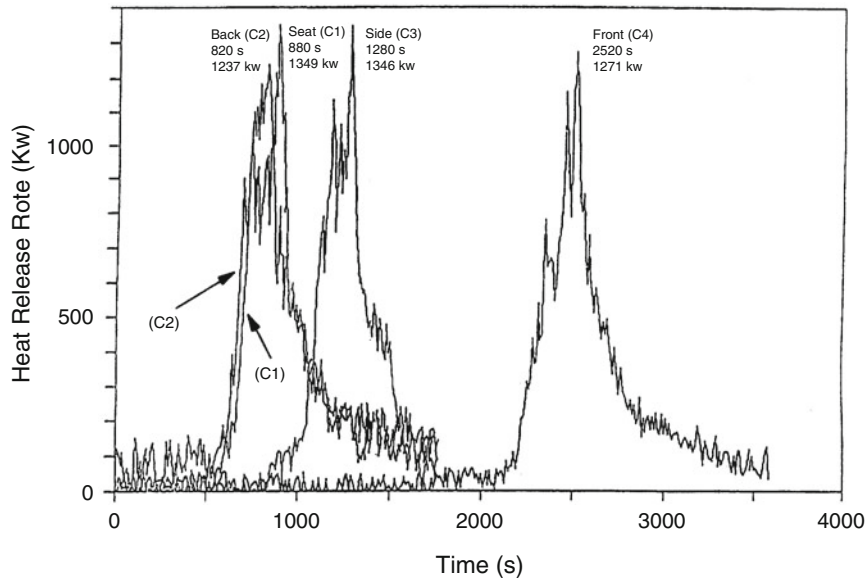

Fig. 26.115 Effect of ignition source location on the HRR curve of upholstered chairs [214]

Foams with fire retardant chemical additives (FR) improve the fire performance only if large loadings are used. Furniture made for the State of California had been required to use FR foams since 1975, but the loading of FR chemicals used was very small (3–5 %). For furniture with a HRR high enough to be a room fire hazard, such minimal FR levels have no effect on HRR [219]. A recent study with a very small ignition source compared the performance of furniture with non-FR foams and with TB117 foams using cotton upholstery [220]. Using specially constructed, non-commercial furniture for testing, no effect was found for three-seater sofas, and an effect was only seen for single-seat chairs. But the latter were of a design where even the

non-FR version showed HRR values so low (approx. 400 kW) as to not comprise a room fire hazard.

Interestingly, the same study reported test results for a large number of commercial chairs and sofas burned for comparison. With few exceptions, the latter showed peak HRR values in the range of 900–2500 kW (Fig. 26.115), indicating that the custom-made furniture was not representative of the retail residential furniture market. Furniture made to the 1975 TB117 standard was actually not intended to have lower HRR values but, rather, to resist small-flame ignitions. However, studies also showed that it was ineffective for that purpose [221]. During recent years, concerns have emerged that the 1975 TB117 standard, while ineffective from a fire safety point of view, resulted in use of noxious chemicals which have been found to have environmental toxicology problems [222]. Consequently, in 2012 the State of California replaced the 1975 TB117 regulation with TB117-2012. The latter is a cigarette-ignition (smolder resistance) test and will not require use of toxic FR chemicals to meet test requirements.

A Cone Calorimeter-based prediction method was proposed by Babrauskas and Walton, based on data obtained in 1982 [223]. This was the earliest effort, and was based on a data set comprising materials primarily from the 1970s. Since that time, the materials in use by the furniture makers changed substantially and, especially, some highly improved materials became available to the contract furniture market. In addition, predictive techniques readily available in the early 1980s were less sophisticated than those developed more recently. Thus, during the course of the European fire research program CBUF, two new predictive models were developed [10, 145]. 'Model I' is a relatively simple model and is described below briefly. A more advanced model was also developed and its details are provided in the above references.

To use the CBUF Model I, Cone Calorimeter data must first be obtained at an irradiance of 35 kW m^{-2}. A well-controlled specimen preparation method is needed, and this is provided in ASTM E 1474 [224]. Then, one determines if the furniture item is likely to sustain a propagating fire, or whether a moderate external flame source will simply result in limited burning and no propagation. This is determined from the 180 s average of Cone Calorimeter HRR results. If $\dot{q}''_{180} < 65$ kW m^{-2}, then no propagation is assumed to occur; otherwise further calculations are made to estimate the peak HRR. The scheme is as follows:

If

$$(x_1 > 115) \; or \; \left(\dot{q}''_{35-tot} > 70 \; and \; x_1 > 40\right) \; or \; (style = \{3,4\} \; \text{and} \; x_1 > 70)$$

then $\dot{q}_{fs} = x_2$

Else,

If $x_1 < 56$

then $\dot{q}_{fs} = 14.4\, x_1$

Else, $\dot{q}_{fs} = 600 + 3.77 x_1$

where $x_1 = (m_{soft})^{1.25}$ (style factor A) $\left(\dot{q}''_{35-pk} + \dot{q}''_{35-300}\right)^{0.7} (15 + t_{ig-35})^{-0.7}$

and the subscript *35* denotes that the Cone Calorimeter HRR tests run at a 35 kW m^{-2} irradiance. The m_{soft} is the mass of the 'soft' = combustible parts of the item (kg); it includes fabric, foam, interliner, dust cover, etc., but does not include the frame nor any rigid support pieces.

And, $x_2 = 880 + 500\left(m_{soft}\right)^{0.7}$(style factor A) $\left(\frac{\Delta h_{c,eff}}{\dot{q}''_{35-tot}}\right)^{1.4}$

Here, $\Delta h_{c,eff}$ is the test-average effective heat of combustion in the Cone Calorimeter (MJ kg^{-1}), and $\dot{q}''_{35-tot}$ is the total heat released

Table 26.32 Style factors used in the CBUF model for predicting upholstered furniture heat release rates

Type of furniture	Style factor A	Style factor B
Armchair, fully upholstered, average amount of padding	1.0	1.0
Sofa, 2-seat	1.0	0.8
Sofa, 3-seat	0.8	0.8
Armchair, fully upholstered, highly padded	0.9	0.9
Armchair, small amount of padding	1.2	0.8
Wingback chair	1.0	2.5
Sofa-bed (convertible)	0.6	0.75
Armchair, fully upholstered, metal frame	1.0	0.8
Armless chair, seat and back cushions only	1.0	0.75
Two-seater, armless, seat and back cushions only	1.0	1.0

at a flux of 35 kW m^{-2}. Another correlation predicts the total heat release:

$$q_{tot} = 0.9\, m_{soft} \times \Delta h_{c,eff} + 2.1\left(m_{comb,\,tot} - m_{soft}\right)^{1.5}$$

where $m_{\mathrm{comb,tot}}$ denotes the total combustible mass of the item (kg), that is, everything except metal parts.

Finally, the time to peak, t_{pk} (s) for the full-scale item is estimated as:

$$t_{pk} = 30 + 4900(\text{style factor B})\left(m_{soft}\right)^{0.3}\left(\dot{q}''_{pk\#2}\right)^{-0.5}\left(\dot{q}''_{trough}\right)^{-0.5}\left(t_{pk\#\,1} + 200\right)^{0.2}$$

where the 'peak' and 'trough' notations refer to the fact that, in the general case, the Cone Calorimeter HRR of furniture composites shows two main peaks and one trough in between them. The style factors are obtained from Table 26.32.

With these values computed, a triangular HRR curve can then be constructed. The peak HRR and the time to peak are given directly, while the base width of the triangle is determined from the calculated total heat release of the furniture item.

Video Games

Edenburn [225] tested the joystick controller from video game console having a plastic enclosure made from ABS (UL 94 V-2 rated). When ignited with a needle flame, the unit showed a peak HRR of 6.7 kW and a total heat release of 2.52 MJ. HRR results for the main portion (console) were not provided.

Wall/Ceiling Lining Materials

Combustible interior finish materials are substantially more difficult to treat than free-standing combustibles. They cannot be measured in a device such as the furniture calorimeter, and require any full-scale study to be a room fire. The materials cover a large area, but the area of active flame involvement is generally not predictable, except after flashover, when in many cases it can be assumed that all surfaces are involved. In the early 1980s, a series of wall materials was studied by Lee at NIST [15] in full-scale room fires, and also in bench-scale, with the Cone Calorimeter. This work comprised the first attempted correlation between bench scale and full scale for wall lining materials. For several materials in the test series, which included both cellulosics and plastics, it was found that, after flashover, the per-unit-area full-scale heat release rates, were approximately

the same as the values obtained from the Cone Calorimeter. Lee's work did not yet lead to a predictive method, since no technique for estimating the flame-covered area, A(t) was found.

At about the same time, Babrauskas found that full-scale fire development on wall/ceiling linings could be approximated [226] by the expression $\dot{q}''_{bs-pk}/t_{ig}$, where the HRR value and the ignition time were obtained from the Cone Calorimeter. The $1/t_{ig}$ factor effectively represented the growth of A(t), but such a scheme was only semi-quantitative.

The first successful quantitative method came with the work of Wickström and Göransson in 1987 [227]. The model was based on the premise that the full-scale scenario involves the combustible materials located on the walls and ceiling of the ISO 9705 room. Note that the same material is expected to be placed on both walls and ceiling. The model uses the principle of area convolution and elaborates on Babrauskas' assumption that $1/t_{ig}$ controls the growth of the burning area. The model was later extended and extensively validated in the European research program EUREFIC, EUropean REaction to FIre Classification [228]. The primary assumptions in the model are:

1. The burning area growth rate and the HRR are decoupled.
2. The burning area growth rate is proportional to the ease of ignition, i.e. the inverse of the time to ignition in small scale.
3. The history of $\dot{q}''$ at each location in the full scale is to be the same as in the Cone Calorimeter test.

The model pays mind to the observation that burning patterns on wall/ceilings can be very different and, especially, that some products stop spreading fire under certain conditions, while others continue. The basic area growth regimes are illustrated in Fig. 26.117, where the regimes are marked in Roman numerals. The fire spread may follow three different routes. At points 'A' and 'B' fire spread may or may not continue, based on whether a calculated fictitious surface temperature is higher than a critical value. The calculation is based on data from the Cone Calorimeter. Within the different flame spread regimes, the burning area growth rate depends on ignitability, i.e. time to ignition in the Cone Calorimeter. Once the flame spread rate

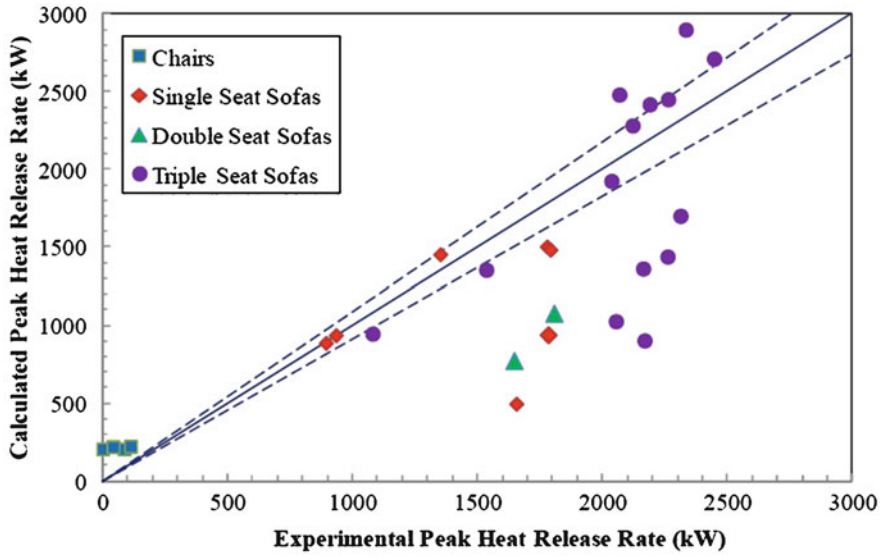

Fig. 26.116 SwRI test results on commercial residential furniture showing that peak HRR values are primarily in the range of 900–2500 kW

is determined, the HRR is calculated assuming that $\dot{q}''$ is the same in small and large scale. This is understood to be a simplification. The HRR depends on the actual heat flux level received by the product as a function of time. Experience showed, however, that the errors average out and can be included in empirical constants. The method is only of moderate difficulty to apply, but the description is somewhat lengthy. Details are available [23]. This reference also contains graphs illustrating the kind of agreement that is obtained between predictions and experiments.

While highly successful for its intended purpose, the EUREFIC model does have notable limitations. It:

- Can only treat the standard ISO 9705 room, with the standard doorway for ventilation
- Only predicts the ISO 9705 100/300 kW burner
- Requires that the material be on both walls and ceiling
- Cannot deal with products that do not ignite in the Cone Calorimeter at a 25 kW m^{-2} irradiance.

It must be remembered that the primary purpose for developing this model was to predict product performance categories to be obtained in the ISO 9705 test, while only using bench-scale Cone Calorimeter data. For its intended purpose, it has been an unquestionable success.

The above limitations indicate that the EUREFIC model, while a major breakthrough, was certainly not the final answer to modeling needs for wall/ceiling products. Two extensions have been proposed to generalize the applicability of this model. Göransson, one of the developers of the EUREFIC model, proposed an extension [229] to encompass a 'huge-scale' room. Such a test room was constructed at VTT. Its dimensions were 6.75 m by 9.0 m, with a ceiling height of 4.9 m. The door opening, 0.8 by 2.0 m high, however, was the same as for the ISO 9705 room. The burner operation was at the 100 kW level for 10 min, then at 300 kW for another 10 min, finally at 900 kW for 10 more minutes. An extended model was created for this situation by introducing a new set of regimes to correspond to the 900 kW burner level. In addition, it was found that the constant had to be modified for the 100 and 300 kW time periods. The agreement between model and prediction was very good, but only five tests were available for validation at the huge scale.

A second extension was developed by Sumathipala and coworkers [230, 231]. This model extends the applicability to the case of the room fire test studied by Lee [15]. The dimensions of that room are almost identical to the ISO room. The differences arise because (a) the two burner regimes are 40 and 160 kW, (b) the burner face size is different, and (c) the product is normally mounted on walls only, rather than walls and ceiling. The authors, however, in their development work, included tests of both rooms in both mounting configurations. The success of these extension confirms that the basic ideas behind the EUREFIC model are sound and can potentially have flexibility. On the other hand, it must be borne in mind that even the extensions are 'hard-wired' configurations and do not yet approach a technique which could be applicable towards user-selected room sizes, burner levels, and product configurations.

Perhaps the most ambitious model so far for wall/ceiling products has been one developed by Karlsson and coworkers [232–234]. Karlsson's model incorporates much more of current concepts of plumes, flame length calculations, ceiling jets, and similar constructs than does the EUREFIC model. The model has the same 'hard-wired' limitations that the EUREFIC model has in terms of ignition sources, product configuration, and room size being fixed. Another wall/ceiling model was developed by Quintiere and Cleary [235–237] and extended by Janssens and coworkers [238].

Wardrobes

Information on the HRR of wardrobes is available from a NIST study [239]. The test wardrobes are illustrated in Fig. 26.118; data

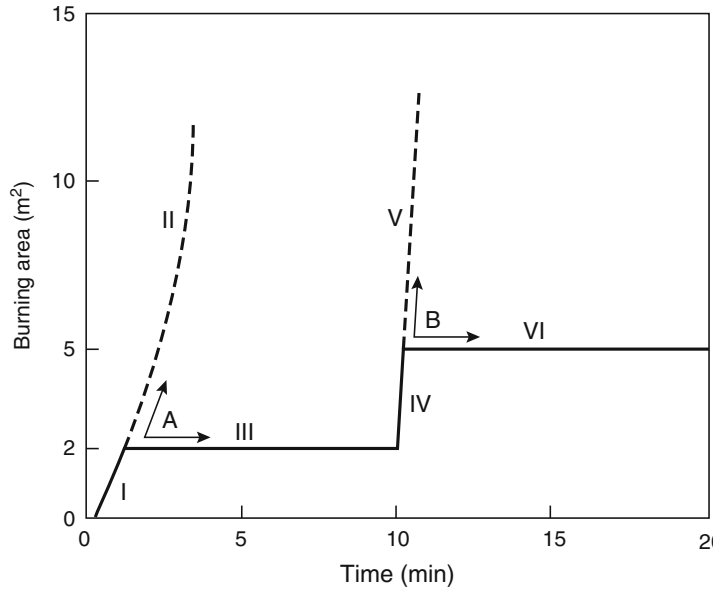

Fig. 26.117 EUREFIC fire spread regimes

Table 26.33 The HRR properties of wardrobes

Test No.	Construction	Wardrobe combustible mass (kg)	Clothing and paper (kg)	Peak HRR (kW)	Total heat released (MJ)	Avg. heat of combustion (MJ kg^{-1})
21	Steel	0	1.93	270	52	18.8
43	Plywood, 12.7 mm thick	68.3	1.93	3100	1068	14.9
41	Plywood, 3.2 mm thick, unpainted	36.0	1.93	6400	590	16.9
42	Plywood, 3.2 mm thick, 1 coat FR paint	37.3	1.93	5300	486	15.9
44	Plywood, 3.2 mm thick, 2 coats FR paint	37.3	1.93	2900	408	14.2
61	Particleboard, 19 mm thick	120.3	0.81	1900	1349	17.5

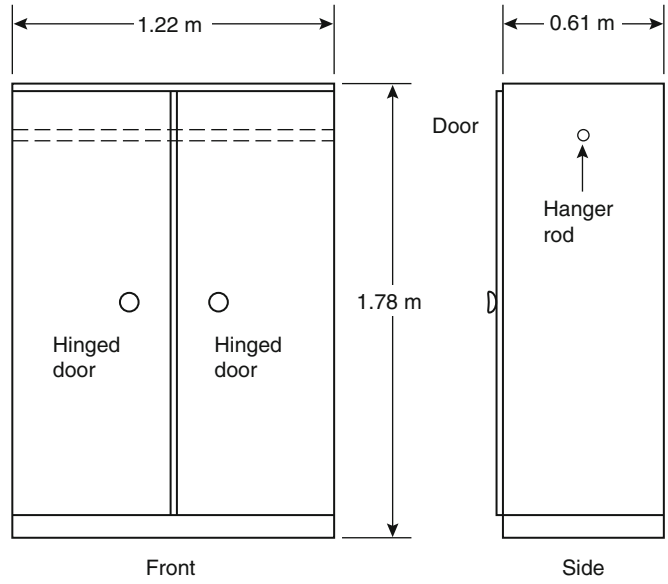

Fig. 26.118 Configuration of the tested wardrobes

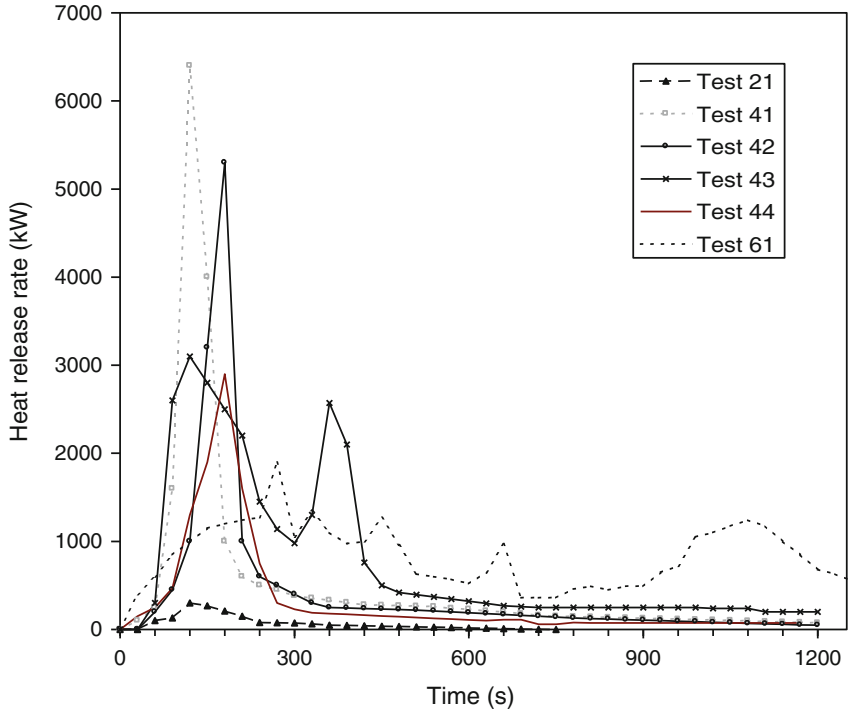

Fig. 26.119 HRR of various wardrobes

Table 26.34 European washing machines tested by VTT

Specimen	W1	W2	W3
Ignition source (kW)	1	1	300–550
Initial mass (kg)	69.3	69.9	63.3
Mass loss (kg)	10.1	10.4	12.3
Peak HRR (kW)	345	431	221
Total heat (MJ)	259	245	383

are given in Table 26.33 and Fig. 26.119. The wardrobes were outfitted with a small amount of clothing, or simulated clothing, and some paper. Tests were not run on the clothes items by themselves. However, since in the case of the steel wardrobe, the only other combustible present was the paint on the metal, it is reasonable to assign a value of about 270 kW peak for the 1.93 kg clothes load. The most important conclusion, however, was that, for combustible constructions, the peak HRR is inversely dependent on wardrobe panel thickness (and, by contrast, no simple connection to combustible specimen mass is seen). Thus, while the total heat content of the 19 mm particleboard specimen is high (see Table 26.33), its peak HRR is quite low, since flame spread and fire involvement proceed more slowly over a thick material (Fig. 26.120).

Washing Machines

VTT tested [105] European washing machines. The specimens are described in Table 26.34, while test results are shown in Fig. 26.120. The specimens were extinguished before the ultimate peak burning would have occurred. These results must not be applied to appliances used in North America, since European appliance styles are different from North American ones and also because local standards are such as to permit appliances of greater flammability in Europe (Fig. 26.120). HRR data on North American washing machines are not available.

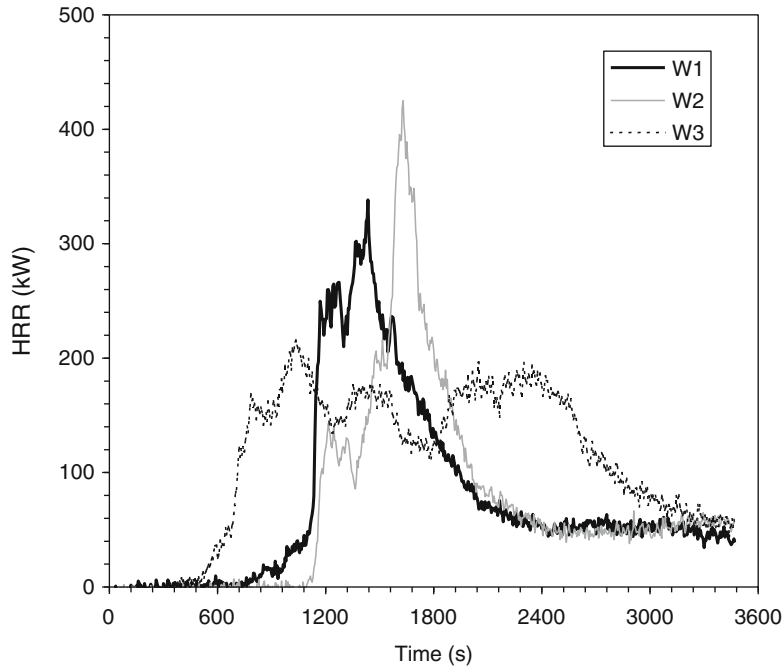

Fig. 26.120 HRR of European washing machines tested by VTT

Windows, Plastic

In applications where vandal resistance is needed, polycarbonate windows are sometimes used. This material is combustible, and limited testing was reported by Peacock et al. [240]. The tests indicated that it is hard to derive an 'innate' HRR value. The windows do not burn unless a sustained flame or heat source is applied. In that case, the HRR of the product increases with increasing severity of the ignition source. For a 50 kW exposure source, a test window showed an additional 50 kW HRR, with a burning time of ca. 80 s. For a 200 kW exposure source, the window peak HRR was about an additional 250 kW, but with a longer duration of about 200 s, at progressively diminishing HRR values.

Estimating the HRR for General Combustibles

The previous edition of the Handbook suggested a hypothetical method for estimating the HRR for general combustibles. This was based on some very simplified assumptions, especially that flame spread could, in the first approximation, be ignored. Further experience gained with additional classes of combustibles, as discussed above, suggests that such a condition will only very rarely hold. Furthermore, the user has no way of knowing when it might hold. Thus, prudent design practice should now demand that first recourse be made to the specific sections above which may address the modeler's needs. If they do not, then testing is indicated. For the modeler wishing to start up a major research activity, the schemata outlined for upholstered furniture, mattresses, and wall/ceiling lining should serve as illustrations of appropriate starting points in theory and practice. It must be pointed out, however, that such research programs have proven to be complex and that quick or inexpensive results cannot be expected.

Uncertainty of HRR Measurements

As in any engineering measurement, uncertainty in HRR measurements can be subdivided into:
1. Bias,

Table 26.35 The 95 % confidence limits for HRR test apparatuses as determined from recent round robins

				Peak HRR		Total HRR	
Apparatus	Year	Labs	Levels	r (%)	R (%)	r (%)	R (%)
Cone calorimeter	2000	4	16	17	23	8	15
ICAL	1999	3	8	56	67	72	118
SBI	1997	16	30	38	54	47	71
Room calorimeter	1994	12	5	65	79	25	41

2. Random error, sometimes termed 'precision uncertainty.'

Bias is properly minimized by use of calibration standards; for HRR testing this often comprises a metered flow of a calibration gas of high purity. Another source of bias that can be minimized, when appropriate, is specific to oxygen-consumption calorimetry bases measurements. For most testing, a standard oxygen consumption constant value of 13.1 MJ per kg of oxygen consumed is used. A small number of substances of fire-safety interest show oxygen consumption constants substantially different from this standard value. If the molecular composition of the substance is known, a correction can always be made to eliminate this source of bias.

Most of the instruments in which the HRR measurements are made have been subjected to round robins ("inter-laboratory trials") to quantify the magnitude of random error that can be expected. Comparative values have been compiled by Janssens [241], as shown in Table 26.35. For a number of them, several round robins have been conducted, thus the data shown are identified by year. SBI denotes the European Single Burning Item test [242], which is a regulatory HRR test for building products that uses two wall panels in a corner configuration, without ceiling. The values tabulated refer to the 95 % confidence intervals; standard deviations can be obtained by dividing the figures shown by 2.8.

References

1. Babrauskas, V., and Peacock, R. D., Heat Release Rate: The Single Most Important Variable in Fire Hazard, *Fire Safety J.* **18**, 255-272 (1992).
2. Babrauskas, V., Lawson, J. R., Walton, W. D., and Twilley, W. H., Upholstered Furniture Heat Release Rates Measured with a Furniture Calorimeter (NBSIR 82-2604), U. S. Natl. Bur. Stand. (1982).
3. Heskestad, G., A Fire Products Collector for Calorimetry into the MW Range (FMRC J. I. OC2El.RA), Factory Mutual Research Corp., Norwood (1981).
4. Standard Test Method for Fire Testing of Real Scale Upholstered Furniture Items (ASTM E 1537), ASTM, West Conshohocken PA.
5. Standard Test Method for Fire Testing of Real Scale Mattresses (ASTM E 1590), ASTM, West Conshohocken PA.
6. Pipe Insulation: Fire Spread and Smoke Production--Full-scale Test (NT FIRE 036), NORDTEST, Espoo (1988).
7. Upholstered Furniture: Burning Behaviour--Full Scale Test (NT FIRE 032), 2nd ed., NORDTEST, Espoo, Finland (1991).
8. Standard Fire Test of Limited-Smoke Cables (UL 1685), Underwriters Laboratories, Northbrook, IL (1991).
9. Hirschler, M. M., Use of Heat Release Calorimetry in Standards, pp. 69-80 in Fire Calorimetry (DOT/FAA/CT-95/46), Federal Aviation Administration, Atlantic City Intl. Airport, NJ (1995).
10. Sundström, B., ed., Fire Safety of Upholstered Furniture--The Final Report on the CBUF Research Programme (Report EUR 16477 EN). Directorate-General Science, Research and Development (Measurements and Testing). European Commission. Distributed by Interscience Communications Ltd, London (1995).
11. Babrauskas, V., and Wickström, U. G., Thermoplastic Pool Compartment Fires, *Combustion and Flame* **34**, 195-201 (1979).
12. Dahlberg, M., Error Analysis for Heat Release Rate Measurement With the SP Industry Calorimeter (SP Report1994:29), Swedish National Testing and Research Institute, Borås (1994).
13. Cooper, L. Y., Some Factors Affecting the Design of a Calorimeter Hood and Exhaust, *J. Fire Prot. Engineering* **6**, 99-112 (1994).
14. Fisher, F. L., and Williamson, R. B., Intralaboratory Evaluation of a Room Fire Test Method (NBS-GCR-83-421), U.S. Natl. Bur. Stand. (1983).

15. Lee, B.T., Standard Room Fire Test Development at the National Bureau of Standards, pp. 29-44 in Fire Safety: Science and Engineering (ASTM STP 882), T. Z. Harmathy, ed., American Society for Testing and Materials, Philadelphia (1985).
16. Sundström, B., Room Fire Test in Full Scale for Surface Products (Rapport SP-RAPP 1984:16). Statens Provningsanstalt, Borås, Sweden (1984).
17. Surface Products: Room Fire Tests in Full Scale (NORDTEST Method NT FIRE 025). NORDTEST, Espoo, Finland (1986).
18. International Standard--Fire Tests--Full scale room test for surface products. ISO 9705:1993(E). International Organization for Standardization, Geneva (1993).
19. Standard Test Method for Room Test of Wall and Ceiling Materials Assemblies (ASTM E 2257), ASTM Intl., West Conshohocken PA.
20. Babrauskas, V., Development of the Cone Calorimeter--A Bench Scale Heat Release Rate Apparatus Based on Oxygen Consumption, *Fire and Materials* 8, 81-95 (1984).
21. Standard Test Method for Heat and Visible Smoke Release Rates for Materials and Products using an Oxygen Consumption Calorimeter (ASTM E 1354), ASTM, West Conshohocken PA.
22. International Standard -- Fire Tests -- Reaction to Fire -- Part 1: Rate of Heat Release from Building Products (Cone Calorimeter method). ISO 5660-1:1993(E). International Organization for Standardization, Geneva (1993).
23. Babrauskas, V., and Grayson, S. J., eds., Heat Release in Fires, Elsevier Applied Science Publishers, London (1992).
24. Urbas, J., and Luebbers, G. E., The Intermediate Scale Calorimeter Development, *Fire and Materials* 19, 65-70 (1995).
25. Standard Test Method for Determining of Fire and Thermal Parameters of Materials, Products, and Systems using an Intermediate Scale Calorimeter (ICAL), (ASTM E 1623), ASTM, West Conshohocken PA.
26. Babrauskas, V., A Closed-Form Approximation for Post-Flashover Compartment Fire Temperatures, *Fire Safety J.* 4, 63-73 (1981).
27. Kokkala, M., Göransson, U., and Söderbom, J., Five Large-Scale Room Fire Experiments. Project 3. EUREFIC Fire Research Program (VTT Publications 104), VTT-Technical Research Center of Finland, Espoo (1992).
28. Schleich, J.-B., and Cajot, L.-G., Natural Fire Safety for Buildings, pp. 359-367 in *Interflam 2001—Proc. 9th Intl. Conf.*, Interscience Communications Ltd., London (2001).
29. Simonson, M., Blomqvist, P., Boldizar, A., Möller, K., Rosell, L., Tullin, C., Stripple, H., and Sundqvist, J. O., Fire-LCA Model: TV Case Study, Swedish National Testing and Research Institute, Borås (2000).
30. Tests for Flammability of Plastic Materials for Parts in Devices and Appliances (UL 94), Underwriters Laboratories, Northbrook IL.
31. Dembsey, N. A., Compartment Fire Measurements and Analysis for Near Field Entrainment, Model Validation and Wall Lining Fire Growth (Ph.D. dissertation), Univ. California, Berkeley (1995).
32. Sherratt, J., and Drysdale, D. D., The Effect of the Melt-Flow Process on the Fire Behaviour of Thermoplastics, pp. 149-159 in *Interflam 2001—Proc. 9th Intl. Conf.*, Interscience Communications Ltd., London (2001).
33. Parker, W. J., Prediction of the Heat Release Rate of Wood (Ph.D. dissertation). George Washington University, Washington, DC (1988).
34. Hirata, T., Kashiwagi, T., and Brown, J. E., Thermal and Oxidative Degradation of Poly (methylmethacrylate): Weight Loss, *Macromolecules* 18, 1410-1418 (1984).
35. Kashiwagi, T., Hirata, T., and Brown, J. E., Thermal and Oxidative Degradation of Poly (methylmethacrylate): Molecular Weight, *Macromolecules* 18, 131-138 (1985).
36. Vovelle, C., Delfau, J. L., Reuillon, M., Bransier, J., and Laraqui, N., Experimental and Numerical Study of the Thermal Degradation of PMMA, pp. 43-66 in *Papers of ITSEMAP International Meeting of Fire Research and Test Centers*, Avila, Spain (October 7-9, 1986).
37. Holland, K. A., and Rae, I. D., Thermal Degradation of Polymers. Part 3. Thermal Degradation of a Compound Which Models the Head-to-Head Linkage in Poly(Methyl Methacrylate), *Australian J. Chemistry* 40, 687-692 (1987).
38. Manring, L. E., Thermal Degradation of Saturated Poly(methylmethacrylate), *Macromolecules* 21, 528-530 (1988).
39. Inaba, A., Kashiwagi, T., and Brown, J. E., Effects of Initial Molecular Weight on Thermal Degradation of Poly(methyl methacrylate). Part 1, *Polymer Degradation and Stability* 21, 1-20 (1988).
40. Steckler, K. D., Kashiwagi, T., Baum, H. R., and Kanemaru, K., Analytical Model for Transient Gasification of Noncharring Thermoplastic Materials, pp 895-904 in *Fire Safety Science—Proc. 3rd Intl. Symp.*, International Association for Fire Safety Science. Elsevier Applied Science, New York, (1991).
41. McGrattan, K., Hostikka, S., McDermott, R., Floyd, R., Weinschenk, C., and overholt, K., Fire Dynamics Simulator Technical Reference G uide. Vol. 1: Mathematical Model (NISTSP 1018) NIST, Gaithersburg MD (2013).
42. Babrauskas, V., Specimen Heat Fluxes for Bench-scale Heat Release Rate Testing, *Fire and Materials* 19, 243-252 (1995).
43. Basic Considerations in the Combustion of Hydrocarbon Fuels in Air (NACA Report 1300), National

Advisory Committee for Aeronautics, Washington (1957).
44. Babrauskas, V., Ignition Handbook, Fire Science Publishers/Society of Fire Protection Engineers, Issaquah WA (2003).
45. Babrauskas, V., and Krasny, J. F., Fire Behavior of Upholstered Furniture (NBS Monograph 173), U.S. Natl. Bur. Stand. (1985).
46. Kokkala, M., and Heinilä, M., Flame Height, Temperature, and Heat Flux Measurements on a Flame in an Open Corner of Walls, Project 5 of the EUREFIC fire research programme, Valtion Teknillinen Tutkimuskeskus, Espoo, Finland (1991).
47. Quintiere, J. G., A Simulation Model for Fire Growth on Materials Subject to a Room-Corner Test, *Fire Safety J*. 20, 313-339 (1993).
48. Parker, A. J., Wenzel, A. B., and Al-Hassan, T., Evaluation of Passive Fire Protection by Jet Fire Test Procedure, paper 4-d in *29th Loss Prevention Symp*., American Institute of Chemical Engineers, New York (1995).
49. Söderbom, J., EUREFIC--Large Scale Tests according to ISO DIS 9705. Project 4 of the EUREFIC fire research programme (SP Report 1991:27). Statens Provningsanstalt, Borås, Sweden (1991).
50. Lee, B.T., Standard Room Fire Test Development at the National Bureau of Standards, pp. 29-44 in *Fire Safety: Science and Engineering* (ASTM STP 882), T. Z. Harmathy, ed., American Society for Testing and Materials, Philadelphia (1985).
51. Hasemi, Y., Experimental Wall Flame Heat Transfer Correlations for the Analysis of Upward Wall Flame Spread, *Fire Science and Technology* 4, 75-90 (1984).
52. Quintiere, J. G., The Application of Flame Spread Theory to Predict Material Performance, *J. of Research of the National Bureau of Standards* 93, 61-70 (1988).
53. **53.,** Kulkarni, A. K., Kim, C. I., and Kuo, C.H., Turbulent Upward Flame Spread for Burning Vertical Walls Made of Finite Thickness (NIST-GCR-91-597), Natl. Inst. Stand. and Technol., Gaithersburg, MD (1991).
54. Fang, J. B., and Breese, J. N., Fire Development in Residential Basement Room (NBSIR 80-2120), U.S. Natl. Bur. Stand., Gaithersburg, MD (1980).
55. Babrauskas, V., and Williamson, R. B., The Historical Basis of Fire Resistance Testing, Part I, *Fire Technology* 14, 184-194, 205 (1978). Part II, *Fire Technology* 14,304-316 (1978).
56. Rhodes, B. T., Burning Rate and Flame Heat Flux for PMMA in the Cone Calorimeter (M.S. thesis, University of Maryland). NIST-GCR-95-664. Natl. Inst. Stand. and Technol., Gaithersburg (1994).
57. Hopkins, D. jr., and Quintiere, J. G., Material Fire Properties and Predictions for Thermoplastics, *Fire Safety J*. 26, 241-268 (1996).
58. Gore, J., Klassen, M., Hamins, A., and Kashiwagi, T., Fuel Property Effects on Burning Rate and Radiative Transfer from Liquid Pool Flames, pp. 395-404 in *Fire Safety Science—Proc. 3rd Intl. Symp*., Elsevier Applied Science, London (1991).
59. Janssens, M., Cone Calorimeter Measurements of the Heat of Gasification of Wood, pp. 549-558 in *Interflam '93: Sixth Intl. Fire Conf. Proc*., Interscience Communications Ltd., London (1993).
60. Sorathia, U., Dapp, T., Kerr, J., and Wehrle, J., Flammability Characteristics of Composites (DTRC SME 89/90), US Navy, David Taylor Research Center, Bethesda MD (1989).
61. Rowen, J. W., and Lyons, J. W., The Importance of Externally Imposed Heat Flux on the Burning Behavior of Materials, *J. Cellular Plastics* 14, 25-32 (1978).
62. Paul, K., unpublished data, RAPRA Technology, Shawbury, England.
63. Elliot, P., Whiteley, R. H., and Staggs, J. E., Steady State Analysis of Cone Calorimeter Data, pp. 35-42 in *Proc. 4th IIntl. Fire and Materials Conf*., Interscience Communications Ltd., London (1995).
64. Tsantaridis, L., Reaction to Fire Performance of Wood and Other Building Products (Ph.D. dissertation), Kungliga Tekniska Högskolan, Stockholm (2003).
65. Cleary, T. G., and Quintiere, J. G., Flammability Characterization of Foam Plastics (NISTIR 4664), Natl. Inst. Stand. Technol., Gaithersburg, MD (1991).
66. Nussbaum, R. M., and Östman, B. A.-L., Larger Specimens for Determining Rate of Heat Release in the Cone Calorimeter, *Fire and Materials* 10, 151-160 (1986); and 11, 205 (1987).
67. Janssens, M., and Urbas, J., Comparison of Small and Intermediate Scale Heat Release Data, pp. 285-294 in *Interflam '96*, Interscience Communications Ltd, London (1996).
68. Orloff, L., Modak, A. T., and Alpert, R. L., Burning of Large-Scale Vertical Wall Surfaces, pp. 1345-54 in *16th Symp. (Intl.) on Combustion*, The Combustion Institute, Pittsburgh (1976).
69. Babrauskas, V., Cone Calorimeter Annotated Bibliography, 2003 edition, Fire Science Publishers, Issaquah WA (2004).
70. Beard, A., and Goebeldecker, S., Fire Behaviour of Household Appliances towards External Ignition, European Fire Retardants Assn., Brussels (2007).
71. Ohlemiller, T. J., Shields, J. R., McLane, R. A., and Gann, R. G., Flammability Assessment Methodology for Mattresses (NISTIR 6497), Nat. Inst. Stand. and Technol., Gaithersburg MD (2000).
72. Bwalya, A. C., Characterization of Fires in Multi-Suite Residential Dwellings: Phase 1 – Room Fire Experiments with Individual Furnishings (IRC-RR-302), National Research Council Canada, Ottawa (2010).

73. Klitgaard, P. S., and Williamson, R. B., The Impact of Contents on Building Fires, *J. Fire and Flammability/Consumer Product Flammability Supplement* 2, 84-113 (1975).
74. White, J. A. jr, Western Fire Center, Inc., Kelso WA, unpublished test results (2003).
75. Huczek, J. P., Southwest Research Institute, San Antonio TX, unpublished test results (2003).
76. Tu, K. M., and Davis, S., Flame Spread of Carpet Systems Involved in Room Fires (NBSIR 76-1013), U. S. Natl. Bur. Stand., Washington (1976).
77. Vandevelde, P., and Van Hees, P., Wind Aided Flame Spread of Floor Coverings, Development and Evaluation of Small and Large Scale Tests, pp. 57-67 in *Interflam '96*, Interscience Communications Ltd., London (1996).
78. Ames, S., Colwell, R., and Shaw, K., The Fire Behaviour and Fire Testing of Carpet Used as a Stair Covering, pp. 69-77 in *Interflam '96*, Interscience Communications Ltd., London (1996).
79. Williamson, R. B., and Dembsey, N. A., Advances in Assessment Methods for Fire Safety, *Fire Safety J.* 20, 15-38 (1993).
80. Stroup, D. W., DeLauter, L., Lee, J., and Roadarmel, G., Fire Tests of Men's Suits on Racks (FR 4013), Nat. Inst. Stand. and Technol., Gaithersburg MD (2001).
81. Satoh, H., and Mizuno, T., Fire Source Model Based on the Ignited Material and Its Burning Property in the Early Stages of Fire in Residential Accommodation, *Fire Science & Technology* 25, 163-188 (2006).
82. Simonson, M., Report for the Fire Testing of One Printer and Two CPUs, (P008664), Swedish National Testing and Research Institute, Borås (2000).
83. Bundy, M., and Ohlemiller, T., Full-Scale Flammability Measures for Electronic Equipment (Tech. Note 1461), Nat. Inst. Stand. and Technol., Gaithersburg MD (2004).
84. Edenburn, D., Burning Mouse, Albemarle Corp. [n. p.] (2003).
85. Bliss, D., and Simonson, M., Fire Performance of IT Equipment Studied in the Furniture Calorimeter, pp. 171-179 in *Interflam 2001—Proc. 9th Intl. Conf.*, Interscience Communications Ltd., London (2001).
86. Steel, J. S., unpublished data, Natl. Inst. Stand. and Technol., Gaithersburg (1985).
87. Zicherman, J. and Stevanovic, A., unpublished test results, Fire Cause Analysis, Inc., Richmond CA, (20035).
88. Babrauskas, V., Harris, R. H., Jr., Gann, R. G., Levin, B. C., Lee, B. T., Peacock, R. D., Paabo, M., Twilley, W., Yoklavich, M. F., and Clark, H. M., Fire Hazard Comparison of Fire-Retarded and Non-Fire-Retarded Products (NBS Special Publication SP 749), U. S. Natl. Bur. Stand. (1988).
89. Mangs, J., and Keski-Rahkonen, O., Full Scale Experiments on Electronic Cabinets (VTT Publications 186), Valtion Teknillinen Tutkimuskeskus, Espoo, Finland (1994).
90. Mangs, J., and Keski-Rahkonen, O., Full Scale Experiments on Electronic Cabinets II (VTT Publications 269), Valtion Teknillinen Tutkimuskeskus, Espoo, Finland (1996).
91. Keski-Rahkonen, O., and Mangs, J., Maximum and Minimum Rate of Heat Release during Flashover in Electronic Cabinets of NPPs. Paper presented at *Fire Safety in Power Plants and Industrial Installations, SMiRT 13 Post Conference Seminar No. 6*, Gramado, Brazil. Valtion Teknillinen Tutkimuskeskus, Espoo, Finland (1995).
92. Rigollet, L., and Mélis, S., Fires of Electrical Cabinets, Paper no. 023 in *11th Intl. Topical Meeting on Nuclear Reactor Thermal-Hydraulics (NURETH-11)*, Avignon, France; publ. by American Nuclear Society, LaGrange Park, IL (2005).
93. Folke, F., Experiments in Fire Extinguishment, *NFPA Quarterly* 31, 115 (1937).
94. Nilsson, L., The Effect of Porosity and Air Flow on the Rate of Combustion of Fire in an Enclosed Space (Bulletin 18), Lund Institute of Technology, Lund, Sweden (1971).
95. Yamashika, S., and Kurimoto, H, Burning Rate of Wood Crib, *Rept. of Fire Res. Inst. Japan,* No. 41, 8 (1976).
96. Harmathy, T.Z., Experimental Study on the Effect of Ventilation on the Burning of Piles of Solid Fuels, *Combustion and Flame* 31, 259 (1978).
97. Quintiere, J.G., and McCaffrey, B.J., The Burning of Wood and Plastic Cribs in an Enclosure, Vol. 1 (NBSIR 80-2054), [U.S.] Natl. Bur. Stand., Washington (1980).
98. Fons, W.L., Clements, H.B., and George, P.M., Scale Effects on Propagation Rate of Laboratory Crib Fires, in *9th Symp. (Intl.) on Combustion,* The Combustion Institute, Pittsburgh (1962).
99. Delichatsios, M.A., Fire Growth Rates in Wood Cribs, *Combustion and Flame* 27, 267 (1976).
100. Moore, L. D., Full-scale Burning Behavior of Curtains and Drapes (NBSIR 78-1448), [U.S.] Nat. Bur. Stand., Washington (1978).
101. Wetterlund, I., and Göransson, U., A Full Scale Fire Test Method for Free-Hanging Curtain and Drapery Textiles (SP Report 1988:45),Swedish National Testing Institute, Borås (1988).
102. Yamada, T., Yanai, E., and Naba, H., A Study of Full-Scale Flammability of Flame Retardant and Non-Flame Retardant Curtains, pp. 463-473 in *Proc. 4th Asia-Oceania Symp. on Fire Science & Technology*, Asia-Oceania Assn. for Fire Science & Technology/Japan Assn. for Fire Science & Engineering, Tokyo (2000).
103. Urban Wildland Interface Building Test Standards (12-7A-5), Fire Resistive Standards for Decks and

Other Horizontal Ancillary Structures, California Office of State Fire Marshal, Sacramento (2004).
104. Chow, W. K., Han, S. S., Dong, H., Gao, Y., and Zou, G. W., Full-Scale Burning Tests on Heat Release Rates of Furniture, *Intl. J. of Engineering Performance-Based Fire Codes* 6, 168-180 (2004).
105. Hietaniemi, J., Mangs, J., and Hakkarainen, T., Burning of Electrical Household Appliances—An Experimental Study (VTT Research Notes 2084), Valtion Teknillinen Tutkimuskeskus, Espoo, Finland (2001).
106. NIST, unpublished data.
107. Tewarson, A., Lee, J.L., and Pion, R.F., Categorization of Cable Flammability. Part I. Experimental Evaluation of Flammability Parameters of Cables Using Laboratory-scale Apparatus, EPRI Project RP 1165-1, Factory Mutual Research Corp., Norwood (1979).
108. Sumitra, P.S., Categorization of Cable Flammability. Intermediate-Scale Fire Tests of Cable Tray Installations, Interim Report NP-1881, Research Project 1165-1, Factory Mutual Research Corp., Norwood (1982).
109. Lee, B.T., Heat Release Rate Characteristics of Some Combustible Fuel Sources in Nuclear Power Plants, NBSIR 85-3195, [U.S.] Nat. Bur. Stand., Washington (1985).
110. Arvidson, M., Potato Crisps and Cheese Nibbles Burn Fiercely, *Brandposten* [SP] No. 32, 10-11 (2005).
111. Madrzykowski, D., unpublished test results (2012).
112. Persson, H., Evaluation of the RDD-measuring Technique. RDD-Tests of the CEA and FMRC Standard Plastic Commodities (SP Report 1991:04), SP, Borås, Sweden (1991).
113. Babrauskas, V., unpublished test results (1997).
114. Heskestad, G., Flame Heights of Fuel Arrays with Combustion in Depth, pp. 427-438 in *Fire Safety Science—Proc. 5th Intl. Symp.,* Intl. Assn. for Fire Safety Science (1997).
115. Heskestad, G., Flame Heights of Fuel Arrays with Combustion in Depth, FMRC J.I. 0Y0J3.RU (2), Factory Mutual Research Corp., Norwood MA (1995).
116. Dean, R. K., Stored Plastics Test Program (FMRC Serial No. 20269), Factory Mutual Research Corp., Norwood MA (1975).
117. Yu, H.-Z., and Kung, H.-C., Strong Buoyant Plumes of Growing Rack Storage Fires, pp. 1547-1554 in *20th Symp. (Intl.) on Combustion*, Combustion Institute, Pittsburgh PA (1984).
118. Yu, H.-Z., and Kung, H.-C., Strong Buoyant Plumes of Growing Rack Storage Fires, FMRC J.I. 0G2E7.RA(1), Factory Mutual Research Corp., Norwood MA (1984).
119. Commodities and Storage Arrangements, *Record* 66:3, 13-18 (May/June 1989).
120. Guide for Smoke and Heat Venting (NFPA 204), National Fire Protection Assn., Quincy MA (1998).
121. Kung, H.-C., Spaulding, R. D., and You, H.-Z., Response of Sprinkler Links to Rack Storage Fires. FMS J.I.0G2E7.RA(2). FMRC (1984).
122. Chicarello, P. J., and Troup, J. M. A., Fire Collector Test Procedure for Determining the Commodity Classification of Ordinary Combustible Products. FMRC J.I. 0R0E5.RR. FMRC (1990).
123. Yu, H.-Z., and Stavrianidis, P., The Transient Ceiling Flows of Growing Rack Storage Fires. FMRC J.I. 0N1J0.RA(3). FMRC (1989).
124. Yu, H.-Z., A Sprinkler-Response-Prediction Computer Program for Warehouse Applications. FMRC J.I. 0R2E1.RA. FMRC (1992).
125. Newman, J., and Troup, J. M. A., The Building Calorimeter: FM Global's Novel Approach to Large-Scale Fire Testing, NFPA World Safety Conf. and Expo., Las Vegas (2005).
126. Yu, H.-Z., RDD and Sprinklered Fire Tests for Expanded Polystyrene Egg Crates, FMRC J.I. 0R2E3.RA(1), Factory Mutual Research Corp., Norwood MA (1990).
127. Sleights, J. E., SPRINK 1.0—A Sprinkler Response Computer Program for Warehouse Storage Fires (M.S. thesis), Worcester Polytechnic Institute, Worcester MA (1993).
128. Lee, J. L., and Dean, R. K., Fire Products Collector Tests of Polyethylene Terephthalate (PET) Plastic Bottles in Corrugated Carton, FMRC J.I. 0N0J6. RA070(A), Factory Mutual Research Corp., Norwood MA (1986).
129. Lee, J. L., Combustibility Evaluation of Shredded Newsprint Commodity and an Improved Polyurethane Foam Packaging Product Using the Fire Products Collector, FMRC J.I. 0K0E6.RANS, Factory Mutual Research Corp., Norwood MA (1984).
130. Khan, M. M., Evaluation of the Fire Behavior of Packaging Materials, presented at Defense Fire Protection Symp., Annapolis (1987).
131. Hasegawa, H., Alvares, N. J., and White, J. A., Fire Tests of Packaged and Palletized Computer Products, *Fire Technology* 35, 294-307 (1999).
132. Hasegawa, H., private communication (2000).
133. Dillon, S. E., Janssens, M. L., and Garabedian, A. S., A Comparison of Building Code Classifications and Results of Intermediate-Scale Fire Testing of Stored Plastic Commodities, pp. 593-604 in *Interflam 2001—Proc. 9th Intl. Conf.*, Interscience Communications Ltd., London (2001).
134. Roberts, T. A., Merrifield, R., and Tharmalingam, S., Thermal Radiation Hazards from Organic Peroxides, *J. Loss Prevention in the Process Industries* 3, 244-252 (1990).
135. Babrauskas, V., unpublished test data (1997).
136. Yu, H.-Z., and Stavrianidis, P., The Transient Ceiling Flows of Growing Rack Storage Fires, FMRC J.I. 0N1J0.RA(3), Factory Mutual Research Corp., Norwood MA (1989).

137. Mitler, H. E., Input Data for Fire Modeling, pp. 187-199 in Thirteenth Meeting of the UJNR Panel on Fire Research and Safety, March 13-20, 1996 (NISTIR 6030, vol. 1), Nat. Inst. Stand. and Technol., Gaithersburg MD (1997).
138. Messa, S., Designing Fires for FIRESTARR, LSF Fire Laboratories, Montano Lucino, Italy (2000).
139. Chow, W. K., Zou, G., Dong, H., and Gao, Y., Necessity of Carrying out Full-Scale Burning Tests for Post-Flashover Retail Shop Fires, *Intl. J. on Engineering Performance-Based Fire Codes* 5, 20-27 (2003).
140. Madrzykowski, D., and Kerber, S, Fire Fighting Tactics under Wind Driven Conditions: Laboratory Experiments (TN 1618), Nat. Inst. Stand & Technol., Gaithersburg MD (2009).
141. Babrauskas, V., Bench-Scale Predictions of Mattress and Upholstered Chair Fires, pp. 50-62 in *Fire and Flammability of Furnishings* (ASTM STP 1233). American Society for Testing and Materials, Philadelphia (1994).
142. Damant, G. H., and Nurbakhsh, S., Heat Release Tests of Mattresses and Bedding Systems, State of California, Bureau of Home Furnishings and Thermal Insulation, North Highlands, CA (1991).
143. Holmstedt, G., and Kaiser, I., Brand I vårdbäddar (SP-RAPP 1983:04), Swedish National Testing and Research Institute, Borås, Sweden (1983).
144. Andersson, B., Fire Behaviour of Beds and Upholstered Furniture--An Experimental Study (LUTVDG/ISSN 0282-3756),Lund University, Dept. of Fire Safety Engineering, Lund, Sweden (1985).
145. Babrauskas, V., Baroudi, D., Myllymäki, J., and Kokkala, M., The Cone Calorimeter Used for Predictions of the Full-scale Burning Behaviour of Upholstered Furniture, *Fire and Materials* 21, 95-105 (1997).
146. Hansen, R., and Ingason, H., Heat Release Rate Measurements of Burning Mining Vehicles in an Underground Mine, *Fire Safety J.* 61, 12-25 (2013).
147. Walton, W. D., and Budnick, E. K., Quick Response Sprinklers in Office Configurations: Fire Test Results (NBSIR 88-3695), [U. S.] Natl. Bur. Stand., Gaithersburg, MD (1988).
148. Madrzykowski, D., and Vettori, R. L., Sprinkler Fire Suppression Algorithm for the GSA Engineering Fire Assessment System (NISTIR 4833), Natl. Inst. Stand. Technol., Gaithersburg, MD (1992).
149. Madrzykowski, D., Office Work Station Heat Release Rate Study: Full Scale vs. Bench Scale, pp. 47-55 in *Interflam '96*, Interscience Communications Ltd., London (1996).
150. Madrzykowski, D., and Walton, W. D. Cook County Administration Building Fire, 69 West Washington, Chicago, Illinois, October 17, 2003: Heat Release Rate Experiments and FDS Simulations (NIST SP 1021), Nat. Inst. Stand. & Technol., Gaithersburg MD (2004).
151. Kakegawa, S., et al., Design Fires for Means of Egress in Office Buildings Based on Full-scale Fire Experiments, pp. 975-986 in *Fire Safety Science—Proc. 7th Intl. Symp.*, International Association for Fire Safety Science (2003).
152. Krasner, L. M., Burning Characteristics of Wooden Pallets as a Test Fuel (Serial 16437), Factory Mutual Research Corp., Norwood (1968).
153. Babrauskas, V., Pillow Burning Rates, *Fire Safety J.* 8, 199-200 (1984/85).
154. Pipe Insulation: Fire Spread and Smoke Production--Full-scale Test (NT FIRE 036), NORDTEST, Espoo, Finland (1988).
155. Wetterlund, I., and Göransson, U., A New Test Method for Fire Testing of Pipe Insulation in Full Scale (SP Report 1986:33), Swedish National Testing Institute, Borås (1986).
156. Babrauskas, V., Toxic Fire Hazard Comparison of Pipe Insulations: The Realism of Full-scale Testing Contrasted with Assessments from Bench-scale Toxic Potency Data Alone, pp. 439-452 in *Asiaflam '95*, Interscience Communications Ltd, London (1995).
157. Ahonen, A., Kokkala, M. and Weckman, H., Burning Characteristics of Potential Ignition Sources of Room Fires (Research Report 285), Valtion Teknillinen Tutkimuskeskus, Espoo, Finland (June 1984).
158. Damant, G., and Nurbakhsh, S., Christmas Trees--What Happens When They Ignite? *Fire and Materials* 18, 9-16 (1994).
159. Babrauskas, V., Chastagner, G., and Stauss, E., Flammability of Cut Christmas Trees, IAAI Annual General Meeting and Conference, Atlantic City NJ (2001).
160. Evans, D. D., Rehm, R. G., Baker, E. S., McPherson, E. G., and Wallace, J. B., Physics-Based Modeling of Community Fires, pp. 1065-1076 in *Interflam 2004*, Interscience Communications Ltd., London (2004).
161. Stroup, D. W., DeLauter, L., Lee, J., and Roadarmel, G., Scotch Pine Christmas Tree Fire Tests (FR 4010), Nat. Inst. Stand. and Technol., Gaithersburg MD (1999).
162. Madrzykowski, D., Impact of a Residential Sprinkler on the Heat Release Rate of a Christmas Tree Fire (NISTIR 7506), Nat. Inst. Stand & Technol., Gaithersburg MD (2008).
163. Jackman, L., Finegan, M., and Campbell, S., Christmas Trees: Fire Research and Recommendations (LPR 17:2000), Loss Prevention Council, London (2000).
164. Stephens, S. L., Gordon, D. A., and Martin, R. E., Combustibility of Selected Domestic Vegetation Subjected to Desiccation, pp. 565-571 in *Proc. 12th Intl. Conf. on Fire and Forest Meteorology*, Society of American Foresters, Bethesda MD (1994).

165. Etlinger, M. G., Fire Performance of Landscape Plants (M.S. thesis), Univ. California, Berkeley (2000).
166. Outline of Investigation for Artificial Christmas Trees (Subject 411), 2nd ed., Underwriters Laboratories Inc., Northbrook IL (1991).
167. Babrauskas, V., to be published.
168. McCaffrey, B., Flame Height, pp. 2-1 to 2-8 in SFPE Handbook of Fire Protection Engineering, 2nd ed., National Fire Protection Assn., Quincy MA (1995).
169. McCaffrey, B. J. Momentum Implications for Buoyant Diffusion Flames, *Combustion and Flame 52*, 149-167 (1983).
170. Särdqvist, S., Initial Fires: RHR, Smoke Production and CO Generation from Single Items and Room Fire Tests (LUTVDG/TVBB-3070-SE), Lund University, Dept. of Fire Safety Engineering, Lund, Sweden (1993).
171. Blinov, V. I., and Khudiakov, G. N., Diffusion Burning of Liquids. U.S. Army Translation. NTIS No. AD296762 (1961).
172. Hottel, H.C., Review Certain Laws Governing Diffusive Burning of Liquids, by V. I. Blinov and G. N. Khudiakov, *Fire Research Abstracts and Reviews* 1, 41-44 (1958).
173. Babrauskas, V., Tables and Charts, pp. A-1 to A-17 in Fire Protection Handbook, 18th ed., National Fire Protection Assn., Quincy, MA (1997).
174. Babrauskas, V., Estimating Large Pool Fire Burning Rates, *Fire Technology* 19, 251-261 (1983).
175. Gosse, A., BG Technologies Ltd., private communication (2000).
176. Putorti, A. D. jr., Flammable and Combustible Liquid Spill/Burn Patterns (NIJ 604-00), National Institute of Justice, U.S. Department of Justice, Washington (2001).
177. Modak, A. T., Ignitability of High-Fire-Point Liquid Spills (EPRI NP-1731), Electric Power Research Inst., Palo Alto, CA (1981).
178. Gottuk, D. T., Scheffey, J. L., Williams, F. W., Gott, J. E., and Tabet, R. J., Optical Fire Detection (OFD) for Military Aircraft Hangars: Final Report on OFD Performance to Fuel Spill Fires and Optical Stresses (NRL/MR/6180--00-8457), Naval Research Lab., Washington (2000).
179. DeHaan, J. D., The Dynamics of Flash Fires Involving Flammable Hydrocarbon Liquids, *Amer. J. Forensic Medicine and Pathology* 17, 24-31 (1996).
180. Babrauskas, V., COMPF2—A Program for Calculating Post-Flashover Fire Temperatures (Tech Note 991), [U. S.] Natl. Bur. Stand., Gaithersburg MD (1979).
181. Gore, J. P., Klassen, M., Hamins, A., and Kashiwagi, T., Fuel Property Effects on Burning Rate and Radiative Transfer From Liquid Pool Flames, pp. 395-404 in *Fire Safety Science—Proc. 3rd Intl. Symp.*, International Association for Fire Safety Science, Elsevier Applied Science, New York (1991).
182. Hamins, A., Fischer, S. J., Kashiwagi, T., Klassen, M. E., and Gore, J. P., Heat Feedback to the Fuel Surface in Pool Fires, *Combustion Science and Technology* 97, 37-62 (1994).
183. Adiga, K. C., Ramaker, D. E., Tatem, P. A., and Williams, F. W., Modeling Pool-Like Gas Flames of Propane, *Fire Safety J.* 14, 241-250 (1989).
184. Adiga, K. C., Ramaker, D. E., Tatem, P. A., and Williams, F., Modeling Thermal Radiation in Open Liquid Pool Fires, pp. 241-250 in *Fire Safety Science—Proc. 2nd Intl. Symp.*, International Association for Fire Safety Science, Hemisphere Publishing Corp., New York (1989).
185. Koseki, H., and Mulholland, G. W., Effect of Diameter on the Burning of Crude Oil Pool Fires, *Fire Technology* 27, 54-65 (1991).
186. Koseki, H., Boilover and Crude Oil Fire, *J. Applied Fire Science* 3, 243-272 (1993/1994).
187. Chow, W. K., Necessity of Testing Combustibles under Well-developed Fires, *J. Fire Sciences* (2005).
188. Troitzsch, J. H., Flammability and Fire Behaviour of TV Sets, pp. 979-990 in *Fire Safety Science—Proc. 6th Intl. Symp.*, Intl. Assn. of Fire Safety Science (2000).
189. Nam, D.-G., Hasemi, Y., and Kamikawa, D., Investigation of an Apartment Fire—Experiments for Estimating the Cause and Mechanism of the Fire, pp. 389-400 in *Fire & Materials 2005*, Interscience Communications Ltd., London (2005).
190. Hoffmann, J. M., Hoffmann, D. J., Kroll, E. C., and Kroll, M. J., Full Scale Burn Tests of Television Sets and Electronic Appliances, *Fire Technology* 39, 207-224 (2003).
191. Shipp, M., and Spearpoint, M., Measurements of the Severity of Fires Involving Private Motor Vehicles, *Fire and Materials* 19, 143-151 (1995).
192. Mangs, J., and Keski-Rahkonen, O., Characterization of the Fire Behaviour of a Burning Passenger Car. Part I: Car Fire Experiments, *Fire Safety J.* 23, 17-35 (1994).
193. Steinert, C., Experimentelle Untersuchhungen zum Abbrand-und Feuerubersprungsverhalten von Personenkraftwagen, *VFDB-Zeitschrift*, No. 4, 63-172 (2000).
194. Ingason, H., Gustavsson, S., and Werling, P., Brandförsök i en bergtunnel—Naturlig ventilation. Delrapport II (SP AR 1995:45), Swedish National Testing and Research Institute, Borås (1995).
195. Okamoto, K., Watanabe, N., Hagimoto, Y., Chigira, T., Masano, R., Miura, H., Ochiai, H., Tamura, Y., Hayano, K., Maeda, Y., and Suzuki, J., Burning Behavior of Sedan Passenger Cars, *Fire Safety J.* 44, 301-310 (2009).
196. Okamoto, K., Otake, T., Miyamoto, H., Honma, M., and Watanabe, N., Burning Behavior of Minivan Passenger Cars, *Fire Safety J.* 62, 272-280 (2013).
197. Ohlemiller, T. J., and Shields, J. R., Burning Behavior of Selected Automotive Parts from a Minivan

(NISTIR 6143), Nat. Inst. Stand. & Technol., Gaithersburg MD (1998).
198. Ohlemiller, T. J., Influence of Flame-Retarded Resins on the Burning Behavior of a Heating, Ventilating and Air Conditioning Unit from a Sports Coupe (NISTIR 6748), Nat. Inst. Stand. & Technol., Gaithersburg MD (2003).
199. Ingason, H., Gustavsson, S., and Dalhberg, M., Heat Release Rate Measurements in Tunnel Fires (SP Report 1994:08), Swedish National Testing & Research Institute, Borås (1994).
200. Steinert, C., Smoke and Heat Production in Tunnel Fires, pp. 123-137 in *Proc. Intl. Conf. on Fires in Tunnels* (SP Report 1994:54), Swedish National Testing & Research Institute, Borås (1994
201. Göransson, U., and Lundqvist, A., Fires in Buses and Trains: Fire Test Methods (SP Report 1990:45). Swedish National Testing and Research Institute, Borås (1990).
202. Peacock, R. D., Reneke, P. A., Averill, J. D., Bukowski, R. W., and Klote, J. H., Fire Safety of Passenger Trains. Phase II: Application of Fire Hazard Analysis Techniques (NISTIR 6525), Nat. Inst. Stand. & Technol., Gaithersburg MD (2002).
203. Hansen, P. A., Fire in Tyres: Heat Release Rate and Response of Vehicles (STF25 A95039). SINTEF NBL, Norwegian Fire Research Laboratory, Trondheim (1995).
204. Shipp, M. P., Fire Spread in Tyre Dumps, pp. 79-88 in Interflam '96. Interscience Communications Ltd., London (1996).
205. Murrell, J., and Briggs, P., Developments in European and International Fire Test Methods for Composites Used in Building and Transport Applications, pp. 21-32 in *Proc. 2nd Intl. Conf. on Composites in Fire*, Conference Design Consultants, Newcastle upon Tyne, England (2001).
206. Ingason, H., and Lönnermark, A., Heat Release Rates from Heavy Goods Vehicle Trailer Fires in Tunnels, *Fire Safety J*. 40, 646-668 (2005).
207. Fires in Transport Tunnels. Report on Full-Scale Tests (EUREKA Project EU 499: FIRETUN), Studiengesellschaft Stahlanwendung e.V., Düsseldorf, Germany (1995).
208. Proceedings of the International Conference on Fires in Tunnels, SP - Swedish National Testing and Research Institute, Borås (1994). Distributed by Interscience Communications Ltd, London.
209. Ingason, H., An Overview of Vehicle Fires in Tunnels, pp. 425-434 in *Intl. Conf. on Tunnel Fires and Escape from Tunnels*, Madrid (2001).
210. Mehaffey, J. R., Craft, S. T., Richardson, L. R., and Batista, M., Fire Experiments in Furnished Houses, pp. 163-174 in *Proc. 4th Intl. Symp. on Fire and Explosion Hazards*, FireSERT, Univ. Ulster, Northern Ireland (2004).
211. Stroup, D. W., and Madrzykowski, D., Heat Release Rate Tests of Plastic Trash Containers (FR 4018), Nat. Inst. Stand. & Technol., Gaithersburg MD (2003).
212. Zicherman, J. B., Fire Cause Analysis, Berkeley CA; unpublished tests conducted at the Western Fire Center, Inc. (2008).
213. Fire Tests for Foamed Plastics Used for Decorative Purposes (UL 1975), Underwriters Laboratories Inc., Northbrook IL.
214. Babrauskas, V., Upholstered Furniture Heat Release Rates: Measurements and Estimation, *J. Fire Sciences* 1, 9-32 (1983).
215. Flammability Information Package (Contains Technical Bulletins 116, 117, 121, 133, 106 and 26). Bureau of Home Furnishings, Dept. of Consumer Affairs, State of California, North Highlands (1987).
216. Babrauskas, V., Full-Scale Burning Behavior of Upholstered Chairs (Tech Note 1103), [U. S.] Natl. Bur. Stand., Gaithersburg MD (1979).
217. Mitler, H. E., and Tu, K.-M., Effect of Ignition Location on Heat Release Rate of Burning Upholstered Furniture, pp. 121-122 in Annual Conf. on Fire Research. Book of Abstracts. October 17-20, 1994 (NISTIR 5499), Nat. Inst. Stand. & Technol., Gaithersburg MD (1994).
218. Collier, P. C. R., and Whiting, P. N., Timeline for Incipient Fire Development (Study Report 194), BRANZ, Judgeford, New Zealand (2008).
219. Babrauskas, V., Lawson, J. R., Walton, W. D., and Twilley, W. H., Upholstered Furniture Heat Release Rates Measured with a Furniture Calorimeter (NBSIR 82-2604), [U. S.] Natl. Bur. Stand., Gaithersburg MD (1982).
220. Janssens, M. L., Gomez, C., Huczek, J. P., Overholt, K. J., Ewan, D. M., Hirschler, M. M., Mason, R. L., and Sharp, J. M., Reducing Uncertainty of Quantifying the Burning Rate of Upholstered Furniture (SwRI Project No. 01.15998), Prepared for National Institute of Justice, Southwest Research Institute, San Antonio TX (2012).
221. Medford, R. L., and Ray, D. R., Upholstered Furniture Flammability: Fires Ignited by Small Open Flames and Cigarettes, CPSC, Washington (Oct. 24, 1997).
222. Babrauskas, V., Blum, A., Daley, R., and Birnbaum, L., Flame Retardants in Furniture Foam: Benefits and Risks, pp. 265-278 in *Fire Safety Science—Proc. 10th Intl. Symp.*, Intl. Assn. for Fire Safety Science, London (2011).
223. Babrauskas, V., and Walton, W. D., A Simplified Characterization for Upholstered Furniture Heat Release Rates, *Fire Safety J*. 11, 181-192 (1986).
224. Standard Test Method for Determining the Heat Release Rate of Upholstered Furniture and Mattress Components or Composites Using a Bench-Scale Oxygen Consumption Calorimeter (E 1474-96a). American Society for Testing and Materials, Philadelphia (1996).
225. Edenburn, D., Burning Video Game System (Technical Report), Albemarle Corp., [n.p.] (2003).

226. Babrauskas, V., Bench-Scale Methods for Prediction of Full-Scale Fire Behavior of Furnishings and Wall Linings, SFPE Technical Report 84-10, Society of Fire Protection Engineers, Boston (1984).
227. Wickström, U., and Göransson, U., Prediction of Heat Release Rates of Surface Materials in Large-Scale Fire Tests Based on Cone Calorimeter Results, *J. Testing and Evaluation* 15, 364-370 (1987).
228. Proceedings of the International EUREFIC Seminar 1991, Interscience Communications Ltd, London (1991).
229. Göransson, U., Model, Based on Cone Calorimeter Results, for Explaining the Heat Release Rate Growth of Tests in a Very Large Room, pp. 39-47 in *Interflam '93: Sixth Intl. Fire Conf. Proc.*, Interscience Communications Ltd., London (1993).
230. Sumathipala, K., Kim, A. K., and Lougheed, G. D., A Comparison of ASTM and ISO Full-scale Room Fire Test Methods, pp. 101-110 in *Proc. Fire and Materials, 2nd Intl. Conf.*, Interscience Communications Ltd, London (1993).
231. Sumathipala, K., Kim, A. K., and Lougheed, G. D., Configuration Sensitivity of Full-scale Room Fire Tests, pp. 237-246 in *Proc. Fire and Materials, 3rd Intl. Conf.*, Interscience Communications Ltd, London (1994).
232. Karlsson, B., and Magnusson, S.-E., An Example Room Fire Model, pp. 159-171 in Heat Release in Fires, *op cit.*
233. Karlsson, B., Models for Calculating Flame Spread on Wall Lining Materials and the Resulting Heat Release Rate in a Room, *Fire Safety J.* 23, 365-386 (1994).
234. Magnusson, S. E., and Sundström, B., Combustible linings and room fire growth – A first analysis, pp. 45-69 in Fire Safety Science and Engineering (ASTM STP 882), American Society for Testing and Materials, Philadelphia (1985).
235. Cleary, T. G., and Quintiere, J. G., A Framework for Utilizing Fire Property Tests, pp. 647-656 in *Fire Safety Science--Proc. of the 3rd Intl. Symp.*, Elsevier Applied Science, London (1991).
236. Quintiere, J. G., A Simulation Model for Fire Growth on Materials Subject to a Room-Corner Test, *Fire Safety J.* 20, 313-339 (1993).
237. Quintiere, J. G., Haynes, G., and Rhodes, B. T., Applications of a Model to Predict Flame Spread over Interior Finish Materials in a Compartment, *J. Fire Prot. Engineering* 7, 1013 (1995).
238. Janssens, M., Grexa, O., Dietenberger, M., and White, R., Predictions of ISO 9705 Room/corner Test Using a Simple Model, pp. 73-83 in *Proc. 4th Intl. Fire and Materials Conf.*, Interscience Communications Ltd., London (1995).
239. Lawson, J. R., Walton, W. D., and Twilley, W. H., Fire Performance of Furnishings as Measured in the NBS Furniture Calorimeter. Part 1 (NBSIR 83-2787), U.S. Natl. Bur. Stand., Gaithersburg MD (1983).
240. Peacock, R. D., Reneke, P. A., Averill, J. D., Bukowski, R. W., and Klote, J. H., Fire Safety of Passenger Trains, Phase II: Application of Fire Hazard Analysis Techniques (NISTIR 6525), Nat. Inst. Stand. and Technol., Gaithersburg MD (2002).
241. Janssens, M. L., Heat Release Rate, FORUM Workshop on Measurement Needs for Fire Safety, Nat. Inst. Stand. and Technol., Gaithersburg MD (2000).
242. Smith, D. A., and Shaw, K., Single Burning Item (SBI) Test: The Euroclasses and Transitional Arrangements, pp. 1-9 in *Interflam '99*, Interscience Communications Ltd., London (1999).

Dr. Vytenis Babrauskas is the President of Fire Science and Technology Inc., Issaquah, WA, a company specializing in fire safety research, fire testing issues, and fire science applications to fire investigations and litigations.

Calorimetry

27

Marc Janssens

Introduction

Heat release rate is the single most important variable in fire hazard assessment [1]. Various test methods for measuring the heat release rate of materials and products under different conditions have therefore been developed. This chapter is dedicated to these test methods. An apparatus used for measuring heat release rate is referred to as a *calorimeter* and the measurement of heat release rate is called *calorimetry*.

The importance of heat release rate in fire hazard assessment was first recognized in the early 1970s by Smith at Ohio State University [2]. Smith and coworkers developed one of the first small-scale test methods for measuring the heat release rate of planar products exposed to radiant heat [3]. They also proposed various procedures to assess compartment fire hazard on the basis of the small-scale data. These procedures ranged from simple calculation methods [4] to a relatively complex computer model [5]. This work was initiated at a time when the most accurate measuring techniques for heat release rate were not available and when computer fire modeling was still in its infancy. Moreover, Smith advocated a practical approach based on engineering judgment rather than detailed science. Hence, his test and fire hazard assessment methods were far from perfect and received major criticism [6, 7]. Nevertheless, Smith deserves recognition as one of the pioneers of heat release rate calorimetry.

With compartment fire hazard assessment as the primary application, there is a need for high-quality heat release rate data and, consequently, for devices and methods to measure it accurately. The first of two basic approaches to assess the fire hazard of a material consists of an experimental evaluation in full scale. Typically, this approach requires multiple large-scale fire tests covering all relevant fire scenarios and end-use conditions. The second option is the use of small-scale data, primarily heat release rate, in conjunction with a calculation procedure to estimate full-scale fire performance. The second approach is significantly more versatile, and time- and cost-effective. With the continuous improvement of the predictive capability and accuracy of fire models and calculation methods, the latter has become the preferred approach.

This chapter begins with a brief discussion of the oxygen bomb calorimeter, which is used to measure the maximum amount of heat that can be released from combustion of a material. The oxygen bomb calorimeter has significant limitations. For example, materials and products are not evaluated under realistic fire conditions. Also, the total heat released is measured as opposed to the heat release rate as a function of time, that is, no information is obtained concerning the dynamic behavior of the material.

M. Janssens (✉)
Southwest Research Institute, San Antonio, TX 78238, USA

M.J. Hurley (ed.), *SFPE Handbook of Fire Protection Engineering*,
DOI 10.1007/978-1-4939-2565-0_27, © Society of Fire Protection Engineers 2016

Various heat release tests have been developed to address these limitations. These test methods all rely on one of four measuring techniques, which are described in detail in the next section. This is followed by a discussion of the effect on the measurements of various small-scale calorimeter features and construction details. In the next section a brief description is provided of commonly used calorimeters ranging in size from small to industrial scale. The chapter concludes with a discussion of the use and application of heat release rate data and a section on uncertainty of heat release rate measurements.

Oxygen Bomb Calorimetry

Oxygen Bomb Calorimeter Test

The maximum amount of heat that can be released during combustion of a material can be determined in an oxygen bomb calorimeter. An oxygen bomb calorimeter consists of a sealed stainless steel container (the "bomb") in which a small quantity of material (approximately 1 g) is combusted at high pressure (30 bar) in pure oxygen (Fig. 27.1). The heat released is measured on the basis of the temperature rise of the surrounding water vessel (adiabatic method) or the heat loss needed to keep the water temperature constant (isoperibol method). Standard procedures for measuring the gross heat of combustion of solid materials are described in ASTM D5865 and ISO 1716.

The building and life safety codes promulgated by the National Fire Protection Association (NFPA) make a distinction between noncombustible and limited combustible materials. Limited combustible materials must have a potential heat of 8.2 MJ/kg or less as determined by NFPA 259, *Standard Test Method for Potential Heat of Building Materials*. According to this method, the potential heat of a material is determined as the difference between the gross heat of combustion of the material measured with an oxygen bomb calorimeter and the gross heat of combustion of its residue after heating in a muffle furnace at 750 °C for 2 h.

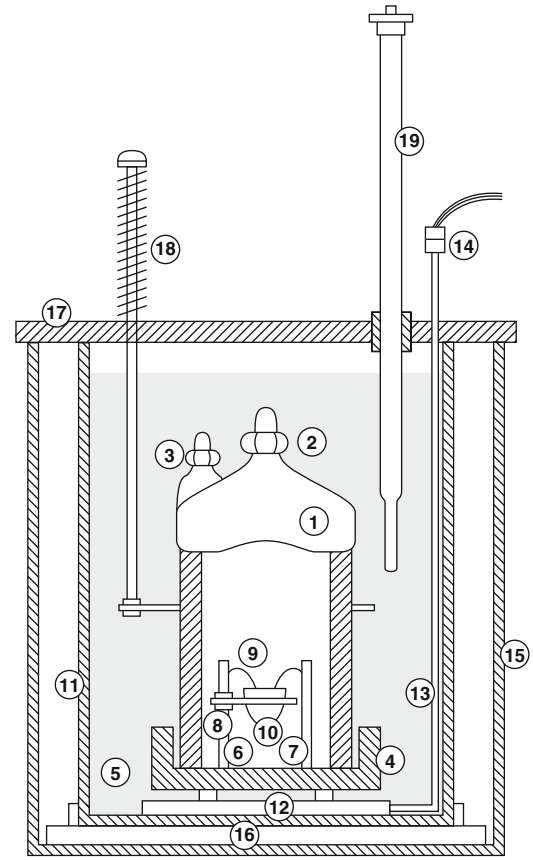

1 High pressure cylinder
2 Oxygen admission valve
3 Pressure release valve
4 Base cap
5 Rubber washer
6 Pillar
7 Pillar
8 Support ring
9 Fuse wire
10 Quartz crucible
11 Water container
12 Calorimeter mount
13 Wire
14 Plug and socket
15 Outer can
16 Wooden platform
17 Cover plate
18 Stirrer
19 Thermometer

Fig. 27.1 Oxygen bomb calorimeter

Gross Versus Net Heat of Combustion

The gross heat of combustion of a solid or liquid fuel is measured in an oxygen bomb calorimeter as described in the previous section. Because the cooling water temperature remains close to ambient during a test, all water vapor generated in the combustion process fully condenses. The measured gross heat of combustion therefore includes the heat released due to condensation

of the water vapor. In practice, combustion products are usually removed from the system at a temperature above the dew point. It is therefore more realistic to quantify the potential heat released in a fire assuming that all water vapor remains in the gaseous state. The corresponding heat released per mass unit of fuel burnt is referred to as the net heat of combustion. It is equal to the gross heat of combustion measured in an oxygen bomb calorimeter minus the heat of vaporization of the water in the products of combustion, which is a function of the moisture and hydrogen content of the fuel:

$$\Delta h_{c,\text{net}} = \Delta h_{c,\text{gross}} - (8.936 Y_H + Y_W)\Delta h_v \tag{27.1}$$

where

$\Delta h_{c,\text{net}}$ = Net heat of combustion (kJ/g)
$\Delta h_{c,\text{gross}}$ = Gross heat of combustion (kJ/g)
Y_H = Mass fraction of hydrogen in the fuel (g/g)
Y_W = Moisture content of the fuel (g/g)
Δh_v = Latent heat of vaporization of water (2.442 kJ/g at 25 °C)

ASTM has developed test standards to determine the moisture content and hydrogen content in a variety of solid fuels, e.g., ASTM D3173 and ASTM D5373, respectively.

The gross heat and net heat of combustion are usually reported at a standard temperature of 25 °C. Gross heat and net heat of combustion values for a wide range of materials can be found in Appendix C, "Fuel Properties and Combustion Data."

Techniques for Measuring Heat Release Rate

The development of the oxygen consumption technique in the late 1970s was a major breakthrough in the accurate measurement of heat release rate in fire tests. Inferior methods had been used prior to that. The most practical of the older methods is still used today for applications that do not require the highest accuracy. The older methods and the oxygen consumption technique (and the related carbon oxide generation technique) are described in this section.

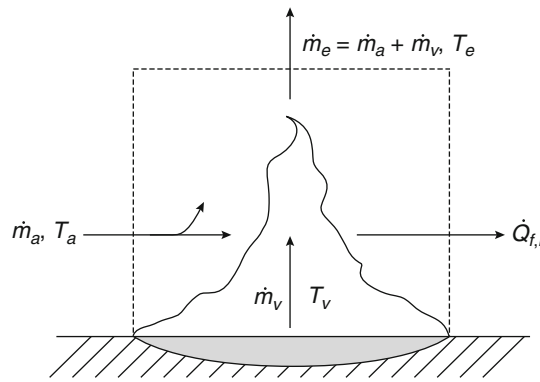

Fig. 27.2 Gas-phase energy balance

Sensible Enthalpy Rise Method

Consider the energy balance of a gas-phase control volume enclosing the flame of a burning specimen (Fig. 27.2). Air enters the control volume at a flow rate $\dot{m}_a$ and temperature T_a. The enthalpy of this air can be written as

$$h_a = h_a^0 + c_p(T_a - T_0) \tag{27.2}$$

where

h_a = Enthalpy of air at temperature T_a(kJ/g)
h_a^0 = Enthalpy of air at reference temperature T_0(kJ/g)
c_p = Average specific heat of air between T_0 and T_a(kJ/g · K)
T_a = Temperature of the air entering the combustion zone(K)
T_0 = Reference temperature (K)

Part of the heat flux that strikes the exposed surface is conducted into the specimen. The resulting heat flow raises the temperature of the solid and decomposes some fraction into combustible fuel vapors. The vapors are generated at a rate $\dot{m}_v$ and enter the control volume at temperature T_v. Assuming that the specific heat of all gases is approximately constant and temperature independent (a reasonable approximation), the enthalpy of the fuel vapors can be written as

$$h_v = h_v^0 + c_p(T_v - T_0) \tag{27.3}$$

where
h_v = Enthalpy of volatiles at temperature T_v (kJ/g)
h_v^0 = Enthalpy of volatiles at reference temperature T_0 (kJ/g)
T_v = Temperature of volatiles entering the combustion zone (K)

The fuel vapors mix with air and are converted in the flame to products of combustion. The total flow rate, $\dot{m}_e$, of combustion products, which includes some excess air, has a temperature T_e and enthalpy given by

$$h_e = h_e^0 + c_p(T_e - T_0) \tag{27.4}$$

where
h_e = Enthalpy of combustion products at temperature T_e (kJ/g)
h_e^0 = Enthalpy of combustion products at reference temperature T_0 (kJ/g)
T_e = Temperature of combustion products leaving the control volume (K)

T_e is higher than the mass-weighted average of T_a and T_v because of the heat released by combustion in the flame, $\dot{Q}$. However, only a fraction of this heat contributes to the temperature rise of the gases. This fraction is referred to as the convective fraction of the heat release rate. The remaining fraction of $\dot{Q}$ is lost and is denoted as $\dot{Q}_{f,1}$. For the most part $\dot{Q}_{f,1}$ is lost in the form of thermal radiation to the walls of the calorimeter (closed configuration) or to the environment (open configuration). A small part of $\dot{Q}_{f,1}$ consists of convective and radiative feedback to the fuel surface. Assuming that gas-phase transients and pressure gradients can be neglected, application of the first law of thermodynamics for the control volume in Fig. 27.2 results in

$$\dot{Q}_{f,1} = \dot{m}_a h_a + \dot{m}_v h_v - \dot{m}_e h_e \tag{27.5}$$

where
$\dot{Q}_{f,1}$ = Convection and radiation heat loss rate from the flame(kW)
$\dot{m}_a$ = Mass flow rate of air entering the combustion zone(g/s)
$\dot{m}_v$ = Generation rate of fuel volatiles(g/s)
$\dot{m}_e$ = Mass flow rate of combustion products leaving the control volume(g/s)

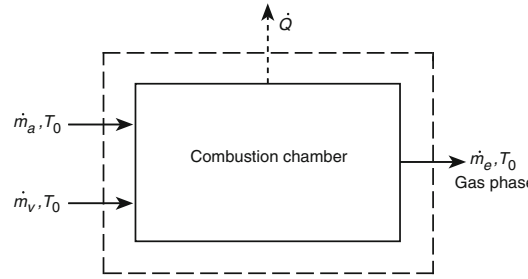

Fig. 27.3 Hypothetical combustion chamber

Suppose now that the same flow rates of air and volatiles, both at temperature T_0, are mixed in a hypothetical combustion chamber. Furthermore, assume the combustion reactions in the chamber are identical to those in the flame in Fig. 27.2, and the products of combustion are cooled down to the reference temperature T_0 without condensing water. This hypothetical situation is shown in Fig. 27.3.

Application of the first law of thermodynamics for the combustion chamber control volume in Fig. 27.3 leads to

$$\dot{Q} = \dot{m}_a h_a^0 + \dot{m}_v h_v^0 - \dot{m}_e h_e^0 \tag{27.6}$$

where $\dot{Q}$ is the total rate of heat released by combustion in the flame (kW).

$\dot{Q}$ is identical in Figs. 27.2 and 27.3 but is distributed in different ways. By expressing the heat released per unit mass of volatiles, an effective heat of combustion can be defined as

$$\dot{m}_v \Delta h_{c,eff} \equiv \dot{Q} \tag{27.7}$$

or per unit exposed area

$$\dot{m}_v'' \Delta h_{c,\mathrm{eff}} \equiv \dot{Q}'' \tag{27.8}$$

where
$\dot{m}_v''$ = Generation rate of fuel volatiles per unit area of fuel surface$(\mathrm{g/m^2 \cdot s})$
$\Delta h_{c,\mathrm{eff}}$ = Effective heat of combustion$(\mathrm{kJ/g})$
$\dot{Q}''$ = Total rate of heat released per unit area of fuel surface$(\mathrm{kW/m^2})$

$\Delta h_{c,\mathrm{eff}}$ is for the combustion reactions as they take place in the calorimeter. $\Delta h_{c,\mathrm{eff}}$ must be

distinguished from the net heat of combustion, $\Delta h_{c,\text{net}}$. The difference between $\Delta h_{c,\text{eff}}$ and $\Delta h_{c,\text{net}}$ is very significant for charring materials such as wood. In an oxygen bomb calorimeter; nearly all the mass of wood is consumed, leaving a small fraction of noncombustible ash (usually less than 1 % by mass). The net heat of combustion, $\Delta h_{c,\text{net}}$, of dry wood is in the range of 16–18 MJ/kg. When exposed under real fire conditions, only 70–80 % of the mass is converted to volatiles that burn almost completely. The heat of combustion of the volatiles, $\Delta h_{c,\text{eff}}$, measured in a small-scale calorimeter is only 12–13 MJ/kg. A solid char residue remains, primarily consisting of carbon, with a net heat of combustion of approximately 30 MJ/kg. In an oxygen bomb calorimeter, most of this char is also burnt, explaining why $\Delta h_{c,\text{net}}$ exceeds $\Delta h_{c,\text{eff}}$ by 25–50 %. Even for materials that do not form a char, $\Delta h_{c,\text{eff}}$ can be significantly lower than $\Delta h_{c,\text{net}}$ if combustion of the volatiles in the small-scale calorimeter is incomplete. In this case, the products of combustion contain measurable amounts of combustible components such as CO, soot, unburnt hydrocarbons, and so forth. The ratio of $\Delta h_{c,\text{eff}}$ to $\Delta h_{c,\text{net}}$ is defined as combustion efficiency, χ. For clean-burning gaseous fuels, such as methane, χ is close to unity. For fuels that produce sooty flames, including gases, χ can be significantly lower. For example, χ for acetylene is approximately 0.75. χ values for a number of gases, liquids, and solids are listed in Chap. 36, "Combustion Characteristics of Materials and Generation of Fire Products."

Substitution of Equations 27.2, 27.3, 27.4, and 27.6 into Equation 27.5 leads to

$$\dot{Q} - \dot{Q}_{f,1} = c_p \dot{m}_e (T_e - T_0) - c_p \dot{m}_a (T_a - T_0) - c_p \dot{m}_v (T_v - T_0) \tag{27.9}$$

The stoichiometric air-to-fuel ratio ranges between 3 and 16 for most fuels. Moreover, small-scale calorimeters are usually operated with excess air. For example, the standard initial flow rate in the cone calorimeter is 30 g/s. Based on the oxygen consumption principle (see below), the stoichiometric flow rate of air for a 10 kW fire (practical upper limit in the cone calorimeter) can be calculated as 10 kW/3 kJ per g of air = 3.3 g/s. Thus, the air supply in the cone calorimeter is at least nine times stoichiometric, or at least $9 \times 3 = 27$ times the generation rate of volatiles. Usually, the ratio is much greater. Hence, $\dot{m}_v$ is negligible compared to $\dot{m}_a$ and Equation 27.9 can be approximated as

$$\dot{Q} - \dot{Q}_{f,1} \approx \dot{m}_a c_p (T_e - T_a) \tag{27.10}$$

This equation is the basis for the sensible enthalpy method. Heat release rate is calculated from the temperature rise $T_e - T_a$ of the gases flowing through a calorimeter. A schematic of a calorimeter based on this principle is shown in Fig. 27.4.

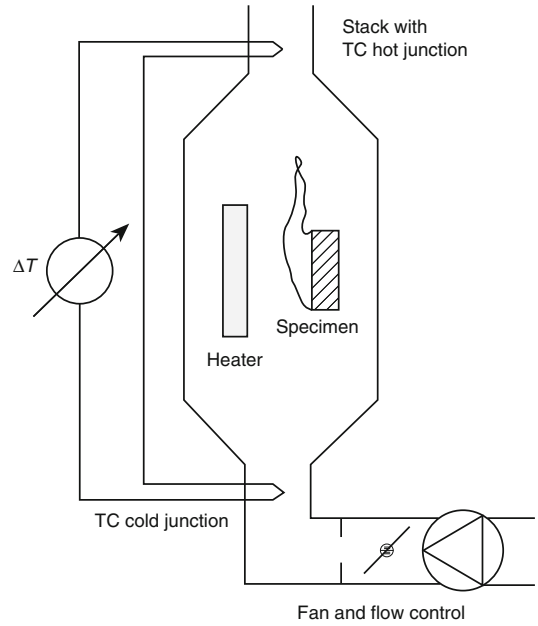

Fig. 27.4 Sensible enthalpy rise calorimeter

There are a few problems with the practical implementation of this technique. The main concern is that only a fraction of the heat released in the flame is used to raise the sensible enthalpy or temperature of the gases. Therefore, it is necessary to recover or measure the loss term $\dot{Q}_{f,1}$. Some calorimeters have water-cooled walls that trap most of the losses. These losses can be estimated by measuring the enthalpy rise of the cooling water. However, due to the additional

hardware and instrumentation, such calorimeters are rather complex and difficult to operate.

A more popular method relies on a gas burner calibration to determine $\dot{Q}_{f,1}$ in the assumption that the losses are fuel independent. Defining the loss fraction, χ_r, by

$$\dot{Q} - \dot{Q}_{f,1} \equiv (1 - \chi_r)\dot{Q} \qquad (27.11)$$

where χ_r is the fraction of total heat release rate lost by radiation.

The symbol χ_r is chosen for this fraction because $\dot{Q}_{f,1}$ consists primarily of radiation. If the calorimeter is operated with a constant airflow rate $\dot{m}_a$, Equation 27.11 can be written as

$$\dot{Q} \approx \frac{\dot{m}_e c_p}{1 - \chi_r}(T_e - T_a) \equiv k(T_e - T_a) \qquad (27.12)$$

where k is the calibration constant (kW/K).

The calibration factor, k, is determined from a gas burner calibration with known $\dot{Q}$. By repeating the calibration over a range of heat release rate levels, k can be determined as a function of $\dot{Q}$ or T_e. If the specimen is enclosed with the heater, Equation 27.12 is still valid, provided a reference temperature T_r is used instead of T_a. The temperature difference $T_r - T_a$ results from the heat transfer between the heater and the airflow through the enclosure. T_r is therefore a function of heater setting, to be determined via calibration.

Ed Smith's rate of heat release test developed at Ohio State University is the most well-known and most widely used calorimeter based on the sensible enthalpy rise method [3]. The test method is described in detail in a separate section.

Substitution Method

For practical reasons, calorimeters based on the sensible enthalpy rise method use a closed configuration. The specimen and heater(s) are located inside a metal box, which may be (partly) insulated. The dynamic response of the enclosure to changes in the thermal environment creates problems in the practical implementation of the sensible enthalpy rise method. After ignition, part of the heat released by a burning specimen is transferred by radiation to the enclosure walls. A fraction of this heat is stored in the walls, causing an increase of their temperature, in turn resulting in an enhanced heat transfer with the air flowing through the box. The result is that, for a material that quickly reaches steady burning conditions, there is a delay for T_e to reach the corresponding steady temperature. A similar phenomenon occurs when the heat release rate from the specimen decreases or after the specimen burns out and the heat release rate goes back to zero. Under unsteady burning conditions, T_e constantly lags behind the temperature corresponding to the instantaneous heat release rate. Several methods have been suggested to mathematically address this problem, but none are completely satisfactory [8–12].

The substitution method was developed to eliminate problems associated with thermal lag. The method requires two runs to determine the heat release rate of a material under a given set of conditions. The first run uses a similar arrangement as shown in Fig. 27.4. The temperature difference $T_e - T_a$ is measured as a function of time. The second run uses the same apparatus, airflow rate, and radiant heat flux. However, the specimen is replaced by a noncombustible dummy specimen and a substitution gas burner. The flow of gas to the burner is controlled in such a way that the temperature difference $T_e - T_a$ closely follows the curve measured during the first run. Figure 27.5 shows a schematic of the substitution run.

Presumably, the dynamics are identical in both runs. Hence, problems with thermal lag have been eliminated, and the heat release rate of the specimen can be determined from the fuel flow rate to the burner in the second run. Unfortunately, implementation of this method is not trivial, because a sophisticated control system is needed for the second run. Moreover, due to the addition of substitution runs, the number of tests required to evaluate a material is doubled.

The substitution method was first implemented at Factory Mutual [13]. The apparatus was designed to measure the heat release

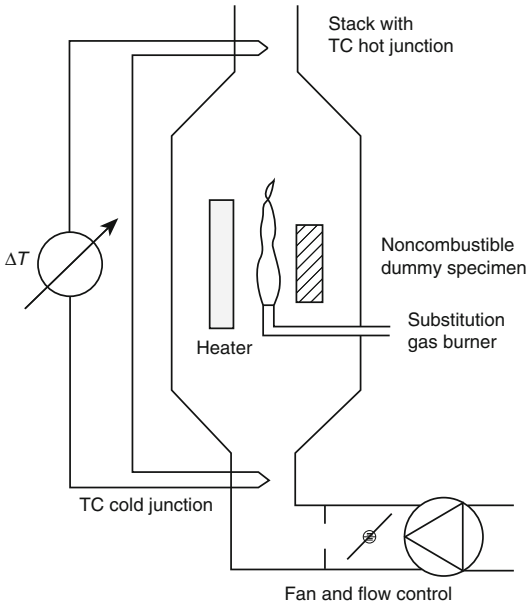

Fig. 27.5 Second run with substitution burner

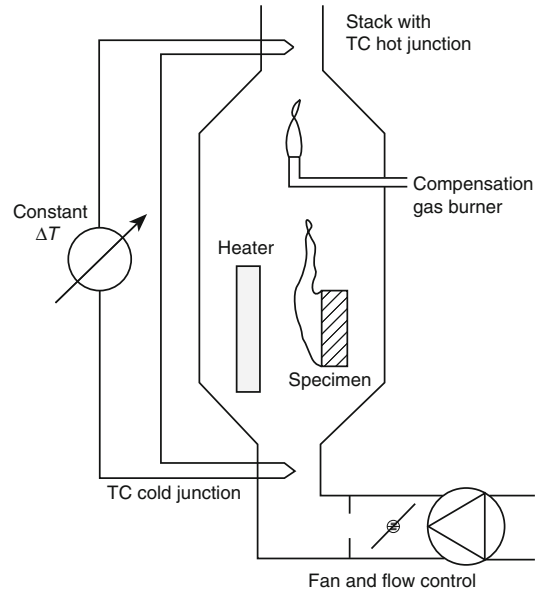

Fig. 27.6 Compensation calorimeter

rate from roof assemblies. A small-scale substitution calorimeter was developed at the Forest Products Laboratory [14].

Compensation Method

A compensation calorimeter is similar to a substitution calorimeter, except that the burner is operated while a specimen is exposed. A schematic is shown in Fig. 27.6. Initially, the burner flow rate is chosen so that the corresponding heat release rate exceeds that of any material to be tested. During a test, the gas flow rate to the burner is controlled so that $T_e - T_a$ remains constant. The heat release rate corresponding to the reduction in flow rate to the burner is equal to the heat release rate from the specimen.

The compensation method also eliminates problems with the dynamic response of the calorimeter enclosure. In theory, a compensation calorimeter is operated at a constant temperature. This would resolve another problem associated with the assumption that $\dot{Q}_{f,1}$ is fuel independent, whereas in reality it is not ($\dot{Q}_{f,1}$ is a strong function of the sootiness of the flame).

In practice, however, the specimen and burner have to be separated to avoid that radiation from the burner flame enhances radiant heat flux to the specimen. Hence, the calorimeter enclosure is not truly isothermal, and the problem remains unresolved. As with substitution calorimeters, the burner flow control system makes compensation calorimeters rather complex and difficult to operate. As a result, they are suitable only for research and not for routine testing.

Compensation calorimeters were developed at the National Bureau of Standards [15, 16] and Stanford Research Institute [17].

Oxygen Consumption Method

In 1917, Thornton showed that for a large number of organic liquids and gases, a nearly constant net amount of heat is released per unit mass of oxygen consumed for complete combustion [18]. Huggett found this also to be true for organic solids and obtained an average value for this constant E of 13.1 MJ/kg of oxygen [19]. This value may be used for practical applications and is accurate with very few exceptions to within ±5 %. Thornton's rule

implies that it is sufficient to measure the oxygen consumed in a combustion system in order to determine the net heat released. This is the basis for the oxygen consumption method for measuring heat release rate in fire tests.

The first application of the oxygen consumption technique in fire research was by Parker on the ASTM E84 tunnel test. [20] During the late 1970s and early 1980s, the oxygen consumption technique was refined at the National Bureau of Standards (NBS, currently the National Institute of Standards and Technology, or NIST). The oxygen consumption method is now recognized as the most accurate and practical technique for measuring heat release rates from experimental fires. It is widely used throughout the world, for both small-scale and large-scale applications.

Thornton's Rule

The exact value of E for a specific fuel is equal to the net heat of combustion of the fuel divided by the mass of oxygen needed for complete combustion of a mass unit of fuel. The mass of oxygen required for complete combustion of a mass unit of fuel can be determined from the stoichiometry of the combustion reactions. Consider, for example, the following equation to describe complete combustion of methane:

$$CH_4 + 2O_2 \rightarrow CO_2 + 2H_2O \qquad (27.13)$$

This equation indicates that 64 g of oxygen are required for complete combustion of 16.04 g of methane. Hence, the mass of oxygen needed to burn 1 g of methane is $r_0 = 64/16.04 = 3.99$ g O_2/g CH_4. Because the net heat of combustion of methane is 50.04 kJ/g, the net heat released per mass unit of oxygen consumed is equal to $E = \Delta h_{c,\text{net}}/r_0 = 50.04/3.99 = 12.54$ kJ/g O_2.

An extensive list of E values can be found in Chap. 36; in Tables C2–C4 and in the literature [21, 22]. A summary of average values for different categories of fuels and polymers based on the data in Chap. 36 is given in Table 27.1. This table also lists values for the amount of heat released per mass unit of CO_2 and CO generated (E' and E'', respectively). Although there is more variation between different categories, these values are also reasonably constant within a given category of fuels or polymers.

Volatiles or Condensed Phase?

An interesting question is whether the oxygen consumption technique measures heat release rate for the volatiles or the solid fuel. Thermal methods approximately measure heat release rate from the volatiles. However, Huggett's constant of 13.1 kJ/g is based on the average net heat of combustion for a large set of materials. Hence, one would expect that oxygen consumption calorimetry gives the heat released by the fuel in its natural state at ambient temperature, because that is how the fuel is supplied in an oxygen bomb calorimeter.

The question can be examined in more detail for some synthetic polymers by comparing the net heat of combustion of the polymer to that of the corresponding monomer. If one were to burn a monomer in an oxygen consumption calorimeter, the products of complete combustion would be the same as for the corresponding polymer, provided test conditions are identical. Therefore, measured heat release rate would be the same in the two cases. However, the net heat of combustion is higher for the monomer. The difference with the net heat of combustion of the polymer is the net heat released in the polymerization process.

Table 27.2 gives values for the net heat of combustion of nine polymers and their monomers. The former are taken from Huggett; [19] the latter are obtained by adding the heat of polymerization as reported in the literature [23]. Table 27.2 confirms that the oxygen consumption technique measures net heat release rate of a solid fuel. The heat release rate from the volatiles is always higher, but not by as much as indicated in the last column of the table, because only a fraction of polymeric fuels decomposes back into the monomer (see Chap. 7, "Thermal Decomposition of Polymeric Materials").

Table 27.1 E, α, E' and E'' values for different fuel and polymer categories

Category	E (kJ/g O_2)	α	E′ (kJ/g CO_2)	E″ (kJ/g CO)
Fuels containing C and H				
Normal alkanes	12.7	1.079	14.6	12.9
Substituted alkanes	12.6	1.076	14.6	12.8
Cyclic alkanes	12.7	1.069	13.8	11.6
Normal alkenes	13.2	1.070	14.2	12.4
Cyclic alkenes	13.0	1.062	13.4	11.1
Dienes	13.5	1.057	13.5	11.2
Normal alkynes	13.3	1.060	14.0	12.0
Arenes	13.0	1.049	12.4	9.4
Fuels containing C, H and O				
Alcohols	13.3	1.104	14.5	12.8
Aldehydes	14.2	1.108	13.3	10.6
Ketones	13.2	1.088	13.2	11.1
Acids	14.2	1.245	9.7	5.4
Esters	13.0	1.118	12.5	9.7
Others	13.9	1.076	12.2	8.9
Fuels containing C, H, N and S				
C-H-N fuels	11.5	1.063	15.4	14.1
C-H-S fuels	11.3	1.055	13.1	11.5
Polymeric materials				
C and H in the structure	12.5	1.051	12.4	9.5
C, H, O and N in the structure	12.5	1.085	10.9	7.2
C, H and Cl in the structure	12.8	1.124	12.1	9.6
C, H and F in the structure	11.3	1.293	9.2	–
C, H and Si in the structure	13.7	1.083	14.8	13.3

Table 27.2 Net heat of combustion of some polymers and their monomers

Polymer	$\Delta h_{c,\text{net}}$ (kJ/g fuel)	E (kJ/g O_2)	Monomer (state)	$\Delta h_{c,\text{net}}$ (kJ/g fuel)	E (kJ/g O_2)	ΔE (%)
Polyethylene	43.3	12.65	C_2H_4 (g)	47.2	13.78	8.9
Polypropylene	43.3	12.66	C_3H_6 (g)	45.8	13.39	5.8
Polybutadiene	42.8	13.14	C_4H_6 (L)	44.1	13.56	3.2
Polystyrene	39.9	12.97	C_8H_8 (L)	40.5	13.19	1.7
Polyvinylchloride	16.4	12.84	C_2H_3Cl (g)	18.0	14.10	9.8
Polyvinylidene chloride	8.99	13.61	$C_2H_2Cl_2$ (L)	9.77	14.79	8.7
Polyvinylidene fluoride	13.3	13.32	$C_2H_2F_2$ (g)	15.6	15.61	17.2
Polymethylmethacrylate	24.9	12.98	$C_5H_8O_2$ (L)	25.4	13.26	2.2
Polyacrylonitrile	30.8	13.61	C_3H_3N (L)	32.2	14.25	4.7
Average		*13.09*			*13.99*	*6.9*

Implementation of the Oxygen Consumption Method

The basic requirement to use the oxygen consumption technique is that all combustion products are collected and removed through an exhaust duct. At a distance downstream sufficient for adequate mixing, both flow rate and composition of the gases are measured. A schematic of an oxygen consumption calorimeter is shown in Fig. 27.7. It is not necessary to measure the inflow of air, provided the flow rate is

measured in the exhaust duct. Therefore, oxygen consumption calorimeters are typically open, to avoid that part of $\dot{Q}_{f,1}$ that is reflected by the calorimeter walls and reaches the specimen surface. This would result in an uncontrolled radiant heat flux, in addition to that from the heater.

The practical implementation of the oxygen consumption technique is not straightforward. Application of Thornton's rule to the combustion system shown in Fig. 27.8 leads to the following equation for the heat release rate:

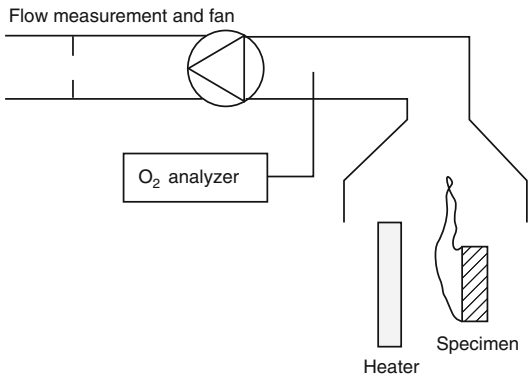

Fig. 27.7 Oxygen consumption calorimeter

$$\dot{Q} = E\left(\dot{m}_a Y^a_{O_2} - \dot{m}_e Y^e_{O_2}\right) \tag{27.14}$$

where

E = Heat release per mass unit of oxygen consumed ($\approx 13.1\text{kJ/g}$)
$Y^a_{O_2}$ = Mass fraction of oxygen in the combustion air(0.232 g/g in dry air)
$Y^e_{O_2}$ = Mass fraction of oxygen in the combustion products(g/g)

There are three problems with the practical implementation of Equation 27.14. First, oxygen analyzers measure the mole (volume) fraction and not the mass fraction of oxygen in a gas sample. Mole fractions can be converted to mass fractions by multiplying the mole fraction with the ratio between the molar mass of oxygen and the molar mass of the gas sample. The latter is usually close to the molar mass of air (≈29 g/mol). Second, water vapor is removed from the sample before it passes through a paramagnetic analyzer, so that the resulting mole fraction is on a dry basis. Third, flow meters measure volumetric rather than mass flow rates. The volumetric flow rate in the exhaust duct, normalized to the same pressure and temperature, is usually slightly different

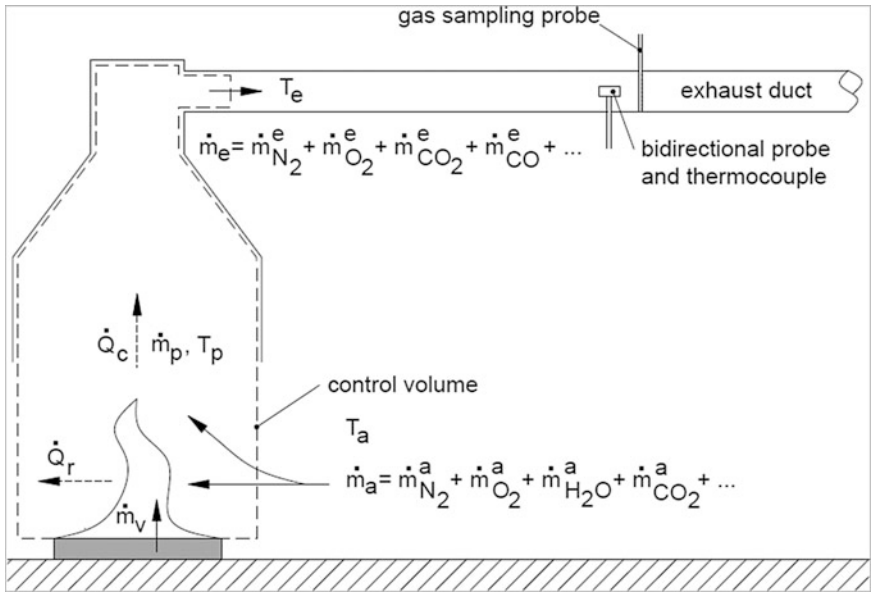

Fig. 27.8 Mass flow rates in oxygen consumption calorimeter

from the inflow rate of air because of expansion due to the combustion reactions.

Parker [24] and Janssens [25] solved these problems and developed equations for calculating rate of heat release by oxygen consumption for various applications. The equations are a function of the extent of the gas analysis. The oxygen concentration must be measured as a minimum. However, the accuracy can be improved by adding instrumentation for measuring the concentration of other gases.

Equations for the two most common configurations of gas analyzers are discussed below. Detailed derivations are not repeated here and can be found in the aforementioned references. Modified equations to address specific circumstances or problems, such as heat release rate measurements during suppression experiments, from fires with significant soot yields, or during experiments conducted in a vitiated (reduced O_2) environment, can also be found in the literature [26–28]. Derivation of detailed equations for carbon oxide calorimetry, a technique that is used extensively by FM Global, can also be found in the literature [29, 30]. Carbon oxide calorimetry is discussed in section "Carbon Oxide Calorimetry".

Only O_2 Measured

In this case all water vapor (by a chiller and moisture sorbent) and CO_2 (by a chemical sorbent) must be removed from the exhaust gas sample stream before O_2 is measured. This leads to the assumption that the sample gas consists of only O_2 and N_2. The resulting equation for calculating heat release rate is

$$\dot{Q} = E\frac{\phi}{1+\phi(\alpha-1)}\dot{m}_e\frac{M_{O_2}}{M_a}\left(1-X^a_{H_2O}-X^a_{CO_2}\right)X^{A^a}_{O_2} \tag{27.15}$$

with

$$\phi = \frac{X^{A^a}_{O_2}+X^{A^e}_{O_2}}{\left(1-X^{A^e}_{O_2}\right)X^{A^a}_{O_2}} \tag{27.16}$$

where

ϕ = Oxygen depletion factor
α = Volumetric expansion factor
$\dot{m}_e$ = Mass flow rate in the exhaust duct of the calorimeter(g/s)
M_{O_2} = Molecular mass of oxygen(28 g/mol)
M_a = Molecular mass of the combustion air(29 g/mol for dry air)
$X^a_{H_2O}$ = Actual mole fraction of water vapor in the combustion air
$X^a_{CO_2}$ = Actual mole fraction of carbon dioxide in the combustion air
$X^{A^a}_{O_2}$ = Measured mole fraction of oxygen in the combustion air
$X^{A^c}_{O_2}$ = Measured mole fraction of oxygen in the exhaust flow

As the composition of the fuel is usually not known, some average value has to be used for α. Complete combustion of carbon in dry air results in $\alpha = 1$. If the fuel is pure hydrogen, α is equal to 1.21. A commonly-used value for α is therefore 1.105. The average value and standard deviation for the fuels in Table 27.1 is 1.093 ± 0.066. $X^a_{H_2O}$ can be calculated from the relative humidity and temperature in the laboratory. Typically it is of the order of 1–2 % in a temperature-controlled laboratory.[1] $X^a_{CO_2}$ in dry air is approximately 390 ppm.[2] Note that the symbols for oxygen mole fraction measured in the combustion air (prior to a test) and the exhaust flow include a superscripted *A*. This is to make a distinction between the actual and measured mole fractions of oxygen, because the latter are for a dry gas sample.

Equation 27.15 is expected to be accurate to within ±10 %, provided combustion is complete; for example, all carbon is converted to CO_2. The error may be larger if CO or soot production is

[1] For example, air at 20 °C, 1013 mbar and a relative humidity of 50 % contains 1.2 % of water vapor by volume.

[2] The concentration of carbon dioxide in the atmosphere is measured at the Mauna Loa Observatory in Hawaii. The average concentration measured in 2010 was 390 ppm. The concentration varies annually by about 3–9 ppm, but the annual average has steadily increased by about 74 ppm since 1958, when the measurements were first recorded.

considerable, or if a significant amount of combustion products consists of species other than CO_2 or H_2O (e.g., HCl). The error is partly due to the uncertainty of E and α. If more exact values are available, accuracy can be improved by using those instead of the generic values of 13.1 kJ/g and 1.105.

O_2, CO_2, and CO Measured

In this case, only water vapor is trapped before the exhaust gas sample reaches the analyzers. CO in many cases is negligible. The rate of heat release in those cases can be calculated from Equation 27.15 with the minor modification that $X^a_{CO_2}$ is not included in the expression inside parentheses. In addition, ϕ is slightly different and follows from

$$\phi = \frac{X^{A^a}_{O_2}\left(1 - X^{A^e}_{CO_2}\right) - X^{A^e}_{O_2}\left(1 - X^{A^a}_{CO_2}\right)}{\left(1 - X^{A^e}_{O_2} - X^{A^e}_{CO_2}\right)X^{A^e}_{O_2}} \tag{27.17}$$

where

$X^{A^a}_{CO_2}$ = Measured mole fraction of carbon dioxide in the combustion air

$X^{A^c}_{CO_2}$ = Measured mole fraction of carbon dioxide in the exhaust flow

Generally, adding CO_2 does not greatly improve the accuracy of measuring heat release rate. However, adding a CO_2 analyzer eliminates the need for an expensive sorbent to scrub CO_2 from the gas sample.

If a significant fraction of carbon in the fuel is converted to CO instead of CO_2, the equations can be corrected to take incomplete combustion into account. Heat release rate is then calculated from

$$\dot{Q} = \left[E\phi - (E_{CO} - E)\frac{1-\phi}{2}\frac{X^{A^e}_{CO}}{X^{A^e}_{O_2}}\right] \frac{\dot{m}_e}{1+\phi(\alpha-1)}\frac{M_{O_2}}{M_a}\left(1 - X^a_{H_2O}\right)X^{A^e}_{O_2} \tag{27.18}$$

with

$$\phi = \frac{X^{A^a}_{O_2}\left(1 - X^{A^e}_{CO_2} - X^{A^e}_{CO}\right) - X^{A^e}_{O_2}\left(1 - X^{A^a}_{CO_2}\right)}{\left(1 - X^{A^e}_{O_2} - X^{A^e}_{CO_2} - X^{A^e}_{CO}\right)X^{A^a}_{O_2}} \tag{27.19}$$

where

E_{CO} = Heat release per mass unit of oxygen consumed for CO(17.6 MJ/g)

$X^{A^c}_{CO}$ = Measured mole fraction of carbon monoxide in the exhaust flow

One might wonder under what conditions the CO correction becomes significant. Figure 27.9 shows the ratio of heat release rate obtained by ignoring CO to the actual heat release rate, as a function of the ratio of measured CO to CO_2 mole fractions in the exhaust flow for methane and for a gaseous fuel of composition $(CH_2O)_n$. According to Roberts, the molecular formula of

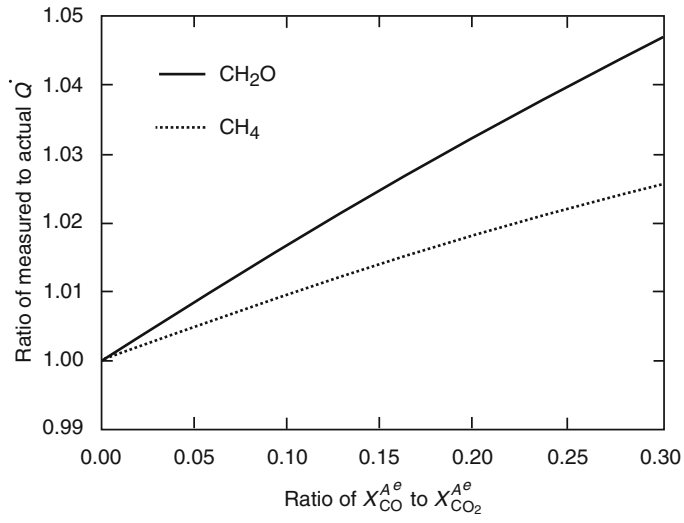

Fig. 27.9 Effect of ignoring CO on $\dot{Q}$ error

the latter represents the thermal degradation products of beech wood [31]. For the CO effect examined here, this fuel represents a "worst case" because it contains enough oxygen for combustion of all hydrogen. Methane gives a practical lower limit for the error, because it is the hydrocarbon with the highest hydrogen-to-carbon ratio.

There is some experimental evidence that the yield of CO in underventilated fires reaches an upper limit approximately equal to 0.2 kg of CO per kg of fuel, when the equivalence ratio exceeds unity [32]. For the fuels considered here, the limit corresponds to a CO/CO_2 mole fraction ratio of 0.27. Figure 27.9 indicates that, even under the worst conditions, the error by ignoring CO generation is less than 5 %.

Carbon Oxide Calorimetry

An alternative method for measuring heat release rate is based on the fact that amount of heat released per mass unit of carbon dioxide and carbon monoxide generated is also relatively constant within a category of fuels or polymers (see Table 27.1). This method is particularly useful for oxidizers [33]. Application to the combustion system shown in Fig. 27.8 leads to the following equation for the heat release rate:

$$\dot{Q} = E'\left(\dot{m}^{e}_{CO_2} - \dot{m}^{a}_{CO_2}\right) + E''\dot{m}^{e}_{CO} = E'\left(\dot{m}_e Y^{e}_{CO_2} - \dot{m}_a Y^{a}_{CO_2}\right) + E''\dot{m}_e Y^{e}_{CO} \tag{27.20}$$

where

E' = Heat released per mass unit of carbon dioxide generated(kJ/g);
E' = Heat released per mass unit of carbon monoxide generated(kJ/g);
$\dot{m}^{e}_{CO_2}$ = Exhaust flow rate of carbon dioxide (g/s);
$\dot{m}^{a}_{CO_2}$ = Inflow rate of carbon dioxide from ambient environment (g/s);
$\dot{m}^{e}_{CO}$ = Exhaust flow rate of carbon monoxide (g/s);
$Y^{e}_{CO_2}$ = Carbon monoxide mass fraction in the exhaust flow(−);
$Y^{a}_{CO_2}$ = Ambient carbon monoxide mass fraction (−); and
Y^{e}_{CO} = Carbon monoxide mass fraction in the exhaust flow(−).

Khan et al. give values for E' and E'' of 13.3 kJ/g ± 11 % and 11.1 kJ/g ± 18 %, respectively (Chap. 36). Practical implementation of Equation 27.20 faces the same challenges as that of Equation 27.14. The following equations can be used to calculate the generation rates of carbon dioxide and carbon monoxide [34]:

$$\dot{m}^{e}_{CO_2} - \dot{m}^{a}_{CO_2} = \frac{X^{A^e}_{CO_2}\left(1 - X^{A^a}_{O_2}\right) - X^{A^a}_{CO_2}\left(1 - X^{A^e}_{O_2} - X^{A^e}_{CO}\right)}{1 - X^{A^e}_{O_2} - X^{A^e}_{CO_2} - X^{A^e}_{CO}} \frac{\dot{m}_e}{1 + \phi(\alpha - 1)} \frac{M_{CO_2}}{M_a}\left(1 - X^{a}_{H_2O}\right) \tag{27.21}$$

with

$$\dot{m}^{e}_{CO} = \frac{X^{A^e}_{CO}\left(1 - X^{A^a}_{O_2} - X^{A^a}_{CO_2}\right)}{1 - X^{A^e}_{O_2} - X^{A^e}_{CO_2} - X^{A^e}_{CO}} \frac{\dot{m}_e}{1 + \phi(\alpha - 1)} \frac{M_{CO}}{M_a}\left(1 - X^{a}_{H_2O}\right) \tag{27.22}$$

Practical Considerations

The equations presented in the previous sections are rather complex and it is very easy to make mistakes. To illustrate the point, Lattimer and Beitel reviewed 17 different standard test methods for measuring heat release rate based on oxygen consumption calorimetry [35]. They found errors in the equations for 12 of the 17 standards. In total, 22 equations were found to be in error. Because it is difficult to avoid

errors in transcribing to a spreadsheet program even with the correct equations, it is essential to do so very carefully and to double-check the results.

Improper setup and maintenance of the gas sampling and analysis system is another common cause for errors. The proper sorbent columns have to be installed depending on the configuration of gas analyzers used. It is necessary to use three columns in series when only oxygen is measured. The first column contains a drying agent. The second column contains a sorbent to scrub the CO_2 from the gas sample. The third column also contains a drying agent and is necessary to remove water vapor that is generated by the CO_2 scrubber. If carbon oxide analyzers are used, a drying column is all that is needed.

Silica gel is a commonly used drying agent in chemistry labs. However, it is not suitable for most oxygen consumption calorimetry applications because of the generation of CO_2 [36]. Drierite® is commonly used instead of silica gel, but some batches seem to have the same problem. Ascarite® is the most commonly used CO_2 scrubbing agent.

Finally, the analyzers are calibrated with certified zero and span gases at the start of each testing day and sometimes more than once a day. It is absolutely essential that flows and pressures during these calibrations are the same as during testing.

Factors Affecting Small-Scale Heat Release Measurements

This section examines the effects of some calorimeter construction details on quality and accuracy of the measurements. The discussion results in some guidelines for building the "ideal" small-scale calorimeter for a specific application.

Open or Closed Configuration

Calorimeters that utilize a measuring technique other than oxygen consumption consist of a closed "box" configuration. Combustion air is supplied to one side of the box, and combustion products are removed from the opposite side. Specimen, heater, and ignition device typically are located inside the box. Advantages of a closed configuration are that airflow rate can be measured at the inlet under clean and soot-free conditions, the combustion air can be heated, and the oxygen concentration in the air can be increased (by adding O_2) or decreased (by adding N_2) from ambient. Disadvantages are thermal lag due to heating or cooling of the enclosure walls and uncontrolled radiation feedback from the enclosure walls to the specimen.

To address the first disadvantage, various numerical procedures have been proposed for correcting the temperature signal measured with calorimeters based on the sensible enthalpy rise method [8–12]. These procedures are based on a mathematical model of the calorimeter consisting of two first-order systems in series. The first system has a rather small time constant (between 8 and 30 s for various calorimeters) and is related to the heat capacity of the gases flowing through the calorimeter. The second system has a large time constant (200–930 s for various calorimeters), which is associated with the heat capacity of the calorimeter walls. The correction procedures adjust the output signal for thermal lag, using discrete forward and inverse Laplace transform techniques.

In spite of the complex calculations, the resulting correction may not always be accurate due to the crude mathematical model for the calorimeter. A more convenient, and perhaps equally accurate, correction method relies on an electronic compensator as described in ASTM E906 and ASTM E1317. The compensator electronically corrects the output signal of the exhaust thermocouples, based on the negative feedback of a wall temperature signal.

The oxygen consumption method also has a time delay, but with properly adjusted sampling flows and oxygen analyzer, this delay consists almost entirely of the transport time for a gas sample from the combustion zone to the analyzer [37]. Because flow rates in the exhaust duct and sampling lines do not change significantly during a test, this delay time is approximately constant.

It can be determined with gas burner calibrations and can be easily addressed by shifting the gas analysis data over the appropriate time interval.

To obtain accurate measurements for thin materials that produce a heat release vs. time curve that has the form of a single sharp peak, it is necessary to make corrections for the response time of the oxygen analyzer [12]. An oxygen analyzer is modeled as a first order system and its time constant is obtained from gas burner step response measurements.

The second disadvantage can be eliminated only by using blackened water-cooled calorimeter walls. If the walls are allowed to heat or cool freely, they emit radiation, which varies with time. Part of this radiation reaches the specimen surface and enhances the radiant heat flux from the heater in an uncontrolled fashion. Obviously, the need for water-cooled walls makes the apparatus much more complex and costly.

Problems with thermal lag and radiation feedback to the specimen can be eliminated by using an open configuration. Solid objects must be water cooled or sufficiently remote from heater and specimen so that they do not interfere with the controlled radiant heat flux to the specimen. A closed configuration can be recommended only for specialized applications, for example, to study the effect of oxygen concentration or temperature of the combustion air on heat release rate and burning behavior.

Type of Heater

Heat release rates must be measured at constant heat flux levels over a range that is relevant for the fire scenario of interest. The heat flux can be provided with a gas burner flame in contact with the specimen or with a radiant panel remote from the specimen.

Incident heat flux from impinging gas burner flames can be adjusted only over a narrow range. To increase the heat flux from a gas burner, either the flame size has to be increased, or a fuel with higher soot yield has to be used. Usually, these parameters can be adjusted only slightly or not at all. It is very difficult to set and maintain a specific heat flux level because a major fraction of the heat transfer is convective. Moreover, the burner gas and combustion products mix with fuel volatiles, which affects burning behavior. In short, impinging flames are not desirable as the external heat source in heat release rate calorimeters.

It is much easier to create constant and uniform exposure conditions if the incident heat flux is primarily radiative. Porous gas panels as well as electrical heating elements are used for this purpose. The radiant heat flux can be adjusted by changing the power of the heater or by changing the distance between heater and specimen. If the second method is used, practical upper and lower limits to the range of radiant heat flux levels can be created. If the heater is too close to the specimen, convective heat transfer becomes significant. Therefore, the upper limit corresponds to the minimum distance that has to be maintained in order to ensure predominantly radiative heat transfer. The lower limit is determined by the uniformity of the incident radiant heat flux, which drops with increasing distance between heater and specimen. The exact limits depend on the geometrical configuration, the power of the heater, and the degree of nonuniformity of the incident heat flux profile that is deemed acceptable.

Another important aspect is the ability of the heater to maintain the radiant heat flux at a constant level during a test. If the heater is operated at a constant power level, incident radiant heat flux changes during testing. At the start of a test, a cold specimen is inserted. The specimen acts as a heat sink, resulting in a decrease of the heater temperature and consequently a decrease of the incident radiant heat flux. After ignition, the heat released by the specimen results in an increase of the heater temperature and incident radiant heat flux.

To maintain incident radiant heat flux during a test, it is therefore necessary to keep the temperature of the heater constant. This is very difficult with a gas panel, but relatively straightforward for electrical heating elements. With the oxygen consumption method, another drawback of using a gas panel is that its products of combustion

result in an oxygen depletion that is usually much larger than the oxygen consumed for combustion of the specimen. Thus, small fluctuations in panel flow can result in significant error of the measured heat release rate. This "baseline" problem can be avoided by using a separate exhaust system for the heater.

It is clear from the preceding discussion that an electrical heater is preferable over a gas panel. Two types of electrical heaters are used: high and low temperature. The former are commonly tungsten filament lamps that operate at temperatures close to 2600 K. According to Wien's displacement law, peak radiant heat flux from such lamps is at a much shorter wavelength than for real fires, with temperatures in the range of 600–1400 K. Piloted ignition studies on plastics and wood have shown that these materials absorb much less radiation in the visible and near-infrared range than at higher wavelengths [38, 39]. On the basis of these findings, it can be concluded that commercially available low-temperature elements are preferable over high-temperature lamps. Such elements typically operate between 800 and 1200 K, a range that is representative of real fire exposure conditions.

Type of Ignition Pilot

Heat release rate tests are usually conducted with an ignition pilot. The use of a pilot reduces the variation in time to sustained flaming between multiple tests conducted under identical test conditions. Because the duration of the preheat period prior to ignition affects burning rate after ignition, use of a pilot also improves repeatability of heat release rate measurements. Furthermore, piloted ignition is used because it is representative of most real fires and conservative in other cases.

The ignition pilot in small-scale fire tests consists of a small gas burner flame, a glowing wire, or an electric spark. An impinging flame should not be used because it locally enhances the incident heat flux to the specimen. Another problem with pilot flames is that they are sometimes extinguished by fire retardants or halogens in the fuel volatiles. A glowing wire is not an efficient method for igniting fuel volatiles, sometimes leading to poor repeatability. An electric spark remains stable when fire retardants or halogens are present. However, it occupies a small volume, so that the positioning of the spark plug is more critical than with other types of ignition pilots.

Specimen Size

The ideal situation would be if small-scale heat release rate data could be used directly to predict burning rate in real-scale fires. Unfortunately, the minimum specimen size that is required to allow for such a straightforward prediction is not practical. As described earlier, the burning rate of a specimen is a direct function of the net heat flux transferred to the fuel. The net flux is equal to the total of external heat flux, flame convection, and flame radiation, minus radiative heat losses from the fuel surface and heat losses (or gains) at the specimen edges.

The Russian work on the effect of diameter on pool fire burning rate by Blinov and Khudiakov gives some insight into this problem. A detailed discussion of this work and its implications is given by Drysdale [40]. If the pool diameter is less than 0.03 m, flame convection is laminar and burning rate increases with decreasing diameter. If the pool diameter exceeds 1 m, flame convection is turbulent and burning rate is independent of diameter. There is a transition region between these two limits, with a minimum burning rate for a pool diameter of approximately 0.1 m. This work indicates that specimen size in a heat release rate calorimeter must be at least 1 m for the results to be independent of scale. This is indeed not feasible in practice. The Russian pool fire data also indicate that heat transfer at the edges becomes excessive at diameters below 0.1 m. Therefore, specimen size in small-scale calorimeters should be at least 0.1 m.

To predict real-scale burning rates, differences in flame heat transfer, and up to a lesser extent heat transfer at the edges, have to

be considered. Östman and Nussbaum reported ignition and heat release data for 13 materials and two specimen sizes [41]. Increase in specimen size from 0.1 m × 0.1 m to 0.2 m × 0.2 m resulted in a slight reduction of piloted ignition time. Average heat release rate over the first minute after ignition on a per-unit-area basis increased by approximately 12 % at exposure levels exceeding 25 kW/m^2. Larger increases were observed at the 25 kW/m^2 exposure level and for peak heat release rate.

Janssens and Urbas presented a comparison of heat release rate data for nine wood products obtained in the cone and an intermediate-scale calorimeter [42]. A 100-fold increase in specimen size resulted in only a 10 % increase of the heat release rate. This modest effect can be explained by the fact that the heat feedback from the flame is relatively insensitive to specimen area for testing in the vertical orientation, in particular for materials, such as wood, that do not produce very luminous flames.

Depending on the specimen size in a small-scale test, there is a limit on the degree of non-uniformity and irregularity of the product being tested, if the test conditions are to be representative of end-use conditions. Therefore, there might be some merit in choosing a specimen size that exceeds the minimum of 0.1 m. However, the main trade-off is that a larger specimen requires a larger and more powerful heater to achieve uniform incident radiant heat flux to the specimen. It should be recognized that, no matter what the specimen size is, there are assemblies and composites for which it is not possible to prepare representative small-scale specimens. Intermediate-scale or full-scale tests are needed to evaluate the fire performance of such assemblies and composites.

Edge Effects

An issue that is closely related to specimen size is that of edge effects. These effects have been studied extensively in the cone calorimeter. ASTM and ISO standards of the cone calorimeter prescribe that, except for calibrations with polymethylmethacrylate (PMMA), the specimen is to be wrapped with aluminum foil on the sides and bottom. The main purpose of the foil is to eliminate mass transfer along all boundaries except the exposed face of the specimen. Furthermore, the ISO standard requires all tests be conducted in the horizontal orientation with the stainless steel retainer frame.

Toal et al. tested several materials with and without foil wrapping, and with and without the retainer frame [43, 44]. They found that the retainer frame reduces peak heat release rate, and lengthens the burning time. This is to be expected because the retainer frame is a relatively large mass of steel that acts as a heat sink, reducing the energy transferred to the specimen.

Urbas and Sand were also concerned with the heat sink effect of the retainer frame [45]. They designed an alternative retainer frame, composed of an insulating collar made of medium-density or high-density refractory material. Their conclusion was that the best edge conditions were obtained using the insulating frame with insulation material that most closely resembles the specimen in thermal properties. Researchers at FM Global proposed a similar approach to address edge effects in a small-scale calorimeter [46].

Babrauskas et al. conducted a very extensive study of the effects of specimen edge conditions on heat release rate [47]. The objective of this study was to further examine the issues raised by Toal et al. and by Urbas and Sand, and to develop definitive recommendations. Specimens of 10 materials were tested in the horizontal orientation at 50 kW/m^2 using three configurations: without retainer frame, with retainer frame, and with an insulated retainer frame akin to that developed by Urbas and Sand [45]. All specimens were wrapped in aluminum foil. The study concluded that the use of an insulated frame gives heat release rate values that are slightly closer to the expected true values. However, the insulated frame makes the test procedure significantly more complicated, so that it is not recommended for routine testing.

If the standard retainer frame is used, Babrauskas et al. recommended that heat release rate data be expressed on the basis of an effective exposure area of 0.0081 m^2. The standard retainer frame reduces the actual exposed area from 0.1 m × 0.1 m to 0.094 m × 0.094 m, or from 0.01 to 0.0088 m^2. The recommendation by Babrauskas et al. [47] to further reduce the exposed area to an effective value of 0.0081 m^2 indicates that the heat sink effect of the retainer frame reduces heat release rate values by approximately 8 %.

Östman and Tsantaridis tested 11 products in the cone calorimeter in the horizontal orientation at 50 kW/m^2, with and without the retainer frame [48]. They also found that the use of the retainer frame results in a reduction of heat release rate greater than what can be explained by the reduction of the exposed area. For the average heat release over the first 3 min following ignition, they found an average reduction of 8 %, identical to Babrauskas et al. [47] However, for maximum heat release rate, they found reductions as high as 25 %.

It can be concluded from these studies that the specimen holder configuration in a small-scale heat release rate test may have a significant effect on the measurements. This effect should be addressed if the test data are used to predict performance in real fires.

Specimen Orientation

Products do not necessarily have to be tested in the same orientation as they are used. For practical reasons, the preferred orientation for small-scale testing is horizontal facing upward. The vertical orientation might be preferable for collecting specialized data for research purposes.

Airflow

Standard rate of heat release test methods are operated under overventilated conditions. Plenty of excess air is supplied, so that the measurements are not affected by lack of oxygen. However, specialized studies have been conducted to evaluate the effect of ventilation and vitiation and to determine the 'Limiting Oxygen Concentration', which is an important parameter in the design of fire protection systems that rely on a reduction of oxygen concentration in the room [49, 50]. Such studies require a closed configuration.

Other Measurements

Heat release rate calorimeters often include additional instrumentation to measure parameters that are important in characterizing the fire performance of materials. Perhaps the most important additional measurement is that of mass loss rate. Most calorimeters can be provided with a load cell to measure specimen mass loss, but this can be very difficult in a closed configuration. Mass loss rate is obtained from numerical differentiation of the mass loss measurements. Smoke meters are added to measure smoke obscuration in the exhaust duct. Both white light and laser light systems are being used. Toxic gas species can be measured in the exhaust duct with additional gas analysis equipment. Such equipment ranges from standard infrared CO and CO_2 analyzers to complex online Fourier transform infrared (FTIR) instrumentation. Whether instrumentation can be added depends mainly on the design and construction details of the calorimeter.

Commonly Used Small-Scale Calorimeters

Ohio State University (OSU) Calorimeter

This apparatus, originally designed by Ed Smith at Ohio State University, is one of the most widely used and best-known small-scale calorimeters [3]. The test method was first published as a proposed ASTM standard in 1980. In 1983, it was adopted as ASTM E906. The standard was recently amended to include two configurations of the test apparatus. Configuration A is that which the Federal Aviation

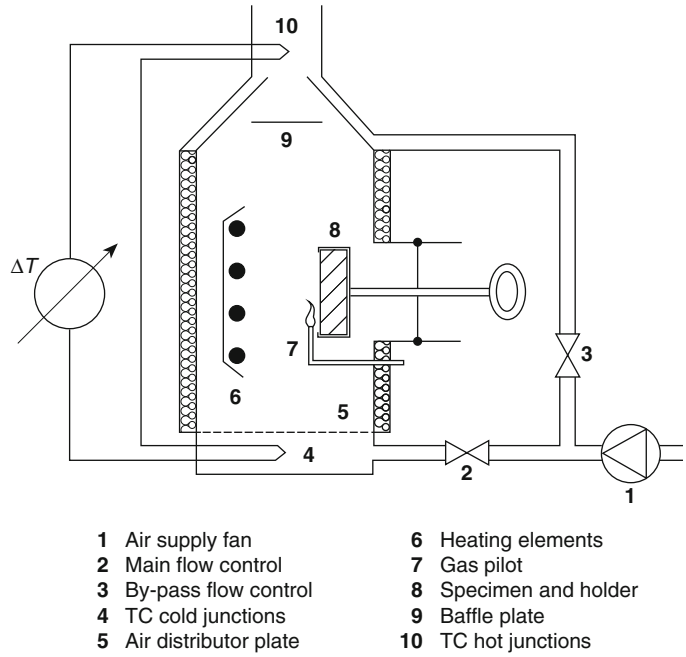

Fig. 27.10 Ohio State University (OSU) calorimeter

Administration (FAA) uses for assessing aircraft cabin materials at a radiant heat flux of 35 kW/m^2. The test procedure in this configuration is also described in the FAA *Aircraft Material Fire Test Handbook* [51]. Configuration B is the original configuration. Both configurations rely on thermopile measurements. Several laboratories have modified the OSU calorimeter to measure heat release rate based on oxygen consumption.

Thermopile Versions

A schematic view of the apparatus is shown in Fig. 27.10. The apparatus consists of an insulated metal box. The conical wall section between the combustion chamber and the stack is hollow. Air flows through this cavity and mixes with the combustion products downstream of the thermocouple hot junctions. However, recovery of the wall heat losses is not fully accomplished. The main features of the OSU apparatus are described below.

Measuring technique. Heat release rate is determined by the sensible enthalpy rise method. The temperatures of inflowing air and outflowing gases are measured with a thermopile of three type K thermocouples. The hot junctions are located symmetrically along a diagonal of the stack cross section, above the baffle plate. The cold junctions are located below the air distributor plate. An electrical compensator is used to correct the temperature signals for thermal lag. The factor k in Equation 27.12 is obtained from line burner calibration runs.

Configuration. Heater and specimen are located inside a box with approximate dimensions of 0.2 m $\times$ 0.41 m $\times$ 0.64 m. The side walls of the box are insulated, and the hollow top wall section is cooled with air.

Heater. The vertical radiant heat source measures approximately 0.3 m $\times$ 0.3 m and consists of four silicon carbide heating elements. A steel masking plate is located in front of the elements to improve uniformity of the incident heat flux distribution over the specimen. The maximum incident heat flux to a vertical specimen is approximately 65 kW/m^2.

Ignition pilot. The optional ignition source is a pilot flame of 2 mL/s methane, premixed with 14 mL/s air. The pilot flame either impinges on

the specimen at the bottom (point ignition), is located in the gas phase at the top of the specimen (pilot ignition), or is not used.

Specimen size and orientation. For testing in the vertical orientation, specimens with an exposed area of 0.15 m × 0.15 m are positioned parallel to the heating elements. Specimens can be tested in the horizontal orientation with the aid of an aluminum reflector foil, which reflects the radiation from the heating elements to the specimen. In this case, the maximum radiant heat flux is reduced to 50 kW/m^2 and the specimen size is 0.11 m × 0.15 m. The use of the reflector plate is awkward and cumbersome, so that testing in the horizontal orientation with the OSU apparatus is not recommended.

Airflow. Total airflow rate is 40 L/s, of which only 10 L/s passes through the combustion chamber and the remaining 30 L/s flows through the upper hollow wall section. Nevertheless, the airflow rate through the combustion chamber contains enough oxygen to feed a 36 kW fire. Because the heat release rate from test specimens rarely exceeds 20 kW, burning conditions in the OSU apparatus are always overventilated. The airflow rates are measured accurately with standard orifices.

Additional measurements. The ASTM E906 standard does not include a mass loss measurement but has a smoke measuring system with a white light source in the stack.

The FAA established a committee in 1978 to examine the factors affecting the ability of aircraft cabin occupants to survive in a postcrash environment. The committee recommended research to evaluate the fire performance of cabin materials and development of a method using radiant heat for testing cabin materials. As a result, the FAA conducted an extensive series of full-scale fire tests and evaluated numerous small-scale tests for their capability to provide results that correlate well with full-scale performance.

The OSU apparatus, standardized as ASTM E906, was found to be the most suitable for material qualification. Improved flammability standards and requirements for airplane cabin interior materials based on ASTM E906 first went into effect in 1986 [52]. The limits for acceptance were based on heat release rate measured at a radiant heat flux level of 35 kW/m^2. Peak heat release rate could not exceed 100 kW/m^2, and average heat release rate over the first 2 min following ignition had to be 50 kW/m^2 or less.

Originally, the test method used by the FAA was identical to ASTM E906. More recently, some significant modifications have been made [11]. The FAA method now uses a thermopile of five thermocouples, a lighter specimen holder, and a modified test procedure to minimize problems associated with thermal lag [52]. The FAA criteria for acceptance were revised in 1990 to 65 kW/m^2 for peak heat release rate during the 5 min test and to 32.5 kW/m^2 for average heat release rate over the first 2 min following ignition [52].

Oxygen Consumption Versions

When oxygen consumption calorimetry became the preferred method for measuring heat release rate, fire research laboratories in the United States, Canada, and Sweden modified their OSU apparatus. These modifications typically consisted of the elimination of the original thermopile, the addition of a gas sampling probe and gas analysis equipment, and some adjustments to the airflow rates [6, 53–55].

The Forest Products Laboratory (FPL) made two additional significant modifications [54]. An auxiliary heat flux meter was added beneath the specimen to monitor incident radiant heat flux during a test. Measurements obtained with this auxiliary meter indicated that the incident radiant heat flux to a burning wood specimen increases significantly during a test. For example, the incident radiant heat flux to a Douglas fir plywood specimen at the end of a 10-min burning period increased by 20 % over the 35 kW/m^2 baseline. This is due to the fact that the heater elements in the OSU calorimeter are supplied with constant power and are not temperature controlled, and

that the calorimeter walls are allowed to heat up (or cool down) during testing.

The fact that exposure conditions in the OSU calorimeter are not constant is a major weakness of the apparatus. It is nearly impossible to remedy this problem. The addition of an auxiliary heat flux meter is highly recommended to record and account for the time-varying exposure conditions.

The second modification at FPL was the addition of a load cell to measure specimen mass loss during a test. This was a rather difficult task due to the geometry of the apparatus and the mechanism for inserting specimens. The FPL load cell design seemed to be satisfactory, demonstrating the feasibility of measuring mass loss in the OSU apparatus.

Cone Calorimeter

The cone calorimeter was developed at the National Bureau of Standards (NBS) by Dr. Vytenis Babrauskas in the early 1980s [37]. It is presently the most commonly used small-scale calorimeter. The apparatus and test procedure are standardized in the United States as ASTM E1354 and NFPA 271, *Standard Method of Test for Heat and Visible Smoke Release Rates for Materials and Products Using an Oxygen Consumption Calorimeter,* and internationally as ISO 5660. Standard cone calorimeter specimens are exposed in an open environment with abundant supply of ambient air for combustion. Some laboratories have used a modified version of the standard apparatus to conduct studies in vitiated or oxygen-enriched atmospheres.

Standard Version

A schematic view of the apparatus is shown in Fig. 27.11. The main features are summarized below.

Measuring technique. Heat release rate is determined by the oxygen consumption method. The gas flow rate in the exhaust duct is calculated from the pressure drop across and temperature at an orifice plate in the duct. A methane burner calibration is performed to determine the orifice constant.

Configuration. Cone heater, spark igniter, specimen holder, and load cell are located beneath the hood. The standard configuration is open, with free access of air to the combustion zone.

Heater. The heater consists of a 5 kW electrical heating element wound inside an insulated stainless steel conical shell. The heater can be oriented horizontally or vertically to perform tests in either orientation. When tests are performed in the horizontal orientation, the specimen is positioned approximately 25 mm below the bottom plate of the cone heater. Flames and products of combustion rise and emerge through a circular opening at the top of the heater. Maximum radiant heat flux to the specimen exceeds 100 kW/m^2.

Ignition pilot. An electric spark is used as the ignition pilot at the top of vertical specimens and over the center of horizontal specimens.

Specimen size and orientation. Specimen size in both orientations is 0.1 m × 0.1 m. The optional retainer frame in the horizontal orientation and the standard specimen holder in the vertical orientation reduce the exposed area to 0.094 m × 0.094 m.

Airflow. Combustion products and dilution air are extracted through the hood and exhaust duct by a high-temperature fan. The initial flow rate can be adjusted between 10 and 32 L/s. Volumetric flow rate remains relatively constant during testing. Some cone calorimeters include additional instrumentation to optionally control and maintain the mass flow rate through the exhaust duct.

Additional measurements. The specimen is mounted on a load cell. Most cone calorimeters include instrumentation for measuring light extinction in the exhaust duct (using a laser light source, described in ASTM E1354 and ISO 5660-2). Instrumentation to measure concentrations of soot, carbon dioxide, carbon monoxide, and other gases is commonly added.

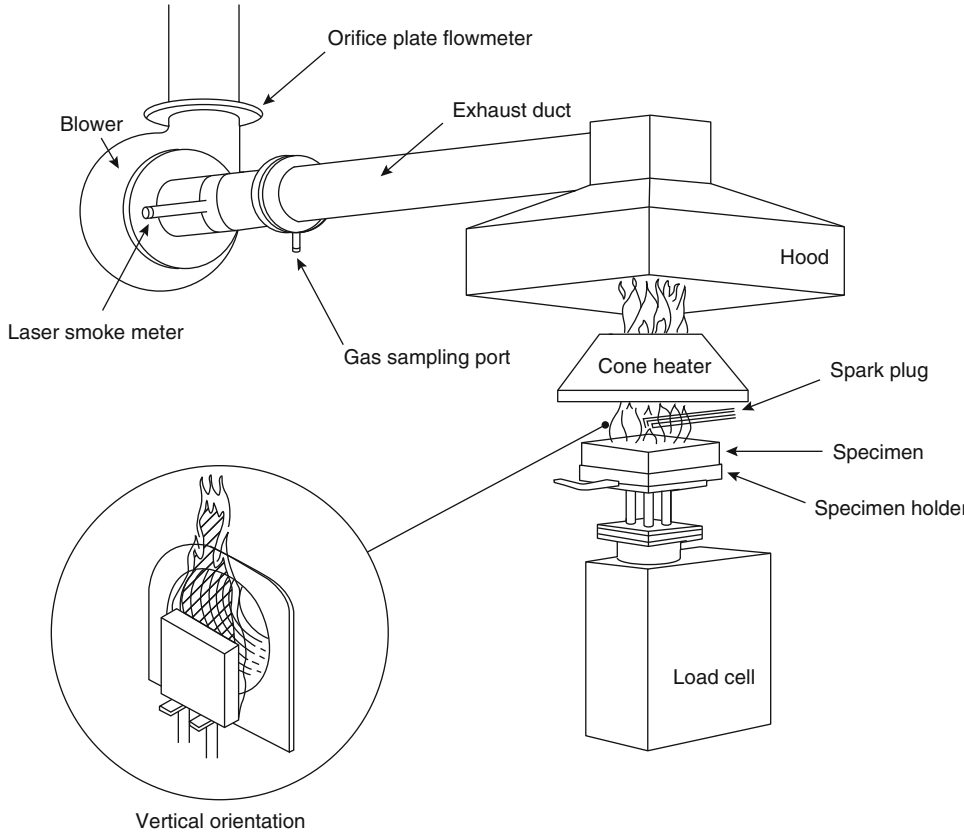

Fig. 27.11 Cone calorimeter

Modified Versions

A number of laboratories have used the cone calorimeter to study the effect of reduced or increased oxygen on the burning behavior of materials [28, 49, 56–59]. An enclosure was built around the heater and load cell and a mixture of nitrogen and oxygen, or air, was supplied to create the desired environment.

Fire Propagation Apparatus

Factory Mutual Research Corporation (FMRC, currently FM Global Research) developed the fire propagation apparatus (originally referred to as the combustibility apparatus) to measure heat release rate and generation rates of smoke and combustion products [60]. A schematic of the apparatus is shown in Fig. 27.12.

Originally, only convective heat release rate was measured on the basis of enthalpy rise of the exhaust gases. Test results reported since the late 1970s also include total heat release rates calculated from oxygen consumption or carbon dioxide generation. Several industrial laboratories in France, Germany, and the United States constructed the apparatus in the 1980s.

Tewarson used the apparatus to determine fire hazard indices [61] and material properties for fire modeling [62]. He also investigated the effect of environmental conditions (such as oxygen concentration in the combustion air) on heat release rate and burning behavior. The results of his extensive research are summarized Chap. 36. The fire propagation apparatus is standardized as ASTM E2058 and has the following main features:

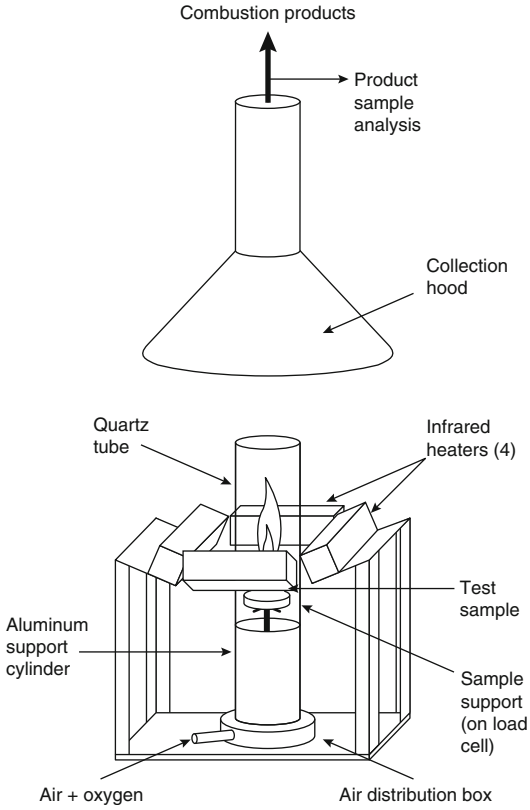

Fig. 27.12 Fire propagation apparatus

Measuring technique: Total heat release rate is determined by the oxygen consumption method. Tewarson also used carbon dioxide generation to calculate heat release rate. However, the amount of energy generated per mass unit of carbon monoxide generated is much more fuel dependent than the amount of energy produced per mass unit of oxygen consumed. Therefore, this technique is not as universally accepted as the oxygen consumption method.

Configuration: Tests are conducted in a semiopen environment. The specimen is located inside a segmented quartz tube, 0.66 m in length and 0.17 m in diameter. A mixture of oxygen and nitrogen is supplied at the bottom of the tube. A stainless steel funnel and vertical exhaust duct are located at some distance above the tube. Dilution air is entrained in the area between the tube and the exhaust system. The total flow of gases through the exhaust duct is determined by measuring pressure drop across a precalibrated orifice. The original apparatus had a vertical exhaust duct. A commercial version with a horizontal duct was recently developed.

Heater: Four heaters, which are located coaxially outside the quartz tube, are used to generate an incident heat flux to the specimen with a maximum of 65 kW/m^2. The electrical heaters operate at high temperatures so that the spectral distribution of the emitted radiation is not representative of that present in most fires. This problem is discussed elsewhere in this chapter.

Ignition pilot: The ignition pilot burner consists of a 6.35-mm stainless steel tube. The burner is supplied with a mixture of 60 % ethylene and 40 % air by volume, at a flow rate to create a stable flame length of 10 mm. The flame is located 10 mm above the horizontal specimen surface or 10 mm from the vertical specimen surface.

Specimen size and orientation: Horizontal specimens measure 0.1 m × 0.1 m or 0.1 m in diameter. ASTM E2058 also describes a procedure for upward flame spread experiments on 0.1 m × 0.3 m vertical planar specimens or 0.8-m-long cable specimens in an environment of 40 % oxygen in nitrogen.

Airflow: Total gas flow rate supplied to the bottom of the quartz tube is 3.3 L/s. Oxygen content of the combustion air can varied between 0 % and 60 %. Oxygen concentrations below ambient are used for simulating ventilation-controlled fires. Oxygen concentrations above ambient are used to increase flame radiation simulating larger fires [63]. Pure nitrogen is used to determine the heat of gasification.

Additional measurements: The apparatus includes instrumentation to measure specimen mass loss, smoke obscuration, and concentrations of O_2, CO_2, and CO in the exhaust flow. An optional hydrocarbon analyzer can be attached as well.

FAA Microscale Combustion Calorimeter

Recently, the U.S. Federal Aviation Administration (FAA) developed the Microscale Combustion Calorimeter (MCC) to assist with the development of fire-resistant polymers for use in commercial passenger aircraft. A schematic of this micro-scale calorimeter is shown in Fig. 27.13.

The apparatus is described in ASTM D7309. A milligram-size specimen is heated at a constant rate between 0.2 and 2 K/s. Decomposition can take place in nitrogen (method A) or in a mixture of nitrogen and oxygen (method B). When method A is used, char-forming specimens do not decompose completely and leave a solid residue. In this case the volatiles are mixed with a metered supply of oxygen in the combustor to obtain the heat release rate of the volatiles. When method B is used, the specimen is completely consumed. The temperature of the combustor is set at approximately 900 °C to completely oxidize all specimen gases. Oxygen consumption calorimetry with E = 13.1 kJ/g is used to measure heat release rate.

The MCC is different from the calorimeters described in the previous three subsections because the primary result is the heat release rate per mass unit of fuel volatiles as a function of time or pyrolysis chamber temperature (as opposed to the heat release rate per unit exposed specimen area as a function of time). The heat release rate per mass unit of fuel volatiles is referred to as the specific heat release rate, $Q(t)$, and is expressed in W/g. A typical result of an MCC test is shown in Fig. 27.14. The following five parameters are calculated when method A is used:

1. The heat release capacity $\eta_c \equiv Q_{max}/\beta$ in J/g·K, where Q_{max} is the maximum value of $Q(t)$ and β is the heating rate in K/s.
2. The heat release temperature T_{max} in K as the pyrolysis chamber temperature at which $Q(t) = Q_{max}$.
3. The specific heat release h_c in J/g as the area under the $Q(t)$ curve.

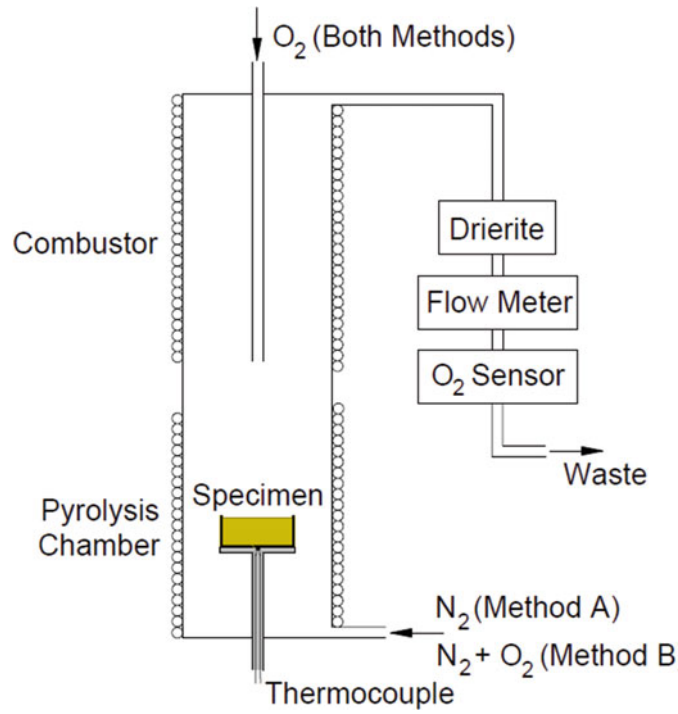

Fig. 27.13 Fire propagation apparatus

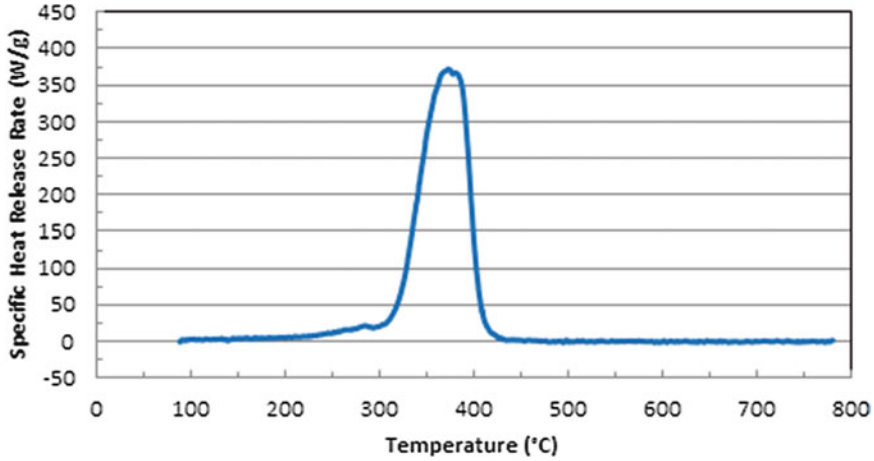

Fig. 27.14 Specific heat release rate versus MCC pyrolysis chamber temperature for PMMA

4. The pyrolysis residue $Y_p \equiv m_p/m_o$ in g/g, where m_p is the residual mass of the specimen at the end of the test.
5. The specific heat of combustion of the specimen gases $h_{c,gas} \equiv h_c/(1-Y_p)$ in J/g.

For method B only three parameters are calculated:

1. The combustion temperature T_{max} in K as the pyrolysis chamber temperature at which the specific heat release rate is a maximum, i.e., $Q(t) = Q^0_{max}$.
2. The combustion residue $Y_c \equiv m_c/m_o$ in g/g, where m_c is the residual mass of the specimen at the end of the test.
3. The net calorific value h_c^0 in J/g as the area under the $Q(t)$ curve.

Comparative Studies Between Different Small-Scale Tests

A number of comparisons are reported in the literature on how results obtained with different calorimeters for the same material compare. Östman et al. reported on a comparison of heat release data for 13 building materials obtained with the modified OSU, the cone calorimeter, and an open calorimeter developed by Sensenig at NBS [64]. Agreement was remarkably good with a correlation coefficient exceeding 90 % for average heat release rate over the first minute following ignition.

Babrauskas compared peak heat release rate from various calorimeters for five aircraft wall paneling materials [65]. He found good agreement between the fire propagation apparatus and the cone calorimeter. However, he also found that the peak heat release rate from the OSU apparatus was approximately 50 % of the peak from the cone calorimeter. Whether thermopile or oxygen consumption were employed seemed to have only a minor effect on the results from the OSU apparatus. Unfortunately, correlation of average heat release rate was not reported, so that a comparison with the work of Östman et al. is not possible.

Tran compared heat release rate curves for Douglas fir plywood from the cone calorimeter, and the OSU apparatus modified for oxygen consumption [54]. First and second peaks agreed well, but the OSU data exceeded the cone calorimeter data by up to 20 % between the peaks. The increased burning rate can be explained by the enhanced radiant heat flux to the specimen due to temperature rise of the calorimeter walls and heater during a test. Tran tested the same material in the OSU apparatus with the vertical specimen holder from the cone calorimeter and found no effect.

Kandola et al. tested several aircraft interior fabrics in the OSU calorimeter according to the

FAA specification and in the cone calorimeter [66]. They found that the specimens ignited much earlier in the OSU apparatus and that the heat release rates were significantly lower in the cone calorimeter. The heat flux in the cone calorimeter had to be increased to 50 kW/m^2 to obtain comparable heat release rates as measured in the OSU calorimeter at 35 kW/m^2.

Two comparative studies were conducted involving electrical cables. Gandhi et al. measured shorter ignition times and lower heat release rates in the fire propagation apparatus than in the cone calorimeter for communication cables [67]. Carman et al. compared oxygen consumption and thermopile measurements for six different types of cables [68]. Good agreement was obtained between the two measurement techniques under flaming conditions.

The thermal combustion properties measured in the MCC are related to flammability characteristics of the material [69–73]. For example, the heat release temperature from method A approximates the surface temperature at ignition. The net calorific value from method B approximates the net heat of combustion measured in an oxygen bomb calorimeter.

Heat release data from small-scale calorimeters are always apparatus dependent. Differences in geometry, test conditions, and mounting methods explain discrepancies between the results from different calorimeters. Apparatus-specific factors must be considered and addressed in a comparison between different calorimeters or when the data are used to predict performance in real fire conditions.

Intermediate- and Large-Scale Calorimeters

This section covers commonly used intermediate- and large-scale calorimeters. Collection and extraction of the products of combustion generated in these calorimeters are usually accomplished in a specific manner. The standard hood and exhaust duct are described before the main features of different intermediate- and large-scale calorimeters are summarized.

Standard Hood and Exhaust Duct

To measure heat release rate in a fire test based on the oxygen consumption technique, it is necessary to collect all combustion products and to measure the oxygen concentration and flow rate of the effluents. A properly designed hood and exhaust duct with the necessary instrumentation are used for this purpose. Various intermediate- and large-scale calorimeters described in subsequent sections use the same standard hood and exhaust duct setup shown in Fig. 27.15.

The square opening of the hood is approximately 2.4 m × 2.4 m and the bottom of the hood is 2.4–3.0 m above the floor of the laboratory. Skirts can be hung down from the hood to minimize spilling. Baffle plates in the plenum or an orifice plate at the entrance of the exhaust duct are used to provide proper mixing of the exhaust gases.

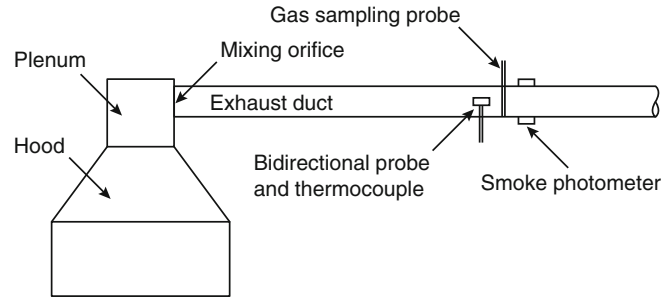

Fig. 27.15 Standard calorimeter hood and exhaust duct

The instrumentation section is located at a distance from the entrance to the exhaust duct of at least 10 times the diameter, that is, 4.0 m for the standard 0.4-m-diameter exhaust duct. The measuring section consists of a combination of a bidirectional probe and thermocouple, a gas sampling probe, and a light extinction measurement system. A straight section of pipe of a length at least six times the diameter is located downstream of the measuring section.

The distance between the base of the fire and the bottom of the hood determines the peak heat release rate that can be measured for a burning object located beneath the hood [74]. On the one hand, the hood has to be sufficiently elevated above the fire to avoid flame impingement. Flame impingement has two undesirable effects. First, flames impinging on a relatively cold surface are quenched, which adversely affects completeness of combustion. Second, radiation from hot metal surface enhances the burning rate of an object located beneath the hood above that of a free burn.

The maximum heat release rate without flame impingement on the standard hood is approximately 1 MW. This is consistent with the fact that the flame height of a 1 MW fire with an effective diameter of 1.5 m is approximately 2.2 m based on Heskestad's flame height correlation (see Chap. 13, "Fire Plumes, Flame Height, and Air Entrainment"):

$$L_f = 0.235\dot{Q}^{2/5} - 1.02D = 0.235(1000)^{2/5} - 1.02(1.5) \approx 2.2\text{m} \quad (27.23)$$

where
L_f = Flame length(m)
$\dot{Q}$ = Heat release rate(kW)
D = Effective diameter of the fire(m)

On the other hand, the hood cannot be located too high above the burning object to avoid spilling. The skirts are helpful in this respect.

An ideal exhaust system extracts combustion products at the same rate as the flow rate in the plume when it enters the hood. This results in the highest and most accurate measurement of oxygen depletion because no additional air above what is entrained in the plume is drawn into the exhaust duct. The plume flow rate at a height of 2.2 m above a fire with an effective diameter of 1.5 m can be estimated from the simple equation developed by Thomas et al. [75] (see Chap. 13):

$$\dot{m}_p = 0.188\frac{\pi}{4}D^2z^{3/2} = 0.188\frac{3.14159}{4}1.5^2 2.2^{3/2} = 1.08\,\text{kg/s} \quad (27.24)$$

where
$\dot{m}_p$ = Plume flow(kg/s)
z = Height above the fire(m)

Assuming a radiative loss fraction of 30 %, which is a typical value for many fuels (see Chap. 36), this corresponds to a volumetric flow rate of 2.8 m^3/s at a temperature of 650 °C. Intermediate- and large-scale calorimeter test standards that specify the hood and exhaust system described in this section typically require an exhaust fan with a capacity of 3.5 m^3/s.

Intermediate-Scale Calorimeter (ICAL)

One of the limitations of the cone calorimeter is that only relatively small samples can be evaluated. As a result, products that have joints or layered materials with a thickness exceeding 50 mm can generally not be tested in the cone calorimeter in a representative manner. For those types of products or assemblies, a larger calorimeter, such as the intermediate-scale calorimeter (ICAL) described in ASTM E1623, is required.

The ICAL apparatus consists of an array of gas heaters, forming a vertical radiant panel with an approximate height and width of 1.33 m and 1.54 m, respectively (Fig. 27.16). The standard test specimen measures 1 m × 1 m and is positioned parallel to the radiant panel. The heat flux to the specimen is preset in the range of 10–60 kW/m^2 by adjusting the distance to the panel. Gas flow to the panel is controlled to

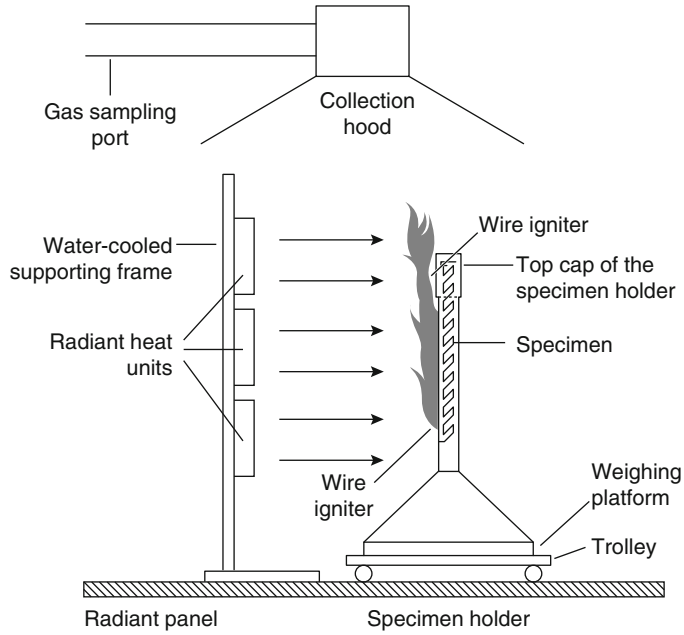

Fig. 27.16 ICAL apparatus

maintain the temperature to the panel and consequently the heat flux to the specimen during a test. The products of pyrolysis from the specimen are ignited with hot wires located close to, but not in contact with, the specimen at its top and bottom. The specimen is placed in a holder that is put on a load cell to measure mass loss during testing.

Panel and specimen are positioned beneath the standard hood described in the previous subsection. Measurements of oxygen concentration, flow rate, and light transmission in the exhaust duct are used to determine the heat release rate and smoke production rate from the specimen as a function of time. Because the combustion products from the radiant panel are also captured in the hood, it is necessary to subtract the corresponding heat release rate or smoke production rate to determine the contribution from the specimen.

Furniture Calorimeter

Often it is very difficult to determine the burning behavior of complex objects on the basis of the fire performance of their individual components. For example, it is very hard to determine the burning behavior of upholstered furniture on the basis of the fire characteristics of the foam, fabric, and framing materials and to account for the geometry and configuration of the furniture and how it is ignited. It is much more practical to measure the heat release rate and related properties for the complete object.

Furniture calorimeters were developed in the 1980s in several laboratories to obtain this kind of data [76, 77]. The first furniture calorimeter test standard was published in 1987 in the Nordic countries as NT Fire 032.

A furniture calorimeter consists of a weighing platform that is located on the floor of the laboratory beneath the standard hood (Fig. 27.17). The object is placed on the platform and ignited with the specified ignition source. The products of combustion are collected in the hood and extracted through the exhaust duct. Measurements of oxygen concentration, flow rate, and light transmission in the exhaust duct are used to determine the heat release rate and smoke production rate from the object as a function of time.

Furniture calorimeter test standards have been developed in ASTM for chairs (ASTM E1537),

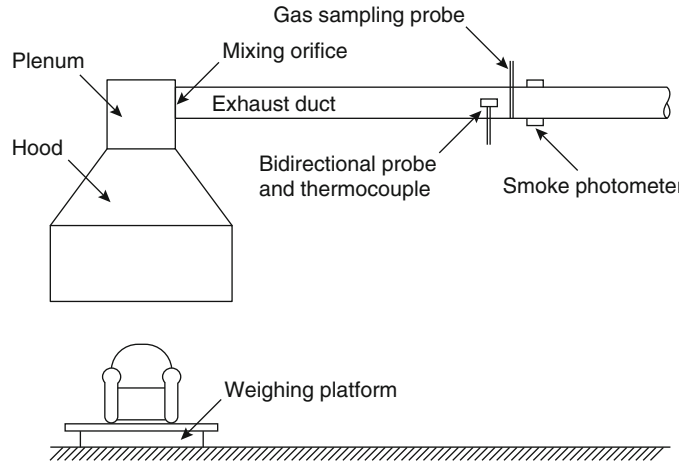

Fig. 27.17 Furniture calorimeter

Table 27.3 Ignition sources specified in fire tests for chairs and mattresses

		Gas burner ignition source			
Test method	Specimen	No.	Type	Heat output	Location of application
ASTM E1537 CAL TB 133	Single chair	1	Square	19 kW for 80 s	Horizontal seating surface
ASTM E1822	Stacked chairs	1	Line	18 kW for 80 s	Bottom chair front edge
ASTM E1590	Mattress (set)	1	Line	18 kW for 180 s	Front bottom edge
CAL TB 603	Mattress (set)	2	Line	19 kW for 70 s	Top surface
16 CFR 1633			Line	10 kW for 50 s	Vertical along side

mattresses (ASTM E1590), and stacked chairs (ASTM E1822). The California Bureau of Home Furnishings and Thermal Insulation (CBHFTI) published California Technical Bulletins (CAL TB) 133 and 603. These documents describe fire test procedures to qualify seating furniture and mattresses, respectively, for use in public occupancies in the state of California. Acceptance is primarily based on a peak heat release rate and 10-min total heat release limits of 80 kW and 25 MJ for chairs (CAL TB 133) and 200 kW and 25 MJ for mattresses (CAL TB 603). The primary difference between the different fire test methods for chairs and mattresses is the ignition source, which has been demonstrated to affect heat release rate [78]. The main features of the gas burner ignition source specified in different methods are given in Table 27.3.

All mattresses sold in the United States must comply with the heat release requirements specified in 16 CFR 1633. The method and requirements are identical to CAL TB 603, except that the 10-min total heat release limit is reduced to 15 MJ. The fire test method for mattresses and mattress/box spring sets described in this document was developed at the National Institute of Standards and Technology (NIST) in a research program sponsored by the Sleep Products Safety Council (SPCS), an affiliate of the International Sleep Product Association (ISPA) [79–81].

The original version of CAL TB 133 specified that the test specimen be located in a corner against the back wall of a 3.7 m × 3.0 m × 2.4 m room with a 1.0 m × 2.1 m open doorway in the front wall. The ignition source consisted of five double sheets of loosely-wadded newspaper inside a chicken wire cage placed on the back of the seat. Acceptance was based primarily on a maximum temperature rise of 111 °C just below the ceiling above the chair. Subsequent NIST research resulted in the development of the

presently used gas burner as an alternative ignition source [82]. The gas burner flame generates an equivalent thermal insult but is much more repeatable and reproducible than the original ignition source.

The NIST research project also resulted in an equivalent heat release rate criterion and demonstrated that the room effects are negligible for heat release rates below 600 kW [83]. Later studies found significant effects at lower heat release rates and proposed a threshold of 460 kW [84]. Because this is still much higher than peak heat release rate limits specified in regulations, all furniture and mattress test standards discussed here permit the use of an open furniture calorimeter configuration as an alternative to the room configuration. In fact, all test standards except 16 CFR 1633 allow two room configurations: the original CAL TB 133 room and a smaller 3.7 m $\times$ 2.4 m $\times$ 2.4 m room commonly used for room/corner testing (see below).

Room/Corner Test

Room/corner tests are by far the most frequently conducted large-scale fire experiments throughout the world. This section provides a historical overview of the development of room/corner test protocols and summarizes the resulting test standards in use today.

Historical Overview

Much of the work toward the development of a standard room/corner test was performed in the United States in the late 1970s and early 1980s. The need for a standard room fire test and some aspects of its design were discussed by Benjamin in 1977 [85]. Subsequent research in North America to arrive at a standard full-scale test was conducted primarily by Fisher and coworkers at the University of California (UCB) [86] and by Lee at the National Bureau of Standards (NBS) [87].

Considerable seminal research was also performed in the Nordic countries. An extensive project to construct a full-scale room calorimeter was conducted in Sweden [88, 89]. No oxygen consumption measurements were made at that time. A heat balance was obtained by comparing the theoretical heat release from combustion of gaseous fuel to the sum of the heat losses. The heat losses consisted of convection through the doorway, conduction through the walls and ceiling, and radiation through the doorway.

Heat convection through the doorway was estimated by measuring gas velocity and temperature at many points in the doorway. Heat conduction through the surrounding surfaces was calculated based on total heat flux, radiation, and surface temperature data. Heat loss by radiation through the door was calculated from radiometer measurements.

Initially, a series of quasi-steady calibration tests were conducted in an inert room. Three different circular propane gas burners were used with diameters of 0.2, 0.3, and 0.4 m, respectively. Heat balance calculations showed reasonable agreement, with convection losses being dominant. In subsequent tests with surface finishes, a heptane pool fire with a heat release rate of approximately 50 kW was used as the ignition source.

Ahonen et al. at the Technical Research Center of Finland (VTT) studied the effects of different gas burner ignition sources on room/corner fire growth [90]. Tests were conducted for each combination of three burner sizes (0.17 m $\times$ 0.17 m, 0.305 m $\times$ 0.305 m, and 0.5 m $\times$ 0.5 m) and three square wave heat release rates (40, 160, and 300 kW). Oxygen consumption calorimetry was used for measuring heat release rate. The burner was placed in a corner in the back of the room. Ceiling and all walls except the front wall were lined with 10-mm-thick particleboard with a density of 720 kg/m^3.

The following six criteria were used to determine the time to flashover:

- Flames emerging through the door (flameover)
- Total heat release rate of 1 MW
- Total heat flux to the floor of 20 kW/m^2
- Specified rate of smoke production
- Temperature of 600 °C at the geometric center of the room
- Total heat flux to the floor of 50 kW/m^2

With the time to flashover defined as the average of the six criteria, the following remarkable results were obtained:

- At the 40 kW level, the medium-sized burner resulted in flashover first, followed by the smaller burner, and then the larger burner.
- At 160 kW, the largest burner resulted in flashover first, quickly followed by the other two configurations.
- At 300 kW, the trend was the same as at 160 kW with an even smaller spread between the three results.

The effect of burner size was most significant at the lowest heat release rate, with the medium-sized burner being the most severe. At higher exposure levels, the size of the burner had no significant effect. Radiative and convective heat transfer from the burner flame were shown to depend on burner size and heat release rate and had a significant effect on the performance of the material tested. On the basis of the results, the medium burner size and heat release rate were recommended.

Room/Corner Test Standards

Several standard room/corner test protocols are now available and are specified in codes and regulations for qualifying interior finishes. For example, U.S. model building codes require that textile wall coverings for use in unsprinklered compartments meet specific performance requirements when tested according to NFPA 265, *Standard Methods of Fire Tests for Evaluating Room Fire Growth Contribution of Textile Coverings on Full Height Panels and Walls*. The principal requirement of these tests is that flashover does not occur. The same codes also require that all other interior wall and ceiling finish materials comply with requirements based on NFPA 286, including a limit on the total smoke released.

The Safety Of Life At Sea (SOLAS) convention, promulgated by the International Maritime Organization (IMO), permits the use of combustible bulkhead and ceiling linings on high-speed craft, provided they meet stringent fire performance requirements based on assessment according to ISO 9705. ASTM E2257 is the American version of ISO 9705.

The test apparatus and instrumentation described in the NFPA and ISO room/corner test standards are very similar (Fig. 27.18). However, some significant differences exist in terms of specimen configuration and ignition source.

The apparatus consists of a room measuring 3.6 m deep by 2.4 m wide by 2.4 m high, with a single ventilation opening (open doorway) measuring approximately 0.8 m wide by 2.0 m high in the front wall. Walls and ceiling are lined for tests according to ISO 9705. For tests according

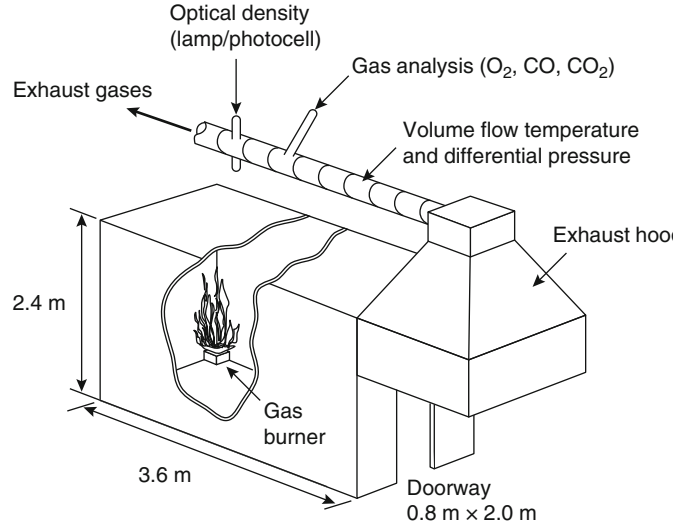

Fig. 27.18 Room/corner test

to the NFPA standards, the interior surfaces of all walls (except the front wall) are covered with the test material. NFPA 286 is also suitable for evaluating ceiling finishes (see below).

The test material is exposed to a propane burner ignition source, located on the floor in one of the rear corners of the room opposite the doorway. The burner is placed directly against (ISO 9705 and NFPA 286) or at a distance of 50 mm from (NFPA 265) the walls. The ISO burner consists of a steel sandbox measuring 0.17 m × 0.17 m × 0.145 m, with the top surface 0.145 m above the floor of the room. Propane is supplied to the burner at a specified rate such that a net heat release rate of 100 kW is achieved for the first 10 min of the test, followed by 300 kW for the remaining 10 min (20-min test duration unless terminated when flashover occurs). The NFPA burner consists of a steel sandbox measuring 0.305 m × 0.305 m × 0.152 m, raised so that the top surface is 0.305 m above the floor of the room. Propane is supplied at a specified rate so that a net heat release rate of 40 kW is achieved for the first 5 min of the test, followed by 150 kW (NFPA 265) or 160 kW (NFPA 286) for the remaining 10 min (15-min test duration unless terminated when flashover occurs). A fundamental difference between NFPA 265 and NFPA 286 is the fact that the flame from the burner alone just touches the ceiling in NFPA 286. This makes it suitable for assessing the fire performance of interior ceiling finish, an application for which NFPA 265 is unsuitable. This effect is partly due to the higher energy release rate of the NFPA 286 burner, but primarily because of the burner being in direct contact with the walls, thereby reducing the area over which the flames can entrain air and increasing the overall flame height.

All combustion products emerging from the room through the open doorway are collected in the standard hood. Instrumentation is provided in the exhaust duct for measuring heat release rate based on the oxygen consumed (ISO and NFPA standards) and smoke production rate (ISO 9705 and NFPA 286 only). The room contains a single heat flux meter located in the center of the floor. The NFPA standards also specify that seven thermocouples be installed in the upper part of the room and doorway to measure the temperature of hot gases that accumulate beneath the ceiling and exit through the doorway. In addition to quantitative heat release and smoke production rate measurements, time to flashover (if it occurs) is one of the main results of a room/corner test. Different criteria are commonly used to define flashover; for example, upper layer temperature of 600 °C, flames emerging through the doorway, heat flux to the floor of 20 kW/m^2, heat release rate of 1 MW, and so forth.

Single Burning Item Test

The European reaction-to-fire classification system for construction products except floor coverings (EN 13501) is based primarily on performance in this test. An SBI test in progress is shown in Fig. 27.19. Two specimens of the material to be tested are positioned in a specimen holder frame at a 90° angle to form an open corner section. Both specimens are 1.5 m high. One specimen is 1 m wide and is referred to as the long wing. The other specimen is 0.5 m wide and is referred to as the short wing. During a test,

Fig. 27.19 SBI test in progress (Photo courtesy SwRI.)

the specimens are exposed for 20 min to the flame of a triangular-shaped diffusion propane gas burner operating at 30 kW. The specimen holder and primary gas burner are mounted on a trolley that can be moved in and out of an enclosure of 3 m ± 0.6 m wide, 3 m ± 0.6 m deep, and 2.4 m ± 0.1 m high. The enclosure walls consist of noncombustible materials (concrete block, calcium silicate board, etc.) and/or gypsum board, and have windows to allow the operator to observe the test. The mean height and maximum heat flux from the 30 kW burner flame are approximately 0.8 m and 35 kW/m^2, respectively [91].

Prior to a test, the specimens are placed in the holder, and the trolley is rolled into the enclosure and positioned under an insulated hood. During a test, the products of combustion are collected in the hood and are extracted through an exhaust duct. Instrumentation is provided in the duct to measure temperature, velocity, gas composition (O_2, CO_2, and CO), and smoke obscuration.

The velocity and gas composition data are used to determine heat release rate on the basis of the oxygen consumption technique. Materials are tested in triplicate. Classification is based primarily on fire growth (FIGRA) and smoke development (SMOGRA) indices that are equal to the peak heat release and smoke production rate, respectively, divided by the time to reach the peak. FIGRA and SMOGRA limits were established based on performance in the ISO 9705 room/corner test as the reference scenario [92].

Industrial-Scale Calorimeters

Industrial-scale calorimeters consist of a larger version of the hood and exhaust duct shown in Fig. 27.15. To handle fires up to 10 MW in size for a short duration, the hood must be at least 6 m × 6 m in size or 6 m in diameter and is typically located 6.5 m or higher above the floor of the laboratory. The fan must be capable of extracting combustion products through a 0.9-m-diameter exhaust duct at a minimum rate of 15 m^3/s. A larger calorimeter and higher fan capacity are needed to handle more severe experimental fires.

Cooper presented useful guidelines to address the special challenges associated with the design of an industrial-scale calorimeter [74]. ASTM E2067 is a standard practice for conducting accurate heat release rate measurements at the multi-megawatt level.

The first industrial-scale calorimeter for fires into the multi-megawatt range was built at Factory Mutual around 1980 [93]. This calorimeter, also referred to as the FM fire products collector, was designed to measure heat and other fire products from test fires up to a size associated with sprinkler activation in commodity warehouse storage and other representative occupancies.

Approximately 10 years later, a similar industrial-size calorimeter for heat release rate measurements up to 10 MW was constructed at the National Testing Laboratory (SP) in Sweden [94]. Since then several other laboratories—such as the National Research Council of Canada, the Fire Research Station in the United Kingdom, the Bureau of Alcohol, Tobacco, Firearms and Explosives (ATF) Fire Research Laboratory, the National Institute of Standards and Technology (NIST), Southwest Research Institute and Underwriters Laboratories in the United States—developed the capability of measuring heat release rate from large fires into the megawatt range.

Use and Application of Heat Release Rate Data

The primary use of heat release rate data is in support of fire hazard assessment of materials and products. Small- and intermediate-scale data can be used in conjunction with mathematical models to predict the performance of materials and products in real fire scenarios. Heat release rates measured in large- and industrial-scale calorimeters can be used directly in support of a fire hazard assessment.

Small-Scale Calorimeter Data

Predictive models that are available for fire hazard assessment on the basis of small- or intermediate-scale heat release rate data vary widely in complexity. The extent of the heat release rate data that are needed varies according to the complexity of the model. Room/corner testing is a widely accepted approach to assess the fire hazard of interior finish materials. The room/corner scenario is used here to illustrate the different types of predictive models and corresponding requirements for input data from small-scale calorimeters.

There are three distinct types of room/corner test models: regression models, analytical models, and physics-based models. Regression models express a relationship between a particular room/corner test performance characteristic, for example, the time to flashover, and small-scale fire test data for the same product. Regression models are based on a statistical analysis of room/corner and small-scale test data for a set of products and can be used as a screening tool. Analytical models predict fire growth but do not simulate the room environment. Physics-based models predict how the room environment varies as a function of time and how flames spread over the walls and ceiling of the compartment. There is a strong interaction between regression and physics-based models because the conditions in the room determine the heat that is transferred back to the wall and ceiling surfaces, which affects the flame spread and the heat release and smoke production rate of burning wall and ceiling sections.

Regression Models

The least sophisticated models are based on regression analyses. The following equation, obtained by Östman et al. based on an analysis of test data for 28 materials in the cone calorimeter and according to ISO 9705, serves as a good example of this type of room/corner test modeling [95].

$$t_{fo} = 0.0716 \frac{t_{ig}^{0.25} \rho^{1.72}}{\left(Q_{300}''\right)^{1.30}} + 57.4 \qquad (27.25)$$

where

t_{f0} = Time to flashover (s)

t_{ig} = Time to ignition in the cone calorimeter at 50 kW/m^2 (s)

ρ = Density of the material (kg/m^3)

Q_{300}'' = Total heat released at 50 kW/m^2 during 300 s following ignition (MJ/m^2)

This equation can be used to predict room/corner test performance on the basis of small-scale data for materials that have not been tested in the room. With this approach the dynamics of the heat release curve are lost entirely. There is no difference in the prediction of full-scale performance for two materials with heat release curves of very different shapes, provided the heat release rate parameter and ignition time used in the correlation are identical. The predictions are valid for one scenario and geometry only. For example, Equation 27.25 cannot be used to predict the time to flashover for the NFPA 265 and NFPA 286 room/corner tests. The main advantage of this approach is that a minimal amount of small-scale testing is needed to obtain the necessary input data.

Analytical Models

The approach outlined in the preceding subsection can be improved by using a heat release curve at a single radiant heat flux level. Thus, the dynamic effects of the room fire on the exposure level are ignored while the dynamics of the heat release curve are largely maintained. The radiant heat flux level is chosen so that it is a representative average (over space and time) for the fire scenario that is being modeled [96]. Representative heat flux levels for the room/corner test scenario range from 25 to 50 kW/m^2.

The single heat release curve is used in combination with a flame spread algorithm to predict heat release rate as a function of time in the room/corner test. The flame spread algorithm can be very simple but needs at least some

ignition data for the material. The burning area expands as time proceeds and new sections of the material are ignited. The heat release rate is calculated at discrete time increments, Δt. The flame spread algorithm calculates the expansion of the burning area at every time step. The heat release rate in the room/corner test at a particular time is then obtained by adding the contributions from all incremental areas to the heat release rate from the ignition burner at that time:

$$\dot{Q}_t(t_N) = \dot{Q}_b(t_N) + \sum_{i=0}^{N} A_i \dot{Q}''(t_N - t_i) \quad (27.26)$$

where

$\dot{Q}_t$ = Total heat release rate in the room/corner test(kW)
t_N = Time after N time increments Δt from the start of the test, equal to$N\Delta t$(s)
$\dot{Q}_b$ = Heat release rate from the ignition burner(kW)
A_i = Incremental area ignited at time t_i(m^2)
$\dot{Q}''$ = Heat release rate measured in the cone calorimeter(kW/m^2)
t_i = Time afteritime increments Δt from the start of the test, equal to $i\Delta t$(s)

This method automatically accounts for burnout. The most widely known room/corner test model of this type was developed by Wickström and Göransson [97].

Physics-Based Models

Direct Use of Heat Release Rate Measurements at Multiple Heat Fluxes

The modeling approach described in the preceding subsection can be refined by using heat release rate curves obtained at multiple heat fluxes. This makes it possible to account for the fact that the incident heat flux to each incremental area varies with time. The problem, however, is that the heat release rate of an incremental area at a particular time cannot be determined from direct interpolation of the heat release rate curves measured in the calorimeter. This is because it takes more time at lower heat fluxes to completely consume the material than at higher heat fluxes. To address this problem, heat release rate has to be expressed as a function of a progress variable that is consistent at different radiant heat flux levels.

Smith and Green conducted experiments in the OSU calorimeter at different heat flux levels and tested the same material at time-varying heat fluxes [98]. They were able to reconstruct the heat release rate curve measured under dynamic exposure conditions from interpolation between the curves obtained at fixed radiant heat fluxes using total heat release as the progress variable. Mitler used total mass loss as the progress variable [99]. Janssens suggested using char depth as a suitable progress variable for wood [100].

The following modification to Equation 27.26 represents an improved room/corner test model that accounts for the effect of incident heat flux on heat release rate. Total heat release rate is used as the progress variable.

$$\dot{Q}_t(t_N) = \dot{Q}_b(t_N) + \sum_{i=0}^{N} A_i \dot{Q}''\left[\dot{q}_{e,i}''(t_N), Q_i''(t_N)\right] \quad (27.27)$$

where

$\dot{q}_{e,i}''$ = Incident heat flux to A_i(kW/m^2)
$\dot{Q}_i''$ = Total heat release from A_i(MJ/m^2)

The model calculates the incident heat flux and keeps track of the total heat release rate for each incremental area. A room/corner test model of this type was developed by Smith et al. at Ohio State University [5].

The primary limitations of using this type of model are that (1) it is based on the assumption that the heat flux from the material's own flame in the small-scale calorimeter is comparable to that in the room/corner test, and (2) Equation 27.27 is assumed to be valid regardless whether the incident heat flux is purely radiative (as in the small-scale calorimeter) or partly convective (as, for example, in areas of the room

where the material is exposed to the flame of the ignition source). These limitations can be addressed, at least in an approximate manner, but not without making the approach much more complex.

Use of Heat Release Properties

A more fundamental approach to account for the effects of time-varying heat fluxes on heat release rate is based on two material properties that can be measured in a small-scale calorimeter. These properties are the effective heat of combustion, $\Delta h_{c,\text{eff}}$, and the heat of gasification, Δh_g. Both properties have the units of kJ/g or MJ/kg.

The effective heat of combustion is the ratio of heat release rate to mass loss rate measured in a small-scale calorimeter.

$$\Delta h_{c,\text{eff}} \equiv \frac{\dot{Q}''}{\dot{m}''} \tag{27.28}$$

where

$\dot{Q}''$ = Heat release rate per unit exposed area(kW/m^2)
$\dot{m}''$ = Mass loss rate per unit exposed area$(\text{g}/\text{m}^2 \cdot \text{s})$

The effective heat of combustion at a particular time t can be calculated by substituting the values for $\dot{Q}''$ and $\dot{m}''$ at that time in Equation 27.28. A curve of $\Delta h_{c,\text{eff}}$ as a function of time can be determined in this manner. Unfortunately, mass loss rate data are often very noisy and the calculated time-varying heat of combustion values may not have any physical meaning. More meaningful values are obtained by calculating an average $\Delta h_{c,\text{eff}}$, over a specified time period by substituting average values of $\dot{Q}''$ and $\dot{m}''$ over that time period in Equation 27.28.

Dillon et al. proposed three methods to calculate the effective heat of combustion [101]. The first value is equal to the ratio of the first peak heat release rate and mass loss rate at the same time. The second value is obtained as the ratio of the average heat release rate over the peak burning period and the mass loss rate over the same period. The peak burning period is defined as the period around the first peak heat release rate during which the heat release rate is at least 80 % of the first peak heat release rate. The third value is equal to the ratio of total heat released and total mass loss over the entire flaming period.

The heat of gasification is defined as the net heat flow into the material required to convert one mass unit of solid material to volatiles. The net heat flux into the material can be obtained from an energy balance at the surface of the specimen. Typically, a sample exposed in a small-scale calorimeter is heated by external heaters and by its own flame. Heat is lost from the surface in the form of radiation. A schematic of the heat balance at the surface of a burning specimen in the cone calorimeter is shown in Fig. 27.20. Hence, Δh_g is defined as

$$\Delta h_g \equiv \frac{\dot{q}''_{\text{net}}}{\dot{m}''} = \frac{\dot{q}''_e + \dot{q}''_f - \dot{q}''_l}{\dot{m}''} \tag{27.29}$$

where

$\dot{q}''_e$ = Heat flux to the specimen surface from external sources(kW/m^2)
$\dot{q}''_f$ = Heat flux to the specimen surface from the flame(kW/m^2)
$\dot{q}''_l$ = Heat losses from the exposed surface (kW/m^2)

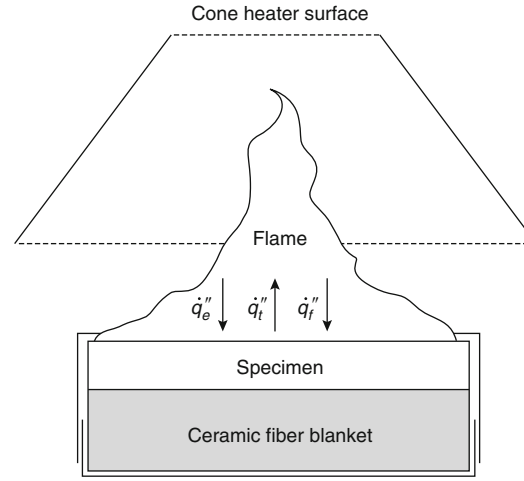

Fig. 27.20 Heat balance at the surface of a burning cone calorimeter specimen

If the flame is approximated as a homogeneous gray gas volume, the heat flux from the flame can be expressed as follows:

$$\dot{q}_f'' = \dot{q}_{f,c}'' + \dot{q}_{f,r}'' = h^*(T_f - T_s) + \sigma \varepsilon_f T_f^4 \tag{27.30}$$

where

$\dot{q}_{f,c}''$ = Convective fraction of the flame flux $(\mathrm{kW/m^2})$
$\dot{q}_{f,r}''$ = Radiative fraction of the flame flux $(\mathrm{kW/m^2})$
h^* = Convection coefficient corrected for blowing $(\mathrm{kW/m^2 \cdot K})$
T_f = Flame temperature (K)
T_s = Surface temperature (K)
σ = Boltzmann constant $(5.67 \cdot 10^{-11} \mathrm{kW/m^2 \cdot K^4})$
ε_f = Emissivity of the flame

The flow of combustible volatiles emerging through the exposed surface of the specimen adversely affects the convective heat transfer between the flame and the surface. This effect is referred to as "blowing." The flame flux in a small-scale calorimeter is primarily convective, in particular in the vertical orientation, and flame absorption of external heater and specimen surface radiation can be neglected.

The heat losses from the surface can be expressed as

$$\dot{q}_l'' = \sigma \varepsilon_s (T_s^4 - T_\infty^4) \tag{27.31}$$

where

ε_s = Surface emissivity of the specimen
T_∞ = Ambient temperature (K)

Some materials exhibit nearly steady mass loss rates when exposed to a fixed radiant heat flux. T_s for these materials reaches a steady value after a short initial transient period and all terms in Equation 27.29 are approximately constant. Δh_g can then be obtained by measuring steady mass loss rates at different radiant heat flux levels and by plotting $\dot{m}''$ as a function of $\dot{q}_e''$. The reciprocal of the slope of a straight line fitted through the data points is equal to Δh_g. The intercept of the line with the abscissa is equal to $\dot{q}_l'' - \dot{q}_f''$. Tewarson et al. [62] and Petrella [102] have used this technique to obtain average Δh_g values for a large number of materials. Tewarson et al. also conducted tests in vitiated O_2-N_2 mixtures and found $\dot{q}_f''$ to decrease linearly with decreasing oxygen concentration. Analysis of these additional experiments made it possible to separate $\dot{q}_f''$ and $\dot{q}_l''$.

Many materials, in particular those that form an insulating char layer as they burn, take a long time to reach steady burning conditions or may never reach steady conditions. Equation 27.29 is still valid for such materials, but the heat and mass fluxes and resulting Δh_g values vary with time. Tewarson and Petrella have used the method described in the preceding paragraph to determine average Δh_g values for nonsteady burning materials using average mass loss rates. They found that average $\dot{m}''$ is still an approximately linear function of $\dot{q}_e''$. However, the average heat of gasification values obtained in this manner may not have any physical meaning. For example, Janssens demonstrated that the values based on average mass loss rates are too high for wood and suggested a method to determine Δh_g as a function of char depth [103].

Dillon et al. proposed six methods to calculate the heat of gasification [101]. The first three values are derived from Equation 27.29 and are equal to the reciprocal of the slope of a linear fit through data points of peak mass loss rate, average mass loss rate over the peak burning period, and average mass loss rate over the entire flaming period respectively plotted as a function of heat flux. The other three values are equal to the appropriate heat of combustion times the reciprocal of the slope of a linear fit through data points of first peak heat release rate, average heat release rate over the peak burning period, and average heat release rate over the entire flaming period respectively plotted as a function of heat flux.

Physically meaningful nonsteady values for Δh_g can be obtained from Equation 27.29, with $\dot{q}_f''$ and $\dot{q}_l''$ calculated from Equations 27.30 and

27.31, respectively. These calculations require values for h^*, ε_f, T_f, ε_s, and T_s. All parameters, except T_s, do not vary greatly during a test and can be estimated relatively easily [104]. T_s, however, may change significantly as a function of time. The surface temperature can be measured, but that presents some major challenges. Janssens obtained T_s as a function of time for wood specimens exposed in the cone calorimeter by solving the equation for heat conduction through the char layer using an integral technique. [100] The resulting values for Δh_g are consistent with a theoretical analysis [105] and calculated Δh_g values based on measured surface temperatures [106]. A drawback of this approach is that thermal properties of the material's char are needed.

The discussion in this subsection is useful in clarifying a common misconception. Often it is believed that materials used in a particular end-use orientation should be tested in that orientation. This is not necessarily correct. Heat release rate is independent of specimen orientation. However, the heat release rate in a calorimeter under otherwise identical conditions is higher in the horizontal than in the vertical orientation. This is because the heat feedback from the flame is much greater in the horizontal orientation. In that orientation, the flame is a relatively large volume of hot gas located above the specimen. The flame is a thin sheet in front of a vertical specimen, leading to a much lower heat feedback. However, neither of these situations is comparable to that in a real fire, where burning areas and flame volumes are much larger and heat flux from the flame is much higher regardless of orientation of the fuel surface.

Hence, the best approach is to interpret small-scale measurements in terms of material properties that are independent of the test apparatus. These material properties can then be used to predict full-scale performance using a method that accounts for the effect of the enhanced heat flux from large flames. The preceding reasoning indicates that small-scale testing in the vertical orientation is preferable, because the heat feedback to the flame is smaller and errors of flame flux estimates are relatively less important. However, for practical reasons, it is often preferable to run small-scale tests in the horizontal orientation to avoid problems with, for example, melting and dripping of the specimen.

The equation to calculate the total heat release rate in a room/corner test based on a model that relies on heat release rate properties has the following form:

$$\dot{Q}_t(t_N) = \dot{Q}_b(t_N) + \sum_{i=0}^{N} A_i \frac{\dot{q}''_{\text{net},i}(t_N)}{\Delta h_g} \Delta h_{c,\text{eff}} \tag{27.32}$$

where $\dot{q}''_{\text{net},i}$ is the net heat flux to A_i (kW/m^2). A room/corner test model of this type was developed by Quintiere [107].

Intermediate-Scale Calorimeter Data

Products that have joints or layered materials with a thickness exceeding 50 mm can generally not be tested in a small-scale calorimeter in a representative manner. The ICAL is suitable to obtain heat release rate data for these products. The ICAL also has some practical advantages over small-scale calorimeters for measuring $\Delta h_{c,\text{eff}}$ and Δh_g [106]. The four approaches discussed in the previous section can be used in support of a hazard assessment of such products based on ICAL data.

Furniture Calorimeter Data

The primary application of furniture calorimetry is to obtain heat release rate data for input into zone models such as CFAST. [108] Furniture calorimeters are designed to obtain data under free burning conditions. However, the heat release rate of a burning object inside a room might be higher due to heat feedback from the hot upper smoke layer and heated walls and ceiling. Although this effect is not very significant during the early stages of a compartment fire, it can become significant as the fire approaches flashover. Zone models are typically

not capable of accounting for this effect, except for some simple geometries for which the effect of external heat flux on burning rate can be calculated.

Industrial-Scale Calorimeter Data

Industrial-scale calorimeters can be used to obtain heat release rate data from large objects in support of the design of passive fire protection of structures. For example, heat release rates from motor vehicles have been measured in several laboratories throughout the world [109–115]. The data obtained in these tests were used to develop guidelines for passive fire protection of structural steel in parking garages.

Industrial-scale calorimeters are also used to determine the hazard classification of commodities. The level of active fire protection required to protect a warehouse is based on the hazard classification of the commodity stored in the warehouse. Standard methods for commodity classification have been developed in the United States and Sweden [116]. For example, FM 3995 describes a protocol to determine the hazard class of plastic pallets and other products. The commodity configuration consists of eight pallet loads of products, each measuring 1.1 m × 1.1 m × 1.1 m. The commodities are placed on a double-row rack segment in a standard 2 × 2 × 2 array with each pallet separated by 150 mm. The commodities are ignited at the bottom in the center of the array. Water is applied to the fire by a special applicator located 200 mm above the top surface of the commodity. The water is applied at the time that a sprinkler system located in a warehouse at 3 m above the commodity would activate. The activation time is calculated based on the convective heat release rate measured during the test and a sprinkler activation program akin to DETACT-QS [117]. Tests are performed at three different water application rates in the range of 0.11–0.39 gpm/ft^2 (4.5–15.9 mm/min) and the commodity is classified based on the heat release rates measured in the tests. The FM Global commodity classification system in ascending order of hazard is as follows:

- Class I: noncombustible products on wood pallets
- Class II: Class I products in slatted wooden crates, solid wooden boxes, multiple thickness corrugated cartons, or equivalent combustible packaging material on wood pallets
- Class III: packaged or unpackaged wood, paper, natural fiber cloth or products therefrom on wood pallets
- Class IV: Class I, II, or III products containing no more than 25 % by volume of expanded plastic or polyurethane or 15 % by weight of unexpanded plastic or polyurethane in ordinary corrugated cartons on wood plastic pallets
- Cartoned Group B unexpanded plastics
- Cartoned Group A expanded or unexpanded plastics
- Idle wood pallets

Uncertainty of Heat Release Rate Measurements

The objective of a measurement is to determine the value of the measurand, that is, the physical quantity that needs to be measured. Every measurement is subject to error, no matter how carefully it is conducted. The true value of a measurand is therefore unknowable because it cannot be measured without error. However, it is possible to estimate, with some confidence, the expected limits of error. This estimate, referred to as the uncertainty of the measurement, provides a quantitative indication of its quality.

The value of the measurand is generally not obtained from a direct measurement but is determined as a function (f) from N input quantities $X_1, X_2, \ldots, X_N$:

$$Y = f(X_1, X_2, \ldots, X_N) \tag{27.33}$$

where

Y = True value of the measurand

f = Functional relationship between measurand and input quantities

X_i = True values of the input quantities ($i = 1 \ldots N$)

The input quantities may be categorized as

- Quantities whose values and uncertainties are directly determined from single or repeated observation
- Quantities whose values and uncertainties are brought into the measurement from external sources such as reference data obtained from handbooks

An estimate of the value of the measurand, y, is obtained from Equation 27.34 using input estimates $x_1, x_2, \ldots, x_N$ for the values of the N input quantities:

$$y = f(x_1, x_2, \ldots, x_N) \tag{27.34}$$

The standard uncertainty of y is obtained by appropriately combining the standard uncertainties of the input estimates $x_1, x_2 \ldots, x_N$. If all input quantities are independent, the combined standard uncertainty of y is given by

$$u_c(y) = \sqrt{\sum_{i=1}^{N} \left[\left. \frac{\partial f}{\partial X_i} \right|_{x_i} \right]^2 u^2(x_i)} \equiv \sqrt{\sum_{i=1}^{N} [c_i u(x_i)]^2} \tag{27.35}$$

where

u = Standard uncertainty
u_c = Combined standard uncertainty
c_i = Sensitivity coefficients

The standard uncertainty of an input estimate x_i is obtained from the distribution of possible values of the input quantity X_i. There are two types of evaluations depending on how the distribution of possible values is obtained:

- A type A evaluation of standard uncertainty of x_i is based on the frequency distribution, which is estimated from a series of n repeated observations $x_{i,k}$ ($k = 1 \ldots n$):

$$u(x_i) \approx \sqrt{s^2(\overline{x}_i)} = \sqrt{\frac{s^2(x_i)}{n}} = \sqrt{\frac{\sum_{k=1}^{n} (x_{i,k} - \overline{x}_i)^2}{n(n-1)}} \tag{27.36}$$

- A type B evaluation of standard uncertainty of x_i is not based on repeated measurements but on an a priori frequency distribution. In this case, the uncertainty is determined from previous measurements, experience or general knowledge, manufacturer specifications, data provided in calibration certificates, uncertainties assigned to reference data taken from handbooks, and so on.

Equation 27.35 is referred to as the law of propagation of uncertainty and is based on a first-order Taylor series approximation of $Y = f(X_1, X_2, \ldots, X_N)$. When the nonlinearity of f is significant, higher-order terms must be included. When the input quantities are correlated, Equation 27.35 must be revised to include the covariance terms. The combined standard uncertainty of y is then calculated from

$$u_c(y) = \sqrt{\sum_{i=1}^{N} [c_i u(x_i)]^2 + 2 \sum_{i=1}^{N-1} \sum_{j=i+1}^{N} c_i c_j u(x_i) u(x_j) r(x_i, x_j)} \tag{27.37}$$

where $r(x_i, x_j)$ is the estimated correlation coefficient between X_i and X_j.

Because the values of the input quantities are not known, the correlation coefficient is estimated on the basis of the measured values of the input quantities. The combined standard uncertainty in Equation 27.37 is usually multiplied by a coverage factor to raise the

confidence level. A multiplier of 2 is often used, which corresponds to a confidence level of approximately 95 %.

Equation 27.37 can be used to calculate the uncertainty of heat release rate measurement based on oxygen consumption calorimetry. For example, Equation 27.15 provides the functional relationship between the measurand (heat release rate) and the input quantities. Assuming the mass flow rate in the exhaust duct is calculated from the differential pressure of and temperature at an orifice plate or bidirectional probe, the output and input quantities are defined as follows:

$$Y \equiv \dot{Q}, \quad X_1 \equiv E, \quad X_2 \equiv X_{O_2}^{A^e}, \quad X_3 \equiv \alpha, \\ X_4 \equiv C, \quad X_5 \equiv \Delta P, \quad X_6 \equiv T_e \tag{27.38}$$

C is the calibration coefficient, which relates the mass flow rate in the exhaust duct to the differential pressure and gas temperature measurements. In a test $\dot{Q}$ is calculated as a function of time based on the input quantities measured at discrete time intervals Δt. The uncertainty of the heat release rate measured at each time interval is estimated from Equation 27.37.

Dahlberg used this approach to determine the uncertainty of heat release rate measured in the industrial-size calorimeter at SP and reported values of ±7 % and ±12 % depending on the use of the CO correction, that is, for Equations 27.18 and 27.15, respectively [118]. Enright and Fleischmann reported an uncertainty of ±5 % for the cone calorimeter [119]. These uncertainties are significantly below the precision obtained from interlaboratory trials involving oxygen consumption calorimeters.

For example, a cone calorimeter round robin resulted in estimates for the peak heat release rate repeatability and reproducibility of 17 % and 23 %, respectively [120]. The discrepancies can be explained by the fact that the uncertainty analyses did not account for dynamic errors and specimen, operator, and heat flux variations. This is consistent with the calculations performed by Janssens, who accounted for the contribution from specimen variations and heat flux measurement errors and obtained an uncertainty of ±11 % for the peak heat release rate of a glass fiber–reinforced plastic measured in the cone calorimeter at a heat flux of 50 kW/m^2 [121].

Summary

Heat release rate is the single most important variable in fire hazard assessment. Various test methods have therefore been developed for measuring heat release rate of materials and products under different conditions. This chapter dealt with calorimeters of various sizes and the use and application of heat release measurements.

The discussion started with a description of the oxygen bomb calorimeter. The most significant limitation of this test is that it does not provide a quantitative measure of heat generation under realistic fire conditions.

The next section described four techniques that have been used to measure heat release rate in fire tests. The sensible enthalpy rise method is the least complicated. The substitution and compensation methods partly address the problem of thermal lag associated with sensible enthalpy rise measurements but require sophisticated control instrumentation. The oxygen consumption method, based on Thornton's rule, was developed in the late 1970s. It is currently the most popular method for measuring heat release rate in fire tests.

The effects of some calorimeter construction details on quality and accuracy of small-scale heat release rate measurements were discussed. Factors examined include configuration (open vs. closed), type of heater, type of ignition pilot, specimen size and orientation, edge effects, and airflow. Four commonly used small-scale calorimeters were briefly described: the Ohio State University calorimeter, the cone calorimeter, the fire propagation apparatus, and the microscale combustion calorimeter. This discussion was followed by a review of studies comparing different small-scale calorimeters.

The chapter continued with a description of the hood and exhaust duct that is specified in many intermediate- and large-scale calorimeter standards. This was followed by a description of

different calorimeters for measuring the heat release rate from chairs, mattresses, and other objects and from wall and ceiling finishes in a corner configuration. Some historical background was provided for the room/corner test. Industrial-scale calorimeters that can be used to measure multimegawatt heat release rates from large objects and commodities were also briefly discussed.

The next section discussed common applications of heat release rate data. Heat release rate data are used primarily in support of fire hazard assessment of materials and products. Small- and intermediate-scale data must be used in conjunction with a mathematical model to predict performance of materials and products in real fire scenarios. General concepts of four types of models were discussed using the room/corner test as an example of a real fire scenario:

- Correlations
- Models based on heat release rate data obtained at a single heat flux
- Models based on heat release rate data obtained at multiple heat fluxes
- Models based on heat release rate properties

Heat release rates measured in large- and industrial-scale calorimeters can be used directly in support of fire hazard assessment. For example, furniture calorimeter measurements can be used to generate heat release rate curves for input in zone models. Industrial-scale calorimeter data can be used to support the design of passive fire protection for structures or to obtain a hazard classification of a commodity.

The chapter concluded with a brief discussion of uncertainty of heat release rate measurements.

References

1. V. Babrauskas and R. Peacock, "Heat Release Rate: The Single Most Important Variable in Fire Hazard," *Fire Safety Journal,* 18, pp. 255–272 (1992).
2. E. Smith, "An Experimental Determination of Combustibility," *Fire Technology,* 7, pp. 109–119 (1971).
3. E. Smith, "Heat Release Rate of Building Materials," in *Ignition, Heat Release and Noncombustibility of Materials, ASTM STP 502,* American Society of Testing and Materials, Philadelphia, PA, pp. 119–134 (1972).
4. E. Smith, "Application of Release Rate Data to Hazard Load Calculations," *Fire Technology,* 10, pp. 181–186 (1974).
5. E. Smith and S. Satija, "Release Rate Model for Developing Fires," *ASME Journal of Heat Transfer,* 105, pp. 282–287 (1981).
6. V. Babrauskas, "Performance of the OSU Rate of Heat Release Apparatus Using PMMA and Gaseous Fuels," *Fire Safety Journal,* 5, pp. 9–20 (1982).
7. M. Janssens, "Critical Analysis of the OSU Room Fire Model for Simulating Corner Fires," in *Fire and Flammability of Furnishings and Contents, ASTM STP 1233,* American Society of Testing and Materials, Philadelphia, PA, pp. 169–185 (1994).
8. D. Evans and J. Breden, "Time Delay Correction for Heat Release Rate Data," *Fire Technology,* 14, pp. 85–96 (1978).
9. D. Bluhme and R. Getka, "Rate of Heat Release Test—Calibration, Sensitivity and Time Constants of ISO RHR Apparatus," NORDTEST Project 115-77, National Institute for Testing of Materials, Copenhagen, Denmark (1979).
10. P. Vandevelde, "An Evaluation of Heat Release Criteria in Reaction-to-Fire Tests," *Fire and Materials,* 4, pp. 157–162 (1980).
11. Abramowitz and R. Lyon, "Effect of Instrument Response Time on Heat Release Rate Measurements," *Fire and Materials,* 19, pp. 11–17 (1995).
12. R. Filipczak, and R. Lyon, "The Correlation of Heat Release Calorimetry Measurements," *DOT/FAA/AR-TN02/104*, FAA William J. Hughes Technical Center, Atlantic City International Airport, NJ (2002).
13. N. Thompson and E. Cousins, "The FM Construction Materials Calorimeter," *NFPA Quarterly,* 52, pp. 186–192 (1959).
14. J. Brenden, "Apparatus for Measuring Rate of Heat Release from Building Products," *Journal of Fire and Flammability,* 6, pp. 50–64 (1975).
15. W. Parker and M. Long, "Development of a Heat Release Rate Calorimeter at NBS," in *Ignition, Heat Release and Noncombustibility of Materials, ASTM STP 502,* American Society of Testing and Materials, Philadelphia (1972).
16. J. Tordella and W. Twilley, "Development of a Calorimeter for Simultaneously Measuring Heat Release and Mass Loss Rate," *NBSIR 83-2708,* National Bureau of Standards, Gaithersburg, MD (1983).
17. S. Martin, "Characterization of the Stanford Research Institute Large-Scale Heat Release Rate Calorimeter," *NBS-GCR 76-54,* National Bureau of Standards, Gaithersburg, MD (1975).
18. W. Thornton, "The Relation of Oxygen to the Heat of Combustion of Organic Compounds," *Philosophical Magazine and Journal of Science,* 33 (1917).
19. C. Huggett, "Estimation of the Rate of Heat Release by Means of Oxygen Consumption," *Fire and Materials,* 12, pp. 61–65 (1980).

20. W. Parker, "An Investigation of the Fire Environment in the ASTM E84 Tunnel Test," *NBS Technical Note 945,* National Bureau of Standards, Gaithersburg, MD (1977).
21. R. Walters, S. Hackett and R. Lyon, "Heats of Combustion of High Temperature Polymers," *Fire and Materials*, 24, pp. 245-252 (2000).
22. C. Gomez and M. Janssens, "Thornton's Constant Revisited," in *Proceedings of the 11th International Fire and Materials Conference*, Interscience Communications Limited, London, England, (2009).
23. H. Sawada, *Thermodynamics of Polymerization,* Marcel Dekker, New York (1976).
24. W. Parker, "Calculations of the Heat Release Rate by Oxygen Consumption for Various Applications," *NBSIR 81-2427,* National Bureau of Standards, Gaithersburg, MD (1982).
25. M. Janssens, "Measuring Rate of Heat Release by Oxygen Consumption," *Fire Technology,* 27, pp. 234–249 (1991).
26. S. Brohez, C. Delvosalle, G. Marlair, and A. Tewarson, "Soot Generation in Fires: An Important Parameter for Accurate Calculation of Heat Release," in *Proceedings of the 6th International Symposium,* International Association of Fire Safety Science, London, UK (2000).
27. B. Dlugogorski, J. Mawhinney, and V. Duc, "Measurement of Heat Release Rates by Oxygen Consumption Calorimetry in Fires under Suppression," in *Proceedings of the 4th International Symposium,* International Association for Fire Safety Science, London, UK (1994).
28. M. Werrel1, J. Deubel, S. Krüger, A. Hofmann and U. Krause, "The Calculation of the Heat Release Rate by Oxygen Consumption in a Controlled-Atmosphere Cone Calorimeter," *Fire and Materials,* 38, pp. 204-226, (2014).
29. P. Beaulieu and N. Dembsey, "Enhanced Equations for Carbon Dioxide and Oxygen Calorimetry," in *Proceedings of the 9th Fire and Materials Conference*, Interscience Communications, London, England., (2005).
30. S. Brohez and C. Delvosalle, "Carbon Dioxide Generation Calorimetry-Errors Induced by the Simplifying Assumptions in the Standard Test Methods," *Fire and Materials*, 33, pp. 89-97 (2009).
31. A. Roberts, "Ultimate Analysis of Partially Decomposed Wood Samples," *Combustion and Flame,* 8, pp. 345–346 (1964).
32. V. Babrauskas, "The Generation of CO in Bench-Scale Fire Tests and the Prediction for Real-Scale Fires," in *Proceedings of the 1st International Fire and Materials Conference,* Interscience Communications, London, UK (1992).
33. E. Buc, "Oxidizer Classification Research Project: Tests and Criteria," Fire Protection Research Foundation, Quincy, MA (2009).
34. M. Janssens, D. Ewan, C. Gomez, M. Hirschler, J. Huczek, R. Mason, K. Overholt and J. M. Sharp, "Reducing Uncertainty of Quantifying the Burning Rate of Upholstered Furniture", Final Report for Award No. 2010-DN-BX-K221, National Institute of Justice, Washington, DC (2012).
35. B. Lattimer and J. Beitel, "Evaluation of Heat Release Rate Equations Used in Standard Test Methods," *Fire and Materials,* 22, pp. 167–173 (1998).
36. V. Babrauskas and P. Thureson, "Short Communication: Drying Agents' Effects on CO_2 Readings," *Fire and Materials,* 18, pp. 201–268 (1994).
37. V. Babrauskas, "Development of the Cone Calorimeter—A Bench-Scale Heat Release Rate Apparatus Based on O_2 Consumption," *Fire and Materials,* 8, pp. 81–95 (1984).
38. J. Hallman, *Ignition of Polymers by Radiant Energy,* University of Oklahoma, Norman, OK (1971).
39. A. Koohyar, *Ignition of Wood by Flame Radiation,* University of Oklahoma, Norman, OK (1967).
40. D. Drysdale, *An Introduction to Fire Dynamics,* 2nd ed., John Wiley and Sons, Chichester, UK (1998).
41. B. Östman and R. Nussbaum, "Larger Specimens for Determining Rate of Heat Release in the Cone Calorimeter," *Fire and Materials,* 10, pp. 151–160 (1986).
42. M. Janssens and J. Urbas, "Comparison of Small and Intermediate Scale Heat Release Rate Data," in *Proceedings of Interflam '96,* Interscience Communications, London, UK (1996).
43. B. Toal, T. Shields, and G. Silcock, "Observations on the Cone Calorimeter," *Fire and Materials,* 14, pp. 73–76 (1989).
44. B. Toal, T. Shields, and G. Silcock, "Suitability and Preparation of Samples for the Cone Calorimeter," *Fire Safety Journal,* 16, pp. 85–88 (1990).
45. J. Urbas and H. Sand, "Some Investigations on Ignition and Heat Release of Building Materials Using the Cone Calorimeter," in *Proceedings of Interflam '90,* Interscience Communications, London, UK (1990).
46. J. deRis (2000). "Sample Holder for Determining Material Properties.," *Fire and Materials*, 24, pp. 219-226 (2000).
47. V. Babrauskas, W. Twilley, and W. Parker, "The Effect of Specimen Edge Conditions on Heat Release Rate," *Fire and Materials,* 17, pp. 51–63 (1993).
48. B. Östman and L. Tsantaridis, "Communication: Retainer Frame Effects on Cone Calorimeter Results for Building Products," *Fire and Materials,* 17, pp. 43–46 (1993).
49. V. Babrauskas, W. Twilley, M. Janssens, and S. Yusa, "A Cone Calorimeter for Controlled Atmosphere Studies," *Fire and Materials,* 16, pp. 37–43 (1992).
50. Y. Xin and M. Khan, "Flammability of Combustible Materials in Reduced Oxygen Environment," in *Proceedings of the 10th Fire and Materials Conference*, Interscience Communications, London, England (2007).
51. *Aircraft Material Fire Test Handbook,* DOT/FAA/CT-89/15, U.S. Department of Transportation,

Federal Aviation Administration, Atlantic City, NJ (1990).
52. In *Federal Register,* 51, Federal Aviation Administration, Washington, DC, pp. 26206–26221 (1986).
53. J. Blomqvist, "Rate of Heat Release of Building Materials, Experiments with an OSU Apparatus Using Oxygen Consumption," *LUTVDG/(TVBB-3017),* Lund University, Lund, Sweden (1983).
54. H. Tran, "Modifications to an Ohio State University Apparatus and Comparison with Cone Calorimeter Results," in *HTD,* Vol. 141, *Proceedings of the AIAA/ASME Thermophysics and Heat Transfer Conference,* American Society of Mechanical Engineers, New York (1990).
55. Y. Tsuchiya, "Methods of Determining Heat Release Rate," *Fire Safety Journal,* 5, pp. 49–57 (1982).
56. F. Hshieh and R. Buch, "Controlled-Atmosphere Cone Calorimeter Studies of Silicones," *Fire and Materials*, 21, pp. 265-272 (1997).
57. J. Leonard, P. Bowditch and V. Dowling, "Development of a Controlled-Atmosphere Cone Calorimeter," *Fire and Materials*, 24, pp. 143-150 (2000).
58. C. Gomez, A. Zalkin and M. Janssens, "Using the Cone Calorimeter for Quantifying Toxic Potency," in *Proceedings of Interflam 2010,* Interscience Communications, London, England (2010).
59. C. Gomez, M. Janssens and A. Zalkin, "Measuring Yields of Toxic Gases from Materials during Different Stages of Fire Development," in *Proceedings of the 12th Fire and Materials Conference,* Interscience Communications, London, England (2011).
60. A. Tewarson, "Heat Release Rates from Burning Plastics," *Journal of Fire and Flammability,* 8, pp. 115–130 (1977).
61. A. Tewarson, "Reliable Small-Scale Fire Testing Apparatus," *Modern Plastics,* 57, 11, pp. 58–62 (1980).
62. A. Tewarson and R. Pion, "Flammability of Plastics. I. Burning Intensity," *Combustion and Flame,* 26, pp. 85–103 (1976).
63. A. Tewarson, J. Lee, and R. Pion, "The Influence of Oxygen Concentration on Fuel Parameters for Fire Modeling," in *Proceedings of the 18th Symposium (International) on Combustion,* Combustion Institute, Pittsburgh, PA (1981).
64. B. Östman, G. Svensson, and J. Blomqvist, "Comparison of Three Test Methods for Measuring Rate of Heat Release," *Fire and Materials,* 9, pp. 176–184 (1985).
65. V. Babrauskas, "Comparative Rates of Heat Release from Five Different Types of Test Apparatuses," *Journal of Fire Sciences,* 4, pp. 148–159 (1986).
66. B. Kandola,, A. Horrocks, K. Padmore, J. Dalton and T. Owen, "Comparison of Cone and OSU Calorimetric Techniques to Assess the Flammability Behaviour of Fabrics Used for Aircraft Interiors," *Fire and Materials*, 30, pp. 241-255 (2006).
67. P. Gandhi, L. Caudill, and T. Chapin, "Comparison of Cone Calorimeter Data with FM 3972 for Communication Cables," in *Proceedings of the 5th International Fire and Materials Conference and Exhibition,* Interscience Communications, London, UK (1998).
68. J. Carman, D. Price, G. Milnes, and D. Purser, "Comparison of Heat Release Rates as Measured by Oxygen Depletion and Thermopile Techniques," in *Proceedings of Interflam'99,* Interscience Communications, London, UK (1999).
69. R. Lyon, "Heat Release Kinetics," *Fire and Materials,* 24, pp. 179-186 (2000).
70. R. Lyon, "Plastics and Rubber," in *Handbook of Building Materials for Fire Protection*, (C. Harper, ed.), McGraw-Hill.: New York, NY, pp. 3.1-3.51 (2004).
71. R. Lyon and M. Janssens, "Polymer Flammability" in *Encyclopedia of Polymer Science & Engineering (On-line Edition)*, John Wiley & Sons: New York, NY (2005).
72. R. Lyon, R. Walters and S. Stoliarov, "A Thermal Analysis Method for Measuring Polymer Flammability," *Journal of ASTM International*, 3, pp. 1-18 (2006).
73. R. Lyon, R. Walters, N. Safronava and S. Stoliarov, "In A Statistical Model for the Results of Flammability Tests," in *Proceedings of the 11th International Fire and Materials Conference*, Interscience Communications Limited, London, England, pp. 141-159 (2009).
74. L. Cooper, "Some Factors in the Design of a Calorimeter Hood and Exhaust," *Journal of Fire Protection Engineering,* 6, pp. 99–112 (1994).
75. P.H. Thomas, P.L. Hinkley, C.R. Theobald, and D.L. Simms, *Fire Technical Paper No. 7,* H.M. Stationary Office, Joint Fire Research Organization, London, UK (1963).
76. V. Babrauskas, J. Lawson, W. Walton, and W. Twilley, "Upholstered Furniture Heat Release Rates Measured with a Furniture Calorimeter," *NBSIR 82-2604,* National Bureau of Standards, Gaithersburg, MD (1982).
77. S. Ames and S. Rogers, "Large and Small Scale Fire Calorimetry Assessment of Upholstered Furniture," in *Proceedings of Interflam '90,* Interscience Communications, London, UK (1990).
78. J, Ezinwa, J. Rigg, D. Torvi and E. Weckman "Effects of Ignition Location on Flame Spread and Heat Release Rates in Furniture Calorimeter Tests of Polyurethane Foams," in Proceedings of the 11th International Fire and Materials Conference, pp. 645-656 (2009).
79. T. Ohlemiller, "Flammability Tests of Full-Scale Mattresses: Gas Burners versus Burning Bedclothes," *NISTIR 7006,* National Institute of Standards and Technology, Gaithersburg, MD (2003).
80. T. Ohlemiller and R. Gann, "Effect of Bed Clothes Modifications on Fire Performance of Bed Assemblies," *NIST Technical Note 1449,* National

Institute of Standards and Technology, Gaithersburg, MD (2003).
81. T. Ohlemiller, T. Shields, A. McLane, and R. Gann, "Flammability Assessment Methodology for Mattresses," *NISTIR 6497,* National Institute of Standards and Technology, Gaithersburg, MD (2000).
82. T. Ohlemiller and K. Villa, "An Investigation of the California Technical Bulletin 133 Test, Part II: Characteristics of the Ignition Source and a Comparable Gas Burner," *NBSIR 90-4348,* National Bureau of Standards, Gaithersburg, MD (1990).
83. W. Parker, K. Tu, S. Nurbakhsh, and G. Damant, "An Investigation of the California Technical Bulletin 133 Test, Part III: Full Scale Chair Burns," *NBSIR 90-4375,* National Bureau of Standards, Gaithersburg, MD (1990).
84. J. Krasny and W. Parker, "Impact of the Room Enclosure on the Peak Heat Release Rates of Upholstered Furniture," in *Proceedings of the Fire and Materials 4th International Conference and Exhibition,* Interscience Communications, London, UK (1995).
85. I. Benjamin, "Development of a Room Fire Test," in *Fire Standards and Safety, ASTM STP 614,* American Society of Testing and Materials, Philadelphia (1977).
86. F. Fisher and R. Williamson, "Intralaboratory Evaluation of a Room Fire Test Method," *NBS GCR 83-421,* National Bureau of Standards, Gaithersburg, MD (1983).
87. C. Lee, "Standard Room Fire Test Development at the National Bureau of Standards," in *Fire Safety: Science and Engineering, ASTM STP 882,* American Society of Testing and Materials, Philadelphia, pp. 29–42 (1985).
88. B. Sundström and U. Wickström, "Fire: Full Scale Tests," *SP-RAPP,* 14, National Testing Institute (SP), Borås, Sweden (1980).
89. B. Sundström and U. Wickström, "Fire: Full Scale Tests, Calibration of Test Room," *SP-RAPP,* 48, National Testing Institute (SP), Borås, Sweden (1981).
90. A. Ahonen, C. Holmlund, and M. Kokkala, "Effects of Ignition Source in Room Fire Tests," *Fire Science and Technology,* pp. 1–13 (1987).
91. J. Zhang, M. Delichatsios and, M. Colobert, "Assessment of Fire Dynamics Simulator for Heat Flux and Flame Heights Predictions from Fires in SBI Tests," *Fire Technology*, 46, pp. 291-306 (2010).
92. E. Smith, N. Marshall, K. Shaw, and S. Colwell, "Correlating Large-Scale Fire Performance with the Single Burning Item Test," in *Proceedings of Interflam'01, 9th International Fire Conference,* Interscience Communications, London, UK (2001).
93. G. Heskestad, "A Fire Products Collector for Calorimetry into the MW Range," *Technical Report FMRC J.I0C2E1.RA,* Factory Mutual Research Corporation, Norwood, MA (1981).
94. M. Dahlberg, "The SP Industry Calorimeter—For Rate of Heat Release Rate Measurements up to 10 MW," *SP Report,* 43, National Testing Institute (SP), Borås, Sweden (1992).
95. B. Östman and L. Tsantaridis, "Correlation Between Cone Calorimeter Data and Time to Flashover in the Room Fire Test," *Fire and Materials,* 18, pp. 205–209 (1994).
96. V. Babrauskas, "Specimen Heat Fluxes for Bench-Scale Heat Release Rate Testing," *Fire and Materials,* 19, pp. 243–252 (1995).
97. U. Wickström and U. Göransson, "Full-Scale/Bench-Scale Correlations of Wall and Ceiling Linings," *Fire and Materials,* 16, pp. 15–22 (1992).
98. E. Smith and T. Green, "Release Rate Tests for a Mathematical Model," in *Mathematical Modeling of Fires, ASTM STP 983,* American Society of Testing and Materials, Philadelphia (1987).
99. H. Mitler, "Predicting the Spread Rates of Fires on Vertical Surfaces," in *Proceedings of the 23rd Symposium (International) on Combustion,* Combustion Institute, Pittsburgh, PA (1991).
100. M. Janssens, "Cone Calorimeter Measurements of the Heat of Gasification of Wood," in *Proceedings of Interflam '93,* Interscience Communications, London, UK (1993).
101. S. Dillon, W. Kim, and J. Quintiere, "Determination of Properties and the Prediction of the Energy Release Rate of Materials in the ISO 9705 Room-Corner Test," *NIST-GCR-98-753,* National Institute of Standards and Technology, Gaithersburg, MD (1998).
102. V. Petrella, "The Mass Burning Rate of Polymers, Wood and Liquids," *Journal of Fire and Flammability,* 11, pp. 3–21 (1980).
103. M. Janssens, *Thermophysical Properties of Wood and Their Role in Enclosure Fire Growth,* University of Ghent, Ghent, Belgium (1991).
104. J. Urbas and W. Parker, "Surface Temperature Measurements on Burning Wood Specimens in the Cone Calorimeter and Effect of Grain Orientation," *Fire and Materials,* 17, pp. 205–208 (1993).
105. M. Sibulkin, "Heat of Gasification for Pyrolysis of Charring Materials," in *Proceedings of the 1st International Symposium on Fire Safety Science,* International Association for Fire Safety Science, London, UK (1985).
106. J. Urbas, "Non-Dimensional Heat of Gasification Measurements in the Intermediate Scale Rate of Heat Release Apparatus," *Fire and Materials,* 17, pp. 119–123 (1993).
107. J. Quintiere, "A Simulation Model for Fire Growth on Materials Subject to a Room-Corner Test," *Fire Safety Journal,* 20, pp. 313–339 (1992).
108. R. Peacock, P. Reneke, W. Jones, R. Bukowski, and G. Forney, "A User's Guide for CFAST: Engineering Tools for Fire Growth and Smoke Transport," *Special Publication 921,* National Institute of Standards and Technology, Gaithersburg, MD (2000).

109. J. Mangs and O. Keski-Rahkonen, "Characterization of the Fire Behavior of a Burning Passenger Car. Part I: Car Fire Experiments," *Fire Safety Journal,* 23, pp. 17–35 (1994).
110. M. Shipp and M. Spearpoint, "Measurements of the Severity of Fires Involving Private Motor Vehicles," *Fire and Materials,* 19, pp. 143–151 (1995).
111. C. Joyeux, "Natural Fires in Closed Car Parks," INC-96/294d-DJ/NB, Centre Technique Industriel de la Construction Métallique (CTICM), Saint-Aubin, France (1997).
112. C. Steinert, "Experimental Investigation of Burning and Fire Jumping Behavior of Automobiles (in German)," *VFDB Journal*, 49, pp. 163–172 (2000).
113. C. Joyeux, J. Kruppa, L. Cajot, J. Schleich, P. van de Leur, and L. Twilt, "Demonstration of Real Fire Tests in Car Parks and High Buildings," Centre Technique Industriel de la Construction Métallique (CTICM), Saint-Aubin, France (2002).
114. Y. Shintani, N. Kakae, K. Harada, H. Masuda, and W. Takahashi, "Experimental Investigation of Burning Behavior of Automobiles," in *Proceedings of the 6th Asia-Oceania Symposium on Fire Science and Technology,* International Association for Fire Safety Science, London, UK (2004).
115. B. Zhao and J. Kruppa, "Structural Behavior of an Open Car Park Under Real Fire Scenarios," *Fire and Materials,* 28 (2004).
116. H. Persson, "Commodity Classification—A More Objective and Applicable Methodology," *SP Report,* 70, National Testing Institute (SP), Borås, Sweden (1993).
117. D. Evans and D. Stroup, "Methods to Calculate the Response Time of Heat and Smoke Detectors Installed Below Large Unobstructed Ceilings," *NBSIR 85-3167,* National Bureau of Standards, Gaithersburg, MD (1985).
118. M. Dahlberg, "Error Analysis for Heat Release Rate Measurements with the SP Industry Calorimeter," *SP Report,* 29, National Testing Institute (SP), Borås, Sweden (1994).
119. P. Enright and C. Fleischmann, "Uncertainty of Heat Release Rate Calculation of the ISO 56601—Cone Calorimeter Standard Test Method," *Fire Technology,* 35, pp. 153–169 (1999).
120. J. Urbas, "BDMC Interlaboratory Cone Calorimeter Test Program," *Fire and Materials,* 26, pp. 29–35 (2002).
121. M. Janssens, "Uncertainty of Fire Test Results," in *Proceedings of Interflam '07,* Interscience Communications, London, UK (2007).

Codes and Standards

16 CFR 1633, *Standard for the Flammability (Open Flame) of Mattresses and Mattress/Foundation Sets,* Consumer Products Safety Commission, Washington, DC (2006).
ASTM D3173, *Standard Test Method for Moisture in the Analysis Sample of Coal and Coke*, ASTM International, West Conshohocken, PA.
ASTM D5373, *Standard Test Methods for Instrumental Determination of Carbon, Hydrogen, and Nitrogen in Laboratory Samples of Coal*, ASTM International, West Conshohocken, PA.
ASTM D5865, *Standard Test Method for Gross Calorific Value of Coal and Coke,* ASTM International, West Conshohocken, PA (2007).
ASTM D7309, *Standard Test Method for Determining Flammability Characteristics of Plastics and Other Solid Materials Using Microscale Combustion Calorimetry,* ASTM International, West Conshohocken, PA (2007).
ASTM E906, *Standard Test Method for Heat and Visible Smoke Release Rates for Materials and Products,* ASTM International, West Conshohocken, PA (2007).
ASTM E1317, *Standard Test Method for Flammability of Marine Surface Finishes,* ASTM International, West Conshohocken, PA (2008).
ASTM E1354, *Standard Test Method for Heat and Visible Smoke Release Rates for Materials and Products Using an Oxygen Consumption Calorimeter,* ASTM International, West Conshohocken, PA (2008).
ASTM E1537, *Standard Test Method for Fire Testing of Upholstered Furniture,* ASTM International, West Conshohocken, PA (2007).
ASTM E1590, *Standard Test Method for Fire Testing of Mattresses,* ASTM International, West Conshohocken, PA (2007).
ASTM E1623, *Test Method for Determination of Fire and Thermal Parameters of Materials, Products, and Systems Using an Intermediate Scale Calorimeter (ICAL),* ASTM International, West Conshohocken, PA (2004).
ASTM E1822, *Standard Test Method for Fire Testing of Stacked Chairs,* ASTM International, West Conshohocken, PA (2007).
ASTM E2058, *Standard Test Methods for Measurement of Synthetic Polymer Material Flammability Using a Fire Propagation Apparatus,* ASTM International, West Conshohocken, PA (2006).
ASTM E2067, *Standard Practice for Full-Scale Oxygen Consumption Calorimetry Fire Tests,* ASTM International, West Conshohocken, PA (2008).
ASTM E2257, *Standard Test Method for Room Fire Test of Wall and Ceiling Materials and Assemblies,* ASTM International, West Conshohocken, PA (2008).
CAL TB 133, *Flammability Test Procedure for Seating Furniture for Use in Public Occupancies,* California Bureau of Home Furnishings and Thermal Insulation, North Highlands, CA (1991).
CAL TB 603, *Requirements and Test Procedure for Resistance of a Mattress/Box Spring Set to a Large Open-Flame,* California Bureau of Home Furnishings and Thermal Insulation, North Highlands, CA (2004).

EN 13501, *Fire Classification of Construction Products and Building Elements—Part 1: Classification Using Test Data from Reaction-to-Fire Tests,* European Committee for Standardization (CEN), Brussels, Belgium (2002).

EN 13823, *Reaction to Fire Tests for Building Products—Building Products Excluding Flooring Exposed to the Thermal Attack of a Single Burning Item,* European Committee for Standardization (CEN), Brussels, Belgium (2002).

FM 4995, *Approval Standard for Commodity Classification of Idle Plastic Pallets,* FM Global Research, Norwood, MA (1992).

ISO 1716, *Reaction to Fire Tests for Building Products—Determination of the Calorific Value,* International Organization for Standardization, Geneva, Switzerland (2002).

ISO 5660-1, *Reaction-to-Fire Tests—Heat Release, Smoke Production and Mass Loss Rate—Part 1: Heat Release Rate (Cone Calorimeter Method),* International Organization for Standardization, Geneva, Switzerland (2002).

ISO 5660-2, *Reaction-to-Fire Tests—Heat Release, Smoke Production and Mass Loss Rate—Part 2: Smoke Production Rate (Dynamic Measurement),* International Organization for Standardization, Geneva, Switzerland (2002).

ISO 9705, *Fire Tests—Reaction-to-Fire—Room Fire Test,* International Organization for Standardization, Geneva, Switzerland (1993).

NFPA *101®, Life Safety Code®,* National Fire Protection Association, Quincy, MA (2006).

NFPA 220, *Standard on Types of Building Construction,* National Fire Protection Association, Quincy, MA (2006).

NFPA 259, *Standard Test Method for Potential Heat of Building Materials,* National Fire Protection Association, Quincy, MA (2003).

NFPA 265, *Standard Methods of Fire Tests for Evaluating Room Fire Growth Contribution of Textile Coverings on Full Height Panels and Walls,* National Fire Protection Association, Quincy, MA (2007).

NFPA 271, *Standard Method of Test for Heat and Visible Smoke Release Rates for Materials and Products Using an Oxygen Consumption Calorimeter,* National Fire Protection Association, Quincy, MA (2004).

NFPA 286, *Standard Methods of Fire Tests for Evaluating Contribution of Wall and Ceiling Interior Finish to Room Fire Growth,* National Fire Protection Association, Quincy, MA (2006).

NFPA 5000®, Building Construction and Safety Code®, National Fire Protection Association, Quincy, MA (2006).

NT Fire 032, *Upholstered Furniture, Burning Behavior—Full-Scale Test,* NORDTEST, Helsinki, Finland (1991).

Dr. Marc Janssens is a Senior Engineer at Southwest Research Institute in San Antonio, Texas. His research has focused on computer fire modeling, fire hazard and risk assessment, fire test standards development, and the experimental and theoretical evaluation of material flammability with emphasis on heat release calorimetry.

The Cone Calorimeter

28

Vytenis Babrauskas

Introduction

Chapter 27 describes the history and development of techniques for measuring heat release rate (HRR). This chapter outlines features and details of today's preferred instrument for measuring bench-scale HRR—the cone calorimeter. Other cone calorimeter measuring functions are

1. Effective heat of combustion
2. Mass loss rate
3. Ignitability
4. Smoke and soot
5. Toxic gases

The cone calorimeter is based on the concept of oxygen consumption calorimetry, which is also presented in Chap. 27.

This chapter provides both an introduction to and description of cone calorimeter measurement technology. The cone calorimeter has recently assumed a dominant role in bench-scale fire testing of various products; therefore, an emphasis will be placed on the *why* of various design features. When conducting tests, the cone calorimeter operator needs to consult several other documents. Testing will presumably be in conformance with either ISO 5660 [1] or ASTM E1354 [2]. In addition, the "User's Guide for the Cone Calorimeter" [3] should be consulted. This chapter does not emphasize the operational aspects documented in these references but instead provides the reader with an overall feel for the equipment. Space is not available in this handbook to fully discuss the applications of cone calorimeter data, apart from the review of data given in Chap. 26. Extensive guidance on using cone calorimeter data is given in a textbook on this subject [4]. It also provides example data compilations and information on using cone calorimeter data for predictions of fires.

Summary of Features

A schematic view of the cone calorimeter is shown in Fig. 28.1. Figure 28.2 shows a commercial instrument, and Fig. 28.3 identifies some of the major components. The more salient operational features and limits of the apparatus are

Specimen size	100 × 100 mm, thickness of 6–50 mm
Specimen orientation	Horizontal, face up (standard testing) or vertical (reserved for exploratory studies)
Specimen back-face conditions	Very low loss insulating ceramic fibrous material
Load cell live load capacity	500 g
Load cell tare capacity	3.5 kg
Load cell resolution	0.005 g
Ignition	Electric spark
Heating flux range	0–110 $kW \cdot m^{-2}$
Flux uniformity, horizontal	Typically 2 %
Flux uniformity, vertical	Typically 7 %

(continued)

V. Babrauskas (✉)
Fire Science and Technology Inc.

M.J. Hurley (ed.), *SFPE Handbook of Fire Protection Engineering*,
DOI 10.1007/978-1-4939-2565-0_28, © Society of Fire Protection Engineers 2016

Sensing principle	Oxygen consumption, only
Maximum instantaneous output	In excess of 20 kW
Normally calibrated range	0–12 kW
Linearity over 0–12 kW range	5 %
Noise intrinsic to oxygen meter	20 ppm O_2
Noise in HRR measurement, over 0–12 kW range	2.5 %
Smoke meter operating range	0–20 m^{-1} (linear)
Smoke meter resolution	0.01 m^{-1}
Soot sampler mass fraction range	0–1 part in 200 (of exhaust gas flow)

Uses of Cone Calorimeter Data

Cone calorimeter data are primarily used for four purposes:

1. comparative evaluation of materials;
2. obtaining of thermophysical constants (fire properties) of materials;
3. as input data to fire models or engineering calculation;
4. for regulatory compliance.

Comparative Evaluation of Materials

Comparative evaluation of materials is the easiest and simplest use of cone calorimeter data. This, in fact, is also where the largest amount of published literature involving cone calorimeter data is found, of which the fire retardants field is a prominent example. There have been hundreds of papers published examining fire retardant formulations with the use of the cone calorimeter. For such studies, modeling or large-scale testing is inappropriate, since the

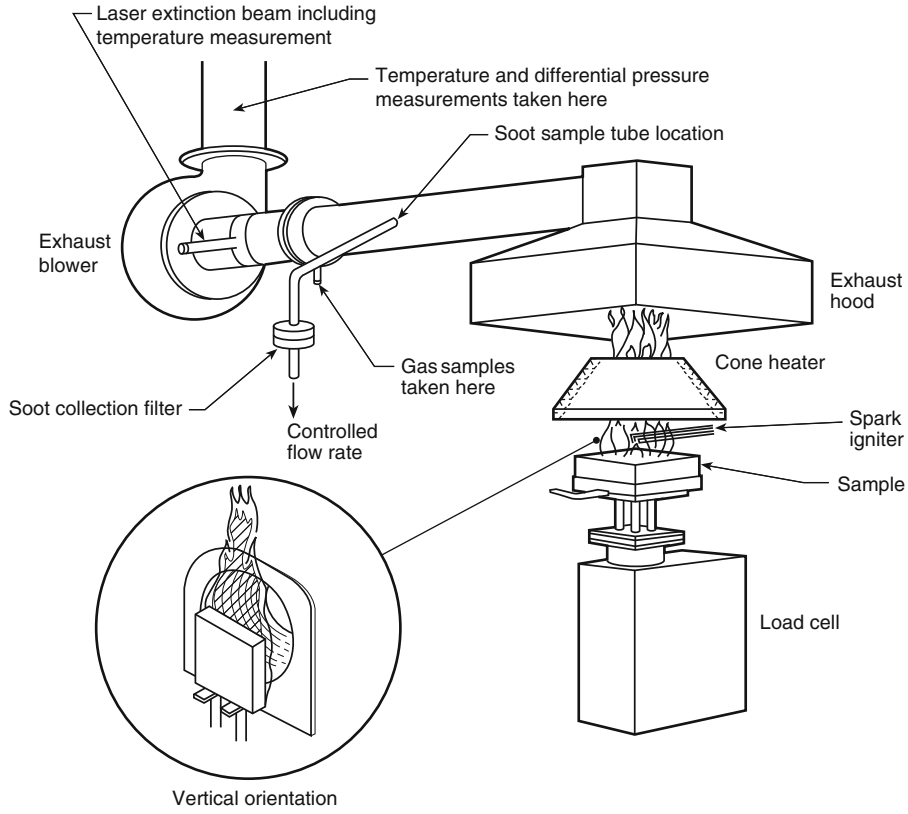

Fig. 28.1 Schematic view of the cone calorimeter

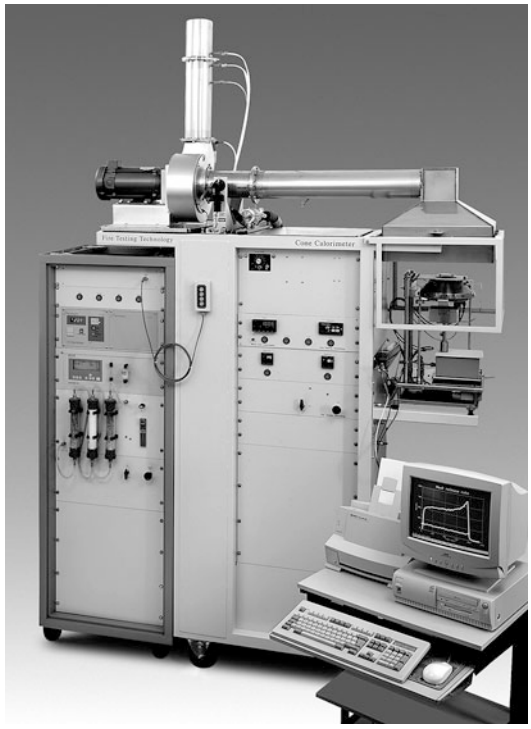

Fig. 28.2 A commercial cone calorimeter (Photo courtesy Fire Testing Technology, Ltd.)

same polymer formulation can be used for a wide array of products. Thus, cone calorimeter data are normally used and a comparative evaluation is made. Most commonly, candidate materials are evaluated simply by comparing their peak HRR values. This approach is not adequate if flame spread in the real-life environment is significant, i.e., if the material is not quickly ignited over its entire face. For taking flame spread into account, albeit in a simplified way, Babrauskas [5] proposed in 1984 that the variable $\dot{q}''/t_{ig}$ be used, which is the ratio of the HRR value to the ignition time. The ignition time was shown to be correlated to flame spread rate, thus, this hazard parameter increases with both increasing HRR and increasing propensity for rapid flame spread. A reasonable semi-quantitative prediction of the time to flashover was possible using this ratio for various wall lining materials. Petrella [6] later proposed a modified rating system where $\dot{q}''/t_{ig}$ is plotted on one axis, while total heat released is plotted on the other. Materials of better performance have both a low $\dot{q}''/t_{ig}$ value and a low total heat release. The most refined scheme

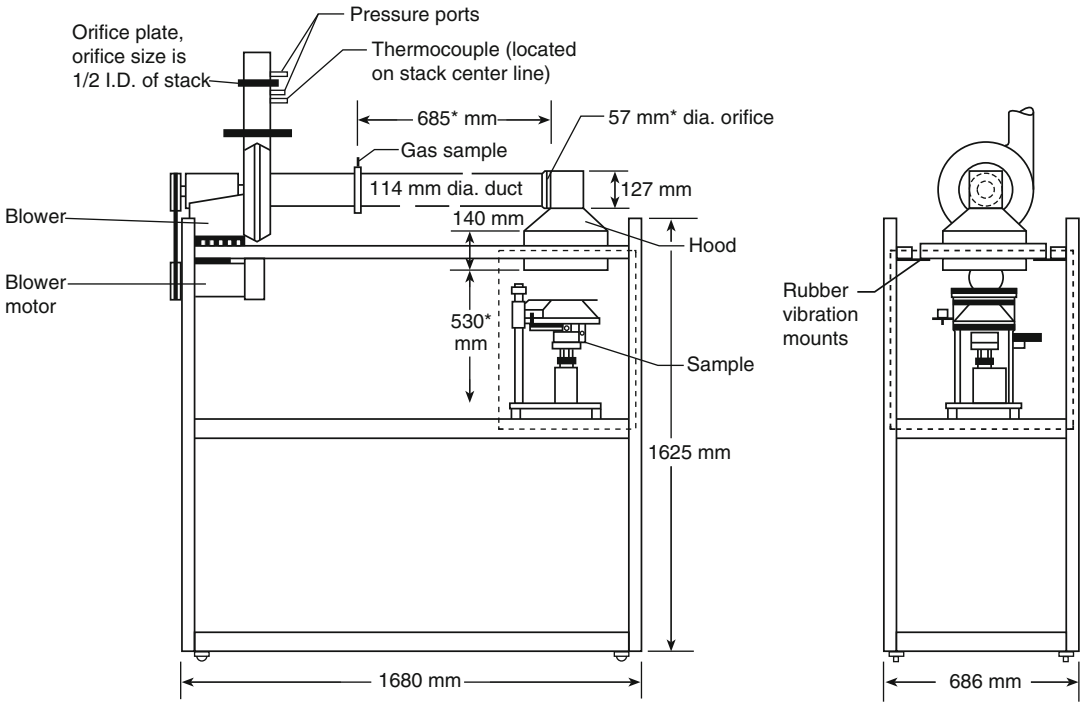

*Indicates a critical dimension

Fig. 28.3 View of major components of the cone calorimeter

which is still simple is the one put forth in 1991 by Cleary and Quintiere [7]. They introduced a parameter b:

$$b = 0.01\dot{q}''_{avg} - 1 - \frac{t_{ig}}{t_b} \qquad (28.1)$$

where $\dot{q}''_{avg}$ = average HRR (kW m^{-2}) at a 50 kW m^{-2} irradiance, t_{ig} = ignition time (s), and t_b = duration of flaming (s). They showed that materials which show $b < -0.4$ have negligible propensity to spread fire, while those with progressively higher values show increased hazard in full-scale applications. The Cleary/Quintiere b is not to be confused with Spalding's B number, sometimes use to characterize hazards of burning liquids.

Obtaining Thermophysical Constants of Materials

The HRR of materials cannot be computed from some ostensibly simple material fire properties, but is rather a complex relationship governed by chemical (reaction kinetics), thermal (heat transfer properties), and mechanical (cracking, delamination, etc.) properties. Thus, in general, it is not possible to deduce some underlying material fire properties from HRR data. However, the situation is more amenable for ignition data, where it is possible to obtain fire properties from cone calorimeter data. This topic is treated at length in the *Ignition Handbook* [8], but here the most useful computation will be identified. For thermally thick materials, Janssens derived the relationship:

$$\dot{q}''_e = \dot{q}''_{cr}\left[1 + 0.73\left(\frac{\lambda\rho C}{h^2_{eff}t_{ig}}\right)^{0.55}\right] \qquad (28.2)$$

According to this, if experimental data are plotted (Fig. 28.4) such that $\dot{q}''_e$ is put on the x-axis and $t_{ig}^{-0.55}$ on the y-axis, then the data will fall in a straight line, with the x-axis intercept being $\dot{q}''_{cr}$. Here $\dot{q}''_e$ = irradiance (kWm^{-2}), $\dot{q}''_{cr}$ = x-axis intercept, t_{ig} = ignition time (s), and $\lambda\rho C$ is the thermal inertia (kJ^2 m^{-4} s^{-1} K^{-2}) of the specimen. From such a plot, the value of thermal inertia can be computed, which is an effective fire property of importance in both ignition and flame spread problems.

Input Data for Fire Models or Calculations

A number of correlational schemes for making engineering calculations on various types of commodities have been developed which are

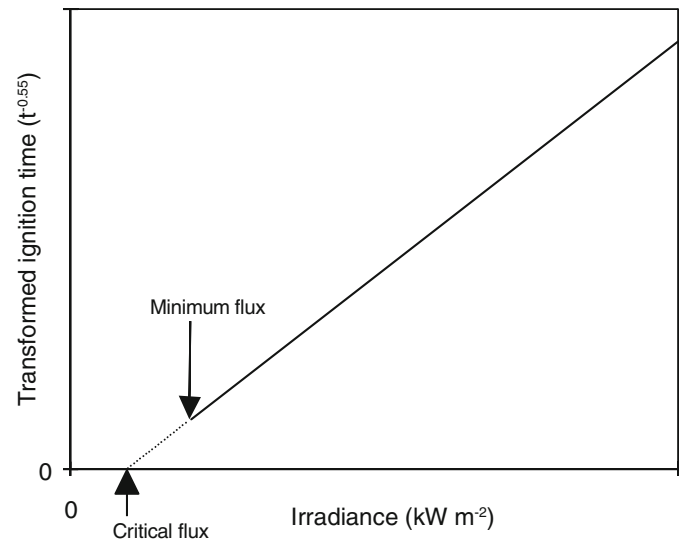

Fig. 28.4 The main variables of the ignitability plot

based on Cone Calorimeter data. These are reviewed in Chap. 26. For more refined models, i.e., zone or CFD models for room fires, the application is more difficult. This is because the HRR is strongly a function of the irradiance. But in most real fires, the irradiance received by any particular locale is a dynamic function of time and is not a constant. Because of this difficulty, it has become more common for modern-day computer codes, e.g., FDS, to adopt a pyrolysis model, rather than using small-scale experimental HRR data as an input. A pyrolysis model effectively is a scheme where the HRR of a small area of material is computed from some sort of input data. But, as discussed above, for realistic materials there generally is no simple series of expression that would be able to predict the HRR, based on the input of a modest collection of constants. Even if the constants can be defined, they must in turn be obtained from experiments, and this is already known to be difficult in the first place. CFD models however may have an option to input small-scale HRR data; typically in that case the HRR at a fixed irradiance is used. Capote et al. [9] illustrated such an approach in modeling train fires with FDS. Aksit et al. [10] described use of cone calorimeter input data for modeling cable tray fires with SOFIE, while Andersson [11] described a more general effort with SOFIE. Tsai et al. [12] described a proprietary CFD model using cone calorimeter data; the model was used solely for calculating ignition behavior of materials.

For zone fire models, the most successful example has been the BRANZfire model of Wade [13–15]. Lattimer et al. [16] described a module for CFAST based on cone calorimeter input data. Janssens and Dillon [17] described a simple room fire model based on cone calorimeter data. Cone calorimeter data have also been used in an application simpler than room fires, the prediction of upward flame spread on vertical panels [18–23].

For some models, it is necessary to know the total heat flux incident on the specimen, not just the external heat flux; the total heat flux is comprised of the external heat flux, plus the flame flux. Hostikka and Axelsson [24] showed an interesting example of CFD modeling by predicting the flame flux in the cone calorimeter.

Regulatory Compliance

The New Zealand building code specifies use of the ISO version of the cone calorimeter standard, ISO 5660 [1], for external wall cladding products. The Building Code of Australia uses cone calorimeter testing to assess fire retardant treated wood for use in bushfire-prone areas. The building code of Japan uses cone calorimeter testing extensively, as a primary measure of the fire performance of surface lining materials [25]. In their application, tests are run at 50 kW m^{-2} irradiance for a duration of 5, 10, or 20 min, depending on the classification sought. In each case, a peak HRR value below 200 kW m^{-2} must be found, with the total heat release being less than 8 MJ m^{-2}, with the latter being a particularly onerous requirement. Taiwan has also adopted similar provisions. IMO, the International Maritime Organization, which provides the regulations for constructing of sea-going vessels, uses cone calorimeter testing for acceptance of "fire restricting material" for high-speed craft in the case of furniture and related materials.

Operating Principle

It is emphasized at this point that the cone calorimeter has been designed to use *only* oxygen consumption calorimetry as its measurement principle [26]. Other calorimeters that on occasion use oxygen consumption principles, for example, the Factory Mutual Research Corporation (FMRC) flammability apparatus (Chap. 27), sometimes incorporate a sensible enthalpy flow measurement technique to arrive at the *convective component* of the heat release rate. In the design of the cone calorimeter, such an approach was deemed to be misleading. The implicit assumption behind this type of measurement is that the fraction of the total heat release being

manifest as the sensible flow enthalpy is a property of the material being tested. Such is not, in fact, the case. The convective fraction is dependent on details of the apparatus design and also on the scale of the specimen [27].

Where high-quality results are required, such as in the cone calorimeter, current-day practice demands that a paramagnetic oxygen analyzer be used. The various manufacturers use measuring schemes that differ in detail, but all rely on the same paramagnetic principle whereby the sensing element is sensitive to the partial pressure of oxygen in the cell. The most significant interferents to this detection principle are NO and NO_2, both of which show a strong paramagnetic response, but not as strong as that of oxygen. Interferents are never a problem in fire testing, however, since O_2 levels measured are 10–21%, whereas concentrations of NO_x are rarely above 100 ppm.

Unlike in applications where oxygen levels are monitored as simply one of many indications of fire hazard, in HRR work it is essential that the instrumentation be designed for the highest possible resolution. Thus, both the ASTM and ISO standards specify that the short-term noise + drift of the oxygen analyzer must be less than or equal to 50 ppm O_2. The best-grade commercial instruments are able to meet a 20 ppm O_2 limit. In addition, the standards provide a significant amount of detail on the layout of the gas sampling system, including desiccation, mass flow control, and bypass flows. All of these aspects have to be in conformance with the specifications for good repeatability and reproducibility performance (see Fig. 28.3) to be achieved.

Because the detection principle responds to oxygen partial pressure, there needs to be a compensation for changes in atmospheric pressure, either with a mechanical back-pressure regulator or by measuring the pressure and correcting electrically. Without compensation, there can be significant error in the calculated heat release rate. Carbon dioxide, the other major component expected to be in the oxygen analyzer, causes less than 0.3 % error in the oxy-gen reading. Extensive practice advice on selecting, setting up, and calibrating oxygen analysis systems is given in Twilley and Babrauskas [3] and in Babrauskas and Grayson [4].

The Radiant Heater

After establishing the operating principle, the next most important feature is the type of heater. In general, such a heater should be able to achieve adequately high irradiances, have a relatively small convective heating component, present a highly uniform irradiance over the entire exposed face of the specimen, and be designed so as not to change its irradiance when the main voltage varies, when heater element aging occurs, or when the apparatus retains some residual heat from the exposure given to a prior specimen.

Range of Heat Fluxes Needed for Testing A room fire burning near its maximum rate can show gas temperatures over 1000 °C, producing corresponding irradiances to walls and contents of 150 $kW \cdot m^{-2}$. Testing under such extreme conditions may not be required; nonetheless, if postflashover fires are to be simulated, irradiances of over 75 $kW \cdot m^{-2}$ should be available, and preferably closer to 100 $kW \cdot m^{-2}$. A significant convective component would negate the purpose of having a radiant ignition test. Rather low convective fluxes can be achieved for specimens oriented horizontally, face up, and with the prevailing airflow being upwards. For vertical specimens, orientation is considered, and it becomes evident that a boundary layer will normally be expected to develop that will add some convective component. The convective boundary layer component is not uniform over the height of a specimen; thus it is seen that better uniformity can also be expected under conditions where the convective component is minimized.

Choice of Heater Type In a real fire, the ignition source is, in most cases, in the vicinity of a combustible. The radiation spectrum depends on the size of the fire. A very small fire can show a substantial fraction of its radiation at

wavelengths characteristic of H_2O, CO_2, and other combustion products [28]. For larger fires—certainly for room fires reaching a hazardous condition—the radiation from the soot tends to dominate. The result is an approximation to a graybody radiation [29]. For such a graybody radiation the temperature is typically in the vicinity of 1000 °C [30]. Experimentally, heater choices for test apparatuses have included gas-fired panels, electric resistance heaters, flames, and high-temperature lamps. Electrical heaters tend to have a near-graybody characteristic and, assuming a dull or oxidized surface condition, a high emissivity. Gas-fired panels derive a substantial portion of their radiation from the ceramic face; thus, while there are discrete molecular wavelength peaks, overall the radiation shows a graybody continuum, typically in the range of 700–1000 °C [31]. High-temperature lamps, which have been used by several investigators [28, 32], typically have radiating temperatures of 2200–3000 °C. The spectral distribution of such a source—further limited by a translucent enclosure—is much different from one operating at 1000 °C. Whether this change in spectral characteristics is important depends on the surface of the material to be ignited. For a material with a radiant absorbance independent of wavelength, this source variation would not matter. Hallman, however, has reported data for a large number of plastics and shows that although there are some specimens with negligible wavelength dependence to their absorbance, the majority shows strong variations [28]. Hallman also measured ignition times of plastics with both a flame source and high-temperature lamps. The effect on ignition times ranges from negligible to more than an order of magnitude, depending on the specimen. For a general-purpose test, flames would probably be the least desirable source of heating. For a bench-scale test, flame size has to be kept small. This means that such flames are optically thin, their emissivity is low, and higher heat fluxes cannot be achieved unless a strong convective component is added.

Design Details Once an electrical radiant heater had been decided upon, design details were also influenced by work at NIST with earlier types of calorimeters. One of the primary requirements of the heater is that it not change the irradiance impressed on the specimen when the specimen ignites. This undesired event is, of course, exactly what happens with several of the older types of calorimeters. The specimen's flames directly heat nearby ironwork, which, in turn, radiates to the specimen. The heater, which had been viewing a cold specimen prior to ignition, also starts to view a hot flame afterwards. The result is that its efficiency increases drastically, giving a rise to its radiating temperature. Based on these observations, guidelines were formulated so that the specimen must, as much as possible, view only

1. A temperature-controlled heater
2. A water-cooled plate
3. The open-air, ambient-temperature environment

Reliance on item 2 increased costs significantly; thus, it was more desirable to use only items 1 and 3. Prior to the development of the cone calorimeter, fire test apparatuses typically controlled the power (or fuel rate) into the heater, but did not maintain it at a fixed temperature.

The Conical Shape The cone calorimeter derives its name from the conical shape of the heater (Fig. 28.5). The decision had been made to use an electric resistance heater, running at a realistic maximum temperature of about 950 °C, but its material and shape still had to be determined. Based on poor experiences with exposed-wire resistance heaters and with silicon carbide rod–type heaters, the tube heater was chosen. The tube heater consists of a resistive wire element inside a protective tube, swaged over a packing of inorganic insulation. The tube is made of Incoloy™ and can be bent to a desired shape.

To determine the best shape, the conical heater used in the ISO 5657 ignitability apparatus [33] was examined. This seemed to be a promising shape. The proper shape had to have a hole in the middle, since otherwise a hot spot would occur at the sample center, where the radiation view factor is the highest. The same

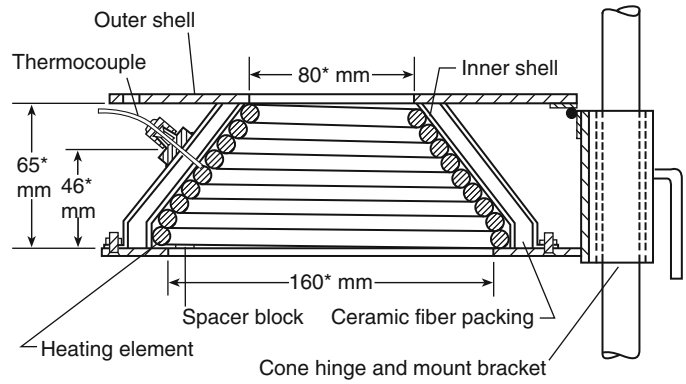

Fig. 28.5 Cross-sectional view through the cone heater

heater had to serve in both horizontal and vertical orientations. In the horizontal orientation, it was essential that all the products of combustion flow out the hole in the middle, and not "splash" on the heater coil itself, nor escape from the underside. The original ISO 5657 design proved to be unsuitable in the former respect. It also had problems with durability and assembly. Thus a totally new design was created, which, however, looked superficially similar to the ISO 5657 cone. With the actual cone calorimeter design, the flames from the specimen do not splash on the heater coil. Instead, a sheath of cold air is pulled up, surrounding the flame plume. Thus, there is not a concern that any surface reactions occur on the heater coil.

The space between the inner and outer cones is packed with refractory fiber. This arrangement helps keep the outside of the unit cool and also helps bring the heater up to operating temperature rapidly.

Emissivity of the Heater The emissivity was characterized by Janssens [34]. The heater coil, once installed and operated a few times, becomes essentially radiatively black. The emissivity itself cannot be directly measured; however, it is possible to compute an approximate view factor, F, for the cone heater. The possibility of measurements is based on a simultaneous determination of the heater surface temperature and the heat flux falling on the heat flux meter, with the meter held in place at the same location where a specimen is situated. Over the range of fluxes of 10–90 kW $\cdot$ m^{-2}, Janssens determined the $\varepsilon \times F$ product to be 0.73, with F being computed as 0.78. Then, solving for ε gives $\varepsilon = 0.91$. Since the temperatures of the heater closely resemble those in room fires, and the emissivity approaches 1.0, this means that the spectral distribution is likely to be very close to that expected from room fires (neglecting the molecular radiation contribution from CO_2 and H_2O). It is important that the heater element be kept in good repair, in order that expected uniformity be achieved. Aging may cause the coil windings to separate and sag. If this occurs, poorer uniformity has been shown to occur [35].

Convective Fraction of the Heating Flux During the development of the cone calorimeter at NIST, a study was conducted to determine the fraction of the heating flux accounted for by the convective contribution [36]. When measured with respect to a water-cooled heat flux meter, the results showed that, in the horizontal specimen orientation, the convective contribution was immeasurably small. In the vertical orientation, the fraction was typically 8–12 %. Janssens later remeasured the vertical configuration [34] using a more accurately calibrated heat flux meter and found that, even for the vertical orientation, the convective transfer is immeasurably small. Thus, it can be stated that the objective of having a test method where the heating is primarily radiant was successfully

met. For modeling of test results, however, one may be more interested in the possibility of convective heat transfer to a specimen that is heated, or even burning, not to a calibration meter constrained by its water-cooling jacket at near-room temperature. Janssens also made some determinations of such actual specimen heating. The direction of the heat transfer was such as to represent a heat loss from the specimen in all cases. A single convective heat transfer coefficient could not be derived, however, since the value was dependent on the irradiance level from the heater. Janssens's results could be represented by:

Irradiance from heater ($kW \cdot m^{-2}$)	Convective heat transfer coefficient h_c ($W \cdot m^{-2} \cdot K^{-1}$)
20	9.0
40	18.0
60	27.0

For practical work, Janssens recommended that an average value of $h_c = 13.5\ W \cdot m^{-2} \cdot K^{-1}$ should be appropriate for work over the common irradiance range of 20–40 $kW \cdot m^{-2}$. The actual details of this small amount of convective heat transfer are pertinent only to certain specialized studies. For most work, it is entirely adequate to assume that the specimen heating is entirely radiative.

Uniformity of the Heating Flux The uniformity of the heating flux over the face of the specimen in the cone calorimeter has been described [36]. Over the range of irradiances from 25 to 100 $kW \cdot m^{-2}$, the ratio of the flux at the specimen center to average flux varied only from 1.00 to 1.06. The peak deviations from average were typically 2 % in the horizontal orientation and 7 % in the vertical. Deviations are higher in the vertical orientation, since the effect of convective fluxes, due to the boundary layer flow, is more pronounced there. Additional measurements have been made in the specimen-depth plane. Control of the surface of the specimen was a special concern to the designers of the ISO apparatus, where a special compressive loading mechanism is provided that attempts to relevel the exposed surface, in case the specimen recedes due to melting. In the cone calorimeter, measurements have been made in the horizontal orientation using a small, 6-mm-diameter Gardon-type heat flux gauge. A flux mapping was obtained starting at the initial surface, and progressing down to the maximum depth of a specimen, which is 50 mm. A normal aluminum foil rectangular specimen wrap was used for these tests, but without any specimen. The results show that, at heating fluxes of both 25 and 50 $kW \cdot m^{-2}$, the deviations over the entire specimen depth are less than 10 %, and can, therefore, be neglected (Fig. 28.6). At the lower depths, reflection from the aluminum foil probably assists in maintaining this uniformity.

Orientation of the Heater and Specimen The normal orientation of the specimen should be

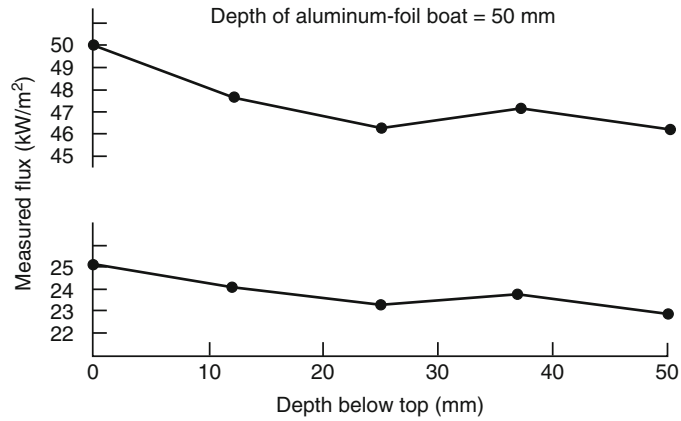

Fig. 28.6 Measured flux at various positions below the top surface of a specimen

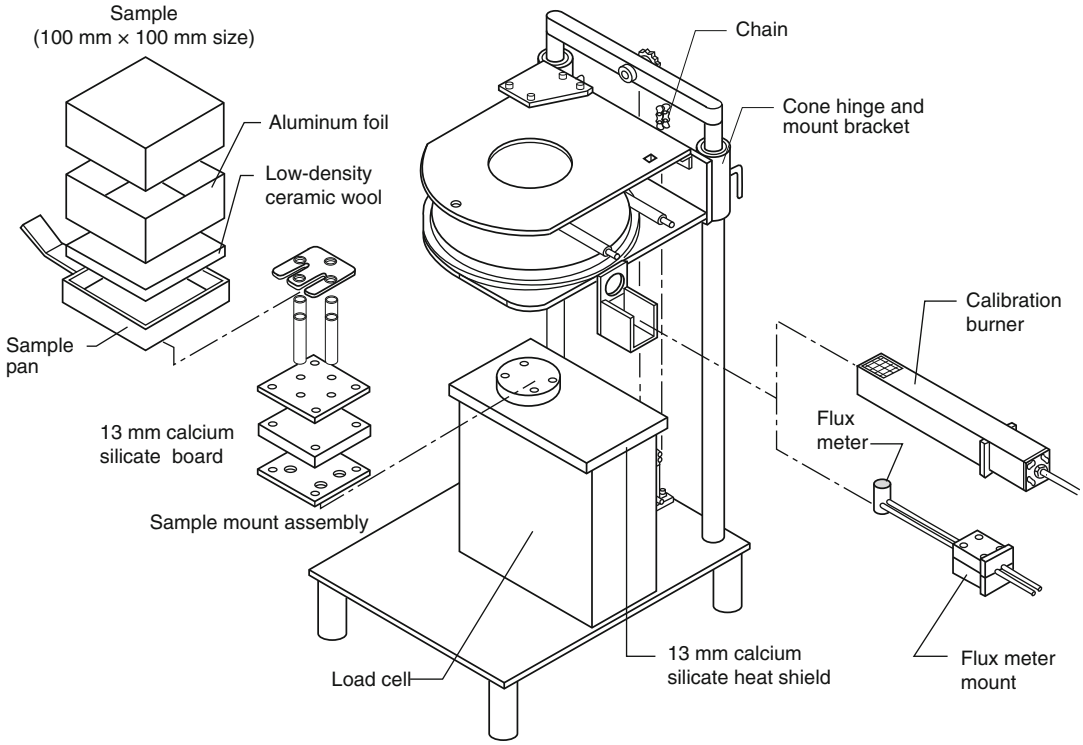

Fig. 28.7 Heater in the horizontal (standard) orientation

horizontal, face up, with the heater being parallel, face down. This allows thermoplastics, liquids, and other melting or dripping samples to be successfully tested. Because it was considered desirable to allow testing in a vertical orientation for certain application exploratory studies, provision was made to swing the heater 90° into a vertical orientation. Vertical orientation testing may be preferable when probing the flame regions or measuring specimen surface temperatures is desired. Figures 28.7 and 28.8 show the comparative horizontal and vertical heater orientations, respectively. It is especially emphasized that no standard testing should be specified for the vertical orientation, *even for products that are normally used in a vertical orientation*. The ASTM standard [2] was amended in 1992 to clarify that the vertical orientation is only for special research studies and not for product testing.

The Shutter

The original NIST design for the Cone Calorimeter did not include a shutter. The operator would just quickly drop the specimen holder on top of the mount plate at the top of the load cell. This was satisfactory for most building products and plastics. However, in 1993 researchers at SP (Technical Research Institute of Sweden) found that there were some reproducibility issues when testing upholstered furniture specimens that ignited very quickly. Thus, they designed a shutter (originally described as "heat shield" and later as "radiation shield") to be interposed between the heater and the specimen surface; this was originally described in a 1996 SP report [37]. The use of a shutter makes it possible to (a) get the load cell to equilibrate before commencing exposure, and (b) provide an nearly step-function initiation of radiant heat flux to the specimen.

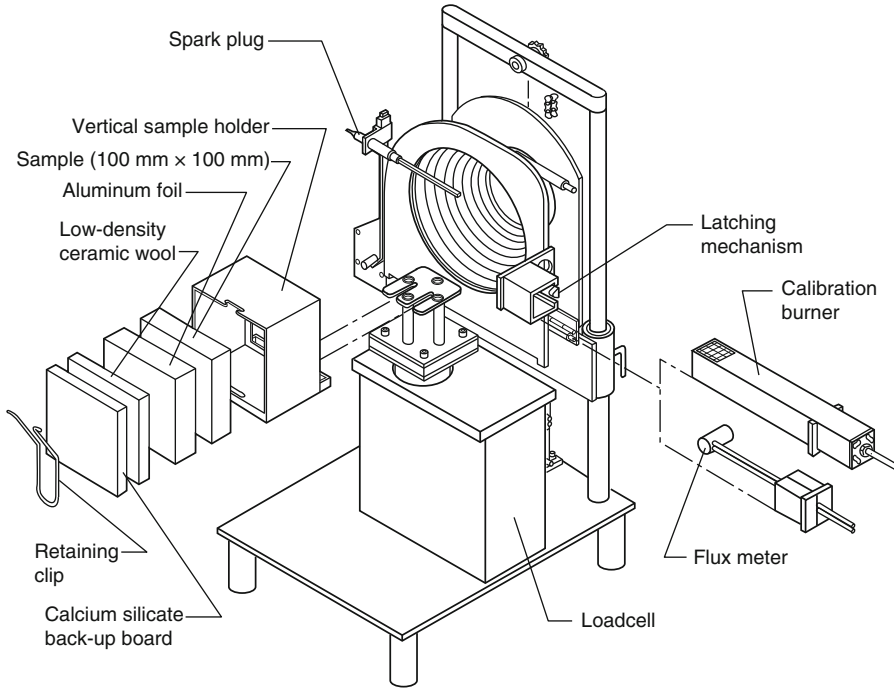

Fig. 28.8 Heater in the vertical orientation

However, with the use of a shutter there is potentially a different type of error that is introduced. A shutter will reflect some heat back to the heater, and will also rise in temperature and reradiate heat flux to the heater. Both of these would cause the heater's temperature to rise. The solution adopted by ASTM [2] and ISO [1] standards was that the shutter should be in place for no longer than 10 s prior to start of test, and that it be either water-cooled with a black coating, or else not water-cooled, but with made of ceramic material or made of reflective metal. The reflective metal option is the least satisfactory, because, while radiation towards the specimen gets eliminated by reflection, the reflection towards the heater does cause its temperature to rise. Thus, the best accuracy is attained with a minimal duration of the shutter's closure. This change was made in the 1997 edition of ASTM E 1354 and in the second edition (2002) of ISO 5660-1.

Airflow

The feasible airflow rate through the system is bound by certain limits. It must not be so fast that ignition results are improperly affected. It must also not be so slow that products of combustion spill out of the hood. If this were a closed system, one would also be concerned about airflow being so slow that the air/fuel ratio drops into the fuel-rich regime. The standard cone calorimeter, however, has been designed for ambient air testing, and this consideration does not apply.

Systematic guidance in this area was not available. However, as an example of the effect of airflow, measurements were made at NIST using the OSU apparatus. Specimens of black polymethyl methacrylate (PMMA) were exposed in the horizontal orientation to a heating flux of 35 kW · m^{-2}. With an airflow rate of 12 L·s^{-1} through the combustion chamber, the ignition time was 209 s. When the airflow rate was doubled to 24 L·s^{-1}, the specimen ignition time increased to 403 s. By contrast, Table 28.1 shows comparative results with the cone calorimeter; it can be seen a flow rate of 24 L·s^{-1} was found to be satisfactory. That flow rate was also about a factor of 2 greater than the minimum at which no spill out of the hood occurs.

The exhaust system uses a high-temperature cast-iron blower to exhaust the gases and an

Table 28.1 Effect of exhaust hood airflow on ignition times in the cone calorimeter[a]

Material	Thickness (mm)	Orientation	Fan setting	Ignition time[b] (s)
PMMA	13	Horizontal	No fan	71
PMMA	13	Horizontal	24 $L \cdot s^{-1}$	76
PMMA	13	Horizontal	41 $L \cdot s^{-1}$	67
PMMA	13	Vertical	No fan	86
PMMA	13	Vertical	24 $L \cdot s^{-1}$	84
PMMA	13	Vertical	41 $L \cdot s^{-1}$	77
Redwood	13	Horizontal	No fan	23
Redwood	13	Horizontal	24 $L \cdot s^{-1}$	24
Redwood	13	Horizontal	41 $L \cdot s^{-1}$	31
Redwood	13	Vertical	No fan	22
Redwood	13	Vertical	24 $L \cdot s^{-1}$	27
Redwood	13	Vertical	41 $L \cdot s^{-1}$	29

[a]At an irradiance of 35 $kW \cdot m^{-2}$
[b]Typical ignition time scatter was on the order of ± 10 % (1σ, $N = 3$)

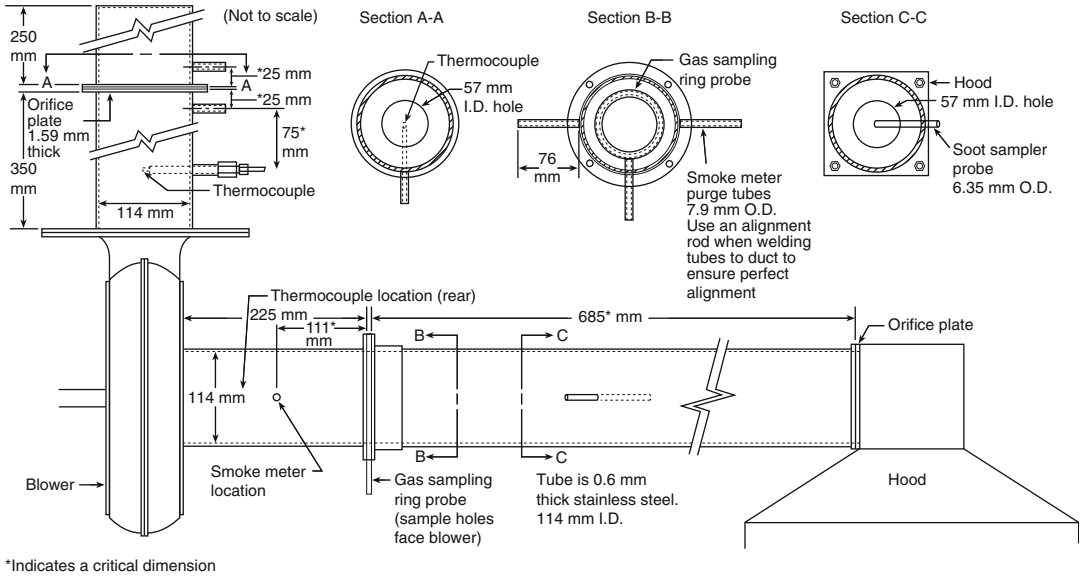

Fig. 28.9 Exhaust duct

orifice plate flowmeter (Fig. 28.9). The orifice plate flowmeter is instrumented with a differential pressure transducer and a thermocouple. For specialized studies, where the entire combustion system is glass enclosed [38], it is possible to go to flow rates below 12 $L \cdot s^{-1}$. With such enclosed systems, accurate measurements can be made down to about 9 $L \cdot s^{-1}$ using the standard orifice plate. For lower flow rates, down to about 5 $L \cdot s^{-1}$, the standard orifice plate is replaced by one with a smaller opening.

Means of Ignition

In some cases no external ignition source is desired, and specimen testing is to be done solely on the basis of autoignition. In most cases, however, an external ignition source is desirable. This ignition source should, in general, not impose any additional localized heating flux on the specimen. Apparatus designs have been developed, with impinging pilots that can, in some cases, produce such high localized

heat fluxes as to burn a hole through the specimen at the point of impingement, yet not ignite it outside of that region [39]. Applications for such devices tend to be specialized, since the general objective of radiant ignition testing is to produce data that can be analyzed in the context of an assumed one-dimensional heat flow. A design using an impinging pilot has an additional difficulty. Since most of the specimen face is not yet heated to the ignition temperature when ignition first begins in the vicinity of the pilot, no unique ignition time can be determined. Instead, there is a significant time spread between when ignition first occurs at the initial location, to when the final portions of the face have been ignited.

The ignitor should reliably ignite a combustible gas mixture in its vicinity. Thus, the location of the ignitor must be chosen so that it is near the place where maximum evolution of pyrolysate gases is expected. Some materials are highly fire-retardant treated, and, when heated, emit vapors that tend to extinguish a pilot flame. The ignitor has to be designed so as not to be extinguished by fire-retardant compounds coming from the specimen, nor by airflows within the test apparatus.

The ISO 5657 apparatus was designed with a "dipping" gas pilot, which is periodically thrust for a short while down close to the specimen face, then retracted. This solution, however, introduces an uncertainty into ignition times and provides further complexity. A gas pilot, based on experience, also requires oxygen premix to achieve a flame that is both small and resistant to blowout [40]. With products high in fire retardant, even such precautions are not likely to lead to a reliable pilot; thus, for instance, the ISO 5657 apparatus uses a second pilot to reignite the main pilot. Pilot stability also tends to be crucially dependent on the physical condition of the pilot tube tip, and significant maintenance can be necessary. Finally, if used in a heat release apparatus, a gas pilot can add noise to the baseline of the heat release measurement. Experimental efforts at the National Bureau of Standards (NBS) had success using the NBS-II calorimeter, a more tractable alternative (i.e., electric spark ignition). This spark plug arrangement for ignition was successful, and so a similar electric pilot was designed for the cone calorimeter. The location of the ignitor should be at the place where the lower flammable limit is expected to first be reached when the specimen begins its pyrolysis. It should, however, not be so close to the specimen surface that minor swelling of the specimen would interfere with the ignition function. In the cone calorimeter, the ignitor locations were chosen so that, when testing in the horizontal orientation, the spark plug gap is located 13 mm above the *center* of the specimen; in the vertical orientation, the spark plug gap is located at the specimen plane and 5 mm above the *top* of the specimen holder.

The actual spark plug arrangement is shown in Fig. 28.10. The spark plug is provided by a special-purpose 10-kV ignition transformer. The spark plug is moved in and out by remote control, operated by an air motor that rotates the shaft on which the spark plug rests. A reversible lock bar is used to adjust the spark-plug-to-heater distance when changing from the horizontal to the vertical orientation (the spark gap is 13 mm away from the heater baseplate in the horizontal orientation, but 25 mm away in the vertical).

Specimen Area and Thickness

Both specimen area and thickness may be expected to have some effect on the ignitability and the heat release rate. The main practical size and thickness limitations come from the fact that the specimens to be tested should exhibit primarily one-dimensional heat transfer. Thus, the configuration should be such that excessive edge effects are not seen. If the specimen thickness is such that it is thermally thick (the heat wave penetration depth being less than the physical depth), then further increases in thickness are not expected to change ignitability results. For thinner specimens, however, there can be expected to be a thickness effect, and the backing or substrate material's thermophysical properties can be of importance.

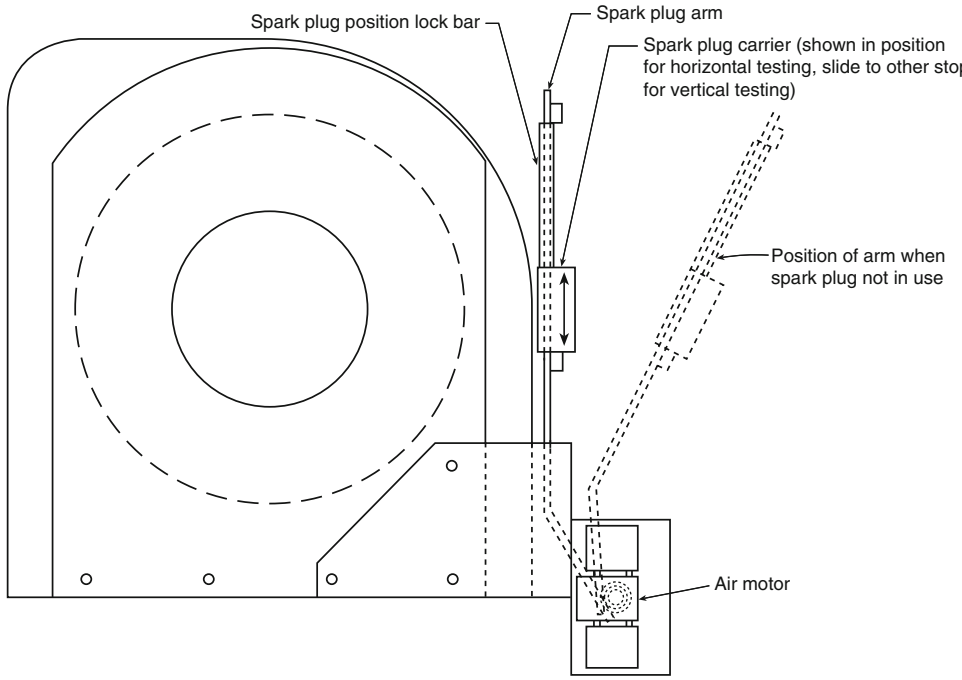

Fig. 28.10 Spark plug, carrier, and air motor

Specimen Area Janssens [34] studied in some detail the general problem of area effect on ignition. The effect is seen to be smaller when irradiances are high rather than low. The exact magnitude of the effect is also dependent on the specimen's thermophysical properties. For specimens of area 0.01 m^2 or larger, however, his results show an increase in ignition time of only about 10 % over what would be seen with a specimen of infinite area. Later, Nussbaum and Östman [41] studied specimens in an experimental apparatus somewhat similar to the cone calorimeter, but accommodating 200 × 200 mm specimens. Their comparison of the ignition times of these larger specimens against the standard 100 × 100 mm ones shows that quadrupling the specimen area decreases the ignition time by about 20 %.

For heat release rate, the specimen size affects the measurement, since flame volume is larger over larger specimens; consequently the flame radiation tends to approach a value of higher emissivity. Nussbaum and Östman also examined heat release rates from larger specimens; the differences were generally of the same order of magnitude as the repeatability of the results. Babrauskas, in commenting on these data [42], discussed tests on larger size, horizontal PMMA samples, where each doubling of the specimen's area increased the heat release rate, per unit area, by about 10 %. The more general treatment of the horizontal specimen, of course, is as a liquid pool. Chapter 26 gives details on the size effect for burning pools. It can be seen that the diameter has to be greater than about 1 m before the specimen area effect becomes negligible.

The effect of specimen size for vertical samples was examined at Factory Mutual Research Corporation (FMRC) in a series of experiments on PMMA walls [43, 44]. The FMRC studies showed little size effect for specimen heights up to 200 mm; beyond 200 mm there was approximately a linear dependence of $\dot{q}''$ on the height. This was true up to the maximum height tested, that is, 3.56 m. Unlike horizontal pools, the rate of heat release was not leveling off at even these sizes, and estimates suggested that the specimen size would have to be increased by

another order of magnitude before a leveling off would be seen.

The conclusion from the above studies was that 100 × 100 mm was a suitable size for bench-scale testing, but that the bench-scale $\dot{q}''$ rates will always be somewhat lower than for full-scale fires.

Specimen Thickness The cone calorimeter is intended for testing actual commercial products. Thus the specimen thickness should be, as much as possible, the thickness of the finished product. There are limitations at both ends of the scale, however. The instrument is restricted to testing specimens not thicker than 50 mm. For products that in their finished state are greater than 50 mm thick, it can readily be seen that, for almost any realizable combination of thermophysical properties and incident radiant fluxes, a 50 mm specimen is thermally thick, and increasing thickness would not change the ignition times [45, 46]. By making calculations for various densities and heat fluxes, it was found that for particleboard the minimum thickness required to ensure that the specimen is thermally thick can be represented by

$$\ell = 0.6\,\frac{\rho}{\dot{q}''} \tag{28.3}$$

where

$$\ell = \text{Thickness}\,(\text{mm})$$
$$\rho = \text{Density}\,(\text{kg}\cdot\text{m}^3)$$
$$\dot{q}'' = \text{Heat flux}\,(\text{kW}\cdot\text{m}^2)$$

This is probably a reasonable rule of thumb for other materials as well. The proportionality of the required thickness to $\rho/\dot{q}''$ is derived from classical heat conduction theory by equating the time for the front surface to reach ignition temperature to the time the rear surface's temperature begins to rise, assuming that the thermal conductivity is proportional to the density. Numerical calculations were necessary to determine a suitable constant because of the impact of front surface heat losses.

For materials that are not thermally thick at the time of ignition, the nature of the backing material or substrate can influence the measured value of the ignition time. In the cone calorimeter, the substrate is a blanket of refractory ceramic fiber material, having a nominal density of 65 $\text{k}\cdot\text{gm}^{-3}$. In use, the material assumes a more compacted density of roughly 100 $\text{kg}\cdot\text{m}^{-3}$. Whenever possible, materials whose thicknesses are less than the minimum suggested in the above formula should be mounted on that substrate material over which they will actually be used. As a practical guide for testing unknown commercial samples, it is desirable to specify that any specimens less than 6 mm thick should always be considered as needing to be tested over their in-use substrate.

Fabrics are a special case. Thin fabrics are sometimes used for constructing air-supported structures; these should be tested with an air space in back, simulating the usage conditions. A special holder has been constructed that allows the fabrics to be pulled taut and held above a dead-air space (Fig. 28.11).

Sample Testing Specifications

Specimen Orientation and Specimen Holders

The specimen holders in Figs. 28.12 and 28.13 show the two specimen holders, respectively. With proper precautions, the horizontal orientation can be used for testing liquids and melting materials, whereas the vertical orientation's small melt trough can only catch a very small amount of molten material. Also, some specimens, when tested in the vertical orientation, show a tendency to lose physical strength and fall out of the holder, which does not happen in the horizontal orientation.

In the vertical orientation, there are several layers of rigid millboard behind the blanket, sufficient in thickness to fill out the depth of the specimen holder. The specimen is wrapped in a single sheet of aluminum foil, covering the sides and bottom. The aluminum foil serves to limit the flow of molten material and prevent it from seeping into the refractory blanket.

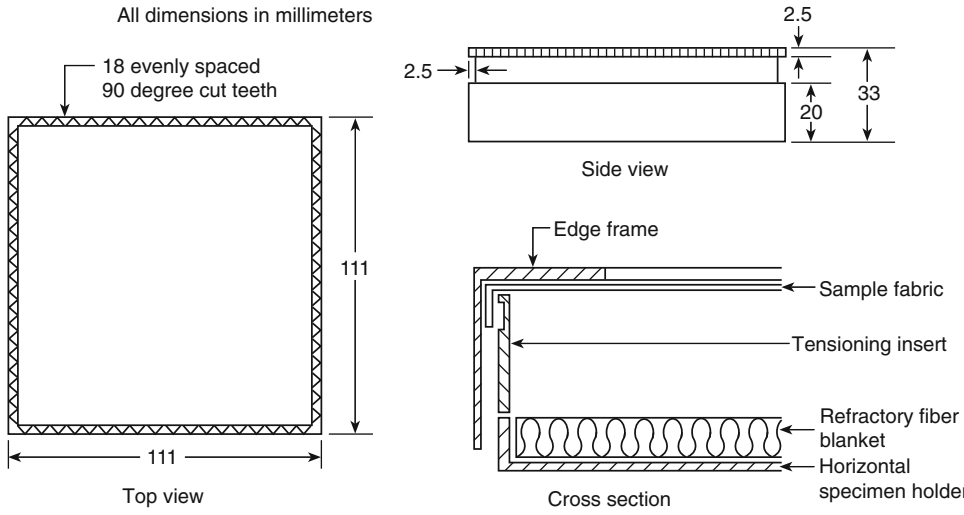

Fig. 28.11 Special holder for testing fabrics and similar thin materials

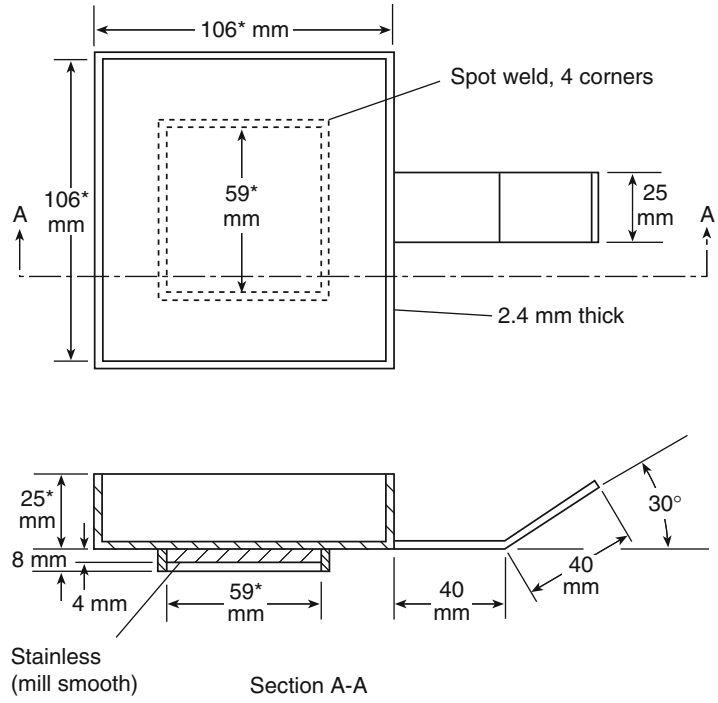

Fig. 28.12 Horizontal orientation specimen holder

Load Cell

Many ancillary measurements made in the cone calorimeter (such as yields of various gas species) require the use of a load cell. Transducers had been tried in various earlier apparatuses, but most suffered because they were not designed for purely single-axis linear motion. That is, if the weight of the specimen was not well balanced, or differential heating stresses occurred, it was

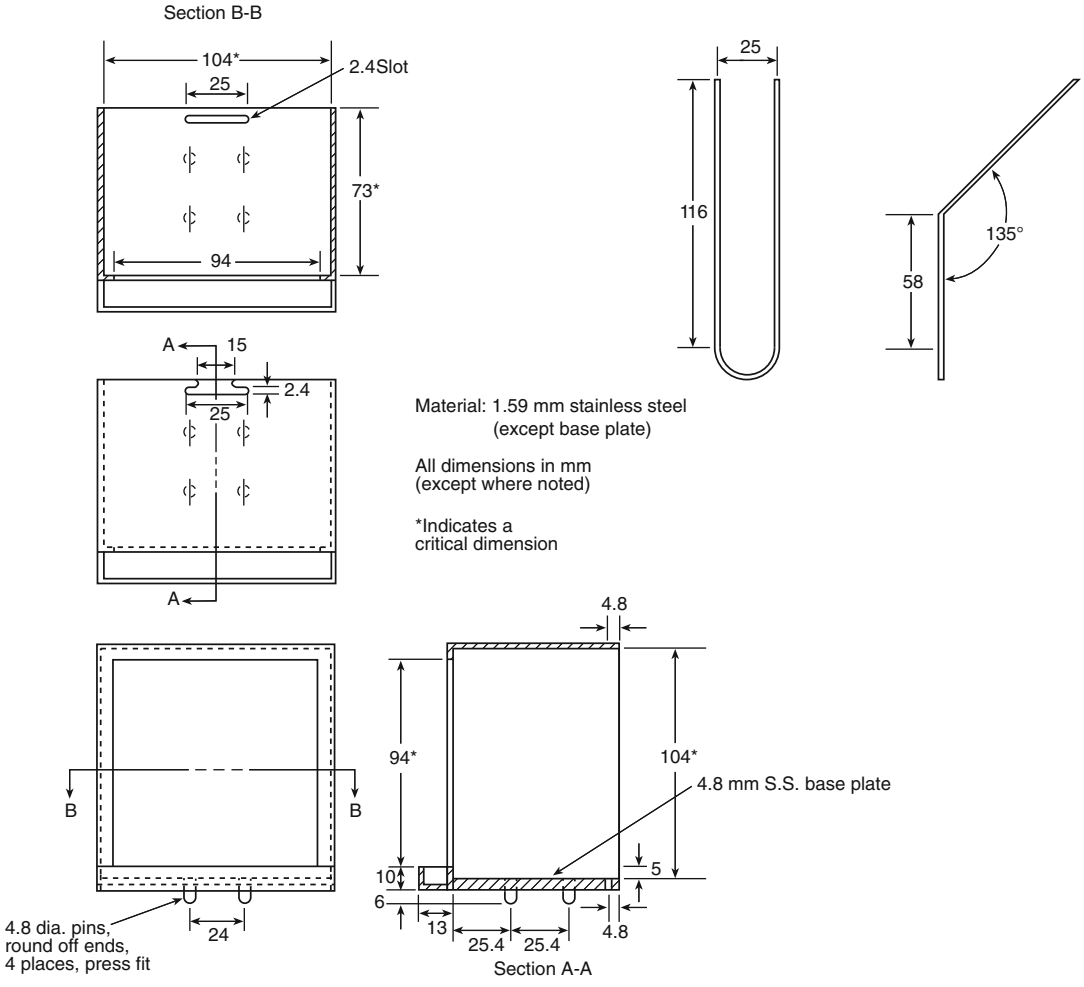

Fig. 28.13 Vertical orientation specimen holder

likely that a mechanical moment (or *torque*) would be applied to the device, with the transducer then being prone to jamming. For the cone calorimeter, a commercial-design load cell was found that permits only up-and-down axial motion while being insensitive to torques or forces from other directions.

The load cell has to accommodate two differently oriented specimen holders and may need to hold additional fixtures. All of these can have substantial—and different—weights, yet must allow accurate mass determination for low-density specimens. The solution adopted was a weighing system that has a large (3.5 kg) mechanical tare adjustment range, along with a sensitive weighing range (500 g). A resolution of 0.005 g is readily achievable.

Figures 28.7 and 28.8 show, respectively, how the horizontal and vertical orientation specimen holders are accommodated on the load cell. The horizontal holder has a square recess on the bottom and simply is placed straight down. The vertical holder is more conveniently inserted directly toward the heater, correctly locating the specimen by four mounting pins on the bottom. In both cases there is a positive specimen location, and the operator does not have to be concerned with how far to insert the holder.

Edge Conditions

Edge Effects In an apparatus such as the cone calorimeter, it is desired that the small-scale test specimen would behave, as much as is possible, like a correspondingly sized element of the full-scale object. If one is dealing with relatively large, flat, full-scale objects, then heat and mass transfer will occur only in the direction perpendicular to the exposed face. There will be no heat or mass flow along either of the face directions. The guidance to be derived from this conceptual model in designing the bench-scale test environment is clear: there should be a minimum of heat or mass transfer at the specimen edges. The aluminum foil used to wrap the specimen usually serves to minimize any mass transfer that may occur. The heat transfer situation, however, is more complicated.

In the vertical specimen orientation, the specimen has to be restrained against falling out; therefore, the vertical specimen holder incorporates a small lip extending 3 mm along the edges. In the horizontal orientation, no special measures need to be taken against falling out. Thus, for many specimens it is satisfactory to simply cover the edges and bottom with aluminum foil, leaving the top exposed in its entirety.

Some categories, however, present special problems—specimens that either have a propensity to ignite first along the outside edge or that, when ignited, burn disproportionately vigorously near the edges. Such behavior is often found with wood specimens and with certain composites. This problem is alleviated by using a stainless steel edge frame for the horizontal orientation, which like the vertical holder provides a 3 mm lip around the edge of the specimen face (Fig. 28.14).

Specimens showing unrepresentative edge burning can be viewed as having a spurious heat gain along the edges when compared against a hypothetical ideal situation of exactly zero heat loss or gain at the edges. When an edge frame is applied, the opposite situation can tend to result, that is, an observed net heat loss from the specimen [47]. The ideal situation of a specimen prevented from showing unrepresentative increased edge burning but equally not sustaining any losses to an edge frame may be difficult to approach in practice. This is still a topic of active study at several institutions.

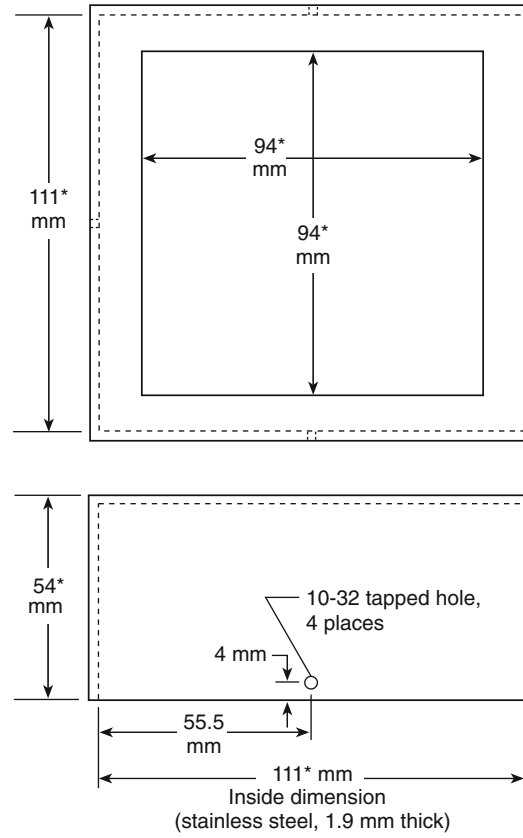

Fig. 28.14 Edge frame for the horizontal specimen holder

In some cases, an edge frame is needed for thermostructural reasons. Some specimens, especially certain composites, can show pronounced edge warping and curling when subjected to heat. The burning of such a specimen would be highly nonuniform if its edges were not held down with an edge frame. In many cases, an edge frame is all that is required. In some cases, however, additional measures such as a wire grid (see below) are required.

Intumescing Samples Intumescence is a common difficulty with fire test specimens, either before ignition or during the burning. The simplest solution used in the cone calorimeter,

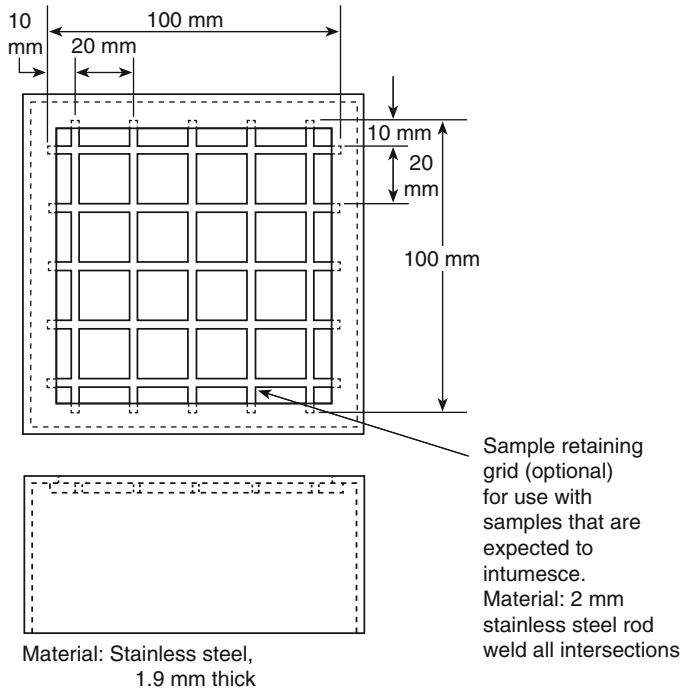

Fig. 28.15 Wire grid

sufficient in many, but not all, cases, is a wire grid placed on top of the specimen. Figure 28.15 shows a medium-weight grid. To minimize effects on measurements, the grid weight should be the smallest possible consistent with providing adequate mechanical restraint to the tested specimen. Effects on measurements will be negligible if the average grid mass is less than 0.6 $kg \cdot m^{-2}$ of specimen face area. This mass corresponds to quite a thin, small grid and will practically be usable only in occasional cases. Additional guidance is given in the NBS "User's Guide for the Cone Calorimeter" [3], but testing laboratories will, on occasion, be required to devise their own special schemes for mounting and restraint.

Smoke Measurement

One of the most essential ancillary measurements performed with the cone calorimeter is smoke obscuration. Widespread dissatisfaction with older, closed-box types of smoke tests [48, 49] caused by the large number of both practical and theoretical difficulties were successfully resolved by developing a flow-through smoke measuring system, using a helium-neon laser as the light source and a sophisticated quasi-dual-beam measuring arrangement. Figure 28.16 shows the overall arrangement of the laser photometer. It is mounted on the exhaust duct at the location shown in Fig. 28.9. A thermocouple is also mounted nearby, since the calculations require a determination of the actual volume flow rate in the duct at the photometer location. The user should consult Geake [49] for details explaining the operation of the laser photometer. Briefly, the light from the laser goes, via two beam splitters, into two detectors. The light reaching the compensation detector is not attenuated by smoke; its signal serves as the reference to cancel out fluctuations in laser output power. The main beam detector measures a signal that is attenuated by the smoke. The optical path is purged by a minute flow of room air through a purge system. The flow is maintained by the pressure differential in the exhaust duct.

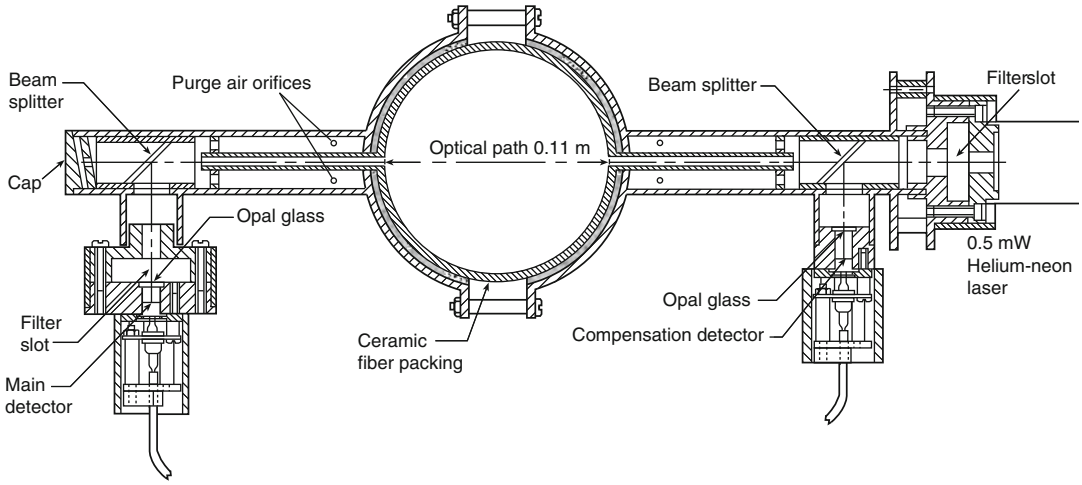

Fig. 28.16 Laser photometer

For certain research purposes, it is advantageous, in addition to obtaining optical smoke obscuration measurement, also to record the gravimetric soot yield by measuring grams of soot evolved per gram of specimen burned. A soot mass sampler is connected to the port indicated in section C-C of Fig. 28.9, and a known mass fraction of the exhaust duct flow is passed through a measuring filter and is weighed before and after the test.

Calibration Equipment

Two basic calibrations are needed: (1) the calibration of the temperature controller for the conical heater and (2) the actual heat release rate calibration. The temperature controller is calibrated using a Schmidt-Boelter-type heat flux meter equipped with a locating collar and inserted in place of the specimen, with its face where the specimen face would be located. No specimen holder is used for this operation. Figures 28.7 and 28.8 show the insertion of the heat flux meter.

The heat release rate is calibrated with a calibration burner inserted into the same bracket used for the heat flux meter (Fig. 28.17). The calibration burner, however, instead of being inserted facing the heater, is inserted so that the discharge opening faces upward. Calibration is accomplished by controlling the flow of high-purity methane going to the burner and comparing it to a known value and using the net heat of combustion for pure CH_4 as 50 MJ · kg^{-1}.

The laser photometer is calibrated by neutral-density glass filters. These are inserted into a filter slot in front of the main beam detector. An auxiliary filter slot is provided in front of the laser. This serves to check the correct balancing of the dual-beam system's common mode rejection ratio.

The NBS "User's Guide to the Cone Calorimeter" [3] details how calibrations are performed.

Miscellaneous Details

Ring Sampler

The combustion products flowing through the exhaust system can be heavily laden in soot, which would cause rapid clogging of the oxygen measurement system if precautions were not taken. The most important precaution is the specially designed ring sampler (Fig. 28.18), which is installed in the exhaust duct with the intake holes facing away from the direction of airflow. A number of small holes are used so as to provide a certain degree of smoothing with respect to duct flow turbulence.

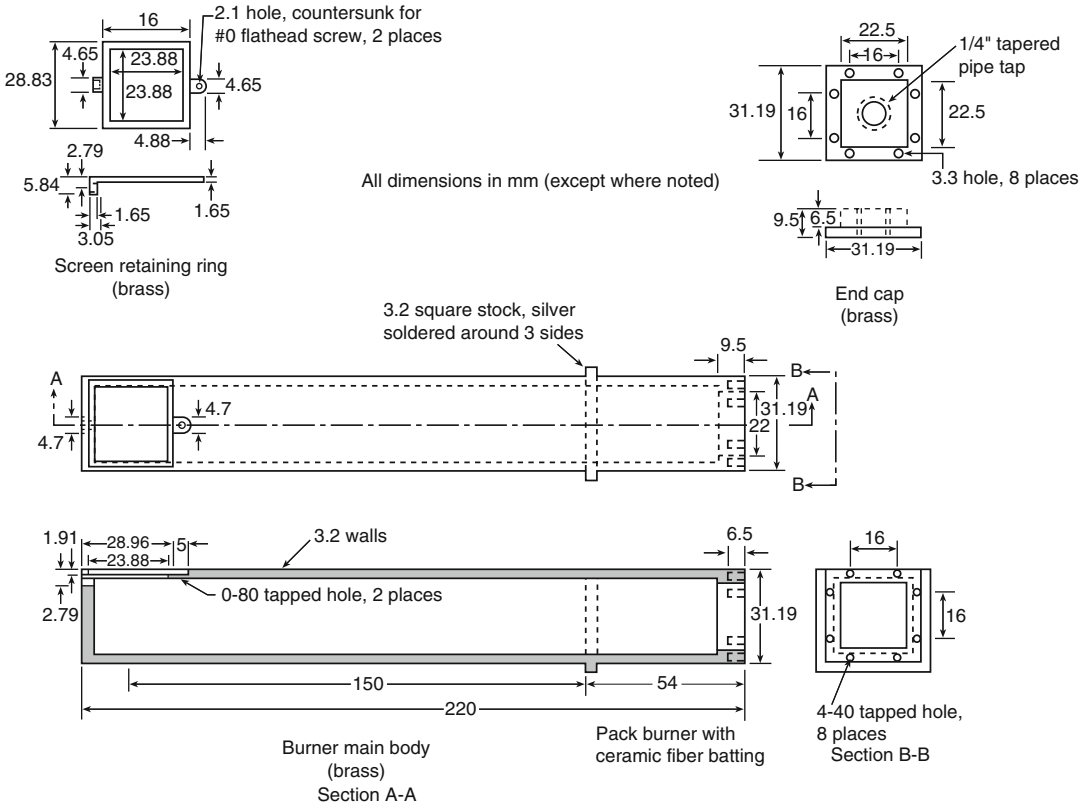

Fig. 28.17 Calibration burner

Additional Gas Analyzers

Many users of cone calorimeters provide not just an oxygen analyzer but also additional gas analyzers to help determine combustion chemistry and toxicity. CO and CO_2 analyzers are simply fitted into the same sampling line serving the oxygen analyzer. Other analyzers, for example, H_2O, HCI, and total unburned hydrocarbons, require a completely separate, heated sampling line system. Such a system also needs to have a heated soot filter at the front.

Special Issues with Product Testing

The cone calorimeter has been used for studying a very wide range of products and materials. In this section, some items of interest are considered where special care needs to be exerted in configuring the samples or in testing.

Liquids

The HRR of liquids is generally not the quantity of interest to regulators and other individuals charged with enforcing fire safety provisions for liquids. In addition, there is no easy way to scale from bench-scale results to large-scale applications. However, some research studies on liquids using the cone calorimeter have been reported. In such studies, use of a circular dish is generally more convenient than using a square specimen. For example, Hayakawa et al. [50] used a 113 mm diameter dish, while Iwata et al. [51] used a 90 mm dish. Liu et al. [52] conducted a study of liquids in the cone calorimeter, accompanied by water mist extinguishment. A number of other studies [53–57] have been reported.

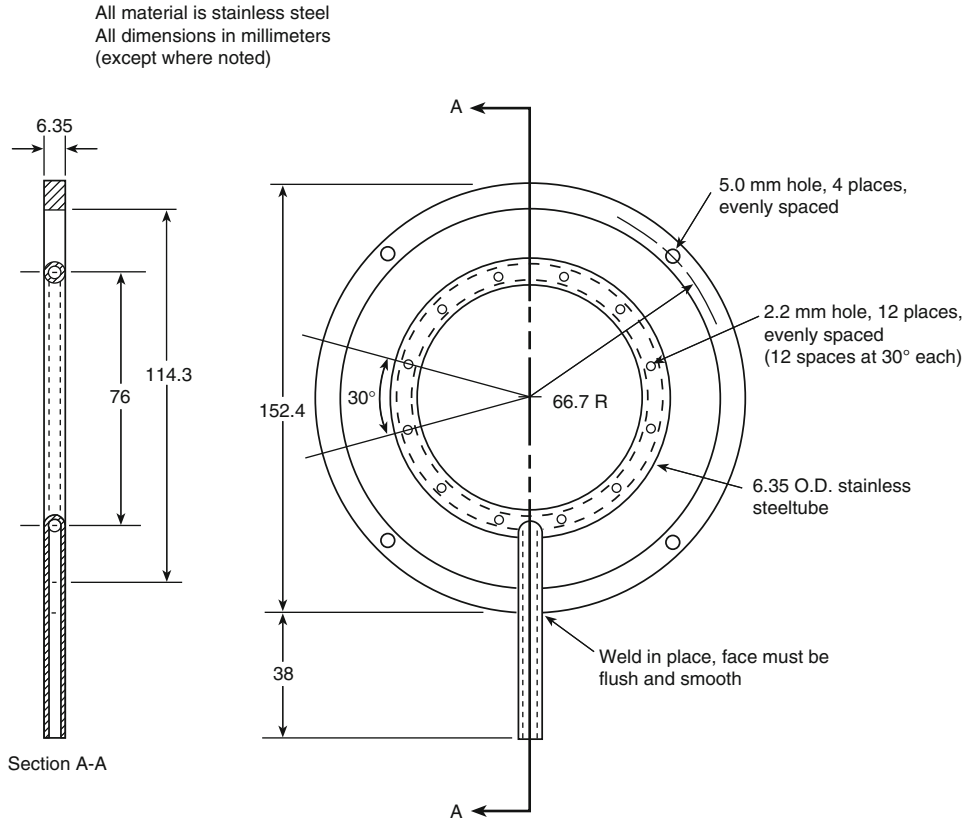

Fig. 28.18 Ring sampler

Electrical Cables

In testing electric cables, pyrolysis gases have a pronounced tendency to flow along the length of the cable interior and burn only at the edges rather than uniformly over the surface. For such specimens, it has often been found useful to coat the cable ends with a sodium silicate cement, such as Insa-Lute Adhesive Cement Paste No. 1, produced by the Sauereisen Cements Co. When the ends are sealed in such a manner, a knife puncture must be made in the face of each piece of cable to avoid pressure buildup and rupture.

Even though electrical cables are circular rather than flat, it has been found that they can be successfully tested in the cone calorimeter. Normally, 100 mm long cable sections are cut and placed side by side, filling up the specimen holder. For this to be practical, the diameter should not be excessive, say less than 15 mm or so.

ASTM has issued a standard [58] on the testing of electrical cables with the cone calorimeter. In the ASTM standard, the cables may either be cut into sections, or else the insulation material alone is to be tested as a flat plaque. The latter will generally not be practical, since cable manufacturers do not produce the plastic in this form. The ASTM standard also permits the ends to be sealed, or unsealed, when actual cable sections are tested.

Grayson et al. [59] documented the results of the FIPEC research program, where electrical cable testing and modeling was done using a wide array of techniques. A very extensive cone calorimeter testing effort is described in this connection. The FIPEC researchers concluded that the best results are obtained when the ends are sealed, except for very small cables

(<4 mm dia.). The sealing did not affect the magnitude of the results, but did improve the repeatability. They also conducted plaque tests on some individual materials.

Intumescing Materials

Intumescing materials can present special problems for testing. Most substances do not intumesce significantly during testing. The exceptions are, of course, intumescent coatings, but also some grades of PVC show a strong tendency to intumesce, as do some a few other materials. The first problem encountered is if the specimen rises sufficiently to contact the spark plug and cause a short. More extreme intumescing can actually result in contacting the heater coil, although this has rarely been seen. Apart from problems with the spark plug (which can be avoided by improvising another ignition arrangement), there is the issue of flux non-uniformity—as the specimen surface rises, it encounters a locale with higher radiant flux.

The original solution for intumescing materials, incorporated into the ASTM [2] and ISO [1] standards, has been to provide a wire retaining grid, which is placed on top of the specimen and held down the edge frame. This generally sufficiently reduces the intumescence to eliminate technical problems. However, this has caused concern for some manufacturers, who considered that their product may not able to achieve the optimal performance that it might in its end-use application, where a thicker layer of intumesced material would be developed.

A procedure was suggested [60] whereby the specimen surface is placed at 60 mm below the base of the heater, instead of 25 mm, in order to allow ample height for expansion. This however also has drawbacks. The heat flux uniformity at such a spacing becomes poor across the face of the specimen. In addition, if a tall hemispherical or elongated configuration is allowed to arise, there is very limited heat flux incident upon the sloped sides of such a specimen.

Low HRR Materials and Noncombustibility

Many building codes, including all in North America, have long taken the stance that materials are to be divided into two kinds: combustible and noncombustible. This kind of categorical yes/no distinction basically reflects the fire knowledge of the nineteenth century, and not the twenty-first, where fire safety engineering is acknowledged to be a profession capable of quantitative assessment of hazards. While codes have numerous and complex provisions on this subject, the most important application, by far, is in regards to materials that are used as either structural members or as lining materials, e.g., wall or ceiling linings. Babrauskas and Janssens recently examined this question in detail [61]. It was concluded that the concept of noncombustibility has no reasonable relationship to life safety, as pertains to sub-surface construction materials, that is, everything except the surface materials. The HRR of surface materials, on the other, is crucial to life safety. But noncombustibility is not useful metric for hazard. It was recommended that a solution which is consistent with fire safety engineering concepts and is presented in a practical way is the Cleary/Quintiere calculation of the '*b*' parameter, in Equation 28.1. A comparison to large-scale room fire test results showed a very good ability of this parameter to distinguish materials which led to hazardous fire conditions, versus ones which did not.

In addition, low HRR materials may show up in the form of composites, where the top layer is highly resistant to burning, while the layer (s) underneath are less so. Such constructions present issues which are discussed in the next section.

Composites

The cone calorimeter is inherently designed to be able to test composite products, provided the layers are can adequately be represented by an

assembly no more than 50 mm deep. In practice, this allows for a reasonable representation of products which are even much thicker, provided that there are not additional layers which are both deep and producing a high HRR. In some cases, however, special precautions need to be taken.

For example, upholstered furniture composites cannot be tested in a representative manner unless the outer layers are constrained to stay in place, instead of crumpling due to exposure to heat. In view of this need, a special test method, ASTM E 1474 [62], was developed for preparing and testing such composites.

Some high-pressure laminates explosively delaminate when subjected to heating. These can only be tested if the use of the wire grid and edge frame eliminates this problem, which it normally does. Another special category of products are ones where the surface layer has a low HRR, while layers underneath show a much higher HRR. If tested simply as a cut specimen, the edges are likely to get involved early, and this may produce unrepresentative burning. The problem was studied by Canadian researchers [63, 64] who developed a special holder which protects the edges of such specimens. The latter was incorporated into the Canadian CAN/ULC S135 standard [65].

Measurements Taken with the Cone Calorimeter

The relevant ISO [1] or ASTM [2] standards mandate certain minimum variables to be recorded. In practice, it is normally desired to make the data from the test be as complete as possible. Cone calorimeter data are normally handled as data tables and files standardized according to the Fire Data Management System (FDMS) prescription [66]. A complete set of data from the cone calorimeter are illustrated there. Here the more important of these are given, somewhat augmenting the ISO and ASTM set. Note that most items must be reported for each test run, and a complete test consists of three runs.

Identification	Various data items must be included here
Preparation	Any nonstandard specimen preparation details must be reported
Test number	Serial number of test; also information on testing laboratory, operator, and so forth
Irradiance	The heating flux set for the test ($kW \cdot m^{-2}$)
Exhaust flow rate	Recorded for completeness, usually the standard value of 24 $L \cdot s^{-1}$
Orientation	Horizontal or vertical
Spark ignition	Yes or no
Edge frame	Yes or no
Wire grid	Yes or no
Area of specimen	(m^2), since may be nonstandard in special cases
Specimen initial mass	(g)
Specimen final mass	(g)
Time to ignition	According to the ISO and ASTM standards, "sustained flaming" (s)
Time to flameout	(s)
Peak $\dot{q}''$	($kW \cdot m^{-2}$)
Peak $\dot{m}''$	($g \cdot s^{-1} \cdot m^{-2}$)
Total q''	($MJ \cdot m^{-2}$)
O_2 consumption	($kJ \cdot kg^{-1}$); this is set to a specific constant value if known, otherwise to 13,100
Effective heat of combustion	($MJ \cdot kg^{-1}$), reported for period of entire test run
Specific extinction rate	($m^2 \cdot kg^{-1}$), reported for period of entire test run
Average mass loss rate	Computed over period starting when 10 % of the ultimate specimen mass loss rate has occurred and ending at the time when 90 % of the ultimate specimen mass loss has occurred ($g \cdot s^{-1} \cdot m^{-2}$)
Average $\dot{q}''$ (60 s)	Computed for the first 60 s after ignition ($kW \cdot m^{-2}$)
Average $\dot{q}''$ (180 s)	Computed for the first 180 s after ignition ($kW \cdot m^{-2}$)
Average $\dot{q}''$ (300 s)	Computed for the first 300 s after ignition ($kW \cdot m^{-2}$)

Note in the above 60, 180, and 300 s averages that, if the test is ended before having burned, say, 300 s, a proper average can still be correctly computed (i.e., at the end of the averaging period a number of zeroes are used for data points past

the end of the test). Since users are often confused by this point, it must be emphasized: it is not sensible to report an "average heat-release rate" without specifying the time interval. The reason has to do with the question of determining the end of the test. The ISO and ASTM standards specify that the end of the test is considered to be

1. After all flaming and other signs of combustion cease
2. While there may still be vestigial combustion evidence, but the mass loss rate has become very small (less than 150 $g \cdot m^{-2}$ being lost during any 1 min)
3. 60 min have elapsed

These rules are needed for establishing some uniformity among testing laboratories. They do not, however, mean that it is technically sound to compare the average of one material that may have burned for 10 min with another that may have burned for 5 min. It is technically sound, however, to compare their burning over the first one, three, and so forth, minutes of test.

Further information on the form, units, and usage of fire properties measured in the cone calorimeter can be found in Babrauskas [67]; specific information on the smoke and soot properties measured in the cone calorimeter is given in Babrauskas and Mulholland [48].

Repeatability and Reproducibility

The repeatability, r, and reproducibility, R, of the cone calorimeter were studied in two sets of interlaboratory trials, one sponsored by ISO and one by ASTM. According to the ISO instructions [68], the definitions of repeatability and reproducibility were taken as

$$r = 2.8\sigma_r$$
$$R = 2.8\sigma_R$$

where σ_r is the repeatability standard deviation, σ_R is the reproducibility standard deviation, and the 2.8 factor comes from specifying the probability level of 95 %.

From the results of the interlaboratory trials, values for r and R were calculated for six variables. These variables, chosen as being representative for the test results, were t_{ign}, $\dot{q}''_{max}$, $\dot{q}''_{180}$, q_{tot}'', $\Delta h_{c,eff}$, and σ_f. A linear regression model was used to describe r and R as functions of the mean overall replicates and overall laboratories for each of the six variables. The regression equations given below also indicate the range of mean values over which the fit was obtained.

The results for time to sustained flaming, t_{ign}, in the range of 5–150 s were

$$r = 4.1 + 0.125 t_{ign}$$
$$R = 7.4 + 0.220 t_{ign}$$

The results for peak heat release rate, $\dot{q}''_{max}$, in the range of 70–1120 $kW \cdot m^{-2}$ were

$$r = 13.3 + 0.131 \dot{q}''_{max}$$
$$R = 60.4 + 0.141 \dot{q}''_{max}$$

The results for 180 s average heat release rate, $\dot{q}''_{180}$, in the range of 70–870 $kW \cdot m^{-2}$ were

$$r = 23.3 + 0.037 \dot{q}''_{180}$$
$$R = 25.5 + 0.151 \dot{q}''_{180}$$

The results for total heat released, $\dot{q}''_{tot}$, in the range of 5–720 $MJ \cdot m^{-2}$ were

$$r = 7.4 + 0.068 q''_{tot}$$
$$R = 11.8 + 0.088 q''_{tot}$$

The results for effective heat of combustion, $\Delta h_{c,eff}$, in the range of 7–40 $kJ \cdot g^{-1}$ were

$$r = 1.23 + 0.050 \Delta h_{c,eff}$$
$$R = 2.42 + 0.055 \Delta h_{c,eff}$$

The results for average specific extinction area, σ_f, in the range of 30–2200 $m^2 \cdot kg^{-1}$ were

$$r = 59 + 0.076 \sigma_f$$
$$R = 63 + 0.215 \sigma_f$$

A comparison of the cone calorimeter repeatability and reproducibility to the values obtained for the ISO 5657 radiant ignition test showed the cone calorimeter results to be about a factor of 2 better.

Fig. 28.19 The NIST controlled-atmosphere cone calorimeter

Special Cone Calorimeters

The standard cone calorimeter has been designed to use room air for combustion. All standard testing is done under such conditions. For special combustion studies, however, it can be of interest to explore the burning of materials at oxygen levels other than 21 %. Such a unit, constructed at NIST, is described in Babrauskas et al. [38]. This controlled-atmosphere unit has already been used for studies of the burning of materials in air supplies with less than 21 % oxygen, with N_2 or CO_2 being mixed into the air stream (Fig. 28.19). It has also been used for pyrolysis studies under pure nitrogen flow conditions. In principle, it could also be used for studies of enriched-oxygen atmospheres; however, the necessary safety procedures for handling high-concentration oxygen streams are required. A unit for handling O_2 mixtures greater than 21 % has been constructed for NASA, but data are not yet available from it. A controlled-atmosphere unit is also appropriate for use when airflow rates of less than 12 $L \cdot s^{-1}$ are required.

All of the present cone calorimeter designs, both standard and otherwise, have been designed for use only under ambient pressures. There is interest at this time from at least one research group to design and construct a unit for aerospace studies that would function under nonambient pressures.

Nomenclature

$\boldsymbol{b}$	Parameter
$\boldsymbol{F}$	View factor (-)
$\boldsymbol{h_c}$	Convective heat transfer coefficient ($W \cdot m^{-2} \cdot K^{-1}$)
ℓ	Thickness (mm)
$\dot{m}''$	Mass loss rate ($g \cdot s^{-1} \cdot m^{-2}$)
$\dot{q}$	Total energy released per unit area ($MJ \cdot m^{-2}$)
$\boldsymbol{q''}$	Total energy released per unit area ($MJ\ m^{-2}$)
$\dot{q}''$	Heat flux ($kW \cdot m^{-2}$)
$\dot{q}''_{180}$	180 s average heat release rate ($kW \cdot m^{-2}$)
$\dot{q}''_{avg}$	Average heat release rate ($kW\ m^{-2}$)
$\dot{q}''$	Irradiance ($kW\ m^{-2}$)
$\dot{q}''_{\max}$	Maximum heat release rate ($kW\ m^{-2}$)
$\dot{q}''_{\text{tot}}$	Total heat released ($MJ \cdot m^{-2}$)

$\dot{q}''_{cr}$	Critical heat flux (kW m^{-2})
r	Repeatability (units dependent on quantity investigated)
R	Reproducibility (units dependent on quantity investigated)
t_b	Duration of flaming (s)
t_{ig}	Ignition time (s)
$\Delta h_{c,eff}$	Effective heat of combustion (MJ · kg^{-1})
ε	Emissivity (-)
$\lambda \rho C$	Thermal inertia (kJ^2 m^{-4} s^{-1} K^{-2})
ρ	Density (kg·m^{-3})
σ_r	Repeatability standard deviation (units dependent on quantity investigated)
σ_R	Reproducibility standard deviation (units dependent on quantity investigated)
σ_f	Average specific extinction area (m^2 · kg^{-1})

References

1. ISO 5660, International Standard, "Reaction-To-Fire Tests—Heat Release, Smoke Production and Mass Loss Rate," International Organization for Standardization, Geneva (2002).
2. ASTM E1354, *Standard Test Method for Heat and Visible Smoke Release Rates for Materials and Products Using an Oxygen Consumption Calorimeter,* American Society for Testing and Materials, West Conshohocken, Pennsylvania (2011).
3. W.H. Twilley and V. Babrauskas, "User's Guide for the Cone Calorimeter," *NBS Special Publication SP 745,* U.S. National Bureau of Standards, Gaithersburg, MD (1988).
4. V. Babrauskas and S.J. Grayson, eds., *Heat Release in Fires,* Elsevier, London (1992). Distributed in the U.S. by NFPA.
5. Babrauskas, V., Bench-Scale Methods for Prediction of Full-Scale Fire Behavior of Furnishings and Wall Linings (SFPE Technical Report 84-10), Society of Fire Protection Engineers, Boston (1984).
6. Petrella, R. V., Assessment of Full-Scale Fire Hazards and Cone Calorimeter Data, *J. Fire Sciences* **12**, 14–43 (1994).
7. Cleary, T. G., and Quintiere, J. G., Framework for Utilizing Fire Property Tests, pp. 647–656 in *Proc. 3rd Intl. Symp. on Fire Safety Science*, Intl. Assn. for Fire Safety Science. Elsevier Applied Science, New York (1991).
8. Babrauskas, V., **Ignition Handbook**, Fire Science Publishers/Society of Fire Protection Engineers, Issaquah WA (2003).
9. Capote, J. A., Alvear, D., Lazano, M., and Espina, P., Heat Release Rate and Computer Fire Modelling vs. Real-Scale Fire Tests in Passenger Trains, *Fire & Materials* **32**, 213–229 (2008).
10. Aksit, I. M., Moss, J. B., and Rubini, P. A., CFD Simulation of Cable Tray Fires, pp. 1129–1140 in *Interflam 2001—Proc. 9th Intl. Conf.*, Interscience Communications Ltd., London (2001).
11. Andersson, J., and Persson, F., Datostöd simulering av pyrolysförlopp [Computer supported simulation of pyrolysis], Examensarbete, Dept. of Chemical Engineering, Chalmers Lindholmen University College, Göteborg, Sweden (2001).
12. Tsai, T.-H., Li, M.-J., Shih, I-Y., Jih, R., and Wong, S.-C., Experimental and Numerical Study of Autoignition and Pilot Ignition of PMMA Plates in a Cone Calorimeter, *Combustion and Flame* **124**, 466–480 (2001).
13. Wade, C., A Room Fire Model Incorporating Fire Growth on Combustible Linings (M.S. thesis), Dept. of Fire Protection Engineering, Worcester Polytechnic Institute, Worcester MA (1996).
14. Wade, C. A., LeBlanc, D., Ierardi, J., and Barnett, J. R., A Room-Corner Fire Growth and Zone Model for Lining Materials, pp. 106–117 in *Proc. 2nd Intl. Conf. on Fire Research and Engineering*, Society of Fire Protection Engineers, Bethesda MD (1998).
15. Wade, C. A., A Theoretical Model for Fire Spread in a Room Corridor Configuration, pp. 295–306 in *Proc. 3rd Intl. Conf. on Performance-Based Codes and Fire Safety Design Methods*, Society of Fire Protection Engineers, Bethesda MD (2000).
16. Lattimer, B. Y., Hunt, S. P., Wright, M., and Sorathia, U., Modeling Fire Growth in a Combustible Corner, *Fire Safety J.* **38**, 771–796 (2003).
17. Janssens, M. L., and Dillon, S. E., Balanced Approach to the Fire Performance Evaluation of Interior Finish Materials, pp. 43–50 in Fifteenth Meeting of the UJNR Panel on Fire Research and Safety, March 1–7, 2000 (NISTIR 6588), S. L. Bryner, ed., Nat. Inst. Stand. & Technol., Gaithersburg MD (2000).
18. Karlsson, B., Models for Calculating Flame Spread on Wall Lining Materials and the Resulting Heat Release Rate in a Room, *Fire Safety J.* **23**, 365–386 (1994). Published in 1995.
19. Grant, G., and Drysdale, D., Numerical Modelling of Early Flame Spread in Warehouse Fires, *Fire Safety J.* **24**, 247–278 (1995).
20. Kokkala, M., Baroudi, D., and Parker, W. J., Upward Flame Spread on Wooden Surface Products: Experiments and Numerical Modelling, pp. 309–320 in *Fire Safety Science—Proc. 5th Intl. Symp.*, Intl. Assn. for Fire Safety Science (1997).
21. Beyler, C. L., Hunt, S. P., Iqbal, N., and Williams, F. W., A Computer Model of Upward Flame Spread on Vertical Surfaces, pp. 297–308 in *Fire Safety Science—Proc. 5th Intl. Symp.*, Intl. Assn. for Fire Safety Science (1997).

22. North, G. A., An Analytical Model for Vertical Flame Spread on Solids: An Initial Investigation (Fire Engineering Research Report 99/12), School of Engineering, University of Canterbury, New Zealand (1999).
23. Wright, M. T., Flame Spread on Composite Materials for Use in High Speed Craft (M.S. thesis), Worcester Polytechnic Institute, Worcester MA (1999).
24. Hostikka, S., and Axelsson, J., Modeling of the Radiative Feedback from the Flames in the Cone Calorimeter (TR 540), Nordtest, Espoo, Finland (2003).
25. Hakkarainen, T., and Hayashi, Y., Comparison of Japanese and European Fire Classification Systems for Surface Linings, *Fire Science & Technology (Japan)* **21**:1, 19–42 (2001).
26. International Code for Application of Fire Test Procedures, 2010 (2010 FTP Code), International Maritime Organization, London (2011).
27. B.J. McCaffrey and G. Cox, "Entrainment and Heat Flux of Buoyant Diffusion Flames," *NBSIR 82-2473,* U.S. National Bureau of Standards (1982).
28. J.R. Hallman, "Ignition Characteristics of Plastics and Rubber," Ph.D. Dissertation, University of Oklahoma, Norman (1971).
29. B. Hägglund and L.-E. Persson, "The Heat Radiation from Petroleum Fires," FOA Rapport C 20126-D6 (A3), Försvarets Forskningsanstalt, Stockholm, Sweden (1976).
30. V. Babrauskas, "Estimating Large Pool Fire Burning Rates," *Fire Technology,* 19, pp. 251–261 (Nov. 1983).
31. J.J. Comeford, "The Spectral Distribution of Radiant Energy of a Gas-Fired Radiant Panel and Some Diffusion Flames," *Combustion and Flame,* 18, pp. 125–132 (1972).
32. A. Tewarson, "Physico-Chemical and Combustion/Pyrolysis Properties of Polymeric Materials," *NBS-GCR-80-295,* U.S. National Bureau of Standards, Gaithersburg, MD (1980).
33. ISO 5657, "Reaction to Fire Tests—Ignitability of Building Products Using a Radiant Heat Source," International Organization for Standardization, Geneva (1997).
34. M.L. Janssens, "Fundamental Thermophysical Characteristics of Wood and Their Role in Enclosure Fire Growth," Ph.D. Dissertation, University of Gent, Belgium (1991).
35. Boulet, P., et al., Characterization of the Radiative Exchanges When Using a Cone Calorimeter for the Study of Plywood Pyrolysis, *Fire Safety J.* **51** 53–60 (2012).
36. V. Babrauskas, "Development of the Cone Calorimeter—A Bench-Scale Heat Release Rate Apparatus Based on Oxygen Consumption," *Fire and Materials,* 8, pp. 81–95 (1984).
37. Babrauskas, V., and Wetterlund, I., The CBUF Cone Calorimeter Test Protocol: Results from International Round Robin Testing (SP Report 1996:12), Swedish National Testing and Research Institute, Borås (1996).
38. V. Babrauskas, W.H. Twilley, M. Janssens, and S. Yusa, "A Cone Calorimeter for Controlled-Atmospheres Studies," *Fire and Materials, 16,* pp. 37–43 (1992).
39. ASTM E906, *Standard Test Method for Heat and Visible Smoke Release Rates for Materials and Products Using a Thermopile Method,* American Society for Testing and Materials, West Conshohocken, Pennsylvania (2010).
40. V. Babrauskas, "Combustion of Mattresses Exposed to Flaming Ignition Sources, Part II. Bench-Scale Tests and Recommended Standard Test," *NBSIR 80-2186,* U.S. National Bureau of Standards (1981).
41. R.M. Nussbaum and B.A.-L. Östman, "Larger Specimens for Determining Rate of Heat Release in the Cone Calorimeter," *Fire and Materials,* 10, pp. 151–160 (1986).
42. V. Babrauskas, Letter to the editor, *Fire and Materials,* 11, p. 205 (1987).
43. L. Orloff, J. deRis, and G.H. Markstein, "Upward Turbulent Fire Spread and Burning of Fuel Surfaces," in *Fifteenth Symposium (International) on Combustion,* The Combustion Institute, Pittsburgh, PA, pp. 183–192 (1974).
44. L. Orloff, A.T. Modak, and R.L. Alpert, "Burning of Large-Scale Vertical Wall Surfaces," in *Sixteenth Symposium (International) on Combustion,* The Combustion Institute, Pittsburgh, PA, pp. 1345–1354 (1976).
45. W.D. Weatherford, Jr. and D.M. Sheppard, "Basic Studies of the Mechanism of Ignition of Cellulosic Materials," *Tenth Symposium (International) on Combustion,* The Combustion Institute, Pittsburgh, PA, pp. 897–910 (1965).
46. H.R. Wesson, J.R. Welker, and C.M. Sliepcevich, "The Piloted Ignition of Wood by Thermal Radiation," *Combustion and Flame,* 16, pp. 303–310 (1971).
47. J. Urbas and H. Sand, "Some Investigations on Ignition and Heat Release of Building Materials Using the Cone Calorimeter," in *Interflam'90, Fifth International Fire Conference Proceedings,* Interscience Communications, Ltd., London, pp. 183–192 (1990).
48. V. Babrauskas and G. Mulholland, "Smoke and Soot Data Determinations in the Cone Calorimeter," in ASTM STP 983, *Mathematical Modeling of Fires,* American Society for Testing and Materials, Philadelphia, pp. 83–104 (1987).
49. P.J. Geake, "Smoke Characterisation by Laser Diffraction," Ph.D. Dissertation, Polytechnic of the South Bank, London (1988).
50. Hayakawa, T., Sakurai, Y., and Yoshida, K., Development of New Test Method of Cone Calorimeter for Liquid Substances, National Maritime Research Institute, Tokyo (2004).
51. Iwata, Y., Koseki, H., Janssens, M. L., and Takahashi, T., Comparison of Combustion Characteristics of Crude Oils, *Fire and Materials* **25**, 1–7 (2001).

52. Liu, J., Liao, G., Fan, W., and Yao, B., Study of Liquid Pool Fire Suppression with Water Mists by Cone Calorimeter, *J. Fire Sciences* **20**, 465–477 (2002).
53. Hshieh, F.-Y., and Julien, C. J., Experimental Study on the Radiative Ignition of Silicones, *Fire and Materials* **22**, 179–185 (1998).
54. Armand, Y., Delfau, J. L., and Vovelle, C., Kinetics of Thermal Degradation of Solid or Liquid Components under a Radiative Flux, pp. 205–221 in *Industrial Fires II—Workshop Proceedings* (Report EUR 15967 EN), European Commission, Luxembourg (1995).
55. Breulet, H., and Desmet, S., Characterization of Industrial Liquids by Means of the Cone Calorimeter, pp. 223–235 in *Industrial Fires II—Workshop Proceedings* (Report EUR 15967 EN), European Commission, Luxembourg (1995).
56. Grand, A. F., and Trevino, J. O., Flammability Screening and Fire Hazard of Industrial Fluids Using the Cone Calorimeter, pp. 157–173 in Fire Resistance of Industrial Fluids (ASTM STP 1284), ASTM, Philadelphia (1995).
57. Elam, S. K., Altenkirch, R. A., Saito, K., and Arai, M., Cone Heater Ignition Tests of Liquid Fuels, *Fire Safety J.* **16**, 65–84 (1990).
58. Standard Test Method for Using a Cone Calorimeter to Determine Fire-Test-Response Characteristics of Insulating Materials Contained in Electrical or Optical Fiber Cables (ASTM D 6113), ASTM Intl., West Conshohocken PA.
59. Grayson, S. J., et al., Fire Performance of Electric Cables—New Test Methods and Measurement Techniques (Contract no. SMT4-CT96-2059), final report to the European Commission. Interscience Communications Ltd., London (2000).
60. Gensous, F., and Grayson, S., Improved Procedure for Testing Intumescent Materials Using the Cone Calorimeter, pp. 977–981 in *Interflam'96*, Interscience Communications Ltd, London (1996).
61. Babrauskas, V., and Janssens, M., Quantitative Variables to Replace the Concept of 'Noncombustibility,' pp. 77–90 in *Proc. Fire & Materials 2009*, Interscience Communications Ltd, London (2009).
62. ASTM E 1474, *Standard Test Method for Determining the Heat Release Rate of Upholstered Furniture and Mattress Components or Composites Using a Bench-Scale Oxygen Consumption Calorimeter*, ASTM Intl., West Conshohocken PA (2010).
63. Richardson, L. R., Determining Degrees of Combustibility of Building Materials—National Building Code of Canada, *Fire and Materials* **18**, 99–106 (1994).
64. Richardson, L. R., and Brooks, M. E., Combustibility of Building Materials, *Fire and Materials* **15**, 131–136 (1991).
65. Standard Method of Test for Determination of Degrees of Combustibility of Building Materials using an Oxygen Consumption Calorimeter (Cone Calorimeter), National Standard of Canada, CAN/ULC-S135, Underwriters' Laboratories of Canada, Scarborough, Ont., Canada.
66. V. Babrauskas, R.D. Peacock, M. Janssens, and N.E. Batho, "Standardizing the Exchange of Fire Data—The FDMS," *Fire and Materials,* 15, pp. 85–92 (1991).
67. V. Babrauskas, "Effective Measurement Techniques for Heat, Smoke, and Toxic Fire Gases," in *Fire: Control the Heat . . . Reduce the Hazard,* QMC Fire & Materials Centre, London, pp. 4.1–4.10 (1988).
68. ISO 5725, "Accuracy (Trueness and Precision) of Measurement Methods and Results," International Organization for Standardization, Geneva (1986).

Vytenis Babrauskas is the president of Fire Science and Technology Inc., a company specializing in fire safety research, fire testing issues, and fire science applications to fire investigations and litigations.

Compartment Fire Modeling

29

James G. Quintiere and Colleen A. Wade

Introduction

An approach for predicting various aspects of fire phenomena in compartments has been called *zone* modeling. Based on a conceptual representation for the compartment fire process, it is an approximation to reality. Any radical departure by the fire system from the basic concept of the zone model can seriously affect the accuracy and validity of the approach. The zone model represents the system simply as two distinct compartment gas zones: an upper volume and a lower volume resulting from thermal stratification due to buoyancy. Conservation equations are applied to each zone and serve to embrace the various transport and combustion processes that apply. The fire is represented as a source of energy and mass manifested as a plume, which acts as a pump for the mass from the lower zone to the upper zone through a process called *entrainment*.

The zone modeling approach emerged in the mid-1970s when the effort to study the developing fire in a compartment intensified. Careful measurements and observations revealed characteristics of the compartment fire system. The upper and lower layers (zones) were deemed relatively uniform in temperature and composition. Distinct phenomena were discerned that could be studied in isolation, enabling better predictions of their roles in the compartment fire system.

Fowkes [1], in his work with Emmons on the Home Fire Project, was the first to publish a basis for the zone model approach in his description of the "Bedroom Fire" series conducted at Factory Mutual Research Corporation (FMRC). Almost simultaneously, computer models based on the zone model approach were produced by Quintiere [2], Pape and Waterman [3], and Mitler [4] working with Emmons. Since then the development of such computer models has been prolific, extending early efforts on single rooms to computer codes that can address a number of interconnected rooms, using a number of new fire phenomena and computer features. These advances in fire science, together with computer development, have given the engineer convenient tools for investigating the fire hazard in buildings. A notable illustration of such a tool is the Hazard I software developed by the National Institute of Standards and Technology (NIST) [5], only one of numerous current computer codes and software packages based on the zone model approach. In 1992, Friedman [6] cited 21 zone models in use around the world. In 2003, Olenik and Carpenter [7] revisited the survey and summarised the available computer models and their general capabilities. For a discussion of specific zone computer fire models, see Chap. 31.

J.G. Quintiere (✉) • C.A. Wade

M.J. Hurley (ed.), *SFPE Handbook of Fire Protection Engineering*,
DOI 10.1007/978-1-4939-2565-0_29, © Society of Fire Protection Engineers 2016

This chapter outlines the basic conservation equations for the gas zones and describes the various transport and combustion processes that make up the system, referred to as the submodels of the system. As such, they can contribute subroutines to computer codes, which implement the mathematical solution. Discussion of submodels will be limited, but the reader will be referred to appropriate references. In most cases, other chapters of *The SFPE Handbook of Fire Protection Engineering* will be cited. No discussion of a computer code or its numerical solution algorithm will be addressed, since these are issues more of style and mathematics. The presentation will elucidate the mathematical basis of the zone model, its assumptions, its features, and its scope of application. Each user of this approach must sufficiently understand its basis to assess its accuracy and validity. When used correctly, zone models predict the average macroscopic features of compartment fires. There are many examples of comparisons to data that illustrate their level of accuracy, and these will not be repeated here. The user must be skilled in assessing the quality of the data and submodels that directly influence the variables of the problem of interest. It is hoped that the discussion that follows will make the user more knowledgeable or sensitive in making these quality assessments.

Conservation Equations

The building block of the zone model is the conservation equations for the upper and lower gas zones. These equations are developed either (1) by using fundamental equations of energy, mass, and momentum transport in control volume form as applied to the zones, or (2) by using differential equations that represent the conservation laws and integrating them over the zones. However, the momentum equation will not be explicitly applied, since information needed to compute velocities and pressures is based on assumptions and specific applications of momentum principles at vent boundaries of the compartment. An extensive review of control volume equations for mass, species, and energy conservation in a combustion system has been presented by Quintiere [8] and serves as a reference for the equations that follow.

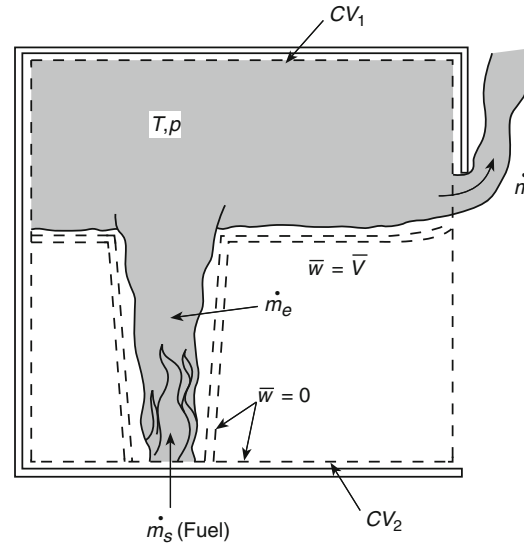

Fig. 29.1 Control volumes selected in zone modeling

Figure 29.1 illustrates a typical zone model for a compartment fire process. It shows a fire plume and a door vent. The hot combustion gases that collect in the upper space of the room and spill out of the vent constitute the upper-layer zone. A control volume, CV_1, is defined to enclose the gas in this upper layer and the fire plume. The lower interface of the upper layer moves with the control volume such that no mass is transferred across this thermally stratified region. The velocity of the control volume along this interface, $\overline{w}$, is equal to the fluid velocity, $\overline{v}$. The temperature of the upper layer is greater than that in the lower layer (zone) which includes all the remaining gas in the room, and is delineated by a second control volume, CV_2. It has been assumed in zone modeling that the volume of the fire plume is small relative to the gas layer or zone volumes, and therefore its effect has been ignored. In general, multiple fire plumes can occur at any height in the room, and multiple vents or mass transport can take place between the zones (CV_1 and CV_2) and the surroundings. In each case mass transport must be appropriately

described in terms of the system variables; however, this may not always be easy or known. The properties of the upper and lower zones are assumed to be spatially uniform, but can vary with time. Thus, temperature, T, and species mass concentration, Y_i, are properties associated with ideal upper and lower homogeneous gas layers. Other assumptions in the application of the conservation laws to the zones are listed below:

1. The gas is treated as an ideal gas with a constant molecular weight and constant specific heats: c_p and c_v.
2. Exchange of mass at free boundaries is due to pressure differences or shear mixing effects. Generally these are caused by natural or forced convection, or by entrainment processes.
3. Combustion is treated as a source of mass and energy. No mechanism from first principles is included to resolve the extent of the combustion zone.
4. The plume instantly arrives at the ceiling. No attempt is made to account for the time required to transport mass vertically or horizontally in the compartment. Hence, transport times are not explicitly accounted for in zone modeling.
5. The mass or heat capacity of room contents is ignored compared to the enclosure wall, ceiling, and floor elements; that is, heat is considered lost to the structure, but not to the contents. Where room contents shield boundary structural surfaces, some compensations can occur in the analysis, but for cluttered rooms this assumption may be poor.
6. The horizontal cross section of the enclosure is a constant area, A. In most cases of zone modeling, rectilinear compartments have been considered. However, this is not a necessary assumption, and enclosures in which A varies with height can easily be handled.
7. The pressure in the enclosure is considered uniform in the energy equation, but hydrostatic variations account for pressure differences at free boundaries of the enclosure; that is, $p \gg \rho gH$. In general, the enclosure pressure, p, is much greater than the variations due to hydrostatics. For example, for $p = 1$ atm $= 14.7$ psi $= 10^2$ kPa (kN/m^2) $= 10^5$ Pa, the hydrostatic variation for a height, $H = 1$ m, gives a pressure difference of $\rho gH = 1.2$ kg/m^3 $\times$ 9.8 m/s^2 $\times$ 1 m $= 10$ kg/m·s^2 $= 10$ Pa (N/m^2).
8. Mass flow into the fire plume is due to turbulent entrainment. Entrainment is the process by which the surrounding gas flows into the fire plume as a result of buoyancy. Empirically, the inflow velocity linearly depends on the vertical velocity in the plume.
9. Fluid frictional effects at solid boundaries are ignored in the current models.

Conservation of Mass

The conservation of mass for a control volume states that the rate of change of mass in the volume plus the sum of the net mass flow rates out for J flow streams is zero

$$A\frac{d}{dt}(\rho z_l) + \sum_{\substack{j=1 \\ (\text{netout})}}^{J} \dot{m}_j = 0 \qquad (29.1)$$

where

ρ = Density of the gas in the control volume (or zone)

z_l = Height of the zone

For the illustration in Fig. 29.1, applying Equation 29.1 to the upper layer (CV_1) would give

$$\sum_{j=1}^{3} \dot{m}_j = \dot{m} - \dot{m}_e - \dot{m}_s \qquad (29.2)$$

where

$\dot{m}$ = Mass flow rate out of the door

$\dot{m}_e$ = Mass rate of entrainment into the fire plume

$\dot{m}_s$ = Mass rate of gaseous fuel supplied

Mass flows at the boundaries can occur due to many phenomena. Therefore, the user or designer of a zone model must include the appropriate mass flow phenomena. For example, in addition to the mass rates in Equation 29.2, mass flows can occur due to forced convection from wind or ventilation effects, from shear entrainment as flows affect layer interfaces, or from cold plumes that could plunge through hot layers.

Conservation of Species

The mass concentration of species i is given by Y_i. By using Equation 29.1 and applying the conservation of mass for species i to a control volume, it follows that

$$\rho z_l A \frac{dY_i}{dt} + \sum_{j=1}^{J} \dot{m}_j \left(Y_{ij} - Y_i\right) = \dot{\omega}_i \qquad (29.3)$$

Where

Y_{ij} = Mass concentration of species i leaving the control volume through the j flow stream

$\dot{\omega}_i$ = Mass concentration rate of species due to combustion

The production term, $\dot{\omega}_i$, in principle, can be described through a knowledge of the chemical equation of the reaction or its particular stoichiometry. Thus, stoichiometric coefficients can be used to represent the production of species and the consumption of oxygen in terms of the mass rate of fuel *reacted*. Stoichiometry is not easily determined, and the fuel gases as they emerge from the pyrolysis of solids can take many chemical forms that differ from the solid fuel's original molecular composition. A partial way to overcome these complications has been to represent the mass production of species for fire in terms of the rate of mass *loss* for the pyrolyzing fuel. Hence, one must be careful to distinguish between the mass of fuel lost and that reacted, and to relate available species yield data to the particular fire conditions of the application. Yield is defined as the mass ratio of species to fuel lost. The yields or production rates may change with fire conditions, and therefore, in general, will not be consistent with data from small-scale tests. For example, the production rate of CO changes markedly with air-to-fuel ratio.

Conservation of Energy

The conservation of energy for the control volume is applied along with Equation 29.1 and the equation of state, $p = \rho RT$, to give

$$\rho c_p z_l A \frac{dT}{dt} - z_l A \frac{dp}{dt} + c_p \sum_{j=1}^{J} \dot{m}_j \left(T_j - T\right) = \dot{\omega}_F \Delta H - \dot{Q}_{\text{net loss}} \qquad (29.4)$$

where

T = Temperature of the gases within the control volume

T_j = Temperature of the gases in the j flow stream crossing the control volume boundary

$\dot{Q}_{\text{net loss}}$ = Net rate of heat transfer lost at the boundary

ΔH = Heat of combustion (taken as a positive quantity)

$\dot{\omega}_F$ = Rate at which the fuel supplied is *reacted*

Usually in zone models it is assumed that all of the fuel supplied can react, provided there is sufficient oxygen available. One assumption on the sufficiency of oxygen is to consider that all the fuel supplied is reacted as long as the oxygen concentration in that control volume is greater or equal to zero, that is,

$$\dot{\omega}_F = \dot{m}_s \quad \text{if} \quad Y_o \geq 0 \qquad (29.5)$$

Thereafter, an excess rate of fuel can exist that can be transported into adjoining zones or control volumes where a decision must be made about whether it can continue to react. At this condition, all of the net oxygen supplied to the control volume is reacted, so that, as long as $Y_o = 0$

$$\dot{\omega}_F = r \times (\text{net mass rate of oxygen supplied}) \qquad (29.6)$$

where r is the stoichiometric fuel-to-oxygen mass ratio. This condition when $Y_o = 0$ in compartment fires is termed the ventilation-limited condition. At this moment, significant changes take place in the nature of the chemical reaction. Notably, incomplete combustion is more likely, and for hydrocarbon fuels this leads to a significant increase in the yield of carbon monoxide and soot. Thus, care must be used in interpreting the results of zone models once ventilation-limited conditions arise, particularly with respect

to the prediction of species concentrations and the extent of burning. Material data used for well-ventilated conditions will no longer apply.

A flame extinction condition can be defined by a flammability line that is based on a critical flame temperature below which extinction occurs and no energy is contributed to the system [9]. Based upon a extinction flame temperature of 1300°C, and incorporating Equations 29.5 and 29.6, the criteria for energy release (or burning rate) is expressed as:

$$\dot{\omega}_F = \begin{cases} \dot{m}_s & ; Y_o > 0 \text{ and } T_f > 1300°\text{C} \\ r\ \dot{m}_o Y_o & ; Y_o = 0 \text{ and } T_f > 1300°\text{C} \\ 0 & ; \quad T_f \leq 1300°\text{C} \end{cases} \tag{29.7}$$

The first term on the left side of Equation 29.4 arises due to the change of internal energy within the control volume. If the temperature is not changing rapidly with time, this term can be small and its elimination gives rise to a quasi-steady approximation for growing fires that allows a more simple analysis. The second term arises from the rate of work done by pressure as the gas layer expands or contracts due to the motion of the thermal stratification interface. Having been rearranged, this term now is expressed as rate of pressure, p, increase for the compartment and is essentially caused by net heat or mass additions to the compartment gases. Except for the rapid accumulation of mass or energy, for compartments with small openings to the surroundings this pressure rise is small, and the pressure nominally remains at nearly the ambient pressure. For example, an addition of 100 kW to a 40 m^3 gas volume in a room with a 0.1 m^2 vent area gives rise to roughly an increase of 10 Pa in less than 10^{-2} s over normal ambient pressure of 10^5 Pa [8]. Any increase in pressure within the compartment could give rise to a flow of mass through a vent, and this term in Equation 29.4 may be associated with a *volumetric expansion* effect. Conversely, a reduction in energy release rate will cause the pressure to drop relative to the ambient. This phenomenon, when cycling between heating and cooling, explains the *breathing effect* for fires in closed buildings.

The third term of Equation 29.4 accounts for the enthalpy flow rates and only applies to j flow streams that enter the control volume, since $T_j = T$ for all flow streams leaving, as long as the uniform temperature assumption still applies.

Summary

The zone model for the compartment fire system consists of two zones: the upper and lower gas layers. The solution process for the layer properties can be visualized by considering the conservation Equations 29.1, 29.3, and 29.4 applied to each zone. The species equation can yield the Y_i for each layer. The mass and energy equations comprise four equations (two for each layer) that permit the determination of the two layer temperatures, one layer height (since the height of the other layer is directly found by difference from the total height of the compartment), and the compartment pressure (which is assumed uniform by Equation 29.4). The densities are found from the ideal gas equation of state in which ρT is approximately a constant. To complete this solution process, each source or transport term in the equations must be given in terms of the above layer properties, or auxiliary relationships must be included for each new variable introduced. The source terms are associated with the $\dot{\omega}_i$ terms, and the transport terms include the j mass flow rates and the boundary heat transfer rates. The extent to which source and transport relationships are included reflects the sophistication and scope of the zone model. Some source and transport terms are essential to a basic zone model, others can be specified as approximations to reality, and others can be ignored when physically irrelevant. These source and transport relationships can comprise subroutines of a zone model computer code. The nature of these submodels is discussed below.

Source Term Submodels

The principal source term for the zone model is the rate of fuel supplied. In an experimental fire this can be known if the fire source is simulated by a gas burner. At the other extreme, the mass of fuel supply can result from a fire spreading over an array of different solid fuels. In general,

$$\dot{m}_s = f(\text{fuel properties, heat transfer}) \quad (29.8)$$

in which the heat transfer to the fuel results from the flame configuration and the heated compartment. The fuel properties are still not completely defined or conventionally accepted for fire applications, since no general theory exists for pyrolysis, and theories of flame spread and ignition are couched in terms of effective fire properties, which are modeling parameters. Nevertheless, data exist for fuel fire properties and can enable approximate models for $\dot{m}_s$ of reasonable accuracy. For example, Tewarson describes how the mass supply and energy release can be determined from fuel properties and tabulates properties for a number of solid fuels (Chap. 36). For realistic items under well-ventilated conditions, Babrauskas has compiled results that could serve as initial estimates for $\dot{m}_s$ in compartment fires (Chap. 26). In under-ventilated compartment fires particularly during the fully developed stage, a more complete submodel should address the fuel response to the thermal feedback from the smoke and compartment walls, and the vitiated oxygen effect on the flame heat flux. The mass of fuel supply (the fuel mass loss rate) can be given as [10],

$$\dot{m}_s = \dot{m}''_s A_{F,b} \frac{Y_{o,l}}{Y_o} + \frac{\dot{q}_{\text{external}}}{L} \quad (29.9)$$

where $\dot{m}''_s$ is the free burning rate per unit area, $A_{F,b}$ is the fuel burning area, $Y_{o,l}$ is the local mass fraction of oxygen feeding the flame, Y_o is the mass fraction of oxygen (ambient), L is the fuel heat of gasification and $\dot{q}_{\text{external}}$ is the total external heat flux feedback from the smoke and the compartment surfaces. The first term on the right hand side of Equation 29.9 represents the vitiated oxygen effect on the flame heat flux while the second term is responsible for the thermal feedback from the smoke and compartment surfaces.

The rate of energy release, $\dot{\omega}_F \Delta H$, required by Equation 29.4 has already been discussed through Equations 29.5, 29.6, and 29.7. The point should be made that the heat of combustion, ΔH, employed must be with respect to the mass of fuel gases pyrolyzed, given by such data as Tewarson's, and is not the theoretical oxygen bomb value for the solid fuel (Chap. 36). Due to incomplete combustion, ΔH will be less than the theoretical value, in general.

The production of species can be described in terms of species yield, γ_i, such that

$$\dot{\omega}_i = \gamma_i \dot{m}_s \quad (29.10)$$

For well-ventilated fires, γ_i may be reasonably constant for a given fuel, as tabulated by Khan et al. (see Chap. 36). In general, it can vary with time and can significantly vary as ventilation-limited conditions are approached and achieved. For example, Tewarson shows that γ_i for CO can vary with equivalence ratio, Φ, where

$$\Phi = \frac{\text{Mass of fuel available}/\text{Mass of oxygen available}}{r} \quad (29.11)$$

where r is the stoichiometric value for complete combustion. Zukoski et al. [11] have shown how this relationship may be applied to compartment fires. The equivalence ratio, Φ, may be computed in a zone (or upper layer) where combustion has occurred by computing the mass concentrations of the "available" fuel and oxygen in the zone. This is done by Equation 29.3 in which $\dot{\omega}_i$ is set equal to zero for both the fuel and oxygen, since this yields the available Y_F and Y_o values, not their actual concentrations in the layer following combustion. The generality of considering $\gamma_i = \gamma_i(\Phi)$ for zone models is still under study, and its use must be considered as exploratory. Nevertheless, it currently offers the only practical approach for estimating species, such as CO, under ventilation-limited conditions in compartment fires.

Mass and Heat Transport Submodels

Entrainment

An essential feature of a zone model is the mass rate of entrainment, $\dot{m}_e$, relationship for the fire plume. This relationship allows the principal mechanism for flow between the lower and upper stratified gas layers. Considerable work has been performed to develop entrainment relationships for pool fires or axisymmetric gas burner fires. Unfortunately both the ideal theoretical plume models and correlations based on data vary widely, and no consensus exists among zone models in practice for the optimum pool fire entrainment model. Rockett [12] illustrates the variations in results he found using different fire entrainment models in the Harvard/NIST Mark VI compartment fire zone model. He found that the layer height, entrainment rate, and layer gas temperature varied by roughly a factor of two among the various models. More useful data rather than ideal mathematical models are clearly needed to resolve this issue of accuracy for a simple pool fire. Yet even a perfect entrainment relationship for an axisymmetric pool fire would not necessarily be perfect in a zone model, because a plume in a compartment can be subject to nonsymmetric airflows that can bend the plume and thus affect its entrainment rate. These wind effects can increase the entrainment rate by as much as two or three times [13], however it is also reported that even small ambient disturbances could provide 20–50 % increases in the measured plume mass flows compared to the 'still' conditions in a laboratory [14].

Rockett [12] has shown that the effect of the entrainment model is crucial to predictions for the developing fire. This research suggests that the entrainment model must be representative of the actual object burning and its location within the enclosure. However while correlations have been developed for axisymmetric plumes and for plumes contacting a wall or corner, no entrainment models exist for an item of furniture; this illustrates a need for further research in this area. Yet this does not mean that the zone model has a fatal flaw; it simply means more systematic data are necessary to expand the versatility of the zone model and its accuracy. Moreover, if a zone model with its selected entrainment relationship tracks well with data from an experimental fire scenario, it can be assumed accurate for simulating the process and can be used with some assurance for that scenario. A catalogue of empirical entrainment relationships for various object fires developed from specialized entrainment apparatus would help resolve the entrainment issue. This apparatus could be developed from the large calorimeter intended to measure energy release rate in which the fire plume is collected in a hood-duct system and the total flow rate is recorded. The reader is referred to Chap. 13 for a more detailed discussion of plume entrainment.

Vent Flows Through Openings in Vertical Partitions

Classic models of fire in a room or building represent the structure with an opening, such as a door or window, to the ambient surroundings. Fire-induced flows through such openings have been well studied, and a widely accepted model exists to compute these flows based on the temperature distribution of the gases on either side of the opening. The theoretical basis of the computation is orifice flow utilizing Bernoulli's equation along a streamline, as illustrated in Fig. 29.2. The velocity at station two is given by

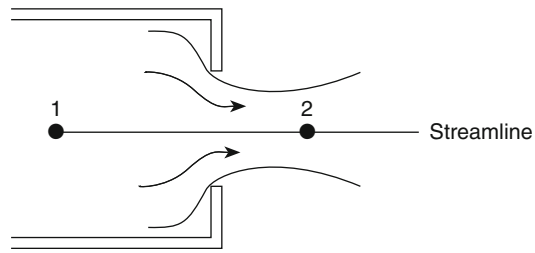

Fig. 29.2 Orifice flow

$$v_2 = \sqrt{\frac{2(p_1 - p_2)}{\rho_1}}. \tag{29.12}$$

where v_1 is assumed to be zero. The mass flow rate is computed by integration over the flow area, A, adjusted by a flow coefficient, C:

$$\dot{m} = C\int \rho_1 v_2 dA \tag{29.13}$$

Emmons suggests that a value of 0.68 for C has an accuracy of ±10 %, except at very low flow rates at the beginning of a fire (see Chap. 15). In general, C will depend on the Reynolds number. Figure 29.3 depicts examples of typical vent flows through an opening in a vertical partition. In both cases Equations 29.12 and 29.13 apply, but the pressure distribution must be described appropriately. For example, in the pure natural convection case shown in Fig. 29.3a, the pressure is determined by the static pressure with respect to the floor pressure, $p(0)$. Actually it is the floor pressure that applies in Equation 29.4 and in the perfect gas equation of state.

The assumption is that the flow velocities are small compared to the vent flow velocities, justifying the static pressure computation. Thus, the vertical pressure distribution on either side of the opening is computed as

$$p(z) = p(0) - \int_0^z \rho g\, dz \tag{29.14}$$

McCaffrey and Rockett [15] illustrate the accuracy of the hydrostatic assumption in Fig. 29.4. The sign of the pressure difference across the opening determines the flow direction. Emmons presents the general equations that enable this computation to be included in a zone model (see Chap. 15). It is by far the most accurate of the submodels, providing the basis for linking rooms together in a zone model, which allows smoke and fire growth computations for a large building.

The flow through an opening in a horizontal partition can be compared to that for the vertical partition, provided the pressure difference is large enough. If there is only a single vent from the fire compartment through a horizontal partition, such as a ceiling, the flow must be oscillatory or bidirectional. The latter case implies a zero pressure difference, with gravity solely determining the flow. A theory for this case has been developed by Epstein [16] and has been implemented by Cooper [17]. For orifice-like vents with zero pressure difference, the volumetric exchange flow rate, V, given by Epstein [16], is approximately

$$\dot{V} = 0.055\left[D^5 g(\rho_1 - \rho_2)\left(\frac{\rho_1 + \rho_2}{2}\right)\right]^{1/2} \tag{29.15}$$

where D is the diameter of the vent and ρ_1 and ρ_2 are the corresponding fluid densities on either side of the vent. For vents of significant depth, L, the coefficient in Equation 29.15 depends on L/D.

Convective Heat Transfer to Surfaces

The $\dot{Q}_{\text{net loss}}$ term in Equation 29.4 is composed of the convective and radiative heat loss to the

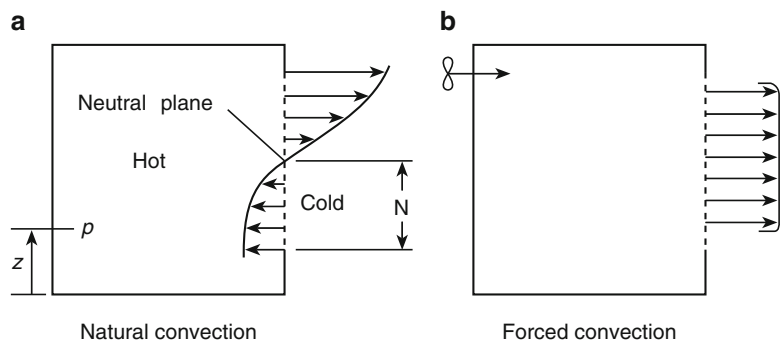

Fig. 29.3 Typical vent flows

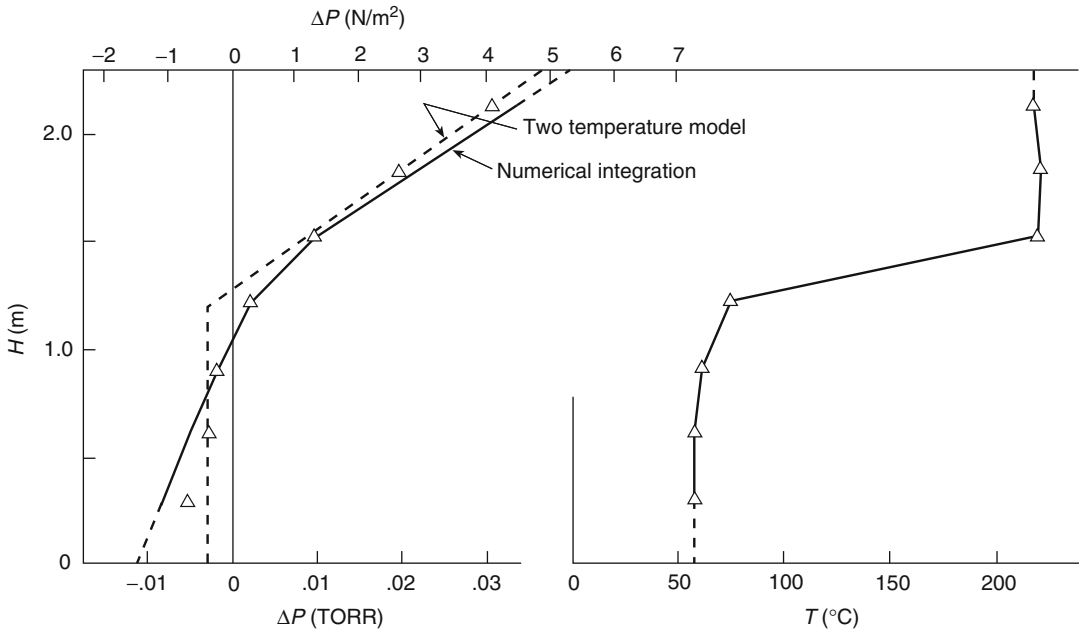

Fig. 29.4 Vertical pressure difference across a room vertical partition compared to a computation based on room fire temperature distribution and a two-temperature zone model approximation using the hydrostatic pressure assumption [15]

boundary surfaces of the layer control volumes. This involves both heat transfer from the gas layers at their bulk temperatures and the heat transfer from the flame. Consistent treatment of the flame and layer gas heat transfer must be carried out for the zone model. If the flame becomes large and fills the upper layer, one cannot count the flame and gas heat transfer without being redundant.

Convective heat transfer to a ceiling by a fire plume has been widely studied at modest scales, such that flame radiation may have been insignificant. Alpert [18] specifically examined only convective heating in contrast to studies by You and Faeth [19] and Kokkala [20] who included flame effects.

In general, convective effects will vary along the ceiling, walls, and floor, and depend on the nature and position of the fire. In some cases an *adiabatic wall temperature* has been appropriately introduced since the driving force for convective heat transfer locally is not the bulk gas layer temperature but rather the local boundary layer temperature, which is not explicitly computed. Convective heat transfer data for the walls and floor of a fire compartment or for rooms beyond the fire compartment have not been developed. Hence, most zone models use estimates from natural convection correlations.

Radiative Heat Transfer

The theory of radiative heat transfer is adequate to develop the needed components for the zone model. However, the theory is not sufficiently developed to predict flame radiation from first principles without very sophisticated modeling of the soot and temperature distributions. Hence, flame radiation is relegated to empirical practices. Radiation from a smoke layer is easier to deal with within the context of a uniform property gas layer for the zone model. One difficulty still is the availability of property data to determine the contribution of smoke particulates to the layer radiation properties. The discussion presented by Tien et al. can be used to begin a development of the radiative equations needed

by the zone model (see Chap. 4). Also, the presentation by Beyler gives empirical approaches to dealing with flame radiation (see Chap. 66). The paper by Forney [21] lays out the theory and equations describing radiation exchange between the gas layers and boundary surfaces.

Conduction Heat Transfer

The radiative and convective heat transfer from the gas must be balanced by conduction heat transfer through the boundary surfaces. This balancing requires a numerical solution to a partial differential equation in conjunction with the ordinary differential equations in time describing the conservation of energy and mass for the gas layers. Usually zone models have considered only one-dimensional conduction, which should be adequate for most applications. Most multiple-compartment models do not consider communication by conduction into the next compartment, treating the structural elements as thermally thick instead. In principle, there is no difficulty with developing an accurate algorithm for conduction through the boundary elements for any conditions. For more information, the reader is referred to the discussion by Rockett and Milke (see Chap. 2).

Mixing Between the Layers

The primary exchange of fluid between the lower and upper gas layers is due to the buoyant effect of the fire plume. Secondary but significant mixing processes can occur due to the other effects. These are shown in Fig. 29.5 and include three phenomena:

1. Exchange due to a cold flow injected into the hot layer
2. Exchange due to shear mixing associated with vent flows
3. Exchange due to wall flows

Phenomenon 1 is the inverse of the hot fire plume penetrating the upper layer. In both cases the fluid at the edge of the plume may not be buoyant enough to penetrate the respective layer. A comparable situation is a cold forced jet introduced vertically into the lower layer. Depending on the relative temperatures, it may not escape the lower layer and, therefore, may not penetrate into the upper layer. These are issues that can be resolved to some extent by research available in the literature on buoyant plumes and jets.

Phenomenon 2 requires the near vent mixing behavior to be characterized. Data suggest that the flow rate of the mixed stream can be significant relative to the vent flow rate, especially for small vents [22]. A correlation for the mixing

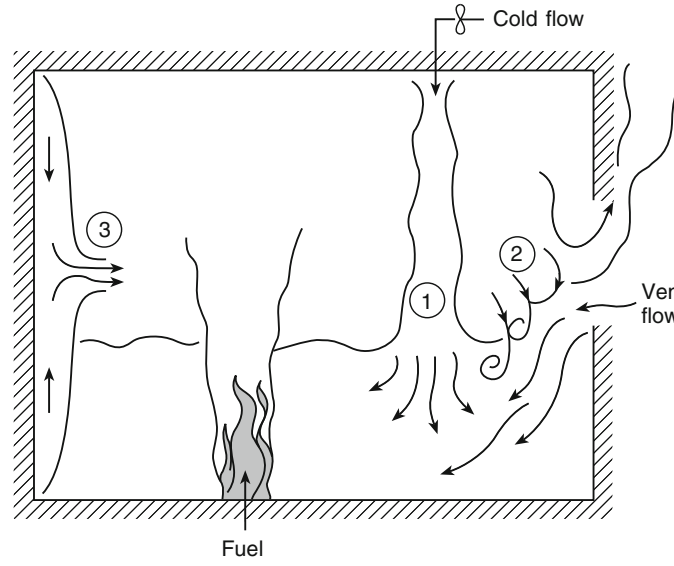

Fig. 29.5 Secondary flows—mixing phenomena. *1*. A cold plume descending from the upper layer into the lower layer. *2*. Shear mixing of an entering vent flow stream. *3*. Wall flows due to local buoyancy effects

rate has been developed from saltwater simulation experiments [23] based on the less than ideal assumption that the cold incoming flow through the opening would behave like a point source buoyant plume. More recently a mixing model has been proposed by Utiskul [24] where the incoming cold air behaves like a jet entering the doorway with a characteristic velocity and diffusing downward because of buoyancy. While the cold air descends, the surrounding hot gas is entrained with a velocity that is proportional to the incoming flow characteristic velocity. An equation for the ratio of mass entrained to the total incoming mass flow was given and single-vent compartment fire experiments were conducted to establish the correlation for the mixing at the quasi-steady state. The correlation exhibited a linear relationship up to an apparent asymptote for the mixing ratio of about 1.3.

Phenomenon 3 has been discussed by Jaluria [25]. He presents relationships that allow the estimation of the rate of transfer of cold fluid adjacent to the wall in the hot upper gas layer into the cold lower gas layer or vice versa.

All of these flows tend to blur the sharp distinction between the upper and lower gas layers, reducing their degree of stratification. Obviously, if sufficient mixing occurs, the layer may appear to become well-mixed or destratified. Destratification should occur naturally in the context of the zone model, and one should not have to switch to a well-mixed compartment model under these conditions.

Relationships for all of these secondary flows have not been developed with confidence nor with full acceptance. However they are important for improving the accuracy of a zone fire model, and additional research is still needed to further establish their validity.

Forced Flow Effects

The effect of forced airflow on fire conditions and smoke spread due to mechanical or natural wind forces has always been an issue in large building fires. Wind effects and the resultant pressure distribution around a tall building have become standard data elements for structural design but have not been utilized for fire safety design. The movement of smoke through a building due to the mechanical ventilation system has been simulated by network models that treat the compartment volume as uniform in properties, including the pressure losses due to vents and duct friction. A two layer zone model has not been linked to the mechanical ventilation system in a building. To create a link, one must include the full-pressure-flow characteristics of fans in both directions to allow for the possibility of the backflow of smoke against the direction of airflow in the ducts. An attempt at this linkage has been presented by Klote and Cooper [26], who hypothesize a fan characteristic relationship. Ultimately an experimental study will be needed to lay a foundation for this analysis.

Fire Growth Rate

In most all zone models, the fire source is considered an input quantity, based on some experimental or empirical data. This limits the simulation capability of a zone model, since fire growth and spread are not modeled. Also the effects of compartment feedback due to thermal and vitiation (oxygen depletion) effects are not taken into account. The versatility and utility of a zone model can only be improved by developing techniques for accommodating realistic fire growth characteristics for building contents and architectural elements. This process will also have an impact on the use and development of flammability tests for hazard analysis and product acceptability.

Embedded Submodels

The detailed physics that one can include in a zone model are only limited by current research and imagination. The zone model can be versatile in accommodating new phenomena, even if they appear inconsistent with the uniform property

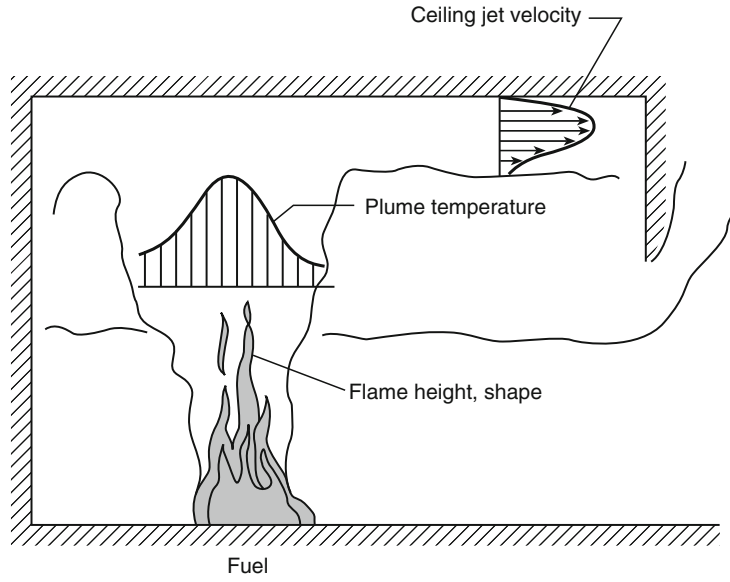

Fig. 29.6 Examples of embedded phenomena

layer assumption. By analogy to the relationship between inviscid flow and boundary layer flow in the analysis of aerodynamic bodies, the layer properties can be regarded as a first-order approximation for higher order analysis. Flame and boundary layer phenomena within the compartment can be computed by regarding the layer properties as infinite reservoirs. These phenomena can be computed after the primary layer properties are computed. Examples of embedded phenomena are shown in Fig. 29.6. Although the combustion region is assumed to be of negligible volume in the zone model formulation, the flame height can be computed along with the velocity and temperature distributions in an axisymmetric fire plume [27]. Other potential embedded phenomena are (1) the ceiling jet, (2) the computation of temperature distributions over the ceiling, (3) the deposition of soot and other products of combustion on surfaces, (4) the heating and degradation of structural elements, (5) balcony spill plumes, (6) flame spread and fire growth for surface linings, and (7) the response of detectors and/or sprinklers.

Unresolved Phenomena

Some significant phenomena are not addressed by the zone modeling approach for fire, such as vent flames, transient flow in corridors, shaft flows (see Fig. 29.7). These phenomena require more research and new strategies to enable them to be included into a zone model. Vent flames are significant for fire growth into the next compartment and usually follow flashover. Information about their rate of heat transfer and extent needs to be computed. Transient corridor flows are important in the analysis of smoke transport through long corridors. The current zone model methodology yields an instantaneous layer that would descend, but the actual process produces a transient ceiling jet. Flows in vertical shafts involve the interaction of plumes with walls, pressure-driven effects, and turbulent mixing.

Selected Reading and Comments

Zone models provide the integrating framework for the phenomena of fire and its fire protection engineering components. Many zone models have been constructed for fire predictions in compartments. They involve the basic conservation equations, submodels describing the particular phenomena included, and the mathematical algorithms for solutions. Some have developed user-friendly interfaces. Most provide documentation on the model and its use. The interested

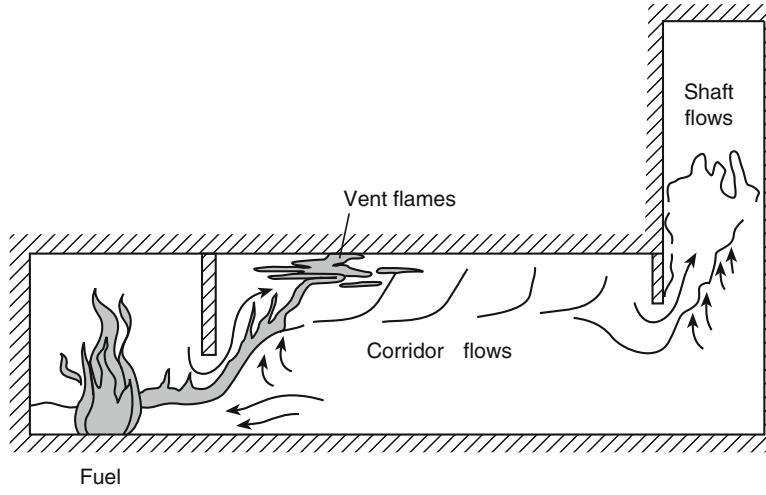

Fig. 29.7 Examples of significant phenomena absent from zone models

reader is referred to some published models for more detailed information [28–31]. Many zone-based computer models exist, similar both in substance and the ability to analyze fire effects in buildings. They can stimulate needed research. However, more effort appears to have gone into the computer code developments rather than the experimental research needed for improvement in the model.

Nomenclature

A	area compartment floor
C	flow coefficient
c_p	specific heat at constant pressure
c_v	specific heat at constant volume
g	acceleration due to gravity
H	compartment height
J	number of flow streams in control volume
m	mass
p	pressure
Q	heat transfer
r	stoichiometric fuel-to-oxygen mass ratio
R	ideal gas constant
t	time
T	temperature
v	fluid velocity
V	volume
w	control volume velocity
Y	mass fraction
z_l	height of control volume or zone
ΔH	heat of combustion
γ_i	yield of species i
ρ	density
Φ	equivalence ratio
$\dot{\omega}_F$	consumption rate of fuel
$\dot{\omega}_i$	production rate of species

Subscripts

e	entrained
f	flame
F	fuel
i	species
j	flow stream
o	oxygen
s	supplied

Superscripts

$(\dot{})$	per unit time

References

1. N.D. Fowkes, "A Mechanistic Model of the 1973 and 1974 Bedroom Test Fires," in *A Study of Room Fire Development: The Second Full-Scale Bedroom Fire Test of the Home Fire Project (*P.A. Croce, ed.), (July 24, 1974), Vol. II, FMRC Technical Report No. 21011.4, pp. 8–50 (1975).
2. J. Quintiere, "Growth of Fire in Building Compartments," in *Fire Standards and Safety (*A.F Robertson, ed.), ASTM STP614, American Society for Testing and Materials, pp. 131–167 (1977).
3. R. Pape and T. Waterman, "Modification to the FIRES Pre-Flashover Room Fire Computer Model," *IITRI Project J6400,* IIT Research Institute, Chicago (1977).
4. H.E. Mitler, "The Physical Basis for the Harvard Computer Fire Code," *Home Fire Project Technical Report No. 34,* Harvard University, Cambridge, MA (1978).
5. R.W. Bukowski, R.D. Peacock, W.W. Jones, and G.P. Forney, "HAZARD I: Technical Reference Guide," *NIST Handbook 146,* Vol. II, National Institute of Standards and Technology, Gaithersburg, MD (1989).
6. R. Friedman, "An International Survey of Computer Models for Fire and Smoke,: *Journal of Fire Protection Engineering*, Vol. 4., No. 3., 1992, pp. 81–92.
7. S.M. Olenik and D.J. Carpenter, "Updated International Survey of Computer Models for Fire and Smoke," *Journal of Fire Protection Engineering*, 13, 2, pp. 87–110 (2003).
8. J.G. Quintiere, "Fundamentals of Enclosure Fire Zone Models," *Journal of Fire Protection Engineering,* 1, 3 (1989).
9. J.G. Quintiere and A.S. Rangwala, "A Theory of Flame Extinction Based on Flame Temperature." *Fire and Materials*, 28, pp. 387–402 (2004).
10. Y.P. Utiskul, and J.G. Quintiere, "An Application of Mass Loss Rate Model with Fuel Response Effects in Fully-Developed Compartment Fires" *Proceedings of the 9th International Symposium on Fire Safety Science,* pp. 827–838 (2008).
11. E.E. Zukoski, S.J. Toner, J.H. Morehant, and T. Kubota, "Combustion Processes in Two-Layered Configurations," *Proceedings of the 2nd International Symposium on Fire Safety Science,* Hemisphere Publishing Corporation, New York, pp. 255–304 (1989).
12. J.A. Rockett, "Using the Harvard/NIST Mark VI Fire Simulation," *NISTIR 4464,* National Institute of Standards and Technology, Gaithersburg, MD (1990).
13. J. Quintiere, W.J. Rinkinen and W.W. Jones, "The Effect of Room Openings on Fire Plume Entrainment." *Combustion Science and Technology*, 26, pp. 193–201 (1981).
14. B.M. Cetegen, E.E. Zukoski, and T. Kubota, "Entrainment in the Near and Far Field of Fire Plumes," *Combustion Science and Technology*, 39, pp. 305–331 (1984).
15. B.J. McCaffrey and J.A. Rockett, "Static Pressure Measurements of Enclosure Fires," *Journal of Research of the National Bureau of Standards,* 82, 2, pp. 107–117 (1977).
16. M. Epstein, "Buoyant-Driven Exchange Flow Through Small Openings in Horizontal Partitions," *Journal of Heat Transfer,* 110 (1988).
17. L.Y. Cooper, "An Algorithm and Associated Computer Subordinate for Calculating Flow Through a Horizontal Ceiling Flow Vent in a Zone-Type Compartment Fire Model," *NISTIR 4402,* National Institute of Standards and Technology, Gaithersburg, MD (1990).
18. R.L. Alpert, "Convective Heat Transfer in the Impingement Region of a Buoyant Plume," *Journal of Heat Transfer,* 109 (1987).
19. H.Z. You and G.M. Faeth, "Ceiling Heat Transfer During Fire Plume and Fire Impingement," *Fire and Materials,* 3, 3 (1979).
20. M.A. Kokkala, "Experimental Study of Heat Transfer to Ceiling from an Impinging Diffusion Flame," *Proceedings of the 2nd International Symposium on Fire Safety Science,* G. Cox and B. Langford, eds., Elsevier Applied Science, London (1991).
21. G.P. Forney, "Computing Radiative Heat Transfer Occurring in a Zone Model," *Fire Science & Technology,* 14, pp. 31–47 (1994).
22. B.J. McCaffrey and J.G. Quintiere, "Buoyancy-Driven Countercurrent Flows Generated by a Fire Source," *Heat Transfer and Turbulent Buoyant Convection,* Vol. II (D.B. Spalding and N. Afgan, eds.), Hemisphere Publishing, pp. 457–472 (1977).
23. C.S. Lim, E.E. Zukoski, and T. Kubota, "Mixing in Doorway Flows and Entrainment in Fire Flames," California Institute of Technology, Pasadena, CA (1984).
24. Y. Utiskul, "Theoretical and Experimental Study on Fully-Developed Compartment Fires" *NIST GCR 07-907,* National Institute of Standards and Technology, Gaithersburg, MD (2007).
25. Y. Jaluria, "National Convection Wall Flows," in *SFPE Handbook of Fire Protection Engineering* (P.J. DiNenno et al., eds.), National Fire Protection Association, Quincy, MA, pp. 2-50–2-63 (1995).
26. J.H. Klote and L.Y. Cooper, "Model of a Simple Fan-Resistance Ventilation System and Its Application to Fire Modeling," *NISTIR 89-4141,* National Institute of Standards and Technology, Gaithersburg, MD (1989).
27. B. McCaffrey, "Flame Height," in *SFPE Handbook of Fire Protection Engineering* (P.J. DiNenno et al., eds.), National Fire Protection Association, Quincy, MA, pp. 2-1–2-8 (1995).

28. H.W. Emmons, H.E. Mitler, and L.N. Trefethen, "Computer Fire Code III," *Home Fire Project Technical Report No. 25,* Harvard University, Cambridge, MA (1978).
29. T. Tanaka, "A Model of Multicompartment Fire Spread," *NBSIR 83-2718,* National Bureau of Standards, Washington, DC (1983).
30. R.D. Peacock, W.W. Jones, R.W. Bukowski, and G.P. Forney, "CFAST- Consolidated Model of Fire Growth and Smoke Transport. (Version 6): Technical Reference Guide," *SP-1026*, National Institute of Standards and Technology, Gaithersburg, MD (2005).
31. C. Wade, G. Baker, K. Frank, A. Robbins, R Harrison, M. Spearpoint, and C. Fleischmann, "B-RISK User Guide and Technical Manual". *BRANZ Study Report No 282*. BRANZ Ltd, New Zealand (2013).

James G. Quintiere is Professor Emeritus, Ph.D. of Fire Protection Engineering at the University of Maryland. His research has focused on fire dynamics, fire growth and flame spread.

Colleen A. Wade is a senior scientist with BRANZ Ltd in New Zealand. Her research and expertise includes fire modeling, flame spread and performance-based design.]

Estimating Temperatures in Compartment Fires

30

William D. Walton, Philip H. Thomas, and Yoshifumi Ohmiya

Introduction

The ability to predict temperatures developed in compartment fires is of great significance to the fire protection professional for protection of human life and property. There are many uses for a knowledge of compartment fire temperatures, including the prediction of (1) the onset of hazardous conditions, (2) property and structural damage, (3) changes in burning rate, pyrolysis rate and heat (energy) release rate, (4) ignition of objects,(5) the onset of flashover and so on.

The fundamental principles underlying compartment fires are presented in Chap. 29. This chapter gives a number of simplified solution techniques.

Fire Stages

In this chapter, compartment fires are defined as fires in enclosed spaces, which are commonly thought of as rooms in buildings, but may include other spaces such as those found in transportation vehicles such as ships, planes, trains, and the like.

Compartment fires are often discussed in terms of growth stages [1]. Figure 30.1 shows an idealized variation of temperature with time along with the growth stages. Fire safety design in terms of evacuation and fire resistance was examined by taking into account fire stage. The stage of ignition and growth are very significant to estimate the time for fire detectors and suppression systems to activate. The stage of fully-developed fire is important for the fire resistance of building loadbearing elements and separating elements.

1. Ignition
2. Growth
3. Flashover
4. Fully-developed fire
5. Decay

Although many fires will not follow this idealization, it provides a useful framework for the discussion of compartment fires. All fires include an ignition stage but, beyond that, may fail to grow, or they may be affected by manual or automatic suppression activities before going through all of the stages listed above.

Growth Stage Definitions

Ignition Stage The period during which the fire begins in a compartment.

Growth Stage Following ignition, the fire initially grows primarily as a function of the fuel itself, with little or no influence from the compartment. The fire can be described in terms of its rate of energy and combustion product generation. A discussion of energy

W.D. Walton (✉) • P.H. Thomas • Y. Ohmiya

M.J. Hurley (ed.), *SFPE Handbook of Fire Protection Engineering*,
DOI 10.1007/978-1-4939-2565-0_30, © Society of Fire Protection Engineers 2016

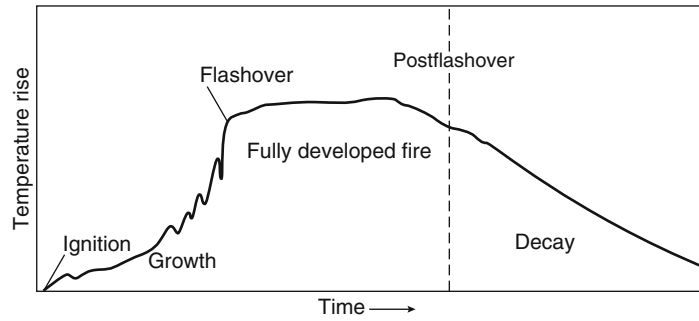

Fig. 30.1 General description of room fire in absence of fire control

generation or burning rate can be found in Chap. 26. If sufficient fuel and oxygen are available, the fire will continue to grow, causing the temperature in the compartment to rise. Fires with sufficient oxygen for combustion are said to be fuel controlled or well-ventilated.

Flashover Flashover is generally defined as the transition from a growing fire to a fully developed fire in which all combustible items in the compartment are involved in fire. During this transition there are rapid changes in the compartment environment. Flashover is not a precise term, and several variations in definition can be found in the literature. However the onset of flashover should be estimated for considering fire safety. Most have criteria based on the temperature at which the radiation from the hot gases in the compartment will ignite all of the combustible contents. Gas temperatures of 300–650 °C have been associated with the onset of flashover, although temperatures of 500–600 °C are more widely used [2]. The ignition of unburnt fuel in the hot fire gases, the appearance of flames from openings in a compartment, or the ignition of all of the combustible contents may actually be different phenomena all related to flashover.

Fully Developed Fire During this stage, the heat release rate of the fire is the greatest. The fire behavior in this stage is influenced by conditions of enclosure such as the size and construction materials, size and form of openings, type amount and distribution of fuel in the enclosure. Frequently during this stage more fuel is pyrolized than can be burned with the oxygen available in the compartment. In this case, the fire is said to be ventilation controlled. If there are openings in the compartment, the unburned fuel will leave the compartment in the gas flow and may burn outside of the compartment. It will cause fire spread to upper floors and neighboring buildings. During the fully developed stage, the environment within the compartment has a significant effect on the pyrolysis rate of the burning objects.

Decay Stage Decay occurs as the fuel becomes consumed, and the heat release rate and temperature within a compartment decline. The fire may change from ventilation to fuel controlled during this period.

Compartment Fire Phenomena

Compartment Fire Model

In order to calculate or predict the temperatures and other properties generated in a compartment fire, a description or model of the fire phenomena must be created. This model will be described in terms of physical equations that can be solved to predict the temperature in the compartment. Such a model is, therefore, an idealization of the compartment fire phenomena. Consider a fire that starts at some point below the ceiling. It releases energy and products of combustion at a rate that may change with time. The hot products of combustion form a plume that, due to buoyancy, rises toward the ceiling above heat source. As the

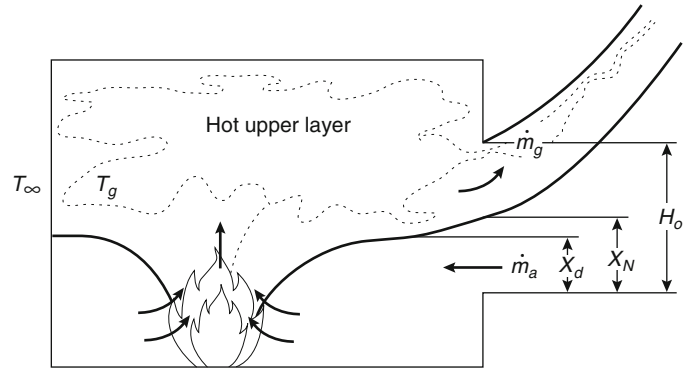

Fig. 30.2 Two-layer model with no exchange between layers except the plume

plume rises, it draws in cool air from within the compartment, decreasing the plume's temperature and increasing its volume flow rate. When the plume reaches the ceiling, it spreads out under ceiling. When the extension of hot current under ceiling reaches the walls, the flow turns downward and forms a hot gas layer that descends with time as the plume's gases continue to flow into it. There is a relatively sharp interface between the hot upper layer and the air in the lower part of the compartment. The only assumed interchange between the air in the lower part of the room and the hot upper layer comprised of products of combustion is through the plume. As the hot layer descends and reaches openings in the compartment walls (e.g., doors and windows), hot gas will flow out the openings and outside air will flow into the openings. This description of compartment fire phenomena is referred to as a two-layer or zone model. The basic compartment fire phenomena are shown schematically in Fig. 30.2.

The two-layer concept assumes that the compositions of the layers are uniform, that is, that the temperature and other properties are the same throughout each layer. Although the temperature of the lower layer will rise during the course of the fire, the temperature of the upper layer will remain greater and is the most important factor in compartment fires. The assumptions may be less valid for very large spaces or for long, narrow spaces such as corridors and shafts. To describe the vertical distribution, multi-layer models were being developed [3].

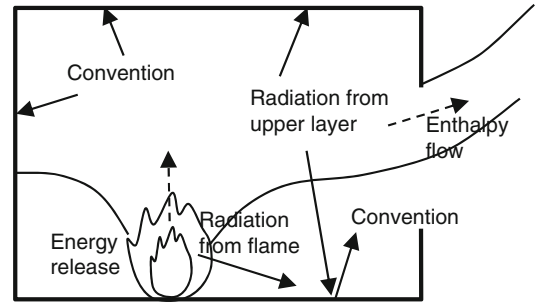

Fig. 30.3 Energy balance of compartment fire during Two-layer condition

Calculation of Compartment Fire Temperatures

The basic principle used to calculate the temperature in a compartment fire is the conservation of energy. In order to estimate the temperature in enclosure, energy balance can be assumed as shown in Fig. 30.3.

As applied to the hot upper layer, the conservation of energy can be simply stated as follows: the energy added to the hot upper layer by the fire equals the energy lost from the hot layer plus the time rate of change of energy within the hot upper layer. From the time rate of change of energy within the hot layer, the temperature of the layer can be computed. Conservation of energy can also be applied to the lower layer. Since the volume of the upper layer changes with time, and mass flows in and out of the upper layer, conservation of mass must be used along with the conservation of energy. Because the

energy generated by the fire and the temperatures in the compartment vary as a function of time, the application of conservation of energy will result in a series of differential equations. For the purposes of examining the components of the conservation of energy, the steady-state expressions for the conservation of energy in the hot upper layer will be used.

The transport of energy in a compartment fire is a very complex process. In order to formulate expressions for the conservation of energy in a practical way, a number of assumptions must be made. It is possible to formulate the equations in a number of ways, based on the level of detail desired. The expressions and assumptions used in this chapter are based on those commonly found in the fire research literature and represent a somewhat simplified description of the phenomena. Additional details may be found in the references cited.

The steady-state conservation of energy for the hot upper gas layer in a compartment can be simply stated as follows: the energy generated by the fire and added to the hot layer equals the energy lost from the hot layer through radiation and convection plus the energy convected out of the compartment openings.

Energy Generated by the Fire

The energy generated by the fire is the primary influence on the temperature in a compartment fire, and much research has been conducted in predicting the energy release rate of many fuels under a variety of conditions. This discussion will focus on flaming combustion, as it is most important in generating a significant temperature rise in a compartment. A discussion of non-flaming combustion is found in Chap. 19. As a fuel is heated it releases pyrolysis products. The amount of pyrolysis products depends on fuel properties, incident heat flux to surface of fuel, oxygen mass fraction in the enclosure and so on. The fortmula to estimate the mass burning rate of the fuel can be given as follows,

$$\dot{m}_f = qA/L \tag{30.1}$$

where

$\dot{m}_f$ = Mass burning rate of the fuel (kg/s)
q = Heat flux to the fuel surface(kW/m^2)
A = Suraface area of the fuel(m^2)
L = Heat of gasification (kJ/kg)

At initial stage in compartment fire, the heat flux to surface of the fuel is due to the flame generated above the fuel. In case that compartment fire reached flashover, it is due to the gas around fuel. If there are oxygen in the enclosure, pyrolysis products react with oxygen, generating heat and producing flames. The rate of energy release is equal to the mass loss rate of the fuel times the heat of combustion of the fuel:

$$\dot{Q} = \dot{m}_f \Delta h_c \tag{30.2}$$

where

$\dot{Q}$ = Energy release rate of the fire (kW)
$\dot{m}_f$ = Mass burning rate of the fuel (kg/s)
Δh_c = Effective heat of combustion of the fuel (kJ/kg)

The effective heat of combustion is the heat of combustion expected in a fire where incomplete combustion takes place. This amount is less than the theoretical heat of combustion as measured in the oxygen bomb calorimeter [4].

The effective heat of combustion is often described as a fraction of the theoretical heat of combustion. The effect of fluctuations is largely neglected.

In fuel-controlled fires, there is sufficient air to react with all the fuel within the compartment. In ventilation-controlled fires, there is insufficient air within the compartment, and some of the pyrolysis products will leave the compartment, possibly to react outside the compartment. For calculating the temperatures produced in compartment fires, the primary interest is the energy released within the compartment.

The pyrolysis rate of the fuel depends on the fuel type, its geometry, and the fire-induced environment. The energy generated in the compartment by the burning pyrolysis products then depends on the conditions (temperature, oxygen concentration, etc.) within the compartment. The processes involved are complex, and some are

not well understood, but for two fire types some simplifying assumptions can lead to useful methods for approximating the energy released by the fire.

Fuel-controlled fires are defined as those in which the pyrolysis rate and the energy release rate are affected only by the burning of the fuel itself and not by the room environment, analogous to a fire burning outdoors on a calm day. Babrauskas has provided data on free-burning fires in Chap. 26. This data is most useful for estimating burning rates of primarily horizontal fuels in preflashover fires, where the primary heating of the fuel is from the flames of the burning item itself. Vertical fuels, such as wall linings and fuels located in the upper hot gas layer, will likely be influenced by the preflashover room environment.

Ventilation-controlled fires are defined as those in which the energy release rate in the room is limited by the amount of available oxygen. The mass flow rate of air or oxygen into the room through a door or window can be calculated from the expressions described below and in Chap. 23. For most fuels [5], the heat released per mass of air consumed is a constant approximately equal to 3000 KJ/kg. Therefore, the rate of energy release of the fire can be approximated from the air inflow rate.

The amount of energy released by the fire that enters the hot upper layer is a function of the fire, layer conditions, and geometry. For most fires, approximately 35 % of the energy released by the fire leaves the fire plume as radiation [6]. (A discussion of flame radiation can be found in Chap. 23.) In a compartment fire, a fraction of the radiated energy reaches the upper layer. The majority of the remaining energy released by the fire is convected into the upper layer by the plume. As the plume rises, it entrains air from the lower layer, thus reducing its temperature and increasing the mass flow rate. For a first approximation, it can be assumed that all of the energy generated by the fire is transported to the upper layer. For a complete discussion of fire plumes see Chap. 13.

Conservation of Mass

The mass flow into the compartment and the flow out are related by

$$\dot{m}_g = \dot{m}_a + \dot{m}_f \tag{30.3}$$

where $\dot{m}_f$ is the mass burning rate of the fuel (kg/s).

The mass flow rate of hot gas out of a window or door is given by Rockett as [7]:

$$\dot{m}_g = \frac{2}{3} C_d W_o \rho_\infty \left[2g \frac{T_\infty}{T_g} \left(1 - \frac{T_\infty}{T_g} \right) \right]^{1/2} (H_o - X_N)^{3/2} \tag{30.4}$$

where

$\dot{m}_g$ = Mass flow rate of hot gas out an opening (kg/s)
C_d = Orifice constriction coefficient (typically ≈ 0.7)
W_o = Width of opening (m)
H_o = Height of opening (m)
ρ_∞ = Ambient air density (kg/m^3)
g = Acceleration due to gravity, 9.8 m/s^2
X_N = Height of neutral plane (m)
T_g = Temperature of the hot upper gas layer (K)
T_∞ = Ambient temperature (K)

The mass flow rate of air into a door or window is given by

$$\dot{m}_g = \frac{2}{3} C_d W_o \rho_\infty \left[2g \left(1 - \frac{T_\infty}{T_g} \right) \right]^{1/2} (X_N - X_d)^{1/2} \times (X_N + X_d/2) \tag{30.5}$$

where

X_d = Height of the interface (m).

The expressions for mass flow in and mass flow out cannot be solved directly for T_g since the height to the neutral plane and interface are unknown. The complete solution of these equations requires expressions for plume entrainment and additional energy equations and is normally carried out only in computer fire models. If the mass burning rate of the fuel is small compared with the mass flow rate of air into the compartment, the mass flow out of the opening may be approximated as equal to the mass inflow

rate. Flows out of vents in the ceiling are discussed in Chap. 66.

For preflashover fires in compartments with typical doors or windows, the neutral plane and interface can be approximated at the midlevel of the opening. This approximation can only be made after the initial smoke filling of the compartment is complete, and flow in and out of the opening is established.

For fires nearing flashover and postflashover fires, the interface between the upper and lower layers is located near the floor, and the flow reaches a maximum for a given upper gas temperature. Rockett [7] has shown the temperature dependence on the flow becomes small above 150 °C and the flow into the compartment can be approximated as a constant multiplied by $A_o\sqrt{H_o}$.

Rockett calculated values for this constant of 0.40–0.61 kg/s · $m^{5/2}$, depending on the discharge coefficient of the opening. Thomas and Heselden estimate the value of this constant at 0.5 kg/s · $m^{5/2}$, which is the value most commonly found in the literature [8]. The resulting approximation is then

$$\dot{m}_a = 0.5A_o\sqrt{H_o} \tag{30.6}$$

where

A_o = Area of opening (m^2)

H_o = Height of opening (m)

The term $A_o\sqrt{H_o}$ is commonly known as the ventilation factor. The first use of this type of opening flow analysis for evaluating postflashover fire test data is attributed to Kawagoe [9]. From early work analyzing such data, the empirical observation was made that wood fires in rooms with small windows appeared to burn at an approximate stoichiometric rate. Although flames emerging from the windows implied that some fuel was burning outside, calculations often suggested that enough air was entering the fire for stoichiometric burning. Empirical observations on wood fires [9] led to

$$\dot{m}_f = 0.09A_o\sqrt{H_o} \tag{30.7}$$

There is now a body of data [10] that modifies this simple proportionality between $\dot{m}_f$ and $A_o\sqrt{H_o}$.

The Conseil International du Bâtiment (CIB) experiments upon which Law [11] has based her method shows a dependence on A_T. It seems possible that the wide use of Equation 30.7 is a result of a concentration of experimental fires in rooms of a limited range of

$$\frac{A_T}{A_o\sqrt{H_o}}$$

where

A_T = Total area of the compartment enclosing surfaces (m^2)

Traditionally, energy balances were often stated in terms of the energy produced by the burning fuel and, thereby, led to an effective heat of combustion of the fuel. However, this practice in principle leads to the same result—the energy produced is related to the air flow for ventilation-controlled fires. Kawagoe [9] and Magnusson and Thelandersson [12] used 10.75 MJ/kg for the effective heat of combustion of wood in the flaming phase for fully developed compartment fires. With 16.4 MJ/kg for the heat of combustion of wood volatiles, this setup corresponds to a combustion efficiency of 10.75/16.4, which is virtually identical to the 0.65 used in several computer models.

By far most data are based on experiments in which the fuel was cellulosic, and much of the experimental data are based on wood in the form of cribs. For the post-flashover burning of a different fuel with a different chemistry, the burning rate expressions may still be used, as long as the fuel is a hydrocarbon producing approximately 3000 kJ for each kg of air consumed in the combustion process. Because different fuels react differently to the thermal environment and will pyrolyze at different rates according to the energy requirements to produce volatiles, one can only estimate temperatures by evaluating the differences or obtain maximum temperatures by using stoichiometry. Fuels more volatile than wood will probably produce lower temperatures inside a compartment, even if the excess fuel produces a greater hazard outside the compartment. The assumptions that the energy is related to the air flow and that the fuel is in stoichiometric proportion will give an upper estimate of

temperatures for ventilation-controlled fires. Since Equation 30.7 is close to stoichiometric, it could, coupled with the effective heat of combustion of wood, give results close to an upper temperature limit for other fuels.

Conservation of Energy

The heat generated by burning materials within a compartment is absorbed by the enclosing surfaces of the compartment and any other structural surfaces, by the surfaces of the fuel, and by the incoming air and any excess fuel. Heat is lost to the exterior in the flames and hot gases that exit from the openings in the compartment enclosing surfaces and by radiation through the openings. Table 30.1 gives an example of an experimental heat balance measured in a small compartment, for which unglazed windows provided ventilation from the start of the fire.

Table 30.1 illustrates the significant amount of heat loss in the effluent gases and shows that, with decreasing window area, a larger proportion of the heat released will be absorbed by the enclosing surfaces. The total heat released, assuming a complete burnout, is directly proportional to the amount of the fire load, but the rate of heat release may also be controlled by the ventilation. In this example, with the lower fire load, both window areas give sufficient ventilation for the fuel to burn at its maximum (free-burning) rate but, with the doubled fire load, the burning rate is not doubled, because the window area restricts the ventilation rate.

Methods for Predicting Preflashover Compartment Fire Temperatures

The solution of a relatively complete set of equations for the conservation of energy requires the solution of a large number of equations that vary with time. Although individual energy transport equations may be solved, in general there is not an explicit solution for a set of these equations. As a result, one of two approaches can be taken. The first is an approximate solution accomplished by hand using a limiting set of assumptions. The second is a more complete solution utilizing a computer program. In either case, a number of methods have been developed. The methods presented are those with the widest apparent acceptance in the fire protection community, each with different assumptions and limitations that should be understood before employing the method. The methods presented in this chapter predict average temperatures and are not applicable to cases where prediction of local temperatures are desired. For example, these methods should not be used to predict detector or sprinkler actuation or the temperatures of materials as a result of direct flame impingement.

Method of McCaffrey, Quintiere, and Harkleroad

McCaffrey, Quintiere, and Harkleroad have used a simple conservation of energy expression and a correlation with data to develop an

Table 30.1 Heat balance measured in experimental fires in a compartment of 29 m^2 floor area with a fire load of wood cribs

			Heat loss from hot gases (%)			
Fire load (kg)	Window area (m^2)	Heat release (kcal/s)	Effluent gas	Structural surfaces	Feedback to fuel	Window radiation
877	11.2	1900	65	15	11	9
	5.6	1900	52	26	11	11
1744	11.2	3200	61	15	11	13
	5.6	2300	53	26	12	9
	2.6	1600	47	30	16	7

approximation of the upper layer temperature in a compartment [13]. Applying the conservation of energy to the upper layer yields

$$\dot{Q} = \dot{m}_g c_p \left(T_g - T_\infty\right) + q_{\text{loss}} \tag{30.8}$$

where
$\dot{Q}$ = Energy (heat) release rate of the fire (kW)
$\dot{m}_g$ = Gas flow rate out the opening (kg/s)
c_p = Specific heat of gas (kJ/kg · K)
T_g = Temperature of the upper gas layer (K)
T_∞ = Ambient temperature (K)
q_{loss} = Net radiative and convective heat transfer from the upper gas layer (kW)

The left-hand side of Equation 30.8 is the energy generated by the fire. On the right-hand side, the first term is the heat transported from the upper layer in the gas flow out an opening. The second term is the net rate of radiative and convective heat transfer from the upper layer, which is approximately equal to rate of heat conduction into the compartment surfaces. The rate of heat transfer to the surfaces is approximated by

$$q_{\text{loss}} = h_k A_T \left(T_g - T_\infty\right) \tag{30.9}$$

where
h_k = Effective heat transfer coefficient (kW/m^{2}K)
A_T = Total area of the compartment enclosing surfaces (m^2)

Substituting Equation 30.9 into Equation 30.8 yields the non-dimensional temperature rise in terms of two dimensionless groups:

$$\frac{\Delta T_g}{T_\infty} = \frac{\dot{Q}/\left(c_p T_\infty \dot{m}_g\right)}{1 + h_k A_T/\left(c_p \dot{m}_g\right)} \tag{30.10}$$

where ΔT_g is the upper gas temperature rise above ambient $(T_g - T_\infty)$(K).

The mass flow rate of hot gas out of a window or door can be rewritten from Equation 30.4:

$$\dot{m}_g = \frac{2}{3} C_d W_o H_o^{3/2} \rho_\infty \left[2g \frac{T_\infty}{T_g}\left(1 - \frac{T_\infty}{T_g}\right)\right]^{1/2} \times \left(1 - \frac{X_N}{H_o}\right)^{3/2} \tag{30.11}$$

where
C_d = Orifice constriction coefficient
W_o = Width of opening (m)
H_o = Height of opening (m)
ρ_∞ = Ambient air density (kg/m^3)
g = Acceleration due to gravity, 9.8 m/s^2
X_N = Height of neutral plane (m)

Since X_N primarily depends on T_g, $\dot{Q}$, and geometric factors (H_o and W_o), $\dot{m}_g$ may be replaced by $\sqrt{g\rho_\infty} A_o \sqrt{H_o}$ in the two dimensionless variables in Equation 30.11, without any loss in generality. The effects of T_g and $\dot{Q}$ are incorporated into the correlation via other terms. Based on an analysis of test data, Equation 30.10 was written as a power-law relationship:

$$\Delta T_g = 480 \left(\frac{\dot{Q}}{\sqrt{g} c_p \rho_\infty T_\infty A_o \sqrt{H_o}}\right)^{2/3} \times \left(\frac{h_k A_T}{\sqrt{g} c_p \rho_\infty A_o \sqrt{H_o}}\right)^{-1/3} \tag{30.12}$$

where
A_o = Area of opening (m^2)
H_o = Height of opening (m)

The numbers 480, 2/3, and −1/3 were determined by correlating the expression with the data from over 100 experimental fires. These data included both steady-state and transient fires in cellulosic and synthetic polymeric materials and gaseous hydrocarbon fuels. Compartment height ranged from 0.3 to 2.7 m and floor areas from 0.14 to 12.0 m^2. The compartments contained a variety of window and door sizes. The term raised to the 2/3 power in Equation 30.12 represents the ratio of the energy released to the energy convected, and the term raised to the −1/3 power represents the energy lost divided by the energy convected.

Substituting the values for ambient conditions of
g = 9.8 m/s^2
c_p = 1.05 kJ/kg · K
ρ_∞ = 1.2 kg/m^3
T_∞ = 295 K
into Equation 30.12 yields [14, 15]

$$\Delta T_g = 6.85\left(\frac{\dot{Q}^2}{A_o\sqrt{H_o}h_k A_T}\right)^{1/3} \qquad (30.13)$$

The heat transfer coefficient can be determined using a steady-state approximation when the time of exposure, t, is greater than the thermal penetration time, t_p, by

$$h_k = k/\delta \quad \text{for} \quad t > t_p \qquad (30.14)$$

The thermal penetration time is defined as

$$t_p = \left(\frac{\rho c}{k}\right)\left(\frac{\delta}{2}\right)^2 \qquad (30.15)$$

where

ρ = Density of the compartment surface (kg/m^3)
c = Specific heat of the compartment surface material (kJ/kg·K)
k = Thermal conductivity of compartment surface (kW/m · K)
δ = Thickness of compartment surface (m)
t = Exposure time (s)
t_p = Thermal penetration time (s)

When the time of exposure is less than the penetration time, an approximation based on conduction in a semi-infinite solid is

$$h_k = \left(\frac{k\rho c}{t}\right)^{1/2} \text{ for } \quad t \le t_p \qquad (30.16)$$

If there are several wall and/or ceiling materials in the compartment, an area-weighted average for h_k should be used.

The limitations as stated by McCaffrey et al. on the use of this method for estimating temperatures are as follows:

1. The correlation holds for compartment upper-layer gas temperatures up to approximately 600 °C.
2. It applies to steady-state as well as time-dependent fires, provided the primary transient response is the wall conduction phenomenon.
3. It is not applicable to rapidly developing fires in large enclosures in which significant fire growth has occurred before the combustion products have exited the compartment.
4. The energy release rate of the fire must be determined from data or other correlations.
5. The characteristic fire growth time and thermal penetration time of the room-lining materials must be determined in order to evaluate the effective heat transfer coefficient.
6. The correlation is based on data from a limited number of experiments and does not contain extensive data on ventilation-controlled fires nor data on combustible walls or ceilings. Most of the fuel in the test fires was near the center of the room.

Example of McCaffrey et al. Method Calculate the upper-layer temperature of a room 3 × 3 m in floor area and 2.4 m high with a door opening 1.8 m high and 0.6 m wide. The fire source is a steady 750 kW fire. The wall-lining material is 0.016 m (5/8 in.) gypsum plaster on metal lath. Perform the calculation at times of 10, 60, and 600 s after ignition. Using Equation 30.12,

$$\Delta T_g = 480\left(\frac{\dot{Q}}{\sqrt{g}c_p\rho_\infty T_\infty A_o\sqrt{H_o}}\right)^{2/3} \times \left(\frac{h_k A_T}{\sqrt{g}c_p\rho_\infty A_o\sqrt{H_o}}\right)^{-1/3}$$

where

$c_p = 1$ kJ/kg·K
$T_\infty = 27$ °C (300 K)
$\rho_\infty = 1.18$ kg/m^3
$A_o = 1.8$ m · 0.6 m = 1.08 m^2
$g = 9.8$ m/s^2
$H_o = 1.8$ m
$\dot{Q} = 750$ kW

$$\begin{aligned} A_T &= A_{walls} + A_{floor} + A_{ceiling} - A_{openings} \\ &= 4 \times (3 \times 2.4) + (3 \times 3) + (3 \times 3) - 1.08 \\ &= 28.8\,m^2 + 9m^2 + 9m^2 - 1.08m^2 \\ &= 45.72m^2 \end{aligned}$$

The wall heat loss coefficient, h_k, is a function of time.

(a) Calculate the thermal penetration time, t_p.

$$t_p = \left(\frac{\rho c}{k}\right)\left(\frac{\delta}{2}\right)^2$$

where
ρ = Wall material density (1440 kg/m^3)
$k = 0.48 \times 10^{-3}$ kW/m·K
$c = 0.84$ kJ/kg·K
$\delta = 0.016$ m
$t_p = 161.3$ s

(b) Calculate h_k at 10, 60, and 600 s.
For $t<t_p$ (10, 60 s),

$$h_k = \left(\frac{k\rho c}{t}\right)^{1/2} \quad k\rho c = 0.581$$

1. At $t = 10$ s,

$$h_k = \left(\frac{0.581}{60}\right)^{1/2} = 0.24 \text{ kW/m}^2\text{·K}$$

2. At $t = 60$ s,

$$h_k = \left(\frac{0.581}{60}\right)^{1/2} = 0.098 \text{ kW/m}^2\text{·K}$$

3. For $t > t_p$ (600 s) at $t = 600$ s,

$$h_k = \frac{k}{\delta} = \frac{0.48 \times 10^{-3}}{0.016} = 0.03 \text{ kW/m}^2\text{·K}$$

(c) Calculate the compartment temperature at the three times using Equation 30.12.
1. At $t = 10$ s,

$$\Delta T_g = 480\left[\frac{750}{(\sqrt{9.8})\,(1)\,(1.18)\,(300)\,(1.08)\,(\sqrt{1.8})}\right]^{2/3} \cdot \left[\frac{(0.24)\;(45.72)}{(\sqrt{9.8})\;(1)\;(1.18)\;(1.08)\;(\sqrt{1.8})}\right]^{-1/3}$$
$$= 480(0.47)^{2/3}(2.05)^{-1/3}$$
$$= 227 \text{ K}$$

2. At $t = 60$ s,

$$\Delta T_g = 480(0.47)^{2/3}(0.837)^{-1/3} = 307 \text{ K}$$

3. At $t = 600$ s,

$$\Delta T_g = 480(0.47)^{2/3}(0.26)^{-1/3} = 453 \text{ K}$$

Method of Foote, Pagni, and Alvares

The Foote, Pagni, and Alvares method follows the basic correlations of McCaffrey, Quintiere, and Harkleroad and adds data for forced-ventilation fires. Using Equation 30.10 and not introducing an expression for doorway flow results in the expression [16]

$$\frac{\Delta T_g}{T_\infty} = 0.63\left(\frac{\dot{Q}}{\dot{m}_g c_p T_\infty}\right)^{0.72}\left(\frac{h_k A_T}{\dot{m}_g c_p}\right)^{-0.36} \tag{30.17}$$

where
ΔT_g = Upper gas temperature rise above ambient (K)
T_∞ = Ambient air temperature (K)
$\dot{Q}$ = Energy (heat) release rate of the fire (kW)
$\dot{m}_g$ = Compartment mass ventilation rate (kg/s)
c_p = Specific heat of gas (kJ/kg·K)
h_k = Effective heat transfer coefficient (kW/m^{2}K)
A_T = Total area of the compartment-enclosing surfaces (m^2)

The coefficient and exponents are based on data from well-ventilated tests in a compartment with a 6 × 4 m floor area and a height of 4.5 m with ventilation rates of 110–325 g/s. The compartment exhaust was through a 0.65 × 0.65 m duct located 3.6 m above the floor. Four air inlet openings were 0.5 × 0.12 m high, with centerlines 0.1 m above the floor. A methane gas burner fire in the center of the floor with heat release rates of 150–490 kW resulted in upper gas temperatures of approximately 100–300 °C.

Foote et al. have shown that the correlation for forced-ventilation fires agrees well with the data presented by McCaffrey et al. for free ventilation fires with

$$\dot{m} \approx 0.1\left(\rho_\infty \sqrt{g} A_o \sqrt{H_o}\right)$$

Example of Foote et al. Method Estimate the temperature in a 5 × 5 m floor area and 4-m-high compartment having 0.025-m (1-in.) thick concrete walls. The forced-ventilation rate is

2.4 m^3/s of air (5000 cfm). Perform the calculation for $t > t_p$. The fire size is given as 1000 kW; ambient air conditions at 300 K. Using Equation 30.17,

$$\frac{\Delta T_g}{T_\infty} = 0.63\left(\frac{\dot{Q}}{\dot{m}_g c_p T_\infty}\right)^{0.72}\left(\frac{h_k A_T}{\dot{m}_g c_p}\right)^{-0.36}$$

where

$\dot{Q} = 1000$ kW
$T_\infty = 300$ K
$c_p = 1.0$ kJ/kg·K
$A_T = 4 \times (5 \times 4) + 2\,(5 \times 5) = 105$ m^2
$\dot{m}_g = (2.4\ m^3/s)\ (1.18\ kg/m^3) = 2.8$ kg/s

Calculate h_k for $t > t_p$. For 0.025-m-thick concrete,

$\delta = 0.025$ m
$\rho = 2000$ kg/m^3
$k = 1.4 \times 10^{-3}$ kW/m·K
$c_p = 0.88$ kJ/kg·K

$$t_p = \left(\frac{\rho c}{k}\right)\left(\frac{\delta}{2}\right)^2 = \left[\frac{(2,000)\cdot(0.88)}{1.4\times 10^{-3}}\right]\left(\frac{0.025}{2}\right)^2 = 196\text{s} \quad \text{for} \quad t > t_p$$

$$h_k = \frac{k}{\delta} = \frac{1.4\times 10^{-3}}{0.025} = 0.056\ \text{kW}/m^2\cdot\text{K}$$

$$\frac{\Delta T_g}{T_\infty} = (0.63)\left[\frac{1,000}{(2.8)\,(1)\,(300)}\right]^{0.72} \times \left[\frac{(0.056)\,(105)}{(2.8)\,(1)}\right]^{-0.36}$$

$$\Delta T_g = (0.14)\,(T_\infty) = 164\ \text{K}$$
$$T_g = 164 + 300\ \text{K} = 464\ \text{K}$$

Method of Beyler and Deal

Beyler and Deal compared a number of methods for naturally ventilated compartments to test data and recommend the method of McCaffrey, Quintiere, and Harkleroad for naturally ventilated compartments. Beyler offers an improved correlation for compartments where the forced-ventilation flow rate is known [17, 18]. This method begins by applying the conservation of energy in the upper layer of a compartment. Combining Equations 30.8 and 30.9 yields

$$\dot{Q} = \dot{m}_g c_p\left(T_g - T_\infty\right) + h_k A_T\left(T_g - T_\infty\right) \tag{30.18}$$

where:

$\dot{Q}$ = Energy (heat) release rate of the fire (kW)
$\dot{m}_g$ = Gas flow rate out the opening (kg/s)
c_p = Specific heat of gas (kJ/kg·K)
T_g = Temperature of the upper gas layer (K)
T_∞ = Ambient temperature (K)
h_k = Effective heat transfer coefficient (kW/m^2K)
A_T = Total area of the compartment enclosing surfaces (m^2)

Rearranging Equation 30.18 yields

$$\Delta T_g = \frac{\dot{Q}}{\dot{m}_g c_p + h_k A_T} \tag{30.19a}$$

or

$$\frac{\Delta T_g \dot{m}_g c_p}{\dot{Q}} = \frac{1}{1 + (h_k A_T)/\dot{m}_g c_p} \tag{30.19b}$$

where $\Delta T_g = T_g - T_\infty$.

A nondimensional temperature rise is defined as

$$\Delta T^* \equiv \frac{\Delta T_g \dot{m}_g c_p}{\dot{Q}} \tag{30.20}$$

and the ratio of the bounding surface loss to the ventilation losses is defined as

$$Y^* \equiv 1 + \frac{h_k A_T}{\dot{m}_g c_p} \tag{30.21}$$

By plotting ΔT^* as a function of ΔY^* for data with experiments with known ventilation rates Beyler and Deal developed a correlation for the effective heat transfer coefficient of

$$h_k = 0.4\max\left(\sqrt{\frac{k\rho c}{t}}, \frac{k}{\delta}\right) \tag{30.22}$$

where
k = Thermal conductivity of the compartment surface (kW/m·K)
ρ = Density of the compartment surface (kg/m^3)
c = Specific heat of the compartment surface material (kJ/kg·K)
δ = Thickness of the compartment surface (m)
t = Exposure time (s)

The expression switches from transient to steady state at a thermal penetration time of $t_p = (\rho c/k)\delta^2$ rather than $t_p = (\rho c/k)(\delta/2)^2$ used by McCaffrey et al. and Foote et al. For the data set Beyler and Deal evaluated, the standard error for their method was 29 K as compared to 51 K for the method of Foote et al., even though the equation uses only one fitting constant.

Beyler and Deal demonstrated that this method works for ventilation to the lower part of the compartment (with or without a plenum) as well as for ventilation to the upper part of the compartment. The Beyler and Deal method was based on data up to 2000 s into fire tests. At longer times, the heat loss model breaks down.

Example of Beyler and Deal Method Estimate the temperature in a 5 × 5 m floor area and 4-m-high compartment with 0.025-m (1-in.) thick concrete walls. The forced-ventilation rate is 2.4 m^3/s of air (5000 cfm). Perform the calculation for $t > t_p$. The fire size is given as 1000 kW; ambient air conditions at 300 K. Using Equation 30.19a,

$$T_g - T_\infty = \frac{\dot{Q}}{\dot{m}_g c_p + h_k A_T}$$

where
$\dot{Q} = 1000$ kW
$\dot{m}_g = (2.4\ \text{m}^3/\text{s})\ (1.18\ \text{kg/m}^3) = 2.8$ kg/s
$c_p = 1.0$ kJ/kg·K
$T_\infty = 300$ K
$A_T = 4(5 \times 4) + 2(5 \times 5) = 105$ m^2

(a) Calculate h_k for $t > t_p$. For 0.25-m-thick concrete,

$\delta = 0.25$ m
$\rho = 2000$ kg/m^3
$k = 1.4 \times 10^{-3}$ kW/m·K
$c = 0.88$ kJ/kg·K

$$h_k = 0.4\left(\frac{k}{\delta}\right) = 0.4\left(\frac{1.4 \times 10^{-3}}{0.25}\right)$$
$$= 0.0224\ \text{kW/m}^2 \cdot \text{K}$$

(b) Calculate the compartment temperature using Equation 30.19a.

$$T_g - 300 = \frac{1000}{(2.8)\,(1.0) + (0.224)\,(105)}$$
$$T_g = 494\ \text{K}$$

Method of Peatross and Beyler

The correlations used in the McCaffrey, Quintiere, and Harkleroad method and the Beyler and Deal method are based on the assumption of normal insulating wall materials. For highly conductive walls such as steel, Peatross and Beyler suggest the use of an alternative heat transfer coefficient [19]. Using a lumped mass analysis for heat transfer through the wall that is appropriate for a highly conductive wall yields

$$m_w'' c \frac{dT_w}{dt} = h_g\left(T_g - T_w\right) - h_\infty T_w \tag{30.23}$$

where
m_w'' = Mass per unit area of the wall (kg/m^2)
c = Specific heat of the wall (kJ/kg·K)
T_w = Wall temperature (K)
t = Time (s)
h_g = Heat transfer coefficient on the hot side of the wall (kW/m^{2}K)
T_g = Upper layer temperature (K)
H_∞ = Heat transfer coefficient on the ambient side of the wall (kW/m^{2}K)

Solving for the wall temperature with the initial condition of the wall at ambient temperature yields

$$T_w = \frac{h_g T_g}{h_g + h_\infty}\left[1 - \exp\left(-\frac{h_g + h_\infty}{m_w'' c} t\right)\right] \tag{30.24}$$

The heat transfer through the wall, $\dot{q}''$, may be expressed in terms of the heat transfer to the hot side of the wall or in terms of an overall effective heat transfer coefficient, h_k.

$$\dot{q}'' = h_g(T_g - T_w) = h_k(T_g - T_\infty) \quad (30.25)$$

Solving for h_k yields

$$h_k = h_g - \frac{h_g^2}{h_g + h_\infty}\left[1 - \exp\left(-\frac{h_g + h_\infty}{\rho\delta c}t\right)\right] \quad (30.26)$$

where
ρ = Density of the wall material (kg/m^3)
δ = Thickness of the wall (m)
h_k = Overall effective heat transfer coefficient W/m^2·K

From the above equations it can be seen that

$$h_k = \frac{h_g h_\infty}{h_g + h_\infty} \quad \text{at} \quad t = \infty$$

$$h_k = h_g \quad \text{at} \quad t = 0$$

From a number of experiments, Peatross and Beyler found the heat transfer coefficients of 30 W/m^2·K for h_g and 20 W/m^2·K for h_∞. Substituting these values yields

$$h_k = 30 - 18\left[1 - \exp\left(-\frac{50}{\rho\delta c}t\right)\right] \quad (30.27)$$

The h_k calculated with this method can be used directly in the Beyler and Deal method. It must be multiplied by 2.5 for use in the McCaffrey, Quintiere, and Harkleroad method to account for the 0.4 fitting constant in the h_k in the Beyler and Deal method.

Example of Peatross and Beyler Method for Forced Ventilation Estimate the temperature in a 5 × 5 m floor area and 4-m-high compartment having 0.00635-m (0.25-in.) thick, 0.5 % carbon steel walls. The forced-ventilation rate is 2.4 m^3/s of air (5000 cfm). Perform the calculation for t = 200 s. The fire size is given as 1000 kW; ambient air conditions at 300 K. Using Equation 30.19a,

$$T_g - T_\infty = \frac{\dot{Q}}{\dot{m}_g c_p + h_k A_T}$$

where
$\dot{Q}$ = 1000 kW
$\dot{m}_g$ = (2.4 m^3/s) (1.18 kg/m^3) = 2.8 kg/s
c_p = 1.0 kJ/kg·K
T_∞ = 300 K
A_T = 4(5 × 4) + 2(5 × 5) = 130 m^2

(a) Using Equation 30.27, calculate h_k for t = 200 s. For 0.25-m-thick, 0.5 % carbon steel,
δ = 0.00635 m
ρ = 7833 kg/m^3
c = 0.465 kJ/kg·K

$$h_k = 30 - 18\left[1 - \exp\left(-\frac{50}{\rho\delta c}t\right)\right]$$
$$= 30 - 18\left\{1 - \exp\left[-\frac{50}{(7833)(0.00635)(0.465)}200\right]\right\}$$
$$= 23.7 \ \text{W/m}^2 \cdot \text{K}$$

(b) Calculate the compartment temperature using Equation 30.19a.

$$T_g - 300 = \frac{1,000}{(2.8)(1.0) + (0.0237)(130)}$$
$$T_g = 470 \ \text{K}$$

Method of Beyler

For compartments with no ventilation the quasi-steady approximation used in many of the methods is not appropriate since the conditions in the compartment will not reach steady state.

Beyler applied a nonsteady energy balance to the closed compartment expressed by the differential equation [17]

$$mc_p \frac{dT}{dt} = \dot{Q} - h_k A_T \Delta T_g \tag{30.28}$$

where

$\dot{Q}$ = Energy (heat) release rate of the fire (kW)
m = Mass of the gas in the compartment (kg)
c_p = Specific heat of gas (kJ/kg·K)
$\Delta T_g = T_g - T_\infty$
T_g = Temperature of the upper gas layer (K)
T_∞ = Ambient temperature (K)
h_k = Effective heat transfer coefficient (kW/m^{2}K)
A_T = Total area of the compartment enclosing surfaces (m^2)
ρ = Density of the compartment surface (kg/m^3)
δ = Thickness of the compartment surface (m)
t = Exposure time (s)

In this case a "closed" compartment has sufficient leaks to prevent pressure buildup, but the leakage is ignored. The mass of the fuel is ignored, and the initial temperature is assumed to be ambient temperature. For constant heat release rate, the solution to Equation 30.28 is

$$\Delta T_g = \frac{2K_2}{K_1^2}\left(K_1\sqrt{t} - 1 + e^{-K_1\sqrt{t}}\right) \tag{30.29}$$

where

$$K_1 = \frac{2(0.4\sqrt{k\rho c})A_T}{mc_p} \tag{30.30}$$

$$K_2 = \frac{\dot{Q}}{mc_p} \tag{30.31}$$

where

k = Thermal conductivity of the compartment surface (kW/m·K)
c = Specific heat of the compartment surface material (kJ/kg·K)

which include the fitting coefficient. Beyler used data with a maximum temperature rise of 150 °C to develop this correlation.

Example of Beyler Method Estimate the temperature in a 5 × 5 m floor area and 4-m-high "closed" compartment having 0.025-m (1-in.) thick concrete walls. Perform the calculation for t = 120 s. The fire size is given as 100 kW; ambient air conditions at 300 K. Using Equation 30.29,

$$\Delta T_g = \frac{2K_2}{K_1^2}\left(K_1\sqrt{t} - 1 + e^{-K_1\sqrt{t}}\right)$$

where

T_∞ = 300 K
t = 120 s

(a) Calculate K_1 using Equation 30.30.

$$K_1 = \frac{2(0.4\sqrt{k\rho c})A_T}{mc_p} = \frac{2\left(0.4\sqrt{(1.4\times10^{-3})(2{,}000)(0.88)}\right)(130)}{(118)(1.0)} = 1.3834$$

where

$m = (100\ \text{m}^3)(1.18\ \text{kg/m}^3) = 118$ kg
c_p = 1.0 kJ/kg·K
ρ = 2000 kg/m^3
$k = 1.4 \times 10^{-3}$ kW/m·K
c = 0.88 kJ/kg·K
A_T = 130 m^2

(b) Calculate K_2 using Equation 30.31.

$$K_2 = \frac{\dot{Q}}{mc_p} = \frac{100}{(118)(1.0)} = 0.84746$$

where

$m = (100\ \text{m}^3)(1.18\ \text{kg/m}^3) = 118$ kg
c_p = 1.0 kJ/kg·K

(c) Calculate the compartment temperature using Equation 30.29.

$$T_g - 300 = \frac{(2)(0.84746)}{(1.3834)^2}\left((1.3834)\sqrt{120} - 1 + e^{-(1.3834)\sqrt{120}}\right)$$

$$T_g = 312.5\ \text{K}$$

Methods for Predicting Postflashover Compartment Fire Temperatures

Method of Babrauskas

The following method is based on the work of Babrauskas [20, 21]. The upper gas temperature, T_g, is expressed according to a series of factors, each one accounting for a different physical phenomenon:

$$T_g = T_\infty + (T^* - T_\infty) \cdot \theta_1 \cdot \theta_2 \cdot \theta_3 \cdot \theta_4 \cdot \theta_5 \tag{30.32}$$

where T^* is an empirical constant = 1725 K, and the factors θ are in Equations 30.38, 30.43, 30.45, 30.46, 30.48 and 30.49.

Burning Rate Stoichiometry, θ_1 The dimensionless stoichiometric coefficient ϕ is defined as

$$\phi = \frac{\dot{m}_f}{\dot{m}_{f,st}} \tag{30.33}$$

where $\dot{m}$ is the fuel mass pyrolysis rate (kg/s), and $\dot{m}_{f,st}$ is the stoichiometric mass burning rate (i.e., no excess fuel and no excess oxygen).

$$\dot{m}_{f,st} = \frac{0.5 A_o \sqrt{H_o}}{r} \tag{30.34}$$

where the ratio r is such that 1 kg fuel + r kg air → (1 + r) kg products. The value of r is readily computable for fuels containing carbon, hydrogen, and/or oxygen from the chemical formula of the fuel, taking the products to be CO_2, H_2O, and N_2.

$$C_x H_y O_z + wO_2 + w\left(\frac{79}{21}\right)N_2 \rightarrow xCO_2 + \frac{y}{2}H_2O + w\left(\frac{79}{21}\right)N_2 \tag{30.35}$$

where

$$w = \frac{2x + 2y/2 - z}{2} \tag{30.36}$$

and

$$r = \frac{[w + w(3.76)]28.97}{12.01x + 1.00y + 16.00z} \tag{30.37}$$

At stoichiometry ϕ = 1, and it is greater than 1 for fuel-rich burning and less than 1 for fuel-lean conditions.

The effect of ϕ on gas temperatures was evaluated by numerical computations using the COMPF2 computer program [22]. The efficiency factor, θ_1, accounts for deviation from stoichiometry and is shown in Fig. 30.4. It is seen that the fuel-lean and the fuel-rich regimes exhibit a very different dependence. For the fuel-lean regime, the results can be approximated by

$$\theta_1 = 1.0 + 0.51 \ln \phi \quad \text{for} \quad \phi < 1 \tag{30.38}$$

Similarly, in the fuel-rich regime a suitable approximation is

$$\theta_1 = 1.0 - 0.05(\ln \phi)^{5/3} \quad \text{for} \quad \phi > 1 \tag{30.39}$$

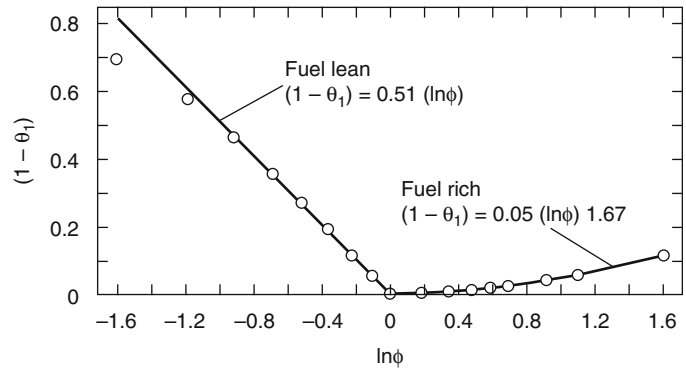

Fig. 30.4 Effect of equivalence ratio

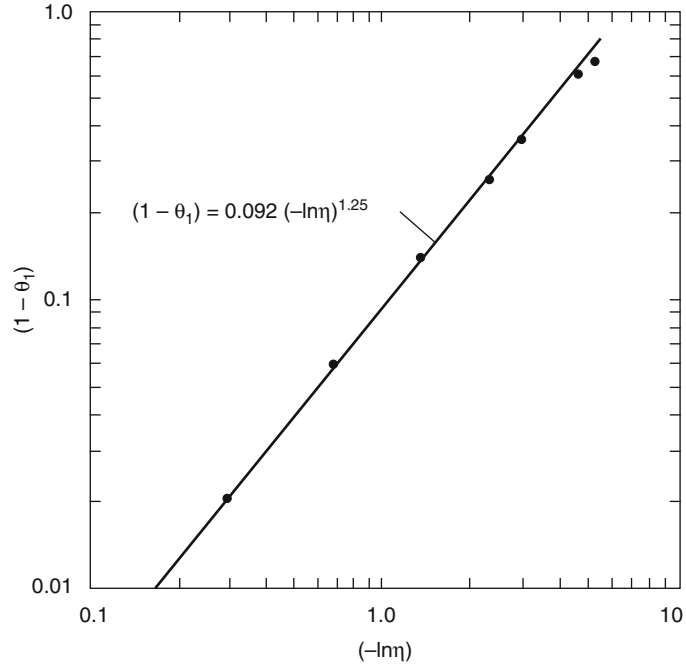

Fig. 30.5 Effect of pool diameter

If heat release rate, $\dot{Q}$, rather than mass loss rate, $\dot{m}$, is used, then

$$\phi = \frac{\dot{Q}}{\dot{Q}_{\text{stoich}}} \tag{30.40}$$

And since the stoichiometric heat release rate is

$$\dot{Q} = 1,500 A_o \sqrt{H_o} \tag{30.41}$$

then

$$\phi = \frac{\dot{Q}}{1,500 A_o \sqrt{H_o}} \tag{30.42}$$

The value of $\dot{Q}$ can be determined from Chap. 26.

A separate procedure is necessary for pool fires, due to the strong radiative coupling. Here

$$\theta_1 = 1.0 - 0.092(-\ln \eta)^{1.25} \tag{30.43}$$

where

$$\eta = \left(\frac{A_o \sqrt{H_o}}{A_f}\right) \frac{0.5 \Delta h_p}{r\sigma\left(T_g^4 - T_b^4\right)} \tag{30.44}$$

where

Δh_p = Heat of vaporization of liquid (kJ/kg)

A_f = Pool area (m^2)

σ = Stefan-Boltzmann constant (5.67×10^{-11} $kW/m^2 \cdot K^4$)

T_b = Liquid boiling point temperature (K)

This expression unfortunately requires an estimate for T_g to be made, so for the pool fire case, a certain amount of iteration is necessary. The relationship above is plotted in Fig. 30.5.

Wall Steady-State Losses, θ_2 The next efficiency factor, θ_2, accounts for variable groups of importance involving the wall surface (which is defined to include the ceiling) properties: area $A_T(m^2)$, thickness L (m), density ρ (kg/m^3), thermal conductivity k (kW/m·K), and heat capacity c_p(kJ/kg·K). This factor is given as

$$\theta_2 = 1.0 - 0.94 \exp\left[-54\left(\frac{A_o \sqrt{H_o}}{A_T}\right)^{2/3}\left(\frac{L}{k}\right)^{1/3}\right] \tag{30.45}$$

and is shown in Fig. 30.6.

Wall Transient Losses, θ_3 For the transient case, Equation 30.45 predicts the asymptotic temperature value. An additional time-dependent factor, however, is needed (Fig. 30.7).

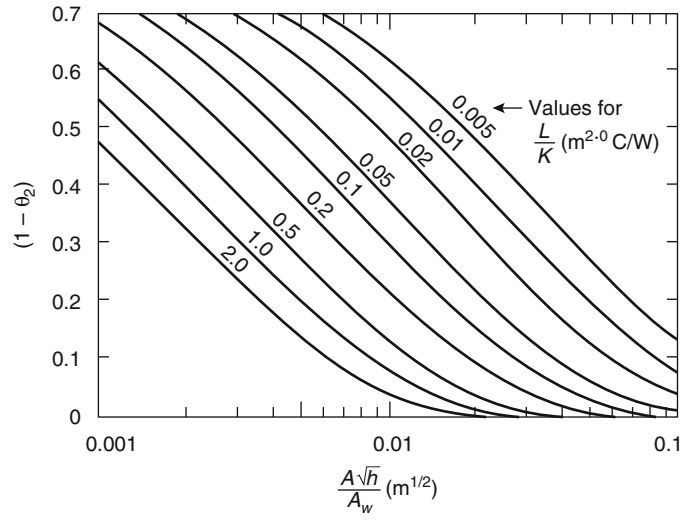

Fig. 30.6 Effect of wall steady-state losses

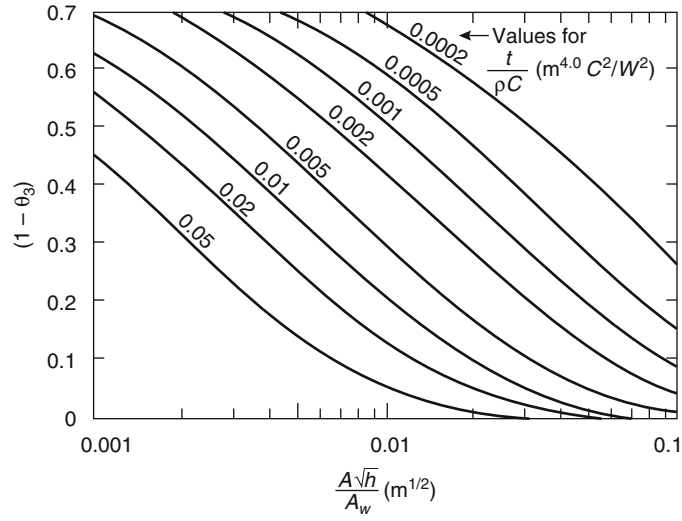

Fig. 30.7 Effect of wall transient losses

$$\theta_3 = 1.0 - 0.92 \exp\left[-150\left(\frac{A_o\sqrt{H_o}}{A_T}\right)^{0.6}\left(\frac{t}{\kappa\rho c}\right)^{0.4}\right] \tag{30.46}$$

where

κ = Thermal conductivity of wall (W/m·K)

c = Specific heat of wall (J/kg·K)

If only steady-state temperatures need to be evaluated, then $\theta_3 = 1.0$.

Wall effects for t just slightly greater than zero are not well modeled with the above relationships for $\theta_2 \cdot \theta_3$; however, this condition is not a serious limitation, since the method is only designed for postflashover fires.

For transient fires, the possibility of two separate effects must be considered. First, the wall loss effect, represented by Equation 30.46, in all fires exhibits a nonsteady character. Second, the fuel release rate may not be constant. Since in the calculational procedure the previous results are not stored, it is appropriate to restrict consideration to fires where $\dot{m}_f$ does not change drastically over the time scale established by θ_3. This "natural" time scale can be determined as the

time when the response has risen to 63 % of its ultimate value, that is, at $\theta_3 = 0.63$, and is

$$t = 2.92 \times 10^{-6}(\kappa\rho c)\left(\frac{A_T}{A_o\sqrt{H_o}}\right)^{1.5} \quad (30.47)$$

Opening Height Effect, θ_4 The normalization of burning rate and wall loss quantities with the ventilation factor $A_o\sqrt{H_o}$ does not completely determine the total heat balance. An opening of a given $A_o\sqrt{H_o}$ can be tall and narrow or short and squat. For the shorter opening, the area will have to be larger. Radiation losses are proportional to the opening area and will, therefore, be higher for the shorter opening. By slight simplification, a representation for θ_4 can be made as

$$\theta_4 = 1.0 - 0.205H_o^{-0.3} \quad (30.48)$$

as shown in Fig. 30.8.

Combustion Efficiency, θ_5 The fire compartment is viewed as a well, but not perfectly, stirred reactor. Thus a certain "unmixedness" is present. A maximum combustion efficiency, b_p, can be used to characterize this state. Since the model assumes infinitely fast kinetics, any limitations can also be included here. Data have not been available to characterize b_p in real fires, but agreement with measured fires can generally be obtained with b_p values in the range 0.5–0.9. The effect of b_p variation can be described by

$$\theta_5 = 1.0 + 0.5 \ln b_p \quad (30.49)$$

as shown in Fig. 30.9.

Method of Law

The area of structural surface to which heat is lost is expressed by $(A_T - A_o)$. For a given fire load, compartments with different values of A_T, A_o, and height H_o will have a different heat balance, and thus the temperatures in the compartments will differ. This is illustrated in Fig. 30.10, which shows how temperature varies with

$$\Omega = \frac{(A_T - A_o)}{A_o\sqrt{H_o}}$$

For low values of Ω (i.e., high ventilation), the rate of heat release is at a maximum, but the heat loss from the window is also large and the resultant temperature is low. For high values of Ω (i.e., low-ventilation areas), there is little heat loss to the outside, but the rate of heat release is also small and the resultant temperature is, again, low.

The curve in Fig. 30.11 has been derived from many experimental fires conducted internationally by CIB [10]. For design purposes, Law has defined it as follows:

$$T_{g(max)} = 6,000\frac{(1 - e^{-0.1\Omega})}{\sqrt{\Omega}} \quad (^\circ C) \quad (30.50)$$

where

$$\Omega = \frac{(A_T - A_o)}{A_o\sqrt{H_o}}$$

and

A_T = Total area of the compartment enclosing surfaces (m^2)
A_o = Area of opening (m^2)
H_o = Height of opening (m)

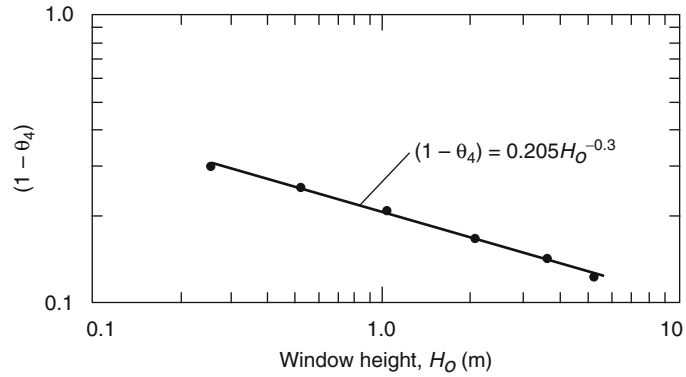

Fig. 30.8 Effect of window height

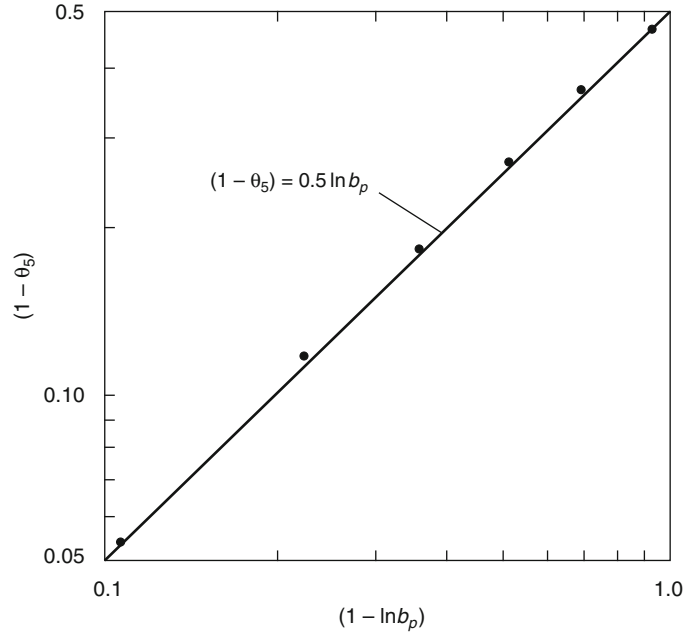

Fig. 30.9 Effect of b_p, the maximum combustion efficiency

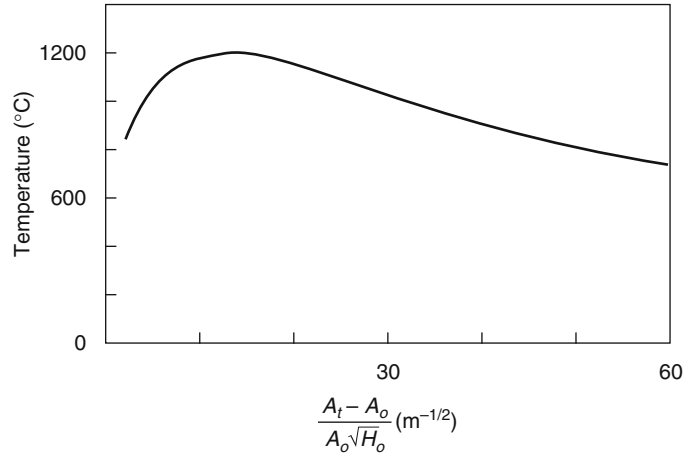

Fig. 30.10 Average temperature during fully developed period measured in experimental fires in compartments

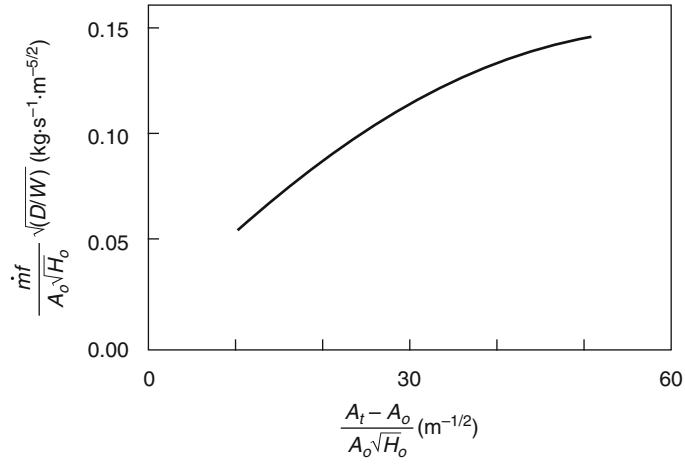

Fig. 30.11 Variation of a rate of burning during fully developed period measured in experimental fires in compartments

This equation represents an upper limit of fire temperature rise for a given Ω. However, if the fire load is low, this value may not be obtained. The importance of the effect of fire load also depends on A_o and A_T, and can be expressed as

$$T_g = T_{g(max)}\left(1 - e^{-0.05\Psi}\right) \ (^\circ C) \qquad (30.51)$$

where

T_g = Average temperature in the compartment (°C)

where

$$\Psi = \frac{L}{[A_o(A_T - A_o)]^{0.5}}$$

where L is the fire load (wood) in kg.

The effect of the fire on the structure depends not only on the value of T_g but also on the duration of heating. The effective fire duration, τ, in seconds, is given by

$$\tau = \frac{L}{\dot{m}_f} \qquad (30.52)$$

where $\dot{m}_f$ is the rate of burning measured in kg/s.

Equation 30.7 implies that the smaller the value of $A_o\sqrt{H_o}$ the lower the rate of burning and the longer the duration. Assuming a complete burnout, therefore, the effect on the structure tends to be more severe for large values of Ω given for small $A_o\sqrt{H_o}$.

For design purposes the following equation has been developed to express the correlation of experimental results [11]:

$$\dot{m}_f = 0.18A_o\sqrt{H_o(W/D)}\left(1 - e^{-0.036\Omega}\right) \quad \xi < 60 \qquad (30.53)$$

where

W = Compartment width (m)

D = Compartment depth (m)

$$\xi = \frac{\dot{m}_f}{A_o\sqrt{H_o}}\left(\frac{D}{W}\right)^{1/2}$$

Equation 30.53 is shown in Fig. 30.11 over the range where the data lie. Both equations are for ventilation-controlled fires. When there is ample ventilation, so that the fuel is free burning, the value of $\dot{m}_f$ depends on L and the type of fuel. For example, domestic furniture has a free-burning fire duration of about 20 min, giving $\tau = 1200$ s and $\dot{m}_f = L/1200$.

The temperatures discussed above are averages measured during the fully developed period of the fire. It is assumed that all fires are ventilation controlled, with the simple relationship for rate of burning given by Equation 30.53, which is near stoichiometric burning, and it is assumed that combustion of 1 kg of wood releases 18.8 MJ in total.

Method of Delichatsios et al.

Delichatsios' proposed a method assuming that [23];

1. determination of uniform maximum gas temperature in the compartment for adiabatic conditions
2. determination of an average heat flux to the compartment boundary during the development of the fire
3. a transient thermal model for the response of the compartment boundary to account for heat losses to the boundary of the compartment.

First, gas temperature in the compartment is defined from the following equation at quasi-steady conditions:

$$\dot{Q}_c = \dot{m}_g c_p\left(T_g^* - T_\infty\right) + \sigma A_o\left(T_g^{*4} - T_\infty^4\right) \qquad (30.54)$$

where

$\dot{Q}_c$ = Heat release rate inside the compartment (kW)

$\dot{m}_g$ = Flow rate of gases out of the compartment (kg/s)

T_g^* = Adiabatic temperature leaving through the opening (K)

T_∞ = Ambient temperature (K)

A_o = Area of the opening (m^2)

Assuming ventilation controlled fire, the heat release rate inside the enclosure can be calculated using following equation.

$$\dot{Q}_c = 1,500A_o\sqrt{H_o} \qquad (30.55)$$

The mass flow rate of hot gas out of the opening can be given by the equation below.

$$\dot{m}_g = 0.5 A_o \sqrt{H_o} \tag{30.56}$$

where

H_o = Height of opening (m)

Substituting Equations 30.55 and 30.56 into Equation 30.54, the following energy balance equation is obtained for the case of ventilation controlled fires.

$$1,500 A_o \sqrt{H_o} = \left(0.5 A_o \sqrt{H_o}\right) C_p \left(T_g^* - T_\infty\right) + \sigma A_o \left(T_g^{*4} - T_\infty^4\right) \tag{30.57}$$

Equation 30.57 can be solved by using simple numerical inversion to obtain the adiabatic temperature. As for Equation 30.57, the adiabatic temperature depends only on $A_o\sqrt{H_o}$.

From the dimensional analysis,

$$\frac{T_g - T_\infty}{T_g^* - T_\infty} = function\left(\frac{\sqrt{t}}{\sqrt{(k\rho c)_w}}\ \frac{\dot{Q}_c}{A_T\left(T_g^* - T_\infty\right)}\right). \tag{30.58}$$

where

A_T = Total area of the compartment enclosing surfaces (m^2)

Compared to the experimental data, the model for gas temperature in the enclosure is proposed below for the growing period of fire before burnout occurs,

$$\frac{T_g - T_\infty}{T_g^* - T_\infty} = 0.5\left(\frac{\sqrt{t}}{\sqrt{(k\rho c)_w}}\ \frac{\dot{Q}_c}{A_T\left(T_g^* - T_\infty\right)}\right)^{1/2} \tag{30.59}$$

Swedish Method

The Swedish method, developed by Magnusson and Thelandersson [12], is based on the conventional mass and energy balance equations. The fire itself is not modeled; heat release rate curves are provided as input and, in all instances, the energy release must be less than stoichiometric. The method does not take into account that the actual mass loss rate may be greater than stoichiometric, with the excess fuel burning outside the compartment. A computer program, SFIRE (versions 1 through 3), is available to perform this method. The results from the computer program have been compared with a large number of full-scale fire experiments, both in the fuel- and ventilation-controlled regimes, with good agreement between theory and experiment. It should be added, however, that most of the experiments involved wood crib fires, which inherently burn slower and produce less excess fuel load than furnishings and other combustibles found in practical fire loads. In the Swedish method, the fire load is expressed in relation to A_T as $\dot{Q} = 18.8\ L/A_T\ \mathrm{MJ/m^2}$.

The design curves approved by the Swedish authorities were computed on the basis of systemized ventilation-controlled heat-release curves taken from Magnusson and Thelandersson [12]. Figure 30.12 shows some typical curves. The curves are calculated for wall, floor, and ceiling materials with "normal" thermal properties from an energy balance which assumes a uniform temperature in the compartment.

Japanese Method

The McCaffery's method (Equation 30.12) was originally derived for fuel-controlled fires [24]. However, the formula was extended to calculate the temperature of ventilation controlled fires as well [25]. The fire temperature in the compartment and fire duration are calculated by

$$T_f = 1,280\left(\frac{Q}{\sqrt{A_T\sqrt{k\rho c}}\sqrt{A_o\sqrt{H_o}}}\right)^{2/3} t^{1/6} + T_\infty \tag{30.60}$$

where

$$t_D = \frac{1}{60}\frac{F_L A_r}{Q} \tag{30.61}$$

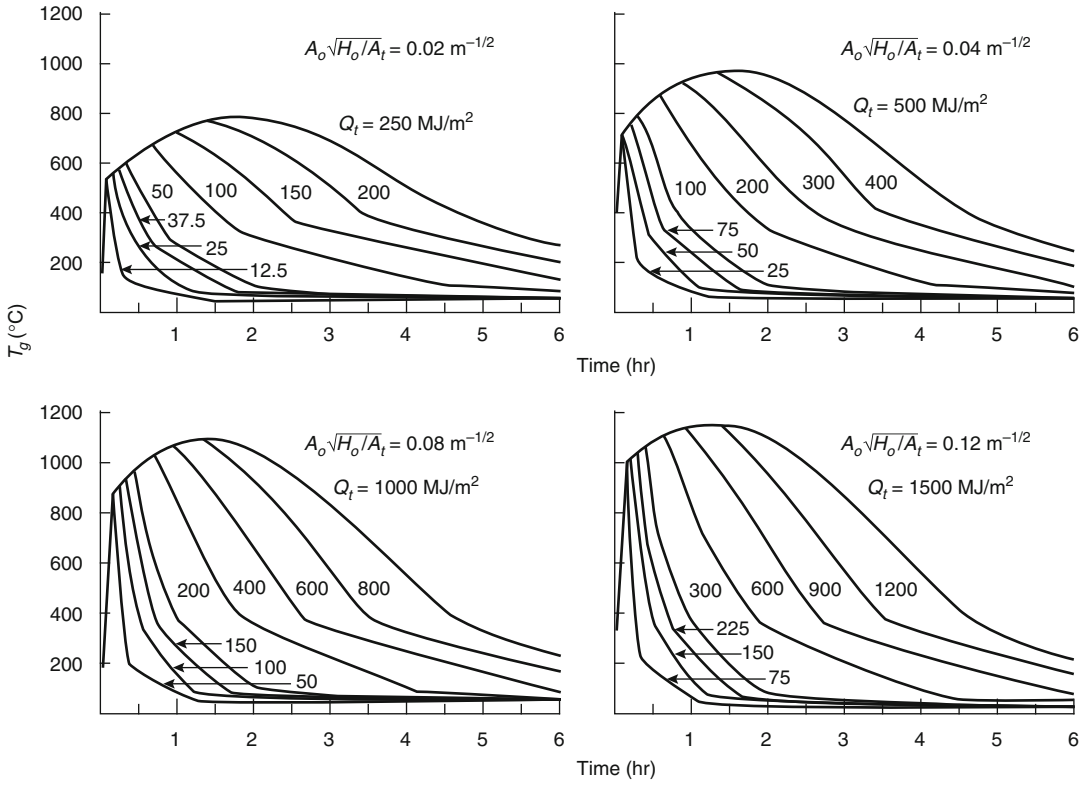

Fig. 30.12 Examples of gas temperature-time curves of postflashover compartment fires for different values of the fire load density $\dot{Q}_t$ MJ per unit of total internal surface area, A_t, and the opening factor $A_o\sqrt{H_o/A_t}$. Fire compartment, type A—from authorized Swedish standard specifications [12]

Q = Heat release rate by combustion (MW)
A_T = Internal surface area of compartment enclosure (m^2)
$\sqrt{k\rho c}$ = Thermal inertia of compartment enclosure (kW·s$^{1/2}$/m^2·K)
A_o = Area of window opening (m^2)
H_o = Height of window opening (m)
T_∞ = Initial and ambient temperatures (°C)
F_L = Fire load density (MJ/m^2)
A_r = Floor area of the room (m^2)
t_D = Fire duration (min.)

The heat release rate is calculated by the burning type index (fraction of ventilation factor to surface area of fuel),

$$\chi = \frac{A_o\sqrt{H_o}}{A_{fuel}}. \tag{30.62}$$

The fuel surface area was assumed to follow the following formula [26].

$$A_{fuel} = 0.26F_L^{1/3}A_{room} \tag{30.63}$$

Using burning type index, the heat release rate is calculated by

$$Q = A_{fuel} \times \begin{cases} 1.6\chi & (\chi \le 0.081) \\ 0.13 & (0.081 < \chi \le 0.1) \\ 2.5\chi\exp(-11\chi) + 0.048 & (0.1 < \chi) \end{cases} \tag{30.64}$$

Example of Japanese Method Calculate the maximum temperature of a room; 3 m width × 3 m in floor depth × 2.4 m high with a door opening installed at 1.8 m high × 0.6 m wide. The internal surface area is 31.32 m^2. The fire load density is 720 MJ/m^2.

The compartment enclosure is made of concrete with $\sqrt{k\rho c} = 1.75$ kW $s^{1/2}/m^2K$. Perform calculation until burnout.

The fuel surface area and ventilation factors are

$$A_{fuel} = 0.26\, F_L^{1/3} A_{room} = 0.26 \times 720^{1/3} \times (3 \times 3) = 21.0\ \text{m}^2$$

$$A_o\sqrt{H_o} = 0.6 \times 1.8 \times \sqrt{1.8} = 1.45\ \text{m}^{5/2}$$

The burning type index is

$$\chi = \frac{A_o\sqrt{H_o}}{A_{fuel}} = \frac{1.45}{21.0} = 0.069$$

As $\chi < 0.081$, fire is ventilation-controlled. The heat release rate and fire duration are

$$Q = A_{fuel} \times 1.6\chi = 21.0 \times 1.6 \times 0.069 = 2.32\text{MW}$$

$$t_D = \frac{1}{60}\frac{F_L A_r}{Q} = \frac{1}{60}\frac{720 \times 3 \times 3}{2.32} = 46.6\ \text{min.}$$

Combining the results, the fire temperature in the compartment can be calculated by the following equation as shown in Fig. 30.13.

$$T_f = 1,280\left(\frac{Q}{\sqrt{A_T\sqrt{k\rho c}}\sqrt{A_o\sqrt{H_o}}}\right)^{2/3} t^{1/6} + T_0$$

$$= 1,280\left(\frac{2.32}{\sqrt{31.32 \times 1.75}\sqrt{1.45}}\right)^{2/3} t^{1/6} + 20$$

$$= 522t^{1/6} + 20$$

For example, the fire temperature at fire duration is

$$T_f = 522 \times 46.6^{1/6} + 20 = 1,009°\text{C}$$

Predicting Flashover

One use of predicted compartment fire temperatures is estimating the likelihood of flashover. The methods used are similar to those used in the prediction of temperature. In one case, that of McCaffrey et al., the method is simply an extension of the temperature calculation.

Method of Babrauskas

Babrauskas uses the energy balance for the upper layer given in Equation 30.8, where the gas flow rate out of the opening is approximated by [27]

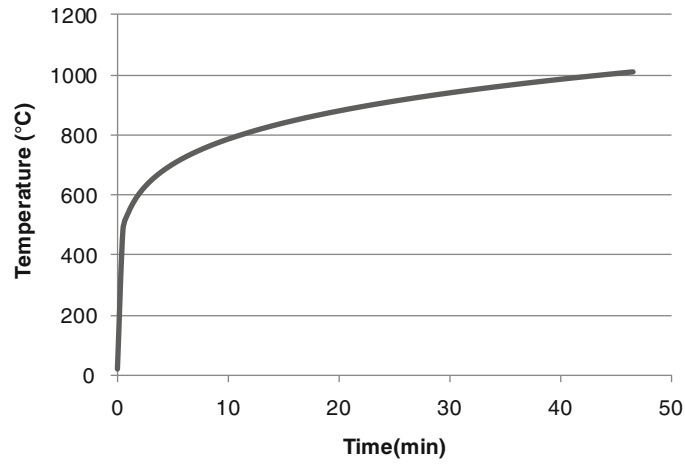

Fig. 30.13 Example of temperature-time curve calculated by Japanese method

$$\dot{m}_g \approx 0.5 A_o \sqrt{H_o} \tag{30.65}$$

The primary energy loss is assumed to be radiation to 40 % of the wall area, which is at approximately ambient temperature:

$$q_{\text{loss}} = \varepsilon\sigma\left(T_g^4 - T_\infty^4\right)(0.40 A_T) \tag{30.66}$$

where
ε = Emissivity of the hot gas
σ = Stefan-Boltzmann constant 5.67×10^{11} kW/m^2·K^4

Combining Equations 30.8, 30.65 and 30.66, using a gas temperature for flashover of 873 K, a specific heat of air of 1.0 kJ/kg·K, an emissivity of 0.5, and assuming the correlation between compartment wall and opening area of

$$\frac{A_T}{A_o\sqrt{H_o}} \approx 50$$

yields a minimum $\dot{Q}$ required for flashover,

$$\dot{Q} = 600 A_o \sqrt{H_o} \tag{30.67}$$

The airflow into the compartment has been approximated as

$$0.5 A_o \sqrt{H_o}$$

The maximum amount of fuel that can be burned completely with this air is known as the stoichiometric amount. For most fuels, the heat released per mass of air consumed is a constant approximately equal to 3000 kJ/kg. Therefore, the stoichiometric heat release rate can be $\dot{Q}_{\text{stoich}}$ calculated:

$$\begin{aligned}\dot{Q}_{\text{stoich}} &= 3{,}000\ \dot{m}_g = 3{,}000\left(0.5 A_o \sqrt{H_o}\right) \\ &= 1{,}500 A_o \sqrt{H_o}\end{aligned} \tag{30.68}$$

From this derivation, it is shown that the minimum $\dot{Q}$ required for flashover equals $0.4\ \dot{Q}_{\text{stoich}}$. Comparing these results with fire tests, Babrauskas found that the data fall within a range of $\dot{Q} = 0.3\ \dot{Q}_{\text{stoich}}$ to $\dot{Q} = 0.7\ \dot{Q}_{\text{stoich}}$. A best fit of the data suggests

$$\dot{Q} = 0.5\ \dot{Q}_{\text{stoich}}$$

which, substituting into Equation 30.68 yields

$$\dot{Q} = 750 A_o \sqrt{H_o} \tag{30.69}$$

The 33 test fires used had energy release rates from 11 to 3840 kW, with fuels primarily of wood and polyurethane. Ventilation factors $A_o\sqrt{H_o}$ ranged from 0.03 to 7.51 m$^{5/2}$, and surface area to ventilation factor ratios

$$\frac{A_T}{A_o\sqrt{H_o}}$$

ranged from 9 to 65 m$^{-1/2}$.

Example of Babrauskas's Method Calculate the heat release rate necessary to cause flashover, using the method of Babrauskas. Assume the same room as in the McCaffrey et al. method example for predicting compartment fire temperatures. From Equation 30.69

$$\dot{Q} = 750 A_o \sqrt{H_o}$$

where
$A_o = 1.08$ m^2
$H_o = 1.8$ m
$\dot{Q} = (750)(1.08)(1.8)^{1/2} = 1087$ kW

Method of McCaffrey, Quintiere, and Harkleroad

The method of McCaffrey, Quintiere, and Harkleroad for predicting compartment fire temperatures may be extended to predict the energy release rate of the fire required to result in flashover in the compartment.

Equation 30.12 can be rewritten as

$$\dot{Q} = \left[\sqrt{g} c_p \rho_\infty T_\infty^2 \left(\frac{\Delta T_g}{480}\right)^3\right]^{1/2} \left(h_k A_T A_o \sqrt{H_o}\right) \tag{30.70}$$

Selecting an upper gas temperature of 522 °C and ambient temperature of 295 K or $\Delta T_g =$ 500 °C for flashover, and substituting values for the gravitational constant ($g = 9.8$ m/s^2), the

specific heat of air ($c_p = 1.0$ kJ/kg·K), and the density of air ($\rho_\infty = 1.18$ kg/m^3), and rounding 607.8–610 yields

$$\dot{Q} = 610\left(h_k A_T A_o \sqrt{H_o}\right)^{1/2} \tag{30.71}$$

where

h_k = Effective heat transfer coefficient (kW/m^{2}K)
A_T = Total area of the compartment surfaces (m^2)
A_o = Area of opening (m^2)
H_o = Height of opening (m)

Using Equation 30.13 yields a slightly different value, 623.6 rounded to 620, of the leading coefficient because of the difference in the value used for the specific heat of air:

$$\dot{Q} = 620\left(h_k A_T A_o \sqrt{H_o}\right)^{1/2} \tag{30.72}$$

The use of either 610 or 620 is acceptable within the accuracy of the expression.

Example of McCaffrey et al.'s Method Estimate the energy release rate required for flashover of a compartment. Assume the same room as in the McCaffrey et al. method example for predicting compartment fire temperatures. Assuming $\Delta T_g = 500$ °C as a condition for flashover, and air properties at 295 K, use Equation 30.71 and assume the compartment has heated for a period of time that exceeds the thermal penetration time.

$$\dot{Q} = 610\left(h_k A_T A_o \sqrt{H_o}\right)^{1/2}$$

where

$$h_k = \frac{k}{\delta} = \frac{0.48 \times 10^{-3}}{0.016} = 0.03 \text{ kW/m}^2\text{K}$$

$A_T = 45.72$ m^2
$A_o = 1.08$ m^2
$H_o = 1.8$ m

Therefore,

$$\dot{Q} = 610\left[(0.03)(45.72)(1.08)\left(\sqrt{1.8}\right)\right]^{1/2} = 860 \text{ kW}$$

Method of Thomas

Thomas uses the energy balance for the upper layer shown in Equation 30.8, where the gas flow rate out of the opening is approximated by [2]

$$\dot{m}_g \approx 0.5 A_o \sqrt{H_o} \tag{30.73}$$

Thomas develops an expression for $\dot{q}_{\text{loss}}$ which assumes the area for the source of radiation for roughly cubical compartments is $A_T/6$:

$$\dot{q}_{\text{loss}} \approx h_c\left(T_g - T_w\right)\frac{A_T}{2} + \varepsilon\sigma\left(2T_g^4 - T_{\text{floor}}^4\right)\frac{A_T}{6} \tag{30.74}$$

where

A_T = Total area of the compartment-enclosing surfaces (m^2)
h_c = Convective heat transfer coefficient (kW/m^2·K)
T_w = Temperature of the upper walls (K)
T_{floor} = Temperature of the floor (K)

From experimental data, Thomas developed an average for $\dot{q}_{\text{loss}}$ of 7.8 A_T. Using an upper layer temperature of 577 °C or a ΔT_g of 600 °C for flashover criterion and $c_p = 1.26$ kJ/kg·K yields an expression for the minimum rate of energy release for flashover:

$$\dot{Q} = 7.8 A_T + 378 A_o \sqrt{H_o} \tag{30.75}$$

Comparison of Methods for Predicting Flashover

Babrauskas has compared the effect of room wall area on the energy release required for flashover, using the above methods [28]. The results of his comparisons, along with some experimental data for rooms with gypsum board walls, are shown in Fig. 30.14. The graph shows the energy required for flashover as a function of compartment wall area, both normalized by the ventilation factor $A_o\sqrt{H_o}$. The method of Babrauskas used in this graph is based on Equation 30.32 with $T_\infty = 25$ °C and $T_g = 600$ °C. Babrauskas observes that over the range of compartment sizes of most

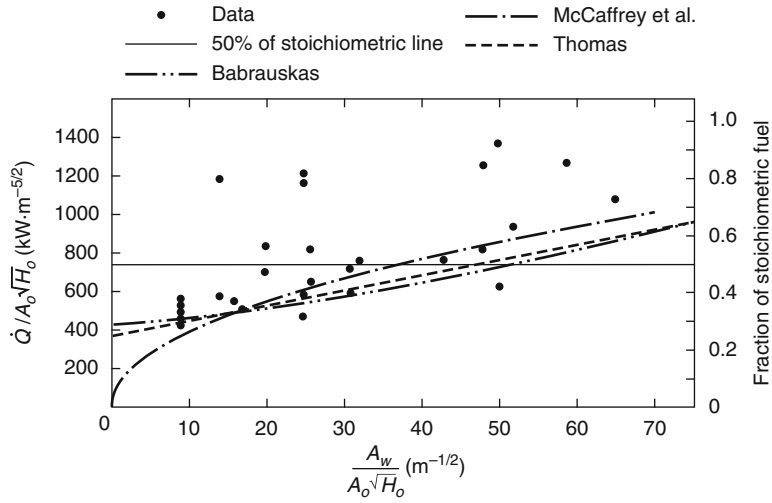

Fig. 30.14 The effect of room wall area (gypsum walls) on the heat required for flashover

interest, all of the methods produce similar results. The method of McCaffrey et al. diverts from the others for small room sizes. Babrauskas notes that all of the methods are a conservative representation of the data.

Nomenclature

$A_{ceiling}$	area of compartment ceiling (m^2)
A_f	pool fire area (m^2)
$A_{\mathbf{floor}}$	area of compartment floor (m^2)
$A_{\mathbf{o}}$	area of openings (m^2)
A_T	total area of the compartment enclosing surfaces (m^2)
$A_{\mathbf{walls}}$	area of compartment walls (m^2)
b_p	maximum combustion efficiency
c	specific heat of the wall (kJ/kg·K)
C_d	orifice constriction coefficient
c_p	specific heat of gas (kJ/kg·K)
D	compartment depth (m)
g	acceleration due to gravity, 9.8 m/s^2
h_c	convective heat transfer coefficient
Δh_c	effective heat of combustion of the fuel (kJ/kg)
h_g	heat transfer coefficient on the hot side of the wall (kW/m^{2}K)
h_k	effective heat transfer coefficient (kW/m^{2}K)
h_∞	heat transfer coefficient on the ambient side of the wall (kW/m^{2}K)
H_o	height of opening (m)
k	thermal conductivity of the wall (kW/m·K)
L	fire load, wood (kg)
m	mass of the gas in the compartment (kg/s)
$\dot{m}_a$	mass flow rate of air into an opening (kg/s)
$\dot{m}_g$	gas flow rate out the opening (kg/s)
$\dot{m}_f$	mass burning rate of fuel (kg/s)
$\dot{m}_{f,st}$	stoichiometric mass burning rate of fuel (kg/s)
$\dot{m}''_w$	mass per unit area of the wall (kg/m^2)
$\dot{q}_{\mathbf{loss}}$	net radiative and convective heat transfer from the upper gas layer (kW)
$\dot{Q}$	energy (heat) release rate of the fire (kW)
$\dot{Q}_{\mathbf{stoich}}$	stoichiometric heat release rate (kW)
t	time (s)
t_p	thermal penetration time (s)
T_b	liquid boiling point (K)
$T_{\mathbf{floor}}$	temperature of the floor (K)
T_g	temperature of the upper gas layer (K)
T_p	thermal penetration time (s)
T_w	wall temperature (K)
T_∞	ambient temperature (K)
W	compartment width (m)
W_o	width of opening (m)
X_d	height of the interface (m)
X_N	height of neutral plane (m)

Greek Letters

δ	thickness of the wall (m)
ε	emissivity of the hot gas
ρ	density of the wall (kg/m^3)
ρ_∞	ambient air density (kg/m^3)
σ	Stefan-Boltzmann constant, 5.67×10^{-11} kW/m^2·K^4

Subscripts

a	air
b	boiling
d	thermal discontinuity
f	fuel
g	gas
N	neutral plane
o	opening
stoich	stoichiometric
T	total
w	wall
∞	ambient

Superscripts

.	per unit time (s^{-1})
$''$	per unit area (m^{-1})

References

1. D. Drysdale, "The Pre-Flashover Compartment Fire," *An Introduction to Fire Dynamics,* John Wiley and Sons, Chichester, UK, pp. 278–303 (1985).
2. P.H. Thomas, "Testing Products and Materials for Their Contribution to Flashover in Rooms," *Fire and Materials,* 5, 3, pp. 103–111 (1981).
3. K. Suzuki, K. Harada, T. Tanaka, "A Multi-Layer Zone Model for Predicting Fire Behavior in a Single Room", Fire Safety Science - Proceedings of the 7th International Symposium on Fire Safety Science, Worcester, June 2002, pp. 851–862, 2003
4. NFPA 259, *Standard Test Method for Potential Heat of Building Materials*
5. C. Huggett, "Estimation of Rate of Heat Release by Means of Oxygen Consumption Measurements," *Fire and Materials,* 4, 2, pp. 61–65 (1980).
6. J. de Ris, *Fire Radiation—A Review,* Tech. Report FMRC, RC78-BT-27, Factory Mutual Research Corporation, Norwood, MA, pp. 1–41 (1978).
7. J.A. Rockett, "Fire Induced Gas Flow in an Enclosure," *Combustion Science and Technology,* 12, pp. 165–175 (1976).
8. P.H. Thomas and A.J.M. Heselden, "Fully Developed Fires in Single Compartments," *Fire Research Note No. 923,* Fire Research Station, Borehamwood, UK (1972).
9. K. Kawagoe, "Fire Behaviour in Rooms," Report of the Building Research Institute, No.27, Building Research Institute, Ministry of Contruction, Japan (1958).
10. P.H. Thomas and A.J.M. Heselden, "Fully Developed Fires in Single Compartments," *CIB Report No. 20,* A Co-operating Research Programme of the Conseil International du Batiment, Joint Fire Research Organization Fire Research Note 923/197.
11. M. Law, *Structural Engineering,* 61A, 1, p. 25 (1983).
12. S.E. Magnusson and S. Thelandersson, "Temperature-Time Curves of Complete Process of Fire Development. Theoretical Study of Wood Fuel Fires in Enclosed Spaces," *Civil Engineering and Building Construction Series No. 65,* Acta Polytechnica Scandinavia, Stockholm, Sweden (1970).
13. B.J. McCaffrey, J.G. Quintiere, and M.F. Harkleroad, "Estimating Room Fire Temperatures and the Likelihood of Flashover Using Fire Test Data Correlations," *Fire Technology,* 17, 2, pp. 98–119 (1981).
14. J.G. Quintiere, "A Simple Correlation for Predicting Temperature in a Room Fire," *NBSIR 83-2712,* National Bureau of Standards, Washington, DC (June 1983).
15. J.R. Lawson and J.G. Quintiere, "Slide-Rule Estimates of Fire Growth," *NBSIR 85-3196,* National Bureau of Standards, Washington, DC (June 1985).
16. K.L. Foote, P.J. Pagni, and N.J. Alvares, "Temperature Correlations for Forced-Ventilated Compartment Fires," in *Proceedings of the First International Symposium,* International Association for Fire Safety Science, Hemisphere Publishing, Newport, Australia, pp. 139–148 (1986).
17. C. Beyler, "Analysis of Compartment Fires with Forced Ventilation," *Fire Safety Science—Proceedings of the Third International Symposium,* Elsevier Science, New York, pp. 291–300 (1991).
18. S. Deal and C. Beyler, "Correlating Preflashover Room Fire Temperatures," *Journal of Fire Protection Engineering*, 2, 2, pp. 33–88 (1990).
19. M.J. Peatross and C.L. Beyler, "Thermal Environmental Prediction in Steel-bounded Preflashover Compartment Fires," in *Fire Safety Science—Proceedings of the Fourth International Symposium,* International Association for Fire Safety Science, Boston, pp. 205–216 (1994).
20. V. Babrauskas, "A Closed-Form Approximation for Post-Flashover Compartment Fire Temperatures," *Fire Safety Journal,* 4, pp. 63–73 (1981).
21. V. Babrauskas and R. B. Williamson, "Post-Flashover Compartment Fires: Basis of a Theoretical Model," *Fire and Materials,* 2, 2, pp. 39–53 (1978).

22. V. Babrauskas, "COMPF2—A Program for Calculating Post-Flashover Fire Temperatures," *NBS TN 991,* National Bureau of Standards, Washington, DC (1979).
23. M. Delichatsios, Y. P. Lee, P. Tofilo (2009) A new correlation for gas temperature inside a burning enclosure. Fire Safety Journal 44(8):1003–1009
24. Ministry of construction of Japan, Notification 1430, 2000
25. K. Matsuyama, T. Fujita, H. Kaneko, Y. Ohmiya, T. Tanaka, T. Wakamatsu, "A Simple Predictive Method for Room Fire Behavior", Fire Science and Technology, Vol. 18 (1998) No. 1
26. K. Aburano, H. Yamanaka, Y. Ohmiya, K. Suzuki, T. Tanaka, T. Wakamatsu, "Survey and Analysis on Surface Area of Fire Load", Fire Science and Technology, Vol. 19 (1999) No. 1
27. V. Babrauskas, "Estimating Room Flashover Potential," *Fire Technology,* 16, 2, pp. 94–104 (1980).
28. V. Babrauskas, "Upholstered Furniture Room Fires—Measurements, Comparison with Furniture Calorimeter Data, and Flashover Predictions," *Journal of Fire Science,* 2, pp. 5–19 (1984).

William D. Walton is retired from the Building and Fire Research Laboratory, National Institute of Standards and Technology.

Philip H. Thomas was with the Fire Research Station, Borehamwood, England.

Yoshifumi Ohmiya is a professor in the department of architecture, graduate school of science and technology, Tokyo University of Science.

Zone Computer Fire Models for Enclosures

31

William D. Walton, Douglas J. Carpenter, and Christopher B. Wood

Introduction

Understanding the behavior of fire in compartments is of interest to the fire protection engineer for both fire safety design and postfire reconstruction. Such understanding may be obtained by examining experimental fires (full or reduced scale) or by *fire models* using mathematical techniques to represent the processes encountered in compartment fires by interrelated expressions based on physics and chemistry. The two major classes of fire models for analyzing enclosure fire development are stochastic and deterministic.

Stochastic or *probabilistic fire models* generally treat fire growth as a series of sequential events or states. Mathematical rules are established to govern the transition from one event to another (e.g., from ignition to established burning). Probabilities are assigned to each transfer point based on analysis of relevant experimental data, historical fire incident data, and computer model results. *Deterministic fire models* represent the processes encountered in fire by interrelated mathematical expressions based on physics and chemistry. These models may also be referred to as *room* or *compartment fire* models or *mathematical fire* models. Ideally, deterministic models represent the ultimate capability: the evaluation of discrete changes in any physical parameter in terms of the effect on fire hazard. The emphasis in this chapter is on deterministic fire models and, more specifically, zone fire models for enclosures.

Although manual or "hand calculation" methods provide reasonable estimates of specific fire effects (e.g., prediction of time to flashover), they are not well suited for comprehensive analyses involving the time-dependent and highly-coupled interactions of multiple physical and chemical processes present in growing compartment fires. With the advent of the personal computer in the 1980s came the development of computer fire models with increasing complexity. *Computer fire models* perform large numbers of tedious and lengthy calculations (in a fraction of the time required by "hand calculations") and can provide analytical solutions to problems that are impractical to solve manually or for which no simple closed form analytical solution exists. As early as 1985, it had become widely accepted that the future of fire engineering would include various levels of modeling aided by the modern computer [1]. Today, computer models are used in many areas of fire protection engineering, including suppression system design, smoke control system design, and egress analysis that all provide an engineering approximation of the time-varying conditions associated with fires.

The state of the art in computer fire modeling is evolving for two reasons: increases in fundamental knowledge or understanding of the processes and

W.D. Walton (retired)
National Institute of Standards and Technology

D.J. Carpenter (✉)
Combustion Science and Engineering

C.B. Wood
FireLink LLC

M.J. Hurley (ed.), *SFPE Handbook of Fire Protection Engineering*,
DOI 10.1007/978-1-4939-2565-0_31, © Society of Fire Protection Engineers 2016

increases in computer processing speeds. Increased understanding of the processes involved in fire growth improves the technical basis for the models. The capabilities, documentation, and support for a given model can change dramatically over a short period of time. In addition, computer technology itself (both hardware and software) is advancing rapidly. In the past, a large mainframe computer was required to use most available computer fire models. Today, most computer fire models can be run on personal computers. Despite the increased awareness and practical application of fire modeling, current computer-based models are not substantially different from their predecessors; they are just more complex and possess greater capabilities. This chapter will provide a description of the characteristics of zone models, an overview of selected models, and a discussion of the selection, validation, and application of such models.

Zone Models

The most common type of physically based fire model is the *zone* or *control volume* model, which solves the conservation equations (i.e., conservation of mass and energy) for discrete and relatively large control volumes. Although many zone models use two control volumes corresponding to an upper (hot) layer and lower (cool) layer, other zone models may have different approaches for specific problems such as a single control volume for postflashover modeling. A complete discussion of the fundamental principles behind the zone fire model formulation can be found in Chap. 29.

The beginnings of preflashover zone fire modeling can be traced to the mid-1970s with the publication of a description of the fundamental equations by Quintiere [2]. Based on these equations, the first zone fire model published was RFIRES by Pape, Waterman, and Eichler [3], followed shortly by the Harvard model by Emmons and Mitler [4, 5]. Following the publication of these two models, a number of zone fire models for mainframe computers were introduced. In 1985 ASET-B, the first zone model written specifically for the newly available IBM-compatible personal computer, was introduced by Walton [6]. Since that time additional models have been introduced, and most of the models written for mainframe computers have been converted for use on personal computers.

Zone models allow for relatively inexpensive parametric studies by providing results very quickly on modern computers. This capability allows for the combination of engineering judgment and deterministic modeling to isolate particular scenarios of interest when more in-depth field modeling is required to answer the ultimate questions posed for the modeling activity. This section discusses more specific characteristics of zone models that may assist the modeler in making an appropriate model selection.

The dominant characteristic of a zone fire model is the division of the compartment(s) or room(s) into a hot, upper layer and a cooler, lower layer (Fig. 1). The model calculations

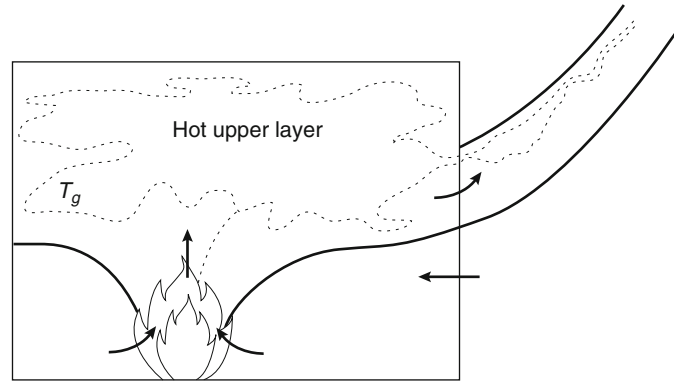

Fig. 1 Two-layer model with no exchange between layers except the plume

provide estimates of key conditions for each of the layers as a function of time. Zone modeling has proved to be a practical method for providing estimates of fire effects in enclosures.

The fundamentals of zone modeling require that a space, room, or compartment be broken up into various zones or control volumes to account for mass and energy driven by the fire. In addition to the room or compartment of origin, some models provide multiroom capability. In these cases, in addition to accounting for control volumes in the room of origin for heat and mass transfer as affected by the fire plume, a multiroom model also accounts for flows out of vents from one room into another or to the "atmosphere." In the room being exposed to fire conditions, where the mass and energy now flow from the compartment of fire origin, the vent plume adds mass and energy to a new control volume in this compartment being exposed.

Heat transfer within zone models focuses on buoyancy-driven flows. In most cases, this flow calculation is implicit as the hot gases produced by the fire are assumed to be instantaneously transported from the fire to the upper layer. Intrinsically, this implies that transport time details are lost in zone models. Some models also calculate the convective heat transfer from the hot layer to the surrounding compartment boundaries whereas others treat this as a lumped-mass loss coefficient, demonstrating how treatment of heat loss from the hot gases may be handled through multiple approaches.

Vent flow handling in zone models often only supports vents that carry horizontal flow and thus do not model holes in floors and ceilings. This restriction does not usually cause difficulty for many commonly occurring fire scenarios. Very early models often did not support vent flows at all. Vents were implicitly handled in the lower layer mathematically so that no pressure buildup occurred within the modeled space, which would have violated a variety of the basic assumptions. These early models were generally only applicable during the early phases of a fire or other limited situations. In addition to natural vents, some models support simulated heating, venting, and air conditioning (HVAC) duct work, in some cases supporting actual interconnections between rooms while in others only approximating overall supply and extraction without specifying interchange between rooms.

Some models attempt to overcome zonal limitations with specialized submodels in addition to the zonal approach. One example is the implementation of detection activation algorithms and the tracking of detection devices, such as fusible links, to predict activation. Other submodels include the switching of the employed governing equations based on the burning regime, such as fuel versus ventilation limited. This is an example of a conversion from a two-zone to a single-zone approach.

Some models add a variety of combustion and fire-related submodels. Pyrolysis and combustion products may be tracked in addition to oxygen to determine whether combustion can occur given the compartment conditions. If combustion is not possible due to lack of oxygen, for example, then these combustion products may ignite if they retain sufficient heat and progress to another compartment where the requisite oxygen is available. Similarly, models sometimes calculate radiative and convective heat transfer along with ignition temperatures of specific objects to predict involvement of additional fuel packages.

Overview of Selected Models

Although the state of the art in understanding fire processes has not yet developed the *ultimate* model, a number of available computer models provide reasonable estimates of selected fire effects. The reader is referred to Friedman [7] and Olenick and Carpenter [8] for a summary of available computer fire models and their general capabilities. The following brief summaries will focus on a representative selection of zone models rather than providing an exhaustive review of the changing state of the art in available computer models.

ASET

ASET (Available Safe Egress Time) is a program for calculating the temperature and position of the hot smoke layer in a single room with closed doors and windows [6]. ASET can be used to determine the time to the onset of hazardous conditions for both people and property. The required program inputs are the heat loss fractions, the height of the fuel above the floor, criteria for hazard and detection, the room ceiling height, the room floor area, a heat release rate, and a species generation rate of the fire (optional). The program outputs are the temperature, thickness, and (optional) species concentration of the hot smoke layer as a function of time and the time to hazard and detection. ASET, written in FORTRAN by Cooper and Stroup [9], can examine multiple cases in a single run. ASET-B is a compact version of ASET written by Walton [6] that was designed to run on personal computers. Species concentrations and time to hazard and detection calculated by ASET are not calculated in the compact ASET-B version.

COMPBRN III

COMPBRN III is primarily used in conjunction with probabilistic analysis for the assessment of risk in the nuclear power industry. The model is based on the assumption of a relatively small fire in a large space, or a fire involving large fuel loads during the early preflashover fire growth period. The model's strengths are (1) emphasis on the thermal response of elements within the enclosure to a fire within the enclosure, and (2) model simplicity. The temperature profile within each element is computed, and an element is considered ignited or damaged when its surface temperature exceeds the user-specified ignition or damage temperature. The model outputs include the total heat release rate of the fire, the temperature and depth of the hot gas layer, the mass burning rate for individual fuel elements, the surface temperatures, and the heat flux at user-specified locations. COMPBRN III was written by Ho et al. [10]

COMPF2

COMPF2 is a computer program for calculating the characteristics of a postflashover fire in a single building compartment, based on fire-induced ventilation through a single door or window. It is intended both for performing design calculations and for the analysis of experimental burn data. Wood, thermoplastics, and liquid fuels can be evaluated. A comprehensive output format is provided that gives gas temperatures, heat-flow terms, and flow variables. The documentation includes input instructions, sample problems, and a listing of the program. The program was written in FORTRAN by Babrauskas [11].

CONTAM

CONTAM is a multizone (nodal) indoor air quality and ventilation analysis computer program designed to predict: (1) airflows in building systems driven by mechanical means, wind pressures acting on the exterior of the building, and buoyancy effects induced by the indoor and outdoor air temperature difference; (2) the dispersal of airborne contaminants transported by airflows; and (3) the exposure of occupants to airborne contaminants. Unlike other fire models, zones in CONTAM are typically building areas connected by airflow paths. CONTAM was developed principally to predict nonfire related conditions within a building and does not have a fire routine; however, the user may specify the temperature in a zone. CONTAM can be useful for evaluating smoke management methods including compartmentation, dilution, pressurization, airflow, and buoyancy. CONTAM consists of two components, a graphical user interface (GUI) and a simulation engine. Once a building representation is developed with the GUI, it is passed to the simulation engine to calculate zone pressures, airflow rates, and contaminant concentrations. The interface also provides a means to graphically review results. CONTAM was written in C by Walton and Dols [12].

CSTBZ1

CSTBZ1 is a computer program for postflashover fires, based on similar basic assumptions as those of COMPF2. The equations of mass and energy conservation are written without neglecting the fuel source term, and several vertical openings in a room can be considered. The equation of heat diffusion into the walls is solved either by a classical explicit finite difference method, or by a new modal approach that offers the capability of storing in a file a few numbers characterizing a given wall, leading to a rapid calculation of the superficial wall temperatures. A sophisticated numerical algorithm was used to solve the equations through uncoupling. The program was written by Curtat and Bodart [13].

CFAST

CFAST (Consolidated model of Fire growth And Smoke Transport) is an upgrade of the FAST program [14] and incorporates numerical solution techniques originally implemented in the CCFM program [15]. CFAST is a multiroom model that predicts conditions within a structure resulting from a user-specified fire. CFAST Version 6 can accommodate up to 30 compartments with multiple openings between compartments and to the outside. The required program inputs are the geometry data describing the compartments and connections; the thermophysical properties of the ceiling, walls, and floors; the fire as a rate of mass loss; and the generation rates of the products of combustion. The program's outputs are temperature, thickness, and species concentrations in the hot, upper layer and the cooler, lower layer in each compartment. Also given are the surface temperatures and heat transfer and mass flow rates. CFAST also includes very limited mechanical ventilation capabilities, a ceiling jet algorithm, capability of multiple fires, heat transfer to targets, detection and suppression systems, and a flame spread model. The CFAST model was developed and is maintained by NIST [16, 17].

BRANZFIRE

BRANZFIRE is a two-zone fire model for predicting the fire environment in an enclosure resulting from a room-corner fire involving walls and ceilings. The zone fire model uses conservation equations based on those found in CFAST. BRANZFIRE predicts ignition, flame spread, and the resultant heat released by the wall and ceiling lining material subjected to a burner fire. The model considers upward flame spread on the walls and beneath the ceiling, lateral flame spread on the walls, and downward flame spread from the ceiling jet. Wall and ceiling flame spread properties are computed from cone calorimeter data. Program outputs include layer height, species concentrations, gas temperatures, visibility, wall temperatures, and heat release rate. BRANZFIRE was written in Visual Basic by Wade [18–20].

JET

JET is a two-zone single compartment model where the compartment is enclosed by a combination of draft curtains and walls. The ceiling may contain fusible links and vents where the vents operate in response to the fusing of the links. The ceiling vents remove hot, upper-layer gas from the compartment. The fire is characterized by a time-dependent heat release rate, a time-dependent radiative fraction, and either a constant or variable fire diameter, which is determined using a heat release rate per unit area for the burning material. Inputs also include the thermal properties of the ceiling. Program outputs include the ceiling jet temperature and velocity, link temperature, and activation times. JET was written in FORTRAN by Davis [21].

FIRST

FIRST is the direct descendant of the Harvard V5 program developed by Emmons and Mitler [4]. The program predicts the development of a fire

and the resulting conditions within a room given a user-specified fire or user-specified ignition. It predicts the heating and possible ignition of up to three targets. The required program inputs are the geometrical data describing the rooms and openings and the thermophysical properties of the ceiling, walls, burning fuel, and targets. The generation rate of soot must be specified, and the generation rates of other species may be specified. The fire may be entered either as a mass loss rate or in terms of fundamental properties of the fuel. Among the program outputs are temperature, thickness, and species concentrations in the hot, upper layer and the cooler, lower layer in each compartment. Also given are surface temperatures and heat transfer and mass flow rates. The FIRST program was written in FORTRAN by Mitler and Rockett [22].

FIRE SIMULATOR

FPETOOL is the descendant of the FIREFORM program [23]. It contains a computerized selection of relatively simple engineering equations and models useful in estimating the potential fire hazard in buildings. The calculations in FPETOOL are based on established engineering relationships. The FPETOOL package addresses problems related to fire development in buildings and the resulting conditions and response of fire protection systems. The subjects covered include smoke filling in a room, sprinkler/detector activation, smoke flow through (small) openings, temperatures and pressures developed by fires, flashover and fire severity predictions, fire propagation (in special cases), and simple egress estimation. The largest element in FPETOOL is a zone fire model called FIRE SIMULATOR. FIRE SIMULATOR is designed to estimate conditions in both pre- and postflashover enclosure fires. The inputs include the geometry and material of the enclosure, a description of the initiating fire, and the parameters for sprinklers and detectors being tracked. The outputs include the temperature and volume of the hot smoke layer; the flow of smoke from openings; the response of heat-actuated detection devices, sprinklers, and smoke detectors; oxygen, carbon monoxide, and carbon dioxide concentrations in the smoke; and the effects of available oxygen on combustion. FPETOOL was written in BASIC by Nelson [24].

FSSIM

FSSIM [25] is a single-zone model originally designed for fire hazard analysis of ships. It includes most of the features of the popular two-zone models but within a single zone fire environment description. It includes HVAC system model components, stack effect, prediction of compartment temperatures, and smoke and gas concentrations, as well as compartment to compartment fire spread, detection, and suppression. It has been applied to ships and buildings with several thousand compartments. Calculations are slower than CONTAM but still much faster than two-zone models and CFD models.

LAVENT

LAVENT (Link-Actuated VENT) is a two-zone model developed to simulate the environment and the response of sprinkler elements in compartment fires with draft curtains and fusible-link actuated ceiling vents. The zone model used to calculate the heating of the fusible links includes the effects of the ceiling jet and the upper layer of hot gases beneath the ceiling. The required program inputs are the geometrical data describing the compartment, the thermophysical properties of the ceiling, fire elevation, the time-dependent heat release rate of the fire, the fire diameter or the heat release rate per unit area of the fire, the ceiling vent area, the fusible-link response time index (RTI) and activation temperature, the fusible-link positions along the ceiling, the link assignment to each vent, and the ambient temperature. A maximum of five ceiling vents and 10 fusible links are permitted in the compartment. The program outputs are the temperature

and height of the hot layer, the temperature of each link, the ceiling jet temperature and velocity at each link, the radial temperature distribution along the interior surface of the ceiling, the activation tie of each link, and the area opened. LAVENT was written in FORTRAN by Cooper [26].

MAGIC

MAGIC is a two-zone fire model for simulations that predict the fire environment as a function of time resulting from a fire in single- or multicompartment geometries, based on a combination of macroscopic conservation equation and empirical correlations for specific phenomena [27]. The required program inputs include the compartment geometry; natural and mechanical ventilation; parameters describing the fire characteristics such as location, fuel type, footprint area, and stochiometric fuel-oxygen ratio; thermophysical properties and location; and any inputs for sprinklers or detectors. The extensive program outputs are customized by the user, but typically include environmental conditions, heat transfer–related outputs, oxygen effects, and flow velocities [28]. MAGIC is being extended to include nonrectangular rooms, convex and sloping ceilings, rooms cluttered with objects, spread of fire through ventilation ducts, and extinction. Although the program can be used for general fire modeling, it was originally intended for nuclear power plant applications. The program is developed and maintained by Electricité de France (EdF).

WPI/FIRE

WPI/FIRE is a direct descendant of the Harvard V [4] and FIRST [22] programs. It includes all of the features of the Harvard program version 5.3 and many of the features of the FIRST program. WPI/FIRE also includes the following additional features: improved input routine, momentum-driven flows through ceiling vents, two different ceiling jet models for use in detector activation, forced ventilation for ceiling and floor vents, and an interface to a finite difference computer model for the calculation of boundary surface isotherms and hot spots. The WPI/FIRE program was written in FORTRAN by Satterfield and Barnett [29], and additions to the program continue to be developed by graduate students at the Center for Fire Safety Studies, Worcester Polytechnic Institute.

BRI2

BRI2 is a two-layer, multi-compartment model to predict smoke spread through large buildings. In addition to conventional zone equations, it includes radiative and convective heat transfer between layers and wall enclosures and species yield prediction using equivalence ratio. For practical purposes, users can input the time-based events such as smoke vent activation, door opening by evacuees etc. The BRI2 program was written in FORTRAN by Tanaka et al. [30].

Selection, Validation, and Application of Zone Models

Selection

The appropriate selection of a zone fire model for a particular application requires significant attention since no existing zone fire model is best for all applications. Although most zone fire models are based on the same fundamental principles, available models can vary significantly in features and capabilities. Appropriate selection of a zone fire model requires sufficient understanding of the assumptions and limitations for any particular model. Frequently, experienced users will employ more than one model to evaluate a particular situation. If several models provide similar results this can increase (although not generally guaranteed) confidence in the results. A significant issue in selecting a zone fire model is model validation, a process by which to assess the predictive capabilities and accuracy of a fire model.

The predictive capability of any model depends on the underlying scientific knowledge and understanding of the phenomenon being modeled and the translation of that knowledge and understanding into a mathematical model. This knowledge may be based upon well-established fire science, secure empirical correlations, or, if these are not available, then the best engineering judgment that can be made [1]. Due to its complexity, there remain substantial voids and shortcomings in the scientific understanding of combustion and fire and associated processes. Obviously, the current level of knowledge supports the development of mathematical models with sufficient predictive capabilities. It is not necessary to understand a phenomenon in every respect in a pure scientific context to exploit the current level of understanding for design and practice purposes. In fact, zone fire models take advantage of "imperfect" knowledge and simplifying assumptions to yield practical and useful results.

Despite imperfect knowledge and simplifying assumptions, properly applied zone models have been shown to be a source of good engineering approximations of fire development within enclosures. Thus, comparison of zone fire modeling results with experimental data is valuable for determining the applicability of a model to a particular situation in the model selection process. As with any fire model, published comparisons of zone fire model results with experimental data are somewhat limited when compared to the range of possible applications.

Validation

With respect to the validation of fire models, ASTM 1355, "Standard Guide for Evaluating the Predictive Capability of Deterministic Fire Models," [31] sets forth a methodology for analyzing a computer fire model, examining two broad conceptual categories. The first category relates to the foundation of the model—its theoretical basis, mathematical equations, and numerical methods. The second category relates to sensitivity, comparison between data and predictions, and actual calculations performed by users. This analysis is ideally performed by the model developer but is sometimes undertaken by other individuals or organizations, such as the Society of Fire Protection Engineers analysis of the thermal detector actuation model DETACT [32]. A critical use of the methodology in ASTM 1355 is to identify sensitive variables associated with the model and to consider those sensitive variables that may have a significant effect in a fire safety design application. They therefore allow an analyst to consider the commensurate uncertainty in the predicted values relating to the input uncertainty and further allow designers to determine safety factors on a more considered basis.

Application

Zone models have enjoyed wide application and general acceptance due to their relatively simplified approach to the modeling problem. Zone fire models have been used or commissioned by engineers and architects, building officials, the fire service, fire investigators, building and fire code developers, materials and systems manufacturers, fire researchers, and educators. Application and use of zone fire modeling include performance-based fire safety design, postfire reconstruction, and fire risk assessment.

With respect to performance-based fire safety design, some fire protection engineers have been able to develop alternative equivalent approaches to meeting the prescriptive requirements of codes through the use of zone fire models. Other applications have utilized zone fire models in fire hazard analyses to develop engineered fire mitigation strategies for unique situations in which a prescriptive approach would not have met specific fire loss criteria. The problem of postfire reconstruction lends itself readily to the use of fire models. Several fire reconstruction case studies of fire incidents using computer models have been published [33–36].

Although zone models have experienced the lion's share of practical applications, the use of

more complex computer fire models has and will continue to increase. This evolution will not render zone models obsolete in everyday practice due to their significant advantages in solving a subset of engineering problems.

In 2011, the Society of Fire Protection Engineers published its engineering guide titled "Guidelines for Substantiating a Fire Model for a Given Application" [37]. Similar to the SFPE's guide on performance-based design, the document recommends a workflow for the modeler. This workflow is captured in a flowchart shown in the document's introduction. As is true with the scientific method, generally, the first step is to define the problem. This is, in fact, a critical step to successful computer fire modeling.

In the absence of a well-defined problem and the applicable parameters that apply to that problem, the next step of selecting a candidate model is unlikely to be properly performed. Running the wrong model may leave the modeler to inaccurate, unreliable, or inapplicable results. However, one of the benefits of using zone models on modern computers is to generally be able to run multiple models in a very short period of time. This can also be done to get preliminary results to better develop the parameters and boundary conditions for use in a fire model requiring much greater time to run, such as a field or CFD model.

The guide goes further to discuss uncertainty and user effects related to model results. Some key studies are discussed as representative of the type of analysis to be considered by the modeler during the work. Some of this work comes out of verification and validation performed by modelers as well as independent studies considering model accuracy. Beyond the specific studies cited, the guide provides recommendations for addressing the uncertainty and user effects. For example, sensitivity and bounding analyses, among others, are methods for examining user effects and their impact on a particular analysis.

Finally, the Guide suggests documenting the findings from this work for use by reviewers, AHJs, and future users of the model results. It addresses the specific concepts of problem definition, candidate model evaluation, verification and validation of the key physics, and evaluating user effects and uncertainties. Good documentation of the modeler's activities in this regard and using the Guide's framework, while helping future reviewers for users of the work, will also benefit the modeler in providing completeness and thoroughness of the model activities.

References

1. H.W. Emmons, "The Needed Fire Science," *Proceedings of the 1st International Symposium on Fire Safety Science* (C.E. Grant and P.J. Pagni, eds.), International Association for Fire Safety Science, October 7–11, 1985, Gaithersburg, MD, pp. 33–54 (1986).
2. J. Quintiere, "Growth of Fires in Building Compartments," *ASTM STP 614,* American Society for Testing and Materials, Philadelphia (1977).
3. R. Pape, T.E. Waterman, and T.V. Eichler, "Development of a Fire in a Room from Ignition to Full Room Involvement—RFIRES," *NBS-GCR-81-301,* National Bureau of Standards, Washington, DC (1981).
4. H.E. Mitler, and H.W. Emmons, "Documentation for CFC V: The Fifth Harvard Computer Fire Code," *NBS GCR 81-344* (Home Fire Project Technical Report 45), National Bureau of Standards, Gaithersburg, MD (1981).
5. H.E. Mitler, "The Harvard Fire Model," *Fire Safety Journal,* 9, pp. 7–16 (1985).
6. W.D. Walton, "ASET-B: A Room Fire Program for Personal Computers," *NBSIR 85-3144,* National Bureau of Standards, Washington, DC (1985).
7. R. Friedman, "An International Survey of Computer Models for Fire and Smoke," *Journal of Fire Protection Engineering,* 4, 3, pp. 83–92 (1992).
8. S.M. Olenick and D.J. Carpenter, "Updated International Survey of Computer Models for Fire and Smoke," *Journal of Fire Protection Engineering,* 13, 2, pp. 87–110 (2003).
9. L.Y. Cooper and D.W. Stroup, "ASET: A Computer Program for Calculating Available Safe Egress Time," *Fire Safety Journal,* 9, pp. 29–45 (1985).
10. V. Ho, N. Siu, and G. Apostolakis, "COMPBRN III—A Fire Hazard Model for Risk Analysis," *Fire Safety Journal,* 13, 2–3, pp. 137–154 (1988).
11. V. Babrauskas, "COMPF2—A Program for Calculating Post-Flashover Fire Temperatures," *NBS TN 991,* National Bureau of Standards, Washington, DC (1979).
12. G.N. Walton and W.S. Dols, "CONTAM 2.4 User Guide and Program Documentation," *NISTIR 7251,* National Institute of Standards and Technology, Gaithersburg, MD (2005).
13. M.R. Curtat and X.E. Bodart, "Simple and Not So Simple Models for Compartment Fires," *Proceedings of the 1st International Symposium on Fire Safety*

Science (C.E. Grant and P.J. Pagni, eds.), International Association for Fire Safety Science, October 7–11, 1985, Gaithersburg, MD, pp. 637–646 (1986).
14. W.W. Jones, "A Multicompartment Model for the Spread of Fire, Smoke and Toxic Gases," *Fire Safety Journal,* 9, pp. 55–79 (1985).
15. G.P. Forney and L.Y. Cooper, "The Consolidated Compartment Fire Model (CCFM) Computer Application. VENTS, Part I, Physical Basis," *NISTIR 4342,* National Institute of Standards and Technology, Gaithersburg, MD (1990).
16. R.D. Peacock, W.W. Jones, P.A. Reneke, and G.P. Forney, "CFAST—Consolidated Model of Fire Growth and Smoke Transport (Version 6): Technical Reference Guide," *SP-1026,* National Institute of Standards and Technology, Gaithersburg, MD (2005).
17. R.D. Peacock, W.W. Jones, P.A. Reneke, and G.P. Forney, "CFAST—Consolidated Model of Fire Growth and Smoke Transport (Version 6): User's Guide," *SP-1041,* National Institute of Standards and Technology, Gaithersburg, MD (2005).
18. C.A. Wade, D. LeBlanc, J. Ierardi, and J.R. Barnett, "A Room-Corner Fire Growth and Zone Model for Lining Materials," Second International Conference on Fire Research and Engineering (ICFRE2), National Institute of Standards and Technology and Society of Fire Protection Engineers, Gaithersburg, MD, pp. 106–117 (1998).
19. C. Wade and J. Barnett, "A Room-Corner Fire Model Including Fire Growth on Linings and Enclosure Smoke-Filling," *Journal of Fire Protection Engineering,* 8, 4, pp. 183–193 (1997).
20. C. Wade, "Branzfire-Engineering Software for Evaluating Hazard of Room Lining Materials," in *Conference Proceedings on the Eighth International Interflam Conference,* Interscience Communications Ltd., London, pp. 1147–1152 (1999).
21. W.D. Davis, "The Zone Fire Model Jet: A Model for the Prediction of Detector Activation and Gas Temperature in the Presence of a Smoke Layer," *NISTIR 6324,* National Institute of Standards and Technology, Gaithersburg, MD (1999).
22. H.E. Mitler and J.A. Rockett, "User's Guide to FIRST, A Comprehensive Single-Room Fire Model," *CIB W14/88/22,* National Bureau of Standards, Gaithersburg, MD (1987).
23. H.E. Nelson, "FIREFORM—A Computerized Collection of Convenient Fire Safety Computations," *NBSIR 86-3308,* National Bureau of Standards, Gaithersburg, MD (1986).
24. H.E. Nelson, "FPETOOL: Fire Protection Engineering Tools for Hazard Estimation," *NISTIR 4380,* National Institute of Standards and Technology, Gaithersburg, MD (1990).
25. J.E. Floyd, S.P. Hunt, F.W. Williams, and P.A. Tatem, "A Network Fire Model for the Simulation of Fire Growth and Smoke Spread in Multiple Compartments with Complex Ventilation," *Journal of Fire Protection Engineering,* 15, 3, pp. 199–229 (2005).
26. Y.L. Cooper, "Estimating the Environment and the Response of Sprinkler Links in Compartment Fires with Draft Curtains and Fusible-Link-Actuated Ceiling Vents Theory," *Fire Safety Journal,* 16, pp. 137–163 (1990).
27. L. Gay, C. Epiard, and B. Gautier, "MAGIC Software Version 4.1.1: Mathematical Model," *EdF HI82/04/024/B,* Electricité de France, Paris, France (2005).
28. L. Gay, "User Guide of the MAGIC Software V4.1.1" *EdF HI82/04/23/A,* Electricité de France, Paris, France (2005).
29. D.B. Satterfield and J.R. Barnett, "User's Guide to WPI-FIRE Version 2 (WPI-2)—A Compartment Fire Model," Center for Fire Safety Studies, Worcester Polytechnic Institute, Worcester, MA (1990).
30. T. Tanaka, S. Yamada, "BRI2002: Two layer Zone Smoke Transport Model", *Fire Science and Technology*, 23(1), special issue, Tokyo University of Science, 2004.
31. "Standard Guide for Evaluating the Predictive Capability of Deterministic Fire Models," *ASTM E1355-97,* American Society for Testing and Materials, West Conshohocken, PA (1997).
32. "SFPE Engineering Guide to the Evaluation of the Computer Model DETACT-QS," Society of Fire Protection Engineers, Bethesda, MD (2002).
33. H.E. Nelson, "An Engineering Analysis of Fire Development in the Hospice of Southern Michigan, December 15, 1985," *Proceedings of the 2nd International Symposium on Fire Safety Science,* Hemisphere Publishing, New York (1989).
34. R.S. Levine and H.E. Nelson, "Full-Scale Simulation of a Fatal Fire and Comparison of Results with Two Multiroom Models," *NISTIR 90-4268,* National Institute of Standards and Technology, Gaithersburg, MD (1990).
35. N. Alvares, "Defining Fire and Smoke Spread Dynamics in the DuPont Plaza Fire of 31 December 1986," *Proceedings of the International Conference on Fire Research and Engineering,* Society of Fire Protection Engineers, September 10–15, 1995, Boston, MA (1995).
36. R.W. Bukowski, and R.C. Spetzler, "Analysis of the Happy Land Social Club Fire with HAZARD I," *Journal of Fire Protection Engineering,* 4, 4, (1992).
37. *Guidelines for Substantiating a Fire Model for a Given Application*, Society of Fire Protection Engineers, Bethesda, MD, 2011

William D. Walton retired from the Building and Fire Research Laboratory, National Institute of Standards and Technology.

Douglas J. Carpenter is vice president and principal engineer with Combustion Science & Engineering, Inc., in Columbia, Maryland.

Christopher B. Wood is a member of Fire Link, LLC, in Tewksbury, Massachusetts.

Modeling Fires Using Computational Fluid Dynamics (CFD)

32

Kevin McGrattan and Stewart Miles

Introduction

It was in the early 1920s that Lewis Richardson first demonstrated the feasibility of solving, using numerical methods, the governing equations of fluid flow [1] for the purpose of weather prediction. It was not for another 50 years that what is now known as computational fluid dynamics (CFD) emerged as a general analysis tool for the full breadth of fluid flow problems including those associated with fire.

In contrast to zone models, the techniques of CFD evolved outside the fire community and were subsequently imported into it. The same basic CFD technology is being developed, applied, verified, and validated for a wide range of applications. Problems and successes demonstrated elsewhere can often be exploited in the fire context, although there are many issues that are unique to fire that can only be the responsibility of the fire community. The same tools that are used to study, for example, heat transfer in an internal combustion engine can also be used to evaluate indoor air movement, early detection of smoke, and the dispersion of combustion products within the atmospheric boundary layer.

K. McGrattan (✉)
Fire Research Division, National Institute of Standards and Technology Gaithersburg, Gaithersburg, MD, USA

S. Miles
International Fire Consultants Ltd., Buckinghamshire, UK

CFD provides the potential to study these complicated problems that are only partially amenable to reduced-scale physical modeling because of the large number of non-dimensional groups that need to be preserved to simulate full-scale behavior. Furthermore, CFD has emerged as an important tool because the assumptions employed in zone models limit their range of application to relatively simple fire scenarios that can be described in terms of a small number of idealized components (e.g., unperturbed fire plume, unconfined ceiling jet, uniform hot gas layer).

The starting point for CFD models is the set of partial differential equations that assert conservation of mass, momentum, and energy within the fire and throughout the space surrounding it. These equations are solved numerically to yield time-varying predictions of temperature, gas velocity, gas species concentrations, and so forth, on a three dimensional mesh of control volumes that spans the geometry being modeled. Unlike two zone models, CFD models enforce the conservation laws in each of the thousands or millions of relatively small control volumes. However, the exact solution of the governing equations, resolving fully the length and time scales that occur in the turbulent flows associated with fire, is still beyond the capabilities of even the largest computers currently available. To capture the details of the chemical processes of a fire would require spatial resolution of less than 1 millimeter. As a consequence, it is necessary to modify the governing equations to model the

M.J. Hurley (ed.), *SFPE Handbook of Fire Protection Engineering*,
DOI 10.1007/978-1-4939-2565-0_32, © Society of Fire Protection Engineers 2016

unresolvable turbulence. Two main approaches are currently employed in CFD simulations of fire: large eddy simulation (LES) and Reynolds-averaged Navier-Stokes (RANS) equations, which are described later in this chapter.

In addition to the uncertainties associated with the modeling of turbulent flow, others are introduced by the description of combustion chemistry; radiation; and mass, momentum, and heat transfer at solid boundaries. Further complexity is introduced in the numerical solution of the equation set in which the choice of numerical schemes and the resolution of the numerical mesh strongly influences the quality of the CFD solution. An appreciation of all these issues is important in the successful exploitation of CFD to solve fire problems. It should be recognized that this topic is rapidly evolving and that this chapter can only represent a "snapshot" in time. Whereas a thousand mesh points constituted a detailed CFD solution in the early 1980s, simulations using millions of mesh points are now routine. This number can be expected to increase further, especially as parallel processing becomes more widespread. However, although the modeling of smoke transport may be considered reasonably mature, there remains considerable research and development still to be done with some of the more complex issues related to the underlying combustion and fire science (e.g., flame spread, oxygen vitiation, soot formation, and water suppression). Here the challenges remain considerable and will not be satisfactorily solved for some time yet.

This chapter does not provide a comprehensive description of CFD. There are already numerous introductory textbooks on the subject [2, 3, 4, 5, 6]. Depending on the background of the author(s), these books tend to emphasize techniques developed for particular fields of science and engineering, such as aerospace, meteorology, or combustion. Discussion of issues related to the modeling of fire can be found in review articles by Cox [7, 8] and Novozhilov [9]. Finally, a comprehensive description of the specific algorithms used by a particular CFD model can only be found within the manuals that accompany the software. A recent review by Olenick and Carpenter [10] lists about a dozen CFD models developed specifically for fire. Some of these models were developed for specific fire scenarios or phenomena. Others were developed to handle a variety of fire scenarios, including JASMINE from the Fire Research Station (UK), the Fire Dynamics Simulator (FDS) from NIST (US) and VTT (Finland), SMARTFIRE from the University of Greenwich (UK), and SOFIE, the product of a European consortium. A more recent development is the FireFOAM model from FM Global, which is based on the open source CFD code OpenFOAM. There are also general-purpose CFD models that have been used for fire simulations. These computer programs contain tens to hundreds of thousands of lines of instructions, along with manuals that contain hundreds of pages of documentation of the development, algorithms, and validation of the models.

This chapter provides an introduction to the theory and practice of computational fluid dynamics as applied to the study of fire. Although the mathematical framework for the subject is more than 100 years old, it is only in the past 20 years that computers have become fast enough to make the models practical.

Governing Equations

This section presents the conservation equations of mass, momentum, and energy that constitute the core of any CFD model. The derivation of these equations can be found in any textbook on the subject and will not be included here. Instead, a discussion of the various techniques used to make these equations tractable for numerical solution will follow. The most important of these is the turbulence model, a subject of considerable study and debate.

Conservation Equations

The conservation equations for mass, momentum, and energy for a mixture of gases are briefly

described here. A particularly useful reference for a more detailed description of the equations, the notation used, and the various approximations employed is Anderson et al. [2].

Conservation of Mass

The conservation equation for mass is

$$\frac{\partial \rho}{\partial t} + \nabla \cdot \rho \mathbf{u} = 0 \tag{32.1}$$

This equation is nothing more than a statement that mass is neither created nor destroyed. In words, the change in the density, ρ, at a given point in the flow field is equal to the net mass flux, $\rho\mathbf{u}$, across the boundary of a small control volume surrounding the point. For fire simulations, it is usually necessary to account explicitly for various individual gaseous species, for example, fuel and oxygen. Thus, the mass conservation equation is often written as a set of transport equations for the mass fractions of the individual gaseous species, Y_α:

$$\frac{\partial (\rho Y_\alpha)}{\partial t} + \nabla \cdot (\rho Y_\alpha \mathbf{u}) = \nabla \cdot (\rho D_\alpha \nabla Y_\alpha) + \dot{m}'''_\alpha \tag{32.2}$$

When all of the species equations are added together, the mass diffusion and production terms on the right-hand side sum to zero, leaving the original mass conservation equation.

Conservation of Momentum

The conservation equation for momentum is

$$\frac{\partial (\rho \mathbf{u})}{\partial t} + \nabla \cdot (\rho \mathbf{u}\mathbf{u}) = -\nabla p + \mathbf{f} + \nabla \cdot \tau \tag{32.3}$$

The momentum equation is written in compact notation here to emphasize that it is essentially Newton's Second Law of Motion, or simply Force = Mass × Acceleration. The forces that drive the fluid consist of the pressure gradient, ∇p, friction (in the form of the viscous stress tensor, τ), and external force terms, $\mathbf{f}$, such as buoyancy. A complete expansion of the various terms can be found in the appendix.

Conservation of Energy

The conservation equation for energy is

$$\frac{\partial (\rho h)}{\partial t} = \nabla \cdot (\rho h \mathbf{u}) = \frac{Dp}{Dt} + \dot{q}''' - \nabla \cdot \mathbf{q} + \varepsilon \tag{32.4}$$

As in the mass conservation equation, the sensible enthalpy, h, at a given point changes according to the net energy flux across the boundary of a small control volume surrounding the point. Now, however, there are additional source terms on the right-hand side of the equation related to the pressure, combustion heat release rate, radiation and conduction, and kinetic energy dissipation, respectively. For fire applications, the contributions from the pressure term and the dissipation term are negligible, except in situations where the compartment of interest is sealed and the pressure rises substantially.

Equations 32.1 through 32.4 constitute a set of partial differential equations for the density (or component mass fractions), velocity, pressure, and sensible enthalpy of the fluid. The momentum equation is actually three equations for the three components of velocity: u, v, and w making five equations for six unknowns. To close the system, an *equation of state* is needed to relate the pressure, p, and sensible enthalpy, h. The latter is a function of the specific heat and temperature of the fluid:

$$h = \int_{T_0}^{T} c_p \, dT \tag{32.5}$$

For most fire applications, it is sufficient to assume a *perfect gas*:

$$p = \frac{\rho \Re T}{\overline{W}}; \quad \overline{W} = \frac{1}{\sum (Y_\alpha / W_\alpha)} \tag{32.6}$$

where $\Re$ is the universal gas constant and $\overline{W}$ is the average molecular weight of the gas mixture.

Additional Assumptions

The foregoing equations form the basis for a wide variety of engineering applications but not

without the further application of simplifying assumptions unique to each field. The only assumptions made thus far are that the fluid is a perfect gas and that the viscous stress is linearly dependent on the strain. A further approximation can be made here, exploiting the fact that fire-driven flows are substantially slower than the speed of sound. By assuming that the pressure is constant (or at most a time-varying average) in the equation of state and the energy equation, the number of unknowns is reduced from six to five, as temperature can now be found from the density. More importantly, there is no longer a need to account for pressure fluctuations that propagate at the speed of sound, a fact that makes the numerical solution of the equations more tractable because the time step size is limited only by the flow speed, not the sound speed [11].

In the sections to follow, additional assumptions will be imposed on the governing equations to apply them to fire and other low-speed thermal processes. Most important is the treatment of the diffusive and source terms that distinguishes one type of CFD model from another.

Turbulence Modeling

The governing conservation equations describe the transport of mass, momentum, and energy via convection and diffusion (material diffusivity, viscosity, thermal conductivity). In large-scale fire applications, convection is the primary mode of transport of heat and combustion products, but the diffusive processes play a significant role in the flames and in boundary layers near solid surfaces. Capturing the large-scale convective transport and the small-scale diffusive processes in the same simulation requires too much computation, even for current-generation computers. Consequently, most practical fire simulations employ models to describe subgrid-scale, or "unresolvable," phenomena. The most important of these are the turbulence models.

The most popular numerical techniques for approximating the governing equations are roughly categorized according to their spatial and temporal fidelity: direct numerical simulation (DNS), Reynolds-averaged Navier-Stokes (RANS), and large eddy simulation (LES). DNS is really nothing more than a direct numerical solution of the governing equations. RANS and LES employ models of the unresolved subgrid dissipative processes. RANS averages over relatively large spatial and temporal scales than those that are characteristic of the given numerical grid or the fundamental frequency of the fire, whereas LES attempts to compute as much of the "resolvable" length and time scales (i.e., the "large eddies") as possible.

Direct Numerical Simulation (DNS)

Direct numerical simulation (DNS) means that the governing equations are solved numerically with no modifications to the form presented above, which implies that all of the relevant temporal and spatial scales are resolved directly without invoking any models to represent the diffusive terms, like the viscosity, thermal conductivity, and material diffusivity. Because this technique demands very fine spatial and temporal resolution (less than 1 mm and 1 ms, respectively), it is limited to small laminar flames and sometimes small turbulent jets. DNS is still not practical for large-scale fire simulations, and nothing more is included in this chapter on the subject.

Reynolds-Averaged Navier-Stokes (RANS)

The approach to modeling turbulence in many commercial and fire-specific CFD models is to solve a statistically time-averaged form of the conservation equations, often referred to as the Reynolds-averaged Navier-Stokes (RANS)[1]

[1] A density-weighted variant of Reynolds averaging (Favre averaging) is often necessary for the treatment of regions where density fluctuations have a significant effect. This variant is not usually necessary for smoke movement studies but can be important close to the fire source. This treatment is not presented here but can be found in, for example, Cox [7].

equations after Osborne Reynolds who introduced the idea over a century ago. The starting point in Reynolds averaging is to decompose the velocity components, enthalpy, and species mass fractions, into a time-averaged component (denoted by an overbar) and a fluctuating component (denoted by a prime):

$$\phi(\mathbf{x},t) = \bar{\phi}(\mathbf{x},t) + \phi'(\mathbf{x},t) \tag{32.7}$$

Notice that for transient flows the time-averaged component is still a function of time, representing the evolution of the mean flow field. In typical fire simulations, the time scale associated with the time-averaged component is on the order of several seconds, whereas that of the fluctuating component is on the order of milliseconds. Substituting the decomposed primitive variables into the conservation equations (Eqs. 32.1, 32.3, and 32.4) and then applying the same time-averaging process to the entire system of equations yields a set of equations that is similar in form to the original equations, with the mass conservation equation remaining unchanged:

$$\frac{\partial(\rho\bar{\mathbf{u}})}{\partial t} + \nabla\cdot(\rho\bar{\mathbf{u}}\bar{\mathbf{u}}) = -\nabla p + \mathbf{f} + \nabla\cdot\bar{\tau} - \nabla\cdot\rho\overline{\mathbf{u}'\mathbf{u}'} \tag{32.8}$$

$$\frac{\partial(\rho\bar{h})}{\partial t} + \nabla\cdot(\rho\bar{h}\bar{\mathbf{u}}) = \frac{Dp}{Dt} + \dot{q}''' - \nabla\cdot\bar{\mathbf{q}} + \bar{\varepsilon} - \nabla\cdot\rho\overline{\mathbf{u}'h'} \tag{32.9}$$

Notice that the Reynolds-averaging process has introduced additional terms on the right-hand sides of the equations and increased the number of unknowns. Thus, the system of equations is no longer closed (i.e., there are more unknowns than equations). The additional terms are referred to as the Reynolds stresses and the turbulent scalar flux, respectively. The scalar, h, is the sensible enthalpy, and similar equations can be derived for the other scalars (e.g., gas species mass fractions). Note that the pressure and density in the preceding equations refer to their time-averaged components.

The majority of commercial and fire-specific CFD models that employ the RANS approach use an eddy viscosity turbulence model to close the set of equations. The basic idea is that the unresolved, turbulent fluctuations can be modeled with diffusive terms that effectively represent the dissipation of turbulent energy:

$$-\rho\overline{u_i'u_j'} = \mu_t\left(\frac{\partial\bar{u}_i}{\partial x_j} + \frac{\partial\bar{u}_j}{\partial x_i}\right) - \frac{2}{3}\delta_{ij}\rho k$$
$$\delta_{ij} = \begin{cases} 1 \text{ if } i = j \\ 0 \text{ if i} \neq \text{j} \end{cases} \tag{32.10}$$

$$-\rho\overline{u_j'h'} = \lambda_t\frac{\partial\bar{h}}{\partial x_j} \tag{32.11}$$

Here μ_t is the turbulent (eddy) viscosity, k the turbulent kinetic energy, and λ_t the turbulent diffusivity, which is related to the eddy viscosity by the expression

$$\lambda_t = \frac{\mu_t}{\sigma_t} \tag{32.12}$$

where σ_t is known as the turbulent Prandtl or Schmidt number, depending on whether the scalar quantity is an energy or species variable. It is usually assigned a constant value depending on the scalar variable in question.

For fire simulations, a two-equation eddy viscosity model is commonly used. This model, in effect, allows the turbulence to be characterized by a velocity and a length scale that varies at each grid cell in the computational domain. The two equation model that is employed in the majority of RANS applications in fire engineering is the k-ε model. Here two additional transport equations are solved; one for the turbulent kinetic energy, k, and one for its rate of dissipation, ε. These quantities form the turbulent viscosity in Eq. 32.10:

$$\mu_t = \rho C_\mu\frac{k^2}{\varepsilon} \tag{32.13}$$

The factor C_μ is an empirical constant. Details of these equations are provided in CFD textbooks. Note that a modification of the basic k-ε model is often made in fire applications, in which buoyancy source terms for the k and ε equations are added. These terms ensure that the effects of

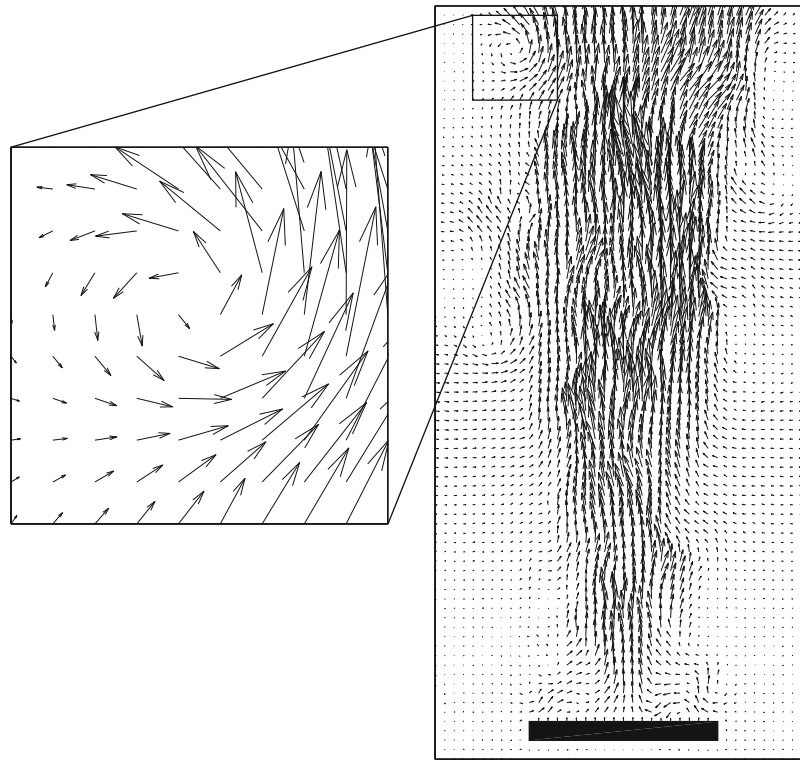

Fig. 32.1 What is meant by "resolvable." At *right* is an instantaneous map of the flow vectors for an LES simulation of a helium plume. the *inset* shows the smallest "eddy" that can be supported by the numerical grid, the spacing of which is indicated by the distance between the *arrows*

stable stratification in hot gas layers and the destabilizing thermal gradients in rising plumes are adequately described. Details are discussed by Cox [8].

The k-ε model has been used successfully for many engineering applications. Its limitation in treating, for example, swirling flows, flow separation, and so on is due partly to the inherent assumption that the modeled turbulence is isotropic, that is, that the unresolved flow field has no cohesive structure. There are a number of variants of the k-ε model, available in commercial CFD models, that claim to provide improved results for some flows (e.g., the RNG k-ε model [12] and the k-ω model [13]). Research into nonlinear eddy viscosity turbulence models that attempt to incorporate directional effects is being undertaken within the CFD community but, as far as the authors are aware, have not been applied to fire problems. Another approach, applied mainly outside of fire, is to solve individual differential equations for Reynolds stresses and turbulent scalar fluxes that appear in Eqs. 32.8 and 32.9. However, the standard k-ε model remains the most commonly used RANS technique in fire applications.

Large Eddy Simulation (LES)

The derivation of LES models is very similar to that of the RANS models, albeit with subtle differences in the interpretation of the decomposition of the primitive variables. RANS emphasizes temporal averaging, whereas LES emphasizes spatial averaging, or *filtering*. Regardless, the mechanics of the derivation are essentially the same, and the simplest of the LES models makes the same "eddy viscosity" argument in replacing the unresolved convection terms with diffusion terms. The key difference between the techniques lies in the magnitude of the diffusive coefficient, the "eddy" viscosity. With LES, one attempts to resolve the flow field as faithfully as possible on a given numerical grid. In other words, flow structures, like swirling

eddies, can span just a few grid cells (Fig. 32.1). To achieve this result, the eddy viscosity must be small enough to avoid smoothing out these small, but resolvable, eddies, but large enough to ensure numerical stability and account for the dissipation of energy at sub-grid scales.

To better understand the eddy viscosity model, the original Navier-Stokes equations are examined. An evolution equation for the kinetic energy of the gas is formed by taking the dot product of the momentum from Eq. 32.3 and the velocity vector **u**:

$$\rho \frac{D\mathbf{u}}{Dt} \cdot \mathbf{u} \equiv \rho \frac{D(|\mathbf{u}|^2/2)}{Dt} = \cdots - \epsilon \qquad (32.14)$$

A term emerges on the right-hand side known as the dissipation rate (see appendix for details):

$$\epsilon \equiv \tau \cdot \nabla \mathbf{u} = \mu \left[2 \left(\frac{\partial u}{\partial x} \right)^2 + \cdots \right] \qquad (32.15)$$

which appears as a source term in the energy conservation equation 32.4:

$$\frac{D}{Dt}(\rho h) = \cdots + \epsilon \qquad (32.16)$$

Extra terms have been hidden to make the point more clearly, and no approximations have been introduced thus far to the Navier-Stokes equations. This exercise merely explains in mathematical terms how the kinetic energy of the flow is converted into thermal energy by the action of the viscosity, μ. In the early 1960s, a meteorologist named Smagorinsky [14] suggested, based mainly on dimensional arguments, that the effect of the viscosity could modeled by a "turbulent" viscosity coefficient:

$$\mu_t = \rho (C_s \Delta)^2 \left[2 \left(\frac{\delta \bar{u}}{\delta x} \right)^2 + \cdots \right]^{\frac{1}{2}} \qquad (32.17)$$

where C_s is an empirical constant, Δ is a filter length comparable to the size of a grid cell, and the expression in brackets has the same functional form as the kinetic energy dissipation rate. The notation $\delta\bar{u}/\delta x$ emphasizes that the turbulent viscosity is calculated from finite difference approximations of the gradients of the computed velocity components. The other diffusive parameters, the thermal conductivity and material diffusivity, are related to the eddy viscosity through the expressions

$$k_t = \frac{\mu_t c_p}{\mathrm{Pr}_t}; \quad D_t = \frac{\mu_t}{\rho \, \mathrm{Sc}_t} \qquad (32.18)$$

The "turbulent" Prandtl and Schmidt numbers are assumed to be constant and of order unity. The appeal of LES is that no additional equations need be solved, as in the RANS k-ε model, and that the dynamics of the fire are captured in the simulation, rendering a more realistic-looking flow field than the time-averaged RANS model. The drawback of LES is that it demands that the model user pay close attention to the choice of numerical grid because the accuracy of the technique can be degraded significantly if there are not enough grid cells to describe the flow field adequately. Various perspectives on LES in general can be found in Pope [15].

Other Approaches

Detached eddy simulation (DES), formulated originally by Spalart et al. [16], combines the RANS and LES approaches discussed above. At solid boundaries and locations where the turbulent length scale is less than the mesh dimension the RANS treatment for turbulence is employed. At other locations, where the mesh is suitably resolved, LES modeling is employed. This approach has the potential benefit of reducing the overall mesh requirement to achieve a given level of turbulent flow resolution. The mesh generation process, however, tends to be more challenging.

A fundamentally different approach to CFD is provided by the so-called Lattice-Boltzmann method (LBM). Instead of the Navier-Stokes equations, the discrete Boltzmann equation is solved in which the fluid is treated as a set of particles rather than as a continuum. These particles are tracked numerically through a

discrete lattice mesh that encompasses the domain of interest, and are allowed to collide with each other and the bounding surfaces. While LBM models offer some advantages over traditional CFD, in particular in respect to complex geometries and parallel computing, the authors are not aware of the application of the Lattice-Boltzmann method to fire problems, and it is not discussed any further.

Source Terms and Boundary Conditions

The governing conservation equations discussed previously do not pertain only to fire scenarios. What constitutes a "fire model" are the conservation equations plus a set of boundary conditions and source terms describing mass, momentum, and energy exchange between hot gases and compartment walls, the reaction of fuel and oxygen, the redistribution of energy by thermal radiation, the spray of water from a sprinkler, the activation of a smoke detector, and dozens of other phenomena that occur in a burning building. Describing these phenomena mathematically is what modeling is all about. In the sections to follow are brief discussions of the boundary conditions and source terms found in the governing equations.

Combustion

The reaction of fuel and oxygen and the associated entrainment of air into the fire plume is the driving source term in the model. The simplest approach to modeling combustion is to ignore the chemistry and assume that the heat is released within a prescribed volume. This may suffice for some applications (e.g., smoke movement associated with a well-ventilated fire), provided a reasonable volume is selected for the release of heat. However, for fire scenarios where the combustion region cannot be predefined or the chemistry becomes important, a combustion model should be employed. The calculation of chemical species is required, for example, where oxygen availability is an important factor or where the composition of the gas mixture is required for the radiation model.

Most engineering models assume that the combustion process can be represented as a single, one-step reaction between fuel and oxygen forming a mixture of products including the major species CO_2 and H_2O and minor species like soot and CO:

$$\mathrm{F} + s\,\mathrm{O_2} \rightarrow \mathrm{P} \tag{32.19}$$

This model is appropriate provided that the detailed kinetics are not important and that the product yields are known from experiment. If the prediction of minor product species such as CO is required, then the assumption of fast, single-step chemistry is no longer valid and a more sophisticated approach is required. An example of such an approach is given at the end of this section.

The most widely used combustion models for fire applications are the Eddy Break-Up (EBU) model of Spalding [17], and the closely related Eddy Dissipation Concept (EDC) devised by Magnussen and Hjertager [18]. The models assume that the consumption of fuel, $\dot{m}_f'''$, is controlled by the rate of molecular mixing of reactants, which in turn is proportional to the rate of dissipation of turbulent eddies:

$$\dot{m}_f''' = -\frac{C\,\rho}{\tau_{\mathrm{mix}}}\min\left\{Y_f, \frac{Y_{\mathrm{O_2}}}{s}\right\} \tag{32.20}$$

C is a dimensionless empirical constant and $\tau_{mix} \approx k/\epsilon$ is the mixing time. RANS and LES models treat the turbulent kinetic energy, k, and the dissipation rate, ε, differently, but the basic idea is the same in both types of models. The heat release rate is obtained by multiplying the fuel mass consumption rate by an effective heat of combustion. Equation 32.20 may be augmented by an additional term involving the products of combustion and also by an Arrhenius expression to limit the rate of reaction in cold mixtures. The EBU and EDC models have the merit of simplicity while permitting heat to be released over a distributed volume determined by the enclosure

geometry and availability of air. Furthermore, the phenomenon of flame lengthening as a consequence of ventilation control is incorporated by this modeling approach. It has been applied with reasonable success by Miles et al. [19] and Holen et al. [20] as it has been in other areas of combustion engineering.

The hazard posed by high temperatures and the loss of visibility due to fire may be compounded by exposure to toxic gases such as carbon monoxide or hydrogen cyanide. Although advanced combustion models may include the capability to predict some of these toxic gas species, it is generally necessary in fire engineering to prescribe the species yields. In other words, the production rate of smoke and other combustion products is usually specified by the user based on experimental measurements. Predicting, rather than specifying, the generation of species such as CO, HCN, and soot requires finite rate chemistry to be included in the combustion model. An approach that has been exploited in a number of fire studies is to assume that the flame is a statistical ensemble of thin laminar flamelets that incorporates detailed chemistry from either experimental measurements or detailed kinetic calculations. Details of this approach may be found in Peters [21] and in the references of Cox [8] and Novozhilov [9]. Magnussen and Hjertager [18] extended the eddy breakup model to include soot formation and oxidation, using the mechanisms suggested by Tesner et al. [22]. This involved the solution of two further transport equations. Soot modeling is, however, difficult and not generally included within current CFD fire computations and remains a topic for research.

Radiation Heat Transfer

The governing conservation equations of mass, momentum, and energy describe the convection and diffusion of hot gases from a fire. However, the redistribution of energy via thermal radiation is very important and needs to be included in the energy transport equation 32.4. What makes radiation heat transfer particularly difficult from a numerical point of view is that radiant energy is propagated at the speed of light, as opposed to the speed of the gas flow or the speed of sound. Numerical flow solvers typically advance the solution of the governing equations using time steps that are constrained either by the flow speed (low Mach number LES) or time steps that are consistent with large-scale changes in the environment (RANS). In either case, the speed of light is essentially infinite; thus, radiant energy is assumed to redistribute itself instantaneously. The simplest model of radiation transport assumes that the gases are non-scattering (the gases only absorb or emit thermal radiation) and gray (the radiation has no spectral dependence). Under these assumptions, the governing equation can be written as

$$\mathbf{s} \cdot \nabla I(\mathbf{x}, \mathbf{s}) = \kappa(\mathbf{x}) \left[I_b(\mathbf{x}) - I(\mathbf{x}, \mathbf{s}) \right] \qquad (32.21)$$

Here, I is the *radiant intensity*, a function of both position, $\mathbf{x}$, and direction, $\mathbf{s}$. The gray-gas assumption neglects the fact that I is also a function of the wavelength, as are the absorption coefficient, κ, and the source term, I_b. To account for wavelength dependence, Eq. 32.21 must be solved over discrete "bands" of the electromagnetic spectrum [23]. However, in fires, soot is the principal emitter and absorber of thermal radiation. Because its radiation spectrum is continuous, it is often assumed that there is no spectral dependence; that is, the participating medium is gray.

Even in its simplest form, the radiation transport equation poses two challenges to the modeler: (1) the prescription of the spatially dependent absorption coefficient, $\kappa(\mathbf{x})$; and (2) the numerical solution. As for the latter, a number of methods have emerged that involve discretizing the equation into a finite number of solid angles and sweeping over the numerical grid until the radiant energy is redistributed. The process is often done gradually over several time steps of the flow solver, depending on the level of temporal fidelity desired. Usually, equivalent or greater temporal resolution is demanded by the flow solver, easing the computational burden of the radiation solver [24].

The prescription of the absorption coefficient, $\kappa(\mathbf{x})$, is challenging because it combines the contributions of soot and gaseous exhaust products. Soot is the main emitter and absorber in practical fire scenarios; thus, any model for must account for it. This requirement has caused difficulties over the years because contributions from the combustion community often emphasize the spectrally dependent properties of CO_2 and H_2O rather than the spectrally independent properties of soot. The dominance of soot in the radiation calculation simplifies the prescription of κ, but at the same time it demands a better description of soot growth and oxidation than the current practical fire models are able to provide.

Regardless of the choice of absorption coefficient and numerical method, the solution of the radiation transport equation is added to the overall solution via a source term in the energy equation 32.4:

$$-\nabla \cdot \mathbf{q}_r(\mathbf{x}) = \kappa(\mathbf{x})\,[U(\mathbf{x}) - 4\pi I_b(\mathbf{x})];$$
$$U(\mathbf{x}) = \int_{4\pi} I(\mathbf{x}, \mathbf{s})\, d\Omega \tag{32.22}$$

The integrated intensity, U, multiplied by κ represents the rate of energy absorbed per unit volume, whereas $4\pi\ \kappa\ I_b$ is the rate of energy emitted per unit volume. The source term is usually assumed to be a blackbody radiator: $I_b = \sigma\ T^4/\pi$. Within the fire itself, the emission term dominates, and there is a net loss of energy from the region, whereas within the relatively cool, smoke-laden upper layer, there is a net gain of energy due to absorption. Because of the uncertainty in the near flame temperature and soot concentration, it is still common practice to prescribe, rather than predict directly via the source term, the fraction of energy lost from the fire via thermal radiation. Typically, 30–40 % is chosen, depending on the fuel type and fire size.

Mass Exchange at Boundaries

Rarely are fire simulations performed for compartments that are completely sealed off from the outside. In most cases, air and smoke pass through open doors or windows, fans blow and extract gases, and items burn and introduce fuel gases into the space. For the modeler, all these phenomena are known as boundary conditions that supplement the governing equations.

Free (or open) boundaries are located where the modeled domain interfaces with the external world beyond. Generally the pressure is specified, typically to a reference or ambient value, and the velocity derivatives normal to the boundary are set to zero. Furthermore, where outflow occurs the normal derivatives of the scalar fields will be set to zero, and where inflow occurs their ambient (atmospheric) values will be assumed. To achieve realistic predictions of air entrainment and smoke exhaust, it may be necessary to locate these boundaries well away from the compartment of fire origin.

Mass inlet boundaries are located where a prescribed source of air enters the computational domain. One example is at mechanical ventilation supplies. Other examples include external wind boundaries and the fuel bed itself if pyrolysis is included in the model in DiBlasi [25]. As for free boundaries where inflow occurs, it is critical that appropriate values are assigned to the sensible enthalpy (temperature) and other scalar fields.

Momentum Exchange at Boundaries

Where the fluid comes into contact with solid objects (compartment walls, for example) boundary conditions are required for the momentum equations and, where appropriate, for the solved turbulence variables. For most applications the no-slip velocity condition is assumed at solid surfaces (i.e., zero flow directly adjacent to the surface). However, the proper specification of boundary conditions is complicated by the fact that the inner region of the turbulent boundary layer adjacent to a solid surface has very sharp velocity gradients. A large number of grid points are required to resolve this region, making the simulation computationally expensive and

impractical for realistic compartments. An alternative, widely used approach to resolving the boundary layer is to use a so-called *wall function* [26], which assumes that the tangential velocity is a logarithmic function of the normal distance from the surface. An empirical relationship relates the wall shear-stress to the resolved variables at the first grid point, and appropriate source terms can be derived for each solved equation. Details are provided in standard textbooks [13].

Care is required in using the wall-function approach to ensure that the first grid point is positioned such that the empirical relationships are valid. Guidance should be taken from the model developer or the model documentation on the appropriate numerical grid to employ at surfaces. Commercial CFD models may offer advanced wall treatments that adapt automatically depending on the grid point and the flow regime, and these should generally be employed if available.

Energy Exchange at Boundaries

Conventional CFD models devote considerable attention to the velocity boundary conditions, but for fire, the energy exchange at solid surfaces is paramount, especially when the surfaces are burning. In fact, pyrolysis modeling is a subject unto itself and is touched on only briefly here. Suffice it to say that almost any treatment of a solid object can be incorporated in a CFD fire model because of the fairly loose coupling that exists between the gas and solid phases.

Hot gases lose heat to the structure at a rate determined by both the thermal properties of the bounding solids and the evolution of conditions within the gas phase. Early in the fire, the walls are nearly at ambient temperature and the rate of heat transfer will, all other things being equal, be at its greatest. Later, as the walls and other surfaces heat up, the rate of heat transfer decreases. In some situations it may be appropriate to treat the solid surfaces as adiabatic (i.e., no heat transfer). However, care must be taken when adopting this approach as heat loss to the surfaces is likely to be an important mechanism. For example, in large compartments or tunnels this heat loss may account for most of the heat losses from the fire, and ignoring it will generate erroneous predictions.

Where there is heat transfer, it is necessary to provide boundary conditions for the enthalpy and radiation equations, which in turn requires the temperature of the solid surface (T_w) be defined at each location adjoining the CFD grid. The surface temperature, together with its emissivity, establishes the radiative heat transfer rate for the radiation transfer equation. For the enthalpy equation the source term is the rate of convective heat transfer ($\dot{q}''_c$) to the surface from the adjoining grid point

$$\dot{q}''_c = h_c \left(T_w - T_g\right) \tag{32.23}$$

where T_g is the gas temperature at the nearest grid point and h_c is the convective heat transfer coefficient. This coefficient can be defined as a constant as in a zone model or, alternatively, a more realistic approach is to compute the coefficient as a function of the local flow regime making use of an empirical wall function akin to that done for the momentum equations and turbulence model.

The definition of the surface temperature is trivial in the case of isothermal boundaries where the surface is maintained at a fixed temperature. In general, however, the conduction of heat into the walls needs to be modeled. If it is assumed that conduction occurs only in the normal direction, then it may be treated by solving a one-dimensional heat conduction equation at each location on the surface adjoining the gas phase grid. The net conduction heat flux into the solid is given by the sum of the net radiation and convection fluxes at the surface.

A more sophisticated solution may be provided by coupling the CFD model with a separate solid phase calculation of the thermal conduction within the solid structure(s). This calculation could take the form of a fully coupled gas and solid-phase model, or a coupling of boundary conditions between a CFD model and a separate solid-phase model. In general, the

required information to be passed from the solid-phase model to the CFD model is the surface temperature and pyrolysis rate and, in the other direction, the convective and radiative heat fluxes.

Open Boundary Conditions

The results of a CFD fire analysis can be sensitive to the location of the "free" (ambient or open air) boundaries at the edge of the computational domain. These should be located at a sufficient distance from the fire source and regions of interest so that they do not incorrectly influence the solution. The setting of ambient values in relation to other boundary conditions may require special attention (e.g., it can dictate whether smoke can be expected to vent naturally in an air-conditioned atrium). Heat losses to solid boundaries can also have a significant influence on smoke movement, particularly where the smoke has cooled down and the amount of heat transferred to walls and ceilings can determine the degree of buoyancy and stratification of the smoke gases.

Visibility

Fire protection applications often require an estimate of visibility, the distance through smoke that a person is expected to be able to see, say, an exit sign. Visibility distance may be derived from a CFD solution using the predicted concentration of soot particulates. The correspondence between smoke concentration and visibility is based on the work of Jin [27] and Mullholland [28] and is commonly implemented into CFD models using the following (or similar) expression for visibility distance:

$$S = \frac{K_1}{K_2 m_s} \tag{32.24}$$

Here K_1 is a constant usually set to 3 for reflecting signs and 8 for illuminated ones, K_2 is the specific extinction coefficient (often taken as 7.6 m^2/g for flaming combustion), and m_s is the mass concentration of soot particles in units of g/m^3. The fire model predicts this latter quantity. Visibility distance calculated in this way at a CFD grid cell represents the visibility corresponding to a homogenous smoke layer and assumes the smoke density at the cell applies everywhere in the domain. Using the CFD solution data, it is possible to perform a more realistic "line of sight" calculation using the computed data at each grid cell along this line [29].

Sprinklers and Fire Suppression

It is fairly straight forward to include a sprinkler activation algorithm within a CFD fire model, based on the RTI (Response Time Index) concept of Heskestad and Bill [30]. This algorithm requires the gas temperature and velocity in the vicinity of the device. Following sprinkler activation, the water spray interaction with the hot gases can be modeled in a variety of ways. It is most often done using a Lagrangian particle tracking sub-model, in which statistically representative water particles are tracked numerically through the gas phase. The impact on the fire gases from the transfer of mass, momentum and heat associated with the trajectories and evaporation of the water particles is included as source terms in the underlying fluid dynamics equations. A good summary of this approach is given by Makhviladze et al. [31]. Water suppression and extinguishment, however, are far more difficult to model, and these phenomena are not generally a practical option for most fire engineering applications.

Fire-Structure Interface

While the modeling of the transport of smoke and heat within the gas phase remains the primary role of a CFD fire model in the majority of fire engineering applications, there are others where the coupling with the compartment boundaries and supporting structures is the main focus. For example, the absorption and

transmission of heat through elements of glazing, possibly to predict the likelihood of failure or to calculate the irradiance where people may be escaping on the unexposed side, might be required. Another example would be to investigate the response of concrete linings to fully developed fire conditions, for example in a road tunnel.

The area where the coupling of CFD and structural response has been considered in most detail is arguably in relation to the fire protection of supporting steel structures. By conducting CFD calculations of reasonably worst case fire scenarios, the thermal conditions to which the steel elements would be exposed can be applied as a boundary condition to the solid phase model describing the transfer of heat and mechanical forces within the structure. In the simplest approach, the analysis would ascertain whether the temperature of the steel elements reaches a critical level beyond which the structure might become unstable or even collapse. The methodology adopted to transfer the information, i.e. surface temperature and convective and radiative thermal fluxes, between the CFD and structural model is non-trivial, and is an area of on-going research, see for example [32].

Numerical Solution

The equations described in the previous sections are all written in continuous form; that is, they are exact representations of the governing conservation laws. Unfortunately, they have no closed form solution except in very limited cases. Therefore, numerical techniques are required to obtain approximate solutions. Even on the fastest computers available, these techniques can be costly in terms of the time consumed by the computer's central processing unit (CPU) and the size of the computer's random-access memory (RAM). Calculation times can range from several hours to several weeks. Memory requirements can range from hundreds of megabytes to tens of gigabytes. In the end, the calculations will produce an enormous amount of data, the processing of which would be impossible if not for graphical tools that have been developed specifically to visualize the computed results in various ways.

Finite Difference Approximation

A commonly used technique for solving the governing conservation equations is known as finite-differencing. The three-dimensional volume of interest, say a room in a building, is subdivided with a mesh made up of many small grid cells, with each cell containing an average value of each flow variable. In general, more grid cells produce a more accurate approximation of the true solution but at increasing computational cost. The simplest meshes consist of cells that are box-shaped with the dimensions of the boxes either fixed or varying. Such a mesh is described as rectilinear. Meshes that conform to the boundaries of complicated objects are known as body-fitted. Fire models that are intended for building applications most often use rectilinear meshes, whereas special applications, like furnaces and combustors, often employ body-fitted coordinate systems.

As an example of how finite-differencing works, consider the discretization of the mass conservation Eq. 32.1 on a three-dimensional rectilinear mesh. The cells are typically indexed by the integers i, j, and k. Each flow variable is represented as an average over the cell volume, $\delta x \ \delta y \ \delta z$, and over the time step, δt. At the start of the simulation, all the flow variables in each grid cell are assigned an initial value, and as the simulation progresses in time, these values are updated at each discrete time step. A common discretization technique is to define scalar quantities at the center of each cell and vector components at their respective cell faces. For example, ρ^n_{ijk} represents the average density in the cell with indices $i\ j\ k$ at the nth time step, whereas u^n_{ijk} and $u^n_{i-1,jk}$ represent the averages of the velocity component u over the faces of the cell that point in the positive and negative directions of x in the standard Cartesian coordinate system. A simple way to advance the density of each cell in time is to write the mass

conservation equation in an approximate form as follows:

$$\rho_{ijk}^{n+1} = \rho_{ijk}^{n} - \delta t\left(\frac{\rho_{i+\frac{1}{2},jk}^{n} u_{ijk}^{n} - \rho_{i-\frac{1}{2},jk}^{n} u_{i-1,jk}^{n}}{\delta x} + \frac{\rho_{i,j+\frac{1}{2},k}^{n} v_{ijk}^{n} - \rho_{i,j-\frac{1}{2},k}^{n} v_{i,j-1,k}^{n}}{\delta y} + \frac{\rho_{ij,k+\frac{1}{2}}^{n} w_{ijk}^{n} - \rho_{ij,k-\frac{1}{2}}^{n} w_{ij,k-1}^{n}}{\delta z}\right) \tag{32.25}$$

Notice that even the simplest of the conservation equations approximated with the simplest of differencing schemes on the simplest of meshes is still fairly difficult to express in a succinct way. In fact, to save space, the density at the respective cell faces, computed as an average of its values in the adjoining cells, is denoted by the $\pm\frac{1}{2}$ in the appropriate subscript. The momentum and energy conservation equations are far more complicated than this one, even though the basic ideas are the same. It is easy to understand why CFD software consists of tens of thousands of lines of computer instructions and that calculations can take hours to weeks to complete, depending on the number of grid cells in the mesh and the complexity of the differencing scheme.

CFD models employ various types of differencing schemes, meshes, physical and numerical assumptions, and so on. No two models are exactly alike, but many have common traits. An informal classification system has evolved within the community of developers to distinguish one model from another. For example, the simple scheme for updating the previous density would be described as a three-dimensional, explicit, conservative, staggered finite-difference scheme that is first order accurate in time and second order accurate in space. Consider each descriptor in turn:

Explicit Versus Implicit Schemes

To say that a numerical scheme is explicit means that the flow variables may be advanced in time based solely on their values at the current time step. In Eq. 32.25, notice that all the values of the density and the velocity components on the right-hand side are taken at the nth time step; thus, advancing the solution in time is merely a matter of computing these terms. An implicit scheme uses values of the flow variables at both the current and next time steps, meaning that there is no direct way of updating the values. Rather, a linear system of equations must be solved. Although they require more computational effort per time step, implicit schemes typically are more numerically stable and permit larger time steps than explicit schemes. In fact, the most commonly used numerical scheme in commercial CFD packages is known as SIMPLE (Semi-Implicit Method for Pressure-Linked Equations). Details may be found in Patankar [4].

Conservative Versus Nonconservative Schemes

A numerical scheme that is described as conservative has the following property: If the right-hand side of Eq. 32.25 were summed over all grid cells, the intermediate mass fluxes would cancel exactly, leaving only the mass fluxes at the boundary of the computational domain. This is the discrete analogue of the Divergence Theorem:

$$\int_V \nabla \cdot \rho \mathbf{u}\, dV = \oint_{\partial V} \rho \mathbf{u} \cdot d\mathbf{S} \tag{32.26}$$

This very desirable property in a numerical scheme ensures that mass is globally conserved, regardless of inaccuracies related to the grid cell size, differencing scheme, or other local effects.

Staggered Versus Co-located Variables

Assigning various flow variables to different locations within the grid cell is a strategy adopted by the developer based on the particular application of the model and the convenience of prescribing boundary conditions, obstructions, and other special features. Suffice it to say that the strategy adopted in Eq. 32.25 is not unique. Other techniques are discussed in Anderson et al. [2] and Ferziger and Peric [3].

Order of Accuracy of the Scheme

A common misconception about numerical schemes is that those with a high order of

accuracy are better than those of lower order. A finite difference is an approximation of a partial derivative, and the order of accuracy relates the degree of approximation. For example, the scheme described in Eq. 32.25 is first order accurate in time because the time derivative of the density at the nth time step is approximated as

$$\frac{\partial \rho}{\partial t} = \frac{\rho^{n+1} - \rho^n}{\delta t} + \mathcal{O}(\delta t) \tag{32.27}$$

The symbol $\mathcal{O}(\delta t)$ represents the *discretization error*—neglected terms from the Taylor series expansion of the density that are proportional to the first and higher powers of the time step size. Another way of characterizing this approximation is to say that it has a forward bias in time. The spatial derivatives in Eq. 32.25 are known as central differences, having neither a forward nor backward bias in the respective coordinate directions. Such differences that incorporate values from the nearest adjacent grid cells are typically second order accurate. Higher-order accuracy requires information beyond nearest neighbors, adding to the cost of computing the finite differences. The potential increases in accuracy are often offset by the decrease in computational efficiency and ease of implementation. A popular trade-off is to use more grid cells with a second-order accurate scheme rather than less grid cells with a higher-order scheme.

Spatial Dimension of the Scheme

There are some fire scenarios where it may not be necessary to solve the fully three-dimensional form of the governing equations. Sometimes, flows through ducts or tunnels can be approximated in two spatial dimensions. Also, where there is a symmetry in the fire scenario (e.g., a simple compartment with a fire in the middle of the room), the computational effort can be reduced by a factor of two by modeling one-half of the geometry. The plane of symmetry is then defined as a symmetry boundary condition at the corresponding edge of the modeled domain. Tunnels are another application in which a vertical symmetry plane is often used, running along the length of the tunnel. Care is required in using symmetry boundaries to ensure that the imposed condition of symmetry is physically realistic. For example, in an LES calculation, it is generally undesirable to use a symmetry boundary because the methodology does not assume the fire to be symmetric (in a time-averaged sense).

Finite Volume Method

A popular alternative to finite-differencing employed in both commercial and fire-specific CFD models is the finite volume method. This method has some of the characteristics of the finite element method employed in structural and solid-phase thermal analysis programs and can be employed with either structured or unstructured meshes. Rather than working with the conservation equations in their differential form, as in Eqs. 32.1–32.4, the finite volume method takes as its starting point the equations in their integral form. For example, integrating equation 32.2 over a control volume V and applying the Divergence Theorem (Eq. 32.26) yields an integral form of the equation:

$$\begin{aligned} &\frac{\partial}{\partial t}\int_V \rho Y_\alpha \, dV + \oint_{\partial V} \mathbf{n}\cdot(\rho Y_\alpha \mathbf{u})\, d\mathbf{S} \\ &= \oint_{\partial V} \mathbf{n}\cdot(D_\alpha \nabla Y_\alpha)\, d\mathbf{S} + \int_V \dot{m}'''_\alpha \, dV \end{aligned} \tag{32.28}$$

The solution domain is subdivided into a finite number of control volumes (cells) in much the same way as in the finite difference method described previously. The crux of the finite volume method is in determining the surface and volume integrals in Eq. 32.28, which in turn requires that the surface values of the solved variables be expressed in terms of the neighboring control volume (node) values, using an appropriate interpolation scheme. A system of algebraic equations is developed as in the finite difference method, the solution of which provides the mean value of the solved variable at each control volume (generally assigned to the

node points). Although the finite volume method was originally employed with structured grids, the trend with modern commercial models has been toward unstructured grids consisting of hexahedral or tetrahedral elements.

The finite volume method is intrinsically conservative (provided the surface fluxes are defined appropriately). It may be explicit or implicit and the mesh may be staggered or co-located. Depending on the numerical approximation of the integrals, the solution may be formally any order of accuracy. For the diffusion terms, a second order (central difference) approach is generally adopted. For the convection terms, matters are more complicated, and the use of central differencing can produce erroneous results in convection-dominated flows when a RANS turbulence formulation is used. First order, or "up-wind," schemes remove the instabilities caused by central differencing, but they can be inaccurate if the grid is not sufficiently fine. A common approach has been to use the so-called "hybrid" scheme [33] in calculating the surface fluxes, which produces stable solutions that are generally more accurate than those provided by a pure first order, upwind approach but not formally as accurate as a second order approach.

Alternative Solution Methods

The finite element method (FEM) is well established for solving the partial differential equations of structural mechanics and solid phase heat transfer, and shares some of the underlying mathematics associated with finite difference and finite volume methods. An unstructured numerical mesh, often composed of tetrahedra, is employed, which makes the method particularly suited to complex geometries. While the finite element method has been applied to fluid flows, its application in the fire field has to date been limited. Other numerical methods that have been employed by the CFD community include spectral methods and boundary elements.

Computer Hardware and Software

CFD solvers are written in a variety of computer languages, most notably Fortran or C. They will run, or execute, on any computer for which a compiler is available to translate the source code into the native machine language. Usually, CFD models consist of three basic parts: an interface that allows the user to input parameters, the flow solver, and a graphical program to display results. It is not unusual for the user interface, flow solver, and graphics utility to be three separate computer programs, sometimes written in different languages, and sometimes run on different computers. For example, the flow solver itself can be run on a remote machine because it does not require any interaction with the user. While a calculation runs somewhere else, the user is free to set up new calculations or process results from a previous one. What were once referred to as "supercomputers" are now simply clusters of conventional computers that are dedicated to running CFD calculations, either serially or in parallel.

The input interface can be a graphical user interface (GUI), a simple text editor, or some combination of the two. Some of the more complex interfaces allow for input data to come from other sources, like a computer-aided design (CAD) program. This is an increasingly important consideration in CFD, as the most time-consuming part of a simulation (for the user, not the computer) is the description of the geometry. It is now possible to simulate the flow of fire-driven gases through entire buildings, but without some automated method of input, the setup process can be tedious.

CFD is becoming more and more routine as computers get cheaper and faster. In addition to the availability of doubly fast CPUs every 18 months, an emerging trend in the industry is to use more than one CPU (and the associated memory) for a single simulation. The technique, known as parallel processing, has been made possible by the development of software that allows data to be transferred rapidly between two or more computers that are working on the

same calculation. The most popular data-passing protocol is message passing interface (MPI). To the CFD developer, MPI is nothing more than a set of "call" statements that can be written into the source code, instructing computer A to send a packet of numbers to computer B and vice versa. The formats of the call statements have been standardized by a committee of interested industry experts, and several very good, and free, implementations of MPI have been released into the public domain. Although writing and running a good, efficient parallel CFD model is still a daunting task, parallel processing does not significantly increase the cost of hardware or software. It is possible to exploit the computers that a company already owns to run CFD models in parallel.

Visualization

As computers get faster and calculations get bigger, there is a tremendous need to render the output of the simulations in some useful form. Certainly, time histories of individual quantities at discrete locations can be saved and readily plotted, much like thermocouple data from a real experiment. But this only tells part of the story. To better understand the flow dynamics, it is necessary to render pictures or animations of the entire computational domain, either in the form of contour plots, flow vectors, streamlines, or tracer particles. This type of output is invaluable to the numerical analyst but still only partially satisfying to the lay person. Perhaps spurred on by the current generation of computer-animated films, some want to see the results of the simulations rendered in a lifelike way, considerably different than conventional CFD output.

This trend to realism is more than superficial. In both design and forensic applications, the realistic rendering of smoke is very valuable, but it requires graphical techniques that stretch the limits of even the best video cards available. Visibility is a key consideration in the design of any large structure, especially given the current trend of open architecture. Unlike temperature or species concentration, visibility is not defined at a point but rather integrated over a path connecting the virtual occupant and the virtual exit sign. The CFD model can produce a spatially and temporally varying smoke density field, but it is difficult or impossible to integrate a priori the density over every possible path between the sign and the moving occupant. Fortunately, graphical techniques are now available that can process the smoke density data and produce at any given time and any given place in any given direction a realistic view through the smoke, allowing the viewer to assess whether or not the sign (or whatever is of interest) would be visible in the event of a real fire.

Verification and Validation

The use of fire models currently extends beyond the fire research laboratories and into the engineering, fire service, and legal communities. Sufficient evaluation of the models is necessary to ensure that users can judge the adequacy of its technical basis, appropriateness of its use, and confidence level of its predictions. The model evaluation process consists of two main components: verification and validation [34]. Verification is a process to check the correctness of the solution of the governing equations. Verification does not imply that the governing equations are appropriate, only that the equations are being solved correctly. Validation is a process to determine the appropriateness of the governing equations as a mathematical model of the physical phenomena of interest. Typically, validation involves comparing model results with experimental measurement. Differences that cannot be attributed to uncertainty in the experimental measurements are attributed to the assumptions and simplifications of the physical model.

It is commonly assumed by model users, particularly those who have purchased expensive CFD software, that verification and validation is the responsibility of the model developers. Certainly, CFD developers do a considerable amount of this type of work, in particular verification, but it is impossible to ensure that the model is

"validated" for every conceivable application. Indeed, the very point of numerical modeling is to predict the outcome of fire scenarios that have not, or cannot be, replicated in a controlled laboratory environment. Thus, the burden of verification and validation must be shared by the model developer and user. The benefit to the user is twofold: first, it confirms that the user can use the software properly, at least for the given application; and second, it assures the user that the model can address the given fire scenario, even providing the user with some estimate of its accuracy.

Verification

The most important task for a CFD modeler is to perform a *grid resolution study* for the particular application at hand. The accuracy of a CFD calculation is dependent on the resolution of the underlying numerical grid. As discussed in Sect. 32, the order of accuracy of a numerical algorithm indicates the rate at which the solution of the discretized governing equations converges towards the solution of the exact equations. For example, if the scheme is second-order accurate in space and time, the error due to the finite difference/volume approximation will decrease by a factor of 4 if the grid cell and time step decrease by a factor of 2. Demonstrating this for a particular application of the model is known as a grid resolution study. Selection of an appropriate grid size should be based on whether or not a particular level of accuracy is achieved for a particular grid cell size.

In addition to a grid resolution study, there are a variety of other tests that a model user should perform to ensure that the model is solving the governing equations correctly, and that the model user is running the model properly. What tests to perform depends on the application. For example, if the application involves a pressure rise in a relatively tight compartment, simple tests should be performed to ensure that the pressure increase obeys the basic laws of thermodynamics. If water droplets are involved, simple tests should be performed to ensure that mass and energy conservation laws are properly applied in the model.

Validation

The typical way to validate a CFD fire model is to compare its results to experimental measurements. This involves two important tasks: (1) selecting appropriate experiments and (2) quantifying the accuracy of the model's prediction of the outcome of these experiments. The following two sections address these two tasks.

Applicability of Validation Experiments

How can one determine if a particular application of the model has been validated? For example, suppose the problem at hand is a fire in a warehouse with a 10 m ceiling, sprinklers, roof vents, and HVAC system. There is probably no experimental data set that is exactly like it, and it would be too expensive to conduct new experiments. How does one determine if any validation work is appropriate for this scenario? The approach taken in a fire model validation study conducted by the US Nuclear Regulatory Commission (NRC) and the Electrical Power Research Institute (EPRI) was to characterize the experiments used in the study in terms of a handful of commonly used non-dimensional quantities from the fire literature [35]. This essentially defines the "parameter space" for which the model was validated. The model users are warned that the models should only be applied within this parameter space. This prevents the tendency by users to simply declare that the model has been validated and can be used for any application. The non-dimensionalized parameters used in the NRC/EPRI study are:

1. *Fire Froude Number,* $\dot{Q}^*$: A convenient way to express the heat release rate of the fire relative to its base area is by way of the non-dimensionalized quantity:

$$\dot{Q}^* = \frac{\dot{Q}}{\rho_\infty c_p T_\infty \sqrt{gD}\, D^2} \tag{32.29}$$

where $\dot{Q}$ is the peak heat release rate of the fire and D is the equivalent diameter of the base of the fire. The Fire Froude Number is a useful quantity for plume correlations and flame height estimates. A large value ($\dot{Q}^* \gg 1$) describes a fire for which the energy output is relatively large compared to its physical diameter, like an oil well blowout fire. A low value ($\dot{Q}^* \ll 1$) describes a fire for which the energy output is relatively small compared to its diameter, like a brush fire.

2. *Flame Height Relative to Ceiling Height, L_f/H*: This ratio is a convenient way to express the physical size of the fire relative to the size of the room. A value greater than one indicates that there is flame impingement on the ceiling, an important consideration when evaluating devices such as sprinklers and smoke detectors. The Flame Height, L_f, is the height of the visible flame, based on Heskestad's correlation [36]:

$$L_f = D\left(3.7\,(\dot{Q}^*)^{2/5} - 1.02\right) \tag{32.30}$$

3. *Global Equivalence Ratio, ϕ*: A convenient way to determine whether a compartment fire is limited by fuel or oxygen is to estimate the ratio of the fuel supply rate, $\dot{m}_f$, to the oxygen supply rate, $\dot{m}_{O_2}$, divided by the stoichiometric ratio, r:

$$\phi = \frac{\dot{m}_f/\dot{m}_{O_2}}{r} = \frac{\dot{Q}}{\Delta h_{O_2}\,\dot{m}_{O_2}} \quad ;$$
$$\dot{m}_{O_2} = \begin{cases} \frac{1}{2}0.23\,A_0\sqrt{H_0} & \text{Natural} \\ 0.23\,\rho\,\dot{V} & \text{Mechanical} \end{cases} \tag{32.31}$$

Here, Δh is the heat of combustion, $\dot{Q} = \dot{m}_f\,\Delta h$ is the peak heat release rate of the fire, $\Delta h_{O_2} = r\,\Delta h$ is the heat of combustion per unit mass oxygen consumed, A_0 is the area of the compartment opening, H_0 is the height of the opening, ρ is the density of air, and $\dot{V}$ is the volume flow of air into the compartment due to a ventilation system. The factor 0.23 is the mass fraction of oxygen in air. If $\phi < 1$, the compartment is considered "well-ventilated" and if $\phi > 1$, the compartment is considered "under-ventilated." In general, under-ventilated fire scenarios are more challenging for the models because the combustion physics are more complicated.

4. *Relative Distance Along the Ceiling, r_{cj}/H*: This ratio indicates the distance from the fire plume of a sprinkler, smoke detector, etc., relative to the compartment height, H. The maximum ceiling jet temperature, important in determining device activation, has been shown to be a function of this ratio.
5. *Relative Distance from the Fire, r_{rad}/D*: This ratio indicates whether a "target" is near or far from the fire. In general, it is more challenging to predict the radiative heat flux to objects near the fire.
6. *Room Length and Width Relative to the Ceiling Height, L/H and W/H*: These ratios are useful mainly when assessing an empirical or zone model because most of the correlations used by these models are limited in terms of compartment aspect ratio. For CFD, extreme values of these ratios might indicate unusual fire behavior.
7. *Ceiling Height Relative to the Fire Diameter, H/D^**: This ratio is a non-dimensional measure of the height of the fire plume. D^* is a length scale that incorporates the heat release rate of the fire:

$$D^* = \left(\frac{\dot{Q}}{\rho_\infty c_p T_\infty \sqrt{g}}\right)^{2/5} \tag{32.32}$$

The larger the ratio H/D^*, the more important the plume becomes in the overall scenario. For empirical and zone models, it indicates whether or not the plume entrainment correlation is appropriate. For CFD, it indicates how "high" the plume actually is, in non-dimensional terms.

Quantifying Model Uncertainty

Having determined the appropriateness of the chosen experiments, it is now necessary to quantify the accuracy of the model in predicting the

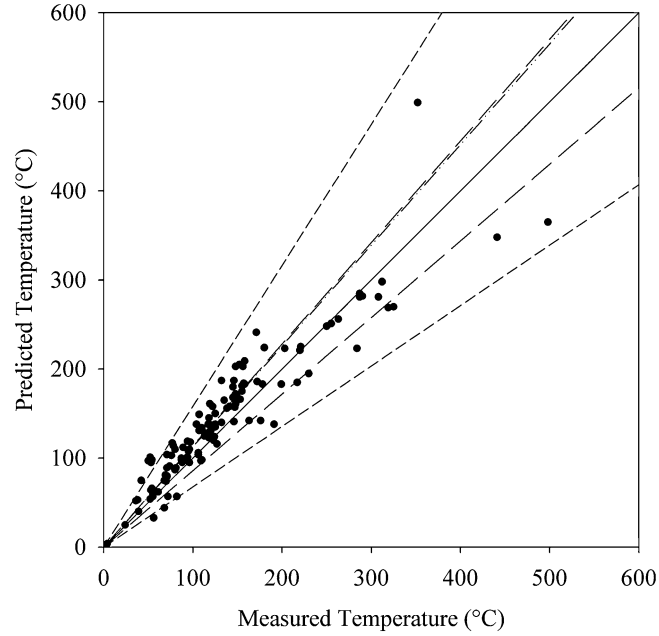

Fig. 32.2 A comparison of measured versus predicted wall temperature. The *off-diagonal lines* indicate the $2\widetilde{\sigma}$ bounds for the experiments (*long dash*) and the model (*short dash*)

outcome of these experiments. For each quantity of interest, a summary plot of the results should be constructed like the one shown in Fig. 32.2. The accuracy of the model can be expressed in terms of two statistical parameters. The first, δ, is the bias factor. It indicates the extent to which the model, on average, under or over-predicts the measurements. For example, the bias factor for the data shown in Fig. 32.2 is 1.13. This means that the model over-predicts wall temperatures by 13 %, on average, and this is shown graphically by the dash-dot line. The second statistic is the relative standard deviation of the model, $\widetilde{\sigma}_M$. This indicates the degree of scatter of the points. Referring again to Fig. 32.2, there are two sets of off-diagonal lines. The first set, shown as long-dashed black lines, indicate the estimated experimental uncertainty. The slopes of these lines are $1 \pm 2\widetilde{\sigma}_E$, i.e. the 95 % confidence interval for the measurements. In this case, $\widetilde{\sigma}_E = 0.07$. The second set of off-diagonal lines, shown as short-dashed lines, indicates the model uncertainty. The slopes of these lines are $\delta(1 \pm 2\widetilde{\sigma}_M)$. In this case, $\widetilde{\sigma}_M = 0.2$. If the model were as accurate as the measurements against which it is compared, the two sets of off-diagonal lines would merge and the dash-dot bias line would overlap the solid diagonal line. The extent to which the data scatters outside of the experimental bounds is an indication of the degree of model uncertainty.

The derivation of these uncertainty statistics is described in [37], and it is summarized here. First, a few assumptions are made:

1. The experimental measurements are assumed to be unbiased, and their uncertainty is assumed to be normally distributed with a constant relative standard deviation, $\widetilde{\sigma}_E$.
2. The model uncertainty is assumed to be normally distributed about the predicted value divided by a bias factor, δ. The relative standard deviation of the distribution is denoted as $\widetilde{\sigma}_M$.

Now, given a set of experimental measurements, E_i, and a corresponding set of model predictions, M_i, compute the following:

$$\overline{\ln(M/E)} = \frac{1}{n}\sum_{i=1}^{n} \ln(M_i/E_i) \qquad (32.33)$$

The relative standard deviation of the model, $\widetilde{\sigma}_M$, can be computed from the following equation:

$$\widetilde{\sigma}_M^2 + \widetilde{\sigma}_E^2 = \frac{1}{n-1}\sum_{i=1}^{n}\left[\ln(M_i/E_i) - \overline{\ln(M/E)}\right]^2 \tag{32.34}$$

The bias factor is:

$$\delta = \exp\left(\overline{\ln(M/E)} + \frac{\widetilde{\sigma}_M^2}{2} - \frac{\widetilde{\sigma}_E^2}{2}\right) \tag{32.35}$$

For a given model prediction, M, the "true" value of the quantity of interest is assumed to be a normally distributed random variable with a mean $\mu = M/\delta$ and a standard deviation of $\sigma = \widetilde{\sigma}_M(M/\delta)$. Using these values, the probability of exceeding a critical value, x_c, is:

$$P(x > x_c) = \frac{1}{2}\,\mathrm{erfc}\left(\frac{x_c - \mu}{\sigma\sqrt{2}}\right) \tag{32.36}$$

Note that the complimentary error function is defined as follows:

$$erfc(x) = \frac{2}{\sqrt{\pi}}\int_t^\infty e^{-t^2}dt \tag{32.37}$$

It is a standard function in most mathematical or spread sheet programs.

As an example of the procedure, suppose that the model whose results are plotted in Fig. 32.2 has predicted that the wall temperature within a compartment would peak at a value of 300 °C due to a given design fire. Suppose also that the failure criterion for the wall lining material is 325 °C. What is the probability that the wall temperature could reach 325 °C? First, it is best to work in terms of temperature rise. The ambient temperature is 20 °C; thus, the predicted temperature rise, ΔT_p, is 280 °C and the critical temperature rise, ΔT_c, is 305 °C. From Eq. 32.36, the probability that the temperature could exceed the critical value is:

$$\begin{aligned} P(\Delta T > \Delta T_c) &= \frac{1}{2}\,\mathrm{erfc}\left(\frac{\Delta T_c - (\Delta T_p/\delta)}{\widetilde{\sigma}_M\,(\Delta T_p/\delta)\sqrt{2}}\right) \\ &= \frac{1}{2}\,\mathrm{erfc}\left(\frac{305 - (280/1.13)}{0.2\,(280/1.13)\sqrt{2}}\right) \cong 0.12 \end{aligned} \tag{32.38}$$

It must be emphasized that this estimated probability of failure is based only on the model uncertainty. It does not account for parameter uncertainty; that is, the uncertainty in the input parameters.

Applications

This section presents examples of how CFD fire models are used in practice. These applications can be divided into three general categories—research, design, and forensic. For research, the models can help explain basic fire phenomena. For design, the models are used to predict the spread of smoke and heat from a hypothetical fire in a real or planned building. For forensics, the models aid in the reconstruction of an actual fire. For a design application, the fire is usually specified; that is, the ignition, growth, and eventual decay of the fire are not predicted by the model but rather specified by the design engineer and reviewed by the code enforcing authority. For a reconstruction, the model is usually used to explain how a small fire grew and spread to cause serious damage or injury. Rarely are fire models of the type described in this chapter used to show how a fire was actually ignited, as the physical mechanism of this event (electrical short, arcing fault, arson, etc.) is usually not included in the model.

Fundamental Fire Dynamics

CFD, in particular large eddy simulation, provides a convenient means to study basic fire behavior. The most obvious application is the study of fire plumes; for example, predicting the height of the visible flame, the centerline velocity and temperature, and the pulsation frequency. Heskestad's empirical flame height correlation (Eq. 32.30) is valid for values of $\dot{Q}^*$ between 0.1 and 10,000, characterizing intermittent grass fires all the way to oil well blowout fires. Figure 32.3 compares FDS predictions with Heskestad's correlation. Note that the

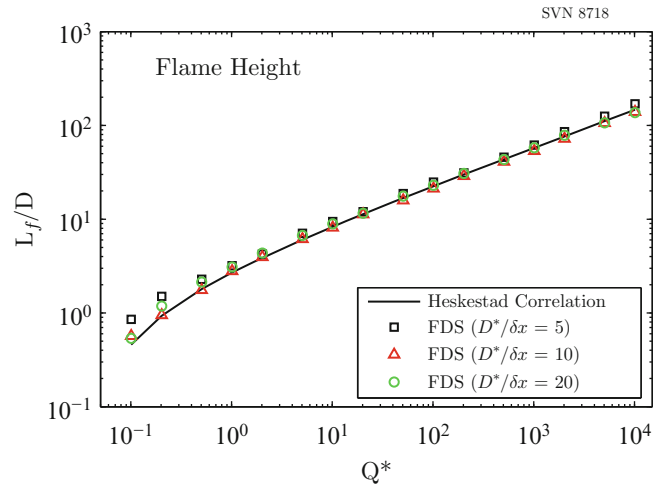

Fig. 32.3 Comparison of FDS predictions of flame height from a 1 m square pan fire for Q* values ranging from 0.1 to 10,000

simulations were run at three different grid resolutions. A useful way to characterize the grid resolution of a fire simulation is via the ratio $D^*/\delta x$, where D^* (Eq. 32.32) is a measure of the effective fire diameter, based on heat release rate, and δx is the size of a grid cell. In effect, $D^*/\delta x$ is the number of grid cells spanning the effective fire diameter.

The fundamental, or "puffing," frequency is a quantity that the fire model also ought to predict accurately. Figure 32.4 displays sequential flame images for a single puff from a simulation of a 1 m methane fire experiment conducted at Sandia National Laboratories [38]. The dominant puffing mode shows good agreement with the measured puffing frequency of 1.65 Hz. Higher frequency fluctuations from the simulation exhibit the classic $-5/3$ scaling of Kolmogorov turbulence [39].

Smoke Movement

A significant proportion of fire fatalities can be attributed to the inhalation of smoke particulates and toxic gases. Furthermore, the effects of reduced visibility, high temperature, radiative flux, and oxygen depletion may add to the hazard associated with the smoke generated by an enclosure fire. Means to control the movement of smoke include physical barriers, natural or mechanical smoke exhaust, and pressurization of protected spaces. In routine applications, the design of the smoke control measures may often be achieved by recourse to various guidance publications and empirical correlations [40, 41]. Network airflow and zone fire models are also available to assist in the design process. However, where the building space is large or complex in shape, or where a novel ventilation system is proposed, CFD can be a useful tool. Covered shopping malls, atria in hotels and office buildings, leisure complexes, airport terminals, and large warehouses are just some examples of where CFD is being increasingly employed.

Many of the earliest examples of the application of CFD to fire engineering were in smoke movement applications [42, 43]. Simulations were at that time restricted to a few tens of thousands of grid cells. Although this number has increased to hundreds of thousands or even millions of cells, many of the modeling issues remain the same and are discussed later [44].

Smoke Transport in a Mechanically Ventilated Library

In collaboration with Olof Granlund Oy, ANSYS Europe Ltd. conducted a CFD analysis of the movement of smoke generated by a fast-growing fire, with a peak heat release rate of 550 kW, inside a library for which the ventilation system was left running in its normal mode of operation.

Fig. 32.4 Snapshots of the flame envelope from a simulation of the Sandia 1 m diameter methane pool fire using 1.5 cm grid resolution. The images span a single "puff"

The building has a pitched, vented glass roof and diffusers at various elevations. ANSYS CFX is a general purpose, commercial CFD model that has a history in fire modeling dating back to the investigation of the 1987 Kings Cross fire in London [45]. Because it is designed to handle virtually any type of geometry, a model like this one can employ a numerical mesh that conforms to the unusual shape of the building. In this case, an unstructured mesh with 3.2 million mesh elements was used. Figure 32.5 shows a contour map of visibility distance after 3 min in a vertical slice through the building.

Smoke Transport in a Historic Landmark

CFD fire modeling is commonly used during the renovation of historic buildings. Often at issue is the inclusion or exclusion of a fire protection system (sprinklers, exhaust fans, etc.) that might require a variance from the local building code requirements. For example, as part of an overall effort in modernizing the Rhode Island Statehouse (the rotunda is the fourth largest self-supporting dome in the world), the LES model FDS was used to model a number of fire scenarios within the structure. The building supervisors wished to avoid having to disrupt the historical fabric of the rotunda while updating the building's fire protection systems. The model was used to examine a number of fire scenarios and how they might impact the ability of occupants to evacuate the building. Note in Fig. 32.6 the use of rectangular obstructions to approximate the very complicated geometry of the building—a simple alternative to the more CPU intensive body-fitted coordinate system.

Smoke Transport in a Multistory Residential Building

To assist means of escape and fire fighter access in high rise residential buildings it is common practice to provide some form of smoke control to the stairwells, which could take the form of a sophisticated pressurization scheme or a relatively simple natural ventilation provision. There may be cases where smoke protection is required also in the corridors and lobbies at each story, possibly as a compensatory measure for extended travel distances. Another approach, adopted in some parts of the world, is to provide

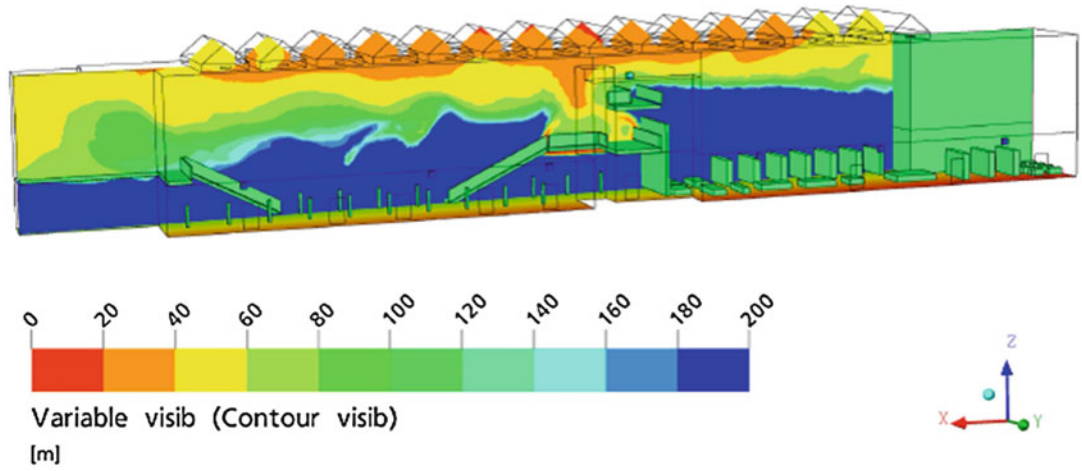

Fig. 32.5 Map of visibility in a vertical plane at time = 3 min for a fire in a library building (Figure courtesy: ANSYS Europe Ltd)

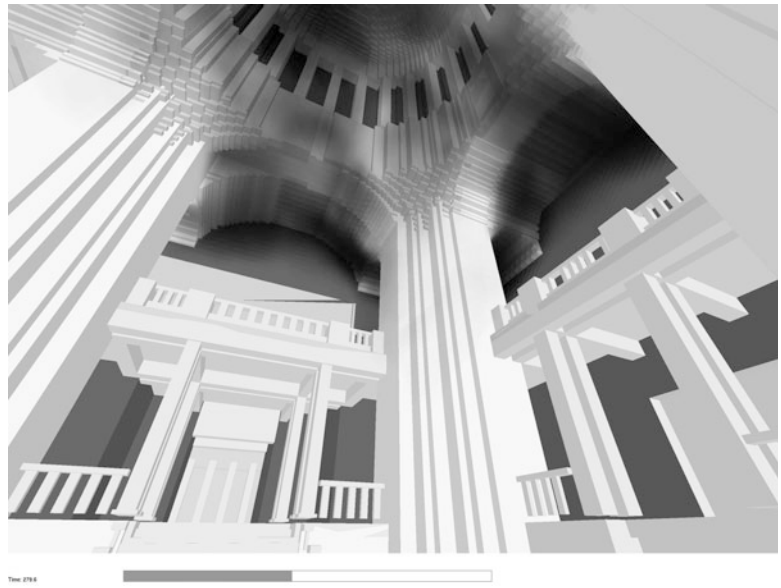

Fig. 32.6 Smoke filling analysis of the Rhode island State capitol (Figure courtesy: Hughes Associates)

mechanical ventilation in the corridor. In the event of a fire in an adjoining apartment smoke is purged from the corridor, while at the same time the ventilation system provides smoke protection to the stairwell by the combined action of pressure differentials and open-door airflows akin to a stair pressurization system. CFD modeling of the air and smoke transport in the corridor and stairwell is often required in support of the design, in particular where the corridors and lobbies have a more complicated layout or the ventilation inlets and outlets cannot be installed in ideal locations.

Tunnels

Historically, smoke control inside tunnels was often considered as an afterthought to design of ventilation for the provision of fresh air. Where natural ventilation was insufficient, mechanical ventilation was designed using network flow

theory aided in recent years by network models. As a two-layer description is generally not valid within a tunnel environment, fire zone models have been applied to tunnels in only a limited number of cases. CFD, however, is now finding increasing application to fire hazard analysis for road tunnels in particular. In recent years a number of major tunnel fire incidents such as the tragedy in the Mont Blanc tunnel in 1999, resulting in 39 deaths, have highlighted the need to understand better the mechanism of fire development and spread inside tunnels. In particular, heat transfer to the tunnel walls is important to account for correctly as this has a strong influence on the distribution of heat along the tunnel, the degree of stratification that can be expected, and the threat to the integrity of the structure.

One area where CFD has been applied successfully is in the analysis of the critical velocity required in a longitudinally ventilated tunnel to control the spread of heat and smoke so that it is forced in the downstream direction, providing safe conditions upstream [46]. Another area currently receiving much attention is the choice of design fire for tunnel fire safety design. In the light of the recent tunnel fire incidents and full-scale fire tests [47], the size of the fire load that can be generated from what were previously considered as nonhazardous cargoes has been revised. Heat release rates well in excess of 100 MW have been measured for heavy-goods vehicles carrying commercial merchandize.

CFD was used in the investigation into the Mont Blanc tunnel fire incident in 1999. One of the modeling studies involved the use of the JASMINE fire model to re-construct conditions inside the tunnel during the first 30 min, during which time most of the fatalities would have occurred. Using information available on the ventilation settings and the location of vehicles, the model predicted the transport of smoke and heat along the length of the tunnel. The data were then fed into a model for fractional effective dose to enable an assessment of when and how the fatalities occurred. Subsequent parametric simulations were performed to investigate whether alternative tunnel ventilation measures would have helped on the day of the incident [48].

Parking Garages

The application of CFD to the analysis and design of smoke control systems in basement car parks may share elements that apply also to road tunnels. Not only is the potential fire source similar, the ventilation strategies and performance criteria may well overlap. Two ventilation strategies that might be considered in a basement car park include dilution (purging by fresh air) and the directional control of smoke by the application of applied air flows.

While diluting smoke and vehicle emissions can in principle be achieved by ventilating at a specified air change rate, in many cases additional ventilation provisions will be required in order to ensure an even mixing of fresh air and the elimination of stagnant regions. This is commonly achieved by the strategic location of impulse (jet) fans on the underside of the ceiling, which assist the movement of air from the inlet points to the exhaust locations. CFD may be usefully employed to determine the number and location of these fans.

The directional control of smoke in the event of a fire, with the objective of providing a relatively smoke free access to the location of the fire for fire fighting personnel, presents a greater challenge than simply purging smoke from the car park. Here careful design of the ventilation system is required, with the impulse fans operating akin to the case of a longitudinally ventilated tunnel, directing the smoke and heat in a direction away from the approaching personnel.

Fire Investigation

CFD is increasingly used to reconstruct actual fires, providing fire service personnel and fire investigators with a better understanding of the events that led to injury, loss of life, or loss of the structure. In any reconstruction, the time line of events provided by the first responders and other eyewitnesses is as crucial as the model input, but it is also invaluable in assessing the results. Rendering the results of the simulation as realistically as possible facilitates the synthesis of

Fig. 32.7 Comparison of photographs of the Charleston furniture store fire with a numerical simulation. Figure courtesy of NIST

model simulation with photographic and visual evidence. Most people at the fire scene are certainly not experts in CFD, but they are very experienced with fire. Examples of how CFD has been used in actual fire reconstructions are available [49, 50, 51, 52, 53].

As an example, NIST researchers used the Fire Dynamics Simulator to analyze a fire that occurred on the evening of June 18, 2007, in a furniture store in Charleston, South Carolina [54]. Using evidence collected at the scene and eyewitness accounts, the investigators put together a plausible sequence of events that led to the deaths of nine fire fighters. Figure 32.7 presents a snapshot of the numerical simulation compared to a photograph of the actual fire.

Outdoor Applications and Wind

Buoyant windblown plumes have been studied since the early 1960s. A summary of the early work together with a useful bibliography is given by Turner [55]. Most of the models described in these works are integral models, where the profiles of physical quantities in cross-sectional planes perpendicular to the wind direction are assumed, together with simple laws relating entrainment into the plume to macroscopic features used to describe its evolution.

The potential shortcomings of these types of models are that they were designed for typical industrial sources, like smokestacks, that are much smaller in terms of energy output than a large fire. The plume from an oil or forest fire will rise higher into the atmosphere, and it is difficult to predict the rise based on empirical correlations. If the plume rise is not calculated correctly, substantial errors in downwind concentration can result. In the case of smoke-stack emissions, the plume does not rise appreciably high, reducing the uncertainty of the results. Most of the assumptions required by integral models can be removed by taking advantage of the advances in CFD over the past few decades. For example, as part of the process of evaluating the feasibility of using in situ burning as a remediation tool for large oil spills, NIST developed a numerical model, ALOFT (A Large Out-door Fire plume Trajectory), to predict the concentration of smoke and other combustion products downwind of a large fire [56]. The model is simply a variant of the large eddy simulation model FDS, with a simplified plume rise model coupled with a coarsely gridded wind calculation spanning tens of kilometers (Fig. 32.8). This combination of models is not unusual for outdoor application, as the range of length scales spans at least three orders of magnitude.

Virtual Experiments

Many codes and standards for fire protection are based upon simple room geometries. For example, the spacing for smoke detectors has historically been based upon smooth, level ceilings with some additional rules for beams, slope, and height. Under those rules a single story room with a 30 m by 30 m smooth ceiling could be protected by a grid of nine smoke detectors, but a ceiling of waffle concrete construction (Fig. 32.9) with structural deep beams 1 m on center, could, under a strict interpretation

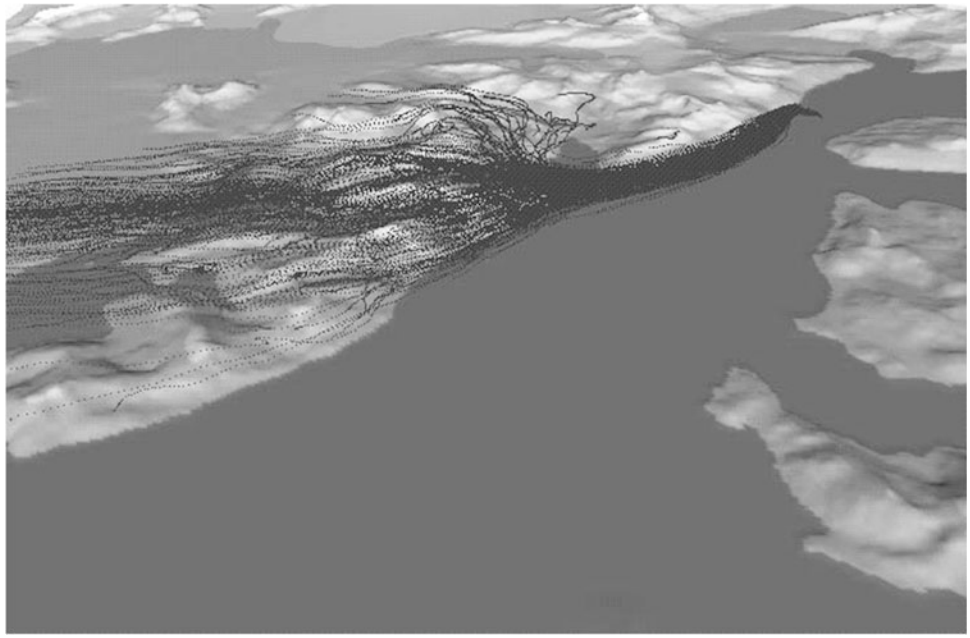

Fig. 32.8 Simulation of smoke from a large oil fire in the Valdez narrows, Alaska (Figure courtesy of NIST)

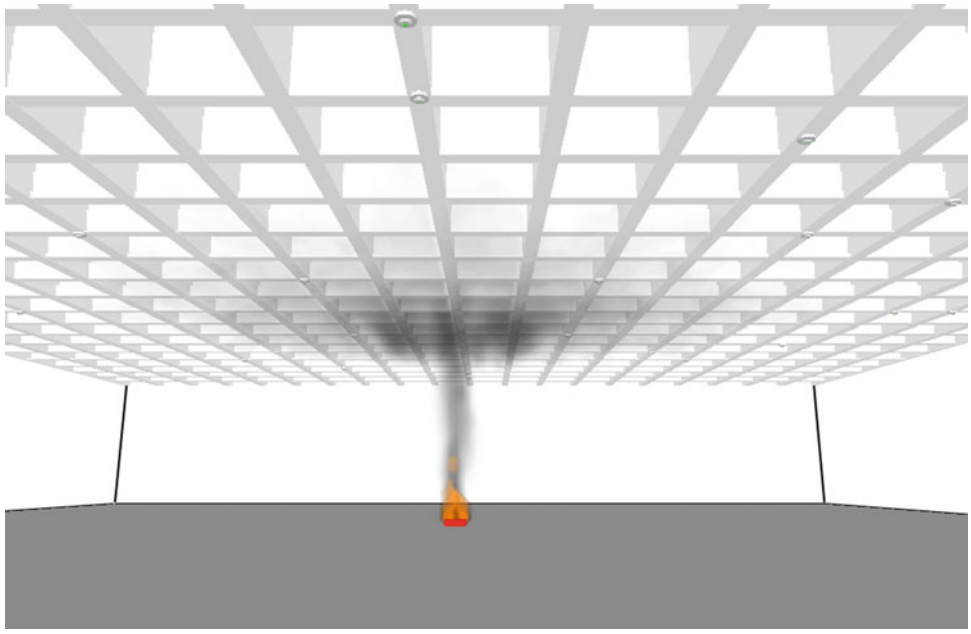

Fig. 32.9 Simulation of smoke filling under a coffered ceiling (Figure courtesy: Aon Fire Protection Engineering Corp.)

of the guidelines, require 900 detectors, one in each beam pocket. While this is obviously unreasonable, making a change to the building code requires evidence. In lieu of a large number of costly full-scale experiments, a small set of full-scale experiments was combined with a large set of "virtual" experiments done with CFD [57, 58]. The researchers evaluated the

appropriateness of the prescriptive provisions and identified ceiling structure parameters, which if altered, would cause significant differences in smoke detection performance as compared to a smooth level ceiling. It had been believed that such beam projections would significantly delay the activation time. The use of CFD modeling showed this expectation to be incorrect and a subsequent full-scale experimental study proved the general findings of the CFD analysis [59]. The final result of the study led to an exception, under some circumstances, to the code requirement of a smoke detector in every beam pocket.

The Role of CFD in the Design Process

As discussed elsewhere in this chapter, CFD has an ever increasing role to play in the development of fire safety science, and has an important contribution to make in better understanding the fundamentals such as flame spread and chemical species production where it is being used in parallel with physical experiments. However, it is as a fire engineering design tool that CFD is probably of most relevance to the majority of readers. Here a few words of caution are worth noting.

CFD modeling has a useful, and sometimes critical, role in developing safe and robust fire engineering solutions where the control of smoke and heat generated by fire forms part of the fire safety strategy. It allows architectural designs to be adopted that in previous eras would have been difficult to justify, for example in respect to smoke control in large and complicated building atria or where a reduced level of structural fire protection is desired. It should, however, be seen as a contributing component to the overall design process, and not as a "black box" that faithfully provides the correct answers regardless of the inputs and assumptions made. A great deal of care and experience is required in order to sensibly use CFD in support of fire engineering designs, and it should be employed alongside simpler calculation and design methods wherever possible to confirm that the CFD results are comparable to the empirical correlations that have traditionally been applied in fire protection engineering.

It is as a parametric design tool that CFD is often most gainfully employed, allowing the impact of varying the input and boundary conditions to be examined. For example, how sensitive is the smoke control solution to the design fire size, or how much influence does a change in wind direction have on a natural smoke ventilation strategy? The reader is encouraged to consult the guidance documents available on the best practice use of CFD in the various application areas and to consult the guidance documentation provided with the CFD model being employed. For example, the guidance document prepared by the US Nuclear Regulatory Commission and the Electrical Power Research Institute (EPRI) on fire modeling for nuclear power plants [60] includes useful information on the appropriate role and application of CFD in the fire safety design process, and is relevant also to fire scenarios outside the nuclear field.

Summary

Computational fluid dynamics modeling of fire has made tremendous progress over the past few decades as our understanding of fire improves and as computers get ever faster. However, although it appears to many that CFD is the cutting edge of fire protection engineering, many non-modelers are surprised to learn that our ability to reproduce fire phenomena via computer simulation lags our empirical understanding by about 10 years. Indeed, current-generation models address transport phenomena reasonably well, making them useful for many engineering applications. However, they have not yet reached the point of reliably predicting, for large-scale applications, such important phenomena as flame spread, extinction, suppression, and CO and smoke production, all of which demand more detailed chemistry and physics than are currently incorporated in the models.

Moving forward will require a new generation of engineers who have expertise in fire physics, mathematics, and computer science to build on

the knowledge possessed by the current generation of modelers. This chapter sets forth the basic elements to lay the foundation of further study for future modelers, and it also provides the current practitioner with a better understanding of the models being used.

Nomenclature

c_p	Specific heat
D_α	Material diffusivity of species α
$\mathbf{f}$	External body force
h	Sensible enthalpy
h_c	Convective heat transfer coefficient
I	Radiant intensity
k	Thermal conductivity; turbulent kinetic energy
$\dot{m}_\alpha'''$	Mass production (destruction) rate of species α per unit volume
p	Pressure
Pr	Prandtl number
$\mathbf{q}$	Heat flux vector
$\dot{q}''$	Heat release rate per unit area
$\dot{q}'''$	Heat release rate per unit volume
$\mathcal{R}$	Universal gas constant
$\mathbf{s}$	Direction vector
s	Stoichiometric air requirement of the fuel
S_{ij}	Strain tensor
Sc	Schmidt number
t	Time
T	Temperature
$\mathbf{u} = (u, v, w)$	Velocity vector
$\overline{W}$	Average molecular weight
$\mathbf{x} = (x, y, z)$	Position vector
Y_α	Mass fraction of species α

Greek Letters

ε	Rate of dissipation of turbulent kinetic energy
κ	Radiation absorption coefficient
λ	Generalized diffusion coefficient
μ	Dynamic viscosity
μ_t	Turbulent viscosity (in eddy viscosity turbulence model)
ρ	Density
σ	Stefan-Boltzmann constant
τ	Stress tensor

Appendix

Much of the difficulty in learning and applying computational fluid dynamics is the complexity of the governing equations. In this appendix, some of the common terms found in the mass, momentum, and energy equations are expanded. Many of the variables and operators can be represented as 3×3, 1×3, or 3×1 matrices, and the expansions can be carried out following the rules of linear algebra. For example, the divergence of the flow vector, $\nabla \cdot \mathbf{u}$, is a scalar formed by multiplying the 1×3 gradient operator ∇ and the 3×1 vector $\mathbf{u}$. On the other hand, the product of the velocity vectors, $\mathbf{u}\,\mathbf{u}$, is found by multiplying a 3×1 vector by a 1×3 vector:

$$\mathbf{uu} = \begin{pmatrix} u \\ v \\ w \end{pmatrix} (u, v, w) = \begin{pmatrix} u^2 & uv & uw \\ vu & v^2 & vw \\ wu & wv & w^2 \end{pmatrix} \tag{32.39}$$

Thus, the convection term in the momentum conservation equation can be expanded as follows:

$$\begin{aligned} \nabla \cdot (\rho \mathbf{uu}) &= \left(\frac{\partial}{\partial x} \frac{\partial}{\partial y} \frac{\partial}{\partial z} \right) \begin{pmatrix} \rho u^2 & \rho uv & \rho uw \\ \rho vu & \rho v^2 & \rho vw \\ \rho wu & \rho wv & \rho w^2 \end{pmatrix} \\ &= \begin{pmatrix} (\rho u^2)_x + (\rho vu)_y + (\rho wu)_z \\ (\rho uv)_x + (\rho v^2)_y + (\rho wv)_z \\ (\rho uw)_x + (\rho vw)_y + (\rho w^2)_z \end{pmatrix}^T \end{aligned} \tag{32.40}$$

The result is a vector whose components form the convective terms of the three component momentum equation. Note that here the subscripts x, y, and z denote partial derivatives with respect to that particular coordinate direction.

The term for the viscosity in the momentum equation, $\nabla\cdot\tau$, is deceptively simple. In reality, it is not, and because it constitutes the heart of the debate over turbulence models, some attention must be paid to it. Using customary tensor notation, the viscous stress tensor is defined as

$$\tau_{ij} = \mu\left(\frac{\partial u_i}{\partial x_j} + \frac{\partial u_j}{\partial x_i} - \frac{2}{3}\delta_{ij}\nabla\cdot\mathbf{u}\right);$$
$$\delta_{ij} = \begin{cases} 1 \text{ if } i = j \\ 0 \text{ if } i \neq j \end{cases} \tag{32.41}$$

These expressions assert that the viscous stresses are linearly related to the strains, the very definition of a Newtonian fluid. The proportionality constant, μ, is called the dynamic viscosity of the fluid. The viscous stress tensor can also be represented as a 3×3 matrix:

$$\tau = \mu\begin{pmatrix} 2u_x & u_y+v_x & u_z+w_x \\ v_x+u_y & 2 & v_yv_z+w_y \\ w_x+u_z & w_y+v_z & 2w_z \end{pmatrix} - \frac{2}{3}\begin{pmatrix} \nabla\cdot\mathbf{u} & 0 & 0 \\ 0 & \nabla\cdot\mathbf{u} & 0 \\ 0 & 0 & \nabla\cdot\mathbf{u} \end{pmatrix} \tag{32.42}$$

The dissipation function, ε, is a scalar formed by the dot product of two 3×3 matrices:

$$\varepsilon \equiv \tau\cdot\nabla\mathbf{u} = \mu\Big(2u_x^2 + 2v_y^2 + 2w_z^2 + (v_x+u_y)^2 + (w_y+v_z)^2 + (u_z+w_x)^2 - \frac{2}{3}(\nabla\cdot\mathbf{u})^2\Big) \tag{32.43}$$

References

1. P.G. Drazin, editor. *Collected Papers of LF Richardson, Volume 1: Meteorology and Numerical Analysis*. Cambridge University Press, Cambridge, UK, 1993.
2. D.A. Anderson, J.C. Tannehill, and R.H. Pletcher. *Computational Fluid Mechanics and Heat Transfer*. Hemisphere Publishing Corporation, Philadelphia, PA, 1984.
3. J.H. Ferziger and M. Peric. *Computational Methods for Fluid Dynamics*. Springer-Verlag, Berlin, second edition, 1999.
4. S.V. Patankar. *Numerical Heat Transfer and Fluid Flow*. Hemisphere Publishing, New York, 1980.
5. R. Peyret and T.D. Taylor. *Computational Methods for Fluid Flow*. Springer-Verlag, New York, 1983.
6. K. Versteeg and W. Malalasekera. *An Introduction to Computational Fluid Dynamics – The Finite Volume Method*. Longmann, Essex, UK, 1995.
7. G. Cox. *Combustion Fundamentals of Fire*, chapter Compartment Fire Modelling. Academic Press, London, 1995.
8. G. Cox. Turbulent closure and the modelling of fire using computational fluid dynamics. *Phil. Trans. R. Soc. Lond. A*, 356:2835–2854, 1998.
9. V. Novozhilov. Computational Fluid Dynamics Modeling of Compartment Fires. *Progress in Energy and Combustion Science*, 27:611–666, 2001.
10. S. Olenick and D. Carpenter. An Updated International Survey of Computer Models for Fire and Smoke. *Journal of Fire Protection Engineering*, 13:87–110, May 2003.
11. R.G. Rehm and H.R. Baum. The Equations of Motion for Thermally-Driven, Buoyant Flows. *Journal of Research of the National Bureau of Standards*, 83:297–308, 1978.
12. V. Yakhot, S.A. Orszag, S. Thangam, T.B. Gatski, and C.G. Speziale. Development of Turbulence Models for Shear Flows by a Double Expansion Technique. *Physics of Fluids A*, 4:1510–1520, 1992.
13. D.C. Wilcox. *Turbulence Modeling for CFD*. DCW Industries, La Cañada, CA, third edition, 2006.
14. J. Smagorinsky. General Circulation Experiments with the Primitive Equations. I. The Basic Experiment. *Monthly Weather Review*, 91(3):99–164, 1963.
15. S.B. Pope. Ten Questions Concerning the Large-Eddy Simulation of Turbulent Flows. *New Journal of Physics*, 6:1–24, 2004.
16. P.R. Spalart, W.H Jou, M. Stretlets, and S.R. Allmaras. Comments on the Feasibility of LES for Wings and on the Hybrid RANS/LES Approach. In *Proceedings of the First AFOSR International Conference on DNS/LES*, Louisiana Tech University, 1997. Air Force Office of Aerospace Research.
17. D.B. Spalding. Mixing and Chemical Reaction in Steady State Confined Turbulent Flames. In *13th Symposium (International) on Combusion*, pages 649–657, Pittsburgh, PA, 1971. The Combustion Institute.
18. B.F. Magnussen and B.H. Hjertager. On Mathematical Modelling of Turbulent Combustion with Special Emphasis on Soot Formation and Combustion. In *16th*

Symposium (International) on Combustion, pages 719–729, Pittsburgh, PA, 1976. The Combustion Institute.

19. S.D. Miles, S. Kumar, and G. Cox. Comparison of 'Blind Predictions' of a CFD Model with Experimental Data. In *Proceedings of the 6th International Symposium on Fire Safety Science*, pages 543–554. International Association of Fire Safety Science, 2000.
20. J. Holen, M. Brostrom, and B.F. Magnussen. Finite Difference Calculation of Pool Fires. In *23rd Symposium (International) on Combustion*, pages 1677–1683, Pittsburgh, PA, 1990. The Combustion Institute.
21. N. Peters. Laminar Flamelet Concepts in Turbulent Combustion. In *21st Symposium (International) on Combustion*, pages 1231–1250, Pittsburgh, PA, 1986. The Combustion Institute.
22. P.A. Tesner, T.D. Snegirova, and V.G. Knorre. Kinetics of Dispersed Carbon Formation. *Combustion and Flame*, 17:253–260, 1971.
23. R. Siegel and J.R. Howell. *Thermal Radiation and Heat Transfer*. Taylor and Francis, New York, fourth edition, 2002.
24. S. Hostikka and K.B. McGrattan. Numerical Modeling of Radiative Heat Transfer in Water Sprays. *Fire Safety Journal*, 41:76–86, 2006.
25. C. DiBlasi. Modeling and Simulation of Combustion Processes of Charring and Non-Charring Solid Fuels. *Progress in Energy and Combustion Science*, 19:71–104, 1993.
26. B.E. Launder and D.B. Spalding. The Numerical Computation of Turbulent Flows. *Computer Methods in Applied Mechanics and Engineering*, 3:269–289, 1974.
27. T. Jin. *SFPE Handbook of Fire Protection Engineering*, chapter Visibility and Human Behaviour in Fire Smoke. National Fire Protection Association, Quincy, MA, fourth edition, 2008.
28. G.W. Mulholland. *SFPE Handbook of Fire Protection Engineering*, chapter Smoke Production and Properties. National Fire Protection Association, Quincy, MA, fourth edition, 2008.
29. B.P. Husted, J. Carlsson, and U. Goransonn. Visibility Through Inhomogeneous Smoke Using CFD. In *Proceedings of Interflam 2004*, pages 697–702, Edinburgh, 2004.
30. G. Heskestad and R.G. Bill. Quantification of Thermal Responsiveness of Automatic Sprinklers Including Conduction Effects. *Fire Safety Journal*, 14:113–125, 1988.
31. G.M. Makhviladze, J.P. Roberts, O.I. Melikhov, and V.I. Melikhov. Numerical Simulation of Sprinkler Jet-Fire Interaction for Compartment Fires. In *Proceedings of the 2nd International Seminar on Fire and Explosion Hazard of Substances and Venting of Deflagrations*, pages 485–496, Moscow, August 1997. All-Russian Institute for Fire Proection.
32. S. Welch, S. Miles, S. Kumar, T. Lemaire, and A. Chan. FIRESTRUC – Integrating Advanced Three-dimensional Modelling Methodologies for Predicting Thermo-mechanical Behaviour of Steel and Composite Structures Subjected to Natural Fires. In *Proceedings of the 9th International Symposium on Fire Safety Science*, pages 1315–1326, Karlsruhe, Germany, September 2008. International Association of Fire Safety Science.
33. D.B. Spalding. A Novel Finite Difference Formulation for Differential Expressions Involving Both First and Second Derivatives. *International Journal for Numerical Methods in Engineering*, 4:551–559, 1972.
34. Society of Fire Protection Engineers, Bethesda, Maryland. *Guidelines for Substantiating a Fire Model for a Given Application*, 2011.
35. K. Hill, J. Dreisbach, F. Joglar, B. Najafi, K. McGrattan, R. Peacock, and A. Hamins. Verification and Validation of Selected Fire Models for Nuclear Power Plant Applications. NUREG 1824, United States Nuclear Regulatory Commission, Washington, D.C., 2007.
36. G. Heskestad. Luminous Heights of Turbulent Diffusion Flames. *Fire Safety Journal*, 5:103–108, 1983.
37. K. McGrattan and B. Toman. Quantifying the predictive uncertainty of complex numerical models. *Metrologia*, 48:173–180, 2011.
38. S. R. Tieszen, T. J. O'Hern, R. W. Schefer, E. J. Weckman, and T. K. Blanchat. Experimental study of the flow field in and around a one meter diameter methane fire. *Combustion and Flame*, 129:378–391, 2002.
39. Stephen B. Pope. *Turbulent Flows*. Cambridge University Press, 2000.
40. J.H. Klote and J.A. Milke. *Principles of Smoke Management*. American Society of Heating, Refrigerating and Air Conditioning Engineers (ASHRAE), Atlanta, GA, 2002.
41. National Fire Protection Association, Quincy, MA. *NFPA 92B, Standard for Smoke Management Systems in Malls, Atria and Large Spaces*, 2005.
42. K.A. Pericleous, D.R.E. Worthington, and G. Cox. The Field Modelling of Fire in an Air-Supported Structure. In *Proceedings of the 2nd International Symposium on Fire Safety Science*, pages 871–880, Tokyo, 1988. Hemisphere Publishing Corporation.
43. G. Cox, S. Kumar, P. Cumber, V. Thomson, and A. Porter. Fire Simulation in the Design Evaluation Process: An Exemplification of the Use of a Computer Field Model. In *Proceedings of the 5th Interflam Conference*, pages 55–66, Canterbury, UK, 1990.
44. S. Kumar and G. Cox. Some Guidance on Correct Use of CFD Models for Fire Applications with Examples. In *Proceedings of Interflam 2001*, pages 823–834, Edinburgh, 2001.
45. S. Simcox and N.S. Wilkes. Computer Simulation of the Flows of Hot Gases from the Fire at King's Cross Underground Station. *Fire Safety Journal*, 18:49–73, 1992.

46. C.C. Hwang and J.C. Edwards. The Critical Ventilation Velocity in Tunnel Fires – A Computer Simulation. *Fire Safety Journal*, 40:213–244, 2005.
47. H. Ingason and A. Lönnermark. Heat Release Rates from Heavy Goods Vehicle Trailer Fires in Tunnels. *Fire Safety Journal*, 40:646–668, 2005.
48. S. Miles and S. Kumar. Computer Modelling to Assess the Benefits of Tunnel Sprinkler and Ventilation Fire Safety Measures. In *Proceedings of 5th International Conference on Tunnel Fires*, pages 23–32, London, 2004. Tunnel Management International.
49. W.L. Grosshandler, N. Bryner, D. Madrzykowski, and K. Kuntz. Report of the Technical Investigation of The Station Nightclub Fire. NIST NCSTAR 2, National Institute of Standards and Technology, Gaithersburg, MD, 2005.
50. K.B. McGrattan, C. Bouldin, and G.P. Forney. Federal Building and Fire Safety Investigation of the World Trade Center Disaster: Computer Simulation of the Fires in the WTC Towers. NIST NCSTAR 1-5F, National Institute of Standards and Technology, Gaithersburg, MD, 2005.
51. D. Madrzykowski and R.L. Vettori. Simulation of the Dynamics of the Fire at 3146 Cherry Road NE, Washington, D.C., May 30, 1999. NISTIR 6510, National Institute of Standards and Technology, Gaithersburg, MD, 2000.
52. D. Madrzykowski and W.D. Walton. Cook County Administration Building Fire: Heat Release Rate Experiments and FDS Simulations. NIST Special Publication 1021, National Institute of Standards and Technology, Gaithersburg, MD, 2004.
53. A.M. Christensen and D.J. Icove. The Application of NIST's Fire Dynamics Simulator to the Investigation of Carbon Monoxide Exposure in the Deaths of Three Pittsburgh Fire Fighters. *Journal of Forensic Sciences*, 49(1):1–4, 2004.
54. N.P. Bryner, S.P. Fuss, B.W. Klein, and A.D. Putorti. Technical Study of the Sofa Super Store Fire - South Carolina, June 18, 2007. NIST Special Publication 1118, National Institute of Standards and Technology, Gaithersburg, MD, 2011.
55. J.S. Turner. *Buoyancy Effects in Fluids*. Cambridge University Press, Cambridge, UK, 1973.
56. H.R. Baum, K.B. McGrattan, and R.G. Rehm. Simulation of Smoke Plumes from Large Pool Fires. In *Proceedings of the 25th (International) Symposium on Combustion*, pages 1463–1469, Pittsburgh, PA, 1994. The Combustion Institute.
57. D.J. O'Connor, E. Cui, M.J. Klaus, C.H. Lee, C. Su, Z. Sun, M. He, Y. Jiang, J. Vythoulkas, and T. Al-Farra. Smoke Detector Performance for Level Ceilings with Deep Beams and Deep Pocket Configurations. Fire Protection Research Foundation report, National Fire Protection Association, Quincy, MA, 2006.
58. C. Mealy, J. Floyd, D. Gottuk, and S. Riahi. Smoke Detector Spacing Requirements for Complex Beamed and Sloped Ceilings. Fire Protection Research Foundation report, National Fire Protection Association, Quincy, MA, 2008.
59. D. Gottuk, C. Mealy, and J. Floyd. Smoke Transport and FDS Validation. In *Fire Safety Science – Proceedings of the 9th International Symposium*, pages 129–140, Karlsruhe, Germany, September 2008. International Association of Fire Safety Science.
60. D. Stroup and R. Wachowiak. Nuclear Power Plant Fire Modeling Analysis Guidelines. NUREG 1934, United States Nuclear Regulatory Commission, Washington, D.C., 2012.

Kevin McGrattan is a mathematician in the Fire Research Division at the National Institute of Standards and Technology in Gaithersburg, Maryland. He is the principal developer of the Fire Dynamics Simulator (FDS)

Stewart Miles, qualified originally as a physicist, is currently a practicing fire engineer at International Fire Consultants Ltd. in the UK. Previously he worked in fire research and engineering at the UK Building Research Establishment, where he contributed to the development of the CFD fire model JASMINE

Enclosure Smoke Filling and Fire-Generated Environmental Conditions

33

Frederick W. Mowrer

Introduction

Fires in buildings and other structures are distinguished from outdoor fires by the confinement effects associated with enclosure boundaries and by the ventilation effects associated with openings in these boundaries. The confinement of heat and smoke released by a fire in an enclosure gives rise to the evolution of fire-generated environmental conditions that can threaten life safety and cause thermal and nonthermal damage to the structure and its contents. For performance-based building fire safety analysis and design, it is important to be able to calculate the environmental conditions generated by fires in enclosures in order to evaluate the threat levels posed by anticipated fire scenarios. This chapter addresses the enclosure smoke-filling process and the fire-generated environmental conditions that develop within an enclosure during this process.

The concept of available safe egress time (ASET) has become a fundamental aspect of performance-based analysis of life safety from fire. In general, life safety from fire is achieved if the required safe egress time (RSET) is shorter than the available safe egress time (i.e., RSET $<$ ASET) for the range of expected fire scenarios. The time it takes to evacuate a space, the RSET, is addressed by Boyce and Gwynne (see Chap. 64) and Gwynne and Rosenbaum (Chap. 59). The available safe egress time is addressed in this chapter in terms of the time it takes for the smoke layer to descend and immerse people located within the fire enclosure and in terms of the hazards associated with fire-generated conditions within the smoke layer.

The control volume, or zone modeling, approach presented by Wade (Chap. 29) is used as the basis for the analyses presented here. A number of explicit equations for evaluating the smoke layer interface position and the average conditions within a smoke layer are presented in this chapter for certain idealized fire scenarios. These closed-form equations, sometimes called "hand calculations" because they can be solved without the aid of a computer, are useful for estimating smoke layer interface position and average smoke layer conditions for the range of applications for which these equations are valid.

For more detailed analyses and for scenarios where hand calculations are impractical or not valid, use of either a computer-based zone model or a computational fluid dynamics (CFD) model may be warranted to evaluate fire-generated conditions in an enclosure. Such computer-based models will generally be needed to evaluate multiroom fire scenarios and may be preferred to evaluate single room scenarios. The concepts presented here are relevant to the computer-based zone fire models, but the complexities associated with keeping track of multiroom fire scenarios are not addressed.

F.W. Mowrer (✉)
Director of Fire Protection Engineering Programs, California Polytechnic State University, San Luis Obispo, CA, USA

M.J. Hurley (ed.), *SFPE Handbook of Fire Protection Engineering*,
DOI 10.1007/978-1-4939-2565-0_33, © Society of Fire Protection Engineers 2016

Computer-based zone models are addressed by Walton, Carpenter, and Wood (see Chap. 31), whereas computer-based CFD models are addressed by McGrattan and Miles (see Chap. 32).

Background

The first efforts to characterize the enclosure smoke-filling process and the environmental conditions generated by a fire in a closed room can be traced to the late 1970s and early 1980s. The seminal paper on this topic was published in 1978 by Zukoski [1], who applied thermodynamic control volume concepts to evaluate mass and energy balances within a closed room subjected to a fire. Shortly thereafter, Cooper applied Zukoski's concepts to develop the available safe egress time (ASET) model [2, 3], a computer-based fire model designed to calculate the evolution of the descending smoke layer interface position and the average temperature and smoke concentration conditions within the smoke layer in response to specified fires. During the early 1980s, Walton [4] converted the original ASET model from FORTRAN to BASIC and simplified the numerical methods used in the model to allow its convenient application on the desktop personal computers that were just then starting to be used in engineering practice; this version of the model was known as ASET-B. Since its original development, various versions of the ASET model have been incorporated into different fire modeling suites, such as FPETOOL [5]. Hurley [6] has compared ASET-B model predictions with large-scale experimental test data.

During the early 1990s, Mowrer [7] addressed the evolution of fire and smoke conditions in a closed room as part of the development of the FIVE Methodology [8] (see Chap. 89) for evaluating fire-induced vulnerabilities in commercial nuclear power plants. Subsequently, Milke and Mowrer [9] expanded this analysis for application to smoke management systems in atria and covered malls. This application has been incorporated into the NFPA 92B, *Standard for Smoke Management Systems in Malls, Atria and Large Spaces* [10] and is discussed further by Milke (see Chap. 51). More recently, Mowrer [11] has revisited the enclosure smoke-filling process, recasting its formulation in terms of the volumetric flow rates generally used for ventilation system design. Mowrer [12] has also addressed the role of mechanical ventilation on smoke filling and management in terms of these volumetric flow rates. Matsuyama et al. [13] and Delichatsios [14] have developed closed-form solutions for enclosure smoke filling, whereas Delichatsios [15] has also addressed tenability conditions and filling times for fires in large spaces.

Stages of Enclosure Fires

Enclosure fires go through a series of stages that depend on the size and shape of the enclosure, the thermal properties of the boundary materials, the sizes and locations of ventilation pathways through the enclosure boundaries, and the development of the fire. Mowrer [11] has identified the four stages of enclosure fires as

- Fire plume/ceiling jet stage
- Enclosure smoke filling stage
- Preflashover vented stage
- Postflashover vented stage

Fire Plume/Ceiling Jet Stage

During the first stage of an enclosure fire, the fire plume/ceiling jet stage, air is entrained into the flame region, where it mixes with fuel being released from the fuel surface and burns, typically in a nonpremixed (diffusion) flame. The energy released by the combustion reaction causes the temperature of the combustion products to increase and their density to decrease. Because these combustion products are less dense than the surrounding air, they rise through the surrounding air in a buoyant coherent stream known as the fire plume, as shown in Fig. 33.1. As the buoyant gases rise in the fire plume, additional air is entrained into the fire

plume, causing the temperature and smoke concentration within the plume to decrease while causing the volume of smoke, which is defined to include the actual combustion products as well as the entrained air, to increase with increasing height above the fire source. Phenomena associated with fire plumes are addressed in more detail by Heskestad (see Chap. 13).

When the fire plume impinges on a smooth horizontal ceiling, the buoyant gases turn and spread out radially beneath the ceiling in a relatively thin layer known as the ceiling jet, as shown in Fig. 33.1. These gases continue to spread radially beneath the ceiling until they are confined by the enclosing walls of the fire room. The impingement of the plume at the ceiling and the confinement of flow beneath the ceiling constitute the first significant distinction between an enclosure fire and an outdoor fire. Ceiling jets are addressed in more detail by Alpert (see Chap. 14).

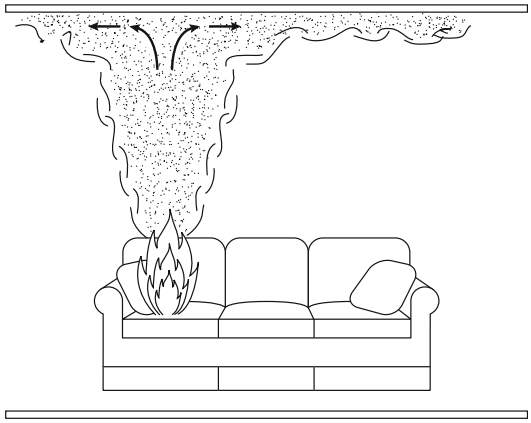

Fig. 33.1 The fire plume/ceiling jet stage of an enclosure fire

Enclosure Smoke-Filling Stage

Once the ceiling jet reaches the wall boundaries, the smoky gases in the ceiling jet turn downward and begin to accumulate beneath the ceiling, as shown in Fig. 33.2. This begins the second stage of enclosure fires, the smoke-filling stage. During the smoke-filling stage, smoke is injected via the fire plume into the developing smoke layer, where the buoyant smoke accumulates beneath the ceiling. The smoke layer interface descends within the enclosure as a result of continued smoke injection via the plume.

If no sizable vents are available in the enclosure boundaries, the smoke layer will continue

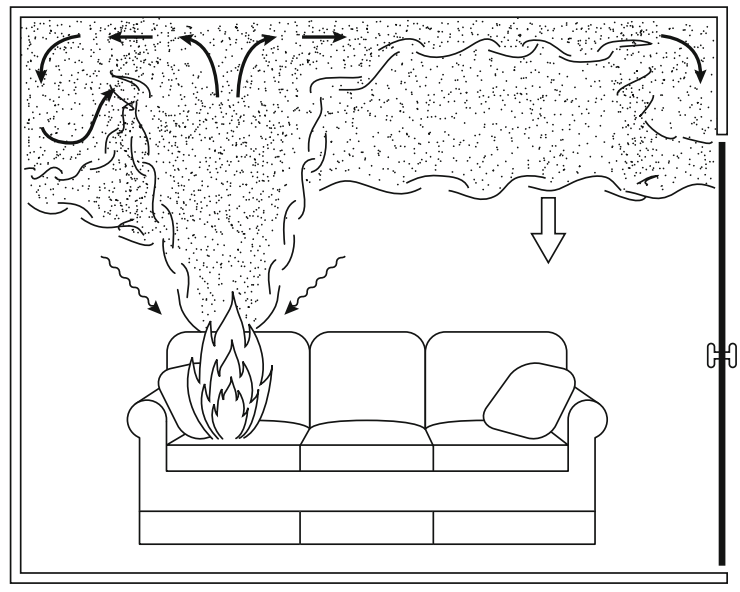

Fig. 33.2 The smoke-filling stage of an enclosure fire

to descend until it reaches either the elevation of the fire source or the floor. Enclosure boundaries in buildings are generally leaky enough to prevent significant pressure increases as a result of the gas expansion associated with enclosure fires. In a closed room, the smoke layer may descend to the level of the fire and act to suppress the fire due to oxygen depletion within the smoke layer, much as a candle flame will extinguish when placed beneath an inverted jar. On the other hand, if a vent is opened, such as a window that breaks from heat-induced stresses or a door that is opened by fire fighters, such a fire may rapidly redevelop due to the influx of fresh air. With an influx of fresh air, a backdraft explosion [16] may occur if sufficient unburned fuel vapors have accumulated within the room.

Preflashover Vented Stage

If one or more open wall vents are provided from the fire space, such as a window to the outside or a doorway to an adjacent space, then the smoke will flow from the enclosure into the adjacent space once the smoke layer descends to the level where a wall vent is available, as illustrated in Fig. 33.3. This begins the third stage of enclosure fires, the preflashover vented stage. During this stage, the smoke layer will descend to the elevation where the flow of air into the fire room is balanced by the flow of smoke out of the fire room. In many cases, both the inflow of air and the outflow of smoke will be through the same wall vent, as illustrated in Fig. 33.3. Vent flows are addressed in more detail by Tanaka (see Chap. 15).

Postflashover Vented Stage

The fourth stage of enclosure fires, the postflashover vented stage, occurs if the fire intensifies to the point where the smoke layer reaches a temperature sufficient to cause the radiant ignition of exposed combustible surfaces within the fire enclosure, as illustrated in Fig. 33.4. Either an average smoke layer temperature of approximately 600 C or an incident heat flux of approximately 20 kW/m [2] at floor level is often used as an indication of the onset of flashover. Methods for estimating the heat release rates necessary to cause flashover and for estimating smoke layer temperatures resulting from pre- and postflashover vented fires are addressed by Walton, Thomas and Ohmiya (see Chap. 30).

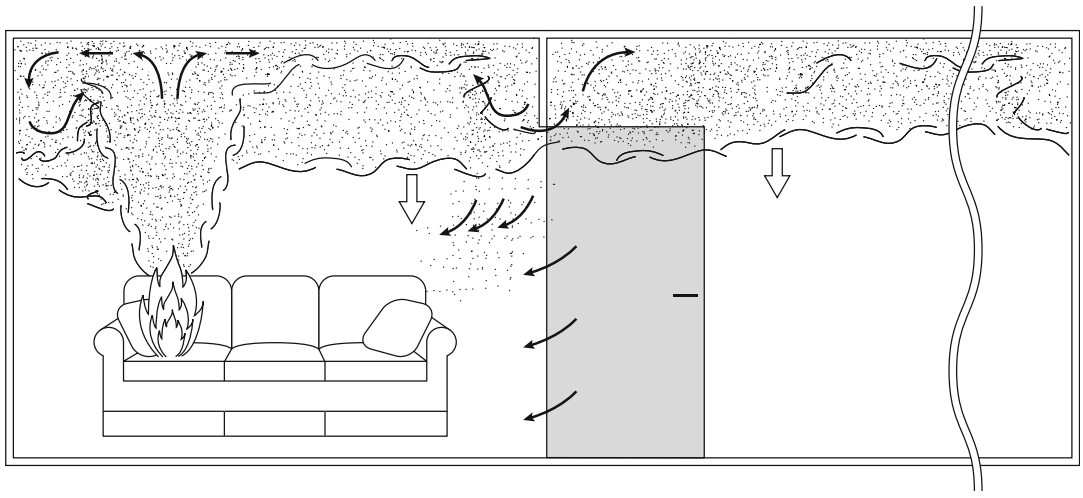

Fig. 33.3 The preflashover vented stage of an enclosure fire

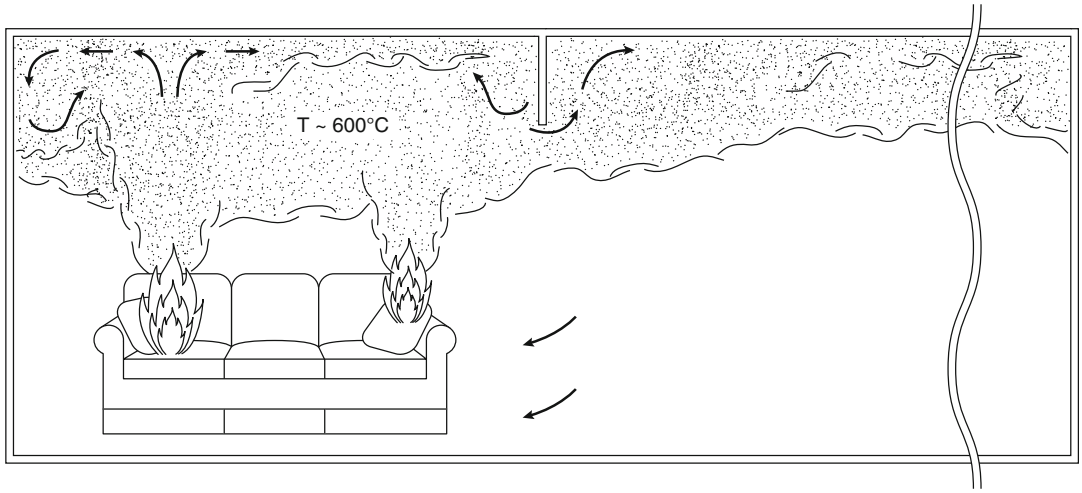

Fig. 33.4 The postflashover vented stage of an enclosure fire

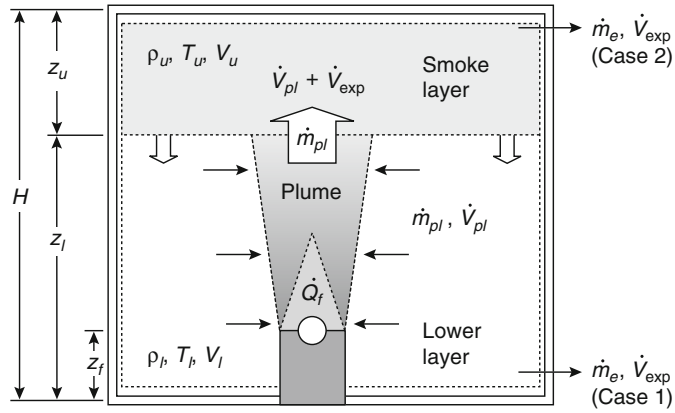

Fig. 33.5 Control volumes and phenomena associated with enclosure smoke filling

Phenomena Associated with Modeling of Enclosure Smoke Filling

Phenomena associated with the modeling of enclosure smoke filling are described in this section. The basic phenomena associated with this stage of enclosure fires are illustrated in idealized form in Fig. 33.5. A fire located at some arbitrary elevation, z_f, above the floor of a room is represented as a point source of heat addition, $\dot{Q}_f$, to the space. A fraction, χ_l, of the heat released by the fire is lost by heat transfer to the boundaries of the enclosure or to other surfaces within the enclosure, while the remaining fraction, $(1 - \chi_l)$, causes heating and expansion of gases within the enclosure. Of the heat released by the fire, a fraction, χ_r, is radiated away from the combustion zone, while the remaining fraction, $\chi_c = 1 - \chi_r$, is convected in the buoyant plume that rises from the fire source to the ceiling.

The plume entrains surrounding air as it rises through the atmosphere. Combustion products and entrained air are transported along with convected heat to the ceiling, where the plume turns to form a ceiling jet that spreads radially beneath the ceiling. When the ceiling jet reaches the wall boundaries of the enclosure, it is deflected downward. For purposes of modeling enclosure smoke filling, it is common to neglect the ceiling jet altogether and to assume that the

enclosure begins to fill uniformly with smoke from the ceiling down due to the injection of smoke into the smoke layer via the fire plume. This is the approach taken here.

The developing smoke layer is normally treated as a distinct control volume with uniform properties for zone modeling purposes. As a modeling idealization, the upper and lower layer control volumes are assumed to be separated by a distinct thermal discontinuity at the interface between the two layers. This interface is known as the smoke layer interface. The smoke layer descends within the enclosure due to the entrainment of fresh air from the lower layer into the fire plume and, depending on the location of leakage paths from the enclosure to surrounding spaces, the expansion of heated gases in the upper layer. Mechanical ventilation will also influence the development of the smoke layer and the conditions within the smoke layer; it is not included in this discussion of general phenomena, but the influence of mechanical ventilation on the development of the smoke layer and the conditions within the smoke layer is addressed in a subsequent section of this chapter.

The expansion of gases within the enclosure due to heat addition pressurizes the enclosure relative to adjacent spaces and forces the flow of gases from the enclosure through available leakage paths. Three different cases are addressed to consider these pressure effects for different leakage flow cases. First, a global analysis is presented where the entire enclosure is treated as a single, fixed control volume assumed to have uniform conditions throughout. The primary purpose of this global analysis is to address pressure effects, but this global analysis is also instructive with respect to temperature and smoke concentration effects, providing a basis for comparison of the more detailed smoke layer descent analyses. This global analysis is followed by two smoke layer descent analyses, designated as Cases 1 and 2, that address the descending smoke layer explicitly in terms of upper and lower layer control volumes. Leakage paths are assumed to be at floor level only in Case 1 and at ceiling level only in Case 2, as illustrated in Fig. 33.5. Case 1 is the scenario addressed by the ASET model [2]. As shown in the subsequent analysis of these two cases, the location of leakage paths does not have a large influence on smoke layer development or conditions.

Once the smoke layer descends to the elevation of the fire source, the fire source becomes immersed in the smoke layer, and further entrainment of fresh air from the lower layer is assumed to cease. After this time, the fire will entrain and recirculate smoke from within the smoke layer, as illustrated in Fig. 33.6, and the smoke layer will continue to descend due only to gas expansion. Because fresh air is no longer being entrained into the fire, the intensity of the fire will eventually diminish due to oxygen depletion within the smoke layer.

As a fire in a closed compartment diminishes due to oxygen depletion, the rate of heat losses to enclosure boundaries will become greater than

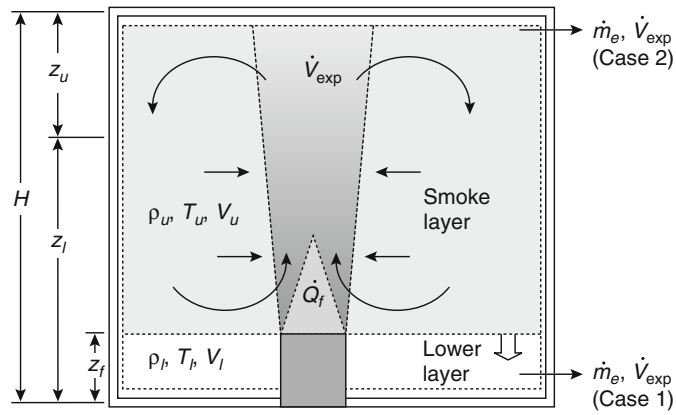

Fig. 33.6 Smoke recirculation associated with smoke layer descent to fuel surface

the rate of heat addition due to the fire. The smoke will cool and contract as a consequence, causing the fire enclosure to depressurize relative to adjacent spaces. This depressurization will draw air into the enclosure from surrounding spaces, which in turn may allow the fire to reintensify and repressurize the enclosure. This cycle of depressurization and repressurization, sometimes called *puffing* behavior, can repeat indefinitely and is one of the warning signs of an underventilated fire, which may result in a backdraft if a large ventilation opening is suddenly provided in an enclosure boundary.

Global (One-Zone) Analysis

In this section, the entire enclosure gas volume is treated as a fixed control volume, as shown in Fig. 33.7. Zukoski [1] addressed the pressure rise that would occur in both sealed and leaky enclosures by considering this global control volume. In both the sealed and leaky cases, a general energy balance for the enclosure control volume can be written as

$$\frac{dU}{dt} = \dot{Q}_{\text{net}} + \dot{m}_i h_i - \dot{m}_o h_o - P\frac{dV}{dt} \qquad (33.1)$$

where U is the total internal energy in the control volume and $\dot{Q}_{\text{net}}$ is the net rate of heat addition into the space; it is equal to the difference between the actual heat release rate of the fire, $\dot{Q}_f$, and the rate of heat loss, $\dot{Q}_l$, to boundaries and other solid surfaces, such as equipment located within the space.

Many fire models calculate boundary heat losses explicitly, usually in terms of one-dimensional heat transfer through a slab. For the present discussion, a constant heat loss fraction, χ_l, is used to represent boundary heat losses, such that

$$\dot{Q}_{\text{net}} = \dot{Q}_f - \dot{Q}_l = \dot{Q}_f(1 - \chi_l) \qquad (33.2)$$

This is the approach taken by Cooper [2, 3], who suggests values for χ_l in the range of 0.6–0.9 for most situations. Cooper suggests that values near the low end of this range are appropriate for spaces with smooth ceilings and large ceiling area to height (A/H^2) ratios. Values near the high end of the range would be appropriate for spaces with irregular ceiling shapes, with small ceiling area to height ratios, or where fires are located near walls. Mowrer [7] found that a value of 0.7 for the heat loss fraction provided good agreement with experimental temperature data for a series of fire tests [17] conducted in a room with a floor area of 223 m^2, a smooth ceiling, an aspect ratio (A/H^2) of 6, and a dimensionless heat release rate, Q^*, defined as

$$Q^* \equiv \dot{Q} / \left(\rho_a c_p T_a \sqrt{gH} H^2\right)$$

of approximately 1.7×10^{-4}.

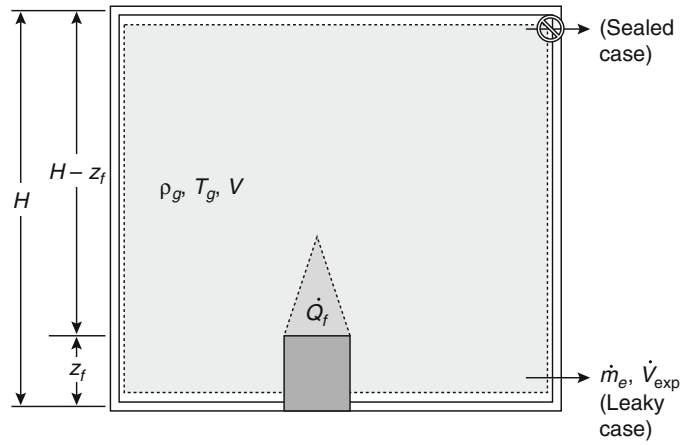

Fig. 33.7 Single control volume and leakage flows used for global analysis

It should be recognized that temperature predictions are sensitive to the selection of the heat loss fraction when using this approach. Because the heat retained in the gas volume is proportional to $(1-\chi_l)$, a seemingly small change in the heat loss fraction from 0.9 to 0.8 represents a twofold difference in the net heat addition term.

Sealed Compartment

Neglecting fuel vapor addition to the enclosure control volume associated with the fire, the mass flow rates into and out of the enclosure are assumed to be nil for the sealed compartment. The volume of the compartment does not change and the total mass within the compartment remains constant. Assuming ideal gas behavior and constant specific heat with properties of air, for the sealed compartment Equation 33.1 reduces to

$$\rho V\frac{du}{dt}=\rho c_v V\frac{dT}{dt}=\frac{c_v V}{R}\frac{dP}{dt}=\dot{Q}_{\text{net}} \tag{33.3}$$

Through manipulation of the ideal gas law, the normalized pressure and temperature rise in a sealed compartment subject to a net change of energy, but without a change in mass or molar quantity, can be expressed as

$$\frac{\Delta P}{P_o}=\frac{\Delta T}{T_o}=\frac{\int_o^t \dot{Q}_{\text{net}}dt}{\rho_o c_v T_o V}=\frac{Q_{\text{net}}}{Q_{o,v}} \tag{33.4}$$

where

$Q_{o,v}(\equiv \rho_o c_v T_o V)$ = Total internal energy of the control volume
P_o = Absolute ambient pressure
T_o = Absolute temperature of the control volume

The product of $\rho_o c_v T_o$ can be treated as a constant with a value of approximately 252 kJ/m^3, assuming air properties at standard temperature and pressure.

Application of Equation 33.4 to representative building fires demonstrates how quickly typical building boundaries would fail due to overpressurization if the boundaries were in fact hermetically sealed to prevent mass flow through enclosure boundaries. The following example illustrates this point. Pressure changes may be a significant issue for fires in airtight vessels, including submarines and space vehicles, but are not usually significant for typical building spaces, which are leaky by nature.

Example 1 Determine the pressure rise and average temperature increase associated with combustion of 1 L of gasoline within a sealed enclosure with dimensions of 10 m by 10 m by 3 m. Assume a heat loss fraction of 0.90. Assuming ordinary window glass can withstand a pressure differential of approximately 1013 Pa (0.01 atm) before failing [18], would this pressure rise be likely to cause window failure?

Solution First, estimate the enthalpy of reaction associated with the gasoline:

$$Q_f=m_f\Delta H_c=\rho_f V_f\Delta H_c=(760\,\text{kg/m}^3)\cdot\left(10^{-3}\text{m}^3\right)\cdot(44{,}000\,\text{kJ/kg})=33{,}440\,\text{kJ}$$

Then, calculate the net heat release associated with the burning of the gasoline:

$$Q_{\text{net}}=Q_f(1-\chi_l)=33{,}440\,\text{kJ}\cdot(1-0.9)=3344\,\text{kJ}$$

Next, calculate the ambient internal energy level associated with the enclosure gases:

$$Q_{o,v}=\rho_o c_v T_o V=\left(252\,\text{kJ/m}^3\right)\cdot\left(300\,\text{m}^3\right)=75{,}600\,\text{kJ}$$

Next, calculate the dimensionless pressure and temperature changes using Equation 33.4:

$$\frac{\Delta P}{P_o} = \frac{\Delta T}{T_o} = \frac{Q_{\text{net}}}{Q_{o,v}} = \frac{3344\ \text{kJ}}{75,600\ \text{kJ}} = 0.044$$

Finally, calculate the dimensional pressure and temperature changes:

$$\Delta P = 0.044 P_o = 0.044(101,325\ \text{Pa}) = 4482\text{Pa}$$

$$\Delta T = 0.044 T_o = 0.044(293\ \text{K}) = 13\ \text{K}$$

Thus, the calculated pressure increase is more than four times the specified pressure differential associated with window breakage, despite the following: the fuel source is only 1 L of gasoline, 90% of the heat release is assumed to be lost to the boundaries, the room volume is relatively large at 300 m^3, and the average temperature change is only 13 K. The fact that such small fires do not routinely cause overpressure failures of enclosure boundaries can be viewed as de facto evidence that real building enclosures are leaky by nature.

Leaky Compartment

For the global analysis of the leaky compartment, the entire enclosure volume is again considered as a fixed control volume, just as it was for the sealed compartment. In this case, the pressure rise in the compartment caused by the release of energy is assumed to force flow out of the enclosure through available leakage paths while at the same time preventing mass flow into the compartment through these same leakage paths. Consequently, for the leaky case, the energy balance expressed by Equation 33.1 reduces to

$$\frac{d(\rho u V)}{dt} = \dot{Q}_{\text{net}} - \dot{m}_o h_o \qquad (33.5)$$

As for the sealed compartment analysis, the left-hand side of Equation 33.5 can be expressed, for an ideal gas, as

$$\frac{d(\rho u V)}{dt} = \frac{c_v V}{R}\frac{dP}{dt} \qquad (33.6)$$

Substituting Equation 33.6 into Equation 33.5 permits the rate of pressure change to be calculated as

$$\frac{dP}{dt} = \frac{R}{c_v V}\left(\dot{Q}_{\text{net}} - \dot{m}_o h_o\right) = \frac{(k-1)}{V}\left(\dot{Q}_{\text{net}} - \dot{m}_o h_o\right) \qquad (33.7)$$

where $k \equiv c_p/c_v$ (≈ 1.4 for air).

Equation 33.7 generally requires numerical solution because the mass outflow term on the right-hand side is a function of the pressure differential between the fire enclosure and surrounding spaces, while the net heat release rate term can vary with time. Zukoski [1] examined the assumption that the rate of pressure change is negligible by comparing the time for the pressure to rise to 86% of its equilibrium value with the time for the smoke layer to descend to the floor. For most scenarios, he found the ratio of these times to be on the order of 10^{-2}; for relatively large fires or relatively small leakage areas, this ratio was on the order of 10^{-1}. Based on this analysis, Zukoski concluded that an assumption of quasi-steady pressure would be satisfactory for most fire scenarios. In all the cases considered by Zukoski, the pressure rise was so small that gas density and pressure were virtually unaffected. This quasi-steady pressure assumption is employed here.

From a practical standpoint, the overall pressure rise relative to atmospheric pressure, $\Delta P/P_o$, is generally very small for fires in leaky enclosures, typically on the order of 10^{-3} to 10^{-5}, depending on the heat addition rate and the area of leakage paths. Pressure differences of this magnitude are significant with respect to the flows they cause through leakage paths in the enclosure boundaries, but can be considered as negligible with respect to the energy equation. Consequently, for most enclosure fire scenarios, the pressure can be treated as quasi-steady (i.e., $dP/dt \to 0$ in Equation 33.7) and the quasi-steady global energy balance for the leaky compartment can then be expressed as

$$\dot{Q}_{\text{net}} = \dot{m}_o h_o = \rho_e c_p T_e \dot{V}_{\text{exp}} \qquad (33.8)$$

Equation 33.8 can be rearranged to solve for the volumetric flow rate of gases from a compartment due to expansion. Using air properties with the customary assumptions of constant specific heat, standard atmospheric pressure, and ideal

gas behavior, this volumetric flow rate caused by expansion can be expressed as

$$\dot{V}_{\exp}\left(\mathrm{m}^3/\mathrm{s}\right) = \frac{\dot{Q}_{\mathrm{net}}}{\rho_e c_p T_e} \cong \frac{\dot{Q}_{\mathrm{net}}(\mathrm{kW})}{353(\mathrm{kJ/m}^3)} \quad (33.9)$$

As illustrated in Figs. 33.5 and 33.6, Equation 33.9 also represents the volumetric expansion rate of the smoke layer.

The quasi-steady pressure rise associated with this volumetric expansion rate can be calculated using classical orifice flow theory as discussed by Tanaka (see Chap. 15):

$$\dot{V}_{\exp} = C_d A_{\mathrm{leak}} v_e = C_d A_{\mathrm{leak}} \sqrt{\frac{2\Delta P}{\rho_e}} \quad (33.10)$$

Equations 33.9 and 33.10 can be combined to solve for the quasi-steady pressure rise, ΔP, within the fire enclosure:

$$\Delta P = \frac{1}{2}\rho_e \left(\frac{\dot{Q}_{\mathrm{net}}}{\left(\rho_e c_p T_e\right) C_d A_{\mathrm{leak}}}\right)^2 \quad (33.11)$$

Equation 33.11 can be used to check the assumption that the pressure rise in a compartment fire is negligible relative to the ambient pressure level.

Example 2 Calculate the volumetric expansion rate and quasi-steady pressure rise that would be associated with a fire with a heat release rate of 500 kW, a heat loss fraction of 0.7, a discharge coefficient of 0.65, and a leakage area of 0.04 m^2. Assume air with a density of 1.20 $\mathrm{kg/m}^3$ is being expelled from the fire room.

Solution First, calculate the net heat release rate:

$$\dot{Q}_{\mathrm{net}} = \dot{Q}_f \cdot (1 - \chi_l) = (500\ \mathrm{kW}) \cdot (1 - 0.7) = 150\ \mathrm{kW}$$

Then, calculate the volumetric expansion rate associated with this net heat release rate:

$$\dot{V}_{\exp} = \frac{\dot{Q}_{\mathrm{net}}}{\rho_e c_p T_e} = \frac{(150\,\mathrm{kW})}{(353\,\mathrm{kJ/m}^3)} = 0.42\ \mathrm{m}^3/\mathrm{s}$$

Finally, calculate the quasi-steady pressure rise associated with this flow rate:

$$\Delta P = \frac{1}{2}\rho_e \left(\frac{\dot{V}_{\exp}}{C_d A_{\mathrm{leak}}}\right)^2 = \frac{(1.2\ \mathrm{kg/m}^3)}{2}\left(\frac{0.42\ \mathrm{m}^3/\mathrm{s}}{(0.65)\,(0.04\ \mathrm{m}^2)}\right)^2 = 157\mathrm{Pa}$$

Thus,

$$\frac{\Delta P}{P_o} = \frac{157\ \mathrm{Pa}}{101,325\ \mathrm{Pa}} \sim O\left(10^{-3}\right)$$

which supports the assumption of negligible effect on the energy equation. Based on measurements of pressure differentials during enclosure fire tests, this is a relatively high pressure differential, suggesting that real enclosures tend to be even more leaky than was assumed for this example.

Temperature Rise

The average temperature rise of the fixed control volume associated with a leaky compartment is considered in this subsection. First, the mass balance for the fixed control volume is introduced, recalling that the pressurization of the control volume caused by heat release from the fire is assumed to prevent mass inflow:

$$\dot{m}_o = -\frac{d(\rho V)}{dt} = -V\frac{d\rho}{dt} \quad (33.12)$$

Substituting Equation 33.12 into Equation 33.8 yields

$$\dot{Q}_{\mathrm{net}} = \dot{m}_o h_o = -c_p T V \frac{d\rho}{dt} \quad (33.13)$$

For an ideal gas at constant pressure, the density is related to the temperature as $\rho = \rho_o T_o / T$. Consequently, the rate of change of density can be related to the rate of temperature change as

$$\frac{d\rho}{dt} = -\frac{\rho_o T_o}{T^2}\frac{dT}{dt} \quad (33.14)$$

Substituting Equation 33.14 into Equation 33.13 yields

$$\dot{Q}_{\mathrm{net}} = \left(\rho_o c_p T_o V\right)\frac{dT}{T dt} = \frac{Q_{o,p}}{T}\frac{dT}{dt} \quad (33.15)$$

The term $Q_{o,p}$ ($\equiv \rho_o c_p T_o V$) is analogous to the $Q_{o,v}$ term for the sealed compartment case; this term represents the ambient enthalpy level for a fixed control volume at constant pressure. Assuming that gases within the control volume have the properties of air, the product of $\rho_o c_p T_o$ can be treated as a constant with a value of approximately 353 kJ/m^3 over the temperature range of interest for preflashover enclosure fires. Equation 33.15 can be rearranged and integrated as

$$\int_0^t \dot{Q}_{\text{net}} dt = Q_{o,p} \int_{T_o}^{T_g} \frac{dT}{T} \tag{33.16}$$

The solution to Equation 33.16 can be expressed in terms of the dimensionless average temperature rise in the fixed control volume:

$$\frac{\Delta T}{T_o} = \exp\left(\frac{Q_{\text{net}}}{Q_{o,p}}\right) - 1 \tag{33.17}$$

where

$Q_{\text{net}} = \int_0^t \dot{Q}_{\text{net}} dt$ = Net energy addition to the control volume as before

T_o = Absolute ambient temperature

The relationship expressed by Equation 33.17 is illustrated in Fig. 33.8.

Equation 33.17 permits calculation of an average temperature rise caused by a fire within an enclosure. Equation 33.17 is particularly useful for fire hazard screening purposes, because it allows thermal hazards to be estimated without the need to track conditions in the descending smoke layer by numerical integration. Global temperatures calculated with Equation 33.17 are compared with smoke layer temperatures for Case 1 and Case 2 descending layer scenarios in a subsequent section of this chapter.

Example 3 Determine the average global temperature rise in an enclosure with dimensions of 18.3 m by 12.2 m by 6.1 m in response to a fire that grows as a *t*-squared fire to a heat release rate of 500 kW in 240 s, then burns at a constant heat release rate of 500 kW for another 360 s. Estimate the average temperature rise within the enclosure at 240 s and at 600 s based on this heat release rate history, assuming a constant heat loss fraction of 0.70 and an ambient temperature of 20 °C (293 K).

Solution First, calculate the net heat release for the two selected times:

$$Q_{\text{net}} = \int_o^t \dot{Q}_{\text{net}} dt = \int_o^t \dot{Q}_f (1 - \chi_l) dt$$

During the period up to 240 s, the fire heat release rate follows the specified *t*-squared

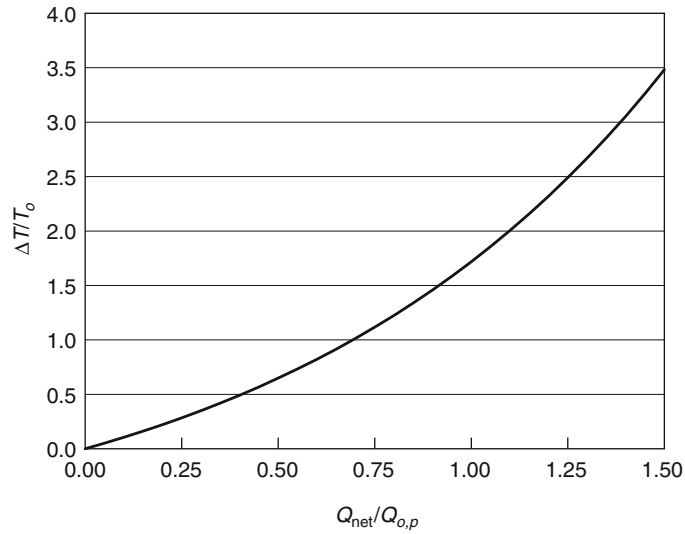

Fig. 33.8 Average dimensionless temperature rise in a closed room as a function of the dimensionless net energy addition

growth, and the net heat release during this period is calculated as

$$Q_{\text{net}}(@240\text{ s}) = \int_o^{240} \left(\frac{500}{(240)^2}\right)(1-0.7)t^2 dt$$
$$= \left(\frac{500}{(240)^2}\right)(0.3)\left(\frac{(240)^3}{3}\right)$$
$$= 12,000\text{ kJ}$$

The net heat release at 600 s is equal to this value plus the net heat release during the period from 240 s to 600 s, when the fire heat release rate is constant:

$$Q_{\text{net}}(@600\text{ s}) = Q_{\text{net}}(@240\text{ s}) + \int_{240}^{600} 500\,(1-0.7)dt$$
$$= 12,000\text{ kJ} + 54,000\text{ kJ}$$
$$= 66,000\text{ kJ}$$

Next, the ambient enthalpy level within the enclosure is calculated:

$$Q_{o,\,p} = \rho_o c_p T_o V = \left(353\text{ kJ/m}^3\right)\cdot\left(1362\text{ m}^3\right)$$
$$= 480,746\text{ kJ}$$

Then, the average dimensionless temperature rise at each time is calculated as

$$\frac{\Delta T}{T_o} = \exp\left(\frac{Q_{\text{net}}}{Q_{o,\,p}}\right) - 1 = \exp\left(\frac{12,000}{480,746}\right) - 1 = 0.025 \text{ at } 240\text{ s}$$

$$\frac{\Delta T}{T_o} = \exp\left(\frac{Q_{\text{net}}}{Q_{o,\,p}}\right) - 1 = \exp\left(\frac{66,000}{480,746}\right) - 1 = 0.147 \text{ at } 600\text{ s}$$

Finally, the dimensional temperature changes are calculated at each time as

$$\Delta T = 0.025 \cdot T_o = 0.025 \cdot 293\text{ K} = 7.3\text{ K at } 240\text{ s}$$

$$\Delta T = 0.147 \cdot T_o = 0.147 \cdot 293\text{ K} = 43.1\text{ K at } 600\text{ s}$$

Note that the ambient enthalpy level has been based on the entire volume of the enclosure, as illustrated in Fig. 33.7, not just on the volume above the fire source, as illustrated in Fig. 33.6. Rather than apply Equation 33.17 based on the entire enclosure volume, it makes sense to consider the fixed control volume defined as the volume between the base of the fire source and the ceiling, as illustrated in Fig. 33.6. Assuming that air entrainment occurs only laterally, this control volume will not have mass inflow across the lower control volume boundary. For this scenario, air entrained into the fire plume is simply recirculated from within the fixed control volume, with some gases forced out of this control volume through its lower face due to expansion. With the smaller control volume defined in this way, the temperature rise expressed by Equation 33.17 will increase more rapidly for elevated fires than if it is based on the entire enclosure volume, assuming the heat loss fraction does not change significantly for elevated fires. This will produce a more conservative estimate of temperature hazards based on application of Equation 33.17.

Example 4 For the previous example, estimate the average temperature rise within the upper layer at the same times (240 s and 600 s) assuming the fire source is located at an elevation of 3.0 m and assuming the same constant heat loss fraction of 0.70. How do these values compare with the results in the previous example?

Solution The only difference in this case compared with the previous example is that the size of the control volume has decreased by a factor of two. Therefore, the ambient enthalpy level within the control volume is calculated as

$$Q_{o,\,p} = \rho_o c_p T_o V = \left(353\text{ kJ/m}^3\right)\cdot\left(681\text{ m}^3\right)$$
$$= 240,373\text{ kJ}$$

For this case, the average dimensionless temperature rise at each time is calculated as

$$\frac{\Delta T}{T_o} = \exp\left(\frac{Q_{\text{net}}}{Q_{o,p}}\right) - 1 = \exp\left(\frac{12,000}{240,373}\right) - 1 = 0.051 \text{ at } 240 \text{ s}$$

$$\frac{\Delta T}{T_o} = \exp\left(\frac{Q_{\text{net}}}{Q_{o,p}}\right) - 1 = \exp\left(\frac{66,000}{240,373}\right) - 1 = 0.316 \text{ at } 600 \text{ s}$$

Finally, the dimensional temperature changes are calculated at each time as

$$\Delta T = 0.051 \cdot T_o = 0.51 \cdot 293 \text{ K} = 14.9 \text{ K at } 240 \text{ s}$$

$$\Delta T = 0.316 \cdot T_o = 0.316 \cdot 293 \text{ K} = 92.6 \text{ K at } 600 \text{ s}$$

Note that these values for the temperature rise are slightly more than twice the respective values in the previous example. The reason for this is that as the smoke layer heats up, more mass is expelled from the smoke layer, leaving less mass within the smoke layer to absorb additional heat input. That is why the temperature relationship expressed by Equation 33.17 increases exponentially with heat input rather than linearly as in the sealed enclosure case, where the mass within the control volume remains constant.

Concentrations of Smoke and Other Species

The conservation of different chemical species (e.g., O_2, N_2, CO_2, CO, H_2O, soot) within a control volume can be expressed generally as

$$\frac{d(mY_i)}{dt} = (\dot{m}_i Y_{i,in}) - (\dot{m}_o Y_i) + \dot{m}_{i,\text{gen}} \quad (33.18)$$

Y_i is the mass fraction of species i within the control volume. For the fixed control volume shown in Fig. 33.7, it is assumed that mass inflow is precluded by pressurization of the enclosure (i.e., this analysis does not address the "puffing" behavior noted previously), so the first term on the right-hand side of Equation 33.18 is negligible. Furthermore, the left-hand side of Equation 33.18 can be expanded to

$$\frac{d(mY_i)}{dt} = m\frac{dY_i}{dt} + Y_i\frac{dm}{dt} = m\frac{dY_i}{dt} - \dot{m}_o Y_i \quad (33.19)$$

The production of a particular species can generally be described in terms of the product of a species yield factor, f_i, by the fuel mass loss rate, $\dot{m}_f$, such that

$$\dot{m}_{i,\text{gen}} = f_i \dot{m}_f = \frac{\dot{Q}_f}{(\Delta H_c / f_i)} \quad (33.20)$$

Equations 33.18, 33.19, and 33.20 can then be combined and simplified to

$$\frac{dY_i}{dt} = \frac{\dot{m}_{i,\text{gen}}}{m_{cv}} = \frac{\dot{m}_{i,\text{gen}}}{(\rho V)_{cv}} = \frac{\dot{Q}_f}{(\rho V)_{cv}(\Delta H_c / f_i)} \quad (33.21)$$

Equation 33.21 applies under scenarios where the fire is fuel limited, such that the heat release rate of the fire can be expressed as $\dot{Q}_f = {}_i\dot{m}_f \Delta H_c$. The term $(\Delta H_c / f_i)$ in Equation 33.21 represents a "species heat of combustion;" it is the quantity of heat released per unit mass of species i produced (or consumed in the case of oxygen). The species heat of combustion can be estimated based on stoichiometry for products of complete combustion (i.e., CO_2 and H_2O) or based on experimental yield data for products of incomplete combustion (i.e., CO and soot). Extensive yield data for a range of fuels is provided by Tewarson

(see Chap. 36). Equation 33.21 can be integrated with appropriate limits to yield

$$(Y_i - Y_{i,o}) = \frac{\int_0^t \dot{Q}_f dt}{(\rho V)_{cv}(\Delta H_c/f_i)} = \frac{Q_f}{(\rho V)_{cv}(\Delta H_c/f_i)} \tag{33.22}$$

$Y_{i,o}$ is the initial mass fraction of species i in the control volume. For most products of combustion, the initial species mass fraction, $Y_{i,o}$, is nil. For this case, the species mass concentration can be expressed as

$$\rho Y_i = \frac{(Q_f/V)}{(\Delta H_c/f_i)} \tag{33.23}$$

where

ρY_i = Mass concentration of species i (kg_i/m^3)
(Q_f/V) = Fire heat release per unit volume of the control volume (kJ/m^3)
$(\Delta H_c/f_i)$ = Species heat of combustion (kJ/kg_i)

Example 5 Assume propylene (C_3H_6) is the fuel burned in the previous examples. Assume propylene has a heat of combustion of 46.4 MJ/kg of fuel and a soot yield of 0.095 g of soot per g of fuel. Estimate the average mass concentration of soot within the 18.3 m by 12.2 m by 6.1 m enclosure at 240 s and 600 s after ignition of a fire that grows as a t-squared fire to a heat release rate of 500 kW in 240 s, then burns at a constant heat release rate of 500 kW for another 360 s.

Solution First, calculate the fire heat released up to the 240 s and 600 s times, respectively:

$$\begin{aligned} Q_f(@240\text{ s}) &= \int_o^{240} \left(\frac{500}{(240)^2}\right) t^2 dt \\ &= \left(\frac{500}{(240)^2}\right)\left(\frac{(240)^3}{3}\right) \\ &= 40,000\text{ kJ} \end{aligned}$$

$$\begin{aligned} Q_f(@600\text{ s}) &= Q_f(@240\text{ s}) + \int_{240}^{600} 500\, dt \\ &= 40,000\text{ kJ} + 180,000\text{ kJ} \\ &= 220,000\text{ kJ} \end{aligned}$$

The volume of the space is calculated as 18.3 m × 12.2 m × 6.1 m = 1362 m^3. Therefore, the heat release per unit volume is calculated at each time as

$$Q_f/V(@240\text{ s}) = 40,000\text{ kJ}/1382\text{ m}^2 = 28.9\text{kJ/m}^3$$
$$Q_f/V(@600\text{ s}) = 220,000\text{ kJ}/1382\text{ m}^2 = 159.2\text{ kJ/m}^3$$

The species heat of combustion is calculated from the given data as

$$\Delta H_c/f_i = \frac{46.4\text{ MJ/kg}_f}{0.095\text{ kg}_{soot}/\text{kg}_f} = 488.42\text{ MJ/kg}_{soot}$$

Finally, the soot mass concentration at each time is calculated as

$$\begin{aligned} \rho Y_{soot}(@240\text{ s}) &= \frac{28.9\text{ kJ/m}^3}{488.42\times10^3\text{ kJ/kg}_{soot}} \\ &= 5.92\times10^{-5}\text{ kg}_{soot}/\text{m}^3 \\ \rho Y_{soot}(@600\text{ s}) &= \frac{159.2\text{ kJ/m}^3}{488.42\times10^3\text{ kJ/kg}_{soot}} \\ &= 3.26\times10^{-4}\text{ kg}_{soot}/\text{m}^3 \end{aligned}$$

As discussed in a subsequent subsection, the visibility through smoke can be related directly to the soot mass concentration.

For oxygen in air under standard conditions, the initial species mass fraction is $Y_{i,o} = 0.233$ and the species heat of combustion can be taken as the well-known "oxygen heat of combustion," for a wide range of representative fuels, with a value of approximately $\Delta H_c/f_{O_2} = -13,100\text{ kJ}/kg_{O_2}$, where the negative sign indicates that oxygen is consumed rather than produced in the combustion reaction. For these values, the oxygen mass fraction within the fixed control volume can be estimated as

$$\begin{aligned} Y_{O_2} &= Y_{O_2,o} + \frac{Q_f}{\rho V(\Delta H_c/f_{O_2})} \\ &= 0.233 - \frac{(Q_f/V)}{(13,100)\rho} \end{aligned} \tag{33.24}$$

Example 6 Assume propylene (C_3H_6) is the fuel burned in the previous examples. Assume propylene has a heat of combustion of 46.4 MJ/kg of

fuel and a soot yield of 0.095 g of soot per g of fuel. Estimate the average oxygen mass fraction within the 18.3 m by 12.2 m by 6.1 m enclosure at 240 s and 600 s after ignition of a fire that grows as a *t*-squared fire to a heat release rate of 500 kW in 240 s, then burns at a constant heat release rate of 500 kW for another 360 s.

Solution From the previous example, the fire heat released up to the 240 s and 600 s times is, respectively:

$$\begin{aligned} Q_f(@240\text{ s}) &= \int_o^{240} \left(\frac{500}{(240)^2}\right) t^2 dt \\ &= \left(\frac{500}{(240)^2}\right)\left(\frac{(240)^3}{3}\right) \\ &= 40,000\text{ kJ} \\ Q_f(@600\text{ s}) &= Q_f(@240\text{ s}) + \int_{240}^{600} 500\, dt \\ &= 40,000\text{ kJ} + 180,000\text{ kJ} \\ &= 220,000\text{ kJ} \end{aligned}$$

The volume of the space was calculated as 18.3 m × 12.2 m × 6.1 m = 1362 m^3 and the heat release per unit volume was calculated at each time as

$$Q_f/V(@240\text{ s}) = 40,000\text{ kJ}/1382\text{m}^3 = 28.9\text{ kJ/m}^3$$
$$Q_f/V(@600\text{ s}) = 220,000\text{ kJ}/1382\text{m}^3 = 159.2\text{ kJ/m}^3$$

The oxygen heat of combustion is assumed to be

$$\Delta H_c/f_i = -13,100\text{ kJ/kgO}_2$$

The average temperature in the enclosure was previously calculated at each time to be

$$T = T_o + \Delta T = 293\text{ K} + 14.9\text{ K} = 307.9\text{ K at 240 s}$$
$$(\text{so } \rho = \rho_o T_o/T = 353/307.9 = 1.15\text{kg/m}^3)$$
$$T = T_o + \Delta T = 293\text{ K} + 92.6\text{ K} = 385.6\text{ K at 600 s}$$
$$(\text{so } \rho = \rho_o T_o/T = 353/385.6 = 0.92\text{kg/m}^3)$$

Finally, the oxygen mass fraction at each time is calculated as

$$Y_{O_2}(@240\text{ s}) = 0.233 - \frac{(28.9)}{(13,100)\,(1.15)} = 0.231$$
$$Y_{O_2}(@240\text{ s}) = 0.233 - \frac{(159.9)}{(13,100)\,(0.92)} = 0.220$$

Thus, for these examples, the oxygen concentration is relatively close to the ambient concentration and consequently would not be expected to have a significant effect on the fire heat release rate. As discussed in the following subsection, however, this is not always the case.

Oxygen Limitations on Heat Release in a Closed Room Fire

There is a limit to how much heat can be released by combustion within a closed room because the release of heat is coupled with consumption of a finite amount of oxygen from the air in the enclosure. It is assumed that oxygen does not enter from outside due to pressurization of the compartment, so the fire must eventually die down due to oxygen depletion, much like the familiar candle flame trapped inside an inverted jar. Equation 33.17 will result in nonphysical and incredible temperatures if applied indefinitely because it does not account for the effect of oxygen depletion on limiting heat release within an enclosed space.

Mowrer [11] has addressed the issue of oxygen limitations on heat release in unventilated enclosure fires. The heat released by combustion in a room fire is related directly to the oxygen consumed. This relationship can be expressed as

$$Q_{f,\lim} = \frac{Q_{o,p}}{(1-x_l)} \ln\left[1 + \frac{\rho_o V}{Q_{o,p}} \frac{\Delta H_c}{r_{air}} \chi_{O_2,\lim}(1-\chi_l)\right] \tag{33.25}$$

Equation 33.25 can be inserted into Equation 33.17 to yield the limiting temperature rise associated with the oxygen-limited heat release in an enclosure:

$$\Delta T_{g,\lim} = \frac{\Delta H_c}{r_{air}} \frac{\chi_{O_2,\lim}(1-\chi_l)}{c_p} \tag{33.26}$$

where $\chi_{O_2,\lim}$ represents the fraction of oxygen that can be consumed before extinction; it is given in general as

$$\chi_{O_2,\lim} = \frac{\left(Y_{O_{2_o}} - Y_{O_2,\lim}\right)}{Y_{O_{2_o}}} = \frac{\left(X_{O_{2_o}} - X_{O_2,\lim}\right)}{X_{O_{2_o}}} \tag{33.27}$$

$\chi_{O_2,\lim}$ is normally evaluated at a limiting extinction value of X_{O_2} or Y_{O_2}. A representative value for X_{O_2} at extinction under normal ambient conditions is approximately 13% for a range of hydrocarbon fuels when the oxygen is diluted with nitrogen (see Chap. 17). For an ambient oxygen mole fraction $X_{O_{2,0}}$ of 21%, a representative value for $\chi_{O_2,\lim}$ would therefore be about 0.4.

Example 7 Determine the oxygen-limited average temperature rise in an enclosure fire for heat loss fractions of 0.6 and 0.9, respectively. Assume a value of $\chi_{O_2,\lim} = 0.4$.

Solution

$$\Delta T_{g,\lim} = \frac{3000(\text{kJ/kg})}{1.0(\text{kJ/kg}\cdot\text{K})}\cdot 0.4\cdot(1-0.6) = 480\ \text{K for}\ \chi_l = 0.6$$

$$\Delta T_{g,\lim} = \frac{3000(\text{kJ/kg})}{1.0(\text{kJ/kg}\cdot\text{K})}\cdot 0.4\cdot(1-0.9) = 120\ \text{K for}\ \chi_l = 0.9$$

Although these temperatures are potentially significant from a thermal injury or damage standpoint, they are below the temperature rise of approximately 580 K commonly associated with flashover conditions. This simple analysis suggests the difficulty of attaining flashover conditions in an unventilated, fully enclosed compartment fire. Lower heat loss fractions and higher oxygen consumption fractions would be needed to achieve temperature increases associated with flashover. On the other hand, these calculated global temperature increases might be sufficient to cause the fracture and collapse of ordinary plate glass windows [19–21] if present, providing new pathways for the introduction of oxygen to the enclosure and consequent escalation of the fire intensity.

Light Attenuation and Visibility Through Smoke

Light attenuation and visibility through smoke can be estimated based on the soot mass concentration within the smoke layer. The light extinction coefficient, K, is directly proportional to the soot mass concentration as

$$K = K_m \rho Y_{\text{soot}} \tag{33.28}$$

K_m is the specific light extinction coefficient. Seader and Einhorn [22] suggested a value of $K_m = 7600\ \text{m}^2/\text{kg}$ for flaming combustion and $K_m = 4400\ \text{m}^2/\text{kg}$ for smoke produced by pyrolysis. These values have been widely used for light attenuation and visibility calculations, but more recently Mulholland and Croarkin [23] have suggested a value of $K_m = 8700\ \text{m}^2/\text{kg}$ for flaming combustion of wood and plastic fuels.

Light attenuation within the smoke layer is calculated in accordance with Bougher's law for monochromatic light:

$$I/I_o = \text{e}^{-KL} \tag{33.29}$$

Visibility through smoke is expected to vary inversely with the light extinction coefficient, with this inverse relationship generally expressed as

$$\text{S} = \text{C}/K \tag{33.30}$$

where

S = Visibility distance (m)
C = Nondimensional constant associated with the object being viewed through the smoke

Mulholland [24] suggests a value of $C = 8$ for light-emitting signs and a value of $C = 3$ for light-reflecting signs based on the work of Jin (see Chap. 61). These values suggest that light-emitting signs can be observed when the light attenuation is $I/I_o = \text{e}^{-8} = 3.35 \times 10^{-4}$, that is, the transmitted light is much less than 1% of the unattenuated light intensity; whereas

light-reflecting signs can be observed when the light attenuation is $I/I_o = e^{-8} = 0.05$, that is, the transmitted light is reduced to 5% of the unattenuated light level.

Example 8 Estimate the visibility of a light-reflecting sign through the smoke layer based on the soot mass concentrations determined in a previous example.

Solution For this example, the soot mass concentration at each time was calculated to be

$$\rho Y_{soot}(@240\text{ s}) = \frac{28.9\text{ kJ/m}^3}{488.42 \times 10^3\text{ kJ/kg}_{soot}} = 5.92 \times 10^{-5}\text{ kg}_{soot}/\text{m}^3$$

$$\rho Y_{soot}(@600\text{ s}) = \frac{159.2\text{ kJ/m}^3}{488.42 \times 10^3\text{ kJ/kg}_{soot}} = 3.26 \times 10^{-4}\text{ kg}_{soot}/\text{m}^3$$

Using these values of soot mass concentration along with the specific light extinction coefficient of 8700 m^2/kg suggested by Mulholland and Croarkin, the extinction coefficient is determined to be

$$K(@240\text{ s}) = K_m \rho Y_{soot} = (8700\text{ m}^2/\text{kg}_{soot}) \times \left(5.92 \times 10^{-5}\text{kg}_{soot}/\text{m}^3\right) = 0.52\text{ m}^{-1}$$

$$K(@600\text{ s}) = K_m \rho Y_{soot} = (8700\text{ m}^2/\text{kg}_{soot}) \times \left(3.26 \times 10^{-4}\text{kg}_{soot}/\text{m}^3\right) = 2.83\text{ m}^{-1}$$

The visibility distance for a light-reflecting sign is then estimated at each time as

$$S\ (@240\text{ s}) = 3/0.52\text{ m}^{-1} = 5.8\text{ m (19.0 ft)}$$

$$S\ (@600\text{ s}) = 3/2.83\text{ m}^{-1} = 1.1\text{ m (3.6 ft)}$$

This concludes the global analysis of fire-induced conditions in a closed room. In the next section, methods to analyze fire-induced conditions within the descending smoke layer are addressed. These can then be compared with the global analysis results presented in this section.

Descending Smoke Layer Analysis

In this section, the descending smoke layer is treated as a distinct control volume, as illustrated in Fig. 33.5. Two limit cases are addressed based on the location of leakage paths in the enclosure boundaries, following the approach originally taken by Zukoski [1]:

- Case 1—Leakage paths near the floor (from the lower layer)
- Case 2—Leakage paths near the ceiling (from the upper layer)

In Case 1, the expansion of gases in the upper layer pushes fresh air at ambient temperature from the lower layer until the smoke layer descends to the floor. At that point, smoke at the upper layer temperature and composition would be expelled and the analysis would be the same as for Case 0, the global analysis presented in the previous section. The Case 1 scenario is the case addressed by Cooper [2, 3] in the development of the ASET model. In Case 2, the expansion of gases from the compartment is assumed to occur directly from the upper layer. Cooper does not address this scenario, but, as demonstrated by the following analysis, the differences between the two scenarios are minor.

Mass balances on the lower layer for the respective cases can be written as

$$\text{Case 1}: \quad \frac{d(\rho V)_l}{dt} = \rho_l \frac{dV_l}{dt} = -\left(\dot{m}_{pl} + \dot{m}_e\right) \tag{33.31}$$

$$\text{Case 2}: \quad \frac{d(\rho V)_l}{dt} = \rho_l \frac{dV_l}{dt} = -\left(\dot{m}_{pl}\right) \tag{33.32}$$

These mass balances for the lower layer can be converted to volumetric filling rates for the upper layer by noting that $dV_u = -dV_l$ and by dividing through by the lower layer density, ρ_l , assumed to remain constant at the ambient air density.

$$\text{Case 1}: \quad \frac{dV_u}{dt} = \frac{\left(\dot{m}_{pl} + \dot{m}_e\right)}{\rho_l} = \left(\dot{V}_{pl} + \dot{V}_{\exp}\right) \tag{33.33}$$

$$\text{Case 2}: \quad \frac{dV_u}{dt} = \frac{\left(\dot{m}_{pl}\right)}{\rho_l} = \dot{V}_{pl} \tag{33.34}$$

Equations 33.33 and 33.34 show that the volumetric growth rate of the smoke layer is due to both plume entrainment and gas expansion in Case 1 and due to entrainment only in Case 2. This difference occurs because the expanding gases are being expelled directly from the smoke layer rather than the lower layer in Case 2, and consequently gas expansion does not contribute to smoke layer development in Case 2.

The rate of smoke layer descent for the two cases derives directly from Equations 33.33 and 33.34 by noting that $dV_u = A_s dz_u$. For rooms with vertical walls and horizontal ceilings, the horizontal area of the space, A_s, remains constant with height, assuming no physical obstructions are located within the space. In general, Equation 33.33 must be integrated numerically to determine the smoke layer interface position as a function of time because analytical solutions do not exist for most realistic scenarios. Equation 33.34 does have an analytical solution for the case of a power law fire, where the fire heat release rate is assumed to vary with time as

$$\dot{Q}_f = \alpha_n t^n$$

and axisymmetric plume entrainment [25], where the plume volumetric flow rate varies as

$$\dot{V}_{pl} = k_v \dot{Q}_c^{1/3} z^{5/3}$$

For these conditions, Equation 33.34 can be rearranged and expressed as

$$\int_0^{z_u} \frac{dz_u}{(H - z_u)^{5/3}} = \frac{k_v}{A_s} \int_0^t (\alpha_n t^n)^{1/3} dt \tag{33.35}$$

The solution to Equation 33.35 can be expressed nondimensionally as

$$\frac{z_u}{H} = 1 - \left[1 + \frac{2t}{(n+3)\tau_V}\right]^{3/2} \tag{33.36}$$

where

$$\tau_V = \frac{V}{\dot{V}_{pl,H}} = \frac{A_s H}{k_v \dot{Q}_c^{1/3} H^{5/3}} = \frac{\left(A_s/H^2\right)}{\left(k_v (\alpha_n t^n)^{1/3}/H^{4/3}\right)} \tag{33.37}$$

τ_V is a characteristic smoke filling time constant, represented as the volume above the fire source divided by the volumetric entrainment rate evaluated at the ceiling height. Note that this *time constant* is actually only constant in the case of a steady fire ($n = 0$). The elevation of the smoke layer interface above the fire source derives directly from Equation 33.36:

$$\frac{z_L}{H} = 1 - \frac{z_u}{H} = \left[1 + \frac{2t}{(n+3)\tau_V}\right]^{-3/2} \tag{33.38}$$

The solution represented by Equation 33.38 is shown in Fig. 33.9 for the cases of a steady fire ($n = 0$) and a t-squared fire ($n = 2$). This solution is also approximately accurate for Case 1 scenarios where $\dot{V}_{pl} \gg \dot{V}_{\exp}$, such that $\dot{V}_{pl} + \dot{V}_{\exp} \approx \dot{V}_{pl}$.

Qualitatively, Fig. 33.9 illustrates the fact that smoke layer descent is initially very rapid, then slows down and asymptotically approaches the fuel surface. This is because the air entrainment rate for axisymmetric plumes varies with the 5/3 power of the elevation between the fuel surface and the smoke layer interface. As the smoke layer descends, the plume entrains less and less air, causing the descent rate to slow down as shown in Fig. 33.9.

The nondimensional representation of smoke layer descent given in Equation 33.38 and shown in Fig. 33.9 is useful to generalize the smoke layer descent analysis, but is not as useful for the computation of specific fire scenarios. This is particularly so for the case of growing t-squared fires because the characteristic time constant given in Equation 33.37 is a function of time for cases other than steady fires (i.e., other than when $n = 0$). For such computations it is more useful to represent the smoke layer descent in dimensional terms. To calculate the time for the

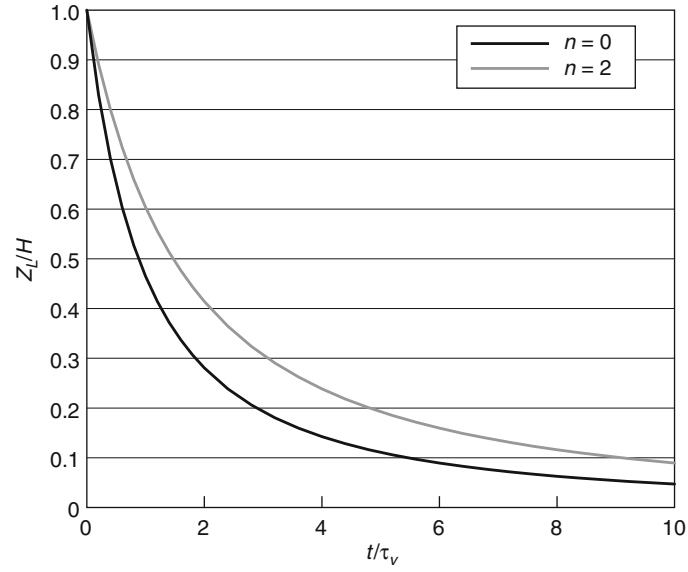

Fig. 33.9 Relative smoke layer interface position as a function of normalized time due to entrainment only in an axisymmetric fire plume

smoke layer to reach a particular elevation relative to the fuel to ceiling distance (z_L/H) for a t-squared fire, Equation 33.37 is substituted into Equation 33.38 and the resulting equation is solved for t. The result is

$$t = \left\{ \frac{(n+3)}{2} \frac{(A_s/H^2)H^{4/3}}{k_v \alpha_n^{1/3}} \left[\left(\frac{z_L}{H} \right)^{-2/3} - 1 \right] \right\}^{1/(1+n/3)} \tag{33.39}$$

Similarly, for a t-squared fire, the relative smoke layer elevation can be expressed explicitly as a function of time as

$$\frac{z_L}{H} = \left[1 + \frac{2k_v \alpha_n^{1/3} t^{(5/3)}}{5(A_s/H^2)H^{4/3}} \right]^{-3/2} \tag{33.40}$$

Example 9 For the previous enclosure fire example, determine how long it would take for the smoke layer interface to descend to elevations of 3.0 m and 1.5 m above the floor for the 6.0-m-high enclosure.

Solution For this example, the enclosure area is $A_s = 18.3\ \text{m} \times 12.2\ \text{m} = 223.3\ \text{m}^2$ and the enclosure height above the fire source is $H = 6.0$ m. The fire grows as a t-squared fire to reach a heat release rate of 500 kW in 240 s, then remains constant at 500 kW for an additional 360 s. Thus, during the growth stage,

$$\alpha_n = \frac{500\ \text{kW}}{(240\ \text{s})^2} = 8.68 \times 10^{-3} \text{kW/s}^2$$

and $n = 2$. Assuming an axisymmetric plume, the entrainment coefficient is taken to be

$$k_v = 0.064\ \text{m}^{4/3}/\text{kW}^{1/3} - s$$

For the smoke layer interface elevation of 3.0 m, the relative smoke layer interface elevation is

$$\frac{z_L}{H} = \frac{3.0\ \text{m}}{6.0\ \text{m}} = 0.5$$

Substituting these values into Equation 33.39 yields the time for the smoke layer to reach the 3.0 m elevation in the enclosure:

$$\text{t}(3.0\ \text{m}) = \left\{ \frac{2+3}{2} \frac{\left(223.3/6.0^2 \times 6.0^{4/3}\right)}{0.064 \times \left(8.68 \times 10^{-3}\right)^{1/3}} \left[\left(\frac{3.0}{6.0} \right)^{-2/3} - 1 \right] \right\}^{1/(1+2/3)}$$
$$= 212\ \text{s}$$

Because this time is less than the growth time of 240 s, the smoke layer will descend to the 3.0 m elevation during the growth period. From this analysis, it appears likely that the fire will stop growing before the smoke layer descends to the 1.5 m elevation. This can be confirmed by substituting this elevation of 1.5 m into Equation 33.39:

$$\begin{aligned} t(1.5\text{ m}) &= \left\{ \frac{(2+3)}{2} \frac{\left(223.3/6.0^2\right) \cdot 6.0^{4/3}}{0.064 \cdot \left(8.38 \times 10^{-3}\right)^{1/3}} \left[\left(\frac{1.5}{6.0} \right)^{-2/3} - 1 \right] \right\}^{1/(1+2/3)} \\ &= 375\text{ s} \end{aligned}$$

Because the fire stops growing at 240 s, it is necessary to apply Equation 33.40 to determine the smoke layer interface position at the end of the growth period, then use this elevation as the enclosure height H in Equation 33.39 to determine the additional time needed for the smoke layer interface to reach the 1.5 m elevation as a result of the steady 500 kW fire. Applying Equation 33.40 with a time of 240 s yields

$$\begin{aligned} \frac{z_L}{H}(@240\text{ s}) &= \left[1 + \frac{2(0.064)\left(8.68 \times 10^{-3}\right)^{1/3} 240^{(1+2/3)}}{(2+3)\left(223.3/6.0^2\right)6.0^{4/3}} \right]^{-3/2} \\ &= 0.44 \\ z_L(@240\text{ s}) &= 0.44 \cdot H = 0.44 \cdot 6.0 = 2.64\text{ m} \end{aligned}$$

This value then becomes the starting height (i.e., H) for the steady fire following 240 s:

$$\begin{aligned} t(1.5\text{ m}) &= 240 + \left\{ \frac{0+3}{2} \frac{\left(223.3/2.64^2 \times 2.64^{4/3}\right)}{0.064 \times (500)^{1/3}} \left[\left(\frac{1.5}{2.64} \right)^{-2/3} - 1 \right] \right\}^{1/(1+0/3)} \\ &= 240 + 159 = 399\text{ s} \end{aligned}$$

In other words, the smoke layer interface reaches the 2.64 m elevation at the end of the 240-s fire growth period, then takes another 159 s to reach the 1.5 m elevation during the ensuing steady fire period.

Conditions in the Descending Smoke Layer

The average temperature in the smoke layer is calculated by invoking the ideal gas law relationship for a constant pressure process, $\rho_o T_o = \rho_u T_u$,

and by noting that the average smoke layer density, ρ_u, is simply the mass of the upper layer divided by the volume of the upper layer. For the two cases, the average temperature of the upper layer is then evaluated as
Case 1:

$$T_u(t) = \frac{\rho_l T_l}{\rho_u} = \frac{\rho_l T_l V_u}{m_u} = \rho_l T_l \left(\frac{\int_o^t \frac{dV_u}{dt} dt}{\int_o^t \frac{dm_u}{dt} dt} \right) = T_l \frac{\int_o^t \left(\dot{V}_{pl} + \dot{V}_{\exp} \right) dt}{\int_o^t \dot{V}_{pl} dt} \tag{33.41}$$

Case 2:

$$T_u(t) = \frac{\rho_l T_l}{\rho_u} = \frac{\rho_l T_l V_u}{m_u} = \rho_l T_l \left(\frac{\int_o^t \frac{dV_u}{dt} dt}{\int_o^t \frac{dm_u}{dt} dt} \right) = \frac{\rho_l T_l \int_o^t \left(\dot{V}_{pl} \right) dt}{\int_o^t \left(\rho_l \dot{V}_{pl} - \rho_u \dot{V}_{\exp} \right) dt} \tag{33.42}$$

The mass fraction of oxygen in the smoke layer is calculated for the two cases as
Case 1:

$$Y_{O_2,u}(t) = \frac{m_{O_2,u}}{m_u} = \frac{\int_o^t \left[\left(\rho_l \dot{V}_{pl} Y_{O_2,o} \right) - \left(\frac{\dot{Q}_f}{\Delta H_c / r_{O_2}} \right) \right] dt}{m_u} \tag{33.43}$$

Case 2:

$$Y_{O_2,u}(t) = \frac{m_{O_2,u}}{m_u} = \frac{\int_0^t \left[\left(\rho_l \dot{V}_{pl} Y_{O_2,o} \right) - \left(\frac{\dot{Q}_f}{\Delta H_c / r_{O_2}} \right) - \left(\rho_u \dot{V}_{\exp} Y_{O_2,u} \right) \right] dt}{m_u} \tag{33.44}$$

The mass fractions of different products of combustion in the smoke layer are calculated for the two cases as
Case 1:

$$Y_{i,u}(t) = \frac{m_{i,u}}{m_u} = \frac{\int_0^t \left[\left(\rho_l \dot{V}_{pl} Y_{i,o} \right) + \left(\frac{\dot{Q}_f}{\Delta H_c / f_i} \right) \right] dt}{m_u} \tag{33.45}$$

Case 2:

$$Y_{i,u}(t) = \frac{m_{i,u}}{m_u} = \frac{\int_0^t \left[\left(\rho_l \dot{V}_{pl} Y_{i,0} \right) - \left(\frac{\dot{Q}_f}{\Delta H_c / f_i} \right) - \left(\rho_u \dot{V}_{\exp} Y_{i,u} \right) \right] dt}{m_u} \tag{33.46}$$

The denominators in Equations 33.43 through 33.46 are evaluated in the same way as in Equations 33.41 and 33.42, respectively. In general, Equations 33.41 through 33.46 do not have analytical solutions and therefore require numerical integration. Numerical methods are discussed in a subsequent section.

Influence of Mechanical Ventilation on Smoke Layer Conditions

The introduction of mechanical ventilation changes the analysis of enclosure smoke filling in a number of ways. As illustrated in Fig. 33.10, with mechanical ventilation, flow may be injected into or extracted from either the upper layer or the lower layer. This will depend on the type of mechanical ventilation system employed, the elevations of injection and extraction vents, and the elevation of the smoke layer interface at a particular time. Smoke layer descent may be either accelerated or retarded relative to the unventilated scenario as a result of mechanical ventilation. Conditions within the smoke layer will also be affected. A quasi-steady smoke layer interface position will develop if the flow rates balance properly. Indeed, the purpose of a dedicated mechanical smoke extraction system is normally to prevent the smoke layer interface position from descending past a certain elevation within a space, for example, to prevent smoke from reaching the highest elevation of human occupancy.

Global Effects of Mechanical Ventilation

Global conditions within a mechanically ventilated enclosure are first considered in terms of a one-zone analysis, as illustrated in Fig. 33.11. This global analysis assumes that conditions throughout the enclosure can be treated as uniform outside the fire-plume/ceiling-jet sublayer as a result of mixing caused by the mechanical ventilation and plume entrainment. One-zone approaches have been used previously to evaluate average fire conditions in mechanically ventilated spaces [7, 26–28].

Volumetric flow rates associated with a fire in a mechanically ventilated enclosure are illustrated in Figs. 33.10 and 33.11. Because the total volume of the enclosure remains essentially constant, the rate at which flow is forced through leakage paths in the boundaries of the enclosure can be expressed as

$$\dot{V}_{\text{net}} = \dot{V}_{\text{inj}} + \dot{V}_{\text{exp}} - \dot{V}_{\text{ext}} \tag{33.47}$$

$\dot{V}_{\text{net}}$ can be either positive or negative, depending on the values for the terms on the right-hand side (RHS) of Equation 33.47. As defined here, $\dot{V}_{\text{net}}$

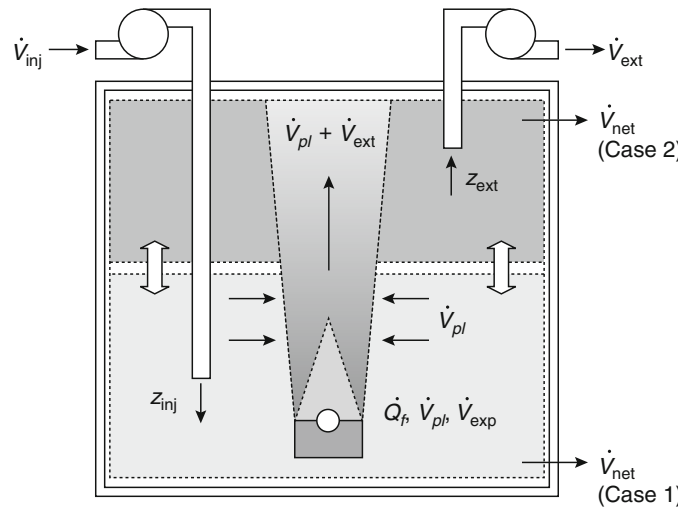

Fig. 33.10 Mechanical ventilation in a two-layer environment

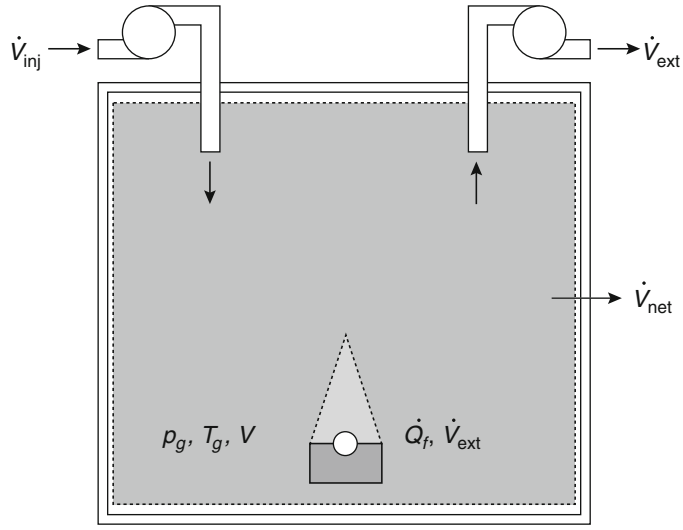

Fig. 33.11 Mechanical ventilation in a one-layer environment

will be positive if flow is forced from the enclosure to surrounding spaces and negative if flow is drawn from surrounding spaces into the enclosure.

The injection and extraction rates, $\dot{V}_{\text{in j}}$ and $\dot{V}_{\text{ext}}$, will depend on the design of the ventilation system. For present purposes, it is assumed that the user specifies the injection and extraction volumetric flow rates, although it should be recognized that these flow rates may be influenced by fan characteristics and space pressures. Under the quasi-steady pressure conditions assumed here, the volumetric expansion rate of gases can be related directly to the net rate of heat addition resulting from the fire, as shown in Equation 33.9.

A global mass balance for the enclosure can be expressed in terms of the volumetric flows across the enclosure boundaries. For situations where $\dot{V}_{\text{net}}$ is positive, flow is forced from the enclosure to adjacent spaces through available leakage paths. For this situation, the global mass balance can be expressed as

$$\begin{aligned}\frac{dm_{gl}}{dt} &= \rho_o \dot{V}_{\text{inj}} - \rho_{gl}\left(\dot{V}_{\text{net}} + \dot{V}_{\text{ext}}\right) \quad \dot{V}_{\text{net}} > 0 \\ &= \rho_o \dot{V}_{\text{inj}} - \rho_{gl}\left(\dot{V}_{\text{inj}} + \dot{V}_{\text{exp}}\right)\end{aligned} \tag{33.48a}$$

For situations where $\dot{V}_{\text{net}}$ is negative, air is drawn into the enclosure through leakage paths and the mass balance becomes

$$\begin{aligned}\frac{dm_{gl}}{dt} &= \rho_o\left(\dot{V}_{\text{inj}} - \dot{V}_{\text{net}}\right) - \rho_{gl}\dot{V}_{\text{ext}} \qquad \dot{V}_{\text{net}} < 0 \\ &= \rho_o\left(\dot{V}_{\text{ext}} + \dot{V}_{\text{exp}}\right) - \rho_{gl}\dot{V}_{\text{ext}}\end{aligned} \tag{33.48b}$$

For any individual species to be tracked, such as O_2, CO_2, CO, or soot, a global species balance also depends on the sign of $\dot{V}_{\text{net}}$. This global species balance can be expressed as

$$\begin{aligned}\frac{dm_i}{dt} &= \rho_o Y_{i,o}\dot{V}_{\text{inj}} - \rho_{gl}Y_i\left(\dot{V}_{\text{inj}} + \dot{V}_{\text{exp}}\right) \\ &\quad + \dot{m}_{i,\text{gen}} \quad \dot{V}_{\text{net}} > 0\end{aligned} \tag{33.49a}$$

$$\begin{aligned}\frac{dm_i}{dt} &= \rho_o Y_{i,o}\left(\dot{V}_{\text{ext}} - \dot{V}_{\text{exp}}\right) - \rho_{gl}Y_i\dot{V}_{\text{ext}} \\ &\quad + \dot{m}_{i,\text{gen}} \quad \dot{V}_{\text{net}} < 0\end{aligned} \tag{33.49b}$$

This global species balance can also be expressed in terms of the mass fraction for each chemical species of interest:

$$\frac{dY_i}{dt} = \frac{1}{m_{gl}}\left[\rho_o \dot{V}_{\text{inj}}(Y_{io} - Y_i) + \dot{m}_{i,\text{gen}}\right] \quad \dot{V}_{\text{net}} > 0 \tag{33.50a}$$

$$\begin{aligned}\frac{dY_i}{dt} &= \frac{1}{m_{gl}}\left[\rho_o\left(\dot{V}_{\text{ext}} - \dot{V}_{\text{ext}}\right)(Y_{io} - Y_i) + \dot{m}_{i,\text{gen}}\right] \\ &\quad \dot{V}_{\text{net}} < 0\end{aligned} \tag{33.50b}$$

The generation (or consumption) rate of a species, $\dot{m}_{i,\,\mathrm{gen}}$, can be expressed in terms of the fuel mass loss rate or the fire heat release rate, as shown in Equation 33.20.

The global temperature in the enclosure is calculated, assuming ideal gas behavior, constant pressure, and properties of air, as

$$T_{gl} = \frac{\rho_o T_o}{\rho_{gl}} = \frac{\rho_o T_o V}{m_{gl}} \tag{33.51}$$

Under quasi-steady conditions, the rate of change of mass in the enclosure goes to zero as the inflow and outflow equilibrate. For an injection-only mechanical system, $\dot{V}_{\mathrm{net}}$ will always be positive and the quasi-steady mass balance expressed by Equation 33.48a becomes

$$\rho_{gl}\left(\dot{V}_{\mathrm{inj}} + \dot{V}_{\mathrm{exp}}\right) = \rho_o \dot{V}_{\mathrm{inj}} \tag{33.52}$$

For this situation, the quasi-steady global temperature can be expressed in dimensionless form as

$$\frac{T_{gl}}{T_o} = \frac{\rho_o}{\rho_{gl}} = \frac{\left(V_{\mathrm{inj}} + \dot{V}_{\mathrm{exp}}\right)}{\dot{V}_{\mathrm{inj}}} = 1 + \frac{\dot{V}_{\mathrm{exp}}}{\dot{V}_{\mathrm{inj}}} \tag{33.53}$$

Alternatively, the quasi-steady global dimensionless temperature rise above ambient can be expressed simply as the ratio of the expansion flow rate to the injection flow rate:

$$\frac{\Delta T_{gl}}{T_o} = \frac{\dot{V}_{\mathrm{exp}}}{\dot{V}_{\mathrm{inj}}} \tag{33.54}$$

Example 10 Determine the quasi-steady average global temperature rise in a mechanically ventilated enclosure with dimensions of 18.3 m by 12.2 m by 6.1 m with an air injection rate of ten air changes per hour in response to a fire with a constant heat release rate of 500 kW. Assume a constant heat loss fraction of 0.70 and an ambient temperature of 20 °C (293 K).

Solution For this example, the volumetric expansion rate, $\dot{V}_{\mathrm{exp}}$, is calculated as in previous examples as

$$\dot{V}_{\mathrm{exp}} = \frac{\dot{Q}_{\mathrm{net}}}{\rho_e c_p T_e} = \frac{(500\ \mathrm{kW})\ (1 - 0.7)}{(353\ \mathrm{kJ/m^3})} = 0.42\ \ \mathrm{m^3/s}$$

The volumetric injection rate, $\dot{V}_{\mathrm{inj}}$, is calculated based on the compartment volume and the specified air exchange rate as

$$\dot{V}_{\mathrm{inj}} = \frac{10(18.3 \times 12.2 \times 6.1)\mathrm{m^3}}{3600\ \mathrm{s}} = 3.78\ \ \mathrm{m^3/s}$$

The quasi-steady global temperature rise is calculated by applying Equation 33.54:

$$\Delta T_{gl} = \left(\frac{\dot{V}_{\mathrm{exp}}}{\dot{V}_{\mathrm{inj}}}\right) T_o = \left(\frac{0.42}{3.78}\right) \cdot 293\ \ \mathrm{K} = 32.5\ \ \mathrm{K}$$

For an extraction only system, the analysis depends on the rate of extraction relative to the expansion rate. If the extraction rate is less than the expansion rate, then the extraction will serve simply to relieve a fraction of the expansion flow, with the remaining fraction forced through available leakage paths. This situation can be treated using the same global analysis as for an unventilated enclosure. There is not a quasi-steady solution for this situation.

For the situation where the extraction rate is greater than the expansion rate, $\dot{V}_{\mathrm{net}}$ will be negative, so air will be drawn into the enclosure through available leakage paths. From Equation 33.48b, the quasi-steady mass balance for this situation is

$$\rho_{gl}\dot{V}_{\mathrm{ext}} = \rho_o\left(\dot{V}_{\mathrm{ext}} - \dot{V}_{\mathrm{exp}}\right) \tag{33.55}$$

For this situation the temperature ratio is calculated to be

$$\frac{T_{gl}}{T_o} = \frac{\rho_o}{\rho_{gl}} = \frac{\dot{V}_{\mathrm{ext}}}{\left(\dot{V}_{\mathrm{ext}} - \dot{V}_{\mathrm{exp}}\right)} \tag{33.56}$$

The dimensionless temperature rise above ambient for this extraction scenario is

$$\frac{\Delta T_{gl}}{T_o} = \frac{\dot{V}_{\text{exp}}}{\left(\dot{V}_{\text{ext}} - \dot{V}_{\text{exp}}\right)} \tag{33.57}$$

Note the similarity between Equations 33.54 and 33.57. The extraction case is analogous to the injection scenario with an effective injection rate equal to the difference between the extraction and expansion rates. This difference is the rate at which air is being drawn into the enclosure when the extraction rate exceeds the expansion rate.

Example 11 Determine the quasi-steady average global temperature rise in a mechanically ventilated enclosure with dimensions of 18.3 m by 12.2 m by 6.1 m with an air extraction rate of ten air changes per hour in response to a fire with a constant heat release rate of 500 kW. Assume a constant heat loss fraction of 0.70 and an ambient temperature of 20°C (293 K).

Solution This example is the same as the previous example, except that the mechanical ventilation system is extracting smoke at ten changes per hour instead of injecting air at this rate. For this case, the volumetric extraction rate, $\dot{V}_{\text{ext}}$, is the same as the volumetric injection rate from the previous example:

$$\dot{V}_{\text{ext}} = \frac{10(18.3 \times 12.2 \times 6.1)\ \text{m}^3}{3600\ \text{s}} = 3.78\ \text{m}^3/\text{s}$$

The quasi-steady global temperature rise is calculated by applying Equation 33.57:

$$\Delta T_{gl} = \left[\frac{\dot{V}_{\text{exp}}}{\left(\dot{V}_{\text{ext}} - \dot{V}_{\text{exp}}\right)}\right] T_o = \left[\frac{0.42}{(3.78 - 0.42)}\right] \cdot 293\ \text{K} = 36.6\ \text{K}$$

The extraction scenario results in a slightly higher average temperature rise than the injection scenario because the airflow rate is lower for the extraction scenario. This assumes that the ventilation rates remain constant and the heat loss fractions remain the same for both scenarios.

Scenarios with both injection and extraction can be considered as variations on the injection only and extraction only analyses. If $\dot{V}_{\text{net}}$ is positive, which will occur if $\dot{V}_{\text{inj}} + \dot{V}_{\text{exp}}$ is greater than $\dot{V}_{\text{ext}}$, then the global temperature rise can be calculated with Equation 33.52. If $\dot{V}_{\text{net}}$ is negative, which will occur if $\dot{V}_{\text{ext}}$ is greater than $\dot{V}_{\text{inj}} + \dot{V}_{\text{exp}}$, then the global temperature rise can be calculated with Equation 33.57.

Neglecting the injection of fuel into the enclosure, the quasi-steady limits for different species can be evaluated by setting the left-hand side of Equation 33.50a to zero and solving for the mass fraction, Y_i:

$$Y_i = \frac{\rho_o Y_{i,o} \dot{V}_{\text{inj}} + \dot{m}_{i,\text{gen}}}{\rho_{gl}\left(\dot{V}_{\text{inj}} + \dot{V}_{\text{exp}}\right)} = Y_{i,o} + \frac{\dot{m}_{i,\text{gen}}}{\rho_o \dot{V}_{\text{inj}}} \tag{33.58}$$

Example 12 Assume propylene (C_3H_6) is the fuel burned in the previous mechanically ventilated examples. Assume propylene has a heat of combustion of 46.4 MJ/kg of fuel and a soot yield of 0.095 g of soot per g of fuel. Estimate the quasi-steady average mass concentration of soot within the 18.3 m by 12.2 m by 6.1 m enclosure for a fire that burns at a constant heat release rate of 500 kW, assuming the enclosure is mechanically ventilated with an injection system at ten air changes per hour. Based on this soot mass concentration, estimate the visibility distance for a light-reflecting sign.

Solution For this example, the ambient mass fraction of soot is assumed to be zero and the soot mass generation rate is calculated with Equation 33.20 as

$$\dot{m}_{i,\text{gen}} = f_i \dot{m}_f = \frac{\dot{Q}_f}{(\Delta H_c / f_i)} = \frac{500\ \text{kW}}{\left(46,400\ \text{kJ/kg}_f\right) / \left(0.095\ \text{kg}_{\text{soot}}/\text{kg}_f\right)} = 1.02 \times 10^{-3} \text{kg}_{\text{soot}}/\text{s}$$

Then the soot mass fraction is calculated with Equation 33.58 as

$$Y_{soot} = 0 + \frac{1.02 \times 10^{-3} kg_{soot}/s}{(1.20\ kg/m^3)\ (3.78\ m^3/s)}$$
$$= 2.26 \times 10^{-4} kg_{soot}/kg_{mix}$$

The average soot mass concentration is calculated based on the average temperature and density within the enclosure as

$$\rho Y_{soot} = \left(\frac{353}{(293 + 32.5)}\right) kg/m^3$$
$$\times \left(2.26 \times 10^{-4}\ kg_{soot}/kg\right.$$
$$= 2.45 \times 10^{-4}\ kg_{soot}/m^3$$

Using this value for the soot mass concentration, along with the specific light extinction coefficient of 8700 m^2/kg suggested by Mulholland and Croarkin, the extinction coefficient is determined to be

$$K = K_m \rho Y_{soot}$$
$$= (8700\ m^2/kg_{soot})\ \left(2.45 \times 10^{-4}\ kg_{soot}/m^3\right)$$
$$= 2.13\ \ m^{-1}$$

The visibility distance for a light-reflecting sign is then estimated as

$$S = 3/2.13\ m^{-1} = 1.4\ \ m\ (4.6\ ft)$$

As a final comment on the global analysis of mechanically ventilated enclosure fires, it is worth noting that $\dot{V}_{net}$ can switch during the course of a fire scenario from negative to positive, for example, for the case of a growing fire where $\dot{V}_{exp}$ increases with time; or from positive to negative, for example, for the case where an extraction system is started at some time after the fire starts. As a consequence, the appropriate equations used to calculate transient and quasi-steady conditions may change over the course of a fire scenario.

Smoke Layer Analysis with Mechanical Ventilation

In this section, conditions within the descending smoke layer are addressed in terms of the two limit cases illustrated in Fig. 33.10. These are

Case 1—Leakage paths near the floor (to and from the lower layer)

Case 2—Leakage paths near the ceiling (to and from the upper layer)

In Case 1, ambient air is expelled from, or drawn into, the enclosure through leakage paths near the floor until the smoke layer descends to the floor. At that point, smoke at the upper layer temperature and composition would be expelled if $\dot{V}_{net}$ were positive. In Case 2, smoke at the upper layer temperature and composition would be expelled from the upper layer through the leakage paths if $\dot{V}_{net}$ were positive, whereas ambient air would be drawn into the smoke layer through these leakage paths if $\dot{V}_{net}$ were negative.

The rate of smoke layer descent and conditions within the smoke layer will depend on the elevations of vents and the injection and extraction rates of the ventilation systems. For the present discussion, it is assumed that all injection vents are located at one elevation, z_{inj}, whereas all extraction vents are located at another unique elevation, z_{ext}. Multiple elevations for either injection or extraction vents are not addressed.

The elevation of the injection vents determines whether air is being injected into the upper layer $\left(\dot{V}_{inj,u}\right)$ or the lower layer $\left(\dot{V}_{inj,l}\right)$, depending on the current elevation of the smoke layer interface. If the elevation of the injection vents is below the smoke layer interface position, then air is injected into the lower layer; otherwise, it is injected into the upper layer. As the smoke layer interface position moves during a fire scenario, injection can shift between the upper and lower layers. Similarly, the elevation of the extraction vents determines whether smoke is being extracted from the upper layer $\left(\dot{V}_{ext,\ u}\right)$ or air is being extracted from the lower layer $\left(\dot{V}_{ext,\ l}\right)$. For the analysis presented here, it is assumed that no mixing occurs between the upper and lower layers.

Floor Leak (Case 1) Analysis

The rate of change of the upper layer volume can be expressed in terms of the volumetric flow rates into and out of the smoke layer. For Case 1, it is

assumed that there is no leakage from the upper layer until the smoke layer descends to floor level. The rate of change of the smoke layer volume or depth can be expressed as

$$\frac{dV_u}{dt} = A_s \frac{dz_u}{dt} = \dot{V}_{pl} + \dot{V}_{\exp} + \dot{V}_{\text{inj},u} - \dot{V}_{\text{ext},u} \tag{33.59}$$

The last two terms on the right-hand side of Equation 33.59 distinguish the mechanically ventilated Case 1 from the unventilated Case 1. If air is injected into the upper layer, then the rate of smoke layer descent will be faster than for the unventilated case. If smoke is extracted from the upper layer, then the rate of smoke layer descent will be slower than for the unventilated case. The injection or extraction of air from the lower layer does not influence the smoke layer descent rate for the Case 1 scenario. These flows simply affect the net flow rate through the leakage path in the lower layer boundary for this scenario.

Provided the upper layer extraction rate is at least large enough to offset the expansion and injection rates, the smoke layer interface will eventually equilibrate at the elevation where a balance is struck between the rates of flow into and out of the smoke layer:

$$\dot{V}_{\text{ext},u} = \dot{V}_{pl} + \dot{V}_{\exp} + \dot{V}_{\text{inj},u} \tag{33.60}$$

Equation 33.60 represents the typical situation for a smoke management system designed according to the *exhaust method*. For this situation, air is not typically injected into the upper layer because this would require higher extraction rates, so the last term on the right-hand side of Equation 33.60 would normally be zero. The upper layer extraction rate needed to maintain the smoke layer interface at a distance z_i above the floor can be determined from Equation 33.60 provided the relationship between plume entrainment, fire intensity, and elevation is known and the fire intensity can be estimated. For the case of an axisymmetric plume, this relationship is normally represented as

$$\dot{V}_{pl} = k_v \dot{Q}_c^{1/3} \left(z_i - z_f\right)^{5/3} \tag{33.61}$$

Based on the Zukoski [25] entrainment correlation, the value for k_v will be approximately 0.064 $\text{m}^{4/3}\ \text{s}^{-1}\ \text{kW}^{-1/3}$. For other plume geometries, such as window plumes, balcony spill plumes, or line plumes, other entrainment rate relationships exist [10]. Further information on plume entrainment is provided by Beyler [29], who prepared a comprehensive review of fire plume and ceiling jet correlations, and by Quintiere and Grove [30], who more recently reviewed the literature on different types of plumes and developed correlations for fire plumes of different geometries.

Once the extraction rate needed to maintain the smoke layer interface at an elevation z_i above the floor is determined, Equations 33.52 through 33.58 can be used to evaluate the global effects of this extraction rate. These effects will included the makeup air requirements $\left(-\dot{V}_{\text{net}}\right)$ to balance the design exhaust rate as well as the leakage opening area requirements to prevent excessive pressure drop and flow velocities across the enclosure boundaries. As indicated by Equation 33.47, mechanical injection of air into the lower layer can be used to reduce the makeup air requirements and consequently the pressure drop and flow velocities across openings in the enclosure boundaries.

At this point, conditions within the smoke layer are considered. For Case 1, mass conservation for the upper layer can be expressed in terms of the various volumetric flow rates into and out of the smoke layer:

$$\frac{dm_u}{dt} = \rho_l \left(\dot{V}_{pl} + \dot{V}_{\text{inj},u}\right) - \rho_u \dot{V}_{\text{ext},u} \quad \text{if } V_1 > 0 \tag{33.62a}$$

$$\frac{dm_u}{dt} = \rho_l \left(\dot{V}_{pl} + \dot{V}_{\text{inj},u}\right) - \rho_u \left(\dot{V}_{\text{ext},u} + \dot{V}_{\text{net}}\right) \quad \text{if } V_l = 0 \tag{33.62b}$$

The additional term in Equation 33.62b compared with Equation 33.62a accounts for the leakage flow from the upper layer that occurs once the upper layer completely fills the enclosure.

Similarly, different species can be tracked in terms of a species balance, which can be expressed for this case as

$$\frac{dm_{i,u}}{dt} = \rho_l Y_{i,o}\left(\dot{V}_{pl} + \dot{V}_{\text{inj},u}\right) - \rho_u Y_{i,u}\dot{V}_{\text{ext},u} + \dot{m}_{i,\text{gen}} \quad \text{if} \quad V_l = 0 \tag{33.63a}$$

$$\frac{dm_{i,u}}{dt} = \rho_l Y_{i,o}\left(\dot{V}_{pl} + \dot{V}_{\text{inj},u}\right) \quad \text{if} \quad V_l > 0 - \rho_u Y_{i,u}\left(\dot{V}_{\text{ext},u} + \dot{V}_{\text{net}}\right) + \dot{m}_{i,\text{gen}} \tag{33.63b}$$

Similar to the global analysis, the rate of change of the mass fraction of a species in the upper layer is calculated as

$$\frac{dY_{i,u}}{dt} = \frac{1}{m_u}\left[\rho_l\left(\dot{V}_{pl} + \dot{V}_{\text{inj},u}\right)\left(Y_{i,o} - Y_i\right) + \dot{m}_{i,\text{gen}}\right] \tag{33.64}$$

The generation, or consumption, rate of different species is expressed in terms of a yield factor, f_i, as given by Equation 33.20 for the global case. All products generated by the combustion reaction are assumed to enter the upper layer via the fire plume.

Finally, the temperature of the upper layer is calculated from the mass and volume of the upper layer as

$$T_u = \frac{\rho_o T_o}{\rho_u} = \frac{\rho_o T_o V_u}{m_u} \tag{33.65}$$

This assumes that the upper layer can be treated as an ideal gas at constant pressure with the properties of air. The mass, volume, and species mass fractions in the upper layer change with time in accordance with Equations 33.59, 33.62, and 33.64. Numerical integration is generally necessary to evaluate these differential equations. Once they are evaluated at a particular time, the upper layer temperature at that time can be calculated using Equation 33.65.

Ceiling Leak (Case 2) Analysis

All leakage is assumed to occur from the upper layer for Case 2. The rate of change of the smoke layer volume or depth can be expressed in terms of the upper layer flow terms shown in Fig. 33.10 as

$$\frac{dV_u}{dt} = A_s\frac{dz_u}{dt} = \dot{V}_{pl} + \dot{V}_{\text{exp}} + \dot{V}_{\text{inj},u} - \dot{V}_{\text{ext},u} - \dot{V}_{\text{net}} \tag{33.66}$$

Because $\dot{V}_{\text{net}} = \dot{V}_{\text{inj}} + \dot{V}_{\text{exp}} - \dot{V}_{\text{ext}}$, $\dot{V}_{\text{inj}} = \dot{V}_{\text{inj},u} + \dot{V}_{\text{inj},l}$, and $V_{\text{ext}} = V_{\text{ext},u} + V_{\text{ext},l}$, Equation 33.66 can be rewritten as

$$\frac{dV_u}{dt} = A_s\frac{dz_u}{dt} = \dot{V}_{pl} + \dot{V}_{\text{ext},l} - \dot{V}_{\text{inj},l} \tag{33.67}$$

The relationship expressed by Equation 33.67 may seem counterintuitive because it shows that, for Case 2, smoke layer descent is affected by injection and extraction in the lower layer but not in the upper layer. Noting that $dV_u = dV_l$, an analysis of flow terms can be conducted on the lower layer to reach the same result expressed by Equation 33.67. Alternatively, this result can be explained as follows. Because all leakage flow from the enclosure in Case 2 is assumed to occur via leakage paths from the upper layer, any injection of air into the upper layer will simply be forced through these paths rather than contribute to the descent of the upper layer. Similarly, all expansion is assumed to be forced through these leakage paths from the upper layer rather than contribute to the smoke layer descent, as in the unventilated Case 2 scenario. Finally, extraction from the upper layer will first act to relieve some of the expansion flow from the enclosure. If the extraction rate is less than the combination of the injection and expansion rates, then additional smoky gases will be forced through the leakage paths from the upper layer. On the other hand, if the extraction rate is greater than the combination of the injection and expansion rates, then

fresh air will be drawn through the leakage paths into the upper layer. Although these factors all influence the composition and temperature of the upper layer, they do not affect the smoke layer descent rate expressed by Equation 33.67.

With leakage occurring from the upper layer in Case 2, the injection of air into the lower layer will act to "push" smoke through leakage paths from the upper layer, reducing the rate of smoke layer descent in the process. In contrast, the extraction of air from the lower layer will act to draw the smoke layer down. If the extraction rate is greater than the combination of the injection and expansion rates, air will be drawn into the upper layer through the leakage paths, contributing to the smoke layer descent while at the same time diluting the smoke in the upper layer. For a scenario where there is no injection and the extraction rate is exactly equal to the expansion rate, then the net flow through leakage paths will be nil. In essence, this is the same scenario as the unventilated Case 1, with the expansion flow from the lower layer replaced by extraction from the lower layer at the same rate. In the unventilated Case 1 scenario, expansion contributes to the smoke layer descent just as an equivalent rate of extraction from the lower layer will in the ventilated scenario.

Equations 33.66 and 33.67 demonstrate that no amount of extraction from the upper layer will prevent the smoke layer from eventually descending to the elevation of the fire in Case 2 scenarios. Similarly, due to the location of the leakage paths in the upper layer, no amount of injection into the upper layer will affect the rate of smoke layer descent. Such injection or extraction will affect only the composition and temperature of the smoke layer.

For Case 2 scenarios, a quasi-steady smoke layer interface position can be achieved only by injecting more air into the lower layer than is extracted from it. The smoke layer will stop descending when the following flow balance is achieved:

$$\dot{V}_{\text{inj},l} = \dot{V}_{pl} + \dot{V}_{\text{ext},l} \tag{33.68}$$

The air injection rate needed to maintain the smoke layer interface at a distance z_i above the floor can be determined by Equation 33.68, provided the extraction rate is known and the relationship between plume entrainment and elevation is known. For the case of an axisymmetric plume, this relationship was given in Equation 33.61. For other plume geometries, other entrainment relationships are available in the literature [10, 29, 30].

The concept of injecting air low in an enclosure while providing ventilation openings high is the basis for the positive pressure ventilation (PPV) technique [31, 32] sometimes employed in fire-fighting operations. This technique is not used as often in building smoke management systems, in part because this technique places the fire enclosure at positive pressure relative to adjacent spaces. Although boundaries adjacent to the smoke layer are assumed to be perfectly tight for the limiting analyses presented here, in reality such boundaries will leak and smoke will be forced from the fire enclosure into adjacent spaces. In contrast, with the exhaust method described in the Case 1 analysis, the extraction of smoke causes the fire enclosure to be at a slightly negative pressure relative to adjacent spaces. Under these conditions, leakage tends to be from the adjacent spaces to the fire enclosure, thus reducing the likelihood and degree of smoke contamination in the adjacent spaces.

At this point, conditions within the smoke layer are addressed for the Case 2 scenario. Mass conservation for the upper layer can be expressed in terms of the various volumetric flow rates across the upper layer boundaries:

$$\frac{dm_u}{dt} = \rho_l\left(\dot{V}_{pl} + \dot{V}_{\text{inj},u}\right) - \rho_u\left(\dot{V}_{\text{ext},u} + \dot{V}_{\text{net}}\right) \quad \text{if } \dot{V}_{\text{net}} > 0 \tag{33.69a}$$

$$\frac{dm_u}{dt} = \rho_l\left(\dot{V}_{pl} + \dot{V}_{\text{inj},u} - \dot{V}_{\text{net}}\right) - \rho_u\left(\dot{V}_{\text{ext},u}\right) \quad \text{if } \dot{V}_{\text{net}} < 0 \tag{33.69b}$$

Similarly, different species can be tracked in terms of a species balance, expressed as

$$\frac{dm_{i,u}}{dt} = \rho_l Y_{i,o}\left(\dot{V}_{pl} + \dot{V}_{\text{inj},u}\right) - \rho_u Y_{i,u}\left(\dot{V}_{\text{ext},u} + \dot{V}_{\text{net}}\right) + \dot{m}_{i,\text{gen}} \quad \text{if } \dot{V}_{\text{net}} > 0 \tag{33.70a}$$

$$\frac{dm_{i,u}}{dt} = \rho_l Y_{i,o}\left(\dot{V}_{pl} + \dot{V}_{\text{inj},u} - \dot{V}_{\text{net}}\right) \quad \text{if } \dot{V}_{\text{net}} < 0$$
$$- \rho_u Y_{i,u} \dot{V}_{\text{ext},u} + \dot{m}_{i,\text{gen}} \tag{33.70b}$$

As for the other cases, these species balances can also be expressed in terms of mass fractions:

$$\frac{dY_{i,u}}{dt} = \frac{1}{m_u}\left[\rho_l\left(\dot{V}_{pl} + \dot{V}_{\text{inj},u}\right)\ \left(Y_{i,o} - Y_i\right)\right.$$
$$\left. + \dot{m}_{i,\text{gen}}\right] \quad \text{if } \dot{V}_{\text{net}} < 0 \tag{33.71a}$$

$$\frac{dY_{i,u}}{dt} = \frac{1}{m_u}\left[\rho_l\left(\dot{V}_{pl} + \dot{V}_{\text{inj},u} - \dot{V}_{\text{net}}\right)\ \left(Y_{i,o} - Y_i\right)\right]$$
$$+ \dot{m}_{i,\text{gen}}\Big] \quad \text{if } \dot{V}_{\text{net}} < 0 \tag{33.71b}$$

Finally, the temperature of the upper layer is calculated from the mass and volume of the upper layer by Equation 33.65. For Case 2, the upper layer volume, mass, and species mass fractions change with time in accordance with Equations 33.67, 33.69a, 33.69b, and 33.71a, 33.71b. Numerical integration is generally necessary to evaluate these differential equations. Once they are evaluated at a particular time, the upper layer temperature at that time is calculated by Equation 33.65.

Numerical Methods for Solving Initial Value Problems

In the previous sections of this chapter, the enclosure smoke-filling process has been described in terms of a number of ordinary differential equations to describe the rate of change of volume, mass, and species within the smoke layer. The enclosure smoke filling process is in the class of problems known as initial value problems. This type of problem is also sometimes referred to as a *time marching* problem, because the objective is to determine the time history of the parameters of interest, given the initial values for these parameters along with equations describing how these parameters change with time as a result of specified boundary conditions.

As noted previously, the differential equations describing the smoke-filling process can be solved analytically for only a few idealized fire scenarios. For most realistic fire scenarios, these equations must be solved approximately using appropriate numerical methods. Computer models of the smoke-filling process, such as ASET and ASET-B, use a variety of similar numerical methods to develop approximate solutions for the enclosure smoke-filling process. Some of these methods are discussed briefly in this section. For a more comprehensive treatment of numerical methods, readers are referred to texts on this topic (e.g., Ferziger and Peric [33]).

Note that most of the equations presented in previous sections are expressed in the form

$$\frac{d\phi(t)}{dt} = f[t, \phi(t)] \tag{33.72}$$

where $\phi(t)$ represents the different parameters of interest, such as the smoke layer interface position and the smoke layer temperature and composition. In general, the objective is to predict values for the parameters of interest as a function of time based on the rate of change of the different parameters, $d\phi(t)/dt$, over each time interval, Δt, being evaluated. Mathematically, this is represented as

$$\phi(t_{n+1}) = \phi(t_n) + \int_{t_n}^{t_{n+1}} f[t, \phi(t)]dt$$
$$\cong \phi(t_n) + f[t, \phi(t)]\,\Delta t \tag{33.73}$$

The question is how to efficiently and accurately approximate the function, $f[t,\phi(t)]$ over a time increment, Δt.

The simplest approach to solving Equation 33.73 numerically, known as the explicit or forward Euler method, evaluates the derivative function at the current time, t_n, that is,

$$f[t, \phi(t)] \cong f[t_n, \phi(t_n)]$$

The forward Euler method is known as an explicit method because the value of the parameter at the future time, $\phi(t_{n+1})$, is evaluated based

on the values of parameters evaluated at the current time, t_n. For many applications, particularly those in which the function is changing rapidly with time, such an approximation may not be very accurate. This will depend to some extent on the time step selected and the nature of the function being evaluated.

The next level of complexity, as well as accuracy, is introduced by methods known as predictor-corrector methods. The simplest of these, known as the improved Euler method or as Heun's method, uses the explicit Euler method to predict the value of the derivative function; this predicted value is represented as $\phi^*(t_{n+1})$. This predicted value is then used to estimate the slope of the function at the endpoint. The average slope over the time step is then taken as the average of the slopes evaluated at the beginning and endpoints, that is, at times t_n and t_{n+1}. Heun's method can be expressed mathematically as

$$\phi^*(t_{n+1}) = \phi(t_n) + f[t_n, \phi(t_n)]\Delta t \tag{33.74a}$$

$$\phi(t_{n+1}) = \phi(t_n) + \frac{1}{2}\left\{f[t_n, \phi(t_n)] + f[t_{n+1}, \phi^*(t_{n+1})]\right\}\Delta t \tag{33.74b}$$

An iterative form of this predictor-corrector method was used in the development of the ASET-B model [4].

The explicit Euler method and Heun's method are single point methods because they use information at only the current time step to evaluate conditions at the future time step. Beyond these simple methods, multipoint methods have been developed that use information that has already been computed at previous time steps to fit a polynomial to a number of points. The Adams-Bashforth method is an explicit method that uses information at the current time step and the previous two time steps to evaluate the derivative function:

$$\phi(t_{n+1}) = \phi(t_n) + \frac{\Delta t}{2}\left\{23f[t_n, \phi(t_n)] - 16f[t_{n-1}, \phi(t_{n-1})] + 5f[t_{n-2}, \phi(t_{n-2})]\right\} \tag{33.75}$$

A disadvantage of multipoint methods is that they cannot be started using only data at the initial point because they require data from multiple points prior to the current one. Consequently, other methods must be used to start a calculation. Once started, the advantage of explicit multipoint methods is that they require only one evaluation of the derivative function per time step because the function has already been evaluated at previous time steps.

Runge-Kutta methods overcome the difficulties in starting multipoint methods by using additional points between times t_n and t_{n+1} rather than earlier points to evaluate the derivative function. The most popular Runge-Kutta method is the fourth-order method, which involves multiple evaluations over the time step:

$$\phi^*\left(t_{n-1/2}\right) = \phi(t_n) + f[t_n, \phi(t_n)]\Delta t/2 \tag{33.76a}$$

$$\phi^{**}\left(t_{n+1/2}\right) = \phi(t_n) + f\left[t_{n+1/2}, \phi\left(t_{n+1/2}\right)\right]\Delta t/2 \tag{33.76b}$$

$$\phi^*(t_{n+1}) = \phi(t_n) + f\left[t_{n+1/2}, \phi^{**}\left(t_{n+1/2}\right)\right]\Delta t \tag{33.76c}$$

$$\phi(t_{n+1}) = \phi(t_n) + \frac{\Delta t}{6}\left\{f[t_n, \phi(t_n)] + 2f\left[t_{n+1/2}, \phi^*\left(t_{n+1/2}\right)\right] + 2f\left[t_{n+1/2}, \phi^{**}\left(t_{n+1/2}\right)\right] + f[t_{n+1}, \phi^*(t_{n+1})]\right\} \tag{33.76d}$$

The fourth-order Runge-Kutta method was used in the development of the original ASET model [2].

Treatment of Enclosure Smoke Filling in Different Fire Models

A number of fire models have been developed over the past three decades to address the enclosure smoke-filling process. The best known of these include the ASET model developed by Cooper [2] during the early 1980s and the ASET-B adaptation of this model developed by Walton [4] during the mid-1980s.

Zone models, such as CFAST, address the enclosure smoke-filling process as a subset of the more general enclosure fire process. Through appropriate specification of vent sizes and locations, users can use these models to address enclosure smoke-filling scenarios. With such vent specifications, the smoke layer will descend within the enclosure until a balance occurs between inflows and outflows.

Similar to the more comprehensive zone models, computational fluid dynamics (CFD) models such as the Fire Dynamics Simulator (FDS) address the enclosure smoke-filling process as a subset of the more general enclosure fire process. As with the more comprehensive zone models, users can address enclosure smoke-filling scenarios by specifying appropriate vent sizes and locations along with appropriate fire parameters.

Comparisons with Experimental Data

The equations describing enclosure smoke filling and conditions presented in the previous sections of this chapter are amenable to solution with spreadsheet templates. A spreadsheet template has been developed [11, 12] based on the explicit Euler numerical method described in a previous section. This spreadsheet template includes calculations and graphs for the global case (Case 0), the floor leak case (Case 1), and the ceiling leak case (Case 2). The parameters calculated in the template include

$V_{ul}(t)$ Upper layer volume (m^3)
$z_{ul}(t)$ Smoke layer interface height above the floor (m)
$m_{ul}(t)$ Upper layer mass (kg)
$T_{ul}(t)$ Smoke layer average temperature (°C)
$Y_{O_2,ul(t)}$ Smoke layer oxygen mass fraction (kg O_2/kg total)

These parameters are calculated for both Case 1 and Case 2. The global temperature rise associated with Case 0 is calculated using Equation 33.17, with the net rate of energy addition, $\dot{Q}_{\text{net}}$, calculated using Equation 33.2. For comparison purposes, the smoke layer descent rate expressed by Equation 33.38 is identified as the global calculation of smoke layer position (Case 0) in the template. This represents the analytical solution for Case 2 for power law fires, permitting evaluation of the accuracy of the Case 2 numerical solution for smoke layer descent.

In the spreadsheet template, the fire is represented as a user-specified power law fire, $\dot{Q}_f = \alpha_n t^n$, which can be used to represent a wide range of fire growth scenarios, including the commonly used steady ($n = 0$) and t-squared ($n = 2$) fire growth rates. The maximum fire size is also specified. The fire grows according to the specified power law relationship until it reaches the maximum fire size and remains constant at the maximum size thereafter. Decay and burnout are not considered in the current implementation of the spreadsheet template.

The calculations performed by the spreadsheet template have been compared with experimental data. The first comparison is based on a fire test conducted by Hagglund et al. [34] in a 5.62 m by 5.62 m by 6.15 m high space with a reported steady fire size of 186 kW located 0.2 m above the floor. $Q^* = 1.6 \times 10^{-3}$ for this scenario, based on a heat release rate of 186 kW, a radiative fraction of 0.35, and a height $z = 5.4$ m. Karlsson and Quintiere [35] note that for this experiment there was a delay of up to 1 min for the fire to reach its steady value of 186 kW. To evaluate the effect of this delay, the fire was ramped up as a t-squared fire to reach a heat release rate of 186 kW at 60 s ($\alpha = 0.052$ kW/s^2), then maintained at a steady value 186 kW for the rest of the 300 s simulation. Results of this simulation are shown along with experimental data in Fig. 33.12.

Figure 33.12 shows that there is little difference between the two numerical cases (Cases 1 and 2) and the analytical solution (Equation 33.38) for the predicted smoke layer descent rates or among the three cases (Cases 0, 1, and 2) for the average smoke layer temperatures. At later times, the smoke layer descends slightly more rapidly for Case 1 than for the other two cases. This is due to the increasingly important role of expansion in Case 1 as the smoke layer

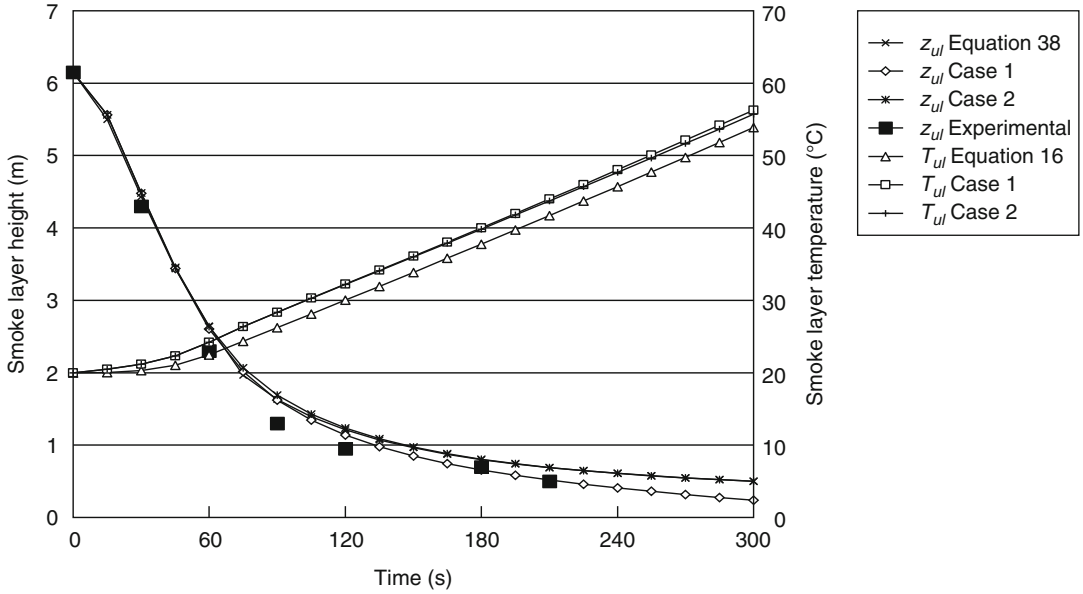

Fig. 33.12 Experimental and predicted results for smoke filling in a 6 m cube [34]

nears the fuel surface. Cooper [3] has previously noted the increasing importance of expansion as the smoke layer approaches the fuel surface. The smoke layer interface positions for Case 2 and the analytical solution are virtually identical at all times; this serves to verify the accuracy of the numerical solution. The smoke layer temperatures for Cases 1 and 2 are a few degrees Celsius higher than for the global case (Case 0), but for most hazard analysis purposes, these differences are not significant.

As a second comparison, an experiment conducted at the Building Research Institute (BRI) in Japan by Yamana and Tanaka [36] is considered. This experiment was conducted in an enclosure with a height of 26.3 m and a plan area of 720 m^2 ($A/H^2 = 1.0$). The enclosure was not mechanically ventilated for the experiment considered here. The fire source was a methanol pool with an area of 3.24 m^2, estimated to develop a steady heat release rate of approximately 1.3 MW after a 60 s period of initial growth assumed to follow a *t*-squared profile. $Q^* = 3.0 \times 10^{-3}$ for this fire, based on the maximum heat release rate of 1.3 MW, a radiative fraction of 0.10 for the methanol pool and a height of 26.3 m. For the calculations, the heat loss fraction was set to 0.50, a relatively low value. This value was selected on the basis that heat losses due to radiation from the flame would be lower than usual due to the relatively low luminosity of the methanol flame.

Results of the comparison with the BRI experiment are shown in Fig. 33.13. For the experimental temperature data, measurements made at an elevation of 16 m above the floor are shown. The experimental smoke layer interface position shown in Fig. 33.13 represents a composite of thermocouple and photometer measurements as well as visual observations reported for this experiment. Figure 33.13 shows generally good agreement between calculated results and measured data for this experiment.

Summary

Enclosure smoke filling and smoke layer conditions have been subjects of interest in the fire protection engineering community at least since Zukoski [1] first described the smoke-filling process in terms of thermodynamic control

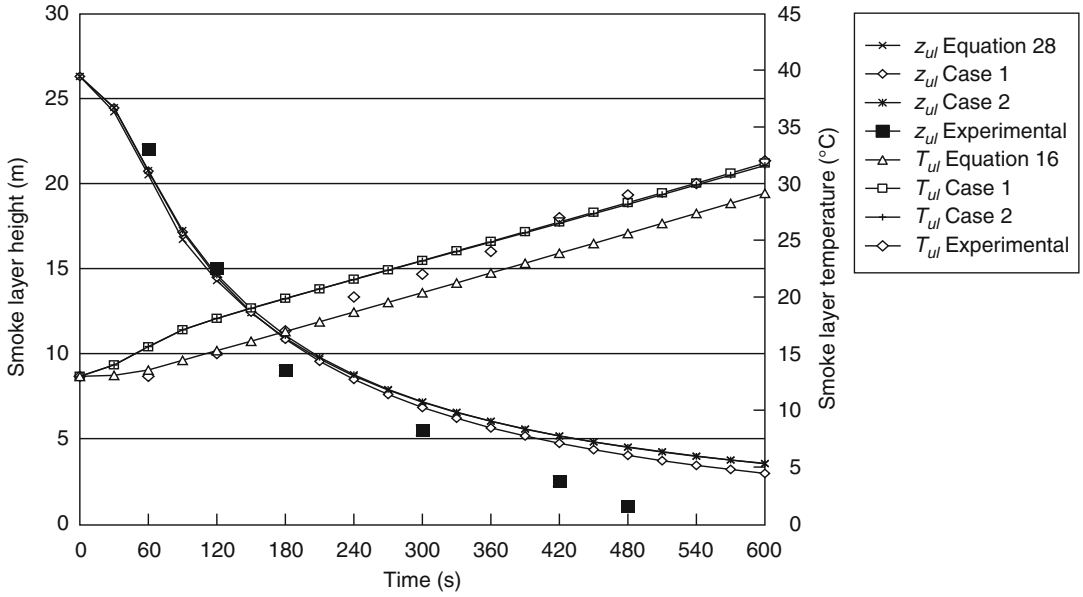

Fig. 33.13 Experimental and predicted smoke-filling results for BRI experiment [36]

volumes and plume flow rates more than 25 years ago. These concepts are now fundamental premises for performance-based consideration of available safe egress time (ASET) [2, 3] and smoke management in large spaces (e.g., NFPA 92B [10]).

This chapter reviewed the concepts of enclosure smoke filling first described by Zukoski [1] and addressed extensively by Cooper [2, 3]. It extended these concepts in a number of ways. First, the smoke-filling process was expressed in terms of volumetric flow rates, consistent with the normal practice of ventilation system design. This analysis also showed that the smoke-filling process can be described simply in terms of two distinct volumetric flow processes: plume entrainment and gas expansion. It further showed that the volumetric rate of gas expansion can be treated as a source term that is directly proportional to the net rate of heat addition to a space.

The relevant set of ordinary differential equations were shown for describing smoke layer descent, temperature, and composition for both unventilated and mechanically ventilated enclosure fire scenarios. In general, these equations must be solved numerically for realistic fire scenarios. Appropriate numerical methods were described briefly.

A number of example calculations were provided to demonstrate application of the enclosure smoke-filling equations. Such calculations are useful for performing preliminary analyses of enclosure smoke-filling fire scenarios. They can be supplemented by the use of computer-based zone and CFD models described in other chapters.

Nomenclature

A	area (m^2)
c_p	specific heat at constant pressure (kJ/kg · K)
c_v	specific heat at constant volume (kJ/kg · K)
C_d	orifice flow coefficient (–)
dm_{O_2}	mass of oxygen consumed by combustion (kg)
h	specific enthalpy (kJ/kg)
H	height of space from floor to ceiling (m)
k_v	volumetric entrainment coefficient ($m^3/s \cdot kW^{1/3} \cdot m^{5/3}$)

m	mass (kg)
$\dot{m}$	mass flow rate (kg/s)
P	pressure (Pa)
P_o	atmospheric pressure (101,325 Pa)
Q_f	heat released by combustion (kJ)
$\dot{Q}$	heat release rate (kW)
Q^*	dimensionless heat release rate—$\dot{Q}/\left(\rho_a c_p T_a \sqrt{gH}H^2\right)$
$r_{\mathbf{air}}$	air stoichiometric ratio (kg air/kg fuel)
r_{O_2}	oxygen stoichiometric ratio (kg oxygen/kg fuel)
R	ideal gas constant of air (287.0 J/kg · K)
t	time (s)
T	temperature (K or °C)
u	specific internal energy (kJ/kg)
U	total internal energy (kJ)
v	velocity (m/s)
V	volume (m^3)
$\dot{V}$	volumetric flow rate (m^3/s)
X_i	mole fraction of species i (n_i/n_{total}) ($moles_i/moles_{total}$)
Y_i	mass fraction of species i (m_i/m_{total}) (kg_i/kg_{total})
z	elevation variable (m)

Greek Letters

α_n	power law fire growth coefficient (kW/s^n)
χ_l	heat loss factor $\left(\dot{Q}_l/\dot{Q}_f\right)$ (–)
χ_{O_2}	oxygen consumption fraction (–)
ΔH_c	fuel heat of combustion (kJ/kg)
ΔT	temperature rise above ambient (K or °C)
ρ	density (kg/m^3)
τ	time constant (s)

Subscripts

atm	atmospheric
c	convective
e	exit
exp	expansion
ext	extraction
f	fire
g	global
i	in, interface
l	loss, lower layer
net	net
o	ambient, reference
$\mathbf{O_2}$	oxygen
p	constant pressure
pl	plume
r	radiative
s	space
tot	total
u, ul	upper layer
v	constant volume

References

1. E.E. Zukoski, "Development of a Stratified Ceiling Layer in the Early Stages of a Closed-Room Fire," *Fire and Materials,* 2, pp. 54–62 (1978).
2. L.Y. Cooper, "A Mathematical Model for Estimating Available Safe Egress Time from Fires," *Fire and Materials,* 6, pp. 135–143 (1982).
3. L.Y. Cooper, "The Development of Hazardous Conditions in Enclosures with Growing Fires," *Combustion Science and Technology,* 33, pp. 279–297 (1983).
4. W.D. Walton, "ASET-B: A Room Fire Program for Personal Computers," *Fire Technology,* 21, pp. 293–309 (1985).
5. H.E. Nelson, "FPETOOL: Fire Protection Engineering Tools for Hazard Estimation," *NISTIR 4380*, National Institute of Standards and Technology, Gaithersburg, MD, General Services Administration, Washington, DC (Oct. 1990).
6. M. Hurley, "ASET-B: Comparison of Model Predictions with Full-Scale Test Data," *Journal of Fire Protection Engineering,* 13, 1, pp. 37–65 (2003).
7. F.W. Mowrer, "Methods of Quantitative Fire Hazard Analysis," *TR-100443*, Electric Power Research Institute, Palo Alto, CA (May 1992).
8. Professional Loss Control, "Fire Induced Vulnerability Evaluation (FIVE)," *TR-100370*, Electric Power Research Institute, Palo Alto, CA (Apr. 1992).
9. J.A. Milke and F.W. Mowrer, "A Design Algorithm for Smoke Management Systems in Atria and Covered Malls," *Report No. FP93–04,* Department of Fire Protection Engineering, University of Maryland (May 1993).
10. NFPA 92B, *Standard for Smoke Management Systems in Malls, Atria, and Large Spaces,* National Fire Protection Association, Quincy, MA (2005).
11. F.W. Mowrer, "Enclosure Smoke Filling Revisited," *Fire Safety Journal,* 33, pp. 93–114 (1999).
12. F.W. Mowrer, "Enclosure Smoke Filling and Management with Mechanical Ventilation," *Fire Technology,* 38, 1, January pp. 33–56 (2002).
13. K. Matsuyama, Y. Misawa, T. Wakamatsu, and K. Hamada, "Closed-Form Equations for Room

Smoke Filling During an Initial Fire," *Fire Science and Technology,* 19, pp. 1–27 (1999).
14. M.A. Delichatsios, "Closed Form Approximate Solutions for Smoke Filling in Enclosures Including the Volume Expansion Term," *Fire Safety Journal,* 38, pp. 97–101 (2003).
15. M.A. Delichatsios, "Tenability Conditions and Filling Times for Fires in Large Spaces," *Fire Safety Journal,* 24, pp. 643–662 (2004).
16. C.M. Fleischmann and K.B. McGrattan, "Numerical and Experimental Gravity Currents Related to Backdrafts," *Fire Safety Journal,* 33, 1, pp. 21–34 (1999).
17. S.P. Nowlen, "Enclosure Environment Characterization Testing for the Base Line Validation of Computer Fire Simulation Codes," *NUREG/CR-4681, SAND86–1296,* Sandia National Laboratories, Albuquerque, NM (Mar. 1987).
18. R. Zalosh, "Explosion Protection," in *SFPE Fire Protection Handbook* (P.J. DiNenno et al., eds.), National Fire Protection Association, Quincy, MA, pp. 3-402–3-421 (2003).
19. M. Skelly, R. Roby, and C. Beyler, "An Experimental Investigation of Glass Breakage in Compartment Fires," *Journal of Fire Protection Engineering,* 3, 1, pp. 25–34 (1991).
20. P.E. Sincaglia and J.R. Barnett, "Development of a Glass Window Fracture Model for Zone-Type Computer Fire Codes," *Journal of Fire Protection Engineering,* 8, 3, pp. 101–118 (1997).
21. F.W. Mowrer, "Window Breakage Induced by Exterior Fires," *NIST GCR 98–751*, National Institute of Standards and Technology, Gaithersburg, MD (1998).
22. J.D. Seader and I.N. Einhorn, "Some Physical, Chemical, Toxicological, and Physiological Aspects of Fire Smokes," in *16th Symposium (International) on Combustion,* Combustion Institute, Pittsburgh, PA, pp. 1423–1445 (1977).
23. G.W. Muholland and C. Croarkin, "Specific Extinction Coefficient of Flame Generated Smoke," *Fire and Materials,* 24, 5, pp. 39–55 (2000).
24. G. W. Mulholland, "Smoke Production and Properties," SFPE Handbook of Fire Protection Engineering, *National Fire Protection Association,* Quincy, MA, 2008.
25. E.E. Zukoski, T. Kubota, and B. Cetegen, "Entrainment in Fire Plumes," *Fire Safety Journal,* 3, pp. 107–121 (1980/1981).
26. V. Ho, N. Siu, and G. Apostolakis, "COMPBRN III—A Fire Hazard Model for Risk Analysis," *Fire Safety Journal,* 13, pp. 137–154 (1988).
27. K.L. Foote, P.J. Pagni, and N.J. Alvares, "Temperature Correlations for Forced-Ventilation Compartment Fires," *Fire Safety Science—Proceedings of the First International Symposium,* International Association for Fire Safety Science, London, UK (1986).
28. C. Beyler, "Analysis of Compartment Fires with Overhead Forced Ventilation," *Fire Safety Science—Proceedings of the Third International Symposium,* International Association for Fire Safety Science, London, UK (1991).
29. C.L. Beyler, "Fire Plumes and Ceiling Jets," *Fire Safety Journal,* 11, 53, pp. 53–75 (1986).
30. J.G. Quintiere and B.S. Grove, "Correlations for Fire Plumes," *NIST GCR 98–744,* National Institute of Standards and Technology, Gaithersburg, MD (1998).
31. P.S. Ziesler, F.S. Gunnerson, and S.K. Williams, "Advances in Positive Pressure Ventilation: Live Fire Tests and Laboratory Simulation," *Fire Technology,* 30, 2, pp. 269–277 (1994).
32. S. Kerber and W.D. Walton, "Full-Scale Evaluation of Positive Pressure Ventilation In a Fire Fighter Training Building," *NISTIR 7342* National Institute of Standards and Technology, Gaithersburg, MD (2006).
33. J.H. Ferziger and M. Peric, *Computational Methods for Fluid Dynamics,* 3rd ed., Springer-Verlag, New York (2002).
34. B. Hagglund, R. Jansson, and K. Nireus. "Smoke Filling Experiments in a $6 \times 6 \times 6$ Meter Enclosure," *FOA Report C 20585-D6,* National Defense Research Establishment, Stockholm, Sweden (1985).
35. B. Karlsson and J. Quintiere, *Enclosure Fire Dynamics,* CRC Press, Boca Raton, FL (2000).
36. T. Yamana and T. Tanaka, "Smoke Control in Large Scale Spaces (Part 2: Smoke Control Experiments in a Large Scale Space)," *Fire Science and Technology,* 5, 1, pp. 41–54 (1985).

Frederick W. Mowrer is the Director of Fire Protection Engineering Programs at the California Polytechnic State University in San Luis Obispo, CA. He is also an emeritus faculty member of the Department of Fire Protection Engineering at the University of Maryland. Dr. Mowrer has served as the president of the Society of Fire Protection Engineers and currently serves as the chair of the SFPE Technical Steering Committee.

Methods for Predicting Temperatures in Fire-Exposed Structures

34

Ulf Wickström

Introduction

The fire resistance of structural elements is traditionally determined by standard fire endurance tests. However, there is also a need to be able to predict the response of structures of various designs when exposed to alternative design fire conditions. Accurate and robust analytical methods are then needed. Such methods may also be used for predicting standard tests of, for example, structural elements that cannot be tested due to their size or for extending test results to modified structures.

It is necessary when using analytical methods, as well as when interpreting test results and their relations to real fires, to understand the fundamental physics governing the thermal behavior of fire-exposed structures. The focus in this chapter is to meet these needs. The content is based on textbooks on heat transfer theory (e.g., Holman [1] and others) and from various publications in the field of fire safety engineering.

Analytical methods for the design of fire resistance of structures have the following three main components:

1. Determining the duration and level of thermal fire exposure
2. Calculating the heat transfer and the internal temperature distribution
3. Estimating the structural response and the load-bearing capacity

U. Wickström (✉)

The first step is in general very complex and requires somewhat uncertain assumptions. Most often the fire exposure is assumed according to standardized time-temperature curves, as specified in ISO 834, ASTM E119, or EN 1363-1. Time-temperature developments determined by fire models or measured at ad hoc tests are seldom applied. The next step is very crucial as the deterioration of material strength depends on the temperature obtained. This chapter focuses on this second step. More information on the first and third steps of an analytical design procedure is outlined elsewhere in this section of the handbook.

The temperature calculation methods presented here disregard in general any mechanical failures that may occur that could alter the thermal conditions. Protection systems may, for example, fall off in case of fire exposure and completely change the thermal conditions. Such phenomena must be investigated by full-scale tests and, therefore, new types of structural systems must in general be tested in full scale in standard furnace tests as a basis for type approval and so on. Calculation methods can, however, be used for generalizations or extensions of test results to various dimensions and configurations.

Heat Transfer to Structures

Heat is transferred from hot fire gases to structures by convection and radiation. The

M.J. Hurley (ed.), *SFPE Handbook of Fire Protection Engineering*,
DOI 10.1007/978-1-4939-2565-0_34, © Society of Fire Protection Engineers 2016

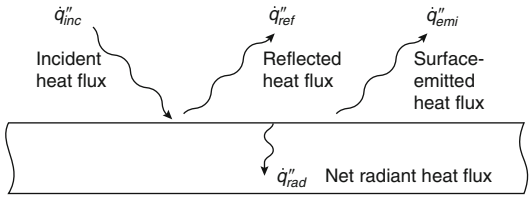

Fig. 34.1 Heat transfer by radiation to a surface, which depends on incident radiation, surface absolute temperature, and surface emissivity

contributions of these two modes of heat transfer are in principal independent and must be treated separately. The convective heat transfer depends on the temperature difference between the target surface and the surrounding gas and the velocity of the gas masses in the vicinity of the exposed surface, whereas the incident heat radiation on a surface originates from surrounding flames and gas masses as well as other surrounding surfaces.

Thus, the total heat flux $\dot{q}''_{\mathrm{tot}}$ to a surface is

$$\dot{q}''_{\mathrm{tot}} = \dot{q}''_{\mathrm{rad}} + \dot{q}''_{\mathrm{con}} \tag{34.1}$$

where $\dot{q}''_{\mathrm{rad}}$ is the net radiation heat flux and $\dot{q}''_{\mathrm{con}}$ is the heat transfer to the surface by convection. Details of these two contributions to follow.

Radiation

The net radiation heat flux $\dot{q}''_{\mathrm{rad}}$ depends on the incident radiation $\dot{q}''_{\mathrm{inc}}$, on the surface emissivity/absorptivity, and on the fourth power of the absolute temperature T_s of the targeted surface. The heat exchange at a surface is illustrated in Fig. 34.1.

Part of the incident radiation is absorbed and the rest $\dot{q}''_{\mathrm{ref}}$ is reflected. Then the surface emits heat by radiation $\dot{q}''_{\mathrm{emi}}$ depending on the emissivity and the surface absolute temperature to the fourth power. Thus, the net radiative heat can be written

$$\dot{q}''_{\mathrm{rad}} = \alpha_s \dot{q}''_{\mathrm{inc}} - \varepsilon_s \sigma T_s^4 \tag{34.2}$$

where α_s and ε_s are the target surface absorptivity and emissivity, respectively. In this presentation the surface emissivity and absorptivity are assumed equal according to the Kirchhoff's identity. Thus,

$$\dot{q}''_{\mathrm{rad}} = \varepsilon_s \left(\dot{q}''_{\mathrm{inc}} - \sigma T_s^4 \right) \tag{34.3}$$

The incident radiation to a surface is emitted by surrounding gas masses and in case of fire by flames and smoke layers and/or by other surfaces. It depends on the fourth power of the absolute temperature. The emissivity and absorptivity of gas masses and flames increase with depth and become, therefore, in general more important in large-scale fires than in, for example, small-scale experiments. In real fires surfaces are exposed to radiation from a large number of sources (surfaces, flames, gas masses, etc.) of different temperatures and emissivities. The heat fluxes are then in general very complicated to model. A simple summation of the main contributions yields in general a good estimate; that is,

$$\dot{q}''_{\mathrm{inc}} = \sum \varepsilon_i F_i \sigma T_i^4 \tag{34.4}$$

where ε_i is the emissivity of the ith source, F_i and T_i are the corresponding view factor (see Chap. 4, "Radiation Heat Transfer," of this handbook) and temperature, respectively. Equation 34.4 may then be inserted in Equation 34.3 to get

$$\dot{q}''_{\mathrm{rad}} = \varepsilon_s \sigma \left(\sum \varepsilon_i F_i T_i^4 - T_s^4 \right) \tag{34.5}$$

or

$$\dot{q}''_{\mathrm{rad}} = \varepsilon_s \sigma \left(T_r^4 - T_s^4 \right) \tag{34.6}$$

where T_r is here termed the black body radiation temperature or just the radiation temperature. T_r is a weighted average identified as

$$T_r^4 \equiv \sum \varepsilon_i F_i T_i^4 \tag{34.7}$$

The emissivities as used above are surface properties, in principle independent of the fire conditions.

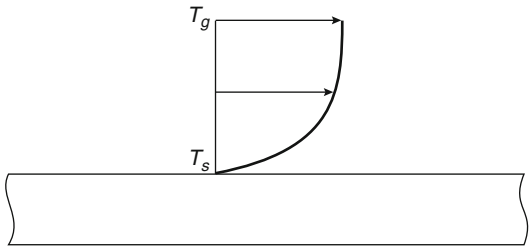

Fig. 34.2 Gas velocity profile, with the heat transfer by convection depending on the temperature difference between the adjacent gases and the target surface and on the gas velocity

Convection

The heat transferred by convection from adjacent gases to a surface varies a lot depending on adjacent gas velocities and geometries (Fig. 34.2).

In most cases it may be written as

$$\dot{q}''_{con} = h\left(T_g - T_s\right)^n \tag{34.8}$$

where h is the convective heat transfer coefficient and T_g is the gas temperature adjacent to the exposed surface. In cases of surfaces heated or cooled by natural or free convection a value of n greater than unity is motivated depending on flow conditions [1].

In fires the heat transfer conditions by convection may vary a lot and the parameters h and n are very hard to determine accurately. However, as radiation heat transfer dominates and the convective conditions are not decisive for the total heat transfer to fire exposed structures, the exponent n is assumed equal to unity for simplicity in most fire engineering cases. Thus,

$$\dot{q}''_{con} = h\left(T_g - T_s\right) \tag{34.9}$$

The convective heat transfer coefficient h depends mainly on flow conditions in the vicinity of the surface and not so much on the surface or the material properties.

Total Heat Transfer and Adiabatic Surface Temperature

The total heat transfer to a surface may now be obtained by adding the contributions by radiation and convection. Thus, by inserting Equations 34.6 and 34.9 into Equation 34.1, the total heat flux to a surface becomes

$$\dot{q}''_{\text{tot}} = \varepsilon_s\sigma\left(T_r^4 - T_s^4\right) + h\left(T_g - T_s\right) \tag{34.10}$$

In most fire engineering design cases the radiation temperature T_r and the gas temperature T_g are assumed equal to a fire temperature T_f. Then the total heat transfer may be calculated as

$$\dot{q}''_{\text{tot}} = \varepsilon_s\sigma\left(T_f^4 - T_s^4\right) + h\left(T_f - T_s\right) \tag{34.11}$$

or

$$\dot{q}''_{\text{tot}} = h_{\text{tot}}\left(T_f - T_s\right) \tag{34.12}$$

where the combined total heat transfer coefficient h_{tot} may be identified from Equations 34.11 and 34.12 as

$$H = \varepsilon_s\sigma\left(T_f^2 - T_s^2\right)\left(T_f + T_s\right) + h \tag{34.13}$$

Alternatively the two boundary temperatures in Equation 34.10, T_r and T_g, may be combined to one effective temperature T_{AST}, the adiabatic surface temperature. This temperature is defined as the temperature of a surface of an ideally perfectly insulating material, i.e. a surface which cannot absorb any heat [2]. Thus, T_{AST} is defined by the surface heat balance equation

$$\varepsilon_s\sigma\left(T_r^4 - T_{AST}^4\right) + h\left(T_g - T_{\text{AST}}\right) = 0 \tag{34.14}$$

The value of T_{AST} is always between T_r and T_g.

Then the total heat transfer may be written as

$$\dot{q}''_{\text{tot}} = \varepsilon_s\sigma\left(T_{AST}^4 - T_s^4\right) + h\left(T_{AST} - T_s\right) \tag{34.15}$$

The adiabatic surface temperature T_{AST} can in many cases be measured, and it may be used for calculating heat transfer to fire-exposed surfaces based on practical tests, as discussed later. It can also be obtained from numerical CFD modeling of fires using computer codes like FDS [2, 3].

Heat Transfer to Fire-Exposed Structures

Based on Equations 34.11 and 34.12 the heat transfer to a fire-exposed surface can be calculated for given fire and surface temperatures T_f and T_s. The emissivity ε_s is a surface property, which can be assumed to equal 0.8 for most building materials except for shiny steel where a lower value may be assumed. The convection coefficient h is not decisive for the temperature development near a fire-exposed surface of a structure as the radiative heat transfer dominates at high temperatures. In Eurocode 1 [4] a value of 25 W/m^2 K is recommended at fire-exposed surfaces. The temperature on the nonexposed side of a separating structure will, on the other hand, depend very much on the heat transfer conditions including the convection coefficient. In Eurocode 1 in this case a convective heat transfer coefficient value of 4 W/m^2 K is recommended.

In many cases, however, a fire-exposed surface will get temperatures very close to the fire temperature (i.e., $T_f \approx T_s$). This approximation applies for insulation materials with a low density and a low thermal conductivity. It may facilitate calculations considerably and is here applied on calculating temperature in insulated steel structures (as discussed later). Even a normal weight concrete surface will get a temperature of 90 % of the fire temperature after 30 min (as shown in Fig. 34.19, later in the chapter).

The heat transfer conditions may be very decisive for the temperature development in a fire-exposed bare steel structure (see discussion on unprotected steel structures later in the chapter). They are also very important for the temperature development on the back side of a fire-separating element. This is in particular the case for light weight structures where the thermal insulation properties are decisive rather than the thermal inertia.

Calculating Heat Transfer Using Plate Thermometer Temperatures

So-called *plate thermometers* are used to monitor the temperature in fire resistance furnaces according to the international standard ISO 834 and the European standard EN 1363-1. A plate thermometer (PT) consisting of an Inconel (trade name for a nickel-based superalloy) plate insulated on its back side is shown in Fig. 34.3. A thermocouple fixed to the plate registers its temperature. Figure 34.4 shows plate thermometers

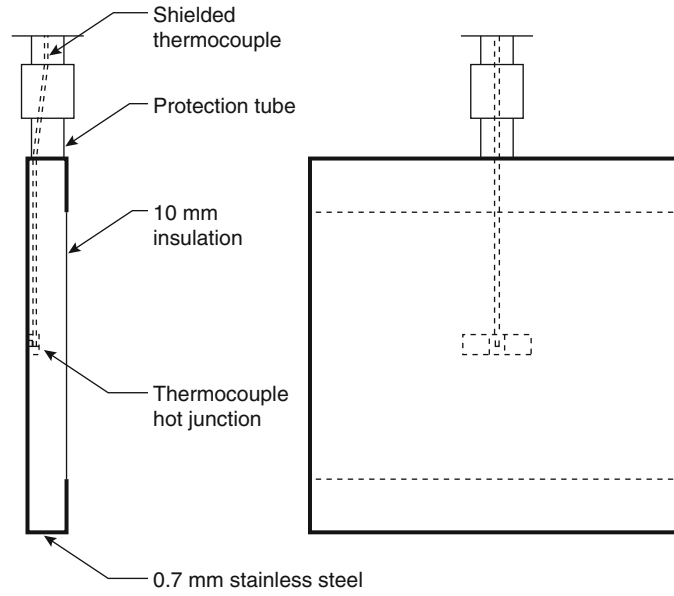

Fig. 34.3 The plate thermometer according to ISO 834 and EN 1363-1 is made of a shielded thermocouple welded to the center of a 0.7-mm-thick Inconel plate, which is insulated on its back side. The exposed front face is 100 mm by 100 mm

Fig. 34.4 Plate thermometers being mounted around a steel girder for measuring local thermal exposures. Note that the plate thermometers are mounted so that the front sides of the steel plates are exposed to roughly the same incident radiation as the girder and the back sides are insulated

being mounted at a steel girder with the insulated back side facing the specimen. The front side of the plate thermometer is exposed to approximately the same heating, including radiation conditions, as the specimen. The exposed surface of the plate thermometer is relatively large and, therefore, its sensitivity to convective heat transfer is about the same as that of the specimen surface. The steel plate is thin, only 0.7 mm, and thus responds quickly to temperature changes. As a matter of fact the plate thermometer in a standard fire resistance test measures approximately the temperature of an adiabatic surface (i.e., the temperature of an ideally perfect insulator exposed to the same heating conditions as the specimen surface, as discussed earlier).

The plate thermometer was introduced mainly to harmonize fire endurance tests (see Wickström and Hermodsson [5]), but the measured temperatures are also well suited as input for calculating heat transfer by radiation and convection to fire-exposed surfaces.

As any surface, the plate thermometer surface exchanges heat by radiation and convection. The sum of these equals the transient heat for raising the temperature of the Inconel plate and the backing insulation. Because the plate is thin and does not lose much heat on its back side, this sum is small and can be neglected except for the very first few minutes of a standard test. Thus, the heat balance of the plate can be written as

$$\varepsilon_{\mathrm{PT}}\left(\dot{q}''_{\mathrm{inc}} - \sigma T_{\mathrm{PT}}^4\right) + h_{\mathrm{PT}}\left(T_g - T_{\mathrm{PT}}\right) = 0 \tag{34.16}$$

or

$$\varepsilon_{\mathrm{PT}}\sigma\left(T_r^4 - T_{\mathrm{PT}}^4\right) + h_{\mathrm{PT}}\left(T_g - T_{\mathrm{PT}}\right) = 0 \tag{34.17}$$

The index PT refers to plate thermometer. This means the plate thermometer yields the adiabatic temperature of the specimen for a given surface emissivity and a given convective heat transfer coefficient.

An approximate alternative expression of the net heat transfer $\dot{q}''_{\text{tot}}$ to a specimen surface can now be obtained in terms of one effective temperature only by deducting Equation 34.17 from Equation 34.10:

$$\dot{q}''_{\text{tot}} = \varepsilon_s \sigma \left(T_{\text{PT}}^4 - T_{\text{s}}^4\right) + h(T_{\text{PT}} - T_{\text{s}}) \quad (34.18)$$

In other words the adiabatic surface temperature is approximated by the plate thermometer temperature. This rewriting of Equation 34.10 facilitates the calculations in many cases. The error $\Delta\dot{q}''$ introduced can be quantified by a simple algebraic analysis as

$$\begin{aligned}\Delta\dot{q}'' = {} & (\varepsilon_s - \varepsilon_{\text{PT}})\sigma\left(T_r^4 - T_{\text{PT}}^4\right) \\ & + (h_s - h_{\text{PT}})\left(T_g - T_{\text{PT}}\right)\end{aligned} \quad (34.19)$$

Thus, the error is small when the surface emissivity of the plate thermometer and the specimen are nearly the same and when the convective heat transfer coefficients are nearly the same. Therefore, the surfaces of the plate thermometers are blasted and heat-treated before being used to get an emissivity of about 0.8. It also has a relatively large surface, 100 mm by 100 mm, to obtain a convection heat transfer coefficient similar to a specimen. Because T_{PT} always has a value between T_r and T_g, the error vanishes when these two temperatures are close.

Modeling of Heat Conduction in Materials

Heat Conduction in Solid Materials

Heat or energy is conducted in solid materials due to temperature gradients. In one dimension in the x-direction the rate of heat transfer or heat flux is expressed according to Fourier's law as

$$\dot{q}''_x = -k\frac{\partial T}{\partial x} \quad (34.20)$$

where k is the thermal conductivity.

In fire problems the most usual objective is to determine the temperature distribution in a structure resulting from conditions imposed on its boundaries. Because these conditions vary with time, the temperature field will be transient or unsteady. It is then governed by the *heat diffusion equation*, which in one dimension is expressed as

$$\frac{\partial}{\partial x}\left(k\frac{\partial T}{\partial x}\right) = \rho c\frac{\partial T}{\partial t} \quad (34.21)$$

where ρ is density, c is specific heat of the material.

If the conductivity k is constant, Equation 34.21 may be written as

$$\frac{\partial T^2}{\partial^2 x} = \frac{1}{\alpha}\frac{\partial T}{\partial t} \quad (34.22)$$

where α is the thermal diffusivity defined as $\alpha = k/\rho c$.

At the boundaries Fourier's law applies and may be expressed as

$$\dot{q}''_x(0) = -k\left.\frac{\partial T}{\partial x}\right|_{x=0} \quad (34.23)$$

Three types of boundary conditions may occur.

1. Given surface temperature: $T(0,t) = T_s$
2. Given surface heat flux: $-k\frac{\partial T}{\partial x}\big|_{x=0} = \dot{q}''_s$
3. Given convection and radiation conditions, for example: $-k\frac{\partial T}{\partial x}\big|_{x=0} = h\left(T_f - T_s\right) + \varepsilon\sigma\left(T_f^4 - T_s^4\right)$

All the specified boundary conditions, T_s, q_s, and T_f, may vary with time. A special type of heat flux boundary condition is the adiabatic or perfectly insulated surface where q_s is equal to zero.

The heat diffusion equation can be solved analytically only in some uncomplicated cases (see Chap. 2, "Conduction of Heat in Solids," of this book). Numerical methods are usually needed as boundary conditions in general are nonlinear and material properties vary with temperature. There are mainly two types of numerical methods, finite difference and finite element methods, depending on how the geometry is approximated and how the temperature field is

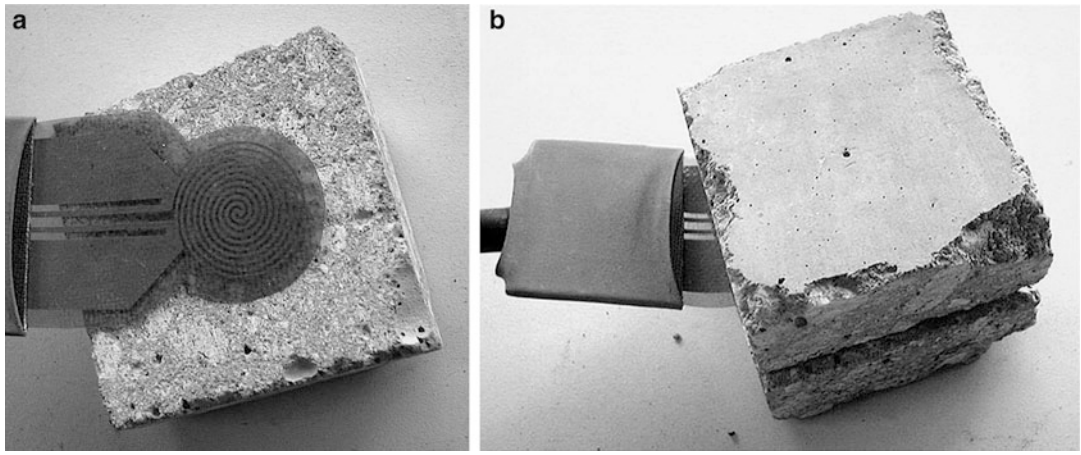

Fig. 34.5 The TPS sensor placed between two pieces of a concrete specimen

expressed by a limited number of discrete temperatures. The finite element method is described briefly later for the one-dimensional case.

Measurement of Thermal Properties

There are a number of techniques to measure thermal properties, each of them suitable for a limited range of materials, depending on thermal properties and temperature level (e.g., see Flynn [6]). However, only a few of the measuring techniques can be used at high temperature levels relevant for fire conditions. They can be divided into steady-state and transient techniques.

The steady-state techniques perform the measurements when the material is in complete equilibrium. Disadvantages of these techniques are that it generally takes a long time to reach the required equilibrium and that at low temperature the measurements are influenced by moisture migration. For moist materials like concrete, it is therefore often preferable to determine the apparent conductivity or thermal diffusivity with transient techniques. These techniques perform the measurements during a process of small temperature changes and can be made relatively quickly.

The guarded hot plate is the most common steady-state method for building materials with a relatively low thermal conductivity [7]. It is quite reliable at moderate temperatures up to about 400 °C.

Because transient thermal processes dominate in fire safety engineering, the thermal diffusivity, a measure of the speed at which temperature is propagating into a material, is the most interesting parameter. It is naturally best measured with transient methods. One of the most interesting techniques is the transient plane source method (TPS). In this method a membrane, TPS sensor, is located between two specimen halves and acts as a heater as well as a temperature detector (Fig. 34.5). By using this technique, thermal diffusivity, thermal conductivity, and volumetric specific heat can be obtained simultaneously for a variety of materials like metals, concrete, mineral wool, and even liquids and films [8].

Finite Element Calculations of Temperature in Fire-Exposed Structures

When calculating temperature in fire-exposed structures nonlinearities must in most cases be considered. The boundary conditions are nonlinear varying dramatically with temperature as shown above, and also the thermal properties of most materials vary significantly within the wide temperature span that must be considered in fire safety engineering problems. Therefore, numerical methods must be employed. The most general

and powerful codes today are based on the so-called finite element method (FEM).

Basic Equations Derived for One-Dimensional Case

The basic equations that follow are derived for a simple one-dimensional case as an illustration. The same type of equation may be derived for two and three dimensions.

Figure 34.6 shows a wall that has been divided into a number of one-dimensional elements. The temperature between the nodes is assumed to vary linearly along the length.

In any element, interior or at the surface, with length L, conductivity k, and a section area A (Fig. 34.7), the heat flow at the nodes can then be calculated as

$$q_1 = -kA/L^*(T_1 - T_2)$$

and

$$q_2 = -kA/L^*(-T_1 + T_2)$$

or in matrix format as

$$\overline{q}^e = \overline{k}^e \overline{T}^e \tag{34.24}$$

where $\overline{q}^e$ is the element node heat flow vector, $\overline{k}^e$ is the element heat conduction matrix, and $\overline{T}^e$ is the element node temperature vector. The element heat conduction matrix may then be identified as

$$\overline{k}^e = \begin{Bmatrix} k^e_{1,1} & k^e_{1,2} \\ k^e_{2,1} & k^e_{2,2} \end{Bmatrix} = (kA/L)\begin{Bmatrix} 1 & -1 \\ -1 & 1 \end{Bmatrix} \tag{34.25}$$

and the element nodal temperature and heat flow vectors as $\overline{T}^e = \begin{Bmatrix} T_1 \\ T_2 \end{Bmatrix}$ and $\overline{Q}^e = \begin{Bmatrix} Q_1 \\ Q_2 \end{Bmatrix}$ respectively.

In a similar way an element heat capacity matrix can be defined by lumping the heat capacity of the element in the nodes. Thus, an element heat capacity matrix may be obtained as

$$\overline{c}^e = \frac{ALcp}{2}\begin{Bmatrix} 1 & 0 \\ 0 & 1 \end{Bmatrix} \tag{34.26}$$

When several elements are combined, the global thermal conductivity matrix $\overline{K}$ can be assembled. In the very simple case of three one-dimensional elements the global heat conduction matrix becomes

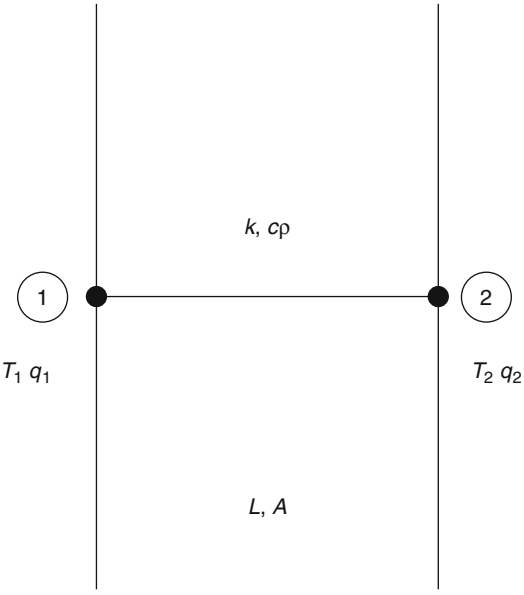

Fig. 34.7 A one-dimensional element with local element node numbers *1* and *2*, length L, and a section area A. The element is given a thermal conductivity k, a specific heat capacity c, and a density ρ

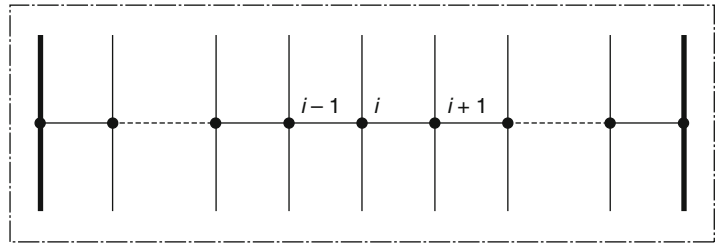

Fig. 34.6 A wall divided into one-dimensional elements

$$\overline{K} = \begin{Bmatrix} k^1_{1,1} & k^1_{1,2} & 0 & 0 \\ k^1_{2,1} & \left(k^1_{2,2} + k^2_{1,1}\right) & k^2_{1,2} & 0 \\ 0 & k^2_{2,1} & \left(k^2_{2,2} + k^3_{1,1}\right) & k^3_{1,2} \\ 0 & 0 & k^3_{2,1} & k^3_{2,2} \end{Bmatrix} \tag{34.27}$$

where the superscripts 1–3 denote element numbers. The global heat capacity matrix $\overline{C}$ may be assembled in a similar way as the global conductivity matrix. Notice that both the thermal conductivity and the heat capacity matrices are symmetric and dominated by their diagonal elements, and that the global heat capacity matrix assembled from element matrices according to Equation 34.26 will have nonzero elements only in the diagonal. This will have a decisive influence on how the global algebraic heat balance equation can be solved as shown below.

In global form the heat balance equation may now be written as

$$\overline{C}\,\dot{\overline{T}} + \overline{K}\,\overline{T} = \overline{Q} \tag{34.28}$$

where $\dot{\overline{T}}$ is the time derivative of the node temperatures. Each row in this equation system represents the heat balance of a node. For each equation or each node either the temperature or the heat flow given in the corresponding rows in the vectors $\overline{T}$ and $\overline{Q}$, respectively, is known. In principle three options are possible for each equation/row:

1. The node temperature T_i is prescribed.
2. The node heat flow Q_i is prescribed.
3. The node heat flow Q_i can be calculated as a function of a given gas temperature and the surface temperature.

In the first case the corresponding equation vanishes as the unknown quantity is prescribed. The most common case for internal nodes is the second case (i.e., the external flow is zero).

A typical boundary condition when calculating temperature in fire-exposed structures is according to the third option. Based on, for example, Equation 34.11, the external heat flow to the ith node becomes

$$Q_i = A_i\left\{\varepsilon\sigma\left(T_f^4 - T_i^4\right) + h\left(T_f - T_i\right)\right\} \tag{34.29}$$

where A_i is the section area of the ith node. The differential equation given in Equation 34.28 can be solved numerically by approximating the time derivative as

$$\dot{\overline{T}} = \frac{\left(\overline{T}^{j+1} - \overline{T}^{j}\right)}{\Delta t} \tag{34.30}$$

where $\overline{T}^{j}$ is the node temperature vector at time step j and Δt is a chosen time increment. Now the heat balance equation in matrix format (Equation 34.28) can be written as

$$\overline{C}\left(\overline{T}^{j+1} - \overline{T}^{j}\right)/\Delta t + \overline{K}\,\overline{T} = \overline{Q} \tag{34.31}$$

In this differential equation the temperature vector is known at time increment j. The new temperature vector at time $j + 1$ is obtained either explicitly based on the conditions at time step j as

$$\overline{T}^{j+1} = \overline{C}^{-1}\left(\overline{Q}^{j} - \overline{K}\,\overline{T}^{j}\right)\Delta t + \overline{T}^{j} \tag{34.32}$$

or implicitly as

$$\overline{T}^{j+1} = \left(\overline{C}/\Delta t + \overline{K}\right)^{-1}\left(\overline{Q}^{j} + \overline{C}\,\overline{T}^{j}/\Delta t\right) \tag{34.33}$$

Combinations of the solution schemes according to Equations 34.32 and 34.33 are also possible. All such schemes require the solution of an equation system containing as many unknowns as there are unknown node temperatures. Most finite element computer codes use such types of implicit solution schemes. They are numerically more stable than the explicit techniques (i.e., longer time increments may be used).

The explicit solution according to Equation 34.32 may be very simple when the heat capacity matrix $\overline{C}$ is diagonal (i.e., it contains only nonzero elements in the diagonal as shown for a one-dimensional element in Equation 34.26). The solution of the equation system

then becomes trivial because each nodal temperature can be obtained directly/explicitly one at a time. This solution scheme is numerically stable only when the time increment Δt is less than a critical value proportional to the heat capacity over the thermal conductivity of the material times the square of an element length dimension Δx (see Equation 34.34). This requirement applies to all the equations of the entire system. If violated in any of the equations (i.e., at any point of the finite element model), the incremental solution equation will turn unstable.

$$\Delta t_{cr} \approx \frac{c\,p}{k}(\Delta x)^2 \qquad (34.34)$$

A similar condition applies to boundaries of type 3 (e.g., according to Equation 34.29).

This means that short time increments are needed for materials with a low density and a high conductivity and when small elements are used. For information on critical time increments, see Sterner and Wickström [9].

In practice, when calculating temperature in fire-exposed structures, numerical stability is only a problem when modeling sections of thin metal sheets with high thermal conductivity. Then according to Equation 34.34, very short time increments are required. The problem may, however, be avoided by prescribing that nodes close to each other shall have the same temperature. This technique has been applied in the code TASEF [9]. In this code a technique is also developed in which the critical time increment is estimated and thereby acceptable time increments can be calculated automatically at each time step.

Available Computer Codes for Temperature Calculations

Several computer codes are commercially available for calculating temperature in fire-exposed structures. In general modern codes are based on the finite element method. Some are specifically developed and optimized for calculating temperature in fire-exposed structures whereas others are more general-purpose codes.

TASEF [10, 11] and SAFIR [12] are examples of programs that have been developed for fire safety problems. They both for temperature-dependent material properties and boundary conditions. TASEF employs a forward difference solving technique, which makes it particularly suitable for problems in which latent heat due to, for example, evaporation of water must be considered. It yields in most cases very short computing times, in particular for problems with a large number of nodes. Both TASEF and SAFIR have provisions for modeling heat transfer by convection and radiation in internal voids. TASEF can be obtained from TASEF Ltd., UK and SAFIR from the University of Liège, Belgium.

There are many very advanced general-purpose finite element computer codes commercially available such as ABAQUS [13], ANSYS [14], ADINA [15], HEATING [See www.oecd-nea.org/tools/abstract/detail/psr-0199/] and Comsol [16]. The main advantage of using such codes is that they can be used in combination with structural codes and that they come with advanced graphical user interfaces and postprocessors.

Accuracy of Finite Element Computer Codes

At the least the following three steps must be considered when estimating the accuracy of computer codes for numerical temperature calculations:

1. Validity of calculation model
2. Accuracy of material properties
3. Accuracy and reliability of the numerical algorithms of the computer code

The first point is, of course, important. For example, the effects of spalling or water migration cannot be accurately predicted with a code based on just heat transfer according to the Fourier heat transfer equation.

The second point is also crucial. Errors in material property input will be transmitted into output errors. Methods for measuring material properties at high temperature were briefly discussed earlier.

Finally, the numerical verification of the computer code itself is also important. By definition, *verification* is the process of determining that a model implementation accurately represents the developer's conceptual description of the model and the solution to the model [17]. If correctly used, most codes yield results with acceptable accuracy. A scheme to follow including a number of reference cases of various levels of complexity have recently been presented in an SFPE standard [Standard on calculation methods to predict the thermal performance of structural and fire resistive assemblies, please ask Chris Jelenewicz for advice on the status of the standard] partly based on cases earlier suggested by Wickström and Pålsson [18] and Wickström [19]. It is mainly developed for finite element codes but it may also be used for codes based on finite difference principles. The first reference example is a linear problem that can be solved analytically. When increasing the number of elements the results should converge to one correct value. Codes yielding results that converge smoothly when increasing the number of elements are generally deemed reliable for the type of problems considered. The scheme suggested employs problems that are relevant for fire safety engineering, including effects of conductivity varying with temperature, latent heat, radiant heat transfer boundary conditions, and combinations of materials, concrete, steel, and mineral wool. For the development of the SFPE standard the computer codes ABAQUS and TASEF were used to obtain solutions which were deemed reliable as these codes use different solutions algorithms.

Calculation of Temperature in Steel Structures

Metals in general conduct heat very well. The thermal conductivity of steel is on the order of 30 times higher than the corresponding value for concrete and 100–1000 times higher than that of insulation products. Therefore, the temperature field in a steel section may in many fire engineering cases be assumed uniform. In particular the temperature across the thickness of a steel sheet will be uniform, whereas the temperature in the plane of the sheet may vary considerably, depending on boundary conditions. The methods presented in Chap. 53, "Analytical Methods for Determining Fire Resistance of Steel Members," assume uniform steel section temperatures. Then zero- or one-dimensional calculation techniques may often be used. For more general two- and three-dimensional cases, numerical computer codes are needed.

Thermal Properties of Steel

The thermal conductivity of carbon steel as a function of steel temperature according to Eurocode 3 [20], is shown in Fig. 34.8. It can also be obtained from Table 34.1.

The specific heat capacity is in most cases more important than the conductivity. In many cases it is accurate enough and convenient to assume a constant specific heat capacity. However, for more accurate calculations the variations with temperature as shown in Fig. 34.9 [20] or given in Table 34.2 are recommended in Eurocode 3 [20]. This specific heat capacity varying with temperature yields in general lower calculated temperatures than when a constant value of 500 J/(kg K) is assumed.

Insulated Steel Structures

In particular in the case of *insulated steel sections* the steel temperature over a section may be assumed uniform. Then the surface heat transfer resistance $1/h_{tot}$ is in most cases negligible in comparison with the heat resistance (i.e., the thickness over the conductivity of the insulation d_i/k_i). h_{tot} is the combined heat transfer coefficient due to radiation and convection as given in Equation 34.13. The fire-exposed surface temperature is then approximately the same as the

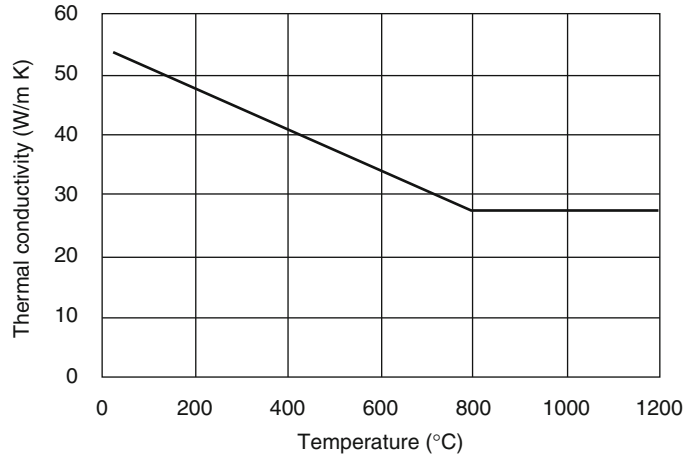

Fig. 34.8 Thermal conductivity of steel as a function of the temperature

Table 34.1 Thermal conductivity of carbon steel as a function of the temperature [20]

Temperature (°C)	Conductivity (W/m K)
$20 < T_{st} < 800$	$54 - 3.33 \times 10^{-2}\, T_{st}$
$800 < T_{st} < 1200$	27.3

fire temperature, and the heat transfer to the steel may under steady-state conditions be approximated as

$$q_{\text{tot}} = A_s(k_i/di)\left(T_f - T_s\right) \tag{34.35}$$

where A_s is the fire-exposed area, and T_f and T_s are the fire and steel temperatures, respectively. If the heat capacity of the insulation is negligible in comparison to that of the steel, transient steel temperature can be obtained from the heat balance equation

$$As(k_i/di)\left(T_f - T_s\right) = c_s\rho_s V_s(\partial T_s/\partial t) \tag{34.36}$$

where c_s and ρ_s are the specific heat capacity and density, respectively, of steel and V_s is the volume per unit length of the considered steel section. In case of heavy insulations when the heat capacity of the insulation cannot be neglected, see the following section on heavily insulated steel structures.

A very simple solution can be obtained if a constant fire temperature rise and constant material properties are assumed; that is,

$$(T_s - T_0) = \left(T_f - T_0\right)\left[1 - \mathrm{e}^{-(t/\tau)}\right] \tag{34.37}$$

where the characteristic response time or time constant τ of the section is identified as

$$\tau = c_s\rho_s V_s/A_s(k_i/d_i) = (d_i/k_i)(c_s\rho_s)/(A_s/V_s) \tag{34.38}$$

The relation A_s/V_s is denoted the section factor or the shape factor that has the dimension one over length. Instructions on how to obtain this factor for various configurations are given in Table 34.3.

For a fire temperature T_f arbitrarily varying with time or when the material properties vary with temperature, the steel temperature may be obtained (e.g., from the numerical scheme derived from Equation 34.36) as

$$\Delta T_s/\Delta t = \left(T_f^i - T_s^i\right)/\tau \tag{34.39}$$

where ΔT_s equals $\left(T_s^{i+1} - T_s^i\right)$ and Δt are the steel temperature rise and the time increment, respectively. The superscripts i and $i + 1$ denote the numerical order of the time increments. When the thermal properties vary with temperature, the time constant τ as defined by Equation 34.38 needs to be updated at each time increment. A forward difference solution scheme can be obtained as

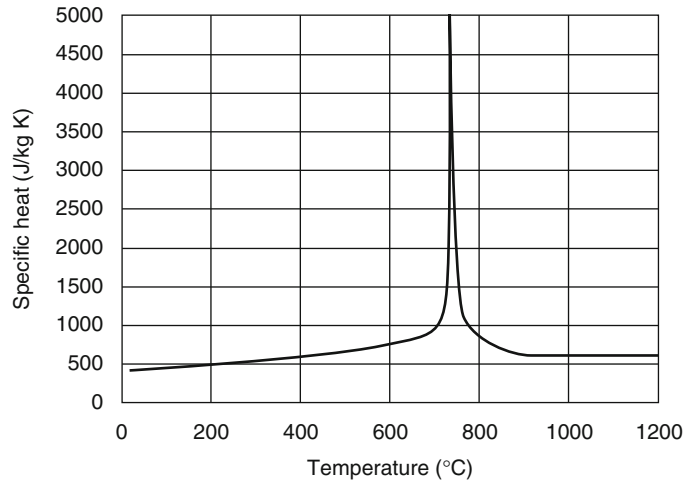

Fig. 34.9 Specific heat of steel as a function of the temperature [20]

Table 34.2 Specific heat capacity of carbon steel as a function of the temperature [21]

Temperature (°C)	Specific heat capacity (J/[kg K])
$20 < T_{st} < 600$	$425 + 7.73 \times 10^{-1}\, T_{st} - 1.69 \times 10^{-3}\, T_{st}^2 + 2.22 \times 10^{-6}\, T_{st}^3$
$600 < T_{st} < 735$	$666 + 13{,}002/(738 - T_{st})$
$735 < T_{st} < 900$	$545 + 17{,}820/(T_{st} - 731)$
$900 < T_{st} < 1200$	650

$$T_s^{i+1} = \Delta t/\tau \cdot T_f^i + (1 - \Delta t/\tau) \cdot T_s^i \qquad (34.40)$$

This forward difference scheme is, however, numerically stable only if

$$\Delta t \leq \tau = (d_i/k_i)(c_s\rho_s)/(A_s/V_s) \qquad (34.41)$$

This condition must be fulfilled at each time increment. In practice time increments Δt longer than 10 % of that critical value should not be used to ensure accurate results.

Heavily Insulated Steel Structures

The heat capacity of the insulation normally has an insignificant influence on the steel temperature rise rate. However, it will considerably reduce the steel temperature rise of sections protected with relatively heavy insulation. A simple approximative approach is then to lump a third of the heat capacity of the insulation to the steel [22–24]. Equation 34.39 may then be modified as

$$\Delta T_s/\Delta t = \left(T_f^i - T_s^i\right)/[\tau(1 + \mu/3)] + [exp(\mu/10) - 1]\Delta T_f/\Delta t \qquad (34.42)$$

where μ is the relation between the heat capacity of the insulation and the steel,

$$\mu = (A_i d_i \rho_i c_i)/(V_s \rho_s c_s) \qquad (34.43)$$

and where ρ_i and c_i are the density and the specific heat capacity of the insulation, respectively. When the material properties vary with temperature, they may be updated at each time increment. The latter term of Equation 34.42 represents a time delay due to the heat capacity of the insulation. ΔT_f is the fire temperature rise between two time increments. Notice that when the heat capacity of the insulation is much smaller than that of the steel, μ vanishes and Equation 34.42 becomes identical to Equation 34.39.

Table 34.3 Section factor A_s/V_s for steel members insulated by fire protection material [20]

Sketch	Description	Section factor (A_s/V_s)
	Contour encasement of uniform thickness	Steel perimeter / Steel cross-sectional area
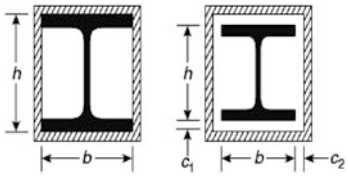	Hollow encasement of uniform thickness[a]	$2(b + h)$ / Steel cross-sectional area
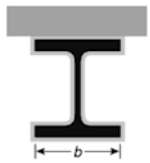	Contour encasement of uniform thickness, exposed to fire on three sides	Steel perimeter – b / Steel cross-sectional area
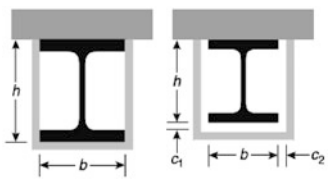	Hollow encasement of uniform thickness, exposed to fire on three sides[a]	$2h + b$ / Steel cross-sectional area

[a]The clearance dimensions c_1 and c_2 should not normally exceed $h/4$

Equation 34.42 has been adopted by Eurocode 3 [20]. The steel temperature can then be obtained, for example, by a forward difference scheme derived from Equation 34.42 as

$$T_s^{i+1} = T_s^i + \Delta t\left(T_f^i - T_s^i\right)/[\tau(1+\mu/3)] - [exp(\mu/10) - 1]\Delta T_f \tag{34.44}$$

As an illustration of the importance of considering the heat capacity of the insulation, a simple example of a steel section is analyzed considering the relative heat capacity μ of the insulation and for comparison neglecting it (i.e., $\mu = 0$). A section factor $A_i/V_s \approx A_s/V_s = 500\ \mathrm{m}^{-1}$ and an insulation thickness $d_i = 0.05$ m, a conductivity $k_i = 0.2$ W/m K, and a specific heat capacity $c_i = 800$ Ws/kg are assumed. Calculated steel temperature developments applying Equation 34.44 considering and not considering the heat capacity of the insulation ($\mu = 0$) are shown in Fig. 34.10. For comparison, temperature rises obtained by accurate finite element calculations are shown as well. Notice how well the temperatures calculated by FEM match the temperatures obtained using the scheme according to Equation 34.44 considering the heat capacity of the insulation. On the other hand, the calculated temperature becomes much higher if the heat capacity of the insulation is not considered. In this case the predicted time to reach a steel temperature of 500 °C is on the

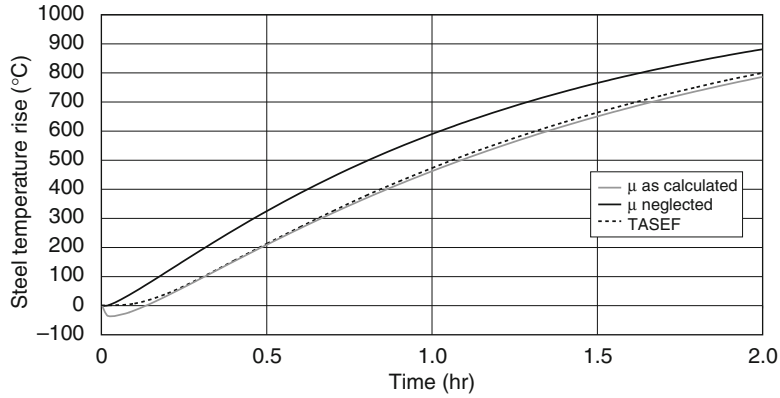

Fig. 34.10 Comparison of calculated steel temperature rise of an insulated steel section when exposed to a standard ISO 834 fire exposure, considering and neglecting the heat capacity of the insulation, respectively

order of a quarter of an hour shorter when the heat capacity is not considered. Notice also that Equation 34.44 predicts a negative temperature change for the first 5–10 min, which of course is a numerical error embedded in the equation.

Insulated Steel Structures Exposed to Parametric Fires

Eurocode 3 [20] (EN1991-2-1) has introduced the concept of parametric fires as a convenient way of expressing a set of postflashover design fires. The fire temperature T_f is then expressed as (see Eurocode 1 [4])

$$T_f = 20 + 1325\left(1 - 0.324e^{-0.2t^*} - 0.204\mathrm{e}^{-1.7t^*} - 0.472\mathrm{e}^{-19t^*}\right) \quad (34.45)$$

where the modified or scaled time is expressed as

$$t^* = \Gamma t \quad (34.46)$$

and where Γ is a function of the compartment properties (i.e., sizes of openings and thermal properties of enclosure surfaces). A Γ-value approximately equal to unity yields the ISO 834 standard fire, whereas Γ less than unity yields a more slowly growing fire and Γ greater than unity a faster growing fire. The fire duration depends on the fuel density in the fire compartment (see Eurocode 3 [20]). Below it is demonstrated how these types of design fires can facilitate the calculation and the presentation of temperature in fire-exposed insulated steel sections. The concept of parametric fires can also be used for concrete structures using the technique outlined later in this chapter.

Table 34.4 Constants in the analytical expression of the parametric fire curve

i	0	1	2	3
B_i (°C)	1325	−430	−270	−625
β_i (h^{-1})	0	−0.2	−1.7	−19

When using parametric design fires, the temperature of insulated steel sections can, of course, be obtained by numerical calculations according to Equation 34.40. Then nonlinear phenomena such as temperature-dependent material properties may be considered. However, if the thermal properties are assumed constant and the fire temperature is expressed by exponential terms as in Equation 34.45, then the steel temperature rise as a function of time can be obtained by integration as a closed-form analytic expression [25].

For convenience Equation 34.45 is first written in the form

$$T_s = 20 + \sum_{i=0}^{3} B_i \exp(-\beta_i t^*) \quad (34.47)$$

where the constants B_i and β_i are given in Table 34.4.

Then the steel temperature can be obtained as a function of the modified fire duration t^* and the modified time constant τ^* of the steel section as

$$T_s - 20 = \sum_{i=0}^{3} \frac{B_i}{1 - \beta_i \tau^*}\left[exp(-\beta_i t^*) - exp(-t^*/\tau^*)\right] \quad (34.48)$$

where

$$\tau^* = \Gamma\tau \tag{34.49}$$

The insulated steel section time constant τ is given in Equation 34.38. The relation between the temperature rise as a function of modified time as expressed in Equation 34.48 is also given in the diagram shown in Fig. 34.11 for various modified time constants τ^*. The diagram in Fig. 34.11 is particularly easy to use for ISO 834 standard fire exposures when Γ by definition is equal to unity.

As an example, consider a steel section with a section factor $A_{st}/V_{st} = 200\ \mathrm{m}^{-1}$ insulated with a 25-mm-thick protection board with a constant thermal conductivity of 0.1 W/(m K). The steel density and specific heat capacity are 7800 kg/m^3 and 500 J/(kg K), respectively. The section time constant may then be obtained from Equation 34.38 as $\tau = 4875$ s or 1.35 h. Then if the section is exposed to standard fire ($\Gamma = 1$), a temperature rise of 418 °C may be obtained from Equation 34.48 or from Fig. 34.11. If the same section is exposed to a more slowly growing fire with $\Gamma = 0.5$, then $\tau^* = \Gamma\tau = 0.68$ h and the temperature rise after 1 h may be found for a modified time of $t^* = \Gamma t = 0.5$ h to be 363 °C. On the other hand, if the section is exposed to a fast-growing fire with $\Gamma = 3.0$, then $\tau^* = (3.0) \cdot (1.35) = 4.05$ h and $t^* = (3.0) \cdot (1.0) = 3.0$ h, and the steel temperature rise can be obtained from Equation 34.47 or from Fig. 34.11 as 505 °C. Notice that the maximum steel temperature for a given fire exposure time increases considerably with an increasing Γ-factor. It must, however, also be kept in mind that the fire duration for a given fuel load is proportional to the inverse of the opening factor included in the Γ-factor. For more information see, for example, Eurocode 1 [4].

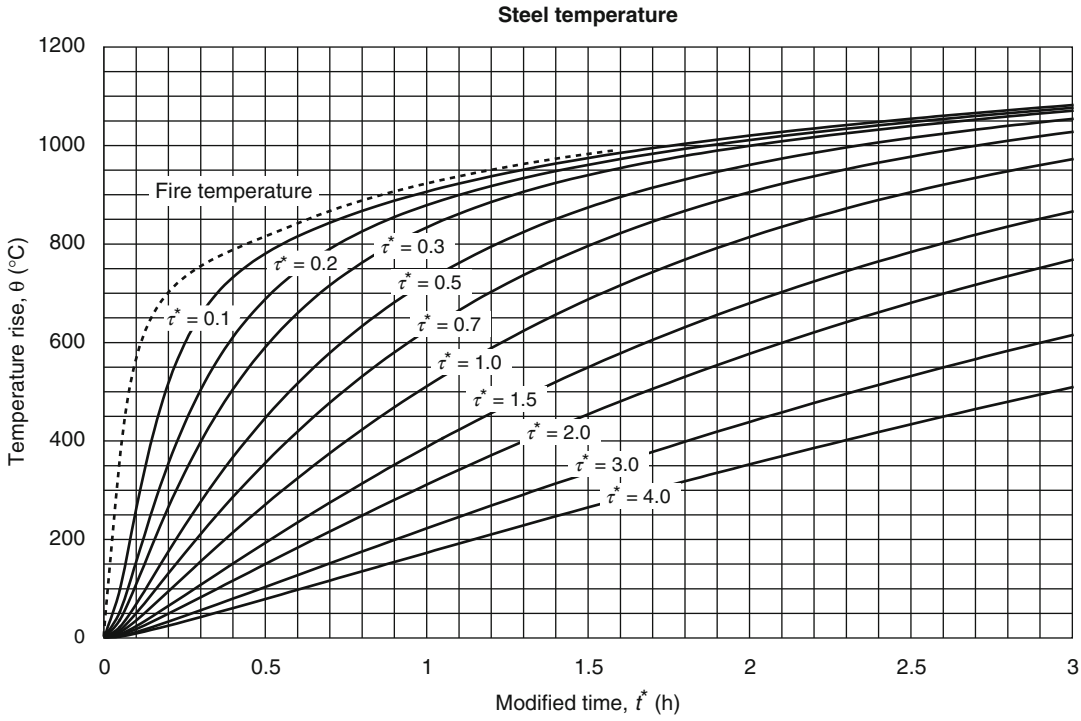

Fig. 34.11 Temperature of various insulated steel sections exposed to parametric fires in the heating phase as a function of modified time t^*. The thermal properties of the steel sections are expressed in modified time constants τ^* [25]

Unprotected Steel Structures

The temperature of unprotected steel structures is numerically more difficult to calculate as the highly nonlinear heat transfer is decisive for the temperature development of the steel. The total heat transfer q_{tot} may be obtained from Equation 34.11 or Equation 34.12. Then the steel temperature can be obtained from the differential heat balance equation in a similar way as for insulated steel sections (see also Equation 34.36).

$$h_{tot}\left(T_f - T_s\right) = c_s\rho_s(V_s/A_s)(\partial T_s/\partial t) \quad (34.50)$$

where the total heat transfer coefficient h_{tot} may be obtained from Equation 34.13. This equation can be solved numerically with a forward difference scheme in a similar way as for insulated sections as

$$T_s^{i+1} = (\Delta t/\tau)T_f^i + (1 - \Delta t/\tau)T_s^i \quad (34.51)$$

where the characteristic response time τ of the steel section in this case is defined as

$$\tau = c_s\rho_s V_s/A_s h_{tot} = (c_s\rho_s)/[h_{tot}(A_s/V_s)] \quad (34.52)$$

Notice that the thermal properties of the steel may vary with temperature, and in particular the total heat transfer coefficient h_{tot} will increase substantially with the temperature level. It would, therefore, be misleading to call τ a time constant in this case.

The stability criterion for the explicit numerical scheme according to Equation 34.51 may then be expressed as

$$\Delta t \leq \tau = (c_s\rho_s)/[h_{tot}(A_s/V_s)] \quad (34.53)$$

Thus, the critical time increment decreases considerably as h_{tot} increases with time and increasing temperature levels.

Principles for calculating the section factors for various types of configurations of unprotected steel can be found in Table 34.5 [20].

Shadow Effects

When an open section such as an I-section is exposed to fire, the heat transfer by radiation will be partly shadowed (Fig. 34.12). That means the section will only receive as much heat from the fire as if it had the same circumference as a boxed section. Therefore, it is appropriate to replace the area per unit length A_s with the so-called boxed area $A_\square$ in Equations 34.50 and 34.52 as the radiation heat transfer mode dominates at elevated temperature. The boxed area $A_\square$ is typically for an I-section 30 % less than the corresponding area A_s, which means a proportional increase of the section response time τ. Alternatively, a section with a 40 % higher section factor would yield the same temperature if the concept of shadow effects is applied. This means that by considering the shadow effects in the calculations many more open steel sections can be accepted without thermal protection.

The principal of shadow effects is particularly important for bare, unprotected steel sections, although the concept can be applied to other types of structures as well.

Example of Steel Temperatures Calculated Using Finite Element Codes

The preceding steel temperature calculations assume uniform steel temperatures in the section analyzed as a crude approximation. It leads indeed in general to solutions on the safe side (i.e., the temperatures are overestimated and often overdesigned, leading to unnecessary costs). For more precise analyses numerical calculations are needed employing, for example, finite element computer codes. An example is given below.

An encased I-section beam is carrying a concrete slab. It is exposed to standard fire conditions according ISO 834 (Fig. 34.13). Heat transfer conditions according to Equation 34.11 are assumed with $\varepsilon = 0.8$ and $h = 25$ W/m^2 K. The thermal properties of steel and concrete are

Table 34.5 Section factor A_s/V_s for unprotected steel members [20]

Open section exposed to fire on all sides:

$$\frac{A_s}{V_s} = \frac{\text{Perimeter}}{\text{Cross-sectional area}}$$

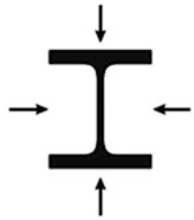

Tube exposed to fire on all sides:

$$A_s/V_s = 1/t$$

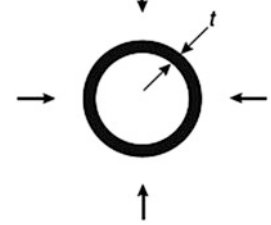

Open section exposed to fire on three sides:

$$\frac{A_s}{V_s} = \frac{\text{Surface exposed to fire}}{\text{Cross-sectional area}}$$

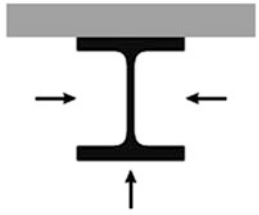

Hollow section (or welded box section of uniform thickness) exposed to fire on all sides:

If $t \ll b$: $A_s/V_s \approx 1/t$

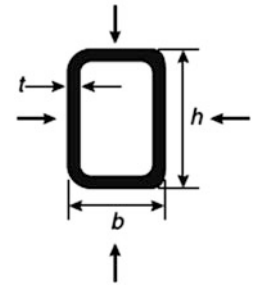

I-section flange exposed to fire on three sides:

$$A_m/V = (b + 2t_f)/(bt_f)$$

If $t \ll b$: $A_s/V_s \approx 1/t_f$

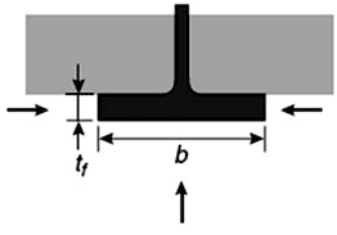

Welded box section exposed to fire on all sides:

$$\frac{A_s}{V_s} = \frac{2(b+h)}{\text{Cross-sectional area}}$$

If $t \ll b$: $A_m/V \approx 1/t$

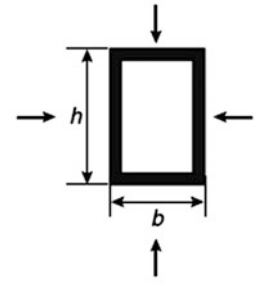

(continued)

Table 34.5 (continued)

Angle exposed to fire on all sides:

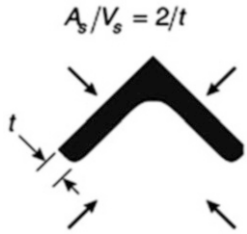

I-section with box reinforcement, exposed to fire on all sides:

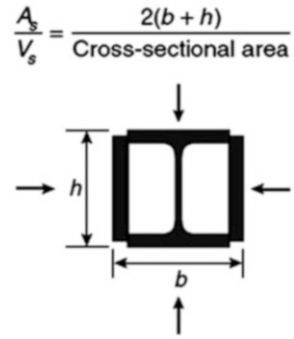

Flat bar exposed to fire on all sides:

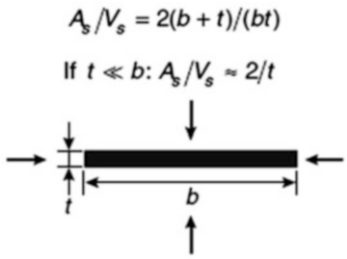

Flat bar exposed to fire on three sides:

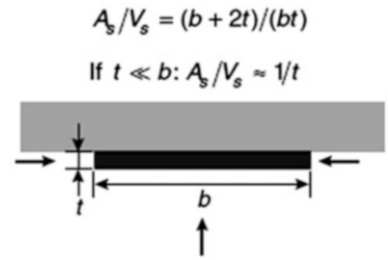

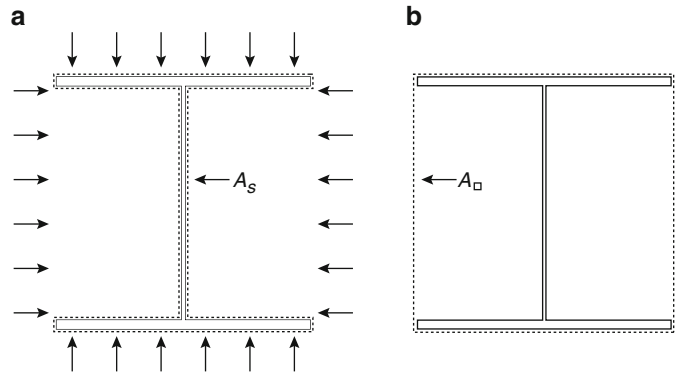

I-section exposed to fire from four sides. The surfaces between the flanges will be partly shadowed.

The boxed area of the I-section, $A_\square$, will have a shorter periphery than the original section.

Fig. 34.12 Illustration of the shadow effect. The boxed value area per unit length $A_\square$ of a steel section represents the area exposed to heating conditions from the fire

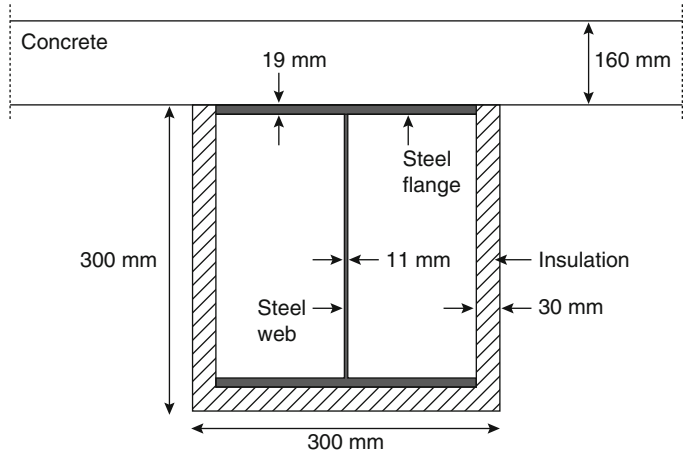

Fig. 34.13 Encased I-section steel (HE 300B) beam carrying a concrete slab. Slab thickness 160 mm, insulation thickness 30 mm, steel height and width 300 mm, flange thickness 19 mm, and web thickness 11 mm

as given in Eurocodes 2 and 3, respectively, shown above and below. The encasement boards are assumed to have a thermal conductivity (k) of 0.2 W/m K and a volumetric specific heat capacity ($c\rho$) of 40 kJ/m^3. The finite element discretization model is shown in Fig. 34.14. Heat transfer inside the void is assumed to be by radiation only with an internal surface emissivity of 0.8.

The calculated temperature histories in the steel flanges are shown in Fig. 34.15. For comparison the temperature calculated assuming uniform temperature is also included. Notice that the temperature difference between the minimum and maximum steel temperatures are on the order of 130 °C due to uneven heating and steel mass distribution and in particular due to the cooling of the top flange by the concrete slab. A simple approximate calculation can be obtained assuming a uniform steel section temperature, according to the discussion on insulated steel structures, with the section factor calculated as shown in Table 34.3. A time constant τ equal to 6460 s or 1.8 h can then be calculated (Equation 34.38) and a uniform steel temperature after 2 h of about 635 °C can be obtained from Fig. 34.10. Notice that this temperature is considerably higher than the average temperature obtained with the much more accurate finite element model.

Calculation of Temperature in Concrete Structures

Reinforced concrete structures are sensitive to fire exposure for mainly two reasons. They may spall due to combinations of internal water pressure and high thermal stresses, and they may gradually lose their load-bearing capacity when the reinforcement bars get hot, reaching temperature levels above 400 °C. Prestressed steel may even lose strength below that level. In addition the concrete loses both strength and stiffness at elevated temperature. When occurring, spalling usually starts within 30 min of severe fire exposure. Because the spalling phenomenon is very complex and cannot be predicted with simple mathematical temperature models, it will not be further discussed here. Thus, the procedures presented below presume that no spalling occurs that could considerably influence the temperature development.

In general, temperatures in fire-exposed structures may be obtained from tabulated values (see, e.g., Eurocode 2 [26]) or by more or less advanced calculations. Below some simple calculation methods are given. For more general situations, finite element calculations are needed.

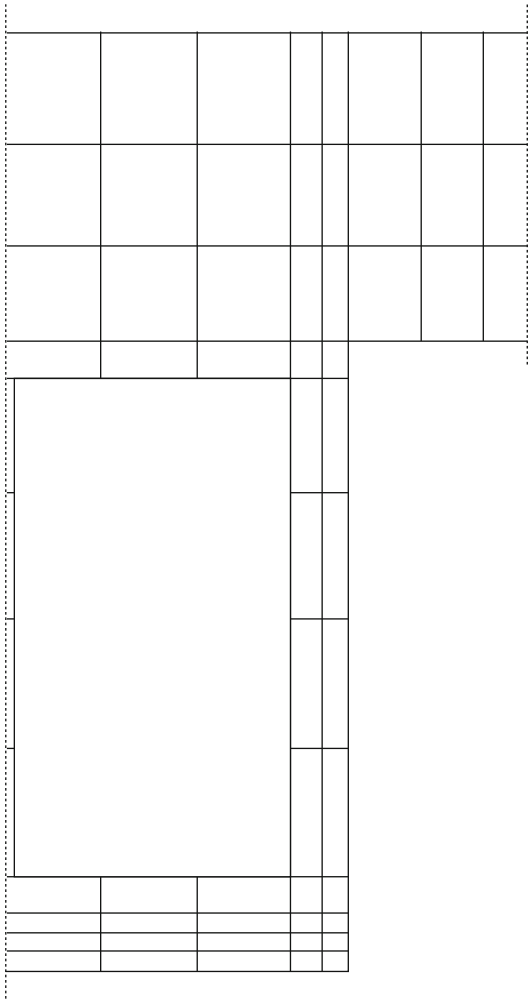

Fig. 34.14 Finite element discretization used to calculate the temperature development of the steel beam shown in Fig. 34.13 when exposed to a standard fire exposure according to ISO 834

Thermal Properties of Concrete

The thermal conductivity of concrete decreases in general with rising temperature. It depends on concrete quality and type of ballast. For design purposes curves as shown in Fig. 34.16 may be used according to Eurocode 2 [26]. For more accurate calculations with alternative concrete qualities more precise material data may be needed, as discussed earlier.

The specific heat of dry concrete does not vary much with temperature. However, in reality concrete structures always contain more or less physically bound water. This water will evaporate at temperatures above 100 °C and constitute a heat sink as the evaporation consumes a lot of heat. Thus, the specific heat capacity for normal weight concrete according to Eurocode 2 is as shown in Fig. 34.17.

The emissivity of concrete surfaces may be assumed to be 0.8 and the convective heat transfer coefficient may, when simulating fully developed fires, be assumed equal to 25 W/m^2 K. See, for example, Eurocode 1 [4]. In general the assumed values of these parameters have little influence on calculated temperatures inside concrete structures.

Penetration Depth in Semi-Infinite Structures

Concrete is a material with relatively high density and low conductivity. Therefore, it takes a

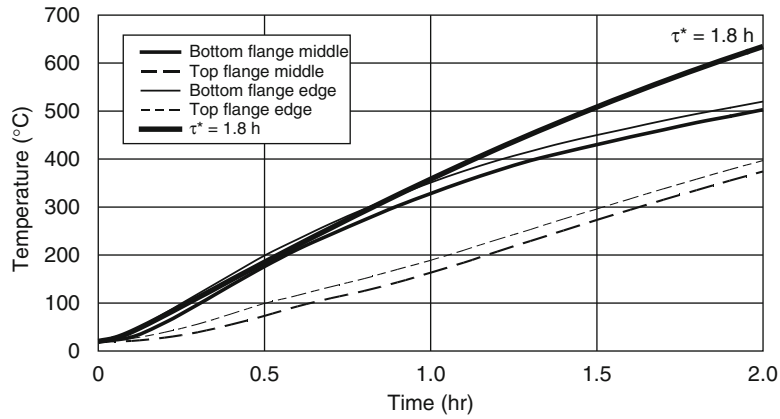

Fig. 34.15 Temperature history of bottom and top flanges, middle and corner points

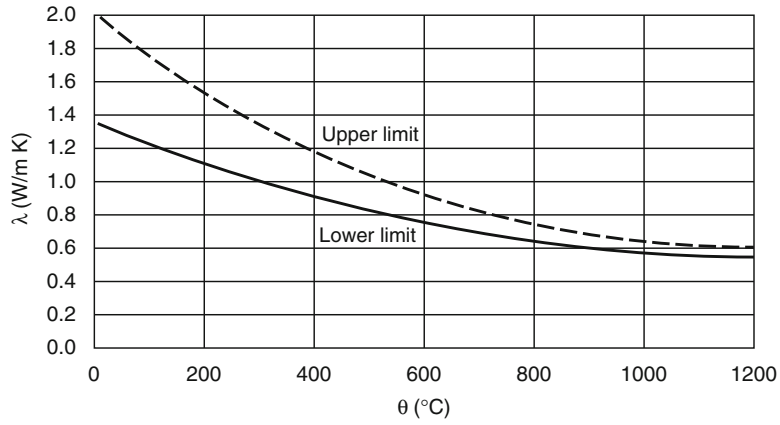

Fig. 34.16 Upper and lower limits of thermal conductivity as a function of temperature of normal weight concrete according to Eurocode 2 [26]

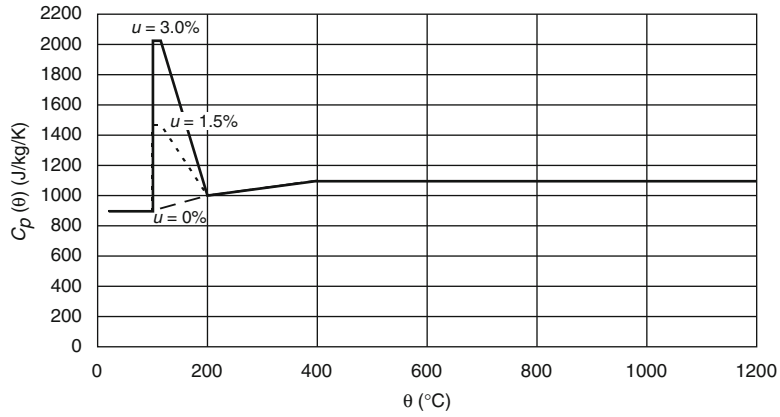

Fig. 34.17 Specific heat capacity of concrete as a function of temperature at three different moisture contents, 0 %, 1.5 %, and 3 %, for siliceous concrete according to Eurocode 2 [26]

long time for heat to penetrate into the structure and raise its temperature, or in other words it takes time before a temperature change at one point is noticeable at another point. Thus, in many cases a concrete structure may then be assumed semi-infinite.

For the idealized case of a semi-infinite body at a uniform initial temperature T_i where the surface temperature momentarily is changed to a constant level of T_s, the temperature rise $(T - T_i)$ inside the body at a depth x at a time t may be written as a function of the normalized group $\eta = x / \left[2\sqrt{(\alpha t)}\right]$ where α is an assumed constant thermal diffusivity as defined in Equation 34.22. The relative temperature rise may then be written as

$$\frac{(T - T_i)}{(T_s - T_i)} = erfc(\eta) = 1 - erf(\eta) \qquad (34.54)$$

The Gauss complementary error function *erfc* is shown in Fig. 34.18. Tabulated values of the Gauss error function may be found in textbooks such as Holman [1]. For values of η greater than a value of 1.4 the relative rise is less than 5 %. Thus, depending on accuracy, the temperature penetration depth δ at a given time may be estimated as

$$\delta = 2.8\sqrt{\alpha t} \qquad (34.55)$$

As an example, the temperature rise can be estimated to penetrate only about 0.11 m into a concrete structure after 1 h, assuming a

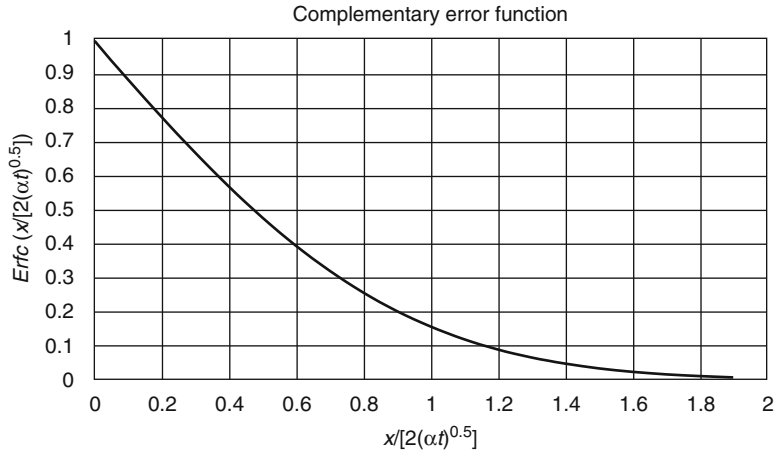

Fig. 34.18 Normalized temperature distribution in a semi-infinite body according to the Gauss complementary error function erfc as in Equation 34.54

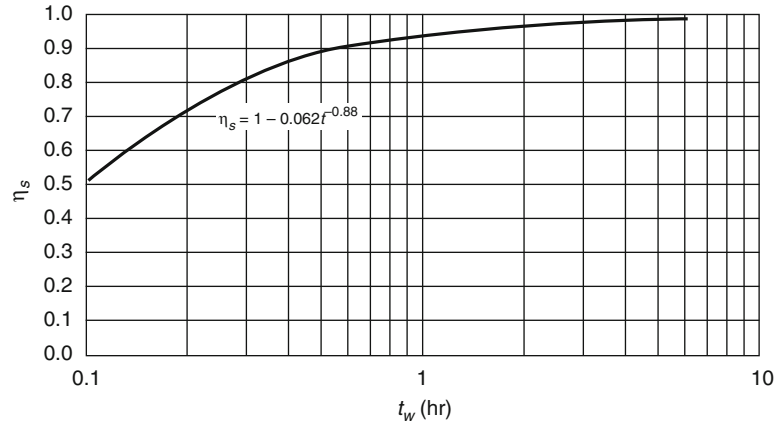

Fig. 34.19 Ratio η_s between concrete surface temperature T_s and the fire temperature T_f as a function of time for a normal weight concrete with thermal properties, according to Eurocode 2 [26], exposed to standard fire conditions, according to ISO 834

conductivity of a 1 W/m K, a density of 2300 kg/m^3, and a specific heat capacity of 1000 J/(kg K).

Penetration depth can actually be applied to steel as well. A temperature change at one point of a steel member will not be noticeable beyond a distance corresponding to the penetration depth.

Simple One-Dimensional Calculations

With the thermal properties of concrete as given in the earlier discussion on measurement of thermal properties, the temperature can be calculated in structures exposed to fires. In general, numerical procedures such as finite element methods need to be employed. Wickström [27–29] has, however, shown, based on numerous finite element calculations, that in one-dimensional cases the temperature inside concrete structures exposed to standard fire conditions according to ISO 834 may be obtained from the diagrams shown in Figs. 34.19 and 34.20. These diagrams apply to normal weight concrete with thermal properties, according to Eurocode 2 [26], as shown in the earlier section on measurement of thermal properties.

In Wickström [27–29] it is shown that the same type of diagrams can be used more generally considering both various parametric fires and various material properties. In these references techniques are also presented on how temperatures can be obtained in walls exposed from two sides and in simple two-dimensional cases by superpositioning based on the same

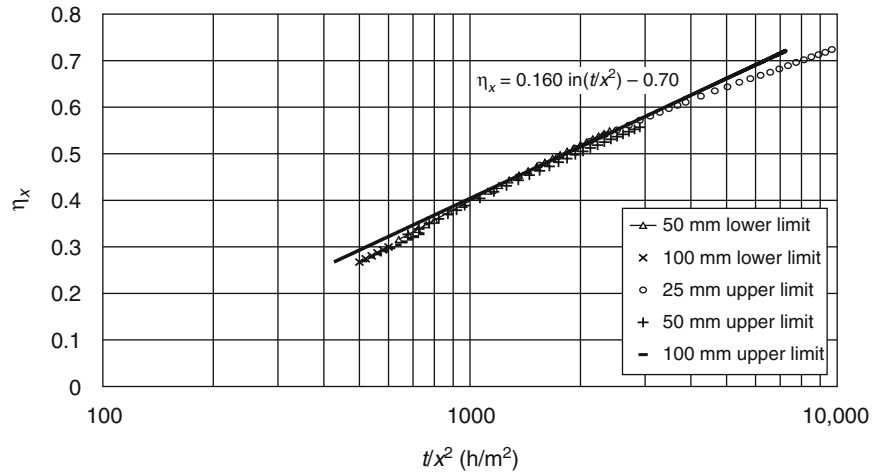

Fig. 34.20 Ratio η_x between internal concrete temperature T_x and the surface temperature T_s as a function of time divided by depth squared t/x^2 for normal weight concrete with thermal properties, according to Eurocode 2 [26], exposed to standard fire conditions, according to ISO 834. Calculations are made assuming the upper and lower limits of the conductivity as shown in Fig. 34.16

simple one-dimensional approximations as outlined below.

Thus, the diagram given in Fig. 34.19 shows the ratio η_s between the concrete surface temperature and the standard fire temperature, according to ISO 834, (see Equation 34.63) as a function of time.

$$\eta_s = \frac{T_s}{T_f} \tag{34.56}$$

The coefficient η_s is in general a function of the group time t over thermal inertia $\sqrt{(k\rho c)}$ of the concrete. In Fig. 34.19 normal weight concrete with thermal properties according to Eurocode 2 [26] is assumed.

Figure 34.20 shows in turn the ratio between the internal temperature T_x at a depth x and the surface temperature T_s. Thus,

$$\eta_x = \frac{T_x}{T_w} \tag{34.57}$$

The coefficient η_x is in principle a function of the Fourier number (i.e., the thermal diffusivity $k/(c\rho)$ of the concrete times the fire duration t over the depth x squared). Results from computer calculations are shown in Fig. 34.20. In these calculations thermal properties of concrete with a water content of 1.5 % are assumed according to Eurocode 2. Both upper and lower limit values of the conductivity (see Fig. 34.16) are included in the finite element calculations as well as depths of 25, 50, and 100 mm. A straight line is drawn in the logarithmic-linear diagram, which yields approximate temperatures slightly higher than would be obtained with more accurate finite element calculations.

The internal concrete temperature may now be written as

$$T_x = \eta_s \eta_x T_f \tag{34.58}$$

The graphs in Figs. 34.19 and 34.20 can be approximated by simple expressions. Thus,

$$\eta_s = \left(1 - 0.062 t^{-0.88}\right) \tag{34.59}$$

and

$$\eta_x = \left[0.16 ln\left(t/x^2\right) - 0.70\right] \tag{34.60}$$

respectively, where t is time in hours and x is distance in meters from the surface.

Then, in summary, for standard fire exposure according to ISO 834 and normal weight concrete according to Eurocode 2 [26] (see earlier section on thermal properties), a very simple closed-form solution may be obtained for the

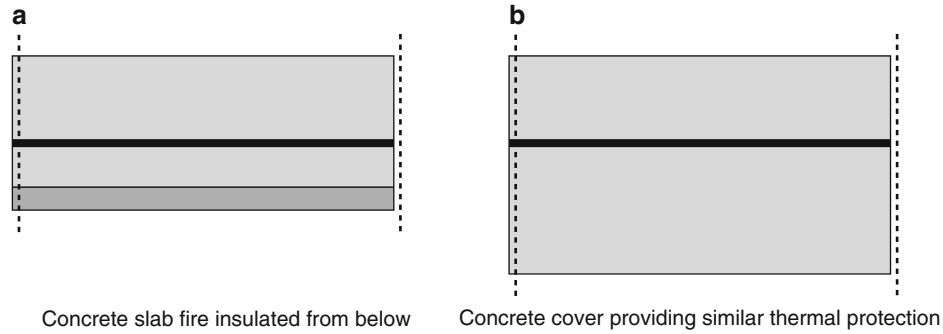

Fig. 34.21 Protection of a concrete structure layer with thickness d_i, which gives an equivalent thermal protection as a concrete layer with thickness d_c

temperature at arbitrary times and depths by inserting Equations 34.59 and 34.63 in hours 34.60 into Equation 34.58:

$$T_x = (1 - 0.062t^{-0.88})\left[0.16\,ln(t/x^2) - 0.70\right]345\log(480t + 1) \quad (34.61)$$

As an illustration, the temperature in a slab of normal weight concrete is calculated at a depth of 4 cm when exposed to an ISO 834 standard fire for 1 h. At first η_s is obtained from Fig. 34.19 to be 0.94 for $t = 1$ h. Then for $t/x^2 = 1.0/(0.04)^2 = 625$ h/m^2, Fig. 34.20 yields $\eta_x = 0.33$. As the standard time temperature rise after 1 h is 925 °C, the concrete surface temperature rise is obtained from Equation 34.56 as 0.94*925 = 870 °C and Equation 34.61 yields the temperature rise at a depth of 4 cm to be $T_x = 0.94*0.33*925$ °C = 287 °C. A corresponding accurate finite element calculation yields a temperature rise of $T_x = 277$ °C.

Fire-Insulated Concrete Structures

In some applications, it may be advantageous to insulate concrete structure surfaces to prevent them from fast temperature rises. This insulation may either be to avoid spalling or to give the concrete-embedded reinforcement bars additional thermal protection (Fig. 34.21). Behind the protection the temperature of the concrete surface will not rise as quickly as when directly exposed to fire. Some insulation materials undergo chemical transformations requiring a lot of heat (latent heat) to raise the temperature whereas others work just as passive thermal barriers. Only the latter type of insulation systems is further discussed here and the formula given below only applies to this type of inert material.

The thermal efficiency of a protection layer is sometimes expressed as the thickness of an additional concrete coverage that would yield the same protection. Wickström and Hadziselimovic [30] have shown that the same effect is approximately obtained when the thermal resistance of the insulation is the same as that for the concrete (i.e., $d_i/k_i = d_c/k_c$ where d is thickness and k conductivity, respectively, and the indices i and c stand for insulation and concrete, respectively). Thus, the equivalent concrete layer thickness can be calculated as

$$d_c = k_c d_i / k_i \quad (34.62)$$

which indicates that the influence of the specific heat capacity and density of the protecting material is negligible in the case of protecting concrete structures. The thermal inertia of the concrete is totally dominating over the inertia of the insulation.

As an example, a 10 mm board of vermiculite with a thermal conductivity of 0.2 W/m K corresponds to a concrete protection layer of 50 mm, assuming the concrete has a conductivity

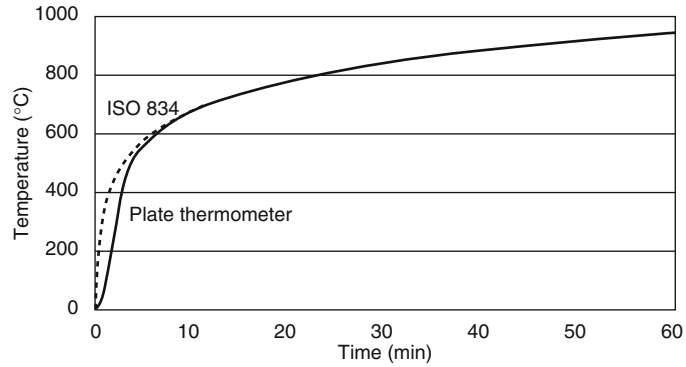

Fig. 34.22 Calculated response of a plate thermometer when exposed to standard fire test conditions, according to ISO 834, Equation 34.63

of 1.0 W/m K for the temperature interval considered. This could mean considerable savings in both weight and space for a concrete structure.

Calculation of Temperature in Timber Structures

Modeling the thermal behavior of wood is complicated by phenomena such as moisture evaporation and migration, and the formation of char has a decisive influence on the temperature development. Nevertheless, it has been shown that general finite element codes such as SAFIR, TASEF, and COMSOL can be used to predict temperature in fire-exposed cross sections of glued laminated beams [31] provided apparent thermal material properties and appropriate boundary conditions are used. Other specialized numerical codes for timber structures have been developed by Fung [32] and Gammon [33].

More commonly empirical rules are used to estimate the penetration of the charring layer and the loss of strength of timber structures (see, e.g., Eurocode 5 [34]).

Heat Transfer in Fire Resistance Furnaces

Nominal time-temperature relations are clearly defined in fire resistance test standards such as ISO 834, EN 1363-1, and ASTM E119. However, furnaces have various characteristics depending on the difference between the black body radiation temperature T_r (Equation 34.7) and the gas temperature T_g. In addition there is a time delay of the temperature recording due to the thermal inertia of the monitoring thermocouples. Therefore, when theoretically simulating fire resistance tests, it must be considered how the temperature has been measured in the various standards.

Furnaces Controlled According to ISO 834 and EN 1363-1

In ISO 834 and EN 1363-1 the nominal furnace temperature T_f is given as

$$T_f = 20 + 345\log_{10}(8t + 1) \qquad (34.63)$$

The furnace temperature shall be monitored with plate thermometers (see ISO 834-1 and EN 1363-1). The time delay or, in other words, the time constant of the plate thermometers in a furnace test is negligible, which is indicated in Fig. 34.22, where the calculated temperature response of a plate thermometer exposed to uniform furnace temperature according to ISO 834 is shown. The heat transfer is then calculated according to Equation 34.11 assuming the emissivity ε and the convection heat transfer coefficient h equal to 0.9 and 25 W/m^2 K, respectively.

Notice that the plate thermometer temperature follows the nominal curve very closely except for the first few minutes. Thus, the time delay of the plate thermometer temperature recordings due to inertia in a standard fire test may be neglected

and the heat transfer to a specimen surface can accurately be calculated according to Equation 34.18.

Sometimes it is of interest to know the *incident radiation* level under a furnace test. This level can be measured directly with heat flux meters, but in the section below it is shown how this radiation level may be obtained from plate thermometer measurements.

The incident radiation heat flux q_{inc} may be obtained from Equation 34.16, and plate thermometer temperature recordings given the gas temperature T_g, the emissivity ε_{PT}, and the convection heat transfer coefficient h_{PT} of the plate thermometer are known as

$$q_{inc} = \sigma T_{PT}^4 - h_{PT}\left(T_g - T_{PT}\right)/\varepsilon_{PT} \qquad (34.64)$$

The latter term in Equation 34.64 is relatively small and may be treated as an error term. For values of the emissivity ε_{PT} and the convection heat transfer coefficient h_{PT} equal to 0.8 and 25 W/m^2 K, respectively, a temperature level of 1000 K and a gas temperature T_g deviating from the plate thermometer temperature T_{PT} by as much as 50 K yields the latter term of Equation 34.64 to be less than 3 %. At higher temperature levels and at minor deviations between gas and radiation temperatures this error is much smaller and probably seldom greater than must be anticipated when measuring incident radiation directly with heat flux meters.

Furnaces Controlled According to ASTM E119

In the American test standard ASTM E119 the nominal furnace temperature is specified according to the time-temperature relation given in Table 34.6.

The standard thermocouple for monitoring the furnace temperature is, however, very thick and, therefore, very slow. According to ASTM E119, it shall have a time constant within the range of from 5.0 to 7.2 min. To eliminate the effects of the time delay the thermocouples may be analyzed as bare steel sections. Thus, by applying Equation 34.51, the effective fire temperature T_f can be derived from the corresponding thermocouple measurements T_{tc} as

Table 34.6 Standard Fire Time-Temperature Relation According to ASTM E119

Time (min)	Temperature rise (°C)	Time (min)	Temperature rise (°C)
0	0	90	986
5	556	120	1029
10	659	180	1090
15	718	240	1133
30	821	360	1193
60	925		

$$T_f^{i+1} = T_{tc}^{i+1} + \tau/\Delta t\left(T_{tc}^{i+1} - T_{tc}^{i}\right) \qquad (34.65)$$

The furnace thermocouple time constant, as referred to in the ASTM E119 standard, is rather imprecisely specified as the heat transfer by radiation that is nonlinear and increases by the temperature level raised to the fourth power. More realistic is to assume a time constant of 6 min (in the middle of the range from 5.0 to 7.2 min) at a furnace temperature level of perhaps 1000 K, and then obtain the heat transfer to the thermocouple by calculating the heat transfer according to Equation 34.11 assuming ε and h equal 0.9 and 50 W/m^2 K, respectively. Then match a surface-to-volume ratio obtained from Equations 34.52 and 34.13 to obtain the stipulated time constant. (As a comparison, the corresponding time constant for a plate thermometer at the same temperature level is on the order of 15 s.)

Figure 34.23 shows the actual furnace temperature rise in a furnace controlled ideally precisely according to ASTM E119. Notice that the real or effective furnace temperature is much higher than indicated by the slowly responding ASTM type of shielded thermocouples. It must, however, be noted that the above analysis assumes that the furnace radiation and gas temperatures are equal, which is seldom the case. The gas temperature may be higher than the radiation temperature and, therefore, the differences in practice between the ASTM thermocouple and the plate thermometer may be much less, as the

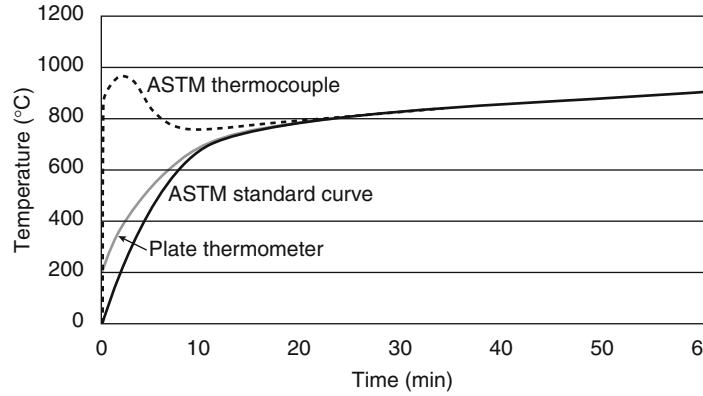

Fig. 34.23 Temperatures ASTM E119 and ISO 834 (plate thermometer), respectively, must follow to obtain the effective furnace temperature T_f according to ASTM E119 due to time delay

ASTM thermocouple is more sensitive to convective heat transfer than the plate thermometer. The general observation from this theoretical analysis agrees with the test results reported by Sultan [35]. The difference between the ASTM type of thermocouples and the plate thermometer is insignificant after 10 min.

References

1. J.P. Holman, *Heat Transfer,* 4th ed., McGraw Hill, New York (1976).
2. U. Wickström, D. Duthinh, and K.B. McGrattan, "Adiabatic Surface Temperature for Calculating Heat Transfer to Fire Exposed Structures," Interflam, Interscience Communications, London, UK (2007).
3. K.B. McGrattan, S. Hostikka, J.E. Floyd, H.R. Baum, and R.G. Rehm, *Fire Dynamics Simulator (Version 5), Technical Reference Guide,* NIST SP 1018–5, National Institute of Standards and Technology, Gaithersburg, MD (2005).
4. EN 1991–1-2, "Eurocode 1: Actions on structures—Part 1–2: General Actions—Actions on Structures Exposed to Fire," European Committee for Standardization (CEN), Brussels, Belgium (2002).
5. U. Wickström and T. Hermodsson, T., "Comments on Paper by Kay, Kirby, and Preston, 'Calculation of the Heating Rate of an Unprotected Steel Member in a Standard Fire Resistance Test'," *Fire Safety Journal,* 29, 4, pp. 337–343 (1997).
6. D. Flynn, "Response of High Performance Concrete to Fire Conditions: Review of Thermal Property Data and Measurement Techniques," NIST GCR 99–767, National Institute of Standards and Technology, Gaithersburg, MD (Mar. 1999).
7. ISO 8302:1991, Thermal insulation -- Determination of steady-state thermal resistance and related properties -- Guarded hot plate apparatus.
8. B. Adl-zarrabi, L. Boström, and U. Wickström, "Using the TPS Method for Determining the Thermal Properties of Concrete and Wood at Elevated Temperature," *Fire and Material,* 30, pp. 359–369 (2006).
9. E. Sterner and U. Wickström, "TASEF—Temperature Analysis of Structures Exposed to Fire," SP Report 1990:05, Swedish National Testing and Research Institute, Borås, Sweden, (1990).
10. U. Wickström, "TASEF-2—A Computer Program for Temperature Analysis of Structures Exposed to Fire," Ph.D. Dissertations, Lund Institute of Technology, Department of Structural Mechanics, Report No. 79-2, Lund, Sweden (1979).
11. E. Sterner and U. Wickström, "TASEF—Temperature Analysis of Structures Exposed to Fire," SP Report 1990:05, SP Technical Research Institute of Sweden, Borås, Sweden (1990).
12. J.M. Fransén, V.K.R. Kodur, and J. Mason, "A Computer Program for Analysis of Structures Submitted to Fire," *User's Manual of SAFIR 2001*, University of Liege, Belgium (2000).
13. *ABAQUS Standard User's Manual, volumes I–III, version 6.2,* Hibbit, Karlsson and Sörensen, Inc., Pawtucket, RI (2001).
14. ANSYS, Inc., 275 Technology Drive, Canonsburg, Pennsylvania (http://www.ansys.com).
15. K.J. Bathe, *Finite Element Procedures,* Prentice Hall, Upper Saddle River, NJ (1996).
16. See website http://www.comsol.com.
17. *Guide for Verification and Validation of Computational Fluid Dynamics Simulations,* AIAA, Guide G-077–1998, American Institute of Aeronautics and Astronautics, Reston, VA (1998).
18. U. Wickström and J. Pålsson, "A Scheme for Verification of Computer Codes for Calculating Temperature in Fire Exposed Structures," SP Report 1999:36, Swedish National Testing and Research Institute, Borås, Sweden (1999).
19. U. Wickström, "An Evaluation Scheme of Computer Codes for Calculating Temperature in Fire Exposed Structures," Interflam (1999).
20. EN 1993-1-2, "Eurocode 3: Design of Steel Structures—Part 1–2: General Rules—Structural

Fire Design," European Committee for Standardization (CEN), Brussels, Belgium (2005).
21. J. Hamann, R. Müller, R. Rudolphi, R. Schriever, and U. Wickström, "Anwendung von Temperatur-Berechnungsprogrammen auf kritische Referenz-beispiele des Brandschutzes," Bundesanstalt für Materialforschung und -prüfung, Berlin (1999).
22. U. Wickström, "Temperature Analysis of Heavily-Insulated Steel Structures Exposed to Fire," *Fire Safety Journal,* 5, pp. 281–285 (1985).
23. S.J. Melinek and P.H. Thomas, "Heat Flow to Insulated Steel," *Fire Safety Journal,* 12, pp. 1–8 (1987).
24. Z.H. Wang and H.T. Kang, "Sensitivity Study of Time Delay Coefficient of Heat Transfer Formulations for Insulated Steel Members Exposed to Fires," *Fire Safety Journal,* 41, pp. 31–38 (2006).
25. U. Wickström, "Temperature Calculation of Insulated Steel Columns Exposed to Natural Fire," *Fire Safety Journal,* 4, pp. 219–225 (1981).
26. EN 1992-1-2, "Eurocode 2: Design of Concrete Structures—Part 1–2: General Rules—Structural Fire Design," European Committee for Standardization (CEN), Brussels, Belgium (2004).
27. U. Wickström, "A Very Simple Method for Estimating Temperature in Fire Exposed Concrete Structures", in *Proceedings of New Technology to Reduce Fire Losses & Costs,* (S.J. Grayson and D.A. Smith, eds.), Elsevier, New York (1986).
28. U. Wickström, "Application of the Standard Fire Curve for Expressing Natural Fires for Design Purposes," *Fire Safety: Science and Engineering,* ASTM STP 882, American Society of Testing and Materials, Philadelphia, pp. 145–159 (1985).
29. U. Wickström, "Natural Fires for Design of Steel and Concrete Structures—A Swedish Approach," *International Symposium on Fire Engineering for Building Structures and Safety, the Institute of Engineers, Australia,* National Conference Publication No. 89/16, Melbourne (1989).
30. U. Wickström and E. Hadziselimovic, "Equivalent Concrete Layer Thickness of a Fire Protection Insulation Layer Paper," Fire Sa, Brandteknik, Odense, Denmark (1996).
31. B.L. Badders, J.R. Mehaffey, and L.R. Richardson, "Using Commercial FEA software Packages to Model the Fire Performance of Exposed Glulam Beams," *Fourth International Workshop "Structures in Fire,"* Aveiro, Portugal (2006).
32. F.C.W. Fung, "A Computer Program for the Thermal Analysis of the Fire Endurance of Construction Walls," *NBSIR 77.1260*, National Bureau of Standards, Washington, DC (1977).
33. B.W. Gammon, "Reliability Analysis of Wood-Frame Wall Assemblies Exposed to Fire," Ph.D. Dissertation, University of California, Berkeley (1987).
34. EN 1995-1-2, "Eurocode 5, Design of Timber Structures—Part 1–2: General Rules—Structural Fire Design," European Committee for Standardization (CEN), Brussels, Belgium (2004).
35. M.A. Sultan, "A Comparison of Heat Exposure in Fire Resistance Test Furnaces Controlled by Plate Thermometers and by Shielded Thermocouples," Interflam 2004, Edinburgh, Scotland, pp. 219–229 (2004).

Professor Ulf Wickström is teaching heat transfer in fire technology at Luleå University of Technology, Sweden. He is a former head of the Department of Fire research at SP Technical Research Institute of Sweden. Professor Wickström has a PhD from Lund University of Technology in fire technology and a master of science from the University of California, Berkeley. For his thesis research he developed the computer program TASEF for calculating temperature in fire-exposed concrete and steel structures. His focus of scientific interest is heat transfer analysis of structures exposed to fire, on which he has published several papers.

Fire Load Density

35

Mario Fontana, Jochen Kohler, Katharina Fischer, and Gianluca De Sanctis

Introduction

The fire load has a strong influence on the temperature development during a compartment fire. Therefore, the assessment of the fire load as an input to model the time-temperature relationship, is an important task in structural fire design.

In combination with the available oxygen and the combustion properties of the material, the fire load density determines the heat release rate *HRR* of a fire.

Figure 35.1 illustrates the qualitative behaviour of the heat release rate as a function of time during a fire. The fire growth phase (including potential flashover), the fully developed state and the decay phase are qualitatively shown for the two burning regimes of fuel (4) or ventilation (3) controlled fires. The area under both curves corresponds to the energy released by the available fire load in the room. The duration of a fire depends on the amount of fire load and the burning regime. For ventilation controlled fires the heat release rate is limited by the available oxygen. In a fuel controlled fire the maximal heat release rate in the room is achieved and the duration of the fire is usually shorter (1).

M. Fontana (✉) • G. De Sanctis
Institute of Structural Engineering, ETH Zurich, Stefano-Franscini-Platz 5, 8093 Zurich, Switzerland

J. Kohler
Department of Structural Engineering, Norwegian University of Science and Technology, 7491 Trondheim, Norway

K. Fischer
Matrisk GmbH, Alte Obfelderstrasse 50, 8910 Affoltern am Albis, Switzerland

Definitions

The **fire load** [MJ] is defined as the quantity of energy which is released by the complete combustion of all combustible material in a fire compartment. The fire load is often subdivided into variable (movable or mobile) and permanent (fixed or immobile) fire load.

The **net heat of combustion** [MJ/kg] is defined as the potential combustion energy per kilogram contained in the material.

The **fire load density** is defined as the fire load per unit floor area [MJ/m^2] or per unit volume [MJ/m^3].

A **fire compartment** is defined as the enclosed space, which is separated from adjoining spaces by adequate fire barriers.

Representation of Fire Load

Basic Representation

The fire load in buildings consists of the energy content of combustible materials, generally comprising furniture, equipment and stored objects and goods (variable fire load) as well as combustible components of the structural elements (permanent fire load) which can burn during a fire. The variable fire load depends

M.J. Hurley (ed.), *SFPE Handbook of Fire Protection Engineering*,
DOI 10.1007/978-1-4939-2565-0_35, © Society of Fire Protection Engineers 2016

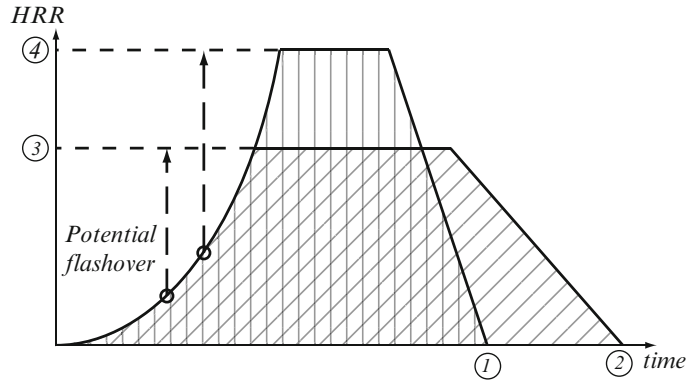

Fig. 35.1 Illustration of the heat release rate (HRR) development as a function of time during a compartment fire

mainly on the occupancy of the room or building, as e.g. residential buildings, hospitals, hotels, stores, storage buildings, industrial facilities, etc.

The fire load the also be represented by the fire load density or the distributed fire load by dividing the fire load by the room area. According to CIB W14 [1], the fire load density can be related to the total floor area of the fire compartment [MJ/m^2] including aisles and local empty spaces. In some literature [2], the area is related to the total interior area of the surfaces within the compartment including all openings [MJ/m^2]. For some building occupancies–especially for storage or industrial buildings–the relation to the volume [MJ/m^3] can be more efficient in order to address the effect of storage height on the fire load.

The fire load density of a fire compartment containing different combustible materials is defined as:

$$q = \frac{\sum_i m_i \cdot H_i}{A} \qquad (35.1)$$

m_i: the mass of a combustible material i [kg]
H_i: heat of combustion or specific energy released from combustion per mass unit of material i [MJ/kg]
A: area of fire compartment [m^2]

Stochastic Representation

The fire load density in a compartment varies in time and in space. In general, it is sufficient to represent the variation in time with a simple time independent random variable $\boldsymbol{q}(t,x,y) = \boldsymbol{q}(x,y)$.

The variation of the fire load density in space (x,y) can be represented in analogy to the approach proposed in CIB W81 [3] by a stochastic field $\boldsymbol{q}(x,y)$ as:

$$\boldsymbol{q}(x,y) = \exp(LN(\hat{q}) + \boldsymbol{V} + \boldsymbol{U}(x,y)) \qquad (35.2)$$

where $\hat{q}$ is the overall median fire load density (e.g. specified for a specific occupancy category), $\boldsymbol{V}$ is a zero mean normal distributed variable representing the variation between different structures and different points in time and $\boldsymbol{U}(x,y)$ is a zero mean random field representing the variation within the compartment. The quantities $\boldsymbol{V}$ and $\boldsymbol{U}$ are considered as stochastically independent.

Fire Load Density in Fire Safety Design

For localized fire models the spatial distribution of the fire load in space should be taken into account e.g. by the random field in Equation 35.2. Depending on the type and purpose of an analysis, the stochastic representation of the fire load can be simplified. For zone fire models the variability in space can usually be neglected. Then the random variable $\boldsymbol{q}$ can be represented as a simple lognormal distributed random variable with mean value μ_q and standard deviation σ_q.

In fire safety design the stochastic representation of the fire load is often simplified. Usually, characteristic values for the fire load are used. These characteristic values are chosen according to the safety format of the corresponding code format. In general, the characteristic values

Table 35.1 Calculation of characteristic values

Distribution type	Lognormal			Gumbel		
Fractile	80 %	90 %	95 %	80 %	90 %	95 %
k-value	0.84	1.28	1.64	0.72	1.30	1.87
Characteristic value	$q_k = \frac{\overline{q}}{\sqrt{v^2+1}} \cdot \exp\left(\sqrt{\ln(v^2+1)} \cdot k\right)$ with $v = {}^{\sigma_q}/_{\overline{q}}$			$q_k = \overline{q} + k \cdot \sigma_q$		

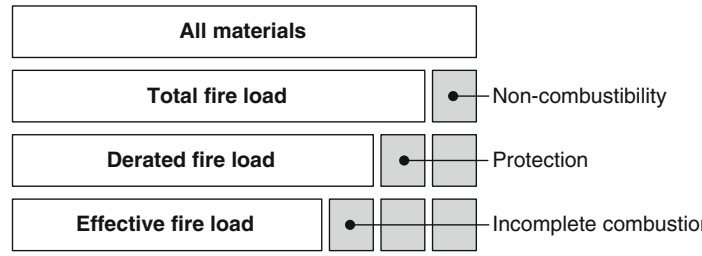

Fig. 35.2 Overview on the assessment of the fire load

correspond to a specific fractile value of the underlying distribution of $\boldsymbol{q}$. Fractile values are calculated depending on the distribution type and the mean $\overline{q}$ and standard deviation $\sigma_{\overline{q}}$ of the distributions according to Table 35.1.

It is suggested to represent the fire load density as a Lognormal distributed random variable. In some fire safety regulations the Gumbel distribution is prescribed. From a theoretical point of view the Gumbel distribution belongs to the family of extreme value distributions while the fire load is considered as a point in time realization of a random process. However, due to the usually large coefficient of variation of the fire load, it is acceptable to use a Gumbel distribution instead of a Lognormal distribution. Table 35.1 contains information for the use of both distributions.

Assessment of the Fire Load for Fire Safety Design

The fire load that is used for design purposes can be assessed as shown in Fig. 35.2: Among all materials only the combustible materials contribute to the potential energy that can be released by a fire. The fire load density of these materials can be assessed by Equation 35.1 using their mass and their heat of combustion and is denoted as of the total fire load (Fig. 35.2 second line). A part of total fire load is protected against direct participation in a fire through encapsulation (Fig. 35.2 third line). Derating factors can be used to account for those protected fire loads. The characteristic value that is used for design purposes is usually derived from the probability distribution of the derated fire load. Because the combustion under natural fire conditions is usually incomplete, the effective contribution of the fire load to the energy released during a fire is smaller than the derated fire load (Fig. 35.2 bottom line).

The design value of the fire load is related to the effective fire load and is usually calculated by multiplying the characteristic fire load with other factors like partial safety factors (e.g. taking account of the rate of fire occurrence, fire fighting measures etc.).

For the design of new buildings the design fire load is estimated based on statistical data of existing buildings with similar occupancies, size and regional tradition. The fire load in an existing compartment or building can be assessed by in situ surveys.

Estimation of Fire Loads Based on In Situ Surveys

The main task in an in situ survey is to identify and to assess the mass and the heat of combustion of all combustible materials and to determine the characteristic fire load for design purposes and can be conducted by different survey methods.

Survey Methods

In the literature (e.g. Zalok [4], Culver and Kushner [5]) several fire load survey methods can be identified:

- *weighing method*: direct measurement of weight of the combustible materials
- *inventory method*: indirect estimation of the weight by measuring the dimension and/or the density of the combustible items
- *questionnaire method*: distribution of questionnaires and estimation of the combustible material through photographic selection and inventory tables.

Common to all approaches is the attempt to assess the fire load density by the mass of the combustibles and their heat of combustion. The methods differ from each other e.g. in terms of the uncertainties associated with the survey method with the time needed for the survey, with the possibility to verify the results, and with privacy concerns and disruption of business.

Based on a study comparing the weighing and the inventory method, Culver and Kushner [5] estimated the relative error to approximately 10 % when using the inventory method instead of the weighing method. The uncertainty in the inventory method is caused mainly by the estimation of the dimensions by the surveyor. On the other hand, also the mass of combustible material estimated based on the weighing method has some inherent uncertainties, e.g. when assessing the individual weights of a composite material. Surveys conducted in the last years constitute that the combination of the inventory and the weighing method leads to results with smallest uncertainties and is therefore considered to be the most appropriate fire load survey method, see Zalok [4].

The advantage of the questionnaire method is that surveys can be carried out with relatively little effort and even without physically entering the building.

Assessment of Weight

The mass can be directly assessed by weighing the material. In some cases weighing of a material can be complicated because the item is too big for weighing or the item is composed of different materials. In the latter case, weighing of the item without destroying the item is often not possible. In those cases, the weight must be estimated indirectly by assessing the volume and the density of the individual components. As mentioned above the indirect estimation of the mass may lead to an error due to simplification made by the assessment of the volume, especially for irregularly shaped objects. In addition, the actual density of a material can deviate from tabulated or estimated values.

Heat of Combustion

The heat of combustion–also known as the calorific value or heating value–is the total amount of heat released when a quantity of a fuel is oxidized completely under standard temperature conditions and (atmospheric) pressure (see also Drysdale [6]). The heat of combustion is related to different units. The most commonly used unit in fire safety engineering is the SI unit [MJ/kg]. For some items values can be established with units like [MJ/m^2], [MJ/m^3], [MJ/l] or [MJ/piece]. For example the calorific value for a carpet can be defined per square meter [MJ/m^2] or for a wooden pallet per piece [MJ/piece]. This can simplify the assessment of the fire load and save time during a survey (see inventory method above). In some (older) surveys the fire load was converted to wood equivalent, e.g. the fire load in [MJ] was converted in kg of wood [kg of wood equivalent] by dividing the fire load by the heat

of combustion of wood. As the heat of combustion of wood is given by different values in different sources (see e.g. Appendix 3) this may lead to differences among different surveys.

The heat of combustion of the material depends on the aggregate state of the reactants and products after combustion. If the reactants and products are in their standard states, the heat of combustion is defined as the gross heat of combustion (or the gross calorific value). Rules how to determine the gross heat of combustion are given in standards e.g. ISO 1716 [7]. The net heat of combustion H_u (or net calorific value) refers to the case where especially water is in vapour state after the combustion. If solid materials are completely dry the gross heat of combustion corresponds to the net heat of combustion. The influence of the moisture content on the net heat of combustion of a material can be considered by accounting the latent heat of evaporation of water as follows [1]:

$$H_u = H_{u0}(1 - 0.01 \cdot u) - 0.025 \cdot u \qquad (35.3)$$

H_u: net heat of combustion [MJ/kg]
u: the moisture content expressed as mass percentage of dry weight
H_{u0}: the net calorific value of dry materials [MJ/kg]

The net heat of combustion of a mixed material $\overline{H}_u$ can be assessed by the mass and the net heat of combustion of the individual components:

$$\overline{H}_u = \frac{1}{M_{tot}} \sum_{i=1}^{n} M_i \cdot H_{u,i} \qquad (35.4)$$

M_i: mass of the material i [kg]
$H_{u,i}$: net heat of combustion of material i [MJ/kg]
M_{tot}: total mass of the mixed material [kg]

Values for the heat of combustion per kilogram can be found in the literature [1, 8–13] in the form of tabulated data for different materials and items. Data on the heat of combustion for some products and composites can be found in Appendix 3.

Total Fire Load

The total fire load is defined as the sum of the products of the mass and the heat of combustion of all combustible materials in the fire compartment (see Equation 35.1). In general, permanent (or fixed) and variable (or movable) fire load is distinguished. Combustible materials which are part of the structure or the confining elements (e.g. the walls, the floor or the ceiling) contribute to the permanent fire load. Combustible material that is moveable and typically varies in time (e.g. daily, weekly, monthly or during the service life of the building) contributes to the variable fire load. The energy released by the permanent and variable fire loads depends on their reaction to fire or combustibility. For this reason many national standards subdivide the combustibility of building materials (permanent fire load) in different reaction to fire classes. According to the Euroclass system EN 13501 [14], building materials are grouped into seven combustibility classes on the basis of their reaction-to-fire properties (see Table 35.2).

All combustible building material and building contents contributing energy to the fire should be accounted for in the fire load assessment.

Materials can be neglected if the energy required for pyrolysis is higher than the energy which is released from the material during the combustion. This means that those materials consume more energy than they release under fire exposure. According to Beilicke [8] this applies to materials with homogeneous or quasi-homogeneous properties that have a heat of combustion smaller than 8.5 MJ/kg. If favourable condition for the combustions apply, lower values are possible.

Materials (protected and unprotected) that are able to explode under fire exposure, e.g. combustible gases, should be considered separately and are not part of the fire load assessment.

Table 35.2 Euroclass system for classification of the combustibility of building materials, EN 13501 [14]

Class		Performance description	Possible test methods	Examples of products
Non combustible	**A1**	No contribution to fire	ISO 1182 [15] ISO 1716 [7]	Products of natural stone, concrete, bricks, ceramic, glass, steel, and many metallic products
	A2	No significant contribution to fire	ISO 1182 [15] ISO 1716 [7]	Products similar to those of class A1, including small amounts of organic compounds
Combustible	**B**	Very limited contribution to fire	ISO 11925-2 [16]	Gypsum boards with different (thin) surface linings Fire retardant wood products
	C	Limited contribution to fire	ISO 11925-2 [16]	Phenolic foam, gypsum boards with different surface linings (thicker than in class B)
	D	Contribution to fire	ISO 11925-2 [16]	Wood products with thickness $\geq$ about 10 mm and density $\geq$ about 400 kg/m^3 (depending on end use)
	E	Significant contribution to fire	ISO 11925-2 [16]	Low density fibreboard, plastic based insulation products
	F	Incapable of achieving Class E	—	Products not tested (no requirements)

Derated Fire Load

A building material will contribute to a fire depending on its combustibility and its reaction to fire. Non-combustible materials (class A1 and A2 according to EN 13501 [14]–e.g. gypsum boards) and materials with limited reaction to a fire (class B and C) are often used to protect combustible building materials (encapsulation of permanent fire load) and variable fire loads against ignition (e.g. steel containers with combustible content).

Whether protected material should be accounted for the fire load assessment should be related to the reliability of the protection under fire exposure. A failure of the protection leads to an ignition of the protected combustible material. Possible reasons include falling off of the protection, cracks or excessive heat transfer. If the combustible material is preheated at the time of ignition its combustibility may be increased. The failure of the protection is assessed considering the exposure of the protection during a fire. Because of the stochastic behaviour of a fire, the failure of the protection is an uncertain event. This uncertainty can be considered by assigning a failure probability to the protection.

CIB W14 [1] propose a semi-probabilistic approach to account for protected fire loads by introducing derating factors $\psi_{p,i}$. These factors represent the probability for a participation of the protected combustible material in the fire. The derated fire load density q may be written as:

$$q = q_{unprotected} + \sum_i \psi_{p,i} \cdot q_{i,protected} \quad (35.5)$$

$q_{unprotected}$ fire load density for the unprotected combustible materials [MJ/m^2]

$q_{i,protected}$ fire load density for the protected combustible material i [MJ/m^2]

$\psi_{p,i}$ derating factor for the protected combustible material i [-]

There is no generally agreed procedure for deriving the derating factor $\psi_{p,i}$. In an informative annex of the Eurocode 1991-1-2 [17] it is proposed that the protected fire load can be neglected (i.e. $\psi_{p,i} = 0$) when the largest protected fire load (minimum 10 % of the whole protected fire load) plus the unprotected fire load are not able to ignite the protected fire load. In other cases, the specific value of $\psi_{p,i}$ for a protected material should be assessed individually.

For a survey it is important to clarify whether derating factors were used or not. Both the underrated and the derated value of the fire load (especially with regard to the permanent fire load, e.g. encapsulated combustible insulation or structural elements) should be reported, to identify how much combustible material was considered as protected.

Effective Fire Load

The combustion behaviour of a material under real fire exposure depends on the material properties, the surface to volume ratio and the thermal action on the material. Material and geometrical properties, e.g. size, location, etc., will affect the heat release rate (HRR) during a fire and the combustion of the material itself. In most fires there will be no complete combustion of all materials in a room. To consider the incomplete combustion a combustion factor χ can be introduced. The combustion factor χ is defined as the ratio of the effective heat released q_{eff} and the theoretically maximal possible heat released q:

$$\chi = \frac{q_{eff}}{q} \tag{35.6}$$

This ratio describes the degree of combustion and has a value between 0 and 1. A combustion factor of 1 means that a complete combustion takes place, while a factor of 0 implies that no combustion of the material takes place.

The combustion efficiency depends on the quantity of the material burned and is mainly influenced by the fire exposure of the item (oxygen supply) and the ability of the material to protect itself against thermal actions (e.g. charring of wood). Another important factor which affects the combustion efficiency is the density of storage of the goods, e.g. wood-wool will burn fast and nearly completely, while a massive block of wood may self-extinguish and only burn partially on its surface.

Whether the combustion factor χ is considered in the fire load data of a survey should be stated clearly. However, the fire load under full combustion and under incomplete combustion should be reported to address the range of the maximal potential heat release during a fire. In the context of design this factor is typically used to estimate the design fire load.

A general assessment of the combustion factor does not exist yet. EN 1991-1-2 [17] proposes a combustion factor of 0.8 for materials which are mainly composed of cellulosic materials.

Defining Characteristic and Design Values from In Situ Surveys

It should be noted that the fire load assessed in an in situ survey represents only a momentary situation. Variation of the fire load over time should be considered (e.g. fire load before or after delivering products and daily, weekly, monthly, yearly variations). Fire loads that are supposed to remain unchanged during the service life time of the building should be accounted for their expected value. The fire loads that strongly vary in time should be considered depending on their frequency of occurrence. For design purposes, often a characteristic value of the fire load is used, e.g. an 80 % fractile value. Such a value denotes the fire load that is not exceeded during 80 % of the service time of the building.

For fire load surveys involving many buildings within the same occupancy class, the momentary fire load for each building can be assessed. Then, the variation of the fire load in time is characterized by the different momentary situation in the different buildings. The accuracy of predicting the fractile value for the characteristic fire load increases by increasing the number of rooms or buildings that are surveyed.

The design value for the fire load depends on the format of the fire safety design codes. It is usually defined as a function of the characteristic value of the fire load and the combustion efficiency. In the design fire load also additional factors can be considered e.g. the occurrence rate of a fire, the fire fighting measures and the required safety level for the structure (see EN 1991-1-2 [17]). It is therefore important to clearly state how design values of the fire load were established.

Fire Load Density for Different Occupancy Classes

If an in situ survey is not possible (e.g. during the design phase of a building) the mean and standard deviation of the fire load density can be

estimated based on data from fire load surveys in buildings within the same occupancy class. Such a statistical approach is especially valuable for common occupancy classes like residential buildings, offices, hotels, schools or hospitals. Choosing an upper fractile (characteristic) value of the statistical distribution, as required by many regulations, allows for future rearrangements as long as the occupancy class remains the same (e.g. different department stores in a shopping mall). In some occupancy classes, e.g. industrial buildings, the variability of the fire load density is very high. Nevertheless, even for industrial buildings information from fire load surveys in rooms of the same occupancy class can be helpful, e.g. for a preliminary analysis in the design phase or for comparison with the fire load estimate obtained by an in-situ survey. Due to the limited available statistical data and the high variability, the fire load density in industrial buildings will be discussed separately from the distributions for the more common situations.

Common Occupancy Classes

Due to socioeconomic and cultural characteristics specific to different countries or regions of the world, it is not possible to provide universal estimates for the distribution of the fire load density in different occupancies. For Europe, mean and fractile values have been defined for common occupancy classes in Annex E of EN 1991-1-2 [17]. The annex is informative only; allowing different values to be defined in the national annexes. Outside of Europe, guidance on fire load densities in common occupancy classes can be found in the International Fire Engineering Guidelines [18].

The mean values and standard deviations provided in Table 35.3 have been derived from EN 1991-1-2 [17]. Characteristic values (e.g. an 80 % fractile) can be estimated based on Table 35.1. The Eurocode assumes a Gumbel distributed fire load density, but Table 35.3 can also be applied assuming a Lognormal distribution. Another assumption is that the coefficient of variation of the fire load density is equal to 0.3 for all occupancy classes. No permanent fire load is included. The permanent fire load has to be estimated separately based on the methodology described in the in situ survey section above. Combustion factors still have to be applied if incomplete combustion is not treated elsewhere in the fire model.

Table 35.3 Mean and standard deviation of the variable fire load density for different occupancy classes according to the EN 1991-1-2 [17]

Variable fire load density [MJ/m^2]		
Occupancy	Mean	Standard
Dwelling	780	234
Hospital (room)	230	69
Hotel (room)	310	93
Library	1500	450
Office	420	126
Classroom of a school	285	85.5
Shopping centre	600	180
Theatre (cinema)	300	90
Transport (public space)	100	30

The information on the statistical distribution of the fire load density provided in Table 35.3 is valid for rooms of typical use for each occupancy class; special rooms have to be treated separately. At any rate, tabulated values should be used as a first estimate only.

An international overview on fire load surveys conducted before 1986 is given in CIB W14 [1]. However, when referring to older data sources one should bear in mind that today's furnishing materials and building contents are different to what was observed several decades ago. Therefore, older data may not be used unreflectingly and reference should be made to more recent studies. Since 1986, a number of fire load studies have been conducted in different parts of the world, including Canada [9, 12, 19, 20], India [21, 22], Japan [23, 24], Hong Kong [25, 26], Brazil [27] and Europe [28, 29].

Differences between data collected in different studies can be attributed to the fact that the studies were conducted in different geographical regions and within a time frame of several decades; also that the assumptions and methods

used for the different surveys can have large effects on the results. Based on the published reports, differences could be identified in the following areas:

- *Treatment of permanent fire loads*: The information published on the composition of the total (permanent and variable) fire loads is not always sufficient for comparison with studies focusing on variable fire loads only.
- *Fire load units*: The fire load is sometimes estimated in terms of "wood equivalent" [kg wood/m^2]. The conversion to the "fire load energy density" [MJ/m^2] or [Mcal/m^2] is ambiguous due to different assumptions for the net calorific value of wood.
- *Reference area*: In some older studies, the total internal surface area of the fire compartment is used as reference area for the fire load. The conversion to fire load per floor area requires assumptions on the geometrical properties of the fire compartment.
- *Derating factors and combustion efficiency*: Some studies use derating factors to account for protected fire loads and/or incomplete combustion while others estimate the full fire loads.
- *Sampling strategy*: The sample of buildings or rooms assessed during the individual studies may be more or less representative for the occupancy group mentioned in the report.
- *Survey method*: The uncertainty of the estimated values depends largely on the survey method (see discussion in the section on in situ surveys).
- *Simplifying assumptions*: The assumptions made e.g. for assessing the heat of combustion or the weight of the surveyed items can lead to a bias in the values provided by different studies.

Industrial Buildings

In occupancy classes with high variability (e.g. industrial buildings), the in situ survey method is preferred. Nevertheless, in this section some tentative values are proposed for several types of industrial buildings. This information may be used for a preliminary analysis or for comparison with the results of an in situ survey. Production and storage rooms are treated separately.

Even more than in other occupancy classes, the fire load densities in industrial buildings have to be expected to be changing in time. In 2005, a fire load survey in 95 Swiss industrial and commercial buildings was performed by ETH Zürich. Table 35.4 gives an overview on fire load densities surveyed in production rooms. Details of the survey methodology are described in Köhler et al. [30] (see also Thauvoye et al. [28]). Table 35.4 uses the same occupancy classification as proposed by Klein [31]. Only groups with five or more observations in at least

Table 35.4 Summary of fire load densities observed in Swiss industrial buildings (production rooms)

	Recorded fire load densities [MJ/m^2]				
Occupancy (production)	Sample size	Range	Mean	Standard deviation	Coefficient of variation
Wood processing	**17**	**80–4923**	**1488**	**1220**	**0.82**
Wood products	8	345–4923	1959	1522	0.78
Wooden furniture	9	80–1985	1070	731	0.68
Paper, cardboard	**24**	**201–2674**	**1071**	**783**	**0.73**
Paper/cardboard goods	15	201–2674	1037	792	0.76
Printing shop	9	322–2406	1127	813	0.72
Polymer processing	**23**	**68–2779**	**1032**	**716**	**0.69**
Goods made of plastics	17	68–2779	1106	779	0.70
Insulated cables	6	364–1713	824	496	0.60
Metal processing	**8**	**81–532**	**246**	**161**	**0.66**
Pharmaceutics	**5**	**90–3306**	**1006**	**1335**	**1.33**

Table 35.5 Summary of fire load densities per room area observed in Swiss industrial buildings (storage rooms)

	Recorded fire load densities [MJ/m^2]				
Occupancy (storage)	Sample size	Range	Mean	Standard deviation	Coefficient of variation
Wood processing	**18**	**1048–39,679**	**10,594**	**10,021**	**0.95**
Wood products	12	1393–39,679	12,546	11,394	0.91
Wooden furniture	6	1048–13,512	6691	5328	0.80
Paper, cardboard	**27**	**1262–48,458**	**14,602**	**11,378**	**0.78**
Polymer goods	**25**	**755–40,808**	**8545**	**9041**	**1.06**
Metal processing	**6**	**128–4747**	**2024**	**1761**	**0.87**
Building materials	**10**	**166–5734**	**1554**	**1678**	**1.08**
Pharmaceutics	**6**	**932–26,207**	**13,557**	**11,372**	**0.84**
Textiles	**5**	**380–2754**	**1285**	**928**	**0.72**
Sugar goods	**5**	**8271–23,572**	**13,219**	**6461**	**0.49**
Special rooms					
Paint storage	5	530–7825	4907	3095	0.63
Solvent storage	15	112–27,168	8686	7995	0.92
Packaging materials	8	372–6424	2229	1995	0.90

two different companies are included. Nevertheless, also for the remaining groups it should be kept in mind that with a coefficient of variation around 0.7, the statistical uncertainty becomes very high if the sample size is small.

The fire loads in storage rooms tend to be much higher than in production areas, see Table 35.5. Predicting the fire load density in one specific fire compartment based on data seems to be very difficult because of the high variability within each occupancy group.

The fire load density in storage rooms depends not only on the type of materials and goods stored, but also on the storage height and type (e.g. packing density). In the Swiss fire load study, both the gross storage volume (calculated from the total room area and the storage height) and the net storage volume (after subtraction of traffic areas etc.) were recorded. Herein, the fire load in a compartment is referred to the gross storage volume.

Based on this fire load survey, values for specific industrial occupancies (production and storage rooms) have been proposed by VKF [11] (available in German, French and Italian) as input data for a Swiss risk evaluation index method. In addition to a range of fire load "suggested values" are proposed derived on the detailed survey protocols of the fire load study summarized in Tables 35.4 and 35.6 and expert judgement. Due to the limited data sample and the large variability of the fire load density in industrial buildings, the estimates could not be defined mathematically, e.g. in terms of characteristic values. The values given in VKF [11] can thus only provide information on the order of magnitude of fire load densities in different industrial production and storage rooms. The older values given in SIA Dok 81 [32] should be interpreted in a similar way. Today these values should be used with care as the data was collected in the 1960s and cannot be assumed to represent well the present situation in buildings.

Besides the Swiss survey, fire load data for industrial buildings have also been reported in Germany by Schneider and Max [33] (see also CIB W14 [1]) and Halfkann and Wiese [34] (see also Schneider and Max [35]). Both studies recorded fire load densities that were quantified based on the 1978 (prestandard) version of the German DIN 18230 [36]. With a maximum of 20 observations per occupancy group, the sample size in the fire load study by Schneider and Max [33] is comparable to the Swiss study. A much larger sample of industrial buildings could be observed by Halfkann and Wiese [34]. However, their data is often related to specific fire design projects.

Table 35.6 Summary of fire load densities per gross storage volume (room area and storage height) observed in Swiss industrial buildings (storage rooms)

	Recorded fire load densities [MJ/m^3]				
Occupancy (storage)	Sample size	Range	Mean	Standard deviation	Coefficient of variation
Wood processing	**18**	**210–6613**	**1904**	**1505**	**0.79**
Wood products	12	696–6613	2268	1617	0.71
Wooden furniture	6	210–3003	1178	998	0.85
Paper, cardboard	**27**	**421–6873**	**2511**	**1696**	**0.68**
Polymer goods	**25**	**326–5056**	**2075**	**1549**	**0.75**
Metal processing	**6**	**37–922**	**433**	**396**	**0.91**
Building materials	**10**	**37–1220**	**412**	**439**	**1.06**
Pharmaceutics	**6**	**386–3679**	**1180**	**1247**	**1.06**
Textiles	**5**	**172–542**	**337**	**144**	**0.43**
Sugar goods	**5**	**2298–4911**	**3866**	**982**	**0.25**
Special rooms					
Paint storage	5	265–4347	2152	1517	0.70
Solvent storage	15	56–6792	2850	2114	0.74
Packaging materials	8	207–1457	616	423	0.69

References

1. CIB W14. Design Guide Structural Fire Safety. Fire Safety Journal. 1986;10:76–137.
2. Petterson O, Magnusson SE, Thor J. Fire Engineering Design of Steel Structures. Swedish Institute of Steel Construction; 1976.
3. CIB W81. Actions on Structures - Fire. CIB Report 1993.
4. Zalok E. Validation of Methodologies to Determine Fire Load for Use in Structural Fire Protection. The Fire Protection Research Foundation; 2011.
5. Culver C, Kushner J. A program for survey of fire loads and live loads in office buildings 1975.
6. Drysdale D. An Introduction to Fire Dynamics, 2nd Edition: John Wiley & Sons; 2002.
7. ISO 1716:2010. Reaction to fire tests for products—Determination of the gross heat of combustion (calorific value). International Organization for Standardization.
8. Beilicke G. Zusammenstellung von Heizwerten für die Brandlastberechnung: Staatsverlag der Deutschen Demokratischen Republik; 1987.
9. Bwalya AC. An Extended Survey of Combustible Contents in Canadian Residential Living Rooms. In: National Research Council Canada, editor. Ottawa, Canada: Institute for Research in Construction; 2004.
10. Krasny JF, Parker WJ, Babrauskas V. Fire behavior of upholstered furniture and mattresses: Noyes Publications; 2001.
11. VKF. Brandschutzerläuterung: Bewertung von Brandabschnittsgrössen—Sicherheitsnachweis bei industriellen und gewerblichen Nutzungen, Berechnungsverfahren. In: Feuerversicherungen VK, editor. 115-03d. Bern, Switzerland 2003.
12. Bwalya AC, Lougheed GD, Kashef A, Saber HH. Survey Results of Combustible Contents and Floor Areas in Multi-Family Dwellings. In: National Research Council Canada, editor. Ottawa, Canada: Institute for Research in Construction; 2008.
13. Di Nenno PJ. SFPE Handbook of Fire Protection Engineering, 3 ed., Quincy, MA, National Fire Protection Association, 2002.
14. EN 13501. Fire classification of construction products and building elements—Part 1: Classification using data from reaction to fire tests. 2010.
15. ISO 1182:2010. Reaction to fire tests for products—Non-combustibility test. International Organization for Standardization.
16. ISO 11925-2:2010. Reaction to fire tests—Ignitability of products subjected to direct impingement of flame—Part 2: Single-flame source test. International Organization for Standardization.
17. EN 1991. Eurocode 1: Actions on structures—Part 1-2: General actions—Actions on structures exposed to fire. 2002.
18. National Research Council Canada, International Code Council (USA), New Zealand. Dept. of Building and Housing, Australian Building Codes Board. International Fire Engineering Guidelines. In: ABCB, editor. Canberra 2005.
19. Hadjisophocleous GV, Chen Z. A Survey of Fire Loads in Elementary Schools and High Schools. Journal of Fire Protection Engineering. 2010;20:55–71.

20. Zalok E, Hadjisophocleous GV, Mehaffey JR. Fire loads in commercial premises. Fire and Materials. 2009;33:63–78.
21. Kumar S, Rao CVSK. Fire Loads in Office Buildings. Journal of Structural Engineering. 1997;123:365–8.
22. Kumar S, Rao CVSK. Fire load in residential buildings. Building and Environment. 1995;30:299–305.
23. Aburano K, Yamanaka H, Ohmiya Y, Suzuki K, Tanaka T, Wakamatsu T. Suvrvey and Analysis on Surface Area of Fire Load. Fire Science and Technology. 1999;19:11–25.
24. Kose S, Motishita Y, Hagiwara I, Tsukagoshi I, Matsunobu S, Kawagoe K. Survey of Movable Fire Load in Japanese Dwellings. Fire Safety Science—Proceedings of the Second International Symposium 1989.
25. Chow WK, Ngan SY, Lui GCH. Movable fire load survey for old residential highrise buildings in Hong Kong. Safety and Security Engineering 2007. p. 215–22.
26. Chow WK. Zone Model Simulation of Fires in Chinese Restaurants in Hong Kong. Journal of Fire Sciences. 1995;13:235–53.
27. Claret AM, Andrade AT. Fire Load Survey of Historic Buildings: A Case Study. Journal of Fire Protection Engineering. 2007;17:103–12.
28. Thauvoye C, Zhao B, Klein J, Fontana M. Fire Load Survey and Statistical Analysis. Proceedings of the Ninth International Symposium on Fire Safety Science. Karlsruhe, Germany. 2008.
29. Korpela K, Keski-Rahkonen O. Fire Loads in Office Buildings. In: Society of Fire Protection Engineers, editor. 3rd International Conference on Performance-Based Codes and Fire Safety Design Methods. Lund, Sweden 2000. p. 278–86.
30. Köhler J, Klein J, Fontana M. Die Erhebung von Brandlasten in 95 Industrie- und Gewerbebauten. Bauphysik. 2006;28:360–7.
31. Klein J. Zum Verhalten von Tragwerken bei natürlicher Brandeinwirkung unter Berücksichtigung technischer Massnahmen. Zürich: ETH Zürich; 2008.
32. SIA Dok 81. Brandrisikobewertung—Berechnungsverfahren / Evaluation du risque d'incendie—Méthode de calcul. Schweizerischer Ingenieur- und Architekten-Verein, Brand-Verhütungs-Dienst für Industrie und Gewerbe, Vereinigung Kantonaler Feuerversicherungen; 1984.
33. Schneider U, Max U. Brandlasterhebungen in Industrie-Stahlhallen. In: Studiengesellschaft für Anwendungstechnik von Eisen und Stahl e.V., editor. 1984.
34. Halfkann K-H, Wiese J. Brandlastberechnung im Industriebau—Statistische Auswertung von über 3000 bearbeiteten Projekten—Einfluss der Neufassung der Norm DIN 18230 (Ausgabe 5/98)—Zukünftige Entwicklung von rechnerischen Verfahren. Erkelenz, Germany: Halfkann + Kirchner Sachverständigenbüro—Brandschutzingenieure; 1998. p. 34.
35. Schneider U, Max U. Baulicher Brandschutz im Industriebau—Kommentar zur DIN 18230 und Industriebaurichtlinie. 3 ed: Beuth Verlag; 2003.
36. DIN V 18230. Baulicher Brandschutz im Industriebau—Structural fire protection in industrial buildings. Berlin: DIN Deutsches Institut für Normung; 1987.

Mario Fontana is a professor at ETH Zurich in Switzerland at the Institute of Structural Engineering. His research activity have included structural fire safety, composite, steel and timber structures.

Jochen Kohler is a professor in NTNU in Norway in the Department of Structural Engineering. His research activities have included probabilistic design and analysis, of structures, risk analysis, probabilistic modelling, code calibration. Before becoming Prof. at NTNU Prof. Kohler was senior scientist at the Institute of Structural Engineering, ETH Zürich.

Katharina Fischer is a consulting engineer at Matrisk GmbH in Switzerland with expertise in risk analysis, probabilistic modelling and code calibration. Before her engagement at Matrisk, she made a PhD at ETH Zürich, focusing on fire risk assessment and societal decision-making.

Gianluca De Sanctis is a senior researcher at ETH Zurich in Switzerland. His research activities have included quantitative fire risk assessment for rational decision-making, assessment and probabilistic modelling of basic design parameters for fire safety and performance evaluation and optimization of fire safety design provisions.

Combustion Characteristics of Materials and Generation of Fire Products

36

Mohammed M. Khan, Archibald Tewarson, and Marcos Chaos

Abbreviations

ABS	acrylonitrile-butadiene-styrene
CDG	carbon dioxide generation calorimetry
CPVC	chlorinated polyvinylchloride
CR	neoprene or chloroprene rubber
CSP (or CSM)	chlorosulfonated polyethylene rubber (Hypalon)
CTFE	chlorotrifluoroethylene (Kel-F)
E-CTFE	ethylene-chlorotrifluoroethylene (Halar)
EPR	ethylene propylene rubber
ETFE	ethylenetetrafluoroethylene (Tefzel)
EVA	ethylvinyl acetate
FEP	fluorinated polyethylene-polypropylene (Teflon)
FPA	Fire Propagation Apparatus
GTR	gas temperature rise calorimetry
IPST	isophthalic polyester
OC	oxygen consumption calorimetry
PAH	polyaromatic hydrocarbons
PAN	polyacrylonitrile
PC	polycarbonate
PE	polyethylene
PEEK	polyether ether ketone
PES	polyethersulfone
PEST	polyester
PET	polyethyleneterephthalate (Melinex Mylar)
PFA	perfluoroalkoxy (Teflon)
PMMA	polymethylmethacrylate
PO	polyolefin
POM	polyoxymethylene
PP	polypropylene
PS	polystyrene
PTFE	polytetrafluoroethylene (Teflon)
PU	polyurethane
PVC	polyvinylchloride
$PVCl_2$	polyvinylidene chloride (Saran)
PVDF	polyvinylidenefluoride (Kynar)
PVEST	polyvinylester
PVF	polyvinyl fluoride (Tedlar)
PVF_2	polyvinylidene fluoride (Kynar Dyflor)
SBR	styrene-butadiene rubber
TFE	tetrafluoroethylene (Teflon)
XLPE	cross-linked polyethylene

M.M. Khan (✉) • M. Chaos
FM Global Research, Norwood, MA 02062, USA

A. Tewarson
Retired from FM Global Research, Norwood, MA 02062, USA

Introduction

Hazards associated with fire are characterized by the generation of calorific energy and products, per unit of time, as a result of the chemical reactions of surfaces and material vapors with oxygen from air. Thermal hazards constitute those scenarios where the release of heat is of major concern. On the other hand, nonthermal hazards are characterized by fire products (smoke, toxic, corrosive, and odorous compounds.) Generation rates of heat and fire products (and their nature) are governed by

M.J. Hurley (ed.), *SFPE Handbook of Fire Protection Engineering*,
DOI 10.1007/978-1-4939-2565-0_36, © Society of Fire Protection Engineers 2016

(1) fire initiation (ignition); (2) fire propagation rate beyond the ignition zone; (3) fire ventilation; (4) external heat sources; (5) presence or absence of fire suppression/extinguishing agents; and (6) materials: (a) their shapes, sizes, and arrangements; (b) their chemical natures; (c) types of additives mixed in; and (d) presence of other materials. In this handbook most of these areas have been discussed from fundamental as well as applied views. For example, the mechanisms of thermal decomposition of polymers, which govern the generation rates of material vapors, are discussed in Chap. 7, generation rate of heat (or heat release rate) from the viewpoint of thermochemistry is discussed in Chap. 5, Flaming ignition of the mixture of material vapors and air is discussed in Chap. 21, and surface flame spread in Chap. 23.

In this chapter emphasis is placed on small scale experiments and how such testing can be used to determine the generation per unit of time of (1) the calorific energy, defined as the heat release rate, and (2) fire products. From these tests, measurements of so-called "fire properties" are made that can be used in models to predict, under a variety of conditions, (1) heat release rate, to assess thermal hazards; and (2) generation rates of fire products, to assess nonthermal hazards. Fire properties are defined herein that help characterize the flammability of a given material and relationships are derived, based on empirical evidence, that elucidate the effect of environmental factors (such as external heat flux and ventilation) on the properties. Also important, and discussed in this chapter, is the connection of these properties to the behavior of large-scale fire phenomena under well ventilated as well as vitiated conditions (i.e., compartment fires.). Lastly, with the advent and quick development of computer modeling as applied to large scale fires, this chapter also discusses the value of small scale testing in determining material flammability parameters specific to such models.

Several other chapters in this handbook relate to the subjects discussed here and should be consulted for complete information and context. The chapters are as follows: Chaps. 27, 28, 16, and 24. Physical and combustion properties of selected fuels in air and heats of combustion and related properties of pure substances, plastics, and miscellaneous materials listed in Appendix 3 should be consulted for information that may not be included in this chapter. This chapter presents the applications of the principles discussed in several chapters in this handbook to determine the fire properties of materials. Simple calculations have been included in the chapter to show how the properties can be used for various applications.

Flammability Apparatuses and Measurement Capabilities

At the scales of relevance to this chapter, there are mainly three heat release rate apparatuses available: (1) The Ohio State University (OSU) Heat Release Rate Apparatus; (2) FM Global's Fire Propagation Apparatus (previously known as "Small-Scale Flammability Apparatus"); and (3) NIST's Cone Calorimeter. These apparatuses are briefly described below.

In 1972, gas temperature rise (GTR) calorimetry (details are given in section "Heat Release Rate" of this chapter) was used by the Ohio State University (OSU) to determine heat release rate [1, 2]. The apparatus used is now known as the OSU heat release rate apparatus; it is shown in Fig. 36.1. The OSU apparatus is an ASTM [3] and an FAA [4] standard test apparatus. In GTR calorimetry, it is assumed that almost all the thermal radiation from the flame is transferred to the flowing fire products-air mixture, as the flames are inside an enclosed space and heat loss by conductive heat transfer is negligibly small. Oxygen consumption (OC) calorimetry (details are given in section "Heat Release Rate" of this chapter) has now been adapted to the OSU apparatus [5].

Calorimetry methodologies based on carbon dioxide generation (CDG, details are given in section "Heat Release Rate" of this chapter), OC, and GTR calorimetries were used during the mid-1970s by FM Global Research

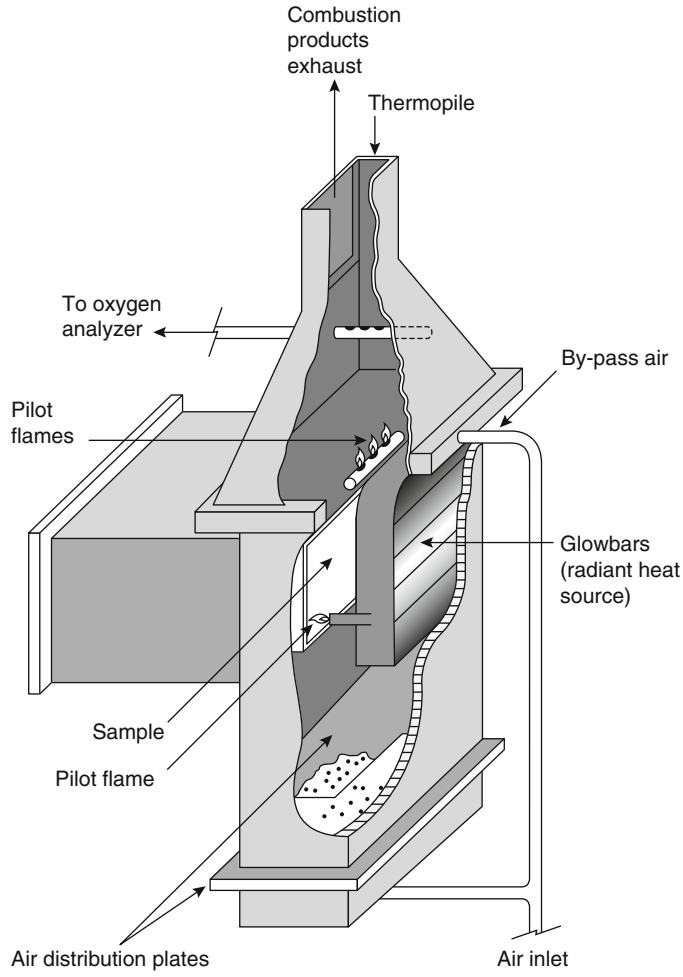

Fig. 36.1 Ohio State University's (OSU, ASTM E906) heat release rate apparatus [1–4]

(formerly, Factory Mutual Research Corporation—FMRC) to determine chemical, convective, and radiative heat release rates [6–9]. The apparatus used is now known as the Fire Propagation Apparatus (FPA) and is an ASTM [10] and ISO [11] standard; it is shown in Figs. 36.2 and 36.3. Heat release rate from CDG and OC calorimetries in the FPA was originally defined as the "actual heat release rate" until 1986 [9, 12–15]; thereafter, however, it was changed to "chemical heat release rate" to account for the effects of (1) the chemical structures of the materials and additives; (2) fire ventilation; (3) the two dominant modes of heat release, that is, convective and radiative; and (4) the effects of flame extinguishing and suppressing agents. The FPA is a standard test apparatus for electrical cables [16, 17], for wall and ceiling insulation materials, replacing the 7.6 m (25-ft) corner test (as described in section "Fire Propagation" of this chapter) [18], for clean room materials used in the semiconductor industry [19], and for conveyor belts [20].

In 1982 the National Institute of Standards and Technology (NIST) used OC calorimetry, following the methodology described by Hugget [21]. The apparatus developed to use this methodology, known as the cone calorimeter [22, 23], is shown in Fig. 36.4. The cone calorimeter became an ASTM standard [24] test apparatus in 1990. Details about the cone calorimeter are given in Chap. 28.

Sampling ducts have been designed for the FPA and the cone calorimeter to measure the mass generation rates of CO_2 and CO and mass consumption rate of oxygen for use in the

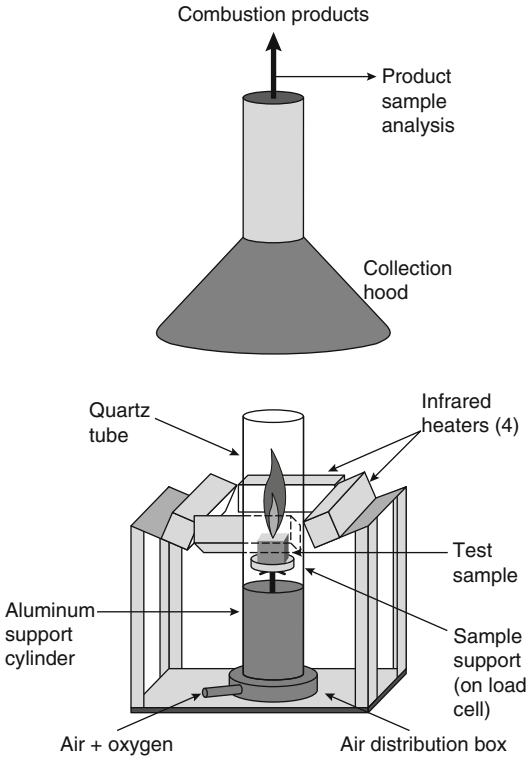

Fig. 36.2 Fire Propagation Apparatus (FPA) [10, 11] designed by FM Global Research. Sample configuration for ignition, pyrolysis, and combustion tests

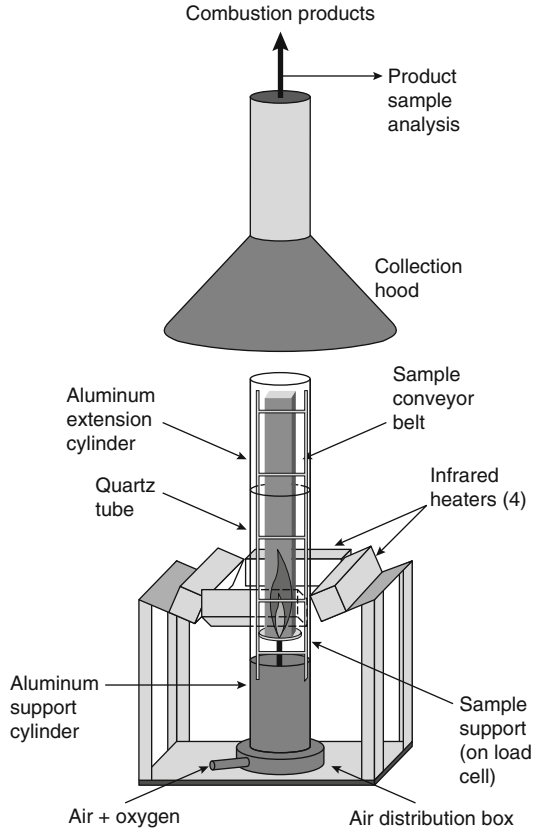

Fig. 36.3 Fire Propagation Apparatus (FPA) [10, 11] designed by FM Global Research. Sample configuration for fire propagation tests; a conveyor belt sample is shown

calorimetric equations (see section "Heat Release Rate" of this chapter). CDG and OC calorimetries are used in the FPA. In the OSU apparatus and the cone calorimeter, only the OC calorimetry is used. For application of GTR calorimetry, a thermopile located in the flue gas chimney is used in the OSU apparatus, and a thermocouple located in the sampling duct is used in the FPA, where heat losses by conduction are negligibly small. The cone calorimeter has not been designed to use GTR calorimetry. The FPA provides the advantage of determining the radiative heat release rate from the difference between the chemical (determined by CDG or OC) and convective (determined by GTR) heat release rates [25]. Details on sample preparation, sample holders, and measurement procedures are provided for each apparatus [3, 10, 11, 24]. The design features, test conditions, and types of measurements for the three apparatuses are listed in Table 36.1. As shown in the table, the Fire Propagation Apparatus measures flammability characteristics of materials under various air flow (ventilation) conditions, in enhanced or reduced oxygen environments, and also has the ability to determine flame extinction by extinguishing agents. Much of the data presented in this chapter takes advantage of all of these capabilities.

Figure 36.5 shows an example of typical heat release rate profiles measured in the FPA. These profiles correspond to the chemical heat release rate of polymethylmethacrylate, determined from CDG and OC calorimetries, as well as the convective heat release rate, determined by GTR. The polymethylmethacrylate (PMMA) sample was 100 mm in diameter and 9.53 mm in

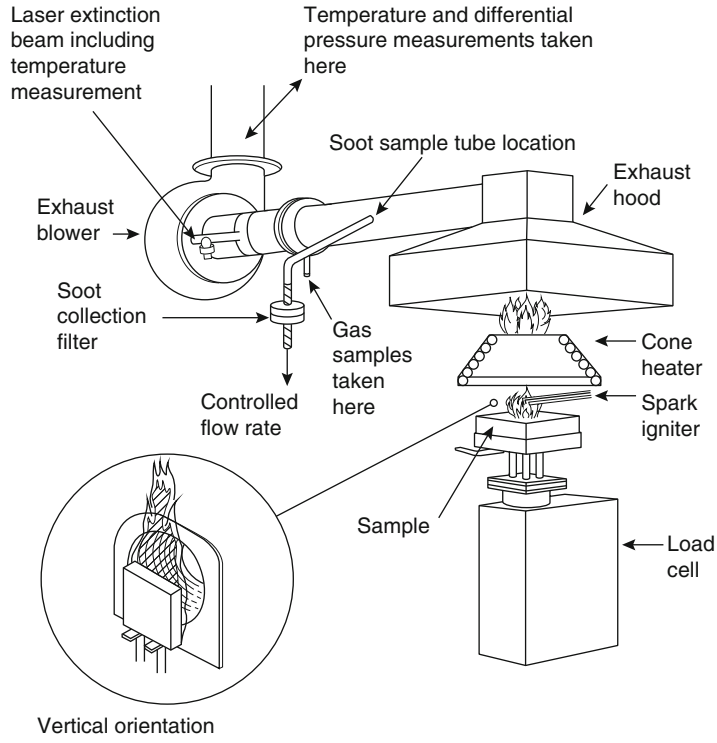

Fig. 36.4 The cone calorimeter [22–24] designed at the National Institute of Standards and Technology (NIST)

thickness. It was exposed to an external heat flux of 50 kW/m^2 under co-flowing normal air. The chemical heat release rate profiles from the CDG and OC calorimetries in the FPA are very similar, as expected.

Combustion Characteristics of Materials: Engineering and Modeling Applications

Ignition (Fire Initiation)

The fundamental ignition principles are described in detail in Chap. 21. These principles suggest that, for fire initiation, a material has to be heated above its critical heat flux (CHF, described below) for ignition. Generally speaking, ignition of a combustible solid, heated by an external source, starts with solid-phase thermal decomposition and evolution of combustible gases from the surface leading to gas-phase combustion, resulting in a sustained diffusion flame.

When a solid material is exposed to an external heat flux, it behaves either as thermally thin or thermally thick, depending on its material properties, dimensions and the magnitude of the incident heat flux. Materials typically behave as thermally thick at high heat fluxes (i.e., at high heating rates); and behave thermally thin at low heat fluxes (i.e., at low heating rates) near their critical heat flux for ignition. A thermally thick material is one having a physical thickness greater than the depth of thermal diffusion at the time of ignition, while the physical thickness of a thermally thin sample is less than the depth of thermal diffusion at ignition.

The equation for piloted ignition time of solids under thermally thick conditions may be expressed as [26, 27]:

$$t_{ig(thick)} = \frac{\frac{\pi}{4} k\rho c_p \left(T_{ig} - T_0\right)^2}{\left(\dot{q}''_e - \chi \dot{q}''_{cr}\right)^2} \qquad (36.1)$$

where, $t_{ig(thick)}$ is the time to piloted ignition (s); k, ρ and c_p are, respectively, thermal conductivity (kW/m/K), density (kg/m^3), and specific heat

Table 36.1 Design features, test conditions, and types of measurements for the OSU heat release rate apparatus, the Fire Propagation Apparatus, and the NIST Cone Calorimeter

Design and test conditions	OSU[a]	ASTM E2058 Fire Propagation Apparatus[b]	Cone[c]
Inlet gas flow	Co-flow	Co-flow/natural	Natural
Oxygen concentration (%)	21	0–40	21
Co-flow gas velocity (m/s)	0.49	0–0.146	NA
External heaters	Electrical resistance elements	Tungsten-quartz	Electrical coils
External heat flux (kW/m^2)	0–80	0–110	0–100
Exhaust product flow (m^3/s)	0.04	0.035–0.364	0.012–0.035
Horizontal sample dimensions (mm)	110 × 150	100 × 100	100 × 100
Vertical sample dimensions (mm)	150 × 150	100 × 600	100 × 100
Ignition source	Pilot flame	Pilot flame	Spark plug
Heat release rate capacity (kW)	8	50	8
Measurements			
Time to ignition	Yes	Yes	Yes
Material gasification rate	No	Yes	Yes
Fire propagation rate	No	Yes	No
Generation rates of fire products	Yes	Yes	Yes
Light obscuration by smoke	Yes	Yes	Yes
Smoke yield	No	Yes	No
Effective (chemical) heat of combustion	No	Yes	Yes
Chemical heat release rate	Yes	Yes	Yes
Convective heat release rate	Yes	Yes	No
Radiative heat release rate	No	Yes	No
Flame extinction	No	Yes	No

NA not available
[a]As specified in ASTM E906 [3] and by DOT/FAA [4]
[b]As specified in ASTM E2058 [10] and ISO 12136 [11]
[c]As specified in ASTM E1354 [24]

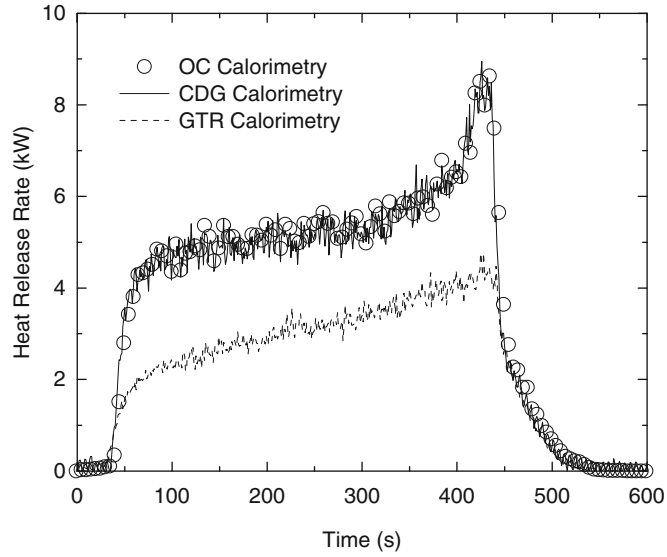

Fig. 36.5 Heat release rates determined employing the methodologies described in the text (CDG, OC, and GTR) for a 9.53-mm thick slab of polymethylmethacrylate (PMMA) exposed to an external heat flux of 50 kW/m^2 and 0.09 m/s co-flowing normal air in the Fire Propagation Apparatus

(kJ/kg/K) of the solid; their product represents the thermal inertia of the solid. T_{ig} and T_0 are the surface ignition temperature (K) and ambient temperature (K), respectively, $\dot{q}''_e$ and $\dot{q}''_{cr}$ are the incident heat flux (kW/m^2) and the critical heat flux for ignition (CHF) (kW/m^2), and χ is the average heat loss as a fraction of the critical heat flux and takes into account the fact that heat losses are initially zero and increase as the solid is heated to its ignition temperature. The square root of the term in the numerator of the right hand side of Equation 36.1 is sometimes referred to as the Thermal Response Parameter (TRP) [28]:

$$\mathrm{TRP} = \left(\frac{\pi}{4} k\rho c_p\right)^{1/2} \left(T_{ig} - T_0\right) \tag{36.2}$$

Under thermally thin conditions for solids of thickness d (m), the time to piloted ignition, $t_{ig(thin)}$, is based on the energy required to heat the material to its ignition temperature assuming a uniform temperature throughout the material:

$$t_{ig(thin)} = \frac{\rho c_p d \left(T_{ig} - T_0\right)}{\dot{q}''_e - \chi \dot{q}''_{cr}} \tag{36.3}$$

T_{ig} in Equations 36.1 and 36.3 is evaluated here assuming that reradiation heat losses dominate the ignition process so that $\dot{q}''_{cr} = \sigma\left(T_{ig}{}^4 - T_0{}^4\right)$ for a black surface, where σ is the Stephan-Boltzmann constant (kW/m^2/K^4).

The value of χ approximates the effect of heat losses during heat up of the solid. It was recommended [27] that $\chi = 0.64$ for thermally thick conditions assuming surface re-radiation losses close to $\dot{q}''_{cr}$ are dominant. After analyzing various materials, and considering both radiant and convective losses Khan et al. [29] proposed a single value of $\chi = 1.0$ for both thermally thin and thermally thick solids. A thermal diffusion time, τ_{th} (s), can be defined to demarcate the transition between thermally thick and thermally thin responses as [26, 29]:

$$\tau_{th} = \frac{4\rho c_p d^2}{\pi k} \tag{36.4}$$

Using Equations 36.1 and 36.4, the relationship between thermally thick and thin ignition behavior is given by [29]:

$$\begin{aligned} t_{ig(thin)} &= \left(\tau_{th} t_{ig(thick)}\right)^{1/2} \\ &= \frac{\left(\frac{\pi}{4} k\rho c_p\right)^{1/2} \left(T_{ig} - T_0\right)}{\dot{q}''_e - \chi \dot{q}''_{cr}} \left(\frac{4\rho c_p d^2}{\pi k}\right)^{1/2} \\ &= \frac{\rho c_p d \left(T_{ig} - T_0\right)}{\dot{q}''_e - \chi \dot{q}''_{cr}} \end{aligned} \tag{36.5}$$

A generalized form applicable to both regimes is [29]:

$$t_{ig(thick/thin)} = \left\{ \left[\frac{\dot{q}_e'' - \chi \dot{q}_{cr}''}{\left(\frac{\pi}{4} k\rho c_p\right)^{1/2} (T_{ig} - T_0)} \right]^4 \frac{1}{\tau_{th}{}^2} + \left[\frac{\dot{q}_e'' - \chi \dot{q}_{cr}''}{\left(\frac{\pi}{4} k\rho c_p\right)^{1/2} (T_{ig} - T_0)} \right]^8 \right\}^{-1/4} \tag{36.6}$$

The exponents ¼, 4, and 8 in Equation 36.6 provide a good fit to exact numerical solutions for transition between thermally thin and thick behavior [29]. In Equation 36.6, if t_{ig} is less than τ_{th} the response of the material becomes thermally thick; whereas, if t_{ig} is greater than τ_{th} the response becomes thermally thin. Thus τ_{th} provides the transition between thermally thin and thermally thick behaviors.

Critical Heat Flux (CHF)

The ignition and subsequent burning of a solid sample is sensitive to heat losses from the rear surface of the sample being tested. This heat loss depends on the sample holder and its surrounding environment. Theoretical studies of ignition and pyrolysis in flammability apparatuses show that the construction of the sample holder has a surprisingly large effect on measured parameters, especially for solids having thermally thin behavior near the critical heat flux [30]. This makes flammability measurements apparatus dependent. One naturally wishes to minimize any such heat losses, but to whatever extent such losses remain, they must be made reproducible and quantifiable so that one can correct for their presence. To minimize apparatus dependencies, de Ris and Khan have designed an insulated sample holder [30] that minimizes heat losses from the rear and sides of the sample being heated. The holder ensures that thermal processes remain one-dimensional so as to conform to most theoretical analyses used to interpret data.

The critical heat flux may provide a measure of the ignition temperature of a given material if, as stated above, one assumes that all heat losses near the CHF are dominated by radiation; this, again, reinforces the need for a well-insulated sample. Empirically, the CHF is obtained by collecting piloted ignition data in a flammability apparatus, such as the FPA, over a range of (low) heat fluxes. By plotting the inverse of time to ignition versus heat flux and using Equation 36.3, the intercept of a best-fit line on the heat flux axis corresponds to the CHF. Alternatively, ignition tests may be also performed in search of the heat flux for which no ignition occurs after a specified threshold (e.g., 15 min).

Thermal Response Parameter (TRP)

TRP is a very useful parameter for engineering calculations to assess resistance to ignition and fire propagation. For thermally thick materials, the inverse of the square root of time to ignition is expected to be a linear function of the external heat flux away from the CHF value (see Equation 36.1). The inverse of the slope of the line is the TRP (see Equations 36.1 and 36.2). Most commonly used materials behave in a thermally thick manner at practical fire conditions and, thus, satisfy Equation 36.1. This behavior is shown in Fig. 36.6 for polymethylmethacrylate (PMMA) [31]; in Fig. 36.7 for heavy corrugated paper sheets; and in Fig. 36.8 for cone calorimeter data [32].

The TRP value is determined, for example, in the Fire Propagation Apparatus, by (1) measuring the time to ignition for 100 mm × 100 mm square or 100-mm diameter and up to 25-mm-thick samples at different external heat flux values. The sample surfaces are blackened with a very thin layer of black paint or fine graphite powder to avoid errors due to differences in the radiation absorption characteristics of the materials, and (2) performing a linear regression analysis of the data away from the critical heat

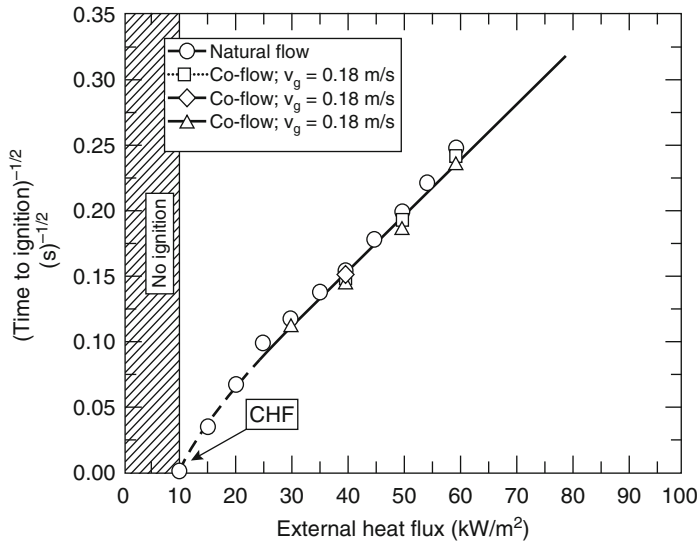

Fig. 36.6 Square root of the inverse of time to ignition versus external heat flux for 100-mm × 100-mm × 25-mm-thick polymethylmethacrylate (PMMA) slab with a blackened surface. Data measured in the Fire Propagation Apparatus [31]

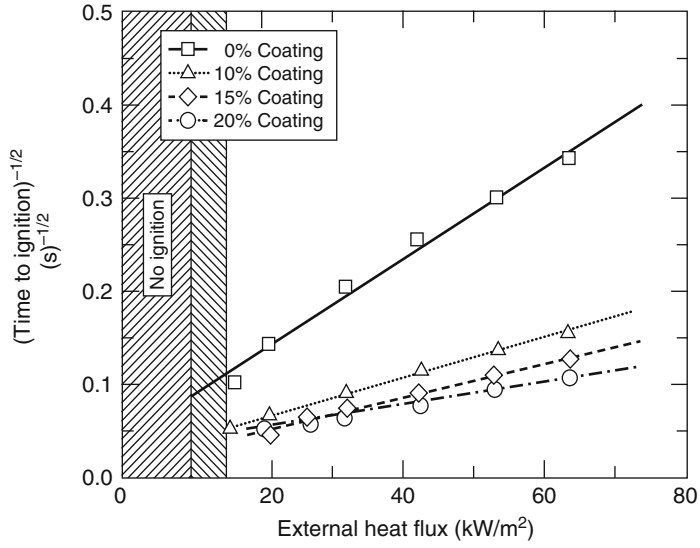

Fig. 36.7 Square root of the inverse of time to ignition versus external heat flux for two 100-mm × 100-mm × 11-mm-thick sheets of heavy corrugated paper with various levels of fire protection coating. Data measured in the Fire Propagation Apparatus. Lines are linear fits to the data; TRP values derived from the fits are given in Table A.35

flux condition, following Equation 36.1, and recording the inverse of the slope of the line.

The TRP for a surface may vary depending on whether or not it is blackened. For example, for nonblackened and blackened surfaces of polymethylmethacrylate (PMMA), TRP = 434 and 274 kW · s$^{1/2}$/m^2, respectively [31]. The TRP value for a blackened surface of PMMA is close to the value calculated from the known T_{ig}, k, ρ, and c_P values for PMMA [31]. These results highlight the importance of a well-defined boundary condition, provided by an appropriate high absorptivity surface coating, in ignition tests. Uncoated samples may be subject to other phenomena such as in-depth radiation [33] as well as the spectral characteristics of both sample surface and radiation source [34, 35]. It is for these reasons that standard FPA tests [10, 11] require that samples be coated with high emissivity paint to ensure surface absorption of imposed heat flux.

TRP depends on the chemical as well as the physical properties of materials, such as the

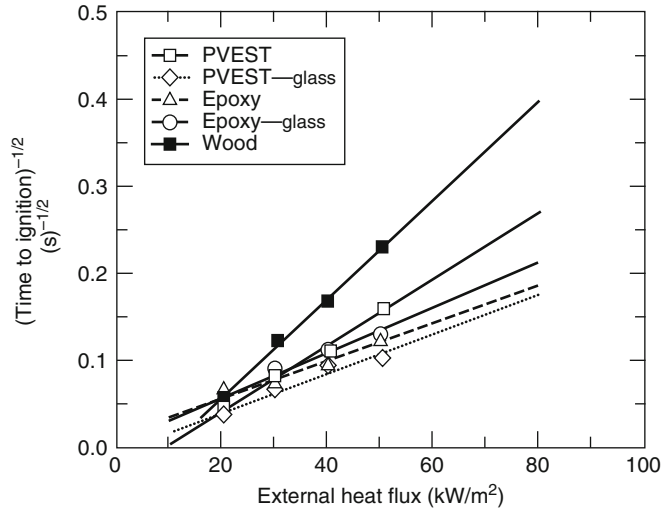

Fig. 36.8 Square root of the inverse of time to ignition versus external heat flux for 100-mm × 100-mm nonblackened surfaces of 10-mm × 11-mm-thick polyvinyl ester (PVEST), 11-mm-thick epoxy, and 6-mm-thick wood (hemlock). Data measured in the cone calorimeter [32]

chemical structure, fire retardants, etc. For example, Fig. 36.9 shows that TRP increases with sample thickness for a composite material (polyester/fiberglass) and increases in the amount of passive fire protection agent used, such as that provided by a surface coating to a heavy corrugated paper sheet (see Fig. 36.7). The TRP response versus thickness shown in Fig. 36.9 is counterintuitive given that TRP is strictly defined for thermally thick materials; this response is a result of the composite material considered and evidences the effect of physical structure and nonhomogeneity of the material.

CHF and TRP values for several materials derived from data for time to ignition versus external heat flux are listed in Table A.35. The ranges of CHF and TRP values in Table A.35 are due to differences in the compositions of materials having similar generic natures and differences in the test procedures, such as the use of an insulated sample holder, as described above.

Examples of calculated TRP values, using available T_{ig}, k, ρ, and c_p data and Equation 36.2, and those measured are listed in Tables A.36 and A.37. The calculated and measured TRP values (TRP_{cal} and TRP_{meas}, respectively) are plotted in Fig. 36.10. For ordinary polymers that do not contain halogen atoms and do not char significantly, the TRP_{cal} value is only about 17 % lower than the TRP_{meas} value, but for highly charring, high-temperature, engineered polymers and highly halogenated polymers, the TRP_{cal} values are significantly lower than the TRP_{meas} values. There is strong flame retardation by the fuel vapors of the highly halogenated polymers with a significant reduction in the fuel vapor concentration due to charring. Thus, for the ordinary polymers, thermal arguments to describe the ignition behavior (Equations 36.1 and 36.2) are sufficient, but not for the highly charring, high-temperature, engineered polymers and highly halogenated polymers.

The effects of the fuel vapors of the highly charring, high-temperature, engineered polymers and highly halogenated polymers on the ignition behavior can be compensated by performing the ignition experiments under enhanced oxygen concentration and, thus, thermal arguments again can be used to describe the ignition behavior. This is supported by the data reported by Khan and de Ris [36], which are listed in Table 36.2.

Example 1 In a fire, newspaper and polypropylene are exposed to a heat flux value of 50 kW/m^2. Estimate which material will ignite first, assuming physical conditions to be very similar for both the materials.

Solution From Table A.35, for newspaper and polypropylene, CHF = 10 and 15 kW/m^2, respectively, and TRP = 108 and 193 kW · s$^{1/2}$/m^2,

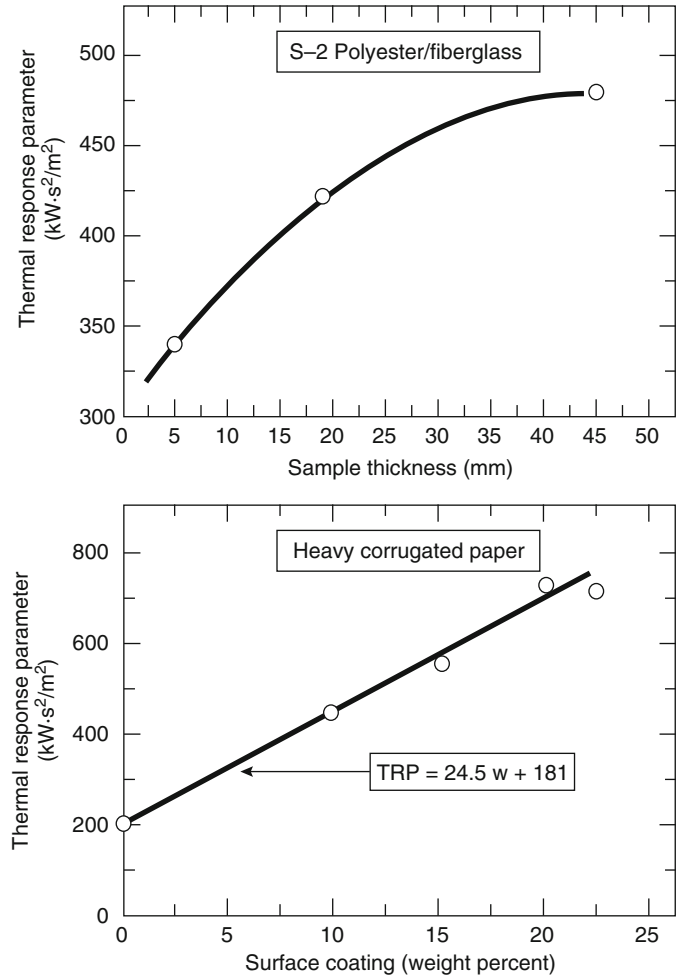

Fig. 36.9 Thermal response parameter versus thickness for S-2 polyester/fiberglass sample and weight percent of surface coating for the heavy corrugated paper (see Fig. 36.7). Data measured in the Fire Propagation Apparatus. *w* weight %

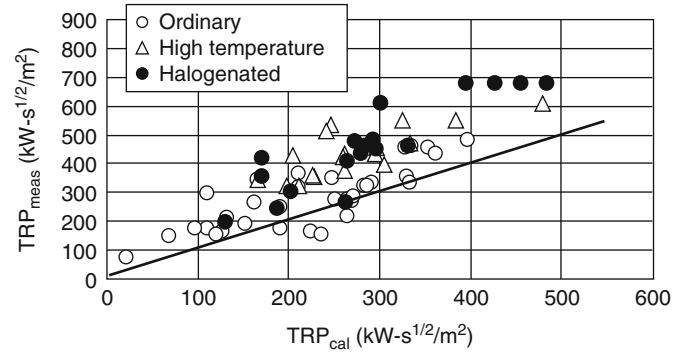

Fig. 36.10 Calculated versus measured values of the thermal response parameter

respectively. Substituting these values in Equation 36.1 with $\dot{q}_e'' = 50$ kW/m^2, the times to ignition are calculated to be 6 and 24 s for newspaper and polypropylene, respectively. Thus, newspaper will ignite first.

Example 2 Halogenated materials are obtained by replacing hydrogen atoms with halogen atoms in the chemical structures of the materials. For example, a unit in polyethylene (PE) consists of C_2H_4. If a hydrogen atom (H) is replaced by a

Table 36.2 Thermal response parameter values measured in normal air and 40 % oxygen concentration and calculated from physical properties [23, 37]

Polymer	TRP_{meas} (kW·s$^{1/2}$/m^2)		TRP_{cal} (kW·s$^{1/2}$/m^2)
	Normal air	40 % oxygen	
Ordinary polymers			
Polymethylmethacrylate (PMMA)	239	230	264
Polyoxymethylene (POM)	252	260	269
Polypropylene/fire retarded	276	301	242
Halogenated polymers			
Polyvinylchloride (PVC)—rigid	498	200	171
Chlorinated PVC (CPVC)—rigid	435[a]	230	280
Polyvinylchloride (PVDF)	447–508	324	301

[a]Data from Table A.35

chlorine atom (Cl) in a PE unit, it becomes a unit of rigid polyvinylchloride (PVC), that is, C_2H_3Cl. If two H atoms are replaced by two fluorine atoms (F) in a PE unit, it becomes a unit of Tefzel (ethylene tetrafluorethylene), that is, $C_2H_2F_2$. If all the hydrogen atoms are replaced by four F atoms in a PE unit, it becomes a unit of Teflon (polytetrafluoroethylene), that is, C_2F_4. Show how the replacement of hydrogen atoms by the halogen atoms affects the ignitability of the materials.

Solution From Table A.35, for PE (high density), PVC (rigid), Tefzel, and Teflon, the CHF values are 15, 15, 27, and 38 kW/m^2, respectively, and the TRP values are 321, 406, 356, and 682 kW · s$^{1/2}$/m^2, respectively. In the calculations, it is assumed that these materials are exposed to a uniform heat flux of 60 kW/m^2 in a fire under very similar physical conditions. From Equation 36.1, using $\dot{q}_e'' = 60$ kW/m^2, the times to ignition for PE (high density), PVC (rigid), Tefzel, and Teflon are calculated to be 40, 64, 91, and 755 s, respectively. Thus, resistance to ignition increases as the hydrogen atom is replaced by the halogen atom in the chemical structure of PE. The higher the number of hydrogen atoms replaced by the halogen atoms in the structure, the higher the resistance to ignition. When all the hydrogen atoms are replaced by the fluorine atoms, the material becomes highly resistant to ignition.

Fire Propagation

The fundamental surface flame spread principles are described in Chap. 23. According to these principles, the fire propagation process, as indicated by surface flame spread, can be explained as follows. As a material is exposed to heat flux from internal and/or external heat sources, a combustible mixture is formed that ignites, and a flame anchors itself on the surface in the ignition zone. As the vapors of the material burn in the flame, they release heat with a certain rate, defined as the chemical heat release rate. Part of the chemical heat release rate is transferred beyond the ignition zone as conductive heat flux through the solid and as convective and radiative heat fluxes from the flame. If the heat flux transferred beyond the ignition zone satisfies CHF, TRP, and gasification requirements of the material, the pyrolysis and flame fronts move beyond the ignition zone, increasing the burning surface area. Consequently, flame height, chemical heat release rate, and heat flux transferred ahead of the pyrolysis front all increase. The pyrolysis and flame fronts move again, and the process repeats itself further increasing the burning area. Fire propagation on the surface continues as long as the heat flux transferred ahead of the pyrolysis front (from the flame or external heat sources) satisfies CHF, TRP, and gasification requirements of the material.

The rate of movement of the pyrolysis front is generally used to define the fire propagation rate:

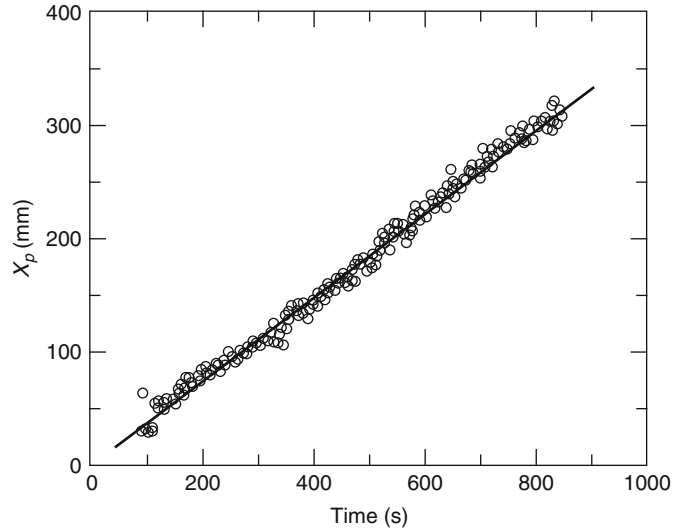

Fig. 36.11 Pyrolysis front versus time for downward fire propagation for a 300-mm-long, 100-mm-wide, and 25-mm-thick PMMA vertical slab under opposed airflow conditions in the Fire Propagation Apparatus. Airflow velocity = 0.09 m/s. Oxygen mass fraction = 0.334 (Figure is taken from Ref. [31])

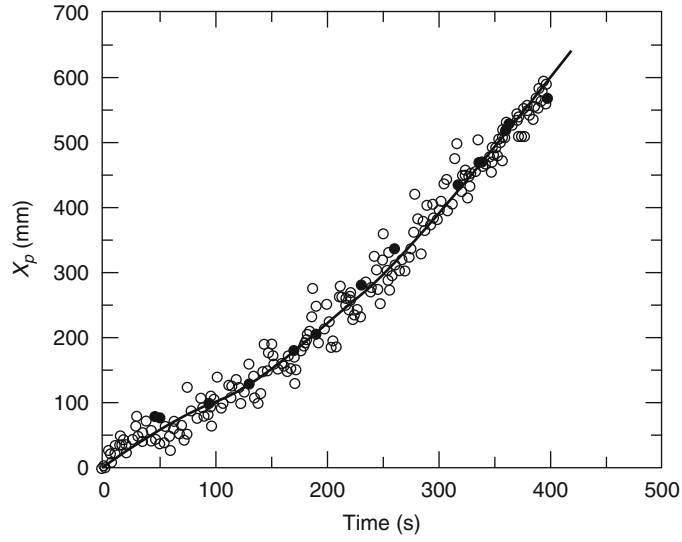

Fig. 36.12 Pyrolysis front versus time for upward fire propagation for a 600-mm-long, 100-mm-wide, and 25-mm-thick PMMA vertical slab under co-airflow conditions in the Fire Propagation Apparatus. Airflow velocity = 0.09 m/s. Oxygen mass fraction = 0.233 (Figure is taken from Ref. [31])

$$u = \frac{dX_p}{dt} \tag{36.7}$$

where u is the fire propagation rate (mm/s or m/s), and X_p is the pyrolysis front length (mm or m).

The fire propagation rate can be determined in one of several apparatuses: (1) the LIFT [37] described in Chap. 23; (2) the Fire Propagation Apparatus [10, 11] shown in Fig. 36.3. Examples of the type of data obtained from the FPA are shown in Figs. 36.11, 36.12, 36.13, and 36.14. In Fig. 36.14, heat release rates increase linearly with time during downward fire propagation, very similar to the pyrolysis front values for the downward fire propagation in Fig. 36.11.

The trends of the lines in Figs. 36.11, 36.12, 36.13, and 36.14 represent fire propagation rates. The upward fire propagation rate is much faster than the downward fire propagation rate. For downward fire propagation, linear increases in the pyrolysis front and heat release rates indicate decelerating fire propagation behavior. For upward fire propagation, nonlinear increases

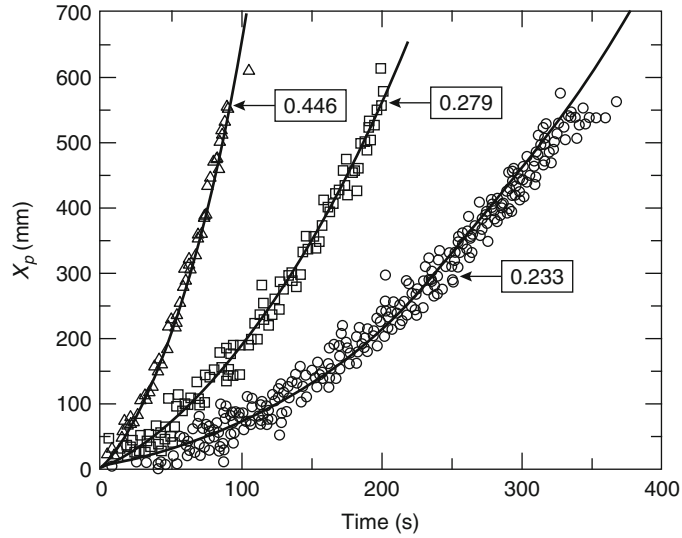

Fig. 36.13 Pyrolysis front height versus time for upward fire propagation for a 600-mm-long and 25-mm-thick diameter PMMA cylinder under co-airflow conditions in the Fire Propagation Apparatus. Airflow velocity = 0.09 m/s. *Numbers* inside the frames are the mass fractions of oxygen in air (Figure is taken from Ref. [31])

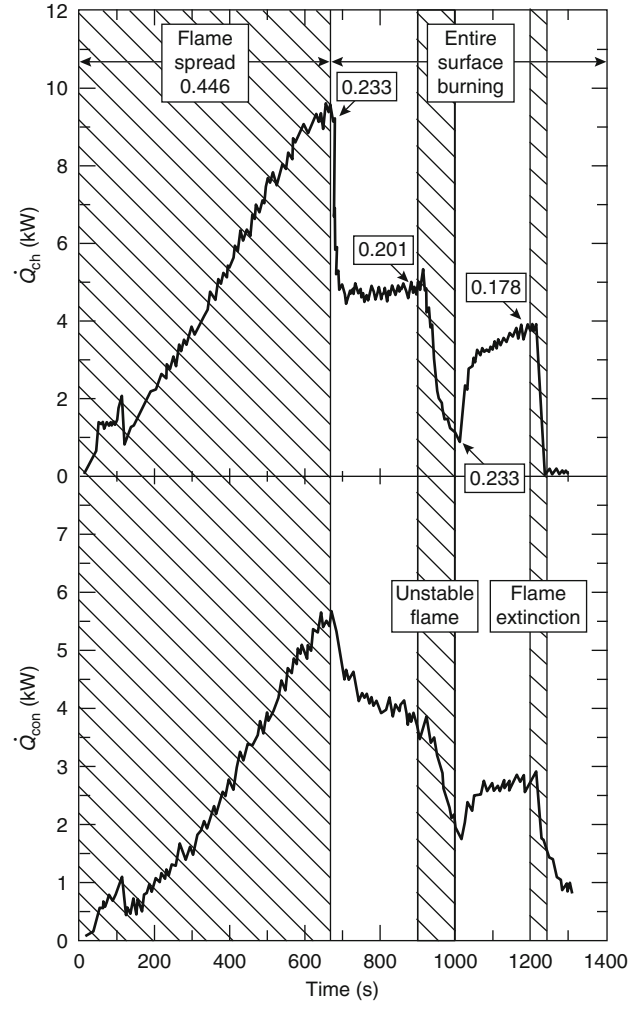

Fig. 36.14 Chemical (*top*) and convective (*bottom*) heat release rate versus time for downward fire propagation, combustion, and flame extinction for a 300-mm-long, 100-mm-wide, and 25-mm-thick PMMA vertical slab under opposed airflow conditions in the Fire Propagation Apparatus. Airflow velocity = 0.09 m/s. *Numbers* inside the frames are the mass fractions of oxygen in air (Figure is taken from Ref. [31])

in the pyrolysis front indicate accelerating fire propagation behavior.

Empirical Relationship Between Fire Propagation Rate, Flame Height, Pyrolysis Front, and Heat Release Rate

Numerous researchers have found the following relationship between the flame height and pyrolysis front (as discussed in Chap. 13, and reviewed in Refs. [31, 38]):

$$X_f = aX_p^n \tag{36.8}$$

where
X_f = Flame height (m)
$a = 5.35$
$n = 0.67–0.80$
for steady wall fires [31]. X_p is in m.

Fire propagation data for PMMA from the FPA and for electrical cables from several standard tests (ICEA [39], CSA FT-4 [40], and UL-1581 [41]) satisfy Equation 36.8, as shown in Fig. 36.15, with $a = 5.32$ and $n = 0.78$. The visual measurement of the pyrolysis front as damage length is used for the acceptance criterion in many of the standard tests for electrical cables. For example, for upward fire propagation in the CSA FT-4, a damage length of less than 60 % of the total length of the cable tray for a 20-min exposure is used as the acceptance criterion. For horizontal fire propagation in the UL-1581 test, a flame length of less than 40 % of the total length of the cable tray is used as the acceptance criterion.

The relationship between the flame height and the chemical heat release rate, expressed as the normalized chemical heat release rate (NCHRR), is defined as

$$\text{NCHRR} = \frac{\dot{Q}'_{\text{ch}}}{\rho c_p T_a g^{1/2} X_p^{3/2}} \tag{36.9}$$

where
$\dot{Q}'_{\text{ch}}$ = Chemical heat release rate per unit width (kW/m)
ρ = Density of air (g/m^3)
c_p = Specific heat of air (kJ/g · K)
T_a = Ambient temperature (K)
g = Acceleration due to gravity (m^2/s)
X_p is in m.

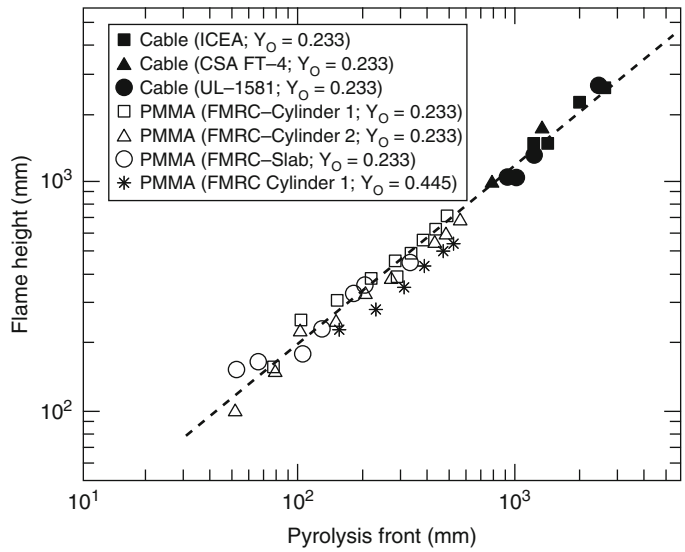

Fig. 36.15 Flame height versus pyrolysis front height for upward fire propagation in normal air. Data are for the vertical fire propagation for electrical cables contained in 2.44-m-long, 310-mm-wide, and 76-mm-deep trays in standard tests for electrical cables (ICEA, CSA FT-4, and UL-1581) and for 600-mm long PMMA slabs (100-mm-wide and 25-mm-thick) and cylinders (25-mm diameter) in the Fire Propagation Apparatus. Data for fire propagation in an oxygen mass fraction of 0.445 are also included (Figure is taken from Ref. [31])

Many researchers have shown that the height ratio of the flame to the pyrolysis front is a function of the heat release rate, such as the following relationship (as discussed in Chap. 13, and reviewed in Refs. [31, 38]):

$$\frac{X_f}{X_p} = a(\text{NCHRR})^n \tag{36.10}$$

where a and n are constants. This relationship reported in the literature (as reviewed in Ref. [31]) for methane, ethane, and propylene is shown in Fig. 36.16. The data for the upward fire propagation for PMMA [31] and for electrical cables from several standard tests (ICEA [39], CSA FT-4 [40], and UL-1581 [41]) also satisfy this relationship as indicated in Fig. 36.16.

In Fig. 36.16, data in the lower left-hand corner are for low-intensity polyvinylchloride (PVC) electrical cable fire propagation in standard tests for cables. These data show that for NCHRR < 0.2, $X_f/X_p < 1.5$ and $n = 1/10$. This is a characteristic property of materials for which there is either no fire propagation or limited fire propagation beyond the ignition zone. The data for higher-intensity fire propagation in Fig. 36.16 show that (1) for $0.2 <$ NCHRR < 5, $n = 2/3$ and $1.5 < X_f/X_p < 20$ (PMMA fire propagation and methane combustion); and (2) for NCHRR > 5, $n = 1/2$ and $X_f/X_p > 20$ (ethane and propylene combustion). Thus, the ratio of the flame height to pyrolysis front height is a good indicator of the fire propagation characteristics of the materials. Materials for which flame height is close to the pyrolysis front location during fire propagation can be useful indicators of decelerating fire propagation behavior.

Researchers have also developed many correlations between the flame heat flux transferred ahead of the pyrolysis front and heat release rate for downward, upward, and horizontal fire propagation (as discussed in Chap. 23, and reviewed in Refs. [31, 38]). For example, small- and large-scale fire propagation test data suggest that, for thermally thick materials with highly radiating flames, the following semiempirical relationship is satisfied [28]:

$$\dot{q}''_f \propto \left(\frac{\chi_{\text{rad}}}{\chi_{\text{ch}}}\dot{Q}'_{\text{ch}}\right)^{1/3} \tag{36.11}$$

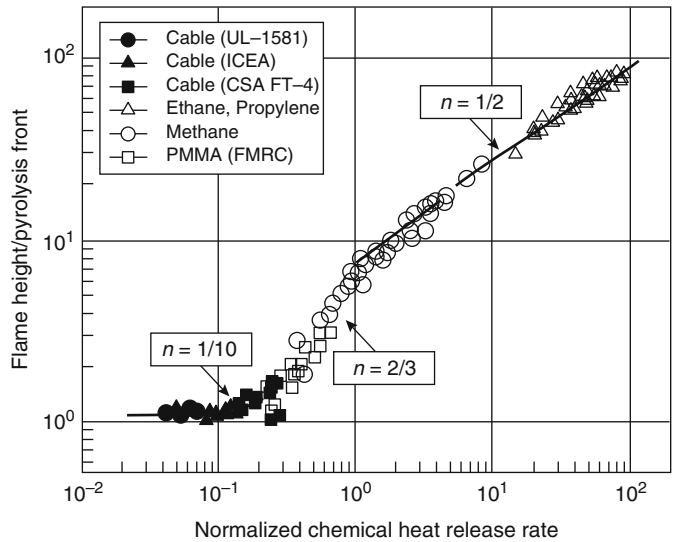

Fig. 36.16 Ratio of flame height to pyrolysis front height versus the normalized chemical heat release rate for upward fire propagation in normal air. Data for diffusion flames of methane, ethane, and propylene are from the literature. Data for cables are from standard tests for electrical cables (ICEA, CSA FT-4, and UL-1581). Data for PMMA are from the Fire Propagation Apparatus for 600-mm-long vertical PMMA slabs (100-mm-wide, 25-mm-thick) and cylinders (25-mm-diameter) [31]

where $\dot{q}''_f$ is the flame heat flux transferred ahead of the pyrolysis front (kW/m^2) and χ_{rad} is the radiative fraction of the combustion efficiency, χ_{ch}. The fire propagation rate is expressed as [28]

$$u^{1/2} \propto \frac{1}{TRP}\left(\frac{\chi_{rad}}{\chi_{ch}}\dot{Q}'_{ch}\right)^{1/3} \tag{36.12}$$

On the basis of the discussion above, an emprical parameter termed *fire propagation index* (FPI) [16, 17, 28, 42–46] has been defined:

$$FPI = 750\frac{\dot{Q}'^{1/3}_{ch}}{TRP} \tag{36.13}$$

FPI describes the fire propagation behavior of materials under flame-radiating conditions prevalent in large-scale fires. Small- and large-scale fire propagation test data of various materials along with understanding of fire propagation phenomena suggest that the FPI values can be used to classify materials as either propagating (fire propagates rapidly beyond ignition zone) and non-propagating (there is no fire propagation beyond the ignition zone) [28, 31, 43–46]. These FPI-based determinations have been validated by using intermediate-scale parallel panel tests (e.g., [19]) as shown in Figs. 36.17 and 36.18 and described below.

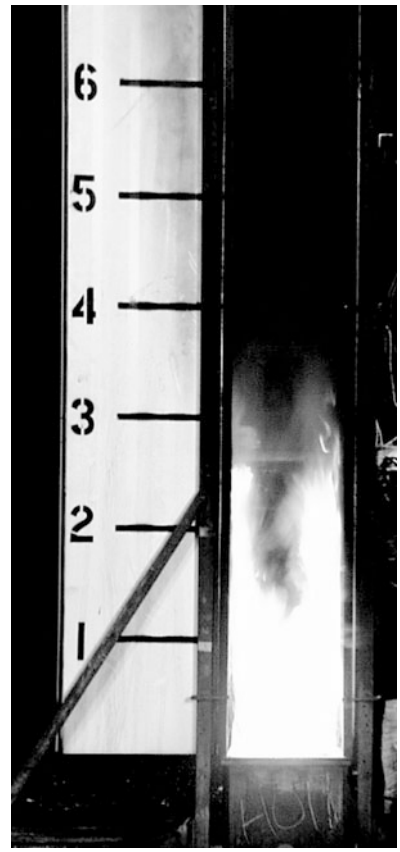

Fig. 36.17 Nonpropagating fire between two vertical parallel panels of a polymer (FPI < 6) for a test duration of 15 min [19]. The panels are about 0.61 m (2 ft) wide, 2.44 m (8 ft) high, and 25 mm (1 in) thick separated by 0.30 m (1 ft). The ignition source is a 60-kW, 0.30-m-wide, 0.61-m-long, and 0.30-m-high propane sand burner. The tip of the flame from the burner reaches a height of about 0.91 m (3 ft). Marks on the scale are in feet

Application of the Fire Propagation Index (FPI) to Classify Materials

The FPI values for the upward fire propagation, under flame-radiating conditions, have been determined for numerous materials at reduced scales in the Fire Propagation Apparatus. The highly radiating conditions, representative of large-scale fires, are created in the FPA by burning the materials in an enhanced oxygen environment (0.40 oxygen mass fraction). Two sets of tests are performed:

1. ***Thermal response parameter test:*** Ignition tests are performed in the FPA (materials are arranged as in Fig. 36.2), and the TRP value is determined from the time to ignition versus external heat flux as described in the subsection "Thermal Response Parameter (TRP)".
2. ***Upward fire propagation test:*** Fire propagation tests for vertical slabs, sheets, or cables are performed in the FPA (materials are arranged as in Fig. 36.3). About 300–600-mm-long, up to about 100-mm-wide, and up to about 100-mm-thick samples are used. The bottom 120–200 mm of the sample is in the ignition zone, where it is exposed to 50 kW/m^2 of external heat flux in the presence of a pilot flame. Beyond the ignition zone, the fire propagates by itself under co-airflow condition with an oxygen mass fraction of 0.40. During upward fire propagation, the chemical heat release rate is measured as a function of time.

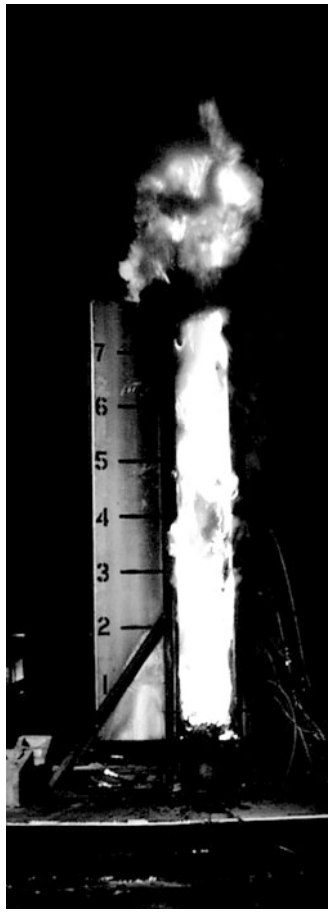

Fig. 36.18 Rapidly propagating fire between two vertical parallel panels of a polymer (FPI > 20) [19]. The panels are about 0.61 m (2 ft) wide, 2.44 m (8 ft) high, and 25 mm (1 in.) thick separated by 0.30 m (1 ft). The ignition source is a 60-kW, 0.30-m-wide, 0.61-m-long, and 0.30-m-high propane sand burner. The tip of the flame from the burner reaches a height of about 0.91 m (3 ft). Marks on the scale are in feet. The photograph was taken a few seconds before flames extended far beyond the top of the panels

The TRP value and the chemical heat release rate so determined are used in Equation 36.13 to calculate the FPI; the maximum (peak) measured chemical heat release rate value is used in the calculation.

Electrical Cables The FM Approval standard for cable fire propagation [17] is used to classify electrical cables, based on their upward fire propagation behavior, under highly flame-radiating conditions (0.40 oxygen mass fraction). A parallel panel intermediate scale test configuration was first introduced in 1988 [28] to verify the fire propagation behavior of electrical cables based on the fire propagation index (FPI), derived from bench-scale FPA measurements. It consists of two parallel panels of test material, each 0.61 m wide and 4.9 m long facing each other with a separation of about 0.31 m (keeping an aspect ratio of the panel width to the separation distance as 0.5). A 60 kW propane sand burner continuously provides an exposure fire at the base of the two panels. This intermediate scale test scenario contains the essential features of fire phenomena expected at larger scales, most notably enhanced radiant fluxes due to the radiation feedback between the panels. This test configuration provides sufficient size and confinement of flames to yield realistic flame heat transfer to the materials (see Figs. 36.17 and 36.18).

The nonpropagating fire condition is satisfied for FPI $\leq$ 10.0 for electrical cables (classified as Group 1) [17] that do not exhibit flame propagation beyond the vicinity of the ignition source in the parallel panel tests. In a recent study [46], plenum rated cables, having FPI values of $\leq$7.0, did not exhibit flame propagation in the parallel panel tests. Table 36.3 lists FPI values for selected electrical cables and conveyor belts.

Example 3 What type of fire behavior is represented by a 300-mm-wide, 8-m-high, and 25-mm-thick vertical cable array with a TRP value of 95 kW $\cdot$ $s^{1/2}/m^2$ if the peak chemical heat release during upward fire propagation is 50 kW?

Solution Fire propagation behavior is assessed by the FPI value. For the cable material, the chemical heat release rate per unit width, $\dot{Q}'_{ch} = 50/0.3 = 167$ kW/m. Substituting this value in Equation 36.13, with TRP = 95 kW $\cdot$ $s^{1/2}/m^2$, FPI = 43. The cable material will propagate fire.

Conveyor Belts A conveyor belt standard has been developed at FM Global [20]. In this

Table 36.3 Fire propagation index for cables and Conveyor belts, determined in the Fire Propagation Apparatus

	Diameter/ thickness (mm)	FPI
Power cables		
PVC/PVC	4–13	11–28
PE/PVC	11	16–23
PVC/PE	34	13
Silicone/PVC	16	17
Silicone/XLPO	55	6–8
EP/EP	10–25	6–8
XLPE/XLPE	10–12	9–17
XLPE/EVA	12–22	8–9
XLPE/neoprene	15	9
XLPO/XLPO	16–25	8–9
XLPO, PVF/XLPO	14–17	6–8
EP/CLP	4–19	8–13
EP, FR/none	4–28	9
Communications cables		
PVC/PVC	4	36
PE/PVC	4	28
PXLPE/XLPO	22–23	6–9
Si/XLPO	28	8
EP-FR/none	28	12
PECI/none	15	18
ETFE/EVA	10	8
PVC/PVF	5	7
FEP/FEP	8	4
FEP/FEP	10	5
Conveyor belts[a]		
Styrene-butadiene rubber (SBR)		8–11
Chloroprene rubber (CR)		5
CR/SBR		8
PVC		4–10

[a]3–25 mm thick

standard, as with the cable standard [17], TRP and upward fire propagation tests are performed, and Equation 36.13 is used to calculate the FPI.

Conveyor belts are classified as propagating or non-propagating. For an approximately 600-mm-long and 100-mm-wide vertical conveyor belt, the data measured in the FPA under highly flame-radiating conditions show that the nonpropagating fire condition is satisfied for FPI $\leq$ 7.0 for belts that show limited fire propagation in the large-scale fire propagation tests [45, 47]. Table 36.3 lists FPI values for selected conveyor belts taken from Refs. [45, 47].

Example 4 Conveyor belts are made of solid woven or piles of elastomers, such as styrene-butadiene rubber (SBR), polychloroprene rubber (CR), polyvinylchloride (PVC), reinforced with fibers made of polymers, such as nylon. In large-scale fire propagation tests in a tunnel, fire on the surface of a CR-based conveyor belt was found to be nonpropagating, whereas for a CR/SBR-based conveyor belt fire was found to be propagating. Small-scale tests showed that the CR- and CR/SBR-based conveyor belts had the following fire properties, respectively: (1) CHF = 20 and 15 kW/m^2, (2) TRP = 760 and 400 $kW \cdot s^{1/2}/m^2$, and (3) peak $\dot{Q}'_{ch}$ = 114 and 73 kW/m under highly flame-radiating conditions (0.40 oxygen mass fraction). Show that small-scale test results are consistent with the large-scale fire propagation behaviors of the two conveyor belts, using the criterion that, for nonpropagating fire behavior, the FPI is equal to or less than 7.

Solution Substituting the TRP and $\dot{Q}'_{ch}$ values in Equation 36.13, the FPI values for the CR- and CR/SBR-based conveyor belts are 5 and 8, respectively. Thus, the CR-based conveyor belt is expected to have a nonpropagating fire behavior, whereas the CR/SBR-based conveyor belt is expected to have a propagating fire behavior. The small-scale test results, therefore, are consistent with the large-scale fire propagation behaviors of the two conveyor belts.

Polymeric Materials For Cleanrooms - Microchip devices are manufactured, in bulk, on wafers of semiconducting materials. Wafers are manufactured in several stages: material preparation, crystal growth and wafer preparation, wafer fabrication, and packaging. Wafers are fabricated in cleanrooms where cleanliness is highly controlled in order to limit the number of contaminants to which the wafer is exposed. The stringent requirements of the solid-state devices define levels of cleanliness that far exceed those of almost any other industry. Contamination in a cleanroom is defined as anything that interferes with the production of wafers and/or their performance. The overall cleanroom

design principle is to build a sealed room that is supplied with clean air, is built with polymeric materials that are noncontaminating, and includes systems to prevent accidental external contamination, interactions of the polymeric materials and wafer cleaning liquids, operator error, and accidental fires.

In 1997, FM Global Research introduced a new methodology, identified as the FM Approval Standard 4910 Test Protocol [19], for testing the fire propagation and smoke development behaviors of polymeric materials for use in cleanrooms for the semiconductor industry. For the acceptance of polymeric materials, two criteria need to be satisfied: (1) Fire Propagation Index FPI ≤ 6 $(m/s^{1/2})/(kW/m)^{2/3}$ and (2) Smoke Development Index SDI ≤ 0.4 (g/g) $(m/s^{1/2})/(kW/m)^{2/3}$.

In the 4910 Test Protocol [19], the Fire Propagation Index (FPI) is formulated from (1) the thermal response parameter (TRP), which relates the time to ignition to the net heat flux, and (2) the chemical heat release rate measured during the upward fire propagation in air having a 40 % oxygen concentration to simulate flame heat transfer at large scale, as described above. SDI is related to the smoke release rate and is obtained by multiplying the FPI value by the smoke yield as shown in Fig. 36.19. The smoke yield is defined as the ratio of the total mass of smoke released per unit mass of burned vapors from the polymeric material (see section "Generation of Fire Products and Smoke Yields" of this chapter). The FPI and SDI values for various polymeric materials (including composites) determined from FPA tests are listed in Table 36.4 [19, 43, 44, 48, 49].

It can be noted from Table 36.4 that specialty polymeric materials (highly halogenated thermoplastics and high temperature thermosets) have low FPI and SDI values and several of them satisfy the 4910 test protocol criteria (FPI ≤ 6 $(m/s^{1/2})/(kW/m)^{2/3}$ and SDI ≤ 0.4 $(g/g)(m/s^{1/2})/(kW/m)^{2/3}$) for acceptance as cleanroom materials [19]. These polymeric materials have high thermal stability with reduced release of carbon, hydrogen, and halogen atoms, as can be noted from their decomposition temperatures listed in Table 36.5 [50]. Ordinary thermoplastics (such as PE, PP, and PVC) can also be modified such that they behave similarly to the specialty polymeric materials and have low FPI and SDI values to satisfy the 4910 Test Protocol criteria for acceptance as cleanroom materials.

Composites and Fiberglass-Reinforced Materials Composites and fiberglass-reinforced materials are very attractive because of their low weight and high strength characteristics and have found practical applications in a large number of sectors such as in aircrafts, submarines, naval ships, military tanks, public transportation vehicles including automobiles, space vehicles, tote boxes, pallets, chutes, and so forth. Fire propagation, however, is one of the major concerns for

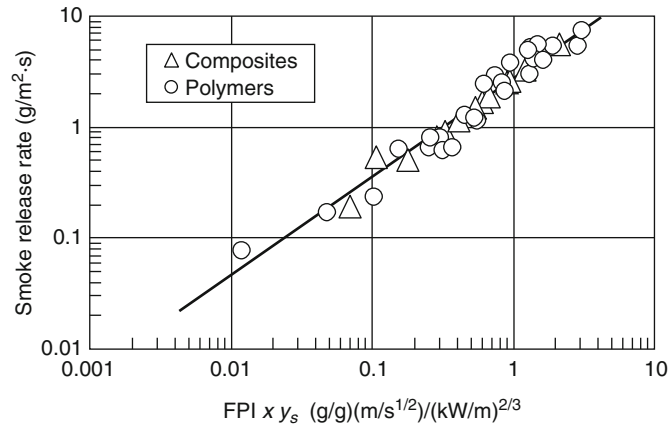

Fig. 36.19 Peak smoke release rate measured in combustion tests in normal air with imposed external heat flux of 50 kW/m^2 versus peak FPI values from the propagation tests in 40 % oxygen environments multiplied by the smoke yields from the combustion tests. Tests were performed in the Fire Propagation Apparatus

Table 36.4 Fire propagation index and smoke development index for polymeric materials

Polymeric material	FPI $(m/s^{1/2})/(kW/m)^{2/3}$	SDI $(g/g)(m/s^{1/2})/(kW/m)^{2/3}$
Fire-retarded or unmodified electrical cables		
Polyvinyl chloride(PVC/polyvinylchloride PVC)	36	4.1
Polyethylene (PE)/polyvinyl chloride (PVC)	28	3.8
Silicone/polyvinyl chloride (PVC)	17	2.0
Modified electrical cables		
Polyvinylchloride (PVC)	8	1.2
High-temperature polyvinylchloride (PVC)	7	0.69
Polyethylene (PE)/ethylvinylacetate (EVA)	5	0.40
Ordinary polymeric materials		
Fire-retarded polystyrene (FR-PS)	34	5.60
Fire-retarded polybutyleneterephthalate (FR-PBT)	32	2.20
Unmodified polymethylmethacrylate (U-PMMA)	23	1.1
Unmodified polyoxymethylene (U-POM)	15	0.03
Fire-retarded (FR) vinyl ester	10	2.5
Unmodified wood slab	14	0.20
Unmodified polyethylene (U-PE)	30	1.4
Polyethylene with 25 % chlorine	15	1.7
Polyethylene with 36 % chlorine	11	1.5
Polyethylene with 48 % chlorine	8	1.9
Modified polyethylene (M-PE)-1	7	0.64
Modified polyethylene (M-PE)-2	6	0.65
Unmodified polypropylene (U-PP)	31	1.7
Fire-retarded polypropylene (FR-PP)	30	2.1
Modified polypropylene (M-PP)-1	11	3.0
Modified polypropylene (M-PP)-2	7	0.95
Modified polypropylene (M-PP)-3	7	0.35
Modified polypropylene (M-PP)-4	6	0.41
Modified polypropylene (M-PP)-5	5	0.40
Modified polypropylene (M-PP)-6	5	0.19
Modified polypropylene (M-PP)-7	5	0.21
Modified polypropylene (M-PP)-8	4	0.19
Fire-retarded flexible polyvinylchloride (FR-PVC)	16	1.6
Unmodified rigid polyvinylchloride (U-PVC)-1	8	0.86
Unmodified rigid polyvinylchloride (U-PVC)-2	7	1.2
Modified rigid polyvinylchloride (M-PVC)-1	6	0.31
Modified rigid polyvinylchloride (M-PVC)-2	5	0.64
Modified rigid polyvinylchloride (M-PVC)-3	4	0.15
Modified rigid polyvinylchloride (M-PVC)-4	3	0.16
Modified rigid polyvinylchloride (M-PVC)-5	3	0.29
Modified rigid polyvinylchloride (M-PVC)-6	2	0.11
Modified rigid polyvinylchloride (M-PVC)-7	2	0.04
Modified rigid polyvinylchloride (M-PVC)-8	2	0.06
Modified rigid polyvinylchloride (M-PVC)-9	1	0.03
Chlorinated rigid polyvinylchloride (CPVC, Corzan)	3	0.13

(continued)

Table 36.4 (continued)

Polymeric material	FPI $(m/s^{1/2})/(kW/m)^{2/3}$	SDI $(g/g)(m/s^{1/2})/(kW/m)^{2/3}$
Highly halogenated specialty polymeric materials		
Unmodified polyvinylidenefluoride (U-PVDF Kynar)-1	5	0.14
Unmodified polyvinylidenefluoride (U-PVDF)-2	4	0.08
Unmodified ethylenechlorotrifluoroethylene (U-ECTFE, Halar)	4	0.15
Unmodified ethylenetetrafluoroethylene (U-ETFE, Tefzel)	7	0.17
Unmodified perfluoroalkoxy (U-PFA, Teflon)	2	0.01
Unmodified fluorinated ethylene-propylene (U-FEP, Teflon)	3	0.01
High-temperature specialty polymeric materials		
Phenol formaldehyde	5	0.06
Polyether ether ketone (PEEK)	4	0.03
Melamine	7	0.24
Unmodified polycarbonate (U-PC)	14	4.2
Modified polycarbonate (M-PC)-1	10	4.2
Modified polycarbonate (M-PC)-2	7	4.0
Unmodified polysulfone (U-POS)	18	1.49
Modified polysulfone (M-POS)-1	11	1.4
Modified polysulfone (M-POS)-2	11	0.32
Modified polysulfone (M-POS)-3	7	1.2
Modified polysulfone (M-POS)-4	7	0.25
Modified polyetherimide (M-PEI)-1	6	0.24
Modified polyetherimide (M-PEI)-2	6	0.04
Modified polyetherimide (M-PEI)-3	5	0.46
Unmodified polyphenyleneoxide (U-PPO)	9	1.6
Glass fiber–reinforced ordinary polyesters		
Glass fiber–reinforced fire-retarded polyester (FR-PES)-1	21	5.4
Glass fiber–reinforced fire-retarded polyester (FR-PES)-1	16	7.4
Glass fiber–reinforced fire-retarded polyester (FR-PES)-1	14	4.0
Glass fiber–reinforced modified polyester (M-PES)-1	11	5.5
Glass fiber–reinforced modified polyester (M-PES)-1	10	5.2
Glass fiber–reinforced modified polyester (M-PES)-1	9	3.1
Composites		
Fire-retarded polyester (30 %)/glass fibers (70 %)-1	13	0.91
Fire-retarded polyester (30 %)/glass fibers (70 %)-2	10	0.68
Unmodified phenolic (16 %)/Kevlar fibers (84 %)	8	0.33
Modified phenolic (20 %)/glass fibers (80 %)	3	0.07
Fire-retarded epoxy (35 %)/glass fibers (65 %)-1	11	2.1
Fire-retarded epoxy (35 %)/glass fibers (65 %)-2	10	0.94
Fire-retarded epoxy (35 %)/glass fibers (65 %)-3	9	1.2
Modified epoxy (24 %)/glass fibers (76 %)-1	5	0.61
Modified epoxy (29 %)/graphite fibers (71 %)	5	0.54
Modified epoxy and phenolic (18 %)/glass fibers (82 %)	2	0.18
Modified polyphenylenesulfide (16 %)/glass fibers (84 %)	3	0.29
Modified cyanate (27 %)/graphite fibers (73 %)	4	0.41

Note: Data taken from Refs. [19, 43, 44, 48, 49]

Table 36.5 Decomposition temperature, char yield, and limiting oxygen index for polymeric materials

Polymeric material	Decomposition temperature (°C)	Char yield (%)	Limiting oxygen index (%)
Polybenzobisoxazole (PBO)	789	75	56
Polyparaphenylene	652	75	55
Polybenzimidazole (PBI)	630	70	42
Polyamideimide (PAI)	628	55	45
Polyaramide (Kevlar)	628	43	28
Polyetherketoneketone (PEKK)	619	62	40
Polyetherketone (PEK)	614	56	40
Polytetrafluoroethylene (PTFE)	612	0	95
Polyether ether ketone (PEEK)	606	50	35
Polyphenylsulfone (PPSF)	606	44	38
Polypara(benzoyl)phenylene (PX)	602	66	41
Fluorinated cyanate ester	583	44	40
Polyphenylenesulfide (PPS)	578	45	44
Polyetherimide (PEI)	575	52	47
Polypromellitimide (PI)	567	70	37
Polycarbonate (PC)	546	25	26
Polysulfone (PSF)	537	30	30
Polyethylene (PE)	505	0	18
Polyamide 6 (PA6)-nylon	497	1	21
Polyethyleneterephthalate (PET)	474	13	21
Acrylonitrile-butadiene-styrene (ABS)	470	0	18
Polyurethane elastomer (PU)	422	3	17
Polymethylmethacrylate (PMMA)	398	2	17
Polychlorotrifluoroethylene	380	0	95
Polyvinylchloride (PVC)	370	11	50
Polystyrene (PS)	364	0	18
Polyoxymethylene (POM)	361	0	15
Polyvinylidenefluoride (PVDF)	355	0	44

Note: Data are taken from Ref. [50]

composites and fiberglass-reinforced materials; therefore, the FPI concept discussed above for electrical cables and conveyor belts can also be applied to these materials [43, 44]. In the case of composites and fiberglass-reinforced materials the nonpropagating fire condition is satisfied for FPI $\leq$ 6.0, for about 600-mm-long and 100-mm-wide vertical composites and fiberglass-reinforced materials, under highly flame-radiating conditions (0.4 oxygen mass fraction), very similar to the conveyor belts. Table 36.4 lists FPI values for selected composites and fiberglass-reinforced materials [43, 44].

Interior Finish Wall/Ceiling Materials Since 1971, FM Global Research has used the 25-ft (7.6 m) corner test as a standard test to evaluate the burning characteristics of interior finish wall and ceiling materials [18]. The 25-ft (7.6 m) corner test is performed in a 7.6-m (25-ft)-high, 15.2-m (50-ft)-long and 11.6-m (38-ft)-wide building corner configuration [51, 52]. The materials tested are typically panels with a metal skin over an insulation core material. The materials installed in the corner configuration are subjected to a growing exposure fire (peak heat release rate of about 3 MW) comprised of about 340 kg (750 lb) of 1.2-m (4-ft) $\times$ 1.2-m (4-ft) wood (oak) pallets stacked 1.5 m (5 ft) high at the base of the corner. The material is considered to have failed the test if within 15 min either (1) fire propagation on the wall or ceiling extends to the limits of the structure,

or (2) flame extends outside the limits of the structure through the ceiling smoke layer.

The fire environment within the 25-ft (7.6 m) corner test structure has been characterized through heat flux and temperature measurements [51, 52]. It has been shown that the fire propagation boundary (pyrolysis front) measured by visual damage is very close to the critical heat flux (CHF) boundary for the material, as shown in Fig. 36.20 [52]. This relationship is in agreement with the general understanding of the fire propagation process. Through small- and large-scale fire propagation tests for low-density, highly char-forming wall and ceiling insulation materials, a semi-empirical relationship has been developed for fire propagation rate for a 15-min test in the 25-ft (7.6 m) corner test [51, 52].

$$\frac{X_p}{X_t} = \frac{\dot{Q}''_{\text{con}}}{\text{TRP}} \tag{36.14}$$

where

X_p = Average fire propagation length along the eaves (Fig. 36.20) of the 25-ft (7.6 m) corner test (pyrolysis front) measured visually (m)

X_t = Total available length [11.6-m (38 ft)] in the 25-ft (7.6 m) corner test

$\dot{Q}''_{\text{con}}$ = Convective heat release rate (kW/m^2) measured in the small-scale test

The right-hand side of Equation 36.14 with the convective heat release rate measured (through GTR, see above) for a material exposed to 50 kW/m^2 of external heat flux in the Fire Propagation Apparatus is defined as the convective flame spread parameter (FSP$_c$) [51, 52]. Figure 36.21 shows a correlation between the convective flame spread parameter obtained from the FPA and the normalized fire propagation length in the FM Global 25-ft (7.6 m) corner test. Pass/fail regions, as determined from the 25-ft (7.6 m) corner test, are indicated in the figure. Materials for which FSP$_c \leq 0.39$ pass the 25-ft (7.6 m) corner test, and materials for which FSP$_c \geq 0.47$ are judged to be unacceptable (i.e., fail); the region where the FSP$_c$ values are greater than 0.39 but less than 0.47 is uncertain [18, 51, 52].

The correlation and pass/fail criterion shown in Fig. 36.21 have been adopted in the

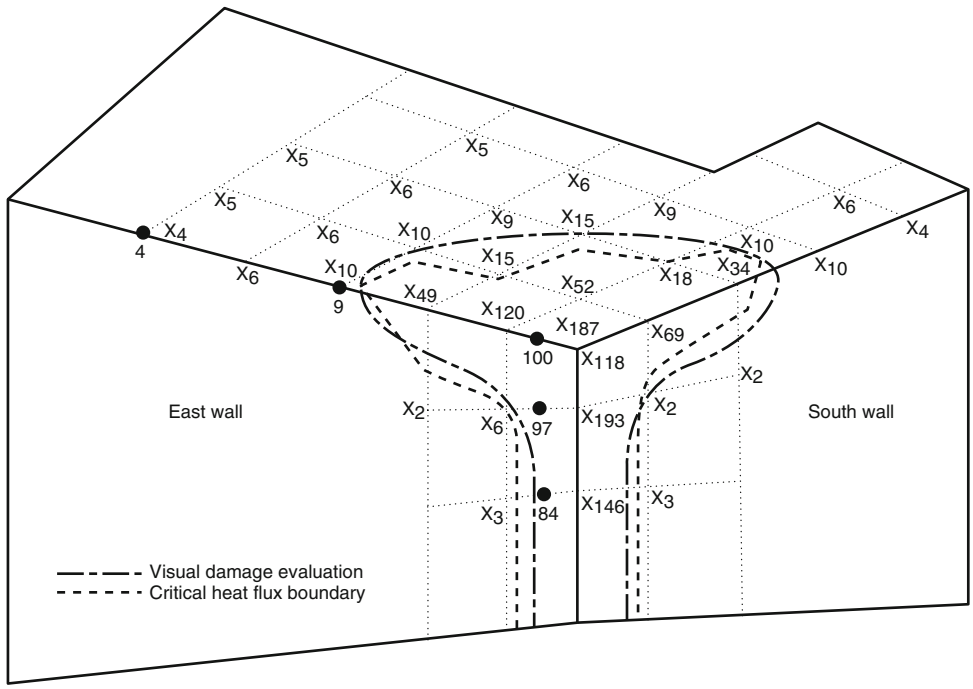

Fig. 36.20 Critical heat flux boundary and visual observations for the extent of fire propagation in the FM Global 25-ft corner test for a product that passes the tests [52]

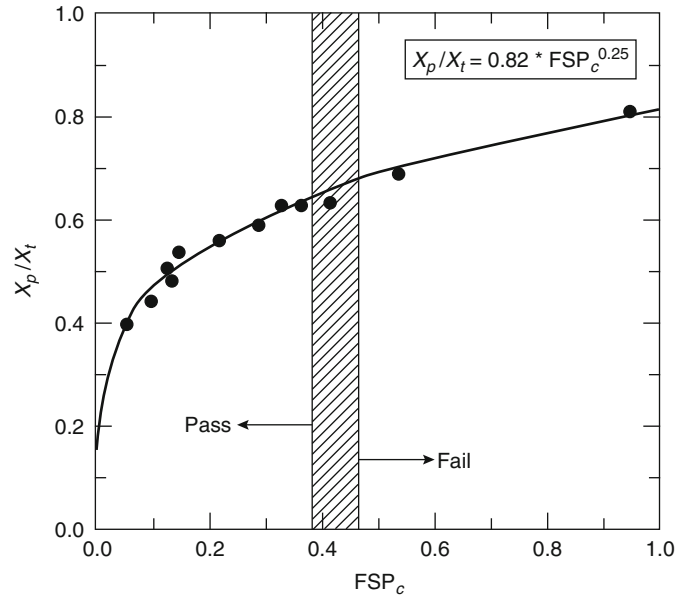

Fig. 36.21 Normalized fire propagation length measured in the 25-ft corner test versus the convective flame spread parameter obtained from the ASTM E2058 fire propagation apparatus (Figure is taken from Refs. [51, 52])

FM Approval Standard Class No. 4880 for insulated wall or wall and ceiling panels [18]. In this standard, the 25-ft (7.6 m) corner test has been replaced by the Fire Propagation Apparatus tests along with a new intermediate-scale parallel panel test [53], which are a cost-effective alternative and considerably simplify the test protocol. Two sets of tests are performed in the FPA [18, 51, 52]:

1. ***Thermal response parameter test:*** Ignition tests are performed using approximately 100-mm × 100-mm and up to 100-mm-thick samples. Times to ignition at various external heat flux values are measured to determine the TRP as described earlier.
2. ***Convective heat release rate test:*** Combustion tests are performed using about 100-mm × 100-mm and up to 100-mm-thick samples. Samples are burned in normal air under an external heat flux exposure of 50 kW/m^2. During the test, measurement is made for the convective heat release as a function of time.

Flaming and Nonflaming Phenomena

During fire propagation, the surface of the material regresses in a transient fashion with a rate slower than the fire propagation rate [31]. The surface regression becomes steady after fire propagates throughout the available surfaces. The surface regression continues until all the combustible components of the material are exhausted. During fire propagation and surface regression, the material generates vapors at a transient or steady rate. The generation rate of the material vapors is measured by the mass loss rate. In the presence of a flame and/or external heat flux, the mass loss rate, under steady state, is expressed as [14, 31, 44]:

$$\dot{m}'' = \frac{\dot{q}''_e + \dot{q}''_{fr} + \dot{q}''_{fc} - \dot{q}''_{rr}}{\Delta H_g} \tag{36.15}$$

where

$\dot{m}''$ = Mass loss rate (g/m^2 · s)

$\dot{q}''_{fr}$ = Flame radiative heat flux transferred to the surface (kW/m^2)

$\dot{q}''_{fc}$ = Flame convective heat flux transferred to the surface (kW/m^2)

$\dot{q}''_{rr}$ = Surface re-radiation loss (kW/m^2)

ΔH_g = Heat of gasification (kJ/g)

total flame heat flux to the surface $\dot{q}''_f = \dot{q}''_{fr} + \dot{q}''_{fc}$

According to Equation 36.15, the generation rate of material vapors is governed by the

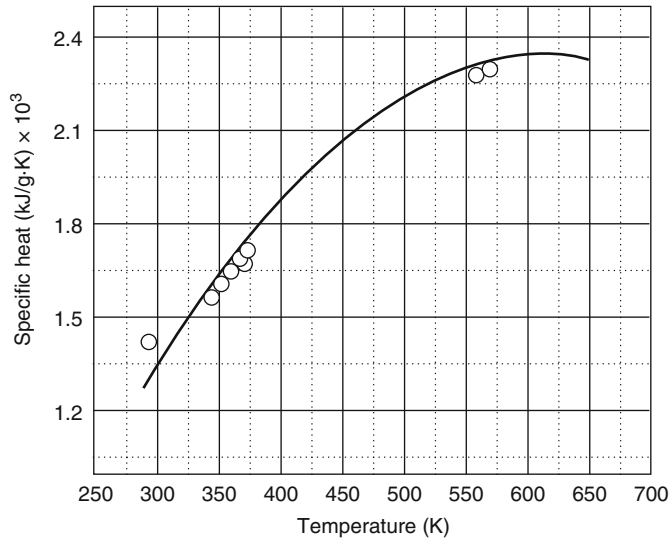

Fig. 36.22 Specific heat of polymethylmethacrylate versus temperature measured by a differential scanning calorimeter at the flammability laboratory of FM Global Research

external and flame heat flux, surface re-radiation loss, and the heat of gasification.

Heat of Gasification The heat of gasification for a melting material is expressed as [6]

$$\Delta H_g = \int_{T_a}^{T_m} c_{p,s} dT + \Delta H_m + \int_{T_m}^{T_v} c_{p,l} dT + \Delta H_v \tag{36.16}$$

where

ΔH_g = Heat of gasification (kJ/g)
$c_{p,s}$ = Specific heat of solid in kJ/g·K
$c_{p,l}$ = Specific heat of molten solid in kJ/g·K
ΔH_m = Heat of melting at melting temperature in kJ/g
ΔH_v = Heat of vaporization at vaporization temperature in kJ/g
T_a = Ambient temperature
T_m = Melting temperature
T_v = Vaporization temperature in K

For materials that do not melt, but sublime, decompose, or char, Equation 36.16 is modified accordingly. The heat of gasification can be determined from (1) the parameters on the right-hand side of Equation 36.16, which can be quantified by thermal analysis techniques or calculated from the properties listed in the literature; and (2) nonflaming tests using apparatuses, such as the OSU heat release rate apparatus, the FPA, or the cone calorimeter. The following are some examples of the techniques:

1. ***Heats of gasification of polymers from differential scanning calorimetry:*** *Values for* $c_{p,s}$, $c_{p,l}$, ΔH_m, and ΔH_v for polymers have been quantified in the FM Global Research Flammability Laboratory [6]. The techniques involve measurement of the specific heat as a function of temperature, such as shown in Fig. 36.22 for polymethylmethacrylate. Further measurements are also made of the heats of melting and vaporization. Some examples of the data measured at FM are listed in Table 36.6.
2. ***Heat of gasification from literature data for the heats of gasification for various molecular weight hydrocarbons (alkanes):*** The *CRC Handbook of Chemistry and Physics* [54] listing for the heats of gasification for liquid and solid hydrocarbons (alkanes) satisfies the following relationship in the molecular weight range of 30–250 g/mol:

$$\Delta H_g = 0.164 + 0.0042M - 3.72 \times 10^{-6} M^2 \tag{36.17}$$

where M is the molecular weight of the hydrocarbon (g/mol).

Table 36.6 Surface re-radiation and heats of gasification of various materials

Materials	Surface re-radiation (kW/m^2)	Heat of gasification (kJ/g)			
		Flam. App.[a]	Cone[b]	DSC[c]	Cal[d]
Distilled water	0.63	2.58	–	2.59	2.58
Hydrocarbons (alkanes)					
Hexane	0.50	–	–	–	0.50
Heptane	0.63	–	–	–	0.55
Octane	0.98	–	–	–	0.60
Nonane	1.4	–	–	–	0.64
Decane	1.8	–	–	–	0.69
Undecane	2.3	–	–	–	0.73
Dodecane	2.8	–	–	–	0.77
Tridecane	3.0	–	–	–	0.81
Tetradecane	3.0	–	–	–	0.85
Hexadecane	3.0	–	–	–	0.92
Natural materials					
Filter paper	10	3.6	–	–	–
Corrugated paper	10	2.2	–	–	–
Wood (Douglas fir)	10	1.8	–	–	–
Plywood/FR	10	1.0	–	–	–
Particleboard	–	–	3.9	–	–
Synthetic materials					
Epoxy resin	–	–	2.4	–	–
Polypropylene	15	2.0	1.4	2.0	–
Polyethylene (PE) (low density)	15	1.8	–	1.9	–
PE (high density)	15	2.3	1.9	2.2	–
PE foams	12	1.4–1.7	–	–	–
PE/25 % chlorine (CI)	12	2.1	–	–	–
PE/36 % CI	12	3.0	–	–	–
PE/48 % CI	10	3.1	–	–	–
Rigid polyvinylchloride (PVC)	15	2.5	2.3	–	–
PVC/plasticizer	10	1.7	–	—	–
Plasticized PVC, LOI = 0.20	10	2.5	2.4	–	–
Plasticized PVC, LOI = 0.25	–	–	–	–	–
Plasticized PVC, LOI = 0.30	–	–	2.1	–	–
Plasticized PVC, LOI = 0.35	–	–	2.4	–	–
Rigid PVC, LOI = 0.50	–	–	2.3	–	–
Polyisoprene	10	2.0	–	–	–
PVC panel	17	3.1	–	–	–
Nylon 6/6	15	2.4	–	–	–
Polyoxymethylene (Delrin)	13	2.4	–	2.4	–
Polymethylmethacrylate (Plexiglas)	11	1.6	1.4	1.6	–
Polycarbonate	11	2.1	–	–	–
Polycarbonate panel	16	2.3	–	–	–
Isophthalic polyester	–	–	3.4	–	–
Polyvinyl ester	–	–	1.7	–	–
Acrylonitrile-butadiene-styrene (ABS)	10	3.2	2.6	–	–
Styrene-butadiene	10	2.7	–	–	–
Polystyrene (PS) foams	10–13	1.3–1.9	–	–	–
PS (granular)	13	1.7	2.2	1.8	–

(continued)

Table 36.6 (continued)

Materials	Surface re-radiation (kW/m^2)	Heat of gasification (kJ/g)			
		Flam. App.[a]	Cone[b]	DSC[c]	Cal[d]
Polyurethane (PU) foams					
Flexible polyurethane (PU) foams	16–19	1.2–2.7	2.4	1.4	–
Rigid polyurethane (PU) foams	14–22	1.2–5.3	5.6	–	–
Polyisocyanurate foams	14–37	1.2–6.4	–	–	–
Phenolic foam	20	1.6	–	–	–
Phenolic foam/FR	20	3.7	–	–	–
Ethylenetetrafluoroethylene (Tefzel)	27	0.9	–	–	–
Fluorinated ethylene propylene (FEP, Teflon)	38	2.4	–	–	–
Tetrafluoroethylene (TFE, Teflon)	48	0.8–1.8	–	–	–
Perfluoroalkoxy (PFA, Teflon)	37	1.0	–	–	–
Composite and fiberglass-reinforced materials					
Polyether ether ketone–30 % fiberglass	–	–	7.9	–	–
Polyethersulfone–30 % fiberglass	–	1.8	–	–	–
Polyester 1–fiberglass	–	–	2.5	–	–
Polyester 2–fiberglass	10	1.4	–	–	–
Polyester 3–fiberglass	10	6.4	–	–	–
Polyester 4–fiberglass	15	5.1	–	–	–
Polyester 5–fiberglass	10	2.9	–	–	–
Phenolic fiberglass (thick sheet)	20	7.3	–	–	–
Phenolic Kevlar (thick sheet)	15	7.8	–	–	–

[a]From the Fire Propagation Apparatus under nonflaming conditions
[b]Calculated from the cone calorimeter data reported for the mass loss rate at various external heat flux values in flaming fires [13, 32]
[c]From the flammability laboratory using the differential scanning calorimetry
[d]Calculated from the data reported in the *CRC Handbook* [54]

The heats of gasification calculated from Equation 36.17 for various alkanes are listed in Table 36.6.

3. ***Heat of gasification from literature data for the specific heats and heats of vaporization:*** Water will be used as an example. The specific heat of liquid water, $c_{p,l}$, which is assumed constant, is 0.0042 kJ/g-K [55] and the heat of vaporization of water at 373 K is 2.26 kJ/g [54]. Assuming the ambient temperature to be 298 K and the vaporization temperature to be 373 K, the heat of gasification of water from Equation 36.16 is calculated as follows:

$$\Delta H_g = \int_{T_a}^{T_v} c_{p,l} dT + \Delta H_v$$
$$= c_{p,l}(T_v - T_a) + \Delta H_v$$
$$= 0.0042(373 - 298) + 2.26 = 2.58 \text{ kJ/g}$$

Using differential scanning calorimetry, the heat of gasification of water determined in the FM Global Research Flammability Laboratory is 2.59 kJ/g, which is in excellent agreement with the calculated value. These two values for the heat of gasification of water are listed in Table 36.6.

4. ***Heat of gasification from nonflaming tests using the Fire Propagation Apparatus:*** The measurement for the heat of gasification from the nonflaming tests in the ASTM E2058 [10] fire propagation apparatus was introduced in 1976 [6]. In the absence of flames, $\dot{q}''_f = 0$, and Equation 36.15 simplifies to:

$$\dot{m}'' = \frac{\dot{q}''_e - \dot{q}''_{rr}}{\Delta H_g} \tag{36.18}$$

where mass loss rate is now extrictly a linear function of the external heat flux. Therefore,

this equation provides a convenient method to determine the heat of gasification in nonflaming tests, where mass loss rate of the sample is measured at various external heat flux values. The heat of gasification is determined from linear regression analysis of the average steady-state mass loss rate as a function of external heat flux, using Equation 36.18. In the Fire Propagation Apparatus, samples can be exposed to radiant fluxes in 100 % nitrogen atmospheres, allowing the application of this methodology

Figure 36.23 shows a plot of the vaporization rate (i.e., mass loss rate), as a function of time, of water in a 0.0072 m^2 Pyrex glass dish exposed to 50 kW/m^2, measured in the Fire Propagation Apparatus. The figure also includes the predicted mass loss rate using Equation 36.18, where

$$\dot{q}''_{rr} = \varepsilon\sigma\left(T_v^4 - T_a^4\right) \tag{36.19}$$

where ε is the emissivity of water (0.95–0.963 in the temperature range 298–373 K), [56] and σ is the Stefan-Boltzmann constant (56.7×10^{-12} $kW/m^2\text{-}K^4$). For water, $T_v = 373$ K and $T_a = 298$ K, and thus $\dot{q}''_{rr} = 1$ kW/m^2. From Equation 36.18, using $\dot{q}''_e = 50$ kW/m^2, $\dot{q}''_{rr} = 1$ kW/m^2, and $\Delta H_g = 2.59$ kJ/g, $\dot{m}'' = 19.0$ $g/m^2{\cdot}s$. There is excellent agreement between the measured and predicted values at the steady state in Fig. 36.23.

Heats of gasification determined from mass loss rate as a function of external heat flux at nonflaming conditions in the FPA are listed in Table 36.6 for selected materials. Excellent agreement can be noted between the heats of gasification determined from the FPA data and those obtained from differential scanning calorimetry.

Heat of gasification can also be determined from flaming fires if high external heat flux values are used such that $\dot{q}''_e >> \dot{q}''_{fr} + \dot{q}''_{fc} - \dot{q}''_{rr}$ in Equation 36.15. This method has been used to calculate the heat of gasification from cone calorimeter data using mass loss rates measured in flaming fires reported in the literature [13, 32]. The values calculated from the cone calorimeter data are also listed in Table 36.6 and show a general agreement with the values from the FPA.

Example 5 Estimate the ignition temperature of a material with a CHF of 11 kW/m^2. Assume its surface emissivity to be unity, ambient temperature to be 20 °C, and vaporization temperature to be approximately equal to the ignition temperature.

Solution Following the assumption that at the CHF reradiation is the only mode of heat loss, from Equation 36.19,

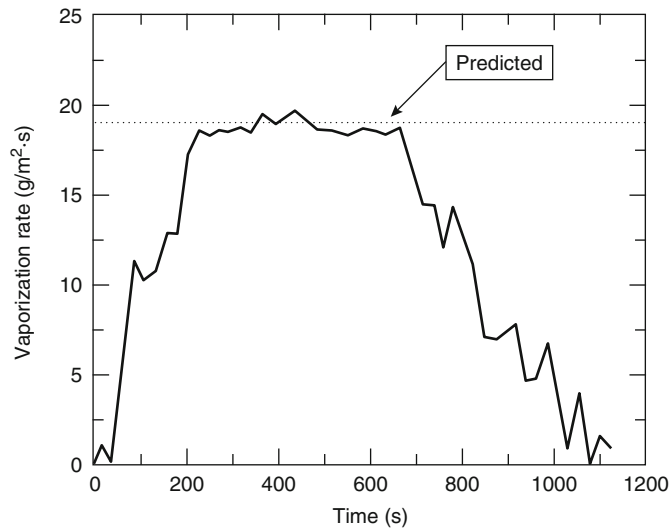

Fig. 36.23 Vaporization rate of water versus time measured in the Fire Propagation Apparatus using 99.69 g of water in a Pyrex dish with an area of 0.0072 m^2. Water was exposed to an external heat flux of 50 kW/m^2

$$\dot{q}''_{rr} = \text{CHF} = \varepsilon\sigma\left(T_v^4 - T_a^4\right)$$

$$T_v = T_{ig} = \left(\frac{\text{CHF}}{\varepsilon\sigma} + T_a^4\right)^{1/4}$$

$$T_{ig} = \left[\frac{11\frac{\text{kW}}{\text{m}^2}}{56.7 \times 10^{-12}\frac{\text{kW}}{\text{m}^2\text{K}^4}} + (298\text{K})^4\right]^{1/4}$$

$$T_{ig} = 670\text{K}$$

Example 6 A material with a surface re-radiation loss of 10 kW/m^2 and heat of gasification of 1.8 kJ/g was found to be involved in a fire with an exposed area of 2 m^2. The combined flame and external heat flux exposure to the material was estimated to be 70 kW/m^2. Estimate the peak mass loss rate at which the material may have been burning in the fire in terms of g/m^2 · s and g/s.

Solution From Equation 36.15,

$$\dot{m}'' = \frac{\dot{q}''_e + \dot{q}''_{fr} + \dot{q}''_{fc} - \dot{q}''_{rr}}{\Delta H_g}$$

$$\dot{q}''_e + \dot{q}''_{fr} + \dot{q}''_{fc} = 70\frac{\text{kW}}{\text{m}^2}$$

$$\dot{m}'' = \frac{(70-10)\frac{\text{kW}}{\text{m}^2}}{1.8\frac{\text{kJ}}{\text{g}}} = 33\frac{\text{g}}{\text{m}^2\text{s}}$$

The estimated peak mass loss rate of the burning material is 33 g/m^2/s, or 33 × 2 = 67 g/s.

Flame Heat Flux For flaming fires, in the absence of external heat flux, from Equation 36.15

$$\dot{m}'' = \frac{\dot{q}''_{fr} + \dot{q}''_{fc} - \dot{q}''_{rr}}{\Delta H_g} \tag{36.20}$$

The results from numerous small- and large-scale fire tests show that, as the surface area of the material increases, the flame radiative heat flux increases and reaches an asymptotic limit, whereas the flame convective heat flux decreases and becomes much smaller than the flame radiative heat flux at the asymptotic limit in large-scale fires [57]. It is also known that, in small-scale fires of fixed size with buoyant turbulent diffusion flames, as the oxygen mass fraction is increased, the flame radiative heat flux increases and reaches an asymptotic limit comparable to the asymptotic limit in large-scale fires, whereas the flame convective heat flux decreases and becomes much smaller than the flame radiative heat flux [13].

The effect of the mass fraction of oxygen on the flame radiative and convective heat fluxes in small-scale fires is shown in Fig. 36.24 for 100-mm × 100-mm square × 25-mm-thick slabs of polypropylene. The data were measured in the Fire Propagation Apparatus [13]. The increase in the flame radiative heat flux with increase in the mass fraction of oxygen is due to the increase in the flame temperature and soot formation and decrease in the residence time in the flame [13]. The oxygen mass fraction

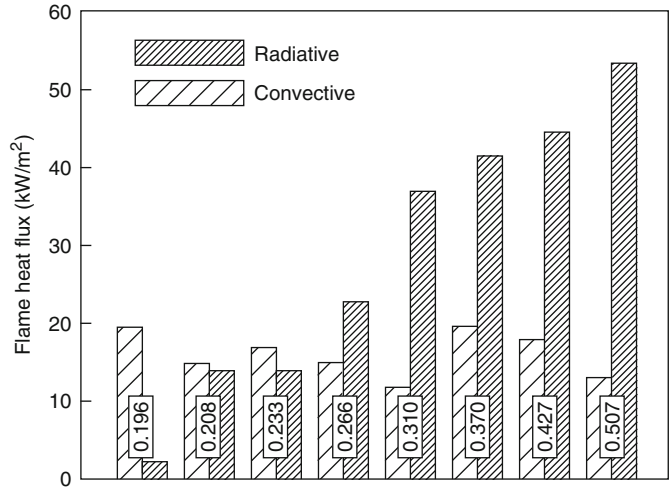

Fig. 36.24 Flame radiative and convective heat fluxes at various oxygen mass fractions for the steady-state combustion of 100-mm × 100-mm square × 25-mm-thick slabs of polypropylene in the FPA under co-airflow velocity of 0.09 m/s (Data taken from Ref. [13]). Mass fractions of oxygen are indicated by the numbers inside the frames

variation technique to simulate large-scale flame-radiative heat flux conditions in small-scale fires is defined as the *flame radiation scaling technique* [44]. This methodology forms the basis for the approaches described above regarding the flame propagating behavior of materials using the FPI concept.

In the flame radiation scaling technique, the flame radiative and convective heat fluxes are determined from (1) mass loss rate measurements at various oxygen mass fractions in the range of 0.12 (close to flame extinction) to about 0.60, under co-airflow conditions; (2) the convective heat transfer coefficient for the FPA, derived from the combustion of methanol; (3) the mass transfer number; and (4) Equation 36.20. In the Fire Propagation Apparatus, the asymptotic limit is reached for oxygen mass fractions in excess of 0.30. At the asymptotic limit, Equation 36.20 can be expressed as

$$\dot{m}''_{\text{asy}} = \frac{\dot{q}''_{f,\text{asy}} - \dot{q}''_{rr}}{\Delta H_g} \tag{36.21}$$

where subscript *asy* represents the asymptotic limit. The asymptotic values for mass loss rate and flame heat flux determined using the flame radiation scaling technique in the FPA are listed in Table 36.7. The measured asymptotic values for mass loss rate reported in the literature and flame heat flux in large-scale fires are also listed in Table 36.7. Flame heat flux values for the large-scale fires are derived from the asymptotic values of the mass loss rate and known values of surface re-radiation losses and heats of gasification.

The data in Table 36.7 show that asymptotic flame heat flux values, determined in the FPA using the flame radiation scaling technique, are in good agreement with the values measured in large-scale fires. The asymptotic flame heat flux values vary from 22 to 77 kW/m^2, depending primarily on the mode of decomposition and gasification rather than on the chemical structures of the materials. For example, for liquids, which vaporize primarily as monomers or as very low molecular weight oligomers, the asymptotic flame heat flux values are in the range of 22–44 kW/m^2, regardless of their chemical structures. For polymers, which vaporize as high molecular weight oligomers, the asymptotic flame heat flux values increase substantially to the range of 49–71 kW/m^2, regardless of their chemical structures. The independence of the asymptotic flame heat values from the chemical structures of materials is consistent with the dependence of flame radiation on optical thickness, soot concentration, and flame temperature in large-scale fires.

Example 7 Calculate the peak mass loss rate for polypropylene in large-scale fires, burning in the open, with no external heat sources in the surroundings.

Solution In the calculation Equation 36.21 will be used. From Table 36.6, $\dot{q}''_{rr} = 15$ kW/m^2 and $\Delta H_g = 2.0$ kJ/g, and from Table 36.7, $\dot{q}''_{f,\text{asy}} = 67$ kW/m^2. Using these values in Equation 36.21,

$$\dot{m}''_{\text{asy}} = \frac{\dot{q}''_{f,\text{asy}} - \dot{q}''_{rr}}{\Delta H_g}$$

$$\dot{m}''_{\text{asy}} = \frac{(67-15)\frac{\text{kW}}{\text{m}^2}}{2.0\frac{\text{kJ}}{\text{g}}} = 26\frac{\text{g}}{\text{m}^2\text{s}}$$

Example 8 Calculate the peak mass loss rate for polypropylene in large-scale fires burning in the open in the presence of a burning object, which provides 20 kW/m^2 of heat flux to the polypropylene surface, in addition to its own flame heat flux of 67 kW/m^2.

Solution In the calculation, Equation 36.15 will be used with $\dot{q}''_e = 20$ kW/m^2. From Table 36.6, $\dot{q}''_{rr} = 15$ kW/m^2 and $\Delta H_g = 2.0$ kJ/g and from Table 36.7, $\dot{q}''_{f,\text{asy}} = 67$ kW/m^2. Using these values in Equation 36.15,

$$\dot{m}'' = \frac{\dot{q}''_e + \dot{q}''_{fr} + \dot{q}''_{fc} - \dot{q}''_{rr}}{\Delta H_g}$$

$$\dot{q}''_e + \dot{q}''_{fr} + \dot{q}''_{fc} = (67+20)\frac{\text{kW}}{\text{m}^2}$$

$$\dot{m}'' = \frac{(87-15)\frac{\text{kW}}{\text{m}^2}}{2.0\frac{\text{kJ}}{\text{g}}} = 36\frac{\text{g}}{\text{m}^2\text{s}}$$

Table 36.7 Asymptotic values of mass loss rate and flame heat flux

Material	$\dot{m}_{asy}''$ (g/m^2/s)		$\dot{q}_{f,asy}''$ (kW/m^2)	
	S[a]	L[b]	S[a]	L[b]
Aliphatic carbon-hydrogen atoms[c]				
Polyethylene	26	–	61	–
Polypropylene	24	–	67	–
Heavy fuel oil (2.6–23 m)	–	36	–	29
Kerosene (30–80 m)	–	65	–	29
Crude oil (6.5–31 m)	–	56	–	44
n-Dodecane (0.94 m)	–	*36*	–	30
Gasoline (1.5–223 m)	–	62	–	30
JP-4 (1.0–5.3 m)	–	67	–	40
JP-5 (0.60–17 m)	–	55	–	39
n-Heptane (1.2–10 m)	~66	75	32	37
n-Hexane (0.75–10 m)	–	77	–	37
Transformer fluids (2.37 m)	27–30	25–29	23–25	22–25
Aromatic carbon-hydrogen atoms[c]				
Polystyrene (0.93 m)	36	34	75	71
Xylene (1.22 m)	–	67	–	37
Benzene (0.75–6.0 m)	–	81	–	44
Aliphatic carbon-hydrogen-oxygen atoms[c]				
Polyoxymethylene 16	–	50	–	–
Polymethylmethacrylate (2.37 m)	28	30	57	60
Methanol (1.2–2.4 m)	20	25	22	27
Acetone (1.52 m)	–	38	–	24
Aliphatic carbon-hydrogen-oxygen-nitrogen atoms				
Flexible polyurethane foams	21–27	–	64–76	–
Rigid polyurethane foams	22–25	–	49–53	–
Aliphatic carbon-hydrogen-halogen atoms				
Polyvinylchloride	16	–	50	–
Tefzel (ETFE)	14	–	50	–
Teflon (FEP)	7	–	52	–

Note: Mass loss rates are from the data reported in the literature
[a]Small-scale fires, pool diameter fixed at 0.10 m, flame radiation scaling technique was used in the Fire Propagation Apparatus, $Y_O \geq 0.30$
[b]Large-scale fires in normal air
[c]Numbers in m in *parentheses* are the pool diameters used in large-scale fires

Pyrolysis and Determination of "Model-Specific" Material Properties

One of the most prevailing observations made with the bench-scale apparatuses discussed in section "Flammability Apparatuses and Measurement Capabilities" of this chapter is the rate of thermal degradation of condensed phase materials under a prescribed heating scenario. This behavior is captured in the tests through the measurement of a mass loss rate (MLR). In the context of this chapter such behavior is referred to as pyrolysis. Pyrolysis is a complex process that involves a number of coupled physical and chemical phenomena, which include, among many others, phase changes, char formation, water desorption/migration (e.g., in cellulosic fuels), gas diffusion, gas-solid heat exchange, oxidation, etc. (refer to Chaps. 21 and 23). These processes determine the formation of gradients (thermal, species, etc.) within a given material which control ignition, heat release, and flame propagation in fires.

There is strong and continued interest in the fire community in the development of predictive fire modeling capabilities for practical large-scale fires through the use of new-generation computational fluid dynamics (CFD) tools [58–60]. Such modeling can provide measures to interpret, interpolate, and extrapolate information obtained from limited experimental data as well as providing cost-effective alternatives by reducing the number of large-scale tests necessary to develop fire protection requirements or standards. To reach this objective, physical models for fluid mechanics, gas phase combustion, soot formation and oxidation, radiation, solid phase heat transfer and pyrolysis, and suppression need to be incorporated into an appropriate CFD solver to properly represent the multi-scale, multi-physics phenomena taking place in large-scale fires. Given the mathematical complexity of these CFD tools, it is important that such fire models be verified and validated against experimental data [59, 60].

Of relevance to the present chapter is how bench-scale experiments may contribute to the development of pyrolysis models to be used in the CFD tools described above. Models have become recently available [61–64] which represent the current state of the art of pyrolysis modeling; these are comprehensive models which share similar robust mathematical and numerical frameworks. These models, due to their complexity, require a potentially large number of adjustable input parameters, i.e., material properties. Many applications (e.g., large-scale industrial fires) involve fuels for which such properties are unknown. In certain cases (e.g., [65–67]) detailed property measurements may be performed (via thermogravimetric analyses, TGA, and differential scanning calorimetry, DSC, for example) and successfully used in the comprehensive models. However, experimental venues such as TGA and DSC, although extremely useful in providing fundamental material information, are often not representative of practical applications as they feature relatively slow heating rates and preclude the formation of mass and thermal gradients within the material. Furthermore, properties measured in this manner may not be directly used even in the most advanced models since they cannot reflect the true complexity and heterogeneity of the physical processes taking place during pyrolysis. To some degree models must always conceptualize and aggregate complex interactions by the use of only relatively simple mathematical equations. Therefore, in that sense, pyrolysis models cannot use "true" material properties if all the physics are not fully captured. Finally, in the context of large CFD simulations, use of comprehensive and complex models may be computationally prohibitive.

On the basis of the above discussion, then, one of the major challenges posed to the end user of CFD pyrolysis models is to make simplifications and approximations to keep the number of parameters manageable and the model computationally efficient while maintaining sufficient model generality and applicability to a given practical scenario. By following this approach the input parameters to the model can be considered "effective" or "model-specific" material properties which are sensitive to the physical processes included in the model. The methodology by which these model-specific properties are obtained is detailed in the following sections.

Optimization

The main requirement regarding the performance of CFD pyrolysis models is that they should properly reproduce aspects of the condensed-phase material behavior, such as pyrolysis gas (i.e., fuel) generation rates, surface temperatures, etc., which may be critical to the successful performance of the CFD fire simulation. These material response characteristics can in principle be measured via bench-scale tests such as those conducted in the Fire Propagation Apparatus. The model-specific material properties alluded to above are obtained by coupling a simplified pyrolysis model to optimization algorithms and the input parameters (i.e., the material properties) are adjusted in order to obtain the best possible agreement between model outputs and experimental bench-scale pyrolysis data. In the general framework of flammability properties this approach has been seldom used [68, 69]

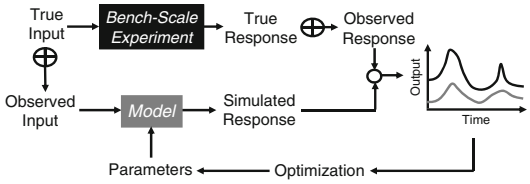

Fig. 36.25 Optimization approach

although it has recently received renewed attention [70–76]. Numerous similar efforts, though, exist in the literature mostly aimed at determining a limited set of thermal properties and for specific applications [77–82].

A schematic of the optimization approach is shown in Fig. 36.25. An experimental process is captured via a numerical model subject to a driving input (e.g., external radiation) and a set of parameters ("material properties"). In the figure, an important distinction is made between the true input to and true response of the experiment and what is actually observed, or measured, in order to represent experimental uncertainty. It is because of this uncertainty that parameters determined through optimization procedures such as the one discussed herein are sensitive to the accuracy of the experimental data used as optimization targets. As can be expected, the optimization problem is complex and highly non-linear. Therefore, local search methods such as direct search [83] and gradient search [84] algorithms are not applicable; however, such methods have been used widely for property estimation [68, 69, 77, 81, 82]. Global methods are needed which can tackle the major complications of high-dimensionality optimization such as local optima, multiple attraction basins, discontinuities, etc.

An optimization algorithm with high efficiency and robustness is needed if one is to perform multiobjective and multivariable optimization as little or no a priori knowledge is available of the structure of the model response surface. Furthermore, these qualities allow optimization algorithms to be easily generalized so as to provide consistent performance over a wide range of problems, even if optimization target data are limited. Here, the selected optimization algorithm is the Shuffled Complex Evolution (SCE) [85]. This is a method that has been mostly applied to hydrological problems [86] but, as will be shown below, it is general and robust enough to show considerably good performance in flammability applications. Chaos et al. [73–75] found SCE to be superior to other global optimization tools, such as genetic algorithms, a finding that has been confirmed by other researchers [87].

A schematic flowchart of the SCE algorithm is shown in Fig. 36.26. Similar to genetic algorithms, SCE is based on a process of natural evolution. A population of s points (i.e., vectors of "material properties" in the present context) is randomly sampled from the feasible parameter space (given the bounds for each parameter) and the value of the objective function to be optimized (e.g., minimization of the sum of squares between model outputs and experimental data) is computed. The points are ranked from smallest to highest objective function value and are then partitioned into p complexes each containing m points (note $s = p \times m$) so that the first complex contains every $(l-1)p + 1$ ranked point, the second every $(l-1)p + 2$ ranked point, etc. where $l = 1, 2, \ldots, m$. Each of these complexes is then allowed to evolve independently according to a competitive complex evolution (CCE) algorithm [85], described below. After the CCE process, all the points in each complex are combined back into a single population, ranked according to their objective function value, and re-partitioned following the procedure above; this effectively "shuffles" the complexes. This procedure is iteratively repeated until specified convergence criteria are met. SCE allows for more extensive (i.e., in different directions) and freer exploration of the feasible space due to the partition of complexes. Shuffling enhances survivability by sharing information about the space gained independently by each complex.

The key component of the SCE method is the CCE algorithm which is based on the Nelder-Mead simplex downhill search scheme [83]. In the CCE algorithm q points are randomly selected within each complex according to a

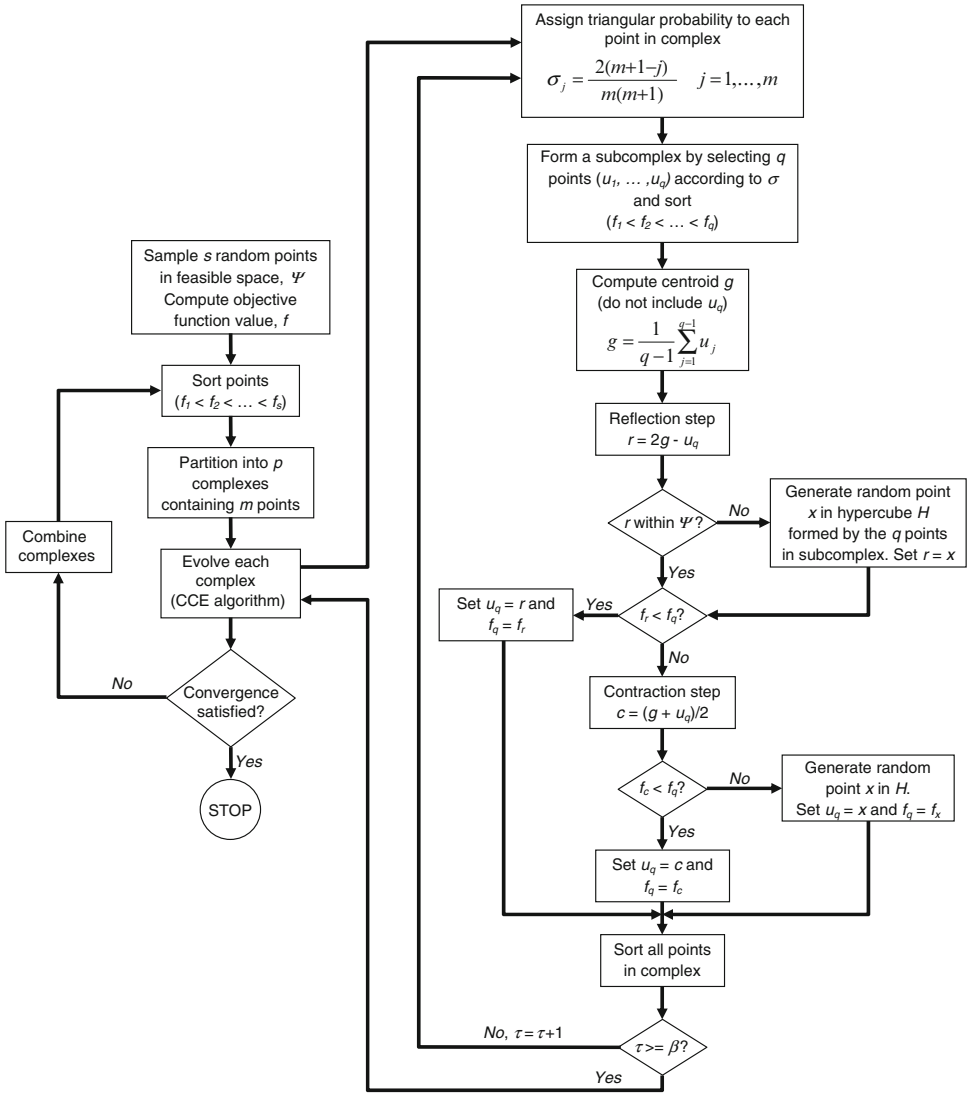

Fig. 36.26 The Shuffled Complex Evolution algorithm

trapezoidal probability distribution so that the best and worst points in the complex have the highest and lowest chance, respectively, of being chosen. The centroid of the subcomplex formed by the set of q points is calculated without considering the worst point in the subcomplex; then, this worst point is reflected through the centroid. If the new point so computed is better (i.e., its objective function value is improved) than the worst point, the worst point is replaced. Otherwise a point is computed halfway between the centroid and the worst point; if this point is better than the worst point, the worst point is replaced. In the case that the latter two steps do not generate a better point or if the reflection through the centroid yields a point outside the feasible space, a point is generated randomly which replaces the worst point. This procedure is repeated a specific number of times, β, before the complexes are shuffled as described above. In this manner, each complex evolves independently as a whole.

The SCE process is shown graphically in Fig. 36.27 by using a two-dimensional example. A test function was generated (left pane in

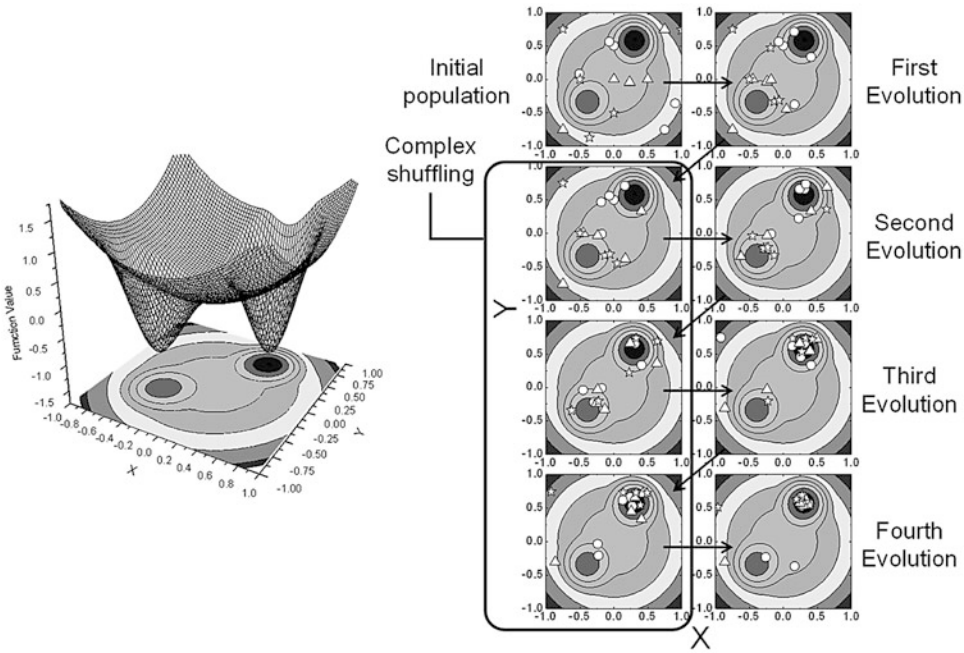

Fig. 36.27 SCE application to a two-dimensional problem

Fig. 36.27) by distorting selected regions of a convex quadratic function so as to introduce local minima with varying regions of attraction, following the methods of Gaviano and Lera [88]. A three-minima function was generated with one global minimum located at (X,Y) = (0.312,0.598). SCE was run with three complexes (denoted by stars, circles, and triangles in Fig. 36.27) consisting of 5 points each (i.e., $p = 3$, $m = 5$, $s = 15$). Note the effect of shuffling in Fig. 36.27. The overall distribution of points from the end of an evolution to the beginning of the next is unchanged; however, the distribution within each complex changes. Also note that some points converge towards the local minimum at (X,Y) = (-0.412,-0.351) in the first two evolutions but shuffling efficiently directs their convergence towards the global minimum.

Application

Synthetic Data and Target Selection

Foremost, it is important to illustrate the features and limitations of the SCE optimization algorithm when applied to problems of practical interest herein. In order to do this, a simplified one-dimensional pyrolysis model was used to generate synthetic experimental data for a supposed charring material. One-dimensionality is assumed as this is representative of tests conducted in the Fire Propagation Apparatus or cone calorimeter where the thickness of samples tested is small compared to their diameter and edge effects can be considered negligible. The specific details of the pyrolysis model used are beyond the scope of this chapter, and the reader is referred to [63, 64, 73–75] for further information; only the simplifications made to the model are described here for brevity. The model employs a control volume approach and the governing mass and energy conservation equations are solved numerically using a fully implicit scheme. Only three species are treated: virgin solid, char, and pyrolytic gas and it is assumed that the virgin solid decomposes to char and/or gas through a single heterogeneous nth-order Arrhenius-type reaction. Pyrolysis gas is assumed to be in thermal equilibrium with the solid and to immediately escape once formed. All material properties are assumed to be temperature-independent.

Table 36.8 Parameters used to generate synthetic data (Fig. 36.28) and parameters returned by optimization

			SCE optimization					
Property		Synthetic	LB	UB	Case 1	Case 2	Case 3	Case 4
Virgin	Thermal conductivity (W/m/K)	0.10	0.01	1.00	0.04	0.09	0.10	0.10
	Density (kg/m^3)	500	100	1000	521	571	660	510
	Heat capacity (J/kg/K)	1500	500	5000	684	1390	1210	1470
	Emissivity	0.5	0.0	1.0	0.30	0.49	0.59	0.50
Char	Thermal conductivity (W/m/K)	0.25	0.01	1.00	0.21	0.30	0.33	0.25
	Density (kg/m^3)	100	50	500	120	169	260	95
	Heat capacity (J/kg/K)	1000	500	5000	5000	1166	2071	1053
	Emissivity	0.9	0.0	1.0	0.49	0.99	1.00	0.90
Arrhenius decomposition	Log [pre-exponential factor (s^{-1})]	10	6	12	10.7	7.6	8.9	10.0
	Activation energy (kJ/mol)	150	50	250	160	119	141	150
	Reaction order	2	0	5	1.3	1.8	1.5	2
	Log [heat of pyrolysis (J/kg)]	5.81	4	7	5.52	5.87	5.85	5.81
Average deviation (%)					57.8	17.1	35.2	1.2

The synthetic dataset consists of mass loss rate and surface temperature data generated for a 5-mm thick material subjected to external radiation levels of 25, 50, and 100 kW/m^2. For simplicity, the back boundary of the material was assumed to be perfectly insulated (adiabatic) and a constant convective heat transfer coefficient of 15 W/m^2/K was assumed for the front surface. The material properties used in the model to generate the data are listed in Table 36.8. The model-generated curves were modified by adding Gaussian error with standard deviations representative of experimental uncertainty: 100 mg for mass loss and 15 K for temperature measurements [75, 89], In order to obtain mass loss rate, the modified mass loss curve was differentiated using Savitsky-Golay filters [37, 90, 91]. As opposed to previous applications of this methodology [36, 91] in which a fixed filter window size was recommended, the window size of the filter was kept between one and two times the full-width-half-magnitude size of the narrowest transient peak of interest [92] in order to avoid introducing unwanted bias in the derived MLR data. This approach ensured that the magnitude of these peaks was preserved after application of the filter. Figure 36.28 shows plots of the synthetic data prior to and after adding Gaussian error. Also in the figure, the effect of varying the smoothing filter size is shown for the 100 kW/m^2 case. Note that by increasing the filter window size by a factor of two the first mass loss rate peak, which is narrower, is "washed out" whereas the second peak is still properly captured.

Several optimization runs were preformed by selecting specific subsets of the data shown in Fig. 36.27. This was done in order to test the robustness of the SCE algorithm as it is often the case, especially with complex practical materials, that target experimental data may be limited and/or difficult to measure accurately. An algorithm that can reach the global optimum with the least amount of target data can be extremely useful as it can allow one to limit the target metrics to only those data that can presumably be measured more accurately without considering data with higher uncertainty. Four target data subsets were selected: Case 1—mass loss rate at 50 kW/m^2; Case 2—mass loss rate, cumulative mass loss, and surface temperature at 50 kW/m^2; Case 3—mass loss rate at 25, 50, and 100 kW/m^2; and Case 4—mass loss rate, cumulative mass loss, and surface temperature at 25, 50, and 100 kW/m^2. SCE was run subject to the property bounds shown in Table 36.8 and with algorithmic parameters (i.e., p, m, q, and β, see above) selected according to the guidelines of [86]; the population size was 150.

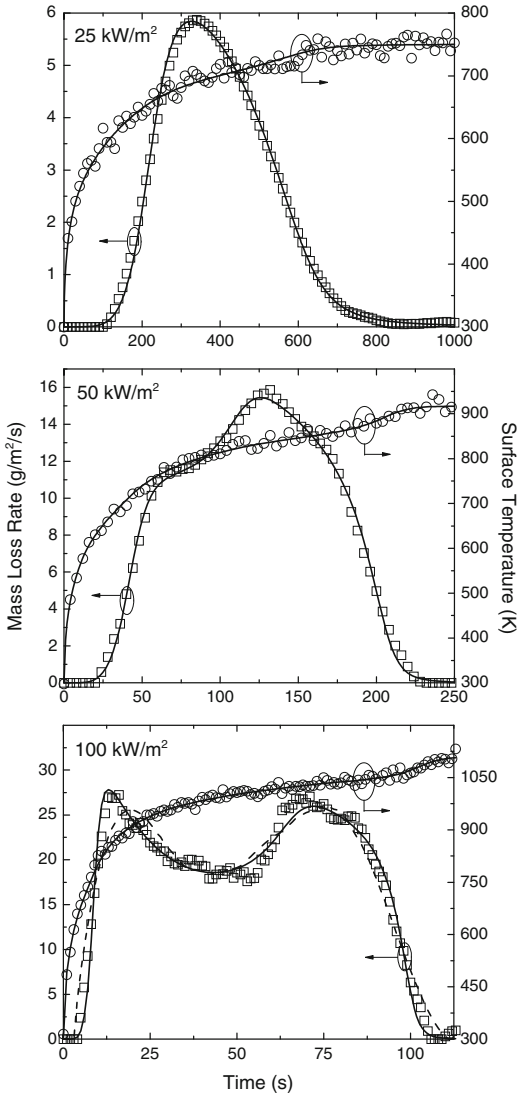

Fig. 36.28 Synthetic data. *Lines* show model outputs and symbols denote the model data after Gaussian error was added (see text). The *dashed line* for mass loss rate at 100 kW/m^2 shows the effect of varying the smoothing filter window size from 25 s to 50 s (see text)

The values for the optimized property parameters obtained for each of the four cases are listed in Table 36.8. For the sake of brevity and in lieu of showing plots it is noted that for all cases a near perfect match was obtained against each of the corresponding datasets used for optimization; the R-squared values for all cases were in excess of 0.99. However, regardless of the good agreement obtained, the original parameters are not recovered in most cases. A clear trend can be observed, nonetheless; the deviation from the original parameters is reduced when more target metrics are added (compare Case 1 to Case 2 and Case 3 to Case 4) and when more heat fluxes are considered for the same target metric (compare Case 1 to Case 3 and Case 2 to Case 4). This trend is an obvious manifestation of how the target data are able to constrain the model and, thus, the optimization algorithm. By considering mass loss rate alone (Case 1 and Case 3) parameters, most notably physical properties such as thermal conductivity and heat capacity, cannot be accurately determined. This is to be expected as these parameters are coupled through the thermal inertia and thermal diffusivity of the material. Introducing temperature as an optimization target improves agreement against these properties and the same can be said about considering additional heat flux levels. It is noted that, in a similar synthetic data exercise as that discussed here, SCE was found to recover the input parameters using datasets consisting of mass loss rate, front and back surface temperatures at two heat flux levels [87]; back surface temperature measurements may present a experimental challenge, however.

The discussion above should persuade the reader that the process of obtaining model-specific properties through optimization will be most successful when considering multiple experimental data (mass loss rate, temperature, etc.) over as wide a range of practical conditions as possible [60]. Furthermore, availability of properties that can be easily measured (e.g., virgin density) will further improve the results by reducing the dimensionality of the problem. Yet, there are cases in the literature (e.g., [76]) where optimization is performed against very limited datasets. As a last word of caution it is reiterated that the "material properties" obtained using the methodology described herein depend on the choice of pyrolysis model as well as the accuracy of the experimental data and are not universally applicable to other models or to scenarios that considerably depart from the experimental conditions used to derive the model-specific properties.

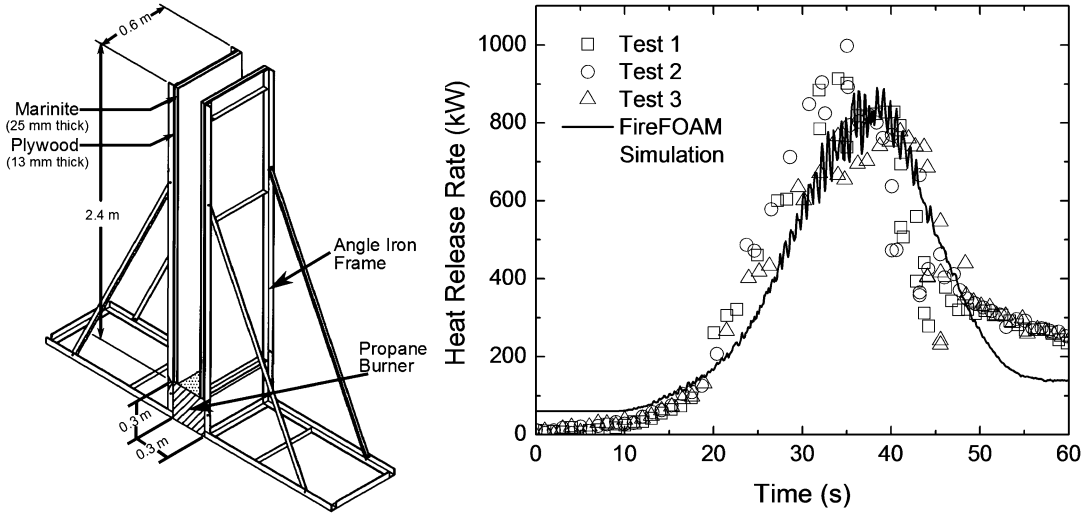

Fig. 36.29 Experimental (*symbols*) and computed (*lines*) parallel panel heat release rates for single-wall corrugated cardboard [96]. The experimental configuration is shown on the *left panel*

FPA Data and Intermediate-Scale Fire Growth Simulations

The approach outlined above has been extensively used and applied to the simulation of the vertical spread of fire between parallel panels at an intermediate scale [60, 93–97]. For this application, model-specific properties were determined using the pyrolysis model included in FireFOAM [98, 99], a Large Eddy Simulation (LES) solver. The target data used for optimization were collected in the Fire Propagation Apparatus in inert environments (i.e., 100 % nitrogen); this is a unique feature of the apparatus (see section "Flammability Apparatuses and Measurement Capabilities") which allows for the decoupling of flame heat flux from the pyrolysis process. Following the recommendations of the previous section, the data consisted of mass loss rates and surface temperatures over heat fluxes spanning the 20–110 kW/m^2 range. The model-specific material properties were shown to successfully predict, at least qualitatively, flame propagating and non-propagating behavior of several materials when used in the LES simulation [60].

Further experience with the application of the methodologies described herein has elucidated the importance of properly characterizing boundary conditions in the FPA experiments and the relative importance of oxidative pyrolysis in certain applications [35, 89, 97]. Considerable progress has been made in the predictive abilities of FireFOAM when compared against flame spread experiments in the parallel panel configuration [97]. An example is shown in Fig. 36.29 where the heat release rate of single-wall corrugated cardboard collected during three separate parallel panel tests (a schematic of the test is also shown in the figure, for more details refer to [93–97] as well as section "Fire Propagation") is compared against simulations. A considerably good agreement can be observed. This is an encouraging result which confirms that the approach described in this section for the characterization of material flammability is promising and may lead to cost-effective modeling alternatives to large-scale testing.

Heat Release Rate

The determination of heat release rate in fires has been influenced by the principles and techniques used for controlled combustion in the heating and power industries. Heat in the flowing combustion products (convective heat) and thermal radiation are used to generate steam, heat a furnace or space, produce mechanical power in internal

combustion engines or gas turbines, and so forth. Heat is generated by injecting fuel (gas, liquid, or solid) into a hot environment, where it undergoes evaporation, gasification, and thermal decomposition or pyrolysis.

Fuel vapors react chemically with oxygen and produce heat and products, such as carbon monoxide (CO), carbon dioxide (CO_2), hydrocarbons, water (H_2O), and soot and other particulates. The theoretical amount of air required for complete combustion is estimated from an empirical guide [100], which suggests that, for every 10.6 kJ of heat in the fuel burned, 3.4 g of air are required for complete combustion [101]. Equivalently, the heat of combustion per unit mass of molecular oxygen consumed (ΔH_0^*) is 13.4 kJ/g. Using $\Delta H_0^* \approx 13.4$ kJ/g to determine the heat release rate in fires from the mass consumption rate of oxygen is discussed in Refs. [14, 21]. This technique forms the basis of oxygen consumption (OC) calorimetry.

A combustion process is characterized by its *combustion efficiency*, χ_{ch}, defined as the fraction of heat of complete combustion released in the chemical reactions, which is the ratio of the chemical heat of combustion to the net heat of complete combustion. The calorific energy generated in chemical reactions leading to complete combustion per unit mass of fuel, with water produced being in the vapor state, is defined as the *net heat of complete combustion*. The calorific energy generated in chemical reactions leading to varying degrees of incomplete combustion per unit mass of fuel consumed is defined as the *chemical heat of combustion*. In the heating and power industries, combustion efficiency is determined routinely from the analysis of waste products (flue gas), especially for CO, CO_2, and O_2, and from the measurements of temperature in the combustion products-air mixture and thermal radiation. For higher combustion efficiency, *mass fuel-to-air ratio* relative to the *stoichiometric fuel-to-air mass ratio* or the *equivalence ratio* is controlled by maintaining the desired primary and secondary airflow.

The net heat of complete combustion can be measured in the oxygen bomb calorimeter [102] (see Chap. 27) and is calculated from the standard heats of formation of the materials, CO_2, and H_2O (the standard heat of formation of O_2 in its standard state being zero).

In fires, complete combustion is rarely achieved and products of incomplete combustion, such as CO and smoke, are quite common. An example of incomplete combustion is given in Table 36.9, where chemical heat of combustion and combustion efficiency decrease as CO, carbon, and ethylene are formed at the expense of CO_2 and H_2O with reduced O_2 consumption, a typical condition found in ventilation-controlled fires [103]. The upper limit of the combustion efficiency is 1.00, corresponding to complete combustion, and the lower limit is 0.46, corresponding to unstable combustion leading to flame extinction for combustion efficiency $\leq$0.40 [103, 104].

Table 36.9 Chemical heat of combustion and combustion efficiency of polymethylmethacrylate

Reaction stoichiometry	ΔH_{ch} (kJ/g)[a]	χ_{ch}
$C_5H_8O_2$ (g) + 6.0 O_2 (g) =		
5CO_2 (g) + 4H_2O (g)	24.9	1.00
$C_5H_8O_2$ (g) + 5.5 O_2 (g) =		
4CO_2 (g) + 4H_2O (g) + CO (g)	22.1	0.89
$C_5H_8O_2$ (g) + 4.5 O_2 (g) =		
3CO_2 (g) + 4H_2O (g) + CO (g) + C (s)	18.2	0.73
$C_5H_8O_2$ (g) + 3.0 O_2 (g) =		
2CO_2 (g) + 3H_2O (g) + CO (g)		
+ C (s) + 0.50 C_2H_4 (g)	11.5	0.46

[a]Standard heat of formation in kJ/mol: PMMA ($C_5H_8O_2$) (g) = −442.7; O_2 (g) = 0; CO_2(g) = 393.5; H_2O (g) = −241.8; CO (g) = −110.5; C (s) = 0; and C_2H_4 (g) = +26.2, where g and s stand for gaseous and solid states, respectively

Chemical Heat Release Rate

As described in section "Flammability Apparatuses and Measurement Capabilities" of this chapter, chemical heat release rate in bench scale apparatuses such as the Fire Propagation Apparatus and cone calorimeter can be determined from CDG and OC calorimetries.

CDG Calorimetry The chemical heat release rate is determined from the following relationships [14, 28, 31, 43, 44, 103, 105]:

$$\dot{Q}''_{ch} = \Delta H^*_{CO_2} \dot{G}''_{CO_2} + \Delta H^*_{CO} \dot{G}''_{CO} \tag{36.22}$$

$$\Delta H^*_{CO_2} = \frac{\Delta H_T}{\psi_{CO_2}} \tag{36.23}$$

$$\Delta H^*_{CO} = \frac{\Delta H_T - \Delta H_{CO} \psi_{CO}}{\psi_{CO_2}} \tag{36.24}$$

where

$\dot{Q}''_{ch}$ = Chemical heat release rate (kW/m^2)
$\Delta H^*_{CO_2}$ = Net heat of complete combustion per unit mass of CO_2 generated (kJ/g)
ΔH^*_{CO} = Net heat of complete combustion per unit mass of CO generated (kJ/g)
ΔH_T = Net heat of complete combustion per unit mass of fuel consumed (kJ/g)
ψ_{CO_2} = Stoichiometric yield for the maximum conversion of fuel to CO_2 (g/g)
ψ_{CO} = Stoichiometric yield for the maximum conversion of fuel to CO (g/g)
$\dot{G}''_{CO_2}$ = Generation rate of CO_2 (g/m^2/s)
$\dot{G}''_{CO}$ = Generation rate of CO (g/m^2/s)

The values for the net heats of complete combustion per unit mass of fuel consumed and CO_2 and CO generated are listed in Table A.38. The values depend on the chemical structures of the materials. With some exceptions, the values remain approximately constant within each generic group of fuels. The average values are also listed in the tables. From the average values, $\Delta H^*_{CO_2} = 13.3 \pm 1.5$ kJ/g and $\Delta H^*_{CO} = 11.1 \pm 2$ kJ/g. In CDG calorimetry, the CO correction (which accounts for the heat generated for incomplete combustion) for well-ventilated fires is very small because of the small amounts of CO generated. The variations of 11 % and 18 % in the $\Delta H^*_{CO_2}$ and ΔH^*_{CO} values, respectively, would reduce significantly if values for low molecular weight hydrocarbons with small amounts of O, N, and halogen were not used in averaging. For the determination of the chemical heat release rate, generation rates of CO_2 and CO are measured and either the actual values (if material composition is known) or the average values of the net heat of complete combustion per unit mass of CO_2 and CO generated are used. The measurements for the generation rates of CO_2 and CO are described in section "Generation of Fire Products and Smoke Yields" of this chapter.

Care must be taken in the application of CDG calorimetry depending on the scenario of interest. For example, in fires where incomplete combustion is ubiquitous and copious amounts of unburned hydrocarbons, soot, and other particulates are generated, the equations above will not yield an accurate measure of heat release rate as corrections for the formation of these species have to be included (much like is done above for CO). One more example is a scenario where a fire is suppressed by water (i.e., a sprinkler) and a large amount water vapor is present in the combustion-product-air mixture. Some correction procedures are available (e.g., [106]) to account for these effects.

OC Calorimetry The chemical heat release rate is determined from the following relationships [13, 21–24, 28, 31, 43, 44, 103, 105, 107]:

$$\dot{Q}''_{ch} = \Delta H^*_O \dot{C}''_O \tag{36.25}$$

$$\Delta H^*_O = \frac{\Delta H_T}{\psi_O} \tag{36.26}$$

where

ΔH^*_O = Net heat of complete combustion per unit mass of oxygen consumed (kJ/g)
$\dot{C}''_O$ = Mass consumption rate of oxygen (g/m^2/s)
ψ_O = Stoichiometric oxygen-to-fuel mass ratio (g/g)

The values for the net heats of complete combustion per unit mass of oxygen consumed are listed in Table A.38 along with the values for the

net heats of complete combustion per unit mass of fuel consumed and CO_2 and CO generated. The average values of the net heat of complete combustion per unit mass of oxygen consumed are also listed in the tables. The values depend on the chemical structures of the materials. With some exceptions, the values remain approximately constant within each generic group of fuels. From the average values, $\Delta H_O^* = 12.8 \pm 0.9$ kJ/g. The ΔH_O^* value of 12.8 kJ/g is in good agreement with the value 13.1 ± 0.7 kJ/g reported in Ref. [21]. The variation of ±0.9 kJ/g (7 %) would reduce significantly if values for low molecular weight hydrocarbons with small amounts of O, N, and halogen were used in averaging. For the determination of chemical heat release rate, mass consumption rate of oxygen is measured, and either the actual values or the average values of the net heats of complete combustion per unit mass of oxygen consumed are used. The measurement for the consumption rate of oxygen is described in section "Generation of Fire Products and Smoke Yields" of this chapter.

As discussed above for CDG calorimetry, in situations where incomplete combustion is prevalent, the equations above will have to be corrected for the formation of products such as soot and unburned hydrocarbons [108, 109]. Furthermore, for materials that have bound oxygen in their chemical structures, oxygen may be released as a product of combustion which will affect the OC methodology [110]. Thus, chemical structure plays an important role in the determination of heat release rate [111].

Convective Heat Release Rate

The convective heat release rate is determined from GTR calorimetry, where the following relationship is used [1–3, 13, 14, 28, 31, 44, 103]:

$$\dot{Q}''_{\text{con}} = \frac{\dot{W} c_p (T_g - T_a)}{A} \tag{36.27}$$

where

$\dot{Q}''_{\text{con}}$ = Convective heat release rate (kW/m^2)
c_P = Specific heat of the combustion product-air mixture at the gas temperature (kJ/g/K)
T_g = Gas temperature (K)
T_a = Ambient temperature (K)
$\dot{W}$ = Total mass flow rate of the fire product-air mixture (g/s)
A = Total exposed surface area of the material (m^2)

Radiative Heat Release Rate The chemical heat release rate consists of a convective and a radiative component [25]. Some fraction of the chemical heat release rate may be lost as conductive heat. In systems where such conductive heat losses are negligibly small, the radiative heat release rate can be obtained from the difference between the chemical and convective heat release rates [14, 25, 28, 31, 44, 103]:

$$\dot{Q}''_{\text{rad}} = \dot{Q}''_{\text{ch}} - \dot{Q}''_{\text{con}} \tag{36.28}$$

where $\dot{Q}''_{\text{rad}}$ is the radiative heat release rate (kW/m^2).

Energy Released in a Fire The total amount of heat generated as a result of chemical reactions in the combustion of a material is defined as chemical energy. The chemical energy has a convective and a radiative component:

$$E_{\text{ch}} = E_{\text{con}} - E_{\text{rad}} \tag{36.29}$$

where

E_{ch} = Chemical energy (kJ)
E_{con} = Convective energy (kJ)
E_{rad} = Radiative energy (kJ)

The chemical energy and its convective and radiative components are calculated by the time integration of the respective heat release rates, expressed here by a numerical summation:

$$E_i = A \sum_{n=t_{ig}}^{n=t_{ex}} \dot{Q}''_i(t_n) \Delta t_n \tag{36.30}$$

where

E_i = Chemical, convective, or radiative energy (kJ)
A = Total surface area of the material burning (m^2)
t_{ig} = Ignition time (s)
t_{ex} = Flame extinction time (s)

The total mass of the material lost during combustion can be measured directly from the initial and final mass or calculated by the time integration of the mass loss rate, expressed here by a numerical summation:

$$W_f = A\sum_{n=t_{ig}}^{n=t_{ex}} \dot{m}''(t_n)\Delta t_n \qquad (36.31)$$

where W_f is the total mass of the material lost (g) in the combustion process.

Heat release rate can also be expressed as the product of the mass loss rate and the heat of combustion of the material, if it is known a priori:

$$\dot{Q}_i'' = \Delta H_i \dot{m}'' \qquad (36.32)$$

where ΔH_i is the chemical, convective, or radiative heat of combustion (kJ/g). In turn, the average chemical, convective, or radiative heats of combustion can be calculated from the calorimetry relationships based on Equations 36.22 (or 36.25), 36.27, 36.28, and 36.30 so that:

$$\Delta\overline{H}_i = \frac{E_i}{W_f} \qquad (36.33)$$

where $\Delta\overline{H}_i$ is the average chemical, convective, or radiative heat of combustion (kJ/g). The average chemical heat of combustion determined in the cone calorimeter is defined as the effective heat of combustion [22–24].

Heat Release Parameter (HRP) From Equations 36.15 and 36.32 the amount of energy generated per unit amount of energy absorbed can be expressed as:

$$\dot{Q}_i'' = \left(\frac{\Delta H_i}{\Delta H_g}\right)\left(\dot{q}_e'' + \dot{q}_{fr}'' + \dot{q}_{fc}'' - \dot{q}_{rr}''\right) \qquad (36.34)$$

where the ratio $\Delta H_i/\Delta H_g$ is defined as the Heat Release Parameter (HRP) and, as the heat release rate itself, has chemical, convective, and radiative components (HRP_{ch}, HRP_{con}, and HRP_{rad}, respectively) [44]. The HRP values are characteristic fire properties of materials but depend on fire ventilation. The chemical HRP is independent of fire size.

Experimental data support Equation 36.34, as shown in Figs. 36.30, 36.31, and 36.32, where the average peak or steady-state chemical heat release rates are plotted against the net heat flux. A clear linear relationship between the chemical heat release rate and net heat flux can be discerned. For the condition $\dot{q}_e'' >> \dot{q}_{fr}'' + \dot{q}_{fc}'' - \dot{q}_{rr}''$, the average HRP value can be calculated from

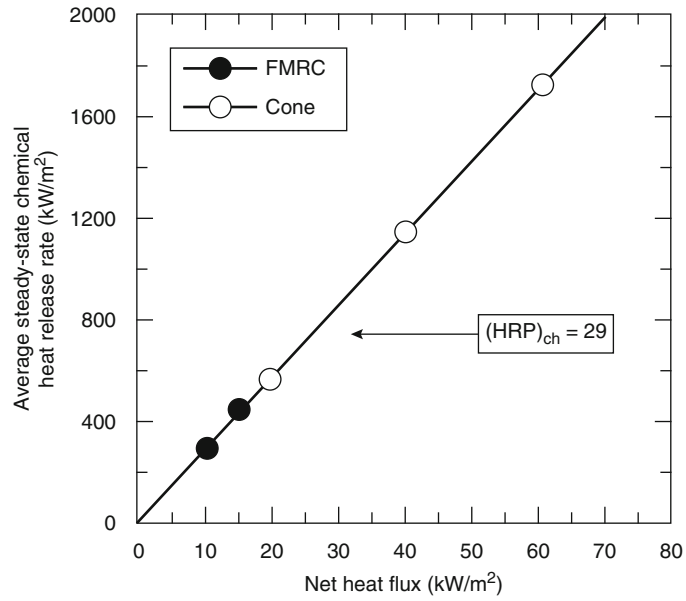

Fig. 36.30 Average steady-state chemical heat release rate versus net heat flux for a polystyrene sample. Net heat flux is the sum of the external and flame heat fluxes minus the surface re-radiation

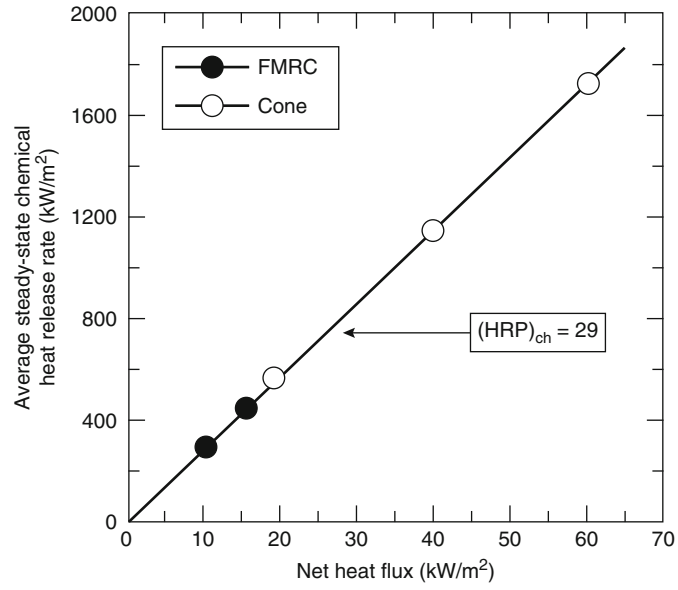

Fig. 36.31 Average steady-state chemical heat release rate versus the net heat flux for a high molecular weight hydrocarbon liquid burning in a 100-mm-diameter dish. The cone calorimeter data were measured at the research laboratory of the Dow-Corning Corporation, Midland, Michigan. Net heat flux is the sum of the external and flame heat fluxes minus the surface re-radiation

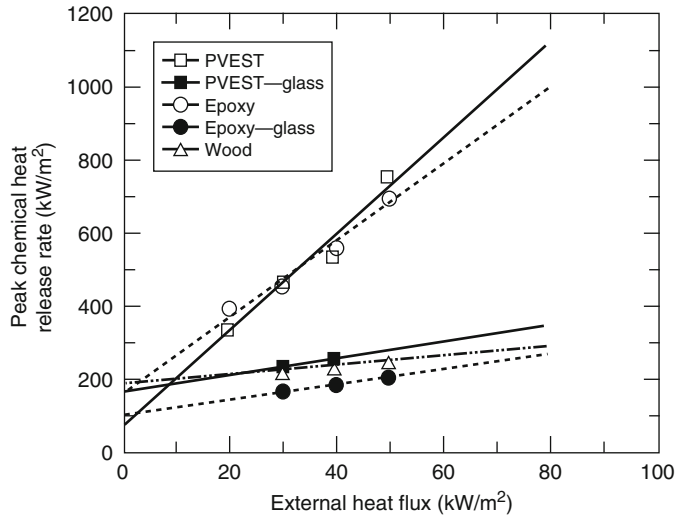

Fig. 36.32 Peak chemical heat release rate versus the external heat flux for a 100-mm × 100-mm × 3-mm to 11-mm-thick slab of polyvinyl ester (PVEST), PVEST/fiberglass, epoxy, epoxy/fiberglass, and wood (hemlock). Data measured in the cone calorimeter are shown [32]

the summation of the heat release rate and the external heat flux:

$$\overline{\mathrm{HRP}}_i = \frac{E_i}{A\int \dot{q}_e'' dt} = \frac{\sum_{n=t_{ig}}^{n=t_{ex}} \dot{Q}_i''(t_n)\Delta t_n}{\sum_{n=t_{ig}}^{n=t_{ex}} \dot{q}_e''(t_n)\Delta t_n} \qquad (36.35)$$

Incompleteness of Combustion In fires, combustion is never complete. Thus, the chemical heat release rate or the chemical heat of combustion are less than the heat release rate for complete combustion or the net heat of complete combustion, respectively. The ratio of the chemical heat release rate to the heat release rate for complete combustion or the ratio of the chemical heat of combustion to net heat of complete combustion is defined as combustion efficiency [13, 14, 28, 31, 44, 102]:

$$\chi_{\mathrm{ch}} = \frac{\dot{Q}_{\mathrm{ch}}''}{\dot{Q}_T''} = \frac{\dot{m}''\Delta H_{\mathrm{ch}}}{\dot{m}''\Delta H_T} = \frac{\Delta H_{\mathrm{ch}}}{\Delta H_T} \qquad (36.36)$$

where χ_{ch} is the combustion efficiency and $\dot{Q}_T''$ is the heat release rate for complete combustion (kW/m^2). The convective and radiative components of the combustion efficiency are defined in a similar fashion [13, 14, 28, 31, 44, 103]:

$$\chi_{con} = \frac{\dot{Q}_{con}''}{\dot{Q}_T''} = \frac{\dot{m}''\Delta H_{con}}{\dot{m}''\Delta H_T} = \frac{\Delta H_{con}}{\Delta H_T} \tag{36.37}$$

$$\chi_{rad} = \frac{\dot{Q}_{rad}''}{\dot{Q}_T''} = \frac{\dot{m}''\Delta H_{rad}}{\dot{m}''\Delta H_T} = \frac{\Delta H_{rad}}{\Delta H_T} \tag{36.38}$$

where χ_{con} is the convective component of the combustion efficiency and χ_{rad} is the radiative component of the combustion efficiency [25]. From the definitions,

$$\Delta H_{ch} = \Delta H_{con} + \Delta H_{rad} \tag{36.39}$$

$$\chi_{ch} = \chi_{con} + \chi_{rad} \tag{36.40}$$

The chemical, convective, and radiative heat release rates, heats of combustion, and combustion efficiencies depend on the chemical structures of the materials and fire ventilation. The distribution of the chemical heat into convective and radiative components changes with fire size. The larger the fire size, the larger the fraction of the chemical heat distributed into the radiative component.

Chemical, convective, and radiative heats of combustion and HRP values for several materials under well-ventilated fire conditions are listed in Tables A.38 and A.39, respectively. Comparisons between the limited data from the OSU apparatus, Fire Propagation Apparatus, and cone calorimeter are satisfactory. Data were taken from Refs. [32, 112–117].

Example 9 Heptane was burned in a 2-m-diameter pan, and measurements were made for the mass loss rate, mass generation rates of CO and CO_2, and mass consumption rate of O_2. The average values in g/m^2/s for the mass loss rate, mass generation rates of CO and CO_2, and mass consumption rate of O_2 were 66, 9, 181, and 216, respectively. For large-scale fires of heptane, the literature values are and $\chi_{ch} = 0.93$, $\chi_{con} = 0.59$, and $\chi_{rad} = 0.34$. The net heat of complete combustion for heptane reported in the literature is 44.6 kJ/g. Calculate the chemical heat release rate and show that it is consistent with the rate based on the literature value of the combustion efficiency. Also calculate the convective and radiative heat release rates.

Solution From Table A.38, for heptane, the net heat of complete combustion per unit mass of oxygen consumed is 12.7 kJ/g; the net heat of complete combustion per unit mass of CO_2 generated is 14.5 kJ/g; and the net heat of complete combustion per unit mass of CO generated is 12.8 kJ/g. From CDG calorimetry (Equation 36.22),

$$\dot{Q}_{ch}'' = \Delta H_{CO_2}^* \dot{G}_{CO_2}'' + \Delta H_{CO}^* \dot{G}_{CO}''$$

$$\dot{Q}_{ch}'' = \left(14.5\,\frac{kJ}{g}\right)\left(181\,\frac{g}{m^2 s}\right) + \left(12.8\,\frac{kJ}{g}\right)\left(9\,\frac{g}{m^2 s}\right)$$

$$\dot{Q}_{ch}'' = 2740\frac{kW}{m^2}$$

From OC calorimetry (Equation 36.25),

$$\dot{Q}_{ch}'' = \Delta H_O^* \dot{C}_O''$$

$$\dot{Q}_{ch}'' = \left(12.7\frac{kJ}{g}\right)\left(216\frac{g}{m^2 s}\right)$$

$$\dot{Q}_{ch}'' = 2743\frac{kW}{m^2}$$

The chemical heat release rate from the CDG and OC calorimetries are in excellent agreement, the average being 2742 kW/m^2.

The chemical heat of combustion can be obtained from Equation 36.36:

$$\chi_{ch} = \frac{\Delta H_{ch}}{\Delta H_T}$$

$$\Delta H_{ch} = \chi_{ch}\Delta H_T$$

$$\Delta H_{ch} = (0.93)\left(44.6\,\frac{kJ}{g}\right)$$

$$\Delta H_{ch} = 41.5\,\frac{kJ}{g}$$

The chemical heat release can now be obtained from the product of the mass loss rate

and chemical heat of combustion, as in Equation 36.32:

$$\dot{Q}''_{\text{ch}} = \Delta H_{\text{ch}} \dot{m}''$$
$$\dot{Q}''_{\text{ch}} = \left(41.5 \frac{\text{kJ}}{\text{g}}\right)\left(66 \frac{\text{g}}{\text{m}^2\text{s}}\right)$$
$$\dot{Q}''_{\text{ch}} = 2739 \frac{\text{kW}}{\text{m}^2}$$

Compare this result the averaged value 2742 kW/m^2 from the CDG and OC calorimetries. Thus, the chemical heat release determined from the measurements is consistent with the rate obtained from the literature values of the combustion efficiency.

Finally, the convective heat release rate can be computed much in the same manner as above. Here, for simplicity, Equations 36.32 and 36.36 are combined to yield the convective heat release rate:

$$\dot{Q}''_{\text{con}} = \chi_{\text{con}} \Delta H_T \dot{m}''$$
$$\dot{Q}''_{\text{con}} = (0.59)\left(44.6 \frac{\text{kJ}}{\text{g}}\right)\left(66 \frac{\text{g}}{\text{m}^2\text{s}}\right)$$
$$\dot{Q}''_{\text{con}} = 1737 \frac{\text{kW}}{\text{m}^2}$$

In a similar fashion, the radiative heat release rate is calculated to be 1001 kW/m^2.

Example 10 From the flame radiation scaling technique, the asymptotic mass loss rate values in g/m^2/s expected in large-scale fires, as listed in Table 36.7, for polyethylene, polystyrene, polyvinylchloride, and Teflon are 26, 36, 16, and 7, respectively. The chemical heats of combustion in kJ/g listed in Table A.38 for these materials are 38.4, 27.0, 5.7, and 4.1, respectively. Estimate the chemical heat release rates expected in large-scale fires of polyethylene, polystyrene, polyvinylchloride, and Teflon. (In this chapter Teflon refers mainly to FEP, except in cases where it is identified otherwise.)

Solution The chemical heat release rate is calculated from Equation 36.32. The chemical heat release rates estimated in the large-scale fires are (1) polyethylene: 26 × 38.4 = 998 kW/m^2; (2) polystyrene: 36 × 27.0 = 972 kW/m^2; (3) polyvinylchloride: 16 × 5.7 = 91 kW/m^2; and (4) Teflon: 7 × 4.1 = 28 kW/m^2.

Example 11 Heat release rate is the product of the HRP and the net heat flux absorbed by the material, as indicated in Equations 36.34 and 36.35. This concept is used in various models to predict fire propagation and heat release rates, whereas values for the HRP are taken from a handbook such as this handbook, and net heat flux is estimated through correlations. The lower the HRP value for a fixed value of net heat flux, the lower the heat release rate.

The values for the surface re-radiation, flame heat flux for large-scale fires, and chemical HRP are listed in Tables 36.6, 36.7, and 36.10, respectively. Calculate the chemical heat release rates expected in large-scale fires of heptane, kerosene, polyethylene, polypropylene, polystyrene, polymethylmethacrylate, polyvinylchloride, and Teflon.

Solution The chemical heat release rates are calculated from Equation 36.34:

$$\dot{Q}''_{\text{ch}} = \left(\frac{\Delta H_{\text{ch}}}{\Delta H_g}\right)\left(\dot{q}''_e + \dot{q}''_{fr} + \dot{q}''_{fc} - \dot{q}''_{rr}\right)$$

In this specific example, there is no external heat flux sources. Recognizing that $(\Delta H_{\text{ch}}/\Delta H_g) = \text{HRP}_{\text{ch}}$, and setting the asymptotic flame heat flux values from 7 to the relationship $\dot{q}''_{fr} + \dot{q}''_{fc}$ one obtains:

$$\dot{Q}''_{\text{ch}} = \text{HRP}_{\text{ch}}\left(\dot{q}''_{f,\text{asy}} - \dot{q}''_{rr}\right)$$

Therefore:

1. heptane: (75)(37 – 1) = 2700 kW/m^2
2. kerosene: (47)(29 – 1) = 1316 kW/m^2
3. polyethylene: (17)(61 – 15) = 782 kW/m^2
4. polypropylene: (19)(67 – 15) = 988 kW/m^2
5. polystyrene: (16)(75 – 13) = 992 kW/m^2
6. polymethylmethacrylate: (15)(57 – 11) = 690 kW/m^2
7. polyvinylchloride: (2)(50 – 15) = 70 kW/m^2
8. Teflon: (2)(52 – 38) = 28 kW/m^2

Table 36.10 Chemical and convective heat release parameters

Materials	$(HRP)_{ch}$			$(HRP)_{con}$		
	ASTM E2058 Fire Propagation Apparatus	ASTM E1354[a]	Cal[b]	ASTM E2058 Fire Propagation Apparatus	ASTM E906[c]	Cal[b]
Liquids and gases (hydrocarbons, alkanes)						
Hexane	–	–	83	–	–	56
Heptane	–	–	75	–	–	50
Octane	–	–	68	–	–	46
Nonane	–	–	64	–	–	42
Decane	–	–	59	–	–	39
Undecane	–	–	55	–	–	36
Dodecane	–	–	52	–	–	34
Tridecane	–	–	50	–	–	32
Kerosene	–	–	47	–	–	17
Hexadecane	–	–	44	–	–	28
Solids (abbreviations/names in the nomenclature)						
ABS	–	14	–	–	–	—
Acrylic sheet	–	6	–	–	–	–
Epoxy	–	11	–	–	–	–
IPST	–	6	–	–	–	–
Polyamide	21	–	–	–	–	–
Polypropylene	19	–	–	11	–	–
Polyethylene	17	21	–	12	–	–
Polystyrene	16	19	–	6	–	–
Polymethylmethacrylate	15	14	–	10	–	–
Nylon	12	–	–	7	–	–
Polyamide-6	–	21	–	–	–	–
Filled phenolic foam–50 % inert	–	1	–	–	–	–
Polycarbonate	9	–	–	–	–	–
Polyoxymethylene	6	–	–	5	–	–
Polyethylene/25 % CI	11	–	–	5	–	–
Plasticized-PVC-3, LOI 0.25	–	5	–	–	–	–
Plasticized-PVC-4, LOI 0.30	–	5	–	–	–	–
Plasticized-PVC-5, LOI 0.35	–	5	–	–	–	–
Polyethylene/35 % CI	4	–	–	2	–	–
Rigid PVC-1, LOI 0.50	–	3	–	–	–	–
Rigid PVC-2	2	3	–	1	–	–
PVC panel	2	–	–	–	–	–
Polyethylene/48 % CI	2	–	–	–	–	–
PVEST	–	13	–	–	–	–
ETFE (Tefzel)	6	–	–	–	–	–
PFA (Teflon)	5	–	–	–	–	–
FEP (Teflon)	2	–	–	–	–	–
TFE (Teflon)	2	–	–	–	–	–
Wood (hemlock)	–	1	–	–	–	–
Wood (Douglas fir)	7	–	–	5	–	–
Wool	–	5	–	–	–	–

(continued)

Table 36.10 (continued)

Materials	$(HRP)_{ch}$			$(HRP)_{con}$		
	ASTM E2058 Fire Propagation Apparatus	ASTM E1354[a]	Cal[b]	ASTM E2058 Fire Propagation Apparatus	ASTM E906[c]	Cal[b]
Composites and fiberglass-reinforced materials (FGR) (abbreviations/names in the nomenclature)						
Bismaleimide/graphite/ceramic (CC)	–	1	–	–	–	–
Epoxy/FGR	–	2	–	–	–	–
Epoxy/graphite	2	–	–	–	–	–
Epoxy/graphite/CC	2	–	–	–	–	–
Epoxy/graphite/intumescent (IC)	2	–	–	–	–	–
IPST/FGR	–	1	–	–	–	–
PEEK/FGR	–	3	–	–	–	–
PES/FGR	–	1	–	–	–	–
PEST-1/FGR	3	–	—	–	–	–
PEST-2/FGR	8	–	–	–	–	–
PEST-3/FGR	10	–	–	–	–	–
PEST-4/FGR	3	–	–	–	–	–
PEST-5/FGR	3	–	–	–	–	–
PEST-6-FGR	3	–	–	–	–	–
Phenol/FGR	–	1	–	–	–	–
Phenolic/Kevlar	2	–	–	–	–	–
Phenol/graphite	1	–	–	–	–	–
PVEST-1/FGR	3	–	–	–	–	–
PVEST-1/FGR/CC	3	–	–	–	–	–
PVEST-1/FGR/IC	1	–	–	–	–	–
PVEST-2/FGR	7	–	–	–	–	–
PVEST-3/FGR	2	–	–	–	–	–
Aircraft panel materials						
Epoxy fiberglass	4	4	–	2	1	–
Epoxy Kevlar	4	4	–	2	2	–
Phenolic Kevlar	5	4	–	2	–	–
Phenolic graphite	4	3	–	1	–	–
Phenolic fiberglass	4	3	–	2	1	–
Polycarbonate panel	9	–	–	–	–	–
Foams						
Polystyrene						
GM53	20	–	–	6	–	–
GM49	19	–	–	8	–	–
GM51	18	–	–	9	–	–
Flexible polyurethane						
GM 21	7	–	–	3	3	–
GM 23	9	–	–	5	6	–
GM 25	14	–	–	6	4	–
GM 27	9	–	–	4	2	–
Phenolic	–	1	–	–	–	–
Electrical cables (abbreviations/names in the nomenclature)						
PVC/PVC-1 (Group 3)	15	–	–	–	–	–
PE/PVC (Group 3)	19	–	–	–	–	–

(continued)

Table 36.10 (continued)

Materials	$(HRP)_{ch}$			$(HRP)_{con}$		
	ASTM E2058 Fire Propagation Apparatus	ASTM E1354[a]	Cal[b]	ASTM E2058 Fire Propagation Apparatus	ASTM E906[c]	Cal[b]
PP, PEST/PVC (Group 3)	11	–	–	–	–	–
PVC/PVC-2 (Group 3)	14	–	–	–	–	–
Chlorinated PE (Group 2)	5	–	–	–	–	–
PVC/PVC-3 (Group 2)	4	–	–	–	–	–
EPR/PVC (Group 2)	6	–	–	–	–	–
PVC/EPR (Group 2)	4	–	–	–	–	–
XLPE/XLPE (Group 2)	6	–	–	–	–	–
EPR/hypalon-1 (Group 2)	6	–	–	–	–	–
EPR/hypalon-2 (Group 2)	4	–	–	–	–	–
EPR/hypalon-3 (Group 1)	3	–	–	–	–	–
EPR/hypalon-4 (Group 1)	3	–	–	–	–	–
EPR/EPR-1 (Group 1)	3	–	–	–	–	–
EPR/EPR-2 (Group 1)	3	–	–	–	–	–
EPR/EPR-3 (Group 1)	2	–	–	–	–	–
XLPE-EVA-1 (Group 1)	3	–	–	–	–	–
XLPE-EVA-2 (Group 1)	3	–	–	–	–	–
ETFA (Group 1)	3	–	–	–	–	–
PVC/PVF_2 (Group 1)	1	–	–	–	–	–
FEP/FEP-1 (Group 1)	2	–	–	–	–	–
FEP/FEP-2 (Group 2)	2	–	–	–	–	–

[a]Calculated from the data reported in Refs. [32, 113]
[b]Calculated from the data in Refs. [112, 114]
[c]From Ref. [115]

The example shows the importance of the chemical HRP, flame heat flux, and surface re-radiation.

Heat Release Rate and Fire Ventilation For the most part, fire hazards are due to fires occurring in enclosed spaces. In early stages, a building fire is well ventilated and is easy to control and extinguish. However, if the fire is allowed to grow, especially with limited enclosure ventilation and large material surface area, it becomes a ventilation-controlled fire and can lead to flashover, a very dangerous condition. In ventilation-controlled fires, the chemical reactions between oxygen from air and products of incomplete combustion from the decomposed and gasified material (e.g., smoke, CO, hydrocarbons, and other intermediate products) remain incomplete and heat release rate decreases [103].

In ventilation-controlled fires, heat release rate depends on the air supply rate and the mass loss rate, in addition to other factors. For ventilation-controlled fires, the effects of mass flow rate of air and fuel mass loss rate are characterized, most commonly, by the local equivalence ratio:

$$\Phi = \frac{S\dot{m}'' A}{\dot{m}_{\text{air}}} \tag{36.41}$$

where
Φ = Equivalence ratio
S = Stoichiometric air-to-fuel mass ratio (g/g)
$\dot{m}''$ = Mass loss rate ($g/m^2 \cdot s$)
A = Exposed area of the burning material (m^2)
$\dot{m}_{\text{air}}$ = Mass flow rate of air (g/s)

Generalized-state relationships between mass fractions of major species (O_2, fuel, CO_2, H_2O, CO, and H_2) and temperature as functions of local equivalence ratios for hydrocarbon-air diffusion flames are available [118]. The relationships suggest that the generation

efficiencies of CO, fuel vapors, water, CO_2, and H and the consumption efficiency of O_2 are in approximate thermodynamic equilibrium for well-ventilated combustion but deviate from equilibrium for ventilation-controlled combustion. This concept has been used for fires of polymeric materials [103]. In the tests, chemical and convective heat release rates, mass loss rate, and generation rates of fire products were measured for various equivalence ratios in the Fire Propagation Apparatus (Fig. 36.2) and in the Fire Research Institute's (FRI) 0.022 m^3 enclosure in Tokyo, Japan [103]. The combustion efficiency and its convective component were found to decrease as fires become fuel rich, due to an increase in the equivalence ratio. The ratio of the combustion efficiency and its convective component or chemical and convective heats of combustion for ventilation-controlled to well-ventilated combustion is expressed as [103]

$$\zeta_{\mathrm{ch}} = \frac{(\chi_{\mathrm{ch}})_{vc}}{(\chi_{\mathrm{ch}})_{wv}} = \frac{(\Delta H_{\mathrm{ch}}/\Delta H_T)_{vc}}{(\Delta H_{\mathrm{ch}}/\Delta H_T)_{wv}} = \frac{(\Delta H_{\mathrm{ch}})_{vc}}{(\Delta H_{\mathrm{ch}})_{wv}} \tag{36.42}$$

$$\zeta_{\mathrm{con}} = \frac{(\chi_{\mathrm{con}})_{vc}}{(\chi_{\mathrm{con}})_{wv}} = \frac{(\Delta H_{\mathrm{con}}/\Delta H_T)_{vc}}{(\Delta H_{\mathrm{con}}/\Delta H_T)_{wv}} = \frac{(\Delta H_{\mathrm{con}})_{vc}}{(\Delta H_{\mathrm{con}})_{wv}} \tag{36.43}$$

where ζ_{ch} is the ratio of the combustion efficiency for ventilation-controlled (vc) combustion to that for well-ventilated (wv) combustion; similarly, ζ_{con} is the ratio of the convective component of the combustion efficiency for ventilation-controlled combustion to that for well-ventilated combustion. These ratios can be represented by the ratio of the chemical or convective heats of combustion for ventilation-controlled to well-ventilated combustion.

The experimental data for the ratios of the chemical and convective heats of combustion for ventilation-controlled to well-ventilated fires at various equivalence ratios are shown in Figs. 36.33 and 36.34. The data and measurement details are described in Ref. [103]. The data for the polymers indicated in the figures satisfy the following general empirical correlations, regardless of their chemical structures:

$$\frac{(\Delta H_{\mathrm{ch}})_{vc}}{(\Delta H_{\mathrm{ch}})_{wv}} = 1 - \frac{0.97}{\exp\left[\left(\frac{\Phi}{2.15}\right)^{-1.2}\right]} \tag{36.44}$$

$$\frac{(\Delta H_{\mathrm{con}})_{vc}}{(\Delta H_{\mathrm{con}})_{wv}} = 1 - \frac{1.0}{\exp\left[\left(\frac{\Phi}{1.38}\right)^{-2.8}\right]} \tag{36.45}$$

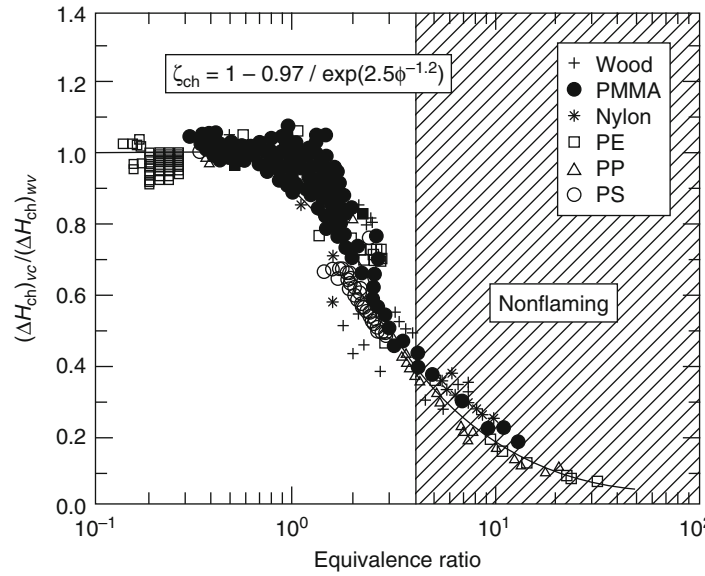

Fig. 36.33 Ratio of ventilation-controlled to well-ventilated chemical heat of combustion versus equivalence ratio (Data are taken from Ref. [103]). Subscript vc represents ventilation-controlled fires, and subscript wv represents well-ventilated fires

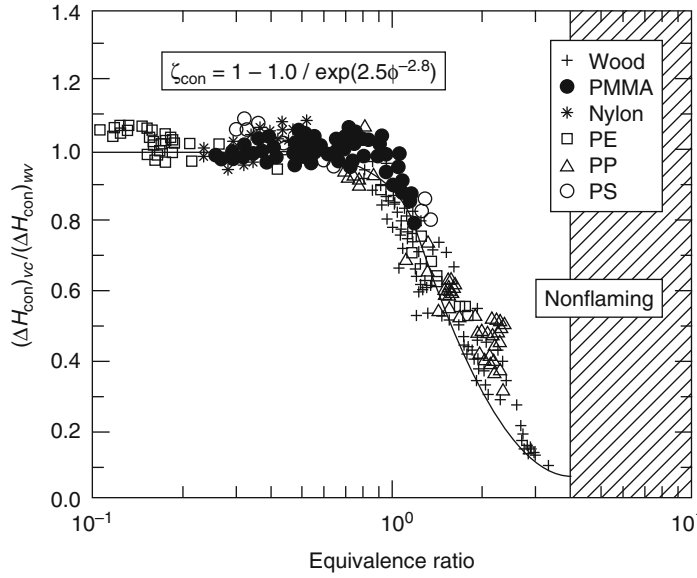

Fig. 36.34 Ratio of the ventilation-controlled to well-ventilated convective heat of combustion versus the equivalence ratio (Data are taken from Ref. [103]). Subscript *vc* represents ventilation-controlled fires, and subscript *wv* represents well-ventilated fires

The effects of ventilation on the chemical and convective heats of combustion are reflected by the magnitudes of the expressions within the parentheses on the right-hand sides of Equations 36.44 and 36.45. For a well-ventilated fire, $\Phi \ll 1.0$, $(\Delta H_{ch})_{vc} = (\Delta H_{ch})_{wv}$, and $(\Delta H_{con})_{vc} = (\Delta H_{con})_{wv}$.

As a fire changes from well ventilated to ventilation controlled, the equivalence ratio increases and the magnitudes of the expressions within the parentheses on the right-hand sides of Equations 36.44 and 36.45 increase. Thus, with increasing equivalence ratio, the chemical and convective heats of combustion decrease. The decrease in the convective heat of combustion is higher than that for the chemical heat of combustion because the coefficients for the equivalence ratios are different. The correlation suggests that a higher fraction of the chemical heat of combustion is expected to be converted to the radiative heat of combustion as fires change from well ventilated to ventilation controlled. This is in general agreement with observations for ventilation-controlled fires in buildings.

Equations 36.44 and 36.45 can be used in models for the assessment of the ventilation-controlled fire behavior of materials, using chemical and convective heats of combustion for well-ventilated fires such as from Table A.39.

Example 12 Calculate the chemical heats of combustion at equivalence ratios of 1, 2, and 3 for red oak, polyethylene, polystyrene, and nylon using Equation 36.44 and data from Table A.39 for well-ventilated fires.

Solution

	Chemical heats of combustion (kJ/g)			
Material	$\Phi \ll 1.0$	$\Phi = 1.0$	$\Phi = 2.0$	$\Phi = 3.0$
Red oak	12.4	11.4	8.3	6.2
Polyethylene	38.4	35.3	25.9	19.3
Polystyrene	27.0	24.9	18.2	13.6
Nylon	27.1	24.9	18.2	13.6

Generation of Fire Products and Smoke Yields

Chemical compounds (smoke, toxic, corrosive, and odorous compounds) are the main contributors to nonthermal hazards and, thus, the assessments of their chemical natures and generation rates are of critical importance for the protection of life and property.

In fires, compounds are generated as a result of gasification and decomposition of materials involved in the fire and burning of the species in the gas phase with air in the form of a diffusion flame. In general, generation of fire products and

consumption of oxygen in diffusion flames occur in two zones [103].

1. *Reduction zone*. In this zone, the material melts, decomposes, gasifies, and/or generates species that react to form smoke, CO, hydrocarbons, and other intermediate products. Very little oxygen is consumed in this region. The extent of conversion of the material to smoke, CO, hydrocarbons, and other products depends on the chemical nature of the material.
2. *Oxidation zone*. In this zone, the reduction zone products (smoke, CO, hydrocarbons, and other intermediates) react with varying degrees of efficiency with the oxygen from air and generate chemical heat and varying amounts of products of complete combustion, such as CO_2 and H_2O. The lower the reaction efficiency, the higher the amounts of reduction zone products emitted from a fire. The reaction efficiency of the reduction zone products with oxygen depends on the concentrations of the products relative to the oxygen concentration, temperature, and mixing of the products and air. For example, in laminar diffusion flames, smoke is emitted when the temperature of the oxidation zone falls below about 1300 K.

The hot ceiling layer in a building fire may be considered in terms of oxidation and reduction zone products. In building fires with plenty of ventilation, the concentrations of the reduction zone products are higher in the central region of the ceiling layer, whereas the concentrations of the oxidation zone products are higher closer to the room opening. As the air supply rate, or oxygen concentration available to the fire, decreases due to restrictions in the ventilation, the ceiling layer expands and starts occupying a greater room volume accompanied with an increase in the concentrations of reduction zone products. Under these conditions, large amounts of reduction zone products are released within the building increasing the nonthermal hazard.

The generation rate of a fire product is directly proportional to the mass loss rate, the proportionality constant being defined as the yield of the product (e.g., [9, 112]):

$$\dot{G}_j'' = y_j \dot{m}'' \tag{36.46}$$

where $\dot{G}_j''$ is the mass generation rate of product j (g/m^2/s), and y_j is the yield of product j (g/g). The total mass of the product generated is obtained by the summation of the generation rate:

$$W_j = A \sum_{n=t_0}^{n=t_f} \dot{G}_j''(t_n) \Delta t_n \tag{36.47}$$

where

W_j = Total mass of product j generated from the flaming and/or nonflaming processes involving the material (g)

t_0 = Time when the sample is exposed to heat(s)

t_f = Time when there is no more product formation

From Equations 36.31, 36.46, and 36.47, the average value of the yield of product j is

$$\overline{y}_j = \frac{W_j}{W_f} \tag{36.48}$$

Similarly, the mass consumption rate of oxygen is also directly proportional to the mass loss rate (e.g., [9, 112]):

$$\dot{C}_{\mathrm{O}}'' = c_{\mathrm{O}} \dot{m}'' \tag{36.49}$$

Where $\dot{C}_{\mathrm{O}}''$ is the mass consumption rate of oxygen (g/m^2/s), and c_{O} is the mass of oxygen consumed per unit mass of fuel (g/g).

In the bench-scale apparatuses described in this chapter, the mass generation rates of fire products and mass consumption rate of oxygen are determined by measuring the volume fractions of the products and oxygen and the total volumetric or mass flow rate of the fire products-air mixture (e.g., [10, 11, 28, 31]):

$$\dot{G}_j'' = \frac{f_j \dot{V} \rho_j}{A} = f_j \dot{W} \left(\frac{\rho_j}{\rho_g A} \right) \tag{36.50}$$

$$\dot{C}_{\mathrm{O}}'' = \frac{f_{\mathrm{O}} \dot{V} \rho_{\mathrm{O}}}{A} = f_{\mathrm{O}} \dot{W} \left(\frac{\rho_{\mathrm{O}}}{\rho_g A} \right) \tag{36.51}$$

where

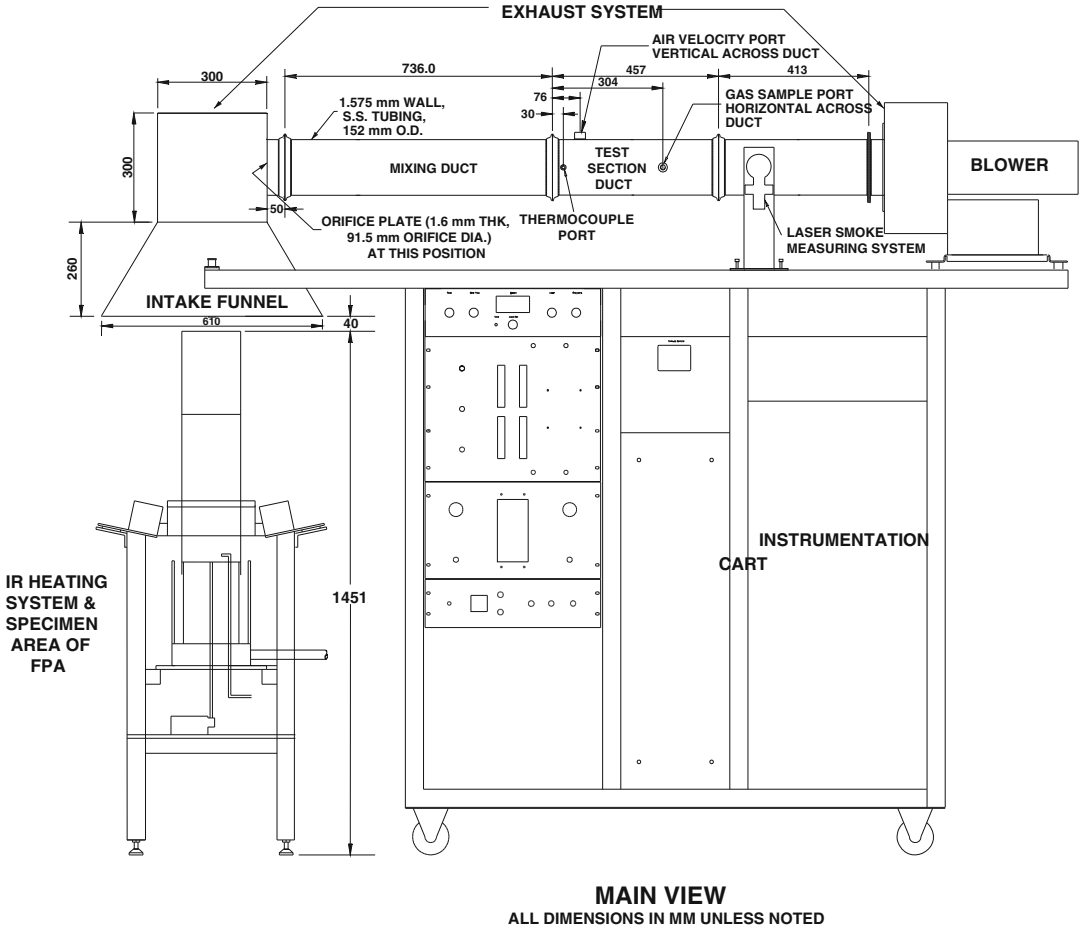

Fig. 36.35 Schematic of the commercial version [119] of the Fire Propagation Apparatus showing locations where measurements are made for product concentration, optical transmission, particulate concentration, and corrosion

f_j = Volume fraction of product j
f_O = Volume fraction of oxygen
$\dot{V}$ = Total volumetric flow rate of the fire product-air mixture (m^3/s)
$\dot{W}$ = Total mass flow rate of the fire product-air mixture (g/s)
ρ_j = Density of product j at the temperature of the fire product-air mixture (g/m^3)
ρ_g = Density of the hot fire product-air mixture (g/m^3)
ρ_O = Density of oxygen at the temperature of the fire product-air mixture (g/m^3)
A = Total area of the material burning (m^2)

For volume fraction measurements, sampling ducts are used where fire products and air are well mixed, such as in the Fire Propagation Apparatuses (Figs. 36.2, 36.3, and 36.35) and in the cone calorimeter (Fig. 36.4). Figure 36.35 shows the measurement locations in the sampling duct of a commercial version [119] of the Fire Propagation Apparatus. The volume fractions are measured by various types of instruments; for example, in the Fire Propagation Apparatus, they are measured continuously by (1) commercial non-dispersive infrared analyzers for CO and CO_2; (2) a high-sensitivity commercial paramagnetic analyzer for oxygen; (3) a commercial flame ionization analyzer for the mixture of low molecular weight gaseous hydrocarbons; and (4) by a laser (wavelength: 0.6328 μm) smoke measuring system.

The optical density at the measurement location in the sampling duct is determined from the following equation:

$$D = \frac{\ln(I_0/I)}{l} \tag{36.52}$$

where, D is the optical density (m^{-1}) at a laser wavelength of 0.6328 μm; I/I_0 is the fraction of monochromatic light transmitted through smoke; and l is the optical path length (m). The volume fraction of smoke f_s is obtained from the following expression [120]:

$$f_s = \frac{D\lambda \times 10^{-6}}{\Omega} \tag{36.53}$$

where, λ is the wavelength of the light source (μm) and Ω is the coefficient of smoke extinction taken as 7 [120]. The mass generation rate ($kg/m^2/s$) of smoke is given by:

$$\dot{G}_s'' = \frac{f_s \dot{V} \rho_s}{A} = \left(\frac{D\lambda \times 10^{-6}}{7}\right)\left(\frac{\rho_s \dot{V}}{A}\right) \tag{36.54}$$

Incorporating the value of smoke density, $\rho_s = 1.1 \times 10^6$ g/m^3, as determined in Ref. [120] and the laser wavelength of 0.6328 μm in Equation 36.54 then gives the following result:

$$\dot{G}_s'' = 9.944 \times 10^{-2}\left(\frac{D\dot{V}}{A}\right) \tag{36.55}$$

Equation 36.55 can then be used along with Equations 36.31, 36.47, and 36.48 to calculate the average smoke yield, $\overline{y}_s$, for a given material. The average value of smoke yield, can also be obtained from the average mass-specific extinction area [24, 121], $\overline{\tau}$ (m^2/g), at the same laser wavelength of 0.6328 μm:

$$\overline{\tau} = \frac{1}{W_f}\int \dot{V} D dt = \frac{1}{W_f}\sum_{n=t_0}^{n=t_f} \dot{V}(t_n) D(t_n) \Delta t_n \tag{36.56}$$

The average smoke yield is, in this case, calculated from the following expression:

$$\overline{y}_s = 9.944 \times 10^{-2}\overline{\tau} \tag{36.57}$$

The average data for the yields of CO, CO_2, mixture of gaseous hydrocarbons, and smoke for well-ventilated fires are listed in Table A.39.

Example 13 For a fiberglass-reinforced material, the following data were measured for combustion in normal air at an external heat flux value of 50 kW/m^2:

Total mass of the sample lost (g)	229
Total mass generated (g)	
CO	0.478
CO_2	290
Hydrocarbons	0.378
Smoke	6.31
Total energy generated (kJ)	3221

Calculate the average yields of CO, CO_2, hydrocarbons, and smoke and the average chemical heat of combustion.

Solution The average yields are calculated from Equation 36.48, and the average chemical heats of combustion are calculated from Equation 36.33.

Average yields (g/g)	
CO	0.0021
CO_2	1.27
Hydrocarbons	0.002
Smoke	0.028
Average chemical heats of combustion (kJ/g)	14.1

Example 14 A circular sample of polystyrene, about 0.007 m^2 in area and 25 mm in thickness, was burned in normal air in the presence of external heat flux. In the test, measurements were made for the mass loss rate and light obscuration by smoke in the sampling duct with an optical path length of 0.149 m. The total volumetric flow rate of the mixture of fire products and air through the sampling duct was 0.311 m^3/s, and the wavelength of light source used was 0.6328 μm. At the steady-state combustion of polystyrene, the measured mass loss rate was 33 $g/m^2/s$ with smoke obscuring 83.5 % of the light. Calculate the yield of smoke from the data using a value of 1.1×10^6 g/m^3 for the density of smoke.

Solution The optical density from Equation 36.52 is

$$D = \frac{\ln(I_0/I)}{l} = \frac{\ln(1/0.835)}{0.149} = 1.21 \ \text{m}^{-1}$$

The smoke generation rate from Equation 36.55 is

$$\dot{G}_s'' = 9.944 \times 10^{-2} \frac{\text{g}}{\text{m}^2} \left(\frac{D\dot{V}}{A}\right)$$

$$\dot{G}_s'' = 9.944 \times 10^{-2} \frac{\text{g}}{\text{m}^2} \left[\frac{\left(1.21 \frac{1}{\text{m}}\right)\left(0.311 \frac{\text{m}^3}{\text{s}}\right)}{0.007 \ \text{m}^2}\right]$$

$$\dot{G}_s'' = 5.35 \frac{\text{g}}{\text{m}^2\text{s}}$$

The smoke yield from Equation 36.46 is

$$\dot{G}_s'' = y_s \dot{m}''$$

$$y_s = \frac{\dot{G}_s''}{\dot{m}''} = \frac{5.35 \frac{\text{g}}{\text{m}^2\text{s}}}{33 \frac{\text{g}}{\text{m}^2\text{s}}}$$

$$y_s = 0.162$$

Efficiencies of Oxygen Mass Consumption and Mass Generation of Products

A chemical reaction between oxygen (air) and a fuel monomer of a material can be expressed as

$$F + \nu_O O_2 + \nu_N N_2 = \nu_N N_2 + \sum_i \nu_{j_i} J_i \tag{36.58}$$

where

F = Fuel monomer of a material

ν_O = Stoichiometric coefficient for oxygen

ν_N = Stoichiometric coefficient for nitrogen

ν_{j_i} = Stoichiometric coefficients for the maximum possible conversion of the fuel monomer to products J_i

The stoichiometric mass oxygen-to-fuel ratio for the maximum possible conversion of the fuel monomer is expressed as

$$\Psi_O = \frac{\nu_O M_O}{M_f} \tag{36.59}$$

where

Ψ_O = Stoichiometric oxygen-to-fuel mass ratio for the maximum possible conversion of the fuel monomer to products

M_O = Molecular weight of oxygen (32 g/mol)

M_f = Molecular weight of the fuel monomer of the material (g/mol)

M_f is calculated from its elemental composition which may be determined from microanalytical techniques.

The stoichiometric yield for the maximum possible conversion of the fuel monomer of the material to a product is expressed as

$$\Psi_j = \frac{\nu_j M_j}{M_f} \tag{36.60}$$

where Ψ_j is the stoichiometric yield for the maximum possible conversion of the fuel monomer of the material to product j, and M_j is the molecular weight of product (g/mol).

The stoichiometric yields for some selected materials, calculated from the elemental composition data from the flammability laboratory, are listed in Table 36.11 for fuel monomer conversion to CO, CO_2, hydrocarbons, smoke, HCl, and HF. The yields provide an insight into the nature of products and the amounts of products expected to be generated in flaming and nonflaming processes, when expressed as the stoichiometric oxygen mass consumption rate and stoichiometric mass generation rates of products:

$$\dot{C}_{\text{stoich,O}}'' = \Psi_O \dot{m}'' \tag{36.61}$$

$$\dot{G}_{\text{stoich},j}'' = \Psi_j \dot{m}'' \tag{36.62}$$

where $\dot{C}_{\text{stoich,O}}''$ and $\dot{G}_{\text{stoich},j}''$ are the stoichiometric oxygen mass consumption rate and stoichiometric mass generation rate of product j for the maximum possible conversion of the fuel monomer to the product, respectively (g/m^2/s).

In fires, due to incompleteness of combustion as discussed above, the actual oxygen mass consumption rate and the mass generation rates of products may be significantly less than the stoichiometric rates. The ratio of the actual oxygen mass consumption rate to stoichiometric rates is

Table 36.11 Stoichiometric yields of major products[a]

Material	Formula	Ψ_O	Ψ_{CO_2}	Ψ_{CO}	Ψ_s	Ψ_{hc}	Ψ_{HCI}	Ψ_{HF}
Carbon-hydrogen atoms in the structure								
PE	CH_2	3.43	3.14	2.00	0.857	1.00	0	0
PP	CH_2	3.43	3.14	2.00	0.857	1.00	0	0
PS	CH	3.08	3.38	2.15	0.923	1.00	0	0
Expanded polystyrene								
GM47	$CH_{1\cdot1}$	3.10	3.36	2.14	0.916	1.00	0	0
GM49	$CH_{1.1}$	3.10	3.36	2.14	0.916	1.00	0	0
GM51	CH	3.08	3.38	2.15	0.923	1.00	0	0
GM53	$CH_{1.1}$	3.10	3.36	2.14	0.916	1.00	0	0
Carbon-hydrogen-oxygen-nitrogen atoms in the structure								
POM	CH_2O	1.07	1.47	0.933	0.400	0.467	0	0
PMMA	$CH_{1.6}O_{0.40}$	1.92	2.20	1.40	0.600	0.680	0	0
Nylon	$CH_{1.8}O_{0.17}\ N_{0.17}$	2.61	2.32	1.48	0.634	0.731	0	0
Wood (pine)	$CH_{1.7}O_{0.83}$	1.21	1.67	1.06	0.444	0.506	0	0
Wood (oak)	$CH_{1.7}O_{0.72}\ N_{0.001}$	1.35	1.74	1.11	0.476	0.543	0	0
Wood (Douglas fir)	$CH_{1.7}O_{0.74}\ N_{0.002}$	1.32	1.72	1.10	0.469	0.536	0	0
Polyester	$CH_{1.4}O_{0.22}$	2.35	2.60	1.65	0.709	0.792	0	0
Epoxy	$CH_{1.3}O_{0.20}$	2.38	2.67	1.70	0.727	0.806	0	0
Polycarbonate	$CH_{0.88}O_{0.19}$	2.26	2.76	1.76	0.754	0.872	0	0
PET	$CH_{0.80}O_{0.40}$	1.67	2.29	1.46	0.625	0.667	0	0
Phenolic foam	$CH_{1.1}O_{0.24}$	2.18	2.60	1.65	0.708	0.773	0	0
PAN	$CHN_{0.33}$	2.87	2.50	1.59	0.681	0.681	0	0
Flexible polyurethane foams								
GM21	$CH_{1.8}O_{0.30}\ N_{0.05}$	2.24	2.28	1.45	0.622	0.715	0	0
GM23	$CH_{1.8}O_{0.35}\ N_{0.06}$	2.11	2.17	1.38	0.593	0.682	0	0
GM25	$CH_{1.7}O_{0.32}\ N_{0.07}$	2.16	2.22	1.41	0.606	0.692	0	0
GM27	$CH_{1.7}O_{0.30}\ N_{0.08}$	2.21	2.24	1.43	0.612	0.698	0	0
Rigid polyurethane foams								
GM29	$CH_{1.1}O_{0.23}\ N_{0.10}$	2.22	2.42	1.54	0.660	0.721	0	0
GM31	$CH_{1.2}O_{0.22}\ N_{0.10}$	2.28	2.43	1.55	0.662	0.729	0	0
GM37	$CH_{1.2}O_{0.20}\ N_{0.08}$	2.34	2.51	1.60	0.685	0.753	0	0
Rigid polyisocyanurate foams								
GM41	$CH_{1.0}O_{0.19}\ N_{0.11}$	2.30	2.50	1.59	0.683	0.740	0	0
GM43	$CH_{0.93}O_{0.20}\ N_{0.11}$	2.25	2.49	1.58	0.679	0.732	0	0
Carbon-hydrogen-oxygen-silicone atoms in the structure								
Silicone-1[b]	$CH_{1.3}O_{0.25}Si_{0.18}$	1.98	1.97	1.25	0.537	0.595	0	0
Silicone-2[c]	$CH_{1.5}O_{0.30}Si_{0.26}$	1.86	1.72	1.09	0.469	0.528	0	0
Silicone-3[d]	$CH_3O_{0.50}Si_{0.50}$	1.73	1.19	0.757	0.324	0.405	0	0
Carbon-hydrogen-oxygen-chlorine-fluorine atoms in the structure								
Fluoropolymers								
PVF (Tedlar)	$CH_{1.5}\ F_{0.50}$	1.74	1.91	1.22	0.522	0.587	0	0.435
PVF2 (Kynar)	CHF	1.00	1.38	0.875	0.375	0.406	0	0.594
ETFE (Tefzel)	$CH_{1.0}\ F_{0.99}$	1.01	1.38	0.880	0.377	0.409	0	0.622
E-CTFE (Halar)	$CHF_{0.75}CI_{0.25}$	0.889	1.22	0.778	0.333	0.361	0.257	0.417
PFA (Teflon)	$CF_{1.7}O_{0.01}$	0.716	1.00	0.630	0.270	0	0	0.765
FEP (Teflon)	$CF_{1.8}$	0.693	0.952	0.606	0.260	0	0	0.779
TFE (Teflon)	CF_2	0.640	0.880	0.560	0.240	0	0	0.800
CTFE (Kel-F)	$CF_{1.5}CI_{0.50}$	0.552	0.759	0.483	0.207	0	0.310	0.517

(continued)

Table 36.11 (continued)

Material	Formula	Ψ_O	Ψ_{CO_2}	Ψ_{CO}	Ψ_s	Ψ_{hc}	Ψ_{HCl}	Ψ_{HF}
Chloropolymers								
PE-25 % Cl	$CH_{1.9}Cl_{0.13}$	2.56	2.38	1.52	0.650	0.753	0.254	0
PE-36 % Cl	$CH_{1.8}Cl_{0.22}$	2.16	2.05	1.30	0.558	0.642	0.368	0
Neoprene	$CH_{1.25}Cl_{0.25}$	1.91	2.00	1.27	0.546	0.602	0.409	0
PE-42 % Cl	$CH_{1.8}Cl_{0.29}$	1.94	1.84	1.17	0.501	0.576	0.424	0
PE-48 % Cl	$CH_{1.7}Cl_{0.36}$	1.73	1.67	1.06	0.456	0.521	0.493	0
PVC	$CH_{1.5}Cl_{0.50}$	1.42	1.42	0.903	0.387	0.436	0.581	0
$PVCl_2$	CHCl	0.833	0.917	0.583	0.250	0.271	0.750	0

[a]Calculated from the data for the elemental compositions of the materials; subscript hc is total gaseous hydrocarbons; s is soot
[b]$\eta SiO_2 = 0.483$
[c]$\eta SiO_2 = 0.610$
[d]$\eta SiO_2 = 0.811$

thus defined as the efficiency of oxygen mass consumption or product mass generation (e.g., [103]):

$$\eta_O = \frac{\dot{C}''_{\text{actual,O}}}{\dot{C}''_{\text{stoich,O}}} = \frac{c_O \dot{m}''}{\Psi_O \dot{m}''} = \frac{c_O}{\Psi_O} \tag{36.63}$$

$$\eta_j = \frac{\dot{C}''_{\text{actual},j}}{\dot{C}''_{\text{stoich},j}} = \frac{y_j \dot{m}''}{\Psi_j \dot{m}''} = \frac{y_j}{\Psi_j} \tag{36.64}$$

Where η_O is the efficiency of oxygen mass consumption and η_j is the generation efficiency of product j.

Example 15 A material is made up of carbon, hydrogen, and oxygen. The weight of the material is distributed as follows: 54 % as carbon, 6 % as hydrogen, and 40 % as oxygen. Calculate the chemical formula of the fuel monomer of the material.

Solution From the atomic weights and the weight percent of the atoms, the numbers of atoms are as follows: carbon (C): 54/12 = 4.5; hydrogen (H): 6/1 = 6.0; and oxygen (O): 40/16 = 2.5. Thus, the chemical formula of the fuel monomer of the material is $C_{4.5}H_{6.0}O_{2.5}$ or, dividing by 4.5, $CH_{1.33}O_{0.56}$.

Example 16 For the material in Example 15, calculate the stoichiometric oxygen-to-fuel mass ratio, stoichiometric air-to-fuel mass ratio, and stoichiometric yields for maximum possible conversion of the fuel monomer of the material to CO, CO_2, hydrocarbons, water, and smoke. Assume smoke to be pure carbon, and hydrocarbons as having the same carbon-atom-to-hydrogen-atom ratio as the original fuel monomer.

Solution

1. For stoichiometric yields of CO_2 and water and the stoichiometric oxygen- and air-to-fuel mass ratio for the maximum possible conversion of the fuel monomer of the material to CO_2 and H_2O, the following expression is used:

$$CH_{1.33}O_{0.56} + 1.06\,O_2 = CO_2 + 0.67\,H_2O$$

The molecular weight of the fuel monomer of the material is $1 \times 12 + 1.33 \times 1 + 0.56 \times 16 = 22.3$ g/mol, the molecular weight of oxygen is 32 g/mol, the molecular weight of CO_2 is 44 g/mol, and the molecular weight of H_2O is 18 g/mol. Thus, from Equation 36.59:

$$\Psi_{CO_2} = \frac{44}{22.3} = 1.97$$

$$\Psi_{H_2O} = \frac{0.67 \times 18}{22.3} = 0.54$$

$$\Psi_O = \frac{1.06 \times 32}{22.3} = 1.52$$

The stoichiometric air-to-fuel mass ratio can be obtained by dividing Ψ_O by 0.233 (i.e., the

mass fraction of oxygen in air); that is, 1.52/0.233 = 6.52.

2. For stoichiometric yields of CO, hydrocarbons, and smoke for the maximum possible conversion of the fuel monomer of the material to these products, different chemical reactions have to be written, as follows:
For CO,

$$CH_{1.33}O_{0.56} + zO_2 = CO + x(HO)$$
$$\Psi_{CO} = 28/22.3 = 1.26$$

For hydrocarbons (same H/C ratio as fuel monomer),

$$CH_{1.33}O_{0.56} + zO_2 = CH_{1.33} + x(HO)$$
$$\Psi_{hc} = 13.3/22.3 = 0.60$$

For smoke (i.e., pure carbon),

$$CH_{1.33}O_{0.56} + zO_2 = C + x(HO)$$
$$\Psi_s = 12/22.3 = 0.54$$

Example 17 For the material in Examples 15 and 16, the generation efficiencies of CO_2, CO, hydrocarbons, and smoke are 0.90, 0.004, 0.002, and 0.036, respectively. The heat of gasification is 1.63 kJ/g, the surface re-radiation loss is 11 kW/m^2, and the predicted asymptotic flame heat flux value for large-scale fires is 60 kW/m^2. Calculate the yields and asymptotic values for the generation rates of CO_2, CO, hydrocarbons, and smoke expected in large-scale fires.

Solution

1. Yields from Equations 36.63 and 36.64 and data from Example 16:

$$y_{CO_2} = \eta_{CO_2}\Psi_{CO_2} = 0.90 \times 1.97 = 1.77 \ \text{g/g}$$
$$y_{CO} = \eta_{CO}\Psi_{CO} = 0.004 \times 1.26 = 0.005 \ \text{g/g}$$
$$y_{hc} = \eta_{hc}\Psi_{hc} = 0.002 \times 0.60 = 0.001 \ \text{g/g}$$
$$y_s = \eta_s\Psi_s = 0.036 \times 0.54 = 0.019 \ \text{g/g}$$

2. Asymptotic values for the mass loss rate from Equation 36.15:

$$\dot{m}'' = \frac{\dot{q}''_{f,asy} - \dot{q}''_{rr}}{\Delta H_g} = \frac{60 - 11}{1.63} = 30 \frac{\text{g}}{\text{m}^2\text{s}}$$

3. Asymptotic values for the mass generation rates of products from Equation 36.46 and the above data:

$$\dot{G}''_{CO_2} = y_{CO_2}\dot{m}'' = 1.77 \times 30 = 53 \ \text{g/m}^2\text{/s}$$
$$\dot{G}''_{CO} = y_{CO}\dot{m}'' = 0.005 \times 30 = 0.159 \ \text{g/m}^2\text{/s}$$
$$\dot{G}''_{hc} = y_{hc}\dot{m}'' = 0.001 \times 30 = 0.036 \ \text{g/m}^2\text{/s}$$
$$\dot{G}''_{hc} = y_{hc}\dot{m}'' = 0.019 \times 30 = 0.584 \ \text{g/m}^2\text{/s}$$

Generation Rates of Fire Products and Fire Ventilation Effects

As discussed previously, the effects of decreasing fire ventilation, as characterized by the increase in the local equivalence ratio, are reflected by an increase in the generation rates of the reduction zone products (smoke, CO, hydrocarbons, and others). For example, for flaming wood crib enclosure fires, as the equivalence ratio increases, the combustion efficiency decreases, flames become unstable, and the generation efficiency of CO reaches its peak for the equivalence ratio between about 2.5 and 4.0 [103].

Ventilation-controlled building fires are generally characterized by two layers: (1) a vitiated ceiling layer, identified as *upper layer,* and (2) an uncontaminated layer below, identified as *lower layer*. Incorporation of these two layers is the classical two-zone modeling of fires in enclosed spaces. Under many conditions, the depth of the upper layer occupies a significant fraction of the volume of the enclosed space. Eventually, the interface between the upper layer and the lower layer positions itself so that it is very close to the floor, very little oxygen is available for combustion, and most of the fuel is converted to the reduction zone products, that is, smoke, CO, hydrocarbons, and others.

Ventilation-controlled large- and small-enclosure and laboratory-scale fires and fires in the vitiated upper layer under experimental hoods have been studied in detail and reviewed [103, 122–125]. The results from these types of fires are very similar. Detailed studies [103] performed for the generation rates of fire products for various fire ventilation conditions

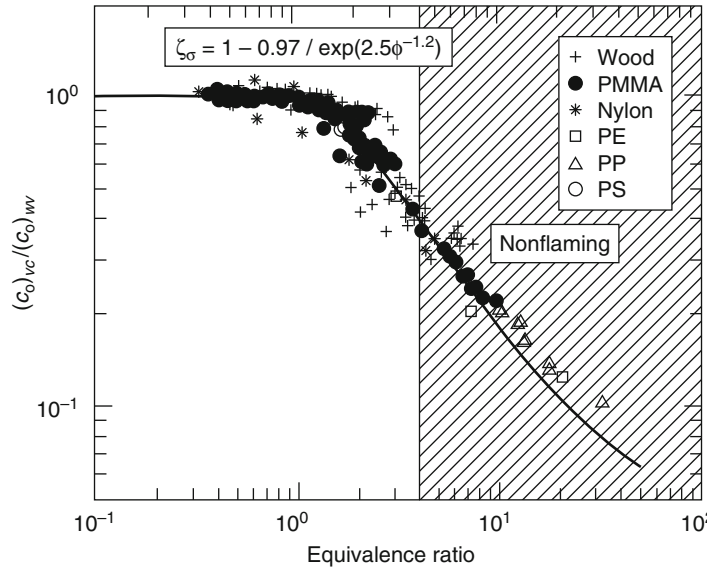

Fig. 36.36 Ratio of the mass of oxygen consumed per unit mass of the fuel for ventilation-controlled to well-ventilated fires (Data are taken from Ref. [103]). Subscript *vc* represents ventilation-controlled fires, and subscript *wv* represents well-ventilated fires

in the Fire Propagation Apparatus and in the Fire Research Institute's (FRI) enclosure, show that with an increase in the equivalence ratio (1) generation efficiencies of oxidation zone products, such as CO_2, and reactant consumption efficiency (i.e., oxygen) decrease, and (2) generation efficiencies of the reduction zone products, such as smoke, CO, and hydrocarbons increase.

Generalized correlations have been established between the generation efficiencies and the equivalence ratio for the oxidation and reduction zone products. The changes in the consumption or generation efficiencies of the products are expressed as ratios of the efficiencies for the ventilation-controlled (*vc*) to well-ventilated (*wv*) fires:

Reactants (oxygen)

$$\zeta_O = \frac{(\eta_O)_{vc}}{(\eta_O)_{wv}} = \frac{(c_O/\Psi_O)_{vc}}{(c_O/\Psi_O)_{wv}} = \frac{(c_O)_{vc}}{(c_O)_{wv}} \quad (36.65)$$

Oxidation zone products (carbon dioxide, water, etc.*)*

$$\zeta_{oxid} = \frac{(\eta_j)_{vc}}{(\eta_j)_{wv}} = \frac{\left(y_j/\Psi_j\right)_{vc}}{\left(y_j/\Psi_j\right)_{wv}} = \frac{\left(y_j\right)_{vc}}{\left(y_j\right)_{wv}} \quad (36.66)$$

where ζ_{oxid} is the oxidation zone product generation efficiency ratio.

Reduction zone products (smoke, carbon monoxide, hydrocarbons, etc.)

$$\zeta_{red} = \frac{(\eta_j)_{vc}}{(\eta_j)_{wv}} = \frac{\left(y_j/\Psi_j\right)_{vc}}{\left(y_j/\Psi_j\right)_{wv}} = \frac{\left(y_j\right)_{vc}}{\left(y_j\right)_{wv}} \quad (36.67)$$

where ζ_{red} is the reduction zone product generation efficiency ratio.

The relationships between the ratios of the mass of oxygen consumed per unit mass of fuel, the yields of the products for the ventilation-controlled to well-ventilated fires, and the equivalence ratio are shown in Figs. 36.36, 36.37, 36.38, 36.39, and 36.40. The ratios for oxygen and CO_2 (an oxidation zone product) do not depend on the chemical structures of the materials, whereas the ratios for the reduction zone products do depend on the chemical structures of the materials.

Oxygen and CO_2 The relationships for oxygen consumed and carbon dioxide generated are shown in Figs. 36.36 and 36.37, respectively. The relationships are very similar to the relationships for the chemical and convective

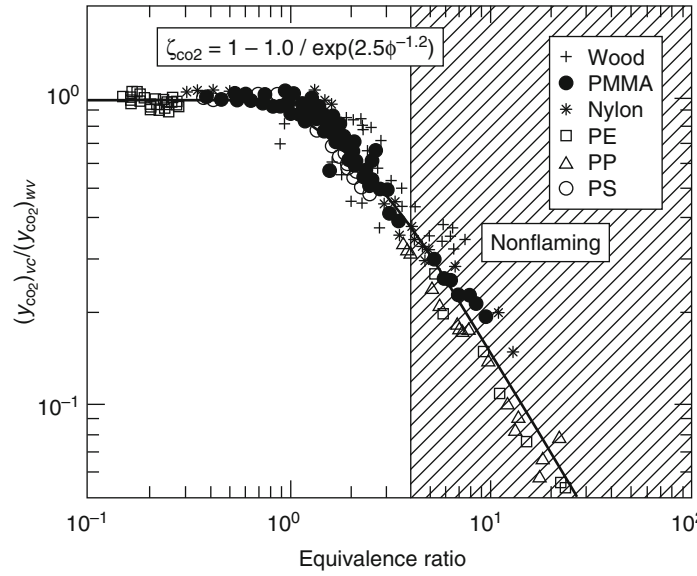

Fig. 36.37 Ratio of the mass of carbon dioxide generated per unit mass of the fuel for ventilation-controlled to well-ventilated fires (Data are taken from Ref. [103]). Subscript *vc* represents ventilation-controlled fires, and subscript *wv* represents well-ventilated fires

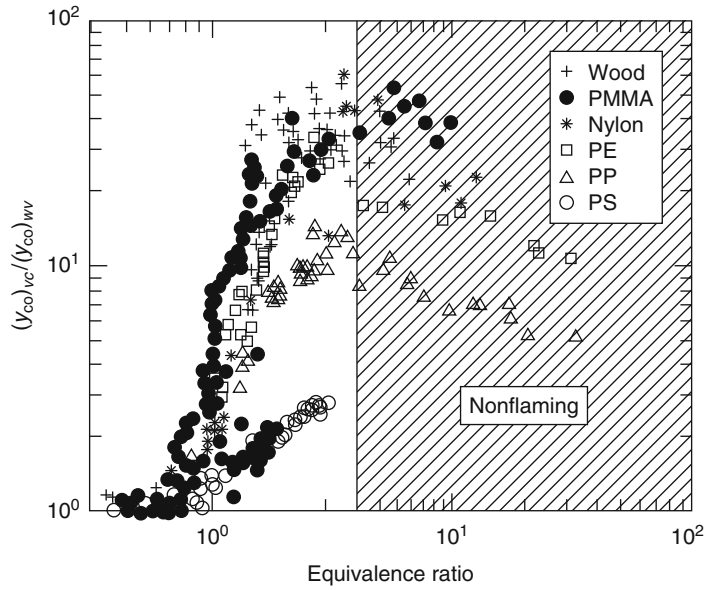

Fig. 36.38 Ratio of the mass of carbon monoxide generated per unit mass of the fuel for ventilation-controlled to well-ventilated fires (Data are taken from Ref. [103]). Subscript *vc* represents ventilation-controlled fires, and subscript *wv* represents well-ventilated fires

heats of combustion ratios (Equations 36.44 and 36.45), as expected:

$$\frac{(c_{\mathrm{O}})_{vc}}{(c_{\mathrm{O}})_{wv}} = 1 - \frac{0.97}{\exp\left[\left(\frac{\Phi}{2.14}\right)^{-1.2}\right]} \tag{36.68}$$

$$\frac{(y_{\mathrm{CO_2}})_{vc}}{(y_{\mathrm{CO_2}})_{wv}} = 1 - \frac{0.97}{\exp\left[\left(\frac{\Phi}{2.15}\right)^{-1.2}\right]} \tag{36.69}$$

Carbon Monoxide The relationship between the ratio of the CO yields for ventilation-controlled to well-ventilated fires and the equivalence ratio is shown in Fig. 36.38. The data suggest the following relationship [103]:

$$\frac{(y_{\mathrm{CO}})_{vc}}{(y_{\mathrm{CO}})_{wv}} = 1 + \frac{\alpha}{\exp\left(2.5\Phi^{-\xi}\right)} \tag{36.70}$$

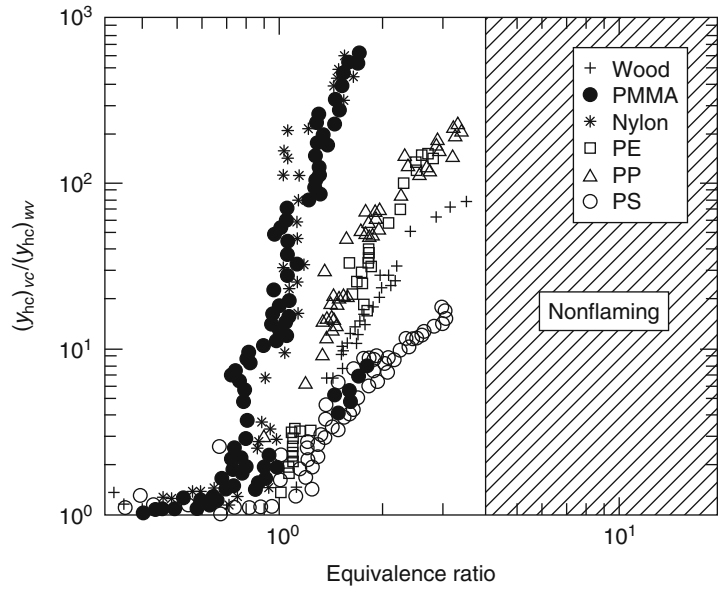

Fig. 36.39 Ratio of the mass of hydrocarbons generated per unit mass of the fuel for ventilation-controlled to well-ventilated fires (Data are taken from Ref. [103]). Subscript *vc* represents ventilation-controlled fires, and subscript *wv* represents well-ventilated fires

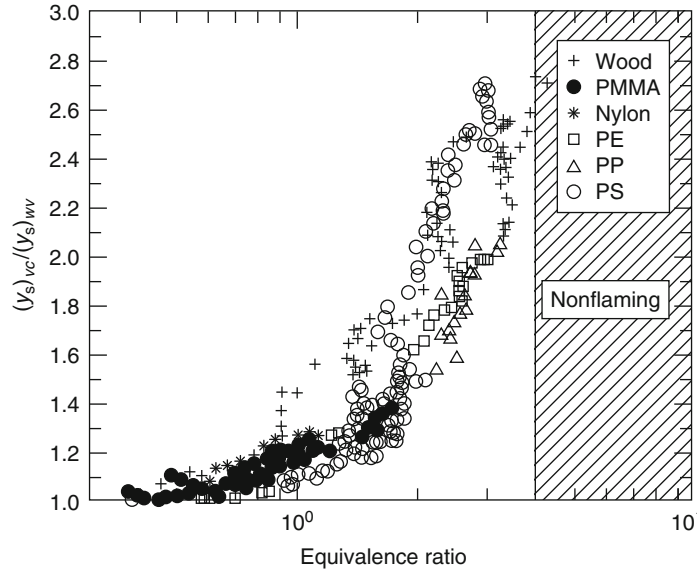

Fig. 36.40 Ratio of the mass of smoke generated per unit mass of the fuel for ventilation-controlled to well-ventilated fires (Data are taken from Ref. [103]). Subscript *vc* represents ventilation-controlled fires, and subscript *wv* represents well-ventilated fires

where α and ξ are the correlation coefficients, which depend on the chemical structures of the materials. The values for the correlation coefficients for CO are listed in Table 36.12.

The increase in the ratio of the carbon monoxide yields for the ventilation-controlled to well-ventilated fires with the equivalence ratio is due to the preferential conversion of the fuel carbon atoms to CO. The experimental data show the following order for the preferential conversion: wood (C-H-O aliphatic structure) > PMMA (C-H-O aliphatic structure) > nylon (C-H-O-N aliphatic structure) > PE (C-H aliphatic linear unsaturated structure) > PP (C-H aliphatic branched unsaturated structure) > PS (C-H aromatic structure). A similar trend is found for the liquid and gaseous fuels, such as shown in Table 36.13 [103]. The presence of O

and N atoms in the fuels with aliphatic C-H structure appears to enhance preferential fuel carbon atom conversion to CO.

Hydrocarbons The relationship between the ratio of the hydrocarbon yields for ventilation-controlled to well-ventilated fires and the equivalence ratio is shown in Fig. 36.39. The data suggest the following relationship [103]:

$$\frac{(y_{hc})_{vc}}{(y_{hc})_{wv}} = 1 + \frac{\alpha}{\exp\left(5.0\Phi^{-\xi}\right)} \tag{36.71}$$

The correlation coefficient values for hydrocarbons are listed in Table 36.12. The numerator in the second term on the right-hand side of Equation 36.71 is 10–40 times that of CO, whereas the denominator is twice that for CO. This relationship suggests that there is a significantly higher preferential fuel conversion to hydrocarbons than to CO, as the equivalence ratio increases. The order for the preferential fuel conversion to hydrocarbons is very similar to CO, except for wood; that is, PMMA > nylon > PE = PP > wood > PS. The exception for wood may be due to the char-forming tendency of the fuel, which lowers the C-to-H ratio in the gas phase.

Table 36.12 Correlation coefficients to account for the effects of ventilation on the generation rates of CO, hydrocarbons, and smoke

	CO			Hydrocarbons			Smoke		
Material	α	β	ξ	α	β	ξ	α	β	ξ
PS	2	1.44	2.5	25	2.45	1.8	2.8	2.02	1.3
PP	10	1.39	2.8	220	1.90	2.5	2.2	2.50	1.0
PE	26	1.39	2.8	220	1.90	2.5	2.2	2.50	1.0
Nylon	36	1.36	3.0	1200	1.65	3.2	1.7	3.14	0.8
PMMA	43	1.33	3.2	1800	1.58	3.5	1.6	4.61	0.6
Wood	44	1.30	3.5	200	2.33	1.9	2.5	2.15	1.2
PVC	7	0.42	8.0	25	0.42	1.8	0.38	2.02	8.0

Smoke The relationship between the ratio of the smoke yields for ventilation-controlled to well-ventilated fires and the equivalence ratio is shown in Fig. 36.40. The data suggest the following relationship: [103]

$$\frac{(y_s)_{vc}}{(y_s)_{wv}} = 1 + \frac{\alpha}{\exp\left(2.5\Phi^{-\xi}\right)} \tag{36.72}$$

The correlation coefficient values for smoke are listed in Table 36.12. The values of the correlation coefficients in the second term on the right-hand side of Equation 36.72 suggest that, with increasing equivalence ratio, the preferential fuel conversion to smoke is lower than it is to hydrocarbons and CO. Also, the order for the preferential conversion of the fuel carbon atom to smoke is opposite to the order for the conversion to CO and hydrocarbons, except for wood. The order is PS > wood > PE = PP > nylon > PMMA, suggesting that the order is probably due to a decrease in the preference for the reactions between OH and CO compared to the reactions between OH and soot.

Table 36.13 Carbon monoxide generation efficiency for ventilation-controlled and well-ventilated combustion[a]

		Ventilation-controlled (vc) $\Phi \approx 4.0$		
Fuel	Well-ventilated (wv)[b] $\Phi < 0.05$	Beyler [123]	Beyler [124]	$(y_{CO})_{vc}/(y_{CO})_{wv}$
Methane	0.001	0.10	–	100
Propane	0.001	–	0.12	120
Propylene	0.004	0.10	–	25
Hexane	0.002	0.10	0.52[c]	50 (260[c])
Methanol	0.001	0.27	1.00[c]	270 (1000[c])
Ethanol	0.001	0.18	0.66[c]	180 (660[c])
Isopropanol	0.002	0.21	–	105
Acetone	0.002	0.21	0.63[c]	105 (315[c])

[a]Table taken from Ref. [103]
[b]Data taken in the Fire Propagation Apparatus
[c]Nonflaming

Other Reduction Zone Products Since the sum of the generation efficiencies of all the products for a material cannot exceed unity, the generation efficiency of products other than CO, CO_2, hydrocarbons, and smoke is

$$\eta_{\text{other}} = 1 - \left(\eta_{\text{CO}} + \eta_{\text{CO}_2} + \eta_{\text{hc}} + \eta_{\text{s}}\right) \quad (36.73)$$

where η_{other} is the generation efficiency of products other than CO, CO_2, hydrocarbons, and smoke. The generation efficiency of other products can be calculated from Equations 36.68, 36.69, 36.70, 36.71 and 36.72 using correlation coefficients from Table 36.12. The generation efficiency values for other products calculated in this fashion for various equivalence ratios are shown in Fig. 36.41. The figure shows that, for equivalence ratios greater than 4, where fires are nonflaming, about 10–60% of fuel carbon is converted to products other than CO, CO_2, soot, and hydrocarbons.

The order for the preferential conversion of fuel carbon to other products in the nonflaming zone is PS (C-H aromatic structure) < PE & PP (C-H aliphatic structure) < wood (C-H-O aliphatic structure) < nylon (C-H-O-N aliphatic structure) < PMMA (C-H-O aliphatic structure). It thus appears that, in nonflaming environments, fuels with C-H structures are converted mainly to CO, smoke, and hydrocarbons, rather than to other products, whereas fuels with C-H-O and C-H-O-N structures are converted mainly to products other than CO, CO_2, smoke, and hydrocarbons. Some of the products include formaldehyde (HCHO) and hydrogen cyanide (HCN) [103].

Generation Efficiencies of Formaldehyde, Hydrogen Cyanide, and Nitrogen Dioxide The experimental data for the generation efficiencies of formaldehyde, hydrogen cyanide, and nitrogen dioxide versus the equivalence ratio are shown in Figs. 36.42 and 36.43.

Formaldehyde is generated in the pyrolysis of wood (C-H-O structure). It is attacked rapidly by oxygen (O) and hydroxyl (OH) radicals in the flame, if unlimited supply of oxygen is available. Thus, only traces of formaldehyde are found in well-ventilated fires. The generation efficiency of formaldehyde, however, increases with the equivalence ratio, indicating reduced concentrations of O and OH radicals and gas temperature due to lack of oxygen available for combustion.

In fires, hydrogen cyanide is formed in the reduction zone from materials with hydrogen

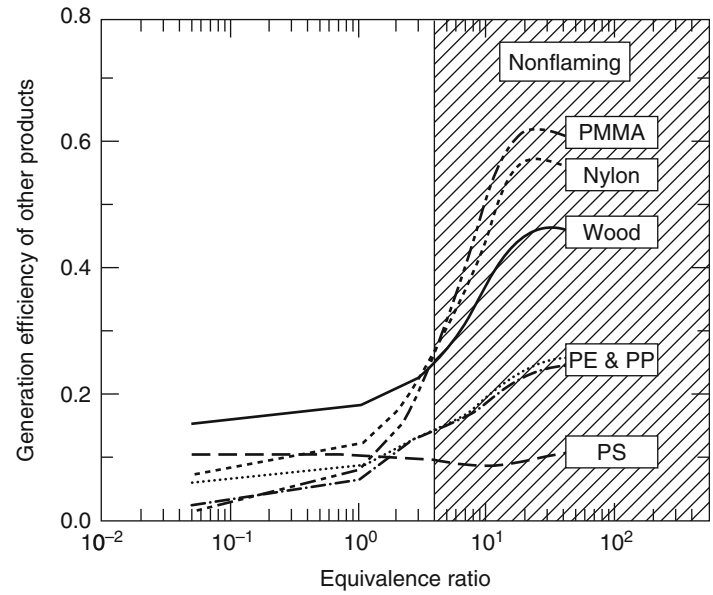

Fig. 36.41 Generation efficiency of products other than CO, CO_2, hydrocarbons, and smoke versus the equivalence ratio

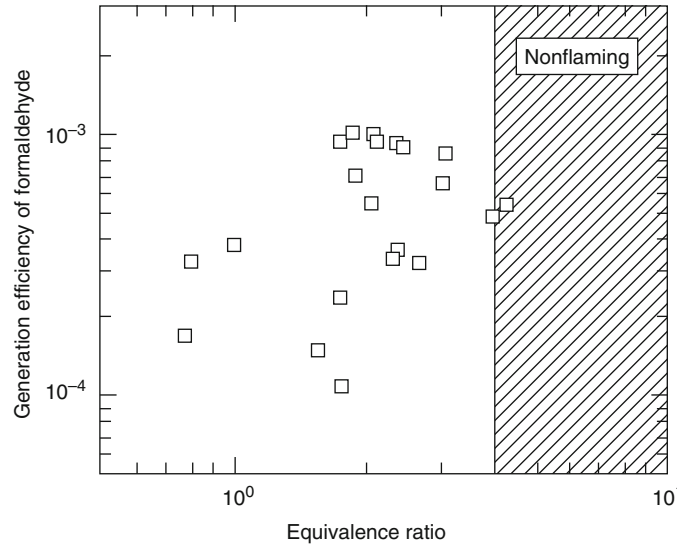

Fig. 36.42 Generation efficiency of formaldehyde generated from wood versus the equivalence ratio

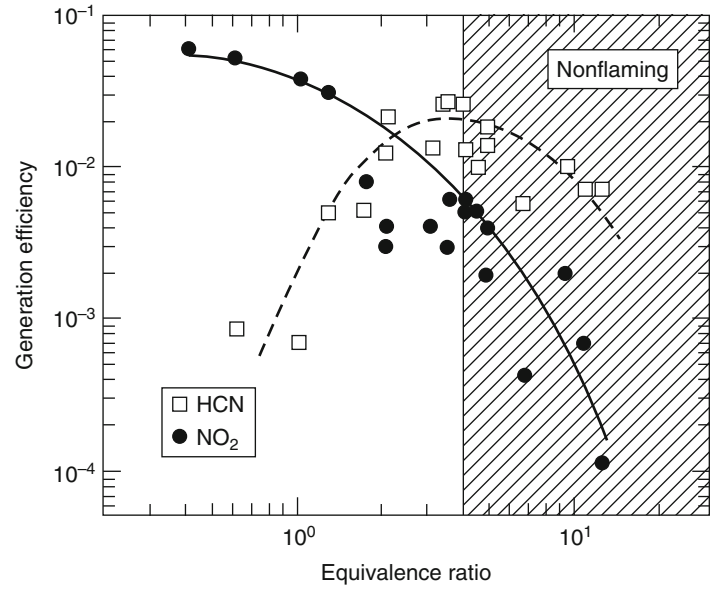

Fig. 36.43 Generation efficiencies of hydrogen cyanide and nitrogen dioxide generated from nylon versus the equivalence ratio

and nitrogen atoms in the structure, such as nylon (C-H-O-N structure). Nitrogen dioxide (NO_2), on the other hand, is formed in the oxidation zone, as a result of the oxidation of hydrogen cyanide. The data in Fig. 36.40 show that the generation efficiency of hydrogen cyanide increases and the generation efficiency of NO_2 decreases with the equivalence ratio. This observation supports that O and OH radical concentrations decrease with increase in the equivalence ratio. The decrease in the generation efficiency of hydrogen cyanide in nonflaming environments suggests a decrease in the fuel mass transfer rate.

Relationship Between the Generation Efficiencies of CO_2 and CO The relationship between the generation efficiencies of CO_2 and CO is shown in Fig. 36.44, where the data are taken from Ref. [103]. CO is generated in the reduction zone of the flame as a result of the

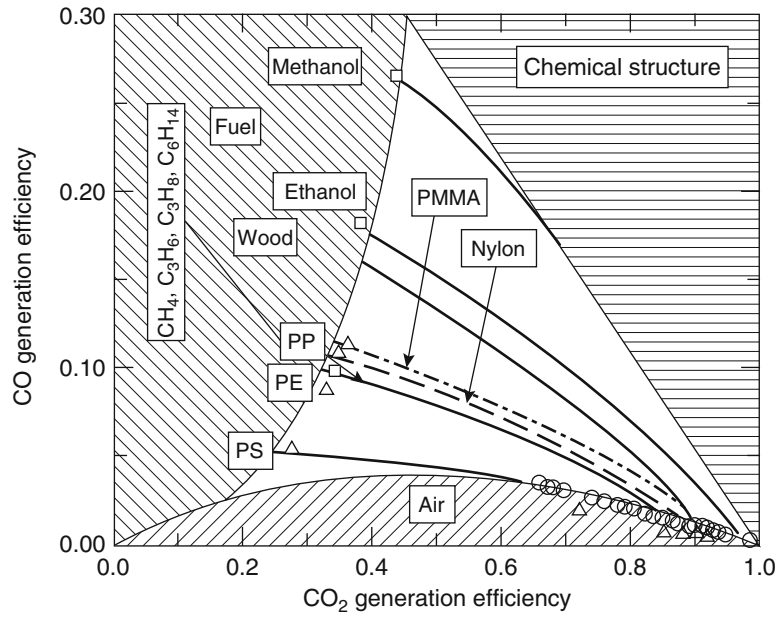

Fig. 36.44 Relationship between the generation efficiencies of CO_2 and CO (Data taken from Ref. [103])

oxidative pyrolysis of the fuel, and is oxidized to CO_2 in the oxidation zone of the flame. The generation efficiency of CO_2 is independent of the chemical structure of the fuel (Fig. 36.37), whereas the generation efficiency of CO depends on the chemical structure of the fuel (Fig. 36.38). In Fig. 36.44, the curves represent approximate predictions based on the correlation coefficients from Table 36.12 and Equations 36.69 and 36.70.

The relationship between the generation efficiencies of CO_2 and CO is quite complex. The boundary of the shaded region marked *air* in Fig. 36.44 is drawn using the data for the well-ventilated combustion for equivalence ratios less than 0.05. The boundary of the *air* region may be considered as equivalent to the lower flammability limit. No flaming combustion is expected to occur in this region, as the fuel-air mixture is below the lower flammability limit; however, nonflaming processes, generally identified as smoldering, may continue. The boundary of the shaded region marked *fuel* is drawn using the data for the ventilation-controlled combustion for equivalence ratio of 4.0, and may be considered as equivalent to the upper flammability limit. In the *fuel* region, no flaming combustion is expected to occur, as the fuel-air mixture is above the upper flammability limit; however, nonflaming processes may continue. The shaded region marked *chemical structure* and drawn to the right of the methanol curve is an imaginary region as it is not expected to exist, because there are no stable carbon-containing fuel structures below the formaldehyde with a structure of HCHO. For the stable fuels with C-H-O structures, formaldehyde (HCHO) and methanol (CH_3OH) have the lowest molecular weights (30 and 32, respectively). Thus, data for HCHO and CH_3OH probably would be comparable.

The curves in Fig. 36.44 show that, in flaming combustion, with increase in the equivalence ratio, the preference for fuel carbon atom conversion to CO, relative to the conversion to CO_2, follows this order: methanol (C-H-O structure) > ethanol (C-H-O structure) > wood (C-H-O structure) > PMMA (C-H-O structure) > nylon (C-H-O-N structure) > PP (C-H aliphatic unsaturated branched structure) ≥ (CH_4, C_3H_6, C_3H_8, C_6H_{14}) ≥ PE (C-H aliphatic unsaturated linear structure) > PS (C-H aromatic unsaturated structure). Thus, for fires in enclosed spaces, generation of higher amounts of CO relative to CO_2 at high local equivalence ratios is expected for fuels with C-H-O structures compared to the

fuels with C-H structures. The reason for higher amounts of CO relative to CO_2 for fuels with C-H-O structures is that CO is easily generated in fuel pyrolysis, but is oxidized only partially to CO_2 due to limited amounts of oxidant available.

Relationship Between the Generation Efficiencies of CO and Smoke The relationship between the generation efficiencies of CO and smoke is shown in Fig. 36.45, where data are taken from Ref. [103]. CO and smoke are both generated in the reduction zone of the flame as a result of the oxidative pyrolysis of the fuel, and their generation efficiencies depend on the chemical structure of the fuel (Figs. 36.38 and 36.40). In Fig. 36.45, the curves represent approximate predictions based on the correlation coefficients from Table 36.11 and Equations 36.70 and 36.72.

The relationship in Fig. 36.45 is quite complicated. The boundary of the shaded region marked *air* is drawn using the data for the well-ventilated combustion for equivalence ratios less than 0.05. The boundary of the shaded region marked *fuel* is drawn using the data for the ventilation-controlled combustion for equivalence ratio of 4.0. The boundary for the region marked *air* may be considered as equivalent to the lower flammability limit, and the boundary for the region marked *fuel* may be considered as equivalent to the upper flammability limit.

In Fig. 36.45, the order for the preference for fuel carbon atom conversion to smoke relative to conversion to CO is wood (C-H-O structure) < PMMA (C-H-O structure) < nylon (C-H-O-N structure) < PP (C-H aliphatic unsaturated branched structure) ≈ PE (C-H aliphatic unsaturated linear structure) < PS (C-H aromatic structure). The generation efficiency of smoke for PS, which is a polymer with aromatic C-H structure, is the highest. The generation efficiency of smoke for wood, which is a polymer with aliphatic C-H-O structure, is the lowest.

Generalized Relationships to Calculate Chemical, Convective, and Radiative Heats of Combustion and Yields of Products at Various Equivalence Ratios

Equations 36.44, 36.45, and 36.68, 36.69, 36.70, 36.71, and 36.72 can be generalized as follows:

$$fp = fp_{\infty}\left\{1 + \frac{\alpha}{\exp\left[\left(\frac{\Phi}{\beta}\right)^{-\xi}\right]}\right\} \qquad (36.74)$$

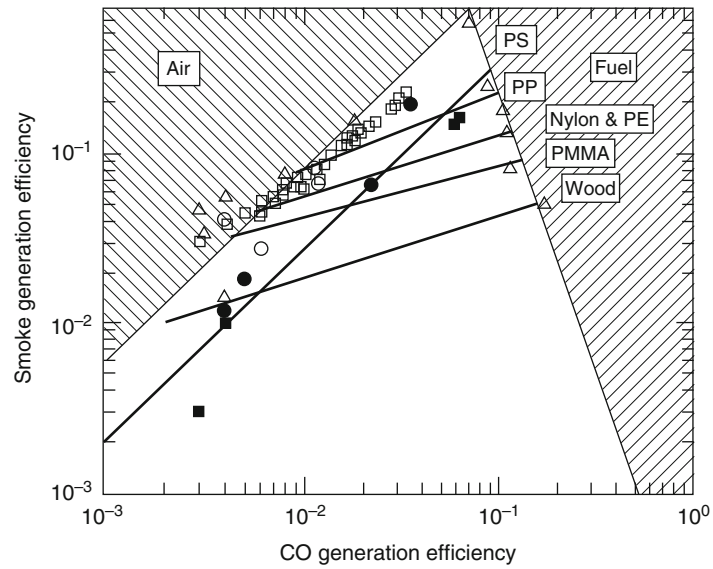

Fig. 36.45 Relationship between the generation efficiencies of CO and smoke (Data taken from Ref. [103])

where
fp = Fire property
α, β, and ξ = Correlation coefficients characteristic of the chemical structures of the polymers
subscript ∞ = Infinite amount of air (i.e., well ventilated conditions)

It is noted that this relationship is applicable under turbulent flame conditions where a given fire property remains constant (i.e., it is not a function of flow conditions). Fire properties to consider include heat of combustion (or combustion efficiency) and yields (or generation efficiencies) of products. Three conditions can be identified: (1) for $\Phi \gg \beta$, $fp = fp_\infty(1 + \alpha)$; (2) for $\Phi \ll \beta$, $fp = fp_\infty$; and (3) $\Phi \approx \beta$, $fp \approx fp_\infty(1 + \alpha/2.7)$. Thus, the parameter α is associated primarily with the magnitude of the fire properties in nonflaming processes (high Φ values). The parameter β is associated with the fire properties in the transition region between fires with an infinite amount of air and fires with a very restricted amount of air. The parameter ξ is associated with the range of Φ values for the transition region. A high value of α is indicative of a strong effect of ventilation on the fire and its properties and vice versa. High values of β and ξ are indicative of rapid change from flaming to nonflaming conditions by a small change in the equivalence ratio, such as for the highly fire-retarded or halogenated materials for which flaming combustion in normal air itself is unstable.

Chemical Heat of Combustion Versus Equivalence Ratio for Nonhalogenated Compounds From Equation 36.74,

$$\Delta H_{ch} = \Delta H_{ch,\infty}\left\{1 - \frac{0.97}{\exp\left[\left(\frac{\Phi}{2.15}\right)^{-1.2}\right]}\right\} \tag{36.75}$$

This equations stems from Equation 36.44. As stated above, this relationship is found to hold for a variety of compounds regardless of their chemical structure (Fig. 36.33). The values of $\Delta H_{ch,\infty}$ can be found in Table A.39.

Chemical Heat of Combustion Versus Equivalence Ratio for Halogenated Polymers (PVC) The effect of ventilation on the burning of halogenated materials is dramatically different from that shown in Equation 36.75,

$$\Delta H_{ch} = \Delta H_{ch,\infty}\left\{1 - \frac{0.30}{\exp\left[\left(\frac{\Phi}{0.53}\right)^{-11}\right]}\right\} \tag{36.76}$$

As can be noted from the terms inside the brackets in Equations 36.75 and 36.76, the effect of ventilation on the chemical heat of combustion is much stronger for PVC than it is for nonhalogenated materials. The effect for PVC occurs at $\Phi \geq 0.4$, which is significantly lower than $\Phi \geq 2.0$ found for nonhalogenated compounds [103, 126]. For PVC homopolymer, flaming combustion changes transitions to nonflaming for $\Phi \geq 0.70$, which is also significantly lower than $\Phi \geq 4.0$ found for nonhalogenated materials. This attribute is consistent with the highly halogenated nature of PVC and its mode of decomposition. The decomposition of PVC is characterized by the release of HCl, which is initiated at temperatures as low as about 100 °C. At temperatures of up to between 200 °C and 220 °C, HCl is the major effluent. The presence of oxygen in the air enhances HCl release. The generation of HCl from PVC leads to the formation of double bonds and release of various aromatic/unsaturated hydrocarbons (benzene, ethylene, propylene, butylene, etc.).

Convective Heats of Combustion Versus Equivalence Ratio for Nonhalogenated Compounds From Equation 36.74,

$$\Delta H_{con} = \Delta H_{con,\infty}\left\{1 - \frac{1.0}{\exp\left[\left(\frac{\Phi}{1.38}\right)^{-2,8}\right]}\right\} \tag{36.77}$$

Similar to the chemical heat of combustion this equation stems from Equation 36.45 and is applicable to a large number of materials, regardless of

their chemical structure (Fig. 36.34). Values for $\Delta H_{con,\infty}$ are listed in Table A.39.

Radiative Heats of Combustion Versus Equivalence Ratio Radiative heats of combustion are obtained from the difference between the chemical and the convective heats of combustion:

$$\Delta H_{rad} = \Delta H_{ch} - \Delta H_{con} \tag{36.78}$$

Consumption of Oxygen for Nonhalogenated Compounds As shown in Fig. 36.36 and similarly to the findings for chemical and convective heat release rates, ventilation effects on oxygen consumption are similar regardless of chemical structure. Therefore in generalized form. Equation 36.68 becomes:

$$c_O = c_{O,\infty}\left\{1 - \frac{0.97}{\exp\left[\left(\frac{\Phi}{2.14}\right)^{-1.2}\right]}\right\} \tag{36.79}$$

Yield of Carbon Dioxide for Nonhalogenated Compounds The generation of CO_2 follows similar trends with respect to equivalence ratio, as discussed above (see Fig. 36.37). Therefore, the generalized form of Equation 36.69 is:

$$y_{CO_2} = y_{CO_2,\infty}\left\{1 - \frac{1.0}{\exp\left[\left(\frac{\Phi}{2.15}\right)^{-1.2}\right]}\right\} \tag{36.80}$$

$y_{CO_2,\infty}$ values for well ventilated fires are listed in Table A.39.

Yield of Carbon Dioxide for Halogenated Polymers (PVC) Lastly, as indicated above for the chemical heat of combustion of PVC, ventilation effects are markedly different for halogenated materials compared to their nonhalogenated counterparts. In this case the generalized equation for CO_2 yield is:

$$y_{CO_2} = y_{CO_2,\infty}\left\{1 - \frac{0.30}{\exp\left[\left(\frac{\Phi}{0.53}\right)^{-11}\right]}\right\} \tag{36.81}$$

From the terms inside the brackets in Equations 36.80 and 36.81, a stronger effect of ventilation on the yield of CO_2 for PVC than for nonhalogenated compounds can be noted. $y_{CO_2,\infty}$ values are listed in Table A.39.

Yields of Carbon Monoxide, Hydrocarbons, and Smoke for Selected Nonhalogenated Materials As discussed above and shown in Figs. 36.38, 36.39, and 36.40, yields of CO, hydrocarbons, and smoke are affected by the chemical structure the given material involved in the fire. In this case the generalized correlation, Equation 36.74, will take different values for the parameters α, β, and ξ depending on the specific material considered, Parameters for polystyrene, polypropylene, polyethylene, nylon, PMMA, wood, and PVC are given in Table 36.12; these are to be used in Equation 36.74 along with the well ventilated values (i.e., fp_∞) for yields of CO, hydrocarbons, and soot listed in Table A.39 for the materials in Table 36.12.

For PVC, the relationships indicate that for $0.40 \geq \Phi \geq 1.0$, the maximum CO and smoke yields reach about 60 % of the stoichiometric yields, listed in Table 36.11. For the nonhalogenated materials, the maximum CO and smoke yields reach $\leq$30 % of the stoichiometric yields for $\Phi \geq 2.0$. Polystyrene is the only polymer, within the above group of polymers, for which the smoke yield exceeds that of PVC. These trends suggest that CO and smoke are generated much more readily from PVC than from the nonhalogenated materials, possibly due to the formation of double bonds, as HCl is eliminated at temperatures as low as 100 °C from the PVC structure, and formation of various compounds occurs with aromatic/unsaturated bonds.

For the nonhalogenated materials considered with $\Phi \geq 4.0$, the CO yield is lowest and the smoke yield is highest for polystyrene, an aromatic ring-containing polymer; whereas, for polymethylmethacrylate, an aliphatic carbon-hydrogen-oxygen-atom-containing polymer, the CO yield is highest and smoke yield is lowest. This result suggests that aromatic ring structure promotes smoke formation, whereas the strong C-O bond in the structure remains intact as ventilation is reduced.

Example 18 Following Example 12, calculate the yields of CO and smoke at equivalence ratios of 1, 2, and 3 for polystyrene, polyethylene, wood, and nylon using Equation 36.74 and the data in Tables A.39 and 36.12.

Solution

	Yield (g/g)							
	$\Phi \ll 1.0$ (Table A.39)		$\Phi = 1.0$		$\Phi = 2.0$		$\Phi = 3.0$	
Material	CO	Smoke	CO	Smoke	CO	Smoke	CO	Smoke
Polystyrene	0.060	0.164	0.070	0.202	0.137	0.331	0.162	0.417
Polyethylene	0.024	0.060	0.074	0.071	0.459	0.098	0.580	0.117
Wood	0.004	0.015	0.018	0.018	0.145	0.028	0.171	0.034
Nylon	0.038	0.075	0.149	0.086	1.040	0.105	1.280	0.120

Smoke Point

Smoke emission characteristics of fuels have been expressed for decades by smoke point, defined as a minimum laminar axisymmetric diffusion flame height (or fuel volumetric or mass flow rate) at which smoke just escapes from the flame tip [112, 114, 127–145]. More recently, the smoke point concept has been applied to develop subgrid soot formation, oxidation, and radiation models for CFD simulations [146, 147]. Smoke-point values have been measured for numerous gases, liquids, and solids [112, 114, 127–145].

Almost all the knowledge on smoke formation, oxidation, and emission from diffusion flames is based on the combustion of fuels containing carbon and hydrogen atoms (hydrocarbons) [128, 129, 134, 136, 141]. On the basis of the chemical structure, hydrocarbons are divided into two main classes: (1) aliphatic and (2) aromatic. Fuels containing both aliphatic and aromatic units are known as arenes. Aliphatic fuels have open-chain structure, and aromatic fuel structures consist of benzene rings. Aliphatic hydrocarbons are divided into three families: (1) alkanes (C_nH_{2n+2}) where n is an integer—the suffix *ane* indicates a single bond; (2) alkenes (C_nH_{2n})—the suffix *ene* indicates a double bond, and *diene*, two double bonds between carbon-carbon atoms; and (3) alkynes (C_nH_{2n-2})—the suffix *yne* indicates a triple bond. The integer n can vary from one in a gas, such as methane, to several thousands in solid polymers, such as polyethylene. In cyclic aliphatic fuels, carbon atoms are also arranged as rings. Dienes are classified as (1) conjugated—double bonds alternate with single bonds, (2) isolated—double bonds separated by more than one single bond, and (3) allenes—double bonds with no separation. Conjugated dienes are more stable than other dienes.

Solid carbonaceous particles present in smoke are defined as soot [129, 134]. Soot is generally formed in the fuel-rich regions of the flame and grows in size through gas-solid reactions, followed by oxidation (burnout) to produce gaseous products, such as CO and CO_2. Flame residence time available for soot formation is on the order of a few milliseconds. Soot particle inception occurs from the fuel molecule via oxidation and/or pyrolysis products, which typically include unsaturated hydrocarbons, especially acetylene, polyacetylenes, and polycyclic aromatic hydrocarbons (PAH). Acetylene, polyacetylenes, and PAH are relatively stable with respect to decomposition. Acetylene and PAH are often considered the most likely precursors for soot formation in flames. PAH have the same role in diffusion flames for both aliphatic and aromatic fuels. In all flames, regardless of the fuel, initial detection of soot particles takes place on the centerline when a temperature of approximately 1400 K [134] is encountered. Thus, even though the extent of conversion of a fuel into soot may significantly change from fuel to fuel, a common mechanism of soot formation is suggested.

Soot production in the flame depends on the chemical structure, concentration, and

temperature of the fuel and flame temperature, pressure, and oxygen concentration [128, 129, 134, 136, 141]. The diffusion-controlled flame ends when fuel and oxidant are in stoichiometric ratio on the flame axis. The flame is followed by a soot after-burning zone, which is partially chemically controlled. The soot oxidation zone increases from about 10–50 % of the visible flame length as the soot concentration increases. Flame luminosity and smoke emission in the plume depend on overall soot production and oxidation. Flames emit soot when soot temperature in the oxidation zone falls below 1300 K [134]. The soot temperature decreases downstream because of radiation losses and diffusion of fresh cold air, both of which quench soot oxidation. At high soot concentrations, flame emissivity approaches unity, and flame luminosity becomes independent of the amount of soot.

Smoke point, carbon-to-hydrogen ratio, aromaticity, and flame temperature have been suggested as useful parameters to assess relative smoke emission characteristics of fuels in laminar diffusion flames [112, 114, 127, 133–135, 140, 143]. The soot-forming tendency of fuels is inversely proportional to smoke point. General trends observed for smoke points for hydrocarbon fuels in laminar diffusion flames are aromatics < alkynes < alkenes < alkanes.

Smoke-point values have been correlated with flame radiation, combustion efficiency and its convective and radiative components, and generation efficiencies of products [112, 114, 127, 133–135, 140, 143]. Figures 36.46, 36.47, and 36.48 show the relationships between the smoke point and the combustion efficiency and its convective and radiative components, and generation efficiencies of CO and smoke. The data were measured in the Fire Propagation Apparatus (Fig. 36.2) and reported in Refs. [112, 114]. Smoke-point data measured for a number of polymers, as well as wood, are listed in Table 36.14. The following relationships can be discerned from the data [112, 114]:

$$\chi_{\mathrm{ch}} = 1.15 L_{sp}^{0.10} \tag{36.82}$$

where χ_{ch} is the combustion efficiency (−), and L_{sp} is the smoke point (m) as measured in the Fire Propagation Apparatus [112, 114].

$$\chi_{\mathrm{rad}} = 0.41 - 0.85 L_{sp} \tag{36.83}$$

where χ_{rad} is the radiative component of the combustion efficiency (−). This correlation is very similar to the one reported by Markstein [135]. The convective component of the combustion efficiency, χ_{con}, can now be obtained using Equation 36.40:

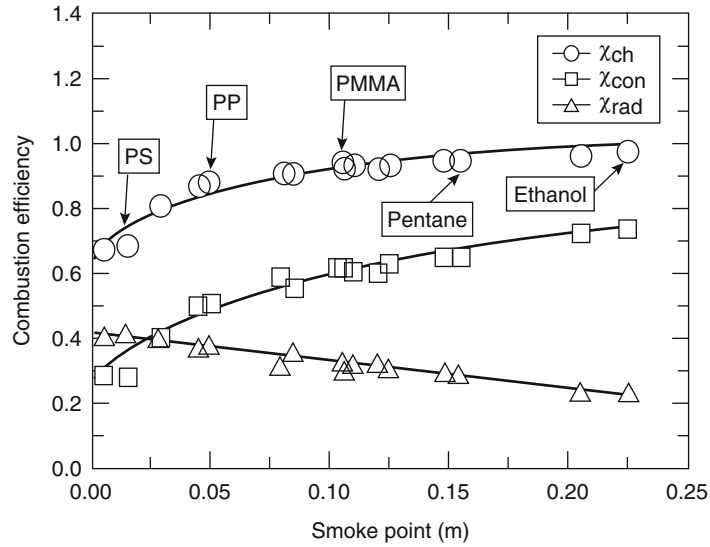

Fig. 36.46 Relationships between combustion efficiency, its convective and radiative components, and the smoke point (Data were measured in the Fire Propagation Apparatus and reported in Refs. [112, 114])

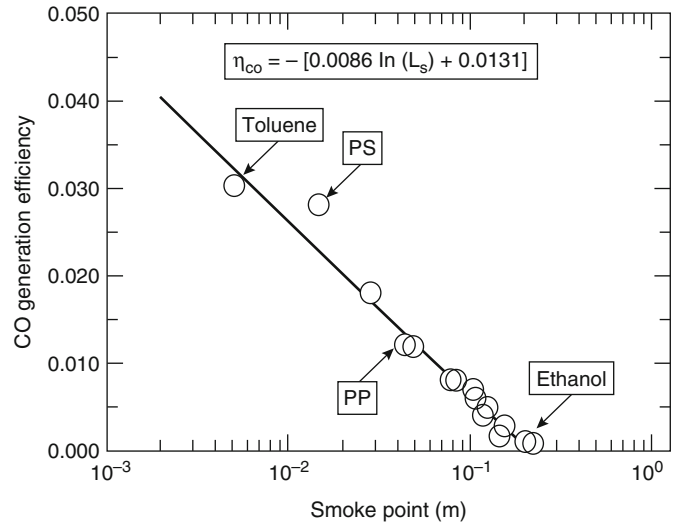

Fig. 36.47 Relationships between CO generation efficiency and smoke point (Data were measured in the Fire Propagation Apparatus and reported in Refs. [112, 114])

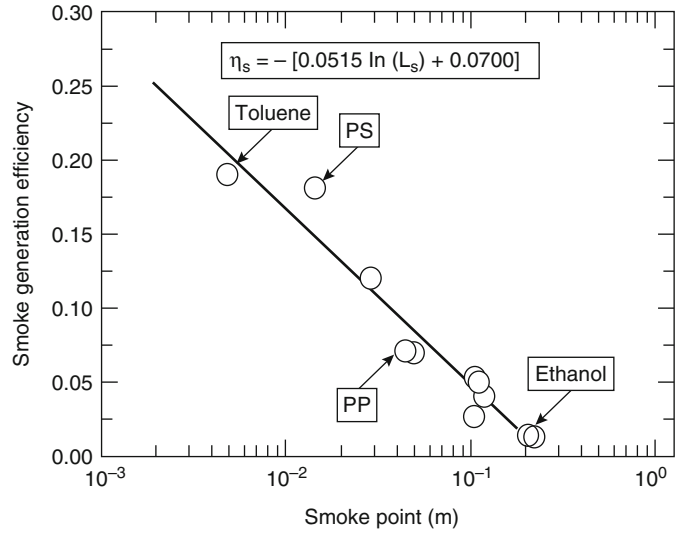

Fig. 36.48 Relationships between the smoke generation efficiency and the smoke point (Data were measured in the Fire Propagation Apparatus and reported in Refs. [112, 114])

$$\chi_{con} = \chi_{ch} - \chi_{rad}$$
$$\chi_{con} = 1.15 L_{sp}^{0.10} + 0.85 L_{sp} - 0.41 \quad (36.84)$$

For the generation efficiency of CO (η_{CO})

$$\eta_{CO} = 0.0086 \ln\left(\frac{0.218}{L_{sp}}\right) \quad (36.85)$$

For the generation efficiency of smoke (η_s)

$$\eta_s = 0.0515 \ln\left(\frac{0.257}{L_{sp}}\right) \quad (36.86)$$

Smoke points were estimated using Equations 36.82, 36.83, 36.84, 36.85 and 36.86 for the materials listed in Table 36.14 using properties (i.e., chemical combustion efficiency, smoke yield, etc.) measured in the Fire Propagation Apparatus and listed in Table A.39; in general, good agreement is observed. It is noted that the highest value of L_{sp} that has been measured is 0.24 m for ethane. Although methane and methanol would be expected to have smoke points higher than 0.24 m, they have not been measured experimentally. Since combustion efficiency cannot exceed unity and the generation efficiencies of CO and smoke cannot be negative, the relationships in Equations 36.82, 36.83, 36.84, 36.85 and 36.86 are valid for

Table 36.14 Smoke point data[a]

Polymer	Smoke point (m)	
	Measured	Estimated[b]
Wood (oak)	0.080	0.085
Wood (fir)	0.080	0.085
Polyoxymethylene (POM)	NM	0.225
Polymethylmethacrylate (PMMA)	0.105	0.139
Polyethylene (PE)	0.045	0.046
Polypropylene (PP)	0.050	0.057
Polystyrene (PS)	0.015	0.012
Polyester	NM	0.009
Nylon	0.120	0.070
GM21	NM	0.013
GM23	NM	0.022
GM25	NM	0.011
GM27	NM	0.013
GM29	NM	0.008
GM31	NM	0.008
GM35	NM	0.009
GM41	NM	0.009
GM43	NM	0.009
GM47	NM	0.009
GM49	NM	0.010
GM51	NM	0.011
GM53	NM	0.011
PE +25 % Chlorine (Cl)	NM	0.013
PE +36 % Cl	NM	0.004
PE +48 % Cl	NM	0.003
PVC	NM	0.015
Polyethylene-tetrafluoroethylene (ETFE, Tefzel®)	NM	0.121
Polytetrafluoroethylene-perfluoro ether (PFA, Teflon®)	NM	0.120
Fluorinated ethylene propylene (FEP, Teflon®)	NM	0.110
Polytetrafluoroethylene (PTFE, Teflon®)	NM	0.110

NM not measured
[a]Data taken from Refs. [112, 114]
[b]Estimated from the polymer properties measured in the Fire Propagation Apparatus and their relationships with smoke point

$0 < L_{sp} \leq 0.24$ m. The correlations show that emissions of CO and smoke are very sensitive to changes in the smoke point values compared to combustion efficiency and its convective and radiative components. This condition is expected from the understanding of the relationship between the smoke point and chemical structures of fuels. For example, a decrease of 33 % in the smoke-point value from 0.15 to 0.10 m produces a decrease of 4 % and 12 % in the combustion efficiency and its convective component, respectively, and an increase of 14 % in the radiative component of the combustion efficiency; however, the generation efficiencies of CO and smoke increase by 89 % and 67 %, respectively.

Equations 36.82, 36.83, 36.84, 36.85 and 36.86 can be used to estimate the fire properties of gases, liquids, and solids from their smoke point values. The smoke point values, however, depend strongly on the apparatus used and cannot be used as reported. One of the approaches is to establish correlations between the smoke-point

values measured in different apparatuses and a single apparatus for which relationships such as those given in Equations 36.82, 36.83, 36.84, 36.85 and 36.86 are available. This type of approach has been described in Refs. [112, 114] for the Fire Propagation Apparatus, where smoke-point values for 165 fuels, reported in the literature, were scaled based on measurements performed in the FPA for 16 common fuels. Fire properties (chemical, convective, and radiative heats of combustion and yields of CO and smoke) were then estimated, using the scaled smoke-point-data, from Equations 36.82, 36.83, 36.84, 36.85 and 36.86, and are listed in Table A.40. In the table, molecular formula and weight, stoichiometric air-to-fuel mass ratio, and net heat of complete combustion have also been tabulated. The estimated data in the table have been validated by direct measurements in small- and large-scale fires using several fuels [112, 114].

Smoke point decreases with increasing molecular weight for a given molecular subgroup. The smoke point values for monomers and polymers, however, show different types of dependencies [112]: (1) the smoke-point values for ethylene and polyethylene are 0.106 and 0.045 m, respectively; (2) the smoke point values for propylene and polypropylene are 0.029 and 0.050 m, respectively; and (3) the smoke point values for styrene and polystyrene are 0.006 and 0.015 m, respectively. The smoke-point data for polymers support the accepted vaporization mechanisms of polymers [148]; that is, polyethylene, polypropylene, and polystyrene vaporize as higher molecular weight oligomers rather than as monomers, and thus, their smoke point values are different than the values for the monomers. The smoke point values suggest that polyethylene is expected to have higher smoke emission than ethylene, whereas polypropylene and polystyrene are expected to have lower smoke emissions than propylene and styrene.

The data in Table A.40 exhibit linear dependencies of the different fire properties on the molecular weight of the fuel monomer within each group [114]:

$$\Delta H_i = h_i + \frac{m_i}{M} \tag{36.87}$$

$$y_j = a_j + \frac{b_j}{M} \tag{36.88}$$

where

ΔH_i = Net heat of complete combustion or chemical, convective, or radiative heat of combustion (kJ/g)

y_j = Yield of product j (g/g)

M = Molecular weight of fuel monomer (g/mol)

h_i = Mass coefficient for the heat of combustion (kJ/g)

m_i = Molar coefficient for the heat of combustion (kJ/mol)

a_j = Mass coefficient for the product yield (g/g)

b_j = Molar coefficient for the product yield (g/mol)

The reader is referred to [114] for listings of h_i, m_i, a_j, and b_j for each fuel class. The coefficients depend on the chemical structures of the fuel; m_i and b_j become negative with the introduction of oxygen, nitrogen, and sulfur atoms into the chemical structure [114]. Relationships in Equations 36.87 and 36.88 support the suggestion [128] that generally smaller molecules offer greater resistance to smoke formation and emission. The relationships also indicate that for gases, liquids, and solids gasifying as high molecular weight fuels, $\Delta H_i \approx h_i$ and $y_j \approx a_j$. The variations of chemical, convective, and radiative heats of combustion as well as yields of CO and smoke with the chemical structures of the fuels are similar to the smoke point variations.

Example 19 The following smoke point values have been reported in Ref. [112]:

Polymer	PE	PP	PMMA	PS
Smoke point (m)	0.045	0.050	0.105	0.015

For well-ventilated conditions, estimate (1) the chemical, convective, and radiative heats of combustion using Equations 36.82, 36.83, and 36.84 and data for the net heat of complete combustion from Table A.39; and (2) yields of CO and smoke using Equations 36.64, 36.85, and 36.86 and stoichiometric yields from Table 36.10.

Solution

1. From Equations 36.82, 36.83, and 36.84 and ΔH_T from Table A.39,

Polymer	PE	PP	PMMA	PS
ΔH_T (kJ/g)	43.6	43.4	25.2	39.2
ΔH_{ch} (kJ/g)	36.8	37.0	23.1	29.6
ΔH_{con} (kJ/g)	20.6	21.1	15.0	14.0
ΔH_{rad} (kJ/g)	16.2	15.9	8.1	15.6

2. From Equations 36.64, 36.85, and 36.87 and Table 36.11,

Polymer	PE	PP	PMMA	PS
Ψ_{CO}	2.00	2.00	1.40	2.15
Ψ_s	0.857	0.857	0.600	0.923
y_{CO} (g/g)	0.027	0.025	0.009	0.050
y_s (g/g)	0.077	0.072	0.028	0.135

Ignition Resistance

Ignition resistance is provided by (1) modifying the chemical structures of the materials for high resistance to ignition and fire propagation, (2) incorporating fire retardants within the materials, (3) coating and wrapping the surfaces, (4) separating materials by inert fire barriers, (5) modifying configuration and arrangement of materials, and so forth. In the context of the concepts introduced and discussed in this chapter, ignition resistance may be interpreted as follows:

Increasing the Resistance to Ignition and Fire Propagation by Increasing the Critical Heat Flux (CHF) and Thermal Response Parameter (TRP) Values

As discussed in section "Ignition (Fire Initiation)" of this chapter, the critical heat flux (CHF) can be expressed as

$$\text{CHF} \approx \sigma\left(T_{ig}{}^4 - T_0{}^4\right) \tag{36.89}$$

where

σ = Stefan-Boltzmann constant (56.7×10^{-12} kW/m^2·K^4)
T_{ig} = Ignition temperature (K)
T_a = Ambient temperature (K)

In turn, the Thermal Response Parameter (TRP) is defined in Equation 36.2, and its relationship to fire propagation in Equations 36.12 and 36.13. The relationships between time to ignition, fire propagation rate, Fire Propagation Index (FPI), and TRP (Equations 36.2, 36.12, and 36.13) show that the time to ignition is directly proportional to the square of the TRP value and the fire propagation rate and FPI are inversely proportional to the TRP value to the power 2 and 1, respectively. Thus, the higher the TRP value, the longer the time to ignition, the slower the fire propagation rate, and the lower the FPI value. For high TRP values with relatively low FPI values, there is empirical evidence [28, 31, 43–46] that no fire propagation beyond the ignition zone will occur, defined as the nonfire-propagating behavior. Also, for materials with high CHF values, higher heat flux exposure is required to initiate a fire.

The CHF and TRP values can be increased by modifying the pertinent parameters, such as an increase in the chemical bond dissociation energy and a decrease in thermal diffusion (combination of the density, specific heat, and thermal conductivity). Figures 36.49 and 36.50 show the CHF and TRP values for a tri-wall corrugated paper sheet containing various amounts of a passive fire protection agent (identified as agent "A" here); the data were obtained from ignition experiments in the Fire Propagation Apparatus. Similarly, Fig. 36.51 shows the TRP value for a single-wall corrugated paper sheet containing various amounts of the passive fire protection agent A. The CHF and TRP values increase with increasing amount of agent; thus, the passive fire protection agent would complement active fire protection agents. Corrugated paper boxes treated with higher amounts of the passive fire protection agent are expected to require reduced amounts of active fire protection agents for fire control, suppression, or extinguishment compared to the amounts of active fire protection agents required for the untreated boxes [149]. The passive fire protection requirements for various materials can be assessed from the data for CHF and TRP listed in Table A.35.

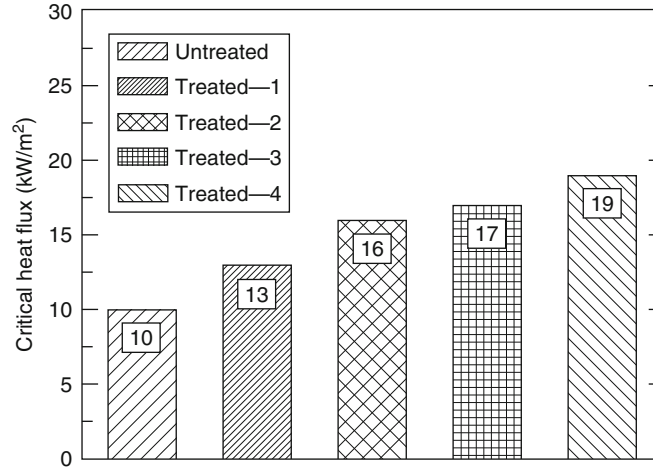

Fig. 36.49 Critical heat flux for untreated and treated tri-wall corrugated paper sheet. The amount of passive fire protection agent is increasing from Treated 1–4. Data obtained from ignition experiments in the Fire Propagation Apparatus. *Numbers* indicated on top of each bar are the critical heat flux values

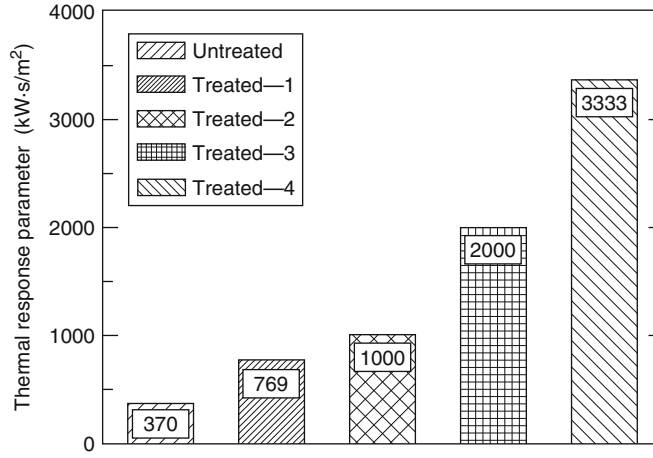

Fig. 36.50 Thermal response parameter for untreated and treated tri-wall corrugated paper sheet. The amount of passive fire protection agent is increasing from Treated 1–4. Data obtained from ignition experiments in the Fire Propagation Apparatus. *Numbers* indicated on top of each bar are the TRP values

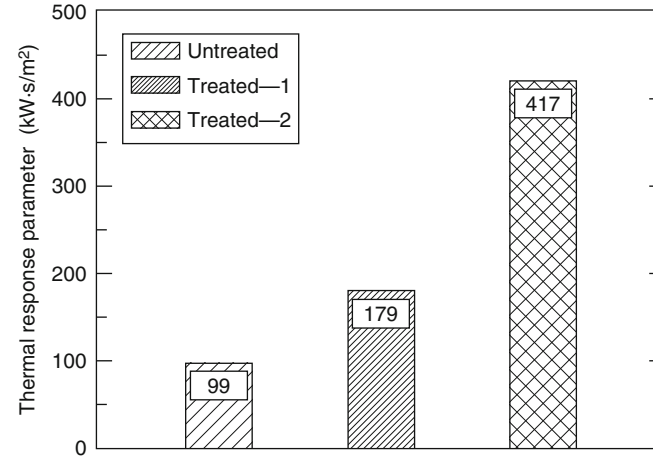

Fig. 36.51 Thermal response parameter for untreated and treated single-wall corrugated paper sheet. The amount of passive fire protection agent is increasing from Treated 1–2. Data obtained from ignition experiments in the Fire Propagation Apparatus. *Numbers* indicated on top of each bar are the TRP values

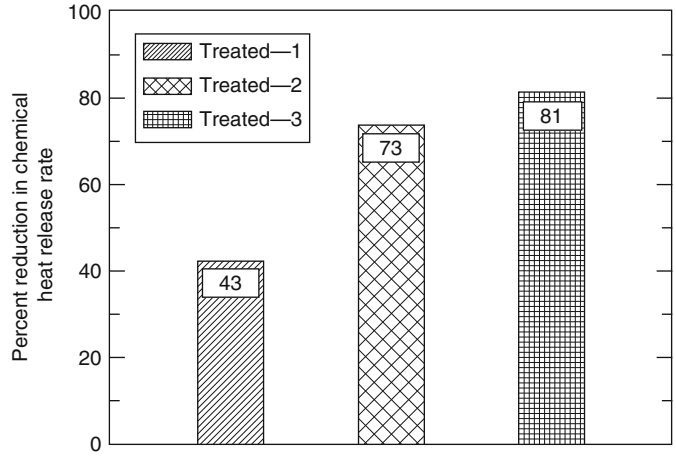

Fig. 36.52 Percent reduction in the chemical heat release rate of untreated tri-wall corrugated paper sheet by a passive fire protection agent. The amount of the passive fire protection agent is increasing from Treated 1–3. Data from combustion experiments in the Fire Propagation Apparatus. *Numbers* indicated on top of each bar are the percent reductions in the chemical heat release rate

Decreasing the Values of the Heat Release Parameter (HRP) and the Flame Heat Flux

Heat release rate is equal to the heat release parameter (HRP) times the net heat flux (Equation 36.34). HRP is the ratio of the heat of combustion to heat of gasification, and thus the HRP value can be decreased by decreasing the heat of combustion and/or increasing the heat of gasification by various chemical and physical means. An examination of data in Table A.39 for heats of combustion shows that introduction of oxygen, nitrogen, sulfur, halogen, and other atoms into the chemical structures of the materials reduces the heat of combustion. For example, the heat of combustion decreases when hydrogen atoms attached to carbon atoms in polyethylene are replaced by halogen atoms, such as by fluorine in Teflon. The chemical heat of combustion decreases from 38.4 kJ/g to 4.2 kJ/g (Table A. 39), and the chemical HRP value decreases from 17 to 2 (Table 36.10).

HRP values can also be reduced by increasing the heat of gasification and decreasing the heat of combustion by retaining the major fraction of the carbon atoms in the solid phase, a process defined as charring. Several passive fire protection agents are available commercially to enhance the charring characteristics of materials.

Figure 36.52 shows the reduction in the chemical heat release rate as a result of an increase in charring of a tri-wall corrugated paper sheet by the passive fire protection agent A; the data were obtained from combustion experiments in the Fire Propagation Apparatus. The amount of agent A increases from Treated 1 to 3 in Fig. 36.52. There is a very significant decrease in the chemical heat release rate of the tri-wall corrugated paper sheet by the passive fire protection agent A, which will complement active fire protection agents. Corrugated paper boxes treated with higher amounts of passive fire protection agent are expected to require reduced amounts of active fire protection agents for fire control, suppression, or extinguishment compared to the one required for the untreated boxes.

The effect on flame heat flux by passive fire protection is determined by using the radiation scaling technique ([44], described in section "Flaming and Nonflaming Phenomena" of this chapter), where combustion experiments are performed in environments with oxygen concentration levels higher than the ambient values. Very little is known about this subject. Table 36.7 lists some of the flame heat flux values derived from the radiation scaling technique, but no systematic study has been performed for the

effectiveness of passive fire protection. From the discussion in section "Flaming and Nonflaming Phenomena" of this chapter, materials that vaporize as species of low molecular weight tend to yield lower flame heat fluxes. Therefore, passive fire protection agents that can reduce the molecular weight of the vaporized materials would be effective in reducing the flame heat flux and complement the active fire protection agents.

Changing the Nature of Fire Products

Nonhalogenated passive fire protection agents or agents that reduce or eliminate the release of halogenated and highly aromatic products and enhance release of aliphatic products, rich in hydrogen and oxygen atoms but poor in carbon atoms, are effective in reducing the nonthermal damage due to smoke and corrosion. Some of the passive fire protection agents, available commercially, interact with the materials in the solid as well as in the gas phase during pyrolysis and combustion.

The critical parameter that needs to be examined in the presence and absence of the passive fire protection agents is the ratio of the generation rate of products (such as for smoke, CO, corrosive products [HCl], and others) to heat release rate. The effectiveness of the passive fire protection agent is reflected in the small values of the ratios at fire control, suppression, and/or extinguishment stages.

Flame Extinction

Flame extinction is achieved by applying agents to the flame and/or to the surface of the burning material. Fire control, suppression, and extinguishment have been described by the firepoint concept [150, 151]. According to the firepoint theory, the convective heat flux from the flame to the burning surface as the flame extinction condition is reached is expressed as [150, 151].

$$\dot{q}''_{fc} = \Phi \Delta H_T \dot{m}''_{\mathrm{cr}} \tag{36.90}$$

where

$\dot{q}''_{fc}$ = Convective flame heat flux from the flame to the surface as the extinction condition is reached (kW/m^2)

ϕ = Maximum fraction of combustion energy that the flame reactions may lose to the sample surface by convection without flame extinction and is defined as the kinetic parameter for flame extinction

ΔH_T = Net heat of complete combustion (kJ/g)

$\dot{m}''_{\mathrm{cr}}$ = Critical mass loss rate for flame extinction (g/m^2/s)

The kinetic parameter is defined as [150, 152]

$$\varphi = \frac{\Delta H_{g,\mathrm{con}}}{\Delta H_T} \tag{36.91}$$

where $\Delta H_{g,\mathrm{con}}$ is the flame convective energy transfer to the fuel per unit mass of fuel gasified (kJ/g). The kinetic parameter is expected to be higher for fast-burning material vapors and lower for slower-burning material vapors, such as materials containing halogens, sulfur, and nitrogen. It is suggested that, at flame extinction, combustion is controlled primarily by convective heat transfer, and thus the critical mass loss rate would follow Spalding's mass transfer number theory [152]:

$$\dot{m}''_{\mathrm{cr}} = \frac{h}{c_p} \ln(B_{\mathrm{cr}} + 1) \tag{36.92}$$

where

h = Convective heat transfer coefficient (kW/m^2/K)

c_P = Specific heat of air (kJ/g/K)

B_{cr} = Critical mass transfer number

The critical mass transfer number is defined as

$$B_{\mathrm{cr}} = \frac{Y_{\mathrm{O}} \Delta H^*_{\mathrm{O}} - c_p(T_s - T_a)}{\Delta H_{g,\mathrm{con}}} \tag{36.93}$$

where

Y_{O} = Oxygen mass fraction

ΔH^*_{O} = Net heat of complete combustion per unit mass of oxygen consumed (kJ/g), which is approximately constant

T_s = Surface temperature (K)

T_a = Ambient temperature (K)

Table 36.15 Critical mass loss rate for ignition and kinetic parameter for flame extinction

Material	Critical mass loss rate ($g/m^2/s$)		Kinetic parameter	
	Ref. [14][a]	Ref. [155][b]	Ref. [14][a]	Ref. [155][b]
Polyoxymethylene	4.5	1.7	0.43	1.05
Polymethylmethacrylate	3.2	1.9	0.28	0.53
Polyethylene	2.5	1.3	0.27	–
Polypropylene	2.7	1.1	0.24	0.50
Polyethylene foams				
1	2.6	–	0.24	–
2	2.6	–	0.25	–
3	2.5	–	0.25	–
4	2.6	–	0.25	–
Chlorinated polyethylenes				
25 % chlorine	6.6	–	0.15	–
36 % chlorine	7.5	–	0.09	–
48 % chlorine	7.6	–	0.08	–
Polystyrene	4.0	0.80	0.21	0.78
Polystyrene foams				
GM47	6.3	–	0.11	–
GM49	4.9	–	0.14	–
GM51	6.3	–	0.10	–
GM53	5.7	–	0.11	–
Polyurethane foams (flexible)				
GM21	5.6	–	0.16	–
GM23	5.3	–	0.17	–
GM25	5.7	–	0.15	–
GM27	6.5	–	0.12	–
$1/CaCO_3$	7.2	–	0.19	–
Polyurethane foams (rigid)				
GM29	7.9	–	0.10	–
GM31	8.4	–	0.09	–
GM35	6.9	–	0.11	–
Polyisocyanurate foams (rigid)				
GM41	6.8	–	0.12	–
GM43	5.5	–	0.15	–
Phenolic foam	5.5	–	0.17	–

[a]Ignition data measured in the Fire Propagation Apparatus
[b]Ignition data measured at the University of Edinburgh, U.K.

For ambient conditions, $Y_O \Delta H_T \gg c_p (T_s - T_a)$. From Equations 36.91, 36.92 and 36.93,

$$\Phi = \frac{Y_O \Delta H_O^*}{\Delta H_T \left[\exp\left(\frac{c_p}{h} \dot{m}''_{cr} \right) - 1 \right]} \tag{36.94}$$

Firepoint theory [150, 151] and experimental data show that the critical mass loss rate for flame extinction is similar to the critical mass loss rate for ignition [14, 122, 153–155] The data for the critical mass loss rate for ignition and flame extinction and the kinetic parameter for flame extinction are listed in Table 36.15. The values for the critical mass loss rate for ignition from the Fire Propagation Apparatus [14] were measured at the time period where the sustained flame is just being established and, thus, are higher than the values from Ref. [155] which were probably measured just before the establishment of a sustained flame. For polymethylmethacrylate,

the critical mass loss rate for ignition from Ref, [14] agrees with the critical mass loss rate for flame extinction from Ref. [154].

The data in Table 36.15 show that the values of the kinetic parameter are higher for the aliphatic materials than the values for the aromatic and chlorinated materials, which is opposite to the trend for the heat of combustion (Table A.39). The data suggest that the materials can be arranged in the following decreasing order of the kinetic parameter values (using data from Ref. [14]): polyoxymethylene ($\phi = 0.43$) > polymethylmethacrylate ($\phi = 0.28$) > polyethylene, polypropylene, and polyethylene foams ($\phi = 0.27$ to 0.25) > polystyrene ($\phi = 0.21$) > polyurethane, polystyrene, and polyisocyanurate foams and chlorinated polyethylenes ($\phi = 0.09$ to 0.19). As expected from the firepoint theory [150, 151], the reactivity of the vapors in the gas phase follows the kinetic parameter.

The combustion efficiency and product generation efficiencies follow the reactivity of the vapors in the gas phase, such as shown in Fig. 36.53 for the combustion efficiency. The lower the value of the kinetic parameter (Equation 36.94), the lower the reactivity of the material vapors, which is reflected in the (1) reduced values of the combustion efficiency (Equations 36.36, 36.37 and 36.38), (2) reduced values of the generation efficiencies (Equation 36.66) of the oxidation zone products (such as CO_2), and (3) increased values of the generation efficiencies (Equation 36.67) of the reduction zone products (such as smoke, CO, and hydrocarbons).

Flame extinction can also be expressed in terms of the critical heat release rate:

$$\dot{Q}''_{\mathrm{cr},i} = \Delta H_i \dot{m}''_{\mathrm{cr}} \tag{36.95}$$

where $\dot{Q}''_{\mathrm{cr},i}$ is the critical heat release rate (chemical, convective, or radiative in kW/m^2), and ΔH_I is the heat of combustion (chemical, convective, and radiative in kJ/g). Table 36.16 lists the critical chemical, convective, and radiative heat release rates for flame extinction, where critical mass loss rate values are taken from Table 36.15 and heats of combustion from Table A.39.

The data in Table 36.16 suggest that the critical heat release rate for flame extinction is weakly dependent on the chemical nature of the material, contrary to the critical mass loss rate. The critical heat release rates thus can be averaged, which are 100 ± 7, 53 ± 9, and 47 ± 10 kW/m^2 for the chemical, convective, and radiative heat release rates, respectively. For materials with highly reactive vapors, such as polyethylene, large amounts of extinguishing agent are needed to reduce the heat release rate to the critical value. For materials with highly

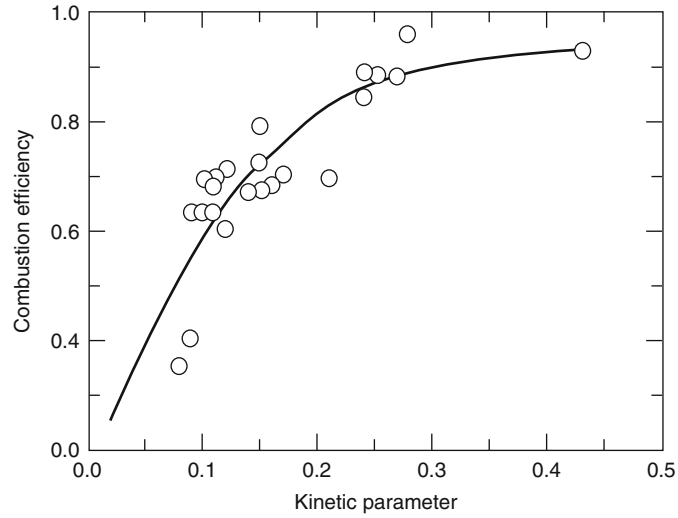

Fig. 36.53 Combustion efficiency versus kinetic parameter for flame extinction versus. Data were measured in the Fire Propagation Apparatus

Table 36.16 Critical chemical, convective, and radiative heat release rates for flame extinction

	Critical heat release rate (kW/m^2)		
Material	Chemical	Convective	Radiative
Polyoxymethylene	(65)	50	(14)
Polymethylmethacrylate	77	53	24
Polyethylene	96	55	42
Polypropylene	104	61	43
Polyethylene foams	88	51	38
Chlorinated polyethylenes	95	48	47
Polystyrenes	108	44	64
Polyurethane foams (flexible)	101	48	53
Polyurethane foams (rigid)	102	44	58
Average	96 ± 10	51 ± 6	46 ± 12

Note: Critical mass loss rates from Table 36.15, and heats of combustion from Table A.39

nonreactive vapors, such as Teflon, it is difficult to reach the critical heat release rate values unless high external heat flux is applied.

The energy balance at the surface as the flame extinction condition is reached can be represented by modifying Equations 36.15 and 36.34 [156]

$$\dot{m}'' = \frac{\Phi \Delta H_T \dot{m}''_{\text{cr}} + \dot{q}''_e - \dot{q}''_{rr} - \dot{q}''_{\text{agent}}}{\Delta H_g} \tag{36.96}$$

$$\dot{Q}''_i = \frac{\Delta H_i}{\Delta H_g}\left(\Phi \Delta H_T \dot{m}''_{\text{cr}} + \dot{q}''_e - \dot{q}''_{rr} - \dot{q}''_{\text{agent}}\right) \tag{36.97}$$

where

$\dot{q}''_e$ = External heat flux (kW/m^2)

$\dot{q}''_{rr}$ = Surface re-radiation loss (kW/m^2)

$\dot{q}''_{\text{agent}}$ = Heat flux removed from the surface or from the flame by the agent as the flame extinction condition is reached (kW/m^2)

ΔH_i = Chemical, convective, or radiative heat of combustion (kJ/g)

ΔH_g = Heat of gasification (kJ/g)

$\Delta H_i/\Delta H_g$ is defined as the heat release parameter (HRP) (see section "Heat Release Rate" of this chapter).

Flame Extinction by the Processes in the Gas Phase

The process of flame extinction by gaseous, powdered, and foaming agents and by an increase in the local equivalence ratio is predominantly a gas-phase process and, thus, is different from the process of flame extinction by water, which occurs predominantly in the solid phase at the surface of the material. The kinetic parameter for flame extinction defined in Equation 36.94, however, is still applicable [156]:

$$\Phi = \frac{\Phi_0 - \kappa Y_{j,\text{ex}}\left[\dfrac{1 + \Delta_{c_p}(T_{ad} - T_a) + \Delta H_D}{Y_{\text{O}} \Delta H^*_{\text{O}}}\right]}{1 - Y_{j,\text{ex}}} \tag{36.98}$$

where

ϕ = Kinetic parameter in the presence of the extinguishing agent

ϕ_0 = Kinetic parameter in the absence of the extinguishing agent

κ = Ratio between the kinetic parameters at the flame temperature and at the adiabatic flame temperature

$Y_{j,\text{ex}}$ = Mass fraction of the extinguishing agent

Δ_{cp} = Difference between the heat capacities of the extinguishing agent and the fire products (kJ/g/K)

T_{ad} = Adiabatic flame temperature at the stoichiometric limit (K)

T_a = Initial temperature of the reactants (K)

ΔH_D = Heat of dissociation (kJ/g)

Equation 36.98 shows that the addition of an extinguishing agent reduces the kinetic parameter from its normal value and includes the effects of four flame extinction mechanisms

[156]: (1) dilution, effects are included in the $\kappa Y_{j,\mathrm{ex}}$ term; (2) added thermal capacity, effects are included in Δ_{cp}; (3) chemical inhibition, effects are included through T_{ad}; and (4) kinetic chain breaking and endothermic dissociation through Δc_P and ΔH_D terms.

From Equation 36.96, in the presence of an extinguishing agent that works in the gas phase,

$$\dot{m}'' = \frac{\varphi \Delta H_T \dot{m}''_{\mathrm{cr}} + \dot{q}''_e - \dot{q}''_{rr}}{\Delta H_g} \tag{36.99}$$

For fixed values of external heat flux, the addition of an extinguishing agent reduces the normal value of the kinetic parameter by one or more of the four mechanisms expressed by Equation 36.98; the mass loss rate decreases and approaches the critical value at which the flame is extinguished. Increasing the external heat flux would increase the mass loss rate, and further addition of the extinguishing agent would be needed to reduce the mass loss to its critical value and to reestablish the flame extinction condition. Continued increases in the extinguishing agent for increasing external heat flux will result in the denominator of Equation 36.98 to approach zero, at which point it would represent a nonflaming condition.

For a fixed airflow rate, as is generally the case in enclosure fires where the extinguishing agent working in the gas phase is used, an increase in the mass loss rate due to increasing external heat flux results in an increase in the equivalence ratio, defined in Equation 36.41. As the equivalence ratio increases and approaches values of 4.0 and higher, the combustion efficiency approaches values less than or equal to 0.40 (see Fig. 36.33), flames are extinguished, and nonflaming conditions become important [103, 104]. Thus, the upper limit for the application of the extinguishing agent working in the gas phase is dictated by the equivalence ratio ≥ 4.0 and/or the combustion efficiency ≤ 0.40. Under nonflaming conditions, an increase in the external heat flux increases the generation rate of the fuel vapors and the reduction-zone products.

Flame Extinction by Reduced Mass Fraction of Oxygen

Flame extinction by reduced mass fraction of oxygen can be the result of (1) dilution and heat capacity effects due to the addition of inert gases, such as N_2 and CO_2; and (2) chemical effects due to the retardation of chemical reactions and reduction in the flame heat flux to the surface, especially the radiative component.

Theoretical and experimental analyses have been performed for flame extinction by reduced oxygen mass fractions. For example, for polymethylmethacrylate (PMMA), an oxygen mass fraction value of 0.180 is predicted for flame extinction [157] compared to the experimental values of 0.181 for a 70-mm-wide, 190-mm-high, and 19-mm-thick vertical PMMA slab [158] and 0.178 for a 100-mm-wide, 25-mm-thick, and 300- and 610-mm-high vertical slabs of PMMA, and 25-mm-diameter and 610-mm-high vertical cylinder of PMMA [31]. The critical values of the chemical, convective, and radiative heat release for PMMA are 106, 73, and 33 kW/m^2 [31], respectively, showing a trend similar to one reported in Table 36.16. At oxygen mass fractions equal to or less than 0.201, flames are unstable and faint blue in color [31].

The effect external heat flux on flame extinction due to reduced oxygen mass fraction has been examined for buoyant turbulent diffusion flames [159]. For example, for rectangular and circular horizontal PMMA slabs, 0.06–0.10 m^2 in area and 0.03–0.05 m in thickness, exposed to external heat flux values of 0, 40, 60, and 65 kW/m^2, flame extinction is found at oxygen mass fractions of 0.178, 0.145, 0.134, and 0.128, respectively [6]. The data support Equation 36.99 and show that, for buoyant turbulent diffusion flames, flaming can occur up to relatively low oxygen mass fraction values. The only condition is that, in the gas phase, the reactant-oxidizer mixture is within the flammability limit.

The effect of reduced oxygen mass fraction on flame extinction of materials in a three-dimensional arrangement, where flame heat flux is enhanced, has been examined. Figure 36.54 shows an example where chemical heat release

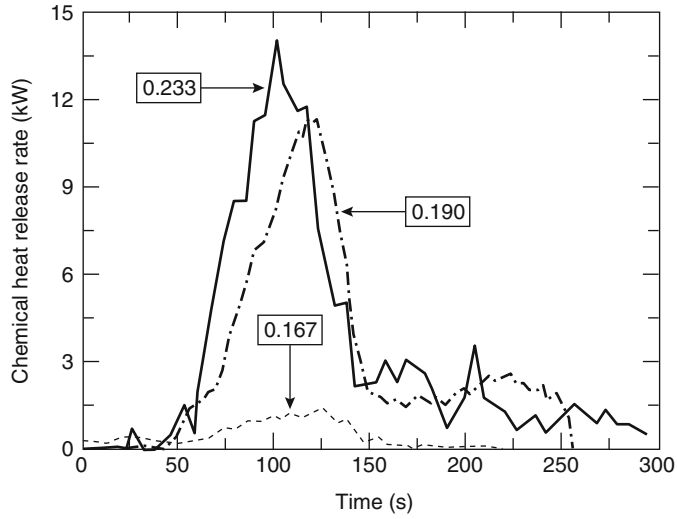

Fig. 36.54 Chemical heat release rate versus time for 50-mm empty corrugated paper boxes in a 2 × 2 × 2 arrangement (two boxes along the length × two boxes along the width × two layers, for a total of eight boxes separated by about 12 mm). Measurements were made in the Fire Propagation Apparatus with no external heat flux under co-flow conditions and at various oxygen mass fractions, which are indicated in the figure

rates at oxygen mass fractions of 0.233, 0.190, and 0.167 versus time are shown for the combustion of 50-mm cubes of empty corrugated paper boxes in a 2 × 2 × 2 arrangement. The weight of each box is about 13 g (839 g/m^2). The measurements were taken in the Fire Propagation Apparatus.

In Fig. 36.54, at an oxygen mass fraction of 0.167, the flame is close to the extinction condition, only 10.5 % of the initial weight of the boxes is consumed, which is equivalent to consumption of a single box with a surface area of about 0.0155 m^2. The peak chemical heat release rate close to flame extinction, in Fig. 36.54, is about 1.5 kW or 97 kW/m^2, using a surface area of 0.0155 m^2. This value is in excellent agreement with the average value in Table 36.16, derived from the critical mass loss rates for ignition. The data in Fig. 36.54 for the three-dimensional arrangement of the corrugated boxes thus support the firepoint theory [150, 151], independent of the critical heat release rate for flame extinction from the geometrical arrangement and surface areas of the materials, and Equations 36.98 and 36.99 as originally formulated in Ref. [156].

Definitions

Chemical heat of combustion	calorific energy generated in chemical reactions leading to varying degrees of incomplete combustion per unit fuel mass consumed
Convective heat of combustion	calorific energy carried away from the flame by the fire products-air mixture per unit fuel mass consumed
Heat of gasification	energy absorbed to vaporize a unit mass of fuel originally at ambient temperature
Heat release parameter	calorific energy generated per unit amount of calorific energy by the fuel
Kinetic parameter for flame extinction	maximum fraction of combustion energy that the flame reactions may lose to the sample surface by convection without flame extinction
Net heat of complete combustion	calorific energy generated in chemical complete reactions leading to combustion, with water as a gas, per unit fuel mass consumed

Radiative heat of combustion	calorific energy emitted as thermal radiation from the flame per unit fuel mass consumed

Nomenclature

A	total exposed surface area of the material (m^2)
a_j	mass coefficient for the product yield (g/g)
b_j	molar coefficient for the product yield (g/mol)
B_{cr}	critical mass transfer number
CHF	critical heat flux (kW/m^2)
$\dot{C}''_O$	mass consumption rate of oxygen ($g/m^2/s$)
$\dot{C}''_{stoich,O}$	stoichiometric mass consumption rate of oxygen ($g/m^2/s$)
c_O	mass of oxygen consumed per unit mass of fuel (g/g)
c_P	specific heat (kJ/g/K)
Δc_P	difference between the heat capacities of the extinguishing agent and the fire products (kJ/g/K)
D	optical density (1/m)
E_i	total amount of heat generated in the combustion of a material (kJ)
f_j	volume fraction of a product
fp	fire property
FPI	Fire Propagation Index
FSP_c	convective flame spread parameter
$\dot{G}''_j$	mass generation rate of product j ($g/m^2/s$)
$\dot{G}''_{stoich,j}$	stoichiometric mass generation rate of product j ($g/m^2/s$)
ΔH_i	heat of combustion per unit mass of fuel vaporized (kJ/g)
ΔH_D	heat of dissociation (kJ/g)
ΔH_g	heat of gasification at ambient temperature (kJ/g)
$\Delta H_{g,con}$	flame convective energy transfer to the fuel per unit mass of fuel gasified (kJ/g)
ΔH_m	heat of melting at the melting temperature (kJ/g)
ΔH_T	net heat of complete combustion per unit of fuel vaporized (kJ/g)
ΔH_v	heat of vaporization at the vaporization temperature (kJ/g)
ΔH^*_{CO}	net heat of complete combustion per unit mass of CO generated (kJ/g)
$\Delta H^*_{CO_2}$	net heat of complete combustion per unit mass of CO_2 generated (kJ/g)
ΔH^*_O	net heat of complete combustion per unit mass of oxygen consumed (kJ/g)
HRP	heat release parameter
h_i	mass coefficient for the heat of combustion (kJ/g)
I/I_0	fraction of light transmitted through smoke
j	fire product
k	thermal conductivity (kW/m/K)
L_{sp}	smoke point (m)
l	optical path length (m)
$\dot{m}''$	mass loss rate ($g/m^2/s$)
M	molecular weight (g/mol)
m_i	molar coefficient for the heat of combustion (kJ/mol)
$\dot{m}_{air}$	mass flow rate of air (g/s)
$\dot{q}''_e$	external heat flux (kW/m^2)
$\dot{q}''_f$	flame heat flux (kW/m^2)
$\dot{Q}''_i$	heat release rate per unit sample surface area (kW/m^2)
$\dot{Q}'_i$	heat release rate per unit sample width (kW/m)
S	stoichiometric mass air-to-fuel ratio (g/g)
t	time (s)
t_f	time at which there is no more vapor formation (s)
t_0	time at which the sample is exposed to heat (s)
T	temperature (K)
ΔT_{ig}	ignition temperature above ambient (K)
TRP	thermal response parameter ($kW \cdot s^{1/2}/m^2$)
u	fire propagation rate (mm/s or m/s)
$\dot{V}$	total volumetric flow rate of fire product-air mixture (m^3/s)
$\dot{W}$	total mass flow rate of the fire product-air mixture (g/s)

W_f	total mass of the material lost in the flaming and nonflaming process (g)
W_j	total mass of product j generated in the flaming and nonflaming process (g)
X_f	flame height (m or mm)
X_p	pyrolysis front (m or mm)
X_t	total length available for fire propagation (m or mm)
y_j	yield of product j
$Y_{j,\mathrm{ex}}$	mass fraction of extinguishing agent
Y_{O}	mass fraction of oxygen

Greek Letters

α	correlation coefficient (nonflaming fire)
β	correlation coefficient (transition region)
ϕ	kinetic parameter for flame extinction
ξ	correlation coefficient (transition region)
Φ	equivalence ratio
χ_{ch}	combustion efficiency
χ_{con}	convective component of the combustion efficiency
χ_{rad}	radiative component of the combustion efficiency
η_j	generation efficiency
κ	ratio between the kinetic parameters for the flame temperature and adiabatic flame temperature
λ	wavelength of light (μm)
σ	Stefan-Boltzmann constant (56.7×10^{-12} kW/m^2/K^4)
$\overline{\tau}$	average specific extinction area (m^2/g)
ρ	density (g/m^3)
ν_j	stoichiometric coefficient of product j
ν_{O}	stoichiometric coefficient of oxygen
Ψ_j	stoichiometric yield for the maximum conversion of fuel to product j
Ψ_{O}	stoichiometric mass oxygen-to-fuel ratio (g/g)
ζ	ratio of fire properties for ventilation-controlled to well-ventilated combustion
ζ_{oxid}	oxidation zone product generation efficiency ratio
ζ_{red}	reduction zone product generation efficiency ratio

Subscripts

a	air or ambient
ad	adiabatic
asy	asymptotic
ch	chemical
con	convective
cr	critical
e	external
ex	extinguishment
f	flame or fuel
fc	flame convective
fr	flame radiative
g	gas
g,con	flame convective energy for fuel gasification
i	chemical, convective, radiative
ig	ignition
j	fire product
n	net
0	initial
oxid	oxidation zone of a flame
rad	radiation
red	reduction zone of a flame
stoich	stoichiometric for the maximum possible conversion of fuel monomer to a product
rr	surface re-radiation
s	surface, smoke
vc	ventilation-controlled fire
wv	well-ventilated fire
∞	infinite amount of air

Superscripts

$\cdot$	per unit time (s^{-1})
$'$	per unit width (m^{-1})
$''$	per unit area (m^{-2})

References

1. Smith, EE (1972) Measuring Rate of Heat, Smoke, and Toxic Gas Release. Fire Technol 8:237–245. doi:10.1007/BF02590547
2. Smith, EE (1972) Heat Release Rate of Building Materials. In: Robertson AF (ed) Ignition, Heat Release, and Non-combustibility of Materials,

ASTM Special Technical Publication 502, pp. 119–134. doi:10.1520/STP502-EB
3. ASTM E906/E906M-14 (2014) Standard Test Method for Heat and Visible Smoke Release Rates for Materials and Products. ASTM International, West Conshohocken, PA. doi:10.1520/E0906_E0906M, www.astm.org.
4. Sarkos CP, Filipczak RA, Abramowitz A (1989) Preliminary Evaluation of an Improved Flammability Test Method for Aircraft Materials. Technical Report DOT/FAA/CT-89/15, Federal Aviation Administration, Atlantic City, NJ.
5. Tsuchiya Y, Mathieu JF (1991) Measuring Degrees of Combustibility Using an OSU Apparatus and Oxygen Depletion Principle. Fire Saf J 17:291–299. doi:10.1016/0379-7112(91)90024-S
6. Tewarson A, Pion RF (1976) Flammability of Plastics. I. Burning Intensity. Combust Flame 26:85–103. doi:10.1016/0010-2180(76)90059-6
7. Tewarson A (1976) Heat Release Rates from Samples of Polymethylmethacrylate and Polystyrene Burning in Normal Air. Fire Mater 1:90–96. doi:10.1002/fam.810010303
8. Tewarson A, Tamanini F. (1976) Research and Development for a Laboratory-Scale Flammability Test Method for Cellular Plastics. Technical Report No. 22524, RC76-T-64, National Institute of Standards and Technology, Gaithersburg, MD.
9. Tewarson A (1977) Heat Release Rate in Fires. J Fire Flammabl 8:115–121.
10. ASTM E2058-13a (2013) Standard Test Methods for Measurement of Synthetic Polymer Material Flammability Using a Fire Propagation Apparatus (FPA), ASTM International, West Conshohocken, PA. doi:10.1520/E2058, www.astm.org.
11. ISO 12136:2011 (2011) Reaction to Fire tests – Measurement of Material Properties Using a Fire Propagation Apparatus. International Organization for Standardization, Geneva, Switzerland.
12. Tewarson A. (1980) Physico-Chemical and Combustion/Pyrolysis Properties of Polymeric Materials, Technical Report NBS-GCR-80-295, National Institute of Standards and Technology, Gaithersburg, MD.
13. Tewarson A, Lee JL, Pion RF (1981) The Influence of Oxygen Concentration on Fuel Parameters for Fire Modeling, Proc Combust Inst 18:563–570. doi:10.1016/S0082-0784(81)80061-6
14. Tewarson A. (1982) Experimental Evaluation of Flammability Parameters of Polymeric Materials. In: Lewin M, Atlas SM, Pearce EM (eds) Flame Retardant Polymeric Materials, Plenum Press, New York, pp. 97–153.
15. Tewarson A. (1986) Prediction of Fire Properties of Materials Part 1: Aliphatic and Aromatic Hydrocarbons and Related Polymers. Technical Report NBS-GCR-86-521, National Institute of Standards and Technology, Gaithersburg, MD.
16. Tewarson A, Khan MM (1992) A New Standard Test Method for the Quantification of Fire Propagation Behavior of Electrical Cables Using Factory Mutual Research Corporation's Small-Scale Flammability Apparatus. Fire Technol 28:215–227. doi:10.1007/BF01857691
17. FM Approval Class Number 3972 (2009) Test Standard for Cable Fire Propagation. FM Approvals, Norwood, MA. http://www.fmglobal.com/assets/pdf/fmapprovals/3972.pdf. Accessed August 2015.
18. FM Approval Class Number 4880 (2010) Approval Standard for Class 1 Fire Rating of Insulated Wall or Wall and Roof/Ceiling Panels, Interior Finish Materials or Coatings and Exterior Wall Systems. FM Approvals, Norwood, MA. http://www.fmglobal.com/assets/pdf/fmapprovals/4880.pdf. Accessed August 2015.
19. ANSI/FM Approvals 4910 (2013) American National Standard for Cleanroom Materials Flammability Test Protocol. FM Approvals, Norwood, MA. http://www.fmglobal.com/assets/pdf/fmapprovals/4910ansi1.pdf. Accessed August 2015.
20. FM Approval Class Number 4998 (1995) Approval Standard for Class 1 Conveyor Belting. FM Approvals, Norwood, MA. http://www.fmglobal.com/assets/pdf/fmapprovals/4998.pdf. Accessed August 2015.
21. Hugget C (1980) Estimation of Rate of Heat Release by Means of Oxygen Consumption Measurements. Fire Mater 4:61–65. doi:10.1002/fam.810040202
22. Babrauskas V (1982) Development of the Cone Calorimeter - A Bench-Scale Heat Release Rate Apparatus Based on Oxygen Consumption. Technical Report NBSIR 82–2611, National Institute of Standards and Technology, Gaithersburg, MD.
23. Babrauskas V (1992) The Cone Calorimeter, In: Babrauskas V, Grayson SJ (eds) Heat Release in Fires, Elsevier Publishing Company, London, UK, pp. 61–92.
24. ASTM E1354-15 (2015) Standard Test Method for Heat and Visible Smoke Release Rates for Materials and Products Using an Oxygen Consumption Calorimeter, ASTM International, West Conshohocken, PA. doi:10.1520/E1354-15, www.astm.org.
25. Tewarson, A. (2004) Combustion Efficiency and Its Radiative Component. Fire Saf J 39:131–141. doi:10.1016/j.firesaf.2003.07.004
26. Mikkola E, Wichman IS (1989) On the Thermal Ignition of Combustible Materials. Fire Mater 14:87–96. doi:10.1002/fam.810140303
27. Delichatsios MA, Panagiotou Th, Kiley F (1991) . The Use of Time to Ignition Data for Characterizing the Thermal Inertia and the Minimum (Critical) Heat Flux for Ignition or Pyrolysis. Combust Flame 84:323–332. doi:10.1016/0010-2180(91)90009-Z
28. Tewarson A, Khan MM (1988) Flame Propagation for Polymers in Cylindrical Configuration and Vertical Orientation. Proc Combust Inst 22:1231–1240. doi:10.1016/S0082-0784(89)80134-1

29. Khan MM, de Ris JL, Ogden SD (2008) Effect of Moisture on Ignition Time of Cellulosic Materials. Fire Saf Sci 9:167–178. doi:10.3801/IAFSS.FSS.9-167
30. de Ris JL, Khan MM (2000) A Sample Holder for Determining Material Properties. Fire Mater 24:219–226. doi:10.1002/1099-1018(200009/10)
31. Tewarson A, Ogden SD (1992) Fire Behavior of Polymethylmethacrylate. Combust Flame 89:237–259. doi:10.1016/0010-2180(92)90013-F
32. Scudamore MJ, Briggs PJ, Prager FH (1991) Cone Calorimetry - A Review of Tests Carried Out on Plastics for the Association of Plastics Manufacturers in Europe. Fire Mater 15:65–84. doi:10.1002/fam.810150205
33. Jiang F, de Ris JL, Khan MM (2009) Absorption of Thermal Energy in PMMA by In-Depth Radiation. Fire Saf J 44:106–112. doi:10.1016/j.firesaf.2008.04.004
34. Bal N, Raynard J, Rein G, Torero JL, Försth M, Boulet M, Parent G, Acem Z, Linteris G (2013) Experimental Study of Radiative Heat Transfer in a Translucent Fuel Sample Exposed to Different Spectral Sources. Int J Heat Mass Transf 61:742–748. doi:10.1016/j.ijheatmasstransfer.2013.02.017
35. Chaos, M (2014) Spectral Aspects of Bench-Scale Flammability Testing: Application to Hardwood Pyrolysis. Fire Saf Sci 11. http://www.iafss.org/publications/fss/11/160
36. Khan MM, de Ris JL (2005) Operator Independent Ignition Measurements. Fire Saf Sci 8:163–174. doi:10.3801/IAFSS.FSS.8-163
37. ASTM E1321-13 (2013) Standard Test Method for Determining Material Ignition and Flame Spread Properties, ASTM International, West Conshohocken, PA. doi:10.1520/E1321, www.astm.org
38. Fernández-Pello AC, Hirano T (1983) Controlling Mechanisms of Flame Spread. Combust Sci Technol 32:1–31. doi:10.1080/00102208308923650.
39. ICEA T-29-520 (1986) Conducting Vertical Cable Tray Flame Tests with Theoretical Heat Input Rate of 210,000 B.T.U./Hour, Insulated Cable Engineers Association, Englewood, CO
40. CAN/CSA-C22.2 (2009) Optical Fiber Cable and Communication Cable Raceway Systems, CSA Group, Toronto, ON
41. UL 1581 (2001) Reference Standard for Electrical Wires, Cables, and Flexible Cords, Underwriters Laboratories, Northbrook, IL
42. Tewarson A, Chin W, Shuford R (2004) Materials Specifications, Standards, and Testing. In: Harper CA (ed) Handbook of Building Materials for Fire Protection. McGraw-Hill, New York, pp. 2.1-2.54 .
43. Tewarson A, Macaione D (1993) Polymers and Composites - An Examination of Fire Spread and Generation of Heat and Fire Products. J Fire Sci 11:421–441. doi:10.1177/073490419301100504199 3
44. Tewarson A (1994) Flammability Parameters of Materials: Ignition, Combustion, and Fire Propagation. J Fire Sci 12:329–356. doi:10.1177/073490419401200401
45. Khan MM (1999) Fire Propagation Characteristics of Conveyor Belts. Proceedings of the Third International Conference on Fire Research and Engineering, pp. 205-216, Society of Fire Protection Engineers, Bethesda, MD.
46. Khan MM, Bill RG Jr, Alpert RL (2006) Screening of Plenum Cables Using a Small-Scale Fire Test Protocol. Fire Mater 30:65–76. doi:10.1002/fam.899
47. Tewarson A (2003) Flammability of Polymers. In: Andrady AL (ed) Plastics and Environment. John Wiley & Sons, Inc., Hoboken, NJ, pp. 403–489.
48. Tewarson A (1994) Fire Hardening Assessment (FHA) Technology for Composite Systems. Technical Report ARL-CR-178, Army Research Laboratory, Aberdeen Proving Ground, MD.
49. Tewarson A, Khan MM, Wu PK, Bill RG Jr (2001) Flammability of Clean Room Polymeric Materials for the Semiconductor Industry. Fire Mater 25:31–42. doi:10.1002/1099-1018(200101/02)25:1<31::AID-FAM755>3.0.CO;2-A
50. Lyon RE, Janssens ML (2005) Polymer Flammability. Final Report DOT/FAA/AR-05/14, Office of Aviation Research, Washington, D.C.
51. Newman JS, Tewarson A (1991) Flame Spread Behavior of Char-Forming Wall/Ceiling Insulations. Fire Saf Sci 3:679–688. doi:10.3801/IAFSS.FSS.3-679
52. Newman JS (1993) Integrated Approach to Flammability Evaluation of Polyurethane Wall/Ceiling Materials. Polyurethanes World Congress, Society of the Plastics Industry, Washington, D.C.
53. Nam S, Bill RG Jr (2009) A New Intermediate-scale Fire Test for Evaluating Building Material Flammability. J Fire Prot Eng 19:157–176. doi:10.1177/1042391508101994
54. Haynes WM (ed) (2012) CRC Handbook of Chemistry and Physics, 93rd ed. CRC Press, Inc., Boca Raton, FL.
55. Paul MA (1962) Physical Chemistry. D.C. Heath and Company, Boston, MA, p. 46.
56. Kern DQ (1950) Process Heat Transfer. McGraw-Hill Book Company, New York, NY, p. 72.
57. Hottel HC (1959) Review of Certain Laws Governing Diffusive Burning of Liquids. Fire Res Abstr Rev 1:41–44.
58. Croce P (2001) The FORUM for International Cooperation on Fire Research: A Position Paper on Evaluation of Products and Services for Global Acceptance. Fire Saf J 36:715–717. doi:10.1016/S0379-7112(01)00034-0
59. Gritzo LA, Senseny PE, Xin Y, Thomas JR (2005) The International FORUM of Fire Research Directors: A Position Paper on Verification and Validation of Numerical Fire Models. Fire Saf J 40:485–490. doi:10.1016/j.firesaf.2005.02.001.
60. Dorofeev SB, Chaos M, Khan MM, Krishnamoorthy N, Chatterjee P, Wang Y, Bill RG

Jr (2011) An Approach for Evaluation of Material Flammability Via Bench-Scale Testing and CFD Simulations. Proceedings of the 12th International Conference on Fire and Materials, San Francisco, CA, pp. 321–332.
61. McGrattan K, Hostikka S, McDermott R, Floyd J, Weinschenk C, Overholt K (2015) Fire Dynamics Simulator Technical Reference Guide Volume 1: Mathematical Model. NIST Special Publication 1018-1, 6th ed, National Institute of Standards and Technology, Gaithersburg, MD. doi:10.6028/NIST.SP.1018-1
62. Stoliarov SI, Lyon RE (2008) Thermo-Kinetic Model of Burning. Technical Report DOT/FAA/AR-TN08/17, Federal Aviation Administration, Atlantic City, NJ.
63. Lautenberger CW (2007) A Generalized Pyrolysis Model for Combustible Solids. PhD Dissertation, University of California, Berkeley, CA. http://escholarship.org/uc/item/7wz5m7dg. Accessed August 2015.
64. GPyro. http://reaxengineering.com/trac/gpyro. Accessed August 2015.
65. Lattimer BY, Ouellette J (2006) Properties of Composite Materials for Thermal Analysis Involving Fires. Compos: Part A 37:1068–1081. doi:10.1016/j.compositesa.2005.01.029
66. Stoliarov SI, Crowley S, Lyon RE, Linteris GT (2009) Prediction of the Burning Rates of Non-Charring Polymers. Combust Flame 156:1068–1083. doi:10.1016/j.combustflame.2008.11.010
67. Stoliarov SI, Crowley S, Walters RN, Lyon RE (2010) Prediction of the Burning Rates of Charring Polymers. Combust Flame 157:2024–2034. doi:10.1016/j.combustflame.2010.03.011
68. de Ris JL, Yan Z (1998) Modeling Ignition and Pyrolysis of Solid Fuels. Proceedings of the 5th International Conference on Fire and Materials, San Antonio, TX, pp. 111–121.
69. Theuns E, Merci B, Vierendeels J, Vandevelde P (2005) Critical Evaluation of an Integral Model for the Pyrolysis of Charring Materials. Fire Saf J 40:121–140. doi:10.1016/j.firesaf.2004.09.003
70. Lautenberger C, Rein G, Fernández-Pello C (2006) The Application of a Genetic Algorithm to Estimate Material Properties for Fire Modeling from Bench-Scale Fire Test Data. Fire S J 41:204–214. doi:10.1016/j.firesaf.2005.12.004
71. Lautenberger C, Kim E, Dembsey N, Fernández-Pello C (2008) The Role of Decomposition Kinetics in Pyrolysis Modeling – Application to a Fire Retardant Polyester Composite. Fire Safety Science 9:1201–1212. doi:10.3801/IAFSS.FSS.9-1201
72. Webster RD (2009) Pyrolysis Model Parameter Optimization Using a Customized Stochastic Hill-Climber Algorithm and Bench Scale Fire Test Data. MS Thesis, University of Maryland, College Park, MD. http://hdl.handle.net/1903/10004. Accessed August 2015.
73. Chaos M, Khan MM, Krishnamoorthy N, de Ris JL, Dorofeev SB (2010) FPA Bench-Scale Flammability Tests and Extraction of Solid Fuel Properties for Fire Models. Proceedings of the 6th International Seminar on Fire and Explosion Hazards, Leeds, UK, paper 161. doi:10.3850/978-981-08-7724-8_15-01
74. Chaos M, Khan MM, Krishnamoorthy M, de Ris JL, Dorofeev SB (2010) Bench-Scale Flammability Experiments: Determination of Material Properties Using Pyrolysis Models for Use in CFD Fire Simulations. Proceedings of the 12th International Fire Science and Engineering Conference, Interflam2010, Nottingham, UK, pp. 697–708.
75. Chaos M, Khan MM, Krishnamoorthy N, de Ris JL, Dorofeev SB (2011) Evaluation of Optimization Schemes and Determination of Solid Fuel Properties for CFD Fire Models using Bench-scale Pyrolysis Tests. Proc Combust Inst 33:2599–2606. doi:10.1016/j.proci.2010.07.018
76. Matala A, Hostikka S (2011) Pyrolysis Modelling of PVC Cable Materials. Fire Saf Sci 10:917–930. doi:10.3801/IAFSS.FSS.10-917
77. Huang CH, Özisik MN (1991) Direct Integration Approach for Simultaneously Estimating Temperature Dependent Thermal Conductivity and Heat Capacity. Numer Heat Transf A 20:95–110. doi:10.1080/10407789108944811
78. Jurkowski T, Jarny Y, Delaunay D (1997) Estimation of Thermal Conductivity of Thermoplastics under Moulding Conditions: An Apparatus and an Inverse Algorithm. Int J Heat Mass Transf 40:4169–4181. doi:10.1016/S0017-9310(97)00027-6
79. García S, Guynn J, Scott EP (1998) Use of Genetic Algorithms in Thermal Property Estimation: Part II – Simultaneous Estimation of Thermal Properties. Numer Heat Transf A 33:149–168. doi:10.1080/10407789808913931
80. Loulou T (2007) Combined Parameter and Function Estimation with Application to Thermal Conductivity and Surface Heat Flux. J Heat Transf 129:1309–1320. doi:10.1115/1.2755064
81. Veiseh S, Hakkaki-Fard A, Kowsary F (2009) Determining of the Air/Fiber Conductivity of Mineral Wool Insulations in Building Applications Using Parameter Estimation Methods. J Build Phys 32:243–260. doi:10.1177/1744259108099431
82. Molavi H, Pourshaban I, Hakkaki-Fard A, Molavi M, Ayasoufi A, Rahmani RK (2009) Inverse Identification of Thermal Properties of Charring Ablators. Numer Heat Transf B 56:478–501. doi:10.1080/10407790903508129
83. Nelder JA, Mead R (1965) A Simplex Method for Function Minimization. Comput J 7:308–313. doi:10.1093/comjnl/7.4.308
84. Coleman TF, Li Y (1996) An Interior, Trust Region Approach for Nonlinear Minimization Subject to

Bounds. SIAM J Optim 6:418–445. doi:10.1137/S1052623494240456
85. Duan Q, Gupta VK, Sorooshian S (1993) Shuffled Complex Evolution Approach for Effective and Efficient Global Minimization. J Optim Theory Appl 76:501–521. doi:10.1007/BF00939380
86. Duan Q, Sorooshian S, Gupta VK (1994) Optimal Use of the SCE-UA Global Optimization Method for Calibrating Watershed Models. J Hydrol 158:265–284. doi:10.1016/0022-1694(94)90057-4
87. Lautenberger C, Fernández-Pello C (2011) Optimization Algorithms for Material Pyrolysis Property Estimation. Fire Saf Sci 10:751–764. doi:10.3801/IAFSS.FSS.10-751
88. Gaviano M, Lera D (1998) Test Functions with Variable Attraction Regions for Global Optimization Problems. J Glob Optim 13:207–223. doi:10.1023/A:1008225728209
89. Chaos M, Khan MM, Dorofeev SB (2012) Pyrolysis of Corrugated Cardboard in Inert and Oxidative Environments. Proc Combust Inst 34. doi:10.1016/j.proci.2012.06.031
90. Savitzky A, Golay MJE (1964) Smoothing and Differentiation of Data by Simplified Least Squares Procedures. Anal Chem 36:1627–1639. doi:10.1021/ac60214a047
91. Staggs JEJ (2005) Savitzky-Golay Smoothing and Numerical Differentiation of Cone Calorimeter Mass Data. Fire Saf J 40:493–505. doi:10.1016/j.firesaf.2005.05.002.
92. Bromba MUA, Ziegler H (1981) Application Hints for Savitzky-Golay Digital Smoothing Filters. Anal Chem 53:1583–1586. doi:10.1021/ac00234a011
93. Krishnamoorthy N, Chaos M, Khan MM, Chatterjee P, Wang Y, Dorofeev SB (2010) Experimental and Numerical Study of Flame Spread in Parallel Panel Geometry. Proceedings of the 6th International Seminar on Fire and Explosion Hazards, Leeds, UK, paper 155. doi:10.3850/978-981-08-7724-8_03-07
94. Krishnamoorthy N, Chaos M, Khan MM, Chatterjee P, Wang Y, Dorofeev SB (2010) Application of Bench-Scale Material Flammability Data to Model Flame Spread in Medium-Scale Parallel Panel Test. Proceedings of the 12th International Fire Science and Engineering Conference, Interflam2010, Nottingham UK, pp. 709–720.
95. Chaos M, Khan MM, Krishnamoorthy N, Chatterjee P, Wang Y, Dorofeev SB (2011) Experiments and Modeling Of Single- and Triple-Wall Corrugated Cardboard: Effective Material Properties and Fire Behavior. Proceedings of the 12th International Conference on Fire and Materials, San Francisco, CA, pp. 625–636.
96. Krishnamoorthy N, Chaos M, Khan MM, Chatterjee P, Wang Y, Dorofeev SB (2011) Numerical Modeling of Flame Spread over Corrugated Cardboard on Vertical Parallel Panels. Proceedings of the 7th US National Technical Meeting of the Combustion Institute, Atlanta, GA, Paper 1 F16.
97. Chaos M, Wang Y, Dorofeev SB (2012) CFD Modeling of Flame Spread over Corrugated Cardboard Panels. Proceedings of the International Congress on Fire and Computer Modeling, Oct. 18–19, 2012, Universidad de Cantabria, Spain.
98. Wang Y, Chatterjee P, de Ris JL (2011) Large Eddy Simulation of Fire Plumes. Proc Combust Inst 33:2473–2480. doi:10.1016/j.proci.2010.07.031
99. http://www.fmglobal.com/modeling. Accessed August 2015.
100. Thornton WM (1917) The Relation of Oxygen to the Heat of Combustion of Organic Compounds. Philos Mag Ser 6 33:196–203. doi:10.1080/14786440208635627
101. Macrae JC (1966) An Introduction to the Study of Fuel. Elsevier Publishing Company, London, UK.
102. ASTM D4809-13 (2013) Standard Test Method for Heat of Combustion of Liquid Hydrocarbon Fuels by Bomb Calorimeter (Precision Method). ASTM International, West Conshohocken, PA. doi:10.1520/D4809-13, www.astm.org.
103. Tewarson A, Jiang FH, Morikawa T (1993) Ventilation-Controlled Combustion of Polymers. Combust Flame 95:151–169. doi:10.1016/0010-2180(93)90058-B
104. Tewarson A, Khan MM (1993) Extinguishment of Diffusion Flames of Polymeric Materials by Halon 1301. J Fire Sci 11:407–420. doi:10.1177/073490419301100503
105. Costa C, Treand G, Moineault F, Gustin J-L (1999) Assessment of the Thermal and Toxic Effects of Chemical and Pesticide Pool Fires Based on Experimental Data Obtained Using the Tewarson Apparatus. Process Saf Environ Prot 77:154–164. doi:10.1205/095758299529974
106. Brohez S, Delvosalle C (2009) Carbon Dioxide Generation Calorimetry - Errors Induced by the Simplifying Assumptions in the Standard Test Methods. Fire Mater 33:89–97. doi:10.1002/fam.988
107. Tewarson A, Marlair G (2004) Liquids and Chemicals. In: Harper CA (ed) Handbook of Building Materials for Fire Protection. McGraw-Hill, New York, pp. 8.1–8.43.
108. Brohez S, Delvosalle C, Marlair G, Tewarson A. (2000) The Measurement of Heat Release from Oxygen Consumption in Sooty Fires. J Fire Sci 18:327–353. doi:10.1177/073490410001800501
109. Brohez, S (2005) Uncertainty Analysis of Heat Release Rate Measurement from Oxygen Consumption Calorimetry. Fire Mater 29:383–394. doi:10.1002/fam.895
110. Biteau H, Fuentes A, Marlair G, Brohez S, Torero JL (2009) Ability of the Fire Propagation Apparatus to Characterise the Heat Release Rate of Energetic Materials. J Hazard Mater 166:916–924. doi:10.1016/j.jhazmat.2008.11.100
111. Biteau H, Steinhaus T, Schemel C, Simeoni A, Marlair G, Bal N, Torero JL (2008) Calculation Methods for the Heat Release Rate of Materials of

Unknown Composition. Fire Saf Sci 9:1165–1176. doi:10.3801/IAFSS.FSS.9-1165
112. Tewarson A (1986) Prediction of Fire Properties of Materials Part 1: Aliphatic and Aromatic Hydrocarbons and Related Polymers. Technical Report NBS-GCR-86-521, National Institute of Standards and Technology, Gaithersburg, MD.
113. Hirschler MM (1987) Fire Hazard and Toxic Potency of the Smoke from Burning Materials. J Fire Sci 5:289–307. doi:10.1177/073490418700500501
114. Tewarson A (1988) Smoke Point Height and Fire Properties of Materials. Technical Report NBS-GCR-88-555, National Institute of Standards and Technology, Gaithersburg, MD.
115. Tewarson A, Zalosh RG (1989) Flammability Testing of Aircraft Cabin Materials, Paper 33 in AGARD Conference Proceedings No. 467 - Aircraft Fire Safety; Propulsion and Energetics Panel 73rd Symposium, Sintra, Portugal, May 22–26, 1989.
116. Tsantarides L, Ostman B (1989) Smoke, Gas, and Heat Release Data for Building Products in the Cone Calorimeter. Technical Report I 8903013, Swedish Institute for Wood Technology Research, Stockholm, Sweden.
117. Khan MM (1992) Characterization of Liquid Fuel Spray Fires. In: Cho P, Quintiere J (eds) Heat and Mass Transfer in Fire and Combustion Systems, American Society of Mechanical Engineers, New York, NY.
118. Sivathanu YR, Faeth GM (1990) Generalized State Relationships for Scalar Properties in Nonpremixed Hydrocarbon/Air Flames. Combust Flame 82:211–230. doi:10.1016/0010-2180(90)90099-D
119. Khan MM, Bill RG Jr (2003) Comparison of Flammability Measurements in Vertical and Horizontal Exhaust Duct in the ASTM E-2058 Fire Propagation Apparatus. Fire Mater 27:253–266. doi:10.1002/fam.830
120. Newman JS, Steciak J (1987) Characterization of Particulates from Diffusion Flames. Combust Flame 67:55–64. doi:10.1016/0010-2180(87)90013-7
121. Mulholland GW, Choi MY (1998) Measurement of the Mass Specific Extinction Coefficient for Acetylene and Ethene Smoke Using the Large Agglomerate Optics Facility. Proc Combust Inst 27:1515–1522. doi:10.1016/S0082-0784(98)80559-6
122. Drysdale D (1985) An Introduction to Fire Dynamics. Wiley, New York, NY, pp. 278–400.
123. Beyler CL (1986) Major Species Production by Diffusion Flames in a Two-Layer Compartment Fire Environment. Fire Saf J 10:47–56. doi:10.1016/0379-7112(86)90031-7
124. Beyler CL (1991) Analysis of Compartment Fires with Overhead Forced Ventilation. Fire Saf Sci 3:291–300. doi:10.3801/IAFSS.FSS.3-291
125. Morehart JH, Zukoski EE, Kubota T (1991) Characteristics of Large Diffusion Flames Burning in a Vitiated Atmosphere. Fire Saf Sci 3:575–583. doi:10.3801/IAFSS.FSS.3-575
126. Tewarson A, Chu F, Jiang FH (1994) Combustion of Halogenated Polymers. Fire Saf Sci 4:563–574. doi:10.3801/IAFSS.FSS.4-563
127. ASTM D1322-08 (2008) Standard Test Method for Smoke Point of Kerosine and Aviation Turbine Fuel, ASTM International, West Conshohocken, PA. doi:10.1520/D1322-08, www.astm.org.
128. Haynes BS, Wagner HGg (1981) Soot Formation. Prog Energy Combust Sci 7:229–273. doi:10.1016/0360-1285(81)90001-0
129. Kent JH, Wagner HGg (1984) Why Do Diffusion Flames Emit Soot. Combust Sci Technol 41:245–269. doi:10.1080/00102208408923834
130. Olson DB, Pickens JC, Gill RJ (1985) The Effects of Molecular Structure on Soot Formation, II. Diffusion Flames. Combust Flame 62:43–60. doi:10.1016/0010-2180(85)90092-6
131. Markstein GH (1985) Relationship between Smokepoint and Radiant Emission from Buoyant Turbulent and Laminar Diffusion Flames. Proc Combust Inst 20:1055–1061. doi:10.1016/S0082-0784(85)80595-6
132. Kent JH (1986) A Quantitative Relationship Between Soot Yield and Smoke Point Measurements. Combust Flame 63:349–358. doi:10.1016/0010-2180(86)90004-0
133. Kent JH (1987) Turbulent Diffusion Flame Sooting - Relationship to Smoke-Point Tests. Combust Flame 67:223–233. doi:10.1016/0010-2180(87)90098-8
134. Glassman I (1989) Soot Formation in Combustion Processes. Proc Combust Inst 22:295–311. doi:10.1016/S0082-0784(89)80036-0
135. Markstein GH (1989) Correlations for Smoke Points and Radiant Emission of Laminar Hydrocarbon Diffusion Flames. Proc Combust Inst 22:363–370. doi:10.1016/S0082-0784(89)80042-6
136. Gülder ÖL (1989) Influence of Hydrocarbon Fuel Structure Constitution and Flame Temperature on Soot Formation in Laminar Diffusion Flames. Combust Flame 78:179–194. doi:10.1016/0010-2180(89)90124-7
137. Shivathanu YR, Faeth GM (1990) Soot Volume Fractions in the Overfire Region of Turbulent Diffusion Flames. Combust Flame 81:133–149. doi:10.1016/0010-2180(90)90060-5
138. Köylü ÜÖ, Sivathanu YR, Faeth GM (1991) Carbon Monoxide and Soot Emissions from Buoyant Turbulent Diffusion Flames. Fire Saf Sci 3:625–634. doi:10.3801/IAFSS.FSS.3-625
139. Köylü ÜÖ, Faeth GM (1991) Carbon Monoxide and Soot Emissions from Liquid-Fueled Buoyant Turbulent Diffusion Flames. Combust Flame 87:61–76. doi:10.1016/0010-2180(91)90027-9
140. Orloff L, de Ris JL, Delichatsios MA (1992) Radiation from Buoyant Turbulent Diffusion Flames. Combust Sci Technol 84:177–186. doi:10.1080/00102209208951852

141. Gülder ÖL (1992) Soot Formation in Laminar Diffusion Flames at Elevated Temperatures. Combust Flame 88:75–82. doi:10.1016/0010-2180(92)90008-D
142. Köylü ÜÖ, Faeth GM (1992) Structure of Overfire Soot in Buoyant Turbulent Diffusion Flames at Long Residence Times. Combust Flame 89:140–156. doi:10.1016/0010-2180(92)90024-J
143. de Ris JL, Cheng X (1994) The Role of Smoke-point in Material Flammability Testing. Fire Saf Sci 4:301–312. doi:10.3801/IAFSS.FSS.4-301
144. Linteris GT, Rafferty JP (2008) Flame Size, Heat Release, and Smoke Points in Materials Flammability. Fire Saf J 43:442–450. doi:10.1016/j.firesaf.2007.11.006
145. Tran MK, Dunn-Rankin D, Pham TK (2012) Characterizing Sooting Propensity in Biofuel-Diesel Flames. Combust Flame 159:2181–2191. doi:10.1016/j.combustflame.2012.01.008
146. Lautenberger CW, de Ris JL, Dembsey NA, Barnett JR, Baum HR (2005) A Simplified Model for Soot Formation and Oxidation in CFD Simulation of Non-Premixed Hydrocarbon Flames. Fire Saf J 40:141–176. doi:10.1016/j.firesaf.2004.10.002
147. Chatterjee P, de Ris JL, Wang Y, Dorofeev SB (2011) A Model for Soot Radiation in Buoyant Diffusion Flames. Proc Combust Inst 33:2665–2671. doi:10.1016/j.proci.2010.06.112
148. Madorsky SL (1964) Thermal Degradation of Organic Polymers. Interscience Publishers, John Wiley & Sons, Inc., New York, NY, p. 192.
149. Tewarson A, Khan MM (1991) The Role of Active and Passive Fire Protection Techniques in Fire Control, Suppression and Extinguishment. Fire Saf Sci 3:1007–1017. doi:10.3801/IAFSS.FSS.3-1007
150. Rasbash DJ (1976) A Flame Extinction Criterion for Fire Spread. Combust Flame 26:411–412. doi:10.1016/0010-2180(76)90095-X
151. Rasbash DJ (1986) The Extinction of Fire with Plain Water: A Review. Fire Saf Sci 1:1145–1163. doi:10.3801/IAFSS.FSS.1-1145
152. Spalding DB (1960) A Standard Formulation of the Steady Convective Mass Transfer Problem. Int J Heat Mass Transf 1:192–207. doi:10.1016/0017-9310(60)90022-3
153. Heskestad G (1980) The Role of Water in Suppression of Fire: A Review. J Fire Flammabl 11:254–262.
154. Magee RS, Reitz RD (1975) Extinguishment of Radiation Augmented Plastic Fires by Water Sprays. Proc Combust Inst 15:337–347. doi:10.1016/S0082-0784(75)80309-2
155. Thomson HE, Drysdale DD (1989) Critical Mass Flowrate at the Firepoint of Plastics. Fire Saf Sci 2:67–76. doi:10.3801/IAFSS.FSS.2-67
156. Beyler C (1992) A Unified Model of Fire Suppression. J Fire Prot Eng 4:5–16. doi:10.1177/104239159200400102
157. Kodama H, Miyasaka K, Fernández-Pello AC (1987) Extinction and Stabilization of a Diffusion Flame on a Flat Combustible Surface with Emphasis on Thermal Controlling Mechanisms. Combust Sci Technol 54:37–50. doi:10.1080/00102208708947042
158. Kulkarni AK, Sibulkin M (1982) Burning Rate Measurements on Vertical Fuel Surfaces. Combust Flame 44:185–186. doi:10.1016/0010-2180(82)90072-4
159. Xin Y, Khan MM (2007) Flammability of Combustible Materials in Reduced Oxygen Environment. Fire Saf J 42:536–547. doi:10.1016/j.firesaf.2007.04.003

Mohammed M. Khan is a Senior Lead Research Scientist (retired) (in place of Senior Research Specialist). He has more than 30 years of flammability research experience. He is recognized for his work on ignition, flame spread, and material flammability characterization.

Archibald Tewarson retired from FM Global. His major specialization is in chemical aspects of fires.

Marcos Chaos is a Senior Lead Research Scientist at the Research Division of FM Global. He has specialized in pyrolysis modeling and optimization algorithms as well as experimental aspects of flammability testing.

Performance-Based Design

37

Morgan J. Hurley and Eric R. Rosenbaum

Introduction

The *SFPE Engineering Guide to Performance-Based Fire Protection* [1] defines performance-based design as "an engineering approach to fire protection design based on (1) agreed upon fire safety goals and objectives, (2) deterministic and/or probabilistic analysis of fire scenarios, and (3) quantitative assessment of design alternatives against the fire safety goals and objectives using accepted engineering tools, methodologies, and performance criteria."

This definition identifies three key attributes of performance-based design. The first is a description of the desired level of fire safety in a building (or other structure) in the event of a fire. The second attribute includes definition of the "design basis" of the building. The "design basis" is an identification of the types of fires, occupant characteristics, and building characteristics for which the fire safety systems in the building are intended to provide protection. In the vernacular of performance-based design, these fires are referred to as "design fire scenarios." The third element involves an engineering analysis of proposed design strategies to determine whether or not they provide the intended level of safety in the event of the design fire scenarios.

M.J. Hurley (✉) • E.R. Rosenbaum

The purpose of this chapter is to provide an overview of performance-based design and to serve as insight into how other chapters in this handbook can be used as resources.

In most cases, utilizing performance-based design goes beyond code application to analysis of how a building and its occupants will be affected by fire. This generally requires consideration of the science of fire and human physiology and psychology. That is why performance-based design potentially utilizes many sections of the *SFPE Handbook of Fire Protection Engineering*.

Types of Performance

For performance-based design, Nelson [2] identifies the following four types of "performance" that may be evaluated.

Component Performance

Component performance identifies the intended performance in fire of individual building systems or components, such as doors, structural framing, or individual protection systems such as detection. In component performance analysis, individual components and systems are designed in isolation without considering how their performance may impact, or be impacted by, the performance of other systems or components. Any

M.J. Hurley (ed.), *SFPE Handbook of Fire Protection Engineering*,
DOI 10.1007/978-1-4939-2565-0_37, © Society of Fire Protection Engineers 2016

system or component that meets the stated performance would be considered to be acceptable.

An example of a component-performance-based approach would be a structural element that is designed to achieve a 1-h fire resistance rating when exposed to the "standard" fire. In this case, the intended performance would involve maximum acceptable point and average temperatures, and the design fire scenario would be the standard time-temperature curve. Although building codes typically require this performance to be achieved through fire testing, calculation methods are available as well [3]. Any assembly that achieves the intended performance when exposed to the design fire scenario would be acceptable.

Another example would be an individual sprinkler used in a sprinkler system. Sprinkler design standards and component standards might require a maximum actuation temperature and thermal response characteristics. Any sprinkler that meets the performance identified would be acceptable.

It is noteworthy that the codes and standards that govern fire-resistant structural elements and sprinklers contain specific requirements that are not performance based, such as limitations on the types of materials that can be used in fire-resistant assemblies and sprinklers.

Environmental Performance

Environmental performance involves identification of the maximum permissible fire conditions within a building or portion thereof. The specification of environmental conditions could involve temperature, heat flux, or products of combustion. Environmental performance approaches identify conditions that are tolerable if a fire were to occur. It is not possible to include fire prevention strategies within an environmental performance approach.

An example of an environmental performance approach would be a requirement that the smoke layer within an atrium not descend below a given elevation above the highest occupied level. Any design that would achieve this criterion would be acceptable, and the performance requirement does not specify or limit how this can be achieved.

Threat Potential Performance

Threat potential performance involves identification of the maximum acceptable threat to life, property, business continuity, or the natural environment. Unlike environmental performance requirements, which involve statements of maximum acceptable conditions in the environment surrounding items that are desired to be protected from fire, threat potential performance involves a statement of the maximum tolerable conditions of the item or items being protected.

An example of a threat potential performance requirement would be a fractional effective incapacitation dose (see Chap. 63). Another example would be an identification of the maximum permissible temperature of an object. As with environmental performance requirements, threat potential performance requirements do not specify or limit how the conditions can be achieved.

Risk Potential Performance

In risk potential performance, the summation of the products of probabilities of occurrence of fire events and their consequences are specified. An example of a risk potential performance requirement would be that the average permissible property loss in a facility resulting from fire must not exceed an average of $10,000 in value per year. When applying this type of approach, a designer would evaluate all possible fire events and their potential consequences. This can be expressed mathematically as [1]:

$$\text{Risk} = \sum \text{Risk}_i = \sum (\text{Loss}_i \cdot P_i)$$

where

Risk_i = Risk associated with scenario i
Loss_i = Loss associated with scenario i
P_i = Frequency of scenario i occurring

Nelson [2] also identifies the typical "prescriptive" approach, which he defines as

"specification." "Specification" involves strict definition of dimensions, construction methods, and other features. An example of "specification" would be some of the requirements in NFPA *101®, Life Safety Code®,* [4] applicable to stairway construction. NFPA *101* identifies specific dimensional requirements for stairs and handrails.

History of Performance-Based Fire Protection Design

Early (pre-1900s) fire protection requirements largely fit into the category of "specification," with such requirements including the permissible materials from which building exteriors could be constructed or the minimum acceptable spacing between buildings. However, most modern building and fire code requirements have some element of performance associated with them.

Performance-based approaches for designing building fire protection can be traced to the early 1970s, when the goal-oriented approach to building fire safety was developed by the U.S. General Services Administration [5]. Other major developments in performance-based design include the following:

- Publication of the performance-based British Regulations in 1985
- Publication in 1988 of the first edition of the *SFPE Handbook of Fire Protection Engineering*
- Publication of the performance-based New Zealand building code in 1992 and the New Zealand *Fire Engineering Design Guide* in 1994
- Publication of the Performance Building Code of Australia and the Australian *Fire Engineering Guidelines* in 1995
- Publication of the *Performance Requirements for Fire Safety and Technical Guide for Verification by Calculation* by the Nordic Committee on Building Regulations in 1995
- Publication of the performance option in the NFPA *101, Life Safety Code,* in 2000
- Publication of the *SFPE Engineering Guide to Performance-Based Fire Protection Analysis and Design of Buildings* in 2000
- Publication of the Japanese performance-based Building Standard Law in 2000
- Publication of the *ICC Performance Code for Buildings and Facilities* in 2001
- Publication of the performance option in the *NFPA 5000®, Building Construction and Safety Code®,* in 2003

The foregoing documents represent only the formalization of performance-based design. Performance-based design has long been practiced through the use of "equivalency" or "alternate methods and materials" clauses found in most, if not all, prescriptive codes and standards. These clauses permit the use of approaches or materials not specifically recognized in the code provided that the approach or material can be demonstrated to provide at least an equivalent level of safety as that achieved by compliance with the code or standard.

However, "equivalency" or "alternate methods and materials" clauses typically do not provide any detail as to how an equivalent level of safety can be achieved. Therefore, the approaches used by individual designers or regulatory officials were frequently developed on an ad hoc basis, with approaches varying among designers and among regulatory officials. The effect of the documents identified in the preceding text was to standardize the practice of performance-based design.

The development of performance-based design has followed an evolution in the quantitative understanding of fire. Before fire science was well understood, proven technologies would be codified into regulations. Similarly, as major fires occurred, and the causes and contributing factors of those fires were identified, codes and standards were modified to prevent similar major fires from occurring in the future.

Specification codes have the following two disadvantages:

- They potentially only protect against events of a type that have occurred in the past. Major

fires are low-probability, high-consequence events. Because of their stochastic nature, some types of rare events have not yet occurred.
- They potentially stifle innovation. By specifying certain types of methods and materials, it can be difficult to introduce new methods and materials into the marketplace.

As the science of fire has become better understood, performance-based fire protection design has become possible. Other engineering disciplines have evolved in a similar manner—as the underlying science has become better understood, their design approaches have become more performance based.

Advantages and Disadvantages of Performance-Based Design

Performance-based design offers a number of advantages and disadvantages over specification-based prescriptive design. As the design approach used moves from specification based toward risk based, these advantages and disadvantages are magnified.

Advantages

One advantage of performance-based design is that it allows the designer to address the unique features and uses of a building. For example, the stores in a shopping mall might have an identical occupancy classification under prescriptive building and fire codes and, hence, require similar fire protection strategies. However, the stores could contain significantly different fire hazards. Some could contain flammable liquids, whereas others might contain few or no combustible items at all. A corollary to this advantage is increased cost-effectiveness of performance-based designs.

Another advantage is that performance-based design promotes a better understanding of how a building would perform in the event of a fire. Compliance with prescriptive codes and standards is intended to result in a building that is "safe" from fire. However, what constitutes "safe" is generally not defined. Similarly, the types of fires against which the building is intended to achieve fire safety are not identified. Although most common fire scenarios would likely result in acceptable performance, the low-frequency scenarios that are not envisioned may not.

Two fire scenarios can be used to illustrate this. Carelessly discarded smoking materials would likely be within the design basis for a code that is intended to apply to a high-rise residential building. However, a gasoline tank truck that accidentally crashes into the building's lobby likely is not. Within these two extremes is a large range of possible events. A corollary to this advantage is that increased thought and engineering rigor are brought to solving fire protection problems.

Disadvantages

A disadvantage of performance-based design is that it requires more expertise to apply and review than does prescriptive-based design. Generally, application of prescriptive codes only requires the selection of building features and systems that fit within the code's requirements. Verification of the acceptability of a prescriptive-based design is equally straightforward. Performance-based design can take more time to conduct and review than prescriptive-based design.

Another disadvantage of performance-based design is that it can be more sensitive to change than prescriptive-based design. Changes in use of a building or portion thereof can result in unacceptable performance in the event of a fire if the effect of the change on fire safety is not contemplated in the design. With prescriptive-based designs, changes in use may be acceptable if the portion modified stays within the original occupancy or hazard classification.

This is not to say that prescriptive designs are completely tolerant to changes; even if a modification remains with the original occupancy

classification, some types of changes could result in the modification not being compliant with prescriptive codes. For example, movement of walls during tenant renovations in an office building could result in the sprinkler system no longer being in compliance with governing codes and standards. If a building is designed according to a performance basis, then some changes in use may result in increased vulnerability in the event of a fire.

The process that is identified in the subsequent section provides methods of overcoming the limitations.

Process of Performance-Based Design [1]

The *SFPE Engineering Guide to Performance-Based Fire Protection* [1] provides a process, or framework, for performance-based design. This process is identified in the flowchart in Fig. 37.1. The process is intended to be flexible, so that it can be tailored to the individual requirements of individual performance-based design projects. This flowchart identifies the steps that are involved in performance-based design without specifying which methods or models should be used to perform specific calculations relating to the development or evaluation of an individual design.

Defining the Project Scope

The performance-based design process identified in the *SFPE Engineering Guide to Performance-Based Fire Protection* begins with developing the project scope. (Defining the project scope is Step 1 in the process section later in the chapter.)

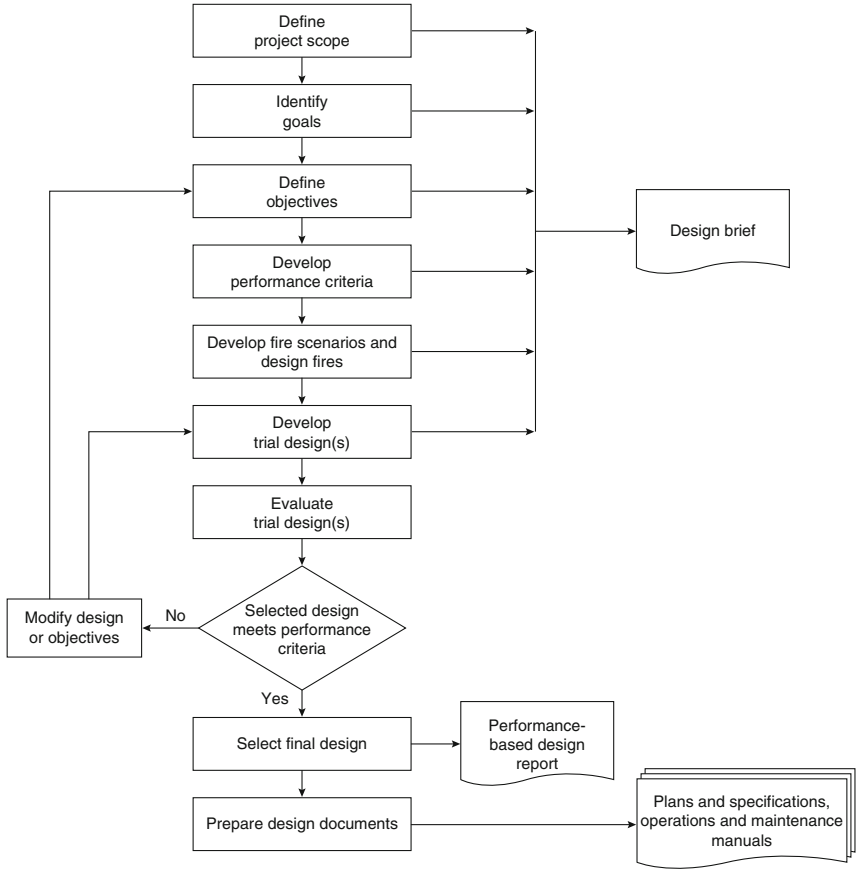

Fig. 37.1 Performance-based design process [1]

Project scopes for performance-based designs are frequently not highly different than project scopes for prescriptive-based designs, although unique features may be identified that might be difficult or impossible to achieve through compliance with prescriptive-based codes.

The project scope identifies the portions of a building or facility that will be considered by the design, the desired features of the design, the intended characteristics of the building, and the regulations that are applicable to the design. The scope also includes identification of the project stakeholders—those that have an interest in the success of the design. Stakeholders may include building owners or their representatives, regulatory authorities, insurance providers, building tenants, fire officials, or other parties. From the scope, a clear understanding can be gained of the needs of the project.

Identifying Goals

Once the scope is identified, the next steps involve the definition of goals and objectives for the design project. (Identifying goals is Step 2 in the process section later in the chapter.) The *SFPE Engineering Guide to Performance-Based Fire Protection* defines goals as the "desired overall fire safety outcome expressed in qualitative terms." Goals are intended to be stated in broad terms that can easily be understood by people who do not have engineering expertise. The purpose of identifying goals is to facilitate understanding and agreement on how the building is intended to perform in the event of a fire.

Laypeople would likely not be able to understand the significance of keeping the upper-layer temperature below a certain temperature, but they could understand what it means to provide for life safety in the event of a fire.

The *SFPE Engineering Guide to Performance-Based Fire Protection* identifies four fundamental goals for fire safety: life safety, property protection, mission continuity, and environmental protection. Although these types of statements are entirely qualitative in nature, they point the direction of the design process. For example, an unattended, fully automated warehouse may have property protection and mission continuity as its primary design goals. A hotel would likely have life safety as its primary fire safety goal.

Goals can come from a variety of sources. Some codes identify goals. For example, NFPA *101* specifies the following fire safety goal [5]:

4.1.1 Fire. A goal of this *Code* is to provide an environment for the occupants that is reasonably safe from fire by the following means:
(1) Protection of occupants not intimate with the initial fire development
(2) Improvement of the survivability of occupants intimate with the initial fire development

4.1.2 Comparable Emergencies. An additional goal is to provide life safety during emergencies that can be mitigated using methods comparable to those used in case of fire.

4.1.3 Crowd Movement. An additional goal is to provide for reasonably safe emergency crowd movement and, where required, reasonably safe nonemergency crowd movement.

NFPA 5000 [6] provides the following goals:

4.1.1 Goals. The primary goals of this *Code* are safety, health, building usability, and public welfare, including property protection as it relates to the primary goals.

NFPA 5000 specifies more goals than NFPA *101* does, which is due to the fact that *NFPA 5000* has a broader scope than NFPA *101*. NFPA *101* addresses only life safety, whereas *NFPA 5000* addresses many additional aspects of building safety. The *ICC Performance Code for Buildings and Facilities* [7] identifies goals that are similar to those contained in *NFPA 5000*.

Designs that comply with the prescriptive option of NFPA *101* or *NFPA 5000* are "deemed" to comply with the goals specified by those codes. Similarly, designs that comply with the ICC family of codes are deemed to comply with the goals of the *ICC Performance Code for Buildings and Facilities*. However, designers

who prepare performance-based designs would have to demonstrate that they achieve the goals of the applicable code.

In some cases, project stakeholders may specify their own goals. See the section on "Application of Performance-Based Design" later in this chapter.

As qualitative statements, goals are insufficient by which to judge the adequacy of a design. Therefore, they will have to be quantified as measurable values. The next two steps of the process outlined in the *SFPE Engineering Guide to Performance-Based Fire Protection* are intended to facilitate translating these broad statements into specific numerical criteria that can be predicted using engineering methods.

Defining Objectives

The next step in this process is the development of objectives. (Defining objectives is Step 3 in the process section later in the chapter.) The *SFPE Engineering Guide to Performance-Based Fire Protection* identifies two types of objectives: stakeholder objectives and design objectives. Stakeholder objectives provide greater detail of maximum allowable levels of damage than goals do.

Stakeholder objectives might be expressed in terms of maximum allowable levels of injury, damage to property, damage to critical equipment, or length of loss of operations. Stakeholder objectives facilitate agreement among the stakeholders of the maximum level of damage that would be tolerable if a fire were to occur.

After the stakeholder objectives have been developed, the *SFPE Engineering Guide to Performance-Based Fire Protection* recommends developing design objectives. Design objectives focus on the items that are intended to be protected from fire and describe the maximum or minimum acceptable fire conditions necessary to achieve the stakeholder objectives.

As with goals, stakeholder objectives could be specified by a performance-based code. For example, NFPA *101* [5] provides the following objectives:

4.2.1 Occupant Protection. A structure shall be designed, constructed, and maintained to protect occupants who are not intimate with the initial fire development for the time needed to evacuate, relocate, or defend in place.

4.2.2 Structural Integrity. Structural integrity shall be maintained for the time needed to evacuate, relocate, or defend in place occupants who are not intimate with the initial fire development.

4.2.3 Systems Effectiveness. Systems utilized to achieve the goals of Section 4.1 shall be effective in mitigating the hazard or condition for which they are being used, shall be reliable, shall be maintained to the level at which they were designed to operate, and shall remain operational.

NFPA 5000 provides additional objectives resulting from the additional goals of the code.

If they are not specified by a code, stakeholder objectives will need to be developed by the engineer in consultation with project stakeholders based on the goals. In most cases, design objectives would be developed by an engineer based on the goals and stakeholder objectives agreed to by the stakeholders.

Developing Performance Criteria

Performance criteria are threshold values that, if exceeded, indicate that unacceptable damage has occurred. (Developing performance criteria is Step 4 in the process section later in the chapter.) Although design objectives provide more detail than the goals or stakeholder objectives, they are not sufficiently detailed for the evaluation of trial designs.

Performance criteria might include temperatures of materials, gas temperatures, smoke concentration or obscuration levels, carboxyhemoglobin levels, or radiant heat flux levels. Performance criteria should be predictable with engineering tools such as fire models.

Table 37.1 Examples fire protection goals, stakeholder objectives, design objectives, and performance criteria [1]

Fire protection goal	Stakeholder objective	Design objective	Performance criteria
Minimize fire-related injuries and prevent undue loss of life	No loss of life outside of the room or compartment of fire origin	Prevent flashover in the room of fire origin	Upper-layer temperature not greater than 200 °C
Minimize fire-related damage to the building and its contents	No significant thermal damage outside of the room or compartment of fire origin	Minimize the likelihood of fire spread beyond the room of fire origin	Upper-layer temperature not greater than 200 °C
Minimize undue loss of operations and business-related revenue due to fire-related damage	No downtime exceeding 8 h	Limit the smoke exposure to less than would result in unacceptable damage to the target	HCl not greater than 5 ppm
			Particulate not greater than 0.5 g/m^3
Limit environmental impacts of fire and fire protection measures	No water contamination by fire suppression water runoff	Provide a suitable means for capturing fire protection water runoff	Impoundment capacity at least 1.20 times the design discharge

The *SFPE Engineering Guide to Performance-Based Fire Protection* divides the types of performance criteria that may need to be developed into two categories: life safety criteria and non–life safety criteria.

Life safety criteria address the survivability of people exposed to fire or fire products. The values selected as performance criteria might vary depending on the physical and mental conditions of building occupants and length of exposure. Performance criteria may need to be developed in the areas of thermal effects to people (e.g., exposure to high gas temperatures or thermal radiation), toxicity of fire products, or visibility through smoke.

Non–life safety criteria may need to be developed to assess the achievement of goals relative to property protection, mission continuity, or environmental protection. Performance criteria relative to these goals may relate to thermal effects, such as ignition, melting, or charring; fire spread, smoke damage, fire boundary damage, structural integrity, damage to exposed items, or damage to the environment.

Given that performance criteria can vary widely depending on the specific design situation, the *SFPE Engineering Guide to Performance-Based Fire Protection* does not provide specific performance criteria. Rather, the guide identifies a number of reference sources that can be used to assist with the development of design-specific performance criteria. Table 37.1 contains examples of goals, objectives, and performance criteria.

Some performance-based codes provide performance criteria. NFPA *101* [5] provides the following performance criterion:

5.2.2 Performance Criterion. Any occupant who is not intimate with ignition shall not be exposed to instantaneous or cumulative untenable conditions.

Since "instantaneous or cumulative untenable conditions" is not defined, this performance criterion is more akin to an objective. However, additional specificity can be found in the annex of NFPA *101*. The options outlined in the annex deal with prevention of incapacitation from smoke or prevention of exposure to smoke.

In many cases, the engineer will need to develop performance criteria from the goals and objectives. To develop performance criteria, the engineer will need to understand the mechanism of harm to the object being protected. Chapter 63 addresses the mechanisms of harm to people in detail.

Developing Fire Scenarios

A second input needed to evaluate whether a trial design is acceptable is the design fire scenario, which describes the conditions of exposure, such

as types of fires and building and occupant conditions for which a design is intended to provide protection. (Developing fire scenarios is Step 5 in the process section later in the chapter.)

The *SFPE Engineering Guide to Performance-Based Fire Protection* suggests a two-step process for identifying design fire scenarios. The first step is considering all possible fire scenarios that could occur in the building or portion of the building that is within the scope of the design. The second step is to reduce the population of possible fire scenarios to a manageable set of design fire scenarios.

Both fire scenarios and design fire scenarios comprise three sets of characteristics: building characteristics, occupant characteristics, and fire characteristics. Building characteristics describe the physical features, contents, and ambient environment within the building. They can affect the evacuation of occupants, growth and spread of fire, and the movement of combustion products. Occupant characteristics determine the ability of building occupants to respond and evacuate during a fire emergency and the potential impact a fire will have on the occupants. Fire characteristics describe the history of a fire scenario, including first item ignited, fire growth, flashover, full development, and decay and extinction.

The *SFPE Engineering Guide to Performance-Based Fire Protection* identifies a number of methods that can be used to identify possible scenarios, including the following:

- Failure modes and effects analysis, where the different types of failures that could occur are studied, and the effects of those failures are analyzed.
- Failure analysis, where potential causes of failures are identified and the expected system performance is investigated.
- "What if" analysis, where expert opinion is used to consider possible events and the consequences of those events.
- Historical data, manuals, and checklists, where past events in a building or a similar building are studied to consider whether similar events could occur in the building that is being designed or modified. Manuals and checklists can be studied to consider warnings, cautions, or operational sequences that could lead to a fire if not followed.
- Statistical data of fires across broad classifications of buildings.
- Other analysis methods such as hazards and operability studies, preliminary hazard analysis, fault tree analysis, event tree analysis, cause-consequence analysis, and reliability analysis.

Given the large number of possible fire scenarios for a given performance-based design project, it is usually necessary to reduce the possible fire scenario population to a manageable number of design fire scenarios for evaluating trial designs. If the design is being done on a deterministic basis, this can be accomplished in part by excluding scenarios that are highly unlikely to occur or that would result in an acceptable outcome regardless of the trial design strategy that is used. However, for a fire scenario to be excluded from further analysis because it is considered too unlikely, all stakeholders must recognize and accept that if the scenario were to occur, an unacceptable outcome may result.

Another method of reducing the number of fire scenarios is to select bounding scenarios, where if the performance criteria can be achieved in these scenarios, it can be safely assumed that they would be achieved in the scenarios that are not specifically considered.

For risk-based analyses, it would only be acceptable to exclude a fire scenario from further reconsideration if it could be established that no design could handle the scenario. Scenarios can be grouped into clusters of like scenarios according to common defining characteristics (e.g., all fires that start in a single room) [8].

When scenarios are clustered, the scenario cluster will be analyzed as a single, aggregate scenario. The probability that will be used for analysis will be the sum of the probabilities of all of the scenarios in the cluster. The consequence that will be used is an average of the consequences of the scenarios in the cluster.

Some performance-based codes provide fire scenarios. Even when such a code is applicable to a design, the fire protection engineer should work with project stakeholders to determine if there are other scenarios that should be considered. For example, NFPA *101* [5] and *NFPA 5000* [7] specify fire scenarios that must be addressed for performance-based designs. These fire scenarios include elements of fire characteristics, building characteristics, and occupant characteristics. However, these elements are not defined explicitly for all of the scenarios. The New Zealand building code [9] provides a verification method that includes fire scenarios in a similar manner as NFPA 101, but also provides information needed to quantify design fire scenarios. The Japanese building code also provides quantitative design fire scenarios. The *ICC Performance Code for Buildings and Facilities* [8] provides general classifications of fire events.

Developing Trial Designs

Trial designs are fire protection strategies that are intended to achieve the goals of the project. (Developing trial designs is Step 6 in the process section later in the chapter.) To be considered acceptable, trial designs much achieve each of the performance criteria when subjected to the design fire scenarios.

The *SFPE Engineering Guide to Performance-Based Fire Protection* groups the types of methods that might be used in trial designs into six subsystems. Attributes from one or more subsystems would be used in a trial design. The six subsystems identified in the guide are the following:

- Fire initiation and development, where methods are used to reduce the likelihood that ignition would occur or reduce the rate of fire development if a fire were to occur.
- Spread, control, and management of smoke, where smoke hazards are reduced by limiting smoke production, controlling smoke movement, or reducing the amount of smoke after it has been produced.
- Fire detection and notification, where the presence of a fire would be detected for purposes of notifying building occupants or first responders, or to activate a fire suppression system.
- Fire suppression, including automatic or manual systems.
- Occupant behavior and egress, where the travel to a place of safety prior to the onset of untenable conditions is facilitated.
- Passive fire protection, including limiting fire spread though construction or preventing premature collapse of all or part of a structure.

When developing trial designs, the engineer should refer back to the goals of the analysis and decide what types of strategies would best achieve those goals. NFPA 550, *Guide to the Fire Safety Concepts Tree* [10], can assist with the development of trial design strategies. The top branches of the tree may closely align with the objectives of the design. In these cases, the protection methods that are identified below the objectives that align with the design goals could be used as trial designs.

Trial design strategies involve the same types of building components and systems that would generally be included in a prescriptive design. In fact, compliant prescriptive system designs may be appropriate as part of a trial design strategy. However, in some cases, augmented performance may be needed beyond that which would be achieved by a prescriptive-compliant system.

Fire Protection Engineering Design Brief

The preceding steps constitute the qualitative portion of the design, and agreement of all stakeholders should be attained prior to proceeding to the quantitative analysis. A mechanism that is suggested by the *SFPE Engineering Guide to Performance-Based Fire Protection* for achieving this agreement is a fire protection engineering design brief.

Evaluating and formally documenting performance-based designs can require extensive effort, and if fundamental aspects of the design change after detailed evaluation, significant

rework may be required. For example, if a design is completed and evaluated based on achieving life safety goals, and after the design is evaluated property protection goals are identified, then effort previously expended may be wasted. Similarly, if project stakeholders insist on certain types of design strategies being used, then these should be identified before other types of design strategies are developed and evaluated. The purpose of the fire protection engineering design brief is to facilitate agreement on the qualitative portions of the design prior to conducting detailed engineering analysis.

The contents of the fire protection engineering design brief will typically include the project scope, goals, objectives and performance criteria, design fire scenarios, and trial design strategies proposed for consideration. The form of the fire protection engineering design brief is intended to be flexible, based on the needs of the project and the relationship of the engineer performing the design to other stakeholders. In some cases, a verbal agreement may be sufficient. In other cases, formal documentation, such as minutes of a meeting or a document that is submitted for formal review and approval, may be prudent.

Once the design team and stakeholders have agreed on the approach that is proposed for the performance-based design, the detailed analysis work begins. This includes quantification of the design fire scenarios, evaluation of trial designs, and development of project documentation.

Quantifying Design Fire Scenarios

After the design fire scenarios have been agreed upon by the stakeholders, they need to be quantified. (Quantifying design fire scenarios is Step 7 in the process section later in the chapter.) The building characteristics, occupant characteristics, and fire characteristics will need to be quantified as necessary to adequately evaluate the trial designs.

The *SFPE Engineering Guide to Performance-Based Fire Protection* identifies several types of characteristics. These characteristics are intended to include a listing of any item that might need to be quantified. However, for most design situations, it will not be necessary to quantify all of the characteristics.

Quantifying Building Characteristics Building characteristics describe the physical features, contents, and internal and external environments of the building. Building characteristics can affect the evacuation of occupants, the growth and spread of fire, and the movement of combustion products. The *SFPE Engineering Guide to Performance-Based Fire Protection* identifies the following building characteristics that may need to be quantified:

- Architectural features, such as compartment geometry, interior finish, construction materials, and openings
- Structural components, including any protection characteristics
- Fire load
- Egress components
- Fire protection systems
- Building services, such as ventilation equipment
- Building operational characteristics
- Fire-fighting response characteristics
- Environmental factors (interior and exterior temperatures, wind speeds, etc.)

Occupant Characteristics For any design in which life safety or occupant response is considered, it will be necessary to consider the occupant characteristics. The *SFPE Engineering Guide to Human Behavior in Fire* [11] identifies the following fundamental occupant characteristics that could influence the response of building occupants to a fire:

- Population (number and density)
- Alone or with others
- Familiarity with the building
- Distribution and activities
- Alertness
- Physical and cognitive ability
- Social affiliation
- Role and responsibility
- Location
- Commitment
- Focal point

- Occupant condition
- Gender
- Culture
- Age

Occupant characteristics provide information as to how people might respond when subjected to fire cues, where fire cues include seeing fire or smoke, smelling smoke, hearing a fire alarm audible signal, or other cues. This includes actions people may take as well as physical effects of fire products.

Design Fire Curves Fire characteristics will typically be quantified as design fire curves, which provide a history of the size of a fire as a function of time. Typically, the "size" of a fire is measured in terms of heat release rate. Figure 37.2 shows an example of a design fire curve.

The *SFPE Engineering Guide to Performance-Based Fire Protection* divides design fire curves into five stages. Depending on the scope of the design, it may not be necessary to quantify each stage of the design fire curve. For example, it may only be necessary to quantify the growth stage for evaluation of a detection system. Similarly, evaluation of structural integrity may only require quantification of the fully developed stage. The guide provides suggestions on how to quantify each stage of the design fire curve.

For most designs, ignition will be assumed to occur. Typically, the design team will consider different first items ignited. If information is known about an item and an energy source, it is possible to predict whether the item will ignite.

After an item ignites, the fire might grow in size. The rate at which a fire grows is a function of the first item ignited and the location of the item within a compartment. As the fire grows, additional items may be ignited and the fire may spread outside of an enclosure.

Flashover occurs when all combustible items within an enclosure ignite. Compartment geometry, compartment ventilation, fire heat release rate, and the thermal properties of the enclosure influence whether and when flashover occurs in a compartment.

If there is no intervention, a fire may reach a maximum size, which is a function of either the amount of fuel in the compartment or the amount of available ventilation. The fully developed stage of the fire is typically used to determine radiation through openings, failure of the structure, fire spread to other enclosures, or failure of compartmentation.

Fires will decay and eventually burn out. Decay can occur due to depletion of fuel, lack of ventilation, or suppression.

When developing design fire curves, it is important to realize that design fires need not be exact or should not be presented as precise predictions of what will happen in a fire. Design fires are meant to be a representation of anticipated fires. Current modeling technology and data make it unnecessary and impractical to create exact predictions of how a potential fire will burn.

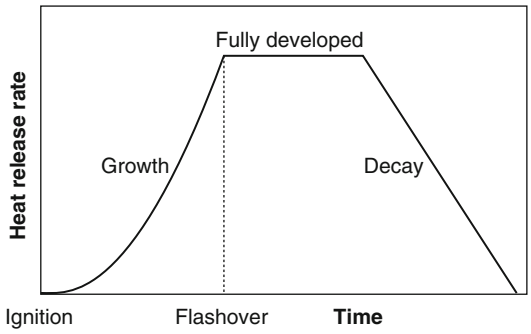

Fig. 37.2 Sample design fire curve

Evaluating Trial Designs

Evaluation is the process of determining if a trial design meets all of the performance criteria in each of the design fire scenarios. (Evaluating trial designs is Step 8 in the process section later in the chapter.) The *SFPE Engineering Guide to Performance-Based Fire Protection* states that the level, or detail, of an evaluation is a function of factors such as the complexity of geometry, level of subsystem interaction, and the margin between evaluation output and the performance

criteria. In some cases, a relatively simple evaluation may be appropriate, whereas in others, an in-depth evaluation would be required.

The levels of evaluation identified in the guide are (1) subsystem, (2) system, and (3) whole building.

Subsystem A subsystem performance evaluation typically consists of a simple comparative analysis in which the performance of a design that involves a single component or subsystem (e.g., egress, detection, suppression, fire resistance, etc.) is compared to the performance of a similar component or subsystem. This type of analysis is frequently employed when using the equivalency provision in a prescriptive code. For an alternate design strategy to be acceptable, it must provide equal or greater performance than that which is required by the code or standard.

System A system performance evaluation might consist of a comparison to prescriptive requirements or an analysis based on specific performance requirements. A system performance evaluation is used when more than one fire protection system or feature is involved. It is more complex than a subsystem evaluation because the analysis must account for the interaction between various subsystems.

Whole Building In a building performance analysis, all subsystems used in the protection strategy and their interactions are considered. A performance-based design that analyzes total building fire safety can provide more comprehensive solutions than subsystem or system performance analysis because the entire building-fire-target (where "targets" are the items being protected, such as people, property, etc.) interaction is evaluated.

The "levels of performance" describe the complexity of a design, whereas the types of performance identified by Nelson [2] in the Introduction describe approaches that a code or standard could use to state desired fire performance.

Typically, engineering tools such as fire models will be used to evaluate trial designs. The tools that are selected must provide information that can be used to determine whether or not the performance criteria have been achieved. Additionally, uncertainty is always present in any design or analysis.

Documenting the Design Process

Following completion of the evaluation and selection of the final design, thorough documentation of the design process should be prepared. This documentation serves three primary purposes: (1) to present the design and underlying analysis such that it can be reviewed and understood by project stakeholders, such as regulatory officials; (2) to communicate the design to the tradespeople who will implement it; and (3) to serve as a record of the design in the event that it is modified in the future or if forensic analysis is required following a fire.

The *SFPE Engineering Guide to Performance-Based Fire Protection* provides detailed descriptions of the types of documentation that should be prepared by the design team. This material includes the documentation associated with the fire protection engineering design brief (discussed previously), a performance-based design report, specifications and drawings, and operations and maintenance manuals.

The guide suggests that a detailed performance-based design report should be prepared that describes the quantitative portions of the design and evaluation. Every model or calculation method that was used should be identified, including the basis for selection of the model or calculation method. Similarly, any input data for the model or calculation method should be documented, including the source of the input data and the rationale of why the data are appropriate for the situation being modeled.

All fire protection analyses have some uncertainty associated with them. This uncertainty may come from limited ranges of applicability of a model or simplifications within models or calculation methods, applicability of data sources to the scenarios modeled, limitations of scientific understanding, or other sources. The design should include methods of compensating

for this uncertainty, and how this was accomplished should be documented.

As with prescriptive designs, performance-based designs use specifications and drawings to communicate to tradespeople how to implement the design. However, master specifications may not be applicable to performance-based designs without significant editing. Similarly, any features of a design that differ from typical prescriptive designs should be clearly identified on drawings.

One feature of documentation of performance-based designs that differs significantly from prescriptive-based designs is the operations and maintenance manual. The operations and maintenance manual communicates to facility managers the limitations that are placed on the design. These limitations stem from decisions made during the design process. For example, heat release rates used as input data place a limitation on the use of a space. Any furnishings placed within a space that could have higher heat release rates than the heat release rates used during fire modeling could result in greater consequences than the model predicted.

The operations and maintenance manual should be written in a format that can be easily understood by people who are not fire safety professionals, since most building owners and facility managers will not have this type of background.

Application of Performance-Based Design

Performance-based design can be applied in one of three situations: with prescriptive regulations, with performance-based regulations, and as a stand-alone design methodology [1]. It is noteworthy that many codes are not wholly performance based or prescriptive; many codes contain a mixture of performance-based and prescriptive requirements. For example, a performance-based code may contain a "deemed to satisfy" prescriptive option. Similarly, a prescriptive code may contain some performance-based requirements. As an example, the requirements for atrium smoke control systems in prescriptive codes are typically performance based.

Use with Prescriptive-Based Regulations

Prescriptive-based regulations provide requirements for broad classifications of buildings. These requirements are generally stated in terms of fixed values, such as maximum travel distances, minimum ratings of boundaries, and minimum features of required systems (e.g., detection, alarm, suppression, and ventilation).

In addition, most prescriptive-based regulations contain a clause that permits the use of alternative means to meet the intent of the prescribed provisions. This provides an opportunity for a performance-based design approach. Through performance-based design, it can be demonstrated whether or not a design is satisfactory and complies with the implicit or explicit intent of the applicable regulation.

When applying performance-based design in this manner, the scope of the design is equivalency with the prescriptive provision(s) for which equivalency is sought. The "intent," or performance achieved by compliance with the prescriptive code provision(s), is identified to provide the goals and objectives for the design.

Use with Performance-Based Regulations

Performance-based codes and standards provide goals, objectives, and performance criteria for buildings or other structures that fall within the scope of the code or standard. Performance-based codes generally either provide specific fire scenarios that must be addressed or information that is intended to identify the types of fire scenarios that must be addressed. Performance-based codes may also provide additional administrative provisions, such as review or documentation requirements.

Use as a Stand-Alone Methodology

In some cases, a building owner or insurer may have additional fire safety goals beyond the minimum requirements of applicable prescriptive codes and standards. In these cases, additional or complementary fire safety goals and objectives might be identified, thus requiring additional fire protection engineering analysis and design. For example, property protection and continuity of operations might be goals of a building owner or insurer, and these goals might not be fully addressed in applicable regulations. The performance-based design process can be used to identify and address these additional goals.

Hazard Versus Risk

In performance-based design, all scenarios must be considered in some manner. There are two ways that can be used to consider the universe of possible scenarios: risk based and deterministic.

Risk-Based and Deterministic Analyses

Risk-based analysis looks at the big picture of all of the possible scenarios—the consequences of each scenario are analyzed; however, these consequences are weighted by the probability of the event occurring. If the sum of the products of the probability of the scenarios occurring and the consequences of the scenarios (e.g., value of property lost, deaths or injuries, length of business interruption, etc.) are below some threshold value, then the design is considered acceptable.

In deterministic analysis, scenarios that are expected to occur with a frequency above a threshold value are analyzed to determine their consequences. If the consequences of those scenarios are within the design objectives, then the design is considered to be acceptable.

Although deterministic analyses are typically used in performance-based fire protection, it may be difficult to use deterministic analysis to judge the superiority of one type of system against another, particularly when the systems protect against fires differently. In deterministic analysis, any scenario that is expected to occur more frequently than a threshold frequency would be analyzed. If the probability of system failure is found to be below the established threshold, this scenario would not be addressed and it would be concluded the system being considered could be used without redundancy. Conversely, if the probability of system failure is found to be above the established threshold, then the scenario in which the system fails would be analyzed, and it would likely be concluded that both must be installed.

Deterministic analysis does not provide a complete evaluation of the fire safety in buildings. Although the probabilities of failure were considered, and the consequences determined by evaluation, probabilities and consequences were considered separately on a pass/fail basis.

Risk assessments differ from traditional, hazard-based assessments in that frequencies or probabilities of fires and the reliability of fire protection systems are explicitly addressed and used to weight the expected consequences. Hazard-based assessments evaluate the consequences given a set of conditions (e.g., a fire starts and sprinklers activate).

Event Trees

Event trees can be used to illustrate the possible courses of action of a fire following ignition. An event tree is a graphical means of identifying all possible outcomes following an initiating event [12]. Event trees are often used to analyze complex situations with several possible scenarios or where several fire or life safety systems are in place or are being considered [13].

Event trees are constructed by identifying an initiation event (the start of a fire) and branching out with the subsequent events that could occur. Possible successes and failures following an initiating event are identified on branches of an event tree. The branches follow a temporal sequence, based on which items would be expected to occur soonest following the fire start. For an event tree to be complete, all possible events should be identified. Figure 37.3 shows an example of an event tree for the possible course of action for a fire that starts in a room [14].

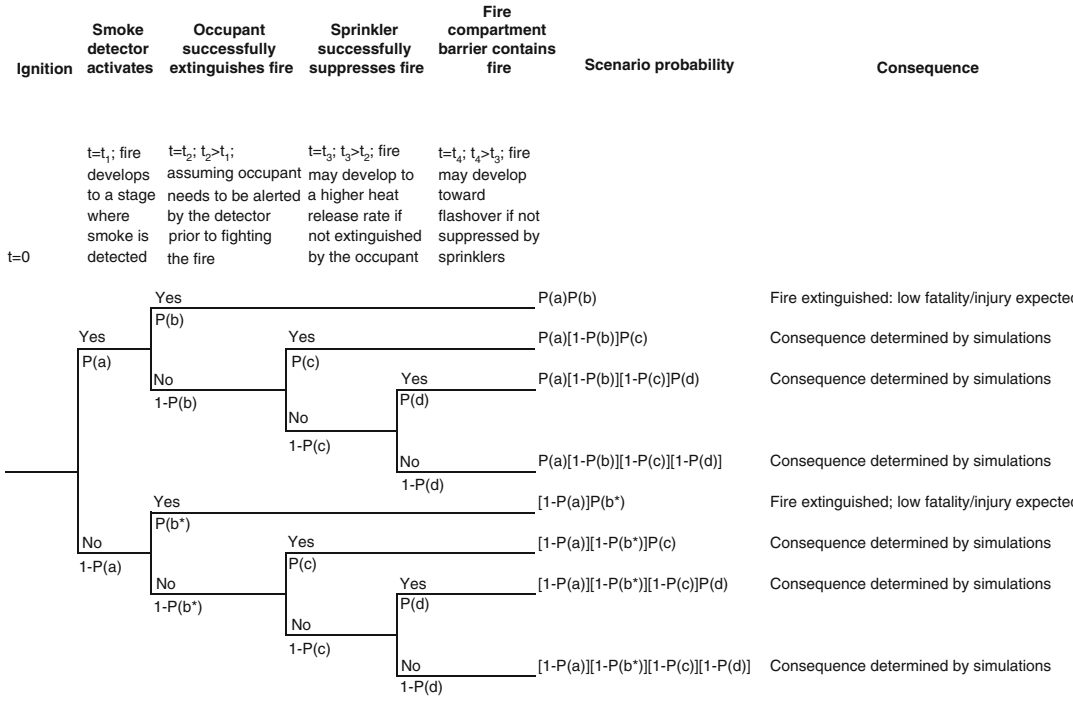

Fig. 37.3 Example of an event tree [14]

Following the ignition event in Fig. 37.3, the smoke detector that protects the room could either activate or not activate. Similarly, the room occupant could either successfully extinguish the fire or not. If the occupant does not extinguish the fire, the sprinkler that is installed in the room could either control the fire or not. Finally, if the sprinkler is not successful, the room compartmentation could either contain the fire or the fire could spread beyond the room of origin. Detector operation, occupant extinguishment, sprinkler activation, and barrier containment are all subsequent events that could occur (or not occur) following the initial fire initiation event.

From the single ignition event in the room, there are eight possible scenarios that could result. Each scenario occurs with a different probability that can be determined by multiplying the probabilities along each branch of the tree leading to an outcome. If the probabilities of the mitigation strategies being successful are high, then the overall probability that the fire will not be controlled or contained within the room of origin is low.

There would likely be a number of event trees that could be prepared for the room shown in Fig. 37.3. Figure 37.3 illustrates the possible scenarios that could occur following a specific ignition event, for example, a carelessly discarded cigarette. There are likely many other ignition events that could occur in this room, and each would have its own event tree associated with it. In some cases, the event tree for other ignition events might be identical or similar to Fig. 37.3. Identical would mean that the same possible subsequent events could occur with the same probabilities. Similar would mean that the same subsequent events could occur, but with different probabilities. However, for other ignition scenarios, the event trees might be much different.

If Fig. 37.3 illustrates the possible scenarios that could occur if smoking materials are carelessly discarded in a wastebasket, then other fire initiation events that start in the wastebasket might have similar or identical event trees. However, if the fire ignition event is a Christmas tree fire, then the event tree for this event would likely be much different—the occupant might

not be capable of extinguishing the fire, and the probability of success of the other mitigation methods would likely be different.

Additionally, the room in Fig. 37.3 would likely be located within a larger building, meaning that the event tree could be expanded to include other events that could occur if the fire is not contained within the room of origin.

Event trees might be prepared to evaluate different fire protection strategies. If so, one or more event trees could be developed for each strategy.

Each scenario that is a terminus on the right-hand side of an event tree represents a series of events that could occur. Each series of events occurs with a different probability, and the probabilities of some scenarios occurring are higher than others.

Model Use in Performance-Based Design

Fire models take a variety of forms. The simplest are algebraic models, which are mathematical equations used to estimate the value of one or more variables as a function of space and/or time. More complex are zone or lumped parameter models, which simplify the behavior of a system by making the approximation that a particular volume or region is homogeneous, uniform, or well-mixed. The most complex are computational fluid dynamics (CFD) models, which are also known as field models. CFD models provide a method for calculating the fluid flow through a volume using numerical solutions of the governing equations for conservation of total mass, chemical species, momentum and energy.

The use of fire models has flourished over the last few decades. Models are used to simulate fire phenomena to determine if a proposed design strategy is acceptable, to test hypotheses developed during fire investigations, or to simulate tests as part of fire research. Each of these applications has potential impacts on public health, safety or welfare, so it is incumbent on model users to make sure that they can have confidence in model results.

The American Society of Testing and Materials (ASTM) published a guide for evaluating fire models in 1990. The Guide is identified as ASTM E-1355. These guidelines provide an approach to evaluating models that consists of defining the model and the scenarios for the evaluation, verification of the appropriateness and the theoretical basis of the model, verifying the mathematical and numerical robustness of the model, and quantifying the uncertainty and accuracy of model results.

The ASTM guidelines are useful where someone wishes to evaluate a model for a broad range of applications. However, the methodology requires a level of effort that is prohibitive for specific, individual project applications. For example, the Society of Fire Protection Engineers evaluated DETACT-QS using the ASTM E-1355 methodology. DETACT-QS is one of the simplest fire models that have been published (it has under 200 lines of code); the evaluation required over a person-year of effort, and the report is 140 pages in length.

The standard of care that is applied to the use of model predictions is that the model should either be accepted by the relevant professional community or the user should demonstrate that the model is acceptable. Only a few models have been formally evaluated using the ASTM E-1355 process—including DETACT-QS and five models that were evaluated for application in nuclear power plants [15] (Fire Dynamics Tools, Fire Induced Vulnerability Evaluation, CFAST, MAGIC and FDS.)

In 2003, 168 fire models were identified [16], and several more have been published since then. Additionally, the published evaluations do not address every possible application of the models that were evaluated, so in most cases it will fall to the person who uses a model to show that the model is appropriate for the intended use.

In 2011, the Society of Fire Protection Engineers published the Guide to Substantiating a Fire Model for a Given Application to provide a framework for determining if a fire model is suitable for use for a specific fire protection application.

The Guide to Substantiating a Fire Model for a Given Application provides a five step process for determining the suitability of a fire model. These steps include defining the problem, selecting a candidate model, verifying and validating the model, determining the impact of uncertainty and user effects on the model results,

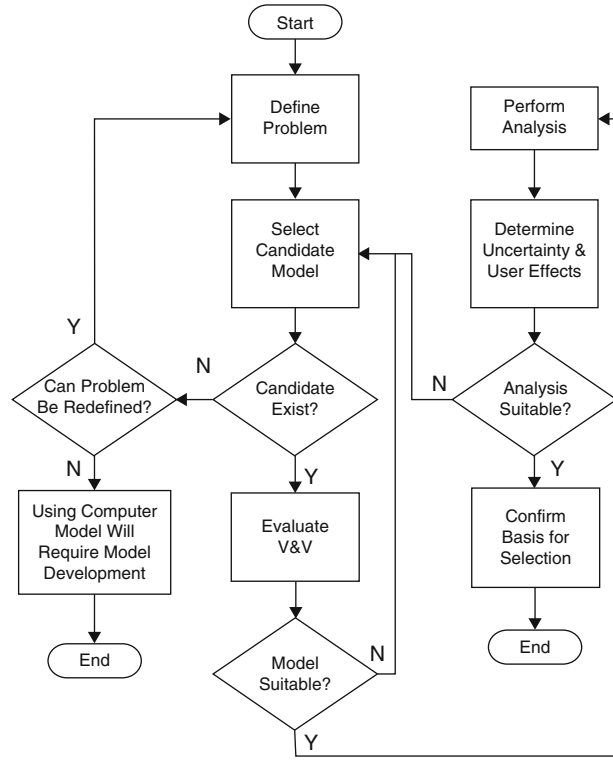

Fig. 37.4 Fire model selection flow chart

and finally, documenting of the model evaluation. This process is illustrated in Fig. 37.4.

Any of these steps may require repetition. If a candidate model is determined to be unsuitable, then another candidate may be selected for evaluation. If no suitable candidate models exist for a given application, then there are several options. These options include:

1. Reevaluate the application to determine if the problem being solved can be reposed to allow the use of another model.
2. Develop, verify, and validate either a new model or a modified version of an existing model.
3. Use an alternate method that does not use a fire model—such as fire testing.

Definition of the Problem of Interest

The first step described in the Guide to Substantiating a Fire Model for a Given Application is to define the problem of interest. The problem of interest should be clearly defined by identifying the relevant phenomena and key physics, collecting available information and determining the analysis objectives.

Commonly encountered key physics in fire modeling generally relate to thermodynamics, fluid dynamics, heat transfer, combustion, or material response. Identification of relevant phenomena and key physics requires knowledge of the details of the problem of interest as well as the underlying chemical and physical processes involved. The appropriate level of knowledge is required to prevent users from treating a fire model as a black-box tool, which can result in using a fire model beyond the scope of its capability.

Defining the problem of interest encompasses several elements. First, the geometry needs to be established. The geometry includes the spatial domain and the objects involved within the spatial domain. For a room or a facility such as a warehouse or office building, the spatial domain is often defined by the physical boundaries like walls, ceilings and floors. For open domain problems, e.g. outdoor pool fires of flammable liquids, a sufficiently large domain should be selected to avoid significant impact along the

boundaries. Detailed geometries should be provided for fuels, building structures, protection devices and other important objects in the spatial domain; however, some specific details may depend upon the type of model utilized.

Next, Guide to Substantiating a Fire Model for a Given Application recommends establishing a timeline. The timeline for the problem of interest includes the duration of the problem and the sequence of events. The problem of interest can be either transient, steady-state, or at a specific point along the timeline.

Events should be included in the information collection process unless they are deemed unimportant to the problem of interest. Examples of events are ignition, closing or opening of doors and windows, actuation of sprinklers or smoke exhaust fans, and collapse of furniture and building structures. Some events will occur at specific points on the timeline, while others will be modeled.

A list of materials relevant to the problem of interest should be generated and relevant material properties should be assigned to each material. The incorporation of specific material properties may depend upon the type of model used in the analysis. The most important properties for most fire problems are often whether the material is combustible and the products of combustion. Other relevant material properties may include, but are not limited to, viscosity, specific heat, heat of combustion, thermal conductivity, heat of gasification and heat of vaporization.

The initial and boundary conditions should be established. This type of information is often needed to start numerical simulations in time and space, respectively. Examples of initial conditions are room temperature and door and window status, while examples for boundary conditions are openings that allow free air passage or an air conditioner on the ceiling blowing at an established flow rate.

Lastly, the analysis objectives should be established. Analysis objectives define what the modeler hopes to achieve by using the fire model. The most important objective related to the use of a fire model is a list of quantities that should be determined to address the problem of interest.

Select a Candidate Model

The next step identified in the Guide to Substantiating a Fire Model for a Given Application is to select a candidate model. A wide variety of models are available for predicting a range of fire phenomena. A number of factors should be considered before selecting a particular model for a problem, including computational resources, time limitations, required level of accuracy, and most importantly, whether or not the governing equations and assumptions in the model are appropriate for the problem of interest.

The guide recommends three major considerations for selecting a candidate model: determining the available model inputs, identifying the desired model outputs, and determining the available resources.

Determining the available model inputs requires the model user to identify the inputs that are available for a given problem and to identify the inputs that are not available but must be acquired before proceeding with an analysis. To perform this analysis of available data, it is often helpful to list each relevant input, along with its value (or range of values) and an indication of any uncertainty that may be involved in the measurement of that input value. In addition to the known input variables, there may be unknown inputs that can be estimated through use of past research or engineering judgment; these inputs should also be listed, along with appropriate references or assumptions that were used to obtain a value.

In some cases, not all of the input data required by a model will be available. In such cases, the guide recommends three possible options:

- Perform preliminary calculations aimed at identifying the value of that specific variable.
- Make a reasonable assumption as to the range of values that the input could have and then perform a sensitivity analysis to determine the effect on the model results of changing that variable.
- Conduct experiments to obtain a value for the input.

After analyzing the available model inputs, but before proceeding with the selection of a fire model, it is important to define the accuracy that is required in the final model output. The acceptable level of resolution of the model output values will vary depending on the problem. It is up to the user of the fire model to determine how much detail is required to appropriately address a problem and to convey this decision to those who will review or make use of the results of the simulations.

When evaluating potential candidate fire models, some consideration should be given to the sensitivity of the desired output values to both the available input variables and to the type of model that is chosen. While this is not always a formal process, it is something that should be taken into account.

There is often more than one model available that may provide a sufficiently accurate solution to a problem. In such cases, model selection can be based upon the resources that are available to run the model. While a CFD model may provide benefits, such as the ability to more exactly represent the geometry of a space and better visualization tools than a zone model, it may not always provide a more accurate solution to a problem. If time constraints and lack of computer resources prohibit a thorough sensitivity analysis using CFD, then for some problems it might be more appropriate to use a zone model or algebraic model in order to more thoroughly address uncertainty.

The guide suggests developing a resourcing plan that follows the following steps before starting large fire modeling projects:

1. Determine the number of simulations needed to address any sources of uncertainty.
2. Determine the amount of time required to run a simulation on the available computational resources.
3. Determine whether or not several simulations can be run simultaneously.
4. Determine the available time before the project must be completed.

After following the steps noted above, the user should make a decision as to whether a candidate model is appropriate for the given problem. The modeler might select an algebraic model, a zone or lumped parameter model, or a computational fluid dynamics model.

Verification and Validation

Prior to using a model for a particular problem, the model user needs to determine if the model is capable of generating a useful result. The formal process by which this is demonstrated is verification and validation (V&V). Model verification serves two purposes. First, it ensures that the mathematical equations have been properly implemented. Second, it ensures that the model user understands the assumptions of the model. Verification ensures that the model is working as designed, i.e., that the equations are being properly solved. It essentially is a check of the mathematics.

The Guide to Substantiating a Fire Model for a Given Application suggests that, at a minimum, model users should read the model documentation that describes efforts made by the developers to verify the model. Then, the user should supplement the work performed by the developers to better address the specific application under consideration. The guide suggests a number of exercises that the model user can perform to supplement the verification efforts of the developers:

- *Verify the basic functionality of the model*—This typically involves creating simple test cases and comparing the model results to known analytical solutions.
- *Verify consistency of input parameters*—The user should address the appropriateness of input values, especially as they are used collectively.
- *Verify that the input parameters are appropriately used*—This generally involves studying the model documentation and diagnostic output.
- *Verify the range of validity for input parameter values*—Some values of the input parameters are only valid within a certain range. The model user should confirm that the input values are consistent with the underlying physical assumptions or experimental conditions.

- *Verify consistency of results*—In short, this involves demonstrating that the results make sense.

Verification ensures that the model is working as designed; that the equations are being properly solved. It essentially is a check of the mathematics. Validation is a check of the physics, i.e., whether the equations are an appropriate description of the fire scenario. Most often, validation takes the form of comparisons with experimental test data. Validation does not mean that a model makes perfect predictions, only that the predictions are good enough for its intended use. The meaning of "good enough" is up to the model user, and to say a model has been validated only means that an end user has decided that the model is sufficiently accurate for a particular application.

The Guide to Substantiating a Fire Model for a Given Application suggests the following procedure for validating a model for a given application:

Select Experiments

The guide provides the following considerations for selecting experiments that will be used as the basis for model validation:

- *Relevance to the application*. The organizations that perform model validation usually have a particular application in mind, which limits the scope, scale and measurements.
- *Comprehensive documentation*. The experimental results should be available and fully documented, or not needed, otherwise implies or interested modelers cannot replicate what was done in the validation study or attempt to do their own validation study.
- *Experimental uncertainty*. There are two major forms of experimental uncertainty to consider in a validation study. The most obvious is the measurement uncertainty. This is the uncertainty of the measurement of the quantity under consideration. The second form of uncertainty is the model uncertainty, which reflects the uncertainty in the model predictions that are due to the uncertainty of the physical parameters that are input into the model. The uncertainty in the input parameters needs to be propagated through the model to ascertain its impact on the final prediction.

Choose a Metric to Quantify Accuracy

Measurements can vary in space and time. Comparisons with model predictions can be based on extreme values, like peak temperatures, or spatial or temporal averages. The decision to use a particular metric is made by the organization doing the validation study based on the particular use of the model. Usually, it is convenient to express these comparative values in terms of a relative difference.

Report Results

The Guide to Substantiating a Fire Model for a Given Application recommends that the validation report provide sufficient detail about the experiments and the model inputs such that an interested reader could repeat the calculations. Specifically, the guide recommends providing the following information:

- Person or organization responsible for the validation study
- References to model documentation and reports of experimental measurements
- Description of the fire scenarios that the experiments were designed to address
- Quantification of the model accuracy
- Conclusion, including limitations of the model and its potential for extension for other fire scenarios

Typically, model validation involves a large amount of data—both in terms of model predictions and experimental measurements—and it can be difficult to succinctly display the results of the study. If all the experimental measurements can be quantified by the same total uncertainty, then a simple graph can be made to summarize the validation exercise. The graphs can indicate the experimental uncertainty in the experimental data. If the model predictions lie within the band defined by the experimental uncertainty, then it cannot be said that the model

predictions differ significantly from the measured data.

If the model predictions lie outside the uncertainty interval, this does not necessarily mean that the model is unsuitable. In such cases, the trend in the model's predictive ability needs to be evaluated in the context of the intended use.

User Effects

Once the verification and validation have been conducted, the next step identified in the Guide to Substantiating a Fire Model for a Given Application is to focus on the uncertainty that arises in model predictions due to the use of a predictive model. Possible sources of uncertainty include definition of the model space or computational domain, simplifying assumptions (in the application of the model), and the choice of input parameters. The result is a propagation of "error" or uncertainty through the model that should be understood, at minimum, at a qualitative level, but preferably, quantitatively.

Input Uncertainty

In addition to uncertainty that exists within the model, the input data can introduce uncertainty into the model calculation.

Predictive models require a description of the model space, often a simplified representation of the actual physical space. The choice of the model extents is a function of the model type and the available computational resources. Choice of the model domain and how boundary conditions—the physical conditions at the model boundaries—are defined can impact the analysis outcome.

The resolution of the model can also affect the analysis outcome. The analysis outcome should be independent of the definition of the domain or the grid resolution.

Input data, often based on assumed values or experimental data, is subject to many sources of uncertainty, including uncertainty in theory (for deriving the parameter) and measurement. Such uncertainty in input imposes a limit on the confidence in model output. It is important to understand the limitations of the input values and of the means by which they were derived in order to quantify or estimate the uncertainty or possible range of the property value. Variation in one or a combination of input parameters may substantially alter the model outcome. Treatment of uncertainty in the assumptions and input that define a problem is an important component of analysis that the modeler should address.

Implications for the Design Process

The Guide to Substantiating a Fire Model for a Given Application suggests several methods of dealing with uncertainty introduced through the use of models.

- Performance Criteria. Fire models are often used as part of a design process in which the results are evaluated against threshold performance criteria. The conclusions that may be drawn from an analysis are limited by the predictive accuracy of the model as well as the potential uncertainty in the input parameters. Performance criteria thresholds should account for limitations in the models and input.
- Safety Factors. Safety factors and margins of safety are used to provide a buffer to allow for uncertainty in the design process. A safety factor is a multiplier of a prediction for reference against a threshold or criterion. Safety margins are additive, not multiplicative.
- Sensitivity Analysis. A sensitivity analysis determines the relationships between the uncertainty in the input variables and the uncertainty in the resultant output. A sensitivity analysis provides information regarding how the uncertainty in the output of a model can be apportioned to different sources of variation in the input of a model. Sensitivity analysis allows the identification of those parameters that are most important to the outcome. It does not necessarily provide information regarding the value that should be used, but it can show the impact of using different values.

- Parametric Analysis. In a parametric analysis, a special form of a sensitivity analysis, detailed information of the effect of a certain input variable on model output is examined by systematically varying the input value of that variable, while holding others constant. A parametric analysis may be useful if detailed information regarding the potential variation of the input variable is unknown.
- Bounding. Bounding is a form of sensitivity study that evaluates the consequences of the extremes of possible values of an uncertain input quantity. If the outcome values at both extreme ends of the range of the uncertain input are acceptable relative to some criteria, further sensitivity analysis may be avoided. Bounding can be applied to not only input parameters but also selections for boundary conditions.
- Differential Analysis. For some models or systems, it is possible to solve directly for the partial derivative of the predicted values with respect to each of the input variables. The set of partial derivatives measures the sensitivity of the solution with respect to changes in the input parameters. A differential analysis has the advantages of being very quick and requiring very few resources to implement.
- Power Dependence. Less formal than differential analysis, power dependence assesses the proportionality or power-dependence of a model target output to an input parameter. By examining the relationship of model outcome to input, the user will be able to identify the relative importance of the input. As a result, the user may be able to focus on refining the estimate for a "more" important input variable, while accepting perhaps a higher variability in a "less" important variable.

Documentation

Finally, the results of the evaluation should be documented so that they can be understood by people who wish to understand how it was determined that the model is appropriate for its intended use.

SFPE Handbook Use in the Step-by-Step Process of Performance-Based Design

Publication of the first edition of the *SFPE Handbook of Fire Protection Engineering* in 1988 was one of the key events that supported the development of performance-based fire protection designs. Earlier in this chapter, the following steps in the performance-based design process as outlined in the *SFPE Engineering Guide to Performance-Based Fire Protection* were identified:

Step 1—Defining project scope
Step 2—Identifying goals
Step 3—Defining objectives
Step 4—Developing performance criteria
Step 5—Developing fire scenarios
Step 6—Developing trial designs
Step 7—Quantifying design fire curves
Step 8—Evaluating trial designs
Step 9—Documenting design process

Chapters within this edition of the *SFPE Handbook of Fire Protection Engineering* can be used to support design development and evaluation. This section identifies typical applications of the information contained in the *SFPE Handbook of Fire Protection Engineering* in the performance-based design process.

Step 1—Defining Project Scope

The project scope is generally defined as part of discussions between the engineer and the project stakeholders. One of the aspects that is determined to be part of the project scope is how the analysis will be conducted. Chapter 72 provides an overview of fire risk analysis that can be referenced when determining if the project will be done on a deterministic or a risk basis and, if the project will be done on a risk basis, the techniques that will be used.

Where risk assessments are to be used, Chap. 82 addresses fire risk index methods. Chapter 75 addresses the general subject of

building fire risk analysis. Specific applications of fire risk assessment can be found in the following chapters: Chaps. 83, 89, 90, and 85.

Step 2—Identifying Goals

The project goals are generally stated by or inferred from applicable codes and standards or through discussions between the engineer and other stakeholders.

Step 3—Defining Objectives

Since they represent a refinement of the amount of loss that is tolerable, objectives are typically developed by the engineer through discussions with the project stakeholders.

Step 4—Developing Performance Criteria

Performance criteria are quantitative values that are used to determine whether or not a trial design achieves the project goals and objectives. Developing performance criteria requires understanding the mechanism(s) of harm of the items that the design will protect from fire.

When people are to be protected from fire, performance criteria generally involve one or more of the following:

- Prevention of incapacitation by fire or smoke
- Prevention of thermal damage
- Providing sufficient visibility such that people can navigate means of egress

Chapter 63 provides information that can be used to set performance criteria associated with prevention of incapacitation by fire products. Additionally, Chap. 63, provides information that can be used to set performance criteria associated with thermal damage from heat exposure.

Several researchers have published suggested maximum values of limiting extinction coefficients or optical densities that could be used as performance criteria associated with maintaining visibility. For more information, see the following chapters: Chaps. 24, 61, and 63. However, these limiting values have embedded within them desired minimum visibility distances, and hence, these values should only be used when the geometry of interest correlates with the minimum visibility distances embedded within the limiting extinction coefficients or optical densities.

In some cases, avoidance of exposure to smoke altogether (either by keeping the smoke layer above a defined elevation or keeping smoke from entering a space) may be selected as a performance criterion.

When things other than people are protected, performance criteria may take one or more of the following forms:

- Prevention of ignition
- Prevention or minimization of flame spread
- Maintenance of fire barrier integrity or structural stability
- Avoidance of nonthermal damage due to exposure to smoke

Prevention of ignition of solid items is typically accomplished by keeping the incident radiant flux to a combustible object below a minimum value, typically the minimum heat flux for ignition ($\dot{q}''_{\min}$) or the critical heat flux for ignition ($\dot{q}''_{\text{crit}}$), depending on how it is measured. In some cases, values might be expressed as the minimum temperature at ignition. Values for a variety of fuels can be found in Appendix 3. The mechanism of ignition of solid fuels is described in Chap. 21.

For prevention of ignition of liquid fuels, performance criteria would typically involve keeping the liquid below its flashpoint. The flashpoint is not a fundamental material property and will vary depending on the test method used to measure it. More information and flashpoints for a variety of fuels can be found in Chap. 18.

For gases, performance criteria generally relate to keeping a gas/air mixture outside of its flammable range, which is discussed in more detail in Chap. 17. This chapter on flammability limits also contains flammability data for several gases.

Flame spread is a process of continuous ignition, as the flame front progresses from portions that are burning to unburned material. This is discussed in Chap. 23.

Performance criteria related to maintenance of barrier integrity is generally limited to specific

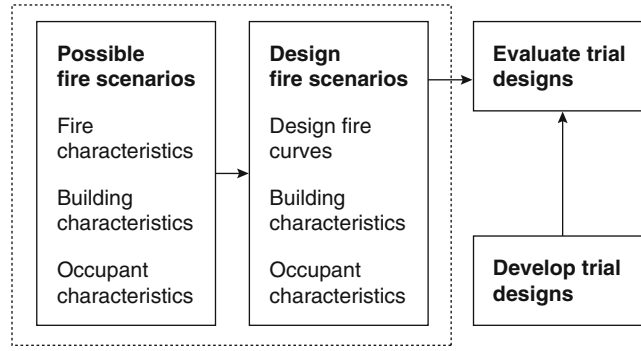

Fig. 37.5 Process for identifying design fire scenarios

assemblies. Chapter 55 provides information for gypsum board on wood studs. Chapter 54 discusses concrete assemblies. In many cases, the methodologies in the chapters referenced are limited to the standard time-temperature exposure.

Information related to structural integrity can also be found in Chap. 55, and Chap. 54, for wood and concrete structural materials, respectively. Steel assemblies are addressed in Chap. 53. Performance criteria associated with exposure of items to smoke can be developed using Chap. 36.

Step 5—Developing Fire Scenarios

A performance-based design requires the evaluation of fire safety based on various design fire scenarios. The *SFPE Engineering Guide to Performance-Based Fire Protection* provides a two-step process for identifying design fire scenarios. As depicted in Fig. 37.5, the first step is considering all possible fire scenarios that could occur in the building or portion of the building that is within the scope of the design. The second step is to reduce the population of possible fire scenarios into a manageable set of design fire scenarios. The design fire scenarios will be used to evaluate trial designs.

Fire scenarios are comprised of three elements: building characteristics, occupant characteristics and fire characteristics. Building characteristics are determined either by surveying an existing building, reviewing architectural design plans, or as part of a trial design strategy. Chapter 38 discusses fire scenarios. Fire load is frequently considered as part of a fire scenario, and this topic is addressed in Chap. 35. Chapter 57 provides information on occupant characteristics that can be used when developing fire scenarios.

Step 6—Developing Trial Designs

Several chapters in this *Handbook* relate to the design and evaluation of trial designs. When developing a trial design, an initial design is usually created. The initial design would be evaluated, and if it achieved the performance criteria when tested using the design fire scenarios, it would be considered acceptable. However, if the design did not achieve the performance criteria, it could either be eliminated or refined and revaluated. In this sense, the process of design development and evaluation can be iterative.

Several chapters can be used in both the development and evaluation of trial designs. These chapters generally do not articulate what must be done for strictly code-compliant designs but rather provide methods and engineering calculations that can be used to support system designs.

Chapter 39 provides a broad overview of the considerations involved with selecting a fire safety system as a trial design approach. System activation is addressed in Chap. 49.

Chapter 40 provides calculation methods for the design of heat detection systems, smoke detection systems, and radiant energy detection systems. That chapter also provides methodologies for designing fire alarm audibility. Approaches for developing occupant egress strategies are presented in Chap. 56.

For automatic sprinkler systems, Chap. 41, can be used to support the design of water supplies. Chapter 42 provides information relating to hydraulic calculations and also provides calculation methods relative to hanging and bracing and to sprinkler performance.

Water mist systems, which are water-based systems that utilize very small droplets, are covered in Chap. 46.

Foam systems are addressed in Chaps. 47 and 48. The former provides a basic description of foam agents and foam extinguishment. This chapter also discusses aviation fire protection considerations, foam water sprinkler systems, and environmental considerations associated with fire-fighting foams. Chapter 48, provides calculation methods associated with foam system design.

Clean agents are addressed in Chaps. 43 and 44. Chapter 43 would generally be used in the evaluation or modification of existing halon systems, since they are rarely used in new construction. Chapter 44 provides an overview of the halon replacements that are available and information that can be used in the design of halon replacement systems. Chapter 36 also provides information associated with fire control, suppression, and extinguishment. Chapter 45 addresses carbon dioxide system design.

Fundamental information relative to systems that employ fluids can be found in Chap. 1.

Several chapters provide information that is generally used in fire resistance design. Fire resistance design is comprised of three steps: determination of the thermal boundary conditions to the structure or portion thereof, determination of the heating of the structure that results from the thermal boundary conditions, and determination of the structural response of the structure at elevated temperature.

Chapter 53 provides an introduction to structural fire protection design. Chapter 30 provides methods for calculating the fire exposures that could be used in fire resistance design. These fire exposures form the thermal boundary conditions. Chapter 34 discusses heat transfer to the structure. Chapter 52 provides an overview of structural systems and frame effects. Chapters 53, 54, and 55 cover the design of fire resistance of steel members, concrete members, and timber members, respectively.

Chapters 54 and 55 address fire barrier design to a limited extent for concrete and timber-framed assemblies, respectively.

Smoke control is addressed in two chapters. Chapter 50 provides an overview, methodologies, and calculation methods for smoke control systems. Chapter 51 focuses on smoke management systems in covered malls, atria, and other similar large spaces.

Step 7—Quantifying Design Fire Curves

The design fire curve consists of many elements, including ignition, fire growth, fully developed burning, and decay. For information on ignition, consult the *SFPE Engineering Guide to Piloted Ignition of Solid Materials Under Radiant Exposure* [17], Chaps. 18 and 21.

There are a number of ways the fire curve can be produced, including testing (large and small scale) and correlations as well as analytical approaches. Information on flame spread and the effect on fire growth rates is provided in Chaps. 23 and 25. Chapter 65 provides information associated with liquid fuel fires. This chapter addresses determination of pool size, growth rate of pool fires, and fire size.

In many evaluations, one of the most critical tasks is estimating the size or heat release rate of a fire. The heat release rate that is estimated affects several other calculations that are used in the evaluation. Chapter 26 provides methodologies for estimating heat release rates and a tremendous amount of heat release rate data for a variety of commodities. In some cases, heat release rate data from small-scale test methods will be used in estimations of heat release rates. Chapters 27 and 28 provide overviews of bench-scale methods.

Compilations of fire data for many forms of fuel, including furniture and storage materials, can be found in Chaps. 26, 36, and 40. The information specifies material burning characteristics, fire growth curves, fire growth rates, and/or maximum heat release rates as well as other information that will assist in

estimates of design fires. Chapter 65, can also be used to calculate fully developed fire sizes for pool fires.

Fire is a dynamic phenomenon influenced by changes in air, fuel, and heat. Modification of any of these factors can increase or decrease the size of the fire. Chapter 16 discusses these effects.

Step 8—Evaluating Trial Designs

The evaluation of trial designs will usually involve performing fire dynamics calculations and hazard calculations. Several chapters address these types of calculations.

Calculations involving fire plumes (temperature, velocity, and mass entrainment), flame heights, and ceiling jets are included in Chaps. 13 and 14. These types of calculations are typically used in the analysis of detection systems and smoke control systems.

Chapter 15 addresses the flows through vents, where vents are any type of opening. These types of calculations are used in modeling the movement of smoke from or into enclosures, such as smoke flows through doorways.

Chapter 61 addresses visibility and human behavior in smoke. The calculation methods in this chapter would be used in any design in which people movement through smoke is contemplated. Equations and graphs are provided for estimating the effect of smoke on visibility and on the reduction on movement speed that could occur in smoky environments.

Chapter 58 provides an overview of behavioral response to fire and smoke. Chapters 64 and 59 provide methodologies and calculation methods for estimating evacuation times. Evacuation times consist of two components: the time for people to determine that there is a need to evacuate and the time necessary to move through building egress components. Evacuation models are addressed in Chap. 60.

In cases in which people may be exposed to smoke, it may be necessary to estimate the concentrations of combustion products. Chapter 16 identifies means of performing these analyses, and Chap. 24 provides additional information. The impact of the combustion products on people can be determined using the methodologies in Chap. 63. The information in Chap. 16, and in Chap. 24, is also useful in cases in which it is desired to consider the effect of constituents as part of a smoke detection analysis.

If an analysis involved determining whether or not an item will ignite, Chap. 17, 18, and 21, provide methods of determining if and when gases, liquids, and solids will ignite, respectively. Spontaneous combustion (self-heating that leads to combustion) is discussed in Chap. 20.

Chapter 19 covers smoldering combustion, including propagation of smolder through media and transition from smoldering combustion to flaming combustion. Chapter 23 addresses the spread of flaming combustion along the surface of solids and liquids.

The heat flux from local fires can be determined using Chap. 25. This type of analysis is typically performed in determinations of the heat flux from a local fire to part of a structure or to a fire barrier. This type of analysis could also be performed in calculations involving the ignition of items from exposure to a localized fire.

Chapter 66 presents methods of performing hazard calculations associated with large hydrocarbon pool fires.

Fire modeling is frequently used in the evaluation of trial designs. Chapter 36 and Appendix 3 provide a tremendous amount of data that can be used in fire modeling. Chapter 29 provides an overview of compartment fire modeling techniques. Chapter 30 provides closed-form equations that can be used for estimating compartment fire temperatures. Chapter 31 provides a discussion of zone modeling, and Chap. 32, addresses CFD, or field models. Smoke filling of enclosures is discussed in Chap. 33, these types of calculations are frequently employed in cases where it is desired to keep a smoke layer above a critical elevation. A broad overview of computer modeling can also be found in Chap. 80.

For designs in which protection from explosions is an objective (either prevention, suppression, or response), Chaps. 69 and 70, provide methods and data that can be used.

Once the engineering calculations have been completed, a decision must be made as to whether or not a design is acceptable. For most cases, acceptability will be judged by seeing if the results of the analyses do not exceed the performance criteria. Chapter 77 provides information where more complex decision analysis is needed.

Most fire protection strategies used will have a reliability that is less than 100 %, and the effects of imperfect reliability should be addressed. Chapter 74 addresses the subject of reliability.

Uncertainty will be introduced in many of the steps of the process. Chapter 76 provides several uncertainty analysis techniques.

Almost all analyses will require data of some sort as input into calculations or models. In some cases, the needed data will be readily available. However, in others, it will be difficult to find. Chapter 78 provides an overview of data types, sources, and issues associated with data.

In some cases, it will be desirable to measure all fire consequences using a single metric. Chapter 79 discusses measuring fire consequences in economic terms. Engineering economics, which are frequently considered in design decisions, are summarized in Chap. 81.

Step 9—Documenting Design Process

All aspects of the design are generally documented. Documentation is provided as a way for stakeholders, regulatory officials, and tradespeople to review, understand, and be able to implement the design. Documentation also serves as a record in case modification or analysis following a fire is required in the future.

Summary

Performance-based design, while drawing increased attention recently, has been evolving over the last several decades. The *SFPE Engineering Guide to Performance-Based Fire Protection* [1] provides a process for conducting performance-based designs. Information in the *SFPE Handbook of Fire Protection Engineering* can be used to support engineering designs and calculations associated with developing and evaluating performance-based designs.

References

1. *SFPE Engineering Guide to Performance-Based Fire Protection,* National Fire Protection Association, Quincy, MA (2006).
2. H. Nelson, "Performance-Based Fire Safety," in *Proceedings: 1996 International Conference on Performance-Based Codes and Fire Safety Design Methods, Society of Fire Protection Engineers, Bethesda, MD (1996).*
3. ASCE/SFPE 29-05, *Standard Calculation Methods for Structural Fire Protection,* American Society of Civil Engineers, Reston, VA (2005).
4. NFPA *101®, Life Safety Code®,* National Fire Protection Association, Quincy, MA (2012).
5. R. Custer and B. Meacham, *Introduction to Performance-Based Fire Safety,* National Fire Protection Association, Quincy, MA (1997).
6. *NFPA 5000®, Building Construction and Safety Code®,* National Fire Protection Association, Quincy, MA (2012).
7. I*CC Performance Code® for Buildings and Facilities,* International Code Council, Falls Church, VA (2012).
8. *Engineering Guide—Fire Risk Assessment,* Society of Fire Protection Engineers, Bethesda, MD (2006).
9. Verification Method: Framework for Fire Safety Design Fire New Zealand Building Code Clauses C1-C6 Protection from Fire, Department of Building and Housing, Wellington, New Zealand, 2012.
10. NFPA 550, *Guide to the Fire Safety Concepts Tree,* National Fire Protection Association, Quincy, MA (2012).
11. *Engineering Guide—Human Behavior in Fire,* Society of Fire Protection Engineers, Bethesda, MD (2003).
12. J. Watts and J. Hall, "Introduction to Fire Risk Analysis," *SFPE Handbook of Fire Protection Engineering,* Springer, New York (2015).
13. B. Meacham, "Building Fire Risk Analysis," *SFPE Handbook of Fire Protection Engineering,* Springer, New York (2015).
14. M. Hui, "How Can a Fire Risk Approach Be Applied to Develop a Balanced Fire Protection Strategy," *Fire Protection Engineering,* 30, pp. 12–21 (Spring 2006).

15. NUREG-1824 and EPRI 1011999, "Verification and Validation of Selected Fire Models for Nuclear Power Plant Applications," Vols. 1-7, U.S. Nuclear Regulatory Commission, Washington, DC and Electric Power Research Institute, Palo Alto, CA, 2007.
16. Olenick, S., and Carpenter, D., "An Updated International Survey of Computer Models for Fire and Smoke," *Journal of Fire Protection Engineering*, 13 (2), 2003, p. 87–110.
17. *Engineering Guide—Piloted Ignition of Solid Materials Under Radiant Exposure,* Society of Fire Protection Engineers, Bethesda, MD (2002).

Morgan J. Hurley is a project director with Aon Fire Protection Engineering. He is also adjunct faculty at the University of Maryland and California Polytechnic University. He holds bachelor's and master's degrees in fire protection engineering from the University of Maryland and is a licensed professional engineer.

Eric R. Rosenbaum is the director of architectural and engineering services for JENSEN HUGHES, Inc. Mr. Rosenbaum is the chair of the Society of Fire Protection Engineers Task Group on Performance-Based Analysis and Design.

Fire Scenarios

38

George V. Hadjisophocleous and Jim R. Mehaffey

Introduction

The engineering approach to fire safety design requires the selection and evaluation of fire scenarios that may occur in a building. Each fire scenario represents a unique combination of events and circumstances that influence the outcome of a fire in a building, including the impact of fire safety measures. The *SFPE Engineering Guide to Performance-Based Fire Protection* [1] refers to fire scenarios as "a set of conditions that defines the development of fire and the spread of combustion products throughout a building or part of a building."

It is obvious that the total number of fire scenarios that may occur in a building can be very large; hence it is not possible to analyze each scenario separately. To reduce the number of scenarios to a manageable number, it is necessary to follow a scenario identification and selection process in a systematic fashion to ensure that the outcome of the engineering analysis is credible and acceptable to all stakeholders. The scenario identification and selection process can be performed by considering both the expected frequency of occurrence of each scenario and its expected consequences. This must be done so that the selected fire scenarios yield a fire protection design that provides acceptable levels of safety for the building occupants and property.

The *SFPE Engineering Guide* [1], the *International Fire Engineering Guidelines* [2], and other publications that provide guidance on the design process clearly indicate that the task of identifying and selecting fire scenarios is an integral part of the design process. Figure 38.1 is a section of the performance-based design process described in the *SFPE Engineering Guide*. The figure shows that developing fire scenarios follows the tasks of defining the project scope, goals, and objectives, and developing performance criteria.

Project scope, goals, and objectives inform the scenario identification and selection process. The project scope identifies whether the design is for a new building or an existing building, specific building components for the whole or part of a building, or repairs to the whole or part of a building. The fundamental fire safety goals for a building can be to

- Provide life safety for building occupants and emergency responders
- Protect property
- Provide for continuity of operations
- Limit the environmental impact of the fire
- Protect the heritage and cultural value of the property.

Although the fire safety goals are expressed in general terms, the fire safety objectives delineate more specific ways of attaining these goals. Quantifiable performance criteria can then be chosen to provide the basis for assessing whether fire protection designs achieve these objectives.

G.V. Hadjisophocleous (✉)
Carlton University

J.R. Mehaffey
CHM Fire Consultants

M.J. Hurley (ed.), *SFPE Handbook of Fire Protection Engineering*,
DOI 10.1007/978-1-4939-2565-0_38, © Society of Fire Protection Engineers 2016

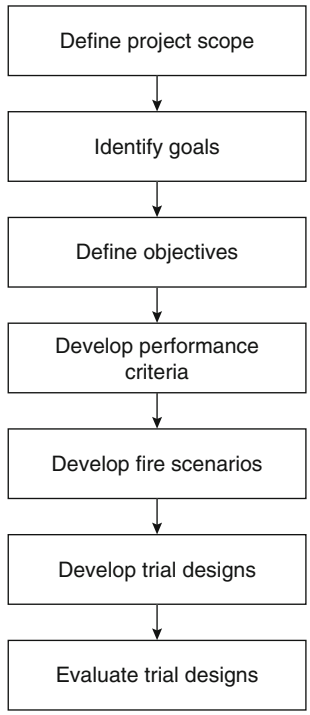

Fig. 38.1 Performance-based design process [1]

To ensure that the design will satisfy the above goals/objectives, the selected fire scenarios should be such that they challenge the proposed fire protection designs. Details on these steps can be found in the *SFPE Engineering Guide* [1].

A useful approach to the process of identifying and selecting fire scenarios has been developed by the International Organization for Standardization (ISO) [3], and it is summarized in Table 38.1.

Development of Fire Scenarios

Before one can identify potential fire scenarios, a significant amount of information about the project must be assembled. The types of information that may be required are described in this chapter.

Building Characteristics

Building characteristics need to be well documented, as they have a profound impact on potential fire scenarios. The physical layout of

Table 38.1 Steps used for identifying and selecting fire scenarios

Steps of ISO/TS 16733	Comments
1. Location of fire	Characterize the space in which fire begins as well as the specific location within the space
2. Type of fire	Characterize the ignition, initial intensity, and growth of potential fires
3. Potential fire hazards	Identify fire scenarios that could arise from fire hazards associated with the intended use of the property or the design
4. Systems impacting on fire	Identify the fire safety systems and features that are likely to have a significant impact on the course of the fire or development of untenable conditions. Characterize the initial status of each system or feature
5. Occupant response	Identify actions that people take that can have significant impact, favorable or otherwise, on the course of the fire or the movement of smoke
6. Event tree	Construct an event tree that represents alternative event sequences from fire ignition to outcome associated with fire scenarios
7. Consideration of probability	Estimate the probability of occurrence of each event using available data and/or engineering judgment
8. Consideration of consequence	Estimate the consequence of each scenario using available loss data and/or engineering judgment
9. Risk ranking	Rank the scenarios in order of relative risk. The relative risk can be evaluated by multiplying the consequence (step 8) by the probability of occurrence (step 7) of the scenario
10. Final selection and documentation	For each fire safety objective, select the highest ranked fire scenarios for quantitative analysis. Selected scenarios should represent the major portion of the cumulative risk (sum of the risk of all scenarios)

the building and the choice of building materials affect fire growth and severity within the compartment of fire origin. The building layout also plays major roles in fire and smoke spread through the building, occupant evacuation, and fire fighter access.

The detail required to describe building characteristics depends on the nature and complexity of the engineering analysis to be undertaken. Not all of the characteristics discussed below need to be quantified for every project.

The proposed layout and construction of compartments of interest, as well as interconnections among them, must be known. The information required could include

- Number of stories above and below grade
- Physical dimensions of compartments
- Construction materials and design of all building assemblies (walls, floors, etc.)
- Flammability and thermal properties of interior finish (density, thermal conductivity, specific heat, etc.)
- Location and dimensions of potential openings that could provide ventilation to the fire (doors, windows, areas of low fire resistance, etc.)
- Interconnections among compartments.

Other features of the construction of the building need to be considered as well, such as

- Location, dimensions, and properties of structural components (materials, thermal properties, mechanical properties, anticipated loads, etc.)
- Location and size of fire compartments (spaces enclosed by fire-resistant assemblies)
- Location and nature of concealed spaces
- Description of the proposed egress routes.

The nature and properties of proposed building services must be determined. This could include HVAC, electrical distribution, and plumbing systems as well as fire protection equipment related to automatic or manual fire suppression, smoke control, and fire detection. Plans for use of firestopping materials and dampers for such systems must also be considered.

Where the potential for fire spread to neighboring buildings is an issue, the location of the building on the site in relation to site boundaries must be determined. The properties of the exterior walls must also be known including their fire-resistant capabilities, the flammability of their claddings, and the size and nature of unprotected openings.

Fuel Loads

The combustible contents of a building can play a more significant role in fire development and severity than building products. It is therefore necessary to estimate the quantity of fuel in each compartment of interest as well as the types of fuel that may be present.

The quantity of fuel (combustible contents) is commonly expressed as a fuel load density; that is, fuel load per unit floor area in MJ/m^2. Statistical data derived from surveys are available for many occupancy types [4]. When a severe but credible representation of the quantity of fuel is desired, it is advisable to choose the 80th or even 95th percentile in the distribution of fuel load densities.

Although the fire load density concept implicitly assumes a uniform distribution of combustibles in compartments, it should be recognized that the actual distribution of combustibles may need to be addressed in some buildings.

Types of Combustibles

Different types of combustibles burn at different rates and exhibit different yields of various products of combustion as they burn. Characterizing the fuel in terms of the fuel load density, that is, in terms of its energy content, is often not sufficient. It can be important to know how much of the fuel is cellulosic, how much is plastic, how much is combustible liquid, and so forth. Some recent surveys provide such detailed data for selected occupancy types [5, 6].

Often the contents of a compartment come in the form of specific fuel packages. For example, an upholstered chair may be constructed of several combustible materials arranged in a unique configuration. It is challenging to model the burning of such a chair based on the flammability characteristics of each component. A simpler and reliable alternative is to rely on experimental data available in the literature [7–9].

Functions in Building

For many occupancy types, statistics are available to draw conclusions concerning likely sources of ignition and first items ignited. Statistics may also indicate which combinations of ignition sources and first item ignited lead to the most serious fire losses [10].

To supplement such statistics, an assessment of potential ignition sources and vulnerable combustibles can be undertaken for the proposed building layout and activities. This may be particularly important in an industrial building where several different manufacturing processes may be carried out, raw materials may be stored, finished products may be warehoused, and office space may be provided for staff. Although statistical data may not be available for the specific functions, the owner, operator, and perhaps even the insurance provider can be very helpful in identifying potential ignition sources and vulnerable combustibles.

Passive Fire Protection Systems

To inhibit fire spread through a building, it can be subdivided into fire compartments enclosed by fire-resistant assemblies. Commonly referred to as compartmentalization, this is a passive fire protection strategy. Although wall and floor/ceiling assemblies can be designed to be sufficiently fire resistant to meet the objectives of the design, the challenge is often to ensure connections between fire compartments are also sufficiently fire resistant.

Details and the statuses of closures intended to protect connections between fire compartments and to ensure the integrity of fire compartments in the event of fire must be determined. Doors can often be assumed to be closed and can be chosen to be sufficiently fire resistant; for example, doors between an apartment and a public corridor. In some occupancies or locations, fire-resistant doors may be held open for operational reasons and must be prompted to close in the event of fire. Detection systems can cut the current to electromagnetic "hold-open" devices and the doors will close. Thus the passive fire protection strategy is ensured by an automatic fire protection system. Similarly, ducts connecting fire compartments may need to be protected by dampers that operate by the use of fusible links or by other means.

Although most passive fire protection systems can be assumed to be very reliable, one must be confident that the design (resistance) of the system is adequate for the risk and that the system will not be compromised by modification (planned or accidental) through the years.

Detection and Suppression Systems

In the analysis of an existing building, the type (smoke detection, heat detection, UV/IR) of an automatic detection system must be documented. The location of detectors and their response time index (RTI) and activation temperatures (if appropriate) also must be noted [11]. The type of alarm notification, the location of alarm devices, and their acoustical performance should be noted. Of course, in the design of a new building the same information is required for the proposed (or trial) detection system(s).

Similarly, whether in an analysis of an existing building or in the design of a new building, the characteristics of automatic suppression systems must be documented. Information such as the types and locations of discharge devices is required. The activation characteristics (RTI and activation temperature) as well as the agent discharge density and distribution must be known [12].

Estimates of the reliability of detection and suppression should be made. Independently, one might also need to consider whether the anticipated fire development is such that these devices cannot be activated.

Occupant Load and Characteristics

Life safety is a common fire safety objective. Many of the variables affecting occupant behavior are either qualitative or difficult to quantify [13–15]. Nonetheless, whether the fire safety strategy involves evacuation or provision of safe areas of refuge, the following "occupant factors" must be considered:

- Occupant load (number and distribution of occupants)
- Familiarity with the building
- Alertness (sleeping or awake)
- Physical and mental ability.

Actions Taken by Occupants

The actions that occupants take can have significant impact, favorable or otherwise, on the course of the fire or the movement of smoke and should be considered. Depending on the nature of the building, trained staff or a well-equipped in-house fire brigade can have a profound influence on a fire in the early stages of development. In many facilities, fire wardens may play a significant role in assisting with evacuation. On the other hand, poorly trained staff or casual visitors could leave key doors open, allowing for rapid fire development and smoke transport. Any of these effects could introduce new potential fire scenarios.

Actions Taken by the Fire Department

A decision can be taken to ignore the beneficial actions taken by the fire department despite the fact that these actions can have a dramatic impact on fire spread within and between buildings. Whether fire department actions are explicitly modeled or not, the location, capability (types of equipment, training, etc.), and response time of the fire department need to be determined [16, 17]. The method of and hence inherent delay in alerting the fire department must be noted. The access of fire fighting appliances to the site and the access of fire fighters to the building must also be noted.

Identification of Potential Fire Scenarios

Having collected the data described in the preceding sections, it is now important to identify potential fire scenarios. One way to proceed is to follow the first five steps in the ISO methodology outlined in Table 38.1.

Step 1—Location of Fire The most likely locations for fire may often be determined by the review of statistics or from the assessment of potential ignition sources and vulnerable combustibles. Identification of the most adverse or challenging locations for fire normally entails the use of engineering judgment.

ISO/TS 16733 provides guidance on selecting challenging locations for fire [3]. Where life safety is the primary objective, Chap. 5 of NFPA *101*®, *Life Safety Code*®, identifies eight "required" design fire scenarios [18]. Most of these scenarios identify what are considered to be challenging locations.

As a minimum, the engineer should give consideration to modeling fires in the following locations:

- Fires in or its spread to "rooms" with a large number of occupants or vulnerable property
- Fires that render part(s) of the means of egress unusable
- Fires that commence within building assemblies and remain undetected while they grow in intensity (e.g., within concealed spaces, sandwich panels, etc.)
- Localized fires and/or postflashover fires that could challenge the structure and compartmentation in the building
- Fire locations that are challenging for proposed active measures (e.g., fires that are

shielded from sprinkler sprays, fires at floor level in the center of a space that generate large volumes of smoke that must be exhausted, etc.)

Step 2—Type of Fire At this point in the analysis, the type of fire refers to a qualitative description of the ignition, initial intensity, and growth of a fire. Much insight can often be gained from perusing statistics. For a given occupancy, one may be able to identify the most common ignition sources and the associated first item(s) ignited. One may also identify those combinations of ignition sources and associated first item(s) ignited that cause the largest percentage of deaths, the largest property losses, the largest percentage of fires that spread beyond the room (or compartment) of fire origin, and so forth [10].

Often Step 1 and Step 2 can be combined. Cooking fires take place on stoves in kitchens, and specific industrial fires take place at certain stages in the manufacturing process associated with specific equipment.

Step 3—Potential Fire Hazards Statistics give information of past and current fire problems but may not shed light on problems in the future as new designs, products, or hazards are introduced. It is therefore important to employ engineering judgment to identify potential fires that may not be identified by reviewing statistics.

For some occupancy types, for example, industrial buildings, the assessment of potential ignition sources and vulnerable combustibles undertaken in the section "Functions in Building" of this chapter may suggest types of fires that must be considered.

Step 4—Systems Affecting Fire The fire safety systems that are proposed for the building or facility, and that are likely to have a significant impact on fire development and the generation of untenable conditions, should be identified. For each system, consider the possibilities that it is operational and that it is not operational (due to routine maintenance, degradation over the years, etc.).

Passive systems that may play an important role are

- Fire separations such as walls and floors (ratings, penetrations, etc.)
- Closures in fire separations (fire doors, dampers, etc.)
- Structural members (rating, status of protection, etc.)
- Protection of means of egress.

Active systems that may play an important role are

- Suppression systems (sprinklers, CO_2, etc.)
- Smoke management systems (mechanical, natural venting, etc.)
- Fire detection systems (smoke, heat, etc.)
- Hold-open devices.

Step 5—Occupant Response Identify actions that people could take that can have significant impact, favorable or otherwise, on the course of the fire or the movement of smoke. Actions of occupants might also impact significantly on evacuation choices.

It may also be possible to consider the impact that in-house fire brigades or municipal fire fighters could have, particularly early in fire development while occupants are still evacuating. This may entail search and rescue efforts as well as suppression and smoke venting.

Selection of Design Fire Scenarios

In principle, all of the fire scenarios identified above should be used to evaluate trial fire protection designs. Such an approach is used by fire risk assessment models such as FiRECAM [19], which is applicable to typical apartment and office buildings. An example of the scenarios used by FiRECAM is described in Appendix 1 at the end of the chapter. In practice, it is not possible to evaluate all possible fire scenarios due to the large number for a given performance-based project. It is therefore necessary to filter possible fire scenarios to reduce their numbers to manageable levels. The selected scenarios are known as the design fire scenarios. The scenario

screening process is done using engineering judgment and a variety of deterministic and probabilistic tools such as event trees or qualitative analysis and risk ranking. Steps 6–10 of Table 38.1 can be followed to screen and select fire scenarios for quantitative analysis.

Event Trees

Step 6 of Table 38.1 deals with event trees, which are a useful tool for identifying and screening fire scenarios. An event tree can be constructed to explicitly display the possible states and alternative event sequences from ignition to burnout or extinguishment for each identified fire scenario. Some of the factors to be considered include the activation (or not) of detection and suppression systems, the presence of occupants in the fire area, the success of manual fire fighting, and fire department response and actions. In addition, factors such as the attainment of flashover, the status (open or closed) of fire doors in the compartment of fire origin, and the status (awake, asleep, infirm, etc.) of occupants of the building can also be considered.

An example of an event tree is shown in Fig. 38.2 for fire scenarios starting at a specified location. The frequency of fire of a specific type starting at this location, P_1, is an important factor that will influence the selection of design fire scenarios. Following ignition is the event "manual suppression," which has a conditional probability of success $P_{1,1}$ and of failure $P_{1,2}$ (equal to $1 - P_{1,1}$). The tree then considers the event "automatic suppression," with probability of success $P_{1,2,1}$ and of failure $P_{1,2,2}$ ($1 - P_{1,2,1}$). As can be seen from Fig. 38.2, the paths with successful events are not expanded for subsequent events, as these events will not have an impact on the final outcome of these paths. The tree considers two additional events, "venting effective" and "barriers effective," in a similar manner.

For each of the resulting paths, a path probability can be computed using the product of the probabilities of events found along that path.

$$P_{S11} = P_1 P_{1,1}$$

$$P_{S12} = P_1 P_{1,2} P_{1,2,1}$$

$$P_{S13} = P_1 P_{1,2} P_{1,2,2} P_{1,2,2,1}$$

$$P_{S14} = P_1 P_{1,2} P_{1,2,2} P_{1,2,2,2} P_{1,2,2,2,1}$$

$$P_{S15} = P_1 P_{1,2} P_{1,2,2} P_{1,2,2,2} P_{1,2,2,2,2}$$

For each path, the consequences in terms of life safety or property damage may be roughly estimated and placed in the last column of Fig. 38.2. Knowledge of the probabilities and

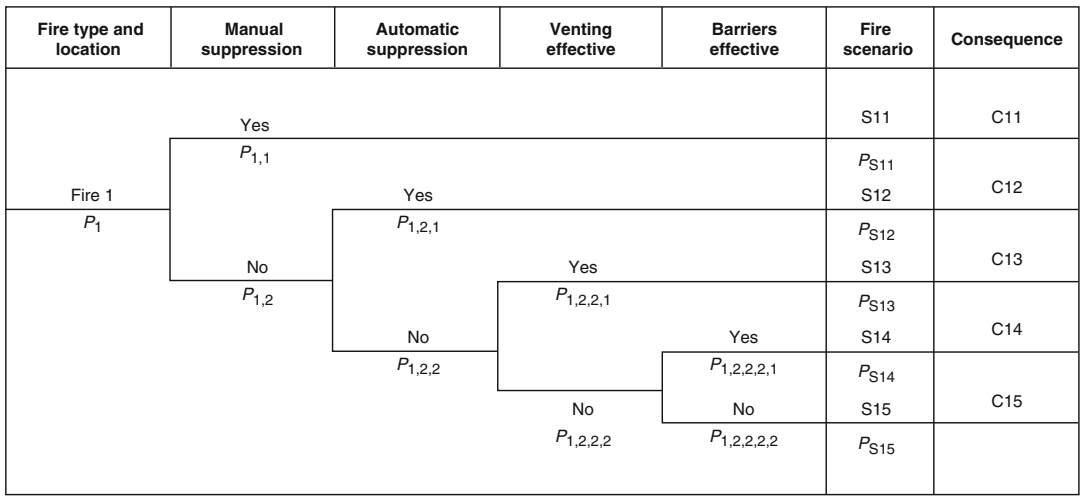

Fig. 38.2 Event tree for a given fire type occurring in a given location

consequence of each fire scenario (each path) can then be used to decide which scenarios should be considered as the design fire scenarios for more detailed analysis.

Frequency Calculation

Step 7 of Table 38.1 deals with the probability of occurrence of scenarios. Each fire scenario has a frequency of occurrence, which is the product of the frequency that this fire type occurs at a given location, P_1, and the probabilities of the occurrence of the different events associated with that scenario. In other words, it is the probability of the branch representing the fire scenario. Values required in determining fire scenario frequencies include the frequency that this fire type occurs at a given location; the reliability and effectiveness values of the active fire protection systems such as detection and alarm systems, suppression systems, and smoke control systems; as well the probability of failure of passive fire protection systems such as walls, floors, and rated doors. Data for estimating these values can be found from statistical databases, from expert judgment, and from mathematical models that may themselves include event and fault trees analysis.

Statistics and Historical Information

Statistical databases of past fire incidents contain data that could be analyzed to determine the most likely areas of ignition, item first ignited, and fuel source, as well as the probability of fire reaching various stages of severity and spreading to areas beyond the compartment of fire origin. Data can be found for various occupancies and can be used to determine frequency of ignition and the availability of active systems and their probability of activation and effectiveness [10].

Consideration of Consequence

In this step of the scenario selection process, Step 8 of Table 38.1, the expected consequences of each scenario or cluster of scenarios are estimated using available loss data and/or engineering judgment. This is a preliminary estimate of consequence for scenario screening purposes only using a risk-ranking matrix, as discussed below. A more detailed consequence analysis is done for each of the selected (design) fire scenarios as part of the quantitative engineering assessment.

Risk Ranking

Risk ranking, which is Step 9 in Table 38.1, is a useful method for screening scenarios because it allows comparison of scenarios based on both their frequencies and their consequences. Risk ranking can be used to perform either a quantitative or a qualitative analysis.

For a quantitative screening process, the probabilities and consequences of each potential scenario must be estimated and then the risk computed as the probability times the consequence. Design fire scenarios are chosen as those that represent the greatest risk. Two examples of how to select scenarios using this technique are provided in the annexes of ISO/TS 16733.

To perform a qualitative analysis, the identified scenarios can be grouped based on their expected consequences in order to implement a "risk binning" method. The *SFPE Engineering Guide* [1] suggests four consequence levels: negligible, low, moderate, and high. Consequences can reflect threat to life, property damage, downtime, environmental damage, and so on. Separate risk matrices can be developed for each type of consequence.

A description of the impact on occupants of the four consequence levels is as follows:

Negligible:	Negligible injuries
Low:	Minor injuries, no permanent disabilities
Moderate:	Serious injuries, permanent disabilities, hospitalization required
High:	Sudden fatalities, acute injuries, immediately life-threatening situations, permanent disabilities.

In terms of the impact on property and operations the four groups are described as follows:

Negligible: Minimum damage to building, minimal operational downtime

Low: Damage less than a specified dollar value $YY, reparable damage to building, significant operational downtime, no impact on surroundings

Moderate: Damage greater than $YY and less than a specified dollar value $XX million, major equipment destroyed, minor impact on surroundings

High: Damage greater than $XX million, building destroyed, surrounding property damaged.

Following the estimation of the consequences of the various scenarios, the risk binning method requires an estimate of the frequency level of each of the scenarios. In a similar fashion to the evaluation of the consequences, the frequencies can be determined using a qualitative or a quantitative approach. The *SFPE Engineering Guide* [1] suggests the following levels of frequencies:

- Anticipated, expected: incidents that might occur several times during the lifetime of the building $\left(f > 1 \times 10^{-2}/\text{yr}\right)$
- Unlikely: events that are not anticipated to occur during the lifetime of the facility $\left(1 \times 10^{-4}/\text{yr} < f \leq 1 \times 10^{-2}/\text{yr}\right)$
- Extremely unlikely: events that will probably not occur during the life cycle of the building $\left(1 \times 10^{-6}/\text{yr} < f \leq 1 \times 10^{-4}/\text{yr}\right)$
- Beyond extremely unlikely: all other incidents $\left(f \leq 1 \times 10^{-;6}/\text{yr}\right)$.

With these scales a risk-ranking matrix is constructed, as shown in Fig. 38.3. Once the risk matrix has been constructed, scenarios with high or moderate risk can be selected as the design fire scenarios for further analysis.

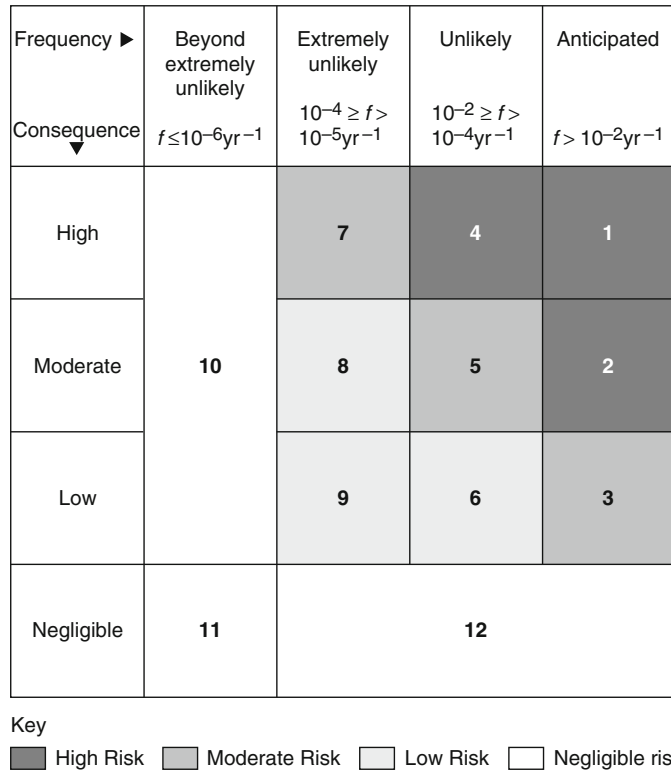

Fig. 38.3 Risk-ranking matrix (Adapted from SFPE Design Guide [1])

Scenario Selection

In Step 10 of Table 38.1, the selection of fire scenarios for quantitative analysis is done and documented. These are the highest ranked scenarios for each fire safety objective. Documentation should include a clear scenario description that includes the design fire associated with each selected scenario and the condition of the active and passive fire protection systems.

Quantifying Design Fire Scenarios

The process of quantifying the selected design fire scenarios is the essence of a fire protection engineering analysis. This process involves the quantification of the fire and smoke characteristics from ignition to outcome (referred to as the design fires) and their impact on property and building occupants (the consequences). In addition, it may involve the quantification of the frequencies of the various scenarios that can assist in selecting appropriate cost-effective designs. Although this process is very broad, it covers all aspects of fire safety engineering and utilizes computer models and other tools in the analysis. In the following sections, some guidelines are provided to assist fire protection engineers.

Design Fires

Following identification of the design fire scenarios, it is necessary to describe the assumed characteristics of the fire on which the scenario quantification will be based. These assumed fire characteristics are referred to as the "design fire." This section provides guidance on characterization of design fires in terms of time-dependent heat release rates.

In principle, a design fire may progress from an incipient phase to a growth phase to a fully developed phase and finally to a decay phase. Depending on the nature of the fire safety engineering assessment, one may not need to model every phase of the fire.

Modeling Preflashover Fire Growth The preflashover growth phase could consist of a smoldering and/or flaming stage. As smoldering produces heat at a slow rate, it is not considered here, but some models, such as FiRECAM [19], do address this phenomenon. For preflashover fires or fires that remain localized, the rate of heat release as discussed in this section, as well as the location of the fire, forms the fundamental description of the design fire.

Rate of Heat Release Modeling preflashover fire growth involves estimating the rate of heat release, $\dot{Q}$, of the fire as a function of time. Several methods are available for the purpose.

The first method is the *generic t^2 model*. When combustible items of varying composition are present, it is often not practical to attempt to model early fire growth by identifying the first item ignited and modeling fire spread from the first item to involve an increasing quantity of fuel. In such cases, it is more appropriate to use a generic fire growth curve that represents the general types of combustible material in the enclosure. Fires that do not involve flammable liquids or gases often grow relatively slowly at the outset. As the fire grows, the rate of growth accelerates. Such fires often grow proportionately to the square of the time.

$$\dot{Q} = (t/t_{1000})^2 \,(\text{kW}) \qquad (38.1)$$

where

t = time (s)

t_{1000} = time (s) to reach a heat release rate of 1000 kW (1 MW)

Analyses of the results of fire tests and real fires have provided a basis for estimating t_{1000}. Four fire growth rates, appropriate for design, are identified in Table 38.2. Each of these fire growth rates is characterized by a specific value of t_{1000} as depicted in the table. Table 38.2 also identifies examples of fuel configurations known to fit into each of the four fire growth categories.

Another method is the *experimental data method*. If it is possible to identify the first item likely to be ignited, the initial rate of fire growth can be determined from test data. Results from

calorimeter or large-scale tests may be used, provided the limitations are considered. Most information on burning rates for single items has been collected from items burning in a large enclosure. These data will be appropriate for the early stages of fire in large enclosures, but if the fire grows large or if it takes place in a small enclosure, the free-burning rate must be adjusted to account for

- Radiative feedback from the hot smoky layer or from enclosure surfaces
- Restriction of fire by an inadequate supply of oxygen.

Based on such large-scale tests, analytical models have been developed [20] to predict the rate of heat release when the burning item is a wooden crib, wooden pallets, or liquid (or thermoplastic) pool fires. Data are also available for a number of other products [7, 9, 20].

Another method is by *calculations from first principles*. In some circumstances, where the relative orientation and spacing of fuel packages are well known, it is possible to undertake calculations from first principles. Once the rate of heat release of the first item ignited has been determined from specific data or models, an analysis should be performed to ascertain whether the fire is likely to spread to neighboring items. This can be accomplished by considering the radiant heat transfer from flames to adjacent fuel items. The radiant flux incident on the adjacent packages should be compared with critical levels for the relevant materials to determine whether secondary ignition (fire spread) is likely. As the fire spreads from item to item, fire modeling can be used to estimate fire growth curves representative of the cumulative heat release rate due to the burning of multiple fuel packages. This should be considered an approximation since the nature and strength of the ignition source could differ from the ignition source used in the specific fire tests where the fire growth curves for the adjacent items were measured.

When modeling the preflashover growth phase as a t^2 fire (Equation 38.1), it should kept in mind that the fire may not be able to grow without limit. There may be a *maximum rate of heat release* that can be realized. If so, the heat release rate could be modeled employing Equation 38.1 until the maximum rate is reached and then assumed to level off at the maximum value. This is depicted in Fig. 38.4, where, in the growth phase, the fire grows as t^2, but levels off at a steady-burning rate. Several examples of this type of behavior follow.

At the point in time when sprinklers activate, if shielding of combustibles from the water spray can be expected, it might be advisable to assume that sprinklers prevent the fire from growing but do not suppress it. In such cases one could assume the heat release rate remains at the level

Table 38.2 Categories of t^2 fires

Growth rate	t_{1000} (s)	Typical real fires
Slow	600	Densely packed wood products
Medium	300	Solid wood furniture (desks) Individual furniture items with small amounts of plastic
Fast	150	High stacked wood pallets Cartons on pallets Some upholstered furniture
Ultrafast	75	Upholstered furniture High stacked plastic materials Thin wood furniture (wardrobes)

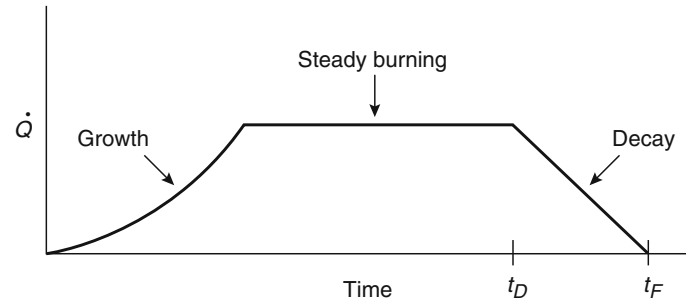

Fig. 38.4 Depiction of the three phases of fire: growth, steady burning, and decay

when sprinklers activated. For many scenarios, the activation of sprinklers will cause the heat release rate to drop; however, for some shielded fires, the heat release rate may continue to rise even after sprinklers activate.

In the absence of sprinkler activation, the amount, type, and configuration of burning items that can become involved in fire may also impose an upper limit on the rate of heat release. The maximum heat release rate then would be given by the maximum free-burning value.

The available ventilation can also impose an upper limit on the rate of heat release in the absence of sprinkler activation. If the available ventilation is restricted, the fire may not even reach flashover. Many computer models automatically account for the possibility of ventilation control. If hand calculations are to be undertaken and there is only one principal opening, the maximum rate of heat release can be predicted as

$$\dot{Q} = 1400A\sqrt{H}\,(\mathrm{kW}) \qquad (38.2)$$

Where A is the area of the opening in m^2 and H the height of the opening in m.

Modeling Postflashover Fires The discussion above does not account for the possibility of flashover. Flashover can be considered to occur when the

- Temperature of the hot gas layer under the ceiling reaches 500 °C
- Heat flux at the floor (or the level of combustibles) reaches 20 kW m^{-2}.

These criteria can be used along with two-zone fire models to predict whether or when flashover is expected to occur in an enclosure. Simple analytical models are also available to predict whether flashover is likely [21].

If flashover occurs, Fig. 38.4 would still apply, but the steady-burning rate would now be defined by the postflashover value predicted below.

Following flashover, the rate of heat release increases rapidly until it reaches the maximum value for the enclosure. The rate of consumption of fuel is approximately constant and is limited by the quantity and nature of the fuel or by the available ventilation. The rate of consumption for both fuel-bed-controlled and ventilation-controlled regimes should be calculated and the lesser value taken as representing the fully developed fire. To simplify design, the growth period between flashover and the maximum heat release rate is usually ignored, and it is assumed that the rate of heat release instantaneously increases to the steady-state level after flashover.

As with preflashover fires, the maximum rate of heat release for ventilation-controlled fires can, in general, be predicted employing Equation 38.2. With fuel-bed-controlled fire, the combustibles are able to burn freely. The rate of heat release is limited by the amount, type, and configuration of the burning items.

Modeling the Decay Phase of the Fire The decay phase of the fire commences at time t_D, which can be defined as the time when about 70–80% of the design fire load has been consumed. In the decay phase it can be assumed that the heat release rate exhibits a linear decrease with time.

Quantifying the Fire and Its Impacts

The process of quantifying the fire and its impacts on life safety and property for each fire scenario, also known as hazard analysis, involves calculations of all the subsystems of the fire safety system. Subsystems include fire initiation development and spread, smoke movement, activation of detection and suppression systems, impact on structure, occupant response and evacuation, and fire department intervention. These calculations may involve simple correlations such as plume calculations or the use of complex mathematical models such as computational fluid dynamics (CFD) models. The following sections consider each subsystem and discuss the various calculation approaches that may be used. The purpose is to provide guidance on the available calculation methods and refer the reader to the appropriate sources for more detailed analysis.

Smoke Movement Smoke movement from the compartment of fire origin to other areas in the building is the main cause of deaths and injuries in building fires. In addition to the life safety impacts of smoke due to toxic gases and high temperature, smoke spread may decrease visibility in the building causing disorientation, reducing traveling speeds, and rendering exits routes untenable, thereby preventing occupants from evacuating safely. The conditions in a building during a fire in terms of temperature, concentration of toxic gases, and visibility can be determined using a number of available computer models. In general, these models fall into three broad categories: network models, two-zone models, and computational fluid dynamics (CFD), or field, models. Network models, such as CONTAMW [22], can be used for large high-rise multicompartment buildings with hundreds or even thousands of compartments. Two-zone models, such as CFAST [23], can be used for buildings with a small number of compartments of typically small size in which the two-zone concept is valid. CFD models, such as the Fire Dynamics Simulator [24], are used for buildings with large compartments and complex geometries where a more detailed spatial resolution is required.

Criteria can be used to determine the impact of smoke conditions on occupants and can be related to the level of the hot layer in compartments or the dosage of toxic gases received by occupants. Details of how to determine impacts of smoke on life safety can be found in Purser [25].

Detection and Suppression Systems Detection and suppression systems may have a significant impact on the outcome of a fire. Detection systems may activate smoke management systems, initiate the activation of suppression systems, and trigger alarm systems. Early warning to building occupants of the fire may lead to its extinguishment if the fire it is still in the early stages of development and will initiate building evacuation. Activation of suppression systems will affect fire development leading to its control or extinguishment. In fire scenarios that consider the impact of detection or suppression systems, it is necessary to predict the activation time of these systems.

The prediction of the activation time depends on the type of system, the rate of growth of the fire, and the location of the fire in relation to the detector. In the case where computer models such as CFAST or FDS are used to predict fire development, the activation time can be predicted by these models. Simple calculations can also be done to predict detection times by following the procedures outlined in Schifiliti et al. [26] or by using simple computer models such as DETACT [27].

The effect of the activation of suppression systems such as sprinklers on the fire depends on the fire size at the time of activation, whether the fire is shielded so that the suppression agents do not reach it, and the spray density of the agent. If the system has no effect, then we can assume that the fire will continue to grow as if the system were not present. In the case when the suppression system controls the fire, we can assume that the fire will continue to burn at the same intensity as at the time of activation. In the case of fire extinguishment by the suppression system, the equation derived by Madrzykowski and Vittori [28] can be used to predict the heat release rate after activation time.

$$Q(t) = Q_{\text{act}} \mathrm{e}^{-0.023\Delta t}$$

where
$Q(t)$ = Heat release rate at time t (kW)
Q_{act} = Heat release rate at activation time (kW)
Δt = Time after sprinkler activation (s)
t = Time (s)

Impact on Structure The fire impact on structures can be used not only to estimate consequences based on structural damage but also to determine fire spread from the compartment of fire to other compartments in the building as a result of failure of compartment barriers to contain the fire. Typically fire attack on structures for most buildings begins after flashover has occurred. The duration of the attack depends on fire duration, which is a function of the total fire

load in the compartment and the postflashover heat release rate. In certain instances, the structure may be subjected to direct flame impingement; hence it would be necessary to include this in the calculations. Direct flame impingement may cause greater damages to the structure due to the fact that flame temperatures are higher than hot layer temperatures.

Occupant Response and Evacuation Occupant response to a fire depends on the warnings received by the occupants during fire development. These in turn depend on the relative location of the occupants to the fire and the availability and operation of fire detection and alarm systems. The earliest occupants can respond to a fire is by receiving fire cues at their location such as seeing the fire, smelling smoke, and hearing fire noises. As not all occupants receive and respond to the various warnings at the same time, an event tree can be constructed, as shown in Fig. 38.5, that considers the types of warnings and response to such warnings. The three different warnings occur at different times as shown in the figure. The response of occupants to the fire cues is denoted as "Occupant response I" in Fig. 38.5 and occurs at time t(I). If a fire detection and alarm system is available, it will detect the fire and warn occupants at a later time. The response to the alarm signals is denoted as "Occupant response II" in the figure and occurs at t(II). Occupants that responded to the various warnings would notify other occupants in the buildings. The response to these warnings is denoted as "Occupant response III" and occurs at t(III). The probability associated with each response type depends on the probability of receiving the warning and the probability that occupants will respond to that warning.

$$P(\mathrm{I}) = P(\mathrm{cues}) \times P(\mathrm{resp})$$

where

P(I) = Probability of response at time t(I)

P(cues, I) = Probability of cues at time t(I)

P(resp, I) = Probability of response to cues

For example, if the probability of smoke detector activation given a fire is 0.7 and the

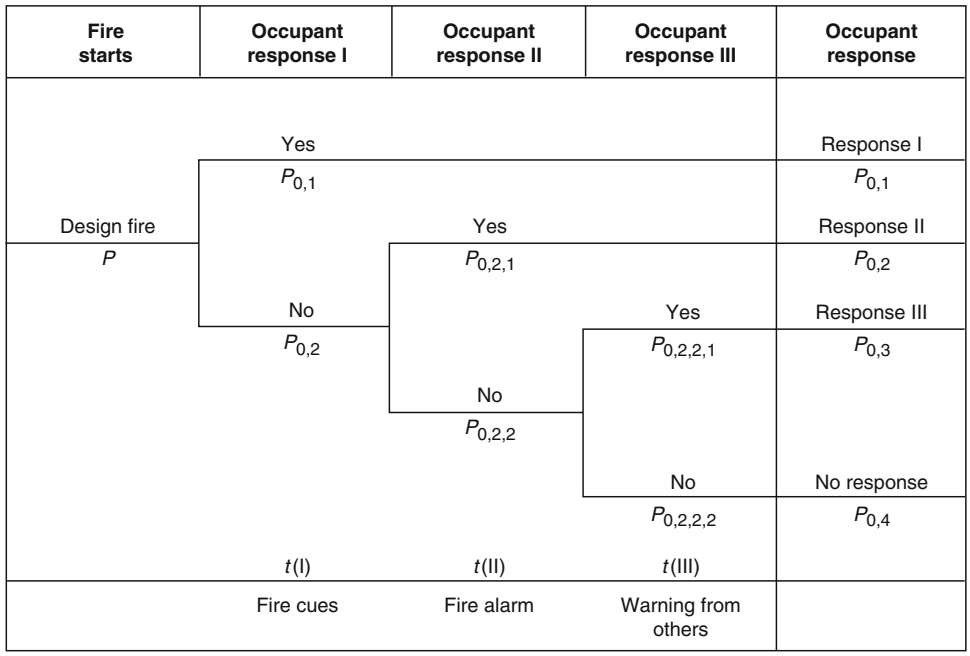

Fig. 38.5 Event tree for occupant response

probability that occupants will respond to the alarm issued by the smoke detector is 0.8, the probability of responding to this warning is $0.7 \times 0.8 = 0.56$. As these probabilities may be different for occupants in the compartment of fire and for occupants in remote compartments, event trees may be constructed for different groups of occupants.

Occupants who respond to the various warnings will commence evacuation. The time required for evacuation depends on the location of occupants in the building, the number of occupants, and the number of available egress routes. The total time required for evacuation can be computed using

$$t_e = t_w + t_r + t_d + t_m$$

where
t_e = Evacuation time (s)
t_w = Time of receiving warning (s)
t_r = Time to respond to warning (s)
t_d = Delay time, preparing to evacuate (s)
t_m = Movement time (s)

Fire Department Intervention Fire department intervention will have a significant impact on the outcome of the fire and the response and evacuation of occupants. This impact, however, is considered as a additional safety feature, and it is usually not explicitly considered in the design calculations.

Consequence Analysis

The consequence of a particular design fire scenario can be determined from information on the fire, its heat and smoke production rates, and fire spread and smoke movement from the location of the fire to other locations. The outcome of the consequence analysis includes injuries and fatalities and property damages to both the building and its contents, as well as damages to the environment and losses resulting from business interruption.

Injuries and Fatalities Injuries and fatalities are caused by the inhalation of toxic products of combustion, exposure to thermal radiation, or direct contact with flames. The impact of a fire scenario on life safety can be determined by tenability analysis. This analysis involves not only calculations of fire development and spread and smoke movement but also an occupant response and evacuation analysis that determines the location of occupants at different times during the fire scenario and the effect of the exposure on occupants. Criteria for determining the effect of the exposure can be found in Purser [25].

Damages to Building and Contents Property damage is a result of exposure to thermal loads, exposure to soot, and corrosive gases. In addition, water damage should be considered as water is the most common fire-extinguishing agent. Thermal loads that include both radiation heat fluxes and convective heat fluxes can be computed from the available information on fire development and spread. Similarly, damage from smoke can be estimated using information on smoke movement and concentration of toxic gases in the building. The level of damage to contents depends to a great extent on the sensitivity of contents to heat, smoke, and water. Information on thermal damages for many materials obtained from results of standard tests can be used to determine threshold damage levels.

Business Interruption Losses from business interruption refer to loss of income as a result of the fire. These losses can be estimated based on expected downtimes caused by the fire. An exact estimate of this may not be easily determined, however, good estimates can be determined. For example, total damage to process equipment may require its replacement. Knowledge of the time for the manufacture, delivery, and installation of this equipment is necessary in estimating downtimes.

Environmental Damage Damage to the environment can be a result of the release of toxic products of combustion or contaminated runoff water. The potential for damage is great especially when dealing with chemical process plants that store significant amounts of chemicals,

the release of which into surface or groundwater reservoirs may have a great impact on aquatic life and the health of people using these resources. Deposition of toxic products of combustion on vegetables and other vulnerable plants and animals may also cause large damages.

Example An example that demonstrates the use of the described methodology for identifying and selecting fire scenarios for a multi-use building is included in Appendix 2 at the end of the chapter.

Summary

The development of fire scenarios is an integral part of the performance-based fire protection design process. The process of identifying and quantifying fire scenarios is described in this chapter. This process requires knowledge of building characteristics, fuel loads and types of combustibles, functions of building, passive and active fire protection systems, and occupant load characteristics. Based on this information all potential fire scenarios can be identified, the number of which may be too large for further analysis. To reduce the number of the identified fire scenarios to those that merit further analysis a selection process is described that involves the use of event trees and other tools to estimate the frequency and consequence of the identified scenarios. Information on the frequency and consequence of the identified scenarios can then be put into a risk-ranking matrix that facilitates the selection of scenarios. The selected fire scenarios can then be quantified using engineering analysis to determine fire severity and impact on occupants and property, as well downtime and impact on environment.

Appendix 1: Fire Scenarios in Risk Model FiRECAM

FiRECAM™ is a fire risk and cost assessment model developed by the National Research Council of Canada [19, 29]. As a result of simplifying assumptions made, the model is applicable to apartment and office buildings. FiRECAM calculates the expected risk to life and fire cost expectation based on a hazard analysis of a number of scenarios. These scenarios and their probability of occurrence are hard coded in the model.

The approach employed in FiRECAM is to consider only three generic fire types that represent the three distinct types of fires that may occur. They are (1) smoldering fires where only smoke is generated, (2) nonflashover flaming fires where a small amount of heat and smoke is generated, and (3) flashover fires where a significant amount of heat and smoke is generated with a potential for fire spread to other parts of the building. The design fires can occur on each floor of the building, and each fire could happen with the apartment door open or closed. In addition, scenarios are considered with occupants being awake or asleep, and suppression systems being effective in extinguishing the fire or not. Within each fire scenario analysis, the times of occupant response and evacuation are based on analysis of the impact of fire detection systems, alarm systems, and other possible perceptions that occupants may receive during the fire.

The probabilities of these three fire types, for both apartment and office buildings, were obtained for Australia, the United States, and Canada [30]. They were obtained based on independent analyses of fire statistics in these three countries. The definition of fire type is based on the severity of the fire when it was observed and recorded by the fire fighters on their arrival. Obviously, small fires can develop into fully developed, postflashover fires if they are given enough time and the right conditions. For risk assessment purposes, however, the fire conditions at the time of fire department arrival are the appropriate ones to use. They represent the fire conditions that the occupants are exposed to prior to fire department extinguishment and rescue operations. In the event of no fire department response, then the eventual conditions of the fire at extinguishment, either by itself or by occupant intervention, are the ones to be used.

Table 38.3 Probabilities of fire types for apartment buildings

Type of fire	Australia (%)	United States (%)	Canada (%)
Smoldering fire	24.5	18.7	19.1
Nonflashover fire	60.0	63.0	62.6
Flashover fire	15.5	18.3	18.3

The reason why fires can develop into different types with different probabilities is because they are governed by a number of random parameters that cannot be predicted, such as the type of ignition source, the point of ignition, and the arrangement of the combustibles. Table 38.3 shows the probabilities of the three fire types, after ignition, for apartment buildings. It is interesting to note that the probabilities are quite similar among the three countries, even though there is no reason that these numbers should be the same due to climatic and cultural differences. Table 38.3 also clearly demonstrates the importance of considering all fire types. For example, flashover fires, which can pose significant hazards to the occupants, have a relatively low probability of occurrence; whereas nonflashover and smoldering fires, which pose lower hazards to the occupants, have a higher probability of occurrence.

Design Fires

In addition to the random parameters, described in the previous section, that govern the type of fire that can develop, the condition of the door to the compartment of fire origin is another random parameter that also affects the fire growth. The fire type and the door condition can be combined to create six design fires that allow all the random parameters that govern fire growth to be easily considered. These six design fires are (1) smoldering fire with the fire compartment entrance door open, (2) smoldering fire with the fire compartment entrance door closed, (3) flaming nonflashover fire with the fire compartment entrance door open, (4) flaming nonflashover fire with the fire compartment entrance door closed, (5) flashover fire with the fire compartment entrance door open, and (6) flashover fire with the fire compartment entrance door closed. The probability of each of these design fires is the product of the probability of the fire type (Table 38.3) and the probability of the door to the compartment of fire origin being open or closed. The probability of the door being open or closed can be estimated based on experience. For example, the entrance door to an apartment unit can be assumed to be mostly closed (for security and privacy reasons), whereas the entrance door to an office room can be assumed to be mostly open (to allow work interaction).

The scenarios used in FiRECAM are shown in Fig. 38.6, which demonstrates the various parameters used that may impact fire development and smoke movement as well as occupant response. The model does not attempt to decrease the number of scenarios, although it is evident from the results that some scenarios such as the smoldering scenarios and flaming nonflashover scenarios contribute less to the overall risk to life. Important scenarios, as identified by the model, are the flashover scenarios with door open and sprinklers nonfunctioning.

Appendix 2: Example Demonstrating Selection of Fire Scenarios

Example The fire protection team is in the process of performing a performance-based design for a complex building with multiple occupancies, including a parking garage on the four floors below grade and shopping areas on the first four floors, which are interconnected through an atrium and a 20 story hotel tower. The complex is fully sprinklered with a central alarm and voice communication, and the atrium has a smoke exhaust system.

Solution The ten steps identified in Table 38.1 are followed for the solution of this example.

Step 1—Location of Fire

A brainstorming session has identified the following fire locations to be considered in the analysis:

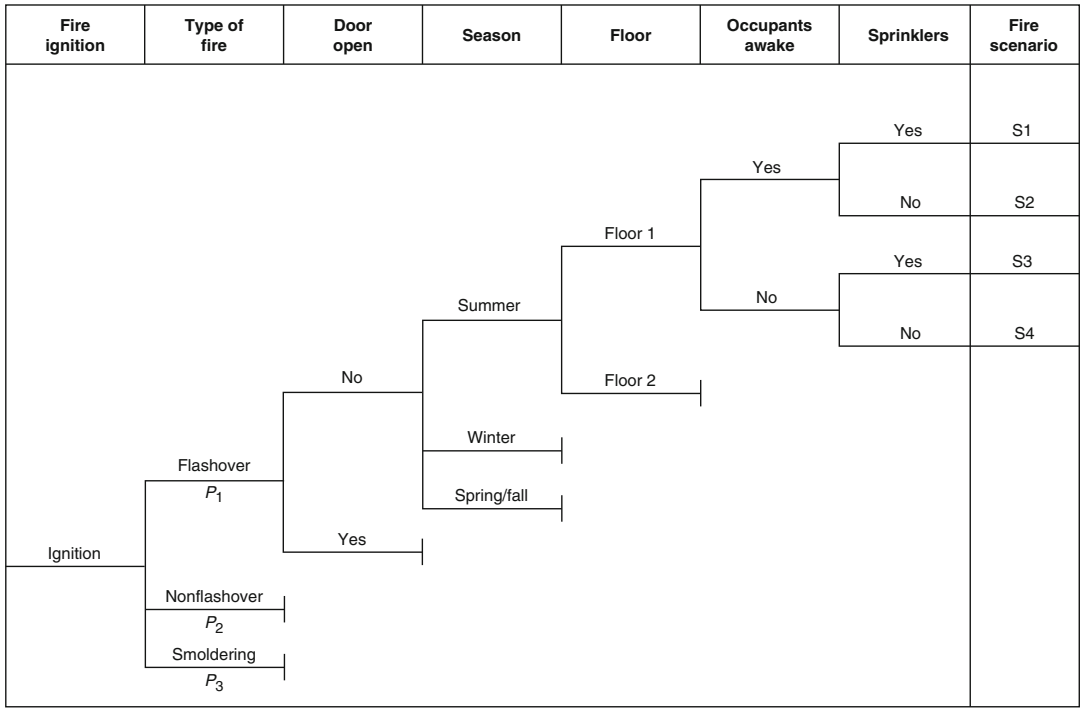

Fig. 38.6 Event tree showing fire scenarios in FiRECAM

- Fire in a hotel room
- Fire in the underground parking garage
- Fire in the atrium
- Fire in the restaurant of the hotel adjacent to the hotel lobby
- Fires in stores of the commercial area

Step 2—Type of Fire

The type of fire that may start at each location depends on the type of combustibles, fuel load, and ignition sources.

Hotel Room One type of fire that may be expected in a hotel room are those that start with a cigarette thrown into a garbage container that ignites curtains and then spreads to a couch and bed. Another type of fire may start in a garbage can but then ignites the wood cabinet with a TV and clothing items in the drawers. Fire development for these two fires may be different, although after flashover both fires may have similar characteristics.

Underground Parking Garage The type of fire expected in an underground garage is one that involves a car and then spreads to adjacent cars.

Atrium In the atrium area, the expected fire could be a fire of a Christmas tree that is placed there during the holidays or a fire involving couches and tables located there.

Restaurant In the case of restaurants, the fire may start in the kitchen area or it may start in the sitting area. These two types of fire are different.

Commercial Area Fire in this area could potentially start in any store. This may result in different types of fires depending on the combustible materials and fire loads in each store as well the size and ventilation characteristics. Examples of different fires in stores are fires in clothing stores, bookstores, and shoe stores. A survey of commercial stores done in 2004 has identified a number of different types of fires that should be considered for commercial areas [5, 6].

Due to space limitations and to avoid repetition, only the fires in the hotel room, the parking

garage, and the atrium are considered in the remainder of the example.

Step 3—Potential Fire Hazards

For this type of occupancy, no special hazards are anticipated. However, the authorities having jurisdiction may request consideration of arson or hazards as a result of functions or events that may be held in the atrium space. This could include exhibitions and displays of goods and merchandise.

Step 4—Systems Affecting Fire

The building is fully sprinklered with central alarm with voice communication. In addition, the atrium and the parking garage have smoke management systems. The effects of these systems should be considered.

Step 5—Occupant Response

Consideration is given here to the response of the occupants to the various warnings and their likelihood to extinguish the fire. For this example, a probability of response and effectiveness in extinguishing the fire is assigned as 0.3 for all fire scenarios.

Step 6—Event Tree

For each fire location, an event tree is constructed so that the different fire scenarios can be identified. Figure 38.7 shows the event tree for fire starting in a hotel room. As the figure shows, four scenarios are associated with this fire type. The probability of occurrence of this fire type could be obtained from statistics. For this example, however, it is assumed that the probability of fire starting at the three locations is the same. Probabilities for each of the events shown in the tree can also be obtained from statistical data; however, because this is a qualitative analysis, expert judgment can be used.

Figure 38.8 shows the event tree for the fire starting in the parking garage. This tree considers the events of manual suppression, sprinkler activation and effective control of the fire, effective smoke ventilation, and barriers that are effective in containing the fire. The fire in this location results in six fire scenarios.

Figure 38.9 shows the event tree for the atrium fire. It considers the same events as the parking garage fire, so it results in six scenarios. (Although it is possible that sprinklers operate but venting does not, for brevity, this potential scenario is not considered here.)

Step 7—Consideration of Probability

The probabilities of the various events shown in the event trees produced in Step 6 can be determined from statistical data and other sources. However, because at this stage of the process the analysis is qualitative, expert

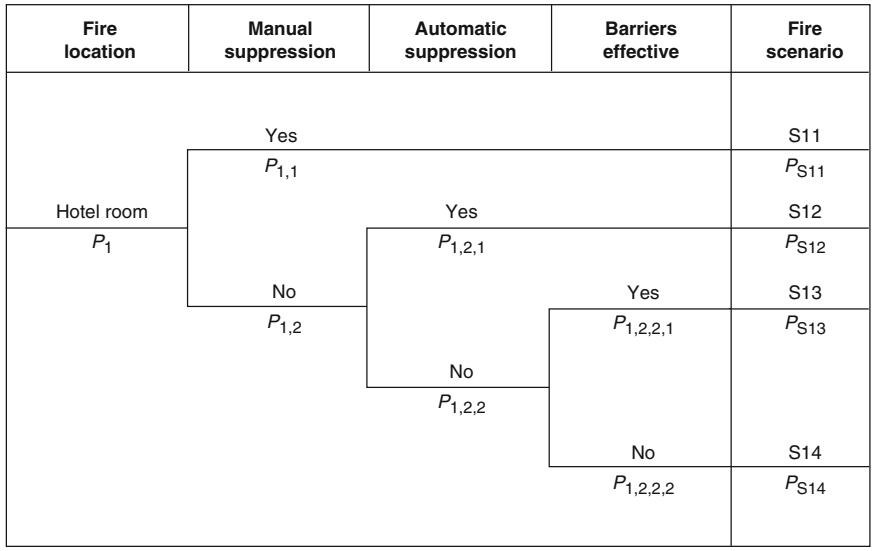

Fig. 38.7 Event tree for hotel room fire

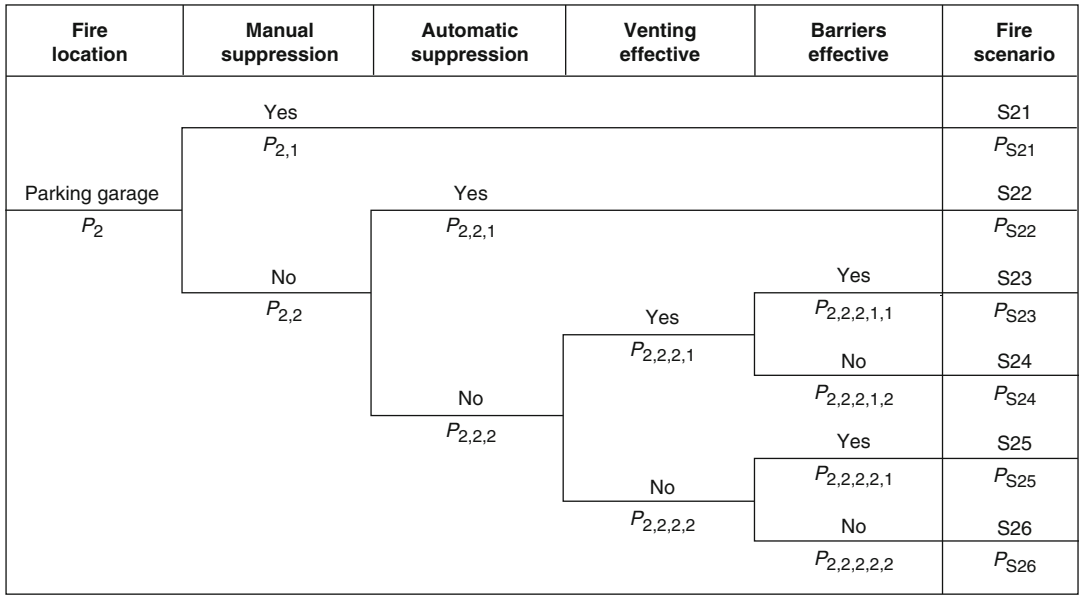

Fig. 38.8 Event tree for parking garage fire

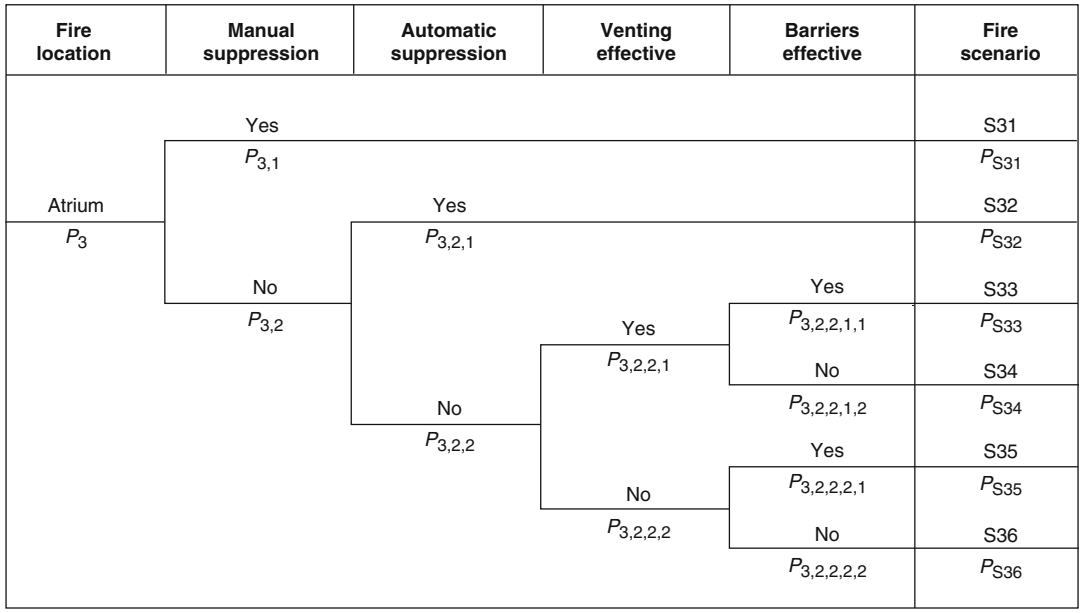

Fig. 38.9 Event tree for atrium fire

judgment can be used for the initial screening of the fire scenarios. For this example, the probabilities of each of the events will be described in qualitative terms and then converted to probability values to facilitate the calculation of the scenario probabilities. For this, the descriptions and values shown in Table 38.4 are used.

The very high value of 0.95 corresponds to the probability of effectiveness of sprinkler

systems in hotel rooms, whereas the value of 0.7 is associated with the probability of smoke detector activation. Using these values, the probabilities of the events of the event trees are assigned and the scenario probabilities are calculated, as shown in Figs. 38.10, 38.11, and 38.12.

Step 8—Consideration of Consequence

In this step, a qualitative evaluation of the consequence of each of the scenarios is performed. This evaluation is done using engineering judgment based on the type of fire, the location of the fire, and the effectiveness of the active fire protection systems. This evaluation considers the impact of the fire on both property as well as life safety. To facilitate this assessment, Table 38.5 shows the different consequence levels that are chosen for this example. The level is determined by considering both the property losses and the occupant impact. For example, the consequence level of a scenario with $30,000 in losses and serious injuries is "high."

Based on the levels shown in Table 38.5 and considering the fire type, fire location, and effectiveness of the active fire protection systems, the consequences of the scenarios in the three event trees are determined as shown in Figs. 38.13, 38.14, and 38.15.

Step 9—Risk Ranking

Figure 38.16 presents the risk-ranking matrix developed based on the results of Steps 7 and 8. The matrix has six levels of probabilities of occurrence, from extremely low to very high, and five levels of consequence estimates. The levels for the probabilities of scenario occurrence for this example have been set as shown in Table 38.6.

The three levels of shaded areas in Fig. 38.16 represent areas of different risk levels, with the darker area representing high risk and the lighter area representing low risk. The white areas represent very low-risk scenarios.

Table 38.4 Values associated with probability descriptions

Quantitative description	Associated value
Very low	0.05
Low	0.3
Moderate	0.5
High	0.7
Very high	0.95

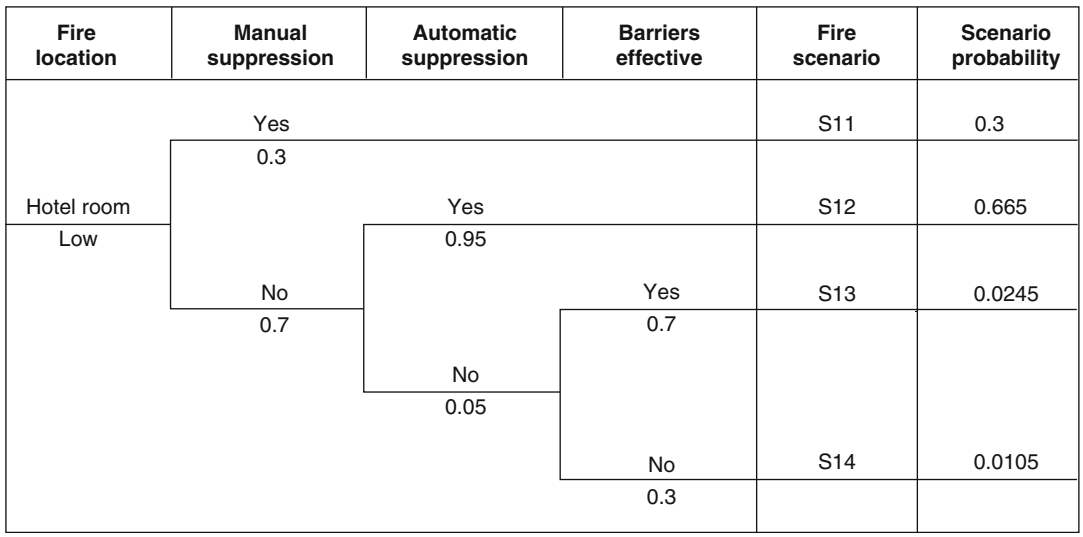

Fig. 38.10 Probabilities of scenarios for hotel room fire

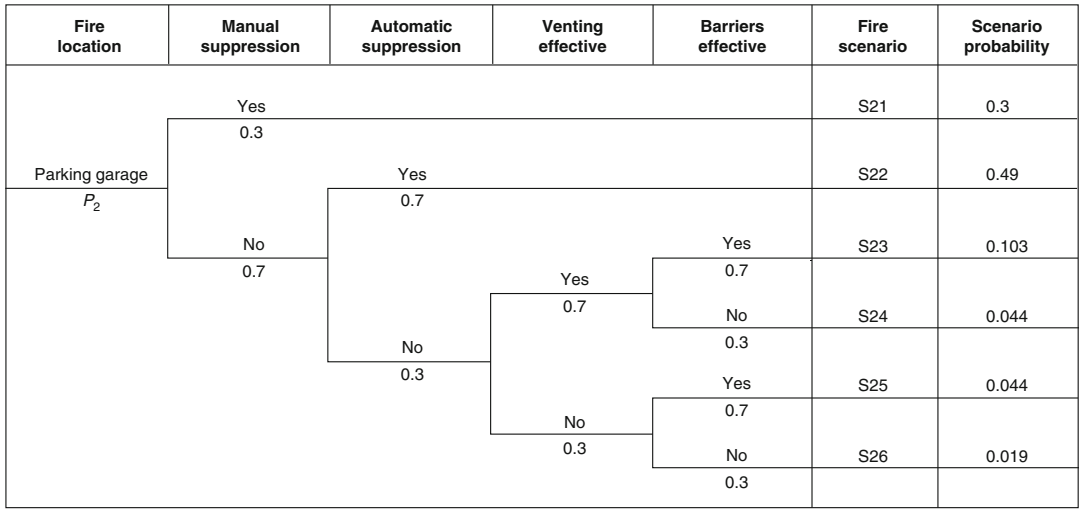

Fig. 38.11 Probabilities of scenarios for parking garage fire

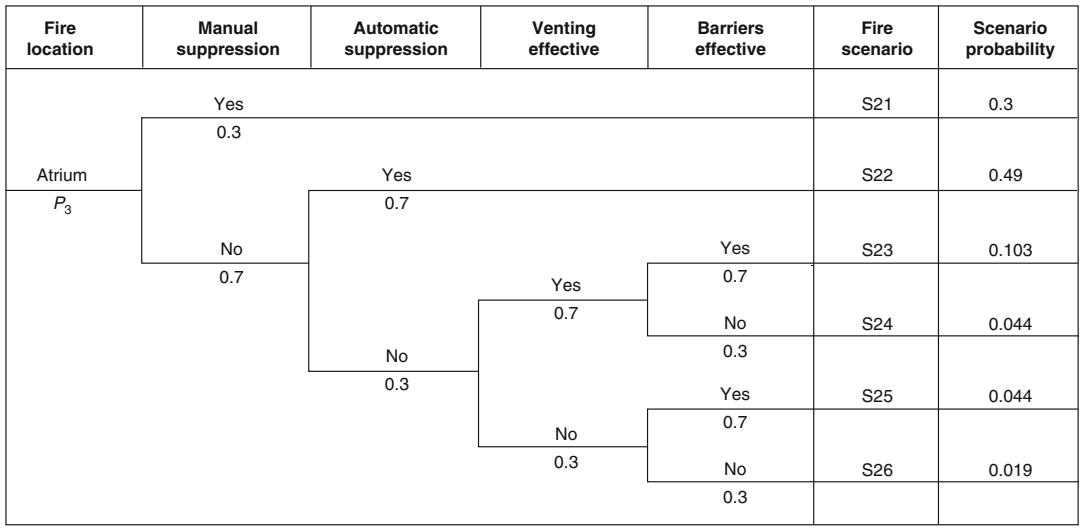

Fig. 38.12 Probabilities of scenarios for atrium fire

Table 38.5 Consequence levels and associated loss estimates

	Associated loss estimate	
Qualitative description	Property losses ($1000)	Occupant impact
Very low	0–5	No deaths or injuries
Low	5–20	No deaths or injuries
Moderate	20–100	No deaths, minor injuries
High	100–1000	No deaths, serious injuries
Very high	1000–10,000	Small number of deaths and injuries
Extremely high	>10,000	Multiple deaths and injuries

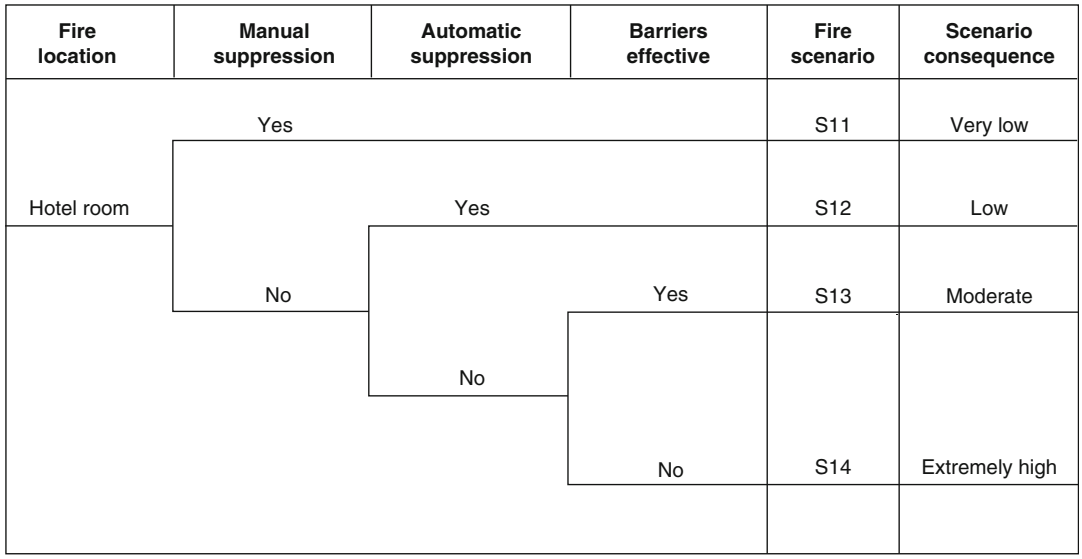

Fig. 38.13 Consequence of hotel room fire scenarios

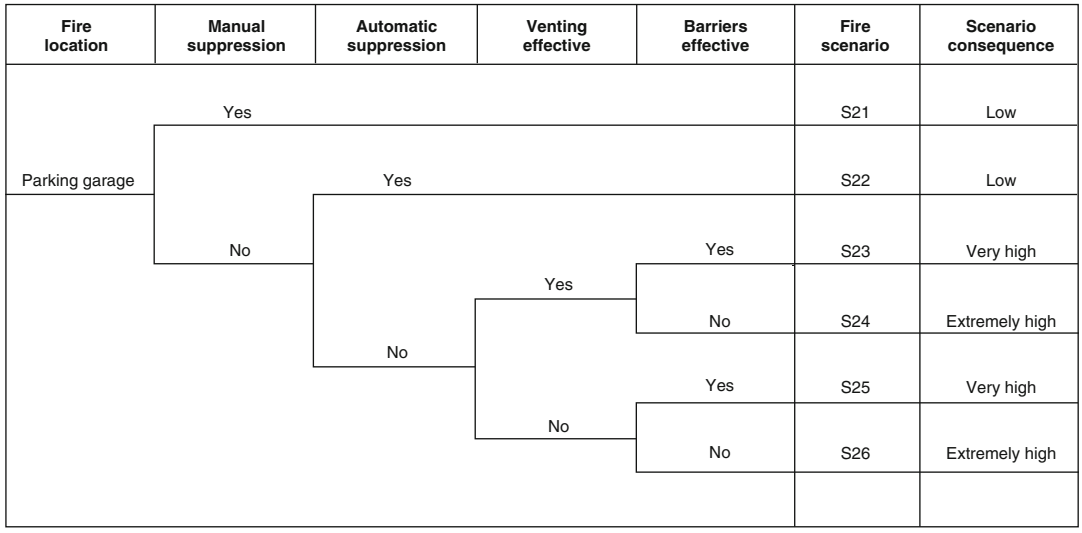

Fig. 38.14 Consequence of parking garage fire scenarios

As shown in Fig. 38.16, no scenario falls in a high-risk area. Scenarios S23 and S24 are moderate-risk scenarios and should be considered for quantitative analysis. Scenarios S25, S33, and S34 are low-risk scenarios that can also be considered further. In addition, Scenario S14, although it falls into a very low-risk area, may be considered for further analysis, as it is a scenario in a different section of the building with different fire protection

Fire location	Manual suppression	Automatic suppression	Venting effective	Barriers effective	Fire scenario	Scenario consequence
Atrium	Yes				S31	Low
	No	Yes			S32	Moderate
		No	Yes	Yes	S33	High
				No	S34	Very high
			No	Yes	S35	High
				No	S36	Extremely high

Fig. 38.15 Consequence of atrium fire scenarios

	Probability of scenario occurrence					
Consequence	Extremely low	Very low	Low	Moderate	High	Very high
Extremely high	S26, S36, **S14**		**S24**			
Very high			**S25** **S26**	**S23**		
High			S35	**S33**		
Moderate		S13			S32	
Low				S21	S22	S12
Very low				S11, S31		

Fig. 38.16 Risk-ranking matrix of identified scenarios

Table 38.6 Scenario probability values used for risk-ranking matrix

Probability level	Scenario probability
Extremely low	0.0–0.02
Very low	0.02–0.04
Low	0.04–0.1
Moderate	0.1–0.3
High	0.0–0.5
Very high	0.5–1.0

systems and different impacts, and it has an extremely high consequence. All other scenarios do not require further analysis and can be dropped.

Step 10—Final Selection and Documentation

The final selection of the design fire scenarios is done in this step, and the fire scenarios are documented in detail. As indicated in Step 9, scenarios S14, S23, S24, S25, S33, and S34 should be considered for further analysis. To facilitate the quantitative analysis, Table 38.7 describes the characteristics of these scenarios. The quantitative analysis of these scenarios should consider both the impact of the fires on life safety and property. The procedure outlined in the section "Development of Fire Scenarios" in this chapter can be followed for the analysis.

Table 38.7 Description of design fire scenarios

Scenario ID	Location	Design fire	Description
S14	Hotel room	Fire involving curtains and mattress	Fire started in a garbage container and spread to the curtain and mattress. Nobody was in the room of fire origin. The sprinkler system did not activate because the water supply was turned off for repairs. The fire spread from the room door to the corridor of the hotel. For life safety calculations, assume that occupants were asleep when the fire started
S23	Parking garage	Vehicle fire	Fire started in a vehicle parked in the parking garage. The sprinkler systems activated but could not control the fire. The exhaust ventilation system operated, and it was effective in removing smoke from the parking garage to the outside. The barriers were effective in containing the fire on the floor of fire origin
S24	Parking garage	Vehicle fire	Fire started in a vehicle parked in the parking garage. The sprinkler systems activated but could not control the fire. The exhaust ventilation system operated, but it was not effective in removing smoke from the parking garage to the outside. The barriers failed to contain the fire on the floor of fire origin
S25	Parking garage	Vehicle fire	Fire started in a vehicle parked in the parking garage. The sprinkler systems activated but could not control the fire. The exhaust ventilation system operated, but it was not effective in removing smoke from the parking garage to the outside. The barriers were effective in containing the fire on the floor of fire origin
S33	Atrium	Christmas tree fire	Fire started involving a Christmas tree and stage at the center of the atrium. The sprinklers failed to control the fire. The smoke management system was effective in maintaining smoke levels to the design level, and the fire was contained in the atrium
S34	Atrium	Christmas tree fire	Fire started involving a Christmas tree and stage at the center of the atrium. The sprinklers failed to control the fire. The smoke management system was not effective in maintaining smoke levels to the design level; however, the fire was contained in the atrium

References

1. Society of Fire Protection Engineers, *SFPE Engineering Guide to Performance-Based Fire Protection,* 2nd ed., Society of Fire Protection Engineers and National Fire Protection Association, Quincy, MA (2007).
2. ICC, *International Fire Engineering Guidelines,* International Code Council, Washington, DC (2005).
3. ISO/TS 16733, *Fire Safety Engineering—Selection of Design Fire Scenarios and Design Fires,* International Organization for Standardization, Geneva, Switzerland (2006).
4. A.H. Buchanan, *Fire Engineering Design Guide,* Centre of Advanced Engineering, University of Canterbury, New Zealand (2001).
5. G. Hadjisophocleous and E. Zalok, "A Survey of Fire Loads in Commercial Premises," *4th International Seminar on Fire and Explosion Hazards,* Londonberry, Northern Ireland (2003).
6. G. Hadjisophocleous and E. Zalok, "Development of Design Fires for Commercial Buildings," *Fire Safety Engineering: Issues and Solutions,* FSE International Conference 2004, Sydney, Australia (2004).
7. V. Babrauskas, J.R. Lawson, W.D. Walton, and W.H. Twilley, "Upholstered Furniture Heat Release Rates Measured with a Furniture Calorimeter," *NBSIR 82–2604,* National Institute of Standards and Technology, Washington, DC (1982).
8. M. Janssens, "Calorimetry," in *SFPE Handbook of Fire Protection Engineering,* 3rd ed. (P.J. DiNenno et al., eds.), National Fire Protection Association, Quincy, MA, pp. 3-38–3-62 (2002).
9. *CBUF, Fire Safety of Upholstered Furniture—The Final Report on the CBUF Research Programme* (B. Sundstrom, ed.), Interscience Communications Ltd., London (1996).
10. J.R. Hall and M.J. Aherns, "Data for Engineering Analysis," in *SFPE Handbook of Fire Protection Engineering,* 3rd ed. (P.J. DiNenno et al., eds.),

National Fire Protection Association, Quincy, MA, pp. 5-65–5-78 (2002).
11. R.P. Schifiliti, B.J. Meacham, and L.P. Custer, "Design of Detection Systems," in *SFPE Handbook of Fire Protection Engineering,* 3rd ed. (P.J. DiNenno et al., eds.), National Fire Protection Association, Quincy, MA, pp. 4-1–4-43 (2002).
12. ISO/TR 13387–7, *Fire Safety Engineering—Part 7: Detection, Activation and Suppression,* International Organization for Standardization, Geneva, Switzerland (1999).
13. J. Bryan, "Behavioral Response to Fire and Smoke," in *SFPE Handbook of Fire Protection Engineering,* 3rd ed. (P.J. DiNenno et al., eds.), National Fire Protection Association, Quincy, MA, pp. 3-315–3-341 (2002).
14. G. Proulx, "Movement of People: The Evacuation Timing," in *SFPE Handbook of Fire Protection Engineering,* 3rd ed. (P.J. DiNenno et al., eds.), National Fire Protection Association, Quincy, MA, pp. 3-347–3-366 (2002).
15. H.E. Nelson and F.W. Mowrer, "Emergency Movement," in *SFPE Handbook of Fire Protection Engineering,* 3rd ed. (P.J. DiNenno et al., eds.), National Fire Protection Association, Quincy, MA, pp. 3-367–3-380 (2002).
16. R. Marchant, K. Nabeel, and S. Wise, "Development and Application of the Fire Brigade Intervention Model," *Fire Technology,* 37, pp. 263–278 (2001).
17. N. Bénichou, A. Kashef, and G. Hadjisophocleous, "Fire Department Response Model (FDRM) and Fire Department Effectiveness Model (FDEM) Theory Report," *Internal Report No. 842,* Institute for Research in Construction, National Research Council of Canada, Ottawa (2002).
18. NFPA *101®, Life Safety Code®,* National Fire Protection Association, Quincy, MA, 2006 edition.
19. D. Yung, G.V. Hadjisophocleous, and G. Proulx, "Modelling Concepts for the Risk-Cost Assessment Model FiRECAM and Its Application to a Canadian Government Office Building," *Proceedings of the Fifth International Symposium on Fire Safety Science,* Melbourne, Australia, p. 619 (1997).
20. V. Babrauskas, "Heat Release Rates," in *SFPE Handbook of Fire Protection Engineering,* 3rd ed. (P.J. DiNenno et al., eds.), National Fire Protection Association, Quincy, MA, pp. 3-1–3-37 (2002).
21. W.D. Walton, P.H. Thomas and Ohmiya, "Estimating Temperatures in Compartment Fires," in *SFPE Handbook of Fire Protection Engineering,* 5tf ed. (M. J. Hurley et al., eds.), Springer, (2015).
22. G.N. Walton, *CONTAMW96 User Manual, NISTIR 6056,* National Institute of Standards and Technology, Gaithersburg, MD (1997).
23. W.W. Jones, "A Multi-Compartment Model for the Spread of Fire, Smoke and Toxic Gases," *Fire Safety Journal,* 9, 55 (1985).
24. K.B. McGrattan, G.P. Forney, F.E. Floyd, S. Hostikka, and K. Prasad, *Fire Dynamics Simulator (Version 3)—User Guide, NISTIR 6784,* National Institute of Standards and Technology, Gaithersburg, MD (2002).
25. D.A. Purser, "Toxicity Assessment of Combustion Products," in *SFPE Handbook of Fire Protection Engineering,* 3rd ed. (P.J. DiNenno et al., eds.), National Fire Protection Association, Quincy, MA, pp. 2-83–2-171 (2002).
26. R.P. Schifiliti, B.J. Meacham, and R.L.P. Custer, "Design of Detection Systems," in *SFPE Handbook of Fire Protection Engineering,* 3rd ed. (P.J. DiNenno et al., eds.), National Fire Protection Association, Quincy, MA, pp. 4-1–4-43 (2002).
27. D.D. Evans and D.W. Stroup, "Methods to Calculate the Response Time of Heat and Smoke Detectors Installed Below Large Unobstructed Ceilings," *NBSIR 85–3 167,* Building and Fire Research Laboratory, U.S. Department of Commerce, Gaithersburg, MD (1985).
28. D. Madrzykowski and R. Vittori, "A Sprinkler Fire Suppression Algorithm," *Journal of Fire Protection Engineering,* 4, pp. 151–164 (1992).
29. G.V. Hadjisophocleous and D.T. Yung, "Parametric Study of the NRCC Fire Risk-Cost Assessment Model for Apartment and Office Buildings," *Fourth International Symposium on Fire Safety Science,* Ottawa, Canada, pp. 829–840 (1994).
30. J. Gaskin and D. Yung, "Canadian and U.S.A. Fire Statistics for Use in the Risk-Cost Assessment Model," *IRC Internal Report No. 637,* National Research Council of Canada, Ottawa, (Jan. 1993).

George V. Hadjisophocleous is a professor at Carleton University and holder of the Industrial Research Chair in Fire Safety Engineering and President of CHM Fire Consultants Ltd. Prior to moving to Carleton University, he was a senior research officer and group leader at the Fire Risk Management Program of the National Research Council of Canada. He holds a PhD in Mechanical Engineering from the University of New Brunswick and he is the author of over 150 publications in the areas of fire research, fire risk assessment, performance-based codes, and CFD modeling. His research areas include fire risk analysis and fire and smoke movement modeling using CFD and zone models. Dr. Hadjisophocleous is a Fellow of SFPE and member of NFPA, IAFSS, ASHRAE, and CIB W14 and a Registered Professional Engineer in the Provinces of Ontario and British Columbia.

Jim R. Mehaffey From 1980 to 1987, Dr. Jim R. Mehaffey was a research scientist at the National Research Council where he developed models to predict the growth and severity of building fires. From 1988 to

2009, he was a research scientist with FPInnovations (Forintek) where he modeled the performance of wood-frame assemblies exposed to fire. From 1993 to 1997, he was seconded to the University of British Columbia where he was director and associate professor in UBC's Fire Protection Engineering Program. He is currently an adjunct professor in the Department of Civil and Environmental Engineering at Carleton University and a Principal with CHMfire Consultants. He holds a PhD in physics from the University of Toronto and is the author of over 80 scientific publications.

Engineering Considerations for Fire Protection System Selection

39

Milosh Puchovsky and Craig Hofmeister

Introduction

A fundamental responsibility of an engineer is the design of systems that satisfy the overall goals and objectives for a given facility. When it comes to fire and life safety, the fire protection engineer (FPE) is called upon to design those systems deemed necessary to meet the performance objectives for the project. However, before specific protection systems can be designed, decisions must be made regarding what systems are most appropriate and necessary in light of the fire events of concern, and the overall outcomes to be achieved at the conclusion of these events.

While FPE's may not always make the final decision about system type, their decision making approach, input and recommendations are vital to the overall success of the enterprise. Ideally, the ultimate choice about system type is given the proper priority, is well informed, and is made well before any system design work or construction commences. Furthermore, such a decision needs to fit into the overall fire safety strategy, which addresses the fire related concerns specific to site conditions, operations and personnel in question.

When considering a specific fire fighting agent and accompanying system, numerous questions that impact the selection arise. The more obvious pertains to the agent's effectiveness and compatibility with the types of fuels and fires events, i.e., can the agent extinguish, suppress or control the fire in the time period needed. However, other considerations must also be dealt with.

For instance, can the agent be discharged on electrically energized components? Can a fire be detected and an agent discharged in the timeframe necessary to be effective? Does agent discharge sound frequency affect electronic and computer equipment performance? Will the discharged agent leave a residue or otherwise impact the equipment or contents it is intended to protect? Is the agent chemically and physically compatible with the fuel, e.g. physical reaction of water on tissue paper, or chemical reaction of discharge on metal fires involving aluminum or magnesium? Does the agent decompose in the presence of the fire or heat and do such agent decomposition products have an affect on the components to be protected? Can the agent be discharged in an occupied area and/or are there health or environmental concerns associated with the agent? Should the agent once discharged be reclaimed or otherwise contained? What are the costs for the overall system including those associated with necessary maintenance activities? How quickly can the agent supply be replenished? Has the fire protection system operation been sufficiently coordinated with facility operations and other equipment? If multiple systems are utilized to protect specific areas or hazards, how are the systems interconnected to operate effectively? Does system operation

M. Puchovsky (✉)
Department of Fire Protection Engineering, Worcester Polytechnic Institute, Worcester, MA, USA

C. Hofmeister
(registered in NC and GA), The Fire Consultants, Inc.,

M.J. Hurley (ed.), *SFPE Handbook of Fire Protection Engineering*,
DOI 10.1007/978-1-4939-2565-0_39, © Society of Fire Protection Engineers 2016

require specialized training of building staff and emergency responders? As should be appreciated, the above only presents a partial list of possible considerations that require attention.

Additionally, the necessary comprehensive approach in addressing fire protection and life safety can at times be met with resistance due to cost and other factors. Some owners view fire protection systems as a cost without a direct return on investment, unless they have experienced a previous fire event or truly understand the associated risks. Similarly, some design team members might view fire protection as a required inconvenience and do not want to spend time or effort beyond the simplest path to meet minimum code requirements. Therefore it is important to open lines of communication with the stakeholders early in the process and discuss the importance and benefits of developing the most appropriate protection schemes.

A generic prescribed approach for selecting the most effective system does not exist within a regulatory document or general application guides. Neither does any comprehensive guidance exist that facilitates the decision as to why one type of agent or system should be chosen over another. The responsible FPE typically needs to develop their own approach that guides and influences their final recommendations.

This chapter puts forth, in a single reference, a collection of topics and other information pertaining to various types of fire fighting agents and their associated systems that can impact a FPE's approach and final recommendations about selecting a specific type of fire protection system. The material presented here should not be interpreted as a formalized step-by-step procedure, but rather an assembly of information that can underpin an FPE's decision-making process. Further to this point, the order of subjects presented is not intended to represent the only sequence in which they can be considered.

Structuring the Decision Making Process

A comprehensive and coordinated decision making process is the basis for selecting the appropriate fire protection system(s) for a given application. The FPE needs to possess a thorough knowledge of the facilities under consideration and the limitations and uses of the various types of fire protection systems he or she might consider as part of the overall fire protection package. As noted above, it often falls upon the individual FPE to develop his or her own approach for selecting and recommending the most appropriate system to meet the overall objectives. While approaches may differ, the key concepts are relatively typical regardless of the application.

Information from applicable building, fire and safety regulations and relevant system design and installation standards as well as from other sources such as system manufacturer materials, listing protocols and fire tests is essential in developing an effective approach. Ideally, a comprehensive fire risk assessment should serve as the basis for structuring any application guide or method for recommending a specific fire protection system. As a minimum the decision process should be at least risk-informed.

A fire risk assessment is a process used to characterize the risk associated with fire for specific scenarios. Both the probability of the scenarios occurring, and their potential consequences are addressed. Within the context of the risk assessment, fire protection systems largely serve to mitigate or moderate the consequences. However, fire protection systems could also be used to decrease the likelihood of an undesirable event from occurring, i.e. inerting an atmosphere before an ignition source occurs.

In undertaking a fire risk assessment, the level of acceptable fire risk needs to be sufficiently considered and articulated, i.e. the desired outcome or consequence at the conclusion of a fire event or scenario. The fire risk assessment will help crystalize the overall intent and purpose of any fire protection system, and how it fits into the overall fire safety strategy, i.e. will the system be used to protect the overall facility or just specific areas or operations. Preferably, the fire protection systems need to be linked to the overall goals and objectives of not only the building owners, but also all key stakeholders involved with the project.

Certain fire protection standards specifically call out the use of fire risk assessments. For example, NFPA 75, *Standard for the Fire Protection of Information Technology Equipment*, indicates that a fire risk analysis can be used to determine the construction, fire protection and fire detection requirements for information technology equipment, information technology rooms, and information technology areas [1]. NFPA 75 identifies factors such as the effect of loss of function of information technology equipment on life safety, e.g. process controls; life safety functions controlled by particular equipment; threat of fire from burning equipment to occupants and other property; and economic impact from loss of function, loss of records or loss of physical assets, among others that need to be considered to determine the level of acceptable fire risk. Numerous resources on fire risk assessments including several chapters in this Handbook, the SFPE Engineering Guide to Fire Risk Assessment [2], and NFPA 551, *Guide for the Evaluation of Fire Risk Assessments* [3] are available to the FPE in this regard.

Another resource available for structuring the decision making process is NFPA 550, *Guide to the Fire Safety Concepts Tree*. The "Tree" can be used to develop and analyze the potential impact of fire safety strategies, and help identify gaps or areas of redundancy. The logic of the "Tree" is directed toward the achievement of specified fire safety objectives that need to be sufficiently articulated. Strategies for achieving the objectives are divided into two general categories: "Prevention of Fire Ignition" and "Managing Fire Impact". Active fire protection systems can be employed to address both categories: preventing a fire from starting, e.g., inerting the atmosphere once a certain concentration of flammable vapors of a particular fuel are detected, and by managing the impact of the fire once ignition has occurred, e.g., suppressing or controlling the fire, and/or safeguarding exposure concerns. The Guide can be used to protect the entire facility or just specific areas or operations [4].

The decision methodology or structure of the analysis can be similar to other types of fire protection engineering analysis such as performance-based design or a particular calculation methodology. The structure of such analyses as outlined in documents including the SFPE Performance-Based Design Guide or the SFPE Guide to Substantiating a Fire Model as Appropriate for a Given Application can provide good reference for a coordinated decision making process.

Considering Stakeholders Concerns

It is important that the various stakeholders are involved in the decision making process leading to the selection of the appropriate fire protection system. Each stakeholder may not provide direct guidance or information to the FPE, but it is important that the FPE have an understanding of the goals and objectives of each stakeholder or their perspective. Typically, the stakeholders will include representatives from the owner, facility operators, tenants, insurer(s), other members of the design team, and the authorities having jurisdiction, but may also include others depending on the facility type and use. See the SFPE Performance-Based Design Guide for more specific information on the role of stakeholders in a coordinated decision making process.

The active participation of each of the individual stakeholder categories may vary from project to project but the FPE should consider the viewpoint for each category in the decision making process. The individual viewpoints may vary significantly and the FPE should consider and address each as it relates to the overall fire safety objectives and the expected role of fire protection system(s). Some stakeholders may view fire protection systems as a cost without a direct return and would therefore want to minimize the process. Other stakeholders may have experienced a previous fire event or have specific operational or business interruption goals that make them more sensitive to the impact of a fire event. Ideally, the different viewpoints can be discussed in a meeting or conference and the general impact of each viewpoint on the systems purpose can be addressed.

As an example, a large multi-tenant data center design would likely have a variety of stakeholders and viewpoints as it relates to the fire protection systems performance for the facility. The owner may have specific goals related to facility and space flexibility, cost, and potential liability, the facility operators and tenants may have specific goals related to equipment protection and business continuity, the insurer may have specific goals related to structure and maximum loss, the design team may have specific goals related to sustainable design and energy usage, and the authorities having jurisdiction may have specific goals related to not only code compliance but also the operations and safety of responding emergency personnel safety. The FPE is then responsible for understanding, considering and integrating the individual stakeholders concerns and objectives in the decision making process, and addressing each in the establishment of system performance criteria and in the selection of the most appropriate fire protection system(s).

Given that many projects and applications will include a variety of viewpoints from the relevant stakeholders, good communication and documentation throughout the process is critical. Ideally, the FPE is leading, organizing, and taking responsibility for the process to ensure that all stakeholder concerns are addressed and sufficiently satisfied, and each stakeholder subsequently understands the reasoning for the final decisions.

Understanding the Facility's Intended Purpose and Operation

Any building project and commercial enterprise is a significant investment and undertaken with specific design and end-use goals and outcomes in mind. Once built, the structure serves the purposes and needs of its owners. The building and its associated systems enable the operations of the overall enterprise contained within, i.e. provide a workplace, facilitate heath care services, support manufacturing processes, shelter people and assets, etc.

Before any fire safety concerns can be properly addressed, the fire protection engineer must possess a functional understanding of the facility operations, their purpose and what the owners expect from their investment. The detail of the facility and operational review may vary but should include features including the site configuration, geographical location and climate; building construction and materials; equipment and/or industrial/manufacturing processes; storage configuration and commodities; presence and categories of hazardous materials; utilities location and configuration; occupancy/occupant loading, occupant locations and responsibilities; and overall building operations. Additionally, seasonal variances should also be reviewed and considered. Do manufacturing or processing operations ramp up due to market conditions? Is there an increase in occupants, including temporary occupants less familiar with their surroundings at different times of the year? Is there a different procedure or an increase in storage at a specific time of the year? Is weather or an accumulation of snow an additional consideration? Are seasonal decorations a notable fire load that needs to be considered, etc? Regardless of the facility type, the operational conditions can vary significantly and therefore it is important that the review and analysis are specific to the subject facility and not a "typical" facility type.

As an example, if the facility is a wood working operation, the details of the site layout and building construction should be reviewed as a baseline; however, the FPE should also invest the time to gain sufficient knowledge about the associated workflow, processes, storage configuration, equipment, materials, operation and configuration, and occupant loading and locations. The operations in each wood working facility will differ to some degree and therefore it is important the FPE understand the specific operation and configuration of the subject facility, such as the type of wood species processed, raw material delivery and storage, cutting, drying, veneer preparation, panel manufacturing, milling, laminating, sanding, finishing, final product storage and distribution, and wood waste management. Further, does the facility have additional

operation shifts or modified hours at different times of the year or during periods of equipment maintenance or outage? Do the materials or storage methods/configuration change for peak or slow operational periods? Are there peak times for raw material or hazardous material delivery? Are there weather or other environmental considerations for the specific facility location?

The full appreciation of the facility, its key processes and configuration, and the operational considerations provides the background to identify and properly understand potential hazards and fire scenarios.

Characterizing How Fire Can Impact the Facility and Its Operations: Defining Fire Hazards and Scenarios

Once the make-up and purpose of the facility is properly understood, the potential fires that could affect its occupants, operations, and contents can be addressed. An important step is to conduct a general hazard assessment to define potential fire events or scenarios. After reviewing the details of the construction and operation as outlined above, a review of potential fire hazards can be conducted specific to the facility and its operations. In general, the hazard assessment should be conducted without considering any protection systems, as the ultimate intent is to identify the most appropriate system to eliminate, mitigate or manage the associated fire hazards. The assessment should consider fire hazards associated with the processes contained within, with specific attention given to the likely range of combustible contents, fuel loads and ignition sources. Potential hazards associated with normal and abnormal operational functions need to be considered, i.e. various failure modes of process equipment and their effects should be investigated.

Overall, the assessment would include a review of potential fire scenarios pertaining to the contents and equipment located within the facility; normal processes and operations; and events resulting from malfunctioning equipment. General fire scenarios should consider all combustible materials and fuel loading locations, and would likely involve building construction materials, storage and packaging materials, furniture and equipment, and other transient items such as trash, decorations, and normal use items. The operations related scenarios would involve a thorough review of potential fire hazards associated with the various aspects of the process housed within the facility and would consider the production or release of dusts, ignitable liquids, flammable gases, etc. Failure scenarios should include a review of reasonable potential events as a result of a single failure of a piece of equipment, process, or even in some cases a malicious event such as arson or security concern.

For example, a fire hazard assessment for a laboratory facility may consider scenarios involving the ignition of general combustibles such as a trash receptacle, a furniture grouping, a computer station, material storage, etc. Operational related scenarios for the laboratory may consider an ignitable liquid spill due to a dropped container or liquid transfer operation, a bench fire resulting from an experiment or non-compatible materials, etc. Failure scenarios may consider a flammable gas line and/or fitting leak, a ruptured flammable liquid container, failure of a critical ventilation fan, etc.

The depth and detail of the hazard assessment is often related to the complexity of the facility use and operation, its range and type of occupants, the value of its contents, and the magnitude of potential loss. As an example, the assessment for a small office building would likely focus more on general combustible scenarios while the assessment for a manufacturing and production facility would include a wider range of operational and failure scenarios. The assessment may also need to consider the potential for outside influences, which may range from exposure from a fire event in an adjacent structure to a wildland fire to a terrorist event. However, regardless of the scenario type, the hazard assessment should include a review of fuel and oxidizer arrangements, ignition sources, and environmental conditions, as well as, the degree to which the outcome of the scenario could impact occupant life safety,

property, operations, responding emergency personnel safety, etc.

The assessment should also consider the timelines for the development and impact of potential fire scenarios. For instance does the scenario involve a smoldering fire that would provide a longer time frame for detection and active protection measures or does the scenario involve an explosive hazard which would result in a very limited time frame for detection and active measures? Further, does the scenario involve isolated combustibles or does it include adjacent fuel sources that can result in accelerated fire spread, significantly increasing the potential for severe consequences? In the laboratory example, a trash receptacle fire may have a relatively slow growth rate; however, if the fire is not initially controlled, fire spread to other items such as flammable liquids may significantly increase the fire growth rate, size, and severity. Scenarios can be represented as a function of fire effect such as fire size and time, i.e. the fire is expected to become larger as time from ignition increases. The details of the developed scenarios should include a complete timeline to better define the potential outcomes. In general, if the scenario is terminated earlier along its potential timeline, less damage would result.

The development of fire scenarios is a well-established technique for FPE's and is often used in the design process. However, it should also be employed when deciding on which type of fire protection system to use. Fire scenarios are typically developed to encompass a range of events that often include smaller more likely scenarios with limited potential consequences to larger less likely scenarios that could result in significant consequences. In the laboratory example previously discussed, a small trash receptacle fire scenario may have a higher likelihood of occurrence but also may have a lesser potential for severe consequences, while a flammable gas line leak scenario may have a lower likelihood of occurrence but may have much higher potential for severe consequences. The resulting time frame for the development of these two scenarios is also quite different.

Describing the Desired Outcomes and Consequences If a Fire Should Occur: Defining Overall Fire Safety Goals

The description of the range and likelihood of specific fire scenarios in combination with the established goals of the stakeholders helps outline the necessary protection scheme. It is important to recognize that the establishment of the potential fire scenarios and their outcomes articulates how and what could go wrong in a particular facility if the scenario is allowed to run its full course. The degree to which a particular scenario runs its course is dependent, in part, upon the overall risk tolerance of the stakeholders, i.e. their fire safety goals, and the recommended fire protection system(s). In other words, a fire protection system should be selected to ensure that the fire scenario is terminated at some specific point along its timeline. This termination point should align with and represent the goals and desired outcomes of the stakeholders. The review of the potential hazards and the development of the fire scenarios and timelines, along with the establishment of stakeholder goals, facilitate the quantification of specific performance objectives for the fire protection systems.

An initial stakeholder viewpoint may be to prevent all potential fire scenarios and, therefore, eliminate any potential detrimental consequences. Realistically however, the associated costs and/or operational tradeoffs might make such a strategy unattainable. Further, some fire outcomes are the result of a combination of a long string of unlikely events that sometimes cannot be reasonably accounted for ahead of time. Therefore it is important that the developed fire scenarios encompass a range of reasonably expected fuel loads, ignition sources and events that adequately capture the relevant and agreed upon concerns.

As discussed above, each of the stakeholders is likely to also have distinct objectives and concerns based upon their responsibilities, perspective and experience. Some of these objectives and concerns may be in general alignment such as those pertaining to occupant safety

and structural protection and which are generally addressed by applicable building and fire regulations. However there may also be differences among some of the stakeholders concerns and objectives such as those relating to preservation of historic fabric and culturally significant items, business continuity and protection of physical assets such as equipment, finished product or raw materials. Even when stakeholders are in general agreement about their respective concerns and objectives, the best means by which to address them can be a topic of debate. In any event, the overall goals and objectives need to be assimilated and quantified as performance criteria for the fire protection systems in light of the relevant hazards and fire scenarios for the facility under consideration. For instance, typical objectives such as the assurance of life safety for occupants not intimate with initial fire growth, isolation of a fire to the room or area of origin, or limiting business interruption to a specific length of time need to be expressed as measurable and quantifiable performance criteria that can be associated with fire protection system performance. This process might involve an iterative approach in which initial objectives and performance criteria are assessed and refined.

Articulating Goals and Objectives

Ideally, the objectives necessary to achieve the stated goals will be quantified in some manner and translated into performance criteria, i.e. expressed as a maximum permitted fire size or a specific concentration of products of combustion that can be achieved within some time period. In other words, how big a fire and for what duration can the owner or other stakeholder (s) tolerate and still achieve the life safety or property protection goals? From a fire protection engineering perspective, especially through the application of performance-based design approaches, the fire can be quantified in terms of heat release rate as a function of time, i.e. a timeline as was previously discussed.

Target maximum fire size and growth rate, factors not explicitly described in building regulations and most design standards, will help inform the decision as to whether extinguishment, suppression or control of the fire is needed; and by when how soon after ignition fire signatures must be detected and system activation is to be initiated; and what quantity and flow of agent will be needed. The type of fuel including its location and orientation, ignition source, enclosing construction, if any, availability of oxygen and ventilation, greatly influence a fire's growth and heat release rate and need to be addressed when considering the previously discussed fire scenarios.

With respect to the various types of systems that can be used, some systems are more appropriate for fire suppression after a relatively short period of agent discharge followed by a longer time period in which the concentration of agent is held in the vicinity or room of the fire. Other systems are better suited for fire control in which the agent is directly applied to the burning and adjacent surfaces for an extended period of time. For many of these systems a supplemental detection system may be necessary to activate and control discharge. Such detection systems and devices need to be integrated into the overall fire safety strategy, and selected and designed so that they initiate fire protection system discharge within the time period necessary to achieve the overall fire safety goals and objectives.

Associating Fire Event Outcomes with Building and Fire Regulations

Governmental building, fire and safety regulations are typically applicable to most new facility and renovation projects and must be adhered to. One of the principle needs and goals of the stakeholders is identification of and compliance with the relevant regulations. Failing to comply with the applicable rules can prevent occupancy, delaying or interrupting the use of the facility, and significantly impacting the overall return on investment for the facility.

The intent of most regulations is to establish the minimum requirements for safeguarding

public health, safety, and general welfare. The key term here being "minimum", and most regulations are based upon establishing the minimum level of safety for building occupants and responding emergency personnel with limited application to property protection, business interruption, and similar related fire protection goals. So the following questions need to be addressed. Do the minimum requirements of the applicable regulations align with the expected outcomes of the stakeholders, and the intended operations of the enterprise? Has it been determined that the "minimum" requirements provide the desired level of life safety, property protection, continuity of business operations or preservation of cultural resources should a fire occur? They might, but has this decision been given proper priority and consideration, and have the overall fire safety goals and objectives of the operation been adequately articulated?

As previously noted, building regulations have traditionally only addressed property protection to the extent necessary for occupant and fire fighter safety. How might this realization impact the overall implementation of the fire protection strategy during not only the design and construction process but throughout the life of the building and its operations? Conversely, how does any modification to the fire protection strategy account for specific goals such as business continuity or equipment protection, and how does this compare to the baseline applicable code requirements and subsequently the basic goal of occupant and fire fighter safety? A typical example is the use of a special total flooding or local application suppression system for a critical computer room. Oftentimes the building owner, operator, or designer may have a goal to use the special suppression system in place of otherwise required sprinkler protection for the room. Most building codes allow the installation of a special suppression system to protect the room and/or specific equipment; however, a sprinkler system is often still required to protect the building and in turn the occupants throughout the remainder of the building. The combination of systems must then be integrated to ensure proper operation and coordination.

It is worthy to note that while model codes and standards serve as the basis for building regulations in various locations, many jurisdictions and governmental agencies amend the various adopted versions of the model regulations, or enact bylaws that override one or more rules of the adopted model codes and standards. Thus, a uniform level of safety from fire is not necessarily prescribed nor implemented. The FPE must be aware of this and clearly identify the applicable rules of the jurisdiction in which the facility is located.

Addressing Property Protection, Business Continuity and Historic Preservation Goals

Depending upon the facility or operation under consideration, certain fire protection codes and standards do indeed address fire safety beyond life safety, and include provisions for property protection, business continuity and historic preservation. However, these codes and standards are not necessarily mandated and referenced by the applicable building, fire and safety regulations. The FPE needs to be aware of these other documents and how they could possibly impact the overall project, and serve to satisfy the overall fire protection goals of the stakeholders.

An example of one such document is NFPA 76, *Standard for the Fire Protection of Telecommunications Facilities,* which has three identified goals. As noted in its purpose, NFPA 76 establishes a minimum level of fire protection in telecommunications facilities to: (1) provide a minimum level of life safety for occupants; (2) protect the telecommunications equipment; and (3) preserve service continuity of the equipment.

Another example is NFPA 914, *Code for Fire Protection of Historic Structures.* This code addresses ongoing operations, renovation, and restoration of historic structures, and acknowledges the need to preserve historically significant and character-defining building features. Additionally, the code provides provisions for the continuity of

operations of historic structures. The code covers those construction, protection, operational, and occupancy features that are necessary to minimize danger to life, structures, and historic fabric from the effects of fire, including smoke, heat, and fumes.

These types of reference documents can provide valuable information for developing the specific protection scheme including the need for specific types of fire fighting systems, however, as noted above the FPE must be cognizant of the integration and coordination of the different protection goals, and provisions of the applicable regulations.

Insurance Company Objectives

The FPE also needs to understand and address any specific insurance company requirements. Insurance loss control and underwriting recommendations often serve to address property protection and business continuity concerns and can have specific requirements for operations or processes deemed too hazardous or with significant loss potential. For example, one insurance company's guidelines state that typically, special protection systems are recommended where the potential property damage and business interruption from fire for a particular process or occupancy is considered unacceptably high. It is further stated that the above protection rationale applies whether automatic sprinklers are provided as backup protection or not. Occasionally, a special protection system may be acceptable as sole protection without backup sprinkler protection to achieve an acceptable loss potential [5].

Considering the above, the owner's desired level of fire protection for the facility needs to be considered and gauged with that of any applicable insurance interests and recommendations. The degree of property protection recommended by the insurance company is normally based upon the policy purchased and the overall philosophy of the insurer, not necessarily the long-term objectives and needs of the building owner and other stakeholders. The degree to which the insurance company policy is based on the expected fire events and desired outcomes specific to the facility in question requires prudent consideration.

Identifying Candidate Fire Fighting Agents

Various types of fire fighting and/or inerting agents are available for achieving specific fire safety goals and objectives under certain scenarios. A brief overview of such agents follows. The agents can take the form of liquids, solids and gases, with the physical form of some agents changing as they flow from the storage container through a piping network and discharge nozzle, and are delivered to the fire area. Each agent, whether water, an aqueous solution, gas, or chemical powder, possesses certain characteristics and limitations. A proper understanding of the various agents, their means of fighting the fire, diluting vapor concentrations, associated system operations and corresponding system design principles is essential in making the correct decision about which type of agent and system to recommend.

When considering fire-fighting agents, the following qualities should be investigated as noted by Friedman [6].

1. Flammability
2. Heat of vaporization
3. Boiling point with respect to the pyrolysis temperatures of solid fuels under consideration
4. Ability to be transported through distribution networks at expected ambient temperatures
5. Toxicity
6. Formation and effect of decomposition products
7. Potential to cause property damage
8. Ability to conduct electricity

Other factors associated with the agent also come into play and deserve appropriate consideration. These include but are not limited to:

1. Environmental concerns and/or limitations.
2. Cost
3. Availability
4. Storage requirements

5. Means of generating the necessary system flow and pressure
6. Ease of reaching the combustion zone
7. Ability to achieve and maintain design discharge concentrations
8. Effect of discharge sound frequency on protected equipment
9. Overall clean up
10. Containment once discharged
11. Compatibility with other agents, fuels and surrounding equipment,
12. Corrosive effects with respect to system piping and components,

Water

Water, the most common fire-fighting agent, is generally low in cost and normally readily available. It possesses many of the qualities noted above that make it uniquely desirable. Its heat of vaporization is relatively high, allowing for the greater absorption of energy from the fire. Water possesses a rather ideal boiling point because it is well above most ambient room temperatures and well below the decomposition temperature of most solid combustibles. It is also considered nontoxic. The two most common means of applying water are: (1) manually through a hose nozzle, and (2) through an automatic sprinkler system. The practical aspects of fire protection hydraulics and automatic sprinkler system design calculations are addressed elsewhere in this handbook.

Water as a fire fighting agent can take the form of a solid stream when discharged from a firefighter's nozzle, a range of relatively course droplets when discharged from an automatic sprinkler or water spray nozzle, as finely divided droplets when discharge from a water mist nozzle, or as a fog when discharged from a fog generating device. Depending upon the form in which it is applied, water may extinguish a fire by a combination of mechanisms—cooling the solid or liquid combustible; diluting water-soluble flammable liquids; cooling the flame itself; generating steam that prevents oxygen access; and as fog, blocking radiative heat transfer. Although all of these mechanisms may contribute to extinguishment, probably the most important is cooling a gasifying or vaporizing combustible [7]. Most fuels, whether liquid or solid, need to gasify in order for combustion to occur.

There are situations, however, where water might not be the best fire-fighting agent for the application in question. Water freezes below 32 °F (0 °C), and does conduct electricity. It can irreversibly damage some items, although, in certain cases, it is possible to salvage wet items. When applied in bulk or in sprays consisting of large droplets, water can have limited positive effect on ignitable liquid fires, especially for those liquids such as hydrocarbons that are insoluble and float on water. Water is also not compatible with certain hot metals, where it can yield hydrogen, and certain chemicals. The application of water to some substances such as food-stuffs and pharmaceuticals can also initiate undesirable reactions. In some cases, excessive corrosion concerns for system piping exist with water. While this can be a function of the water supply and type of system and its installation, it warrants proper attention.

It is possible to improve the properties of water by using additives. For example, introducing antifreeze such as ethylene glycol or glycerin can lower the freezing point of water. However, at certain concentrations and discharge pressures the solution of antifreeze and water can become flammable [8]. Restrictions have been placed on the use of antifreeze with sprinkler systems. The use of dry-pipe or pre-action systems provides a potential alternative to using antifreeze additives where cold temperatures are a concern. However, there is a water delivery time delay with some of these systems that needs to be considered.

Other additives are intended to improve other qualities of water as a fire-fighting agent. For instance NFPA 18A, *Standard on Water Additives for Fire Control and Vapor Mitigation*, notes that water additives might provide enhanced cooling, emulsification, foaming and insulating characteristics of water [9].

Other additives, referred to "wetting agents" can reduce the surface tension of water and improve water's ability to penetrate porous materials and spread across surfaces [10]. A recent Fire Protection Research Foundation Project has been initiated to provide a comprehensive evaluation of water additives used for fire control and vapor mitigation, with the intent to clarify the fire protection benefit of using water with additives for fire suppression versus water without additives [11]. As noted in the report, "various water additives are available in today's marketplace that claim to provide advantageous performance characteristics for fire control and vapor mitigation. Of particular interest are additives that report to provide superior fire suppression capabilities through emulsification or encapsulation. However, a scientific assessment of these various additives is lacking, and the fire protection community would benefit from an evaluation of the various available water additives for fire control and vapor mitigation".

Emulsification can be described as a forced mixture of two or more liquids that are normally immiscible. From a fire protection standpoint, the two liquids could be a hydrocarbon and water, with or without additives. The water is applied to the surface of the hydrocarbon with some energy so that the two liquids are agitated together and the water is dispersed within in the hydrocarbon, in the vicinity of its surface, in the form of droplets which in some cases appear as a froth. This solution of dispersed droplets within the hydrocarbon is referred to as an emulsion. The presence of the emulsion serves to cool the hydrocarbon surface mitigating the release of flammable vapors, thus rendering the hydrocarbon less flammable or more benign [12]. In some cases, depending upon the agents used, usually not just plain water, the emulsion hardens forming a crust. This process is referred to as saponification.

The fire protection qualities of water might also be improved for specific applications without the use of additives. Misting systems have received attention especially since the initiation of the phase-out of halons in the late 1980s. Mist systems typically deliver water in finely divided droplets so that some drops remain suspended in the air entrained with the spray and fire plume, and others fall due to gravity. Water mist system standards such as NFPA 750, *Standard on Water Mist Fire Protection*, set limits on the size of water droplets produced.

For some applications, water mist serves to control or extinguish fire by various mechanisms. The mist droplets evaporating near the combustion zone, can remove heat, either at the surface of the combustible potentially reducing pyrolysis or vapor generation, or within the flame, reducing the flame temperature. The mist droplets evaporating in the hot environment might do so before reaching the combustion zone, generating steam, which could displace air and dilute the oxygen concentration. Before they evaporate, the mist droplets might block the radiative heat transfer from the flame to the combustible fuel. Various system designs utilizing a range of operating pressures, droplet sizes, and discharge nozzles have been developed and are discussed elsewhere in this Handbook. The limits and specific applications of mist systems need to be confirmed with system manufacturers and third party testing organizations.

Aqueous Foams

Fire-fighting foam consists of a mass of bubbles formed by various methods from aqueous solutions consisting of specially formulated foaming agents and water. Some foams are intended to be gently applied to the surface of ignitable liquids, and float on the liquid surface, creating an air-excluding, cooling, continuous layer of vapor-sealing, water-bearing material that can terminate or prevent combustion. Other foams expand rapidly and are intended for use as large volumes of wet gas cells for inundating spaces and filling cavities. Yet other foams are thick, pasty and viscous, and when applied through a nozzle form a tough heat-resistant blanket covering three-dimensional burning areas and vertical surfaces. Foam concentrates can also be added to sprinkler and water spray systems to aid in the control of certain types of ignitable liquid and storage commodity fires. It needs to be noted that as foam systems are

largely water-based, many of the concerns associated with water and fuel interactions previously discussed also apply.

Fire-fighting foams are usually formulated by mechanical means in which a certain percentage of foam concentrate is added to a flow of water to form a foam solution. Air is then induced into the foam solution by various means such as foam generators or discharge nozzles, and the foam solution is created and applied. Different types of foam concentrates exist and are intended for certain types of applications and fuels. Foam concentrate types are described as: (1) protein, which contain natural protein polymers; (2) flouroprotein, which in addition to the natural protein polymers contains surface-active agents; (3) aqueous film-forming, which consists entirely of synthetic materials; (4) alcohol-resistant types; (5) high-expansion foams; and (6) Class A foams. A further description of the foams produced by these concentrates, and the various methods for applying them are addressed in other chapters of this Handbook.

It needs to be recognized that foam breaks down because it is a rather unstable air-water emulsion. The water content is vaporized when exposed to heat and flame. In the case of liquid surface fires, the foam should be applied at a sufficient rate and volume to compensate for this loss, and to provide an additional amount to ensure that a residual foam layer remains over the extinguished portion of the fuel. Sufficient quantities of foam concentrate and water need to be available to form and sustain a cohesive foam blanket of some depth over the entire anticipated burning surface for some time period. Failing to do so can result in only partial extinguishment, allowing the fire to reach its original intensity after the foam supply has been depleted.

In addition to foam breakdown by heat, physical or mechanical forces can also break down the foam concentrate. As an example, certain chemical vapors or fluids can destroy foam quickly and where certain other extinguishing agents are used in conjunction with foam, severe breakdown of the foam can occur. Turbulent air or violently convective combustion gases can divert light foam from its intended area of application.

As with some other agents, consideration of foam needs to extend beyond the fire fighting characteristics. The growing awareness of environmental issues in many parts of the world has focused on the potential adverse impact of foam solution discharge. Primary areas of concern pertain to toxicity, biodegradability, persistence, treatability in wastewater treatment plants, and nutrient loading when foam solutions reach natural or domestic water systems. While the release of foam solutions into the environment can occur with fire suppression system discharge, all manufacturers are required to address foam retention, clean-up and disposal procedures in Material Safety Data Sheets (MSDS). Therefore, fire fighting foams should be used in a responsible manner to limit the associated environmental concerns associated with their use [13].

Inert Gases and Carbon Dioxide

Inert gases serve to extinguish fires or prevent ignition by displacing the combustion air in the vicinity of the reaction zone and diluting the concentration of oxygen below that necessary for combustion, typically below 12 %. Inert gases can also have an effect on increasing the heat capacity of the atmosphere supporting the flame. Application of an inert gas in sufficient quantity can extinguish the flame over a liquid or solid. Upon their release, inert gases leave no residue and therefore no clean up of agent after a fire incident is needed. Additionally, inert gases do not form potentially harmful decomposition products when subject to high temperatures. Another potential advantage of inert gases is their suitability for suppressing fires in the presence of physical barriers or obstructions. Inert gases in the context of this chapter pertain to the agent's affect on the combustion chemical reaction, i.e. rendering it chemically inactive due largely to the displacement of oxygen. Depending upon the specific design standard or regulation applied, different definitions of the term inert gas might be employed.

Inert gases for fire protection use consist largely of carbon dioxide, nitrogen and certain

formulations of inert gas mixtures classified as clean agents. Note that carbon dioxide is not considered a clean agent because of its toxic effects. In this instance, carbon dioxide is not inert with respect to human physiology. Quantity and unit cost are usually the driving factors when considering a specific inert gas agent. Certain agents are more efficient on a volume and weight basis due to their heat capacity. The use of inert gases becomes problematic in occupied areas necessitating additional safeguards, as the premise is to reduce oxygen concentrations below that necessary to support combustion, which is typically below the level required to sustain human life. However certain inert gas mixtures have been approved and shown safe for occupied spaces [14].

Depending upon the fuel and the type of inert gas used, specific concentrations of inert gas are to be achieved and maintained near the reaction zone for a period of time. This time duration is referred to as hold time. In sufficient quantity, an inert gas will prevent the combustion of most fuels with the exception of certain metals or unstable chemicals such as pyrotechnics, solid rocket propellants, etc. Inert gases generally have limited affect on fuels that contain or liberate oxygen during combustion such as nitrates for the former and conjugated ketones for the latter. Deep-seated fires of ordinary cellulosic fuels also require prudent consideration, as extinguished surface fires can be re-ignited.

Inerting concentrations can be achieved and maintained due to the presence of an enclosure around the anticipated combustion zone. In this case, successful extinguishment is tied to the integrity and ventilation aspects of the enclosure in which the agent is discharged. Inerting concentrations can also be maintained by continuously saturating the combustion zone with the inert gas for some specified period of time. If the necessary concentration of inert gas cannot be maintained and dissipates before the fire is completely extinguished and the reaction zone does not cool, remaining glowing embers or hot surfaces could reignite any lingering flammable vapors. Depending upon the value of the equipment or contents to be protected, providing a reserve supply of agent or a redundant system serves to minimize the associated risk.

Minimum design concentrations for specific inert gases are fuel dependent, but the lowest referenced concentration for most is about 34 %. Even at these minimum design concentrations, the oxygen level in the vicinity of the agent discharge will be reduced to levels that are generally hazardous to exposed humans with some exceptions. In the case of carbon dioxide, an additional serious physiological effect will occur at concentrations much lower than that necessary to extinguish a fire [15]. Minimum design concentrations must be confirmed with design standards and system manufacturer's data.

See Chap. 44 and Chap. 45 for more discussion on inerting agents.

Halocarbon Clean Agents

Clean agents were developed in response to the Montreal Protocol, which called for the phase-out of the production of chlorofluorocarbon agents (halons) in the late 1980s. With respect to fire protection, Halon 1301 and Halon 1211 were the most notable agents affected. Clean agents are generally described as electrically non-conducting fire extinguishing agents that vaporize readily and leave no residue. They are subject to specific evaluation with regard to their hazards to personnel and their potential effect on the environment, specifically Ozone Depletion Potential (ODP) and Global Warming Potential (GWP) [14]. Depending upon the agent, they are stored under high pressure as a liquid or a gas, and are utilized in their gaseous state when released from their storage containers. Clean agent halon replacements fall into two broad categories: (1) halocarbon compounds and (2) inert gas mixtures.

Halocarbon clean agents include compounds containing carbon, hydrogen, bromine, chlorine, fluorine, and iodine. They extinguish fires by a combination of chemical and physical mechanisms depending on the compound. Chemical suppression mechanisms of certain compounds are similar to Halon 1301 in that the bromine and iodine species scavenge flame

radicals and interrupt the chemical combustion chain reaction. However, such compounds of clean agents are not widely used.

Most halocarbon compounds suppress fires primarily by extracting heat from the flame reaction zone, reducing the flame temperature below that necessary to sustain combustion. Halocarbon agents also decompose which further absorbs energy from the combustion reaction. As noted in Chap. 44, decomposition products of halocarbons merit consideration. Oxygen depletion by halocarbons also plays a role in reducing flame temperature and extinguishing the fire, similar to the effect that inert gases have. The lack of significant chemical reaction inhibition in the flame zone by most halocarbon compounds results in reduced performance on a volumetric basis and requires higher extinguishing concentrations relative to Halon 1301.

Halocarbon agents can be considered for applications similar to those intended for carbon dioxide and other inert gases. One potential advantage of halocarbons over inert gases is that halocarbons are effective in lower volumetric concentrations so that sufficient oxygen necessary to support human life remains in area of discharge. As with inert gases, a certain concentration of the halocarbon needs to be maintained in the vicinity of the combustion reaction zone. The potential drawbacks to using halocarbons relate to their potential toxicity, and the toxicity and corrosive nature of potential decomposition products during a fire. In general, halocarbon agents are not appropriate for use on certain burning metals such as, but not limited to, aluminum, magnesium, iron, chromium, cobalt, copper, nickel and the alkali metals. These fuels reduce the extinguishing agent to liberate halogenated acids, metal salts, organometallic compounds and metal carbonyls, all of which can pose consequential hazards to both occupants and property. Therefore, in addition to a halocarbon's fire extinguishing characteristics, consideration also needs to be given to the agent's impact on safety to exposed personnel, its decomposition products and its environmental impact.

Dry Chemicals

A dry chemical is a finely divided powdered material that has been specially treated to be water repellent and capable of being fluidized and free-flowing so that it can be discharged through piping under expellant gas pressure. Dry chemicals are sodium bicarbonate, potassium or mono-ammonium phosphate-based, and certain agents are more effective than others on specific types of fires. For example, potassium-based dry chemicals are not generally recommended for the extinguishment of fires involving ordinary, Class A, combustibles [16]. Once discharged, dry chemical will settle on and coat surrounding surfaces and objects.

It is generally understood that dry chemicals act to suppress the flame of a fire by chemical mechanism that stops the chain reaction taking place in the flame combustion. It is presumed that the dry chemical interacts with the flame to form volatile species that react with hydrogen atoms or hydroxyl radicals similar in some ways to the effect of halon. Dry chemicals also discourage combustion by absorbing heat, by blocking radiative energy transfer, and in the case of mono-ammonium phosphate, by forming a surface coating [7].

Dry chemicals have been used to effectively protect hazards involving flammable and combustible liquids and gases, combustible solids, electrical hazards, such as oil-cooled transformers and circuit breakers, textile operations subject to flash surface fires, and ordinary combustibles such as wood, paper and cloth [17]. Surface coating by dry chemical can be especially effective on elevated objects and vertical surfaces. In cases where other agents would run-down vertical surfaces, dry chemical is more likely to adhere to surfaces, and provide a coating and insulation of the object.

Upon discharge, dry chemical residue will remain on surrounding objects and potential corrosion and staining concerns exist. Prompt cleanup will minimize these concerns. Certain dry chemicals can corrode metals such as steel, cast iron, and aluminum among others. In most

cases, dry chemical agents can be readily removed from surfaces by wiping, vacuuming or washing exposed surfaces. Consideration of environmental restrictions is prudent if dry chemical residue is washed away into bodies of water or wastewater systems. Some dry chemicals will require scraping and washing if the exposed surfaces were hot when the chemical was applied.

Health affects of dry chemicals also warrant attention. While dry chemicals are considered non-toxic from a physiological perspective, they are finely divided powders and can produce irritation affects when discharged, especially in enclosed areas. Discharge can reduce visibility, and cause breathing difficulty and irritation to the eyes. Suitable safeguards should be provided to ensure prompt evacuation of any exposed occupants during discharge [16].

While there are specific types of dry chemicals based on certain chemical compounds, they are produced by different manufacturers. As such, dry chemicals produced by different manufacturers are usually not identical in all characteristics, and each manufacturer develops equipment for use with a specific dry chemical. System design principles applicable to the products of one manufacturer are not applicable to the products of another manufacturer.

Wet Chemicals

A wet chemical fire-fighting agent consists of organic or inorganic potassium-based salts or both, mixed with water to form an alkaline solution capable of being discharged through piping or tubing when pressurized by an expellant gas. The primary use of wet chemical agents is for the protection of fires in cooking oils and fats [18].

Upon discharge, the wet chemical results in a vapor-suppressing foam-like substance that rapidly spreads across the fuel known as saponification. The wet chemical application extinguishes and secures the flame by forming a barrier between the liquid fuel and the surrounding air. The barrier prevents oxygen from reaching the combustion reaction zone, and mitigates the release of flammable vapors from the fuel surface. The cooling affect of the wet chemical also lowers the temperature of the oil or fat further decreasing the release of ignitable vapors.

Wet chemicals are usually discharged in the form a fine spray. As such some of the agent can settle on surrounding surfaces and can have a corrosive effect on electrical components and cooking equipment. As with dry chemicals, prompt clean-up will minimize staining or corrosion.

Similar to dry chemicals, wet chemicals produced by various manufacturers are usually not identical in all characteristics, and each manufacturer develops equipment for use with a specific wet chemical. Therefore, system design principles applicable to the products of one manufacturer are not applicable to the products of another manufacturer.

Aerosols

Aerosols are a relatively new type of fire fighting agent first appearing in the marketplace in the mid 1990s. Two types of aerosol agents exist: condensed aerosols and dispersed aerosols. Condensed aerosols are described as an extinguishing medium consisting of finely divided solid particles, generally less than 10 microns in diameter, and a gaseous matter, generated by a combustion process of a solid aerosol-forming compound. Dispersed aerosols are described as an extinguishing medium consisting of finely divided solid particles, generally less than 10 microns in diameter, already resident inside a pressurized agent storage container, suspended in a halocarbon or inert gas [19]. At the time of the writing of this chapter, dispersed aerosol systems are not commercially available.

Fixed condensed aerosol extinguishing system units include condensed aerosol generators with mounting brackets, actuating mechanisms,

and other accessory equipment (as applicable). Condensed aerosol generators are normally non-pressurized devices incorporating an aerosol-forming compound consisting of a mixture of oxidant(s) and combustible component(s) that, when pyrotechnically actuated, produces an aerosol extinguishing agent of gaseous matter and finely divided solid particles that flow through a cooling mechanism within the device prior to exiting through discharge port(s) and into the protected space.

The primary mechanism of fire extinguishment by condensed aerosols is reported to be the interruption of the chemical combustion chain reaction taking place in the flame, similar to the affects of halon and dry chemicals. Some cooling near the combustion zone also occurs due to heat absorption by the aerosol particles.

For total flooding applications, the hazard is surrounded by a fixed enclosure to enable the required aerosol extinguishing agent concentration to be achieved and maintained for the required hold time to effectively extinguish the fire within the enclosure. Aerosol-generating extinguishing system units, when assembled into a system with one or more condensed aerosol generators, are designed for automatic and manual actuation. Aerosol-generating automatic extinguisher units are self-contained units designed for automatic thermal actuation and do not have a manual means of actuation. The extinguisher units are also limited to a single protected enclosure.

The use of condensed aerosol agents might present hazards to personnel. The discharge of aerosol extinguishing systems to extinguish a fire could create a hazard to personnel from the natural form of the aerosol or from certain products of aerosol generation, including combustion products and trace gases from condensed aerosols. Acid by-products, such as hydrofluoric acid, can also be formed and present a hazard to exposed personnel. Unnecessary exposure of personnel to either the natural agent or the decomposition products should be avoided. Potential hazards associated with noise, turbulence, reduced visibility, cold temperature, toxicity, thermal hazards and irritation to persons in the protected spaced and other areas where the aerosol agent can migrate should to be evaluated [19].

Code Mandated Fire Protection Systems

Building regulations mandate active fire protection systems, largely automatic sprinkler systems, based upon the occupancy types associated with the building, the size and location of the fire area, and the expected occupant load. For instance the *International Building Code* (IBC) requires automatic sprinkler systems in Group A-2 occupancies, e.g. restaurants, where one of the following conditions exist: i) the fire area exceeds 5000 sq ft; ii) the fire area has an occupant load of 100 or more; or iii) the fire area is located on a floor other than the level of exit discharge. Similar requirements are found in NFPA 5000, *Building Construction and Safety Code,* and NFPA 101, *Life Safety Code*. Additionally, model codes require sprinkler systems for certain types of buildings regardless of the occupancy type. For example, sprinkler systems are required for all high-rise buildings.

The basis for mandating such fire protection systems is largely based on the premise that the building owner is obligated to provide a safe environment for the building occupants, or the public at large. In general, building regulations do not force a building owner to protect his or her own property.

Fire regulations typically have more specific occupancy related requirements that can include specific requirements for special fire protection systems. As an example, the *International Fire Code* (IFC) contains requirements for the application of foam systems for flammable and combustible liquid storage tank protection for certain configurations. However, similar to building regulations, the detail of such requirements are typically limited and based upon the goal of occupant and emergency personnel safety.

Building regulations also allow for "Alternative Automatic Fire-Extinguishing Systems" or "Other Automatic Extinguishing Equipment",

but provide limited direction on when such systems are needed, or should be considered. Although, the terms "Alternative" and "Other" with respect to fire protection systems are not specifically defined, it is often interpreted that such systems are used to protect against "special hazards". Harrington [20] describes special hazards as a fuel array that for one or more reasons cannot be effectively protected by standard spray sprinkler systems. Numerous alternatives to standard spray sprinkler systems have been developed to protect special hazards, each having certain characteristics uniquely suited to effectively protect specific aspects of certain special hazards. Special hazard fire protection systems employ various types of agents including water as previously described. The term "special protection system" is also sometimes used to describe these systems.

Depending upon the model code, these "Alternative" or "other" systems are identified as wet chemical, dry chemical, foam, carbon dioxide, halon, clean-agent, water spray, foam-water, and water mist. Reference is normally made to the associated NFPA standards for the specific type of system under consideration for relevant design, installation and related provisions, i.e. NFPA 2001, *Standard for Clean Agent Fire Extinguishing Systems,* or NFPA 17, *Standard on Dry Chemical Extinguishing Systems*.

It needs to be recognized that when a building or fire regulation references an "alternative" or "other" system it is usually done so in the context of providing life safety for building occupants, usually as an alternative to the requirement for installing an automatic sprinkler system. It needs to be further recognized that although building and fire regulations typically mandate the installation of sprinkler systems for life safety, sprinkler systems were initially invented and developed for property protection and business continuity concerns and they continue to serve this purpose for various types of commercial, residential and industrial applications. For instance, the provisions of NFPA 13 pertaining to the protection of storage facilities were developed specific to property protection goals. However, certain types of systems have been developed and are intended primarily to enhance life safety, e.g., residential sprinkler systems.

Facility Specific Standards

In addition to regulatory provisions found in applicable building and fire codes, other fire protection related documents specific to certain types of facilities and operations exist and might provide some insight as to the type of fire protection system to be used. Examples of such documents include NFPA 34, *Standard for Dipping, Coating, and Printing Processes Using Flammable or Combustible Liquids*; NFPA 45, *Standard for Laboratories Using Chemicals*; NFPA 76, *Standard for the Fire Protection for Telecommunications Facilities*; and NFPA 409, *Standard on Aircraft Hangers* among others. The FPE needs to confirm whether or not these facility specific standards are mandated by the jurisdiction in which the facility is located or if any governmental regulations come into play. A summary of the relevant provisions of NFPA 34, NFPA 76 and NFPA 409 pertaining to fire protection systems follows.

NFPA 34 specifically states that processes are to be protected with any of the following approved automatic fire protection systems: (1) a water spray extinguishing system especially on liquids having flash points above 60 °C (140 °F); (2) a foam extinguishing system; (3) a carbon dioxide system; (4) a dry chemical extinguishing system; and (5) a gaseous clean agent extinguishing system. It is further noted that fixed, automatic carbon dioxide systems historically have been provided to protect: (a) Flexograph presses and rotogravure presses using Class I and Class II inks, with CO2 nozzles arranged to protect printing heads, ink reservoirs, and other areas likely to contain flammable liquid-based inks; and (b) presses using flammable liquid-based inks having shielded spaces where automatic sprinkler installation is impractical. Additional considerations for CO2 systems include providing a connected reserve supply for high-pressure carbon dioxide systems, and

sufficient agent for two complete discharge cycles for low-pressure carbon dioxide systems. It is further noted that if a foam extinguishing system is used, hoods and ducts are to be protected by other approved fire protection systems.

NFPA 34 also allows for the use of standard automatic sprinkler system protection for certain components of the associated coating, dipping and printing processes. These components specifically include tanks containing liquids having flash points above 93 °C (200 °F) and their associated process hazards, and tanks equipped with covers arranged to close automatically in the event of fire.

NFPA 45 requires, and assumes as a baseline, that all laboratory units be provided with full automatic sprinkler protection, and provides guidance on the hazard classification dependent upon the laboratory unit classification. The standard also recognizes that other types of special hazard extinguishing systems and non-water automatic extinguishing systems may be used and provides reference to the appropriate design standards, but provides no specific design criteria. In the standard's purpose section, it states that "This standard is designed to control hazards and protect personnel from the toxic, corrosive, or other harmful effects of chemicals to which personnel might be exposed as a result of fire or explosion [21]. " Given the types of hazards that may be present in a laboratory, the protection scheme must include a comprehensive fire protection strategy to ensure that the utilized system does not result in unintended consequences, i.e. the use of a standard sprinkler system for a laboratory with notable and/or exposed quantities of water reactive chemicals, or the use of a fire protection system that may produce a hazardous atmosphere as part of the extinguishing process.

NFPA 45 provides guidance on the fire protection systems as noted above, and also provides guidance on construction, ventilation, chemical storage, handling, and disposal, chemical container sizes, and laboratory operations to result in a coordinated protection approach. It is the FPE's responsibility to understand the various requirements and controls to review the impact on the fire protection system decision making process.

As part of its fire protection provisions, NFPA 76 makes reference to several types of automatic fire suppression systems, but does not specifically mandate their use. Some commentary is provided on when a particular type of system could be used. For instance, NFPA 76 notes that automatic or manual fire suppression equipment should be considered as an element in the overall fire protection plan for a telecommunications facility. However, the standard seems to caution on the use of such suppression systems, as it states that telecommunications facilities have experienced an excellent fire loss record due to the high standards of construction, compartmentation of hazards, and high quality of telecommunications equipment, mostly without the use of automatic extinguishing systems. The standard notes that automatic suppression should be considered when other fire protection elements cannot be employed. Furthermore, the potential impact of the suppression agent on energized telecommunications equipment requires thorough evaluation as accidental discharge of agents can cause damage to equipment or otherwise harm personnel. The standard also states that fire suppression agents are not to cause severe damage to the telecommunications equipment, and those agents containing dry chemicals or corrosive wet chemicals in fixed systems should not be used in any area containing telecommunications equipment.

NFPA 76 states that wet pipe, dry pipe, and pre-action systems are acceptable for use in the protection of technical support, administrative and building service areas, and support areas of telecommunications facilities, but they are not recommended for the power area, main distributing frame (MDF) areas, signal processing area, and standby power areas. The need to introduce water piping into telecommunications power areas, MDF areas, or signal-processing areas needs thorough evaluation, as water is a risk to telecommunications signal-processing equipment and, by extension, to public safety. The use of special sprinkler configurations, such

as double-interlock pre-action systems, can minimize the risk of inadvertent water discharge.

With regard to aircraft hangers, NFPA 409 states that the protection of aircraft storage and servicing areas of Group II aircraft hangars is be with any one of the following systems: (1) foam-water deluge systems with or without air-aspirating discharge devices; (2) a combination of automatic sprinkler protection and an automatic, low-level, low-expansion foam system; (3) a combination of automatic sprinkler protection and an automatic, high-expansion foam system; or (4) a closed-head foam-water sprinkler system.

As can be observed, the four referenced facility standards noted above that pertain to four very different types of facilities and hazards, make no clear recommendation on the type of fire protection system to be used, or whether fire control, suppression or extinguishment are intended. However, even in the absence of a stated fire protection goal, the selection of a specific fire protection system will usually imply the overall objective of fire suppression or fire control. Naturally, any decision needs to be coordinated with the overall outcomes to be achieved for the expected fire scenarios.

Rather than providing specific recommendations, each facility standard provides options on the types of systems that could be used, and in some cases includes additional commentary or precautionary statements about the use of the various types of fire suppression systems. Specifically, NFPA 34 cautions about the flash points of liquid fuels, the position and location of certain types of discharge nozzles, the need for reserve supply of fire fighting agent and the limitation of certain types of systems. NFPA 76 cautions about accidental system discharge, the affect of agent discharge on equipment, and the corrosive affects of certain types of agents. NFPA 409 identifies four different types of systems for a specific type of aircraft hangar. NFPA 484 specifically cautions against the use of automatic sprinkler protection where certain types of metals are produced or handled. It should be obvious that in many cases, the stakeholders and the FPE cannot rely solely on the on the facility standards or the applicable building and fire regulations for a prescriptive mandate on the most appropriate type of system to be used.

Insurance Company Guidelines

Some insurance companies issue guidelines that address the use of special hazard or special protection systems. One company notes that such systems are used to extinguish or control fires in easily ignitable, fast-burning substances such as flammable liquids, some gases and chemicals. It is further stated that the systems can also be used to protect ordinary combustibles in certain high-value occupancies especially susceptible to damage and in certain high-piled storage occupancies. The quick action of these systems can keep production downtime at a minimum [5].

Insurance company recommendations for application of special protection systems include dip tanks, drainboards, flow coaters, engine test rooms, foil mills, electronic computer installations, storage tanks of flammable liquid or liquefied gas, fur vaults, oil-filled transformers, rotating electrical equipment, aircraft hangars, rubber tire storage, and chemical processing equipment. In certain cases, recommendations for specific types of systems for specific applications are identified. In other cases, options are provided.

Depending upon the insurance company, special protection systems might only be considered a supplement to automatic sprinkler systems, and not a substitute for them. Sprinkler systems are usually designed to operate for longer periods of time than most special protection systems, and can be restored to service more quickly. Special protection systems are more complex than conventional sprinkler systems, and consequently subject to more electrical and mechanical failure modes. Reflash or reignition potential is also a concern, especially for total flooding systems and certain types of extinguishing agents. However, sprinkler systems are usually designed for fire control over a longer period of time, where as special protection systems are usually designed for suppression or extinguishment in a much shorter time frame.

Fire Protection System Reference Standards

As previously noted, standards addressing certain types of fire protection systems are referenced by building and fire regulations and specific facility standards. These system reference standards, especially those promulgated by NFPA, are generally intended for use by those responsible for purchasing, designing, installing, testing, inspecting, approving, listing, operating, and maintaining such systems, and contain various information in this regard.

System reference standards usually make it clear that it is not within their purview to identify where such systems are required to be used, e.g. NFPA 11, *Standard for Low-, Medium-, and High-Expansion Foam,* specifically states that it is not the intent of this standard to specify where foam protection is required. However, such system reference standards might include some information about the fire hazards and conditions under which the systems could be used. For example, NFPA 12, *Standard on Carbon Dioxide Systems*, includes Annex B, *Examples of Hazard Protection,* in which five applications of Carbon Dioxide Systems are specifically identified. These applications include (1) Commercial/Industrial Food Processing Deep-Fat (Hot Oil) Cookers; (2) Restaurant Range Hoods, Connected Ducts, and Associated Equipment, (3) Newspaper Printing and Rotogravure Presses; (4) Open-Top Pits and (5) Below Raised Floors.

Another example includes NFPA 2001, which provides advisory annex language indicating that clean agent fire extinguishing systems are useful within certain limits for extinguishing fires in specific hazards or equipment, and in occupancies where an electrically non-conductive medium is essential or desirable, or where cleanup of other media presents a problem. Such total flooding clean agent systems are used primarily to protect hazards that are enclosed or equipment that in itself includes an enclosure to contain the agent. A list of typical hazards that could be suitable for protection by clean agent systems is provided and includes (1) electrical and electronic hazards, (2) subfloors and other concealed spaces, (3) flammable and combustible liquids and gases, (4) high-value assets, and (5) telecommunications facilities. NFPA 2001 also states that clean agent systems could be used for explosion prevention and suppression where flammable materials collect in confined areas. Again, the standard does not explicitly prescribe where such systems are to be used but rather provides some commentary about their potential application.

Even when a system reference standard does not explicitly identify the application of such a system, the standards might include design and installation requirements that address the types of hazards or fuels for which the fire protection agent and system could be used and oftentimes includes reference data such as fuel specific extinguishing and/or inerting concentrations. Referring again to NFPA 12, provisions about the design of carbon dioxide systems for specific hazards are provided and can be applied once a decision has been made to install a carbon dioxide system. Specifically, CO2 design concentrations for certain fuels such as acetone, gasoline and propane among others are identified.

Other reference standards do not directly identify the hazards they are intended to protect, but rather tie the appropriateness of the system to specific listing and testing requirements. For example, NFPA 750, *Standard on Water Mist Fire Protection Systems*, states that water mist protection systems are to be designed and installed for the specific hazards and protection objectives specified in the listing. An Annex note in NFPA 750 includes a list of fire test protocols and the associated listing organizations. It should be obvious that the FPE needs to be sufficiently familiar with the application and limits of the listing protocols, as well as the design and installation manual for each type of water mist system that might be under consideration. More discussion on listing protocols is discussed below.

It is important to recognize that with many of these "alternative" or "other" systems, not just water mist systems, a generic design approach such as for automatic sprinkler systems as outlined in NFPA 13, *Standard for the*

Installation of Sprinkler Systems, does not exist. Many of these "alternative" systems are of a proprietary nature and the design and installation provisions are specific to the manufacturer of each type of system. For a given hazard, the design, installation and operational details of one manufacturer's water mist system is likely to be significantly different from that of another manufacturer. It is worth noting, that even with sprinkler systems more specialized devices are entering the marketplace.

Manufacturer's Literature

It should not be concluded, that the only applications appropriate for a certain type of special hazard system are those identified in a particular system reference standard or a specific facility document. System and component manufacturer literature typically includes information on the possible applications of such systems. However, any claims on system appropriateness for specific hazards needs to be verified by the FPE. The question is how?

If a system manufacturer's literature state that its system is appropriate for use in addressing specific fire scenarios, it is reasonable to expect that the system manufacturer possesses specific fire test data and, therefore, more detailed and comprehensive information about such system performance and the verification of such performance. This information, which can take the form of test reports and other evaluation protocols, should be requested by the FPE and examined during the system selection process.

Key considerations in the examination of such information include the degree to which evaluation protocols, acceptance criteria, overall hazard dimensions, etc. correlate with those of the desired outcomes and identified hazards of the specific facility and operation in question. Simply relying on the manufacturer's marketing information should not be considered adequate justification by the FPE that the system is appropriate for the specific scenarios under consideration. More discussion of listing protocols and system testing is provided in the next section.

Listing Protocols

The majority of fire protection systems and their components, including special hazard systems, are associated with some type of listing requirements. A generally accepted definition of the term "listed" means equipment, materials, or services included in a list published by an organization that is acceptable to the authority having jurisdiction and concerned with evaluation of products or services, that maintains periodic inspection of production of listed equipment or materials or periodic evaluation of services, and whose listing states that either the equipment, material, or service meets appropriate designated standards or has been tested and found suitable for a specified purpose [22].

When a fire protection system or its components are "listed" as noted above, it is understood that such equipment has been evaluated for a specified purpose, and that such evaluation has been done in accordance with appropriate standards or has been otherwise tested and found suitable. Therefore an examination of listing protocols will provide some insight as to the appropriateness and applicability of a certain system for a specific hazard. Here again, the FPE needs to confirm that the information presented in the listing protocols correlates with that of the facility operation in question, the fire hazards to be protected against and the desired outcomes.

Listing organizations usually contain on-line databases and other recourses that FPE's and others can use to verify if a particular manufacturer's system or equipment has been evaluated and "listed" by the organization. However, the fact that a system or piece of equipment is listed does not serve as validation that the system or equipment is appropriate for the given situation or application. As noted above, the listing protocols and evaluation reports should be further examined. Even within a given listing organization, the evaluation and testing protocols for the various types of fire protection systems and equipment differ. Depending upon the system and equipment, attributes about their associated performance vary.

Listing organizations might provide some detail about the application or intended use of the system. Referring to Factory Mutual Global (FM) Approvals on-line guide [23] with respect to CO2 systems, it notes that carbon dioxide discharge falls into two broad categories, total flooding and local application. The approvals guide further states that total flooding systems are intended to protect enclosed special hazards such as rooms or spaces involving flammable liquids or containing electrical equipment, records, furs, or other storage where a fire would be extinguished. Local application systems are intended to protect flammable liquids in unenclosed special hazards such as dip tanks and drain boards by discharging carbon dioxide directly on the burning material.

Further information might be found in the listing organization's published listing protocol. For instance, FM Approvals Standard 5420 on Carbon Dioxide Extinguishing Systems [24] includes specific fire tests for carbon dioxide extinguishing systems for the protection of wet benches and similar processing equipment. Additional criteria pertain to other performance characteristics such as those associated with salt fog corrosion, thermal shock and areas of coverage among others.

In some cases, system reference standards refer directly to any associated listing protocols for information about system application. As previously noted, NFPA 750, requires that water mist protection systems be designed and installed for the specific hazards and protection objectives specified in the listing. NFPA 750 goes on to state that the characteristics of the specific application, e.g. compartment variables and hazard classification, are to be consistent with the listing of the system. Furthermore, an evaluation of the compartment geometry, fire hazard, and system variables are to be performed to ensure that the system design and installation are consistent with the system listing. As such, the listing of water mist fire protection systems are to be based on a comprehensive evaluation designed to include fire test protocols, system components, and the contents of the manufacturer's design and installation manual.

While the following concepts are paraphrased from NFPA 750, they are pertinent to any fire protection system for which no generalized application guide and design method are readily available. Listings about system performance should be obtained through full-scale fire tests and thorough system component evaluations conducted by recognized laboratories to demonstrate that performance objectives can be met. Where full-scale assessments are not possible or practical, an extrapolation and assessment of available data and information might be appropriate. However, the setting of practical limits of any extrapolated data needs to be well informed with good intuitive reasoning applied.

Where fire tests are employed as part of a listing protocol, they should reflect, to the extent possible, the intended conditions under which the special hazard system is expected to operate. It needs to be verified that the fire tests are sufficiently and appropriately challenging so that the performance of the system can be adequately assessed. It also needs to be confirmed that any performance objectives outlined in a listing protocol are consistent with those of the intended application of the system.

New potential applications of fire protection systems can occur. In these cases, existing listing protocols might not necessarily address the intended application of the system. Ad hoc test procedures for such applications could be developed and completed. Where ad-hoc tests protocols are developed, they should adequately address the associated concerns and be: (1) based on an evaluation of the fire hazard, the compartment and space conditions where the fire hazard is located, and the performance objectives for the system; and (2) developed, executed, and interpreted by recognized fire testing professionals acceptable to the stakeholders. Only those ad-hoc test protocols developed in such a manner should be recognized.

Listing evaluations typically consist of an approval report describing the results of the fire testing and component evaluations, and are associated with the manufacturer's design, installation, maintenance and operations manual. For special hazard systems, nozzle characteristics;

spacing between nozzles; distances from ceilings, walls, or obstructions; minimum operating pressures; and agent supply requirements, among other criteria are all usually documented in the listing report. Again, where the listing protocols for such system component performance cannot be correlated with the intended outcomes and scenarios under consideration, it is incumbent on the responsible FPE to make appropriate assessments.

Long Term System Performance

When deciding on those fire protection systems that best serve the intended fire and life safety purposes, the long-term effectiveness, reliability and performance of the systems should be incorporated into the decision making process. Once the systems are commissioned, the occupancy certificate is issued and the building is in operation, the design team moves on. It is now the owner's responsibility to keep the building and the respective fire and life safety systems in proper working order. The applicable fire code, which normally applies to existing buildings, will address the need to maintain an appropriate level of safety. As previously noted, most regulations primarily address life safety rather than property protection. Nonetheless, any provision promulgating effective system performance should be translated and implemented into an effective inspection, testing and maintenance program for the installed fire and life safety systems. Details of this program should be incorporated into the early stages of the system selection and design process, as it will have a distinct impact on the building's overall operational costs.

Most design and installation standards contain some information about the necessary inspection, testing and maintenance activities. For instance NFPA 2001 includes a chapter entitled Inspection, Testing, Maintenance and Training. However, these provisions can be generic in nature. When it comes to specific types of proprietary or pre-engineered systems, the design, installation and operation manual furnished by the system manufacturer should be obtained and evaluated before any system is selected. While these manuals tend to be tailored for each individual system installed, sample manuals for the types of applications under consideration can be requested and made available.

Designing the system to facilitate the work of inspection, testing and maintenance personnel, as well as contemplating the availability of replacement parts and system supplies should also receive proper priority. Designing the system to best facilitate testing and maintenance activities is not necessarily a provision mandated by the applicable design and installation standard, but doing so will help ensure more cost-effective long-term performance of the system. Additionally, if replacement parts and supplies are not readily available but are needed, the resulting disabled or impaired system means that life safety and the owner's investment are unduly compromised. While not within the scope of routine inspection and maintenance, consideration of future building expansion and anticipated changes in building operations also deserve attention. Can the fire protection system once installed be expanded or otherwise modified to address the related change in fire hazard, or will an entirely new replacement system be necessary?

Concluding Remarks

In the absence of any standardized generic application guides for the selection of fire protection systems, validating one's choice is not always a straightforward matter. Providing the appropriate systems will often require more than just code consulting and compliance with the applicable regulations. As has been discussed, building and fire regulations are often not likely to give much guidance on the selection and use of systems other than sprinkler systems for life safety

concerns. Where other types of systems are permitted in place of, or in combination with sprinkler systems, or needed for other purposes, limited guidance is provided with regard to the conditions under which such so called special hazard systems could be used, and the reasons why such systems should be used.

A comprehensive fire and life safety strategy needs to be developed and implemented with the overall long-term goals of the stakeholders clearly articulated, agreed upon and properly documented. A competent fire safety analysis and assessment will facilitate the overall strategy, identify if the applicable regulations adequately serve the fire and life safety needs over the expected lifespan of the facility, and more effectively address any gaps in protection. Specific attention needs to be given to any property protection, business continuity and historic preservation goals that might not be sufficiently addressed by the prescribed solutions embodied in applicable building and fire regulations.

The FPE needs to be knowledgeable and well versed with the application and limitations of the different types of fire protection systems that could be used to satisfy the overall fire and life safety goals and objectives. This requires not only an unbiased in-depth grasp of the applicable rules, regulations, available technologies, design principles and testing protocols, but also a sufficient understanding of the operations for the planned building and the associated fire and life safety risks. Information about the appropriateness of the proposed system, especially if it is a special hazard system, typically needs to be obtained from a combination of building and fire regulations; stakeholder viewpoints; system design, installation and testing standards; insurance company recommendations; listing protocols and evaluations; manufacturer's information and in certain cases the completion of calculations.

In the end, the FPE needs to confirm that all applicable regulations are complied with, and that the proposed system will satisfy the goals and objectives of the stakeholders under the conditions specified, i.e. validation that the expected outcomes can be achieved for the fire scenarios to be considered. Naturally, the right choice is predicated on the assumption that the recommended system is properly designed, installed, and maintained.

References

1. NFPA 75, *Standard for the Fire Protection of Information Technology Equipment,* National Fire Protection Association, Quincy, MA, 2011.
2. Engineering Guide to Fire Risk Assessment, Society of Fire Protection Engineers, Bethesda, MD, 2006.
3. NFPA 551, *Guide for the Evaluation of Fire Risk Assessments*, National Fire Protection Association, Quincy, MA, 2010.
4. Watts, J. "Systems Approach to Fire-Safe Building Design," *Fire Protection Handbook,* 20th Edition, National Fire Protection Association, Quincy, MA: 2008.
5. FM Global Property Loss Prevention Data Sheet 4-0, Special Protection Systems, Factory Mutual Insurance Company, Johnston, RI, 2002.
6. Friedman, R., "Fire Fighting Procedures," *Principles of Fire Protection Chemistry and Physics*, 3rd Edition, Jones and Bartlett, Sudbury, MA, 2009.
7. Yu, H.Z. & Newman, J.S., "Theory of Fire Extinguishment," *Fire Protection Handbook,* 20th edition, National Fire Protection Association, Quincy, MA, 2008.
8. Updated NFPA Alert Regarding Antifreeeze – April 5, 2011, National Fire Protection Association, Quincy, MA.
9. NFPA 18A, *Standard on Water Additives for Fire Control and Vapor Mitigation*, National Fire Protection Association, Quincy, MA, 2011.
10. NFPA 18, *Standard on Wetting Agents*, National Fire Protection Association, Quincy, MA, 2011.
11. Scheffey, J.L, Forssell, E.W. & Childs, J.T., *Evaluation of Water Additives for Fire Control and Vapor Mitigation, Phase 1, Final Report,* Fire Protection Research Foundation, Quincy, MA, June 2013.
12. Frank, J.A., "Characteristics and Hazards of Water and Water Additives for Fire Suppression," *Fire Protection Handbook,* 20th Edition, National Fire Protection Association, Quincy, MA, 2008.
13. NFPA 11, *Standard for Low-, Medium-, and High-Expansion Foam*, National Fire Protection Association, Quincy, MA, 2010.
14. NFPA 2001, *Standard on Clean Agent Fire Extinguishing Systems,* National Fire Protection Association, Quincy, MA, 2012.
15. NFPA 12, *Standard on Carbon Dioxide Extinguishing Systems*, National Fire Protection Association, Quincy, MA, 2011.

16. NFPA 17, *Standard for Dry Chemical Extinguishing Systems*, National Fire Protection Association, Quincy, MA, 2013.
17. Hague, D.R., *Fire Protection Systems for Special Hazards*, National Fire Protection Association, Quincy, MA, 2004.
18. NFPA 17A, *Standard for Wet Chemical Extinguishing Systems*, National Fire Protection Association, Quincy, MA, 2013.
19. NFPA 2010, *Standard for Fixed Aerosol Fire-Extinguishing Systems*, National Fire Protection Association, Quincy, 2010.
20. Harrington, J. "Application of Gaseous Agents to Special Hazards Fire Protection," *Fire Protection Handbook*, 20th edition, National Fire Protection Association, Quincy, MA 2008.
21. NFPA 45, *Standard on Fire Protection for Laboratories Using Chemicals*, National Fire Protection Association, Quincy, MA 2011.
22. "NFPA Glossary of Terms," National Fire Protection Association, Quincy, MA 2013.
23. FM Approvals Guide, http://www.approvalguide.com (Accessed August 2013)
24. Approval Standard for Carbon Dioxide Systems, Class Number 5420, FM Approvals, Norwood, MA, 2007.

Milosh Puchovsky P.E., FSFPE is Professor of Practice in the Department of Fire Protection Engineering at Worcester Polytechnic Institute in Worcester, MA, USA, where his efforts focus on the application, design, installation and maintenance of active and passive fire protection systems. His e-mail is milosh@wpi.edu.

Craig Hofmeister P.E., FSFPE, LEED AP is a Principle at the fire protection engineering firm The Fire Consultants, Inc., where he consults on a variety of project types including fire protection systems design and review, code compliance, and performance-based design/alternate design analysis. His e-mail is chofmeister@the-fireconsultants.com.

Design of Detection Systems

40

Robert P. Schifiliti, Richard L.P. Custer,
and Brian J. Meacham

Introduction

Fire detection and alarm systems are recognized as key features of a building's fire prevention and protection strategy. This chapter presents a systematic technique to be used by fire protection engineers in the design and analysis of detection and alarm systems. The majority of discussion is directed toward systems used in buildings. However, many of the techniques and procedures also apply to systems used to protect planes, ships, outside storage yards, and other nonbuilding environments.

Scientific research on fire growth and the movement of smoke and heat within buildings provides fire protection engineers with information and tools that are useful in the design of fire detection systems. Also, studies of sound production and transmission allow communication systems to be engineered, thus eliminating the uncertainty in locating fire alarm sounders. All of this information allows engineers and designers to design systems that meet specific, identifiable goals.

R.P. Schifiliti (✉)
Schifiliti Associates, Inc., Fire Protection Engineers, 297MA 01867, USA

R.L.P. Custer
Associates, Inc. Fire Protection Engineers, P.O. Box 297 Reading, MA 01867, USA

B.J. Meacham
Fire Protection Engineering and Architectural Engineering, Worcester Polytechnic Institute, 50 Prescott Street, MA 01609, Worcester

Previous chapters in this handbook introduced and discussed a series of concepts and tools for use by fire protection engineers. This chapter shows how some of these tools can be used collectively to design and evaluate detection and alarm systems.

A Note About Precision

When solving multiple equations with numerous variables from many sources, it is often easy to overlook the importance of precision and confidence in the final answer. This acknowledgment is particularly true since engineers have progressed from slide rulers to calculators to computers in a relatively short span of time. Most calculations in this chapter have been done using a computer—most often with a simple spreadsheet. The generally accepted practice for these types of tools is to round off only the final answer to the correct number of significant digits.

The standard and most widely taught rule for rounding is to round off using the same number of significant digits as the least precisely known number used in the calculation. An alternate rule suggests using one more significant figure than suggested by the standard rule. It has been shown that the alternate rule is more accurate and does not lead to loss of data as does the standard rule [1, 2]. The alternate rule for rounding has been used in this chapter. For more information or to refresh your knowledge of precision, rounding, and significant figures, consult the references or

M.J. Hurley (ed.), *SFPE Handbook of Fire Protection Engineering*,
DOI 10.1007/978-1-4939-2565-0_40, © Society of Fire Protection Engineers 2016

a standard text on engineering and scientific measurements.

Overview of Design and Analysis

To design a fire detection and alarm system, it is first necessary to establish the system's goals. These goals are established by model codes, the property owner, risk manager, insurance carriers, and/or the authority having jurisdiction. Ultimately, the goals of the system can be put in the following four basic categories:

1. Life safety
2. Property protection
3. Business protection
4. Environmental concerns

Some designers include heritage conservation in the list of goals. However, the protection of historic property is really another form of property and mission protection, although the methodology and extent for protection may vary.

When designing for life safety, it is necessary to provide early warning of a fire condition. The fire detection and alarm system must provide a warning early enough to allow complete evacuation of the danger zone before conditions become untenable. The fire detectors or fire alarm system may be used to activate other fire protection systems, such as special extinguishing systems and smoke control systems, that are used to help maintain a safe environment during a fire.

In some situations, the life safety mission of a detection system is enhanced by providing information to occupants. This situation is often the case in *stay-in-place* or *defend-in-place* strategies or partial evacuation/relocation strategies. The detection system is used to provide information about the location and extent of the fire. Instructions are then given to the target audience.

Property protection goals are principally economic. The objective is to limit damage to the building structure and contents. Maximum acceptable losses are established by the property owner or risk manager. The goal of the system is to detect a fire soon enough to allow manual or automatic extinguishment before the fire exceeds acceptable damage levels.

Goals for the protection of a mission or business are determined in a manner similar to that used in property protection. Here fire damages are limited to prevent undesirable effects on the business or mission. Some items that need to be considered are the effects of loss of raw or finished goods, loss of key operations and processes, and loss of business to competitors during downtime. Other concerns include the availability and lead time for obtaining replacement parts. If the equipment to be protected is no longer available or requires several months for replacement, the ability to stay in business during and after an extended period of downtime may be jeopardized.

Protection of the environment is also a fire protection concern. Two examples are (1) toxicity of products of combustion and (2) contamination by fire protection runoff water. Should large quantities of contaminants be expected from a large fire, the goal of the system may well be to detect a fire and initiate appropriate response prior to reaching a predetermined mass loss from burning materials or quantity of fire suppression agent discharged.

Once the overall goals have been set, specific performance and design objectives for a performance-based design can be established [3–5]. Performance-based fire protection design requires that specific performance objectives, rather than generic prescriptive requirements, be met. A typical prescriptive requirement would be to provide a smoke detector for every 84 m^2 (900 ft^2) or 9-m (30-ft) spacing. In prescriptive design, speed of detection and the fire size at detection for such an installation are not known or considered explicitly. In addition, if some action must be taken in response to the alarm in order to control the fire, the expected damage is also unknown.

Implementation of a fire safety performance objective requires that the objective be stated first by the client in terms of acceptable loss. The client loss objectives must then be (1) expressed in engineering terms that can be quantified using fire dynamics, and (2) related to design fires, design fire environments, and the performance characteristics of fire suppression equipment. For example, the client loss objective may be to prevent damage to essential electronic equipment in the compartment of origin. To meet this objective, one must first define what *damage* is. This

damage could be expressed in terms of the thickness of the smoke layer. Other criteria, such as temperature or concentration of corrosive combustion products, or a combination of criteria, could also be used.

Based on a study of the likelihood of ignition and fire growth scenarios, a design fire needs to be established. The design fire is characterized by its heat release rate, $\dot{Q}$, at any moment in time; its growth rate, dq/dt; a combustion product rate, dcp/dt, such as smoke particulate, toxic or corrosive species, and so forth; and production rate, dp/dt. The design fire may be determined by (1) a combination of small- and large-scale testing specific to the application or (2) analysis of data taken from studies reported in the literature.

For a given fire safety design objective, there will be a point, $\dot{Q}_{do}$, on the design fire curve where the energy and product release rates will produce conditions representative of the design objective. Given that there will be delays in detecting the fire, notifying the occupants, accomplishing evacuation, or initiating suppression actions, the fire will need to be detected at some time in advance of $\dot{Q}_{do}$. In order to account for these delays, a critical fire size, $\dot{Q}_{cr}$, can be defined as the point on the design fire curve at which the fire must be detected in order to meet the design objectives for a given spacing or radial distance from the fire.

There are two types of delays that influence the size of the fire at detection: (1) those that are variable and (2) those that are fixed. Variable delays represent transport lag and are related to radial distance of the detector from the fire, ceiling height, and the convective heat release rate of the fire. Fixed delays are associated with system characteristics, such as alarm verification time. Adding the fixed delays to $\dot{Q}_{cr}$ defines another point on the design fire curve: $\dot{Q}_i$ or the *ideal* fire; that is, the fire that would be detected with no transport delay.

The design fire, $\dot{Q}_{do}$, has been defined as the fire size (in terms of peak heat release and given growth rate history) that corresponds to the maximum acceptable loss fire, and the critical fire, $\dot{Q}_{cr}$, as the maximum fire size at time of detection that allows actions to be taken to limit the continually growing fire to the design fire limit. The time needed to take the limiting actions is the response lag. The total system response time, then, is the amount of time required between the critical fire and the design fire for all the actions to take place before $\dot{Q}_{do}$ is reached, and is the sum of the fixed and variable delays and the response lag. The various design and evaluation points on a design fire curve are shown in Fig. 40.1.

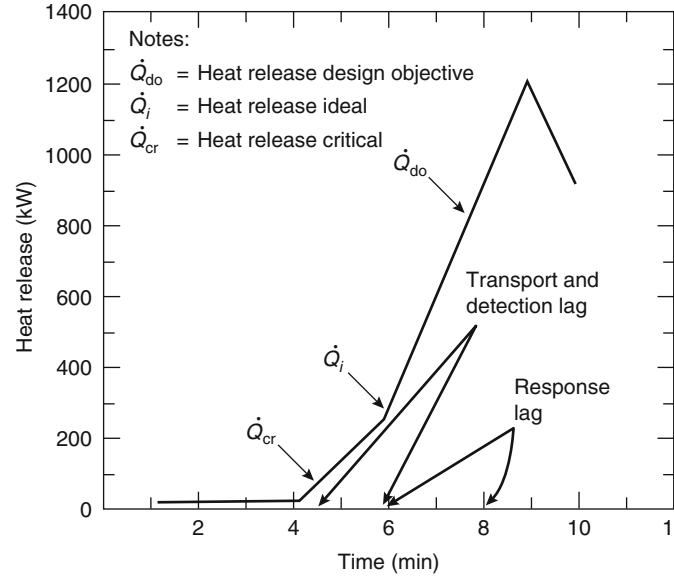

Fig. 40.1 Design fire curve

For example, if the design fire is determined to be 1500 kW and manual suppression will be employed, the critical fire can be selected at a moment in time that permits detection, notification, and response before the 1500 kW fire size is reached. If the total system response time is estimated to be 3 min, the critical fire would be at the size determined at 3 min prior to reaching 1500 kW using the estimated fire growth rate.

Expressing fire size or fire load as an energy release and growth rate may be thought of in the same way that structural engineers use earthquake zone maps to design for potential earthquakes. Electrical engineers might compare fire loads to fault currents used in designing overcurrent protection devices. At the present time, design fire, critical fire, and total system response time requirements are not established by any building codes. It is the job of the design engineer to work with the building owner and local code officials to establish the performance requirements for a given system application.

Once the goals of a system have been established, several probable fire scenarios should be outlined. The occupancy of the building and the expected fuels should be analyzed to establish an expected fire growth rate and an expected maximum heat release rate. Fire loss reports and fire test data can be used to help estimate heat release rates and the production of smoke and fire gases. It is important that different fire scenarios be evaluated to establish how the system design or response might change as a result of varying fire conditions. Several possible fire scenarios should be outlined using the techniques presented elsewhere in this handbook.

When designing a system, select the most likely fire scenario as the basis of the design. Once the design requirements for spacing and detector type are established, the system's response can be analyzed using the other possible fire scenarios. If the alternate fire scenarios cause the design not to meet the established goals, design changes can be made and retested, if warranted.

The several fire scenarios used when analyzing a system will produce upper and lower bounds or a range of system performance characteristics. The fire scenarios selected should include best- and worst-case fires as well as several likely scenarios for the particular building characteristics and occupancy.

For the purposes of design or analysis, detection and alarm systems have three basic elements: detection, processing, and signaling. The first, detection, is that part of the system that senses fire. The second element involves the processing of signals from the detection portion of the system. Finally, the processing section of the system activates the signaling portion in order to alert occupants and perform other auxiliary signaling operations. Auxiliary functions may include smoke control, elevator capture, fire department signaling, and door closing.

This chapter focuses on the detection and signaling elements of a fire alarm system. Engineering methods for the design and analysis of heat detector response are presented along with several examples. A method to calculate the audibility of fire alarm sounders is also presented. The selection of a system's control panel and the design of auxiliary functions is beyond the scope of this chapter.

Detection

To design the detection portion of a fire alarm system, it is necessary to determine where fire detectors should be placed in order to respond within the goals established for the system. Several different detector types might respond to the expected fire, so it may be necessary to develop several candidate system designs, using various combinations of detector types in order to optimize the system's performance and cost.

A fire signature [6] is some measurable or sensible phenomenon present during combustion. Table 40.1 is a cross-reference of fire signatures and commercially available detector types. The table shows the predominant fire signature to which the detector responds.

Table 40.1 Fire signatures and commercially available detectors

Fire signature/ detector type	Electromagnetic radiation wave length 1700–2900 angstroms	Electromagnetic radiation (thermal) 6500–8500	Invisible products of combustion less than 0.1 μm	Visible smoke and products of combustion more than 0.1 μm	Rapid change in temperature	High temperature
Ultraviolet detector	X	—	—	—	—	—
Infrared detector	—	X	—	—	—	—
Submicron particle detector						
Wilson cloud chamber	—	—	X	—	—	—
Infrared particle detector	—	—	—	—	—	—
Smoke detector						
Photoelectric	—	—	—	X	—	—
Ionization	—	—	X	—	—	—
Photo beam	—	—	—	X	—	—
Rate-of-rise heat detector	—	—	—	—	X	—
Rate anticipation heat detector	—	—	—	—	—	X
Fixed temperature heat detector	—	—	—	—	—	X

Heat Detection

This section discusses an engineering method for determining the placement of heat detectors on a large flat ceiling.

The present practice in designing fire detection systems using heat detectors is to space the detectors at intervals equal to spacings established by tests at Underwriters Laboratories Inc. Listed spacings are determined in full-scale fire tests [7].

In the Underwriters Laboratories Inc. (UL) test, a burning pan of 190-proof denatured alcohol is located in the center of a test room. Sprinkler heads having a 160 °F (71 °C) rated operating temperature are located on the ceiling in a square array having 10 ft (3 m) sides. The fire is in the center of the square. The distance between the fire and the ceiling is varied so that the 160 °F (71 °C) sprinkler head being used operates in approximately 2 min.

As shown in Fig. 40.2, detectors of the type being tested are located at the corners of squares having 20, 30, 40, and 50 ft (6.1, 9.1, 12.2, and 15.2 m) sides. The spacing of the last detector to operate prior to a sprinkler head operating becomes the detector's listed spacing. A similar test procedure is employed by Factory Mutual Research Corporation (FMRC) to arrive at an approved detector spacing.

Most codes require that detectors be spaced at intervals equal to the UL or FMRC spacing. *NFPA 72®*, *National Fire Alarm Code®* [8], 2007 edition, requires that the installed spacing be less than the listed spacing to compensate for high ceilings, beams, and air movement. High ceilings mean that the fire plume will entrain more ambient air as it rises. This condition has the effect of cooling the gases and reducing the concentration of fire products. Beams, joists, walls, or sloped ceilings alter the flow of combustion products. This situation can serve to restrict or enhance the operation of a fire

detector. For instance, consider the case where a fire detector is located on a ceiling between two parallel beams and a fire occurs at floor level between the beams. If the distance between the beams is small compared to the horizontal distance from the fire to the detector, the beams will act as a channel directing the flow of hot gas to the detector, thus speeding operation. *NFPA 72* allows detector spacing to be increased beyond the listed spacing in areas, such as corridors, with narrow walls to confine the smoke and heat produced by the fire. Systems can be designed using this type of code approach; however, this approach will not permit quantitative assessment of detector response or measure the ability of a given system design to meet specific design goals relating to fire size, allowable damage, or hazard.

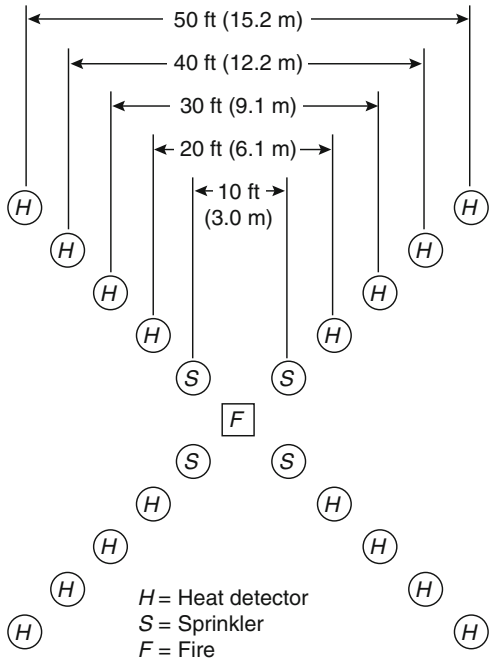

Fig. 40.2 Detector test layout

The best possible location for a heat detector is directly over the fire. If there are specific hazards to be protected, the design should include detectors directly overhead or inside of the hazard. In areas without specific hazards, detectors should be spaced evenly across the ceiling. When detectors are evenly spaced, as shown in Fig. 40.3, the point that is farthest from any detector will be in the middle of four detectors. The spacing between detectors is

$$S = 2^{1/2}r \tag{40.1}$$

For a given detector, the problem is to determine the maximum distance the detector can be located from the fire and still respond within the

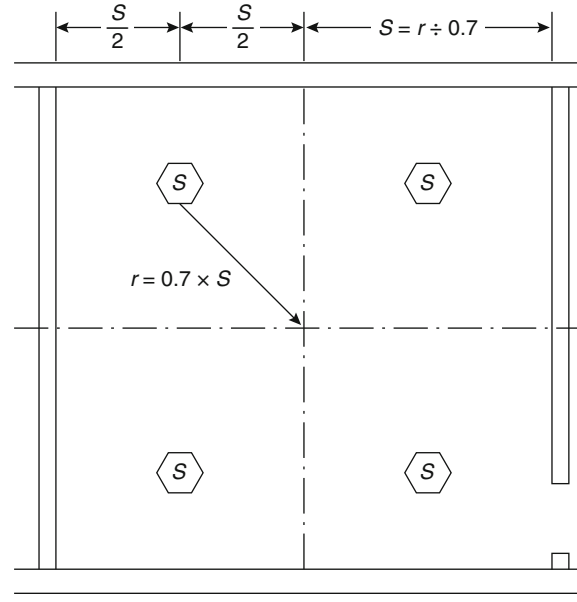

Fig. 40.3 Detector spacing

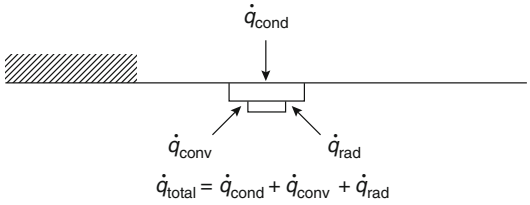

Fig. 40.4 Heat transfer to a ceiling-mounted detector

design goals of the system. This determination requires a method for predicting detector response, based on fire size and growth rate, ceiling height, and detector characteristics.

Fire plume and ceiling-jet models can be used to estimate the temperature and velocity of fire gases flowing past a detector. The heat transfer can be calculated, and the response of the detector can be modeled.

Figure 40.4 describes the heat transfer taking place between a heat detector and its environment. The total heat transfer rate to the unit, $\dot{q}_{\text{ltotal}}$, can be expressed by the relationship

$$\dot{q}_{\text{total}} = \dot{q}_{\text{cond}} + \dot{q}_{\text{conv}} + \dot{q}_{\text{rad}} (\text{kW or Btu/s}) \tag{40.2}$$

where

$\dot{q}_{\text{cond}}$ = Conduction
$\dot{q}_{\text{conv}}$ = Convection
$\dot{q}_{\text{rad}}$ = Radiation heat transfer rates

During the initial stage of fire growth, radiation heat transfer can be neglected. Also, the elements of most commercially available heat detectors are thermally isolated from the remainder of the unit. In these cases, it can be assumed that the heat lost from the heat-sensitive element by conduction to other parts of the detector, and to the ceiling by conduction, is negligible in comparison to the convection heat transfer taking place. This exclusion leaves a net rate of heat transfer to the detector equal to $\dot{q}_{\text{conv}}$. The convective heat transfer rate to the detector is described by

$$\dot{q} = q_{\text{conv}} = hA\left(T_g - T_d\right) \ (\text{kW or Btu/s}) \tag{40.3}$$

where

h = Convective heat transfer coefficient in kW/(m^2 · °C) or Btu/(sft^2 · °F)
A = Area being heated
T_d = Detector temperature
T_g = Temperature of the gas heating the detector

Treating the detector element as a lumped mass, m (kg or lbm), the change in its temperature is found by

$$\frac{dT_d}{dt} = \frac{\dot{q}}{mc} \text{deg/s} \tag{40.4}$$

where c is the specific heat of the element being heated and has units of kJ/(kg · °C) or Btu/(lbm · °F) and $\dot{q}$ is the heat transfer rate. This equation leads to the following relationship for the change in temperature of the detector with respect to time:

$$\frac{dT_d}{dt} = \frac{hA\left(T_g - T_d\right)}{mc} \tag{40.5}$$

Heskestad and Smith [9] have proposed use of a time constant, τ, to describe the convective heat transfer to a particular detector element:

$$\tau = \frac{mc}{hA} \text{s} \tag{40.6}$$

$$\frac{dT_d}{dt} = \frac{T_g - T_d}{\tau} \tag{40.7}$$

Note that is a function of the mass, area, and specific heat of the particular detector element being studied. For a given fire-gas temperature and velocity and a particular detector design, an increase in mass increases τ. A larger τ results in slower heating of the element.

The convective heat transfer coefficient, h, is a function of the velocity of the gases flowing past the detector element and the shape of the detector element. For a given detector, if the gas velocity is constant, h is constant. It has been shown [10] that the convective heat transfer coefficient for spheres, cylinders, and other objects similar to a sprinkler or heat detector element is approximately proportional to the square root of the Reynolds number, Re:

$$\text{Re} = \frac{ud}{v} \tag{40.8}$$

where
u = Gas velocity
d = Diameter of a cylinder or sphere exposed to convective heating
v = Kinematic viscosity of the gas

For a given detector, this equation means that h and, hence, τ, is approximately proportional to the square root of the velocity of the gases passing the detector. This relationship can be expressed as a characteristic response time index, RTI, for a given detector:

$$\tau u^{1/2} \simeq \tau_0 u_0^{1/2} = \text{RTI} \qquad (40.9)$$

Thus, if τ_0 is measured in the laboratory at some reference velocity u_0, this expression is used to determine the τ at any other gas velocity, u, for that detector. The product, $\tau^{1/2}$, is the response time index, RTI.

The use of RTI as a heat transfer function is a simplification. The determination of RTI assumes that τ (and, therefore, h) is proportional to the square root of the gas velocity, regardless of the magnitude of the velocity. The flow of gases past irregularly shaped objects such as detectors and sprinklers is very complex. Even the flow past cylinders is too complex to use a simple relationship for the heat transfer coefficient (i.e., constant RTI). Hollman showed that the heat transfer coefficient (and, therefore, τ) is actually proportional to the Reynolds number raised to a fractional power, n, that varies from 0.330 to 0.805 depending on the value of the Reynolds number [10]. For values of Re between 40 and 4000, which is probably the range for most fire detection scenarios, the value of n is given as 0.466. This value is close to 0.5 (square root), but may explain some of the variation found in the experimental determination of τ and RTI.

Plunge tests performed on a variety of heat detectors by Bissell [11] show variations in τ and RTI, whereas other tests produced reasonable results for a variety of test parameters. It is possible that further analysis may show that an RTI based on $n = 0.5$ is reasonable and that the potential errors are insignificant in the context of fire and detector modeling. On the contrary, it may be found that some other value for n produces better results.

The exponent n may vary over ranges of Reynolds numbers less than those reported by Hollman. Some detector geometries are aerodynamically designed to channel fire gases to the detector element. The ability to affect the gas flow is a function of both the flow velocity and whether the flow is turbulent or laminar. These effects introduce additional variables that complicate the determination of a heat transfer function.

An added source of error in heat transfer modeling is that the temperature-sensing element of a heat detector is never completely isolated from the detector body. This setup results in conductive heat loss that may not be accounted for when using only one time constant. Kokkala has shown that for some detectors as much as 10 % of the heat gained by convection is lost by conduction to the detector body [12]. A two-time-constant approach, similar to the C parameter used in modeling the response of sprinkler heads, is suggested by Kokkala. In a plunge test, the velocity may be high enough so that the conduction heat loss is negligible when compared to the heat gain by convection. In actual fire conditions, this conduction heat loss may contribute to the variation in RTI as it is currently used.

The magnitude of the potential error resulting from the assumption that RTI is constant has not been investigated. Future research and analysis should also consider the possibility that it might be best to test and report several discrete values for τ (hence, h) [13]. An example is using a plunge test to find τ at three different velocities. The slow, medium, and fast velocities should be representative of the range of possible fire-gas velocities.

A continuous curve of τ versus u for every model detector would be ideal. However, the economic feasibility of testing must be considered. At the present time, heat detectors are tested in ovens to determine their operating temperatures and are tested in full-scale fire tests to determine their listed spacing (relative sensitivity). A single oven could be used to test for operating temperature and τ at several different velocities as discussed above. This type of

testing would be more repeatable (precise), have a lower environmental impact, and give results that can be directly used by engineers in performance-based analysis and design. The test data could be used to calculate a listed spacing comparable to that determined in the present full-scale test so that current code-based design methods could continue to be used.

The remainder of the calculations in this chapter will be made using RTI as a heat transfer function. The user will readily see how other functions, when available, can be incorporated into the equations to effect other solutions.

Heskestad and Smith [9] developed a test apparatus at Factory Mutual Research Corporation to determine the RTI of sprinkler heads. In the test, called a *plunge test*, the sprinkler head is suddenly lowered into the flow of a hot gas. The temperature and velocity of the gas are known and are constant during the test. The equation for the change in the detector temperature is then

$$\frac{dT_d}{dt} = \left(\frac{1}{\tau}\right)\left(T_g - T_d\right) \tag{40.10}$$

Since the gas temperature is constant during the test, the solution to this equation is

$$T_d - T_g = \left(T_g - T_a\right)\left[1 - \exp\left(\frac{-t}{\tau}\right)\right] \tag{40.11}$$

where T_a is the ambient, or initial, temperature of the sprinkler or detector at time $t = 0$. T_d is the temperature of the detector at time t. Rearranging the equation gives

$$\tau = \frac{t}{\ln\left[\left(T_g - T_a\right)/\left(T_g - T_d\right)\right]} \tag{40.12}$$

By measuring the response time, t_r, of the unit in the plunge test, this equation can be used to calculate τ_0 at the test velocity u_0. This calculation is done by substituting the response temperature and time for T_d and t. The sensitivity of the detector or sprinkler can then be expressed as

$$\tau_o(at\,u_0) = \frac{t}{\ln\left[\left(T_g - T_a\right)/\left(T_g - T_r\right)\right]}(s) \tag{40.13}$$

In terms of the response time index, this equation becomes

$$\mathrm{RTI} = \frac{t_r u_0^{1/2}}{\ln\left[\left(T_g - T_a\right)/\left(T_g - T_r\right)\right]} \tag{40.14}$$

The RTI has units of $\mathrm{m}^{1/2}\mathrm{s}^{1/2}$ or $\mathrm{ft}^{1/2}\mathrm{s}^{1/2}$.

A plunge test can be used to determine the RTI for a heat detector or a sprinkler. Knowing the RTI, the change in temperature of similar units can be calculated for any history of fire gases flowing past it. The form of the heat transfer equation is

$$\frac{dT_d}{dt} = \frac{u^{1/2}\left(T_g - T_d\right)}{\mathrm{RTI}} \tag{40.15}$$

This equation is used to calculate the temperature of a fixed-temperature heat detector or sprinkler exposed to fire gases. The equation can be used to determine the time at which the unit reaches its operating temperature.

The use of a lumped mass model may not hold for rate-of-rise heat detectors and rate-compensated heat detectors. The heat transferred to a fixed-temperature heat detector either heats a sensing element until it melts, or it heats two dissimilar metals of a snap disk. In each case, the element itself is exposed to the hot gases. This result is not true for rate-of-rise heat detectors or rate-compensated heat detectors.

Most commercial rate-of-rise heat detectors operate when the expansion of air in a chamber exceeds the rate at which the air can escape through a small vent hole. For this type of detector, it is also necessary to model heat transfer from the detector body to the air in its chamber. Then the expansion of the air and its escape through a vent hole must be accounted for. The response time index determined in a plunge test may not be constant as fire-gas velocities or temperatures vary. Hence, RTI is only an approximation of how the detector responds. Also, it has been hypothesized, but not tested, that rate-of-rise detectors may be modeled by simply comparing the rate of change of gas temperature to their rated response threshold [13]. This hypothesis may be true since their rated response in

degrees per minute or degrees per second is actually the measured rate of gas temperature change in the test apparatus. Thus, it would be expected that if the velocity of the fire gases was on the same order of magnitude as in the test, the rate of change of gas temperature would be the measure for detector response.

A rate-compensated detector consists of a metallic shell surrounding two bowed metal struts. There are electrical contacts on the struts. The struts and shell expand at different rates as the detector is heated. When heated fast, the outer shell expands and causes the bowed struts to straighten and close the contacts, signaling an alarm. This condition usually occurs at temperatures below the rated operating temperature. However, if the unit is heated more slowly, the difference between the expansion rates of the inner and outer parts is such that the contacts close at or near the unit's rated temperature. For rates of temperature rise up to approximately 22 °C/min (40 °F/min), rate-compensated detectors tend to respond when the surrounding gas temperature reaches the unit's rated operating temperature [14].

Obviously, the rate-compensated type of heat detector cannot be treated as a lumped mass when calculating its response to a fire. However, at rates of temperature rise less than approximately 22 °C/min (40 °F/min), they can be modeled by simply assuming that they respond when the surrounding gas temperature reaches their operating temperature.

From the discussion above, it is evident that the response of fixed-temperature heat detectors can be modeled. It is necessary to know the temperature at which the detector is rated to operate. For rate-of-rise heat detectors, it is necessary to know the rate of change in the detector's temperature at which it will alarm. The RTI or τ_0 and u_0 for the detector are also needed.

In order to calculate the response of a heat detector, it is necessary to know the temperature and velocity of the gases flowing past it. Some fire plume models or ceiling-jet models may give functional relationships for temperature and velocity that can be substituted into the heat transfer equation and integrated. Other models may not be suitable for an analytical solution. In this case, the fire model should be used to produce data on time-versus-temperature and time-versus-gas velocities. These data can then be used to numerically solve the detector heat transfer equation.

Most fire and ceiling-jet models do not model the temperature and velocity profile as a function of distance from the ceiling. This lapse introduces error and uncertainty in the results. Marrion [15] showed that maximum temperature and velocity occurs between 1 and 3 in. (25 and 76 mm) below the ceiling for small (5- to 7-in. [127- to 178-mm] diameter) gasoline pan fires with a ceiling clearance of about 14 ft (4.3 m). Others have reported maximums at a distance down from the ceiling of approximately one-tenth the distance from the fuel to the ceiling. Alpert [16] reports ceiling-jet thickness to be approximately 5–12 % of the ceiling to fuel distance. Users are cautioned when modeling detector mechanisms that are not within this range.

When the responses of multiple detectors or sprinklers are modeled, no provisions are made to account for sprinkler spray cooling of the room and, therefore, the activation of additional elements (beyond the first) may be inaccurately predicted. For more information on this topic the reader is referred to the references for works by Cooper [17], Delichatsios and Alpert [18], and Heskestad [19].

Heat Detection: Steady-State Fires

Alpert [16] presented the following series of equations to calculate temperature and velocity of fire gases in a ceiling jet as a function of heat release rate and position for steady-state fires:

$$T_g - T_a = \frac{\left[5.38\left(\dot{Q}/r\right)^{2/3}\right]}{H}\,^{\circ}\mathrm{C} = \frac{\left[4.74\left(\dot{Q}/r\right)^{2/3}\right]}{H}\,^{\circ}\mathrm{F}$$

where $r/H > 0.18$, and

$$T_g - T_a = \frac{\left[16.9\dot{Q}^{2/3}\right]}{H^{5/3}}\,^{\circ}\mathrm{C} = \frac{\left[14.9\dot{Q}^{2/3}\right]}{H^{5/3}}\,^{\circ}\mathrm{F}$$

where $r/H \leq 0.18$, and

$$u = \frac{\left(0.20\dot{Q}^{1/3}H^{1/2}\right)}{r^{5/6}}\,\mathrm{m/s} = \frac{\left(0.25\dot{Q}^{1/3}H^{1/2}\right)}{r^{5/6}}\,\mathrm{ft/s}$$

where $r/H > 0.15$, and

$$u = 0.95\left(\frac{\dot{Q}}{H}\right)^{1/3}\mathrm{m/s} = 1.2\left(\frac{\dot{Q}}{H}\right)^{1/3}\mathrm{ft/s}$$

where $r/H \leq 0.15$.

In the above series of equations,

T_g = Maximum, near ceiling, fire-gas temperature in °C or °F

T_a = Ambient temperature in °C or °F

$\dot{Q}$ = Total heat release rate of the fire in kW or BTU/min

r = Radial distance from the axis of the fire plume in m or ft

H = Height above the origin of the fire in m or ft

u = Maximum, near ceiling, fire-gas velocity in m/s or ft/s

This model assumes that the temperature and velocity of the fire gases at a point away from the source are related to the instantaneous heat release rate of the fire. This assumption neglects the time required for transport of the fire gases from the source to the detector. Also, because the correlations are based on the total heat release rate rather than only the convective heat release rate, errors will be introduced when the convective fraction differs from that in the tests used to develop the correlations.

For a constant gas temperature and constant gas velocity, the basic heat transfer equation can be solved:

$$\frac{dT_d}{dt} = \frac{T_g - T_d}{\tau}$$

$$dT_d = \int_0^t \frac{1}{\tau}\left(T_g - T_d\right)dt$$

$$\Delta T_d = T_d - T_a - \left(T_g - T_a\right)\left[1 - \exp\left(\frac{-t}{\tau}\right)\right]^{\circ}\mathrm{C} \tag{40.7}$$

or, substituting the equation for RTI

$$\Delta T_d = T_d - T_a = \left(T_g - T_a\right)\left[1 - \exp\left(\frac{-tu^{1/2}}{\mathrm{RTI}}\right)\right]^{\circ}\mathrm{C}$$

The response of heat detectors to fires with ceiling jets having a near constant gas temperature and velocity can be modeled using the above equations.

Heat Detection, Growing Fires, and Quasi-Steady-State Modeling

A growing fire can be modeled by assuming the fire to be composed of a series of increasing steady heat release rates. This model is referred to as quasi-steady-state modeling. The first step is to break the heat release rate curve into a series of small time intervals. For each interval, use the average heat release rate for that interval to calculate the fire-gas temperature and velocity. Then, starting at ambient temperature, calculate the change and resulting temperature of the detector at the end of the first interval. Using that new detector temperature at the start of the next interval, use the next gas temperature and velocity to calculate the detector temperature at the end of the interval. Continue until you have reached the time of interest or until the detector temperature exceeds its operating temperature.

Example 1 A stack of wood pallets is burning under a flat ceiling that is 6 m high. Table 40.2, showing heat release rates, is given below. The ambient temperature is 20 °C. What would be the temperature of a ceiling-mounted heat detector having an RTI of 55 $\mathrm{m}^{1/2} \cdot \mathrm{s}^{1/2}$ after a 180-s exposure if it were located 6 m from the center of the plume?

Solution The detector is located in the developed ceiling jet. The first step is to calculate the change in temperature and the velocity for each heat release rate in the table. For the period 0 to 10 s, the heat release rate is given as 5 kW. The change in temperature and the velocity of the ceiling jet at the detector are

Table 40.2 Example 1: heat release rates

Δt	$\dot{Q}$	Δt	$\dot{Q}$
0	0	100	469
10	5	110	567
20	19	120	675
30	42	130	792
40	75	140	919
50	117	150	1055
60	169	160	1200
70	230	170	1355
80	300	180	1519
90	380		

$$T_g - T_a = \frac{\left[5.38\left(\frac{\dot{Q}}{r}\right)^{2/3}\right]}{H}\,^{\circ}\mathrm{C}$$

$$T_{g,1} - T_a = \frac{\left[5.38\left(\frac{5}{6}\right)^{2/3}\right]}{6} = 0.794^{\circ}\mathrm{C}$$

$$T_{g,1} = 20.794^{\circ}\mathrm{C}$$

$$u = \frac{\left(0.20\dot{Q}^{1/3}H^{1/2}\right)}{r^{5/6}}\,\mathrm{m/s}$$

$$u_1 = \frac{\left[0.20(5)^{1/3}(6)^{1/2}\right]}{6^{5/6}} = 0.188\,\mathrm{m/s}$$

Next calculate the change in detector temperature ΔT_d as a result of that exposure by assuming the temperature and velocity to be steady over short intervals;

$$\frac{dT_d}{dt} = \frac{T_g - T_d}{\tau} = \frac{u^{1/2}\left(T_g - T_d\right)}{\mathrm{RTI}}$$

$$\Delta T_d = T_{d,n} - T_{d,n-1} = \frac{u_n^{1/2}\left(T_{g,n} - T_{d.n-1}\right)}{\mathrm{RTI}}\Delta t^{\circ}\mathrm{C}$$

$$T_{d,n} = \left[\frac{u^{1/2}\left(T_{g,n} - T_{d,n-1}\right)}{\mathrm{RTI}}\Delta t\right] + T_{d,n-1}{}^{\circ}\mathrm{C}$$

Initially, the detector is not exposed to hot gases and is at ambient temperature. For the first step or interval, the detector is exposed and the resulting detector temperature at the end of the interval ($T_{d,1}$) is calculated:

$$T_{d,1} = \left[\frac{u^{1/2}\left(T_{g,1} - T_{d,0}\right)}{\mathrm{RTI}}\Delta t\right] + T_{d,0}{}^{\circ}\mathrm{C}$$

$$T_{d,1} = \left[\frac{(0.188)^{1/2}(20.794 - 20)}{50}10\right] + 20$$

$$= 20.063^{\circ}\mathrm{C}$$

To simplify the process, set up a table or a spreadsheet, as shown in Table 40.3, to complete the calculations. Rounding to two significant digits is done last.

After 180 s of exposure, the detector temperature is approximately 46 °C. If the detector were rated at 57 °C, it would not have responded.

Heat Detection: Potential Errors: Steady-State and Quasi-Steady-State Modeling

There are many sources of potential error in these calculations. These include uncertainty in the operating temperature, uncertainty in the ambient temperature, and inaccuracies in the fire-gas temperature and velocity correlations. Because the magnitude of these potential errors is unknown or unreported, a tolerance or confidence interval for the answer cannot be estimated.

In addition, it has been assumed that use of the ceiling-jet model is valid for the previous example. The model assumes an infinite ceiling for the ceiling jet to flow outward without encountering walls and developing a layer. In the example, the velocity of the ceiling jet for each interval can be used to estimate the approximate position of the leading edge of the ceiling jet. If the ceiling jet is a sufficient size to have reached the bounding walls or draft curtains in a space, a layer will begin to develop. This analysis can be used as a test to determine if additional error is possible because limitations of the model have been exceeded.

Evans and Stroup [20] published a computer program called DETACT-QS, which uses Alpert's equations to calculate the response of heat detectors. That program requires the

Table 40.3 Example 1: spreadsheet calculations

Step, n	t	Q	ΔT_g	T_g	u	ΔT_d	T_d
0	0	0	0	—	0	0	20
1	10	5	0.794	20.794	0.188	0.063	20.063
2	20	19	1.934	21.934	0.294	0.184	20.247
3	30	42	3.281	23.281	0.383	0.341	20.588
4	40	75	4.830	24.830	0.464	0.525	21.114
5	50	117	6.496	26.496	0.538	0.718	21.832
6	60	169	8.301	28.301	0.609	0.918	22.749
7	70	230	10.194	30.194	0.674	1.112	23.861
8	80	300	12.170	32.170	0.737	1.297	25.158
9	90	380	14.247	34.247	0.797	1.476	26.633
10	100	469	16.393	36.393	0.855	1.641	28.274
11	110	567	18.603	38.603	0.911	1.792	30.066
12	120	675	20.896	40.896	0.965	1.935	32.001
13	130	792	23.246	43.246	1.018	2.063	34.064
14	140	919	25.669	45.669	1.070	2.183	36.247
15	150	1055	28.143	48.143	1.120	2.289	38.536
16	160	1200	30.666	50.666	1.170	2.385	40.921
17	170	1355	33.252	53.252	1.218	2.474	43.396
18	180	1519	35.884	55.884	1.265	2.554	45.950

following input: ceiling height, H; ambient temperature, T_a; distance from fire axis to detector, r; detector response or activation temperature, T_r; and detector response time index (RTI). The user must also input history of time versus heat release rate for the fire. The program uses the quasi-steady-state method demonstrated above to calculate the detector response.

Heat Detection: Power-Law Fires

Heskestad and Delichatsios [8] presented functional relationships for modeling the temperature and velocity of fires whose heat release rates grow according to the power-law relationship:

$$\dot{Q} = \alpha t^p \text{ kW}$$

where

α = Constant for a particular fuel describing the growth of the fire (kW/s^2)
t = Time (s)
p = Positive exponent
$\dot{Q}$ = Heat release rate (kW)

NFPA 72, Appendix B, uses a constant called the *fire growth time*, t_g, in lieu of α to describe the fire intensity. The fire growth time is defined as the time at which a power-law fire would reach a heat release rate of 1055 kW (1000 Btu/s). In terms of t_g, the power-law equation becomes

$$\dot{Q} = \left(\frac{1055}{t_g^2}\right) t^p \text{ kW}$$

The nondimensional functional relationships given by Heskestad and Delichatsios [21] for temperature and velocity of fire gases in a ceiling jet are

$$u_p^* = \frac{u}{\left(A^{1/(3+p)} \alpha^{1/(3+p)} H^{(p-1)/(3+p)}\right)}$$
$$u_p^* = f\left(t_p^*, \frac{r}{H}\right) \tag{40.16}$$

$$\Delta T_p^* = \frac{\Delta T}{A^{2/(3+p)} (T_a/g) \alpha^{2/(3+p)} H^{-(5-p)/(3+p)}}$$
$$\Delta T_p^* = g\left(t_p^*, \frac{r}{H}\right) \tag{40.17}$$

where

$$A = \frac{g}{C_p T_a \rho_o} \tag{40.18}$$

$$t_p^* = \frac{t}{A^{-1/(3+p)} \alpha^{-1(3+p)} H^{4/(3+p)}} \tag{40.19}$$

All variables are described in this chapter's nomenclature section.

For $p = 2$ power-law fires, the above nondimensional equations reduce to the following:

$$u_2^* = \frac{u}{\left(A^{1/5} \alpha^{1/5} H^{1/5}\right)}$$

$$\Delta T_2^* = \frac{\Delta T}{A^{2/5} (T_a/g) \alpha^{2/5} H^{-3/5}}$$

$$t_2^* = \frac{t}{A^{-1/5} \alpha^{-1/5} H^{4/5}}$$

Heskestad and Delichatsios [21] presented correlations to the functional relationships for fires whose release rates vary according to the power-law equation, with $p = 2$. These fires are referred to as t^2 fires. It has been shown [22, 23] that the $p = 2$ power-law fire growth model can be used to model the heat release rate of a wide range of fuels. The original correlations were used in several publications and popular calculation programs for ceiling-jet and heat-detector modeling, including the first two editions of this handbook [8, 9, 20, 23–26].

Subsequently Heskestad and Delichatsios found that an incorrect value for the heat of combustion of wood resulted in the correlations being in error. All examples in this chapter that use these correlations have been updated or replaced. The corrected data correlations are as follows: [27]

$$t_{2f}^* = 0.861 \left(1 + \frac{r}{H}\right)$$

t_{2f}^* is the nondimensional time at which the heat front reaches the detector. When $t_2^* < t_{2f}^*$, the heat front has not reached the detector position. Therefore, $\Delta T_2^* = 0$.

For $t_2^* < t_{2f}^*$,

$$\Delta T_{2f}^* = \left[\frac{\left(t_2^* - t_{2f}^*\right)}{(0.146 + 0.242 r/H)}\right]^{4/3}$$

This relationship may also be expressed as

$$\Delta T_2^* = \left[\frac{\left(t_2^* - t_{2f}^*\right)}{D}\right]^{4/3}$$

where

$$D = 0.146 + 0.242 \frac{r}{H}$$

$$\frac{u_2^*}{\left(\Delta T_2^*\right)^{1/2}} = 0.59 \left(\frac{r}{H}\right)^{-0.63}$$

The above correlations assume that the convective heat release rate is approximately 75 % of the total heat release rate.

When the convective fraction differs from 75 %, the following equations are more useful forms and are used with the nondimensional equations for ΔT_2^* and u_2^* by first multiplying α by the convective fraction X: [2]

$$\begin{aligned} \alpha_c &= X\alpha \ \text{kW/s}^2 \\ t_{2f}^* &= 0.813 \left(1 + \frac{r}{H}\right) \end{aligned} \tag{40.20}$$

When $t_2^* < t_{2f}^*$ $\Delta T_2^* = 0$

For $t_2^* \le t_{2f}^*$,

$$\Delta T_2^* = \left[\frac{\left(t_2^* - t_{2f}^*\right)}{(0.126 + 0.210 r/H)}\right]^{4/3} \tag{40.21}$$

This may also be expressed as

$$\Delta T_2^* = \left[\frac{\left(t_2^* - t_{2f}^*\right)}{D}\right]^{4/3}$$

where

$$D = 0.126 + 0.210 \frac{r}{H} \tag{40.22}$$

$$\frac{u_2^*}{\left(\Delta T_2^*\right)^{1.2}} = 0.59 \left(\frac{r}{H}\right)^{-0.63} \tag{40.23}$$

Beyler found that these correlations for temperature and velocity could be substituted into the heat transfer equation and integrated [28].

Beyler's analytical solution was published in *Fire Technology* [29] and is repeated here.

The analytical solution for the instantaneous rate of change of detector temperature is

$$\frac{dT_d(t)}{dt} = \frac{4}{3}\frac{\Delta T}{\Delta T_2^*}\Delta T_2^{*1/4}\frac{(1-e^{-\gamma})}{(t/t_2^*)D} \tag{40.24}$$

The analytical solution for change in detector temperature is

$$\begin{aligned}\Delta T_d &= T_d(t) - T_d(0) \\ &= \frac{\Delta T}{\Delta T_2^*}\Delta T_2^*\left[1 - \frac{(1-e^{-\gamma})}{\gamma}\right]\end{aligned} \tag{40.25}$$

where

$$\gamma = \frac{3}{4}\sqrt{\frac{u}{u_2^*}}\sqrt{\frac{u_2^*}{(\Delta T_2^*)^{1/2}}}\left(\frac{\Delta T_2^*}{\mathrm{RTI}}\right)\left(\frac{t}{t_2^*}\right)D \tag{40.26}$$

and as previously defined,

$$D = 0.126 + 0.210\frac{r}{H} \tag{40.22}$$

In a design situation, the objective is to determine the spacing of detectors required to respond to a specific fire scenario. The detector must respond when the fire reaches a certain threshold heat release rate or in a specified amount of time. Time and heat release rate are interchanged using the fire growth model. The steps in solving this type of problem using the $p = 2$ power-law model are outlined below and are discussed in more detail in the examples following this section. The referenced equation numbers assume that the correlations used are the ones for a variable convective fraction. The procedure would be the same if using the correlations for the fixed, 75 % convective fractions except that α is not multiplied by the convective fraction when used in the equations. For design problems,

1. Determine the environmental conditions of the area being considered.
   (a) ambient temperature, T_a (convert to absolute temperature)
   (b) ceiling height or height above fuel, H
2. Estimate the fire growth characteristic α or t_g for the fuel expected to be burning. If t_g is used, calculate the corresponding α. Multiply α by the convective fraction to get α_c before using in the equations.
3. Establish the goals of the system: required response time t_r or maximum permitted threshold heat release rate $\dot{Q}_T$.
4. Select the detector type to be used. For fixed-temperature units, this choice establishes the detector response temperature T_r and its RTI, or τ_0 and u_0.
5. Make a first estimate of the distance, r, from the fire to the detector necessary to meet the system goals.
6. Assume that the fire starts obeying the power-law model at time $t = 0$.
7. Set the initial temperature of the detector and its surroundings at ambient temperature.
8. Using Equation 40.20, calculate the nondimensional time, t_{2f}^*, at which the initial heat front reaches the detector.
9. Calculate the factor A defined in Equation 40.18.
10. If the equations for a variable convective fraction are used, multiply α by the convective fraction X to get α_c and use result that with the required response time in Equation 40.19 to calculate the corresponding value of t_2^*.
11. If t_2^* is greater than t_{2f}^*, continue with Step 12. If not, try a new detector position, r, closer to the fire and return to Step 8.
12. Calculate the ratio u/u_2^* using Equation 40.16.
13. Calculate the ratio $\Delta T/\Delta T_2^*$ using Equation 40.17.
14. Use Equation 40.21 to calculate ΔT_2^*.
15. Equation 40.23 is used to calculate the ratio $u_2^*/(\Delta T_2^*)^{1/2}$.
16. Use Equations 40.22 and 40.26 to calculate D and Y.
17. Equation 40.25 can now be used to calculate the resulting temperature of the detector.
18. If the temperature of the detector is below its operating temperature, this procedure must be repeated using a smaller r. If the

temperature of the detector exceeds its operating temperature, a larger r can be used.

19. Repeat this procedure until the detector temperature is about equal to its operating temperature. The required spacing of detectors is then $S = 141r$.

This same procedure is used to estimate the response of rate-of-rise heat detectors. The difference is that in Step 17, Equation 40.24 is used to calculate rate of change of the detector temperature. This result is then compared to the rate at which the detector is designed to respond.

The discussion and procedure so far has centered around the solution of a design problem. The question asked was, How far apart must detectors of a specific design be spaced to respond within specific goals to a certain set of environmental conditions and a specific fire scenario?

The second type of problem that must be addressed is the analysis of an existing system or the analysis of a proposed design. Here the spacing of detectors or sprinklers is known. The engineer must still estimate the burning characteristics of the fuel and the environmental conditions of the space being analyzed. The equations can then be solved in a reverse fashion to determine the rate of heat release or the time to detector response. The technique is as follows:

1. Determine the environmental conditions of the area being considered.
   (a) ambient temperature, T_a (convert to absolute temperature)
   (b) ceiling height or height above fuel, H
2. Estimate the fire growth characteristic α or t_g for the fuel expected to be burning. If t_g is used, calculate the corresponding α. Multiply α by the convective fraction to get α_c before using in the equations.
3. Determine the spacing of the existing detectors or sprinklers. The protection radius is then $r = S/\sqrt{2}$.
4. Determine the detector's rated response temperature and its RTI, or τ_0 and u_0.
5. Make a first estimate of the response time of the detector or estimate the heat release rate at detector response and calculate the corresponding response time using the power-law equation.
6. Assume that the fire starts obeying the power-law model at time $t = 0$.
7. Set the initial temperature of the detector and its surroundings at ambient temperature.
8. Using Equation 40.20, calculate the nondimensional time, t^*_{2f}, at which the initial heat front reaches the detector.
9. Calculate the factor A defined in Equation 40.18.
10. Use the estimated response time along with Equation 40.19 to calculate the corresponding value of t^*_2.
11. If t^*_2 is greater than t^*_{2f}, continue with Step 12. If not, try a longer estimated response time or a larger estimated heat release rate and return to Step 8.
12. Calculate the ratio u/u^*_2 using Equation 40.16.
13. Calculate the ratio $\Delta T/\Delta T^*_2$ using Equation 40.17.
14. Use Equation 40.21 to calculate ΔT^*_2.
15. Equation 40.23 is used to calculate the ratio $u^*_2/(\Delta T^*_2)^{1/2}$.
16. Use Equations 40.22 and 40.26 to calculate D and Y.
17. Equation 40.25 can now be used to calculate the resulting temperature of the detector.
18. If the temperature of the detector is below its operating temperature, this procedure must be repeated using a longer estimated response time. If the temperature of the detector exceeds its operating temperature, a smaller t_r can be used.
19. Repeat this procedure until the detector temperature is about equal to its operating temperature. The resulting response time, t_r, can be used to calculate either the total heat release rate or the convective heat release rate at response using the power-law equation.

As in the design problem, this technique can be used to estimate the response of existing systems of rate-of-rise heat detectors. The difference is that in Step 4 the set point or rate of temperature rise at which the detector will

respond must be determined from the manufacturer's data. In Step 17, Equation 40.24 is used to determine the rate at which the temperature of the detector is changing.

Heat Detection: Potential Errors: Power-Law Fire Modeling

When the exact conditions of velocity and temperature of fire gases flowing past a detector are not known, errors are introduced in the design and analysis of fire detector response. Graphs in Heskestad and Delichatsios's report show the errors in calculated fire-gas temperatures and velocities [22]. An exact treatment of these errors is beyond the scope of this chapter, though some discussion is warranted.

Plots of actual data and calculated data show that errors in ΔT_2^* can be as much as 50 %, though generally there appears to be much better agreement [22, 23]. The maximum errors occur at r/H values of about 0.37. All other plots of actual and calculated data, for various r/H, show much smaller errors. In terms of the actual change in temperature over ambient, the maximum errors are on the order of 5–10 °C. The larger errors occur with faster fires and lower ceilings.

At $r/H = 0.37$, the errors are conservative when the equations are used in a design problem. That is, the equations predicted lower temperatures. Plots of data for other values of r/H indicate that the equations predict slightly higher temperatures.

Errors in fire-gas velocities are related to the errors in temperatures. The equations show that the velocity of the fire gases is proportional to the square root of the change in temperature of the fire gases [22]. In terms of heat transfer to a detector, the detector's change in temperature is proportional to the change in gas temperature and the square root of the fire-gas velocity. Hence, the expected errors bear the same relationships.

Based on the discussion above, errors in predicted temperatures and velocities of fire gases will be greatest for fast fires and low ceilings. Sample calculations simulating these conditions show errors in calculated detector spacings on the order of plus or minus 1 m, or less [23].

Similar to Alpert's steady-state model, the power-law ceiling-jet model assumes a flat infinite ceiling. If the leading edge of the ceiling jet has passed the detector position and not reached a wall or other obstruction, then the model is within its stated parameters. The nondimensional time that the heat front reaches some position, r/H, is given by the equation for t_{2f}^*. The corresponding nondimensional time at response is given by the equation for t_2^*. Setting these equal to each other and solving for r at $t = t_r$ gives the radial distance from the fire to the leading edge of the heat front. Using the equations for a user-entered convective fraction,

$$t_{2f}^* 0.813\left(1 + \frac{r}{H}\right)$$

and

$$\begin{aligned} t_2^* &= \frac{t_r}{A^{-1/5}\alpha_c^{-1/5}H^{4/5}} \\ t_{2f}^* &= t_2^* \\ 0.813\left(1 + \frac{r}{H}\right) &= \frac{t_r}{A^{-1/5}\alpha_c^{-1/5}H^{4/5}} \\ r &= \left\{\left[\left(t_r/ = A^{-1/5}\alpha_c^{-1/5}H^{4/5}\right)/0.813\right] - 1\right\}H \\ r &= \left(t_2^*/0.813 - 1\right)H \end{aligned}$$

Selection of Data for Design and Analysis

In order to calculate the required spacing of heat detectors or sprinklers to respond to a given fire, the following information is required:

1. *System goals*: desired fire size (heat release rate) at response or time to detector response from the start of open flaming
2. Fire growth constant α or t_g
3. Ambient temperature
4. Height above the fuel or ceiling height

In addition to the above, the heat capacity of air at constant pressure, C_p, the density of air, ρ, and the gravitational constant, g, are used in the calculations. It is also necessary to know the characteristics of the detector for which the spacing calculations are being made. Specifically, the response temperature and the RTI of the detector must be known.

Establishing system goals is not within the scope of this chapter. However, it should be pointed out that, no matter what the goals are, they must be expressed in terms of heat release rate or time to detector response. The system's goals may actually be to limit damages to some dollar value, provide adequate escape time, or limit the production of toxic gases. In order to calculate required detector spacing using this system, these goals would have to be translated. For instance, as the fire grows, at what time or heat release rate must the detector respond so that the fire department can be summoned and extinguish the fire before damage levels are exceeded or conditions become untenable due to toxic gases?

Table 40.4 is a list of furniture calorimeter tests done at the National Bureau of Standards [16, 24]. The tests provide a database of heat release rate, particulate production, and radiation from a variety of common furnishings. The table provides the corresponding α or t_g for the calorimeter tests [23]. The virtual time data in the table is the approximate time at which the heat release rate in the test began to follow the $p = 2$ power-law model ($\dot{Q} = \alpha t^2$ kW). Prior to this time, the behavior of the fire cannot be predicted with this model. Figure 40.5 shows some test data along with a power-law curve superimposed.

The data in Table 40.4 can be used to select α or t_g for use in spacing calculations. However, in many cases the data in this table will not match the scenario being studied. If the heat release rate versus time history can be obtained or approximated for the expected fuel, the α or t_g can be calculated using curve-fitting techniques [23].

In most cases, since the exact fuel that will be involved in a fire cannot be known, the rigorous calculation of α is not warranted. Engineering judgment can be used to select α or t_g that approximates the severity of the fire. The data in Table 40.4 suggest a range of 50–500 s for t_g. Only a few rapidly developing fires had a t_g below 50 s. Three slow fires had values above 500 s for t_g.

Table 40.4 also lists the maximum heat release rate reached during the power-law growth. The heat release rate model $\dot{Q} = \alpha t^2$ does not predict when a fuel package stops following the model or when the fuel is depleted. This task is an important point often missed by many designers. A simple test is to calculate the mass of fuel consumed from $t = 0$ to the time of interest. For $p = 2$ power-law fire growth rate, the total energy consumed is

$$E = \int_{t=0}^{t} \dot{Q} = \int_{t=0}^{t} \alpha t^2 \ \text{kJ}$$

$$E = \frac{\alpha t^3}{3} \text{kJ}$$

Knowing the heat of combustion, H_c, for the fuel permits calculation of the mass of fuel necessary to release a given amount of energy in the time period:

$$E = mH_c \ \text{kJ}$$

$$m = \frac{E}{H_c} \text{ g or kg (depending on the units for } H_c)$$

When doing a design or analysis, try several different fire growth rates to determine the effect of their variance on the calculations. In some

Table 40.4 Summary of NBS calorimeter tests

Test no.	Description	Fire growth time (s) (t_g)	α (kW/s^2)	Virtual time (s)	Maximum heat release rate (kW)
Test 15	Metal wardrobe 41.4 kg (total)	50	0.4220	10	750
Test 18	Chair F33 (trial loveseat) 39.2 kg	400	0.0066	140	950
Test 19	Chair F21 28.15 kg (initial stage of fire growth)	175	0.0344	110	350
Test 19	Chair F21 28.15 kg (later stage of fire growth)	50	0.4220	190	2000
Test 21	Metal wardrobe 40.8 kg (total) (average growth)	250	0.0169	10	250
Test 21	Metal wardrobe 40.8 kg (total) (later growth)	120	0.0733	60	250
Test 21	Metal wardrobe 40.8 kg (total) (initial growth)	100	0.1055	30	140
Test 22	Chair F24 28.3 kg	350	0.0086	400	700
Test 23	Chair F23 31.2 kg	400	0.0066	100	700
Test 24	Chair F22 31.9 kg	2000	0.0003	150	300
Test 25	Chair F26 19.2 kg	200	0.0264	90	800
Test 26	Chair F27 29.0 kg	200	0.0264	360	900
Test 27	Chair F29 14.0 kg	100	0.1055	70	1850
Test 28	Chair F28 29.2 kg	425	0.0058	90	700
Test 29	Chair F25 27.8 kg (later stage of fire growth)	60	0.2931	175	700
Test 29	Chair F25 27.8 kg (initial stage of fire growth)	100	0.1055	100	2000
Test 30	Chair F30 25.2 kg	60	0.2931	70	950
Test 31	Chair F31 (loveseat) 39.6 kg	60	0.2931	145	2600
Test 37	Chair F31 (loveseat) 40.40 kg	80	0.1648	100	2750
Test 38	Chair F32 (sofa) 51.5 kg	100	0.1055	50	3000
Test 39	$^1/_2$-in. Plywood wardrobe w/ fabrics 68.8 kg	35	0.8612	20	3250
Test 40	$^1/_2$-in. Plywood wardrobe w/ fabrics 68.32 kg	35	0.8612	40	3500
Test 41	$^1/_8$-in. Plywood wardrobe w/ fabrics 36.0 kg	40	0.6594	40	6000
Test 42	$^1/_8$-in. Ply. wardrobe w/ fire-ret. (int. fin. initial)	70	0.2153	50	2000
Test 42	$^1/_8$-in. Ply. wardrobe w/ fire-ret. (int. fin. later)	30	1.1722	100	5000
Test 43	Repeat of $^1/_2$-in. Plywood wardrobe 67.62 kg	30	1.1722	50	3000
Test 44	$^1/_8$-in. Ply. wardrobe w/ F-R., latex paint 37.26 kg	90	0.1302	30	2900
Test 45	Chair F21 28.34 kg (large hood)	100	0.1055	120	2100
Test 46	Chair F21 28.34 kg	45	0.5210	130	2600
Test 47	Chair adj. back metal frame, foam cush. 20.8 kg	170	0.0365	30	250
Test 48	Easychair CO7 11.52 kg	175	0.0344	90	950
Test 49	Easychair 15.68 kg (F-34)	200	0.0264	50	200
Test 50	Chair metal frame minimum cushion 16.52 kg	200	0.0264	120	3000
Test 51	Chair molded fiberglass no cushion 5.28 kg	120	0.0733	20	35
Test 52	Molded plastic patient chair 11.26 kg	275	0.0140	2090	700
Test 53	Chair metal frame w/ padded seat and back 15.5 kg	350	0.0086	50	280
Test 54	Loveseat metal frame w/ foam cushions 27.26 kg	500	0.0042	210	300
Test 55	Group chair metal frame w/ foam cushion 6.08 kg	Never exceeded 50 kW heat release rate			
Test 56	Chair wood frame w/ latex foam cushions 11.2 kg	500	0.0042	50	85
Test 57	Loveseat wood frame w/ foam cushions 54.60 kg	350	0.0086	500	1000
Test 61	Wardrobe $^3/_4$-in. particleboard 120.33 kg	150	0.0469	0	1200
Test 62	Bookcase plywood w/ aluminum frame 30.39 kg	65	0.2497	40	25
Test 64	Easychair molded flexible urethane frame 15.98 kg	1000	0.0011	750	450
Test 66	Easychair 23.02 kg	75	0.1876	3700	600
Test 67	Mattress and boxspring 62.36 kg (later fire growth)	350	0.0086	400	500
Test 67	Mattress and boxspring 62.36 kg (initial fire growth)	1100	0.0009	90	400

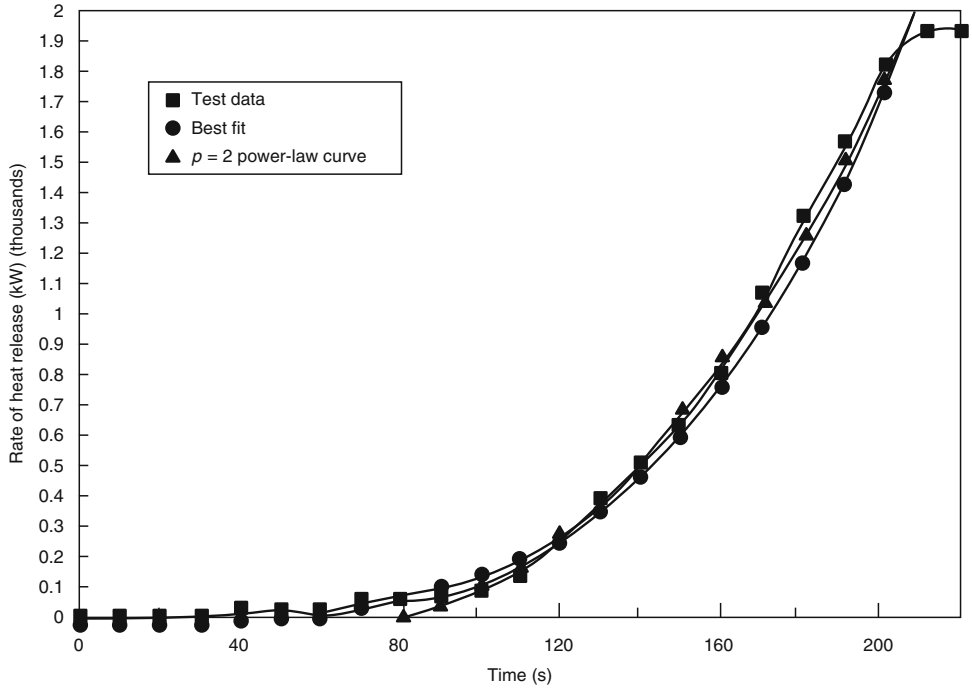

Fig. 40.5 Test 27 chair

cases, the effect will be minimal. In other cases, this type of sensitivity analysis will show that a more thorough analysis of the possible fuels and fire scenarios is warranted.

The selection of an ambient temperature can have a measurable effect on the calculations. The calculations assume that the detector or sprinkler starts out at the same temperature as the ambient air when the fire starts. Hence, if a temperature of 20 °C is assumed for the spacing calculations and the actual temperature at the time of the fire is 10 °C, the system's goals will not be met. For design calculations to be conservative, the lowest expected ambient temperature should be used.

The relationships presented by Heskestad and Delichatsios [21] are correlated to fire test data using the ceiling height above the fuel surface for H. If this height varies, the larger value of H will produce more conservative results in the calculations for detector spacing or response. The most conservative results are obtained when the floor-to-ceiling height is used, since this height is the maximum vertical distance from fuel to detector.

The values for C_p, ρ_0, and g should be 1.040 kJ/(kg·K), 1.1 kg/m^3, and 9.81 m/s^2, respectively. Slight variations in these constants have negligible effects on the calculations.

As previously mentioned, the design or analysis calculations are done for a particular detector or sprinkler. Therefore, it is necessary to know the unit's operating temperature. The response time index or τ_0 and u_0 are also needed. Operating temperature is obtained from manufacturer's data. The detector's sensitivity is best determined by conducting a plunge test [9].

In the absence of plunge test data, a detector's UL-listed spacing can be used as a measure of detector sensitivity. Heskestad and Delichatsios analyzed UL test data and calculated time constants, τ_0, for various combinations of UL-listed spacing and detector operating temperature [22]. The Appendix Subcommittee of *NFPA 72* expanded the table to include a larger selection of detectors [8]. That table is reproduced here as Table 40.5.

Table 40.5 Time constants for any listed detector τ_0 (s)[a]

	UL (°F)						
Listed spacing (ft)	128°	135°	145°	160°	170°	196°	FMRC all temp.
10	400	330	262	195	160	97	195
15	250	190	156	110	89	45	110
20	165	135	105	70	52	17	79
25	124	100	78	48	32		48
30	95	80	61	36	22		36
40	71	57	41	18			
50	59	44	30				
70	36	24	9				

Reproduced from *NFPA 72* (1993, Appendix B [8])
These time constants are based on an analysis of the Underwriters Laboratories Inc. and Factory Mutual Research Corporation listing test procedures
Plunge test results performed on the detector to be used will give a more accurate time constant
[a]At a reference velocity of 5 ft/s

Heat Detection Design and Analysis Examples Using the Power-Law Fire Model

Analysis and design problems will be used to show how fire protection engineers can use the techniques presented in this chapter. The examples show the sensitivity of these techniques to changes in variables and input parameters. A design problem is first worked by hand to solve the equations presented earlier in the section on heat detection. The remaining examples were worked using a spreadsheet written to solve the equations.

Example 2 A fire detection system is being designed for an unsprinklered manufacturing building. The area being considered has a large, flat ceiling 5.0 m high. Ambient temperature is normally 20 °C, but on weekends it is cut back to 10 °C. It will be assumed that the fire scenario involves the ignition of a stack of wood pallets. The pallets are stacked 1.5 m (5 ft) high. Fire tests [8] show that this type of fire follows the $p = 2$ power-law equation with a t_g of approximately 150 s. The corresponding α can be calculated:

$$\dot{Q} = \alpha t^2 \text{ kW}$$

$$\alpha = \frac{1055}{t_g^2} = \frac{1055}{150^2} = 0.047 \text{ kW/s}^2$$

The goal is to detect the fire before it reaches a total heat release rate of 2500 kW. Fixed-temperature heat detectors will be used. The detectors have a 57 °C (135 °F) operating temperature and a UL-listed spacing of 30 ft. From Table 40.5 the time constant is found to be 80 s. This time constant is referenced to a gas velocity of 1.5 m/s and can be used with Equation 40.9 to calculate the detector's RTI.

First, use the power-law equation to calculate the time that the fire would reach a total heat release rate of 2500 kW:

$$\dot{Q} = \alpha t^2 \text{ kW}$$

$$t = \sqrt{\frac{\dot{Q}}{\alpha}} = \sqrt{\frac{2500}{0.047}} = 231 \text{ s}$$

The RTI is calculated using Equation 40.9 and a reference velocity, u_0, of 1.5 m/s (5 ft/s):

$$\text{RTI} = \tau_0 u_0^{1/2} = 80\sqrt{1.5} = 98 \text{ m}^{1/2}\text{s}^{1/2}$$

As described previously in Step 5 for design of a proposed system, it is necessary to make a first guess at the required detector spacing. In this case, try using $r = 6.0$ m. Use Equation 40.20 to calculate the nondimensional time, t_{2f}^*, at which the initial heat front reaches the detector. Use the distance from the top of the fuel package to the ceiling for H.

$$t_{2f}^{*} = 0.813\left(1 + \frac{r}{H}\right)$$

$$t_{2f}^{*} = 0.813\left(1 + \frac{6.0}{3.5}\right) = 2.207$$

Next, Equation 40.18 is used to calculate A. Note that in this equation the ambient temperature, T_a, must be expressed as an absolute temperature. In this case add 273 to °C to get K (Kelvin).

$$A = \frac{g}{C_p T_a \rho_o}$$

$$A = \frac{9.81}{1.040(10 + 273)1.1} = 0.030$$

The nondimensional time corresponding to the required response time is now calculated. However, first we must calculate α_c. Assuming a convective fraction of 70 %:

$$\alpha_c = X\alpha = 0.70(0.047) = 0.033\ \text{kW/s}^2$$

$$t_2^{*} = \frac{t}{A^{-1/5}\alpha_c^{-1/5}H^{4/5}}$$

$$t_2^{*} = \frac{231}{(0.030)^{-1.5}(0.033)^{-1/5}(3.5)^{4/5}} = 21.256$$

Since $t_{2f}^{*} > t_2^{*}$, we know that the heat front has passed the detector location. Next, the ratio of the velocity to the nondimensional velocity is calculated:

$$u_2^{*} = \frac{u}{\left(A^{1/5}\alpha_c^{1/5}H^{1/5}\right)}$$

$$\frac{u}{u_2^{*}} = A^{1/5}\alpha_c^{1/5}H^{1/5}$$

$$\frac{u}{u_2^{*}} = (0.030)^{1/5}(0.033)^{1/5}(3.5)^{1/5} = 0.322$$

The ratio of the change in gas temperature to the nondimensional gas temperature is calculated:

$$\Delta T_2^{*} = \frac{u}{A^{2/5}(T_a/g)\alpha_c^{2/5}H^{-3/5}\big)}$$

$$\frac{\Delta T}{\Delta T_2^{*}} = A^{2/5}\left(\frac{T_a}{g}\right)\alpha_c^{2/5}H^{-3/5}$$

$$\frac{\Delta T}{\Delta T_2^{*}} = (0.030)^{2/5}\left(\frac{283}{9.81}\right)(0.033)^{2/5}(3.5)^{-3/5} = 0.855$$

The nondimensional change in gas temperature is now calculated:

$$D = 0.126 + 0.210\left(\frac{6.0}{3.5}\right) = 0.486$$

$$\Delta T_2^{*} = \left[\frac{\left(t_2^{*} - t_{2f}^{*}\right)}{D}\right]^{4/3}$$

$$\Delta T_2^{*} = \left[\frac{(21.256 - 2.207)}{0.486}\right]^{4/3} = 133.142$$

Next, the ratio $u_2^{*}/(\Delta T_2^{*})^{1/2}$ is calculated:

$$\frac{u_2^{*}}{\left(\Delta T_2^{*}\right)^{1/2}} = 0.59\left(\frac{r}{H}\right)^{-0.63}$$

$$\frac{u_2^{*}}{\left(\Delta T_2^{*}\right)^{1/2}} = 0.59\left(\frac{6.0}{3.5}\right)^{-0.63} = 0.420$$

Y is now calculated:

$$\Upsilon = \frac{3}{4}\sqrt{\frac{u}{u_2^{*}}}\sqrt{\frac{u_2^{*}}{(\Delta T_2)^{1/2}}}\left(\frac{\Delta T_2^{*}}{\text{RTI}}\right)\left(\frac{t}{t_2^{*}}\right)D$$

$$\Upsilon = \frac{3}{4}\sqrt{0.322}\sqrt{0.420}\left(\frac{133.142}{98}\right)\left(\frac{231}{21.256}\right)(0.486) = 1.979$$

The resulting temperature of the detector at $t = 231$ s, $T_d(t)$, can now be calculated. Assume that the temperature of the detector at the start of the fire, $T_d(0)$, is the same as ambient temperature, T_a.

$$\Delta T_d = T_d(t) - T_d(0)$$
$$= \frac{\Delta T}{\Delta T_2^*} \Delta T_2^* \left[1 - \left(\frac{1 - e\Upsilon}{\Upsilon}\right)\right]$$
$$\Delta T_d = T_d(t) - T_d(0)$$
$$= 0.855(133.142)\left[1 - \left(\frac{1 - e^{-1.979}}{1.979}\right)\right]$$
$$\Delta T_d = T_d(t) - T_d(0) = 64.264$$
$$T_d(t) = \Delta T_d = T_d(0) = 64.264 + 10$$
$$= 74.264 = 74°C$$

After 231 s, when the heat release rate has reached 2500 kW, the detector located 6 m from the fire axis has reached an approximate temperature of 74 °C. Note that the answer has been rounded to two significant digits, one more than the least precision of any of the variables. This rule is the alternate rule for rounding as discussed in the introduction of this chapter.

The detector actuation temperature is 57 °C. This result indicates that the detector has responded before the fire has reached 2500 kW. Since the calculated temperature is higher than the actuation temperature, a larger r can be tried. The calculations should be repeated until the calculated detector temperature is approximately equal to the actuation temperature.

For this example the answer converges on a radial distance of approximately 7.4 m. The spacing between detectors is

$$S = r\sqrt{2} = 7.4\sqrt{2} = 10.5 \text{ m}$$

Example 3 This example will show how an existing heat detection system or a proposed design can be analyzed to determine its response time or fire size at response. The scenario used in Example 2 will be repeated, except that the manufacturing building has an existing system of heat detectors, which are spaced evenly on the ceiling at 15.0-m intervals. The detector characteristics are the same as above. The actuation temperature is 57 °C and the RTI is 98 $m^{1/2} \cdot s^{1/2}$. The ceiling height is 5 m, and the height of the pallets is 1.5 m. Ambient temperature is 10 °C. α is 0.047 kW/s^2 (t_g = 150 s) and α_c is 0.033 kW/s^2.

The maximum radial distance from the fire axis to a detector is calculated first, using Equation 40.5.

$$S = r\sqrt{2} \text{ m}$$
$$r = \frac{S}{\sqrt{2}} = \frac{15.0}{\sqrt{2}} = 10.6 \text{ m}$$

The next step in the analysis is to estimate the response time of the detector or the fire size at response. In the design above, the fire grew to about 2500 kW in 231 s when the detector at a distance of 7 m responded. The radial distance in this example is larger and should result in a slower response and larger fire size at response. A first guess at response time might be 6 min or 360 s. The fire size (total heat release rate) at 360 s is

$$\dot{Q} = \alpha t^2 \text{ kW}$$
$$\dot{Q} = 0.047(360)^2 = 6091 \text{ kW}$$

The remaining calculations for the resulting detector temperature are similar to those in Example 2. Rather than show the detail, a spreadsheet was used to complete the calculations. The resulting detector temperature at 360 s was calculated to be approximately 84 °C.

This result indicates that the detector response time is less than the estimated 6 min. Therefore, a smaller response must be tried. If the calculated temperature were lower than the actuation temperature, a larger t would be tried. The calculations are repeated until the calculated detector temperature is approximately equal to the actuation temperature. In this case, the response time converges at 295 s. This result corresponds to a fire size at response of 4070 kW. It is at this time and heat release rate that the detector temperature reaches its actuation temperature of 57 °C.

This example assumes that the fire continues to follow the power-law relationship through the burning period. If there is not enough fuel available, it is possible for the heat release rate curve to flatten out before reaching 4070 kW. These calculations do not predict when this development will happen. These calculations also do

not predict how the detector temperature changes after the fire stops following the power-law relationship. It may be that sufficient heat continues to be released and the detector eventually responds. It is also possible for the fire gases to cool sufficiently to preclude detector actuation unless additional fuel becomes involved in the fire.

Comparing Example 2 with Example 3 shows how detector spacing affects response time. A difference in spacing of 4.4 m (15–10.6 m) results in a difference of approximately 64 s in the detector response time. Because the fire is accelerating according to the $p = 2$ power-law relationship, the resulting difference in fire size at response is 1570 kW.

Example 4 A warehouse is used to store sofas and other furniture. The sofas are similar to one tested by the National Bureau of Standards in their furniture calorimeter [30]. Burning characteristics are assumed to be similar to the sofa used in Test 38: [23, 30] $\alpha = 0.1055\ \text{kW/s}^2$, $t_g = 100$ s; peak heat release rate = 3000 kW. The sofas are stored one or two high. Assume a convective fraction of 65 %.

The building has a flat roof and ceiling. The distance from the floor to the ceiling is 4.6 m. When the sofas are stacked two high, the distance from the top of the fuel package to the ceiling is 2.4 m. Ambient temperature in the warehouse is kept above 10 °C (Fig. 40.6).

Based on maximum allowable property loss goals established by the owner, it is desirable to detect a fire and notify the fire department prior to a second fuel package becoming involved. The original NBS report [30] contains data on radiation measured during Test 38. This information can be used along with other techniques presented in this handbook to determine when a second item might ignite. For instance, it might be determined that furniture across a 2-m aisle might ignite when the fire reaches a total heat release rate of 3000 kW. The objective would then be to detect the fire soon enough so that the fire can be extinguished or controlled before the fire reaches a total of 3000 kW. In this example, it is assumed that the fire must be detected when it reaches a total heat release rate of about 2000 kW.

The fire detection system will consist of fixed-temperature heat detectors connected to a control panel that is, in turn, connected to the local fire department. The detector to be used has a fixed-temperature rating of 57 °C and an RTI of $42\ \text{m}^{1/2} \cdot \text{s}^{1/2}$.

The problem is determining the spacing of detectors required to detect this fire. When the computer program runs, the user is prompted for all of the above information. In this example, the data are fixed except for the distance from the ceiling to the flame origin. If the distance between the top of the fuel and the ceiling (2.4 m) is used, the calculations indicate that the

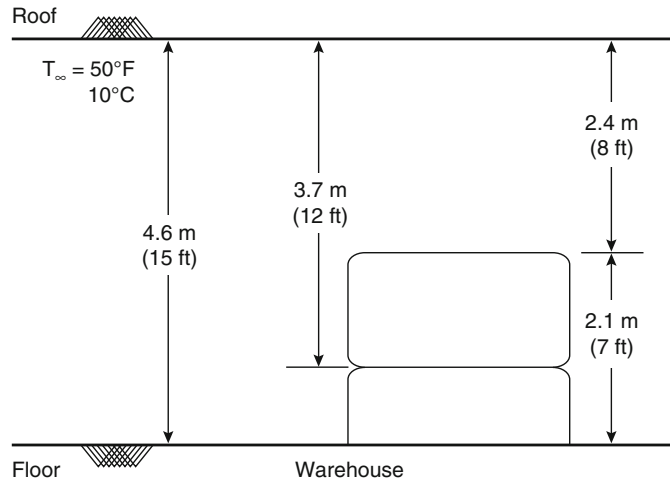

Fig. 40.6 Example 4: warehouse

detectors must be spaced 7.3 m apart to respond when the fire reaches a heat output of 2000 kW.

For a worst-case analysis, the distance from the floor to the ceiling (4.6 m) is used. This distance results in a required detector spacing of 5.9 m.

A more realistic worst-case scenario would be when the sofas are not stacked two high. With one sofa on the floor, the distance from the fuel to the ceiling would be about 3.7 m. The required detector spacing would then be 6.5 m.

These results are summarized in Table 40.6. This table clearly shows the relationship between ceiling height and detector response. The greater the distance from the fire to the ceiling, the closer the detectors must be spaced to respond within the goals of the system. Designs based on the floor-to-ceiling distance are conservative and representative of a worst-case condition. More realistic designs are based on the most probable or the greatest expected vertical clearance between fuel and detector.

Example 5 For the same conditions in Example 4, if the detector spacing is fixed at 10.3 m ($r = 7.3$ m), how does the ceiling height affect the response time of the system?

Using the spreadsheet, the results, after rounding, are summarized in Table 40.7.

Example 6 This example will show how to select a detector type to economically meet the system's goals. The fire scenario and goals used in Examples 4 and 5 will be used: $H = 2.4$ m; $T_a = 10$ °C; RTI = 42 $m^{1/2} \cdot s^{1/2}$; X = 65 %, $t_g = 100$ s.

Table 40.6 Example 4: ceiling height or height above fuel versus detector spacing

Ceiling height, H (m)	Required spacing, S (m)
2.4	10.3
3.7	9.2
4.6	8.4

Table 40.7 Example 5: ceiling height or height above fuel versus response time

Ceiling height, H (m)	Required spacing, t_r (s)
2.4	140
3.7	150
4.6	160

In Example 4, it was found that heat detectors with a fixed temperature rating of 57 °C and an RTI of 42 $m^{1/2} \cdot s^{1/2}$ must be spaced 10.3 m apart to meet the system's goals—a response at 2000 kW. Here, the spacing of rate-of-rise heat detectors will be estimated.

The detector to be used is rated to respond when its temperature increases at a rate of 11 °C minutes or more. The detector's RTI will be assumed to be the same as the detector in Example 4. The calculation procedure is the same as for fixed temperature detectors except that, in the last step, the equation for the rate of temperature change is used:

$$\frac{dT_d(t)}{dt} = \frac{4}{3}\frac{\Delta T}{\Delta T_2^*}\Delta T_2^{*1/4}\frac{\left(1 - e^{-\Upsilon}\right)}{\left(t/t_2^*\right)D}$$

Solving the equations, it is found that the rate-of-rise heat detectors can be spaced up to 25 m apart and respond at approximately 2000 kW total heat release rate.

If the total area of the warehouse is 5000 m^2, approximately 48 fixed-temperature heat detectors would be required to meet the established goals. The same goals can be met with approximately eight rate-of-rise heat detectors. Additional detectors might be required due to obstructing beams or walls. It should also be pointed out that the use of m^2 for calculating the required number of units is only an estimate. The detector does not cover an area that is 625 m^2 (25 m × 25 m). It is covering a circular area having a radius no more than about 17.7 m. That is, all points on the ceiling must be within the protection radius of a detector for the calculations to be valid. If one used a "rated area" for a detector rather than a radial measurement, it could be concluded that a single detector in this example could cover a space that was 125 m long if it were only 5 m wide.

By trying different detector types or detectors with higher sensitivities, project goals might be met with a fewer number of detectors. The scenario in this example shows that, to detect the

same fire, a much greater number of fixed-temperature heat detectors than rate-of-rise heat detectors is required. This conclusion is not always the case. Many fires will develop slowly and cause high ceiling temperatures without ever exceeding the rate of temperature rise necessary to actuate a rate-of-rise heat detector. As a backup, most commercially available rate-of-rise heat detectors have a fixed-temperature element also. The rate-of-rise element and the fixed-temperature element should be considered separately when designing or analyzing a system.

Example 7 In this example, a combination fixed-temperature and rate-of-rise heat detector will be analyzed and the response of the two elements will be compared. For an installed spacing of 10.0 m ($r = 0.707$ m), the effect of fire growth rate on response time will be shown. The following conditions from Examples 4, 5, and 6 will be repeated: $H = 2.4$ m; $T_a = 10\,^{\circ}\text{C}$; RTI $= 42\ \text{m}^{1/2} \cdot \text{s}^{1/2}$; X = 65 %. The fixed-temperature element response threshold is $T_r = 57\,^{\circ}\text{C}$, and the rate-of-rise threshold is $dTr/dt = 11\,^{\circ}\text{C/min}$.

The results are shown in Table 40.8 and Fig. 40.7. For fire growth times up to $t_g = 509$ s, the rate-of-rise element responds faster. For fires that grow slower (increasing t_g), the fixed-temperature element will respond faster.

For larger installed spacings, such as the 25 m spacing calculated in the previous example for the spacing of the rate-of-rise detector, the cross-over point occurs sooner. The results for a 25 m spacing are shown in Table 40.9 and Fig. 40.8. For fire growth times up to $t_g = 228$ s, the rate-of-rise element responds faster. For fires that grow slower (increasing t_g), the fixed-temperature element will respond faster.

Table 40.8 Response time as a function of fire growth time, t_g

	Response time, t_r (s)	
t_g	Fixed temperature	Rate of rise
50	85	31
100	135	53
200	219	98
300	297	155
400	373	241
500	447	426
509	454	454
600	521	835

Example 8 In this example, the effects of fire growth rate on detector spacing will be examined. The scenario used in Examples 4 through 7 will be used again. The following conditions from these examples will be repeated: $H = 2.4$ m; $T_a = 10\,^{\circ}\text{C}$; RTI $= 42\ \text{m}^{1/2} \cdot \text{s}^{1/2}$; X = 65 %. The fixed-temperature element response threshold is $T_r = 57\,^{\circ}\text{C}$ and the rate-of-rise threshold is $dT_r/dt = 11\,^{\circ}\text{C/min}$.

In Examples 4, 5, and 6, the rate of fire growth followed the power-law equation with an α of 0.1055 kW/s^2 or $t_g = 100$ s. Calculations were done for several values of t_g. The results are summarized in Table 40.10 and Fig. 40.9.

For fixed-temperature detectors, if the fire grows at a faster rate (smaller t_g), a smaller spacing is required to meet the system's goals. If the fire grows at a slower rate, a larger detector spacing is allowed. This relationship clearly shows the effects of thermal lag on detector response. At slow rates of growth, the detector is immersed in the hot fire gases and, despite thermal lag, has time to absorb the heat before the fire reaches the maximum permissible heat release rate. The effects of thermal lag are less important at slow rates of fire growth.

The rate-of-rise detector also experiences thermal lag. However, the curve peaks at approximately $t_g = 110\ \text{m}^{1/2} \cdot \text{s}^{1/2}$ and $S = 25$ m. For the rate-of-rise detector, as the fire growth rate slows (larger t_g), thermal lag decreases as it did for the fixed-temperature detector. However, as the rate of fire growth slows, so does the rate of change of the detector's temperature. For this particular detector and fire scenario, at fire growth times greater than about 110 s, the detector spacing must be reduced so that the threshold rate of change of the detector temperature is reached before the maximum permissible heat release rate is reached.

Example 9 In this example a detector is exposed to the ceiling jet for a fire with $t_g = 150$ s and a 75 % convective fraction. Ambient temperature is 10 °C. The ceiling is 4 m high, and the detector is located at a radial distance of 5 m from the fire.

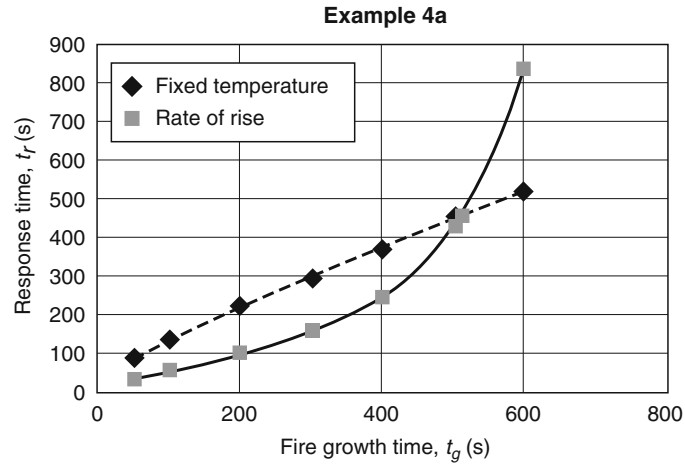

Fig. 40.7 Response time as a function of fire growth time, tg

Table 40.9 Response time as a function of fire growth time, t_g

	Response time, t_r (s)	
t_g	Fixed temperature	Rate of rise
50	168	77
100	269	140
200	448	355
228	497	497
300	619	1330

The RTI of the detector is 50. Plot the detector temperature and the fire-gas temperature at the detector location for t up to 240 s.

The detector remains at ambient temperature until the ceiling jet first reaches the detector position. At what time does the ceiling jet first reach the detector? This result is found by setting $t_{2f}^* = t_2^*$ and solving for t. First, α_c is calculated:

$$\alpha = \frac{t_g^2}{1055} = \frac{1055}{150^2} = 0.047\ \text{kW/s}^2$$

$$\alpha_c = X\alpha = 0.75(0.047) = 0.035\ \text{kW/s}^2$$

$$t_{2f}^* = t_2^*$$

$$0.813\left(1 + \frac{r}{H}\right) = \frac{t}{A^{-1/5}\alpha_c^{-1/5}H^{4/5}}$$

$$t = 0.813\left(1 + \frac{r}{H}\right) = A^{-1/5}\alpha_c^{-1/5}H^{4/5}\ \text{s}$$

$$t = 0.813\left(1 + \frac{5}{4}\right)$$

$$= \left(0.030^{-1/5}\right)\left(0.035^{-1/5}\right)\left(4^{4/5}\right)$$

$$= 21.86 = 22\ \text{s}$$

The heat front reaches the detector at about 22 s, and heating begins. Prior to this point, the detector and gas temperature surrounding the detector are at ambient temperature.

The method to calculate the detector temperature is the same as in previous examples. To calculate the change in ceiling-jet gas temperature, combine the following equations and solve to ΔT:

$$\Delta T_2^* = \frac{\Delta T}{A^{2/5}(T_a/g)\alpha_c^{2/5}H^{-3/5}}$$

and

$$\Delta T_2^* = \left[\frac{\left(t_2^* - 2_{2f}^*\right)}{(0.126 + 0.210r/H)}\right]^{4/3}$$

$$\Delta T = A^{2/5}\left(\frac{T_a}{g}\right)\alpha_c^{2/5}H^{-3/5} \times \left[\frac{\left(t_2^* - 2_{2f}^*\right)}{(0.126 + 0.210r/H)}\right]^{4/3}$$

A spreadsheet solution is shown in Table 40.11 and graphed in Fig. 40.10.

Example 10 A sprinkler system is being installed in a large exhibition hall. The building has a flat roof deck supported by open space frame trusses. The distance from the underside

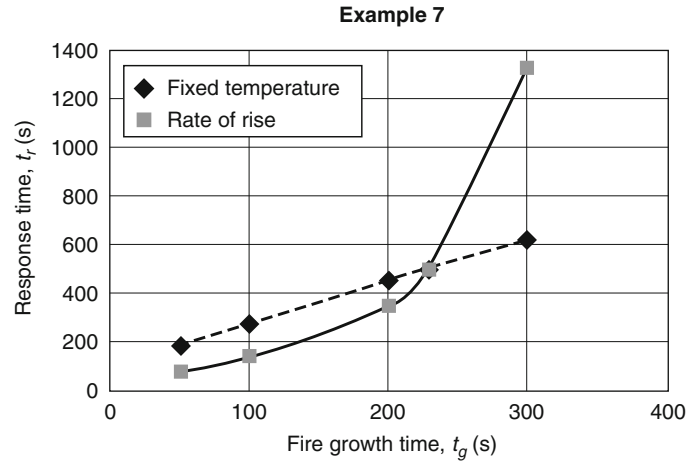

Fig. 40.8 Response time as a function of fire growth time, tg

Table 40.10 Required detector spacing as a function of fire growth time, t_g

	Required spacing (m)	
t_g	Fixed temperature	Rate of rise
50	7.2	23
75	9	24
100	10	25
110	11	25
120	11	24
150	12	24
200	14	22
300	15	18
400	16	14
500	17	12
600	18	10

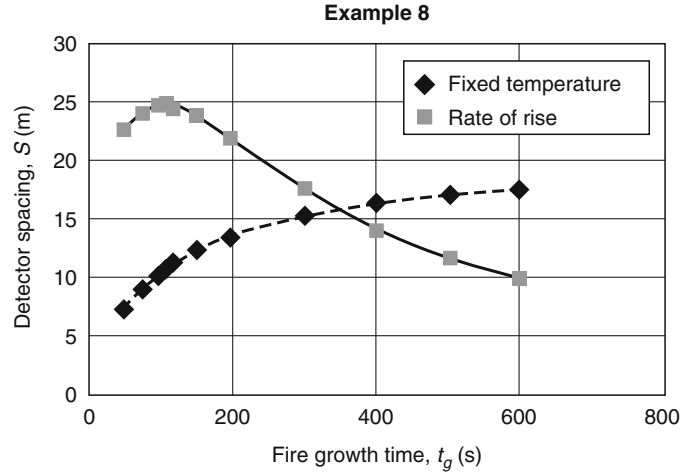

Fig. 40.9 Required detector spacing as a function of fire growth time, tg

of the roof deck to the floor is 12 m. Ambient temperatures do not usually fall below 5 °C.

Three different designs for the sprinkler system have been proposed. All three are designed to provide the same water density over a specified area. Each proposal uses a sprinkler with a temperature rating of 74 °C and an RTI of 110 $m^{1/2} \cdot s^{1/2}$. The only difference among the three systems is the spacing of the sprinklers and the branch lines that feed them. The first proposal uses a square array with a spacing of 3.0 m. The second and third proposals are based on square array spacings of 3.7 m and 4.6 m, respectively.

Table 40.11 Example 9: ceiling jet and detector temperature as a function of time

t (s)	T_g (s)	T_d (s)
22	10	10
30	12	10
40	15	10
50	19	11
60	24	13
70	29	15
80	34	18
90	39	21
100	45	25
110	51	30
120	58	35
130	64	40
140	71	46
150	78	52
160	85	59
170	93	66
180	100	73
190	108	81
200	116	88
210	124	96
220	132	104
230	140	112
240	148	120

What effect will the three different spacings have on the size of the fire when the system responds? Assume two different fire scenarios. In the first, the fire grows at a moderate rate with $t_g = 200$ s. The second fire scenario has a slower fire growth rate with $t_g = 500$ s. For both, assume a convective fraction of 75 %. Results of the calculations are shown in Table 40.12 after rounding.

The calculations show an increase of about 25 % in the fire size at response when the spacing is increased 50 % from 3.0 to 4.6 m. The increased spacing may result in a lower system cost. However, closer spacings mean that the sprinkler system will probably respond sooner. The fire protection engineer can use this type of analysis to assist in choosing a system that best meets the project's overall goals.

Example 11 A fire impacting elevator machinery can result in passengers or fire fighters being carried to a fire floor or being trapped between floors. Elevator safety codes generally do not require any sprinkler protection or detection at

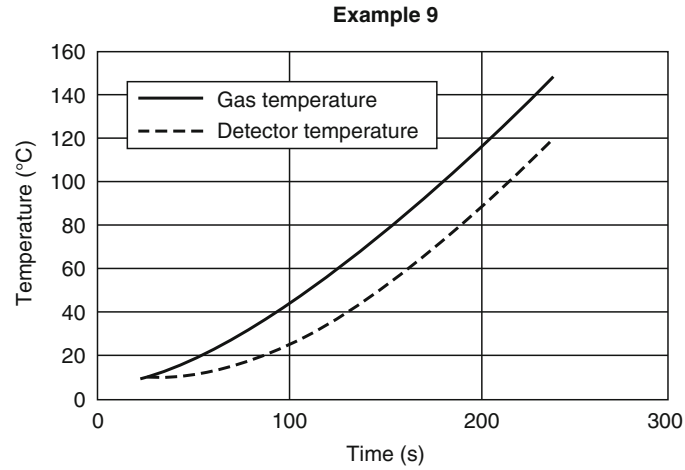

Fig. 40.10 Example 9: ceiling jet and detector temperature as a function of time

Table 40.12 Example 10: effects of sprinkler spacing on fire size at response and time to response

	$t_g = 200$ s		$t_g = 200$ s	
S (m)	t_r (s)	$\dot{Q}_T$(kW)	t_r (s)	$\dot{Q}$(kW)
3.0	350	3300	800	2700
3.7	370	3600	840	3000
4.6	400	4100	890	3400

the top of shafts since the fuel load is typically insufficient to actuate a sprinkler or affect persons in the cars.

Smoke detection is used in elevator lobbies and machine rooms to recall elevators to a safe level when smoke threatens the elevator shaft. The presence of sprinklers in the elevator machine room presents another risk: the possibility of water discharge on energized controllers and motors and on the elevator brakes. To reduce this risk, in addition to smoke detection, heat detectors may be used to ensure that equipment is de-energized on or prior to the discharge of water. To accomplish this task, some codes may require a heat detector with a lower temperature rating and a lower RTI within 0.61 m of every sprinkler in an elevator machine room. Are these requirements sufficient to assure response before the sprinkler to a range of possible fire scenarios?

Solution For this example, use an ambient temperature of 15 °C and a ceiling height or clearance of 4 m. Assume the actuation temperature of the sprinklers is 74 °C and the actuation temperature of the heat detectors is 57 °C. The RTI of the sprinklers is 110 $m^{1/2} \cdot s^{1/2}$, and the RTI of the detectors is 42 $m^{1/2} \cdot s^{1/2}$. Spacing of the sprinklers is 3.0 m. Calculate the response of the sprinkler and the heat detector to a fast fire, $t_g = 50$ s, and a slow fire, $t_g = 600$ s. Assume a 75 % convective fraction.

A sprinkler spacing of 3.0 m results in a worst-case radial distance of 2.12 m. The heat detector could be an additional 0.61 m beyond at $r = 2.73$ m. The results of the calculations are summarized in Table 40.13.

These calculations show that the heat detector will respond before the sprinkler. Depending on the actual conditions, additional calculations should be tried for different fire scenarios and for changes in other variables such as RTI, ambient temperature, ceiling clearance, and so forth.

Table 40.13 Example 11: sprinkler and heat detector response to different fire growth rates

	Response time (s)	
	$t_g = 50$ s	$t_g = 600$ s
Sprinkler	65	370
Heat detector	50	300

Smoke Detection

In order to determine whether or not a smoke detector will respond to a given $\dot{Q}_{cr}$, a large number of factors must be evaluated. These include smoke aerosol characteristics, aerosol transport, detector aerodynamics, and sensor response.

Smoke aerosol characteristics at the point of generation are a function of the fuel composition, the combustion state (smoldering or flaming), and the degree of vitiation of the combustion air. The characteristics considered include particle size and distribution, particle number or concentration at various sizes, composition, color, and refractive index. Given the dynamic nature of fire growth and spread and fuels involved, ventilation conditions will change over time, thus affecting the smoke produced.

Transport considerations include (1) changes to the aerosol characteristics that occur with time and distance from the source and (2) transport time. Changes in the aerosol largely relate to the particle size and concentration and result from the processes of sedimentation, agglomeration, and coagulation. Transport time is a function of the characteristics of the travel path from the source to the detector, which include ceiling height and configuration (sloped, beamed, etc.), intervening barriers such as doors, and buoyancy effects such as layering and thermal inversions.

Once smoke reaches the detector, other factors become important, namely the

aerodynamic characteristics of the detector and the type of sensor. The aerodynamics of the detector relate to the ease with which smoke can pass through the detector housing and enter the sensor. In addition, the location of the entry portion of the housing relative to the velocity profile of the detector normal to the plane of the ceiling is also a factor. Finally, different sensing modes (e.g., ionization or photoelectric) will respond differently, depending on the characteristics of the transported aerosol. Within the family of photoelectric devices, there will be variations depending on the wavelengths of light and the scattering angles employed. Also, algorithms used to sample and weight the sensor's response are introduced by the manufacturer and affect the detector's response.

Standard practice for the design of smoke detection systems is much the same as that for heat detection systems. Recommended spacing criteria are established based on detector response to a specific parameter, such as the optical density within an enclosure. A variety of smoke tests are used to verify that the detector responds between defined upper and lower activation thresholds and within required response times to a range of different types of smoke. This information translates into recommended spacing criteria intended to ensure that the detector responds within defined parameters. In some cases, the recommended spacing can be increased, or must be decreased, depending on factors such as compartment configuration and air flow velocity [8].

In applications where estimating the response of a detector is not critical, the recommended spacing criteria provide sufficient information for the design of a basic smoke detection system. If the design requires detector response within a certain time frame, optical density, specified heat release rate, or temperature rise, then additional analysis may be required. In this case, information concerning the expected fuel, fire growth, sensor, and compartment characteristics is required. The following examples show various performance-based approaches to evaluating smoke detector response.

Modeling Smoke Detector Response: General

The response of smoke detectors to fire conditions is not easily modeled. The response characteristics of smoke detectors vary widely compared with thermal detectors. In addition, less is known about the production and transport of smoke in the early stages of a fire. Natural and forced air currents have a larger effect on the movement of smoke at the time of interest (very early in the fire) than they do on the stronger thermal currents required to alarm heat detectors.

A comparison of how smoke detectors operate with the smoke measurement methods most often employed and reported by researchers shows that smoke measurements do not generally include the factors that we need to model smoke detector response [13]. Thus, there is a gap between the data generated by fire researchers and the data needed to model smoke detector response.

For example, fire researchers most often measure and report data on heat release rate, temperature and velocity of fire gases, and the optical density or obscuration per unit distance of the smoke at various locations. Of these, only optical density and obscuration relate to smoke. Although called *obscuration*, it is more accurately called *attenuation* since the light beam may be absorbed, reflected, or refracted by the smoke. These are calculated as follows:

Percent obscuration, O:

$$O = 100\left(I - \frac{I}{I_0}\right)$$

Percent obscuration per unit distance, O_u

$$O_u = 100\left[1 - \left(\frac{I}{I_0}\right)^{1/I}\right]$$

Optical density, D

$$D = \log_{10}\left(\frac{I_0}{I}\right) = -\log_{10}\left(\frac{I}{I_0}\right)$$

Optical density per unit distance, D_u (m^{-1})

$$D_u = \frac{D}{l} = \frac{1}{l}\log_{10}\left(\frac{I_0}{I}\right) = -\log_{10}\left(\frac{I}{I_0}\right)\mathrm{m}^{-1}$$

where I_0 is the initial intensity of a light beam reaching a photocell, I is the intensity of the light beam in the presence of smoke, and l is the distance between the source and the photocell.

Optical density and obscuration are useful data for evaluating visibility. However, the only commercially available smoke detector that operates by sensing the attenuation of a light beam is the projected-beam-type smoke detector. Further, these measurements are sensitive to the wavelength of light used. Thus, to be valuable for estimating the response of a projected-beam smoke detector, the data must be measured and reported using the same wavelength as the light source used by the detector.

The two most common types of smoke detectors are ionization type and photoelectric type. Neither type operates using light attenuation. Without a correlation between the optical density data and the response characteristics of a particular detector, accurate modeling is not possible.

In addition, detectors often use complex response algorithms rather than simple threshold or rate-of-change response levels. The algorithms are used to reduce false and nuisance alarms and to enhance fire signature matching. These algorithms vary from detector to detector and are generally not published by the manufacturers. Thus, even if correlations between optical density and the response of scattering- and ionization-type smoke detectors were available, the actual response of each model is affected by the signal sampling algorithm.

Nevertheless, there are methods that can be used to grossly estimate smoke detector response. These estimation methods may not provide accurate prediction of time to detector response because the potential errors in the estimation methods are not generally known and the response algorithms for a particular detector are not known. Without knowledge of the accuracy of the models and the potential errors, these estimation methods should not be used to compare detector response to other model calculations such as egress time calculations or time to untenability. Estimation methods are best used to compare changes in the response of a particular detector as a result of changes in spacing or location, while holding all other variables constant.

In addition to these estimation methods, actual fire tests with detectors present may provide information to compare smoke detector response to other factors such as egress time, structural response, heat release rate, and so forth. Product performance tests may be sources of data. Although the actual response may not be reported in manufacturer's literature, the minimum and maximum permissible performance imposed by the test standard provides ranges of possible response.

Modeling Smoke Detector Response: Light Obscuration Smoke Detectors

For projected-beam-type detectors, fire or smoke models that calculate the optical density per unit length, D_u, in a space or the total optical density in the path of the detector, D, may be used to determine when the detector would respond. Manufacturer specifications will typically indicate at what levels of total obscuration or total optical density the detectors respond. Projected-beam smoke detectors generally have adjustable response thresholds.

Many fire models estimate the unit optical density, D_u, in a uniform upper layer or volume. This method is referred to as zone modeling. The optical density over the entire length of the beam is then determined by multiplying D_u by the path length, l. The path length is the distance between the source and receiver or the projected-beam smoke detector. This method assumes homogenous distribution of smoke throughout the path, an assumption that may not be valid.

Another method to model the response of projected-beam obscuration-type detectors is to calculate the unit optical density, D_u, at several discrete points or in several discrete segments between the source and the receiver of the projected-beam smoke detector. This approach

is a form of field modeling. The optical density per unit length is then multiplied by the length of that particular segment. The total optical density of the path is then the sum of all of the densities for the individual segments.

Modeling Smoke Detector Response: Light Scattering (Photoelectric) Smoke Detectors

The amount of light scattered by smoke is very complex and is related to factors such as the particle number density and size distribution, refractive index, the wavelength of the light source, and the angle between the source and the receiver. Some of these variables can be described by the manufacturer for a particular detector. Some require information about the smoke produced by the fuel and its transport to the detector location.

Information about smoke properties related to light scattering is presently limited to a few types of fuels and is not readily available to practicing fire protection engineers. In addition, the data may not be in a useable format. For instance, the data must match the wavelength of the light source used in the detector being modeled. Scattering data at other wavelengths introduces errors and uncertainties.

Meacham has shown that it is possible to model the response of light-scattering detectors using information about smoke properties obtained by small-scale testing of various fuels [31, 32]. However, the recommended test methods have not been further developed, tested, or incorporated into fire test programs.

At the present time, there are no practical methods available to directly model the response of light-scattering-type detectors. However, obscuration or optical density modeling, as discussed above for obscuration-type detectors, can be used in a limited way to estimate scattering-type smoke detector response.

A scattering-type detector responds at different optical densities for different types of smoke. For example, a scattering-type smoke detector that responds at an optical density of .029 m^{-1} (2.0 %/ft obscuration) to smoke produced by a smoldering gray cotton lamp wick may not respond until an optical density of 0.15 m^{-1} (10 %/ft) is reached for smoke from a kerosene fire. At the response threshold, both types of smoke are scattering the same amount of light to the receiver of the scattering photoelectric smoke detector. There are many factors involved in this effect. One is that the darker smoke from the kerosene fire does not reflect as much light as the lighter colored smoke from the lamp wick.

Another way to understand the differing response of a scattering-type detector to two types of smoke is to consider the amount of light being scattered when both smoke samples have the same optical density. Both samples of smoke equally block our vision of the light reflected by an object. One type of smoke may be composed of large, highly reflective smoke particles that cause the incident light to scatter in many directions. Thus, it reduces the amount of light in the forward direction. The other type of smoke may consist of a smaller number of larger particles that absorb light more readily than they reflect it. Though they have equal optical densities, one is more likely to scatter light and set off a scattering-type detector.

In order to model the response of a scattering-type detector using obscuration or optical density, it is necessary to know the optical density required for a particular type of smoke to alarm a particular model detector. For example, many manufacturers label their smoke detectors with a unit optical density, D_u, or unit obscuration, O_u, based on a calibration test that is part of UL standard number 268 [33]. That number indicates the unit optical density required for that detector to respond to smoke having very specific characteristics. The optical density required to alarm a particular detector as quoted by the manufacturer is just one value for a given particle size distribution, concentration, color, and so on used in the laboratory calibration test of that model detector. If the smoke and conditions are similar to that used in the test of the detector, the specified alarm threshold can be used in calculations.

It is not sufficient to have data for a particular fuel and detector combination. It is known that smoke changes as it moves away from a fire [34]. There may be changes in the number, size, shape, and velocity of the particles. The optical density at response to any smoke signature other than the laboratory calibration test will be different and will vary with different fuels and burning modes.

Threshold response data to various fuels for a particular detector are not readily available. Some manufacturers may provide data if available and when requested. Product performance and safety tests as well as fire tests with detectors present are useful sources of limiting performance data. Product standards typically test detectors in rooms with specified fuels and smoke buildup rates and velocities. The detectors must respond at certain levels or within certain time limits. Although the exact performance data may not be made available, the test limits are useful for estimating the range of possible detector response.

Geiman and Gottuk [35] have provided further guidance on selecting general optical density (OD) at alarm thresholds. This guidance was developed from data collected from full-scale tests conducted by the U.S. Navy [36, 37], the Fire Research Station [38], and the Indiana Dunes Tests [39] using a wide variety of ion and photoelectric smoke detectors with smoldering and flaming fires. Table 40.14 presents the arithmetic means of the cumulative 20, 50, and 80 % of the OD at alarm thresholds for each combination of detector and fire type. The data represent nominal sensitivity values ranging from 0.0071 to 0.0288 OD/m (0.5–2 %/ft) for ionization detectors and from 0.0071 to 0.0508 OD/m (0.5–3.5 %/ft) for photoelectric detectors. These ranges capture most alarm settings for which the detectors will be used in practice.

Geiman and Gottuk also investigated using the "nominal" detector sensitivity, that determined by a standard laboratory test such as UL. They determined that using the nominal sensitivity as the alarm threshold provides extremely poor results. They found the majority of the 20 % OD alarm thresholds were greater than the nominal sensitivity levels of the detectors indicating that premature detector response was predicted. Except for ionization detectors with flaming fires, using the nominal sensitivity of the detector as the alarm threshold with OD/m data would only have been approximately 21 % effective at signifying an actual alarm based on the data studied. The use of the nominal detector sensitivity as an alarm threshold will generally result in predicting alarms before they actually occur. However, their results suggested that typical responses (i.e., 50 %) of ionization detectors with flaming fires could be reasonably predicted using the nominal sensitivity.

The Geiman and Gottuk work evaluated the use of an alarm threshold of 0.14 OD/m (9.4 %/ft) for modeling. This OD/m value represents the upper bound in the UL smoke detector tests [40, 41] and was compared to the optical density measurements at the time of alarm for all cases in the test data set. They found that, using the nominal detector sensitivity, the alarm threshold of 0.14 OD/m provided a much higher level of certainty that a detector will have alarmed. At a measured smoke optical density of 0.14 OD/m in the tests, 91 % of the ionization detectors alarmed for flaming fires and

Table 40.14 Average OD alarm thresholds for all test series and nominal detector sensitivities

OD alarm threshold (%)	Fire type	Ionization detectors (OD/m)	Photoelectric detectors (OD/m)
20	Flaming fires	0.007 ± 0.004	0.031 ± 0.016
	Smoldering fires	0.045 ± 0.028	0.032 ± 0.016
50	Flaming fires	0.021 ± 0.005	0.063 ± 0.029
	Smoldering fires	0.113 ± 0.048	0.059 ± 0.019
80	Flaming fires	0.072 ± 0.027	0.106 ± 0.039
	Smoldering fires	0.176 ± 0.052	0.110 ± 0.034

Source: Geiman and Gottuk [35, p. 204]

65 % for smoldering fires. Similarly, 86 % of the photoelectric detectors alarmed for flaming fires and 85 % for smoldering fires at a measured smoke optical density of 0.14 OD/m. For all but one case, over 75 % of the photoelectric detectors alarmed for both flaming and smoldering fires.

According to Geiman and Gottuk [35], an alarm threshold of 0.14 OD/m provides a relatively high level of confidence in predicting detector alarms. However, that value is not necessarily optimized or narrowly defined. For example, many detectors alarmed at OD/m values less than 0.14 OD/m. The use of this alarm threshold will lead to estimated alarm response times that are potentially longer than would actually occur [35].

Modeling Smoke Detector Response: Ionization Smoke Detectors

The signal produced by the chamber of an ionization detector has been shown to be proportional to the product of the number of particles and their diameter [42–45]. The exact signal produced by an ionization smoke detector is given by a more complex equation in the literature and requires an additional number called the chamber constant. The chamber constant varies with each different model of detector.

Given the quantity and size distribution of smoke particles and the chamber constant (from the manufacturer), it is possible to model the ionization smoke detector. Unfortunately, there are no fire models that provide the required detector model input. In addition, manufacturer specifications do not presently include chamber constants.

Newman modified the chamber theory to account for ionization detector sensitivity to the small electrical charge carried by some fire aerosols [46]. Newman also developed a method to model ionization smoke detector sensitivity as a function of the soot yielded by a particular fuel. Using his method, the change in a detector's signal, ΔI, can be related to the optical density of smoke measured at a particular wavelength, $D_{u\lambda}$.

To use the method proposed by Newman it is necessary to know what change in detector chamber signal, ΔI, will cause a detector or system to alarm. Although manufacturers do not presently provide these data, they may be persuaded to do so in the future.

Newman's work was done using a small-scale apparatus and three ionization smoke detectors. A wider range of tests, including some full-scale testing, is needed to verify this method. Presently, the only way to model ionization detector response is to use the optical density estimations as discussed for scattering-type photoelectric smoke detectors.

Modeling Smoke Detector Response: Entry Resistance

In addition to smoke characteristics and the detector's operating mechanism, the ability to get the smoke into the chamber affects the response of the unit. For spot-type photoelectric- and ionization-type smoke detectors, entry resistance is caused by bug screens, chamber design, and the detector's aerodynamic characteristics.

In a scenario where the optical density at the detector location is increasing with time, the optical density inside the detector chamber will always be less than that outside the detector chamber. Similarly, if a detector is placed in a smoke stream having a constant optical density, there will be a time delay before the optical density inside the chamber approaches that outside the detector. As with heat transfer to heat detectors, smoke entry resistance can be characterized by a detector time constant, τ:

$$\frac{dD_{\mathrm{ui}}}{dt} = \frac{1}{\tau}(D_u - D_{\mathrm{ui}})\mathrm{s}^{-1} \cdot \mathrm{m}^{-1}$$

where

$D_{\mathrm{ui}}(\mathrm{m}^{-1})$ = Optical density per unit length inside the detector chamber
$D_u(\mathrm{m}^{-1})$ = Optical density per unit length outside the detector
τ = Detector time constant (s)

If the time constant and the rate of change of optical density outside the detector are constant,

then this equation can be solved. Further, substituting D_{ur} for the optical density outside the detector at response and D_{uo} for the optical density required inside the detector to produce response yields the following: [47, 48]

$$D_{ur} = D_{uo} + \tau\left(\frac{dD_u}{dt}\right) \times \left\{1 - \exp\left[-D_{ur}\frac{1}{\tau}\left(\frac{dD_u}{dt}\right)\right]\right\} \mathrm{m}^{-1}$$

Heskestad proposed that the time constant could be represented by the following:

$$\tau = \frac{L}{u} \mathrm{s}$$

where L is the detector's characteristic length and u is the velocity of the ceiling jet flowing past the detector.

The characteristic length is thought to be a property of the detector that is independent of the smoke and ceiling-jet properties. It is interpreted as the distance the smoke would travel at the velocity u before the optical density inside the detector reaches the value outside of the detector. Combining the equations,

$$D_{ur} = D_{uo} + \frac{L}{u}\left(\frac{dD_u}{dt}\right) \times \left\{1 - \exp\left[-D_{ur}\frac{u}{L}\left(\frac{dD_u}{dt}\right)\right]\right\} \mathrm{m}^{-1}$$

The exponential term is small compared to the rest of the equation, allowing the equation to be simplified [47]. Simplification of the equation is not necessary when calculations are made using a computer. However, the simplified form clearly shows the effect of entry resistance:

$$D_{ur} = D_{uo} + \tau\left(\frac{dD_u}{dt}\right) m^{-1}$$

or

$$D_{ur} = D_{uo} + \frac{L}{u}\left(\frac{dD_u}{dt}\right) m^{-1}$$

This form of the entry resistance equation clearly shows that when the optical density outside a detector is increasing with time, the optical density inside the detector will lag behind if there is any entry resistance.

Heskestad and, later, Bjorkman et al. [49] have plotted test data to determine the L number for a variety of smoke detectors. Additional work has been done by Marrion and by Oldweiler to study the effects of detector position and gas velocity on the L number [15, 50].

Bjorkman et al., Marrion, and Oldweiler all observed variations in L that may be attributed to a dependence on velocity. Marrion's and Oldweiler's data also imply that there may also be a dependence on the characteristics of the smoke. Table 40.15 below summarizes the results from the works cited above.

Examination of the data and analysis work cited above shows that more work needs to be done to study the effects of low velocities

Table 40.15 Range of characteristic length (L) numbers

Researcher	Ionization detector L (m)	Scattering detector L (m)
Heskestad [47]	1.8	15[a]
Bjorkman et al. [49]	3.2 ± 0.2[b]	5.3 ± 2.7[c]
Marrion [15]	Not tested	7.2,[d] 11.0–13.0[e] 18.4[f]
Oldweiler [50]	4.0–9.5[g]	Not tested
	4.3–14.2[h]	

[a]Older style detector with more elaborate labyrinth
[b]L determined by best fit for three test velocities
[c]L based on a single test velocity and a limited number of tests (complete equation used)
[d]Low L number at low test velocity
[e]Range of L for several fuels and detector positions
[f]L increased by adding "fence" to further restrict smoke entry
[g]Range of L for a variety of velocities using simplified equation for entry resistance
[h]Range of L for a variety of velocities using simplified equation for entry resistance

and smoke characteristics on detector entry characteristics. The sharp increase in L at lower velocities appears to indicate that entry resistance may be related to smoke particle size. It is also possible that L is a function of the smoke momentum at low velocities. Thus, the time lag would be inversely proportional to the velocity squared.

Engineers can use L as a measure of entry resistance and the resulting time lag. However, in scenarios where the ceiling-jet velocity is low, there will be greater uncertainty in the results.

Without validation of L as a measure of lag time, manufacturers and test laboratories are not measuring or reporting L in their literature. Nevertheless, the range of L numbers reported in Table 40.15 can be used to estimate possible errors in detector response time.

Smoke Detection Calculation Examples

Example 12 The smoke level measured outside of a detector at the time of response in a laboratory calibration test is listed on manufacturers' specifications as the optical density or obscuration required to alarm the unit. Because of entry resistance, the smoke level inside the detector will be less. The specified response is for a particular type of smoke and is measured in a laboratory test apparatus. An example of one calibration test is the gray smoke test listed in the UL 268 smoke detector test standard [33].

In the test, the smoke detector response threshold must not exceed 0.0581 m^{-1} (4.0 %/ft). Velocity in the test chamber is 9.8 m/min. The test starts with clear air. A smoldering cotton lamp wick is used to increase the optical density in the test chamber. The rate of increase of optical density in the chamber must fall within the following limits:

$$3.7 \times 10^{-3} \leq \frac{dD_u}{dt} \leq 5.3 \times 10^{-3}\ \mathrm{m}^{-1} \cdot \mathrm{min}^{-1}$$

What is the range of optical density inside of the detector at the time of response (D_{uo}) if the detector has an L of 3 m? What would it be if the detector had an L of 14 m?

Solution For $L = 3$ m and $dDu/dt = 3.7 \times 10^{-3}\ \mathrm{m}^{-1} \cdot \mathrm{min}^{-1}$,

$$D_{\mathrm{ur}} = D_{\mathrm{uo}} + \frac{L}{u}\left(\frac{dD_u}{dt}\right)\ \mathrm{m}^{-1}$$

$$D_{\mathrm{uo}} = D_{\mathrm{ur}} - \frac{L}{u}\left(\frac{dD_u}{dt}\right)\ \mathrm{m}^{-1}$$

$$D_{\mathrm{uo}} = 0.0581 - \frac{3}{9.8}\left(3.7 \times 10^{-3}\right) = 0.057\ \mathrm{m}^{-1}$$

For $L = 3$ m and $dD_u/dt = 3.7 \times 10^{-3}\ \mathrm{m}^{-1} \cdot \mathrm{min}^{-1}$,

$$D_{\mathrm{uo}} = 0.0581 - \frac{3}{9.8}\left(5.3 \times 10^{-3}\right) = 0.056\ \mathrm{m}^{-1}$$

For $L = 14$ m and $dD_u/dt = 3.7 \times 10^{-3}\ \mathrm{m}^{-1} \cdot \mathrm{min}^{-1}$,

$$D_{\mathrm{uo}} = 0.0581 - \frac{14}{9.8}\left(3.7 \times 10^{-3}\right) = 0.053\ \mathrm{m}^{-1}$$

For $L = 14$ m and $dD_u/dt = 5.3 \times 10^{-3}\ \mathrm{m}^{-1} \cdot \mathrm{min}^{-1}$,

$$D_{\mathrm{uo}} = 0.0581 - \frac{14}{9.8}\left(5.3 \times 10^{-3}\right) = 0.051\ \mathrm{m}^{-1}$$

These calculations indicate that the actual quantity of this particular type of smoke required to alarm the detector varies from 0.051 to 0.057 m^{-1} or from 3.5 to 3.9 %/ft.

Smoke Production and Characteristics The fuel characteristics of primary concern for smoke detection are (1) material and (2) mode of combustion. These two parameters are important for determining pertinent features of expected products of combustion, such as particle size, distribution, concentration, and refractive index. The importance of these features with regard to smoke detection are well documented [6, 31, 32] and are discussed by Mulholland [34] Assuming a well-mixed smoke-filled volume, data on smoke characteristics for given fuels can provide an estimation of detector response.

Example 13 The design objective is to detect the smoke from a flaming 200 g (0.5 lb)

polyurethane pillow in less than 2 min. The pillow is located in a 36 m^2 room with a ceiling height of 2.5 m (8 ft). Assume that the pillow is burning at a steady rate of 50 g/min. Can the design objective be met? What assumptions are required?

Solution The total mass loss at 2 min is 100 g. Given this information, the optical density in the room can be calculated from the relationship [34]:

$$D_u = \frac{D_m M}{V_c} \tag{40.27}$$

where D_m (mass optical density [m^2/g]) can be taken from Mulholland [34] as 0.22 m^2/g.

$$D_u = \frac{(0.22\ \text{m}^2/g)\,(100\ \text{g})}{(36\ \text{m}^2)\,(2.5\ \text{m})} = 0.244\ \text{m}^{-1}$$

Assuming the detector will respond at the UL upper sensitivity limit of 0.14 m^{-1} (black smoke) [33], it can be assumed that the detector will respond within 2 min. This approach is simplified, however, and assumes that the smoke is confined to the room, is well mixed, can reach the ceiling level, and can enter the detector.

Example 14 Polyurethane mattresses are stored in a room that is 50 m × 75 m × 10 m high. A goal has been set to detect a flaming fire before approximately 350 g of fuel has been consumed. Using a projected beam smoke detector with sensitivity settings that can vary from 20 % to 70 % total obscuration in 10 % increments, what is the minimum sensitivity setting for response to this fire? Assume the smoke is mixed evenly throughout the space.

Solution The mass optical density, D_m, for a flaming polyurethane mattress is given in this handbook on page 2–298 as 0.22 m^2/g. The volume of the room is 37,500 m^3.

From the equation for mass optical density, calculate the resulting unit optical density in the room when 350 g of fuel is consumed:

$$D_m = \frac{D_u V}{\Delta m}\ \text{m}^2/\text{g}$$

$$D_u = \frac{\Delta m D_m}{V}\ \text{m}^{-1}$$

$$D_u = \frac{350(0.22)}{37,500} = 0.002\ \text{m}^{-1}$$

Knowing D_u and assuming the path length of the beam to be 75 m, the ratio of light reaching the receiver of the unit can be calculated:

$$\frac{I}{I_0} = 10^{-D_u I}$$

$$\frac{I}{I_0} = 10^{-0.002(75)} = 0.708$$

Next, the percent obscuration caused by the smoke is calculated:

$$O - 100\left(1 - \frac{I}{I_0}\right)$$

$$O = 100(1 - 0.708) = 29.2$$

Thus, a projected-beam smoke detector would have to be set to respond at about 30 % total obscuration or less to meet the design objective.

Discussion Related to the Use of D_m The previous two examples used the mass optical density, D_m, to calculate the expected optical density, D_u, in a space when a certain mass of fuel was consumed. D_m data are typically measured in small-scale tests due to the need for accurate measurements of mass loss and optical density. The use of D_m from small-scale tests to calculate the resulting D_u in a large-scale scenario introduces error. Some comparisons show qualitative correlation. However, it has been reported that the correlation breaks down with complex fires [34].

Stratification In the context of this chapter, smoke dilution refers to a reduction in the quantity of smoke available for detection at the location of the detector. This dilution can occur either through natural convection (entrainment in the plume or the ceiling jet) or by effects of a heating or ventilation system. In many cases, forced

ventilation systems with high exchange rates cause the most concern. In the early stages of fire development, when smoke production rate is small and the plume is weak, smoke can easily be drawn out of the room and away from area smoke detectors. In addition, high velocity air flows out of supply and into return vents creating defined patterns of air movement within a room. Such flows can either keep smoke away from detectors that are located outside of these paths, or, in some cases, inhibit smoke from entering a detector located directly in the air flow path.

Although there currently are no quantitative methods for estimating either smoke dilution or air flow effects on smoke detector siting, these factors must be considered qualitatively. It should be clear, however, that the air flow effects become larger as the required fire size at detection, $\dot{Q}_{cr}$, gets smaller. If the application warrants, it may be useful to obtain velocity profiles of the air movement within a room or to perform small-scale smoke tests under various conditions to aid in the smoke detector placement analysis.

The potential for smoke stratification is another concern in the detection of low-energy fires and fires in rooms or volumes with very high ceilings. Stratification occurs when the temperature within the plume equals that of the surrounding air, and there is insufficient thermal energy from the fire to force the smoke higher. Once this point of equilibrium is reached, the smoke layer will maintain its height above the fire, regardless of the ceiling height, until additional energy is provided.

Unlike the effects of air flow on smoke dilution, stratification effects can be calculated using the relationship [51]

$$\dot{q}_{\text{conv}} > 0.352 H^{5/2} T_s^{3/2} \qquad (40.28)$$

where

$\dot{q}_{\text{conv}}$ = Convective heat release rate in W

H = Distance from the top of the fuel package (base of the fire) to the ceiling level in m

T_s = Difference in ambient gas temperature in °C between the fuel location and ceiling level

This same relationship can also be found in NFPA 92B, *Standard for Smoke Management Systems in Malls, Atria, and Large Areas*, 2005 edition [52]. A more through treatment of stratification can be found in Chapter 2-1 of this handbook.

Example 15 The design objective is to detect the pyrolysis of overheated PVC cable insulation in a 7-m (23-ft) high, 100 m^2 (1076 ft^2) room. The room is air conditioned with a temperature differential of 10 °C (18 °F) between the base of the switch equipment and the ceiling. The proposed design has smoke detectors mounted at the ceiling level. Assuming the critical fire size is 1000 W, will there be sufficient thermal energy to force the smoke to the ceiling level?

Solution In this case, one can rearrange Equation 40.28 and solve for H:

$$H < \left(\frac{\dot{q}_{\text{conv}}}{0.352 T_s^{3/2}} \right)^{2/5}$$

where $\dot{Q}_{cr} = 1000$ W, and $T_s = 10$ °C (18 °F). This result indicates that the highest level of smoke rise is estimated to be 6 m (20 ft). As a result, the design objective may not be achieved by the proposed design. This approach is also valid for evaluating the effects of stratification in a high-ceiling room where a larger fire might be expected. However, the effects of heating and air conditioning systems and warm or cold walls are not considered.

Example 16 The design objective is to detect the flaming combustion of a chair located in the lobby of an office building in order to initiate smoke management functions. The lobby is located at the lowest level of a 20-m (64-ft) high atrium. The atrium has offices on three sides and a glass facade to the outside on the other. The atrium is air conditioned with a temperature differential of 20 °C (36 °F) between the lobby and the ceiling level. The proposed design is for smoke detectors to be mounted at the ceiling level. Is there sufficient thermal energy to force the smoke to the ceiling level?

Solution First, a value for $\dot{Q}_{cr}$ must be selected for the burning chair. From an analysis of the

chair and a review of published heat release data, it is determined that the chair most closely resembles the metal frame chair with padded seat used in Test 53 of the NIST furniture heat release rate tests [8]. This chair had a maximum heat release rate of 280 kW, which can be used as $\dot{q}_{\text{conv}}$ (or in this case $\dot{Q}_{cr}$, the critical fire) in Equation 40.28. Equation 40.28 can then be rearranged to solve for H:

$$H < \dot{Q}_{cr} / \left(0.352 T_{\text{s}}^{3/2}\right)^{2/5}$$

where $\dot{Q}_{cr} = 280{,}000$ W and $T_s = 20$ °C (36 °F). In this case, the highest point of smoke rise is estimated to be 38 m (125 ft). Thus, the smoke would be expected to reach the ceiling-mounted detector.

It should be noted that air flow concerns were not considered in Examples 10, 11, and 12. In some cases, a system supplying air at a low level and exhausting at an upper level may actually help transport the smoke to the upper levels of a room, where in other cases it may serve to inhibit smoke movement. It should also be noted that, simply because the smoke reaches the level of the detector, there is no guarantee that it can enter the sensor chamber.

Velocity Analog Spot-type smoke detectors, whether commercial or residential, or ionization- or light-scattering type, all require smoke to enter the detection chamber in order to be sensed. This requirement is another factor that must be considered when attempting to estimate smoke detector response. Smoke entry into the detector can be affected in several ways, for example, due to insect screens, chamber configuration, and proximity of the detector to the ceiling.

As previously discussed in this chapter, Heskestad [53] introduced the concept of smoke detector lag to explain the difference between the optical density outside (D_{ur}) and inside (D_{uo}) of a detector at the time of activation. Although studies of this relationship have provided useful information concerning smoke detector lag [15, 48], the difficulty in quantifying L for different detectors and relating it to siting requirements has limited its usefulness. In its stead, the concept of critical velocity (u_c) has been introduced [4, 54].

Critical velocity, in this context, refers to the lowest gas velocity required for smoke entry into the sensor chamber at a level to sound an alarm at a given threshold. Experimental work has shown this requirement to be in the range of 0.15 m/s for the detectors tested in one study [54]. When velocities fell below this value, the smoke level outside the detector at the time a specified analog output level was reached rose dramatically compared to levels when the velocity was above the critical value. This figure can be useful for design and evaluation purposes, as it is close to the low-velocity value (0.16 m/s) at which a detector must respond in the UL smoke detector sensitivity chamber in order to be listed [33]. Thus, the location of a velocity of 0.16 m/s in the ceiling jet for a given fire and ceiling height can be considered as a first approximation design radius for detector siting purposes. It should be noted that the ceiling-jet velocity correlations assume a horizontal, smooth ceiling. A detailed discussion of ceiling-jet flows by Alpert is presented in Chap. 14, "Ceiling Jet Flows." The critical velocity approach can be illustrated with a simplified example.

Example 17 The new owners of a hotel have established a fire detection design objective that the smoke detection system in the grand ballroom must be able to detect a 50 kW fire. The ballroom is 50 m (160 ft) long by 30 m (96 ft) wide with a 7.1-m (23-ft) high smooth ceiling. The existing smoke detectors are installed at a listed spacing of 10 m on center and have a critical velocity of 0.15 m/s. Assuming the fire starts at a point equally spaced between the existing smoke detectors, will the velocity of the ceiling jet from a 50 kW fire be sufficient to force smoke into the detection chamber? Assume there will be no ventilation system effects.

Solution The stated design objective is to detect a 50 kW fire. Because it is not stated whether the fire is steady state or growing, this solution will assume a steady-state fire of 50 kW. This

assumption allows the use of Alpert's [16] velocity correlations for a steady-state fire. Alpert provides two equations that can be used: one for $r/H = 0.15$, and the other for $r/H > 0.15$. This correlation is generally considered to be valid when r/H is between 0.15 and 2.1. Therefore, the ratio r/H must be determined first. In addition, the fire source should be at a distance of at least 1.8 times the ceiling height from the nearest enclosure wall.

The installed spacing is 10 m (32 ft) on center. Using the relationship $S = 2^{1/2}r$, the radial distance is found to be approximately 7.1 m (23 ft). Given that H is also 7.1 m (23 ft), the ratio r/H is found to be 1.0. This value is greater than 0.15; thus, the following equation can be used:

$$u = \frac{0.195\dot{Q}^{1/3}H^{1/2}}{r^{5/6}}$$

By entering the values of $\dot{Q} = 50$ kW, $H = 7.1$ m (23 ft), and $r = 7.1$ m (23 ft), a velocity of 0.37 m/s is calculated. This indicates that, for a steady-state 50 kW fire, there will be sufficient velocity to force smoke into the detectors at their existing locations.

However, if the 50 kW fire as stated is the design fire, $\dot{Q}_{do}$, and it was determined that the critical fire, $\dot{Q}_{cr}$, was only 5 kW, the resulting velocity using the steady-state correlation at 5 kW would be 0.17 m/s—very close to the critical velocity of 0.16 m/s. Furthermore, with a relatively small fire and a relatively high ceiling, stratification is likely to be a factor and should be considered. Assuming the room is air conditioned, with a temperature differential of 10 °C from the top of the fuel package to the ceiling level, the smoke from a 5 kW fire would stratify at a level of about 7.3 m (23.4 ft)—very close to the ceiling height of 7.1 m (23 ft). Given probable dilution of smoke and errors in approximations, it could be considered unlikely that a 5 kW fire would be detected under the defined conditions.

In addition to illustrating how the concept of critical velocity can be used for the design of smoke detection systems, it clearly points out the need to adequately define performance and design objectives, and to select correlations that fit those objectives. First, the objectives should be stated in terms of both the design fire and the critical fire. A 50 kW design fire is significantly different from a 50 kW critical fire, and the design for one may not meet the requirements for the other. Second, care should be taken in selecting a ceiling-jet velocity correlation that most closely fits the design objectives. Unless the hazard analysis indicates that the maximum fire size of $\dot{Q}_{do}$ will be 50 kW, it may be better to apply a ceiling-jet velocity correlation, based on a growing fire. In this case, the fire growth rate must also be estimated as part of the evaluation. The following example shows the importance of these factors by using the same ballroom as described in Example *17*, and provides more specific performance and design parameters.

Example 18 After additional consultation, the owners of the hotel described in Example 17 have modified their objectives as follows: assuming that a fire will begin in a chair, the smoke detection system for the grand ballroom must be able to detect the fire and initiate an internal response before it spreads beyond the chair of origin. The typical fuel load within the room consists of metal-framed chairs with padded seats and backs and plywood tables with cotton tablecloths.

The response time from when the alarm signal is indicated at the annunciator until the first staff member arrives is estimated to be 60 s. The delay time from detector activation until alarm initiation, as measured at the sensor, is 10 s. Because of the potential for nuisance alarms, the detection system employs an alarm verification feature that has a minimum delay time of 15 s and a maximum delay time of 60 s.

The existing smoke detectors are installed at a UL-listed spacing of 10 m on center and have a critical velocity of 0.15 m/s. Assuming the fire starts at a point equally spaced between the existing smoke detectors, and there are no ventilation system effects, can the existing smoke detection system be expected to meet the design objectives?

Solution The complete solution to a problem like this one may require several steps; for example, determination of the design fire, determination of the critical fire, estimation of ceiling jet velocity at $\dot{Q}_{cr}$, estimation of smoke production or optical density, and analysis of possible stratification effects. In all cases, however, determination of the design fire and the critical fire is essential.

Given that the goal is to detect the fire while in the chair of origin, a first step might be to estimate the fire size within the chair that could ignite the cotton tablecloth. From analysis of the chair and a review of published heat release data, it is determined that the chair most closely resembles the metal frame chair with padded seat and back used in Test 53 of the NIST furniture heat release rate tests [8]. This chair had a maximum heat release rate of 280 kW; a fire growth rate of ≈ 0.0086 kW/s^2; a growth time, t_g, of 350 s; and a virtual start time, t_v, of 50 s.

Assuming that the fire would likely grow up the seatback of the chair and that the seatback is located approximately 0.5 m from the tablecloth, an estimate of the energy output required for ignition of the tablecloth can be made. In this case, using the radiant ignition routine in FIREFORM [55] and assuming the fuel is easy to ignite (ignition flux of 10 kW/m^2) with a separation distance of 0.5 m, it is estimated that the tablecloth will ignite when the total energy output from the burning chair reaches 139 kW. These parameters define the design fire.

The next step is to calculate the time for the design fire to reach the threshold limit of 139 kW. Using the relationship $\dot{Q} = \alpha t^2$, a time of 118 s (about 2 min) is calculated. This calculation is growth time of the fire after it begins to follow an exponential growth rate until the design fire size is reached. Given that the fire would probably start as smoldering combustion, the actual growth time could be considerably larger (1 to 2 h possible).

The critical fire size can then be estimated by subtracting the various response times and estimating the heat release rate at that moment in time. In this regard, reasonable time delays should be used based on the information provided. The focus should be on obtaining the "most reasonable" worst-case delay for the situation. From the problem statement, this delay is estimated based on the response times given, using the following equation:

$$t_{\text{response}} = t_{\text{transport}} + t_{\text{verify}} + t_{\text{system}} + t_{\text{staff}}$$

where

$t_{\text{transport}}$ = Smoke transport time (unknown)
t_{verify} = Verification time (60 s maximum)
t_{system} = System response time (10 s)
t_{staff} = Staff response time (60 s)

Momentarily ignoring the smoke transport time and assuming prompt staff response, the result is a maximum detection system response time of 130 s. However, in an actual fire situation, the smoke detector verification time should be at its minimum of 15 s, and not at its maximum of 60 s. Making this assumption, the total response time (still ignoring smoke transport time) is 85 s. This result is less than the 127 s time to ignition of the tablecloth and is used to help define the critical fire size ($\dot{Q}_{cr}$).

Here, the 85 s is subtracted from the 127 s (that defines the design fire), and the relationship $\dot{Q} = \alpha t^2$ is used to calculate the heat release rate at that moment in time. The result is a heat release rate of 15 kW. Assuming no smoke transport time, this result would be the critical fire size at which detection must occur in order to detect the fire and cause the required response before the design fire size is reached.

The next step is to factor in a lag due to the smoke transport time. In order to account for smoke transport lag, Brozovsky [54] suggests a safety factor that is equivalent to a heat release rate that is 80 % of the maximum fire size at the time of detection. This factor would result in a critical fire size of 12 kW and a corresponding response time of 37 s. These values can then be used to determine if the ceiling-jet velocity will exceed 0.16 m/s.

Although several simplifications have been made, this example outlines a methodology for

estimating the potential for detector response, given the concepts of design fire and critical fire. In addition, the cross-checking utilized points out the importance of understanding the limitations and boundary conditions of correlations and empirical relationships (i.e., simply because one condition can be met, it does not automatically mean that all others will be met as well, and the complete scenario should be considered). Engineering of smoke detection, especially for low-energy fires, can be a difficult task, and the application of any method for this purpose should include clear statements of all assumptions made.

Temperature Approximation Method for Modeling Smoke Detection The temperature approximation theory is another method used to estimate the optical density produced by flaming fires. The theory hypothesizes that the mass concentration of smoke particles at a point is proportional to the change in temperature due to the fire (at that point) [56]. The following assumptions are necessary:

1. Particle size distribution is constant in space and time.
2. Mass generation rate is proportional to mass burning rate.
3. There is no heat transfer between particles or between the particles and the confining surfaces.
4. The smoke does not continue to react as it travels.

Heskestad then hypothesized that the ratio of optical density to temperature rise would be a constant for a particular fuel and burning mode (flaming, smoldering, vertical combustion, horizontal combustion, etc.). There are actually three parts to this hypothesis.

The first is that each fuel and burning mode results in a unique optical density required to alarm a particular model and type of detector. This aspect was discussed previously regarding photoelectric, ionization, and projected-beam smoke detectors. This phenomenon is regularly observed, explained by theory, and accepted by the scientific and engineering community.

The second part of the hypothesis is that for each fuel and burning mode the optical density at a point is proportional to the mass concentration of particles:

$$D_u \propto C$$

The final part of the hypothesis is that, for each fuel and burning mode, the mass concentration of particles is proportional to the change in temperature at a point:

$$C \propto \Delta T$$

Combining these proportionalities, optical density is proportional to the change in gas temperature for a given fuel and combustion mode:

$$D_u \propto \Delta T$$

Therefore, the ratio of optical density to temperature rise is constant for a given fuel:

$$\frac{D_u}{\Delta T_g} = \text{Constant}$$

This hypothesis assumes that the only way to move the smoke particles from the source to the detector at the ceiling is by buoyant forces.

Heskestad and Delichatsios examined experimental data for obscuration and temperature rise at various locations on a ceiling for different fuels. They concluded that while the data showed some variation in time at different radial positions relative to the fire source, the ratio could be approximated as a constant. Table 40.16 lists the ratios recommended by Heskestad and Delichatsios for various fuels.

Examining the original data, the last column has been added to show the range of values for each fuel. Averages have also been calculated and listed in the last row of the table for reference.

Others experiments have resulted in data that differ from that of Heskestad and Delichatsios. Bjorkman et al. reported values for polyurethane that are approximately one half that reported by Heskestad and Delichatsios [49]. The data produced by Heskestad and Delichatsios show the ratio of optical density to temperature rise was

Table 40.16 Ratios recommended by Heskestad and Delichatsios for various fuels

Material	$D_u/\Delta T$ (1/m °C)	Range of values
Wood	1.2×10^{-3}	8.9×10^{-4} to 3.2×10^{-3}
Cotton	$5.9 \times 10^{-4}/1.2 \times 10^{-3}$	3.0×10^{-4} to 1.8×10^{-3}
Paper	1.8×10^{-3}	Data not available
Polyurethane	2.4×10^{-2}	1.2×10^{-2} to 3.2×10^{-2}
Polyester	1.8×10^{-2}	Data not available
PVC	$3.0 \times 10^{-2}/5.9 \times 10^{-2}$	5.9×10^{-3} to 5.9×10^{-2}
Foam rubber PU	7.7×10^{-2}	Data not available
Average	2.4×10^{-2}	3.0×10^{-4} to 7.7×10^{-2}

not constant. The authors concluded that the variation was the result of slowly changing characteristics of the smoke particles as they left the flaming source and traveled in the plume and ceiling jet. Nevertheless, they concluded that a constant value could be used as a rough approximation to allow engineers to model optical density produced by a fire. Although it has not yet been done, it is possible to examine their original data and place error bars on the values recommended in Table 40.16.

A fire model can be used to calculate the temperature rise at a smoke detector location or in a layer. Then, using the ratios reported by researchers, the optical density at that location as a function of time can be approximated.

Discussion Related to the Use of fire Models for Heat and smoke Detector Modeling Some computer fire models or sets of computational tools include routines for calculating heat or smoke detector response. It is important for users to understand the underlying detector models being used so that limitations and potential errors can be understood. For heat detection, most computational tools use a lumped mass model as described in this chapter. However, for smoke detection some use a temperature rise model, and some use a mass optical density or specific extinction area model. The specific extinction area is similar to the mass optical density except that it is based on calculations using the natural log, e, rather than $\log_{10}$. Most do not include entry resistance modeling. Some permit the use of fuel-specific parameters for smoke yield and mass optical density. Others use preset values.

Radiant Energy Detection

During the combustion process, electromagnetic radiation is emitted over a broad range of the spectrum. Currently, however, fire detection devices operate only in one of three bands: ultraviolet (UV), visible, or infrared (IR), where the wavelengths are defined within the following ranges: [8]

Ultraviolet	0.1–0.35 μm
Visible	0.35–0.75 μm
Infrared	0.75–220 μm

Selection of a specific sensor type for fire detection is based on a number of factors, including fuel characteristics, fire growth rate, ambient conditions, resulting control or extinguishing functions, and environmental conditions in the detection area. More specifically, it includes evaluation of the radiant energy absorption of the atmosphere, presence of nonfire-related radiation sources; the electromagnetic energy of the spark, ember, or fire to be detected, the distance from the fire source to the sensor; and characteristics of the sensor.

These factors are important for several reasons. First, a radiation sensor is primarily a *line-of-sight* device, and must "see" the fire source. If there are other radiation sources in the area, or if atmospheric conditions are such that a large fraction of the radiation may be absorbed in the atmosphere, the type, location, and spacing of the sensors may be affected. In addition, the sensors react to specific wavelengths, and the fuel must emit radiation in

the sensors' bandwidth. For example, an infrared detection device with a single sensor tuned to 4.3 μm (the CO_2 emission peak) cannot be expected to detect a noncarbon-based fire. Furthermore, the sensor must be able to respond reliably within the required time, especially when activating an explosion suppression system or similar fast-response extinguishing or control system.

Once the background information has been determined, the detection system can be designed. Standard practice for the design of radiant energy detection devices is based on application of generalized fire size versus distance curves that are derived using the inverse square law: [8]

$$S = \frac{kP\exp^{\zeta d}}{d^2}$$

where

S = Radiant power reaching the detector (W)
k = Proportionality constant for the detector
P = Radiant power emitted by the fire
ζ = The extinction coefficient of air
d = The distance between the fire and the detector

This relationship is used to produce sensor response information for specific fuels. By then plotting the normalized fire size versus the normalized distance, the resulting curve defines the maximum distance at which the tested sensor can be expected to consistently detect a fire of a defined size (usually provided in m^2). By testing a sensor using various fuels, a family of curves can be developed to assist in system design. These curves (sometimes given in tabular form) are usually provided by the sensor manufacturer.

Before applying the distance obtained from such a curve, one must also consider the sensor's field of view. Because the radiation sensor is a line-of-sight device, the sensitivity of the device to a defined fire size decreases as the fire location is moved off the optical axis of the device. This result means that a fire of X m^2, which is detectable at a distance Y m on axis from the sensor, may not be detectable at the same distance Y m if it is located 30° off axis. Limitations of viewing angles are also provided by manufacturers.

Ambient conditions should also be considered as part of the evaluation and design process. Factors such as humidity and dust can affect the absorption of radiation in the atmosphere, thus limiting the amount of radiation reaching the sensor for a given fire size. Similarly, temperature can affect the relative sensitivity of a sensor. As the ambient temperature increases, the relative sensitivity can decrease. Even if the decrease is small, it can affect the response of the sensor to the expected fire.

Radiation Detection Example

Example 19 The design objective is to detect a 1.0 m^2 (11 ft^2) pool fire of JP4 aircraft fuel in a large hangar in order to activate a fixed suppression system. The hangar dimensions are 50 m (160 ft) by 80 m (257 ft) with a 20 m (64 ft) ceiling height. The ambient temperature at the ceiling level varies between 15 °C (59 °F) and 60 °C (140 °F), depending on time of day and season. The humidity also varies by season, with relative humidity of 90 % possible. What steps should be taken during system design?

Solution The first step should be selection of a detection device. Because the hazard is carbon based, IR detection at 4.3 μm is suitable. Also, because IR detectors generally provide a larger surveillance area per device than UV detectors, they could be more cost effective than UV detection in this case.

One should then determine possible sources of interfering radiation and select a device that is resistant to these extraneous sources. Such resistance to false response can be obtained by filtering, use of multiple sensors (e.g., two- or three-channel detector), or a combination.

The next step is to review the manufacturer's data to determine mounting criteria based on the size of the critical fire [1.0 m^2 (11 ft^2)]. Generally, this step begins with the fire size versus distance curve or table. If only a curve is provided, one must then determine the mounting height and lateral distance limits of the detector. Lateral distances are important as related to the sensors' field of view.

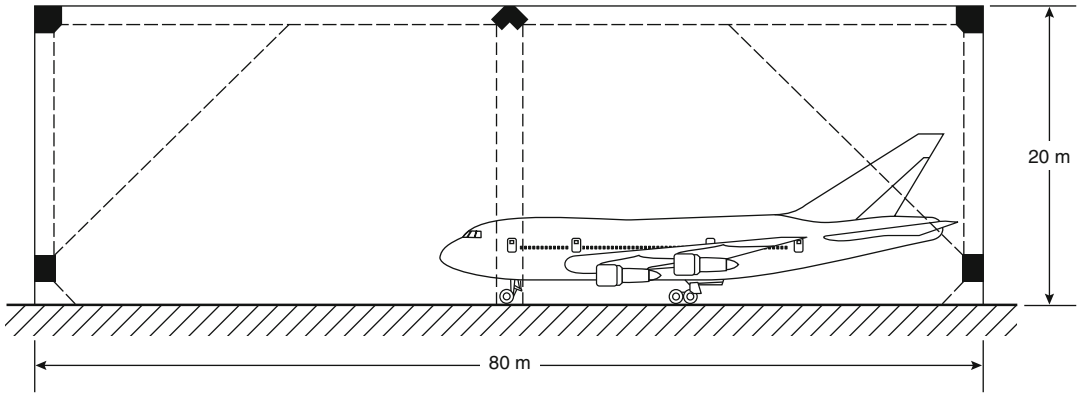

Fig. 40.11 IR detector layout for an aircraft hangar

Given this information, a device layout design can be made. This design should consider all possible obstructions, and result in all parts of the hangar being monitored. One such design is illustrated in Fig. 40.11.

As part of the layout, one should consider the possible effects of reduced device sensitivity due to angular displacement, temperature, and humidity. Because manufacturers' criteria vary on these parameters, typical values are used in this solution to illustrate their effects.

For example, the proposed layout has devices utilizing a field of view of 45°. Assuming the nominal sensitivity is such that a 1.0 m^2 (11 ft^2) fire can be detected at 40 m (128 ft), and there is a reduction in sensitivity of 30 % due to angular displacement, the distance at which a 1.0 m^2 (11 ft^2) fire can be detected at 45° is reduced to 28 m (90 ft). If the manufacturers' data indicate a further reduction in sensitivity for temperature, for example 3 % at 50 °C (122 °F) the distance is reduced to about 26.8 m (86 ft). If there are further reductions due to humidity, for example a 3% reduction at 90% relative humidity, the resulting detection distance at 45° is about 25.6 m (82 ft).

In this example, the viewing distance at 45° is a maximum of 20 m (64 ft), and the design can be considered valid. Had the sensitivity decreased such that the distance dropped below 20 m (64 ft), an alternative layout or different devices must be used. In all cases, the manufacturers' literature should be consulted to determine all pertinent increases or reductions in detector sensitivity due to fuel, distance, angular displacement, and environmental conditions.

Designing Fire Alarm Audibility

In most cases, the purpose of a fire detection and alarm system is to alert the occupants of a building that an emergency exists and to initiate evacuation. In situations such as high-rise or industrial buildings, it may be desirable to provide the occupants with more information, such as the nature and location of the fire. In either case, the purpose of the system is defeated if the signal is not heard and understood by the occupants.

This section demonstrates a method for fire protection engineers to estimate the relative effectiveness and cost of various fire alarm alerting systems during the design process. In the past, the selection and location of fire alarm devices has been based on experience and engineering judgment. The use of this simplified methodology can save thousands of dollars in retrofit costs required to correct deficiencies in an alarm system.

The transmission of sound from a source to a target is a function of many factors, such as humidity; air viscosity and temperature; the frequency of the signal; the location of the source relative to the target; the construction of walls, floors, and ceilings; and the furnishings in the

area. *Architectural Acoustics* [57] contains a good discussion of these and many other factors affecting sound transmission and loss.

Sound power and sound pressure levels are expressed in decibels (dB) relative to a reference. It is assumed that the reader is familiar with this system of measurement. Throughout this chapter sound power level (SWL or L_W) in decibels is referenced to 10^{-12} W. Sound pressure level (SPL or L_P) in decibels is referenced to 2×10^{-5} Pa. This discussion also assumes that the reader is familiar with the concept of A-weighting. The purpose of A-weighting is to adjust sound pressure level measurements to correspond as closely as possible to the way humans perceive the loudness of the many different frequencies we hear. For instance, a 1000 Hz signal at an SPL of 20 dB would be clearly audible. A 100 Hz signal at the same SPL would not be heard. A-weighting allows a single number to describe the SPL produced by a signal containing frequencies between 20 and 20,000 Hz. The weighting of the various frequencies is established by an internationally accepted A-weighting curve [58].

Typical fire alerting systems consist of a combination of audible and visual signals activated by fire detection systems. The audible devices are usually horns, bells, chimes, or speakers. The visual indicators are usually strobe lights, incandescent lamps, or, occasionally, revolving beacons.

In residential occupancies, fire alerting systems should be capable of awakening a sleeping person and informing him or her that a fire emergency exists. Several studies have been done to establish the sound pressure level required to achieve this goal [59, 60]. These studies suggest an SPL between 55 and 70 dBA will awaken a college-age person with normal hearing. The minimum required SPL is also a function of the background noise or signal-to-noise ratio. These levels establish the SPL required to alert or be audible. They do not address the problem of how the person will perceive the sound or react to it.

Until recently, fire codes did not set forth the SPL that a fire alarm system must produce within a building. *NFPA 72* [8] requires signals to be 15 dBA above ambient in areas where people may be sleeping. British standards require fire alarm signals to produce a sound pressure level of 65 dBA or 5 dBA above ambient noise in areas where occupants are not sleeping [61]. A sound pressure level of 75 dBA at the head of the bed is required in occupancies where people may be sleeping.

The audible design requirements listed above and the remaining discussion and examples in this section all use dBA as a measure of audibility. However, it should be pointed out that for a sound to be perceived as audible, it need only penetrate or be greater than the background noise level at one particular frequency bandwidth. For example, certain facilities such as manufacturing plants may have a background noise level in excess of 85 dBA. An installed fire alarm may produce only 75 dBA at a certain location. Nevertheless, occupants will hear and respond to the fire alarm system. Why? The reason is because the background noise that contributes to the 85 dBA is mostly low frequency sound and the fire alarm is mostly high and midrange frequencies. Figure 40.12 illustrates this concept. Like two picket fences, one behind the other, only one picket or octave band must be taller for us to perceive the presence of the second fence or signal. More discussion on this approach can be found in the *National Fire Alarm Code*. While the balance of this section uses dBA, the procedure and methods apply equally well to work done in a single frequency band.

Visual signals are located to assist people in deciphering potentially confusing alarm signals. The visual signals also help alert occupants in high background noise environments.

Butler et al. [58] have described a method to estimate sound pressure levels at some location remote from the sound source. Formulas presented in their study are analogous to standard sound attenuation formulas found in other references [59, 62]. They have been simplified by replacing complex terms with constants for which they have provided tables of data (see Tables 40.17, 40.18, 40.19, 40.20, 40.21, 40.22, 40.23, 40.24, 40.25, 40.26, 40.27, 40.28, 40.29, and 40.30). The equations and data presented in

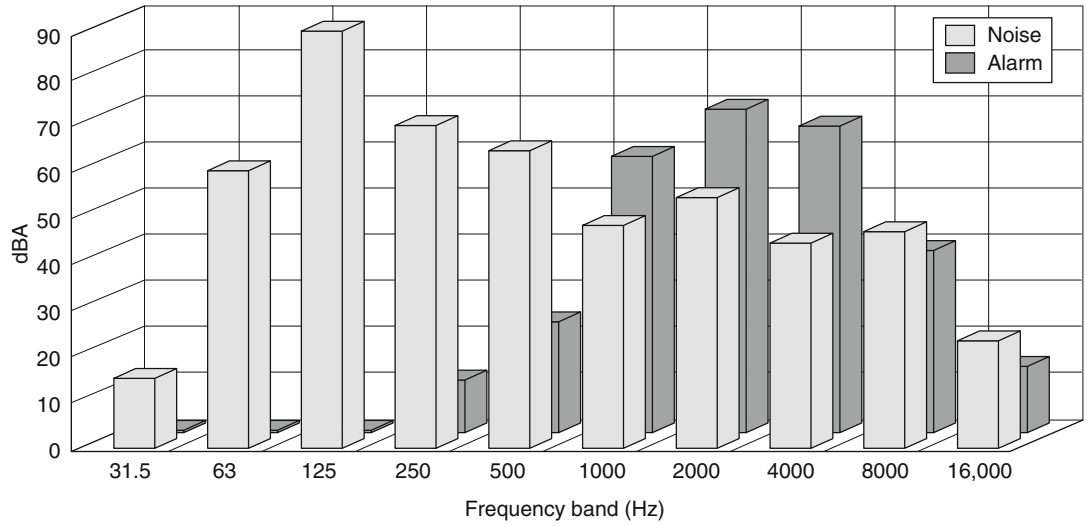

Fig. 40.12 Penetration of noise by alarm

Table 40.17 Adjustment for mounting position of sounder (C_1)

Sounder position	C_1
Wall/ceiling mounted (more than 1 m from any other major surface)	+5
Wall/ceiling mounted (closer than 1 m to one other major surface)	+7

Table 40.18 Adjustment for distance (C_2) with distance from source (m)

Distance from source (m)	C_2
1	−11
2	−17
3	−21
6	−27
12	−33
15	−35
20	−37
25	−39
30	−41
40	−43
50	−45
60	−47
80	−49
100	−51

their study provide a straightforward method for analyzing proposed designs. The same equations and data can be used to determine the power requirement and maximum allowable spacing of signaling devices required to achieve a specified sound pressure level. The technique presented in their study is suitable for acoustically simple buildings only and may not be suitable on their own for voice alarm systems. Complex building arrangements and materials may require a more rigorous analysis using other methodologies which are beyond the scope of this chapter.

In assessing signaling system design, one may have to consider estimating required sound levels for devices located within a space, external to the space, or in combination. With respect to the sound at a point within an enclosed space, one may need to consider direct and reverberant components [58]. The direct component is a function of the sound pressure level (SWL or L_W) and distance from the source. The reverberant component is affected by the characteristics and contents of the enclosure, including type and quantity of finishes and furnishings, with acoustically soft materials absorbing sound waves and acoustically hard materials reflecting them. In large open spaces, such as open plan offices or ballrooms, it has been found for sound power

Table 40.19 Adjustment for number of directions of sound propagation (C_3)

Number of directions	C_3
Single direction (e.g., positioned at one end of a corridor)	0
Two-directional (e.g., positioned in the length of a corridor)	−3
Three-directional (e.g., positioned at a T junction of corridors)	−5

Table 40.20 Adjustment based on the finishes in the corridor (C_4)

Surface finishes	C_4
Hard (e.g., walls and ceiling with solid surfaces and terrazzo floor)	0
Medium (e.g., acoustic ceiling, plastered solid walls with 5 % coverage of soft surfaces and floor of composite tiles)	−8
Soft (e.g., acoustic ceiling, plastered solid walls with 5 % coverage of soft surfaces and carpets on felt on concrete floor)	−9

Table 40.21 Adjustment for distance from source to midpoint of the partition (C_5)

Distance from source (m)	C_5
1	0
3	−4
6	−8
10	−10
12	−11
15	−12
20	−14
30	−15
50	−17

Table 40.22 Addition of two sound pressure levels

Difference between the two levels (dB to be added)	Add to the higher level (dB)
0	3
1	2
2	2
3	2
4	2
5	1
6	1
7	1
8 or more	0

Table 40.23 Factor for area of partition between sounder and receiver (C_6)

Partition area (m^2)	C_6
2	+3
4	+6
8	+9
10	+10
15	+11.5
20	+13
30	+15
50	+17
80	+19
100	+20
200	+23

Table 40.24 Adjustment for frequency of maximum output of sounders (C_7)

Frequency of sounder (Hz)	C_7
500	0
1000	−3
2000	−5
4000	−9

assessment of nonvoice signals, the reverberant component has little contribution and can be effectively ignored (note: this does not apply to voice signals where intelligibility is a concern and reverberation does play a role). For basic analysis of the situation where the alarm sounding device is located within the enclosed space, the sound pressure level needed at a defined point from the source can be determined by the following relationship:

$$L_P = L_W + C_1 + C_2 \text{ dBA}$$

where C_1 is a function of the mounting position of the sounder and C_2 is a function of the distance

Table 40.25 Second reduction indices (dB) for a selection of typical structures (100–3150 Hz frequency range)

Building element	Weight of partition (kg/m^2)	Average attenuation (dB)
Walls and partitions		
1. 100-mm-dense concrete with or without plaster	250	45
2. 150-mm "no fines" concrete with 12-mm plaster on both faces	250	45
3. 115-mm brickwork with 12-mm plaster on both faces	250	45
4. 115-mm brickwork unplastered	195	42
5. 300-mm lightweight concrete precast blocks with well-grouted joints	190	42
6. 75-mm clinker blockwork with 12-mm plaster on both faces	115	40
7. 50-mm-dense concrete	120	40
8. 25.4-mm plasterboard (two layers) separated by timber studding (75 mm) and mineral fiber blanket	—	40
9. 200-mm lightweight concrete precast blocks with well-grouted joints	122	40
10. 150-mm lightweight concrete precast blocks with well-grouted joints	93	37
11. 50-mm clinker blocks with 12-mm plaster on both faces	—	35
12. 63-mm hollow clay blocks with 12-mm plaster on both faces	—	35
13. 9.5-mm plasterboard (two layers) separated by timber studding (75-mm with 12-mm) with plaster on both faces	—	35
14. 6-mm plywood/hardboard (two layers) separated by timber studding (50- and 50-mm) mineral fiber blanket	—	30
15. 19-mm chipboard on a supporting frame	—	25
16. 0.8-mm sheet steel	—	25
17. 21-mm tongued and grooved softwood boards tightly clamped on a support frame	—	20
18. 3.2-mm hardboard (two layers) separated by 44-mm polystyrene core	—	20
Doors		
19. Flush panel, hollow core, hung with one large air gap	9	14
20. Flush panel, hollow core, hung with edge sealing	9	20
21. Solid hardwood, hung with edge sealing	28	26
Windows		
22. Single glass in heavy frame	15	24
23. Double-glazed 9-mm panes in separate frames 50-mm cavity	62	34
24. Double-glazed 6-mm panes in separate frames 100-mm cavity	112	38
25. Double-glazed 6-mm and 9-mm panes in separate frames 200-mm cavity, absorbent blanket in reveals	215	58

from the sounder to the point of concern. The values for C_1 and C_2 are given in Tables 40.17 and 40.18.

If the space of concern is large enough that the receiver (e.g., person in the room) can receive alarm signals (noise, sound) from more than one source, the combined noise level should be estimated. The combined noise level is not the arithmetic sum of the individual sound pressure levels (dBA); rather, it will be a level that corresponds to the arithmetic addition of the individual sound powers in watts. For the purpose of this methodology, the combined noise level at a particular receiver position can be estimated by first estimating the noise level from each sounder in the space (ignoring the existence of the other sounders) and then combining the noise level based on the difference in sound pressure levels using the values in Table 40.22. For example, if an estimated sound pressure level from one device is 65 dBA and is 63 dBA from another, the resulting total sound pressure level will be 67 dBA (from Table 40.22, the difference in noise level between the two sounders is 2 dBA, so 2 dBA is added to the higher sound pressure level value).

Table 40.26 Average sound reduction indices (dB) of partitions incorporating a door of 26 dB attenuation (i.e., heavy door with edge sealing) (100–3150 Hz frequency range)

Door representing percentage of total area of partition (%)	Sound reduction index of partition without glazing					
	25 dB	30 dB	35 dB	40 dB	45 dB	50 dB
100	26	26	26	26	26	26
50	25	27	28	28	28	28
25	25	28	30	31	31	31
10	25	28	32	34	35	35
5	25	28	33	36	38	38

Table 40.27 Average sound reduction indices (dB) of partitions incorporating a door of 14 dB attenuation (i.e., one with large air gaps) (100–3150 Hz frequency range)

Door representing percentage of total area of partition (%)	Sound reduction index of partition without glazing					
	25 dB	30 dB	35 dB	40 dB	45 dB	50 dB
100	14	14	14	14	14	14
50	16	16	16	16	17	17
25	19	19	19	19	20	20
10	21	23	23	23	23	23
5	23	25	26	26	26	26

Table 40.28 Average sound reduction indices (dB) of partitions incorporating a door of 20 dB attenuation (i.e., light door with edge sealing) (100–3150 Hz frequency range)

Door representing percentage of total area of partition (%)	Sound reduction index of partition without glazing					
	25 dB	30 dB	35 dB	40 dB	45 dB	50 dB
100	20	20	20	20	20	20
50	21	22	22	22	22	23
25	23	24	25	25	25	26
10	24	27	28	29	29	29
5	24	28	30	32	32	32

Table 40.29 Combined sound reduction indices for combination of standard doors and glazing (100–3150 Hz frequency range)

	Sound reduction index for standard size door (1.54 m^2)		
	14 dB	20 dB	26 dB
Area of (24 dB) glazing (m^2)	Insulation values for combined door and glazing		
1	16	21	25
2	17	22	25
4	18	22	24
6	19	23	24
8	20	23	24
10	20	23	24
12	21	23	24
16	21	23	24
20	22	23	24

Table 40.30 Average sound reduction indices for a partition whose surface is a combination of glass, door, and wall partition (100–3150 Hz frequency range)

Door + glazing as percentage of total partition area	Sound reduction value of partition without glazing or door											
	30 dB			35 dB			40 dB			45 dB		
	Insulation value of combined door and glazing (dB) (from Table 40.29)											
	15	20	25	15	20	25	15	20	25	15	20	25
5	26	28	30	28	31	33	28	32	36	28	33	37
10	24	27	29	24	29	32	25	30	34	25	30	35
20	22	25	28	21	26	31	22	27	32	22	27	32
30	20	24	28	20	25	29	20	25	30	20	25	30
50	18	23	27	18	23	28	18	23	28	18	23	28
75	16	21	26	16	21	26	16	21	26	16	21	26
100	15	20	25	15	20	15	15	20	25	15	20	25

For sounders located outside of the space of concern, one needs to consider additional factors, particularly if the arrangement is from a corridor to another space, such as an office, a hospital suite, or a hotel guest room. If the sounder is located in a corridor, for example, there may be directional considerations for the sounder, and consideration must also be given to the distance from the sounder to the partition separating the corridor and space of concern, in addition to the acoustical characteristics of the corridor. One then needs to consider the attenuation of the sound through the partition and the distance to the receiver. These factors are addressed in more detail in the following examples.

To demonstrate how signaling systems can be designed and analyzed, two scenarios will be considered. Both scenarios are based on a typical dormitory or office layout. The building has long corridors with rooms of equal size on each side. Each room is approximately 5 m wide by 6 m deep. The walls consist of two layers of Sheetrock (total of 25.4 mm thick) separated by wood studs. The wall cavities contain 75-mm-thick mineral fiber insulation. The floors are concrete with carpeting. The ceiling is 3 m high and consists of acoustical tiles. The room doors are solid core with good edge seals. The alerting systems will be designed to achieve a 75 dBA sound pressure level at the farthest point in the rooms.

In the first scenario, wall-mounted fire alarm speaker/light combinations are spaced equally in the corridor with a nonvoice alarm signal being transmitted. Calculations determine the maximum allowable spacing of the speakers in order to achieve the design goal of 75 dBA in the rooms.

In the second scenario, speakers are placed in each room as well as in the corridor. Calculations determine the size of the speaker and the power needed to drive that speaker to achieve the design goal of 75 dB. Calculations are also presented to determine the required spacing of speakers in the corridor to achieve a sound level of 65 dB.

Unless otherwise noted, the following formulas and data are from Butler, Bowyer, and Kew [58].

Scenario A In this scenario, the fire alerting system, or sounder, will consist of wall-mounted speaker/light combinations in the corridors only.

L_W is the sound power level of a horn, bell, speaker, or any sounder (dBA referenced to 10^{-12} W).

$$L_W = L + 20 \log_{10} r + 11 \text{ dB}$$

where L is the manufacturer's stated output in dBA at a distance r meters. A typical compression driver-type fire alarm speaker powered at 2 W has an L equal to 94 dBA at 3.05 m [63]. Therefore,

$$L_W = 94 + 20 \log_{10}(3.05) + 11$$

$$L_W = 115 \text{ dB}$$

L_{P1} is the sound pressure level (dBA referenced to 2×10^{-5} Pa) produced outside of a room wall from one speaker.

$$L_{P1} = L_W + C_3 + C_4 + C_5$$

where

C_3 = Correction for the number of directions that the sounder propagates

C_4 = Correction for the characteristics of the corridor walls, ceiling, and floor

C_5 = Function of the distance from the sounder to the center of the bedroom wall

From Table 40.19 [58] C_3 is −3 dB, because the speaker propagates in two directions along the corridor; from Table 40.20 is C_4 is −9 dB, because the floor and ceiling are acoustically soft; and C_5 is unknown since the required spacing of the corridor speakers has not yet been determined. Table 40.21 provides C_5 values for determined distances.

A worst-case condition exists for a room located farthest from a speaker. In this situation the room is located equally between two speakers. Since each unit propagates sound to the room, the sound pressure level outside of the room is higher than if there were only one speaker. The sound pressure level is not double that for a single speaker. For equally spaced sounders, Table 40.22 indicates to add 3 dB to the level expected from a single unit. Therefore,

$$L_{P1} = 115 - 3 - 9 + C_5 + 3$$
$$L_{P1} = 106 + C_5$$

L_{P2} is the sound pressure level at the farthest point in a room. To achieve the established goals, L_{P2} must be 75 dBA. In this situation, with the speaker located outside of the occupied space,

$$L_{P2} = L_{P1} - R + C_2 + C_6 + C_7 + 11 \text{ dBA}$$

where

R = Average sound reduction index for the wall

C_2 = Function of the distance from the wall to the point of interest

C_6 = Function of the area of the room wall (see Table 40.23)

C_7 = Function of the frequency of the sound reaching the wall (see Table 40.24)

In this case, from data presented by Butler, Bowyer, and Kew [58], the sound reduction index R for the wall is about 40 dB (see Table 40.25). This value is based on incident sound in the range of 100–3150 Hz. Sound attenuation through the door is about 26 dB (see Table 40.25). The average sound reduction index, R, for the combined door and wall is 34 dB, if the door is 10 % of the area (see Table 40.26). C_2 is found to be −27 dB, because there are 6.5 m from the center of the wall to the corner of the room (see Table 40.26). Since the wall is 15 m^2, C_6 is +11.5 dB (see Table 40.23). If it is assumed that the sound reaching the wall is at a maximum at a frequency of 2000 Hz, $C_7 = 15$ dB (see Table 40.24). Therefore,

$$L_{P2} = (106 + C_5) - 34 - 27 + 11.5 - 5 + 11 \text{ dBA}$$
$$L_{P2} = 62.5 + C_5 \text{ dBA}$$

If there were no loss of sound pressure level between the speaker and the room wall due to distance, C_5 would be zero and L_{P2} would be 62.5 dBA. This result shows that even if the two speakers were right outside the room, the goal of 75 dBA in the room would not be met. In fact, the resultant noise level in the room would be slightly less than the 65 dBA required by British standards [61] to alert nonsleeping persons. The sound level of 62.5 dBA would exceed the 55 dBA reported by Nober et al. [32] to alert sleeping college-age persons in a quiet ambient setting.

To meet the goal of 75 dBA in the room, either the sound system or the environment would have to be changed. Fire alarm speakers are normally available with multiple power taps such as 4, 2, 1, 1/2, and 1/4 W. A single unit may allow choice of two or three different power levels, which allows balancing of the system after installation.

If a 4-W power input were used, this would be a doubling of the 2 W originally tried in the previous calculation. Because decibels are logarithmic, a doubling of power results in a change of 3 dB in L_W ($10 \times \log_{10} 2 = 3$).This action alone would not be sufficient to meet the 75-dBA goal. In addition, the higher sound pressure level

in the immediate vicinity of the speaker might be discomforting. If the fire alarm system were also used for voice communication, a speaker tapped at 4 W in a small corridor might sound very distorted and be unintelligible.

It is also possible to change the sound pressure level in dBA by changing the frequency of the source. In general, the higher the frequency, the higher the attenuation as the sound waves pass through a wall. Hence, a lower frequency would increase the sound pressure level in the room. In the calculations above, it was assumed that the predominant frequency of the source was 2000 Hz. This frequency resulted in a C_7 of −5 dBA. According to Table 40.24, if this frequency were 500 Hz, C_7 would be 0 dBA. This adjustment would increase the SPL in the room by 5 dBA.

Changes could be made to the building design that would make it possible to meet the design goal. For instance, the use of a lighter-weight door or one without good edge sealing could increase sound transmission to the room by as much as 12 dBA (see Tables 40.27, 40.28, 40.29, and 40.30). However, changes such as this one would tend to defeat other goals such as fire resistance and resistance to smoke spread. If the floor and ceiling were hard surfaces without carpeting or tiles, C_4 could be increased from −9 to 0 dBA (Table 40.31). Changes such as this would probably be resisted for reasons other than fire safety. The only remaining alternative is to provide speakers in each of the rooms.

Scenario B In this case, a speaker in each room powered at only 1/4 W will be tried in addition to the speaker in the corridor. The building use is a dormitory space. The problem, then, is to select a speaker with a sound power output that can meet the goal of 75 dB at the pillow.

$L = ?$ $r =$ at 305 m (3.05 m is a commonly used reference point).

$$L_W = L + 20 \log_{10} r + 11 \text{ dB}$$

$$L_W = L + 20 \log_{10}(3.05) + 11 \text{ dB}$$

$$L_W = L + 21 \text{dB}$$

L_{P2} is the sound level at the bed. In this case, with the speaker in the occupied space,

$$L_{P2} = L_W + C_1 + C_2 \text{ dBA}$$

where C_1 is a correction for how close the sounder is to an adjacent surface, and C_2 is a correction for the distance from the speaker to the bed. In this case, the speaker is on the wall and close to the ceiling. Therefore [58], C_1 is +7 dB, and C_2 is −27 dB (approximately 6.5 m from the speaker to the bed) (see Tables 40.17 and 40.18). Therefore,

$$L_{P2} = (L + 21) + 7 - 27 \text{ dBA}$$

$$L_{P2} = L + 1 \text{ dBA}$$

To get $L_{P2} = 75$ dBA, L must be at least 74 dBA. The smallest and least expensive fire alarm speaker available is a 4-in. paper cone speaker. A typical speaker of this size and type, powered at 1/4 W, has an L equal to 75 dB at 3.05 m [64]. This speaker would meet the design goal in the room, without even

Table 40.31 Average sound reduction indices (dB) of partitions incorporating single glazing (100–3150 Hz frequency range)

Percentage of glazing (24 dB) (%)	25 dB	30 dB	35 dB	40 dB	45 dB	50 dB
100	24	24	24	24	24	24
75	24	25	25	25	25	25
50	24	26	27	27	27	27
33	25	27	28	29	29	29
25	25	27	29	30	30	30
10	25	29	31	33	34	35
5	25	29	33	35	36	37
2½	25	30	34	37	39	40
—	25	30	35	40	45	50

considering any sound contribution from corridor-mounted speakers.

For the corridor speakers in Scenario B, L_{P1} is the sound pressure level at a point farthest from a speaker.

$$L_{P1} = L_W + C_3 + C_4 + C_5 \text{ dBA}$$

where C_3 and C_4 are the same as in Scenario A (-3 and -9 dB, respectively). C_5 is a function of the spacing, which is to be determined. If a single corridor speaker tapped at only 1/4 W is used, with an L of 85 dB at 3.05 m [63],

$$L_W = L + 20 \log_{10} r + 11 \text{ dB}$$
$$L_W = 85 + 20 \log_{10}(3.05) + 11 \text{ dB}$$
$$L_W = 106 \text{ dB}$$
$$L_{P1} = 106 - 3 - 9 + C_5 \text{ dBA}$$
$$L_{P1} = 94 + C_5$$

The goal is to maintain a 65 dBA sound pressure level in the corridors (L_{P1}).

Therefore, C_5 must be -29 dBA or more for L_{P1} to be 65 dBA or higher. From Table 40.20 [58], it is found that distance of 50 m between source and target in the corridor could be exceeded and still meet the 65 dBA goal.

Earlier in this section it was noted that designing for alarm audibility alone is not always sufficient, especially when voice alarm signals are involved. This is because speech is not necessarily intelligible simply because it is audible: adding more sound level to speech that has been blurred by reverberation, echoes, or distortion does not make it more intelligible [65]. A sufficiently loud but overly reverberant speech signal can be almost completely unintelligible. There are many examples of this in airports, train stations, and other large spaces, particularly those with hard acoustical surfaces.

When considering intelligibility, there are a variety of factors which are important, starting with the person who is speaking, the mode and features of the transmission system, the characteristics of the space wherein the signal is received, and the listener. This is illustrated in Fig. 40.13.

For fire alarm signaling system design, major facility use concerns include the characteristics of the space and the intended occupant population. The population matters from the perspective of understanding the message (e.g., language and abilities). The space matters from the perspective of how the signal, once introduced into the space, may become distorted or otherwise affected such that intelligibility is diminished. Factors that can corrupt the integrity of a voice signal on its path from talker to listener are summarized below [65].

- *Speech-signal-to-noise ratio*. Noise has the effect of masking or obscuring the voice signal. Remarkably, we are able to tolerate a great deal of noise before intelligibility

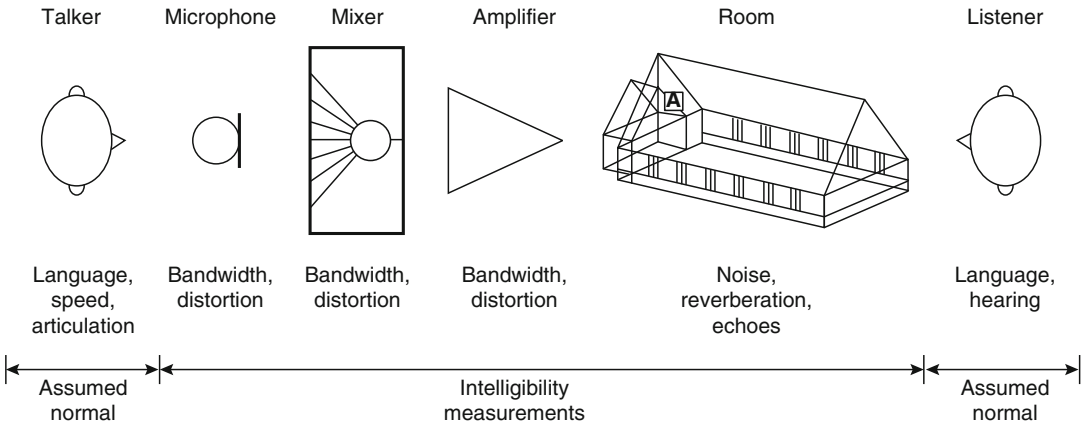

Fig. 40.13 Talker-to-listener transmission path [65]

diminishes appreciably, but once it begins to diminish, it diminishes rapidly.

- *Reverberation*. Most are familiar with how difficult it can be to understand speech in a reverberant environment such as a cathedral or gymnasium. Reverberation is made up of sound reflections that have the effect of smearing or blurring speech, making it less clear and distinct and therefore more difficult to understand.
- *Echoes*. If echoes arrive much later in time than the first arrival of sound, they can harm intelligibility. In continuous speech, the echo from a previously uttered syllable masks or obscures the sound of subsequent syllables, making speech more difficult to understand. The time delay and level of the echo are key variables in determining the impact of echoes on intelligibility.
- *Distortion*. If one of the electrical or electro-acoustical components in the sound system is distorting, it is generating a form of noise that masks the original speech signal. Severe amplifier clipping, for example, can make an otherwise perfect speech signal at the input to the amplifier more difficult to understand at the output.

To accurately account for the effect of the above factors, they must be measured in at least octave-band resolution; a single broadband measurement is insufficient and more than octave-band resolution is almost always unjustified. Various documents exist for guiding the measurement of intelligibility [66–69], and appropriate instrumentation is available for obtaining the speech transmission index (STI) and other acoustical data necessary for better siting speakers for emergency voice communication. Descriptions of how to collect and use these data can be found in the literature (e.g., Woycheese [70]).

Cost Analysis

Scenario A For comparison purposes, assume that sufficient changes could be made to the building and alarm system to allow speakers to be mounted in the corridor only at a spacing of 3 m. A typical dormitory with about 30 bedrooms per floor requires approximately 24 speakers per floor in the corridors. In a building with seven floors, this requirement amounts to 168 speakers. At 2 W per speaker, the result would be 336 W. This setup requires three 125 W power amplifiers at an installed cost of about $3500.00 each. This amount does not include other fixed costs, such as control equipment and detectors, that are the same for each of the scenarios.

Assume each corridor unit to be a speaker/light combination. The average installed cost, including backbox, wiring back to a control panel on the first level, and conduit, would total to about $250.00 per unit. The total cost is then

$$\text{TOTAL} = (3 \times \$3500.00) + (168 \times \$250.00)$$
$$\text{TOTAL} = \$52,500$$

Scenario B In this case, there are thirty 4-in. paper cone speakers per floor at an average cost of $200.00, installed. Assume a total of four speaker/light units per floor in the corridors. The calculations show that the system goals are met with only one or two units in the corridors. However, the halls may be split by smoke doors or they may be irregular in shape. Also, system reliability is increased by using more than one unit.

Each bedroom speaker and corridor speaker is powered at 1/4 W. For seven floors, this setup gives a total power requirement of 59.5 W. Therefore, one 60 W amplifier, at a unit cost of $1500.00, is needed. The total cost is then

$$\text{TOTAL} = (3 \times \$1500.00) + (7 \times 30 \times \$200.00) + (7 \times 4 \times \$250.00)$$
$$\text{TOTAL} = \$50,500.00$$

The estimates show the relative costs of the different scenarios, not the actual costs. The real costs of the systems are affected by factors such as whether the building is new or existing. If existing, the price is affected by the extent of other renovations. Also, the estimates do not reflect the cost of other parts of the system. The balance of the system includes such items as

smoke and heat detectors, equipment for elevator capture, and air handler controls.

The relative costs of the two systems in Scenarios A and B under "Cost Analysis" differ by only about 4 %. In a building of this size and type, such a small margin cannot be considered significant enough to conclude that one system is more economical than the other.

The small difference in the costs of the two systems is due to the additional cost of amplifiers needed to power the system that has only corridor units. The total number of units (corridor + room) in Scenario B is 70 more than in Scenario A. The reduced power requirement offsets the added cost of their installation.

Scenario A has a higher equipment cost but a lower installation cost than Scenario B. This result means that the relative costs of the two systems will be slightly sensitive to the type of equipment used and the cost of installation labor. By changing the figures used in the cost estimates, it can be shown that the variance is only a few percent and probably not significant.

If the building were four stories or less in height, the difference in relative cost rises to about 5 %. Again, this amount is not considered to be a significant difference.

By increasing the size of the building to 12 stories, Scenario B becomes significantly less expensive than Scenario A. Above this height, the combined use of room and corridor units becomes increasingly economically attractive.

Changing the size of each floor has about the same effect as changing the height of the building. Therefore, increasing the floor area makes Scenario B more viable. A reduction in floor area and building height does not make the corridor-only system attractive, unless the building is only a few stories in height. Then a voice system is probably not needed. From an economics standpoint, a corridor-only horn/light system is probably best, since the cost of these units is generally less than that of speakers. Again, this conclusion assumes that sufficient changes could be made to the building design to increase the level of sound penetrating the corridor walls.

Obviously, if the sound loss from the corridor to the individual rooms is less, Scenario A starts to look better. This situation has the effect of raising the height above which Scenario B becomes significantly less expensive. However, changing construction features to reduce sound loss may reduce the passive fire resistance of the structure below an acceptable level as well as decrease the privacy level.

There are other factors to consider when choosing between different systems. In Scenario A, the quantity of speakers in the corridors and the high power levels driving each speaker (2 W each) can cause sound distortion. Voice messages may not be intelligible in the bedrooms even though there is enough sound to wake a sleeping occupant. Also, the high sound levels (106 dBA plus) in the corridors approach uncomfortable levels.

It is clear from the discussions above that a system with room speakers in conjunction with corridor units is the most desirable case. That system has the added advantage of eliminating most of the uncertainties in the design of the system. It is easier and more accurate to calculate sound levels at a point in the same room as the sound source than it is to estimate sound losses through composite walls.

This cost-benefit analysis shows that a fire alarm alerting system with units in each office or bedroom can be installed at about the same cost or less than a corridor-only system. In addition, there is a higher confidence level that the system with the sounders in each room will perform its intended function: to awaken and alert sleeping occupants.

Designing Fire Alarm Visibility

Visual alarm notification is an important part of a fire alarm system. This visual aspect is especially important in cases where the ambient noise level is high, building occupants may be sleeping, or building occupants or their visitors may have hearing impairments. In these cases, it should be expected that the visual alarm will be required to alert occupants and initiate evacuation or

relocation. As such, one first needs to determine a suitable intensity required to obtain this function.

In many cases, a suitable intensity can be obtained from regulatory documents, such as building codes, fire codes, or the Americans with Disabilities Act. These references typically give a required appliance intensity and a maximum size space that can be covered by an appliance with that intensity. If additional guidance is needed, reference can be made to appropriate documentation on alerting of persons by visual means [71]. It is also possible that a reference may cite a required level of illumination to alert someone. This requirement should not be confused with the intensity of the lamp providing the signal. The two are related by the inverse square law where E is the illumination (lumens per unit area), I is the intensity of the light source (candela), and d is the on-axis distance between the light source and the point where the illumination is measured (Fig. 40.14).

$$E = \frac{I}{d^2}$$

In cases where flashing signals are required, the source strength or output is cited as *effective intensity*. Effective intensity is used to equate the perceived brightness of a flashing light to that of a steady light. It can be calculated using the relationship [64],

$$I_e = \frac{\left(\int_{t_1}^{t_2} I\,dt\right)}{(a + t_2 - t_1)} \tag{40.29}$$

where

I_e = Effective intensity
I = Instantaneous intensity
t_1 = The time (s) of the beginning of that part of the flash where I exceeds I_e
t_2 = The time (s) of the ending of that part of the flash where I exceeds I_e

In the United States, the value of 0.2 is usually used for the constant a. This relationship is shown graphically in Fig. 40.15.

There are two ways to use light as a notification method. The first is direct viewing where the person must be "see" the appliance in their direct or peripheral vision. The second is indirect viewing where the person is alerted by light reflected off of adjacent surfaces.

Equation 40.29 is referred to as the Blondel-Rey equation and was adopted as a product metric in the early 1990s. This allowed different light sources to be evaluated as being equivalent. The research by Blondel and Rey was published in 1912 and is based on direct viewing of a flashing light in a dark environment [72]. Equation 40.29 has worked as a metric to compare two light sources that use the same technology and that have similar pulse durations and pulse shapes.

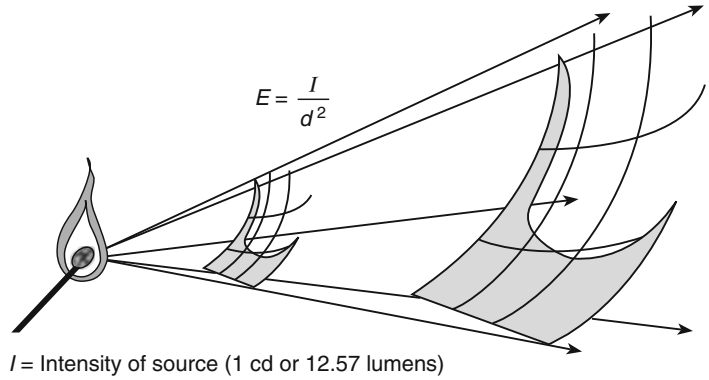

I = Intensity of source (1 cd or 12.57 lumens)

E = Illumination (1 lumen/ft^2 or 1 footcandle [1 lumen/m^2 or 1 lux or 0.0926 footcandle])

d = Distance from source to object (ft or m)

Fig. 40.14 Relationship between intensity of lamp and level of illumination required to alert someone

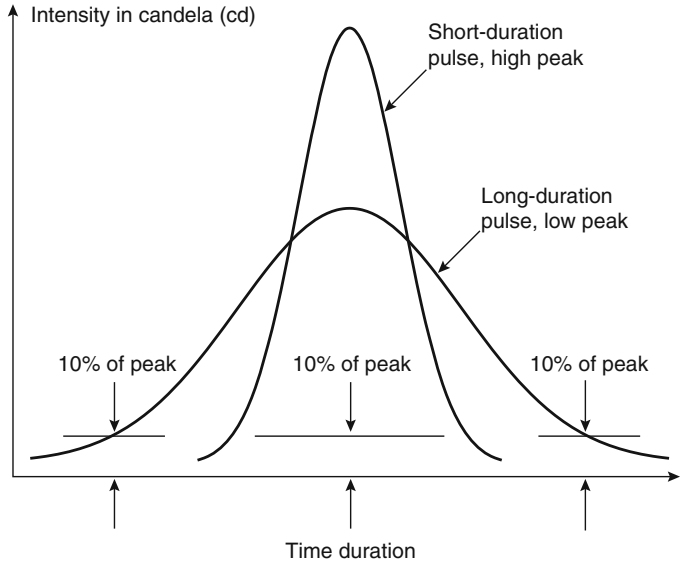

Fig. 40.15 Peak versus effective intensity (Source: R.P. Schifiliti Associates, Inc., Reading, MA)

Until recently, all lights used for occupant notification in the fire alarm industry have been based on Xenon flash tubes. These strobe lights all have pulse durations less than 1 millisecond (ms) and have the similarly shaped response curves.

Recent research has indicated that Equation 40.29 it is not suitable for comparing the detection of indirect flashing lights or for comparing different light technologies, such as Xenon strobes versus LED lights that have rectangular pulse curves [73]. Additional research is being done to define a new metric that allows different technologies to be compared and that is well correlated to actual indirect alerting effectiveness. The examples that follow are valid only for strobe lights that use Xenon flash tube technology.

If the duration of the flash is less than 1 millisecond, Equation 40.29 can be further simplified to [64]

$$I_e = 5\int I \; dt$$

where the integration is performed over the complete flash cycle.

As part of a test program to determine signaling applications for the hearing impaired, UL determined that an illumination of 0.398 lm/m^2 (0.037 lm/ft^2) as viewed on axis from a single flashing light source located in the center of one wall of a 6.1 m by 6.1 m (20 ft by 20 ft) room was the minimum required by their objective. It was also determined that, by increasing the "square" dimensions in increments of 3 m (10 ft) in both directions (length and width), the minimum illumination value of 0.398 lm/m^2 could be used to extrapolate the required signal intensity as the room size increased.

For example, if the room size were increased to 12.2 m by 12.2 m (40 ft by 40 ft), the effective intensity, cd eff, of the flashing strobe signal could be determined using the inverse square law and solving for I:

$$E = \frac{I}{d^2}; \text{ therefore}$$

$$I = Ed^2 = (0.398 \text{ lumens/m}^2)(12.2 \text{ m}^2)$$

$$= 59.2 \text{ candela}$$

Thus, one signal rated at 60 cd eff would be sufficient for the space. Using the same approach, but smaller squares, one would also find that two signals rated at 30 cd eff, or four signals rated at 15 cd eff each, would also be applicable.

Designers should check with the authority having jurisdiction or the current edition of *NFPA 72* regarding the use of multiple flashing lights.

Example 20 The design objective is to evaluate the visual alarm notification system installed in a large open space for suitability in providing signals for the hearing impaired. The space is 21 m (70 ft) by 37 m (120 ft), with a 6.5 m (20 ft) ceiling height. The notification appliances are located 2 m (6.5 ft) above floor level and are spaced as shown in Fig. 40.16. The signals are rated at 45 cd eff each. Is the required illumination of 0.398 lm/m^2 currently provided?

Solution The first step is to section off the space into blocks that are anticipated to be covered for each signal. In this case, the result is six blocks, each 12.2 m (40 ft) long by 10.5 m (34 ft) wide. This step is illustrated in Fig. 40.17.

Given these dimensions, one could calculate the illumination at point A, where

$$E = \frac{45 \text{ cd}}{(10.5 \text{ m}^2)} = 0.41 \text{ lumens/m}^2$$

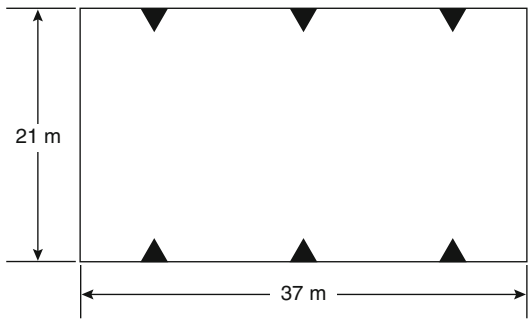

Fig. 40.16 Notification appliance (▲) locations

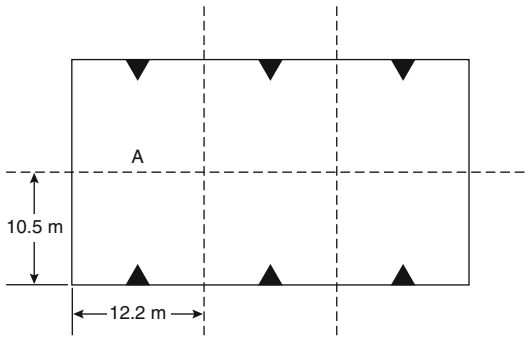

Fig. 40.17 Sections for anticipated signal (▲) coverage

This illumination is greater than the minimum required of 0.398 lm/m^2. However, application of this method requires the blocks of coverage by a signal to be square with the lateral distance (90°) being equal to one-half the coverage distance on-axis. In this case, the lateral distance is 12.2 m (40 ft), and this is the figure that should be used to calculate the illumination throughout the entire block. In doing this, one finds that the illumination provided is

$$E = \frac{45 \text{ cd eff}}{(10.5 \text{ m}^2)} = 0.29 \text{ lumens/m}^2$$

which is below the minimum required 0.398 lm/m^2. This outcome results in areas of the space not having the required illumination. This outcome is illustrated in Fig. 40.18.

To determine what intensity is required for the signals in order to provide the required 0.398 lm/m^2, the inverse square law can be applied using the value $d = 12.3$ m. This application results in a required incident intensity of 60 cd eff for each existing signal location.

By applying this method of dividing spaces into squares and applying the inverse square law, the intensity of signals and their required spacing can be calculated for spaces of any shape and size. Trade-offs can be made between the number of signals and the intensity of signals to best fit the application (e.g., one signal of 60 cd eff

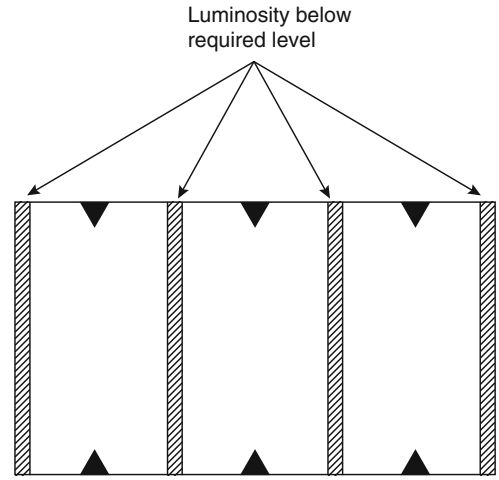

Fig. 40.18 Diagram of subadequate luminosity intensity

versus four properly spaced signals of 15 cd eff each).

In cases where a minimum required illumination at all points in a space is specified (as opposed to the minimum effective intensity on-axis within a square), the illumination can be calculated using the inverse square law, the cosine law, and the cosine cubed law. In this case, the inverse square law provides the illumination on-axis, application of the cosine law provides the illumination at a perpendicular surface within the same plane as the signal, and application of the cosine cubed law provides the illumination at parallel surfaces within the same plane as the signal.

With this information, it should be possible to calculate visual fire alarm signals for most situations. In all cases, a value for the required effective intensity at some point within the room is required. If not provided at the beginning of the design process, one should determine an effective intensity based on the specific application and the condition of the occupants being alerted.

Nomenclature

α	Fire intensity coefficient (Btu/s^3 or kW/s^2)
A	Area (m^2 or ft^2)
A	$g/(C_pT_a\rho_0)$ [m^4/(s^2·kJ) or ft^4/(s^2·Btu)]
c	Specific heat of detector element [Btu/(lbm·R) or kJ/(kg·K)]
C_p	Specific heat of air [Btu/(lbm·R) or kJ/(kg·K)]
d	Diameter of sphere or cylinder (m or ft)
D	Nondimensional change in gas temperature
Δt	Change in time (s)
ΔT	Increase above ambient in temperature of gas surrounding a detector (°C or °F)
ΔT_d	Increase above ambient in temperature of adetector (°C or °F)
ΔT_p^*	Change in reduced gas temperature
f	Functional relationship
g	Functional relationship
g	Gravitational constant (m/s^2 or ft/s^2)
h_c	Convective heat transfer coefficient [kW/(m^2·°C) or Btu/(ft^2·s·°F)]
H	Ceiling height or height above fire (m or ft)
ΔH_c	Heat of combustion (kJ/mol)
H_f	Heat of formation (kJ/mol)
L_p	Sound pressure level
L_W	Sound power level
m	Mass (lbm or kg)
p	Positive exponent
$\dot{q}$	Heat release rate (Btu/s or kW)
$\dot{q}_{cond}$	Heat transferred by conduction (Btu/s or kW)
$\dot{q}_{conv}$	Heat transferred by convection (Btu/s or kW)
$\dot{q}_{rad}$	Heat transferred by radiation (Btu/s or kW)
$\dot{q}_{total}$	Total heat transfer (Btu/s or kW)
$\dot{Q}$	Heat release rate (Btu/s or kW)
$\dot{Q}_{cr}$	Critical heat release rate
$\dot{Q}_{do}$	Design heat release rate
$\dot{Q}_i$	Ideal heat release rate
$\dot{Q}_p$	Predicted heat release rate (Btu/s or kW)
$\dot{Q}_T$	Threshold heat release rate at response (Btu/s or kW)
r	Radial distance from fire plume axis (m or ft)
ρ_0	Density of ambient air (kg/m^3 or lb/ft^3)
Re	Reynolds number
RTI	Response time index (m$^{1/2}$·s$^{1/2}$ or ft$^{1/2}$·s$^{1/2}$)
S	Spacing of detectors or sprinkler heads (m or ft)
t	Time (s)
t_c	Critical time—time at which fire would reach a heat release rate of 1000 Btu/s (1055 kW) (s)
t_r	Response time (s)
t_v	Virtual time of origin (s)
t_{2f}	Arrival time of heat front (for $p = 2$ power-law fire) at a point r/H (s)
t_{2f}^*	Reduced arrival time of heat front (for $p = 2$ power-law fire) at a point r/H (s)
t_p^*	Reduced time
T	Temperature (°C or °F)
T_a	Ambient temperature (°C or °F)
T_d	Detector temperature (°C or °F)
T_g	Temperature of fire gases (°C or °F)
T_s	Rated operating temperature of a detector or sprinkler (°C or °F)

U Velocity (m/s)
u Instantaneous velocity of fire gases (m/s or ft/s)
u_0 Velocity at which τ_0 was measured (m/s or ft/s)
u_p^* Reduced gas velocity
v Kinematic viscosity (m^2/s or ft^2/s)
x Vectorial observation point (m or ft)
Y Defined in Equation 40.26
τ Detector time constant—$mc/(hA)$ (s)
τ_0 Measured at reference velocity u_0 (s)

References

1. C. Mulliss and W. Lee, "On the Standard Rounding Rule for Multiplication and Division," *Chinese Journal of Physics,* 36, 3, pp. 479–487 (1998).
2. W. Lee, C. Mulliss, and H.-C. Chiu, "On the Standard Rounding Rule for Addition and Subtraction," *Chinese Journal of Physics,* 38, 1, pp. 36–41 (2000).
3. R. Custer, "Selection and Specification of the 'Design Fire' for Performance-Based Fire Protection Design," in *Proceedings, SFPE Engineering Seminar,* Phoenix, AZ, Society of Fire Protection Engineers, Boston (1993).
4. R. Custer, B. Meacham, and C. Wood, "Performance-Based Design Techniques for Detection and Special Suppression Applications," in *Proceedings of the SFPE Engineering Seminars on Advances in Detection and Suppression Technology,* San Francisco, Society of Fire Protection Engineers, Boston (1994).
5. *SFPE Engineering Guide to Performance-Based Fire Protection,* Society of Fire Protection Engineers, National Fire Protection Association, Quincy, MA (2000).
6. R. Custer and R. Bright, "Fire Detection: The State-of-the-Art," *NBS Tech. Note 839,* National Bureau of Standards, Washington, DC (1974).
7. UL 521, *Standard for Safety Heat Detectors for Fire Protective Signaling Systems,* Underwriters Laboratories Inc., Northbrook, IL (1993).
8. *NFPA 72®, National Fire Alarm Code®,* National Fire Protection Association, Quincy, MA (2007).
9. G. Heskestad and H. Smith, *FMRC Serial Number 22485,* Factory Mutual Research Corp., Norwood, MA (1976).
10. J.P. Hollman, *Heat Transfer,* McGraw-Hill, New York (1976).
11. W. Bissell, "An Investigation into the Use of the Factory Mutual Plunge Tunnel and the Resulting RTI for Fixed Temperature Fire Detectors," Master's Thesis, Worcester Polytechnic Institute, Worcester, MA (1988).
12. M. Kokkala, "Thermal Properties of Heat Detectors and Sprinklers," *Nordtest Brand Symposium,* Boras, Sweden (1986).
13. R.P. Schifiliti and W.E. Pucci, "Fire Detection Modeling: State of the Art," The Fire Detection Institute, Bloomfield, CT (1996).
14. "Discussion of a New Principle in Fire Detection, Rate Compensation," Fenwal, Inc., Ashland, MA (1951).
15. C. E. Marrion, "Lag Time Modeling and Effects of Ceiling Jet Velocity on the Placement of Optical Smoke Detectors," Master's Thesis, Worcester Polytechnic Institute, Center for Firesafety Studies, Worcester, MA (1989).
16. R. Alpert, *Fire Technology,* 8, p. 3 (1972).
17. L.Y. Cooper, "Interaction of an Isolated Sprinkler and a Two Layer Compartment Fire Environment," National Institute of Standards and Technology, Gaithersburg, MD (1991).
18. M. Delichatsios and R. L. Alpert, "Calculated Interaction of Water Droplet Sprays with Fire Plumes in Compartments," *NBS-GCR 86-520,* Center for Fire Research, National Bureau of Standards, Washington, DC (1986).
19. G. Heskestad, "Sprinkler/Hot Layer Interaction," *NIST-GCR 91-590,* National Institute of Standards and Technology, Gaithersburg, MD (1991).
20. D.D. Evans and D.W. Stroup, "Methods to Calculate the Response Time of Heat and Smoke Detectors Installed Below Large Unobstructed Ceilings," *NBSIR 85-3167,* National Bureau of Standards, Gaithersburg, MD (1985).
21. G. Heskestad and M.A. Delichatsios, "The Initial Convective Flow in Fire," *17th Symposium on Combustion,* Combustion Institute, Pittsburgh, PA (1978).
22. G. Heskestad and M.A. Delichatsios, "Environments of Fire Detectors—Phase I: Effect of Fire Size, Ceiling Height, and Material," Volume I: "Measurements" (NBS-GCR-77-86), (1977), Volume II: "Analysis" (NBS-GCR-77-95), National Technical Information Service (NTIS), Springfield, VA (1977).
23. R.P. Schifiliti, "Use of Fire Plume Theory in the Design and Analysis of Fire Detector and Sprinkler Response," Master's Thesis, Worcester Polytechnic Institute, Center for Firesafety Studies, Worcester, MA (1986).
24. D.W. Stroup, D.D. Evans, and P. Martin, *NBS Special Publication 712,* National Bureau of Standards, Gaithersburg, MD (1986).
25. *SFPE Handbook of Fire Protection Engineering,* National Fire Protection Association, Quincy, MA (1988 and 1995).
26. *NFPA 72®, National Fire Alarm Code®,* National Fire Protection Association, Quincy, MA, 1984 through 1996 editions.
27. G. Heskestad and M. Delichatsios, "Update: The Initial Convective Flow in Fire," *Fire Safety Journal,* 15, pp. 471–475 (1989).

28. C. Beyler, personal communication (1985).
29. C. Beyler, "A Design Method for Flaming Fire Detection," *Fire Technology,* 20, 4, pp. 9–16 (1984).
30. J.R. Lawson, W.D. Walton, and W.H. Twilley, *NBSIR 83-2787,* National Bureau of Standards, Washington, DC (1983).
31. B.J. Meacham, "Characterization of Smoke from Burning Materials for the Evaluation of Light Scattering-Type Smoke Detector Response," Master's Thesis, Worcester Polytechnic Institute, Center for Firesafety Studies, Worcester, MA (1991).
32. B.J. Meacham and V. Motevalli, "Characterization of Smoke from Smoldering Combustion for the Evaluation of Light Scattering-Type Smoke Detector Response," *Journal of Fire Protection Engineering, SFPE,* 4, 1, p. 17 (1992).
33. UL 268, *Standard for Safety Smoke Detectors for Fire Protective Signaling Systems,* Underwriters Laboratories, Inc., Northbrook, IL (1989).
34. G. Mulholland, "Smoke Production and Properties," *SFPE Handbook of Fire Protection Engineering,* 4th ed., National Fire Protection Association, Quincy, MA, (2008).
35. J. Geiman and D.T. Gottuk, "Alarm Thresholds for Smoke Detector Modeling," *Fire Safety Science—Proceedings of the Seventh International Symposium,* International Association for Fire Safety Science, Worcester, MA, pp. 197–208 (2003).
36. D.T. Gottuk, S.A. Hill, C.F. Schemel, B.D. Strehlen, S.L. Rose-Phersson, R.E. Shaffer, P.A. Tatem, and F.W. Williams, "Identification of Fire Signatures for Shipboard Multicriteria Fire Detection Systems," Naval Research Laboratory, Memorandum Report, 6180-99-8386, Washington, DC, June 18, 1999.
37. H.W. Carhart, T.A. Toomey, and F.W. Williams, "The Ex-USS SHADWELL Full-Scale Fire Research and Test Ship," NRL Memorandum Report 6074, revised January 20, 1988, reissued 1992.
38. M.J. Spearpoint and J.N. Smithies, "Practical Comparison of Domestic Smoke Alarm Sensitivity Standards," Fire Research Station, Home Office Fire Research and Development Group, FRDG Publication No. 4.97 (1997).
39. R.W. Bukowski, T.E. Waterman, and W.J. Christian, "Detector Sensitivity and Siting Requirements for Dwellings," Final Technical Report, IITRI Project J6340, Contract No. 4-36092, NBS-GCR-75-51, National Bureau of Standards, Gaithersburg, MD (1975).
40. UL 217, *Standards for Single and Multiple Station Smoke Alarms,* Underwriters Laboratories Inc., Northbrook, IL (1999).
41. UL 268, *Standard for Smkie Detectors for Fire Protective Signaling Systems,* Northbrook, IL (1996).
42. J. Hoseman, "Uber Verfahren zur Bestimmung der Korngrossenverteilung Hokkonzentrierter Polydispersionen von MiePartikeln," Ph.D. Thesis, Aachen, Germany (1970).
43. C.D. Litton, "A Mathematical Model for Ionization Type Smoke Detectors and the Reduced Source Approximation," *Fire Technology,* 13, 4, pp. 266–281 (1977).
44. R.W. Bukowski and G.W. Mulholland, "Smoke Detector Design and Smoke Properties," TN 973, U.-S. Department of Commerce, National Bureau of Standards, Washington, DC (1978).
45. C. Helsper, H. Fissan, J. Muggli, and A. Scheidweiler, "Verification of Ionization Chamber Theory," *Fire Technology,* 19, 1, p. 14 (1983).
46. J. Newman, "Modified Theory for the Characterization of Ionization Smoke Detectors," in *Fire Safety Science—Proceedings of the Fourth International Symposium,* International Association for Fire Safety Science, Ottawa, Ontario (1994).
47. G. Heskestad, "Generalized Characteristics of Smoke Entry and Response for Products-of-Combustion Detectors," in *Proceedings, 7th International Conference on Problems of Automatic Fire Detection,* Rheinish-Westfalischen Technischen Hochschule, Aachen, Germany (1975).
48. M. Kokkala et al., "Measurements of the Characteristic Lengths of Smoke Detectors," *Fire Technology,* 28, 2, p. 99 (1992).
49. J. Bjorkman, O. Huttunen, and M. Kokkala, "Paloilmaisimien toimintaa kuvaavat laskentamallit (Calculation Models for Fire Detector Response)," *Research Notes 1036,* Technical Research Center of Finland (1989).
50. A. Oldweiler, "Investigation of the Smoke Detector L Number in the UL Smoke Box," Master's Thesis, Worcester Polytechnic Institute, Worcester, MA (1995).
51. M.A. Delichatsios, "Categorization of Cable Flammability, Detection of Smoldering, and Flaming Cable Fires," Interim Report, Factory Mutual Research Corporation, Norwood, MA (1980).
52. NFPA 92B, *Guide for Smoke Management Systems in Malls, Atria, and Large Areas,* National Fire Protection Association, Quincy, MA (2005).
53. G. Heskestad, *FMRC Serial Number 21017,* Factory Mutual Research Corp., Norwood, MA (1974).
54. E.L. Brozovsky, "A Preliminary Approach to Siting Smoke Detectors Based on Design Fire Size and Detector Aerosol Entry Lag Time," Master's Thesis, Worcester Polytechnic Institute, Center for Firesafety Studies, Worcester, MA (1991).
55. S. Deal, "Technical Reference Guide for FPEtool Version 3.2," *NISTIR 5486,* National Institute for Standards and Technology, Gaithersburg, MD (1994).
56. G. Heskestad and M.A. Delichatsios, "Environments of Fire Detectors, Phase I: Effects of Fire Size, Ceiling Heights, and Material," Volume II, *Analysis Technical Report Serial Number 11427,* RC-T-11, Factory Mutual Research Corp., Norwood, MA (1977).
57. K.B. Ginn, *Architectural Acoustics,* Bruel and Kjaer (1978).
58. H. Butler, A. Bowyer, and J. Kew, "Locating Fire Alarm Sounders for Audibility," Building Services Research and Information Association, Bracknell, UK (1981).

59. E.H. Nober, H. Pierce, A. Well, and C.C. Johnson, *NBS-GCR-83-284,* National Bureau of Standards, Washington, DC (1980).
60. M.J. Kahn, "Detection Times to Fire-Related Stimuli by Sleeping Subjects," *NBS-GCR-83-435,* National Bureau of Standards, Washington, DC (1983).
61. *British Standard Code of Practice CP3,* British Standards Institution, London (1972).
62. C. Davis and D. Davis, *Sound System Engineering,* Howard H. Sams and Co., Inc., Indianapolis, IN (1975).
63. *Product Catalog,* Fire Control Instruments, Newton, MA (1986).
64. "Nomenclature and Definitions for Illuminating Engineering," *IES RP-16-1987,* Illuminating Society of North America, New York (1987).
65. K. Jacobs, *Understanding Speech Intelligibility and the Fire Alarm Code,* presented at the NFPA Congress, Anaheim, CA, copyright Bose corporation (2001).
66. Accredited Standards Committee S3 (Bioacoustics), "Method for Measuring the Intelligibility of Speech over Communications Systems," *ANSI S3.2*, Acoustical Society of America, Melville, NY (1995).
67. International Organization for Standardization, "Acoustics—The Construction and Calibration of Speech Intelligibility Tests," *ISO TR 4870*, Geneva, Switzerland (1991).
68. International Electrotechnical Commission, "Sound Systems for Emergency Purposes," *IEC 60849,* 2nd ed., IEC, Geneva, Switzerland (1998).
69. International Electrotechnical Commission, "Sound System Equipment—Part 16: Objective Rating of Speech Intelligibility by Speech Transmission Index," *IEC-60268-16*, 3rd ed., IEC, Geneva, Switzerland (2003).
70. J.P. Woycheese, "Speech Intelligibility Measurements in an Office Building," *Journal of Fire Protection Engineering,* 17, 4, pp. 245–269 (2007).
71. UL 1971, *Standard for Safety Signaling Devices for the Hearing Impaired,* Underwriters Laboratories, Inc., Northbrook, IL (1992).
72. A. Blondel, and J. Rey, "The perception of lights of short duration at their range limits". *Transactions of the Illuminating Engineering Society*, 7, 625–662 (1912).
73. J.D. Bullough, N.P. Skinner, and Y. Zhu, "Parameters for Indirect Viewing of Visual Signals Used in Emergency Notification" The Fire Protection Research Foundation, Quincy, MA, September 2013.

Further Readings

V. Babrauskas, J.R. Lawson, W.D. Walton, and W.H. Twilley, *NBSIR 82-2604,* National Bureau of Standards, Washington, DC (1982).

Robert P. Schifiliti is a fire protection consultant specializing in fire detection and alarm systems design and analysis. Located in Reading, Massachusetts, he is a licensed Fire Protection Engineer and holds a Master of Science degree in Fire Protection Engineering from Worcester Polytechnic Institute. Mr. Schifiliti is a fellow of the Society of Fire Protection Engineers.

Richard L.P Custer is senior fire consultant for Arup Fire located in Massachusetts. Mr. Custer is a fellow of the Society of Fire Protection Engineers.

Brian J. Meacham is an associate professor in the Department of Fire Protection Engineering at Worcester Polytechnic Institute (WPI) in the United States. He is a licensed Professional Engineer, a Chartered Engineer, and a fellow of the Society of Fire Protection Engineers.

Hydraulics

41

Kenneth E. Isman

Introduction

Hydraulics may be regarded as the application of knowledge about how liquids behave in static and flowing conditions to solve practical fluid related problems. It is generally held to describe the behavior and effects of water in motion in both closed conduits and open channels. In the field of fire protection we are concerned primarily with the closed conduit flow regime. In this chapter we will restrict our discussion to the behavior and properties of water flowing in pipes as the phenomenon of paramount interest, although other fluids such as antifreezes at room temperature and foam/water solutions are similar enough to water that the discussion will be applicable to them as well. Additionally some of the principles presented here also apply to system designs utilizing other fluids such as foam concentrate or antifreeze at low temperatures.

A significant portion of this chapter was written by John J. Titus. Editorial and technical updates were incorporated and additional information on pumps and water supplies have been provided for this edition.

K.E. Isman (✉)

Physical Properties of Fluids

The solution of any flow problem requires a basic knowledge of the physical properties of the fluid being considered. A brief description of the most basic properties follows.

Density

The density of a fluid (ρ) is the mass of the fluid (m) per unit volume (V) as shown in the equation below:

$$\rho = \frac{m}{V}$$

Density is expressed in SI units as kg/m^3 and in English, or U.S. customary, units as slugs/ft^3 (or lbf · s^2/ft^4). The density of water at 4 °C (~40 °F) is 1000 kg/m^3 (1.94 lbf · s^2/ft^4).

Specific Weight

The specific weight of a fluid (γ) is the representation of the force exerted by gravity on a unit volume of the fluid. The specific weight can also be calculated by multiplying the density of a fluid (ρ) by the gravitational constant (g) as shown below:

$$\gamma = \rho g$$

Specific weight takes on units of weight per unit volume, which in SI units would be kN/m^3 and in

M.J. Hurley (ed.), *SFPE Handbook of Fire Protection Engineering*,
DOI 10.1007/978-1-4939-2565-0_41, © Society of Fire Protection Engineers 2016

English customary units would be lb/ft^3. At 4 °C, the specific weight of water is 9.81 kN/m^3 (62.4 lb/ft^3) [1].

Specific Gravity (Relative Density)

Specific gravity (SG) is the ratio of a liquid's density (ρ) or specific weight (γ) to that of water (ρ_{water} or γ_{water}) as shown by the following formulas:

$$SG = \frac{\rho}{\rho_{water}} \quad \text{or} \quad SG = \frac{\gamma}{\gamma_{water}}$$

Where the specific gravity of a fluid is greater than 1.0, it means that the fluid is heavier than water. Where the specific gravity of a fluid is less than 1.0, it means that the fluid is lighter than water. If the fluid is also not miscible with water, it will float or settle on top of the water creating a defined interface.

Viscosity

The term *viscosity* refers to a proportionality constant in the equation relating cross-sectional velocity variations (or rate of fluid deformation) to shear stresses developed in the fluid flow. (See the subsection of this chapter titled "Fluid Flow Energy Loss Equations" to see how viscosity is used.) Viscosity can be considered a measure of a fluid's resistance to deformation or shear or, alternatively, its readiness to flow when acted upon by an external force. In engineering analyses it is useful to think of viscosity as a momentum diffusivity term.

Viscosity is commonly expressed in one of two forms: absolute (or dynamic) viscosity (μ), which is the proportionality constant referred to above, or kinematic viscosity (ν), which is related to the absolute viscosity divided by the density (ρ) as follows:

$$\nu = \frac{\mu}{\rho}$$

Note that the kinematic viscosity is expressed with the Greek letter "nu", which looks like a "v", but is not a "vee". This means that the kinematic viscosity often gets mixed up with the velocity. Engineers must understand and distinguish the meanings of the variables in the equations that they use. For this reason, some engineers use the Greek letter kappa (κ) for kinematic viscosity.

A wide variety of units is used to express absolute (or dynamic) viscosity, depending not only on U.S. customary or SI formulations but also on older English and metric conventions as well as on the type of instrument used to measure this fluid property. In S.I. units, absolute (or dynamic) viscosity is measured in kilograms per meter-seconds (kg/(m-sec)). In customary English units, absolute or dynamic viscosity is measured in pounds per foot-seconds (lb/(ft-sec)). A unit based on the c.g.s. (centimeter, gram, second) convention of the old metric system has gained wide favor in the representation of absolute (or dynamic) viscosity. This unit, called the *poise,* has dimensions of dyne · seconds per square centimeter or grams per centimeter · second. The centipoise, which equals 0.01 P, is the form of preference for many engineers because the viscosity of water at 20 °C (68 °F) is very close to one centipoise. One centipoises is equal to 6.72×10^{-4} lb/(ft-sec).

For kinematic viscosity, there is also a wide variety of units used. In the S.I. system, the units of kinematic viscosity are square meters per second (m^2/s) and in the customary English system the units are square feet per second (ft^2/s). Another unit has also gained favor in the engineering community called the centistoke (named after George Gabriel Stokes, a late nineteenth century English mathematician and physicist). One centistoke is equal to 0.000001 m^2/s or 0.0000107639 ft^2/s.

Fluid Pressure

Pressure is a force per unit area that arises when a fluid is subjected to a compressive stress. Units may be newtons/m^2, lb/ft^2, lb/in.^{2}, or any similar equivalent of force over area. Pascal's law states that the pressure in a fluid at rest is the same in all directions, a condition different from that for a

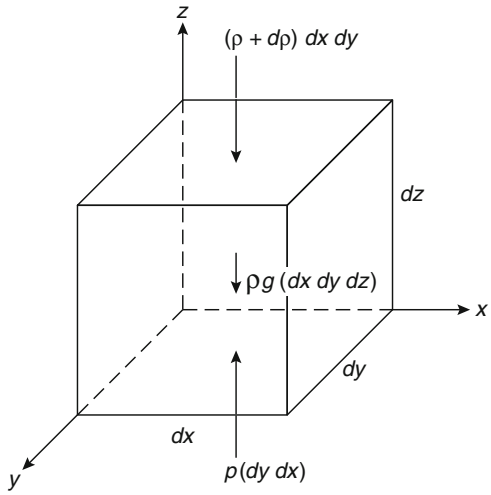

Fig. 41.1 Notation for basic eq. of fluid statics

stressed solid where the stress on a plane depends upon the orientation of that plane. For an infinitesimal fluid element in a larger static body of fluid, a free body diagram of the vertical forces can be drawn as shown in Fig. 41.1. The pressure difference $[(p + dp) - p]$ is due only to the weight of the fluid element. Since the weight of the element is given by $mg = \rho g\, dz\, dA$, a summing of forces in the vertical direction gives:

$$dp\ dA = -\rho g\ dz\ dA \tag{41.1a}$$

$$dp = -\rho g dz \tag{41.1b}$$

In integral form, Equation 41.1b becomes

$$\int_1^2 \frac{dp}{\rho g} = -\int_1^2 dz = -(z_2 - z_1) \tag{41.2}$$

where the path endpoints 1 and 2 refer to different elevation levels.

To integrate Equation 41.2, it is necessary to establish a functional relation between the pressure p and the product of the density times the gravitational constant (ρg). Where density varies with pressure, the fluid is considered compressible, and the functional relation may be complex. For fluids that may be considered incompressible, such as water, ρ is a constant at any specified temperature. Equation 41.2 then becomes

$$p_2 - p_1 = -\rho g(z_2 - z_1) \tag{41.3}$$

The term (z_2–z_1) may be called a static *pressure head,* which can be expressed in units of length such as feet, inches, or meters of water. A simplified form of Equation 41.3 is often written

$$\rho = \gamma h \tag{41.4}$$

where h is height (elevation) of the column of liquid above a reference surface (i.e., (z_2–z_1). For water at 60 °F (15.6 °C), γ is taken to equal 62.4 lb/ft^3 (16.02 kg/m^3). The pressure corresponding to a head of h feet, then, is 0.433 h lb/in.^{2} (psi), or approximately 3 kPa per meter elevation. The head corresponding to a pressure of 1 psi (0.07 bar) is, inversely, 2.3 ft (0.7 m). Note that Equation 41.4 is valid only for a homogeneous, noncompressible fluid at rest, and that regardless of the shape of the container, points in the same horizontal plane experience the same pressure.

The vertical distance h is termed the *head* of a fluid. A pressure due only to the weight of a column of fluid is called a static pressure and can be measured by a standard Bourdon-type gauge (see Fig. 41.4). Such a measure is generally referred to as *gauge pressure*. The term *absolute pressure* takes into account the pressure exerted by the atmosphere as well, which at sea level is approximately 14.7 psi (1 bar), equivalent to a 33.9 ft (10.3 m) column of water. A pressure less than atmospheric is called a vacuum pressure, a perfect vacuum being zero absolute pressure. Since most fluid properties of interest are not significantly affected by small changes in atmospheric pressure, most fluids calculations are in terms of gauge pressure, although this fact is not often indicated in standard calculation nomenclature. When they are explicitly identified, gauge pressure is denoted by the term psig and absolute pressure by psia. If not stated otherwise, psi may be taken to designate gauge pressure.

Pressure Measuring Devices

Manometer Tube

Pressure measurement in a manometer tube is obtained by measuring the vertical displacement of a relatively heavy fluid (usually mercury),

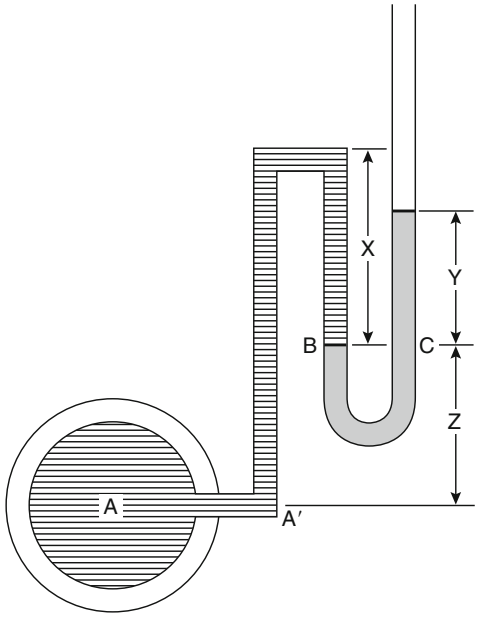

Fig. 41.2 Manometer

which will rise a smaller vertical distance than water in proportion to the ratio of its specific weight to that of water. Depending on the actual arrangement of the manometer tubing, a gauge equation can be written to solve for the pressure head. For the manometer shown in Fig. 41.2, the gauge equation is written by proceeding from the open end through the tube to point A', adding terms when descending a column and subtracting when ascending. Using mercury as the manometer fluid, we can write

$$(y+z)\gamma_{H_g} - z\gamma_{H_g} - x\gamma + (x+z)\gamma = p_A \quad (41.5)$$

Combining terms, generalizing the result, and expressing in terms of feet of water (head),

$$\frac{P_A}{\gamma} = ys + z \quad (41.6)$$

where s is the specific gravity of the manometer fluid.

Piezometer Tube

Literally a *pressure measuring tube,* a piezometer consists essentially of a narrow tube rising from a container enclosing a fluid under pressure (Fig. 41.3). Through the relation among pressure, height, and specific weight, the height to which the fluid rises in the tube represents the pressure of the contained fluid. While useful for some laboratory work, piezometer tubes are not generally feasible in practical applications.

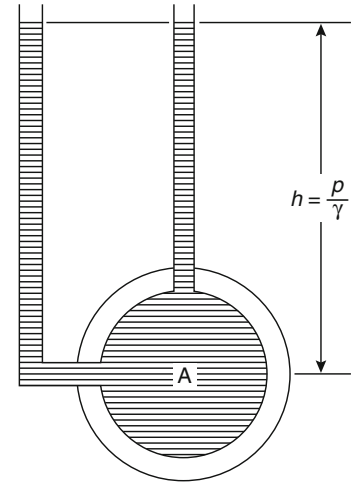

Fig. 41.3 Piezometer

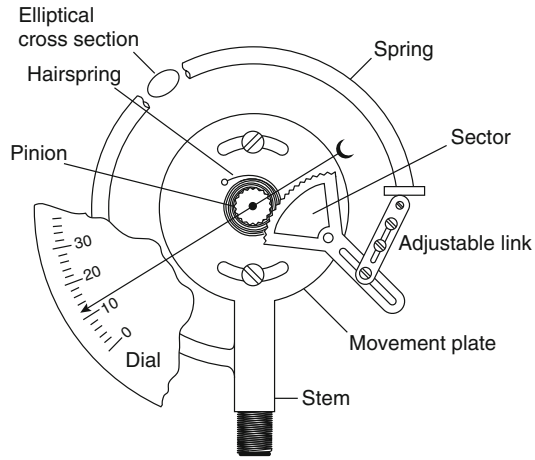

Fig. 41.4 Standard Bourdon gauge

Bourdon Gauge

The standard pressure measuring device used in a wide variety of fluid pressure measurement applications is the Bourdon gauge (Fig. 41.4).

The gauge contains a curved tube of elliptical cross section that undergoes a change in curvature with change in pressure. A dial hand, connected to the inner tube through a linkage system, indicates gauge pressure on a numerical dial face. Bourdon gauges are factory calibrated and reasonably accurate instruments if not damaged by pressure surge or impact force. A field reading, unless known to be correct, cannot be assumed to be accurate and should be checked by independent means.

Forces on Submerged Plane Areas due to Fluid Pressure

It is sometimes of interest to determine the magnitude of the resultant force on a submerged area and the location of the center of pressure where the resultant force can be assumed to act. Consider the following example of a tank that has a plate in a vertical wall (Fig. 41.5). The magnitude of the resultant force can be determined from

$$F_R = \gamma h_c A \tag{41.7}$$

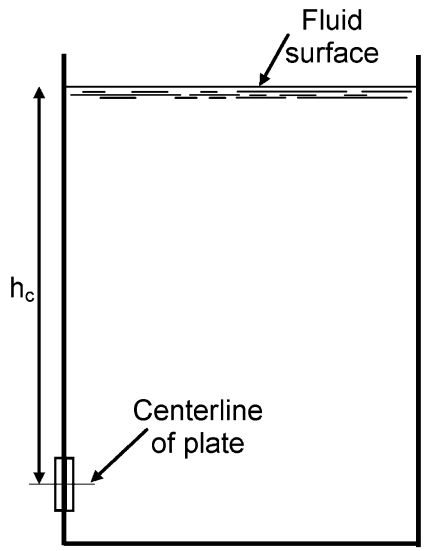

Fig. 41.5 Tank with a plate in a vertical wall

Fluid Dynamics

While the study of fluids in a static condition (at rest) yields some interesting information, it is the study of fluids in motion that is the most relevant to the fire protection engineer. Water, the most common fluid for fire protection needs to be available at the location of the fire, and therefore, needs to be moved from its source of supply though a series of conduits, typically pipes and hoses. The study of fluids in motion is called Fluid Dynamics.

Conservation Laws in Fluid Flows

Fluid flow may be characterized as uniform or nonuniform, steady or unsteady, compressible or incompressible, laminar or turbulent, rotational or irrotational, and one-, two-, or three-dimensional or some combination thereof. Real flows may be modeled as approximations of ideal flows when real properties do not depart significantly from the ideal characteristics defined by these terms.

For example, uniform flow occurs when the average velocity of a fluid does not change in either magnitude or direction anywhere along the flow path. Thus, liquid flow in a constant head pipeline of unchanging diameter is considered uniform flow. Steady flow, on the other hand, is determined with reference to a stationary point in the flow path. For steady flow to occur, the velocity of flow at that point must remain constant with time. This condition implies that the fluid density, the pressure head, and the volume rate of flow also are invariant with time. Thus, liquid flow in a constant head pipeline of varying diameter may be considered steady, nonuniform flow. It is important to note that a flow may be considered uniform (no change in magnitude or direction of the velocity) in a curved pipeline as long as the reference direction of the velocity vector is taken in the direction of the flow. We can then say that the velocity of the fluid does not change direction with respect to its enclosing boundaries.

We can also consider this flow one-dimensional whenever it is permissible to say that velocities or accelerations normal to the general direction of the flow are negligible. Clearly, real flow in a real-world structure has three dimensions, but a one-dimensional analysis is highly desirable as it represents a considerable mathematical simplification. Fortunately, a very large number of practical engineering flow problems involving water can be modeled as one-dimensional, steady flow problems, particularly many pipeline flows. In such cases it is possible to apply basic physical principles of conservation of mass and conservation of energy in the direction of flow to obtain the energy balance at any point in the flow. In fire flow hydraulics, it is common practice to introduce additional simplifying assumptions, such as the requirements that the fluid be incompressible and that flow properties be invariant with temperature and pressure. It then follows directly that with no flow additions or subtractions, the volumetric flow rate at any point in a fluid stream must be a constant. This statement of mass conservation, known as the equation of continuity, can be expressed mathematically as

$$\rho_1 A_1 v_1 = \rho_2 A_2 v_2 = \text{Constant} \tag{41.9}$$

If the fluid is considered incompressible, as is the case with water, the density will not change with respect to the fluid at different locations in the flow, so Equation 41.9 becomes

$$A_1 v_1 = A_2 v_2 = \text{Constant} = Q \tag{41.9a}$$

By applying the principal of conservation of energy to a flowing fluid, an expression can be derived that gives the theoretical net energy balance of the fluid at any point along its flow path. This is known as the Bernoulli equation, which can be written as:

$$\frac{p_1}{\gamma} + \frac{v_1^2}{2g} + z_1 = \frac{p_2}{\gamma} + \frac{v_2^2}{2g} + z_2 \tag{41.10}$$

In Equation 41.10, p_1, v_1, and z_1 represent the pressure, velocity, and elevation (above a given data plane) of the fluid at one location in the flow stream while p_2, v_2, and z_2 represent the pressure, velocity, and elevation of the same fluid at a second point in the same flow stream. In this form, units are feet (or meters) of fluid. Each term thus represents a fluid head with the addition of the three terms representing the total head (or energy) of the fluid at any point. Multiplying each term by the specific weight, γ, converts the equation to units of pressure. Changes in internal energy of the fluid are ignored and are assumed to be negligible. The form of Equation 41.10 suggests that the flow of liquid (or transport of fluid energy) results from three principal causes: pressure difference, gravity, and inertia. Equation 41.10 expresses an ideal condition fulfilled by the three components of head corresponding to these three causes.

The assumption of incompressibility (i.e., constant density) requires that the product of the velocity of flow and the cross-sectional area of the flow of any conserved portion of the stream be constant; the ideal flow streamlines, therefore, converge as the velocity increases and diverge as the velocity decreases. If it could be assumed that the total Bernoulli head were, indeed, constant or, equivalently, if it were possible to obtain total head simply as a function of the coordinates of the moving fluid element, then many hydrokinetic problems could be solved theoretically by mathematically manipulating and extrapolating the Bernoulli equation. Unfortunately, this is not the case. Other energy transfers are possible, and these require use of a more general form of the equation. In addition to the pressure, velocity, and position (elevation) energies possessed by the fluid at sections 1 and 2, energy may be added to the fluid (work done on the fluid by a pump), lost by the fluid (through friction), or extracted from the fluid (work done by the fluid). Therefore, we write the Bernoulli energy conservation expression in the more general form:

$$\left(\frac{p_1}{\gamma} + \frac{v_1^2}{2g} + z_1\right) + h_A - h_L - h_E = \left(\frac{p_2}{\gamma} + \frac{v_2^2}{2g} + z_2\right) \tag{41.10a}$$

In Equation 41.10a, the value of h_A represents the energy being added to the fluid, h_L represents the

energy lost from the fluid due to friction loss, and h_E represents the energy taken from the fluid. An example of how the Bernoulli equation can be used to solve a simple water flow problem follows as Example 1.

Example 1 Water flows from a reservoir through a pipeline as shown in the following diagram. The flow is considered frictionless and discharges freely at point *C*.

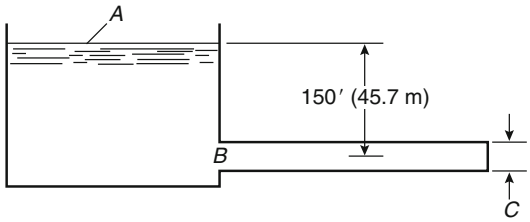

(a) What is the total head (total specific energy) at point *A*?
(b) What is the total head (total specific energy) at point *B*?
(c) What is the discharge velocity at point *C*?

Solution

(a) At *A*, both the velocity and gauge pressures are considered to be zero. Assuming that the plane at the middle of the discharge outlet at *C* is the reference data place, by Bernoulli, then, the total head would be written as:

$$h_A = 0 + 0 + 150 \text{ ft} = 150 \text{ ft}$$

or, in SI unit equivalents,

$$h_A = 0 + 0 + 45.7 \text{ m} = 45.7 \text{ m}$$

(b) At *B*, the fluid has a nonzero velocity head and is under hydrostatic pressure. As long as we consider the flow frictionless, the total head is constant. Therefore,

$$h_B = h_A = 150 \text{ ft } (45.7 \text{ m})$$

(c) At *C*, the pressure head is again zero, since the discharge is at atmospheric pressure and the discharge of the water is at the reference data elevation, so it is also zero. Once more by Bernoulli,

$$h_C = 0 + \frac{v^2}{2g} + 0$$

Since the total energy at one point in the flow is equal to the total energy at another point, we know that h_C is also equal to h_A and h_B, which are 150 ft. Using this knowledge, we can solve the equation for "v" as follows:

$$150 = \frac{v^2}{2g}$$
$$v^2 = (150)2g = (150)2(32.2) = 9,660$$
$$v = 98.3$$

or, in SI unit equivalents,

$$v^2 = 2(9.81)(45.7)$$
$$v = 29.9 \text{ m/s}$$

Note that we could calculate the actual values of the pressure and velocity heads at point *B* if we had more information about the system. For example, we could determine the flow at the discharge point (*C*), if we knew the area and type of discharge opening (see section "Free Discharge at an Opening"). This determination is simply an application of the continuity equation. Knowing the pipeline diameter at point *B* allows us to apply continuity constraints once again to calculate v_B from which the velocity head may be determined. The pressure head at *B* is simply a function of the weight of the vertical column of water.

The components of the Bernoulli equation may be expressed graphically in terms of energy levels existing at any points in the flow regime. In Fig. 41.6 a simple system representing a realistic flow is shown. Water flows from a reservoir (with presumed constant surface elevation) to atmosphere. The flow is accompanied by losses of energy represented by h_L. The losses may occur in many places such as at valves, bends, and sudden changes in pipe diameter. Generally, the most important loss is that due to friction between the moving fluid and the pipe wall. Since there are always energy losses in real flows, the total energy of the system decreases in the direction of flow. Graphically, the linear curve in Fig. 41.6 connecting all points

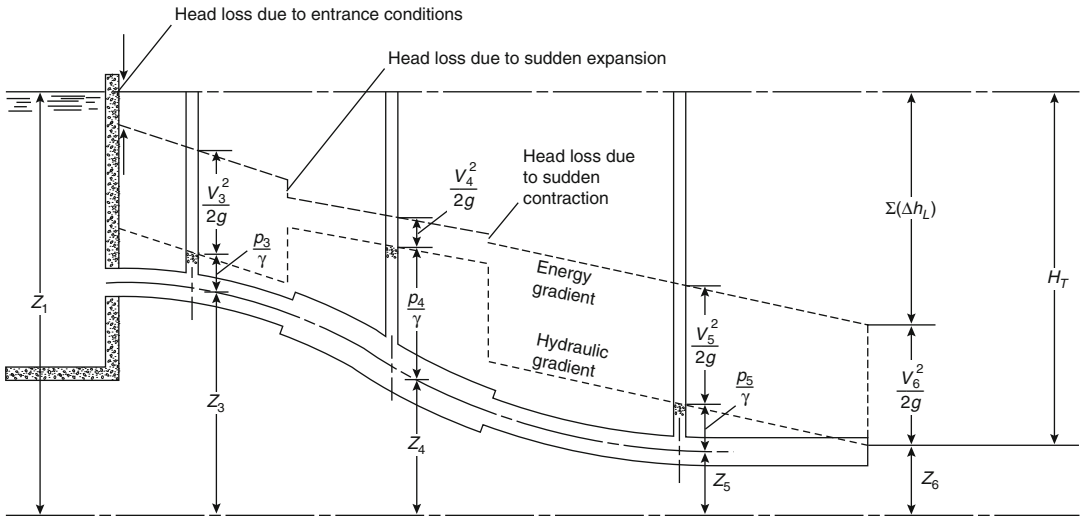

Fig. 41.6 Realistic flow characteristics

represents the total energy in the piping system and is referred to as the *energy gradient* (EG). It must always decrease in the direction of flow unless energy is added to the system such as by a pump. The *hydraulic gradient* (HG) connects the points representing the sum of static pressure and elevation energies (i.e., the heights to which water in piezometer tubes would rise in a flow path). Note that the hydraulic gradient may increase in the direction of flow if velocity head is converted to pressure head at a given point in the system (such as at an increase in pipe diameter). Thus, the relationship between the energy and hydraulic gradients can be written as

$$\mathrm{EG} = \mathrm{HG} + \frac{v^2}{2g} \tag{41.11}$$

General Considerations for Fluid Energy Losses in Pipe Flows

Energy losses in fluids due to friction in piping are of key importance in fire protection engineering. Losses due to friction are due to shear stresses set up within a moving fluid in a conduit by an imposed pressure gradient. Flow driven by the pressure force is restrained by drag forces acting at the conduit wall. To better visualize this phenomenon, it is useful to introduce the concept of the boundary layer. For many fluids, such as air or water, motion through a stationary conduit or pipe is characterized in most practical situations by a nearly constant velocity cross section everywhere except in a very thin layer near the wall of the pipe. This layer may be as little as 0.1 mm thick, but may vary significantly with the nature of the fluid, the velocity of flow, and the surface roughness of the conduit. We may visualize boundary layer flow in terms of a velocity profile (Fig. 41.7). Theories developed primarily by Prandtl [2, 3] hold that a very thin (molecular) layer of fluid sticks to the conduit wall. The tendency of the next fluid layer to move due to an imposed force creates a shearing stress, τ, between the layers. If the boundary is thought of as many thin fluid plates (lamina) sliding on each other, then we can expect the velocities of these lamina to increase with distance y from the wall until, at the edge of the boundary layer, the local velocity reaches the free-stream velocity of the fluid. The factor relating the velocity profile to the developed stress in the fluid is termed the fluid viscosity. The relationship was expressed mathematically by Newton as

$$\tau = \mu \frac{du}{dy} \tag{41.12}$$

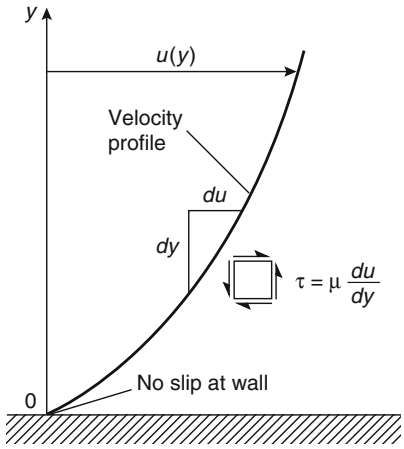

Fig. 41.7 Velocity profile

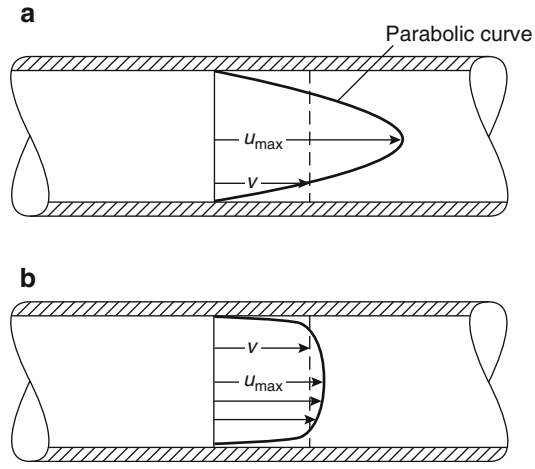

Fig. 41.8 Laminar (**a**) and turbulent (**b**) pipe flow velocity profiles for the same volume

The smaller the value of fluid viscosity, the thinner the boundary layer will be. The first layer of fluid sticks or adheres to the surface of the conduit while lamina above it successively slide on each other, exerting drag forces that, for most fluids, are proportional to the viscosity (so-called Newtonian fluids). The rate of change of the velocity between successive lamina is a measure of the unit shearing force between them. A curve joining the tips of velocity vectors plotted for the different lamina in the boundary layer is called a velocity profile. Laminar (smooth, streamline) flow (Fig. 41.8a) is characterized by a parabolic velocity profile with maximum velocity attained at the theoretical centerline of the flow. Turbulent flow, by contrast, is rough (nonstreamline) flow (Fig. 41.8b), characterized by an essentially uniform average velocity across the flow section, with only a very thin boundary layer close to the wall where viscous forces predominate. The velocities associated with laminar flows are generally so low that they are not representative of typical velocities in fire protection systems. Most flows of interest are turbulent, and the use of an approximated uniform or average velocity in calculating kinetic energy and velocity pressures does not introduce notable errors. In those situations where relatively large velocity heads are involved (such as where a pump adds a large amount of energy), a correction factor may be used to relate the actual average kinetic energy to the kinetic energy calculated using average velocity. From continuity considerations,

$$\mathrm{KE} = \int_A \rho u^3 dA = \alpha\rho \int_A v^3 dA \qquad (41.13)$$

where

KE = True kinetic energy of the flow

v = Average velocity of flow

α = Kinetic energy correction factor

For incompressible fluids, α can be represented by the following:

$$\alpha = \frac{1}{A}\int_A \left(\frac{u}{v}\right)^3 dA \qquad (41.14)$$

The value of α is approximately 1.1 for most turbulent flow problems. However, since the velocity head in most water distribution fire protection piping systems is relatively small, this correction factor is usually ignored.

While the development of boundary layer theory and the theory of viscous forces has led to an improved theoretical understanding of the mechanics of pipe flows, most flows of interest in fire protection cannot be fully analyzed from theoretical considerations alone. Fire protection flows are almost always turbulent flows. Despite a great expenditure of effort to develop a general predictive theory of turbulent flow phenomena, a fully descriptive theory does not yet exist.

While it is postulated that head losses arise because of friction between the fluid and the pipe wall, there is an additional head loss contribution due to turbulence within the flowing fluid. In turbulent flows the rate of head loss, unfortunately, is not simply a function of fluid velocity but depends also on pipe wall roughness. The determination of head loss is further complicated by the changing interaction among these variables at different flow velocities, interior pipe surface roughness and actual pipe sizes. Within the last century, however, a large body of empirical flow data has been collected, analyzed, and reproduced by several investigators. The major features and limits of applicability of the more important results are presented in the following paragraphs.

Fluid Flow Energy Loss Equations

Chezy Equation

Theoretical development of the physical relationships describing pipe flows dates from about the middle of the nineteenth century, when Chezy postulated a fundamental proportionality between volumetric flow and pipe size based on the continuity equation. His formula is commonly given as

$$Q = \frac{\pi D^2}{4} v = \frac{\pi D^2}{4} \frac{C}{2} \sqrt{DS} \tag{41.15}$$

and may also be written as

$$S = \left(\frac{8Q}{\pi C}\right)^2 D^{-5} \tag{41.16}$$

where D and S are pipe diameter and slope of the energy gradient, respectively. The factor, C, is a proportionality factor incorporating a significant degree of physical uncertainty. Since, by definition

$$S = \frac{h_L}{L}$$

the equation can be rewritten as an expression for pipe flow head loss as a function of pipe diameter and discharge as follows:

$$h_L = \left(\frac{8}{\pi C}\right)^2 \frac{L}{D^5} Q^2 \tag{41.17}$$

Use of the Chezy equation was limited by uncertainties relating to evaluations of the C-factor, which is not, in fact, a constant for a given size conduit or wall condition as was originally thought.

Darcy-Weisbach Friction Loss

A theoretically more satisfying approach was taken by Darcy, Weisbach, and others. Their formula, which bears the names of the two primary investigators, is generally written as:

$$h_L = f \frac{L}{D} \frac{v^2}{2g} \tag{41.18}$$

It postulates a basic proportionality between head loss and the kinetic energy of the flow, as well as to pipe length and diameter. The proportionality factor f, known as the friction factor, became the subject of extensive theoretical and experimental investigation. The value of f for laminar flow can be shown theoretically to be a simple linear function of the Reynolds number, Re, where:

$$\mathrm{Re} = \frac{D_e v \rho}{\mu}$$

The term D_e is the equivalent flow diameter, which is the actual inside diameter of a circular pipe. The equivalent diameter, D_e, can be found from the hydraulic radius, r_h, which is defined as the area in flow divided by the wetted perimeter. The wetted perimeter does not include the free fluid surface.

$$D_e = 4 r_h$$

For Re less than about 2000 (corresponding to low velocity flows or fluids of high viscosity) the relation is

$$f = \frac{64}{\mathrm{Re}} \tag{41.19}$$

In turbulent flows (higher Reynolds numbers) the roughness of the pipe walls becomes a much more significant factor, and a simple expression to determine f is unavailable.

A systematic investigation of the actual characteristics of piping inner wall surfaces was first performed by Nikuradse in 1933. To simulate varying degrees of roughness in commercial pipes due to corrosion or surface finish, Nikuradse glued sand grains of known sizes to the inside walls of test pipes. The resulting logarithmic plot of friction factor versus Re is shown in Fig. 41.9. Although the tests are from Nikuradse, the plot is called Stanton's diagram in recognition of his earlier (1914) elucidation of the relation between friction factor and Reynolds number. Note that at sufficiently high Re, the friction factor depends almost entirely on pipe roughness and is essentially independent of Re. In these plots the roughness parameter is expressed as the ratio of the root mean square grain diameter to the pipe diameter. The resulting ratio is termed the relative roughness and is represented mathematically as ε/D. Typical values for the roughness (ε) of new commercial pipes are shown in Table 41.1. However, fire protection engineers are expected to build safety factors into their calculations, so the use of pipe roughness values that correspond to new pipe should not be used. To be consistent with fire protection standards, values for aged pipe should be used. Also shown in Table 41.1 are a number of recommended roughness values that should be considered for aged pipe in fire protection system calculations.

Moody plotted various solutions for the friction factor (f) using different Reynolds numbers and relative roughness of pipes on a graph. The resulting Moody diagram (Fig. 41.10) is widely used today in conjunction with the Darcy-Weisbach equation to compute friction losses for water flowing in pipe. Figure 41.11 presents relative roughness values for use with the Moody diagram over a wide range of conditions. Other diagrams have been developed for use with the Darcy-Weisbach equation [6, 7] when parameters other than h_L are sought. Essentially, the alternative graphical formulations employ a rearrangement of variables to facilitate solving for some other unknown variables such as Q or D.

Both experimental and theoretical investigations have yielded uncertain results in

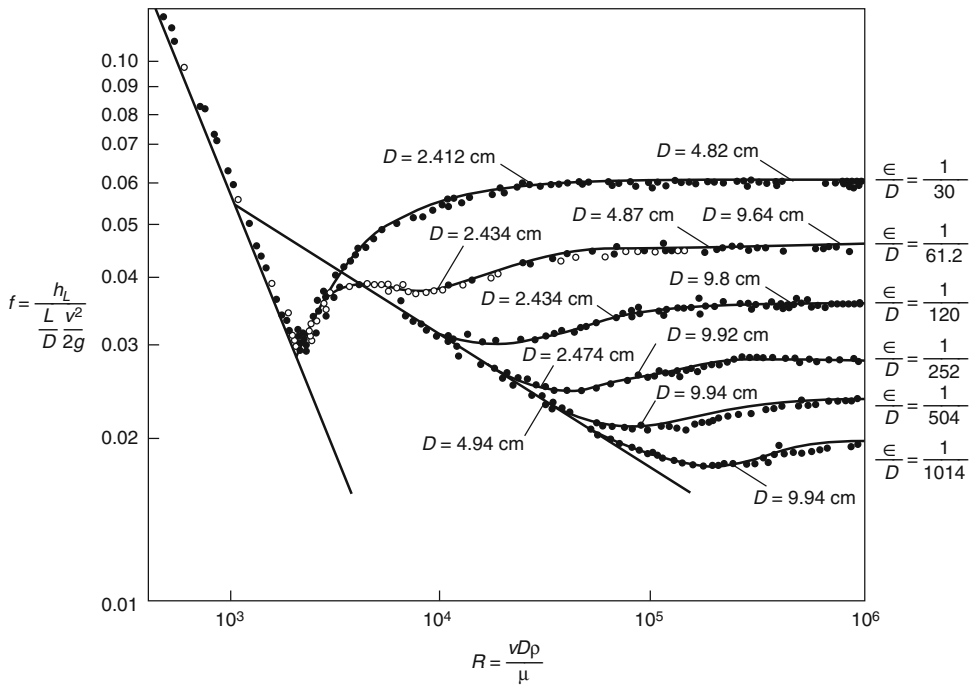

Fig. 41.9 Nikuradse's sand-roughened-pipe tests

Table 41.1 Values of absolute roughness of commercial pipes

Type of pipe or tubing	ε in ft × 10^{-6} Range	Design	Probable maximum variation of f from design (%)
New clean pipe [4]			
Asphalted cast iron	400	400	−5 to +5
Brass and copper	5	5	−5 to +5
Concrete	1000–10,000	4000	−35 to +50
Cast iron	850	850	−10 to +15
Galvanized iron	500	500	0 to +10
Wrought iron	150	150	−5 to +10
Steel	150	150	−5 to +10
Riveted steel	3000–30,000	6000	−25 to +75
Wood stave	600–3000	2000	−35 to +20
Aged pipe [5]			
Steel, dry system		1250	
Steel, wet system		333	
Plastic		7	
Copper		7	

Notes: For ε values in meters, multiply the above numbers by 0.3048
For ε values in inches, multiply the above numbers by 12

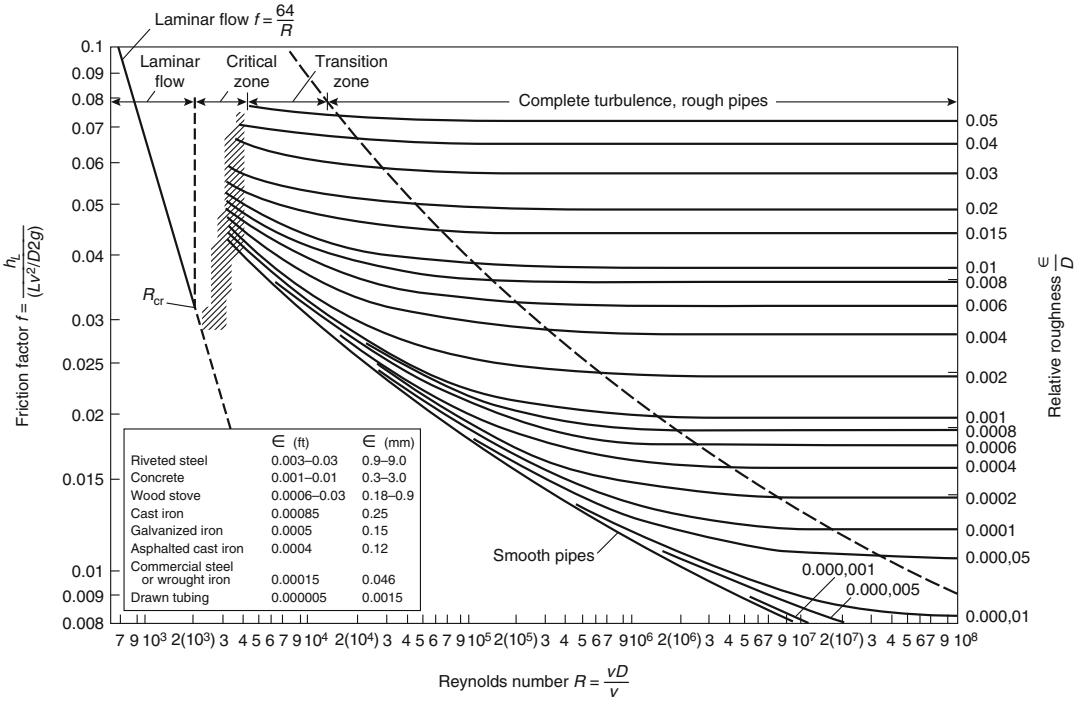

Fig. 41.10 Moody diagram

the region known as the *critical zone,* wherein the flow changes from laminar to turbulent. Uncertainty may be expected since the transition point is difficult to define precisely and, in fact, varies over a considerable range of Re depending upon the direction of the transition (i.e., flow going from laminar to turbulent or from turbulent to laminar) and the local

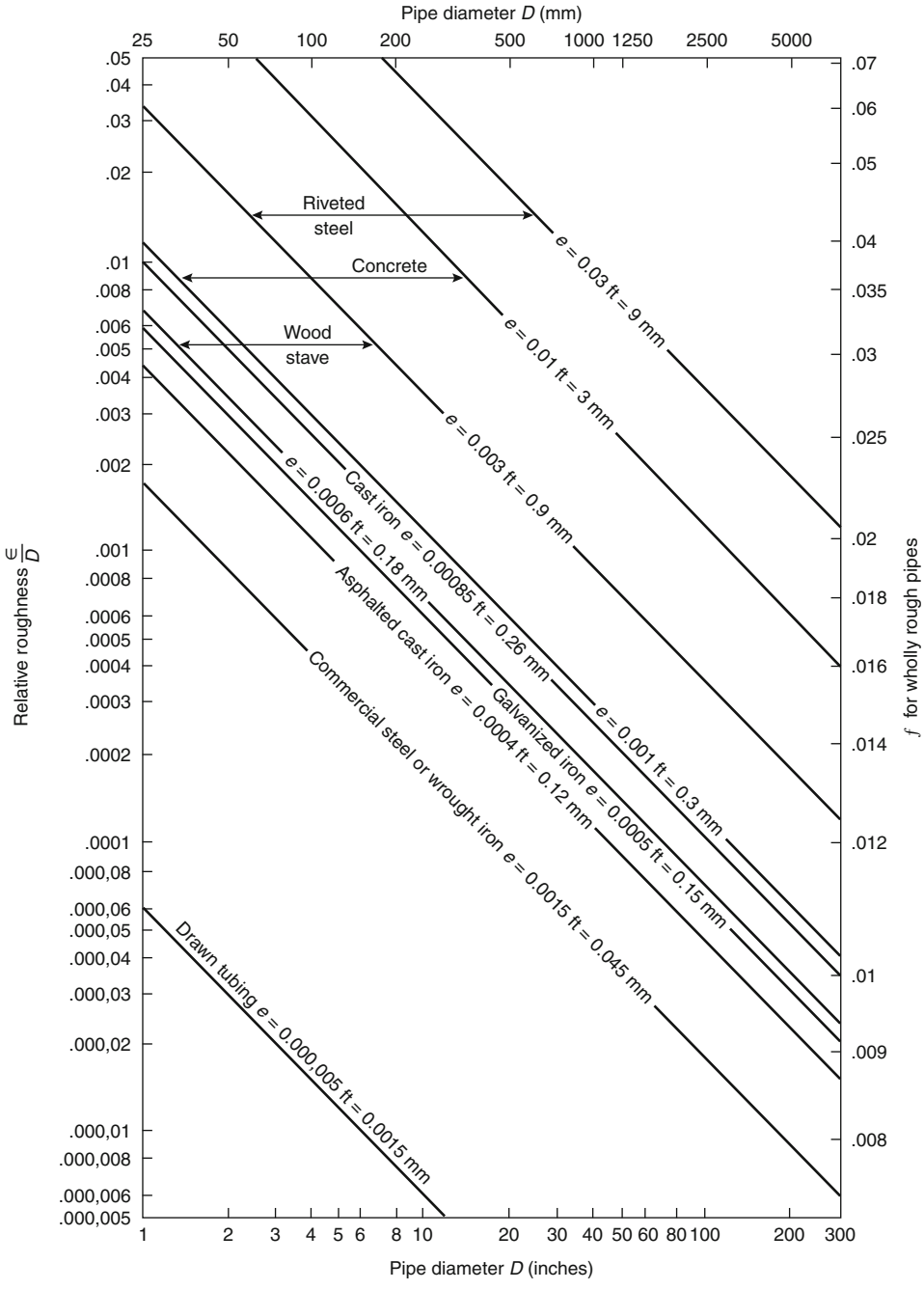

Fig. 41.11 Relative roughness chart

conditions affecting flow stability. As a practical consideration, however, this uncertainty is of little importance in fire protection, since most real flows of interest fall well into the turbulent range.

Colebrook developed an empirical transition function for the region between smooth flow and complete turbulence. Flow in this region is sometimes referred to as hydraulically smooth or turbulent smooth. The equation has been presented

in various forms, the following expression being commonly used:

$$\frac{1}{\sqrt{f}} = -0.86 \ln\left(\frac{\varepsilon/D}{3.7} + \frac{2.51}{\mathrm{Re}\sqrt{f}}\right) \qquad (41.20)$$

An alternate and equivalent expression is

$$f = \left[1.14 - 2\log\left(\frac{\varepsilon}{D} + \frac{9.35}{\mathrm{Re}\sqrt{f}}\right)\right]^{-2} \qquad (41.20a)$$

This relation forms the primary basis for the Moody diagram.

VonKarman used boundary layer theory to derive an expression characterizing the friction factor for fully turbulent flow within rough-walled pipes. The final numerical form of the equation

$$\frac{1}{\sqrt{f}} = 1.4 + 2\log\frac{D}{\varepsilon} \qquad (41.21)$$

was adjusted to agree more closely with Nikuradse's experimental results. As pipe roughness decreases, this expression approaches Colebrook's equation.

The Darcy-Weisbach equation and the Reynolds number calculation both force the engineer to utilize variables in unusual units. Typically, engineers deal with flow in gallons per minutes instead of cubic feet per minute or velocity in feet per second. Similarly, the diameter of the pipe is typically in inches and not in feet. The formulas for the Darcy-Weisbach equation and the Reynolds number can be rewritten in terms of variables that are much more commonly used (ΔP is friction loss in psi, Q is flow in gpm, d is the internal diameter of the pipe in inches, and μ is the viscosity in centipoises) as follows:

$$\Delta P = 0.000216 f \frac{l\rho Q^2}{d^5} \quad \mathrm{Re} = \frac{50.6 Q\rho}{d\mu}$$

Hazen-Williams Friction Loss

While the Darcy-Weisbach method of friction loss calculation yields sufficiently accurate results for a broad range of flow conditions, it can be difficult to use because of the associated variables that need to be determined. The density and viscosity of a fluid are not always known at every temperature at which the fluids are going to be used. In addition, since the friction factor cannot be solved for directly, it needs to be obtained from the Moody diagram, which introduces some potential error into the use of the technique because the engineer can arrive at some widely different friction factors based on very small changes in how the curves on the Moody diagram are interpreted.

A much more straight forward calculation technique was developed by Hazen and Williams (two civil engineers affiliated with the University of Michigan) around the turn of the nineteenth to the twentieth Century. Due to its simplicity, this technique has become one of the most widely used flow-energy loss relations. The empirically based Hazen-Williams formula was developed from observations of a very large number of pipeline flows. The Hazen-Williams equation was originally written in the form

$$V = 0.113 C D^{0.63} S^{0.54} \qquad (41.22)$$

where V is the average velocity in feet per second, S is the slope of the energy gradient—that is, the loss of energy per unit length of the pipe—and D is the actual internal pipe diameter in inches. The coefficient C is a *friction* factor introduced as a constant to represent the roughness of the pipe walls. Table 41.2 presents a representative list of C coefficients for various piping materials. Note that the value of C can vary significantly with the piping material, the age of the pipe, and the corrosive qualities of the water.

The Hazen-Williams formula is also encountered in the form

$$Q = 0.285 C D^{2.63} S^{0.54} \qquad (41.22a)$$

where Q is volumetric flow rate in gpm and D is in inches. Yet another form, also in the same units for Q and D, is widely used in automatic sprinkler system design. It is arranged to solve for the pressure drop in psi per linear foot of pipe:

$$p = \frac{4.52 Q^{1.85}}{C^{1.85} D^{4.87}} \qquad (41.22b)$$

Table 41.2 Values of C in Hazen-Williams formula[a]

Type of pipe	*C values for certain pipe diameters*					
	2.5 cm (1 in.)	7.6 cm (3 in.)	15.2 cm (6 in.)	30.5 cm (12 in.)	61 cm (24 in.)	122 cm (48 in.)
Uncoated cast iron—smooth and new	—	121	125	130	132	134
Coated cast iron—smooth and new	—	129	133	138	140	141
30 years old						
Trend 1—slight attack	—	100	106	112	117	120
Trend 2—moderate attack	—	83	90	97	102	107
Trend 3—appreciable attack	—	59	70	78	83	89
Trend 4—severe attack	—	41	50	58	66	73
60 years old						
Trend 1—slight attack	—	90	97	102	107	112
Trend 2—moderate attack	—	69	79	85	92	96
Trend 3—appreciable attack	—	49	58	66	72	78
Trend 4—severe attack	—	30	39	48	56	62
100 years old						
Trend 1—slight attack	—	81	89	95	100	104
Trend 2—moderate attack	—	61	70	78	83	89
Trend 3—appreciable attack	—	40	49	57	64	71
Trend 4—severe attack	—	21	30	39	46	51
Miscellaneous						
Newly scraped mains	—	109	116	121	125	127
Newly brushed mains	—	97	104	108	112	115
Coated spun iron—smooth and new	—	137	142	145	148	148
Old—take as coated cast iron of same age						
Galvanized iron—smooth and new	120	129	133	—	—	—
Wrought iron—smooth and new	129	137	142	—	—	—
Coated steel—smooth and new	129	137	142	145	148	148
Uncoated steel—smooth and new	134	142	145	147	150	150
Coated asbestos-cement—clean	—	142	149	150	152	
Uncoated asbestos-cement—clean	—	142	145	147	150	
Spun cement-lined and spun bitumen-lined—clean	—	147	149	150	152	153
Smooth pipe (including lead, brass, copper, polythene, and smooth PVC)—clean	140	147	149	150	152	153
PVC wavy—clean	134	142	145	147	150	150
Concrete—Scobey						
Class 1—$C_s = 0.27$; clean	—	69	79	84	90	95
Class 2—$C_s = 0.31$; clean	—	95	102	106	110	113
Class 3—$C_s = 0.345$; clean	—	109	116	121	125	127
Class 4—$C_s = 0.37$; clean	—	121	125	130	132	134
Best—$C_s = 040$; clean	—	129	133	138	140	141
Tate relined pipes—clean	—	109	116	121	125	127
Prestressed concrete pipes—clean	—	—	—	147	150	150

[a]The above table has been compiled from an examination of 372 records. It is emphasized that the Hazen-Williams formula is not suitable for the coefficient *C* values appreciably below 100, but the values in the above table are approximately correct at a velocity of 0.9 m/s (3 ft/s)

For other velocities the following approximate corrections should be applied to the values of *C* in the table above [8]

Values of *C* at 0.9 m/s	Velocities below 0.9 m/s for each halving Rehalving of velocity relative to 0.9 m/s	Velocities above 0.9 m/s for each doubling Redoubling of velocity relative to 0.9 m/s

(continued)

Table 41.2 (continued)

Values of C at 0.9 m/s	Velocities below 0.9 m/s for each halving Rehalving of velocity relative to 0.9 m/s	Velocities above 0.9 m/s for each doubling Redoubling of velocity relative to 0.9 m/s
C below 100	Add 5 % to C	Subtract 5 % from C
C from 100 to 130	Add 3 % to C	Subtract 3 % from C
C from 130 to 140	Add 1 % to C	Subtract 1 % from C
C above 140	Subtract 1 % from C	Add 1 % to C

In SI units,

$$p = \frac{6.05Q^{1.85}}{C^{1.85}D^{4.87}} \times 10^5 \qquad (41.22c)$$

where the units of Q are L/min, D is in mm, and p is in bars per meter of pipe.

Many manufacturers of fire protection equipment, many fire underwriters, and others have published Hazen-Williams-based pipe friction loss data (usually in tabular format) over applicable ranges of pipe sizes, flow rates, and C-factors. A useful calculation aid in a more compact format is the Hazen-Williams nomograph (Fig. 41.12), which is reproduced here in its generalized form.

The Hazen-Williams formula is most appropriate for water flow at or around 60 °F (15.6 °C), as it does not contain any factors relating to the physical properties of the fluid. The formula gives acceptable results in practice with a judicious choice of the C-factor. Fundamentally, the C-factor is a proportionality constant and, as such, its *true* value depends as much upon the values chosen for the associated exponent in the accompanying formula as it does upon actual pipe roughness. The suggested values are the result of curve-fitting exercises and cannot be expected to accurately and evenly represent flow parameter relationships across the full range of observed flow velocities. Allowing fpr the desirability of retaining constant exponent values for D and S (i.e., a presumed theoretically stable correlation among all flow parameters in the equation), the value of C for any given flow scenario becomes a narrowly bounded variable that reflects the pipe roughness. Although, as in the Chezy formula, C is not actually a constant, for practical use it is assigned a constant value for a given presumed roughness. Unfortunately, as Table 41.2 shows, the Hazen-Williams equation is a much better model of smooth pipe flow than of rough pipe flow. As long as the flow velocity is close to that at which C was measured and as long as the pipe roughness is not excessive, the Hazen-Williams relation can be expected to give reliable results. It has been noted, however, that in rough pipes head loss varies with flow (and velocity) to the power of 2 rather than the power of 1.85 characteristic of smooth pipes [9]. This observation introduces a significant element of uncertainty into the hydraulic analysis of rough pipe with higher velocity flows.

Example 2 Water at 50 °F (10 °C) flows through 4 in. (102 mm) Schedule 40 welded steel pipe at a rate of 500 gpm (1892.7 l/m). Compare the friction head losses calculated by the Darcy-Weisbach and Hazen-Williams equations for flow through 100 ft of pipe.

Solution

Basic Data:

For 50 °F water, kinematic viscosity, $\nu = 1.41 \times 10^{-5}\text{ft}^2/\text{s}$

Pipe flow area $= 0.0884\ \text{ft}^2$

$\varepsilon = 0.0002$ (very close to new pipe)

Pipe inside diameter $= 0.3355\ \text{ft} = 4.026\ \text{in.}$

Using the Darcy approach, we first determine the Reynolds number (Re), and then we determine the relative roughness of the pipe as a ratio of the roughness to the diameter (ε/D). After obtaining these values, we enter the Moody diagram (Fig. 41.10) to get the friction factor (f). In order to get the Reynolds number, we need the velocity associated with the flow:

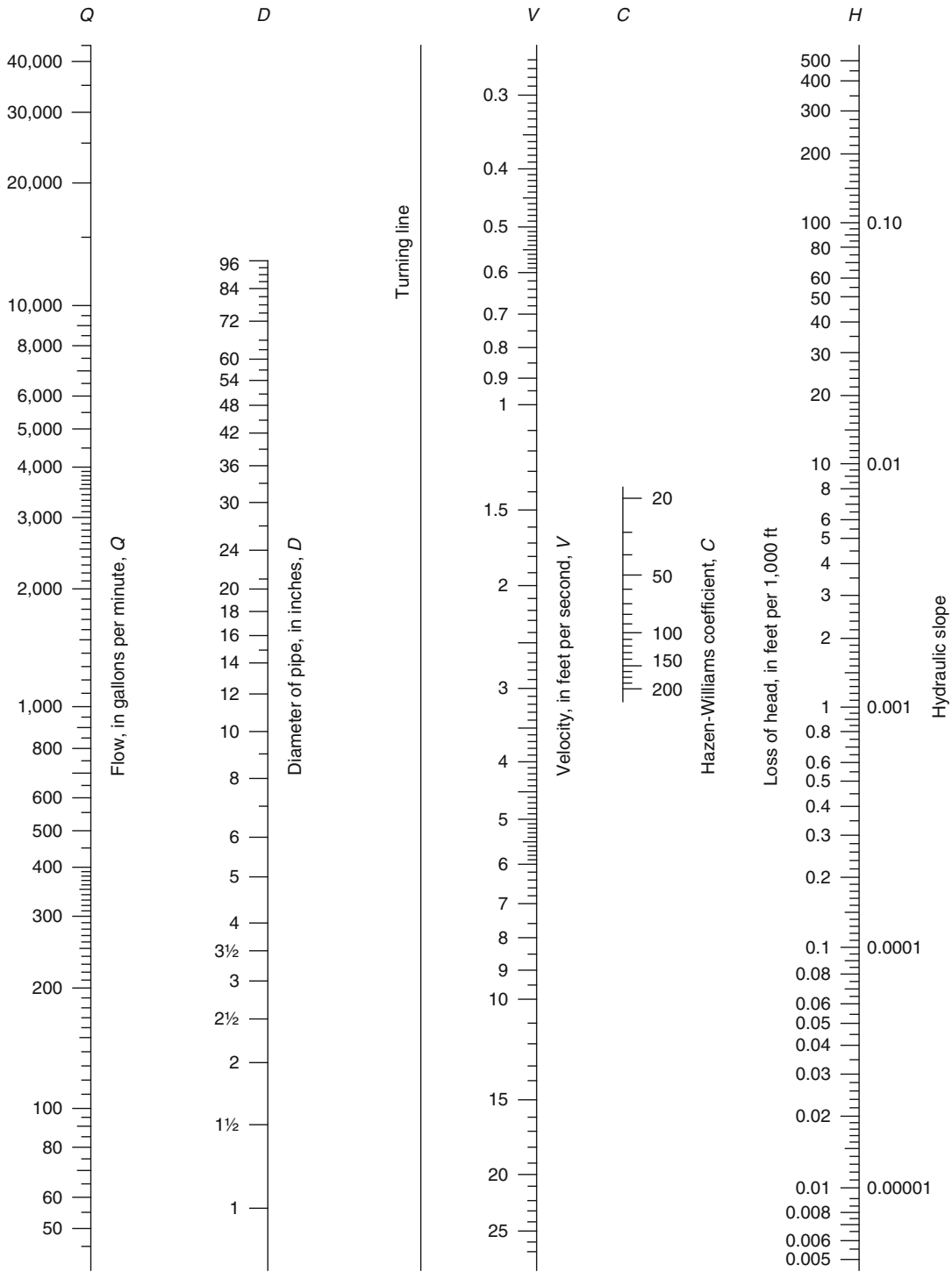

Fig. 41.12 Nomograph for solution of the Hazen-Williams formula

$$\text{Flow quantity} = Q = 500 \text{ g pm}$$
$$\equiv 1.1140 \text{ cfs } (31.54 \text{ L/s})$$
$$\text{Velocity} = v = \frac{Q}{A} = \frac{1.1140}{0.0884}$$
$$= 12.60 \text{ fps } (3.8 \text{ m/s})$$

$$\text{Re} = \frac{Dv}{\nu} = \frac{0.3355(12.60)}{1.41 \times 10^{-5}} = 3.0 \times 10^5$$
$$\frac{\varepsilon}{D} = \frac{0.0002}{0.3355} = 0.0006$$

From the Moody friction chart, $f = 0.0188$.

From Equation 41.18,

$$h_L = \frac{0.0188(100)\ (12.60)^2}{2(0.3355)\ (32.2)} = 13.8 \text{ ft}$$
$$= 5.98 \text{ psi } (0.41 \text{bar})$$

For the Hazen-Williams approach (Equation 41.22b) a C-factor for the pipe needs to be selected. Since the Darcy-Weisbach method used an ε value associated with new pipe, it would make sense to use a C-factor for new pipe in order to make an accurate comparison. As Table 41.2 shows, new steel pipe has C-factors between 134 and 150. If we assume $C = 140$,

$$\Delta p = \frac{4.52(100)\ (500)^{1.85}}{(140)^{1.85}(4.026)^{4.87}}$$
$$\Delta p = 5.40 \text{ psi } (0.37 \text{ bar})$$

The Hazen-Williams formula comes within 10 % of the value obtained using the Darcy-Weisbach equation, with significantly less effort. This is considered to be within the range of acceptable values in an engineering exercise involving fire protection system piping. Note that the system design and installation standards such as NFPA 13 do not allow the use of C-factors for new pipe for this very reason. Using a C-factor of 100, to simulate the aged pipe associated with dry-pipe systems and solve directly for pressure drop in psi per 100 ft we would obtain:

$$\Delta p = \frac{4.52(100)\,(500)^{1.85}}{(100)^{1.85}(4.026)^{4.87}} = 10.06 \text{ psi } (0.69 \text{ bar})$$

Note that the friction loss with the aged pipe is nearly twice what would have been predicted with the use of the value for new pipe. Accuracy in using Hazen-Williams clearly depends on a careful choice of C-factor. The Darcy-Weisbach result does not seem to be so sensitive to choice of roughness.

Minor Losses

Flows through pipe fittings, valves, or other pipeline fixtures generate additional turbulence and, therefore, additional energy losses. These losses, although termed minor, can be rather significant fractions of the total energy loss. In particular, losses due to pipeline obstructions such as swing-type check valves and certain types of flow meters are equivalent to adding many feet (or meters) of piping to the system. Thus, in some instances minor losses may have to be considered major, particularly in systems where there are many fittings, valves, or other appurtenances. Empirical methods are used to determine these losses for a range of flow or obstruction geometries. One common method is to define a *minor loss coefficient* to express head loss as a function of velocity head. Thus,

$$h_L = k\frac{v^2}{2g} \tag{41.23}$$

where k is a dimensionless loss coefficient. It is sometimes convenient to express such losses in terms of *equivalent length of straight pipe*, or as pipe diameters that produce the same head loss. Thus, by Darcy-Weisbach,

$$\frac{L}{D} = \frac{k}{f} \tag{41.24}$$

Table 41.3 shows local loss coefficients for a number of fittings and flow patterns. Wherever possible, manufacturers' data should be used, particularly for valves because of the wide variety of designs for the same generic valve type. Such data are often published in the form of flow coefficient or C_v values, which may be used in the equation

Table 41.3 Local loss coefficients

Use the equation $h_L = kv^2/2g$ unless otherwise indicated. Energy loss E_L equals h_v head loss in feet.

1

Perpendicular square entrance:
$k = 0.50$ if edge is sharp

2

Perpendicular rounded entrance:

$R/d =$	0.50	0.1	0.2	0.3	0.4
$k =$	0.25	0.17	0.08	0.05	0.04

3

Perpendicular re-entrant entrance:
$k = 0.8$

4

Additional loss due to skewed entrance:
$k = 0.505 + 0.303 \sin \alpha + 0.226 \sin^2 \alpha$

5

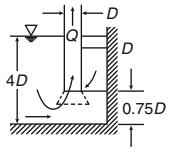

Suction pipe in sump with conical mouthpiece:

$$E_L = D + \frac{5.6Q}{\sqrt{2g}D^{1.5}} - \frac{v^2}{2g}$$

Without mouthpiece:

$$E_L = 0.53\ D + \frac{4Q}{\sqrt{2g}D^{1.5}} - \frac{v^2}{2g}$$

Width of sump shown: $3.5D$

(After I. Vágás)

6

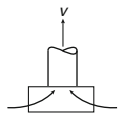

Strainer bucket:
$k = 10$ with foot value
$k = 5.5$ without foot value

(By Agroskin)

7

Standard tee, entrance to minor line:
$k = 1.8$

8

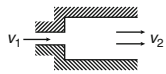

Sudden expansion:

$$E_L = \left(1 - \frac{v^2}{v^1}\right)^2 \frac{v_1^2}{2g} \quad \text{or} \quad E_L = \left(\frac{v^1}{v^2} - 1\right)^2 \frac{v_2^2}{2g}$$

9

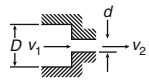

Sudden contraction:

$(d/D)^2 =$	0.01	0.1	0.2	0.4	0.6	0.8
$k =$	0.5	0.5	0.42	0.33	0.25	0.15

10

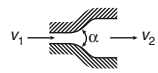

Diffusor:

$$E_L = k(v_1^2 - v_2^2)/2g$$

$\alpha^\circ =$	20	40	60	80
$k =$	0.20	0.28	0.32	0.35

(continued)

Table 41.3 (continued)

11

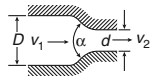

Confusor:

$E_L = k(v_1^2 - v_2^2)/2g$

$\alpha^\circ =$	6	10	20	40	60	80	100	120	140
k for $D = 3d$	0.12	0.16	0.39	0.80	1.0	1.06	1.04	1.04	1.04
$D = 1.5d$	0.12	0.16	0.39	0.96	1.22	1.16	1.10	1.06	1.04

12

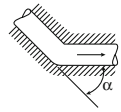

Sharp elbow:

$k = 67.6 \times 10^{-6}(\alpha^\circ)^{2.17}$

(By Gibson)

13

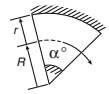

Bends:

$k = [0.13 + 1.85(r/R)^{3.5}]\sqrt{\alpha^\circ/180^\circ}$

(By Hinds)

14

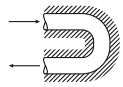

Close return bend:

$k = 2.2$

15

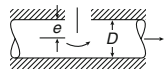

Gate valve:

$e/D =$	0	1/4	3/8	1/2	5/8	3/4	7/8
$k =$	0.15	0.26	0.81	2.06	5.52	17.0	97.8

16

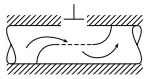

Global value:

$k = 10$ when fully open

17

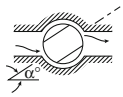

Rotary valve:

$\alpha^\circ =$	5	10	20	30	40	50	60	70	80
$k =$	0.05	0.29	1.56	5.47	17.3	52.6	206	485	¥

(By Agroskin)

18

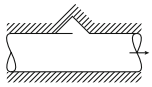

Check valves:

Swing type $k = 2.5$ when fully open

Ball type $k = 70.0$

Lift type $k = 12.0$

19

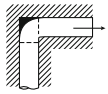

Angle valve:

$k = 5.0$ if fully open

20

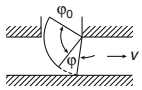

Segment gate in rectangular conduit:

$k = 0.3 + 1.3\left[\left(\frac{1}{n}\right)\right]^2$

where $n = \varphi/\varphi_0$ = the rate of opening with respect to the central angle

(By Abelyev)

21

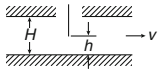

Sluice gate in rectangular conduit:

$k = 0.3 + 1.9\left[\left(\frac{1}{n}\right) - n\right]^2$

where $n = h/H$

(By Burkov)

$$Q = C_v\sqrt{h_L} \tag{41.25}$$

C_v is determined from the relation

$$C_v = \pi D^2\sqrt{\frac{g}{8k}} \tag{41.26}$$

which results directly from a combination of the continuity equation with the equations above.

Use the equation $h_L = kv^2/2g$ unless otherwise indicated. Energy loss EL equals h_v head loss in feet.

Table 41.4 Typical equivalent lengths of schedule 40 straight pipe for screwed steel fittings and valves for any fluid in turbulent flow

	Equivalent length		
	Pipe size (ft)		
Fitting type	1 in. (25.4 mm)	2 in. (50.8 mm)	4 in. (101.6 mm)
Regular 90° elbow	5.2	8.5	13.0
Long radius 90° elbow	2.7	3.6	4.6
Regular 45° elbow	1.3	2.7	5.5
Tee, flow through line (run)	3.2	7.7	17.0
Tee, flow through stem	6.6	12.0	21.0
180° return bend	5.2	8.5	13.0
Globe valve	29.0	54.0	110.0
Gate valve	0.84	1.5	2.5
Angle valve	17.0	18.0	18.0
Swing check valve	11.0	19.0	38.0
Coupling or union	0.29	0.45	0.65

Example 3 Table 41.4 lists a number of equivalent lengths of standard Schedule 40 pipe for screwed steel fittings and valves. Using the table determine the equivalent length of the 2-in.-diameter pipe network shown below.

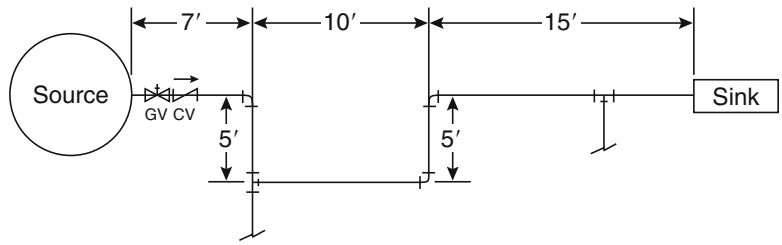

Solution The line comprises

1 check valve	19.0 ft (5.7 m)
3 90° standard elbows	$3 \times 8.5 = 25.5$ ft (7.7 m)
1 tee (flow through run)	7.7 ft (2.4 m)
1 tee (flow through branch or stem)	12.0 ft (3.7 m)
1 gate valve	1.5 ft (0.5 m)
1 straight pipe	42.0 ft (12.8 m)
	$L_e = 107.7$ ft (32.8 m)

The Darcy equation for determining friction losses through the network would then have the form

$$h_L = \frac{fL_e v^2}{2Dg}$$

Alternately, the loss coefficient approach may be used, where

$$h_L = k\frac{v^2}{2g}$$

This method must be used to find entrance and exit losses. For this example, however, we either refer to manufacturer's data for valve and fitting C_v values or calculate k from the relation

$$k = \frac{fL_e}{D}$$

Energy Losses in Pipe Networks

Flow networks can consist of pipes arranged in series, parallel, or combinations or multiples thereof. In any case, an evaluation of friction losses for the flows is based on energy conservation principles applied to the flow junction points. Methods of solution depend on the particular piping configuration. In general, however, they involve establishing a sufficient number of simultaneous equations or employing a friction loss formula where the friction coefficient depends only on the roughness of the pipe (e.g., Darcy-Weisbach or Hazen-Williams).

Pipes in Series When two pipes of different sizes or roughnesses are connected in series (Fig. 41.13a), head loss for a given discharge, or discharge for a given head loss, may be calculated by applying the energy equation between the bounding points, taking into account all losses in the interval. Thus, head losses are cumulative.

Series pipes may be treated as a single pipe of constant diameter to simplify the calculation of friction losses. The approach involves determining an equivalent length of a constant diameter pipe which has the same friction loss and discharge characteristics as the actual series pipe system. Minor losses due to valves and fittings are also included. Referring again to Example 3, we note that application of the continuity equation to the solution allows the head loss to be expressed in terms of only one pipe size.

The lost head in equivalent feet of 6-in. pipe is then given in Darcy-Weisbach form by

$$h_L = f\left(\frac{L_e}{D}\right)\left(\frac{v2}{2g}\right)$$

L_e can be obtained if f is known. Exact hydraulic equivalence in the velocity head terms depends upon f being a constant over the range of velocities applicable to the problem. In fact, f is not a constant over wide ranges of velocity. Since it varies only slightly with Reynolds number, however, solutions are sufficiently accurate.

Pipes in Parallel Two or more pipes connected as in Fig. 41.13b, so that flow is first divided among the pipes and is then rejoined, comprise a parallel pipe system. Flows in pipes arranged in parallel are also determined by application of energy conservation principles—specifically, energy losses through all pipes connecting

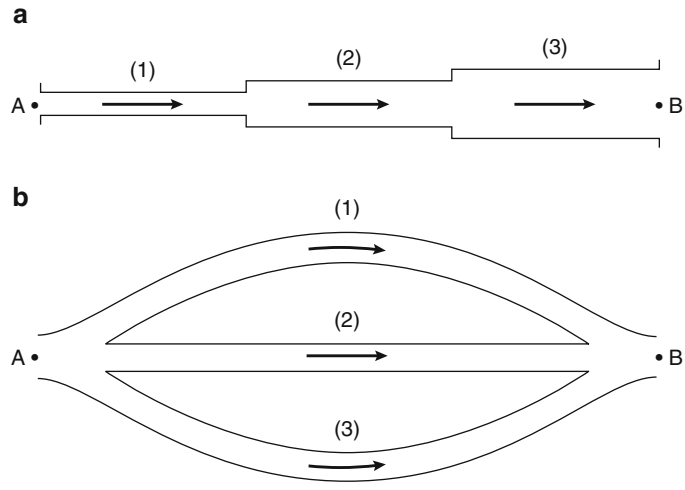

Fig. 41.13 Energy losses in pipe network: (**a**) pipes in series, (**b**) pipes in parallel

common junction points must be equal. Each leg of the parallel network is treated as a series piping system and converted to a single equivalent length pipe. The friction losses through the equivalent length parallel pipes are then considered equal and the respective flows determined by proportional distribution. For a given Q, an outline of the procedure is as follows:

1. Express each branch of the parallel system as an equivalent length of a single pipe size, including all minor losses between the bounding junction points.
2. Assume a discharge Q_1' through pipe branch 1.
3. Solve for h_L, using Q_1'.
4. Using h_L, find Q_2' and Q_3' for the remaining branches.
5. Knowing the proportional distribution of flow among the legs, Q_1', Q_2', and Q_3' are adjusted so that their sum equals the known Q; thus,

$$Q_1 = \frac{Q_1'}{\sum Q'} Q \quad Q_2 = \frac{Q_2'}{\sum Q'} Q \quad Q_3 = \frac{Q_3'}{\sum Q'} Q \tag{41.27}$$

6. h_{L_1}, h_{L_2}, and h_{L_3} are computed for the values of Q_1, Q_2, and Q_3 as a check for correctness.

For judicious choice of assumed discharges, solutions are obtained rapidly that agree within a few percent, well within the range of accuracy of the assumed friction factors.

In the case where the head loss is known between points A and B, Q for each branch is found simply by solution of the equation for pipe discharge. The discharges are added to obtain the total flow through the system.

Compound Piping Networks Energy loss calculations in compound piping configurations or networks employ the same basic physical principles as for single pipes. That is, conservation of energy and conservation of mass (continuity) must be satisfied throughout the network. In particular, at each pipe junction

$$\sum Q = Q_1 + Q_2 + \cdots + Q_n = 0 \tag{41.28}$$

and around each closed loop or circuit

$$\sum h_L = h_{L_1} + h_{L_2} + \cdots + h_{L_n} = 0 \tag{41.29}$$

The general solution procedure involves setting up a sufficient number of independent equations of these two types and solving simultaneously for the unknowns. For complicated networks, straightforward algebraic solution is clearly impractical. A very widely used relaxation method for systematic solution of large networks was developed by Hardy Cross in 1928. The method is well suited for solution by hand and is readily adaptable for machine computation.

We have seen that loss of head in a pipe may be represented generally by an equation of the form $h_L = KQ^n$ (where, for the Hazen-Williams formula, $n = 1.85$). For any single pipe in a network, we may write

$$Q = Q_0 + \Delta \tag{41.30}$$

where
Q = Corrected flow
Q_0 = Assumed flow
Δ = Flow correction

The problem, so stated, reduces to finding Q to a desired degree of accuracy by successive evaluations of Δ based on updated estimates of Q_0. We solve for Δ as follows:

$$\begin{aligned} h_L &= KQ^n = K(Q_0 + \Delta)^n \\ &= K\left(Q_0^n + nQ_0^{n-1}\Delta + \cdots\right) \end{aligned} \tag{41.31}$$

If Δ is small relative to Q_0, the higher-order terms in the expansion may be neglected. Since, for any circuit, $\Sigma h_L = 0$, we may write

$$\sum KQ^n = 0 = \sum \left(KQ_0^n + KnQ_0^{n-1}\Delta\right) \tag{41.32}$$

to a good approximation. Solving for Δ we have

$$\Delta = \frac{-\sum KQ_0^n}{n\sum KQ_0^{n-1}} = \frac{\sum h_{L_0}}{n\sum \left(h_{L_0}/Q_0\right)} \tag{41.33}$$

The overall formulation is made algebraically consistent by designating clockwise flows positive and counterclockwise flows negative.

The calculation procedure is controlled by the requirement that the algebraic sum of all assumed flows must equal zero at each pipe junction. The originally assumed flows are repeatedly and cyclically corrected until the Δ values are negligible, indicating that a hydraulic balance has been reached. Note that pipes common to two circuits are corrected twice in each cycle, once for each circuit. For a system where total head loss is known, flows can be balanced by correcting assumed head losses instead of flows.

Several other methods exist for determining flows and head losses in compound pipe networks. Many can be performed manually, although computer analysis is desirable and necessary for the more complex methods, particularly those involving unsteady flow. For a review of alternative methods, the reader is referred to Stephenson [10] and Walski [9].

Flow Measurement and Discharge

Flow Measuring Devices

This section deals primarily with the basic principles of operation of some flow measuring devices in common use and, in particular, with the pitot tube and the pipeline differential flow meters that have been standardized by the ASME (American Society of Mechanical Engineers): namely, the Venturi, the flow nozzle, and the square-edge thin-plate concentric orifice.

In general, an incompressible fluid of density ρ, viscosity μ, flows with average velocity v through a metering element of diameter d. The metering element is located in a horizontal metering tube of roughness ε and diameter D. The flow through the element produces a pressure differential Δp sensed by pressure taps located a distance L apart. It can be shown by dimensional analysis that the fundamental parameters involved in fluid metering, namely L, ε, v, ρ, μ, d, D, and Δp, yield relational solutions conventionally formulated as follows:

$$\frac{d\rho v}{\mu} = \mathrm{Re}_d \quad \text{Metering element Reynolds number}$$

$$\frac{L}{D} \quad \text{Tap location ratio}$$

$$\frac{d}{D} = \beta \quad \text{Beta ratio}$$

$$\frac{\varepsilon}{D} \quad \text{Relative roughness}$$

$$\frac{v}{\sqrt{2g\Delta p/\rho}} = \overline{K} \quad \text{Flow coefficient (pressure coefficient)}$$

Since $v = \overline{K}\sqrt{2g\Delta p/\rho}$, the continuity equation allows the volumetric flow rate measured by the meter to be expressed as

$$Q = \overline{K} A_d \sqrt{2g\Delta p/\gamma} \tag{41.34}$$

where A_d is the flow area of the metering element.

Typically, flow meter calculations are based on the idealized flow of a one-dimensional, frictionless, incompressible fluid in a horizontal metering tube. Real conditions require corrections to the ideal formulation. Conventional corrections for the effects of variations from ideal geometry and flow velocity profile are achieved through the use of modification factors. Thus, in Equation 41.34 above, $\overline{K}$ includes pressure and flow modifications which are conventionally defined as

$$\overline{K} = CE \tag{41.35}$$

where C is the coefficient of discharge defined as the ratio of actual flow rate to ideal flow rate and

$$E = \frac{1}{\sqrt{1-\beta^4}}$$

where E is known as the velocity of approach factor, since it accounts for the one-dimensional kinetic energy at the inlet tap.

The general volumetric flow metering equation is then given as,

$$Q = \overline{K} A_d \sqrt{\frac{2g\Delta p}{\gamma}} = CEA_d \sqrt{\frac{2g\Delta p}{\gamma}} \tag{41.36}$$

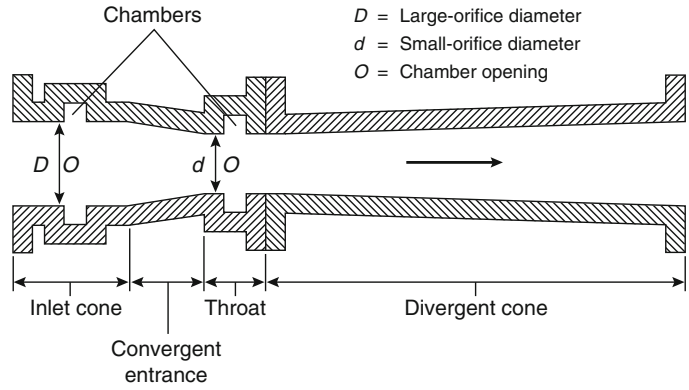

Fig. 41.14 Venturi tube

Table 41.5 ASME coefficients for venturi tubes

	Re_2			
Type of inlet cone	Minimum	Maximum	Value of C	Tolerance (%)
Machined	—	1,000,000	0.995	±1.00
Rough welded sheet metal				
	500,000	2,000,000	0.985	±1.50
Rough cast	—	—	0.984	±0.70

Venturi Flow Meter Figure 41.14 shows a schematically typical Venturi-type flow tube. The divergent cone section reduces the overall pressure loss of the meter. Pressure is sensed through a series of holes in the inlet cone and throat. These holes lead to an annular chamber, and the two chambers are connected to a pressure differential sensor such as a U-tube manometer. Standardized discharge coefficients, C, as reported by ASME are given in Table 41.5. Venturi tubes must be individually calibrated to obtain coefficients outside range identified in the table.

Determination of volumetric flow rate is a simple calculation employing the general flow metering formula—Equation 41.36—where C is obtained from Table 41.5 based on Re_d, and E is calculated directly from the beta ratio.

ASME Flow Nozzle This nozzle is depicted in Fig. 41.15. The pressure differential is sensed by either throat taps or appropriately located pipe wall taps. Coefficients of discharge for ASME flow nozzles may be accurately computed from the following equation:

$$C = 0.9975 - 0.00653\left(\frac{10^6}{\mathrm{Re}_d}\right)^a \qquad (41.37)$$

where

$$a = \frac{1}{2} \quad \text{for } \mathrm{Re}_d < 10^6$$

$$a = \frac{1}{5} \quad \text{for } \mathrm{Re}_d < 10^6$$

Volumetric flow rates are calculated in the same manner as for the Venturi tube.

ASME Orifice Meters Fluid flowing through a thin, square-edged orifice plate experiences a contraction of the flow stream some distance downstream from the orifice. The minimum cross sectional area of flow is called the *vena contracta* and its location is a function of the beta ratio. Figure 41.16 shows the relative pressure difference due to the presence of the orifice plate and the location of the *vena contracta* with respect to beta. By inspection of Fig. 41.16 it is clear that the actual location of the pressure taps is critical. Three distinct arrangements for tap locations are specified by the ASME for

accurately measuring the pressure differential. These types of tap arrangements are called the flange, *vena contracta,* and the 1*D* and ½*D*. Each has certain advantages and disadvantages and affects the value of the discharge coefficient.

Discharge coefficients for orifice metering plates may be calculated from the equation

$$C = C_o + \frac{\Delta C}{\mathrm{Re}_d^a} \tag{41.38}$$

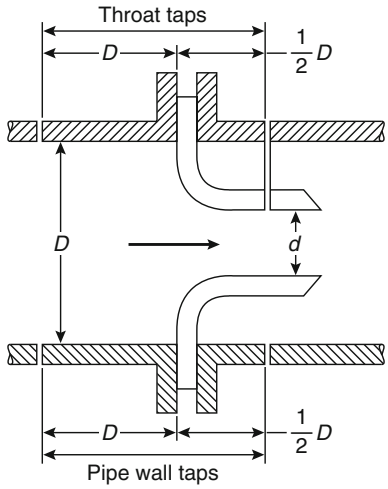

Fig. 41.15 ASME flow nozzle

where C_o and α are obtained from Table 41.6. Since the jet contraction downstream of the orifice can amount to nearly half of the orifice area, orifice discharge coefficients are in the order of 0.6 compared to the near-unity coefficients obtained with Venturi tubes and flow nozzles.

Pitot Tube A pitot tube is a device designed to sense stagnation or total pressure for the determination of velocity and volumetric flow rate. A number of commercial devices are available, some of which include a static pressure tap, that are designed for insertion into a water main under pressure through a standard pipe tap or corporation cock. The installed pitot tube measures velocity at a point in the fluid. Conventional practice assumes that the conversion of kinetic energy to flow work in the tube is frictionless. Thus, applying the energy equation to the generalized pitot tube diagram (Fig. 41.17) we obtain

$$\frac{u_s^2 - u_i^2}{2g} + \frac{p_s - p_0}{\rho_0 g} = 0 \tag{41.39}$$

where
u_s = Stagnation point velocity
u_i = Ideal streamtube velocity
p_s = Stagnation pressure
p_0 = Static pressure

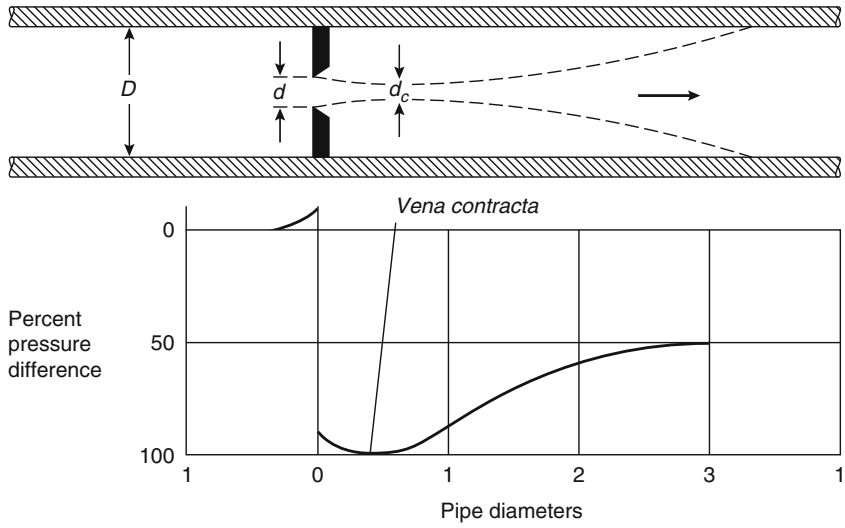

Fig. 41.16 Relative pressure changes due to flow through an orifice

Table 41.6 Values of Co, DC, and a for use in Equation 41.38

	$D = 2$ in. $= 50$ mm		$D = 4$ in. $= 100$ mm		$D = 8$ in. $= 200$ mm		$D = 16$ in. $= 400$ mm	
β	C_o	ΔC	C_o	ΔC	C_o	ΔC	C_o	ΔC
Flange taps α = 1								
0.20	0.5972	127	0.5946	200	0.5951	327	0.5955	551
0.30	0.5978	144	0.5977	209	0.5978	307	0.5980	457
0.40	0.6014	181	0.6005	256	0.6002	362	0.6001	514
0.50	0.6050	260	0.6034	386	0.6026	584	0.6022	903
0.60	0.6078	392	0.6055	622	0.6040	1015	0.6032	1710
0.70	0.6068	573	0.6030	953	0.6006	1637	0.5991	2898
Vena contracta taps α = ½								
0.20	0.5938	1.61	0.5928	1.61	0.5925	1.61	0.5924	1.61
0.30	0.5939	1.78	0.5934	1.78	0.5933	1.78	0.5932	1.78
0.40	0.5970	2.01	0.5954	2.01	0.5953	2.01	0.5953	2.01
0.50	0.5994	2.29	0.5992	2.29	0.5992	2.29	0.5991	2.29
0.60	0.6042	2.68	0.6041	2.68	0.6041	2.69	0.6041	2.70
0.70	0.6069	3.34	0.6068	3.37	0.6067	3.44	0.6068	3.57
1*D* and ½*D* taps α = ½								
0.20	0.5909	2.03	0.5922	1.41	0.5936	1.10	0.5948	0.94
0.30	0.5915	2.02	0.5930	1.50	0.5944	1.24	0.5956	1.12
0.40	0.5936	2.17	0.5951	1.72	0.5963	1.49	0.5974	1.38
0.50	0.5979	2.40	0.5978	1.99	0.5999	1.79	0.6007	1.69
0.60	0.6036	2.67	0.6040	2.31	0.6044	2.12	0.6048	2.11
0.70	0.6078	3.19	0.6072	2.98	0.6068	3.07	0.6064	3.51

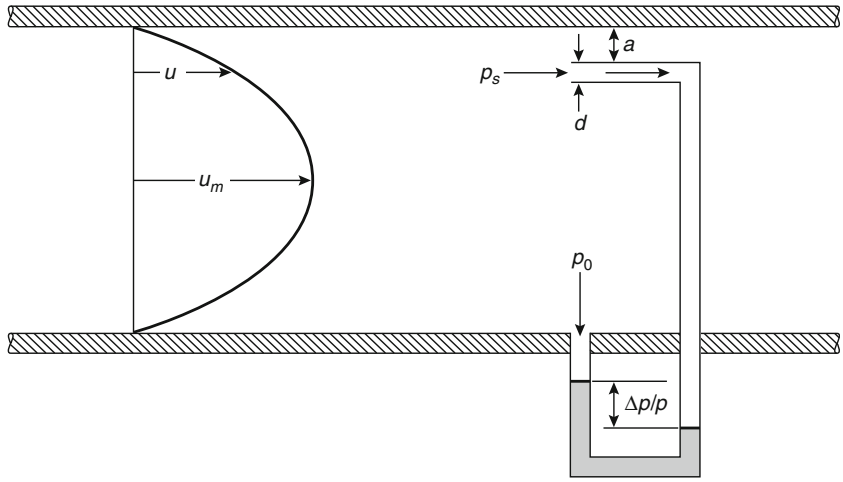

Fig. 41.17 Pitot tube study

Since, by definition $u_s = 0$, solving for u_i we obtain

$$u_i = \sqrt{\frac{2g(p_s - p_0)}{\gamma_0}} = \sqrt{\frac{2g\Delta p}{\gamma_0}} \qquad (41.40)$$

Typically, a pipe coefficient, C_p, which is independent of the geometry of the velocity profile, is defined as

$$C_p = \frac{\text{Average velocity}}{\text{Centerline velocity}}$$

For typical velocity profiles, C_p, varies from about 0.75 to 0.97 but usually lies within a narrower range of about 0.80–0.90. Knowing the centerline velocity, the flow can be obtained simply by

$$Q = C_p A v_{CL} \tag{41.41}$$

In situations where pipe velocity profiles are unknown, and therefore average velocities are not available, it may be necessary to obtain velocity measurements at many individual points. Given n velocities, the flow is then

$$Q = \sum_{i=1}^{n} v_i A_i \tag{41.42}$$

where

v_i = Velocity at the ith point

A_i = Area of annular ring of flow cross section for which velocity v_i is accurate

Detailed procedures for obtaining accurate pitot traverses are available in the literature along with suggestions for assessing the reliability of water audits, C-factor tests, and so forth, based on pitot gauge measurements [6, 9]. See the next section for a discussion of discharge measurements using pitot tubes.

Free Discharge at an Opening

Flow discharging to the atmosphere from a tank, hydrant, nozzle, or open conduit is affected by the area and shape of the opening. The total energy of the fluid is converted into kinetic energy at the orifice according to an appropriate form of the Bernoulli equation. In the most general case of a closed pressurized tank,

$$\frac{v_0^2}{2g} = z_1 + \frac{p_1}{\rho} \tag{41.43}$$

$$v_0 = \left[2g\left(z_1 + \frac{p_1}{\rho}\right)\right]^{1/2} \tag{41.44}$$

Accounting for losses at the point of discharge,

$$v_0 = C_v\sqrt{2gh} \tag{41.45}$$

where C_v, the coefficient of velocity, is determined from the coefficients of discharge and contraction

$$C_v = \frac{C_d}{C_c}$$

Commonly used values of orifice coefficients for water are given in Table 41.7. The orifice discharge can then be expressed as

Table 41.7 Orifice coefficients for water

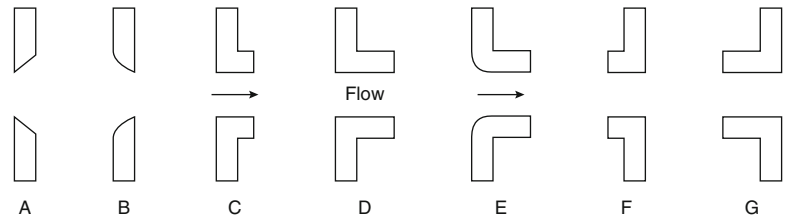

Illustration	Description	C_d	C_c	C_v
A	Sharp-edged	0.62	0.63	0.98
B	Round-edged	0.98	1.00	0.98
C	Short tube (fluid separates from walls)	0.61	1.00	0.61
D	Short tube (no separation)	0.82	1.00	0.82
E	Short tube with rounded entrance	0.97	0.99	0.98
F	Reentrant tube, length less than one-half of pipe diameter	0.54	0.55	0.99
G	Reentrant tube, length 2–3 pipe diameters	0.72	1.00	0.72
Not shown	Smooth, well-tapered nozzle	0.98	0.99	0.99

$$Q_o = C_d A_0 \sqrt{2gh} \tag{41.46}$$

and the head loss due to turbulence at the orifice as

$$h_L = \left(\frac{1}{C_v^2} - 1\right)\frac{v_0^2}{2g} \tag{41.47}$$

where

$\left(\frac{1}{C_v^2} - 1\right)$ = Minor loss K-factor

For the general case of a tank of varying cross-sectional area being replenished with inflow, $\dot{Q}_{IN}$, the time to empty from height z_1 to z_2 is given by

$$t = \int_{z_1}^{z_2} \frac{A_t dz}{c_d A_o \sqrt{2gh} - \dot{Q}_{\mathrm{IN}}} \tag{41.48}$$

where A_t is expressed as a function of z.

For a tank of constant cross section this simplifies to

$$t = \frac{2A_t\left(\sqrt{z_1} - \sqrt{z_2}\right)}{C_d A_o \sqrt{2g}} \tag{41.49}$$

Example 4 A 15-ft-diameter tank discharges water at 50 °F through a 2-in.-diameter sharp-edged orifice. If the initial water depth in the tank is 10 ft and the tank is continuously pressurized to 50 psig, how long will it take to empty the tank?

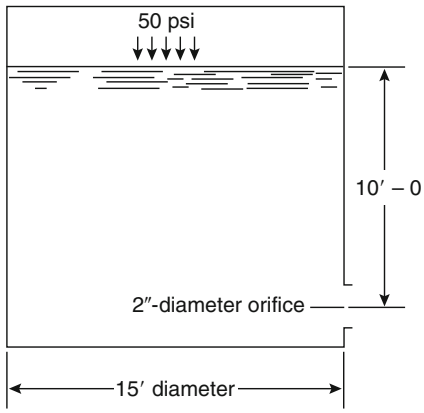

Solution At 50 °F (10 °C),

$$\gamma = 62.4 \text{ lbm/ft}^3 \ \left(16.02 \text{ kgm/m}^3\right)$$

For the orifice:

$$A_o = \frac{\pi D^2}{4} = 3.14 \text{ ft}^2 \left(0.29 \text{ m}^2\right)$$

$$C_d = 0.62 \text{ (sharp-edged orifice)}$$

For the tank:

$$A_t = \frac{\pi D^2}{4} = 176.7 \text{ ft}^2 \left(16.4 \text{ m}^2\right)$$

$$h_0 = 10 + \frac{50(144)}{62.4} = 125.38 \text{ ft } (38.2 \text{ m})$$

$$h_1 = 0 + \frac{50(144)}{62.4} = 115.38 \text{ ft } (35.2 \text{ m})$$

The total pressure head on the discharging fluid results from both an elevation and a static pressure head. Therefore,

$$t = \frac{2A_t\left[(z_0 = p_0/\gamma)^{1/2} - (z_1 + p_1/\gamma)^{1/2}\right]}{C_d A_o \sqrt{2g}}$$

$$t = 10.4 \text{ s}$$

Discharge stream coordinates are given by

$$x = v_0 t = v_0 \sqrt{\frac{2y}{g}} = 2C_v \sqrt{zy} \tag{41.50a}$$

$$y = \frac{gt^2}{2} \tag{41.50b}$$

For the simpler case of a hydrant discharging to atmosphere, the flow can be determined by an appropriate form of Equation 41.36,

$$Q = 29.8 D^2 C_d \sqrt{p} \tag{41.51}$$

where

Q = Discharge (gpm)

D = Outlet diameter (in.)

p = Pressure detected by pitot gauge (psi)

C_d = Coefficient based on hydrant outlet geometry (usually taken to be 0.90 for full flow across a standard 2½-in. outlet)

In the absence of a pitot gauge, hydrant flows may be estimated by observing the trajectory of the discharge stream. The horizontal component of the velocity does not change appreciably over time, thus allowing calculation of the velocity

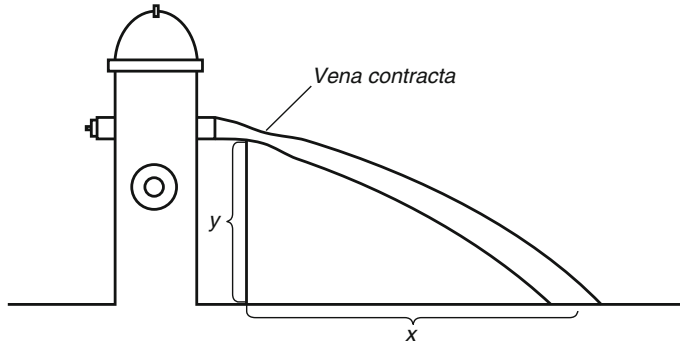

Fig. 41.18 Determining discharge by the trajectory method

based on the height of the outlet and the distance traveled by the stream. Figure 41.18 presents the basic parameters. The velocity determined in this manner is at the *vena contracta* and is given by

$$v = \frac{x}{\sqrt{2y/g}} \tag{41.52}$$

The discharge is simply the product of this velocity and the area of the *vena contracta*. The method is relatively inaccurate due to the obvious difficulty of measuring the required area and the distance x. It is a useful bounding guide, however, in the absence of precision measuring devices.

Water Hammer

Water hammer in a pipeline is caused by a sudden stoppage of flow and is characterized by loud noise and vibration.[1] The kinetic energy from the interrupted flow is transferred to the walls of the enclosing pipe or equipment. Associated pressures, or shock waves, can be severe enough to damage the pipe network and attached equipment.

Density changes due to pressure are assumed zero for nearly all hydraulic calculations, as water is considered incompressible for practical purposes even though it is about 100 times more compressible than steel. When shock waves arise in confined water, however, the compressibility of water becomes very significant, and water's elastic properties must be taken into account. The primary property of interest is the bulk modulus of elasticity, E, which is defined as the ratio of pressure change to the corresponding change of volume as determined by compression tests on volumes. (The bulk modulus is analogous to Young's modulus in solid mechanics, which is the ratio of linear stresses to linear strains as determined by tension tests.) The formula expressing the relationship between pressure and volume is

$$\Delta p = -E\frac{\Delta V}{V_0} \tag{41.53}$$

where the minus sign indicates that a positive change in pressure produces a decrease in volume. A modulus of compressibility, K, is also defined as the inverse of E.

Under normal conditions, water confined and flowing under pressure in a pipeline exerts pressure on the pipe walls according to the pressure-energy term of the energy equation. Any change in discharge within the system (due to valve closure, pump stoppage, etc.) results in a change of flow momentum. By virtue of the impulse-momentum relation, the momentum change will cause an impulse force to be created. This force in a pipeline is commonly referred to as water hammer.

The theory of water hammer, as developed by Zhukovsky, can be briefly illustrated as follows: a valve in a pipeline is closed instantaneously;

[1] This discussion is patterned after the theory of water hammer as developed by N. J. Zhukovsky and as presented in Andrew L. Simon's *Practical Hydraulics,* 2nd ed. [6].

the fluid impacts the closed gate and is decelerated to zero velocity, thereby creating a pressure shock. By Newton, pressure shocks in fluids of infinite extent travel at a velocity given by

$$c^* = \sqrt{\frac{KE}{\rho}} \tag{41.54}$$

where c^* is called the celerity (velocity) of the shock wave, KE is the kinetic energy of the fluid, and ρ is the fluid density. The pipe, however, also posses certain elastic properties. Therefore, if the fluid in the pipe is subject to a sudden force, the force will be transmitted to the pipe and associated equipment and fittings. Depending upon the magnitude of the force, the pipe and fittings will resist the force as they remain rigid, expand and compress, based upon the associated limits of elasticity of the pipe and fitting materials, or fail via a rupture. The modulus of elasticity, E_c, of a system composed of fluid and pipe may be determined from the equation

$$\frac{1}{E_c} = \frac{1}{E} + \frac{D}{E_p w} \tag{41.55}$$

where
D = Pipe diameter
w = Thickness of the pipe wall
E_p = Modulus of elasticity of the pipe material

Table 41.8 gives the modulus of elasticity for common pipe materials. The celerity of a shock wave in a pipe system of finite extent can then be computed from

$$\frac{c}{c^*} = \frac{1}{\sqrt{1 + ED/(E_p w)}} \tag{41.56}$$

which is plotted in Fig. 41.19. The graph indicates the considerable influence of pipe rigidity on the velocity of the shock.

The shock waves that travel upstream and downstream from the valve closure eventually reach points in the system that correspond to large stationary energy stores (e.g., reservoirs) or other sudden closure points, which may vary in their ability to absorb or reflect the shock wave. If the shock is absorbed into a larger energy field it will disappear, and it will do so in a certain amount of time as indicated by Equation 41.57,

$$t = \frac{L}{c} \tag{41.57}$$

where L is the distance from the energy reservoir to the shock wave point of origin. At the instant of shock absorption the compressed fluid, that is no longer balanced, begins to flow backward, creating a relief pressure shock that travels back to the valve. The time period T that the initial shock or impulse pressure acts on the valve is, therefore, the time required for the pressure wave to travel away from and back to the valve. T can be determined as follows:

Table 41.8 Modulus of elasticity Ep of various pipe materials

	E_p		
Pipe material	(psi)	(lb/ft^2)	(kg/m^2)
Lead	0.045 × 106	6.48 × 106	31.64 × 106
Lucite (at 73 °F)	0.4 × 106	57.6 × 106	281.23 × 106
Rubber (vulcanized)	2 × 106	288 × 106	1406 × 106
Aluminum	10 × 106	1440 × 106	7030 × 106
Glass (silica)	10 × 106	1440 × 106	7030 × 106
Brass, bronze	13 × 106	1872 × 106	8489 × 106
Copper	14 × 106	2016 × 106	9842 × 106
Cast iron, gray	16 × 106	2304 × 106	11,249 × 106
Cast iron, malleable	23 × 106	3312 × 106	16,170 × 106
Steel	28 × 106	4023 × 106	19,685 × 106

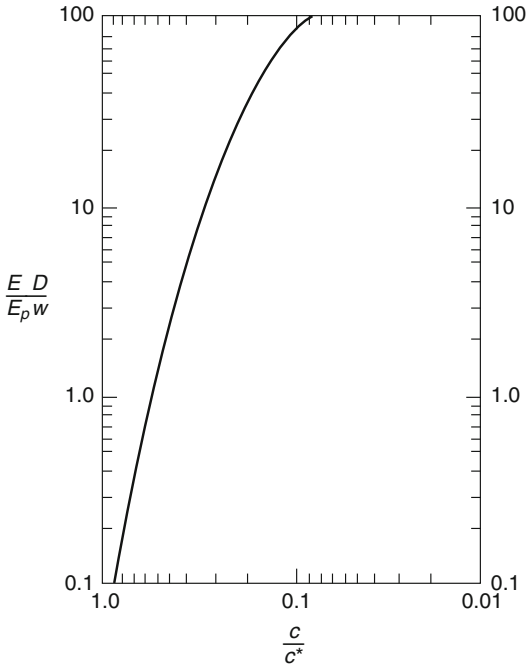

Fig. 41.19 Celerity of pressure waves in pipes, c equals celerity in elastic pipe; c* equals celerity in fluid of infinite extent

$$T = 2t = \frac{2L}{c} \tag{41.58}$$

At time T, all the fluid is moving backward at some velocity v. Since the valve is closed, there is no supply for this flow. A negative pressure shock is created at the valve. The shock travels to and back from the reservoir, as the flow is reversed. Such oscillations of pressure and periodic flow reversals persist until the kinetic energy is dissipated by friction. The process described will occur both upstream and downstream from the point of origin, though the initial shock will be positive upstream and negative downstream and the periodicities would not likely be equal.

The theoretical magnitude of the pressure shock at instantaneous valve closure can be determined directly from

$$p^* = \rho c \Delta v \tag{41.59}$$

and the pressure will oscillate in the pipe within the range

$$p = p_0 \pm p^* \tag{41.60}$$

In actuality, the time of closure of a valve is not zero but some finite time period which we may call T_c. The water hammer pressure increases gradually with the rate of closure of the valve. Depending on whether T_c is smaller or larger than T, we distinguish between quick and slow closure. For T_c less than T, the shock pressure will attain its maximum value p^*. (In this sense, quick closure is equivalent to instantaneous closure.) For T_c greater than T, maximum pressure will be somewhat less than p^* and may be calculated by the Allievi formula

$$p = p_0 \left(\frac{N}{2} + \sqrt{\frac{N^2}{4} + N} \right) \tag{41.61}$$

in which

$$N = \left(\frac{Lv\rho}{p_0 T_c} \right)^2 \tag{41.61a}$$

In general the calculation of water hammer pressure rises, regardless of method, will tend to underestimate the actual values. Real systems will tend to experience superimposition of positive or negative pressure waves due to complex piping configurations. Discontinuities introduced by a variety of auxiliary valving and metering equipment complicate the analysis considerably. Other methods are available for analyzing water hammer effects on systems that may not be reasonably handled by the above idealized method [11]. Since water hammer can be extremely detrimental, often resulting in complete loss of the system, it is desirable to perform an analysis wherever such effects are of concern. Control over the development of damaging shock waves is achieved through use of slow-closing valves, pressure relief valves, or shock-absorbing devices.

Water Supplies

An adequate supply of water is essential to any water-based fire protection system. Water can be provided from a number of sources: public

mains, private mains, elevated tanks, ground level tanks, pressure tanks, ponds, rivers, or oceans. Each of these sources has its advantages and disadvantages.

Public mains, private mains, elevated tanks, and pressure tanks are typically associated with a positive pressure, that in certain cases can be sufficient to supply the flow and pressure demands for the water-based fire protection system for some specified period of time. In other cases, a means of providing supplemental pressure, such as through a fire pump, or augmenting the quantity of water is needed.

Ground level tanks, ponds, rivers, or oceans are typically not associated with a positive pressure capable of forcing the water through a pipe network. This, however, is dependent upon the relative elevation of the water supply with respect the fire protection system. These water supplies usually need to be served by a fire pump.

Water Mains

Water mains can be either public or private. The only real difference between the two is ownership. Public mains are owned and operated by municipalities or public utilities that serve the citizens of a particular community. Generally any tax-paying entity in the associated community has a right to access to the mains, albeit through a fee. Private mains are generally owned and operated by a single property owner or cooperative group that makes the water available for their own use.

Before deciding whether a water main (public or private) can be used as a water supply for a fire protection system, two questions need to be addressed. The first pertains to whether or not the water supply is "reliable". There are no universal measurements or criteria to determine whether or not a water supply is "reliable". This is a judgment to be made by the stakeholders of a given project after evaluating the availability of waterflow while considering the length and frequency of any potential disruption of service. Factors to consider in this regard are associated with the means of supplying and ensuring pressure for the mains including the reliance on pumps, availability of power supply for any electrically motor driven pumps, fuel supplies and condition of any diesel engine driven pumps, use of elevated tanks and the overall condition and maintenance of the water mains.

The second question pertains to the adequacy of the supply. In other words, can the supply provide the necessary flow and pressure to meet the demand of the fire protection system? Testing of the water supply along with detailed hydraulic calculations are undertaken to assess if the main can meet the demand of the fire protection system. In assessing water supplies, the system demand in terms of flow, pressure and duration are needed. As exact system layouts and designs are not usually finalized until the later stages of a project, a series of assessments might need to be made during the design process, and possibly even during the installation phase of the project. Engineers can use an estimating technique to facilitate the process.

The simplest technique for estimating the flow demand for the system is to first determine the number of sprinklers that are expected to operate should a fire occur. The number of sprinklers can be determined from design and installation standards based upon the occupancy, commodity or fire hazard under consideration. Additional factors also need to be considered including the type of sprinkler used, its spacing, and required discharge density or discharge pressure. From this basic information, the minimum flow from each sprinkler can be determined.

The minimum estimated total flow (Q_d) needed for the sprinkler system will then be the number of sprinklers (N) multiplied by the minimum flow necessary from each sprinkler (q) multiplied by an "overage factor" (O) as indicated in Equation 41.62. The overage factor is an approximation of the added pressure that needs to be introduced into the system to overcome the pressure losses associated with waterflow through the system. It accounts for the extra flow that occurs at sprinklers closer to the water supply due to the fact that higher pressures are expected closer to the water supply and this condition will produce a greater flow

discharge. Average "overage factors" are about 15 %, but consideration needs to be given to relative pipe sizes, piping arrangements, i.e. tree, looped or gridded, and piping elevation changes.

$$Q_d = N \times q \times O \tag{41.62}$$

The estimation of the required system pressure will involve consideration of two pressure components. As previously noted, the water supply needs to possess sufficient pressure to overcome friction and other losses, and elevation changes while meeting the demand of the fire protection system. To estimate the pressure demand for a sprinkler system (P_d), add an estimate of the total friction loss in the system (P_f) to an estimate of the pressure due to elevation (P_e) to the pressure needed by the most demanding sprinkler (P_s).

$$P_d = P_f + P_e + P_s \tag{41.63}$$

To determine P_f an estimate of the average friction loss per foot from the main to the most remote sprinkler is needed. A value sometimes used is 0.15 psi/ft. However, smaller pipes in tree systems would have larger friction losses and larger pipes in looped and gridded systems would have smaller friction losses.

The above formulas can be used to generate a rough "ball-park" approximation of the system demand when assessing an available water supply. Any early estimates would need to be confirmed by the completion of more detailed hydraulic calculations usually completed with the aid of a computer. The following example illustrates the estimation technique.

Example 5 Estimate the demand of a sprinkler system utilizing 12 ESFR (K25.2) sprinklers requiring a discharge pressure of 25 psi. (each discharging at least 126 gpm) where The sprinklers are located 40 ft above the elevation where the water supply was measured. The piping system will be installed in a gridded arrangement under the flat roof of the building. The total pipe length from the water supply to the most remote sprinkler is about 400 ft. This includes equivalent lengths for pipe fittings and valves.

Solution The minimum flow demand for each sprinkler is 126 gpm ($25.2 \times (25)^{1/2}$)). The flow demand can be estimated by multiplying the number of sprinklers in the design area (12 for ESFR's) times the minimum flow per sprinkler (126 gpm) times an overage factor. Given the flat roof and the gridded piping arrangement, the overage factor is likely to be less than the average of 15 %. However, as a conservative estimate a value of 15 % is used. The flow demand is estimated to be 1739 gpm ($12 \times 126 \times 1.15$).

The friction loss that is likely to occur in the system can be estimated by first estimating the average friction loss per linear foot for waterflow through the system. Given that the piping is going to be gridded, the average friction loss is likely to be less than 0.15 gpm per ft. However, as conservative estimate, the value of 15 gpm/ft will be used. The friction loss associated with water flowing from the main to the most remote sprinkler can be estimated at 60 psi (0.15 gpm/ft $\times$ 400 ft). The change in elevation will be responsible for another 17 psi (0.433 psi/ft $\times$ 40 ft = 17 psi). The hydraulically most remote sprinkler requires a minimum of 25 psi to operate properly. The pressure demand can then be estimated as 102 psi (60 + 17 + 25). The demand for this sprinkler system can be estimated at 1739 gpm at 102 psi.

To determine whether a the main can sufficiently meet the demand of a fire protection system, some analysis of the water supply needs to take place. One way to analyze the water supply is to conduct a water flow test in close proximity to the project and apply appropriate safety factors to account for daily and seasonal fluctuations that might occur. Another way to analyze the water supply without physical testing is to use existing data about the main and a computer model to determine the flow and pressure available at any location along the main. Certain models might account for daily and seasonal fluctuations in water usage, so additional adjustments would not be necessary.

Whether the information is obtained from a specific flow test or a computer model, the engineer is looking for at least two data points: a static pressure (pressure when no water is flowing out of the main) and a residual pressure at a known flow out of the main. These points can be plotted to characterize the water supply over a range of flows and pressures. The relationship between flow and pressure is exponential (to the 1.85 power). Therefore, the water supply curve can be drawn as a line if the associated graph is scaled to log-1.85 as shown in Fig. 41.20. The figure shows four different flow scales. Other scales can be created by picking one of the scales and multiplying the number on it by a consistent factor. The correct or applicable flow scale needs to be clearly indicated. Example 6 illustrates the graphing technique.

Example 6 A proposed sprinkler system for a specific building is estimated to have a flow demand of 750 gpm. The main that will serve as the sprinkler system supply has recently been tested. The test locations are relatively close to the effected building. Test results, which have been adjusted for reasonable worse-case daily and seasonal fluctuations, are a static pressure of 50 psi and a residual pressure of 35 psi at 1600 gpm. Plot the water supply curve and determine what pressure is available at a flow of 750 gpm.

Solution The water supply curve is plotted as shown on Fig. 41.21. The "X" on the curve is approximately at the location of 750 gpm, showing that the pressure at this flow would be about 46 psi, but it is difficult to tell exactly which pressure is associated with the flow due to the inaccuracies involved in reading numbers on graphs, especially when one of the axes is not linear.

Rather than representing the water supply as a graph, the water supply can also be expressed as a function of the flow as shown in Equation 41.64

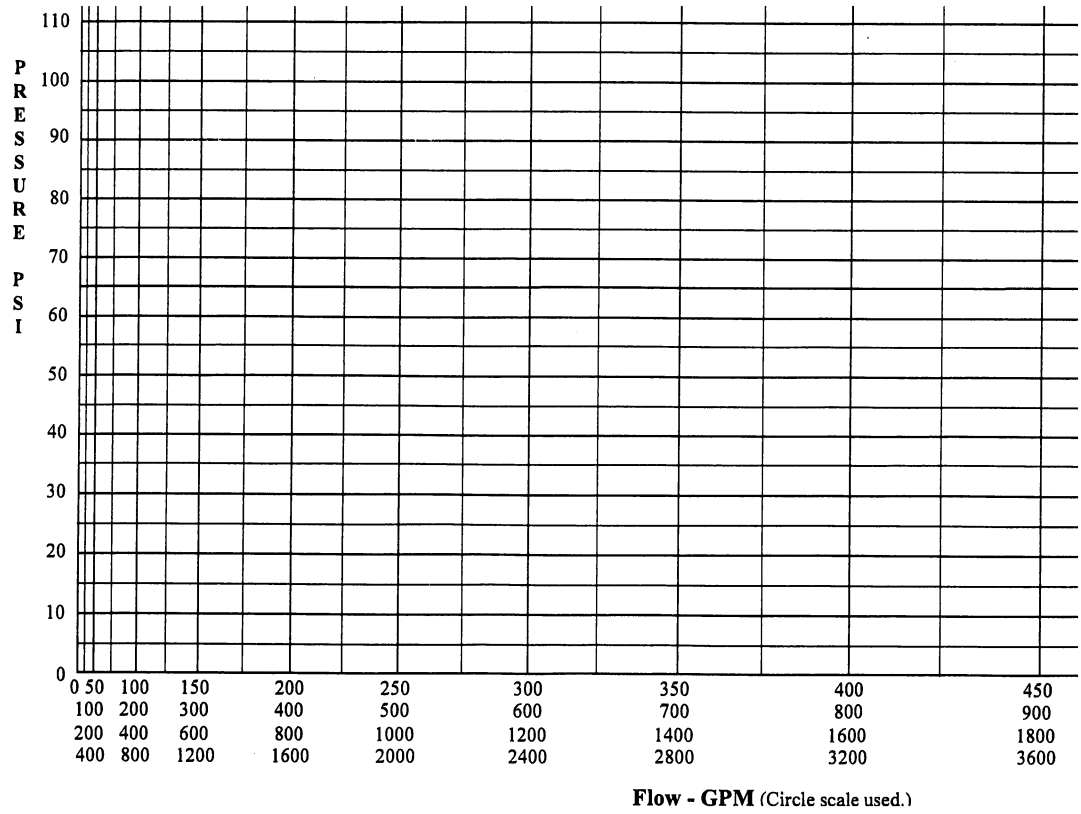

Fig. 41.20 Log-1.85 graph paper

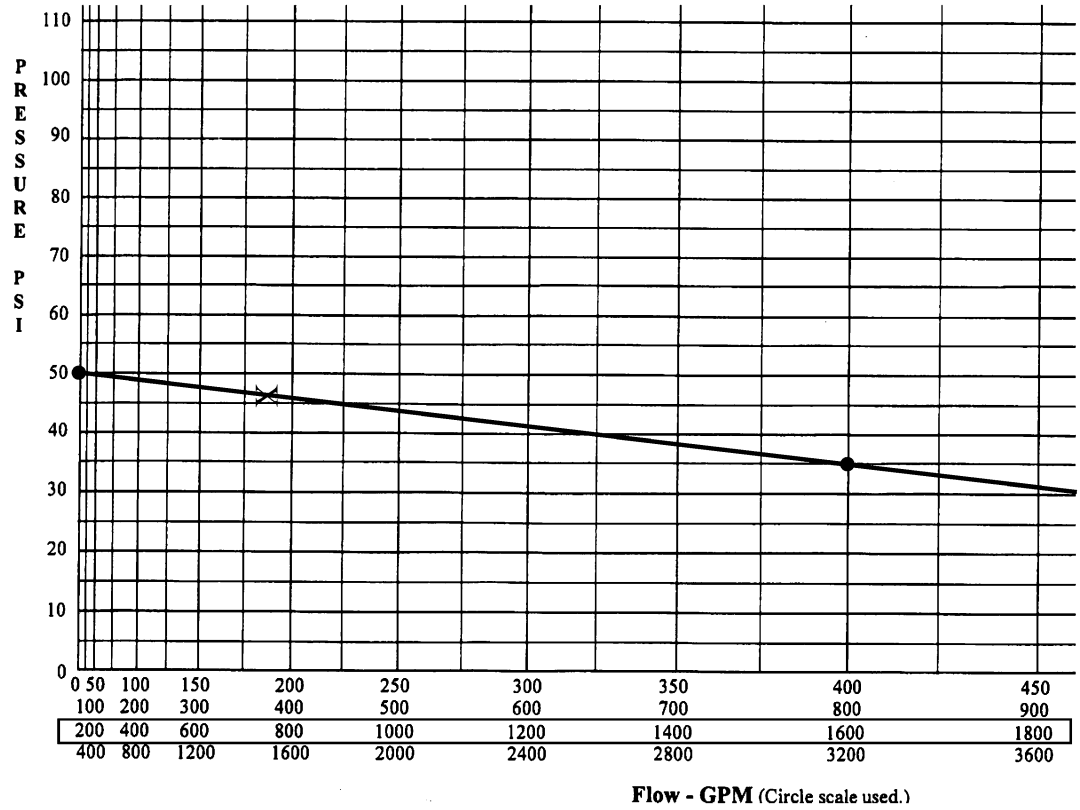

Fig. 41.21 Water supply graph for Example 6

where P is the pressure that you want to know at some flow (Q), P_S is the static pressure from the test, P_R is the residual pressure from the test and Q_R is the residual flow from the test.

$$P = (P_R - P_S)\left(\frac{Q}{Q_R}\right)^{1.85} + P_S \qquad (41.64)$$

Equation 41.64 can be used to develop an equation for a given water supply. For example, the water supply in Example 6 can be represented as follows:

$$P = (35 - 50)\left(\frac{Q}{1{,}600}\right)^{1.85} + 50$$

$$P = -15\left(\frac{Q^{1.85}}{(1{,}600)^{1.85}}\right) + 50 \qquad (41.65)$$

$$\mathrm{P} = 50 - 1.77 \times 10^{-5}\mathrm{Q}^{1.85}$$

Equation 41.65 represents the water supply in Example 6. The pressure at 750 gpm can be calculated by inserting 750 into Equation 41.65 as Q and solving for P as follows:

$$\mathrm{P} = 50 - 1.77 \times 10^{-5}(750)^{1.85}$$

$$\mathrm{P} = 50 - 3.7 = 46.3$$

When evaluating a water supply, it is sometimes advantageous to determine the flow that will be available at a certain pressure. In these cases, Equation 41.64 can be solved for Q and rewritten as shown in Equation 41.66.

$$Q = \left(\frac{P - P_S}{P_R - P_S}\right)^{0.54} Q_R \qquad (41.66)$$

Elevated Tanks

There are at least four basic situations, as noted below, where a tank or some other stored body of water such as a pond, reservoir, river or ocean

might be considered as the water supply for a fire protection system:

1. Where a public or private main is not available.
2. Where a public or private main is available, but does not produce sufficient flow for the fire protection system.
3. Where a public or private main is available and sufficient, but a redundant supply is desired improve overall reliability of the fire protection system.
4. Where a public or private main is available and sufficient, but a redundant supply is required such as in active seismic zones.

Once it has been determined that a tank or other body of water is needed, an elevated tank might be considered. The advantage of an elevated tank is that it is inherently associated with potential energy without the need for any pumps or supplemental pressurization. The amount of energy is function of the height of the tank. As discussed earlier in this chapter, water will develop 0.433 psi for every foot that it raised above some datum plane, i.e. the base of a sprinkler riser. As a further example, if a tank is elevated so that its bottom discharge flange is 150 ft above the location where the water from the tank will be used (such as the outlet of a hydrant), the water in the tank will posses a static pressure head of 65 psi (150 ft × 0.433 psi/ft). Of course, friction losses associated with waterflow need to be considered in determining the available pressure at the hydrant. The further from the tank the hydrant is located, the greater the friction losses and less of a residual pressure would be available at a hydrant.

While some elevated tanks are actually built some distance above the ground, other elevated tanks are built at ground level but located on hilltops at higher elevations that the building and systems they are intended to serve. Similarly, tanks can be located un upper floors of tall buildings where the water is used for fire protection systems on lower floors.

There are situations when it is necessary to determine the maximum flow that can be generated from an elevated tank. To accomplish this, an energy balance needs to be established by equating the energy gained from gravity to the energy lost due to friction and flow effects. Using the Hazen-Williams friction loss method of calculation, Equation 41.67 can be set up with P_E representing the energy gained from elevation and L representing the length of pipe between the tank and the location where the water will be used for fire protection:

$$P_E = \frac{4.52LQ^{1.85}}{C^{1.85}d^{4.87}} \tag{41.67}$$

P_E is equal to 0.433 multiplied by the height of the elevation of the tank (H in feet). Equation 41.67 can be rewritten and solved for Q so that the flow can be determined as shown in Equation 41.68.

$$Q = \frac{0.28CH^{0.54}d^{2.63}}{L^{0.54}} \tag{41.68}$$

Example 7 A tank is going to be installed at the top of a hill to serve an industrial park located at the base of the hill. The bottom of the tank is estimated to be 200 ft above the point of connection to the water main in the industrial park served by the elevated tank. It is further estimated that the pipe from the tank to the center of the industrial park will be 500 ft in length including equivalent lengths for fittings and valves. What is the maximum fire flow that would be available at the center of the industrial park if the pipe material is lined ductile iron (Hazen-Williams C-factor of 140) with an actual inside diameter of 8.27 in.? Note that no other pressure producing devices, such as pumps, will be used.

Solution Using Equation 41.68, the maximum flow that could develop from this tank on the hill is 6186 gpm, calculated as follows:

$$Q = \frac{0.28CH^{0.54}d^{2.63}}{L^{0.54}}$$

$$= \frac{0.28(140)\,(200)^{0.54}(8.27)^{2.63}}{(500)^{0.54}} = 6,186$$

The duration for which the above flow can be maintained will depend upon the size of the tank. The above solution assumes that the flow is

taking place at a pressure of about 86 psi (200 ft × 0.433 psi/ft) not including friction losses. As the tank drains, the flow and available pressure will decrease until they both reach a value of zero once the tank is drained. Many public utilities and operators of water mains require that pressures within the main not drop below a certain value, typically 20 psi. Some private operates might allow lower pressures. Equation 41.69 is a variation of Equation 41.68 with P_M representing the minimum pressure that needs to be maintained in the piping system:

$$Q = \frac{Cd^{2.63}[(0.433H) - P_M]^{0.54}}{2.26L^{0.54}} \qquad (41.69)$$

Example 8 For the situation is Example 7, what is the available fire flow if the plan is to keep a minimum pressure of 20 psi in the main?

Solution

$$Q = \frac{Cd^{2.63}[(0.433H) - P_M]^{0.54}}{2.26L^{0.54}}$$
$$= \frac{(140)(8.27)^{2.63}[(0.433(200)) - 20]^{0.54}}{2.26(500)^{0.54}}$$
$$= 5,399$$

As the solution above shows, for the situation described in Example 7, the available fire flow drops from 6186 to 5399 gpm when the decision is made to maintain a minimum of 20 psi in the mains.

While elevated tanks inherently posses some amount of potential energy so that water can be discharged from them, the adequacy of the elevated tank with respect to any associated fire protection systems still needs to be properly accessed to ensure that the elevated tank can meet the flow and pressure demands of the fire protection system.

Pumps and Tanks

For tanks that are not elevated, a supplemental means of adding pressure is needed to provide and maintain the proper water flow rate from the tank into the fire protection system. Depending upon the size of the tank, a fire pump usually serves this purpose.

Fire pumps serve to increase the pressure in a given fluid system, thereby increasing the flow rate. While fire pumps can increase the flow rate, they cannot increase the capacity of a water supply, i.e. they cannot create water. If a given water supply consisting of a public main cannot produce the necessary flow anywhere along its representative water supply curve or can only produce the necessary flow at a point below the pressure permitted by the water utility, i.e. at less than 20 psi, a fire pump on it own will not solve the problem. A pump and a tank will likely be needed.

Brief details on selecting fire pumps and designing a fire protection system with a fire pump are included later in this chapter. More detailed information on fire pumps is available from a number of sources including the text *Pumps for Fire Protection Systems.*.

Pumps and Other Stored/Static Water Sources

As previously stated, other relatively static water sources such as ponds, reservoirs, rivers, lakes and even oceans can be used for fire protection. From a hydraulic design perspective, these sources are very similar to tanks. However, these water sources also challenge the engineer with additional considerations for corrosion protection and concerns for sediment and other particulate in the water being deposited in the fire protection system. Typically, screens and strainers are used to minimize the amount of sediment and other debris from entering the system. Cleaning of these screens is critical to good performance of such systems. In addition, it is also common to use upright sprinklers on such systems, so that sediment does not accumulate on the sprinkler orifice, or pendent sprinklers on return bends. A return bend is a pipe that is connected to the top of a branch line with an elbow, a lateral piece of pipe, and then another elbow to a drop in order to feed a pendent

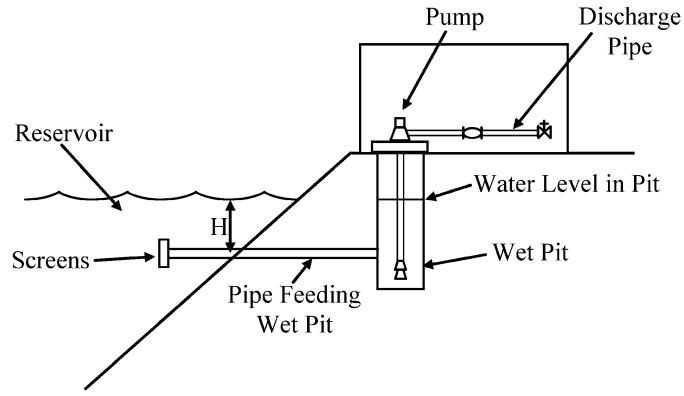

Fig. 41.22 Vertical shaft turbine pump taking suction from a reservoir

sprinkler. In this manner, sediment in the water is more likely to settle at the bottom of the branch line rather than at the sprinkler.

When a pump takes suction from a static source such as a pond or reservoir, that is located below the pump, vertical shaft turbine type pumps, as shown in Fig. 41.22, is typically used. In some cases, a pipe arrangement can be used to feed a pit with water from the pond or reservoir, and a fire pump is then arranged with the pit.

In situations where a pipe is used to feed the wet pit as shown in Fig. 41.22, it is necessary to ensure that the pump will receive a sufficient amount of water to continuously operate at maximum flow, which is typically defined as 150 % of the rated pump flow. A calculation needs to be completed to ensure that the maximum flow will occur between the reservoir and the pit. Equation 41.68 can be used to determine whether the flow will be acceptable.

Example 9 For a situation where a 1500 gpm rated vertical shaft turbine pump is installed similar to Fig. 41.22 with the pipe at least 10 ft under the lowest expected water level in the reservoir and a 50 ft long lined ductile iron pipe with an internal diameter of 8.27 in. used to feed the wet pit, will the maximum flow needed for the pump ($1500 \times 1.5 = 2250$ gpm) be achieved for this arrangement?

Solution Using Equation 41.68, the maximum flow that can be achieved with this arrangement is 4255 gpm (as shown below), which well exceeds the requirement for the pump of 2250 gpm. This arrangement would be acceptable (assuming that the friction loss for the strainer was accounted for in the 50 ft of pipe through an equivalent length assumption).

$$Q = \frac{0.28CH^{0.54}d^{2.63}}{L^{0.54}} = \frac{0.28(140)\,(10)^{0.54}(8.27)^{2.63}}{(50)^{0.54}} = 4,255$$

Pumps

Pump Operating Characteristics

Pumps are mechanical devices that convert electrical or mechanical energy into hydraulic energy (net pressure). There are many types of pumps—for example, reciprocating, rotary, jet, ram, centrifugal—with each type name referring to the different means by which the pump increases the energy of the liquid. The most common type of pump used for fire protection is the centrifugal pump due to its simplicity and reliability. However, for some applications such as high pressure water mist systems and foam concentrate pumps, centrifugal pumps are not ideal and rotary gear or other types of positive displacement pumps are used.

For centrifugal pumps, the impeller (the rotating component) imparts energy to the water

using centrifugal force. Vanes within the impeller improve the efficiency to which energy is transferred. Centrifugal pumps may be divided into several categories. Turbine or radial flow centrifugal pumps force water outward at right angles to the rotating axis. Mixed flow pumps force water in both radial and axial directions. Propeller pumps move water in the axial direction only. Any of these types may be single or multistage with the stage number referring to the number of impellers on the pump's rotating shaft. For example, a two-stage pump has two impellers on the same shaft whereas a four-stage pump would have four impellers on the same shaft. The orientation of the shaft may be vertical or horizontal. The following discussion, while broadly applicable, is directed mainly to centrifugal pumps.

Figure 41.23 illustrates several of the terms commonly used to describe pump performance conditions. In general, pumping of liquids requires that the pressure at any point in the intake line be greater than the vapor pressure of the liquid to avoid the loss of prime (water entering the pump due to its own pressure head) and the highly destructive phenomenon known as cavitation. The pressure gradient that causes a liquid to move through the intake line to the pump impeller is termed the net positive suction head (NPSH). In pump selection, it is essential to determine that the *available* NPSH of the water supply exceeds the *required* NPSH for the pump under consideration so that prime is provided. Required NPSH depends upon many factors relating to pump geometry and construction and intake system operating conditions, but it is defined simply as the difference between net suction head and vapor pressure at a given flow, or the energy needed to fill the pump on the intake side and overcome intake system head

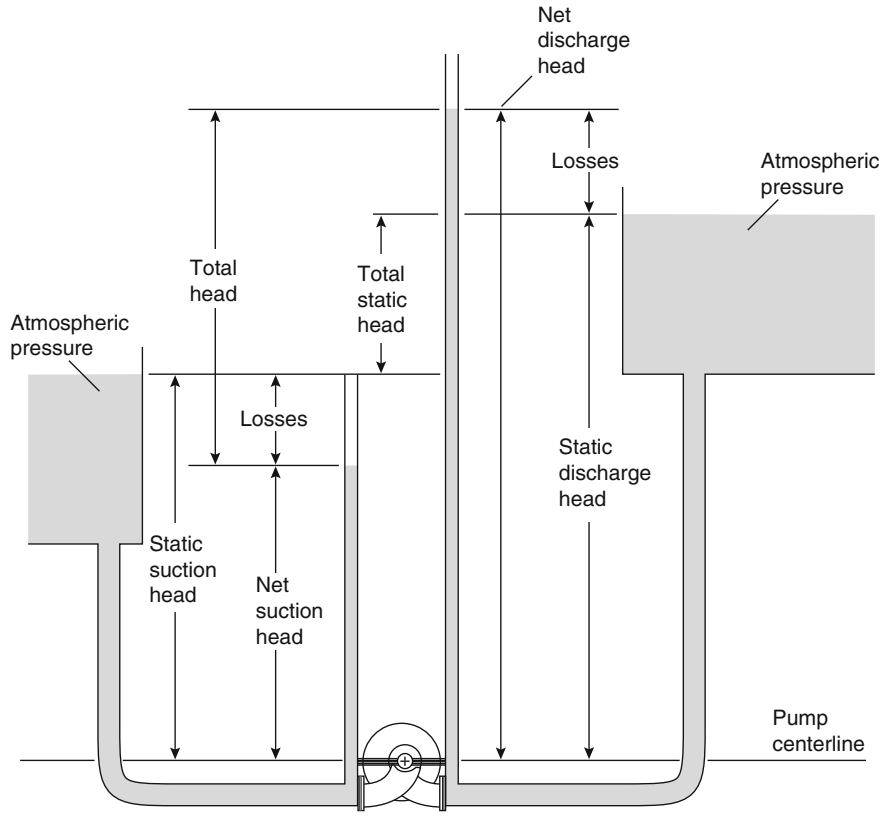

Fig. 41.23 Pump head definitions

losses. If the net suction head is less than the vapor pressure of the incoming water, the water will form small vapor bubbles or cavities within the pump. Where the small vapor bubbles formed in the low-pressure region collapse violently upon entering regions of high pressure, they cause localized stress concentrations and vibrations, ultimately leading to mechanical failure of the pump. This phenomenon is referred to as cavitation.

The required net positive suction head ($NPSH_{req}$) for any pump can be obtained from the manufacturer. The available net positive suction head ($NPSH_{av}$) must be calculated for each system. Because the total energy of a system is constant, the available NPSH may be determined at any point in the system. The general expression at the pump centerline follows from Bernoulli as

$$NPSH_{av} = \frac{(p_{gauge} + p_{atm})}{\rho g} + z - h_L - \frac{p_{vp}}{\rho g} \tag{41.70}$$

where

h_L = Friction head loss in intake system piping (in feet of water)

p_{vp} = Vapor pressure (0.256 psia for water at 20 °C)

Knowing the pressure and pipe friction loss terms, the pump can be set at a height, z, which will ensure that $NPSH_{av}$ is greater than $NPSH_{req}$.

Where a free surface exists on the intake side (such as at the surface of an intake reservoir) and the velocity at a point on the surface is negligible, the above expression simplifies to

$$NPSH_{av} = z - h_L + \frac{(p_{atm} - p_{vp})}{\rho g} \tag{41.71}$$

For pumps of relatively low heads and large discharge capacities (common in fire protection applications) the available NPSH may be less than zero (h_L is large). These pumps should be installed well below the reservoir water level to eliminate the possibility of cavitation. For this reason and also to avoid accidental loss of prime, authorities having jurisdiction generally require *positive suction* installation. In such instances the pump should be of the vertical shaft type so that the pump impellors sit in the water supply and the pump driver is installed at an elevation above any possible flood level.

The useful work done by a pump is the product of the weight of the liquid pumped and the head developed by the pump. The work per unit time in this context is the hydraulic horsepower, commonly called the water horsepower (WHP). For discharge, Q, in gpm, total dynamic head, h, in feet, and specific weight, γ, for water at 20 °C (68 °F),

$$WHP = \frac{Qh}{3,960} \tag{41.72}$$

The power required to actually drive the pump is the brake horsepower (BHP). The difference between water horsepower and brake horsepower is the power lost within the pump due to mechanical and hydraulic friction. The ratio of WHP to BHP is the pump efficiency, η_p. Similarly, the ratio of BHP to electrical or engine horsepower (EHP) is the motor efficiency, η_m . The overall efficiency is, then, the pump efficiency multiplied by the motor efficiency:

$$\eta = (\eta_p)(\eta_m) = \frac{WHP}{BHP} \cdot \frac{BHP}{EHP} \tag{41.73}$$

Although WHP should be calculated using the specific weight of the fluid at known conditions of temperature and pressure, the variation for water is very small; it should be noted that pump motor and engine sizes are chosen from standard available sizes in any case.

The interrelations of head, capacity, power, and efficiency for a given pump are known as the characteristics of the pump. They can be expressed graphically in the form of pump characteristic curves. Figure 41.24 shows a standard plot of the several variables at constant impeller speed (N). Note that the point of maximum operating efficiency on the head-capacity curve corresponds to the maximum value of the efficiency curve. The actual operating point of the

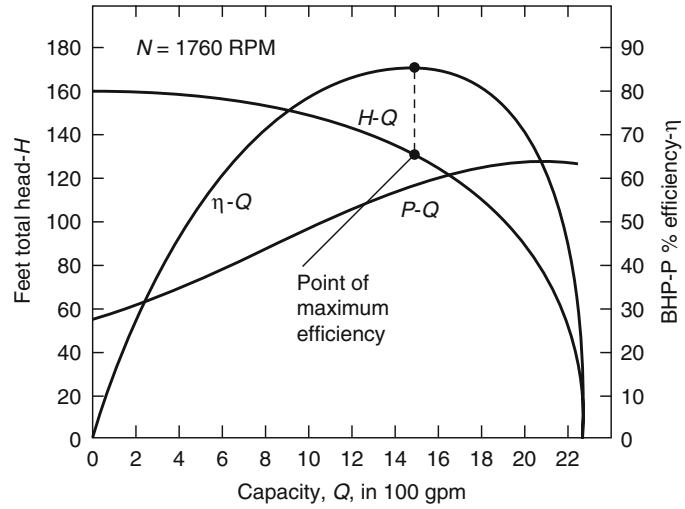

Fig. 41.24 Centrifugal pump characteristics

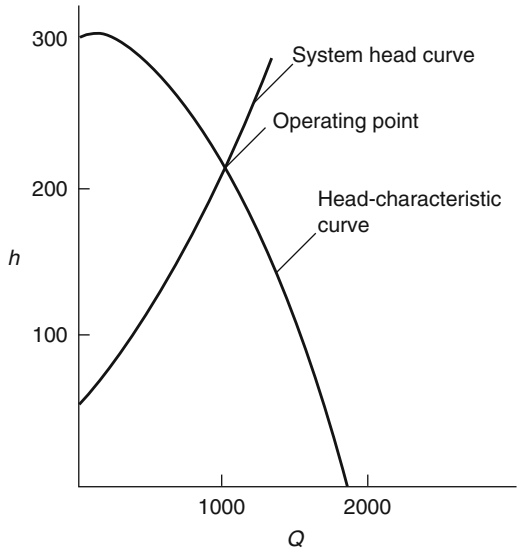

Fig. 41.25 Graphical determination of operating point

pump, however, depends on the system demand (or system head) curve. The system head loss for any flow rate is the sum of the system friction head loss at that rate plus the total static head to be overcome in the system. Figure 41.25 illustrates the relationship. Recall from Fig. 41.23 that the total static head is the difference in elevation between the discharge level and the suction level. System friction losses may be determined by calculations methods given in previous sections.

Pump Selection

Economical pump selection for fire protection applications requires consideration of the following factors:

1. The maximum discharge rate required under the most demanding design conditions
2. The total head-capacity relation (characteristic curve)
3. The suction head—in particular, the net positive suction head available
4. Pump speed and power source requirements
5. Pump spatial and environmental requirements
6. The maximum allowable system head downstream of the pump discharge

The usual design condition is that a system will be given or will be chosen from a very limited range of possibilities, and the proper pump must be selected. As shown in Fig. 41.25, when the system demand curve and the pump head-capacity curve are superimposed, their intersection will determine the operating point of the pump. This point also locates the efficiency and, therefore, the power requirements. It is often economically desirable to select a pump such that its operating point is at or near its peak efficiency. In many fire protection applications, however, a pump may be called upon to operate very infrequently. Power consumption may, therefore, not be a significant factor relative to initial cost. Common practice in fire protection applications

is to select a pump to operate at 150 % of rated capacity at 65 % of rated head (see NFPA 20[8])—that is, an operating point farther out along the characteristic curve. A pump is chosen such that its operating point so defined meets or exceeds the system demand curve at that point.

If the pump is to be used as a *booster* to increase supply main pressure, it must be confirmed that when selecting a pump having a maximum discharge head at zero flow (also known as *churn* head), which, when added to the maximum water main's supply head, does not exceed the maximum allowable working pressure on the system. The maximum allowable working pressure typical for many components in fire sprinkler systems is 175 psig [12], although higher rated components are available.

Centrifugal Pump Affinity Relations

The abstract concept of *pump specific speed* has been developed to simplify the description of pump performance characteristics. It consolidates the discharge, head, and speed (rpm) at optimum performance into a single number. For a single stage, single suction pump, specific speed may be calculated from

$$N_s = \frac{NQ^{1/2}}{H^{3/4}} \tag{41.74}$$

where Q (in gpm) is taken at pump rpm, N, and total dynamic head, H. The specific speed of a pump is not actually a speed for that pump in any physical sense; it is defined as the speed in revolutions per minute at which a homologous (geometrically similar) pump would run if constructed to deliver 1 gpm against 1 ft total head at its peak efficiency. For pump impeller designs of identical proportions but different sizes, the specific speed is a constant performance index. That is, the performance of any impeller can be predicted from knowledge of the performance of any other geometrically similar impeller.

Changing the impeller diameter results in changes in discharge, total head, and delivered power. These changes occur according to the follow relations:

$$\frac{Q_1}{Q_2} = \left(\frac{D_1}{D_2}\right)^3 \frac{n_1}{n_2} \tag{41.75a}$$

$$\frac{H_1}{H_2} = \left(\frac{D_1}{D_2}\right)^2 \left(\frac{n_1}{n_2}\right)^2 \tag{41.75b}$$

$$\frac{Q_1}{Q_2} = \left(\frac{H_1}{H_2}\right)^{1/2} \left(\frac{D_1}{D_2}\right)^2 \tag{41.75c}$$

$$\frac{\mathrm{BHP}_1}{\mathrm{BHP}_2} = \left(\frac{D_1}{D_2}\right)^5 \frac{\rho_1}{\rho_2} \frac{n_1^3}{n_2^3} \tag{41.75d}$$

Since

$$\frac{N_1}{N_2} = \frac{D_1}{D_2} \tag{41.76}$$

a change in motor speed only will yield similar results. That is, a change in impeller size has the same effect on pump performance as a change in speed provided, of course, that there is no marked change in operating efficiency.

Example 10 A 6 in. (152.4 mm) pump operating at 1770 rpm discharges 1500 gpm (5678 l/m) of water at 40 °F against a 120 ft (36.6 m) head.

(a) What discharge capacity and total head can be expected from a homologous 8 in. (203 mm) pump operating at 1170 rpm?

(b) If the pumps operate at an overall 80 % efficiency, what is the 8 in. (203 mm) pump power requirement?

Solution

(a) From Equation 41.75b,

$$H_2 = \left[\frac{8^2(1,170)^2}{(6)^2(1,170)^2}\right](120) = 93.2 \text{ ft } (28.4\,\text{m})$$

From Equation 41.75a,

$$Q_2 = \left[\frac{8^3(1,170)}{(6)^3(1,170)}\right](1,500)$$
$$= 2,350 \text{ gpm } (8,895.5\,\text{L/m})$$

(b) From Equation 41.72,

$$\mathrm{WHP} = \frac{2,350(93.2)}{3,960} = 55.3 \text{ HP}$$

Therefore,

$$\text{BHP} = \frac{55.3}{0.8} = 69.1 \text{ HP}$$

The motor chosen would be the next highest standard horsepower rating.

If more discharge or more head is required than a single pump can provide, two or more pumps may be combined to provide the necessary output. For example, when discharge is too little, pumps may be installed in parallel, sharing the same suction and inlet conditions. Figure 41.26 illustrates the principle. If a pump provides sufficient discharge but too little head, a second pump may be installed in series, the output of the first pump being fed directly into the suction of the second pump. Figure 41.27 depicts the

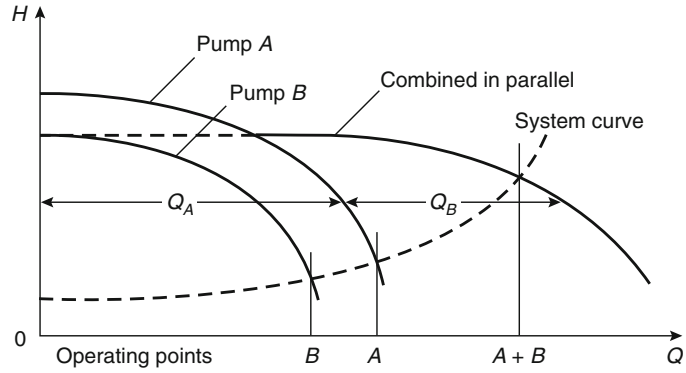

Fig. 41.26 Two pumps combined in parallel

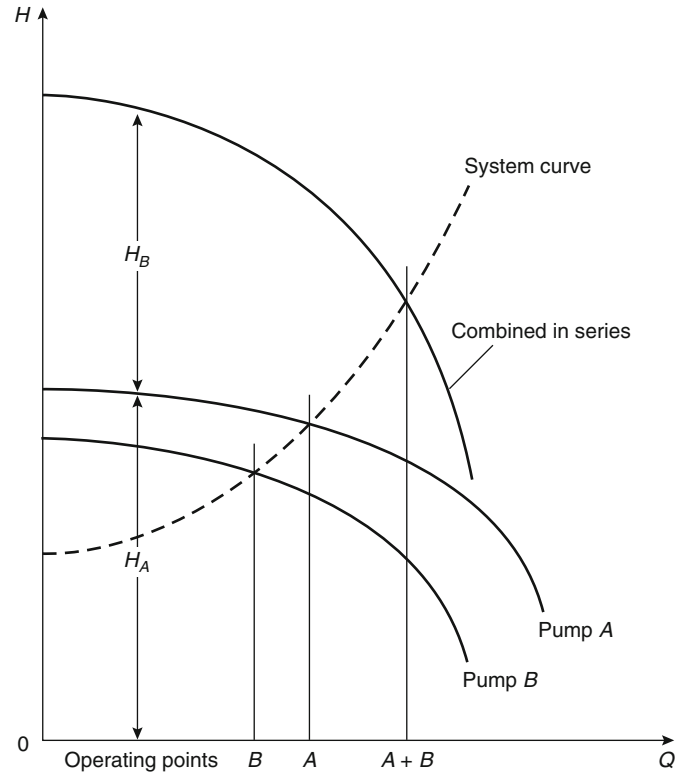

Fig. 41.27 Two pumps combined in series

series arrangement. A variety of compound arrangements are possible, depending on details of actual supply and demand, with economics being the prime arbiter.

Nomenclature

A	area
C	proportionality constant or flow coefficient, Hazen-Williams C-factor
c	celerity of a shock wave
D	pipe diameter
d	element diameter
E	velocity of approach factor, bulk modulus of elasticity
f	Darcy-Weisbach friction loss factor
G	gravitational acceleration constant, 9.8 m/s^2
H	head of water
h	head
h_c	height of centroid
h_L	head loss
I	moment of inertia
K	proportionality constant or flow coefficient
k	proportionality constant or flow coefficient
L	length of conduit (in friction loss equations)
l	length or distance
m	mass
N	pump rpm
p	pressure
Q	volumetric discharge rate
Re	Reynolds number
S	slope of energy gradient
s	specific gravity
u	stream velocity at a given point in flow cross section
V	volume
v	average stream velocity
z	height above a reference datum (potential head)
α	kinetic energy correction factor
β	beta ratio
γ	specific weight
Δ	increment
ε	pipe wall absolute roughness
η	efficiency
μ	absolute (dynamic) viscosity
ν	kinematic viscosity
ρ	density
τ	fluid shear stress

References

1. H.E. Hickey, *Hydraulics for Fire Protection,* National Fire Protection Association, Quincy, MA (1980).
2. R.P. Benedict, *Fundamentals of Pipe Flow,* Wiley-Interscience, New York (1980).
3. V.L. Streeter and E.G. Wylie, *Fluid Mechanics,* McGraw-Hill, New York (1979).
4. *Pipe Friction Manual,* 3rd ed. Hydraulic Institute (1961).
5. Isman, K. "Darcy Weisbach Friction Loss", *Sprinkler Quarterly*, National Fire Sprinkler Association, Winter 2001, pp 27–30.
6. A.L. Simon, *Practical Hydraulics,* John Wiley & Sons, New York (1981).
7. F.M. White, *Fluid Mechanics,* McGraw-Hill, New York (1986).
8. *Journal AWWA,* 73, 5 (1981), by permission. Copyright © 1981, The American Water Works Association.
9. T.M. Walski, *Analysis of Water Distribution Systems,* Van Nostrand Reinhold, New York (1984).
10. D. Stephenson, *Pipeflow Analysis,* Elsevier, Amsterdam (1984).
11. NFPA 20, *Installation of Centrifugal Fire Pumps,* National Fire Protection Association, Quincy, MA (2013).
12. NFPA 13, *Installation of Sprinkler Systems,* National Fire Protection Association, Quincy, MA (2013).

Kenneth E. Isman has been a Clinical Professor in Fire Protection Engineering at the University of Maryland since 2014. Prior to that, he worked for 28 years for the National Fire Sprinkler Association where he established an expertise in pumps, hydraulics, water supplies, and the design and installation of fire sprinkler systems and other water-based fire protection systems.

Automatic Sprinkler System Calculations

42

Russell P. Fleming

Introduction

Applications Where Water Is Appropriate

Water is the most commonly used fire fighting agent, mainly due to the fact that it is widely available and inexpensive. It also has very desirable fire extinguishing characteristics such as a high specific heat and high latent heat of vaporization. A single gallon of water can absorb 9280 Btus (2586.5 kJ) of heat as it increases from a 70 °F (21 °C) room temperature to become steam at 212 °F (100 °C).

Water is not without limits as an extinguishing agent, however, and is considered inappropriate for the protection of certain water reactive materials. In some cases, the application of water can exacerbate the production of heat, flammable or toxic gases, or cause an explosive reaction. The quantities and arrangement of such products must be considered, however, because the sufficient application of water can overcome the combustion reaction in some cases.

Another drawback of water is that it is more dense than most liquid hydrocarbon fuels, and immiscible with these liquids as well. Therefore, water will not effectively cover the burning liquid hydrocarbons, nor will it mix with them and dilute the volatile concentrations to the point where they will no longer sustain combustion. Instead, the hydrocarbons will float on top of the water, continuing to burn. In certain cases, the application of water could spread unconfined ignitable liquids and the associated fire. However, water additives such as foam concentrates can be added to the water discharge to produce foams that will float on the hydrocarbon surfaces to provide an effective cover and smother the fire. Applying water in a fine mist has also been successful for certain types of fires involving ignitable liquids. Other types of additives and discharge methods are also available to improve the effectiveness of water for specific applications.

Even when water from sprinklers will not suppress the fire, its cooling ability can protect structural elements of a building by controlling the fire until it can be extinguished by other means.

Types of Sprinkler Systems

For the majority of applications, automatic sprinkler systems are considered to be the most effective and economical way to apply water to control, suppress, or extinguish a fire. There are four basic types of sprinkler systems:

1. A *wet pipe* system is by far the simplest and most common type of sprinkler system. It consists of a network of piping containing water under pressure. Automatic sprinklers activated by internal heat responsive elements are connected to the piping such that each

R.P. Fleming (✉)

M.J. Hurley (ed.), *SFPE Handbook of Fire Protection Engineering*,
DOI 10.1007/978-1-4939-2565-0_42, © Society of Fire Protection Engineers 2016

sprinkler protects an assigned horizontal building area, usually a floor area. The application of heat to any sprinkler will cause that single sprinkler to operate, permitting water to discharge over its area of protection.

2. A *dry pipe* system is similar to a wet system, except that water is held back from the piping network by a special dry pipe valve. The valve is kept closed by air or nitrogen pressure maintained in the system piping. The operation of one or more sprinklers will allow the air pressure to escape, causing operation of the dry valve, which then permits water to flow into the piping network to control or suppress the fire. Dry systems are used where the water in the piping would be subject to freezing.
3. A *deluge* system is one that does not use automatic sprinklers, but rather open sprinklers. A special deluge valve holds back the water from the piping, and is activated by a separate fire detection system. When activated, the deluge valve admits water to the piping network, and water flows simultaneously from all of the sprinklers comprising the system. Deluge systems are used for protection against rapidly spreading, high heat release fires.
4. A *preaction* system is similar to a deluge system except that automatic sprinklers rather than open sprinklers are used. A small amount of air pressure is usually maintained in the piping network to ensure that the system is air tight. As with a deluge system, a separate detection system is used to activate a deluge valve, admitting water into the piping network. However, because automatic sprinklers are used, the water is only discharged from activated sprinklers, i.e. those that were fused by heat from the fire. Some special arrangements of preaction systems permit variations on detection system interaction with sprinkler operation. Preaction systems are generally used where there is special concern for accidental discharge of water, as in data processing computer rooms or flash freeze warehouses.

These four basic types of systems differ in terms of the most fundamental aspect of how the water is discharged into the fire area. There are other variations of sprinkler system arrangements, classified according to the hazard they protect (such as residential, in-rack, or exposure protection); additives to the system (such as antifreeze or foam concentrate); or special connections to the system (such as multipurpose piping). However, all sprinkler systems can still be categorized as one of the basic four types.

Applicable Standards

Various sprinkler system design and installation standards are in use around the world. NFPA 13, *Standard for the Installation of Sprinkler Systems* (hereafter referred to as NFPA 13), is the most widely used, and is referenced by most building and life safety codes in the United States and Canada [1]. This standard, in turn, references other NFPA standards for design and installation requirements relating to water supply or interconnection with other systems. These standards include NFPA 14, *Standard for the Installation of Standpipe and Hose Systems*, NFPA 20, *Standard for the Installation of Stationary Pumps for Fire Protection*, and NFPA 22, *Standard for Water Tanks for Private Fire Protection*.

For protection of warehouse storage, NFPA 13 traditionally referenced special storage standards that contained sprinkler system design criteria, including NFPA 231, *Standard for General Storage Materials*, NFPA 231C, *Standard for Rack Storage of Materials*, NFPA 231D, *Standard for Storage of Rubber Tires*, and NFPA 231F, *Standard for Storage of Roll Paper*. However, beginning with the 1999 edition of NFPA 13 these standards were all merged into NFPA 13 to produce a consolidated sprinkler system design and installation standard.

Other standards contain design and installation criteria for specific types of facilities or water-based systems, including NFPA 13D, *Standard for the Installation of Sprinkler Systems in One- and Two-Family Dwellings and*

Manufactured Homes, NFPA 15, *Standard for Water Spray Fixed Systems for Fire Protection*, NFPA 16, *Standard for the Installation of Foam-Water Sprinkler and Foam-Water Spray Systems*, NFPA 30, *Flammable and Combustible Liquids Code*, NFPA 30B, *Code for the Manufacture and Storage of Aerosol Products*, and NFPA 409, *Standard on Aircraft Hangars*.

The European standard addressing sprinkler system design and installation is EN 12845—*Fixed Firefighting Systems, Automatic Sprinkler Systems, Design, Installation and Maintenance*. The standard was first published in 2004, but is the successor to European insurance standards that in turn were based on sprinkler design and installation rules originally published by the Fire Offices Committee of the United Kingdom.

Insurance companies may also develop and enforce their own standards for their customers. For example, FM Global has developed Property Loss Prevention Data Sheet 2-0, *Installation Guidelines for Automatic Sprinklers*. In Europe, may insurers reference the use of CEA 4001-*sprinkler systems: planning and installation*. In some cases insurance companies or other authorities might modify the provisions or a given standard such as NFPA 13. While this chapter addresses the calculations and engineering considerations associated with the general design of sprinkler systems, the reader needs to confirm the applicable rules and regulations in effect for the particular project under consideration.

Trends in Sprinkler System Development

Since the 1970s, there have been a number of new developments in a technology with more than a century of performance history. Hydraulic calculations allowed system designers to take advantage of strong water supplies in order to use smaller pipe sizes. More aesthetically pleasing sprinklers entered the marketplace to appeal to architects and owners as sprinkler system installation spread from factories and warehouses to public spaces and private homes. New types of piping offered options. Fast response sprinklers enhanced safety to life while reducing design areas and water supplies based on fewer sprinklers expected to open during a fire event. Larger sprinkler orifice sizes were developed to better address the hazards of high challenge industrial and storage fires.

Almost all of these developments were aimed at equal or better fire protection at less cost, made possible through improved allocation of resources. The more efficient use of resources remains a challenge today, with a great deal of focus on sustainability. Because fire sprinklers systems utilize water for periodic testing as well as fire suppression, conservation will increase in importance, and the potential impact of reduced available water supplies on sprinkler system performance will need to be monitored [2]. Proposed environmental solutions such as the use of gray water supplies must be evaluated for their potential to reduce the long-term performance and reliability of fire sprinkler systems. For this reason, NFPA 13 requires that any source of recycled or reclaimed water and its proposed treatment process be analyzed before being made available to the sprinkler system, with a specific concern for compatibility with system components.

Limits of Calculation in an Empirical Design Process

Engineering calculations are best performed in areas where an understanding exists as to relationships between parameters. This is not the case with the technology of automatic sprinkler systems. Calculation methods are widely used with regard to only one aspect of sprinkler systems: water flow through piping. There are only very rudimentary calculation methods available with regard to the most fundamental aspect of sprinkler systems, that is, the ability of water spray to suppress fires.

The reason that calculation methods are not used is simply the complexity of the mechanisms by which water suppresses fires. Water-based fire suppression has to this point not been thoroughly

characterized to permit application of mathematical modeling techniques. As a result, the fire suppression aspects of sprinkler system design are empirical at best.

Some, but not all, of the current sprinkler system design criteria are based on full-scale testing, including the criteria originally developed for NFPA 231C, NFPA 13D, and parts of NFPA 13, such as the provisions pertaining to the use of CMSA (control mode specific application) and ESFR (early suppression fast response) sprinklers. Most of the protection criteria of NFPA 13 and other sprinkler system design standards, however, are the result of the evolution and application of experienced judgment and intuitive reasoning. In the 1970s, the capabilities of pipe schedule systems, which had demonstrated a hundred years of satisfactory performance, were codified into a system of density/area curves [3]. This permitted the introduction of hydraulic calculations to what had become a cookbook-type method of designing sprinkler systems. Hydraulic calculations allowed system designers to take advantage of strong water supplies to produce more economical systems. It also permitted the determination of specific flows and pressures available at various points of the system, opening the door to the development and use of new types of sprinklers. The number of different types of sprinklers available in the global marketplace has increased dramatically in the past few decades, and the fire protection engineer needs to be knowledgeable with regard to the variety of fire sprinkler products.

Even where design criteria were developed on the basis of full-scale testing, the number and sequence of operating sprinklers has been found to be variable. Some of this variability is due to the variability in fire growth itself and prevailing air currents within a building, but there are also observed phenomena such as "sprinkler skipping," in which a sprinkler will operate substantially prior to a nearby sprinkler that is closer to the fire plume. Generally associated with high challenge fire scenarios, skipping has been attributed to water drop impingement from nearby operating sprinklers [4], and there is evidence that steps can be taken to shield a sprinkler's heat sensing element from such impingement [5].

Because of this history, the calculation methods available to the fire protection engineer in standard sprinkler system design are only ancillary to the true function of a sprinkler system. The sections that follow in this chapter address hydraulic calculations of flow through piping, simple calculations commonly performed in determining water supply requirements, and optional calculations that may be performed with regard to hanging and bracing of system piping. The final section of this chapter deals with the performance of a system relative to a fire, and the material contained therein is totally outside the realm of standard practice. This material is not sufficiently complete to permit a full design approach, but only isolated bits of total system performance. The technical reference guide to the current version of the Fire Dynamics Simulator (FDS), a computational fluid dynamics model that has become the most popular tool in fire protection engineering, includes the statement that "simulating the effects of a sprinkler spray involves a number of elements beyond just activation: computing the droplet trajectories and tracking the water as it drips onto the burning surface" [6]. Efforts are underway to develop a mathematical model of sprinkler spray discharge based on first principles [7], with the hope of ultimately being able to model the impact of a fire sprinkler system on a fire.

Hydraulic Calculations

Density-Based Sprinkler Demand

Occupancy hazard classification, or commodity classification in the case of protecting storage, is the most critical aspect of the sprinkler system design process. If the hazard or commodity class is underestimated, it is possible for fire to overpower the sprinklers, conceivably resulting in a large loss of property or life. Hazard classification is not an area in which calculation methods are presently in use, however. The proper classification of hazard requires experienced judgment

and familiarity with relevant design and installation standards, and an understanding of sprinkler system performance. Commodity classification is also not possible by means of calculation, but intermediate scale fire testing is sometimes used as the basis of classifying a specific product.

Once the hazard or commodity classification is determined and a sprinkler spacing and piping layout has been proposed in conformance with the requirements of the applicable standard, the system designer can initiate a series of calculations to demonstrate that the delivery of a prescribed rate of water application will be accomplished for the maximum number of sprinklers that might be reasonably expected to operate. This number of sprinklers, which must be supplied regardless of the location of the fire within the building, is the basis of the concept of the remote design area. The designer needs to demonstrate that the shape and location of the sprinkler arrangement in the design area will be adequately supplied with water in the event of a fire. Adequacy of water relates to flow, pressure and quantity of water available through the sprinklers expected to operate in response to the fire.

Prior to locating the design area, there is the question of how many sprinklers are to be included in the expected maximum simultaneous flow area. This question is primarily addressed by the occupancy hazard classification, but the designer also has some freedom to decide this matter.

For example, in the 2013 edition of NFPA 13, Figure 11.2.3.1.1 contains density/area curves from which the designer can select a design area and density appropriate for the occupancy hazard classification. Any point on or to the right of the curve in the figure is acceptable. The designer may select a high density over a small area, or a low density over a large area. In either event, the fire is expected to be controlled by the sprinklers within that design area, without opening any additional sprinklers. For the protection of storage, similar curves or individual density/area specifications can be found in Chaps. 12, 13, 14, 15, 16, 17, 18, 19, 20, and 21. Chapter 22 of NFPA 13 (2013) contains some sprinkler design density/area specifications or hazard classifications from other NFPA codes and standards relating to the protection of specific occupancies.

Example 1 Using the sample density/area curve shown in Fig. 42.1, many different design criteria could be selected, ranging from a density of

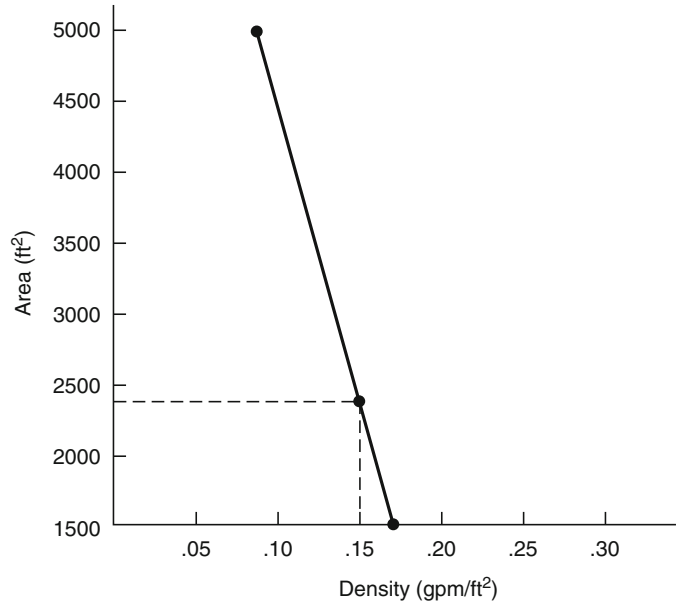

Fig. 42.1 Sample density/area curve

0.1 gpm/ft^2 (3.7 mm/min) over 5000 ft^2 (500 m^2) to 0.17 gpm/ft^2 (6.9 mm/min) over 1500 ft^2 (139 m^2). Either of these two points, or any point to the right of the curve (such as 0.16 gpm/ft^2 [6.5 mm/min] over 3000 ft^2 [276 m^2]) would be considered acceptable. A selection of 0.15 gpm/ft^2 (6.1 mm/min) over 2400 ft^2 (221 m^2) is indicated.

Water is provided only for the number of sprinklers in the design area, since no water is needed for the sprinklers that are not expected to open. The design area will be located in the hydraulically most demanding portion of the system. The actual number of sprinklers in the design area depends, of course, on the spacing of the individual sprinklers. NFPA 13 requires that the design area be divided by the maximum sprinkler spacing used, and that any fractional result be rounded up to the next whole sprinkler, as illustrated below.

Example 2 Based on the point selected from the sample density/area curve above and the proposed maximum spacing of sprinklers, the number of sprinklers to be included in the design area can be determined. If sprinklers are spaced at 12 × 15 ft (3.66 × 4.57 m) so as to each protect an area of 180 ft^2 (16.72 m^2), the design area of 2400 ft^2 (221 m^2) would include.

$$\frac{2,400}{180} = 13.33 = 14 \text{ sprinklers}$$

The remote design area is required to have a rectangular shape, with the long side of the rectangle parallel to the branch lines. The length of the long side of the design area needs to be determined to calculate the number of sprinklers to be included on each branch line in the design area. This length is normally determined by multiplying the square root of the design area by a factor of 1.2 in accordance with the rules of NFPA 13. Again, any fractional result is rounded to the next whole sprinkler as indicated below. Note that other standards or design methods may use multiplication factors other than 1.2. The higher the factor, the more conservative the design, since it requires more water to be available through individual branch lines.

Example 3 If the 14 sprinklers from Example *2* were spaced 12 ft (3.66 m) along the branch lines and the branch lines were spaced 15 ft (4.57 m) apart, the number of sprinklers along the length of the branch lines in the design area would be

$$\frac{1.2(2,400)^{1/2}}{12} = \frac{1.2(49)}{12} = 4.9 = 5 \text{ sprinklers}$$

If the sprinklers were spaced 15 ft (4.57 m) along the branch lines with the branch lines spaced 12 ft (3.66 m) apart, the design area rectangle would include only 4 sprinklers along its length.

NFPA 13 (2013) contains some exceptions to this method of locating a remote design area and determining the number of sprinklers to be supplied. Chapters 11 and 12 of the standard include special adjustments to the design area based on factors such as the use of a dry system, the use of quick response sprinklers under flat smooth ceilings of limited height, and the existence of nonsprinklered combustible concealed spaces within the building. These chapters also contain rules for the use of a room design method, which can reduce the number of sprinklers expected to operate in a highly compartmented occupancy. Also, beginning in 1985, the standard adopted a four sprinkler design area for dwelling units and their adjacent corridors when residential sprinklers are installed in accordance with their listing requirements. Listing requirements are specific to the applicable standard but normally pertain to the independent laboratory evaluation of performance of a product, system or service, in this case a residential sprinkler.

A step-by-step hydraulic calculation procedure is usually applied. For example, see Chapter 23 of the 2013 edition of NFPA 13. The starting point is the most remote sprinkler in the design area. For tree systems, in which each sprinkler is supplied from only one

direction, the most remote sprinkler is generally the end sprinkler on the farthest branch line from the system riser. This sprinkler, and all others in the design area, must be provided with a sufficient flow of water to meet the density appropriate for the point selected on the density/area curve.

Where a sprinkler protects an irregular area, NFPA 13 prescribes that the area of coverage for the sprinkler must be based on the largest sides of its coverage. In other words, the area which a sprinkler protects for calculation purposes is equal to

$$\text{Area of coverage} = S \times L$$

where S is twice the larger of the distances to the next sprinkler (or wall for an end sprinkler) in both the upstream and downstream directions, and L is twice the larger of the distances to adjacent branch lines (or wall in the case of the last branch line) on either side. This reflects the need to flow more water with increasing distance from the sprinkler, since increased flow tends to expand the effective spray umbrella of the sprinkler.

The minimum flow from a sprinkler must be the product of the area of coverage multiplied by the minimum required density

$$Q = \text{Area of coverage} \times \text{Density}$$

Most of the special listed sprinklers and residential sprinklers have a minimum flow requirement associated with their listings, which is often based on the spacing at which they are used. These minimum flow considerations override the minimum flow based on the density/area method.

Example 4 If a standard spray sprinkler protects an area extending to 7 ft (2.1 m) on the north side (half the distance to the next branch line), 5 ft (1.5 m) on the south side (to a wall), 6 ft (1.8 m) on the west side (half the distance to the next sprinkler on the branch line), and 4 ft (1.2 m) on the east side (to a wall), the minimum flow required for the sprinkler to achieve the density requirement selected in Example *1* can be found by completing two steps. The first step involves determining the area of coverage. In this case:

$$S \times L = 2(6\text{ ft}) \times 2(7\text{ ft}) = 12\text{ ft} \times 14\text{ ft} = 168\text{ ft}^2\ (15.6\text{ m}^2)$$

The second step involves multiplying this coverage area by the required density:

$$Q = A \times \rho = 168\text{ ft}^2 \times 0.15\text{ gpm/ft}^2 = 25.2\text{ gpm}\ (95.4\text{ L/min})$$

Pressure Requirements of the Most Remote Sprinkler

When flow through a sprinkler orifice takes place, the energy of the water changes from the potential energy of pressure to the kinetic energy of flow. A formula can be derived from the basic energy equations to determine how much water will flow through an orifice based on the water pressure inside the piping at the orifice:

$$Q = 29.83 c_d d^2 P^{1/2}$$

This formula contains a factor, c_d, which is a discharge coefficient characteristic of the sprinkler orifice that is determined by laboratory testing. For sprinklers, the product listing organizations determine the orifice discharge coefficient for each particular model of sprinkler. To simplify matters, all physical factors of the sprinkler orifice are lumped into what is experimentally determined as the K-factor of a sprinkler, such that

$$Q = \text{K} \times P^{1/2}$$

where K has units of gpm/(psi)$^{1/2}$ [L/min/(bar)$^{1/2}$].

Since the required minimum flow at the most remote sprinkler is known, determined by either the density/area method or the special sprinkler listing, the minimum pressure needed at the most remote sprinkler can easily be calculated.

Since $Q = \text{K}(P)^{1/2}$ then $P = (Q/\text{K})^2$

Many sprinklers require a minimum operating pressure of 7 psi (0.48 bar) to ensure proper spray pattern development.

Example 5 The pressure required at the sprinkler in Example 4 can be determined using the above formula once a specific sprinkler is selected. The K-factor for any sprinkler needs to be confirmed with the manufacturer and listing organization. For the purposes of this example, a K-factor of 5.6 is assumed, since this is a common value for what are considered standard ½-inch orifice sprinklers.

$$P = \left(\frac{Q}{\mathrm{K}}\right)^2 = \left(\frac{25.2}{5.6}\right)^2 = 20.2 \text{ psi} (1.4 \text{ bar})$$

Once the minimum pressure at the most remote sprinkler is determined, the hydraulic calculation method proceeds backward toward the source of water supply. If the sprinkler spacing is regular, it can be assumed that all other sprinklers within the design area will be flowing at least as much water, and the minimum density is assured. If sprinkler spacing is irregular due to walls and obstruction, or sprinklers with different K-factors are used, it must be verified that each sprinkler is provided with sufficient flow.

As the calculations proceed toward the system riser and water supply, the minimum pressure requirements increase, because additional pressures are needed to overcome losses associated with elevation changes, pipe friction, and turbulence caused by fittings, so that the minimum design densities for all sprinklers in the design area are maintained. The determination of the friction and elevation losses are discussed below, with their values added to the total pressure requirements.

It should be noted that each sprinkler closer to the source of supply will show a successively greater flow rate, since a higher total pressure is available at that point in the system piping. This effect on the total water demand is termed hydraulic increase, and is the reason why the total water demand of a system is not simply equal to the product of the minimum density and the design area. When calculations are complete, the sprinkler system demand will be known, stated in the form of a specific flow at a specific pressure. A hose demand is also sometimes added to the sprinkler system demand. The total quantity of water will be determined based upon the duration of required flow that will be specified by applicable standards.

Pressure Losses Through Piping, Fittings, and Valves

Friction losses resulting from water flow through piping can be estimated by several engineering approaches, but the most common is the Hazen-Williams method. This approach is based on the formula developed empirically by Hazen and Williams:

$$p = \frac{4.52Q^{185}}{C^{1.85}d^{4.87}}$$

where
p = Friction loss per ft of pipe in psi
Q = Flow rate in gpm
d = Internal pipe diameter in in.
C = Hazen-Williams coefficient

The choice of C is critical to the accuracy of the friction loss determination, and is therefore normally stipulated by design standards. C values for various types of pipe materials are shown in Fig. 42.1. The values assigned for use are intended to simulate the expected interior roughness of aged pipe (Table 42.1).

Rather than make the Hazen-Williams calculation for each section of piping, it has become standard practice, when doing hand calculations, to use a friction loss table, which contains all values of p for various values of Q and various pipe sizes. In many cases the tables are based on

Table 42.1 C values for pipes

Type of pipe	Assigned C factor
Steel pipe—dry and preaction systems	100
Steel pipe—wet and deluge systems	120
Galvanized steel pipe—dry and preaction systems	100
Galvanized steel pipe—wet and deluge systems	120
Cement lined cast or ductile iron	140
Copper tube	150
Plastic (listed)	150

the use of Schedule 40 steel pipe for wet systems. The use of other pipe schedules, pipe materials, or system types may require the use of multiplying factors. Most commercially available sprinkler system hydraulic calculation programs have these values programmed into the software.

Once the value of friction loss per foot is determined using either the previous equation or friction loss tables, the total friction loss through a section of pipe is found by multiplying p by the length of pipe, L. Since some standards use p to designate loss per foot, total friction loss in a length of pipe can be designated by p_f, where

$$p_f = p \times \mathrm{L}$$

In the analysis of complex piping arrangements, it is sometimes convenient to lump the values of all factors in the Hazen-Williams equation (except flow) for a given length of pipe into a constant, K, identified as a friction loss coefficient. To avoid confusion with the nozzle coefficient K, this coefficient can be identified as FLC, friction loss coefficient.

$$\mathrm{FLC} = \frac{(L \times 4.52)}{\left(C^{1.85} d^{4.87}\right)}$$

The value of p_f is therefore equal to

$$p_f = \mathrm{FLC} \times Q^{1.85}$$

Example 6 If the most remote sprinkler on a branch line requires a minimum flow of 25.2 gpm (92.1 L/min) for a minimum pressure of 20.2 psi (1.4 bar) as shown in Examples 4 and 5, and the second sprinkler on the line is connected by a 12 ft (3.6 m) length of 1 in. (25.4 mm) Schedule 40 steel pipe, with both sprinklers mounted directly in fittings on the pipe (no drops or sprigs), the minimum pressure required at the second sprinkler can be found by determining the friction loss caused by a flow of 25.2 gpm (92.1 L/min) through the piping to the end sprinkler. Typically, pressure losses associated with straight-through fittings can be ignored in the calculation process if there is no change in flow direction. Also, the fitting directly attached to each sprinkler is generally ignored, since K-factors of sprinklers are determined with such a fitting in place.

Using the Hazen-Williams equation with values of 25.2 for Q, 120 for C, and 1.049 for d (the inside diameter of Schedule 40 steel 1 in. pipe) results in a value of $p = 0.20$ psi (0.012 bar) per foot of pipe. Multiplying by the 12 ft (3.6 m) length results in a total friction loss of $p_f = 2.4$ psi (0.17 bar). The total pressure required at the second sprinkler on the line is therefore 20.2 psi + 2.4 psi = 22.6 psi (1.6 bar). This will result in a flow from the second sprinkler of $Q = \mathrm{K}(P)^{1/2} = 26.6$ gpm (100.7 L/min).

Minor losses through fittings and valves are not friction losses but energy losses, caused by turbulence in the water flow, which increase as the velocity of flow increases. Nevertheless, it has become standard practice to simplify calculation of such losses through the use of "equivalent lengths," which are added to the actual pipe length in determining the pipe friction loss. NFPA 13 contains a table of equivalent pipe lengths for this purpose (Table 42.2). As an example, if a 2 in. (50.8 mm) 90-degree long turn elbow is assigned an equivalent length of 3 ft (0.914 m), this means that the energy loss associated with turbulence through the elbow is expected to approximate the energy loss to friction through 3 ft of 2 in. pipe (0.914 m of 50.8 mm pipe). As with the friction loss tables, the equivalent pipe length chart is based on the use of steel pipe with a C-factor of 120, and the use of other piping materials requires multiplying factors. The equivalent pipe length for pipes having C values other then 120 should be adjusted using the following multiplication factors: 0.713 for a C value of 100; 1.16 for a C value of 130; 1.33 for a C value of 140; 1.51 for a C value of 150.

Example 7 If the 12 ft (3.6 m) length of 1 in. (25.4 mm) pipe in Example 6 had contained four elbows so as to avoid a building column, the pressure loss from those elbows could be approximated by adding an equivalent length of pipe to the friction loss calculation. Table 42.2 gives a value of 2 ft (0.610 m) as the appropriate equivalent length for standard elbows in 1 in. (25.4 mm) Schedule 40 steel pipe. For four elbows, the equivalent fitting length would be 8 ft (2.4 m). Added to the actual pipe length of

Table 42.2 Equivalent pipe length chart (for C = 120)

	Fittings and valves expressed in equivalent feet of pipe													
Fittings and valves	¾ in.	1 in.	1¼ in.	1½ in.	2 in.	2½ in.	3 in.	3½ in.	4 in.	5 in.	6 in	8 in.	10 in.	12 in.
45° elbow	1	1	1	2	2	3	3	3	4	5	7	9	11	13
90° standard elbow	2	2	3	4	5	6	7	8	10	12	14	18	22	27
90° long turn elbow	1	2	2	2	3	4	5	5	6	8	9	13	16	18
Tee or cross (flow turned 90°)	3	5	6	8	10	12	15	17	20	25	30	35	50	60
Butterfly valve	—	—	—	—	6	7	10	—	12	9	10	12	19	21
Gate valve	—	—	—	—	1	1	1	1	2	2	3	4	5	6
Swing check[a]	—	5	7	9	11	14	16	19	22	27	32	45	55	65

For SI units: 1 ft = 0.3048 m

[a]Due to the variations in design of swing check valves, the pipe equivalents indicated in the above chart are to be considered average

12 ft (3.6 m), the total equivalent length would be 20 ft (6 m). This results in a new value of $p_f = 20$ ft × 0.20 psi/ft = 4.0 psi (0.28 bar). The total pressure at the second sprinkler would then be equal to 20.2 psi + 4.0 psi = 24.2 psi (1.67 bar). The total flow from the second sprinkler in this case would be $Q = K(P)^{1/2} = 27.5$ gpm (100.4 L/min).

Some types of standard valves, such as swing check valves, are included in Table 42.2, the equivalent pipe length chart. Equivalent lengths for pressure losses through system alarm, dry, and deluge valves are determined by the approval laboratories at the time of product listing.

Use of Velocity Pressures

The value of pressure, P, in the sprinkler orifice flow formula can be considered either the total pressure, P_t, or the normal pressure, P_n, since design standards typically permit the use of velocity pressures at the discretion of the designer. Total pressure, normal pressure, and velocity pressure, P_v, have the following relationship:

$$P_n = P_t - P_v$$

Total pressure is the counterpart of total energy or total head, and can be considered the pressure that would act against an orifice if all of the energy of the water in the pipe at that point were focused toward flow out of the orifice. This is the case where there is no flow past the orifice in the piping. Where flow does take place in the piping past an orifice, however, normal pressure is the portion of the total pressure acting perpendicular to the direction of flow in the piping, and therefore acting in the direction of flow through the orifice. The amount by which normal pressure is less than total pressure is velocity pressure, which is acting in the direction of flow in the piping. Velocity pressure corresponds to velocity energy, which is the energy of motion. There is no factor in the above expression for elevation head, because the flow from an orifice can be considered to take place in a datum plane.

When velocity pressures are used in calculations, it is recognized that some of the energy of the water is in the form of velocity head, which is not acting normal to the pipe walls (where it would help push water out the orifice), but rather in the downstream direction. Thus, for every sprinkler (except the end sprinkler on a line), slightly less flow takes place than what would be calculated from the use of the formula $Q = K(P_t)^{1/2}$ (Fig. 42.2).

Design standards typically permit the velocity pressure effects to be ignored, however, since they are usually rather minor for most sprinkler system configurations. Additionally, ignoring the effects of velocity pressure tends to produce a more conservative design in that the calculated system demand (flow and pressure) increase when velocity pressures are not taken into account.

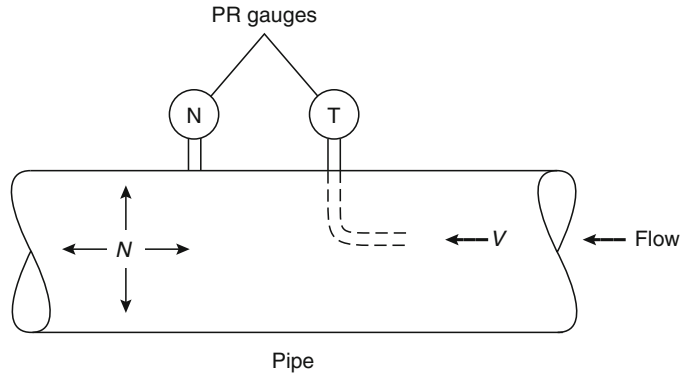

Fig. 42.2 Velocity and normal pressures in piping

If velocity pressures are considered, normal pressure rather than total pressure is used when determining flow through any sprinkler except the end sprinkler on a branch line, and through any branch line except the end branch line on a cross main. The velocity pressure, P_v, which is subtracted from the total pressure in order to determine the normal pressure, is determined as

$$P_v = \frac{v^2}{2g} \times 0.433 \text{ psi/ft } (0.098 \text{ bar/m})$$

or

$$P_v = 0.001123Q^2/d^4$$

where Q is the upstream flow through the piping to an orifice (or branch line) in gpm and d is the actual internal diameter of the upstream pipe in inches.

Because design standards typically mandate the use of the upstream flow, an iterative approach to determining the velocity pressure is necessary. The upstream flow cannot be determined unless the flow from the sprinkler (or branch line) in question is known. Since the flow from the sprinkler (or branch line) is affected by the velocity pressure resulting from the upstream flow, an estimate of the upstream flow is needed to start the iteration.

Example 8 If the pipe on the upstream side of the second sprinkler in Example 6 were 3 in. Schedule 40 steel pipe with an inside diameter of 1.38 in. (35 mm), the flow from the second sprinkler would be considered to be 26.6 gpm (100.2 L/min) as determined at the end of Example 6, if velocity pressures were not included.

If velocity pressures were to be considered, an upstream flow would first be assumed. Since the end sprinkler had a minimum flow of 25.2 gpm (95.2 L/min) and the upstream flow would consist of the combined flow rates of the two sprinklers, an estimate of 52 gpm (196.8 L/min) appears reasonable. Substituting this flow and the pipe diameter into the equation for velocity pressure gives

$$\begin{aligned} P_v &= \frac{0.001123Q^2}{d^4} \\ &= \frac{0.001123(52)^2}{(1.38)^4} \\ &= 0.8 \text{ psi } (0.06 \text{ bar}) \end{aligned}$$

This means that the actual pressure acting on the orifice of the second sprinkler is equal to

$$\begin{aligned} P_n &= P_t - P_v \\ &= 22.6 \text{ psi} - 0.8 \text{ psi} \\ &= 21.8 \text{ psi } (1.50 \text{ bar}) \end{aligned}$$

This would result in a flow from the second sprinkler of

$$\begin{aligned} Q &= \mathrm{K}(P)^{1/2} \\ &= 26.1 \text{ gpm } (98.7 \text{ L/min}) \end{aligned}$$

Combining this flow with the known flow from the end sprinkler results in a total upstream flow of 51.3 gpm (194.2 L/min). To determine if the initial guess was close enough, determine the velocity pressure that would result from an upstream flow of 51.3 gpm (194.2 L/min).

This calculation also results in a velocity pressure of 0.8 psi (0.06 bar), and the process is therefore complete. It can be seen that the second sprinkler apparently flows 0.5 gpm (1.9 L/min) less than the estimated flow due to velocity pressures.

Elevation Losses

Variation of pressure within a fluid at rest is related to the density or unit (specific) weight of the fluid. The unit weight of a fluid is equal to its density multiplied by the acceleration of gravity. The unit weight of water is 62.4 lbs/ft^3 (1000 kg/m^3).

This means that one cubic foot of water at rest weighs 62.4 lbs (1000 kg). The cubic foot of water, or any other water column one foot high, thus results in a static pressure at its base of 62.4 lbs/ft^2 (304.66 kg/m^2). Divided by 144 in.^{2} per ft^2 (1.020 $\times$ 10^4 kg/m^2 bar), this results in a pressure of 0.433 lb per in.^{2} per ft (0.099 bar/m) of water column.

A column of water 10 ft (3.048 m) high similarly exerts a pressure of 10 ft $\times$ 62.4 lbs/ft^2 $\times$ 1 ft^2/144 in.^{2} = 4.33 psi (3.048 m $\times$ 999.5 kg/m^2 $\div$ 1.020 $\times$ 10^4 kg/m^2 bar = 0.299 bar). The static pressure at the top of both columns of water is equal to zero (gauge pressure), or atmospheric pressure.

On this basis, additional pressure must be available within a sprinkler system water supply to overcome the pressure loss associated with elevation, i.e. when water flow is acting against the force of gravity. This pressure is equal to 0.433 psi/ft (0.099 bar/m) of elevation of the sprinklers above the level where the water supply information is known.

Sometimes the additional pressure needed to overcome elevation is added at the point where the elevation change takes place within the system. If significant elevation changes take place within a portion of the system that is likely to be considered as a representative flowing orifice (such as a single branch line along a cross main that is equivalent to other lines in the remote design area), then it is considered more accurate to wait until calculations have been completed, and simply add an elevation pressure increase to account for the total height of the highest sprinklers above the supply point.

Example 9 The pressure that must be added to a system supply to compensate for the fact that the sprinklers are located 120 ft (36.6 m) above the supply can be found by multiplying the total elevation difference by 0.433 psi/ft (0.099 bar/m).

$$120 \text{ ft} \times 0.433 \text{ psi/ft} = 52 \text{ psi} \ (3.62 \text{ bar})$$

Loops and Grids

Hydraulic calculations become more complicated when piping is configured in loops or grids, such that water feeding any given sprinkler or branch line can be supplied through more than one route. A number of computer programs that can quickly complete the repetitive calculations have therefore been developed specifically for fire protection systems, and are being marketed commercially.

Determining the flow split that takes place in the various parts of any loop or grid is accomplished by applying the basic principles of conservation of mass and conservation of energy. For a single loop, it should be recognized that the energy loss across each of the two legs from one end of the system to the other must be equal. Otherwise, a circulation would take place within the loop itself. Also, mass is conserved by the fact that the sum of the two individual flows through the paths is equal to the total flow into (and out of) the loop (Fig. 42.3).

Applying the Hazen-Williams formula to each leg of the loop

$$p_f = L_1 \frac{4.52 Q_1^{1.85}}{C_1^{1.85} d_1^{4.87}} = L_2 \frac{4.52 Q_2^{1.85}}{C_2^{1.85} d_2^{1.85}}$$

Substituting the term FLC for all terms except Q,

$$p_f = \text{FLC}_1 Q_1^{1.85} = \text{FLC}_2 Q_2^{1.85}$$

This simplifies to become

$$\left(\frac{Q_1}{Q_2}\right)^{1.85} = \frac{\text{FLC}_2}{\text{FLC}_1}$$

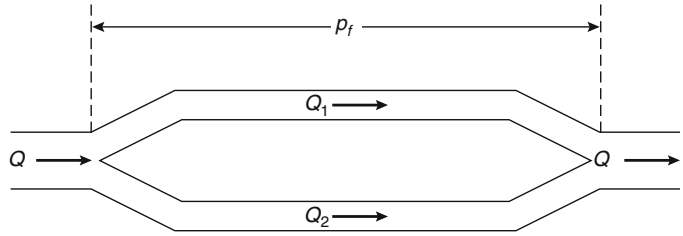

Fig. 42.3 Example of a simple loop configuration

Since Q_1 and Q_2 combine to create a total flow of Q, the flow through one leg can be determined as

$$Q_1 = \frac{Q}{\left[(\mathrm{FLC}_1/\mathrm{FLC}_2)^{0.54} + 1\right]}$$

For the simplest of looped systems, i.e. a single loop, hand calculations are not complex. Furthermore, sometimes a seemingly complex piping system can be simplified by substituting an "equivalent pipe" for two or more pipes in series or in parallel.

For pipes in series

$$\mathrm{FLC}_e = \mathrm{FLC}_1 + \mathrm{FLC}_2 + \mathrm{FLC}_3 + \cdots$$

For pipes in parallel

$$\left(\frac{1}{\mathrm{FLC}_e}\right)^{0.54} = \left(\frac{1}{\mathrm{FLC}_1}\right)^{0.54} + \left(\frac{1}{\mathrm{FLC}_2}\right)^{0.54} + \cdots$$

For gridded systems, which involve flow through multiple loops, computers are generally used since it becomes necessary to solve a system of nonlinear equations. When hand calculations are performed, the Hardy Cross [8] method of balancing heads is generally employed. This method involves assuming a flow distribution within the piping network, then iterating, i.e. applying successive corrective flows until differences in pressure losses through the various routes are nearly equal.

The Hardy Cross solution procedure applied to sprinkler system piping is as follows:

1. Identify all loop circuits and the significant parameters associated with each line of the loop, such as pipe length, diameter, and Hazen-Williams coefficient. Reduce the number of individual pipes where possible by finding the equivalent pipe for pipes in series or parallel.
2. Evaluate each parameter in the proper units. Minor losses through fittings should be converted to equivalent pipe lengths. A value of all parameters except flow for each pipe section should be calculated (FLC).
3. Assume a reasonable distribution of flows that satisfies continuity, proceeding loop by loop.
4. Compute the pressure (or head) loss due to friction, p_f, in each pipe using the FLC in the Hazen-Williams formula.
5. Sum the friction losses around each loop with due regard to flow direction, i.e. assume clockwise flow positive and counter-clockwise flow as negative. Flows are correct when the sum of the losses, dp_f, is as small as desirable, typically 0.5 psi (0.03 bar).
6. If the sum of the losses is not sufficiently small for each loop, divide each pipe's friction loss by the presumed flow for the pipe, p_f/Q.
7. Calculate a correction flow for each loop as

$$dQ = \frac{-dp_f}{\left[1.85 \sum \left(p_f/Q\right)\right]}$$

8. Add the correction flow values to each pipe in the loop as required, thereby increasing or decreasing the earlier assumed flows. For cases where a single pipe is in two loops, the algebraic difference between the two values of dQ must be applied as the correction to the assumed flow.
9. With a new set of assumed flows, repeat steps 4–7 until the values of dp_f are sufficiently small.

10. As a final check, calculate the pressure loss by any route from the initial to the final junction. A second calculation along another route should give the same value of pressure loss within the range of accuracy expected, again typically 0.5 psi (0.03 bar).

Design standards typically require that pressures be shown to balance within 0.5 psi (0.03 bar) at hydraulic junction points. The designer, with or without the use of a computer program, must continue to make successive guesses as to how much flow takes place in each section of pipe until the pressure loss from the design area back to the source of supply is approximately the same (within 0.5 psi [0.03 bar]) regardless of the path chosen.

Example 10 For the small two-loop grid shown in Fig. 42.4, the total flow in and out is 100 gpm (378.5 L/min). It is necessary to determine the flow taking place through each pipe section. The system has already been simplified by finding the equivalent pipe for all pipes in series and in parallel. The following values of FLC have been calculated:

$$\begin{aligned} &Pipe\ 1\ FLC = 0.001 \\ &Pipe\ 2\ FLC = 0.002 \\ &Pipe\ 3\ FLC = 0.003 \\ &Pipe\ 4\ FLC = 0.001 \\ &Pipe\ 5\ FLC = 0.004 \end{aligned}$$

Recall that FLC pertains to the length, internal diameter, and Hazen-Williams C-factor for each pipe segment.

Under step 3 of the Hardy Cross procedure, flows that would satisfy conservation of mass are estimated as shown in Fig. 42.5. Steps 4–9 are then carried out in a tabular approach as shown in Table 42.3.

As the difference between dp_f for loop 1 and loop 2 is greater than 0.5 psi (0.03 bar), at least another iteration is necessary to balance flows. Using the calculated flow estimates from the first iteration, another set of calculations is completed as shown in Table 42.4. Revised flows after the first iteration are shown in Fig. 42.6.

With regard to the flow in pipe #3, which is common to both loops, the first iteration indicates that the estimated flow should be reversed. For loop 1, the flow calculates to −11.4 gpm but was estimated to be +5 gpm.

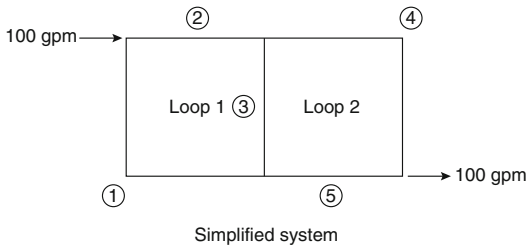

Fig. 42.4 Simplified system, pipe in series

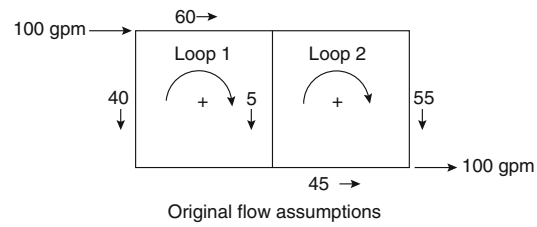

Fig. 42.5 Original flow assumptions

Table 42.3 First iteration

Loop	Pipe	Q	FLC	p_f	dp_f	(p_f/Q)	$dQ = -dp_f/1.85[\Sigma(p_f/Q)]$	$Q + dQ$
1	1	−40	0.001	−0.92		0.023	$dQ = -16.4$	−56.4
	2	60	0.002	3.90		0.065		+43.6
	3	5	0.003	0.06		0.012		−11.4
					=3.04	0.100		
2	3	−5	0.003	−0.06		0.012	$dQ = 11.2$	+6.2
	4	55	0.001	1.66		0.030		+66.2
	5	−45	0.004	−4.58		0.102		+33.8
					$= -2.98$	0.144		

Table 42.4 Second iteration

Loop	Pipe	Q	FLC	p_f	dp_f	(p_f/Q)	$dQ = -dp_f/1.85[\Sigma(p_f/Q)]$	$Q + dQ$
1	1	−56.4	0.001	−1.74		0.031		−54.0
	2	43.6	0.002	2.16		0.050		+46.0
	3	−22.6	0.003	−0.96		0.042	$dQ = 2.4$	−20.2
					$= -0.54$	0.123		
2	3	22.6	0.003	0.96		0.042		+20.5
	4	66.2	0.001	2.34		0.035		+64.1
	5	−33.8	0.004	−2.69		0.080		+35.9
					=0.61	0.157	$dQ = -2.1$	

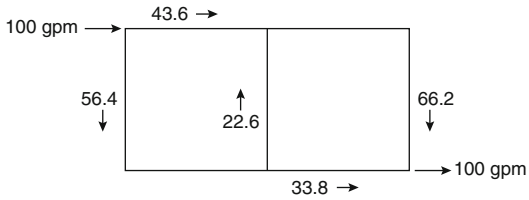

Fig. 42.6 Corrected flows after first iteration

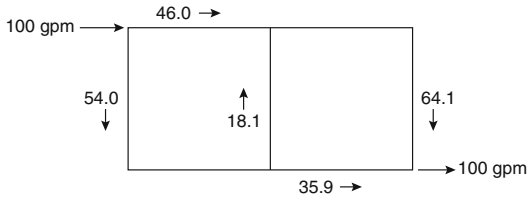

Fig. 42.7 Corrected flows after second iteration

For loop 2, the flow calculates +6.2 gpm but was estimated to be −5 gpm. As indicated in step 8, where a pipe segment is common to another loop, the algebraic difference between the two values of dQ is to be applied as the correction to the assumed flow. In other words, the flow correction for the common pipe is the net effect of the corrections for both loops. For pipe #3, the algebraic difference in dQ for loops 1 and 2 is 27.6 gpm (16.4 gpm + 11.2 gpm). This results is a corrected flow for pipe #3 of 5–27.6 = −22.6 gpm for loop 1 and +22.6 for loop 2.

After completion of the second iteration, the difference in dp_f between loops 1 and 2 is still too large, so a third iteration is needed. The flows after the second iteration are shown in Fig. 42.7. The third iteration calculations, as shown in Table 42.5, indicate that the In starting the pressure losses around both loops are balanced within 0.5 psi. Therefore, the flow split assumed after two iterations can be accepted. As a final check, step 10 of the above procedure calls for a calculation of the total pressure loss through two different routes, requiring that they balance within 0.5 psi (0.03 bar):

Water flow route through pipes 1 and 5:

$$\begin{aligned} &\mathrm{FLC}_1\,(Q_1)^{1.85} + \mathrm{FLC}_2(Q_2)^{1.85} \\ &= 0.001(54.0)^{1.85} + 0.004(35.9)^{1.85} \\ &= 1.6 + 3.0 = 4.6 \text{ psi } (0.32 \text{ bar}) \end{aligned}$$

Water flow route through pipes 2 and 4:

$$\begin{aligned} 0.002(46.0)^{1.85} + 0.001(64.1)^{1.85} &= 2.4 + 2.2 \\ = 4.6 \text{ psi } (0.32 \text{ bar}) & \end{aligned}$$

This is acceptable. Note that this example required less than three full iterations to achieve a successful solution, i.e. correctly balanced flow, despite the fact that the initial flow assumption called for reverse flow in pipe #3. The initial assumption was for a clockwise flow of 5 gpm (18.9 L/min) in pipe 3, but the final solution shows a counterclockwise flow of 18.1 gpm (68.5 L/min).

Water Supply Calculations

Determination of Available Supply Curve

Depending upon the location of the sprinkler system, public or private water main networks might be available to serve as the water supply

Table 42.5 Third iteration

Loop	Pipe	Q	FLC	p_f	dp_f	(p_f/Q)	$dQ = -dp_f/1.85\left[\Sigma\left(p_f/Q\right)\right]$	$Q + dQ$
1	1	−54.0	0.001	−1.60				
	2	46.0	0.002	2.38				
	3	−18.1	0.003	−0.64				
					=0.14			
2	3	18.1	0.003	0.64				
	4	64.1	0.001	2.20				
	5	−35.9	0.004	−3.01				
					= −0.17			

for the system. For instance, the municipal underground water mains of many large cities in North America are permitted to be used for fire protection purposes.

Flow testing of public or private water supply mains permits an evaluation of the strength of the available water supply in terms of both quantity of flow and available pressures. The strength of a water supply is the key to whether it will adequately serve a sprinkler system.

Each test of a water supply must provide at least two pieces of information—a static pressure and a residual pressure at a known flow. The static pressure is sometimes referred to as the "no flow" condition, as no water is being discharged from the main in the vicinity of the test. However, it must be recognized that rarely is any public water supply network in a true no flow condition. This condition is intended represent a situation where the fire protection system is not creating an additional flow demand beyond that which is ordinarily placed on the system. The residual pressure reading is taken with an additional flow being taken from the system, preferably a flow that approximates the likely maximum system demand.

Between the two (or more) points, a representation of the water supply (termed a water supply curve) can be made. For the most part, this water supply curve is a fingerprint of the system supply and piping arrangements, since the static pressure tends to represent the effect of elevated tanks and operating pumps in the system, and the drop to the residual pressure represents the friction and minor losses through the piping network that result from the increased flow during the test.

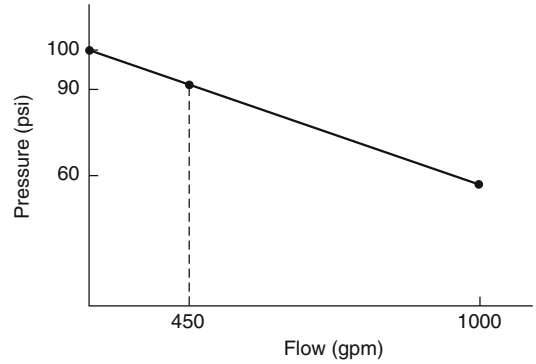

Fig. 42.8 Pressure available from 450 gpm flow water supply

The static pressure is read directly from a gauge attached to a hydrant. The residual pressure is read from the same gauge while a flow reading is taken from another hydrant, preferably downstream. A pitot tube is usually used in combination with observed characteristics of the nozzle through which flow is taken in order to determine the amount of flow.

Figure 42.8 is an example of a plot of water supply information. The static pressure is plotted along the *y*-axis, reflecting a given pressure under zero or no-flow conditions. The residual pressure at the measured flow is also plotted, and a straight line is drawn between these two points. Note that the *x*-axis is not linear, but rather shows flow as a function of the 1.85 power. This corresponds to the exponent for flow in the Hazen-Williams equation. Using this semi-exponential graph paper demonstrates that the residual pressure effect is the result of friction loss through the system, and permits the water supply curve to be plotted as a straight line.

Since the drop in residual pressure is proportional to flow to the 1.85 power, the available pressure at any flow can be read directly from the water supply curve.

For adequate design, the system demand point, including hose stream allowance, should lie below the water supply curve.

Example 11 If a water supply is determined by test to have a static pressure of 100 psi (6.9 bar) and a residual pressure of 80 psi (5.5 bar) at a flow of 1000 gpm (3785 L/min), the pressure available at a flow of 450 gpm (1703 L/min) can be approximated by plotting the two known data points on the hydraulic graph paper as shown in Fig. 42.8. At a flow of 450 gpm (1703 L/min), a pressure of 90 psi (6.2 bar) is indicated.

Pump Selection and Testing

Specific requirements for pumps used in sprinkler systems are normally contained in separate design and installation standards such as NFPA 20.

Fire pumps provide a means of making up for pressure deficiencies where an adequate volume of water is available at a suitable net positive suction pressure. Plumbing codes or municipal water supply regulations sometimes set a minimum allowable net positive suction pressure of 10–20 psi (0.69–1.38 bar) for water taken from public mains. If insufficient water is available at such pressures from such sources, then it becomes necessary to use a stored water supply.

Listed centrifugal fire pumps are available with either diesel or electric drivers, and with capacities ranging from 25 to 5000 gpm (95–18,927 L/min), although fire pumps are most commonly found with capacities ranging from 250 to 2500 gpm (946–9463 L/min) in increments of 250 up to 1500 gpm (946 up to 5678 L/min) and 500 gpm (1893 L/min) increments beyond that point. Each pump is specified with a rated flow and rated pressure. Rated pressures vary extensively, since manufacturers can control this feature with small changes to impeller design.

Pump affinity laws govern the relationship between impeller diameter, D, pump speed, N, flow, Q, pressure head, H, and brake horsepower, bhp. The first set of affinity laws assumes a constant impeller diameter.

$$\frac{Q_1}{Q_2} = \frac{N_1}{N_2} \quad \frac{H_1}{H_2} = \frac{N_1^2}{N_2^2} \quad \frac{\text{bh p}_1}{\text{bh p}_2} = \frac{N_1^3}{N_2^3}$$

These affinity laws are commonly used when correcting the output of a pump to its rated speed, such as during a fire pump acceptance test when the installed pump is not operating precisely at its rated speed.

The second set of the affinity laws assumes constant speed with change in impeller diameter, D.

$$\frac{Q_1}{Q_2} = \frac{D_1}{D_2} \quad \frac{H_1}{H_2} = \frac{D_1^2}{D_2^2} \quad \frac{\text{bh p}_1}{\text{bh p}_2} = \frac{D_1^3}{D_2^3}$$

Pumps are selected to fit the system demands on the basis of three key points relative to their rated flow and rated pressure (Fig. 42.9). Fire pump standards such as NFPA 20 specify that centrifugal fire pumps meet these three points as noted below, and the listing laboratories verify this and establish pump performance curves for each pump.

1. A minimum of 100 % of rated pressure at 100 % of rated flow
2. A minimum of 65 % of rated pressure at 150 % of rated flow (overload)
3. A maximum of 140 % of rated pressure at 0 % of rated flow (churn)

While each fire pump has its individual performance curve, a pump specifier knows the basic performance characteristics of a pump even before the performance curve is available, since it must meet the three points described above. It is usually possible to have more than one option when choosing pumps, since the designer is not limited to using a specific point on the pump performance curve.

There are limits to flexibility in pump selection, however. For example, it is not permitted to install a pump in a situation where it would be expected to operate with a flow exceeding 150 % of rated capacity, since the performance is not a

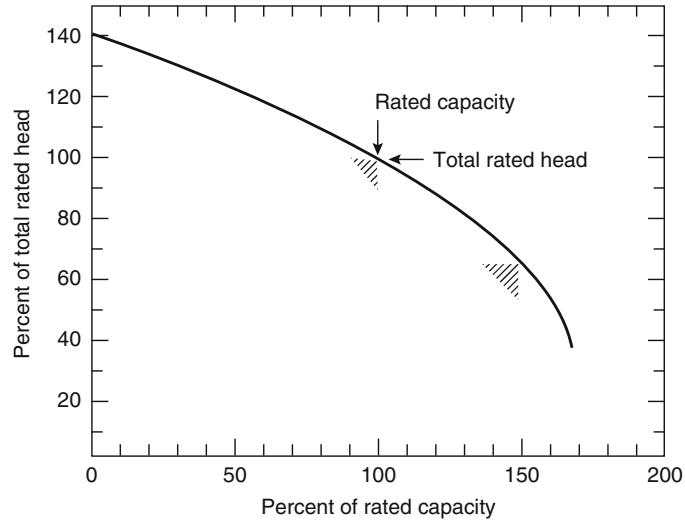

Fig. 42.9 Pump performance curve

known factor, and indeed available pressure is usually quick to drop off beyond this point.

NFPA 20 has traditionally provided guidance on what part of the pump curve to use. A centrifugal fire pump should be selected in the range of operation from 90 % to 150 % of its rated capacity. The performance of the pump when applied at capacities over 140 % of rated capacity may be adversely affected by the suction conditions, but if suction conditions can be properly assured, the pump can operate at any point on its characteristic curve from shutoff to 150 % of its rated capacity.

Application of the pump at capacities less than 90 % of the rated capacity is not recommended.

Where specific pump performance curve is not available, the adequacy of a pump can be determined on the basis of the required performance points. For design capacities below the rated capacity, the rated pressure should be used. For design capacities between 100 % and 150 % of rated capacity, the pressure used should be found by the relationship made apparent by similar triangles.

$$\frac{0.35P}{0.5Q} = \frac{P' - 0.65P}{1.5Q - Q'}$$

where P and Q are the rated pressure and capacity, and P' is the minimum available pressure at capacity, Q', where $Q < Q' < 1.5Q$.

Example 12 A pump is to be selected to meet a demand of 600 gpm (2271 L/min) at 85 psi (5.86 bar). To determine whether a pump rated for 500 gpm (1893 L/min) at 100 psi (6.90 bar) would be able to meet this point without having an actual pump performance curve to work from, the above formula can be applied, with $P = 100$, $Q = 500$, and $Q' = 600$.

Inserting these values gives

$$\frac{(0.35)(100)}{(0.5)(500)} = \frac{\left[P' - (0.65)(100)\right]}{\left[(1.5)(500) - 600\right]}$$

$$\frac{35}{250} = \frac{\left(P' - 65\right)}{(750 - 600)}$$

$$P' = 65 + 21 = 86 \text{ psi } (5.93 \text{ bar})$$

Since the value of P' so calculated is greater than the 85 psi (5.86 bar) required, the pump will be able to meet the demand point.

Tank Sizing

Tank selection and sizing are relatively straightforward compared to fire pump selection. The most basic question is whether to use a standalone elevated storage (gravity) tank, or a pressure tank, or a suction tank in combination with a fire pump. Standards such as NFPA 22 describe the types of tanks in terms of suitable

construction materials, and provide design and installation requirements.

From a calculation standpoint, tanks must be sized to provide the minimum durations specified by NFPA 13 or other applicable standards for the system design. Required pressures must still be available when the tanks are nearly depleted of their water supplies. Durations are based on consideration of the full hydraulic demand (i.e., all sprinklers flowing in the design area). This is a conservative assumption for an automatic sprinkler system, due to the fact that the design area itself is considered to include some conservatism, with the additional understanding that sprinkler operations take place incrementally. Because of this conservatism, it is not necessary that the duration also be provided for a hydraulically less demanding design area, which would be a design area closer to the tank. Minimum durations are generally based on hazard classification, with shorter minimum durations allowed for systems with remote alarm service to a constantly attended location.

If the tank is intended to provide the needed supply without the use of a fire pump, the energy, i.e. pressure for the sprinkler system must be available due to the height of the bottom of a gravity tank or the air pressure held within a pressure tank.

An important factor in gravity tank calculations is the requirement that the pressure available from elevation (calculated using 0.433 psi per foot [0.099 bar/m]) must be determined using the lowest expected level of water in the tank. This is normally the point at which the tank would be considered empty.

In sizing pressure tanks, the percentage of air in the tanks must be controlled so as to ensure that the last remaining quantity of water leaving the tank will be flowing at an adequate pressure. While a common rule of thumb has been that one-third of the tank's volume consist of air at a minimum pressure of 75 psi (5.17 bar), this rule does not hold true for systems with high pressure demands or where the tank is located a considerable distance below the level of the highest sprinkler.

For pipe schedule systems, two formulas have traditionally been used, based on whether the tank is located above the level of the highest sprinkler or some distance below.

For the tank above the highest sprinkler

$$P = \frac{30}{A} - 15$$

For the tank below the highest sprinkler

$$P = \left(\frac{30}{A} - 15\right) + \left(\frac{0.434H}{A}\right)$$

where

A = Proportion of air in the tank
P = Air pressure carried in the tank in psi
H = Height of the highest sprinkler above the tank bottom in ft

It can be seen that these formulas are based simply on the need to provide a minimum pressure of 15 psi (1.03 bar) to the system at the level of the highest sprinkler, and an assumption of 15 psi (1.03 bar) atmospheric pressure.

Using the same approximation for atmospheric pressure, a more generalized formula has come into use for hydraulically designed systems:

$$P_i = \frac{P_f + 15}{A} - 15$$

where

P_i = Tank air pressure to be used
P_f = System pressure required per hydraulic calculations
A = Proportion of air in the tank

Example 13 A pressure tank is to be used to provide a 30 min water supply to a system with a hydraulically calculated demand of 140 gpm (530 L/min) at a pressure of 118 psi (8.14 bar). Due to nearby component pressure ratings, it is important that air pressure in the tank not exceed 175 psi (12.0 bar). To determine the minimum size tank that can be used, it is important not only to consider the total amount of water needed, but also the amount of air necessary to keep the pressures within the stated limits of 118 and 175 psi.

The above equation for hydraulically designed systems can be used to solve for A.

$$P_i = \left[\frac{(P_f + 15)}{A}\right] - 15$$

If

$$A = \frac{(P_f + 15)}{(P_i + 15)}$$
$$A = \frac{(118 + 15)}{(175 + 15)} = \frac{133}{190} = 0.70$$

then

This means that the tank will need to be 70 % air if the air pressure in the tank is to be kept to 175 psi (12.0 bar).

The minimum water supply required is 30 min $\times$ 140 gpm = 4200 gal (15,898 L).

Thus, the minimum tank volume will be such that 4200 gal (15,898 L) can be held in the remaining 30 % of volume.

$$0.3V = 4,200 \text{ gal}$$
$$V = \frac{4,200}{0.3} = 14,000 \text{ gal tank } (53,000\,\text{L})$$

Hanging and Bracing Methods

Hangers and Hanger Supports

Sprinkler design standards such as NFPA 13 contain a great deal of specific guidance relative to hanger spacing and sizing based on pipe sizes. It should be recognized that performance-based approaches are also often permitted. Different criteria can exist for individual hangers and their connection to the supporting building structure. For example, NFPA 13 considers any hanger and installation method is acceptable if certified by a registered professional engineer to meet the following criteria:

1. Hangers are capable of supporting five times the weight of the water-filled pipe plus 250 lb (114 kg) at each point of piping support.
2. Points of support are sufficient to support the sprinkler system.
3. Spacing between hangers does not exceed the limits within the standard for the various types of piping materials.
4. Ferrous materials are used for hanger components.
5. Detailed calculations are submitted when required by the reviewing authority.

The building structure itself must be capable of supporting the weight of the water-filled pipe plus 250 lbs (114 kg) applied at the point of hanging. The 250 lb (114 kg) weight is intended to represent the extra loading that would occur if a relatively heavy individual were to hang on the piping.

Trapeze Hangers

Trapeze hangers are used where structural members are not located, so as to provide direct support of sprinkler lines or mains. This can occur when sprinkler lines or mains run parallel to structural members such as joists or trusses.

Because they are considered part of the support structure, the criteria within NFPA 13 call for the hangers to support the weight of 15 ft (5 m) of water-filled pipe plus 250 lbs (114 kg) applied at the point of hanging. An allowable bending stress of 15 ksi (103 MPa) is used for steel members. Two tables are provided in the standard, one of which presents required section moduli based on the span of the trapeze and the size and type of pipe to be supported, and the other of which presents the available section moduli of standard pipes and angles typically used as trapeze hangers.

In using the tables, the standard allows the effective span of the trapeze hanger to be reduced if the load is not at the midpoint of the span. The equivalent length of trapeze is determined from the formula

$$L = \frac{4ab}{(a + b)}$$

where L is the equivalent length, a is the distance from one support to the load, and b is the distance from the other support to the load.

Example 14 A trapeze hanger is required for a main running parallel to two beams spaced 10 ft (3.048 m) apart. If the main is located 1 ft 6 in. (0.457 m) from one of the beams, the equivalent span of trapeze hanger required can be determined by using the formula

$$L = \frac{4(1.5\,\text{ft})\,(8.5\,\text{ft})}{(1.5\,\text{ft} + 8.5\,\text{ft})} = 5.1\ \ \text{ft}(1.554\,\text{m})$$

Earthquake Braces

Protection for sprinkler systems in earthquake areas is provided in several ways. Flexibility and clearances are added to the system where necessary to avoid the development of stresses that could rupture the piping. Too much flexibility could also be dangerous, however, since the momentum of the unrestrained piping during shaking could result in breakage of the piping under its own weight or on collision with other building components. Therefore, lateral and longitudinal bracing is required for all mains and lateral bracing is required for branch lines exceeding 2 in. (50 mm) in diameter. Smaller branch lines are required to be restrained against movement, which involves a less rigorous means of holding the piping in place.

Calculating loads for earthquake braces is based on the assumption that the normal hangers provided to the system are generally capable of handling vertical forces. However, the upward vertical component of strong horizontal forces must be addressed where braces are insufficiently angled from the horizontal. Traditionally, horizontal forces were conservatively approximated by a constant acceleration equal to one-half that of gravity.

$$a_h = 0.5g$$

Due to advances in earthquake engineering, more specific mapping of expected earthquake accelerations is now available. Current codes call for the design of mechanical building systems to be based on maximum short-period (0.2 s) accelerations expected for the 500 year earthquake. NFPA 13 (2013) contains a seismic coefficient table that allows a simplified method by which these accelerations can be converted to the horizontal seismic load for braces using the formula

$$F_{pw} = C_p W_p$$

where F_{pw} is the force acting on the brace, C_p is the seismic coefficient selected in the table on the basis of short period response, and W_p is 1.15 times the weight of water-filled piping supported by the brace.

Table 42.6 contains some of the NFPA 13 seismic coefficients based on short period accelerations, where the horizontal accelerations S_s are expressed relative to gravity. The seismic coefficients are based on the assumption of fairly soft soil and other conservative assumptions.

Since the braces can be called on to act in both tension and compression, it is necessary not only to size the brace member to handle the expected force applied by the weight of the pipe in its zone of influence, but also to avoid a member that could fail as a long column under buckling.

The ability of the brace to resist buckling is determined through an application of Euler's formula. Tables provide loads based on maximum slenderness ratios of 100, 200, and 300. The 300 value corresponds to the maximum slenderness ratio generally used under steel construction codes for secondary framing members. This is expressed as

Table 42.6 Seismic coefficient table

Ss	*Cp*
0.33 or less	0.35
0.50	0.40
0.75	0.42
0.95	0.50
1.00	0.51
1.25	0.58
1.50	0.70
2.00	0.93
2.40	1.12
3.00	1.40

Source: NFPA 13, Table 9.3.5.9.3 (2013)

$$\frac{\ell}{r} \leq 300$$

where ℓ is the length of the brace and r is the least radius of gyration for the brace.

The least radius of gyration for some common shapes is as follows:
pipe

$$r = \frac{\left(r_0^2 + r_i^2\right)^{1/2}}{2}$$

rod

$$r = \frac{r}{2}$$

flat

$$r = 0.29h$$

Special care must be taken in the design of earthquake braces so that the load applied to any brace does not exceed the capability of the fasteners of that brace to the piping system or the building structure, and that the braces are attached only to structural members capable of supporting the expected loads.

Performance Calculations

Sprinkler Response as a Detector

Automatic sprinklers serve a dual function as both heat detectors and water distribution devices. As such, the response of sprinklers can be estimated using the same methods as for response of heat detectors (see Chap. 40). Care should be taken, however, that these calculations are used within their limitations. Factors pertaining to sprinkler orientation, air flow deflection, radiation effects, heat of fusion of solder links, and convection within glass bulbs are all considered to introduce minor errors into the calculation process. Heat conduction to the sprinkler frame and distance of the sensing mechanism below the ceiling have been demonstrated to be significant factors affecting response, but are ignored in some computer models. Efforts have been made to quantify the prediction capability of the models, including DETACT-QS and the more recent Fire Dynamics Simulator (FDS) [9].

Modeling of sprinkler response can be useful, particularly when used on a comparative basis. Beginning with the 1991 edition, an exception within NFPA 13 permitted variations from the rules on clearance between sprinklers and ceilings "...provided the use of tests or calculations demonstrate comparable sensitivity and performance."

Example 15 Nonmetallic piping extending 15 in. (0.38 m) below the concrete ceiling of a 10-ft (3.048 m) high basement 100 ft by 100 ft (30.48 × 30.48 m) in size makes it difficult to place standard upright sprinklers within the 12 in. (0.30 m) required by NFPA 13 for unobstructed construction. Using the LAVENT [10] computer model, and assuming RTI values of 400 $ft^{1/2} \times s^{1/2}$ (221 $m^{1/2} \times s^{1/2}$) for standard sprinklers and 100 $ft^{1/2} \times s^{1/2}$ (55 $m^{1/2} \times s^{1/2}$) for quick-response sprinklers, it can be demonstrated that the comparable level of sensitivity can be maintained at a distance of 18 in. (0.457 m) below the ceiling. Temperature rating is assumed to be 165 °F, and maximum lateral distance to a sprinkler is 8.2 ft (2.50 m) (10 ft × 13 ft [3.048 m × 3.962 m] spacing). Assuming the default fire (empty wood pallets stored 5 ft [1.52 m] high), for example, the time of actuation for the standard sprinkler is calculated to be 200 s, as compared to 172 s for the quick-response sprinkler. Since the noncombustible construction minimizes concern relative to the fire control performance for the structure, the sprinklers can be located below the piping obstructions.

Dry System Water Delivery Time

Total water delivery time consists of two parts. The first part is the trip time taken for the system air pressure to bleed down to the point where the system dry valve opens to admit water to the piping. The second part is the transit time for

the water to flow through the piping from the dry valve to the open sprinkler. In other words

$$\text{Water delivery time} = \text{Trip time} + \text{Transit time}$$

where water delivery time commences with the opening of the first sprinkler.

Sprinkler standards such as NFPA 13 have traditionally not contained a maximum water delivery time requirement if system volume is limited, generally to no more than 750 gal (2839 L). Larger systems were permitted only if water flow from a remote inspector's test connection took place within 60 s. As such, the rule of thumb for dry system operation is that no more than a 60-s water delivery time should be tolerated, and that systems should be divided into smaller systems if necessary to achieve this 1-min response. Beginning with the 2007 edition of NFPA 13, the 60-s water delivery time was mandated for dry pipe systems protecting dwelling unit portions of any building. Dry system response is simulated in field testing by the opening of an inspector's test connection. The inspector's test connection is required to be at the most remote point of the system from the dry valve, and is required to have an orifice opening of a size simulating the smallest orifice sprinkler installed on the system.

The water delivery time of the system is recorded as part of the dry pipe valve trip test that is conducted using the inspector's test connection. However, it is not a realistic indication of actual water delivery time for two reasons:

1. The first sprinkler to open on the system is likely to be closer to the system dry valve, reducing water transit time.
2. If additional sprinklers open, the trip time will be reduced since additional orifices are able to expel air. Water transit time may also be reduced since it is easier to expel the air ahead of the incoming water.

FM Global researchers have shown [11] that it is possible to calculate system trip time using the relation

$$t = 0.0352 \frac{V_T}{A_n T_0^{1/2}} \ln\left(\frac{p_{a0}}{p_a}\right)$$

where

t = Time (s)
V_T = Dry volume of sprinkler system (ft^3)
T_0 = Air temperature (°R)
A_n = Flow area of open sprinklers (ft^2)
p_{a0} = Initial air pressure (absolute)
p_a = Trip pressure (absolute)

Calculating water transit time is more difficult, but may be accomplished using mathematical models. FM Global researchers developed the first such model in the 1970s. In 2003 a dry system water delivery model was introduced to the commercial marketplace [12], following the incorporation of acceptance criteria into the 2002 edition of NFPA 13. A literature review conducted in 2007, intended to develop data to assist in the evaluation of the traditional 60-s water delivery requirement of NFPA 13, observed that "the water delivery time limit of 60 s has some, but not overwhelming data to support requiring or not requiring a time limitation for small systems" [13].

Droplet Size, Penetration and Motion

For geometrically similar sprinklers, the median droplet diameter in the sprinkler spray has been found to be inversely proportional to the $^1/_3$ power of water pressure and directly proportional to the $^2/_3$ power of sprinkler orifice diameter such that

$$d_m \propto \frac{D^{2/3}}{p^{1/3}} \propto \frac{D^2}{Q^{2/3}}$$

where

d_m = Mean droplet diameter
D = Orifice diameter
P = Pressure
Q = Rate of water flow

The relationship of droplet size production to pressure and orifice diameter has been confirmed using high-magnification shadow imaging [14].

A sprinkler "penetration ratio" has likewise been observed to be proportional to the median droplet diameter, which is needed for fire plume penetration when the sprinkler spray is in the

gravity mode [15]. However, fire plumes can also be penetrated by water sprays using a momentum mode. Fire plume penetration is considered essential to the early suppression of the fire by automatic sprinklers, as compared to fire control, in which the spread of the fire is stopped and the impact mitigated.

Total droplet surface area has been found to be proportional to the total water discharge rate divided by the median droplet diameter

$$A_s \propto \frac{Q}{d_m}$$

where A_s is the total droplet surface area.

Combining these relationships, it can be seen that

$$A_s \propto \left(Q^3 pD^{-2}\right)^{1/3}$$

When a droplet with an initial velocity vector of **U** is driven into a rising fire plume, the one-dimensional representation of its motion has been represented as [16]

$$\frac{m_1 d\mathrm{U}}{dt} = m_1 g - \frac{C_D \rho_g (\mathrm{U} + V)^2}{2S_f}$$

where

U = Velocity of the water droplet
V = Velocity of the fire plume
m = Mass of the droplet
ρ_g = Density of the gas
g = Acceleration of gravity
C_D = Coefficient of drag
S_f = Frontal surface area of the droplet

The first term on the right side of the equation represents the force of gravity, while the second term represents the force of drag caused by gas resistance. The drag coefficient for particle motion has been found empirically to be a function of the Reynolds number (Re) as [17]

$$C_D = 18.5\,\mathrm{Re}^{-0.6} \text{ for } \mathrm{Re} < 600$$
$$C_D = 0.44 \text{ for } \mathrm{Re} > 600$$

Mathematical modeling comparing the drag force of a sprinkler spray to the buoyancy of a smoke layer in the vicinity of sprinklers, validated by full scale experiments, has been used recently to address the long-standing question of the value of automatic smoke vents in sprinklered buildings. The modeling indicated that increases in sprinkler operating pressure eventually lead to ineffective smoke venting, and that the area of smoke venting has very little influence on smoke flow once sprinkler operation causes a loss in smoke flow efficiency [18].

Spray Density and Cooling

The heat absorption rate of a sprinkler spray is expected to depend on the total surface area of the water droplets, A_s, and the temperature of the ceiling gas layer in excess of the droplet temperature, T. With water temperature close to ambient temperature, T can be considered excess gas temperature above ambient.

Chow [19] has developed a model for estimating the evaporation heat loss due to a sprinkler water spray in a smoke layer. Sample calculations indicate that evaporation heat loss is only significant for droplet diameters less than 0.5 mm. For the droplet velocities and smoke layer depths analyzed, it was found that the heat loss to evaporation would be small (10–25 %), compared to the heat loss from convective cooling of the droplets.

FM Global researchers [20] have developed empirical correlations for the heat absorption rate of sprinkler spray in room fires, as well as convective heat loss through the room opening, such that

$$\dot{Q} = \dot{Q}_{\mathrm{cool}} + \dot{Q}_c + \dot{Q}_l$$

where

$\dot{Q}$ = Total heat release rate of the fire
$\dot{Q}_{\mathrm{cool}}$ = Heat absorption rate of the sprinkler spray
$\dot{Q}_c$ = Convective heat loss rate through the room opening
$\dot{Q}_l$ = Sum of the heat loss rate to the walls and ceiling, $\dot{Q}_s$, the heat loss rate to the floor, $\dot{Q}_f$, and the radiative heat loss rate through the opening, $\dot{Q}_r$

Test data indicated that

$$\dot{Q}_{\text{cool}}/\dot{Q} = 0.000039\Lambda^3 - 0.003\Lambda^2 + 0.082\Lambda$$

For

$$0 < \Lambda \leq 33/\left(\text{min} \times \text{kW}^{1/2} \times \text{m}^{5/4}\right)$$

where Λ is a correlation factor incorporating heat losses to the room boundaries and through openings as well as to account for water droplet surface area.

$$\Lambda = \left(AH^{1/2}\dot{Q}_l\right)^{-1/2}\left(W^3PD^{-2}\right)^{1/3}$$

for

$$P = \frac{p}{(17.2\ \text{kPa})} \quad \text{and} \quad D = \frac{d}{0.0111\,\text{m}}$$

where

A = Area of the room opening (m)
H = Height of the room opening (m)
P = Water pressure at the sprinkler (bar)
d = Sprinkler nozzle diameter (m)
W = Water discharge (L/min)

The above correlations apply to room geometry with length-to-width ratio of 1.2–2 and opening size of 1.70–2.97 m^2.

Suppression by Sprinkler Sprays

In 1993, researchers at the National Institute of Standards and Technology (NIST) developed a "zeroth order" model of the effectiveness of sprinklers in reducing the heat release rate of furnishing fires [21]. Based on measurements of wood crib fire suppression with pendant spray sprinklers, the model was described as conservative. The model assumed that all fuels have the same degree of resistance to suppression as a wood crib, despite the fact that tests have shown furnishings with large burning surface areas can be extinguished easily compared to the deep-seated fires encountered with wood cribs.

The recommended equation, which relates to fire suppression for a 610-mm-high crib, has also been checked for validity with 305 mm crib results. The equation is

$$\dot{Q}(t - t_{\text{act}}) = \dot{Q}(t_{\text{act}})\exp\left[\frac{-(t - t_{\text{act}})}{3.0\left(\dot{w}''\right)^{-1.85}}\right]$$

where

$\dot{Q}$ = Heat release rate (kW)
t = Any time following t_{act} of the sprinklers (s)
$\dot{W}''$ = Spray density (mm/s)

The NIST researchers claimed the equation was appropriate for use where the fuel is not shielded from the water spray, and the application density is at least 0.07 mm/s (4.2 mm/min [0.1 gpm/ft^2]). The method does not account for variations in spray densities or suppression capabilities of individual sprinklers.

The model must be used with caution, since it was developed on the basis of fully involved cribs. It does not consider the possibility that the fire could continue to grow in intensity following initial sprinkler discharge, and, for that reason, should be restricted to use in light hazard applications.

Sprinklers are assumed to operate within a room of a light hazard occupancy when the total heat release rate of the fire is 500 kW. The significance of an initial application rate of 0.3 gpm/ft^2 (0.205 mm/s) as compared to the minimum design density of 0.1 gpm/ft^2 (0.07 mm/s) can be evaluated by the expected fire size after 30 s. With the minimum density of 0.07 mm/s (0.1 gpm/ft^2), the fire size is conservatively estimated as 465 kW after 30 s. With the higher density of 0.205 mm/s (0.3 gpm/ft^2), the fire size is expected to be reduced to 293 kW after 30 s. Corresponding values after 60 s are 432 and 172 kW, respectively.

More recent efforts to model suppression by automatic sprinklers have taken place as part of the NIST's development of the Fire Dynamics Simulator (FDS) computational fluid dynamics model. Within that model, simulating the effects of a sprinkler spray involves predicting activation, computing droplet trajectories, and tracking water as it drips onto the burning fuel. In order to compute droplet trajectories, the initial size and velocity of each droplet must be estimated, a process that is one of the limiting factors in the use of the model for practical applications. As stated earlier, efforts have been under way to

develop atomization models for integration with FDS to better characterize the formation and distribution of droplets from the impact of a water stream on a sprinkler deflector [22, 23]. The effect of droplets on burning surfaces is another area in which additional work is needed. When dealing with liquid droplets hitting a solid surface, the current Version 5 of FDS assigns a random horizontal direction and moves at a fixed velocity on the order of 0.5 m/s until it reaches the edge, at which point it is assumed to drop down at the same velocity. While on the surface, the droplet is assumed to contribute to the formation of a surface film of water that participates in heat transfer. If the surface is burning, assumptions need to be made about the extent to which the water reduces the pyrolysis rate of the fuel. Most of the available correlations are based on fires involving rack storage of standard commodities in corrugated cartons. Work at Factory Mutual [24] has led to the following expression:

$$\dot{Q} = \dot{Q}_o e^{k(t-to)}$$

where $\dot{Q}_o$ is the total heat release at the time of water application t_o and k is a fuel-dependent constant, which in turn is dependent on the rate of water application.

Nomenclature

C	coefficient of friction
FLC	friction loss coefficient
Q	flow (gpm)
$\dot{Q}$	heat release rate (kW)
$\dot{W}''$	spray density (mm/s)
C_p	seismic coefficient
K	fuel-dependent constant

References

1. *NFPA Codes and Standards,* National Fire Protection Association, Quincy, MA (2013).
2. Thomas, R., "Water Conservation and Sustainable Use in Fire Suppression Systems," SUPDET 2009 Suppression & Detection Conference, Fire Protection Research Foundation (2009).
3. Palenske, G. and O'Connor, D., "Single Point Design Criteria vs. Traditional Density-Area Curves," Fire Protection Research Foundation, (2007).
4. Croce, P., Hill, J., and Xin, Y., "An Investigation into the Causative Mechanism of Sprinkler Skipping," *Journal of Fire Protection Engineering*, Vol. 15, No. 2 (2005).
5. Ditch, B., de Ris, J., and Yu, H.Z., "Development and Experimental Evaluation of a Sprinkler Resistant to Skipping," SUPDET Suppression and Detection Conference, Fire Protection Research Foundation (2009).
6. K. McGrattan, S. Hostikka, J. Floyd, H. Baum, and E. Rehm, "Fire Dynamics Simulator (Version 5) Technical Reference Guide," NIST Special Publication 1018–5, National Institute of Standards and Technology, Gaithersburg, MD (2007).
7. A. Marshall, "Unraveling Fire Suppression Sprays," International Association of Fire Safety Science, College Park, MD, (2011).
8. H. Cross, *Analysis of Flow in Networks of Conduits or Conductors,* University of Illinois Engineering Experiment Station, Urbana, IL (1936).
9. M. J. Hurley and A. Munguia, "Analysis of Prediction Capability of FDS for Response of Thermal Detectors," *Journal of Fire Protection Engineering*, Vol. 20, No. 2 (2010)
10. W.D. Davis and L.Y. Cooper, "Estimating the Environment and Response of Sprinkler Links in Compartment Fires with Draft Curtains and Fusible-Link Actuated Ceiling Vents, Part 2: User Guide for the Computer Code LAVENT," *NISTIR/89-4122,* National Institute of Standards and Technology, Gaithersburg, MD (1989).
11. G. Heskested and H. Kung, *FMRC Serial No. 15918,* Factory Mutual Research Corp., Norwood, MA (1973).
12. Golinveaux, J., "Taking the Guesswork out of the Numerous Variables That Impact the Water Delivery Time of Dry-Pipe Sprinkler Systems," *NFPA Journal*, March/April (2004).
13. O'Connor, D., Pennel, G., Cohn, B., Cul, E., Sun, Z., and Gummersail, M., "Review of NFPA 13 Dry System Water Delivery Provisions," Fire Protection Research Foundation, (2007).
14. M. Avila, H. Boham, Z. Magnone, R. Winsten, C. Yueshan, and N. Dembsey, "Droplet Characterization Using Direct Imaging Techniques," SupDet Conference March 8, 2012, Fire Protection Research Foundation, (2012).
15. C. Yao, C., "Overview Of Sprinkler Technology Research," *Fire Safety Science* 5: 93–110.doi:10.3801/IAFSS.FSS.5-93, (1997)
16. C. Yao and A.S. Kalelkar, "Effect of Drop Size on Sprinkler Performance," *Fire Technology,* 6, 4 (1970).
17. C.L. Beyler, "The Interaction of Fire and Sprinklers," *NBS GCR 77–105,* National Bureau of Standards, Washington, DC (1977).

18. K.Y. Li, M. J. Spearpoint, J. Ji, R. Huo, Y.Z. Li and L. H. Hu, "A Mathematical Model of the Drag Component of a Sprinkler Spray Adjacent to Horizontal Smoke Vents," *Journal of Fire Protection Engineering*, Vol. 20, No. 1 (2010)
19. W.K. Chow, "On the Evaporation Effect of a Sprinkler Water Spray," *Fire Technology,* pp. 364–373 (1989).
20. H.Z. You, H.C. Kung, and Z. Han, "Spray Cooling in Room Fires," *NBS GCR 86–515,* National Bureau of Standards, Washington, DC (1986).
21. D.D. Evans, "Sprinkler Fire Suppression Algorithm for HAZARD," *NISTIR 5254,* National Institute of Standards and Technology, Gaithersburg, MD (1993).
22. D. Wu, D. Guillemin, and A.W. Marshall, "A Modeling Basis for Predicting the Initial Sprinkler Spray," *Fire Safety Journal,* 42, pp. 283–294 (2007).
23. Tabaddor, M., Dubriel, D., Troolin, D., and Hart, P., "Complex Spray Pattern Measurements for Fire Sprinkler Modeling," SUPDET Suppression, Detection and Signaling Conference, Fire Protection Research Foundation, (2011).
24. H.Z. Yu, J.L. Lee and H. C. Kung, "Suppression of Rack-Storage Fires by Water," *Fire Safety Science—Proceedings of the Fourth International Symposium,* pp. 901–912, International Association for Fire Safety Science (1994).

Russell P. Fleming is Managing Director of the International Fire Sprinkler Association, Patterson, New York. Mr. Fleming has served as a member of 20 different NFPA technical committees, including 30 years as a member of the Committee on Automatic Sprinklers. He is a past president of SFPE, past chair of the Standards Council and past member of the Board of Directors of NFPA.

Halon Design Calculations

43

Casey C. Grant

Introduction

Fire protection systems using halogenated extinguishing agents provide a classic example of a fire protection technology with a comprehensive evolutionary lifespan. These systems are a relatively recent innovation in fire protection, but, despite this, they already face extinction. As of January 1, 1994, the production of fire protection halons in most countries ceased, based on international treaties.

The phase-out of halon agent production has obviously created significant limitations on the proliferation of this technology. Yet despite this phase-out numerous systems still exist today based on agent reserves. Although global production of fire protection halons essentially ceased on January 1, 1994, this technology continues to linger. Accordingly, a need remains to address the modification and maintenance of existing systems, and new essential systems that will use recycled surplus stock of halon.

The stratospheric ozone layer depletion issue is a problem confronting the global community unlike any other. Late in 1987, the United States and 24 other countries (including the European Economic Community) signed the Montreal Protocol to protect stratospheric ozone [1]. Originally, the protocol restricted the consumption of ozone-depleting chlorofluorocarbons (CFCs) to 50% of the 1986 use levels by 1998, and halon production was to be frozen in 1993 at 1986 production levels. But the November 1992 Copenhagen revision to the Montréal Protocol accelerated this, such that all production of the chemicals ceased worldwide as of January 1, 1994.

The Montreal Protocol is based on unprecedented trade restrictions and is the first time nations of the world have joined forces to address an environmental threat in advance of fully established effects. The trade restrictions concern nations not participating in the agreement (the nonsignatories). Within 1 year of the agreement taking effect, each party shall ban the import of the bulk chemicals from the nonsignatory nations. About 4 years after the effective date of the agreement, imports of products containing the identified chemicals from nonsignatory nations are banned. Within 5 years, products made with the chemicals (but not containing them) are banned or restricted. This is truly significant since many products, including many electronic components, are currently manufactured using some of these chemicals.

Characteristics of Halon

Background, Definition, and Classifications of Halon Compounds

Although there are a variety of methods available for applying halogenated agents, the most common is the total flooding system. The most

C.C. Grant (✉)
Executive Director of the Fire Protection Research Foundation

M.J. Hurley (ed.), *SFPE Handbook of Fire Protection Engineering*,
DOI 10.1007/978-1-4939-2565-0_43, © Society of Fire Protection Engineers 2016

popular halogenated agent is Halon 1301, with its superior fire extinguishing characteristics and low toxicity.

Halogenated extinguishing agents are hydrocarbons in which one or more hydrogen atoms have been replaced by atoms from the halogen series: fluorine, chlorine, bromine, or iodine. This substitution confers flame extinguishing properties to many of the resulting compounds that made them ideal for certain fire protection applications.

The halogenated extinguishing agents are currently known simply as halons, and are described by a nomenclature that indicates the chemical composition of the materials without the use of chemical names. This simplified system was proposed by James Malcolm at the U.S. Army Corps of Engineers Laboratory in 1950 and avoids the use of possibly confusing names [2]. The United Kingdom and parts of Europe have been known to use the initial capital "alphabet" system, that is, bromotrifluoromethane (Halon 1301) is BTM and bromochlorodifluoromethane (Halon 1211) is BCF. The number definition for the chemical composition of Halon 1301, perhaps the most widely recognized halogenated extinguishing agent, is 1 (carbon), 3 (fluorine), 0 (chlorine), 1 (bromine), and 0 (iodine).

By definition, the first digit of the number represents the number of carbon atoms in the compound molecule; the second digit, the number of fluorine atoms; the third digit, the number of chlorine atoms; the fourth digit, the number of bromine atoms; and the fifth digit, if any, the number of iodine atoms. Trailing zeros in this system are not expressed. Figure 43.1 graphically demonstrates this concept by illustrating Halon 1301 in comparison to methane.

There are three halogen elements commonly found in halon extinguishing agents used for fire protection: fluorine (F), chlorine (Cl), and bromine (Br). Compounds containing combinations of fluorine, chlorine, and bromine can possess varying degrees of extinguishing effectiveness, chemical and thermal stability, toxicity, and volatility. In general, the relevant properties of these three halogen elements are characterized as shown in Table 43.1.

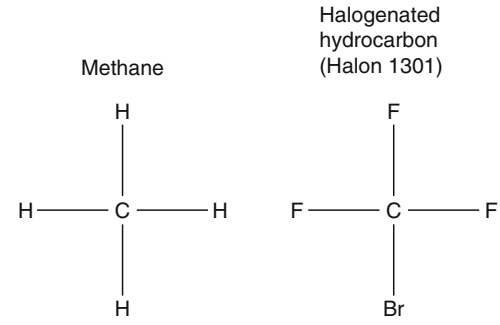

Fig. 43.1 Molecular composition of methane and Halon 1301

Table 43.1 Contributing characteristics of fluorine, chlorine, and bromine

	Fluorine	Chlorine	Bromine
Stability to compound	Enhances	—	—
Toxicity	Reduces	Enhances	Enhances
Boiling point	Reduces	Enhances	Enhances
Thermal stability	Enhances	Reduces	Reduces
Fire extinguishing Effectiveness	—	Enhances	Enhances

Due to the many chemical combinations available, the characteristics of halogenated fire extinguishing agents differ widely. It is generally agreed that the agents most widely used for fire protection applications are Halon 1301, Halon 1211, Halon 1011, and Halon 2402. Also somewhat common is Halon 122, which has been used as a test gas because of its economic advantages. However, because of its widespread use as a test agent, many individuals have wrongly assumed that Halon 122 is an effective fire extinguishing agent. Table 43.2 illustrates the halogenated hydrocarbons most likely to be used today.

History

The earliest halogenated fire extinguishing agent known to be used for industrialized fire protection was carbon tetrachloride (Halon 104) [3]. First becoming available as early as 1907, it was most widely used in handpump portable extinguishers and was popular due to its low electrical conductivity and lack of residue

following application. Also referred to as "pyrene" extinguisher fluid, Halon 104 caused a number of accidental deaths and serious injuries due to its toxicity, and eventually its use was halted during the 1950s.

Methyl bromide (Halon 1001) gained popularity after it was discovered in the late 1920s to be a more effective extinguishing agent than carbon tetrachloride. Due to its high toxicity, it was never used in portable extinguishers even though it was used extensively in British and German aircraft and ships during World War II. Interestingly, methyl bromide possesses a narrow flammability range between 13.5 % and 14.5 % in air, though above and below this range it is an efficient fire extinguishant. Germany developed bromochloromethane (Halon 1011) in the late 1930s to replace methyl bromide, but it failed to enjoy widespread use until after World War II [4].

Table 43.2 Halons commonly used for fire protection

Chemical name	Formula	Halon number
Methyl bromide	CH3Br	1001
Methyl iodide	CH3I	10001
Bromochloromethane	CH2BrCl	1011
Dibromodifluoromethane	CF2Br2	1202
Bromochlorodifluoromethane	CF2BrCl	1211
Dichlorodifluoromethane*	CF2Cl2	122
Bromotrifluoromethane	CF3Br	1301
Carbon tetrachloride	CCl4	104
Dibromotetrafluoroethane	C2F4Br2	2402

*A previously popular test gas without substantial fire extinguishing properties

Thus, prior to World War II, three halogenated fire extinguishing agents were available: Halon 104, Halon 1001, and Halon 1011. Yet because of their inherently high toxic nature, these agents slowly disappeared from typical system applications. By the mid-1960s Halon 104 and Halon 1001 were no longer being used, and Halon 1011 was only in limited use for specialized explosion suppression applications. Figure 43.2 represents a chronology chart that indicates the usage of these early halons as well as the halons more commonly used today.

Joint research was undertaken in 1947 by the U.S. Army Chemical Center and the Purdue Research Foundation to evaluate the fire suppression effectiveness and toxicity of the large number of available agents [2]. After testing more than 60 new agents, 4 were selected for further study: dibromodifluoromethane (Halon 1202), bromochlorodifluoromethane (Halon 1211), bromotrifluoromethane (Halon 1301), and dibromotetrafluoromethane (Halon 2402). Further testing revealed that Halon 1202 was the most effective yet also most toxic, while Halon 1301 was the second most effective and least toxic. As a result of this testing, the use of halon to provide fire protection for modern technology took on new dimensions. Halon 1202 was used by the U.S. Air Force for military aircraft engine protection while the Federal Aviation Administration (FAA) selected Halon 1301 for a similar application in commercial aircraft engine nacelles [5]. Portable extinguishers using Halon 1301 were implemented by the U.S. Army. The use of total flooding systems

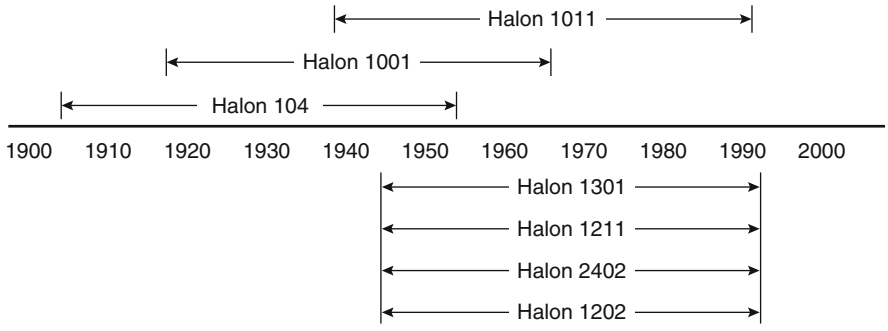

Fig. 43.2 Time span usage of selected halons

originated in 1963, and in the following 5 years several total flooding systems were installed based on carbon dioxide system technology.

In 1966, attention began to focus on the use of Halon 1301 for the protection of electronic data processing equipment. That year, the NFPA organized a Technical Committee (NFPA 12A) to standardize the design, installation, maintenance, and use of halon systems. Their resulting work was officially adopted by the NFPA membership as a standard in 1968 [6]. Subsequent recognition that there were differences among the halon agents made it apparent that separate standards would be necessary. The initial halon standard, NFPA 12A, *Standard for Halon 1301 Fire Extinguishing Systems* (hereinafter referred to as NFPA 12A), focused on the use of Halon 1301 due to its high desirability and growing popularity [7]. Work on an additional standard, NFPA 12B, *Standard on Halon 1211 Fire Extinguishing Systems,* concerning the use of Halon 1211, was started in 1969 and was officially adopted by the NFPA as a standard in 1972 [8]. A tentative standard on the use of Halon 2402 (NFPA 12CT) was developed, but was never officially adopted [9].

Another NFPA committee directly concerned with the use of halon is the NFPA Committee on Electronic Computer/Data Processing Equipment (NFPA 75, *Standard for the Protection of Information Technology Equipment*) [10]. Even though this standard was adopted in 1961, the use of halon was not considered until after 1972, when extensive testing by several major companies demonstrated that the use of Halon 1301 was suitable for protecting electronic computer and data processing equipment [11]. Halon 1301 eventually became the most widely used extinguishing agent for this purpose in the United States and throughout much of the world. However, certain areas of Europe have preferred Halon 1211 and 2402.

In anticipation of the worldwide production phase-out of fire protection halons, which eventually settled at January 1, 1994, a new committee was established during 1992 within the NFPA codes- and standards-making system designated as the Technical Committee on Alternative Protection Options to Halon, and later renamed the Technical Committee on Halon Alternative Protection Options. The committee's first document is NFPA 2001, *Standard on Clean Agent Fire Extinguishing Systems,* which addresses the design, installation, maintenance, and operation of total-flooding fire extinguishing systems that use halon replacement agents [12].

Halon 1301

Attributes and Limitations

Of all the halogenated extinguishing agents used in fire protection, Halon 1301 was by a wide margin the most commonly used. The primary use of this agent is for the protection of electrical and electronic equipment, flammable liquids and gases, and surface-burning flammable solids such as thermoplastics. Areas normally or frequently occupied, air and ground vehicle engines, and other areas where rapid extinguishment is important or where damage to equipment or materials or cleanup after use must be minimized were also ideally protected by this agent. However, Halon 1301 was not a panacea, and it is appropriate to recognize its limitations as well as its attributes. The benefits of Halon 1301 are: fast chemical suppression, penetrating vapor, clean (no residue), noncorrosive, compact storage volumes, nonconductive, and colorless (no obscuration). There are also limitations to using Halon 1301: it has minimal extinguishing effectiveness on reactive metals and rapid oxidizers, it may have unfavorable side effects on deep-seated Class A fires, the agent is expensive, and it is potentially harmful to the environment. Obviously, the most significant limitation is the detrimental effect that the halons have on the earth's stratospheric ozone layer.

Because Halon 1301 inhibits the chain reaction of the combustion process, it chemically suppresses the fire very quickly, unlike other extinguishing agents that work by removing the fire's heat or displacing oxygen or air in close proximity to the combustion zone. Stored as a liquid under pressure and released at normal room temperature as a vapor, Halon 1301 gets

into blocked and baffled spaces readily and leaves no corrosive or abrasive residue after use. A high liquid density permits compact storage containers, which on a comparative weight basis, makes Halon 1301 approximately 2.5 times more effective as an extinguishing agent than carbon dioxide. Since it is virtually free of electrical conductivity, Halon 1301 is highly suitable for electrical fires. Halon 1301 is a colorless vapor when discharged into a hazard volume, though it sometimes temporarily clouds the volume due to the chilling of any moisture in the air. But of all its attributes, the most attractive is that of people compatibility; unlike other extinguishing agents, Halon 1301 is essentially nontoxic in the concentrations usually required for fire suppression.

There are several types of flammable materials on which Halon 1301 is ineffective and not recommended. Reactive metals such as potassium, Nak eutectic alloy, magnesium, sodium, titanium, and zirconium burn so intensely that they overpower the agent's extinguishing abilities [5]. Included with these are the metal hydrides such as lithium hydride, and petroleum solvents such as butyl-lithium. Autothermal decomposers and fuels that contain their own oxidizing agent will also burn freely in the presence of halon agents. These latter substances, such as gunpowder, rocket propellants, and cellulose nitrate, have an oxidizer physically too close to the fuel, and the agent cannot penetrate the fire zone fast enough. Halon is also not effective in preventing the combustion or reaction of chemicals capable of autothermal decomposition such as hydrazine or organic peroxides. Even though Halon 1301 is effective with certain surface-burning flammable solids such as thermoplastics, deep-seated Class A fires typically require relatively high agent concentrations for long soaking periods. When exposed to deep-seated fires for long periods of time, Halon 1301 may decompose into toxic and corrosive products of decomposition. Therefore, it is important that the agent be dispersed while the fire is small. The expense necessary to purchase, install, and maintain a properly functioning Halon 1301 system for more specific Class A hazards is often not economically justified. Halon 1301 fire suppression systems are usually not associated with everyday commodities, but instead are found in applications pertaining to highly valued risks.

Properties

Physical Properties

On the average, Halon 1301 requires 10% less agent on a gas-volume basis than does Halon 1211 to extinguish any given fuel [2]. However, both agents are approximately 2.5 times more effective on a weight-of-agent basis than carbon dioxide. Halon 1301 is a gas at 70 F (21 C) with a vapor pressure of 199 psig. Although this pressure would adequately expel the material, it decreases rapidly to 56 psig (4 bar) at 0 F (−18 C) and to 17.2 psig (1.2 bar) at −40 F (−40 C). Therefore, it is necessary to increase the container pressure with dry nitrogen either to 360 or 600 psig (25 or 41 bar) at 70 F (21 C), ensuring adequate performance at all temperatures. Figure 43.3 demonstrates the temperature-pressure profile for Halon 1301 and Halon 1301 superpressurized with dry nitrogen.

Halon 1301 is normally stored in a pressure vessel as a liquid before it is released to occupy the hazard volume as a vapor. With a boiling point of −72 C (−58 C), it is approximately 1.5 times more dense than water in its liquid phase and approximately 5 times heavier than air in its vapor phase. Thus, Halon 1301 vapor will typically escape through openings in the low portions of a totally flooded volume. Other physical properties are shown in Table 43.3.

Traditionally, there were three distinct elements assumed for combustion: heat, fuel, and oxygen. Known as the fire triangle, this theory had to be modified as halons became more widely used and better understood. Typical fire extinguishment involves either removing the fuel from the fire, limiting oxygen to the fire (smothering), or removing the heat (quenching). The halons do not extinguish fire in any of these ways, but instead break up the uninhibited chain reaction of the combustion process. The tetrahedron of the fire, as it is called, is shown in Fig. 43.4.

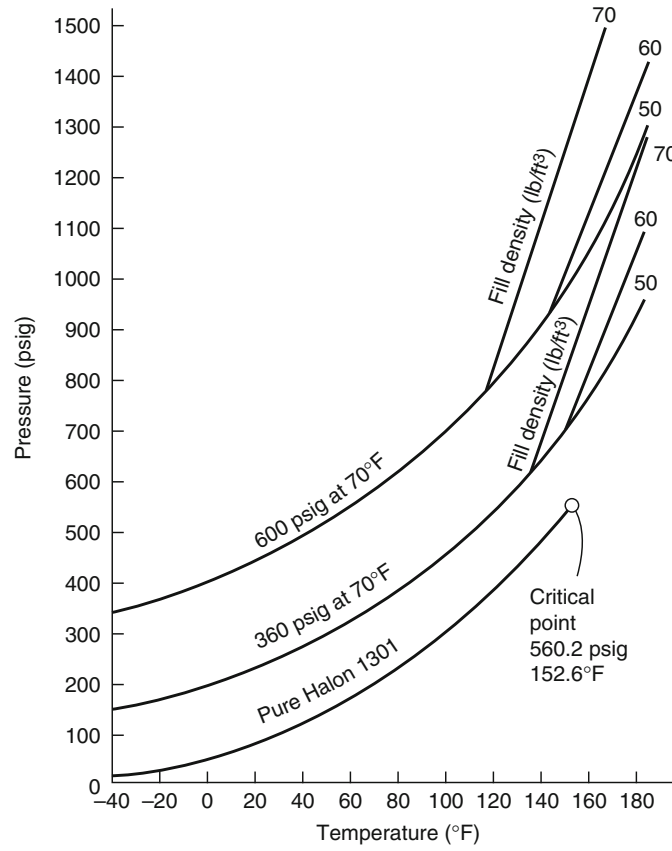

Fig. 43.3 Temperature-pressure relationship for pure Halon

Table 43.3 Selected physical properties of Halon 1301

Boiling point	−72.0 F
Freezing point	−270.4 F
Specific gravity of liquid (@70 F)	1.57
Specific gravity of vapor (@70 F)	5.14
Liquid density @70 F	98.0 lb/ft3
Vapor density @70 F	7.49 lb/ft3 (standard)
Critical temperature	152.6 F
Critical pressure	575 PSIA

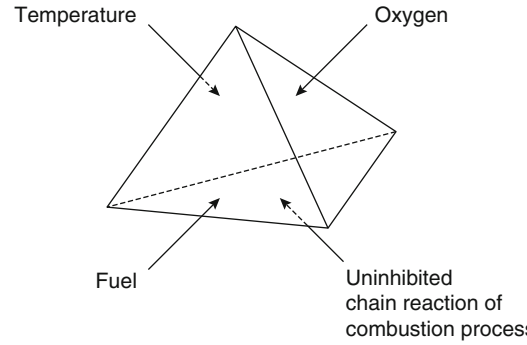

Fig. 43.4 The tetrahedron of fire

The extinguishing mechanism of the halogenated agents is not completely understood, yet there is definitely a chemical reaction that interferes with the combustion process. The halogen atoms act by removing the active chemical species involved in the flame chain reaction. While all the halogens are active in this way, bromine is much more effective than chlorine or fluorine. With Halon 1301 (54% by weight bromine), it is the bromine radical that acts as the inhibitor in extinguishing the fire. Yet the fluorine in the molecule also serves a specific task since it is the fluorine that gives the agent thermal stability and keeps Halon 1301 from decomposing until approximately 900 F (480 C) [13].

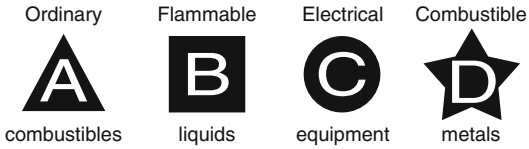

Fig. 43.5 The four classes of fire

Extinguishing Effectiveness

As shown in Fig. 43.5, the four types of fire are ordinary combustibles (Class A), flammable liquids and gases (Class B), electrical (Class C), and reactive metals (Class D) [5].

It was previously mentioned that Halon 1301 is ineffective on Class D fires and is not as desirable as other agents in extinguishing deep-seated Class A fires. The effectiveness of Halon 1301 on Class A fires is not as predictable as with other classes of fire. It depends to a large extent upon the burning material, its configuration, and how early in the combustion cycle the agent is applied. Most plastics behave as flammable liquids and can be extinguished rapidly and completely with 4–6% concentrations of Halon 1301 [14].

Other materials, particularly cellulosic products, can in certain forms develop deep-seated fires in addition to flaming combustion. The flaming portion of such fires can be extinguished with low 4–6% Halon 1301 concentrations, but the glowing deep-seated portion of the fire may continue under some circumstances. Even so, the deep-seated fire can be controlled since its rate of burning and consequent heat release will be reduced. Considerably higher concentrations (18–30%) of Halon 1301 are required to achieve complete extinguishment, but these levels are seldom economical to apply and their application may result in unwanted products of decomposition. However, the concept of controlling deep-seated fires with halogenated agents has been accepted in the respective NFPA standards [14].

It is Class B and Class C fires for which halon is particularly well suited. The most common applications involve Class C electrical hazards, with the increase in popularity of Halon 1301 keeping well in stride with the development of high technology. Typically, electrical and electronic equipment are protected with a concentration of 5% Halon 1301 by volume, though a significantly lower concentration will suitably extinguish a potential fire [15]. The concentrations necessary to extinguish Class B fires have been the subject of much testing with results that vary widely. The effectiveness of halogenated agents on flammable liquid and vapor fires is quite dramatic, especially in total flooding systems. Rapid and complete extinguishment is obtainable with low concentrations of the agent [14]. To be effective, the fire must be contained (such as inside a room or chamber) so that the agent can react with it; Halon 1301 applied to large exterior running pool fires dissipates into the atmosphere without penetrating the flame zone.

Corrosive Effects of Undecomposed Halons

Unlike Halon 1301 and Halon 1211, the early nonfluorinated halogenated agents had significant corrosive problems. Laboratory tests by DuPont in a 44-month exposure period with aluminum, magnesium, steel, stainless steel, titanium, and brass exposed to undecomposed Halon 1301 support the fact that this agent will not corrode these metals, which may all commonly be used in fixed fire extinguishing systems. [13] This is not surprising from a chemical standpoint because the presence of the fluorine atom in a molecule generally reduces its chemical reactivity and corrosive properties and increases its stability.

The presence of free water in systems containing Halon 1301 should be avoided. Free water is defined as the presence of a separate water phase in the liquid halon. When present in a small quantity, free water can provide a site for concentrating acid impurities into a corrosive liquid [16]. Free water should not be confused with dissolved water, which is not a problem in a Halon 1301 system.

Halon 1301 is inert toward most elastometers and plastics. In general, rigid plastics that are normally unaffected include polytetrafluorethylene, nylon, and acetal copolymers. Most of the commonly used plastics undergo little, if any, swelling in the presence of Halon 1301, with the

exception of ethyl cellulose and possibly cellulose acetate/butyrate. Elastomers are particularly suitable when exposed to Halon 1301 for extended periods of time with the notable exception of silicone rubber [13]. Halons decomposed at high temperatures during suppression produce halogen acids such as HF and HBr and free halons that can be corrosive.

Toxicity

General Toxic Properties

The relative safety of Halon 1301 has been established through more than 30 years of medical research involving both humans and test animals. No significant adverse health effects have been reported from the proper use of Halon 1301 as a fire extinguishant since its original introduction into the marketplace [14].

Early studies by the U.S. Army Chemical Center on Halon 1301 determined the approximate lethal concentration for a 15 min exposure to be 83% by volume [2]. Animals exposed to concentrations below lethal levels exhibit two distinct types of toxic effects. Concentrations greater than 10% by volume produce cardiovascular effects such as decreased heart rate, hypotension, and occasional cardiac arrythmias [17]. Concentrations of Halon 1301 greater than 30% by volume result in central nervous system changes including convulsions, tremors, lethargy, and unconsciousness. Effects are considered transitory and disappear after exposure [18].

Human exposure to concentrations of Halon 1301 greater than 10% by volume have shown indications of pronounced dizziness and a reduction in physical and mental dexterity [19]. With concentrations between 7% and 10% by volume, subjects experienced tingling of the extremities and dizziness, indicating mild anesthesia. Exposure to Halon 1301 concentrations less than 7% by volume have little effect, with the exception of a deepening in the tone of voice caused by a higher density in the medium between the vocal chords. The effects at all levels of concentration disappear quickly after removal from the exposure. Testing of Halon 1301 for potential teratogenic (i.e., altering the normal process of fetal development) and mutagenic (a carcinogen in humans) effects has indicated that no serious problems exist. [5]

Table 43.4 Permitted exposure time for Halon 1301

Concentration (percent by volume)	Permitted time of exposure
Normally occupied areas	
0–7 %	15 min
7–10 %	1 min
Above 10 %	Not permitted
Normally unoccupied areas	
0–7 %	15 min
7–10 %	1 min
10–15 %	30 s
Above 15 %	Prevent exposure

Most fire protection applications today have a design concentration of 5% by volume, thus the question of toxicity is usually not a serious concern. Exposure limitations for Halon 1301 (indicated by NFPA 12A) are summarized in Table 43.4 [14].

In addition to possible toxic effects, liquid Halon 1301 (including the spray in the immediate proximity of a discharge) may freeze the skin on contact and cause frostbite. However, direct contact is necessary for this to occur and is unlikely, since with engineered Halon 1301 fire extinguishing systems the discharge nozzles are typically distant from all occupants.

Products of Decomposition

Consideration of the life safety of Halon 1301 must also include the effects of breakdown products which have a relatively higher toxicity than the agent itself. Upon exposure to flames or hot surfaces above approximately 900 F (480 C), Halon 1301 decomposes to form primarily hydrogen bromide (HBr) and hydrogen fluoride (HF) [20]. Trace quantities of bromine (Br2), carbonyl fluoride (COF2), and carbonyl bromide (COBr2) have been observed, but the quantities are generally too small to be of concern. Although small amounts of carbonyl halides (COF2 and COBr2) were reported in early tests, more recent studies have failed to confirm the

Table 43.5 Predominant Halon 1301 decomposition products

Compound	Formula	ALC* for 15 min exposure ppm by volume in air
Hydrogen fluoride	HF	2500
Hydrogen bromide	HBr	4750
Bromine	Br2	550
Carbonyl fluoride	COF2	1500
Carbonyl bromine	COBr2	—

* = acute lethal exposure

Table 43.6 Selected physical properties of typical halogenated fire extinguishing agents

Halon number	Type of agent	Approximate boiling point (°F)	Approximate freezing point (°F)	Specific gravity of liquid (@70 F)
104	Liquid	170	−8	1.59
1001	Liquid	40	−135	1.73
1011	Liquid	151	−124	1.93
1202	Liquid	76	−223	2.28
1211	Liquefied gas	25	−257	1.83
1301	Liquefied gas	−72	−270	1.57
2402	Liquid	117	−167	2.17

presence of these compounds. Table 43.5 summarizes the predominant products of decomposition for Halon 1301 [21].

The primary toxic effect of the decomposition products is irritation. Even in concentrations of only a few parts per million, the decomposition products have characteristically sharp, acrid odors. This characteristic provides a built-in warning system since the irritation becomes severe well in advance of truly hazardous levels. In addition, the odor also serves as a warning that carbon monoxide and other potentially toxic products of combustion may be present. Prompt detection and rapid extinguishment of a fire will produce the safest postextinguishment atmosphere.

Other Halons

Physical Properties

The predominant halogenated agent still in existence today for total flooding fire extinguishing systems is Halon 1301, though some areas of Europe have utilized Halon 1211 for this purpose. One reason for this use of Halon 1301 (besides low toxicity) is the ability of the agent to vaporize and penetrate all portions of the hazard volume. Table 43.6 shows that Halon 1301 has the lowest boiling point and Halon 1211 has the second lowest.

With the discharge of a halon system at ambient temperature, Halon 1301 flashes to a vapor almost instantaneously, while Halon 1211 tends to pool momentarily. Agents with boiling points exceeding the temperature of the hazard volume will stay liquid until heated by the fire itself. These high boiling point halogenated agents have two distinct attributes: they can be projected in a liquid stream and they have a quenching effect in addition to breaking the uninhibited chain reaction. Thus, portable extinguishers generally use Halon 1301 as a propellant for other halon agents.

Toxicity

One of the primary reasons that Halon 1301 is the most preferred of the halogenated agents is its relatively low toxicity, as discussed earlier. Table 43.7 compares the approximate lethal concentration of both the natural and decomposed vapors for a variety of fire extinguishing halon

Table 43.7 Approximate lethal concentrations (ppm) for 15 min exposure to vapors of various fire extinguishing agents

Formula	Halon number	Natural vapor	Decomposed vapor
CCl4	104	28,000	300
CH3Br	1001	5900	9600
CH2ClBr	1011	65,000	4000
CF2Br2	1202	54,000	1850
CF2ClBr	1211	324,000	7650
CF3Br	1301	832,000	14,000
C2F4Br2	2402	126,000	1600
CO2	—	658,000	658,000

Table 43.8 Necessary control measures for computer room fire stage sequence

Fire stage	Control	Serious danger concern
1. Pre-ignition	Good housekeeping practices, control combustible furnishings and interior finish	
2. Initial pyrolysis	Smoke detection system	Occupants and business interruption
3. Incipient	Portable fire extinguishers, Halon 1301 automatic suppression system	Occupants and contents
4. Preflashover	Automatic sprinklers	Occupants and structure
5. Postflashover	Fire walls, compartmentalization	Surrounding structures

agents and carbon dioxide (CO2). For sake of comparison, carbon dioxide is included with this list of halon agents. As a natural vapor, Halon 1301 is the least toxic halogenated agent. Carbon dioxide may appear to compare favorably with Halon 1301, yet high concentrations of carbon dioxide are necessary for fire extinguishment, which also makes the hazard volume lethal to human occupants.

Halon in the Fire Protection Spectrum

Halogenated agent extinguishing systems are only one segment of the total fire protection spectrum. Good engineering judgment is necessary when trying to determine the applicability of halon and whether it should be used instead of, or in addition to, other fire protection measures. It must be clearly understood that halogenated agent extinguishing systems are not the panacea for all fire hazards, yet they do offer a safe method to extinguish certain fires in their very early stages. Thus, these systems have been commonly applied to situations where even the smallest fire is absolutely unthinkable.

As an example, total computer room fire protection might involve several different control measures addressing different possible fire conditions. Table 43.8 illustrates this concept, based on the different stages of a growing fire. The table is not a rigid description of the fire protection requirements of every computer room, but instead an example of how total fire protection is the overall objective when approaching a design situation.

An important factor of developing halogenated agent extinguishing systems is the interaction of all concerned individuals. To design, install, maintain, and operate a halon system requires a cooperative effort from a number of different groups. As shown in Fig. 43.6, these individuals include the end users, consultants, manufacturers, installers, insurance representatives, and other selected authorities. Representatives from all these groups work together to develop and enhance model codes, which provide guidance and understanding for proper halon system usage.

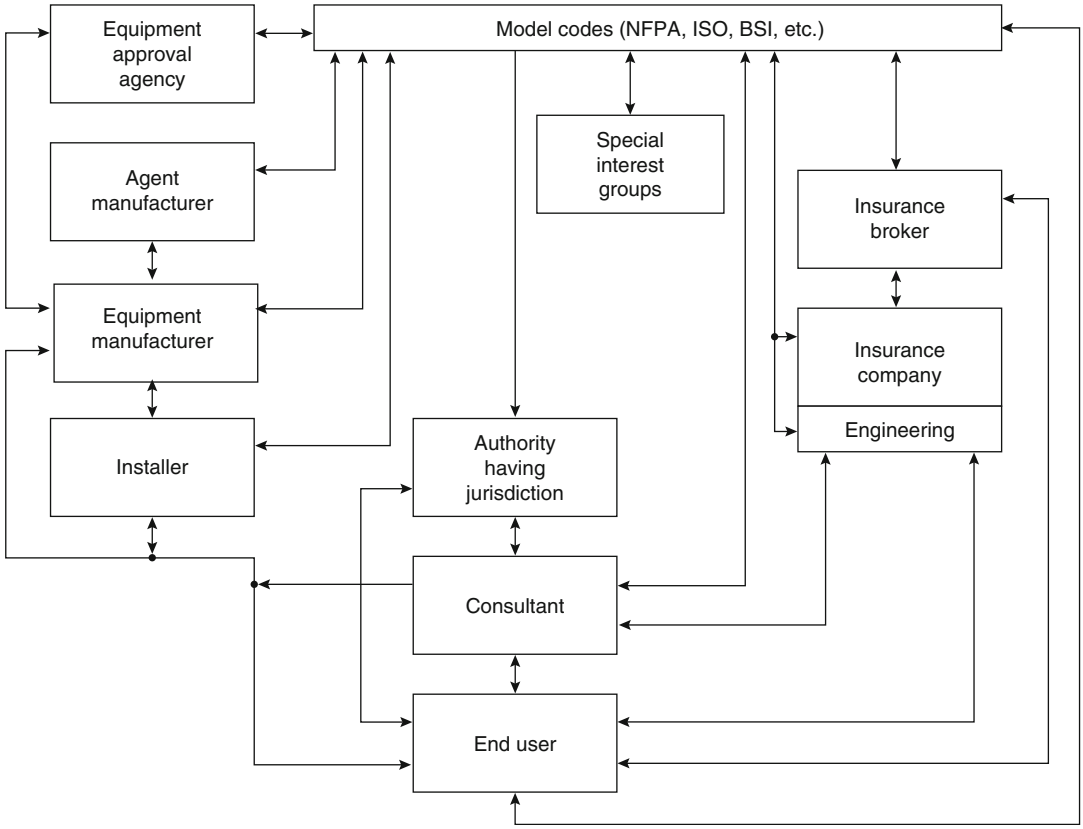

Fig. 43.6 Typical interrelationship of halon fire protection interests

System Configurations

Detection

The three primary parts of every halogenated agent extinguishing system are detection, control panel, and agent delivery. Since there is no single type of detector that offers the ultimate for every application, consideration must be given to the best detection made for the types of combustibles and combustion that are likely to occur in the protected area and the required response time (see the section on design of detection).

Photoelectric and ionization smoke detectors have different response characteristics to fires, depending on the situation, and can be susceptible to certain types of false or unwanted alarms. Thermal detectors, although more reliable, react more slowly to fire conditions. In certain applications, speed is critical and optical detectors would be required.

To optimize the speed and reliability of detection systems, it is important to use two different types of detectors on two separate detection loops within the hazard area. This method is referred to as cross-zone detection. Each detection loop functions independently to provide both added reliability and a comforting degree of redundancy [22].

Control Panels

Features

As its name implies, the control panel is the device that controls system operation and allows the system to function as designed. When a control panel protects more than one area, each individual area is referred to as a zone of

Table 43.9 Typical control unit features

	Halon zone	Fire alarm zone
Initiating circuit	Two cross-zone detection circuits	One circuit for detection
Signaling circuit	Multiple signaling sequence	Multiple signaling sequence
Release circuit	One circuit	None

Table 43.10 Modes of control panel operation

Unpowered condition	Off
Normal condition	On
Alarm condition:	
Prealarm	One detector activates.
Prerelease	Two cross-zoned detectors activate.
	Time delay starts.
Release	Time delay ends or manual pull station activates. Halon is released.
Postrelease	Halon has been released.
Trouble condition	Failure or disruption of field wiring.
	Insufficient power input.

protection. Each zone of every halon control panel has three different types of circuits: initiating, signaling, and release. A fire alarm zone and halon zone are compared in Table 43.9 to illustrate the differences between these circuit types. It is unusual for a single halon control panel to protect more than five zones at once due to the high number of circuits required. Fire alarm control panels, on the other hand, may have dozens of individual zones.

Initiating circuits provide the input into the panel and support automatic detectors, manual pull stations, and other initiating devices. Automatic detectors are normally cross-zoned, which implies two separate detection circuits. One circuit is required for prealarm and both circuits are necessary for halon release. The signaling circuits, sometimes referred to as bell or auxiliary circuits, are used for audible/visual alarms and other auxiliary functions. The release circuits allow the halon to release from the containers and are sometimes referred to as firing, solenoid, initiator, dump, or halon circuits.

Modes of Operation

At any time, a halon control panel and the halon system could be in one of four modes of operation; as shown in Table 43.10 these include unpowered, normal, alarm, and trouble condition. The alarm condition is further definable with prealarm, prerelease, release, and postrelease conditions. Typical systems utilizing cross-zoning detection activate, when required, into prealarm and/or release condition, but this often becomes more complicated with time delays, abort switches, and other auxiliary functions. Unless otherwise specified, manual pull stations activate all alarm conditions, override abort switches, if present, and immediately release the halon. These different alarm conditions provide a convenient mechanism for sequential operation of audible/visual signaling, equipment shutdown, fire service notification, and other auxiliary functions.

Control Panel Economics

Large-scale projects with multiple halon zones in a single facility are not uncommon. For example, in the past entire data processing centers and telecommunications buildings were protected throughout with Halon 1301 systems. To protect a large building with many halon zones, it may appear that the most effective way of configuring the system is by using a single large control panel with the capacity for all required halon zones. This is not true, since there is a limitation to the number of halon zones that any one halon panel can effectively manage. Figure 43.7 illustrates an

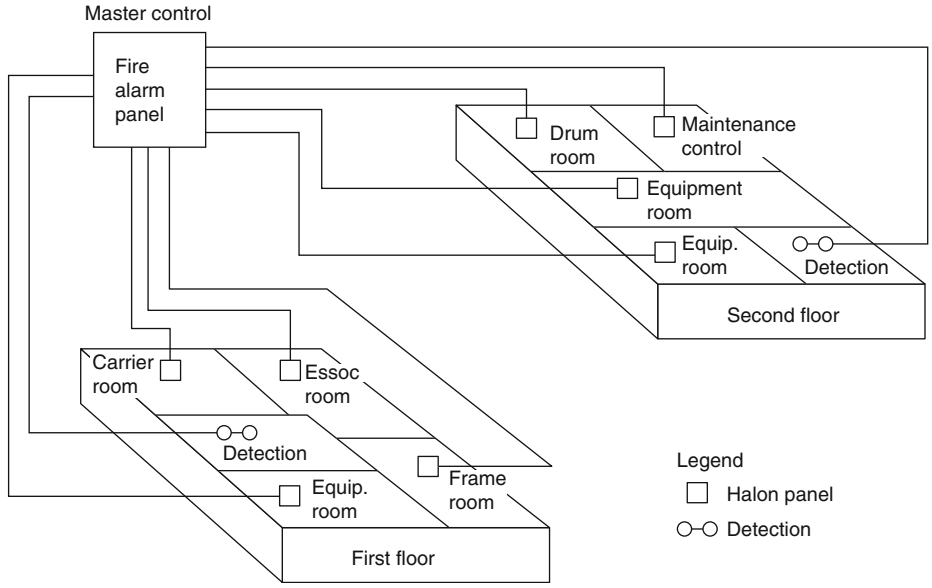

Fig. 43.7 The network concept of control panel interface for a typical halon application

alternative method, where the individual halon zones of a large building each have their own halon panel wired to give an alarm or trouble signal to a central fire alarm panel.

A typical halon zone required an average of 12 wires to support all the necessary system functions. Thus, the cost of running multiple wires and large conduit instead of only two wires (for interpanel communication) often offsets the cost of smaller, more numerous panels located near the halon zones. This configuration offers flexibility for future consolidations or additions, which are common for high-technology facilities. Aesthetics are enhanced at the master control location, and system operation is simplified. Installation checkout and servicing is easier when the halon control panel is within the hazard area. Finally, the overall system is more reliable due to less wiring, lack of design complexity, simplified maintenance, and multi-source dependence.

Agent Delivery

In addition to the control panel and detection, the other primary part of every halogenated agent extinguishing system is agent delivery. The agent delivery includes the discharge nozzles, agent storage container(s), release mechanism, and associated piping. As shown in Table 43.11, three methods of agent delivery exist: (1) central storage, (2) modular, and (3) shared supply. Central storage has the container(s) centrally located, with the agent piped accordingly. This method is popular due to its similarity with carbon dioxide system technology (which helped develop early systems), along with usually having the lowest initial cost. Modular systems use smaller containers strategically located throughout the hazard area, with minimal piping. The high reliability of modular systems is based on lack of dependency on piping integrity, negligible piping calculations, total system supervision, multi-source dependence, and the inherent ability to be heat actuated regardless of catastrophic system failure. Modular systems are simple to design, are relatively easy to install, and have a high degree of future flexibility. Systems utilizing shared supply are essentially central storage systems with a container(s) shared by more than one hazard volume. Even though fewer containers are used, directional valves and extensive piping do not often allow shared

Table 43.11 Comparison of different methods of agent delivery

	Central storage	Modular	Shared supply
Hardware cost	Moderate	High	Moderate
Installation cost	Moderate	Low	Moderate
Design simplicity	Difficult	Simple	Difficult
Installation simplicity	Difficult	Medium	Difficult
Operation and maintenance simplicity	Medium	Medium	Medium
Reliability	Moderate	High	Low
Future flexibility	Low	High	Low

supply systems to be cost effective. Adding to its unpopularity are its design and installation complexity, low reliability, and impaired future flexibility. When a shared supply halon system activates for one hazard, the remaining hazards become unprotected until the system is completely recharged.

Design Concepts and Methodology

Definitions and Terminology

Halogenated agent extinguishing systems are typically classified as either total flooding or local application systems. A total flooding system is designed to develop and maintain a concentration of halon that will extinguish fires in combustible materials located in an enclosed space. Local application systems are designed to apply the agent directly to a fire that may occur in an area or space that is not immediately enclosed. In addition to these, there are specialized applications, which may include combination total flooding/local application or partial flooding. The vast majority of existing halon systems today are the total flooding type using Halon 1301.

The definitions of halon system and halon zone are often confusing. This is especially true to individuals closely associated with the fire alarm industry, since fire alarm terminology is similar. Figure 43.8 defines the basic features of a halon system and halon zone and offers a comparison with each respective fire alarm counterpart.

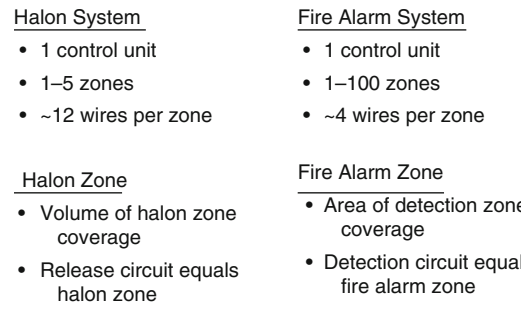

Fig. 43.8 Halon/fire alarm differences

A halon zone usually equates to an area of halon coverage functioning on a single release circuit, while the zones in a fire alarm system typically are each detection circuit. As an example, one halon zone could be a single computer room, whereas a fire alarm zone could be the entire floor of a building. A halon system also has much fewer (though more comprehensive) zones than a fire alarm system.

Halon Design Guidelines

The design process necessary for total flooding systems is easily quantified. The procedure can be separated into five definable steps: (1) hazard identification, (2) determination of agent quantity, (3) specification of operating requirements, (4) determination of hardware requirements, and (5) generation of postdesign information.

The initial step is to provide a definition of the hazard. This includes determining the fuels involved, the dimensions and configuration of the enclosure, the maximum and minimum net volumes, the status of occupancy, the expected

hazard area temperature range, and possible unclosable openings. Based on this information, the minimum design concentration can be established. Next, the agent quantity is determined based upon the design concentration, the volume, minimum expected temperature, leakage due to ventilation or unclosable openings, and altitude above sea level. Usually, the gross volume is used to calculate the agent quantity to allow for extra agent to replace that lost through normal building leakage. However, agent concentrations must conform with the applicable toxicity criteria with respect to the minimum net volume and maximum temperature. The operating specifications are then required if they have not already been established. These will indicate how the system is to operate, the modes of operation, the type of agent delivery, and so forth. When these are known, the necessary hardware requirements must be obtained and the design of the system completed. The final step is to generate the postdesign information necessary for others to install, test, operate, and maintain the system. Postdesign information should contain all design calculations (including hydraulic calculations), complete blueprint drawings, and detailed information describing the testing, operation, and maintenance of the system.

Local Application and Special Systems

Local application systems were typically installed to extinguish fires involving flammable liquids, gases, and surface burning solids. Such systems are designed to apply the agent directly to a fire that may occur in an area or space not immediately enclosed. They must be designed to deliver halon agent to the hazard being protected in such a manner that the agent will cover all burning surfaces during discharge of the system. Because of its lower volatility, Halon 1211 may be better suited than other forms of halon for local application systems. The lower volatility, plus a high liquid density, permits the agent to be sprayed as a liquid and thus propelled into the fire zone to a greater extent than is possible with other vaporized agents. Examples of areas protected by local application are spray booths, dip and quench tanks, oil-filled electric transformers, printing presses, heavy construction equipment, and vapor vents. An example of a local application system is shown in Fig. 43.9.

Traditionally, NFPA standards have not set a minimum limit on the discharge time for a local application design. The rate of discharge and the amount of agent required for a given application must be determined by experimentation and evaluation. The most critical components of these systems are the discharge nozzles; the discharge velocity and rate must be sufficient to penetrate the flames and produce extinguishment but not be so great as to cause splashing or spreading of fuel and thus increase the fire hazard. The minimum design discharge quantity should not be less than 1.5 times the minimum quantity required for extinguishment at any selected design rate [21]. Also of critical importance are type and location of detectors.

As with other types of gaseous suppression systems, local application systems have been designed according to the rate-by-volume

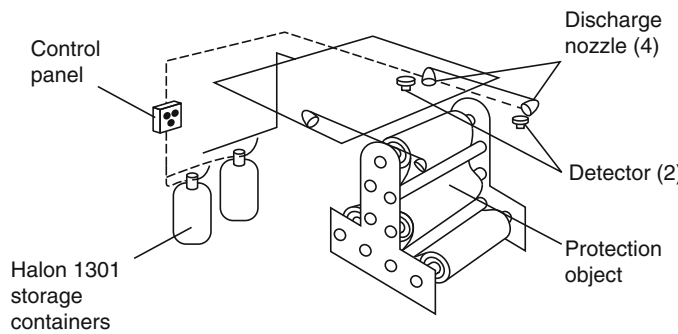

Fig. 43.9 Local application system

method or the rate-by-area method. The rate-by-area method determines nozzle discharge rates based on the exposed surface area of the hazard being protected. This method is less popular than the rate-by-volume method, which requires discharge rates sufficient to fill (within the discharge time) a volume whose imaginary boundaries extend a limited distance from the protected hazard. This method is favored since it performs similarly to total flooding systems. Important factors to be considered in the design of a local application system are the rate of agent flow, the distance and area limitations of the nozzles, the quantity of agent required, the agent distribution system, and the placement of detectors.

Unlike total flooding systems, only the liquid portion of the discharge is effective for local application systems. The computed quantity of agent needed for local application must be increased to compensate for the residual vapor in the storage container at the end of liquid flow. An additional 25% storage capacity is required in the absence of an enclosure that would prevent gas dissipation. Systems should also compensate for any agent vaporized in the pipe lines due to heat absorption from the piping. The heat transfer is important when the piping is at a higher temperature than the agent. The following equation determines the amount of agent increase necessary to compensate for this effect: [14]

$$W_x = \frac{2\pi kL\left(T_p - T_a\right)(t)}{3600h(\ln r_o/r_i)} \qquad (43.1)$$

where

Wx = Amount of agent increase, kg (lb)
k = Thermal conductivity of the piping, W/m · K (Btu · t/h · ft2 · F)
L = Linear length of the piping, m (ft)
Tp = Pipe temperature, C (°F)
Ta = Agent temperature, C (°F)
t = System discharge time
h = Heat of vaporization of the agent at Ta, kJ/kg (Btu/lb)
ro = Outside pipe radius, mm (in.)
ri = Inside pipe radius, mm (in.)

Specialized systems using a variety of agents are in wide use throughout the world to protect hazards such as aircraft engine nacelles, military vehicles, emergency generator motors, earth moving equipment, and racing cars. The characteristic common to all these systems is that they can only be applied to the specific hazard for which they were designed and tested. One unusual concept used to protect aircraft flight simulator areas is known as partial flooding, where only the volume containing the simulator equipment receives the total flooding concentration, and not the expansive open areas above it. A design concentration of 7% is recommended to achieve a 5% concentration in the hazard area and should provide for a minimum agent height level relative to the agent concentration of approximately 1.5 m (5 ft) above the highest part of the hazard. The placement of the nozzle is critical and should be designed to direct agent discharge approximately 30° below the horizontal plane. As shown in Fig. 43.10, the savings associated with partial flooding systems can be substantial, especially in areas with very high ceilings [20].

Agent Requirements: Total Flooding

Design Concentrations: Solid Fuels

Flammable solids may be classified as those that do not develop deep-seated fires and those that do. Class A combustible solids that develop deep-seated fires do so after exposure to flaming combustion for a certain length of time, which varies with the material. Some materials may begin as deep seated through internal heating such as spontaneous ignition. With respect to Halon 1301 total flooding systems, a fire is considered deep seated if a 5% concentration will not extinguish the fire within 10 min after agent discharge [14]. Materials that do not become deep seated undergo surface combustion only and may be treated much the same as those in a flammable liquid fire.

The presence of Halon 1301 in the vicinity of a deep-seated fire will extinguish the flame and reduce the rate of burning, yet the quantity of agent required for complete extinguishment of

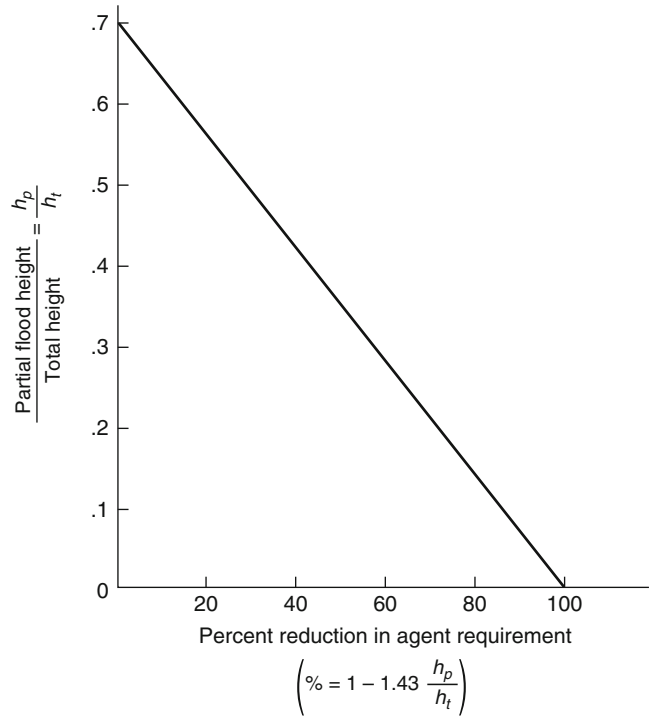

Fig. 43.10 Agent reduction associated with partial flooding systems

all embers is difficult to assess. Often it is impractical to maintain an adequate concentration of Halon 1301 for a sufficient time to ensure the complete extinguishment of a deep-seated fire. Factors affecting this concentration include:

1. Nature of fuel
2. Time during which it has been burning
3. Availability of oxygen within the enclosure
4. Ratio of burning surface area to the volume of the enclosure
5. Geometric characteristics of the fuel
6. Fuel distribution within the enclosure

Table 43.12 illustrates the extinguishing concentrations of selected flammable solid fires as indicated by six different halon industry groups [23].

Even where the fire has inadvertently become deep seated, application of a low Halon 1301 concentration has two benefits. First, all flaming combustion is halted, preventing rapid spread of the fire to adjacent fuels. Second, the rate of combustion is drastically reduced. These two characteristics justify the ability of Halon 1301 to control, if not extinguish, deep-seated fires. However, Halon 1301 systems that are specifically designed to extinguish deep-seated fires are seldom economical to apply and may not be as effective in these fires as other types of extinguishing systems.

Design Concentrations: Liquid and Gas Fires

There are two general types of flammable liquid or gas fires. First, a flammable or explosive mixture of vapors exists that must be prevented from burning; and second, fuel is burning that must be extinguished. Associated with each of these conditions is a minimum level of Halon 1301 extinguishing concentration, respectively known as inerting and flame extinguishment. When determining the halon design concentration, proper consideration must be given to the quantity and type of fuel involved, the conditions under which it normally exists in the hazard, and any special conditions of the hazard itself. If certain hazards have explosion potential either before or following a fire due to the presence of volatile, gaseous, or atomized fuel, then special

Table 43.12 Extinguishing concentrations of selected flammable solid fires

	Halon 1301 concentration (percent by volume)					
	Factory mutual	Fenwal	Ansul	DuPont	Safety first	Underwriter labs
Surface fires						
Polyvinyl chloride	—	2.0	—	2.6	3.8	—
Polystyrene	—	3	—	—	—	—
Polyethylene	—	3	—	—	—	—
Stacked computer printout	—	—	5.1	—	—	—
Polyester computer tape	—	5	—	—	3.8	—
Wood crib 30 pcs. 3/4″ × 7/8 ″	3	—	—	—	—	—
Wood crib 24 pcs. 2″ × 2″ × 18″	—	—	—	—	3.8	—
Wood crib 1A 50 pcs. 2″ × 2″ × 18″	—	—	—	—	3.8	3.88
Excelsior loose on floor	—	—	—	—	3.8	6.0
Shredded paper loose on floor	—	—	—	—	3.8	—
Polyurethane foam	—	—	—	3	3.8	—
Cotton lint	—	—	—	—	3.8	—
Crumpled paper	3	6	—	—	3.8	—
Wood pallets—stack of 10	3	—	—	—	—	—
Deep-seated fires						
Shredded paper in wire basket	—	—	—	—	20	18.0
Polyester computer tape loose in open wire basket	—	10	—	—	—	—
Charcoal	13	—	—	—	—	—
Parallel wood blocks	20	—	—	—	—	—
Glazed fox fur	—	—	—	—	6.5	—

consideration should be given to vapor detection and explosion suppression measures.

As its name implies, the flame extinguishment concentration assumes that the given fuel is burning and that Halon 1301 injected into the air surrounding the fuel at the stated concentration will extinguish the fire [14]. Design concentrations for flame extinguishment are given in Table 43.13. These concentrations are not considered effective with premixed flames or explosive mixtures of fuel vapor in air, but instead apply to diffusion flames, where the flames emanate from pure fuel vapor, and oxygen suffuses into the flame zone from the outside. If the possibility of a subsequent reflash or explosion exists, then the flame extinguishing concentration is not sufficient. NFPA 12A [14] defines these conditions as "when both:

1. The quantity of fuel permitted in the enclosure is sufficient to develop a concentration equal to or greater than one-half of the lower flammable limit throughout the enclosure, and
2. The volatility of the fuel before the fire is sufficient to reach the lower flammable limit in air (maximum ambient temperature or fuel temperature exceeds the closed cup flash point temperature) or the system response is not rapid enough to detect and extinguish the fire before the volatility of the fuel is increased to a dangerous level as a result of the fire."

Most fuels exhibit about a 30–40% higher concentration for inerting than for flame extinguishment. The minimum inerting concentration suppresses the propagation of the flame front at the "flammability peak" or stoichiometric fuel/air composition and inerts the enclosure so that any fuel/air mixture will not burn. The higher inerting concentration is often considered safer to use even if the flame extinguishment concentration is feasible, yet the sacrifices include

Table 43.13 Design concentration for flame extinguishment

Fuel	Minimum design concentration (percent by volume)
Acetone	5.0
Benzene	5.0
Ethanol	5.0
Ethylene	8.2
Methane	5.0
n-Heptane	5.0
Propane	5.2

Table 43.14 Halon 1301 design concentrations for inerting

Fuel	Minimum concentration (percent by volume)
Acetone	7.6
Benzene	5.0
Ethanol	11.1
Ethylene	13.2
Hydrogen	31.4
Methane	7.7
n-Heptane	6.9
Propane	6.7

Note: Includes a safety factor of 10% added to experimental values

higher system cost and higher concentrations to which personnel may be exposed (Table 43.14).

It is possible to calculate whether the flame extinguishing concentration is acceptable by determining if the fuel present in the hazard will permit attainment of the one-half lower flammable limit of the fuel. The equation to determine the maximum allowable fuel loading (MFL) for flame extinguishment concentrations is

$$\mathrm{MFL} = \frac{(K_c)(LFL)(\mathrm{MW})}{T} \qquad (43.2)$$

where

MFL = Maximum allowable fuel loading, kg/m3 (lb/ft3)

Kc = Conversion factor, 0.06093 (0.00685)

LFL = Lower flammable limit of fuel in air, percent volume

MW = Molecular weight of fuel

T = Temperature, K (R)

This can be compared with the actual fuel loading (FL), which is calculated by

$$\mathrm{FL} = \frac{(VF)(W_{h_2O})(SG)}{V} \qquad (43.3)$$

where

FL = Fuel loading, kg/m^3 (lb/ft^3)

VF = Volumetric quantity of fuel, m^3 (ft^3)

W_{h_2C} = Specific weight of water, 997.9 kg/m^3 (62.3 lb/ft^3)

SG = Specific gravity of fuel

V = Volume of enclosure, m^3 (ft^3)

If the fuel loading, FL, exceeds the maximum allowable fuel loading, MFL, then the inerting concentration for the particular fuel should be used. Most applications involve a variety of fuels within a single enclosure. If the sum of the actual fuel loadings, FL, is greater than any single maximum allowable fuel loading, MFL, then the most stringent inerting concentration is recommended. If it is determined that a flame extinguishment concentration is sufficient, the value for the fuel requiring the greatest concentration is most applicable.

Calculation of Agent Quantity

The calculations necessary for determining the Halon 1301 total flooding quantity are dependent on temperature, volume of the enclosure, agent concentration, altitude with respect to sea level, and losses due to ventilation and leakage. Most applications are based on a static volume enclosure with all openings sealed and all ventilation systems shut down prior to discharge. This simplifies the calculation significantly. Often the ventilation system does not shut down but instead is dampered to allow recirculating air (without makeup air) to continue cooling sensitive electronic equipment and promote the mixing of halon and air. Total flooding quantities are still based on a static volume for these applications. However, in this instance, it may be necessary to include the volume of the ventilation ductwork in addition to the volume of the

Table 43.15 Correction factors for altitudes

Altitude		
Feet	Meters	Correction factor
3000	914	0.90
4000	1219	0.86
5000	1524	0.83
6000	1829	0.80
7000	2134	0.77
8000	2438	0.74
9000	2743	0.71
10,000	3048	0.69
11,000	3353	0.66
12,000	3658	0.64
13,000	3962	0.61
14,000	4267	0.59
15,000	4572	0.56

enclosure. The equation to determine the Halon 1301 total flooding quantity is

$$W = \frac{(V)(C)(A_c)}{S(100 - C)} \tag{43.4}$$

where

W = Weight of Halon 1301 required, kg (lb)
C = Halon 1301 concentration, percent by volume
Ac = Altitude correction factor (Table 43.15)
S = Specific vapor volume based on temperature, m3/kg (ft3/lb)
$S = 0.14781 + 0.000567\ T$; T = temperature C
$S = 2.2062 + 0.005046\ T$; T = temperature F

Application Rate

Discharge Time and Soaking Period

When designing a Halon 1301 total flooding system, it is important to determine the system discharge time and soaking period.

As indicated in NFPA 12A, "the agent shall be completed in a nominal 10 s or as otherwise required by the authority having jurisdiction." [14] The reasons for a rapid discharge time include keeping unwanted products of decomposition to a minimum and achieving complete dispersal of agent throughout the enclosure. Sometimes a much faster application rate is required due to the possibility of a fast spreading fire; yet, discharge times longer than 10 s are sometimes necessary for areas such as museums requiring that turbulence be kept to a minimum, or areas with unavoidably difficult piping configurations.

The soaking time is another important requirement for a Halon 1301 total flooding system. This is especially true for deep-seated fire or fires that may reflash. The most common application today for total flooding systems is the protection of valuable electronic equipment. Fires in these applications are almost always extinguished within a few seconds by the Halon 1301 agent, yet a 10-min soaking period is usually required. This estimated time period allows responsible individuals to arrive at the scene to take follow-up action. It is important to remember that halogenated agent extinguishing systems in most cases have only a single chance to control an unwanted fire.

Effects of Ventilation

When Halon 1301 is discharged into a total flooding enclosure that is ventilated, some agent will be lost with the ventilating air. Assuming that ventilation must continue during and after discharge, a greater amount of agent is required to develop a given concentration. Also, to maintain the concentration at a given level requires continuous agent discharge for the duration of the soaking period. If an enclosure initially contains pure air, the Halon 1301 discharge rate required to develop a given concentration for agent at any given time after the start of discharge is [14]

$$R = \frac{(C)(E)}{(S)(100 - C)[1 - e^{(-Et_1/V)}]} \tag{43.5}$$

where

R = Halon 1301 discharge rate, kg/s (lb/s)
E = Ventilation rate, m3/s (ft3/s)
$t1$ = Discharge time, s
e = Natural logarithm base, 2.71828

The Halon 1301 discharge rate necessary to maintain a given concentration of agent is [14]

$$R = \frac{(C)(E)}{(S)(100 - C)} \tag{43.6}$$

After the agent discharge is stopped, the decay of the agent concentration with respect to time is [14]

$$C = C_0 e^{(-Et_2/V)} \tag{43.7}$$

where

C_0 = Agent concentration at end of discharge, percent volume

t_2 = Time after stopping discharge, s

Compensation for Leakage

Occasionally a Halon 1301 total flooding system is designed for an enclosure that has openings that cannot be closed. An example may be a conveyor belt penetrating an enclosure wall, yet even these openings can sometimes be closed using inflatable seals. Halon 1301 discharged into an enclosure for total flooding will result in an air/agent mixture that has a higher specific gravity than the air surrounding the enclosure. Therefore, any openings in the lower portions of the enclosure will allow the heavier air/agent mixture to flow out and the lighter outside air to flow in. Fresh air entering the enclosure will collect toward the top, forming an interface between the air/agent mixture and fresh air. As the leakage proceeds, the interface will descend toward the bottom of the enclosure. The space above the interface will be completely unprotected, whereas the lower space will essentially contain the original extinguishing concentration. There are two methods of compensating for unclosable openings: initial overdose and extended discharge.

The initial overdose method provides for an adequate overdose of Halon 1301 to ensure a pre-established minimum of agent at the end of the desired soaking period. Mechanical mixing is required within the enclosure to prevent stratification of agent concentration and a descending interface. Also, caution must be used to prevent personnel exposure to the high initial concentrations. The necessary initial concentration depends upon the extended protection time required, the opening height, the opening width, and the volume of the enclosure. Referring to Fig. 43.11, the equation used to determine the initial concentration for a final concentration of 5% is [14]

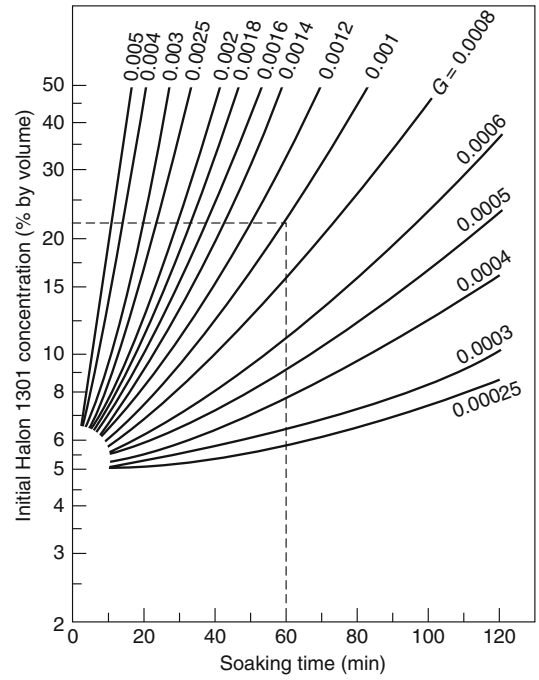

Fig. 43.11 Initial amount of Halon 1301 to produce a 5% residual concentration in enclosures equipped for mechanical mixing

$$\mathrm{G} = \frac{(K)(W_o)\left(2g_c H^3\right)^{1/2}}{3V} \tag{43.8}$$

where

G = Geometric constant

K = Orifice discharge coefficient, 0.66

W_o = Opening width, m (ft)

g_c = Acceleration due to gravity, 9.81 m/s^2 (32.2 ft/s^2)

H = Opening height, m (ft)

The other method used to compensate for unclosable openings is extended discharge. This involves at least two separate piping systems: one to achieve the initial agent concentration, and the other to provide a continuous addition

of Halon 1301 at a rate which will compensate for leakage out of the enclosure during the soaking period. The agent must be discharged in such a way that uniform mixing of agent and air is obtained. This mixing is often difficult due to the extremely low flow rates being discharged over the entire soaking period, occasionally resulting in small nozzles freezing due to air moisture. Based on the design concentration and opening height, Fig. 43.12 can be used to determine the Halon 1301 makeup rate per unit opening width.

Assuming the design concentration of Halon 1301 is established in the enclosure initially, the time required for the interface to reach halfway down the enclosure height can be calculated. Referring to Fig. 43.13, the geometric constant previously calculated for initial overdose is used to find the soaking time based on the initial design concentration.

Flow Calculations

Piping Theory

The overall objective of designing a Halon 1301 piping system is to properly disperse the required concentration of Halon 1301 throughout the hazard volume within the specified time period. Systems must be engineered to operate quickly and effectively. The discharge time (usually a nominal 10 s as indicated by NFPA 12A) is a critical system constraint and is measured as the interval between the first appearance of liquid at the nozzle and the time when the discharge becomes predominantly gaseous [14]. The hydraulic calculations are considered to be the most difficult part of the entire design process, and are almost always calculated with the aid of computer programs due to the tedious nature of manual calculations.

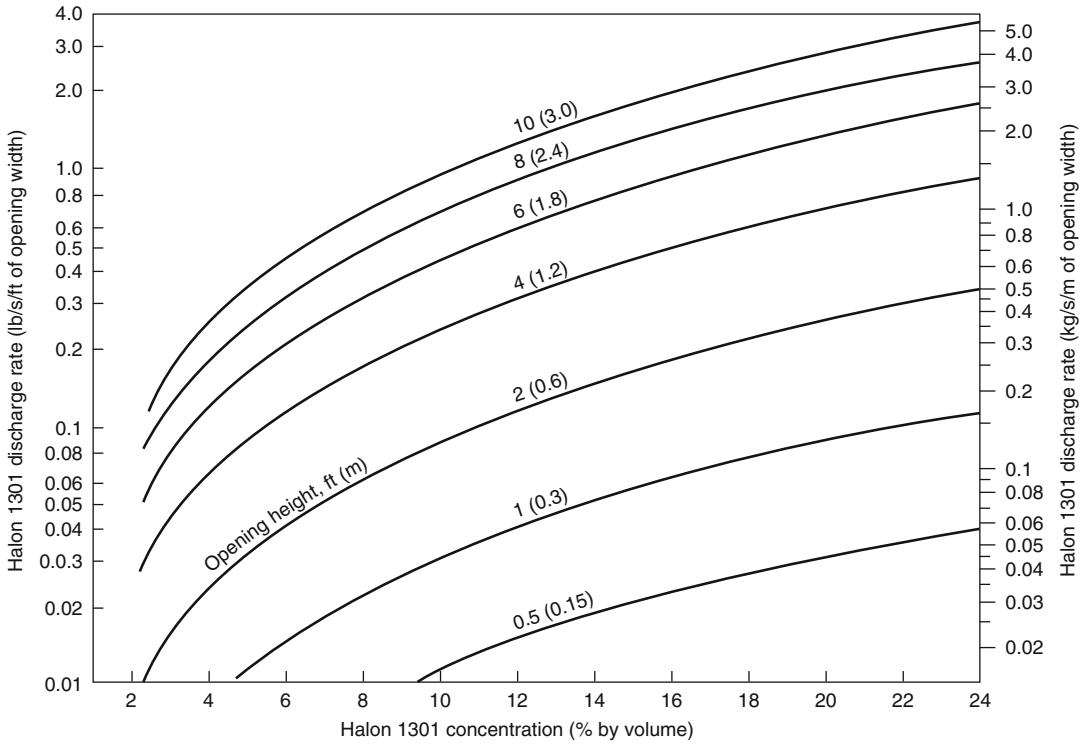

Fig. 43.12 Extended discharge rate of Halon 1301 to maintain constant concentrations in enclosures with openings

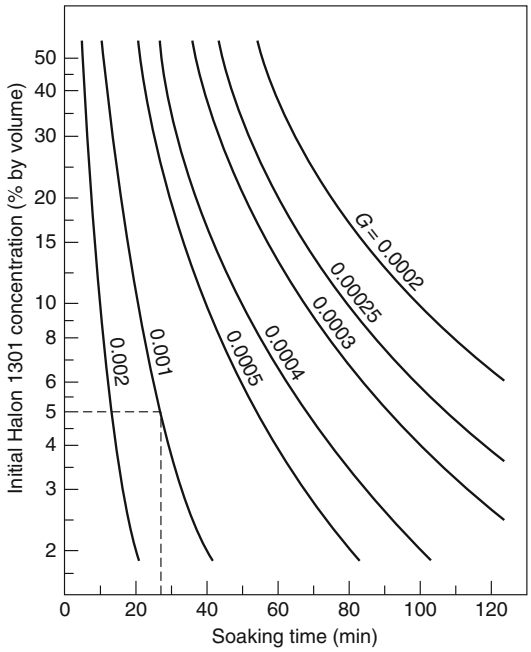

Fig. 43.13 Time required for interface between effluxing Halon 1301/air mixtures and influxing air to descend to center of enclosures not equipped for mixing

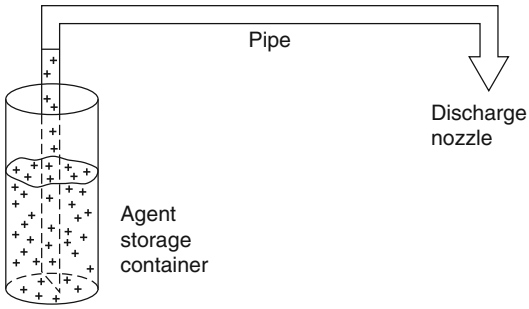

Fig. 43.14 Primary components of a Halon 1301 piping system

As illustrated in Fig. 43.14, the primary components of a Halon 1301 piping system are the agent storage container, the discharge nozzle, and the pipe. Often, more than one nozzle is required, complicating the calculations significantly. An attempt should always be made to keep the piping system simple and if possible, balanced. A balanced system has the actual and equivalent pipe lengths from container to each nozzle within ±10% of each other and has equal design flow rates at each nozzle [14].

As with sprinkler systems or other systems involving fluid flow, the methodology for solving Halon 1301 piping calculations involves seeking terminal characteristics based on property changes encountered due to the movement of the fluid. The system hydraulics are controlled by the selection of the orifice area at the discharge nozzle. This orifice area is calculated from the nozzle pressure, which is based on the starting pressure in the container and pressure losses in the pipe. Because the flow of Halon 1301 is nonsteady and has a change in phase from liquid to vapor, the calculations become highly complex. To simplify calculations, the average discharge conditions are determined so that they might reasonably represent the entire discharge time span. This time-independent model is based on the moment in time when half the liquid phase of the agent has left the nozzle. All the calculations for a 10 s discharge condition shown in Fig. 43.15 would be solved at the mid-discharge condition (5 s). Hence, the critical characteristics that vary with discharge, such as the storage container pressure and the pressure-density relationship in the pipeline, are replaced with average time-independent values [24].

By the time half of the liquid agent is out of the nozzle, the original pressure in the storage container has dropped considerably. To calculate the mid-discharge storage container pressure, the percent of agent still within the pipe must be determined. Also, the initial drop in pressure immediately after the start of discharge is nonlinear. As seen in Fig. 43.16, the pressure recovery is due to the nitrogen vigorously boiling out of the halon/nitrogen mixture within the storage container.

Unlike water-based fluid flow, the pressure drop occurring when Halon 1301 flows through a pipe is nonlinear and is dependent on the pipeline agent density, not the distance traveled. The pipeline flow is two phase, with a mixture of liquid and vapor agent. As the agent travels in the pipe, the pressure and density decrease, which increases the velocity and the amount of halon vapor. Interestingly, the evolution of the nitrogen from the halon/nitrogen mixture in the storage container causes the halon to drop in

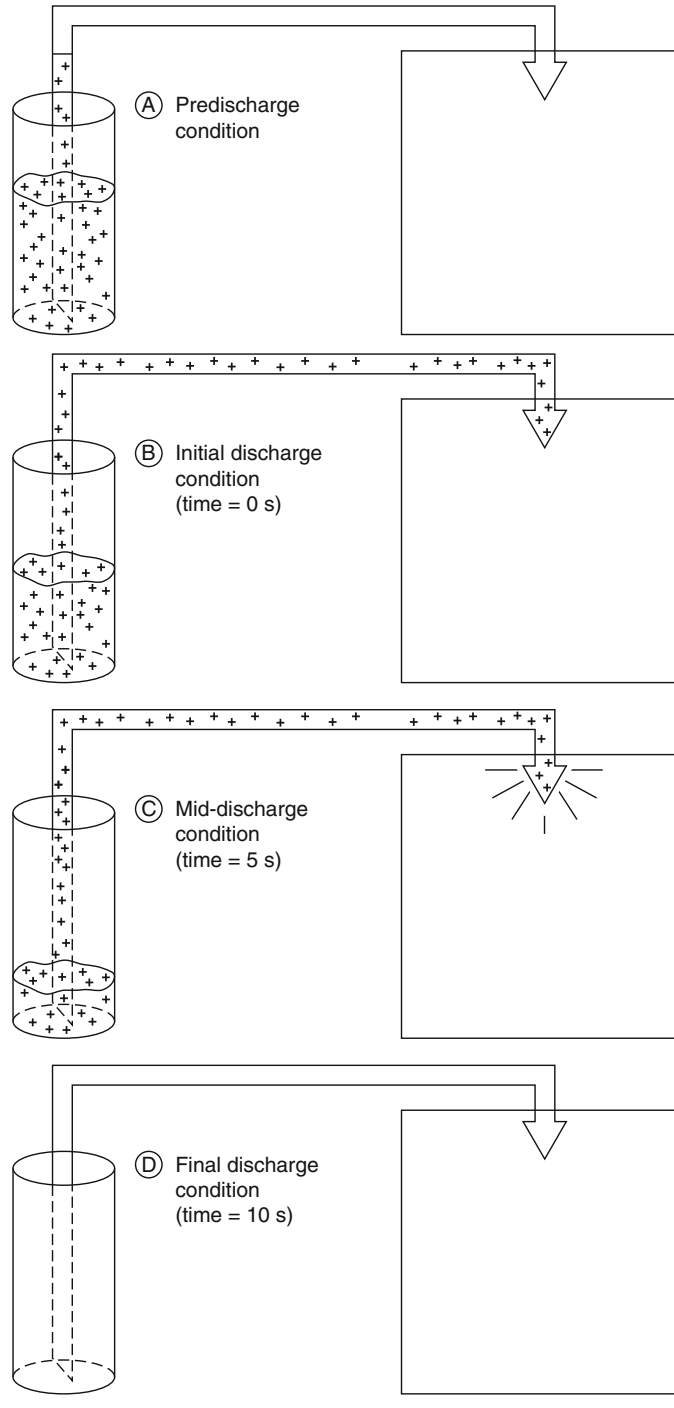

Fig. 43.15 Summary of Halon 1301 discharge conditions based on a 10 s discharge

temperature and become more dense. This phenomenon fortunately is not a factor in the calculations since a time-independent model is being used. The increase in density at any one location over the entire time span should not be confused with the decrease in density that occurs when the agent flows from one location to another.

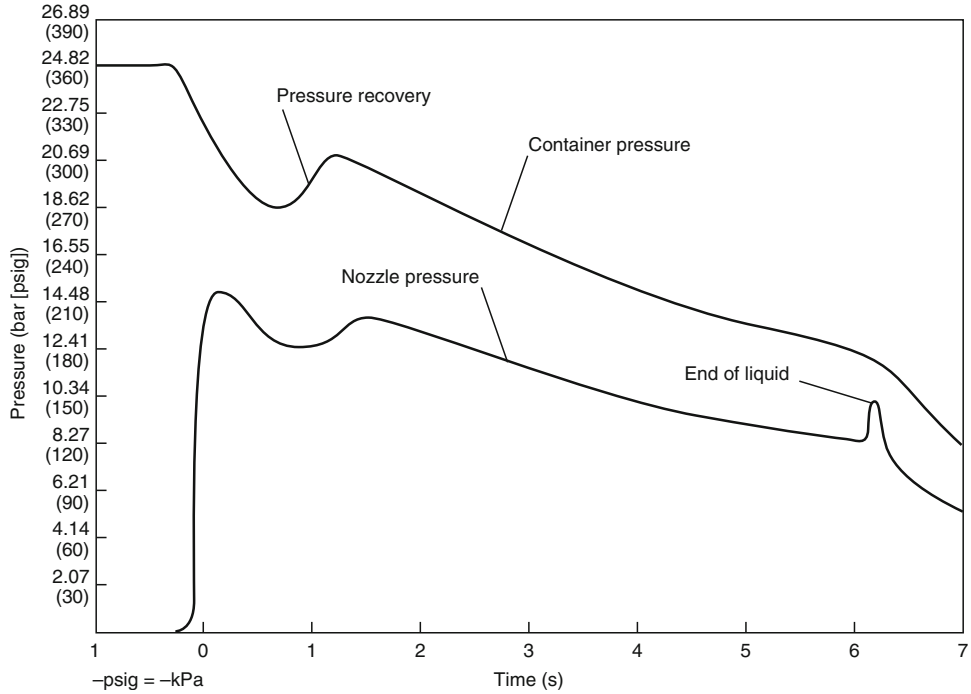

Fig. 43.16 Pressure profile during system discharge

Guidelines and Limitations

Unrealistic distribution networks often fail to perform to specifications and are difficult if not impossible to predict from a calculation standpoint. As the piping system becomes more unrealistic, the calculations become more unreliable. To aid in the development of accurate calculations, certain fundamental limitations are necessary to ensure proper system design. These limitations are especially important with respect to computer programs since these programs have a tendency to be operated abusively with high expectations. Summarized below are the design constraints for Halon 1301 hydraulic calculations [25].

1. Good design practice
2. Discharge time $\leq$10 s
3. Favorable system temperature
4. Initial container pressure = 2482.2 kPa (360 psig) or 4137.0 kPa (600 psig)
5. Initial container fill density $\leq$1121.4 kg/m3 (70 lb/ft3)
6. Percent in pipe $\leq$ maximum value
7. Turbulent flow $\geq$ minimum value
8. Nozzle pressure $\geq$ minimum value
9. Actual nozzle area $\leq$ percentage of feed pipe area
10. Actual nozzle area = calculated nozzle $\pm$5%

Good design practice includes such items as favoring balanced systems, keeping the degree of flow/split imbalance below a maximum value, avoiding vertically installed tees, and avoiding nozzles on different floor levels which may separate the halon gas/vapor mixture. The values for some of the constraints are determined by the individuals developing computer programs that are verified by approval agencies through testing.

Calculation Procedure

The piping calculations comprise four steps:

1. Determining the necessary input data
2. Calculating the average storage container pressure

3. Calculating the nozzle pressure at each nozzle
4. Calculating the nozzle orifice areas

Pipeline calculations are performed for each segment of pipe having both a constant flow rate and a uniform pipe diameter; thus the piping network is divided into sections called *junctions*. Each discharge nozzle is also identified. The forms necessary for the input data, pressure calculations, and nozzle calculations are contained in Figs. 43.17 and 43.18. Assuming the appropriate input data are known, the average storage container pressure is determined from Fig. 43.19 based on the percent agent in pipe, which itself is determined by [14]

$$\%\,\text{in pipe} = \frac{K_1}{(W_i/V_p) + K_2} \tag{43.9}$$

where

W_i = Initial charge weight of Halon 1301, lb
V_p = Internal pipe volume, ft^3 (Table 43.16)
K_1 and K_2 = Constants (Table 43.17)

Once the average storage container pressure is known, Figs. 43.18 and 43.20 and Equations 43.10 through 43.22 can be used to determine the nozzle orifice areas for a 360 psig system. Usually the calculations are based on a 10 s discharge time, though this is sometimes changed

System Halon weight _____ lb
Container fill density _____ lb/ft^3
Discharge time _____ s

Form I: System summary

N1: _____ lb N3: _____ lb N5: _____ lb
N2: _____ lb N4: _____ lb N6: _____ lb

A	B	C	D	E	F	G	H	I	W	X	Y
Inputs									Outputs		
Junction number	Nozzle number	Flow rate *Q*	Pipe type	Pipe diameter *D*	Actual pipe length *L*	Fittings, equivalent length *L*	Total length *L*	Elevation change *h*	Junction pressure *P* (starting of from Form II)	Density at orifice *r* (Fig. 4-6.20)	Orifice area *F* (Eq. 22)

Fig. 43.17 Halon 1301 piping calculation summary form

Form II: Pressure calculations

J	K	L	M	N	O	P	Q	R	S	T	U	V
Initial pressure				Final pressure								
	Elevation			Pipe size factors								
Junction pressure	Density r (Fig. 4-6.20)	Pressure P_e (Eq. 10)	Corrected starting pressure P_0	A (Eq. 11)	B (Eq. 12)	1st Y factor Y_1 (Table 4-6.19, Eq.13)	1st Z factor Z_1 (Eqs. 14–17)	Temporary Y factor Y_t (Eq. 18)	Temporary pressure P_t (Table 4-6.19, Eq.19)	2nd Z factor Z_2 (Eqs.14–17)	2nd Y factor Y_2 (Eq. 20)	Final junction pressure P (Table 4-6.19, Eq. 21)

Fig. 43.18 Halon 1301 pressure calculation summary form

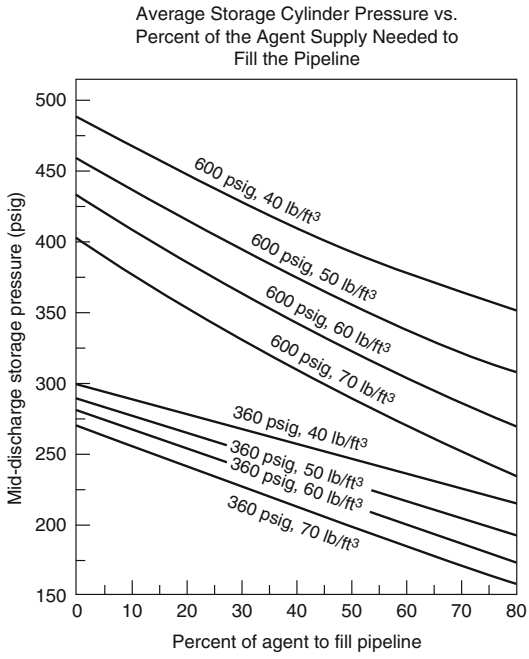

Fig. 43.19 Mid-discharge storage container pressure

slightly to produce flow rates in accordance with Table 43.18. Turbulent pipeline flow can also be achieved by using smaller pipe sizes. Pipe diameters that are too small result in unacceptably high pressure losses; therefore, care must be used in pipe size selection. It is important to recognize that approximations have been made for Y and Z factors and nozzle coefficients. The calculation procedure presented here is only intended to demonstrate the current methodology and not to provide a rigorous solution. The necessary equations are [14, 26]

$$P_e = \frac{rL_e}{144} \tag{43.10}$$

where
P_e = Elevation pressure, psig
r = Agent density, lb/ft^3
L_e = Pipe elevation length, ft

$$A = 1.013D^{5.25} \tag{43.11}$$

Table 43.16 Internal volume of steel pipe

Nominal pipe diameter (in.)	Schedule 40 inside diameter (in.)	ft3/ft	Schedule 80 inside diameter (in.)	ft3/ft
1/4	0.364	0.0007	0.302	0.0005
3/8	0.493	0.0013	0.423	0.0010
1/2	0.622	0.0021	0.546	0.0016
3/4	0.824	0.0037	0.742	0.0030
1	1.049	0.0060	0.957	0.0050
11/4	1.380	0.0104	1.278	0.0089
11/2	1.610	0.0141	1.500	0.0123
2	2.067	0.0233	1.939	0.0205
21/2	2.469	0.0332	2.323	0.0294
3	3.068	0.0513	2.900	0.0459
31/2	3.548	0.0687	3.364	0.0617
4	4.026	0.0884	3.826	0.0798

Table 43.17 Constants to determine percent of agent in piping

Storage (psig)	Filling density	K1	K2
600	70	7180	46
600	60	7250	40
600	50	7320	34
600	40	7390	28
360	70	6730	52
360	60	6770	46
360	50	6810	40
360	40	6850	34

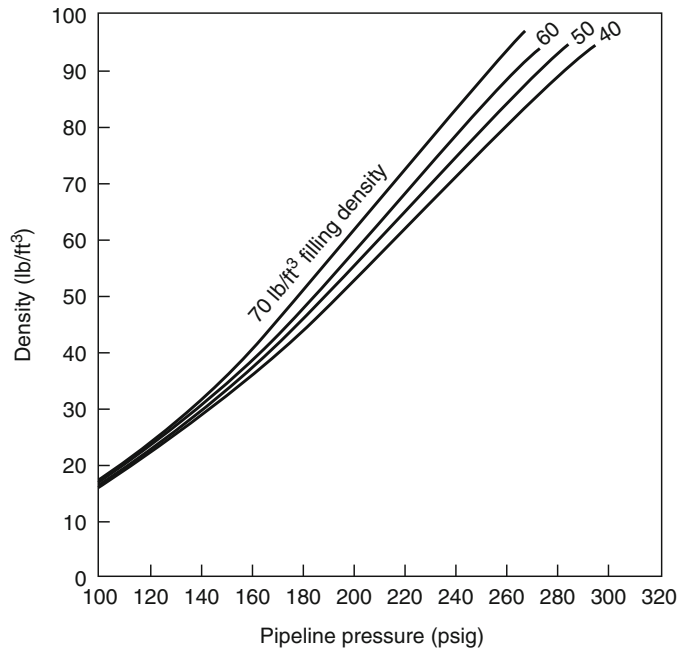

Fig. 43.20 Pipeline density/pressure relationship for a 360 psig system

Table 43.18 Minimum design flow rates to achieve turbulent pipeline flow

Nominal pipe diameter (in.)	Schedule 40 minimum flow rate (lb/s)	Schedule 80 minimum flow rate (lb/s)
1/8	0.20	0.11
1/4	0.34	0.24
3/8	0.68	0.48
1/2	1.0	0.79
3/4	2.0	1.9
1	3.4	2.8
11/4	5.8	4.8
11/2	8.4	7.5
2	13	13
21/2	19.5	17
3	33	26
4	58	48
5	95	81
6	127	109

Table 43.19 Constant for Y factor/pressure equations

P storage (psig)	Fill density (lb/ft3)	a	b	c	d
360	70	$3.571 \times 10 - 4$	0.6971	−63.50	−5921
360	60	$4.018 \times 10 - 4$	0.6913	−64.01	−6333
360	50	$3.125 \times 10 - 4$	0.6238	−56.90	−7386
360	40	$3.720 \times 10 - 4$	0.6187	−55.55	−8120

where
A = Pipe size factor
D = Actual pipe diameter, in.

$$B = \frac{7.97}{D^4} \tag{43.12}$$

where
B = Pipe size factor

$$Y_1 = \left(\frac{\mathrm{a}}{3}p_0^3 + \frac{\mathrm{b}}{2}p_0^2 + \mathrm{c}P_0 + \mathrm{d}\right) \tag{43.13}$$

where
Y_1 = First Y factor
P_0 = Junction starting pressure, psig
a, b, c, and d = Constants (Table 43.19)

$$Z = 1.01790 - 0.01179(P - 160) \quad \text{for 70 lb/ft}^3 \text{ fill density} \tag{43.14}$$

$$Z = 0.96913 - 0.01098(P - 170) \quad \text{for 60 lb/ft}^3 \text{ fill density} \tag{43.15}$$

$$Z = 0.96412 - 0.01051(P - 175) \quad \text{for 50 lb/ft}^3 \text{ for 40 lb/ft}^3 \tag{43.16}$$

$$Z = 0.95900 - 0.01008(P - 180) \quad \text{fill density} \tag{43.17}$$

where
Z = Z factor
P = Pressure, psig

$$Y_T = Y_1 + L\left(\frac{Q^2}{A}\right) \tag{43.18}$$

where
Y_T = Temporary Y factor
Q = Flow rate, lb/s

$$P_T^3 + \left(\frac{3b}{2a}\right)P_T^2 + \left(\frac{3c}{a}\right)P_T = -\left(\frac{3}{a}\right)Y_T - \left(\frac{3d}{a}\right) \tag{43.19}$$

where
P_T = Temporary pressure, psig

$$Y_2 = Y_T + B(Z_2 - Z_1)Q^2 \tag{43.20}$$

where
Y_2 = Second Y factor

$$P^3 + \left(\frac{3b}{2a}\right)P^2 + \left(\frac{3c}{a}\right)P = -\left(\frac{3}{a}\right)Y_2 - \left(\frac{3d}{a}\right) \tag{43.21}$$

$$F = 1.5Q\left[1/f(rp)^{1/2}\right] \tag{43.22}$$

where
F = Nozzle orifice area, in.^{2}
f = Nozzle coefficient (approximately 0.7)

Postdesign Considerations

Postdesign considerations are divided into two categories: system documentation and inspection/acceptance practices. Good halon system design is not complete until full documentation is provided for installation, acceptance, and eventual end user operation. Proper documentation is especially important to prevent the inadvertent discharge of a halon system for other than a fire, since replacement of the halon agent could be very difficult with future availability being dependent on recycled stock.

System Documentation

System documentation should include the items listed below. This material is necessary for others to install, test, operate, and maintain the system. Information can be recorded entirely on system drawings or in both a written manual and system drawings.

System Manual

1. Design Data
   (a) Functional and operational description
   (b) Halon 1301 weight calculations
   (c) Hydraulic piping calculations
   (d) Special considerations
2. Installation, Maintenance, and Inspection Instructions

As-Built System Drawings

1. Floor Plan Layout
   (a) Suitable dimensions
   (b) Equipment locations
   (c) Special installation details
2. Electrical Schematic
3. Equipment Identification
4. Special Notes

Inspection and Acceptance

After installation, each system should be inspected and tested by technicians trained by the equipment manufacturer covering the items listed below:

1. Test system wiring for proper connection, continuity, and resistance to ground.
2. Check system control unit in accordance with factory recommended procedures.
3. Calibrate and test each detector in accordance with factory recommended procedures.
4. Test each releasing circuit for proper resistance by means of a current-limiting meter.
5. Test the operation of all ancillary devices such as alarms, dampers, magnetic closers, and so on.
6. Obtain a certificate of inspection signed and dated by the installing contractor and the authority having jurisdiction.

An installation checklist is often used, which expands on the above items in complete detail [27]. These checklists are available from agent

and equipment manufacturers, installers, insurance groups, and consultants.

When accepting a newly installed halon system, it is important to determine compliance with design specifications. In previous years, a full discharge test was required to provide unquestionable evidence of performance, yet this could be a costly and sometimes unnecessary burden carried by the end user. End users with multiple systems would often prove system acceptance based on the performance characteristics of their other systems.

The primary reason for discharge test failure, when it was performed, was because the hazard enclosure would not hold the design concentration over the entire soaking period [28]. Checking the enclosure for possible halon leakage points has always been difficult and is the only questionable part of the acceptance/inspection procedure. A method referred to as the enclosure integrity test has proved to be very effective for this problem, and validates the integrity of the protected enclosure [14]. This technique shows much promise and has potential for substantially enhancing the reliability of proper system operation.

The most effective use of fan pressurization techniques for these types of applications is for leakage path indication [29]. This involves pressurizing or depressurizing the enclosure with the fan pressurization apparatus and using an indicating device, such as a smoke pencil or acoustic sensor, to determine leakage paths. The installers' visual inspection of the enclosure now becomes very effective since even the smallest cracks can be located. Due to low cost and simplicity, a smoke source is usually the most desirable method for locating leaks, but an excellent alternative is the use of a directional acoustic sensor that can be selectively aimed at different sound sources [30]. Highly sensitive acoustic sensors are available that can detect air as it flows through an opening and are sensitive enough to clearly hear a human eye blink [31]. Openings can also be effectively detected by placing an acoustic source on the other side of the barrier and searching for acoustic transmission. Another method is to use an infrared scanning device if temperature differences across the boundary are sufficient [32]. These techniques are not quantitative, but they are effective, inexpensive, and easily performed.

Environmental Considerations

Scientific evidence indicates that fire protection Halon 1301 is one of several man-made substances adversely affecting the earth's ozone layer [33]. Ozone exists naturally as a thin layer of gas in the stratosphere that blocks the sun's harmful ultraviolet rays and thus is vital to life on earth. Several adverse environmental and direct health effects are linked to ozone layer depletion, and its preservation is of paramount concern to mankind. It's believed that Halon 1301 (and other chlorofluorocarbons) chemically destroy ozone when emitted into the atmosphere.

Earlier, the phase-out of full system discharge tests that were used to verify enclosure integrity received special attention since they accounted for a proportionately large percentage of fire protection halon emissions. Fortunately, the amount of fire protection Halon 1301 released for actual fires is relatively small. Testing a system by performing a full discharge test allows the release of Halon 1301, which on a cumulative basis may be potentially harmful to the environment and depletes relatively precious stocks of halon agent that should be dedicated to suppressing fires. The release of Halon 1301 should be minimized.

With regard to ozone layer depletion, halons used for fire protection are different than halons used for other industrial applications [34]. Fire protection halons are unique because of their essential mission to prevent the loss of life, minimize the loss of irreplaceable property, assure the continuity of vital operations, and reduce the amount of fire by-products polluting the atmosphere. Efforts have been made to minimize the release of fire protection halons for noncritical tasks such as training, testing, and research. It is assumed that existing halon systems will remain in existence for an undetermined time into the

future, despite the present worldwide restriction on their production.

Nomenclature

a	constant (see Table 43.19)
A	pipe size factor
Ac	altitude correction factor (see Table 43.15)
b	constant (see Table 43.19)
B	pipe size factor
c	constant (see Table 43.19)
C	Halon 1301 concentration, percent by volume
*C*0	agent concentration at end of discharge, percent by volume
d	constant (see Table 43.19)
D	actual pipe diameter, in.
e	natural logarithm base, 2.71828
E	ventilation rate, m3/s (ft/s)
f	nozzle coefficient (approximately 0.7)
F	nozzle orifice area, in [2].
FL	fuel loading, kg/m3 (1b/ft3)
gc	acceleration due to gravity, 9.81 m/s2 (32.2 ft/s2)
G	geometric constant
h	heat of vaporization of the agent at *Ta,* kJ/kg (Btu/lb)
H	opening height, m (ft)
k	thermal conductivity of the piping, W/m · K (Btu · t/h · ft2 · f)
K	orifice discharge coefficient, 0.66
K*c*	conversion factor, 0.06093 (0.00685)
L	linear length of piping, m (ft)
Le	pipe elevation length, ft
LFL	lower flammable limit of fuel in air, percent volume
MFL	maximum allowable fuel loading, kg/m3 (lb/ft3)
MW	molecular weight of fuel
P	pressure, psig
*P*0	junction starting pressure, psig
Pe	elevation pressure, psig
PT	temporary pressure, psig
Q	flow rate, lb/s
r	agent density, lb/ft3
R	Halon 1301 discharge rate, kg/s (lb/s)
ri	inside pipe radius, mm (in.)
ro	outside pipe radius, mm (in.)
S	specific vapor volume of Halon 1301 based on temperature, m3/kg (ft3/lb)
SG	specific gravity of fuel
t	system discharge time
T	temperature, K (R)
*t*1	discharge time, s
*t*2	time after stopping discharge, s
Ta	agent temperature, C (F)
Tp	pipe temperature, C (F)
V	enclosure volume, m3 (ft3)
VF	volumetric quantity of fuel, m3 (ft3)
Vp	internal pipe volume, ft3 (see Table 43.16)
Wx	amount of agent increase, kg (lb)
W_{h_2O}	specific weight of water, 997.9 kg/m3 (62.3 lb/ft3)
W	weight of Halon 1301 required, kg (lb)
Wo	opening width, m (ft)
Wi	initial charge weight of Halon 1301, lb
*Y*1	first *Y* factor
*Y*2	second *Y* factor
YT	temporary *Y* factor
Z	factor

References

1. C.C. Grant, "Fire Protection Halons and the Environment: An Update Symposium," Fire Technology, 24, p. 1 (1988).
2. "The Halogenated Extinguishing Agents," NFPA Quarterly, 48, 8, Part 3 (1954).
3. D. Wharry and R. Hirst, Fire Technology: Chemistry and Combustion, Institute of Fire Engineers, Leicester, England (1974).
4. R. Strasiak, "The Development of Bromochloromethane (CB)," WADC Technical Report 53–279, Wright Air Development Center, Dayton, OH (1954).
5. Fire Protection Handbook, 17th ed., National Fire Protection Association, Quincy, MA (1991).
6. NFPA 12A-T, Standard on Halogenated Fire Extinguishing Agent Systems, National Fire Protection Association, Quincy, MA (1968).
7. NFPA 12A, Standard on Halon 1301 Fire Extinguishing Systems, National Fire Protection Association, Quincy, MA (1992).

8. NFPA 12B, Standard on Halon 1211 Fire Extinguishing Systems, National Fire Protection Association, Quincy, MA (1990).
9. NFPA 12C-T, Tentative Standard on Halon 2402 Fire Extinguishing Systems, National Fire Protection Association, Quincy, MA (1983).
10. NFPA 75, Standard for the Protection of Electronic Computer/Data Processing Equipment, National Fire Protection Association, Quincy, MA (1992).
11. C. Ford, Halon 1301 Computer Fire Test Program—Interim Report, DuPont Co., Wilmington, DE (1972).
12. NFPA 2001, Standard on Clean Agent Fire Extinguishing Systems, National Fire Protection Association, Quincy, MA (1994).
13. "DuPont Halon 1301 Fire Extinguishant," Technical Bulletin B-29E, DuPont Co., Wilmington, DE.
14. NFPA 12A, Standard on Halon 1301 Fire Extinguishing Systems, National Fire Protection Association, Quincy, MA (2004).
15. Evaluation of Telephone Frame Fire Protection, GTE/Fenwal, Holliston, MA (1970).
16. "Handling and Transferring 'Freon' FE 1301 Fire Extinguishing Agent," Technical Bulletin FE-2, DuPont Co., Wilmington, DE (1969).
17. D.G. Clark, The Toxicity of Bromotrifluoromethane (FE 1301) in Animals and Man, Ind. Hyg. Res. Lab., Imperial Chemical Industries, Alderley Park, Cheshire, England (1970).
18. R.D. Stewart, P.E. Newton, A. Wu, C. Hake, and N.D. Krivanek, Human Exposure to Halon 1301, Medical College of Wisconsin, Milwaukee, unpublished (1978).
19. The Hine Laboratories, Inc., Clinical Toxicologic Studies on Freon Fe-1301, Report No. 1, San Francisco, CA, unpublished report (1968).
20. J.L. Bryan, Fire Suppression and Detection Systems, Macmillan, New York (1982).
21. N. Sax, Dangerous Properties of Industrial Materials, Section 12, 2nd ed., Reinhold, New York (1963).
22. G.J. Grabowski, Fire Detection and Actuation Devices for Halon Extinguishing System, An Appraisal of Halogenated Fire Extinguishing Agents, National Academy of Sciences, Washington, DC (1972).
23. C. Ford, "Extinguishment of Surface and Deep-Seated Fires with Halon 1301," Symposium of an Appraisal of Halogenated Fire Extinguishing Agents, National Academy of Sciences, Washington, DC (1972).
24. H.V. Williamson, Halon 1301 Flow Calculations—An Analysis of a Series of Tests Conducted by FEMA at the Fenwal Test Site, Chemetron Corp., Hanover, PA (1975).
25. C.C. Grant, "Computer-Aided Halon 1301 Piping Calculations," Fire Safety Journal, 9, 2, pp. 171–179 (1985).
26. Flow in Pipes—Pyroforane Halon 1301, Produits Chimiques Ugine Kuhlmann, Corbevoie, France.
27. J.J. Brenneman and M. Charney, "Testing a Total Flooding Halon 1301 System in a Computer Installation," Fire Journal, 68, p. 6 (1974).
28. S.A. Chines, "Halon System Discharge Testing—An Authority Having Jurisdiction Point of View," Seminar Paper for Fire Protection Halons and the Environment, NFPA Annual Meeting, Cincinnati (1987).
29. C.C. Grant, "Controlling Fire Protection Halon Emissions," Fire Technology, 24, p. 1 (1988).
30. D.N. Keast, and H.S. Pei, "The Use of Sound to Locate Infiltration Openings in Buildings," Proceedings of the ASHRAE-DOE Conference on the Thermal Performance of the Exterior Envelope of Buildings, Orlando, FL, p. 85 (1979).
31. Ultraprobe 2000 Data Sheet (acoustic sensor), UE Systems, Elmsford, NY (2000).
32. A.K. Blomsterberg, and D.T. Harrje, "Approaches to Evaluation of Air Infiltration Energy Losses in Buildings," in ASHRAE Transactions, Vol. 85, Pt. 2, p. 797 (1979).
33. S.O. Andersen, "Halons and the Stratospheric Ozone Issue," Fire Journal, p. 56 (May/June 1987).
34. G. Taylor, "Achieving the Best Use of Halons," Fire Journal, 81, 3, p. 69 (1987).

Casey C. Grant is Executive Director at the Fire Protection Research Foundation and was previously secretary of the NFPA Standards Council. He is a former member of the NFPA Technical Committee on Halogenated Fire Extinguishing Agent Systems and was previously supervisor of systems design engineering at Fenwal Incorporated.

Clean Agent Total Flooding Fire Extinguishing Systems

44

Philip J. DiNenno and Eric W. Forssell

Introduction

Total flooding clean agents and systems were developed in response to the regulation of Halon 1301 under the Montreal Protocol and its amendments, which culminated in the phase-out of production of halons in the developed countries on December 31, 1993. This regulation engendered tremendous research and development efforts across the world in a search for replacements and alternatives. Since that time, on the order of 15 total flooding clean agent alternatives to Halon 1301 have been commercialized and development continues on others. In addition to clean total flooding gaseous alternatives, new technologies, such as water mist and fine solid particulate, are being introduced. This chapter focuses on total flooding clean agent halon replacements.

Table 44.1 is a summary of common halocarbon and inert gas extinguishing agents developed to date. The most widely used commercialized total flooding agents include HFC-227ea, HFC-125, FK-5-1-12 and all of the inert gases. Perfluorocarbons (PFC) and Hydrochlorofluorocarbons (HCFC) agents are essentially no longer used due to environmental regulations. The best performing replacement agent in terms of effectiveness per unit mass is the Trifluoroiodide but concerns regarding toxicity precluded that agent from widespread commercialization and adoption. The table gives the chemical name; trade name; American Society of Heating, Refrigerating, and Air Conditioning Engineers, Inc. (ASHRAE) designation (for halocarbons); and the chemical formula.

Characteristics of Clean Agents

Clean fire suppression agents are generally defined as electrically nonconducting fire extinguishants that vaporize readily and leave no residue [1]. They are subject to specific evaluation with regard to their hazards to personnel and their effect on the environment. Depending upon the agent, they are stored under high pressure as a liquid or a gas, and are utilized in their gaseous state when released from their storage containers. Clean agent halon replacements fall into two broad categories: (1) halocarbon compounds and (2) inert gases and mixtures.

Halocarbon clean agents include compounds containing carbon, hydrogen, bromine, chlorine, fluorine, and iodine. They are grouped into five categories: (1) hydrobromofluorocarbons (HBFC), (2) hydrofluorocarbons (HFC), (3) hydrochlorofluorocarbons (HCFC), (4) perfluorocarbons (FC or PFC), and (5) fluoroiodocarbons (FIC) and Fluoroketones (FK). The recent introduction of Fluoroketones has enabled the use of halocarbon agents with near zero global warming potential in normally occupied areas.

P.J. DiNenno • E.W. Forssell (✉)
Jensen Hughes (Formerly Hughes Associates, Inc.),
3610 Commerce Drive, Suite 817, Baltimore,
MD 21227

M.J. Hurley (ed.), *SFPE Handbook of Fire Protection Engineering*,
DOI 10.1007/978-1-4939-2565-0_44, © Society of Fire Protection Engineers 2016

Table 44.1 Commercialized halon replacement nomenclature

Chemical name	Trade name	ASHRAE designation	Chemical formula
Heptafluoropropane	FM-200	HFC-227ea	CF_3CHFCF_3
Trifluoromethane	FE-13	HFC-23	CHF_3
Chlorotetrafluoroethane	FE-24	HCFC-124	$CHClFCF_3$
Pentafluoroethane	FE-25	HFC-125	CHF_2CF_3
Dodecaflouro-2-methylpentan-3-one	Novec 12330	FK-5-1-12mmy2	$CF_3CF_2C(O)(CF(CF_3))_2$
Hexaflouropropane	FE-36	HFC-236fa	$CF_3CH_2CF_3$
Triflouroiodide	Triodide	FIC-13I1	CF_3I
$N_2/Ar/CO_2$	Inergen	IG-541	N_2 (52 %)
			Ar (40 %)
			CO_2 (8 %)
N_2/Ar	Argonite	IG-55	N_2 (50 %)
			Ar (50 %)
Argon	Argon	IG-01	Ar (100 %)
Nitrogen	Nitrogen	IG–100	N_2

Although the characteristics of halocarbon clean agents vary widely, they share several of the following common attributes:

1. All are electrically nonconductive,
2. All are clean agents; that is, they vaporize readily and leave no residue,
3. All are liquefied gases or display analogous behavior (e.g., compressible liquid),
4. All can be stored and discharged from typical Halon 1301 hardware (with the possible exception of HFC-23, which more closely resembles 600 psig [40 bar] superpressurized halon systems),
5. All (except HFC-23) use nitrogen superpressurization in most applications for discharge purposes,
6. All are less efficient fire extinguishants than Halon 1301 in terms of storage volume and agent weight. The use of most of these agents requires increased storage capacity.
7. All are total flooding gases after discharge. Many require additional care relative to nozzle design and mixing,
8. All produce more decomposition products (primary HF) than Halon 1301, given similar fire type, fire size, and discharge time,
9. All halocarbon agents except FK-5-1-12mmy2 and FIC-13I1 have substantial greenhouse warming characteristics; FK-5-1-12mmy2, a Fluoroketone, has a near zero global warming potential,
10. All of the halocarbon agents have a near zero ozone depletion potential, (ODP) and,
11. All halocarbon agents must be evaluated with respect to health and safety concerns, which are primarily related to cardiac sensitization, as discussed later in this chapter.

Inert gas clean agents include nitrogen and argon and blends of these. One inert gas replacement has a small fraction of carbon dioxide. Carbon dioxide is not an inert gas because it is physiologically active and toxic at low concentrations. However, the approximately 8 % of carbon dioxide used as a component of IG-541 is not considered to pose a safety concern in terms of toxicity. Inert gas clean agents share the following common attributes:

1. All are electrically nonconductive.
2. All are clean agents; that is they leave no residue.
3. All are stored as compressed gases utilizing low capacity high pressure cylinders,
4. All are less efficient fire extinguishants than Halon 1301 in terms of storage volume and agent weight. Storage volumes are much greater than Halon 1301 or the halocarbon clean agents due to the need for high pressure cylinders,

Table 44.2 Comparisons of systems in 500–5000 m^3 range of volumes [2]

	Percentage additional weight when compared to a Halon 1301 system						
	Halon 1301	CO_2	FE-13	FM-200	Novec 1230	Inergen	Water mist
Weight comparison							
500 m^3	0	150	200	50	50	400	625
1000 m^3	0	163	188	38	50	450	613
3000 m^3	0	200	219	48	71	529	671
5000 m^3	0	186	211	36	58	497	522
Footprint comparison							
500 m^3	0	84	105	20	20	327	1119
1000 m^3	0	82	94	20	20	365	889
3000 m^3	0	118	122	19	43	459	1030
5000 m^3	0	99	107	6	19	404	636
Percentage cost comparison							
500 m^3	0	108	315	202	259	277	1032
1000 m^3	0	140	406	267	368	330	723
3000 m^3	0	200	553	351	513	449	478
5000 m^3	0	204	585	361	515	460	376

5. Inert gases do not produce more decomposition products,
6. Inert gas agents have zero global warming potentials,
7. All of the halocarbon agents have a zero ozone depletion potentials, and,
8. All inert gas agents must be evaluated with respect to health and safety concerns, which are primarily related to oxygen depletion, as discussed later in this chapter.

Wickham [2] has provided comparative values for cost and footprint of potential halon, replacement systems for use in marine applications. These comparisons are given for weight, footprint, and cost in Table 44.2. Note that all clean agents require at least 50 % more agent by weight than halon as a consequence of the elimination of bromine in the compounds and subsequent level of catalytic recombination of flame radicals. These data should be taken as representative values, as there are variations among hardware manufacturers. The storage volume equivalent does not translate directly to a required area or volume for storage cylinders. The relative footprint of these storage volume equivalents will vary with the volume of the space protected and the maximum storage cylinder size offered by a manufacturer for a particular gas.

Extinguishing Mechanisms

Halocarbon clean agents extinguish fires by a combination of chemical and physical mechanisms depending on the compound. Chemical suppression mechanisms of HBFC and FIC compounds are similar to Halon 1301; that is, the Br and I species scavenge flame radicals, thereby interrupting the chemical chain reaction. FIC-13I1 is the only HBFC or FIC compound listed in Table 44.1. Other replacement compounds suppress fires primarily by extracting heat from the flame reaction zone, thereby reducing the flame temperature below that which is necessary to maintain sufficiently high reaction rates by a combination of heat of vaporization, heat capacity, and the energy absorbed by the decomposition of the agent. Oxygen depletion also plays a role in reducing flame temperature.

The energy absorbed in decomposing the agent by breaking fluorine and chlorine bonds is quite important, particularly with respect to decomposition production formation. There is undoubtedly some degree of "chemical" suppression action in flame radical combustion with halogens, but it is considered to be of minor importance since it is not catalytic (e.g., one F radical combines with one H flame radical).

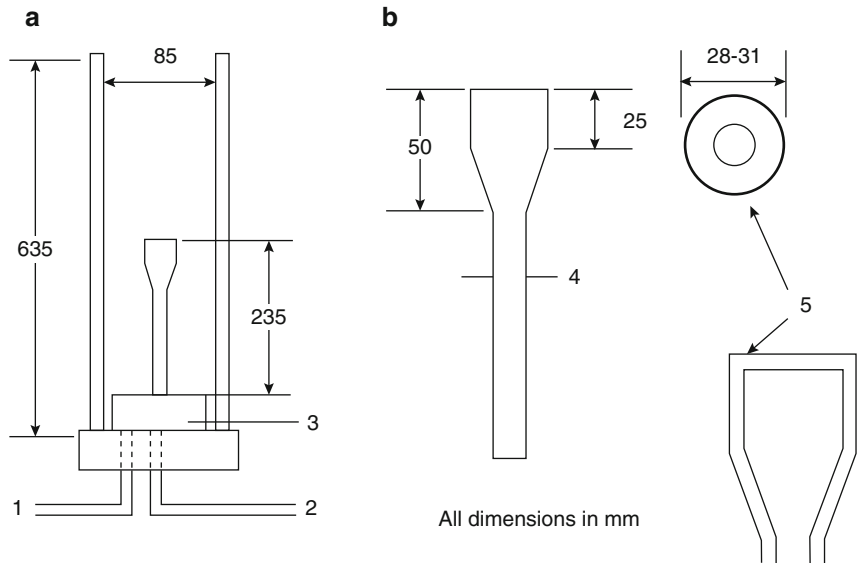

Fig. 44.1 Schematic of cup burner apparatus [3]

The lack of significant chemical reaction inhibition in the flame zone by HCFC, HFC, and FC compounds results in higher extinguishing concentrations relative to Halon 1301. The relative importance of the energy sink represented by breaking halogen species bonds results in higher levels of agent decomposition relative to Halon 1301.

Inert gas clean agents act by reducing the flame temperature below thresholds necessary to maintain combustion reactions. This condition is created by reducing the oxygen concentration and by raising the heat capacity of the atmosphere supporting the flame. The addition of a sufficient quantity of inert gas to reduce the oxygen concentration below 12 % (in air) will extinguish flaming fires. The agent concentration required is also a function of the heat capacity of the inert gas added. Hence, there are differences in minimum extinguishing concentration between inert gases.

Flammable Gas and Liquid Extinguishing Concentration

Flame suppression effectiveness of total flooding clean agents has been evaluated in a number of ways. The predominant small-scale test method for establishing flame extinguishing concentrations for liquid and gaseous fuels is the cup burner or variations thereof.

Figure 44.1 is a schematic of the cup burner apparatus as specified in ISO 14520 [3]. A small laminar flame is established above a "cup" of fuel surrounded by a cylindrical chimney. An air-agent mixture flows up the chimney surrounding the flame. The minimum concentration of agent (in air) at which the flame is extinguished is the minimum extinguishing concentration (MEC). There are many variations of the basic device as used by different laboratories. These variations include cup and chimney diameter, different mixing and measuring methods, chimney height, and agent-air mixture velocity past the flame [3]. Since about 2005, cup burner devices and test procedures have been standardized to the point where very little variation is seen between devices and laboratories. Users are cautioned that older data may not have been obtained using the standardized apparatus and procedures. The current n-heptane cup burner extinguishing values using the more recent standardized device are given Table 44.3. In addition, the validity and utility of the cup burner test apparatus has been verified in part by a theoretical model of the flame extinction process [4].

Table 44.3 n-Heptane cup burner extinguishing values from various investigators

Reference	Halon 1301	FK-5-1-12	HFC-125	HFC 227ea	IG-541	IG-55
NFPA 2001[1]	~3.2	4.5	8.7	6.7	31	35

From NFPA 2001[1]

Table 44.4 Agent fraction in the oxidizer stream at extinction of n-heptane cup burner flames [5]

Agent type	Agent	Mass percent	Volume percent
Inert	N_2	31	32
	CO_2	32	23
	He	6.0	31
	Ar	38	41
Nitrogen containing	NF_3	[a]	[a]
Silicon containing	SiF_4	36	13
Sodium containing	$NaHCO_3$ (10–20 μm)	3.0	[b]
Hydrofluorocarbons	CF_3H	25	12
	CF_2H_2	[c]	[c]
	CF_2H_2/C_2HF_5	30	15
	CH_2FCF_3	29	10
	CHF_2CF_3	29	8.7
	$CF_3CH_2CF_3$	27	6.5
Fluorocarbons	C_3HF_7	28	6.2
	CF_4	37	16
	C_2F_6	30	8.1
	C_3F_6	29	7.3
	C_3F_8	30	6.3
	c-C_4F_8	32	6.3
Chlorine containing	C_4F_{10}	32	5.3
	CHF_2Cl	28	12
	$CHCl_2F$	32	11
	CH_3CF_2Cl	[c]	[c]
	$CF_2 = CHCl$	[c]	[c]
	$CF_2 = CFCl$	31	10
Bromine containing	$CHFClCF_3$	26	7.0
	CF_3Br	14	3.1
	CF_2Br_2	16	2.6
	CH_2BrCF_3	17	3.5
	$CH_2 = CHBr$	[c]	[c]
	$CF_2 = CFBr$	27	6.3
Iodine containing	$CF_2 = CHBr$	24	6.0
	CF_3I	18	3.2

[a]Acted as an oxidizer, promoted flame stability
[b]Solid powder not expressed in volume percent
[c]Agent observed to be flammable

The cup burner concentration for IG-541 is 31 % as given in Table 44.3. This result is in contrast to concentrations of 32, 41, and 23 % by volume measured by the National Institute of Standards and Technology (NIST) for nitrogen, argon, and carbon dioxide, the components of Inergen. NIST has conducted investigations on a wide range of halon replacement chemicals for aviation use. In order to give a wider perspective on the type and range of chemicals being evaluated for fire suppression use, Table 44.4 is included. The table gives cup burner n-heptane

Table 44.5 Cup burner minimum extinguishing concentrations [5–9]

	Cup burner extinguishment concentration (Vol %)				
Fuel	HFC-227eab	FC-3-1-10	HFC-23	HCFC Blend A	N2
Acetone	6.8[e]	5.5[a]			
Acetonitrile	3.7[e]				
AV gas	6.7[e]				
n-Butanol	7.1[e]				
n-Butyl acetate	6.6[e]				
Cyclopentanone	6.7[e]				
Diesel no. 2	6.7[e]				
Ethanol	8.1[e]	6.8[a]			
Ethyl acetate	5.6[e]				
Ethylene glycol	7.8[e]				
Gasoline (unleaded)	6.5[e]				
n-Heptane	6.0[b]	5.2[c]	12.0[c]	12.6[d]	32[b]
	5.8–6.6[c]	5.0[d]	12.6[d]		
Hydraulic fluid	5.8[b]	4.3–4.5[b]			22–26[b]
JP-4	6.6[e]				
JP-5	6.0[b]	4.8[b]			27[b]
	6.6[c]				
Methane	6.2[e]				
Methanol	10.0[e]	9.4[a]			
Methyl ethyl ketone	6.7[e]				
Methyl isobutyl ketone	6.6[e]				
Morpholine	7.3[e]				
Propane	6.3[e]	6.0[b]			32.5[b]
i-Propanol	7.3[e]				
Pyrrolidine	7.0[e]				
Tetrahydrofuran	7.2[e]				
Toluene	5.8[e]				
Turbo hydraulic oil 2380	5.1[e]				
Xylene	5.3[e]				

[a]From Ferreira et al. [9]
[b]From Hamins et al. [5]
[c]From Sheinson et al. [7]
[d]From Moore et al. [8]
[e]From Robin [6]

flame extinction data for a wide range of potential halon replacements.

Table 44.5 presents cup burner MEC for a range of fuels and agents taken from various sources [5–9]. Where multiple values of the MEC were found, they are given. The nitrogen data are presented as representative inert gas values. Argon/N2 blend MEC values would be higher. These data were not all developed using the standardized cup burner device. These data should not be used for design purposes without ensuring that the concentrations are consistent with system manufacturer requirements and third-party approvals.

Table 44.6 presents cup burner and full-scale data from VdS [10]. Table 44.7 is a compilation of "best values" of cup burner data from a range of sources compiled by Tapscott [11].

In addition to the cup burner apparatus, researchers at NIST have utilized an opposed-flow diffusion flame (OFDF) apparatus to rank clean agents (halon replacements) for fire

Table 44.6 Inert gas extinguishing concentration data from VdS [10]

		ISO cup burner			Room fire	
Extinguishant gas	Fuel	Fuel unheated (percent by volume gas)	Fuel heated (percent by volume gas)	VdS large cup burner (percent by volume gas)	Extinguished (percent by volume gas[a])	Not extinguished (percent by volume gas[a])
CO_2	Acetone	18.7	19.4	21.4		
	Diethyl ether	–	23.0			
	Ethanol	20.8	23.0			
	n-Heptane	19.6	21.1	23.3	24.1	23.1
	n-Hexane	20.4	21.3			
	Methanol	27.5	28.5	31.3		
	n-Pentane	–	21.6			
	Toluol	15.9	16.7			
	Polypropylene			21.5		
	Polyethylene			20.8		
	Wood crib				26.8	24.4
Argon	Acetone	37.8	38.8	43.7		
	Diethyl ether	–	44.8			
	Ethanol	41.4	44.1			
	n-Heptane	40.9	41.4	45.0	40.8	38.7
	n-Hexane	40.0	41.5			
	Methanol	52.2	55.6	54.5		
	n-Pentane	–	41.7			
	Toluol	32.7	35.5			
	Polypropylene			40.6		
	Polyethylene			37.8		
	Wood crib				30.7	29.0
Inergen	Acetone	29.4	31.7	35.9		
	Diethyl ether	–	35.7			
	Ethanol	32.8	35.5			
	n-Heptane	33.0	33.8	37.2		
	n-Hexane	31.6	34.8			
	Methanol	41.1	43.8	47.3		
	n-Pentane	–	32.9			
	Toluol	25.7	28.1			
	Polypropylene			35.8		
	Polyethylene			31.3		
	Wood crib				28.1	26.6
Nitrogen	Acetone	28.5	29.9	33.2		
	Diethyl ether	–	33.8			
	Ethanol	32.1	34.5			
	n-Heptane	30.9	32.3	35.6	36.6	33.8
	n-Hexane	30.6	32.6			
	Methanol	38.5	41.2	44.8		
	n-Pentane	–	32.4			
	Toluol	22.2	28.0			
	Polypropylene			34.7		
	Polyethylene			30.8		
	Wood crib				28.6	27.7

[a]Calculated on the basis volume of discharge extinguishant

Table 44.7 "Best values" of cup burner concentrations (vol %) [11]

Fuel	Halon 1301	FC-3-1-10	FIC 13I1	HCFC Blend A	HCFC 124	HFC 125	HFC 227ea	HFC-23	HFC 236fa	IG-01	IG-100	IG-541	IG-55
70 % isopropanol in water													26 (1)
80 % methanol/ 20 % n-heptane	5.8 (1)*	5.2 (1)					8.3 (1)*						
Acetone				10.0 ± 0.7 (2)*			6.8 ± 0.1 (2)*			38 (1)	29 (1)	29 ± 0.90 (3)	31 (1)
Acetonitrile				7.0 (1)*						33 (1)*			16 (1)
Aviation gas, 100 octane, low lead				11.4 ± 0.1 (2)*						32 (1)*		30 (1)	26 (1)
Benzene	2.4 (1)	3.4 (1)					4.8 (1)	10.6 (1)			31(1)		
n-Butanol				12.2 (1)*						36 (1)*			33 (1)
n-Butyl acetate				9.8 (1)*									36 (1)
Carbon disulfide													49 (1)
Cyclohexane				10.1 ± 0.3 (2)*						36 (1)*			32 (1)
n-Decane	3.9 (1)										34 (1)		
Diesel					6.8 (1)*								
Diesel no. 2				8.9 (1)						27 (1)*			26 (1)
Diethyl ether										45 (1)	34 (1)	36 (1)	
n-Dodecane	3.7 (1)										33 (1)		
Ethanol	4.3 ± 0.0 (2)	6.9 ± 0.0 (2)					8.5 ± 0.2 (2)	16.0 ± 0.0 (2)		41 (1)	35 ± 2.7 (3)	35 ± 3.3 (2)	30 (1)
Ethyl acetate				10.6 (1)*						35 (1)*			30 (1)
Ethylene glycol				11.1 (1)*						31 (1)*			30 (1)
Exxon Turbo Oil													16 (1)
Gasoline (unleaded)				9.7 (1)*	7.5 (1)					37 (1)*			26 (1)
Heptane (commercial)	3.2 (1)						6.5 ± 0.2 (1)	12.6 ± 0.5 (2)				32 (1)	
n-Heptane	3.4 ± 0.0 (2)	5.4 ± 0.1 (3)	3.2 (1)	9.9 (1)	6.7 ± 0.3 (3)*	8.9 (1)	6.6 ± 0.0 (5)	13.0 ± 0.2 (3)	6.3 ± 0.4 (3)*	42 ± 1.4 (3)	33 ± 1.6 (3)	31.2 (5)	35 ± 3.7 (2)

n-Hexane				11.0 ± 0.1 (2)*					40 (1)	31 (1)	31 ± 0.4 (2)	29 (1)
Hydraulic oil (Mobil Fluid 350)									26 (1)*			21 (1)
Hydrogen				20 (1)*								
Isobutanol												29 (1)
Isooctane				9.8 (1)*		5.9 (1)	11.3 (1)					
Isopropanol				10.6 (1)*		7.2 ± 0.2 (1)			35 (1)*		28 (1)	28 (1)
Jet A/JP-5				9.0 (1)*	6.9 (1)*				32 (1)*			26 (1)
JP-4				10.1 (1)*					32 (1)*			
JP-8				9.7 (1)								
Kerosene	3.4 (1)	5.0 (1)				6.4 (1)	12.5 (1)			30 (1)	31 (1)	
Methane				13.7 (1)*					35 (1)*			25 (1)
Methanol	7.8 (1)	8.0 (1)		17 (1)		10.2 ± 0.4 (3)	19 (1)	8.0 (1)*	52 (1)	41 ± 3.5 (2)	41 (1)	39 (1)
Methyl isobutyl ketone				9.4 (1)*								
Morpholine				13.7 (1)*					38 (1)*			
Natural gas				12.4 (1)*								
Nitromethane									34 (1)*			32 (1)
n-Octane	3.4 (1)									34 (1)		
n-Pentane										30 (1)*		
Propane				12.6 (1)*					40 (1)*			34 (1)
n-Propanol				10.6 (1)*								
Pyrrolidine				10.1 (1)*								31 (1)
Tetrahydrofuran				12.0 (1)*		4.8 ± 0.3 (4)	9.7 ± 0.0 (2)					32 (1)
Toluene	2.3 ± 0.0 (2)	3.6 ± 0.0 (2)		6.8 (1)		6.6 (1)	12.8 (1)		33 (1)	25 ± 2.0 (3)	25 ± 0.5 (2)	26 (1)
Transformer oil	2.3 (1)	5.4								27 (1)	28 (1)	
n-Undecane			3.8 (1)							33 (1)		
Xylene				8.7 (1)*					26 (1)*			24 (1)

*Not determined with standard cup burner apparatus

extinguishing effectiveness. The OFDF burner is commonly used for combustion research. It has many advantages as a research tool for fundamental combustion studies. Its primary advantage is in its ability to relate the results to fundamental predictions of flame structure and conditions at flame extinction. The oxidizer (and suppressant) stream is forced down onto the fuel surface, exhaust gases are drawn down through an annulus or jacket around the fuel cup, and a flat flame is established. Water cooling is provided for the fuel cup and exhaust gas.

The OFDF burner can vary the turbulence intensity or strain rate of the flame. For most applications of clean agent fire suppression, the strain rate is not a major concern, but in specialized applications, such as engine nacelles with high fuel and oxidizer flow rates or in high-pressure spray or jet fires, the strain rate will substantially impact the minimum condition for extinguishment. Figure 44.2 is a sample plot showing the variation of the mole fraction of extinguishing agent versus the strain rate at extinction for n-heptane fuels for a range of suppressants. For typical natural fires, the strain rate is approximately 25 s^{-1}. At high strain rates, the flame is extinguished at lower agent concentrations.

Figure 44.3 shows the relationship between MEC for the cup burner and OFDF apparatus. As expected, the cup burner concentration is quite similar to the OFDF concentration at a low strain rate (25 s^{-1}), typical of natural fires. In all cases, the MEC of agent is much lower for high strain rate flames, which further reinforces the value of the cup burner and OFDF apparatus for evaluation of minimum extinguishing concentration. The reduction in extinguishing concentration as a function of the velocity of the agent/air mixture across the flame has important ramifications in the evaluation of extinguishment results when the velocity of the agent/air mixture at the flame is not well controlled. This often gives rise to erroneous and misleadingly low extinguishing concentrations obtained from full-scale room test results. When in doubt the higher extinguishing concentration obtained by small-scale tests at low strain rates should be used. This is particularly important because at near flame extinction conditions there is a very strong dependence of extinguishing concentration and velocity of the agent/air mixture. The practical implications of this fact are discussed later in this chapter under design concentrations.

Solid Fuel Extinguishing Concentrations

Extinguishing concentrations for Class A fuels were traditionally developed using wood cribs as

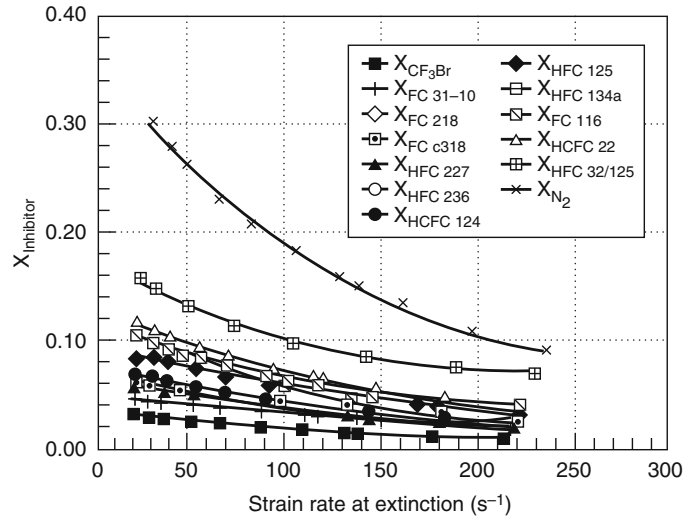

Fig. 44.2 Mole fraction of various suppressants as a function of strain rate at extinction for n-heptane [5]

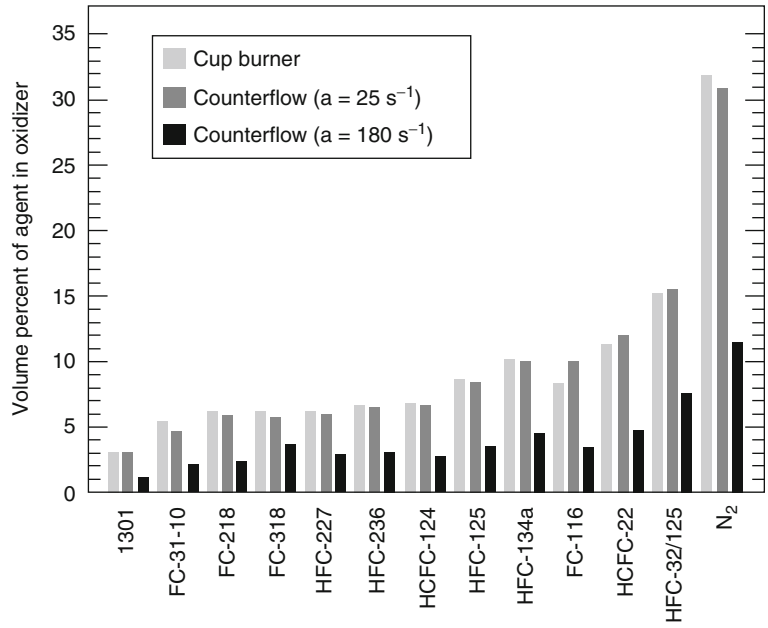

Fig. 44.3 Comparison of n-heptane extinction results for the cup burner and OFDF apparatus at two strain rates [5]

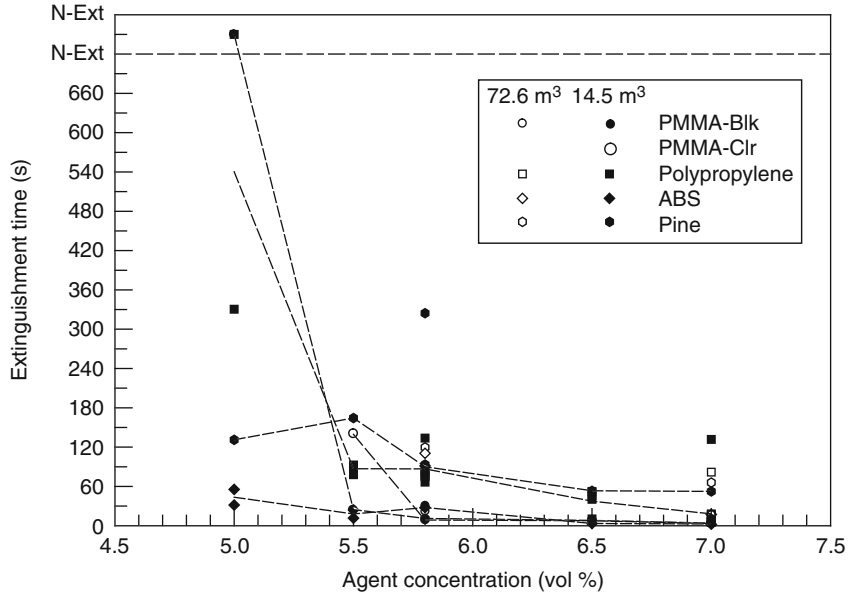

Fig. 44.4 Typical Class A extinguishment results for HFC-227ea

part of the equipment listing/approval process. Further, the minimum Class A extinguishing concentration used for design purposes was required to be greater than or equal to the minimum extinguishing concentration (MEC) for heptane. Additional tests utilizing plastic sheet arrays of polymethylmethacrylate (PMMA), acrylonitrile-butadiene-sytrene (ABS), and polypropylene (PP) have been required [12, 13]. Typical results are shown in Fig. 44.4 for two different room sizes. The results of these tests indicate that for extinguishment times exceeding

3 min, the extinguishing concentrations for these materials are below the heptane cup burner value and in general above the concentration required to cause extinguishment of the wood crib fires. The plastic sheet array fires therefore determine the Class A concentration requirements for these agents. Note that the most recent addition of NFPA 2001[1], imposes a minimum Class A design concentration equal to that of the minimum extinguishing concentration for n-heptane as determined with the cup burner apparatus.

Table 44.8 gives extinguishment and design concentration values for clean agents, using both NFPA 2001, Standard on Clean Agent Fire Extinguishing Systems, and the related UL third-party approval protocols and ISO 14520 installation standard. The extinguishing concentration values designated as test results in the table vary between NFPA 2001 and ISO 14520, primarily due to the slight differences in the test protocols, particularly for Class A solid fuel surface fires. There are differences between some equipment manufacturers for the same agent, which indicates a significant problem with the validity of the test result, in that the extinguishing concentrations should be independent of the system delivery hardware used. To the extent that there are hardware dependencies, the actual extinguishing concentration is, at best, equal to the higher value. Test differences between NFPA 2001 and ISO 14520, particularly for Class A fuels, indicate that the NFPA minimum extinguishing concentrations are artificially low for most agents. This is in part due to efforts by system manufacturers to reduce the minimum extinguishing concentration for Class A fuels with regards to the NFPA 2001 Standard and UL Approval Standards. For example, the HFC-227ea minimum extinguishing concentration for Class A fuels was reduced from 5.8 % to 5.2 % between 1996 and 2010.

At a minimum, the ISO test values for minimum extinguishing concentration should be used. Additional discussion of the design concentration values in the table is presented later in this chapter.

Energized Electrical Equipment Extinguishing Concentrations

Clean agent systems are widely used in electronic equipment areas where fires involving electrically energized cables and equipment are encountered. Extinguishment tests involving PMMA heated externally with Nichrome wire indicated that agent concentrations substantially higher than those typical for plastic fuels were required. For example, minimum extinguishing concentrations of 9.5, 9, 20, and 56.1 % were required for FC-3-1-10, HFC-227ea, HFC-23, and IG-541 respectively at the highest applied energy level (192 W applied to wrapped 7.5 × 5.0 × 0.6 cm (3 × 2 × 0.25 in. block of PMMA). The increase in required concentration was a direct function of the energy applied, consistent with the heat absorption extinguishing mechanism utilized by these agents. Note that increased fire size does not require an increase in agent concentration as the heat flux to the fuel surface does not vary significantly with fire size.

Linteris [14] at NIST obtained similar results that showed that minimum extinguishing concentrations may easily double when even small amounts of external heating are applied, using the Radiant Enhanced Extinguishment Device (REED). For example the minimum extinguishing concentration of Nitrogen more than doubled with the addition of relatively small external heat flux from results reported by Factory Mutual. Additional data from NIST on HFC-23 showed an increase in required extinguishing concentration of 350 %. These data are summarized in Fig. 44.5. Additional data using the same device for the range of current clean agents shows similar results [15].

Extinguishment tests on actual wire and cable materials were reported by McKenna et al. [16]. Three types of tests were conducted: ohmic heating, conductive heating, and printed wiring board arcing. The ohmic heating tests involved deliberate electrical overheating of the conductor. The electrical current applied was just below what would result in melting and breaking the conductor. These results are summarized in

Table 44.8 Summary of the Class a and Class B extinguishing concentrations for various agents and equipment manufacturers

			UL (NFPA 2001)				ISO 14520				
			Class B		Class A		Class B		Class A		
Agent	Trade name	Equipment manufacturer	Test	Design	Test	Design	Test	Design	Min (95 % of Class B)	Test	Design
HFC-227ea	FM-200, FE-227	A	6.7	8.7							
		B	6.7	8.7							
		C	6.7	8.7							
		D	6.7	8.7	5.2	6.2					
		E	6.7	8.7	5.4	6.5					
		F	6.6	8.6			6.9	9.0	8.5	6.1 (4.9 WdCrib)	7.9
HFC-125	FE-25	A			6.7	8.0					
		B								8.6 (6.7 WdCrib)	11.2
		~	8.7	11.3			9.3	12.1	11.5		
	NAF-S-125	C	8.7	11.3	6.7	8.0				6.7	8.7
HFC-23	FE-13	A		18		18					
		B	12.9	16.8			12.6	16.4	15.6	12.5 (10.5 WdCrib)	16.3
FK-5-1-12	Novec-1230										
		A	4.5	5.9	3.5	4.2					
		B	4.5	5.9			4.5	5.9	5.6	4.1 (3.4 WdCrib)	5.3
IG-541	Inergen		28.9	37.6	28.5	34.2	31.7	41.2	39.1	30.7 (28.2 WdCrib)	36.5
IG-55	Argonite						36.5	47.5	45.1	31 (28.7 WdCrib)	40.3
IG-01	Argon						39.2	51.0	48.4	32.2 (30.7 WdCrib)	41.9
IG-100	Nitrogen						33.6	43.7	41.5	31.0 (30 WdCrib)	40.3

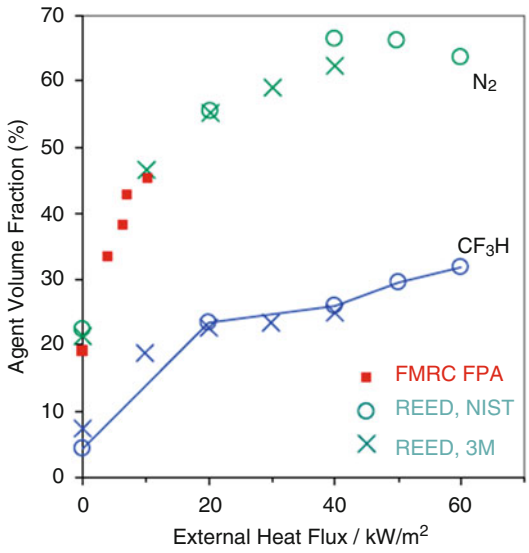

Fig. 44.5 Effect of external applied energy on extinguishment concentration (Linteris [14])

Table 44.9 for HFC-227-ea. This limited testing with low energy single and small cable bundles indicated that for HFC-227ea a concentration of between 6.5 % and 6.8 % was necessary to extinguish small cable bundles or arrays with PVC/PE or PE insulation. These values exceed the minimum Class A extinguishing concentration for HFC-227ea of between 5.2 % and 5.4 % and the design concentration of 6.2–6.5 %, which is supposed to embody a 20 % safety factor.

This dangerous situation has arisen, in part, because the Class A extinguishing concentration for HFC-227ea has been reduced from 5.8 % to 5.2% over time. This further illustrates the weakness of the test method used to determine Class A minimum extinguishing concentrations. A situation now exists in which small energized electrical fires would not be extinguished at either the minimum extinguishing concentration or the design concentration. These same fires would have been expected to be extinguished at the design concentration in 1996. This is due, in part, to poor experimental design of full scale tests where the effects of agent/air velocity at the flame were not sufficiently controlled and erroneous low minimum extinguishing concentrations were obtained.

The 6.5–6.8 % concentration required to extinguish all the test fires in Table 44.9 should be viewed as minimum extinguishing concentration with respect to these fires. A design concentration, suitable for use in actual installations, would incorporate an appropriate safety factor (20–30 % similar to Class A or B applications). This would imply a design concentration between 8.2 % and 8.8 % which would correspond to an approximate 50–60 % increase over the minimum Class A extinguishing concentration for HFC-227ea.

Linteris [14] also included a comprehensive review of suppression of energized electrical equipment and discussed the relevance and weaknesses of various ad hoc electrical equipment tests including those described above. The conclusion of this work is that the current guidance on minimum extinguishing concentrations for energized electrical equipment is inadequate, and insufficient data is available to definitively prescribe these concentrations. It is clear that theoretical and experimental results indicate that substantially higher concentrations than those currently used, are necessary.

These very limited results on small electrically energized conductors are not applicable to large-diameter, high-voltage, and high-power-rated cables, particularly in cable bundles and arrays. Such cables in these arrays have historically required much higher extinguishing concentrations than Class A surface values. For example, Sandia Laboratories and the Nuclear Regulatory Commission required design concentrations of 40 % for carbon dioxide and 6 % for Halon 1301 for such periods of at least 30 min. NFPA 12, Standard on Carbon Dioxide Extinguishing Systems, requires a CO_2 design concentration of >40 % for energized electrical equipment. These values represent increases of at least 20 % (for Halon 1301) over the Class A design value. As indicated in previous discussions, the Class A design value for the Halon 1301 is in the range of 80 % higher than HFC-125 when compared to a common baseline.

ISO 14520 [3], recognizing the more challenging nature of energized electrical fires,

Table 44.9 Summary of ohmic heating tests with HFC-227ea [16]

Test	Sample	Current (A)	Orientation	Ignition source	% C_3HF_7 (FM 200)	Time to extinguish (s)
EEE035	8 AWG XLPE, 5 wire bundle, center wire energized	350	Horizontal	Pilot	5.8	9
EEE036		350	Horizontal	Pilot	5.8	9
EEE046		350	Horizontal	Pilot	5.8	10
EEE049		350	Horizontal	Pilot	5.8	13
EEE037		350	Horizontal	Pilot	5.8	13
EEE038		350		Pilot	5.8	8
EEE039		350		Pilot	5.8	8
EEE054		350		Pilot	5.8	10
EEE055		350		Pilot	5.8	10
EEE040		350		Pilot	5.0	11
EEE047	12 AWG SJTW-A, 6 cable bundle, 4 of 18 conductors energized	600	Horizontal	Pilot	5.8	11
EEE050		600	Horizontal	Pilot	5.8	11
EEE053		600	Horizontal	Pilot	5.8	9
EEE041		600	Horizontal	Pilot	5.5	9
EEE043		600	Horizontal	Pilot	5.5	8
EEE044		600	Horizontal	Pilot	5.0	11
EEE056	8 AWG PVC, 7 cable bundle, center wire energized	325	Horizontal	Pilot	5.8	12
EEE059		325	Horizontal	Pilot	5.8	10
EEE062		325	Horizontal	Pilot	5.8	13
EEE068	18 AWG chrome PVC, over PE, 4 cable bundle, 12 conductors energized	350	Horizontal	Pilot	6.8	12
EEE069		350	Horizontal	Pilot	6.8	13
EEE071		350	Horizontal	Pilot	6.5	15
EEE075		350	Horizontal	Pilot	6.5	11
EEE079		350	Horizontal	Pilot	6.5	16
EEE076		350	Horizontal	Pilot	6.2	DNE
EEE077		350	Horizontal	Pilot	6.2	15
EEE078		350	Horizontal	Pilot	6.2	DNE
EEE058		350	Horizontal	Pilot	5.8	12
EEE061		350	Horizontal	Pilot	5.8	DNE
EEE065		350	Horizontal	Pilot	5.8	10
EEE066		350	Horizontal	Pilot	5.8	11
EEE067		350	Horizontal	Pilot	5.8	DNE
EEE057	16 AWG neoprene over rubber, 9 of 12, conductors energized	500	Horizontal	Pilot	5.8	3
EEE060		500	Horizontal	Pilot	5.8	6
EEE064		500	Horizontal	Pilot	5.8	6
EEE031	18 AWG PE, 4 parallel wire array, all wires energized	475	Horizontal	Self-ignited	6.8	14
EEE033		475	Horizontal	Self-ignited	6.8	14
EEE048		475	Horizontal	Self-ignited	6.8	14
EEE029		475	Horizontal	Self-ignited	6.5	DNE
EEE030		475	Horizontal	Self-ignited	6.5	DNE
EEE028		475	Horizontal	Self-ignited	5.8	DNE
EEE026		475	Horizontal	Self-ignited	5.7	DNE

provides additional guidance for applications involving energized electrical equipment:

> It is recognized that the wood crib and polymeric sheet Class A fire tests may not adequately indicate extinguishing concentrations suitable for the protection of certain plastic fuel hazards (e.g., electrical and electronic type hazards involving grouped power or data cables such as computer and control room under-floor voids, telecommunication facilities, etc.) An extinguishing concentration not less than that determined in accordance with 7.5.1.3 (wood crib and plastic sheet array fire tests), or not less than 95% of that determined from the heptane fire test described in C.6.2 (heptane pan fire test), whichever is the greater, should be used under certain conditions. These conditions may include:
>
> 1. Cable bundles greater than 100 mm in diameter;
> 2. Cable trays with a fill density greater than 20% of the tray cross-section;
> 3. Horizontal or vertical stacks of cable trays (closer than 250 mm);
> 4. Equipment energized during the extinguishment period where the collective power consumption exceeds 5 kW.

Given the uncertainty apparent in the NFPA 2001 Class A and energized electrical equipment values for minimum extinguishing concentrations, designers should consider using ISO 14520 as the basis of any total flooding clean agent system design. Section "Design Concentrations" provides additional guidance and discussion on this topic.

Explosion Inerting

One of the most important application areas of total flooding fire suppressants is explosion inertion. The inerting concentration of an agent is the concentration required to prevent unacceptable pressure increases in a premixed fuel-air-agent mixture subjected to an ignition source. Inertion concentrations are typically measured in small laboratory-scale spheres with an electric spark initiator.

The measured inerting concentration of an agent is dependent on the details of the test apparatus used, particularly the ignition source strength and "allowable" pressure rise. The allowable pressure rise is a surrogate measurement of the distance the flame front travels inside the constant-volume sphere prior to suppression. Inerting concentration is not appropriate for use in explosion suppression either deflagrations or detonations.

Table 44.10 Explosion inerting concentrations, small-scale inertion sphere [6, 17–19]

	Inerting concentration (vol %) of fuel			
Agent	Propane	Methane	i-Butane	Pentane
FC-3-1-10	10.3[a]	~7.8[b]	–	–
	9.5[b]			
HFC-227ea	12.0[b]	8.0[b]	11.3[a]	11.6[c]
	11.6[c]			
HFC-23	20.2[a]	20.2[a]	–	–
	19.8[b]	14.0[b]		
IG-541	49.0[d]	43.0[d]	–	–
HCFC Blend A	18.0[b]	13.3[b]	–	–

[a]From Senecal [17]
[b]From Heinonen [19]
[c]From Robin [6]
[d]From Tamanini [18]

Small-scale sphere data are used to develop flammability diagrams for various fuel-oxidizer-agent concentrations. Chapter 17, which addresses flammability limits, gives an excellent introduction to the subject. There is a wealth of data in the combustion literature on flammability limits of a variety of fuels in the presence of an atmosphere of inert gases, such as nitrogen and argon.

Table 44.10 provides inerting concentration data for several agents and fuels taken from small scale inertion spheres [17–19]. There are some substantial differences in results. Heinonen [20] has identified both ignition source type and strength as important variables with differences of ±40 % for Halon 1301 inerting concentrations reported. Large scale inertion results have been presented by Moore [21]. While the small to large scale agreement is reasonable, there are scale effects.

Explosion Suppression

Explosion suppression systems employ rapid delivery of agent following very early detection of an ignition. Such systems employ significantly

higher agent quantities (than flame suppression or inertion) delivered at higher rates. The total agent delivery time is on the order of 100 ms.

Explosion suppression systems must be specifically designed for a particular application. There are no generic design requirements or standards currently available for such systems. Senecal [22] and Senecal et al. [23] report on explosion suppression testing in occupied armored fighting vehicles and aerosol filling rooms. Results were obtained on premixed fuel droplet (aerosol) sprays. In contrast to flame suppression or inerting, suppression of a deflagration or detonation requires significantly more agent. The tests employed 20 kg of HFC-227ea, FC-3-1-10, and HFC-236fa, and 10 kg of water in an 80 m^3 test room to suppress a 90 g propane release in a simulated aerosol filling station. Suppression of the propane-air deflagration was achieved, and the maximum flame front extension was approximately 1.22 m. Suppression tests of heated diesel fuel droplet cloud deflagrations were also conducted in simulated armored fighting vehicle crew compartments.

Table 44.11 summarizes typical data for flame suppression, inertion, and deflagration suppression concentrations. Note these values are for comparison purposes only. They should not be used in any way for design purposes. Suppression of detonations requires substantially higher agent concentrations than for deflagrations. An excellent discussion on this topic is given in Hamins et al. [5].

Toxicity

A major factor in the use of a clean agent fire suppressant in a normally occupied space is toxicity. Although all halocarbon agents are tested for long-term health hazards, the primary endpoint is acute or short-term exposure. The primary acute toxicity effects of the halocarbon agents described in this chapter are anesthesia and cardiac sensitization. For inert gases, the primary physiological concern is reduced oxygen concentration.

Halocarbon Agents Cardiac sensitization is the primary short-term toxicity problem for fire suppression applications involving halocarbon agents. Cardiac sensitization is an increased potential for cardiac arrhythmia with exposure to the agent in conjunction with the hormone epinephrine or adrenalin. Cardiac arrhythmia is a condition in which the heart beats with an irregular or abnormal rhythm and in an extreme case, can lead to a heart attack. Epinephrine is produced naturally by the body with increased production rates when the body is under stress. Epinephrine can cause arrhythmia on its own at high concentrations. Cardiac sensitization reduces the epinephrine concentration associated with the onset of cardiac arrhythmia when exposed to the agent.

The two toxicity endpoints used to describe cardio-toxicity and allowable exposure levels are (1) no observed adverse effect level (NOAEL) and (2) the lowest observed adverse effect level

Table 44.11 Comparison of concentrations for flame extinguishment, inertion, and deflagration suppression [1, 22]

	Volume (%)		
Agent	Typical value flame suppression	Inerting concentration in propane	Diesel fuel droplet deflagration suppression
Halon 1301	3	6–7	12
FC-3-1-10	5.5	10.3	8
HFC-227ea	5.8	~12	11
HFC-23	12	20.2	–
IG-541	29	49.0	–

(LOAEL). The NOAEL is the highest concentration of an agent at which no "marked" or adverse effect occurred. The LOAEL is the lowest concentration of an agent at which an adverse effect was measured.

The procedures used to evaluate cardiac sensitization vary somewhat. The basic approach involves a stepped method that includes the intravenous dosing of male beagle hounds with epinephrine for 5 min. Continuous inhalation exposure to the agent at a specific concentration follows for 5 min. Following this inhalation exposure, the hound is dosed again with epinephrine and monitored for another 5 min to determine the effect of the agent and epinephrine. The protocol is performed at higher doses until an effect occurs.

Effects are monitored by electrocardiograph (EKG) measurements. An adverse effect is generally considered to be the appearance of five or more arrhythmias or ventricular fibrillation. The data from these tests are evaluated by medical experts, and the appropriate NOAEL and LOAEL values are reported by the United States Environmental Protection Agency (EPA) under the Significant New Alternatives Policy (SNAP) program.

There is no direct correlation between the experimental results from hounds to humans. It is generally accepted, due to the combination of the high doses of epinephrine in the tests and the similarity in cardiovascular function between hounds and humans, that the results can be applied to humans.

For most of the listed halocarbon agents, the concentration where adverse effects are observed is higher than the design concentration required for use in fire suppression. The exceptions to this are FIC-13I1 (CF_3I) and HFC-125 (C_2HF_5). The concentration where cardiac sensitization effects are noted (LOAEL) for FIC-13I1 is 0.4 % by volume [1] while its minimum design concentration for Class B hazards is 4.2 % by volume. For HFC-125, the concentration where cardiac sensitization effects are noted is 10 % by volume which is exceeded by the minimum design concentration for Class B hazards of 11.3 % by volume, however, for Class A hazards, the minimum design concentration is 8.7 % by volume which is less than the LOAEL.

In addition to the short-term chronic exposure limits of interest in fire suppression system design, the EPA evaluates longer-term inhalation data for these compounds. One procedure used to evaluate longer-term effects involves the exposure of a concentration of the halocarbon agent to a population of rats for a period of 4-h. The measure LC_{50} is the concentration of the halocarbon agent lethal to 50 % of the rat population during the 4-h exposure. This is also referred to as the approximate lethal concentration (ALC). Table 44.12 summarizes NOAEL, LOAEL, and

Table 44.12 Toxicity data for halocarbon clean agent fire suppressants [1]

Agent	Trade name	LC_{50} and ALC (%)	NOAEL (%)	LOAEL (%)
FIC-1311	Triodide	>12.8	0.2	0.4
FK-5-1-12	Novec 1230	>10	10	>10
HCFC Blend A	NAFS-III	64	10	>10
HCFC-124	FE-24	23-29	1	2.5
HFC-125	FE-25	>70	7.5	10.0
HFC-227ea	FM-200	>80	9	10.5
HFC-23	FE-13	>65	30	>30
HFC-236fa	FE-36	>45.7	10	15
HFC Blend B	Halotron II	56.7[a]	5.0[a]	7.5[a]

Notes
(1) LC_{50} is the concentration lethal to 50% of a rat population during a 4-h exposure. The ALC is the approximate lethal concentration
(2) The cardiac sensitization levels are based on the observance or non-observance of serious heart arrhythmias in a dog. The usual protocol is a 5 min exposure followed by a challenge with epinephrine
(3) High concentration values are determined with the addition of oxygen to prevent asphyxiation
[a]These values are for the largest component of the blend, HFC Blend B (HFC-134A)

Table 44.13 Exposure limits derived from PBPK modeling for HFC-227ea and HFC-125 [1]

HFC-227ea concentration			HFC-125 concentration		
% V/V	ppm	Human exposure time (min)	% V/V	ppm	Human exposure time (min)
9.0	90,000	5.00	7.5	75,000	5.00
9.5	95,000	5.00	8.0	80,000	5.00
10.0	100,000	5.00	8.5	85,000	5.00
10.5	105,000	5.00	9.0	90,000	5.00
11.0	110,000	1.13	9.5	95,000	5.00
11.5	115,000	0.60	10.0	100,000	5.00
12.0	120,000	0.49	10.5	105,000	5.00
			11.0	110,000	5.00
			11.5	115,000	5.00
			12.0	120,000	1.67
			12.5	125,000	0.59
			13.0	130,000	0.54
			13.5	135,000	0.49

LC_{50} values. Note that the LC_{50} values greatly exceed the NOAEL and typical fire-extinguishing concentrations.

Because the arrhythmia potential is measured in dogs, a means of providing improved human relevance has been established. Physiologically based pharmacokinetic modeling (PBPK) for evaluation of acute exposure to halocarbon agents has been used to establish alternative exposure limits for halogenated agents [1]. PBPK modeling utilizing a computerized tool attempts to account for the time-dependent uptake rate of halocarbons in the body and establishes exposure limits based on the rate of uptake [24–28]. The limits are based on the concentration of agent and the time at which the concentration of agent in the blood equals that of the LOAEL. Typical PBPK results for safe exposure times for HFC227ea and HFC-125 are given in Table 44.13. Note that exposure above the NOAEL limits and up to the LOAEL is permitted.

These limits were derived and supported by the EPA, which has the primary regulatory authority for health and toxicity associated with halon replacements. The use of the PBPK approach partially accounts for the differences between laboratory animal tests and humans. The laboratory results form the basis of the endpoints (NOAEL, LOAEL) and are still conservative due to the nature of epinephrine dosage used during the animal tests [29].

Where PBPK modeling data do not exist, the use of halocarbon agents in occupied areas is subject to the constraint that the design concentration must be less than the NOAEL. Although it is recommended that all systems employ predischarge alarms and that personnel evacuate prior to system actuation, it is understood that inadvertent discharges and short-term exposures will occur, hence, the limitation. It is expected that emergency exposures for up to several minutes at or below the NOAEL are reasonably safe. In no case should systems be designed or installed where intentional exposure of any duration is anticipated. It has been proposed by the EPA that agents be permitted for use at concentrations up to the LOAEL where evacuation will occur in less than 60 s. This proposal has not been integrated into design standards to date due to the uncertainty of accidental exposure conditions. Based on the limitation that the design concentration must be below the NOAEL, it can be seen from Table 44.12 that three agents are acceptable for use in normally occupied areas for flame extinguishant purposes: HFC-227ea, HFC-23, and FK-5-1-12.

Inert Gas Agents Inert gas agents are, in effect, physiologically inert. The primary physiological

problem with these agents is the reduced oxygen concentration caused by the high agent design concentrations. One inert gas blend employs a low concentration of CO_2 (which is not physiologically inert) in order to counter the effects of the reduced oxygen concentration. The mechanism of this effect is discussed in EBRDC Report 10.30.92 [30]. Current limitations on exposure limits for inert gases are as follows: for gas concentrations up to 43 % (a residual oxygen concentration of 12 %), exposure time is limited to 5 min. For agent concentrations between 43 % and 52 % (12 % and 10 % residual oxygen concentration), the exposure time is limited to 3 min. For concentrations greater than 52 %, exposure time is limited to 30 s. There is strong indication that small concentrations of CO_2 added to inert gases (such as IG-541) substantially reduce hypoxic effects and improve human performance at low oxygen levels. Regulatory authorities have not yet differentiated between such agents and other inert gases or blends [30].

Environmental Factors

Two main environmental impacts need to be considered with respect to halocarbon extinguishing agents: (1) ozone depletion and (2) global warming [1]. Another environmental factor, atmospheric lifetime, can be considered in the discussion of each of these environmental impacts. It is also a "stand-alone" environmental concern that needs to be addressed. International, national, state, and local governments currently regulate halocarbon fire-fighting agents based on their effect on ozone depletion. However, the EPA also takes into account atmospheric lifetimes and global warming potentials in the implementation of its SNAP program under Section 612 of the Clean Air Act in the United States, as amended in 1990. Although no specific national environmental regulations cover global warming and atmospheric lifetimes, the consideration of these issues in the EPA's implementation of existing regulations makes these issues of concern.

Ozone Depletion

Ozone (O_3) is a naturally occurring gas that is found in the atmosphere. Most naturally occurring ozone is created by the reaction of O_2 with ultraviolet (UV) light coming from the sun.

$$O_2 + UV \quad O + O$$
$$O + O_2 \quad O_3$$

The UV light causes this reaction to occur. Ozone is also created in nature when the high energy output from lightning initiates a similar reaction.

Ozone is also formed by a number of manufactured sources, mainly as a result of air pollution. When carbon monoxide, methane, and other hydrocarbons meet nitrogen oxide (e.g., from car exhaust) and ordinary sunlight, ozone is produced. It is also produced by laser printers and electric motors and is responsible for the pungent odor often associated with the devices. Man-made ozone is often called "smog" and is a considerable health risk.

Halons, HCFCs, and other halocarbons containing chlorine or bromine have been shown to cause the destruction of stratospheric ozone. The characterization of stratospheric ozone destruction is not a measure of the exact amount of ozone destroyed. Instead, it is the relative amount of ozone destroyed as compared with an arbitrary standard. The standard chosen is trichlorofluoromethane, CFC-11, a compound of chlorine, fluorine and carbon, which has been assigned an ozone depletion potential (ODP) of 1. ODP of all other halocarbons relates to their relative effect on the destruction of ozone as compared with CFC-11. Halon 1301 has an ODP of 12, meaning it will destroy 12 times as much ozone as CFC-11 on a pound-for-pound (kilogram-for-kilogram) basis. A compound having an ODP of 0.1 would have 10 % of the relative ozone-depleting effects of CFC-11. All ODP values are based on mass (weight) and not on moles (numbers of molecules).

The only remaining nonzero ozone-depleting fire-extinguishing gases are HCFC compounds, none of which are widely used for total flooding system applications. All HCFCs are subject to

some degree of environmental regulation in most parts of the world.

Atmospheric Lifetimes

When one thinks of a chemical species lifetime, the term *half-life* is often used. This usage is most common in the nuclear field when calculations are made to determine how long it takes a species to decay to half its original concentration. Atmospheric lifetime values used in the determination of ozone depletion and global warming potentials are *not* half-lives. They are $^1/_e$ lifetimes, sometimes called e-folding lifetimes.

It has been determined that greenhouse gases break down in the atmosphere according to the following equation:

$$C = C_o e^{-kt}$$

where:

C = Concentration at time t
C_o = Initial concentration at time t
k = An experimentally determined rate constant (units = 1/time)

A mathematical manipulation can be made to express this equation as a function of more readily quantifiable terms and is accomplished by defining the atmospheric lifetime, L, as an e-folding lifetime, or the time it takes for the ratio of $C:C_o$ to be equal to $^1/_e$ (e is the base of the natural logarithm system and has a numerical value of approximately 2.718). The resulting equation is as follows:

$$C = C_o e^{-t/L}$$

Although the term *half-life* is most commonly used when describing the decay of a species concentration, the use of the e-folding lifetime allows for quantification of concentration in terms of a compound's atmospheric life-time, as previously shown. A half-life refers to the time it takes for half a given amount of compound to be broken down in the atmosphere; thus, the ratio $C:C_o$ is equal to ½. Using an e-folding lifetime, the ratio is equal to $^1/_e$ or 0.368. After one lifetime, the concentration will be equal to 0.368 times its original value. After two lifetimes, the concentration will be 0.135 or $(0.368)^2$ times its original value. After three lifetimes, the concentration will be 0.0498 or $(0.368)^3$ times its original value, and so on.

An important factor when using the preceding equation to solve for concentration as a function of time is that, no matter what value is used for time, the concentration never equals zero. Some portion will always exist in the atmosphere. When the atmospheric life-time is small, the concentration over hundreds of years may become negligible. When the atmospheric life-time is very large, on the order of tens of thousands of years, the concentration in the atmosphere may not be negligible.

The environmental concern is one of "what if." The halons were believed to be "safe" for many years after their release into the atmosphere began. It was not until many years later that they were linked to ozone depletion. There is a concern that these halocarbons, or other compounds, may cause other environmental impacts that are yet unknown. If the atmosphere is filled with these chemicals and they exist in appreciable amounts for hundreds, thousands, and millions of years, what then? Might the damage we do to our environment be more than humans can cope with? Nature can probably overcome this impact, but it may take tens of millions of years. This is a short time frame for nature but not for man. Current implementation of the EPA SNAP program places restrictions on perfluorocarbons that have very large or "outlying" atmospheric lifetimes as compared with the rest of the halocarbons. This restriction is not based on any known or anticipated environmental problem. It is a response to the "what if" concerns raised previously.

Global Warming Potential

The most important global environmental issue is currently climate change. A basic understanding about the earth's climate and atmosphere is needed to understand what global warming potential (GWP) is and how to attempt its measurement.

Estimates of the average temperature of earth's atmosphere have been made, assuming two theoretical conditions. The first assumes no

atmosphere at all, and the second assumes an atmosphere made up solely of N_2 and O_2 (normally representing 99 % of our atmosphere). In both cases, models have predicted that earth's surface would be some 91 °F (33 °C) cooler than it is. The temperature difference is believed to be a direct result of the very small amounts of trace gases, water vapor, and CO_2. These act very much like the glass on a greenhouse that lets the sunlight in but helps to prevent the heat from escaping, hence, the terms *greenhouse effect and greenhouse gases*. A greenhouse gas is defined as any gas that absorbs infrared (IR) radiation.

Climate change and global warming are not synonymous. Climate change includes cooling and warming of the atmosphere. Global warming only deals with the aspects of climate change that result in warming of the atmosphere.

It is estimated that about one-third of the total solar radiation is reflected off earth's atmosphere. Most of the remaining two-thirds passes through the atmosphere and is absorbed by the earth's surface, causing it to warm [31].

The earth cools itself by releasing heat, or IR. In order for a balance to be maintained, the solar radiation coming in must equal the radiation going out. If more radiation entered the atmosphere than left, the earth would be constantly getting warmer. The opposite would be true if more radiation left the earth than came in; that is, the earth would be constantly getting cooler.

To estimate the amount of global warming expected from a release of a particular greenhouse gas, a scale was developed by the International Panel on Climate Change (IPCC), based on the idea of radiative forcing. This scale is called the global warming potential (GWP) and relates to positive radiative forcing that will cause the atmosphere to heat up. The GWP is the cumulative amount of radiative forcing between the present and some future time caused by a unit mass (weight) of a compound, as compared with the same unit mass (weight) of an arbitrary standard. Carbon dioxide, CO_2, is the most common reference, and 20-year, 100-year, and 500-year time periods, or horizons, are the most common time references cited in the literature. The choice of time horizons is a policy issue and not a technical one.

Since the GWP is a cumulative effect, summed year by year over a given time horizon, the quantity present in the atmosphere must be known year by year over that horizon. The atmospheric lifetime is used to perform these calculations. GWPs are also affected by the specific IR-absorbing capabilities of the chemical. Analogous to ODPs, GWPs are not exact numbers showing the precise effect on global warming. A 100-year horizon GWP of 6200 for Halon 1301 means that 1 lb (0.454 kg) of Halon 1301 will cause as much global warming as 6200 lb (2812 kg) of CO_2. A 500-year horizon GWP for methylene chloride of 0.3 means that 1 lb (0.454 kg) of methylene chloride will cause the same warming as 0.3 lb (0.14 kg) of CO_2.

GWPs are used to determine the future global warming contribution of a substance *over a given time* by multiplying the weight of the greenhouse gas by a specific time-horizon-GWP. The resultant number can be compared with others to decide which will have the least (or greatest) impact *over that time horizon*. Emitting a large quantity of a small GWP greenhouse gas may cause less global warming than a small release of a very large GWP greenhouse gas over a certain time horizon. Different time horizons may lead to different results.

Environmental Regulation of Halon Replacements

The evaluation of clean agent fire suppressants includes a consideration of environmental factors. International, national, and local government regulations control the use of any alternatives in this regard. As described above, a key environmental consideration is ODP. All chemicals with a nonzero ODP are subject to phaseout under the Montreal Protocol and its amendments. Table 44.14 summarizes environmental impact data for halocarbon agents. Note that FC and HFC compounds have zero ODP.

As also discussed above other environmental factors important in a regulatory context are GWP and atmospheric lifetime. The evaluation of GWP is an extremely complex issue, and

Table 44.14 Environmental factors for halocarbon clean agents [31]

Designation	ODP	GWP (100 years)	Atmospheric lifetime (years)
Halon 1301	12.000	7030	65
HFC-227ea	0.000	2900	34.2
HFC-23	0.000	14,310	270
HFC-125	0.000	3450	29
FK-5-1-12	0.000	1	0.038
Inert gas	0.000	0	NA

currently none of these compounds are regulated on that basis in the United States. Long atmospheric lifetime, a measure of the persistence of a chemical in the atmosphere, is of concern not only as it relates to GWP but also due to the uncertainty of the effects of chemicals for long time periods in the atmosphere. The EPA currently has use restrictions on FC-3-1-10 based primarily on its long atmospheric lifetime. These restrictions permit the use of this chemical in applications where no other alternative is technically feasible.

There is regulation of HFCs and PFCs for fire protection use in many parts of the world. There are few blanket prohibitions of HFCs for fire protection use, but regulation relating to minimizing emissions on the basis of global warming currently exists in Europe. As consensus grows at the magnitude and threat posed by global climate change, one would reasonably expect increased regulation worldwide on HFC fire suppressants. Note that some of the inert gases have no GWP impact and that the FK-5-1-12, a halogenated agent, has a GWP of 1; therefore, low climate change impact fire suppression gases currently exist. This agent possesses many of the advantages of a halogenated agent but with an environmental impact similar to inert gases.

It is also important to bear in mind that the total usage relative to total global production of these gases for fire suppression uses is quite low and perhaps more importantly the emissions of these gases relative to other uses is very low. Hence the overall impact of fire suppression agents to climate change can be expected to be minimal if not negligible. The Halon Alternative Research Commission (HARC) estimates that fire protection use of all halocarbons contributes less than .01 % of the impact of all greenhouse gas emissions [32].

Thermophysical Properties

Tables 44.15 and 44.16 give thermophysical properties of clean agent replacements from NFPA 2001 for halocarbon and inert gases. Additional thermophysical and transport property data can be found in Robin [6] for FM-200 and Yang and Bruel [33] for a range of halocarbon alternatives.

Isometric diagrams for halocarbon agents HFC-227ea, pressurized at 360 and 600 psig at 70 °F with nitrogen, and HFC-23 are given in Figs. 44.6, 44.7, and 44.8, respectively. Note that HFC-23 is not pressurized with nitrogen.

Figure 44.9 gives the pressure-temperature relationship for inert gases IG-541, IG-55, and IG-01, pressurized to 2175 psig, at 70 °F. This display is the pressure-temperature relationship for an ideal gas.

Clean Agent System Design

Once an agent has been selected for a specific application, the general discussion on clean agent system design presented in Chapter 43, should be reviewed. Many of the design principles for clean agent systems have been adapted from those principles used for halon systems. The basic process is outlined below:

1. Determine the design concentration.
2. Determine the total agent quantity.
3. Establish the maximum discharge time.

Table 44.15 Physical properties of clean halocarbon agents (Si units) [1]

Physical property	Units	FIC-1311	FK-5-1-12	Blend A	HDFC Blend B	HFC HCFC-124	HFC-125	HFC-227ea	HFC-23	HFC-236fa
Molecular weight	NA	195.91	316.04	92.90	99.4	136.5	120	170	70.01	152
Boiling point at 760 mmHg	°C	−22.5	49	−38.3	−26.1	−12.0	−48.1	−16.4	−82.1	−1.4
Freezing point	°C	−110	−108	<107.2	−103	−198.9	−102.8	−131	−155.2	−103
Critical temperature	°C	122	168.66	124.4	101.1	122.6	66	101.7	26.1	124.9
Critical pressure	kPa	4041	1865	6647	4060	3620	3618	2912	4828	3200
Critical volume	cc/mole	225	494.5	162	198	243	210	274	133	276
Critical density	kg/m^3	871	639.1	577	515.3	560	574	621	527	551.3
Specific heat, liquid at 25 °C	kJ/kg°C	0.592	1.103	1.256	1.44	1.153	1.407	1.184	4.130 at 20 °C	1.264
Specific heat, vapor at constant pressure (1 atm) and 25 °C	kJ/kg°	0.3618	0.891	0.67	0.848	0.742	0.797	0.808	0.730 at 20 °C	0.840
Heat of vaporization at boiling point	kJ/kg	112.4	88	225.6	217.2	165.9	164.1	132.6	239.3	160.4
Thermal conductivity of liquid at 25 °C	W/m °C	0.07	0.059	0.09	0.082	0.0684	0.0592	0.069	0.0534	0.0729
Viscosity, liquid at 25 °C	Centipoise	0.196	0.524	0.21	0.202	0.257	0.14	0.184	0.044	0.286
Relative dielectric strength at 1 atm at 734 mm Hg, 25 °C (N 2 = 1.0)	NA	1.41	2.3	1.32	1.014	1.55	0.955 at 21 ° C	2	1.04	1.0166
Solubility of water in agent	ppm	1.0062 % by weight	<0.001	0.12 % by weight	0.11 % by weight	700 at 25 °C	700 at 25 °C	0.06 % by weight	500 at 10 °C	740 at 20 °C

Table 44.16 Physical properties of clean Inert Gas agents (Si units) [1]

Physical property	Units	IG-01	IG-100	IG-541	IG-55
Molecular weight	NA	39.9	28.0	34.0	33.95
Boiling point at 760 mmHg	°C	−189.85	−195.8	−196	−190.1
Freezing point	°C	−189.35	−210.0	−78.5	−199.7
Critical temperature	°C	−122.3	−146.9	NA	−134.7
Critical pressure	kPa	4903	3399	NA	4150
Specific heat, vapor at constant pressure (1 atm) and 25 °C	kJ/kg °C	0.519	1.04	0.574	0.782
Heat of vaporization at boiling point	kJ/kg	163	199	220	181
Relative dielectric strength at 1 atm at 734 mmHg, 25 °C (N 2 = 1.0)	NA	1.01	1.0	1.03	1.01
Solubility of water in agent at 25 °C	NA	0.006 %	0.0013 %	0.015 %	0.006 %

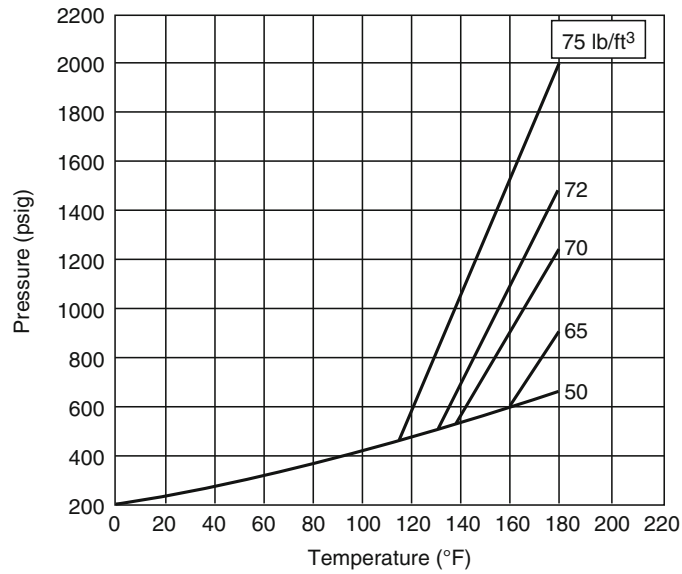

Fig. 44.6 Isometric diagram of HFC-227ea, pressurized to 360 psig with N_2, at 70 °F [6]

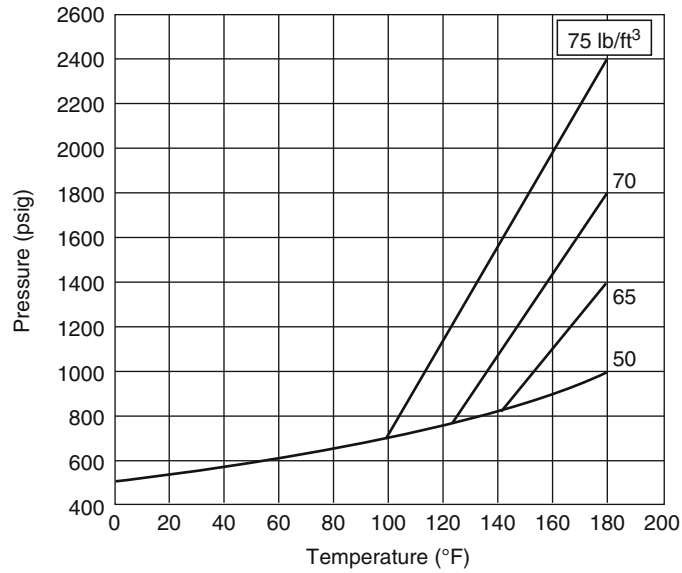

Fig. 44.7 Isometric diagram of HFC-227ea, pressurized to 600 psig with N_2, at 70 °F [6]

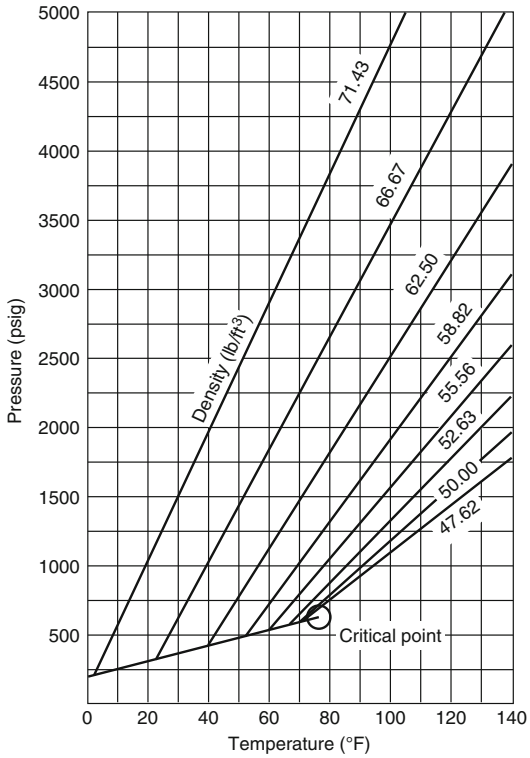

Fig. 44.8 Isometric diagram of HFC-23 [1]

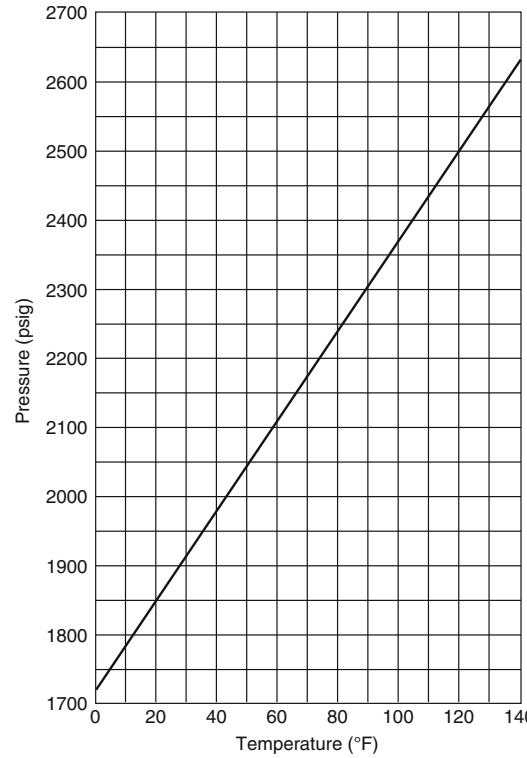

Fig. 44.9 Isometric diagram of inert gases and blends, treated as ideal gases, pressurized to 2175 psig, at 70 °F [1]

4. Select piping material and thickness consistent with pressure rating requirements.
5. Design piping network and select nozzles to deliver required concentration at required discharge time to ensure mixing.
6. Evaluate compartment over/underpressurization and provide venting if required.
7. Establish minimum agent hold requirements and evaluate compartments for leakage.

These attributes apply only to the mechanical design of the system.

The detection and actuation systems are critical and integral parts of a clean agent system design. The detection system should be designed to actuate the system, with appropriate predischarge alarms, before unacceptable thermal or nonthermal damage occurs. This aspect is particularly important where the thermal decomposition products of halocarbon clean agents are a concern. Chapter 40, provides engineering methods and calculation procedures for this purpose.

In addition to the detection, actuation, and alarm systems, the enclosure itself is critical in the design of any total flooding suppression system. The most important considerations are that the enclosure be of sufficient integrity to (1) prevent preferential agent loss during discharge and (2) prevent excessive agent-air mixture loss after discharge to ensure adequate hold time.

As a general rule, all openings, notably doors and ventilation fans and/or openings must be secured prior to discharge in conjunction with the detection and alarm systems. Agent system installation in rooms with unclosable openings should not be attempted unless sufficient test data are available to ensure adequate concentrations. Some enclosures, such as very tightly sealed low EMF emission electronics spaces, require additional care to avoid compartment damage due to over/under pressurization during agent discharge.

Table 44.17 Comparison of design concentrations for Class A fires [1, 3, 34–36]

Agent	Heptane MEC (NFPA 2001, 2008) (%)	Class A design concen. NFPA 2001/UL (%)	Ratio Class A design to MEC (NFPA)	Class A design concen. (ISO 14520) (%)	Ratio Class A design concen. to MEC (ISO 14520)	Ratio Class A design NFPA 2001 to ISO 14520
Halon 1301	3.4[a]	5[b]	1.47	–	–	–
CO_2	23[a]	>34[c]	1.48	–	–	–
HFC-227ea	6.7	6.25–7.0	0.93–1.04	7.9	1.2	0.79–0.88
HFC-125	8.7	8.0	0.92	11.2	1.3	0.71
HFC-23	12.9	16.8–18	1.3–1.4	16.3	1.26	1.03–1.1
FK-5-1-12	4.5	4.2	0.93	5.3	1.17	0.79
IG-541	31	34.2	1.1	36.5	1.17	0.94
IG-55	35	37.9	1.08	40.3	1.15	0.94
IG-01	42	–	–	41.9	1.0	–
IG-100	31	–	–	40.3	1.3	–

[a]From NFPA handbook (mid-range value) [34]
[b]From NFPA 12A [35]
[c]From NFPA 12 [36]

Design Concentration

Flame Extinguishment Design concentrations for various agents and fuel combinations are generally determined by a combination of small-scale testing, large-scale testing, independent laboratory approval of hardware, and addition of design safety factors as discussed above.

Historically, minimum design concentrations for Halon 1301 were set by the cup burner extinguishing concentration plus a 20 % safety factor. A minimum Halon 1301 design concentration of 5 % was also established for all applications. For heptane, the cup burner value ranged from 2.9 % to 3.9 % [34]; with a 20 % safety factor, a design concentration ranging from of 3.5 % to 4.7 % is obtained. At the minimum design concentration set by NFPA 12A, *Standard on Halon 1301 Fire Extinguishing Systems*, 2009 Edition [35], of 5 %, a safety factor ranging from 28 % to 72 % was achieved. For fuels with cup burner extinguishing concentrations greater than 4.2 %, the safety factor remained at 20 %.

Table 44.17 presents the minimum design concentration of clean agents under the requirements of NFPA 2001 [1] and ISO 14520 [3].

The design concentrations required under the ISO 14520 installation standards are significantly higher due to two factors. First, in general, the extinguishing concentrations measured under the ISO protocols are generally higher than those obtained by the methods required by NFPA 2001; these sometimes larger differences are surprising, given the very minor test differences between test protocols. In general, a designer should select the higher of the extinguishing concentrations.

The second and most important difference between the two installation standards is in the safety factor. NFPA 2001 requires a minimum safety factor of 20 %, whereas the ISO minimum is 30 %. The product designer should bear in mind that for typical Class A hazards, Halon 1301 systems designed at 5 % had a minimum effective safety factor of 65 %; for carbon dioxide, it is in the range of 75–100 %.

There has been some full-scale test work that indicates that the 20 % safety factor may be insufficient. Sheinson et al. noted significant improvement in extinguishing time performance with a safety factor of 40 % [7]. Brockway noted similar results with no performance improvement beyond a safety factor of 40 % [37].

Analysis by Schlosser [38] indicated that the probability of failure of a system was reduced

from approximately 15 % to 10 % when the safety factor increased from 20 % to 30%. In addition to these data, the variation in cup burner values used as a basis for design concentration was significant due in part to a lack of standardization in the method. Some full-scale test results [39] also indicated a need for higher design concentrations.

Based on these factors, the first edition of ISO 14520-1 required a minimum safety factor of 30 % [40]. The current edition of NFPA 2001 [1] requires a 30 % safety factor for Class B hazards and for any system actuated by manual means only.

A review of the adequacy of these minimum required design concentrations can be found in Hanauska and DiNenno [41]. In this report weaknesses are identified in the development of the minimum extinguishing concentrations and the safety factors associated with the minimum required design concentration for Class A and energized electrical equipment fires. The current edition of NFPA 2001 increases the safety factor for energized electrical equipment fires to 35 % over the MEC for Class A hazards. This does not fully address this hazard as discussed previously in section "Energized Electrical Equipment Extinguishing Concentrations."

Table 44.17 shows comparison data for Class A design concentrations in both NFPA 2001 and ISO 14520 against the minimum heptane extinguishing concentration for each agent. In addition, data for carbon dioxide and Halon 1301 are presented for comparison. The heptane minimum extinguishing concentration (MEC) is used as a baseline for the following reasons:

1. The value is independent of system delivery hardware, which is a problem for Class A test results.
2. The MEC can and has been determined for each agent by various laboratories with minimum differences among laboratories.
3. The use of a liquid fuel is a reasonable worst case for a diffusion flame over a solid surface.
4. Comparison data exist for Halon 1301 and CO_2 that form the basis of historical total flooding gases.

An analysis of the data in Table 44.17 indicates the following:

1. The UL/NFPA 2001 design concentration differences for Class A surface fires for clean agents are as high as 47 % (for HFC-125) less than the equivalent concentration for carbon dioxide compared to a cup burner baseline. The design concentration for HFC-125 is approximately 62 % of the value one would expect for carbon dioxide if applying the same safety factor and design concentrations (0.92 vs. 1.48).
2. Similarly, the design concentration for HFC-125 is 63 % of that expected for Halon 1301 (0.92 vs. 1.47).
3. The agent faring the best in comparison to Halon 1301 and carbon dioxide is HFC-23.
4. Design values contained in ISO 14520 are much more reasonable in comparison with the NFPA 2001/UL values due, as previously discussed, to higher safety factors and more demanding extinguishing concentration tests for Class A fuels in ISO 14520.
5. The last column in Table 44.17 shows, in very stark terms, the weakness of NFPA 2001 to ISO 14520. The design value for HFC-125 used by NFPA 2001 is only 71 % of the value used in ISO 14520. The design concentration used in NFPA is lower for all agents, except HFC-23.

The analysis presented in Table 44.17 indicates that the Class A extinguishing concentrations used in NFPA 2001 for clean agents are significantly lower (approximately 30 %) than the equivalent values for Halon 1301 and CO_2, relative to a common baseline. Note that these differences do not exist between Halon 1301 and the clean agents for liquid Class B fuels. In addition, the NFPA 2001/UL values for Class A design concentrations are as much as 30 % lower than the equivalent design value under ISO 14520.

From both a historical perspective and current international practice, the design concentrations for Class A surface fires required in NFPA 2001 appear too low.

It has also been noted by several investigators that higher safety factors result in lower thermal

decomposition products [7, 8, 37]. None of the above referenced investigations utilized listed or approved hardware for the specific agents tested; as in most cases, the tests were performed before such hardware was available.

There is an exception in NFPA 2001 to the general rule that a minimum extinguishing concentration be established by the cup burner method. It was alleged that reliable cup burner data were not available for HCFC Blend A due to the fact that (1) the agent was a blend and (2) one of the blend components heats at a low vapor pressure. In the case of this agent, a minimum extinguishing concentration of 7.2 % and, hence, a design concentration of 8.6 % was established through limited full-scale testing for Class A hazards. Since at the time insufficient data were available to evaluate the claim, the exception that requires full-scale testing at minimum extinguishing concentration consistent with UL 2127, *Inert Gas Clean Agent Extinguishing System Units* [12] and UL 2166, *Halocarbon Clean Agent Extinguishing System Units* [13], were invoked. Since that time, reliable cup burner data were obtained for the blend from several laboratories. The data are consistent with MEC values for the blend components, primarily HCFC-22. Furthermore, some full-scale testing has indicated that the design concentration of 8.6 % may be inadequate [42]. This issue is, however, unresolved at the present time.

For Class A fires, NFPA 2001 requires full-scale testing and third-party approval for evaluating design concentration on solid polymeric materials. In many cases, the MEC for heptane is used as a practical minimum.

There has been no systematic evaluation of these agents under so-called "deep-seated" fire scenarios. Part of the problem is the circular definition of deep-seated fires in NFPA 12A [35]. However, the Underwriters Laboratories Inc. (UL) and Factory Mutual Research Corporation (FMRC) listing procedures require testing on wood cribs subsequent to long preburn times (approximately 6 min). Under these tests, surface oxidation and char reactions do occur.

Design concentrations for fire scenarios involving long preburn times in thick arrays of cellulosic fuels will require additional testing. For most applications where incidental quantities of cellulosic materials may be involved and pre-burn times are relatively short time frames (i.e., automatic actuation), the flame extinguishing concentrations for Class A fuels will be less than, or equal to, that of n-heptane and can be used. Surface oxidation or charring reactions do not occur with most polymers; hence, so-called "deep-seated" fires are not a concern when these Class A fuels are involved.

IG-541 is used at 37.5 % minimum design concentration when Class A materials are involved. Other inert gases should have similar or higher minimum design concentrations. As previously discussed, the minimum design concentration is a function of the fuel, the agent, and the delivery systems. Design concentrations for specific hazards must be determined in accordance with the system manufacturer's approval or listing.

As previously discussed the Class A design concentrations are inadequate for energized electrical equipment or in any scenarios where external heating is applied to the combustion system which may be 2–3 times the Class A fuel design concentration. While the 2012 edition of NFPA 2001 increased the minimum design concentration for energized electrical equipment to a value no less than 90 % of the MEC for Heptane, this is clearly inadequate. Designers are referred to the ISO 14520 for the use of more realistic (and higher) design concentrations.

Design Factors In addition to safety factors, the concept of design factors was first introduced into NFPA 2001 for the 2000 edition. A design factor is used to increase the agent quantity for a specific installation or design that has attributes for which the minimum safety factor may not be sufficient. The only variable for which design factors have been quantified is for systems with multiple flow splits protecting multiple enclosures simultaneously. The motivation for a design factor in these cases is the uncertainty in the split of agent mass flow at unbalanced tee junctions. This uncertainty is compounded as the flow is divided at subsequent unbalanced tees.

Table 44.18 Specific volume constants [1]

Generic name	Trade name	k_1 English units	k_2 English units	k_1 Sl units	k_2 Sl units
Halocarbons					
Halon 1301	Halon 1301	2.2062	0.005046	0.1478	0.00057
HFC-23	FE-13	4.7302	0.010699	0.3168	0.0011942
HFC-125	FE-25	2.722	0.006376	0.1828	0.0007085
HFC-227ea	FM 200	1.879775	0.0046625	0.1268	0.0005133
HFC-236fa	FE-36	2.0978	0.00514	0.1413	0.00058
FK-5-1-12	Novec-1230	0.9856	0.002441	0.0664	0.0002743
Inert gases					
IG-01	Argon	8.40299	0.018281	0.5612	0.002054
IG-55	Argonite	9.8809	0.0214956	0.65979	0.0024134
IG-100	NN-100	11.976	0.02606	0.7997	0.002927
IG-541	Inergen	9.858	0.02143	0.659	0.00241

The piping tee design factor is used to provide additional agent to compensate for the uncertainty in the flow division when the flow to a nozzle has passed through more than four tees.

Agent Quantity

Once the design concentration is established, the quantity of agent necessary to achieve that concentration is determined. The quantity of halocarbon agent necessary is determined by the following equation:

$$w = \frac{V}{S}\left(\frac{C}{100 - C}\right)$$

where:
V = Net volume of protected space
C = Design concentration (%)
w = Specific weight of agent required
S = Specific volume (ft^3/lb [m^3/kg]) and is determined by

$$S = k_1 + k_2(T)$$

where T is the minimum ambient temperature of the protected space, and k_1 and k_2 are constants. Values for k_1 and k_2 used in Equation 44.2 are given in Table 44.18. The flooding factor in Equation 44.1, (C/[100 – C]) implies that the agent-air mixture leaking from the enclosure as a result of the addition of the agent, exit the enclosure at the final concentration after mixing with the air initially in the enclosure. As these agents are stored as a liquid and vaporize in the enclosure during the discharge, the enclosure is under a negative pressure relative to ambient, early in the discharge allowing the agent to mix with the air in the enclosure, prior to leaking from the enclosure as the pressure in the enclosure goes positive late in the discharge.

For inert gases, the following formula is used:

$$X = 2.303\frac{V}{S}\log\left(\frac{100}{100 - C}\right)\mathrm{V_s}$$

where
X = Volume of inert gas required at 70 °F
V_s = Specific volume at 70 °F
V = Net protected hazard volume
S = Specific volume at ambient temperature in protected volume (from Equation 2) = k_1 + k_2 (T)

The flooding factor used here log(100/[100 – C]) is derived assuming that leakage from the compartment during discharge occurs with a varying concentration of agent from zero to C from beginning to the end of discharge. As the pressure in the enclosure is positive throughout the discharge for these agents and the relatively long agent discharge, the leakage flow from the enclosure has the agent concentration present at that stage of the discharge. It is identical to the expression used in CO_2 system design.

Discharge Time

The maximum discharge time permitted for halocarbon clean agent systems is 10 s. This discharge time is taken to be the moment when all liquid agent has cleared the nozzles. The total discharge time will be longer as agent vapor and nitrogen are expelled from the system.

The 10-s discharge time limitation for halocarbon agents is designed to aid four objectives:

1. Provide high flow rates through nozzles to ensure adequate mixing of agent with air inside the enclosure.
2. Provide sufficient velocity through pipes to ensure homogeneous flow of liquid and vapor.
3. Limit the formation of agent thermal decomposition products.
4. Minimize direct and indirect fire damage, particularly in fast-developing fire scenarios.

The most important of these objectives relative to discharge time is the minimization of agent thermal decomposition product formulation. Items 1 and 2 alone are determined by the piping system design.

The discharge time requirement for inert gases is currently 120 s for Class A and Class C fires and 60 s for Class B fires [1]. Longer discharge times are typically used for these systems in Europe. The two primary reasons to constrain the discharge time of inert gas agents that form no thermal decomposition products are (1) to limit the direct and indirect fire damage and (2) to minimize the length of time that the fire burns in a depleted oxygen atmosphere.

In some applications, such as flammable liquid hazards and explosion inerting, it is necessary to discharge the agent quickly to minimize direct fire damage or to ensure that the agent concentration is achieved prior to the lower explosive limit (LEL) being reached.

Thermal Decomposition Products

All of the halocarbon replacement agents form higher levels of thermal decomposition products than Halon 1301 under similar conditions. For a given fuel, the two primary variables determining the level of decomposition products are (1) the size of the fire at the time of discharge and (2) the time required to reach an extinguishing concentration in the compartment.

The dependence of thermal decomposition product formulation on discharge time and fire size has been extensively evaluated [8, 42–45]. Figure 44.10 from Back et al. [42] is a plot of peak HF concentration as a function of fire size to room volume ratio. Similar data for

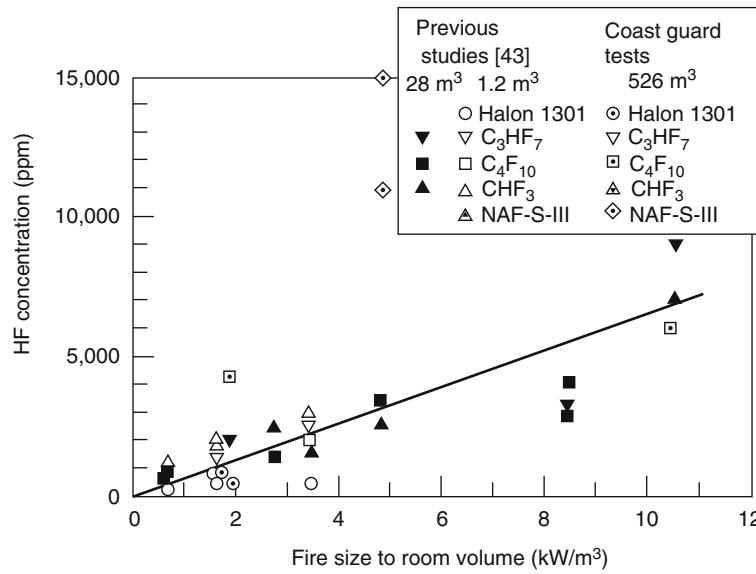

Fig. 44.10 Maximum HF concentration resulting from extinguishment of heptane fires with nominal 10–15 s total discharge times [42]

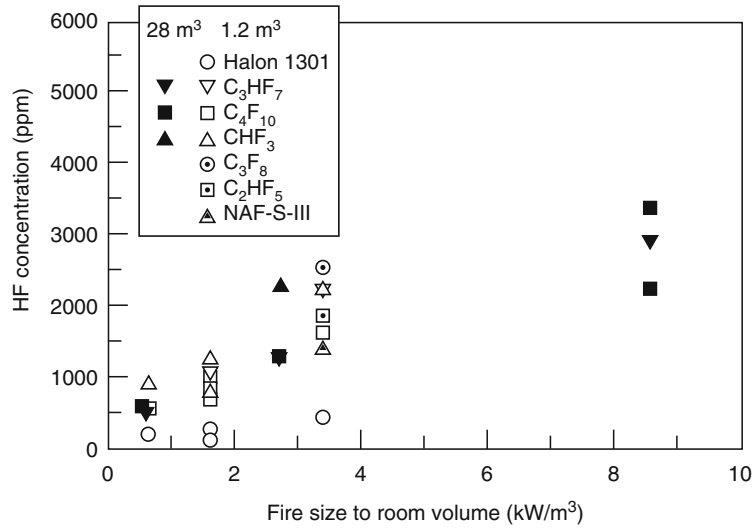

Fig. 44.11 Average HF concentration resulting from extinguishment of heptane pool or heptane pool and spray fires with nominal 15-s total discharge time [43]

10-min average HF concentrations are given in Fig. 44.11. Data are given for Halon 1301, HFC-23, HFC-227ea, FC-3-1-10, and HCFC Blend A from three series of fire tests done at different room scales. The data are for a total discharge time of 15 s, which is analogous to a 10 s discharge time based on nozzle liquid run-out. The data are for heptane pool or heptane pool and spray fires.

The first observation is that the quantity of HF formed is approximately 5–10 times higher for all halocarbon clean agents relative to Halon 1301. There may be differences among the various HFC/HCFC compounds tested, but it is not clear from these data whether such differences (1) occur, (2) are attributable to agent mixing and distribution, or (3) are attributable to locally high velocities or concentrations of agent from the nozzle. In all of the data reported, the fire source, that is, heptane pans of varying sizes, was baffled to prevent direct interaction with the agent jet.

The exception to the similarity of decomposition product formation among the Halocarbon clean agents is the higher concentrations resulting from tests with HCFC Blend A. This agent was tested at the manufacturer's recommended design concentration, which is approximately 40 % lower than the basis for all other agents, which would be expected to correlate with higher decomposition product formation [42].

These data were taken with an FTIR spectrometer at a location approximately 1 m from the floor, or about midflame height, near the wall. The method used was correlated to grab sample and ion-specific electrode (ISE) methods [43]. In all cases, the agreement was good, except for the HCFC blend. In this case, the HF concentration inferred from the treated grab sample was significantly (>50 %) higher than that measured using the FTIR. Since the HCFC blend contains an HF "scrubber," it is postulated that treatment of the grab sample with a basic solution, as required for the ISE measurements, caused formation of additional HF by reentry with F loosely bound up by reaction with the scrubber. Hence, the FTIR data presented for HCFC Blend A represent a significantly lower quantity of HF than would actually be expected if the product were hydrolyzed.

The effect of long discharge times or delayed extinguishing times is shown in Fig. 44.12 [43]. The variation between the HFC/HCFC alternatives and Halon 1301, relative to HF production, is approximately the same as that shown in Fig. 44.11 for different fire sizes.

Although other thermal decomposition products have been identified in some cases, it appears that HF is the primary thermal

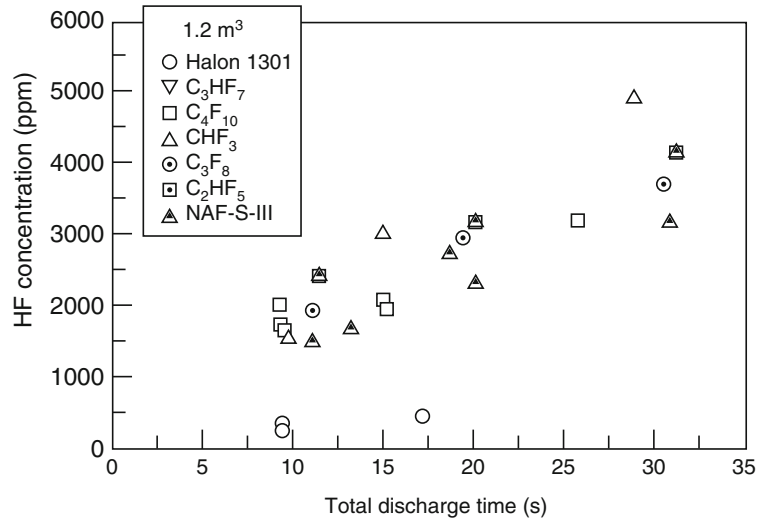

Fig. 44.12 Maximum HF concentration resulting from extinguishment of 4.0-kW heptane fires [43]

Table 44.19 Potential human health effects of hydrogen fluoride in healthy individuals [1]

Exposure time	Hydrogen fluoride (ppm)	Reaction
2 min	<50	Slight eye and nasal irritation
	50–100	Mild eye and upper respiratory tract irritation
	100–200	Moderate eye and upper respiratory tract irritation, slight skin irritation
	>200	Moderate irritation of all body surfaces, increasing concentration may impair escape
5 min	<50	Mild eye and nasal irritation
	50–100	Increasing eye and nasal irritation, slight skin irritation
	100–200	Moderate irritation of skin, eyes, and respiratory tract
	>200	Definite irritation of tissue surfaces, will impair escape at increased concentrations
10 min	<50	Definite eye, skin, and upper respiratory tract irritation
	50–100	Moderate irritation of all body surfaces
	100–200	Moderate irritation of all body surfaces, escape-impairing effects likely
	>200	Escape-impairing effects will occur, increasing concentrations can be lethal without medical intervention

decomposition product of interest relative to human safety and equipment damage. HF, like HCl, is an irritant gas, detectable at very low concentrations. For HF there are very large differences between the approximate lethal concentration (ALC) and human detection and severe sensory irritant thresholds (approximately 2 and 3 orders of magnitude, respectively).

The fire size necessary to generate short-term lethal concentrations of HF in an enclosure (on the order of >1000 ppm) can, in some cases, pose a greater hazard to personnel in the protected space during a discharge in a fire incident, due to the fire and its effects, than the secondary impact of agent thermal decomposition products. This effect, however, should be verified for a particular application under a range of fire scenarios, using engineering methods discussed by Hanauska [46] and Hanauska et al. [47].

The production of HF and other agent decomposition products forms a potential hazard for occupants. Table 44.19 [1] summarizes potential health effects in healthy individuals. Note that

exposures above 200 ppm may begin to impair escape, particularly at exposure times exceeding 5 min.

Emergency Response Planning Guidelines (ERPG) values, developed by the American Industrial Hygiene Association, for 10 min exposures, are as follows: ERPG-2, a level at which mitigating steps such as evacuation should be taken is 50 ppm, and ERPG-3, the maximum nonlethal exposure concentration for 10 min is 170 ppm. The ERPG values are in contrast to an analysis by Meldrum [48] which indicates that a dose of 12,000 ppm/min has 1 % lethality in exposed animals. Additional health-effect and risk-assessment data are given in Dalby [49], Machle and Kitzmiller [50], Machle et al. [51], and Brock [52].

The impact of thermal decomposition products on electronics equipment is another area of concern. There is not sufficient data at present to predict the effects of a given HF exposure scenario on all electronics equipment. Several evaluations of the impact of HF on electronics equipment have been performed relative to the thermal decomposition of Halon 1301, where decomposition products include HF and HBr. One of the more notable was a NASA study where the shuttle orbital electronics were exposed to 700, 7000, and 70,000 ppm HF and HBr [53]. In these tests, exposures up to 700 ppm HF and HBr caused no failures. At 7000 ppm, severe corrosion was noted; there were some operating failures at this level.

Dumayas exposed IBM-PC-compatible multifunction boards to environments produced by a range of fire sizes as part of an evaluation program on halon alternatives [54]. He found no loss of function of these boards following a 15-min exposure to postfire extinguishment atmosphere up to 5000 ppm HF, with unconditioned samples stored at ambient humidity and temperature conditions for up to 30 days. Forssell et al. [55], exposed multifunction boards for 30 min in the postfire extinguishment environment; no failures were reported up to 90 days post-test. HF concentrations up to 550 ppm were evaluated.

Although no generic rule or statement can be made at present, it appears that short-term damage (<90 days) resulting in electronics equipment malfunction is not likely for exposures of between 500 to 1000 ppm HF for up to 30 min. This result, however, is dependent on the characteristics of the equipment exposed, post exposure treatment, exposure to other combustion products, and relative humidity. Important equipment characteristics include its location in the space, existence of equipment enclosures, and the sensitivity of the equipment to damage.

All HCFC and HFC clean agents form more thermal decomposition products than Halon 1301, given similar fire sizes and discharge times. The primary variable controlling the quantity of thermal decomposition products is the size of the fire at the time of agent discharge. Through evaluation of the fire size at the time of system actuation, using engineering methods described in Chap. 40, and subsequent design of the detection system, the potential hazard posed can be managed adequately.

Hanauska [46] and Hanauska et al. [47] have indicated that the degree of thermal decomposition products of agents can be managed safely. Full-scale testing with typical Class A fuel packages, in conjunction with typical detection system installation [55], has shown that the level of thermal decomposition products is acceptable in typical computer/electronics spaces. For installation in hazard areas where very rapidly developing large fires are likely, the degree of thermal decomposition formation should be evaluated in the context of the hazard posed by the fire and the performance of alternative fire protection systems.

System Discharge Effects

When a clean agent system activates, liquid, gas or a two-phase discharge is introduced into the enclosure through a turbulent high velocity jet or spray via a nozzle. The well-known effects of system discharge, including over or under pressurization of the enclosure, and movement of loose objects have been dealt with to a large extent through system and hardware design.

In the case of compartment pressurization it is sometimes necessary to provide relief venting particularly in the case of the use of inert gases.

Another issue might also exist. It has been observed that in certain system configurations used in spaces with sensitive and high speed hard disc computer equipment, the discharge of the clean agent system may cause failure of some of the hard drives in the protected space [56–58]. This has occurred in at least one published case [56] and in this case an inert gas system was involved. It appears from work done by several manufacturers that the failures are caused by acoustic waves resulting from the noise of discharge interacting with hard disc drive storage devices and causing failure of the devices [57, 59]. The problem may be eliminated by the use of longer discharge times and potentially by modified nozzle designs.

Hydraulic Flow Characteristics

All halocarbon replacement agents exhibit two-phase flow behavior. Since all, except HFC-23, are used in cylinders pressurized to 360 or 600 psig, they are also multiple-component flows. Inert gas mixtures are single-phase gas flows with one or more components. As in the case of engineered Halon 1301 systems, all flow calculation procedures used must be listed as further described below or approved by the authority having jurisdiction and be within the limitations of the flow calculation method determined during the engineered system approval and listing process.

The characteristic that differentiates two-phase pipe flow from incompressible fluid (e.g., water) pipe flow is the existence of gas and liquid phases simultaneously in the pipe network. This aspect, coupled with the relatively short flow times, results in significant challenges in correctly predicting the flow. Among the important factors are the change in density of the fluid with pressure, the release of nitrogen in the cylinder and pipe as the fluid pressure and temperature change, differences in agent mass delivered caused by the flow time imbalances between nozzles, and preferential distribution of phases (and subsequently agent mass) at tee splits.

The need for accurate flow predictions is driven by three design requirements:

1. Control of agent discharge time
2. Maintenance of adequate nozzle flow and pressure to ensure agent distribution and mixing at the listed coverage area
3. Delivery of adequate, but not excessive, agent quantities to different rooms within the same protected area, when such rooms are flooded simultaneously.

In addition, agent flow rate and thermodynamic state properties are necessary for estimating compartment pressurization changes during agent discharge.

For pre-engineered systems, those having predetermined flow rates, nozzle pressures, and quantities of agent, limits on discharge time and nozzle pressure are built into the restrictions of piping system geometry. Agent distribution is handled by constraining pre-engineered systems to balanced flow conditions (i.e., the same agent mass is distributed from tee split and each nozzle). For adequate design of engineered systems, accurate methods for predicting these elements are required.

Figure 44.13 is an idealized plot of cylinder and nozzle pressure during discharge. Throughout the discharge process the amount of agent vapor and liquid, as well as dissolved and gaseous nitrogen, varies. As the pressure decreases in the cylinder and piping system, more agent is vaporized and nitrogen is released from the solution in the agent. The formation of additional vapor and nitrogen bubbles lowers the average density of the fluid. The rapid vaporization of agent is more pronounced in low boiling point/high vapor pressure agents. The fluid temperature also varies with time and along the length of the piping network. The fluid temperature also impacts the degree of agent vaporization and nitrogen release as well as liquid agent density. The discharge process can be divided into five sections.

The first is the process of filling the pipe with agent. The rate at which this process occurs is driven by the speed of the agent interface moving

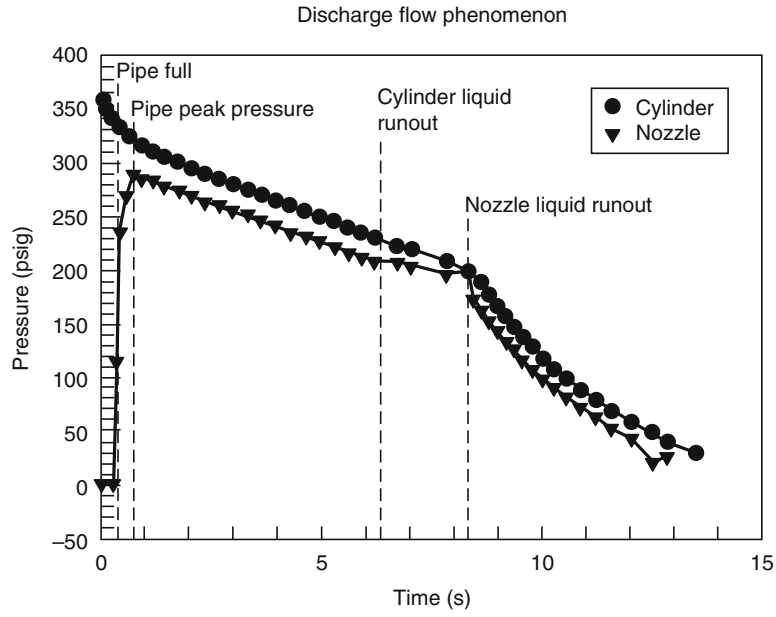

Fig. 44.13 Idealized cylinder and nozzle pressure time curves for halocarbon agents

through the network. This speed is determined by either the sonic velocity at the agent interface or the discharge of displaced air through the nozzle. This phase determines the time at which the agent starts to discharge from each nozzle. For systems with high degrees of imbalance in terms of flow path length or large pipe volume differences between nozzles, there can be significant delay in agent reaching one nozzle before another. This delay has a dramatic effect on the distribution of mass from each nozzle.

Once the agent reaches the nozzle and is compressed in the pipeline, the so-called nozzle peak pressure is reached. At this moment, agent is discharging from each nozzle.

The next step in the discharge process is the so-called quasi-steady agent flow regime. This step is generally the longest portion of the discharge, particularly for systems with low pipe volume to agent volume ratios. This period of the discharge process is the basis for the simplified pressure drop calculations embodied in NFPA 12A for balanced Halon 1301 systems [35].

The next milestone during the discharge process is cylinder liquid runout, where no liquid agent remains in the cylinder. At this moment, an interface between liquid-agent and nitrogen-agent vapor forms and travels through the network.

When the trailing liquid-vapor interface reaches the first nozzle, nozzle liquid run-out occurs. This run-out is important in two ways. First, liquid run-out occurs at different times during the discharge for each nozzle and can significantly impact the quantity of agent flowing from any given nozzle. Second, it is possible in many circumstances to discharge sufficient vapor-gas mixture from the first nozzle at NLRO (nozzle liquid run-out) to reduce the pressure in the piping below that necessary to flow the remaining agent in the network. This aspect is especially important for low vapor pressure agents and for nozzle designs requiring relatively high minimum operating pressures.

Once all of the nozzles have been cleared of liquid agent, the system is discharging a combination of nitrogen and agent vapor. This regime is usually ignored since most (>95 %) of the agent has already been delivered through the nozzles.

The importance of the pipe filling and nozzle run-out with these alternatives is relatively more critical with low vapor pressure alternatives due to (1) the inability of the agent to deliver significant pressure to the system by boiling and (2) the

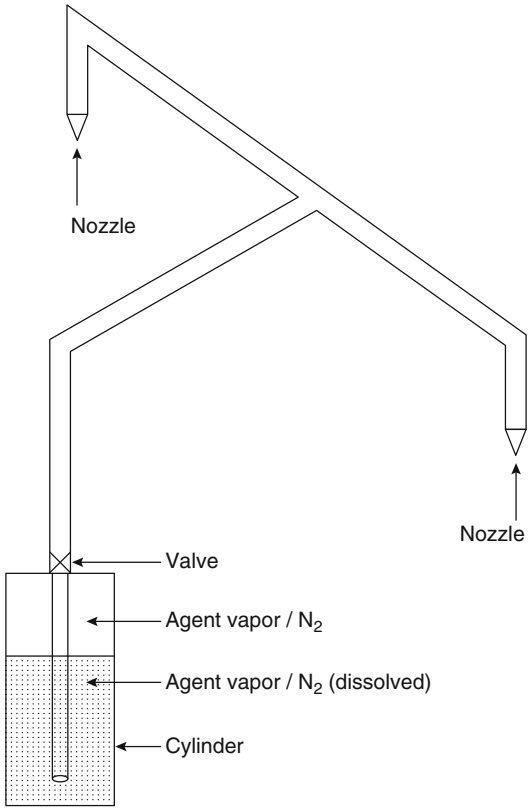

Fig. 44.14 Initial conditions

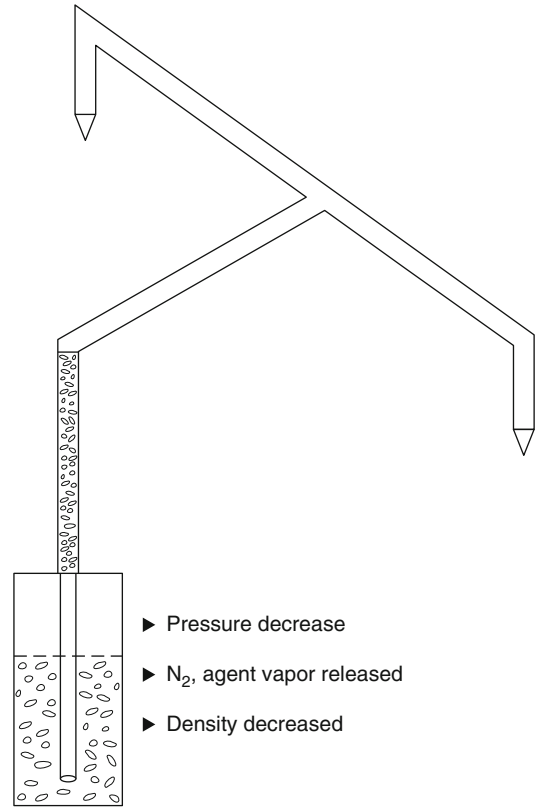

Fig. 44.15 Valve open, pipe filling

higher fluid densities that occur in the piping relative to Halon 1301.

Figures 44.14, 44.15, 44.16 and 44.17 illustrate the stages of the agent discharge network.

Flow Regime If the flow velocity of the agent in the piping is not high enough, the flow may separate into two distinct phases within the piping [60]. This phase separation causes rather unpredictable fluid behavior at tee splits and makes evaluating pressure drop in the piping system more challenging. Therefore, minimum flow rates that ensure a homogeneous mixture of liquid agent and vapor-nitrogen bubbles must be maintained. Various flow regimes are illustrated in Figs. 44.18 and 44.19 for horizontal and vertical pipe, respectively. One of the objectives of approval testing of flow calculation procedures is to ensure that homogeneous flow regimes are maintained in the piping throughout the clean agent discharge process. Figures 44.18 and 44.19 depict the dispersed-bubble and bubble-flow regimes, respectively.

Flow Division at Tees For a single-component (agent only, i.e. no dissolved nitrogen), single-phase flow condition, the flow split at a tee junction can be determined by the flow rate of the nozzles downstream of the tee. For two-phase fluids, flow distribution at the tees is sensitive to four physical conditions: (i) the velocity of the fluid flow along each branch of the tee, (ii) the orientation of the tee, (iii) the pressure at the tee, and (iv) the phase distribution of the fluid (gas or liquid) entering the tee.

The primary cause of preferential flow splits at tees is the inertia of the liquid versus vapor-gas phase. This condition is most readily envisioned for side-flow tees where one branch of the flow is required to turn 90°. Gas-vapor bubbles with lower momentum relative to the liquid agent will make this change of direction more readily.

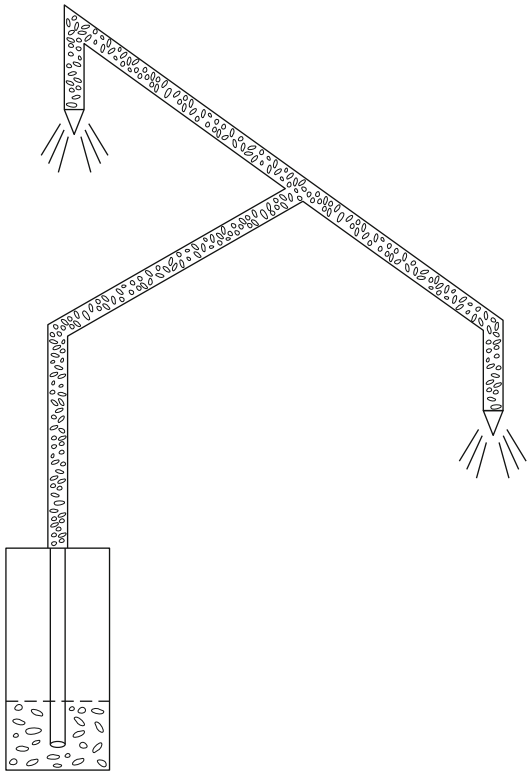

Fig. 44.16 Quasi-steady flow, liquid throughout network

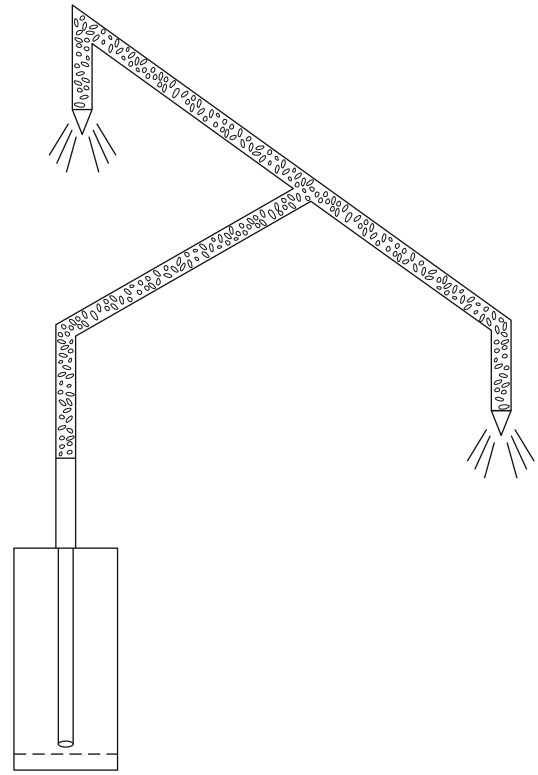

Fig. 44.17 Cylinder liquid runout

Fig. 44.18 Horizontal pipe flow regimes [60]

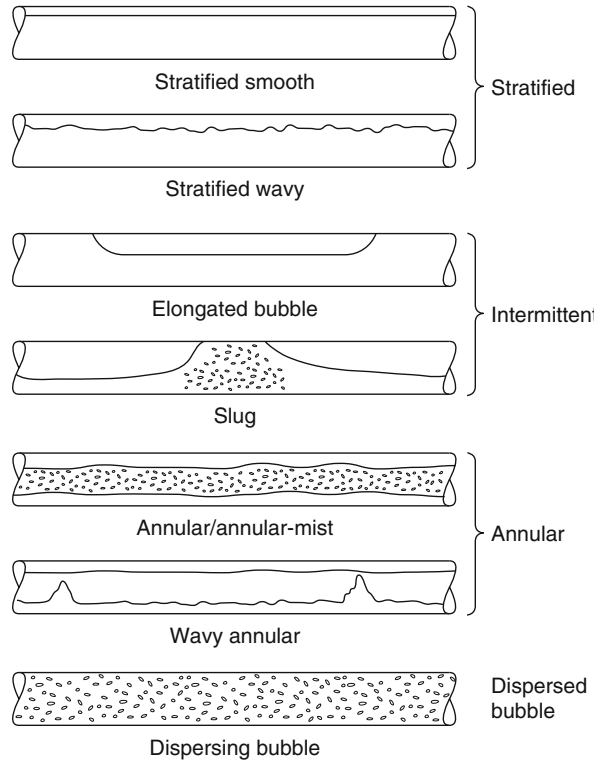

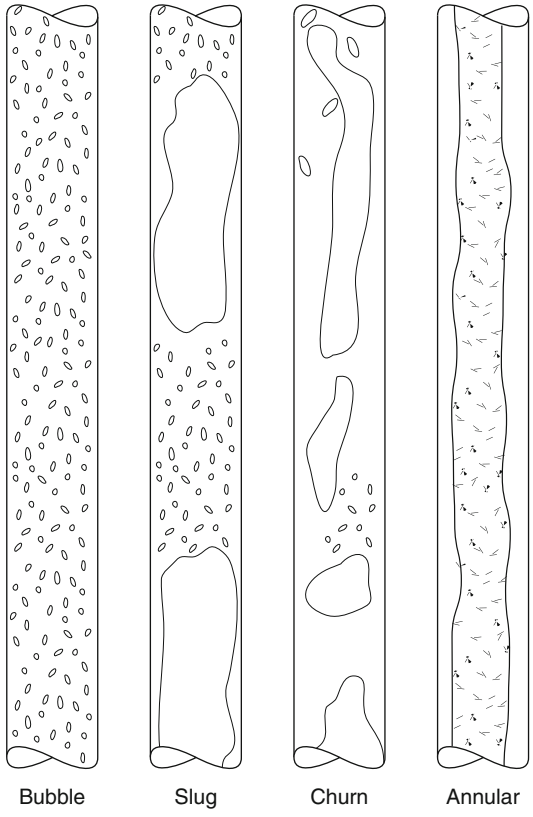

Fig. 44.19 Vertical pipe flow regimes [60]

This change results in relatively less mass flow down the side-flow branch at approximately the same volumetric flow rate or velocity. For bullhead tees, the same phenomenon occurs, except that it is more subtle and involves velocity differences through each branch of the tee. For evenly split (50%/50%) flows, the velocity is identical in both directions, resulting in no flow split correction; as the split becomes greater the velocity differences are greater, and inertial effects of the gas-vapor portion of the fluid relative to the liquid portion cause significant redistribution of mass through each branch of the tee.

The dependence was understood for Halon 1301 and described in detail by Williamson [61]. Similar processes occur in all two-phase flows including air-water, steam- water, and refrigerant flows. In the context of clean agent system design calculations, this flow distribution is dealt with using empirical factors that redistribute the flow relative to the pure pressure-driven flow distribution that would occur without preferential phase distribution at tees.

Figures 44.20 and 44.21 illustrate these correction factors for Halon 1301 flows in bullhead and side-flow tees, respectively [61]. All of the

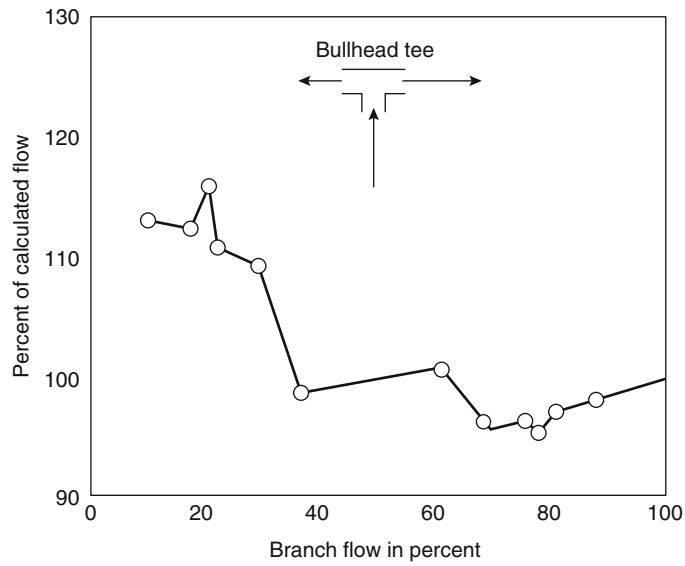

Fig. 44.20 Bullhead-tee-flow split corrections for Halon 1301 [61]

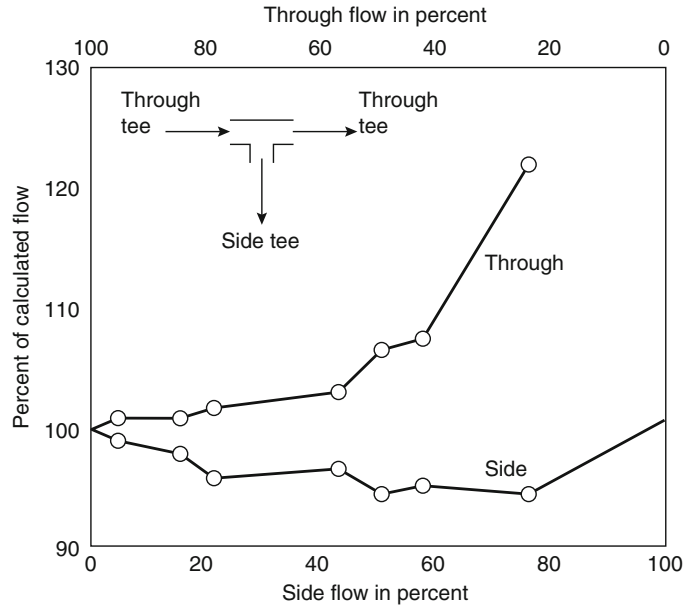

Fig. 44.21 Side- and through tee-flow split corrections for Halon 1301 [61]

halocarbon agent flow predictions require similar treatment. Side-flow tees and bullhead tees require independent empirical correction factors. One of the most important limitations to any flow calculation procedure is the maximum flow split allowed for each type of tee. For a bullhead tee, as one moves farther away from 50%/50% splits, the correction factor becomes greater, and at some point usually in the range of 80%/20%, it becomes so large that the prediction becomes unreliable. For side-allowable flow splits, ranges between 75%/25% and 90%/10% are typical. This correction of flow splits at tees is one reason that final approval of engineered system designs should be constrained to calculation methods that have undergone testing within the range of the flow splits required.

Pressure Drop due to Friction Loss The pressure drop caused by friction in the pipeline is calculated differently for two-phase fluids. The presence of agent vapor and gas affects the pressure drop per unit length of pipe. There are numerous methods for dealing with two-phase fluid pressure drop [62, 63]. Those typically used for fire suppression agent calculations involve either (1) correcting the pressure drop estimated for single-phase fluid as a function of liquid to vapor-gas volume fraction or (2) empirical correlations of the pressure drop to average fluid density. Figure 44.22 illustrates the dependence of pressure drop on liquid volume fraction. In all cases for purposes of design of fire protection systems, the pressure drop is calculated on the basis of a homogeneous flow assumption where changes in the liquid fraction are seen as density changes in the homogeneous fluid.

Testing and Approval of Design Methods The approval or listing of a two-phase flow calculation procedure is part of the overall approval necessary for engineered systems. Since some aspects of two-phase flow calculations are empirically based (e.g., flow regime, pressure drop, and flow splits) and all calculation procedures have some bounds on their validity, testing is performed to verify the predictions and establish the limits of the calculation procedure. These calculation procedure limitations are crucial in helping to ensure overall adequacy of system designs.

One of the most rigorous approval procedures used in verifying design calculation methods for clean agent systems are outlined in UL 2127, *Inert Gas Clean Agent Extinguishing System Unit* [12] and in UL 2166, *Halocarbon Clean*

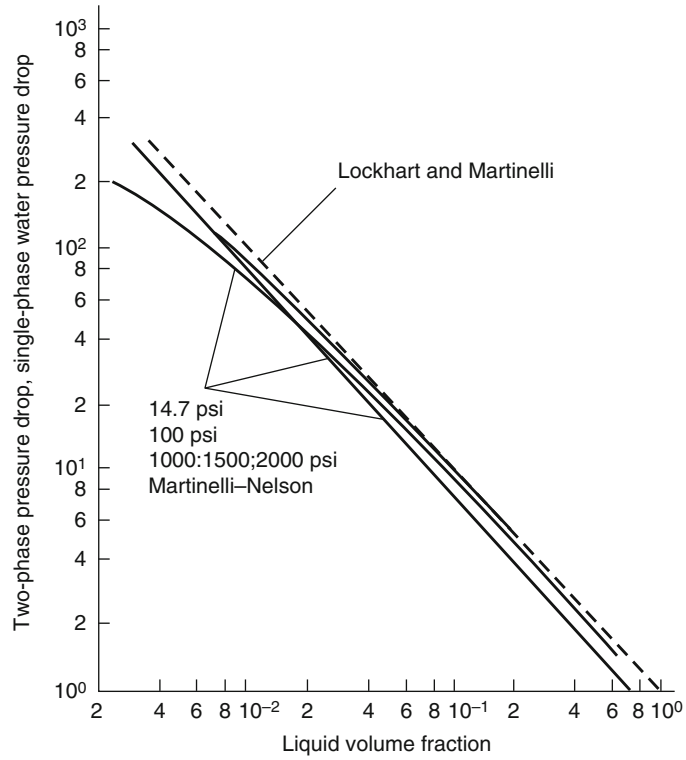

Fig. 44.22 Pressure drop versus liquid volume fraction [62]

Agent Extinguishing System Units [13]. Design method limitations are described by the following 10 parameters:

1. Percentage of agent in piping (maximum)
2. Minimum and maximum discharge times
3. Minimum pipeline flow rates
4. Variance of piping volume to each nozzle
5. Maximum variance of nozzle pressures within a piping arrangement
6. Maximum ratio of nozzle diameter to inlet pipe diameter
7. Arrangement most likely to exhibit vapor time-imbalance condition at nozzle
8. All types of tee splits, including through tees, bullhead tees, and so forth
9. Minimum and maximum container fill density
10. Minimum and maximum flow split for each type of tee.

These parameters are related to the important attributes of the agent discharge process previously discussed. Full-scale testing is performed to evaluate the performance of the design method. The limits on flow calculation method performance are as follows:

1. Actual versus predicted discharge time ±1 s for halocarbon agents and ±10 s for inert gas agents
2. Actual versus predicted nozzle pressure ±10 %
3. Actual versus predicted mass flow through a nozzle, ±10 %

The flow calculation method testing is performed with the specific manufacturer's hardware to ensure that the flow through the hardware is modeled correctly.

Several generic flow calculation routines have been developed [43, 64–67]. Of these, two are directed at single-nozzle systems with very short discharge times [66] or relatively simple balanced networks [65]. It is not recommended that any generic calculation procedure be used for final design purposes unless the procedure has been tested with the specific hardware to be installed, and system performance is within the limitations derived by testing.

In order to preserve a 10 s discharge time, the mass flow rate of these clean agents must be higher than Halon 1301. The increased density of some of the clean agents in the piping, caused by lower vapor pressures and nitrogen solubility differences, may result in high enough mass flow rates to retrofit existing Halon 1301 systems. Although agent cylinders and nozzles will require replacement, it is possible to preserve the existing Halon 1301 pipe network. Preservation often requires the use of lower fill density cylinders to increase the average system pressure throughout the discharge time. Any retrofit using existing Halon 1301 piping must be prudently evaluated with respect to hydraulic performance, with particular attention given to preserving the minimum required nozzle pressures and flow divisions at tees.

Nozzle Area Coverage and Height Limitations

One of the most important requirements of a gaseous total flooding fire suppression system is the ability of the system to deliver a uniform concentration of agent throughout the protected enclosure within the discharge period. The nozzle design and minimum nozzle discharge pressure are critical in ensuring this distribution of agent. The performance of the nozzle is evaluated by full-scale testing, such as through UL 2127 [12] and UL 2166 [13]. The basic testing performed to evaluate nozzles is as follows:

1. Establish minimum nozzle pressure and maximum nozzle height by ensuring extinguishment of heptane fires located throughout a space with a height equal to the maximum allowable, at the minimum allowable nozzle pressure.
2. Establish maximum nozzle coverage area by extinguishing tests in a plenum at the minimum height (generally less than 0.5 m) at the maximum nozzle coverage area (on the order of 100 m^2) and minimum nozzle operating pressure.

There are substantial differences among hardware manufacturers relative to minimum nozzle pressure, maximum ceiling height, and maximum average cover- age. All nozzle anticipated orientations should be evaluated. In general, maximum nozzle heights are on the order of 4–5 m, nozzle area coverage on the order of 90–100 m^2, and minimum nozzle pressure between 3 and 6 bar. It is critical to ensure that the nozzle spacing, height, and minimum pressure limits are not exceeded for a particular manufacturer's hardware in a specific design.

The flow, mixing, and distribution of an agent from a nozzle into an enclosure can be predicted theoretically for relatively simple nozzle designs using sophisticated computer models [65]. Further development of such methods for complex nozzle designs and compartment geometries could eventually form the basis of a design procedure. At present, however, the primary means of ensuring adequate nozzle performance is the hardware approval process and real-scale testing.

Since many of the halocarbon agents have lower vapor pressures than Halon 1301, there is often a much higher percentage of liquid at the nozzle. This liquid makes the task of vaporizing and mixing the agent in the compartment more difficult. In general, nozzle designs used for Halon 1301 systems are not adequate for the halocarbon replacement agents. Due to the increased liquid fraction at the nozzle, it is critical to ensure that no unenclosed openings exist along the trajectory of the nozzle orifices. Increased liquid fraction may result in significant preferential loss of agent through these openings. This condition further emphasizes the need for third-party approval testing and listing of nozzle performance. In any retrofit situation including those of other types of clean agent systems and Halon 1301 systems, the nozzles will need to be replaced even if the piping is adequately sized to deliver proper agent flow rates.

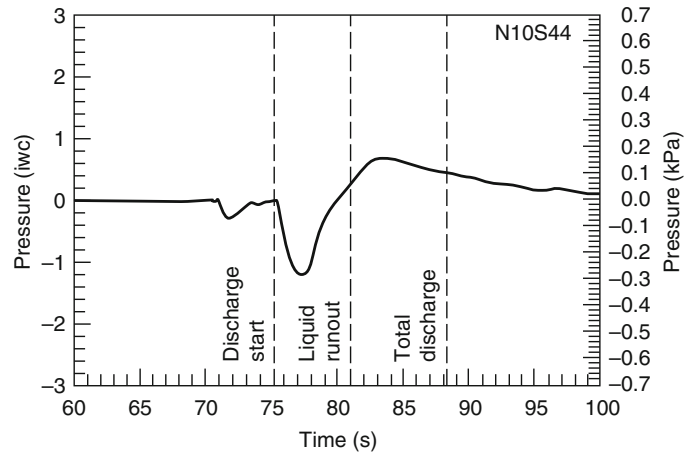

Fig. 44.23 Pressure measured in 28 m^3 enclosure during HFC-227ea (C_3F_7H) discharge, with nominal 15 s discharge time and 5 cm pan of n-heptane [43]

Compartment Pressurization

The rapid discharge of agent into a compartment will cause rapid changes in the compartment pressure. Depending on the agent and rate of discharge, the initial pressure change may be negative. Figure 44.23 is a plot of compartment pressure versus time for the discharge of HFC-227ea into a 28 m^3 room with a 360 cm^2 (56 $in.^2$) leakage area [43]. Immediately after discharge, the pressure in the compartment drops below ambient to a minimum of −0.3 kPa; at approximately 1.5 s after discharge, the pressure then begins to increase to a maximum of approximately 0.14 kPa after nozzle liquid run-out. Similar results were obtained for FC-3-1-10. HFC-23 discharge exhibited much higher compartment overpressurization, without the marked initial negative pressure. The maximum overpressure for HFC-227ea and FC-3-1-10 discharge was similar to that of Halon 1301.

As the halocarbon agent is discharged into the space, it vaporizes rapidly, cooling the compartment and lowering the pressure. As the agent-air mixture gains heat from the walls or other objects in the space, the pressure recovers and, as additional agent is added, the pressure increases over ambient as mass is added to the compartment.

The expected maximum and minimum compartment pressure during discharge will be a function of the following:

1. Thermodynamic state of the agent at the nozzle
2. Nozzle design
3. Compartment volume and wall surface area
4. Size of fire
5. Initial conditions in space
6. Leakage area from compartment
7. Agent flow rate

For inert gases, significant compartment overpressurization can occur during discharge unless adequate free vent area is provided. Calculation of required open area for venting is a part of the design manual for inert gas systems as for IG-541 systems [68].

No generalized design procedure for calculating under/overpressurization has been established. Forssell and DiNenno [43] have developed a procedure for estimating the compartment pressure as a function of agent, agent flow rate, agent thermodynamic state at the nozzle, compartment volume, and surface area and leakage area. However, the method has not been sufficiently tested for general application. The Fire Suppression System Association, FSSA, has developed a guide for estimating the pressure relief vent areas for preventing damage to enclosures during the discharge of clean agent

systems [69]. The guide is based on empirical correlations developed during a experimental research program.

Agent Hold Time and Leakage

Traditionally, total flooding gas systems were required to maintain a minimum concentration for a specified time period (10–20 min) after discharge. The minimum required hold time was based on the following:

1. Soak time required for deep-seated Class A fuels
2. Response time of emergency personnel
3. Prevention of re-flash of the fire due to the presence of hot surfaces, electrical energy and other reignition sources, particularly with flammable and combustible liquid applications.

The absolute minimum hold time requirement is 10 min. The variables described above will vary between installations, and there is no significant database on the performance of these agents on deep-seated fires other than wood cribs. The designer will be required to specify the minimum soak time consistent with the requirements of the hazard being protected.

The ability of a compartment to maintain adequate agent concentrations is a function of the leakage of the compartment. Historically, this was done with Halon 1301 through the use of discharge tests. Discharge testing for this purpose was rendered unnecessary by the introduction of door fan pressurization leakage tests.

The only difference between alternative agents and Halon 1301 in this regard is the density of the agent-air mixture, which is the driving force for leakage in quiescent environments. The mixture density can be estimated as follows [1]:

$$\rho_m = V_d \frac{C}{100} + \left[\frac{\rho_a(100 - C)}{100}\right]$$

where:

ρ_m= Clean agent-air mixture density (kg/m^3)

ρ_a= Air density (1.202 kg/m^3)

C = Clean agent concentration (%)

V_d = Agent vapor density (kg/m^3)

Agent vapor densities are given below:

FC-3-10	$9.85\,kg/m^3\,(0.615\,lb/ft^3)$
HBFC-22B1	$5.54\,kg/m^3\,(0.346\,lb/ft^3)$
HCFC-Blend A	$3.84\,kg/m^3\,(0.240\,lb/ft^3)$
HFC-124	$5.83\,kg/m^3\,(0.364\,lb/ft^3)$
HFC-125	$5.06\,kg/m^3\,(0.316\,lb/ft^3)$
HFC-227ea	$7.26\,kg/m^3\,(0.453\,lb/ft^3)$
HFC-23	$2.915\,kg/m^3\,(0.182\,lb/ft^3)$
IG-541	$1.43\,kg/m^3\,(0.089\,lb/ft^3)$
Halon 1301	$6.283\,kg/m^3\,(0.392\,lb/ft^3)$

All agents, except inert gases, have higher mixture densities than Halon 1301 at 5 % when used at their design concentrations requiring slightly more leak-tight enclosures to maintain the same hold time.

There are several methods available to estimate the hold time of gaseous agent mixtures based on leakage measured by the door fan pressurization method. The first method, initially developed by DiNenno and Forssell [70] and Grant [71], modeled the leakage of a gas-air mixture from a compartment as a two-layer system with a uniform gas-air mixture below a sharp interface and air above the interface. In this idealization, the gas-air mixture leaks out of the bottom of the room and the inter-face descends with time much like a draining bathtub. This method is standardized in NFPA 2001. The interface is modeled as remaining well defined throughout its descent. Spreading of the interface due to diffusion and localized mixing is ignored. Another idealized case treated by DiNenno and Forssell [70] is the case of a uniform mixture of gas and air across the height of the room in which the uniform concentration decays with time as air leaks in and gas-air mixture leaks out. This case is the so-called "uniform mixing" case.

Dewsbury and Whitely [72, 73] also proposed a treatment of a widely spreading interface. In this idealization there are two "zones" in a compartment. At the ceiling, the agent concentration is assumed to be zero and over time a zone where the agent concentration increases from zero at the ceiling to the initial agent concentration at the interface boundary exists. This so-called

spreading interface increases in depth as the agent-air mixture leaves from the bottom of the room. This method is embodied in ISO 14520 and is more conservative than the other methods. Additional refinements to the spreading interface modeling approach have been proposed by Hetrick et al. [74].

A key difference between this wide interface case and the sharp interface case is that the position within the spreading interface, where the agent concentration falls below 70 % or 80 % of the design concentration, is defined to be the position in the room above which the agent concentration is inadequate. In the sharp interface case this position would occur when the agent concentration is 50 % of the initial value (assuming a non-sharp interface actually occurred). Consequently, the allowable leakage will be significantly less than that permitted using the sharp interface model in NFPA 2001. The full-scale data obtained by Dewsbury and Whitely [72, 73] and Klocke [75] for inert gas mixtures indicate widely spreading interfaces are typical.

Additional refinements relying much more on empirical data on interface spread and refinements in the estimation of leakage area were added to the provisions of NFPA 2001.

All of these leakage area measurement methods and leakage calculation estimates are approximate since the precise size and location of the leakage paths are never know. Based on a range of full-scale idealized experiments it appears that the hold time or retention calculations are likely conservative.

Summary

A range of inert gas and halocarbon total flooding clean agents are available. The use of an agent must be consistent with applicable environmental and toxicity regulations. The selection of an agent is driven by its fire performance characteristics, agent and system space and weight concerns, toxicity (particularly for use in occupied areas), and the availability of approved system hardware.

The design of clean agent systems must be thoroughly completed in accordance with third-party listing and approval limitations on the agent, distribution hardware, and hydraulic calculation procedure. Given the specialized knowledge associated with these types of fire protection systems, particular care in the design, installation, inspection, testing, and maintenance of these systems is warranted. It is important to recognize that fire protection standards, such as NFPA 2001, form the minimum requirements for these clean agent technologies.

In the case of all clean agents, system designs are much less robust than those for Halon 1301 systems. Of particular concern is the application of inadequate or unjustified design concentrations particularly where energized electrical equipment is used or deep-seated fires are a concern. Designers and users are encouraged to investigate the means by which the design concentrations are established and consult the ISO 14520 standard for more conservative design concentration requirements.

References

1. NFPA 2001, *Standard on Clean Agent Fire Extinguishing Systems*, National Fire Protection Association, Quincy, MA (2012).
2. R.T. Wickham, "Review of the Use of Carbon Dioxide Total Flooding Fire Extinguishing Systems," Wickham Associates prepared for US EPA, August 8, 2003.
3. ISO 14520-1, "Gaseous Fire Extinguish Systems – Physical Properties and System Design, Part 1: General Requirements," International Standards Organization, 2006.
4. A. Liu and M. Colket, "Modeling Cup-burner Minimum Extinguishing Concentration of Halogenated Agents," Proceedings of 2010 Suppression, Detection and Signaling Research and Applications Symposium, February 16–19, 2012, National Fire Protection Research Foundation, Quincy, MA, (2010).
5. A. Hamins, G. Gmurczyk, W. Grosshandler, R. Rehwoldt, I. Vazquez, and T. Cleary, "Flame Suppression Effectiveness," in *Evaluation of Alternative In-Flight Fire Suppressants for Full-Scale Testing in Simulated Aircraft Engine Nacelles and Dry Bays*, NIST SP 861, National Institute of Standards and Technology, Gaithersburg, MD (1994).
6. M.L. Robin, "Properties and Performance of FM-200™," in *Proceedings of the Halon Options*

Technical Working Conference 1994, New Mexico Engineering Research Institute, Albuquerque, NM, pp. 531–542 (1994).
7. R. Sheinson, H. Eaton, B. Black, R. Brown, H. Burchell, A. Maranghides, C. Mitchell, G. Salmon, and W., "Halon 1301 Total Flooding Fire Testing, Intermediate Scale," in *Proceedings of the Halon Options Technical Working Conference 1994*, New Mexico Engineering Research Institute, Albuquerque, NM, pp. 43–53 (1994).
8. T.A. Moore, D. Dierdorf, and S. Skaggs, "Intermediate Scale (645 ft3) Fire Suppression Evaluation of NFPA 2001 Agents," in *Proceedings of the Halon Options Technical Working Conference 1993*, New Mexico Engineering Research Institute, Albuquerque, NM, pp. 115–127 (1993).
9. M.J. Ferreira, C. Hanauska, and M. Pike., "Thermal Decomposition Product Results Utilizing PFC-410," in *Proceedings of the Halon Options Technical Working Conference 1992*, New Mexico Engineering Research Institute, Albuquerque, NM (1992).
10. "Extinguishing Behavior of Inert Gases," *Final Report*, VdS, Cologne, Germany (1998).
11. R.E. Tapscott, "Best Values of Cup Burner Extinguishing Concentration," in *Proceedings of the Halon Technical Options Technical Working Conference 1999*, New Mexico Engineering Research Institute, Albuquerque, NM, pp. 27–29 (1999).
12. UL 2127, *Inert Gas Clean Agent Extinguishing System Units*, Underwriters Laboratories Inc., Northbrook, IL (1999).
13. UL 2166, *Halocarbon Clean Agent Extinguishing System Units*, Underwriters Laboratories Inc., Northbrook, IL (1999).
14. Linteris, G "Clean Agent Suppression of Energized Electrical Equipment Fires," NIST Technical Note 1622 NIST, Gaithersburg, MD (2009).
15. R. Patel and P. Rivers, "Performance Based Guidance in Specifying Clean Extinguishing Agent Protection Against Energy Augmented Data Center Fire Conditions," Proceedings of 2012 Suppression, Detection and Signaling Research and Applications Symposium, March 5–8, 2012, National Fire Protection Research Foundation, Quincy, MA (2012).
16. L.A. McKenna, D. Gottuk, P. DiNenno; A. Kline, and S. Mehta, "Extinguishment Tests of Continuously Energized Class C Fires," in *Halon Options Technical Working Conference 1998*, New Mexico Engineering Research Institute, Albuquerque, NM (1998).
17. J.A. Senecal, "Agent Inerting Concentrations for Fuel-Air Systems," *CRC Technical Note No. 361,* Fenwal Safety Systems (1992).
18. F. Tamanini, *Determination of Inerting Requirements for Methane/Air and Propane/Air Mixtures by an Ansul Inerting Mixture of Argon, Carbon Dioxide, and Nitrogen*, Factory Mutual Research Corp., Norwood, MA (1992).
19. E. Heinonen, "Laboratory-Scale Inertion Results," *Halon Substitutes Program Review (1993).*
20. E.W. Heinonen, "The Effect of Ignition Source and Strength on Sphere Inertion Results," in *Proceedings of the Halon Options Technical Working Conference 1993*, Albuquerque, NM, pp. 565–576 (1993).
21. T.A. Moore, "Large-Scale Inertion Evaluation of NFPA 2001 Agents," in *Proceedings of the 1993 International CFC and Halon Alternatives Conference*, Washington, DC (1993).
22. J.A. Senecal, "Explosion Protection in Occupied Spaces: The Status of Suppression and Inertion Using Halon and Its Descendants," in *Proceedings of the 1993 International CFC and Halon Alternatives Conference*, Washington, DC, pp. 767–772 (1993).
23. J.A. Senecal, D.N. Ball, and A. Chattaway, "Explosion Suppression in Occupied Spaces," in *Proceedings of the Halon Options Technical Working Conference 1994*, Albuquerque, NM, pp. 79–86 (1994).
24. A. Vinegar and G.W. Jepson, "Cardiac Sensitization Thresholds of Halon Replacement Chemicals Predicted in Humans by Physiologically-Based Pharmacokinetic Modeling," *Risk Analysis,* 16, 4 (1996).
25. A. Vinegar, G.W. Jepson, and J.H. Overton, "PBPK Modeling of Short Term (0 to 5 min) Human Inhalation Exposures to Halogenated Hydrocarbons," *Inhalation Toxicology*, 10, pp. 411–429 (1998).
26. A. Vinegar, *Performance of Monte Carlo Simulations of Exposure to HFC-227ea*, ManTech Environmental Technology, Inc., Dayton, OH (1999).
27. A. Vinegar, G.W. Jepson, M. Cisneros, R. Rubenstein, and W.J. Brock, "Setting Safe Exposure Limits for Halon Replacement Chemicals Using Physiologically Based Pharmacokinetic Modeling," *Inhalation Toxicology*, 12, 8, pp. 751–763 (2000).
28. A. Vinegar and G. Jepson, "Pharmacokinetic Modeling for Determining Egress from Exposure to Halon Replacement Chemicals," in *Proceedings of Halon Options Technical Working Conference 1998*, New Mexico Engineering Research Institute, Albuquerque, NM (1998).
29. A. Vinegar and G. Jepson, "Epinephrine Challenge for Cardiac Sensitization Testing versus Endogenous Epinephrine," in *Proceedings of the Halon Technical Working Conference 1999 New Mexico Engineering Research Institute, Albuquerque, NM (1999).*
30. "Research Basis for Improvement of Human Tolerance to Hypoxic Atmospheres in Fire Prevention and Extinguishment," *EBRDC Report 10.30.92*, Environmental Biomedical Research Data Center, Institute for Environmental Medicine, University of Pennsylvania, Philadelphia, PA (1992).
31. David de Jager, Martin Manning, Lambert Kuijpers, Stephen O. Andersen, Paul Ashford, Paul Atkins, Nick Campbell, Denis Clodic, Sukumar Devotta, Dave Godwin, Jochen Harnisch, Malcolm Ko,

Suzanne Kocchi, Sasha Madronich, Bert Metz, Leo Meyer, Jose Roberto Moreira, John Owens, Roberto Peixoto, Jose Pons, John Pyle, Sally Rand, Rajendra Shende, Theodore Shepard, Stephen Sicars, Susan Solomon, Guus Velders, Dan Verdonik, Robert Wickham, Ashley Woodcock, Paul Wright, and Masaaki Yamabe, "Technical Summary," *Safeguarding the Ozone Layer and the Global Climate System: Issues Related to Hydrofluorocarbons and Perfluorocarbons*, IPCC/TEAP Special Report, United Nations Environment Programme (2005).

32. Halon Alternatives Research Corporation (HARC) (2007), "Report of the HFC Emissions Estimating Program, 2002–2005 Data Collection," HARC, Arlington, VA, November 2007.
33. J.C. Yang and B.D. Bruel, "Thermophysical Properties of Alternative Agents," in *Evaluation of Alternative In-Flight Fire Suppressants for Full-Scale Testing in Simulated Aircraft Engine Nacelles and Dry Bays*, NIST SP 861, National Institute of Standards and Technology, Gaithersburg, MD (1994).
34. P.J. DiNenno, "Direct Halon Replacement Agents and Systems" in *Fire Protection Handbook*, Nineteenth edition, National Fire Protection Association, Quincy, MA (2003).
35. NFPA 12A, *Standard on Halon 1301 Fire Extinguishing Systems*, National Fire Protection Association, Quincy, MA (2009).
36. NFPA 12, *Standard on Carbon Dioxide Extinguishing Systems*, National Fire Protection Association, Quincy, MA (2011).
37. J.C. Brockway, "Recent Findings on Thermal Decomposition Products of Clean Extinguishing Agents," 3 M Report presented to NFPA 2001 Committee, Ft. Lauderdale, FL (1994).
38. I. Schlosser, "Reliability and Efficacy of Gas Extinguishing Systems," in *Proceedings of Conference on Fire Extinguishing Systems,* VdS, Cologne, Germany (1998).
39. *Halon Alternatives, A Report on the Fire Extinguishing Performance Characteristics of Some Gaseous Alternatives to Halon 1301, LPR6: July 1996*, Loss Prevention Council, Hertfordshire, UK (1996).
40. ISO 14520–1, *Gaseous Fire Extinguish Systems—Physical Properties and System Design, Part 1: General Requirements*, International Standards Organization (2000).
41. C. Hanauska and P. DiNenno, "The Adequacy of Guidance on Agent Concentrations for Gaseous Fire Extinguishing Systems," Proceedings of Suppression and Detection Research Applications- A Technical Working Conference, Orlando FL, Feb 24–27, 2009, National Fire Protection Research Foundation, Quincy, MA (2009).
42. G.G. Back, C.L. Beyler, P.J. DiNenno, and M. Peatross, "Draft Report: Full-Scale Machinery Space Testing of Gaseous Halon Alternatives," USCG R&D Center, Groton, CT (1994).
43. E.W. Forssell and P.J. DiNenno, "Evaluation of Alternative Agents for Use in Total Flooding Fire Protection Systems," Contract NAS 10–1181, National Aeronautics and Space Administration, John F. Kennedy Space Center, FL (1994).
44. P.J. DiNenno, E. Forssell, M. Peatross, J. Wong, and M. Maynard, "Thermal Decomposition Testing of Halon Alternatives," in *Proceedings of the Halon Alternatives Technical Working Conference 1993*, New Mexico Engineering Research Institute, Albuquerque, NM (1993).
45. D.S. Dierdorf, T. Moore, and S. Skaggs, "Decomposition Product Analysis During Intermediate Scale (645 ft3) Testing of NFPA 2001 Agents," in *Proceedings of the Halon Alternatives Technical Working Conference 1993*, New Mexico Engineering Research Institute, Albuquerque, NM (1993).
46. C.P. Hanauska, "Hazard Assessment of HFC Decomposition Products," presented at the *1994 International CFC and Halon Alternatives Conference,* Washington, DC (1994).
47. C.P. Hanauska, E. Forssell, and P. DiNenno, "Hazard Assessment of Thermal De- composition Products of Halon Alternatives," in *Proceedings of the Halon Alternatives Technical Working Conference 1993,* New Mexico Engineering Research Institute, Albuquerque, NM (1993).
48. M. Meldrum, *Toxicology of Substances in Relation to Major Hazards: Hydrogen Fluoride,* Health and Safety Executive (HSE) Information Centre, Sheffield, England (1993).
49. W. Dalby, *Evaluation of the Toxicity of Hydrogen Fluoride at Short Exposure Times*, Stonybrook Laboratories, Inc., Pennington, NJ, sponsored by the Petroleum Environmental Research Forum (PERF), PERF Project 92–90 (1996).
50. W. Machle and K.R. Kitzmiller, "The Effects of the Inhalation of Hydrogen Fluoride, II, The Response Following Exposure to Low Concentrations," *Journal of Industrial Hygiene and Toxicology,* 17, pp. 223–229 (1935).
51. W. Machle, F. Tharnann, K.R. Kitzmiller, and J. Cholak, "The Effects of Inhalation of Hydrogen Fluoride, I, The Response Following Exposure to High Concentrations," *Journal of Industrial Hygiene and Toxicology*, 16, pp. 129–145 (1934).
52. W.J. Brock, "Hydrogen Fluoride: How Toxic Is Toxic? (A Hazard and Risk Analysis)," in *Proceedings of the Halon Options Technical Working Conference 1999*, New Mexico Engineering Research Institute, Albuquerque, NM, pp. 27–29 (1999).
53. M.D. Pedley, "Corrosion of Typical Orbiter Electronic Components Exposed to Halon 1301 Pyrolysis Products," NASA TR-339-001, National Aeronautics and Space Administration, 1995.
54. W.A. Dumayas, "Effect of HF Exposure on PC Multifunction Cards," Senior Research Project, University of Maryland, College Park (1992).

55. E.W. Forssell et al., "Draft Report: Performance of FM-200 on Typical Class A Computer Room Fuel Packages," Hughes Associates, Inc., Columbia, MD (1994).
56. "Fire Suppressants Impact on Hard Disks," The Availability Digest, 2011. Earlier article, "WestHost Fire-Suppression Test Fiasco-An Update," The Availability Digest, (2010).
57. Siemens, "Potential Problems with computer hard disks when fire extinguishing systems are released," Siemens Switzerland Ltd. (2010).
58. Ansul, "Impact of System Discharge/Alarm on Sensitive Hard Drives," Bulletin 5651, (2010).
59. Ansul, Bulletin 5688, "Study of System Discharge/Alarm on Sensitive Hard Disc Drives-Update," (2010).
60. D. Barnea and Y. Taitel, "Flow Pattern Transition in Two-Phase Gas-liquid Flows," in *Encyclopedia of Fluid Mechanics, Vol. 3* (N.P. Cheremisinoff, ed.), Gulf Publishing Company, Houston, TX (1986).
61. H.V. Williamson, "Halon 1301 Flow in Pipelines," *Fire Technology*, 13, 1, pp. 18–32 (1976).
62. D. Chisholm, "Predicting Two-Phase Flow Pressure Drop," in *Encyclopedia of Fluid Mechanics, Vol. 3* (N.P. Cheremisinoff, ed.), Gulf Publishing Company, Houston, TX (1986).
63. Y.Y. Hsu and R.W. Graham, *Transport Processes in Boiling and Two-Phase Systems*, Hemisphere Publishing Corporation, Washington, DC (1976).
64. P.J. DiNenno, E. Forssell, M. Ferreira, C. Hanauska, and B. Johnson, "Modeling the Flow Properties and Discharges of Halon Replacement Agents," in *Proceedings of the Halon Options Technical Working Conference 1994*, New Mexico, Engineering Research Institute, Albuquerque, NM, (1994).
65. E.B. Bird, H. D. Giesecke, J.A. Hillaert, T.J. Friderichs, and R.S. Sheinson,, "Development of Computer Model to Predict the Transient Discharge Characteristics of Halon Alternatives," in *Proceedings of the Halon Options Technical Working Conference 1994*, New Mexico, Engineering Research Institute, Albuquerque, NM, (1994).
66. T.G. Cleary, W. Grosshandler, and J. Wang, "Flow of Alternative Agents in Piping," in *Proceedings of the Halon Options Technical Working Conference 1994*, New Mexico Engineering Research Institute, Albuquerque, NM (1994).
67. W.M. Pitts, J. Yang, G. Gmurczyk, L. Cooper, W. Grosshandler, W. Cleveland, and C. Presser, "Fluid Dynamics of Agent Discharge," in *Evaluation of Alternative In-Flight Fire Suppressants for Full-Scale Testing in Simulated Aircraft Engine Nacelles and Dry Bays*, (W. Grosshandler, R. Gann, and W. Pitts., eds.), NIST SP 861, National Institute of Standards and Technology, Gaithersburg, MD (1994).
68. Ansul Co., *Inergen System Design Installation and Maintenance Manual*, Ansul Co., Marinette, WI (1994).
69. FSSA, *Guide to Estimating Enclosure Pressure and Pressure Relief Vent Area for Applications Using Clean Agent Fire Extinguishing Systems*, First Edition, Fire Suppression Systems Association, Baltimore, MD, April 2008.
70. P.J. DiNenno and E.W. Forssell, "Evaluation of the Door Fan Pressurization Leakage Test Method Applied to Halon 1301 Total Flooding Systems," *Journal of Fire Protection Engineering*, 1, 4, pp. 131–140 (1989).
71. C.C. Grant (ed.), "Enclosure Integrity Procedure for Halon 1301 Total Flooding Fire Suppression Systems," National Fire Protection Research Foundation, Quincy, MA, revision 1.0 (1989).
72. J. Dewsbury and R.A. Whitely, "Review of Fan Integrity Testing and Hold Time Standards," *Fire Technology*, 36, 4, pp. 249–265 (2000).
73. J. Dewsbury and R.A. Whitely, "Extensions of Hold Time Standards," *Fire Technology*, 36, 4, pp. 266–278 (2000).
74. T.M. Hetrick, A.S. Rangwala, and P.E. Rivers, "Development and Validation of a Modified Hold Time Model for Total Flooding Fire Suppression," Proceedings of Suppression and Detection Research Applications – A Technical Working Conference, Orlando FL, Feb 24–27, 2009, National Fire Protection Research Foundation, Quincy, MA (2009).
75. M. Klocke, "Door Fan Test," in *Proceedings of Conference on Fire Extinguishing Systems,* VdS, Cologne, Germany (1998).

Philip J. DiNenno was the president of Hughes Associates, Inc., a fire protection engineering research and development firm. He was actively involved in the testing and development of halon replacement chemicals and alternate fire suppression technologies.

Ericis Forsell, PE a Senior Engineer with Jensen Hughes (formerly Hughes Associates, Inc) He has over 25 years experience with design and application research with clean agent systems.

Carbon Dioxide Systems

45

Jeff Harrington and Joseph A. Senecal

Introduction

Carbon dioxide (CO_2) fire extinguishing systems have been in use continuously since the early 1900s. The National Fire Protection Association (NFPA) first published its design standard on carbon dioxide extinguishing systems in 1929. Since this time, carbon dioxide extinguishing systems have gained wide acceptance around the world, and have successfully protected fire hazards in a large variety of configurations and locales, including in land-based industrial environments, and on ships and mobile drilling platforms at sea. Carbon dioxide is electrically non-conductive and, when used at concentrations recommended in design standards, extinguishes fires relatively quickly leaving no residue.

The health risk associated with carbon dioxide extinguishing systems is notable. Carbon dioxide is lethal at the minimum design concentrations (vol.%) required by the various design standards over relatively short durations of exposure. Death occurs from a severe reduction of oxygen in the blood due to hypercapnia. During the long history of carbon dioxide use in fire extinguishing systems, numerous fatal accidents have occurred, especially during the maintenance and testing of the systems. However, the risk of exposure to carbon dioxide resulting from CO_2 system discharge can be effectively managed.

This chapter provides useful information about the design and safe use of carbon dioxide in fire extinguishing systems to protect industrial and marine fire hazards. There are numerous design standards currently in use. No attempt is made to duplicate all of the information contained in those standards. The intention is to supplement and clarify some of the critical concepts these standards address.

Range of System Configurations

Carbon dioxide fire extinguishing systems are most commonly arranged in either of two configurations: total flooding or local application. The appropriate configuration choice is dependent on the nature of the hazard being protected. In both cases, a stationary, connected supply of carbon dioxide is attached to a fixed network of pipes and discharge nozzles that deliver carbon dioxide to the hazard location and discharge it within, on, or about the protected volume, surface, or area in a manner designed to accomplish fire extinguishment or suppression. Either system configuration can be designed to operate automatically and manually, or manually-only.

Carbon dioxide is also used in manual hose applications. The most common configuration consists of a stationary, connected supply of

J. Harrington, P.E., FSFPE (✉)
Harrington Group, Inc., 2400 Meadowbrook Parkway, Suite 250, Duluth 30096, GA

J.A. Senecal
Kidde-Fenwal, Inc., 400 Main Street, Ashland 01721, MA

M.J. Hurley (ed.), *SFPE Handbook of Fire Protection Engineering*,
DOI 10.1007/978-1-4939-2565-0_45, © Society of Fire Protection Engineers 2016

carbon dioxide attached to a fixed network of pipes and manual hose stations.

Carbon dioxide can also be configured with a fixed pipe network known as a standpipe system, which does not have a stationary, connected supply of carbon dioxide attached to it. The carbon dioxide supply is a mobile supply on a cart or truck designed to be towed or driven to the scene and quick-connected to the standpipe system for delivery to the protected hazard.

Total Flooding

A total flooding system discharges carbon dioxide into an enclosure that surrounds the hazard. For example, the enclosure may be the walls, floor and ceiling that form a room, which houses electrical switchgear, flammable liquids storage, or paper archival records. Carbon dioxide is discharged into the enclosure in such a manner that promotes mixing of the enclosure atmosphere, achieving a relatively uniform pre-determined concentration of carbon dioxide throughout the enclosure to achieve extinguishment or suppression of the fire. No matter where the fire is located within the enclosure, it will be extinguished or suppressed by a total flooding system.

Local Application

A local application system discharges carbon dioxide directly onto a hazard that is not surrounded by an enclosure. Two design approaches are used as determined by the spatial orientation of the hazard. Relatively flat, two dimensional hazards where the fire will be of the surface type are protected by rate-by-area local application systems. Three dimensional hazards where the fire will be of the surface type are protected by rate-by-volume local application systems.

Extended Discharge Duration

Extending the duration of carbon dioxide discharge is a strategy that can be incorporated into the design of both total flooding and local application systems where the initial discharge of agent cannot be retained about the hazard long enough to ensure fire extinguishment. This approach is important when the nature of the environment surrounding the hazard allows excessive dissipation of the initial carbon dioxide discharge.

Hand Hose Line System—Fixed Supply

A fixed-supply manual hose system discharges significantly more carbon dioxide through the hand-held hose and nozzle than a hand portable or wheeled carbon dioxide fire extinguisher unit. Each manual hose station consists of a length of hose attached to the fixed pipe network equipped with a discharge nozzle [1]. The hose and attached nozzle are commonly stored on a hose reel or a rack. This system of manual hose stations is used to supplement fixed total flooding or local application systems, or as the sole form of protection for a hazard where fixed total flooding or local application system are deemed unsuitable.

Standpipe System—Mobile Supply

Such a system can be arranged as a total flooding or local application system, and manual hose stations may or may not be employed. The carbon dioxide supply is typically not attached to the pipe network, but is transported to the site using a trailer or truck and attached to the standpipe system using a quick-connect coupling. A mobile supply arrangement can also be used as a non-connected reserve to supplement a connected supply.

Range of Applications

Carbon dioxide has been in use since the early 1900s to protect a wide variety of special fire hazards. One study reports that approximately 20 % of all fire protection applications are considered special hazards, where the use of an automatic sprinkler system is not the best

solution, and about 20 % of the protected special hazards are protected by carbon dioxide systems [2].

Between the 1920s and 1960s, carbon dioxide was the only gaseous fire extinguishing agent commercially available. In the late 1960s, halon 1301 was commercialized and grew in popularity as the preferred gaseous agent for total flooding applications where human exposure was probable, such as in normally occupied spaces. There was a corresponding reduction in the use of carbon dioxide systems for these types of applications.

Halons were found to be potent depleters of stratospheric ozone and were targeted for a phased reduction in production and import by the US Clean Air Act, as amended in 1990. Subsequent rulemaking by the EPA established January 1, 1994 as the date to complete this phase-out [3]. Since the halon phase-out, the decline in the use of carbon dioxide in fire extinguishing systems reversed in some use sectors, most notably the marine sector [4].

Classification of Fire Hazards

One system used to classify various fire hazards is found in NFPA 10, *Standard for Portable Fire Extinguishers* [5]. Fire hazards are grouped into five distinct classes, shown in Table 45.1.

Class A Fires and Type of Burning Fires in ordinary combustible materials, such as wood, cloth, paper, rubber, and many plastics are Class A fires. Class A fuel arrays may burn with a predominant surface flame and negligible smoldering combustion. This type of fire is often referred to as a Class A surface fire. Materials made of plastic or rubber often produce Class A surface fires. A surface flame propagates in the gas phase in close proximity to the fuel surface, but not actually in contact with it [6]. Heat from the flame vaporizes the solid or liquid fuel just ahead of the flame front. The flame then ignites the vaporized fuel at the lower limit flammability of the vapor mixture, and the flame advances. The spreading flame vaporizes more solid or liquid fuel and the process continues. Surface-type flame spread can also occur in liquid-fuel fires (Class B).

In Class A fuel arrays that are comprised of cellulosic material in fibrous or particulate form, smoldering may be the predominant form of combustion, either in the absence of any surface flaming, or after the surface flaming has subsided. Wood, pressed fiber insulation board, corrugated paper board, paper, and natural textile fabrics are examples of cellulosic materials or products that will produce significant smoldering combustion. Smoldering is a form of combustion without flame that occurs in fuel that is comprised of finely divided fibers or particles that have a relatively large surface area to mass ratio [7]. Smoldering combustion is commonly referred to as deep-seated combustion. The fuel aggregate must be permeable allowing oxygen transport to the combustion reaction zone below the surface of the fuel. The fuel aggregate must also be dense enough to form an effective insulation layer that slows down heat losses from the reaction zone. Smoldering combustion can occur only in solid fuels.

Class C Fires Fires that involve energized electrical equipment are Class C fires. Examples of Class C fire hazards include telecommunication switches, satellite uplink transmitters, data

Table 45.1 Fire classification and fuel

Fire classification	Fuel
Class A	Ordinary combustible materials, such as wood, cloth, paper, rubber, and many plastics
Class B	Flammable liquids, combustible liquids, petroleum greases, tars, oils, oil-based paints, solvents, lacquers, alcohols, and flammable gases
Class C	Energized electrical equipment
Class D	Combustible metals, such as magnesium, titanium, zirconium, sodium, lithium, and potassium
Class K	Combustible cooking media (vegetable or animal oils and fats)

processing equipment, and industrial process control rooms. When a fire in such hazards results in a planned interruption of power to the equipment, the fire classification is immediately converted from a Class C to a Class. A-type hazard. The polymeric materials used in electric cable insulation and printed circuit boards are inherently Class A materials. When these materials burn, the flame is predominantly a surface burning phenomenon. Class C hazards with combustibles in dense configurations can promote smoldering combustion due to restricted air circulation combined with a relatively large fuel surface area.

Carbon Dioxide Suitability

Carbon dioxide is effective in extinguishing fires in Class A, Class B, Class C, and Class K fire hazards. Where surface type burning is expected, carbon dioxide in both total flooding and local application configurations is effective. For smoldering type combustion, only total flooding should be used because the design concentration of carbon dioxide must be maintained for at least 20 min.

Carbon dioxide is not suitable as an extinguishant for Class D fire hazards [8]. Carbon dioxide is not effective in extinguishing fires involving combustible metals (e.g., aluminum, magnesium, titanium, zirconium), alkali metals (e.g., lithium, potassium, cesium), and metal hydrides [9]. Use of carbon dioxide to extinguish fires in these materials is ineffective, and in some cases can accelerate the fire, making it more severe [10].

Carbon dioxide is also not suitable as an extinguishant for materials that contain and release oxygen when they burn, such as cellulose nitrate [8].

Industrial Applications

Carbon dioxide extinguishing systems can be designed and configured to effectively protect a wide range and variety of fire hazards. The types of applications that are suitably protected by carbon dioxide systems are virtually limitless. A single document listing all possible industrial applications may not exist. Numerous documents were reviewed that contain authoritative information about common carbon dioxide system applications [1, 2, 8, 11–14]. The following list, which is not all exhaustive, was compiled from the information contained in these documents.

- Battery storage rooms
- Cable trays
- Cargo areas (aircraft)
- Coal storage silos
- Computer room subfloor spaces
- Control rooms, industrial process
- Dip tanks
- Dryers
- Dust collectors
- Electrical cabinets
- Electrical rooms (motor control, switchgear, transformers)
- Flammable liquid/gas storage rooms and lockers
- Industrial fryers (fryers, cookers, roasters)
- Lube oil pits
- Mixing tanks
- Ovens
- Paint spray booths
- Particle board chippers
- Printing presses
- Quench tanks
- Records storage rooms
- Rolling mills
- Transformers (high voltage)
- Turbine generators
- Vehicle parking areas
- Wave solder machines
- Wet chemistry benches

Marine Applications

Carbon dioxide fire extinguishing systems are used extensively in a wide range of marine applications, including cargo, passenger and tank vessels, as well as mobile offshore drilling units. These marine environments contain a myriad of fire hazards which are required by the applicable governing regulations to be protected

by fixed fire extinguishing systems. Carbon dioxide fire extinguishing systems are identified by these regulations as acceptable for many types of marine fire hazards.

Marine vessels involved in international commerce are regulated by Safety of Life at Sea (SOLAS), 1974, as amended, and promulgated by the International Maritime Organization (IMO). Fire protection requirements are included in Chapter II-2 of that document which is titled Fire Protection, Fire Detection, and Fire Extinction [15, 16].

Marine vessels are subject to the rules and regulations of the flag administration under which they are registered, and in addition, for commercial vessels, the vessel's classification society [12].

United States-flagged commercial vessels fall under the jurisdiction of the United States Coast Guard, Department of Homeland Security (USCG). The fire safety regulations enforced by the USCG are contained within the Code of Federal Regulations (CFR) under Title 46, Shipping [15, 17].

American Bureau of Shipping (ABS) is the second largest classification society in the world based upon tonnage [18]. Based in Houston, TX, ABS is the classification society generally used by U.S. manufactured and flagged vessels [12]. ABS publishes rules for constructing vessels of various types and contain detailed requirements covering the application and design criteria for fixed gas fire extinguishing systems, including carbon dioxide. For example see Rules for Building and Classing Steel Vessels, Jan. 1, 2013, Part 4, Chap. 7 [19].

Carbon dioxide fire extinguishing systems are commonly used in total flooding configurations to protect marine vessel fire hazards in the following locations:

1. Cargo Holds
2. Cargo Pump Spaces
3. Electrical Spaces (e.g., electrical propulsion, power generation, power distribution)
4. Machinery Spaces (e.g., engines, pumps, oil-filling stations, heating-ventilating-air condition equipment)
5. Paint and Flammable Liquid Storage Lockers
6. Vehicle Spaces (e.g., automobiles, other self-propelled vehicles)

Characteristics of Carbon Dioxide

Carbon dioxide, which depending upon its physical form and chemical make-up, may also be referred to as carbon anhydride, carbonic acid gas, carbonic anhydride and dry ice. Carbon dioxide has certain characteristics that make it well suited for use as a fire extinguishing agent both in manual firefighting equipment and automatic fire protection systems. It is a gas at atmospheric pressure and the full range of ambient temperatures likely to be encountered when there is a need to suppress a fire. Carbon dioxide does not leave a residue, will not chemically react with the fire, or with objects in the environment being protected, and is electrically nonconductive. Most fires will be extinguished when carbon dioxide is supplied in sufficient quantity to the flame zone. These and other favorable characteristics of carbon dioxide are shown in the following list:

1. Gaseous form at atmospheric pressure and expected range of ambient temperatures
2. Is an effective fire extinguishant
3. Does not leave a residue
4. Is not corrosive or otherwise reactive
5. Is electrically non-conductive
6. Its own vapor pressure provides sufficient discharge force
7. It is widely available
8. It is relatively inexpensive

Carbon dioxide also has certain detrimental characteristics that must be carefully accounted for in system design to effectively mitigate them. These include:

1. Is lethal at fire extinguishing concentrations
2. Discharge can create conditions leading to electrostatic charging
3. Discharge can create high sound pressure levels
4. Discharge can create disruptive turbulence

5. Discharge can create harmful pressure changes within an enclosure

Fire Extinguishing Mechanisms

The discharge of carbon dioxide into air results in two effects: (1) a decrease in oxygen concentration, and (2) an increase in the heat capacity per mol of available oxygen. Understanding the latter point is central to understanding how gaseous agents contribute to flame extinction. The combustion of oxygen and ordinary carbonaceous fuels releases heat at the rate of approximately 406 kJ per mol of oxygen consumed. In the adiabatic case (no heat loss), that heat must be absorbed by the combustion product gases resulting in a rise in temperature. The stoichiometric combustion of a hydrocarbon fuel and air results in an adiabatic flame temperature of about 2400 K. As the concentration of carbon dioxide added to air increases, the flame temperature decreases because the total thermal mass per unit mass of oxygen for the gas mixture increases.

$$\frac{1}{m_{O2}}\sum m_i \cdot C p_i \qquad (45.1)$$

The result is a lower flame temperature. Combustion reaction rates are very sensitive to temperature, decreasing exponentially with decreasing temperature. When the concentration of carbon dioxide in air is sufficiently high, the combustion temperature becomes depressed to the point where the rate of heat release falls below the rate of heat loss to the surroundings and the flame is extinguished (in simple cases) or suppressed (in complex geometries). For example, the flame above heptane burning in the cup-burner apparatus is extinguished when the concentration of carbon dioxide added to the air flowing past the "cup" reaches about 21 vol. % [20].

Carbon dioxide is often called an "efficient" extinguishing gas. One reason for this claim lies in the fact that compared with other extinguishing gases such as nitrogen and argon, carbon dioxide has a much larger heat capacity so less of it is required to extinguish a flame. One study reported the relationship between extinguishing agent gas heat capacity and minimum extinguishing concentration (MEC) for n-heptane in the cup-burner test as shown in Table 45.2 [21].

Table 45.2 Agent gas heat capacity and minimum extinguishing capacity

Agent		Cp (298 K)	MEC
Gas	Composition	J/mol-K	vol.%
IG-01	Argon	20.8	42.5
IG-55	50/50 N2/Ar	24.6	36.4
IG-541	52/40/8 N2/Ar/CO2	26.1	34.3
IG-100	Nitrogen	28.5	31.9
CO2	Carbon dioxide	37.5	20.9

The data in Fig. 45.1 illustrates that the extinguishing effectiveness of inert gas agents is an inverse function of their heat capacity.

Thermo-physical Properties

Carbon dioxide for fire extinguishing systems is stored either as a liquefied compressed gas, usually in U.S. DOT 3AA1800 high-pressure steel cylinders, or as a refrigerated liquid in insulated tanks maintained at approximately 0 ± 2 °F. The amount of carbon dioxide that can be safely stored in a container of a given type and size depends on the vapor pressure and densities of the liquid and gas phases. The thermo-physical properties of carbon dioxide are indicated in Table 45.3.

While carbon dioxide is a gas at normal ambient conditions, 21 °C (70 °F) and 101.3 kPa (14.7 psia), it can assume any of the three usual physical forms—as a liquid, gas, or solid—depending on the prevailing pressure and temperature. The thermodynamic properties (vapor pressure, density, enthalpy, entropy, heat capacity, and heat of vaporization) and physical properties (viscosity and thermal conductivity) also vary widely with temperature as indicated in Tables 45.4 and 45.5.

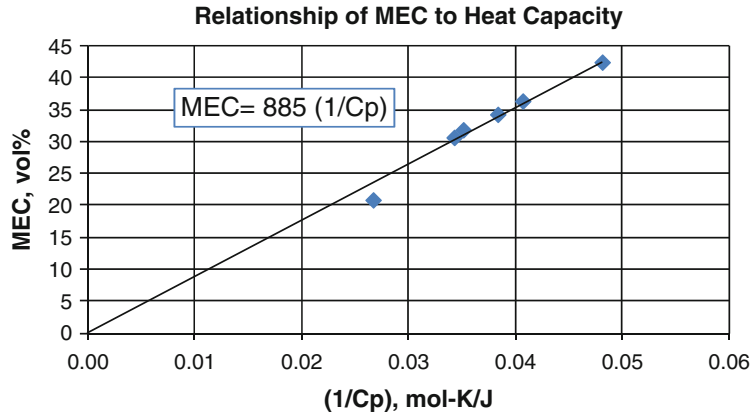

Fig. 45.1 Relationship of MEC to heat capacity

Table 45.3 Reference properties of carbon dioxide [22]

Chemical name	Carbon dioxide
Synonyms	Carbon anhydride; carbonic acid gas; carbonic anhydride; dry ice
CAS Registry No.[a]	124-38-9
Chemical formula	CO2
Property	S.I. units
Molecular weight	44.01 g/mol
Vapor pressure at 2 °F (−16.7 °C)	2181.4 kPa
Specific gravity of gas at 70 °F (21.1 °C) and 1 atm	1.522
Solid to gas expansion ratio at 70 °F (21.1 °C) and 1 atm	0.5457 m3/kg
Gas density at 70 °F (21.1 °C) and 1 atm	1.833 kg/m3
Density of solid (dry ice) at −109.3 °F (−78.5 °C)	1563 kg/m3
Sublimation temperature at 1 atm	−78.5 °C
Critical temperature	31.1 °C
Critical pressure	7381.8 kPa
Critical density	468 kg/m3
Triple point	−56.6 °C at 518 kPa
Latent heat of vaporization at −16.7 °C, 2.18 Mpa	276.8 kJ/kg
Latent heat of fusion at 518 kPa; at −93.8 °C	547 kJ/kg
Latent heat of sublimation at −78.5 °C, 101.3 kPa	571.0 kJ/kg
Specific heat at constant pressure, C_P, gas at 25 °C	0.850 kJ/kg-°C
Specific heat at constant volume, C_V, gas at 25 °C	0.657 kJ/kg-°C
Ratio of gas specific heats, C_P/C_V, at 15 °C	1.304
Solubility in water at 20 °C	0.90 vol/vol
Viscosity of saturated liquid at −16.7 °C	0.000119 kg/m-s

[a]CAS numbers are unique numerical identifiers assigned by the Chemical Abstracts Service to every chemical described in the open scientific literature

The Shomate equations, shown below, and the appropriate coefficients as indicated in Table 45.6, can be used to calculate the heat capacity, molar enthalpy, and molar entropy at specific temperatures. See Table 45.7 for a tabulation of these values for a range of temperatures [24]. The Shomate equation coefficients given in Table 45.6 are for calculations in S.I. units.

Table 45.4 Saturation properties of carbon dioxide [23]

Temp.	Pressure	Density, liquid	Density, vapor	Enthalpy, liquid	Enthalpy, vapor	Heat of vaporization
K	Mpa	kg/m3	kg/m3	kJ/kg	kJ/kg	kJ/kg
218	0.5504	1173	14.58	82.80	430.9	348.1
220	0.5991	1166	15.82	86.73	431.6	344.9
222	0.6510	1159	17.13	90.67	432.3	341.6
224	0.7062	1151	18.53	94.62	432.9	338.3
226	0.7648	1144	20.02	98.59	433.5	334.9
228	0.8270	1136	21.60	102.57	434.1	331.5
230	0.8929	1129	23.27	106.57	434.6	328.0
232	0.9626	1121	25.05	110.59	435.1	324.5
234	1.0363	1113	26.94	114.62	435.5	320.9
236	1.1141	1105	28.93	118.67	435.9	317.2
238	1.1961	1097	31.05	122.74	436.2	313.5
240	1.2825	1089	33.30	126.84	436.5	309.7
242	1.3734	1081	35.67	130.96	436.7	305.8
244	1.4690	1072	38.18	135.10	436.9	301.8
246	1.5693	1064	40.85	139.27	437.0	297.7
248	1.6746	1055	43.66	143.48	437.1	293.6
250	1.7850	1046	46.65	147.71	437.0	289.3
252	1.9007	1037	49.80	151.98	437.0	285.0
254	2.0217	1028	53.14	156.28	436.8	280.5
256	2.1483	1018	56.68	160.62	436.6	276.0
258	2.2806	1009	60.44	165.01	436.3	271.3
260	2.4188	999	64.42	169.44	435.9	266.5
262	2.5630	989	68.64	173.92	435.4	261.5
264	2.7134	979	73.12	178.45	434.9	256.4
266	2.8701	968	77.89	183.04	434.2	251.2
268	3.0334	957	82.97	187.69	433.4	245.8
270	3.2033	946	88.37	192.41	432.6	240.1
272	3.3802	934	94.15	197.21	431.5	234.3
274	3.5642	922	100.33	202.08	430.4	228.3
276	3.7555	910	106.95	207.05	429.1	222.0
278	3.9542	897	114.07	212.12	427.6	215.5
280	4.1607	884	121.74	217.30	425.9	208.7
282	4.3752	870	130.05	222.61	424.1	201.5
284	4.5978	855	139.09	228.06	421.9	193.9
286	4.8289	839	148.98	233.70	419.6	185.9
288	5.0688	823	159.87	239.54	416.9	177.3
290	5.3177	805	171.96	245.63	413.7	168.1
292	5.5761	785	185.55	252.01	410.2	158.2
294	5.8443	764	201.06	258.80	406.0	147.2
296	6.1227	740	219.14	266.10	401.0	134.9
298	6.4121	713	240.90	274.14	394.9	120.8
300	6.7131	679	268.58	283.37	387.1	103.7
302	7.0268	634	308.15	295.02	375.7	80.7
304	7.3555	530	406.42	318.36	347.9	29.6

Table 45.5 Specific heat, thermal conductivity, viscosity [23]

Temp.	Cp, liquid	Thermal cond., liquid	Viscosity, liquid	Cv, vapor	Thermal cond., vapor	Viscosity, vapor
K	J/kg-K	W/m-K	uPa-s	J/kg-K	W/m-K	uPa-s
220	1962	0.1762	242.0	639	0.01130	11.14
225	1977	0.1697	222.2	654	0.01175	11.41
230	1997	0.1633	204.2	670	0.01222	11.69
235	2021	0.1570	187.9	687	0.01274	11.98
240	2051	0.1508	173.0	705	0.01330	12.27
245	2087	0.1446	159.3	725	0.01392	12.58
250	2132	0.1385	146.7	746	0.01461	12.90
255	2187	0.1324	135.1	769	0.01540	13.25
260	2255	0.1264	124.4	794	0.01631	13.61
265	2342	0.1203	114.4	822	0.01738	14.02
270	2454	0.1143	105.0	852	0.01869	14.47
275	2603	0.1082	96.2	885	0.02033	14.99
280	2814	0.1020	87.7	923	0.02247	15.60
285	3133	0.0958	79.5	969	0.02542	16.36
290	3676	0.0895	71.4	1026	0.02982	17.36
295	4794	0.0836	62.9	1106	0.03722	18.79
300	8698	0.0806	53.1	1248	0.05369	21.31

Table 45.6 Shomate equation coefficients for carbon dioxide

Temperature range, K	298–1200	1200–6000
A	24.99735	58.16639
B	55.18696	2.720074
C	−33.69137	−0.492289
D	7.948387	0.038844
E	−0.136638	−6.447293
F	−403.6075	−425.9186
G	228.2431	263.6125
H	−393.5224	−393.5224
MW	0.044	kg/mol

$$\mathrm{Cp^\circ} = \mathrm{A} + \mathrm{B{*}t} + \mathrm{C{*}t^2} + \mathrm{D{*}t^3} + \mathrm{E}/\mathrm{t^2} \quad (45.2)$$

$$\mathrm{H^\circ} - \mathrm{H^\circ 298.15} = \mathrm{A{*}t} + \mathrm{B{*}t^2}/2 + \mathrm{C{*}t^3}/3 + \mathrm{D{*}t^4}/4 - \mathrm{E}/\mathrm{t} + \mathrm{F} - \mathrm{H} \quad (45.3)$$

$$\mathrm{S^\circ} = \mathrm{A{*}ln(t)} + \mathrm{B{*}t} + \mathrm{C{*}t^2}/2 + \mathrm{D{*}t^3}/3 - \mathrm{E}/\left(2{*}\mathrm{t^2}\right) + \mathrm{G} \quad (45.4)$$

where
$\mathrm{Cp^\circ}$ = heat capacity (J/mol-K)
$\mathrm{H^\circ}$ = standard enthalpy (kJ/mol)
$\mathrm{S^\circ}$ = standard entropy (J/mol-K)
t = temperature (K)/1000

Carbon dioxide is soluble in water to an extent that depends on pressure and temperature as shown in Fig. 45.2 below [26].

The dissolution of CO_2 in water (this may be sea water, or the saline water in geological formations) involves a number of chemical reactions between gaseous and dissolved carbon dioxide (CO_2), carbonic acid (H_2CO_3), bicarbonate ions (HCO_3^-) and carbonate ions (CO_3^{2-}) which can be represented as follows:

$$CO_{2(g)} \leftrightarrow CO_{2(aq)} \quad (45.5)$$

$$CO_{2(aq)} + H_2O \leftrightarrow H_2CO_{3(aq)} \quad (45.6)$$

$$H_2CO_{3(aq)} \leftrightarrow H^+_{aq} + HCO^-_{3(aq)} \quad (45.7)$$

$$HCO^-_{3(aq)} \leftrightarrow H^+_{aq} + CO^{2-}_{3(aq)} \quad (45.8)$$

Addition of CO_2 to water initially leads to an increase in the amount of dissolved CO_2. The dissolved CO_2 reacts with water to form carbonic acid. Carbonic acid dissociates to form bicarbonate ions, which can further dissociate into carbonate ions. The net effect of dissolving

Table 45.7 Properties of superheated carbon dioxide at 101.3 kPa

Temp	Heat capacity	Enthalpy	Entropy	Temp	Heat capacity	Enthalpy	Entropy
T	C_P	H	S	T	C_P	H	S
C	kJ/kg-K	kJ/kg	kJ/kg-K	C	kJ/kg-K	kJ/kg	kJ/kg-K
−4	0.81	−8.97	4.75	54	0.87	−8.92	4.90
−1	0.81	−8.97	4.76	57	0.88	−8.92	4.91
2	0.82	−8.96	4.76	60	0.88	−8.92	4.92
4	0.82	−8.96	4.77	63	0.88	−8.91	4.92
7	0.82	−8.96	4.78	66	0.89	−8.91	4.93
10	0.83	−8.96	4.79	68	0.89	−8.91	4.94
13	0.83	−8.95	4.80	71	0.89	−8.91	4.94
16	0.83	−8.95	4.80	74	0.89	−8.90	4.95
18	0.84	−8.95	4.81	77	0.90	−8.90	4.96
21	0.84	−8.95	4.82	79	0.90	−8.90	4.97
24	0.84	−8.95	4.83	82	0.90	−8.89	4.97
27	0.85	−8.94	4.84	85	0.90	−8.89	4.98
29	0.85	−8.94	4.84	88	0.91	−8.89	4.98
32	0.85	−8.94	4.85	91	0.91	−8.89	4.99
35	0.85	−8.94	4.86	93	0.91	−8.88	4.99
38	0.86	−8.93	4.86	96	0.91	−8.88	5.00
41	0.86	−8.93	4.87	99	0.92	−8.88	5.01
43	0.86	−8.93	4.88	102	0.92	−8.88	5.02
46	0.87	−8.93	4.88	104	0.92	−8.88	5.02
49	0.87	−8.92	4.89	107	0.92	−8.87	5.03
52	0.87	−8.92	4.90	110	0.93	−8.87	5.03

Values of the above can be computed for temperatures up to 1600 K, in metric units on a mole basis, using the Shomate equation

anthropogenic CO_2 in water is the removal of carbonate ions and production of bicarbonate ions, with a lowering in pH.

Data on the compatibility of carbon dioxide with specific materials is indicated in Table 45.8 [27]. Although the information has been compiled from what are considered reliable sources (International Standards: Compatibility of cylinder and valve materials with gas content; Part 1: ISO 11114-1 (Jul 1998), Part 2: ISO 11114-2 (Mar 2001), the data should be used with a sufficient degree of prudence. No raw data such as that presented in Table 45.8 can address all scenarios and conditions of concentration, temperature, humidity, impurities and aeration. It is therefore recommended that the data in Table 45.8 be used to initially choose possible materials with a more extensive investigation and testing carried out under the specific anticipated conditions of use. The collected data mainly concern high-pressure applications at ambient temperature and the safety aspect of material compatibility.

Health and Safety

Carbon dioxide is usually described as an asphyxiant gas. However, exposure to atmospheres that contain high concentrations of carbon dioxide result in a condition called hypercapnia (also called hypercarbia). Hypercapnia, is a condition whereby there is too much carbon dioxide in the blood [28]. In severe hypercapnia, generally where the ambient partial pressure of carbon dioxide exceeds approximately 10 kPa, or 10 vol. % at sea level, the symptomatology progresses, over a period of several minutes, to disorientation, panic, hyperventilation, convulsions, unconsciousness, and, eventually, death [29].

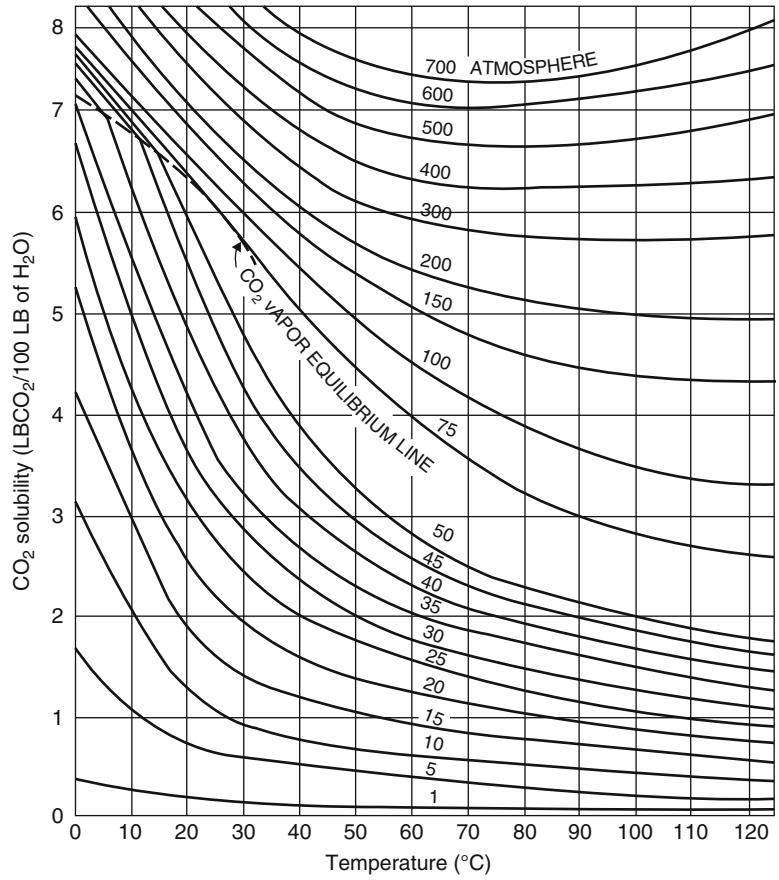

Fig. 45.2 Solubility of carbon dioxide in water [25]

Death will occur because of a lack of oxygen in the blood, leading to complete organ failure as the oxygen has been overtaken by the carbon dioxide. In some cases, victims who have been exposed to very high levels of carbon dioxide in the atmosphere have been known to die almost immediately of asphyxiation, as the carbon dioxide serves to displace, or push out, the oxygen in the air [30].

Treating hypercapnia is best achieved by removing a victim from the exposure to carbon dioxide and providing high concentrations of oxygen. If the exposure was at mild to moderate levels (6–9 kPa), the patient should recover fully. If the exposure was at levels higher than 10 kPa, the patient may suffer from permanent damage of the central nervous system.

The acute physiological effects of exposure to atmospheres containing carbon dioxide depend on the carbon dioxide concentration and the duration of exposure. The effects of exposure have been reported in several sources. Table 45.9 summarizes the effects of exposure to carbon dioxide as reported in three different sources.

Protection standards have been developed for workers who may be exposed to carbon dioxide. (Table 45.10 shows exposure limits as noted in U.S. standards but similar limits are understood to apply in standards of other countries).

A carbon dioxide fire extinguishing system discharges carbon dioxide in sufficient quantity to produce a lethal concentration in a localized or confined atmosphere. Total flooding type systems are required to achieve a minimum design concentration of 34 vol.% [33]. For many fire hazards, the design concentration is required to be substantially higher than 34 vol.%. As indicated in Table 45.9, a carbon dioxide concentration in the range of 17–30 vol.% is lethal to humans within only 1 min of exposure.

Table 45.8 Material compatibility of carbon dioxide [27]

Material	Compatibility
Metals	
Aluminium	Satisfactory
Brass	Satisfactory
Copper	Satisfactory
Ferritic steels (e.g. carbon steels)	Satisfactory but risk of corrosion in presence of CO and/or moisture. cold brittleness
Stainless steel	Satisfactory
Plastics	
Polytetrafluoroethylene (PTFE)	Satisfactory
Polychlorotrifluoroethylene (PCTFE)	Satisfactory
Vinylidene polyfluoride (PVDF) (KYNAR™)	Satisfactory
Polyamide (PA) (NYLON™)	Satisfactory
Polypropylene (PP)	Satisfactory
Elastomers	
Buthyl (isobutene – isoprene) rubber (IIR)	Non recommended, significant swelling
Nitrile rubber (NBR)	Non recommended, significant swelling and significant loss of mass by extraction or chemical reaction
Chloroprene (CR)	Non recommended, significant swelling and significant loss of mass by extraction or chemical reaction
Chlorofluorocarbons (FKM) (VITON™)	Non recommended, significant swelling and significant loss of mass by extraction or chemical reaction
Silicon (Q)	Acceptable but strong rate of permeation
Ethylene – Propylene (EPDM)	Acceptable but important swelling and significant loss of mass by extraction or chemical reaction
Lubricants	
Hydrocarbon based lubricant	Satisfactory
Fluorocarbon based lubricant	Satisfactory

All properly designed total flooding carbon dioxide fire extinguishing systems, therefore, have the potential to be lethal.

In fact there have been numerous incidents with carbon dioxide fire extinguishing systems that have resulted in fatalities and serious injuries. One study by the U.S. Environmental Protection Agency (EPA) reported that between 1975 and 1999, 72 deaths and 145 injuries occurred as a result of 51 incidents involving carbon dioxide fire extinguishing systems [2]. This study also reported on incidents that occurred prior to 1975. Table 45.11, which is reproduced from the EPA study, shows data on deaths and injuries categorized by time frame, geographical region, and military/non-military installations.

The EPA study included a comprehensive data search and analysis of incidents involving carbon dioxide fire extinguishing systems. The search included governmental, public, and private document archives internationally. Many details about each reported incident were collected and presented in the study.

All of the 13 military incidents reported were marine-related. Only 11 of the 49 nonmilitary incidents reported were marine-related. The remaining incidents occurred in a variety of land-based facilities noted below:

- Data processing centers
- Nuclear power plants
- Pilot training centers
- Airplanes
- Bus garages

Table 45.9 Acute health effects of high concentrations of carbon dioxide

	Source	U.S. EPA examining the risks (2004) [2]	Air products (2004) [31]	Rice (2004) [32]
CO2 conc. vol.%	Exposure time	Effects	Effects	Effects
1			Slight increase in breathing rate	Respiratory rate increased by about 37 %
2	Several hours	Headache, dyspnea upon mild exertion	Breathing rate increases to 50 % above normal level. Prolonged exposure can cause headache, tiredness	Ventilation rate raised by about 100 %. Respiratory rate raised by about 50 %; increased brain blood flow
3	1 h	Mild headache, sweating, and dyspnea at rest	Breathing increases to twice normal rate and becomes laboured. Weak narcotic effect. Impaired hearing, headache, increase in blood pressure and pulse rate	Exercise tolerance reduced in workers when breathing against inspiratory and expiratory resistance
4–5	Within a few minutes	Headache, dizziness, increased blood pressure, uncomfortable dyspnea	Breathing increases to approximately four times normal rate; symptoms of intoxication become evident and slight choking may be felt	Increase in ventilation rate by ~200 %. Respiratory rate doubled, dizziness, headache, confusion, dyspnea
5–10	Within minutes		Characteristic sharp odour noticeable. Very labored breathing, headache, visual impairment and ringing in the ears. Judgment may be impaired, followed within minutes by loss of consciousness	
6	1–2 min	Hearing and visual disturbances		
	<16 min	Headache, dyspnea		
	Several hours	Tremors		
7–10	Few minutes	Unconsciousness, near unconsciousness		At 8–10 %, severe headache, dizziness, confusion, dyspnea, sweating, dim vision. At 10 %, unbearable dyspnea, followed by vomiting, disorientation, hypertension, and loss of consciousness
	1.5 min to 1 h	Headache, increased heart rate, shortness of breath, dizziness, sweating, rapid breathing		

(continued)

Table 45.9 (continued)

	Source	U.S. EPA examining the risks (2004) [2]	Air products (2004) [31]	Rice (2004) [32]
CO2 conc. vol.%	Exposure time	Effects	Effects	Effects
10–15	1 to several minutes	Dizziness, drowsiness, severe muscle twitching, unconsciousness		
17–30	<1 min	Loss of controlled and purposeful activity, unconsciousness, convulsions, coma, death		
50–100	<1 min			Unconsciousness occurs more rapidly above 10 % level. Prolonged exposure to high concentrations may eventually result in death from asphyxiation

Table 45.10 Permissible exposure limits—US standards

	Time-weighted average (8 h day/40 h week)	Short-term exposure limit (15 min)	Immediately dangerous to life and health
OSHA permissible exposure limit[a]	5000 ppm (0.5 %)		
NIOSH permissible exposure limit[b]	5000 ppm (0.5 %)	30,000 ppm (3 %)	40,000 ppm (4 %)
ACGIH permissible exposure limit[c]	5000 ppm (0.5 %)		

[a]OSHA—US occupational safety and health administration (1986)
[b]NIOSH—US national institute of occupational safety and health (1997)
[c]ACGIH—American conference of governmental industrial hygienists

Table 45.11 Summary of deaths and injuries from carbon dioxide system incidents

Use category		Number of incidents	Deaths	Injuries
United States and Canada				
1975- present	Military	9	10	15
	Nonmilitary	20	19	73
Before 1975	Military	3	11	0
	Nonmilitary	5	3	3
Total		37	43	91
International				
1975-present	Military	1	4	5
	Nonmilitary	21	39	52
Before 1975	Military	0	0	0
	Nonmilitary[a]	3	33	4
Total		25	76	61
Total		**62**	**119**	**152**

[a]Included in in the total international nonmilitary incidents, deaths, and injuries before 1975 are the 20 deaths resulting from the use of carbon dioxide as a fire suppressant in England from 1945 to the mid 1960s, for which the cause is unknown

- Emergency unit communication centers
- Waste storage facilities
- Underground parking garages
- Steel rolling mills
- Motor vehicle assembly lines
- Other facilities

In another study [4] Wickham analyzed the data collected in the EPA study and concluded that maintenance activities on the carbon dioxide systems, or in their vicinity, are the most common cause categories associated with the incidences evaluated. This data are summarized in Table 45.12.

Wickham also reported on a number of carbon dioxide extinguishing system incidents that occurred subsequent to the EPA study, between 2000 and 2003. This data is summarized in Table 45.13.

Clearly, carbon dioxide fire extinguishing systems have the potential to be lethal and cause serious injury. Great care must be taken in the design, installation, testing and maintenance of carbon dioxide systems to prevent harm to persons present in their immediate and general vicinity.

Carbon Dioxide System Design

Design Standards and Guidelines

Carbon dioxide system design is governed by standards applicable to the type and locale of the system. Land-based industrial system design is governed by the design standard adopted and enforced by the governmental jurisdiction in

Table 45.12 Causes of injuries and deaths associated with carbon dioxide discharges (1975–1999) [4]

Type discharge	Circumstances	Incidents	Deaths	Injured
Accidental	During maintenance on the CO2 system	9	8	10
	During maintenance near the CO2 system	8	19	19
	During testing	1	2	6
	During fire situation	2	10	7
	Faulty component or installation	2	4	13
	Operator error	2	1	4
	False alarm	2	1	15
Intentional	During testing or training	3	2	2
	During fire situation	5	15	8
	False alarm	1	2	1
	Total	35	64	85

Table 45.13 Additional death and injury incidents in the US and Mexico (associated with carbon dioxide total flooding fire extinguishing systems) [4]

Event date	Source	Deaths	Injuries	Summary
07/27/2000	OSHA Technical Information Bulletin 12/22/2001	1	0	"...an employee of a securities firm died from CO2 intoxication. The employee was inside the vault with the vault door closed and locked. When the employee pulled a manual fire alarm actuation device that was located inside the vault space, it activated the warning alarm and the total flooding CO2 system."
02/20/2002	Mr. Donald Murray Ansul 03/31/2003	2	0	A carbon dioxide system prematurely connected and manually discharged in error by workers aboard a ship at the Mexican Navy Shipyard in Salina Cruz Oaxaca Mexico. The engine room was occupied at the time by many workers as ship was being overhauled.
03/31/2002	Honolulu Adviser 04/03/2002	2	0	Two civilian crew members died on the 750-foot Ready Reserve Force ship Cape Horn from apparent suffocation when a fire was put out in the engine room, officials said. "The possibility is that it may have been as a result of a fire suppression system ..... The suppression systems replace oxygen with carbon dioxide to smother a fire."
01/19/2003	Associated Press 01/31/2003	2	0	"A couple found dead aboard their docked 58-foot yacht apparently suffocated when a fire suppression system was accidentally set off, using up all the oxygen in the yacht. Marine experts have determined that John Robertson, a leg amputee who wasn't wearing his prosthesis, fell and grabbed a wire that triggered the carbon dioxide powered fire-suppression system. Andreija was overcome by lack of oxygen when she probably tried to rescue her 260-pound husband. The couple was cleaning the yacht's engine room and had begun painting it when the accident happened, police said."

which the system will be installed. Two of the most widely used standards for these systems are NFPA 12 [34] and ISO 6183 [35].

Marine system design is governed by marine standards. The specific standards that apply depend on the several factors including the flag administration under which the vessel is registered, the vessel's classification society if it is a commercial vessel, and whether or not the vessel is used in international commerce. Unites States flag commercial vessels fall under USCG standards [17]. Vessels involved in international commerce fall under SOLAS which requires compliance with the FSS Code [36] There are also many classification societies which have extensive standards and guidelines that their classified marine vessels must be in compliance with, e.g. ABS [37]. NFPA 12 also contains a chapter that provides marine system design requirements [38].

System Configuration

Storage and Distribution

NFPA 12 recognizes two types of storage for carbon dioxide: high pressure and low pressure. Each type has advantages and disadvantages.

High Pressure High-pressure systems utilize carbon dioxide stored in cylinders at an ambient temperature between −18 °C (0 °F) and 54 °C (130 °F) and at a density of 600–680 kg/m^3 (37–42.5 lb/ft^3). This is usually expressed as a percentage of the cylinder's water capacity, which can range from 60 % to 68 %.

The curve shown in Fig. 45.3 illustrates the relationship between the temperature and the pressure of liquid carbon dioxide. Below 31 °C (87.8 °F), carbon dioxide exists as both liquid and gas. At 21 °C (70 °F), the cylinder pressure is approximately 58.6 bar (850 psi) absolute. As the

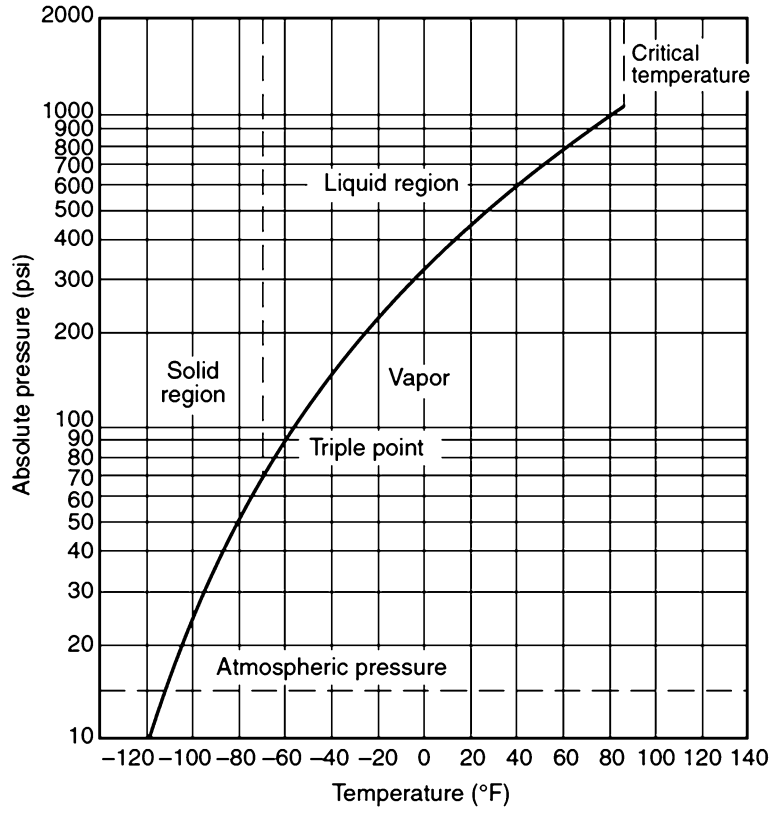

For SI units, 1 psi = 6.89 kPa; °C = ⅝ (°F – 32).

Fig. 45.3 Variation of pressure of carbon dioxide with change in temperature at constant volume (Courtesy of NFPA)

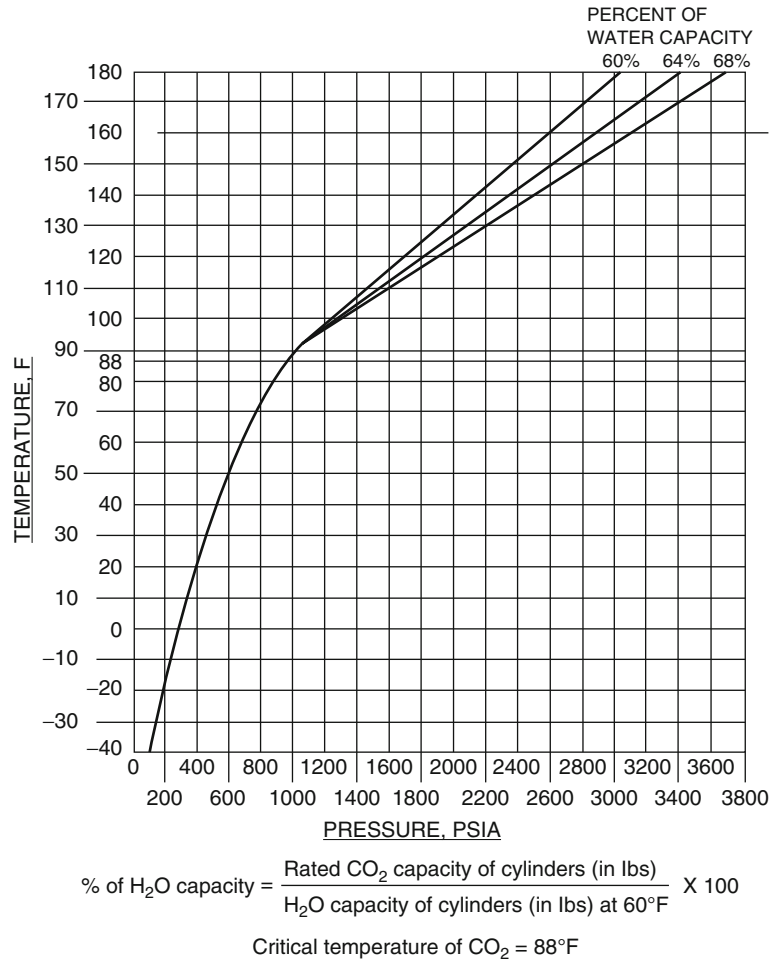

Fig. 45.4 Pressure-temperature curve for carbon dioxide

temperature increases, the vapor pressure and density increase and the liquid density decreases, until the critical temperature is reached. At 31 °C (87.8 °F), the liquid and the vapor have the same density, and the carbon dioxide is in a single-phase.

Above the critical temperature, the relationship between pressure and temperature is dependent on the fill density of the cylinder. Higher fill densities result in a greater rise in pressure with temperature, as demonstrated in Fig. 45.4.

Given such high working pressures, it is generally necessary to use seamless steel cylinders which have pressure strength but relatively small internal volumes. This has traditionally limited the maximum storage capacity of a single cylinder to 120 lb (54.4 kg). However, for most applications, a larger supply of carbon dioxide is required. In order to provide a sufficient quantity of gas, multiple high-pressure cylinders are connected to a manifold and discharged simultaneously through a single pipe network.

All cylinders connected to a common manifold must be of the same design and capacity, such that they are interchangeable. For example, a system that requires a minimum supply of 68 kg (150 lb) of carbon dioxide may be satisfied by two 34.0 kg (75 lb) cylinders, by three 22.6 kg (50 lb) cylinders, or by two 45.3 kg (100 lb) cylinders. However, it is not permissible to connect one 22.6 kg (50 lb) cylinder and one 45.3 kg (100 lb) cylinder to a single pipe network.

It is also permissible to provide a connected reserve supply of carbon dioxide. The reserve supply must be identical to the main supply,

including cylinder size and manifold configuration. The actuation subsystem must be provided with a means, such as a switch or valve, to select between the two cylinder banks. In some cases, the reserve supply is used as a "second shot" in the event that the primary supply does not successfully extinguish a fire. In other cases, the reserve supply is used to provide continuity of protection while the main supply is recharged.

Where the supply consists of a single cylinder, the cylinder valve may be connected directly to the discharge piping. Where multiple cylinders are connected to a manifold, a means, such as a check valve, must be provided at each cylinder connection. This prevents loss of agent in the event that the system is activated while one of the cylinders is removed for service. This requirement also applies where a single main cylinder and a single reserve cylinder are connected to a common system.

High-pressure cylinders must be securely mounted and supported in order to prevent movement during discharge and accidental dislodgement. When multiple cylinders are connected to a manifold, they are required to be mounted in a rack, provided for the purpose and arranged to facilitate inspection and maintenance of the cylinders. To ensure a proper fit, mounting brackets, straps, and/or racking equipment are usually available from the system manufacturer.

Low-pressure systems utilize carbon dioxide stored in refrigerated vessels. The reduced storage temperature results in a lower storage pressure, thus permitting a greater quantity of carbon dioxide to be stored in a single tank. For high capacity systems, this can yield lower installation costs and smaller storage areas, versus high pressure systems.

A carbon dioxide refrigeration system is designed to maintain the carbon dioxide supply at a nominal pressure of 2068 kPa (300 psi). According to Fig. 45.4, this pressure corresponds to a temperature of approximately −18 °C (0 °F). Where the ambient temperature is expected to be lower, a heating system may be required to maintain this temperature/pressure.

The storage vessel is usually designed in accordance with ASME Pressure Vessel Code with a minimum design pressure of 2241 kPa (325 psi) and filled after installation. However, if the container is to be pressurized prior to shipping, it must comply with the laws governing transport of pressurized vessels, such as Section 49 of the U.S. Code of Federal Regulations (Department of Transportation).

Single and Multiple Hazards: Carbon dioxide systems can be designed to protect a single hazard or multiple hazards from a single supply. Further, multiple hazards may be protected simultaneously or independently. See discussion on Selector Valves for more information on using a single supply to independently protect multiple hazards.

System Controls for Industrial Applications

Since carbon dioxide systems are used to protect many different types of hazards, system controls can vary widely and are designed to suit the specific needs of each application. These controls can include automatic detection systems, manual actuation equipment, valve actuators, notification appliances, supervisory switches, and auxiliary controls. Systems may be operated electrically, pneumatically, mechanically, or by a combination of these methods.

Means of Electrical Operation

Electrically operated systems generally offer the greatest flexibility and a high degree of reliability. This control equipment must be installed in accordance with NFPA 72, which generally requires the use of a listed fire alarm control panel (FACP) and listed devices. Ideally, the FACP should be specifically listed for releasing service, which provides additional protection against accidental discharge.

The reliability of electrically operated systems is enhanced by the use of supervised circuits and devices. This provides notification of a system or device fault. In addition, the use of secondary power sources, such as batteries, ensures the continuity of protection in the event of a power outage.

Means of Pneumatic Operation

Pneumatically operated systems use pressure to activate a system component. This includes both pneumatic detection and pneumatic (pressure) actuation.

Pneumatic detection systems are composed of one or more detectors, in the form of an air chamber, connected to a mechanical device through tubing. The device is typically designed with a vent that relieves pressure in the tubing due to normal temperature fluctuations. However, when the air temperature within the chamber increases quickly, as when exposed to a fire, the resulting increase in pressure occurs faster than can be relieved through the vent and causes actuation of the discharge valve, or the master valve in the case of a multi-cylinder system. Because activation relies on the rate of temperature increase, the system may not react to slow-growing fires. The success of pneumatic detection systems is dependent on proper selection of the relief vent size, as well as careful installation practices to ensure that there are no unintended leaks or breaches in the tubing and that the system does not exceed the limitations of the manufacturer's listing and installation instructions. Since the integrity of the tubing cannot be supervised, periodic testing is critically important. Pneumatic detection systems were a historically important component of carbon dioxide systems, particularly in applications involving flammable liquid storage and marine vessels, where the availability of electricity was limited or undesired. This type of detection is less frequently employed in modern systems, as electrical detectors have become more prevalent, but such means of detection still has certain advantages.

Pneumatic (pressure) actuation systems are composed of a stored pressure supply—usually a cylinder filled with nitrogen—connected to a mechanical device through a network of hose, pipe, and/or tubing. When pressure is released into the tubing, a mechanical pressure-operated valve actuator advances an operating pin that causes the discharge valve to open. Frequently, these systems are called "pressure operated", rather than "pneumatic", in order to differentiate them from pneumatic detection systems. This arrangement is typically used as a means to open valves and/or activate auxiliary equipment. There are two primary benefits to this arrangement: (1) the pressure supply can be used to automatically actuate multiple devices from a single manual or automatic control point, (2) the pressure supply can be connected through a pneumatic device that delays activation of the downstream components. Because it relies on activation of the stored pressure supply, this type of system must be coupled with another form of operation. Success is dependent on proper design and installation, the availability of pressure, and the integrity of the network.

Means of Mechanical Operation

Mechanically operated systems rely solely on mechanical advantage to operate a device and are usually used only for manual actuation of the system.

Lever operation is usually encountered as a manual control located directly on a valve or other system component. In some cases, the movement of the lever is translated directly to the actuating element. In other cases, the lever activates a spring-loaded device, which in turn performs the work to open the valve.

Cable operated systems permit a mechanical control to be located remotely from the operating valve. A cable is usually installed inside a protective sheath, such as pipe or conduit, and threaded through pulleys to reduce friction where changes in direction are necessary. Most carbon dioxide systems use a pull-to-trip mechanism, which activates the valve when tension is applied to the cable. Another type, called a release-to-trip mechanism, activates the valve when tension in the cable is relieved.

System Actuation

Actuation of low-pressure systems is usually achieved by the use of an electrically operated valve, located on the discharge port of the storage vessel. Because it is not typically necessary to use more than the contents of one low-pressure

carbon dioxide storage vessel in a single discharge, these controls remain relatively simple, unless multiple independent hazards are protected.

Actuation of high-pressure systems is more complicated because it is usually necessary to actuate more than one cylinder valve. In order to simplify the controls, the cylinder valves are designed (in many but not all cases) to open with back pressure from the manifold. That is, a mechanism in the valve causes the valve to open when a minimum pressure is developed in the manifold pipe. With this arrangement, actuation of the entire system can be achieved by activation of a limited number of pilot cylinders (those that discharge first and serve to pressurize the manifold), thus limiting the number of controls that are required.

Manual Normal Actuation

All carbon dioxide systems are required to be provided with a means of manually actuating the system. This is satisfied by a manual releasing device located on, at, or remotely from the carbon dioxide supply. The manual release must be capable of causing the entire system—including notification and auxiliary devices—to actuate, as intended, as well as initiating the release of carbon dioxide. This can be simplified by the use of a fire alarm control panel to control all of the system functions. However, mechanical and/or pneumatic devices can also be used to ensure the full functionality of the system.

Manual actuation must be accomplished with a pull force of not more than 178 N (40 lb) and a movement of not more than 356 mm (14 in).

Manual Emergency Actuation

All valves that control the release and distribution of carbon dioxide are required to have an emergency manual means of activation. This is a fully mechanical control, located at or near the device being controlled. This is intended only to provide a means of opening the valve in the event that the normal manual and/or automatic controls fail to do so. It is not necessary to achieve full activation of the entire system from this control, as is required for a normal manual control.

Automatic Actuation

All carbon dioxide systems are required to be automatically actuated, unless the authority having jurisdiction approves the use of a manual-only system.

Automatic detection may utilize any listed or approved method or device that is capable of sensing and indicating the presence of heat, flame, smoke, combustible vapors, or an abnormal condition in the protected space such as process trouble that is likely to produce fire.

System Valves

Selector Valves

Selector valves are normally-closed control valves that are used to direct the flow of carbon dioxide to a specific location upon system activation. Selector valves are used where a single supply of carbon dioxide serves more than one protected space. In this arrangement, a single supply of carbon dioxide is piped to a header with multiple branches that can deliver carbon dioxide to a specific location, Each header outlet branch is fitted with a selector valve. Examples are shown in Figs. 45.5 and 45.6. When an automatic detector or manual control in one of the hazards is activated, the control system is designed to open the required quantity of supply cylinders and the appropriate selector valve for that hazard.

Lockout Valves

A lockout valve is a manually-operated normally-open valve that is closed when maintenance is being performed on the system to prevent discharge into the protected space where persons may be present. A lockout valve should be provided with a position switch connected to the Supervisory circuit of the FACP to provide notification of system impairment when the valve is closed. It should also be provided with a means to lock the valve in position, in order to permit use of a lockout/tagout system.

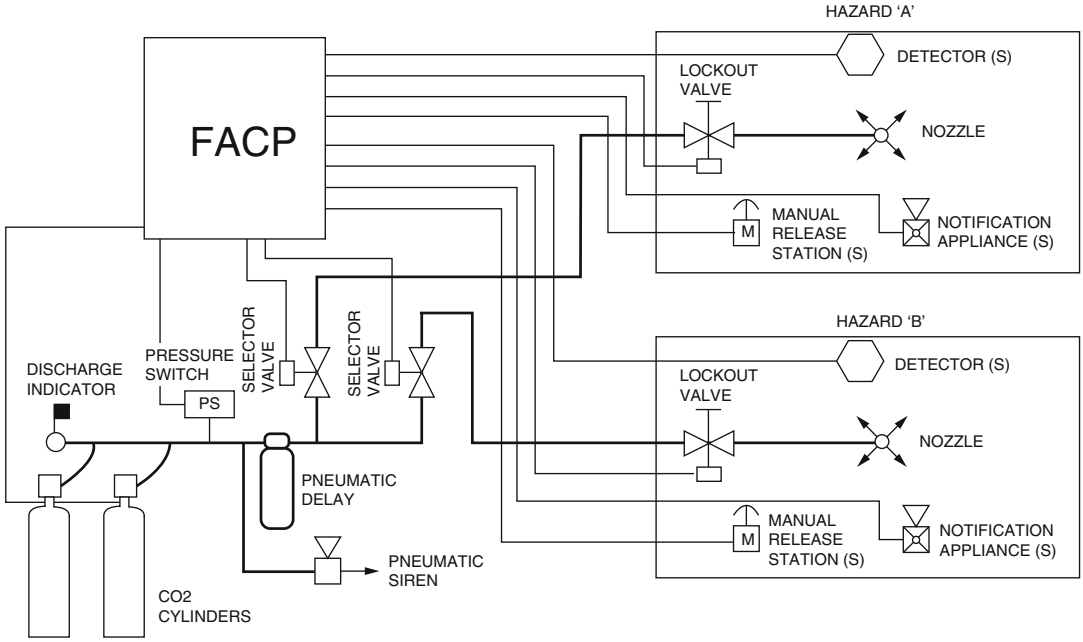

Fig. 45.5 Example of a selector valve arrangement with electric operation

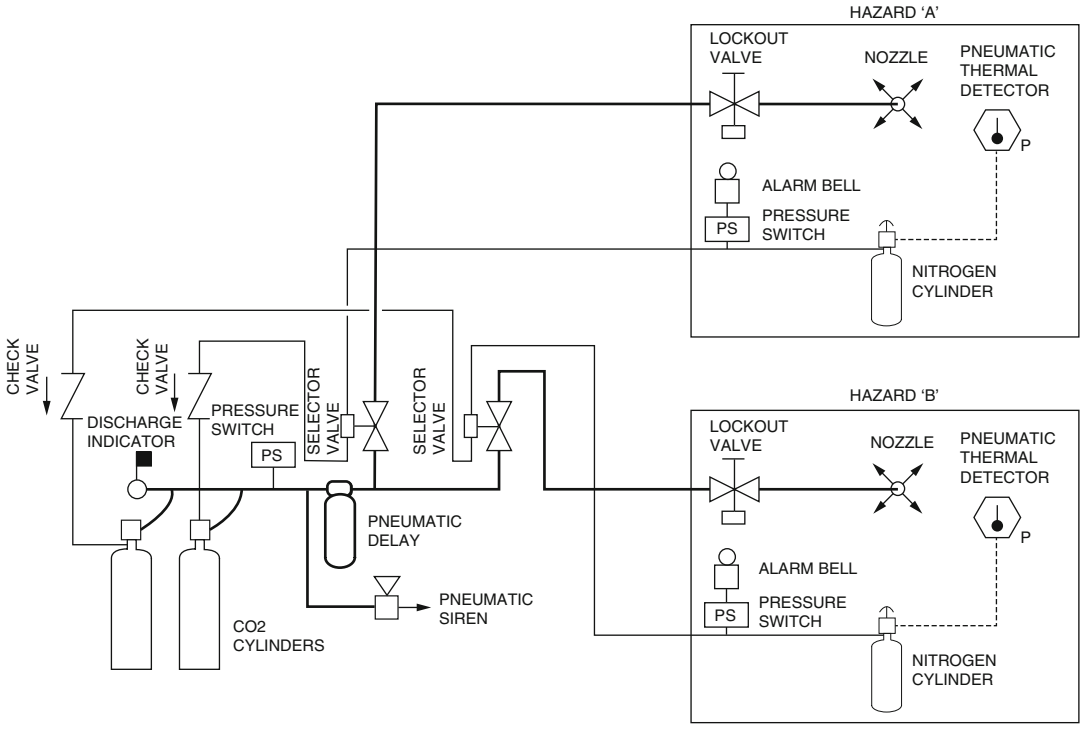

Fig. 45.6 Example of a selector valve arrangement with pneumatic operation

Check Valves

Check valves are frequently used in carbon dioxide systems to isolate main and reserve supplies and to separate pneumatic actuation systems.

Since high-pressure cylinders can be opened by back pressure in the manifold, check valves are required in a system with a reserve supply, in order to prevent the reserve supply from being actuated when the main supply is discharged and vice versa. In addition, the check valve prevents the loss of agent in the event that either supply is discharged while the other supply is disconnected and removed for recharging.

Where multiple pneumatic actuation cylinders are used to actuate a common supply from different locations, check valves are required at the point of connection. This ensures that actuation from either station is not dependent on the condition of the other. In addition, there are practical limitations on the overall size of the actuation piping/tubing system, and the check valves ensure that the entire network does not need to be pressurized.

Notification of System Status

Due to the inherent safety risks associated with carbon dioxide, the role of notification is extremely important in the design of carbon dioxide systems. This encompasses warning and instruction signs, a pre-discharge alarm and discharge time delay, a post-discharge alarm, and discharge indication.

Warning and Instruction Signs

NFPA 12 prescribes a number of warning and instruction signs that are to be placed in various locations, depending on the layout of the building or hazard area. Signs located near or within the hazard provide instruction to evacuate when the alarm sounds; signs located near or outside the hazard provide instruction not to enter the space while the alarm is activated; and signs located at the manual actuation stations indicate the purpose of the release and instruct the user to verify that no personnel are in the protected space before actuating the system.

Pre-discharge Alarm and Time Delay

A pneumatic pre-discharge time delay, and pneumatic pre-discharge alarm, shall be incorporated into any carbon dioxide total flooding system that protects a space that is normally occupied, or that could be occupied even if occasionally. The purpose of this device is to provide a highly reliable means of alerting people within the protected space of an imminent carbon dioxide release, giving them sufficient time to safely egress prior to system discharge.

Certain design standards may allow omission of the time delay under certain conditions where the risk to personnel may be greater with the time delay, or where the physical dimensions of the protected space eliminate the possibility of occupancy at any time.

Certain design standards may also require pre-discharge alarms and time delays for local application systems that present a significant health risks to occupants.

Post-discharge Alarm and Discharge Indication

Visible and audible alarm devices shall be provided outside each entrance to protected spaces that are normally occupied or that could be occupied even if occasionally, where carbon dioxide is discharged directly into the space, or could migrate into the space. These alarm devices should activate prior to system discharge, or at the time of system discharge.

A discharge indicator or alarm shall be provided that alerts personnel to the fact that a carbon dioxide system has discharged and need to be recharged.

System Controls for Marine Applications

Marine carbon dioxide systems generally are arranged for manual release of carbon dioxide into the protected space. A notable exception is a small system of less than or equal to 136 kg (300 lb) carbon dioxide, protecting a normally unoccupied space, whose automatic discharge will not interfere with safe navigation of the vessel.

There are numerous marine carbon dioxide design standards and guidelines, and their requirements regarding the design of carbon dioxide extinguishing systems differ. The design standards that apply to a particular carbon dioxide system to be installed on a marine vessel should be identified and the requirements carefully adhered to.

Manual Operation

It is a common requirement in various marine carbon dioxide design standards that each manually operated system be provided with two separate valves controlling the delivery of carbon dioxide into the protected space. One valve should control discharge from the carbon dioxide storage, while the other controls delivery of carbon dioxide to the protected space.

Each of these two valves should be provided with a manually-operated control device. The set of control devices, one for each valve, should be installed together inside of a single control box. The control box should be located outside of the protected space, in the immediate vicinity of the main egress from the space.

Other Controls and Notification Requirements

Other controls and notification devices are required for marine carbon dioxide systems that are similar to those described for land-based industrial systems. The applicable design standards should be consulted.

Carbon Dioxide Quantity and Rate of Application

The stored quantity, or mass, of carbon dioxide is the amount needed to achieve the design concentration (total flooding) or rate and duration of discharge (local application) in accordance with the applicable system design, plus additional amounts as required for specific design considerations.

Total Flooding Systems, Non-marine Applications

The design principle of a total-flooding system is for carbon dioxide to be discharged into an enclosed space in such manner as to achieve a specific design concentration that will promptly extinguish surface fires under anticipated conditions, or will extinguish deep-seated fires after the concentration is maintained or held within the enclosure for a specified length of time.

Calculation of the design quantity of carbon dioxide assumes (a) that it is discharged into an enclosure as a gas, and (b) that it is well mixed with the enclosure air. The assumption that carbon dioxide enters the enclosure as a gas is an approximation since it leaves the nozzle as a mixture of gas and dry ice snow. The all-gas approximation, however, has been found useful in calculations. In most cases, carbon dioxide discharge causes a rise of pressure in the protected enclosure. Some carbon dioxide is lost from the enclosure as pressurized air escapes through leakage and vent openings, the rate of carbon dioxide loss being progressively greater as its concentration increases during discharge. As such, the quantity of carbon dioxide required to achieve concentration C in an enclosure can be calculated as follows:

$$m = \frac{V}{s}\ln\left(\frac{100}{100 - C}\right) \qquad (45.9)$$

where

m quantity of CO_2, kg
V enclosure volume, m^3
s specific volume of CO_2 vapor at the enclosure temperature, m^3/kg
C CO_2 concentration, vol.%

Carbon dioxide should be discharged in a manner that promotes mixing of the enclosure atmosphere. Under most conditions, the pressure in an enclosure will rise during the discharge period. The displaced atmosphere is exhausted freely from the enclosure through small openings or through a pressure-relief vent if provided. This is referred to as free-efflux flooding [39].

Determining the quantity of agent necessary to achieve fire extinguishment within the protected enclosure is a multistep process, summarized below.

1. Define the fire hazard and the enclosure about the hazard;
2. Determine minimum extinguishing concentration (MEC) for the predominate combustible material;
3. Determine the design concentration (DC);
4. Determine the base design quantity (m_{BD}) of carbon dioxide;
5. Determine additional quantities of carbon dioxide for special conditions;
6. Determine final design quantity (m_{FD}) of carbon dioxide.

The overall process for determining the final design quantity for surface fires and deep-seated fires is the same; however, there are distinct variations within some of the steps. The detailed process for each is, therefore, described separately, first for surface fires, then for deep-seated fires.

Surface Fires

Determining Design Quantity

The detailed steps for determining the final design quantity of carbon dioxide for surface fires are described below.

Step 1: Define the fire hazard and the enclosure about the hazard

Identify the predominate combustible material (fuel) associated with the fire hazard. Determine the type of burning that will characterize the fire; surface or deep-seated (smoldering).

Identify the boundaries of the fixed enclosure about the hazard that is inherently suitable to receive gaseous carbon dioxide and retain it for the required length of time. Calculate the gross volume of the enclosure. The gross volume of all interconnected spaces, wherever free flow of carbon dioxide between them can take place, must be included in the total gross volume calculation. Calculate the total net volume by subtracting the volumes of fixed solid impermeable objects within the enclosure (e.g. pillars). The net volume is the protected volume (V_P) for the purpose of determining the final design quantity of carbon dioxide.

Step 2: Determine minimum extinguishing concentration (MEC) for the predominate combustible material

The minimum theoretical carbon dioxide extinguishing concentration for liquids and gases must be determined by test, or obtained from a recognized source, according to NFPA 12. If the maximum residual oxygen value (O_2) is known, the theoretical carbon dioxide extinguishing concentration may be calculated. The result must be obtained from the following equation [33]:

$$\%CO_2 = \left(\frac{21 - O_2}{21}\right) \cdot 100 \qquad (45.10)$$

NFPA 12 provides a theoretical minimum extinguishing concentration (MEC) value for a number of flammable and combustible liquids [33], and several are given in Table 45.14.

Step 3: Determine the design concentration (DC)

The design concentration (DC) is determined by applying a safety factor, at least 20 %, to the MEC. Furthermore, the design concentration is typically required to be greater than or equal to 34 vol.%. If, after applying the safety factor, the design concentration value is less than 34 vol.%, it must be increased to equal 34 vol.%. NFPA 12 provides a design concentration value for a number of flammable and combustible liquids [33], adjusted to the minimum required 34 vol.% where necessary. Design concentrations for a number of different materials are provided in Table 45.14.

Table 45.14 Minimum extinguishing and design concentrations for selected flammable liquids

Material	MEC, vol.%	DC, vol.%
Acetone	27[a]	34
Acetylene	55	66
Carbon disulfide	60	72
Ethyl alcohol	36	43
Hexane	29	35
Methyl alcohol	33	40
Propane	30	36

MEC minimum extinguishing concentration
DC design concentration
[a]Calculated from accepted residual oxygen values

Table 45.15 Flooding factors vs. hazard volume

Protected volume (V_P), m3	Flooding factor, kg/m^3	Minimum quantity, kg
≤3.96	1.15	–
3.97–14.15	1.07	4.5
14.16–45.28	1.01	15.1
45.29–127.35	0.9	45.4
127.35–1415	0.8	113.5
>1415	0.74	1135

Step 4: Determine the base design quantity (m_{BD}) of carbon dioxide

The base design quantity (m_{BD}) is determined by applying the appropriate carbon dioxide flooding factor provided in Table 45.15 obtained from NFPA 12 [34] to the protected volume (V_P).

$$m_{BD} = V_P \cdot FF \tag{45.11}$$

The result must not be less than the minimum quantity value shown in the appropriate row in the table. If the calculated value of m_{BD} is less than the minimum quantity value, it must be increased to equal the minimum quantity value.

All of the flooding factor values in Table 45.15 were developed based upon a carbon dioxide concentration of 34 vol.%; therefore, the calculated value of m_{BD} for design concentrations exceeding 34 vol.% must be increased by applying a material conversion factor, as described in Steps 5 and 6.

The flooding factors in Table 45.15 are based on a carbon dioxide expansion factor (mass of liquid to volume of gas) of 0.56 m^3/kg (9 ft^3/lb) [39] at a temperature of 30 °C (86 °F). This same value is also inherently or expressly used in other carbon dioxide design standards, including the USCG [17], SOLAS [36] and ABS [37].

The flooding factors in Table 45.15 contain inherent safety factors to account for a reasonable amount of normal leakage [39] for protected volumes equal to 1415 m^3 (50,000 ft^3) or less. For protected volumes greater than 1415 m^3 (50,000 ft^3), no safety factor for normal leakage is included. The reasons for including normal leakage safety factors in the smaller protected volumes is not given in NFPA 12; however, it is assumed to be related to the possibility that the effect of normal leakage on carbon dioxide concentration increases as the volume decreases in proportion to the increasing enclosure surface area to volume ratio.

NFPA 12 has contained the concept of including a normal leakage safety factor in the flooding factors for smaller protected volumes in every edition since the first edition was published in 1929. The flooding factors in the 2015 edition were introduced in the 1955 edition, and have remained unchanged in every edition since.

Step 5: Determine additional quantities of carbon dioxide for special conditions

The base design quantity of carbon dioxide (m_{BD}) determined in the previous steps, may require adjustment based upon the effects of several special conditions. Each of these special conditions must be considered, and adjustments made to the m_{BD} as appropriate, which will lead to the determination of the final carbon dioxide design quantity (m_{FD}).

Step 5a: Material Conversion factor

The base design quantity of carbon dioxide was determined based on a carbon dioxide concentration of 34 vol.%. As such, the calculated value of m_{BD} for design concentrations exceeding 34 vol.% must be increased by applying a material conversion factor (MCF). The MCF for design concentration, C can be determined using Equation 45.12 or from Fig. 45.7. The corrected design quantity of carbon dioxide (m_{cf}) is calculated as the base design quantity (m_{BD}) times the MCF as shown in Equation 45.13.

$$MCF = 2.41 \cdot \ln\left(\frac{100}{100 - C}\right) \tag{45.12}$$

$$m_{cf} = m_{BD} \cdot MCF \tag{45.13}$$

Step 5b: Uncloseable Openings

Determine if the enclosure surrounding the protected volume has openings that cannot be closed. As carbon dioxide is discharged into the

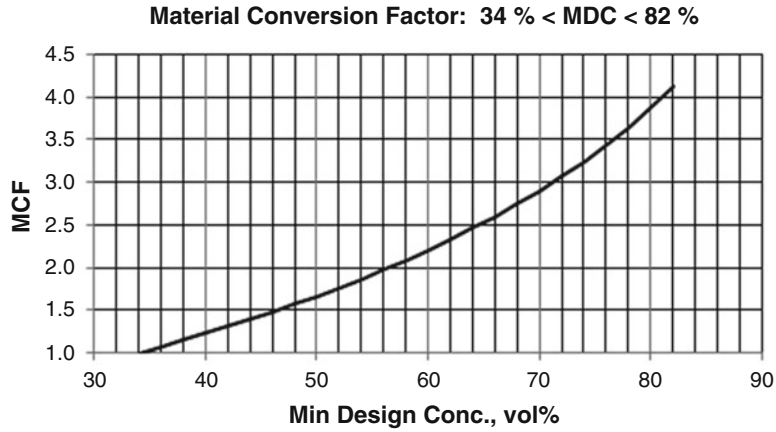

Fig. 45.7 Material conversion factor vs. Minimum design concentration

protected volume, some quantity of carbon dioxide will be expelled through these openings. The quantity of carbon dioxide lost must be calculated so that it can be included in the final design quantity of agent (m_{FD}).

For surface fires, the design concentration must be achieved within 1 min from the start of carbon dioxide discharge. The surface fire is expected to be extinguished during this time period, therefore, it is necessary to account for the loss of carbon dioxide through uncloseable openings during only this time period. It is assumed that the volume of carbon dioxide/air mixture expelled during this 1 min time period will contain carbon dioxide at the design concentration. The total quantity of carbon dioxide lost due to leakage from uncloseable openings (m_{lo}) for a given time period (t) can be estimated by Equations 45.14 (SI units) and 45.15 (U.S. units). A graphical method for estimating the quantity of carbon dioxide lost through uncloseable openings is also provided in NFPA 12 [40].

$$m_{lo} = 116 \cdot A\sqrt{\rho_1 \cdot (\rho_1 - \rho_A)h} \cdot t \qquad (45.14)$$

where

m_{lo} quantity of CO2 leaked through openings, kg
A area of opening, m^2
h height, center of opening to top of protected space, m
ρ_1 density of carbon dioxide-air atmosphere, kg/m^3
ρ_A density of air external to enclosure, kg/m^3
t time duration of leakage, min

At 1 atm pressure (101,300 Pa) and 21 °C

$$\rho_A = 1.202 \ \text{kg/m}^3$$
$$\rho_1 = 0.006220\text{C} + 1.202 \ \text{kg/m}^3$$

$$m_{lo} = 0.6 \cdot C \cdot \rho_{CO2} \cdot A\sqrt{\frac{2g(\rho_1 - \rho_A)h}{\rho_1}} \cdot t \qquad (45.15)$$

where

m_{lo} quantity of CO2 leaked through openings, lb
C CO_2 concentration, vol.%
A area of opening, ft^2
g acceleration of gravity, 32.2 ft/s^2
h height, center of opening to top of protected space, ft
ρ_{CO2} density of carbon dioxide vapor, lb/ft^3
ρ_1 density of carbon dioxide-air atmosphere, lb/ft^3
ρ_A density of air external to enclosure, lb/ft^3
t time duration of leakage, min

At 1 atm pressure, 14.7 psi, and 70 °F

$$\rho_{CO2} = 0.114 \ \text{lb/ft}^3$$
$$\rho_A = 0.0751 \ \text{lb/ft}^3$$
$$\rho_I = 0.000388 \ \text{C} + 0.0750 \ \text{lb/ f}t^3$$

Where an uncloseable opening is on a wall without an opening of comparable size near the

ceiling, the area of the opening (A) in the preceding equations is divided by two since half of the opening acts to allow leakage of carbon dioxide/air mixture while the other half acts to allow ingress of outside makeup air.

Step 5c: Ventilation systems

Mechanical ventilation of a protected volume should be arranged to shut down prior to the discharge of a carbon dioxide system. Where this is not possible, and the ventilation system continues to operate, some quantity of carbon dioxide will be removed from the protected volume. The quantity of carbon dioxide lost due to ventilation (m_{lv}) must be calculated so that it can be included in the final design quantity (m_{FD}). The quantity of carbon dioxide lost is equal to the volume of fresh air introduced into the protected volume by the mechanical ventilation system over a given time period (t) times the flooding factor, as shown in Equation 45.16. For surface fires, the given time period (t) for this calculation is 1 min.

$$m_{lv} = Q_v \cdot t \cdot FF \tag{45.16}$$

where

m_{lv} CO_2 added to compensate for forced ventilation, kg
Q_V ventilation rate, m^3/s
t duration of discharge, s
FF flooding factor, kg/m^3

Step 5d: Temperature Extremes

The quantity of agent must be adjusted to account for extreme temperatures in the protected volume whenever present. Extreme temperatures are those that exceed 93 °C (200 °F) or that are less than −18 °C (0 °F).

SI units: For high temperature extremes, add 0.36 % to carbon dioxide quantity per degree Celsius greater than 93 °C. Refer to Equation 45.17. For low temperatures, add 1.8 % to carbon dioxide quantity per degree Celsius less than −18 °C. Refer to Equation 45.18.

U.S. units: For high temperature extremes, add 1 % to carbon dioxide quantity for each additional 5° Fahrenheit greater than 200 °F. Refer to Equation 45.19. For low temperatures, add 1 % to carbon dioxide quantity for each additional degree Fahrenheit less than 0 °F. Refer to Equation 45.20.

Where the protected volume experiences both high and low extreme temperatures, calculate both the high and low extreme temperature factors, and choose the one with the highest value.

Use the extreme temperature factor in Equation 45.21 to calculate the additional quantity of carbon dioxide required for extreme temperature (m_T), which must be included in the final design quantity (m_{FD}) in Step 6.

$$\tau_H = 0.0036 \cdot (T_H - 93) \tag{45.17}$$

$$\tau_L = -0.018 \cdot (T_L + 18) \tag{45.18}$$

where:

τ_H = Extreme high temperature factor (S.I. units)
T_H = High temperature value (°C)
τ_L = Extreme low temperature factor (S.I. units)
T_L = Low temperature value (°C)

$$\tau_H = 0.002 \cdot (T_H - 200) \tag{45.19}$$

$$\tau_L = 0.01 \cdot (0 - T_L) \tag{45.20}$$

where:

τ_H = Extreme high temperature factor (U.S. units)
T_H = High temperature value (°F)
τ_L = Extreme low temperature factor (U.S. units)
T_L = Low temperature value (°F)

$$m_T = \tau \cdot \left(m_{cf} + m_{lo} + m_{lv}\right) \tag{45.21}$$

where:

m_T = Additional carbon dioxide quantity for extreme temperature
τ = Extreme high or low temperature factor, whichever is greater
m_{cf} = Base quantity of carbon dioxide after applying MCF
m_{lo} = Additional carbon dioxide quantity for leakage through openings
m_{lv} = Additional carbon dioxide quantity for mechanical ventilation

Table 45.16 Design parameters for specific deep-seated fire hazards [41]

Hazard type	Min. design Conc., vol.%	Flooding factor, kg/m^3	Remarks
Dry electrical hazards in general, V < 56.6 m^3	50	1.6	
Dry electrical hazards in general, V > 56.6 m^3	50	1.33	Minimum quantity, 91 kg
Record (bulk paper) storage, ducts, covered trenches	65	2.0	
Fur storage vaults, dust collectors	75	2.66	

Step 6: Determine final design quantity of carbon dioxide

The final design quantity of carbon dioxide is calculated using Equation 45.22, by adding each adjustment quantity determined in Steps 5a through 5d.

$$m_{FD} = m_{cf} + m_{lo} + m_{lv} + m_T \qquad (45.22)$$

Ducts and Covered Trenches

Ducts and covered trenches are a special form of total flooding application. The quantity of carbon dioxide for surface and deep-seated fire hazards in ducts and covered trenches is determined by the protected volume divided by the flooding factor of 2.0 kg/m^3 (0.125 lb/ft^3). The quantity of carbon dioxide so determined will result in a design concentration of approximately 65 vol.%. It is not necessary to further adjust this quantity using the Material Conversion Factor shown in Step 5a. Other special conditions may apply, and if present, should be accounted for as described in Steps 5b through 5d.

Discharge Rate

The discharge rate for surface fires must be sufficient to achieve the design concentration within 1 min from the start of discharge.

Deep-Seated Fires

Determining the Design Quantity

The detailed steps for determining the final design quantity of carbon dioxide for deep-seated fires are described below.

Step 1: Define the fire hazard and the enclosure about the hazard

Identify the predominant combustible material (fuel) associated with the fire hazard. Verify that deep-seated smoldering combustion will characterize the expected fire.

Identify the boundaries of the fixed enclosure about the hazard that is inherently suitable to receive gaseous carbon dioxide and retain it for the required length of time. Calculate the gross volume of the enclosure. Calculate the net volume by subtracting the volumes of any fixed solid, impermeable objects within the enclosure. The net volume is the protected volume (V_P) for the purpose of determining the final design quantity of carbon dioxide.

Step 2: Determine minimum extinguishing concentration (MEC) for the predominate combustible material

There is no theoretical basis for the determination of minimum extinguishing concentrations for deep-seated fires. (See Steps 3 and 4.)

Step 3: Determine the design concentration (DC)

The design concentration (DC) is selected from the Table 45.16. For deep-seated fire hazards not listed in Table 45.16, the DC must be justified to the authority having jurisdiction before the design is finalized and the system is installed.

Step 4: Determine the base design quantity (m_{BD}) of carbon dioxide

There is no theoretical basis for the determination of the base design quantity of carbon dioxide for deep-seated fires. Instead, flooding factors associated with specified design concentrations have been empirically determined by testing and experience for a few common hazards.

Use the flooding factor in Table 45.16 associated with the design concentration selected in Step 3.

For deep-seated fire hazards not listed in Table 45.16, the flooding factor must be justified to the authority having jurisdiction before the design is finalized and the system is installed.

The base design quantity of carbon dioxide is calculated by applying the flooding factor (FF) to the protected volume (Vp) using Equation 45.11.

Step 5: Determine additional quantities of carbon dioxide for special conditions

The base design quantity of carbon dioxide (m_{BD}) determined in the previous steps, may require adjustment based upon the effects of several special conditions. Each of these special conditions must be considered, and adjustments made to the m_{BD} as appropriate, which will lead to the determination of the final carbon dioxide design quantity (m_{FD}).

Step 5a: Material Conversion Factor

The Material Conversion Factor used for surface fires does not apply to deep-seated fires. Proceed to Step 5b.

Step 5b: Uncloseable Openings

Determine if the enclosure surrounding the protected volume has openings that cannot be closed. As carbon dioxide is discharged into the protected volume, some quantity of carbon dioxide will be expelled through these openings. The quantity of carbon dioxide lost must be calculated and added into the final design quantity (m_{FD}).

The total quantity of carbon dioxide lost due to leakage from uncloseable openings (m_{lo}) for a given time period (t) can be estimated by Equations 45.14 and 45.15. For deep-seated fires, time (t) is the entire extinguishing period, which must be a minimum of 20 min, and in some cases may need to be longer. As a result, it is necessary to minimize the normal leakage and close all openings in the enclosures around deep-seated fire hazards. If this is not possible, an extended discharge will likely be required.

Step 5c: Ventilation systems

Mechanical ventilation of a protected volume should be arranged to shut down prior to the discharge of a carbon dioxide system. Where this is not possible, and the ventilation system continues to operate, some quantity of carbon dioxide will be removed from the protected volume. The quantity of carbon dioxide lost due to ventilation (m_{lv}) must be calculated so that it can be included in the final design quantity (m_{FD}). The quantity of carbon dioxide lost is equal to the volume of fresh air introduced into the protected volume by the mechanical ventilation system over a given time period (t) times the flooding factor, as shown in Equation 45.16.

For deep-seated fires, the given time period (t) for this calculation must be a minimum of 20 min, and in some cases may need to be longer. This will normally require the provision of an extended discharge.

Step 5d: Temperature Extremes

The quantity of agent must be adjusted to account for extreme temperatures in the protected volume whenever present. Extreme temperatures are those that exceed 93 °C (200 °F) or that are less than −18 °C (0 °F).

For high temperature extremes, add 0.36 % to carbon dioxide quantity per degree Celsius greater than 93 °C. Refer to Equation 45.17. For low temperatures, add 1.8 % to carbon dioxide quantity per degree Celsius less than −18 °C. Refer to Equation 45.18.

(For high temperature extremes, add 1 % to carbon dioxide quantity for each additional 5° Fahrenheit greater than 200 °F. Refer to Equation 45.19. For low temperatures, add 1 % to carbon dioxide quantity for each additional degree Fahrenheit less than 0 °F). Refer to Equation 45.20.

Where the protected volume experiences both high and low extreme temperatures, calculate both the high and low extreme temperature factors, and choose the one with the highest value.

Use the extreme temperature factor in Equation 45.21 to calculate the additional quantity of carbon dioxide required for extreme temperature (m_T), which must be included in the final design quantity (m_{FD}) in Step 6.

Step 6: Determine final design quantity of carbon dioxide

The final design quantity of carbon dioxide is calculated using Equation 45.22, by adding each adjustment quantity determined in Steps 5a through 5d, where $m_{cf} = 0$.

Discharge Rate

The discharge rate for deep-seated fires must be sufficient to achieve the design concentration within 7 min from the start of discharge, and also achieve a concentration of at least 30 vol. % within 2 min from the start of discharge.

Enclosed rotating electrical equipment: The design concentration of 30 vol.% design concentration must be provided for enclosed rotating electrical equipment, and maintained for the entire deceleration period and not less than 20 min.

This type of equipment is expected to have an enclosure that will leak some carbon dioxide during the deceleration period. This will require an initial discharge followed by an extended discharge of carbon dioxide to maintain 30 vol.% continuously.

For enclosure volumes less than or equal to 56.6 m^3 (2000 ft^3), a flooding factor of 1.6 kg/m^3 (0.1 lb/ft^3) should be used to determine the quantity of carbon dioxide to use for the initial discharge. For enclosure volumes greater than 56.6 m^3 (2000 ft^3), a flooding factor of 1.32 kg/m^3 (0.08 lb/ft^3) should be used.

The values given in Tables 45.17 and 45.18 may be used as a guide in determining the quantity of carbon dioxide for the extended discharge to maintain a carbon dioxide concentration of 30 vol.% as a function of the enclosure volume and equipment deceleration time, and assuming average leakage from the enclosure. For dampered, non-recirculating-type equipment, add 35 % to the quantities indicated.

Example—Total Flooding System What is the CO_2 design quantity and rate of discharge required to protect by total flooding a 500 m^3 (10 m × 12.5 m × 4 m) enclosure of light building construction in which ethyl alcohol is processed?

For combustibles where the MDC is 34 vol.% the flooding factor for a 500 m^3 enclosure is 0.80 kg/m^3 and the basic CO_2 design quantity, m_{BD}, is (500 m^3) (0.80 kg/m^3) = 400 kg CO_2. However, ethyl alcohol has an MDC of 43 % and a corresponding material conversion factor is 1.4. Therefore, the design quantity, m_D, is (400 kg) (1.4) = 560 kg. The design discharge time is 1 min so w = 560 kg/min.

Total Flooding Systems, Marine Applications

Carbon dioxide total flooding systems are used extensively to protect the unique hazards aboard ships and other structures, such as mobile offshore drilling units, that are governed by various marine regulations. These marine systems should be designed to comply with the applicable regulations.

Quantity of Carbon Dioxide

There are several variations in the methods used to determine carbon dioxide design quantity for marine total flooding systems. NFPA 12 specifies a minimum design concentration for several types of hazards, including machinery, vehicle storage and electrical equipment. A flooding factor is specified for general cargo storage hazards rather than a minimum design concentration.

The U.S. Coast Guard specifies flooding factors for all covered hazards, including machinery, general cargo storage, and vehicle storage. SOLAS specifies minimum design concentrations for machinery hazards and a flooding factor for general cargo storage. ABS specifies minimum design concentrations for machinery, general cargo storage and vehicle storage, and does not specify flooding factors for any hazard types.

Tables 45.19 and 45.20 provide the design specifications for various hazard types from NFPA 12, SOLAS, USCG, and ABS.

When a standard specifies a minimum design concentration as the governing design requirement, a calculation method defined by each standard must be followed to determine the final design quantity of carbon dioxide. These design methods vary, so it is important to use the calculation method from the standard being employed.

For example, NFPA 12 specifies a minimum design concentration of 34 vol.% for the

Table 45.17 Extended discharge for enclosed recirculating rotating electrical equipment (cubic meters protected for deceleration time) (S.I. units) [42]

Time (min)								
kg CO_2	5	10	15	20	30	40	50	60
45.4	34.0	28.3	22.6	17.0	14.2	11.3	8.5	5.7
68.1	50.9	42.5	34.0	28.3	21.2	17.0	14.0	11.3
90.8	67.9	55.2	45.3	36.8	28.3	24.1	18.4	14.2
113.5	93.4	69.3	56.6	46.7	36.8	29.7	22.6	17.0
136.2	130.2	87.7	67.9	56.6	46.7	36.8	28.3	19.8
158.9	172.6	116.0	84.9	70.8	56.6	46.7	34.0	25.5
181.6	217.9	152.8	107.5	89.1	70.8	56.6	45.3	34.0
204.3	261.8	192.4	138.7	113.2	87.7	73.6	59.4	45.3
227.0	305.6	229.2	172.6	141.5	110.4	93.4	79.2	62.3
249.7	348.1	268.9	209.4	172.6	138.7	118.9	101.9	87.7
272.4	393.4	308.5	243.4	203.8	169.8	147.2	127.4	110.4
295.1	435.8	348.1	278.8	234.9	199.5	175.5	155.7	135.8
317.8	478.3	384.9	314.1	266.0	229.2	203.8	181.1	158.5
340.5	523.6	424.5	349.5	297.2	258.9	232.1	206.6	184.0
363.2	586.0	464.1	384.9	328.3	288.7	260.4	232.1	206.6
385.9	608.4	502.3	420.3	359.4	319.8	288.7	257.5	229.2
408.6	650.9	540.5	455.6	390.5	349.5	317.0	284.4	254.7
431.3	696.2	580.2	491.0	421.7	379.2	345.3	311.3	277.3
454.0	738.6	619.8	526.4	452.8	410.4	373.6	336.8	302.8
476.7	781.1	659.4	563.2	483.9	441.5	401.9	363.7	325.5
499.4	823.5	696.2	595.7	515.1	469.8	430.2	389.1	350.9
522.1	866.0	735.8	631.1	546.2	500.9	458.5	416.0	373.6
544.8	911.3	772.6	666.5	577.3	532.0	486.8	441.5	399.0
567.5	953.7	812.2	701.8	609.4	561.8	515.1	467.0	421.7
590.2	999.0	851.8	737.2	641.0	591.5	543.4	493.8	447.1
612.9	1041.4	888.6	772.6	672.1	622.6	571.7	520.7	471.2
635.6	1086.7	928.2	808.0	704.7	653.7	600.0	547.6	495.3
658.3	1129.2	967.9	843.3	735.8	684.9	628.3	574.5	519.3
681.0	1171.6	1007.5	878.7	766.9	713.2	656.6	600.0	543.4

protection of machinery spaces based on the gross volume, including the casing. The method specified for calculating the final design quantity of carbon dioxide associated with the specified design concentration includes the concept of free-efflux flooding (Equation 45.5), and quantity adjustments if necessary to account for uncloseable openings, mechanical ventilation and extreme temperatures. Employing the free-efflux flooding concept results in a quantity of carbon dioxide that will achieve an initial carbon dioxide concentration that is higher than the minimum design concentration to account for the loss of some carbon dioxide during discharge through normal enclosure leakage.

In contrast, SOLAS and ABS do not require the calculation of carbon dioxide quantity using the free-efflux flooding equation, when a minimum design concentration is specified. Instead, a carbon dioxide liquid to gas expansion factor (specific volume) is specified, which must be used to calculate the quantity of carbon dioxide required based upon the minimum design concentration specified for the protected volume of the enclosure surrounding the hazard. Equation 45.23 is used for this calculation.

Table 45.18 Extended discharge for enclosed recirculating rotating electrical equipment (cubic feet protected for deceleration time) (U.S. units) [43]

Time (min)								
lb CO_2	5	10	15	20	30	40	50	60
100	1200	1000	800	600	500	400	300	200
150	1800	1500	1200	1000	750	600	500	400
200	2400	1950	1600	1300	1000	850	650	500
250	3300	2450	2000	1650	1300	1050	800	600
300	4600	3100	2400	2000	1650	1300	1000	700
350	6100	4100	3000	2500	2000	1650	1200	900
400	7700	5400	3800	3150	2500	2000	1600	1200
450	9250	6800	4900	4000	3100	2600	2100	1600
500	10,800	8100	6100	5000	3900	3300	2800	2200
550	12,300	9500	7400	6100	4900	4200	3600	3100
600	13,900	10,900	8600	7200	6000	5200	4500	3900
650	15,400	12,300	9850	8300	7050	6200	5500	4800
700	16,900	13,600	11,100	9400	8100	7200	6400	5600
750	18,500	15,000	12,350	10,500	9150	8200	7300	6500
800	20,000	16,400	13,600	11,600	10,200	9200	8200	7300
850	21,500	17,750	14,850	12,700	11,300	10,200	9100	8100
900	23,000	19,100	16,100	13,800	12,350	11,200	10,050	9000
950	24,600	20,500	17,350	14,900	13,400	12,200	11,000	9800
1000	26,100	21,900	18,600	16,000	14,500	13,200	11,900	10,700
1050	27,600	23,300	19,900	17,100	15,600	14,200	12,850	11,500
1100	29,100	24,600	21,050	18,200	16,600	15,200	13,750	12,400
1150	30,600	26,000	22,300	19,300	17,700	16,200	14,700	13,200
1200	32,200	27,300	23,550	20,400	18,800	17,200	15,600	14,100
1250	33,700	28,700	24,800	21,500	19,850	18,200	16,500	14,900
1300	35,300	30,100	26,050	22,650	20,900	19,200	17,450	15,800
1350	36,800	31,400	27,300	23,750	22,000	20,200	18,400	16,650
1400	38,400	32,800	28,550	24,900	23,100	21,200	19,350	17,500
1450	39,900	34,200	29,800	26,000	24,200	22,200	20,300	18,350
1500	41,400	35,600	31,050	27,100	25,250	23,200	21,200	19,200

$$m_{BD} = \frac{V}{s} \cdot \frac{C}{100} \tag{45.23}$$

where

m_{BD} base design quantity of carbon dioxide, kg (lb)

V protected volume, m^3 (ft^3)

C minimum design concentration (vol.%)

s specific volume (expansion factor), 0.56 m^3/kg (9 ft^3/lb)

Equation 45.23 does not account for leakage during discharge. The resulting quantity of carbon dioxide is less than would be determined using the free-efflux model, Equation 45.9. Equation 45.23 is correct only where carbon dioxide-free air is expelled from the protected volume during discharge, which is very unlikely given that the discharge rate requirement under SOLAS and ABS standards is release of 85 % of the design quantity of carbon dioxide in 2 min (Table 45.21). For example, consider a 500 m^3 (17,650 ft^3) enclosure, a design concentration of 35 % (total flooding, machinery spaces, including casing)), and a specific volume, s, of 0.56 m^3/kg (9 ft^3/lb). The required quantity of carbon dioxide by Equation 45.23 is 313 kg (690 lb), and by Equation 45.9 is 385 kg (849 lb). Where gas mixing and leakage occur during discharge (free-efflux model), the quantity of 313 kg (690 lb) would result in a post-discharge carbon dioxide concentration of only

Table 45.19 Marine design criteria comparison (S.I.)

Location	NFPA 12 [38]		SOLAS [36]		US Coast Guard, DHS [17]		Classification society- ABS [37] (vessels 90 m length)	
	Design concentration (vol.%)	Flooding factor by gross vol. (kg/m^3)	Design concentration (vol.%)	Flooding factor by gross volume (kg/m^3)	Design concentration (vol.%)	Flooding factor by gross volume (kg/m^3)	Design concentration (vol.%)	Flooding factor by gross volume (kg/m3)
Machinery spaces								
excluding casing			40 %[a, b]			*See below*	40 %[a, b]	
Including casing	34 %[a]		35 %[a, c]				35 %[a, c]	
0–14.15 m^3 gross volume						1.07		
>14.15–45.28 m^3 gross volume						1.00		
>45.28–127.35 m^3 gross volume						0.89		
>127.35–1415 m^3 gross volume						0.80		
>1415 m^3 gross volume						0.73		
Propulsion machinery-international voyage						0.64		
Cargo spaces		0.53		0.53		0.53	30 %[a, d]	
Vehicle spaces	34 %[a]					0.73	45 %[a, e]	
Electrical equipment spaces								
<56.6 m^3	50 %	1.60						
≥56.6 m^3	50 %	1.33						

[a]0.56 m^3/kg expansion factor
[b]35 % if less than 2000 gross tonnage vessel
[c]30 % if less than 2000 gross tonnage vessel
[d]30 % if less than 2000 gross tonnage vessel
[e]For ro-ro and cargo spaces (other than special category spaces) used for vehicle storage with fuel in tanks

Table 45.20 Marine design criteria comparison

Location	NFPA 12 [38]		SOLAS [36]		US Coast Guard, DHS [17]		Classification society- ABS [37] (vessels 295 ft length)	
	Design concentration (vol.%)	Flooding factor by gross volume (lb/ft^3)	Design concentration (vol.%)	Flooding factor by gross volume (lb/ft^3)	Design concentration (vol.%)	Flooding factor by gross volume (lb/ft^3)	Design concentration (vol.%)	Flooding factor by gross volume (lb/ft^3)
Machinery spaces								
Excluding casing			40 %[a, b]			*See below*	40 %[a, b]	
Including casing	34 %[a]		35 %[a, c]				35 %[a, c]	
0–500 ft^3 gross volume						0.067		
>500–1600 ft^3 gross volume						0.063		
>1600–4500 ft^3 gross volume						0.056		
>4500–50,000 ft^3 gross volume						0.050		
>50,000 ft^3 gross volume						0.045		
Propulsion machinery- international voyage						0.040		
Cargo spaces		0.033		0.033		0.033	30 %[a, d]	
Vehicle spaces	34 %[a]					0.045	45 %[a, e]	
Electrical equipment spaces								
<2000 ft^3	50 %	0.100						
≥2000 ft^3	50 %	0.083						

[a]9 ft^3/lb expansion factor
[b]35 % if less than 2000 gross tonnage vessel
[c]30 % if less than 2000 gross tonnage vessel
[d]30 % if less than 2000 gross tonnage vessel
[e]For ro-ro and cargo spaces (other than special category spaces) used for vehicle storage with fuel in tanks

Table 45.21 Marine system discharge rates

Type of space	NFPA 12 [38]	U.S. Coast Guard, DHS [17]	SOLAS (FSS) [36]	ABS [37]
Machinery	85 % of design concentration (DC) in 2 min	85 % of m_{FD} in first 2 min	85 % of m_{FD} in first 2 min	85 % of m_{FD} in first 2 min
Cargo	No discharge rate given	Specific rate not required	No discharge rate given	No discharge rate given
Vehicle storage >19 L (5 gal) fuel	85 % of design concentration (DC) in 2 min	100 % of m_{FD} in first 2 min[a]	No discharge rate given	N/A[b]
Vehicle storage ≤19 L (5 gal) fuel	2/3 of design concentration (DC) in 10 min	N/A[a]	No discharge rate given	N/A[b]

[a]Requirements are not based upon quantity of fuel in vehicles
[b]Carbon dioxide systems are not allowed in these spaces

29.5 vol.%. The USCG requirement for a space of this size (see Table 45.20) is to use a flooding factor of 0.80 kg/m^3 (0.05 lb/ft^3) giving a required quantity of 400 kg (883 lb) which would result in a concentration of 36.1 vol.% per Equation 45.9.

All referenced marine carbon dioxide system design standards require a flooding factor (FF) be applied to the protected volume (V_P) to determine the quantity of carbon dioxide for one or more hazard types (refer to Equation 45.11).

SOLAS does not require adjustments to the base design quantity of carbon dioxide calculated using Equations 45.23 or 45.9 [44]. ABS requires an additional quantity of carbon dioxide equal to that lost through "non-tight" cargo space hatch covers [45] but provides no guidance to calculate this quantity.

Discharge Rate

Marine total flooding carbon dioxide system discharge rate requirements are dependent on both the specific type of hazard being protected and the governing standard. Table 45.21 illustrates this point by summarizing the discharge rates found in the four referenced standards.

Enclosure Venting for Pressure Control for Total Flooding Systems

Carbon dioxide enters a nozzle as a mixture of cold liquid and vapor and exits as a mixture of vapor and solid-phase "dry ice" or "CO_2-snow." Sublimation (vaporization) of the solid carbon dioxide and exchange of the cold vapor with the air in a room results in a temperature reduction. The net effect on the pressure in a tightly sealed room depends on the storage condition of the carbon dioxide (high-pressure or refrigerated low-pressure), total quantity of gas discharged, the size of the protected volume, and its initial temperature. In most cases the enclosure pressure will rise upon carbon dioxide discharge. It is possible, however, under unusual circumstances for the enclosure pressure to decrease.

Discharge of a large quantity of cold carbon dioxide into a tightly sealed room can result in a pressure decrease. Where such conditions are possible it is recommended that an energy balance evaluation be completed for the enclosure air and the quantity, and storage enthalpy of the carbon dioxide discharged, to determine if there is a risk of pressure decrease.

The pressure rise in an enclosure due to carbon dioxide discharge is capable of causing damage to the enclosure construction due to characteristics common to many system installations. The risk of enclosure damage can be greatly reduced by designing and installing a means of pressure relief.

Enclosure construction, including walls, ceilings and floors, are commonly not tightly sealed. Such enclosures contain numerous locations where pressure would be relieved to

some degree. The aggregate effect of such leakage locations is often referred to as "normal leakage" or "average leakage". Normal leakage should not be relied upon to provide adequate pressure venting to prevent unsafe pressure rise resulting from carbon dioxide discharge. The size of the minimum pressure relief area required is based on the maximum flow rate of carbon dioxide and is calculated using Equation 45.24 [46].

$$A_V = \frac{239 \cdot w}{\sqrt{P}} \qquad (45.24)$$

Where:
A_V = vent area, mm^2
w = carbon dioxide flow rate, kg/min
P = allowable enclosure pressure limit, kPa

The pressure relief (vent) area can be provided by passive (e.g. barometric dampers) or actuated vents (motor-controlled louvers that are opened before the onset of carbon dioxide discharge). Where a minimum concentration of carbon dioxide must be maintained in a room for a specific hold time, vents must be located at the highest point in an otherwise tightly closed room and should be arranged to close after discharge ceases.

Assessment of the allowable pressure limit for an enclosure is often a challenge. Table 45.22 indicates approximate pressure limits for three general types of construction. In the absence of a structural analysis of an enclosure, the user should consider discounting the values in Table 45.22 to provide a safety margin for the design.

Pressure Relief Example What size pressure relief vent is necessary to protect the enclosure described in the total-flooding example given above? Assume the pressure limit is 0.6 kPa (0.09 psi), half of the rated strength for light building construction.

The design rate of discharge is 560 kg/min (1,234.6 lb/min). Light building construction has a rated strength of 1.2 kPa (0.17 psi) as shown in Table 45.22. For this example the design pressure limit is half of the rated value, or (½) (1.2 kPa) = 0.6 kPa (0.09 psi). Using half of the rated value in this manner is a choice of the designer to incorporate a design safety margin. Using Equation 45.24, the required vent area is:

$$A_V = \frac{239 \cdot 560}{\sqrt{0.6}} = 172,787 \ mm^2 = 0.173 \ m^2$$

Table 45.22 Allowable pressure for average enclosures [47]

Construction type	P, kPa	Note
Light building	1.2	Venting sash remains open
Normal building	2.4	Venting sash designed to open freely
Vault building	4.8	

Local Application Systems

A total-flooding system discharges carbon dioxide throughout an entire enclosed volume so that the atmosphere can no longer support combustion. By contrast, a local application system projects carbon dioxide directly onto or in close proximity to a defined surface-fire hazard (flammable gases, liquids, or shallow solids) and maintains an extinguishing atmosphere on or about a precisely define geometric space, but only during the discharge period. Local application systems are designed by either of two methods: rate-by-area or rate-by-volume.

Local application systems are used where the fire hazard is either not confined within an enclosure or the defining enclosure is too large to protect by total flooding in a practical manner. Protected hazards may by completely indoors, partly sheltered, or completely outdoors. The discharge of carbon dioxide must be so arranged that extinguishment of the target fire is not impaired by air currents or wind.

A local application system must be designed to protect the entirety of the hazard which must be sufficiently separated from other hazards so as not to pose a risk of fire spread outside of the protected space. The definition of the protected hazard must include the principal process space or equipment as well as locations or items that can be wetted by splashing, leaking, dripping, or

condensing flammable liquids and associated items or materials such as coated objects, drain boards, hood, or ducts that could serve to propagate a fire into or out of the primary protected space. A series of hazards that expose each other to fire propagation can be can be divided and protected as subgroups or sections with the approval of the local authority having jurisdiction.

The basic design quantity of carbon dioxide required is determined by rate of liquid discharge to protect a defined area or volume times the liquid discharge time. The basic design quantity must be increased based upon consideration of the following factors: high-pressure storage supply; carbon dioxide vaporization in distribution pipe system.

High-Pressure Storage Supply

Where carbon dioxide is supplied from high-pressure storage containers the basic carbon dioxide quantity shall be increased by 40 %, i.e. multiplied by a liquid efficiency factor of 1.4, as these containers discharge only about 70–75 % of their contents as liquid which is deemed, in local application, to be the effective part of the discharge.

Vaporization in Pipe System

Some carbon dioxide is vaporized in the pipe system at the start of discharge. The basic quantity of carbon dioxide must be augmented by the amount so vaporized which can be estimated as follows:

$$m_{CO2.V} = \frac{m_P C_P (T_1 - T_2)}{\Delta H_V} \tag{45.25}$$

where

C_P = specific heat of steel pipe, approximately 0.46 kJ/kg-K

ΔH_V = latent heat of vaporization of liquid CO_2 (149 kJ/kg for high-pressure storage and 279 kJ/kg for low-pressure storage)

$m_{CO2,V}$ = mass of CO2 evaporated in the pipe, kg

m_P = mass of pipe system, kg

T_1 = initial pipe temperature, °C

T_2 = average temperature of liquid CO_2 flowing in pipe, taken as 16 °C for high-pressure storage and −21 °C for low-pressure storage

Assuming that $T_1 = 20$ °C and average values of T_2 °C, the amount of CO_2 vaporized in a pipe system will be approximately:

$$m_{CO2,V} = 0.012 m_P \quad \text{high-pressure storage} \tag{45.26}$$

$$m_{CO2,V} = 0.0678 \cdot m_P \tag{45.27}$$

The total rate of discharge of a local-application system will be the sum of the individual discharge rate of all nozzles or other dispensing points in a system. The number of nozzles for a local application system is determined as described under *Nozzle coverage*, in the Rate-by-Area and Rate-by-Volume methods sections below.

Where part of a hazard is to be protected by total flooding and part by local application the following guidance applies:

The total-flooding design concentration must be achieved not later than the end of discharge for the local-application portion of the system.

The discharge rate for the total-flooding part shall be computed by dividing the quantity required for total flooding by the factor 1.4 and by the time of the local application discharge in minutes. Use the following equation:

$$w_{TF} = \frac{m_{TF}}{1.4 \cdot t_{LA}} \tag{45.28}$$

where

w_{TF} flow rate into total-flood part, kg/s

m_{TF} total quantity of CO2 for the total-flood part, kg

t_{LA} discharge time for local-application part, s

The duration of liquid discharge for computing the basic carbon dioxide quantity for a local-application system, or the local-application portion of a combined system, shall be at least 30 s. Where a liquid fuel has an auto-ignition temperature below its boiling point (e.g., cooking oils, paraffin waxes) the minimum discharge time shall be 3 min. Longer discharge times should

Table 45.23 Example nozzle coverage values

Coated surface		*Nozzle*[a]		*Liquid surface*	
Area, m^2	Side of square, m	Height, m	Flow rate, kg/min	Area, m^2	Side of square, m
1.29	1.14	0.75	16.99	0.92	0.96
1.51	1.22	1.00	21.69	1.08	1.03
1.72	1.31	1.25	27.20	1.22	1.11
1.95	1.39	1.50	32.57	1.38	1.17
2.16	1.46	1.75	37.80	1.53	1.23
2.36	1.53	2.00	42.99	1.68	1.29

[a]Refer to manufacturer's values for actual specific nozzles

be considered to compensate for hazard conditions that may require more time for them to be rendered ineffective as re-ignition sources. For example, additional time may be required to cool hot liquids or heated surfaces to at least 35 °C (95 °F) below the autoignition temperature of exposed flammable liquids or gases. In such cases an engineering analysis may be required to estimate cooling times.

Rate-by-Area Method

The rate-by-area method is used where the fire hazard is primarily characterized by flat surfaces or low-level objects. System designs are based on use of nozzles having approved area coverage based on location and height above the protected surface. Since each nozzle used in the rate-by-area or rate-by-volume method is used to protect a specific portion of a hazard, the flow rate through each nozzle must be within its listed and approved limits.

For each over-head nozzle, its discharge rate is based only on its location and distance from the hazard. The approved discharge rate is determined by testing to establish the design flow rate at which a nozzle should be used for the height at which it is installed above a liquid surface.

The carbon dioxide system manufacturer's manual will contain nozzle tables for each type of nozzle approved for use in local application extinguishing systems. Typically, each table will list a range of nozzle mounting heights. Table 45.23 shows typical format and coverage values for one nozzle type. For each height there will be a corresponding CO_2 flow rate, the maximum coverage area and "side-of-square" for liquid-surface and coated-surface fire hazards. "Side-of-square" is the width of a square corresponding to the allowed area coverage and represents the maximum distance between nozzles, or between rows of nozzles. Table 45.23 (illustrative only) shows how manufacturer's nozzle coverage data would typically be tabulated.

A system protecting multiple hazards can be designed to incorporate both local-application and total-flooding protection. The rate of discharge for the total-flooding portion shall be as described under *Rate of discharge* in the preceding total flooding section.

The discharge rate for a tank-side nozzle is based on its projection of CO_2 required to cover a protected surface. The approved discharge rate is determined by test. Fire tests are conducted to develop curves relating the maximum and minimum flow rates at which a nozzle can be used to the area of fire that the nozzle is capable of extinguishing, with additional limitations regarding maximum width of hazard and spacing requirements between nozzles and to the nearest corner of a hazard.

The rate-by-area method is used to protect fire hazards characterized predominantly by flat surfaces or low-level objects associated with horizontal surfaces. Examples include vats, drip trays, dip tanks, coated rollers or surfaces where liquid drains off and where the area of localized liquid pooling is less than 10 % of the protected area. The maximum area covered by a nozzle is based on its projection distance and maximum rated discharge rate. The shape of area covered by a nozzle is deemed to be square.

Where the area to be protected consists of coated surfaces, and where there is not a heavy accumulation of combustible residue, it is permissible to increase the maximum area coverage of a nozzle by 40 %.

Where a local application nozzle is used to project carbon dioxide across the face of an opening the maximum area coverage of the nozzle may be increased by 20 % over its rated value.

Where flammable liquids having depth are to be protected, a freeboard of at least 152 mm (6 in.) must be provided unless otherwise noted in the approved rating of a nozzle.

The number of nozzles used in an application shall be sufficient to cover the entire hazard area. Tank-side and linear nozzles shall be located within their approved spacing and discharge rate limits. Overhead nozzles must be mounted centered over and perpendicular to the covered hazard area. The nozzle height used to determine the flow rate is based on the distance from the nozzle face to the aiming point.

Nozzles may be installed in non-overhead locations. In such cases nozzles need may be aimed at an angle of 45°–90° (perpendicular) with respect to the plane of the hazard surface provided that the following conditions are met:

- The distance to the nozzle is measured to an aiming point at the near side of the protected area.
- The design area coverage for each nozzle is reduced from its approved rated value by an "aiming factor." See Table 45.24.
- The design nozzle area coverage is calculated as the product of the width of the protected area times the aiming factor.

The flow path from a nozzle to its protected hazard area must be unobstructed. Where an object protects above the protected surface, nozzles shall be arranged to cover the object with an extinguishing atmosphere. The effects of air currents in the protected area shall be compensated for by adjusting nozzle locations or extending the area of coverage beyond the perimeter of the hazard.

Table 45.24 Nozzle aiming factors [48]

Nozzle discharge angle[a]	Aiming factor[b]
45°–60°	0.25
60°–75°	0.25–0.375
75°–90°	0.375–0.50
90°	0.50

[a]From plane of hazard surface
[b]Fractional amount of nozzle area coverage

To summarize, the quantity of carbon dioxide required for a rate-by-area system can be calculated as follows (assuming initial pipe temperature of 20 °C, and average temperature of carbon dioxide liquid flowing in pipe system of 16 °C for high pressure systems and −21 °C for low pressure systems):

High-pressure storage :

$$m_D = 1.4\left[t_D \sum_i n_i w_i + 0.012 m_P\right] \tag{45.29}$$

Low-pressure storage :

$$m_D = \left[t_D \sum_i n_i w_i + 0.127 m_P\right] \tag{45.30}$$

where
n_i = number of nozzles with flow rate w_i
w_i = flow rate i, kg/min
t_D = liquid discharge time, at least 0.5 min
m_P = mass of pipe, kg

Example—Local Application Rate-by-Area Method Consider a quench tank measuring 5 m × 3 m with a 0.15 m free board as shown in Fig. 45.8. The fuel is quench oil. Nozzle heights are limited to 0.6–1.8 m above the liquid. Describe a high-pressure CO_2 system using 45.4 kg capacity cylinders, number type and arrangement of nozzle to protect the quench tank and a spillage perimeter that extends 0.6 m on all sides. Assume 30 s discharge time and a pipe system with a mass of 300 kg.

Hazard dimensions: length = 5 + 0.6 + 0.6 = 6.2 m ; width = 3 + 0.6 + 0.6 = 4.2 m ; area = (6.2)(4.2) = 26.0 m^2.

Nozzle height: initially select 1.5 m (this dimension is a design choice)

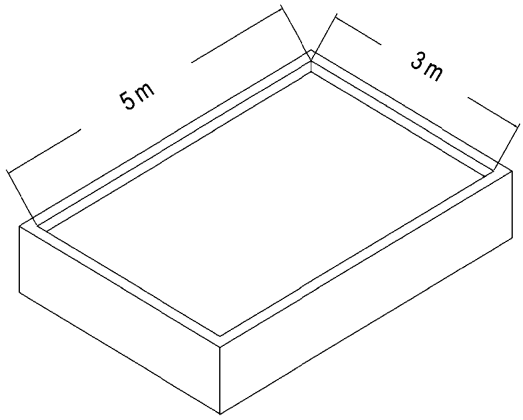

Fig. 45.8 3 m × 5 m quench tank

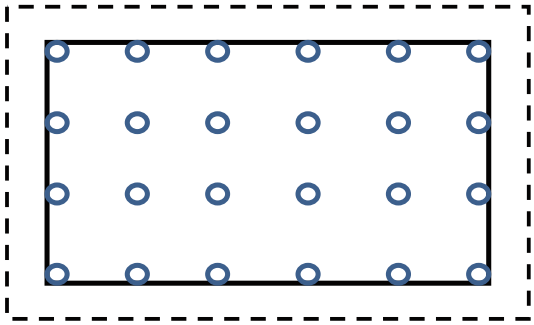

Fig. 45.9 Nozzle arrangement over quench tank hazard

Consult example nozzle table: Flow rate = 32.57 kg/min; side-of-square = 1.17 m

No. nozzle rows parallel to length = 4.2/1.17 = 3.6; round up to 4

No. nozzle rows parallel to width = 6.2/1.17 = 5.3; round up to 6

Total number nozzles = 4 × 6 = 24

CO_2 liquid flow rate = 24 × 32.57 = 781.7 kg/min

Quantity of CO_2: (a) Basic design quantity = rate of discharge x discharge time × high-pressure efficiency factor = 781.7 × 0.5 × 1.4 = 547.2 kg; (b) Quantity to compensate for pipe-cooling: (0.012 kg CO_2/kg-pipe) (300 kg) = 3.6 kg. Total CO_2 requirement = 561 kg. The number of cylinders = 561/45.4 = 12.1, round up to 13 cylinders. The nozzles can be arranged in four rows of six nozzles each centered over the hazard as illustrated in Fig. 45.9.

Rate-by-Volume Method

The rate-by-volume method is used where the fire hazard consists of three-dimensional irregularly shaped objects that cannot be reasonable represented as a simple equivalent surface. The total rate of discharge is based on the gross volume of a virtual hazard enclosure that extends at least 0.6 m beyond the lateral and vertical dimensions of the actual hazard, unless an actual wall or ceiling is closer, and which includes areas of possible spillage, splashing, or leakage. The smallest dimension of the virtual hazard is to be no less than 1.2 m. The floor beneath the virtual volume should be a uniformly closed surface and, if not, special provisions are required to account for openings. If the protected volume is subject to winds or drafts, the virtual hazard volume shall be increased to compensate for losses on the windward sides.

The total discharge rate for the basic system shall be equal to 16 kg/min · m^3 of virtual volume. The discharge rate may be reduced by as much as 12 kg/min · m^3 in proportion to the fraction of the perimeter of the virtual volume that consists of permanent and continuous walls that extend at least 0.6 m above the hazard, and provided that the walls are not actually part of the protected hazard. See Fig. 45.10.

The number of nozzles used to cover the entire protected hazard volume is based on the total discharge rate as determined by the assumed volume. Nozzles are located and aimed so as to promote retention of the discharged carbon dioxide within and throughout the virtual hazard volume to the extent possible and to compensate for the effects of air currents, winds, or forced drafts. The design discharge rates through individual nozzles shall be determined on the basis of location or projection distance in accordance with their approved use for surface fires.

The extinguishing system is to be designed for automatic operation except where the authorities having jurisdiction permit manual operation. The fire detection system should be designed to initiate discharge promptly after ignition to prevent excessive heating of materials within the hazard.

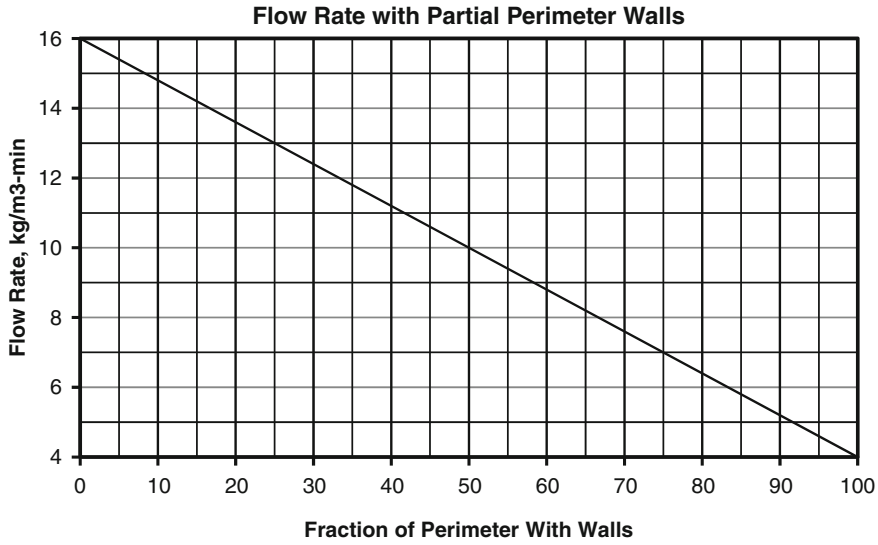

Fig. 45.10 Carbon dioxide flow rate with partial perimeter walls

The carbon dioxide supply should be located as close as practicable to the hazard while not exposing the equipment to a prospective fire. The pipeline should be as short and direct as practicable to minimize the time from cylinder actuation to the onset of carbon dioxide discharge into the protected space. Nozzles shall be used within their approved performance limits (flow rate, range, area coverage), and positioned and aimed in accordance with the system design requirements as previously described.

Example—Rate-by-Volume Method Consider protection of a diesel fuel pumping skid having an equipment arrangement with a footprint measuring 3 m by 4 m and an overall height of 3 m as illustrated in Fig. 45.11. The equipment is located on a solid floor and in a corner where two walls meet at 90°. The ceiling height is 5 m. The equipment is positioned so that each edge of the skid 1 m from a wall. The equipment is not enclosed on the other two sides. Determine the design quantity of carbon dioxide to be delivered from high-pressure storage for a rate-by-volume system assuming a virtual volume that includes the 1 m distance between the equipment and the two walls and a 0.6 m distances above the equipment and beyond the two unenclosed sides. Neglect the amount required to compensate for pipe cooling. The sketch below depicts (a) two confining walls; (b) the equipment volume surrounded by (c) the virtual design volume in dashed lines.

The size of the protected volume is L × W × H = (4 + 0.6 + 1) (3 + 0.6 + 1) (3 + 0.6) = 92.7 m^3. The protected perimeter is (2) [(4 + 0.6 + 1) + (3 + 0.6 + 1)] = 20.4 m. One-half of the protected perimeter, 10.2 m, consists of permanent and impermeable walls. As such, the basic discharge per unit volume can be reduced from 16 kg/min-m^3 by the amount (½) (12 kg/min-m^3) = 6 kg/min-m^3. Thus, the design rate of liquid CO_2 discharge is (92.7 m^3) ([16 – 6] kg/min-m^3) = 927 kg/min. The duration of liquid discharge is 30 s. The total design quantity of CO_2 = rate of discharge × discharge time × high-pressure efficiency factor = 927 × 0.5 × 1.4 = 649 kg. The number of 45.4 kg high-pressure CO_2 cylinders is 649/45.4 = 14.3, rounded up to 15 cylinders.

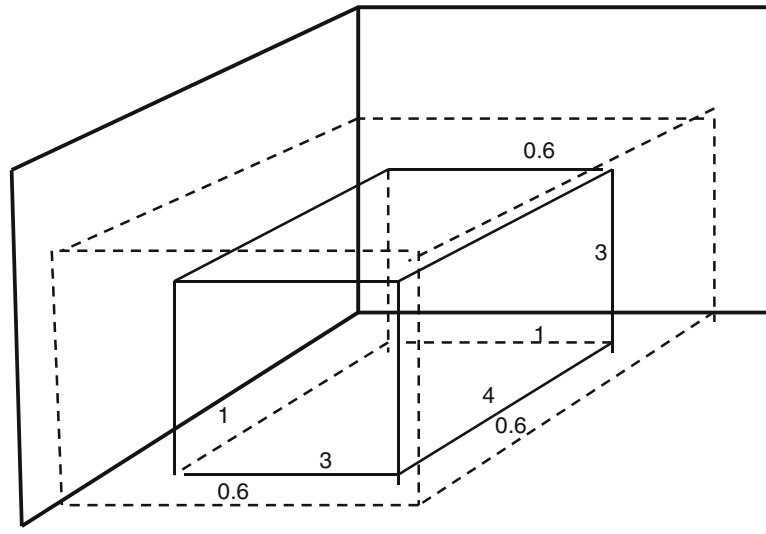

Fig. 45.11 Representation of three-dimensional hazard including virtual boundaries

Carbon Dioxide Hydraulic Calculations to Estimate Nozzle Pressure

Pipeline Pressure Loss due to Flow

A carbon dioxide fire extinguishing system is designed to discharge a certain quantity of carbon dioxide through one or more nozzles within a specified time period as determined by a total flooding or local application system design approach. Each nozzle in a system is selected based on its design flow rate at the average anticipated discharge pressure. The flow rate of carbon dioxide through a nozzle, Q_{NOZ}, is calculated as the product of the mass flow rate per unit of orifice area of the nozzle, i.e. the orifice mass flux, G, times the equivalent nozzle orifice area, A_{NOZ} as indicated in Equation 45.31.

$$Q_{NOZ} = G \cdot A_{NOZ} \qquad (45.31)$$

The equivalent orifice area of a given manufacturer's nozzle is determined through testing. The carbon dioxide orifice mass flux, G, varies depending on the average fluid density which, in turn, depends on the pressure at the discharge outlet. Values of G are tabulated as a function of pressure in Table 45.25.

The design challenge, therefore, is to determine the effective average pressure at each nozzle during discharge. Commercial computer programs are available for facilitating the design and layout of carbon dioxide pipe distribution systems. These programs calculate pressures at key nodes of a pipe network, optimize the pipe-size, nozzle sizes, and determine the mass of liquid and vapor discharged at each nozzle. Flow calculation routines are usually based on, or are at least benchmarked against, the method described in NFPA 12, Annex C. The same method is also documented in ISO 6183 [35]. The following describes how to use the NFPA 12 carbon dioxide flow equation to calculate pressure loss in a pipeline and select nozzle sizes.

As noted previously, carbon dioxide is stored as a liquefied compressed gas in either refrigerated low-pressure tanks, maintained at about −18 °C (0 °F), or in high-pressure cylinders stored at ambient temperatures. Upon discharge, carbon dioxide flows into a pipe system that terminates at one or more nozzles. The average pressure at any point in the pipe system is governed by conservation equations of momentum and energy. The momentum equation relates pressure changes to changes in fluid

Table 45.25 Discharge rate per unit of orifice area

Low-pressure storage				High-pressure storage			
Orifice pressure, psi	G, lb/min-in.^{2}	Orifice pressure, Pa	G, kg/min-mm^2	Orifice pressure, psi	G, lb/min-in.^{2}	Orifice pressure, Pa	G, kg/min-mm^2
300	4220	2068	2.970	750	4630	5171	3.258
290	2900	1999	2.041	725	3845	4999	2.706
280	2375	1931	1.671	700	3415	4826	2.403
270	2050	1862	1.443	675	3090	4654	2.174
260	1825	1793	1.284	650	2835	4481	1.995
250	1655	1724	1.165	625	2615	4309	1.840
240	1525	1655	1.073	600	2425	4137	1.706
230	1410	1586	0.992	575	2260	3964	1.590
220	1305	1517	0.918	550	2115	3792	1.488
210	1210	1448	0.851	525	1985	3620	1.397
200	1125	1379	0.792	500	1860	3447	1.309
190	1048	1310	0.737	475	1740	3275	1.224
180	977	1241	0.688	450	1620	3103	1.140
170	912	1172	0.642	425	1510	2930	1.063
160	852	1103	0.600	400	1400	2758	0.985
150	795	1034	0.559	375	1290	2586	0.908
				350	1180	2413	0.830
				325	1080	2241	0.760
				300	980	2068	0.690

This table combines the data presented in Tables 4.7.5.2.1 and 4.7.5.3.1 from NFPA 12 [34]

density and friction loss along the pipe network. The energy equation accounts for heat exchange between carbon dioxide and the pipe system, particularly during initial flow when the pipe system is cooled to the fluid temperature. Vapor-liquid equilibrium is assumed to prevail everywhere in the pipe system.

The momentum equation is presented as:

$$dp + d\left(\rho u^2\right) + \tfrac{1}{2}\rho u^2 f \cdot \frac{dx}{D} = 0 \qquad (45.32)$$

Here p is pressure, u is velocity, ρ is density, x is distance, D is the internal pipe diameter, and f is the Darcy-Weisbach friction factor. The first term on the left is the pressure change over distance dx; the second term accounts for pressure change due to variations in the fluid density and velocity (e.g. acceleration as liquid vaporizes); and the third term accounts for pressure loss due to friction effects with the pipe wall. The friction factor is a non-linear function of the degree of turbulence in the flow, characterized by the Reynolds number, Re, which is equal to $\rho Du/\mu$, where μ is viscosity, and on the surface roughness, ε, of the pipe [49]. At very high Reynolds numbers the value of f is insensitive to changes in u, ρ, and μ. In this flow regime f is effectively a function of ε and D only. The applicable friction factor relations are assumed to apply during system discharge for three common types of pipe used in carbon dioxide systems:

Uncoated steel pipe	$f = 0.0227\ D^{-0.25}$
Galvanized pipe	$f = 0.032\ D^{-0.35}$
Drawn tubing	$f = 0.011\ D^{-0.117}$

where D is in inches.

The solution of Equation 45.32 over a defined pipe length, L, yields the following governing flow equations for each type of pipe:

$$\text{Uncoated steel pipe} \quad Q^2 = \frac{3647 \cdot YD^{5.25}}{L + 8.08D^{1.25}Z} \qquad (45.33a)$$

$$\text{Galvanized pipe} \quad Q^2 = \frac{2586 \cdot YD^{5.35}}{L + 5.72D^{1.35}Z} \tag{45.33b}$$

$$\text{Drawn tubing} \quad Q^2 = \frac{7524 \cdot YD^{5.117}}{L + 16.66D^{1.117}Z} \tag{45.33c}$$

Where Q is mass flow rate (lb/min), D is inside pipe diameter (in), and L is the equivalent pipe length (ft). Values of Y and Z are non-linear functions of pressure and density defined as follows:

$$Y = -\int_{Po}^{P} \rho dP \tag{45.34}$$

$$Z = -\int_{\rho o}^{\rho} \frac{d\rho}{\rho} \tag{45.35}$$

The values of Y and Z are functions of pressure that depend on the storage method of the carbon dioxide supply which is either as a refrigerated low-vapor pressure liquid or as an ambient-temperature high-vapor pressure liquid. Values of pressure (averaged over the period of discharge) along a pipe system are determined by solving Equations 45.34 and 45.35 for Y and Z and then looking up the corresponding value of pressure in Tables 45.26 and 45.27.[1]

In practice a pipe network is evaluated in sections. A section may be as small as a single pipe fitting or length of pipe, or may consist of multiple lengths of pipe and fittings so long as the pipe diameter is constant. The equivalent length, L, of a section of a pipe system is the sum of the lengths of the included pipe sections and all fittings or flow devices such as valves. Values of equivalent length of manufacturer-supplied components (cylinder discharge valves, check valves, etc.) are determined by testing. Corrections to pressure are made to account for changes in pipe elevation. Values of pipe diameters, equivalent length of standard pipe fittings, and elevation pressure correction factors are indicated in the Tables 45.28, 45.29, 45.30 and 45.31.

Nozzle Selection

A manufacturer's nozzle is characterized by an "equivalent single orifice area" regardless of the actual number of orifices it contains. The standard "Orifice Code No." is equal to the diameter, in increments of 1/32 in., of the equivalent single orifice.

- Orifice Codes 1 to 9.5 are in size increments of 0.5
- Orifice Codes 10 to 64 are in size increments of 1

For example, a nozzle having an equivalent single orifice area of 0.0431 in.^{2} has an equivalent diameter of 15/64 in., or 7.5/32 in., therefore the Orifice Code No. is 7.5. In a design application where a calculated orifice size falls between two standard sizes, choose the nearest size unless the applicable flow rate requirement is a minimum value, in which case choose the next larger size.

Estimation of Nozzle Pressure

The choice of nozzle depends on the estimated value of average pressure at the nozzle. Commercially available computer programs are able to perform the associated calculations to determine average nozzle pressures for complex piping arrangement. While somewhat tedious, the associated calculations can be performed by hand or with the use of a spreadsheet. The procedure for performing hand or spreadsheet calculations is described below.

Calculation of pressure along a pipe network is carried out by solving Equation 45.33 in a stepwise manner, i.e. node-to-node. Here, a node is any component junction and includes: cylinder siphon tube entrance, cylinder valve exit, flex-hose to valve, flex-hose to manifold tee, tee to

[1] Tables 45.26 and 45.27 are expanded versions, in 1 psi pressure increments, of Tables C.1 (a) and C.1 (b) from NFPA 12 [34].

Table 45.26 *Y* and *Z* factors vs. P for 300 psi systems

P, psi	Z	Y	P, psi	Z	Y	P, psi	Z	Y	P, psi	Z	Y
300	0.000	0	260	0.505	1989	220	0.950	3228	180	1.384	4030
299	0.014	63	259	0.517	2027	219	0.961	3253	179	1.395	4046
298	0.027	126	258	0.528	2065	218	0.971	3277	178	1.407	4062
297	0.041	187	257	0.540	2102	217	0.982	3301	177	1.418	4077
296	0.054	248	256	0.551	2139	216	0.993	3325	176	1.429	4093
295	0.068	308	255	0.563	2176	215	1.004	3349	175	1.441	4108
294	0.081	367	254	0.574	2212	214	1.014	3372	174	1.452	4123
293	0.095	426	253	0.586	2248	213	1.025	3395	173	1.463	4138
292	0.108	483	252	0.597	2283	212	1.036	3418	172	1.474	4152
291	0.122	540	251	0.609	2318	211	1.046	3440	171	1.486	4167
290	0.135	596	250	0.620	2352	210	1.057	3462	170	1.497	4181
289	0.148	652	249	0.631	2386	209	1.068	3485	169	1.509	4196
288	0.161	706	248	0.642	2420	208	1.079	3506	168	1.520	4210
287	0.174	760	247	0.654	2454	207	1.089	3528	167	1.532	4223
286	0.187	814	246	0.665	2487	206	1.100	3549	166	1.543	4237
285	0.200	866	245	0.676	2519	205	1.111	3570	165	1.555	4251
284	0.212	918	244	0.687	2552	204	1.122	3591	164	1.566	4264
283	0.225	969	243	0.698	2583	203	1.133	3612	163	1.578	4277
282	0.238	1020	242	0.710	2615	202	1.143	3632	162	1.589	4291
281	0.251	1070	241	0.721	2646	201	1.154	3653	161	1.601	4303
280	0.264	1119	240	0.732	2677	200	1.165	3673	160	1.612	4316
279	0.276	1168	239	0.743	2708	199	1.176	3692	159	1.624	4329
278	0.289	1216	238	0.754	2738	198	1.187	3712	158	1.636	4341
277	0.301	1263	237	0.765	2768	197	1.198	3731	157	1.648	4354
276	0.313	1310	236	0.776	2797	196	1.209	3750	156	1.660	4366
275	0.326	1357	235	0.787	2826	195	1.220	3769	155	1.672	4378
274	0.338	1402	234	0.797	2855	194	1.230	3788	154	1.683	4390
273	0.350	1448	233	0.808	2884	193	1.241	3807	153	1.695	4402
272	0.362	1492	232	0.819	2912	192	1.252	3825	152	1.707	4413
271	0.375	1536	231	0.830	2940	191	1.263	3843	151	1.719	4425
270	0.387	1580	230	0.841	2968	190	1.274	3861	150	1.731	4436
269	0.399	1623	229	0.852	2995	189	1.285	3879			
268	0.411	1666	228	0.863	3022	188	1.296	3896			
267	0.422	1708	227	0.874	3049	187	1.307	3914			
266	0.434	1749	226	0.885	3075	186	1.318	3931			
265	0.446	1790	225	0.896	3102	185	1.329	3948			
264	0.458	1831	224	0.906	3128	184	1.340	3965			
263	0.470	1871	223	0.917	3153	183	1.351	3981			
262	0.481	1911	222	0.928	3179	182	1.362	3998			
261	0.493	1950	221	0.939	3204	181	1.373	4014			
260	0.505	1989	220	0.950	3228	180	1.384	4030			

Table 45.27 *Y* and *Z* factors vs. P for 750 psi systems

P, psi	Z	Y	P, psi	Z	Y	P, psi	Z	Y	P, psi	Z	Y
750	0	0	690	0.205	2733	630	0.393	4993	570	0.609	6840
749	0.004	51	689	0.208	2774	629	0.396	5027	569	0.613	6868
748	0.008	101	688	0.211	2815	628	0.400	5061	568	0.616	6895
747	0.011	151	687	0.214	2856	627	0.403	5095	567	0.620	6922
746	0.015	201	686	0.217	2897	626	0.407	5129	566	0.624	6949
745	0.019	251	685	0.220	2937	625	0.410	5162	565	0.628	6976
744	0.023	300	684	0.223	2978	624	0.413	5196	564	0.631	7003
743	0.027	350	683	0.226	3018	623	0.417	5229	563	0.635	7030
742	0.030	399	682	0.229	3059	622	0.420	5263	562	0.639	7057
741	0.034	448	681	0.232	3099	621	0.424	5296	561	0.642	7084
740	0.038	497	680	0.235	3139	620	0.427	5329	560	0.646	7110
739	0.042	545	679	0.238	3179	619	0.431	5362	559	0.650	7137
738	0.045	594	678	0.241	3219	618	0.434	5395	558	0.653	7163
737	0.049	642	677	0.244	3259	617	0.438	5427	557	0.657	7190
736	0.053	690	676	0.247	3298	616	0.441	5460	556	0.661	7216
735	0.057	738	675	0.250	3338	615	0.445	5493	555	0.665	7242
734	0.060	786	674	0.253	3377	614	0.448	5525	554	0.668	7268
733	0.064	833	673	0.256	3416	613	0.452	5557	553	0.672	7294
732	0.068	881	672	0.259	3455	612	0.455	5589	552	0.676	7320
731	0.071	928	671	0.262	3494	611	0.459	5621	551	0.679	7345
730	0.075	975	670	0.265	3533	610	0.462	5653	550	0.683	7371
729	0.079	1022	669	0.268	3572	609	0.466	5685	549	0.687	7396
728	0.082	1068	668	0.271	3611	608	0.469	5717	548	0.690	7422
727	0.086	1115	667	0.274	3649	607	0.473	5749	547	0.694	7447
726	0.089	1161	666	0.277	3688	606	0.476	5780	546	0.697	7472
725	0.093	1208	665	0.281	3726	605	0.480	5811	545	0.701	7498
724	0.096	1254	664	0.284	3764	604	0.484	5843	544	0.705	7523
723	0.100	1299	663	0.287	3802	603	0.487	5874	543	0.708	7548
722	0.103	1345	662	0.290	3840	602	0.491	5905	542	0.712	7572
721	0.107	1391	661	0.293	3878	601	0.494	5936	541	0.715	7597
720	0.11	1436	660	0.296	3916	600	0.498	5967	540	0.719	7622
719	0.113	1481	659	0.299	3953	599	0.502	5997	539	0.723	7647
718	0.117	1527	658	0.302	3991	598	0.505	6028	538	0.726	7671
717	0.120	1572	657	0.305	4028	597	0.509	6058	537	0.730	7696
716	0.123	1616	656	0.308	4065	596	0.513	6089	536	0.734	7720
715	0.127	1661	655	0.312	4102	595	0.517	6119	535	0.738	7744
714	0.130	1706	654	0.315	4139	594	0.520	6149	534	0.741	7768
713	0.133	1750	653	0.318	4176	593	0.524	6179	533	0.745	7792
712	0.136	1794	652	0.321	4213	592	0.528	6209	532	0.749	7816
711	0.140	1838	651	0.324	4250	591	0.531	6239	531	0.752	7840
710	0.143	1882	650	0.327	4286	590	0.535	6268	530	0.756	7864
709	0.146	1926	649	0.330	4323	589	0.539	6298	529	0.760	7888
708	0.149	1970	648	0.334	4359	588	0.542	6328	528	0.763	7911
707	0.152	2013	647	0.337	4395	587	0.546	6357	527	0.767	7935
706	0.155	2057	646	0.340	4431	586	0.550	6386	526	0.770	7958
705	0.159	2100	645	0.344	4467	585	0.554	6415	525	0.774	7982
704	0.162	2143	644	0.347	4503	584	0.557	6444	524	0.778	8005
703	0.165	2186	643	0.350	4539	583	0.561	6473	523	0.781	8028

(continued)

Table 45.27 (continued)

P, psi	Z	Y	P, psi	Z	Y	P, psi	Z	Y	P, psi	Z	Y
702	0.168	2229	642	0.353	4575	582	0.565	6502	522	0.785	8052
701	0.171	2271	641	0.357	4610	581	0.568	6531	521	0.788	8075
700	0.174	2314	640	0.36	4645	580	0.572	6560	520	0.792	8098
699	0.177	2357	639	0.363	4681	579	0.576	6588	519	0.796	8120
698	0.180	2399	638	0.367	4716	578	0.579	6616	518	0.799	8143
697	0.183	2441	637	0.370	4751	577	0.583	6645	517	0.803	8166
696	0.186	2483	636	0.373	4786	576	0.587	6673	516	0.806	8189
695	0.190	2525	635	0.377	4821	575	0.591	6701	515	0.810	8211
694	0.193	2567	634	0.380	4855	574	0.594	6729	514	0.813	8234
693	0.196	2608	633	0.383	4890	573	0.598	6757	513	0.817	8256
692	0.199	2650	632	0.386	4924	572	0.602	6785	512	0.820	8278
691	0.202	2691	631	0.390	4959	571	0.605	6812	511	0.824	8301
690	0.205	2733	630	0.393	4993	570	0.609	6840	510	0.827	8323
510	0.827	8323	450	1.038	9520	390	1.262	10,486	330	1.518	11,247
509	0.831	8345	449	1.042	9538	389	1.266	10,501	329	1.523	11,258
508	0.834	8367	448	1.045	9556	388	1.270	10,515	328	1.527	11,269
507	0.838	8389	447	1.049	9574	387	1.274	10,529	327	1.532	11,280
506	0.841	8411	446	1.052	9592	386	1.278	10,543	326	1.536	11,291
505	0.845	8433	445	1.056	9609	385	1.282	10,557	325	1.541	11,302
504	0.849	8454	444	1.059	9627	384	1.286	10,571	324	1.546	11,313
503	0.852	8476	443	1.063	9644	383	1.290	10,585	323	1.550	11,323
502	0.856	8497	442	1.066	9662	382	1.294	10,599	322	1.555	11,334
501	0.859	8519	441	1.070	9680	381	1.298	10,613	321	1.559	11,345
500	0.863	8540	440	1.073	9697	380	1.302	10,627	320	1.564	11,356
499	0.867	8562	439	1.077	9714	379	1.306	10,641	319	1.569	11,366
498	0.870	8583	438	1.080	9731	378	1.310	10,654	318	1.573	11,377
497	0.874	8604	437	1.084	9748	377	1.315	10,668	317	1.578	11,387
496	0.877	8625	436	1.087	9765	376	1.319	10,681	316	1.582	11,398
495	0.881	8646	435	1.091	9782	375	1.323	10,695	315	1.587	11,408
494	0.884	8667	434	1.095	9799	374	1.327	10,708	314	1.592	11,418
493	0.888	8688	433	1.098	9816	373	1.331	10,722	313	1.596	11,428
492	0.891	8709	432	1.102	9833	372	1.336	10,735	312	1.601	11,439
491	0.895	8730	431	1.105	9850	371	1.340	10,749	311	1.605	11,449
490	0.898	8750	430	1.109	9866	370	1.344	10,762	310	1.61	11,459
489	0.902	8771	429	1.113	9883	369	1.348	10,775	309	1.615	11,469
488	0.905	8791	428	1.116	9900	368	1.352	10,788	308	1.619	11,469
487	0.909	8812	427	1.120	9916	367	1.357	10,801	307	1.624	11,479
486	0.912	8832	426	1.124	9933	366	1.361	10,814	306	1.629	11,499
485	0.916	8852	425	1.128	9949	365	1.365	10,827	305	1.634	11,509
484	0.919	8873	424	1.131	9966	364	1.369	10,840	304	1.638	11,519
483	0.923	8893	423	1.135	9982	363	1.373	10,853	303	1.643	11,529
482	0.926	8913	422	1.139	9998	362	1.378	10,866	302	1.648	11,539
481	0.930	8933	421	1.142	10,014	361	1.382	10,878	301	1.652	11,548
480	0.933	8953	420	1.146	10,030	360	1.386	10,891	300	1.657	11,558
479	0.936	8973	419	1.150	10,046	359	1.390	10,904			
478	0.940	8993	418	1.154	10,062	358	1.395	10,916			
477	0.943	9012	417	1.157	10,078	357	1.399	10,929			
476	0.947	9032	416	1.161	10,094	356	1.403	10,941			

(continued)

Table 45.27 (continued)

P, psi	Z	Y	P, psi	Z	Y	P, psi	Z	Y	P, psi	Z	Y
475	0.950	9052	415	1.165	10,110	355	1.408	10,954			
474	0.953	9071	414	1.169	10,126	354	1.412	10,966			
473	0.957	9091	413	1.173	10,141	353	1.416	10,978			
472	0.960	9110	412	1.176	10,157	352	1.420	10,991			
471	0.964	9129	411	1.180	10,173	351	1.425	11,003			
470	0.967	9149	410	1.184	10,188	350	1.429	11,015			
469	0.971	9168	409	1.188	10,204	349	1.433	11,027			
468	0.974	9187	408	1.192	10,219	348	1.438	11,039			
467	0.978	9206	407	1.195	10,234	347	1.442	11,051			
466	0.981	9225	406	1.199	10,250	346	1.447	11,063			
465	0.985	9244	405	1.203	10,265	345	1.451	11,075			
464	0.988	9263	404	1.207	10,280	344	1.455	11,087			
463	0.992	9282	403	1.211	10,295	343	1.460	11,099			
462	0.995	9301	402	1.214	10,310	342	1.464	11,110			
461	0.999	9319	401	1.218	10,325	341	1.469	11,122			
460	1.002	9338	400	1.222	10,340	340	1.473	11,134			
459	1.006	9356	399	1.226	10,355	339	1.478	11,145			
458	1.009	9375	398	1.230	10,370	338	1.482	11,157			
457	1.013	9393	397	1.234	10,385	337	1.487	11,168			
456	1.016	9412	396	1.238	10,399	336	1.491	11,180			
455	1.020	9430	395	1.242	10,414	335	1.496	11,191			
454	1.024	9448	394	1.246	10,429	334	1.500	11,202			
453	1.027	9466	393	1.250	10,443	333	1.505	11,214			
452	1.031	9484	392	1.254	10,458	332	1.509	11,225			
451	1.034	9502	391	1.258	10,472	331	1.514	11,236			
450	1.038	9520	390	1.262	10,486	330	1.518	11,247			

pipe, pipe to elbow, pipe to nozzle, etc. Pressure change calculations can be performed at each node or for a pipe segment between several nodes involving the same pipe diameter.

The procedure uses a variant of Equation 45.33 as follows:

$$\frac{L}{D^d} - \frac{a \cdot Y}{\left(\frac{Q}{D^{(b-d)/2}}\right)^2} + c \cdot Z = 0 \qquad (45.36)$$

The constants a, b, c and d for the different types of pipe are shown in the Table 45.32.

For uncoated steel pipe (sometimes called "black" pipe), Equation 45.36 becomes

$$\frac{L}{D^{1.25}} - \frac{3647 \cdot Y}{\left(\frac{D}{D^2}\right)^2} + 8.08Z = 0 \qquad (45.37)$$

In a given pipe section the total equivalent length, L, the flow rate Q, and diameter, D, are known. The terms Y and Z are functions of pressure (tabulated in Tables 45.26 and 45.27). The end-of-segment pressure, P, having Y and Z values that make the left-hand side (LHS) of Equation 45.37 equal to zero is the solution.

The hand or spreadsheet calculation procedure can be performed as follows:

1. Create a sketch of the required pipe system layout showing the carbon dioxide supply (one or more high-pressure cylinders or a low-pressure tank), discharge manifold, pipe type, size and length, elevation changes, fittings (elbows, tees, check valves, etc.). Label all the nodes at which pressure will be calculated as illustrated in Fig. 45.12.

Table 45.28 Size data for ANSI steel pipe

Nominal size, in.	Pipe schedule	D, in.	$D^{1.25}$	D^2
1/4	40	0.364	0.2827	0.1325
3/8	40	0.493	0.4131	0.2430
1/2	40	0.622	0.5524	0.3869
3/4	40	0.824	0.7851	0.6790
1/4	80	0.302	0.2239	0.0912
3/8	80	0.423	0.3411	0.1789
1/2	80	0.546	0.4693	0.2981
3/4	80	0.742	0.6887	0.5506
1	80	0.957	0.9465	0.9158
1–1/4	80	1.278	1.3588	1.6333
1–1/2	80	1.500	1.6600	2.2500
2	80	1.939	2.2881	3.7597
2–1/2	80	2.323	2.8679	5.3963
3	80	2.900	3.7844	8.4100
4	80	3.826	5.3510	14.6383
5	80	4.813	7.1289	23.1650
6	80	5.761	8.9253	33.1891
7	80	6.625	10.6288	43.8906
8	80	7.625	12.6707	58.1406

2. Set up a table to capture data for each pipe segment as indicated in Table 45.33.
3. Determine the equivalent length, L, between nodes. This is the sum of (1) actual pipe length, (2) equivalent length of fittings in the flow path,[2] and (3) the equivalent length of the pipe system upstream of the section being evaluated. "Up-stream" equivalent length is calculated as follows:

$$L = \frac{a \cdot YD^b}{Q^2} - c \cdot D^d Z \qquad (45.38)$$

Where the values of D and Q are for the pipe segment being evaluated and the values of Y and Z are those of the exit end of the previous pipe segment. Values of a, b, and c are indicated in Table 45.32. The remaining steps indicate how the values for D, Q, Y and Z are determined.

4. Specify the quantity of carbon dioxide liquid to be discharged from each nozzle. For high-pressure cylinders, the total carbon dioxide supply is 140 % of the required liquid quantity.
5. Specify the required liquid discharge time in accordance with the requirements of the design approach and applicable standard..
6. The flow rate, Q, in a pipe segment is the liquid quantity passing through the pipe segment divided by the discharge time.
7. Enter data for pipe system components (D, L, fitting equivalent lengths), and segment flow rates, Q.
8. Segment inlet pressure. For first segment use the supply pressure (750 or 300 psi). Otherwise use exit pressure from prior segment.
9. Segment exit pressure, Y, and Z are determined by determining values of Y and Z that satisfy Equation 45.36. Approaches using trial-and-error and spreadsheet methods are described.
   (a) Calculation by trial-and-error approach. Guess a pressure, P, then look up the corresponding values of Y and Z in Table 45.26 and 45.27. Calculate the value of the left-hand side (LHS) of Equation 45.36. If the result is greater than zero then make a second guess at a lower pressure. If the result is less than zero then make a second guess at a higher pressure.
   (b) Spreadsheet calculation approach.
      (i) Prepare lookup table
         1. Copy, in columns 2, 3, and 4 the table of P, Y, and Z to an area of spread sheet.
         2. In column 1 enter Equation 45.36 (in form for pipe type) with reference to the values of Q, D, and L for the segment and to values of Y and Z in col. 3 and 4. Copy equation to each cell in column 1 for this table.
         3. The calculated values in column 1, the "residue," decrease progressively from the 750 psi row (or 300 psi row) from positive to negative numbers.

[2] The equivalent lengths of the custom components (cylinder valve, hose, check valves) must be obtained from the manufacturer.

Table 45.29 Equivalent length of threaded pipe fittings

Pipe size, in.	Std 45 elbow	Std 90 elbow	90° long radius elbow and thru tee	Side tee	Gate valve and union coupling
3/8	0.6	1.3	0.8	2.7	0.3
½	0.8	1.7	1.0	3.4	0.4
¾	1.0	2.2	1.4	4.5	0.5
1	1.3	2.8	1.8	5.7	0.6
1¼	1.7	3.7	2.3	7.5	0.8
1½	2.0	4.3	2.7	8.7	0.9
2	2.6	5.5	3.5	11.2	1.2
2½	3.1	6.6	4.1	13.4	1.4
3	3.8	8.2	5.1	16.6	1.8
4	5.0	10.7	6.7	21.8	2.4
5	6.3	13.4	8.4	27.4	3.0
6	7.6	16.2	10.1	32.8	3.5

Table 45.30 Equivalent length of welded pipe fittings

Pipe size, in.	Std 45° elbow	Std 90° elbow	90° Long-radius elbow and thru tee	Side tee	Gate valve and union coupling
3/8	0.2	0.7	0.5	1.6	0.3
½	0.3	0.8	0.7	2.1	0.4
¾	0.4	1.1	0.9	2.8	0.5
1	0.5	1.4	1.1	3.5	0.6
1¼	0.7	1.8	1.5	4.6	0.8
1½	0.8	2.1	1.7	5.4	0.9
2	1.0	2.8	2.2	6.9	1.2
2½	1.2	3.3	2.7	8.2	1.4
3	1.8	4.1	3.3	10.2	1.8
4	2.0	5.4	4.4	13.4	2.4
5	2.5	6.7	5.5	16.8	3.0
6	3.0	8.1	6.6	20.2	3.5

Table 45.31 Pressure correction factors for pipe elevation changes

300 psi systems		750 psi systems	
Average line pressure, psi	Elevation pressure correction, psi/ft	Average line pressure, Psi	Elevation pressure correction, psi/ft
300	0.443	750	0.352
280	0.343	700	0.300
260	0.265	650	0.255
240	0.207	600	0.215
220	0.167	550	0.177
200	0.134	500	0.150
180	0.107	450	0.125
160	0.085	400	0.105
140	0.067	350	0.085
		300	0.070

4. By inspection, identify the table row and P value where the residue changes from positive to negative. Interpolate to find the exact value of P where the residue is zero. This is the solution for the given pipe segment.

(ii) Set up spreadsheet table. Referring to example below:

1. Col. 1–9. Pipe segment data.
2. Col. 10–12. Segment equivalent length.
3. Col. 13. Segment inlet pressure.
4. Col. 14. Segment exit pressure due to flow (not elevation-corrected). Determined from the Lookup Table described above.
5. Col. 15. Calculate pressure correction to account for elevation change.
6. Col. 16. Calculate exit pressure (Col. 14 + Col. 15).
7. Col 17–18. Lookup segment exit values of Y and Z, needed calculate the Upstream Equivalent Length in next pipe segment.

While rather complex, the procedures strictly follow the NFPA 12 method and yield results as accurate as the overall method allows.

Example Consider a system that is required to discharge 71.4 lb of carbon dioxide liquid from each of two nozzles in the balanced pipe system shown in the figure. The carbon dioxide supply is two 100 lb high-pressure cylinders. The required quantity of carbon dioxide is $2 \times 71.4 \times 140\ \% = 200$ lb. The carbon dioxide supply is two 100 lb high-pressure cylinders. The liquid discharge time is 30 s. This example shows the design input and calculation results for a balanced two-nozzle high-pressure carbon dioxide system. Use the pipe segment sizes shown in Table 45.33.

Nozzle Selection In this example, nozzle pressure at Nodes 8 and 10 is 554.7 psi. The corresponding mass flux, G, interpolated from

Table 45.32 Pipe flow pressure constants

Pipe type	a	b	c	d
Uncoated steel	3647	5.25	8.08	1.25
Galvanized	2586	5.35	5.72	1.35
Drawn tubing	7524	5.117	16.66	1.117

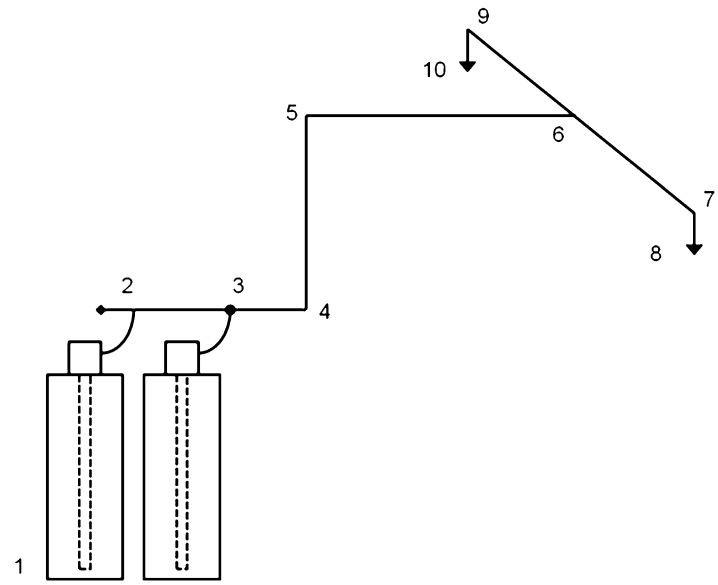

Fig. 45.12 High pressure, 2-nozzle, balanced CO_2 system

Table 45.33 Seven-segment calculation—cylinder and every pipe section

Segment nodes		Flow	Segment parts description					Elev.
1	2	3	4	5	6	7	8	9
Inlet	Exit	Q, lb/min	Segment parts[a]	Pipe size, in.	Pipe Sch	Pipe ID, in.	Pipe L, ft	Elev chng, dh, ft
1	2	142.8	VH	1/2	40	0.622	0	6.28
2	3	142.8	ST; 1/2″P	1/2	40	0.622	1	0
3	4	285.6	TT; 3/4″P	3/4	40	0.824	3	0
4	5	285.6	EL; 3/4″P	3/4	40	0.824	12	12
5	6	285.6	EL; 3/4″P	3/4	40	0.824	30	0
6	7	142.8	ST; 1/2″P	1/2	40	0.622	14	0
7	8	142.8	EL; 1/2″P	1/2	40	0.622	1	−1
6	9	142.8	See 6–7					
9	10	142.8	See 7–8					

[a]Parts: *VH* cylinder valve & hose, *ST* side tee, *TT* thru-tee, *EL* elbow, *P* pipe

Segment nodes		Equivalent flow length			Inlet P	P_{Flow}	Elevation	Segment exit P, Y, Z		
1	2	10	11	12	13	14	15	16	17	18
Inlet	Exit	Fitting equiv L, ft	Up-stream Eq. Len, ft	Total equiv L, ft	Inlet P, psi	Unadjusted exit P, psi	ΔP due to elev. psi	Exit P, psi	Exit Y	Exit Z
1	2	30	0	30.0	750	705.6	−1.92	703.7	2156	0.163
2	3	3.4	31.2	35.6	703.7	696.5	0.00	696.5	2462	0.185
3	4	1.4	38.7	43.1	696.5	689.7	0.00	689.7	2745	0.206
4	5	2.2	43.1	57.3	689.7	667.0	−3.23	663.8	3772	0.284
5	6	2.2	59.2	91.4	663.8	604.2	0.00	604.2	5837	0.483
6	7	3.4	84.2	101.6	604.2	561.8	0.00	561.8	7062	0.639
7	8	1.7	101.6	104.3	561.8	**554.5**	0.18	554.7	7250	0.666

Table 45.25, is 2142 lb/in.^{2}-min. The required flow rate is 142.8 lb/min. A nozzle having an equivalent area of (142.8 lb/min)/(2142 lb/in.^{2}-min) = 0.0667 in.^{2} is required. The corresponding equivalent orifice diameter is 0.291 (9.32-32nd) inch for which the nearest Nozzle Orifice Code is 9.5.

The preceding calculation shows how each of the seven segments of the example carbon dioxide pipe system contributes to the determination of the nozzle pressure. Shown below is an abbreviated, if slightly less accurate, calculation can be used for estimating purposes. The three-row Table 45.34 shows how the calculation can be performed by combining pipe segments of the same diameter. The nozzle pressure in the abbreviated calculation is 566.1 psi as compared to 554.7 psi in the more detailed calculation. The pressure difference of 1.4 psi arises from the difference in reference pressure (663.8 psi vs. 605.5 psi) used to calculate the pressure loss in the 12 ft riser, Nodes 4–5.

Nozzle Selection In this example, nozzle pressure at Nodes 8 and 10 is 556.1 psi. The corresponding mass flux, G, interpolated from Table 45.25, is 2150 lb/in.^{2}-min. The required flow rate is 142.8 lb/min. A nozzle having an equivalent area of (142.8 lb/min)/(2150 lb/in.^{2}-min) = 0.0664 in.^{2} is required. The corresponding equivalent orifice diameter is 0.291 (9.30-32nd) inch for which the nearest Nozzle Orifice Code is 9.5.

Table 45.34 Three-segment calculation—constant pipe diameter

Segment nodes		Flow	Segment parts description					Elev.	Fittings	Equiv length		Inlet P	P_{Flow}	Elevation	Segment exit P, Y, Z		
1	2	3	4	5	6	7	8	9	10	11	12	13	14	15	16	17	18
Inlet	Exit	Q, lb/min	Segment parts	Pipe size, in.	Pipe Sch	Pipe ID, in.	Pipe L, ft	Elev chng, dh, ft	Fitting equiv L, ft	Up-stream Eq L, ft	Total equiv L, ft	Segm't inlet P, psi	Unadjusted exit P, psi	ΔP due to elevation, psi	Exit P, psi	Exit Y	Exit Z
1	3	142.8	V, H, ST, P	1/2	40	0.622	1	6.28	33.4	0	34.4	750	698.4	−1.87	696.5	2462	0.185
3	6	285.6	TT, 2EL, P	3/4	40	0.824	45	12	5.8	38.7	89.5	696.5	608.4	−2.64	605.5	5796	0.478
6	8	142.8	ST, EL, P	1/2	40	0.622	15	−1	5.2	83.6	103.8	605.5	605.5	0.18	556.1	7213	0.660

References

1. Kidde Fire Systems (2007) Engineered carbon dioxide (CO_2) fire suppression systems: design, installation, operation and maintenance manual 190 [3–76]
2. US Environmental Protection Agency Office of Air and Radiation, Stratospheric Protection Division (2000) Carbon dioxide as a fire suppressant: examining the risks: SPA430-R-00-002
3. US Environmental Protection Agency (1998), Federal register, rules and regulations: 40 CFR part 82, final rule 4810–7, vol 63, no 43
4. Wickham RT (2003) Review of the use of carbon dioxide total flooding fire extinguishing systems
5. National Fire Protection Association (2010) NFPA 10 standard for portable fire extinguishers
6. Quintiere J (2012) Surface flame spread. In: SFPE fire protection handbook, 3rd edn
7. Ohlemiler TJ (2008) Smoldering combustion. In: SFPE fire protection handbook, 3rd edn
8. Wysocki TJ (2008) Carbon dioxide and application systems. In: NFPA fire protection handbook, 20th edn, vol 2
9. National Fire Protection Association (2012) NFPA 484 standard for combustible metals
10. Christman (2008) NFPA fire protection handbook, 20th edn, vol 2
11. Ansul (2001) Carbon dioxide systems: components, design, installation, recharge, and maintenance manual
12. Fire Suppression Systems Association (2011) FSSA design guide for use with carbon dioxide total flooding applications, 1st edn
13. Fire Suppression Systems Association (2005) FSSA design guidelines for carbon dioxide local application rate-by-volume
14. Fire Suppression Systems Association (2010) FSSA Design guidelines for carbon dioxide local application systems rate-by-area
15. Eberly, R (2008) Marine Vessels. In: NFPA fire protection handbook, 20th edn, vol 2
16. International Maritime Organization (2007) SOLAS, chapter II-2-Construction - fire protection, fire detection and fire extinction
17. CFR Title 46 Shipping, Chapter 1, Part 76.15-Carbon Dioxide Extinguishing Systems, Details, U.S. Coast Guard, Department of Homeland Security
18. American Bureau of Shipping (2012) Annual review 2011
19. American Bureau of Shipping (2013) Rules for building and classing steel vessels. In: Annual review 2011
20. National Fire Protection Association (2006) NFPA cup-burner inter laboratory study: rev 1
21. Senecal J (2005) Flame extinguishing in the cup-burner by inert gas. Fire Safety Journal 40: 579–591
22. Compressed Gas Association (2009) CGA-G-6 – 2009 Carbon dioxide, 7th edn
23. NIST Chem WebBook, October, 2013. http://webbook.nist.gov/cgi/fluid.cgi?Action = Data&Wide = on&ID = C124389&Type = SatP&Digits = 5&THigh = 304&TLow = 218&TInc = 1&RefState = DEF&TUnit = K&PUnit = MPa&DUnit = mol%2Fl&HUnit = kJ%2Fmol&WUnit = m%2Fs&VisUnit = uPa*s&STUnit = N%2Fm
24. National Institute of Standards and Technology (2011) Carbon dioxide. NIST chemistry web book http://webbook.nist.gov/cgi/cbook.cgi?Formula = co2&NoIon = on&Units = SI&cTG = on&cTC = on&cTP = onAccessed on 5 September 2013
25. Kohl AL, Nielsen RB (2005) Gas purification, 5th edn. Gulf Publishing Company, Houston
26. Bachu S, Freund P, Gupta M, Simbeck D, Thambimuthu K (2005) Annex I: properties of CO_2 and carbon-based fuels. In IPCC special report on carbon dioxide capture and storage. Cambridge University Press, New York
27. Gas encyclopedia. Air Liquide. http://encyclopedia.airliquide.com/Encyclopedia.asp?GasID = 26 Accessed 5 September 2013
28. Hypercapnia. Wikipedia. http://en.wikipedia.org/wiki/Carbon_dioxide_poisoning Accessed on 5 September 2013
29. Documentation for immediately dangerous to life or health concentrations (IDLHs): carbon dioxide. Centers for Disease Control and Prevention. http://www.cdc.gov/niosh/idlh/124389.html Accessed on 5 September 2013
30. Sanders A How does carbon dioxide poisoning kill a human. Ehow. http://www.ehow.com/how-does_4695252_carbon-dioxide-poisoning-kill-human_.html Accessed on 5 September 2013
31. Air Products (1993) Safetygram-18: carbon dioxide. Air Products. http://www.airproducts.com/en/company/Sustainability/environment-health-and-safety/~/media/Files/PDF/company/safetygram-18.pdf Accessed on 5 September 2013
32. Rice SA (2004) Human health risk assessment of CO_2: survivors of acute high-level exposure and populations sensitive to prolonged low-level exposure, Third Annual Conference on Carbon Sequestration, Alexandria, VA
33. National Fire Protection Association (2011) Total flooding systems: flammable materials. In: NFPA 12 standard on carbon dioxide extinguishing systems
34. National Fire Protection Association (2011) NFPA 12 standard on carbon dioxide extinguishing systems
35. International Organization for Standardization (2009) ISO 6183 - Fire protection equipment-carbon dioxide extinguishing systems for use on premises-design and installation
36. International Maritime Organization (2007) SOLAS FSS Code - International code for fire safety systems

37. American Bureau of Shipping (2005) Guidance notes on fire-fighting systems
38. National Fire Protection Association (2011) Marine systems. In: NFPA 12 standard on carbon dioxide extinguishing systems
39. National Fire Protection Association (2011) Annex d total flooding systems. In: NFPA 12 standard on carbon dioxide extinguishing systems
40. National Fire Protection Association (2011) Figure e.1b, calculated CO_2 loss rate. In: NFPA 12 standard on carbon dioxide extinguishing systems
41. National Fire Protection Association (2011) Table 5.4.2.1, flooding factors for specific hazards. In: NFPA 12 standard on carbon dioxide extinguishing systems
42. National Fire Protection Association (2011) Table a.5.5.3(a) extended discharge protection for enclosed recirculating rotating electrical equipment. In: NFPA 12 standard on carbon dioxide extinguishing systems
43. National Fire Protection Association (2011) Table a.5.5.3(b) extended discharge protection for enclosed recirculating rotating electrical equipment. In: NFPA 12 standard on carbon dioxide extinguishing systems
44. International Maritime Organization (2007) Section 2.2.1. In: International code for fire safety systems (FSS)
45. American Bureau of Shipping (2005) Section 3.2.1. In: Guidance notes on fire-fighting systems
46. National Fire Protection Association (2011) Venting consideration. In: NFPA 12 standard on carbon dioxide extinguishing systems
47. National Fire Protection Association (2011) Table a.5.6.2 strength and allowable pressures for average enclosures. In: NFPA 12 standard on carbon dioxide extinguishing systems
48. National Fire Protection Association (2011) Table 6.4.4.3.2 aiming factors for angular placement of nozzles. In: NFPA 12 standard on carbon dioxide extinguishing systems
49. Crane Co (2013) Technical paper no 410, flow of fluids through valves, fittings, and pipe

Jeffrey L. Harrington, P.E., FSFPE, is a registered fire protection engineer and has been actively working since 1977 in fire protection engineering, property loss control, and code consulting. He is the President and Founder of Harrington Group, Inc., one of the oldest and largest firms headquartered in the Southeast dedicated solely to fire protection engineering consulting.

Mr. Harrington has served in a leadership capacity on several National Fire Protection Association (NFPA) technical committees, including the Technical Committee on Gaseous Fire Extinguishing Systems (GFE-AAA), which is responsible for three separate NFPA standards: NFPA 12, Carbon Dioxide Extinguishing Systems; NFPA 12A, Halon 1301 Fire Extinguishing Systems, and NFPA 2001, Clean Agent Fire Extinguishing Systems. Additionally, Mr. Harrington is the first Chair of the NFPA Hybrid (Water and Inert Gas) Fire Extinguishing Systems Technical Committee (HYB-AAA).

Mr. Harrington is a frequent author and lecturer on an array of fire protection engineering topics and is a nationally recognized expert, having received numerous awards for his contributions to the fire protection engineering industry. He is also a leader in activities with the Society of Fire Protection Engineers (SFPE), both locally and internationally He has been an SFPE Fellow since 2006.

Joseph A. Senecal has, since 1987, been an employee of Kidde-Fenwal, Inc., a Buildings & Industrial Systems company of United Technologies Corp. He has a Ph.D. in Chemical Engineering, an MBA, and is a Registered Professional Chemical Engineer. During his Kidde-Fenwal career he has been deeply involved in advancing the technology of special-hazard fire and explosion protection systems including product development, materials flammability testing, process hazards consulting, national and international standards development, and trade association representation with a particular interest in gaseous fire extinguishing systems. He is a charter member of the NFPA standard 2001 committee and has continued to serve actively on the since-merged NFPA "GFE" committee (NFPA 2001, 12, and 12a). In 2008 Joe was appointed to *Senior Fellow* (for UTC Fire & Security, since merged with UTC's Carrier and Otis divisions). Joe is one of only a few recipients of both the U.S. EPA's *Stratospheric Ozone Protection Award* (2004) and the *Climate Protection Award* (2009). Joe has presented or published over 50 articles related to fire and explosion protection technology. He is an inventor on five issued patents and on four current patent applications. His reading preferences include biographies of persons of scientific note, history, and character-rich fiction.

Water Mist Fire Suppression Systems 46

Jack R. Mawhinney and Gerard G. Back III

Introduction

This chapter addresses the engineering of fixed fire suppression systems that discharge water mist. The term *water mist,* as currently understood in the fire protection field, relates to fine water sprays with no drops larger than 1.0 mm, or 1000 μm (micrometers or microns) [1, 2]. Such sprays are not true mists, however. A *mist* in the scientific sense consists of drops somewhere on a continuum between *aerosol* (particles with diameter approximately 5 μm) and *fog* (droplet diameters ranging between 10 and 100 μm). Particles less than 20 μm in diameter take a long time to settle out and, hence, create what is recognized in both literature and science as a "mist." A water mist as intended for fire protection purposes is a fine water spray consisting of a range of droplet sizes, many of which are in the range of true mist particles and some of which are considerably larger. Water mist nozzles produce sprays that have a higher fraction of very fine droplets, in the range of mist, than is typical of standard sprinklers or water spray nozzles.

Fire suppression research performed in the past 60 years typically referred to "fine water sprays" or "finely divided water sprays" as the subject of study. Remarkable success at cooling and extinguishing diffusion flames was documented using fine water sprays with mean diameters less than 0.3 mm (300 μm) [3, 4]. Researchers in the 1950s confirmed the expected improvement in the efficiency of heat absorption due to the increase in surface area available for heat transfer as a spray is divided into smaller and smaller particle sizes. Also, as particles become smaller they settle out less quickly (remain suspended), providing more time for heat absorption and evaporation to take place. More heat is absorbed per unit of mass as the particle size decreases. Thus, it was understood that increasing the fraction of very fine water droplets contained in a water spray could reduce the amount of water needed for fire suppression, or in other words, improve the efficiency of application.

The term *water mist* was adopted by the National Fire Protection Association (NFPA) Technical Committee on Water Mist Fire Suppression systems in the early 1990s as part of the renewed interest in efficient use of water in fire suppression systems. This term distinguishes the technology of NFPA 750, *Standard on Water Mist Fire Protection Systems, 2010 edition,* from that of NFPA 15, *Standard for Water Spray Fixed Systems for Fire Protecting,* 2012 Edition [5], and NFPA 13, *Standard for the Installation of Sprinkler Systems,* 2013 Edition [6]. A more thorough discussion of drop size distribution as a significant spray characteristic is presented later in this chapter.

For technical and economic reasons, the knowledge about the advantages of using fine water sprays for fire suppression did not result in an immediate movement to finer sprays for fire protection. Technical concerns included the

J.R. Mawhinney (✉) • G.G. Back III
Jensen Hughes, 3610 Commerce Drive,
Arbutus, MD 21227

M.J. Hurley (ed.), *SFPE Handbook of Fire Protection Engineering*,
DOI 10.1007/978-1-4939-2565-0_46, © Society of Fire Protection Engineers 2016

negative effects of increasing operating pressures to improve atomization, the potential plugging of small orifices with corrosion products, and doubts about the long-term maintainability of equipment. Economic concerns related to the fact that there were less expensive alternatives: either standard sprinklers or the halogenated hydrocarbons—gaseous agents (halons) such as Halon 1301—could be used. So long as water was an inexpensive resource and halons were available to handle a broad range of special hazards, finer water sprays did not offer enough of a suppression advantage to justify their widespread use.

Three events happened in the 1980s that changed the economic background and revitalized interest in using fine water sprays for fixed fire suppression systems. These were the following:

1. The aviation industry's response to the Manchester air crash in 1984
2. The 1987 signing of the Montreal Protocol, an agreement to phase out the use and manufacture of ozone-depleting substances (halons), and
3. An International Maritime Organization (IMO) ruling that required the installation of marine sprinklers on all existing and new passenger ships capable of carrying more than 35 passengers

The Manchester, England, plane crash in 1984 [7] initiated an international effort to develop a fixed water spray system for passenger compartments on aircraft. The SAVE program, as it was called, was funded by the Civil Aviation Authority in England; the Federal Aviation Administration (FAA) in the United States; Transport Canada; and by the major builders of aircraft, such as Boeing and Airbus. The objective of the program was to increase the time available for evacuation of an aircraft passenger compartment exposed to a ground pool fuel fire after a crash landing. Tests were conducted utilizing water spray to prolong the tenability of the space to allow more time for safe evacuation of passengers. The SAVE program set well-defined performance objectives relating to occupant tenability [8]. The design was constrained by the need to minimize the weight of the system including the stored quantity of fire fighting agent. The choice of a fine water spray to maximize the effectiveness of a small quantity of water was a natural outcome of the work. A water mist system that exceeded all of the performance objectives was accomplished. The system extended tenability for 7 min, within the weight and volume constraints, using approximately 10 L of water. The SAVE study demonstrated that a fine water mist system using a limited supply of water could be custom designed to meet very specific objectives, within the constraints of the industry. The aviation industry regulatory authorities, however, did not make such systems mandatory on aircraft, on the basis that the cost per life saved was unacceptably high [7]. Nevertheless, international awareness of the SAVE research, which was focused on improving the heat absorption qualities of a water spray using a minimum application rate of water, for the purpose of achieving a specific performance objective, meant that the idea of "fine water sprays" was readily picked up by other researchers working on a larger issue that emerged at the same time, that is, the search for an alternative for gaseous fire-extinguishing agents.

The second key event that spurred interest in fine water spray fire suppression systems was the 1987 signing of the Montreal Protocol, an international agreement to reduce the manufacture and use of ozone-depleting substances [9]. Widely used halogenated fire suppression gases were discovered to be ozone-depleting substances. The threat of a phase-out of halon fire-extinguishing agents motivated the release of funds for research into alternative fire suppression agents, water among them. Water at least was not likely to be phased out in the future as an environmentally harmful substance. The high-level research into halon alternatives provided a windfall of improved scientific understanding of the physical and chemical nature of combustion and extinguishment processes. Advances in measurement of suppression phenomena, understanding of fire dynamics, and computer modeling of complex fire scenarios were

applicable to the engineering design of innovative fire suppression systems. The loss of halons as a class of extinguishing agents forced the re-examination of old assumptions about the unsuitability of water for certain types of fires, such as Class B fires in machinery compartments. With improved atomization and reduced flow rates, water could be used where the traditional default had been to use the gaseous clean-agent suppressants. Fine water spray fire suppression systems began to look viable from both performance and economic perspectives as an alternative to gaseous fire suppressants for a number of applications.

A third congruent event that propelled the use of fine water sprays into the realm of practical fire suppression systems was a move by the International Maritime Organization (IMO) to mandate the installation of sprinkler systems on passenger ships. This very influential rule-making body involves the interests of marine shipping societies, marine regulatory authorities (coast guards), and shipping companies worldwide. This regulatory action came about as a result of several large life-loss fires on-board Scandinavian passenger ferries that occurred in the 1980s [10]. In response, the International Maritime Organization mandated the installation of marine sprinklers on all ships capable of carrying 35 or more passengers to come into effect in 1995. Marine architects view marine sprinklers as a negative feature in terms of weight, space, and effects on vessel stability. Adding weight to the upper levels of a ship creates potential stability problems, particularly when sprinklers are retrofitted to an existing ship that was not designed to support the additional weight. There were strong economic and technical incentives to develop a system equivalent to sprinklers that would satisfy the intent of the IMO ruling but use less water and weigh less than traditional marine sprinkler systems. Fine water spray fire suppression systems promised to deliver just that. Research was conducted to develop performance criteria for fine water spray systems that could be impartially evaluated as equivalent to sprinklers installed on Solas II-2/12 [11–13]. The Scandinavian countries Sweden, Norway, and Finland performed development testing that laid the foundation for fire test protocols for marine machinery rooms and for accommodations and public spaces on passenger ships. The Swedish National Testing and Research Institute (SP) in Borås, Sweden; SINTEF, the Norwegian fire research institute in Trondheim, Norway; and VTT Building Technology research facility in Espoo, Finland, were the key centers of development for water mist fire testing. Manufacturers interested in developing water mist nozzles participated in the development of the tests. The test results were discussed, modified, and eventually accepted as consensus test protocols at meetings of the IMO fire protection subcommittees.

The availability of substantial funding to support research for halon alternatives and the creation of a worldwide market for alternatives to marine sprinklers were the two most important factors that changed the economic viability of using fine water sprays for fire suppression systems. Now there was financial incentive to support the cost of overcoming the engineering challenges involved.

As a result of the two distinct origins of renewed interest, there are two basic domains of application for water mist systems. One area of application is as a replacement for gaseous fire suppressants such as Halon 1301. Thus, in applications involving Class B flammable liquid fuels—or where clean agents were used because of concern about water damage—water mist is viewed as a halon system alternative. For applications where the water mist systems are installed for Class A fuels (ordinary cellulosic combustibles), a water mist system is viewed as potential alternative to sprinkler systems.

Water mist systems are not intended to be designed on a “rote” or prescriptive basis. As of 2014, it is becoming evident that water mist systems should be recognized foremost for the opportunity they provide to take a performance based design approach to managing challenging fire hazards. Water mist technology relies on an advanced fire protection engineering understanding of the fire hazard and the fire dynamics that need to be managed. The performance that is

claimed must be verified by conducting fire tests designed by experienced, commercially neutral engineers and testing laboratories. Water mist sytsems present an opportunity for importing types of equipment into fire protection from nontraditional fire protection equipment manufacturers.

Fundamentals of Water Mist Systems

The following review of the fundamentals of water mist system design covers mechanisms of extinguishment and suppression and spray characteristics.

Mechanisms of Fire Extinguishment and Suppression

Excellent discussions of the extinguishing mechanisms of water mist from an engineering perspective can be found in Braidech et al. [3], Rasbash et al. [4], and Mawhinney et al. [14] An understanding of the mechanisms of extinguishment associated with water mist (then called "finely divided water spray") was articulated approximately 50 years ago [3, 4]. Braidech and Rasbash both concluded that fires were extinguished by dilution of the air (oxygen) with water vapor (steam), resulting from evaporation of water droplets in the area local to the flame. They also concluded that the cooling effects of the water may contribute to the extinguishment of flames.

Mawhinney et al. [14] describe five mechanisms associated with extinguishment of hydrocarbon fires. They are the following:

- Gas phase cooling;
- Oxygen depletion and flammable vapor dilution;
- Wetting and cooling of the fuel surface;
- Radiation attenuation; and,
- Kinetic effects

The extinguishing mechanisms apply to extinguishment of Class B liquid fuel fires as well as Class A solid fuels, although with different importance of one mechanism over another. Typically, all mechanisms are involved to some degree in the extinguishment process.

Gas Phase Cooling

Gas phase cooling refers to the removal of heat from the combustion zone due to evaporation of water. The cooling efficacy of water mist is due to the fact that the water is broken up into many fine droplets, which enhances the evaporation rate. The more water that evaporates, the greater the amount of heat that is extracted from the combustion zone, thus reducing the temperature of the flame and hot gases. If the flame temperature is reduced below the critical value necessary to sustain combustion (limiting adiabatic flame temperature), the flame will be extinguished. The limiting adiabatic flame temperature for diffusion flames is approximately 1600 K (1326 °C) [15]. The cooling of the flame also reduces the radiation (thermal feedback) to the fuel surface, thus reducing the pyrolysis or gasification rate of the fuel. Scientific work involving the extinguishment of methane-air counterflow flames has been conducted that has shown that water mist/vapor is more effective on a mass basis than Halon 1301, if it can be delivered at near 100 % efficiency [16, 17]. The reality is that in full-scale compartment fire suppression, the efficiency of application of water is very much less than 100 %.

Various attempts have been made to establish a design relationship between the fire size and amount of water needed to extinguish the fire by gas phase cooling. Wighus [18] defined the term *spray heat absorption ratio* (SHAR), which relates the rate at which heat is absorbed by evaporation of a given mass of water (Q_w), to the rate at which heat is given off by the fire (Q_f).

$$\mathrm{SHAR} = \frac{Q_w}{Q_f} \tag{46.1}$$

Wighus's experiments showed that, for optimized application of mist to an unconfined propane flame, the heat absorption rate in the water needs to be only a fraction of the heat release rate of the fire, as low as 0.3 under optimum conditions. SHAR values in the range of

0.6 were noted for more realistic machinery space conditions, where small flames can persist in shielded areas to cause reignition. (In the absence of reignition sources, only enough heat has to be absorbed from the flame to drop the temperature to the limiting adiabatic flame temperature: it is not necessary to drop the temperature of the compartment or the fuel to ambient.)

On the surface, it seems promising to use a calculation of the amount of water that must be evaporated to extinguish a fire of a certain heat release rate as a design parameter. In real systems, however, the efficiency of delivery of water mist into flame, hence the rate of evaporation of the droplets in the flame zone, is almost unpredictable and certainly uncontrollable over the range of conditions encountered in fire events. The SHAR relationship nonetheless may be useful in a hydrocarbon extinguishment submodel for use in a computational fluid dynamics (CFD) approach to mist system design [19–21].

Andersson et al. [22] present the concept of the required extinguishing medium portion (REMP). This is the ratio of the mass application rate of extinguishing agent required ($\dot{m}_e'$) to the mass rate of fuel consumed ($\dot{m}_g'$). The REMP parameter is similar to the SHAR in that a certain mass of water must be evaporated to extract enough heat to extinguish the flame.

$$\text{REMP} = \frac{\dot{m}_e'}{\dot{m}_g'} \tag{46.2}$$

For propane flames, Andersson et al. [22] measured that the mass application rate of water needed to extinguish a propane flame under laboratory mixing conditions was between 1.2 and 2.2 times the mass burning rate of propane gas. They indicate that this range of REMP values corresponds to a water content volume concentration of 100–200 g/m^3—that is, the mass of water mist suspended in a unit volume of air. Note that both the SHAR and REMP values were measured under conditions of ideal interaction of flame and mist: the mist was discharged downward into the upward rising plume. The velocity vectors of mist and flame were opposite, resulting in the maximum degree of turbulent mixing in the collision zone. The mass flow rate of mist estimated from the REMP values should represent the minimum mass application rate. The mist mass flow rate values for real systems could be expected to be higher to account for inefficiency in delivery of mist to the flame and variability in the directional aspects of interaction.

The REMP parameter suggests that the mass application rate of extinguishing agent would have to be set for the largest expected mass burning rate of fuel. This assumption does not take into account the simultaneous action of other extinguishing mechanisms, however. As will be discussed shortly, for fires in enclosures, it has been observed that larger fires can be extinguished using less water than smaller fires due to the increased efficiency of evaporation attributed to heat confinement in the enclosure and other phenomena. Thus, one would expect the REMP values to go in opposite directions for enclosed fires versus unenclosed fires, indicating that the REMP value is not uniquely a function of the mass rate of fuel consumed.

As was suggested for the SHAR parameter, the REMP parameter is potentially useful in a computer submodel of extinguishment of spray or pool hydrocarbon flame [20]. Today, more complex physical models for evaporation and cooling of hot gases by water sprays are embedded in computational fluid dynamics (CFD) models as will be discussed later in this chapter. The accuracy of the CFD models remains limited by the difficulty of accurately modeling the sprays produced by the different types of water mist nozzles. Furthermore, the ability to model extinguishment of different types of fuels by cooling, wetting and oxygen displacement on principles of physics or chemistry, is limited. The concepts of SHAR and REMP remain conceptually useful for illustrating the principle that not all of the water mass discharged contributes effectively to fire extinguishment.

A number of researchers have sought to estimate a critical extinguishing concentration (in g/m^3) of water mist surrounding a diffusion flame. A number of international laboratories are

able to measure volume concentrations in g/m^3 of mist at various points in a spray, using a phase-Doppler particle size anemometer. Experimental values range from 100 to 200 g/m^3 [21–24] although values as low as 50 g/m^3 have successfully extinguished heptane flames [25]. Newer technology, referred to as "nanomist," generates clouds of suspended ultrafine water droplets with a suspended mass concentration as high as 240 g/m^3, using an ultrasonic transducer assembly and a process technology for aerosolization, extraction, and transport of mist. This technology is likely to be limited by cost to relatively small-scale applications [26–28]. Although the REMP concept appears to be a promising possibility for a universal design parameter, it is difficult to make practical use of this value for selecting spray characteristics or nozzle spacing. It is possible to calculate *nominal* total mass discharge per unit volume values for nozzles discharging into a compartment. On the macroscale of a machinery space, however, it is extremely difficult to predict or control volume concentrations at the point of interaction with flame. There are many randomizing events that alter the local concentrations of water mist at the point of extinguishment.

Oxygen Depletion and Flammable Vapor Dilution

These mechanisms can occur on either a localized or compartmental scale. On the localized scale, as the water droplets are converted to the vapor phase, the volume occupied by the water mist droplets increases over three orders of magnitude. If the vaporization of the water occurs in the flame, the volumetric expansion can disrupt the entrainment of air (oxygen) into the flame. On a compartmental scale, the production of steam resulting from mist interactions with the flame, hot gases, and/or hot surfaces can significantly reduce the oxygen concentration in the space [29]. The oxygen available for combustion is a function of the size of the fire, the compartment volume, and the ventilation conditions in the compartment. As the size of the fire increases, the average temperature in the space increases, and the oxygen concentration decreases due to consumption of the oxygen by the fire and dilution of the oxygen by water vapor. If the combined effects of oxygen depletion due to the fire and dilution by water vapor can reduce the oxygen concentration below the critical value necessary to sustain combustion (i.e., the limiting oxygen concentration [LOC]), the fire will be extinguished [29]. The LOC for most hydrocarbon fuels is approximately 13 % [15].

Wetting and Cooling of the Fuel Surface

Wetting/cooling of the fuel surface will be, in many cases, the dominant extinguishment mechanism for fuels that do not produce combustible mixtures of vapor above the fuel surface at ambient temperatures (i.e., solid fuels and liquid fuels with flashpoints above normal ambient temperatures). Wetting/cooling of the fuel surface reduces the pyrolysis or gasification rate of the fuel. If the vapor-air mixture above the fuel surface is reduced below the lower flammability limit (LFL) of the fuel, the flame will be extinguished.

Radiation Attenuation and Kinetic Effects

Water mist and water vapor measurably reduce radiant heat flux to objects near the fire, which assists in preventing fire spread to unburned fuel. Within the combustion zone, *radiation attenuation* is the result of gas phase cooling and the increase in water vapor concentration between the fuel and the flame. Lowering the flame temperature reduces the radiation feedback to the fuel surface. Also, water vapor in the air above the fuel surfaces acts as a graybody radiator that absorbs radiant energy and reradiates it to the fuel surface at a reduced intensity [19].

Kinetic effects may contribute either to flame intensification or to extinction. Flame intensification has been measured [14] as a flare-up of a flame on first contact with mist. Possibly the turbulence and entrainment associated with the rapid evaporation at the flame surface accelerate the burning rate. Ho [30], who studied the phenomenon in high-flashpoint oils, noted that most of the intensification is due to spray-induced oil splattering, which increased with increasing

Weber number as well as increased oil temperature. He noted that the heat release rate is enhanced by a factor from 2.12 to 5.55 compared to the heat release rate of free burning cooking oil. Kinetic effects may also be involved in flame suppression, the result of both gas phase cooling and oxygen depletion/dilution. When a diluent (in this case water vapor and recycled, vitiated combustion gases) is added to the combustion reaction, combined with flame cooling, it is hypothesized that reaction rates at the molecular level are significantly different from stoichiometric conditions.

Enclosure Effects, Turbulent Mixing, and Cycling

The importance of enclosure effects is described by Mawhinney, Dlugogorski, and Kim [14] and by Liu, Kim, and Su [31]. Enclosure effects maximize the benefits of oxygen depletion and dilution. The hot, vitiated gases collecting in the upper layer of an enclosure are cooled rapidly by the first contact with the water mist. Vitiated gases plus water vapor are forced down by the spray to the seat of the fire and contribute to extinguishment through oxygen depletion. Depending on the temperature and depth of the hot layer, the rapid cooling results in an instantaneous volume reduction, creating a negative pressure that can suck in the windows or walls of a tight enclosure. If the enclosure had reached flashover temperatures before mist activation, assuming that water could flow through the pipes and mist could be introduced, it is hard to say which phenomenon would dominate, the expansion due to steam generation or contraction due to cooling. At least one manufacturer has investigated a means of allowing an initially small injection of spray to initiate cooling, followed by a gradual increase in flow. Such an approach was described as taking the "shock" out of the introduction of mist to the hot enclosure. With reasonably early detection and activation, an automatically activated system will release in the first few minutes of a fire in an enclosure before the upper layer becomes too hot and deep. With systems that are manually activated, some thought should be given to the expected effect on introduction of the water mist into a very hot compartment. The author's experience has shown that the rapid cooling of a deep hot layer (by water mist) in a closed compartment can create a sudden negative pressure pulse strong enough to pull in the walls of the enclosure. The experience is contrary to the often cited but unfounded fear of "steam explosion," that is, a strong positive pressure forcing hot gases out of the compartment.

Some manufacturers have noticed that turning the spray off momentarily and then on again can speed up extinguishment in enclosures. The benefits of pulsing, that is, the on-off action of water sprays, also described as cycling, are well described in Liu et al. [31] and Liu and Kim [32]. Liu et al. [31] showed that pulsing the injection of water mist into an enclosure resulted in more rapid extinguishment, with less total water usage, than continuous application of mist. It was noted that the compartment temperature rose as the fire regrew during the first off-stage, allowing for more evaporation of lingering fine mist. The resurgent fire further reduced the oxygen concentration in the enclosure. The next injection of spray further cooled and mixed the oxygen-depleted gases. In this manner, cycling appeared to lead to greater net evaporation and oxygen reduction than with steady injection. Liu et al. [31] attributed the improvement of the efficacy of water mist in fire suppression using cycling discharges to the faster depletion rate of oxygen in the compartment and the recurrent turbulent mixing created by cycling discharge.

In some systems cycling was used to avoid too rapid cooling of the simulated turbine casing in the FM Global test protocol [33]. That protocol includes a test to ensure that cooling of the turbine casing will not result in damage to the turbine blades. By having spray on for only 50 % of the time, not only was the cooling test passed but also the volume of stored water needed for 10 min of protection was significantly reduced. The manufacturer's design criteria, therefore, incorporated the cycling as an essential element of system performance. Although the repeated off-stages in the cycle had been acceptable for

purposes of passing the FM Global test protocol, the author notes that cycling may not always be acceptable in installations where the equipment cannot tolerate re-exposure to flame during an extended off cycle. Furthermore, the apparent benefit is likely to be very dependent on the volume of the compartment.

Explosion Hazard Mitigation with Water Mist

A number of studies have been done to assess the potential for water mists to mitigate explosion hazards. The interest originates with several plausible hypotheses, such as: (a) that a deflagration flame front in a pre-mixed combustible vapor, moving through a cloud of finely atomized water droplets would be quenched as it encountered sufficiently small water droplets; (b) that the energy of a detonation shock wave moving through a field of water droplets would be "stripped" by the break-up of spherical water drops; and, (c) that the ignition energy required to ignite a vapor/air mixture would be increased by the presence of the water mist.

A review of experimental work performed over the last three decades reveals that there is mixed opinion about "whether application of water spray will quell or invigorate an explosion [34]." In some experiments, the peak overpressure was reduced, although it occurred sooner than if the mist had not been present. In other tests, the peak overpressure was increased by the water mist, presumably due to increased turbulence and stretching of the flame front. Unfortunately, there were major differences in spray characteristics involved in the various experimental programs, so the data are inconclusive. Analytical work supports the idea that benefits of using water mist to mitigate explosions are substantial, provided attention is paid to the details of application [35–38].

Butz et al. [36] investigated the use of water sprays to reduce explosion overpressures from a stoichiometric mixture of hydrogen gas and air released in a test chamber. The test scenario involved creating a mixture of hydrogen and air in a closed chamber, injecting a water spray, and then igniting the mixture. The tests demonstrated that ignition required higher spark energy than without the mist, and the overpressure generated by the deflagration was reduced by about 15 % (Fig. 46.1). Figure 46.1 shows a pressure reduction from 35 to 30 psia "with mist." Butz also measured a significant temperature reduction of the passing flame front, which could reduce the risk of burn injury to personnel who might be exposed to the flash inside a compartment.

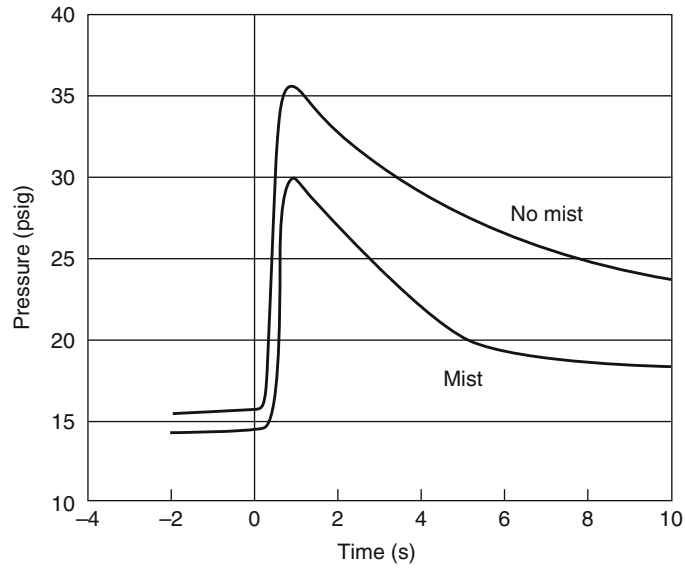

Fig. 46.1 Reduction in explosion chamber overpressure due to presence of water mist [36]

The U.S. Naval Research Laboratory examined the potential for water mist fire suppression systems to perform dual service in suppressing peacetime fires and mitigating blast effects in wartime scenarios [37, 38]. A survey of the use of water (bulk, sprays, mists, etc.) as an agent for blast mitigation was conducted [37]. That survey showed that there are several ways in which the use of water sprays can mitigate the effects of an explosion. It may (1) break up larger droplets into finer mist, (2) directly lead to an attenuation of the shock waves produced, (3) reduce the intensity of secondary shock and pressure waves, (4) slow down or quench the chemical reactions taking place behind the shock waves, and (5) dilute the concentration of explosive gases in the enclosure and, hence, prevent a secondary gas explosion or fire. Studies by Kailasanath and Schwer concluded that water mists will reduce the propagation rate of shock waves. In general, finer droplets increase the attenuation rate. The reduction in propagation rate does not necessarily lead to a reduction in the peak overpressure, however, because the peak overpressure occurs at some distance behind the shock front. In addition, the interaction differs for a shock wave or a flame front.

British Gas (BG) conducted a study aimed at improving the oil industry's confidence in its safety systems with respect to hydrocarbon fires and explosions [39]. A similar study was undertaken at the Christian Mikelson Institute in Norway. In contrast to the results recorded by Butz, the oil industry studies showed that water spray increased the overpressure caused by ignition of a methane-air mixture in a fully enclosed compartment (Fig. 46.2). However, in an open compartment (one wall removed) from the test compartment, a reduction in the overpressure was recorded (Fig. 46.3), but it was a much greater reduction than the 15 % measured by Butz. Both studies also pointed out the role that turbulence plays in accelerating the flame front. Piping clutter and the injection of large drop water sprays increase turbulence in the gas-air mixture and thereby contribute to worsening the deflagration.

There were significant differences in the spray characteristics of the nozzles used in Butz's tests and those used in the BG tests. BG tests used a water deluge nozzle typically used on offshore platforms, which produces spray much coarser than what we now define as water mist. It is believed that subsequent work by Kailasanath and Schwer [38] for example, more accurately

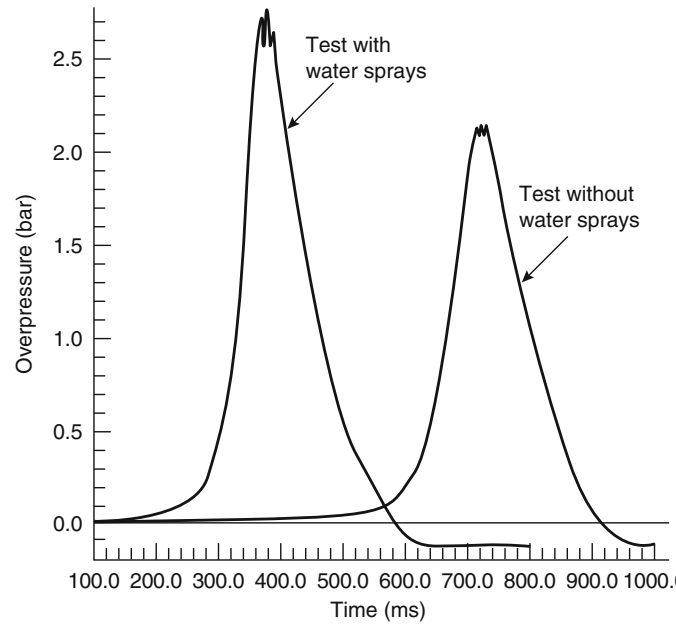

Fig. 46.2 Blast overpressures measured in an enclosure with no open side, with and without water mist, from Selby and Burgan [39]

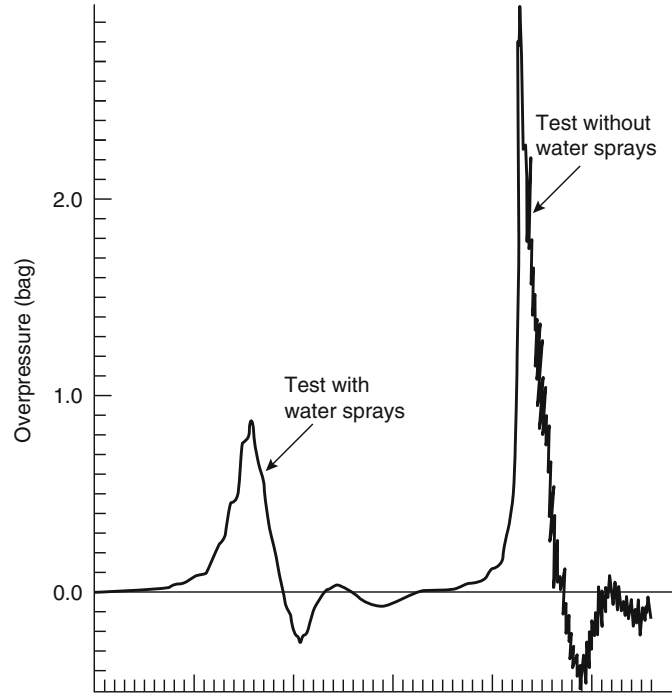

Fig. 46.3 Blast overpressure reduction due to the application of water mist in an enclosure with one open side, from Selby and Burgan [39]

reflects the interaction of blast waves with smaller droplets typical of water mist. The editors of the BG industry report concluded that more work is needed with focus on working with sprays with finer drop size distributions.

During preparation of the first edition of NFPA 750 (1996), a task group of the committee prepared a review of the literature on fine water spray suppression systems. As part of that work, Robert Zalosh of Worcester Polytechnic Institute (WPI) prepared a review of studies on the use of fine water sprays to mitigate explosion hazards [40]. Several relevant conclusions based on his review are summarized as follows:

- In an unconfined environment, high-momentum water spray can entrain air into a gas cloud and dilute it below the lower flammable limit.
- Water vapor can slightly narrow the flammability limits for a gas, and it can dilute the gas-air mixture below the flammability limit. At higher temperatures, higher concentrations of water vapor are possible than at lower temperatures, so warm mist is likely to be more effective than cool mist.
- In near-limit gas-air mixtures, the spray/mist can have either a mitigating effect or an exacerbating effect on flame speeds and pressures depending on the turbulence produced by the spray and the characteristic drop size. The mitigating effect has occurred only with gas concentrations only slightly above the lower flammable limit.
- In the case of a very high flame speed with an accompanying shock wave, the spray/mist can reduce deflagration pressures and possibly extinguish the flame because the shock wave breaks up the drops into a micromist with a characteristic drop size on the order of approximately 1 μm. These tiny drops can evaporate in a sufficiently short time interval to absorb a significant fraction of the combustion energy released during the deflagration.
- The exacerbating effect that occurs in some situations is due to the turbulence produced by the water spray causing the flame speed to increase and/or causing a larger fraction of the flammable gas to burn.
- Generally, drops do not vaporize rapidly enough to absorb the combustion energy

before the deflagration is complete, unless they are very small (i.e., on the order of 1 μm).
- More widespread use of water spray systems for deflagration control will depend on the viability of generating a micromist with sufficiently small drop sizes, which will require water mist systems that are different from those being developed commercially for fire suppression applications.

Spray Characteristics

Measuring and understanding the characteristics of sprays produced by different nozzles are prerequisites for understanding differences in performance. To fully characterize a spray requires information about the following elements:
- Drop size distribution (DSD);
- Cone angle;
- Velocity of the discharge jet(s);
- Mass flow rate; and,
- Spray momentum (product of velocity and mass).

These spray characteristics, which are discussed in more detail below, potentially determine nozzle location and spacing as well as ceiling height limitations.

Drop Size Distribution

Water mist is made up of finely divided water drops of different sizes. Some of the drops may be falling under gravitational force, while other smaller drops may be "floating" in the air entrained with the spray. The drop size distribution of the spray is not yet used explicitly as a parameter in the design of a water mist system. Effective practical application awaits the results of further research. Nevertheless, the drop size distribution of a water spray clearly relates to overall system performance, as it impacts the rate of mist evaporation, how discharge is affected by obstructions, and the momentum of the spray relative to the buoyancy of the fire plume. If the differences in drop size distributions of water sprays are not quantified and understood, an explanation of the differences in performance between different manufacturers' nozzles might not be attainable. When using computer models to approximate the dynamics of suppression with water mist, a quantitative estimation of the drop size characteristics of the mist discharge is essential.

The term *drop size distribution* refers to the range of drop sizes contained in a representative sample of a mist discharge. There is a distribution of small and large drops, which varies with location in the discharge as a function of time. For a continuous discharge, the distribution of drop sizes changes with distance from the source as drops collide, evaporate, or hit surfaces and fall out. For a short burst of discharge, the distribution measured at a point in space changes with time as the larger droplets pass through quickly, leaving increasingly finer drops, which take more time to settle.

There are a number of ways to present data about drop size distributions of sprays [31, 32]. It is customary in some fields to refer to the size of particles in a spray by a single drop size parameter, such as a Sauter mean diameter (SMD) or volumetric median diameter (VMD). Such single-point parameters reveal little about the range of drop sizes in a spray, however. It is important to know the fraction contained in larger drop sizes and the fraction contained in much smaller drop sizes during a given discharge to understand the mist's performance as a fire suppressant.

NFPA 750 has adopted the curve of cumulative percent volume versus diameter to represent the distribution of drop sizes in a water mist. Reasons for this choice are that the cumulative percent volume plot visually reveals the range of sizes, and the volume distribution converts readily to mass distribution, which is the most relevant term for analyzing heat transfer and evaporation rates using computer modeling. The range of drop sizes can be fully described by characteristic parameters such as $D_v0.90$ and $D_v0.50$. The $D_v0.90$ is the drop diameter at which 90 % of the volume of a sample of the spray is contained in drops of that diameter or smaller. Similarly, $D_v0.50$ is the volumetric mean drop diameter; that is, 50 % of the volume of the spray is contained in drops less than that diameter.

Spray Cone Angle

Commercially available nozzles typically produce either 90° or 102° spray cones. Other cone angles are possible but not available as Listed nozzles. Typically the sprays are solid cones, not hollow cone sprays.

Spray Velocity

Velocity is a vector quantity—it has both direction and magnitude. The directions of individual jets define the shape of the spray cone. The magnitude of the jet velocity is the velocity at which water emerges from a small orifice and begins to atomize. There is also a transfer of the velocity of the individual water particles to the surrounding air (through drag effects). In a multijet nozzle, the drag effect of adjacent spray jets pulls surrounding air into the spray cone, adding to the mass flux of the spray cone. It is the combined velocity of the water droplets from all the jets and the air entrained in the flow that contributes to the spray momentum, which dictates the overall impact of the spray on a fire plume.

Discharge Rate

The mass discharge rate of a nozzle is a function of water pressure and the total area of the orifice (s). Ideally the discharge rate per nozzle could be designed around the SHAR or REMP values—theoretical minimum application rates relative to the amount of heat to be absorbed. In reality, discharge rates vary for different manufacturers for the same fire test scenario.

Spray Momentum

Momentum is calculated as mass times velocity. The combination of the mass of water droplets plus the mass of entrained air, multiplied by the velocity of mist particles plus entrained air, constitutes the momentum of a water spray. In general, for a constant mass discharge rate, increasing spray velocity increases the air entrainment rate, which contributes to the spray momentum. Like velocity, momentum has both magnitude and direction—and its direction relative to the fire plume or fuel source has a bearing on its effectiveness. Where the spray direction is opposed to the fire plume direction there is penetration of the flame by the water mist, and any water vapor created in the flame may be carried to the seat of the fire. In contrast, codirectional flows may not create the turbulent flame-mist mixing needed to enhance evaporation and cooling, and the water vapor formed will be carried away from the fuel surface rather than pushed down to it. Studies to evaluate the relative benefits of using high-velocity or low-velocity water mist nozzles must include this directional component of the momentum factor, not only the magnitude of jet velocities. Also, since the entrained air forms a significant proportion of the mass flow rate, it contributes to the momentum of the overall spray cone. Two nozzles with similar initial jet velocities and mass flow rate could have very different degrees of air entrainment—hence, the spray momentum for each could differ significantly. As control over the directional aspects of spray application can be a design choice, spray velocity and spray momentum represent potential first-principles design parameters.

Measurement of Drop Size Distributions

An annex of NFPA 750 describes a methodology for obtaining a statistically meaningful measurement of the drop size distribution of a water spray. Listing organizations typically measure the drop size distribution of a nozzle as part of the component approval process. A phase-Doppler anemometer may be used to measure the drop sizes passing through a small volume of space within the spray cone. The drop size distribution in a spray is not the same at all locations in the spray cone. A single reading taken at one location is not representative of the average drop size in the spray. It is standard practice to take a set of readings and combine them into a statistically representative value [41, 42]. For the purpose of being able to compare water mist sprays, NFPA 750 prescribes the measurement of drop size distribution with the spray cone axis vertically downward over an imaginary plane through the spray cone a distance of 1 m below the nozzle. This distance is usually sufficient so that the atomization process is complete and the average droplet velocity has

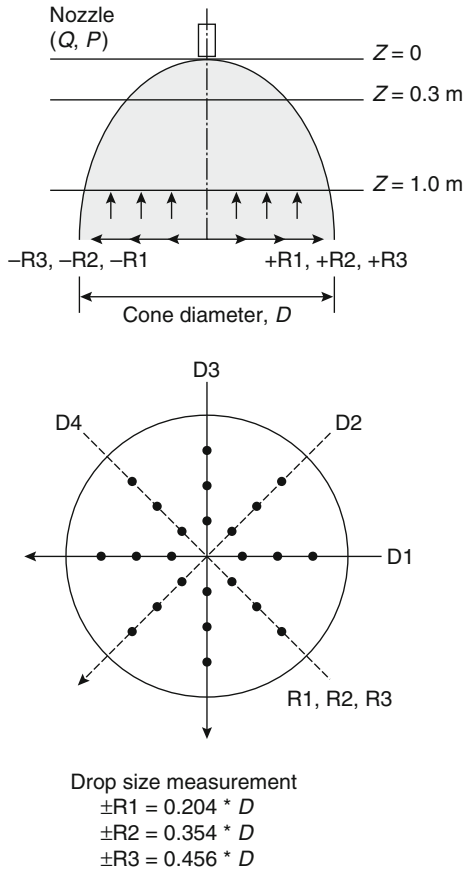

Fig. 46.4 Locations within spray cones for measurement of flux density distribution and drop size distribution. The positions shown are the centroids of segments of equal area [42]

slowed to approximately the velocity of the entrained air.

Figure 46.4 illustrates a setup in which spot readings were taken at 24 locations in the spray, measured on a plane 1 m below the nozzles. The positions for taking a measurement represent the midpoint of sectors of equal area in the circular cross section of a spray cone. A grid of collector pans is used to collect the flux density at each of the measurement locations. It is assumed that the drop size distributions measured in areas of high flux density are more representative of the overall distribution than measurements taken in areas of low flux density. Thus, Equation 46.3 is used to calculate a weighted average drop size distribution curve, weighted according to the flux density measurements at each location.

$$R_k \frac{\sum_i \left(R_{j,i} \times A_i \times V_i\right)}{\sum_i \left(A_i \times V_i\right)} \tag{46.3}$$

where

$R_k =$ Weighted cumulative volume percent readings for sizes equal to and less than d_{upper}

$R_{j,i} =$ Cumulative volume percent readings for sizes equal to and less than d_{upper} at location i

$A_i =$ Area centered at location i in which the size distribution is represented by R_k

$V_i =$ Water flux density measured at location i

The NFPA 750 annex method was used to obtain weighted average cumulative percent volume drop size distribution (DSD) curves for four commercially available water mist nozzles. Figure 46.5 compares the weighted cumulative percent volume DSD curves for the four nozzles investigated [43, 44]. Nozzles A and B were low-pressure single-fluid nozzles; nozzles C and D were high-pressure single-fluid nozzles. It is interesting to note that even the coarsest spray measured (A) had at least 50 % of its volume contained in drop sizes smaller than 300 μm. Spray B shows approximately 80 % of its volume (mass) in drop sizes smaller than 300 μm. However, nozzle B discharged at a rate of 5 l/min (=5 kg/min) whereas nozzle A discharged at a higher rate of 12 kg/min. Therefore, nozzle A, the apparently "coarser" spray, generated about 6 kg/min of drop sizes below 300 μm, whereas nozzle B, the apparently "finer" spray, produced only 4 kg/min of sub-300 m droplets. In terms of potential for heat extraction by rapid evaporation of the smallest droplets, one cannot conclude that one spray is "better" than another on the basis of drop size distribution alone. Factors such as mass flow rate, cone angle, air entrainment, and spray velocity also influence the mixing of mist with fire gases in the compartment.

Spray Velocity

Laboratories involved in measurement of water spray characteristics for research or approvals may use a phase-Doppler anemometer (PDA) instrument to measure drop size distributions and

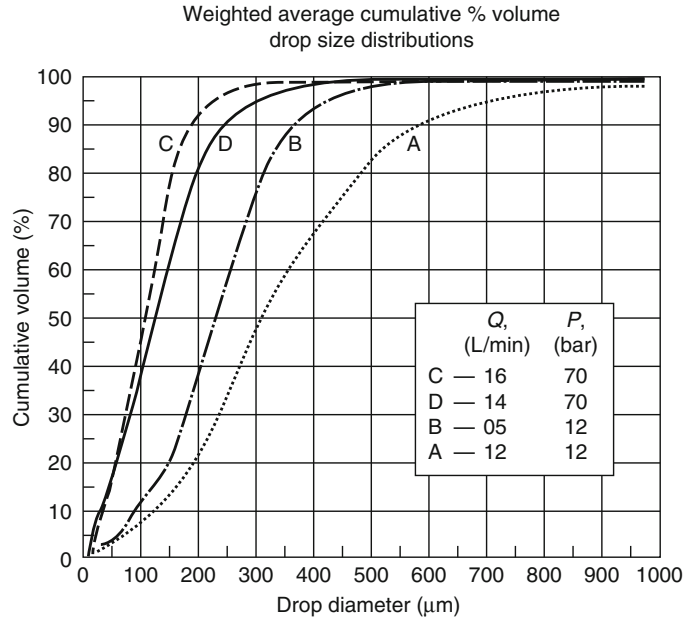

Fig. 46.5 Comparison of statistically weighted cumulative percent volume versus drop size distribution plots for two low-pressure (*A* and *B*) and two high-pressure (*C* and *D*) water mist nozzles

drop velocity, including speed and direction. The PDA may be mounted on a movable structure of vertical and horizontal beams, which can be raised or lowered relative to the position of a nozzle. The PDA measurement focuses two laser beams on a small volume of space and is able to count the number of particles of different sizes at a point inside the spray volume. It determines at least one component of the velocity, using the principle of the Doppler shift that occurs depending on the velocity of the object relative to the viewer. By moving the laser source to different positions around the spray cone, a map of drop size particle size, mass density, and velocity can be constructed.

As part of the same study referred to for the drop size distributions shown in Fig. 46.5, measurements of vertical-downward velocity profiles were taken for two of the nozzles [43, 44]. The velocity was measured by placing a vane-type anemometer horizontally in the spray cone at different locations and at two different distances below the nozzle. The anemometer measured the velocity of the entrained air plus water drops normal to the plane of the anemometer vanes. Individual drops hitting the rotating vane either accelerated or decelerated the vane. It was estimated that the effects of individual water drops on the vane speed approximately canceled out, so that the velocity of the entrained air dominated the measurement. The measured velocity was probably less than the velocity of the fastest-moving drops but close to the average velocity of the entrained air.

Figure 46.6 compares the downward velocity profiles measured 0.3 m and 1.0 m below a high-pressure (C) and a low-pressure (A) nozzle. These data provide a qualitative means of understanding the difference between how a high-pressure and a low-pressure water mist nozzle might interact with the fire plume.

At this time it is not possible to formulate invariable relationships between spray drop size distributions, spray velocity, and the suppression efficiencies of different water mist nozzles. There are many interacting factors involved in suppression, such as enclosure effects and fuel properties. There are, therefore, many possible combinations of spray characteristics and local conditions that will effectively control or extinguish fires. Computational fluid dynamics (CFD) field models present a fruitful means of studying the relative importance of specific spray characteristics. However, it is necessary to measure the physical characteristics of water mist

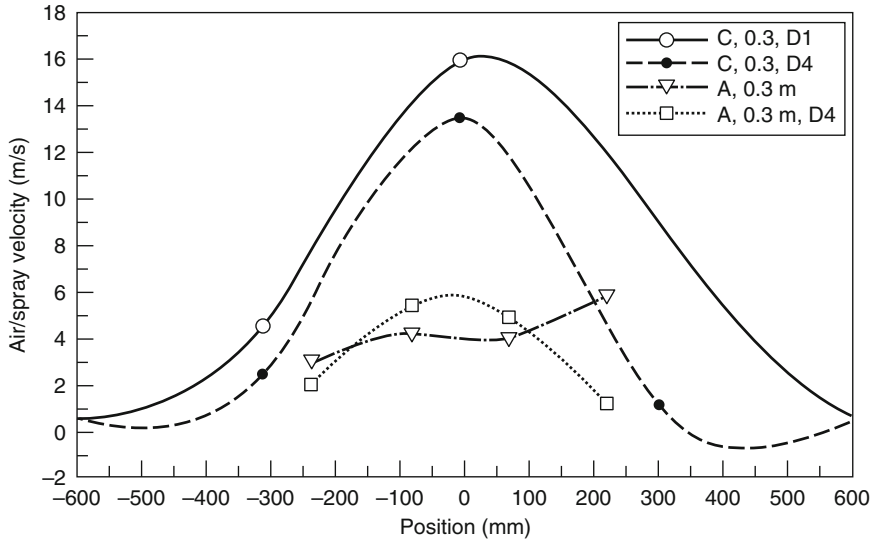

Fig. 46.6 Downward spray velocity profiles, measured 0.3 m and 1.0 m below a high-pressure (*C*) and a low-pressure (*A*) water mist nozzle

sprays as they are needed as input parameters for the field models.

Additives and Health Concerns

In the early 1990s concerns were raised that inhalation of very fine water droplets could cause persons to drown. Various studies were conducted to review the literature on the subject of inhalation of aerosol sized particles into the lungs. Examination of drop size distribution measurements revealed that even the finest water mist sprays do not contain a significant mass of water in drop sizes small enough to be inhaled, and the limited fraction of aerosol-sized particles that could be inhaled are removed as they move through the bronchial tract before reaching the lungs. Consensus was reached that inhalation of "pure" water could be dismissed as a health concern [45]. The use of potentially toxic additives to the water mist, however, was considered to be a potential health concern.

Low concentrations of additives, such as alkali salts and the surfactants in AFFF solution, improve the extinguishment capabilities of water mist [46, 47]. In Class B fires, the surfactant spreads over the liquid pool surface, blocks the generation of fuel vapors, and helps extinguish small flames in hidden corners. Extinguishing the small flames helps break the extinction-reignition cycles that prolong the extinguishment of obstructed pool fires. For enclosed systems, the addition of inert gas (nitrogen) to the spray has been demonstrated to enhance extinguishment by aiding in oxygen depletion [48]. Antifreeze and biocides to prevent algae growth are also potential water mist additives. The use of additives introduces concern about possible negative effects on human health. The U.S. Environmental Protection Agency (EPA) permits the use of water mist as a halon alternative in occupied spaces only when potable water or normal seawater is used [49]. This permission was based on the response of a panel of toxicity experts convened under the Halon Alternatives Research Corporation (HARC) to question the possible adverse health effects of water mist. The report concluded that even the smallest drop sizes in water mist are not present in sufficient quantities to harm humans if breathed into the lungs, provided the water is of potable quality.

The report *Water Mist Fire Suppression Systems Health Hazard Evaluation* (1995) was generated by the Halon Alternatives Research

Corporation (HARC) [45]. Members of the NFPA 750 technical committee provided input to the panel of health experts. The report provided data for discussion of concerns over water mist and additives to the water. The report included a section entitled "Toxicity Profile—Water Mist Spray with Additives" that was prepared for the Army Program Executive Office, Armored Systems Modernization group, by the Toxicology Division, U.S. Army Environmental Hygiene Agency.

The US Army study summarized the available toxicity data on water mist and six potential additives. It identified additives that are the least toxic:

- Propylene and ethylene glycol (antifreeze)—acceptable;
- Potassium acetate and calcium chloride (antifreeze plus fire retardant)—acceptable with reservation; and,
- Potassium iodide and lithium chloride—potentially hazardous to humans.

Since the US Army study was done in the mid-1990s, the fire protection engineering community has become aware that propylene and ethylene glycol antifreeze solutions in excess of 50 % may cause a flash fire deflagration if finely atomized and discharged into an ignition source. If the phenomenon has been observed with sprinkler sprays, it is inadvisable to use such antifreeze solutions in water mist systems, where the fraction of spray that is in very fine droplets is much higher. The army toxicity report does not address the matter of how much additive may be present. Is a product safe at 1 % but unsafe at 5 %? Some antifreeze concentrations may be as high as 30–50 % by weight. The concentrations of biocide needed for bacteria control may be below the harmful threshold for humans. One must distinguish between chronic, or long-term, exposure, and short-term, low-probability exposure that would be less harmful than the exposure to the fire combustion products. At the present time there are no simple answers to such questions.

There are concerns with storage of water in cylinders for water mist systems for crew compartments in military vehicles. The concerns range from toxicology of chemical additives used as antifreeze agents or fire retardants, to bacteriological growth in untreated stored water. The U.S. Environmental Protection Agency (EPA) states that only "pure" (i.e., potable) water or natural seawater can be used without question for water mist systems in occupied spaces. If additives are considered, the onus is on the proponent to prove that there is no toxicological risk. Dr. Martial Pabon, of DuPont de Nemours, France, presented an example of a toxicological study of the effect of a fluorosurfactant additive (2 % Forafac) to water mist at the 2005 conference of the International Water Mist Association [50]. Working with G. LeFort and Dr. André Marshall at the University of Maryland, it was proven that the additive did not alter the atomization process and that the additive improved the extinction capability of the water mist and prevented reignition of a hydrocarbon pool fire [50, 51]. A toxicological study was carried out at Haskell Laboratory by J. Stader and T. Kegelman. This study was based on the "OECD Guideline for the Testing of Chemicals, Section 4: Health Effects, Acute Inhalation Toxicology, Number 403" (1981) [52]. The conclusion of the toxicity study was that "according to the guide for the labeling of dangerous substances published in the Official Journal of the European Communities (EEC Directive 93/21), 2 % (of the Forafac additive) to the water mist is not classifiable ($LC_{50} > 5$ mg/L)."

Addressing health concerns involves not only studying the effect of chemical additives, but also the bacterial content of the water. Heating and air conditioning engineers in the United States have noted that *Legionella* bacteria can be spread to humans by inhalation of fine sprays that may carry the bacteria [53]. In 1976, an unnamed bacterium caused 34 deaths and 221 people at a Legionnaire's convention in Philadelphia to become sick with symptoms of pneumonia. At the time of its discovery and naming as "*Legionella*," it was thought that the bacteria were not present in fresh potable water, but only in stored water associated with the building cooling systems. Experience with worldwide outbreaks since then, however, has shown that *Legionella* bacteria can be present in

potable water systems, particularly in the hot water plumbing systems, and can be spread through any systems involving atomization of water. *Legionella* bacteria thrive in water between 20 °C and 48 °C (68 °F and 108 °F) [53].

Precautions against bacterial growth are also recommended to prevent plugging of the control valves and nozzles by algae growth. Water mist systems often utilize water storage tanks as part of the design. Some marine water mist systems utilize water reservoirs or break tanks. Although in principle only clean potable water goes into the tanks, conditions may change over time, particularly when the tanks are placed in warm machinery rooms. Filtration removes particulates but not bacteria present in the source water. The American Society of Heating, Refrigerating and Air-Conditioning Engineers (ASHRAE) produced a guideline with recommendations for controlling the development of *Legionella* in stored water systems [54]. Careful annual maintenance and cleaning are recommended. It notes that during the release of fire water in a fire emergency, fire department personnel wear breathing apparatus, and non-fire-fighting personnel will exit the fire area. However, appropriate precautions should be taken when testing the fire protection system.

Some water mist systems have been designed to provide a high level of cleanliness in the water supply [55]. The system water is circulated continuously between a reservoir and the system piping. An ultraviolet treatment chamber kills bacteria and filters remove particulates on a continuous basis. Pressure loss across the filters can be monitored to indicate when the filters have reduced flow capacity. High-cleanliness water supply precautions are a solution for any applications where there is concern about maintaining the quality of the water, either for health or functional reasons.

Fire Suppression Modeling

The major difficulties with water mist systems are those associated with a standardized approach to their engineering design. The problems arise from the need to generate, distribute, and maintain an adequate concentration of the proper size drops throughout the compartment or fire area for the necessary time period while accounting for the effects of gravity and water deposition on surfaces, which deplete the overall concentration of mist. There is currently no theoretical basis for considering these parameters in the design process. System design parameters are normally extrapolated from large-scale test data on a case-by-case basis for specific applications. This approach is not necessarily cost effective for water mist system manufacturers and poses difficulties for standards-making and regulating authorities. There has been at least one significant effort at developing and applying physical scaling rules (i.e. Froude number scaling) to water mist system design applications [56]. Although the study showed some applicability, the overall approach is significantly limited.

Over the years, an empirical understanding of how water mist systems extinguish a fire has been bounded. The degree of understanding however is still not yet at the stage where water mist systems can be designed from first principles, although some progress continues to be made. The progress that is currently being made is through the application, development and validation of CFD algorithms for specific applications. Now that water mist technology has been fielded for over 15 years, the trends have shifted from basic/fundamental research to the assessment of specific applications.

A basic understanding of the mechanisms of extinguishment associated with water mist was developed over 45 years ago [3, 4]. Braidech and Rasbash both concluded that fires were extinguished by dilution of the air (oxygen) with water vapor (steam), resulting from evaporation of water droplets in the area local to the flame. They also concluded that the cooling effects of the water with respect to the flame and the fuel might contribute to the extinguishment process. Research conducted to date has not altered this understanding. Recent research has, however, identified the primary mechanism(s) associated with extinguishment for a given set

of conditions as well as some additional less predominant extinguishment mechanisms [14].

The mechanisms of extinguishment can be broken down into two basic groups—direct and indirect flame interaction. Direct flame interaction includes gas phase cooling and localized oxygen depletion, and indirect effects include global oxygen depletion and surface wetting/cooling effects.

Direct flame interaction encompasses a broad range of both chemical and thermodynamic relations associated with the release and distribution of energy during the combustion process. Extinguishment by direct flame interaction (primarily gas phase cooling) is basically the removal of energy from the flame and hot gases. As the energy is removed from the flame, the temperature of the flame is reduced. If the flame temperature is reduced below the critical value necessary to sustain combustion (limiting adiabatic flame temperature), the flame will be extinguished. The limiting adiabatic flame temperature for a number of hydrocarbon fuels is on the order of 1600 K (1326 °C) [15].

Recent investigations have bounded some of the parameters associated with direct flame interaction [20, 22, 57]. Numerous research programs have focused on identifying the critical mist concentrations needed to extinguish diffusion flames [17, 58–62] and to extinguish hydrocarbon pool fires [22, 63–67]. Other research agencies have studied the effects of water vapor as an inerting gas [68, 69], as well as the attenuation of radiation to the fuel surface provided by the mist [70–72].

The difficulty in predicting extinguishment by direct effects is associated with being able to predict and/or measure the amount of mist reaching the fire. The ability of mist to diffuse into all areas in the space in the same manner as the gaseous agents is significantly limited for the range of drop sizes produced by current commercially available hardware [63, 73]. Recent studies have shown that the concentration of mist decreases by more than a factor of two after traveling less than a meter horizontally away from the spray pattern of a nozzle. To compensate for this limitation, the higher performance water mist systems rely on high-velocity sprays to mix the mist throughout the compartment (i.e., to create turbulent conditions in the space). The fire size (heat release rate) and fire location are also variables that need to be considered. The fire tends to alter the mist conditions in the compartment by changing the drop size distribution (vaporization and condensation) and affecting the flow patterns throughout the space due to the plume and ceiling jets.

Additional research has bounded the effects of oxygen depletion and dilution (indirect effects) on extinguishment [18, 74–76]. The production of steam resulting from mist interactions with the flame, hot gases, and/or hot surfaces can significantly reduce the oxygen concentration in the space. The oxygen available for combustion on a compartmental scale is a function of the size of the fire, the compartment volume, and the ventilation conditions in the compartment. As the size of the fire increases, the average temperature in the space increases, and the oxygen concentration decreases due to both the consumption of the oxygen by the fire and dilution of the oxygen by water vapor (steam). If the combined effects of oxygen depletion and dilution can reduce the oxygen concentration below the critical value necessary to sustain combustion (limiting oxygen concentration [LOC]), the fire will be extinguished. The LOC for most hydrocarbon fuels is on the order of 13 % [77].

Fuel surface effects can be the predominant extinguishment mechanism for fuels that do not produce combustible mixtures of vapor above the fuel surface at ambient temperatures, that is, solid fuels and liquid fuels with high flashpoints (i.e., diesel $\approx$ 60 °C). Wetting/cooling of the fuel surface reduces the pyrolysis rate of the fuel. If the vapor-air mixture above the fuel surface is reduced below the lower flammability limit (LFL), the flame will be extinguished. The ability to predict extinguishment based on surface cooling has also been investigated in numerous experimental programs [78–82]. This information includes both Class A materials as well as high-flashpoint hydrocarbon pool fires.

Typically, a combination of mechanisms is involved to some degree in the extinguishment

process. In order to accurately predict the conditions required for extinguishment, the combustion chemistry, combined with thermodynamics and fluid dynamics, needs to be covered in detail. These complex relations are best analyzed using computational models that are based on first principles. The current mathematical models used to predict suppression of fires by water mist systems cover the range of approaches from zone fire modeling to computation fluid dynamics (CFD), which are often referred to as field models. A zone model calculates the fire environment by dividing each compartment into one or two homogeneous zones. The energy balance and conservation of mass equations are solved based on a control volume dictated by the boundaries of the compartment for a single-zone model or by the zonal boundaries for a two-zone model.

The input requirements for zone models vary depending on the model and the desired output. The compartment geometry and opening dimensions are needed to define the space and the surroundings. The thermal properties of the compartment boundaries are needed to estimate the heat loss through the walls, ceiling, and floor. The fire size must be entered, though the model may modify the heat release rate as the oxygen concentration in the compartment is reduced by the fire. Some zone models account for effects of mechanical ventilation, which means that the fan flow rate and the location of the vent inlets and outlets are required as input to the model.

CFD models divide the control volume into a large number of small three-dimensional cells and calculate the fire environment within the control volume by numerically solving the conservation equations (mass, energy, momentum, diffusion, species, etc.) within each cell. Solving these equations is accomplished by using finite difference, finite element, or boundary element methods. The results are three-dimensional in nature and are very refined when compared to a zone-type model. The enormous number of computations performed during these modeling exercises is very time consuming and requires powerful computational equipment.

Like zone models, CFD models require a description of the compartment geometry and the openings within the compartment as input. Depending on the sophistication of the extinguishment/fire model, the fire heat release rate may also need to be specified. Heat losses to the compartment boundaries are calculated using the thermal properties of the bounding materials. CFD models have the capabilities to simulate the conditions that occur within complex compartment geometries as well as unenclosed fires since these models are not strictly limited to compartment fire scenarios.

Zone Models

Zone fire suppression models for water mist have been developed by Back et al. [83], Li and Chow [84], Forssell et al. [85], Vaari [86], and Wighus and Brandt [87]. All five models assume a single zone and vary in sophistication from steady-state predictions to transient computations.

Quasi-Steady-State Zone Models

Two quasi-steady-state models have been developed to predict the effectiveness of water mist systems for extinguishing hydrocarbon fuel fires in machinery space applications. The model developed Wighus and Brandt [86] addresses only pool fires whereas the model developed by Back et al. [83] was developed for both pools and spray fires.

Both models were developed for obstructed fires where extinguishment primarily occurs as a result of a reduction in oxygen concentration (consumption and dilution) and neglects the effects of the interaction of mist with the flame. Consequently, the predictions made by these models serve as the limiting case where obstructions prevent direct spray interactions with the fire. The models are based on conservation of energy and mass and require the following input parameters: fire size, compartment geometry, vent area, and water flow rate. The steady-state compartment temperatures and oxygen

concentrations predicted by these models are used to determine the smallest fire (critical fire size) that will sufficiently reduce the oxygen concentration to below the LOC of the fuel.

The energy balance used in these two zone models can be expressed by the following equation:

$$\dot{Q}_{\text{Fire}} = \dot{Q}_{\text{Boundary}} + \dot{Q}_{\text{Vent}} + \dot{Q}_{\text{Vapor}} + \dot{Q}_{\text{Water}} \tag{46.4}$$

where

$\dot{Q}_{\text{Fire}}$ = Heat release rate of the fire
$\dot{Q}_{\text{Boundary}}$ = Energy lost through the walls, ceiling, and floor
$\dot{Q}_{\text{Vent}}$ = Energy lost out of the vent opening
$\dot{Q}_{\text{Vapor}}$ = Heat absorbed by evaporation
$\dot{Q}_{\text{Water}}$ = Energy absorbed by the mist

The following assumptions were made to simplify the calculation:

- Combustion is complete and takes place entirely within the confines of the compartment
- The heat release rate of the fire is a constant (steady state).
- The temperature is uniform within the compartment at all times (after discharge), and the gases exhausted are assumed to be at the compartment temperature.
- The exhaust gases and the gases contained in the compartment are assumed to be saturated with water vapor.
- A single surface heat transfer coefficient is used for the entire inner surface of the compartment.
- The heat transfer through the compartment boundaries is unidimensional; that is, corners and edges are ignored and the boundaries are assumed to be infinite slabs.
- Mist droplets are assumed to be heated to the compartment gas temperature.

The individual components of Equation 46.4 are calculated as follows: the heat release rate of the fire is an input parameter and is calculated based on the known constant fuel spray or mass burning rate of the fire and the heat of combustion of the fuel. The heat lost through the boundaries of the compartment is determined using an overall heat transfer coefficient developed for preflashover fires. The energy losses by vent gas flow are based on the temperature of the exhaust gases and the exhaust rate determined from a vent flow correlation applicable to well-stirred compartment environments. The heat lost by evaporation is based on achieving the equilibrium vapor pressure (assuming saturation), the vent flow rate, and the heat of vaporization. The heat absorbed by the water is determined from the water mist application rate, assuming all the mist is heated to the compartment temperature.

The computational exercise begins by solving the energy balance to predict the steady-state compartment temperatures in the space and the mass flow rate of air/gases through the vent opening. Once the steady-state temperatures and the mass flow rates are known, the steady-state oxygen concentration is then calculated by first determining the amount of oxygen consumed by the fire and then diluting the remaining oxygen with water vapor until the gases are saturated.

The steady-state oxygen concentrations are then used to predict the critical fire size for the selected compartment configuration and water mist system flow rate. In this context, the critical fire size is defined as the smallest fire that will reduce the oxygen concentration below the LOC of the fuel.

The approach used to predict the time of extinguishment varies between the two models. For the model developed by Back, the extinguishment times are predicted using a coupled energy and mass-transfer correlation. The mass transfer is implicit in the following equation, whereas the energy/temperature dependence is embedded in the volumetric flow rate and predicted steady-state oxygen concentration terms. Assuming that steady-state conditions occur quickly and that the extinguishment of these fires becomes related to the time required to dilute the gases in the compartment, the extinguishment times can be approximated using the following equation:

$$\Delta C_{O_2(t)} = \Delta C_{O_2(\text{ss})}\left(1 - e^{\dot{\nu}t/\nu}\right) \tag{46.5}$$

where

$C_{O_2(t)}$ = Oxygen concentration (percent by volume) in the compartment at time t

$C_{O_2(ss)}$ = Predicted steady-state oxygen concentration

v = Volume of the compartment

$\dot{\nu}$ = Volumetric flow rate of air/gas through the compartment

The extinguishment times are determined by setting $C_{O_2(t)}$ equal to the LOC of the fuel (14 % is typically used during this calculation) and solving Equation 46.5 for t. This approach is a first-order approximation and is best suited to predict the extinguishment times of large fires and loses accuracy as the fire size approaches the critical value.

For the model developed by Wighus and Brandt, the extinguishment times are predicted by iterating through the equations in 0.05-s time steps.

The primary outputs of the model are the steady-state compartment temperature and the extinguishment times for a range of fire sizes for a specific compartment configuration and water mist discharge rate. The predictions made by these models compared favorably to the results of four full-scale machinery space investigations conducted for the U.S. Coast Guard. For the range of compartment sizes (100–3000 m^3) and ventilation conditions (closed compartment, naturally ventilated [1.25–5.7 $m^{5/2}$ ventilation factors], and forced ventilation [25 m^3/min]) included in these investigations, the models were able to accurately predict the steady-state compartment temperatures and oxygen concentrations that occurred during the test. In many cases, the larger fires were extinguished before steady-state conditions were reached. This result was also predicted by these models. The models were also able to accurately predict the smallest fire (critical fire size) that could be extinguished due to a reduction in oxygen concentration in the space. Both models were able to accurately predict the extinguishment times for a wide range of fire sizes but lost accuracy as the fire approached the critical value.

Although these models show promise for predicting the steady-state temperatures and oxygen concentrations in an enclosure for a given set of parameters and provide reasonably accurate fire extinguishment time predictions, more sophisticated models are required to accurately predict the transient conditions that occur in a compartment during the discharge of a water mist system. The analysis of these transient conditions significantly increases the complexity of the computations.

Transient Zone Models

Three transient zone models that predict the effectiveness of water mist systems to extinguish hydrocarbon fires have also been developed [84–86]. The models developed by Vaari [85] and Li and Chow [83] are very similar and use the same basic set of equations as described above for the quasi-steady state zone models. The model developed by Forssell et al. [85] is similar in some respects but different in others.

With respect to similarities, all three models solve the conservation of mass and energy equations as a function of time for a given set of conditions. The conservation of mass equations used in the quasi-steady-state models have been replaced by conservation of species. The mass/volumetric flow rate of air through the vent is determined using an orifice flow correlation and the pressure in the compartment similar to the quasi-steady-state models. The compartment pressure is calculated from the density and gas temperature in the compartment using the equation of state for an ideal gas. New mist concentration, droplet evaporation, and extinguishment algorithms have also been developed.

The models are different with respect to how they handle boundary losses, drop evaporation, and predict extinguishment. The models developed by Vaari and Li and Chow neglect all energy losses to the boundaries, whereas the model developed by Forssell et al. includes a lumped mass boundary heat loss algorithm similar to the quasi-steady-state models.

The evaporation algorithms differ significantly among the models. The algorithm developed by Vaari is fairly detailed, as compared to the simplified versions developed by Li and Chow and Forssell et al. In the algorithm developed by Vaari, it is assumed that the heat transfer between the gas and liquid phases is infinitely fast, making the two phases identical temperatures. As a result, all of the heat absorbed by the drop is utilized in the evaporation process. The algorithm includes drop concentration and drop size subroutines that include drop agglomeration and terminal velocity predictions. Using the Clausius-Clapeyron equation to calculate the vapor pressure near the drop surface, the mass transfer number (B) for a single drop is determined. This mass transfer number is then used to determine the evaporation rate for a single drop, which in turn is applied to the entire spray. The algorithm developed by Li and Chow uses a similar approach that has been significantly simplified. In the algorithm developed by Forssell et al., the evaporation model incorporates a correlation constant that represents the combination of the mass transfer number (B) and the surface area–to-volume ratio of the droplet. Rather than including a set of subroutines based on spray characteristics of the nozzle/system that may or may not be available in the public domain, Forssell et al. chose a single empirically fitted correlation constant.

The extinguishment algorithms are also somewhat different among the models. In the algorithms developed by Vaari and Li and Chow, extinguishment is predicted based on a calculated flame temperature determined based on an energy balance conducted in the flame. For this calculation, a limiting flame temperature must be selected (typical values are on the order of 1550 K). This energy balance calculates the temperature of the gases in the flame region by taking into account the species concentrations in the combustion process as well as the mist entrained into the flame. In order to estimate the amount of water droplets entrained into the flame, a simple mist concentration algorithm was developed based on mist discharge rate, terminal drop velocity, and compartment height. Forssell et al. selected a critical oxygen concentration (14 %) to predict extinguishment, similar to the quasi-steady-state models, which is basically equivalent to the previous approach with the exception that the entrainment of mist into the flame is not included in the computation.

All three transient models provide as output the gas (species) concentrations and temperature histories in a compartment for a given set of input parameters (e.g., compartment configuration, ventilation condition, and fire scenario). Transient models provide the capability to study scenarios that never achieve steady-state conditions and that cannot be represented by the steady-state computations. Two examples of these are growing fires (fires with varying heat release rates) and variable flow rate water mist systems. The transient models include more sophisticated evaporation algorithms, which, in theory, should allow them to predict extinguishment more accurately than the steady-state models. The limitations are associated with the single-zone approximation and the need for experimental data to define the unknown parameters used in the model (namely, the spray characteristics of the system). The single-zone approximation may cause the model to fail if the space is not well mixed or the fire is allowed to burn for a significant duration prior to mist system activation. None of the three transient zone models has been thoroughly validated. However, the limited validation performed by Vaari shows promise with respect to the accuracy of these models.

CFD Models (Field Models)

CFD models are much more sophisticated than the previously described zone models and show promise for handling the complex physical and chemical relations that occur. As stated previously, CFD models divide the computational domain into a large number of small three-dimensional cells and solve the conservation equations (Navier-Stokes) in each cell simultaneously. CFD models can provide detailed information on the mass/energy transfer between the

fire and the water mist and on the distribution of water vapor and mist concentration throughout the compartment.

Like zone models, CFD models require a description of the compartment geometry and the openings within the compartment as input. Compartment contents and boundary materials must also be specified. The model is run for a specific set of conditions (compartment configuration, fire scenario, and water mist system). The outputs are very detailed in nature and consist of data files containing information pertaining to the conditions (temperature, velocity, mist concentration, gas/species concentrations, etc.) for each element and time step in the computation. This detailed information allows a graphical/visual representation of the conditions in the compartment during selected time intervals. For example, color contour temperature images and velocity fields represented by small arrows, with the magnitude of the velocity indicated by the length of the arrow, are typical outputs for CFD modeling runs. These outputs allow the visualization of the conditions that occur in the compartment during a specific scenario.

Some of the CFD models currently in use include ALOFT-FT [88], CFX [89], FDS [90], FIRE [91], FLUENT [92], JASMINE [93], KAMELEON [94], KOBRA-3D [95], MEFE [96], PHOENICS [97], RMFIRE [98], SMARTFIRE (sometimes referred to as FIREDASS) [99], SOFIE [100], SPLASH [101], STAR-CD [102], and UNDSAFE [103], but only a limited number of them have been used to characterize water mist applications. Many of these CFD models contain variants of the K-Epsilon submodel required to handle the turbulent conditions produced in this application. K-Epsilon submodels are two additional differential or algebraic equations (where K is turbulence energy and Epsilon is its dissipation rate) that relate turbulent stresses and fluxes to the flow field.

The limitations for applying CFD modeling to water mist applications include the following three general areas: the inability to accurately model the spray characteristics of the nozzle/system discharge, the inability to accurately predict drop transport and flow around obstructions, and the lack of knowledge/algorithms to accurately predict extinguishment.

The ability of CFD models to accurately predict water sprays needs additional research/development and validation. The difficulty with drop transport is associated with linking the liquid water droplets to the gas phase domain and demonstrating the influence of one on the other. Detailed extinguishment algorithms must include an energy balance conducted in the flame and at the fuel surface during the entire combustion process. The approximation of the combustion process must take into account the following species concentrations: fuel vapor, water vapor, oxygen, nitrogen, combustion gases, and water mist concentration. In most cases, the fuel vapor concentration is driven by the radiation from the flame back to the fuel surface and must be solved simultaneously. Although progress continues to be made in all three areas, more work still needs to be done.

The ability of Fire Dynamics Simulator (FDS), Version 4, to reproduce a measured flux distribution map was recently assessed for two multiple-orifice–high-pressure water mist nozzles at two operating pressures [104]. During the study, several flux density distributions were measured under identical conditions in order to achieve an average value. Experimental data were used to define the drop size distribution, the initial drop velocity, and the directional geometry of the nozzle orifices. The cumulative volume fraction curve was reproduced using a Rosin-Rammler/log-normal distribution equation. The study showed that the current nozzle characterization technique used in FDS that employs sectors on the surface of a sphere as source points, input as a single line in the input file, was problematic and required a new approach. Acceptable agreement was achieved by characterizing each orifice in the multiport nozzle as a single solid cone spray with a separate line of parameters in the input file. The results again showed that accuracy of the modeled distribution is very sensitive to the resolution of the computational grid. It was concluded that if high-resolution predictions of

flux distributions are the goal, the numerical nozzle characterization requires some trial-and-error adjustments of values such as spray cone angle, spray direction, and initial drop velocity. Other recent studies have arrived at the same conclusions [105–107]. Based on these studies, it appears that fine computational grids (i.e. small cell sizes) may be required to accurately predict mist discharge characteristics in the region local to the nozzle. This may prove to be a significant limitation depending on the size of the protected space being modeled and the required resolution of the predictions.

The manner in which the spray characteristics of the nozzle affect drop transport and the transport phenomenon in general also needs additional research. Recent research has focused on both the flow of water droplets through cluttered environments [108–112] and on the effects of fire plumes and ceiling jets on the water droplets [113–119]. However, the problem lies more on a fundamental level. Drop transport and tracking are currently being performed using either Eulerian or Lagrangian formulations [120, 121]. A Eulerian formulation uses a fixed grid and assumes the drops pass through (drops and gases travel at different velocities), whereas the Lagrangian formulation considers the droplets and gases to be a single homogeneous mixture. Research has been conducted using both formulations but the information found throughout the literature is very inconclusive regarding the choice of the appropriate method [122]. The appropriate formulation may depend on the spray characteristics of the nozzle as well as on the application. For example, the transport of larger drops may be better predicted using a Eulerian formulation whereas smaller drops may be better predicted using a Lagrangian tracking model. To make matters more complicated, a specific technique may work better closer to the nozzle (near field) and lose accuracy in the far field. Additional research is needed.

With respect to extinguishment algorithms, the physics and computational issues associated with numerical modeling of fire suppression have been identified [123–125]. Studies found throughout the literature typically focus on specific fire types and scenarios. The National Institute of Standards and Technology (NIST) and the Naval Research Laboratory (NRL) have both recently developed algorithms to predict suppression of opposed flow diffusion flames [126, 127]. A recent study validated the accuracy of these algorithms [128]. Limited research has also been conducted on premixed flames [129]. On a larger scale, extinguishment algorithms have also been developed for pool fires [130–134], spray fires [135] and solid fuels [136–141]. Although these advances are promising, there is still the need to develop an all-encompassing extinguishment algorithm capable of handling a variety of fuel types and configurations to be used with CFD modeling.

With respect to the general use of CFD models to simulate the conditions during a specific application, CFD models are currently being used to evaluate full-scale test results, to assess the effects that the application and system design parameters have on the capabilities of the system (i.e., to conduct a sensitivity analysis on the system and application), to extrapolate results/capabilities to conditions outside the bounds of the approval test, and to bound the capabilities of a system in an application where there is little or no empirical data. Most of this information is proprietary with only a limited amount available to the public.

A limited number of general studies using CFD models for full-scale fire suppression research have been carried out by Hadjisophocleous [108, 142]. The research includes the extinguishment of liquid pool fires in both open and closed compartments and fire suppression in an aircraft cabin. The modeling was performed using the CFD model TASCFLOW with the water spray transport handled using a Lagrangian tracking model. During the initial study [108], water mist system parameters (the number of nozzles, nozzle locations, spray characteristics, and discharge rate) were systematically varied to determine their effect on the extinguishment process. The predicted results showed reasonably good agreement with corresponding experimental data. Recently, a sensitivity analysis on how drop size affects extinguishment was conducted using FDS

[125]. As expected, the results of the study were inconclusive due to the number of potential variables associated with the fuel and fire type, and the extinguishment process.

Studies have also been conducted using the CFD model FDS to augment full-scale fire suppression research programs [143–145]. The research includes the extinguishment of liquid pool fires in both open and closed compartments. In both cases, the water spray transport was handled using a Eulerian tracking model. During the latter study, both sprinkling and water mist systems were included in the study. The predicted results showed reasonably good agreement with corresponding experimental data.

A study was also conducted to assess the capability of the CFD model CFX to predict the suppression of hydrocarbon pool fires in an unobstructed enclosure [146]. The modeling work included a sensitivity study that looked at a number of parameters and compared the predictions to empirical data collected in a 96 m^3 enclosure. The results showed that the accuracy of the predictions was highly dependent on the grid/mesh resolution (finer resolutions produced more accurate results). This was also observed during at least three previous studies conducted with FDS [104, 145, 147].

Over the past few years, a significant amount of research has been conducted with the focus of quantifying the hazard associated with vehicle tunnels. This research includes full scale hazard quantification testing, standards development, mitigation system development and testing, modeling and validation testing [148, 149].

In a paper written by Mawhinney and Trelles [148], large scale fire tests conducted in a tunnel test facility in San Pedro de Anes, Spain were modeled using FDS. The objective was to show that the CFD simulations could be, at minimum, partially validated by demonstrating a reasonable degree of agreement with the conditions measured during the tests. The level of agreement between the fire suppression tests results and the simulated conditions was deemed to be adequate to establish confidence in applying the model to examine the conditions that would occur during an unsuppressed fire (i.e. the free-burn, baseline hazard conditions, which were not tested due to cost and potential damage to the tunnel).

In a paper written by Nilsen and Log, the results of large scale tunnel fire tests were simulated using three different models ranging in complexity from spread sheet level calculations to CDF modeling predictions using the CFD model SOLVENT [150] The results showed good agreement across the board for smaller fires but the larger fires were better simulated using CFD. Although there were deviations in the results for the larger fires, the paper concluded that all three models were acceptable tools for assessing baseline tunnel fire hazards.

The U.S. Navy has been investigating the concept of using water mist to reduce the blast overpressures produced during a weapon hit by activating the ship-board water mist system just prior to weapon impact. A series of tests were conducted to validate the concept. The results of the tests were later successfully modeled using FDS [151, 152]. To increase the accuracy of the predictions, an algorithm was developed to predict droplet breakup caused by the initial pressure wave produced by the blast.

The results obtained using CFD modeling demonstrate its potential for analyzing the complex physical and chemical phenomena of fire suppression by water mist. The primary use of CFD modeling has been to extend the understanding of the relationships between the water mist system design parameters and fire suppression (i.e., CFD modeling has been successfully used to extrapolate large-scale test results and to conduct sensitivity analyses on specific water mist system design parameters). CFD modeling not only has the potential to augment the test and evaluation process as currently being used but also shows promise for approving specific water mist system designs for actual applications in the future. The potential for CFD modeling as a research and design tool is now recognized. CFD modeling is currently being used as a research tool at NRC Canada, NRL, NIST, SP, SINTEF, and at numerous universities.

Modeling Summary

An empirical understanding of how water mist systems extinguish a fire is continuing to emerge. Although progress continues to be made, the degree of understanding is not yet at the stage where water mist systems can be designed from first principles. In order to accurately predict the conditions required for extinguishment, the combustion chemistry, combined with thermodynamics and fluid dynamics, needs to be covered in detail. These complex relations are best analyzed using computational models. The current mathematical models used to predict suppression of fires by water mist systems cover the range of approaches from zone fire modeling to computational fluid dynamics (CFD), which are often referred to as field models.

Five zone models (two steady-state and three transient) have been developed to predict the effectiveness of water mist systems against hydrocarbon fuel fires (both spray and pan fires). The models appear to make reasonably accurate first-order approximations of the extinguishment of a range of fire sizes for a given compartment configuration and set of mist system parameters/characteristics. The strength of the zone models is their ability to bound the capabilities of a water mist system for a given application. The limitation of these zone models is associated with a general lack of detail incorporated in the computation. As a result, these zone models may lose accuracy when applied to complex configurations (geometries).

CFD modeling has been shown to be a promising tool for analyzing the complex physical and chemical phenomena of fire suppression by water mist. The strength of the CFD models is their ability to expand the understanding of how the application and system design parameters affect the performance of the system. The graphical/visual nature of the output can illustrate the physical phenomena occurring during the event. The limitations are associated with the high labor costs required to develop a fine computational grid for a large-scale application and the associated long computer run-times to perform the simulation. Applying CFD modeling to a specific application can be an iterative process and requires a certain level of expertise. Additional research is required to further develop and validate techniques to model the spray characteristics of the nozzle/system, formulations to accurately predict drop transport, and an all-encompassing extinguishment algorithm capable of handling a variety of fuel types and configurations. Only limited progress has been made in these areas over the past few years due to the application specific nature of the latest research and the limited amount of validation test data. In any case, modeling still has the potential not only to augment the test and evaluation process but also to aid in approving specific designs for actual applications in the future.

Approval Testing of Equipment

Creating and delivering water mist as an effective fire suppression agent requires different types of hardware than traditional fire sprinkler equipment. The first decade of water mist development saw the introduction of innovative ideas and hardware from non-fire related industries, such as positive displacement pumps from the hydraulics (machinery) field, and the use of compressed gas as an energy source. By the end of the 1990s there were several distinct types of water mist systems on the world market: low pressure systems operating within the pressure range of conventional fire pumps and sprinkler system fittings; intermediate pressure systems requiring slightly higher pressure than conventional sprinkler systems, and high pressure systems operating at pressures much higher than conventional sprinkler systems. Some systems combined water and compressed gas as the driving force. The types of nozzles differed greatly among manufacturers, as they attempted to develop and patent atomization methods and customized valves and control equipment. Hardware, such as positive displacement pumps and pneumatically-released deluge valves, came

from industrial markets where UL Listings or FM Approvals were not common. Therefore, the only effective way to establish that a particular water mist system design based on non-listed hardware can meet performance objectives for a given application is to conduct specialized component evaluations and fire tests. Consequently, water mist approval protocols have been developed and adopted as a means to allow the introduction of non-traditional equipment to the fire protection industry.

Fire test protocols are designed to match or simulate a specific hazard. Water mist systems that meet performance criteria appropriate for that application, which are specified in a consensus test protocol, receive the approval of the approval or listing agency. Table 46.1 shows a list of formalized fire test protocols produced by approval entities recognized in North America and Europe, and that are widely accepted globally. Ideally, test protocols should test the limits of performance of systems against a realistic range of conditions, including worst-case scenarios, and establish measurable performance objectives that meet the needs of a broad range of potential end users and stakeholders.

For marine applications, consensus test protocols have been developed through the International Maritime Organization (IMO). The IMO test protocols encompass machinery room fire hazards (Class B fuels) and accommodation (sleeping rooms) and public spaces on ships (Class A fuels), where water mist systems are installed in place of marine sprinkler systems. For land-based industrial applications, the IMO test protocols have been adopted and modified by FM Global for turbine enclosures, machinery spaces, and pump rooms where liquid fuel fire hazards exist (see Table 46.1). FM Global has also developed test protocols for light and ordinary hazard classifications as referenced in traditional sprinkler system design, and wet benches in clean room environments. UL has also adopted and modified the IMO marine test protocols for machinery spaces, marine accommodation spaces, and land based ordinary and light hazard occupancy classifications.

Annex C of NFPA 750 [2] describes a number of formalized fire test protocols in detail. Note that the criteria for deciding what constitutes acceptable performance is often decided with a specific situation in mind. Successful performance may not mean extinguishment of the fire in all cases. For example, the IMO test protocols for accommodation spaces and public spaces on ships require that the fire only be controlled for a period of 10 min with a limit to the fire spread during that time period. At the end of 10 min, the fire is manually extinguished and the percentage of burned to unburned fuel is calculated. Fire damage to the test materials must be within certain limits. The fire continues to burn throughout the 10 min discharge, and when the water mist system is shut off, the fire may re-kindle. The IMO machinery space protocol, however, requires extinguishment of all fires within 15 min. To achieve extinguishment, the system designers are permitted to utilize combinations of total flooding ceiling nozzles and screening nozzles over the ventilation opening, as well as the addition of surfactants to the water supply for obstructed bilge areas.

The existence of a listing under one of the formalized test protocols does not eliminate the need for experienced judgment in applying the criteria and results of the listing evaluation to a specific application of a water mist system. It is important to confirm that the application sufficiently correlates with the conditions of the listing, and that the performance criteria used to judge pass or fail in the test protocol are consistent with the end user's needs.

Development of Additional Fire Test Protocols

The formalized fire test protocols presented in Table 46.1 do not include all potential applications for water mist systems. Where there is no existing standardized fire test protocol for an application where water mist could provide important advantages, an ad-hoc hazard-specific test protocol often needs to be developed and implemented. One possible difference between

Table 46.1 Fire test protocols for water mist fire protection systems as of September 2012

Agency	Water mist fire test protocol
1. International Maritime Organization (IMO)	IMO Res. A800 (19): Revised Guidelines for Approval of Sprinkler Systems Equivalent to That Referred to in SOLAS Regulations II-2, Chap. 12 [153, 154]
	Appendix 1, "Component Manufacturing Standards for Water Mist Nozzles"
	Appendix 2, "Fire Test Procedures for Equivalent Sprinkler Systems in Accommodation, Public Space and Service Areas on Passenger Ships," December 1995
	IMO MSC/Circular 668: Alternative Arrangements for Halon Fire Extinguishing Systems in Machinery Spaces and Pump Rooms [155]
	Appendix A: "Component Manufacturing Standards of Equivalent Water-Based Fire Extinguishing Systems," 1994
	Appendix B: "Interim Test Method for Fire Testing Equivalent Water-Based Fire Extinguishing Systems for Machinery Spaces of Category A and Cargo Pump Rooms," 1994
	As amended in MSC/Circ. 728: "Amendments to the Test Method for Equivalent Water-Based Fire-Extinguishing Systems for Machinery Spaces of Category A and Cargo Pump-Rooms contained in MSC/Circ. 668, Annex B," June 1996
	MSC/Circ. 913: "Guidelines for the Approval of Fixed Water-Based Local Application Fire-Fighting Systems for use in Category A Machinery Spaces," June 4, 1999 [156]
	MSC/Circ. 1165, "Revised Guidelines for the Approval of Equivalent Water-Based Fire-Extinguishing Systems for Machinery Spaces and Cargo Pump-Rooms," 10 June 2005 [157]
2. FM Global Research Corporation (formerly FMRC) Norwood, MA, USA	FM Global, Approval Standard for Water Mist Systems, Class Number 5560, 2009 [158]
	(a) Appendix A, B, C: Fire Tests for Water Mist Systems for the Protection of Machinery Spaces, Special Hazard Machinery Spaces, Combustion Turbines with Volumes up to, and including, 2825 ft^3 (80 m^3) (respectively)
	(b) Appendices D, E, and F: Fire Tests for Water Mist Systems for the Protection of Machinery Spaces, Special Hazard Machinery Spaces, Combustion Turbines with Volumes up to and including 9175 ft^3 (260 m^3) (respectively)
	(c) Appendix G: Fire Tests for Water Mist Systems for the Protection of Machinery Spaces and Special Hazard Machinery Spaces with Volumes Exceeding 9175 ft^3 (260 m^3)
	(d) Appendix H: Fire Tests for Water Mist Systems for the Protection of Combustion Turbines with Volumes Exceeding 9175 ft^3 (260 m^3)
	(e) Appendix I: Fire Tests for Water Mist Systems for the Protection of Light Hazard Occupancies
	(f) Appendix J: Fire Tests for Water Mist Systems for the Protection of Wet Benches and Other Similar Processing Equipment
	(g) Appendix K: Fires Tests for Water Mist Systems for the Protection of Local Applications
	(h) Appendix L: Fire Tests for Water Mist Systems for the Protection of Industrial Oil Cookers
	(i) Appendix M: Fire Tests for Water Mist Systems for the Protection of Computer Room Subfloors
	(j) Appendix N: Other Occupancies Which FM Global Has an Interest in Protecting with Water Mist Systems
3. Underwriters Laboratories Inc. (UL) Northbrook, IL	ANSI / UL 2167, Proposed First Edition of the Standard for Water Mist Nozzles for Fire Protection
	Service, June 1998 [159]
	Machinery Spaces
	Passenger Cabin Fire Tests
	Passenger Cabins Greater Than 12 m^2
	Public Space Fire Tests
	Residential Area Fire Tests
	Light Hazard Area Fire Tests
	Ordinary Hazard I and II Tests
	Nozzle Construction Design, Marking, and Performance Requirements

(continued)

Table 46.1 (continued)

Agency	Water mist fire test protocol
4. Verband der Schadenversichen e. V. (VdS) Cologne, Germany	VdS 2498 Guidelines for Water Extinguishing Systems Requirements and Test Methods for
	Fine Spray Nozzles, August 1996 [160]
	Fine Spray Nozzles for Cable Conduits
	Fine Spray Nozzles for Engine Test Cell
	VdS Safety Concept for Road Tunnels: VdS 3502—Leaflet on Fire Protection in Road Tunnels, VdS-Draft 16.10.2006
	VdS 2562en, "Guidelines for Extinguishing Systems, Procedure for the Approval of New Extinguishing Techniques", 1998-xx (01); VdS Schadenverhütung GmbH, Cologne, Germany [161]

an ad hoc test program and a formalized test protocol conducted by a listing organization is the range of expertise and opinions involved in identifying failure conditions and criteria for judging acceptability of the equipment or system being evaluated. Worldwide, many ad hoc water mist test programs have taken place and continue to be undertaken. Examples include local application systems [25], high-voltage cable tunnels [162], railway tunnels [163, 164], heritage properties [165], libraries and archival storage on fixed shelving [166, 167], electronic equipment rooms [168], computer room underfloor areas [48], aircraft cargo bays [169], and outdoor transformers [170].

Water mist standards, such as NFPA 750, provide guidance on what to include and how to develop a meaningful protocol for a specific hazard. Key factors to consider in the development of such a protocol include the following:

- The test protocols are to be based on a fire protection engineering evaluation of the fire hazard, the compartment conditions, and the performance objectives for the system.
- The test protocols are to be developed, carried out, and interpreted by recognized fire testing laboratories.

Specific to the fire test scenario of the ad-hoc protocol, the following factors should be considered:

1. Simulate the compartment conditions and fuel type and geometry (volume, height, width, and elevation of ventilation and exhaust openings).
2. Provide capability to vary the ventilation conditions to determine sensitivity of the performance to ventilation factors.
3. Select the fuel arrangement that simulates the expected combustibility and fire growth rate. This may require conducting a review of the end users' facilities to establish a realistic fuel geometry. Obtain enough fuel packages to do repeatable tests.
4. Establish meaningful and measurable performance objectives appropriate for the risk.
5. Develop an experiment plan to test the range of parameters for the water mist system design: nozzle selection, cone angle, K-factor, operating pressure (hence, flow rate), nozzle locations, spacing, and orientation.

Formalized listing protocols such as VdS 2562 [161], which is referenced in Table 46.1, describes a methodical approach to the approval of new extinguishing techniques similar in principle to that described in NFPA 750. Test protocols developed in the above manner for ad hoc testing may eventually become formalized protocols and the basis of a listing.

All details of the test must be accurately documented so that the test can be repeated (by others) in the future. The full listing process culminates in the following outputs:

- A report showing the results of the fire tests;
- A report summarizing the results of the component evaluations intended to verify the functionality, durability, corrosion, and environmental resistance of the key components; and,
- A design and installation manual explaining the correct application, installation, and maintenance of the specific equipment. The nozzle characteristics; spacing between nozzles and maximum distances from walls, ceilings, or obstructions; minimum operating pressures; and water supply requirements are all documented in the manual.

Water Mist Systems in Tunnels

One of the most active areas involving the development and application of water mist systems has been for highway road tunnels. Until recently, the European and North American standards [171–175] pertaining to fire safety in highway tunnels were opposed to the use of active water-based fire suppression systems in tunnels. To give an example, Annex D of the 2004 edition of NFPA 502, *Standard for Road Tunnels, Bridges, and Other Limited Access Highways* [171], listed the objections to the use of water-based suppression systems long believed to be unassailable truths by the tunnel fire safety community. The information in NFPA 502-2004 echoed the European equivalent standards, PIARC-1999, "Fire and Smoke Control in Road Tunnels [173]." These documents included statements such as "water spray will cause explosions in petrol"; "vaporized steam can hurt people"; and "visibility is reduced due to de-stratification of the smoke layer." Appendix 4 of NFPA 502-2004 went on to recommend that sprinklers definitely not be installed in tunnels, except possibly for tunnels involving dangerous or hazardous cargo, but even for that risk the advice was to carefully consider the advantages and disadvantages of such systems.

After a series of serious highway and rail tunnel fires that occurred between 1995 and 2005, which resulted in a large number of casualties and financial losses totaling in the billions of dollars [176], road tunnel authorities have reconsidered their reluctance to use active water-based fire suppression systems in tunnels. NFPA 502-2004 and PIARC-1999 represented a different understanding of the fuel loads involved and suppression processes available, and the overall risks. Some of the conditions described the standards might be valid for a fleeting moment in a developing fire scenario, but they neither take into account the rapidity with which fire may progress from incipient to "uncontrollable", nor do they consider the catastrophic scale of the consequences of an unmitigated fire in a highway tunnel. When one considers that uncontrolled fire in the Mont Blanc tunnel burned for more than 50 h, involved hundreds of vehicles over a 500 m length of tunnel, caused catastrophic damage to the tunnel structure that cost billions in repair costs and lost revenue, and 39 fatalities [176], the concern about de-stratification of the smoke layer during the first 5 min of a fire is put into perspective.

Conventional practice for fire protection in highway and railway tunnels has been to rely on ventilation to mitigate the hazard associated with fire in a tunnel by attempting to control the flow of smoke. Refractive coverings are applied to concrete and other structural elements to protect against severe time-temperature exposures [176]. To aid in the design of such safety measures, NFPA 502 provides guidance on the expected fire size for different types of vehicles, or which "time-temperature" curve and duration to use for structural protection. For design of tunnel ventilation systems and determination of the critical velocity needed to control smoke conditions, NFPA 502-2004 indicated that a "bus" results in a heat release rate (HRR) of 20 MW; and a heavy goods vehicle (HGV) fire could achieve 20–30 MW [171]. These design-fire sizes were shown to be significant underestimates of the probable size of fires in large vehicles as a result of full-scale fire testing carried out in the Runehamar test tunnel in Norway. The Runehamar tunnel was instrumented to measure heat release rate during the fires [177, 178]. Results reported by Ingason and Lönnermark indicated that HGV's carrying standard household furniture could create fires of 150–200 MW in a tunnel fire scenario [178, 179]. This new information suggested that tunnel ventilation systems and structural fire protection based on a grossly underestimated fire size of 20–30 MW fires could prove inadequate in the event of a HGV fire in an existing tunnel.

As a result of the Runehamar tests, NFPA-502 2008 Edition [172] and PIARC-2008 [174] now indicate much larger estimated heat release rates are to be used in the design of tunnel safety systems. These influential documents have also removed the language discouraging the use of fixed fire fighting systems. Many tunnel

structural engineers now recognize that installation of fixed fire fighting systems should be (re)-considered for existing tunnels as a means to reduce fire severity so that existing ventilation systems and structural protection can survive a foreseeable fire [180].

Since 1997, a number of fire test programs have been carried out in Europe to determine design criteria for water mist systems for tunnels [181–183]. Fire tests carried out in 2003 and in 2005 in the Hagerbach test facility in Switzerland [181] involved the burning of standard passenger cars arranged to simulate an accident involving three vehicles surrounded by stationary vehicles. The tunnel outlet was instrumented to permit measurement of heat release rate of the fires. The ventilation air velocity was initially 6 m/s, but after ignition the wind velocity dropped to 3 m/s over a 2-min period. The reduction simulated the reduced piston effect as vehicles in the tunnel come to a stop on encountering the accident. Fire in the group of three vehicles typically achieved 15 MW in 7 or 8 min, then rapidly grew to 30–35 MW as the first fuel tanks ruptured. Fuel from the ruptured fuel tanks flowed downslope in the tunnel but was easily extinguished by the water mist system, primarily due to the water mist cooling the fuel as it spread into a thin layer on the roadway. Once the water mist system was activated, the fire in the three vehicles first involved was controlled to 5–7 MW, which gradually diminished as fuel inside the vehicles was consumed. The fire did not spread to adjacent vehicles. In cases where flames impinged on target vehicles about 1 m away, fire did not become established in the interiors even when the windows were breeched by heat, as illustrated in the photographs in Fig. 46.7. When the windows fell out, water mist entered the passenger compartment and soaked the plastic and fabric surfaces. Fire was limited to the three vehicles initially involved in the simulated accident.

Although fire did not propagate to the adjacent vehicles, conditions inside the vehicles shown in Fig. 46.7 photographs (a) and (b) would not have been "tenable." Claims have been made by some proponents of water mist systems that water mist provides a "scrubbing" benefit that may improve visibility and create "breathable" conditions in tunnel fires [184, 185]. If we understand tenability to be a function of temperature, soot concentrations affecting visibility, the toxicity of combustion gases such as carbon monoxide, and the duration of exposure, it is primarily the temperature component that is mitigated by the water mist. A fraction of the carbon soot may be washed out of the smoke and some of the soluble gases may be absorbed by water, but not to the extent necessary to render the environment tenable [186]. This dangerous overstatement of the effect of water mist on smoke has been disproven repeatedly in full-scale fire tests.

Fig. 46.7 Photographs showing the benefit of a water mist system in preventing fire propagation to adjacent vehicles in a passenger car tunnel [181]. With three vehicles fully involved in fire, fire did not propagate into adjacent vehicles because of the wetting and cooling effects of the water mist

Fire tests conducted in the San Pedro de Anes test facility near Oviedo in Spain in 2006 confirmed the satisfactory performance of water mist systems in mitigating fire in HGV's [182]. The fuel package consisted of European wood pallets stacked 2.5 m high, 2.5 m wide, and up to 14 m long on a platform, simulating a fully loaded trailer of a heavy goods transport vehicle. There was enough fuel in the fuel array to support a fire of 70 MW or larger if unsuppressed. The water mist system was typically activated when the fires were between 15 and 20 MW and growing. Over a total of 11 tests, the water mist system prevented the fires from growing to their full potential—reducing the peak heat release rates to 50–60 % of their maximum potential. At a distance of less than 10 m downwind of a fire with a sustained heat release rate (HRR) in the range of 20 MW, ceiling temperatures were less than 100 °C. Except in a small zone of flame impingement immediately over the fuel array, gas temperatures were too low to be a threat to the tunnel lining. Fire did not spread to targets located 5 m away from the vehicle [182]. Furthermore, the reduced temperature of the combustion gases made it possible for an air velocity of less than 2 m/s to overcome the backlayering of the smoke and heat [187]. In spite of the fact that there was a sustained 20 MW fire in the tunnel, due to the cooling provided by the mist engulfing the flames, the thermal impact on the tunnel was nothing like what would occur with an uncontrolled 20 MW fire.

The very large simulated HGV fires used in current testing are highly dynamic and rather unpredictable. Large variations in local temperature conditions may occur from one test to the next, under apparently similar conditions. In spite of some unpredictability of spot temperature readings in the near-field of the fire, the water mist consistently reduced the combustion gas temperatures to below the threshold for ignition of targets or thermal damage to concrete, within 5–10 m from the fuel array. It is important to avoid setting performance criteria based on single point measurements, such as a maximum temperature at a particular distance from the fire or elevation in the tunnel. Judgments about adequacy of the fire protection system should reflect the overall ability of the mist system to reduce fire severity [187]. The performance evaluation of a fixed fire protection system should recognize the macro-benefits of cooling and preventing fire propagation to surrounding vehicles, thus protecting the structural elements from catastrophic thermal damage. The benefits should not be viewed as limited to property protection, however. Sprinkler systems are installed in industrial buildings ostensibly for property protection objectives, yet it is widely recognized that there are very few multiple life loss fire events in sprinklered buildings including those that are industrial in nature [188]. This is because the sprinkler system provides a degree of fire control or fire suppression within the time period necessary for occupants to escape, and can prevent the fire from escalating into a life-threatening event. The same logic should apply to fixed fire fighting systems in tunnels: preventing a fire from escalating to uncontrollable intensity reduces the risk to life of persons trying to escape the fire as well as to fire fighters attempting to approach and suppress the fire.

Water mist systems in tunnels are typically open nozzle, deluge-type systems divided into approximately 30 m long zones controlled by a deluge valve. The water supply is designed so that three zones can be activated simultaneously. It is intended that a fire detection system will locate the fire source accurately and automatically activate the water mist system in the zone where the fire is located, plus one zone upstream and one zone downstream. Very seldom do the fire test protocols for water mist systems include testing the ability of the detection system to reliably locate the source of the fire within a given timeframe. In principle, the efficacy of the detection system should be evaluated as part of the performance testing of the system. There are many difficulties inherent in pinpointing the source of heat, smoke or flame in the dynamic, turbulent and dirty environment typical of roadway tunnels.

There is some debate about what the fire size could be when the water mist system is activated in a real roadway tunnel fire scenario. The fire

size will likely depend on the sensitivity of the detection system and the administrative policy regarding manual activation of the suppression system. It is this author's opinion that activating the water mist system will be beneficial at any stage, although it is obviously preferable to do so before damage to critical infrastructure occurs. The most important performance requirement of the detection system is to locate the fire so that the correct water mist zones may be activated. The benefits of the water mist system can be fully realized even if applied when the fire has reached 15 or 20 MW. HGV fires are likely to reach such intensity within 5–10 min. With 20–25 m long water mist zones and an appropriately designed and coordinated detection and releasing strategy, the fire should not activate any more than the three zones allowed for in the hydraulic design of the water supply. It should be relatively straightforward for any detection technology to detect and accurately locate a fire as large as 15 MW in a tunnel. There may be advantages in being able to detect smaller fires in order to initiate emergency response in a tunnel, such as traffic control and dispatch of emergency personnel, but there is little advantage in imposing an unnecessary requirement to detect very small fires on the detection system controlling release of the water mist system. Any gain in ability to detect smaller fires is likely to be at the cost of reduced reliability in determining the location.

A research project to evaluate fire detection technologies for highway tunnels, coordinated by the National Fire Protection Research Foundation and the National Research Council, Canada, was completed in 2007. A part of the study included monitoring four trial detection technologies over a 10-month period in the Lincoln Tunnel between New Jersey and Manhattan, NY. Detection technologies for the study were selected based only on the willingness of the manufacturers to fund their own participation in the study. One optical flame detector, two video imaging detection systems, and an air sampling detection system were evaluated. One finding of the study was that the systems were prone to generating "nuisance" alarms, or their overall reliability in being able to detect the fire source was adversely affected by the grime and other effluent that is characteristic of roadway tunnel environments. At the end of 10 months all of the systems were tested in a fire demonstration. Test fires were approximately 1–2 MW maximum HRR and were ignited inside a passenger van with windows. The two video imaging systems did not detect any of the demonstration fires, whereas the optical detection and the air aspirating systems detected most but not all of the test fires [189]. The NFPRF study did not include any linear heat detection, which is widely specified for tunnel fire detection in Europe and Japan. Linear detection is resistant to the grimy conditions of the tunnel environment. However its ability to accurately locate the fire at high ventilation air velocities can be questioned. It should further be noted that the tunnel fire testing that has been conducted in Europe has focused on the hazard presented by HGV fires, which can reach a HRR in excess of a 20 MW relatively quickly. The detection tests based on 1–2 MW fires are perhaps pertinent to fires in passenger automobiles, which do not typically result in catastrophic damage to tunnels.

More research is needed on selection and evaluation of appropriate fire detection technologies to integrate with water mist systems. However, most highway tunnels that are candidates for installation of fixed fire protection systems are equipped with closed circuit television monitors, control room and trained operators. Where CCTV monitors are present, manual activation of the water mist system by a tunnel operator can be an acceptable alternative to automatic detection.

Engineering Details of Water Mist Systems

Types of Water Mist Systems

Requirements to conduct performance-based testing of water mist systems result in an assessment of the fire fighting capabilities of the system, and promote the evaluation of new types of hardware and assemblies. This testing has

increased the rate of introduction of new equipment and fire control concepts to the generally conservative field of fire protection systems design. Hardware borrowed from non-fire industries (such as positive displacement pumps from the petroleum industry and hydraulics field), and from gaseous fire protection system hardware, can be component tested and receive the equivalent of an assembly approved for fire protection as part of the process of satisfying the testing protocol. Positive displacement pressure pumps, pressure regulating or unloading valves, compressed gas driven equipment, pneumatic and hydraulically actuated deluge valves, high pressure valves, piping and tubing, as well as tube bending and piping support methods not previously employed in fire protection systems are now available. Fire protection engineers need to understand the associated hardware in order to design, specify, test and commission new types of systems. A few of the engineering design and evaluation concepts that have been introduced as a result of water mist system research and development are described below.

Water mist systems can be categorized based on several distinguishing factors. The four most important from a systems engineering perspective are (a) the mode of application of the mist, (b) method of spray generation (c) the pressure regime, and (d) the means of providing the necessary system flow and pressure. There are several subcategories of systems, each with its own specific technical features, such as single-fluid and twin-fluid systems, and constant pressure versus decaying pressure discharges. The mode of application refers to how the system is intended to develop and deploy the mist within a given space or environment, and includes total compartment application (TCA); local application (LA), and zoned application (ZA) systems. With regard to pressure regimes, water mist systems distinguish among Low, Intermediate and High Pressure systems. The means of providing the necessary flow and pressure distinguish between the general categories of pumps either electric or gas driven, or some arrangement of compressed gas cylinders. The latter category can be further divided into systems that operate at a constant pressure, similar to a pumped system, versus those that have a declining pressure.

Mode of Application

Water mist systems can perform well in enclosed compartments where the confinement of heat, water vapor and the oxygen depletion caused by the fire can contribute to the extinguishment of even shielded fires. However, it is not the case that water mist systems only work well in enclosed compartments. They also provide fire control benefits in the open air, and in large, well-ventilated spaces such as tunnels. If the compartment is very large relative to the size of the fire, enclosure effects are diminished, and more attention must be paid to projecting water mist to the seat of the fire and wetting or cooling the flame and the surrounding fuels and surfaces.

TCA systems consist of open nozzles distributed throughout the compartment according to the manufacturer's spacing rules. Water is discharged from all open nozzles on opening of a control valve in the same manner as a deluge sprinkler or water spray system. TCA systems benefit from enclosure effects (capture of heat, confinement of water vapor, and recirculation of oxygen-depleted gases) to varying degrees, depending on the size of the compartment. However, TCA water mist systems can accomplish extinguishment with fairly large openings in the compartment, which is not the case with gaseous total-flooding agents [73]. On the other hand, it is not enough to inject a fixed quantity of mist into a compartment, close the door, and expect the fire to go out immediately. The amount of time needed to extinguish a fire varies according to the compartment volume and the size of fire [83]. Water mist must be injected continuously for a sufficient length of time to bring about control, and the fire must generate enough heat to convert water droplets into water vapor and sustain a relatively high water vapor concentration. The extinguishment time of a hydrocarbon fire can be predicted approximately on the basis of a ratio of HRR to volume

(MW/m^3) ratio, and it has been expressed that there will be a fire size that is too small to be extinguishable [83].

It is generally intended that TCA water mist systems be activated automatically by a fire detection and releasing system. In some marine or military applications, however, manual activation of the system is permitted. Some caution should be observed in the design of a system intended to be manually released. If there is a long delay in activation, the combustion gas layer in the compartment may become quite hot and deep. The empty piping may become so hot that water will boil explosively when water is introduced, potentially rupturing some types of piping systems. If the piping survives, the sudden introduction of water mist into a hot gas layer may result in a very rapid cooling, which creates a strong negative pressure in the compartment. In some experimental work a negative pressure spike of minus 1700 Pascal was measured, which resulted in violent damage to the walls of the test structure [46].

The total water discharged by a TCA system in a large space must be considered. Water mist systems require much less water than sprinkler deluge systems, but they still discharge water which must be collected and treated. On Alaska's North Slope, machinery modules up to 1500 m^3 in volume, may be protected by TCA water mist systems. State of Alaska environmental regulations require that all of the water discharged in the enclosure must be captured and removed to a waste-water treatment facility. The water cannot be simply drained into the natural environment. The retention and removal of runoff from a total compartment application system must be considered as part of the design of the system.

TCA systems may be designed for a range of objectives. The IMO machinery space systems are required in the IMO test protocol to completely extinguish most test fires in a specified period of time (15 min). On the other extreme, TCA systems have been installed in Norwegian historic wood stave churches to achieve flashover suppression [43, 165, 167] at much lower flow rates. For flashover suppression a fine mist is injected into the upper portion of the compartment to cool the fire gases and reduce thermal feedback to the objects in the compartment, which prevents flashover from occurring. The amount of water that strikes the art on the walls is minimized. Extinguishment of the source fire is achieved by installing nozzles at floor level that discharge water spray at a much higher rate than the ceiling nozzles, without damaging the treasured wall paintings. The lower nozzles are local application nozzles that work in concert with the total compartment system.

LA systems are designed to discharge directly on an object or hazard in an enclosed, partially enclosed, or open area. Since there will be no confinement of heat, water vapor, or vitiated gases, extinguishment will depend largely on gas phase cooling or wetting of the fuel. To achieve extinguishment requires projection of mist to all areas in which fire can persist. Local application systems do not necessarily need to be designed to achieve extinguishment. The discharged water mist can act as a screen to block radiant heat transfer, mitigating fire spread or limiting damage to surrounding materials. Local application systems are considered necessary compliments to a TCA system in some machinery room systems on ships [157] and in industrial process buildings. The compartment ceiling may be so high that low level equipment must be surrounded with local application mist nozzles to facilitate fire control. Local application systems may be installed around specific hazards such as diesel engines, flammable liquid or vapor compressors, or large turbines in an open floor area [190].

The IMO prepared IMO MSC/Circ. 913 test protocol for fixed water-based local application systems for marine machinery spaces [156]. FM 5560, FM Global's water mist testing standard, has test protocols for local application water mist systems for industrial food processing burners, deep-fat fryers, outdoor transformers, flammable liquid storage racks, and other special equipment [158]. VdS in Germany has test protocols for local application systems for engine test cells and electric cable tunnels (see Table 46.1) [176].

As discussed for TCA systems, choice of fire detection and system activation strategy for local application systems is an important part of the design of the system. Some systems are intended to be manually activated, whereas others incorporate special detection equipment for automatic activation. The detection system, release, and delivery equipment must be matched to the conditions dictated by the hazard.

ZA systems are designed to protect hazards in a portion of an enclosure, eliminating the need to flood the entire compartment. The concept intends that multiple zones surrounding the fire location will be activated, such that the fire area will be totally engulfed by mist in a manner similar to a deluge system. The incentive for zoning a system is to reduce the overall water flow requirement to a fraction of that required for total compartment flooding.

Recent testing conducted to develop water mist systems for highway tunnels has confirmed the satisfactory fire control performance of zoned water mist systems [181–183]. The water mist system is divided into zones up to 32 m long, each controlled by a local deluge valve. The water supply and pumping capacity are designed to support the activation of three complete zones: the zone in which the fire is located and one zone upstream and one zone downstream. Clearly it is essential that there be either a fixed fire detection system that is suitably precise to correctly locate the fire, or a CCTV system monitored by trained operators with authority to activate the system manually.

Experience with thermally activated sprinklers or nozzles in tunnels has shown that heat from a fire will travel along the ceiling and open sprinklers or nozzles faster than can be controlled by the resulting water discharge. The risk is that more sprinklers may be opened than can be supported by the water supply. For this reason, zoned deluge water mist systems are preferred because the water supply can be designed to supply a fixed, pre-determined number of nozzles, an attractive option for protecting tunnels [183]. It is essential of course that the zones that are opened completely envelope the source of the fire. Thermally activated nozzles (automatic nozzles) have been used in conjunction with a ZA system, to further reduce the amount of water required by the water mist system. Every second nozzle on a line is thermally activated and covered by a protective cap, with an open mist nozzle inbetween. Three zones of nozzle lines are activated by the detection system as for a normal zoned deluge system. There is enough water mist distributed to prevent "runaway" activation of the thermally activated nozzles as hot gases flow along the tunnel prior to activation of the mist system. Once detected and located by a separate detection system normally used in the tunnel, the appropriate zones are activated. The protective caps in the activated zones are released by water pressure, exposing the thermal elements. Then in the hottest areas directly surrounding the fire, the thermally activated nozzles activate and effectively double the mist application rate over the fire. This patented concept has been tested by Marioff Corporation and shown to be as effective at controlling temperatures as the full deluge system, with approximately 60 % of the water discharge rate.

The proper performance of a zoned application water mist system depends critically on the performance of the detection system. Testing of the ability of the detection system to determine the fire location and actuate the correct zone should be made part of the approval test protocol for such systems.

Automatic Sprinkler Alternative Water Mist Systems are a fourth category of mode of application, which is that of a water mist system with closed, thermally activated (automatic) nozzles installed throughout a building in the same manner as a conventional sprinkler system. IMO has long accepted water mist systems with automatic nozzles as equivalent to marine sprinkler systems. Such systems are installed throughout accommodation and public spaces on most passenger ships. It is not surprising that there is interest in providing similar systems in land-based applications. In a number of jurisdictions in Europe, water mist systems have been installed in hotels and office buildings in lieu of conventional sprinkler systems. The concept is

now recognized by the NFPA 750 committee. A new definition has been approved for publication in NFPA 750, 2013 Edition, which defines an "Occupancy Protection System" as "a water mist system utilizing automatic water mist nozzles installed throughout a building or portion of a building and intended to control, suppress or extinguish a fire." The question that remains to be explored is whether the building and fire regulations, which provide substantial trade-offs in building construction requirements in recognition of the benefits of automatic sprinklers, will apply those benefits to water mist systems designed and installed as an automatic sprinkler system alternative. At the present time (2012) water mist systems do not have as broad a range of approval tests as conventional sprinklers. Generic prescriptive design and installation criteria, and standardized listing evaluations exist for conventional sprinkler systems for light hazard to extra hazard applications. Such is not the case for water mist systems, which rely upon manufacturer specific design and installation criteria, and performance-based listing criteria for light and ordinary hazards (OH1 and OH2),. However, efforts are underway to expand testing of water mist systems against as many hazard scenarios in buildings as for sprinkler systems, so that the benefits associated with conventional sprinkler systems can be extended to water mist systems.

Pre-engineered versus *engineered systems*. A pre-engineered water mist system is one that has been developed for a hazard of a limited size and consistent features defining the compartment. For example, a water mist system may be tested in a test structure of a certain volume to represent a turbine or diesel engine enclosure, with specific ceiling height, obstructions, ventilation openings, and fire scenarios. The detection time and the size of fire on detection will be largely predictable. The number of nozzles, their locations, the amount of stored water required for the required duration of flow, and the diameters and maximum lengths of pipe or tubing are all determined by the test protocol. The installer need only match the nozzle spacing and stay within the limits specified for pipe diameter and length of run to install the system properly. No engineering calculations are required to ensure that nozzle pressures are adequate or that flow rates and water storage volume are sufficient for the hazard.

Pre-engineered should not be taken to mean fool-proof or "no engineering required." Pre-engineered water mist systems are sometimes improperly installed and maintained. In the international off-shore oil industry, for example, pre-engineered water mist systems are widely used to protect small turbine enclosures. The nature of the contracting environment is such that installers of the fire protection systems often work for a general piping contractor that is approved to work in the particular oil field, as opposed to a fire protection specialist familiar with the intricacies of the water mist system. Errors that can occur and have occurred, are many. The volume of the enclosure may be outside the limits of the pre-engineered system listing. Nozzles may be improperly placed or oriented; tubing diameters and lengths may be incorrect; the water storage unit may be located too far from the hazard, and specialty pneumatic releasing valves may be improperly set up. The interlocks to accomplish automatic release of the water mist and shut down the fuel pumps and ventilation may not be complete and may never have been tested. The inspecting engineers from the production sector do not have the experience necessary to inspect the systems and identify the faults. Annual maintenance may be performed by personnel unfamiliar with the system hardware, so that the installation faults never get corrected. It is not surprising that fires have occurred in which the pre-engineered system failed to operate.

Engineered systems, on the other hand, are designed in the same manner as traditional sprinkler or water spray system, based on criteria in the manufacturer's design, installation, operation and maintenance manual. The designer applies nozzle spacing rules, pipe or tubing and water flow requirements to a variety of compartment sizes and fire hazards. The pump or compressed gas supply is dimensioned to be able to satisfy

the calculated flow and pressure requirements. An engineer must perform hydraulic calculations to confirm that minimum nozzle pressures and system flow rates are achieved. Problems such as those listed above may still occur during installation, but an engineered system is likely to receive a higher level of construction supervision, acceptance testing and maintenance, than a pre-engineered system.

Methods of Spray Generation

There are numerous ways to generate atomized sprays [41]. Water mist system equipment manufacturers have staked out and filed patent applications for their preferred means of mist generation. Research in the spray and atomization literature discusses exotic technologies such as electrostatic sprays, nebulizers, and ultrasonic devices [27]. However, not all atomization processes are practical for fire protection systems. Some techniques are only suitable for mass flows of milligram/second with projection distances measured in millimeters, whereas sprays suitable for water mist fire suppression systems must have mass flow rates in the kilogram/second, with projection distances measured in meters. Suitable nozzle types include multi-orifice pressure jet nozzles, impingement nozzles, and twin-fluid nozzles. Mass flow rates are typically measured in the range of 0.033–0.667 kg/s (2–40 L/min). Cone diameters and projection distances are typically measured in meters. The atomization process must be sustained for tens of minutes in most cases. This section will highlight some of the engineering features of interest associated with different methods of generating water mist.

Twin-fluid nozzles. Twin-fluid water mist nozzles involve combining two independent streams of fluid, one of water and one of compressed gas, at a nozzle to generate finely atomized spray. By combining the energy stored in the compressed gas with a water stream, finely atomized sprays can be produced at relatively low water pressure. Twin-fluid nozzles generally have separate piping networks for water and compressed gas, which join at the nozzle. They provide a high degree of adjustability between the balance of liquid and gaseous streams—hence, they can be tuned to maximize the quality of the spray. On the small-scale twin-fluid nozzles provide excellent control and versatility in spray production. On the larger scale necessary for general fire protection, practical limits to their applicability are encountered. Designing the piping systems for both liquids involves trying to balance the air-to-liquid mass ratio (ALR) (ratio of the mass flow rate of air to the mass flow rate of water) at each nozzle throughout the discharge. Twin-fluid nozzles can utilize larger orifices than pressure jet nozzles, and are therefore somewhat less vulnerable to plugging. On the negative side, twin-fluid nozzle systems require storage and delivery of media with distinctly different engineering characteristics. Calculations must be done for both compressible and incompressible fluids in two distribution systems. A suggested approach to balancing the distribution of atomizing medium with the water flow is provided in Mawhinney [191].

The NFPA 750, 2013 Edition expands the definition of twin-fluid system to include those that combine both the water and the compressed gas in one piping system. One manufacturer has produced a reciprocating pump driven by compressed nitrogen that discharges water and nitrogen into the piping system. The friction losses in the distribution piping cannot be calculated using either incompressible liquid flow equations (normal hydraulics) or compressible flow equations. Nor is the mix a "two-phase flow" because the mix consists of two fluids, not two phases of the same fluid. The engineering of such systems, including the dimensioning of piping, confirmation of end nozzle pressures, and ensuring balanced discharge through nozzles close to the source and those far from the source, not to mention comparable discharge duration of both water and compressed gas supplies, depends almost entirely on empirical data.

Single-fluid nozzles discharge water only. Most water mist systems utilize single-fluid nozzles. The water is ejected through one or

more orifices and either disintegrates into mist due to velocity differences between the water jet and the surrounding air (pressure jet nozzles) or disintegrates into small particles on impact against an impingement surface such as a deflector plate (impingement nozzles). A more in-depth discussion of the physical mechanisms involved in atomization can be found in Lefebvre [41] and of common water mist nozzles, in Mawhinney [191].

Manufacturers of nozzles for industrial applications have catalogs filled with different nozzle designs, delivery rates, and cone shapes. They have been manufacturing a wide range of nozzles for many years. It is surprising, therefore, how much money and effort have gone into the custom design of nozzles for water mist systems by fire protection specialists. The water mist system manufacturers have developed their preferred nozzle design through in-house research and development. Some off-the-shelf commercial nozzles have been successfully applied in water mist systems, but have required customized selection of individual orifice sizes [23, 33].

Mist generation by flashing of superheated water. Evidence that water mist with sufficiently small drop sizes may quell a dust explosion is found in work conducted at the Irish agricultural research facility involving dusts of dried milk products [192–194]. The mist-generating method involves the flashing of superheated water released from a self-pressurized container [195]. Water is superheated to 175 °C in a closed container up to 70 L (18.5 gal) in volume. As steam tables indicate, this puts the closed container at a pressure of approximately 10 bar (145 psig). When released to atmospheric pressure through a fast-opening valve, a percentage of the water flashes directly to vapor phase and then condenses into fog-sized particles (<20 μm) as the cloud cools. There is a dynamic release of energy as the liquid flashes, which shatters the remainder of the mass of water into relatively fine spray ($D_v0.90$, ~300 μm) (i.e., 90 % of the volume of the spray as contained in drops less than 300 μm in diameter) [195]. The energy exchange also results in intense cooling of the spray, so that 30 cm away from the discharge orifice, the mist temperature may be 35 °C or less [193].

The flashing process does not require a nozzle—simply an open orifice—and it results in a rapid distribution of mist plus fog throughout the protected space. The condensed fog is similar in particle size to NanoMist, that is, an order of magnitude finer than can be achieved by mechanical generation of spray. The phenomenon is very dynamic and allows for the rapid distribution of "fog" and water vapor throughout a space. Full-scale fire suppression tests carried out by Mawhinney et al. [193] determined that the ultrafine mist was not more effective than other mists at extinguishing pool fires in enclosures. It was suggested, however, that its success in dust explosion mitigation may be due to the high mass fraction of very small (~20 μm), closely spaced droplets, suggested by Zalosh [40] to be a prerequisite for explosion mitigation with water mist. Further experimental work is required to validate its potential for vapor-air explosion mitigation [194].

NanoMist is an ultrafine mist with very uniform drop size distribution with a volumetric mean droplet diameter in the 10 μm range [27]. The technology combines an ultrasonic transducer assembly (nebulizer) and a process equipment for aerosolization, extraction, and transport of the mist. The capacity of the mist generator is in the range of 0.25 Lpm (0.06 gpm). The opaque cloud of low momentum mist can achieve suspended mass of water droplets in excess of 240 g/m^3. No conventional water mist nozzle approaches that level of suspended water droplets. The NanoMist is transported by fans through smooth ducts to confined areas. In a series of tests conducted for the U.S. Navy to develop a "hybrid" system (nitrogen plus water mist), NanoMist was tested in a mock computer room subfloor (false-deck) against telltale fires [26–28]. Various combinations of inert gas (nitrogen) and water mist were used to extinguish the test fires. The concentration of nitrogen needed to inert the space and extinguish the fires was first determined. Then water mist was

added to the nitrogen. A conventional fine water mist reduced the concentration of nitrogen needed to extinguish the fires by as much as 40 %. Water mist itself could not extinguish the concealed fires in the subfloor. In contrast, the NanoMist was able to extinguish the telltale fires itself without the addition of nitrogen. One of the problems encountered in trying to apply NanoMist is that of delivery. The fog itself has very little velocity or momentum; the act of trying to force it to flow and to fill spaces causes coalescence and condensation of the suspended water droplets.

Pressure Regimes

NFPA 750 distinguishes between low-, intermediate-, and high-pressure systems. Low-pressure systems operate at pressures below 12.1 bar (175 psi), the same as conventional sprinkler systems. Conventional centrifugal fire pumps can be utilized to achieve system pressures, and standard sprinkler piping and hanging methods can be used. Intermediate-pressure systems have operating pressures that lie between 12.1 and 34.5 bar (175 and 500 psi). High-pressure systems operate above 34.5 bar (500 psig). Pumps, pipe or tubing, fittings, and supports for high-pressure water mist systems require specialized knowledge to design, install and maintain.

Most pre-engineered gas-driven water mist systems require banks of high pressure compressed gas cylinders, therefore at least portions of the system require familiarity with high pressure compressed gas equipment. With twin-fluid systems, some may be high pressure and some low pressure; the extinguishing medium (water) cylinders or tanks may be at low pressure, and regulators may be used to reduce compressed gas from cylinder pressure to match the lower water pressure.

With the NanoMist technology described earlier, the water is delivered to the nebulizer under low pressure, but the mist created does not fit the conventional concept of a piping system delivering water to a nozzle under pressure. It is in effect a "no-pressure" system. A NanoMist system must incorporate a means of transporting the mist to the volume to be protected.

Low- and intermediate-pressure systems. The dividing line between "low" and "intermediate" water mist systems in NFPA 750 is 12.1 bar (175 psi). For standard sprinklers, 12.1 bar (175 psi) is the *maximum* permitted nozzle pressure, whereas many so-called low pressure water mist nozzles were developed for a *minimum* nozzle pressure of 12.1 bar (175 psi). If the minimum nozzle pressure is 12.1 bar (175 psi), basic hydraulic calculations will demonstrate that the upstream piping and the pumps required must produce pressures higher than 12.1 bar (175 psi), i.e., in the "intermediate" pressure range. For this reason, it is preferable to consider the maximum pressure in the piping system, rather than the nozzle, in distinguishing *low* from *intermediate* pressure water mist systems. By that measure, water mist systems that require pump ratings and piping pressures in excess of 12.1 bar (175 psi) but less than 34.5 bar (500 psi) are intermediate pressure water mist systems. For water mist nozzles with a minimum allowable pressure in the 5–8 bar (72.5–116 psi) range, the entire system including the fire pumps can operate at less than 12.1 bar (175 psi), therefore the system is genuinely a low pressure water mist system.

Water mist systems that require pumps rated to 17 and 20 bar (245.5 psi and 290 psi) are intermediate pressure water mist systems. Some approved fire pumps exist for this range of system pressure (20 bar, 290 psi) at least within Europe. The intermediate pressure water mist systems that this author has designed or reviewed to date, operate between 12.1 bar and 20 bar (175 psi and 290 psi).

High-pressure systems. Most high pressure water mist systems operate at pressures in the range of 60–120 bar (870 psi to 1740.5 psi), considerably higher than 34.5 bar (500 psi). Not all of the pressure is needed at the nozzles, which might be Listed with a minimum acceptable pressure of 50 bar. The surplus pressure permits the

use of relatively small diameter piping, which is an advantage for installation in some settings. For example, for heritage buildings, the ability to use small-diameter tubing reduces the impact of the fire suppression system piping on the architecture. Therefore, high pressure systems utilize electrical energy to gain some material advantage over the fire: effective at greater ceiling height; use of smaller diameter tubing and reduced water flow requirements, compared to low pressure water mist systems.

High-pressure water mist systems are installed on passenger cruise ships as an alternative to marine sprinkler systems. The ability to reduce the weight of piping in the superstructure of the ship, compared to marine sprinkler systems, was a major factor favoring the use of high pressure water mist systems. They are widely used in marine and petroleum machinery and equipment spaces on the North Slope of Alaska. Water mist systems have been installed in new highway tunnels up to 10 km in length have been high-pressure systems. They have also been installed in heritage buildings, museums, and art galleries.

High-pressure water mist systems may be gas-driven, pre-engineered systems, or pump-driven engineered systems. Gas-driven systems operate over a declining-pressure range from, for example, 100 bar at first release to 20 bar at the end of a 10 min discharge period. There is also a gas-driven pump that can extend the operation of a gas-driven high-pressure system for up to 1 h without the need for electric-motor or engine-driven pumps [196]. For high-pressure system piping, stainless steel tubing is used in conformance with the ASME/ANSI B31.1, *Power Piping Code* [197]. Good practices for tube bending, cleaning, and swabbing; supports; and makeup of compression fittings must be applied.

Opinions are sometimes expressed regarding whether high-pressure water mist systems are "better" than low-pressure water mist systems. If that were the case, one would expect that the range of successful water mist technologies would have quickly become limited to high pressure systems. The fact that both low pressure and intermediate pressure systems are actively competing with high pressure systems in the market place is because, as extensive testing has shown, acceptable fire suppression can be achieved with both high- and low-pressure water mist systems. The choice of technology for any given application is based primarily on practical matters specific to the application, such as the level of importance placed on minimizing water discharge volume, the cost of electric power, the cost of labor, and the availability of labor with the requisite skills to design, install and maintain the system. In principle, then, the engineering, environmental, and economic issues related to the different technologies will determine the best choice for a given application. However, individual vendors of water mist systems whose equipment is limited to one pressure regime will limit their recommendation for "best choice" to their own equipment.

It is highly beneficial to end users to have an independent fire protection engineer who is familiar with the technical details of all types of water mist systems, assist them in evaluating the best choice for their application. Preliminary layouts of systems with equivalent approvals can be made using different manufacturers' nozzles, and performing hydraulic calculations to determine the total water demand and pump selection. Table 46.2 is presented to illustrate this point. Nozzle and piping layouts were made following the manufacturers' spacing rules and K factors for nozzles or sprinklers. The table lists the type of nozzle or water mist system components, the minimum nozzle pressure required and its K-factor, the total number of nozzles within a design area, and the calculated total water flow rate (with 15 % overage). Hydraulic calculations were performed for each trial layout to determine the discharge pressure at the pump outlet. The pump pressure shown in Column 8 is the nominal rating of the pump that one would select, not the calculated minimum demand pressure.

Table 46.2 illustrates that there are several factors to consider when making a decision about which water mist system to use for a given application. Column 2 identifies the system by the minimum nozzle pressure. Two water mist

Table 46.2 Comparison of water demand and pumping requirements for five different designs for water mist systems using nozzles from three manufacturers, with the demand for conventional sprinklers for the same application

Col 1	Col 2	Col 3	Col 4	Col 5	Col 6	Col 7	Col 8	Col 9	Col 10
Manufacturer/Design	Nozzle pressure regime[a]	Nozzle pressure bar	Nozzle K factor	Spacing m	# Units Op'g	**Total Q L/min**	Pump H Bar	System pressure regime[a]	Power rank[b] kW
Manuf A Linear, Aisle	LP-LWM	6	10.0	2.7	12	**338**	16	IP	9
Manuf A Linear, Aisle + flue	LP-LWM	6	20.0	2.7	12	**676**	16	IP	18
Manuf A OH2 Nozzle Aisle	IPWM	10	14.3	2.4	16	**832**	20	IP	28
Manuf B OH2 Nozzle Aisle	IPWM	13	9.2	2.4	16	**610**	20	IP	20
Manuf C OH2 Nozzle, Aisle	HPWM	70	5.2	2.4	16	**801**	90	HP	120
CONV OH2 Sprinkler, Aisle	LPSS	3	80.7	2.4	16	**2572**	8	LP	34

HPWM High pressure water mist, 34 to 100 bar, *IPWM* Intermediate pressure 12 to 34 bar, *LPWM* Low pressure, <12 bar, *LP-LWM* Low pressure Linear Water Mist system, *LPSS* Low Pressure Standard Sprinkler

[a]Note: the minimum nozzle pressure may be in the low pressure regime, but the **system pressure** is in the intermediate pressure regime

[b]"**Power Rank**" is the hydraulic horsepower (kW) to pump the design flow at the rated pump pressure

nozzles and the sprinkler system are shown as being in the low-pressure regime. Column 9 identifies that all of the water mist systems have system pressures greater than 12.1 bar (175 psi), and should properly be referred to as intermediate-pressure systems. Column 7 shows the calculated total water flow for each system. One water mist system requires only 338 L/min (89 gpm); another requires 832 L/min (220 gpm), while the standard sprinkler system requires a flow of 2572 L/min (680 gpm). If minimizing the total water requirement is of primary importance for the application, the "best" system will be based on Column 7. Column 10 calculates a relative energy requirement factor, referred to as "Power rank" number. This number is simply the "hydraulic horsepower," or hydraulic energy requirement in kilowatts, to move the design flow rate shown in Column 7 at the pump rated pressure shown in Column 8. The numbers shown in the table utilize Equation 46.6 presented in the following section, assuming an efficiency value of 1.0 for all pumps. The resulting number is useful for ranking the different technologies against each other according to energy requirements. The hydraulic energy requirement for the high pressure system is more than 10 times the comparative energy requirement for the water mist system with the lowest water flow and pressure requirement. By completing the preliminary designs and laying out the requirements for the candidate systems, as shown in the table, one can begin to make an informed choice. Although not shown in the table, the relative costs of the different systems will also need to be considered in selecting the best option.

Designing with Positive Displacement Pumps

High-pressure water mist systems can utilize use electric motor- or diesel engine-driven, positive displacement (PD) pumps to achieve the necessary system pressures. This is in contrast to traditional centrifugal fire pumps used in fire protection systems. Unlike centrifugal pumps, which can put out a wide range of flows (Q) at different pressures, PD pumps put out a constant Q at a specific pressure for given rotational speed. The pressure achieved is a function of the power (kilowatts) of the driver, electric motor or diesel engine, that turns the pump shaft. The pump discharges the volume of water contained in each piston chamber or gear void

with each stroke or revolution. If a PD pump operates against a closed system, i.e. no nozzles are discharging water, the pump will cause the pressure in the system to increase until the system piping fails or damage is done to the pump or the driver or both. Unlike centrifugal fire pumps, PD pumps have no "shut-off" head.

Most water-based fire protection systems, including those consisting of automatic sprinklers on a piping grid, generally have a variable demand, which depends on the number of sprinklers or nozzles expected to open in response to a fire. The hydraulic demand in terms of flow rate increases as more sprinklers activate. Thus it is essential to have a water supply with pumping ability that can accommodate the associated range of hydraulic demands of most fire protection systems [198].

There are practical limits to the pressures that can be achieved using centrifugal fire pumps, however. To provide the discharge pressures associated with high pressure water mist systems, the speed of the driver must be significantly increased, or multiple centrifugal pumps must be connected in series. Even with these arrangements though, it is unlikely that centrifugal pumps can provide the necessary pressures in the 60 bar to 120 bar (870 psi to 1740.5 psi) range that might be required for some types of water mist systems.

In order to adapt high-pressure PD pump technology to serve fire protection systems with variable demands, various innovations to traditional fire pump practice from the hydraulics industry have been incorporated. By combining the PD pump with a pressure relief valve, referred to here as an "unloader" valve, it is possible to direct the unused portion of a PD pump discharge to a bypass line, while maintaining a high pressure flow to the water mist system. Some manufacturers of high pressure pumps for water mist systems have chosen to use a single large volume PD pump, such as a gear pump, connected to a discharge header with one or two unloader valves installed to discharge any surplus flow and relieve excess pressures. Figure 46.8 illustrates the latter single-pump configuration for a PD pump with 454 L/min output at 17.2 bar (120 GPM at 250 PSIG).

The power requirement (brake horsepower) of the motor to achieve a particular flow and pressure is calculated as shown in Equation 46.6.

Designing with Positive Displacement Pumps

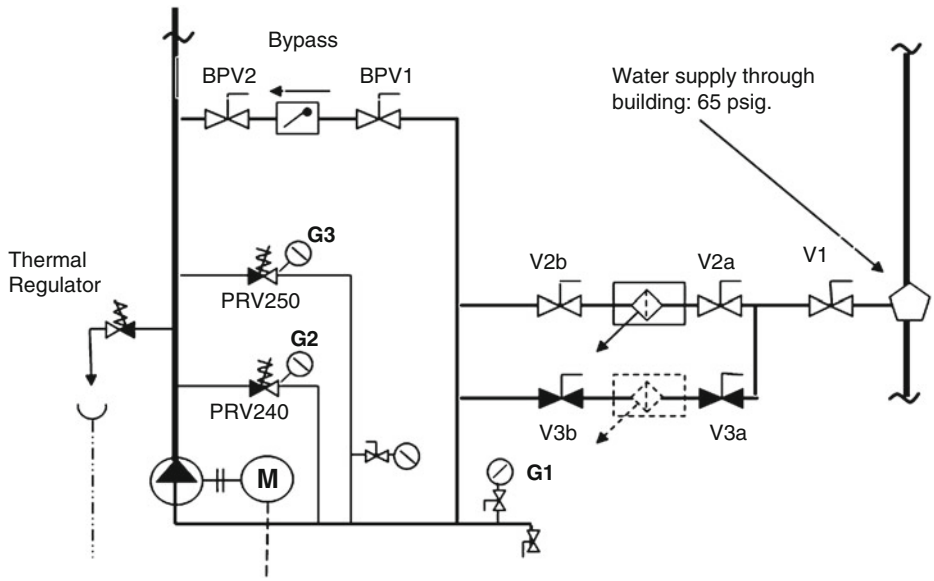

Fig. 46.8 ISO symbol diagram of a single positive-displacement pump with two pressure regulating valves discharging to the suction supply line. The thermal regulator is required by NFPA 20 for relief discharging to suction. The by-pass line is necessary to sustain a minimum standby pressure on the deluge valve manifold

$$P = Q \times H/(600 \times E) \qquad (46.6)$$

Equation 46.7 defines the maximum pressure limit (H) for a given motor-pump combination, as shown in Fig. 46.9.

$$H = (P \times 600 \times E)/Q \qquad (46.7)$$

where

P = Brake Horsepower (kW)
Q = Pump discharge (L/min)
H = Pump discharge head (bar)
E = Combined efficiency of the motor and gear drives ($\eta_d \times \eta_m$)

As a PD pump will produce the same flow at a given speed regardless of discharge pressure, a workable approach to achieving both high pressures and variable water flow rates is to combine multiple PD pumps in parallel, with each pump provided with its own unloader valve. Figure 46.9 illustrates an arrangement of one electric motor driving two PD pumps in parallel. One of the two unloader valves is set to release at a specific pressure, such as 140 bar, while the second unloader valve is set at one half of that, or 70 bar. Regarding Equation 46.6, given that the available Power (P) is constant (e.g., a 17 kW electric motor), the system is capable of discharging either Q × H, or 2Q × ½ H. That is, if each PD pump nominally delivers 50 L/min, the total output from the assembly will be 1 × 50 L/min, at the higher pressure setting of 140 bar, or 2 × 50 L/min or 100 L/min from two pumps at the lower pressure setting of 70 bar. If the system demand calls for a pressure of up to 139 bar, only 50 L/min will flow through the system as the unloader valve set at 70 bar will be discharging all of the flow from the pump it serves, through the low pressure bypass line. If the system demand pressure drops below 70 bar, 100 L/min will be flowing through the system. High-pressure pump skids are manufactured with two, four, six or more electric motors, with each motor driving two PD pumps, in a PD pump assembly. Manufacturers have obtained IMO, FM and UL approvals for such multi-motor, multi-PD pump assemblies for water mist systems.

In order to select a pump for fire protection purposes, fire protection engineers normally follow standardized hydraulic calculation practices [199, 201] to match the system demand to the water supply. NFPA 20, Standard for the Installation of Stationary Pumps for Fire Protection [200] includes a chapter on PD pumps. However, the information provided in the annex of NFPA 20 relating to the performance point for a PD pump, and the data provided by some PD pump manufacturers, is not in an ideal format for conducting conventional hydraulic analysis of

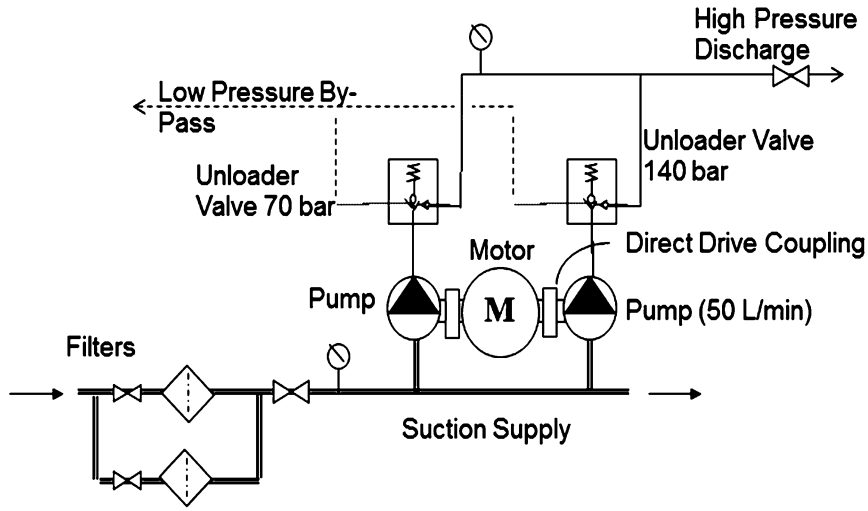

Fig. 46.9 ISO symbol diagram of a positive displacement pump assembly with two PD pumps in parallel, each with a dedicated unloader valve

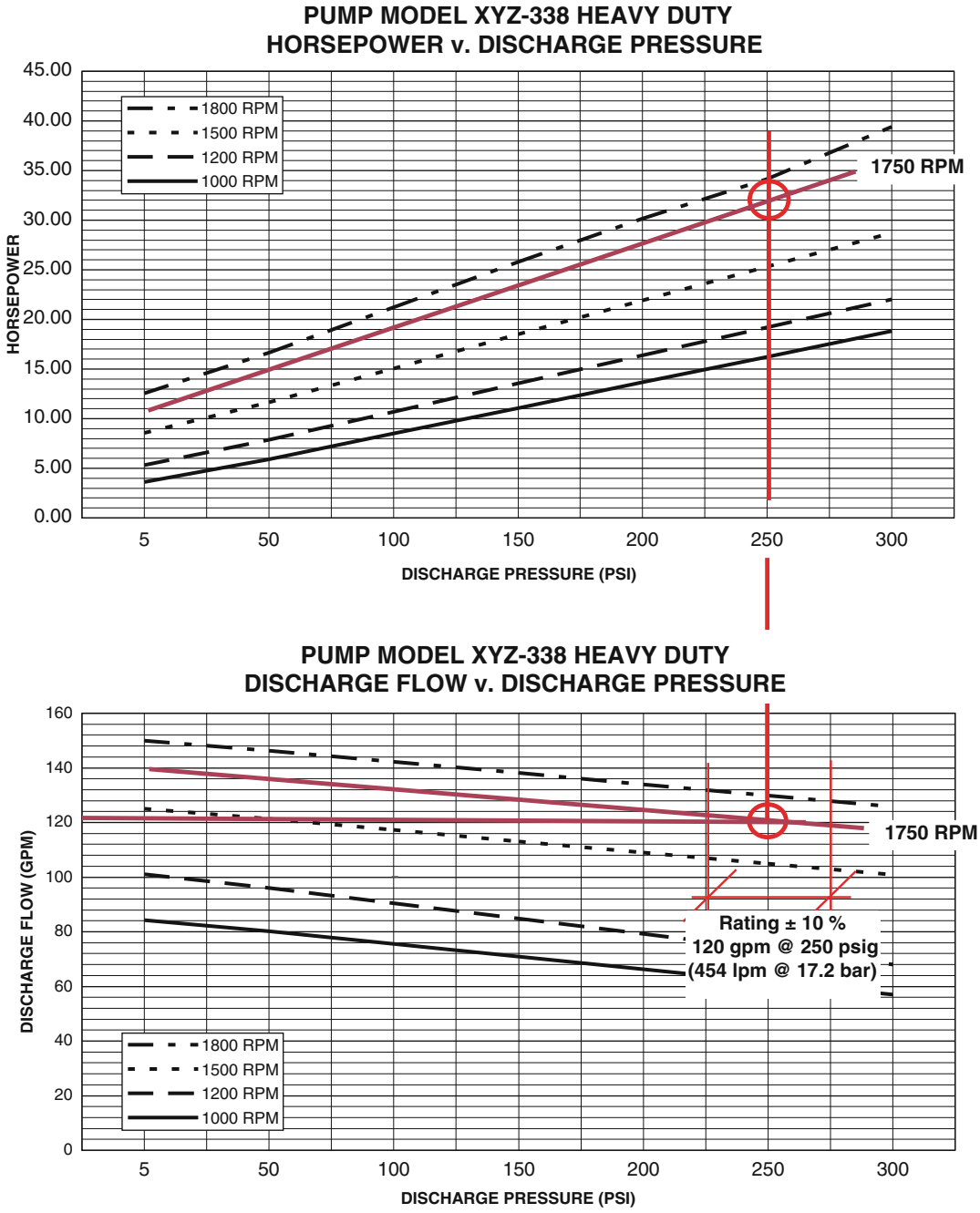

Fig. 46.10 Manufacturer's presentation of performance data for a PD pump approved for intermediate pressure water mist systems

fire protection systems as the information is not presented on a customary hydraulic (N = 1.85) graph. Figure 46.10 illustrates how to determine a specific performance point and an acceptable operating range for a given PD pump. Fluctuations in voltage to the pump motor will cause the pump to deliver slightly more or less than the nominal expected performance.

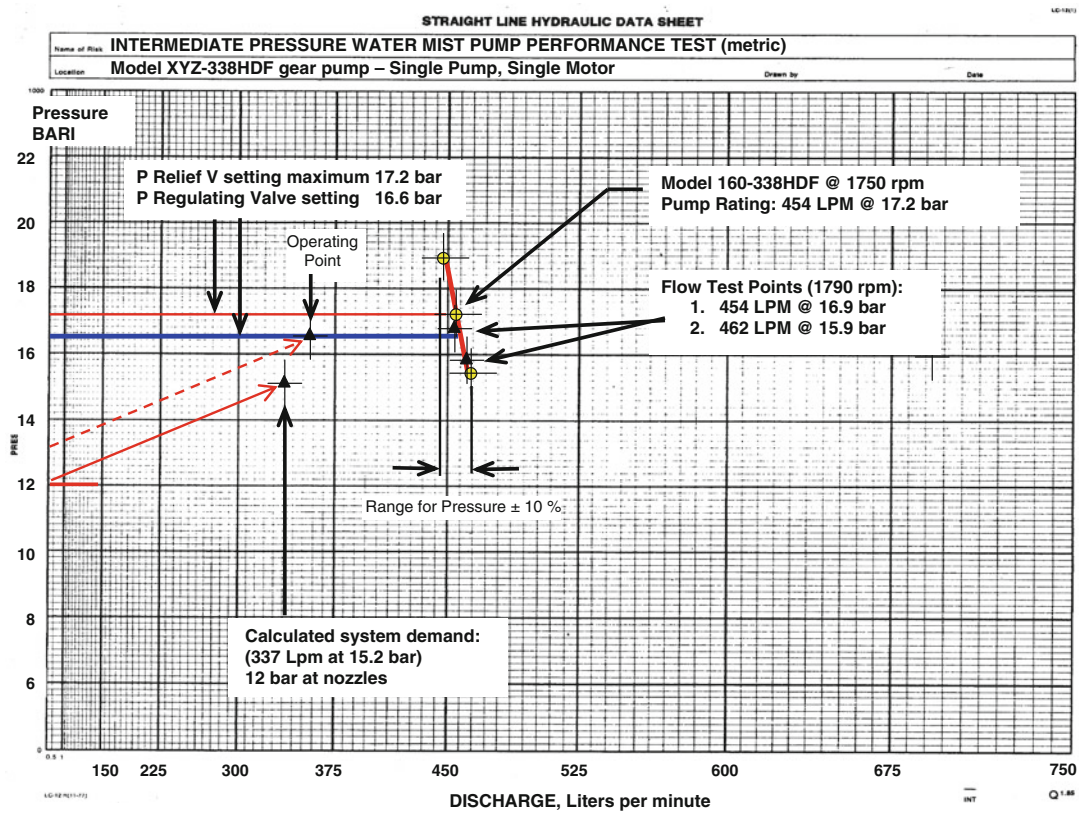

Fig. 46.11 Metric N1.85 straight line hydraulic performance plot for a single PD pump with one motor

Figure 46.10 contains two figures that indicate the available flow, pressure and horsepower for a given PD pump when it operates at different speeds. The circles indicate the necessary performance point for a pump operating at 1750 RPM to provide 454 L/min at 17.2 bar (120 gpm at 250 psi). Note that Fig. 46.10 is presented on a conventional Cartesian grid, whereas fire protection hydraulic calculations typically use N = 1.85 graph paper.

Figure 46.11 presents the information provided by the PD pump manufacturer in Fig. 46.10 on a hydraulic graph (N = 1.85) as this format better facilitates design and analysis of water supplies for fire protection systems [101]. The uppermost horizontal line at 17.2 bar represents the pump's performance "curve" for the given motor size. The pump has a nominal rating of 454 L/min at 17.2 bar (120 GPM at 250 PSI) when operating at 1750 RPM, which is shown as the point in the center of the red circle (Because of voltage fluctuations that affect motor speed, there is an acceptable operating range of approximately ± 10 % with respect to the rating value.).

When combined with an unloader or other pressure regulating valve, the PD pump's narrow performance point or output, in this case 454 L/min at 17.2 bar, can be modified to better accommodate a discharge from the nozzles that is less than the fixed output from the pump. In Fig. 46.11, the horizontal line at the unloader valve setting of 16.6 bar approximates a water supply "curve" capable of accommodating any flow between 0 and 454 L/min to a system of nozzles, while by-passing the unused portion of the pump output. The system pressure relief valve, which is required by NFPA 750 in addition to the unloader valves, is set at 17.2 bar (the upper line). The primary pressure regulating (unloader) valve set to discharge at 16.6 bar will allow a flow of about 360 L/min into the

system. The balance of the pump output, or 454–360 = 94 L/min, will be discharged either back to the suction side of the pump or to a waste line.

The minimum demand for a water mist system, as determined by hydraulic calculation starting with a minimum nozzle pressure of 12 bar, is shown in Fig. 46.11. However, the "system" will operate at the pressure point determined by the setting of the regulating valve(s), as shown in the figure. It is evident that the operating point of the pump assembly exceeds the theoretical fire protection demand, therefore the pump assembly is a satisfactory for the water mist system. The flow test points are discussed later under the Acceptance Testing section.

As noted earlier, Fig. 46.9 shows two PD pumps connected in parallel, each with its own pressure regulating or "unloader" valve. Manufacturers of high pressure water mist systems have FM approved assemblies of PD pumps and motors capable of delivering substantial flow rates at 100 bar pressure or higher. The procedure for plotting the hydraulic performance "curve" for assemblies of PD pumps is extended by summing the volumetric output of the pumps. Figure 46.12 shows a N = 1.85 straight line hydraulic graph for an assembly of six electric motors, each with 2 PD pumps, as previously illustrated in Fig. 46.9. The total flow capability with all six motors and 12 pumps operating is 585 L/min. All 12 unloader valves are nominally set to the same pressure, 100 bar. There is normally some variation in the release pressure setting of unloader valves, so that some of them will "leak" before reaching the 100 bar setting. Therefore, it is not common to achieve a flow test result during an acceptance test that is exactly at

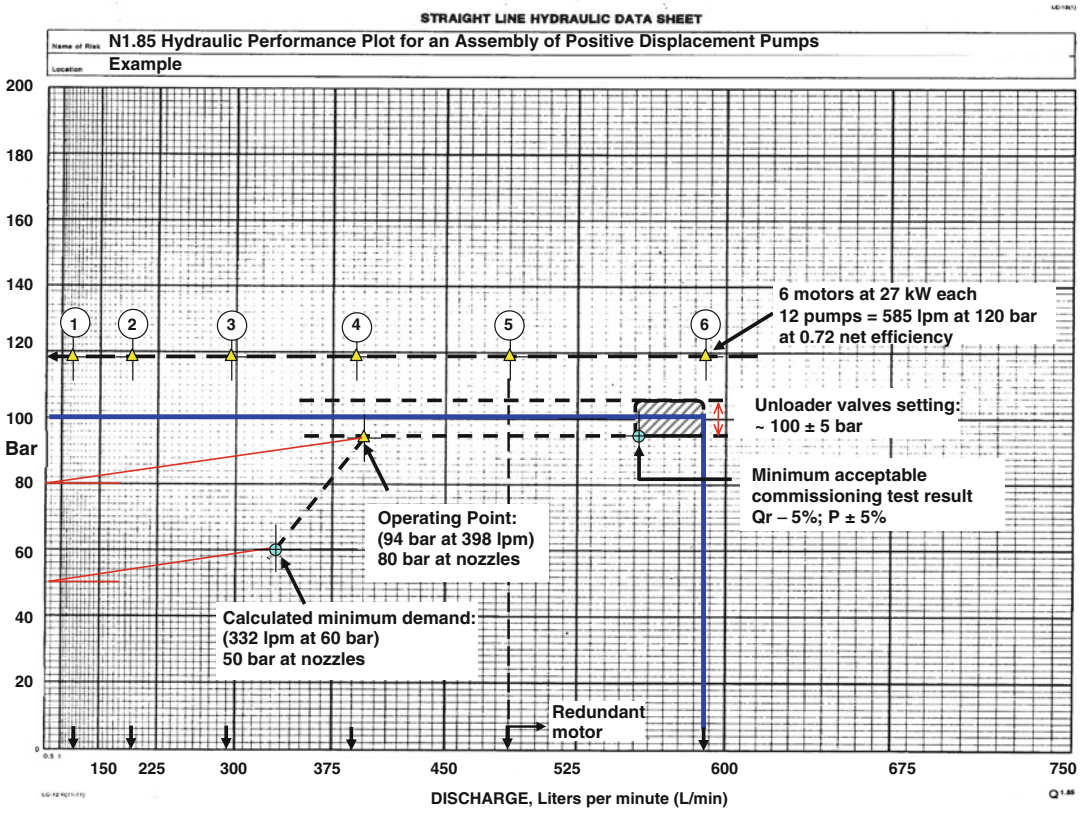

Fig. 46.12 Metric N1.85 straight line hydraulic performance plot for an assembly of six motors and 12 PD pumps connected in parallel

the nominal pressure setting of the unloader valves. For example, in Fig. 46.11 two flow test results are shown, neither of which is exactly at the nominal setting, but both of which fall nicely on the factory curve. Anticipating this, it is wise to state the pump performance at some percentage below nominal setting, so that when the pump is field tested, it delivers at least what it is specified to deliver (flow and pressure). Figure 46.12 shows a possible range within which the flow test results should lie, in order to pass the field test.

The PD pump assembly shown in Fig. 46.12 is capable of delivering 585 L/min with all six motors operating and an unloader setting of 100 bar. However, it is evident in the Figure that the assembly could deliver 487.5 L/min with only 5 motors operating, which also exceeds the system demand. For the multi-motor, multi-pump assembly shown, it is common to specify that the system design demand (Q and P) be met with only five of the six motors operating, i.e., with one of the motor/pump combinations being redundant.

Acceptance Testing of Water Mist Systems

Upon completion of an installation, NFPA 750 requires that a flow test be conducted to confirm the performance of the PD pump or pump assembly. The procedure for flow testing a PD pump or pump assembly differs from standard practice for centrifugal fire pumps as outlined in NFPA 20 [200]. For centrifugal fire pumps, the flow test data must show that the pump performance curve is equal to or better than the "factory curve" for the pump. In contrast, for PD pumps and pump assemblies, which incorporate a pressure relief/regulating or unloader valve, it is the unloader valve settings that determine the discharge pressure, not the factory rating for the pump. Furthermore, the flow test points are often less than the nominal settings of the relief valves. This is particularly the case for multi-pump assemblies, where there are many unloader valves, each with a small deviation from the nominal setting.

Figure 46.11 shows the flow test results for a single PD pump. Although the pump has a performance point of 454 L/min at 17.2 bar when operating at 1750 RPM, the two test points are at 16.9 and 15.9 bar, slightly less than the nominal setting of the regulating valves which are set at 17.2 bar and 16.6 bar. This is considered an acceptable result in spite of the fact that the test points are below 17.2 bar, the pump performance point. With only one relief valve governing the maximum pressure, the two points obtained by means of a full flow test, were very close to the nominal relief valve setting, but they are below the apparent pump rating. To be considered an acceptable test, the engineer and authority having jurisdiction must understand that the pressure regulating valves setting determines the assembly rating.

As shown in Fig. 46.12, the deviation from the nominal unloader valve setting is even greater for multi-pump assemblies than for single PD pump installations. This is because with more unloader valves, there is more "leakage" from the ones with settings slightly below the nominal setting which in Fig. 46.12 is shown as 100 bar. The pressure/flow result for an acceptable field test should be within 5 % of the sum of the output of all pumps, at a pressure not more than five percent less than the nominal setting of the unloader valves. It is important that the test engineer, the vendor and the authority having jurisdiction, be aware of these differences between testing centrifugal pumps and PD pumps, to avoid disputes over interpretation of test results.

Acceptance testing of twin-fluid, declining-pressure, and pumped high-pressure water mist systems involves engineering analysis that is not typical of traditional sprinkler and other fire protection systems. The technology involved in sizing compressed gas supplies for decaying-pressure systems, or designing PD pump assemblies, is sufficiently complicated that discharge testing is required as the final proof of functionality. NFPA 750 requires that a full system discharge test be conducted unless there is an overriding reason not to do so.

Without taking measurements of flow and pressure, it is impossible to judge by visual

indicators alone whether a system is operating properly. Visual inspection of the mist conditions during a discharge can confirm only basic aspects of the system performance, such as the opening and closing of valves, and verifying that pipes or nozzles are not plugged, and are able to produce mist. One can observe that water flows from individual nozzles, but one cannot discern that the spray quality, flow rate and projection are acceptable. Only by measuring pressures over the entire discharge duration can one be sure that the stored quantities of compressed gas and water are sufficient to meet the required discharge duration.

Figures 46.13 and 46.14 are plots of air and water pressure taken during the discharge of a twin-fluid system involving cycled flow at the hydraulically most remote nozzle and at a nozzle very close to the supply tank. The design called for six discharge cycles of 50 s each, with 40 s intervals between them. Air and water pressures at the nozzles should be between 82 and 66 psig. From visual and audio observations in the compartment, six discharges occurred. From the pressure traces, however, it was evident that the sixth discharge did not achieve the minimum nozzle pressures, particularly at the most remote nozzle. For the nozzle closest to the supply tank (Fig. 46.14), the minimum operating air and water pressures were achieved in the fifth but not the sixth discharge. The differences between pressures at the closest and most remote nozzles indicate that the nozzles closest to the source were discharging considerably more air and water than the remote nozzles.

The recorded pressures of the discharge tests demonstrated that the system exhausted the supply of atomizing medium before the end of the fifth discharge, although not the supply of stored water. Additional cylinders of compressed gas were required to achieve the desired six discharges. This test experience demonstrates that a full understanding of the performance of the system and the need for corrective action could not have been identified unless the discharge test had been instrumented so that a true measure of performance could be revealed.

Ultimately, the reliability of water mist systems depends on proper design, installation, acceptance testing and on-going maintenance. Water mist systems have less over-design capacity and more potential failure modes than standard

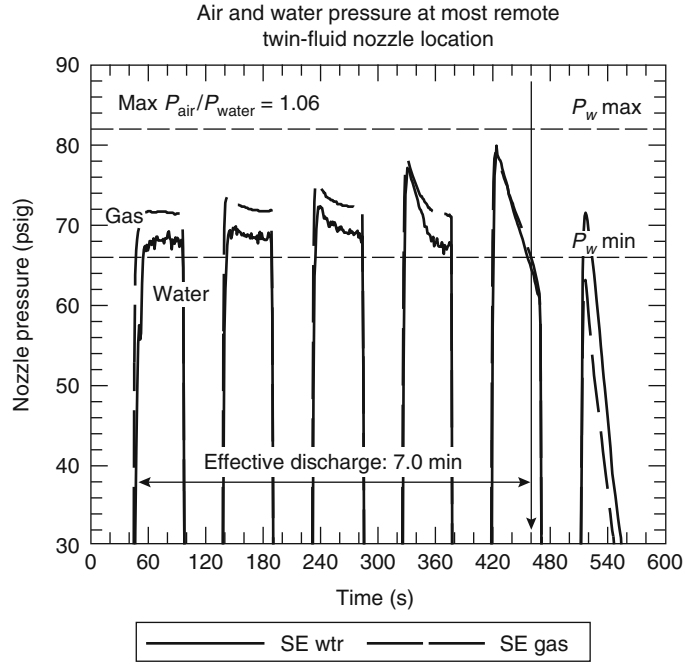

Fig. 46.13 Pressure versus time plot of compressed gas and water pressures at the most remote twin-fluid nozzle location. Acceptable operating range is between 66 and 82 psig, with compressed gas pressure required to be approximately the same as the water pressure ($P_a/P_w = 1.0$)

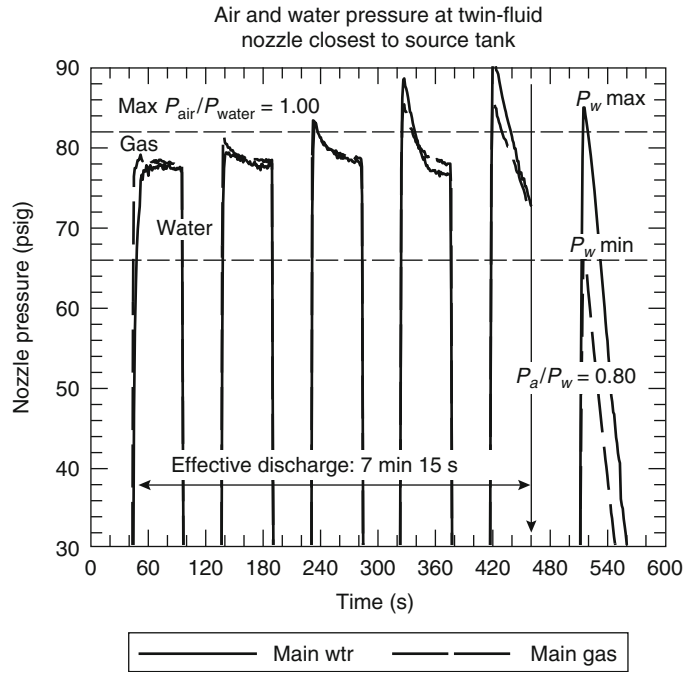

Fig. 46.14 Compressed gas and water pressures measured at a nozzle close to the source tank. Acceptable operating range is between 66 and 82 psig, with compressed gas pressure required to be approximately the same as the water pressure ($P_a/P_w = 1.0$)

sprinkler systems. The importance of applying good engineering practice, starting at the selection and design stage and continuing through the service life of the system, cannot be overstated.

Summary

This chapter provides a review of the history behind recent developments of water mist fire suppression systems. Significant studies on how finely divided water sprays improved the efficiency of fire control, suppression and extinguishment had been done years before, but it was not until the 1990s that additional incentives for considering and employing the technology became apparent. Motivated by interest in finding halon alternatives and developing lightweight suppression systems for ships, manufacturers of fire protection systems began to incorporate new ideas and new hardware into fire protection system design. Water mist emerged as a viable alternative for a number of halon applications, and the improved efficiency in use of water promised major reductions in the weight and volume of system hardware.

Currently design criteria for water mist systems must be based on full-scale fire testing for specific hazards. Interestingly, testing has revealed that the design criteria for different manufacturers' equipment, tested to a formal test protocol, may vary greatly. One water mist system could meet the performance objectives at of the test protocol at one flux density (application rate), but a second manufacturer, using a different type of nozzle or pressure regime, would also succeed, but at a lower or higher average application density. Both systems must be recognized as acceptable for the hazard, but we cannot predict what difference a change in spray characteristics might make to the suppression outcome.

CFD modeling presents a promising tool for analyzing the complex physical and chemical phenomena of fire suppression by water mist. The strength of the CFD models is their ability to expand the understanding of how the application and system design parameters affect the performance of the system. The limitations are associated with the high labor costs required to develop a fine computational grid for a large scale application and the associated long

computer run-times to perform the simulation. Applying CFD modeling to a specific application requires a certain level of expertise. Additional research is required to further develop and validate techniques to model the spray characteristics of the nozzle/system, and an all-encompassing extinguishment algorithm capable of handling a variety of fuel types and configurations. Considering the physical and chemical complexity of extinguishing multi-fuel fires, accomplishing this latter goal is rather ambitious. Only limited progress has been made in these areas over the past few years due to the application specific nature of the latest research and the limited amount of test data available for validation. In any case, modeling still has the potential not only to augment the test and evaluation process but also to aid in approving specific designs for actual applications in the future.

Water mist system technology has become a global fire protection market in the second decade of the twenty-first century. The strongest market first appeared in the international marine sector, where water mist was competitive with marine sprinkler systems on passenger ships. Satisfactory fire protection could be achieved with a fraction of the water requirements of marine sprinkler systems. Penetration of land-based markets has been restrained by a lack of suitable broad range test protocols. After a decade of full-scale fire testing and developments in computer modeling of tunnel fires, water mist systems are now recognized to be capable of preventing catastrophic fire losses in highway and rail tunnels. Water mist systems reduce the heat release rate of fires, provide thermal management to protect the tunnel structure, and prevent propagation of fire to other vehicles. More work is required to integrate the benefits of water mist systems into traditional tunnel design procedures, but water mist systems are presently being installed in many new tunnels in Europe.

Efforts are increasing in both Europe and North America to have water mist systems given the same recognition, in terms of construction trade-offs, as sprinkler systems in building codes. The largest growth potential for water mist technology is to have water mist systems installed throughout commercial and residential buildings as an alternative to standard sprinkler systems. Increasing consciousness of the need to reduce the fire protection demand on urban water systems in regions of water scarcity is one factor that is encouraging the application of water mist systems as equivalent to sprinkler systems. On the other hand, some building safety engineers express concern that the reliability of water mist systems is not equivalent to standard sprinklers, and tend to discourage the idea of treating them as equivalent to sprinkler systems. It is hoped that the water mist system manufacturers will invest in innovative approaches to increasing the reliability of water mist systems, and demonstrating their overall long term performance.

References

1. NFPA 750, *Standard on Water Mist Fire Suppression Systems,* National Fire Protection Association, Quincy, MA (1996).
2. NFPA 750, *Standard on Water Mist Fire Systems,* National Fire Protection Association, Quincy, MA (2010).
3. M.M. Braidech, J.A. Neale, A.F. Matson, and R.E. Dufour, "The Mechanism of Extinguishment of Fire by Finely Divided Water," National Board of Fire Underwriters, New York, p. 73 (1955).
4. D.J. Rasbash, Z.W. Rogowski, and G.W.V. Stark, "Mechanisms of Extinction of Liquid Fuels with Water Sprays," *Combustion and Flame,* 4, pp. 223–234 (1960).
5. NFPA 15, *Standard for Water Spray Fixed Systems for Fire Protection,* National Fire Protection Association, Quincy, MA (2012).
6. NFPA 13, *Standard for the Installation of Sprinkler Systems,* National Fire Protection Association, Quincy, MA (2010).
7. Civil Aviation Authority, "International Cabin Water Spray Research Management Group: Conclusions of Research Programme," *CAA Paper 93012* (1993).
8. R.G. Hill, T.R. Marker, and C.P. Sarkos, "Evaluation and Optimization of an On-Board Water Spray Fire Suppression System in Aircraft," in *Proceedings of Water Mist Fire Suppression Workshop,* NIST, Gaithersburg, MD (1993).
9. The Montreal Protocol on Substances That Deplete the Ozone Layer—Final Act (1984).
10. D.S. Aldenwinckle and D. Prentice, *The Safety Record and Risk Analysis of Ro-ro Passenger*

Ferries, Lloyd's Register Safety Technology Department (1992).
11. Technical Research Centre of Finland (VTT), "Evaluating the Suppression Efficiency of the Hi-Fog Fire Protection System in Accommodation Areas on Passenger Ships According to IMO Res. A.800 (19)," *VTT Test Report No. RTE10320/98,* Espoo, Finland (1998).
12. M. Arvidson, S. Isaksson, and M. Tuomisaari, "Recommended Acceptance Criteria for Sprinkler Systems Equivalent to SOLAS II-2/12," *SP Report 1995:20,* Swedish National Testing and Research Institute, Boras, Sweden (1995).
13. M. Arvidson and S. Isaksson, "Equivalency Sprinkler Fire Tests," *SP Report 1995:19,* Swedish National Testing and Research Institute, Boras, Sweden (1995).
14. J.R. Mawhinney, B.Z. Dlugogorski, and A.K. Kim, "A Closer Look at the Extinguishing Properties of Water Mist," in *Proceedings: International Association for Fire Safety Science (IAFSS) Conference,* Ottawa, Ontario (1994).
15. D. Drysdale, *Fire Dynamics,* 2nd ed., John Wiley & Sons, New York (1999).
16. S.P. Fuss, D.J. Dye, B.A. Williams, and J.W. Fleming, "Inhibition of Premixed Methane Air Flames by Mists of Water and Aqueous Sodium Hydroxide," *Halon Options Technical Working Conference,* Albuquerque, NM (2000).
17. E.J.P. Zegers, B.A. Williams, R.S. Sheinson, and J.W. Fleming, "Water Mist Suppression of Methane/Air and Propane/Air Counterflow Flames," *Halon Options Technical Working Conference,* Albuquerque, NM (2000).
18. R. Wighus, "Engineering Relations for Water Mist Fire Suppression Systems," in *Proceedings: Halon Alternatives Technical Working Conference,* Albuquerque, NM, p. 397 (1995).
19. G.V. Hadjisophocleous, A.K. Kim, and K. Knill, "Physical and Numerical Modeling of the Interaction between Watersprays and a Fire Plume," *8th International Symposium on Transport Phenomena in Combustion,* San Francisco, CA, pp. 1–12 (1995).
20. J.R. Mawhinney and G.V. Hadjisophocleous, "The Role of Fire Dynamics in Design of Water Mist Fire Suppression Systems," *Interflam'96,* Cambridge, UK (1996).
21. K. Prasad, C. Li, K. Kailasanath, C. Ndubizu, R. Ananth, and P. Tatem, "Numerical Modeling of Fire Suppression Using Water Mist," *NRL/MR/6410-98-8102,* Naval Research Laboratory, Washington, DC (1998).
22. P. Andersson, M. Arvidson, and G. Holmstedt, "Small Scale Experiments and Theoretical Aspects of Flame Extinguishment with Water Mist," *Report 3080,* Department of Fire Safety Engineering, Lund University, Lund, Sweden (1996).
23. G.G. Back, P.J. DiNenno, J.T. Leonard, and R.L. Darwin, "Full Scale Tests of Water Mist Fire Suppression Systems for Navy Shipboard Machinery Spaces: Part 2, Obstructed Spaces, September 1993–December 1994," *NRL/MR/6180-96-7831,* Hughes Associates, Inc. (1996).
24. G.G. Back, C.L. Beyler, P.J. DiNenno, R. Hansen, and R. Zalosh, "Full-scale Testing of Water Mist Fire Suppression Systems in Machinery Spaces," *Rpt No. CG-D-26-98,* U.S. Coast Guard, Groton, CT (1998).
25. G.G. Back, "Coast Guard Tests for Local Application Protocols," *Rpt No. CG-D-03-99,* U.S. Coast Guard, Groton, CT (1999).
26. E.W. Forssell, J.L. Scheffey, et al., "False Deck Development Testing of Hybrid Nitrogen—Water Mist Fire Suppression Systems," *Halon Options Technical Working Conference (HOTWC),* New Mexico Engineering Research Institute (NMERI), Albuquerque, NM (2004).
27. E.W. Forssell, J.L. Scheffey, et al. (2004) False Deck Testing of NanoMist Water Mist Systems. Navy Technology Center for Safety and Survivability, Chemistry Division, Washington, DC, pp. 1–53.
28. E.W. Forssell, J.L. Scheffey, et al. (2004) False Deck Development Testing of Hybrid Nitrogen—Water Mist Systems—Interim Report (FY 2003). Hughes Associates, Inc., Baltimore, MD, pp. 1–48
29. G.G. Back III, "A Quasi-Steady-State Model for Predicting Fire Suppression in Spaces Protected by Water Mist Systems," Department of Fire Protection Engineering, University of Maryland, College Park, MD (1996).
30. S.P. Ho, "Water Spray Suppression and Intensification of High Flash Point Hydrocarbon Pool Fires," Ph.D. Dissertation, Faculty of Fire Protection Engineering, Worcester Polytechnic Institute, Worcester, MA (2003).
31. Z. Liu, A. Kim, and J.Z. Su, "Improvement of Efficacy of Water Mist in Fire Suppression by Cycling Discharges," *ICFRE'97,* National Institute of Standards and Technology, Gaithersburg, MD (1997).
32. L. Liu and A.K. Kim, "A Review of Water Mist Fire Suppression Systems—Fundamental Studies," *Journal of Fire Protection Engineering,* 10, 3, pp. 32–50, Bethesda, MD (2000).
33. FM Global, "Approval Standard for Water Mist Systems," Class 5560, Factory Mutual Research Corporation, Norwood, MA (May 2005).
34. A. Jones and G.O. Thomas, "The Action of Water Sprays on Fires and Explosions," *Process Safety Environment,* 71, 1, pp. 41–49 (1993).
35. J.R. Mawhinney and R.L. Darwin, "Protecting against Vapor Explosions with Water Mist," in *Halon Options Technical Working Conference,* Albuquerque, NM (2000).
36. J.R. Butz, P. French, and M. Plooster, "Application of Fine Water Mists to Hydrogen Deflagrations," in *Halon Options Technical Working Conference Proceedings,* Albuquerque, NM, pp. 345–355 (1993).

37. K. Kailasanath, P.A. Tatem, F.W. Williams, and J.R. Mawhinney, "Blast Mitigation Using Water—A Status Report," Naval Research Laboratory, Washington, DC (2002).
38. K. Kailasanath and D. Schwer, "Shock Attenuation Using Water Mists," Naval Research Laboratory, Washington, DC (2004).
39. C.A. Selby and B.A. Burgan, eds., "Joint Industry Project on Blast and Fire Engineering for Topside Structures, Phase 2: Final Summary Report," The Steel Construction Institute, UK (1998).
40. R.G. Zalosh, "Water Mist for Deflagration Control," *NFPA 750 Committee on Water Mist Suppression Systems,* National Fire Protection Association, Quincy, MA (1994).
41. A. Lefebvre, *Atomization and Sprays,* Hemisphere Publishing Corporation, New York (1989).
42. ASTM E799, *Standard Practice for Determining Data Criteria and Processing for Liquid Drop Size Analysis,* American Society for Testing and Materials, West Conshohocken, PA (1992).
43. J.R. Mawhinney, P.J. DiNenno, and F.W. Williams, "Using Fine Water Mist for Flashover Suppression on Navy Ships," *Halon Alternatives Technical Working Conference,* Albuquerque, NM (1999).
44. J.R. Mawhinney, P.J. DiNenno, and F.W. Williams, "Water Mist Flashover Suppression and Boundary Cooling System for Integration with DC-ARM: Volume 1: Summary of Testing," *NRL/MR/6180-99-8400,* Navy Technology Center for Safety and Survivability, Chemistry Division, Washington, DC (1999).
45. T.A. Cortina, ed., *Water Mist Fire Suppression Systems Health Hazard Evaluation: Response to Questions Posed by the US Environmental Protection Agency,* Halon Alternative Research Corporation, Washington, DC (1995).
46. J.R. Mawhinney, "Characteristics of Water Mists for Fire Suppression in Enclosures," *Halon Alternatives Technical Working Conference,* Albuquerque, NM (1993).
47. M. Edwards, S. Watkins, and J. Glockling, "Development of Low Pressure Fine Water Spray for the Royal Navy: Additive Concentration and Spray Fire Testing," *Halon Alternatives Technical Working Conference,* Albuquerque, NM (2000).
48. E.W. Forssell and P.J. DiNenno, "Tests of Marioff Computer Room Fire Protection System," Client Report, Hughes Associates, Inc., Baltimore, MD (2000).
49. U.S. Environmental Protection Agency, "Protection of Stratospheric Ozone: Acceptable Substitutes for the Significant New Alternatives Policy (SNAP) Program," *40 CFR Part 82, U.S. Federal Register,* 60, 145, p. 38731 (1995).
50. M. Pabon, J. Stader, T. Kegelman, "New Additive for Water Mist Systems on Class B Fires: Toxicological Study on Breathable Particles," Presentation at the Annual Meeting of International Water Mist Association, Berlin, Germany (Sept. 29, 2005).
51. G. LeFort, A. W. Marshall, M. Pabon, "Evaluation of Surfactant Enhanced Water Mist Performance," *Fire Technology*, vol. 45, no. 3, pp. 341–354, 2009.
52. Organization for Economic Co-Operation and Development (OECD), "OECD Guideline for the Testing of Chemicals, Section 4: Health Effects, Acute Inhalation Toxicology, Number 403" (1981, 2009).
53. S. Ecker, "Legionnaire's Disease and Plumbing Systems," *Plumbing Engineer* (Sept. 2006).
54. ASHRAE Guideline 12, "Minimizing the Risk of Legionellosis Associated with Building Water Systems," American Society of Heating, Refrigerating, and Air-Conditioning Engineers (ASHRAE), Atlanta, GA (2006).
55. Marioff Corporation Oy, "HI-FOG System for Protection of Light and Ordinary Hazard 1 Occupancies Requiring High Level Cleanliness," Land System Data Sheet LS, Marioff Corporation Oy, Vantaa, Finland (June 21, 2006).
56. Yu, H., Zhou, X., and Ditch, B., "Experimental Validation of Froude Modeling Based Physical Scaling of Water Mist Cooling of Enclosure Fires," *Fire Safety Science*, (2008).
57. A.U. Modak, A. Abbud-Madrid, J.P. Delplanque, and R.J. Kee, "The Effect of Mono-Dispersed Water Mist on the Suppression of Laminar Premixed Hydrogen-, Methane-, and Propane-Air Flames," *Combustion & Flame,* 144, p. 103 (Jan. 2006).
58. A.M. Lentati and H.K. Chelliah, "The Dynamics of Water Droplets in a Counterflow Field and Its Effect on Flame Extinction," in *1996 Proceedings of the Fall Technical Meeting: The Eastern States Section of the Combustion Institute,* Hilton Head, SC, pp. 281–284 (1996).
59. A.K. Lazzarini, R.H. Krauss, H.K. Chelliah, and G.T. Linteris, "Extinction of Counterflow Diffusion Flames with Fine-Water Droplets," in *Proceedings: Halon Alternatives Technical Working Conference,* Albuquerque, NM (2000).
60. S.C. Yang, M.L. Huber, R.A. Bryant, and W.M. Pitts, "Experimental Investigation of Extinguishment of Laminar Diffusion Flames by Thermal Agents," in *Proceedings: Halon Alternatives Technical Working Conference,* Albuquerque, NM (2000).
61. A. Dvorjetski and J.B. Greenberg, "Theoretical Analysis of Polydisperse Water Spray Extinction of Opposed Flow Diffusion Flames," *Fire Safety Journal,* 39, 4, pp. 309–326 (2004).
62. J.W. Fleming, B.A. Williams, R.S. Sheinson, W. Yang, and R.J. Kee, "Water Mist Fire Suppression Research: Laboratory Studies," in *Science, Technology and Standards for Fire Suppression Systems,* National Research Institute of Fire and Disaster, Tokyo, Japan, pp. 117–132 (2002).

63. J.T. Leonard, G.G. Back, and P.J. DiNenno, "Small/Intermediate Scale Studies of Water Mist Fire Suppression Systems," *NRL Ltr Rpt 6180/0869.1,* Naval Research Laboratory, Washington, DC (1994).
64. W.K. Chow, Y. Gao, H. Dong, G. Zou, and L. Meng, "Full-scale Burning Tests on Heat Rate of Gasoline Fire with Water Mist," *Journal of Applied Fire Science,* 11, 1, pp. 21–44 (2002–2003).
65. K. Prasad, C. Li, and K. Kailasanath, "Simulation of Water Mist Suppression of Small Scale Methanol Liquid Pool Fires," *Fire Safety Journal,* 33, 3, pp. 185–212 (1999).
66. J. Richard, J.P Garo, J.M. Souil, and J.P. Vantelon, "On the Flame Structure at the Base of a Pool Fire Interacting with a Water Mist," *Experimental Thermal & Fluid Science,* 27, 4, p. 439 (2003).
67. G. Heskestad, "Extinction of Gas and Liquid Pool Fires with Water Sprays," *Fire Safety Journal,* 38, pp. 301–317 (2003).
68. B.Z. Dlugogorski, R.K. Hichens, E.M. Kennedy, and J.W. Bozzelli, "Water Vapour as an Inerting Agent," in *Proceedings: Halon Alternatives Technical Working Conference,* Albuquerque, NM, p. 7 (1997).
69. J. Suh and A. Atreya, "The Effect of Water Vapor on Counterflow Diffusion Flames," *International Conference on Fire Research and Engineering,* Orlando, FL, pp. 103–108 (1995).
70. T.S. Ravigururajan and M.R. Beltran, "A Model for Attenuation of Fire Radiation Through Water Droplets," *Fire Safety Journal,* 15, pp. 171–181 (1989).
71. T. Log, "Flashover Suppression Using Fine Water Spray," *Interflam'96,* Cambridge, UK (1996).
72. W. Yang, T. Parker, H.D. Ladouceur, and R.J. Kee, "The Interaction of Thermal Radiation and Water Mist in Fire Suppression," *Fire Safety Journal,* 39, 1, pp. 41–66 (2004).
73. P. Andersson and G. Holmstedt, "Limitations of Water Mist as a Total Flooding Agent," *Journal of Fire Protection Engineering,* 9, 4, pp. 31–50 (1999).
74. R.G. Bill, Jr., R.L. Hansen, and K. Richards, "Fine Spray (Water Mist) Protection of Shipboard Engine Rooms," *Fire Safety Journal,* 29, pp. 317–336 (1997).
75. R.G. Bill, Jr., and E.A. Ural, "Water Mist Protection of Combustion Turbine Enclosures," in *Fire Safety Science—Proceedings of the Sixth International Symposium,* International Association for Fire Safety, Poitiers, France (1999).
76. G.G. Back, C.L. Beyler, and R. Hansen, "The Capabilities and Limitations of Total Flooding Water Mist Fire Suppression Systems in Machinery Space Applications," *Fire Technology,* 36, pp. 8–23 (2000).
77. C. Beyler, "Flammability Limits of Premixed and Diffusion Flames," *The SFPE Handbook of Fire Protection Engineering,* National Fire Protection Association, Quincy, MA, Section 1/Chapter 7 (1988).
78. H.C. Kung and J.P. Hill, "Extinction of Wood Crib and Pallet Fires," *Combustion and Flame,* 24, p. 305 (1975).
79. F. Tamanini, "Application of Water Sprays to the Extinguishment of Crib Fires," *Combustion Science and Technology,* 14, pp. 17–23 (1976).
80. R.S. Magee and R.D. Reitz, "Extinguishment of Radiation Augmented Plastic Fires by Water Sprays," in *Proceedings of the 15th International Symposium on Combustion,* Combustion Institute, Pittsburgh, PA, pp. 337–347 (1974).
81. M.B. Kim, Y.J. Jang, and M.O. Yoon, "Extinction Limit of a Pool Fire with a Water Mist," *Fire Safety Journal,* 28, pp. 295–306 (1997).
82. L. Wimin, B. Yao, and J. Qin, "Preliminary Burning Tests on PVC Fires with Water Mist," *Polymer Testing,* 24, 5, p. 583 (2005).
83. G.G. Back, C.L. Beyler, and R. Hansen, "A Quasi-Steady-State Model for Predicting Fire Suppression in Spaces Protected by Water Mist Systems," *Fire Safety Journal,* 35, pp. 327–362 (2000).
84. Y.F. Li and W.K. Chow, "Modeling of Water Mist Fire Suppression Systems by a One-zone Model," *Combustion Theory and Modeling,* 8, 3, pp. 567–592 (2004).
85. E.W. Forssell, G.G. Back, and C.L. Beyler, *A Transient Model for Predicting Fire Suppression in Spaces Protected by Water Mist Systems,* Hughes Associates, Baltimore, MD (1999).
86. J. Vaari, "A Transient One-Zone Computer Model for Total Flooding Water Mist Fire Suppression in Ventilated Enclosures," *VTT Rpt FIN-02044,* VTT Technical Research Center, Espoo, Finland (2000).
87. R. Wighus and A.W. Brandt, "Watmist-A One-zone Model for Water Mist Fire Suppression," *Halon Options Technical Working Conference* (April 2001).
88. K.B. McGrattan, H.R. Baum, W.D. Walton, and J.J. Trelles, "Smoke Plume Trajectory from In Situ Burning of Crude Oil in Alaska–Field Experiments and Modeling of Complex Terrain," NISTIR 5958, National Institute of Standards and Technology (1997).
89. "CFX-5 User Manual," AEA Technology, Harwell, UK (2000).
90. K.B. McGrattan and G.P. Forney, "Fire Dynamics Simulator—User's Manual," NISTIR 6469, National Institute of Standards and Technology (2000).
91. V. Novozhilov, D.J.E. Harvie, A.R. Green, and J.H. Kent, "A Computational Fluid Dynamic Model of Fire Burning Rate and Extinction by Water Sprinkler," *Combustion Science and Technology,* 123, 1–6, pp. 227–245 (1997).
92. *Fluent/UNS and Rampant 4.2 User's Guide,* Fluent Incorporated, Lebanon, NH (1998).
93. G. Cox and S. Kumar, "Field Modeling of Fire in Forced Ventilated Enclosures," *Combustion Science and Technology,* 52, 7 (1986).

94. *Kameleon FireEx 99 User Manual,* SINTEF Energy Research report TRF5119, Trondheim, Norway (1999).
95. V. Schneider, *WinKobra 4.6—User's Guide,* I.S.T. Intefrierte Sischerheits-Technik GmbH, Germany (2001).
96. J.C.G. Viegas, "Seguranca Contra Incendios Em Edificios. Modelacao Matematica De Incenditos E Validacao Experimental (Fire Safety in Buildings, Mathematical Modeling of Fire and Experimental Validation)," Ph.D. Thesis, Insituto Superior Tecnico, Lisbon, Portugal (1999).
97. *PHOENICS User's Guide,* http://www.cham.co.uk/phoenics/d_polis/d_docs/tr326/tr326top.htm.
98. G.V. Hadjisophocleous and A. Yakan, "Computer Modeling of Compartment Fires," *Internal Report No. 613, Institute for Research in Construction,* National Research Council of Canada, Ottawa, ON (1991).
99. *SMARTFIRE V2.0 User Guide and Technical Manual,* Doc Rev. 1.0 (July 1998).
100. P.A. Rubini, "SOFIE—Simulation of Fires in Enclosures," in *Proceedings of the 5th International Symposium on Fire Safety Science,* International Association for Fire Safety Science, London, UK (1997).
101. A.J. Gardiner, "The Mathematical Modeling of the Interaction Between Sprinkler Sprays and the Thermally Buoyant Layers of Gases from Fires," Ph.D. Thesis, South Bank Polytechnic, London, UK (1998).
102. *Star-CD V3.100A User Guide,* Computational Dynamics Ltd., London, UK, http://www.cd.co.uk (2001).
103. K.T. Yang and L.C. Chang, "UNDSAFE-1: A Computer Code for Buoyant Flow in an Enclosure," NBS GCR 77-84, National Bureau of Standards (now National Institute of Standards and Technology), Gaithersburg, MD (1977).
104. J. Trelles, J.R. Mawhinney, and P.J. DiNenno, "Characterization of a High-Pressure Multi-jet Water Mist Nozzle for the Purposes of Computational Fluid Dynamics Modeling," in *Proceedings of the Computational Simulation Models in Fire Engineering and Research,* GIDAI, Universidad De Cantabria, Santander, Spain (Oct. 2004).
105. Ditch, B. and Yu, H., "Water Mist Spray Characterization and Its Proper Application for Numerical Simulations," *Fire Safety Science*, MA (2009).
106. Santangelo, P.E., Tartarini, P., Pulvirenti, B. and Valdiserri, P., "Discharge and Dispersion in Water-Mist Sprays: Experimental and Numerical Analysis," Triennial International Annual Conference on Liquid Atomization and Spray Systems, CO (2009)
107. Santangelo, P.,"Characterization of High-Pressure Water-Mist Sprays: Experimental Analysis of Droplet Size and Dispersion," *Experimental Thermal and Fluid Science*, Italy (2010).
108. P.J. Disimile, J.R. Tucker, B. Croswell, and J.M. Davis, "The Transport of Water Sprays Past Generic Clutter Elements Found Within Engine Nacelles," *Fire Safety Journal,* 40, pp. 65–78 (2005).
109. J.W. Fleming and J. Yang, "Modeling Study of the Behavior of Liquid Fire Suppression Agents in a Simulated Engine Nacelle," in *Halon Options Technical Working Conference Proceedings,* HOTWC 2004, Albuquerque, NM (2004).
110. P.J. Disimile, J.R. Tucker, J. Stern, L. Mehl, and B. Croswell, "Velocity and Drop Size Distributions Downstream Generic Clutter Elements Found Within Engine Nacelles," in *Halon Options Technical Working Conference Proceedings,* HOTWC 2004, Albuquerque, NM (2004).
111. C. Presser, J.F. Widmann, P.E. DesJardin, and L.A. Gritzo, "Measurements and Numerical Predictions of Liquid Agent Dispersal Around Solid Obsticles," in *Halon Options Technical Working Conference Proceedings* (B.L. Daniels and D.G. Cole, eds.), pp. 122–130 (2001).
112. Iannantuoni, L. and Manzini, G., "Water Mist Fire Protection – Research on a Numerical Toolbox for Systems Effectiveness Assessment," *The Open Thermodynamics Journal,* (2010).
113. G.V. Hadjisophocleous and K. Knill, "CFD Modeling of Liquid Pool Fire Suppression Using Fine Water Sprays," *Annual Conference on Fire Research,* Gaithersburg, MD, pp. 71–72 (1994).
114. G.V. Hadjisophocleous, S. Cao, and A.K. Kim, "Modeling the Interaction Between Fine Watersprays and a Fire Plume," in *4th International Conference on Advanced Computational Methods in Heat Transfer,* Udine, Italy (1996).
115. W.K. Chow and B. Yao, *Numerical Modeling for Interaction of a Water Spray with Smoke Layer, Numerical Heat Transfer: Part A—Applications 2/23/2001,* 39, 3, p. 267 (2001).
116. J. Hua, K. Kumar, and B.C. Boo, "A Numerical Study of the Interaction of Water Spray with a Fire Plume," *Fire Safety Journal,* 37, 7, pp. 631–657 (2002).
117. Li, Y. and Chow, W.," Study of Water Droplet Behavior in Hot Air Layer in Fire Extinguishment." *Fire Technology*, (2008).
118. Kumari, N., Bahadur, V., Hodes, M., Salamon, T., Kolodner, P., Lyons, A. and Garimella, S., "Analysis of Evaporating Mist Flow for Enhanced Convective Heat Transfer," *International Journal of Heat and Mass Transfer*, (2010).
119. J. Xia, and K.H. Luo, "Direct Numerical Simulation of Diluted Combustion by Evaporating Droplets," *Proceedings of the Combustion Institute,* UK (2009).
120. A. Adeniji-Fashola and C.P. Chen, "Modeling of Confined Turbulent Fluid-Particle Flows Using Eulerian and Lagrangian Schemes," *International Journal of Heat Transfer,* 33, pp. 691–701 (1990).
121. F. Durst, D. Milijevic, and B. Schonung, "Eulerian and Lagrangian Predictions of Particulate

Two-Phase Flows: A Numerical Study," *Applied Mathematical Modeling,* 8, pp. 101–115 (1984).
122. M.W. An, A.C.M. Sousa, and J.E.S. Venart, "Modeling of Shipboard Waterfog Fire Suppression System," *Contract #991-1042/2045,* National Research Council of Canada, Ottawa (1993).
123. S.R. Tieszen and A.R. Lopez, "Issues in Numerical Simulation of Fire Suppression," in *Proceedings: Halon Alternatives Technical Working Conference,* Albuquerque, NM (1999).
124. Z. Liu, "The Use of Computer Modeling to Evaluate the Performance of Halon Alternatives—A Literature Review," *Internal Report 738,* National Research Council of Canada, Ottawa (1997).
125. Yuh-Ming Ferng and Cheng-Hong Liu, "Numerically Investigating Fire Suppression Mechanisms for the Water Mist with Various Droplet Sizes through FDS Code," *Nuclear Engineering and Design*, (2011).
126. W.M. Pitts and L.G. Blevins, "An Investigation of Extinguishment by Thermal Agents Using Detailed Chemical Modeling of Opposed Flow Diffusion Flames," in *Proceedings: Halon Alternatives Technical Working Conference,* Albuquerque, NM (1999).
127. K. Prasad, C. Li, K. Kailasanath, C. Ndubizu, R. Ananth, and P. Tatem, "Numerical Modeling of Fire Suppression Using Water Mist, 1. Gaseous Methane-Air Diffusion Flames," *NRL/MR/6410-98-8102,* Naval Research Laboratory, Washington, DC (1998).
128. Takahashi, F. and Katta, V., "Extinguishment of Diffusion Flames Around a Cylinder in a Coaxial Air Stream with Dilution or Water Mist," *Proceedings of the Combustion Institute*, (2009).
129. R. Srivastava, T. McKinnon, and J.R. Butz, "Modeling Study of the Effect of Fine Water Mists on Premixed CH_4/Air Flame Propagation," in *Proceedings: Halon Alternatives Technical Working Conference,* Albuquerque, NM, p. 550 (1997).
130. P.E. DesJardin, L.A. Gritzo, and S.R. Tieszen, "Modeling the Effect of Water Spray Suppression on Large Scale Pool Fires," *Halon Options Technical Working Conference,* Albuquerque, NM (2000).
131. G.V. Hadjisophocleous, A.K. Kim, and K. Knill, "Modeling of a Fine Water Spray Nozzle and Liquid Pool Fire Suppression," in *International Conference on Fire Research and Engineering,* Orlando, FL, pp. 1–6 (1995).
132. G. Heskestad, "Extinction of Gas and Liquid Pool Fires with Water Sprays," *Fire Safety Journal,* 38, pp. 301–317 (2003).
133. P.E. DesJardin, L.A. Gritzo, and S.R. Tieszen, "Modeling the Effect of Water Spray Suppression on Large-Scale Pool Fires," in *Halon Options Technical Working Conference Proceedings,* Albuquerque, NM, pp. 262–273 (2000).
134. Beihua, C., Guangxuan, L. and Zhen, H., " Extinction Limit of Diesel Pool Fires Suppressed by Water Mist," *Journal of Fire Sciences*, (2009).
135. Pan, Q. Li, G. Liao, and J. Qin, "Preliminary Experimental Study and Numerical Simulations on Suppressing Spray Bitumen Fire with Water Mist in a Confined Space," *Fire Safety Science*, (2008).
136. C.C. Ndubizu and R. Ananth, "The Effects of Air-Borne Water Mist on the Local Burning Rate of a PMMA Plate in Boundary Layer Combustion," in *Halon Options Technical Working Conference Proceedings,* HOTWC 2004, Albuquerque, NM (2004).
137. F.K. Amon, W. Yang, R.J. Kee, J.T. McKinnon, and A. Abbud-Madrid, "Experimental and Numerical Studies of the Effect of Water Mist on Premixed Gas and Solid Fuel Flames Under Various Burning Conditions," in *Halon Options Technical Working Conference Proceedings,* Albuquerque, NM (May 2003).
138. R. Ananth, C.C. Ndubizu, and F.W. Williams, "A Numerical Model for Water Mist Suppression of a Solid Plate in Boundary Layer Flow," in *Halon Options Technical Working Conference Proceedings,* HOTWC 2004, Albuquerque, NM (2004).
139. A.I. Karpov, V. Novozhilov, V.K. Bulgakov, and A.A. Galat, "Numerical Modeling of the Effect of Fine Water Mist on the Small Scale Flame Spreading Over Solid Combustibles," *Fire Safety Science—Proceedings of the 8th International Symposium,* International Association for Fire Safety Science, London, UK, pp. 753–764 (2005).
140. Yang, P., Liua, T. and Qin, X., "Experimental and Numerical Study on Water Mist Suppression System on Room Fire," *Building and Environment*, (2010).
141. Trelles, J., and Mawhinney, J.R., "CFD Investigation of Large Scale Pallet Stack Fires in Tunnel Protected by Water Mist Systems," Journal of Fire Protection Engineering, 20 (3), Aug. 2010, pp. 149–199.
142. G.V. Hadjisophocleous and S. Cao, "Numerical Simulations of Aircraft Cabin Fire Suppression," in *AGARD Conference Proceedings,* 587, 88th Symposium of the Propulsion and Energetic Panel on Aircraft Fire Safety, Dresden, Germany, pp. 5-1–5-12 (1996).
143. S.C. Kim and H.S. Ryou, "An Experimental and Numerical Study on Fire Suppression Using a Water Mist in an Enclosure," *Building and Environment,* 38, 11, pp. 1309–1316 (2003).
144. F. Tanaka, Y. Ohmiya, S. Sugawara, M. Morita, and K. Matsuyama, "A Study of Fire Behavior in a Compartment with an Activation of Fire Suppression System," in *Proceedings of the Computational Simulation Models in Fire Engineering and Research,* GIDAI, Universidad de Cantabria, Santander, Spain (October 2004).
145. D. LeBlanc, "The Use of Field Models for Determining the Performance of Water Mist Systems: A Preliminary Analysis," in *2nd International Water Mist Conference Proceedings,* Amsterdam, the Netherlands (2002).

146. Y.L. Sinai, P.J. Stopford, M. Edwards, and S. Watkins, "CFD Modeling of Fire Suppression by Water Spray: A Feasibility Study Examining a Pool Fire in a Simple Enclosure," *Interflam 2001,* Interscience Communications, London, UK (2001).
147. Liang, T., Lo, S., Wang, X. and Liao, G., "A Numerical study of the Fire-extinguishing Performance of Water Mist in an Opening Machinery Space," *Procedia Engineering*, (2012).
148. Mawhinney, J.R., Trelles, J.; "Performance Testing of Fire Protection Systems in Tunnels: Integrating Test Data with CFD Simulations", in Proceedings, Fourth International Symposium on Tunnel Safety and Security, Frankfurt am Main, Germany, 17 – 19 March, 2010, Eds. A. Lönnermark, H. Ingason, SP Sweden, pp. 297 – 309.
149. Nmira, F., Consalvi, J., Kaiss, A. Fernandez-Pello, A. and Porterie, B., "A Numerical Study of Water Mist Mitigation of Tunnel Fires," *Fire Safety Journal*, (2009).
150. Nilsen, A. and Log, T., "Results from Three Models Compared to Full-Scale Tunnel Fires Tests," *Fire Safety Journal,* (2009).
151. Adiga, K., Willauer, H., Ananth, R. and Williams, F., "Implications of Droplet Breakup and Formation of Ultra Fine Mist in Blast Mitigation," *Fire Safety Journal*, (2009).
152. Ananth, R., Williauer, H., Farley, J. and Williams, F., "Effects of Fine Water Mist on a Confined Blast," *Fire Technology*, (2012).
153. IMO, *FTP Code,* "International Code for Application of Fire Test Procedures (Resolution MSC. 61C67)," International Maritime Organization, London, pp. 177–230 (1998).
154. International Maritime Organization, "IMO Res. A800 (19), Revised Guidelines for the Approval of Sprinkler Systems Equivalent to that Referred to in SOLAS Regulations II-2, Chapter 12", (1994).
155. IMO, *FTP Code,* "International Code for Application of Fire Test Procedures (Resolution MSC. 61C67)," International Maritime Organization, London, pp. 269–308 (1998).
156. International Maritime Organization, "IMO MSC/Circ. 913, Guidelines for the Approval of Fixed Water-Based Local Application Systems for Use in Category A Machinery Spaces," London (June 2005).
157. International Maritime Organization, "IMO MSC/Circ. 1165, Revised Guidelines for the Approval of Equivalent Water-Based Fire-Extinguishing Systems for Machinery Spaces and Cargo Pump-Rooms," London (June 2005).
158. FM Approvals, Approval Standard for Water Mist Systems, Class Number 5560, Norwood, MA (March 2009).
159. *UL 2167,* "Proposed First Edition of the Standard for Water Mist Nozzles for Fire Protection Service," Underwriters Laboratories Inc., Northbrook, IL (1998).
160. *VdS 2498,* "Guidelines for Water Extinguishing Systems Requirements and Test Methods for Fine Spray Nozzles," Verband der Schadenversichen, Germany (1996).
161. VdS 2562, "Guidelines for Extinguishing Systems, Procedure for the Approval of New Extinguishing Techniques," Verband der Schadenverhütung GmbH, Germany (1998).
162. J.R. Mawhinney, "Mercury Energy CBD Tunnel Project, New Zealand—Performance Based Fire Testing of a Water Mist Fire Suppression System," *InterFlam'99,* Edinburgh, UK, pp. 663–673 (1999).
163. P. Southwood and G. Grant, "Eurotunnel's Full-Scale Fire Suppression Test Programme," *International Conference on Tunnel Fires and Escape from Tunnels 5–7,* Lyon, France (1999).
164. G. Grant and P. Southwood, "Development of an Onboard Fire Suppression System for Eurotunnel HGV Shuttle Trains," *Interflam'99,* Edinburgh, UK, pp. 651–662 (1999).
165. G. Jensen, "A White Paper on Water Mist for Protection of Heritage," Interconsult ASSA, Trondheim, Norway, pp. 1–31 (2004).
166. J.R. Mawhinney, "A Linear Water Mist Fire Suppression System for Fixed Shelving in Archival Vaults," Presented at the International Water Mist Association (IWMA) Annual Conference, Rome, Italy (Oct. 6–8, 2004).
167. T. Log and P. Cannon-Brookes, "Water Mist for Fire Protection of Historic Buildings and Museums," *Museum Management and Curatorship,* 14, 3, pp. 283–298 (1995).
168. Factory Mutual Research Corporation, "Protecting Telephone Central Offices," *FMRC Update—A Progress Report from the Factory Mutual Research Corporation,* 6, 3, pp. 1–4, Norwood, MA (1992).
169. T.R. Marker and J.W. Reinhardt, "Water Spray as a Fire Suppression Agent for Aircraft Cargo Compartment Fires," Technical Note DOT/FAA/AR-TN01/1, Department of Transportation, Washington, DC (June 2001).
170. M. Tuomisaari and M. Kokkala, "Fire Suppression Tests of a Power Transformer in an Outdoor Installation with a Hi-Fog Fire Protection System," *Research Report No. RTE10607/97,* VTT Building Technology Centre, Espoo, Finland (1997).
171. NFPA 502, *Standard for Road Tunnels, Bridges, and Other Limited Access Highways,* Appendix D, National Fire Protection Association, Quincy, MA (2004).
172. NFPA 502, Standard for Road Tunnels, Bridges, and Other Limited Access Highways, Annexes B and E, National Fire Protection Association, Quincy, MA (2008).
173. PIARC, "Fire and Smoke Control in Road Tunnels," World Road Association (1999).
174. PIARC, "An Assessment of Fixed Fire Fighting Systems," World Road Association, Committee on Road Tunnels (C5) (2008).

175. U.S. Department of Transportation, Federal Highway Administration, "Prevention and Control of Highway Tunnel Fires," FHWA-RD-83-032 (1984).
176. R. Carvel, *The Handbook of Tunnel Fire Safety* (A. Beard and R. Carvel, eds.), Thomas Telford Publishing Company, London, chapter 6, p. 119 (2004).
177. H. Ingason, S. Gustavsson, and M. Dahlberg, "Heat Release Rate Measurements in Tunnel Fires," SP Swedish National Testing and Research Institute, SP Report 1994:08, Borås, Sweden (1994).
178. H. Ingason and A. Lönnermark, "Heat Release Rates from Heavy Goods Vehicle Trailers in Tunnels," *Fire Safety Journal,* 40, pp. 646–668 (2005).
179. A. Lönnemark and H. Ingason, "Gas Temperatures in Heavy Goods Vehicle Fires in Tunnels," *Fire Safety Journal,* 40, pp. 506–527 (2005).
180. L. M. Noordjik, P.G. Scholten, A.J. Breunese and C. Both, "Emerging Problems for Immersed Tunnels – Fire Induced Concrete Cracking",", in Proceedings, Fourth International Symposium on Tunnel Safety and Security, Frankfurt am Main, Germany, 17 – 19 March, 2010, Eds. A. Lönnermark, H. Ingason, SP Sweden, pp. 211-222.
181. J.R. Mawhinney, "Approval Testing of a Hi-Fog Water Mist System for Protection of the A86 Passenger Vehicle Highway Tunnel, Paris, France," Client Report HAI-5022-010-1, for Marioff Corporation Oy, Finland, Hagerbach Test Tunnel, Sargans, Switzerland (Oct. 2005).
182. J.R. Mawhinney and H. Ingason, "Full-Scale Fire Testing of Suppressed Heavy Goods Vehicle Fires in Road Tunnels," Client Report HAI 5022-010-2 for Marioff Corporation Oy, Finland, San Pedro de Anes Test Tunnel, Asturias, Spain (Feb. 2006).
183. S. Kratzmeir, "Safety of Life in Tunnels – Research Report, The SOLIT Research Project", FOGTEC Brandschutz GmbH & Co. KG, Germany (2007).
184. P.J. Sturm, K. Pucher, J. G. Rodler, G. Mühlenbruch, and P. Krezschmar, "Test of Water Mist Equipment to increase Escape Chances in Cases of Fire in Tunnels", in Proceedings of the International Water Mist Association Conference, Vienna, Austria, (April 2001).
185. S. Kratzmeir, and M. Lakkonen, "Fixed Fire Fighting Systems in Tunnels – Integration and Compensation", in Proceedings, Fourth International Symposium on Tunnel Safety and Security, Frankfurt am Main, Germany, 17 – 19 March, Eds. A. Lönnermark, H. Ingason, SP Sweden, pp. 283–292 (2010).
186. J.R. Mawhinney, "A Critique of Claims of Smoke Scrubbing by Water Mist," Proceedings of the National Fire Protection Research Foundation, Fire Suppression and Detection Research Application Symposium, Tampa, FL, January 23–25, 2002.
187. J. R. Mawhinney. J. Trelles, "Testing Water Mist Systems against Large Fires in Tunnels: Integrating Test Data with CFD Simulations," Fire Technology, National Fire Protection Association, Quincy, MA, December 30, 2009, DOI: 10.1007/s10694-009-0129-1.
188. J. Mawhinney, "Fixed Fire Protection Systems in Tunnels: Issues and Directions," Fire Technology, April 2011, pp 32, DOI: 10.1007/s10694-011-0220-2.
189. K. Almand, D. Gottuk, and J. Mawhinney, "International Road Tunnel Fire Detection Research Project – Phase II Tasks 5 and 6: Monitoring and Fire Demonstration in the Lincoln Tunnel," Report No. 200803143, National Fire Protection Research Foundation, Quincy, MA, 2008.
190. J.R. Mawhinney, "A Review of Water Mist Fire Suppression Systems at the Phillips Alaska Alpine Site Central Facility, Prudhoe Bay, Alaska," Client Report CR 4814-1, by Hughes Associates, Inc., Baltimore, MD (Aug. 2000).
191. J.R. Mawhinney, "Principles of Water Mist Fire Suppression Systems," *NFPA Handbook* (A. Cote, ed.), National Fire Protection Association, Quincy, MA (2003).
192. J. Keary and R. McGovern, "Characterisation of a Heated Water Extinguishing System," Unpublished manuscript, Department of Experimental Physics, University College Galway, Galway, Ireland (1994).
193. J.R. Mawhinney, B. Taber, and J.Z. Su, "The Fire Extinguishing Capability of Mists Generated by Flashing of Super-Heated Water," in *Proceedings, American Institute of Chemical Engineers, 1995 Summer National Meeting,* Boston, MA (1995).
194. J.R. Mawhinney and R. Darwin, "Protecting against Vapor Explosions with Water Mist," in *Proceedings, Halon Technical Options Working Conference,* Albuquerque, NM (2000).
195. R. Brown and J.L. York, "Sprays Formed by Flashing Liquid Jets," *American Institute of Chemical Engineers Journal,* 8, 21, pp. 149–153 (1962).
196. Technical Research Centre of Finland (VTT), "Evaluating the Extinguishing Effectiveness of the HI-FOG Fire Protection System in a Class 1 Machinery Space According to IMO MSC/CIRC 668," *VTT Test Report No RTE10310/98,* Espoo, Finland (1998).
197. ASME/ANSI B31.1, *Power Piping Code,* American National Standards Institute, New York (1995).
198. J.R. Mawhinney, "Water Mist Fire Suppression Systems," NFPA *Fire Protection Handbook,* 20th ed. (A.E. Cote et al., eds.), National Fire Protection Association, Quincy, MA, pp. 16-135–16-180 (2008).
199. H. S. Wass, Jr, *Sprinkler Hydraulics and What It's All About*, Society of Fire Protection Engineers, Bethesda, MD (2000).
200. NFPA 20, *Standard for the Installation of Stationary Pumps for Fire Protection*, National Fire Protection Association, Quincy, MA (2010).
201. K. Isman, "Hydraulics," *SFPE Handbook of Fire Protection Engineering*, The Society of Fire Protection Engineers, Bethesda, MD (2015).

Jack R. Mawhinney was a senior engineer with Jensen Hughes, previously Hughes Associates, Inc., in Arbutus, Maryland from 1996 until his retirement in 2014. He holds a master's degree (1979) in civil engineering from the University of Alberta. He has 45 years' experience in fire protection construction and research, including 11 years with the National Research Council, Canada, Institute for Research in Construction. Mr. Mawhinney was chair of the NFPA 750, Water Mist Systems, Committee from 1992 to 2002 and a principal member of that committee until his retirement from Jensen Hughes in 2014.

Gerard G. Back III is a senior engineer with Jensen Hughes in Arbutus, Maryland. He has a bachelor's degree (1983) in mechanical engineering and a master's in fire protection engineering (1996), both from the University of Maryland. In 25 years with HAI, Mr. Back has conducted extensive fire testing and analysis of the performance of water mist systems for the U.S. Army, Navy, and Coast Guard research and development programs and for other international clients. He is a member of the NFPA 750 Committee.

Foam Agents and AFFF System Design Considerations

47

Joseph L. Scheffey

Introduction

Foams have been developed almost entirely from experimental work. Although the technologies are rather mature, no fundamental explanations of foam extinguishment performance have been developed based on first principles. As a result, foams are characterized by (1) fire tests for which there is no general international agreement and (2) physical and chemical properties that may or may not correlate with empirical results. This chapter reviews the important parameters associated with foam agents, test methods used to evaluate foams, and relevant data in the literature that can be used to evaluate foam system designs. Because of their superior performance in extinguishing certain types of hydrocarbon liquid fuel fires, the emphasis is on film-forming foams and thin pool fires (e.g., from spills). Situations involving fuels "in depth" are limited to a discussion on foam modeling and small-scale tests to assess oil and petrochemical industry hazards.

Fire-fighting foam consists of air-filled bubbles formed from aqueous solutions. The solutions are created by mixing a foam concentrate with water in the appropriate proportions (typically 1, 3, or 6 % concentrate to water). The solution is then aerated to form the bubble structure. Some foams, notably those that are protein-based, form thick, viscous foam blankets on liquid hydrocarbon fuel surfaces. Other foams, such as film-formers, are much less viscous and spread rapidly on the fuel surface. The film-formers are capable of producing a vapor-sealing film of surface-active water solution on most of the hydrocarbon fuels of interest.

Because the foam is lighter than the aqueous solution that drains from the bubble structure, and lighter than flammable or combustible liquids, it floats on the fuel surface. The floating foam produces an air-excluding layer of aqueous agent, which suppresses and prevents combustion by halting fuel vaporization at the fuel surface, and preventing air from reaching the combustion zone. If the entire surface is covered with foam, the fuel vapor will be completely separated from air, and the fire will be extinguished. Low-expansion foams (i.e., foam volume-solution volume of $\leq$10:1) are quite effective on two-dimensional (pool) flammable and combustible liquid fires, but not particularly effective on three-dimensional fuel fires. This is particularly true of three-dimensional fires involving a low flashpoint fuel. Typically, an auxiliary agent, such as dry chemical, is used with foam where a three-dimensional fire (running fuel or pressurized spray) is anticipated. In enclosed hazard areas, other extinguishing media may be used, such as water mist or high-expansion foam. These agents generally require total flooding of the hazard volume.

J.L. Scheffey (✉)
Vice President. JENSEN HUGHES, Baltimore, MD, USA

M.J. Hurley (ed.), *SFPE Handbook of Fire Protection Engineering*,
DOI 10.1007/978-1-4939-2565-0_47, © Society of Fire Protection Engineers 2016

Description of Foam Agents

There are no universally agreed-on definitions of foam agents or terms associated with fire-fighting foam. For example, where foam is referenced in NFPA standards, definitions vary from document to document. Because foams vary in performance, in terms of application rates and quantities required for extinguishment, agent definitions can be cast to accentuate positive attributes, such as "rapid knockdown" or "superior burnback resistance." Geyer et al. have described the composition of various foam agents, paraphrased as follows [1].

1. *Protein foam.* Protein foam is a "mechanical" foam produced by combining (proportioning) foam concentrate and water and discharging the resulting solution through a mixing chamber. The mixing chamber introduces (aspirates) air, which expands the solution to create foam bubbles. The liquid concentrate consists primarily of hydrolyzed proteins in combination with iron salts. Hoof and horn meal and hydrolyzed feather meal are examples of proteinaceous materials used in protein-foam concentrates. No aqueous film is formed on the fuel surface with this type of agent.
2. *Fluoroprotein.* These agents are basically protein foams with fluorocarbon surface-active agents added. The varying degrees of performance are achieved by using different proportions of the base protein hydrolyzates and the fluorinated surfactants. Although fluoroprotein foams generally have good fuel shedding capabilities and dry chemical compatibility, the solution that drains out from the expanded foam does not form a film on hydrocarbon fuels. However, the addition of the fluorinated surfactants may act to reduce the surface tension of the solution. This reduction may, in turn, decrease the viscosity of the expanded solution, thus promoting more rapid fire control when compared to protein foams.
3. *Aqueous film-forming foam (AFFF).* These agents are synthetically formed by combining fluorine-free hydrocarbon foaming compounds with highly fluorinated surfactants. When mixed with water, the resulting solution achieves the optimum surface and interfacial tension characteristics needed to produce a film that will spread across a hydrocarbon fuel. The foam produced from this agent will extinguish in the same air-excluding fashion as other foams. Further, the solution that results from normal drainage or foam breakdown produces an aqueous "film" that spreads rapidly and is highly stable on the liquid hydrocarbon fuel surface. It is this film formation characteristic that is the significant distinguishing feature of AFFF as it actually results in a seal significantly mitigating the emission of vapors from the liquid.

These definitions are by no means all-inclusive. For example, film-forming fluoroprotein (FFFP) foam is an agent that is produced by increasing the quantity and quality of the surfactants added to a protein hydrolyzate. By doing this, the surface tension of the resulting solution, which drains from the expanded foam, is reduced to the point where it may spread across the surface of a liquid hydrocarbon fuel. An alcohol-resistant concentrate is formulated to produce a floating polymeric skin for foam buildup on water-miscible fuels. This polymeric skin protects the foam from breakdown by polar solvents, for example, acetone, methanol, and ethanol. Hybrid AFFFs are being formulated to reduce or eliminate fluorosurfactants, which may have an adverse environmental impact.

A potential new class of foams, fluorosurfactant-free foam, has been developed in response to the environmental impact of fluorosurfactants (see section on "Foam Environmental Considerations"). This is neither a film forming or protein based foam. Underwriters Laboratories (UL) classifies these foams generically as "synthetic" foams. UL defines synthetic foams as those having as its base other than a fluorinated surfactant or hydrolyzed protein.

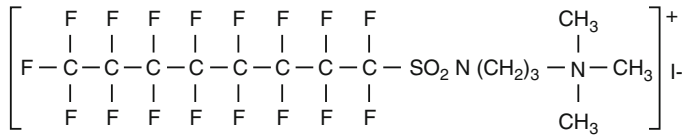

Fig. 47.1 Typical AFFF fluorosurfactant molecule [3]

The descriptions show that there are distinct chemical differences between protein-based foams and AFFF. In general, the surfactants used in aqueous foams are long-chained compounds that have a hydrophobic or hydrophilic (i.e., water repelling or water attracting, respectively) group at one end [2]. The molecular structure of a typical AFFF fluorinated surfactant is shown in Fig. 47.1 [3]. In this molecule, the perfluoroctyl group on the left is the hydrophobic group, while the propyltrimethylammonium group is the hydrophilic group. When these compounds are dissolved into solution with water, they will tend to group near the surface of the solution, aligned so that their hydrophobic ends are facing toward the air/solution interface. The advantage of this is that the perfluoroctyl group found in these compounds is also oliophobic (i.e., oil repelling) as well as hydrophobic [4].

AFFF concentrates also contain hydrocarbon surfactants. These compounds are less hydrophobic than those containing the perfluoroctyl group. However, they do provide greater stability once the solution is expanded into a foam. As a result, the surface tension of the solution is reduced below that of water; the expanded foam produced from the solution is resistive to breakdown from heat, fuels, or dry chemical extinguishing agents; and the solution that drains out from the expanded foam is able to form a film on hydrocarbon fuels.

The importance of both the film formation and foam bubble characteristics of AFFF, resulting from the combination of fluorocarbon and hydrocarbon surfactants, was evaluated in early work by Tuve et al. [5] When a highly expanded, stiff formulation of AFFF was used, these researchers found it difficult to obtain good fire extinguishment and vapor sealing characteristics. The foam resisted flow, and drainage of the aqueous solution (film) was slow. The drainage was corrected by expanding the foam to a lesser degree. This pioneering AFFF formulation, with an expansion ratio of 8:1 and 25 % drainage time of 6 min, appeared to offer the best compromise in characteristics. It provided a readily flowable foam that sealed up against obstructions, promoted the rapid formation of a surface-active film barrier on the fuel, and provided a sufficiently stable foam to resist burnback.

Fire Extinguishment and Spreading Theory

As noted in the *Fire Protection Handbook*® review of suppression theory, the fundamental mechanisms of foam fire extinguishment on two-dimensional pool fires have not been developed [6]. Usually, fire extinguishment is described simply as a factor of the cessation of fuel vaporization at the fuel surface. As the area of fuel vapor production decreases due to the spreading foam, the size of the combustion zone decreases. When the area is totally covered, sufficient amounts of air cannot reach the liquid fuel and extinguishment occurs. As the fuel is covered, cooling must also occur to bring the vapor pressure of the fuel below that of its boiling point. Once the fuel is cooled, a layer of foam must continue to be applied either manually or by spreading to terminate combustion and prevent re-ignition. Hanauska et al. have proposed fundamental extinguishment parameters [7]. A similar foam extinguishment model has been proposed by Persson and Dahlberg [8]. Bench-scale experiments have been combined with correlation/modeling techniques.

Foam Loss Mechanisms

Fire extinguishment by foams can be summarized as shown in Fig. 47.2. Foam having a temperature, T_i, and depth, h, spreads at a rate of V_s along a fuel of temperature, T_s, and vapor pressure, P_v . Fuel is volatized by the fire at a rate of $\dot{m}_{\text{fuel}}$, which is a function of the radiative feedback, $\dot{q}_{\text{rad}}$. The foam is added by the discharge application, $\dot{m}_{\text{add}}$, and lost through evaporation, $\dot{m}_{\text{vap}}$, and drop-through, $\dot{m}_{\text{drop}}$.

The total mass loss of the foam is a function of the loss due to drop-through and the mass loss due to vaporization. The mass loss due to drop-through is at least partially dependent on the drainage of liquid from the foam. Evaporation of the liquid results primarily from radiant energy from the fire. Assuming that most of the radiation results in direct evaporation of the foam, the evaporation of foam can be characterized by

$$\dot{m}''_{\text{vap}} = \frac{\dot{q}''_{\text{rad}}}{\Delta H_v} \tag{47.1}$$

where ΔH_v is the combined latent and sensible heats of vaporization. Using a rough estimate of $\dot{q}''$ from large pool fires of 45–185 kW/m^2 yields an evaporation rate of 18–72 g·m^2/s, assuming a heat of vaporization of 2563 kJ/kg. To account for reflective and absorbed losses, Persson [9] has proposed a calculation method

$$\dot{m}''_{\text{vap}} = \dot{q}''_{\text{rad}} k_e \tag{47.2}$$

where k_e is an experimentally derived constant using different fluxes from a radiant exposure. For $\dot{q}''_{\text{rad}}$ values of 45 and 185 kW/m^2, Equation 47.2 yields values for $\dot{m}''_{\text{vap}}$ of 11 and 46 g·m^2/s, respectively. Because the estimated $\dot{m}''_{\text{vap}}$ values based on Equation 47.1 at the same heat fluxes were 18 and 72 g·m^2/s, the experimental mass loss rate results are about 62 % lower than the theoretical loss. The difference between values is attributable to neglecting the reflected and absorbed losses in Equation 47.1. This indicates that about 48 % of the radiant flux to the foam surface is either reflected from or absorbed into the foam blanket. The division between these two heat transfer mechanisms is not clear and is an area for further study.

Foam loss can likewise be described theoretically, based on the downward force of gravity and the opposing forces due to surface tension and buoyancy. Alternately, a model mass loss due to drainage can be expressed as a time-averaged constant

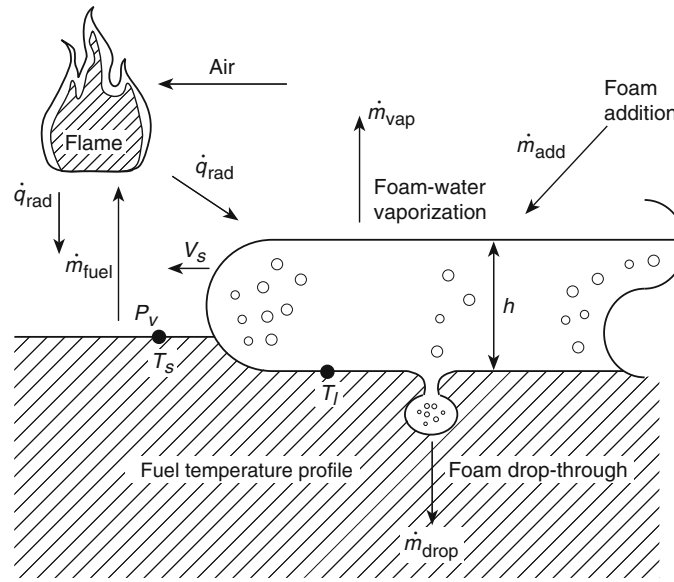

Fig. 47.2 Illustration of the significant parameters affecting a foam's hydrocarbon fuel fire extinguishment capability

$$\dot{m}_{\text{drain}} = k_d \tag{47.3}$$

where k_d is an experimentally determined drainage coefficient. From the data of Persson, the drainage coefficient can be estimated to be 17–25 g·m^2/s [9]. The drainage rate was found to be relatively independent of the radiant heat flux to the foam, but highly dependent on the expansion ratio. Foams with lower expansion ratios will drain faster. For example, decreasing the expansion ratio by about half (11.3–5.3) increased the drainage rate by a factor of about 2 (55–105 g/min). Decreasing the expansion ratio changes fundamental parameters of the foam, which allows it to drain faster.

Experimental work on the foam model, particularly with regard to the effects of incident heat flux on the foam blanket, has been performed in the United States and Europe. Lattimer et al. [10] designed a test apparatus that was used to measure the behavior of foam when exposed to irradiance levels of 0–50 kW/m^2. The apparatus provided data on evaporation rate, drainage rate, foam destruction rate, foam temperature, heat penetration, and time to fuel ignition. The performance of a single AFFF formulation was characterized.

Evaporation rates were measured primarily to be a function of irradiance, making it possible to predict evaporation using the irradiance from the fire and an effective heat of vaporization. The AFFF foam evaluated in this study was determined to have an effective heat of vaporization of 4.87 ± 0.75 MJ/kg. This result is slightly higher than that found by Ikasson and Persson [11], 4.0 MJ/kg. Different AFFF formulations may explain this difference.

Foam drainage rate was measured to be insensitive to the irradiance level or the presence of a fuel layer below the foam. This was consistent with the findings of the Swedish researchers. For foams with expansion ratios ranging from 6.0 to 9.7, drain rate was determined to be a function of foam mass per unit area. A single curve was developed to characterize the drain rate for all foams with a thickness equal to or less than 75 mm. The drainage rate was measured to be constant down to a foam mass per unit area of 3.0 kg/m^2 and decreased linearly to zero by 1.5 kg/m^2. The steady-state drain-rate level decreased from 40 g·m^2/s to 28 g·m^2/s by increasing the expansion ratios from 6.0 to 9.7, respectively.

The drainage rate of low-expansion ratio foams (3.3) was as much as 4–10 times higher than levels measured at higher expansion ratios. The high level was attributed to the fluidity of the foam, which is affected by solution density in foam, breaking and coalescing of bubbles, and solution viscosity. Measurements of foam fluidity for different AFFF foam expansion ratios and temperatures are necessary to further understand these trends in the data at low-expansion ratios.

Foam depletion rate was measured primarily to be a function of the irradiance level incident on the foam. As irradiance increased, the foam depletion rate increased. Foam depletion rate was independent of the initial foam height and expansion ratio.

Heat penetration through the foam was measured to be a function of foam height and foam mass. For all of the different tests where heat penetration was measured, the data indicate that heat begins penetrating through the foam when the foam becomes approximately 50 ± 7 mm thick and has a foam mass of 4.2 ± 1.2 kg/m^2.

Ignition time in tests with JP-5 fuel layers was measured to be a function of both irradiance and initial foam height. Increases in irradiance and decreases in initial foam height were determined to decrease the time to ignition. This result was found to be independent of expansion ratio and initial fuel temperature. At ignition, nearly all of the AFFF (less than 0.8 kg/m^2) had been lost from the fuel surface.

Additional small-scale testing needs to be performed to quantify the foam losses and foam spread characteristics of other foam concentrates. Foam loss and spread data are expected to be concentrate dependent, and these data are necessary to further validate the performance of the foam extinguishment model.

Foam drainage is a complicated phenomenon that is highly time dependent. Besides the forces associated with the bubble structure, drainage is

dependent on the continual changing geometries of the cells and other variable conditions, such as collapsing cells. Even though all aspects of this problem cannot be fully detailed, simplified models have been created that predict the drainage rate for foams. Kraynik has developed one such model that considers the drainage from a column of persistent foam [12]. The model contains no empirical parameters and assumes the foam is dry with very thin walls such that the liquid contained in the cell walls is negligible. Additional modeling has been performed as described in the following paragraphs.

The focus of the tests on the foam by Lattimer et al. [10] was to quantify the evaporation and drainage loss mechanisms, and develop methods for using these data in suppression models. Drain rates were shown to be affected by both expansion ratio and initial foam height. Evaporation rates were primarily affected by the irradiance on the foam. Additional data analysis was conducted to develop methods for expressing the data in a form that could be used in modeling the losses of foam during a fire where the foam may be exposed to a range of irradiance levels. A simple model that monitors the mass of the foam was used to evaluate the proposed methods for predicting evaporation and drainage.

Solution drain rate from foams being heated is extremely difficult to model from first principles due to the complexities that arise from bubbles expanding, coalescing, and bursting. A simple approach for predicting solution drainage was sought for use in fire suppression modeling. Persson et al. [13] found that initial foam height affected drainage rate with time for a particular type and expansion ratio of foam. Empirical relations for drain rate were developed as a function of time and foam height.

In order to avoid having to rely on accurate predictions of foam height in fire suppression calculations, an alternative approach was developed. Through analysis of the data, the mass of the foam was found to be related to the drain rate. Plotting the drain rate versus foam mass essentially collapsed the data for tests with an expansion ratio (ER) of 6 and 10. The relation between drain rate and foam mass was found to be generally unaffected by irradiance or initial foam height.

The second mechanism by which foam will lose solution is through evaporation. The evaporation of solution from the foam surface was modeled as a Lagrangian thin film of solution at a constant temperature of 100°C. The evaporation rate was simplified to

$$\dot{m}''_{\text{evap}} = \left(\frac{\alpha_{\text{foam}}}{\varepsilon_{hfg}}\right)\left(\frac{q''_{hfg}}{\Delta h_v}\right) \tag{47.4}$$

where the $\varepsilon_{hfg} = 0.96$ and the average heat flux is 97 % of the centerline heat flux, $q''_{hfg} = 0.97\ q''_{hfg,cl}$, and the heat of vaporization is that of water at 100°C ($\Delta h_v = 2257\ \text{kJ/kg}$). In the experiments, the mass evaporated was measured directly but the absorptivity of the foam was unknown. Incorporating the constants above, the absorptivity of the foam can be determined by

$$\alpha_{\text{foam}} = 2257\frac{\dot{m}''_{\text{evap}}}{q''_{hfg,cl}} \tag{47.5}$$

This pure radiation model does not account for other phenomena that may affect the evaporation rate such as bubbles bursting, foam density on the surface, and transient heating. Therefore, the absorptivity determined using experimental data would be an effective absorptivity that embodies the radiation properties of the foam and the other phenomena that affect the evaporation rate. This average effective absorptivity is shown in Table 47.1.

These methodologies were used to predict the foam mass drained and evaporated. The mass drained was predicted using a reference curve that related foam mass to drain rate. This function was developed from test data at an irradiance

Table 47.1 Test average effective absorptivity for AFFF at different expansion ratios

Expansion ratio, ER	Effective absorptivity, α foam
3	0.34 ± 0.09
6	0.42 ± 0.06
10	0.41 ± 0.04

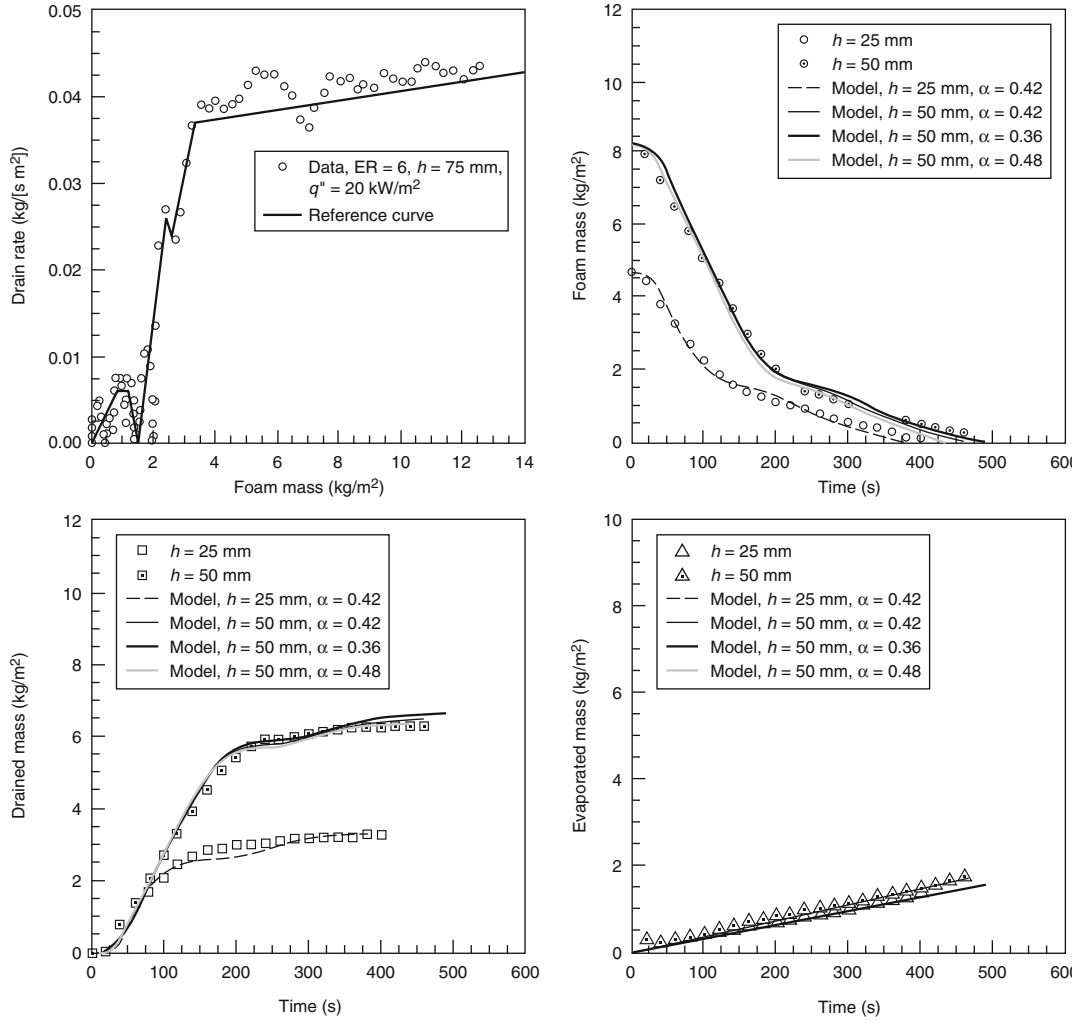

Fig. 47.3 Model predictions for foam with an ER = 6 with h = 25 and 50 mm at q″ = 20 kW/m2

of 20 kW/m^2 with a foam height of 75 mm. The mass evaporated was determined from using the effective absorptivity values provided in Table 47.1. Additional simulations were conducted to evaluate the sensitivity of the results to the range of effective absorptivity stated in Table 47.1.

Predictions of foam having an expansion ratio equal to six are shown in Figs. 47.3 and 47.4 for irradiance levels of 20 and 50 kW/m^2, respectively. Also shown is the reference curve used to predict the drainage rate. The model predicts the masses quite well, particularly near the end of the test where mass of foam on the surface could be used to predict time of fuel ignition. Data from this study indicate that the fuel beneath the foam will ignite when the foam mass per unit area is approximately 0.8 kg/m^2. With good agreement between the model and the data especially near the end of the test when ignition will occur, the model could be used to also predict fuel layer ignition. Also shown in Figs. 47.3 and 47.4 is the effect of varying the effective absorptivity. Because the evaporation represents a small portion of the mass loss, the results were not strongly

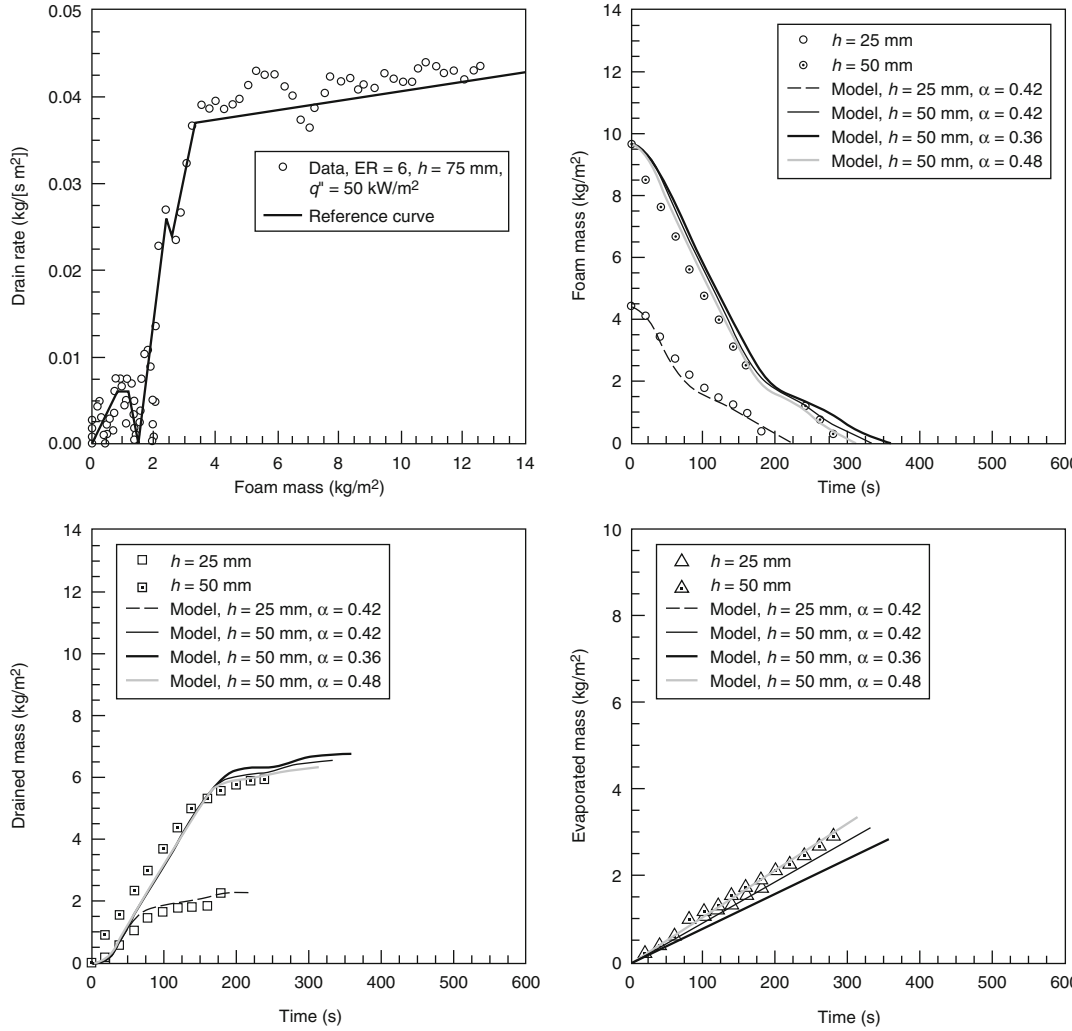

Fig. 47.4 Model predictions for foam with an ER = 6 with h = 25 and 50 mm at q″ = 50 kW/m2

affected by varying this parameter. Similar results were determined for foam at an ER = 10.

Predicted masses for foam at an ER = 3 are shown in Fig. 47.5 along with the reference curve used to predict the drainage rate. Due to the initial surge of drainage in the beginning of these tests, the model does not predict these masses as well in the initial part of the test. After approximately 150 s, the model is within 10 % of the data. Again, the predicted mass of foam near the end of the test agrees well with the data, which indicates that the time of ignition could be predicted using this model even for lower expansion foams.

Foam Spread over Liquid Fuels

In order to predict the extinguishment of a liquid pool fire by fire-fighting foam, it is necessary to describe the process of spreading the foam over the liquid fuel surface. This process of foam spread on a liquid fuel is similar to the spread of a less dense liquid (such as oil) on a more dense liquid (such as water). This

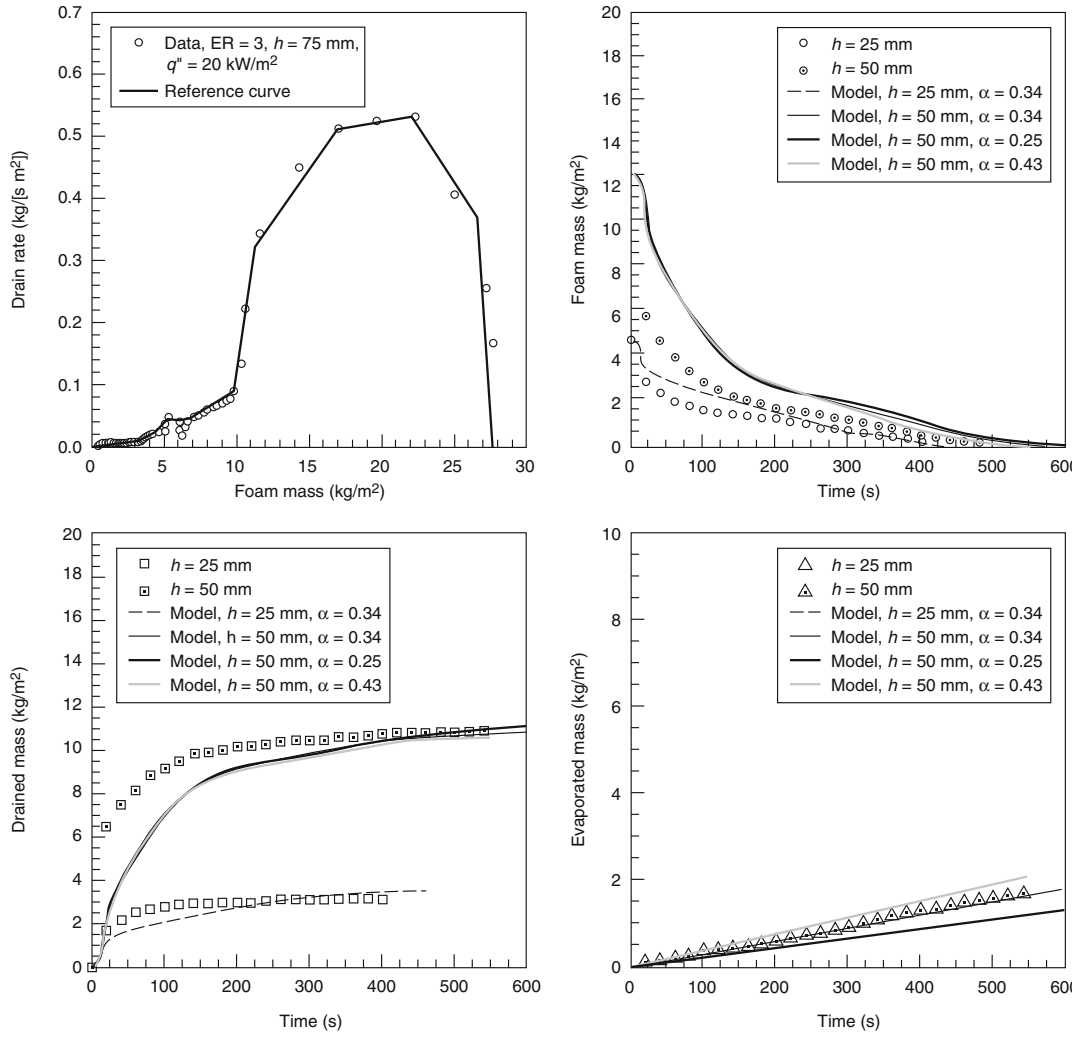

Fig. 47.5 Model predictions for foam with an ER = 3 with h = 25 and 50 mm at $q'' = 20$ kW/m2

phenomenological approach to the spread of foam on a liquid pool fire is appropriate to the extent that foam can be treated as a liquid. Kraynik characterizes foams macroscopically as being Bingham fluids with a finite shear stress and non-Newtonian viscosity [14]. That is, foam displays an infinite viscosity up to some initial shear rate above which it displays a shear-rate dependent viscosity.

Because fuels typically have low viscosities (especially compared to foam viscosities at relatively low shear rates), it may be appropriate to model foam spread across a fuel surface using models developed for oil spread on water. These models assume that the oil spreads as a fluid with a viscosity much higher than the water on which it is spreading. The process of oil spread on water has been described in detail by Fay [15], and Fay and Hoult [16]. Their phenomenologically based model describes three regimes of spread characterized by combinations of spreading forces and retarding forces. The first regime is the gravity-inertia regime, where the outward spread of the oil is driven by a gravity force and

retarded by the inertia required to accelerate the oil. The second regime is the gravity-viscous regime, where the gravity-induced spreading is retarded by viscous dissipation in the water. Because the oil is much more viscous than the water, they assume that there is slug flow in the oil and that the viscous drag force is dominated by the velocity gradient in the water. The third regime is characterized by a surface-tension spreading force opposed by the viscous retarding force. By setting the spreading and retarding forces equal in each of the regimes, they developed equations to estimate the length of the spread as a function of time.

By treating the spread of foam on fuel as similar to the spread of oil on water, the equations developed by Fay and Hoult might be used to describe the spread of a foam blanket over a fuel pool as a function of time [15]. Because foam generally has a much higher viscosity than the fuel on which it is spreading, the assumption of slug flow made for the oil by Fay and Hoult should be reasonably valid for foam spread on fuel as well [16]. The equations are

$$\begin{aligned} &\text{gravity-inertia regime:} && l = (\Delta g V t^2)^{1/4} \\ &\text{gravity-viscous regime:} && l = \left(\frac{\Delta g V^2 t^{3/2}}{\nu^{1/2}}\right)^{1/6} \\ &\text{surface-tension-viscous regime:} && l = \left(\frac{\sigma^2 t^3}{\rho^2 \nu}\right)^{1/4} \end{aligned} \tag{47.6}$$

where

l = Length of spread (cm)
$\Delta = (\rho_{\text{fuel}} - \rho_{\text{foam}})/\rho_{\text{fuel}}$
g = Acceleration of gravity (981 cm/s^2)
V = Foam volume (cm^3)
t = Time (s)
ν = Kinematic viscosity of fuel (cm^2/s)
σ = Spreading coefficient (dynes/cm)
ρ = Density of fuel or foam (g/cm^3)

Equation 47.6 represents an untested theoretical model of foam spread. The equation includes the parameters that are known or suspected to affect foam spread. They are presented here as an initial effort to understand foam flow based on first principles. They are not yet developed for engineering use. The following discussion expands on this theory.

The transition from gravity-dominated spread to surface-tension-dominated spread can be shown to occur at a critical thickness of the foam layer, h_c, given by

$$h_c = \left(\frac{\sigma}{g\Delta\rho_{\text{foam}}}\right)^{1/2} \tag{47.7}$$

The transition from inertia- to viscous-dominated retarding force occurs when the foam thickness, h, is equal to the viscous boundary layer thickness, δ, of the fuel, with

$$\begin{aligned} h &= \frac{\nu}{l^2} \\ \delta &= (\nu t)^{1/2} \end{aligned} \tag{47.8}$$

The equations for length of spread can be used to generate preliminary estimates of the spread distance and area coverage for the placement of a volume of foam on a fuel surface. The equations are only estimates because they consider a force balance between just the dominant forces for each regime. All forces are actually present in each regime. Also, the densities of both fluids are considered to be very nearly equal for the development of the equation for the gravity-viscous regime. This is the case for oil spread on water, but may not be the case for foam on fuel.

Using approximations for fuel and foam characteristics, it can be shown that a positive spreading coefficient does not begin to affect the spread of foam until the foam layer has become very thin. For the placement of a volume of foam on a fuel, this may not occur until after significant time has passed, relative to the time scale for knockdown desired in many fire protection situations.

The equations for foam spread on fuel include many of the parameters known to be important to foam spread. However, the equations are independent of the foam viscosity. Observations indicate that low-viscosity nonrigid foams, such as AFFF, spread faster than high-viscosity rigid protein foams. The inclusion in the model of a term to account for this is desirable.

The equations for spread length so far have assumed that the foam spreads over the fuel as plug flow, with no relative movement within the foam itself. It is easy to conceive that the foam has the capability to flow over itself. The relative movement within the foam is equivalent to the foam flowing over a solid surface. The total foam flow might ultimately be modeled as the combination of the foam plug over the fuel and the flow within the foam layer itself.

According to Cann et al., several regimes exist for spread of a liquid on a solid that are similar to those described for spread of a liquid on a liquid [17]. Most of this spread occurs in a gravity-viscous force regime, where the spread is given by

$$l = \frac{kt}{\mu} \tag{47.9}$$

where k is an empirically determined constant, and μ is the foam viscosity.

Thus, the spread of foam over fuel can be characterized by two scenarios: (1) high-viscosity liquid spreading over a low-viscosity liquid and (2) a liquid spreading over a "solid." The spread of foam can be described by modifying Equation 47.6, as follows:

$$\begin{aligned}
&\text{gravity-inertia regime:} \quad l = \left(\Delta g V t^2\right)^{1/4} + \frac{kt}{\mu} \\
&\text{gravity-viscous regime:} \quad l = \left(\frac{\Delta g V^2 t^{3/2}}{\nu^{1/2}}\right)^{1/6} + \frac{kt}{\mu} \\
&\text{surface-tension regime:} \quad l = \left(\frac{\sigma^2 t^3}{\rho^2 \nu}\right)^{1/4} + \frac{kt}{\mu}
\end{aligned} \tag{47.10}$$

Kraynik describes foams as being characterized by a yield stress and shear thinning viscosity [14]. Thus, the foam viscosity in the equations above is not a constant but is a function of the shear rate. The stress in the foam is a result of the gravity-induced pressure gradient. As the foam flows out and becomes thin, the stress will be reduced. When the stress falls below the yield stress, the viscosity will become infinite and the second term, kt/μ, in the spread length equations will go to zero. The foam will flow simply as plug flow. Above the yield stress, the foam will have a finite viscosity, but this viscosity will be dependent on the yield stress.

An AFFF agent that is very free flowing will have a relatively small yield stress and will retain the second term in the spread length equations until it has flowed out to a very thin layer. A protein foam that is relatively stiff will have a large yield stress, and the second term will go to zero before the foam has spread very far. Above the yield stress, the viscosity of the AFFF will be lower than that of a protein foam, and the second term will provide a greater contribution to foam spread. The rheological properties described appear to have a significant impact on foam spread; however, the properties are not a part of any current specification and are rarely measured.

Foam Extinguishment Modeling

At present, modeling of foam extinguishment cannot be performed because of the large number of remaining uncertainties. A model would have to take into account the addition of foam to the fuel surface, the spread of foam on the fuel surface, and the foam loss mechanisms of evaporation and drop-through. The foam spread length equations can be used to estimate the area of foam coverage at a specific time and for a specific quantity of foam. Modeling at this time is limited because of the lack of established values for k_e (Equation 47.2) and k_d (Equation 47.3). Also, the yield stress and viscosity relationships for fire-fighting foams have not been quantified. Experimental work is needed to complete this modeling effort. Also, the actual method of application (e.g., from a handline nozzle or fixed device such as a sprinkler) must ultimately be taken into account. Even so, preliminary calculations using this methodology are encouraging and support continued development [7].

An attempt has been made to model large tank fires [13]. This included modeling of foam spread with gentle and over-the-top application. The models were based on the assumption that a driving force caused by hydrostatic pressure differences in the foam and a resisting force due

to viscous friction between the foam and the fuel is governing the foam spread. In case of foam flow in a channel, there is also a resisting force due to friction between the foam and the sidewalls. The models take into account ordinary drainage, radiation-induced drainage, and evaporation. Friction data for the models were obtained from cold foam flow tests in laboratory scale. In general, the models for gentle application agree well with the experiments. Due to lack of data, it was not possible to incorporate the destruction of foam at the foam front when it starts to dry out. The effect of this is that the models generally predicted spreading times that were too short. A remaining uncertainty in the models is how to scale the friction data when increasing the length scale by orders of magnitude (e.g., to tank diameters 100–120 m). This is because detailed large-scale data are lacking. Obtaining better experimental observations of large tank fires was recommended.

The model was compared with a few full-scale tank fires ranging from 40 to 80 m in diameter where detailed observations were available. In general, the predicted time to cover is in the range of 10–20 min shorter than the observed time to knockdown. This is because some effects are not included in the model, such as the initial destruction of foam when the foam plunges into the burning fuel, fuel pickup, and foam destruction at the front due to drainage and evaporation. It was concluded that further work is needed to incorporate the destruction of foam at the front, quantify the initial delay phase caused by foam destruction, determine how to scale the friction data when increasing the length scale by orders of magnitude, and obtain more accurate data on foam properties generated by various types of large-capacity foam nozzles.

Surface Tension and Spreading Coefficient

Film-forming foams are defined by the ability of the aqueous solution draining from the foam to spread spontaneously across the surface of a hydrocarbon fuel. The fundamental relationship used to describe the spreading coefficient is

$$S_{a/b} = \gamma_b - \gamma_a - \gamma_l \tag{47.11}$$

where

$S_{a/b}$ = Spreading coefficient (dynes/cm)
γ_b = Surface tension of the lower liquid phase of a hydrocarbon fuel (dynes/cm)
γ_a = Surface tension of the upper layer of liquid using AFFF solution (dynes/cm)
γ_l = Interfacial tension between liquids a and b (dynes/cm)

Surface tension and interfacial tension can be measured using methods such as those described in ASTMD-1331, *Standard Test Methods for Surface and Interfacial Tension of Solutions of Surface-Active Agents*. Reagent-grade cyclohexane is typically used as a reference fuel. A du Nouy tensiometer, having a torsion balance with a 4- or 6-cm-circumference platinum-iridium ring, is lowered into the liquid and slowly pulled out until the liquid detaches from the ring's surface. The force recorded at the point where this separation occurs is the surface tension (dynes/cm) of the pure liquid. Similarly, the interfacial tension is the measurement of tension when the ring is pulled through the boundary layer between two liquids.

The Naval Research Laboratory developed some of the earliest quantitative data on the spreading coefficient of AFFF on hydrocarbons, as shown in Tables 47.2 and 47.3 [18]. As fuel temperature increases, the surface tensions of both the fuel and the solution decrease. The spreading coefficient may go to zero or go negative [18, 19].

Although it has been shown that film-forming foams are superior fire extinguishing agents compared to other foams, there are no one-to-one correlations between bench-scale surface-tension/spreading coefficient data and fire control, extinguishment, and burnback resistance times. Both Scheffey et al. [20] and Geyer [21] have demonstrated that there is no direct correlation between fire extinguishment and spreading coefficient. As such, spreading coefficient data alone

Table 47.2 Surface tension of hydrocarbon liquids and fuels [18]

Hydrocarbon liquid	Grade	Surface tension at 25 °C (dynes/cm)
Cyclohexane	Certified A.C.S.	24.2
n-Heptane	Certified spectroanalyzed	19.8
n-Heptane	Commercial	20.9
Isooctane	Certified A.C.S.	18.3
Avgas	115/145	19.4[a] 19.5[b]
JP-4	Navy specification	22.4[a] 22.8[b]
JP-5	Navy specification	25.6[a] 25.8[b]
Motor fuel	Regular	20.5[a] 21.5[b]
Naphtha	Stove and lighting	20.6

[a]Sample 1
[b]Sample 2

cannot be used as a relative predictor of fire performance.

Because the surface tensions of most AFFFs are approximately equal, there must be a balance between the surface tension of the fuel and the interfacial tension of the two liquids to create a positive spreading coefficient. It can be seen then that, while both the surface tension of the foam solution and the interfacial tension between the liquids have an impact on the spreading coefficient, the interfacial tension is usually the determining factor. For fuels, such as avgas or *n*-heptane, which have surface tensions in the range of 19–20 dyn/cm, either the foam surface tension or the interfacial tension, or both, must be reduced. Normally, the changes resulting from a modification of the formulation will be more significant for the interfacial-tension value than they will be for the foam surface-tension value.

Table 47.3 Interfacial tensions, spreading coefficients, and film formation observations for various surfactant solution–hydrocarbon liquid combinations [18]

Surfactant solution	Hydrocarbon liquid	Interfacial tension (dynes/cm)	Spreading coefficient (dynes/cm)	Film formed
FC-194 (lot 107) (solution surface tension of 15.5 dyn/cm at 25 °C)	Cyclohexane	4.3	4.4	Yes
	n-Heptane, certified	5.5	−1.2	No
	n-Heptane, commercial	4.3	1.1	Yes (very slow spread)
	Avgas[a]	4.6	−0.7	No
	JP-4[a]	3.6	3.3	Yes
	JP-5[a]	4.9	5.2	Yes
	Motor fuel[a]	3.7	1.3	Yes
FC-195 (lot 9) (solution surface tension of 15.6 dyn/cm at 25 °C)	Cyclohexane	3.2	5.4	Yes
	n-Heptane, certified	4.2	0.0	Yes (slow spread)
	Isooctane	2.5	0.2	Yes (slow spread)
	Avgas[a]	0.5	3.3	Yes
	JP-4[b]	3.6	3.6	Yes
	JP-5[b]	4.9	5.3	Yes
	Motor fuel[a]	2.6	2.3	Yes
	Naphtha	2.8	2.2	Yes
FC-195 (lot 10) (solution surface tension of 16.4 dyn/cm at 25 °C)	Cyclohexane	1.5	6.3	Yes
	n-Heptane, certified	3.2	0.6	Yes
	Isooctane	2.8	−1.3	No
	Avgas[a]	2.1	1.0	Yes
	JP-4[a]	2.7	3.3	Yes
	JP-5[a]	4.2	5.0	Yes
	Motor fuel[a]	1.2	2.9	Yes
	Naphtha	0.8	3.4	Yes (slow spread)

[a]Sample 1
[b]Sample 2

Still, a relationship between the two values does exist. [4] Therefore, in reducing the sum of the values to obtain a positive spreading coefficient, a delicate balance must be maintained.

Maintaining this balance and achieving a positive spreading coefficient is accomplished by controlling the amount and type of fluorinated surfactants used to formulate the agent. This at first seems beneficial, because a positive number on a low surface-tension fuel will ensure an even larger value with higher surface-tension fuels (e.g., JP-5 or motor gasoline). But, in reducing the interfacial tension, the foam may lose some of its fuel-shedding capabilities. The effects of adding too much fluorosurfactant to an aqueous solution and the result on foam bubble stability are described by Rosen [4] and Aubert et al. [2] This could be a problem that manifests itself only during actual fire testing. The type and amount of fluorosurfactants also affect the spreading coefficient [20].

Despite the lack of one-to-one correlations between surface-tension spreading coefficient data and fire control, extinguishment, and burnback results, these criteria are useful in categorizing film-forming agents. The spreading coefficient test is used internationally as a standard indicator of aqueous film-forming foams. Although undocumented, it is believed that film formation results in improved viscosity (or associated mechanisms that improve spreading), ultimately resulting in superior extinguishing performance.

Assessment of Fire Extinguishing and Burnback Performance

Standard Test Methods

Because a fundamental model of foam spreading has not been developed, performance of foams is measured using fire tests. The use of bench-scale burning fuel trays (e.g., less than 1 m diameter) results in varying fuel burning rates for the same fuel. This was observed by Chiesa and Alger when they attempted to use a 15-cm by 45-cm pan for foam performance evaluation [22]. Data from their experiments are shown in Fig. 47.6, which correlates control times observed when foam samples were tested using bench-scale apparatus (laboratory) and 4.6 m^2 (50 ft^2) fire tests (field method). Equal control times correspond to a 45° line. Because the majority of the points fall below this line, the laboratory test is more severe (about 35 %) than the field test.

Fire test methods used by regulatory authorities for certification are usually on the order of 2.6 to 9.3 m^2 (28 to 100 ft^2). Foams

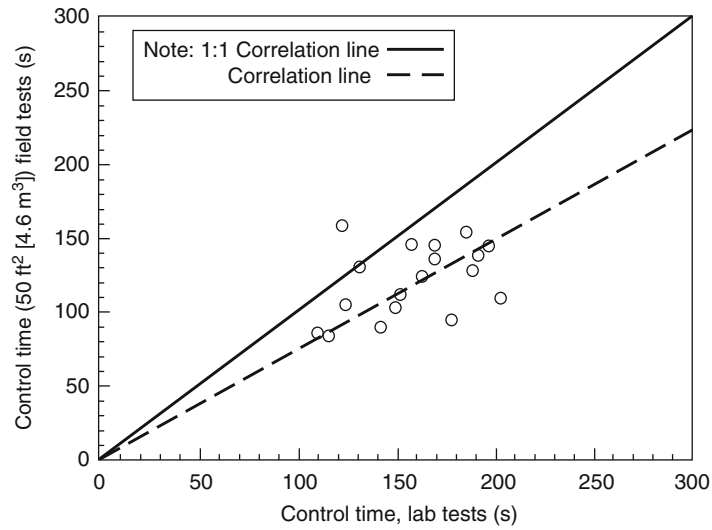

Fig. 47.6 Correlation of control times observed in laboratory and field tests of foam [22]

must also meet additional test parameters related to storage, proportioning, and equipment factors.

Underwriters Laboratories Standard 162 Underwriters Laboratories (UL) 162, *Standard for Foam Equipment and Liquid Concentrates,* is the principal test standard for the listing of foam concentrates and equipment in the United States. Test procedures outlined in this standard have been developed to evaluate specific agent/proportioner/discharge device combinations. When a foam concentrate is submitted for testing, it must be accompanied by the discharge device and proportioning equipment with which it is to be listed. Listed products, including the foam concentrate, discharge device, and proportioner, are then described in the UL *Fire Protection Equipment Directory*.

Listed with a system, foam liquid concentrates are associated with discharge devices classified as Type I, II, or III. Type I devices deliver foam gently onto the flammable liquid fuel surface, for example, a foam trough along the inside of a tank wall. These devices are no longer evaluated in UL 162. Type II discharge devices deliver foam onto the liquid surface in a manner that results in submergence of the foam below the fuel surface, and restricted agitation at the fuel surface. Examples include subsurface injection systems, tank wall–mounted foam chambers, and applications where foam is bounced off the wall of a tank. Type III discharge devices deliver foam directly onto the liquid surface and cause general agitation at the fuel surface, for example, by using handheld nozzles. The flammable liquid fire tests in UL 162 include methods for sprinklers, subsurface injection, and topside discharge devices, including nozzles.

Class B fire test requirements for Types II and III discharge devices and sprinklers are shown in Table 47.4. Commercial grade *n*-heptane is placed in a square test pan. The area of the pan is a minimum of 4.6 m^2 (50 ft^2). The application rates ("densities" in UL 162, *Standard for Foam Equipment and Liquid Concentrates*) for various concentrates are outlined in Table 47.4.

In the test fire, the fuel is ignited and allowed to burn for 60 s. Foam is then discharged for the

Table 47.4 Foam application rates and duration to burnback ignition in UL 162 for hydrocarbon fuels

Application	Foam concentrate	Fuel group	Test application density (L/min/m^2 [gpm/ft^2])	Time of foam application (min)	Maximum extinguishment density (L/m^2 [gal/ft^2])	Duration until burnback ignition (min)	Minimum application rate (L/min/m^2[gpm/ft^2])
Type III discharge outlets	P, FP, S, FFFP[a]	Hydrocarbon	2.5 (0.06)	5	12.2 (0.3)	15	6.6 (0.16)
	AFFF, FFFP[a]	Hydrocarbon	1.6 (0.04)	3	4.9 (0.12)	9	4.1 (0.10)
Type II discharge outlets	P, FP, S, FFFP[a]	Hydrocarbon	2.5 (0.06)	5	12.2 (0.3)	15	4.1 (0.10)
	AFFF, FFFP[a]	Hydrocarbon	1.6 (0.04)	3	4.9 (0.12)	9	4.1 (0.10)
	All	Polar	[b]	5	—	15	[c]
Foam-water sprinklers	P, FP, S	Hydrocarbon	6.6 (0.16)	5	30 (0.8)	15	6.6 (0.16)
Standard orifice sprinkler and spray systems	AFFF, FFFP	Hydrocarbon	4.1 (0.10)	5	20.4 (0.5)	15	6.6 (0.16)
		Polar	[b]	5	—	15	[d]

Source: UL 162, Standard for Foam Equipment and Liquid Concentrates, Mar. 1994, updated Sept. 8, 1999
P protein, *FFFP* film-forming fluoroprotein, *FP* fluoroprotein, *AFFF* aqueous film-forming fluoroprotein, *S* synthetic
[a]Film-forming fluoroprotein is to be tested at application densities of 2.5 and 1.6 L/min/m2 (0.06 and 0.04 gpm/ft^2)
[b]Application rate may vary among polar groups, as specified by the manufacturer
[c]0.10 or 1.67 times test application rate, whichever is greater
[d]0.16 or 1.6 times test application rate, whichever is greater

duration specified in Table 47.4. The foam blanket resulting from the foam discharge must spread over and completely cover the fuel surface, and the fire must be completely extinguished before the end of the foam discharge period.

After all the foam is discharged, the foam blanket formed on top of the fuel is left undisturbed for the period specified in Table 47.4. During the time the foam blanket is left undisturbed, a lighted torch is passed approximately 25.4 mm (1 in.) above the entire foam blanket in an attempt to reignite the fuel. The fuel must not reignite, candle, flame, or flash over while the torch is being passed over the fuel. However, candling, flaming, or flashover that self-extinguishes is acceptable, provided that the phenomenon does not remain in one area for more than 30 s.

After the attempts to reignite the fuel with the lighted torch are completed, a 305-mm (12-in.) diameter section of stovepipe is lowered into the foam blanket. The portion of the foam blanket that is enclosed by the stovepipe is removed with as little disturbance as possible to the remaining blanket outside the stovepipe. The cleared fuel area inside the stovepipe is ignited and allowed to burn for 1 min. The stovepipe is then slowly removed from the pan while the fuel continues to burn. After the stovepipe is removed, the foam blanket must either restrict the spread of fire for 5 min to an area not larger than 0.9 m^2 (10 ft^2) or flow over and reclose the burning area.

When the UL 162 test is passed, the agent, proportioning device, and discharge device become listed together. The fact that foam concentrate has a UL label does not mean it has been tested under all potential end-use conditions. The UL *Fire Protection Equipment Directory* must be referenced to determine with what equipment the concentrate has been tested and approved.

UL 162, *Standard for Foam Equipment and Liquid Concentrates,* is not an agent specification; therefore, there are no requirements for physical properties, such as film formation and sealability and corrosion resistance. Neither are there any provisions to test, on a large scale, the degree of dry chemical compatibility of an agent, or the effects of aging or mixing with agents of another manufacturer. Requirements for a positive spreading coefficient (greater than zero using cyclohexane) for film-forming foams recently have been implemented [23].

As a result of environmental issues related to AFFF, and the removal of products from the marketplace, the U.S. oil industry conducted a series of fire-fighting foam tests [24]. The purpose of the tests was to provide updated data on suitable Class B fire-fighting foam concentrates for use by the oil and petrochemical industry. The foam is used to extinguish large, in-depth flammable liquid fires in both hydrocarbon and polar solvent fuels. These tests were conducted using UL 162 as a guide. The tests were conducted using normal heptane as a baseline model, along with 93 octane gasoline, 93 octane gasoline with 10 % ethanol blend, and isopropanol anhydrous. The objective of the testing was to provide the oil industry with an updated list of foam concentrates that have passed the UL protocol with fuels more commonly found than heptane used in the test standard. This information can then be used to select foams for use at petrochemical facilities and to verify claims by different foam concentrate manufacturers regarding use of their products as suitable for all flammable liquids, including both hydrocarbons and polar solvents, found in the petrochemical industry today. The data from the Chevron Foam Concentrate Team [24] provide comparative results when the UL 162 method is used with different fuel substrates and a range of different concentrates.

U.S. Military Specification The U.S. Military Specification, MIL-F-24385, is the AFFF procurement specification for the U.S. military and federal government. The U.S. military, in all likelihood, is the largest user of foam in the world. It is important to recognize that MIL-F-24385 is a procurement specification as well as a performance specification. Hence, there are requirements for packaging, initial qualification inspection, and quality conformance inspection, in addition to fire performance criteria. Equipment designs unique to the military, in particular

U.S. Navy ships, also impact on the specification requirements (e.g., use of seawater solutions and misproportioning-related fire tests). These requirements have been developed based on research and testing at the Naval Research Laboratory and actual operational experience with protein and film-forming foams.

Table 47.5 summarizes the important fire extinguishment, burnback resistance, film formation, and foam quality requirements established by MIL-F-24385. The fire tests are conducted using 2.6 m^2 (28 ft^2) and 4.6 m^2 (50 ft^2) circular fire test pans. There are specific requirements to conduct a fire test of the agent after it has been subjected to an accelerated aging process (simulating prolonged storage) and after intentionally misproportioning the concentrate with water. In particular, the requirement to conduct a fire test of the agent at one-half of its design concentration is one of the most difficult tests. The 2.6 m^2 (28 ft^2) half-strength fire test must be extinguished in 45 s, only 15 s greater than allowed when the full-strength solution is used.

The physical and chemical properties evaluated for MIL-F-24385 agents are outlined in Table 47.6, along with the rationale for each test. These procedures have been developed based on experience and specific military requirements. For example, MIL-F-24385 requires that the agent be compatible with dry chemical agents. Dry chemical agents may be used as "secondary" agents in aviation and shipboard machinery space fires, for example, to combat three-dimensional fuel fires, where AFFF alone may have limited effectiveness. MIL-F-24385 requires that an agent's compatibility with potassium bicarbonate dry chemical agent (PKP) be demonstrated. The burnback time of the foam in the presence of the dry chemical is measured. Also, the concentrate of one manufacturer must be compatible with concentrates of the same type furnished by other manufacturers, as determined by fire tests and accelerated aging tests.

Table 47.5 Summary of the U.S. Military AFFF specification (MIL-F-24385, revision F) key performance requirements

Test parameter	Revision F
Fire extinguishment	
2.6 m2 (28 ft^2) fire test	
Application rate	2.9 L/min/m^2 (0.71 gpm/ft^2)
Maximum extinguishment time	30 s
Maximum extinguishment density	1.45 L/m^2 (0.036 gal/ft^2)
4.6 m^2 (50 ft^2) fire test[a]	
Application rate	1.6 L/min/m^2 (0.04 gpm/ft^2)
Minimum 40 s summation	320 s
Maximum extinguishment time	50 s
Maximum extinguishment density	1.34 L/m^2 (0.033 gal/ft^2)
Fire extinguishment—over- and underproportioning (2.6 m^2 [28 ft^2] test)	
One-half strength	
Maximum extinguishment time	45 s
Maximum extinguishment density	2.2 L/m^2 (0.054 gal/ft^2)
Quintuple (5 ×) strength	
Maximum extinguishment time	55 s
Maximum extinguishment density	2.7 L/m^2 (0.066 gal/ft^2)
Burnback resistance	
2.6 m^2 (28 ft^2) fire test	25 % maximum at 360 s[b]
4.6 m^2 (50 ft^2) fire test	25 % maximum at 360 s
Foam quality	
Expansion ratio	6.0:1 minimum
25 % drainage	150 s minimum
Film formation	
Spreading coefficient	
Fuel	Cyclohexane
Minimum value	3 dyn/cm
Ignition resistance test	
Fuel	Cyclohexane
Pass/fail criteria	No ignition

[a]Saltwater only
[b]300 s for one-half-strength solutions; 200 s for quintuple-strength solutions

Table 47.6 Physical/chemical properties and procurement requirements of the AFFF Mil spec

Requirement	Rationale
Refractive index	Enables use of refractometer to measure solution concentrations in field; this is most common method recommended in NFPA 412[a]
Viscosity	Ensures accurate proportioning when proportioning pumps are used; for example, balance pressure proportioner or positive displacement injection pumps
pH	Ensures concentrate will be neither excessively basic or acidic; intention is to prevent corrosion in plumbing systems
Corrosivity	Limits corrosion of, and deposit buildup on, metallic components (various metals for 28 days)
Total halides/chlorides	Limits corrosion of, and deposit buildup on, metallic components
Environmental impact	Biodegradability, fish kill, BOD/COD[b]
Accelerated aging	Film formation capabilities, fire performance, foam quality; ensures a long shelf life
Seawater compatibility	Ensures satisfactory fire performance when mixed with brackish or saltwater
Interagent compatibility	Allows premixed or storage tanks to be topped off with different manufacturers' agents, without affecting fire performance
Reduced- and over-concentration fire test	Ensures satisfactory fire performance when agents are proportioned inaccurately
Compatibility with dry chemical (PKP) agents	Ensures satisfactory fire performance when used in conjunction with supplementary agents
Torque to remove cap	Able to remove without wrench
Packaging requirements	Strength, color, size, stackable, minimum pour, and vent-opening tamperproof seal; ensures uniformity of containers and ease of handling
Initial qualification inspection	Establishes initial conformance with requirements
Quality conformance inspection (each lot)	Ensures continued conformance with requirements

[a]NFPA 412, Standard for Evaluating Aircraft Rescue and Fire-Fighting Foam Equipment, 2003 edition
[b]BOD/COD: Biological oxygen demand/chemical oxygen demand

Standards Outside the United States The number of standards developed for foams outside the United States is quite substantial. A brief review of the literature yielded over 17 different standards and test methods [25]. Developments in the European community are reviewed here to provide examples of differences in test standards.

The International Civil Aviation Organization (ICAO) develops crash fire-fighting and rescue documents for its member bodies. The ICAO *Airport Services Guide,* Part 1, "Rescue and Firefighting," describes airport levels of protection to be provided and extinguishing agent characteristics. Minimum usable amounts of extinguishing agents are based on three levels of performance: Level A and Level B. A performance Level C has been adopted. The amounts of water specified for foam production are predicated on an application rate of 8.2 L/min/m^2 (0.20 gpm/ft^2) for Level A, and 5.5 L/min/m^2 (0.13 gpm/ft^2) for Level B. Agents that meet performance Level B require less agent for fire extinguishment. ICAO foam test criteria are described in Table 47.7. Foams meeting performance Level B have an extinguishment application density of 2.5 l/m^2 (0.061 gal/ft^2) and 1.75 l/m^2 (0.043 gal/ft^2) for Level C. There are no surface-tension, interfacial-tension, and spreading coefficient requirements.

The International Organization for Standardization (ISO) has issued a specification for low-expansion foams, EN 1568–3 [26]. The specification includes definitions for protein, fluoroprotein, synthetic, alcohol resistant, AFFF, and FFFP concentrates. A positive spreading coefficient is required for film-forming foams when cyclohexane is used as the test fuel. There are toxicity, corrosion, sedimentation, viscosity, expansion, and drainage criteria. The fire test uses a 2.4-m (8-ft) diameter circular pan with

Table 47.7 ICAO foam test requirements

Fire tests	Performance level A	Performance level B	Performance level C
1. Nozzle (air aspirated)			
(a) Branch pipe	UNI 86 foam nozzle	UNI 86 foam nozzle	UNI 86 nozzle
(b) Nozzle pressure	700 kPa (100 psi)	700 kPa (100 psi)	700 kPa (100 psi)
(c) Application rate	4.1 L/min/m^2 (0.10 gpm/ft^2)	2.5 L/min/m^2 (0.06 gpm/ft^2)	1.75 L/min/m^2 (0.043 gpm/ft^2)
(d) Discharge rate	11.4 L/min (3.0 gpm)	11.4 L/min (3.0 gpm)	11.4 L/min (3.0 gpm)
2. Fire size	≅2.8 m^2 (≅30 ft^2) (circular)	≅4.5 m^2 (≅48 ft^2) (circular)	7.3 m^2 (79 ft^2) (circular)
3. Fuel (on water surface)	Kerosene	Kerosene	Kerosene
4. Preburn time	60 s	60 s	60 s
5. Fire performance			
(a) Extinguishing time	≤60 s	≤60 s	≤60 s
(b) Total application time	120 s	120 s	120 s
(c) 25 % reignition time	≥5 min	≥5 min	≥5 min

Table 47.8 Maximum extinction times and minimum burnback times from ISO/EN specification

		Gentle application test		Forceful application test	
Extinguishing Performance class	Burnback Resistance level	Extinction time (min) Not more than	Burnback time (min) Not less than	Extinction time (min) Not more than	Burnback time (min) Not less than
I	A	—	—	3	10
	B	5	15	3	Not tested
	C	5	10	3	Not tested
	D	5	5	3	Not tested
II	A	—	—	4	10
	B	5	15	4	Not tested
	C	5	10	4	Not tested
	D	5	5	4	Not tested
III	B	5	15	Not tested	Not tested
	C	5	10	Not tested	Not tested
	D	5	5	Not tested	Not tested

heptane as the fuel. The UNI 86 foam nozzle is used for either a "forceful" or "gentle" application method at a flow rate of 11.4 L/min (3 gpm). The application rate is 2.4 L/min/m^2 (0.06 gpm/ft^2). For the greatest performance level, a 3 min extinguishment time is required. This extinguishment time results in an extinguishment application density of 7.6 l/m^2 (0.19 gal/ft^2).

The proposed ISO/EN requirements for extinguishing and burnback are summarized in Table 47.8. There are three levels of extinguishment performance and four levels of burnback performance. For extinguishing performance, Class I is the highest class and Class III the lowest class. For burnback resistance, Level A is the highest level and Level D is the lowest level.

Typical performance classes and levels for different concentrates are provided. Typical anticipated performance for AFFF is noted as Level IC, and Level IB for alcohol-type AFFF. For a fluoroprotein foam, performance is expected to be Level IIA for both alcohol-type and hydrocarbon-only concentrates.

Comparison of Small-Scale Tests Table 47.9 outlines the large number of variables associated with foam performance and testing. These include factors such as foam bubble stability and fluidity, actual fire test parameters (e.g., fuel, foam application method and rate), and environmental effects. Even the fundamental methods of measuring foam performance (i.e., knockdown, control, and extinguishment) vary. For example, Johnson reported that FFFP fails the proposed ISO/EN gentle application tests because small flames persist along a small area of the tray rim [27]. As a result, the foam committees have proposed redefining extinction to include flames.

Given the variations and lack of fundamental foam spreading theory, it follows that tests and specifications for various foams and international standards have different requirements. The differences are reflected in Table 47.10, which compares four key parameters of MIL-F-24385, UL 162, ICAO, and ISO/EN standards for manual application (e.g., handline or turret nozzles). There is no uniform agreement among test fuel, application rate, the allowance to move the nozzle, and the extinguishment application density for AFFF. There is a factor of six difference between the lowest permitted extinguishment application density (MIL-F-24385) and the highest (ISO/EN). This significant difference is attributed, at least in part, to the fixed nozzle requirement in the ISO/EN specification.

No study has been performed to correlate test methods; given the significant differences in performance characteristics and requirements, it is unlikely that correlation between these test methods could be established, even when considering AFFF only. An AFFF that meets the ICAO standard could not be said to meet MIL-F-24385 without actual test data. The problem of correlating differences in small-scale tests was demonstrated by UL in a comparison of UL, MIL-F-24385, O-F-555B (U.S. government protein foam specification), and U.K. test methods [28]. In those tests, differences between different classes of agents (protein vs. AFFF) and between agents within a class (e.g., AFFF) were demonstrated. No correlations between test standards could be established.

The problem of correlation is compounded when a single test method is used in an attempt to assess different classes of foam (e.g., protein and AFFF). Attempts to use a single test method are problematic because of the inherent difference between these foams. That is, protein foams require air aspiration so that the foam floats on the fuel surface. This stiff, "drier" foam is viscous and does not inherently spread well without outside forces (e.g., nozzle stream force). AFFF, because of its film-formation characteristics, does not require the degree of aspiration that protein foams require. This heavier, "wetter" foam is inherently less viscous, which contributes to improved spreading and fluidity on fuel surfaces. This is related, at least in part, to the degree of aspiration of the foam. A more exact description of foam aspiration is appropriate. Thomas has described two levels of foam aspiration: (1) primary aspirated and (2) secondary aspirated [29]. Primary aspirated foam occurs when a foam solution is applied by means of a special nozzle designed to mix air with the solution within the nozzle. The consequence is foam bubbles of general uniformity. *Air-aspirated* foam refers to this primary aspirated foam. Secondary aspirated foam results when a foam solution is applied using a nozzle that does not mix air with the solution within the nozzle. Air is, however, drawn into the solution in-flight or at impact at the fire. Secondary aspirated foam is more commonly referred to as *non-air-aspirated* foam.

The correlation between foam solution viscosity and extinguishment time has been shown by Fiala, but the entire foam spreading and extinguishment theory has yet to be demonstrated based on first principles [30]. Thus, the test standards reference bench-scale methods that measure a factor of foam fluidity (e.g., spreading coefficient), but fail to recognize the total foam spreading system, including viscous effects. Fundamental understanding of foam mechanisms would promote the development of bench- and small-scale test apparatuses that potentially have

Table 47.9 Variables associated with foam performance and testing

I. Physical/chemical properties of foam solution
- A. Bubble stability
  - 1. Measures
    - a. Expansion ratio
    - b. Drainage rate
  - 2. Variables
    - a. Water temperature
    - b. Water hardness/salinity
    - c. Water contamination
- B. Fluidity of foam
  - 1. Measures
    - a. Viscosity
    - b. Spreading rate
    - c. Film formation
  - 2. Variables
    - a. Fuel type and temperature
    - b. Foam bubble stability
- C. Compatibility with auxiliary agents
  - 1. Measures—fire and burnback test
  - 2. Variables
    - a. Other foam agents
    - b. Dry chemical agents
- D. Effects of aging
  - 1. Measures—fire and burnback test
  - 2. Variable—shelf life of agent

II. Test methods to characterize foam performance
- A. Fuel
  - 1. Measures
    - a. Vapor pressure
    - b. Flashpoint
    - c. Surface tension
    - d. Temperature
  - 2. Variables
    - a. Volatility
    - b. Depth and size
    - c. Initial temperature of air and fuel temperature
    - d. Time fuel has been burning (e.g., short versus long, and depth of hot layer)
- B. Foam application method
  - 1. Measures
    - a. Stream reach
    - b. Aspiration of foam
    - c. Foam stability (e.g., contamination by fuel)
    - d. Water content of foam
    - e. Proportioning rate
  - 2. Variables
    - a. Aspiration
      - (1) Effect on stream reach
      - (2) Degree to which foam is aspirated and the need to aspirate based on foam type
    - b. Fixed versus mobile device
    - c. Application technique
      - (1) Indirect, for example, against backboard or sidewall
      - (2) Direct
        - (a) Gentle
        - (b) Forceful
        - (c) Subsurface injection
    - d. Application location
      - (1) High—need to penetrate plume
      - (2) Low
    - e. Application rate of foam
    - f. Wind (as it affects stream reach)
      - (1) Crosswind
      - (2) With and against
    - g. Effect of reduced or increased concentration due to improper proportioning
- C. Fire configuration
  - 1. Measures
    - a. Fuel burning rate, radiation feedback to fire
    - b. Propensity for reignition
    - c. Surface tension
  - 2. Variables
    - a. Pan/containment geometry
    - b. Two-dimensional (pool) versus three-dimensional (running fuel/atomized spray)
    - c. Presence and temperature of freeboard
    - d. Wind (as it affects flame tilt and reradiation)
    - e. Surface on which there is fuel
      - (1) Rough
      - (2) Smooth
      - (3) Water substrate—"peeling" effect of fuel
- D. Measurement of results
  - 1. Measures
    - a. Time to knockdown, control, extinguish, and burnback
      - (1) Actual or estimated time by visual observations
      - (2) Summation values, that is, summation of control at 10, 20, 30, and 40 s
    - b. Heat flux during extinguishment and burnback
  - 2. Variables—qualitative and quantitative methods to determine fire knockdown, extinguishment, and burnback
    - a. 90 % control—measure of ability of foam to quickly control the fire
    - b. 99 % (virtual extinguishment)—all but the last flame or edge extinguished
    - c. Extinguishment—100 %
    - d. Burnback—25 %, 50 %

Table 47.10 Examples of extinguishment application densities of various test standards

Test standard	Fuel	Application rate ($L/min/m^2$[gpm/ft^2])	Nozzle movement permitted	Extinguishment application density (L/m^2 [gal/ft^2])
Mil SPEC	Motor gasoline	1.6 (0.04)	Yes	1.34 (0.033)
UL 162	Heptane	1.6 (0.04)	Yes	4.9 (0.12)
ICAO Level B	Kerosene	2.5 (0.06)	Yes (horizontal plane)	2.5 (0.06)
ICAO Level C	Kerosene	1.6 (0.04)	No	1.6 (0.04)
ISO/EN—Forceful	Heptane	2.5 (0.06)	No	7.6 (0.19)

greater direct correlation for predicting large-scale results.

There has been some criticism of the human element involved in many of the test methods. The human factor occurs when an operator is allowed to apply foam from a handheld nozzle onto the burning test fire. Personnel are also called on in some tests to qualitatively assess the percentage of fire involvement in the test pan during the burnback procedure. Using a fixed nozzle during a specification test eliminates the human element during extinguishment. For sprinkler applications, using a fixed nozzle is entirely appropriate and should yield results comparable to actual installations. For applications where movement is actually involved (e.g., fire-fighting handlines, crash-rescue truck turrets, and movable monitors on ships and at petrochemical facilities), the extinguishment densities in the fixed test application will generally exceed the densities found in actual applications in the field. (See Table 47.10 for differences in extinguishing densities for manual versus fixed applications.) Removal of the human element is certainly advisable from a test repeatability standpoint. However, removing the human element from approval fire tests has proved difficult. Both U.S. and Canadian military authorities have investigated the use of fixed nozzles. Both organizations concluded that tests with human operators resulted in better correlation with large fires and overall repeatability.

Quantitative methods for evaluating burnback performance have been described by Scheffey et al. [20] and been adopted in ISO/EN and Scandinavian (NORDTEST) test methods. These methods involve the use of radiometers to establish a heat flux during full test-pan involvement. After extinguishment, the radiometers measure the increasing flux as the burnback fire grows. This increasing flux due to burnback is compared against the original flux. A cutoff is established so that the maximum burnback time is the time for the burnback flux to reach some percentage (e.g., 25 %) of the original full-burning flux.

Critical Application Rates and Correlations Between Small- and Large-Scale Tests

The previous section described the application rate differences in standard test methods between AFFF, fluoroprotein, and protein foams. These application rate differences were established based on full-scale testing. For sprinklers, much of the fundamental application rate differences were established during testing conducted by Factory Mutual Research Corporation (FMRC). (See section on "Foam-Water Sprinkler Systems.") For manual applications, tests in the aviation fire protection field provide the basis for the fundamental application rates. The application rates specified in test standards are usually rates lower than those used in actual practice (see Table 47.4). There are two reasons for this: (1) a factor of safety is used when specifying rates in actual practice and (2) differences between individual foam agents are more readily apparent at critical application rates. To demonstrate how application rates are developed and how specification tests correlate with large-scale results, an example from aviation fire tests will be used.

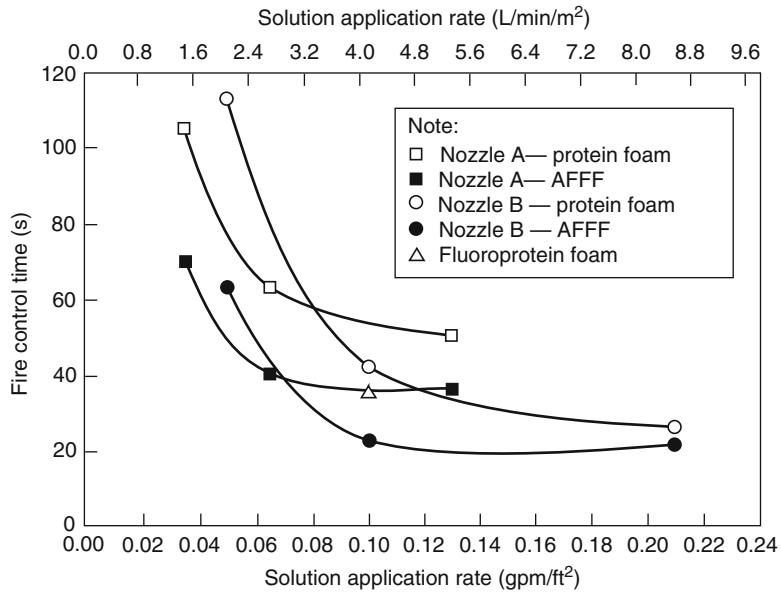

Fig. 47.7 Fire control time as a function of solution application rate using protein foam and AFFF on JP-4 pool fires [31]

This example is based on a review of foam fire test standards performed by Scheffey et al. for the Federal Aviation Administration (FAA) [25].

Tests were conducted by the FAA to determine application rates for a single-agent attack to achieve fire control (e.g., 90 % extinguishment of a fire area) within 1 min under a wide variety of simulated accident conditions. Two factors are important in addition to the application rate required for 1-min fire control: (1) the critical application rate, below which fires will not be extinguished independent of the amount of time an agent is applied; and (2) application density, which is the amount of foam per unit area to control or extinguish a fire.

Minimum application rates were originally developed by Geyer in tests of protein and AFFF agents [31]. These tests involved "modeling" tests with JP-4 pool fires of 21-, 30-, and 43-m (70-, 100-, and 140-ft) diameter. Large-scale verification tests with a B-47 aircraft and simulated shielded fires (requiring the use of secondary agents) were conducted with 34- and 43-m (110- and 140-ft) JP-4 pool fires. All tests were conducted with air-aspirating nozzles. The protein foam conformed to the U.S. government specification, O-F-555b, while the AFFFs used were in nominal conformance with MIL-F-24385 for AFFF. These tests were being performed at the time when the seawater-compatible version of MIL-F-24385 had just been adopted based on large-scale tests.

Figure 47.7 illustrates the results of the modeling experiments. The results show that, for a fire control time of 60 s, the application rate for AFFF was on the order of 1.6 to 2.4 L/min/m^2 (0.04 to 0.06 gpm/ft^2), whereas the application rate for protein foam was 3.3 to 4.1 L/min/m^2 (0.08 to 0.10 gpm/ft^2). The data indicated that the application rate curves become asymptotic at rates of 4.1 L/min/m^2 (0.1 gpm/ft^2) and 8.2 L/min/m^2 (0.2 gpm/ft^2) for AFFF and protein foam, respectively. Above these rates, fire control times are not appreciably improved. Likewise, critical application rates for fire control are indicated when control times increase dramatically. The single test with a fluoroprotein agent indicated that this agent, as expected, fell between AFFF and protein foam.

Large-scale auxiliary agent tests were conducted to identify increases in foam required when obstructed fires with an actual fuselage were added to the scenario. The results indicated that fire control times increased by a factor of 1 to 1.9 for AFFF and 1.5 to 2.9 for protein foams. It was estimated that the most effective foam

solution application rates were 4.9 to 5.7 L/min/m^2 (0.12 to 0.14 gpm/ft^2) for AFFF and 7.5 to 9 L/min/m^2 (0.18 to 0.22 gpm/ft^2) for protein foam. This is the original basis of the recommendations adopted by ICAO of 5.5 L/min/m^2 (0.13 gpm/ft^2) for AFFF and 8.2 L/min/m^2 (0.20 gpm/ft^2) for protein foam. A rate of 7.5 L/min/m^2 (0.18 gpm/ft^2) was subsequently established for fluoroprotein foam. These application rate values are still used by FAA, NFPA, and ICAO to establish minimum agent supplies at airports.

Tests of AFFF alone were conducted by Geyer [32]. These agents, selected from the U.S. Qualified Products List (MIL-F-24385 requirements), were tested on JP-4, JP-5, and aviation gasoline (avgas) fires. Air-aspirating nozzles were used with different AFFF agents. Example results are shown in Fig. 47.8. Similar data were collected by holding the JP-4 fuel fire size constant at 743 m^2 (8000 ft^2) and varying the flow rates to develop application rate comparisons. These data are shown in Fig. 47.9.

Additional tests were conducted by Geyer et al. to verify the continuation of the reduction of water when AFFF agents were substituted for protein foam in aviation situations [1]. In 25-, 31-, and 44-m- (82.4-, 101-, and 143-ft-) diameter Jet A pool fires, AFFF, fluoroprotein, and protein foams were discharged with air-aspirating and non-air-aspirating nozzles. The data, summarized in Fig. 47.10, validated the continued allowance of a 30 % reduction in water requirement at certified U.S. airports when AFFF is substituted for protein foam.

Although some test criteria in standardized methods do not necessarily correlate directly with actual fire and burnback performance, small-scale test data for AFFF formulated to the U.S. military specification (MIL-F-24385) has been shown to correlate with large-scale fire test results. This is based on a comprehensive review of small- and large-scale test data [25]. In these data, a key variable was controlled; that is, all AFFF agents were formulated to meet MIL-F-24385. Ninety percent fire control times were used as the most accurate measure of fire knockdown performance, which were reported in all tests. The use of 90 % control times eliminates the variability of total extinguishment, which

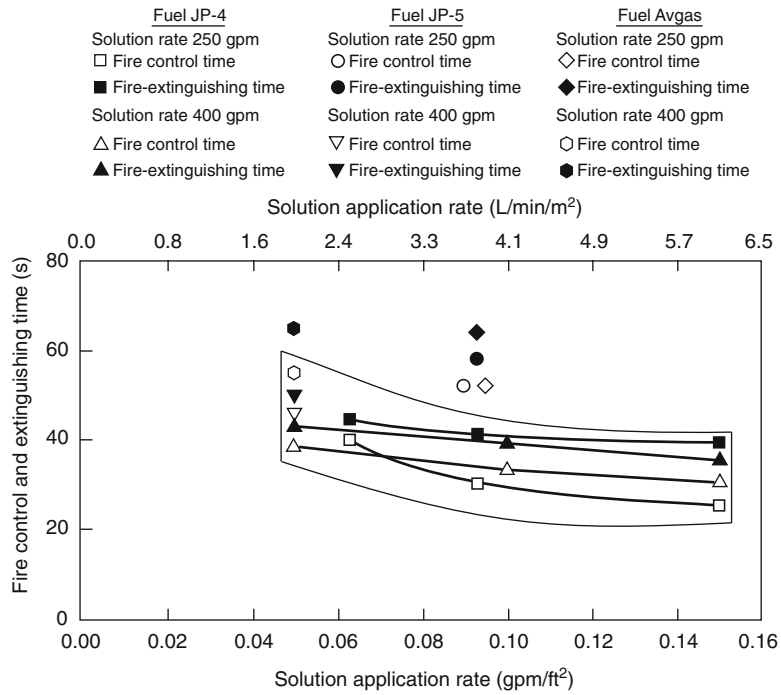

Fig. 47.8 Fire control and extinguishing times as functions of the foam solution application rate using AFFF at 250 gpm (946 L/min), 400 gpm (1514 L/min), and 800 gpm (3028 L/min) on JP-4, JP-5, and avgas fires [32]

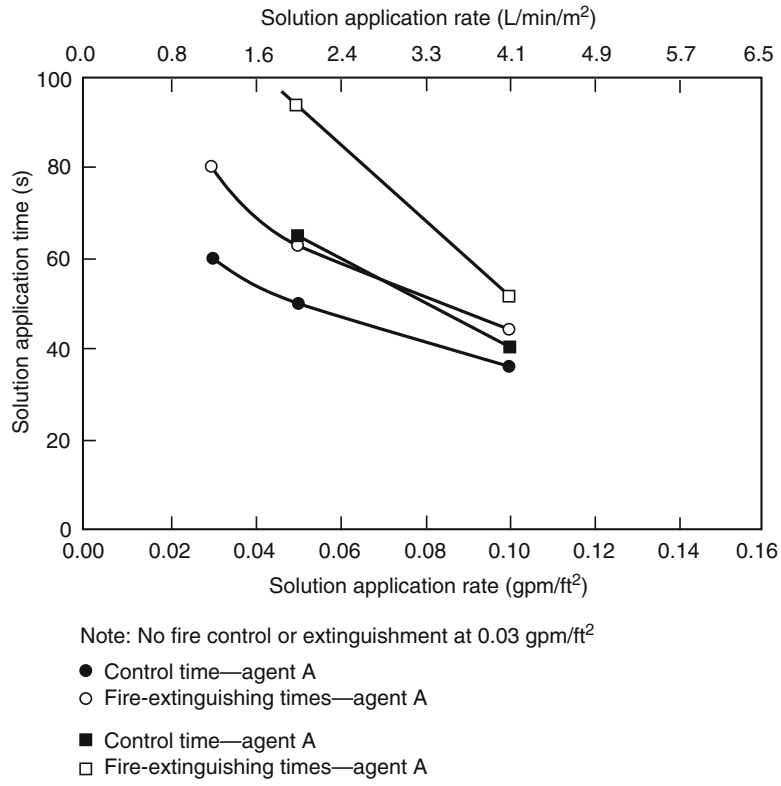

Fig. 47.9 Fire control and extinguishing times as a function of solution application rate using AFFF at 250, 400, and 800 gpm on 743-m2 (8000-ft2) JP-4 fuel fires [32]

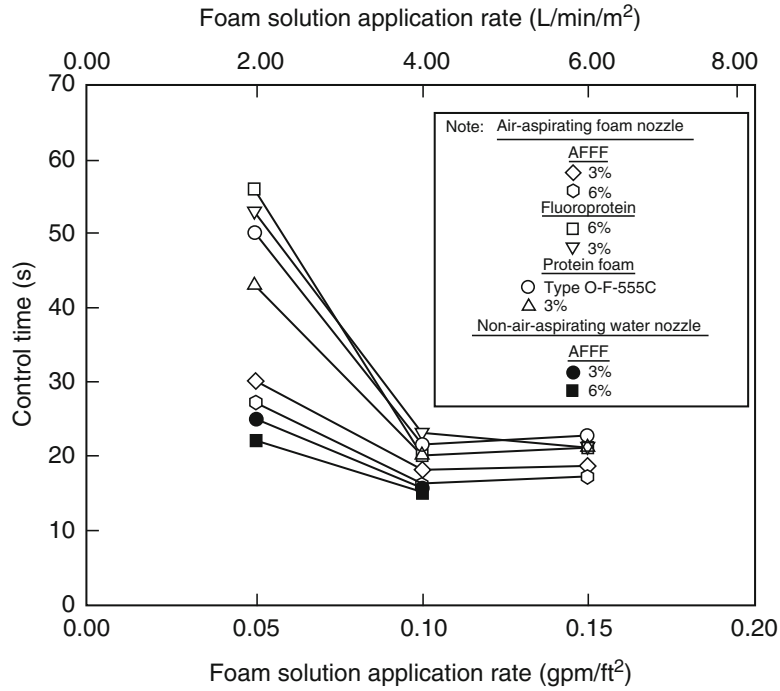

Fig. 47.10 Fire control time as a function of solution application rate for AFFF, fluoroprotein, and protein foams for Jet A pool fires [1]

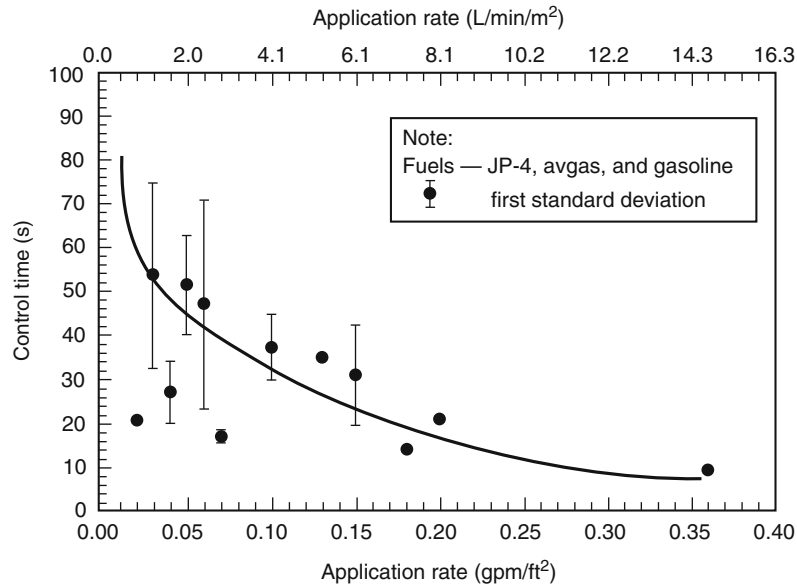

Fig. 47.11 AFFF control time as a function of application rate [25]

might be dependent on test-bed-edge effects or running fuel fire scenarios. Data for tests using air-aspirated or non-air-aspirated nozzles were combined. Low-flashpoint (less than 0°C [32°F]) fuels were evaluated. The evaluation included only tests where manual application was used, eliminating the variable of fixed versus manual application.

The effects of application rate on control and extinguishment times, as demonstrated in Figs. 47.7 through 47.10, were reconfirmed as shown in Fig. 47.11. Control time increases exponentially as application rate decreases, particularly below 4.1 L/min/m^2 (0.10 gpm/ft^2). Variability of the data is shown by the first standard deviation.

The scaling of small fires with large fires is shown in Figs. 47.12 and 47.13, which relate the time needed to control the burning fuel surface as a function of fire size. The time needed to control a unit of burning area (s/ft^2 [s/m^2]), designated as the specific control time, is plotted as a function of fire size. For low (1.2 to 2.5 L/min/m^2 [0.03 to 0.06 gpm/ft^2]) and intermediate (2.8 to 4.1 L/min/m^2 [0.07 to 0.10 gpm/ft^2]) application rates, the specific control times decrease linearly as a function of fire area. These data are in agreement with data from Fiala, which also indicate decreasing specific extinguishment control times as a function of burning area for increasing application rates of AFFF. [30] Also, Fiala showed that, for a constant application rate, AFFFs have lower specific extinguishment times as a function of burning area than those of protein and fluoroprotein foams. Obviously, this linear relationship must change at very large areas; otherwise, the specific control/extinguishment time would go to zero. This is evidenced in Fig. 47.12, where the curve flattens at the high-area end of the plot.

Figures 47.12 and 47.13 show that higher specific control times are required for MIL-F-24385 test fires (2.6 and 4.7 m^2 [50 and 20 ft^2]) compared to large fires. This is readily apparent as actual/control extinguishment times for the small fires are on the same order as results from large fires. FAA and NFPA criteria for minimum quantities of agent are also shown in Figs. 47.12 and 47.13. These criteria are expressed in terms of specific control time as a function of area by using the required control time of 60 s and the practical critical fire areas for airports serving different sizes of aircraft. The data indicate that specific control times with MIL-F-24385 agents are roughly equivalent or less than the specific control times established by NFPA and FAA

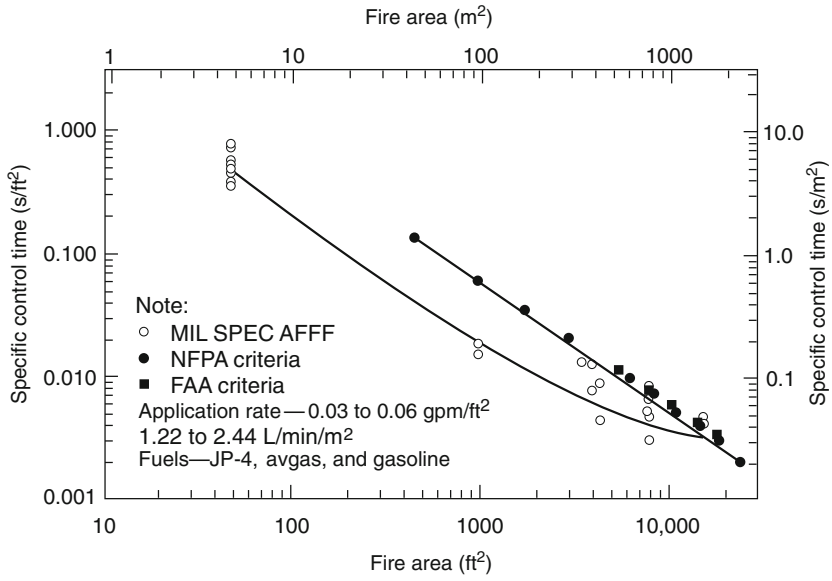

Fig. 47.12 Specific control times for AFFF at low application rates [25]

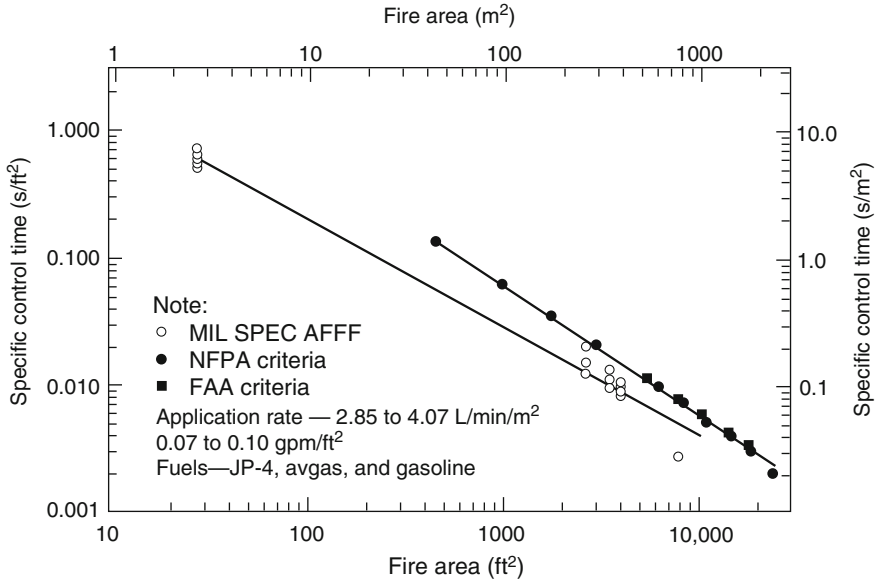

Fig. 47.13 Specific control times for AFFF at intermediate application rates [25]

requirements for large fire areas. This relationship is true even with the AFFF discharged at rates 25–75 % below the minimum NFPA/FAA discharge rate of 5.5 L/min/m^2 (0.13 gpm/ft^2). From these data, it can be concluded that a scaling relationship exists between MIL-F-24385 small-scale tests and actual large-scale crash rescue and fire-fighting applications. The MIL-F-24385 tests are more challenging than the larger tests in terms of specific control time, but

this challenging test produces an agent that can meet NFPA and FAA requirements at less than the design application rate. This factor of safety accounts for variables in actual aviation crash situations, for example, running fuel fires, debris that may shield fires, and crosswinds that may limit foam stream reach.

Aviation Fire Protection Considerations

Historical Basis for Foam Requirements

The underlying principle in aviation fire protection is to temporarily maintain the integrity of an aircraft fuselage after a mishap to allow passenger escape or rescue. When an aircraft is involved in a fuel spill fire, the aluminum skin will burn through in about 1 min. If the fuselage is intact, the sidewall insulation will maintain a survivable temperature inside the cabin until the windows melt out in approximately 3 min. At that time, the cabin temperature rapidly increases beyond survivable levels.

Aircraft rescue and fire-fighting (ARFF) vehicles are designed to reach an incident scene on the airport property in 2–3 min, depending on the standard enforced by the authority having jurisdiction (AHJ). Having reached the scene in this time frame, the agent must be applied to control a fire in 1 min or less. The 1 min critical time for fire control is recognized by FAA, NFPA, and ICAO.

Minimum agent requirements on ARFF vehicles are established using the 1-min critical control time plus the anticipated spill area for the largest aircraft using the airport. A "theoretical critical fire area" has been developed, based on tests, and is defined as the area adjacent to the fuselage, extending in all directions to the point beyond which a large fuel fire would not melt an aluminum fuselage regardless of the duration of the exposure. A function of the size of an aircraft, the theoretical critical fire area was amended to a "practical critical fire area" after evaluation of actual aircraft fire incidents. The practical critical area, two-thirds the size of the theoretical critical area, is widely recognized by the aviation fire safety community, including FAA, NFPA, and ICAO. Vehicles must be equipped with sufficient agent and discharge devices to control a fire in the practical critical area within 1 min. Vehicles must also be equipped with a secondary agent (dry chemical or Halon 1211) for use in combating three-dimensional fuel fires.

The FAA has recently reviewed the basis of airport foam requirements. They considered new large aircraft containing significantly greater jet fuel loads (e.g., Airbus A380), and aircraft containing significantly greater fuselage combustible composite materials (in place of aluminum) [33, 34]. An fire hazard approach which assumed an unlimited size aircraft spill fire was considered, along with loss history. The "critical area" concept was found to be an acceptable and appropriate approach for establishing agent quantities. Research is continuing of the impact of composite materials.

Agent Quantities and Standards

The previous text on critical application rates described the rationale used to develop design application rates used in aviation fire protection. These rates are 5.5 L/min/m^2 (0.13 gpm/ft^2) for AFFF, 7.5 L/min/m^2 (0.18 gpm/ft^2) for fluoroprotein foam, and 8.2 L/min/m^2 (0.28 gpm/ft^2) for protein foam. Using these rates, the practical critical fire area and the 60-s control time criteria, minimum agent quantities are established for airports serving different size aircraft. These criteria are contained in NFPA 403, *Standard for Aircraft Rescue and Fire-Fighting Services at Airports,* and the FAA Advisory Circular 150/5210-6C, "Aircraft Fire and Rescue Facilities and Extinguishing Agents." ICAO uses similar criteria. NFPA 403 has adopted the 4.6 m^2 (50 ft^2) fire extinguishment and burnback criteria from MIL-F-24385 for AFFF agents. UL test criteria are acceptable for protein and fluoroprotein foams. All certified airports in the United States must now use MIL SPEC AFFF when purchasing foam concentrate. Recognizing the limitations of its test methods

for aviation applications, UL has deleted references to crash rescue fire fighting from the scope of UL 162, *Standard for Foam Equipment and Liquid Concentrates*. NFPA 403 recognizes that the standards for foam that it references are widely recognized throughout North America, but may not be recognized in other areas of the world. In particular, the ICAO test method has significantly different test parameters, including test fuel, application rate, and extinguishment density. The NFPA notes that it is incumbent on the national authority having jurisdiction to determine that alternative test methods meet the level of performance established by NFPA 403 test criteria.

NFPA 412, *Standard for Evaluating Aircraft Rescue and Fire-Fighting Foam Equipment,* provides field test methods to determine the adequacy of foam equipment on crash rescue vehicles. It includes criteria for foam expansion and drainage, and methods to determine foam solution concentration.

Expansion and Drainage Foam expansion and drainage requirements of the current version of NFPA 412, *Standard for Evaluating Aircraft Rescue and Fire-Fighting Foam Equipment,* are shown in Table 47.11.

NFPA 412 references a 1600 mL foam sample collector, which was originally adopted by ICAO and ISO/EN. This single method is used to obtain expansion and drainage measurements for all types of foams in hope that similar success could be obtained in using a single fire test method for all foams. The multiple categories of foam test classification in Table 47.8 for the ISO/EN method show how difficult this has been to achieve. Given the different methods of foam flow over a fuel surface, it may not be practical to use a common fire test method predicated on the current means of testing. Further development of fundamental foam-extinguishing principles is recommended.

Table 47.11 Foam quality requirements from NFPA 412

Agent	Minimum expansion ratio	Minimum solution 25 % drainage time (min)
AFFF or FFFP		
Air aspirated	5:1	2.25
Non-air-aspirated	3:1	0.75
Protein	8:1	10
Fluoroprotein	6:1	10

The 1600 mL expansion and drainage test method replaced two other methods where a 1000 mL cylinder or 1400 mL pan was used as the collection device. MIL-F-24385 still uses the 1000 mL collection method. This situation, plus other different test methods, makes direct comparison of expansion and drainage data difficult. Tests performed by Underwriters Laboratories (UL) identified differences among the three test methods based on expansion and drainage results [35]. UL found that expansion ratios remained the same but that drainage was quicker using the 1600 mL method compared to the 1000 mL method for film-forming foams. Drainage time increased (i.e., doubled) for the protein foams when the 1600 mL method was used compared to the 1400 mL pan method.

No direct correlations have been established between expansion, drainage, and fire-extinguishing performance. There is a relationship between foam drainage and burnback. Longer drainage times generally result in longer burnback times. Refer back to the "Fire Extinguishment and Spreading Theory" section for quantitative relationships.

The expansion and drainage data in Table 47.11 indicate the inherent differences between air-aspirated and non-air-aspirated film-forming foams. The data in Fig. 47.10 showed that non-air-aspirated AFFF was more effective at critical application rates than was air-aspirated AFFF. This conclusion was verified by Jablonski in tests with U.S. Air Force crash trucks, as shown in Fig. 47.14 [36]. Even so, there continues to be debate over air-aspirated and non-air-aspirated foam for manual applications involving aviation fuel spills.

Under certain conditions, non-air-aspirated AFFF is not as effective as air-aspirated AFFF. The results of the foam tests in the United Kingdom [37, 38] and the results from DiMaio et al. [39] described situations where

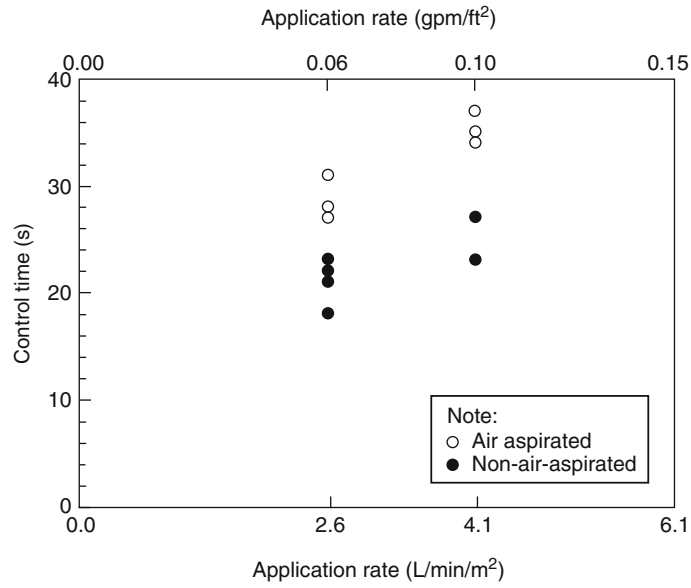

Fig. 47.14 Effects of AFFF aspiration on JP-4 pool fire control times [36]

air-aspirated AFFF resulted in better fire extinguishment performance than non-air-aspirated foam.

Given that one-to-one correlation between expansion, drainage, and fire-extinguishing performance is difficult to identify, there appears to be a lower limit where non-air-aspirated AFFF becomes ineffective. This has not been quantified, but it is speculated that poor performance occurs when the AFFF expansion ratio is less than 2.5:3.0, and drainage is difficult to measure, that is, nearly instantaneous. This is based in part on unpublished data from the Naval Research Laboratory on shipboard bilge AFFF sprinklers [40] and the results of the U.K. tests [37, 38]. The importance of this lower limit of foam aspiration is recognized in NFPA 412 criteria.

Foam Concentration Determination The most common method of determining foam concentration in the field is by use of a handheld refractometer. The refractive index, n, is defined as

$$n = \frac{\sin i}{\sin r} \tag{47.12}$$

where
$\sin i$ = Angle of incidence
$\sin r$ = Angle of refraction

Note:
Refractive index, $n = \dfrac{\sin i \text{ (angle of incidence)}}{\sin r \text{ (angle of refraction)}}$

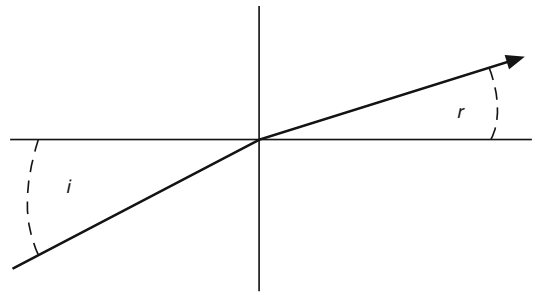

Fig. 47.15 Refractive index of solutions

This is depicted graphically in Fig. 47.15.

Manufacturers report that the glycols in AFFF formulations create the necessary refractive characteristics to determine concentration. However, they also report that glycol has a potential detrimental impact on overall agent performance. Elimination of this compound might improve (slightly) the performance of AFFF, but the glycol is also needed as a fundamental component of agent mixing.

The refractive index of water at 20°C (68°F) is 1.333 (air has a refractive index of 1.0002926). Because the refractive index of a solution is proportional to the inverse of the solution

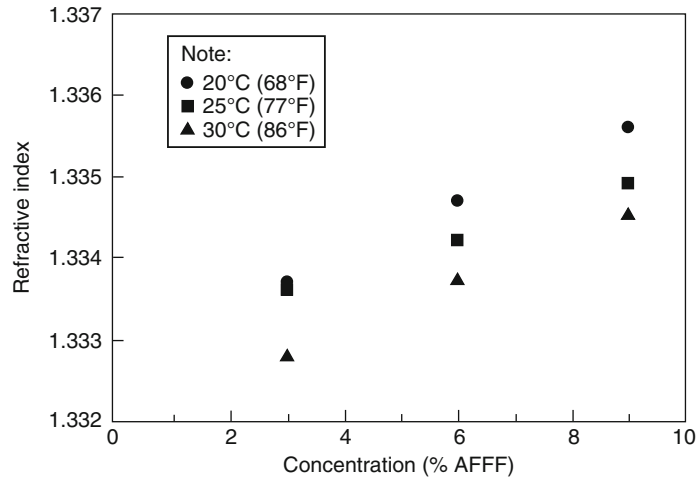

Fig. 47.16 Effects of temperature on refractive index [41]

density, and density is proportional to temperature, then

$$n \propto \frac{1}{T} \tag{47.13}$$

where T is the temperature. This relationship is illustrated in Fig. 47.16. Any refractive index measurements must be made considering temperature. Some handheld measurement devices are temperature compensated. It is good procedure to conduct concentration measurements at a constant temperature.

Other scales may be used. For example, the Brix scale is used as a measure of sucrose weight percent concentration. Units with this scale, commonly found in the food product industry, can be used to measure foam concentration. A typical range of a bench or handheld refractometer is 1.3000 to 1.7000.

NFPA 412, *Standard for Evaluating Aircraft Rescue and Fire-Fighting Foam Equipment,* describes a method to determine foam concentration using the refractive method. In NFPA 412, the preparation of three standard solutions is recommended: one at the nominal concentration, one at one-third more than the nominal concentration, and one at one-third less than the nominal concentration. A plot of the refractive scale reading against the known foam concentration is made on graph paper. This plot establishes a "calibration" curve against which foam samples from a vehicle or system can be judged. Because refractive index is linear, a calibration curve can be created by

$$\text{AFFF}\%_{\text{sample}} = \frac{n_{\text{foam}} - n_{\text{water}}}{n_{\text{concentrate}} - n_{\text{water}}} \times 100 \tag{47.14}$$

This method is used by the U.S. Navy for checking proportioning system accuracy on board ships.

The limitations of the refractive index technique are described by Timms and Haggar [41]. The accuracy of the refractometer can become poor due to the focusing and setting of the refracted light junction on the crosshairs of the viewing window, and the reading of the graduated scale to four decimal places (where the scale is graduated to only three places). This effect is illustrated in Fig. 47.17, where a calibration curve for a 1 % AFFF concentrate was established using a straight line through the 50 % concentration point and the "water" reading by one of the experimenters. Note that the error between readings by the two experimenters at 1 % concentration exceeds 25 %. In this example, differences in the baseline water reading will create substantial error in the calibration curve. These differences are exaggerated with 1 % concentrates. At 3 % or 6 %, the experimental

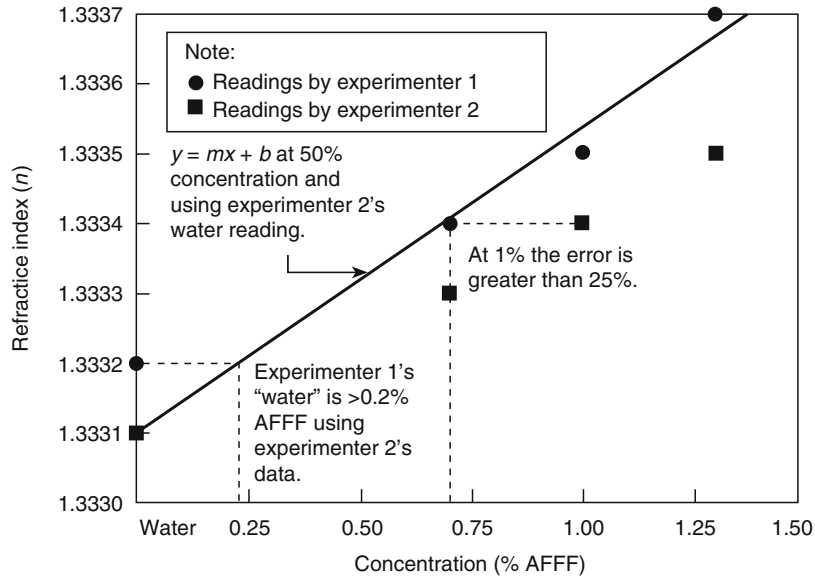

Fig. 47.17 Refractive indices of 1 % AFFF solutions in tap water

error in reading the refractometer, for field testing, is generally accepted as adequate.

Alternative methods for measuring AFFF concentration include total fluorine content, optical absorption methods, and electrical conductivity. Because neither the total fluorine content method nor the optical absorption method is suited to field use, the conductivity method has been proposed. Because foams contain electrolytes, their conductance, G, can be measured and described as

$$G = \frac{1}{R}(mhos) \qquad (47.15)$$

where R is resistance (ohms). Conductivity, σ, is conductance per unit length:

$$\begin{aligned}\sigma &= \mathrm{G/unit\ length}\\ &= \mathrm{mhos/cm}\\ &= \mathrm{siemens/cm}\end{aligned}$$

Because conductivity is directly proportional to temperature, conductivity increases with temperature (Fig. 47.18). Temperature compensation is appropriate when using this method.

Timms and Haggar showed the influence of the substrate water on both refractive index and conductivity [41] (Figs. 47.19 and 47.20). It is important to note the difference of the characteristic curve for a salt solution. AFFF actually reduces the conductivity of this highly conductive water. Note also that, although conductance may exhibit straight-line characteristics in the area of interest (0 to 10 %), the overall curves from 0 to 100 % are nonlinear.

The "sensitivity" of the two methods (i.e., refractive index and conductivity) was shown by these researchers by comparing the difference between readings for solutions of 3 % and 6 % divided by the reading at 6 %. The sensitivities for tap water show that the conductivity method is more sensitive than the refractive index measure (Table 47.12). In repeated readings of refractive index and conductivity, the foam concentration accuracy using conductivity was ±0.1 %, where the accuracy of the refractive index method was ±0.8 % (Table 47.13).

An evaluation was conducted by the U.S. FAA to comparatively test various conductivity meters and retractometers used in testing airport rescue and fire fighting (ARFF) vehicle foam-proportioning systems. [42] During the annual certification inspection of an airport fire department, refractometer and conductivity meter tests are conducted to test the foam concentrate and foam-proportioning systems of the ARFF apparatus. Historically, the refractive

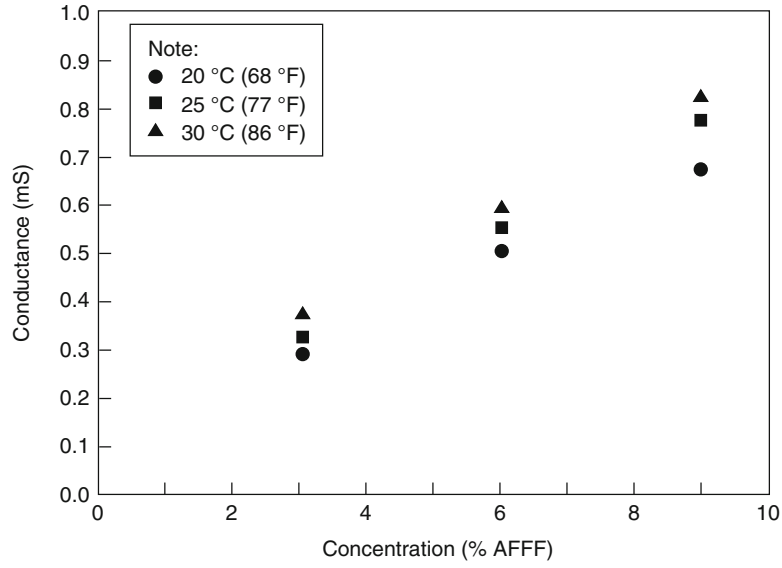

Fig. 47.18 Effects of temperature on the conductance of AFFF solutions [41]

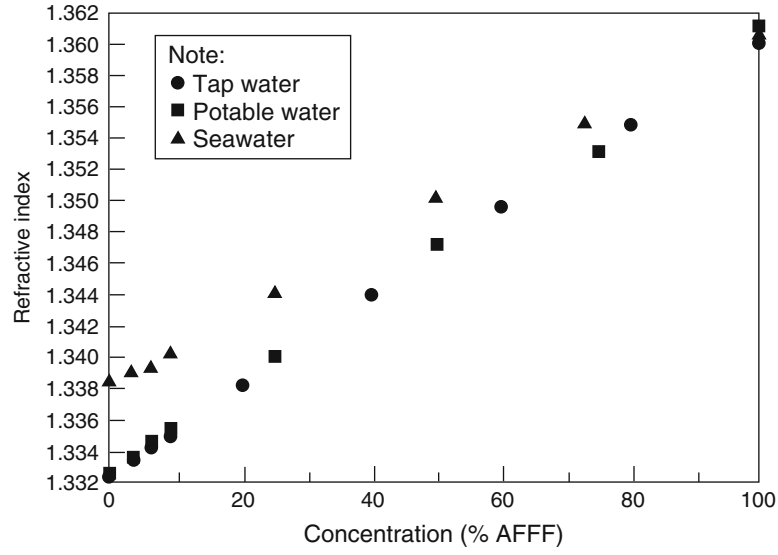

Fig. 47.19 Effect of substrate water on refractive index of AFFF solutions [41]

index method has been used to determine the proportioning of foam-generating systems. Because of the limited accuracy of the refractometer, particularly for assessing systems using 1 % and 3 % concentrates, the conductivity method is gaining more widespread use. Five conductivity meters were evaluated against a standard refractometer. A range of representative 3 % and 6 % foam concentrates were evaluated. Measured standard solutions prepared from the five conductivity meter tests show very close readings to one another. Typically, the units read within 0.2 mS. More importantly, all five conductivity meters exhibited the same trends in the readings from one foam product to the other. The refractometer data were not as consistent. A significant factor in the use of the refractometer is the fact that the readings can be interpreted differently by several evaluators during the same test. The digital readings from the conductivity

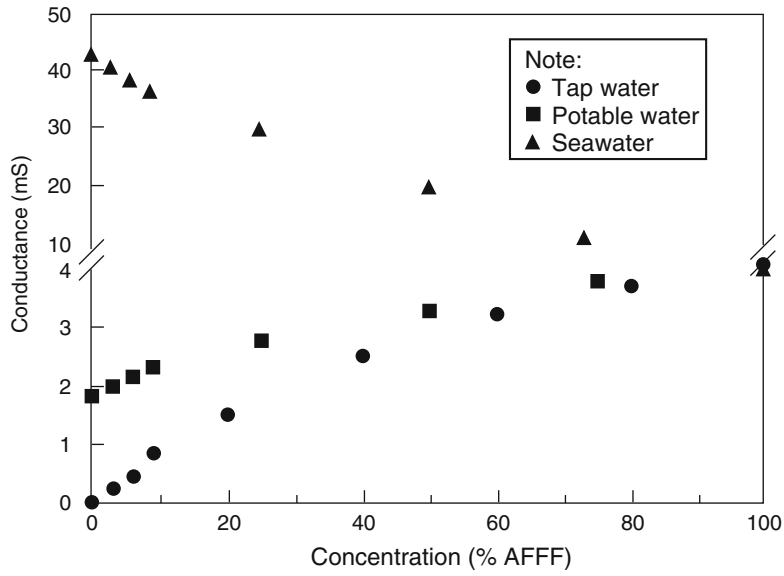

Fig. 47.20 Effect of substrate water on conductivity of AFFF solutions [41]

Table 47.12 Sensitivity of refractive index and conductivity methods for determining foam concentration [41]

	Refractive index	Conductance (mS)
3 %	1.3337	0.318
6 %	1.3343	0.558
Difference	0.0006	0.240
"Sensitivity"	0.0005 (0.5 in 1000)	0.43 (430 in 1000)

Table 47.13 Accuracy of foam test measurements [42]

Solution	Refractive index	Electrical conductance	Actual
A	4.5 % ± 0.8 %	3.5 % ± 0.1 %	3.50 ± 0.01 %
B	5.1 % ± 0.8 %	5.5 % ± 0.1 %	5.50 ± 0.01 %
C	8.7 % ± 0.8 %	8.5 % ± 0.1 %	8.50 ± 0.01 %

meters removed the interpretive errors and proved to have very good repeatability between tests.

When evaluating the various conductivity meters for usability and accuracy, it was determined in the FAA study that all five units were considered better tools for inspecting the foam-proportioning systems than were refractometers. There were some aspects of the various conductivity meters that made some meters slightly better than others. The accuracies of the conductivity meters can be greatly affected by variations between the temperature of the solution and conductivity probe; care should be taken that conductivity measurements are made when the solution and conductivity probe are at the same temperature. One of the units automatically compensated for temperature.

The electrical conductivity method is now recognized in NFPA standards including NFPA 11 and NFPA 412. NFPA 412 cautions against the use of this method for seawater applications. The electrical conductivity method, used for process control in the chemical industry, has recently been adapted for use as a proportioning controller for AFFF systems.

New Airfield Protection Approaches

The U.S. Air Force Research Laboratory (AFRL) has done extensive research and development of novel ARFF-related fire fighting techniques in an attempt to develop smaller, lightweight, air-transportable ARFF vehicles that can be easily carried on cargo aircraft, such as the USAF C-130.

AFRL research has focused on the following technologies:

Ultra High Pressure System (UHPS)—This system utilizes high-pressure positive displacement plunger pumps to deliver AFFF at a

nominal pump discharge pressure of 1500 psi. Turret residual pressures are in the 1100–1200 psi range, which in effect causes AFFF to be delivered as a foam "mist". The applied foam has the characteristics of conventional AFFF delivery. It creates a foam blanket and aqueous film formation on the fuel surface, and may have the added fire suppression feature of small droplet mist, namely cooling, flame stripping, and oxygen displacement via water vapor formation.

Compressed Air Foam System (CAFS)—In a CAFS system air is injected under pressure into AFFF solution between the pump and the nozzle, so that expanded foam discharges from the nozzle. This allows greater control over the resultant foam expansion ratio and provides a uniform, more expanded, foam delivery to the fuel surface.

Combined Agent Fire Fighting System (CAFFS)—Recent testing has focused on the patented "Hydrochem" technology where dry chemical agent, typically PKP, and AFFF are discharged through a concentric nozzle design. PKP is discharged through a central orifice while AFFF, or CAFS, is discharged through the annular opening around the central dry chemical orifice. When flowing simultaneously, the AFFF/CAFS discharge carries the PKP in the center core of the discharge stream providing greater dry chemical discharge range then if discharged separately.

Tri/Quad Agent Systems—As a refinement of the twin agent concept widely used for flammable liquid fire fighting for over 30 years, recent delivery systems have been developed to discharge three or four agents (water, AFFF, dry chemical, gaseous/Halogenated agents) either simultaneous or consecutively, often through a single nozzle. This provides the nozzle man the option of easily selecting the desired agent for the particular fire scenario.

Two recent AFRL reports [43, 44] document testing at Tyndall Air Force Base of UHPS, CAFS, and CAFFS. Testing was conducted on fuel fires on a water substrate, fuel on gravel, fuel on soil/sod, and fuel on a hard surface. Since most tests over the years have been conducted with fuel on water (previously cited Geyer and NRL testing, for example), the fuel-on-water test results are described below.

Table 47.14 USAF new technology testing [42]

Extinguishing method	Number of test fires	Mean application density (gals/ft^2)
P-19	22	0.044
UHPS	20	0.014
CAFs	27	0.028
CAFFS	27	0.027

Agent extinguishment tests were conducted against three different size JP-8 fires: 880, 3500 and 5100 ft^2. Comparative data was generated against the performance of the primary USAF crash truck, the P-19. Agent flow rates were as follows:

• P-19	250/500 gpm AFFF
• UHPS	70–100 gpm AFFF
• CAFs	250–560 gpm AFFF
• CAFFS	125 gpm AFFF/3 pps dry chem.
	220 gpm AFFF/7.5 pps dry chem.

A total of 114 fuel-on-water fire tests were conducted, with the results as shown in Table 47.14:

The UHPS delivery method produced a mean application density based on pool fire extinguishment of 0.014 gals/ft^2, compared to a mean application density with the conventional P-19 of 0.044. The UHPS provided a lower application density. The USAF, after applying an appropriate safety factor to the discharge density, is deploying this technology.

Aircraft Hangar Protection

The two objectives of aircraft hangar protection are (1) protect aircraft and (2) prevent collapse of the hangar roof structure, which is usually unprotected steel. The protection of the aircraft is the principal concern, because its value is generally many times that of the structure. This concern is particularly true for advanced military aircraft. Historically, these protection systems have been

deluge-type sprinkler systems with open-head nozzles. They are activated by rapid-response detection systems. Before the development of foam, water-deluge systems were used. The original foam-water sprinkler systems used protein foam. With the development of AFFF, research was performed to determine appropriate application rates and types of discharge devices. The research work, performed primarily by Factory Mutual Research Corporation (FMRC), provides the basis not only for current aircraft hangar protection criteria but also for other sprinkler suppression system criteria.

Overhead Sprinkler Protection Before the advent of foam, hangars were protected by conventional spray sprinklers using water. Water-deluge systems having discharge rates on the order of 10.4 L/min/m^2 (0.25 gpm/ft^2) were used in conjunction with sloped floors and drains to protect aircraft. Even with these systems, activated by detection systems, burnthrough protection of aircraft fuselages (e.g., 1 min) could not be ensured. Ceiling temperatures in an 18.3-m-(60-ft-) high space on the order of 427 to 816°C (800 to 1500°F) have been recorded for fuel spill fires where this protection was provided. For a 121 m^2 (1300 ft^2) JP-4 fuel fire, 927°C (1700°F) ceiling temperatures have been recorded within 30 s of ignition prior to deluge system discharge.

Protein foam systems, discharging at a rate of 8.2 L/min/m^2 (0.20 gpm/ft^2), were an improvement on the water systems. Air-aspirating sprinklers were required to make effective protein foam. Because of the high centerline velocities of a pool fire plume, the foam flow from the perimeter toward the center of the fire was thought to be the dominant suppression mechanism [41].

With the development of AFFF, FMRC conducted a series of tests for the U.S. military to establish appropriate design parameters. In a series of baseline comparison tests, FMRC compared AFFF with protein foam. The tests consisted of 83.6 m^2 (900 ft^2) JP-4 pool fires in an 18.3-m (60-ft) high space. Air-aspirating, standard upright, and old-style upright sprinklers were evaluated at application rates of 4.1 to 8.2 L/min/m^2 (0.10 to 0.20 gpm/ft^2). In one test, a low-level turret nozzle discharging AFFF was used in conjunction with sprinklers discharging water. Table 47.15 summarizes the results of the AFFF tests. A comparison of Tests 4 and 5 with Test 3 indicates improved results from the use of standard sprinklers compared to foam-water

Table 47.15 Hangar deluge system tests by factory mutual research corporation [45]

Test conditions	Test no. 2	Test no. 3	Test no. 4	Test no. 5	Test no. 6	Test no. 7 (turret nozzle)
Type of head	Foam-water	Foam-water	Standard	Standard	Standard	Old-style sprinkler
Spacing (m^2 $head^{-1}$ [ft^2 $head^{-1}$])	7.4 (80)	9.3 (100)	12.1 (130)	12.1 130	9.3 (100)	9.3 (100)
Application rate (L/min/m^2[gpm/ft^2])	8.2 (0.20)	6.6 (0.16)	6.6 (0.16)	6.6 (0.16)	5.2 to 4.4 (0.125 to 0.105)	6.6 (0.16) (water system)
End head pressure (kPa [psi])	193 (28)	193 (28)	97 (14)	97 (14)	35 (5)	55 (8) (water system)
25 % Drainage time (min)	2.5	2.1	0.5–0.8	1.0–1.3	0.5–0.7	No data recorded
50 % Drainage time (min)	5.0	4.4	1.3–1.8	1.8–2.3	1.2–1.6	No data recorded
Expansion ratio	4.3:1	3.4:1	2.2:1	2.3:1	2.2:1	12:1
Extinguishment time (min:s)	2:22	2:15	1:45	1:25	3:05	≈0:33

Table 47.16 Estimated particle diameter vs. terminal velocity [46]

	Terminal velocity (m/s [ft/s])			
		Foam		
Particle diameter (mm [in.])	Water	Expansion Ratio 2:1	Expansion Ratio 5:1	Expansion Ratio 10:1
12.7 (0.5)	See note[a]	10.1 (33)	6.7 (22)	4.6 (15)
6.3 (0.25)	10.4 (34)	7.3 (24)	4.6 (15)	3.4 (11)
2.5 (0.1)	6.7 (22)	4.6 (15)	2.7 (9)	—

[a]The breakup of water drops greater than about 6.3-mm (0.25-in.) diameter is highly probable due to instability

sprinklers. At application rates of 6.6 L/min/m^2 (0.16 gpm/ft^2), the standard sprinklers were 1.3 to 1.6 times as effective in achieving extinguishment compared to air-aspirating foam-water sprinklers. At an application rate of 8.2 L/min/m^2 (0.20 gpm/ft^2), the extinguishment times with AFFF from foam-water sprinklers were comparable to results from protein foam tests. Rapid suppression with the turret nozzle (at 8.3 L/min/m^2 [0.22 gpm/ft^2]) combined with an overhead water system was demonstrated in Test 7. No adverse effects were evident from the water discharged from the overhead sprinklers after the foam ran out.

The superior performance of the standard sprinklers was attributed to more effective plume penetration by higher density foam particles. The maximum centerline velocities measured were 23.2 m/s (76 ft/s), with 15.2 m/s (50 ft/s) at the centerline of the fire. The fire plumes tended to bend due to air currents within the test building. Because the terminal velocity of the foam agents was estimated to be on the order of 9.1 m/s (30 ft/s) maximum, the droplets near the centerline never reached the fire. This result supports the theory that extinguishment occurs from the outside perimeter inward. Because foam droplets from standard sprinklers are about twice as dense as air-aspirated particles, the terminal velocities are greater. Greater velocities allow greater penetration of the fire plume. The same mechanisms explain why air-aspirated AFFF provides similar performance to protein foam. When the AFFF is air aspirated, there is no longer any advantage of increased droplet terminal velocity.

Additional work by FMRC established estimates for the terminal velocity of foam, as shown in Table 47.16 [46, 47]. Plume theory was used to estimate roughly that velocity on the order of 18.3 m/s (60 ft/s) could be expected in an 18.3-m (60-ft) high space with an 83.6 m^2 (900 ft^2) JP-4 fire. This estimate was in good agreement with the experimental results. Based on an average foam particle diameter of 6.3 mm (0.25 in.), a maximum terminal velocity of 7.3 m/s (24 ft/s) could be expected. For a JP-4 pool fire, this translates into a 0.7-m^2 (8-ft^2) maximum fire size before plume penetration is not possible.

The practical significance of AFFF discharged through non-air-aspirating sprinklers was demonstrated by Breen et al. [46] Air-aspirating sprinklers require 207 kPa (30 psi) nozzle pressure to be effective. Standard sprinklers can discharge effective AFFF solution at pressures as low as 69 kPa (10 psi). This capability had important retrofit considerations where foam-proportioning system losses could be made up through reduced sprinkler pressures.

Additional tests were conducted with closed-head sprinklers in an 18.3-m (60-ft) high hangar [48]. Potential cost benefits would have resulted from reduced hardware costs and unwanted discharges from deluge systems. These tests demonstrated that this concept was not feasible for the hangar scenario because of the large number of sprinklers that opened during the 83.6 m^2 (900 ft^2) fire tests.

The superior performance of standard sprinklers compared to air-aspirating sprinklers is reflected in the criteria of NFPA 409, *Standard*

on Aircraft Hangars. If standard sprinklers are used with AFFF, the design application rate for overhead deluge systems may be reduced to 6.6 L/min/m^2 (0.16 gpm/ft^2) from 8.2 L/min/m^2 (0.20 gpm/ft^2) required for air-aspirated sprinklers. This decrease represents a 20 % reduction in foam required when standard sprinklers are used.

It should be noted that AFFF discharging from sprinklers cannot be assumed to control a three-dimensional Class B fire. In tests conducted by the U.S. Navy, AFFF sprinklers were discharged on a simulated ruptured fuel tank fire [49]. Deluge, air-aspirating sprinklers were discharged at 6.5 L/min/m^2 (0.16 gpm/ft^2) from a 8.5-m (28-ft) high simulated hangar. The three-dimensional fire consisted of 28 L/min (7.5 gpm) of marine diesel (simulating JP-5) flowing down over a shielded cascade assembly. The assembly simulated a ruptured fuel tank below a damaged aircraft wing, which prevented direct AFFF application to the running fuel fire. Although the contiguous pool fire was suppressed, the running fire was not. It was also found that delaying AFFF discharge time for this scenario had an adverse effect on suppression.

Care must be taken in designing AFFF sprinklers for both pool fire suppression and extinguishment of other hazards. In fire tests for shipboard vehicle storage areas, a fire scenario involving a Class B pool fire (marine diesel, simulating vehicle diesel fuel or JP-5) and ordinary combustibles was performed [50]. Tests were conducted in an 8.5-m (28-ft) high space with air-aspirating sprinklers discharging 6.5 L/min/m^2 (0.16 gpm/ft^2). The Class A fuel load was simulated by a 1.6 m (6 ft) stack of wood pallets. The Class B pool fire was readily controlled and extinguished, but the Class A pallet fire was not controlled or suppressed. It was concluded that a higher sprinkler application rate was required to control/suppress the Class A fire. This is consistent with NFPA 13, *Standard for the Installation of Sprinkler Systems,* requirements for a minimum application rate of 8.1 L/min/m^2 (0.2 gpm/ft^2) or greater for wooden pallets stacked 1.8 m (6 ft) high or more. Fires within actual vehicles will likely require a higher sprinkler application rate to prevent spread to adjacent vehicles [51].

Low-Level Application of AFFF With the increase in wingspan areas of large aircraft, it was recognized that significant damage could occur before extinguishment of the pool fire underneath the wing. Using overhead sprinklers only, FMRC demonstrated the times required for the foam to spread and extinguish fires (see Table 47.15). The concept of low-level application of foam, using monitors or turret nozzles, was developed to reduce extinguishment time where shielded fires may occur. This concept was later extended to include side-mounted nozzles and discharge outlets, and flush-mounted nozzles installed in a floor or deck.

These systems are effective because AFFF solution droplets do not have to penetrate the fire plume. They also typically deliver, at spot locations, high densities of foam. A high density allows the foam to gain a "bite" or toehold on the fire. Low-level AFFF systems have been used successfully for over two decades on U.S. Navy air-capable ships, protecting flight decks and special hazard areas.

Table 47.17 summarizes fire test data for low-level application of AFFF. As seen, control and extinguishment times are quite rapid. NFPA 409, *Standard on Aircraft Hangars,* criterion of 4.1 L/min/m^2 (0.10 gpm/ft^2) for low-level applications is based on a fire control time of 30 s and extinguishment in 60 s. Data indicate that a JP-5 pool fire can be 90 % controlled in 60–90 s and 99 % extinguished in 2 min when an application rate of 2.4 L/min/m^2 (0.06 gpm/ft^2) is used. The system can be effective at rates as low as 1.6 L/min/m^2 (0.04 gpm/ft^2). For low-flashpoint fuels (e.g., avgas), control time increases. Control and extinguishment times can be reduced by increasing the application rates on JP-5 fuel fires. Based on these results, the U.S. Navy adopted an AFFF application rate of 2.4 L/min/m^2 (0.06 gpm/ft^2) for protecting aircraft carrier flight decks [56].

Although they may help control a three-dimensional (spill) fire, low-level application systems cannot be assumed to suppress totally a

Table 47.17 Fire test data for low-level application of AFFF

Reference	Test no.	Test area (m^2[ft^2])	Fuel	Nozzle	Nozzle k factory (gal/$psi^{0.5}$)	Maximum spray Height[a] (m [ft])	Spray diameter[a] (m [ft])	Nominal application rate (L/min/m^2[gpm/ft^2])	Control extinguishment times
FMRC 1975[46]	3	83.6 (900)	JP-4	Turret nozzle (monitor)	50.3	50° arc, 8 s cycle time, 15° angle of elevation, 25.9 m (85 ft) from the center of the test pool		4.1 (0.10)	90 % in 10 to 15 s 100 % in 35 to 40 s
	4	83.6 (900)	JP-4	Turret nozzle (monitor)	50.3	50° arc, 8 s cycle time, 15° angle of elevation, 25.9 m (85 ft) from the center of the test pool		4.1 (0.10)	90 % in 1 min 30 s[b] 100 % in ≈ 2 min
	6	83.6 (900)	JP-4	Turret nozzle (monitor)	50.3	50° arc, 8 s cycle time, 15° angle of elevation, 25.9 m (85 ft) from the center of the test pool		4.1 (0.10)	90 % in 20 s 100 % in 25 s
FMRC 1973 [45]	7	83.6 (900)	JP-4	Overhead OSS[c] + turret nozzle	5.0	N/A	N/A	6.6 (0.16)[d] ±9.0 (0.22) 9.5 (0.38)	Controls in 17 s[d] 100 % in 33 s
Australia [52]	1	78.5 (846)	Aviation kerosene	P10 Pop-up	4.1	0.8 (2.6)	4.3 (14.1)	5.5 (0.13)	95 % in 30 s
	2	78.5 (846)	Aviation kerosene	W-1 Pop-up	3.6	1.5 (4.9)	3.3 (10.8)	4.9 (0.12)	≈90 % in 25 se
Naval Weapons Center	5	697 (7500)	JP-5	Type S flush deck	5.5	1.8 (6)	12.2 (40)	1.6 (0.04)	50 % in 30 s 90 % in 60 s
Phase III 1972 [53]	11	697 (7500)	JP-5	Type S flush deck	5.5	1.8 (6)	12.2 (40)	2.4 (0.06)	70 % in 30 s 90 % in 60 s
	9	697 (7500)	Avgas	Type S flush deck + deck edge	5.5 [114 L min (30 gpm)]	1.8 (6)	12.2 (40)	2.4 (0.06) ±1.6 (0.04) 4.1 (0.10)	15 % in 30 s 50 % in 60 s
	15	697 (7500)	Avgas	Type S flush deck + deck edge	5.5 [114 L/min (30 gpm)]	1.8 (6)	12.2 (40)	2.4 (0.06) ±1.6 (0.04) 4.1 (0.10)	40 % in 30 s 70 % in 60 s
Naval Weapons Center	10 and 10 R	372 (4000)	JP-5	Type SB flush deck	5.1	1.8 (6)	9.1 to 12.2 (30 to 40)	2.4 (0.06)	60 to 90 s for 90 % control 99 % in ≈ 2 min
Pop-Up 1985 [54]	5, 5R, and 5R1	372 (4000)	JP-5	Bete pop-up	5.5	1.8 (6)	9.8 (32)	2.4 (0.06)	60 to 90 s for 90 % control 99 % in ≈ 2 min

Naval Weapons Center	18	48.3 (520)	JP-5	Overhead side-mounted spray nozzles	1.9	NA	NA	8.6 (0.21)	90 % in 15 s
									99 % in 52 s
									100 % in 57 s
Staging Area 1988 [55]	11	48.3 (520)	JP-5	Overhead side-mounted spray nozzles	1.9	NA	NA	21.6 (0.53)	90 % in 8 s
									99 % in 15 s
									100 % in 27 s
	16[f]	66.9 (720)	JP-5	Low-level fan	4.7	NA	NA	11.8 (0.29)	90 % in 24 s
									99 % in 52 s
									100 % in 79 s
	12[f]	66.9 (720)	JP-5	Low-level fan	4.7	NA	NA	20.4 (0.50)	90 % in 9 s
									99 % in 16 s

[a]Spray height and diameter at the pressure/flow used in the test
[b]An unplanned 69 kPa (10 psi) pressure drop in FMRC Test 4 caused a 4.6 m (15 ft) reduction in nozzle range, resulting in 90 % control and extinguishment times 3 to 4 times those observed in Tests 3 and 6
[c]No wing obstruction over fire test area
[d]The overhead deluge system discharging ordinary water was accidentally activated 12 s later than the turret nozzle (5 s before control was attained)
The contribution, if any, of the overhead deluge system toward complete extinguishment was judged to be quite small compared to the turret nozzle
[e]Wind-affected results
[f]Deck pool fire area was obstructed with simulated weapons carts

running fuel fire. Running fuel fires at a spill rate of 189 L/min (50 gpm) are typically used in U.S. Navy flight-deck suppression tests using the flush-deck system. The running fuel fire, shielded by simulated aircraft debris, requires aggressive handline attack for extinguishment [57].

Obstructions, such as parked vehicles, may block low-level nozzles. Testing for a flight-deck weapons staging area showed that a side-mounted low-level system could be effective even when nozzles were obstructed [55]. In these tests, 5 of the 12 deck-edge nozzles were obstructed to simulate vehicle tires blocking edge-mounted nozzles. Even with 40 % reduction, the fire was controlled and extinguished in less than 1 min (compared to 15–30 s when unobstructed). As with overhead sprinklers, low-level AFFF nozzles should not be relied on to extinguish three-dimensional Class B fires.

Cost of installation, maintainability, and reliability are factors when considering a low-level application system. Reliability issues with turrets/monitors have been identified by both FMRC and the U.S. Navy. The flush-deck system adopted by the U.S. Navy took considerable effort before a high degree of reliability and maintainability could be achieved. This open deluge nozzle, originally installed as a water washdown nozzle, incorporates a ball-check feature in the nozzle orifice to prevent debris from clogging the nozzle. Clean-out traps are installed in system piping for maintenance. Pop-up nozzles have been proposed as an alternative to flush-deck nozzles. These nozzles have their own reliability and maintainability issues. Unless there are very high costs associated with the loss of an aircraft, in-floor or flush-deck nozzles are generally cost-prohibitive for commercial aviation facilities. For high-risk/cost applications, in-floor nozzles may be justified. This may be the case for advanced military aircraft; for example, research has been performed on an inverted deluge system that not only can suppress a pool fire but also can cool exterior combustible components of the airframe. Initial installations have suffered from design and installation problems. [58] Lack of experience with these types of systems was the significant single cause of problems with these systems. Acceptance testing and maintenance were found to be lacking.

Side-mounted nozzles are the most reliable systems, consisting of open-pipe or -spray nozzles. The spreading rate of foam from an aspirated open-pipe system increases control and suppression time. Open-spray nozzles can be very effective, but their reach is limited.

New Hangar Fire Protection Design Concepts Issues related to asset protection, reliability of fixed systems, and environmental impact led the U.S. Navy to reevaluate its approach to hangar fire protection systems. A goal was established to install reliable and easily maintained fire protection systems that prevent damage to the hangar structure and to aircraft not directly involved in an initial spill fire ignition. This goal resulted in a multidiscipline study to address all associated technical issues.

All military service branches in North America have been plagued with false activation involving foam-water-deluge sprinkler systems over aircraft with open cockpits. These false activations have been caused by numerous sources including lightning strikes that introduced transient voltage spikes into the fire alarm system; water hammers in aging underground water distribution systems; accidental releases by maintenance personnel; deliberate acts of vandalism; accidental activation of manual pull stations; failure of pressure relief valves at pumping stations; roof-water leakage into overhead heat detection systems; and false activation of fire detection systems. This situation prompted the pursuit of alternative fire protection designs that would provide the desired level of protection.

Alternative designs included the use of closed-head AFFF overhead sprinkler systems and greater reliance on low-level monitor nozzle AFFF systems as the primary extinguishing component as described in the previous section. Low-level systems were originally designed to provide supplementary protection for the area shadowed from the overhead system by large

wing areas. In pursuing these alternative designs, technical and operational issues and limitations of both existing and proposed new systems were identified:

- Thermally activated systems may result in unacceptably high damage to assets prior to fire control/extinguishment, particularly in very high bay hangar ceilings (see Gott et al. [59]).
- Although it is readily accepted that conventional hangar fire protection systems were not designed to extinguish a three-dimensional fire, some fire protection engineers believed that AFFF extinguishing systems could be designed to control a spill fire and limit the area of the fire to only those aircraft intimate with the initial ignition source.
- Different aviation fuels are now commonly being used, for example, JP-5 and JP-8 are now the predominant fuels, compared to the lower flashpoint JP-4 previously used.
- Low-level AFFF monitor nozzle systems are
  - Relatively inefficient in terms of pattern distribution
  - Unreliable
  - Susceptible to blockage by equipment
  - Commonly found out of service in the field
- Any new AFFF low-level nozzle should be designed for minimal overspray and should not be significantly impacted by water discharge from any water-only protection system.
- Optical fire detectors are
  - Prone to false alarms
  - Currently tested, listed, and approved using fuels that are not typical in aviation
  - Subjected to few if any sources of false alarms in currently recognized approval standards

A concept was developed by the U.S. Navy to meet the desired performance goals. This concept included the following:

- Use of low-level AFFF deluge nozzles, having minimal overspray, to control/extinguish liquid fuel pool spill fires
- Operation of the low-level AFFF system using improved optical detectors designed to
  - Be highly immune to false alarms
  - Rapidly detect JP-5 fuel spill fires
- Installation of a quick-responding, closed-head, wet-pipe sprinkler system in the hangar ceiling
- Implementation of lessons learned from all military hangar design experiences in a comprehensive, new, improved design

Most of the research and development associated with the process has been completed and is described in Gott et al. [59], Szepezi et al. [60], Back et al. [61], Gottuk et al. [62], Scheffey et al. [63], and Parker [64]. Two aspects of U.S. Navy research and development are germane to the performance of AFFF. The first involves the performance of AFFF when subjected to water spray from sprinklers. The second is a developmental effort initiated to design a reliable, low-profile AFFF nozzle that could be installed in the floors of hangars.

Twenty-three full-scale fire tests were conducted to evaluate the effects of overhead water sprinklers on AFFF foam blankets [61]. One AFFF application rate (4.0 L/min/m^2 [0.1 gpm/ft^2]) and two sprinkler application rates (6.5 and 10.2 L/min/m^2 [0.16 and 0.25 gpm/ft^2]) were included in this evaluation. The tests were conducted on a range of spill fires. The spill fires were produced using either JP-5 or JP-8 aviation fuels and were evaluated on a concrete pad with similar drainage characteristics typical of navy hangars. The spill fires continued to burn (i.e., were shielded) during water/foam application. The heating effect on the burnback resistance of foam, with and without sprinkler water application, was evaluated.

The results show that the use of water sprinklers in conjunction with a low-level AFFF fire suppression system (with an application rate of 4.0 L/min/m^2 [0.1 gpm/ft^2]) had minimal effects on the ability of the system to suppress the fire and resist burnback. In all tests, the low-level AFFF system was capable of quickly

extinguishing the test fire (control ~30 s and extinguishment ~1 min) independent of the sprinkler application rate. The time required for the fire to burnback across the fuel surface was apparently a function of the drainage characteristics of the hangar and was only slightly affected by the application of water through the overhead sprinklers. The tests also show that the flashpoint of the fuel has an effect on the control, extinguishment, and burnback resistance capabilities of the system. Although the burnback times for the lower flashpoint fuels were faster than the higher flashpoint fuels, the duration of protection was not significantly altered. These tests show that overhead water sprinklers have minimal effect on AFFF foam blankets, independent of the test fuel, particular fire, and sprinkler application rate. A combined low-level AFFF extinguishing system operating in conjunction with an overhead water sprinkler system provided adequate burnback protection during AFFF discharge, but this protection may be lost shortly (a few minutes) after the end of AFFF discharge.

The new low-level fire-extinguishing system was designed to discharge AFFF adequately across a hangar floor, to be less likely to be affected by obstructions, and to reduce the likelihood of damage to exposed aircraft electronic equipment [63]. To achieve these objectives, the nozzle was designed to

- Produce a nominal AFFF application rate of 4.0 L/min/m^2 (0.1 gpm/ft^2)
- Operate at a nominal pressure of 2.8 bar (40 psi)
- Provide coverage to a distance of 7.6 m (25 ft) from a hangar floor drainage trench (centerline of two parallel trenches spaced 15.2 m [50 ft] apart)
- Spray AFFF so that the pattern height does exceed 0.3 m (1 ft) above the deck

The nominal AFFF application rate of 4.0 L/min/m^2 (0.1 gpm/ft^2) was selected based on current design practices as described in the previous two sections of the chapter. The nozzle operating pressure was selected based on standard, commercially available pump performance curves and preliminary estimates of friction loss for the system.

Over 50 nozzles were evaluated for this application [64]. Testing of these nozzles indicated that, although a limited number of commercially available nozzles could meet the design requirements, manufacturing, installation, and operation of these nozzles under normal hangar conditions were not feasible. Existing pop-up nozzles were not designed for the high flow rates or spray characteristics required of this application. As a result of these deficiencies, a prototype nozzle was developed. The prototype concept was subsequently developed into a commercially available nozzle. Foam pattern, distribution, and flow tests were conducted by Underwriters Laboratories Inc. on a nozzle with a flow coefficient of 22.6 k (gpm/psi$^{1/2}$).

There is no universal agreement on the proper approach to military hangar fire protection in North America. For example, the U.S. Air Force recognizes the use of high-expansion foam. Many of these systems have recently been installed.

The Canadian Ministry of Defense (MoD) is using compressed-air foam, or CAF. The primary advantage of CAF systems is for situations where there is an extremely limited water supply. Unlike traditional foam systems where air aspiration occurs at or near the discharge device, CAF systems inject air prior to the discharge device [65, 66]. Foam is generated by injecting air under pressure into a foam solution stream. As the solution moves through the piping system, foam is produced by the combined momentum of the foam solution and the injected-air stream in the hose or pipe. In the hangar system, AFFF is used as the foam concentrate, proportioned at 2 % compared to 3 % for traditional foam sprinklers. Also, the effective application rate (foam solution, L/min/m^2 or gpm/ft^2) is lower than similarly listed low-expansion foam sprinkler systems. NFPA 11, *Standard for Low-, Medium-, and High-Expansion Foam,* recognizes this system and provides design and installation requirements.

Additionally, the U.S. Army has evaluated the use of early suppression fast-response (ESFR) closed-head water sprinkler protection for helicopter hangars [67]. FMRC concluded that both 93 °C (200 °F) temperature-rated ESFR sprinklers discharging at 345 kPa (50 psig)

(41 L/min/m^2 [1.0 gpm/ft^2]) and 517 kPa (75 psig) (49 L/min/m^2 [1.2 gpm/ft^2]) and temperature-rated, $k = 5.6$ (gpm/psi^{½}) quick-response sprinklers at 345 kPa (50 psig) (16 L/min/m^2 [0.40 gpm/ft^2]) can provide adequate fire protection for the hangar against a 61-m^2 (200-ft^2), 473 L (125 gal) JP-4 aviation fuel-pan fire. For some tests, fuel depletion was necessary for the fire to be controlled.

New fire detection technology, potentially applicable to hangar fire protection, has become available. Video image flame detection (VIFD) is a software-based method of flame detection that can be implemented by a range of video image analysis techniques. VIFD systems can analyze images for changes in features such as brightness, contrast, edge content, loss of detail, and motion. The detection equipment can consist of cameras producing digital or analog (converted to digital) video signals and processing unit (s) that maintain the software and interface to the fire alarm control unit. The technology potentially speeds detection, while improving immunity to false alarms. *NFPA 72®, National Fire Alarm Code®,* now recognizes this technology.

Foam-Water Sprinkler Systems

This chapter has dealt with foam characteristics, foam concentrate, test standards, and manual application techniques. In particular, applications in the aviation industry were described. The text on aircraft hangar protection addressed the concept of fixed foam protection systems. Much of the foam-water sprinkler system test data was originally developed for aircraft hangars. Herein, foam-water sprinkler system design criteria for other applications are described. Again, emphasis is placed on AFFF systems because they are more effective for extinguishment than protein or fluoroprotein systems.

Codes, Standards, and Regulations

Overhead foam-water sprinkler systems, as specified in the NFPA standards, are generally designed to serve dual purposes: (1) to control and/or suppress a fuel spill fire and (2) when the foam runs out, to cool materials with water. Because the systems are designed to provide protection for flammable/combustible liquid hazards and ordinary combustibles, the specified application rates reflect this dual-protection approach. Table 47.4 shows the fundamental application rates used by Underwriters Laboratories on hydrocarbon fuel fires to evaluate sprinklers discharging foam-water. The fire must be extinguished within 5 min for AFFF discharged at 4.1 L/min/m^2 (0.10 gpm/ft^2) for standard sprinklers and 6.6 L/min/m^2 (0.16 gpm/ft^2) for agents discharged from foam-water sprinklers (air aspirating). However, because most deluge and closed-head sprinkler systems are installed in industrial occupancies for property protection concerns, they must usually meet highly protected risk (HPR) insurance requirements. As a result, the NFPA standard for deluge and closed-head AFFF systems (NFPA 16, *Standard for the Installation of Foam-Water Sprinkler and Foam-Water Spray Systems*) requires 6.6-L/min/m^2 (0.16-gpm/ft^2) minimum water application. This water application rate also provides a safety factor over the 4.1 L/min/m^2 (0.10 gpm/ft^2) rate at which AFFF discharged from sprinklers is effective on pool fires. The safety factor is reflected in Table 47.4 under the column heading Minimum Application Rate.

Table 47.18 summarizes current requirements from NFPA standards. NFPA 11, *Standard for Low-, Medium-, and High-Expansion Foam,* is geared toward petroleum and chemical industry protection. Previous requirements from NFPA 11 allowed 4.1 L/min/m^2 (0.10 gpm/ft^2) for loading racks, for example, tank truck loading facilities. The latest requirements for NFPA 11 eliminate this design criterion and reference NFPA 16 requirements, which require 6.6 L/min/m^2 (0.16 gpm/ft^2). In special situations, 4.1 L/min/m^2 (0.10 gpm/ft^2) is permitted by NFPA 11, but only where there is low-level or manual application for a hydrocarbon fuel spill. NFPA 16 is consistent in requiring 6.6 L/min/m^2 (0.16 gpm/ft^2); it references other NFPA standards for special exceptions, for example, NFPA 409, *Standard on Aircraft Hangars,* and NFPA 30, *Flammable and Combustible Liquids Code*. NFPA 409 requirements were previously

Table 47.18 NFPA standards related to AFFF sprinkler systems

Standard*	Minimum AFFF application rate (L/min/m^2 [gpm/ft^2])	Duration (min)
NFPA 11, (2010) *Standard for Low-, Medium-, and High-Expansion Foam*	Indoor storage tank greater than 37 m^2 (400 ft^2) 6.6 (0.16)	30
	Loading rack monitors 4.1 (0.10)	15
	Diked areas	
	Fixed low level (Class II hydrocarbon) 4.1 (0.10)	20
	Monitor 6.6 (0.16)	20
	Undiked areas for AFFF handlines 4.1 (0.10)	15
NFPA 16, Standard for the Installation of Foam-Water Sprinkler and Foam-Water Spray Systems (2015)	6.6 (0.16)	10 min; 7 min if above minimum design
NFPA 409, Standard *on Aircraft Hangars (2016)*	Overhead deluge 8.2 (0.20) for aspirated AFFF 6.6 (0.16) for non-air-aspirated AFFF	10 min; 7 min if above minimum design
	Supplemental low level (for shielded wing areas) 4.1 (0.10)	10 min

[a]See Additional Readings for complete titles and dates

Table 47.19 Foam application rate for marine hydrocarbon hazards (NFPA 11)

Type of hazard	Calculation of rate
Deck spill	6.50 L/min/m^2 (0.16 gpm/ft^2) or 10 % of the cargo block area
Largest tank	9.78 L/min/m^2 (0.24 gpm/ft^2) of the single largest tank area
Largest monitor	3.0 L/min/m^2 (0.074 gpm/ft^2) of the area protected by the largest monitor (not less than 1250 L/min)

Table 47.20 Foam application rate for marine polar solvent hazards (NFPA 11)

Type of hazard	Calculation of rate
Deck spill	Rate for most hazardous polar solvent × 10 % of the cargo block area
Most demanding	150 % of the highest required foam tank application rate for the single largest tank
Largest monitor	45 % of the highest required foam application rate applied over the area protected by the monitor (not less than 1250 L/min)

discussed. Chapter 48 provides an example for calculating foam quantities based on design application rates and areas to be protected.

With the publication of the 1998 edition of NFPA 11, marine foam application was specifically addressed. Foam application rates are required to be not less than the greatest of that required for deck spills, the largest tank, or the largest monitor solution flow rate as shown in Table 47.19 for hydrocarbon fuels and Table 47.20 for polar solvents. For polar solvents, standardized fire tests are used to determine the minimum foam design application rate for the most difficult extinguishment case. Foam concentrates for hydrocarbon fuels must be approved using a 9.29-m^2 (100-ft^2) fire test similar to UL 162. The fixed-nozzle gasoline fire test has an extinguishment application density of 12.2 l/m^2 (0.30 gal/ft^2).

Model building and fire codes in the United States have adopted AFFF protection criteria for the storage of flammable and combustible liquids. Criteria of insurance companies are usually similar to the NFPA requirements, but this needs to be verified. Insurance authority guidelines should be referenced for specific projects, because there can be differences in protection criteria.

Protection of Stored Flammable and Combustible Liquids

Flammable and combustible liquids are stored in containers ranging in size from less than one quart to several hundred gallons. These liquids may be stored for display in a retail outlet or "superstore," stored for distribution in a general-purpose warehouse housing many different combustibles, or stored in "liquid" warehouses containing large quantities of the liquid. NFPA 30, *Flammable and Combustible Liquids Code,* addresses these situations. This code includes requirements for tank storage, piping systems, containers, and operations. Criteria for suppression system protection is addressed in the sections dealing with container storage.

The protection of flammable and combustible liquids is a function of many factors, including the liquid properties, the ignition (which can be a factor of the storage occupancy), the packaging system (e.g., stored in cardboard cartons), the container design and material (e.g., steel, plastic, glass, fiberboard), and the arrangement of storage (e.g., rack versus pallet, storage height, aisle width, and mixture of other combustibles in the array). Based on these factors, a suppression system is provided to control or suppress the anticipated fire and protect the structure. The system may be designed to (1) control a fire so that the fire department can ultimately extinguish or suppress the burning material or (2) suppress the fire. Variables in suppression system design include application rate, fire fighting agent, and sprinkler orifice size, spacing, response time index (RTI), temperature rating, and use of in-rack sprinkler protection.

The basis of protection criteria in NFPA 30 is now well documented. Fire test references and associated citations in technical literature are now included with all protection criteria [68]. The basis of the protection criteria can now be directly linked to test data or engineering extrapolations of the data. Material in Appendix E of NFPA 30 provides guidance and an example test protocol for evaluating protection of liquids stored in the containers. This includes consideration of the source of the fire, which may be a "point" ignition (i.e., small ignition) or a large spill/three-dimensional fire. Depending on other variables, such as container type and packaging material, one of these scenarios may be more difficult to protect. Annex E of NFPA 30 provides detailed guidance on this subject.

Stored liquids may be protected using water sprinklers, foam, or other approved methods. Figure 47.21 shows a conceptual grouping of water and AFFF protection methods as a function of container type and storage method for water protection of liquids. The reader should consult Nugent [68]. The basis of AFFF protection is described in the following sections.

Protection of Drum and Tank Storage Some of the earliest work using AFFF sprinklers involved the protection of 208 L (55 gal) drums. In work conducted at Factory Mutual Research Corporation, sponsored by Allendale Insurance, Factory Insurance Association (FIA), and the 3 M Company, the effectiveness of standard sprinklers supplied with AFFF for controlling drum fires was determined [69]. Five fire tests were conducted in simulated flammable liquid-drum storage using two types of storage arrangements. Three tests were conducted with two-, three-, and four-high palletized drum storage, respectively. Two tests were conducted with five-tier high-rack storage of palletized drums.

In all tests, a heptane fuel supply simulated leakage from the upper level of storage. Except for one rack-storage test that used a 57 L/min (15 gpm) spill rate, fuel spillage was 7.6 L/min (2 gpm). Ceiling protection employed high-temperature sprinklers at discharge rates of either 12.3 or 24.6 L/min/m^2 (0.30 or 0.60 gpm/ft^2). In-rack supplemental protection for the rack-storage tests was provided at three levels, with ordinary temperature sprinklers each discharging 113 L/min (30 gpm). The success of each test was based on storage stability, that is, no pile collapse, and limitation of drum pressure to 104 kPa (15 psig).

AFFF was effective in controlling spill fires on the floor. The exception was in areas not

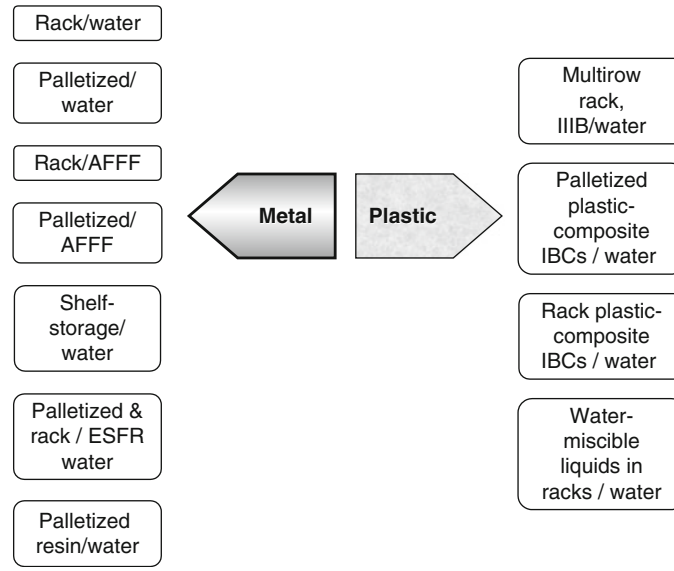

Fig. 47.21 Grouping of NFPA 30 protection criteria for liquids

reached by the discharge from operating sprinklers, where the flow of foam was blocked by pallets. Protection was not effective on the three-dimensional spill fires. Fire exposure and resultant pressure development within drums was more severe with increased clearances between storage and sprinklers due to greater delays in sprinkler operation.

Generally, results were considered good in the rack-storage tests, where in-rack sprinklers were provided in each tier. For palletized storage, the AFFF protection controlled the floor fire although pallets hindered the spread of foam. Ceiling sprinklers alone did not adequately protect palletized storage where an elevated spill resulted in a three-dimensional fire within the pile.

The results of these tests were used, along with engineering judgment, to develop AFFF protection criteria in NFPA 30, *Flammable and Combustible Liquids Code*. AFFF protection of 12.3 L/min/m^2 (0.30 gpm/ft^2) at the ceiling for rack protection of metal drum/tank storage up to 7.6 m (25 ft) high is specified. In-rack protection (e.g., sprinklers in alternating tiers or every tier) is a function of the liquid (flashpoint) container style (relieving vs. nonrelieving), and capacity of the container.

The results of the original Factory Mutual (FM) drum tests were extended in a series of tests conducted by Southwest Research Institute [70]. The objective was to test the effectiveness of relieving-style steel drums and varying degrees of overhead sprinkler protection to mitigate fire hazards associated with the storage of flammable liquids. Nylon plugs inserted in the 5.1 cm (2.0 in.) pour hole and 1.3 cm (0.5 in.) vent hole were designed to melt under fire conditions, allowing the drum to vent any built-up pressure. Heptane, a Class IB flammable liquid, was used as the stored commodity.

Tests were designed to model credible, worst-case loss scenarios involving the 208 L (55 gal) storage of the commodity. The fire modeled the accidental puncture of a full drum, and either an immediate or a delayed ignition source. Sprinkler suppression of the fire was monitored for the duration of the spill, and until flames were either under control or completely extinguished. Commodity was stacked in a 3 × 3 palletized array, to varying heights (2, 3, or 4 high), and protected with varying sprinkler types and densities.

The relieving-style closures were successful at mitigating the hazards associated with overpressurizing drums during a fire. The installed suppression systems were capable of either extinguishing or controlling the fire for the duration of the spill. A summary of the successful protection configurations for the commodity tested is provided in Table 47.21.

Table 47.21 Summary of heptane-palletized drum storage tests [70]

Test	Commodity	Protection (nominal application rates)
2 and 3	3 × 3, 2 high	3 % AFFF at 12.3 L/min/m^2 (0.30 gpm/ft^2)
5	3 × 3, 2 high	ELO water-based at 24.6 L/min/m^2 (0.60 gpm/ft^2)
7	3 × 3, 3 high	ELO, 3 % AFFF at 18.5 L/min/m^2 (0.45 gpm/ft^2)
8	3 × 3, 4 high	ELO, 3 % AFFF at 24.6 L/min/m^2 (0.60 gpm/ft^2)

The fuel spill rate (7.6 vs. 56.8 L/min) was found to have a substantial impact on the fire exposure of the drums. When taken in conjunction with the effect of the ignition scenario, the fuel spill rate had a strong influence on the number of initial heads operating and on the duration of the fire exposure. The ignition of the fuel source also played a role in the number of heads actuated during a test. The immediate ignition of fuel (simulating a spill onto an existing ignition source) resulted in a slower growing fire, actuating fewer sprinkler heads. Alternately, an ignition scenario where a 7.6 L spill was allowed to develop prior to ignition resulted in the actuation of four heads within the first minute of fire exposure. A comparable test with the immediate ignition scenario resulted in only two heads operating in a time in excess of 2 min and 30 s. The involvement of fewer sprinkler heads and the prolonged fire exposure implied that the immediate ignition provided a more challenging scenario.

The AFFF system used in the test program was successful in generating a good blanket of foam within 1 to 2 min of actuation (depending on the number of initial heads actuated). The foam quality was such that it was free to flow over drum heads, providing cooling to the tops and sides of drums, and forming a blanket at the floor to suppress pool fires. The foam system (in Tests 6 through 8) was also effective at limiting the fire at the fuel introduction point, periodically extinguishing the source. In general, by the time fuel flow to the array was complete, the foam system had suppressed all pool fires, leaving only small pallet fires for manual suppression.

An initial survey of closure obstruction versus venting phenomenon indicated that there was little or no effect on the obstruction of a plug and its ability to vent. This is indicated by the low number of drums that exhibited bulging during tests. The bulging of a drum indicates an unusual buildup of pressure. This phenomenon was not consistent, even in drums where both closures were obstructed. It was also noted that even partial venting of either opening was sufficient in reducing the pressure within the drum.

Drum deformation was recorded on a subjective basis. Typical deformation involved bulging of the head of the drum by 1.2 to 2.5 cm (0.5 to 1.0 in.). In some cases, deformations were seen on the order of 7.6 to 10.2 cm (3 to 4 in.) with some unfurling of the head chime.

It is difficult to attribute the level of deformation with a corresponding internal pressure. Several drums were deformed to a degree consistent with hydrostatic pressures of 207 to 241 kPa (30 to 35 psi); however, no pressures of this magnitude were recorded. A possible reason for higher levels of deformation at lower pressures may lie in the exposed temperatures of the drums. Several drums were subjected to uneven heating. The uneven heating phenomenon is present where a drum is located directly above a pallet containing venting drums. This scenario sets the subject drum over an isolated flame source, heating it from below.

The results of these tests have been included in the NFPA 30 protection criteria tables for palletized steel drum storage up to four high when protected using AFFF. The use of listed relieving devices is recommended; the exact details of this listing procedure are being developed.

Liquid Spill and Container Storage Table 47.22 summarizes early closed-head AFFF sprinkler testing on a flammable liquid spill [71]. In a 9.1-m (30-ft) high ceiling room, *n*-heptane was discharged in a simulated spill to create a three-dimensional spill and a two-dimensional pool fire. Fuel spill rate was varied up to 113 L/min (30 gpm). AFFF application rates were 4.5 to 12.3 L/min/m^2 (0.11 to 0.30 gpm/ft^2). The

Table 47.22 Closed-head sprinkler tests [71]

Sprinkler temperature rating (°C [°F])	Nominal application rate (L/min/m^2[gpm/ft^2])	Total heads opened	Sprinkler operation and control times (min:s)
71 (160)	4.5 (0.11)	34	First sprinkler—0:27
			Final sprinkler—1:01
			3:50 Control time
71 (160)	7.4 (0.18)	32	First sprinkler—0:22
			Final sprinkler—1:08
			1:00 to 1:20 for knockdown
			2:20 Control time
138 (280)	7.4 (0.18)	7	First sprinkler—0:33
			Final sprinkler—0:531
			1:50 Control time
138 (280)	7.4 (0.18)	15	First sprinkler—0:28
			Final sprinkler—1:44
			2:20 Control time
138 (280)	7.4 (0.18)	17 to 19	First sprinkler—0:22 to 0:24
			Final sprinkler—1:03 to 1:13
			2:00 Control time
141 (286)	12.3 (0.30)	10	First sprinkler—0:24
			Final sprinkler—1:10
			2:25 Control time

primary variables were the temperature rating of the sprinkler and the application rate. Non-air-aspirating sprinklers were used. The data show that high-temperature-rated sprinklers, activated at about the same time as ordinary temperature sprinklers, controlled the fire in comparable times (roughly 2 min control time), and resulted in significantly fewer sprinklers operating (7 versus 32). An increase in application rate when the high-temperature sprinklers were used resulted in fewer heads operating, but did not decrease overall control and extinguishment time. Fires were controlled, but not totally extinguished as a result of the three-dimensional spill fire. These tests showed the advantage of using high-temperature-rated sprinklers in AFFF closed-head suppression systems.

In response to the concerns related to flammable liquid warehouse protection, the National Fire Protection Research Foundation (NFPRF) initiated the International Foam-Water Sprinkler Research Project. The objectives were to document the performance of foam-water sprinkler systems designed for real-world storage and ignition scenarios and provide a design basis and minimum design parameters for foam-water sprinkler systems. Five tasks were performed, including a literature search, range-finding tests, and large-scale tests involving palletized and rack storage of liquids.

The literature search identified over 1100 sources of information related to flammable liquid fires and foam protection, but a dearth of data related to water and foam-water sprinkler suppression of liquid storage fires [72]. The range-finding tests indicated that the Class IB flammable liquids (heptane) provided a greater challenge than water-miscible fuels (e.g., isopropanol) [73]. Breach of steel containers exposed to a flammable liquid pool fire without sprinkler protection occurred over a range of times between 2 and 7.5 min, depending on the particular type of container. Plastic containers were quickly breached and discharged their contents to the exposing pool fire.

Large-scale tests were conducted under an 8.2-m (27-ft) high ceiling at the Underwriters Laboratories fire test facility in Northbrook, Illinois [74]. A series of 14 fire tests involving the protection of 3.8 and 18.9 L (1 and 5 gal) metal and 18.9 L (5 gal) plastic containers filled with heptane (Class IB flammable liquid) were

conducted. The use of closed-head foam-water sprinkler systems for the protection of these fuel packages was investigated. Quantities of fuel used in the fire tests varied from 605 to 7260 L (1601920 gal); fuel storage densities ranged from 160 to 1907 L/m^2 (3.9–46.5 gal/ft^2); and storage heights ranged from 4.3 to 42.7 m (1.3–13 ft). Each fire test was initiated using a 37.8 L (10 gal) flammable liquid (heptane) spill, recognizing the larger spill ignition scenarios observed in large-loss fires.

Fire tests involving palletized storage of 3.8 L (1 gal) metal F-style containers of heptane, packaged four containers in a corrugated cardboard carton, were conducted. The results indicated that the 37.8 L (10 gal) flammable liquid spill fire could be suppressed by a closed-head foam-water sprinkler system at a 16.4 L/min/m^2 (0.40 gpm/ft^2) design application rate for storage heights up to 3.3 m (10.7 ft) under the 8.2 m (27 ft) ceiling prior to any container breach or fuel loss. Fires involving 18.9 L (5 gal) metal containers of heptane could be suppressed by a closed-head foam-water sprinkler system application rate of 12.3 L/min/m^2 (0.30 gpm/ft^2) for a palletized storage height of up to 3.6 m (12 ft). Plastic pour spouts in the 18.9 L (5 gal) tight-head metal containers safely vented and prevented container breaching.

Fires involving 18.9 L (5 gal) plastic containers of heptane could not be suppressed by a preprimed, closed-head foam-water sprinkler system with an application rate of 12.3 L/min/m^2 (0.30 gpm/ft^2), where containers were stacked one high (483 mm [19 in.]), due to container breaching and flammable liquid spillage prior to foam-water discharge.

Rack-storage tests also conducted in the NFPRF International Foam-Water Sprinkler Research Project did not lead to conclusive results [75].

Based on the results of the NFPRF foam-water sprinkler testing, the FMRC original AFFF drum testing, and engineering judgment/extrapolation, the NFPA 30 Technical Committee adopted protection criteria for palletized and rack storage of liquids in metal containers when protected by AFFF. Variables that affect the specific level of protection include container size, class of liquid stored, inclusion of exterior packaging material, and storage height. Ceiling application rates are on the order of 12.3–16.4 L/min/m^2 (0.30–0.40 gpm/ft^2). Protection criteria shown in Table 47.23 are recommended for palletized storage of small containers that are nonrelieving style (i.e., do not readily vent when exposed to fire). Additional criteria are included in NFPA 30 for foam protection of palletized relieving-style containers based on extrapolation of the NFPRF data and engineering judgment. Where the hazard involves a water-miscible fuel, an alcohol-type foam should be used. The application rate should be at least as great as the rate established by foam listing requirements. AFFF solution should be discharged when four sprinklers are operating.

AFFF protection of flammable and combustible liquids should be used where large spills of low flashpoint fuels are a realistic scenario. Other protection options are available and have recently been adopted or are currently being considered by NFPA 30 and the model building/fire prevention codes. Designers of warehouse protection should have a thorough knowledge of these criteria and the available test data (including water-only protection) when considering design options for the protection of stored combustible and flammable liquids. Nugent [68] and NFPA 30 provide detailed data and guidance for water-only protection. Additional guidance for warehouse protection is available from the Center for Chemical Process Safety [76].

Foam Environmental Considerations

There has been increasing concern about the consequences of the discharge of foam in the environment. This concern affects the users of foam, the manufacturers of foam agents, the fire safety authority having jurisdiction, and environmental authorities. The issue is not a new or unique development but has received increased notice as a result of increased attention to environmental impact of fire-fighting agents.

Factors related to the impact of fire-fighting foam on the environment include

Table 47.23 AFFF sprinkler protection requirements in NFPA 30 for solid-pile and palletized storage of flammable and combustible liquids in non-relieving-style metal containers of 18.9 L (5 gal) capacity or less

Package type	Cartoned	Uncartoned
Class liquid	IB, IC, II	IB, IC, II
Application rate (L/min/m^2 [gpm/ft^2])	16.4 (0.40)	12.3 (0.30)
Area (m^2 [ft^2])	186 (2000)	186 (2000)
Temperature rating (°C [°F])	141 (286)	141 (286)
Maximum spacing (m^2/head [ft^2/head])	9.3 (100)	9.3 (100)
Orifice size (mm [in.])	13.3 (0.53)	12.5 or 13.3 (0.5 or 0.53)
Maximum height (m [ft])	3.4 (11)	3.7 (12)
Hose (L/min [gpm])	1891 (500)	1891 (500)
Water supply duration (min)	120	120
Foam supply duration (min)	15	15

1. Discharge of foam solutions and fuel-contaminated foam solutions to waterways and the potential toxicity to aquatic life
2. Effects on water treatment facilities
3. Persistence and biodegradability of chemicals in foam concentrates and solutions
4. Combustion products of fuel/foam solutions

In the United States, all fire-fighting foams are regulated at some point during their life cycle, and all have the potential to impact the environment. Fire-fighting foams have several intrinsic properties that cause environmental impacts, including foaming, oxygen demand, aquatic toxicity, biodegradability, and oil emulsification. Because of these properties, fire-fighting foams will impact surface water and groundwater if released into the environment. If sent to a wastewater treatment plant, they can cause disruption of the plant, preventing sewage from being treated and forcing the plant to discharge raw sewage.

All fire-fighting foams have these properties because they consist of ingredients that exhibit these properties. The main ingredients in fire-fighting foams are water, surfactants, solvents, and other ingredients used to make the foam work in a particular system or under specified conditions. Some of these ingredients are specifically listed in U.S. environmental laws because of their environmental impacts (e.g., butyl carbitol, dipropylene glycol methyl ether, ethylene glycol, etc.). Although it is easier to highlight these as being regulated because they are specifically named, almost all of the ingredients in fire-fighting foams are regulated due to their properties.

The properties and ingredients of fire-fighting foams make them subject to U.S. federal environmental laws that regulate their manufacture, storage, use, release, cleanup, remediation, and disposal. These laws include the Clean Water Act (CWA); Clean Air Act (CAA/CAAA-90); Comprehensive Environmental Response, Compensation, and Liability Act (CERCLA or Superfund); the Superfund Amendments and Reauthorization Act (SARA); the Emergency Planning and Community Right-to-Know Act (EPCRA); the Resource Conservation and Recovery Act (RCRA); the Hazardous and Solid Waste Amendments of 1984 (HSWA); the Safe Drinking Water Act (SDWA); the Toxic Substances Control Act (TSCA); and the Uniform National Discharge Standard (UNDS). These laws cover the entire life cycle of fire-fighting foams from manufacture to final disposition.

Whether foams are used in fixed facility systems or on crash fire-rescue vehicles, mitigating the environmental impacts is best accomplished through careful planning and management. This forethought may include engineered systems for capture and containment, temporary containment equipment, improved standard operating procedures, and other measures. Simple substitution of one "environmentally friendly" foam for another will not eliminate environmental impacts. In order to make the final decision to use any type of system

for fire protection, it is essential to fully review the fire and environmental risks and benefits of using fire suppression chemicals and their associated systems. The review should involve both fire protection and environmental professionals to ensure a balanced approach that guarantees maximum fire protection and environmental protection at the same time.

Fluorinated Surfactants

AFFF fire fighting agents contain fluorinated surfactants (fluorosurfactants). They are key ingredients that provide AFFF with the required low surface tension and positive spreading coefficient that enables film formation on top of hydrocarbon fuels. This provides for superior fire extinguishment capability as described earlier.

Environmental regulators have investigated AFFF chemicals for their persistence, tendency to bioaccumulate, and toxicity (PTB). As part of this assessment process, the AFFF manufacturing industry has formed a coalition to represent the fire fighting foam industry's interests on all issues related to the environmental acceptability of AFFF agents. The Fire Fighting Foam Coalition (FFFC) provides periodic updates on the status and use of chemicals used to create AFFF [77]. They note that the chemicals used to produce fluorosurfactants can be manufactured by different processes and have different chemical structures. The fluorosurfactants used in AFFF have historically been produced from fluorochemicals manufactured by two methods: electrochemical fluorination and telomerization.

In 2002, the US manufacturer of fluorosurfactants using the electrochemical fluorination process voluntarily stopped production of a number of products including AFFF agents because they contain and degrade into perfluorooctane sulfonate (PFOS). PFOS is considered by environmental authorities to be PBT. Regulations in the United States, Canada, European Union, Australia, and Japan act as a ban on new production of PFOS-based products including foams. These regulations do not currently restrict the use of existing stocks of PFOS-based foam in the US, Australia, or Japan. In the EU and Canada, existing stocks of PFOS-based foam must be removed from service over a set time period. A general overview of this regulatory restriction on PFOS in the US is available in the general fire service literature [78].

Other AFFF agents contain telomer-based fluorosurfactants. Telomer-based AFFF agents do not contain or break down into PFOS. Telomer-based AFFF agents are not made with any chemicals that are currently considered by environmental authorities to be PBT. The US Environmental Protection Agency (EPA) has indicated that some telomer-based fluorochemicals can break down in the environment into perfluorooctanoic acid (PFOA) or other perfluorocarboxylic acids (PFCAs). EPA's concern is focused on long-chain perfluorinated chemicals (LCPFCs) containing eight carbons or more (C8, C10, C12). Existing data shows that shorter-chain compounds (C6 and below) have a lower potential for toxicity and bioaccumulation. Under an EPA stewardship program, fluorochemical manufacturers have voluntarily agreed to reduce both plant emissions and product content of PFOA, PFOA precursors, and related chemicals. This will result in the reformulation of many existing telomer-based AFFF agents.

The restrictions on the manufacture and use of AFFF has resulted in industry creating a new class of foams, "fluorine-free" foam. Preliminary test data show that these non-film forming foams take longer to extinguish fires compared to AFFF [79], but have better fire extinguishing performance than protein or fluoroprotein foams. This is not surprising since the fluorosurfactants used to create the "film" in AFFF have been eliminated. Users may be faced with trade-offs in selecting foams for fire performance and environmental impact. If reduced fire extinguishing performance must be accepted for lower environmental impact, priorities for protecting hazards may have to be established. An example methodology has been published by the U.S. Navy [80].

Perspective on the Use of Foam Agents

In order to assess the impact of foam on the environment, the likely scenarios under which AFFF may be discharged should be considered. Based on these scenarios, the overall impact can be assessed and, where appropriate, potential mitigation strategies can then be developed. Likely scenarios include uncontrolled fires, potential hazardous situations, fire-fighting training evolutions, and fixed or mobile vehicle suppression system discharge testing.

Uncontrolled Fires There are many fires for which foam may be used, including flammable liquid storage, process industry protection, aviation protection, and marine applications. For most fires, the elimination of foam as a suppression agent results in the potential for dramatically increased environmental impact. This impact results from the potential increase in hydrocarbon fuel effluent to the environment (due to smoke from uncontrolled burning and fuel/fire-fighting water effluent). Consider the example shown in Fig. 47.22. A 929 m^2 (10,000 ft^2) section of a warehouse containing combustible and flammable liquids may be protected using traditional water sprinklers discharging at a rate of 12.3 L/min/m^2 (0.30 gpm/ft^2). If these sprinklers fail to control a large spill fire, the fire may develop and spread past the design area of the sprinklers. The example assumes the fire is contained within the fire wall; this may not always be the case for high-challenge fires. If the fire department aggressively combats the fire, a rough estimate of fire-fighting water that may be used is 15 to 50 times the minimum anticipated agent required for suppression [6, 81, 82]. A rough estimate of the potential fuel-contaminated effluent (neglecting the actual quantities of hydrocarbon liquid) is shown in Fig. 47.22. In the alternative situation, a properly specified foam-water sprinkler system designed for a high degree of reliability can control or suppress the fire. Using application rates and discharge times based on recent tests and building code requirements, the anticipated fuel/foam-water effluent for this scenario can be estimated (see Fig. 47.22). The use of the foam-water system reduces the potential effluent by a factor of

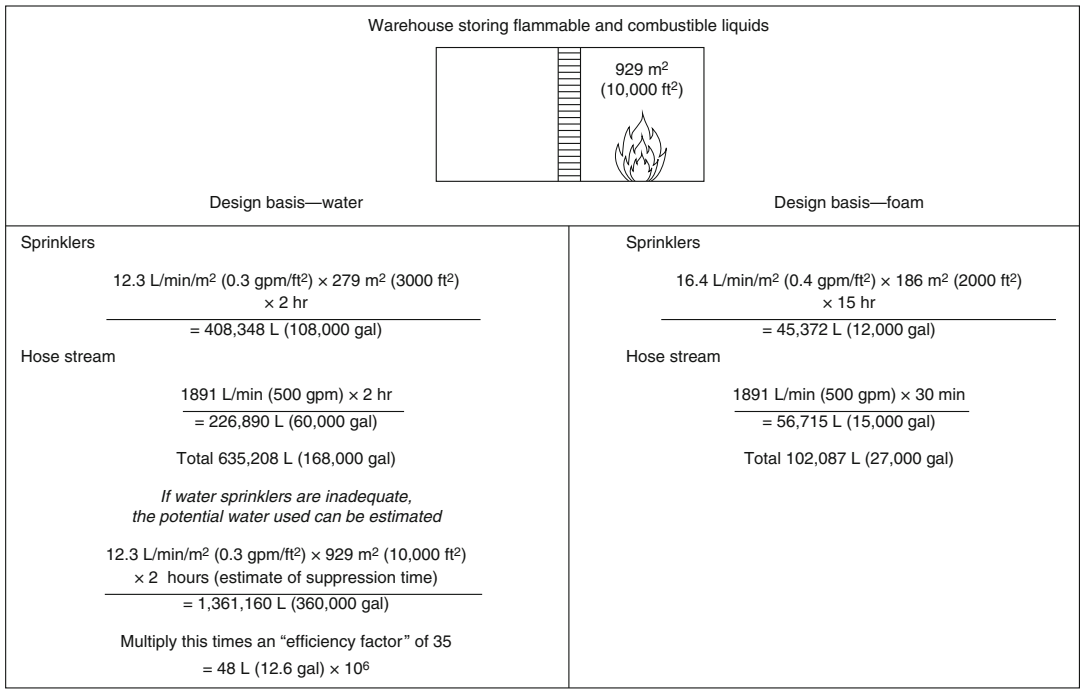

Fig. 47.22 Example of potential effluent from flammable liquid warehouse fire

nearly 500 compared to the "unsuccessful" water sprinkler scenario where handlines are used. This reduction neglects the impact of smoke discharged to the atmosphere during the uncontrolled burning in the water-only scenario.

In some cases, it may be possible to collect the effluent from an uncontrolled fire. In other situations, it may not be possible. Any foam solution that has been used in fire suppression is likely to be contaminated with fuel and diluted with water.

Potential Hazardous Situations Potential hazardous situations may result from a fuel spill where there is a likely ignition source. In this situation, foam may be applied for ignition prevention. The potential impact of ignition and resulting uncontrolled fire must be assessed against the potential additional environmental impact by discharging foam for ignition prevention. The potential environmental effects from an uncontrolled fire should be considered as described in the previous text. Another consideration is the assessment of any additional impact of foam when applied to a fuel spill. For example, would the resulting fuel with foam have any greater impact on the environment than the fuel alone? If so, how is this impact quantitatively determined?

Training Evolutions Fire-fighting training is usually conducted under conditions conducive to collection of fuel, water, and foam. A separation process might be used to recover fuel. Water/foam solution may then be treated or reused. Alternatively, simulated hydrocarbon fuel spill scenarios might be used, with a simulated foam agent. Propane-fired burners are typically used. The disadvantage of these systems is the potential loss of realism of the simulated fire/agent interaction. These techniques may potentially reduce training effectiveness. Quantitative comparisons have not been performed to assess these differences.

System Discharge Testing Facilities protected by foam systems may have containment systems that can hold effluent. Requirements for these containment systems are becoming more widespread in model building and fire codes. An alternative to discharge testing with foam is the use of a simulant that can be measured using concentration determination methods. For example, salt solutions can be used as the "concentrate" to test AFFF systems, with the simulant concentration measured using the conductivity method. Simulators may be more difficult to use for protein-based systems, where viscosity factors influence proportioning system accuracy.

Because of their persistent nature, NFPA 11 recommends that emissions of fluorochemical surfactants to the environment be minimized whenever possible using the following techniques:

1. Use training foams that do not contain fluorochemical surfactants.
2. Provide for containment, treatment, and proper disposal of foam discharges.
3. Follow applicable industry standards on the design, installation, and maintenance of foam systems and extinguishers.
4. Minimize false discharges from fixed foam systems by using approved detection, actuation, and control systems as required by industry standards.
5. When appropriate consider treating collected wastewater with granular activated carbon (GAC) or a membrane process such as reverse osmosis to remove the fluorochemical surfactants prior to disposal.

Methods of Assessment

Biodegradability The primary component of AFFF solution is water. Examples of other components are nonfluorinated surfactants, glycol ethers, and fluorinated surfactants. Freeze-resistant concentrate may contain ethylene or propylene glycol. Alcohol-type foams contain xanthan or similar gums. The fluorinated surfactants are particularly resistant to biodegradation. Further, the less-effective protein-based foams were largely assumed to be nonpolluting because of their "natural" organic base. An early review of the available literature by Factory Mutual Research Corporation indicated that both

types of agents, that is, AFFF and protein-based, present inherent environmental issues and that effluents containing either should be processed in some form of sewage treatment facility or diluted prior to discharge into a stream [47].

A conventional method used to determine the biodegradability of a material is comparison of the chemical oxygen demand (COD) of the material with its biological oxygen demand (BOD). This method is particularly important for waste treatment facilities where the stability of the treatment process may be upset. The method typically used is specified in *Standard Methods for the Examination of Water and Wastewater* [83]. BOD measures the amount of oxygen consumed by microorganisms in breaking down a hydrocarbon. COD measures the maximum amount of oxygen that could theoretically be consumed by microorganisms. Therefore, a BOD/COD ratio is representative of the ability of microorganisms to biodegrade the components in a foam. The higher the BOD/COD ratio, the more biodegradable the foam. Results reported for BOD/COD of AFFF range from 0.60 to 0.99. MIL-F-24385 requires a maximum COD of 500,000 mg/l and a minimum 20-day BOD/COD ratio of 0.65 for 6 % concentrate. AFFF agents have been reported to have higher BOD and COD values than protein foams. [47] AFFF solutions are high-BOD materials compared to the normal influent to treatment plants. Large quantities can "shock load" wastewater treatment facilities.

The fluorochemical-based surfactants in AFFF have a carbon–fluorine chain that apparently does not break down in either the BOD or the COD test. The AFFF might then appear to be completely "biodegradable," even though the carbon-fluorine chain remains.

If nonbiodegradability concerns are based on the persistence of the fluorochemical surfactants, then the environmental impact tests currently used to assess foams do not address this concern. There is speculation that the undegradable material is biologically inert, but no published data confirm this. Because the fluorinated surfactants are required to create surface-tension reduction of the solution, replacement with less persistent chemicals is problematic. There is a need for a more thorough understanding and testing related to the environmental impact of fluorosurfactants and possible alternatives.

The persistence of fluorosurfactants in soil has been quantified in a study of fire-training facilities [84]. In a study of training sites having long-term use, perfluorocarboxylates were detected using gas chromatography/mass spectrometry. These chemicals were detected at sites that were inactive for a period of 7–10 years. The results are consistent with the view that biodegradation of the long chain perfluorocarbon is unlikely. The influence of the perfluorinated compounds on the biotransformation and transport of other cocontaminants (e.g., training fuel) and other site characterization parameters (e.g., dissolved organic carbon and inorganics) is unknown.

Methods for detecting AFFF in aqueous solutions have been investigated [85]. A Fourier Transform Infrared Spectroscopy (FTIR) method and drain-time test were found to be effective in evaluating the level of AFFF contamination in wastewater and soil. The drain-time method was proposed as a simple, easy-to-use field test. Using these methods, procedures were developed to estimate AFFF contamination levels in wastewater and soil. Analysis of wastewater and soil for AFFF contamination was broken into two groups: nonbiodegraded samples and biodegraded samples. Nonbiodegraded samples were screened for AFFF, then analyzed further if deemed necessary. Samples were initially screened using the drain-time test. Samples with no drain time contain less than a 1:240 dilution of AFFF (5 ppm of fluorosurfactant). If the sample had a drain time, it was recommended that the FTIR analysis be performed on the sample. In solutions with fluorosurfactants, FTIR analysis can provide a quantitative level of AFFF in the sample if the fluorosurfactant source solution is available to develop a calibration curve. Otherwise, FTIR provides a qualitative estimate of the AFFF level in the solution.

Biodegraded wastewater samples were difficult to analyze because the hydrocarbon surfactants and a portion of the fluorosurfactant molecule were degraded. With these foam-

making constituents degraded, the drain-time test results were found to be unreliable. However, the fluorine-carbon tail of the fluorosurfactant is not biodegraded, making FTIR analysis on biodegraded samples possible. With biodegraded samples, FTIR analysis can provide a qualitative measure of AFFF levels.

Toxicity In sufficient concentrations, foams may affect aquatic life. A number of fish toxicity studies have been performed. In tests using fathead minnows, the U.S. Air Force found that these fish could live in a simulated effluent stream containing 250 ppm AFFF without fatality for up to 8 days. LC_{50} values (i.e., the concentration causing deaths of 50 % of the fish exposed) at 96 and 24 h were 398 and 650 ppm, respectively [86]. MIL-F-24385 requires AFFF toxicity testing in accordance with ASTM E729, using dynamic procedures with killifish. LC_{50} of 1000 mg/l for 6 % concentrate is permitted.

Alone, these values may be considered as having a low degree of fish toxicity using environmental regulation rating scales. Localized concentrations in ponds or streams may exceed the values cited, if there is limited water movement.

Published data do not exist for the phytotoxicity of foam solutions; however, there have been no published reports of plant kills resulting from foam solution discharges.

Manufacturers report that thermal decomposition products from AFFF do not present a health hazard during fire fighting. Again, there are no data published in the literature. Manufacturers' product environmental data for AFFF include references to a test where a layer of AFFF was burned in a pan of gasoline inside an enclosure. Two measurements of hydrogen fluoride recorded above the sample were 0.23 and 0.16 ppm [87].

Foaming and Emulsification of Fuels The surfactants in AFFF solutions can cause foaming in treatment aeration ponds. This foaming process may suspend high BOD solids in the foam. If these are carried over to the outfall of the treatment facility, nutrient loading in the outfall waterway may result. Foam aeration may also cause foam bubble backup in sewer lines.

In uncontrolled fires, spills, and live fire-training scenarios, foams may contain suspended fuels. The fuel may become emulsified in the foam-water solution.

A bench-scale study has been conducted to evaluate the potential inhibitory effects of untreated AFFF wastewater on the biological nutrient removal process [88]. In this study, bench-scale reactors simulating the nitrification process were loaded at various AFFF concentrations, and the influence on process performance was evaluated. The results indicated that AFFF in concentrations between 10 and 60 ppm did not show any inhibition to biological nitrification, and effluent did not exhibit any pass-through toxicity. These range-finding tests did indicate that nitrification inhibition did occur above 60 ppm AFFF. Some reductions in percent COD removal were observed as AFFF concentrations were increased.

Mitigation Strategies

Foam discharges are more easily handled where there is an in-place collection capability. This situation may be available at warehouses, tank farms, and fire-fighting training facilities. Where these facilities are not available, temporary diking is an alternative where time and resources permit.

Investigations have been conducted to develop foam-water separators using aeration and agitation techniques. To date, these techniques have not been optimized.

Discharge to water treatment facilities is recommended by many foam vendors when the solution is uncontaminated by fuel. Metering or dilution may be required to prevent levels of foam that will upset treatment facility reactions or cause excessive foaming. The use of defoamers to reduce aeration has been suggested.

Where fuels contaminate foam solutions, fuel-water separators might be used to skim off the hydrocarbon fuel. AFFF solutions have a tendency to form emulsions with fuels, potentially reducing the effectiveness of fuel-water separators. An alternative is to hold the solution in a pond or tank until the emulsion breaks and

the separation process can be used. Agitation should be avoided to prevent the emulsion from reforming. In some situations (e.g., training), the fuel and treated water have been reused. Many fire training facilities collect foam solution for ultimate discharge to water treatment facilities.

To ensure that unbalanced conditions do not occur in water treatment facilities, foam discharge should be carefully monitored. Different ranges of discharge rates have been suggested. This is an area requiring further investigation. Manufacturers of the foam solution should be consulted in conjunction with the wastewater treatment operator.

The entire area of environmental aspects of foam discharge requires additional evaluation and development of generally recognized guidance. Until generally recognized guidance is promulgated, users must rely on manufacturers' data and guidance. In all situations, discussions with the operator of the wastewater treatment facility and the environmental regulatory authorities are appropriate. Work is continuing in an effort to identify appropriate policy and criteria covering foam discharge for facilities having foam suppression systems. These efforts are focusing on identifying applicable codes and standards, analyzing environmental impact, and evaluating containment options.

Nomenclature

$\mathbf{AFFF\%_{sample}}$	percentage of AFFF present in the sample
$\boldsymbol{\alpha_{foam}}$	absorptivity of foam
BOD	biological oxygen demand (mg/l)
$\boldsymbol{\gamma_a}$	surface tension of liquid *a* (dynes/cm)
$\boldsymbol{\gamma_b}$	surface tension of liquid *b* (dynes/cm)
$\boldsymbol{\gamma_l}$	interfacial tension between liquids *a* and *b* (dynes/cm)
COD	chemical oxygen demand (mg/l)
ER	expansion ratio
$\boldsymbol{\Delta H_v}$	combined latent and sensible heads of vaporization (kJ/kg)
$\boldsymbol{\delta}$	viscous boundary layer thickness (cm)
$\boldsymbol{G}$	conductance (mhos)
$\boldsymbol{g}$	acceleration of gravity (cm/s^2)
$\boldsymbol{h}$	foam thickness
$\boldsymbol{h_c}$	critical thickness of the foam layer
$\boldsymbol{i}$	angle of incidence
$\boldsymbol{k}$	foam spreading coefficient, dimensionless or nozzle coefficient (L/min/kPa$^{1/2}$)
$\boldsymbol{k_d}$	foam drainage coefficient, dimensionless
$\boldsymbol{k_e}$	foam evaporation coefficient, dimensionless
$\boldsymbol{l}$	length of foam spread
$\boldsymbol{n}$	refractive index, dimensionless
$\boldsymbol{\mu}$	viscosity (cm^2/s)
$\boldsymbol{\dot{m}_{add}}$	foam addition rate
$\boldsymbol{\dot{m}_{fuel}}$	fuel mass loss rate
$\boldsymbol{\dot{m}_{drain}}$	foam mass loss due to drainage
$\boldsymbol{\dot{m}_{drop}}$	foam loss rate due to drop-out
$\boldsymbol{\dot{m}_{vap}}$	foam mass loss rate due to vaporization
mS	milli siemens
$\boldsymbol{v}$	kinetic viscosity (cm^2/s)
$\boldsymbol{n_{water}}$	refractive index of water, dimensionless
$\boldsymbol{n_{foam}}$	refractive index of foam solution, dimensionless
$\boldsymbol{n_{concentrate}}$	refractive index of foam concentrate, dimensionless
$\boldsymbol{P_v}$	vapor pressure of fuel
$\boldsymbol{\rho_{fuel}}$	fuel density (g/cm^3)
$\boldsymbol{\rho_{foam}}$	foam density (g/cm^3)
$\dot{q}''$	rate of heat transfer
$\dot{q}_{rad}$	rate of heat transfer due to radiation
$\boldsymbol{\dot{q}''_{rad}}$	radiative heat release rate from pool fire
$\boldsymbol{R}$	resistance (ohms)
$\boldsymbol{r}$	angle of refraction
$\boldsymbol{\sigma}$	spreading coefficient (dynes/cm) or conductivity (mhos)
$\boldsymbol{S_{a/b}}$	spreading coefficient between liquids *a* and *b* (dynes/cm)
$\boldsymbol{T}$	temperature (°C)
$\boldsymbol{t}$	time (s)
$\boldsymbol{T_i}$	foam temperature (°C)

T_s	fuel temperature (°C)
V	volume (cm^3 or l^3)
v_s	spreading velocity of foam (cm/s)

Subscripts

add	addition of foam
drain	drainage of foam
drop	drop-out of foam
rad	radiation
vap	vaporization

Superscripts

$\cdot$	rate of change, as in $\dot{m}$
$''$	per unit area

References

1. G.B. Geyer, L.M. Neri, and C.H. Urban, "Comparative Evaluation of Fire Fighting Foam Agents," *Report FAA-RD-79-61,* Federal Aviation Administration, Washington, DC (1979).
2. J.H. Aubert, A.M. Kraynik, and P.B. Rand, "Aqueous Foams," *Scientific American,* 19, 1, pp. 74–82 (1988).
3. V.L. Francen, "Fire Extinguishing Composition Comprising a Fluoroaliphatic and a Fluorine-Free Surfactant," U.S. Patent 3,562,156 (1971).
4. M.J. Rosen, *Surfactants and Interfacial Phenomena,* John Wiley and Sons, New York, Chapters 1, 5, 7 (1989).
5. R.L. Tuve, H.B. Peterson, E.J. Jablonski, and R.R. Neill, "A New Vapor-Securing Agent for Flammable Liquid Fire Extinguishment," *NRL Report 6057,* Naval Research Laboratory, Washington, DC (1964).
6. H.-Z. Yu and J.S. Newman, "Theory of Fire Extinguishment," *Fire Protection Handbook,* 20th ed. (A.E. Cote et al., eds.), National Fire Protection Association, Quincy, MA, p. 2–85 (2008).
7. C.P. Hanauska, J.L. Scheffey, R.J. Roby, and D.T. Gottuk, "Improved Formulations of Firefighting Agents for Hydrocarbon Fuel Fires," *SBIR Phase I Final Report,* Hughes Associates, Inc., Baltimore, MD (1994).
8. B. Persson and M. Dahlberg, "A Simple Model of Foam Spreading on Liquid Surfaces," *SP Report 1994:27,* Swedish National Testing and Research Institute, Boras, Sweden (1994).
9. H. Persson, "Fire Extinguishing Foams—Resistance Against Heat Radiation," *SR Report 1992:54,* Swedish National Testing and Research Institute, Boras, Sweden (1992).
10. B.Y. Lattimer, C.P. Hanauska, J.L. Scheffey, and F.W. Williams, "The Use of Small-Scale Test Data to Characterize Some Aspects of Fire Fighting Foam for Suppression Modeling," *Fire Safety Journal,* 38, pp. 117–146 (2003).
11. S. Ikasson and H. Persson, "Fire Extinguishing Foam—Test Method for Heat Exposure Characterisation," *SP Report 1997:09,* Swedish National Testing and Research Institute, Boras, Sweden (1997).
12. A.M. Kraynik, "Foam Drainage," *Sandia Report SAND-83-0844,* Sandia National Laboratories, Albuquerque, NM (1983).
13. B. Persson, A. Lonnermark, H. Persson, D. Mulligan, A. Lancia, and M. Demichela, "FOAMSPEX Large Scale Foam Application–Modelling of Foam Spread and Extinguishment," *SP Report 2001:13,* Boras, Sweden (2001).
14. A.M. Kraynik, "Foam Flows," *Annual Review of Fluid Mechanisms,* 20, pp. 325–357 (1988).
15. J.A. Fay, "The Spread of Oil Slicks on a Calm Sea," in *Oil on the Sea* (D.P. Hoult, ed.), Plenum, New York, pp. 53–64 (1964).
16. J.A. Fay and D.P. Hoult, "Physical Processes in the Spread of Oil on a Water Surface," *Coast Guard Final Report,* Massachusetts Institute of Technology, Cambridge, MA (1971).
17. P. Cann, H.A. Spikes, and G. Caporico, "Spreading of Perfluorinated Fluids on Metal Surfaces," in *4th International Colloquium on Synthetic Lubricants and Operation Fluids,* Oatfildern, Germany, pp. 631–638 (1984).
18. H.E. Moran, J.C. Burnett, and J.T. Leonard, "Suppression of Fuel Evaporation by Aqueous Films of Fluorochemical Surfactant Solutions," *NRL Report 7247,* Naval Research Laboratory, Washington, DC (1971).
19. T. Briggs, and B. Abdo, "Emphasis on Spreading Quality of AFFF Could Be Misleading," *FIRE,* 80, 94 (1988).
20. J.L. Scheffey, R.L. Darwin, J.T. Leonard, C.R. Fulper, R.J. Ouellette, and C.W. Siegmann, "A Comparative Analysis of Film-Forming Fluoroprotein Foam (FFFP) and Aqueous Film-Forming Foam (AFFF) for Aircraft Rescue and Fire Fighting Services," *Hughes Associates, Inc. Report 2108-A01-90,* Hughes Associates Inc., Baltimore, MD (1990).
21. G.B. Geyer, "Status Report on Current Foam Fire Fighting Agents," *International Conference on Aviation Fire Protection,* Interlaken, Switzerland (1987).
22. P.J. Chiesa and R.S. Alger, "Severe Laboratory Fire Test for Fire Fighting Foams," *Fire Technology,* 16, 1, pp. 12–21 (1980).
23. Underwriters Laboratories Inc., *Standard for Foam Equipment and Liquid Concentrates,* 6th ed., Northbrook, IL (1994, with revisions through 2015).
24. Chevron Foam Concentrate Team, "Chevron Firefighting Foam Test Report," Report to the American Petroleum Institute, Washington, DC (2001).
25. J.L. Scheffey, J. Wright, and C. Sarkos, "Analysis of Test Criteria for Specifying Foam Firefighting Agents

for Aircraft Rescue and Firefighting," *FAA Technical Report, DOT/FAA/CT-94/04,* Atlantic City, NJ (1994).
26. International Organization for Standardization, "Fire Extinguishing Media—Foam Concentrates—Part 3: Specification for Low-Expansion Foam Concentrates for Surface Application to Water-Immiscible Liquids," *European Standard EN 1568–3,* ISO, Geneva, Switzerland (2008).
27. B.P. Johnson, "A Comparison of Various Foams When Used Against Large-Scale Petroleum Fires," Home Office Fire Research and Development Group, London, UK (1993).
28. W.M. Carey and M.R. Suchomel, "Testing of Fire Fighting Foam," *Underwriters Laboratories Report No. CG-M-1-81,* Underwriters Laboratories Inc., Northbrook, IL (1980).
29. M.D. Thomas, "UK Home Office Research into Domestic Fire Fighting," *First International Conference on Fire Suppression Research Proceedings,* Stockholm, Sweden, pp. 283–289 (1993).
30. R. Fiala, "Aircraft Post-Crash Firefighting/Rescue," from *AGARD Aircraft Fire Safety Lecture Series No. 123* (1982).
31. G.B. Geyer, "Evaluation of Aircraft Ground Firefighting Agents and Techniques," *Technical Report AGFSRS 71–1,* Tri-Service System Program Office for Aircraft Ground Fire Suppression and Rescue, Wright-Patterson AFB, OH (1971).
32. G.B. Geyer, "Firefighting Effectiveness of Aqueous Film-Forming Foam (AFFF) Agents," *FAA Technical Report FAA-NA-72-48,* DOD Aircraft Ground Fire Suppression and Rescue Unit (ASD-TR-73-13), Washington, DC (1973).
33. J.L. Scheffey, R.L. Darwin, and S. Hunt, "A Technical Review of Methodologies for Calculating Firefighting Agent Quantities Needed to Combat Aircraft Crash Fires," *DOT/FAA/AR-11/29*, Federal Aviation Administration, Atlantic City Int'l Airport, NJ (2012).
34. J.L. Scheffey, R.L. Darwin, and S. Hunt, "Analysis of Suppression Effects on Aviation Fuel Fires Around an Aircraft," *DOT/FAA/AR-11/27*, Federal Aviation Administration, Washington, DC (2011).
35. W.M. Carey, *Improved Apparatus for Measuring Foam Quality,* Underwriters Laboratories Inc., Northbrook, IL (1983).
36. E.J. Jablonski, "Comparative Nozzle Study for Applying Aqueous Film-Forming Foam on Large-Scale Fires," *U.S. Air Force Report, CEEDO-TR-78-22,* Tyndall AFB, FL (1978).
37. J.A. Foster, "Additions for Hosereel Systems: Trials of Foam on 40 m^2 Petrol Fires," *Scientific Research and Development Branch Report 40/87,* Home Office, London (1987).
38. P.L. Parsons, "Trials of Foam on Petrol Fires at the Fire Service Technical College," *Scientific Advisory Branch Report No. 14/75,* Home Office, London (1976).
39. L.R. DiMaio, R.F. Lange, and F.J. Cone, "Aspirating vs. Non-Aspirating Nozzles for Making Fire Fighting Foams—Evaluation of a Non-Aspirating Nozzle," *Fire Technology,* 20, 1, pp. 5–10 (1984).
40. J.L. Scheffey, "Submarine Bilge AFFF Sprinklers," *Naval Research Laboratory Project, 64561N-S1946–2024000,* unpublished data (1988).
41. G. Timms and P. Haggar, "Foam Concentration Measurement Techniques," *Fire Technology,* 26, 1, pp. 41–50 (1990).
42. K. Bagot, "Evaluation of Conductivity Meters for Firefighting Foams," *DOT/FAA/AR-02/115*, Final Report, Federal Aviation Administration, Airport and Aircraft Safety Research and Development Division, Atlantic City International Airport, NJ (2002).
43. M.J. McDonald, D.S. Dierdorf, J.L. Kalberer, and K.D. Barrett, "Fire Extinguishing Effectiveness Tests," *AFRL-ML-TY-TR-2004-4554*, Applied Research Associates, Tyndall AFB, FL (2004).
44. C.P. Menchini, J.L. Kalberer, D. Dierdorf, M.J. McDonald, K.S. Cozart, and A.C. Abildgaard, "The Development and Design of a Prototype Ultra High Pressure P-19 Firefighting Vehicle," *AFRL-ML-TY-TR-2007-4525*, Applied Research Associates, Tyndall AFB, FL (2007).
45. D.E. Breen, "Hangar Fire Protection with Automatic AFFF Systems," *Fire Technology,* 9, 2, pp. 119–131 (1973).
46. D.E. Breen, L.M. Krasner, B.G. Vincent, and P.J. Chicarello, "Evaluation of Aqueous Film Forming Foam for Fire Protection in Aircraft Hangars," *FMRC Technical Report, Serial No. 21032,* Factory Mutual Research Corporation, Norwood, MA (1974).
47. L.M. Krasner, D.E. Breen, and P.M. Fitzgerald, "Fire Protection of Large Air Force Hangars," *AFWL-TR-75-119,* Factory Mutual Research Corporation, Norwood, MA (1975).
48. L.M. Krasner, "Closed-Head AFFF Sprinkler Systems for Aircraft Hangars," *FMRC S. I. 0C6N3.RG, RC 79-T-58,* Factory Mutual Research Corporation, Norwood, MA (1979).
49. J.L. Scheffey, S.M. Bryant, H.V. Pham, M.A. Harrison, J.P. Farley, F.W. Williams, and M.P. Hunstad, "Aircraft Carrier Hangar Bay Test Program–Test Series 3, AFFF System Testing and Manned Firefighting Scoping Tests," *NRL Letter Report, Serial No. 6180/0272,* Naval Research Laboratory, Washington, DC (2004).
50. A.C. Luers, M.A. Harrison, H.V. Pham, J.A. Lynch, J.L. Scheffey, F.W. Williams, J.P. Farley, and M.P. Hunstad, "Test Report for the Well Deck and Vehicle Stowage Area Vulnerability and Fire Model Validation Tests, Series 1—An Evaluation of Aqueous Film Forming Foam (AFFF) Suppression Systems for the Protection of LHA(R) Well Deck and Vehicle Stowage Areas," *NRL Letter Report, Serial No. 6180/0369,* Naval Research Laboratory, Washington, DC (2004).
51. M. Shipp, K. Annable, and C. Williams, "Assessment of the Fire Behaviour of Cargo Loaded on Ro-Ro Vehicle Decks in Relation to the Design Standards for Fire Suppression Systems," *BRE Fire and Security*

Report 227974, prepared for the Maritime and Coastguard Agency, Garston, UK (2006).
52. "Pop-Up-Type Floor-Mounted Foam Sprinklers for Aircraft Hangars," *Technical Record TR44/153/14 (L),* Department of Housing and Construction, Australia.
53. *China Lake CVA Fire Fighting Tests, Phase III,* unpublished data (1972).
54. J.L. Scheffey, "Flow, Pattern, and Fire Performance Characteristics of a Prototype Pop-Up Nozzle for Use on Aircraft Carrier Flight Decks," *Report 2429–17,* Hughes Associates, Inc., Columbia, MD (1985).
55. J.L. Scheffey and J.T. Leonard, "AFFF Protection for Weapons Staging Areas," *Fire Safety Journal,* 14, 14, pp. 47–63 (1988).
56. Department of the Navy, "General Specifications for Ships of the United States Navy, 1991 Edition," *NAVSEA S9AA0-AA-SPN-010/GEN-SPEC, Section 555,* Department of the Navy, Washington, DC (1991).
57. H.W. Carhart, J.T. Leonard, R.L. Darwin, R.E. Burns, J.T. Hughes, and E.J. Jablonski, "Aircraft Carrier Flight Deck Fire Fighting Tactics and Equipment Evaluation Tests," *NRL Memorandum Report 5952,* U.S. Naval Research Laboratory, Washington, DC (1987).
58. Rolf Jensen and Associates, "Comprehensive Aqueous Film Forming Foam Central Fire Suppression System Analysis/Report, B1-B Aircraft Hangars," *Technical Report A6406,* U.S. Air Force, Washington, DC (1989).
59. J.E. Gott, D.L. Lowe, K.A. Notarianni, and W. Davis, "Analysis of High Bay Hangar Facilities for Fire Detector Sensitivity and Placement," *NIST TN1423,* National Institute of Standards and Technology, Gaithersburg, MD (1997).
60. D.B. Szepezi, G.G. Back, J.L. Scheffey, F.W. Williams, and J.E. Gott, "Aircraft Hangar Fire Suppression System Evaluation—Intermediate Scale Studies," *NRL/MR/6180-99-8422,* Naval Research Laboratory, Washington, DC (1999).
61. G.G. Back, F.W. Williams, J.E. Gott, A.J. Parker, and J.L. Scheffey, "Aircraft Hangar Fire Protection System Evaluation Full Scale Study," *NRL Letter Report, Serial No. 6180/0620,* Naval Research Laboratory, Washington, DC (1998).
62. D.T. Gottuk, J.L. Scheffey, F.W. Williams, J.E. Gott, and R.J. Tabet, "Optical Fire Detection (OFD) for Military Aircraft Hangars: Final Report on OFD Performance to Fuel Spill Fires and Optical Stress," *NRL/MR/6180-00-8457,* Naval Research Laboratory, Washington, DC (2000).
63. J.L. Scheffey, A.J. Wakelin, J.E. Gott, R.J. Tabet, and F.W. Williams, "Aircraft Hangar Fire Suppression System Design Study," *NRL/MR 6180-00-8464,* Naval Research Laboratory, Washington, DC (2000).
64. A.J. Parker, G.G. Back, J.L. Scheffey, J.J. Schoenrock, J.P. Ouellette, F.W. Williams, J.E. Gott, and R.J. Tabet, "The Development of a Prototype Low-Level AFFF Nozzle System for U.S. Navy Aircraft Hangars," *NRL Letter Report, Serial No. 6180/0004,* Naval Research Laboratory, Washington, DC (2000).
65. G.P. Crampton, A.K. Kim, and J.K. Richardson, "A New Fire Suppression Technology," *NFPA Journal,* July/Aug. (1999).
66. G. Crampton and A. Kim, "The Comparison of the Fire Suppression Performance of Compressed-Air Foam with Foam Water Sprinklers on Free-Flowing Heptane Spill Fires," *Research Report RR-174,* National Research Council Canada, Ottawa, Canada (2004).
67. B.G. Vincent, H.C. Kung, and P. Stavrianidis, "Fire Protection for U.S. Army Helicopter Hangars," *FMRC J.I.OXON1.RA,* Factory Mutual Research Corporation, Norwood, MA (1993).
68. D.P. Nugent, *Directory of Fire Tests Involving Flammable and Combustible Liquids in Small Containers,* 3rd ed., Schirmer Engineering, Deerfield, IL (2004).
69. R.M. Newman, P.M. Fitzgerald, and J.R. Young, "Fire Protection of Drum Storage Using 'Light Water' Brand AFFF in a Closed-Head Sprinkler System," *FMRC Technical Report, Serial No. 22464, RC 75-T-16,* Factory Mutual Research Corporation, Norwood, MA (1975).
70. Southwest Research Institute, "Performance Testing of Automatic Sprinkler Systems in the Protection of Palletized, 55-Gal Storage of Heptane in Self-Relieving Style, Steel Drums," *SwRI Project No. 01-2016-001,* San Antonio, TX (1999).
71. J.R. Young and P.M. Fitzgerald, "The Feasibility of Using 'Light Water' Brand AFFF in a Closed-Head Sprinkler System for Protection against Flammable Liquid Spill Fires," *FMRC Technical Report RC 75-T-4, Serial No. 22352,* Factory Mutual Research Corporation, Norwood, MA (1975).
72. Schirmer Engineering Corporation, "International Foam-Water Sprinkler Research Project: Task 1—Literature Search," *Technical Report No. 10-90001-04-00,* National Fire Protection Research Foundation, Quincy, MA (1992).
73. J.P. Hill, "International Foam-Water Sprinkler Research Project: Task 3—Range Finding Tests," *Technical Report OTOR6.RR,* National Fire Protection Research Foundation, Quincy, MA (1991).
74. Underwriters Laboratories Inc., "International Foam-Water Sprinkler Research Project: Task 4—Palletized Storage Fire Tests 1 through 13," *Technical Report 91NK14873/NC987,* National Fire Protection Association, Quincy, MA (1992).
75. W.M. Carey, "International Foam-Water Sprinkler Research Project: Task 5—Rack Storage Fire Tests," *Technical Report,* National Fire Protection Research Foundation, Quincy, MA (1992).

76. Center for Chemical Process Safety, *Guidelines for Safe Warehousing of Chemicals,* American Institute of Chemical Engineers, New York, (1998).
77. Fire Fighting Foam Coalition, "Fact Sheet on AFFF Fire Fighting Agents," Arlington, VA, www.fffc.org/AFFF (undated).
78. A. Riecher, "The Day the Bubble Burst: 3M Abandons Class B AFFF Fire Fighting Foam," *Industrial Fire World* (May-June, 2000).
79. B. Williams, T. Murray, C. Butterworth, Z. Burger, R. Sheinson, J. Fleming, C. Whitehurst, and J. Farley, "Extinguishment and Burnback Tests of Fluorinated and Fluorine-free Firefighting Foams with and without Film Formation," Suppression, Detection and Signaling Research and Applications – A Technical Working Conference (SUPDET 2011), Orlando, FL (2011).
80. J.L. Scheffey, R.L. Darwin, W. Leach, S. Fallis, and F.W. Williams, "Performance Analysis of Foam Agents Required to Combat Liquid Fuel Hazards," *NRL/MR/6180-02-8608*, Naval Research Laboratory, Washington, DC (2002).
81. D.J. Rasbash, "The Extinction of Fire with Plain Water: A Review," *Proceedings from the First International Symposium on Fire Safety Science* (C.E. Grant and P.J. Pagni, eds.), National Institute of Standards and Technology, Gaithersburg, MD, pp. 1145–1163 (1986).
82. J.L. Scheffey and F.W. Williams, "The Extinguishment of Fires Using Low-Flow Water Hose Streams—Part II," *Fire Technology,* 27, 4, pp. 291–320 (1991).
83. American Public Health Association, *Standard Methods for the Examination of Water and Wastewater,* 18th ed., Washington, DC (1992).
84. C.A. Moody and J.A. Field, "Determination of Perfluorocarboxylates in Groundwater Impacted by Fire-Fighting Activity," *Environmental Science and Technology,* 33, 16, pp. 2800–2806 (1999).
85. Hughes Associates, Inc., "Development of Detection Method for Aqueous Film Forming Foam (AFFF)," Armstrong Laboratories Environics Directorate, Dayton, OH (1997).
86. National Environmental Health Laboratory, "Biological Treatment of Fire Fighting Foam Waste," *Report No. REHL(K) 67–14,* Kelly AFB, Texas (1967).
87. "Light Water Brand AFFF Waste Disposal Recommendations and Hazard Evaluation," *3M Product Environmental Data Sheet,* 3M Company, St. Paul, MN (1991).
88. M. Enten-Unal, S. Paranjape, G.C. Schafran, and F.W. Williams, "Evaluation of the Effects of AFFF Inputs to the VIP Biological Nutrient Removal Process and Pass-Through Toxicity," *NRL/MR/6180-98-8141,* Naval Research Laboratory, Washington, DC (1998).

Additional Readings

ASTM D1331, *Standard Test Methods for Surface and Interfacial Tension of Solutions of Surface-Active Agents*, American Society for Testing and Materials, Philadelphia, PA (2014).

ASTM E729, "Standard Practice for Conducting Acute Toxicity Tests with Fish, Macroinvertebrates, and Amphibians," American Society for Testing and Materials, Philadelphia, PA (2014).

FAA, "Aircraft Fire and Rescue Facilities and Extinguishing Agents," *FAA Advisory Circular 150/5210-6C*. Federal Aviation Administration, Washington, DC (1985).

ICAO, "Rescue and Firefighting," *Airport Services Guide*, 4th ed., International Civil Aviation Organization, Montréal, Québee (2014).

NFPA 11, *Standard for Low-, Medium-, and High-Expansion Foam*, National Fire Protection Association, Quincy, MA (2010).

NFPA 13, *Standard for the Installation of Sprinkler Systems*, National Fire Protection Association, Quincy, MA (2013).

NFPA 16, *Standard for the Installation of Foam-Water Sprinkler and Foam-Water Spray Systems*, National Fire Protection Association, Quincy, MA (2015).

NFPA 30, *Flammable and Combustible Liquids Code*, National Fire Protection Association, Quincy, MA (2015).

NFPA 72®, National Fire Alarm Code®, National Fire Protection Association, Quincy, MA (2013).

NFPA 403, *Standard for Aircraft Rescue and Fire-Fighting Services at Airports*, National Fire Protection Association, Quincy, MA (2014).

NFPA 409, *Standard on Aircraft Hangars*, National Fire Protection Association, Quincy, MA (2016).

NFPA 412, *Standard for Evaluating Aircraft Rescue and Fire-Fighting Foam Equipment*, National Fire Protection Association, Quincy, MA (2014).

UL 162, *Standard for Foam Equipment and Liquid Concentrates*, Underwriters Laboratories Inc., Northbrook, IL (1994, with revisions through 1999).

UL Fire Protection Equipment Directory. Underwriters Laboratories Inc., Northbrook, IL (2008).

U.S. Military Specification, MIL-F-24385F, Department of the Navy, Washington, DC (1992).

U.S. Government, "Federal Specification, Foam Liquid, Fire Extinguishing, Mechanical." *O-F-55B*, U.S. Government Protein Foam Specification, Washington, DC (1964).

Joseph L. Scheffey, P.E., is Vice President for Jensen Hughes, jscheffeye jensenhughes.com., Baltimore, Maryland.

Foam System Calculations

48

Hamid R. Bahadori

Introduction

Foam is a stable aggregation of gas-filled bubbles formed from a homogeneous mixture of water and foam concentrate in predetermined proportions. Foam fire protection is well suited for the control and extinguishment of specific types of fires especially those involving certain arrangements of flammable and combustible liquids. Foam is generally lighter than flammable/combustible liquids; therefore it floats on the liquid surface producing a layer which has multiple advantageous effects. These effects include vapor-sealing of the liquid, cooling of the liquid surface, and limitation of oxygen to the liquid surface.

In addition to flammable and combustible liquid fires, foam can be used to address other types of fire protection problems. Building and fire regulations and standards such as those promulgated by the NFPA address the application of foam systems for an array of fire protection concerns [1].

This chapter discusses the different types of foam systems and describes the calculation procedures to properly formulate the engineering design and analysis of these systems. Although not all applications of foam systems are discussed, the procedures put forth herein will provide a fundamental overview of the steps and considerations involved.

Fire Protection Objectives for Foam Systems

Foam systems can be used to achieve the following objectives with respect to fire safety. Note that foam system can be used as a means of fire prevention as well as fire protection. Also note that the objectives are specific to certain types of fuels and their physical arrangement. The specific objective for the applicable fire scenario will drive the overall design of the foam system.

Objective 1: Secure the production of ignitable vapors from the surface of flammable or combustible liquids.

Depending upon certain physical conditions such as temperature and pressure, flammable and combustible liquids emit vapors that may form ignitable atmospheres in close proximity to the liquid surface. The presence of an ignition source can result in a fast developing fire. The production of the ignitable vapors prior to the presence of any ignition source can be mitigated and controlled by generating a foam blanket that spreads over and covers the entire liquid surface. This objective can be accomplished for stored quantities of liquids as well as for confined liquid spills.

H.R. Bahadori (✉)
Vice President, Jensen Hughes, Inc., Baltimore, MD, USA

M.J. Hurley (ed.), *SFPE Handbook of Fire Protection Engineering*,
DOI 10.1007/978-1-4939-2565-0_48, © Society of Fire Protection Engineers 2016

Objective 2: Control and extinguish fires involving localized flammable and combustible liquid fuel spills inside buildings.

Flammable and combustible liquids can be stored inside buildings in drums and other types of containers such as intermediate bulk containers (IBC), subject to the limitations of the applicable codes. These stored liquids can also be used in association with other building operations such as manufacturing processes (dip tanks), industrial machinery, heating equipment, and testing activities. The rupture of a container, feed line or hydraulic line can result in the formation of a liquid pool that can release ignitable vapors. The ignition of these vapors will result in localized fires that can be controlled or extinguished by the application of foam.

Objective 3: Extinguish fires in outdoor atmospheric flammable and combustible liquid storage tanks.

Foam agent fire protection has a long track record of successfully extinguishing fires in outdoor vertical atmospheric storage tanks, and the diked areas in the vicinity of tanks to control fuel spills. This type of protection still represents one of the most common uses of foam agents. Foam agent fire protection has been successfully used to extinguish flammable and combustible liquid fires in atmospheric storage tanks with diameters up to 200 ft (61 m).

Objective 4: Extinguish fires in outdoor and indoor processing areas involving flammable liquids

A wide range of industrial processes machines utilize flammable and combustible liquids. In most processing plants, these liquids pass through pipelines and are captured in holding tanks. Foam agents, properly selected for the hazard, are suitable for controlling and extinguishing fires in process equipment by either applying the foam to the liquid fuel surface or filling the entire space containing the hazard with foam. However, foam agents are not generally suitable for protection of burning ignitable liquids flowing down vertical surfaces, or fires where the ignitable liquid is discharging from an orifice under pressure.

Objective 5: Prevent, control, and extinguish fires for fuels other than flammable and combustible liquids.

Foam systems have been found to be effective for fuels that are not in a liquid state such as rubber tire storage and rack storage of plastic commodities.

Basic Types of Foam System Protection

Foam fire protection systems can generally be classified into one of five categories. Each category is briefly described below. Conditions exist where it may be appropriate to use more than one category of foam protection for a given fire problem.

Fixed Foam Systems

These systems are complete installations piped from a central foam station, discharging through fixed delivery outlets to the hazard to be protected. Any required pumping equipment is permanently installed. For example, a fixed system for a vertical atmospheric cone roof storage tank would include the following permanently installed equipment: water supply lines, foam proportioning equipment, a foam liquid storage tank, foam concentrate and solution lines, control valves, riser pipes, and one or more topside foam chambers. Other equipment may be added based on the complexity of the problem and associated hydraulic conditions. Several calculation examples of fixed foam systems will be described within this chapter.

Semifixed Foam Systems

The semifixed foam system concept includes a system where a portion of the total system is permanently installed and the remainder of the system is provided by portable elements. In general, this includes a fire hazard equipped with fixed discharge outlets connected to piping that terminates at a safe distance. The fixed piping installation may or may not include a foam

maker. Necessary foam producing materials are transported to the scene after the incident begins and are connected to the fixed piping.

Mobile Systems

Mobile systems basically consist of a unit on wheels that transports all of the required equipment and foam liquid necessary for making finished foam. This concept includes any foam producing unit which is mounted on wheels, and which may be self-propelled or towed by a vehicle. These units may be connected to an available water supply or may use a premixed foam solution. The original concept of a mobile foam system was called a "foam house on wheels," a mobile piece of fire apparatus with a UL-rated fire pump, an integral part of the pumping network, a foam liquid tank, and fire hose. Essentially this unit can double as a structural fire suppression unit. NFPA 1901, Standard for Automotive Fire Apparatus, covers the specifications and performance criteria for mobile foam fire apparatus [1].

Portable Systems

Portable systems represent a rather economical approach to providing basic foam fire protection for small hazards. This classification considers that the foam producing equipment and materials, including the foam liquid, the proportion device(s), the discharge nozzle, the hose, and other required appliances, are transported by hand from a storage location to the incident scene. While portable systems are simple to operate, they are limited by their foam discharge rate capability; they may also be labor intensive to maintain a continuous foam supply over the required duration of discharge. Foam equipment manufacturers can provide technical information on a range of portable equipment.

Compressed Air Foam Systems

This type of foam fire protection injects pressurized air to the system to generate foam prior to the discharge device. These types of systems are limited to protection of flammable and combustible liquids and are generally not permitted for fires involving chemicals with oxidizing agents, energized unenclosed electrical equipment, water-reactive metals, hazardous water-reactive materials, or liquefied flammable gases.

Protection of Incipient Spills and Related Hazards

Portable fire extinguishers provide one method of protection for small flammable liquid storage hazards, fuel transfer hazards, and incipient spill fires. Although once classified and listed by Underwriters Laboratories (UL), chemical foam extinguishers are now considered obsolete and should not be utilized. The AFFF extinguisher closely resembles the stored pressure water extinguisher in appearance except for the special type of nozzle. NFPA 10, Standard for Portable Fire Extinguishers, should be consulted concerning the selection and placement of portable fire extinguishers [1].

Low-Expansion Foam Systems

Low expansion foam systems are well suited for protection of interior flammable/combustible liquid hazards, outdoor storage tank areas, truck loading racks, diked and non-diked spill areas. These systems may include aqueous film-forming foam (AFFF) agents, alcohol-resistant (AR) type agents, fluoroprotein (FP) agents, and film-forming fluoroprotein (FFFP) agents. This section presents several examples of design calculations.

Protection for Fixed Roof Atmospheric Storage Tanks

Fixed roof atmospheric storage tanks for the storage of flammable/combustible liquids can be protected by fire fighting foam. Several techniques are available for correctly applying foam to a fixed roof tank fire. Each technique should be carefully considered with reference to the size of the storage tank, the flammable or combustible liquid being stored in a given tank, and the foam agent classification that is suitable for the hazard. Some fundamental concepts associated with the proper protection for fixed roof atmospheric storage tanks are discussed below. Each individual topic is further developed through example design problems on cone roof atmospheric storage tanks.

Foam Monitors

One or more foam monitors may be positioned around the periphery of a fixed roof tank to project foam over the tank shell and onto the surface of a burning liquid. These monitors, or cannons, provide a large foam stream and can be fixed in position or moveable. This technique has been successfully used on numerous fires. However, NFPA 11 clearly indicates that foam monitors may not be considered the primary means of protection for fixed roof tanks when the tank is more than 60 ft in diameter. This indication represents a severe limitation on the recommended use of foam monitors for the protection of fixed roof tanks.

If foam monitors are to be utilized, the minimum foam application rate to the surface of the liquid is generally specified at 0.16 gpm/ft^2 (6.5 L/min-m^2). However, the applicable design regulations need to be consulted in this regard. The minimum application rate may need to be increased to account for flammable liquids with lower boiling points (i.e., less than 100 °F), environmental conditions such as wind, or other factors that may lead to potential foam loss. Durations of application are dependent on the fuel and generally range between 50 and 65 min.

Foam Handlines

Similar to the concept of providing protection with monitors, foam handlines may be positioned around the periphery of a fixed roof tank to project foam over the tank shell and onto the surface of a burning liquid. Foam handlines generally have a flow range from 50 gpm (190 lpm) to less than 300 gpm (1136 lpm) and are only suitable for possible protection of fixed roof tanks with a diameter of less than 30 ft (9 m) and a height not greater than 20 ft (6 m). The selection of foam handline nozzles must be carefully considered to provide the appropriate total discharge for the flammable liquid hazard to be protected. Personnel protection also needs to be sufficiently considered when this option as the primary means of protection.

Foam handlines are very important for providing supplemental fire protection. Handlines delivering a minimum of 50 gpm (190 lpm) are very useful for extinguishing small spill fires and dike fires in the vicinity of a storage tank. The number of such supplemental foam hose streams is dependent on the diameter of the largest storage tank in the facility to be protected. Again the applicable design standards and regulations needs to be consulted.

Surface Application of Foam

One common and acceptable method of applying foam to the flammable/combustible liquid surface of a single roof storage tank is through fixed discharge outlets installed on the tank shell. Two distinct types of foam discharge outlets are available based on the hazard and the type of concentrate used. Each type of device may be distinguished as follows:

Type I Outlets These approved discharge outlets deliver foam gently onto the liquid surface without submergence of the foam below the flammable liquid surface and agitation of the surface. This type of device was originally intended to apply special alcohol resistant foams to polar solvent fuels. Today, Type I discharge outlets are generally considered obsolete.

Type II Outlets These approved discharge outlets do not necessarily deliver foam gently onto the liquid surface. However, they do lessen the submergence of the foam or agitation of the surface. An air foam chamber with a Type II outlet may be attached to the top of the tank shell above the level of the liquid within. The chamber is attached to the tank shell so that the displacement of the tank roof will not subject the chamber to damage. The discharge outlet is positioned on the inside of the tank to permit discharge of the foam down the inside of the tank wall surface onto the flammable liquid surface. The number of Type II foam chambers for a given size (diameter) storage tank is presented in design standards such as NFPA 11. Discharge capacity of the chambers is calculated based on the required application rate prescribed by the applicable design, and the foam chamber manufacturer.

Procedure for Determining Foam Supply for Atmospheric Storage Tanks Protected with a Surface Application Low-Expansion System

Through a specific example, this section addresses the design and associated hydraulic calculations for surface application low-expansion foam systems protecting atmospheric storage tanks. The example addresses the topside application of foam using foam chambers for a single flammable liquid storage tank, and presents methods and techniques for computing the foam agent requirements, system hardware requirements, and the necessary hydraulic calculations to properly deliver the required rate of foam discharge onto the liquid fuel surface.

Example 1 A single fixed roof outside storage tank storing gasoline is depicted in Fig. 48.1. The tank is to be protected by a fixed foam system for the purpose of extinguishing a fire that starts on the liquid surface in the tank. A topside foam chamber arrangement is to be used. A municipal water main is the only supply of water for the foam system. The corresponding water supply curve for the municipal main is illustrated in Fig. 48.2. A foam

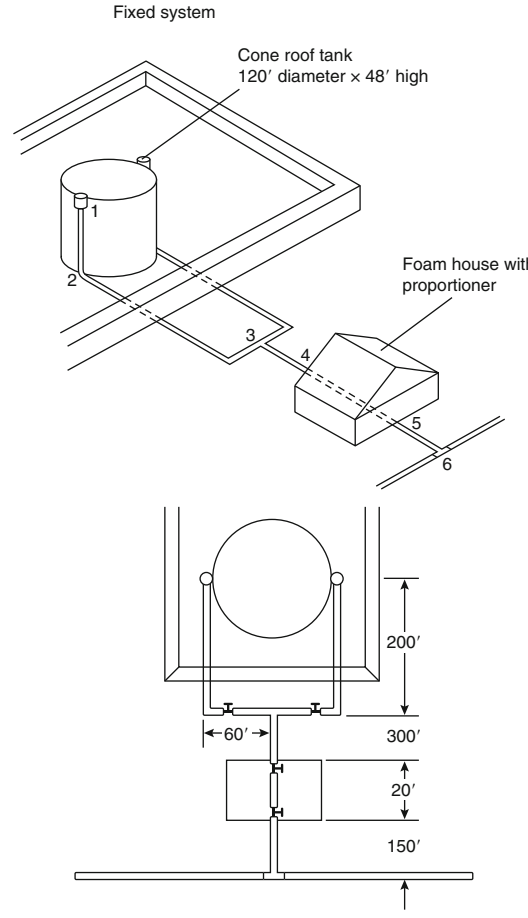

Fig. 48.1 Single storage tank with fixed foam system protection. The numbers 1 through 6 in the top portion of the drawing represent the reference points for hydraulic calculations in Example 1

system design and complete set of hydraulic calculations are to be prepared for this installation. Figure 48.3 provides a summary of the information determined in Steps 1–13 below.

Solution A systematic step-by-step process follows. Reference is made to discharge criteria presented in NFPA 11. Information on specific system components is documented in the referenced problem job sheet (Fig. 48.3) and the associated hydraulic calculation sheet (Fig. 48.4). In addition to the physical layout of the tank, information is needed on the specific type of fuel involved.

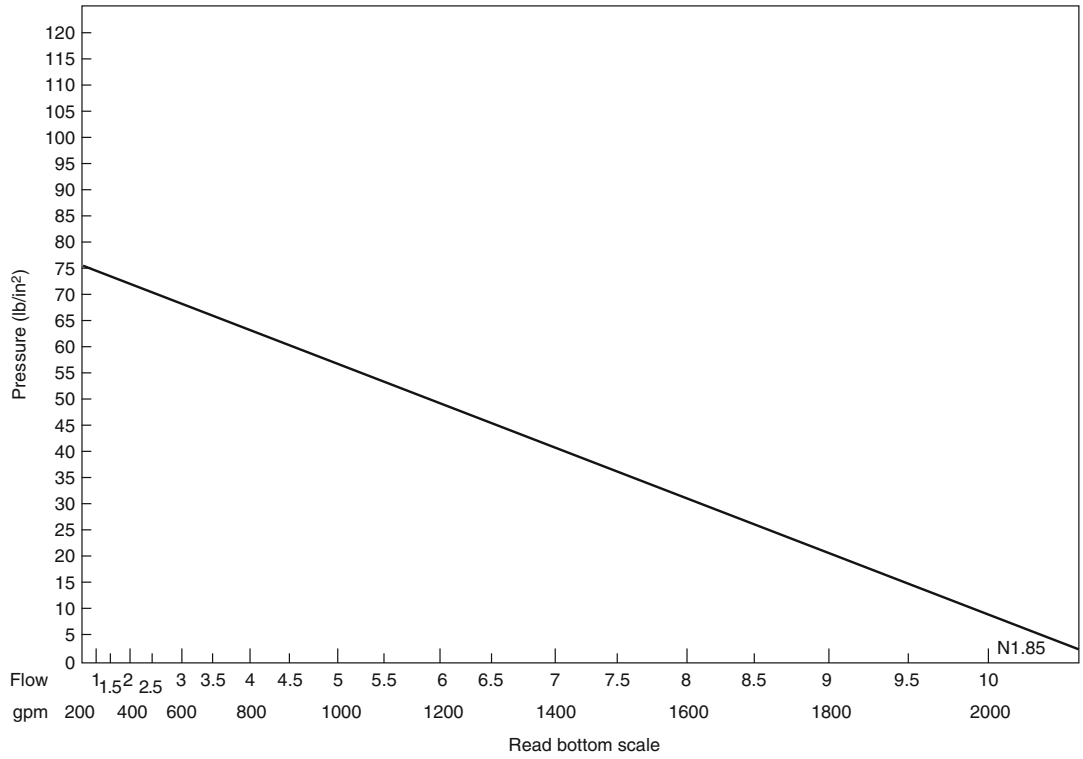

Fig. 48.2 Water supply curve for fixed foam system in Examples 1 and 2

Step 1: Installation identification.

Refer to Fig. 48.1. The evaluation must consider the site conditions of the storage tank and surrounding areas. In this example, a single vertical atmospheric storage tank is positioned in an area surrounded by a dike wall. The tank is to be protected by a fixed foam fire protection system and connected to the domestic water supply.

Step 2: Hazard classification and description.

The specific hazard and storage arrangement need to be identified. In this example, a 120-ft diameter outdoor fixed roof tank is storing a flammable liquid.

Step 3: Flammable/combustible liquid identification.

The characteristics of the stored liquid must be determined in order to select the appropriate type of foam concentrate to be used. In this example, gasoline is stored and has a specific gravity of 0.72. The fire protection engineer needs to be certain of the specific types of liquids to be stored in the tank as some facilities rotate the types of liquids stored in a given tank.

Step 4: Type of protection.

Based on the storage arrangement and contents, an appropriate protection concept must be determined. Fixed protection systems using Type II discharge outlets (foam chambers) will be used. As previously noted Type I outlets are considered obsolete.

Step 5: Surface area of liquid to be protected.

Calculate the liquid surface area to be protected. For the cylindrical storage tank, the area of protection will be equivalent to the area of the top surface:

$$\text{Area} = 1/4\pi d^2$$

$$\text{Area} = 1/4\pi(120)^2 = 11,310\,\text{ft}^2$$

FOAM SYSTEM JOB WORK SHEET

Sheet: 1 of 1

Designer: Staff Date:

Installation identification: Ourville Oil Company

Hazard classification: Flammable liquid atmospheric storage tank

Type of protection: Fixed protection system

Hazard description: 120-ft-diameter outdoor cone roof flammable liquid storage tank

Flammable or combustible liquid area to be protected: 11,310 ft^2

Flammable or combustible liquid identification: Gasoline — SG 0.72

Foam application method: Type II—fixed chambers

Description, number, and placement of foam application devices: 2—Chambers equally spaced

Foam agent selected: Fluoroprotein—3%

Foam solution application rate: 0.1 gpm per ft^2 or 1131 gpm

Foam concentration rate: 34 gpm

Water application rate: 1098 gpm

Duration of discharge: 55 min

Gallons of foam required: 1870 gallons

Gallons of water required: 60,390 gallons

Water supply information: See Figure 4-5.2

Special foam design considerations:

Fig. 48.3 Foam system job worksheet for Example 1

Step 6: Foam agent selected.

Based on the liquid being stored, an appropriate foam concentrate must be selected. Specific manufacturers will need to be consulted to determine the most appropriate foam concentrate for the hazard.

For this example, a 3 % fluoroprotein foam will be selected for the defined hazard. Note that the type of foam agent selected for a particular design will affect other variables and considerations in the foam system design.

Step 7: Description, number, and placement of foam application devices.

Several factors need to be simultaneously considered in developing this step. The selection of foam application devices will be dependent on the foam agent selected. In addition, the flow and pressure characteristics of the discharge device will be a factor or present options for the system design. Manufacturer's literature and the listing evaluation data of foam equipment should be consulted on this matter.

HYDRAULIC CALCULATIONS

Subject: Example problem 1 Job no.:

Sheet no.: of

By: Date:

Chkd by: Date:

Application rate: 0.1 gpm per sq ft Area: 11,130 ft²

Minimum solution rate: 1131 gpm Actual solution rate: 1132 gpm

Foam maker pressure and rate: 50 psi—566 gpm Foam system: Chamber type 2

Water data: Ref. drawing: Figure 4-5.1

Foam maker type and location	Added gpm	Total gpm	Pipe size (in.)*	Pipe & equivalent fitting lgth. (ft)**	Friction		Static psi	Proportioner psi	Req'd pres gpm
					psi/ft C=100	Total psi			
Starting point: 1			Elevation: 48 ft				Pressure at foam maker: 50 psi		
1	566	566							50
1–2		566	5.047	48'+(1E)8.6'=56.6'	0.0420	2.4	20.8		73.2
2–3		566	5.047	260'+(1GV)2'=(1T)25'					—
(2–3)				Σ = 287'	0.0420	12.1	—		85.3
3–4	566	1132	8.071	300'+(1GV)2'=302'	0.154	4.7	—		90.0
4–5		1132	8.071	18'+(1GV)2'=20'	0.154	0.3		4.0	94.3
5–6		#1098	8.071	150'=(1T)35'=185'	0.145	2.7			97.0
Σ at 6		1098							97.0

\# Water only

* "X" indicates extra hvy.—std. wt. otherwise

** See sheet for tabulation of pipe and fittings

Fig. 48.4 Hydraulic calculation work sheet

As previously noted, foam chambers will be used and specific characteristics are associated with each type of chamber, which must be obtained from the manufacturer. For this example, the selected foam chamber is identified as ABC chamber with an operating pressure range of 40–80 psi and a flow range of 300–700 gpm.

Foam standards and manufacturer's design guides provide details on the number of foam chambers need. Referencing NFPA 11,

Table 5.2.5.2.1, a minimum of two foam chambers for a 120-ft diameter tank are required. Additional foam chambers may be used based on hydraulic considerations, or equipment costs. Individual manufacturers of foam equipment must be consulted on these options.

Placement of foam makers should consider equal spacing around the upper tank perimeter to ensure even distribution of foam. A constant and uniform flow and pressure should also be maintained during system discharge.

Step 8: Foam solution application rate.

Foam solution application rates for storage tanks containing liquid hydrocarbons are generally provided in foam standards and manufacturer's design guides. Referencing NFPA 11, Table 5.2.5.2.2, for this example an application rate of at least 0.1 gpm/ft^2 over the liquid surface area is to be provided. Specific types of foam equipment may require different application rates. Also, flammable and combustible liquids not classified as hydrocarbons may require different application rates. Appropriate references should be consulted in this regard.

The total foam solution discharge rate for Example 1 is calculated as follows:

$$\begin{aligned}\text{Rate (g pm)} &= 0.1\ \text{g pm/ft}^2 \times 11,310\ \text{ft}^2 \\ &= 1,131\ \text{g pm}\end{aligned}$$

The total discharge rate can be divided equally between the two required foam chambers. It is appropriate to specify a total foam solution discharge rate of 1132 gpm, with 566 gpm per each of the two foam chambers.

Step 9: Foam concentrate supply rate.

The foam concentrate supply rate is based on the foam agent proportioning rate. As noted in the example, a 3 % fluoroprotein foam has been selected (Step 6). In other words, 3 % of the calculated foam solution rate is the foam concentrate supply rate. This rate may be determined as follows:

$$\begin{aligned}\text{Foam concentrate rate} &= 0.03 \times 1,132\ \text{g pm} \\ &= 34\ \text{g pm}\end{aligned}$$

Therefore, a continuous supply of foam concentrate must be available at a rate of 34 gpm for the required duration of discharge (Step 11).

Step 10: Water supply rate.

The water supply rate is the foam solution rate minus the foam concentrate supply rate. The necessary water supply rate can be calculated as follows:

$$\begin{aligned}\text{Water supply rate} &= 1,132\ \text{g pm} - 34\ \text{g pm} \\ &= 1,098\ \text{g pm}\end{aligned}$$

The water supply rate can also be determined as 97 % of the foam solution rate when using a 3 % foam concentrate.

Step 11: Duration of discharge.

Foam standards and manufacturer's design guides generally specify the duration of foam discharge. Duration of discharge is dependent on the classification of the ignitable liquid stored, and the type of discharge outlet used. Gasoline has a flash point below 100 °F (37.8 °C). Referring to NFPA 11, Table 5.2.5.2.2) a minimum discharge duration of 55 min is required to control and extinguish a fire in a fixed roof storage tank containing gasoline using Type II foam chambers.

Step 12: Quantity of foam required.

The necessary foam supply for any given application should properly consider a primary supply and the availability of a reserve supply. The primary supply is calculated by multiplying the foam concentrate supply rate by the duration of discharge as follows:

$$\begin{aligned}\text{Foam agent required} &= 34\ \text{g pm} \times 55\ \text{min} \\ &= 1,870\ \text{gal}\end{aligned}$$

A risk analysis or the authority having jurisdiction may require that an equal quantity of foam be placed in reserve on site if there is a credible likelihood of a second fire occurring before the foam supply can be replenished.

Step 13: Total quantity of water required.

The basic procedure follows the concept presented in Step 12. The water requirement is the product of the water supply rate multiplied by the duration of discharge. In this case:

$$\text{Minimum Volume of water required} = 1,098\,\text{g pm} \times 55\,\text{min} = 60,390\,\text{gal}$$

Fixed foam protection systems for atmospheric storage tanks require large volumes of water. The total quantity of water must be available at the site to assure foam delivery over the entire required duration.

Step 14: Pipe size determination.

System piping can be sized to minimize friction loss between the supply and the system discharge outlets (foam chambers). Pipe can also be sized on the basis of a targeted mean velocity flow in a given section of pipe. A flow velocity of 10 ft per second is often used in the absence of other specific criteria for the determination of system piping. Hydraulic calculations need to be completed to verify pipe sizes and proper system discharge. Hydraulic calculations for the system in Example 1 are completed later in this chapter.

In addition to system piping flowing water and foam solution, piping for delivery of foam concentrate into the system also needs to be considered. Foam concentrates do not behave as Newtonian fluids, e.g. water, when flowing due primarily to their viscosity and resulting nonproportional viscous stresses. Therefore the calculation approach for foam concentrates differs from that typically used for water and foam solution, which is usually about 97–93 % water.

Step 15: Valve selection and location

Valves need to be listed for the purpose. The laterals to each foam discharge outlet on fixed roof tanks are to be separately valved outside of the dike installation. Valves are to be located where the laterals branch from the common supply line. Valves are to be located a minimum distance of at least one tank diameter from the tank. The water line to each proportioner inlet should be separated by a valve. Appropriate valves locations for the system in Example 1 are shown in Fig. 48.1.

Step 16: Foam proportioner selection.

Several different types of foam proportioners are available from equipment manufacturers. It is important to select foam proportioning equipment that meets the following requirements:

- Proper and uniform proportioning over the range of expected flows and system pressures.
- Minimum or acceptable friction loss across the proportioning device.
- Suitability for the foam concentrate selected.
- Capability of overcoming any back pressures such as might be associated with system elevation changes or subsurface foam applications.

Step 17: Pump Considerations.

To generate the necessary system flow rate and discharge, the pressure in the water supply might need to be augmented by the use of a pump. The need for a pump will be determined though hydraulic analysis. Where a pump is required, consideration must be given to the pump capacity, the pressure profile, the pump horsepower requirement, and the pump intake-discharge positions with respect to the total installation of pipe. Any pump selected for the foam system needs to be listed for the intended purpose. A foam concentrate pump might also be needed to inject the proper concentration of foam into the system. These pumps are usually different from the centrifugal pumps used for water-based system. Positive displacement pumps are usually employed for foam concentrate injection.

Hydraulic Analysis of a Surface Application Foam System Protecting a Flammable Liquids Storage Tank

The following outlines the procedure involved in calculating the hydraulic demand for a surface application foam system. The reader is assumed to posses a fundamental understanding of fire protection water supply analysis, and hydraulic calculations employing the Hazen-Williams

approach. The system in Example 1 as depicted in Fig. 48.1 is used in outlining the procedure. The design parameters and associated calculations are presented in sequential steps, which are summarized on a hydraulic calculation sheet as shown in Fig. 48.4 with reference points identified in Fig. 48.1.

Step 1: Starting point.

The design objective is to provide each of the two foam chambers in Example 1 with the required pressure to discharge the calculated quantity of foam solution. The stated problem requires each foam chamber to discharge 566 gpm of foam solution at 50 psi. An orifice plate is supplied by the foam equipment manufacturer to ensure the correct discharge at the design pressure of 50 psi. The design pressure is a function of the range of pressures that can be used with a specific manufacturer's foam chamber.

Step 2: Determination of supply riser size.

The vertical pipe supplying the foam chambers (reference points 1–2) is sized based on a maximum flow velocity of 10 ft per second. The pipe size is determined as follows:

Formula:

$$Velocity = \frac{0.40852 \times gpm}{d^2}$$

(a) Solve for d using a velocity of 10 ft per second

(b) $10 fps = \frac{0.4085 \times gpm}{d^2}$

(c) $d^2 = 23.12$ in.

(d) $d = 4.8$ in.

(e) A minimum 5-in. pipe is required.

Step 3: Determine friction loss between reference points 1 (top of tank) and 2 (bottom of tank).

1. Friction loss, FL, is determined by the Hazen-Williams formula

$$FL = \frac{4.52 \times Q^{1.85}}{C^{1.85} \times d^{4.87}}$$

Where
Q = 566 gpm
C = 100
d = 5.047 (internal diameter of 5-in Schedule 40 steel pipe)

$$FL = 0.0420 \text{ psi/ft}$$

2. Note: All friction losses and elevation losses are summed in the required pressure column.
3. The elevation loss, H_L, for 48 ft of elevation difference between reference points is computed as follows:

$$H_L = 0.433 \text{ psi/ft} \times 48 \text{ ft} = 20.8 \text{ psi}$$

4. The pipe section includes one standard elbow at reference point 2. For hydraulic calculations, fittings are treated as equivalent feet of pipe in accordance with NFPA13, Standard for the Installation of Sprinkler Systems [1].

Step 4: Determine friction loss between reference point 2 (bottom of tank) and reference point 3.

1. The flow is constant at 566 gpm so the pipe size remains the same at 5 in.
2. Pipe fittings include a gate valve outside the dike area and a standard tee at reference point 3.

Step 5: Determine friction loss between reference point 3 and reference point 4 (foam house).

1. The total foam solution flow (1132 gpm) is supplied by line 2–3.
2. Determine the pipe size based on a maximum flow velocity of 10 ft/s.

$$Velocity = \frac{0.40852 \times gpm}{d^2}$$

$$10 fps = \frac{0.4085 \times 1132 gpm}{d^2}$$

$$d = 6.8 \text{ in.}$$

3. An 8-in. pipe is recommended between the foam house and reference point 3.

4. The friction loss in the stated line includes the linear distance plus the gate valve.
5. It should be observed that the required pressure at the discharge side of the foam house is 90.0 psi.

Step 6: Determine the friction losses in the foam house piping between reference points 4 and 5.

1. The foam house will contain the proportioning equipment. The proportioner selected for this problem has a friction loss of 4 psi at a solution flow rate of 1132 gpm. This information would normally be provided by the manufacturer. The ratio controller takes up a lineal distance of 2 ft leaving 18 ft of straight run pipe within the foam house.
2. The calculations provided do not include provisions for a pump within the foam house.

Step 7: Determine the friction loss from the foam house to the water supply between reference points 5 and 6.

1. The flow rate in line 5–6 is 1098 gpm (water supply rate). Note the change in friction loss.
2. An 8-in. main is used to connect the water supply to the foam house.

Step 8: Summary.

1. The water demand requirement at reference point 6 is 1098 gpm at 97.0 psi.
2. The hydraulic demand has been calculated to provide a foam solution flow of 566 gpm at 50 psi for each designated foam chamber.
3. The water supply curve referenced as Fig. 48.2 shows a flow of 1098 gpm available at 53 psi. This water supply is not sufficient for the foam system. Therefore, a pump is required to boost the pressure from 50 psi (loss of pressure from reference points 6–5 is approximately 3 psi) to 97 psi or approximately 47 psi. A pump can be selected for this specific application.

Subsurface Application of Foam

Another method of applying foam to a fixed roof storage tank is through subsurface injection, usually near the base of the tank but above the level of any water that has accumulated in the bottom in the tank, recalling that many ignitable liquids are lighter than and not miscible with water. The subsurface application technique involves injecting expanded foam under controlled velocity conditions. The buoyancy of the foam allows the foam to slowly rise to the ignitable liquid surface and spread across the surface to effect fire control and then provide extinguishment similar to a surface application.

The subsurface application technique requires design considerations with respect to foam equipment and hydraulic calculations that differ from those of surface applications. There are three important conditions to consider in subsurface application of foam in fixed and semifixed systems.

1. Subsurface foam application is not considered suitable for the protection of Class IA hydrocarbon liquids.
2. Subsurface foam application is not currently suitable for polar solvents.
3. Subsurface and semisubsurface injection systems are not recommended for open top or covered floating roof tanks.

Procedure for Determining Foam Supply for Atmospheric Storage Tanks Protected with a Subsurface Application Low-Expansion System

Through a specific example, this section addresses the design and associated hydraulic calculations for subsurface application low-expansion foam systems protecting atmospheric storage tanks. The example presents methods and techniques for computing the foam agent requirements, system hardware requirements, and the necessary hydraulic calculations to properly deliver the required rate of foam discharge into the fuel tank. The following principles need to be understood in the design of subsurface application foam systems:

1. Foam solution is expanded outside of the dike area by a “high back pressure” foam maker.

A typical foam expansion of 4:1 is achieved at the foam maker.

2. The expanded foam flows through a carefully designed pipeline from the foam maker to an opening in the tank shell just above the water level at the bottom of the tank. In accordance with design standards such as NFPA 11, the foam velocity at the point of discharge into the tank contents is not to exceed 10 ft/s for Class IB liquids and 20 ft/s for other type liquids. An excessive input velocity to the tank can cause the foam to be saturated with fuel as it rises to the liquid surface. This phenomenon is referred to as fuel pickup.
3. Foam entering the product rises to the fuel surface by natural buoyancy.

Example 2 This example considers a 120-ft diameter storage tank storing gasoline that is to be protected with a fixed subsurface application foam system as illustrated in Fig. 48.5. A municipal water main is the only supply of water for the foam system. The water supply information shown in Fig. 48.2 also applies to this example. A foam system design and complete set of hydraulic calculations are to be prepared.

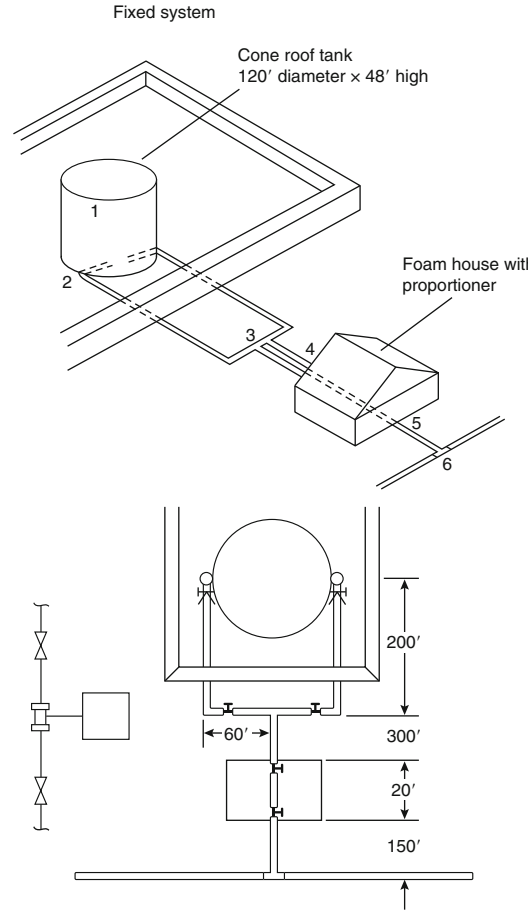

Fig. 48.5 Subsurface application foam system with reference points used in Example 2

Solution A systematic step-by-step solution follows for the design and hydraulic assessment of the associated foam system. Reference is made to provisions documented in NFPA 11 as this standard is often referenced by applicable fire regulations. Relevant information to be determined has been transferred to the work sheet in Fig. 48.6, and the associated hydraulic calculation sheet in Fig. 48.7.

In addition to the physical layout of the tank and the foam system, information about the fuel (hazard) is required as will be discussed below. Some of the steps from Example 1 on surface application are also applicable here and are identified as such.

Step 1: Installation identification.

Referring to Fig. 48.5 the site conditions of the storage tank and surrounding area are to be considered. In this example, a single vertical atmospheric storage tank is positioned in an area surrounded by a dike wall. The tank is to be protected by a fixed subsurface injection foam fire protection system supplied by a municipal water main.

Step 2: Hazard classification and description.

The specific hazard and storage arrangement need to be identified. In this example, a 120-ft diameter outdoor cone roof tank is storing gasoline, a flammable liquid.

Step 3: Flammable/combustible liquid identification.

The characteristics of the stored liquid must be determined in order to select the appropriate type of foam concentrate to be used. Again, gasoline with a specific gravity of 0.72 is stored in the tank.

FOAM SYSTEM JOB WORK SHEET

Sheet: 1 of 1

Designer: Staff Date:

Installation identification: Ourville Oil Company

Hazard classification: Flammable liquid storage tank

Type of protection: Subsurface application to fixed roof storage tank

Hazard description: 120-ft-diameter outdoor cone roof flammable liquid storage tank

Flammable or combustible liquid area to be protected: 11,310 ft^2

Flammable or combustible liquid identification: Gasoline — SG 0.72

Foam application method: Subsurface application to a liquid hydrocarbon

Description, number, and placement of foam application devices: Two subsurface injection points positioned equal and opposite on the tank shell. A PHB foam maker is used.

Foam agent selected: 3%

Foam solution application rate: 1132 gpm

Foam concentration rate: 34 gpm

Water application rate: 1098 gpm

Duration of discharge: 55 min

Gallons of foam required: 1870

Gallons of water required: 60,390

Water supply information: See Figure 4-5.2

Special foam design considerations: Foam injection piping to be sized for a maximum fluid velocity of 10 fps

Fig. 48.6 Foam system job worksheet for Example 2

Step 4: Type of protection.

Based on the hazard and the liquid, an appropriate protection scheme must be determined. Fixed protection systems using subsurface application will be used.

Step 5: Surface area of ignitable liquid in tank to be determined.

11,310 ft^2 (See Example 1 for calculation)

Step 6: Foam agent selected.

Based on the liquid being stored and the subsurface injection method, an appropriate foam must be selected. Specific manufacturers will need to be consulted to determine the most appropriate foam for the hazard.

As with the surface application example, a 3 % fluoroprotein foam is selected for the defined hazard. Note that the type of foam agent selected

HYDRAULIC CALCULATIONS

Subject: Example problem 2 Job no.:

Sheet no.: of

By: Date:

Chkd by: Date:

Application rate: 0.1 gpm per sq ft Area: 11,130 sq ft

Minimum solution rate: 1132 gpm Actual solution rate: 1132

Foam maker pressure and rate: PHB—159 psi—566 gpm Foam system: Subsurface

Water data: Figure 4-5.2 Ref. drawing:

Foam maker type and location	Added gpm	Total gpm	Pipe size (in.)*	Pipe & equivalent fitting lgth. (ft)**	Friction		Static psi	Proportioner psi	Req'd pres psi
					psi/ft C=100	Total psi			
Starting point: 1		Elevation: 48 ft					Pressure at foam maker: 50 psi		
1		2264	10"				15		15
1–2		2264	10"	20	0.20	0.4			15
2–3				560+1CV(55)1GV(5)	0.40	24.8			40
				620					
Σ3									40

Note: The demand pressure at 3 is less than the allowable pressure of 64.0 psi

* "X" indicates extra hvy.—std. wt. otherwise

** See sheet for tabulation of pipe and fittings

Fig. 48.7 Hydraulic calculations for Example 2

for a particular design problem may affect other factors in the foam system design.

Step 7: Description, number, and placement of foam application devices.

Several equipment design factors must be considered simultaneously in this step. Again, reference must be made to a specific foam manufacturer's equipment or a comparative analysis between two or more manufacturers of suitable equipment should be conducted. The manufacturer's literature and the listing information about the foam equipment needs to be consulted in this regard.

Gasoline is a Class IB liquid, and therefore the injection velocity of the expanded foam into the product tank should not exceed 10 ft/s per NFPA 11. This does not mean that the velocity of foam between the foam maker and the injection point has to be controlled to a maximum of 10 ft/s. Rather, the foam velocity at the physical point of entry into the tank is the key consideration.

Remember that the foam is expanded at the entry point into the fuel, i.e. gasoline. Special flow curves must be examined to determine velocity characteristics with expanded foam. These curves are available in the annex of NFPA 11. Manufacturer's literature can also referenced. Figure A.5.2.6.2(a) from NFPA 11 is consulted for this example [1].

Table 5.2.6.2.8 of NFPA 11 indicates that two discharge outlets must be provided for a 120-ft-diameter tank storing gasoline. The foam solution rate for each outlet is given in Step 8 of this example and is equal to the calculations for the surface application example: 566 gpm per outlet. However, the foam is expanded at the high back pressure foam maker using a ratio of 4:1. The expanded foam flow rate at each outlet is 2264 gpm. This is the value to be used when verifying foam velocity.

A 10-in. pipe is required to maintain a foam velocity at less than 10 ft/s when the rate of expanded foam is 2264 gpm (see NFPA 11, Fig. A.5.2.6.2(a)). The pipe length upstream from the discharge point must be at least 20 times the diameter of the pipe to establish uniform velocity. Therefore, a straight run of 10-in. pipe at least 17 ft in length is necessary.

The foam outlet is not required to be at the tank shell. Note that the 10-in. pipe is actually inserted into the tank. This design approach permits economizing the pipe sizes between the tank and the high back pressure foam maker. The high back pressure foam maker is to be positioned outside of the dike area. A gate valve and a check valve are installed adjacent to the tank shell.

Step 8: Foam solution application rate.

For tanks containing liquid hydrocarbons, the foam solution rate must be at least 0.10 gpm/sq ft of liquid surface area of the tank to be protected. The maximum rate must be 0.20 gpm/sq ft. (Ref: NFPA 11, Table 5.2.6.5.1)

The foam solution application rate for this example is the same foam solution rate calculated for the surface application in Example 1, 1132 gpm.

Step 9: Foam concentrate supply rate.

The foam concentrate supply rate is determined in the same manner as set forth for the surface application in Example 1. Using a 3 % fluoroprotein foam, the requirement is 34 gpm for a total solution flow rate of 1132 gpm.

Step 10: Water supply rate.

The water supply rate is also determined in the same manner as set forth in the surface application in Example 1. The water supply rate is the foam solution rate minus the foam concentrate supply rate, which in this case is 1098 gpm.

Step 11: Duration of discharge.

The minimum discharge time for subsurface application of foam is 55 min for a tank storing gasoline (Ref: NFPA 11, Table 5.2.6.5.1)

Step 12: Quantity of foam required.

The volume of required foam is computed in the same manner as set forth in the surface application in Example 1. The primary foam supply is calculated by multiplying the determined rate of foam concentrate by the duration of flow, which indicates a quantity of 1870 gal.

Step 13: Quantity of water required.

The water requirement is the product of the water supply rate times the discharge time, or 60,390 gal.

Step 14: High-back-pressure foam maker.

A high-back-pressure foam maker is designed for the production and discharge of foam against considerable backpressure (from tank contents). The high-back-pressure foam maker selected for Example 2 is designed to operate satisfactorily at inlet pressures of 100–300 psi and produce foam of 2:4 expansion against back pressures not exceeding 40 % of the inlet pressure. With an inlet pressure of 150 psi, for example, 60 psi is available at the discharge for forcing the foam through a hose and/or piping into the storage tank and to overcome the pressure caused by the depth of fuel in the tank. Manufacturers of high-back-pressure foam equipment need to be consulted with regard to the associated flow and pressure characteristics, and back pressure limitations. Two high-back-pressure foam makers are used with this example. They are located in the foam house and are arranged for parallel operation (See Fig. 48.5.).

Step 15: Pipe size determination.

Expanded foam flowing in pipe does not follow the friction loss characteristics expressed by the Hazen-Williams approach. A set of flow curves have been developed for determining friction loss for expanded foam discharge by a high-back-pressure foam maker [1]. A set of these curves is provided in the Annex of NFPA 11.

A flow velocity of 10 ft/s is used for the determination of pipe sizes flowing foam solution and water. If necessary, water supply pipe and foam solution pipe can be sized to minimize friction loss between the water/foam supply and the discharge points.

Step 16: Valve selection and location.

For subsurface application, each foam delivery line must be provided with a valve and check valve, unless the latter is an integral part of the high-back-pressure foam maker or pressure generator to be connected at the time of use. When flammable/combustible liquid product lines are used for foam injection, product valving must be arranged to ensure foam enters only the tank to be protected. The valves need to be listed for the intended purpose.

Step 17: Foam proportioner selection.

The practices and procedures about foam proportioners outlined for the surface application in Example 1 also applies to this example. However, to accommodate the pressure requirements associated with a high-back-pressure foam maker, balanced or water-driven proportioners provide options for providing a reliable level of constant proportioning over the anticipated pressures.

Step 18: Pump Considerations.

For Example 2, the required pressure at the intake to the high-back-pressure device is approximately 150 psi. The static pressure on the water system is only 75 psi. Therefore, a pump is required to boost the water-solution pressure in the foam hose. The most efficient approach to designing a required pump installation is to select or design a pump-driver combination that will boost the available residual pressure to the required residual pressure at the demand flow. In other words, with the right capacity pump, the driver horsepower is calculated to raise the pressure over the differential range.

Hydraulic Analysis for Subsurface Application Foam System Protecting a Flammable Liquids Storage Tank

The following outlines the procedure involved in calculating the hydraulic demand for a subsurface application foam system. The reader is assumed to posses a fundamental understanding of fire protection water supply analysis, and hydraulic calculations employing the Hazen-Williams approach. The system in Example 2 as depicted in Fig. 48.5 is used in outlining the procedure. The design parameters and associated calculations are presented in sequential steps, which are summarized on a hydraulic calculation sheet as shown in Fig. 48.7 with reference points identified in Fig. 48.5.

Step 1: Pre-calculation for high-back-pressure foam maker (Reference Point?).

The hydraulic characteristics of the high-back-pressure foam maker must be considered before initiating the calculations. A high-back-pressure foam maker delivering 550 gpm at 150 psi is selected for each of the two foam lines leading to the tank.

1. Determine a K value for the foam maker:

$$Q = K\sqrt{P}$$

$$K = \frac{Q}{\sqrt{P}} = \frac{550}{\sqrt{150}} = 44.9$$

2. Required discharge per foam maker is 566 gpm.
3. Determine the required input pressure for a flow of 566 gpm:

$$566 gpm = 44.9\sqrt{P}$$

$$P = 159 psi$$

4. The pressure available to adequately account for back pressures associated with the stored fluid in the tank and associated elevation and friction losses in the system piping between the pump house and the tank is therefore 40 % of 159 psi, or 64.0 psi. Recall that from Step 14 in section 1.4.1.4 this type of foam maker was selected.

Step 2: Size foam injection pipe to tank.

Step 7 under problem assessment for Example 2—established that a 10-in. pipe is required to maintain a flow velocity under 10 ft/s.

Step 3: Determine friction loss from production storage.

Finished foam rising through the product must overcome the pressure from the product depth. Gasoline is the product for this series of problems with a specific gravity of 0.72.

$$\text{psi loss} = 48 \text{ ft} \times 0.433 \text{ psi/ft} \times 0.72 \text{ SG}$$

$$\text{psi loss} = 15$$

Step 4: Size the foam supply line from the tank shell to the foam house.

The stated pipe is selected on the basis of the allowable friction loss of 64 psi minus the pressure from the product depth (which equals 15 psi). Therefore, 49 psi (64 psi – 15 psi) can be dissipated from the tank to the foam maker through 500 ft of pipe and be used as an initial estimator; the flow rate is 2264 gpm. NFPA 11, Fig. A.5.2.6.4(a) should be consulted to determine appropriate pipe sizing. In this case, a 6-in. pipe is used. A 6-in. check valve and a 6-in. gate valve will be installed on the foam supply line adjacent to the tank in the dike area. The required friction loss calculations are presented in Fig. 48.7.

Calculation Note Subsurface foam system hydraulics actually divide into two separate calculation sets, as follows: (1) the hydraulics between the high-back-pressure foam maker and the storage tank and (2) the hydraulics between the water supply main and the high-back-pressure foam maker.

Step 5: Water supply main to fire pump calculation.

The lateral supply line will be designed at a velocity of 10 ft/s. Recall that only water is moving through this line.

$$Velocity = \frac{0.4085 \times gpm}{d^2}$$

1. Solve for d
2. $$10 ft/s = \frac{0.4085 \times 1098 gpm}{d^2}$$
3. $d^2 = 44.85$ in.
4. $d = 6.69$ in.
5. Use an 8-in. pipe

Step 6: Piping in foam hose (Reference Points).

Eight inch diameter pipe will be used in the foam house to connect between the pump, the foam proportioner, and the high-back-pressure foam maker.

Semisubsurface Injection Method

A modified form of subsurface foam injection for fixed roof tanks is used in a number of European countries. The modified technique is designated the semisubsurface injection method, based on the equipment used to insert the expanded foam into the tank shell. The semisubsurface injection method has not found any particular application in the United States and is not discussed herein.

Protection for Floating Roof Storage Tanks

Introduction

In contrast to fixed roof tanks, floating roof tanks have a cover or roof over the flammable liquid that floats on the surface of the liquid and moves vertically with the liquid level in the tank. The floating roof may be open to the atmosphere. This physical arrangement of the tank is classified as an "open-top floating roof tank." A permanently installed cover may be placed over the entire tank; this second designation is classified as a "covered floating roof tank."

The floating roof has a perimeter seal between the roof cover perimeter and the tank shell. The seal is necessary to prevent flammable vapors from escaping into the atmosphere and collecting over the floating roof. Foam system standards such as NFPA 11 address seal devices and their physical arrangement. Some devices also require the use of a foam dam when protected by fixed foam systems. The requirements for foam dams are also addressed in design and installation standards.

The fire experience with floating roof tanks is generally favorable. Consequently, fixed foam outlets are not generally called for on either open top floating roof tanks or covered floating roof tanks. When a facility operator or an owner elects to protect these types of tanks or the local fire protection authority requests protection for these types of tanks, three different application techniques are typically used for the fire protection of open top floating roof tanks. A brief description of each technique follows.

Portable Nozzle Method

The basic fire problem associated with floating roof tanks is a fire burning in the seal area between the cover and the tank shell. Typically, the surface area of this fire is quite small. One technique to extinguish this type of fire is to advance a portable hose line to the top of the tank, supply foam to this hose line, and manually apply foam to the seal area. Personnel operating this hose line should be adequately trained for these types of fire fighting operations and be aware of established safety practices.

Catenary System Method

The catenary system consists of a series of foam makers at evenly spaced points in the roof near the seal. These foam makers are connected to a common section of piping which in turn is attached to a flexible hose that rides up and down with the access stairway to the roof cover. The stairway is fixed to the top of the tank shell, and the bottom portion of the stairway rides on a set of tracks attached to the floating cover. This arrangement allows the stairway to move both horizontally and vertically as the cover moves with the flammable liquid level.

At the time of a fire, foam solution is pumped under pressure through a vertical pipe and flexible hose to the foam makers. This system can be designed to discharge foam under the seal directly onto the flammable liquid, or foam can be discharged above the seal. Foam equipment manufacturers producing this type of equipment should be consulted for engineering data on design requirements, installation techniques, and hydraulic calculations.

Fixed Foam Maker Method

The fixed foam maker method consists of installing piping around the outside wall of the tank and connecting a series of foam makers installed on special mounting shields above the storage tank rim. The circumference of the tank will determine the number of points needed for foam application. This method requires a foam dam to retain the foam over the seal or weather shield. This dam is normally 12–24 in.

(305–610 mm) in height. Construction details of the foam dam are addressed in foam system standards such as NFPA 11.

Covered floating roof tanks are generally not protected with fixed foam fire protection systems. However, there might be some cases where local regulations or practices call for protection for these types of tanks. The standards for fixed roof tanks should apply where it is required to protect covered floating roof type tanks with foam systems.

Seal Area Application of Foam

Fires that occur on floating roof tanks are generally limited to the seal between the floating roof and the tank shell. A common method of protection for this type of fire is to apply foam either above the seal or below the seal. This is the type of protection that will be examined in this section.

In certain situations, the possibility may exist that the floating roof will sink within the tank below the surface of the stored liquid. Under this scenario, the protection concept should treat the tank as a fixed roof tank as described previously.

Procedure for Determining Foam and Water Supply for Surface Application Low-Expansion Foam Systems for the Protection of Floating Roof Tank Seals

This section is concerned with the design and associated hydraulic calculations for application of foam fire protection systems protecting the seal of a floating roof storage tank. The material presented is limited to fixed protection systems using fixed discharge devices. A single flammable liquid storage tank problem is presented for developing the appropriate methods and techniques for calculating the foam agent requirements, system hardware requirements, and the necessary hydraulic calculations to properly deliver the required rate of foam to the subject hazard. The single example will be calculated using top of seal application of foam.

Example 3 A single floating roof storage tank is to be protected by a fixed foam system with similar tank characteristics as indicated in Fig. 48.1. The top of seal protection concept is to be used in this installation. A private fire service main will provide water to the foam system. The hydraulic characteristics of the main are illustrated in Fig. 48.2. For this problem, consider that the water available for the foam system is limited to the water supply characteristics shown in Fig. 48.2 (i.e., no additional water sources are available). A foam system design and complete set of hydraulic calculations are to be prepared for this installation.

Solution A systematic step-by-step process follows. Reference is made to criteria established in NFPA 11. In addition to the physical layout of the design problem, information is required on the fuel stored in the tank, i.e. the hazard. The nature of the hazard influences the system design.

Step 1: Installation identification.

The evaluation must consider the site conditions of the storage tank and surrounding areas. In this example, a single floating roof storage tank is positioned in an area surrounded by a dike wall. The seal between the floating roof and the tank shell will be a mechanical shoe seal. The tank is to be protected by a fixed foam fire protection system and connected to a private fire service main.

Step 2: Hazard classification and description.

The specific hazard and storage arrangement need to be identified. In this example, a 120-ft diameter floating roof tank is storing a flammable liquid.

Step 3: Flammable/combustible liquid identification.

The characteristics of the stored liquid must be determined in order to select the appropriate type of foam concentrate to be used. In this example, gasoline is stored in (with a specific gravity of 0.72) is stored in the tank. The designer is cautioned to carefully review the types of liquids to be stored. Facilities sometimes utilize the same tank enclosure for the storage of various types of liquids.

Step 4: Type of protection.

Based on the storage arrangement and contents, an appropriate protection concept must be determined. Fixed protection systems using Type II discharge outlets will be used.

Step 5: Surface area of liquid to be protected.

Calculate the seal surface area to be protected. For the cylindrical storage tank, the area of protection will be equivalent to the area of the tank shell minus the area of the floating roof to the foam dam:

$$\text{Area} = 1/4\pi\left(d_1{}^2 - d_2{}^2\right)$$

$$\text{Area} = 1/4\pi\left((120)^2 - (118)^2\right) = 1,500\ \text{ft}^2$$

Step 6: Foam agent selected.

Based on the liquid being stored, an appropriate foam concentrate must be selected. Specific manufacturers will need to be consulted to determine the most appropriate foam concentrate for the hazard.

For this example, a 3 % fluoroprotein foam will be selected for the defined hazard. Note that the type of foam agent selected for a particular design will affect other variables and considerations in the foam system design.

Step 7: Description, number, and placement of foam application devices.

Several factors need to be simultaneously considered in developing this step. The selection of foam application devices will be dependent on the foam agent selected. In addition, the flow and pressure characteristics of the discharge device will be a factor or present options for the system design. Manufacturer's literature and the listing evaluation data of foam equipment should be consulted on this matter.

For top-of-seal protection, foam system standards such as NFPA 11 require the discharge devices to be spaced at maximum of 40 ft intervals around the perimeter of the tank for 12-in. foam dams and at maximum of 80 ft for 24-in. foam dams. For the purposes of Example 3, a 24-in. foam dam is installed. Therefore, a 120-ft diameter tank has a circumference of approximately 380 ft and requires a minimum of 5 discharge devices spaced around the perimeter of the tank. Additional devices might be appropriate based on hydraulic considerations, or equipment costs. Individual manufacturers of foam equipment must be consulted on these options.

Placement of discharge devices should be equally spacing around the upper tank perimeter to ensure even distribution of foam. If possible, A constant and uniform flow and pressure should also be maintained during discharge.

Step 8: Foam solution application rate.

Foam solution application rates for floating roof storage tanks with a mechanical shoe seal are usually specified by foam system standards and manufacturer's design guides. Referencing NFPA 11, Table 5.3.5.3, at least 0.3 gpm/ft^2 of seal area of the tank to be protected is to be provided. It should be noted that specific types of seal protection may require different application rates. Appropriate references should be consulted in this regard.

The total foam solution discharge rate for Example 3 is calculated as follows:

$$\begin{aligned}\text{Rate (g pm)} &= 0.3\ \text{g pm/ft}^2 \times 1,500\ \text{ft}^2 \\ &= 450\ \text{g pm}\end{aligned}$$

The total discharge rate can be divided equally among the five required discharge devices. It is appropriate to specify a total rate of 450 gpm, with 90 gpm per discharge device or foam maker.

Step 9: Foam concentrate supply rate.

The foam concentrate supply rate is based on the foam agent proportioning rate. As noted in this example, 3 % fluoroprotein foam has been selected for this problem (Step 6). In other words, 3 % of the calculated foam solution rate is the foam concentrate supply rate. This rate may be determined as follows:

$$\begin{aligned}\text{Foam concentrate rate} &= 0.03 \times 450\ \text{g pm} \\ &= 13.5\ \text{g pm}\end{aligned}$$

Therefore, a continuous supply of foam concentrate must be available at a rate of 13.5 gpm for the required duration of discharge (Step 11).

Step 10: Water supply rate.

The water supply rate is the foam solution rate minus the foam concentrate supply rate. The necessary water supply rate can be calculated as follows:

$$\text{Water supply rate} = 450\,\text{g pm} - 13.5\,\text{g pm} = 436.5\,\text{g pm}$$

The water supply rate can also be determined as 97 % of the foam solution rate when using a 3 % foam concentrate.

Step 11: Duration of discharge.

Foam system standards and manufacturer's design guides generally specify the duration of foam discharge. Duration of discharge is dependent on the classification of seal protection. Per NFPA 11, Table 5.3.5.3.1, the requirement for floating roof tanks with a mechanical shoe seal and top-of-seal protection is 20 min. of continuous foam solution discharge. A minimum foam solution discharge time is specified in NFPA 11 (Table 5.3.5.3.1).

Step 12: Quantity of foam required.

The necessary foam supply for any given application should consider a primary supply and the availability of a reserve supply. The primary supply is calculated by multiplying the foam concentrate supply rate by the duration of discharge as follows:

$$\text{Foam agent required} = 13.5\,\text{g pm} \times 20\,\text{min} = 270\,\text{gal}$$

A risk analysis or the authority having jurisdiction may require that an equal quantity of foam be placed in reserve on site if there is a credible likelihood of a second fire occurring before the foam supply can be replenished.

Step 13: Total quantity of water required.

The basic procedure follows the concept presented in Step 12. The water requirement is the product of the water supply rate multiplied by the duration of discharge. In this case:

$$\text{Volume of water required} = 436.5\,\text{g pm} \times 20\,\text{min} = 8,730\,\text{gal}$$

Hydraulic Analysis of a Surface Application Low-Expansion Foam Systems for the Protection of Floating Roof Tank Seals

The hydraulic analysis for this system is similar to that provided for the surface application of foam to the fixed roof storage tank in Example 1. Therefore, the procedure is not repeated here.

Protection of Storage or High-Volume Hazards with High-Expansion Foam

High-expansion foam is an agent for the control and extinguishment of both Class A and Class B fires. The classification of foam also makes is particularly suitable as a flooding agent for use in confined spaces.

The development and application of high expansion foams for firefighting purposes started with the work of the Safety in Mines Research Establishment in England concerning the difficult problem of fires in coal mines. It was found that by expanding an aqueous surface active agent solution to a semistable foam of about 1000 times the volume of the original solution, it was possible to force the foam down relatively long corridors, thus providing a means for transporting water to a fire inaccessible to ordinary hose streams. This work was expanded upon by the United States Bureau of Mines immediately after World War II.

Developmental work in the United States on high expansion foam has led to the refinement of specialized high expansion foam generating equipment for fighting fire in confined spaces, for specific applications to fire control problems in both municipal and industrial fire fighting, and for the protection of special hazard occupancies. Medium-expansion foam was developed to cover the need for a more wind-resistant foam than high expansion foam for outdoor applications.

Concepts and Suitability for Medium and High-Expansion Foams

Medium- and high-expansion foams are aggregations of bubbles that are mechanically generated by the passage of air or other bases

through a net, screen, or other porous medium that is wetted by an aqueous solution of surface active foaming agents. Under proper conditions, fire fighting foams of expansions from 20:1 to 1000:1 can be generated. Such foams provide a unique agent for transporting water to inaccessible places, for total flooding of confined spaces such as basements, and for volumetric displacement of vapor, heat, and smoke. Extensive tests have demonstrated that under certain circumstances high expansion foam, when used in conjunction with water sprinklers, will produce more positive fire control and extinguishment than by either extinguishment system alone. This appears to be especially true with high rack storage of mixed commodities (e.g., high piled storage of paper stock and mixed storage of Class A and Class B materials). Optimum efficiency of high-expansion foam in any one type of hazard is dependent to some extent on the rate of application and also the foam expansion and stability throughout the fire event.

Personal Safety

Persons should not enter a space filled with high expansion foam without wearing full protective gear, self contained breathing apparatus, an attached lifeline, and operating in a "buddy" system. A person who is immersed in high-expansion foam can experience disorientation and other psychological and personal discomforts. Foam entering any of the body cavities may cause severe irritation and membrane swelling.

Special Considerations

The proper design and application of high-expansion foam systems are directly related to a number of unique considerations such as maximum submergence time and location of foam generating equipment.

A maximum submergence time needs to be specified for filling the enclosed space to the proper depth with expanded foam. The time, usually expressed in minutes, is a function of the type of combustible material and the arrangement of the combustible material. An important consideration in maximum submergence time is whether the materials/products to be protected remain at a constant height. Another consideration is the presence of an automatic sprinkler system. The basic objective is to control a developing fire before the fire has an opportunity to spread vertically over the face of a storage pile.

Fixed installations using high-expansion foam will probably involve the use of customized foam generating equipment to produce the necessary rate of volumetric foam discharge. The following factors should be considered in the selection and placement of high-expansion foam generating equipment:

1. Two foam generators positioned remotely from each other are more effective and efficient than a single generator.
2. Foam generating equipment should be top mounted to avoid back pressures on the foam making equipment. Foam generators are normally mounted on external towers or special roof supports.
3. Foam generating equipment should be so positioned as to avoid product-of-combustion air intake. Induced smoke into the generating equipment can significantly reduce the quality and quantity of the foam produced.
4. To effectively dampen convection currents from a developing fire in an area to be protected, the capacity of each required foam generator should be the same.

High-Expansion Foam System Calculations

Many of the fundamental hydraulic concepts presented with low-expansion foam system design problems also apply to high-expansion foam systems. Some similarities and differences between the hydraulic design for high-expansion foam systems and low-expansion foam systems are presented in Table 48.1. In this analysis, a low-expansion foam system using top-mounted

Table 48.1 Comparison of design criteria for low-expansion and high-expansion foam systems

Design/hydraulic step function	Low-expansion foam system—top chamber	High-expansion foam system—top generator
Starting point	Foam chamber(s)	Foam generator(s)
Second determination	Foam solution requirement per chamber (gpm)	Expanded foam requirement per chamber (cfm)
Third determination	Foam solution delivery rate between foam maker and foam house	Same determination
Fourth determination	Size pipe from foam maker(s) to foam house	Size pipe from foam generator (s) to foam house
Fifth determination	Determine type and size of foam proportioner	Same determination
Sixth determination	Determine hydraulic requirements in foam house	Same determination
Seventh determination	Evaluate water supply/demand requirement at foam house	Same determination
Eighth determination	Assess requirement for pump in foam house; recalculate hydraulic requirements in foam house	Same requirement

foam chambers is compared to an elevated high-expansion foam generator installation.

The following example considers the use of a high-expansion foam system in conjunction with automatic sprinkler protection for fire control and suppression in a specified warehouse. Be careful to note the generator flow rates, foam concentrate rates, and water supply rates. One of the advantages for considering high-expansion foam for the protection of confined space hazards is the low rate of foam application and associative water rate when compared to other aqueous types of systems.

Hydraulic Calculation Procedure for High-Expansion Foam Systems

Example 4 An owner has elected to protect a number of warehouse complexes with a combination of automatic sprinklers and high-expansion foam. A typical four-bay warehouse complex is illustrated in Fig. 48.8. The storage item is crude rubber piled 12.5 ft high in 2000 ft^2 pile areas. The installed sprinkler design is 0.2 gpm/ft^2. The location of the high-expansion foam generators is illustrated on the 12-in.-wide brick fire walls. Each foam generator is equipped with a set of remote controlled baffles that permits directional flow of foam into adjacent fire areas. Custom generators are used that have a foam solution rate requirement of 1.83 gpm per 1000 ft^3 of foam production. Three percent foam proportion with listed high-expansion foam is used for this system.

Solution The key consideration in high expansion foam system design is the proper sizing of the foam-generating equipment to be used for the application. A job work sheet is provided to facilitate the system design and identify relevant requirements. (See Fig. 48.9.) Applicable information is transferred from the referenced job sheet to the associated hydraulic calculation sheet. (See Fig. 48.10.) Reference is made to criteria established in foam system standards, specifically NFPA 11. The applicable foam system standards should be referenced for the systematic evaluation of any foam system.

The fundamental considerations of the hazard to be protected against establish the basis for the system design. In the case of high-expansion foam, some subjective criteria need to be established due to the lack of specific details in some foam system standards. Subjective criteria will be specifically noted below. A systematic step-by-step process follows.

Step 1: Installation identification.

Refer to Fig. 48.8, a storage warehouse.

Step 2: Hazard classification.

High density combustibles. The actual storage material is assumed to be crude rubber provided in irregular flat sheets. This commodity is not

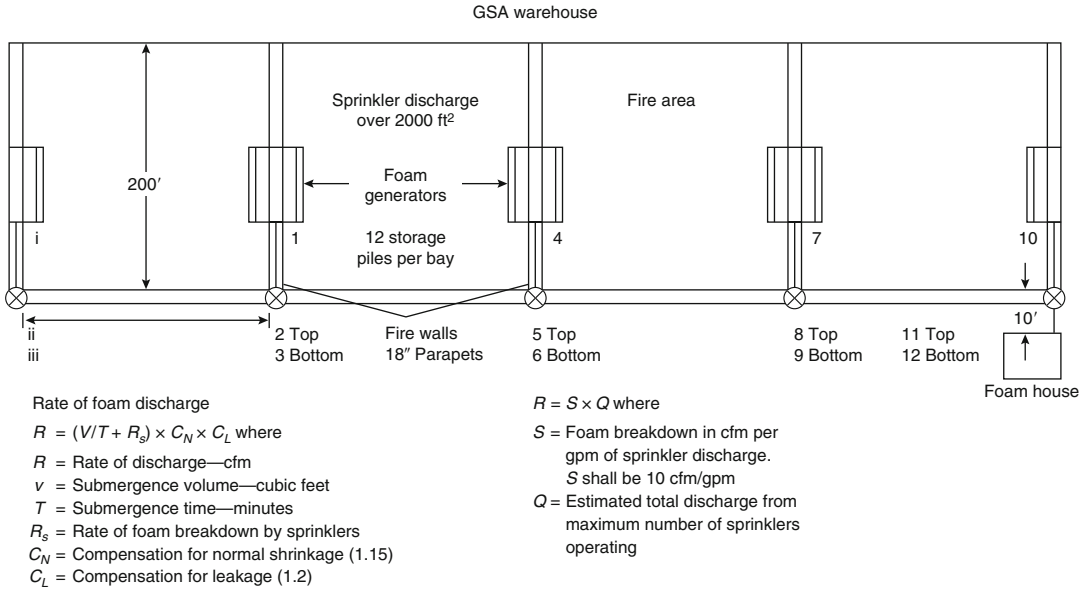

Fig. 48.8 Typical four bay warehouse complex

specifically identified in NFPA 11. Therefore, some judgment must be made when selecting foam submergence time as required for the calculations below.

Step 3: Type of protection.

The warehouse is protected by a dry-pipe automatic sprinkler system with a maximum discharge capability of 0.2 gpm/ft^2 over 2000 ft^2. This discharge density alone is not considered adequate protection for crude rubber in 2000 ft^2 piles. The automatic sprinkler protection is to be supplemented by a fixed high-expansion foam system. The foam generators are mounted on the coping section to the fire walls that divide the warehouse into fire areas. Generators positioned on the internal fire walls are arranged to discharge foam into whichever compartment, as required.

Step 4: Hazard description.

The fundamental considerations associated with the hazard are given under Step 1. It should be further noted that 12 storage piles of 2000 ft^2 each are located in the designated fire areas. Each individual pile is approximately 12.5 ft high. Due to the piling arrangement of the rubber and the burning characteristics of rubber, no deduction is made for "stock volume" in the rate discharge determination.

Step 5: Rate of discharge determination.

The basic design objective is to determine the rate of expanded foam discharge in cubic feet per minute to sub- merge the hazard in a defined period of time. This determination can be accomplished by applying a rate formula developed by the NFPA Foam Committee. The formula is given in NFPA 11, Section 6.12.8.2.3.1. The formula can be applied by first calculating and then assigning values to the formula variables.

1. *Submergence volume* (Re: NFPA 11, Section 6.12.5.2.2).

   Floor area: $200\text{ ft} \times 200\text{ ft} = 40,000\text{ ft}^2$

   Foam Depth:

   $$1.1 \times \text{height} = 1.1 \times 12.5\text{ ft} = 13.75\text{ ft}$$

   $$\text{Height} + 2\text{ ft} = 12.5\text{ ft} + 2\text{ ft} = 14.5\text{ ft}$$

   Use the larger of the two values (14.5 ft) for calculations.

HIGH-EXPANSION FOAM SYSTEM JOB WORK SHEET

Sheet: 1 of 1

Designer: Staff Date:

Installation identification: GSA Defense Materials Warehouse

Hazard classification: High density combustibles

Type of protection: Dry pipe automatic sprinkler—fixed HI-X foam

Hazard description: Crude rubber in piles

Rate of discharge determination:

1. Submergence volume (cubic feet)
   v = floor area 40,000 sq ft × foam depth 14.5 ft = 580,000 cu ft
2. Submergence time (minutes) T = 5
3. Rate of foam breakdown by automatic sprinklers: $R_s = S \times Q$ where
   S shall be 10 cfm/gpm and Q shall be total discharge from operating sprinklers
   R_s = 10 cfm × 400 gpm = 4000 cfm
4. Compensation for normal foam shrinkage—C_N: C_N = 1.15
5. Compensation for leakage—C_L; C_L range is from 1 to 1.2: C_L = 1.1
6. Rate of discharger (cfm) = $(v/T + R_s) \times C_N \times C_L$ = 151,800

Description, number, and placement of foam generators: 2—80,000 cfm foam generators per storage bay. Placement on fire walls as shown

Foam solution rate: 146 gpm/generator × 2 = 292 gpm

Foam concentration rate: 3% proportion × 292 gpm = 9 gpm

Duration of discharge: 15 minutes of full operation

Gallons of foam required: Main and reserve = 270 gals

Gallons of water required: 4,245

Water supply information: Adequate for demand curve

Special foam system design considerations: System is activated by automatic sprinkler system dry pipe trip.

Fig. 48.9 High expansion foam system job work sheet

$$\text{Volume} = \text{area} \times \text{depth}$$

$$\text{Volume} = 40{,}000\ \text{ft}^2 \times 14.5\ \text{ft}$$

$$= 580{,}000\ \text{ft}^3$$

(See Step 4—no deduction is made for stock volume)

2. *Submergence time* (Re: NFPA 11, Section 6.12.7).
   5 min for high density materials with sprinkler protection
3. Rate of foam breakdown for sprinklers (Re: NFPA 11, Section 6.12.8.2.3.2).
   Discharge from sprinklers:

HYDRAULIC CALCULATIONS

Subject: GSA Warehouse
Job no.: Sample problem 3
Sheet no.: 1 of 1
By: Staff Date:
Chkd by: Date:
Application rate: NH gpm per sq ft
Area: 40,000 ft
Minimum solution rate: 1.83 gpm/1000 ft^3
Actual solution rate: 185 gpm/1000 ft^3
Foam maker pressure and rate: 50 psi @ 146 gpm
Foam system: Fixed
Water data:
Ref. drawing:

Foam maker type and location	Added gpm	Total gpm	Pipe size (in.)*	Pipe & equivalent fitting lgth. (ft)**	Friction		Static psi	Proportioner psi	Req'd pres psi
					psi/ft C=100	Total psi			
Starting point: 1			Elevation: 22 ft				Pressure at foam maker: 50 psi		
1	146	146							50
1–2–3		146	3.068	212′+E(7′)=1T(15)	.0387	9.1	9.5		68.6
				234′					
2 @ 3									68.6
3–6		146	4.026	200′	.0103	2.06			70.7
6–9–12	148	294	4.026	400′	.0375	15.0			85.7
Foam house		294						4.0	89.7
System demand		294							90.0

* "X" Indicates extra hvy.—std. wt. otherwise

** See sheet for tabulation of pipe and fittings

Fig. 48.10 Hydraulic calculations for Example 3

$$Q = 0.2\,\text{g pm/ft}^2 \times 2{,}000\ \text{ft}^2 = 400\,\text{g pm}$$

Apply formula:

$$R_s = 10\,\text{c fm/g pm} \times 400\,\text{g pm} = 4{,}000\,\text{c fm}$$

4. *Compensation for shrinkage*. Set at 1.15 as a constant (Re: NFPA 11, Section 6.12.8.2.3.3).
5. *Compensation for leakage*. Use 1.1 to allow for some leakage around doors (Re: NFPA 11, Section 6.12.8.2.3.4).
6. Apply formula:

$$\text{Rate} = (v/T + R_s) \times C_N \times C_L$$

$$\begin{aligned}\text{Rate} &= \left(580{,}000\ \text{ft}^3/5\ \text{min} + 4{,}000\,\text{c fm}\right) \\ &\quad \times 1.15 \times 1.1 \\ &= 151{,}800\,\text{c fm}\end{aligned}$$

Note The foam breakdown from sprinklers is a relatively small value compared to the total cfm rate.

Step 6: Description, number, and placement of generators.

Custom-built foam generators will be required for this problem. Each generator will have a capacity of 80,000 cfm with a foam solution rate of 146 gpm. (See given information with problem statement.) Five generators will be required to protect the entire warehouse. Generators mounted on interior fire walls will be equipped with baffles arranged to discharge foam into either adjacent compartment; electrical controls will be operated from the foam house. Generators are actually mounted 22 ft above the finished floor.

Step 7: Foam solution rate.

The foam solution rate per generator is given in Step 6. The solution rate requirement is 1.83 gpm per 1000 ft^3 of foam production.

$$\begin{aligned}\text{Solution rate} &= 80{,}000\ \text{ft}^3/1000\,\text{ft}^3 \times 1.83\,\text{g pm} \\ &= 146\,\text{g pm}\end{aligned}$$

Two generators require 292 g pm.

Step 8: Foam concentrate rate.

The foam selected for this problem proportions at 3 %. Therefore, the concentrate rate is 3 % × 292 gpm = 9 gpm.

Step 9: Duration of discharge.

Duration of discharge for the foam systems should be checked with the authority having jurisdiction. A basic minimum discharge time is 15 min of continuous operation.

Step 10: Quantity of foam required.

It is assumed that enough foam will be placed in storage to meet both a main and a reserve requirement: 9 gpm × 15 min × 2 = 270 gal.

Step 11: Quantity of water required.

The primary water supply must provide a rate of 283 gpm for 15 min or 4245 gal. A similar quantity is required to be supplied for the secondary demand.

Step 12: The problem considers that the water supply to the foam house is adequate to meet the calculated demand for the system.

Step 13: The foam system is to be activated by the automatic sprinkler system when the dry-pipe valve trips due to a sprinkler operating. The system can also be activated manually.

Hydraulic Analysis for High-Expansion Foam System

The following outlines the procedure involved in calculating the hydraulic demand of a high expansion foam system. The reader is assumed to posses a fundamental understanding of water supply analysis and fire protection hydraulics. The system in Example 4 as depicted in Fig. 48.8 is used in outlining the calculation procedure. The design parameters and associated calculations are presented in sequential steps, which are summarized on a hydraulic calculation sheet as shown in Fig. 48.10 with reference points identified in Fig. 48.8.

Step 1: The inlet pressure requirement for the foam generator is 50 psi.

Step 2: The foam solution line supplying each foam generator and the riser pipe to the top of the fire wall are sized on the basis of a maximum flow velocity of 10 ft/s.

$$Velocity = \frac{0.4085 \times gpm}{d^2}$$

$$10 fps = \frac{0.4085 \times 146 gpm}{d^2}$$

$$10d^2 = 59.64$$

$$d^2 = 5.96$$

$$d = 2.44$$

Use a $3-$ in. pipe

Since the same size pipe is used from the foam generator to ground level, the hydraulic analysis can go from reference point 1 to reference point 3. The elevation head to be considered is 22 ft.

Step 3: The flow and pressure demand at the base of each riser supplying a foam generator is the same, since the generator sizes are equal. It is necessary to calculate a flow constant at this location so the pressure points upstream can be correctly adjusted for higher pressure values developed by friction loss between supply points. The demand constant is calculated as follows (reference point 3):

$$Q = K\sqrt{P}$$

$$146 \text{ g pm} = \text{K } (68.6)^{1/2}$$

Step 4: The ground-level cross-main connecting the foam generator risers is sized on the basis of a maximum flow velocity of 10 ft/s. The flow from two generators is used for the flow computations.

$$Velocity = \frac{0.4085 \times gpm}{d^2}$$

$$V = \frac{0.4085 \times 292 gpm}{d^2}$$

$$10d^2 = 119.282$$

$$d^2 = 11.928$$

$$d = 3.45$$

Use a $4-$ in. pipe

Step 5: Determine the actual flow characteristics for the high-expansion foam generator at reference point 4.

Use the K value (constant) determined in Step 3 to calculate the actual supply to the second foam generator at reference point 4. The new pressure at the riser base (reference point 6) is 70.7 psi from the hydraulic calculation sheet. The higher pressure is used with the K value to determine the actual flow for the second high-expansion foam unit.

$$Q = K\sqrt{P}$$

$$Q = 17.6\sqrt{70.7}$$

$$Q = 148$$

The actual flow increases by 2 gpm for the second generator.

Step 6: Determine the flow and pressure requirements at the foam house. Determine the friction loss for the total flow back to the foam hose and add in 4 psi for the foam proportioner.

Step 7: System demand.

The final system demand is 294 gpm at 90.0 psi at the foam proportioner inlet to supply the two high-expansion foam generators. The water supply to the foam house must meet this demand.

Compressed Air Foam Systems

Compressed Air Foam Systems (CAFS) are recent developments highly dependent on the manufacturer's products and the specific listing

requirements of the particular system. As such, foam system standards such as NFPA 11 do not provide comprehensive design guidance for these types of systems. Instead design standards and regulations mostly indicate that the system design must be in accordance with the manufacturer's design manual, which is required to be part of the listing.

Foam system standards such as NFPA 11 require that compressed air foam systems to provide a minimum discharge density in accordance with applicable occupancy and facility specific standards, but in no case less than 0.04 gpm/ft^2 (1.63 L/min- m^2) for hydrocarbon fuels applications and 0.06 gpm/ft^2 (2.3 L/min-m^2) for alcohol and ketone applications. The CAFS is also to be designed to provide a minimum discharge duration, 5 min for fixed spray systems and 10 min for deluge-type system per NFPA 11.

Limitations of Foam Fire Protection Systems

This section discusses both low- and high-expansion foam systems. The limitations of foam fire protection must be addressed relative to each of these two types of systems. The following factors should be reviewed during the selection and design of fire protection systems generating foam.

Limiting Factors for Low-Expansion Foam Systems

1. Low-expansion foam application is limited to the extinguishment of horizontal or two-dimensional fire problems. This type of foam application is not suitable for three-dimensional fires.
2. Low-expansion foam systems are limited by foam agent suitability for the defined flammable or combustible liquid. Basically, foam agents are suitable for either hydrocarbon fuels or polar solvents. Alcohol resistant-type foams may be approved for both hydrocarbons and polar solvents.
3. Different types and brands of foam concentrates may be incompatible and should not be mixed in storage.
4. Foam solution consists of 90 % or more water. Foam system limitations should be evaluated with respect to the proper use of aqueous based agents on flammable materials and the electrical conductivity of the application method.
5. Foam systems are limited by the equipment appliances and devices used to proportion the foam and to deliver the finished foam onto a given hazard or fire problem. Equipment limitations pertaining to flow rate, operating pressure ranges, and proportioning ranges should be carefully considered in the selection and application of foam systems.

Limiting Factors for Medium- and High-Expansion Foam Systems

1. Medium- and high-expansion foams are finding applications for a broad range of fire protection problems. However, unlike low-expansion foam systems, medium- and high-expansion foam fire protection systems should be specifically evaluated for each type of hazard condition. The fact that each system requires a feasibility study and individual design may be considered a form of limitation when contrasted to the design concepts for low-expansion foam systems.
2. NFPA 11 states that *under certain circumstances, it might be possible to utilize medium- or high-expansion foam systems for control of fires involving flammable liquids or gases issuing under pressure, but no general recommendations can be made in this standard due to the infinite variety of particular situations that can be encountered in actual practice* [1]. This statement is considered to be a design limitation.

3. Medium- and high-expansion foam systems should not be used on fires in the following hazards unless competent evaluation, including tests, indicates acceptability:
   (a) Chemicals, such as cellulose nitrate, which release sufficient oxygen or other oxidizing agents to sustain combustion
   (b) Energized unenclosed electrical equipment
   (c) Water reactive metals, such as sodium and potassium (Na, K)
   (d) Hazardous water reactive materials, such as triethylaluminum and phosphorous pentoxide
   (e) Liquefied flammable gas

The Advent of Class A Foams

Foam agent fire protection systems are also suitable for Class A fires in ordinary combustible materials in addition to Class B fires (flammable and combustible liquids). Historically, portable foam fire extinguishers provided important fire protection for both Class A and Class B problems. The dual consideration of evaluating foam fire protection systems for both Class A and Class B fire protection problems is important. This consideration is especially important for mixed occupancy storage, which may be suitably protected by foam spray systems, foam water sprinkler or spray systems, or closed head sprinkler systems using aqueous film forming foam (AFFF) type foam agents.

Class A foams have been used extensively in wildland fire suppression activities. The success of Class A foam for the confinement, control, and extinguishment of natural cover fuel fires suggests that this type of foam may be effective for structural fire protection as foam solution in fire streams. Initial research has been conducted to quantify the fire fighting efficiency of Class A foams to improve the operating efficiency of these foams when compared to plain water fire streams. The National Fire Protection Research Foundation has published research findings on Class A foam effectiveness: one in December 1993 [2] and one in November 1994 [3]. A synopsis of the findings are presented below.

The National Fire Protection Research Foundation (NFPRF) sponsored a research program with Underwriters Laboratories, Inc. (UL), to investigate the effectiveness of Class A foams by means of three discharge devices: (1) a standard spray nozzle, (2) an air-aspirated spray nozzle, and (3) by injecting compressed air into the Class A foam solution. This research investigation has two objectives: (1) to develop test data related to the fire fighting effectiveness of Class A foam solutions as compared to water only and (2) to conduct laboratory analysis of the Class A foam concentrate used in the performance tests.

Briefly, the initial fire test plan included a Class 20A wood crib fire with foam solution concentrates selected at 0.1 %, 0.3 %, and 0.5 %. Adjunct variables included nominal expansion ratios of 5 for a standard nozzle at 15 gpm, 7.5 for an air-aspirated nozzle at 15 gpm, and 7.5 for injecting compressed air into the Class A foam solution.

The wood crib fire tests were conducted at UL's test facility located in Northbrook, Illinois, and are reported in the December 1993 publication.

In summary, the initial set of fire tests provides support of the following conclusions by the Technical Advisory Committee (TAC):

- Handheld hose lines supplied with Class A foam solutions provide enhanced fire fighting performance when compared to handheld hose lines supplied with water only.
- The best foam quality, as measured by retention and exposure protection tests, was achieved with compressed air foam.
- Results of the wood crib fire tests indicated superior characteristics in terms of fire control time for Class A foams when compared to water application only.
- Fire tests conducted with the air-aspirated test nozzle had the longest reignition times, while

tests conducted with the Compressed Air Foam had the lowest crib weight losses.
- Exposure protection test results demonstrated the ability of the Class A foam to lengthen the ignition time of a combustible surface when compared to cribs protected by the same rate and duration of water.
- Retention-of-weight tests demonstrated that wood cribs exposed to Class A foam retain more weight than cribs treated with water.

The testing program outline above was very controlled in a laboratory setting. Foam applications were not subjected to many real world variables that could include wind, weather conditions, fuel geometry, pre-burn times, and human factors in the foam application. Despite such conditions, the reported testing program clearly supports a number of advantages for using Class A foam on structural type fires.

The Phase II research project report of 1994 reviews the conduct of structural fire suppression tests. These tests were also conducted at UL's test facilities in Northbrook, Illinois. A test cell measuring 30 by 36 by 30 ft was used for the Class A foam comparative analysis tests. Two fuel package scenarios were used as follows:
- The Series I UL 1626 residential fuel package consisted of a wood crib and simulated furniture positioned in one corner of the enclosure.
- The Series II fuel package consisted of a corner upholstered sofa scenario.

Fire test monitoring of the enclosure included measurements of the Class A foam solution or water flow rate; room temperature gradients at distances of 2, 9, 18, 24, 33, 48, and 72 in. below the ceiling; rate of heat release; oxygen content; smoke density; and heat flux. In each test series, observations were made of fire knockdown and damage to the walls of the enclosure and the fuel package.

Upon ignition, the fuel package was allowed to burn until flashover was achieved in the enclosure. Five seconds after flashover, a water application or a Class A foam solution was applied to suppress the fire using either a direct or indirect application method. The direct application method consisted of discharging the agent directly onto the walls of the enclosure and the fuel package. In contrast, the indirect application method consisted of discharging the agent first onto the ceiling and walls and then onto the fuel package.

The 1994 Class A Foam Study Report divides the summary information according to the Series I and II testing programs. The Series I abbreviated findings are summarized as follows:
- Class A foam using a direct application method took less time and quantity of agent to lower heat release to 500 KW than plain water.
- Class A Compressed Air Foam (CAF) using the indirect application method was more effective in reducing heat release values down to 500 KW.

The Series II abbreviated findings are limited to the following selective observations:
- The test results using Class A foam solutions generally provided for a reduced amount of total heat release from the fire and less damage to the sofa.
- Class A Compressed Air Foam applied at 7 gpm using the direct application method demonstrated the shortest time period and the lowest quantity of agent required to reduce the rate of heat released to 500 KW.
- The direct application method provides for a reduced amount of total heat release and less damage to the sofa when compared to the same tests conducted using the indirect application method.

Both reports recommend additional research on the application of Class A Foams with special attention given to hardware devices that include handheld fixed nozzles, proportioning equipment, and foam-generating equipment.

Additional research has been conducted by the National Institute of Standards and Technology [4]. The effectiveness of Class A foams on Class A and Class B fire threats were characterized. Four representative Class A foams were chosen for evaluation. A series of Class B fire suppression tests were conducted in

conformance with UL 162 *Standard for Foam Equipment and Liquid Concentrates*. These tests utilized a 4.6-m^2 (50-ft^2) heptane pool fire and consisted of the suppression of the fire and then testing for reignition and burnback resistance. Agent was applied at 2.44 and 4.88 lpm/m^2 (0.06 and 0.12 gpm/ft^2), which is one and one-half and three times the rate required by the standard for AFFF application. The higher flow rates were used because the agents could not extinguish the fire at the standard AFFF application rate. The four agents had fire knockdown (control) times similar to AFFF, but two of the agents did not completely extinguish the fire in all the tests. AFFF had a higher resistance to burnback and longer time to re-ignition than the other four agents.

Full-scale fire experiments were conducted with 92.9-m^2 (1000-ft^2) gasoline pool fires. Agent application was made with a 454 lpm (120 gpm) hose stream (i.e., 4.88 lpm/m^2 [0.12 gpm/ft^2]). Two application techniques were used with each of the four agents in the large-scale tests. One application was made with a self-aspirating tube nozzle, and one application was made with a nonaspirating adjustable fog nozzle. AFFF and water were used as benchmark agents for these tests. Plain water could not extinguish this fire. AFFF exhibited better fire control and extinguishment characteristics, and substantially better burnback resistance, than those of the Class A foams.

In tests conducted for the U.S. Air Force, the Naval Research Laboratory assessed a compressed air foam system for possible use for aircraft hangar scenarios involving JP-8 fuel [5]. The breadboard unit used AFFF as the fire extinguishing agent. It was found that a commercial off the-shelf non-air-aspirating nozzle was as effective as the air-aspirating nozzle provided with the unit. Air injection for aeration of the AFFF stream before discharge from the nozzle was found to be unnecessary.

Nomenclature

C	Hazen-Williams coefficient (constant)
C_L	Foam leakage correction factor
C_N	Normal foam shrinkage factor
D	Internal pipe diameter (in.)
FL	Friction loss (psi/ft)
K	Nozzle discharge coefficient (gpm/psi1/2)
Q	Flow (gpm)
R	Total foam generator capacity (cfm)
R_s	Total rate of foam breakdown [S × Q] (cfm/gpm)
S	Rate of foam breakdown by sprinklers per gpm of sprinkler discharge (cfm/gpm)
T	Submergence time (min)
V	Velocity (ft/s)
ν	Submergence volume (ft^3)

References

1. NFPA 11, *Standard for Low-, Medium-, and High-Expansion Foam*, National Fire Protection Association, Quincy, MA, 2010.
2. W.M. Carey, *National Class A Foam Research Project Technical Report*, National Fire Protection Research Foundation, Quincy, MA (December 1993).
3. W.M. Carey, *National Class A Foam Research Project Technical Report, Phase II*, National Fire Protection Research Foundation, Quincy, MA (December 1994).
4. D. Madrzykowski and D.W. Stroup, "Demonstration of Biodegradable, Environmentally Safe, Non-Toxic Fire Suppression Liquids," *NISTIR 6191*, National Institute of Standards and Technology Report, Gaithersburg, MD (1998).
5. S.A. Hill, J.L. Scheffey, F. Walker, and F.W. Williams, "Tests of Alternative Fire Protection Methods for USAF Hangars," *NRL/MR/6180-99-8337*, Naval Research Laboratory Report, Washington, DC (1999).

Hamid Bahadori is a Vice President with Jensen Hughes, Inc.

Considerations for Coordinating and Interfacing Fire Protection and Life Safety Systems

49

David Jacoby, David LeBlanc, Jeffrey Tubbs, and Andrew Woodward

Introduction

Fire protection and life safety strategies for modern buildings and facilities are developed to accomplish specific goals and objectives as agreed to by the relevant stakeholders. Effective implementation of such strategies requires not only sound design and installation of the relevant building systems and features, but also the proper integration and coordination of such systems and features. The overall process for properly integrating and coordinating the applicable systems often requires significant effort and focus as the various systems are often designed and installed by different engineering and contracting disciplines, and approved by different enforcement agencies. As such, it is critical that the building system integration and coordination process be appropriately considered throughout the design, installation, *commissioning* (*Cx*), and acceptance testing process, as well as during the life-cycle maintenance of the systems.

System coordination is needed for new buildings, existing building renovations, existing building additions, upgrades to existing building systems, and retrofit installations of new systems in existing buildings. Because the size, functionality and complexity of buildings continue to increase, building and fire regulations require fire protection and *life safety systems* that rely upon proper integration for effective performance. For some buildings and facilities, performance-based solutions, which are permitted by many building and fire regulations, offer the best approach because they allow greater flexibility in the design of the buildings and their supporting systems. However, these performance-based solutions may require even more sophisticated fire protection and life safety system solutions. Whether code-prescribed or performance-based approaches are used, effective integration and coordination of the associated fire protection and life safety systems requires proper attention and knowledge.

Systems and components that typically require *integrated systems* and coordination include those associated with fire detection and alarm, emergency communication, suppression and extinguishing, fire pump and water supply, security and access control, smoke control, HVAC, building management (BMS), emergency and standby power, emergency lighting, exit signage, elevators and escalators, doors, operable windows, fire shutters, and dampers.

Integration and coordination of systems can be accomplished in various ways. The following identifies a systematic approach that can be applied through various types of building design and construction procurement methods,

D. Jacoby
Simpson Gumpertz & Heger, 550 7th Avenue, New York, NY 10018, USA

D. LeBlanc
JENSEN HUGHES, 1661 Worcester Road, Suite 501, Framingham, MA 01701, USA

J. Tubbs (✉) • A. Woodward
Arup, 955 Massachusetts Ave, Fourth Floor, Cambridge, MA 02139, USA

M.J. Hurley (ed.), *SFPE Handbook of Fire Protection Engineering*,
DOI 10.1007/978-1-4939-2565-0_49, © Society of Fire Protection Engineers 2016

e.g. traditional Design Bid Build, Design Build, and Design Assist. The majority of this chapter focuses on steps three thru six below:

1. Develop the design objectives and goals with the stakeholders for the project, incorporating the *Owner's Project Requirements* (*OPR*) and establish the preliminary fire protection and life safety strategy to meet these goals and objectives during the Planning Phase.
2. Implement the strategies into the design, through the *Basis of Design* (*BOD*), fire protection and life safety strategy report, system design reports, design drawings, sequence of operation (i.e. fire alarm input/output functional matrix), specifications, and other documentation during the Design Phase.
3. Updates of the various system designs during the Design Phase, including refinements and integration of systems as described in the reports, design documents, and specifications.
4. Cross reference and verify consistency among the various systems with multiple contractor shop drawings and submittals, and field changes during the Construction Phase of the project.
5. Complete *fire and life safety commissioning* documentation for the individual fire protection and life safety systems including *pre-functional test*.
6. Complete Integrated Testing of all of the integrated fire protection and life safety systems and complete final *acceptance* testing.
7. Periodic Inspection, Testing, and Maintenance of the individual fire protection systems along with periodic integrated system testing for the life of the building.

This chapter overviews *integration*, interfacing, and coordination considerations for systems used to support comprehensive fire protection and life safety design strategies, with a focus on electronic interface among the various installed fire protection and life safety systems. These electronic or physical *interconnections* between systems comprise the interfacing between these systems. *Integration* of fire protection and life safety systems includes the physical or electronic interfaces, and also includes other items such as the trained human intervention in a defined process like a prison guard releasing egress doors in a prison during an emergency. Section "Systems Overview" provides background on fire protection and life safety design and features that may require coordination. Sections "System Integration Considerations During the Design Process", "Systems Coordination During Construction" and "Life of the Building" focus on coordination of these systems and features during design, construction, and post occupancy. The section on "Commissioning and Integrated Systems Testing" overviews commissioning for fire protection and life safety systems. Although the emphasis of the chapter is on active fire protection systems, passive systems support active systems (directly or indirectly) and, as such they are discussed where appropriate. Passive systems are an important component of the overall life safety and fire protection strategy of a building.

A general discussion is provided on considerations that may need to be addressed to ensure that the installed fire and life safety systems perform as a fully integrated and coordinated unit. A full all-inclusive list describing all possibilities is not practical. Various examples and cases are illustrated. There are numerous ways a system can be designed and configured. The specific building, fire protection systems, owner's and project's goals and objectives all impact the design and approach for coordination and integration of fire protection systems. The coordination and integration of the fire protection systems usually need to be customized for each building, and approaches will vary from project to project. Systems may be successfully integrated through other methods than those presented in the Chapter.

Fire Protection Engineers are uniquely qualified to be an integral part of the coordinating, integration, and interfacing fire protection and life safety systems, due their background, experience, and education.

Relevant Documents

Building and fire codes detail prescriptive requirements for fire protection and life safety systems and their components. For example, the International Building Code [11]; International Fire Code [12]; NFPA 101; *Life Safety Code* [17]; NFPA 5000; *Building Construction and Safety Code* [18]; and NFPA 1; *Fire Code* [19] specifically mandate various systems based upon the intended building occupancy classification, function and characteristics. Detailed design and installation provisions concerning the systems, including *acceptance testing*, are included in various reference standards and other regulations such as those published by NFPA, ASHRAE, ASME, and others. However, the general functionality of the systems is outlined in the applicable building or fire code, with specific reference made to the pertinent reference standards. In a growing number of instances, performance-based design approaches are used to develop more holistic strategies for building and infrastructure projects, and such strategies often require unique combinations of systems and their components. Insurance regulations may also mandate or recommend certain features and systems not specifically addressed by the applicable building or fire code.

Commissioning and integrated testing of fire protection and life safety systems are critical functions ideally done during the Design Phase and Construction Phase of the project. The first step in commissioning is the development of the *OPR*, the owner and user developed project requirements and performance criteria developed that describe project goals and criteria for system function, performance and maintainability. The *OPR* may then serve as direction for the *BOD*.

Fire Protection and Life Safety Commissioning is completed on an individual system basis, such that each of the individual systems are commissioned separately. *Integrated Testing* is done to integrated systems to verify the integration or interface between these systems are functioning appropriately. An independent third party owner's representative typically conducts the commissioning and integrated testing activities to verify that the systems have been properly installed, programmed and coordinated and to confirm that the installed systems function as an integrated unit as intended by their design documentation. The owner's representative ideally assists in both the Design Phase and the Construction phase of the project.

In some parts of the world, such as in several European nations, commissioning of building systems including active fire protection systems have occurred for decades and is extremely common. In the United States, commissioning of fire protection systems is a more recent growing trend.

Numerous documents addressing commissioning and integrated testing of fire protection and life safety systems have been published. The following lists specific relevant documents. Section "Commissioning and Integrated Systems Testing" discusses commissioning and the commissioning process in more detail.

NFPA 3, *Recommended Practice for Commissioning and Integrated Testing of Fire Protection and Life Safety Systems* [21], outlines a process for commissioning and integrated testing.

NFPA 4, *Standard for Integrated Testing of Fire Protection and life Safety Systems*, 2015 Edition focuses on providing the minimum requirements for integrated testing of fire protection and life safety systems as an adoptable and enforceable standard.

ASHRAE Guideline 0, *The Commissioning Process* [5] and ASHRAE Guideline 1.5, *The Commissioning Process for Smoke Control Systems* [6] outline a process and provide detail specific to commissioning of smoke control systems.

CAN/ULC-S1001-11 *Integrated Testing of Fire Protection and Life Safety Systems* [35] outlines integrated testing.

D.M.10.03.1998—Decreto Ministeriale—Criteri generali di sicurezza antincendio e per la gestione dell'emergenza nei luoghi di lavoro—Art.4 is the Law in Italy requiring Commissioning of fire protection and life safety systems

Association des Etablissements Cantonaux d'Assurance Incendie (AEAI) has released pamphlets such as NPI8:2012, *Installations techniques de protection incendie—réceptions*

et contrôles [2], which is the Switzerland common insurance requirement requiring commissioning of fire protection systems and periodic testing, with virtually every building requiring insurance.

Système de Sécurité Incendie(*SSI*)—*Fire Safety System* is the National Standard in France requiring Commissioning and Integrated Testing of fire protection systems, with other national standards that indicate what tasks may need to be performed for commissioning and integrated testing depending on the systems and their complexity.

In Australia, the commissioning requirements for fire protection systems are generally found in the individual system standards.

Terminology

When discussing systems coordination and integration, there is sometimes an inconsistency of the meanings of words. Sometimes the same terminology is viewed or understood to mean different things to different people. For example, the term commissioning has become an often used word that has very different meaning to different people, since some people inappropriately use the term *commissioning* to mean *acceptance testing*. A Glossary of Terms can be found at the end of this chapter. The authors have defined these terms to provide a common reference throughout the chapter. Readers should verify these definitions in the code, standards, and regulations in use for a specific project, as definitions may differ from those defined within this chapter.

Systems Overview

Fire protection and life safety strategies are developed to accomplish specific goals and objectives and often rely upon the effective performance and integration of various fire and *life safety systems*. While these goals and objectives guide the design of the various individual safety systems, such systems need to be interconnected and coordinated with other systems for proper implementation of the overall fire protection and life safety strategy. As stated previously, early and continuing coordination of fire protection and life safety systems throughout the design process is critical for the successful integration and performance of the individual systems and the overall approach.

The following provides a general overview of typical fire and life safety systems mandated by building and fire regulations, or otherwise recommended by fire protection strategies. More detail about these individual systems can be found in other chapters of this handbook as well as in other documents. Section "System Integration Considerations During the Design Process" of this chapter outlines integration issues that require attention during the design and construction process.

Egress

The egress strategy usually serves as the basis for the life safety strategy for a facility, and can include evacuation, relocation, or protect-in-place approaches that can be combined or phased depending upon overall goals and objectives. Evacuation plans for a building may include simultaneous full or partial phased evacuation of building occupants during emergencies. For protect-in-place strategies, occupants do not evacuate or even move from their rooms. Phasing strategies can be used to efficiently use the egress components. Evacuation plans need to consider wheel chair users and other persons with disabilities and mobility impairments [34].

Consider a typical high-rise evacuation strategy that calls for the occupant evacuation from three floors during a fire scenario—the alarm floor, one floor above and one floor below. If properly protected from the anticipated fire hazards through various active and passive systems and the fire is controlled or suppressed by the appropriate systems, occupants on other floors can remain in place for some time period and may not even need to be made aware of the fire situation. In this scenario, occupants on other floors would be directed to remain in place, or not notified of the fire situation. If necessary, a

phasing scheme can be used to evacuate the occupants on other floors depending upon the progress of fire suppression activities, or verification of the status of the alarm. Tall buildings can also incorporate specially protected and controlled elevators to efficiently and effectively evacuate occupants from upper floors.

Relocation strategies can be used to direct occupants to move away from the vicinity of the fire hazard to a safer place. This might include staff relocating patients confined to beds to an adjacent fire rated smoke zone in the event of a fire in their smoke zone. Event-based approaches allow flexibility through a selection of pre-planned scenarios, but rely upon real-time accurate information (situational awareness) provided to those in authority so that they can make effective decisions, react appropriately and relay necessary instructions. Pre-planning and training are essential. Regardless of the approach used, the means and type of occupant notification employed need to be coordinated with and appropriate for the overall life safety strategy. Egress strategies rely upon various building components and features such as doors, corridors, stairs, and exit passageways, to facilitate safe evacuation.

The specific strategy for a given facility might require more coordination and integration for certain systems. For example, coordination of fire detection and notification systems with the established evacuation protocols might be of key importance for tall buildings. Fire detection and evacuation zones need to be coordinated with fire zones or smoke compartments and their associated fire barriers. Evacuation or relocation messages need to match the evacuation strategy, and need to provide specific messages tailored to the strategy where relocation or protect-in-place strategies are used. The survivability from fire of the notification and two way communication systems should be considered so that people can continue to receive instructions during a fire regarding when and where to evacuate. Where partial or phased evacuation schemes are used, the communication systems may need to be coordinated to facilitate effective evacuation or relocation. Also, architectural and fire separation features may need to be coordinated with expected egress paths.

Compartmentation

Depending upon the overall goals, compartmentation, which is achieved through fire- and smoke-rated assemblies, and opening and penetration protection, provides necessary safeguards against the spread of fire and smoke within a building. The use of fire barriers is also used to limit or prevent the fire spread to adjacent buildings and structures. Codes and fire protection strategies require fire or fire and smoke rated barriers to separate exits and other portions of the means of egress from the effects of fire. Fire-rated and smoke-rated assemblies are also used to protect essential equipment and isolate more hazardous areas within the building. Table 49.1

Table 49.1 Typical fire-rated separations [11, 17, 18]

Protection goal	Potential protection strategies
Protect exits and limit exposure to vulnerable exit pathways	Exit stairways, exit passageways, exit discharges, horizontal exits, and corridors
Prevent or limit fire and smoke spread in buildings	Shaft enclosures, elevator lobby enclosures, atrium separations, smoke zone separations, tenant separations, storage rooms, waste and linen storage rooms, occupancy separations, floor fire ratings, edge of slab fire and smoke assemblies, hazardous use separations (control areas, paint shops, and certain furnace, boilers, and refrigerant machinery rooms)
Protect essential equipment	Fire separation for: elevator machine rooms, certain electrical transformers rooms, emergency generator rooms, fire pump rooms, fire command center, and survivability of fire alarm notification circuits or fire fighters two-way communication systems
Prevent or limit fire spread to adjacent buildings	Fire walls, party walls, sprinklers, exterior wall and opening protection, and building separation distances

identifies various fire protection goals and typical building spaces and features that require some type of fire separation or compartmentation.

Penetrations through fire-rated and smoke-rated barriers need to be protected with listed fire protection and smoke sealing products. Penetrations of rated walls can take many forms, from mechanical and electrical systems, such as ducts or conduits, to architectural openings or building features, such as lights or fire extinguisher cabinets. Duct penetrations can be protected by fire, smoke or combination dampers. Architectural openings can be protected by swing-type doors, horizontal sliding doors, or roll-downs. Doors held open by listed hold-open devices, and sliding or roll-down doors, need to close as required by the fire alarm function matrix and compartment scheme. The designer must consider the penetration protection and membrane protection for each of these breaches such that these systems do not defeat the passive system.

Detection Systems

Fire detection and supervisory devices combine to initiate critical features of most comprehensive life safety plans. Fire alarm systems are often a key system in the *interconnections* of various other fire protection and life safety systems [14].

Fire and Smoke Detection Selection of specific fire and smoke detection systems and devices should be based upon detection goals and objectives. Detection devices can include spot-type smoke and heat detectors, duct smoke detectors, linear heat detectors, radiant energy sensing devices, air sampling systems and video smoke and fire detection. Devices and systems can be integrated into the fire alarm and signaling system or can be separate, through standalone systems that integrate with the fire alarm and signaling system. Examples of standalone systems include air sampling systems in data centers, video detection systems within road tunnels, and hazardous material detection systems.

Sprinkler Water Flow Alarm-Initiation Sprinklers are heat activated devices that function well as zoned heat detectors. When the sprinklers actuate, water flows within the piping system. Water flow devices monitor sprinkler water flow through the fire alarm system, and initiate a water flow signal.

NFPA 72 allows a 90 s delay for water flow indicating devices to reduce the risk of false activation due to water pressure variations. This delay should be considered if the sprinkler system is used to initiate occupant notification [20].

Gas Detection Specialized detection devices and systems can be used to detect hazardous gases, such as general hydrocarbons, methane, carbon monoxide, chlorine gas, oxygen depletion and other hazardous gases. Detectors need to be calibrated to the specific gas, vapor or mixture expected. For flammable gases, the detector may occur at a pre-determined percentage of the Lower Flammable Level (LFL) or Lower Explosive Level (LEL), for example, 25 % or 50 % of the LFL or LEL. Once a specific gas concentration is detected, a signal is sent to the fire alarm control unit.

Manual Detection Manual fire alarm boxes (i.e. manual pull stations) allow occupants to initiate the signaling system. While these devices are important, relying only upon activation of manual devices in areas accessible to the general public should be limited and can be susceptible to nuisance activations. Consider a zoned healthcare facility with manual pull stations in each zone with an egress plan that calls for the relocation of patients to other zones. In this example, it may be possible for an untrained occupant to activate a manual pull station in a zone adjacent to the event zone. This manual system activation in the adjacent zone could initiate an incorrect sequence. A more appropriate configuration might be to locate manual pull stations at a constantly attended area (such as at

nurse stations), and in areas not accessible to the general public. With proper training, staff would then be able to appropriately and effectively activate the system through these manual devices.

Supervisory Functions A supervisory signal is activated when an off-normal condition occurs in a supervised system, or equipment. Examples include monitoring of sprinkler system control valves, low water pressure, and low and high air pressure in dry-pipe or pre-action sprinkler systems. Areas that are susceptible to freezing could be provided with low temperature alarms. If the fire suppression system is supplied through a water storage tank, the water level in the tank would be monitored.

In some facilities, the fire alarm system could be used to monitor certain aspects of a process such as the status of a pressure vessel. However, building and manufacturing processes are generally not monitored by the fire alarm system, but rather by other separate systems. Such separate systems may need to be integrated with the fire alarm system to initiate notification, means of egress activities or other functions such as the closure of doors, activation of ventilation fans, and similar devices.

Notification Systems

Occupants need to be provided with timely and accurate information so that they can understand the urgency of a particular event and make appropriate egress decisions. Emergency communication systems used for notification provide means for notifying a large group of individuals and for the fire service to communicate with occupants and other first responding personnel. As noted below, a public address system can sometimes be used for this purpose. There are one-way and two-way methods of providing communication.

One way systems include fire alarm notification, mass notification and public address systems. Fire alarm notification is commonly referred to as emergency voice/alarm communication systems and used to evacuate or relocate occupants during an emergency. NFPA 72 identifies four major categories of mass notification methods [20] that include in-building, exterior, personal and public mass notification. Public address systems would be found in airports, stadia and other large public assembly venues for general messaging and emergency notification.

Two way systems include communication between emergency responders, and emergency responders and building occupants. Communication between emergency responders can be either a wired or a wired antenna system that enhances the radio coverage within a building. Two way systems between occupants and emergency responders are used when individuals are unable to escape on their own, such as by being trapped in an elevator, or unable to use the exits.

Fire Alarm Notification Audible and visible notification of a fire situation is typically provided to occupants with horns or speakers and strobes. Alarm signals as well as pre-recorded and live instructions regarding means of egress can be announced. Alerting for hearing impaired individuals is generally provided with strobes for visible notification of an emergency. In some buildings, where a relocation evacuation strategy is used, such as hospitals and jails, chimes, bells or other signals are sometimes used to provide a coded notification to trained staff. In these cases, the audible notification provides a distinctive signal, which is usually only recognizable by staff. The selection and definition of the *Evacuation Signaling Zones* and notification zones are critical for fire alarm notification.

Mass Notification The following four major mass notification methods are available [20].

1. **In-Building Mass Notification** is obtrusive messaging within a building. These systems would not require any interaction from building occupants to receive the message and the building occupants cannot deactivate this system. This category could include a voice fire alarm system that is also used to broadcast mass notification messages, a public address system, a voice paging system that is

dedicated for mass notification, or activation of digital signage.

2. **Exterior Mass Notification** is obtrusive messaging outside the building. The system could be a tone, a voice message or a combination of both. Sirens used for warning during times of war and tornados are examples of exterior notification. High powered speaker arrays such as "Big Voice" systems used in military applications can be used to provide a voice message to broadcast specific instructions during an emergency. Outdoor notification is not intended to notify people within a building. Depending on the building construction, broadcasted messages may or may not be capable of alerting people in buildings.
3. **Public Personal Mass Notification** is personal alerting. Personal alerting messages target specific individuals. Methods of contacting an individual could be through short common message services such as text messaging, email, specific applications that display alert messages on computers or smart phones, and automatic dialing or reverse 911 to provide automated voice phone messages. Personal alerting can target a specific audience and limit the distribution. Personal alerting to a specific group such as emergency response team could provide details of an incident. Providing notification through personal alerting can be rather cost effective because individuals generally own the equipment and the organization is only providing the equipment to broadcast alerts. A challenge of personal alerting is maintenance of a current list of contact information.
4. **Public Mass Notification** is public notification. Previously, public alerts were broadcast solely through television and radio. A majority of the public alerts were weather alerts issued by the National Weather Service. In recent years, the method of transmitting public alerts has evolved. In the United States, the Commercial Mobile Alert System (CMAS) allows authorized national, state or local government officials to send text messages to a targeted geographic area. CMAS alerts are designed to be broadcast from select cellular towers in a geographic area. Systems are designed so that CMAS alerts have a higher priority over normal text messages and voice calls. Social networks allow anyone on the network to broadcast messages of events and users can follow messages from specific organizations (http://www.fcc.gov/guides/commercial-mobile-alert-system-cmas).

Public Address System Certain types of buildings containing public assembly such as airports and stadiums are generally provided with public address systems. Because of the nature of the live voice instructions and messages to be transmitted, these systems usually provide better audio quality than basic fire alarm systems. When properly designed, the public address system can be used for pre-recorded or live voice emergency messages. In addition to audible announcements, visible displays are usually also provided to relay captions of the spoken messages for hearing impaired individuals.

Two-Way Wired Emergency Communication Systems Communication between fire service responders is important during an emergency. Typically, high rise buildings were provided with fixed firefighter telephones or jacks to connect a hand-held phone to communicate with a central location or between multiple locations and the central location. Current codes require a radio enhancement system where most firefighters are equipped with a radio, rather than a wired system.

Two-Way Radio Emergency Enhancement Systems A radio emergency enhancement system is a common alternative to a two-way wired firefighter telephone system and required by model fire codes. A radio enhancement system improves the communication between the firefighters in a building, and dispatchers and command staff outside by boosting the radio signal inside of a building through a distributed antenna system throughout the building. The fire service is equipping a majority of firefighters with a handheld radio and this is their primary method for communicating during an

emergency. The building construction including steel framing and reinforcement prevents the radio signal from penetrating the interior portions of the especially large buildings such as high rise structures, hospitals, and shopping malls [10].

To provide the necessary radio coverage, a two-way radio enhancement system is provided. This system generally consists of an exterior antenna, a booster to enhance the signal and antennas strategically located throughout the building to enhance signals. An antenna system could consist of several single components, or a radiating ("leaky cable") that allows the messages to be received and transmitted through the entire cable.

Occupant Emergency Communication Systems Building occupants that are unable to use stairs can relocate to spaces such as areas of refuge where they are able to summon assistance from emergency responders. A two-way communication would need to be installed at strategic locations such as at areas of refuge to allow communication with emergency responders. Similarly, if stairway doors are arranged to prevent re-entry into the building from the stairway, a means of two way communication might need to be provided at discrete points in the stair.

Elevator Emergency Communication Systems Potential problems with elevator operations necessitate the ability for elevator occupants to communicate with others in the building to summon assistance or receive instructions. ASME A17.1 Safety Code for Elevators and Escalators [4] requires such a two-way communication system. Although not a common occurrence for most buildings, elevators specially designated and arranged for occupant evacuation might require additional features regarding means of communication.

Suppression Systems

Automatic sprinkler systems are required in many buildings as they provide an effective and reliable means of reducing fire hazards. Fire sprinkler systems are designed to suppress or control fires until the fire department arrives to extinguish the fire. Sprinkler systems can be wet pipe, dry-pipe, pre-action, or deluge.

Wet pipe sprinkler systems are connected directly to the water supply and are most common. Dry-pipe systems are used within areas subject to cold or freezing temperature. Dry-pipe systems are pressurized with air or nitrogen, rather than water. Activation of dry-pipe sprinkler systems cause the air or gas pressure to drop in the piping systems, which activates a dry pipe valve and allows water to flow through the sprinkler system.

Pre-action systems provide additional protection against false activation through interlocking the pre-action valve with a detection system. As with dry-pipe systems, the system can be pressurized with air or nitrogen. Through a releasing service fire alarm system, when a fire signature is sensed by a supplemental detection system, the fire alarm panel sends a signal that releases a pre-action valve which then allows water to enter the system piping. Deluge systems use open sprinklers with a deluge valve and a supplemental detection system similar to that for a pre-action system. As deluge systems employ open sprinklers or nozzles, water discharges from all nozzles and sprinklers once the system is activated.

Other special suppression systems, such as those that use or generate foam, carbon dioxide, clean agents, water mist, aerosols, and wet or dry chemicals can be more appropriate for specific hazards. In many cases, building and fire codes require sprinkler protection regardless of the presence of special suppression systems.

Fire detection used with pre-action, deluge, or special suppression systems are connected to releasing service fire alarm control units. These releasing systems are designed to activate the suppression systems upon detection of a certain fire signature. Such fire detection devices and systems need to be coordinated with the fire suppression zoning. The coordination of the releasing sequence is important as the suppression system relies upon the sequence for proper operation.

Table 49.2 Potential suppression systems supervision and monitoring interfaces [24, 27, 28]

System	Potential supervision and monitoring
Wet pipe system	Water flow, valve supervision, low water supply pressure
Dry-pipe system	Water flow, valve supervision, low water supply pressure, low air pressure
Pre-action, deluge, water spray, and special suppression systems	Water flow, valve supervision, low water supply pressure, low air pressure, releasing service fire alarm control unit supervision (alarm, trouble, supervisory, suppression system releasing sequence activated)
Standpipe systems	Water flow, valve supervision
Water supply tank	Low water reservoir, water reservoir empty, low water temperature, valve supervision
Diesel or electric fire pump	Pump running, controller switched to manual control, pump trouble, over speed deactivation, system overpressure, low pump room temperature, relief valve discharge, control valve closure, flow meter bypass condition, pump room intrusion
Diesel fire pump	Engine running low oil pressure, failure to start, high engine temperature, battery failure/missing battery, battery charger trouble, alternate ECM, fuel injector malfunction, low fuel, high fuel, low air pressure (air start engines), low engine temperature, fuel spill
Electric fire pump	Power phase reversal
Special suppression system	Discharge, detection, supervisory, trouble

A reliable water supply system is required for water based systems such as sprinkler, water spray and foam. The water supply can be provided through the municipal water supply with or without a fire pump, or through private fire service. Such private service might consist of private fire service mains, tanks and fire pumps. In some cases a secondary water supply is required such as might be the case for buildings located in certain seismic areas, or where the primary supply is not considered sufficiently reliable. Pressurized or gravity water tanks can provide the necessary water flow and pressure for municipal or private systems. Monitoring of water supply conditions and equipment, as well as detection of water flow and system activation need to be provided and coordinated.

System Supervision Most fire protection and life safety strategies rely upon the proper design, installation and operation of automatic sprinkler and other fire suppression systems. Approximately one-half of automatic fire sprinkler system failures are due to valves being inappropriately closed [9]. Given the reliance upon sprinklers in most fire protection and life safety strategies, control valve monitoring to ensure valves are open where required, is very important.

Generally, control and isolation valves on all sprinkler systems required for life safety purposes are required to be electronically supervised. Additionally, all standpipe supply, isolation, and control valves are normally required to be supervised. Water flow indicating devices are required to be connected to the fire alarm system and initiate an alarm. Table 49.2 lists suppression system equipment and system conditions that may require supervision and monitoring.

High-rise buildings are generally defined as buildings with occupied floors 75 f. above the lowest level of fire department access. These structures require additional reliability for the sprinkler systems, as fire service operations are hindered by the building height. Systems are provided to supervise floor control valves, and initiate supervisory signals to indicate system status. Examples of conditions that pertain to system status and which need to be monitored include valve position, low building temperatures, low water supply pressure, loss of electric fire pump power supplies, and low water tank levels.

Manual fire suppression is provided through standpipe systems and fire extinguishers. Standpipes can be standalone or combined with

sprinkler system risers. As with any water based system, valve position and water flow need to be monitored. Devices used to monitor fire extinguisher pressure and location can also be provided.

Smoke Control

Smoke from fires consists of soot, hot gases, and other products of combustion. Smoke can move through buildings and impact people or property remote from the fire zone. Smoke moves through ventilation systems running during a fire, through normal air currents like the stack effect, and through buoyancy created by the temperature difference between hot gases and ambient air. Smoke control systems are designed and installed to limit or prevent smoke spread, possibly maintain tenability, or to assist with post fire operations. The Handbook of Smoke Control Engineering [13] provides insight and information of the various types of smoke control systems.

The simplest form of smoke control is deactivation of the normal mechanical air-handling equipment through smoke detection and closing of smoke dampers to prevent smoke spread by the HVAC system and through building. Pressurization systems use pressure differences across barriers to keep smoke from moving to other areas of the building. With stair pressurization, stairs are designed as pressurization zones to limit the potential for smoke contamination into the stairs. Stair pressurization systems can incorporate pressurized vestibules, or vestibules with both supply and exhaust to purge smoke. Other pressurization methods involve floor-by-floor pressurization zones or multiple pressurization zones on each floor.

In large open spaces, smoke exhaust systems can be used to limit smoke spread within the space or to connected spaces. Exhaust systems are combined with mechanical supply or openings to provide outside air to remove smoke and limit its impact to people or property. High level vents in a large open space can be used to allow the effect of buoyancy to remove smoke.

Systems can also be provided for non-life safety post fire smoke purging. This can be achieved through manual override controls of the normal mechanical systems, switching the systems into 100 % exhaust and supply mode, or through operable windows or manual breakout windows to vent spaces post fire.

Smoke Control Components Smoke control supply and exhaust fans used to provide pressure differences or to provide the required volumetric air flow need to be controlled and monitored. Dampers may be needed to achieve intended system performance. Strategically located, automatically operated doors and vents are often used to provide make-up air for the smoke control system. Fans, dampers, and make-up air openings need to be controlled, monitored, and configured as necessary.

Mechanical Ventilation Systems Shutdown Mechanical air-handling equipment may need to be deactivated when the smoke control systems is activated. Deactivation of associated fans occurs through interruption of power to the devices or through the building management (BMS) system controls.

HVAC systems that recirculate air beyond the enclosing walls, floors, and ceiling of the room or space of concern are generally required to be deactivated to prevent the spread of smoke during a fire. Generally, a system with a capacity greater than 2000 cfm is required to be deactivated [11, 23].

Smoke Barriers Smoke barriers penetrated by ductwork require smoke dampers that close upon detection of smoke. Smoke detection is provided throughout the entire area served or a duct smoke detector located usually within 5 f. of the smoke damper. On activation of the associated smoke detector, the fire alarm system transmits a signal to close the effected smoke damper or deactivate the HVAC system that controls power for the smoke dampers and fans.

Other Ventilation Systems

Mechanical systems other than those used for smoke control may need to be controlled and monitored and be coordinated with the overall building *life safety systems* to avoid hazardous conditions. For example, mechanical systems may need to be deactivated and dampers closed within spaces using gaseous fire suppression systems, or parking garage exhaust systems that do not operate continuously to save energy may need to be activated to avoid hazardous carbon monoxide levels. Hazardous material exhaust systems are another example. Hazardous exhaust systems for laboratories, fume hoods, fabrication areas, gas storage rooms, process rooms, and similar spaces, are critical and need to remain in operation during a fire. Deactivating hazard exhaust systems during a fire could create a secondary hazard.

Emergency and Standby Power

Emergency and standby power systems are often required to provide reliable alternative power source for essential *life safety systems* during loss of primary power. Emergency power systems serve essential equipment where interruption would cause life-threatening safety or health hazards. Emergency power systems are required to transfer power within 10 s of loss of primary power [29]. Typical systems requiring emergency power include exit signs, means of egress illumination, elevator car lighting, emergency voice/alarm communications systems, automatic fire detection and gas detection systems, fire alarm systems, sprinkler alarm and supervisory system, electrically powered fire pumps, power doors and locks in certain types of occupancies, and essential hazardous material safety systems such as laboratory hoods. Emergency power may be necessary for energy saving lighting controllers and house lighting controls for dimmable arena, theater, and similar lighting to appropriately initiate the emergency lighting sequence.

Standby power is categorized within NFPA 70 as legally required and optional. Legally required standby systems mandate a 60 s transfer time after loss of primary power. The National Electrical Code notes legally required standby power is typically provided for systems that "create hazards or hamper rescue or fire-fighting operations" if interrupted [29]. Legally required standby power systems typically supply elevators, air compressors for dry-type and pre-action suppression systems, inflation systems for membrane structures, accessible means of egress elevators and lifts, evacuation elevators, horizontal sliding doors, and smoke control systems, as well as sewage disposal, critical industrial processes, and similar equipment [25, 29].

In healthcare facilities, a critical supply branch is provided as a subsystem to the emergency power system, and supplies power to critical equipment, and essential electrical systems that could cause immediate danger to patients [22].

Optional standby power is provided for systems that are not required for life safety, but are provided to continue important operations or processes. Owners may elect to supply other equipment and systems through optional standby power [25, 29].

The emergency or standby power systems can be supplied through a battery system, a generator set, an uninterrupted power source (UPS), a separate service (where approved), a fuel cell power system, or through unit equipment (i.e., batteries integral to the equipment). An automatic transfer switch senses the loss of power and switches to emergency or standby power. UPS systems are different from other emergency or standby power systems, as UPS systems provide continuous power without interruption during loss of primary power, for certain design durations. In some cases, the power source status and the automatic transfer switches are required to be monitored [26, 29].

Generator sets are required to be provided with an automatic remote start capability, a "Run-off-automatic" switch, and controls to automatically and manually shut down and lock out the prime mover. Alarms for generators include: over crank, low water temperature,

high engine temperature pre-alarm, high engine temperature, low lube oil pressure, over speed, low fuel main tank, low coolant level, emergency power system supplying load, control switch not in automatic position, high battery voltage, low cranking voltage, low voltage in battery, battery charger power failure, low starting hydraulic pressure, air shutdown damper (when used), and remote emergency stop [25].

Elevators and Escalators

In most buildings and structures, occupants are instructed to use the stairs and not use the elevators as a means of egress in an emergency. Elevators are designed to automatically recall to a lower floor, typically the level of exit discharge, upon dedicated elevator smoke detector activation. This arrangement largely prevents the elevators from being used as a component of means of egress. Elevators used for accessible egress is an exception. The intent is for the accessible egress elevators to be used for assisted rescue. Elevators are equipped with a manual over ride feature for use by the fire service to facilitate assisted rescue operations and to assist fire-fighting and emergency operations.

With the proliferation of tall buildings around the globe and the development of new elevator protection schemes [4, 11, 17], evacuation elevators now are generally permitted. These specially designed evacuation elevators allow occupants to use the elevators under certain emergency conditions. In most cases, evacuation elevators supplement rather than reduce the number and capacity of traditional means of egress components.

Elevator Emergency Recall and Emergency Operation Smoke detector actuation in an elevator lobby, elevator machine room or elevator shaft initiate Phase I emergency recall, which is designed to return elevators to a lower level and open the doors to allow occupants to exit the elevator cab during a fire emergency. Typically, elevators are not recalled by activation of any other detector in the building, but this varies in some jurisdictions. When the elevator is recalled, a special indicator in the elevator car is typically illuminated. When an elevator machine room smoke detector is activated this indicator typically flashes to warn fire fighters in the car of this situation. After recall, the elevators are available for fire service use.

Phase I recall returns all elevators to the lobby on the level of exit discharge. In most buildings, this is the first floor. If the smoke detector in the elevator lobby on the level of exit discharge activates, the elevator would return to the alternate level. Typically, the alternate recall level for the elevator is the second floor or a basement level depending on which level is most accessible to the fire service.

Phase II emergency operation is initiated manually by the fire department. A key operated switch located in the elevator lobby and in the fire command room initiates Phase II emergency operation. A second key operated switch located in the cab allows the fire service to take control of individual elevators.

Elevator Power Shunt Trip In some cases, the applicable building code requires sprinklers to be installed in the elevator machine room or shaft. Elevator equipment power is designed to be disconnected before the sprinkler actuates to prevent damage to the elevator controls, power equipment, and people.

The hoistway heat detector and water flow indicator, combined with elevator recall operations, are designed to allow elevators to be recalled and deactivated before the shaft sprinkler actuates. The flashing special indicator, such as a fireman's hat, warns that smoke has been detected in the elevator machine room, and indicates that the shunt trip may soon activate.

Emergency Evacuation Elevators Walking down many flights of stairs from upper floors of high-rise buildings and tall structures can be difficult for some and impossible for others. Even buildings of modest height pose evacuation issues for a percentage of the population, like

the elderly, injured occupants and occupants with medical conditions and mobility impairments. Emergency evacuation elevators continue to gain acceptance for providing a means of egress in tall buildings for people with mobility impairments or otherwise unable to use the stairs to exit [34].

Both the Life Safety Code [17] and the International Building Code [11] allow emergency evacuation elevators to serve as a means of evacuation with specific limitations. The Life Safety Code limits the use of emergency evacuation elevators to observation, control, operation, and signaling towers. The International Building Code allows evacuation elevators as an alternative to the required additional stair within buildings over 420 f. (128 m) tall. Emergency evacuation elevators only operate prior to Phase I emergency recall, as recall activation indicates that smoke is in the elevator lobby or that responders have determined the evacuation elevators should not be used.

Fire Service Access Elevators In the International Building Code, fire service access elevators are required for high-rise buildings with an occupied floor over 120 f. above the lowest level of fire department access. In these buildings, every floor is required to be accessed by the fire fighter elevator. The fire service access elevators recall under the same conditions and follow the same recall sequences as the other building elevators.

Escalators Deactivation Most building and life safety regulations do not allow the use of escalators as a component of a building's means of egress. There are some exceptions to this general rule such, as where they are needed to meet the objectives of the fire protection and life safety strategy or to meet local requirements. In these cases, escalators typically need to be powered down and slowed to full stop when the fire alarm actuates. NFPA 130 allows for the use of escalators as a component of the means of egress, and requires escalators operating opposite the egress direction to deactivate, slowing to a stop [15].

Access Control Systems

Access control and security system designs need to balance safety with security. Life safety needs to override security in most cases to allow occupants to escape, and access control features that are part of security systems, such as delayed egress locks, stair door locks, detention facility locks, and other security door locking arrangements, need to allow for egress during emergency conditions [11]. Components need to be carefully coordinated and tested to be sure the systems meet the appropriate design criteria and function as intended.

Electrically controlled egress doors may be required to be locked under normal building operations for security, but during an emergency the doors must be unlocked. The interface with the fire alarm system can be completed through a variety of methods. The fire alarm system can provide an output to the access control system. The access control system must be programmed to operate the required doors. For latches that are fail safe, the latches are normally powered and when the power is released, the doors unlock. In this case, the fire alarm system can intercept the power circuit to remove power to the latch. This strategy eliminates the risks associated with changes to the access control system that impact the unlocking of secure doors.

Delayed Egress Locks Delayed egress locks can be an effective means of providing a measure of security while allowing occupants a reasonable level of safety. For these systems, specific doors are normally locked but unlocked within a set amount of time, typically 15 s, after the push-bar hardware is used. Delayed egress doors unlock immediately upon loss of power, sprinkler water flow initiation, and activation of a smoke detection system. Signage is provided to alert and inform occupants of the delay [11].

Stair Door Unlocking Some arrangements require a floor level to be secure from other floors. When this is important, stair doors can be provided with hardware that prevents re-entry from the stair side, securing the floor from other floors. Stair door locking requires a means to simultaneously unlock all doors during an emergency [11].

Secure Facilities Lock-down areas in detention, correction, and healthcare facilities are of particular concern. Since detainees cannot freely exit to the exterior, detainees are moved to adjacent smoke compartments during an event. This arrangement requires smoke and fire barriers to separate compartments, along with a means for guards to quickly unlock doors and for staff control or assist movement [11].

Other Control and Monitoring Systems

The fire and life safety strategy may require interfacing with a wide range of systems, including: process control systems, explosion detection and suppression systems, CBRN (chemical, biological, radiation, and nuclear) detection, carbon monoxide or other hazardous gas detection, medical and other gas shut-down, laboratory system control, SCADA (system control and data acquisition) systems, nurse call systems, and special effects and amusement feature shut-down and control. Process controls may need to regulate and safely shutdown process, reaction vessels, or oven or other heating systems. An extreme example is the safe shutdown of a power plant. Airport baggage systems may need to be deactivated. Lighting control needs to initiate emergency lighting sequences. Explosion or hazardous gas detection systems may need to activate notification sequences, or initiate equipment de-activation, activation, or other sequences. Gas systems may need to shut down. Laboratory control systems may need to initiate exhaust sequences, or de-energize heating or other processes. SCADA systems control and integrate complex road, rail and process systems. As an example, SCADA systems can combine roadway tunnel fire detection, emergency notification, traffic signaling and control, emergency ventilation, normal ventilation, and CCTV into an integrated operator console. Nurses call systems may need to initiate a coded emergency message that without alerting patients.

Emergency (Fire) Command Center

Emergency command centers and fire command centers should be in a central location within a high-rise building that contains information on the status of all of the required fire protection and life safety features. From this location, the fire department and responding personnel can determine the status of the various building systems that could impact life safety, fire department operations, and control certain systems [11, 17]. The following list identifies the features of the emergency command center that require coordination and interfacing.

- Emergency voice/alarm communication system, which provides the ability to select specific areas of the building to be evacuated and provide the ability to broadcast live voice messages to selected areas of the building.
- Fire department communications systems, such as a firefighter telephone or radio system that allows communication within the building.
- Fire alarm system annunciation including the locations of detectors in alarm, off normal conditions with the fire suppression system, and faults with the fire alarm and other systems.
- Status indicators and controls of the air distribution system. This allows the fire department to control the air distribution system if the system is not functioning in the intended state.
- Control panel for the smoke control system in the building is required in many codes. The controls will allow the fire department to activate and deactivate the smoke control system.

The smoke control panel is required to be UL Listed to category UUKL.

- Security is a major concern; therefore, it is very common for the stairway doors to be locked to prevent unauthorized access. To facilitate access for the fire department to each of the floors, controls are necessary to automatically unlock all of the stairway doors.
- Status of the sprinkler water flow and valve equipment is required. Generally, this information would be provided through the fire alarm system, but in some cases the sprinkler system may be monitored by a separate system.
- Emergency and standby power status indicators is required. Typically this information is provided by a remote annunciator from the automatic transfer switch. An alternative is to monitor the transfer switches by the fire alarm system.
- A telephone connected to the public telephone system are required. This allows the fire department to contact responsible parties during an emergency.
- The status of the fire pump system is required. The status will inform the fire department if the fire pump system is running, impaired, or not operating due to a failure or fault.
- Generator monitoring, manual start and transfer indicators are required.
- Public address system to provide voice announcements when required. Generally, a public address system would be found in stadium facilities, conventions centers or similar public assembly facilities. Coordination and integration of the public address system with the fire alarm system and/or the emergency communication system is needed to eliminate conflicting messages.
- Elevator controls that contain recall switch(es) to initiate elevator recall is needed.
- Elevator standby power selector, for elevators provided with emergency power, is required. This allows the elevators to be transferred to emergency power manually if necessary.

Summary

Fire protection and life safety strategies may require a wide range of system coordination and interfaces to accomplish the stated goals and objectives; Table 49.3 summarizes typical system interfaces.

System Integration Considerations During the Design Process

The reliance on active systems to enhance or maintain safety has allowed designers greater flexibility to express architectural vision and meet owner and stakeholder goals. The number of active systems involved has steadily increased over the years. These systems, introduced in section "Systems Overview" above, are largely automated, which has allowed them to be integrated with other systems to better coordinate the response of the overall fire and life safety strategy, and to ensure that one system does not negate the effectiveness of another. For example, a fire alarm system has been permitted to be interconnected via an *emergency control function interface device* (relay) with a sound system for many years [20]. When the fire alarm activates, it shuts down the sound system so that the fire alarm system is audible. As technology has progressed the ability to interconnect various systems has become easier. Although the codes have not kept up with leading edge communication capabilities of these systems, they have recognized the benefits of *interconnected systems* when implemented properly and now allow for more direct communication, interfacing, and interoperability between systems.

Once the goals, and objectives, and strategies related to fire and life safety are developed and agreed to by the design team and stakeholders, the *Basis of Design* (*BOD*) can be developed to identify the concepts and approach of the design. The design team can then design the individual systems and systems integration to meet the *BOD*.

Table 49.3 Coordination and interfacing examples

Systems	Possible components and example features
Egress	Actuate security door unlock sequence, emergency lighting, emergency notification, and exit marking—audible notification,
Compartmentation	Actuate release, rolling and accordion doors release, fire/smoke shutter release, and fire/smoke damper release
Detection and notification systems	Fire and smoke detection, gas detection, actuate emergency notification, smoke control activation, SCADA (System Control and Data Acquisition) control functions, process shut-down, paging/music system shut-down, house lighting controls interface, and special suppression system release
Mass notification systems	Actuate building notification systems, initiate telephone voice messaging or text messaging, initiate textural display devices, initiate computer pop-up messaging, and interface with wide area mass notification system
Emergency communication systems	Actuate building notification systems, area-of-refuge communication systems, elevator communication systems
Fire suppression	Actuate water flow alarms, tamper switches (supervisory), low water pressure monitoring, special suppression releasing service, kitchen hood system monitoring, laboratory hood and duct system suppression monitoring and control, fire pump monitoring, and secondary water storage tank monitoring
Smoke control	System feature control (fan control, damper control, door control, fire/smoke shutter control, and other operable element control), smoke control panel overrides (manual override), and positive status indication (monitoring) of key smoke control components (such as dampers, fans, natural supply openings)
Other ventilation and conditioning systems	Fan deactivation and damper closure, parking enclosure exhaust control, hazardous exhaust and fume hood system control
Emergency and standby power	Generator monitoring and control, power status monitoring, emergency lighting control, solar and other power source shut-down, and providing operating power to various fire protection and life safety systems
Elevator and escalator	Evacuation elevator actuation, elevator recall, elevator power shunt-trip, escalator shut-down
Security systems	Access control, unlock secured doors, emergency lighting activation, emergency notification
Other systems	Building Management Systems, Security Systems, explosion suppression systems, hazardous gas detection, CBRN (Chemical Biological Radiological, and Nuclear) detection, carbon monoxide detection, medical and other gas system shut-down, process and other equipment deactivation, airport baggage system deactivation, laboratory equipment control, nurse call systems, SCADA control and monitoring functions, special effects and amusement feature deactivation and control
Emergency (fire) command centers	Voice fire alarm system panels and controls, fire department two-way telephone communication service, fire detection and fire alarm system annunciation panels, public address system controls, elevator floor location and operation annunciators, elevator fire recall switch, elevator emergency power selector switch(es), sprinkler valve and water flow annunciators, emergency generator status indicators, controls for stairway door unlocking system, fire pump status indicators, and controlled access public telephone for fire department

In large modern buildings, the designer must consider all of the systems and how these systems are intended to interact with each other. The designer must identify the intended function of each system and what, if any, *interconnection* is needed or desired. It is important to note that the system may have multiple desired functions depending on the event. As identified in Table 49.3, various types of building systems can affect fire and life safety.

Proper i*nterconnection* of all these systems requires interaction between many design professionals with the fire protection engineer often serving as the central point of contact and coordination as illustrated in Fig. 49.1. The following identifies design team members that may be involved in the design and coordination process. The degree of involvement depends upon the size and complexity of the project, owner requirements, code requirements, and project requirements:

1. Owner or Owner's Representative
2. Architect
3. Engineer of Record for each discipline
4. Fire Protection Engineer
5. Contractor
6. Sub-contractors installing the various fire protection and life safety systems
7. *Commissioning Authority* (*CxA*)
8. *Fire Commissioning Agent* (*FCxA*)
9. *Integrated Testing Agent* (*ITa*)
10. Insurance Representative
11. Third Party Testing Entity
12. Authority Having Jurisdiction (AHJ)—traditionally building and fire departments.
13. Emergency responders

Various levels of coordination are likely to be needed. The first level is typically among the architect, engineers, and owner. The *FCxA* and *ITa* may also be involved in this first level of coordination, depending on when they are incorporated into the project. The design team develops a strategy and package of information to meet the project objectives and goals. The package may include a Fire Protection and Life Safety Report, Narrative Report, Basis of Design, coordinated drawings (identifying interfaced points, locations, and methodologies), and sequences of operations of the various systems [30]. These documents will likely be updated

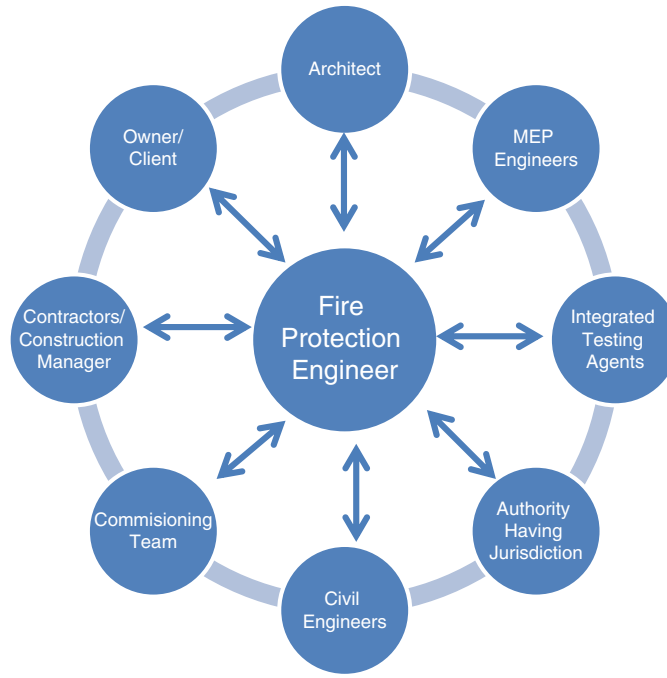

Fig. 49.1 Fire protection and life safety coordination team

throughout each phase of the design process and should incorporate modifications that have occurred in construction.

It may also be prudent at an early stage to meet with the Authorities Having Jurisdiction (AHJ), typically the building and fire official, to review the strategies and goals of the project, particularly if the approach may require a Code Variance, Modification, or Appeal. The overall project strategies, project goals, and *BOD* will eventually be reviewed by the AHJ when permit drawings are submitted. Therefore, it is advisable to meet with the AHJ and obtain their agreement and acceptance of the coordinated design as early in the process as possible. The AHJ may require a third party to support the review process.

The *FCxA* and *ITa*, if part of the project team, should be involved during the design phase of the project to participate, review, and comment on the plans and specifications during the design phase. Their review, as an owner's representative, should incorporate the project's goals and objectives. The goals and objectives should also guide the development of the *commissioning plan* of the individual systems and the integrated commissioning plan of these systems, without designing or redesigning these systems [6].

During the design phase the design documents are updated, refined, and modified based on the coordination and integration of the fire protection and life safety systems from the Engineer of Record or from comments/clarifications from the coordination team members.

Design Considerations

When designing fire protection and life safety systems, an initial step is to identify the purpose and ultimate goal of each system being installed. Identifying this purpose will assist the designer in recognizing what other systems need to be relied upon or what other systems need to be interconnected. For example, providing a total flooding gaseous suppression system in a space that is also provided with an automatic smoke control system may not allow either system to achieve the intended purpose. The smoke control system may be designed for a specific size fire that relies on the special suppression system to control the fire size. Clearly, the smoke control system would remove some of the suppression agent defeating the system's ability to control the fire and potentially overwhelming the smoke control system.

The individual system designer must be aware of the wide range of building systems that can affect the system(s) for which they are responsible and that may need to integrate with their system. To integrate these systems successfully, the designers of each of the systems need to work together to identify when and where *interconnections* will occur, priority of control for each system and shared components, fail safe conditions, *data sharing connections*, and design remediation for when system functions may conflict but cannot be addressed through system operations. One of the first items that needs to be coordinated for all of these systems are space requirements within the building. Each system must have enough space to ensure not only proper operation and function, but also so that adequate access is provided for maintenance and testing activities.

Multiple designers will provide input into the design and integration of the various systems. This information must be assembled and coordinated. Several common systems, although not necessarily integrated in all cases, still require multiple designers to be involved. Figure 49.2 provides examples of systems and the designers that would be involved with their design and integration.

A brief discussion of the decisions concerning integration and coordination of various types of systems is provided below.

Egress The egress system may have several goals ranging from relocation, to shelter in place to full evacuation. Depending on the overall goals, the designer must consider and address several systems. If the facility relies upon trained staff, individual staff responsibilities need to be identified. Coordination is needed among the fire protection engineer, architect, and owner to establish the egress goals and determine what

System \ Discipline	Fire Protection Engineer	Electrical Engineer	Mechanical Engineer	Structural Engineer	Controls Designer	Architect	Acoustician	Security Designer	IT/Comms	Plumbing Engineer	Commissioning/ Integrated Testing Agent
Smoke Control	X	X	X	X	X	X			X	X	X
Stair Pressurization	X	X	X	X	X	X			X		X
Dampers	X	X	X		X				X		X
Elevator Recall	X	X			X				X	X	X
Detection/Notificatio	X	X	X		X	X	X	X	X	X	X
Emergency Standby Power	X	X	X	X					X		X
Sprinkler	X	X		X		X				X	X
Alternative	X	X			X	X			X	X	X
HVAC	X		X		X	X			X		X
Standpipe	X			X		X				X	X
Fire Pump	X	X							X	X	X
Fire Command Center	X	X	X		X	X			x		X
Door locking etc	X	X			X	X		X	X		X
Compartmentation	X			X		X	X				X
Emergency Communications	X	X					X		x		X

Fig. 49.2 Typical coordination responsibilities

active systems will need to be in place to achieve the goals. Individual systems that affect egress can include fire alarm and notification, elevators, stair pressurization, security, and compartmentation. The designers need to address the individual integration concerns for each system but also have a broader view on how each system affects egress.

Doors being held open need to be coordinated to determine if the hold-open device will be on low voltage circuits or standard building circuits. Depending on the jurisdiction, the voltage of the circuit could impact which contractor installs these circuits and equipment. *Emergency control function interface devices* (relay) from the fire alarm needs to be provided to disconnect power to the doors when they need to close. Coordination is needed to determine if each door is individually controlled or controlled through a common circuit serving multiple doors. This also needs to be coordinated with security functions such as turnstiles, gates and locked doors. Power needs to be provided to the powered doors (e.g. shutters, and sliding doors) and the need for emergency power should be considered. Latching conditions need to be considered for both normal power operation and under conditions such as power failure. If the door needs to remain latched but unlocked in the fail safe condition, this needs to be coordinated among the electrical engineer, architect, hardware consultant, fire alarm designer, security designer, and fire protection engineer.

Compartmentation Fire and smoke separations need to coordinate with the overall fire protection and life safety strategy and need to match the egress strategy. Smoke control zones boundaries, and associated fire and smoke separations, need to match the smoke control strategy. Sprinkler zones also need to match the smoke control zones if they are used to activate the smoke control system and evacuation strategies. The overall strategy needs to account for closure of opening protection components, such as doors held open with hold-open devices, roll-down or horizontal sliding doors, fire dampers, smoke dampers, and combination fire and smoke dampers.

Most buildings will have dampers located in rated walls, such as shafts. The architect or fire protection engineer will identify rated walls, and the mechanical engineer will design for dampers at locations where the ductwork penetrates a rated wall. The electrical engineer must consider how power is provided and voltage requirements for the damper circuits, and may need to coordinate with the controls designer depending upon how the damper is controlled. In some cases, placement of the damper position will need to

be coordinated with the structural engineer for cuts or notches in the building structure and the architect to provide access panels.

Generally, a fire damper is activated by a fusible element that melts releasing the fire damper. The activation of a fire damper is similar to a sprinkler. Smoke dampers are required to be powered to control the damper. Typically, a smoke damper is wired fail safe so the damper must be powered to be open.

The designer must coordinate the closure of smoke dampers with the controls for fan operation. The closure of a damper without deactivating the fan could significantly damage the ductwork. The design should deactivate the HVAC system components to prevent potential damage. Duct smoke detectors require a minimum pressure differential for air to flow through the detector sensing chamber per individual manufacturer installation instructions. Typically, when the air system is not operating the pressure differential is not within the equipment listing and the smoke dampers must be closed.

Example: HVAC Shutdown

Mechanical ventilation systems can recirculate air within spaces served by the HVAC system. In a fire, these systems could spread smoke from the room of origin to other areas of the building. The areas remote from a fire could be overwhelmed quickly by smoke. Typically, applicable codes and standards require the HVAC system to be deactivated when a system has a design capacity greater than 2000 cfm. HVAC systems with a larger design capacity and that serve multiple floors, typically 15,000 cfm, may require a smoke detector at the return for each floor.

Duct smoke detectors are necessary to determine if smoke is present in the HVAC system. Smoke detectors are typically located in the return air ducts after the last inlet, and before air is exhausted to the outside or mixed with outside air. These detectors deactivate the associated HVAC system to prevent recirculation of smoke beyond the location of the fire. If smoke dampers are present, additional smoke detectors are generally required within 5 f. of each smoke damper. Generally, all duct smoke detectors are monitored by the fire alarm system. In some instances the smoke detector may be integral with the smoke damper.

After smoke is detected, the mechanical ventilation system serving the area is to be deactivated as a minimum. Additional systems might also need to be deactivated. Depending on the size and use of the building, all of the mechanical systems could be shutdown to simplify programming and testing.

The method upon which the mechanical ventilation system is to be deactivated will depend on how the system components are controlled. The fans that are associated with the mechanical ventilation system may be controlled by a motor starter. The motor starter has a control circuit that activates a contactor that provides the higher voltage and current to a mechanical system component like a fan. The control circuits are typically 120 VAC or 24 VDC. The building management system could control the operation of the HVAC system components.

The following are some potential methods to control an HVAC system.

- An *emergency control function interface device* (relay) controlled by the fire alarm system could be located in the control circuit of the motor starter. The relay may be in series to allow control of the equipment by multiple systems. For example, the control circuit could pass through relays for fire alarm, and building management system.
- If the fans are controlled by a building management system, the fire alarm system could provide an output through an emergency control interface

(continued)

(continued)

(addressable output module or similar) to deactivate the mechanical systems. With this interfacing method, the building management must be programmed to deactivate the mechanical systems when the output is received. Changes to the building management system program could prevent the mechanical systems from deactivating in a fire condition. It is important that if the building management system program is changed, the necessary deactivations are verified similarly to the testing requirements for changes to the site specific software used by the fire alarm system.

- Newer motor starters and variable frequency drives (VFDs) are microprocessor controlled. This equipment generally has a dedicated input for fire shutdown mode. This capability might be an option and therefore must be specified by the design team.
- In older buildings, the control circuit may be required to be powered to deactivate the fan. For these systems, a power circuit is required to be provided to initiate the deactivation. The presence of power must be monitored, typically with a relay and an addressable input module. The addressable output module is typically used to deactivate the fan. This output module is required to be located close to the motor starter to reduce the possibility of wiring damage impacting the shutdown of the ventilation where this wiring is not supervised.

Detection Systems The design of the detection components of the system should consider the technical criteria and equipment selection, and should review device locations so that proper maintenance can occur after they are installed. The owners' property protection goals should be considered and may require additional detectors or types of systems with alternative alarm thresholds. For example, an atrium smoke exhaust system may require smoke detection with an alarm threshold that is lower than typical detectors. Detection zones likely need to match smoke control, egress, and notification zoning.

Gas Detection Systems Gas detection systems need to be coordinated with fire detection and alarm systems. The designer must consider how to make the notification distinct to affect the proper response from occupants. Location, color, and sound of the alarm needs to be considered with respect to other warning devices. There should be special considerations for occupant notification and off premise reporting of these hazardous conditions.

Notification Systems Fire alarm and signaling regulations, such as NFPA 72, continue to change to reflect the multiple modes for notifying occupants. In fact, the title of 2010 Edition of *NFPA 72, National Fire Alarm and Signalling* Code, has changed to represent this broader focus. Items such as Mass Notification (Emergency Communication Systems) use monitors and other text devices, as well as cellular text messaging and phone messages, as means to provide notification. Mass notification systems can take the form of integrated fire alarm systems over multiple locations or be a completely separate and independent system. The design must consider priorities and which parts of the systems will be used simultaneously [20]. For other means of notification, interface is often accomplished via a network and industry standard communication protocols. Manufacturers offer web based applications that can text and phone individuals or large groups of people to notify of an event detected by the fire alarm system. The fire alarm system can also be integrated with other systems, such as public address and public information systems. A common example of this is in sport stadia and arenas where the large display screens or "jumbo-trons" and all of the flat panel displays can be used to indicate a fire or other emergency event and provide instructions for evacuation or other actions. This requires the designer to consider what systems will be

utilized, whether appropriate redundancy and protection is provided, and which system will have priority for any shared equipment.

Interface with other systems such as general sound systems or other displays that could distract occupants from emergency instructions may also need to be deactivated or otherwise controlled. It is critical that the operation and zoning of the fire alarm system is coordinated with the emergency response plans, evacuation procedures, risk analysis, and emergency communication system strategies.

The type and mode of emergency communication needs to be coordinated with the fire and life safety consultant and the Authority Having Jurisdiction. Depending on the system chosen, the engineers and fire alarm manufacturer may need to coordinate locations, distances and number of devices operating at once for a wired system. If a radio system is used, coordination with the IT and Communications consultant will be necessary to provide the necessary infrastructure and to determine if there are conflicts with other radio systems.

The notification strategy for the fire alarm system must be coordinated with the evacuation strategy and the fire and smoke separation strategy. Public address systems require coordination with fire alarm notification systems and Emergency Communication Systems to ensure proper prioritization and avoid several audio systems being used simultaneously to make the emergency message non-intelligible. Similarly, the designer must consider the acoustics of the area being notified. In a building lobby with mostly hard surfaces, providing more, lower wattage devices will likely be necessary to achieve intelligibility. If the notification strategy provides different messages in different areas, the acoustic separation of the areas needs to be considered. In a large concourse or mall, it may be desirable to evacuate an area near to the event while only alerting areas remote from the event. If the space is open, the interface between where people receive the evacuation message and the alert message needs to be designed such that the messages can be distinct and understood.

Coordination is particularly important in high-rise buildings, where generally the fire floor, and one floor immediately above and below are initially evacuated. Emergency Voice/Alarm Communication Systems (EVACS) are required in buildings where relocation instructions are provided to the occupants.

In some cases fire alarm signals can be deactivated in the event of a higher priority mass notification event, when based upon an approved risk analysis and approved emergency response plan. The impact of an in-building mass notification system must be considered when designing a fire alarm notification system [20, 33].

To effectively communicate an emergency message, the notification scheme may need to consist of multiple alerting methods, such as voice, text, and strobes, and be coordinated with the emergency response plan. The emergency response plan should dictate when each of the alerting methods would be used. For example, in the event of an active shooter on a college campus the strategy might be discrete and provide notification through emails, automatic dialing, popups on computers, and text messages. For an immediate threat such a tornado, where individuals should quickly seek shelter, the response might consider obtrusive outdoor alert sirens, automatic dialing, weather radio alerts, and the Commercial Mobile Alert System.

Depending on the equipment configuration, other building systems such as a phone system could provide supplemental notification functions for mass notification. For example a phone system in a building can provide localized obtrusive in-building and personal alerting. Messages can be displayed on the phone if the device is equipped with a display, or each individual phone extension could be called to broadcast a message. Alternatively, current calls can be dropped during an emergency, and the speakers can activate at the maximum volume to broadcast the emergency message.

Emergency Control Functions The fire alarm system may need to provide a variety of control functions. The system may need to interface with

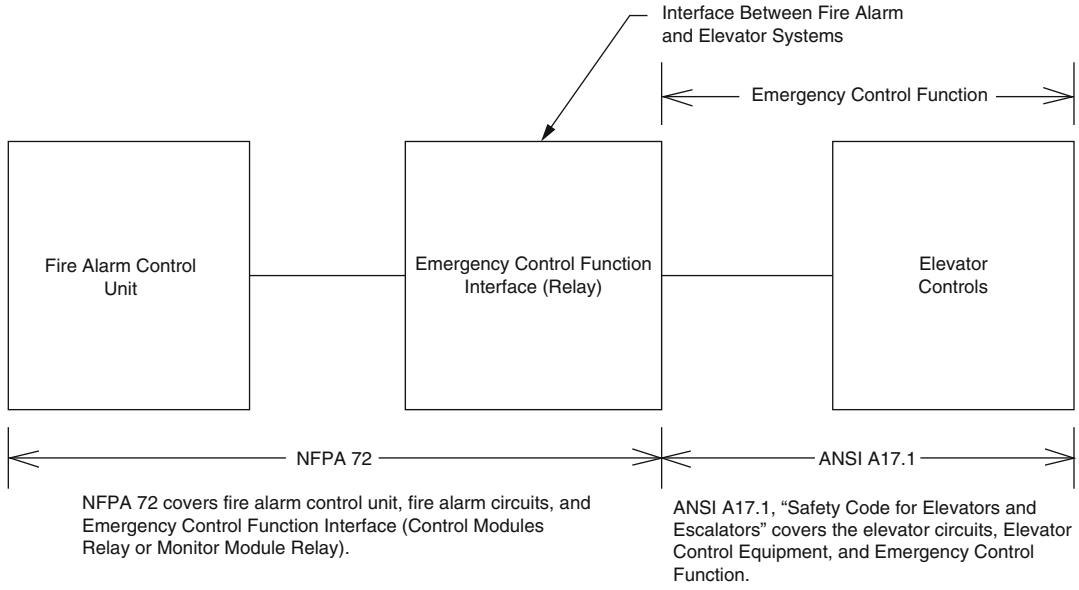

Fig. 49.3 Fire alarm system emergency control for elevator system

the elevator controls to initiate emergency elevator functions, such as elevator fire service recall, or initiate elevator shutdown. Where occupant evacuation elevators are used, the fire alarm system needs to initiate elevator evacuation mode, as well as elevator recall and shutdown. Figure 49.3 illustrates a fire alarm system *emergency control function interface device* (relay) for items such as elevator recall, shunt trip, and recall indicators. Elevator recall would be controlled by the elevator controller. The fire alarm system typically provides relays to the elevator controller. This output can be from addressable output modules or from a relay output card that is installed in the fire alarm control unit. Once elevator recall has been initiated, a key operated switch must be activated to return the elevators to normal service. Restoring the fire alarm system to normal would not automatically return the elevators to normal operation. The system may also need to initiate HVAC system shutdown, initiate door and shutter closure, and release locked doors.

An example of the division of design responsibilities during the design phase for integration of the fire alarm and elevator systems via an *emergency control function interface device* can be seen in Fig. 49.4.

The use of *emergency control function interface devices* (relay) on a fire alarm system to interface elevator controls may include initiation of the following modes:

1. Elevator evacuation sequence
2. Primary Elevator Recall
3. Alternate Elevator Recall
4. Fire service manual recall
5. Fire service notification of elevator shunt trip

Separate relays are needed for each point of information required. For example, if the only interface between the fire alarm and elevator recall was primary elevator recall and secondary elevator recall, two (2) relays would be needed to interface the fire alarm system to the elevator control equipment. Some of the inputs, such as manual fire service recall may be through the elevator control system.

The fire alarm system often needs to be interfaced either through relays or through direct communication with other systems for the sole purpose of shutting them off. As discussed above, this may include items such as lighting, door closure, and performance effects such as

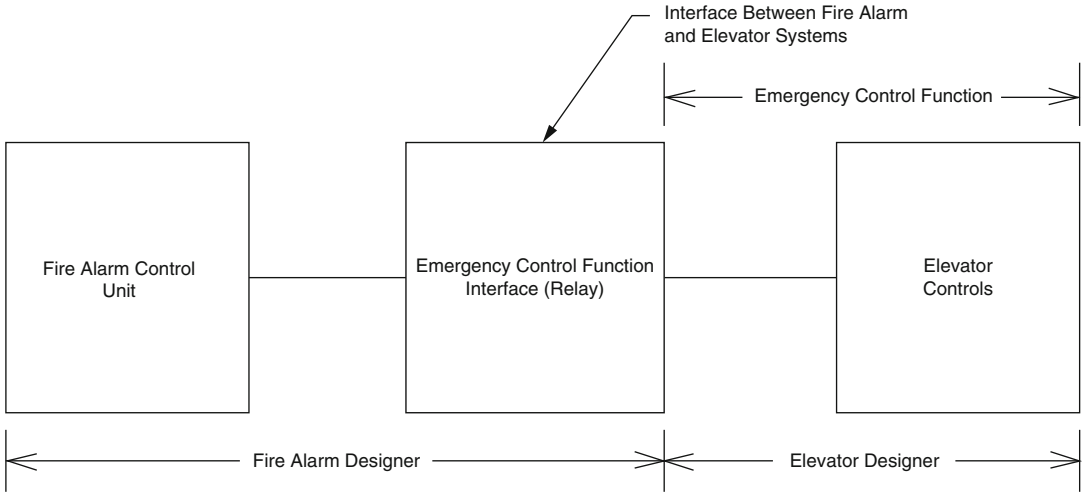

Fig. 49.4 Division of designer responsibilities example

deactivating a sound system or special effects so that the fire alarm system is audible. Other systems that might need to be shutdown include gas shut-off for cooking and heating devices, medical gas systems such as oxygen, hazardous processes, and similar systems. This requires coordination between the architect, fire protection engineer, plumbing engineer and potentially a specialty piping designer. Baggage conveyor systems may also require to be deactivated. Whether in a baggage handling facility or bulk material handling, shutting down the conveyor may be necessary to maintain fire separations or to stop the flow of combustible materials to a fire.

The overall design needs to consider interfacing with other systems such as BMS to turn on a smoke control system. When dealing with hazardous chemicals it may be desirable to interface with specialized systems such as chemical hood controls. Newer systems have multiple set points to address energy saving desires, but upon alarm it may desirable for these systems to return to full operation. This may require special coordination with the mechanical engineer especially if other forms of smoke control such as an exhaust system or stairway pressurization system are present in the building.

Figure 49.5 from NFPA 3 shows a Fire Alarm System Sequence of Operations (input/output matrix), which includes fire protection systems interfaced and the intended outcome. Table 49.3 provides additional systems that may need to interface with the fire alarm system.

Suppression Systems The sprinkler designer often has to coordinate with the architect to achieve a desired function and appearance through specifying concealed or recessed sprinklers or providing a specific design to address concealing pipes or views of the sprinklers. The designer must coordinate with the fire alarm designer to connect water flow and tamper switches, and water level and pump status. If the pump is electric, emergency power must be considered. If a dry pipe or pre-action system is provided, space and power for compressors must be considered. Coordination with the mechanical engineer is necessary to determine if local space heating will be required. The sprinkler design must coordinate with the architect to identify the use of each space such that an appropriate hazard classification can be made [24].

Special suppression systems such as gaseous suppression agents require similar coordination as the sprinkler system. The fire protection engineer may specify the type of system and whether there will be any redundancies in the system.

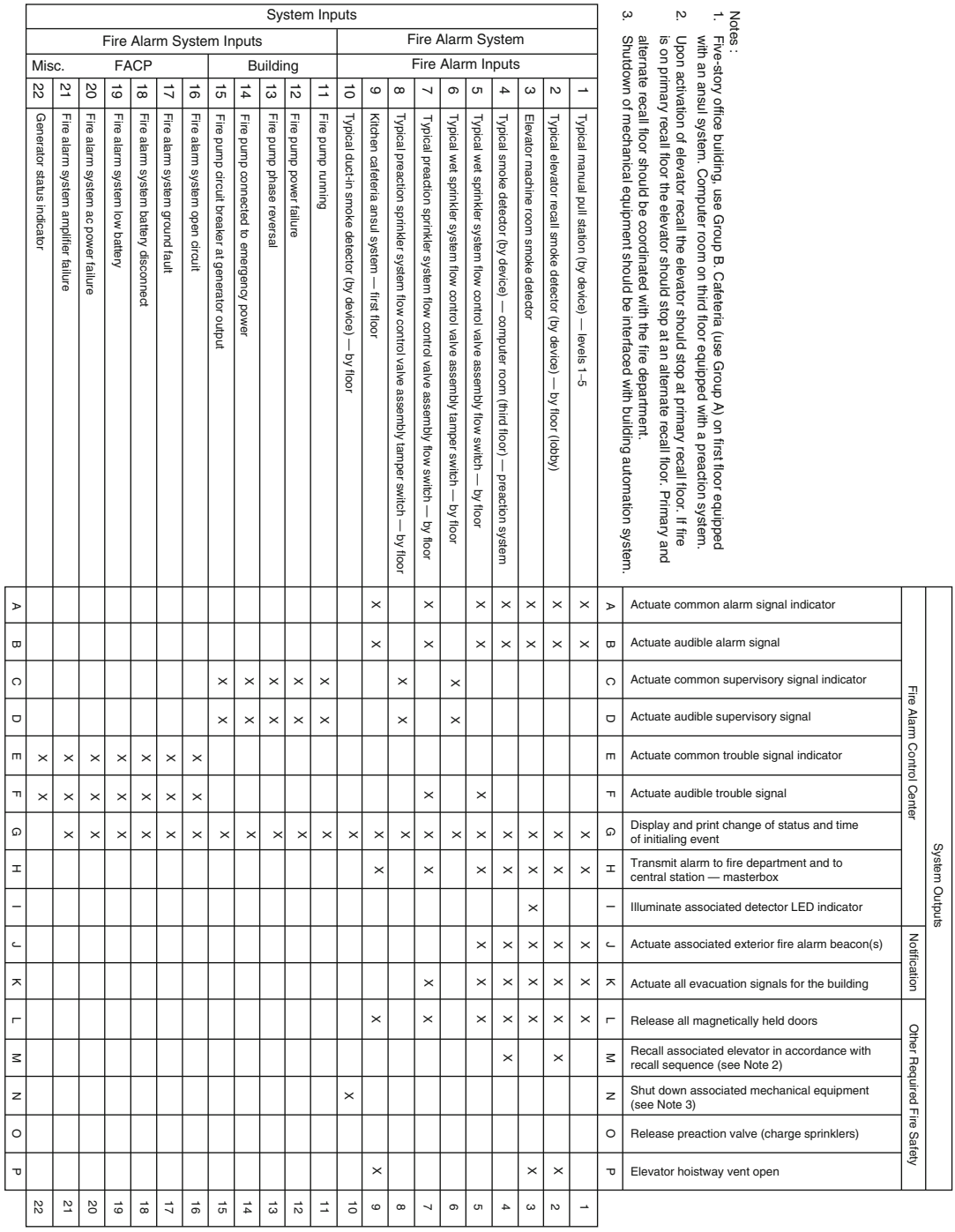

Notes :
1. Five-story office building, use Group B, Cafeteria (use Group A) on first floor equipped with an ansul system. Computer room on third floor equipped with a preaction system.
2. Upon activation of elevator recall the elevator should stop at primary recall floor. If fire is on primary recall floor the elevator should stop at an alternate recall floor. Primary and alternate recall floor should be coordinated with the fire department.
3. Shutdown of mechanical equipment should be interfaced with building automation system.

Fig. 49.5 Fire alarm system sequence of operations (Reproduced with permission from NFPA 3–2012, *Recommended Practice for Commissioning and Integrated Testing of Fire Protection and Life Safety Systems*, Copyright 2011, National Fire Protection Association. This reprinted material is not the complete and official position of the NFPA on the referenced subject, which is represented only in the standard in its entirety)

These systems typically involve smoke or fire detection. The dedicated detection and notification system needs to be coordinated with the overall building fire alarm system so that conflicting messages are not sent and that appropriate notification occurs when the system discharges. Controls need to be coordinated with other system functions, such as HVAC systems shutdown, damper and door closure, so that openings are sealed in order for the suppression agent to work properly. Coordination of the detailed sequencing, such as verification, interlocking, or releasing strategies are important.

In contrast, regulations might restrict the use of software in certain instances due to prior loss history. For example, NFPA 72, since the 2007 edition, does not permit fire alarm system software (programming) as a means to secure a suppression system from a discharge. These software disconnects on fire alarm systems have had previous failures due to programming changes, operating system changes, and power fluctuations, such that NFPA 72 requires a physical switch and does not allow the software disconnect for suppression systems.

Example: Special Suppression System

Special suppression systems might include clean agent, carbon dioxide, dry and wet chemical, foam systems, and interlocking and deluge water-based suppression systems. For these types of systems one or more electronic or mechanical inputs must occur for water or suppression agent to be released. Generally, special suppression systems are controlled by a dedicated fire alarm control unit. In some cases, the system can be controlled by the fire alarm system or a mechanically operated pilot actuated system. This example addresses suppression systems activated by a fire alarm system dedicated to the special suppression system.

The strategy of providing a dedicated fire alarm system for the special suppression system must consider back-up power supply requirements. Depending on the applicable regulations and design standards, and the owner's insurance company's requirements, the back-up power supply may be required to operate the system for 90 h or more. The typical duration of a building fire alarm system generally operates the system for 24 h. Therefore, it is likely that it is more cost effective to provide a dedicated control unit for the special suppression system.

Special suppression systems are likely to have a number of automatic and manual inputs. Automatic inputs may consist of points for air sampling, smoke, heat and gas detectors. The detectors may provide multiple alarm thresholds so that notification is provided at one threshold and then the agent is released when a second higher threshold is reached. Manual input could consist of manual alarm stations (pull stations) and abort switches. Depending on the suppression agent, the system may be programmed with a time delay to allow occupants to leave the area prior to agent discharge or manually preventing the agent release by continuously activating the abort switch.

Occupant notification may include horns, speakers, flashing lights and strobes. The audible notification appliance(s) may be programmed to provide multiple tones or messages. In some cases a bell or horn might pulse to notify of a pending agent discharge and then become steady once the agent has been released. Colored lights may also be used to provide notification in the protected room and at the entrances to notify of pending agent discharge.

Next, the special suppression system must be connected to a solenoid or an actuator to initiate the release of the agent. Typically the fire alarm control unit is connected to a control head that activates a master tank for certain types of systems

(continued)

(continued)

such as clean agents or carbon dioxide. For systems that require multiple tanks of agent, the master tank activates additional secondary tanks through an actuation line. The actuation line is connected from the pilot port of the master tank to each of the pneumatic actuators on the secondary tanks. This configuration allows for release of the secondary tanks only when the main tank is released. For other types of systems, such as deluge and pre-action systems, a solenoid can be operated to activate a larger valve to begin the flow of water.

As part of the commissioning process, the installation must be confirmed to the approved installation instructions. These instructions are reviewed as part of the listing and approval process. Some special suppression systems are approved to operate with a specific solenoid valves therefore the commissioning process must confirm that the appropriate equipment is being selected, designed, and installed to maintain the listing.

The special suppression system must also be interfaced with other systems, such as the mechanical system to compartment the room to maintain the agent concentration. The compartment integrity can occur through a variety of methods, such as using electrically controlled dampers or electrically actuated fusible links to release dampers to hold the agent within the space. Prior to completing the commissioning of the special suppression system, the interface with the dampers must be complete. Depending on the actuation method, replacement fusible links will need to be replaced for the system to maintain operability.

Depending on the distribution of the mechanical ventilation systems, deactivation of the fans needs to be considered to prevent damage to the mechanical systems. Failure to deactivate a fan when the damper is closed could cause high pressures in the ducts that could cause failure of the duct work.

The testing of a special suppression system must be coordinated with the construction of the building. Some authorities will require a flow test of a deluge sprinkler system, therefore this test must occur before specific items are installed and protection would need to be provided to prevent damage to surrounding areas. A discharge test of a clean agent could be cost prohibitive. It is important that the extent of testing is developed and reviewed with the AHJ during the design process. The testing must confirm that the electrically actuated equipment operates and that mechanically operated equipment is properly installed. Another critical test is the room integrity test for gaseous suppression system that is designed to hold a certain design concentration in the room.

Depending on the contractor, multiple contractors may be involved with the installation. For example, a clean agent suppression system may be installed by a separate contractor but their system might need output to the electrical, fire alarm and mechanical systems. The interfaced systems must be designed to receive these inputs and coordinated to provide the intended functionality.

The design team must coordinate the responsibilities of each of the contractors in the design documents. This coordination is necessary because it may be unclear which contractor is responsible for completing a specific activity and may result in scope gaps and delays to occupying the building. Figure 49.6 graphically depicts the various interfacing for inputs and outputs from a special suppression system and the other systems that are commonly found in buildings.

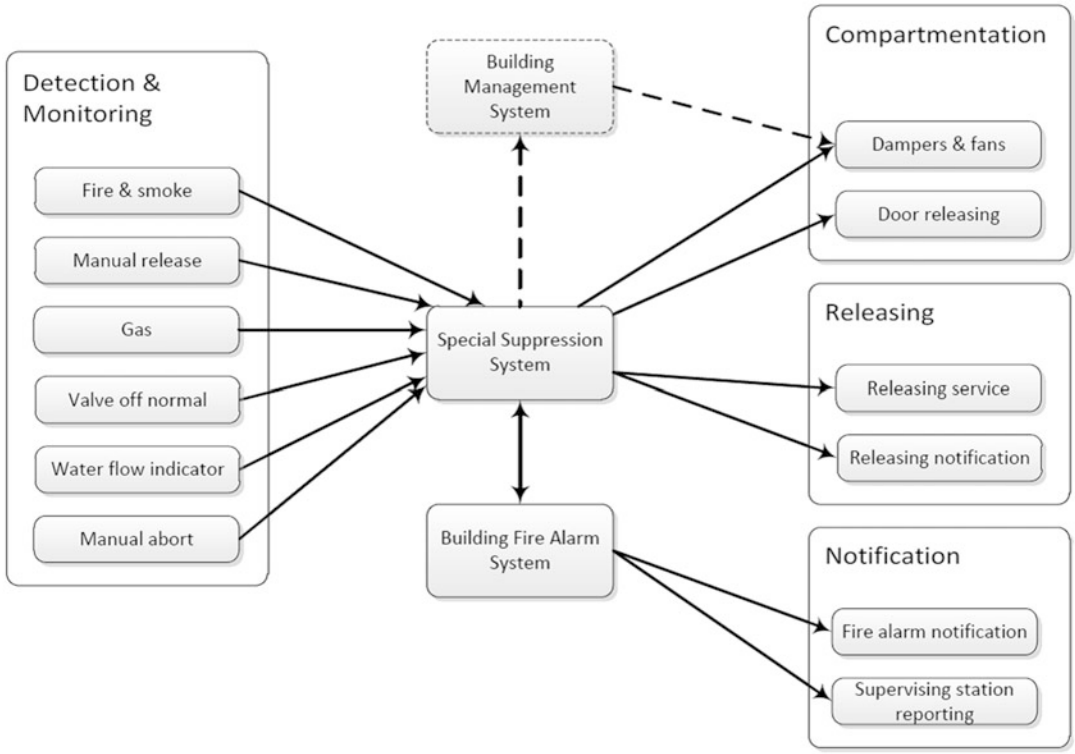

Fig. 49.6 Interconnections with special suppression systems

Smoke Control An atrium requires several systems to function correctly. A three story atrium would require smoke control, which requires coordination decisions to be made early in the process. In larger systems, the supply and exhaust locations need to be coordinated with the architecture, as the amount of louvers or openings can be quite large and getting supply air to the lowest level is often a challenge.

The smoke control system is often an *integrated system* itself, consisting of a fire detection and alarm system, mechanical systems, potentially a BMS, and the sprinkler system. Controls for the smoke control system can be through the fire alarm system, the Building Management Systems (BMS), Building Automation System (BAS), or through a dedicated controls system. The control system selected will determine interfacing and communication needed to control and supervise system components. Regardless of the control system, automatic and manual sequences need to be coordinated to achieve the system goals. Manual inputs typically override automatic smoke control functions.

Smoke control fans, dampers, and make up-air openings need to be monitored to determine if the equipment appropriately configures. Fault conditions should be reported through the control system. In some cases, dampers and make-up air openings need to be properly configured before fans are actuated, to avoid excessive duct pressures or door opening forces.

The designer must consider the activation of the smoke control system. If sprinklers are being used, then the design of the sprinkler system must include having a separate sprinkler zone for the atrium. Non-atrium sprinkler zones cannot be extended into the atrium, as this could cause an improper activation. If stairway pressurization is provided, detection for activation of the system needs to be coordinated. Where the

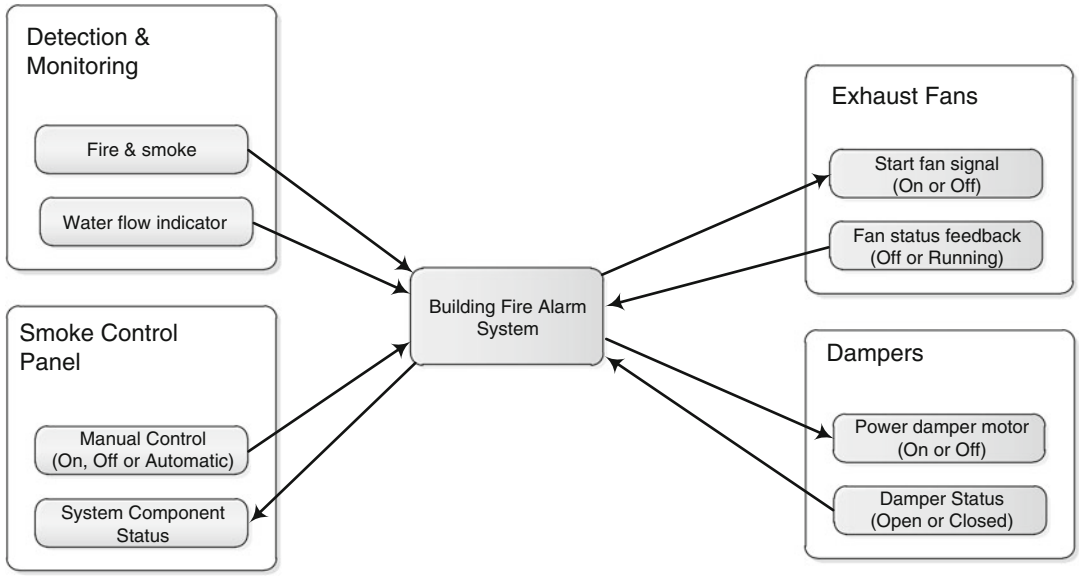

Fig. 49.7 Potential smoke control fan interfacing—option 1 (fire alarm)

smoke is being discharged, where fresh air is coming from and potential impact to surrounding buildings should be considered. The use of the BMS to control the mechanical equipment could reduce redundant wiring to equipment by the fire alarm and BMS systems. If the BMS is used, it must be appropriately listed for smoke control by an approved agency and the designer needs to understand how integrating systems may affect this listing. The interface between the fire alarm (initiating the smoke control system) and the BMS (controlling the mechanical system) also must be considered. Both Fire Alarm and BMS system manufacturers offer communication solutions such as LonWorks <www.echelon.com> or BacNet [3] for communication. These are networking platforms specifically created to address the needs of control applications. These platforms provide more information than dry contacts between the two systems would.

The location of the smoke control system components need to be coordinated with the egress plan, architecture and the computer smoke model if one were utilized. Locating exhaust points to pull smoke away from egress paths or to take advantage of a reservoir can also make the smoke control system more effective.

Figures 49.7 and 49.8 illustrate two potential options for interfacing fan control. Other options are available.

Hazardous Exhaust Systems Utilizing ventilation zones for containment, via negative pressure zones, needs to be reviewed for both construction integrity and for proper operation when a smoke control system is operating or not operating.

Exhaust systems may need to run continuously or to modulate to high-speed exhaust for hazardous atmospheres venting upon carbon monoxide gas, hazardous gas, or hazardous chemical leak detection. The exhaust systems may need to be interfaced with process controls to actuate during unwanted process conditions, such as overheating. Systems that need to run continuously may need to run during other emergency events, including loss of normal power. Exhaust and make-up air need to coordinate with smoke control and other ventilation systems, along with emergency power. These systems may need to be monitored through air flow sensors and alarms.

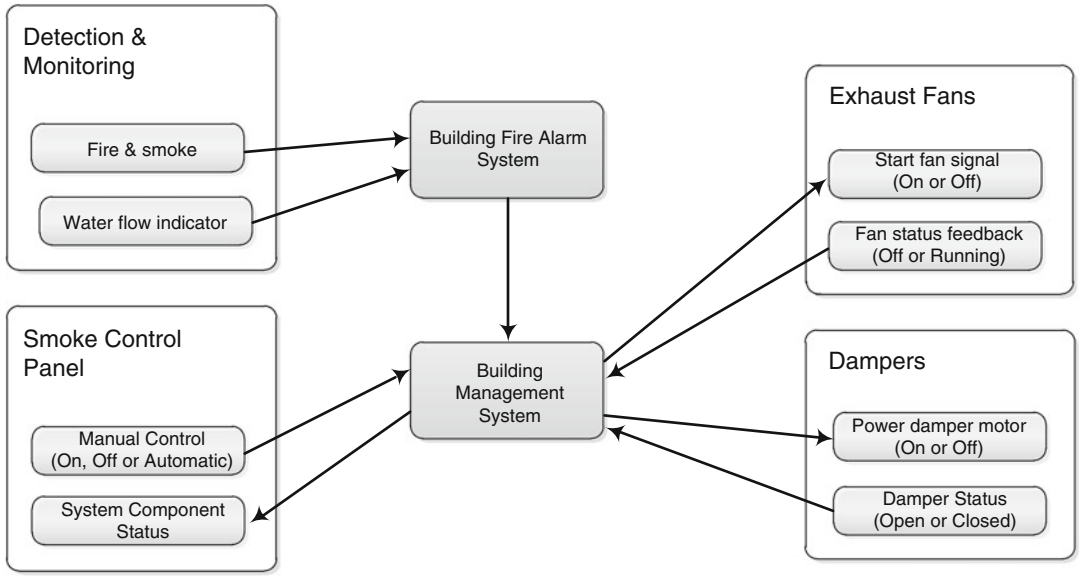

Fig. 49.8 Potential smoke control fan interfacing—option 2 (building management system)

Gas or leak detection can be through the fire alarm system, the BMS/BAS system, or standalone systems. Integrated or separate systems can be used to actuate exhaust or modulate the systems to provide additional exhaust.

Emergency and Standby Power Emergency and Standby power systems require coordination between electrical engineers providing the power system and the fire and life safety consultant in identifying the appropriate forms of emergency/standby power. This design must then be coordinated with controls and the architect to identify which systems will require power such as computer systems or medical systems. Mechanical engineers should identify which building systems will require emergency and standby power and which systems are desired to have optional standby power. In some cases the duration of fuel supply may become a concern as more and more items are added to the emergency and standby power for potentially longer and longer durations.

Required fire resistive rating of power cabling for emergency and standby power feeds to panels also requires coordination [11, 24, 25].

Elevators Interfacing with elevator controls are discussed in the Emergency Control Functions discussion above. Other considerations include building code requirements for sprinklers to be installed in the elevator machine room or shaft. To prevent damage to the elevator control equipment, the fire alarm system would be configured to initiate disconnecting of the power (shunt trip). A heat detector or a water flow switch would initiate disconnection of the power. If a heat detector is used, the device is required to located within 2 f. of each sprinkler with an activation temperature and response rate lower than the sprinkler. When a water flow switch is used, a delay is not permitted.

Generally, this would be accomplished through a shunt trip circuit breaker. The fire alarm system would activate power to initiate the disconnection of power. Most shunt trip breakers require power to initiate disconnect; therefore it is important to monitor the power source to the shunt trip breaker. Usually this is accomplished with an *emergency control function interface device* (relay) that is powered by the shunt trip source and located within 3 f. of the shunt trip breaker. The status of this relay would

be monitored by the fire alarm system and would report a supervisory signal [4, 20]. Depending on the authority, the sprinklers could be removed from these spaces eliminating the need to disconnect power.

Electronic features requiring interfacing and coordination include: elevator evacuation system status indicator in lobby (IBC only), elevator system monitoring to indicate car floor location and direction of travel, two-way communication system between elevator lobby and fire command center, elevator car occupancy status indicator (IBC only), Phase I emergency recall remote control located in fire command center, and status indicator of normal and standby power in fire command center.

Emergency elevator evacuation activation initiates through any sprinkler water flow or any smoke detector activation, other than an elevator lobby detector, and through manual activation. The system is configured to return the elevator cabs to the lobby floor to allow occupants within the cab to exit. The elevators are then prioritized to shuttle occupants from fire floor, and two floors above and below the fire floors, to the lobby floor. The highest priority is given to the fire floor. If elevator recall is initiated manually or automatically after commencing emergency evacuation sequence, the elevators return to the recall floor.

The use of evacuation elevators may be integrated with the CCTV system to detect occupants in an elevator lobby. The CCTV system could be used by an operator to determine which floors need to be evacuated first.

Access Control and Security Access control and security systems often are a challenge to the other *life safety systems* and therefore require special attention. Often a security system design is intentionally kept separate from the rest of the design process. Locking of doors, security gates and other security counter measures must be considered by the designer of the fire alarm and egress systems. Doors can be unlocked upon alarm, but the designer should consider non-fire events that do not trigger a fire alarm. As part of security plan there may be a need to evacuate and area that would normally be locked. Alternative means of egress may need to be developed. Priorities must be understood by the designer as releasing security features in places of detention may not be acceptable and alternative design solutions must be developed.

Some system integration can be done relatively simply, such as integrating a CCTV monitoring system with access control and intrusion detection. This information could also be helpful to first responders for non-security issues so integrating a video feed to a fire alarm control area may be desirable and is proposed as a requirement for high rise buildings with over 4000 occupants. Where these two systems do not conflict, as one is just "observing" the other, the integration is relatively simple. However, with new technology such as video image smoke detection, cameras can now be used for detecting a fire as well as tracking individuals or items of interest. This requires the designers to coordinate locations and view angles of cameras to address both security and fire concerns. If the cameras are being used to detect fires then redundancy, circuit integrity, and listing issues need to be addressed [8].

Lighting Lighting effects may need to be turned off and house lights may need to be brought up to an appropriate level to aid in egress. Often a theater or other performing arts venue or amusement ride has lowered lighting levels in the space. Designers need to coordinate where minimum levels of fixed lighting will be provided as well interfacing systems such that house lights are brought up and theatrical lights are turned off. Exit signs will need to be visible to occupants and their location needs to be coordinated with the architecture.

Matrix of Responsibilities

Depending upon the specific construction procurement method, systems could be installed by a different contractor and at different times. Each system connection presents a potential problem when trying to install, *pre-functional test*, and commission the individual systems and the

Table 49.4 Coordinating the design of integrated building systems

Section reference	Work	Furnish	Install	Wire	Commission
21131X	Sprinkler system	21	21	21	21 and 28
21311X	Fire pump	21	21	21	21
212200	Clean agent suppression system	21	21	26	21 and 28
233300	Fire & smoke dampers	23	23	26	23
283111	Duct smoke detector	28	23	28	23 and 28

integration of these systems. Often, these systems will be covered within different MasterSpec (e.g. standard guide specifications for building systems, equipment, and features) sections and one contractor may not even realize they need to coordinate with another. One tool to minimize these problems is for the designer to develop a responsibilities matrix, as shown in Table 49.4. This matrix identifies each trade, where the interface between systems will occur, and which trade is responsible for each system and system *interconnection* [32].

Another tool for addressing this is coordination drawings. These are drawings prepared by the contractor and reviewed by the designers. The drawings are sometimes used for physical coordination and sometimes are specifically to indicate the coordination between the different trades, and designate all of the *interconnections* and information needed for the *interconnections* [32].

Systems Interfacing Methods

Building systems are increasingly becoming more integrated, with multiple systems performing as one system. Following those trends, the number of systems integrated with the building fire alarm system is increasing, further complicating the commissioning and integrated testing process. Microprocessor based fire alarm systems are being programmed to complete more than detection and notification of occupants in the event of an emergency in a building.

The fire alarm system can be interfaced with a variety of building systems and inform trained personnel. An *Integrated System* is two or more individual systems that work together in achieving an overall fire protection or life safety objective. Figure 49.9 conceptually illustrates the difference between integrated systems and *interconnected systems*. Trained personnel can be, in certain circumstances, a critical part of the integrated fire protection system, since they may be required to evaluate the information received and take action to manually initiate other fire protection systems.

An example is trained personnel, such as a guard at a prison. A prison guard in a prison can be part of an *integrated system*, in which the guard relies on information from the fire alarm system or the emergency communication system in order to determine if manual release of door locking controls is required. This is an example on an *integrated system* that is not an interconnected system.

Wiring Methods

Various wiring methods are available to interface and connect other systems found in buildings with the fire alarm system. A device that is controlled by the fire alarm system is considered an output. The fire alarm system is interfaced with a number of building systems to activate or deactivate depending on the desired state during an emergency. Outputs are also used to initiate off premise reporting (supervising station), fire department reporting, or reporting to a constantly monitored location. Fire alarm outputs can be connected in series or parallel, and configured to be either fail safe or fail secure.

A device that reports status and is controlled by a system is a two-way interface. An example of a two way interface would be a smoke control system, when a fire alarm is initiated, the fire alarm system would activate a smoke exhaust

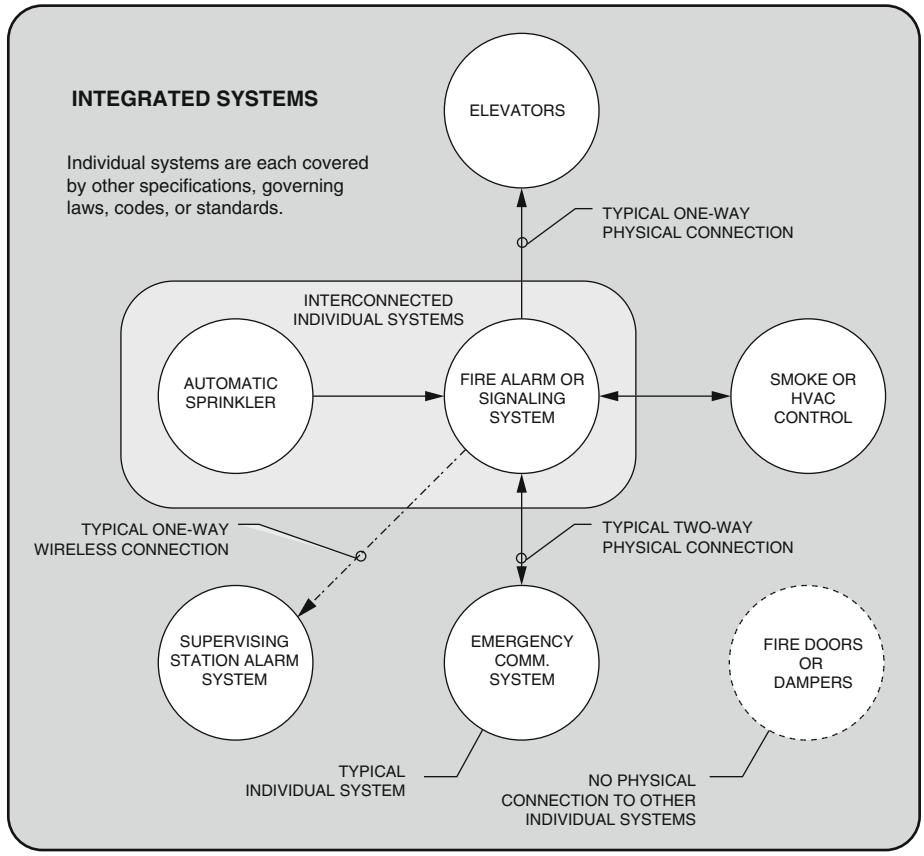

Fig. 49.9 *Integrated system* vs. *interconnected systems* (Reproduced with permission from NFPA 3–2012, *Recommended Practice for Commissioning and Integrated Testing of Fire Protection and Life Safety Systems*, Copyright 2011, National Fire Protection Association. This reprinted material is not the complete and official position of the NFPA on the referenced subject, which is represented only the standard in its entirety)

system. The output might consist of an interface with a motor starter/controller to start a fan and open a damper. The input to the fire alarm system would be positive status indication of the system components operation, such as fan operation and damper position status. Examples of a two-way interface include data communications and building automation protocols.

Series A control circuit wired in a serial method requires all control points to be in the desired state to operate a system. For example, a control circuit for an air handler serving the building heating, ventilation and air conditioning (HVAC) system might be controlled by both the fire alarm and building management systems. In this example, if either the fire alarm controller or the building management system control shuts down the HVAC, the system will shut down. Therefore, the HVAC will not operate if the fire alarm system is in alarm, regardless of the building management system status.

Parallel A parallel circuit permits any of the control points to activate the system. An emergency lighting system that is controlled by the building automation and fire alarm system is an example of a parallel system. In this example, the building automation system includes occupancy sensors to activate lighting. Lighting would also activate when an alarm is initiated on the fire alarm system. Paralleling the control circuit would activate lighting when either system sends the command.

Fail Safe In fail safe wiring, circuit wiring may not be monitored, as the intended operation is performed in the event of circuit failure. A common example would be a motor starter circuit that controls a non-smoke control fan associated with the ventilation system. The motor starter circuit is required to be completed for the fan to operate. The fire alarm system controls the fan through a series connected *emergency control function interface device* (relay), where a control switch is required to be energized for the fan to operate. This switch can be de-energized through the fire alarm sequence or de-energized through interruption of the fire alarm circuit. If the fire alarm wiring fails, the relay would not be energized which would prevent the fan from operating. A second example would be fire or smoke doors held open by magnetic door holders, if power is lost to the electromagnet, the doors are released. Doors are also released through an alarm condition on the fire alarm.

Fail Secure An example of a fail secure component would be an electric door strike. For the door to be unlocked the circuit must be complete and power applied to unlock the door. A fail secure lock is important to maintain security of the building in the event of a power failure in the building. Fail secure locks are not permitted in the path of the means of egress.

Data Communications Complex control systems can be difficult to interface between multiple systems. In the connected world, a majority of equipment is transitioning to communication over internet protocol (IP), through a single connection that uses software to communicate utilizing a standard protocol. This strategy reduces installation and equipment, which reduces the installation and maintenance costs. The integration quickly blurs the demarcation points between multiple connections.

As more and more interfacing is completed through equipment software and firmware, commissioning and integrated testing will continue to become more complicated and involved because the control functions programed into the software of associated equipment also needs to be verified. The sequencing and control of fire alarm equipment is not usually obvious as the associated software and firmware is generally proprietary and controlled by the fire alarm system contractor. With the fire alarm system sending a fire alarm signal to the building automation system, the contractor programming the building automation system is responsible for programming items that impact the input or output from the fire alarm system. Modifications to building automation systems tend to occur more frequently than changes to the fire alarm system. These changes could impact the operation of the life safety system, and may require a partial re-test or a full re-test of the *integrated systems*. A simple software upgrade could create an incompatibility between the control units and the associated equipment they are intended to control.

Building Automation Protocols In buildings with smoke control systems, there may be a number of system components that need to be controlled that are also used for normal building HVAC systems. In some buildings, the fire alarm and building automation system are configured to require a duplication of the interfaced wiring to smoke control equipment. Building automation systems can share equipment status and control the various components through a common protocol interface, connecting to the building fire alarm system. Standard building automation protocols include BACnet, LonWorks, and MODBUS.

Each type of protocol has multiple versions. Some manufacturers customize their communication properties. When integrating the fire alarm system with a building automation protocol, it is important to confirm the type, version, and supervision of the communication, and that both systems support the necessary protocols for the intended functionality. Traditionally, most building automation systems communicated over a proprietary network that require dedicated network infrastructure. The dedicated network consisted of dedicated copper or fiber cabling between each network component. More recently, most building automation systems

support and use the shared TCP/IP network to communicate. Some manufacturers support open protocols, which allow open communication between different manufacturers.

Installation Considerations

The designer must consider the system installation methods when designing the *interconnections* of the systems. Usually a separate contractor installs each system such as fire alarm, sprinkler, HVAC, and low voltage controls. Some of these systems may be design build or fully designed by the sub-contractor. In either case, the sub-contractor often is not aware or does not fully appreciate the overall goals of the *integrated systems*, even though they completely understand their individual system. In order to address this, the designer needs to consider coordination meetings with the sub-contractors early in the process. The use of checklists can assist with coordination and integration of the various systems. In an effort to assist with plan review, many Authorities have developed internal checklists. These checklists are often made available to the designer to speed the review process and provide examples in which system interaction may be desirable. The designer may consider developing a project specific checklist for the contractors to use to verify the *interconnections* between various systems and equipment are done correctly.

Commissioning and Integrated Systems Testing

Commissioning and Integrated Systems Testing are two ongoing activities that are essential in the coordination and interfacing of fire protection and life safety systems during the design and construction phases of a building project. Many building owners recognize the benefits of a comprehensive *commissioning plan* and an *integrated test plan* initiated early in the design process for fire protection and life safety systems regardless of the complexity of their buildings. The total expense of implementing a comprehensive *commissioning* and *integrated test* plan early in the design process is usually recouped due to savings associated with reduced construction costs, delays and change orders, with efficiencies gained from optimized system performance and coordinated maintenance activities [1]. Commissioning can assist in opening a building on time [7]. Commissioning of fire protection and life safety systems is one portion of the overall building commissioning.

NFPA 3 [21] outlines a systematic commissioning process, which is completed through an owner's representative to meet the owner's goals and objectives that have been incorporated into the design and installation of the building. The commissioning process includes verification and documentation. As illustrated in Fig. 49.10 the commissioning process can include the Planning Phase, Design Phase, Construction Phase, and Occupancy Phase for a building. *Commissioning* is much more than *acceptance testing* of each individual system and can also include *integrated testing* of the interfaced systems. *Re-commissioning* (commissioning systems previously commissioned) and *Retro-commissioning* (commissioning systems never commissioned) are also part of commissioning process for existing buildings.

An early step in the commissioning process is for the relevant stakeholders to agree to use a common set of terminology. Industry terminology, which includes terms such as *Commissioning Authority* (*CxA*), Fire Commissioning Agent (*FCxA*), and *Integrated Testing Agent* (*ITa*), must be understood by all parties involved. The commissioning process and integrated testing does not replace or supersede the *acceptance testing* requirements found in individual system standards. Additionally, inspection, testing, and maintenance of the individual fire protection systems still need to be accomplished in accordance with the specific individual standards (e.g. NFPA 25 [16] for sprinkler systems). Commissioning standards and guidelines are generally more detailed in documenting the commissioning process than it is for documentation in other fire protection and

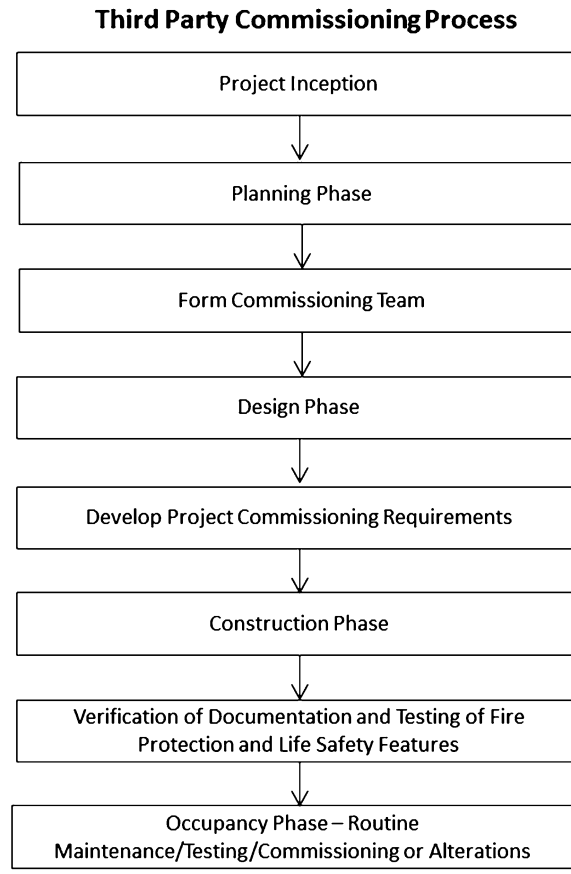

Fig. 49.10 The third party commissioning process

life safety systems codes or standards. In some cases, commissioning has become a building code requirement, for example the smoke control systems special inspector requirements included in the International Building Code (IBC) is essentially commissioning the smoke control system.

Integrated Testing is performed according to the specific *Integrated Test Plan* developed and approved for the project, which may require *end-to-end test* to verify the proper functionality of the various fire protection systems intended to operate as single unit under certain scenarios.

An important aspect of the *Integrated Test Plan* is the development of a set of test scenarios. Such test scenarios are to be agreed to prior to the commencement of any integrated testing, and are developed to articulate the adverse conditions under which the systems are expected to perform as a single unit. Ideally, these scenarios are considered and documented when the overall fire protection strategy for the facility is being developed. Part of the *Integrated Test Plan* is an *interface test*, where the integration and connectivity of the affected systems is tested, the expected performance is demonstrated and verified, and results are documented. A simple building with only a few integrated fire protection and life safety systems would have a rather simple, basic *Integrated Test Plan* with a limited number of scenarios. A larger more complex building may include numerous and expansive integrated fire protection systems, and would typically need a larger number of more complex testing scenarios. Figures 49.11 and 49.12 include excerpts from *Integrated Test Plans* for a simple scenario and a more complex scenario. The *Commissioning Plan* and the *Integrated Test*

Scenario #Y Sprinkler Water Flow Activation (SIMPLE BUILDING)

System Action

Annunciate at the fire alarm panel
Send signal to Central Station Service
Activate audible and visual alarm signals throughout building

Elevators remain in normal operation.

System Verification

Verify alarm received at fire alarm panel within 90 seconds	YES	NO
Audible and visual alarms at the fire alarm panel	YES	NO
Proper alarm annunciation at the fire alarm panel	YES	NO
Verify signal sent to Central Station Service	YES	NO
Audible/visual notification activated throughout building	YES	NO
Verify supervision in event of device failure or signal interruption.	YES	NO

Fig. 49.11 Integrated test plans excerpt– simple scenario

Scenario #X Atrium Waterflow Activation Activation on Level Y (Complex Building)

System Action

Annunciate in the Fire Command Center (F.C.C.)
Send signal to BMS system
Send signal to 24-hr remote station
Activate audible and visual alarm signals (floor of alarm, floor above, and floor below)

Elevators remain in normal operation

Activate smoke control sequence, as follows:

Atrium Exhaust Fans ON	EF-AA and EF-BB
Stair Pressurization Fans ON	SSF CCC, SSF DDD, SSF EEE, SSF FFF
Exhaust Dampers OPEN	FSD FFF and FSD-GGG
Dampers CLOSE	All others
Door Magnetic Hold Opens Release	Zone of Alarm
Release Security Stair Door Locks	All Floors

System Verification

Audible and visual alarms at Fire Command Center (F.C.C.) annunciation panel	YES	NO
Send Signal to BMS system	YES	NO
Send signal to 24-hr remote station	YES	NO
Audible/visual notification activated on floor of alarm, floor below, and floor above	YES	NO
Smoke Control Exhaust Fans ON	YES	NO
Smoke Control Supply Fans ON	YES	NO
Dampers OPEN per the Smoke Control Sequence noted above	YES	NO
Dampers CLOSE per the Smoke Control Sequence noted above	YES	NO
Stairwell Pressurization Fans operate	YES	NO
Vestibule Pressurization Fans operate	YES	NO
Status lights for Stairwell Pressurization Fans on Smoke Control Panel in F.C.C.	YES	NO
Status lights for Smoke Zone at Smoke Control Panel in F.C.C.	YES	NO
Manual override of Smoke Control Mode at the Smoke Control Panel in F.C.C.	YES	NO
Manual initiation of Smoke Control Mode sequence at the Smoke Control Panel in F.C.C.	YES	NO
Manual override of Stair Pressurization Fans at Smoke Control Panel in F.C.C.	YES	NO
Verify supervision in event of device failure or signal interruption.	YES	NO
Toilet exhaust fans ON	YES	NO

Fig. 49.12 Integrated test plans excerpt—complex scenario

Plan should be developed and customized for each individual building, since each building usually has its own unique features and functions.

The contractor and subcontractors are brought in at different times of a project depending on the procurement method of the building (e.g. Design Build, Design Assist, or Design/Bid/Build). The contractor and subcontractors should be involved to some degree with the coordination process as soon as they become involved with the project. Contractor shop drawings, calculations, and equipment submittals of the fire protection and life safety systems provide more detail, including specific manufacturer's equipment proposed for installation. The contractor's shop drawings should be coordinated with all other relevant disciplines' (e.g. mechanical, electrical, plumbing, structural, and other specialists) shop drawings. The Design Team, *FCxA*, and *ITa* review of the contractor's documents needs to include verification of the *BOD*, and the project's strategies and goals. The commissioning process is not intended to alter the installation of fire protection and life safety system components from their listing requirements or the manufacturer's approved installations instructions.

Some government agencies, such as U.S. General Services Administration (GSA), have long standing requirements for a fire protection engineer (FPE) to review the overall design of the building and the various fire protection systems. Such FPE is not necessarily the engineer of record for the individual systems. With an overall understanding of the architectural design, the buildings functionality, and how the various fire protection systems and features are intended to function together, the FPE review during the design and construction phase serves to verify proper performance of the *integrated system*s. Other Agencies have also implemented commissioning requirements which include fire protection and life safety systems.

Individual fire protection and life safety systems need to undergo *acceptance testing* in accordance with the appropriate individual standards (e.g. NFPA 72 ([20]) for fire alarm systems and NFPA 13 [24] for water based suppression systems), prior to Integrated System Testing. The engineer of record for each system is required to review the progress of installation, witness *acceptance testing* of the individual systems and provide engineers approval. The Commissioning Team reviews the progress of the installation, tracks and documents deficiencies, coordinates and witnesses system testing, coordinates and witnesses, along with the *ITa*, the integrated testing of systems, and provides a complete and final fire protection and life safety commissioning team report and integrated test report recommending approval.

Final *acceptance testing* of individual fire protection and life safety systems with the Authority Having Jurisdiction (AHJ) and obtaining *acceptance testing* final approval by the AHJ may be required prior to the Integrated Testing. Discussion and coordination with the AHJ should have taken place during the design phase or early in construction phase, long before the *acceptance* testing to determine if separate individual system acceptance tests are required prior to the Integrated Test. Some AHJ's may require or desire the AHJ final *acceptance testing* to be completed after the Integrated Testing has been completed and documented, to assure the integrated systems work in a coordinated manner with each other prior to issuing a certificate of occupancy. Periodic testing, maintenance, and integrated testing of the various systems should continue to occur over the life of the building. Commissioning may continue over the life of the building for building modifications, system upgrades or major changes to the building and/or fire protection and life safety systems.

Systems Coordination During Construction

The contractor and sub-contractors are involved at different times of the project depending on the procurement method as discussed above. Contractor shop drawings, calculations, and equipment submittals of the fire protection and

life safety systems provide the next level of detail after the design phase drawings, and include specific manufacturers and equipment proposed to be installed. The contractor shop drawings need to be coordinated with the other contractors shop drawings. The Design Team, Engineer of Record, *FCxA*, and *ITa* review of the contractor's documents needs to include verification of the *BOD*, and the project's strategies and goals. All fire protection and life safety system components should be installed per their listing and written manufacturer's recommended procedures. Field changes need to be evaluated for their potential impact on individual fire protection and life safety systems and to the impact on interfaced fire protection and life safety systems. Approved field changes related to fire protection and life safety systems need to be appropriately documented and incorporated for commissioning, testing, and final *acceptance testing*.

Figure 49.13 depicts a possible contractor responsibility diagram for the fire alarm system interface device with the elevator controls via a fire alarm system *emergency control function device* (relay) for items such as elevator recall, shunt trip, fire fighter's hat, and evacuation elevators.

One of the particularly effective tools for coordination is well managed focused coordination meetings with the design team, owner, contractor, subcontractor, *CxA*, *FCxA*, and *ITa* to review interfaced or integrated points between systems, review the overall sequence of operations between the systems, review of the *Commissioning Plan*, and review development of the Integrated Systems Testing Plan. These coordination and review meetings may involve hardcopies of the drawings to review and mark-up drawings, or other times they may use Building Information Management (BIM) software [31] to electronically display the various systems on screen during the meeting.

Other coordination tools for the design team and installing contractor include:

1. Coordination Checklists
2. BIM 3D/4D Modeling
3. Responsibility Matrix (matrix outlining responsible for furnishing and installing each component)
4. Hardcopy set of redlined coordination drawings

BIM software programs, if properly implemented, allow for creation of tag layers for equipment features, such as system interface

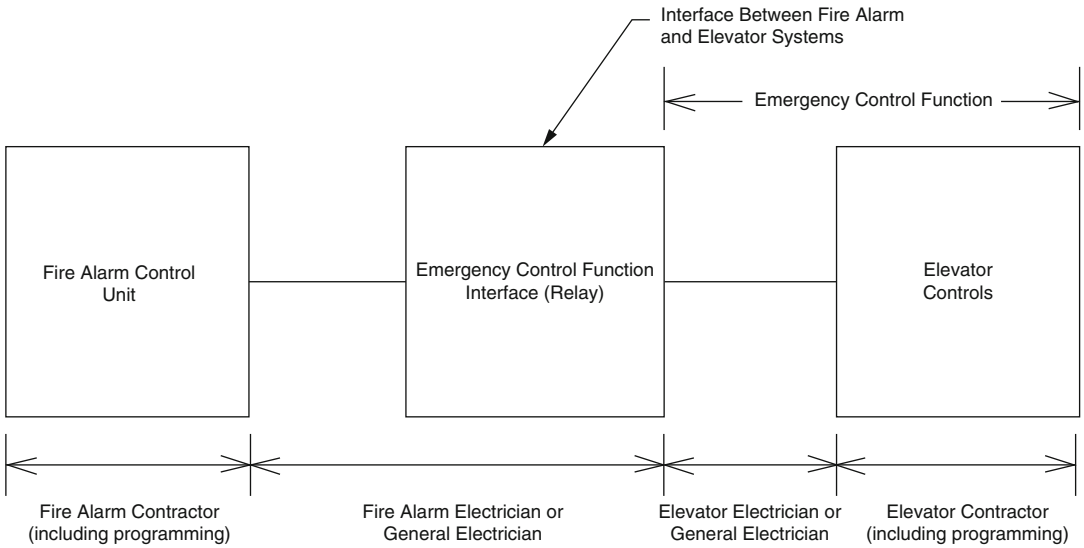

Fig. 49.13 Sample contractor responsibility diagrams

and integration locations, to be easily identified and located for identification and coordination in the future across various disciplines. This also allows reminders or notes to be added for future reference by either the person involved in that particular system, by other designers or engineers, or by other trades.

One example of the division of installation responsibilities for a combination fire/smoke damper serving a non-dedicated smoke control system controlled by a UUKL listed BMS system could be:

1. HVAC Contractor to install ductwork, and combination fire/smoke damper with integral open and closed position end switches.
2. Fire Alarm Electrical Contractor to install system duct smoke detector associated with the smoke damper, output control module to interface with the BMS system and input monitor module for monitoring of combination fire/smoke damper power.
3. BMS Contractor to install control module for the combination fire/smoke damper for initiation of the combination fire/smoke damper, monitor of the closed position switch of the smoke damper, and a monitor module interface between the fire alarm system and the BMS system.
4. Electrical Contractor to install 120 V emergency power to the combination fire/smoke damper and actuator.
5. General contractor to install shaft enclosure and access panel for combination fire/smoke damper.

Routine progress inspection of systems during the installation is required for proper oversight and coordination. Scheduled progress inspection by the Engineer of Record, *CxA*, *FCxA*, and *ITa* is critical in the commissioning and installation process. Of particular importance are specific reviews by Engineer of Record, *CxA*, *FCxA*, *ITa*, and AHJ for proper rough inspections and approvals prior to concealment of parts or all of the fire protection and life safety systems. Interim steps, such as smoke control system duct pressure tests, are critical to be performed during rough inspections, since the ducts are tested in segments as the ducts are constructed.

The Engineer of Record of the fire protection and life safety systems, fire protection engineer, and the *FCxA* review the contractor (or subcontractor) installation of these systems for conformance with the approved documents. The individual fire protection systems *pre-functional test* should be completed by the installing subcontractor, including items such as air balancing for smoke control systems. After a successful contractor *pre-functional test*, the Engineer of Record and the *FCxA* then witness the individual fire protection system *pre-functional test*. Once all the individual fire *interconnected systems* have been successfully tested, an Integrated Test, in accordance with the *Integrated Test Plan*, is conducted by the contractor and various sub-contractors, and witnessed by the Engineer of Record, the *FCxA*, and *ITa*. A final acceptance test by the AHJ would be required for final sign off. In some cases the AHJ testing may be completed at the same time as the Integrated Test. This should be discussed and agreed with the AHJ before the AHJ test.

Below are examples of integrated tests that, ideally, should be completed. Often these are not completed for various reasons:

1. Testing of emergency power on a maximum load, such as interrupting normal building power while the fire pump and smoke control system are operating.
2. *Integrated testing* of fire protection and life safety system without bypassing any of the systems (e.g. complete test without bypassing elevator recall, audio and visual notification devices, fan shutdown, or any other required sequence).
3. *End to End Test* rather than simulated events (e.g. actual sprinkler water flow rather than shorting the fire alarm sprinkler water flow monitor module).

Atrium Smoke Control Example One example, of an integrated fire protection and life safety system is an atrium smoke control system in which CFD analysis was employed to verify the design parameters of the smoke exhaust. The associated fire alarm system, sprinkler system, door operations and HVAC smoke control

equipment all need to be coordinated and integrated to meet the smoke management goals and objectives for the atrium. Improperly coordinated and integrated systems are likely to result in the spread of smoke and fire throughout the building rather than the exhaust of smoke from the space. Although the CFD computer model may have been employed with a specific design fire, it is usually not practical to simulate this design fire in the atrium during testing. However, all other conditions should be simulated during the test. A certified air balancing contractor is a critical member of the team, with responsibility for testing the performance of the smoke control system by taking various measurements, which may include airflow, velocity, and pressure differentials to demonstrate that the installed smoke control system performs as intended and meets the established design parameters.

The testing of a smoke control system is completed in four (4) primary steps.

1. Component verification
2. Component testing
3. Commissioning of and measurements of individual systems
4. *Integrated testing* of the smoke control system

Component verification is an inspection of the installed components to verify they are present and installed per the design documents, listing, and manufacture's instruction. Component testing requires testing of the components of individual systems (e.g. fire alarm, sprinklers, HVAC, dampers, and doors) to verify proper sequencing and function (e.g. smoke damper position). Commissioning tests of the individual fire alarm, sprinkler, and HVAC systems include verification of the sequence of operation, and air balance measurements of exhaust and/or supply capacities. After component verification and component testing is complete, *integrated testing* is performed to verify the proper sequence of components in accordance with the established test scenarios identified in the *Integrated Test Plan*. The *Integrated Test Plan* for a smoke control system typically incorporates test scenarios for: (1) activation an atrium sprinkler water flow (actual water flowing though inspection test connection), which is supervised by the fire alarm system, and (2) activation of an atrium smoke detector. Sequences should include initiating the atrium smoke control system in normal power and standby power. Other items that would be part of the *Integrated Test Plan* test scenarios would be to verify that the smoke control sequence does not activate from non-atrium initiation devices. For instance, tests should verify that non-atrium sprinkler water flow does not initiate the atrium smoke control system as designed.

Documentation Documentation of successful commissioning and *integrated testing* of fire protection and life safety systems should be developed and distributed, upon successful completion, and retained by the building owners.

Documentation of the individual systems and integration of the systems (e.g. shop drawings, as-built drawings, final sequence of operations, identification of location and type of interface points between systems, commissioning records, control drawings, *integrated testing* records, *integrated test plan*, and periodic testing plan) should be gathered and secured by the owner. These documents are essential for the required on-going periodic inspection and testing required by the various building, fire, and codes for the life of the building. Documentation of AHJ approval may include the signed permits, the issuance of the temporary Certificate of Occupancy, or the final Certificate of Occupancy.

Life of the Building

Once all testing is complete, approvals are complete, and occupants occupy the building, the required maintenance and testing cycles of the various fire protection and life safety systems should continue for the life of the building. Similarly, performance-based design elements, narrative basis of designs, *Integrated Test Plans*/Reports, and all critical documentation of fire protection and life safety systems need to be retained, referenced, and maintained for the building. Tenant improvement projects,

additions, alterations, system upgrades, and system replacements should be reviewed for conformance with the original fire protection and life safety documents. These critical documents may also require updates, modifications, and approvals to address changes, additions, alterations, system upgrades, new systems added, or systems being replaced over the life of the building. Periodic inspection, maintenance, and testing of all fire protection and life safety systems are required to be performed over the life of these systems. *Periodic Integrated Test* should also occur over the life of these systems per the *Integrated Test Plan*. *Re-commissioning* (*Re-Cx*) over the life of the systems may also be required due to either changes in the building or on an identified periodic basis.

Glossary[1]

Acceptance Testing Test performed with the local authorities and possibly the engineer of record or owner to show the fire protection or life safety system performs appropriately for final acceptance or approval.

Basis of Design (BOD) A report that documents the criteria of the fire protection and life safety design, which indicate the concepts and approach selected for a project, which should meet the Owner's requirements and applicable codes.

Commissioning (Cx) A formal process during the design and construction phase of a project that provides independent review and documentation that an individual system functions according to the design outlined in the project documentation, meeting the projects goals and objectives and applicable codes.

Commissioning Authority (CxA) The company or firm that is responsible and oversees the entire commissioning process for a building.

Commissioning Plan A project document that outlines the process, tasks, and procedures for implementation of *commissioning*.

Data Sharing Connection One of the methods of sharing information between interconnected fire protection systems via data streams.

End to End Test A test that replicates a real world situation that does not use simulations, such as shorting out a sprinkler water flow switch. For example, consider sprinkler system electrical supervision, the water flow indicating switch can be shorted to simulate water flow. Flowing water through the sprinkler system's inspectors test connection to verify fire alarm supervision represents an end to end test. Another example is visual verification of elevators recalling when an elevator lobby smoke detector is activated.

Emergency Control Function Interface Device The electronic interface, typically *emergency control function interface devices* (relays), between two or more fire protection and life safety systems that is a coordinated signal output to perform a particular control function (e.g. fire alarm system relay for elevator recall).

Evacuation Signaling Zone An area consisting of one or more *notification zone*s where evacuation signals are actuated throughout.

Fire and Life Safety Commissioning A formal process during the design and construction phase of a project that provides independent review and documentation that individual fire protection systems function according to the design outlined in the project documentation, meeting the *Owner's Project Requirements* and applicable codes.

Fire Commissioning Agent (FCxA) An independent company or person, acting as an owner representative, who implements and leads the *commissioning* of fire protection and *life safety systems*. Globally different terms may be

[1] The authors have defined the following terms to provide a common reference throughout the chapter. Readers should verify these definitions in the code, standards, and regulations in use for a specific project, as definitions may differ from those defined within this chapter.

utilized, for example, in France this person is referred to as the Coordonnateur SSI.

Interface Test A test that provides verification of the performance of the systems being interfaced/*interconnected* to meet the project goals and objectives. An *end to end test* or simulating event, through shorting out a *emergency control function interface devices* (relay) to simulate the input, is required.

Integrated System Two or more fire protection and life safety systems that are designed and coordinated to operate together in order to meet the *BOD*, *Owner's Project Requirements*, and applicable code requirements. A prison guard can be part of an integrated system, in which the guard relies on information from the fire alarm system or the emergency communication system in order to determine if he or she will manually release the door locking controls.

Integrated Testing Testing of integrated fire protection and life safety systems to verify the proper operation and sequence of the *integrated systems* (multiple systems) to meet the *BOD*, project goals and objectives, and applicable codes.

Integrated Testing Agent (ITa) An independent company or person selected by the owner who develops, implements, and documents the Integrated Test of the integrated fire protection and life safety systems.

Integrated Test Plan A plan on how and what tests will be performed on to confirm the proper integration of two or more fire protection system or life safety systems.

Interconnected Systems Two or more fire protection and life safety systems that have physical or electronic connections between the systems to meet the *BOD*, project goals and objectives, and applicable codes.

Interconnection The connections between two or more interconnected fire protection and life safety systems. The term interfacing is sometimes also used to describe interconnections.

Life Safety Systems A system that enhances life safety, such as evacuation, tenability (like a smoke control system) or compartmentation.

Notification Zone An area of a building that occupants would receive a common notification signal throughout an area.

Owner's Project Requirements (OPR) Owner and user developed project requirements and performance criteria developed that describe project goals and criteria for system function, performance and maintainability.

Periodic Integrated Test A test to re-verify the proper integration between multiple systems that occurs on an identified recurring period basis.

Pre-functional Testing System tests performed prior to *acceptance testing* to verify the fire protection or life safety system performs per the *BOD*, *OPR*, and applicable codes.

Re-commissioning (Re-Cx) *Commissioning* of existing fire protection and *life safety systems* that have been previously commissioned.

Retro-commissioning (RCx) *Commissioning* of existing fire protection and *life safety systems* that have never been commissioned.

References

1. AIA (2007) AIA Best Practices, Building Commissioning: Analyzing Costs and Benefits, New York, NY: The American Institute of Architects
2. AEAI (2012) NPI8: Installations techniques de protection incendie – réceptions et contrôles Berne, Germany: Association des Etablissements Cantonaux d'Assurance Incendie
3. ANSI/ASHRAE (2012) Standard 135- BACnet - A Data Communication Protocol for Building Automation and Control Networks, Atlanta, GA: American Society of Heating, Refrigerating and Air-Conditioning Engineers
4. ASME (2007) ASME A17.1: Safety Code for Elevators and Escalators, New York, NY: ASME
5. ASHRAE (2005) Guideline 0, The Commissioning Process, Atlanta, GA: American Society of Heating, Refrigerating and Air-Conditioning Engineers
6. ASHRAE (2012) Guideline 1.5: The Commissioning Process for Smoke Control Systems, Atlanta, GA: American Society of Heating, Refrigerating and Air-Conditioning Engineers
7. Brown, T. (2012) "Proper Commissioning of the Fire and Life Safety Systems Will Ensure An On-Time Building" Consulting-Specifying Engineer
8. Gottuk, D. (2008) "Video Image Detection Systems Installation Performance Criteria Research Project" Quincy, MA: Fire Protection Research Foundation

9. Hall, J. (2010) "U.S. Experience with Sprinklers and Other Automatic Fire Extinguishing Equipment." Quincy, MA: National Fire Protection Association
10. IAFC (2005) "Radio Communications for the Fire Service: A Planning Guide for Obtaining the Communications System You Need for Enhanced Safety and Emergency Preparedness." International Association of Fire Chiefs, National Volunteer Fire Council, Congressional Fire Services Institute and National Fallen Firefighters Foundation. (http://www.iafc.org/files/commComm_GuideRadioCommForFireServ.pdf)
11. ICC (2012a) *International Building Code*, Country Club Hills, IL: International Code Council
12. ICC (2012b) *International Fire Code*, Country Club Hills, IL: International Code Council
13. Klote, J., Milke, J., Turnbull, P., Kashef, A., and Ferreira, M. (2012) *Handbook of Smoke Control Engineering*, Atlanta, GA: American Society of Heating, Refrigerating and Air-Conditioning Engineers
14. Leber F. (2008) "Fire Alarm Interconnections", Fire Protection Handbook of Fire Protection Engineers, 20th Edition, Quincy, MA: National Fire Protection Association
15. NFPA (2010) NFPA 750: Standard on Water Mist Fire Protection Systems, Quincy, MA: National Fire Protection Association
16. NFPA (2011) NFPA 25: *Standard for the Inspection, Testing, and Maintenance of Water-Based Fire Protection Systems*, Quincy, MA: National Fire Protection Association
17. NFPA (2012a) NFPA 101: *Life Safety Code*®, Quincy, MA: National Fire Protection Association
18. NFPA (2012b) NFPA 5000®: *Building Construction and Safety Code,* Quincy, MA: National Fire Protection Association
19. NFPA (2012c) NFPA 1: *Fire Code*, Quincy, MA: National Fire Protection Association
20. NFPA (2012d) NFPA 72: National Fire Alarm and Signaling Code, Quincy, MA: National Fire Protection Association
21. NFPA (2012e) NFPA 3: Recommended Practice for Commissioning and Integrated Testing of Fire Protection and Life Safety Systems, Quincy, MA: National Fire Protection Association
22. NFPA (2012f) NFPA 99: Health Care Facilities Code, Quincy, MA: National Fire Protection Association
23. NFPA (2012g) NFPA 90A: *Standard for the Installation of Air-Conditioning and Ventilating Systems*, Quincy, MA: National Fire Protection Association
24. NFPA (2013a) NFPA 13: *Standard for the Installation of Sprinkler Syste*ms, Quincy, MA: National Fire Protection Association
25. NFPA (2013b) NFPA 110: Standard for Emergency and Standby Power Systems, Quincy, MA: National Fire Protection Association
26. NFPA (2013c) NFPA 111: Standard on Stored Electrical Energy Emergency and Standby Power Systems, Quincy, MA: National Fire Protection Association
27. NFPA (2013d) NFPA 20: *Stationary Fire Pumps Handbook*, Quincy, MA: National Fire Protection Association
28. NFPA (2013e) NFPA 24: *Standard for the Installation of Private Fire Service Mains and Their Appurtenances*, Quincy, MA: National Fire Protection Association
29. NFPA (2014) NFPA 70: *National Electrical Code*®, Quincy, MA: National Fire Protection Association
30. Shanahan, A. (2010) "Commissioning Fire Protection Systems" . Engineered Systems, July
31. SFPE (2011) Position Statement P-05-11, Building Information Modeling and Fire Protection Engineering, SFPE
32. Sinopoli, J. (2007) "Coordinating the Design of Integrated Building Technology Systems" Automated Buildings.com
33. Tubbs, J., Meacham, B., Kimball, A. (2009) "Evacuation Design Strategies and Considerations for Tall Buildings: Suggested Best Practices" ASHREA Transactions, Volume 115, Part 1, Atlanta, GA: American Society of Heating, Refrigerating and Air-Conditioning Engineers
34. Tubbs, J. and Meacham B.J. (2007). E*gress Design Solutions: A Guide to Evacuation and Crowd Management Planning*. Hoboken, NJ: John Wiley and Sons
35. ULC (2011) Integrated Systems Testing of Fire Protection and Life Safety Systems, Toronto, ON: Underwriters Laboratories of Canada

David Jacoby is a Principal with Simpson Gumpertz & Heger.

David LeBlanc is a Vice-President with JENSEN HUGHES.

Jeffrey Tubbs is a Principal with Arup.

Andrew Woodward is a Associate with Arup.

Smoke Control

50

John H. Klote

Introduction

In building fires, smoke often flows to locations remote from the fire, threatening life and damaging property. Research has shown that smoke is the major killer in building fires (Harland and Woolley 1979; [37]).

NFPA 92 [29] defines a smoke control system as an engineered system that includes all methods that can be used singly or in combination to modify smoke movement. These methods are the physical mechanisms of smoke control which are discussed later in this chapter. Research in the field of smoke control has been conducted in Australia, Canada, England, France, Japan, the United States, and Germany. This research has consisted of field tests, full-scale fire tests, scale model fire tests, and computer simulations. Many buildings have been built with smoke control systems and numerous others have been retrofitted for smoke control.

The conventional approach to smoke control consists of using the physical mechanisms to prevent people from coming into contact with smoke to the extent possible. A newer approach consists of evaluating the effect of some smoke contact with the intent of providing a tenable environment for occupants. Smoke control systems based on this newer approach are referred to as *tenability systems*. This chapter focuses on the conventional approach, but tenability systems are discussed near the end of the chapter. For an exhaustive treatment of smoke control including weather design data, design fires, conventional systems, tenability systems, and method of analysis see the *Handbook of Smoke Control Engineering* [21].

In this chapter the term *smoke* is used in accordance with the NFPA 92 definition that states that smoke consists of the airborne solid and liquid particulates and gases evolved when a material undergoes pyrolysis of combustion, together with the quantity of air that is entrained or otherwise mixed into the mass. It is important for smoke control purposes that the definition of smoke includes the air that is mixed with the particulates and other gases because smoke control often involves exhausting smoke which is mostly air. Including air as a part of smoke is also important for tenability systems.

Physical Mechanisms of Smoke Control

The physical mechanisms of smoke control are (1) compartmentation, (2) dilution, (3) pressurization, (4) airflow, and (5) buoyancy. For centuries, compartmentation has been recognized as a way of controlling the spread of fire and smoke. When a person closes the door to a burning room, smoke flow from the room decreases considerably. Also, the amount of air available to the fire drops off. Today this passive

J.H. Klote (✉)
consultant specializing in fire in smoke control, Leesburg, VA

M.J. Hurley (ed.), *SFPE Handbook of Fire Protection Engineering*,
DOI 10.1007/978-1-4939-2565-0_50, © Society of Fire Protection Engineers 2016

smoke protection is recognized in many building and fire codes even without a design analysis. Engineered smoke control systems that use only passive smoke barriers are a form of tenability systems that are discussed later in this chapter.

Dilution can occur naturally as when smoke flows away from a fire and mixes with air as it flows or be forced by fan powered flows. Naturally occurring dilution can be analyzed by the methods discussed in the section on tenability systems.

Fan powered dilution can be used to remove smoke from the fire space after a fire has been extinguished, and it can be used to remove smoke from a space connected to the fire space after the connection has been has been closed. Fan powered dilution consists of supplying air to the fire space and either exhausting air (or smoke) from the space or providing a path for a path for air (or smoke) to flow from the space. This kind of fan powered dilution can be analyzed by the methods discussed in the section on tenability systems.

The use of dilution to produce or maintain tenable conditions in the fire space is not recommended because such a system is beyond the current state of the technology. The air supplied to the fire space can increase the burning rate of the fire resulting in increased smoke production. The increased smoke production in the fire space has the potential to result in untenable conditions in the fire space. Because of this failure mode the use of dilution in the fire space is generally not recommended.

Many smoke control systems use mechanical fans to control smoke by pressurization. Pressure difference across a barrier can control smoke movement. The idea is that a pressure difference is produced across a barrier such that the smoke on the low pressure side of the barrier is prevented from migrating to the high pressure side, and this is shown in Fig. 50.1a for a relatively small amount of smoke. However, pressurization can control smoke from a

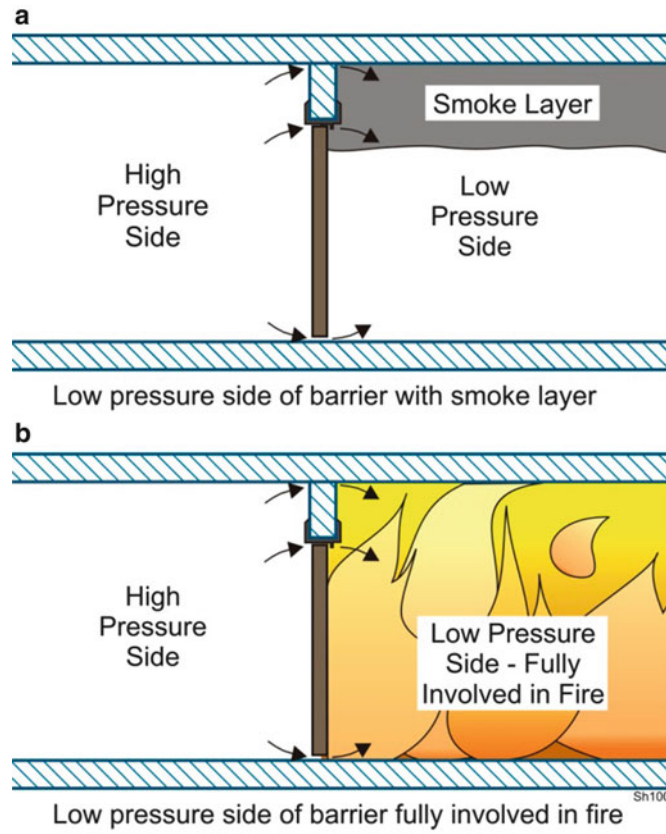

Fig. 50.1 Pressure difference across a barrier can control smoke flow

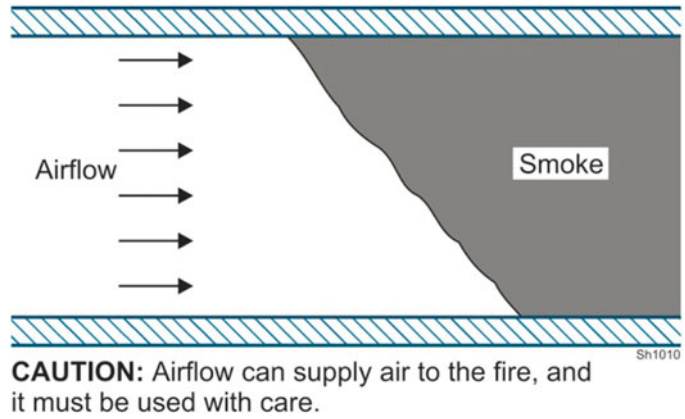

Fig. 50.2 Airflow can control the flow of smoke

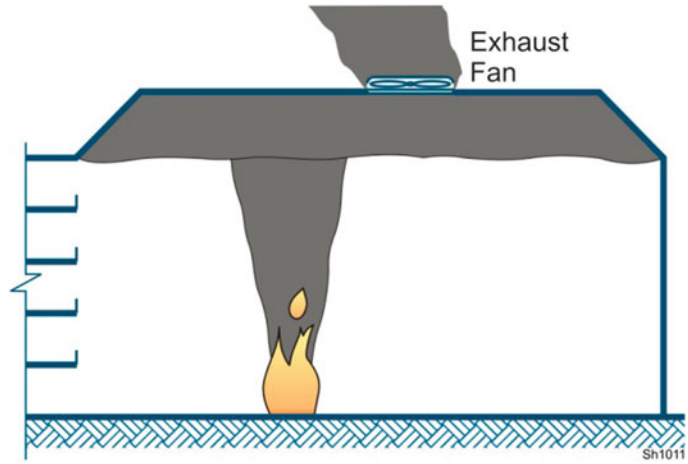

Fig. 50.3 Buoyancy can be used for smoke control as in an atrium smoke exhaust system

large fully developed fire as shown in Fig. 50.1b. In a room with a fully developed fire, everything that can burn is burning. Pressurization smoke control systems are discussed later in this chapter.

Airflow has been used extensively to control smoke flow during fires in subway, railroad and highway tunnels (Fig. 50.2). Airflow can also be used to control smoke between atria and spaces connected to atria. A number of empirical equations have been developed to calculate the air velocity needed for specific applications. Because the large amounts of air are needed for this method can supply additional oxygen to the fire, the use of airflow to control smoke needs to be done with caution.

Atria smoke exhaust systems rely on the buoyancy for a smoke plume to form above the fire and move the smoke away from occupants (Fig. 50.3). This form of smoke control is called atrium smoke management, and it is the subject of Chap. 51.

Pressurization Smoke Control Systems

Commonly used pressurization smoke control systems are (1) stairwell pressurization, (2) elevator pressurization, and (3) zoned smoke control. The concept of stairwell pressurization is to supply air to the stairwell with the intent of maintaining tenable conditions in stairwell. The idea of elevator pressurization is to supply air to the elevator shaft with the intent of preventing smoke flow through elevator shaft to locations

Table 50.1 Activation signals for pressurization smoke control systems

System	Smoke Detector	Heat Detector	Sprinkler Water Flow	Manual Pull Station
Stairwell pressurization	Yes	Yes	Yes	Yes[a]
Elevator pressurization	Yes	Yes	Yes	Yes[a]
Zoned smoke control	Yes	Yes	Yes	No

[a]Manual pull stations are not recommended for activation of stairwell or elevator pressurization systems that rely of fire floor exhaust

remote from the fire floor. The idea of zoned smoke control is to rely on pressurization or passive smoke control with the intent of preventing or minimizing smoke movement beyond the zone where the fire is located.

The primary purpose of pressurization smoke control systems is to maintain a tenable environment in the means of egress. Other purposes of these systems are to control smoke movement between fire area and adjacent spaces, provide conditions to help fire service, reduce property damage, and aid in post-fire smoke removal.

Table 50.1 lists sources of signals that can be used to activate pressurization smoke control systems. Zoned smoke control should not be activated from manual fire alarm pull stations. For proper operation of zoned smoke control needs, the location of the fire needs to be identified. A person who has seen a fire may start to leave the building and some distance away from the fire zone realize that he or she should pull the manual pull station. If zoned smoke control were activated by this manual pull station, the wrong zone would be identified as where the fire was located. Some stairwell pressurization systems and elevator pressurization systems rely on fire floor exhaust, and activation of these systems by manual pull stations can result in the wrong floor being exhausted. For this reason, manual pull stations are not recommended for activation of stairwell or elevator pressurization systems that rely of fire floor exhaust.

Network Modeling

Network models are a class of software that can simulate the flow of air or water through a complex system of paths which is called the network. Network modeling for smoke control application dates back to the 1960s, but these early models were subject to numerical difficulties and data input was extremely cumbersome and time consuming.

Network computer models such as CONTAM [36] have become widely used for analysis of pressurization smoke control systems due to their robust numerical routines and sophisticated data input. While CONTAM was developed for indoor air quality applications, care was taken to assure that it could be used for smoke control applications. Because CONTAM is a product of the US National Institute of Standards and Technology (NIST), it can be downloaded from the NIST website at no cost. In this chapter, when CONTAM is discussed, it should be noted that it may be possible that other network models could be used.

These models represent a building by a network of spaces or nodes, each at a specific pressure and temperature. The stairwells and other shafts can be modeled by a vertical series of spaces, one for each floor. Air flows through leakage paths from regions of high pressure to regions of low pressure. These leakage paths are doors and windows that may be opened or closed. Leakage can also occur through partitions, floors, and exterior walls and roofs. The airflow through a leakage path is a function of the pressure difference across the leakage path.

In network models, air from outside the building can be introduced by a pressurization system into any level of a shaft or into other building spaces. This allows simulation of stairwell pressurization, elevator shaft pressurization, stairwell vestibule pressurization, and pressurization of any other building space. In addition, any building space can be exhausted. This allows analysis of zoned smoke control systems where the fire zone is exhausted and other zones are

pressurized. The pressures and flows throughout the building are obtained by solving the conservation equations for the network. This analysis can include the driving forces of wind, the pressurization system, and inside-to-outside temperature difference.

The primary purpose of network simulations is to determine if a particular smoke control system in a particular building is capable of being balanced such that it will perform as intended. Network models are capable of simulating the pressures and flows throughout very large and complex building networks with high accuracy.

There are many flow paths in buildings including gaps around closed doors, open doors, construction cracks in walls and floors. These flow paths can be approximated for a design analysis, and the results of a network model simulation are approximations. However, these approximate results can be useful in identifying problems with specific smoke control systems. If such problems are identified, the smoke control system can be modified appropriately. A secondary purpose of these simulations is to provide information to help size the system components such as supply fans, exhaust fans, and vents.

Smoke Movement

A smoke control system must be designed so that it is not overpowered by the driving forces that cause smoke movement. For this reason, an understanding of the fundamental concepts of smoke movement is a prerequisite to intelligent smoke control design. The driving forces of air and smoke movement in building are (1) stack effect, (2) buoyancy of combustion gases, (3) expansion of combustion gases, (4) wind, (5) forced ventilation, and (6) elevator piston effect. Forced ventilation consisting of supply air is used for pressurization smoke control. Also, forced ventilation is used in heating, ventilating and air-conditioning (HVAC) systems. Generally, in a fire, smoke movement will be caused by a combination of these driving forces. The following sections discuss of each driving force as it would act in the absence of any other driving force.

Stack Effect

When it is cold outside, there is often an upward movement of air within building shafts such as stairwells, elevator shafts, dumbwaiter shafts, mechanical shafts, or mail chutes. This phenomenon is referred to as a *normal stack effect* as shown in Fig. 50.4. The air in the building has a buoyant force because it is warmer and less dense than the outside air. This buoyant force causes air to rise within the shafts of buildings, and the pressure difference due to normal stack effect is shown in Fig. 50.5. The significance of normal stack effect is greater for low outside temperatures and for tall shafts.

When the outside air is warmer than the building air, downward airflow frequently happens in shafts. This downward airflow is called *reverse stack effect* (Fig. 50.5), and the pressure difference due to reverse stack effect is shown in Fig. 50.5b. At standard atmospheric pressure, the pressure difference due to either normal or reverse stack effect is

$$\Delta p_{SO} = 7.63\left(\frac{1}{T_O + 460} - \frac{1}{T_S + 460}\right)z$$

$$\Delta p_{SO} = 3460\left(\frac{1}{T_O + 273} - \frac{1}{T_S + 273}\right)z \quad \text{for SI} \tag{50.1}$$

where

Δp_{SO} = pressure difference from a shaft to the outside, in. H_2O (Pa),
T_O = temperature outside, °F (°C),
T_S = temperature in the shaft, °F (°C),
z = distance above the neutral plane, ft (m).

The neutral plane is a horizontal plane where the pressure in the shaft is the same as that outdoors. For a shaft 200 ft (60 m) tall, with a neutral plane at the midheight, an outside temperature of 0 °F (−18 °C) and an inside temperature of 70 °F (21 °C), the maximum pressure difference due to normal stack effect would be 0.22 in. H_2O (55 Pa). This means that at the top

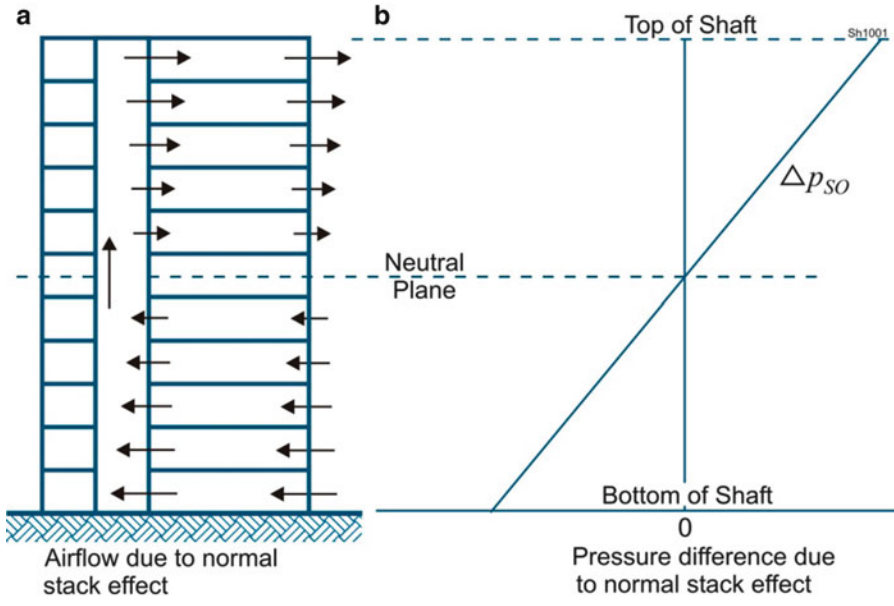

Fig. 50.4 Airflow and pressure differences of normal stack effect

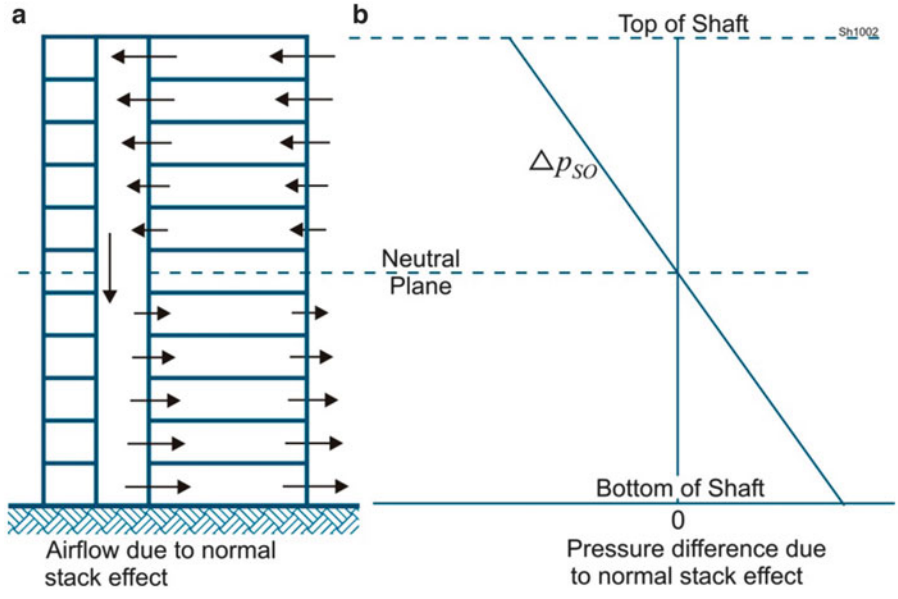

Fig. 50.5 Airflow and pressure differences of reverse stack effect

of the shaft, the shaft would have a pressure of about 0.22 in. H_2O (55 Pa) greater than that outside. At the bottom of the shaft, the shaft would have a pressure of about 0.22 in. H_2O (55 Pa) less than the outside pressure.

Stack effect can have a significant impact on smoke flow during building fires. When it is cold outdoors, the upward airflow in shafts can be enhanced by the buoyancy of the smoke. Figure 50.6 shows smoke flows in a building

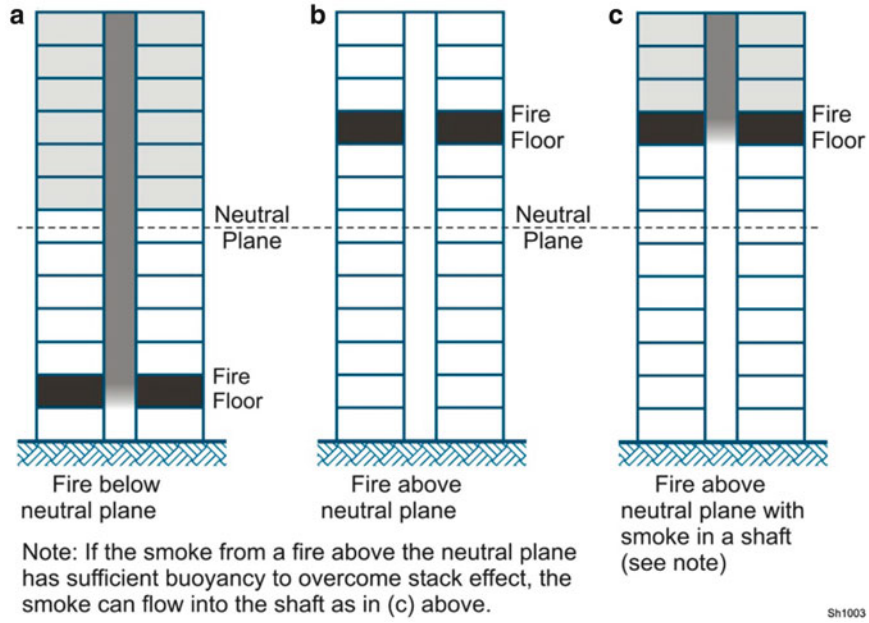

Fig. 50.6 Smoke movement in a high rise building due to normal stack effect

subjected to normal stack effect. For a fire below the neutral plane, smoke tends to enter and flow up shafts, and above the neutral plane this smoke flows from the shaft to building spaces (Fig. 50.6a). Smoke from a fire above the neutral plane can flow through cracks and gaps in the floor to the floor above the fire, but the forces of stack effect work to prevent smoke from entering shafts as shown in Fig. 50.6b. If the smoke from a fire above the neutral plane has sufficient buoyancy to overcome stack effect and flow into a shaft, it will flow up the shaft and infiltrate floors above the fire floor as can be seen in Fig. 50.6c.

For a building with shafts of various heights and different shaft temperatures, the flows can become very complicated. These flows would not look like those of either Fig. 50.4 or Fig. 50.5. Each shaft could have its own neutral plane with respect to the outside, and sometimes a shaft may have more than one neutral plane. Equation (50.1) is not applicable for such complicated buildings, but the flows and pressures in such buildings can be analyzed by CONTAM.

Myth: It is a myth that the pressure difference due to stack effect is nearly proportional to the temperature difference between the building and the outside

Fact: This pressure difference is nearly proportional to the temperature difference between a *shaft* and the outside

Another Meaning of Stack Effect

The term stack effect is often used in a different way from that discussed above. Sometimes engineers will say that a pressurized stairwell (or elevator) needs to be designed to account for the impact of stack effect. If the stairwell (or elevator) is properly pressurized, there is no neutral plane, and the flows do not look like those in Figs. 50.4 or 50.5. Strictly speaking there is no stack effect in the pressurized stairwell (or elevator). What is meant when an engineer says "that a pressurized stairwell (or elevator shaft) needs to be designed to account for the impact of stack effect" is that it needs to be

designed to account for the temperature differences that cause stack effect.

Myth: It is a myth that stack effect is the major factor impacting stairwell and elevator pressurization

Fact: Today the impact of stack effect is a minor factor for most pressurized stairwells and elevators. The pressurization air for many stairwells and elevators is untreated outside air that is not heated or cooled. The temperature of these shafts is often nearly the same as the outside temperature, and the impact of stack effect is significantly reduced as compared to shafts pressurized with air treated to the building temperature

Buoyancy of Combustion Gases

High-temperature smoke from a fire has a buoyancy force due to its reduced density. The pressure difference between a fire compartment and its surroundings can be expressed by an equation of the same form as Equation (50.1) with the variables updated as shown in Equation (50.2).

$$\Delta p_{FS} = 7.63\left(\frac{1}{T_O + 460} - \frac{1}{T_F + 460}\right)z$$

$$\Delta p_{FS} = 3460\left(\frac{1}{T_O + 273} - \frac{1}{T_F + 273}\right)z \quad \text{for SI} \tag{50.2}$$

where

Δp_{FS} = pressure difference from a fire space to the surroundings, in. H_2O (Pa),

T_O = temperature surroundings, °F (°C),

T_F = temperature in the fire space, °F (°C),

z = distance above the neutral plane, ft (m).

For a fire, the neutral plane is the horizontal plane of where the pressure in the fire space is the same as that of the surroundings. For a fire with a fire compartment temperature of 1470 °F (800 °C) and surroundings at 68 °F (20 °C), the pressure difference 5 ft (1.52 m) above the neutral plane can be calculated from Equation (50.2) to be 0.052 in. H2O (13 Pa). Fang [7] has studied pressures caused by room fires during a series of full-scale fire tests. During these tests, the maximum pressure difference reached was 0.064 in. H2O (16 Pa) across the burn room wall at the ceiling.

Expansion of Combustion Gases

In addition to buoyancy, the energy released by a fire can cause smoke movement due to expansion. In a fire compartment with only one opening to the building, building air flows into the fire compartment and hot smoke flows out of the fire compartment. Neglecting the added mass of the fuel (which is small compared to the airflow), the ratio of volumetric flows can simply be expressed as

$$\frac{V_{out}}{V_{in}} = \frac{T_{out} + 460}{T_{in} + 460}$$

$$\frac{V_{out}}{V_{in}} = \frac{T_{out} + 273}{T_{in} + 273} \quad \text{for SI} \tag{50.3}$$

where

V_{out} = volumetric flow of smoke out of the fire compartment, cfm (m^3/s),

V_{in} = volumetric flow of air into the fire compartment, cfm (m^3/s),

T_{out} = temperature of smoke leaving the fire compartment, °F (°C),

T_{in} = temperature of air entering the fire compartment, °F (°C).

For fire gas temperature of 2200 °F (1260 °C), the gas will expand to about five times its original volume. For a fire room with open doors or windows, the pressure difference across these openings due to expansion is negligible because of the large flow areas involved. However, for a fire space without open doors or windows, the pressure differences due to expansion may be important, provided there is sufficient oxygen to support combustion for a significant time.

Wind

In many instances, wind can have a pronounced impact on smoke movement within a building. The pressure that wind exerts on a wall is

$$p_w = 0.00645\, C_w \rho_o U_H^2$$
$$p_w = \frac{1}{2} C_w \rho_o U_H^2 \quad \text{for SI} \tag{50.4}$$

where
p_w = wind pressure, in H_2O (Pa),
C_w = pressure coefficient, dimensionless,
ρ_o = outside air density, lb/ft^3 (kg/m^3),
U_H = velocity at wall height H, mph (m/s).

The pressure coefficients, C_w, depends on wind direction, building geometry and local obstructions to the wind. The pressure coefficients are in range of −0.8 to 0.8, with positive values for windward walls and negative values for leeward walls.

Wind is often measured at airports, and the standard height for measuring velocity and direction is 33 ft (10 m). The Chap. 2 of the *Handbook of Smoke Control Engineering* lists design wind speeds for many locations in the US, Canada, and other countries. The local design wind can be calculated as follows

$$U_H = U_{met}\left(\frac{\delta_{met}}{H_{met}}\right)^{a_{met}}\left(\frac{H}{\delta}\right)^{a} \tag{50.5}$$

where
U_H = wind velocity at wall w/height H, mph (m/s),
U_{met} = measured velocity, mph (m/s),
H_{met} = height of wind measurement, ft (m),
δ_{met} = boundary layer height in the vicinity of the wind anemometer, ft (m),
a_{met} = wind exponent in the vicinity of the wind anemometer, dimensionless,
H = height of wall, ft (m),
δ = boundary layer height at wall, ft (m),
a = wind exponent at wall.

A number of approaches have been developed for categorizing terrain boundary layer and the wind exponent. For additional information about wind see Chap. 3 of the *Handbook of Smoke Control Engineering*, Shaw and Tamura [33], Kandola [12–14], Aynsley [3], and Klote [16]. Some civil engineering texts have useful information about wind [6, 24, 25, 35].

Forced Ventilation

The current code requirements for heating, ventilating and air conditioning (HVAC) systems started with a 1939 report by the National Board of Fire Underwriters [28]. The NBFU examined NFPA fire data from January 1936 to April 1938. Of 25 fires recorded, 19 involved combustion of parts of the air moving system. In five cases of no fire in the HVAC system, smoke was distributed by the system. Modern HVAC systems are built of materials intended to withstand fires. Also modern HVAC systems either shut down in the event of a fire or go into a smoke control mode of operation. This mode of operation is called zoned smoke control, and it is discussed later.

Elevator Piston Effect

The transient pressures and flows produced when an elevator car moves in a shaft are called *piston effect*. Figure 50.7 shows the airflows resulting from an upward-moving elevator car. Such piston effect can pull smoke into a normally pressurized elevator lobby or elevator shaft. In a

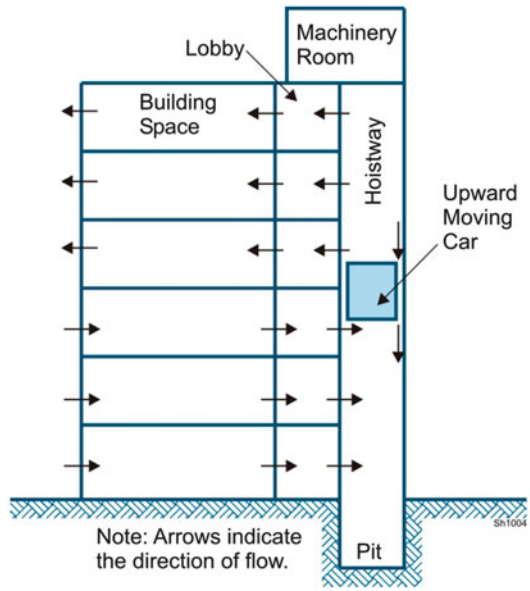

Fig. 50.7 Airflow due to an upward moving elevator car

joint US and Canadian project, an analysis of piston effect was developed and validated [15, 20, 23].

The upper limit of piston effect for an elevator with enclosed lobbies is

$$\Delta p_{u,ir} = \frac{1.66 \times 10^{-6}\rho}{2}\left(\frac{A_s A_e U}{A_a A_{ir} C_c}\right)^2 \qquad (50.6)$$

$$\Delta p_{u,ir} = \frac{\rho}{2}\left(\frac{A_s A_e U}{A_a A_{ir} C_c}\right)^2 \quad \text{for SI}$$

where

$\Delta p_{u,si}$ = upper limit pressure difference from the shaft to the building, in H_2O (Pa),
ρ = air density in hoistway, lb/ft^3 (kg/m^3),
A_s = cross-sectional area of shaft, ft^2 (m^2),
A_{ir} = leakage area between building and lobby, ft^2 (m^2),
A_a = free area around the elevator car, ft^2 (m^2),
A_e = effective area, ft^2 (m^2),
U = elevator car velocity, fpm (m/s),
C_c = flow coefficient for flow around car, dimensionless.

The flow coefficient, C_c, was determined experimentally at about 0.94 for a multiple car hoistway and 0.83 for a single car hoistway. The free area around the elevator car is the cross-sectional area of the shaft less the cross-sectional area of the car. For an elevator with enclosed lobbies, the effective area is

$$A_e = \left(\frac{1}{A_{sr}^2} + \frac{1}{A_{ir}^2} + \frac{1}{A_{io}^2}\right)^{-1/2} \qquad (50.7)$$

where

A_{sr} = leakage area between shaft and lobby, ft^2 (m^2),
A_{io} = leakage area between the building and the outside, ft^2 (m^2).

Figure 50.8 shows the upper limit of piston effect from the lobby to the building for car velocities from 100 to 1000 fpm (1 to 5 m/s). All elevator velocities are in this range with the exception of those of extremely tall buildings. The pressure differences shown in Fig. 50.8 happen for a brief time as the elevator car passes a floor.

Effective Flow Areas

Effective flow areas were essential in the early days of smoke control design to simplify flow networks. With computer network models such as CONTAM, there is much less need for network simplification. However, the effective flow area concept is still used for the following: (1) with the equation approach for analysis of pressurized stairwells, (2) with analysis of elevator piston effect, (3) to reduce data input to

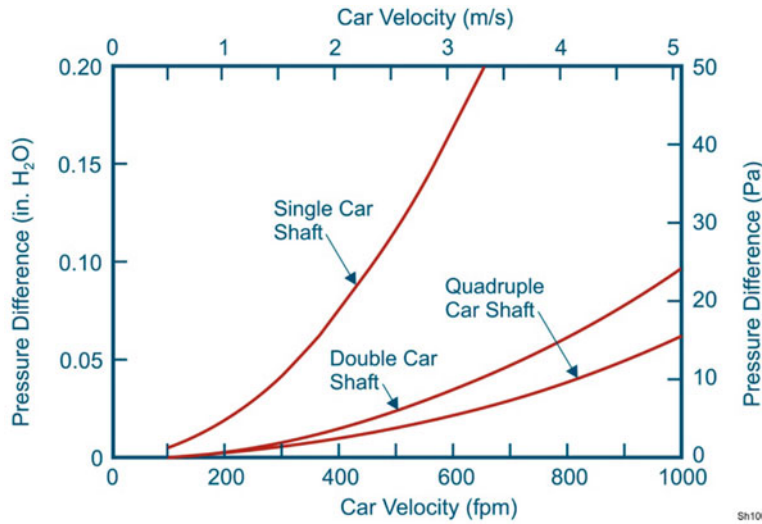

Fig. 50.8 Calculated upper limit of piston effect across elevator lobby doors

network models, and (4) to solve some problems without calculations.

The various paths of air movement in the system can be parallel with one another (Fig. 50.9a), in series with one another (Fig. 50.9b), or a combination of parallel and series paths (Fig. 50.9c). The effective flow area of a given system of flow paths is the area of a single opening that results in the same flow as the given system when subjected to the same pressure difference over the total system of flow paths. This concept is similar to an effective resistance of a system of electrical resistances.

For the three parallel flow paths in Fig. 50.9a, the effective area is

$$A_e = A_1 + A + A_3 \tag{50.8}$$

and for any number of flow paths in parallel the effective area is

$$A_e = \sum_{i=1}^{n} A_i \tag{50.8a}$$

For the three series flow paths in Fig. 50.9b, the effective area is

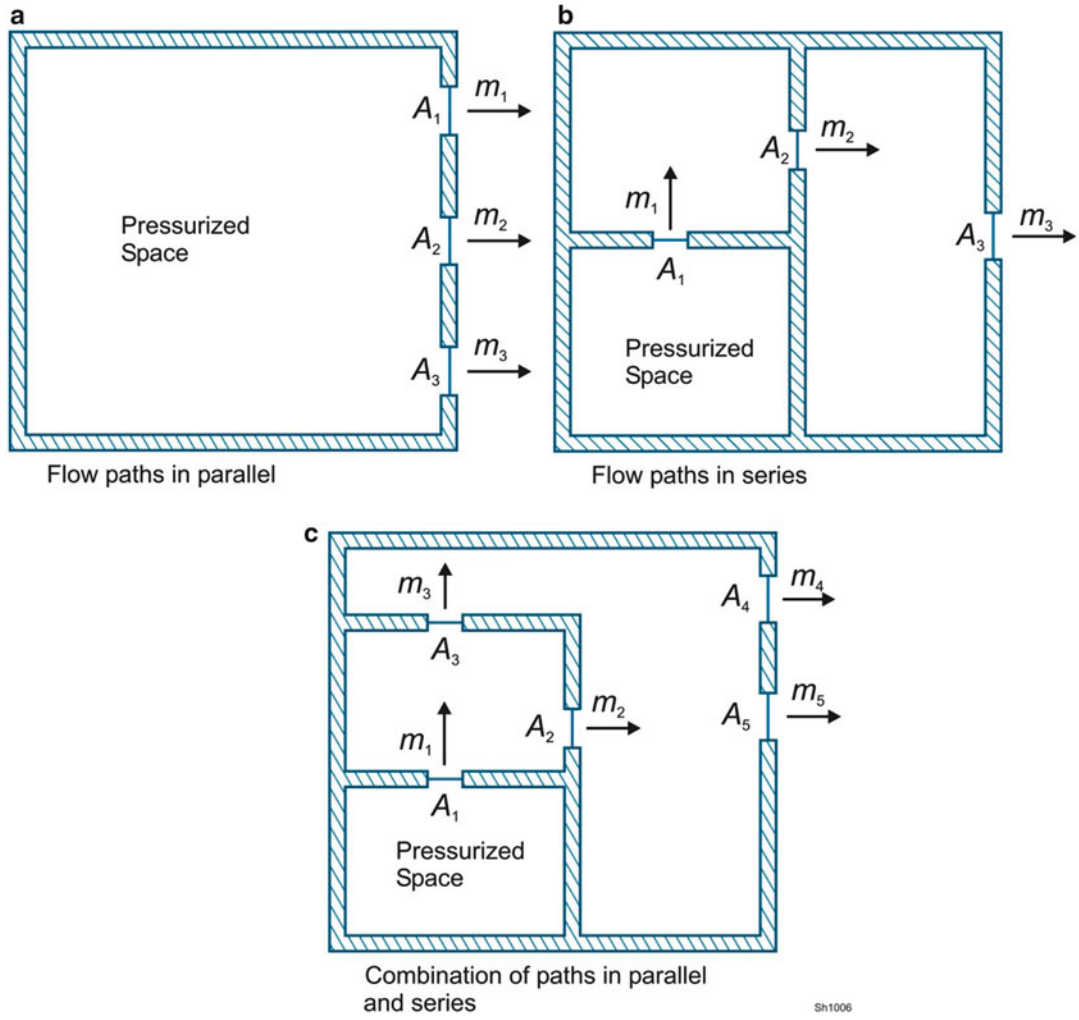

Fig. 50.9 Flow paths in parallel, in series, and a combination of both

$$A_e = \left(\frac{1}{A_1^2} + \frac{1}{A_2^2} + \frac{1}{A_3^2}\right)^{-1/2} \quad (50.9)$$

and for any number of paths in series the effective area is

$$A_e = \left(\sum_{i=1}^{n} \frac{1}{A_i^2}\right)^{-1/2} \quad (50.9a)$$

where
A_e = effective flow area, ft^2 (m^2),
A_i = flow area of path i, ft^2 (m^2).

The above equations for effective flow areas are based on having the same flow coefficients and temperatures for all the paths in the total system of flow paths. For a system with both parallel and series paths, and the method of developing an effective area for the system is to combine parallel paths first and then series paths. Example *1* illustrates calculation of effective flow areas.

Example 1. Effective Flow Areas

Part 1: In Fig. 50.9a, what is the effective flow area if A_1, A_2 and A_3 are 0.1 ft^2?

Because these areas are in parallel, $A_e = A_1 + A_2 + A_3 = 1 + 1 + 1 = 3$ ft^2

Part 2: In Fig. 50.9b, what is the effective flow area if A_1, is 0.1 ft^2 and A_2 and A_3 are both 1 ft^2?

Because these areas are in series, $A_e = \left(\frac{1}{A_1^2} + \frac{1}{A_2^2} + \frac{1}{A_3^2}\right)^{-1/2} = \left(\frac{1}{0.1^2} + \frac{1}{1^2} + \frac{1}{1^2}\right)^{-1/2} = (100 + 1 + 1)^{-1/2} = 0.099$ ft^2

This shows that for a system of flow areas in series with on area much smaller than the others, the effective flow area is slightly less than the smallest area.

Part 3: In Fig. 50.9c, what is the effective flow area if A_1, is 0.1 ft^2 and all the other flow areas are 1 ft^2?

$A_1 = 0.1$ ft^2 and $A_2 = A_3 = A_4 = A_5 = 1$ ft^2.

Because A_2 and A_3 are in parallel, the effective flow are of A_2 and A_3 is $A_{23e} = A_2 + A_3 = 1 + 1 = 2$ ft^2.

Because A_4 and A_5 are in parallel, the effective flow are of A_4 and A_5 is $A_{45e} = A_4 + A_5 = 1 + 1 = 2$ ft^2.

The effective flow area of the system of flow paths in Fig. 50.9c is $A_e = \left(\frac{1}{A_1^2} + \frac{1}{A_{23e}^2} + \frac{1}{A_{45e}^2}\right)^{-1/2} = \left(\frac{1}{0.1^2} + \frac{1}{2^2} + \frac{1}{2^2}\right)^{-1/2} = \left(100 + \frac{1}{4} + \frac{1}{4}\right)^{-1/2} = 0.0998$ ft^2

The reader can look at Fig. 50.9c and see that A_{23e} and A_{34e} are both much larger than A_1, so that for practical purposes, the effective flow area of the system is A_1.

Symmetry

As with effective areas, symmetry was essential in the early days of smoke control design to simplify flow networks, symmetry is also used with the equation approach for analysis of stairwell pressurization. Figure 50.10 illustrates the floor plan of a multistory building that can be

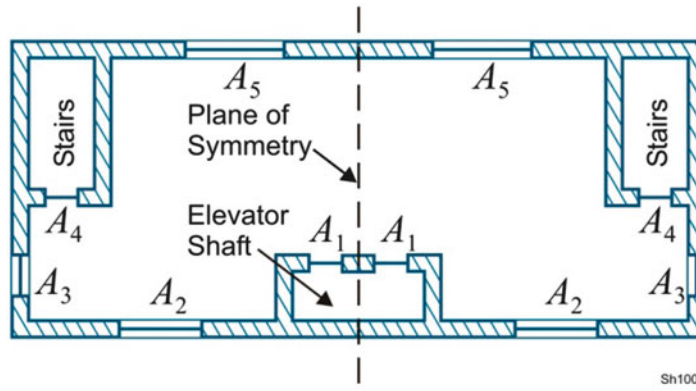

Fig. 50.10 Floor plan of building floor illustrating symmetry

divided in half by a plane of symmetry. Flow areas on one side of the plane of symmetry are equal to corresponding flow areas on the other side. For a building to be so treated, every floor of the building must be such that it can be divided in the same manner by the plane of symmetry. If wind effects are not considered in the analysis or if the wind direction is parallel to the plane of symmetry, then the airflow in only one-half of the building needs to be analyzed. It is not necessary that the building be geometrically symmetric, as shown in Fig. 50.10. A building that is not geometrically symmetric can be symmetric with respect to flow.

Flow and Pressure Difference

The primary equation used for analysis of pressurization smoke control systems is the orifice equation given in Equation (50.10).

$$\begin{aligned} m &= 12.9\, CA\sqrt{2\rho\Delta p} \\ m &= CA\sqrt{2\rho\Delta p} \quad \text{for SI} \end{aligned} \tag{50.10}$$

For mass flow at 70 °F (21 °C) and standard atmospheric pressure, the orifice equation becomes

$$\begin{aligned} m_{sv} &= 2610CA\sqrt{\Delta p} \\ m_{sv} &= 0.839CA\sqrt{\Delta p} \quad \text{for SI} \end{aligned} \tag{50.11}$$

where

m = mass flow through the path, lb/s (kg/s),
m_{sv} = mass flow through the path, scfm (standard m^3/s),
C = flow coefficient, dimensionless,
A = flow area (or leakage area), ft^2 (m^2),
Δp = pressure difference across path, in H_2O (Pa),
ρ = gas density in flow path, lb/ft^3 (kg/m^3).

One standard cubic foot per minute, scfm, equals 0.00125 lb per second, and one standard cubic meter per second (standard m^3/s) equals 1.2 kg per second at 70 °F (21 °C) and standard atmospheric pressure. Alternatively, the orifice equation can be expressed in terms of volumetric flow as shown in Equation (50.12).

$$\begin{aligned} V &= 776\, CA\sqrt{\frac{2\Delta p}{\rho}} \\ V &= CA\sqrt{\frac{2\Delta p}{\rho}} \quad \text{for SI} \end{aligned} \tag{50.12}$$

where V is volumetric flow through the path in cubic feet per minute, cfm (m^3/s).

Equations (50.10), (50.11) and (50.12) are equivalent forms of the same equation, and the label "orifice equation" applies to all of them. The orifice equation gets its name because it is used to calculate the flow through an orifice. For these flow equations, the area term is the cross-sectional area, and the flow coefficient is called the discharge coefficient. A network flow program such as CONTAM uses this flow meter terminology. Flow areas and flow coefficients for building components are discussed later, and Idelchik [10] also is a source of flow data.

Airflow paths must be identified and evaluated in the design of smoke control systems. Some leakage paths are obvious, such as cracks around closed doors, open doors, elevator doors, windows, and air transfer grilles. Construction cracks in building walls are less obvious but no less important.

The flow area of most large openings, such as open windows, can be calculated easily. However, flow areas of cracks are more difficult to evaluate. The area of these leakage paths depends on workmanship (such as how well a door is fitted or how well weatherstripping is installed). A door that is 36 in. by 7 ft (0.9 by 2.1 m) with an average crack width of $^1/_8$ in. (3.2 mm) has a leakage area of 0.21 ft^2 (0.020 m^2). However, if this door is installed with a ¾ in. (19 mm) undercut, the leakage area is 0.32 ft^2 (0.30 m^2). This is a significant difference. The leakage area of elevator doors has been measured in the range of 0.55–0.70 ft^2 (0.051–0.065 m^2) per door.

For many flow paths in buildings, a flow coefficient of 0.65 is used. The open doors of

Table 50.2 Flow areas of walls and floors of commercial buildings

Construction element	Leakage	Area ratio Leakage area per unit wall area in^2/ft^2	 ft^2/ft^2	 m^2/m^2
Exterior Building Walls (includes construction cracks, cracks around windows and doors)	Tight	7.2×10^{-3}	5.0×10^{-5}	5.0×10^{-5}
	Average	2.5×10^{-2}	1.7×10^{-4}	1.7×10^{-4}
	Loose	5.0×10^{-2}	3.5×10^{-4}	3.5×10^{-4}
	Very Loose	1.7×10^{-1}	1.2×10^{-3}	1.2×10^{-3}
Stairwell Walls (includes construction cracks but not cracks around windows or doors)	Tight	2.0×10^{-3}	1.4×10^{-5}	1.4×10^{-5}
	Average	1.6×10^{-2}	1.1×10^{-4}	1.1×10^{-4}
	Loose	5.0×10^{-2}	3.5×10^{-4}	3.5×10^{-4}
Elevator Shaft Walls (includes construction cracks but not cracks around doors)	Tight	2.6×10^{-2}	1.8×10^{-4}	1.8×10^{-4}
	Average	1.2×10^{-1}	8.4×10^{-4}	8.4×10^{-4}
	Loose	2.6×10^{-1}	1.8×10^{-3}	1.8×10^{-3}
		Leakage area per unit floor area		
Floors (includes construction cracks and gaps around penetrations)	Tight	9.5×10^{-4}	6.6×10^{-6}	6.6×10^{-6}
	Average	7.5×10^{-3}	5.2×10^{-5}	5.2×10^{-5}
	Loose[4]	2.4×10^{-2}	1.7×10^{-4}	1.7×10^{-4}

Note: The data in this table are for use with the orifice equation with a flow coefficient of $C = 0.65$. Floor leakage does not account for gaps that sometimes exist between the floor and curtain walls

pressurized stairwells commonly have stationary vortices which reduce the flow significantly [5, 19]. These vortices are thought to be caused by the asymmetric flow from the stairs, and stationary vortices can be expected at many open doors in other locations of smoke control systems. For open doors in stairwells, the geometric area of the opening should be used for the flow area along with a flow coefficient of 0.35.

Typical leakage areas for walls and floors of commercial buildings are tabulated as area ratios as shown in Table 50.2. These data are based from field tests performed by the National Research Council of Canada (Tamura and Wilson 1966; Tamura and Shaw 1976a, 1976b, 1978; [38–40]). Considerable data concerning leakage through building components are also provided in the *Handbook of Smoke Control Engineering*.

The determination of the flow area of a vent is not always straightforward especially when the vent surface is covered by a louver or screen. For vents with louvers, the flow area is referred to as the *free area*, and the free area is smaller than the geometric area (height multiplied by width) of the vent area. Because the slats in louvers are frequently slanted, calculation of the flow area is further complicated. When available, manufacturers' data regarding free are should be used. It is generally considered that the free area of a vent with a louver is about half the geometric area.

The density of air and smoke are expressed by the ideal gas law which is

$$\rho = \frac{144\,p}{R(T+460)} \qquad \rho = \frac{p}{R(T+273)} \quad \text{for SI} \tag{50.13}$$

where

ρ = density, lb/ft^3 (kg/m^3),
p = pressure, lb/in^2 (Pa),
R = gas constant, 53.34 ft lbf/lbm/°R (287 J/kg K)
T = temperature, °F (°C).

Friction Losses in Shafts

The pressure losses due to friction in ducts, stairwells and elevator shafts can be significant when flow rates are high. Tamura and Shaw (1976b) [40] and Achakji and Tamura [1] conducted tests of pressure loss in stairwells. Network computer models such as CONTAM employ algorithms that use this test data to calculate pressure losses due to friction in ducts, stairwells and other flow paths.

Door Opening Forces

The door opening forces resulting from the pressure differences produced by a smoke control system must be considered. Unreasonably high door opening forces can result in occupants having difficulty or being unable to open doors along the egress route such as into a stairwell.

The force to open a side hinged swinging door is shown in Fig. 50.11. The force required to open such a door when the smoke control system is operating can be determined using Equation (50.14).

$$F = F_{dc} + \frac{5.2WA\Delta p}{2(W-d)}$$
$$F = F_{dc} + \frac{WA\Delta p}{2(W-d)} \quad \text{for SI} \tag{50.14}$$

where:
F = total door-opening force, lb (N),
F_{dc} = door closer force, lb (N),
W = door width, ft (m),
A = door area, ft^2 (m^2),
d = distance from doorknob to knob side of door, ft (m),
Δp = pressure difference, in. H_2O (Pa).

Equation (50.14) applies when the door opening force is applied at the knob. Example 2 illustrates calculation of the door opening force.

Example 2. Door Opening Force
What is the door opening force for a side hinged swinging door 3 ft wide by 7 ft high with a door closer that requires 9 lb of force and a pressure difference across it of 0.35 in. H_2O? The knob is 3 in. (0.25 ft) from the edge of the door.

$W = 3$ ft; $F_{dc} = 9$ lb; $A = 3(7) = 21$ ft^2; $d = 0.25$ ft; $\Delta p = 0.35$ in. H_2O

The door-opening force is $F = F_{dc} + \frac{5.2WA\Delta p}{2(W-d)} = 9 + \frac{5.2(3)(21)(0.35)}{2(3-0.25)} = 30$ lb

Design Pressure Differences

Pressurization smoke control systems are designed to operate within a pressure difference range. This range is between the minimum design pressure difference and the maximum design pressure difference. A minimum design pressure difference intended to prevent smoke migration across a barrier of a smoke control system is generally stipulated by the applicable

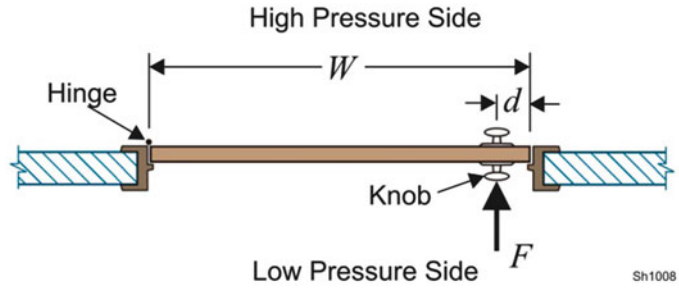

Fig. 50.11 Door-opening force for side hinged door

building and life safety regulations. A smoke control system should be designed to maintain this minimum design pressure difference under likely conditions of stack effect and wind.

The pressure difference across a barrier must not result in door-opening forces that exceed the maximum values stipulated by the applicable building and life safety regulations. For example, in NFPA 101, Life Safety Code [30], this maximum force is 30 lb (133 N). Calculation of door opening forces is discussed above. Acceptable pressurization consists of maintaining pressure differences across the barriers of a smoke control system that are between the minimum and maximum design values.

Stairwell Pressurization

Pressure differences across a stairwell tend to vary over the height of the stairwell. Figure 50.12 shows two pressure profiles for pressurized stairwells during cold winter months. One profile is for an idealized building, and the other is for a more realistic building with vertical leakage through floors and an elevator shaft. When it is cold outside, the pressure differences tend to be less at the bottom of the stairwell than at the top as can be seen in Fig. 50.12. When it is hot outside, the trend is the opposite. For both winter and summer conditions, the pressure profile for an idealized building is a straight line. An idealized building has no vertical leakage through the floors and shafts, and has leakage that is the same from floor to floor.

The pressure profiles of stairs in actual buildings depends on many factors including: (1) the leakage values of the various openings (flow paths) through building elements such as walls and floors, (2) the building floor plans, (3) the size of the elevator shaft or shafts and the number of elevator doors, (4) the presence or absence of elevator vents, and (5) the leakage through other shafts. There are many possible shapes for such pressure profiles in actual buildings.

For a building with vertical leakage, the flows through the floors and shafts act to even out to some extent the highest and lowest pressure differences across the stairwell. The profile for a building with vertical leakage is bounded by the extremes of the pressure profile of the idealized building. This means that other things being equal, the smallest pressure difference of the idealized analysis will be less than that of the actual building, and that the largest pressure difference of the idealized analysis will be more than that of the actual building. This is the reason that the algebraic equation method discussed below is conservative.

An algebraic equation method for analysis of pressurized stairwells is presented in Chap. 10 to the *Handbook of Smoke Control Engineering*. This algebraic equation method is based on

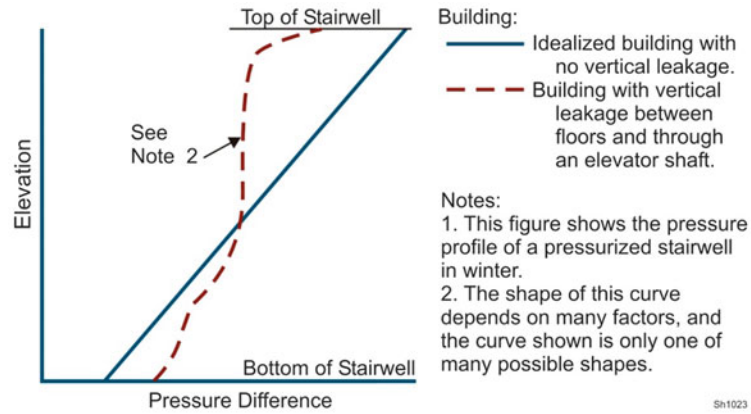

Fig. 50.12 Pressure profile of a pressurized stairwell in winter

(1) the idealized building, (2) flows calculated by the orifice equation, (3) effective flow areas, and (4) symmetry. The algebraic equation method does not account for pressure losses in the stairwell due to friction, but these losses tend to be small for stairwells when all the stair doors are closed.

Network computer models such as CONTAM are capable of analyzing pressurized stairwells much more realistically than the algebraic equation method. CONTAM can simulate the impact of a realistic building flow network based on the performance of pressurized stairwells. As already mentioned, computer network models can also simulate pressure losses in the stairwell due to friction.

Height Limit

For some tall stairwells, acceptable pressurization may not be possible because of the impact of the indoor to outdoor temperature differences. This is more likely with systems with treated supply air than those with untreated supply air.

The height limit is the height above which acceptable pressurization is not possible for an idealized building. For standard atmospheric pressure at sea level, the height limit can be determined by Equation (50.15).

$$H_m = 0.131 \frac{F_R(\Delta p_{\max} - \Delta p_{\min})}{\left| \frac{1}{T_O + 460} - \frac{1}{T_S + 460} \right|}$$

$$H_m = 2.89 \times 10^{-4} \frac{F_R(\Delta p_{\max} - \Delta p_{\min})}{\left| \frac{1}{T_O + 273} - \frac{1}{T_S + 273} \right|} \quad \text{for SI} \tag{50.15}$$

where

H_m = height limit, ft (m),

F_R = flow area factor (dimensionless),

$\Delta p_{\max}$ = maximum design pressure difference, in. H_2O (Pa),

$\Delta p_{\min}$ = minimum design pressure difference, in. H_2O (Pa).

The flow area factor is

$$F_R = 1 + \frac{A_{SB}^2 (T_B + 460)}{A_{BO}^2 (T_S + 460)}$$

$$F_R = 1 + \frac{A_{SB}^2 (T_B + 273)}{A_{BO}^2 (T_S + 273)} \quad \text{for SI} \tag{50.16}$$

where

A_{SB} = flow area between the stairwell and the building, ft^2 (m^2),

A_{BO} = flow area per stairwell between the building and the outside, ft^2 (m^2),

T_S = temperature in stairwell, °F (°C),

T_B = temperature in building, °F (°C).

The area, A_{SB}, is the total flow area between the stairwell and the building, which would typically include the gaps around all the closed doors and the leakage paths in the walls. For a stairwell with an unpressurized vestibule, A_{SB}, is the sum of the effective flow areas for all floors from the stairwell to the building.

The area, A_{BO}, is on a per stairwell basis because of symmetry considerations. For a building with an open floor plan, A_{BO} consists of the total leakage area of the exterior walls divided by the number of stairwells. For more complex floor plans, an effective flow area concept discussed above needs to be used to calculate A_{BO}.

Stairwell Temperature

Today, the supply air for most stairwells in North America is not treated so that pressurized stairwells are hot in the summer and cold in the winter. In many applications, the use of untreated supply air can be justified for the following reasons: (1) fire drills are usually held in the spring or fall when the outside temperature usually is mild, and (2) during a fire emergency being exposed to nearly outdoor temperatures seems reasonable considering occupants are often traveling to the safety of the outdoors.

When pressurization air is untreated in cold climates, there is a concern about the water freezing in sprinkler and standpipe risers in stairwells. To prevent such freezing, listed heat tracing systems can be used on the risers.. Alternately,

pressurization air can be treated to a minimum temperature in the range of 45–50 °F (7–10 °C) to prevent such freezing of water in the riser. ~~Using heat trace systems and untreated pressurization air has the advantage of minimizing the impact of stack effect, but using air treated to a minimum temperature has the advantage of minimizing the potential of freezing water on the stairwell floor during firefighting.~~

When pressurization air is untreated, the stairwell temperature can be expressed as

$$T_S = T_O + \eta(T_B - T_O) \qquad (50.17)$$

where
T_S = temperature in the stairwell, °F (°C),
T_O = temperature outdoors, °F (°C),
T_B = temperature in the building, °F (°C),
η = heat transfer factor (dimensionless).

There has been little research on the heat transfer factor. It is believed that the heat transfer factor is in the range of 0.05–0.15. In the absence of better data for a specific application, a heat transfer factor of 0.15 is suggested as being conservative regarding the impact of stack effect.

For untreated supply air, it takes a few minutes for the temperature in the stairwell to stabilize near that of the outdoors. During this stabilization, excessive pressure differences could be produced. To prevent this, supply air can gradually be increased so that when the stairwell temperature is near that of the building there is insufficient flow to cause excessive pressurization. If needed, the temperature stabilization can be evaluated by a heat transfer analysis.

Simple and Complicated Buildings

For simple stairwell pressurization systems in simple buildings, some designers may know from experience that the pressurized stairwell will work as intended, and the fans can be sized by simple calculations. A simple stairwell pressurization system is one that: (1) has air supplied at a constant (or nearly so) volumetric flow rate, (2) is intended to maintain acceptable pressurization with all the doors closed, and (3) has no features to prevent loss of pressure when stair doors are opened. As discussed later, a compensated stairwell system has features intended to prevent pressure loss when stair doors are opened, but such systems can be rather complex with regard to their design, installation and operation.

Figure 50.13a is an example of a simple building. The algebraic equation method can be used to size the supply fans for a simple building. Some engineers have developed their own rules of thumb that are appropriate for certain kinds of stairwell pressurization systems in some buildings. Rules of thumb are generally in the range of 300–550 cfm (0.14–0.26 m^3/s) per floor. Engineers determining a rule of thumb for stairwell pressurization should take into account the building specifications and the anticipated quality of construction. Of course, experienced engineers develop rules of thumb including an allowance to avoid the expense of replacing fans, motors and electrical wiring in the event that the stairwell would be somewhat more leaky than anticipated. Example *3* illustrates calculations for a simple stairwell system in a simple building.

Example 3. Simple Stairwell Pressurization in a Simple Building

The stairwells in a 20 story open plan office are to be pressurized, and the stairwells are the only pressurization smoke control systems in the building. The building has two stairwells that serve all floors. This building can be considered simple because the stairwells are all the same height and the floors are very similar from floor to floor. The winter design temperature is $T_O = 10$ °F, and the building temperature is $T_B = 70$ °F. The minimum and maximum design pressure differences are $\Delta p_{min} = 0.10$ in. H_2O and $\Delta p_{max} = 0.35$ in. H_2O. The floor-to-floor height is 10 ft, and building height is 200 ft. For a typical

(continued)

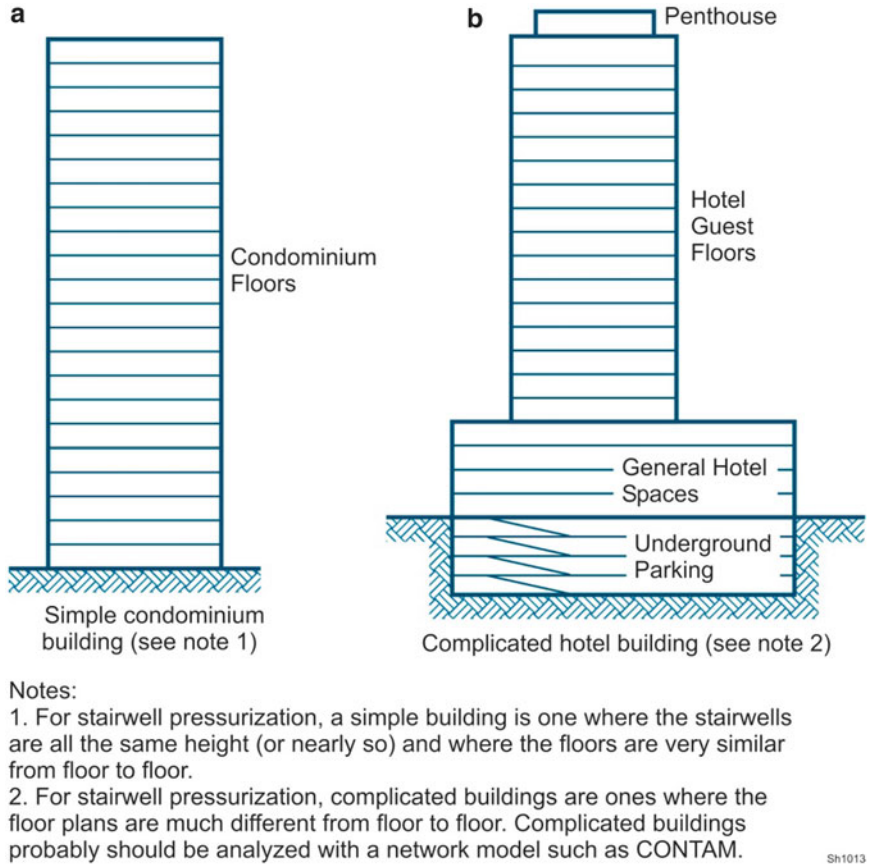

Fig. 50.13 Simple and complicated buildings with respect to stairwell pressurization

(continued)
floor, the flow area between the stairwell and the building is $A_{SB} = 0.34$ ft^2, and the flow area per stairwell between the building and the outside is $A_{BO} = 0.30$ ft^2.

Part 1: The stairwells are pressurized with untreated outside air, can this stairwell be pressurized?

Using a heat transfer factor of $\eta = 0.15$, the stairwell temperature is $T_S = T_O + \eta(T_B - T_O) = 10 + 0.15(70 - 10) = 19\,^\circ$F.

The flow area factor is $F_R = 1 + \frac{A_{SB}^2(T_B+460)}{A_{BO}^2(T_S+460)} = 1 + \frac{0.34^2(70+460)}{0.30^2(19+460)} = 2.42$.

The height limit is $H_m = 0.131 \frac{F_R(\Delta p_{\max} - \Delta p_{\min})}{\left|\frac{1}{T_O+460} - \frac{1}{T_S+460}\right|} = 0.131 \frac{2.42(0.35 - 0.10)}{\left|\frac{1}{10+460} - \frac{1}{19+460}\right|} = 1980$ ft.

Because the stairwells are in a simple building and the height limit is greater than the building height, the stairwells can be pressurized.

Part 2: The stairwells are pressurized with treated air at 70 °F, can this stairwell be pressurized?

The flow area factor is $F_R = 1 + \frac{A_{SB}^2(T_B+460)}{A_{BO}^2(T_S+460)} = 1 + \frac{0.34^2(70+460)}{0.30^2(70+460)} = 2.28$.

The height limit is $H_m = 0.131 \frac{F_R(\Delta p_{\max} - \Delta p_{\min})}{\left|\frac{1}{T_O+460} - \frac{1}{T_S+460}\right|} = 0.131 \frac{2.28(0.35 - 0.10)}{\left|\frac{1}{10+460} - \frac{1}{70+460}\right|} = 310$ ft.

This height limit is much less than that of Part 1. As with part 1, the stairwells can be pressurized, because the stairwells are in a simple building and the height limit is greater than the building height.

Part 3: Each stairwell is to be pressurized with one fan. Choose the capacity of the fan.

(continued)

(continued)

Based on experience with similar construction and buildings, the design engineer chooses 420 cfm per floor for this application. Because the stairwell is 20 stories, the fan capacity is 8400 cfm. Each stairwell needs an 8400 cfm fan.

For buildings that are relatively complicated, computer-based network analysis of the pressurized stairwells is often needed to determine if the stairwell systems are capable of being balanced to perform as intended. For stairwells pressurized with untreated air, building complexity often has more impact than stack effect. Even buildings that are not especially tall are considered complicated when the floors plans vary significantly from floor to floor.

The building indicated in Fig. 50.13b consists of underground parking levels, general hotel floors, guest room floors and a penthouse. It can be difficult to maintain acceptable pressurization of stairwells that extend from the parking levels to the penthouse, because the plans of these floors are so different. Complicated buildings should probably be analyzed with a network analysis model such as CONTAM. Wind effects add complexity to building when there are many openings to the outdoors (operable windows, balconies with doors that open, etc.). For complicated buildings with many openings to the outdoors, analysis of the pressurized stairwell systems with a computer network model is needed.

Single and Multiple Injection

A single injection system has pressurization air supplied at one location. Air can be supplied at the top of the stairwell, the bottom, or at a location in between. Figure 50.14a and b illustrate top and bottom injection systems. When roof-mounted propeller fans are used for stairwell pressurization, propeller fans should have tops that shield the fan from wind effects. Wall-mounted propeller fans should not be used because they can be adversely impacted by the wind unless a wind analysis indicates otherwise.

With a bottom injection system such as illustrated in Fig. 50.14b, some of the supply air can short circuit the system by flowing directly out of the opened exterior bottom doorway reducing system effectiveness. The bottom doorway is expected to be open as occupants egress the building through the stairwell. Simulation of such detailed fluid flow is typically beyond the capability of network models such as CONTAM, but it can be simulated with more sophisticated computations fluid dynamics, CFD, computer models. It is recommended that bottom injection systems be analyzed using CFD to determine the extent to which supply air flows out of an open exterior door. Alternatively, the air can be introduced into the stairwell at least one floor above or below the exterior doors.

For tall stairwells, single injection systems can fail when a few doors near the air injection point are open simultaneously. Much of the pressurization air can be lost through these open doors, and the system will then fail to maintain positive pressures across doors further from the injection point compromising the effectiveness of the overall stairwell pressurization system. To reduce the potential for such failure, multiple injection systems can be used. Multiple injection systems can consist of one fan supplying air through a duct located in a shaft as shown in Fig. 50.14c. Other arrangements of multiple injection systems eliminate the need for a shaft by using more than one fan as shown in Fig. 50.14d.

There has been no research on this subject, but the consensus is that single injection systems for stairwell heights more than 100 ft (30.5 m) need a design analysis using computer network models. For multiple injection systems supplying air through a duct in a shaft, injection points are usually one to three floors apart. Multiple injection systems that have a separate fan at each

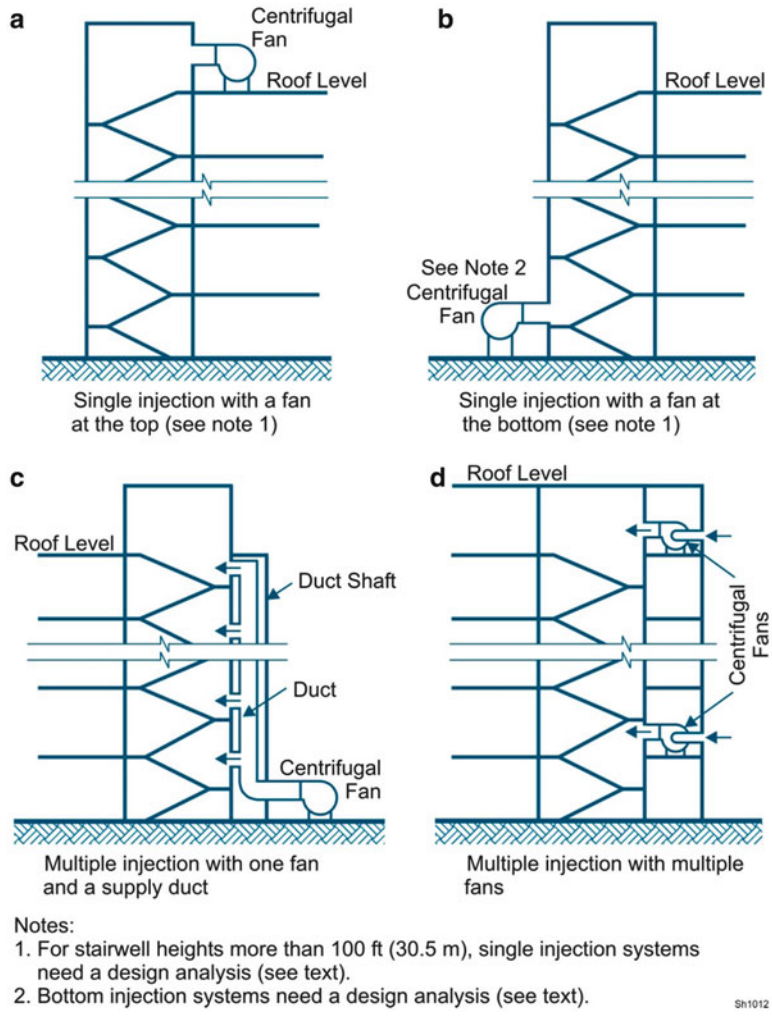

Fig. 50.14 Some single and multiple injection stairwell pressurization systems

injection point can have injection points much further apart. For systems with two injection points, one at the top and another near the bottom, a computer network model analysis is recommended for stairwell heights more than 200 ft (61 m).

Vestibules

Pressurized stairwells with vestibules are occasionally used. The vestibules can be: (1) unpressurized, (2) pressurized, (3) ventilated, or (4) a combination of pressurized and ventilated. Vestibules provide an additional barrier around a stairwell, and vestibules have the potential to reduce the probability of an open-door connection existing between the stairwell and the building.

An evacuation analysis can be performed to determine the extent to which both vestibule doors and stairway doors are likely to be opened simultaneously. For densely populated buildings, it is expected that on many floors both vestibule doors and stairway doors would be opened simultaneously. Therefore, vestibules may provide little benefit of an extra barrier for densely populated buildings.

The algebraic equation method of analysis can be used to analyze a pressurized stairwell with an

unpressurized vestibule. The pressure differences and flows of stairwell systems with any kind of vestibules can be analyzed by computer network model. It is possible to evaluate the benefits of ventilated vestibules using tenability analysis.

System with Fire Floor Exhaust

System employing fire floor exhaust can achieve acceptable pressurization of tall stairwells in very complex buildings. A relatively small amount of air is supplied to the stairs, and the fire floor is exhausted such that acceptable pressurization is maintained on the fire floor where it is needed. It is common to also exhaust one or two floors above and below the fire floor. Fire floor exhaust is a form of zoned smoke control, and stairwell pressurization with such zoned smoke control is discussed later.

Stairwells and Open Doors

When any stair door is opened in a simple stairwell pressurization system, the pressure difference drops significantly. When all doors are closed suddenly in such a simple system, the pressure difference increases significantly. A compensated stairwell pressurization system is one that adjusts for changing conditions either by modulating supply airflow or by relieving excess pressure. The intent of a compensated system is to maintain acceptable pressurization when doors are opening and closing.

In the United States, most building and life safety regulations do not require pressurized stairwells to be compensated, and such stairwells are designed to maintain pressurization only when all the stair doors are closed. Traditionally, some engineers believed that pressurized stairwells need to be compensated, but an incidental finding of a study by Klote [18] casts doubt on this opinion. For two simulations in this study with a closed stair door on the fire floor and some other stair doors open, the stairwell remained tenable. The reason the stairwell remained tenable was that the smoke that leaked into the stairwell was diluted by the large amount of air supplied to the stairwell. In light of this finding, ASHRAE is sponsoring a research project to study the need for compensated stair systems.

Many kinds of compensated stairwell pressurization systems have been used, but the most common are (1) the open exterior door system and (2) the variable air volume (VAV) system. The open exterior door system has "constant-supply" airflow, and an exterior stairwell door that opens automatically upon system activation. This system is sometimes called the Canadian system because it originated in Canada, and it has been used extensively there. The supply air rate is not actually constant, but it varies to some extent with the pressure across the fan. For centrifugal fans this variation in flow is generally small. However, the term "constant-supply" is used to differentiate this system from the systems where the supply air rate is designed to intentionally change.

By keeping the exterior stairwell door open during system operation, the Canadian system eliminates the major source of pressure fluctuations. This system is simple and relatively inexpensive, but there are many locations where opening exterior doors automatically raises issues of building security. For complex buildings, it is recommended that this system be evaluated using a computer network model to assure that it operates as intended.

With the VAV system, the flow rate of supply air to the stairwell is adjusted to account for opening and closing of doors. Tamura (1990) conducted research on VAV systems at the National Research Council of Canada. It was found that the pressure drops when doors are opened, and it took about 3–7 min for the pressure to recover to the initial value. When all the stair open doors in a VAV system are closed, there is a pressure spike. In Tamura's research, the spike had a peak of 0.728 in. H_2O (181 Pa). This spike only lasted about 30 or 40 s, but the peak was much more than any reasonable maximum design pressure difference. Such peaks are a concern. A person encountering such a peak, would probably not be able to open the stair door,

but they could open it a minute or so later provided they knew enough to try. It is possible that a person encountering such a peak would think the stair door was locked, and he or she might not try to open it again.

Wind can have a serious impact on VAV stair pressurization systems. During design analysis of some of these systems, some engineers have encountered very high pressure differences during some wind conditions. For example, when an exterior door is opened during the design wind speed, a compensated stair system may supply so much air that the pressure difference across some stair doors may exceed the maximum design value. It is possible to exceed this design value by as much as 100 %. During such an occurrence, it would be impossible or extremely difficult for occupants to enter the stairwell. For this reason, it is recommended that design analysis of VAV compensated stairwell pressurization systems include computer network model simulations under wind conditions.

Elevator Shaft Pressurization

The elevator pressurization systems discussed in this section are intended to prevent smoke from flowing from the fire floor through an elevator shaft and threatening life on floors away from the fire floor. This section does not address smoke control for elevator evacuation, but elevator evacuation is discussed in Chap. 12 of the *Handbook of Smoke Control Engineering*. Usually pressurized elevator shafts are in buildings that have pressurized stairwells, and the focus of this section is on both of these pressurization systems operating together. In the rare situation where pressurized elevator shafts are the only pressurization smoke control system in a building, the information in this section may also be useful.

The information discussed earlier about piston effect can be used to evaluate the impact of piston effect on the performance of pressurized elevator systems. The piston effect produces a pressure spike when a car passes a particular floor, and this happens for only a few seconds during the run of an elevator car. For elevators in multiple car shafts with car velocities less than 1000 fpm (5 m/s), piston effect should not adversely impact the performance of elevator pressurization. For elevators in single car shafts with car velocities less than 500 fpm (2.5 m/s), piston effect should not adversely impact the performance of elevator pressurization.

Design of pressurized elevator shafts is much more complicated than design of pressurized stairwells, but there are a number of approaches that can deal with this complexity. The reasons for this complexity are: (1) often the building envelope is not capable of effectively handling the large airflow resulting from both elevator and stairwell pressurization, and (2) open exterior doors on the ground floor can cause high pressure differences across the elevator shaft at the ground floor.

Usually a number of exterior doors on the ground floor are open during a building fire. During a fire, the fire service opens a number of exterior doors or keeps these doors open while fighting the fire. Occupants also open exterior doors during evacuation. The shaft pressurization system needs to operate as intended with these exterior doors open.

Generally a computer network model analysis is needed to determine if pressurized elevators and pressurized stairwells in a particular building are capable of being balanced to perform as intended. While it may be theoretically possible to use only a rule of thumb to design these systems, a computer network model analysis is strongly recommended.

The elevator pressurization systems discussed here are: (1) the basic system, (2) the exterior vent (EV) system, (3) the floor exhaust (FE) system, and (4) the ground floor lobby (GFL) system. As mentioned above, these systems are for use in buildings with pressurized stairwells. The results of 36 computer network model simulations using CONTAM were used to study the performance of an elevator shaft pressurization system for a 14-story building illustrated in Fig. 50.15. Further details of this analysis are presented in Chap. 11 of the *Handbook of Smoke Control Engineering*. The following discussion about elevator pressurization

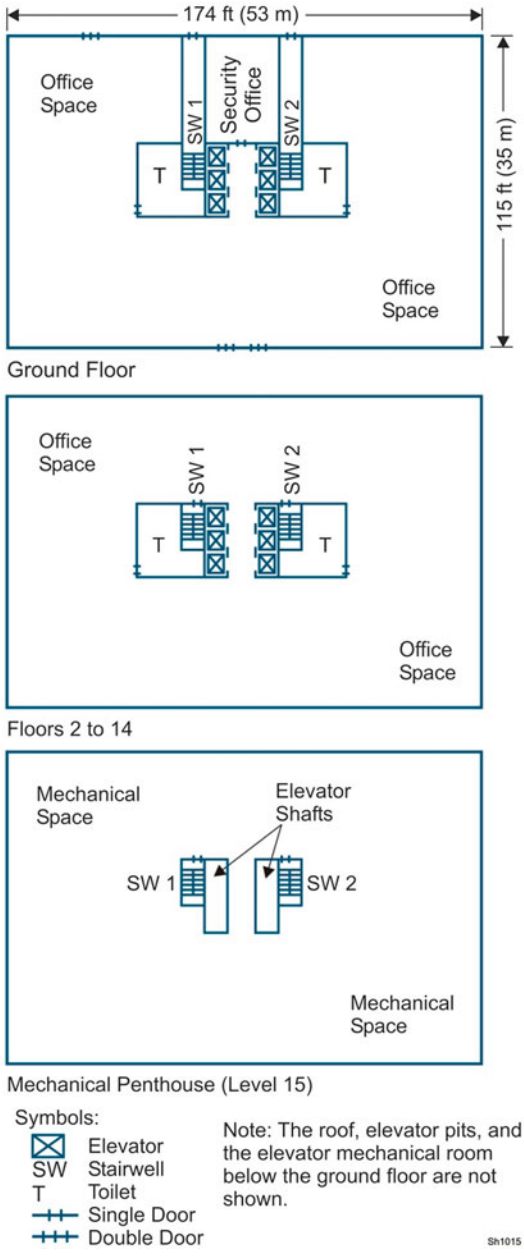

Fig. 50.15 Floor plans of the example 14 story open plan office building for elevator pressurization study

systems is based on these 36 simulations. For these simulations, the pressure difference criteria listed in Table 50.3 were used, and these criteria are consistent with pressure differences requirements in the *International Building Code* (ICC 2012). The leakage values and flow coefficients used for these simulations are listed in Tables 50.4 and 50.5. For the CONTAM simulations of the 14-story building, supply air was injected only at the top of the elevator shafts, but about half the supply air was injected at the top of the stairs and the rest at the second floor.

Table 50.3 Pressure differences criteria for elevator pressurization simulations[a]

	Minimum		Maximum	
System	in. H_2O	Pa	in. H_2O	Pa
Pressurized elevators	0.10	25	0.25	62
Pressurized stairwells	0.10	25	0.35	87

[a]The above criteria are for the elevator simulations discussed Chap. 11 of the *Handbook of Smoke Control Engineering*, and some projects may have different criteria depending on code requirements and requirements of specific applications

Table 50.4 Flow areas and flow coefficients of doors used for elevator pressurization simulations[a]

			Flow area	
Flow path	Path name[b]	Flow coefficient	ft^2	m^2
Single door (closed)	DOOR-SC	0.65	0.25	0.023
Single door (opened)	DOOR-SO	0.35	21	2.0
Double door (closed)	DOOR-DC	0.65	0.48	0.045
Double door (opened)	DOOR-DO	0.35	42	3.9
Elevator door (closed)	DOOR-EC	0.65	0.65	0.06
Elevator door (opened)	DOOR-EO	0.65	6	0.56

[a]The values in this table were chosen for the elevator simulations discussed Chap. 11 of the *Handbook of Smoke Control Engineering*. The flow areas and flow coefficients appropriate for a design analysis of a specific building may be different

[b]The path name is an identifier used in the CONTAM simulations

Basic System

In the basic system, each stairwell and elevator shaft has one or more dedicated fans that supply pressurization air. For reasons mentioned above,

Table 50.5 Flow areas and flow coefficients of leakages used for elevator pressurization simulations

Flow path	Leakage classification	Path name	Flow coefficient	Flow area	
				ft^2 per ft^2 of wall	m^2 per m^2 of wall
Exterior walls	Tight	WALL-EXT	0.65	0.50×10^{-4}	0.50×10^{-4}
	Average			0.17×10^{-3}	0.17×10^{-3}
	Loose			0.35×10^{-3}	0.35×10^{-3}
	Very loose			0.12×10^{-2}	0.12×10^{-2}
Interior walls	Loose	WALL	0.65	0.35×10^{-3}	0.35×10^{-3}
Floor (or roof)	Tight	FLOOR	0.65	0.66×10^{-5}	0.66×10^{-5}
	Average			0.52×10^{-4}	0.52×10^{-4}
	Loose			0.17×10^{-3}	0.17×10^{-3}
				ft^2 per ft of wall	m^2 per m of wall
Curtain wall gap	Tight	FLOORW	0.65	0.002	0.00061
	Loose			0.02	0.0061

See notes on Table 50.4

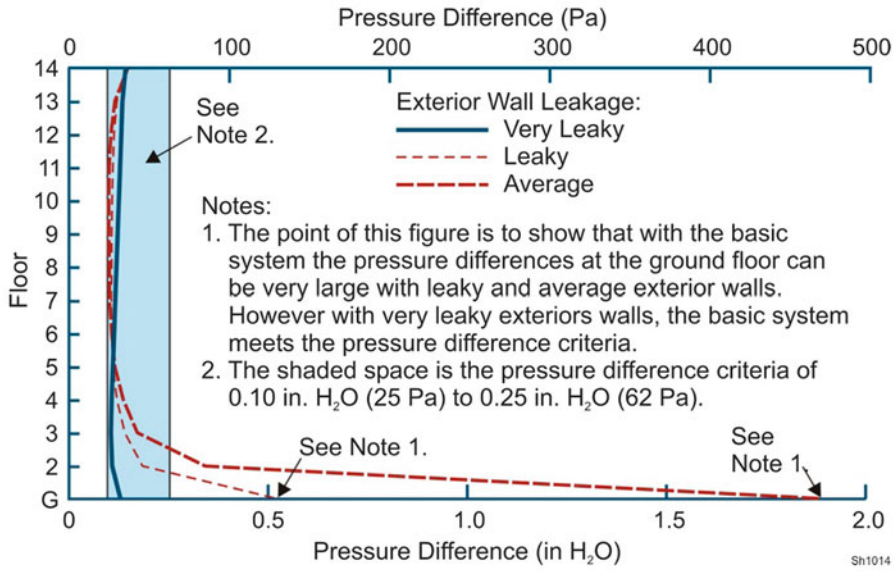

Fig. 50.16 Elevator pressure differences for basic elevator pressurization system

the basic system also includes stairwell pressurization, and the stair subsystems are not compensated systems. In most buildings the basic system does not result in successful pressurization, and the other systems discussed below consist of the basic system plus features to improve performance.

When the 14-story building contained very leaky exterior walls, the CONTAM simulations showed that the basic pressurization system would perform well, but this was not the case with less leaky exterior walls. It can be seen on Fig. 50.16 that for leaky exterior walls, the pressure difference across the elevator doors on the ground floor is about 0.5 in. H_2O (75 Pa). For exterior walls of average leakage the pressure difference across the elevator doors on floor 2 is about 0.35 in. H_2O (52 Pa), and at the ground floor it is about 1.9 in. H_2O (280 Pa). These values exceed the maximum criteria used for elevator doors, which is 0.25 in. H_2O (62 Pa) as indicated in Table 50.3. For average and leaky

exterior walls, there is insufficient leakage in the building envelope to accommodate the large amount of pressurization air supplied to the shafts.

With very leaky exteriors walls, it can be seen on Fig. 50.16 that the basic system meets the pressure difference criteria identified in Table 50.3. Air was supplied to each elevator shaft at 27,700 cfm (13.1 m^3/s), and air was supplied to each stairwell at 6560 cfm (3.09 m^3/s). With very leaky exteriors walls, there is enough wall leakage area to accommodate this large amount of pressurization air. For the few buildings that have very leaky building envelopes, the basic system can be a simple way to pressurize elevators and stairwells. For less leaky buildings, the systems discussed present other options.

Exterior Vent (EV) System

The idea of the EV system is to use vents in the exterior walls to increase the leakiness of the building envelope such that successful pressurization can be achieved. The vents are usually closed, but they open when the pressurization system is activated. The vents should be located in a manner to minimize adverse wind effects, and the supply intakes need to be located away from the vents to minimize the potential for smoke migration into the supply air. These vents may need fire dampers depending on building and fire code requirements.

Figure 50.17a shows a typical floor of the example 14-story building with vents in the exterior walls. For the example building, the vents can be sized to assure the design criteria are met. The vents were sized such that the amount of pressurization used for the basic system produce acceptable pressurization with the EV system in the example building.

The example building has open office plan. For buildings with corridors, the simple EV approach of Fig. 50.17a is not appropriate. The flow resistance of corridor walls and other walls has a negative impact on system performance

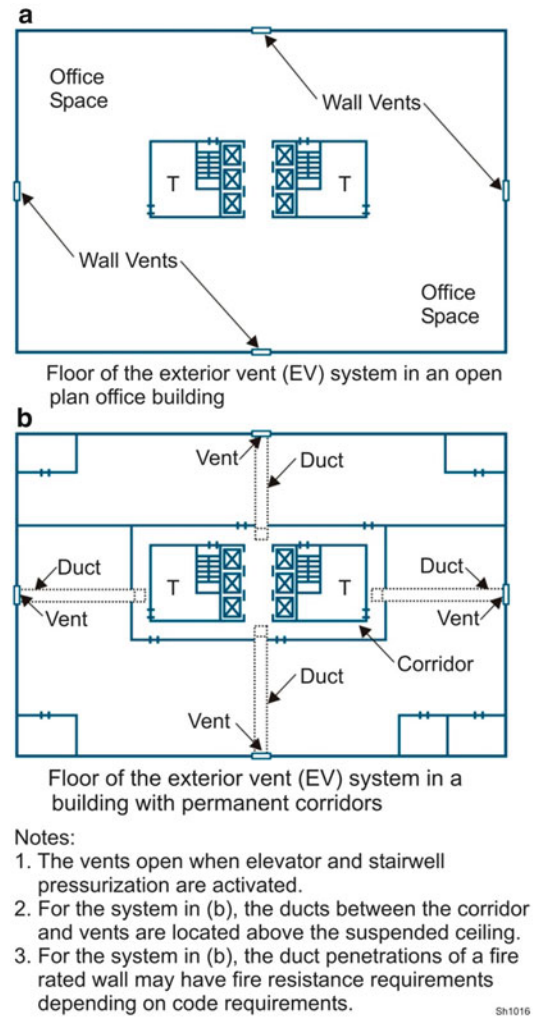

Fig. 50.17 Typical floor plans of buildings with the exterior vent (*EV*) system

when the vents are located in the exterior walls, but this can be overcome by use of ducted vents.

Figure 50.17b shows a ducted EV system that can be used for an office building with permanent corridors. The ducted EV system can be used for other occupancies such as hotels and condominiums. Any duct penetrations of a fire rated wall will need to be firestopped in accordance with applicable building and fire regulations. For a building where the floors can be either open plan or divided by tenant installed partitions, an EV system can be achieved by wall vents above a suspended ceiling and one or more

air transfer grills in the ceiling of the elevator lobby.

With open exterior doors, it is not necessary to have exterior vents on the ground floor. Because the EV system may not be able to achieve acceptable pressurization with some or all the exterior doors closed, it may be necessary to have some of the exterior doors open automatically on system activation. The number of exterior doors that need to be opened automatically can be evaluated by the use of a computer network model.

In Figure 50.17a and b, the vents are in all four exterior walls with the intent of minimizing any adverse impact of the wind. It is suggested that the vent area be proportional to the area of the exterior walls. If fewer vents are used, it is suggested that wind effects be evaluated with the use of a computer network model.

Floor Exhaust (FE) System

The FE system deals with the building envelope issue by reducing the amount of supply air used. In the FE system, a relatively small amount of air is supplied to the elevator shafts and the stairwells, and the fire floor is exhausted such that acceptable pressurization is maintained on the fire floor where it is needed. It is common to also exhaust one or two floors above and below the fire floor.

The FE system is a kind of zoned smoke control. As discussed later, exhausting air from the fire floor and some floors above and below the fire floor has a beneficial impact on shaft pressurization. Often this system can achieve successful pressurization in tall and very complex buildings.

Typically the exhaust is through a shaft with a fan located in a mechanical floor or on the roof, and dampers between the shaft and the floors are closed on all floors when the system is not operating. On system activation, the dampers open on the floors to be exhausted. The outlet of the exhaust fan needs to be located away from the inlets the supply fans to minimize the potential for smoke feedback into supply air.

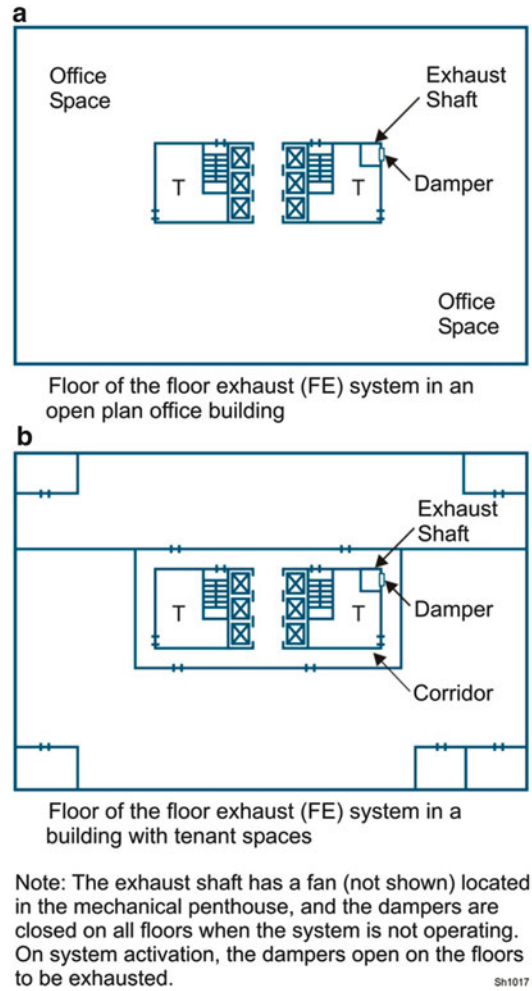

Fig. 50.18 Typical floor plans of buildings with the floor exhaust (*FE*) system

For the 14-story example building, the FE system is shown in Fig. 50.18a. For the simulations of the example building, each elevator shaft needed 15,100 cfm (7.14 m^3/s), and each stairwell needed 3800 cfm (1.79 m^3/s). The floor exhaust needed from the floors ranged from 4800 to 5400 cfm (2.28–2.55 m^3/s). For a building with many interior partitions, the exhaust can be from the corridor that the elevators and stairwells open onto, and this is shown in Fig. 50.18b.

As with the EV system, some of the exterior doors on the ground floor may need to open automatically upon system activation, and the

number of such doors needed can be determined with the use of a computer network model.

Ground Floor Lobby (GFL) System

The GFL system has an enclosed elevator lobby on the ground floor to reduce the tendency of open exterior doors to cause high pressure differences across the elevator shaft at the ground floor. The GFL system often has a vent between the enclosed lobby and the building with the intent of preventing excessive pressure differences across the lobby doors. The lobby doors are the doors between the enclosed lobby and the building.

The pressure difference across the lobby door and the elevator door depend on the area of the vent. There is no established criterion for the maximum pressure difference across the lobby doors, but the pressure should not be so high as to prevent the doors from remaining closed. This value depends on the specific doors and hardware. For discussion here, a maximum pressure difference for the lobby doors was chosen as 0.35 in H_2O (87 Pa), but this value can be much different for specific applications. The vent should have a fire damper and a control damper in series. The control damper can be used to adjust the flow area of the vent so it can be balanced during commissioning. Figure 50.19 shows the ground floor of the example building with a GFL system.

As stated above, the intent of the elevator pressurization systems discussed in this chapter is to prevent smoke from flowing from the fire floor through an elevator shaft and threatening life on floors away from the fire floor. In the GFL system, the enclosed lobby on the ground floor protects the elevator from smoke from a fire on the ground floor. For this reason, the minimum elevator pressure difference criterion of Table 50.3 does not apply to the ground floor for a GFL system. The other criteria of Table 50.3 apply. Table 50.6 identifies the criteria that were used for the GFL system simulations. For the GFL system of the simulations discussed below, successful pressurization consists of meeting the criteria identified in Table 50.6.

For fires in high-rise buildings, frequently the fire service uses the elevators for rescue and for mobilization of firefighting equipment. When ground floor lobby doors are opened, the pressure difference may exceed the maximum pressure difference. If this can happen for a particular design, the fire service should be contacted to determine if this is acceptable to them.

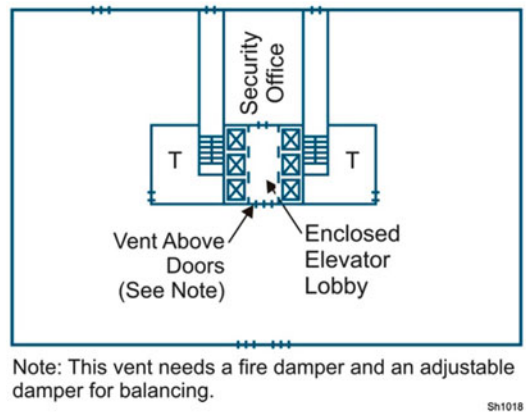

Fig. 50.19 Ground floor of a building with the ground floor lobby (*GFL*) system

Table 50.6 Pressure differences criteria for GFL elevator pressurization simulations[a]

	Criteria	Minimum		Maximum	
Location	Number	in H_2O	Pa	in H_2O	Pa
Pressurized elevators on ground floor	1	NA	NA	0.25	62
Pressurized elevators on other floors	2	0.10	25	0.25	62
Pressurized stairwells on all floors	3	0.10	25	0.35	87
Ground floor elevator lobby door	4	NA	NA	0.35	87

[a]These pressure differences are with stairwell doors closed, the elevator doors closed, and the ground floor lobby door closed. The above criteria are for the GFL simulations discussed in this chapter, and some projects may have different criteria depending on code requirements and requirements of specific applications

The floor-to-floor leakage can have a significant impact on the performance of a GFL system. This leakage consists of the leakage of the floor and that of the curtain wall gap (Table 50.5).

Zoned Smoke Control

The traditional approach for HVAC systems is to shut them down during building fires, but HVAC systems can be designed to operate in a smoke control mode during building fires. Zoned smoke control consists of exhausting the zone of the fire and possibly pressurizing the surrounding zones. For reasons discussed later in this chapter, pressurizing the surrounding zones is not recommended for zoned smoke control systems in tall buildings. For zoned smoke control systems that rely on smoke exhaust only, the zoned smoke control can complement the performance of stairwell pressurization in tall and complex buildings. In addition to using the HVAC system, dedicated equipment can be used for zoned smoke control.

In zoned smoke control, a building is divided into a number of zones each separated from the others by barriers. In the event of a fire, the zone with the fire is called the smoke zone, and the others are called the non-smoke zones. The zones that border on the smoke zone are called the surrounding zones. Passive smoke protection or pressurization smoke protection is used to limit the extent of smoke spread beyond the smoke zone. It is beyond the capability of smoke control to make conditions tenable in the smoke zone, and it is intended that occupants evacuate the smoke zone as soon as possible.

Smoke arrangements of smoke control zones are shown in Fig. 50.20. In this Figure the smoke zone is indicated by a minus sign, and the surrounding zones are indicated by a plus sign. Often the smoke zone is one floor of the building (Fig. 50.20a). A common approach is to make the smoke zone be the fire floor plus the floor directly above and below the fire floor as shown in Fig. 50.20b. In a relatively low sprawling building made of a number of wings, the smoke zone can be part of a floor as in Fig. 50.20c. A surrounding zone can be one floor as in Fig. 50.20a and b, and it can be part of a floor as in Fig. 50.20c. A surrounding zone can also be a number of floors as shown in Fig. 50.20d.

The traditional approach to zoned smoke control is to exhaust the smoke zone and to pressurize the surrounding zones, but many other approaches have been used. The methods that can be used to treat the smoke zone are: (1) fan powered exhaust, (2), passive smoke control using smoke barriers (3) exterior wall vents, or (4) smoke shafts. Fan powered smoke exhaust is the most common method, and passive smoke control using smoke barriers may be satisfactory when fan powered exhaust is not practical. Exterior wall vents and smoke shafts are not commonly used, but they are discussed in Chap. 13 of the *Handbook of Smoke Control Engineering*.

The methods that can be used for the zones surrounding the smoke zone are: (1) fan powered pressurization or (2) passive smoke control using smoke barriers. Fan powered pressurization of the surrounding zones has a negative impact on stairwell pressurization as discussed below. For the rest of this section, fan powered pressurization will be called pressurization, and fan powered exhaust will be called exhaust.

When the floors of a building are divided into many rooms with normally closed doors, these floors do not lend themselves to the traditional concept of zoned smoke control. This can also be said of wings of a building that are divided into many rooms with normally closed doors. For such applications, a form of zoned smoke control can be used that relies on a combination of corridor exhaust and passive smoke control using smoke barriers. Figure 50.21 shows a floor of a condominium building that can be considered a form of a smoke zone. The floor has corridor exhaust, and the other spaces rely on passive smoke protection of the corridor walls and ceiling floor assembly of the other spaces. This passive protection tends to minimize smoke flow through the ceiling floor assembly during a building fire.

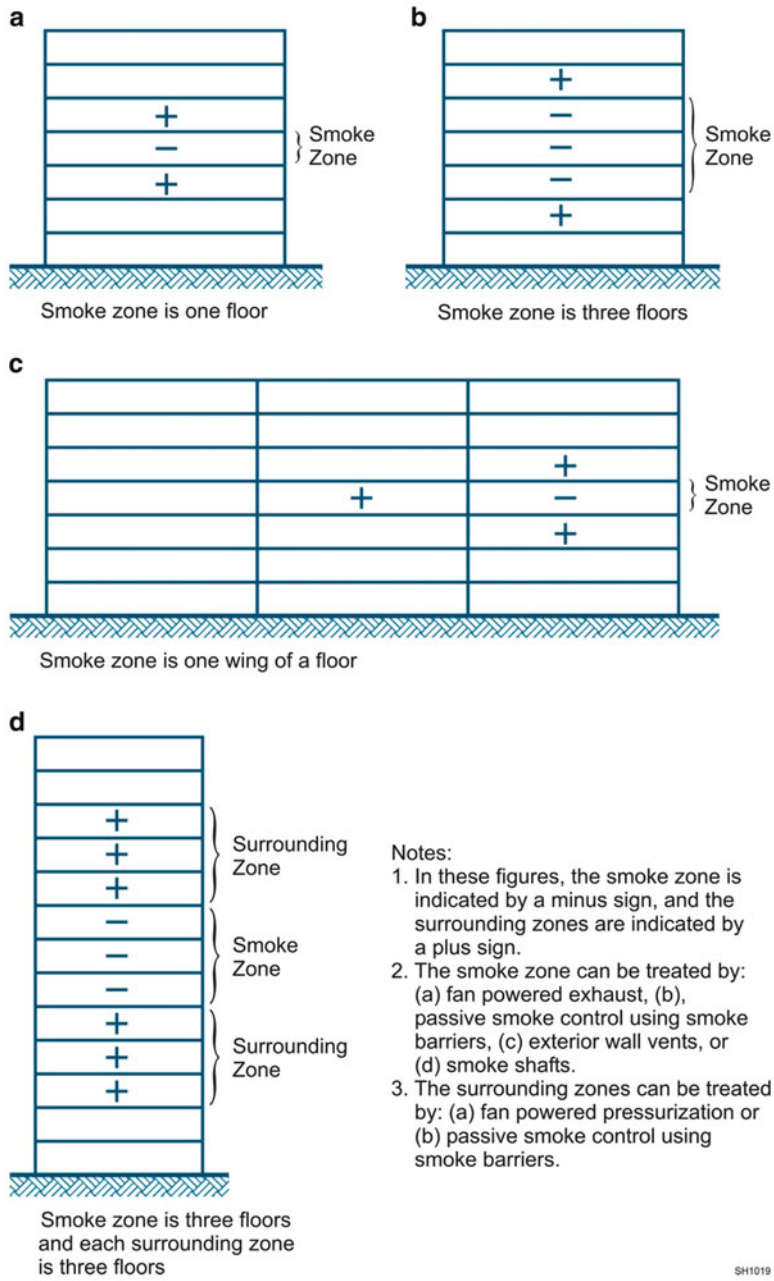

Fig. 50.20 Smoke arrangements of smoke control zones

Interaction with Pressurized Stairs

The interaction of zoned smoke control with pressurized stairwells can have a significant impact on the pressure differences across the stairwell doors. The following discussion is about smoke zones that are comprised of one floor and surrounding zones consisting of one floor above and one floor below. However, the same kind of interactions can happen with smoke zones and surrounding zones that are more than one floor.

Zoned smoke control using both exhaust and pressurization is shown in Fig. Fig. 50.22a, and pressure differences, Δp_{SB}, from the stairwell to the building are shown in Fig. 50.22b and Fig. 50.22c. Exhaust of the smoke zone increases

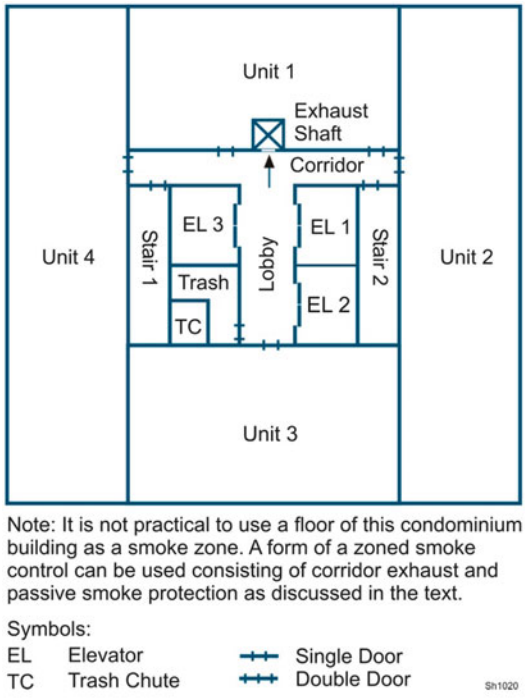

Fig. 50.21 Example of corridor exhaust and passive smoke control

the pressure difference across pressurized stairwell doors on the floor or floors of the smoke zone. Pressurization of the surrounding zones decreases the pressure difference across pressurized stairwell doors on these floors.

The pressure difference, Δp_{SB}, can be positive on all the floors as shown in Fig. 50.22b. This pressure difference can be negative on some floors as shown in Fig. 50.22c. Negative pressurization can happen on the floors that are pressurized, and this negative pressurization has the potential for the significant failure mode discussed below.

In Fig. 50.20a, smoke should be prevented from reaching the floor above the smoke zone, and negative stairwell pressurization should not compromise tenability of the stairwell. The effectiveness of this depends on proper identification of the fire floor. Properly maintained fire detection and alarm systems are very good at identifying the location of a fire, but issues can arise. In some fire scenarios, the first smoke detector to activate has been a floor or so above the fire floor. This can be attributed to any of the following: (1) smoke

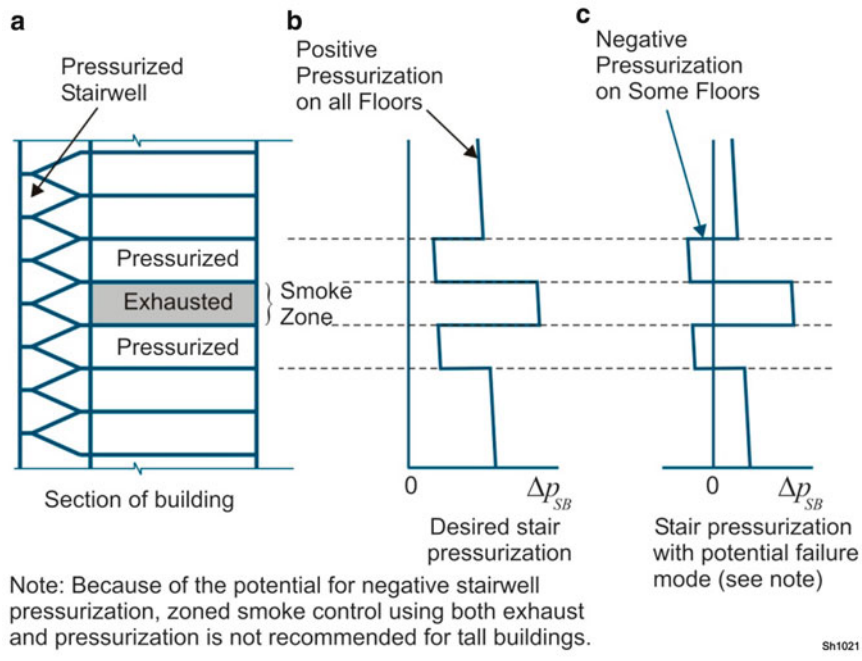

Fig. 50.22 Interaction between pressurized stairwells and zoned smoke control using both exhaust and pressurization

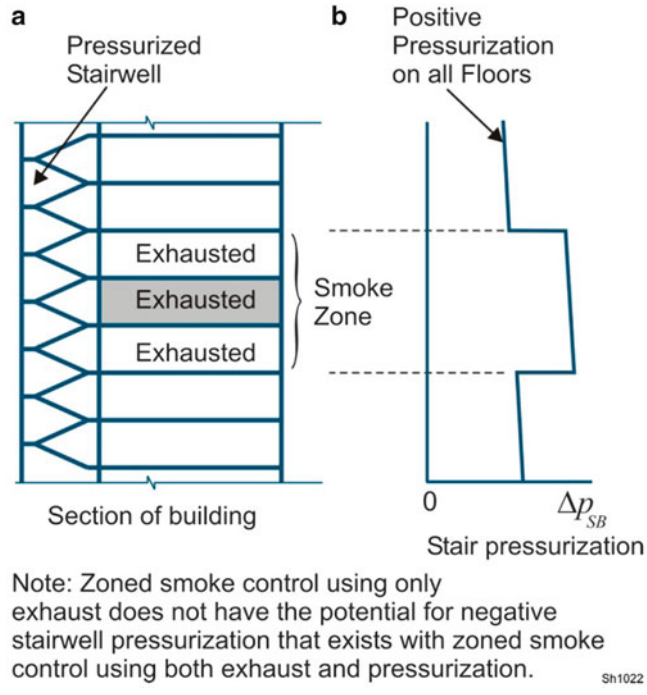

Fig. 50.23 Interaction between pressurized stairwells and zoned smoke control using only exhaust

flowing through a complex route to a floor above the fire, (2) smoke detectors not working properly on the fire floor, and (3) signals from smoke detectors being misidentified.

Regardless of the reason, when a fire floor is incorrectly identified, the smoke zone is incorrectly chosen. In this situation, the failure mode is that inadvertent pressurization of the fire floor can push smoke into the stairwells. An additional concern is that if this failure mode happens, it will probably happen to all the stairwells serving the fire floor. This failure mode is more of a concern for tall buildings because: (1) acceptable pressurization is more difficult in taller buildings than in shorter ones, and (2) stairwell smoke protection is more important in taller buildings than in shorter ones. Occupant density is another factor regarding the importance of stairwell smoke protection. In this context, a tall building might be thought of as one having a minimum of about 10 stories. Because of this failure mode, it is recommended that zoned smoke control using systems employing both exhaust and pressurization not be used for tall buildings where protection of the stairwells is especially important. Alternatively an analysis of this failure mode could be performed that includes factors such as evacuation time, emergency response time, and probability using the Firefighter's Smoke Control Station (FSCS) for corrective action.

The zoned smoke control shown in Fig. 50.23 does not have this failure mode. The zoned smoke control system of Fig. 50.23 consists of a three story smoke zone that is exhausted and the surrounding zones rely on passive smoke protection. The exhaust acts to increase Δp_{SB} for the three floors of the smoke zone (Fig. 50.23b). Because this system does not have pressurization of surrounding zones, Δp_{SB} is not reduced for surrounding zones, and this eliminates the failure mode discussed above.

In Fig. 50.23a the fire floor is shaded, and the smoke zone consists of the fire floor and the floors directly above and below. It is expected that there will be some smoke flow to the floor above the fire floor, and there may be some smoke flow to the floor below the fire floor. This smoke flow is restricted by the floor-ceiling assembly. A floor-ceiling assembly is a passive

smoke barrier that has significant resistance to smoke flow. Even a floor-ceiling assembly not constructed as a passive smoke barrier has considerable resistance to smoke flow provided that the only openings through it are construction cracks and small cracks around pipe and conduit penetrations. This means that there will be some amount of time for occupants of the floors directly above and below the fire floor to evacuate those floors. Further, the small amount of smoke on these floors should act to convince occupants of the serious nature of the fire such that pre-movement time before evacuation will be significantly reduced.

Tenability Systems

As previously stated, the conventional smoke control systems discussed above are based on the approach of preventing occupants from coming into contact with smoke. These conventional systems have some level of smoke contact with the occupant at times when stair doors open for occupant entry or due to natural fluctuations in building pressures. Provided that the contaminates are sufficiently diluted, such smoke contact is usually considered to be of little concern. Tenability systems are designed with the intent of providing a tenable environment for occupants who are exposed to some concentration of smoke.

Analysis Components

Analysis of tenability systems requires consideration of the following components: (1) fire scenario, (2) smoke transport mechanisms, and (3) tenability thresholds.

Fire Scenario A fire scenario can be thought of as the outline of events and conditions that are critical to determining the outcome of alternate designs. In addition to the fire location and heat release rate (HRR), the fire scenario includes the status of the doors, the HVAC systems, and the smoke management system, and other systems. Species (O_2, N_2, CO, CO_2, etc.) generation can be included in the fire scenario. The scenario may also include specifics about the fuel, ignition of multiple fuel packages, and the effect of an fire suppression activities. The selection of the fire scenario can be based on a combination of professional judgment, fire dynamics, historical fire data, or code requirements. An analysis of a smoke control system is likely to include the consideration of a number of fire scenarios.

Smoke Transport Smoke can flow far from a fire and threaten life. The major driving forces that cause smoke movement are naturally occurring stack effect, buoyancy of combustion gases, expansion of combustion gases, wind effect, fan powered ventilation systems, and elevator piston effect.

Tenability Tenability calculations estimate the life hazard of a scenario. Tenability calculations address one or more of the following: exposure to toxic gases, exposure to heat, exposure to thermal radiation, and visibility through smoke. The exposures are time-integrated doses of toxic gases, heat, and thermal radiation. The conservative approach generally used for tenability systems is to make the tenability calculations as if an occupant were to remain at each location under consideration throughout the duration of the fire scenario.

Smoke Transport Calculations

Smoke transport analysis can be done with network models or computational fluid dynamic (CFD) models. Network models have already been discussed. The idea of a CFD model is to divide a space of interest into a large number of volumetric cells, and to solve the governing equations to calculate the flow, temperature, and concentrations of fire products at each cell.

The CFD models are appropriate for analysis of smoke flow in large spaces such as atria, malls, and arenas; and the network models are appropriate for analysis of smoke control systems that involve all or a large part of a large building. Fire dynamics simulator (FDS) is a CFD model that is in the public domain and was developed at the National Institute of Standards and Technology

(NIST) specifically for fire applications [26, 27]. FDS is available from NIST at no cost. FDS can calculate temperatures, concentrations of gases, and visibility; this is a significant aid in the tenability analysis.

Computer network models, such as CONTAM which is available in the public domain, were previously discussed for conventional smoke control systems, but they can also be used for smoke transport calculations. CONTAM has been used to analyze a number of tenability systems ([8, 22], Ferreira 2002; [17, 18]). CONTAM can simulate the transport of contaminants, including the products of combustion. However, CONTAM cannot simulate heat transfer, so it cannot calculate the temperatures. The user needs to supply the temperatures of spaces to CONTAM, and zone fire models have been used to generate such temperature information. The zone fire model, CFAST, has been used for this purpose [11, 31, 32]. CFAST is available from NIST at no cost.

Tenability Calculations

There are a number of models that can be used to evaluate exposure to smoke. For most smoke control applications when smoke is diluted to meet visibility criteria, exposure to it is not life threatening. The fractional effective dose (FED) model is the simplest model for evaluating exposure to smoke, and it can be used to check that smoke is not life threatening.

The FED can be used to obtain an approximate of the effects of exposure to toxic gases.

$$\text{FED} = \frac{\sum_{i=1}^{n} C_i \Delta t_i}{\text{LC}t_{50}} \qquad (50.18)$$

where

FED = fractional effective dose, dimensionless,
$C_{,i}$ = mass concentration of material burned at the end of time interval i, lb/ft^3 (g/m^3),
Δt_i = time interval i, min (min),
$\text{LC}t_{50}$ = lethal exposure dose from test data, lb ft^{-3} min (g m^{-3} min).
n = number of discrete concentration time pairs.

This equation is for uniform time intervals as calculated by computer models, and it evaluates the FED for the exposure time at the end of interval i (exposure time is $n\Delta t$). An FED greater than or equal to one indicates fatality. The concentration is in units mass of the material burned per unit volume. The lethal exposure dose, $\text{LC}t_{50}$, is the product of the LC_{50} and the exposure time. The LC_{50} is the concentration of airborne combustion products that is lethal to 50 % of the subjects exposed for a specified time. The mass concentration of material burned, C_i, can be obtained from the smoke transport calculations.

For any time interval, the visibility can be calculated from

$$S_i = \frac{K}{2.303 \delta_m C_i} \qquad (50.19)$$

where

S_i = visibility, ft (m),
K = proportionality constant,
δ_m = mass optical density, ft^2/lb (m^2/g),
C_i = mass concentration of fuel burned lb/ft^3 (g/m^3).

The proportionality constant, K, is 8 for illuminated signs and 3 for non-illuminated signs. For objects in reflected light (walls, hand rails, stairs, etc.), a value of $K = 3$ is normally used. Because C_i varies from location to location in fires, the visibility calculated from the above equation is considered to be the visibility at the point for which C_i is calculated. For example, if the calculated visibility was 20 ft (6.1 m), it would mean that a person could see 20 ft (6.1 m) through smoke where C_i was uniform.

Alternatively visibility can be calculated along a path through non-uniform smoke. There are many applications where non-uniform smoke happens such as smoke on a balcony in an atrium, smoke in a tunnel, and smoke in a hotel corridor. For example, Fig. 50.24 shows a person looking at an exit sign through non-uniform smoke. The smoke near the exit sign could exceed criteria for visibility at a point, but that does not mean that the person could not see the sign. Calculation of the visibility along the path between the person and the sign can evaluate if the sign can be seen.

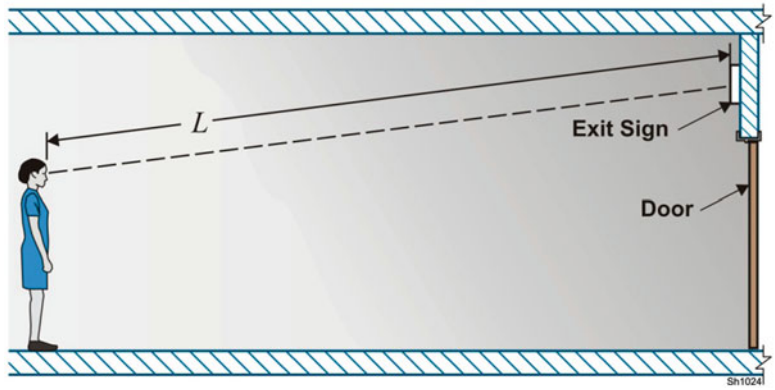

Fig. 50.24 Visibility through non-uniform smoke

Visibility along a path can also be calculated from percent obscuration as

$$S = -\frac{KL}{\log_e(1 - \lambda/100)} \tag{50.20}$$

where
S = visibility, ft (m),
K = proportionality constant,
L = length of path, ft (m),
λ = percent obscuration, dimensionless.

If the visibility is greater than or equal to the length of the path ($S > L$) an object can be seen over the path. When the path length is the same as the visibility ($L = S$), an object at the end of the path can barely be seen by a person with average eyesight. If the object were any farther away such a person could not see it. Percent obscuration, λ, can be calculated by FDS.

Generally, contact with dry air of temperatures greater than 250 °F (121 °C) can be expected to result in skin burns. Also, contact with dry air at a temperature less than approximately 250 °F (121 °C) leads to hyperthermia. For hyperthermia, heat exposure can be estimated from

$$F_{Ith} = \sum_{i=1}^{n} \frac{\Delta t}{\exp(5.67 - 0.0152T_i)}$$
$$F_{Ith} = \sum_{i=1}^{n} \frac{\Delta t}{\exp(5.185 - 0.0373T_i)} \quad \text{for SI} \tag{50.21}$$

where
F_{Ith} = total cumulative dose (dimensionless),
Δt = time interval, min (min),
T_i = temperature of air in interval i, °F (°C).

Incapacitation due to heat exposure would be expected for F_{Ith} greater than or equal to one. If contact with gases does not result in incapacitation due to heat exposure, thermal radiation from those gases would not result in incapacitation for the same exposure time. Generally, exposure to thermal radiation is not an issue for most smoke control applications.

Commissioning and Testing

Commissioning is the means to demonstrate to an owner and other project stakeholders that the installed smoke control system meets the smoke control system design for the project. Commissioning is the process for verifying and documenting that the performance of facilities, systems, and assemblies meets defined fire safety objectives and criteria. Commissioning refers to the process of examining, comparing, testing, and documenting the installation and performance of a smoke control system to ensure that it functions according to an approved design.

Special inspections are a means that an Authority Having Jurisdiction (AHJ) uses to determine that a smoke control system meets the applicable code requirements and regulations. The International Building Code (IBC) has requirements for a special inspection and describes the qualifications required for a special inspector (ICC 2012).

Commissioning Process

The commissioning process begins at the start of the project and continues throughout the project. ASHRAE Guideline 5 provides methods for verifying and documenting that the performance of smoke control systems conforms with respect to the intent of the design [2]. For smoke control systems, an AHJ such as a building official or fire marshal typically enforces a combination of building codes, fire codes, and local standards. The intent of the smoke control system commissioning testing is to determine that the system meets the Owner's Project Requirements (OPR), including code requirements and inspections by the AHJ throughout the delivery of the project

In order to achieve successful commissioning of a system, a number of different people will typically be involved in the process. In addition to the building owner and AHJ, the system designer, general contractor, subcontractors, fire protection engineering consultants, and test and balance technicians can be involved. At the end of the testing, documentation is provided that the system is working properly according to the design.

Commissioning activities can occur at multiple stages during the construction process. Duct inspections, duct leakage testing, and barrier inspections are activities that typically occur early in the construction process when the ducts and barriers are readily visible. Component testing, including air flow measurement, can occur at a mid-point in construction where power is provided to individual devices, but central monitoring and control has not yet been provided. Sequence of operations and final performance testing typically occurs when construction is nearly complete, often just before the building is intended to obtain its permits and open to the public.

Commissioning Testing

Commonly, testing and balancing is required before formal acceptance testing to achieve the expected performance of all the components. Testing and balancing refers to the process where the as-built performance of smoke control systems is tested in the field and compared to the required design conditions. Adjustments to the installed system, such as refining the supply airflow rates, are made to ensure that the smoke control system is functioning as intended in the approved design documentation.

System performance testing is the phase where the code-specified performance parameters appropriate to the smoke control design are measured. For example, building codes require that a minimum pressure difference exist between a pressurized stairwell and other zones in the building, and that door opening force must not exceed a specified amount. In this case, performance testing would focus on measuring the pressure difference across stairwell doors and door opening forces. Some common parameters measured during smoke control system performance testing are: (1) exhaust/supply airflow quantities, (2) airflow velocities at atrium or other large open space perimeters, (3) door-opening forces, and (4) pressure differences between zones.

Smoke Bomb Tests Not Recommended: Chemical smoke from smoke bombs (also called smoke candles) is not recommended for any performance testing because it lacks the buoyancy of hot smoke from a real building fire. Smoke near a flaming fire has a temperature in the range of 1000–2000 °F (540–1100 °C). Heating chemical smoke to such temperatures to emulate smoke from a real fire is not recommended unless precautions are taken to protect life and property

Periodic Testing

After a smoke control system has been commissioned, testing must still be performed periodically so that the system is in the proper operating condition in the event of a fire. Periodic testing needs to be performed over the life of a

building to determine that the installed smoke control systems are capable of operating as designed. Periodic testing includes: (1) manual testing involving ongoing inspection and maintenance and (2) automatic testing to determine that integral equipment is functional and operational. Automatic testing is often performed at a higher frequency than manual testing. Continued inspection and testing helps so that adjustments and repairs can be made to account for unforeseen changes to the building or failure of components.

Until recently, smoke control system reliability has been somewhat compromised because periodic testing was limited to manual testing. Inspections performed years after commissioning showed that some smoke control systems were inoperable, turned off, or made ineffective due to modifications to equipment or the building. It is expected that the reliability of smoke control systems will be significantly improved by the use of automatic weekly self-testing of system components, afforded by listed equipment carrying the appropriate product designations.

Nomenclature

A	Flow area, ft^2 (m^2); or door area, ft^2 (m^2),
a	Wind exponent at wall.
A_a	Free area around the elevator car, ft^2 (m^2),
A_{BO}	Flow area per stairwell between the building and the outside, ft^2 (m^2),
A_e	Effective flow area, ft^2 (m^2),
A_i	Flow area of path i, ft^2 (m^2).
A_{io}	Leakage area between the building and the outside, ft^2 (m^2).
A_{ir}	Leakage area between building and lobby, ft^2 (m^2),
a_{met}	Wind exponent in the vicinity of the wind anemometer, dimensionless,
A_s	Cross-sectional area of shaft, ft^2 (m^2),
A_{SB}	Flow area between the stairwell and the building, ft^2 (m^2),
A_{sr}	Leakage area between shaft and lobby, ft^2 (m^2),
C	Flow coefficient, dimensionless,
$C_{,i}$	Mass concentration of material burned at the end of time interval i, lb/ft^3 (g/m^3),
C_c	Flow coefficient for flow around car, dimensionless.
C_w	Pressure coefficient, dimensionless,
d	Distance from doorknob to knob side of door, ft (m),
F	Total door-opening force, lb (N),
F_{dc}	Door closer force, lb (N),
FED	Fractional effective dose, dimensionless,
F_{Ith}	Total cumulative dose (dimensionless),
F_R	Flow area factor (dimensionless),
g	Acceleration due to gravity, ft/s^2 (m/s^2),
H	Height of wall, ft (m),
H_m	Height limit, ft (m),
H_{met}	Height of wind measurement, ft (m),
K	Proportionality constant,
L	Length of path, ft (m),
LCt_{50}	Lethal exposure dose from test data, lb ft^{-3} min (g m^{-3} min).
m	Mass flow through the path, lb/s (kg/s),
m_{sv}	Mass flow through the path, scfm (standard m^3/s),
n	Number of discrete concentration time pairs.
p	Pressure, lb/in^2 (Pa),
p_{atm}	Absolute atmospheric pressure, lb/ft^2 (Pa),
p_w	Wind pressure, in H_2O (Pa),
R	Gas constant, 53.34 ft lbf/lbm/°R (287 J/kg K)
S	Visibility, ft (m),
T	Temperature, °F (°C).
T_B	Temperature in the building, °F (°C),
T_F	Temperature in the fire space, °F (°C),
T_i	Temperature of air in interval i, °F (°C).
T_{in}	Temperature of air entering the fire compartment, °F (°C).

T_O Temperature outside, °F (°C); temperature surroundings, °F (°C),
T_{out} Temperature of smoke leaving the fire compartment, °F (°C),
T_S Temperature in the shaft, °F (°C),
U Elevator car velocity, fpm (m/s),
U_H Velocity at the upwind wall of height H, mph (m/s),
U_{met} Measured velocity, mph (m/s),
V Volumetric flow through the path, cfm (m^3/s).
V_{in} Volumetric flow of air into the fire compartment, cfm (m^3/s),
V_{out} Volumetric flow of smoke out of the fire compartment, cfm (m^3/s),
W Door width, ft (m),
z Distance above the neutral plane, ft (m).
δ Boundary layer height at wall, ft (m),
ρ Density, lb/ft^3 (kg/m^3),
η Heat transfer factor (dimensionless).
λ Percent obscuration, dimensionless.
δ_m Mass optical density, ft^2/lb (m^2/g),
δ_{met} Boundary layer height in the vicinity of the wind anemometer, ft (m),
ρ_o Outside air density, lb/ft^3 (kg/m^3),
Δp Pressure difference, in. H_2O (Pa).
Δp_{max} Maximum design pressure difference, in. H_2O (Pa),
Δp_{min} Minimum design pressure difference, in. H_2O (Pa).
Δp_{SF} Pressure difference from a fire space to the surroundings, in. H_2O (Pa),
Δp_{SO} Pressure difference from a shaft to the outside, in. H_2O (Pa),
$\Delta p_{u,si}$ Upper limit pressure difference from the shaft to the building, in H_2O (Pa),
Δt Time interval, min (min),

References

1. Achakji, G. Y. and Tamura, G. T. 1988. Pressure Drop Characteristics of Typical Stairshafts in High-Rise Buildings, ASHRAE Transactions, Part 1.
2. ASHRAE 2012. Guide for the Commissioning Process of Smoke Control Systems, ASHRAE, Atlanta, GA.
3. Aynsley, R. M. 1989. The Estimation of Wind Pressures at Ventilation Inlets and Outlets on Buildings, ASHRAE Transactions, Vol. 95, Part 2.
4. Berl, W.G. and Halpin, B.M. 1980. "Human Fatalities from Unwanted Fires," Johns Hopkins APL Technological Digest, 1, p. 129.
5. Cresci, R. J. 1973. Smoke and Fire Control in High-Rise Office Buildings - Part II: Analysis of Stair Pressurization Systems, Symposium on Experience and Applications on Smoke and Fire Control at the ASHRAE Annual Meeting, June 1973, Louisville, KY, Atlanta, GA, pp. 16-23.
6. Dyrbye, C. and Hansen, S. O. 1997. Wind Loads on Structures, Wiley, New York, NY.
7. Fang, J.B. 1980. Static Pressures Produced by Room Fires, NBSIR 80-1984, National Bureau of Standards, Washington.
8. Ferreira, M.J. 1998. Analysis of Smoke Control System Design Using a Computer-based Airflow Analysis, Pacific Rim Conference, Society of Fire Protection Engineers, Bethesda, MD.
9. ICC 2012. International Building Code, International Code Council, Country Club Hills, IL.
10. Idelchik, I. E. 1986. Handbook of Hydraulic Resistance, 2nd Edition, Hemisphere Publishing, New York.
11. Jones W. W., et al. 2009. CFAST – Consolidated Model of Fire Growth and Smoke Transport (Version 6) – Technical Reference Guide. NIST Special Publication 1026, National Institute of Standards and Technology, Gaithersburg, MD.
12. Kandola, B. S. 1986a. A Wind Tunnel Building Model for the Investigation of Smoke Movement Problems, Fire Safety Journal, Vol. 10, No. 3.
13. Kandola, B. S. 1986b. Comparison of Wind Tunnel Pressure Measurements and Smoke Movement Computer Predictions inside a Five-storey Model building, Fire Safety Journal, Vol. 10, No. 3.
14. Kandola, B. S. 1986c. The Effects of Simulated Pressure and Outside Wind on the Internal Pressure Distribution in a Five-storey Building, Fire Safety Journal, Vol. 10, No. 3.
15. Klote, J. H. 1988. An Analysis of the Influence of Piston Effect on Elevator Smoke Control, NBSIR-88-3751, National Bureau of Standards, Gaithersburg, MD.
16. Klote, J. H. 1995. Design of Smoke Control Systems for Elevator Fire Evacuation Including Wind Effects, 2nd Symposium on Elevators, Fire, and Accessibility, Baltimore, MD April 19-21, 1995, ASME, New York.
17. Klote, J. H. 2004a. Hazards Due to Smoke Migration through Elevator Shafts – Vol. I: Analysis and Discussion. Final Report. NIST GCR 04-864-I, National Institute of Standards and Technology, Gaithersburg, MD.

18. Klote, J. H. 2004b. Tenability and Open Doors in Pressurized Stairwells, ASHRAE Transactions, Vol. 110. Part 1.
19. Klote, J. H. and Bodart, X. 1985. Validation of Network Models for Smoke Control Analysis, ASHRAE Transactions, Vol. 91, Part 2b.
20. Klote, J. H. and Tamura, G. T. 1986. Elevator Piston Effect and the Smoke Problem, Fire Safety Journal, Vol. 11 No. 3.
21. Klote, J. H. et al. 2012. Handbook of Smoke Control Engineering. ASHRAE, Atlanta, GA.
22. Klote, J. H., Nelson, H. E., Deal, S. and Levin, B. M. 1992. Staging Areas for Persons with Mobility Limitations, NISTIR 4770, National Institute of Standards and Technology, Gaithersburg, MD.
23. Klote, J.H. and Tamura G.T., 1987. "Experiments of Piston Effect on Elevator Smoke Control," ASHRAE Transactions, 93, 2, pp. 2217–2228.
24. Liu, H. 1991. Wind Engineering – A Handbook for Structural Engineers, Prentice Hall, Englewood, NJ.
25. MacDonald, A. J. 1975. Wind Loading on Buildings, Wiley, New York NY.
26. McGrattan, K. B. et al. 2008a. Fire Dynamics Simulator (Version 5) User's Guide, NIST Special Publication 1019-5, National Institute of Standards and Technology, Gaithersburg, MD.
27. McGrattan, K. B. et al. 2008b. Fire Dynamics Simulator (Version 5) Technical Reference Guide, Volume 1: Mathematical Model, NIST Special Publication 1018-5, National Institute of Standards and Technology, Gaithersburg, MD.
28. NBFU 1939. Smoke Hazards of Air-Conditioning Systems, NFPA Quarterly, Vol. 33, No. 2.
29. NFPA 2012a. Standard for Smoke Control Systems, NFPA 92, National Fire Protection Association, Quincy, MA
30. NFPA 2012b. Life Safety Code, NFPA 101, National Fire Protection Association, Quincy, MA.
31. Peacock, R. D., et al. 2008a. CFAST – Consolidated Model of Fire Growth and Smoke Transport (Version 6) – Software Development and Model Evaluation Guide. NIST Special Publication 1086, National Institute of Standards and Technology, Gaithersburg, MD.
32. Peacock, R. D., et al. 2008b. CFAST – Consolidated Model of Fire Growth and Smoke Transport (Version 6) – User's Guide. NIST Special Publication 1041, National Institute of Standards and Technology, Gaithersburg, MD.
33. Shaw, C. T. and Tamura, G. T. 1977. The Calculation of Air Infiltration Rates Caused by Wind and Stack Action for Tall Buildings, ASHRAE Transactions, Vol. 83, Part 2.
34. Shaw, C. Y., Reardon, J. T. and Cheung, M. S. 1993. Changes in Air Leakage Levels of Six Canadian Office Buildings, ASHRAE Journal, American Society of Heating, Refrigerating and Air Conditioning Engineers, Atlanta, GA, Vol. 35, No. 2.
35. Simiu, E. and Scanlan, R. H. 1996. Wind Effects on Structures: Fundamentals and Application to Design, 3rd Ed., Wiley, New York, NY.
36. Walton, G. N., Dols, W. S. 2005. CONTAM 2.4 User Guide and Program Documentation, NISTIR 7251, Revised December 14, 2010. National Institute of Standards and Technology, Gaithersburg, MD.
37. Harland, W. A., Woolley, W. D. 1979. Fire fatality study – University of Glasgow. Building Research Establishment, Borehamwood Information Paper IP 18/79.
38. Tamura, G.T., and A.G. Wilson. 1966. Pressure differences for a nine-story building as a result of chimney effect and ventilation system operation. ASHRAE Transactions, 72(1).
39. Tamura, G.T., and C.Y. Shaw. 1976a. Studies on exterior wall air tightness and air infiltration of tall buildings. ASHRAE Transactions, 82(1).
40. Tamura, G.T., and C.Y. Shaw. 1976b. Air leakage data for the design of elevator and stair shaft pressurization systems. ASHRAE Transactions, 82(2).
41. Tamura, G.T., and C.Y. Shaw. 1978. Experimental studies of mechanical venting for smoke control in tall office buildings. ASHRAE Transactions, 86(1).
42. Frrreira, M. J. 2002. Use of Multizone Modeling for High-Rise Smoke Control Design. ASHRAE Transactions, 108(2).

John H. Klote is consultant specializing in fire in smoke control in Leesburg, VA

Smoke Control by Mechanical Exhaust or Natural Venting

51

James A. Milke

Introduction

Smoke management in large-volume spaces, such as atria and covered malls, poses separate and distinct challenges from well-compartmented spaces. In particular, smoke control strategies using pressure differences and physical barriers described by Klote in Chap. 50, and NFPA 92, *Standard for Smoke-Control Systems* [1], are infeasible. Without physical barriers, smoke propagation is unimpeded, spreading easily throughout the entire space. The tall ceiling heights in many large-volume spaces pose additional challenges because of the production of substantial quantities of smoke and delayed detection times. However, on the positive side, the combination of large-volume space and tall ceiling height permit the smoke to become diluted and cooled as it spreads vertically and horizontally, thereby reducing the level of hazard posed by the smoke. Even so, there is still a need to ensure that dangerous concentrations of smoke are prevented in large-volume spaces.

In addition to atria and covered malls, there are many other examples of large-volume spaces, including convention centers, airport terminals, sports arenas, and warehouses where smoke management is of concern. The engineering principles governing the design of smoke control systems for all of these various large-volume spaces are the same. However, differences in the smoke control system designs for the variety of large-volume spaces may be found. Differences in designs are a result of differences in fire scenarios and design goals, reflecting the range of building uses and operations and the nature of who or what may be exposed to the smoke. Given the similarities in engineering principles affecting smoke control system design, the term *atrium* will be used throughout this chapter to refer to all types of large-volume spaces.

The discussion presented in this chapter is divided into two sections. First, conditions within the atrium prior to actuation of a smoke control system are discussed. As part of this discussion, the smoke filling process is described along with the time required for actuation of a smoke control system. The second part of the chapter includes a description of conditions within the atrium after actuation of the smoke control system.

As a preface to any discussion on smoke control systems, a definition of smoke must be established (NFPA 92, *Standard for Smoke Control Systems* [1], Section 3.3.13):

> The airborne solid and liquid particulates and gases evolved when a material undergoes pyrolysis or combustion, together with the quantity of air that is entrained or otherwise mixed into the mass.

Although only the combustion products are visible and potentially toxic, what is visually observed as smoke is a mixture of the combustion products and the entrained air. Air is

J.A. Milke (✉)
University of Maryland, Department of Fire Protection Engineering, University of Maryland, College Park, MD, 20742, USA

M.J. Hurley (ed.), *SFPE Handbook of Fire Protection Engineering*,
DOI 10.1007/978-1-4939-2565-0_51, © Society of Fire Protection Engineers 2016

entrained along the entire height of the smoke plume below a smoke layer. Proportionally, the smoke is mostly entrained air. In the space between the base and tip of the flames, most of the entrained air is not consumed in the combustion process and only dilutes the combustion products. Entraining air into the smoke plume increases the mass flow in the plume to increase the quantity of smoke produced. However, the entrained air also dilutes the smoke to decrease the concentration of combustion gases and cool the smoke. In some cases, the smoke may be sufficiently diluted to mitigate the associated hazards.

Hazard Parameters

Smoke can adversely affect building occupants, fire brigade members, property (including the building structure and contents), and mission continuity. Typically, the threat to people or objects is posed when they come into contact with smoke for a sufficient period of time.

People who become exposed to smoke are generally harmed as a result of the exposure to toxic gases or elevated temperature. The toxic effects of smoke on people are described in Purser (see Chap. 63) and Klote et al. [2]. In addition, smoke may reduce visibility. A reduction of visibility may cause people to become disoriented and can in turn increase the amount of time they are exposed to the smoke [3]. A reduction of visibility may also increase the susceptibility of building occupants to trip over obstructions or even fall over balcony railings [4].

Building components can be affected by the elevated temperature due to smoke. Building components heated by smoke are considered in fire resistance analyses. In addition, building contents may be affected by exposure to the elevated temperatures, corrosive gases, or particulate matter. Contents exposed to heated smoke may be melted, distorted, or charred, depending on the temperature of the smoke and the degree of exposure. Contents that are submerged in smoke and come into contact with combustion gases and smoke particles may become stained or emit an odor of smoke. Exposure to smoke can damage electronic equipment, especially if restoration activities are not initiated promptly after the fire [5].

Following a fire, a building or portion thereof may be closed due to restoration, threatening mission continuity. This results in loss of revenue for the building owner, temporary unemployment of workers in the building, and loss of service of the facility to the community, among other outcomes.

Smoke Layer Interface Position

The smoke layer interface position is located a distance, z, above the top of the fuel, as indicated in Fig. 51.1. This parameter is used to assess the danger of people or objects being immersed in a smoke layer. Sole use of this parameter to assess hazard level is conservative by considering any concentration of smoke to be unacceptable. For people, even though the physiological effects due to being submerged in "light" smoke levels may be minor, the psychological effects and extended evacuation time may be appreciable. Being surrounded by smoke of any nature may decrease the speed of evacuation, perhaps until the smoke is no longer relatively benign. In terms of property protection issues, any smoke may be unacceptable because of smoke staining or smoke corrosivity.

Light Obscuration

As with the smoke layer depth parameter, light obscuration is not lethal by itself. Associated with an increase in light obscuration is a reduction in visibility, which is likely to yield a longer evacuation time and extend exposure to the toxins in smoke. In some documented fires, evacuation has been terminated due to a lack of sufficient visibility [6–8]. A fire fighter's injury in an atrium fire was attributed to a significant

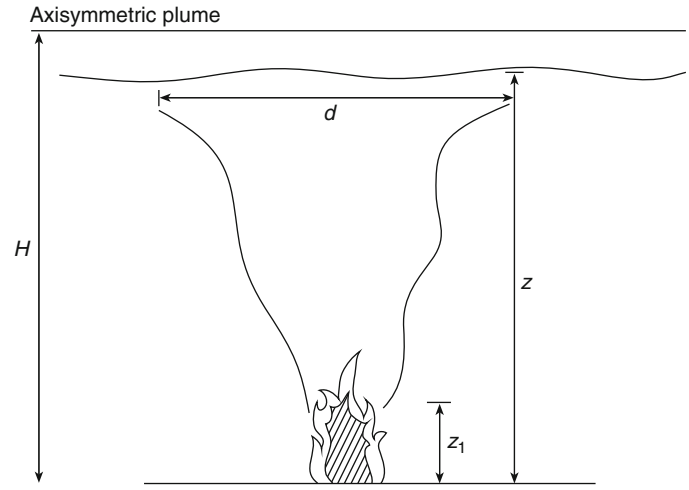

Fig. 51.1 Axisymmetric plume [1]

reduction in visibility due to light obscuration [4]. The fire fighter fell from an upper balcony because he could not see the edge.

Limiting values from 0.23 to 1.2 m^{-1} have been suggested for the extinction coefficient [6–8]. Alternatively, a critical limit may be based on a preferred minimum visibility distance to a particular target. For example, a limit of light obscuration can be suggested such that occupants can see an illuminated exit sign across a room or at the end of a corridor [3, 9].

Temperature and Gas Specie Concentration

The final two parameters, elevated temperature of the smoke layer and gas specie concentration (such as CO, CO_2, and HCN), can be directly related to the potential for harm (see Chap. 63). Critical limits for these two parameters can be suggested based on toxicity studies.

Smoke Management Approaches

The design of a smoke control system for an atrium is influenced by the following three characteristics of the atrium:

1. Geometric shape and dimensions
2. Relative location within the building
3. Separation from communicating spaces

Several approaches are available to achieve smoke management goals in an atrium (e.g., limit the fire size, provide physical barriers, and provide mechanical or natural ventilation). Selection of the best smoke management approach for a particular atrium should consider the use, size, and arrangement of the associated spaces.

Limiting the fire size can be accomplished by controlling the type, quantity, and arrangement of fuel. In addition, the fire size can be controlled through an automatic suppression system.

Physical barriers limit smoke spread to adjacent spaces. The ability of a physical barrier to limit smoke spread is dependent on the leakage of the barrier and pressure difference across the barrier. The barrier needs to withstand the exposure to smoke and an elevated temperature environment. In an atrium with a tall ceiling, the temperature of the smoke layer in the atrium may be only slightly above ambient temperatures in the space.

Mechanical or natural ventilation may be provided to remove smoke from the atrium. Removing smoke from the atrium can be intended to limit the accumulation of heat and smoke within the atrium or arrest the descent of the smoke layer. Mechanical ventilation can be provided to oppose smoke movement induced by the fire to restrict smoke spread to communicating

spaces. Gravity vents may be provided to remove smoke, though their performance can be compromised by environmental factors.

Analytical Approach

Numerous tools are available to aid in the design and evaluate the adequacy of a smoke control system. The selection of a particular tool is dependent on the accuracy needed for the analysis and the applicability of the analytical tools given the characteristics of the large space and selected fire scenarios. The principal characteristics that affect applicability are

- Geometry of the large space: variation of horizontal cross-sectional area, sloped versus flat ceiling
- Transient aspects: unsteady versus steady heat release rate, constant versus transient operation of smoke control system
- Fire development: heat release rate as a function of time (for example, constant, power-law relationship with time, t^n)
- Environmental effects: stack effect, wind
- Interacting systems: other smoke control systems, HVAC, other exhaust systems (for example in laboratories)

The range of design tools available to assess the performance of smoke control system designs can be grouped into the following categories:

- Zone model (algebraic equation based)
- Zone model (computer based)
- Field model
- Physical scale model

The intent of an engineering analysis of smoke conditions in an atrium is to express the level of hazard in terms of physically based parameters, for example, smoke layer interface position, temperature, gas concentration (such as carbon monoxide), and light obscuration. The magnitude of each of these parameters can be predicted based on engineering principles. In addition to being predictable, critical threshold values are available for the hazard parameters in order to properly assess the severity of the threat (See Chap. 63). This chapter will concentrate on the life hazards posed by smoke. The hazards smoke poses to contents, property, and mission continuity are described elsewhere [2–4, 10].

Physical Scale Models

Physical scale models provide a representation of a space, though in a reduced scale. Physical scale models are especially useful in examining atria with irregular shapes or numerous projections. A review of applying physical scale models as a design aid for atrium smoke control systems was provided by Milke and Klote [11].

Quintiere provided a review of scaling relationships based on preserving the Froude number [12]. The Froude number, Fr, is defined as v/gl.

The scaling relations are

Temperature:

$$T_m = T_F \tag{51.1}$$

Geometric position:

$$x_m = x_F \left(\frac{l_m}{l_F}\right) \tag{51.2}$$

Pressure:

$$\Delta p_m = \Delta p_F \left(\frac{l_m}{l_F}\right) \tag{51.3}$$

Velocity:

$$v_m = v_F \left(\frac{l_m}{l_F}\right)^{1/2} \tag{51.4}$$

Time:

$$t_m = t_F \left(\frac{l_m}{l_F}\right)^{1/2} \tag{51.5}$$

Convectiveheat release:

$$\dot{Q}_{c,m} = \dot{Q}_{c,f} \left(\frac{l_m}{l_F}\right)^{5/2} \tag{51.6}$$

Volumetric flow rate:

$$V_{\text{fan},m} = V_{\text{fan},F} \left(\frac{l_m}{l_F}\right)^{5/2} \tag{51.7}$$

Experiments based on Froude modeling may be done with air at atmospheric pressure. Froude modeling does not preserve the Reynolds number. However, appropriate selection of the size of the physical scale model can ensure that fully

developed flow is achieved to minimize the consequences of not preserving the Reynolds number. Because the smoke behavior in only certain areas of the scaled atrium may be of interest, fully developed flow only needs to be achieved in these particular areas. Often a physical scale model with a critical dimension of at least 0.3 m in any areas of interest will be sufficient to achieve fully developed, turbulent flow. As an example, in most shopping malls and atria, the critical dimension in question would be the floor-to-ceiling height of one of the balconies.

In addition, Froude modeling does not preserve the dimensionless parameters concerning heat transfer. Generally, this limitation has little effect because the temperature is the same for the physical scale model and the full-scale facility. Froude modeling does not apply to locations with high temperature and low Reynolds numbers (e.g., near the flame). However, Froude modeling provides useful information about smoke transport away from the fire.

Some surface effects can be preserved by scaling the thermal properties of the construction materials for the model. The thermal properties can be scaled by

Thermal properties:

$$\left(k\rho c_p\right)_{w,m} = \left(k\rho c_p\right)_{w,F}\left(\frac{l_m}{l_F}\right)^{0.9} \tag{51.8}$$

Because scaling thermal properties have only a secondary effect on fluid flow, considerations of convenient construction and flow visualization may require that some or all surface materials in the model are different from those selected based on thermal property scaling.

Example 1 A physical scale model is proposed to determine the equilibrium smoke layer position for the atrium depicted in Fig. 51.2. Because the horizontal cross-sectional area varies with height, algebraic equation and computer-based zone models are of limited value. The overall height of the atrium being studied is 30.5 m and the design fire is steady with a heat release rate of 5 MW. An exhaust fan capacity of 142 m^3/s is proposed. By applying the scaling relationships

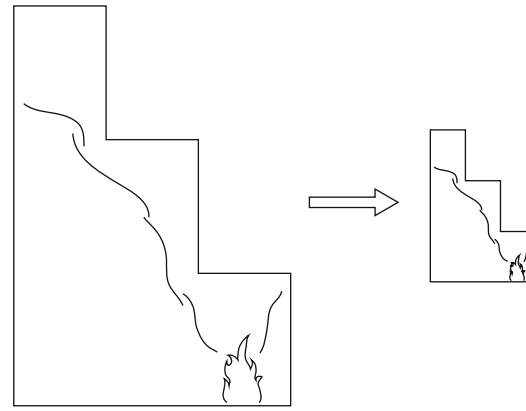

Fig. 51.2 Small-scale model of atrium

to formulate a small-scale model, the basic parameters for the scale model are

- Height: 3.8-m-tall model (1/8 scale)
- Fire size: 28 kW
- Fan capacity: 0.78 m^3/s

Analytical Models

Two categories of analytical models are zone and field models. A description of field models is outside the scope of this chapter. Zone models divide each compartment into a limited number of control volumes, typically an upper and a lower zone. Inherent in the zone approach is the assumption of uniform properties throughout each zone. In spaces with a large floor area, this assumption may be tenuous. Nonetheless, calculations associated with the zone model approach are relatively easy to perform and are often accepted for engineering purposes. Calculations following the zone model approach may be in the form of algebraic equations or a computer algorithm.

The zone model approach assumes that smoke from a fire is buoyant, rises to the ceiling, and forms a smoke layer. The buoyant nature of smoke is due to the decreased density of the heated smoke. As smoke rises in a plume, air is entrained to increase the mass flow rate in the plume. A decrease in the velocity and temperature of the smoke plume results from the increase in the plume mass flow rate, as dictated by

conservation of momentum and energy. In addition, the entrained air dilutes the combustion products in the plume. The entire smoke layer is assumed to have uniform characteristics. As smoke is supplied to the smoke layer from the plume, the interface between the smoke layer and lower clear air zone descends. The additional smoke supplied by the plume also results in an increase in the smoke layer temperature, carbon monoxide concentration, and light obscuration.

Being a simplification, the zone model approach may not be applicable in some situations. One example includes a scenario with operating sprinklers, which may cool the layer and also entrain smoke from the upper layer into the water spray pattern descending into the lower zone. Another example consists of the case where smoke does not reach the ceiling as a result of a loss of buoyancy, where the pre-fire temperature near the ceiling of the atrium is greater than that near the floor. This situation is discussed in more detail later in this chapter. A third situation involves an atrium with a large cross-sectional area where the horizontal variation in conditions from one portion of the atrium to another is important to the analyst. Where localized conditions associated with the smoke plume or smoke layer need to be assessed, field models are more appropriate than zone models.

Two categories of fire scenarios for smoke management design in atria include (1) fires located in the atrium, and (2) fires located in a space adjacent and open to the atrium. This chapter concentrates only on fires within the atrium space. Methods to estimate conditions in any of the adjacent spaces, resulting from fires originating in the atrium or from fires in other adjacent spaces, are addressed elsewhere [2].

Smoke Filling Period

A smoke layer is formed once the smoke plume reaches the ceiling and the ceiling jet spreads horizontally to reach the bounding walls of the space. Subsequently, the smoke layer starts to descend in the space. In relatively small spaces with low ceilings, the smoke layer forms almost immediately. However, in large spaces with tall ceilings, the time required to form a smoke layer may be appreciable. The delay in forming a layer is attributable to the transport lag of the smoke. The smoke filling period continues until the properly sized smoke exhaust fans are actuated.

Transport Lag

The transport lag is composed of the time for a smoke plume to reach the ceiling (plume transport lag) and the time for the ceiling jet to reach the bounding enclosure (ceiling jet transport lag). These two time periods are depicted in Fig. 51.3.

Correlations for the plume and ceiling jet transport lag are available in the literature for both steady and t^2 fires [13, 14]. Because virtually all fires have a growth period before reaching a steady phase, the transport lag correlations for steady fires have little relevance.

Correlations for the plume transport lag for steady and t^2-fires are
Steady files:

$$t_{pl} = 0.67H^{4/3}/\dot{Q}^{1/3} \tag{51.9}$$

t^2 fires:

$$t_{\mathrm{pl}} = 0.1H^{4/5}t_g^{2/5} \tag{51.10}$$

Estimates of the plume transport lag from Equations 51.9 and 51.10 are provided in Fig. 51.4. As indicated in the figure, even the shortest plume transport lag for t^2 fires, associated with the fast t^2 fire, is greater than that for a modest-size steady fire.

Comparable correlations for the ceiling jet transport lag for steady and t^2 fires are
Steady files:

$$t_{\mathrm{cj}} = \frac{r^{11/6}}{1.2\dot{Q}^{1/3}H^{1/2}} \tag{51.11}$$

t^2 fires:

$$t_{\mathrm{cj}} = \frac{0.72rt_g^{2/5}}{H^{1/5}} \tag{51.12}$$

A comparison of the ceiling jet transport lag for a modest-size steady fire and t^2 fires is

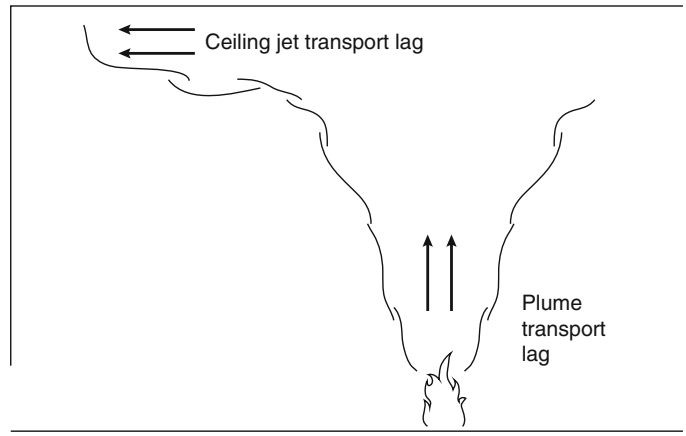

Fig. 51.3 Plume and ceiling jet transport lag

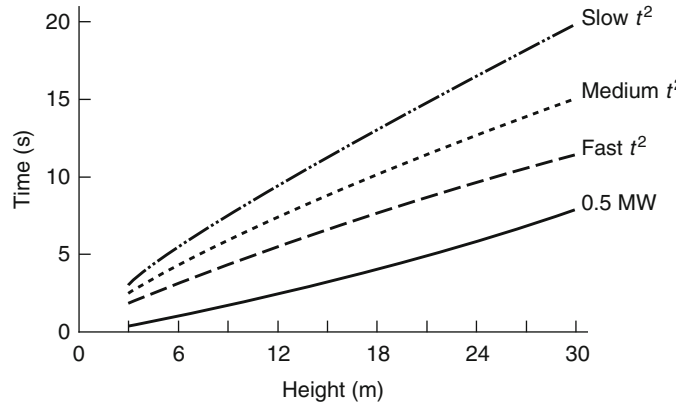

Fig. 51.4 Plume transport lag

presented in Fig. 51.5. Again, the transport lag associated with the steady fire is much less than that associated with any of the t^2 fires.

Many zone models do not account for transport lag. In low-height spaces with small compartments, this is likely to be inconsequential. In tall spaces with large cross-sectional horizontal areas, the lag may be important. In such cases, only models that incorporate transport lag are to be selected.

Smoke Layer Interface Position

Once the smoke layer has formed, the initial rate of descent of the layer is very rapid, slowing as the layer descends. This is attributable to the rate of smoke production being dependent on the height of the plume where entrainment occurs, i.e., the distance from the top of the fuel to the smoke layer.

Both empirical correlations and theoretically based methods are available to address conditions during the smoke filling period using a zone model approach [15]. Theoretically based methods use statements of conservation of mass and energy to determine the volume of the upper layer. Conservation of mass accounts for the smoke mass supplied from the plume to the smoke layer along with any smoke leaving the zone through ventilation openings. Conservation of energy is applied to address the energy being supplied by the plume along with heat losses from the layer.

Generally, the predicted smoke layer interface position determined by the two analytical

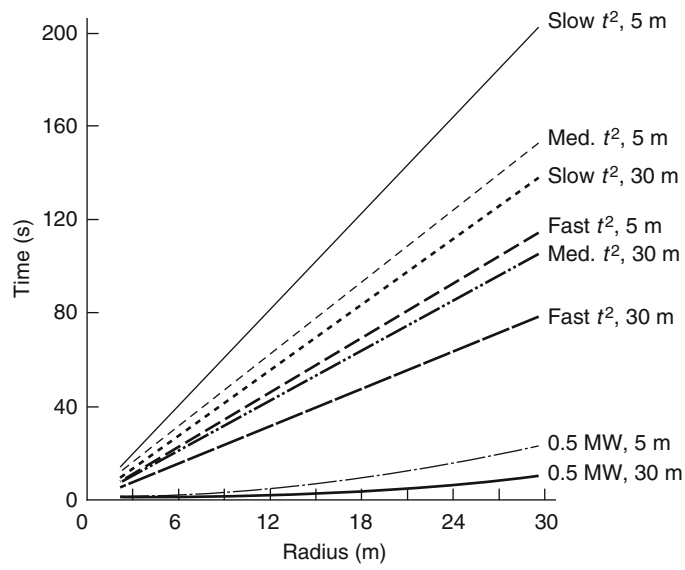

Fig. 51.5 Ceiling jet transport lag

methods differs. The smoke layer is comprised of the uppermost portion of the layer in which the conditions are relatively uniform at any elevation. Below that section is a transition zone, where the conditions decrease until they reach the bottom edge of the layer and are at their minimum value. The predictions from the empirical correlations relate to the position of the bottom edge of the transition zone as determined in an experimental program. In the theoretically based correlations, all of the smoke is considered to be in one layer with uniform properties. Combination of the transition zone and the upper portion into one uniform zone effectively results in the transition zone being compressed so as to have the same properties as the upper portion. As such, the theoretically based correlations relate to a thinner smoke layer than the empirical approach.

Empirical Correlations

Empirical correlations have been developed by Heskestad to determine the smoke layer interface position as a function of time for steady and t^2 fires. These correlations, included in NFPA 92 [1], are based on experimental data in large spaces. In the experimental efforts, the smoke layer interface position was established by a variety of means, including visual observations and measurements of temperature change, carbon dioxide concentration, or light obscuration.

The correlations are simple expressions with easily acquired input and minimal computations. The correlations provide conservative estimates of the smoke layer interface position (i.e., predicting the lower edge of the transition zone of the smoke layer which may include only 'wisps' of smoke) [16]. The correlations are applicable to simplified cases related to the fire and geometry of the space. Fire scenarios must be steady state or, if growing, follow a t^2 profile. The assumed geometrical configuration is a space of uniform cross-sectional area (i.e., rectangular or right cylindrical solids). In addition to the noted simplifications, second-order parameters such as environmental factors (e.g., stack effect, wind) and the effect of HVAC systems are neglected.

Steady Fires The position of the smoke layer interface for steady fires can be estimated using Equation 51.13 [16, 17]. Equation 51.13 is based on experimental data from fires in large-volume spaces with A/H^2 of 0.9–14 [18–20].

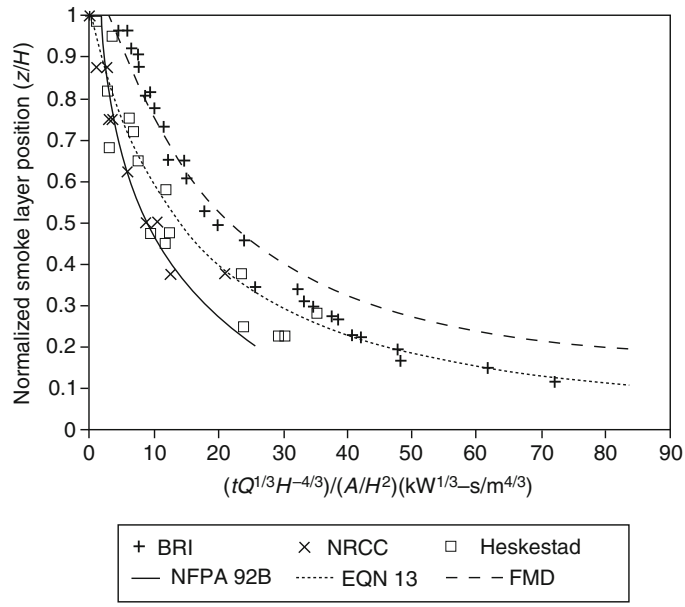

Fig. 51.6 Comparisons of smoke layer position—experimental data versus predictions

$$\frac{z}{H} = 1.11 - 0.28 \ln\left(\frac{t\dot{Q}^{1/3}H^{-4/3}}{A/H^2}\right) \qquad (51.13)$$

Where $z/H \geq 0.2$.

Equation 51.13 is presented in non-dimensional form. The quantity $t\dot{Q}^{1/3}H^{-4/3}$ represents the normalized time from ignition. The significance of the normalized time parameter is to indicate that the same relative smoke layer position occurs for a long duration, low heat release rate fire in a tall ceiling height atrium, as for a short duration, large fire in an atrium with a short ceiling height. Different atrium geometries are accounted for by the non-dimensional shape factor, (A/H^2) [18, 19].

The limits noted for A/H^2 reflect the range of shape factors for the facilities in which the experiments were performed [18, 19]. Examples of atria within the noted range include atria with a cross-sectional area of 10,000 m^2 and a height of 105 m ($A/H^2 = 0.9$) or a height of 27 m ($A/H^2 = 14$). Comparisons of the predictions from Equation 51.13 to experimental data from fires in tall spaces are provided in Fig. 51.6 [20–22].

Transport lag, or the initial time period to form a smoke layer, is implicitly included in Equation 51.13. Evidence of this characteristic is obtained for short time durations where the resulting z/H is greater than 1.0 (otherwise $z/H > 1$ would literally mean that the smoke layer interface is *above* the ceiling). The lower limit for z/H of 0.2 relates to the lowest level where data were taken in any of the referenced experiments.

t^2fires Equation 51.14 provides a correlation of the time-dependent smoke layer interface position for fires following a t^2-type profile [16]. Equation 51.14 is also based on experimental data in spaces with shape factors ranging from 0.9 to 14 [20, 23].

$$\frac{z}{H} = 0.91\left[tt_g^{-2/5}H^{-4/5}\left(A/H^2\right)^{-3/5}\right]^{-1.45} \qquad (51.14)$$

Equations 51.13 and 51.14 both assume that the fire is located near the center of the atrium floor, remote from any walls. Smoke production is greatest for the centered configuration and thereby represents the worst-case condition.

Example 2 For a fast, t^2 fire in an atrium with a cross-sectional area of 800 m^2 and height of 20 m, determine the position of the smoke layer interface after 120 s.

Solution Applying Equation 51.14 with $A/H^2 = 2.0$ and $t_g = 150$ s, z/H is 0.95 or $z = 19$ m.

Example 3 For a fast, t^2 fire in an atrium with a cross-sectional area of 800 m^2 and height of 20 m, determine the time for the smoke layer interface to reach 15 m above floor level.

Solution Re-expressing Equation 51.14 to solve for t,

$$t = 0.94 t_g^{2/5} H^{4/5} \left(A/H^2\right)^{3/5} (z/H)^{-0.69} \quad (51.15)$$

Applying Equation 51.15 with $A/H^2 = 2.0$ and $t_g = 150$ s, t is 140 s.

Reviewing the results from Examples 2 and 3, the smoke layer barely descends below the ceiling in the first 120 s. This is indicative of the lag time required for the plume to reach the ceiling and to form a layer. Then, after only another 20 s, the smoke layer descends 4 m, demonstrating the rapid initial descent rate of the smoke layer interface. The rapid descent is attributable to the significant quantity of smoke produced during the early stage of a fire in a tall ceiling space when the height available for entrainment is at its largest value. The predicted trend of rapid filling during the early stage of a fire has been reported by eye-witness accounts from four fires in atria [4, 24–26].

Theoretically Based Approach

Conservation of mass and energy can be applied to provide an estimate for the position of the theoretical smoke layer interface. Equation 51.16 expresses the conservation of mass, m_u, for the upper smoke layer, assuming no exhaust from the layer.

$$\frac{dm_u}{dt} = \dot{m} \quad (51.16)$$

Approximating the smoke as an ideal gas with properties of heated air, and assuming that the ambient pressure and specific heat are constant, the expression for conservation of energy for the smoke layer is

$$(\rho h)_u \frac{dV_u}{dt} = \dot{Q}_c + \dot{m} h_1 \quad (51.17)$$

Given the previously assumed conditions, ρh is a constant. Substituting the volumetric flow rate for the mass flow rate and simplifying,

$$\frac{dV_u}{dt} = \frac{\dot{Q}_c}{\rho h} + \dot{V} \quad (51.18)$$

The growth rate of the upper layer indicated in Equation 51.18 is dependent on two terms: (1) the volume supplied by the plume and (2) the expansion of the volume due to heating. For the case of an atrium with a constant cross-sectional area, A,

$$\frac{dV_u}{dt} = A \frac{dz_u}{dt} \quad (51.19)$$

As long as the smoke layer interface is well above the flaming region (see discussion later in this chapter), the plume mass entrainment rate can be estimated from [27].

$$\frac{dV_u}{dt} = \frac{\dot{m}}{\rho} = k_v \dot{Q}^{1/3} z^{5/3} \quad (51.20)$$

Several simplifications can be made for large clear heights (i.e., clear heights in excess of 10 m). The clear height is the distance from the top of the fuel to the bottom of the smoke layer. The magnitude of the second term is much less than the first. Generally, z is much greater than z_o. In addition, the volume increase of the upper layer supplied by the plume is appreciably greater than that due to expansion. With these simplifications and by substituting Equations 51.19 and 51.20 into Equation 51.18, an expression for dz_u/dt can be formulated

$$\frac{dz_u}{dt} = \frac{k_v \dot{Q} z^{5/3}}{A} \quad (51.21)$$

In Equation 51.21, k_v is the volumetric entrainment constant, defined as [36].

$$k_v = 0.076/\rho$$

The convective heat release fraction is the ratio of the convective heat release rate to the total heat release rate and is typically assumed

to be on the order of 0.7–0.8. Throughout this chapter, a value of 0.7 is selected for the convective heat release fraction [1]. Assuming a plume entrainment constant of 0.076 kg $kW^{-1/3} \cdot m^{-5/3} \cdot s^{-1}$ and the density of ambient air as 1.2 kg/m^3, the volumetric entrainment constant is 0.064 $m^{4/3}$ $kW^{-1/3}$ s^{-1}.

An expression for the smoke layer position resulting from a steady fire as a function of time can be obtained by integrating Equation 51.9:

$$\frac{z}{H} = \left[1 + \frac{2k_v t \dot{Q}^{1/3}}{3(A/H^2)H^{4/3}}\right]^{-3/2} \tag{51.22}$$

Alternatively, for a t^2 fire

$$\frac{z}{H} = \left[1 + \frac{4k_v t(t/t_g)^{2/3}}{(A/H^2)H^{4/3}}\right]^{-3/2} \tag{51.23}$$

A comparison of the predictions from Equations 51.13 and 51.22 is provided in Fig. 51.6. One principal difference relates to the time delay for the smoke layer to form, i.e., transport lag. Transport lag is included implicitly in Equation 51.13. Equation 51.22 assumes that a smoke layer forms immediately. The transport lag can be accounted for separately [13].

Example 4 For a fast, t^2 fire in an atrium with a cross-sectional area of 800 m^2 and height of 20 m, determine the position of the smoke layer interface after 120 s.

Solution Applying Equation 51.23 with $A/H^2 = 2.0$ and $t_g = 150$ s, z/H is 0.72 or $z = 14.4$ m.

Vented Period

If a smoke control system has the capability to exhaust smoke, the descent of the smoke layer can be arrested if the volumetric rate of smoke exhaust from the smoke layer equals the volumetric rate of smoke supplied to the layer. Neglecting the effect of expansion, the layer descent is stopped when the mass exhaust rate is equal to the mass entrainment rate by the plume. Algebraic equations are available to estimate the properties of the smoke layer, including

1. Position of smoke layer interface
2. Temperature of smoke layer
3. Light obscuration in smoke layer and
4. Gas concentration in smoke layer

Equilibrium Smoke Layer Interface Position

The exhaust rate necessary to arrest the descent of the smoke layer can be estimated based on knowledge of the mass entrainment rate into the plume. The mass entrainment rate depends on the configuration of the plume. Plume configurations reviewed in this chapter are

1. Axisymmetric plume
2. Wall plume
3. Corner plume
4. Balcony spill plume

Axisymmetric Plume Axisymmetric plumes are formed from fires involving fuel packages remote from any walls (i.e., near the center of the atrium floor). Being remote from any walls, air is entrained around all of the plume perimeter along the entire clear height of the plume. The functional relationship of the mass entrainment rate to the heat release rate and clear height is [28].

$$\dot{m} = f\left(\dot{Q}_c^{1/3} z^{5/3}\right) \tag{51.24}$$

One set of equations for the mass entrainment rate was originally derived by Heskestad [27]. One of the equations in the pair developed by Heskestad applies to estimating the entrainment in the flaming portion of the plume and another deals with the overall plume, including flaming portion and upper portion where flames are absent.

The limiting height is defined as the height of the continuous flaming region, (i.e., where flames are present 50 % of the time). The limiting height may be estimated as [27].

$$z_f = 0.166\dot{Q}_c^{2/5} \tag{51.25}$$

For clear heights less than the limiting height, i.e., where flames extend into the smoke layer, the entrainment rate is estimated using Equation 51.26

$$\dot{m} = 0.032\dot{Q}_c^{3/5} z \tag{51.26}$$

For clear heights greater than the limiting height, i.e., where the flaming region ends prior to reaching the smoke layer, the entrainment rate is estimated using Equation 51.27:

$$\dot{m} = 0.071\dot{Q}_c^{1/3} z^{5/3} + 0.0018\dot{Q}_c \tag{51.27}$$

Equation 51.27 is a simplified version of the original expression developed by Heskestad (see Chap. 13, with z_o from the original expression set equal to zero. The validity of neglecting z_o in Equation 51.27 is based on the observation that z_o is typically small, compared to z [2]. The location of the virtual origin of an assumed point source can be estimated as [27].

$$z_o = 0.083\dot{Q}^{2/5} - 1.02d_o \tag{51.28}$$

For noncircular fuels, an equivalent diameter needs to be defined. The definition of an equivalent diameter is based on a circle that has an area equal to the floor area covered by the fuel. Considering a wide range of diameters and heat release rates associated with a variety of typical fuel packages, the virtual origin ranges from 0.5 to −5 m. Negative values are obtained when the second term is greater than the first (i.e., for fuel commodities with modest heat release rates spread over a large area).

Originally, Equations 51.26 and 51.27 were developed to describe plumes from horizontal, circular flammable liquid pool fires. However, these equations have been shown to be applicable to more complex fuels, as long as the limiting height is greater than the diameter of the fuel, and the fire only involves the surface of the material (i.e., is not deep-seated) [27].

The mass rate of smoke production estimated by Equations 51.26 and 51.27 is independent of the type of materials involved in the fire, other than indirectly in terms of the heat release rate. This is due to the mass rate of entrained air being much greater than the mass rate of combustion products generated, which is true as long as sufficient air is available for combustion. As a result of the fire being approximated as a point source in the entrainment equations, the shape or form of the fuel is not of primary importance. Thus, the parameters associated with a detailed description of the fuel package are relegated to a level of secondary importance.

In both Equations 51.26 and 51.27, the mass entrainment rate is dependent on the clear height, where the mass entrainment rate increases with increasing values of the clear height. During the early stages of the fire, the clear height has its maximum value thereby providing the maximum smoke production rate. This is especially true if the flame height is well below the smoke layer, where the smoke production rate is proportional to $z^{5/3}$.

In most engineering applications, the smoke production (or exhaust) rate is expressed in terms of a volumetric rate rather than a mass rate. In order to accommodate this preference, the relationship between the volumetric rate and mass rate is expressed as Equation 51.29.

$$\dot{V} = \frac{\dot{m}}{\rho} \tag{51.29}$$

Assuming smoke to have the same properties as air, the density of smoke may be evaluated as the density of air at the temperature of the smoke layer [3]. Graphs relating the volumetric smoke production rate to the clear height for selected total heat release rates ranging from 1000 to 10,000 kW are provided in Fig. 51.7.

Example 5 A fire has a total heat release rate of 5000 kW and is located at the center of the atrium floor. The smoke layer interface is 35 m above the floor. Determine the mass and volumetric rates of smoke being supplied by the plume to the smoke layer (i.e., at the location of the smoke layer interface).

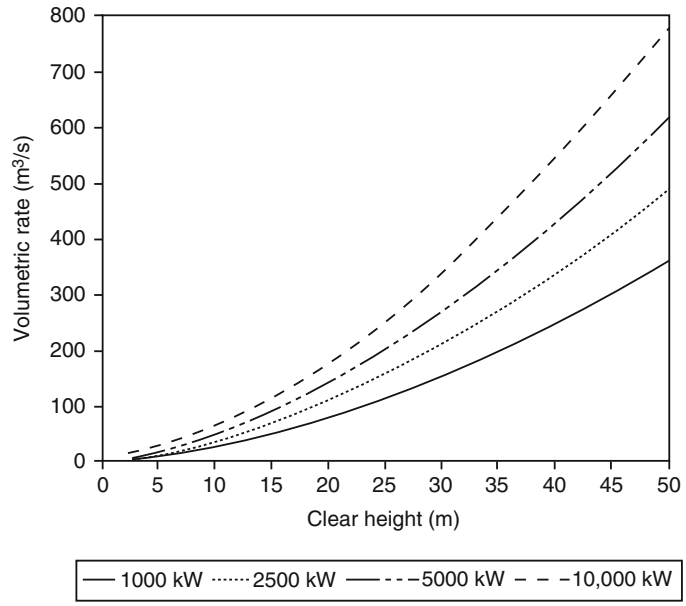

Fig. 51.7 Smoke production rate for axisymmetric plumes

Solution First, the limiting height is evaluated using Equation 51.25 to determine the applicable equation for the mass rate of entrainment, assuming the convective heat release fraction is 0.7, $z_f = 4.3$ m. Because z > z_f, Equation 51.27 is the applicable equation for determining the mass rate of smoke production. Neglecting z_o, the mass smoke production rate is 410 kg/s. The associated volumetric rate (from Equation 51.29, assuming 20 °C and 1 atm pressure) is 340 m^3/s.

Wall and Corner Plumes Fires located near walls and corners principally entrain air only along the surface of the plume away from the walls or corner. Consequently, the amount of smoke production is reduced for these locations, compared to the axisymmetric plume remotely located from the walls. Using the concept of reflection, the smoke production rate from wall and corner plumes can be estimated [29, 30].

A plume generated by a fire located against a wall only entrains air from approximately half of its perimeter, as indicated in Fig. 51.8. According to the concept of reflection, the smoke production rate is estimated as half of that from a fire that is twice as large (in terms of heat release rate) (note: having half of the entrainment does not cancel out the impact of considering twice the fire size as the entrainment is proportional to the one-third power of the heat release rate).

Similarly, a plume generated by a fire located near a corner of a room is referred to as a corner plume (see Fig. 51.8). Using the concept of a reflection, the smoke production rate from corner plumes, where the intersecting walls form a 90° angle, is estimated as one-quarter of that from a fire that is four times as large.

Example 6 A fire located on the floor of an atrium has a total heat release rate of 5000 kW. The smoke layer interface is 35 m above the floor. Compare the mass rates of smoke being supplied by the plume to the smoke layer, given an axisymmetric, wall, or corner plume configuration.

Solution In Example 5, $z_f = 4.3$ m and the smoke production rate for the axisymmetric plume using Equation 51.27 is 410 kg/s. Applying the same equation for the wall plume, the smoke production rate for a fire size of 10,000 kW is estimated as 520 kg/s. Dividing that rate by two provides the smoke production rate for the wall plume (260 kg/s). Similarly, for

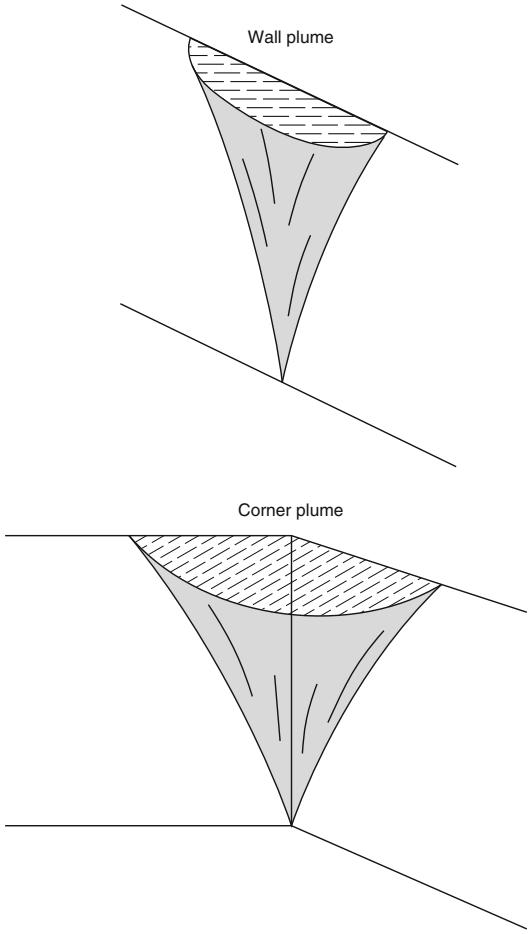

Fig. 51.8 Wall and corner plume diagrams

the case of the corner plume, the smoke production rate is 170 kg/s (considering one-quarter of the smoke production rate from a 20,000 kW fire).

Comparing the smoke production rates for the three plumes (axisymmetric, wall, and corner plumes), the smoke production rate is greatest for the axisymmetric plume (410 kg/s) compared to 260 and 170 kg/s for the wall and corner plumes, respectively. Thus, conservative hazard assessments should assume an axisymmetric plume is developed from a fire that is located away from the walls, near the center of the space.

Balcony Spill Plume A balcony spill plume is generated in cases where smoke reaches an intermediate obstruction, such as a balcony, travels horizontally under the obstruction, and then turns and rises vertically. Scenarios with balcony spill plumes involve smoke rising above a fire, reaching a ceiling, balcony, or other significant horizontal projection, then traveling horizontally toward the edge of the balcony. Characteristics of the resulting balcony spill plume depend on characteristics of the fire, width of the spill plume, and height of the ceiling above the fire. In addition, the path of horizontal travel from the plume centerline to the balcony edge is significant.

Several correlations on air entrainment into balcony spill plumes have been presented in the literature over several decades. A comprehensive review of the proposed correlations is provided by Harrison [31], Lougheed et al. [32] and Lim [33]. The correlations presented in NFPA 92 reflect the results obtained by Lougheed et al. from large-scale experiments and numerical simulations. One of the correlations in NFPA 92 has its roots back to Law's [34] interpretation of small-scale experimental data obtained by Morgan and Marshall [35]. This correlation is presented as:

$$\dot{m} = 0.36\left(\dot{Q}\dot{W}^2\right)^{1/3}(z_b + 0.25H) \qquad (51.30)$$

Lougheed et al. found that their large scale data was well described by this correlation for clear heights (z) in excess of 15 m. For lower heights, Lougheed et al. suggest the following correlation:

$$\dot{m} = 0.59\dot{Q}^{1/3}W^{1/5}(z_b + 0.17\dot{W}^{7/15}H + 10.35W^{7/15} - 15) \qquad (51.31)$$

The correlations presented in Equations 51.30 and 51.31, as well as others presented by numerous previous researchers, apply to balcony spill plumes of a specific configuration. The configuration considered is depicted in Fig. 51.9. As illustrated in the figure, the fire is located in a communicating space and the smoke flows under a soffit out from the room of fire origin, then under a short horizontal obstruction, i.e., balcony. The balcony is oriented perpendicular to the opening from the room. Any variations from

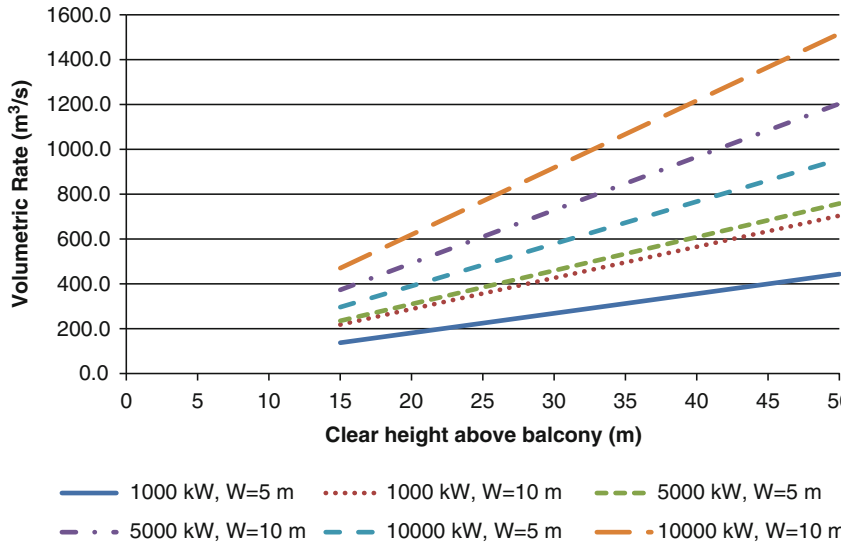

Fig. 51.9 Approximation of a balcony spill plume

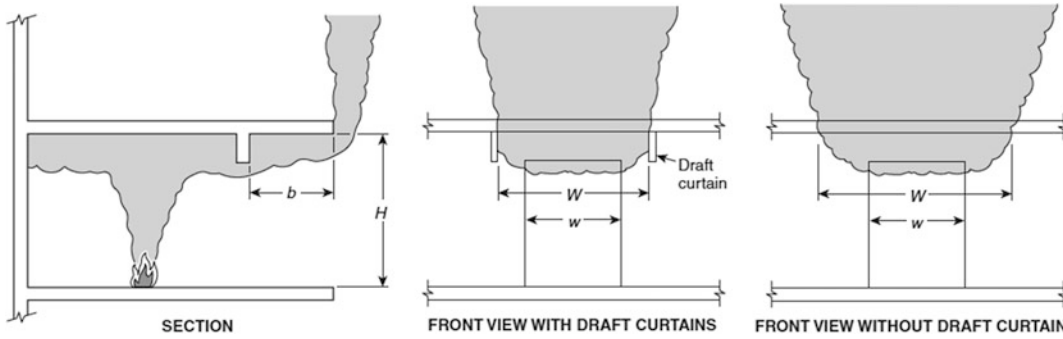

Fig. 51.10 Smoke production rate predictions for balcony spill plumes (H = 3 m)

this specific configuration have not been investigated and thus the balcony spill plume correlations presented as Equations 51.30 and 51.31 should not be applied for those situations. Instead, the application of CFD codes or small-scale models should be applied to assess those situations.

Predictions of the smoke production rate using Equation 51.30 for the balcony spill plume are included in Fig. 51.10. The calculations represented in the figure consider a 3-m height to the underside of the balcony.

Reprinted with permission from NFPA 92-2012, *Standard for Smoke Control Systems*, Copyright© 2011, National Fire Protection Association. This reprinted material is not the complete and official position of the NFPA on the referenced subject, which is represented only by the standard in its entirety.

A comparison of the smoke production rate for axisymmetric and balcony spill plumes is provided in Fig. 51.11. The results from both Equations 51.30 and 51.31 are depicted in Fig. 51.11 and are the reason for the points of inflection at a clear height of 15 m. The heat release rate for both fires is a steady state 5000 kW, and H is 3 m for the balcony spill plume. For short heights, the smoke production

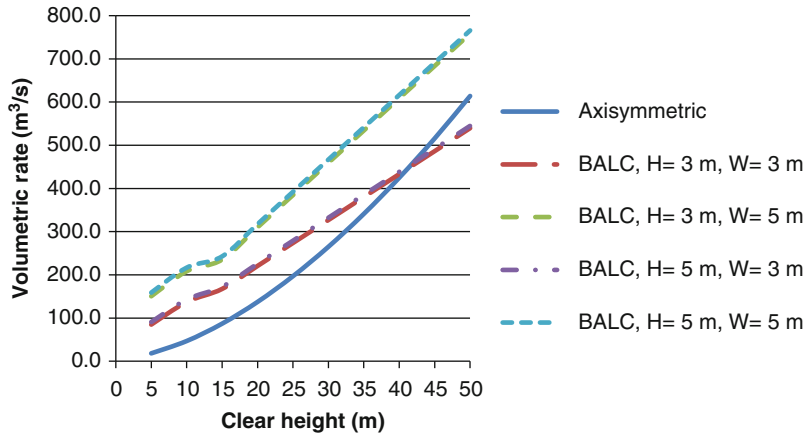

Fig. 51.11 Comparison of smoke production rate for axisymmetric and balcony spill plumes

rate for the balcony spill plume is appreciably greater than that for the axisymmetric plume. However, with increasing height, the smoke production rates from the two plumes become comparable. Eventually, the two curves intersect, suggesting that, at some height, the balcony spill plume behaves in the same manner (i.e., produces the same amount of smoke) as an axisymmetric plume. The point of intersection can be determined by setting the mass flow in Equation 51.27 equal to that in Equation 51.30.

The width of the plume, W, can be estimated by considering the presence of any physical vertical barriers attached to the balcony. The barriers act to restrict dispersion of the horizontal flow of smoke under the balcony. However, in the absence of any barriers, an equivalent width can be defined, based on results from visual observations of the width of the balcony spill plume at the balcony edge from the set of small-scale experiments by Morgan and Marshall [35]. The definition of an *equivalent confined plume width* is the width that entrains the same amount of air as an unconfined balcony spill plume. The equivalent width is evaluated using the following expression

$$L = w + b \tag{51.32}$$

Properties of Smoke Layer

Properties of the smoke layer are of interest both during the filling period of the fire and during the vented period. During the filling period, determination of the smoke layer properties is important to assess the level of hazard prior to actuation of a mechanical smoke control system. During the vented period, smoke layer properties are of interest to assess the level of hazard associated with those cases where occupants are exposed to smoke (i.e., the highest walking level is submerged in the smoke layer). The smoke layer properties of interest include temperature, light obscuration, and gas species concentration.

Temperature Rise in Smoke Layer The temperature of the smoke layer can be determined based on an energy balance for the volume of the smoke layer. Energy is supplied to the layer by the fire. Energy may be lost from the layer to the enclosure (walls, ceiling) of the space. During the filling period, the resulting expression is [1].

$$T = T_o \exp\left(\frac{(1-\chi_l)Q}{Q_o}\right) \tag{51.33}$$

Estimates for χ_l (heat loss fraction from the smoke to enclosure) vary appreciably. Some of the design guides suggest assuming that the smoke layer is adiabatic (i.e., setting $\chi_l = 0$), in order to be conservative [1]. Walton suggested values for χ_l between 0.6 and 0.9 for relatively small spaces of near cubic shape [36]. In many of the large spaces with tall ceiling heights, the temperature rise anticipated for the smoke layer is relatively modest such that convection and radiation heat transfer to an

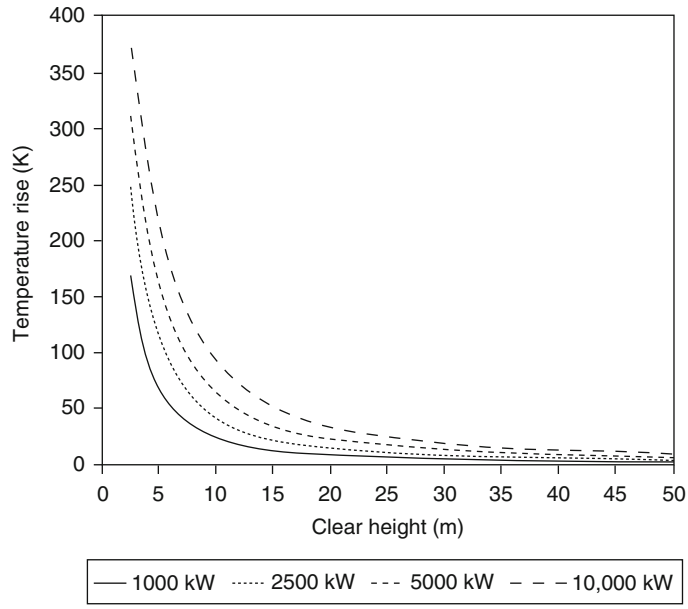

Fig. 51.12 Temperature rise of smoke layer for axisymmetric plumes

enclosure will also be modest. Consequently, in such applications, the adiabatic assumption will provide reasonable predictions of the temperature rise. However, in low ceiling spaces (under approximately 10 m) the temperature may be significantly overestimated by applying the adiabatic assumption.

Similarly, the equilibrium smoke layer temperature during venting can be approximated by applying an energy balance to the smoke layer. In this case, energy is also lost from the layer due to smoke being exhausted from the atrium. Equation 51.34 can be used to determine the temperature rise of the smoke layer under adiabatic conditions.

$$\Delta T = \frac{(1-\chi_l)\dot{Q}_c}{c_p \dot{m}} \tag{51.34}$$

If the adiabatic assumption is applied, the smoke layer temperature will be overestimated, providing a conservative estimate of the hazard. In reality, some heat is lost from the upper smoke layer to the surrounding walls and ceiling. However, no elementary method is available to estimate the overall proportion of heat that is lost to the surroundings [37, 38]. Some zone and field computer fire models account for heat losses to the boundary, thereby avoiding the need to specify the heat loss fraction [19, 39]. The adiabatic smoke layer temperature for a range of fire sizes is presented in Fig. 51.12.

The degree of overestimation can be assessed by comparing the estimated smoke layer temperature with the plume centerline temperature. For thermodynamic reasons, the smoke layer temperature cannot exceed the plume centerline temperature. The plume centerline temperature, T_c, can be evaluated using Equation 51.35 [40]

$$T_c = 0.08 T_o \dot{Q}_c^{2/3} z^{-5/3} + T_o \tag{51.35}$$

The volumetric venting rate for other heat release rates or temperature rises may be determined using Equation 51.36 considering that the specific heat is virtually constant for the expected temperature range of interest

$$\frac{\dot{Q}_{c_1}}{\dot{Q}_{c_2}} = \frac{V_1}{V_2}\frac{\Delta T_{\mathrm{ad}_1}}{T_{\mathrm{ad}_2}}\frac{T_2}{T_1} \tag{51.36}$$

As can be observed from Equation 51.36, doubling the volumetric venting rate for the same size fire reduces the temperature rise by approximately 50 % (the temperature rise is not precisely halved, since the absolute temperature of the smoke layer in both instances is not exactly the same).

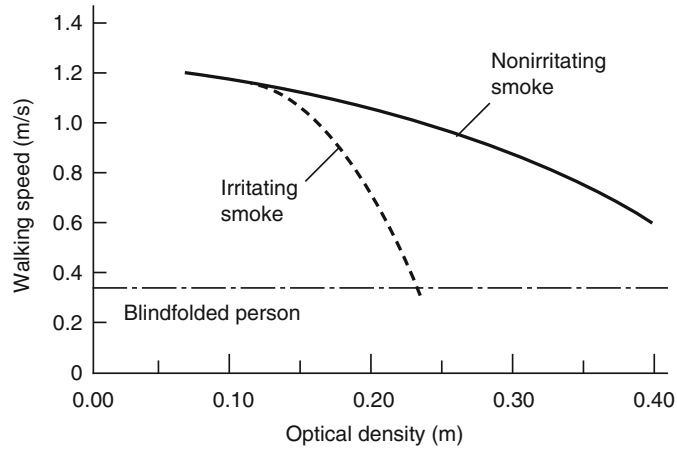

Fig. 51.13 Relationship between visibility through smoke and walking speed

Light Obscuration The visibility distance through smoke can be related to the optical density per unit pathlength via empirical correlations [41, 42]. The experimental basis for the correlations consists of tests with humans viewing objects through smoke. However, the participants were not directly exposed to the irritating effects of smoke. Consequently, the reported correlations are likely to overestimate the visibility distance.

In addition to the light obscuration quality of the smoke, the visibility of an object is dependent on the light source for the object being viewed as well as ambient lighting conditions [42, 43].

The optical density of the smoke layer can be determined considering that all of the particulates generated by the fire are transported to the layer via the plume and accumulate in the layer. Such an approach neglects any deposition of soot on enclosure surfaces, thereby overestimating the optical densities. The expressions for the smoke filling and vented periods are provided as Equations 51.37 and 51.38 [16].

$$\text{Smoke filling}: \quad D = \frac{D_m Q}{\chi_a H_c A (H - z)} \tag{51.37}$$

$$\text{Vented}: \quad D = \frac{D_m \dot{Q}}{\chi_c \Delta H_c \dot{m}/\rho} \tag{51.38}$$

The mass optical density is dependent on the fuel, burning mode, ventilation conditions, and operation of sprinklers. The mass optical density can vary by orders of magnitude for different ventilation conditions.

Although a reduction in visibility is not directly life-threatening, it does reduce the walking speed of individuals, thereby increasing the exposure time to toxic gases and elevated temperatures. In addition, the reduction in visibility may lead to an increased susceptibility to occupants tripping or falling. The relationship between visibility and movement speed is indicated in Fig. 51.13.

Carbon Monoxide Concentration The concentration of gas species contained in the smoke layer can be determined considering that all of the mass that is supplied to the layer via the plume accumulates in the layer. No absorption by the enclosure is assumed. The resulting expressions for the smoke filling and vented periods are [16].

$$\text{Smoke filling}: \quad \Upsilon_i = \frac{f_i Q}{\rho_o \chi_a H_c A (H - z)} \tag{51.39}$$

$$\text{Vented}: \quad \Upsilon_i = \frac{f_i Q}{\dot{m} \chi_a H_c} \tag{51.40}$$

In order to express the gas species concentration in units of ppm, Equation 51.41 needs to be applied

$$ppm_i = \frac{MW_{\text{air}}}{MW_i}\gamma_i \times 10^6 \qquad (51.41)$$

Input for evaluating the gas species concentration includes the yield fraction and heat of combustion, both of which are fuel dependent parameters. The yield fraction is dependent on the burning mode and oxygen concentration. Most of the information tabulated on the yield fraction, such as that by Khan (see Chap. 36), assumes well-ventilated, flaming combustion. Most of the fires of interest in large spaces will involve flaming combustion and are likely to be well ventilated. However, fires in small, connected spaces may become underventilated. Caution needs to be exercised in properly identifying ventilation conditions when predicting these parameters because the yield fraction can vary by orders of magnitude for different ventilation conditions. Also, the yield fractions noted by Tewarson are relevant only to cases where sprinklers are not operating [44].

Example 7 Estimate the steady-state smoke layer properties (temperature, visibility to an internally illuminated exit sign, and CO concentration) during the vented period, given the following situation:

1. The smoke layer interface is maintained 35 m above floor level.
2. The rate of heat release of the flaming fire is a steady state 5000 kW.
3. The fuel is comprised principally of polyurethane foam.

SOLUTION *Smoke Layer Temperature*
Equation 51.34 can be applied to determine the adiabatic smoke layer temperature rise. In Example 5, a mass rate of smoke production of 410 kg/s was determined. Thus, assuming an adiabatic smoke layer, a convective heat release rate fraction of 0.7 and specific heat of air of 1.0 kJ/kg·K, the temperature rise is 8.5 °C.

Visibility Visibility during the vented period is estimated using Equation 51.38. Fuel-related parameters are obtained in Chaps. 36, 24.

$$D_m = 260\ \text{m}^2/\text{kg}$$
$$H_c = 12,400\ \text{kJ/kg}$$

Considering smoke layer density, ρ, at the temperature of the smoke layer to be 1.17 kg/m^3, the optical density is 0.32 m^{-1} and the associated visibility is 8.5 m.

CO Concentration CO concentration for the vented period is estimated using Equations 51.40 and 51.41, with the fuel-related properties again evaluated from, Appendix C.

f_{CO} for polyurethane is ~ $0.030\text{kg}_{\text{co}}/\text{kg}_{\text{fuel}}$

The resulting CO concentration in the smoke layer is 31 ppm.

Comparison of Mechanical Exhaust and Natural Venting Designs

Design Aspects of Mechanical Venting Systems

Most smoke control systems for covered malls and atria in the United States use mechanical venting systems. Mechanical venting systems need to be designed to exhaust the amount of smoke needed to satisfy design objectives. The volumetric flow of smoke needs to be adjusted for temperature, using the methods discussed previously in this chapter.

Mechanical exhaust systems are relatively immune to environmental effects because the energy associated with the fan is able to provide a sufficient force for smoke movement and, thus, is not relying as much on the buoyancy of the smoke or stack effect. Protection from wind effects can be accommodated by hardware.

Response time is a principal limitation for mechanical exhaust systems. The response time is the sum of the time for detection and the time for the system to reach capacity (which may be up to a minute). This combined time may be longer than the time for the smoke layer to reach the critical height established by design goals. Also, because the capacity of a mechanical venting system is sized considering a particular

size of design fire (see Equations 51.26, 51.27, 51.30 and 51.31), if an actual fire has a greater heat release rate than considered in the design, the capacity of the mechanical exhaust will not be sufficient.

In addition, mechanical exhaust systems are susceptible to plugholing, a situation in which a hole is created in the smoke layer below the exhaust inlet by a high-capacity exhaust system. This results in a reduction in efficiency of the exhaust system because air from beneath the smoke layer is being extracted, thereby the desired quantity of smoke is not being extracted, causing the smoke layer to deepen. Plugholing is addressed later in this chapter.

The limitations of mechanical venting systems can be overcome in some cases by providing detection devices that minimize the time required for detection and by using several small capacity exhaust fans to avoid plugholing. However, despite these measures, it is still possible that design goals will not be able to be achieved by mechanical venting designs. Thus, the feasibility of such goals may need to be evaluated. Alternative smoke management approaches may be sought, for example, providing physical barriers at upper levels to reduce the required clear height or considering opposed airflow at openings above the design smoke layer interface position.

Design Aspects of Natural Venting Systems

Natural venting removes smoke by taking advantage of the buoyancy of the smoke. In the United States, natural venting systems are primarily found only in facilities such as industrial or warehouse structures. Outside of the United States, natural venting is often utilized in many applications.

The key advantages of natural venting systems are the self-correcting aspect of the vents in case the design fire is inappropriately defined and the simplicity of the operation of natural vents. These advantages will be described as part of the continuing discussion in this section.

The engineering principles that apply to vent operation addressed in this section consider the scenarios depicted in Fig. 51.14. Because smoke filling along the underside of the ceiling in a curtained area is similar to that in a compartment, additional information on compartment fire scenarios is presented in Chap. 33. If the draft curtains are deep enough, they can be thought of as simulating the walls of a single compartment.

The description of engineering principles of natural vents will be provided from the perspective of a two-layer zone model. The overall building compartment is assumed to have near-floor inlet vents that are large enough to maintain the area below the smoke layer at outside-ambient conditions. The upper smoke-layer thickness will change with time, but at any instant it is assumed to be uniform in space, with absolute temperature, T, and density, ρ.

Mass and energy are transferred continuously to and from the upper and lower layers. Conservation of energy and mass along with the Ideal Gas Law is applied to the layers, which leads to equations that require estimates of components of heat transfer, enthalpy flow, and mass flow to the layers. Qualitative and some key quantitative features of these phenomena are described and presented below. The reader is referred to Chap. 15, for a general discussion on the topic of flow through vents. Considering a vent in a wall or ceiling, flow is driven through such a vent mainly by cross-vent hydrostatic pressure differences from the high- to the low-pressure side of the vent. The traditional means of calculating vent-flow rates is by using an orifice-type flow calculation.

Assuming relatively quiescent conditions in the areas on both sides of the vent, the pressure in each space can be described as the hydrostatic pressure. The mass flow through a vent is derived from Bernoulli's equation, where the buoyancy pressure is related to the dynamic pressure at the vent:

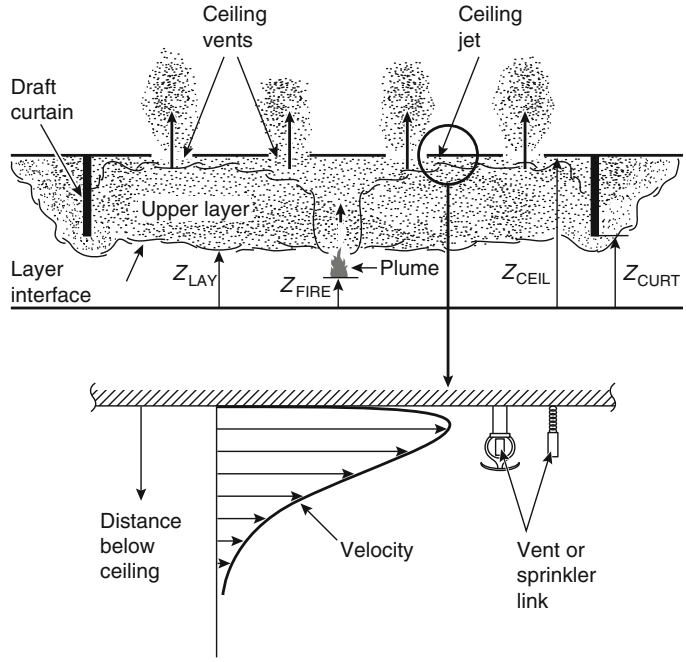

Fig. 51.14 Fire in a building space with draft curtains and ceiling vents

$$\frac{1}{2}\rho_o \mu^2 = \Delta\rho g d \qquad (51.42)$$

where
ρ = Density of smoke (kg/m^3)
ρ_o = Density of ambient air (kg/m^3)
$\Delta\rho = \rho_o - \rho$ (kg/m^3)

Relating the mass flow through the vent to the velocity of the gases

$$\dot{m} = \rho A_v u \qquad (51.43)$$

where
$\dot{m}$ = Mass flow rate through vent (kg/s)
A_v = Flow area of vent (m^2)

Replacing the densities with temperatures using the ideal gas law:

$$\dot{m} = \left(2\rho_o^2 g\right)^{1/2} \left(\frac{T_o \Delta T}{T}\right)^{1/2} A_v d^{1/2} \qquad (51.44)$$

As indicated in Equations 51.42–51.44, the capacity of natural vents is related to the pressure difference caused by the buoyancy of the smoke layer. As such, the flow rate of smoke through the vent increases with increasing smoke-layer temperature and depth.

$$\dot{m} = \left(2\rho_o^2 g\right)^{1/2} \left(\frac{T_o \Delta T}{T^2}\right)^{1/2} \frac{A_v d^{1/2}}{\sqrt{1 + \frac{C_{d,v}^2 A_v^2 T_o}{C_{d,i}^2 A_i^2 T_o}}} \qquad (51.45)$$

For vents installed in sloping roofs, the design position of the smoke layer should be at least below the bottom of the vent. To ensure that only smoke is exhausted from that vent and not any air from below the layer, the smoke layer position should be at least 10 % of the vertical distance from the top of the vent (Fig. 51.15). Then the distances d and z (recall that clear height is imbedded in the consideration of $\dot{m}$) are measured from the center of the vent.

Makeup Air Supply The effect of the inlet area on the flow rate through the vent can be assessed by recognizing that the pressure drop across the inlets associated with the inflow of replacement air must be subtracted from the buoyancy pressure causing the gases to flow through the vents. The effect of inlet pressure may be included in Equation 51.45 by replacing A_v by an effective vent area $\left(A_v^*\right)$ where

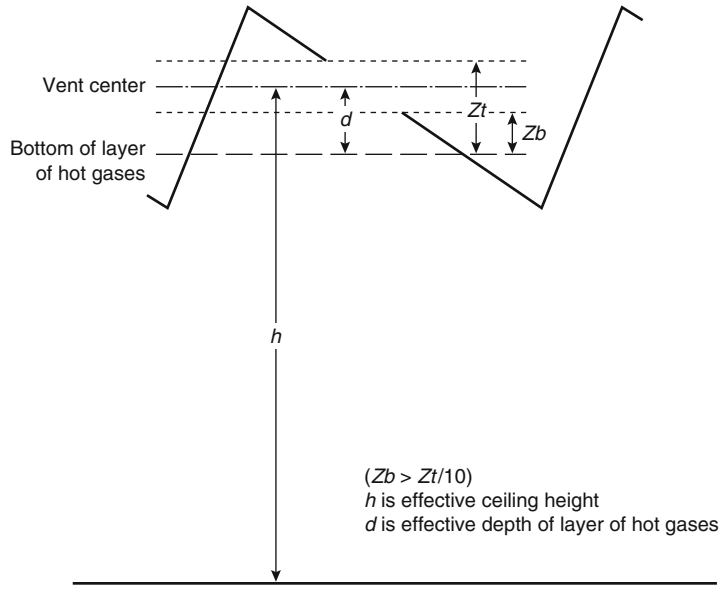

Fig. 51.15 Design position of gas layer versus vent

$$\frac{1}{A_v^{*2}} = \frac{1}{A_v^2} + \frac{1}{A_i^2}\left(\frac{T_o}{T}\right) \tag{51.46}$$

As such, the ratio of the actual vent area to the effective vent area, K, is given as

$$K = \frac{A_v}{A_v^*} = \left[1 + \left(\frac{A_v}{A_i}\right)^2 \frac{T}{T_o}\right]^{1/2} \tag{51.47}$$

The effect of vent ratio (ratio of outlet to inlet areas) on the effectiveness of natural venting is presented in Fig. 51.16 with a design fire of 2.5 MW and a ceiling height of 15 m. As indicated in the figure, with a vent ratio of 0 (having infinite inlet area), the clear height is slightly greater than when the outlet to inlet areas are equal. Thus, as with mechanical systems, the inlet area is an important consideration.

One of the principal advantages of natural venting systems is the relative insensitivity of the equilibrium smoke-layer position with the fire size, as indicated in Fig. 51.15. The graphs in Fig. 51.17 indicate that for two different ceiling heights (15 and 30 m), the equilibrium smoke-layer temperature is virtually identical for the two significantly different fire sizes. This similarity is due to the bigger fire size producing a smoke layer with a greater temperature. The hotter smoke will be more buoyant, thereby increasing the buoyancy force at the vent leading to an increase in the mass flow rate through the vent to reduce the amount of smoke accumulating under the ceiling.

The ability of a vent to perform similarly for two different fire sizes is a significant benefit of natural vents. Unlike mechanical exhaust, for natural vents if an error is made such that an actual fire is greater than the defined "design fire," the natural vents should still able to provide near-satisfactory performance.

Limitations The limitations of natural venting systems are related to the forces affecting smoke movement: principally a lack of buoyancy and wind effects. The smoke must be buoyant relative to the ambient environment in order for natural venting systems to be effective. Smoke may lose its buoyancy either due to cooling from sprinkler operation or dilution from entrained, cool air. Because the mass flow is strongly dependent on the difference in the smoke-layer temperature and outdoor temperature, if the smoke-layer temperature rise is only slightly different than the ambient temperature, then the flow from a vent will also be modest. As such, in tall spaces with relatively small fire sizes, the

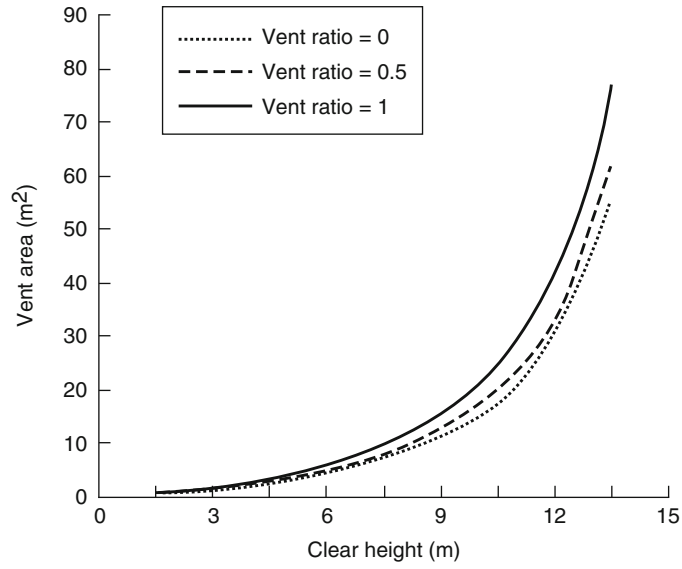

Fig. 51.16 Effect of vent ratio on natural venting

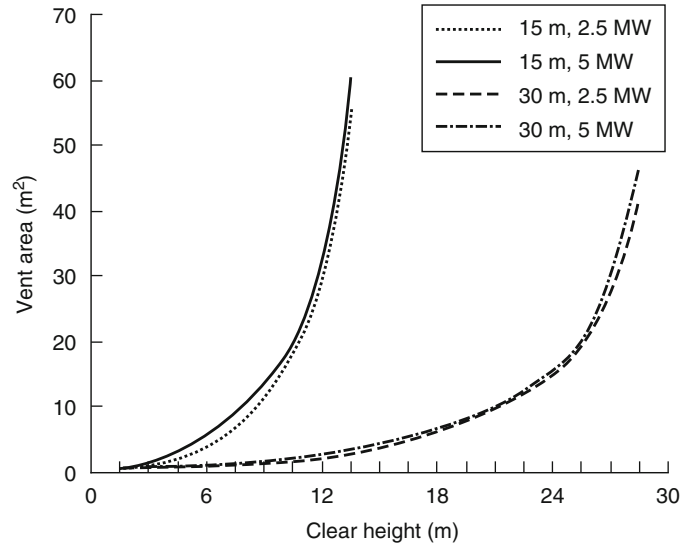

Fig. 51.17 Effect of vent ratio on natural venting for two ceiling heights (15, 30 m) and fire sizes (2.5 MW, 5 MW)

modest capacity of natural vents may constrain the ability to achieve design objectives, necessitating that mechanical ventilation be used.

To consider the effect of outside wind conditions, pressures on the outside of the building in the vicinity of the vent need to be assessed. The pressure on the building depends on the wind speed at the elevation of the vent, wind direction relative to the outside building geometry, and proximity and geometry of neighboring buildings. Wind effects on buildings are addressed in Klote et al. [2].

If the building vents are open and if vent areas are relatively small compared to the building surface area, then pressures near the vent openings will be substantially unchanged from the above-mentioned, closed-vent pressure distribution, except near any local through-vent flows that may develop. Also, although the

exterior pressures generally vary from vent to vent, they will be relatively uniform for any particular vent. Under these conditions, a determination of flow rates into and/or out of vents and through the interior of the building is based on an interior building flow analysis, with pressure-specified boundary conditions at the open vents.

A Single, Open Inlet Vent or Multiple Openings at the Same Pressure If there is only one open inlet vent on the upwind side of the building that experiences a relatively high pressure differential above the local hydrostatic pressure or if there are several open vents, all at locations on the outside surface of the building where pressures are substantially identical, then, the wind will have no effect on the inflow or outflow through the vents. Thus, if the air inside the building is uniformly at the outside air temperature and if there is no mechanical ventilation, then the effect of the wind will be simply to bring the interior hydrostatic pressure at the location of the vent(s) to the aerodynamic-flow-specified value; the interior of the building will be "pressurized" as a result of the open vent(s), but there will be no wind-induced interior flows. If there is a fire in the room with the open vent (e.g., the vent is a broken window), then, in the usual way, there will be fresh air inflow into the room toward the bottom of the vent and buoyant smoke outflow toward the top of the vent, all this taking place at an aerodynamic-flow-specified, elevated hydrostatic pressure within the room.

If the open vent is in a side of the building with a negative wind coefficient (e.g., facing downwind or on roofs near the upwind side), the pressure at the vent will be relatively low, and the local hydrostatic pressure will be *reduced* by an amount only on the order of $\rho_o u^2/2$. Again, no wind-induced flow at the vent is expected.

Two Inlet Vents, One on the Upwind Side and One on the Downwind Side of the Building If there are two inlet vents in the walls of the building, one upwind and one downwind (ignoring heating and mechanical ventilation), then there *will* be wind-induced flow through the vents and within the building. Inlet air will be provided at the high-pressure upwind vent and outlet air at the low-pressure downwind vent, with levels of through-vent flows and of interior hydrostatic pressures determined by an appropriate analysis that accounts for conservation of momentum (i.e., Bernoulli's equation) and mass at the exterior vents and at room-to-room vents within the interior of the building. The changes in hydrostatic pressures within the rooms of the building, over and above the hydrostatic pressures that would be present in a quiescent environment, would be somewhere between the wind-induced pressures at the locations of the high-pressure vent and the low-pressure vent.

Wind-Modified Pressures at Roof Surfaces and Wind-Modified Action of Ceiling Vents Roof surfaces of flat-roofed buildings tend to have negative, wind-induced pressure coefficients, unless the buildings are very long in a direction parallel with the wind direction. Sloping roofs may have pressure coefficients that can be positive or negative, depending on wind direction. Therefore, if the interior, wind-induced hydrostatic pressures are greater than those associated with a quiescent environment (e.g., the result of open vents in the upwind side of the building), then the flow of smoke through ceiling vents can be enhanced significantly by virtue of increased, favorable, cross-vent pressures. However, for reduced interior pressures (e.g., as a result of open vents on the downwind side of the building), the effect of wind conditions can substantially disrupt the desired smoke-removing action of ceiling vents, even reducing the *direction* of the cross-vent pressures and, as a result, the direction of the flow through the vents (i.e., making the flow travel from the outside to the inside).

Thermal Activation of Vents

Convective heating and thermal response of near-ceiling-deployed fusible links or other near-ceiling thermal sensor devices (including thermoplastic vent covers designed to soften

and "drop out" at specified actuation design temperatures) are determined from the local time-dependent distributions of ceiling jet velocity and temperature. These distributions will depend on vertical distance below the ceiling and radial distance from the fire-plume axis. Once the operating temperature of the thermal element is reached, the device or devices operated by the element will be actuated. Characteristics of ceiling jets are described in Chap. 14.

The mathematical fire model LAVENT (fusible-*L*ink-*A*ctuated *VENT*s) [22–24] was developed and is available to simulate most of the phenomena described above. The LAVENT model can be used to simulate on a time-dependent basis and to study parametrically a wide range of scenarios with natural vents. Full documentation for LAVENT, including its theoretical basis [22], a user guide for the computer code [23], and sample problems using the code are included in Annexes B, C, and D of NFPA 204 [45]. In its current form, LAVENT does not account for wind effects, the reduced effectiveness of vents as a result of limited-area inlet vents, or the presence of mechanical systems [22]. Input data on the thermal response characteristics of the link will be needed for such an analysis. The use of LAVENT has not been validated for estimating the response of "drop out" vents.

Sprinklers and Vents

Vents and sprinklers provide different fire safety benefits. The level of fire safety in a facility would be enhanced if both sets of benefits could be achieved systematically. However, simply providing the two technologies following design rules independent of each other will not necessarily lead to a combination of their respective benefits. Potential problems may occur as a result of the interaction of the two technologies (i.e., operation of the smoke and heat vents can modify sprinkler performance and the operation of the sprinklers can modify smoke and heat vent performance). As an example of the latter, consider the case in which water spray from a sprinkler system cools the smoke, thereby reducing the buoyancy of the smoke. The reduced buoyancy reduces the mass flow rate through a vent, thereby resulting in a deeper smoke layer. However, the sprinkler discharge can also dramatically reduce the fire size resulting in a decreased production of smoke.

Numerous research projects have been conducted to address the interaction between vents and sprinklers (see Annex A of NFPA 204 and Beyler and Cooper [46] for a thorough review of the previous research). The previous projects have sought to demonstrate the level of impact that one system has on the other's performance, either by indicating that it is always significant, always insignificant, or significant only if a particular set of conditions is provided. Projects have also attempted to identify design changes necessary if both systems are present (i.e., perhaps larger vent sizes could be installed in sprinklered buildings to counteract the reduced mass flow of cooled smoke). To date, none of the previous projects have been able to provide the conclusive results that provide definitive information illustrating the degree of influence that one system has on the other for all situations.

Past Studies of Combined Vent/Sprinkler Systems A review of 34 papers evaluated the validity of generic claims and counterclaims on the benefits of combined vent/sprinkler systems [46]. A listing of these claims and counterclaims and a summary of conclusions on their validity follow.

Claims and Counterclaims [46] In the literature, claims that have been made in favor of vent/sprinkler systems can be reduced to the following three:

1. Smoke and heat vents limit the distribution of products of combustion in the facility whether deployed sprinklers are operative or inoperative.
2. Smoke and heat vents decrease the number of activated sprinklers.

3. Smoke and heat vents assist the fire department in identifying the location of the fire within the facility and in reducing the need for manual roof venting.

In the literature, claims that have been made *against* vent/sprinkler systems can be reduced to the following four:

1. Smoke and heat vents cause enhanced burning rates.
2. Smoke and heat vents delay sprinkler activation.
3. Smoke and heat vents increase the number of activated sprinklers.
4. Smoke and heat vent flow rates are insufficient to realize any benefit.

Validity of Claims for and Against Combined Vent/Sprinkler Systems After evaluating reports of studies of combined vent/sprinkler systems, Beyler and Cooper [46] came to the following conclusions:

- Venting does not have a negative effect on sprinkler performance.
- If a fire is directly beneath a vent, activation of the first sprinklers may be delayed slightly, but there is no evidence that this delay will have a significant impact on overall sprinkler performance.
- Venting does limit the spread of smoke by removing smoke from the building near the source of the fire (within the curtained compartment of fire origin), improving visibility for building occupants while evacuating and for fire fighters during fire control operations.
- By limiting the spread of smoke and heat, venting reduces smoke and heat damage to the building.
- In the event that sprinklers do not operate, venting remains a valuable aid in controlling the fire manually.
- In many fires, current vent design practices, for example, those of NFPA 204 [45], are likely to limit the number of vents operated to one and, in successful sprinkler operations, vents may not operate at all.
- Design practices should use methods that ensure early operation of vents; vent operation should be ganged so that the benefit of roof vents is fully realized.
- When deployed with vents and draft curtains, a sprinkler design needs to take full account of draft curtains as obstructions to ceiling jet flows and sprinkler discharge.
- Draft curtains should be placed in aisles rather than over storage.

Considerations for the Design of Combined Vent/Sprinkler Systems Taking Beyler and Cooper's conclusions into account and drawing on current knowledge of basic physical phenomena involved in vent/sprinkler interactions, the design of combined sprinkler/vent systems should seek to satisfy the following general criteria:

1. A successful vent design, whether deployed with or without sprinklers, is one that leads to the benefits of improved visibility and safety during a fire by limiting the descent of the upper smoke layer to a specified height (i.e., eye level of occupants and fire fighters).
2. When draft-curtain compartmentation is included in the vent design, a significant additional possible benefit results from the smoke being contained within the curtained compartment of fire origin by action of the venting.

Interaction of Sprinkler Spray and Smoke Layer The action of sprinkler sprays on a smoke layer includes a combination of evaporative cooling and dilution of the smoke. Dilution occurs due to entrainment of the relatively cool and uncontaminated lower-layer gases and the upper layer by the spray [47–59]. Provided the sprinkler spray–reduced smoke temperature and associated loss of buoyancy are not too great, the effect of evaporative cooling of the smoke, even if accompanied by moderate sprinkler spray–driven mixing, could be offset by additional vent capacity. However, even without significant evaporative cooling, sprinkler spray–driven mixing action can be so significant that it leads to a precipitous increase in the volume of smoke and thus a deeper smoke-layer. If and when the latter vigorous mixing occurs, then even impractically large increases in vent capacity are unlikely to lead to any significant

improvement. The latter phenomenon is commonly referred to as *smoke logging*. As such, a vent design that is developed to meet the above general criteria must be based on an analysis that accounts for and avoids the phenomena of smoke logging.

There is experimental evidence that smoke logging can be controlled by venting [60], and a preliminary analysis to explain the phenomenon has been provided [47, 48]. Thus, it has been reported that "preliminary tests in [a] . . . large-scale mall . . . showed that, under some conditions, [a] . . . smoke layer could be brought down by a manually operated sprinkler spray, [and that] smoke logging then occurred rapidly, with a high smoke density at low level. However, under some conditions, the smoke layer was not disturbed by a sprinkler spray" [48].

Computer Simulations of Sprinkler Spray–Driven Cooling, Mixing, and Smoke Logging A computer model could be applied to address the issue of sprinkler spray–driven cooling, mixing, and smoke logging. However, the past experimental studies have not led to an understanding of the complex phenomena of sprinkler spray cooling and sprinkler spray–driven smoke transport and mixing that causes the temperature reduction that could be used as a basis for such a model. What is known through anecdotal accounts of visual observations is that spray-driven mixing and transport of an initially stable and growing upper smoke layer can and often does lead to onset of smoke logging, whereby the mixing actions of sprinkler sprays are so vigorous as to effectively and continuously mix any newly generated smoke from the fire plume with the smoke already present in the smoke layer to fill the entire space.

Analytic fire-modeling has been employed to assess a generic interaction of a downward-directed sprinkler spray and a two-layer fire environment can be used to resolve the above issues [59]. The model simulated the action of the sprinkler spray, including the effects of evaporative cooling and the spray-driven mixing of the elevated-temperature, upper smoke layer and the relatively cool and uncontaminated lower layer. The analysis led to the identification of six possible modes of sprinkler/layer interaction [58, 59]. The mode that prevailed at any time during the development of a particular fire was found to depend mainly on the thickness and temperature of the upper smoke layer and on the momentum, spread angle, and characteristic droplet size of the sprinkler spray. In any particular fire scenario, the action of open vents and/or draft-curtain compartmentation could provide some control of the thickness and temperature of the layer and, therefore, of sprinkler/layer interactions that prevail.

Of the six above-referenced modes of sprinkler/vent interaction, four were found to be particularly favorable in the sense that they would *maximize* the success of a combined sprinkler/vent design. Thus, with proper vent design the favorable modes could lead to the desired control of the smoke-layer depth while minimizing smoke mixing to the lower layer to the point that any smoke there is only in a highly dilute state. Thus, for a given set of sprinkler spray characteristics, if the smoke layer is kept relatively thin and/or not too buoyant (i.e., its temperature is not too high), then the rates of both mass and enthalpy flow entrained into the upper-layer part of the sprinkler's "spray cone of influence" would be relatively insignificant compared to the corresponding rates associated with the fire-plume flow to the upper layer. In the early part of a typical fire scenario and immediately subsequent to one or more rapid-response sprinkler discharges, the condition of a relatively thin and not-too-high-temperature upper smoke layer should be prevalent. As a result, the combined action of cooling and momentum exchange in the spray cone would be strong enough to transport the entrained smoke through the layer interface and well into the depth of the lower layer to be mixed eventually, with negligible consequences, into the rest of the lower-layer gases.

In contrast to the above, there were two particularly *unfavorable* modes of sprinkler/vent interaction that would *minimize* the likely success of a combined sprinkler/vent design. These configurations could lead to relatively vigorous

mixing between the smoke layer and the lower layer, leading to a rapid growth of the upper smoke layer and possibly to smoke logging.

Resolving the Problem of Sprinkler Skipping and Vent Skipping In terms of achieving vent/sprinkler design objectives, it is important to identify a possible means of resolving problems associated with the phenomena known as *sprinkler skipping* and *vent skipping*.

If ceiling jet–convected water droplets strike a sprinkler link or bulb, then, because of effects of evaporative cooling, there will be a significant reduction of its rate of heating, which can lead to a significant delay in sprinkler discharge. It is the resulting, unpredictable, and deleterious delay in sprinkler discharge that is referred to as *sprinkler skipping*.

Although research has been conducted to characterize the spray from sprinklers, a general description of all aspects of the spray is beyond the current state of knowledge. Such a description would be needed to provide a reliable model that can be used to predict the phenomenon.

Accounting for Sprinkler Skipping and Vent Skipping in Design In the design of sprinklers without vents, the effects of sprinkler skipping on the ability of a sprinkler system to control a fire are taken into account by the empirically based design standard, NFPA 204. In contrast, when vents and sprinklers are used *together,* the random and unpredictable effects of vent skipping are not accounted for in the design of automatic vent systems as outlined in NFPA 204.

In terms of combined vent/draft-curtain designs, and as an alternative to traditional automatic, fusible-link-actuated vents, which could involve the problem of vent skipping, a more controllable and reliable means of ensuring timely and effective vent action is available. One generic possibility would involve *ganging,* that is, opening together all or most vent units in the compartment of fire origin [61]. A ganging strategy that could be well integrated into a reliable, consensus sprinkler/vent design is one in which all vents of the fire compartment are ganged to open together immediately following first sprinkler discharge.

A Consensus Approach to the Design of Combined Sprinkler/Vent Systems

Using Mathematical Fire Models to Achieve Design Objectives The above discussion indicates that effective sprinkler/vent systems are feasible and that mathematical fire models with a proven capability for simulating sprinkler/smoke interactions can be used as the basis for a consensus approach to identify and establish effective sprinkler/vent system designs.

The capabilities of mathematical models to simulate sprinkler/smoke interactions have been reviewed [62, 63]. The models considered were those that are complete (i.e., they can simulate both isolated sprinkler/smoke interactions and full fire scenarios, where the latter would be used to establish the success of sprinkler/vent designs). Both zone-type and field model–type simulation approaches were found to be applicable for addressing the problem. In the usual way, the two approaches are complementary in the sense that the zone model approach is more applicable and appropriate for parametric studies and as a practical design tool and the field model approach is more applicable for simulating and studying the details of specific scenarios, for example, the discharge sequence of sprinklers and the effectiveness of a vent design where draft curtains are almost directly above the fire.

A sprinkler/vent design approach that uses zone-type fire model simulations might involve application of an advanced version of LAVENT that would include the sprinkler/smoke-interaction simulation model [59] discussed earlier. A successful preliminary implementation of this approach, with a revised prototype model called LAVENTS (fusible *L*ink-*A*ctuated *VENT*s and *S*prinklers), has already been presented [64]. Applications of the LES (*L*arge *E*ddy *S*imulation) model [65–68], the JASMINE model [69, 70], and others [71, 72] have also been reported.

One of the difficulties in applying the above for design applications is the limited availability of input data to describe the initial sprinkler spray from a wide range of sprinklers and the response characteristics of the vent.

A Set of Example Guidelines for Design of a Consensus Sprinkler/Vent System As a summary to the above discussion, the following example guidelines are provided for the design of a sprinkler/vent system.

1. Establish the sprinkler design in the traditional way; that is, develop design parameters using full-scale testing involving effective, rapid, sprinkler-activation strategies in the absence of vents (in this context, "rapid" means that the design problem involves an effectively unconfined ceiling where smoke-layer buildup is negligible and does not affect the timing or sequence of early sprinkler discharge).
2. Establish a vent design objective. In cases in which sprinkler action is expected to control the fire (i.e., the fire will not exceed a specified, maximum energy-release rate), the design objective for scenarios as shown in Fig. 51.13 might be for the vents to maintain indefinitely the smoke from spreading beyond the curtained compartment of fire origin (i.e., the smoke-layer interface does not descend below the bottom of the draft curtains). If the latter design objective is too ambitious or in cases in which sprinkler action is expected only to slow but not to stop the growth of the fire, then the design objective would be for the vents to maintain the smoke from spreading beyond the curtained compartment of fire origin for a specified time interval (e.g., the time expected for the fire department to respond and initiate an attack on the fire).
3. Adopt a practical/achievable strategy of early opening of all vents in the compartment of fire origin, e.g., ganged operation of all vents in the curtained compartment of fire origin based on and subsequent to first sprinkler activation.
4. Using a fire model with a proven capability of simulating the time-dependent interaction of sprinklers, vents, and draft curtains, develop a vent design that meets the established design objectives.

Special Conditions

There are some aspects of smoke control system design that involve special attention. These aspects, which affect actuation of active smoke control systems and the efficiency of exhaust fans, are the following:

- Intermediate stratification
- Confined flow
- Plugholing
- Makeup air supply

Intermediate Stratification

The upward movement of smoke in the plume is dependent on the smoke being buoyant relative to the surroundings. Delays in activation may be experienced where ceiling-mounted initiating devices are present if the air near the ceiling is warmer than the rising smoke [2, 73]. Dillon [74] reported measurements of the difference in ambient temperature from floor to ceiling to be on the order of 50 °C in some atria with glazed ceilings. A prefire, warm air layer may be created due to a solar load where the ceiling contains glazing materials. In such cases, the smoke will stratify below this warm air layer and not reach the ceiling. Early after ignition, the maximum height to which the smoke plume will rise depends on the convective heat release rate and the ambient temperature variation in the open space.

Algebraic correlations may be applied to address two situations (Fig. 51.18):

1. The temperature of the ambient air is assumed constant up to a height above which there is discrete increase in temperature associated with a layer of warm air. This situation may occur if the upper portion of a mall, atrium, or other large space is unoccupied so that the air in that portion is left unconditioned.
2. The ambient interior air within the large space has a constant temperature gradient

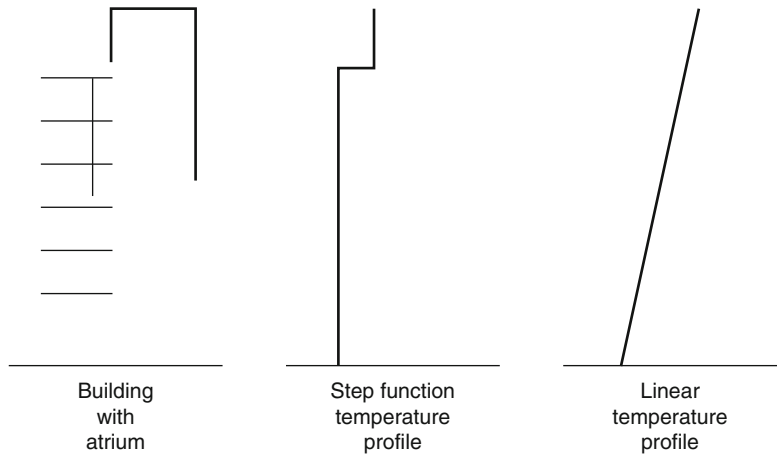

Fig. 51.18 Pre-fire temperature profiles

(temperature change per unit height) from floor level to the ceiling. This case is less likely than the first.

In the first case, where the interior air has a discrete temperature change at some elevation above floor level, then the potential for stratification can be assessed by determining the temperature of the plume at the height associated with the lower edge of the warm air layer. Where the plume centerline temperature is equal to the ambient temperature, the plume is no longer buoyant, loses its ability to rise, and stratifies at that height. One correlation for the plume centerline temperature was presented previously as Equation 51.35.

In the particular case where the ambient, pre-fire temperature increases uniformly along the entire height, the maximum plume rise can be determined from [19].

$$z_m = 3.79F^{1/4}G^{-3/8} \tag{51.48}$$

where

$$F = g\dot{Q}_c/\left(T_o\rho_o c_p\right)$$

$$G = -(g/\rho_o)d\rho_o/dz$$

Assuming standard conditions and that the smoke in the space behaves as an ideal gas, the expressions for F and G are

$$F = 0.0277\dot{Q}_c$$

$$G = 0.0335dT_o/dz$$

Because dT_o/dz is a constant, $\Delta T_o/H$ may be substituted for the derivative. Substituting the simplified expressions for F and G into Equation 51.48 yields [73].

$$z_m = 5.54\dot{Q}_c^{1/4}(\Delta T_o/H)^{-3/8} \tag{51.49}$$

By reformulating Equation 51.49 to solve for $\dot{Q}_c$, a minimum fire size can be determined that is just large enough to force the smoke to the ceiling of an atrium without prematurely stratifying due to the increasing ambient temperature.

$$\dot{Q}_c = 0.00118H^{5/2}\Delta T_o^{3/2} \tag{51.50}$$

The results of an analysis of intermediate stratification are presented in Fig. 51.19. In one case, a step function is assumed to provide a 30 °C change in temperature 15 m above the floor due to the upper portion of the atrium being unconditioned. For the other case, a temperature gradient of 1.5 °C/m is arbitrarily assumed in an atrium with a ceiling height of 20 m. Plume centerline temperatures from two size fires are graphed based on Equation 51.35. As indicated in the figure, for the case with the uniform gradient, smoke is expected to stratify

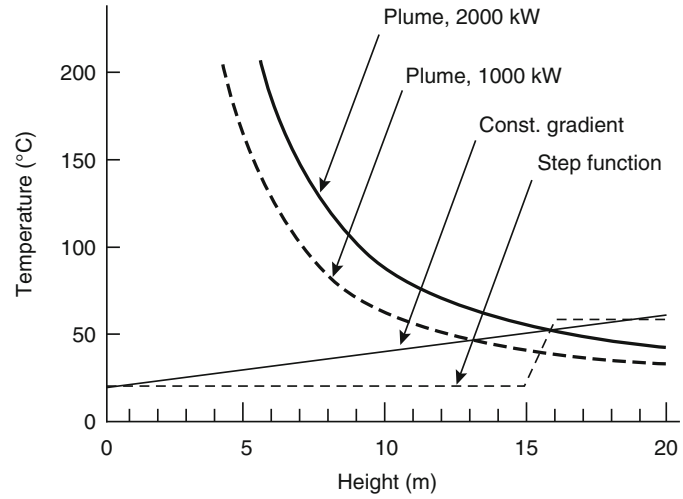

Fig. 51.19 Indoor air and plume temperature profiles with the potential for intermediate stratification

approximately 13 or 15 m above the floor, depending on the fire size. For the case involving the step function change in temperature, the smoke stratifies from both fire sizes at the height of the step change in temperature.

If the smoke is expected to stratify at an intermediate height below the ceiling, then a device other than ceiling-mounted detectors (such as projected beam detectors) needs to be considered to initiate the smoke control system. The beam detectors should be placed below the height of stratification to intercept the rising plume. In general, once the smoke control system operates, the warm air layer should be exhausted to permit the smoke to reach the ceiling.

Plume Width

As a plume rises it also widens as a result of the entrainment of additional mass into the plume. For tall, narrow spaces, the plume may fill the entire cross section of the atrium prior to reaching the ceiling. Above this position, air entrainment into the plume is greatly reduced due to the limited amount of air available. In such situations, initially the bottom of the smoke layer may be assumed to be located at this point of contact. Plume width is also important when determining the location of projected beam detectors intended to intercept the plume.

In order to determine the point of contact of the plume with the walls, the plume width must be expressed as a function of height. The width of the plume has been addressed theoretically and also experimentally.

Based on theory (see Chap. 13), the plume width is expected to be

$$d = 2.4\alpha z \tag{51.51}$$

where $\alpha \cong 0.15$

$$\text{Thus,} \quad d = 0.36z \tag{51.52}$$

Experimentally, the plume width is estimated by examining photographs [75] or the difference between the plume temperature and ambient temperature (i.e., temperature excess at various horizontal distances from the plume centerline) [30]. Using temperature measurements, the plume width is defined as the position where the temperature excess is one-half of the value at the centerline.

Handa and Sugawa [75] developed an empirical correlation of the width of the plume determined from photographs of the visual plume from wood crib fires

$$d = d_o z^{1/2} \tag{51.53}$$

Heskestad [76] noted that the visible plume diameter was greater than that determined from the temperature excess. Consequently, Heskestad

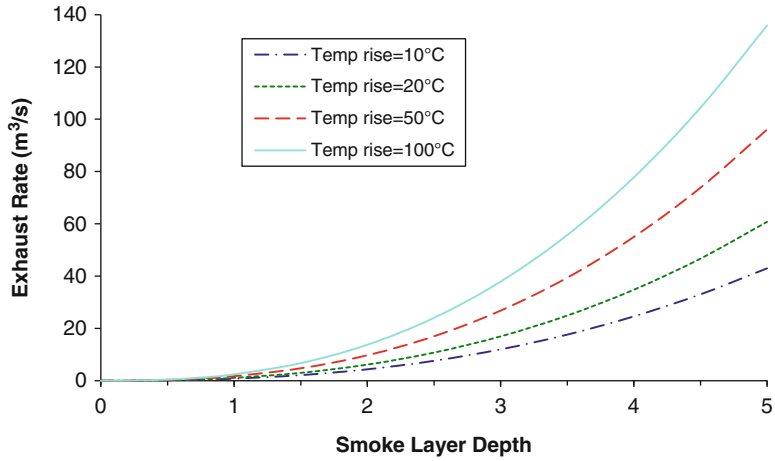

Fig. 51.20 Effect of smoke-layer depth and temperature rise on maximum exhaust capacity

estimated the visible plume diameter to be twice that determined by the excess temperature approach. Thus, the plume diameter is estimated as

$$d = 0.48\left(\frac{T_c}{T_o}\right)^{1/2} z \qquad (51.54)$$

As indicated in Equation 51.35, the plume centerline temperature decreases appreciably with increasing height. Thus, for tall spaces, the plume centerline temperature may be close to ambient. For example, at a height of 30 m with a fire size of 5000 kW and T_o of 293 K, T_c is 312 K. In this case $(T_c/T_o)^{1/2}$ in Equation 51.51 is only 1.03. Because of the rapid decline in T_c with increasing height, for engineering purposes $(T_c/T_o)^{1/2}$ can be approximated as being 1.0. Consequently, in many cases the total plume diameter may be approximated by considering the plume diameter to be approximately one-half of the height.

Considering the variety of analyses for plume width, the plume width is estimated to be 25–50 % of the height above the top of the fuel package, with the 36 % proportion from theory being near the middle of the range.

Plugholing

Plugholing occurs when the exhaust capacity at a single point is sufficiently large to draw air from the lower layer in addition to smoke. As such, less smoke is removed by the exhaust fans and a deeper layer results. Because a simple method to estimate the proportion of air drawn in from below the smoke layer by the fans is unavailable, an elementary method of estimating the smoke layer depth during plugholing is not available. As such, simple calculations can only be performed to assess the occurrence of plugholing, not the effect.

The original research on plugholing was done for natural vents. Recently, Lougheed and Hadjisophocleous demonstrated that the plugholing analysis for natural vents was also applicable to mechanical venting [77]. In order to avoid plugholing, the maximum exhaust capacity at an extract point is:

$$\dot{V}_{max} = 4.16\gamma d^{5/2}\left(\frac{\Delta T}{T_o}\right)^{1/2} \qquad (51.55)$$

Where γ is a factor relating to the location of the vent. If the vent is in the middle of the space, γ = 1 [1].

Results of applying Equation 51.56 are provided in Fig. 51.20 for a range of temperature rise values of the smoke. Where venting capacities greater than the maximum limit are needed to achieve smoke management objectives, multiple extract points need to be provided to avoid plugholing.

Assuming an axisymmetric plume, $\dot{m}$ can be replaced using Equation 51.20, and the smoke

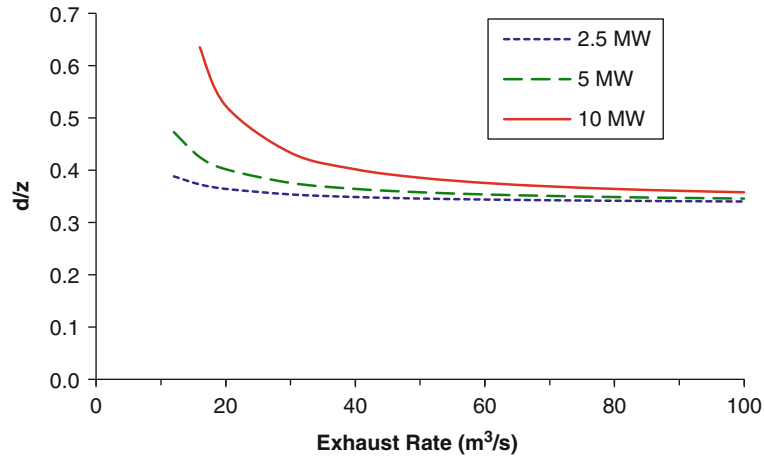

Fig. 51.21 Ratio of smoke-layer depth to clear height for single exhaust point

layer temperature can be replaced using Equation 51.34 (assuming adiabatic conditions) to express the minimum smoke layer depth in terms of the heat release rate and clear height as indicated in Fig. 51.21. For a single extract point, the minimum smoke layer depth is slightly less than 40 % of the clear height.

Makeup Air Supply

The makeup air supplied to the atrium should be

- Uncontaminated
- Introduced below the smoke layer
- Introduced at a slow velocity
- Supplied at a rate less than the required exhaust rate

Air that is not contaminated by smoke can be provided by locating intakes for the makeup air remote from the smoke exhaust discharge, preventing smoke feedback. To address the potential for smoke being introduced into the makeup air supply, a smoke detector should be provided to shut down the makeup air supply system. Selection of a smoke detector for this application should consider the operating conditions, range of temperatures, and installation within a duct.

All makeup air should be provided below the smoke layer interface. Any makeup air provided above the smoke layer interface merely adds mass to the smoke layer, which must be added to the required capacity of the smoke exhaust to prevent an increase in the smoke layer depth. If introduced near the smoke layer interface, the makeup air may increase the amount of mixing of clean air with the smoke to further add to the smoke layer.

Makeup air should be provided at a slow velocity so that the plume, fire, and smoke layer are not adversely affected. Makeup air supplied at a rapid velocity near the plume may deflect the plume to enhance the entrainment rate, thereby increasing the rate of smoke production. In addition, the burning rate of the fire may be increased by makeup air provided at an excessive velocity. Because the entrainment process induces an air velocity of approximately 1 m/s, the maximum makeup air velocity in the vicinity of the plume is often recommended to be 1 m/s. Because of the diffusion of air once past the diffuser, the makeup air velocity at the diffuser may be greater than 1 m/s.

Finally, the mass rate of makeup air supplied must be less than that being exhausted. Failure to follow this guideline may lead to the atrium being pressurized relative to the communicating spaces. Being at a positive pressure, smoke movement will be forced through any unprotected openings in physical barriers into the communicating spaces.

Limited Fuel

In some cases smoke management objectives may be fulfilled without a dedicated smoke control system due to the intrinsic qualities of the atrium. The intrinsic qualities of the atrium include parameters, such as the composition and quantity of fuel and geometry of the atrium. As an example, a limited amount of fuel may be present that is unable to sustain a fire for a sufficient period of time to create conditions beyond the allowable limits. The amount of fuel consumed during the time period of interest depends on whether the fire is steady or unsteady. In the case of a steady fire, the fuel mass consumed in a given period of time is determined as

$$\dot{m}_f = \frac{\dot{Q}_t}{H_c} \tag{51.56}$$

Alternatively, for an unsteady, t^2 profile fire, the fuel mass consumed during a given period of time is given as

$$\dot{m}_f = 333\frac{t^3}{H_c t_g^2} \tag{51.57}$$

When analyzing the inherent ability of the atrium to fulfill the smoke management design goals, the time period should relate either to the performance of a fire protection system or to the development of smoke layer conditions in excess of acceptable levels. For example, in life safety–oriented designs, the time period may be either that required for evacuation, or for untenable conditions to be generated, whichever is less.

Opposed Airflow

Opposed airflow refers to systems where airflow is provided in a direction opposite to the undesired direction of smoke movement. Opposed airflow may be used in lieu of physical barriers to prevent smoke spread from one space to another (i.e., between the communicating space and the atrium). Opposed airflow limits smoke flow by countering the momentum of the smoke attempting to enter the adjoining space. A minimum airflow velocity at all points of the opening must be provided in order to prevent smoke migration through the opening. Empirical correlations to estimate the minimum average velocity for the entire opening are available, based on limited experimental data [78]. The calculated average velocity is greater than the actual minimum velocity required at an opening to oppose smoke propagation to insure that the minimum critical velocity is achieved at all points, considering the effects of turbulence caused by the edges and corners of the opening.

The minimum average velocity to oppose smoke originating in the communicating space is evaluated using Equation 51.59.

$$v_e = 0.64\sqrt{\frac{gH(T_s - T_o)}{T_s}} \tag{51.58}$$

Alternatively, if the smoke at the opening is part of a rising plume that is rising along the side of the atrium wall, then Equation 51.60 is applicable.

$$v_e = 0.057\left(\frac{\dot{Q}}{z}\right)^{1/3} \tag{51.59}$$

The opposed airflow velocity should not exceed 1 m/s. Above that limit, the airflow velocity may deflect the plume away from the wall, making more plume surface area available for entrainment. The increased area for entrainment will enhance the smoke generation rate. Consequently, the problem of propagation to the communicating space may be solved by an excessive average velocity; however, other problems may be created by the increased smoke production rate and a possible increase in the depth of the smoke layer in the atrium. The volumetric capacity of the mechanical equipment required to deliver the necessary velocity for opposed airflow can be approximated as

$$V_{\text{oa}} = A_o v_e \tag{51.60}$$

If several openings are protected with the opposed airflow approach using the same

mechanical equipment, the cross-sectional area should be the sum of the areas for all of the openings. The opposed airflow technique may be infeasible due to the substantial amount of airflow capacity required to protect numerous openings having a large total area.

Where opposed airflow is utilized, the impact of the volume of air being introduced into the space with the fire must be assessed. For example, if the airflow is directed into the atrium and smoke exhaust equipment is also provided to maintain a constant position of the smoke layer interface in the atrium, then all of the additional air used for opposed airflow must also be exhausted. The additional air can be accounted for by increasing the required mass rate of exhaust in the atrium by the amount used for the opposed airflow. The additional air being exhausted will also affect the qualities of the smoke layer within the atrium (see Equations 51.34, 51.38, and 51.40). The smoke layer temperature, T_s(K), can be determined using Equation 51.61, based on an analysis included elsewhere [3].

$$T = 293 + \left[0.0018 + 0.072\dot{Q}_c^{-2/3} z^{5/3} + \frac{712 A_o \sqrt{H(T-293)}}{\dot{Q}_c T^{3/2}}\right]^{-1} \quad (51.61)$$

Equation 51.61 must be applied iteratively to determine the resulting smoke layer temperature. In cases with large clear heights, the temperature of the air used for the opposed airflow strategy will be virtually equal to the temperature of the smoke layer to permit the addition of volumetric rates of air rather than mass rates.

Alternatively, if airflow is directed from the atrium into a communicating space, the communicating space must also be exhausted, otherwise the communicating space will become positively pressurized.

Example 8 Considering the atrium from Example 5. There are five 5-m-wide × 2.5-m-high openings to the communicating space. The bottom of the openings is 30 m above the floor of the atrium. Considering a 5000 kW fire in the center of the floor of the atrium, determine the following:

1. Minimum airflow velocity required for opposed airflow
2. Volumetric rate of air supply for opposed airflow
3. Capacity of the exhaust fans in the atrium to maintain the smoke layer interface at an elevation 25 m above floor level and also to accommodate the additional air from the opposed airflow approach

Solution The minimum opposed airflow velocity can be determined using Equation 51.60. However, the temperature of the smoke layer, T, is unknown. Thus, Equation 51.61 must be applied first. Solving iteratively, T is approximately 305 K. The minimum airflow velocity is 0.20 m/s. The volumetric supply capacity for the opposed airflow strategy for all five openings is 12.5 m^3/s. The associated mass flow rate is 15.0 kg/s.

Without the opposed airflow, the mass rate of smoke exhaust required to maintain the smoke layer interface height in the atrium at a height of 25 m is determined using Equation 51.27 to be 236 kg/s. Thus, the combined mass exhaust rate necessary is 251 kg/s. This mass flow rate corresponds to a volumetric rate of 209 m^3/s.

As a practical issue, this exhaust rate should be compared to that required to keep the smoke layer interface above the top of the openings (i.e., 32.5 m above floor level). Based on Equations 51.27 and 51.29, the required volumetric exhaust rate is 362 kg/s. Thus, in this situation, the combined exhaust rate with the opposed airflow strategy is less than that associated with the strategy to keep the smoke layer interface above the opening.

Nomenclature

A	Cross-sectional area of the atrium (m^2)
A_o	Cross-sectional area of opening (m^2)
b	Distance from the store opening to the balcony edge (m)

C_{CO}	Volumetric concentration of carbon monoxide (ppm)
c_p	Specific heat (kJ/kg-K)
D	Optical density per unit pathlength (m^{-1})
D_m	Mass optical density (m^2/kg)
d	Plume diameter (based on excess temperature) (m)
d_o	Diameter of fire (m)
f_{CO}	Yield fraction of CO (kg_{CO}/kg_{fuel})
f_i	Yield fraction of species i (kg of species i per kg of fuel consumed)
g	Gravitational acceleration (9.8 m/s^2)
H	Height of ceiling above top of fuel surface (m)
H_b	Height of balcony above top of fuel surface (m)
H_c	Heat of combustion (kJ/kg)
$H_{c,conv}$	Convective heat of combustion (kJ/kg)
h	Enthalpy
K	Constant, depending on target being viewed (e.g., = 6 for lighted signs)[3]
k	Thermal conductivity (W/m·K)
k_v	Volumetric entrainment constant (0.065 $m^{4/3}$ kW $\cdot^{-1/3}\cdot$ s^{-1})
L	Width of balcony spill plume (m)
l	Characteristic length (m)
MW_i	Molecular weight of species i (kg)
M_{CO}	Molecular weight of carbon monoxide (28 kg)
M_{air}	Molecular weight of air (29 kg)
m_u	Mass of upper smoke layer (kg)
$\dot{m}$	Mass entrainment rate in plume (kg/s)
m_f	Mass burning rate (kg/s)
Δp	Pressure difference (Pa)
r	Radius (i.e., horizontal distance from plume centerline (m)
Q	$= \frac{1055}{t_g^2}\frac{t^3}{3}$ for t^2 fires (kJ)
Q=	$\dot{Q}\ t$ for steady fires (kJ)
Q_o=	$\rho_o c_p T_o A(H–z)$ (kJ)
$\dot{Q}$	Heat release rate of fire (kW)
$\dot{Q}_c$	Convective portion of heat release rate of fire (kW)
T_c	Temperature at plume centerline (K)
T	Temperature (K)
ΔT_{ad}	Temperature difference between smoke layer and ambient air (°C)
ΔT_o	Prefire temperature change from floor to ceiling of the ambient air (°C)
t	Time (s)
t_{cj}	Ceiling jet transport lag (s)
t_g	Growth time (s)
t_{pl}	Plume transport lag (s)
V	Volumetric flow rate (m^3/s)
V_{oa}	Volumetric capacity required for opposed air-flow (m^3/s)
V_u	Volume of upper layer (m^3)
v	Characteristic velocity (m/s)
v_e	Opposed airflow velocity (m/s)
w	Width of the balcony opening from the area of origin (m)
x	Position (m)
Y_{CO}	Mass fraction of CO (kg of species CO per kg of smoke)
Y_i	Mass fraction of gas species i (kg of species i per kg of smoke)
z	Clear height, position of smoke layer interface above the top of fuel surface (m)
z_b	position of smoke layer interface above top of balcony (m)
z_f	Limiting height above fuel (m)
z_m	Maximum rise of plume (m)
z_o	Virtual origin of plume (m)
χ_a	Combustion efficiency
χ_l	Heat loss fraction from smoke to enclosure
ρ	Density (kg/m^3)

Subscripts

F	Full-scale building
m	Small-scale model
o	Ambient air
w	Wall, ceiling, or floor of enclosure

References

1. NFPA 92, *Standard for Smoke-Control Systems,* National Fire Protection Association, Quincy, MA (2012).***was 92A
2. J.H. Klote, J.A. Milke, P.G. Turnbull, A. Kashef, and M.J. Ferreira, *Handbook of Smoke Control Engineering,* ASHRAE, Atlanta (2012).

3. T. Jin, "Irritating Effects of Fire Smoke on Visibility," *Fire Science and Technology,* 5, 1 (1985).
4. J. Morehart, "Sprinklers in the NIH Atrium: How Did They React During the Fire Last May?" *Fire Journal,* 83, pp. 56–57 (1989).
5. NFPA 75, *Standard for the Protection of Information Technology Equipment,* National Fire Protection Association, Quincy, MA (2009).
6. R.D. Peacock and E. Braun, "Fire Tests of Amtrak Passenger Rail Vehicle Interiors," *NBS Technical Note 1193,* National Bureau of Standards, Gaithersburg, MD (1984).
7. V. Babrauskas, "A Laboratory Flammability Test for Institutional Mattresses," *Fire Journal,* 72, 93, pp. 35–40 (1981).
8. S.W. Harpe, T.E. Waterman, and W.S. Christian, "Detector Sensitivity and Siting Requirements for Dwellings, Phase 2, Part 2 'Indiana Dunes Tests,'" Report No. PB-263882, National Bureau of Standards, Gaithersburg, MD (1977).
9. Milke, J.A., Hugue, D.E., Hoskins, B.L., and Carroll J.P., "Tenability Analyses in Performance-Based Design," *Fire Protection Engineering*, 28, 50-56 (2005),
10. J.L. Bryan, "Damageability of Buildings, Contents, and Personnel from Exposure to Fire," *Fire Safety Journal,* 11, pp. 15–32 (1984).
11. J.A. Milke and J.H. Klote, "Smoke Management in Large Spaces in Buildings," Building Control Commission of Victoria and The Broken Hill Proprietary Company Limited, Melbourne, Australia (1998).
12. J.G. Quintiere, "Scaling Applications in Fire Research," *Fire Safety Journal,* 15, pp. 3–29 (1989).
13. F.W. Mowrer, "Lag Times Associated with Fire Detection and Suppression," *Fire Technology,* 26, 3, pp. 244–265 (1990).
14. J.S. Newman, "Principles for Fire Detection," *Fire Technology,* 24, 2, pp. 116–127 (1988).
15. J.A. Milke, "Smoke Management for Covered Malls and Atria," *Fire Technology,* 26, 3, pp. 223–243 (1990).
16. G. Heskestad and M.A. Delichatsios, "Environments of Fire Detectors—Phase I: Effect of Fire Size, Ceiling Height, and Materials," *Vol. I—Measurements (NBS-GCR-77-86), Vol. II—Analysis (NBS-GCR-77-95),* National Bureau of Standards, Gaithersburg, MD (1977).
17. B.R. Morton, Sir Geoffrey Taylor, and J.S. Turner, "Turbulent Gravitational Convection from Maintained and Instantaneous Sources," in *Proceedings of Royal Society A,* 234, pp. 1–23, London (1956).
18. G. Mulholland, T. Handa, O. Sugawa, and H. Yamamoto, "Smoke Filling in an Enclosure," *Paper 81-HT-8,* The American Society of Mechanical Engineers, New York (1981).
19. L.Y. Cooper, M. Harkleroad, J. Quintiere, and W. Rinkinen, "An Experimental Study of Upper Hot Layer Stratification in Full-Scale Multiroom Fire Scenarios," *Paper 81-HT-9,* The American Society of Mechanical Engineers, New York (1981).
20. G. Heskestad, Letter to the Editor, *Fire Technology,* 27, 2, pp. 174–185 (1991).
21. T. Yamana and T. Tanaka, "Smoke Control in Large Spaces (Part 2—Smoke Control Experiments in a Large-Scale Space)," *Fire Science and Technology,* 5, 1, pp. 41–54 (1985).
22. G.D. Lougheed, Personal Communication, National Research Council of Canada (Mar. 20, 1991).
23. S.P. Nowlen, "Enclosure Environment Characterization Testing for the Baseline Validation of Computer Fire Simulation Codes," *NUREG/ CR-4681, SAND 86–1296,* Sandia National Laboratories, Albuquerque, NM (1987).
24. J.A. Sharry, "An Atrium Fire," *Fire Journal,* 67, 6, pp. 39–41 (1973).
25. J. Lathrop, "Atrium Fire Proves Difficult to Ventilate," *Fire Journal,* 73, 1, pp. 30–31 (1979).
26. D.M. McGrail, "Denver's Polo Club Condo Fire: Atrium Turns High-Rise Chimney," *Fire Engineering,* pp. 67–74 (1992).
27. G. Heskestad, "Engineering Relations for Fire Plumes," *SFPE TR 82-8,* Society of Fire Protection Engineers, Boston (1982).
28. C. Beyler, "Fire Plumes and Ceiling Jets," *Fire Safety Journal,* 11, pp. 53–76 (1986).
29. R.L. Alpert and E.J. Ward, "Evaluation of Unsprinklered Fire Hazards," *Fire Safety Journal,* 7, pp. 127–143 (1984).
30. F.W. Mowrer and B. Williamson, "Estimating Room Temperatures from Fires along Walls and in Corners," *Fire Technology,* 23, 2, pp. 133–145 (1987).
31. Harrison, R., "Entrainment of Air Into Thermal Spill Plumes," PhD Dissertation, University of Canterbury, New Zealand (2009).
32. Lougheed, GD., McCartney, C.J. and Gibbs, E., "Balcony Spill Plumes Final Report, RP-1247, ASHRAE, Atlanta (2007).
33. Lim, J.M.K., "Numerical Modeling of Balcony Spill Plumes Using Fire Dynamics Simulator (FDS)," MS Thesis, University of Maryland (2010).
34. M. Law, "A Note on Smoke Plumes from Fires in Multi-Level Shopping Malls," *Fire Safety Journal,* 10, pp. 197–202 (1986).
35. H.P. Morgan and N.R. Marshall, "Smoke Control Measures in a Covered Two-Story Shopping Mall Having Balconies and Pedestrian Walkways," *BRE CP11/79,* Fire Research Station, Borehamwood, England (1979).
36. W.D. Walton, "ASET-B: A Room Fire Program for Personal Computers," *NBSIR 85-3144,* National Bureau of Standards, Gaithersburg, MD (1985).
37. Lincolne Scott Australia Pty Ltd., *Jupiters Casino—Report on Atrium Smoke Tests,* Lincolne Scott Australia Pty Ltd., Toowong, Australia (1986).

38. G.O. Hansell and H.P. Morgan, "Smoke Control in Atrium Buildings Using Depressurization," *PD 66/88,* Fire Research Station, Borehamwood, UK (1988).
39. R.A. Waters, "Stansted Terminal Building and Early Atrium Studies," *Journal of Fire Protection Engineering,* 1, 2, pp. 63–76 (1989).
40. G. Heskestad, "Similarity Relations for the Initial Convective Flow Generated by Fire," *Paper 72-WA/HT-17,* American Society of Mechanical Engineers, New York (1972).
41. T. Jin, "Visibility Through Fire Smoke (Part 2)," *Report of the Fire Research Institute of Japan, Nos. 33, 31,* Tokyo (1971).
42. J.G. Quintiere, "An Assessment of Correlations Between Laboratory and Full-Scale Experiments for the FAA Aircraft Fire Safety Program, Part 1: Smoke," *NBSIR 82-2508,* National Bureau of Standards, Gaithersburg, MD (1982).
43. G. Heskestad, "Hazard Evaluation," submitted to NFPA Task Group on Smoke Management of Atria, Covered Malls, and Large Spaces, unpublished manuscript (1988).
44. G.D. Lougheed, "Probability of Occurrence and Expected Size of Shielded Fires in Sprinklered Building; Phase 2, Full-Scale Fire Tests," National Research Council of Canada, Ottawa (1997).
45. NFPA 204, *Standard for Smoke and Heat Venting,* National Fore Protection Association, Quincy, MA (2012).
46. C.L. Beyler and L.Y. Cooper, "Interaction of Sprinklers with Smoke Vents," *Fire Technology,* 37, 1, pp. 9–36 (2001).
47. M.L. Bullen, "The Effect of a Sprinkler on the Stability of a Smoke Layer beneath a Ceiling," *Fire Research Note No. 1016,* Department of the Environment and Fire Officers' Committee, Joint Fire Research Organization, Watford, UK (1974).
48. M.L. Bullen, "The Effect of a Sprinkler on the Stability of a Smoke Layer beneath a Ceiling," *Fire Technology,* 13, 1, pp. 21–34 (1977).
49. R.L. Alpert, "Calculated Interaction of Sprays with Large-Scale Buoyant Flows," *Journal of Heat Transfer,* 106, pp. 310–317 (1984).
50. A.J. Gardiner, *First Report on the Interaction between Sprinkler Sprays and the Thermally Buoyant Layers of Gases from Fires,* South Bank Polytechnic, London (1985).
51. A.J. Gardiner, *Second Report on the Interaction between Sprinkler Sprays and the Thermally Buoyant Layers of Gases from Fires,* South Bank Polytechnic, London (1986).
52. A.J. Gardiner, *Third Report on the Interaction between Sprinkler Sprays and the Thermally Buoyant Layers of Gases from Fires,* South Bank Polytechnic, London (1988).
53. A.J. Gardiner, *Fourth Report on the Interaction between Sprinkler Sprays and the Thermally Buoyant Layers of Gases from Fires,* South Bank Polytechnic, London (1988).
54. L.A. Jackman, *Second Report on the Interaction between Sprinkler Sprays and the Thermally Buoyant Layers of Gases from Fires,* South Bank Polytechnic, London (1990).
55. L.A. Jackman, *Third Report on the Interaction between Sprinkler Sprays and the Thermally Buoyant Layers of Gases from Fires,* South Bank Polytechnic, London (1991).
56. L.A. Jackman, P.F. Nolan, A.J. Gardiner, and H.P. Morgan, *Mathematical Model of the Interaction of Sprinkler Spray Drops with Fire Gases,* South Bank University, London, Swedish Fire Research Board, and National Institute of Standards and Technology (NIST), Fire Suppression Research, First International Conference on Fire Suppression Research, May 5–8, 1992, Stockholm, Sweden, (V. Sjolin, D.D. Evans, and N.H. Jason, eds.), pp. 209–227 (1992).
57. G. Heskestad, "Sprinkler/Hot Layer Interaction," *NIST-GCR-91-590,* National Institute of Standards and Technology (NIST), Gaithersburg, MD (1991).
58. L.Y. Cooper, "The Interaction of an Isolated Sprinkler Spray and a Two-Layer Compartment Fire Environment. Phenomena and Model Simulations," *Fire Safety Journal,* 25, 2, pp. 89–107 (1995).
59. L.Y. Cooper, "The Interaction of an Isolated Sprinkler Spray and a Two-Layer Compartment Fire Environment," *International Journal Heat and Mass Transfer,* 38, 4, pp. 679–690 (1995).
60. P.L. Hinkley, "Work by the Fire Research Station on the Control of Smoke in Covered Shopping Centers," *BRE Paper CP 83/75,* Building Research Establishment (BRE), Fire Research Station (FRS), London (1975).
61. A.J.M. Heselden, "The Interaction of Sprinklers and Fire Venting," *Fire Surveyor,* 11, 5, pp. 13–28 (1982).
62. G. Holmstedt, "Sprinkler and Fire Venting Interaction," *Literature Survey on Modeling Approaches and Experiments Available and Recommendations for Further Studies, 92178 AR GH/AB,* Swedish Fire Research Board, Stockholm, Sweden (1992).
63. B. Persson and H. Ingason, "Modeling of Interaction between Sprinklers and Fire Vents," *SP Report 1996:32,* Swedish National Testing and Research Institute, Sweden (1996).
64. L.Y. Cooper, "LAVENTS—A Computer Program to Model the Interaction between Sprinklers, Smoke Layers, and Smoke Vents," presented at the *International Conference on Smoke Ventilation and Sprinklers—Aspects of Combined Use,* Fire Research Station, Borehamwood, UK (1992).
65. K.B. McGrattan, A. Hamins, D.W. Stroup, "Sprinkler, Smoke and Heat Vent, Draft Curtain Interaction—Large-Scale Experiments and Model Development," *NISTIR 6196,* National Institute of Standards and Technology (NIST), Gaithersburg, MD (1998).
66. K.B. McGrattan, H.R. Baum, and R.G. Rehm, "Large Eddy Simulations of Smoke Movement," *Fire Safety Journal,* 30, pp. 161–178 (1998).

67. K.B. McGrattan and D.W. Stroup, "Sprinkler, Vent and Draft Curtain Interaction: Experiment and Computer Simulation," *National Institute of Standards and Technology (NIST),* Gaithersburg, MD (1997).
68. K.B. McGrattan and D.W. Stroup, "Large Eddy Simulations of Sprinkler, Vent and Draft Curtain Performance," *Fire Suppression and Detection Research Application, Symposium, Research and Practice: Bridging the Gap, Proceedings,* National Fire Protection Research Foundation, February 12–14, 1997, Orlando, FL, pp. 59–68 (1997).
69. H. Touvinen, "Validation of Ceiling Jet Flows in a Large Corridor with Vents Using the CFD Code JASMINE," *Fire Technology,* 32, 1, pp. 25–49 (1996).
70. H. Touvinen and L.Y. Cooper, "Validation of Ceiling Jet Flows in a Large Corridor with Vents Using the CFD Code JASMINE: Errata and Additional Remarks," *Fire Technology,* 33, 2, pp. 183–186 (1997).
71. R.N. Mawhinney, E.R. Galea, and M.K. Patel, "Euler-Lagrange Modeling of Fire/Sprinkler Interactions," *Fire Safety Science—Proceedings of the Fifth International Symposium,* International Association of Fire Safety Science (IAFSS), Australia, p. 1336 (1997).
72. W.K. Chow and A.C. Tang, "Experimental Studies on Sprinkler Water Spray Smoke Layer Interaction," *Journal of Applied Fire Science,* 4, 3, pp. 171–184 (1994–95).
73. G. Heskestad, "Note on Maximum Rise of Fire Plumes in Temperature-Stratified Ambients," *Fire Safety Journal,* 15, pp. 271–276 (1989).
74. M. Dillon, "Acceptance Testing and Techniques," presented at *The Roundtable on Fire Safety in Atriums—Are the Codes Meeting the Challenge?,* Washington, DC (1988).
75. T. Handa and O. Sugawa, "Flow Behavior of Plume from Growing Fire Source in High Ceiling Enclosure," *Journal of Fire and Flammability,* 12, 1, pp. 31–50 (1981).
76. G. Heskestad, "Fire Plume Entrainment and Related Problems in Venting of Fire and Smoke from Large Open Spaces," submitted to NFPA Task Group on Smoke Management of Atria, Covered Malls, and Large Spaces, unpublished manuscript (1987).
77. G.D. Lougheed and G.V. Hadjisophocleous, "Investigation of Atrium Exhaust Effectiveness," *ASHRAE Transactions,* 103, 2 (1997).
78. G. Heskestad, "Inflow of Air Required at Wall and Ceiling Apertures to Prevent Escape of Fire Smoke," *FMRC J. I. OQ4E4.RU,* Factory Mutual Research Corporation, Norwood, MA (1989).

James A. Milke is a professor and chair in the Department of Fire Protection Engineering at the University of Maryland. His recent research activities have included assessing the performance of smoke control systems in fires.

Structural Fire Engineering of Building Assemblies and Frames

52

Jean-Marc Franssen and Nestor Iwankiw

Introduction

Use of the temperature-dependent thermophysical material properties, shape geometry, and fundamental heat transfer and structural principles, in combination with available fire test data, can enable several distinct levels of engineering/calculation methods of fire resistance. The simpler computational methods, such as those in ASCE/SFPE 29-05 [1], are semi empirically based on standard fire test results. They provide fire resistance ratings for members and assemblies that do not directly match listed assemblies to meet prescriptive code requirements. Higher-order fire simulations and structural analyses can be used as performance-based design alternatives to achieve a solution to overall fire safety.

Substantial fire-induced damage is expected after a severe (fully developed or post-flashover) fire exposure, not only to the building content and finish but also to the structural elements. It is not uncommon for well-designed, ductile, and properly functioning fire-resistive framing systems to experience visible distortions, cracking, permanent damage, and deflections that, in floors, can be on the order of 12–24 in. (300–600 mm), or more, without collapse.

In the following sections, several computational approaches to the determination of the fire resistance of building construction are summarized, independent of any requirements of a particular building code or design standard. These can be considered generally applicable to any structural material. The specific provisions of the governing building code and design standard(s) for a given project must be consulted for any engineering applications.

Limit States Design

Design for structural fire resistance and safety (i.e., for the possible strength limit states, in general) to avoid collapse requires that the structural resistance be greater than the applied load effects. This strength limit can be symbolically expressed in Equation 52.1 as

$$R_{\text{fire}} \geq L_{\text{fire}} \tag{52.1}$$

where

R_{fire} = Available structural resistance under the particular high-temperature conditions, including the effects of degraded material properties

L_{fire} = Design values of the load effects (direct effects resulting from the applied loads and indirect effects resulting from restrained thermal expansion) expected to be simultaneously acting during the fire event

For critical facilities that need to continue operations immediately after fire events, it is also possible that such an engineering approach

J.-M. Franssen (✉)
University of Liege, Liege, Belgium

N. Iwankiw
Quartier Polytech, Liége, Belgium

M.J. Hurley (ed.), *SFPE Handbook of Fire Protection Engineering*,
DOI 10.1007/978-1-4939-2565-0_52, © Society of Fire Protection Engineers 2016

could be used to not only prevent collapse but to also minimize fire-induced damage. Such an objective could be accomplished through application of more stringent deflection controls in the design, to which conventionally rated fire resistive assemblies would typically not be subjected.

Because of the assumed accidental and extreme nature of this fire load and response condition, the safety/failure check should be conducted only in the ultimate limit state (ultimate strength or load and resistance factor design, LRFD) design realm, and not with the more restricted allowable or working stress design methods.

The simplest fire resistance calculations for individual structural members (beams and columns) and assemblies (walls and floor systems) are developed from best-fit, regression equations of ASTM E119 [2] fire test data and ratings. There are several shortcomings and limitations to standard fire tests and their derived fire resistance ratings, such as ASTM E119. Some are circumstantial as the cost of the tests, the time required to build specimens and do the tests and the limited number of facilities. Some others are more fundamental as the fact that only single elements can be tested as opposed to complete structures, the fact that the size of the tested elements is often smaller than the size or real elements, the fact that it is very difficult to control and have a precise idea of the boundary conditions in an experimental setup (perfect hinges and perfectly fixed supports are not easily realized in practice) and the variability inherent to experimental processes that make it nearly impossible to make controlled parametric analyses.

For a more complete assessment of structural load and response variables, Equation 52.1 provides the essential underlying criterion for strength adequacy under fire conditions, for both structural members and entire framing systems. More sophisticated analyses for members and frames rely on this basic limit state comparison of Equation 52.1 more explicitly. The degradation of the construction material properties at high temperatures; fire time-temperature values; type, thickness, and properties of the fire protection material(s); boundary conditions; connection response; and thermal strains are the key variables that should be included in this type of analysis.

Resistance

The two most important fire effects that alter a structure's resistance from that at ambient are the high-temperature degradation of its mechanical properties (strength and stiffness) and thermally induced strains. These softening, weakening, and damage to even noncombustible construction materials directly lead to a progressive reduction of load-carrying resistance at higher temperatures. Meanwhile, fire-induced thermal elongations can (1) lead to displacements so large that they influence the effects of action (a term used to designate bending moments, axial forces or shear forces) in the structure or, (2) when restrained, generate additional effects of action, typically in the form of compressive forces. These dual responses demonstrate that fire is clearly time dependent with effects on both the load and the resistance sides of Equation 52.1. Similar to the real time–history response of a structure subjected to an earthquake, load-resistance interactions exist that usually give rise to nonlinear structural behavior and permanent distortions/damage.

For example, a floor system may see the load bearing mode changing from bending at ambient temperatures to one with combined bending and axial compression; and, finally, during the large deflection and high-temperature stages of fire exposure, it may experience combined bending, axial tension and compression (catenary action in the beams and membrane action in the slab). This redistribution of the load-carrying capabilities of a typical floor system in a building from simple flexure under service conditions to catenary action at ultimate is schematically illustrated in Fig. 52.1.

The intent of the general design of Equation 52.1 is to verify the adequacy of structural

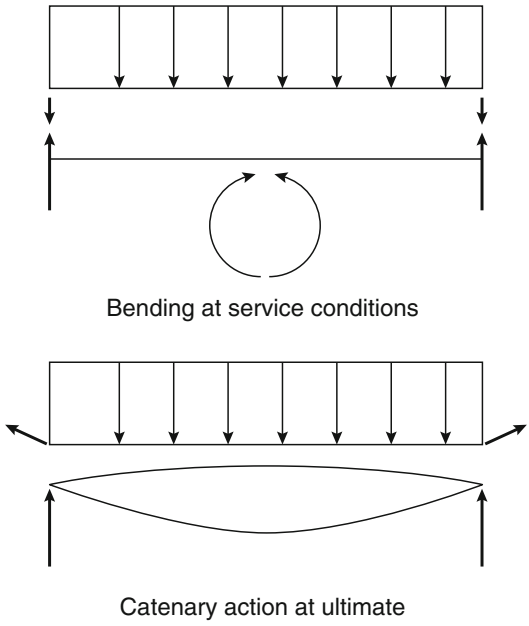

Fig. 52.1 Change in structural resistance of floor beams from bending to catenary action

resistance throughout the entire fire duration and response range or, alternatively, during a required period of performance time. The critical strength condition may not always occur at the maximum fire exposure time, especially with so-called natural design fires that have a burnout or cool-down stage. Member connections adjacent to the fire must also accordingly accommodate the forces, moments, and distortions generated by the event, with adequate ductility to avoid any failure(s); the same holds for all remote elements or parts of the structure that are not directly affected by the fire (in the sense that their temperature remains unchanged). An alternative and generally equivalent limit state formulation to that in the strength domain can be established in the time domain. Use of conventionally pre-established critical member temperatures alone does not provide a totally meaningful or comprehensive solution under fire exposure, because this is only one aspect of the structural response. It does not explicitly address whether the member will fail to support its load demands under such conditions.

Reliability

The general limit states formulation of Equation 52.1 is implicitly based on probability theory and a low, but societally acceptable, failure risk. Such a de minimis risk, or the threshold level below which an event is not of regulatory concern, is a probability of failure of approximately 10^{-6} or less per year [3]. The reliability index to sufficiently control this probability of occurrence is at least about 3.8, which could be used as the target design reliability baseline if one were not using a recognized fire design standard or code. The design reliability includes both the extreme load effects and the lower-bound expected resistance at ultimate strength, as well as the probability of occurrence of an uncontrolled, fully developed fire. The available statistics of the selected or specified load combination, design fire, and structural framing enable a rational calculation of the particular combined reliability of any such design scenario, at least in an approximate sense.

Similar to the empirical fire resistance ratings of building construction elements, fire engineering design of a compartment space is intended to control its vulnerability to localized structural member or assembly failures for a design fire exposure. The potential for fire movement beyond the compartment of origin to other areas or floors can also be duly considered and rationally evaluated, as well as effects of simultaneously occurring fires in multiple compartments and/or floors, relative to potential development of progressive (or disproportional) catastrophic failure of the framing system. For these conditions, a much more complex interaction of thermal and structural action over the affected framing takes place, with significantly greater demands placed on modeling capabilities, computational power, and convergence time for concurrent time–history solutions. The need for suitably customized finite element software, project budget allowances, and computational resources lead to the situation that these types of applications are not usually performed for smaller projects. This more advanced fire

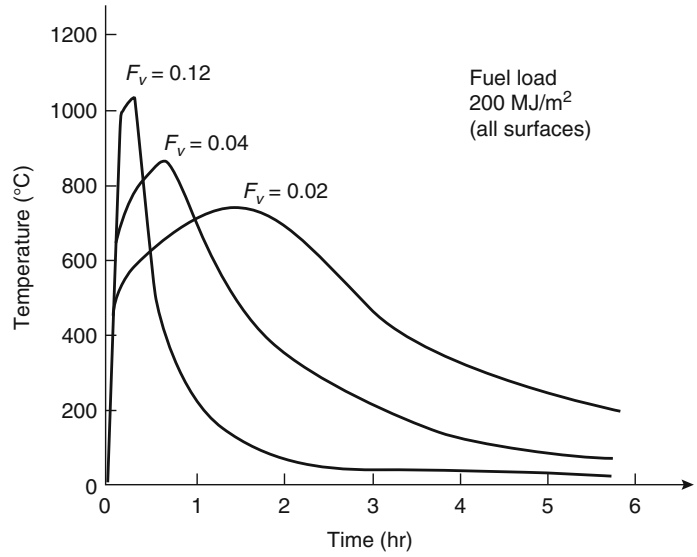

Fig. 52.2 Real time–temperature curves for different ventilation factors, F_v, with a constant fuel load [7]

engineering is essentially applied to higher importance, higher risk, high-rise and/or otherwise unique landmark buildings.

Fire Exposures

This section provides a short introduction to the information covered much more in depth in Chaps. 29, 30, 53, 54, and 55. ASTM E119, *Standard Test Method for Fire Tests of Building Construction and Materials* [2], has long provided (since 1918) the basis for the test fire used in establishing fire ratings of structural building elements in the United States. UL 263, *Fire Tests of Building Construction and Materials* [4], and NFPA 251, *Standard Methods of Tests of Fire Resistance of Building Construction and Materials* [5], are similar documents, as is the international standard ISO 834 [6]. All these standard fire exposure curves can be considered essentially identical. This ASTM E119 standard fire is fast starting, hot, and rising with an equivalent burning temperature of 1000 °F (538 °C) after only 5 min.

An uncontrolled natural fire has distinct stages of growth, fully developed (flashover) burning, and finally decay. In contrast, the ASTM E119 standard fire has no decay or burnout branch but specifies ever-increasing furnace compartment temperatures with time that can reach 2300 °F (1260 °C) at 8 h, if testing were to reach this duration. Normally, ASTM E119 fire tests for listing of building construction elements are not conducted for more than 3–4 h.

A natural fire eventually consumes its combustibles in a finite time that is dependent on the initial quantity and type of fire load and the amount of ventilation in the compartment. Hence, the actual fire load and ventilation present in the room will determine the nature, intensity, and duration of a real fire. Uncontrolled, well-ventilated fires reach higher temperatures than poorly ventilated fires, but they burn faster and have a shorter duration for the same fuel. This is illustrated in Fig. 52.2 [7], in which F_v is a ventilation factor.

In Fig. 52.3, the ASTM E119 standard time-temperature curve is superimposed on several representative real fire curves for various fuel loads and a constant ventilation factor. The maximum fire temperature, its decay phase, and its fire time duration are significantly affected by the fuel content and ventilation, and are quite different from the standard time-temperature curve. As expected, higher fuel loads cause longer and hotter fires under uncontrolled conditions. The standard fire time-temperature curve between

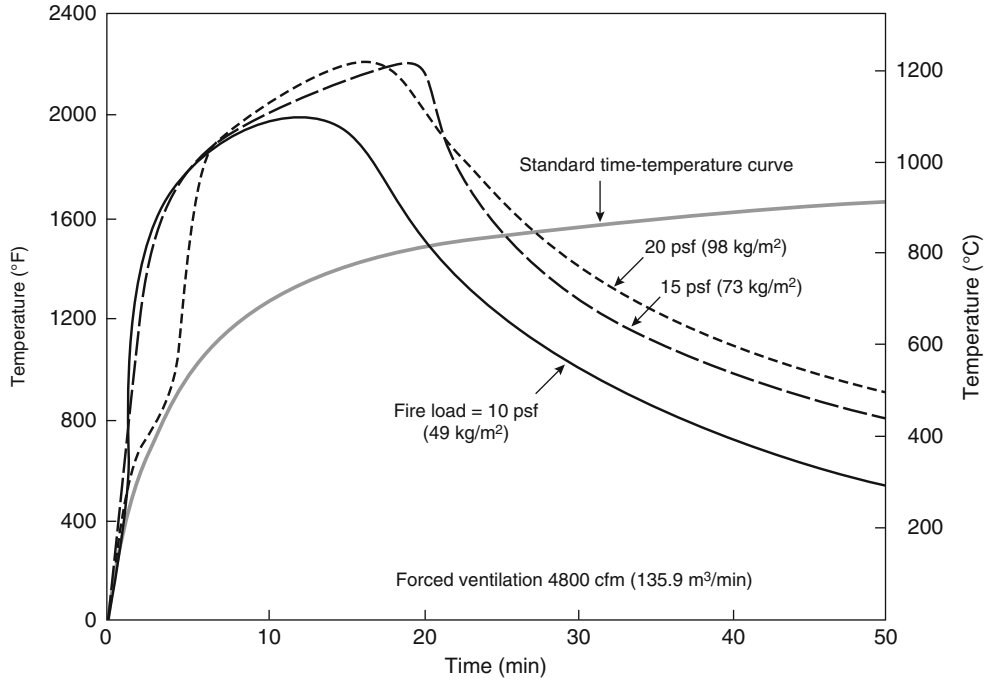

Fig. 52.3 ASTM E119 standard fire and real fire time-temperature curves

1 and 4 h provides a good order of magnitude of the room temperatures that will be encountered in a real conventional fire in many cases. However, in real uncontrolled fires, these high temperatures most likely occur over only a relatively short time interval.

For faster starting and hotter fires, such as those that occur from petrochemicals or other hazardous materials, a standard fire exposure more severe than that given in ASTM E119 may be more appropriate. ASTM E1529 (UL 1709), *Standard Test Method for Determining Effects of Large Hydrocarbon Pool Fires on Structural Members and Assemblies*, defines such a standard fire exposure that reaches and remains at about 2000 °F (1100 °C) after 5 min.

Mathematical representations of the ASTM E119 [2], other standard fire time-temperature curves, and a variety of real compartment fire time-temperature formulations can be made for analysis and design purposes. Various such fire models and parametric curves can be found in the literature, such as the *SFPE S.01 2011 Engineering Standard* [8] and Eurocode 1 [9]. Fire models usually can predict a fire temperature-time history only within a single compartment.

The simplest fire models predict the resulting evolution of the gas temperature within the fire compartment. This is the case for parametric fire models or one zone models. This gas temperature is unique at any time during the fire, which is mostly relevant for a post-flashover situation. More refined models can provide a more detailed picture of the situation in the fire compartment, which is needed if the pre-flashover phase has to be described or in the case of localized fires, such as an axisymmetric fire plume. Two zone models consider a vertical separation between a higher zone containing the hot combustion gases and a lower zone containing cold uncontaminated air. More recent travelling fire models represent the fact that, even in a post-flashover fire, the maximum combustion and maximum gas temperature do not occur simultaneously in the whole compartment [10]. Computational Fluid Dynamics

(CFD) models can also be used to give a very detailed description of the situation in terms of gas temperature, pressure, velocity, in millions of cells of the compartment.

Interior fire extensions through window openings presents another scenario category which analytical modeling can also simulate. Eurocode 1 [9] presents a standard formulation to represent such events.

In performing a structural fire resistance analysis and design, either the well-established standard fire, such as E119, or a natural design fire for the particular building and occupancy can be employed to determine both its R_{fire} and L_{fire} effects. For selection of a natural design fire, surveyed or code-specified fuel loads are an essential demand input. The fuel load can be separated into fixed and variable classifications. The fixed combustibles are those that remain essentially unchanged within the bounded compartment (i.e., interior wall, floor, and ceiling finish, structural framing), whereas the variable fuels are those combustibles that can change over time based on occupancy (furnishings and contents). The fixed fuel load should be determined from a project-specific survey or estimated for noncombustible construction. This fixed fuel load is added to the variable quantity to comprise the total fire design load. Typically, in the absence of a project-specific survey, the variable fuel load could be represented as a nominal design level for the fire demand to provide for suitable overall reliability. Adjustments to higher percentile fuel levels may be specified for selected building conditions, such as lack of automatic suppression/sprinkler systems, larger compartment sizes, occupancy, height/criticality of building, and the risk that the design fire could propagate beyond the compartment of origin to adjacent areas or floors.

As a guide for some typical variable fuel contents expressed in terms of potential heat energy release per unit floor area, Eurocode 1 [9] can provide a reasonable initial reference for common occupancies such as residential, office, commercial, and library. The expected statistical distribution parameters (mean, standard deviation) of the fuel loads are provided as well as values for certain non-exceedance percentiles. Older publications, and some current work, also cite the potential fuel in terms of a weight density per floor area, pounds per square foot (psf), or the like for equivalent amounts of wood combustibles. NFPA 557 [11] is a comparable U.S. fire load standard based on review of the literature and fuel data surveys. The particular design value for variable fire load density depends on the selected or required percentile of non-exceedance, which will vary depending on the height and criticality of the building project, presence of other fire safety measures (including active fire suppression systems), and areas of compartments. Special fuel content surveys may also be undertaken to assess this load density for particular buildings. Hence, selection of the appropriate design fire load, in the absence of a building code requirement, is subject to the responsible professional's judgment and approval by the authority having jurisdiction. For more information, refer to Chap. 35.

High hazard occupancies must be individually determined for each given project.

Overview of Heat Transfer Analysis

The structural behavior of a structure subjected to fire is directly dependent on the temperatures that are induced in this structure by the fire. The determination of the fire resistance of a structure, or of a member, by calculation thus starts with the determination of the temperatures in the structure or in the member. Once a design fire has been selected, a heat transfer analysis is thereby the next step to determine the resulting temperatures in the structure. More discussion of heat transfer is contained in Chap. 34.

Usually, lumped mass single temperature, one-dimensional or two-dimensional analyses will suffice. Most engineered structures are indeed based on linear or planar members, such as beams or columns, frames, floors or walls. If the boundary conditions imposed by the fire to such members are the same along the length of a linear element or on the surface of a planar element, the temperature does not vary along the

length or in the plane of the element. The determination of the temperature distribution is thus usually reduced to a two-dimensional problem on the section of linear elements or to a uniaxial (one-dimensional) problem across the thickness of a planar element (at least for walls and floors that have a constant thickness and are of a single material). Some slabs, like hollow core concrete slabs or composite steel-concrete floors with trapezoidal corrugated steel sheets, require a two-dimensional analysis. The problem in that case is similar to the two-dimensional problem that has to be solved for the beam sections.

Three-dimensional thermal analyses may be performed locally, for example in complex joints between linear elements such as, e.g. beam-column joints. Some walls can in fact be made of concrete blocks with internal cavities or masonry bricks that, together with the mortar joints, form a three-dimensional structure. However, thermal analyses considering the walls with such a level of details are seldom performed.

The size, nature, and type of fire protection (insulation) used for the structural member(s) are essential factors in how quickly, and to what level, the structural material's temperature will rise when subjected to the effects of a fire. Unprotected noncombustible members will heat up most rapidly to eventually reach thermal equilibrium with the fire gas temperature, whereas combustible elements will eventually ignite and be consumed as a fuel.

The heat transfer computation will determine a temperature profile for the higher-order analysis option, within a given structural member at a given fire duration. The one-dimensional heat transfer solution can produce temperature gradients in one direction, commonly through the material thickness. The further simplified, lumped mass analysis is limited to just solution of a single material temperature, hence assumed uniform member temperature. A general flowchart schematically showing the steps and options for this fire and thermal part of the engineering approach is given in Fig. 52.4. Usually, the single fire compartment scenario would govern, as assumed in the standard fire resistance tests and ratings. This scenario is repeated with the fire starting in each possible compartment and/or floor.

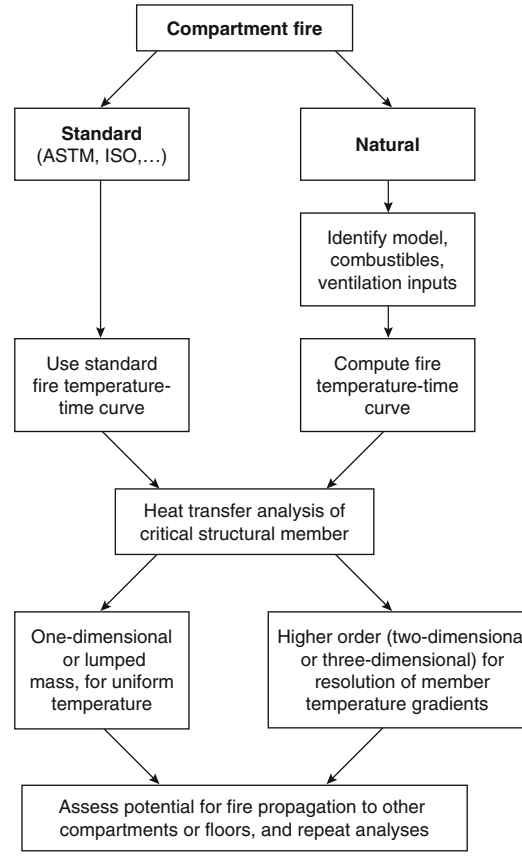

Fig. 52.4 Schematic of fire engineering process to determine maximum temperatures in individual structural members

Most often, a weak coupling is considered between the thermal and the structural analyses. This means that the effects of the temperature variation in the structure on the behavior of the structure are taken into account, whereas the effects of the structural behavior on the temperature development are neglected. One exception could be the failure of partition walls or floors that extend the fire zone.

The longitudinal heat flux that may exist along linear members or in the plane of planar members, the heat flux that may exist from members to members, and the temperature distribution in the joints are briefly discussed in the following section.

Variation of Temperatures along the Members The world in which we live is geometrically three-dimensional. The temperature distribution in construction members is thus three-dimensional in general. Even if the hypothesis of a two-dimensional temperature distribution in linear members is common and practical, longitudinal heat fluxes and temperature gradients will indeed be present in practical situations, essentially in the vicinity of the joints that connect the members and especially in the situation where some members are subjected to the heating of the fire, while some others connected to the same joint are in an adjacent compartment where the cooler ambient situation still prevails.

It is possible to determine the longitudinal heat fluxes, the temperature gradients along the length of the members, as well as the influence of these temperature variations on the mechanical behavior of the members or of the complete structure. Very often, such analyses have been performed for the idealized and somewhat academic situation of prismatic members that have, for example, one part of the length subjected to the fire and the rest surrounded by air at ambient temperature. But these members have, in most studies, the same section along their length and are themselves isolated from the rest of the building.

In reality, each joint is in general a geometrically complex object that extends in all directions (for example, two vertical elements, two horizontal elements spanning in the main direction, and two horizontal elements in the secondary direction). The joint connects members of different types and different sections. It may also be thermally influenced by the presence of nonstructural elements, such as suspended ceilings or vertical walls. Very often, the presence of stiffeners, bolts, and various connecting elements that all have an influence on the heat transfers through the joint will further complicate the situation. This explains why the determination of the true three-dimensional temperature distribution for all the joints in a real building would be an extremely long and expensive process. Performing parametric analyses on various joint typologies and deriving practical design guides about the temperature distribution to be used in everyday design is probably beyond reasonable expectations.

In fact, the information contained in the complex three-dimensional temperature distribution that could eventually be determined in a particular situation could hardly be exploited in the analysis of the adjacent elements. This is because the three-dimensional temperature distribution would be determined on the basis of three-dimensional solid elements, whereas the structural members are usually modeled by oriented elements, either linear (beams and columns) or planar (floors and walls). It would thus be challenging to map the temperature distribution determined in a 3D object into oriented 2D members.

The simplified hypothesis of a temperature distribution in the members that is uniform along the length per segment and that varies abruptly only at the joints is thus normally used. It is somehow justified by the observations made during the analysis of ideal prismatic members. Even if the thermal environment varies abruptly along the length of a prismatic member, the affected zone in terms of temperature variation is quite restricted in length [12]. There is an observable zone in the cold compartment where the temperature in the member is increased, but this temperature increase is smaller than in the adjacent heated part, and failure is not likely to appear here. There is also a short zone in the exposed part where the temperatures are reduced, but it is assumed to be on the safe side to neglect the effects of this colder zone. Typically, the affected zone is twice as long in the cold compartment as in the hot compartment.

The temperature in the joint is of crucial importance if the mechanical behavior of the joint has to be determined. For joints between steel members, the hypothesis is often made that the temperature in the joint is uniform and the mechanical behavior is determined as a function

of this temperature. This temperature can, for example, be determined on the basis of the thermal massivity of the joint as a three-dimensional object, i.e. the ratio between the exposed surface of the joint and the volume of steel. If a slightly more refined thermal model is required, it is possible to calculate the temperature in each component with its own massivity, but this amounts to neglecting the heat flux between the components, which is certainly not true in a thermally composite joint. Numerical tools can be used to derive a very detailed temperature distribution in the joint. To the authors' knowledge, joints have so far been analyzed on the hypothesis that the joint is fully exposed to the fire on all sides. The analysis of joints that are only partly subjected to the fire has yet to be done.

Thermophysical Properties of Fire Protection Materials The variation with high temperatures of key input properties such as conductivity, specific heat, and density for the various spray-on and intumescent coating products, gypsum boards, and the likes will directly affect the analytical predictions of temperatures in the structural members. There are relatively little published data on these, and they are often rather approximate, incomplete, or conflicting. A parametric sensitivity analysis would quantify the range of possible results corresponding to the input variations. Moreover, the adhesion/cohesion of these materials to the substrate and/or the integrity of their protective envelope during the fire are important response characteristics that cannot ordinarily be evaluated solely from analytical models. Experimental evidence of the materials' suitable fire protection performance in this regard is necessary to enable the analytical assumptions that the materials remain in place, as installed, throughout the exposure duration.

The relevant material properties at high temperatures are discussed in Chap. 9 in this handbook.

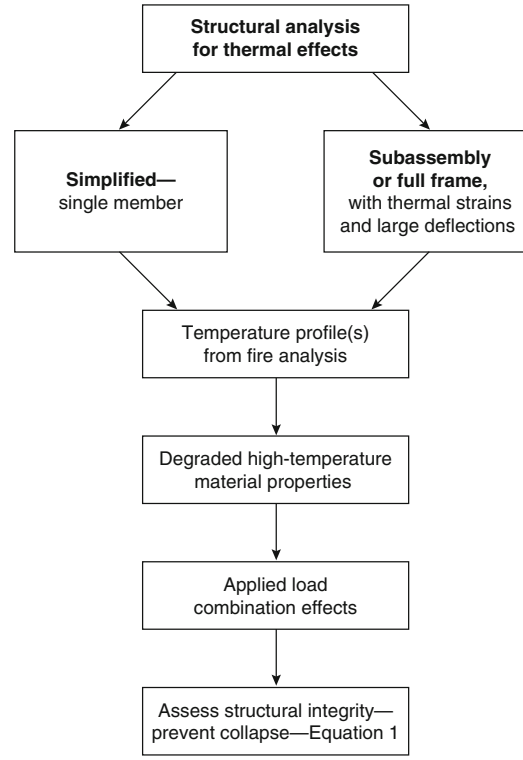

Fig. 52.5 Schematic of structural analysis for fire effects

Overview of Structural Analysis

Figure 52.5 outlines the subsequent structural analysis for loading effects that is performed once the fire-induced temperature(s) in the structural member or system have been determined. A simplified single member-by-member or a subassembly/frame structural analysis can be conducted. The fire-induced thermal expansion and structural restraints are unique features of structural-fire interaction. For the single member assumption, the member boundary conditions and load effects are taken only from the structural analysis at ambient temperatures, thereby neglecting any thermal strain effects on the selected member or the surrounding structure. A subassembly or full-frame structural analysis that includes the thermal response of the fire-exposed member(s) will offer the most complete representation of the response,

including any restraining effects on or by the adjacent framing due to the fire, which would otherwise not become manifest in the single member method. More information on structural analysis is contained in Chaps. 53–55.

Given the complex and advanced nature of the nonlinear structural response under high-temperature exposures, several unique factors that are not routinely considered for most design practice will need to be duly evaluated for analytical solution accuracy.

Local Member or Frame Instability These destabilizing effects due to slenderness of members in compression can be represented by the addition of the geometric stiffness matrix—or comparable idealizations—that accounts for the coupling of axial compressive forces on flexural stiffness. This second-order (or higher) effect can also be described as ensuring the equilibrium of the applied loads on the displaced structure, not its original geometry. The role of structural imperfections for compressively loaded elements may be important in this regard. Initial member crookedness, expected geometrical misalignments, and/or construction tolerances in the building framing or connections may need to be further assessed and studied. These initial imperfections would be reflected as input data to the model(s), in lieu of the perfectly straight original geometry. Larger compressive loads will effectively soften the member or element, which consequently leads to amplified lateral/transverse deformations and bending moments relative to linear elastic assumptions. This structural weakening can eventually progress to the final buckling limit state, when the element becomes unstable and is considered to have failed, at large distortions and with little, if any, residual stiffness. This instability is analytically signaled by the stiffness matrix becoming singular, large displacements, and/or the occurrence of non-convergent numerical solution algorithms. Local buckling instabilities can be analytically modeled and detected only if the structural member is adequately discretized into appropriate beam, plate, brick, or shell elements. If each member is discretized by one single element, only overall member and frame instabilities can be detected in a nonlinear formulation. Linear elastic solutions cannot detect any instability.

Floor Slab Effects The structural effects of the concrete and deck floor slabs on the strength and stiffness of the steel beams and girders, for bracing and composite design with shear studs, must be properly modeled; the steel beams and the concrete slab work together in a composite action.

Thermal Strains The thermal expansion, and structural restraints, must be properly included, since this is a unique feature of structure-fire interaction, as discussed later.

Tensile Membrane Action of Composite Floors [13] Composite floor systems based on profiled steel sheets (decks) are designed for the normal situation to span in one direction, the direction of the ribs. The length of the span is in the order of magnitude of 10 ft, depending on the depth and thickness of the steel deck and on the eventual presence of shoring during casting of the fresh concrete. The traditional approach for ensuring an appropriate fire resistance to such systems was, until the end of the twentieth century, based on additional steel reinforcing bars located in the ribs in order to carry the tension force when the temperature in the steel profiles has increased and their load bearing capacity has vanished. Experimental tests [14, 15] and observations in real fires such as the Broadgate fire in London in 1990 or the Churchill Plaza in Basingstoke in 1991 have shown that a different load transfer mode may develop in the fire situation. Where the load transfer capacity by bending in the slab has been lost, the slab deflects and tension develops in the central part of rectangular slab panels. These tensile forces are supported by the steel reinforcing mesh that must be present in the concrete slab and are equilibrated by a compression ring that forms in the external parts of the slab. This allows leaving some of the infill beams that support the floor unprotected on the condition that the edge beams that form the new

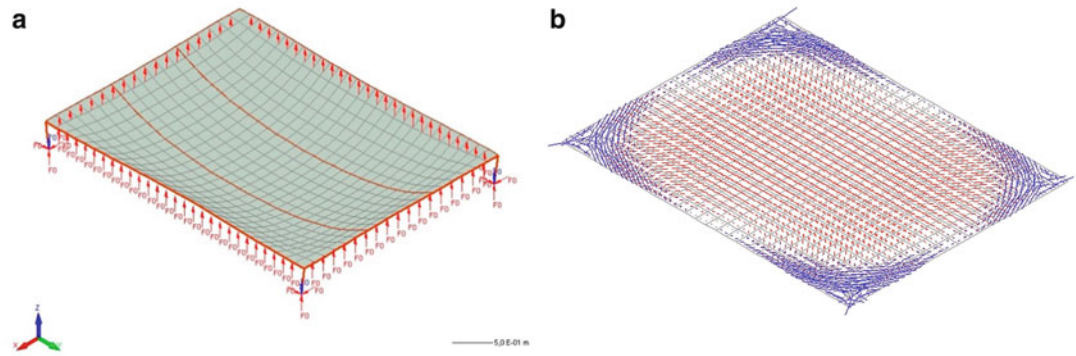

Fig. 52.6 Tensile membrane action. (**a**) Deformed shape of the floor. (**b**) Membrane forces in the floor

slab panel are able to carry the vertical reaction of the system. Figure 52.6 shows: (a) the deformed shape of the new slab panel of increased dimensions that forms during the fire when the two infill steel beams—represented by the **bold** lines—are left unprotected and (b) the distribution of membrane forces in this panel with compression near the edges and tension in the central part of the slab panel.

This mechanism is now well understood and is routinely used for designing composite steel-concrete floor systems, especially in the U.K.

Connection Moment-Rotation Behavior Building framing connections for ordinary design are usually idealized as being either fully rigid-FR (full bending moment transfer and maintain original angles between members) or simple (no bending moment capability and free rotation between members). Depending on the nature of the postulated collapse mechanism and its critical subassembly, it may become necessary to more rigorously model some of these connections with characteristic moment-rotation curves in place of the original simplifying design assumptions, in order to estimate the real joint flexibility and partial rotational restraints. Significant progress has been made in the last decade for understanding and modeling the stiffness and strength characteristics of connections in the fire situation [16]. It has been shown that not only the strength but also the ductility of the joints is essential for ensuring a satisfactory behavior, especially during the cooling phase of a fire [17].

Nonuniform Heating A temperature gradient through the member depth/thickness causes differential thermal strains between the hotter and cooler external surfaces. A temperature gradient will exist, for example, in steel beams with concrete floors under fire exposures, because the floor slab keeps the top of the steel beam cooler. Perimeter columns and truss members will also likely experience some degree of non-uniform heating in a real fire. These thermal effects will depend on whether it is assumed that the fire totally engulfs a given structural member. If so, a similarly uniform heating exposure on all sides can be expected with no temperature gradient or bowing, such as for an interior column. In simply supported members, these thermal gradients give rise to the so-called "thermal bowing." This thermal bowing/curvature will usually be toward the hotter side of the member. These induced thermal curvatures reduce the load-carrying capability of the members in compression due to P-delta effects and, hence, may influence the stability of the columns and truss. Under restrained end conditions, these displacements cannot develop and the effects of actions are modified even at first order (no need of large displacements). A beam that has both ends fixed in rotation and is subjected to a thermal gradient on its depth will experience no bowing in any direction but the bending moment diagram will be changed; if the lower part of the section is hotter than the upper part, negative moments, or hogging, will develop on the whole length of the beam.

Material Strength Limit States Strength (due to ductile yielding, crushing, or tensile rupture) will govern the response of the common construction materials such as steel, concrete, masonry and wood. Yielding, rupture, or stability will often control the ultimate strength of steel members; heavier concrete and masonry have negligible tensile resistance and rely essentially on compressive strength, with steel reinforcement providing the primary tensile capacity and supplemental shear resistance. The extent and type of reinforcing details in concrete and masonry will greatly influence the ductile or brittle nature of subsequent behavior. Plain/unreinforced concrete and masonry will generally be quite brittle and much more susceptible to early cracking failures, whereas heavily reinforced and well-detailed members can perform in a ductile manner at large deformations. Yielding marks the major departure of the structural element's behavior from linear elastic to nonlinear. This nonlinearity is manifest by reduced material stiffness below Young's elastic modulus and by strength that is governed by the constitutive properties of that particular material. Available ambient and temperature-dependent stress-strain relationships for these materials can be used in this regard. Wood structures, with loss-of-section by charring effects, can be reasonably modeled through otherwise linear elastic assumptions. Conversely, steel and concrete structures usually require a full nonlinear analysis. Cracking, potential explosive spalling, and loss of concrete cover to the interior steel reinforcement will affect the reinforced or prestressed concrete member's integrity under fire, but this response is usually well beyond the capabilities of most software.

Collapse Prevention

The primary life safety objective of structural fire resistance is either to avoid collapse during the standard, or design, fire or delay collapse, in a real fire scenario, to a time when all occupants have safely evacuated the building. Collapse can be broadly classified as either local or global. Local collapse is failure of a single member, connection, or limited frame subassembly, whereas global, progressive, or disproportionate collapse produces a major cascading series of related failures triggered by the original local collapse. The latter is the much more dangerous and destructive in terms of both public safety and property loss.

With use of the single member, subassembly, or full-frame structural/fire analyses described earlier, one can determine the source and type of any initial failure. Ordinarily, identification or avoidance of this first structural failure will suffice for compliance with the basic safety requirements of the building codes.

However, more recently with concerns after several terrorist attacks, there is an increased awareness of the risks of disproportionate collapse, particularly for taller or monumental/historical buildings. The analytical determination of whether an initial local/member failure can propagate to further global or disproportionate structural instabilities may be difficult, or impossible, for most finite element software operating in a static analysis mode. Numerical solution convergence for any subsequent catastrophic and complex global collapse mechanisms can be much more easily achieved if the nonlinear software processes the analysis (with resulting large deformations, member failures, singularities, etc.) as a dynamic, rather than static, equilibrium problem, with an appropriate time step [18].

In addition, it may be necessary to conduct such simulations in full three-dimensional space, with adequate and appropriate discretization of the potentially affected members, that is, many more model nodes and elements, to reach the best response fidelity. Such intricate simulations are likely to require extensive computing resources, time, and effort to accomplish.

Structural Load Combinations for Fire Resistance

The applied load effects, L_{fire}, for use in Equation 52.1 need to be determined from the loads

and load combinations required by the applicable building code, and these will constitute the so-called mechanical, or nonthermal, effects on the heated structure. The common building design loads are dead (D), floor live (L), roof live (L_r), roof snow (S), rain (R), wind (W), and earthquake (E), several of which may or may not act simultaneously. Maximum structural stresses or deformations, therefore, will result from the critical combination of the loads. Building codes specify various combinations that must be checked. The most critical load combination may occur when one or more of the loads are not acting. In some codes or standards, provisions for design to withstand an extraordinary, extreme, or accidental event (A_k) may also be given, such as for fire, explosion, and vehicular collisions with building.

For the fire engineering problem, the design values of the loads are based on probabilistic considerations: the probability of failure from the effect of a fire (which must meet a certain target value) is the product of the probability of having a severe uncontrolled post-flashover fire by the probability of failure when this fire occurs. As the first of these two probabilities is much lower than 1, the probability of the second event, the one that is assumed when the fire resistance is calculated, can be higher than the target value. The design value of the load will thus be less in the fire situation than the full design live load that is normally specified for ambient temperatures. In addition to the normal (ambient) design load requirements, ASCE/SEI 7-10 [19] in the United States specifies use of the following extraordinary event gravity load combination for fire design:

$$1.2D + A_k + (0.5L \text{ or } 0.2S) \qquad (52.2)$$

where A_k symbolically represents the fire effects or typically the construction material's strength and stiffness reductions caused by the fire's heating.

This load combination in Equation 52.2 for extreme exposures is intended exclusively for application in limit states design with Equation 52.1.

Other international codes and standards specify comparable reduced load combinations to be used in combination with fire exposures. This contrasts with the full gravity design live load that is used in most standard fire resistance tests, such as ASTM E119. It should be recognized that the frequency of major building fires is relatively low due to the small probability of ignition coupled with flashover, due to occupants or fire department intervention and/or automatic fire suppression system's extinguishment of the fire before it becomes fully developed [3]. However, if flashover occurs, the uncertainties of the actual fire intensity, duration, spread, and localized heat distribution effects to the affected structural members (L_{fire}) are large relative to the variability of the structural fire resistance (R_{fire}). The coefficient of variation (COV) of the fuel load contents that serve as the fire combustibles is considered to be on the order of 0.50 or more, similar to common live gravity and environmental (wind, snow, earthquake) loads [3, 20], whereas the typical structural resistance COV is in the range of 0.10–0.20.

High-Temperature Effects on Structure

The two primary high-temperature effects on structural materials that are not exhibited under typical ambient conditions are thermally induced strains and degradation of the materials' mechanical properties (strength and stiffness). Because of these two effects, deflections of structural members during the longer duration, hot fires (post-flashover) can reach many inches or even several feet. This is at least an order of magnitude greater than the small elastic deflections, usually no more than about 1–2 in. (25–50 mm) that are normally contemplated for design service. These effects are only briefly described in the following sections, as there are existing sources for this detailed information, including other chapters in this handbook. The commonly used structural fire protection materials and systems are generically addressed in the final section.

Table 52.1 Coefficients of thermal expansion for steel and concrete at high temperature [21]

Structural and reinforcing steel	7.8×10^{-6}/°F (1.4×10^{-5}/°C)
Normal-weight concrete (NWC)	1.0×10^{-5}/°F (1.8×10^{-5}/°C)
Lightweight concrete (LWC)	4.4×10^{-5}/°F (7.9×10^{-6}/°C)

Thermal Strains

Strain is defined as change in member length divided by the initial length. In general, the total strain, ε_{total}, in a structural element, can be considered to be primarily composed of mechanical and thermal parts, as given in Equation 52.3.

$$\varepsilon_{total} = \varepsilon_{mechanical} + \varepsilon_{thermal} \tag{52.3}$$

Mechanical strain is related to applied loads and stresses, whereas thermal strain results only from the material's expansion or contraction due to temperature changes. Under fire exposures, the thermal strain is elongation in proportion to the material's coefficient of thermal expansion. For constant temperatures, the total strain is only the mechanical strain, because the thermal strain is zero. However, at elevated temperatures, high mechanical strains can develop even under negligible superimposed and dead loads due to restraint of thermal expansion.

If the member is fully restrained so that no total strain occurs, all the thermal expansion effects are converted into an equal and opposite mechanical strain (compression). These mechanical strains induce internal reaction forces and moments in the structure, which may lead to either material ultimate strength or strain becoming the governing limit state. Similar to seismic design, the ultimate strain, or deformation, rather than strength may become the failure limit for the more brittle construction materials that do not have sufficient ductility. For the opposite extreme, in the case of a simply connected but effectively thermally unrestrained member, all the thermal expansion will freely occur as part of the total strain and will not directly induce any additional mechanical strain (additional mechanical strain can occur because of second-order effects linked to the large displacements that the free thermal expansion produces). Therefore, for totally unconstrained thermal expansion and unloaded elements, total strain equals the thermal strain, with thermally induced mechanical strain and stress being zero.

The real boundary conditions for thermal restraint in buildings lie between these extremes and require a more in-depth analysis for an accurate determination. For such indeterminate framing, this deformation compatibility and force/moment equilibrium analysis under heating and applied loads is the key step in assessing the structural integrity of a member or subassembly.

AISC [21] provides the following thermal elongation strains (coefficients of thermal expansion) in Table 52.1 for material temperatures above 150 °F (65 °C), which are similar to the values given in other major international standards.

Constant coefficients of expansion lead to a thermal expansion that is proportional to temperature. This simplification closely approximates more detailed representations that can be found in the literature, and it is usually both practical and sufficient for design applications of simple elements. The thermal elongation strain resulting from a temperature increase of 500 °C in the material is about 0.004 for lightweight concrete (LWC) and 0.007–0.009 for steel and normal-weight concrete (NWC), which represents an increase of about 0.5 in./10 ft (4 mm/m) for LWC or about 1.0 in./10 ft (8 mm/m) for steel or NWC. These possible levels of elongation during a severe fire are clearly significant.

Thermal Degradation of Construction Material Properties

Combustibility is one broad, and important, fire classification of building materials. Noncombustible materials will degrade under the higher

temperatures of a fire but will not burn. Combustible materials will not only degrade at higher temperatures but also ignite and burn, thereby adding to the fuel contents during a fire.

Building materials serve in the primary, load-bearing elements that are necessary to preserve the structural safety of the building in preventing partial or total collapse. The traditional building materials have been steel, concrete, masonry, and wood. Wood is the only combustible material of these four. In all cases, visible damage/distortions and degradation (potentially including cracking, dehydration, loss of section, charring, etc.) of the mechanical properties of all building materials occur under prolonged elevated temperatures.

Application of more advanced fire resistance solutions will require an explicit representation of the basic thermal and mechanical material properties at elevated temperatures, such as yield and ultimate stress, modulus of elasticity, coefficient of thermal expansion, thermal conductivity, and specific heat. The detailed material response and property variations at high temperatures of fire on concrete, masonry, and wood materials may be readily obtained from Chaps. 54 and 55 in this handbook, as well as from the published literature.

Structural Analysis

For each combination of loads that could be applied to the structure in the fire situation, the effects of actions, namely bending moments, axial and shear forces, and also the support reactions, have to be determined in the structure. This determination is the structural analysis.

Because of the indirect effects of actions, that is, those variations in the effects of actions caused by restrained thermal expansion, it may be necessary to perform the structural analysis continuously during the duration of the fire course. This has then to be made not only for every combination of loads, but also for any fire scenario that is being considered. The fact that large displacements created by unrestrained thermal expansion and the softening of materials vary constantly under increasing temperatures is another reason that may lead to the necessity to perform a structural analysis at every stage of the fire.

There are yet some simplifications that can lead to a less demanding process for the structural analysis. The conditions of these simplifications and the limitations of these simpler procedures are discussed in this section.

Structural Analysis Before the Fire

As a starting point, the effects of actions have to be determined in the structure under the design load combination in case of fire for the moment when the fire starts, a moment that is usually called $t = 0$, or time at zero.

In fact, some simplified methods used to determine the fire resistance member by member are based on the effects of actions calculated at $t = 0$. This is, of course, a gross simplification because any indirect effect of actions is then neglected. Such a simplified procedure is acceptable only when used in conjunction with a simplified representation of the fire environment, typically a nominal or standard time-temperature fire curve. It is accepted in that case because the representation of the fire is conventional and cannot pretend to reproduce or predict the real fire development that could take place. Then the structural analysis can also be done on the basis of a conventional situation for the effects of actions, namely the situation at time $t = 0$. The goal of such a simplified analysis is not to represent the behavior of a real structure in a real fire. Rather, the aim is to predict the result of a standard fire test that would be performed in a laboratory on a simple element subjected to a standardized time-temperature curve.

Even when the structural analysis will be performed in a continuous manner during the course of the fire, it is sound practice for the engineer to have a close look at the results of the structural analysis at time $t = 0$. This provides a good opportunity to verify whether the results obtained match the expected perception of the solution. Any structural engineer

should have enough experience in structural analysis at room temperature in order to judge whether the obtained bending moment diagram and the deflection shape, for example, are consistent with the boundary conditions and loads that were supposed to be applied to the structure. This also allows for checking the stress level that exist in the structure before the fire starts, which gives an idea of the load level and, hence, of the possibility for the structure to present a significant degree of fire resistance.

In practice, the structural analysis at time $t = 0$ can be performed by an elastic analysis, because it is reasonable to assume that the structure will exhibit very little, if any, nonlinear material behavior under the design load combinations in case of fire. Indeed, if the situation that prevails at the beginning of the fire is compared to the situation that has to be taken into account for the design of the structure under normal conditions, the design values of the mechanical loads are lower, as well as the partial safety factor dividing the resistance of the material. For example, a steel structure that has been designed to sustain in normal conditions a design load equal to $1.20D + 1.60\ L$ with a design value of the material strength will exhibit very little plasticity at the beginning of the fire if the load is only $1.20D + 0.50\ L$ and the actual full material strength can be mobilized, where D is the nominal dead load and L is the nominal live load. Additional discussion of limit states design principles was covered earlier in this chapter. Because the effects of actions are determined at time $t = 0$, the stiffness of the material at room temperature is, of course, taken into account. If the structure is simple, the analysis is trivial, but if the structure is complex, it is possible to use one of the numerous numerical tools developed for the analysis of structures at ambient temperature. If the structural analysis is performed continuously during the fire course and a nonlinear method is used for that, it is simpler to use the same method also at time $t = 0$.

Another good practice before performing the analysis of the structure during the fire is to load it until failure. The loads applied in the fire situation are simultaneously and proportionally increased until collapse while the temperature is maintained at ambient. The ratio between the value of the loads in the fire situation and the value of the loads at collapse is the load level. The lower the load level, the higher the fire resistance can be. Here also, the tool of choice for determining the collapse load is the tool that will be used for the analysis under elevated temperatures.

Structural Analysis During the Fire

Except when the structure is analyzed member by member, it is common practice to take into account the effects of indirect actions and of large displacements during the fire. Thus, the structural analysis has to be performed in a continuous manner during the fire exposure.

The procedure is first to apply the loads while the structure is at ambient temperature and then to let the temperature increase in the structure while the external applied loads are usually kept constant. The response of the structure is calculated until failure and, in simple structures, this time of failure may be considered as the fire resistance time for these applied loads.

If the load-bearing capacity at a prescribed fire resistance time has to be calculated, the preceding procedure has to be repeated in an iterative manner with the applied loads being modified until the obtained fire resistance time matches the prescribed resistance time. It is possible to apply a procedure that yields directly the load-bearing capacity at the prescribed fire resistance time, as is described later.

Elastic or Elastoplastic Analysis An elastic or elastoplastic analysis for the combined effects of fire and structural loads is very rarely performed due to the nonlinearities present.

Timber constructions may be an exception, because thermal expansion in wood is normally neglected and no indirect effects of actions take place in a timber structure. A structural analysis method established for the ambient temperature situation could thus be applied in the fire, simply taking into account the fact that the stiffness of

the members subjected to the action of the fire is reduced by loss of cross section, as the charring depth progresses in these members. It should be kept in mind that the effects of large displacements may increase as the fire progresses because of this reduction in stiffness of certain members, and may become crucial in the fire, whereas these could be disregarded in ambient design. The strength of the connection should be checked at every stage during the fire, as well as the decrease of the stiffness of the members and its effect on the load transfer in the structure.

One could envisage performing a thermoelastic analysis of a steel structure by one of the elastic methods normally used at ambient temperature, in which the thermal expansion and the reduction of Young's modulus would simply be introduced in order to reflect the increase of temperature. Such a procedure would have two disadvantages: that (1) the indirect effects of actions would be severely overestimated, because in reality plasticity in the members relaxes the thermal strains, and (2) any benefit from load redistribution by the formation of plastic hinges could not be accounted for.

One could also envisage performing a structural analysis of a steel structure by one of the methods established for normal ambient conditions and based on an elastic–perfectly plastic material model. This would, at least, solve the second disadvantage of the purely elastic models, namely the incapability to consider the formation of plastic hinges. The fact that the "true" nonlinear stress-strain of the material has been approximated by an elastic–perfectly plastic behavior would still lead to an overestimation of the indirect effects of action and to an underestimation of the displacements. This is why such a procedure is rarely applied. It is considered that a structural analysis based on a full nonlinear material model is not that much more complicated and is more suitable to capture the real behavior of the structure during a fire.

One practical and interesting application of elastic or elastoplastic analysis methods for the structural analysis during the fire is in very large structures that are only partially subjected to the fire. It may, in fact, prove to be an efficient procedure to limit the full nonlinear analysis to those parts of the structure that are subjected to the fire or that are in the near vicinity of the fire affected zone, and to rely on a more simple model for those zones that are far away from the fire and deemed to behave elastically. It will, nevertheless, be necessary to verify that the obtained effects of actions in the supposedly elastic part of the structure can indeed be accommodated by the assumed elastic members. Thermal elongation of rather long portions of concrete slabs subjected to the action of two burning cars has, for example, led in 2010 to the collapse in shear of a column that was 12 m away from the fire source in the "Tour d'Ivoire" building in the city of Montreux in Switzerland, see Fig. 52.7 [22].

Fig. 52.7 Concrete columns that failed in shear due to thermal elongation of the ceiling

Nonlinear Analysis The most common procedure for the structural analysis during the course of the fire is to perform a step-by-step, nonlinear analysis of the structure. The basic equations of structural mechanics are used, but most of the simplifications that were, sometimes implicitly, used for the analyses at ambient temperature cannot be used anymore. The use of a numerical program is required.

The temperature in the structure is not uniform. The level of sophistication for the representation of the temperature distribution varies from one particular method to another and from one particular software to another. Some models have a uniform temperature in the sections, with the temperature varying from one section to the other (valid only for metallic materials). Others allow a thermal gradient, linear or nonlinear, across the depth of the section, either a steel section or a concrete slab. Some others have capability for a completely non-uniform, two-dimensional temperature distribution on the sections. Still others, more rarely, may consider a full three-dimensional temperature distribution on the whole structure.

A sophisticated constitutive model represents the behavior of the material at the local level. Most of these models are based on strain decomposition. The total strain, that is, the one resulting from a spatial derivative of the displacements, is decomposed into several components accounting, for example, for elasticity, plasticity, cracking, true creep, transient creep (in concrete), and thermal expansion. All these terms are temperature dependent, most of them in a nonlinear manner. There is, for example, no such thing as a constant coefficient of thermal expansion. The thermal expansion strain is a nonlinear function of the temperature. Most of these strain terms are also stress dependent. Different material models have been developed based on different theories such as plasticity models or damage models or a combination of both [23], some in the pure local form, and some in a nonlocal form. Different models may be used simultaneously in a single analysis for a structure made of different materials. A detailed presentation of all these models is beyond the scope of this chapter.

The finite element technique is probably the most commonly used method for solving the equilibrium equations. Displacements-based elements are commonly used, although other element types are totally suitable. Here also, some care has to be taken in the development of the particular element type for the fire analysis, or in the choice of the element type taken in the library of a program that has been written for the ambient situation if it has to be used for the fire situation. The hypothesis that the neutral axis is at midlevel of a symmetrical section is not generally valid anymore, and, for example, the usual linear expression for the longitudinal displacement field in a beam element may need to be revisited.

When the structural analysis is performed in that manner continuously during the course of the fire, the numerical program tries, at every time step defined by the user or chosen automatically by the program itself, to find a displaced position of the structure that ensures equilibrium with the applied external forces. There is no separate verification of the members. The simulation will continue as long as a position of equilibrium of the structure can be found, although some members may suffer severe distortions, high level of plasticity, or cracking. The whole structure may itself exhibit very large displacements. It is the responsibility of the user to verify whether the displacements depicted by the program are still compatible with the particular serviceability limit states for the given project. A single-level single bay steel portal frame, for example, that hangs in a catenary manner such that the beam is below ground level is certainly physically not acceptable, whereas a computer program with capability for such very large deformations and highly ductile response may see no problem in that situation. Other less trivial situations may also require the attention of the engineer and an assessment decision of the analytical results.

Whereas the example of an excessively ductile result from a computer program has been depicted in the previous paragraph, the user most often faces the opposite situation, especially in complex structures. The simulation

may stop when one of the members of the structure becomes unstable, while the global stability of the structure is still maintained. Such a simulated failure produced by the inability of the software solution to converge while the global load-bearing capacity of the structure has not been exhausted is called a numerical failure. Reducing the time step used for the analysis is of no use for this problem of local failure, even though other numerical failures can be solved by the use of a shorter time step. One of the main reasons of the problems created by local instabilities has been identified in the fact that the step-by-step analysis procedure was until recently based on a series of successive, quasi-static analyses. Time was not really present in the equilibrium equations, except that it changed the material properties. A position of static equilibrium had thus to be found at any time, and such a situation of static equilibrium may not prevail during the few seconds that, for example, a member in compression buckles and its axial force suddenly drops to zero and is redistributed to adjacent members. The situation develops in a highly dynamic manner. It has been shown [18] that the numerical problems created by local failures can be significantly reduced if the dynamic behavior of the structure is taken into account in the basic equations. A significant number of the structural analyses performed in the fire situation are nowadays performed in the dynamic mode, although the final technique that would avoid all numerical failures has yet to be found.

Structural Analysis at the Required Resistance Time

It is possible to calculate directly the load-bearing capacity of a structure at the prescribed fire resistance time. This procedure may be appealing because (1) it allows expressing directly the equivalent of a safety margin in the load domain, whereas the application of the procedure described in the previous section yields a safety margin in the time domain; and (2) the numerical procedure established for the loading of structures at ambient temperature can be almost directly applied, whereas the previous procedure requires more refined theoretical developments.

The procedure is to apply from the beginning of the analysis the temperatures in the structure that prevail at the required fire resistance time. The mechanical properties of the different materials in the structure are adapted at every point of integration in order to reflect the temperature level at that point. A first loading then takes into account the thermal expansion in the materials. The external loads are then applied and increased progressively while the temperature is kept constant until equilibrium is no longer possible.

Although it may be appealing, this type of procedure is much less often applied than is nonlinear analysis during a fire. The reasons follow:

1. The step-by-step nonlinear analysis aims at reproducing the development of events in the order in which the events occur during the course of a fire, namely heating of the structure under load, whereas this procedure, which loads the structure after it has been heated, is more a numerical trick used because it may be more convenient for the designer. Yet, because the physical phenomena in play are highly nonlinear, there are no guarantees that both procedures would yield exactly the same result. In other words, if a load L yields a fire resistance time R with the first procedure, it is not certain that the load-bearing capacity will be exactly equal to L if it is calculated with the second procedure at time R.
2. If the AHJ or the engineer wants to have an idea of the safety margin in the time domain, an iterative application of calculating the load-bearing capacity at the prescribed fire resistance time is then required.
3. The complex sequence of events that ultimately leads to the global collapse of a structure can be examined and may be understood with nonlinear analysis during a fire, for example when the successive failures of

different members in the structure and the load redistribution that they generate are due to different heating rates in these members. The successive failures produced by a progressive application of the external load under isotherm conditions may be completely different and would not give any insight into the real behavior of the structure during the course of the fire.

4. This procedure is, of course, not applicable when the required fire resistance time is in the cooling phase of a real fire. If the required resistance time is sufficiently longer than the heating phase, the temperatures in the structure have significantly decreased at the required fire resistance time and the corresponding load-bearing capacity could be significantly higher than it was when the temperatures in the structure were at their maximum.

Utilization of Substructures

The structure of even a rather simple building is typically composed of tens of members linked together in a way to make a stable assembly that supports the nonstructural elements of the building, the wind, the snow loads, and the live loads. The capabilities of computers have increased tremendously in recent years, and current computer programs can analyze three-dimensional structures. It is, thus, theoretically possible to undertake the three-dimensional analysis of a complete structure; however, it has to be acknowledged that there is still a limit to the size of structures that can be practically analyzed.

For everyday practice, when time and budget constraints are important limitations, it is very rare that the entire structure is analyzed for fire effects. Instead, a substructure can be extracted from the whole system and effectively analyzed. The reason for this is to be found not only in the computer time required to run the analyses but also in the time required by the engineer to develop the computer model and interpret the results.

The quality of the results from the analysis of the substructure, defined as the similarity between the analytical results of the substructure and the total structure, highly depends on the size and on the boundary conditions imposed on the substructure, that is, at the locations where the virtual cut is made between the substructure and the rest of the structure. The decision about the model size and the boundary conditions is the responsibility of the designer. The same is also true in most structural analyses made at ordinary temperatures, but the situation is more critical for an analysis in the fire condition because of the indirect effects of actions.

The most precise results would be obtained if the rest of the structure is represented by equivalent, usually linear, springs. It may be difficult and quite time consuming to determine the stiffness of all the required springs. In most cases, the stiffness's of all the degrees of freedom that form the interface are not independent. A series of independent springs is not sufficient to represent the effect of the surrounding structure; a more or less complete stiffness matrix is required. This necessity is why it is often considered as an approximation that the variables that exist at the interface between the substructure and the rest of the structure are kept constant during the whole fire duration. These variables are—degree of freedom per degree of freedom—either a force or bending moment, or a displacement or rotation.

It is possible to define a systematic procedure that lists the different steps that have to be followed and that highlights the decisions to be taken [24].

1. The effects of actions in the whole structure must be determined at time $t = 0$ under the load combination in the case of the fire under consideration (see section "Structural Analysis Before the Fire").
2. The limits of the substructure have to be chosen. The choice is made with the contradictory objective that not only does the substructure become as simple as possible but also at the same time the hypothesis of constant variables at the boundary conditions during the fire must represent an accurate approximation of

the real situation, with respect to the thermal expansion and load paths that exist in reality. The choice of the limits of the substructure is highly dependent of the location(s) of the fire. Engineering judgment is necessary.

3. All the supports of the structure that belong to the substructure have to be taken into account as supports of the substructure.
4. All the external mechanical loads that are applied on the substructure in case of fire have to be taken into account as acting on the substructure.
5. For each degree of freedom existing at the boundary between the substructure and the rest of the structure, an appropriate choice has to be made in order to represent the situation as properly as possible. The two possibilities are:
   - The displacement (or the rotation) with respect to this degree of freedom is fixed.
   - The force (or the bending moment) deduced from the analysis of the total structure made in step 1 is applied.

   These two possibilities are exclusive because it is not possible to impose simultaneously the displacement and the corresponding force at a degree of freedom. Whatever the choice, these restrictions on the displacements and these forces applied at the boundaries will remain constant during the fire.
6. The substructure that has been defined is then considered as a new structure and a new structural analysis is performed on this new structure. Either the fire resistance is based on the effects of action at time $t = 0$ and the procedure explained in the earlier section "Structural Analysis Before the Fire" is applied, or the structural analysis is performed in a continuous manner during the fire and the procedure explained in the earlier section "Structural Analysis During the Fire" is applied, in which case the indirect actions that can develop within the substructure are taken into account. Displacements (or rotations) will appear at the degrees of freedom where the force (or moment) has been imposed whereas reactions forces (or moments) will appear at the degrees of freedom where the displacement (or rotation) has been fixed.

The necessity to perform a new structural analysis on the substructure even if the fire resistance is based on the effects of action determined at time $t = 0$ comes from the boundary conditions considered at the interface. A simple example is that of a continuous beam, uniformly loaded by p, from which one of the interior spans of length L is extracted as a very simple substructure. The bending moments determined from step 1 are approximately $pL^2/12$ at the supports, with $pL^2/24$ at mid span. If the choice made in step 5 is to consider that these moments at the supports are constant, the consequence is that the end support rotation is free and the substructure is statically determinate; it will fail as soon as the bending moment resistance on the supports decreases to $pL^2/12$ and plastic hinges are formed. If, on the contrary, the choice is to consider that no rotation can develop on the support, a new and very simple structural analysis will show that failure of the fixed-fixed beam can occur only when three plastic hinges have developed, and the bending moment resistance has decreased to $pL^2/16$ at the supports and at mid span.

Fire Resistance of Individual Members

Simple calculation models or design equations are usually able to treat the fire resistance of only individual members such as one column or one beam. Because such simple calculation models have historically been the first to be developed, it has been possible for many years to determine the fire resistance for only individual members. When complex building structures had to be evaluated with regard to their fire resistance, all constitutive members were evaluated separately, and it was traditionally considered that the fire resistance of the global structure was equal to that of the weakest member.

In fact, except for very simple structures, there is no guarantee for that conclusion. Individual members are indeed connected to each other, and there are strong interactions between their individual behaviors. As a matter of fact, these interactions are stronger in the fire than at ambient temperature because of the high levels of thermal expansion that occur at elevated temperatures. These interactions come either from additional indirect effects of actions caused by restrained thermal expansion or from large displacements caused by free thermal expansion. They can have beneficial or unfavorable effects on the fire resistance of the members and their connections and, as a consequence, on the fire resistance of the whole system (see next section, "Fire Resistance of Frames"). Therefore, this simplified member-by-member analysis and design is limited in accuracy because any changes due to the fire in load effect on the members are ignored, not only in magnitude but also in type and direction (e.g., primary bending/shear or compression load effects can change to tension [catenary action] due to thermal effects).

It is easily accepted that, because the interactions are neglected in an analysis of the fire resistance made member by member, the fire resistance of the weakest member is not exactly equal to the real fire resistance time of the whole structure. But most people think that there is at least a relationship between these two values and the correlation is positive. In other words, if the fire resistance of the weakest member is increased, the fire resistance of the whole structure is also increased. If this is true, the analysis made member by member can be used, if not to quantify exactly the time of fire resistance of a complete structure, at least to compare different systems or solutions between each other, which means that it can be used for a grading system, albeit a conventional one. A structure in which all members have a fire resistance of 2 h would necessarily be safer than a structure in which the members have only a 1 h fire resistance.

This is why more general calculation models, usually based on numerical modeling, have been developed. These allow analyzing in a more realistic manner the behavior of complete structures and determining their fire resistance as their true ability to sustain the applied loads during a certain time, and not as the minimum of otherwise independently analyzed elements.

Yet, despite its drawbacks and limitations, the analysis of structures member by member is still widely used today. It will probably continue being used for the foreseeable future and thus is worth consideration for the following three reasons.

First, the utilization of complex computer software requires a high level of education, expertise, and experience, whereas simple models for the analysis of individual members are more easily understood and applied.

Second, the costs of acquiring sophisticated numerical software, learning to use it, creating the numerical model of the structure to be analyzed, running the analysis, and interpreting the results are not always compatible with the size of the project and the resources that can be allocated to the thermal and structural analyses. An approximate conservative answer that can be obtained rapidly may be more valuable than a more precise answer that takes weeks to develop.

Finally, it has to be recognized that, for most usual structures of reasonable size and complexity, the member-by-member analysis provides a reasonable estimation of the fire resistance time of the structure. Also, in many cases, only this resistance time is to be determined, whereas the deeper understanding of the true failure mode is not required.

Most simple design equations used in the fire situation for the analysis of individual members are a direct extrapolation of the methods used for the same member at room temperature in which the stiffness and strength of the material have been adapted in order to reflect the effects of the temperature increase, although some particularities may appear in some design equations at elevated temperature. It is noted that the empirically derived correlations or tabulated data for member fire resistance based on standard fire tests are not considered to be a general structural analysis–design solution in this context and so are not addressed in this section.

Of course, the results of prescriptive fire tests for the standard fire, acceptance criteria and limited assembly conditions, together with their interpolations, can provide some validation benchmarks for the engineering methods outlined.

The design equations that give the structural resistance R_{fire} to be used in Equation 52.1 are different depending on the material type (steel, concrete, composite steel-concrete, or timber), on the type of effect of actions (tension, compression, or bending), as well as on the national building code and/or design standards to be used. The actual formulas or values for the various fire design variables, such as material strength changes with temperature, section reduction criteria, and buckling coefficients, are given by the respective design standards and building codes. Design differences among countries in this representation do exist, even though the underlying heat transfer and structural behavior are identical. The detailed equations for evaluating the fire resistance of individual linear members at elevated temperatures are given in Chaps 52–54. of this Handbook. Only floors and walls will be treated here as their design is not systematically treated in textbooks while their behavior is worth discussion.

Floors

Floor systems are usually assessed in the fire scenario where the fire is applied underneath the floor. This means that the floor evaluated is in fact the ceiling of the fire compartment. The attack from the fire that develops on that floor is usually not considered for various reasons: buoyancy that directs hot gases and diffusion flames toward the upper zone of the fire compartment, eventual presence of a mineral material that covers the floor, or presence of ashes on the floor that obstruct radiative impinging flux.

Many floor systems span in one direction only. This is the case, for example, for hollow core concrete slabs, for composite steel-concrete floors based on corrugated steel sheets, or for traditional timber floors based on simply supported timber beams. In these systems, the load-bearing capacity is assessed by the methods established for beams in bending. Additional requirements are normally imposed in order to ensure the separating function required for these horizontal elements that usually play a role in the compartmentation of the building. These requirements have to do with the thickness in concrete-based floors in order to limit the temperature increase on the upper side of the floor. In timber floors, these requirements may have to do with the thickness of the planks and also with the arrangement of the lateral joints between the planks because these joints are a weak point for the passage of hot gases.

Floor systems that span in two directions were traditionally designed in the fire situation on the basis of the bending yield-line theory, as for the ambient temperature situation. The effective yield strength of reinforcing bars in the lower zones of the slab was simply adapted as a function of their particular temperature, and the compressive zone in concrete was eventually reduced in thickness on the support lines where continuity of the slab exists. Full-scale tests performed in Great Britain [25] have demonstrated that such a design is over conservative. In reality, the load transfer system in a slab is significantly modified when the slab exhibits large deflections. In the fire, the thermal gradient on the thickness of the slab induces such high deflections already in the early course of the fire. At the later stages, when the stiffness of the slab is decreased, the applied loads also induce large deflections. In such a highly deformed position, tensile membrane forces develop in the central part of the floor, whereas a compression ring is established near the supports. If sufficient reinforcing steel is present in both directions, the loads can then be transferred to the supports more by tension in the bars than by bending.

This effect has been demonstrated in the Cardington full-scale test and has been reproduced in smaller scale but better controlled experimental laboratory tests as well as in numerical modeling. A simple method to be used by designers has been established [26], which takes that tensile membrane effect into

account. When the design is performed according to this more realistic load transfer mechanism, the floor slabs can span over wider surfaces in the fire than what the serviceability limit state allows in the ambient situation. It is thus possible to leave some intermediate supporting beams unprotected.

The tensile membrane effect can develop even in systems that are considered at room temperature as spanning in one direction (e.g., in composite floors with corrugated steel deck), provided that sufficient reinforcing is provided in the transverse direction.

Walls

Walls are vertical plane elements commonly found is most building structures. Different types of walls exist, depending on the basic material and on the way they are constructed. For example, brick walls, concrete block walls, concrete walls, steel-stud or timber-stud gypsum plasterboards, and sandwich steel panels are common construction types. Columns may be inserted in the wall in order to provide lateral stability (Fig. 52.8). Walls can also be made of a combination of masonry comprised between concrete columns and beams (Fig. 52.9).

Walls can also be classified depending on the function(s) that they have to fulfill. The main functions of walls follow:

- *Separating function in normal conditions*. A wall may be used in order to separate two rooms in a building visually, thermally, and/or acoustically. Two bedrooms in the same apartment may, for example, be separated by steel-stud gypsum plasterboard that has separating functions only in normal conditions.
- *Separating function in the fire condition*. The wall is used in order to prevent the fire from spreading from one fire compartment to the other.
- *Load-bearing function*. The wall is used in order to carry some structural loads induced in it by horizontal elements that it supports such as the floors and the roof of the building.

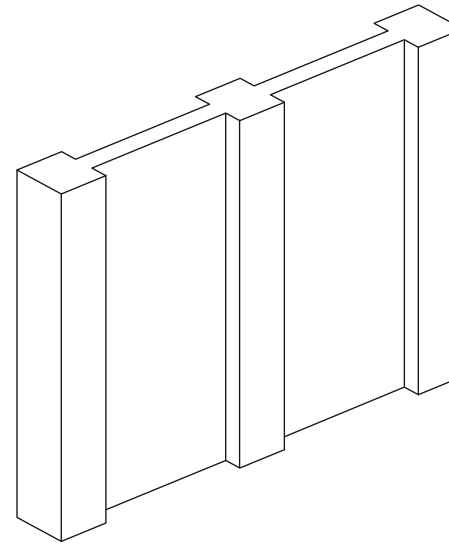

Fig. 52.8 Columns in a wall

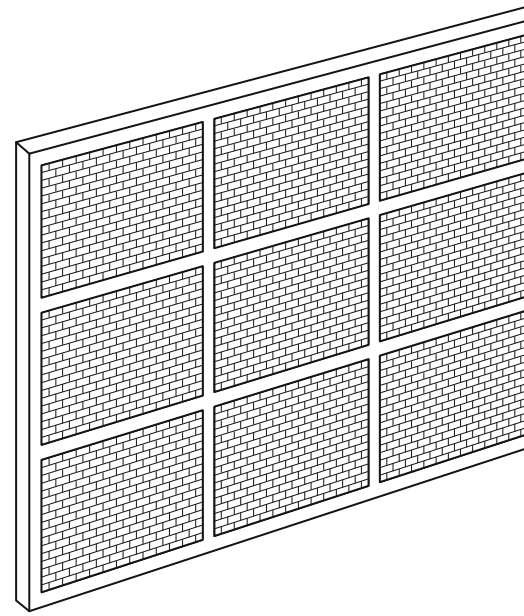

Fig. 52.9 Masonry in a reinforced concrete grid

A wall that has only a separating function in normal conditions but not in a fire is called a nonrated wall. The presence of such walls influences the development of the fire because, if only during the initial stage of the fire, the walls mark the boundaries of the room of origin

of the fire and thus deeply influence the ventilation conditions in this room. Yet, the influence of such walls is normally not considered in the design fire scenario because, first, there is no means to estimate the amount of time during which their influence will persist and, second, there is absolutely neither reliability of the influence of such walls during the fire nor reliability of the presence of the wall when the fire starts.

A wall that has a separating function in the fire is usually rated by a standardized fire test. The wall is exposed to a normalized time temperature-time curve on one side, whereas the conditions on the unexposed side are monitored and compared to defined performance criteria. The temperature is monitored on the unexposed face, and acceptance criteria are imposed on the average temperature increase as well as on the highest temperature increase at any point. Radiation emitted toward the environment by the unexposed surface can also be recorded and compared to a defined level. These criteria allow verification of the insulating property of the wall. The temperatures and the emitted flux must remain sufficiently low so that they do not pose a threat to any nearby fuel (combustibles) that may be present in the vicinity of the wall or to persons who may need to use the compartment as an escape route or as a rescue area. The characteristic of integrity is also verified continuously during the fire. In the test standard ASTM E119 [2], for example, this is done by verifying that "passage of flame or gases hot enough to ignite cotton waste" will not occur near any visible crack, fissure, or opening that appears in the wall's unexposed side. Of course, even if no external load is applied to the wall, it has to carry its own weight; any collapse of the wall from the effect of its own weight automatically leads to the failure of the two previously mentioned criteria.

A wall that has a load-bearing function must support the applied load during the prescribed fire duration. In most situations, such a wall has also a separating function and is tested as exposed to the fire on one side only. It may yet occur that a load-bearing wall is subjected to the fire on both sides. This could be the case, for example, for a shear wall of limited length located within a compartment in order to transfer horizontal loads applied in the plane of the wall. Representing such a situation in an experimental test is not easy, and walls are rarely, if ever, tested with the fire on both sides.

The insulating performance of the wall can be calculated only in very simple configurations. It is, for example, generally considered that the temperature on the unexposed side of a concrete wall can be calculated with sufficient precision by numerical methods. The temperature of masonry walls can also be estimated as long as there is no macro crack in the wall. For most separating walls, however, the insulation and the integrity criteria can only be verified by experimental tests; numerical calculation provides little help. This is because the behavior of these walls made of several components strongly depends on the relative behavior of the different components. The opening of the joints between adjacent gypsum panels in a timber-stud gypsum boards wall, the behavior of connections between a steel panel and a steel stud, the charring in horizontal joints of plane timber walls, or the settlement of fiber-insulating panels inside sandwich walls each have a direct consequence on the insulation and integrity criteria. Yet, these relative behaviors can hardly be predicted for several reasons. First, these are fully coupled phenomena; the temperature field influences the deformations, but the opening of the joints influences the temperature distribution. The scale that should be considered to model these multi-physics phenomena is so small that it is absolutely incompatible with the scale of a complete building wall. Second, these behaviors exhibit a high level of variability because of the overwhelming influence of small local details such as the size and topology of a glued connection or the fact that a mechanical fastener is perfectly perpendicular to the steel sheeting or not. Also, it has to be recognized that a comprehensive constitutive model for, say, gypsum plaster at elevated temperatures has still to be established. For similar reasons, the load-bearing capacity of walls can be calculated only in the same simple configurations.

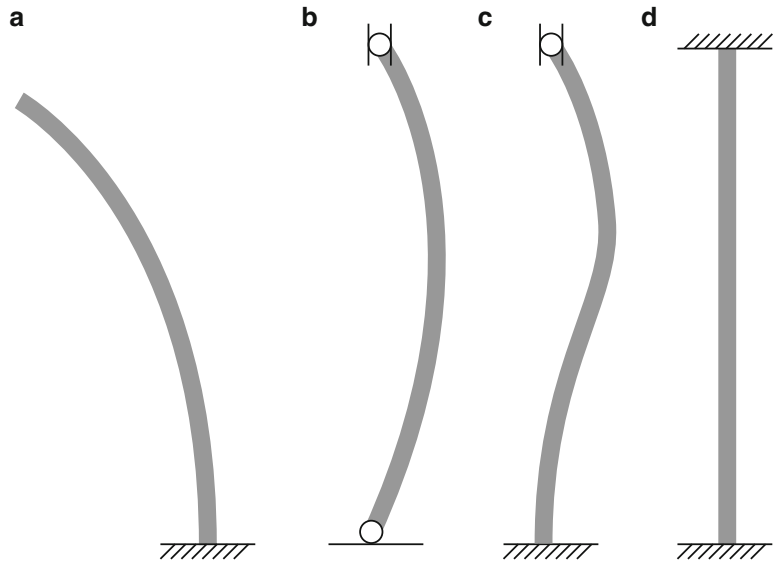

Fig. 52.10 Different lateral supports of a wall (fire on the right-hand side)

As far as the load-bearing capacity is concerned, there is no conceptual difference between a load-bearing and a non-load-bearing wall. The first one has to support an applied design load but the latter one has to support its own weight anyway. The difference is then just in the level of applied load which could affect the wall deflections, damage, integrity and stability during the fire. However, the mechanical behavior and the calculation methods for the two cases are the same.

The biggest difference between a wall and the other types of vertical elements, namely the columns, is that walls are very often heated on one side only. If a wall is heated on both sides, its behavior is similar to that of a column.

When the wall is heated on one side only, a severe thermal gradient appears across the thickness of the wall. Because of the thermal elongation in the material, this leads to a curvature in the section and, hence, to large deformations or, if the deformations are restrained, to indirect effects of actions. Four typical behaviors can be noted, depending on the type of lateral support provided to the wall. Figure 52.10 shows schematically four possibilities with regard to the lateral supports.

The wall may be simply cantilevered from the floor with no lateral support at the top (see a in Fig. 52.10). Such a wall is statically determinate and, in a first-order theory, thermal gradients will not induce a variation of the effects of actions. Yet the lateral displacements of the wall are not restrained and large displacements will indeed occur. The displacement at the top of the wall is proportional, according to a first-order theory, to the curvature induced by the thermal gradient and to the second power of the height of the wall. The displacement at the top of significantly high walls can be very important, easily on the order of several hundreds of millimeters. This important relative displacement between the fire wall and the adjacent structure that supports the rest of the building must be accommodated. The lateral displacements lead to an increase of the bending moment, especially at the base of the wall, because of the eccentricity created for the applied load and for the dead weight. This increase of bending moment will increase the displacements, which, in turn, will increase the bending moments further. The process can converge to a position of equilibrium or can lead to the collapse of the wall. Collapse can occur either because the combined effects of actions at the base of the wall exceed the resistance of the section or because the foundation has not been foreseen to withstand this

increased eccentricity of the load and the rotation of the foundation cannot be prevented.

The wall may be simply supported at the base and at the top (see b of Fig. 52.10). In that case, the wall is still statically determinate and, in a first-order theory, thermal gradients will not induce a variation of the effects of actions. Lateral displacements will also occur but, compared to the cantilevered wall, they are four times smaller. Such walls are thus inherently more stable than the cantilevered walls and, furthermore, there is no danger of rotation of the foundation. The increase of the bending moment due to large displacements is much lower, and the maximum increase occurs at midlevel where only half of the dead weight is applied. A horizontal force will be applied to the supporting structure at the top of the wall because of the eccentricity of the dead weight, but this force should be easily accommodated by the structure that remains on the cold side of the wall. The challenge with this type of wall is that it has to be linked horizontally at the top to the structure on both sides of the wall. The fire may indeed occur on either side, and the support must be provided when the remaining cold structure is the one on either the left side or the right side. But, because the structure on either side is attached to the wall, this means that the collapse of the structure on the fire side may tear the wall down. Some developments have been made in order to disconnect the wall from the heated structure when it collapses; some are based on topological details that transmit the horizontal reaction only in the direction from the wall to the structure but not in the reverse direction, and some are based on plastic materials that are supposed to have melted when the heated structure collapses.

A wall that is fixed in rotation at the top (see d on Fig. 52.10) is not easily realized in practice. Such a wall would see an increase of the bending moment due to thermal gradients that are uniform along the height of the wall. Because of the fixity of the rotation at both ends, no lateral displacement would be induced in the wall, neither toward the fire nor away from the fire.

The wall shown as c in Fig. 52.10 can be constructed. It leads to lower lateral displacements than the simply supported wall B, but the horizontal force induced on the support at the top will be much higher. Such a configuration is not often used.

Structural Steel Design Criteria in the United States

In the United States, ASCE/SEI 7-10 [19] and ANSI/AISC 360-10 [21] are the fundamental design standards for structural steel and composite steel-concrete building construction. The former document specifies the design loads whereas the latter covers the structural design criteria. These documents should be utilized for any implementation of the pertinent design requirements.

It is noteworthy that ANSI/AISC 360-10 [21] includes an Appendix 4, "Structural Design for Fire Conditions," which contains provisions for both advanced and simple analytical methods, as well as acceptance of the traditional prescriptive methods based on standard fire testing.

The major characteristic of the AISC limit states design for fire conditions is substitution of the degraded mechanical properties (yield strength and elastic modulus) at elevated temperatures for their ambient counterparts, assuming elastic–perfectly plastic material response. Special provisions have been added to account for high temperature stability effects on compression members and laterally unbraced beams. Otherwise, the equations for design strength of steel and composite members remain identical to those specified for ambient conditions. The design basis fire may be a standard exposure or a postulated natural/real fire for the given space occupancy and use.

For example, under combined axial compression and bending loads, the AISC interaction equations for doubly and singly symmetric members at elevated temperatures would become the following:

$$\text{For } \frac{P_u}{\phi_c P_n(T)} \geq 0.2 : \frac{P_u}{\phi_c P_n(T)} + \frac{8}{9}\left[\frac{M_{ux}}{\phi_b M_{nx}(T)} + \frac{M_{uy}}{\phi_b M_{ny}(T)}\right] \leq 1.0$$

$$\text{For } \frac{P_u}{\phi_c P_n(T)} < 0.2 : \frac{P_u}{2\phi_c P_n(T)} + \frac{M_{ux}}{\phi_b M_{nx}(T)} + \frac{M_{uy}}{\phi_b M_{ny}(T)} \leq 1.0 \quad (52.4)$$

where P_u and M_u are the required factored axial and flexural strength per ASCE/SEI 7-10 [19] (see earlier section "Structural Load Combinations for Fire Resistance"), respectively; and $\phi_c P_n(T)$ and $\phi_b M_n(T)$ are the design axial compressive strength and flexural strength, respectively, per ANSI/AISC 360-10 [21], inclusive of the material property dependency on the high temperatures. The applied and resisting bending moments are referred to both the strong (x) and weak (y) principal axes of the cross section. In a similar manner, the remaining AISC provisions for ambient design can be readily converted to their corresponding design strength under fire exposure based on the predicted structural member temperature(s). Appendix 4 of ANSI/AISC 360-10 [21] permits the fire load analysis to be simply performed for the same member support and restraint boundary conditions as encountered at ambient.

Given the simplifications of the member by member approach, Appendix 4 of ANSI/AISC 360-10 [21] also allows, in general terms, for more advanced analyses and alternative design solutions that include effects of thermally induced deformations, framing restraint/continuity, and any load redistribution during the fire. Many of the methods cited earlier and in the following section are of this type, including those contained in internationally recognized design standards and in the technical literature. These advanced analysis methods for structural fire engineering will usually require use of computer models with the capability for material and geometric nonlinearities.

Fire Resistance of Frames

A frame is a structural system very often used in building construction. It is defined here as an assembly of several linear elements connected together to form a skeleton that extends vertically (columns) and horizontally (girders and beams) in one (two-dimensional frame) or two (three-dimensional frame) directions. The frame supports other components of the construction such as the floors, the roof, and the walls. In a framed building, the building and the frame are comprised in the same volume; the physical space that exists between the different elements of the frame is the usable space of the building.

Although the discussion in this section will be limited to two-dimensional frames for reasons of simplicity, most of the concepts highlighted here can be extended to a three-dimensional configuration.

Indirect effects of actions appear in a structure during the course of the fire because of thermal expansion. This is at least the case when the elements are made of metal or concrete but not so much for timber elements because this material exhibits very little thermal expansion. The indirect effects of actions come from the combined influence of two opposite sources:

1. Geometrical second-order effects, created by the change in position that the thermal expansion produces in the structure. It has been explained, for example, how severe this effect can be in a cantilevered wall (see the section "Walls" earlier in this chapter). If a high-rise building would be affected by a fire on several floors but on one side only, the situation could develop in a similar manner. Structural elements subjected to an axial force will show an increase of bending moment if lateral displacements are created in the elements by an unsymmetrical temperature distribution in the section. Similar effects are also produced if the displacements are caused by a decrease in stiffness of the elements.
2. Thermal expansion that cannot develop freely in an element will also induce variations in the

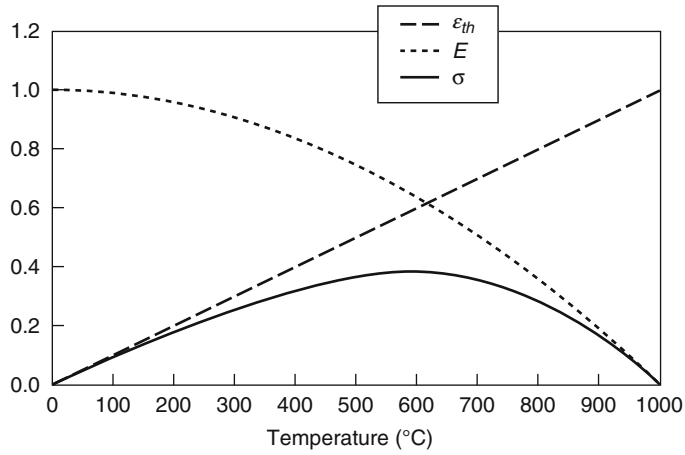

Fig. 52.11 Evolution of the restraint stress with the temperature

effects of action. When a column cannot elongate, an increase in axial force is induced in this element. Because of the variation of axial force in, say, a beam, the columns connected to that beam will consequently see an increase in bending moment. Similarly, a beam subjected to thermal gradients across the thickness will see a variation of the bending moment distribution if the transverse displacement that would be generated is prevented; this is the case, for example, of a continuous beam on more than two supports or of a beam in which the rotation is fixed at the supports.

These combined effects usually are detrimental to the fire resistance of the frame but, in some circumstances, can have a neutral or beneficial influence. This is the case, for example, when tensile forces can be mobilized to withstand the loads that bending cannot accommodate anymore.

If the design fire scenario is based on a nominal fire curve in which the temperature increases continuously, or if failure of the structure occurs during the increasing phase of a more realistic fire scenario, indirect effects of actions created by large displacements have a tendency to increase constantly during the fire. This is because the temperatures of the parts of the structure subjected to the fire increase constantly and, as a consequence, the stiffness of these parts decreases constantly, which leads to a continuous increase of the displacements.

The situation is more complex when the indirect effects of actions are due to restrained thermal expansion. This can be explained quantitatively by the model of a simple element that has a thermoelastic constitutive model and has the elongation totally restrained. The increase of stress $\Delta\sigma$ due to a thermal expansion $\Delta\varepsilon_{th}$ is equal to the amount of thermal expansion that cannot develop. For this case, it equals the whole thermal expansion (because the restraint is total) multiplied by the Young's modulus of the material E in Equation 52.5:

$$\Delta\sigma = E\varepsilon_{thermal} \tag{52.5}$$

Owing to the fact that thermal expansion is usually an increasing function of the temperature and that the Young's modulus is a decreasing function of the temperature, the product of these two variables first increases, passes through a maximum, and then decreases again. This is illustrated schematically by Fig. 52.11 in which the supposedly linear thermal strain has been normalized to 1.0 at 1000 °C and the nonlinear decrease of the modulus E has been normalized to 1.0 at 0 °C. In that hypothetical case, the so-called "thermal stress" would have a peak around 580 °C. If the restraint is not total but the restraining structure behaves elastically, the

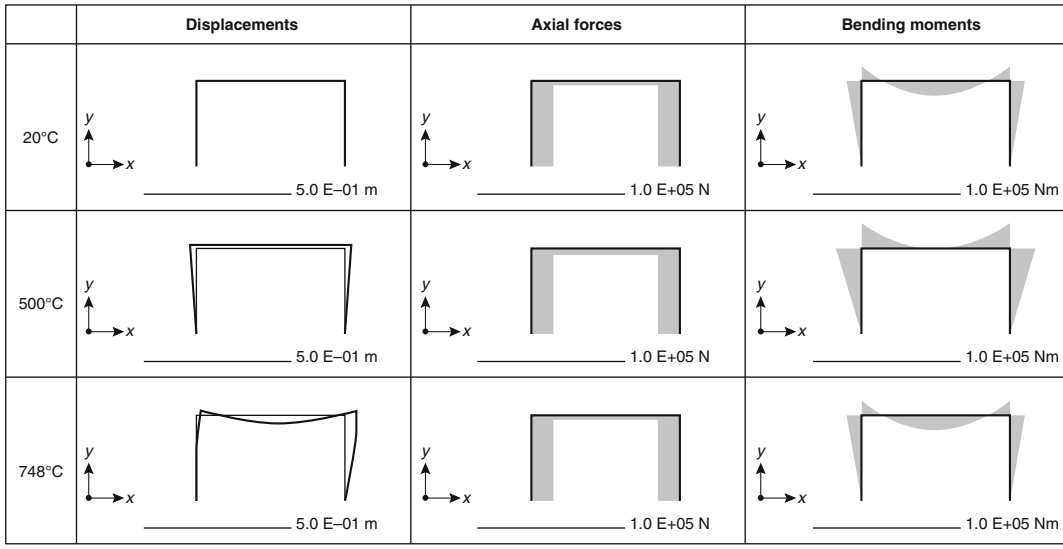

Fig. 52.12 A simple portal frame under increasing temperature

thermal stress will be lower in magnitude, but the maximum will occur for the same temperature of the heated parts.

Even if all elements of the frame are subjected to the action of the fire and in the hypothetical case that all elements have their temperature increasing at the same rate, a restraint to thermal expansion is likely to appear. This is because the supports of the structure on the ground (that is, usually, the bottom of the columns of the first floor) are normally restricted in their horizontal displacement.

Figure 52.12 shows the evolution of the displacements and the effects of actions in a small simple portal frame, 5 m wide by 3 m high, the steel members of which are heated uniformly. If the effects of creep are neglected, the situation can thus be depicted as a function of the steel temperature, independently of the fire scenario. The beam is subjected to a downward uniformly distributed load of 30 kN/m, with an associated horizontal distributed load of 30 N/m introduced as an equivalent initial imperfection. The section on the beam is an IPE400 and the section of the column is HE280B. Steel has yield strength of 235 N/mm^2. The results have been obtained by a nonlinear numerical analysis that takes large displacements, thermal expansion, and nonlinear stress-strain relationships into account.

At room temperature, the displacements can hardly be seen on the picture, although they have been amplified by a factor of 5. The axial force and bending moment diagrams are standard for this type of structure.

When the temperature of the elements increases, the thermal expansion of the columns develops freely, while the thermal expansion of the beam is restrained by the bending stiffness of the columns. The compressive axial force in the beam increases, accompanied by the same increase in horizontal reaction force directed toward the inside of the frame at the two supports. This induces a significant modification in the bending moment diagram.

The axial force in the beam increases until 500 °C and decreases thereafter. It has to be noted that, in this case, not only the stiffness of the restrained member (the beam) decreases as the temperature increases, but also the stiffness of the restraining system (the columns) does.

For temperatures beyond 500 °C and until failure at 748 °C, the indirect effects of actions decrease continuously, and at failure the effects

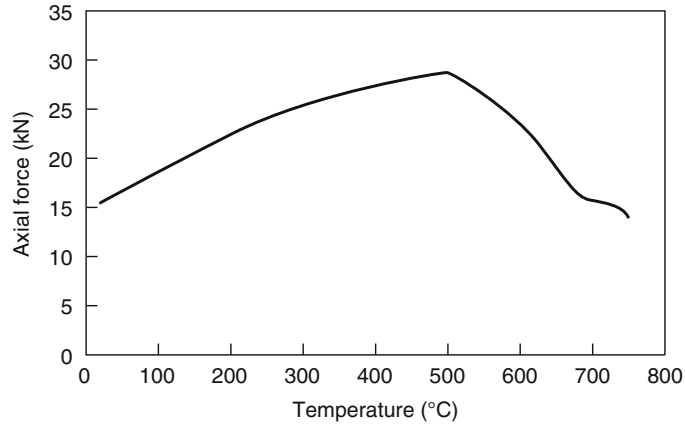

Fig. 52.13 Evolution of the axial force in the beam

of actions have nearly the same pattern as at room temperature. This behavior has been observed on many occasions, especially when the failure temperatures are rather high.

Figure 52.13 shows the evolution of the axial force in the beam as a function of the temperature in the structure. It shows that, although the force has approximately doubled at 500 °C, its value at failure is nearly identical to the value it had at room temperature.

The following example is based on a multi-story, moment-resistant frame in which only one floor is subjected to the fire. The vertical distance between the beams is 3 m; and the columns are separated by 6, 8, and 6 m. The sections and the material model are the same as for the previous example. The steel columns at floor 4 as well as the steel beam that they support are heated at a uniform temperature (Fig. 52.14).

The axial force and bending diagrams at room temperature are typical for this type of structure. The displacements can hardly be seen in Fig. 52.14, although they have been amplified by a factor of 5.

During the first phase of the fire, until a steel temperature of 405 °C, the longitudinal elongation of the heated beam is restrained not only by the bending stiffness of the heated columns that support this beam but also by the bending stiffness of the cold columns just above the beam. A compression force thus develops in that beam with, for equilibrium reasons, tensile forces in the beams directly above and below the heated beam. This is reflected in the bending moment diagram of the columns, especially the outermost ones.

From then on, the compression force in the heated beam decreases, not only because of the decrease of axial stiffness in that restrained beam and in the restraining heated columns but also because of the vertical downward deflection of the beam that provides some relief geometrically to the compression force. Whereas indirect effects of actions were mainly induced by restrained thermal expansion in the first phase of the fire, large displacements will play an increasingly prominent role.

At 633 °C, failure is imminent. A severe downward deflection in the central span of the heated beam is observed. The axial force and bending moment diagrams are not as disturbed as they were at 405 °C but are still not totally equal to the pattern displayed at room temperature.

Total collapse of the frame finally occurs at 634 °C by buckling of the two central columns. The axial force diagram shows that the compression force has nearly totally vanished in the upper part of these two central columns. This is because dynamic effects have been taken into account in this analysis (heating rate = 1 °C/s). An analysis made by a succession of static equilibrium would probably stop one or two degrees earlier, thus with only a marginal difference in critical temperature but a much less complete insight into the failure mode.

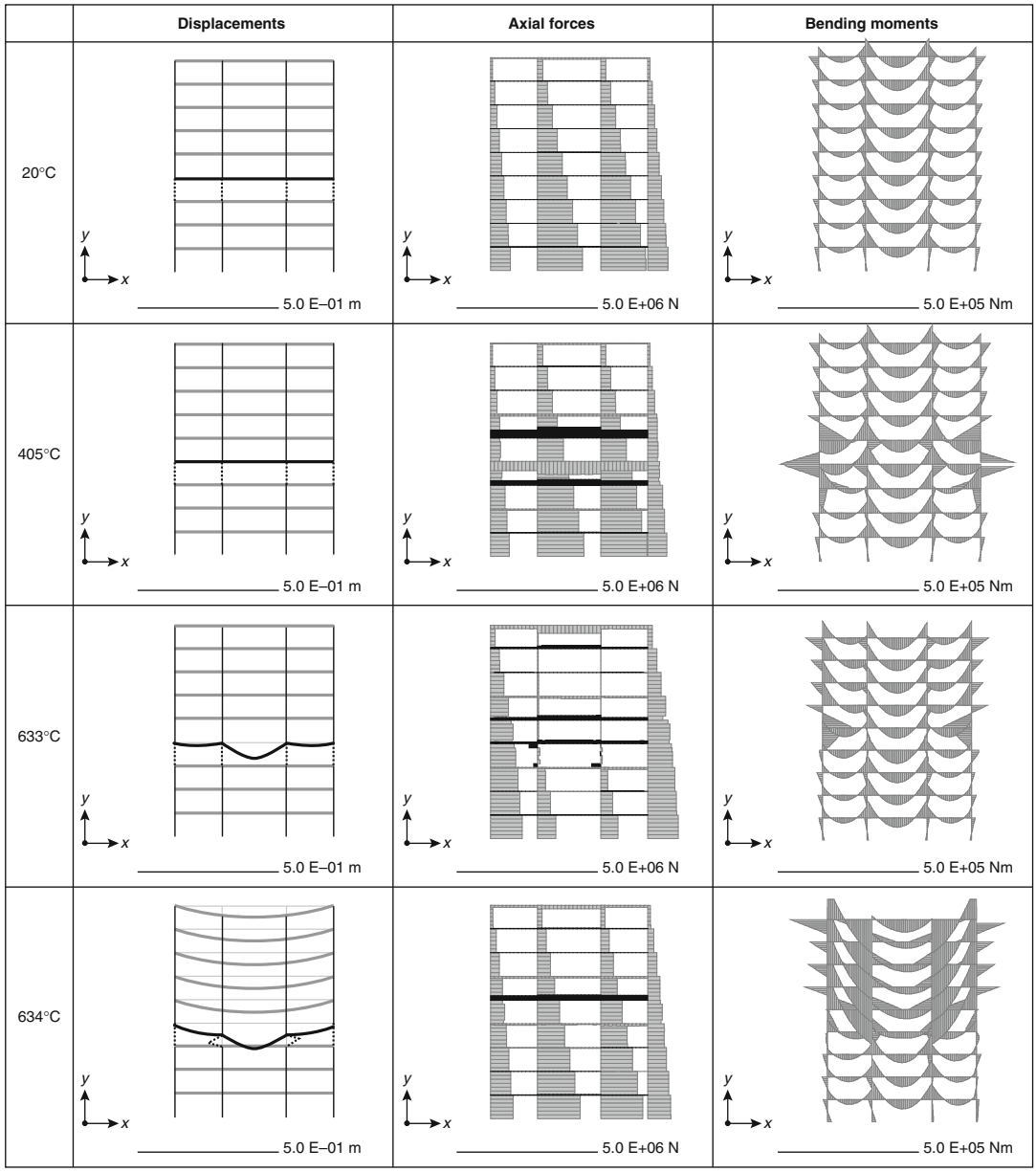

Fig. 52.14 A multistory portal frame under increasing temperature

Figure 52.15 shows the evolution of the axial force at mid length of the heated beam. It shows that, when failure is approaching, the axial force tends to decrease to the same level that it had been at room temperature, with even a sign reversal at the very end, when large displacement effects become predominant.

When the same examples are run with the thermal expansion of steel being artificially turned off, the simple frame of Fig. 52.12 fails exactly at the same critical temperature of 748 °C, whereas the multistory frame of Fig. 52.14 fails at a critical temperature of 613 °C, compared to a value of 634 °C with

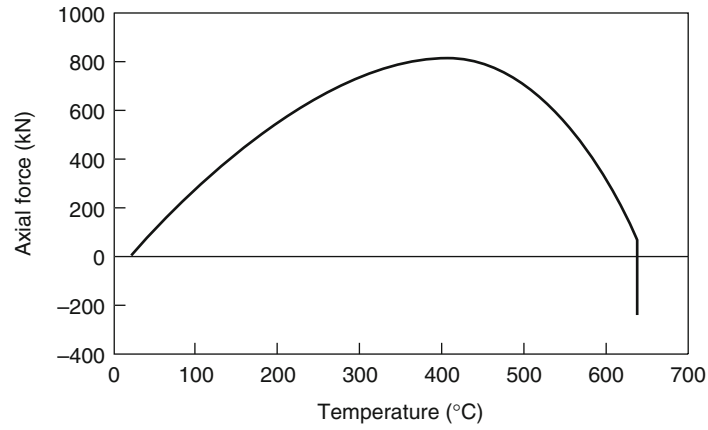

Fig. 52.15 Evolution of the axial force in the heated beam

thermal expansion being considered. This means that, in this particular example, the effects of thermal expansion are somewhat beneficial for the fire resistance.

Input and Modeling Uncertainties

Engineers and scientists are continually working with the reality of the physical world in which we are living. In particular, civil/structural engineers try to understand and quantify the different natural and materials phenomena in order to design safe structures and to protect these structures against any foreseeable loads and actions, including fire. The only way to represent the physical reality is to create analytical and experimental models that best represent it. If the models are realistic and simple enough, the engineer can vary the input of the models and see how the output varies. This allows the engineer to see the influence of different parameters on the behavior and safety of the structure.

Because the models are simplified representations of reality, they have their inherent limitations and uncertainties. Limitations are defined here as approximations that are clearly identified but accepted because of the range of input or response assumptions, or because they are considered to have a negligible influence on the results. On the other hand, uncertainties are defined as a lack of knowledge about a particular physical behavior (model uncertainty) or about the precise value of an input parameter (input uncertainties).

There are essentially two different types of model for representing reality: experimental models and analytical models. Experimental models consist of physical specimens built to represent the real structure. Very often, only a part of the structure can be represented by a specimen and tested as either a full-scale or a small-scale model. In the latter case, it is possible to represent a larger part of the structure, possibly the whole structure. Full-scale experimental models of complete structures are extremely rare in general and for structural fire response, with the one major exception and example being the series of tests performed by BRE at Cardington [25].

Analytical models are defined here as models made of equations and criteria, from the most fundamental force equilibrium, structural mechanics, and design criteria equations used in engineering office practice to the most complex numerical models (finite element), which require huge computing capabilities. A particular family of the analytical models consists of the empirical models, sometimes called the tabulated data. They are not real behavioral models, but the presentation in a simple form (data tables or statistical regression equations) of the results obtained by application of the experimental or analytical models.

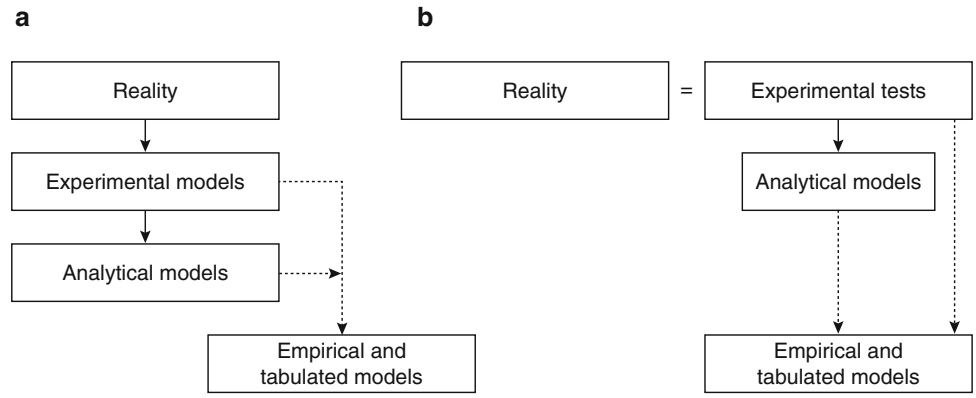

Fig. 52.16 Two common perceptions of the hierarchy in structural fire engineering

It is essential that the limitations and uncertainties of the models are fully understood by the users. If not, there is a high risk that the models may be used in an inappropriate manner or used beyond their intended scope of application. Sensitivity analyses by variation of suspect inputs can provide a more robust, bounded answer, but this is possible only if the uncertainties have been identified.

For some sciences, such as astronomy, experimental models are not feasible and only analytical models can be developed. In the field of structural fire engineering, the first experimental fire tests made on simple elements were conducted in the early 1900s before even the simplest analytical models could be created. At the end of the twentieth century, analytical models were becoming more complex due to the growth of the large historical fire test database and computational capabilities. The initial objective at the time when many of these numerical models appeared was to efficiently complement or replace fire testing of simple elements. Because of this delayed appearance of analytical models, there is a common perception that a hierarchy exists with reality at the top, the experimental models just underneath, and the analytical models at the bottom (Fig. 52.16a). For some, the experimental tests are even incorrectly considered as an exact representation of reality, not as a model of the reality (Fig. 52.16b).

The situation, that is, the relationship between the models and reality, is in fact different. First of all, it has to be realized that, when an engineer has to protect a future building against the effect of possible fires, there is no such a thing as "the reality" (Fig. 52.17).

The fires that occurred in the past provide us with some useful information but it has limited applicability. First, the historical fires may not have occurred on exactly the same structure as the one that is envisaged. Second, and above all, a building is very rarely instrumented with recording devices when a fire starts, and thus it is not easy to derive quantitative conclusions from the general observation of buildings devastated by a fire. The future fire that may occur in the building that is being designed does not belong to reality either, at least not at the time when the design is being made.

Note that one exception to this is when the case that is investigated is a real fire that occurred in a real building, in forensic investigations, for example. In that case, the text in the upper rectangle of Fig. 52.17 should be replaced by "Fire under investigation," and it belongs, indeed and unfortunately, to reality.

Second, regarding the relationship between the models and reality, if it is well accepted that analytical models, and especially the numerical models, have their own limitations, the general perception is that experimental models are a perfect representation of the real building or at least of the element under investigation. The technicians and engineers in charge of experimental fire tests know all too well this is not

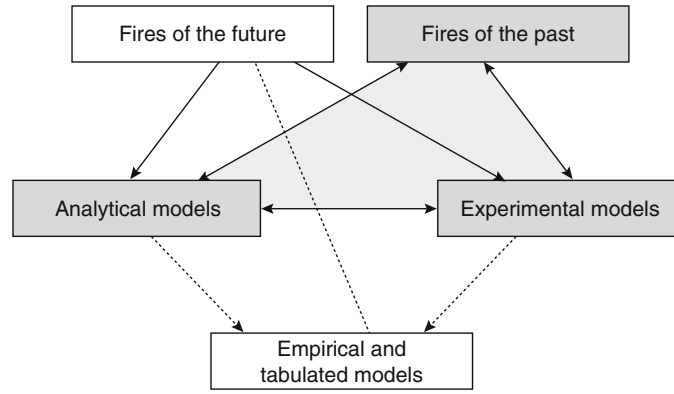

Fig. 52.17 A more correct representation of the relationships between the models

exactly the case. As it is sometimes said in a caricatured manner: "Nobody believes in the results of a numerical model, except the one who made it, but everybody believes in the results of an experimental test, except the one who made it."

Fires of the past, analytical models, and experimental models must be considered as three tools of similar utility, each with its own merits and limitations. They all should be considered on the same level, with no particular one being predominant. All three benefit from the others, as they mutually interact with each other. When analyzing a real fire, analytical models may help trying to explain what happened, and experimental reconstruction may help verifying some hypotheses made about the behavior of the building. When developing analytical models, experimental tests on simple elements are considered as the necessary point of comparison for verification, and comparison with the outcome of real fires may be considered as a good validation. Numerical models are very often used to make the predesign of experimental tests in order to ensure a higher probability of success or in a complementary manner in order to maximize the information obtained from the test.

The main limitations and uncertainties of the models will be briefly mentioned in the following sections. Most of the structures subjected to fire are designed according to the hypothesis of an uncoupling between the mechanical and the thermal problems. The temperatures in the structure are first calculated in the structure without taking the stress level into consideration, and these temperatures are then taken into account in the subsequent mechanical analysis. The limitations related to the determination of the temperature in the structure by analytical models will be discussed first, then the limitations related to the mechanical analysis by analytical models, and finally the limitations of experimental models.

Limitations and Uncertainties of Thermal Calculations

Thermal Properties In order to determine the evolution of the temperature in a structure, the thermal properties of the materials present in the structure must be known.

Generic properties are given in Appendix 2 of this Handbook for the most commonly used building materials such as structural steel, normal strength concrete, gypsum, and so forth. They can be used with a reasonable level of confidence because they have been widely validated and have been in use for several years already with no apparent significant problem. Attention must be paid when the field of application is extended to "similar" materials that may or may not have markedly different properties such as iron steel, stainless steel, high-performance concrete, bricks, mortars, and the like. The ideal situation is when the person determining the temperatures in a structure for a practical application has access

to experimental results made on elements comprising the material that will have to be taken into account in the application. It is then possible to determine by trial and error the thermal properties of the material that allow reproducing the results of the tests, and these properties can be used in subsequent analyses on structures that will not be tested but only calculated. Not only the thermal conductivity and the specific heat have to be determined but also the properties for the boundary conditions, such as the convection heat transfer coefficient and the emissivity. If this cannot be done and thermal properties of similar materials are utilized, the engineer must be aware of the inherent degree of uncertainty introduced in the final results.

For other materials, mainly the thermally insulating products, no generic properties can be given and the information must necessarily be taken from experimental tests. It must be emphasized that most of the thermal properties are highly temperature dependent and a value given for a commercial product for utilization at room temperature (e.g., insulating the walls of houses against heat loss to the outside atmosphere) cannot be used directly in a fire. The thermal conductivity, to name only one, has a tendency to increase significantly with increasing temperatures.

If a producer is able to deliver for his or her product the laws giving the evolution of the thermal properties as a function of the temperature, there is a high probability that these laws have been derived by recalculations of experimental tests by a simplified calculation method in which several hypotheses are included: a uniform temperature in the section, the temperature on the outside of the insulating layer equal to the temperature of the fire, and so on. The given laws are thus suitable for utilization in the same type of simple calculation model. If numerical calculations have to be performed, it is better first to recalculate all the available experimental tests by the use of the numerical model. Because the same simplifications are not present in the numerical analysis, the laws obtained by that method could indeed be slightly different from the laws obtained with the simplified method. It is important that the same model be used for a practical application as the one used to determine the thermal properties.

Fixed Geometry In most if not all methods used for determining the temperatures in structures exposed to fire, the geometry of the sections is given before the calculation starts, and it remains fixed during the whole simulation. Theories and numerical algorithms do exist for calculating temperature distributions in objects with a shape that is continuously changing (e.g., in the ablation process that occurs at the nose of re-entrant space vehicles), but these techniques are not commonly used for designing buildings subjected to fire.

A first situation of changing geometry is the case of intumescent painting, usually applied on steel members. Whereas the dry film has a very limited thickness in the order of some millimeters, the product exhibits an endothermic chemical reaction when heated and expands to a layer of foam-like product with a thickness of several tens of millimeters. Very few attempts have been made to model precisely this expansion (see Butler et al. [27]). The usual procedure is to model the intumescent painting as a purely conductive layer of constant thickness (e.g., the thickness of the dry film) and to determine "equivalent" thermal properties yielding the same temperature evolution for the steel section as the one observed in experimental tests. A peak can be introduced in the curve of specific heat in order to account for the endothermic chemical reaction. It has to be noted that different laws of thermal conductivity should possibly be used for different thicknesses of the dry film because it has been observed that the thermal resistance provided by these products is usually not proportional to the thickness of the dry film.

Another situation is found in timber sections that exhibit shrinkage and cracking after charring. A practical solution very often used is to also consider a constant geometry and equivalent thermal properties.

The phenomenon of concrete cracking and spalling, another situation of evolving geometry, is usually not taken into account when modeling concrete structures subjected to fire. This is acceptable only for materials that are known for not being particularly prone to spalling (e.g., normal-strength concrete with a limited level of free moisture), or if particular provisions have been made in order to prevent the occurrence of spalling (e.g., the addition of polypropylene fibers). In other cases, and especially for high-strength concrete, the behavior of the material against spalling must have been determined experimentally. In case of doubt or for critical situations, it is still possible to neglect from the very beginning of the calculation the presence of the outer layer, this one being assumed to disappear in the early stages of the fire because of spalling. The question is then to decide on the thickness of this sacrificial layer. A usual choice is to limit the spalling to the first layer of reinforcing bars, these being then directly exposed to the influence of the fire, but there is experimental evidence of cases when the spalling did progress beyond the first external layer of reinforcing bars.

Equally unpredictable by analytical models at this time are delaminations or detachment of spray-on materials or gypsum board and other fire-related damage that will accelerate thermal penetration into the structure.

Perfect Contact If two materials are in contact with each other in a section, the usual hypothesis for an analysis is that the contact at the interface between both materials is perfect. This is not always the case, and sometimes initial contact does not persist and disappears during fire tests.

For example, when a concrete slab is cast in situ on the upper flange of a steel beam in order to form a composite steel-concrete section, it is generally accepted that the contact between the concrete slab and the steel beam is nearly perfect and will remain so during the fire because of the eventual shear connectors fastening the slab to the beam. If not, simply the action of the gravity load is assumed to force the slab to follow any downward movement of the beam on which it is laid.

A situation with a similar geometry can arise if a concrete facade element is placed against the external flange of a steel column. In that case, it is not possible to be sure that no gap will be created during the course of the fire between the steel column and the wall element, with each one having its own thermal and structural bowing. If at least a reasonable amount of connectors is provided, it is reasonable to take the effect of the wall elements into account by supposing that the external flange of the steel column is not attacked by the fire. On the other hand, because of the uncertainty of the contact with the concrete element, the concrete element will not be represented in the thermal analysis of the steel column, which will inhibit in the model any heat sink effect from the column to the wall (an adiabatic boundary condition is imposed on the external flange of the column).

In composite steel-concrete slabs using unprotected thin steel decking, it has been observed in experimental tests that the steel sheet very often detaches from the concrete slab after a short duration. The research work performed by Both [28] allowed to take this effect into account in a method presented in Eurocode 4 [29], but this method is an empirical method. This effect is usually neglected in numerical analyses, with the consequences that the temperatures in the steel decking are slightly underestimated. The bare steel deck loses its strength very quickly anyway, and the temperatures in the concrete slab are somewhat overestimated, which is on the safe side.

A similar situation exists in hollow steel sections filled with concrete. The external steel tube has the highest temperatures in the section and exhibits the highest radial thermal expansion. This, plus the effect of the steam pressure from the evaporating water of the concrete, leads to a far from perfect contact, and a thermal resistance does appear at the interface between the concrete core and the steel section. As it was observed that the temperatures measured in the center of the section did not compare well with the temperatures computed on the base of a

perfect contact, it has sometimes been tried in the past to correct this effect by introducing very high levels of evaporable water in the concrete. Levels as high as 10 % in weight are reported in Eurocode 4 [29] although a more reasonable value of 4 % is recommended in the absence of data. It is by far physically more correct to include a thin layer of conductive material between the concrete core and the steel section. In Renaud [30], this contact resistance has been estimated to 0.01 m^2K/W, that is, equivalent to a 16 mm layer of concrete with a thermal conductivity of 1.6 W/mK (but it is geometrically more correct to use a 1 mm layer of a material with a conductivity of 0.1 W/mK)

Effects of Localized Fires The assumption most often used for the design fire scenario utilized for verification of a structure under the effects of fire is a uniform temperature in the compartment. The reasons are probably that, first of all, this is the situation prevailing in the standard fire tests that the numerical programs tried to mimic in the early days and, second, because it is a good approximation for fully developed fires in small compartments, which are the most challenging for the structure. Yet, more and more attention is being paid nowadays to localized fires, which include either any fire in its early stage or a fire in which the available fuel load is concentrated on a limited part of the floor area, such as a registration desk in an otherwise empty atrium or one car burning in a parking garage with no propagation to adjacent cars. These situations have to be considered because of the susceptibility of statically determinate structures to the failure of a single element that could be located just above the localized fire source, and also because this period of time when the situation is still tenable in the compartment is very critical for the evacuation of the occupants and for action of the fire brigade. With these localized fires, the temperature is far from uniform in the compartment and much more of a problem for the numerical programs. The temperature of the gas in the vicinity of the structure is by far not the most important parameter driving the heat transfer to the structure, with radiation from the fire source usually being dominant.

First, consequences are conceptual. The boundary conditions for the determination of the temperature in the structure are much more complex. They are certainly varying with the location of the boundary, and this possibility has to be taken into account in the numerical program. A steel beam located above the fire plume is not subjected to the same thermal attack as a beam located several meters away. Second, the question arises whether an uncoupled determination of the temperatures is still valid. Is it admissible to calculate the temperatures in the compartment using, for example, computational fluid dynamic (CFD) software and, afterward, the temperatures in the structure based on those calculated in the compartment? Or is it necessary to make a fully coupled determination of the temperatures, simultaneously in the compartment and in the structure, taking into account precisely the interaction between the two? The question has even been raised whether the mechanical analysis should not also be part of the same simulation. For example, the deflecting ceiling would modify the interior geometry of the compartment and this would also affect the development of the fire. Whereas the last coupling can probably be neglected in most cases, the thermal coupling from the localized fires to the structure must be considered, and this is not done easily.

A practical problem in which the interaction between the compartment and the structure has to be considered is the difference in size of the meshes used in both problems. Whereas the dimension of the cells can be in the order of 10–50 cm when modeling a compartment, the thickness of the web of a steel beam can be as low as 4 mm. It is not realistically possible to decrease the size of all cells of the compartment down to the size required for a precise determination of the temperatures in the structure. Algorithmic solutions must be derived in order to cope with this geometric discrepancy at the interface.

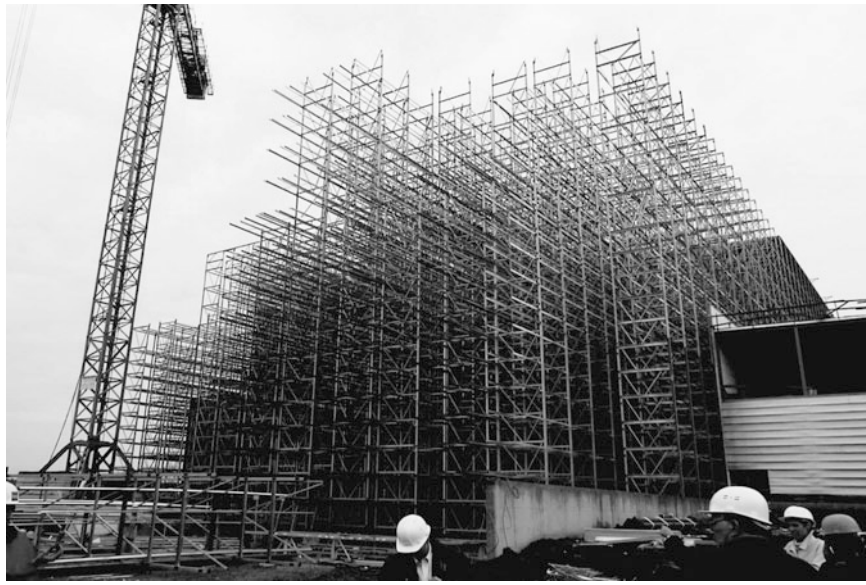

Fig. 52.18 A numerically very large structure

If the structure is subjected to the effects of a localized fire, the temperature distribution inside the structure is inherently a three-dimensional distribution. The precise determination of such a temperature distribution would normally require the utilization of a full three-dimensional model of the structure made of three-dimensional solid elements. The size of such a model would be so huge that it would not be practically feasible. Some approximations have to be made in the model, introducing some additional limitations.

Limitations and Uncertainties of Mechanical Calculations

Very Large Structures Although the geometrical dimensions of a structure are not a problem for numerical modeling, there is still a limit to everything, including the power of our processing units and the patience, schedules, or budgets of the users. Some complex steel structures may easily comprise tens of thousands of elements of different sorts, each experiencing a different temperature history (Fig. 52.18). These structures are not only geometrically big; they are above all numerically big. It is, for example, beyond any reasonable expectation to think that the whole structure of one of the WTC towers could in the foreseeable future be modeled completely in detail, with every member, every slab, and every connection represented. One possible solution in case of very large structures is to limit the analysis to substructures, that is, representative parts of the whole structure. It is also possible to represent with simple elements, possibly elastic ones, the parts of the structure that are far away from the zone affected by the fire and that are expected not to exhibit any nonlinear deterioration.

The most detailed beam finite elements used in numerical modeling allow determining the precise extent of plasticity at every point in the sections and along the members and provide a very precise shape of the deformed members; but several elements are required in order to represent each subassembly, such as a beam or a column. More simple formulations can be used, in which each subassembly is represented by a single element, for example, using the beam-column plastic hinge approach such as in Liew and Ma [31] or Landesmann [32].

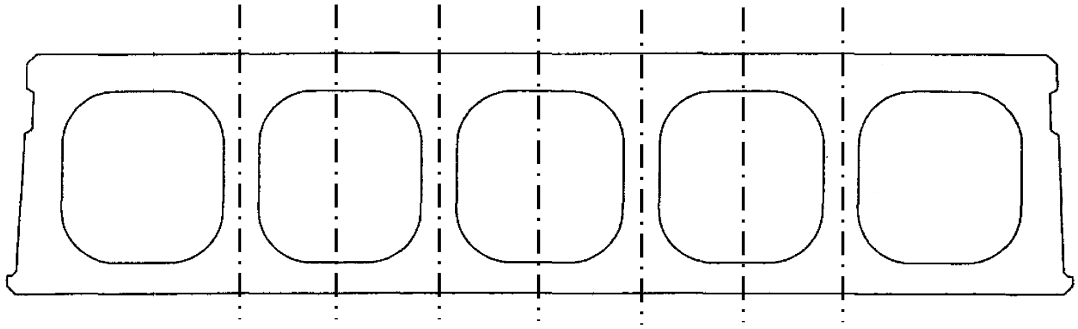

Fig. 52.19 Planes of symmetry in a hollow core slab

It has also to be realized that modeling a building structure, subjected to fire or not, using solid brick elements is far beyond our present possibilities. Only parts of the structure can be analyzed with these types of finite elements. In this case, the limitation explained in the following section will arise, namely the decision on the boundary conditions.

Boundary Conditions The boundary conditions may pose some problems in the discretizations that are particular to the fire. Some are inherent to the three-dimensional stress level in solid-type structures and they cannot be solved easily; others appear in bar-type structures when defining a substructure and selecting the appropriate boundary conditions.

Let us imagine that a simply supported flooring system made of parallel hollow core prefabricated concrete elements has to be modeled and that solid brick elements are used. If the loading is symmetric with respect to the longitudinal axis of the elements, only half of the span of the system needs be modeled. The boundary conditions along this plane of symmetry are standard and not particular to the fire. In the other direction, it is clear that a series of parallel vertical planes of geometrical symmetry do exist; for example, passing through the center of the cavities and also passing through the center of the webs between the cavities (Fig. 52.19).

If the loading is uniform on the floor, one might be tempted to discretize only a part of the structure, limited by a cavity and a web plane of symmetry. The question then arises about the boundary conditions, especially for the displacements perpendicular to the parallel planes of symmetry. If they are left free, no thermal stress will arise in this direction, and this is not correct in the fire situation. If they are completely fixed, a full restraint will be created, and this is also not correct. Even if the slab is laterally not restrained at all, a linear constraint relation between all the nodes located in a plane of symmetry would imply that a Bernoulli condition has been imposed, and this also may not correspond to reality. In fact, in order to obtain a realistic answer, it is impossible to consider all these parallel planes of symmetry. Only the one in the center of the slab can be taken into account. This means that as much as one-quarter of the whole floor has to be discretized. This can prove to create a model that is numerically very big.

In big structures made of bars, the concept of substructure is often used. In this case also, a choice has to be made for the boundary conditions at the interface between the structure and the rest of the structure (Fig. 52.20). The choice is for each degree of freedom between imposing a fixed displacement or imposing a force and leaving the displacement free. In fact, the real boundary conditions are intermediate between these two extreme solutions, dictated by the response of the surrounding structure.

Spalling The same limitations exist during the mechanical analysis as during the thermal

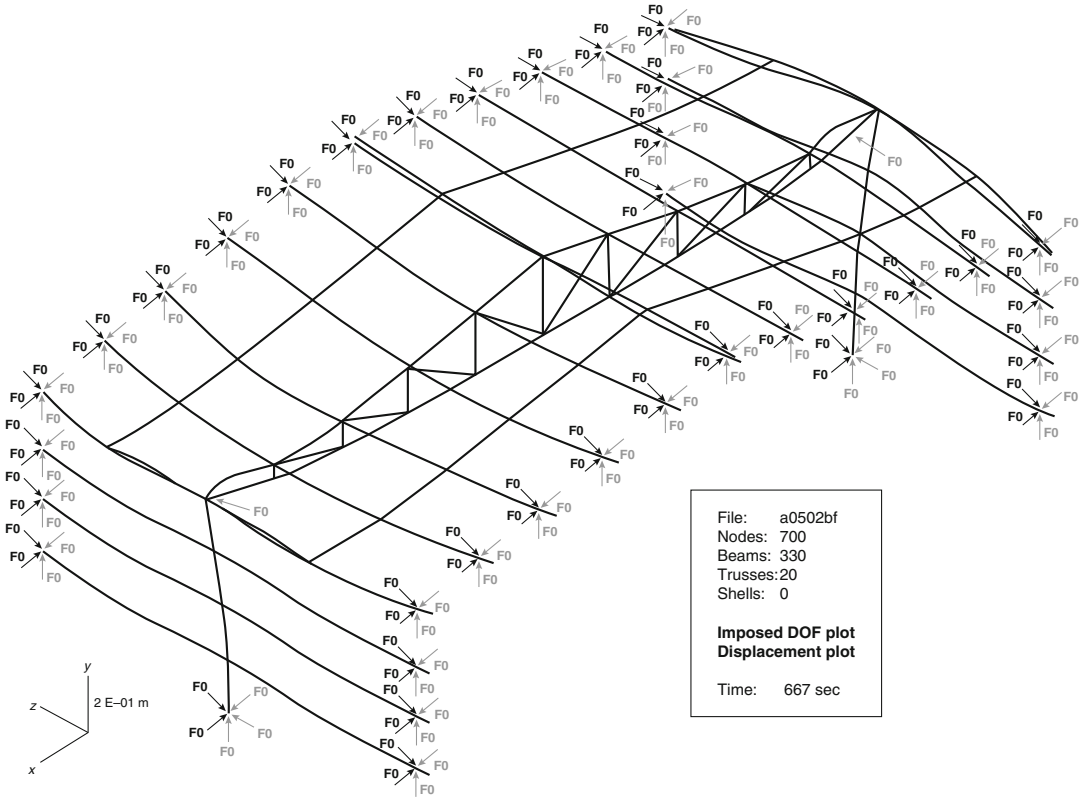

Fig. 52.20 Boundary conditions in a substructure

analysis; if the concrete spalling phenomenon is not taken into account when determining the temperatures, it is also not taken into account in the mechanical model. All comments made above in the section on fixed geometry could be repeated here.

It has to be mentioned that some efforts have indeed been made in order to predict the phenomenon of spalling. This modeling relies on highly sophisticated constitutive and numerical models taking into account the coupling between the mechanical and the thermal problems; mechanical stresses created by applied loads and by thermal restraint interaction with the water pressure. These models provide a unique insight in the phenomena that can help understand the physics and identify the relevant parameters. However, these models have to be provided with a very large number of temperature-dependent input data and the prediction cannot yet provide a complete level of confidence with respect to a phenomenon that is not really deterministic. As a consequence, in a real design situation, it is probably faster, much cheaper, and perhaps more reliable to make a simple experimental test aiming at identifying the susceptibility to spalling for a particular concrete mix/structure situation than to make all the experimental tests that are necessary to feed the model and then try to predict whether spalling is likely to occur or not.

Lack of Convergence The equations that govern the equilibrium of a structure subjected to fire are highly nonlinear, the reasons being in the geometrical as well as in the material behavior. Moreover, these equations express the equilibrium at a given time and, in order to model the evolution of the structure during the course of the fire, they have to be integrated over time. The

integration of these nonlinear equations involves an iterative procedure and experience has shown that, in structures with some level of complexity, convergence of this process is not guaranteed. Depending on the size of the time step or on the value used for the convergence criterium that is used, the simulation of the same case may stop running at different moments in the fire. The simulation may stop at an early stage, when the load-bearing capacity of the structure is not yet exhausted. These failure times produced by a lack of convergence are called *numerical failures*. In some cases, the experience of the user with nonlinear modeling in general and in the computer code used in particular allows the user to find a solution that makes the code run until the real physical time of collapse. But in the most difficult cases, all the algorithmic resources are not sufficient to solve this difficulty; the simulations stop prematurely, and this is certainly a severe limitation of the numerical models.

The biggest danger is that the user may be tempted to modify, in fact to alter, the model in order to facilitate the convergence. Modification of the constitutive models is a common way to achieve this result, with creation of numerical materials that are excessively elastic or with unlimited ductility or, for concrete, with an artificial tensile strength never encountered in reality. The model will then perhaps converge, but to a solution that has an unknown relation to the solution of the original problem. The user should perhaps have the courage to admit that the tool does not do the job that was expected, rather than draw conclusions from an altered model.

There is another problem linked to numerical modeling, which is in fact nearly at the opposite of the problem of numerical failures. In some cases, the deflections of the structure can be so high when the simulation stops that they have no possible physical existence. For example, the vertical deflection of a simply supported beam could exceed the floor to ceiling distance available under the beam. Or the horizontal displacement of a rolling support could reach several hundreds of millimeters.

Because of these two opposite problems, the moment of the last converged time step cannot be considered automatically as the fire resistance time of the structure. The displacements and the evolution of the displacements during the fire are the best indicators to decide about the fire resistance time.

If the displacements at the last converged time step are exceedingly large, it is necessary to observe the displacements at previous time steps and to decide when the fire resistance of the structure was exhausted. Conventional and sometimes arbitrary failure criteria have to be used, for example, based on deflection or deflection rate limits.

If no large displacement is found, it is necessary to judge whether this corresponds to a numerical failure or to the real loss of load-bearing capacity of the structure. Finding one degree of freedom in the structure for which the evolution of the displacement as a function on time shows a vertical asymptote near the end of the simulation is a good indication of real failure (runaway failure), at least when this movement involves a global displacement of the structure. The lateral displacement of an individual bar that buckles in a statically indeterminate structure may not be sufficient to lead to a global collapse. There are yet some cases, on the contrary, when a real failure has a particular fragile character and these are not so easily detected. The experience of the user is here a key factor.

Bernoulli Hypothesis The workhorse for modeling of building structure framing in fire is the Bernoulli beam finite element. It has yet to be understood that the hypothesis of plane sections remaining plane and perpendicular to the longitudinal axis has some consequences; some failure modes are not covered by this type of element. These are namely the shear failures, the slip between reinforcing bars or prestressing tendons and the concrete and the lack of rotational capacity due to local buckling. Any steel section, as thin as it might be, is seen by a Bernoulli beam finite element as a compact section with infinite rotational capacity. If local buckling is expected to be a crucial issue, it is still possible to rely on

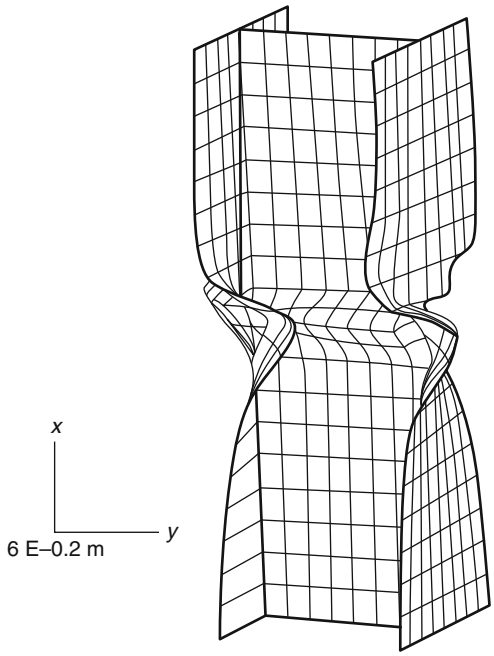

Fig. 52.21 Local buckling in a steel column

shell finite elements, see Fig. 52.21, but these are numerically more expensive elements and they will normally be used to analyze single members or subassemblies as opposed to complete structures.

Connections Connections between bar-type elements are most conveniently modeled on the basis of a simple hypothesis with respect to the relative rotation between the members: the connection is either assumed not to transmit any bending moment at all—hinged or pinned connection—or the relative rotation of the members is supposed to be null—rigid or fully fixed connection. In fact, the real behavior of any connection is between these two extreme situations. Any connection is semi rigid (or partially restrained), with some being more rigid than the others. The situation is more complex in the fire than at room temperature because of possible temperature differences between different components of the same connection and because of the presence of indirect effects of actions inducing axial forces (possibly different in sign between the heating and the cooling phase) and possible reversal in the sign of the applied bending moments. Very large displacements or thermal expansion can even totally modify the behavior of a connection. A connection that is very flexible at room temperature may become much stiffer in the fire if, for example, some gaps between different components are closed and these components enter into contact.

Significant research work has been done and is still being conducted on this topic with the aim of identifying and understanding the behavior of connections subjected to fire, especially of connections between steel, composite steel-concrete, and timber members. Valuable information has been derived, but this topic is still in the research phase and consideration of semi rigid connections in the fire situation is not yet common practice for real projects.

Limitations of Experimental Tests

Experimental tests also have their own limitations. Some are obvious, whereas others are not.

Cost is often mentioned as the first limitation. It is true that, in addition to the cost required by the fire laboratory for performing the test, other costs have to be added for the fabrication, transport, and disposal of the specimen, as well as for the time spent to define the test and assess its results.

The size of the structure is another limitation. Except under very exceptional circumstances, it is not possible to test a long span beam of, say, more than a few meters. Testing full-scale, complete structures is also seldom possible.

Time constraints may be another problem because there may be a significant amount of time between the day when the decision of a test is taken and the day when the results are available. Some time is required for buying the materials for the specimen if they are not available. The specimen has to be built and transported. Several months should be allowed for drying if concrete is involved. A time slot has to be found in the operations of a possibly busy

fire lab, and the results have to be documented and interpreted. For some problems and questions that may appear during the erection phase of a building, time may simply not be available and experimental testing is, therefore, not an option.

Experimental testing has the same problem of boundary conditions as the analytical models but in the opposite direction. Pure and perfectly identifiable boundary conditions—such as perfect hinges and totally fixed supports for a mechanical analysis or an adiabatic condition for a thermal analysis—are easily considered in an analytical model, but they seldom represent the real boundary conditions that may exist in reality. On the contrary, it is very difficult to impose well-defined boundary conditions in an experimental test. Perfectly fixed supports would require an infinitely stiff testing machine. Some precautions that may prove technically complex and financially demanding have to be taken to approach a perfect hinge. It is very difficult to test a column under a perfectly centrically loaded condition. If, and this is often the case, the supports of the specimen are outside the furnace, the longitudinal heat loss along the member is not easily quantified, but may have a significant influence on the result.

The results of experimental testing have variability. Two identical specimens tested in the same laboratory will generally not yield exactly the same result. For example, variability has been observed and documented for concrete elements in which a slight difference in the concrete cover on the reinforcing bars or a difference in spalling may have a significant influence on the results. Variability may be higher in axially loaded columns than in elements with first-order bending moments because of the bigger relative influence of accidental eccentricities in the first case. Assemblies protected with membrane ceilings likewise can exhibit substantial fire performance differences attributable to the gypsum board material and its installation details, as can other assemblies or members that are more susceptible to physical integrity failures of the protection material or system. As a consequence, it is very difficult to make a parametric or sensitivity analysis by experimental testing, because the influence of the parameter that is analyzed may be hidden by the noise produced in the results by the variability linked to other factors. This is not the case, of course, if the number of experimental tests is statistically significant—and this may require a very significant number of tests—or if the influence of the analyzed parameter is overwhelming. Because of this variability, a so-called validation of any analytical model by comparison with the result of one or even a few experimental tests may be inconclusive.

Summary

This chapter reviews the key fundamentals of structural fire engineering and introduces the more advanced analytical methods (finite element–based for computers) that are emerging. It relies on the existing background derived from decades of prescriptive fire resistance testing and design and provides an advanced framework that enables solutions for performance-based objectives. Limit states structural design principles, fire loads and resistance, reliability, heat transfer, and the basics of structural analysis are presented. Several of the important variables affecting response to severe fire exposures are described, all of which can influence potential for major damage and collapse. These include thermal strains; local, member, and frame instability; floor slab effects and catenary action; connection stiffness and strength; nonuniform heating; material properties; and limit states.

The highlight of this chapter is contained in the insights and nuances of higher-order structural fire analysis, including the nonlinear elastoplastic regime, for different types of problems, exposures, primary loads, construction materials and elements, and levels of discretization. This information draws heavily from research, international sources, and engineering experience in the field. Modeling considerations for individual structural elements, substructures, and entire frames are given and further reinforced with a realistic overview of

their advantages, limitations, uncertainties, and possible issues with numerical solution convergence. These advanced analytical methods are also juxtaposed to the typical constraints and limitations of construction fire testing to create a balanced perspective on their capabilities for prediction of actual structural behavior.

Nomenclature

A_k	Structural fire effects, typically the construction material's strength and stiffness reductions caused by the fire's heating
D	Nominal design dead load
E	Youngs modulus of a material
f_y	Minimum specified yield strength
L	Nominal design live load (gravity)
L_{fire}	Design values of the load effects (direct effects resulting from the applied loads and indirect effects resulting from restrained thermal expansion) expected to be simultaneously acting during the fire event
M_n	Nominal flexural strength
M_u	Required (factored) flexural strength
P_n	Nominal axial strength
P_u	Required (factored) axial strength
x	Strong principal axis of the cross section
y	Weak principal axis of the cross section
S	Nominal design snow load
t	Time
T	Temperature
R_{fire}	Available structural resistance under the particular high temperature conditions, including the effects of degraded material properties

Greek Letters

$\Upsilon_{M,1}$	Partial safety factor for material strength
$\Delta\sigma$	Variation of mechanical stress
$\varepsilon_{mechanical}$	Mechanical strain
$\varepsilon_{thermal}$	Thermal strain
ε_{total}	Total strain
ϕ_c	Resistance factor for compression
ϕ_b	Resistance factor for flexure

References

1. ASCE/SFPE 29-05, *Standard Calculation Methods for Structural Fire Protection,* Structural Engineering Institute of the American Society of Civil Engineers, Reston, VA (2005).
2. ASTM, ASTM E119, *Standard Test Method for Fire Tests of Building Construction and Materials,* American Society for Testing and Materials, West Conshohocken, PA.
3. B.R. Ellingwood, "Load Combination Requirements for Fire-Resistant Structural Design," *Journal of Fire Protection Engineering,* 15, 1, pp. 43–61, Society of Fire Protection Engineers, Bethesda, MD (2005).
4. UL 263, *Standard for Fire Tests of Building Construction and Materials,* Underwriters Laboratories Inc., Northbrook, IL.
5. NFPA 251, *Standard Methods of Tests of Fire Resistance of Building Construction and Materials,* National Fire Protection Association, Quincy, MA (2006).
6. International Standards Organization, ISO 834, *Fire Resistance Tests—Elements of Building Construction,* International Organization for Standardization, Geneva, Switzerland.
7. A.H. Buchanan, *Structural Design for Fire Safety,* John Wiley and Sons, New York (2001).
8. SFPE S.01 2011, *SFPE Engineering Standard on Calculating Fire Exposures to Structures,* Society of Fire Protection Engineers, Bethesda, MD (2011).
9. EN 1999-1-2, *Eurocode 1: Actions on Structures Exposed to Fire,* European Committee for Standardization (CEN), Brussels, Belgium (2002).
10. J Stern-Gottfried and G. Rein, "Travelling fires for structural design–Part I : literature review", *Fire Safety Journal,* 54, pp. 74–85 (2012).
11. NFPA 557, Standard for Determination of Fire Loads for Use in Structural Fire Protection Design, National Fire Protection Association, Quincy, MA (2012)
12. J.B. Schleich, L.G. Cajot, M. Pierre, M. Brasseur *et al.*, *Development of design rules for steel structures subjected to natural fires in large compartments*, RFCS research report N° EUR 18868 EN, ECSC Steel Publications, Brussels (1999).
13. J.M. Franssen, "Tensile membrane action in composite floors subjected to fire", in *Advances in steel concrete composite and hybrid structures,* Research Publishing, Singapore, pp 125–154 (2012), http://hdl.handle.net/2268/126889
14. Newman G M, Robinson J T and Bailey C G (2006) *Fire Safe Design: A new approach to multi-storey steel framed buildings,* P288, The Steel Construction Institute

15. Zhao B, Roosefid M and Vassart O (2008), *Full scale test of a steel and concrete composite floor exposed to ISO fire*, Proc. of the 5th Structures in Fire Workshop SiF'08, Singapore
16. K.S. Al-Jabri, J.B. Davison and I.W. Burgess, "Performance of beam-to-columns joints in fire – A review", Fire Safety Journal, Vol. 43-1, pp 50–62 (2008)
17. B. Zhao, M. Roosefid *et al., Connections of steel and composite structures under natural fire conditions (COSSFIRE)*, EU Bookshop, Luxemburg (2011)
18. J.M. Franssen and F. Gens, "Dynamic Analysis Used to Cope with Partial and Temporary Failures," in *SiF04, Structures in Fire—Proceedings of the 3rd International Workshop* (J.M. Franssen, N. Bénichou, V.R. Kodur, and M.A. Sultan, eds.), NRC-CNRC, IRC, Ottawa (May 2004),), http://hdl.handle.net/2268/15030
19. ASCE/SEI 7-10, *Minimum Design Loads for Buildings and Other Structures,* Structural Engineering Institute of the American Society of Civil Engineers, Reston, VA (2010).
20. NIBS/MMC, *Best Practice Guidelines for Fire Safety Design of Concrete and Steel Structures,* Multihazard Mitigation Council of the National Institute of Building Sciences, Washington, DC (draft, in production).
21. ANSI/AISC 360-10, *Specification for Structural Steel Buildings,* American Institute of Steel Construction, Chicago, IL (June 2010).
22. O. Burnier, Reconstitution de l'incendie de deux voitures dans le parking de la Tour d'Ivoire à Montreux, le 9 décembre 2010, Travail de diplôme, heig-vd ed., Yverdon-les-Bains (2011)
23. T. Gernay and A. Millard, "A multiaxial concrete model for applications in structural fire engineering", Proc. 7th intl Conf. on Structures in Fire, 2012, M Fontana, A. Frangi and M. Knobloch ed., ETH Zürich, 531–540, http://hdl.handle.net/2268/115505
24. J.-M. Franssen, V. Kodur, and R. Zaharia, *Designing Steel Structures for Fire Safety,* Taylor & Francis, Leiden, the Netherlands (2009),, http://hdl.handle.net/2268/14870
25. C.G. Bailey, T. Lennon, and D.B. Moore, "The Behaviour of Full-Scale Steel-Framed Buildings Subjected to Compartment Fires," *Structural Engineer,* 77, 8, pp. 15–21 (1999).
26. C.G. Bailey and D.B. Moore, "The Structural Behaviour of Steel Frames with Composite Floor slabs Subject to Fire: Part 1: Theory," *Structural Engineer,* 78, 11, pp. 19–27 (2000).
27. K.M. Butler, H.R. Baum, and T. Kashiwagi, "Three Dimensional Modeling of Intumescent Behavior in Fires," *Fire Safety Science: Proceedings of the 5th International Symposium* (Y. Hasemi, ed.), International Association for Fire Safety Science, Boston, MA, pp. 523–534 (1997).
28. C. Both, *The Fire Resistance of Composite Steel Concrete Slabs,* Ph.D. Dissertation, TU Delft, Delft University Press, Delft, the Netherlands (1998).
29. EN 1994-1-2, *Eurocode 4: Design of Composite Steel and Concrete Structures—Part 1–2: General Rules—Structural Fire Design,* European Committee for Standardization (CEN), Brussels, Belgium (2005).
30. C. Renaud, *Improvement and Extension of the Simple Calculation Method for Fire Resistance of Unprotected Concrete Filled Hollow Columns,* CTICM Report INC-01/262-CR/IM, Centre Technique Industriel de la Construction Métallique, Saint-Aubin, France (2001).
31. J.Y. Liew and K.Y. Ma, "Advanced Analysis of Steel Framework Exposed to Accidental Fire," in *Proceedings of SiF02* (P.J. Moss, ed.), University of Canterbury, Christchurch, New Zealand (2002).
32. A. Landesmann, "Plastic-Hinge Approach for Performance-Based Assessment of RC Columns Under Fire," in fib workshop "Fire Design of Concrete Structures," University of Coïmbra, Portugal, 2007, International Federation for Structural Concrete (fib), Lausanne, Switzerland (in press).

Jean-Marc Franssen is full professor at the University of Liege in Belgium. His field of expertise is research in the behavior of structures subjected to fire and modeling of fire compartments (parametric models and zone models).

Nestor Iwankiw is senior engineer at Quartier Polytech, Liége, Belgium, involved in testing, analyses, product development, and code compliance for structural fire resistance.

Analytical Methods for Determining Fire Resistance of Steel Members

53

James A. Milke

Introduction

Traditionally, fire resistance has been evaluated by subjecting a structural member to a standard test for a specified duration [1]. All members performing acceptably are rated and listed for the duration period of the test (e.g., 1 h, 2 h). Assemblies not listed are assumed to be unable to meet the test criteria and thus have no rating, unless proven otherwise. Providing proof of acceptable performance can be accomplished in one of three manners:

1. Conduct the standard test [1].
2. Conduct a special experiment [2].
3. Apply an analytical technique [3].

The standard test can involve an appreciable turnaround time in order to specify, schedule, and analyze the results of the test. An experimental program can require a substantial amount of effort in order to obtain accurate data. The costs involved in sponsoring a standard test or experimental program can be appreciable. In the case of archaic structural assemblies, materials may no longer be available to reconstruct the design for possible testing.

Because of these drawbacks, calculation methods have been developed to analyze structural designs for fire conditions. The calculation methods have been formulated based on analyses of data from standard tests, experimental programs, and theoretically based investigations.

J.A. Milke (✉)
Department of Fire Protection Engineering, University of Maryland, College Park, MD 20742, USA

A broad-based analytical method for fire resistance will consider three aspects:

1. Fire exposure
2. Heat transfer
3. Structural response

The fire exposing the structure must be characterized using methods described in other chapters of this handbook for the case of a real fire or by assuming the fire exposure specified in the standard test. An SFPE standard provides parameters to describe exposing fires for six fire scenarios [4]. The thermal response of the structural member can be addressed using principles of heat transfer. Heating within the member is treated by a conduction heat transfer analysis (radiation and convection heat transfer may also need to be considered if voids or porous insulation materials are present within the assembly). Typically, radiative and convective boundary conditions are applicable. Finally, the structural response is examined by comparing some or all of the following: deflections, strains, and stress levels to established limits.

The following types of calculation methods are available to assess the fire resistance of steel structural members:

1. Empirical correlations
2. Heat transfer analyses
3. Structural analyses

Empirical correlations are based on the analysis of data resulting from performing the standard test numerous times. A limitation of the empirical correlations is that they can be applied only when considering the fire exposure, loading, and span

M.J. Hurley (ed.), *SFPE Handbook of Fire Protection Engineering*,
DOI 10.1007/978-1-4939-2565-0_53, © Society of Fire Protection Engineers 2016

provided in the standard test. If other conditions apply, then another approach is needed.

The second group of calculation methods consists of heat transfer analyses. The heat exposure conditions may be those associated with the standard test or a specified fire. The purpose of the heat transfer analysis is to determine the time required for the structural member to attain a predetermined critical temperature or to provide input to a structural analysis. The temperature endpoint criteria cited by ASTM E119 [1] are often accepted as the critical temperatures. Typically, inaccuracies of this method are related to the temperature dependence of the material properties or the description of the heating conditions.

Many of the structural analysis–based calculations are similar to those conducted for structural engineering purposes, except the material properties are evaluated at elevated temperatures and thermal expansion is considered. In higher order analyses, creep may also be accounted for. In structural analyses, the loading and end conditions must be known or assumed. Limitations result from uncertainties in characterizing the end conditions and the material properties at elevated temperatures.

This chapter provides an overview of the available calculation methods for determining the fire resistance of steel structural members. The basis of each method will be presented along with sample applications.

Standard Test for Fire Resistance of Structural Members

The standard test method in the United States for determining the fire resistance of columns, floor and roof assemblies, and walls is ASTM E119 [1].[1] Basically, the test involves subjecting the structural component to a heated furnace environment for the desired duration. If the endpoint criteria are not reached prior to the end of the test period, the assembly passes the test and is rated.

[1] Versions of the test method are also published as NFPA 251 [5] and UL 263 [6].

Gas burners are used to heat the furnace in testing laboratories throughout North America. The furnace is heated so that the temperature inside the furnace follows the time-temperature curve illustrated in Fig. 53.1. In principle, the time-temperature curve is intended to relate to a severe exposure from a room fire, though relating the standard exposure to actual fires is difficult. Thus, the applicability of the test method to examine the fire resistance of exterior structural members exposed to fires outside of the building is questionable [4].

Assemblies may be tested with or without load. If tested under load, the assembly is subjected to maximum design stress levels, based on common structural analysis procedures for ambient temperature design. Floor and roof assemblies and bearing walls are always tested under load. Columns are tested with or without a loading. Steel beams and girders may be tested without load if the design loading cannot be achieved in the laboratory.

Structural assemblies may be restrained or unrestrained against thermal expansion. The effect of restraint on the fire resistance of assemblies has been investigated by Bletzacker [7]. The degree of restraint in structural members varies with the geometry, connection method, and framing system, among other factors [6]. The descriptions presented in Table 53.1 relate actual construction conditions to the restrained and unrestrained designation noted in the ASTM E119 test method.

The minimum dimensions of the structural components for testing are specified in ASTM E119. A maximum set of dimensions is established by the size of available test furnaces. Although the test is large scale, the test cannot be considered full scale, given the stipulation of the maximum permissible dimensions. The consequence of not testing full-scale members means that continuous beams, actual floor/roof ASTM assemblies, and long columns are not tested. Consequently, given the scale of the test and furnace exposure conditions, this test is only comparative in nature and cannot be used to assess performance in actual fires.

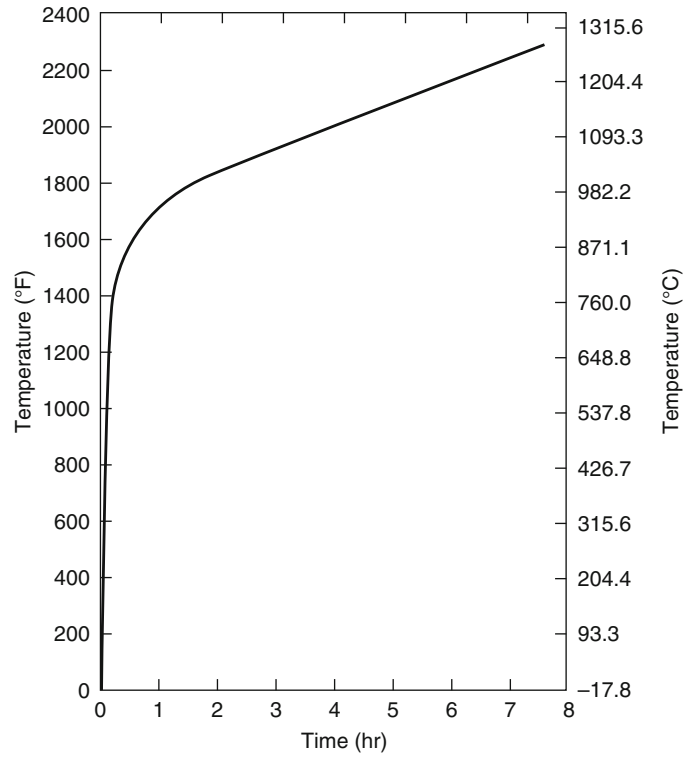

Fig. 53.1 ASTM E119 standard time-temperature curve [1]

The ASTM E119 endpoint criteria for building assemblies consider structural integrity, temperature, passage of flame, ignition of cotton waste, and, in some cases, response to the hose stream. For the tests without loading, the structural integrity endpoint criterion is relaxed to require that the component only remains in place. The structural integrity criterion addresses the need for members to remain in place (supporting self-weight of member) and to continuously support any applied loads. The ignition-of-cotton-waste endpoint addresses the ability of the structural assembly to prevent the transmission of flame and hot gases to the side not exposed to the furnace fire.

The temperature endpoint criteria are noted in Table 53.2. In principle, the endpoint temperatures are based on the maximum allowable reduction in load-bearing capacity of the structural member, considering the reduction in steel strength experienced at elevated temperature and the maximum permissible loads stipulated by structural design standards.

Fire Resistance of Steel Members

Several calculation techniques are available to determine the fire resistance of steel members, including steel columns, beams in floor and roof assemblies, and trusses [8–11]. Three types of techniques are available: empirically derived correlations, heat transfer analyses, and structural analyses.

The equations and models do not eliminate the need for all future testing. Testing is still required, at least to validate the calculation techniques and assess the interaction and mechanical behavior of the constituents of the assembly, such as the steel structural member, insulating materials, or other components. However, the calculation techniques can be used to extend the application of test results and reduce the number of required tests. In addition, experimental methods are essential in determining the material properties at elevated temperatures of the protection materials.

Table 53.1 Restrained and unrestrained construction systems (From ASTM E119 Table X3.1) [1]

Wall bearing	
Single span and simply supported end spans of multiple bays[a]	
Open-web steel joists or steel beams, supporting concrete slab, precast units, or metal decking	Unrestrained
Concrete slabs, precast units, or metal decking	Unrestrained
Interior spans of multiple bays	
Open-web steel joists, steel beams, or metal decking, supporting continuous concrete slab	Restrained
Open-web steel joists or steel beams, supporting precast units or metal decking	Unrestrained
Cast-in-place concrete slab systems	Restrained
Precast concrete where the potential thermal expansion is resisted by adjacent construction[b]	Restrained
Steel framing	
Steel beams welded, riveted, or bolted to the framing members	Restrained
All types of cast-in-place floor and roof systems (such as beam-and-slabs, flat slabs, pan joists, and waffle slabs) where the floor or roof system is secured to the framing members	Restrained
All types of prefabricated floor or roof systems where the structural members are secured to the framing members and the potential thermal expansion of the floor or roof system is resisted by the framing system or the adjoining floor or roof construction[b]	Restrained
Concrete framing	
Beams securely fastened to the framing members	Restrained
All types of cast-in-place floor or roof systems (such as beam-and-slabs, flat slabs, pan joists, and waffle slabs) where the floor system is cast with the framing members	Restrained
Interior and exterior spans of precast systems with cast-in-place joints resulting in restraint equivalent to that which would exist in condition III(1)	Restrained
All types of prefabricated floor or roof systems where the structural members are secured to such systems and the potential thermal expansion of the floor or roof systems is resisted by the framing system or the adjoining floor or roof construction[b]	Restrained
Wood construction	
All types	Unrestrained

[a]Floor and roof systems can be considered restrained when they are tied into walls with or without tie beams, the walls being designed and detailed to resist thermal thrust from the floor or roof system

[b]For example, resistance to potential thermal expansion is considered to be achieved when:

1. Continuous structural concrete topping is used
2. The space between the ends of precast units or between the ends of units and the vertical face of supports is filled with concrete or mortar, or
3. The space between the ends of precast units and the vertical faces of supports, or between the ends of solid or hollow core slab units, does not exceed 0.25 % of the length for normal-weight concrete members or 0.1 % of the length for structural lightweight concrete members

Steel Material Properties

The principal material properties of interest are yield strength, ultimate strength, modulus of elasticity, coefficient of thermal expansion, density, specific heat, and thermal conductivity. The effect of temperature on steel properties has been examined by many researchers [12]. For steel, all of the properties, except for density, are strongly influenced by temperature.

The thermal properties of ASTM A36 steel are provided in the following correlations [8, 13–15]:

$$k = \begin{cases} -0.022T + 48 & (0 \le T < 900^{\circ}\mathrm{C}) \\ 28.2 & (900^{\circ}\mathrm{C} < T) \end{cases}_{[\mathrm{W/m \cdot K}]} \quad (53.1)$$

Table 53.2 ASTM E119 temperature endpoint criteria [1]

Structural member	Location	Maximum temperature °C (°F)
Walls/partitions (bearing and nonbearing)	1. Unexposed side	
	Average	139 (250)[a]
	Single point	181 (325)[a]
Steel columns	1. Average	538 (1000)
	Single point	649 (1200)
Floor/roof assemblies and loaded beams	1. Unexposed side	
	Average	139 (250)[a]
	Single point	181 (325)[a]
	2. Steel beam	
	Average	593 (1100)
	Single point	704 (1300)
	3. Prestressing steel	426 (800)
	4. Reinforcing steel	593 (1100)
	5. Open-web steel joists	593 (1100)
Steel beams/girders (not loaded)	1. Average	538 (1000)
	Single point	649 (1200)

[a]Maximum temperature cited refers to the maximum temperature rise above initial conditions

$$c_s = \begin{cases} 0.51T + 420 & (0 \le T < 650^\circ\text{C}) \\ 8.65T + 4870 & (650^\circ\text{C} < T \le 725^\circ\text{C}) \\ -10.9T + 9340 & (725^\circ\text{C} < T \le 800^\circ\text{C}) \\ 578 & (800^\circ\text{C} < T)_{[\text{J/kg.K}]} \end{cases}$$

$$\rho = 7860 \ \text{kg/m}^3 \tag{53.2}$$

The influence of temperature on the mechanical properties of A36 steel is presented in Fig. 53.2. At 538 °C (1000 °F) the yield strength is approximately 60 % of the value at normal room temperature.

Mathematical expressions describing the relationship of the yield strength, modulus of elasticity, and coefficient of thermal expansion on temperature are [8, 17, 18]

For $0 < T \le 600$ °C,

$$\sigma_{yT} = 1 + \frac{T}{900 \ln(T/1750)}\sigma_{y0}$$
$$E_T = 1 + \frac{T}{2000 \ln(T/1100)}E_0 \tag{53.3, 53.4}$$

For $T > 600$ °C,

$$\sigma_{yT} = \frac{340 - 0.34T}{T - 240}\sigma_{y0}$$
$$E_T = \frac{690 - 0.69T}{T - 53.5}E_0 \tag{53.5, 53.6}$$

For any temperature of interest,

$$\alpha_T = (0.04T + 12) \times 10^{-6} \tag{53.7}$$

where

σ_{yT} = Yield strength at temperature T (MPa) (psi)
σ_{y0} = Yield strength at 20 °C (68 °F) (MPa) (psi)
E_T = Modulus of elasticity at temperature T (MPa) (psi)
E_0 = Modulus of elasticity at 20 °C (68 °F) (MPa) (psi)
α_T = Coefficient of thermal expansion at temperature T (m/m °C)
T = Steel temperature (°C)

Alternatively, values of the yield and tensile strength and modulus of elasticity at elevated temperature are included in Appendix 4 of the AISC Specification [19], and BSI 5950 [20]. In addition to the changes in material properties that occur at elevated temperatures, the crystalline structure of steel also changes, as noted in Fig. 53.3 [21]. However, for the low-carbon steels typically used in building construction, significant changes in crystalline structure begin to occur only at temperatures in excess of 650 °C (1200 °F) [22], above the endpoint temperature noted in the standard test.

Creep, the time-dependent deformation of a material, may be significant in structural steel at temperatures in excess of 460 °C (860 °F) [23]. The rate of creep increases approximately 300 times for ASTM A36 structural steel when the steel temperature is increased from 460 to 520 °C (860–968 °F). In-depth discussions of

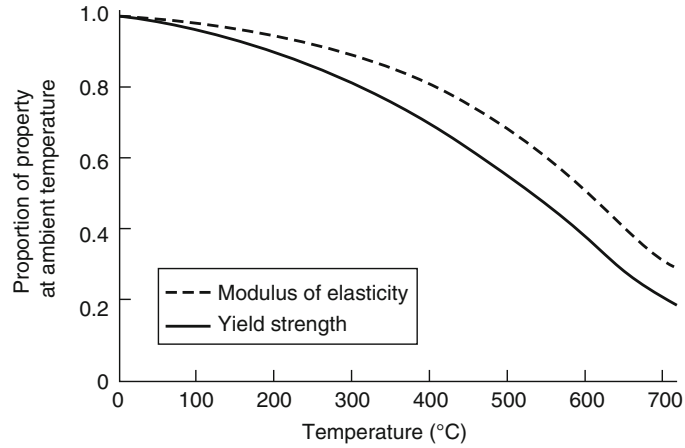

Fig. 53.2 Temperature effects on properties of ASTM A36 steel [13, 16]

creep have been prepared by Harmathy [24, 25]. Because of the complexity in addressing creep explicitly, given its dependence on the stress level, rate of heating, and other factors, often creep is included implicitly in the mechanical properties to simplify the fire resistance calculations [16, 23]. One exception to this approach was in the NIST study of the collapse of the North and South Towers of the World Trade Center. In their study, Gross and McAllister proposed that creep was a significant factor that led to the collapse of the towers [26].

Methods of Protection

The basic intent of the various methods of protection is to reduce the rate of heat transfer to the structural steel. This is accomplished by using insulation, concrete filling, membranes, flame shielding, and heat sinks.

Insulation

Insulation of the steel is achieved by surrounding the steel with materials that preferably have the following characteristics [27]:

1. Noncombustibility and the added attribute of not producing smoke or toxic gases when subjected to elevated temperatures
2. Thermal protective capability when subjected to elevated temperatures
3. Product reliability giving positive assurance of consistent uniform protection characteristics
4. Availability in a form that permits efficient and uniform application
5. Sufficient bond strength and durability to prevent either dislodgement or surface damage during normal construction operations
6. Resistance to weathering or erosion resulting from atmospheric conditions

In addition to the insulating qualities of the protection materials, chemical reactions may occur in the insulation, further reducing the rate of heat transfer. The chemical reactions include calcination, ablation, intumescence, thermal hydrogeneration, and sublimation.

Insulating methods include the use of board products, spray-applied materials, and concrete encasement. A brief review of each method is presented below.

Board Products Four types of board products are commonly used to protect structural steel: gypsum board, fiber-reinforced calcium silicate board, vermiculite-sodium silicate board, and mineral fiber board. In each case, the means of attachment of the boards surrounding the steel is a critical parameter affecting the performance of the assembly. Two commonly used methods of attachment of gypsum wallboard with and without steel covers are illustrated in Fig. 53.4. Detailed descriptions of the attachment mechanisms for the other board products are

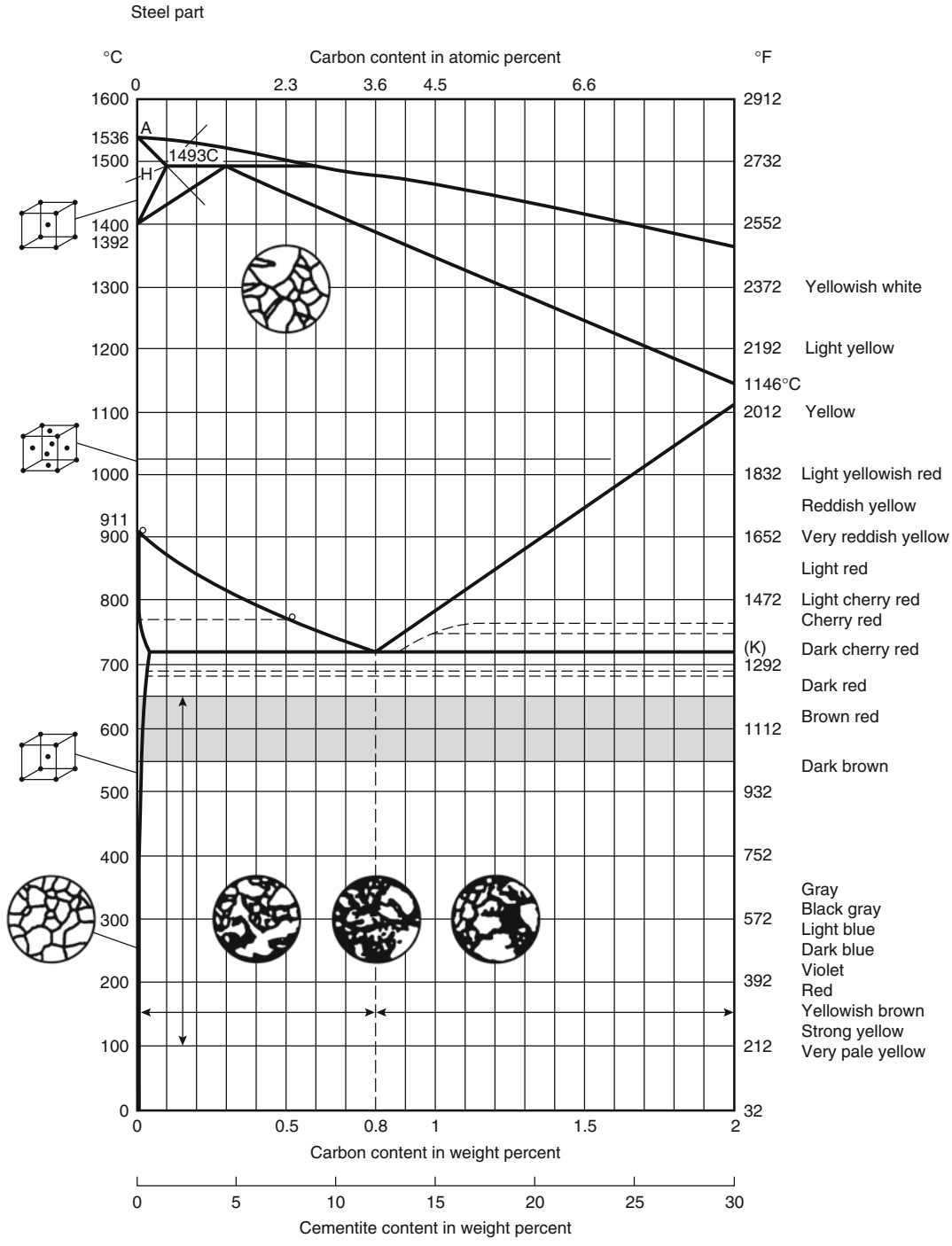

Fig. 53.3 Influence of elevated temperatures versus carbon content in steel [21]

provided elsewhere [29, 30]. Also, board products can be used in wall assemblies to provide an envelope around steel trusses.

Spray-Applied Materials Several types of spray-applied materials are commonly used. These include cementitious plasters, mineral

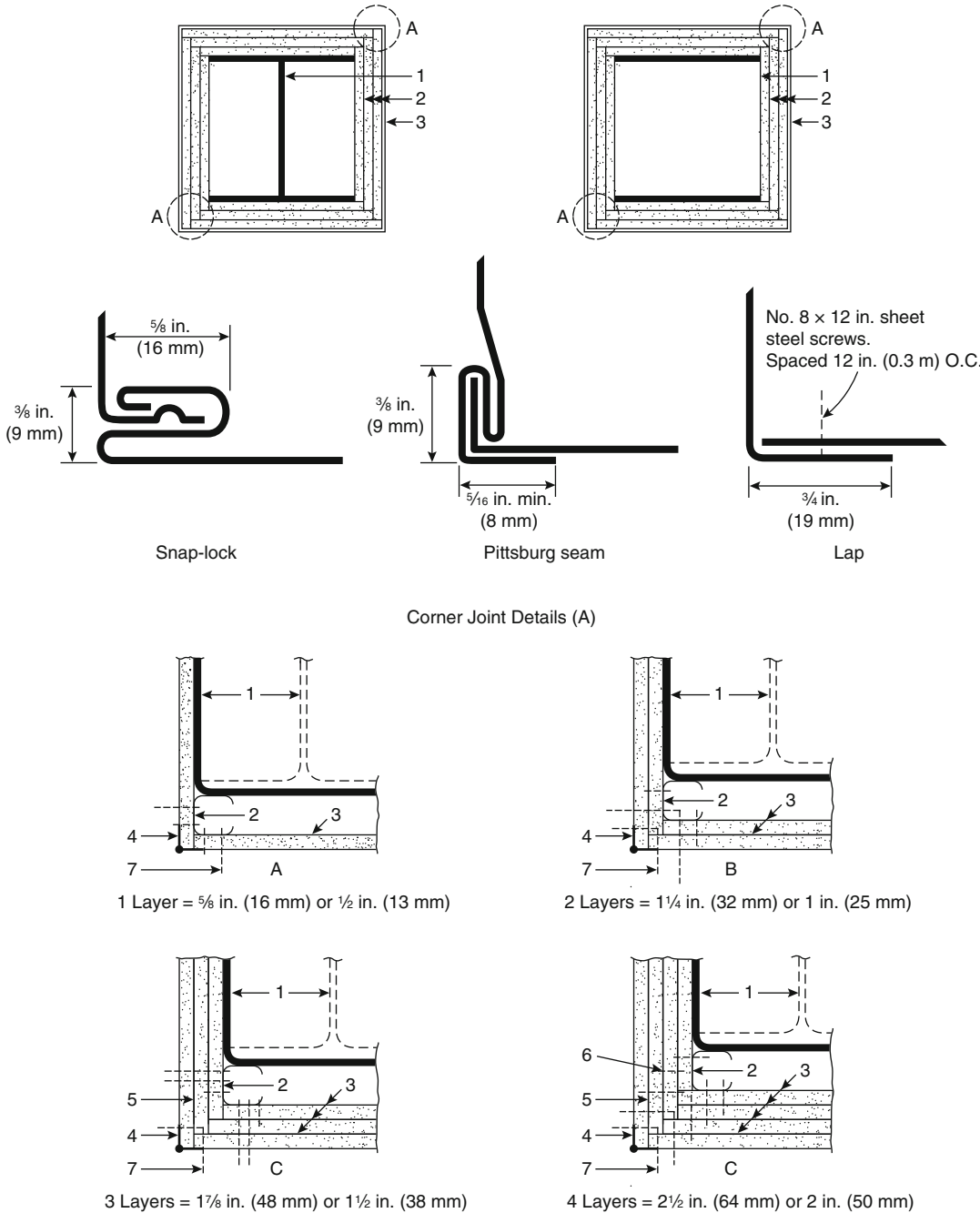

Fig. 53.4 Attachment mechanisms of gypsum wallboard to steel columns [29]

fibers, magnesium oxychloride cements, and intumescents. Sufficient data have been obtained to characterize spray-applied cementitious and mineral fiber materials for the purpose of estimating the fire endurance of structural steel protected with these materials. An illustration of a steel column protected by a spray-applied material is presented in Fig. 53.5.

Concrete Encasement Concrete encasement of steel members to surround and insulate the steel is illustrated in Fig. 53.6. As indicated in

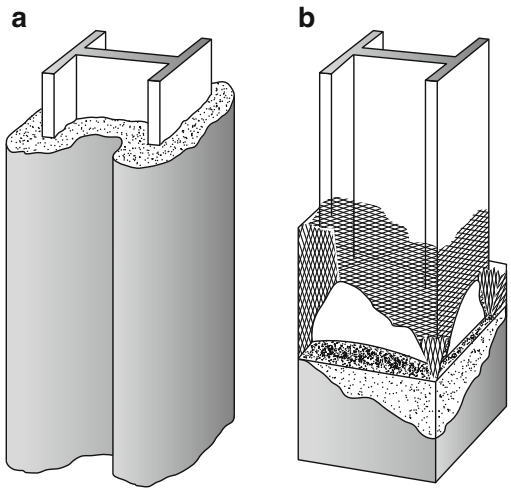

Fig. 53.5 (**a**) Sprayed insulation; (**b**) metal lath and plaster encasement [27]

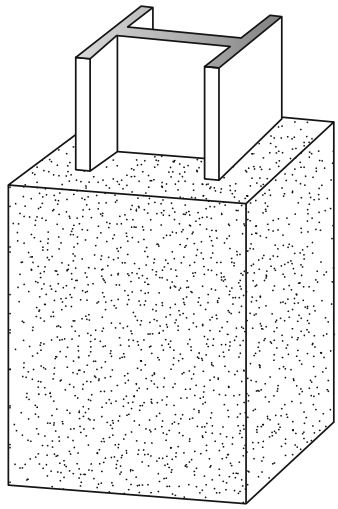

Fig. 53.6 Steel column with concrete encasement [27]

Fig. 53.6, the concrete is cast to fill in all re-entrant spaces. Alternatively, concrete column covers may be used, as illustrated in Fig. 53.7. The concrete is assumed to act only to thermally protect the steel. Some empirical correlations implicitly account for the load-bearing capacity of the concrete and possible steel-concrete composite action.

Concrete Filling

Concrete filling of hollow steel members can also be used to provide a fire-resistant assembly. The concrete may be plain concrete or reinforced concrete [31, 32].

Membrane

Suspended ceiling assemblies are used as membranes to protect structural steel in floor and roof assemblies. The ceiling panels and tiles comprising the ceiling assembly may consist of gypsum, perlite, vermiculite, or mineral fibers. Gypsum wallboard and other board products also fall into this category of protection.

The membrane method of protection is illustrated in Fig. 53.8. Heat transfer to the structural steel is reduced due to the air space above the membrane and the insulating characteristics of the membrane. Also, membranes help prevent the direct impingement of flame on the structural steel.

Flame Shield

Flame shields are intended to reduce the incident radiant heat flux on the steel by preventing direct flame impingement. The effectiveness of flame shields to protect exposed spandrel beams was first examined by Seigel [2, 33]. In this instance, 14-gauge sheet steel was used as the flame shield.

Heat Sinks

The heat sink approach delays the heating of steel by absorbing heat transferred through the steel. The heat sink approach usually involves liquid or concrete filling of the interior of hollow steel members (tubular and pipe sections). Liquid filling can be used to provide a sufficient level of protection for the columns, without any externally applied coating. The liquid used for

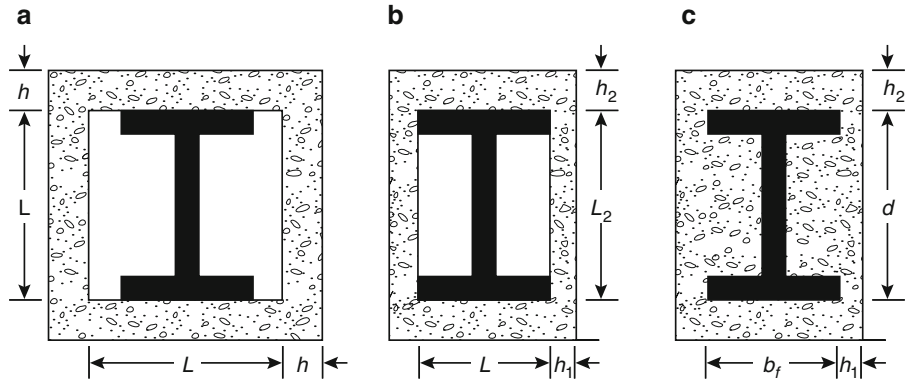

Fig. 53.7 Concrete-protected structural steel columns. (**a**) *Square* shape protection with a uniform thickness of concrete cover on all sides; (**b**) *rectangular* shape with varying thickness of concrete cover; and (**c**) encasement having all re-entrant spaces filled with concrete

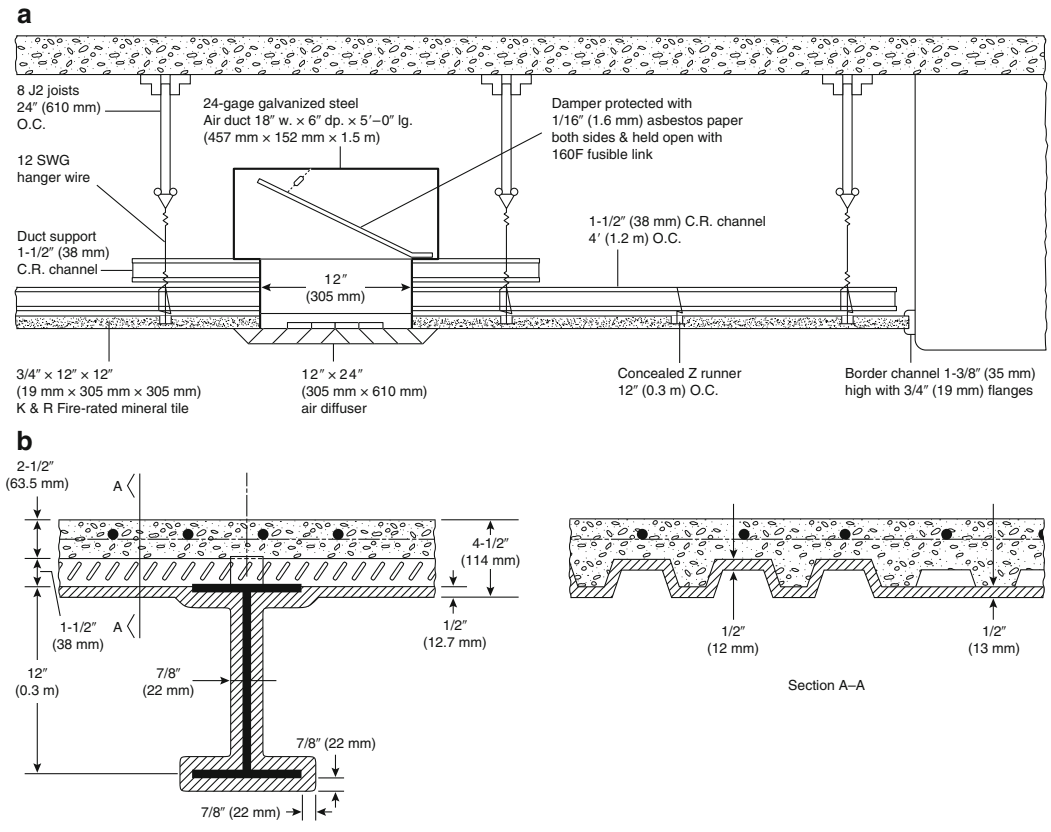

Fig. 53.8 Membrane method of protection [27]. (**a**) Cross-section of a floor-ceiling system with conventional sheet steel fusible-link damper for protecting typical ceiling outlets in galvanized sheet ducts; (**b**) sprayed contact fireproofing applied directly to the underside of formed-steel decking and to a supporting steel beam

protection is an aqueous solution. Additives are provided primarily for antifreeze, corrosion protection, and biological reasons.

A diagram of a typical design for a liquid-filled column fire protection system is presented in Fig. 53.9. The components of this system

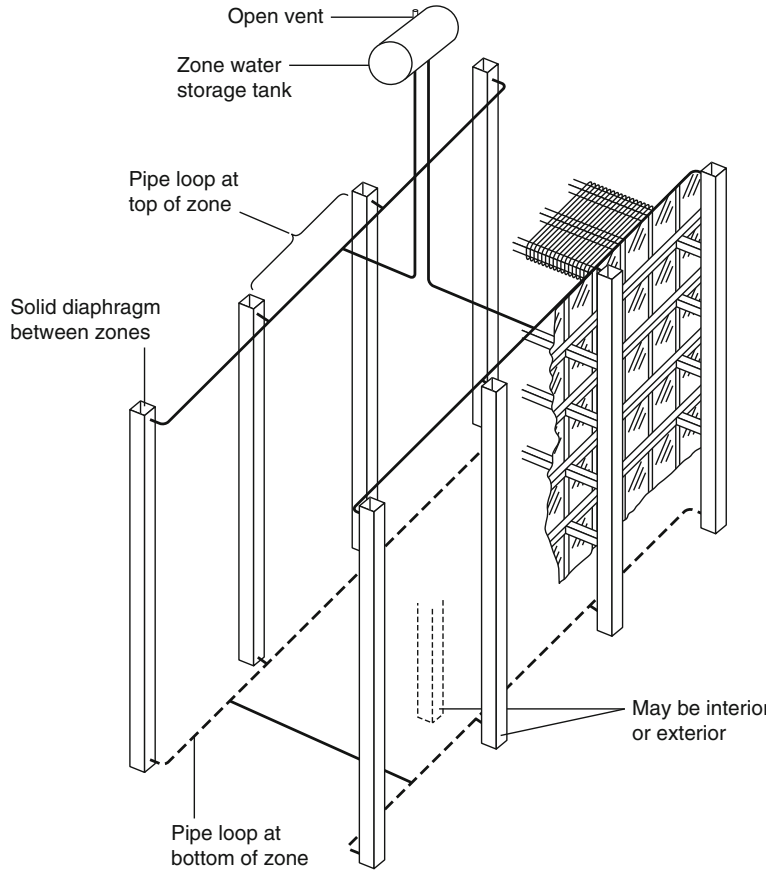

Fig. 53.9 Schematic layout of a typical piping arrangement used in a liquid-filled column fire protection system [33]

include the hollow structural steel columns, piping to connect the columns, a water storage tank, and associated valves.

The system operates on the principle that heat incident on the column is removed by circulation of the liquid. If sufficient heat is delivered to the liquid, boiling can be expected, which enhances the efficiency of the heat removal process. In many tests with liquid filling, steel temperatures have been observed to be well below those required for failure, as long as the column remains full of the liquid.

Another heat sink approach consists of filling the interior of hollow steel columns with concrete. If the concrete is reinforced, load transfer from the steel to the concrete can be expected as the steel weakens with increasing temperature. Calculation methods to determine the fire resistance of concrete-filled steel columns are available [11, 13].

Empirically Derived Correlations

Numerous easy-to-use, empirically derived correlations are available to calculate the fire resistance of steel columns, beams, and trusses. The correlations are based on data from performing the standard test numerous times on variations of a particular assembly. Curve-fitting techniques are used to establish the various correlations. In some cases, a best-fit line has been drawn for the data points, whereas in other cases, lines were placed to provide conservative estimates of the fire endurance by connecting the two lowest points [34].

Steel Columns

The correlations to estimate the fire endurance of unprotected and protected steel columns are given in Table 53.3. Present in each of the equations is *W*/*D* for wide-flange sections and *A*/*P* for hollow sections. The *W*/*D* and *A*/*P* ratios are comparable. The *W*/*D* ratio is the weight per lineal foot to the heated perimeter of the steel at the protection interface (or the perimeter of the steel if unprotected). The *A*/*P* ratio is the cross-sectional area divided by the heated perimeter. Essentially, the *W*/*D* ratio relates to the product of the density of the steel and the *A*/*P* ratio.

The relevance of the *W*/*D* and *A*/*P* ratios was first noted by Lie and Stanzak [35]. *W*/*D* ratios for commonly used wide-flange and tubular shapes for columns and beams are available elsewhere [29, 36–38]. The two factors in the *W*/*D* ratio that affect the rate of heat transfer to the steel (and consequently the rise in temperature of the steel) are (1) shape of the fire protection system, *D*, and (2) steel mass per unit of length, *W*.

The parameter that characterizes the shape of the fire protection system is *D*, the heated perimeter expressed in inches, which is defined as the inside perimeter of the steel at the fire protection material interface. Figure 53.10 illustrates the method for determining *D* in four typical cases. As indicated in the figure, the heated perimeter depends on the dimensions of the column and also on the profile of the protection system. Two different commonly used profiles are (1) contour profile, where all surfaces of the steel column are in contact with the protection material; and (2) box profile, where a rectangular box of protection material is built around the column.

A large value of *W* refers to a column with a large weight per lineal foot. A given amount of energy will raise the temperature of the massive column to a lesser degree than that of a light column. Less surface area is available for heat transfer if the heated perimeter, *D*, is small, thereby inhibiting the temperature rise in the steel. The greater the *W*/*D* ratio, the greater the inherent fire resistance of the assembly is.

Because steel elements with larger *W*/*D* ratios are inherently more fire resistant, substituting shapes with greater *W*/*D* ratios for shapes identified in the listed designs in the UL *Fire Resistance Directory* [3] is permitted while maintaining the same thickness of protection. However, such substitution yields inefficient designs, because shapes with large *W*/*D* ratios actually require less fire protection material than shapes with small *W*/*D* ratios for the same level of fire resistance.

The equation for gypsum wallboard protection is nonlinear. The weight of the gypsum wallboard is included because the heat capacity of gypsum has a considerable impact on the fire resistance of the assembly. The thickness of wallboard required to achieve a particular level of fire resistance as a function of the *W*/*D* ratio of the column is presented in Fig. 53.10.

Based on an elementary heat transfer analysis for spray-applied fire protection materials, Stanzak and Lie conducted a parametric analysis that resulted in correlations of the following form to estimate the thickness of material required to achieve a particular level of fire resistance [29, 30]:

$$R = (C_1 W/D + C_2)h \qquad (53.8)$$

where

R = Fire endurance (min., note: the version in the UL Directory expresses the equation with R in hour.)

W = Steel weight per lineal foot (lb/ft)

D = Heated perimeter of the steel at the insulation interface (in.)

h = Thickness of insulation (in.)

The constants C_1 and C_2 need to be determined for each protection material. The constants take into account the thermal conductivity and heat capacity of the insulation material. Constants for some materials are included in listings in the UL *Fire Resistance Directory* [3].

Considering the equation for the concrete cover column protection method (see Table 53.3), R_0 is the fire endurance of the assembly if the concrete has no moisture content. However, because the fire resistance of concrete cover

Table 53.3 Empirical equations for steel columns [22, 28–30]

Member/protection	Solution	Symbols
Column/unprotected	$R = 10.3(W/D)^{0.7}$, for $W/D < 10$	R = fire endurance time (min)
	$R = 8.3(W/D)^{0.8}$, for $W/D \geq 10$ (for critical temperature of 1000 °F)	W = weight of steel section per linear foot (lb/ft)
		D = heated perimeter (in.)
Column/gypsum wallboard	$R = 130\left(\frac{hW'/D}{2}\right)^{0.75}$ where $W' = W + \left(\frac{50hD}{144}\right)$	h = thickness of protection (in.)
		W' = weight of steel section and gypsum wallboard (lb/ft)
Column/spray-applied materials and some board products—wide flange shapes	$R = [C_1(W/D) + C_2]h$	C_1 and C_2 = constants for specific protection material
Column/spray-applied materials and some board products—hollow sections	$R = C_1\left(\frac{A}{P}\right)h + C_2$	C_1 and C_2 = constants for specific protection material
		The A/P ratio of a circular pipe is determined by $A/P_{\text{pipe}} = \frac{t(d-t)}{d}$ where
		d = outer diameter of the pipe (in.)
		t = wall thickness of the pipe (in.)
		The A/P ratio of a rectangular or square tube is determined by
		$A/P_{\text{tube}} = \frac{t(a+b-2t)}{a+b}$ where
		a = outer width of the tube (in.)
		b = outer length of the tube (in.)
		t = wall thickness of the tube (in.)
Column/concrete cover or encased	$R = R_0(1 + 0.03m)$ where $R_0 = 0.17(^w/_D)^{0.7} + 0.28\left(\frac{h^{1.6}}{k_c^{0.2}}\right) \times \left\{1 + 26\left[\frac{H}{\rho_c c_c h(L+h)}\right]^{0.8}\right\}$	R_0 = fire endurance at zero moisture content of concrete (min)
		m = equilibrium moisture content of concrete (% by volume)
		b_f = width of flange (in.)
		d = depth of section (in.)
		k_c = thermal conductivity of concrete at ambient temperature (Btu/hr·ft·°F)
		H = thermal capacity of steel section at ambient temperature (=0.11 W Btu/ft·°F). If encased, H is defined as: $H = 0.11W + \frac{\rho_c c_c}{144}(b_f d - A_s)$
		c_c = specific heat of concrete at ambient temperature (Btu/lb·°F)
		L = inside dimension of one side of *square* concrete box protection (in.) If encased, $L = (b_f + d)/2$
		As = cross-sectional area of steel column (in.^{2})

over steel columns is known to increase by approximately 3 % for each 1 % of moisture, R_0 is multiplied by the $(1 + 0.03m)$ factor where m is the equilibrium moisture content of concrete. The parameters h and L noted in the equation are shown in Fig. 53.7. If the protection thickness or column dimensions are not the same in the vertical and horizontal directions, average values are used for h and L.

The heat capacity of the concrete must be accounted for in the determination of H if all re-entrant spaces are filled (see Fig. 53.7).

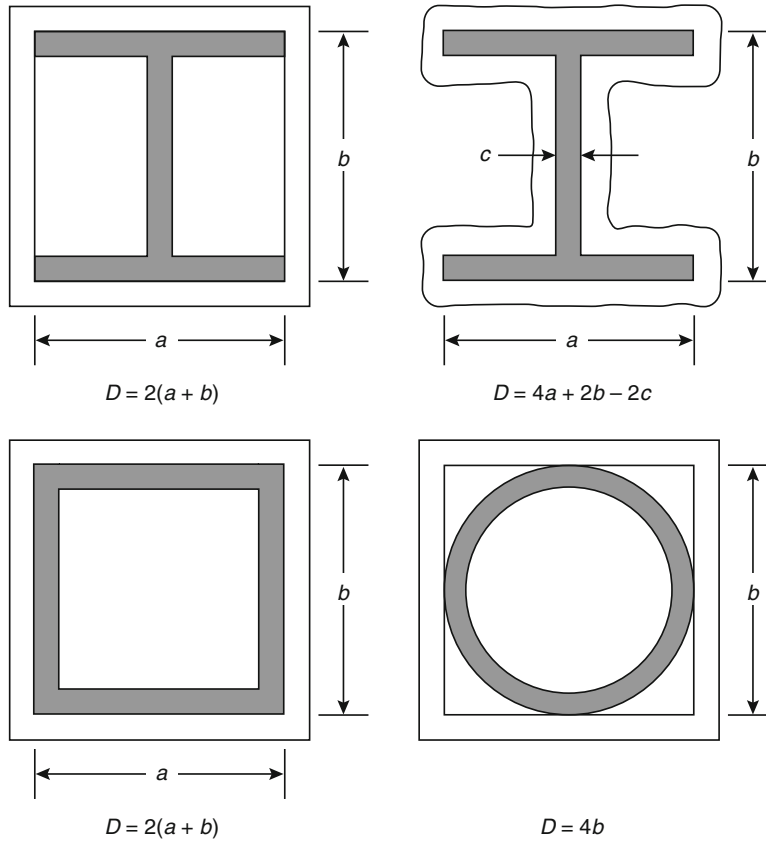

Fig. 53.10 Heated perimeter for steel columns [29]

If specific data on the concrete's thermal properties are not available, values given in Table 53.4 may be used. Typical densities for normal-weight and lightweight concrete are 145 and 110 lb/ft^3 (2320 and 1760 kg/m^3). Also, the typical equilibrium moisture content (by volume) for normal-weight concrete is 4 % and lightweight concrete is 5 %.

Many of the equations cited in Table 53.3 are limited to a range of shapes or protection thicknesses. Before applying any equation from this table, users should consult the original reference and confirm that the equation is being applied properly.

Example 1 Determine the thickness of spray-applied cementitious material to obtain a 2-h fire endurance when applied to a *W* 12 × 106 column.

Solution From UL X772, the applicable equation is

$$R = (1.05W/D + 0.6)h \tag{53.9}$$

Solving for h,

$$h = \frac{R}{1.05W/D + 0.6} \tag{53.10}$$

where

$R = 2$ h

$W/D = 1.44$ lb/ft·in. (0.0844 kg/m^2) for a *W* 12 × 106 with contour profile protection

Substituting,

$$h = \frac{2}{1.05 \times 1.44 + 0.6} = 0.95\,\text{in.} \quad (24.1\text{mm}) \tag{53.11}$$

Example 2 Determine the fire endurance of a *W* 8 × 28 column encased in lightweight concrete (density of 110 lb/ft^3 [176.2 kg/m^3]) with all re-entrant spaces filled. The concrete cover thickness is 1.25 in. (31.8 mm).

Table 53.4 Thermal properties of concrete at 70 °F

	Normal-weight Concrete	Structural Lightweight concrete
Thermal conductivity (k)[a]	0.95 Btu/h·ft·°F (1.64 W/m K)	0.35 Btu/h·ft·°F (0.61 W/m K)
Specific heat (c)[b]	0.20 Btu/lb·°F (835 J/kg K)	0.20 Btu/lb·°F (835 J/kg K)

Solution From Table 53.3, the appropriate equation is

$$R = R_0(1 + 0.03m) \tag{53.12}$$

where

$$R_0 = 10(W/D)^{0.7} + 17\left(h^{1.6}/k_c^{0.2}\right) \times \left\{1 + 26[H/\rho_c c_c h(L+h)]^{0.8}\right\} \tag{53.13}$$

Referring to Fig. 53.7,
h_2=h_1=h=1.25 in. (31.8 mm)
b_f = 6.535 in. (166.0 mm)
d = 8.060 in. (204.7 mm)
W/D = 0.67 lb/ft·in. (39.3 kg/m^2) (contour profile)
A = 8.25 in.^{2} (0.0053 m^2)
From Table 53.4,

$$k_c = 0.35\,\text{Btu/hr}\cdot\text{ft}\cdot{}^\circ\text{F}(0.605\,\text{W/m.K})$$

$$c_c = 0.20\,\text{Btu/lb}\cdot{}^\circ\,\text{F}(836\,\text{J/kg.K})$$

$$\rho_c = 100\,\text{lb/ft}^3\left(1600\,\text{kg/m}^3\right)$$

$$L = \frac{1}{2}\left(b_f + d\right) = 7.30\,\text{in.}\,(185\text{mm}) \tag{53.14}$$

$$\begin{aligned} H &= 0.11W + \frac{\rho_c c_c}{144}\left(b_f D - A_s\right) \\ &= 0.11 \times 28 + \frac{110 \times 0.20}{144} \\ &\quad \times (6.535 \times 8.060 - 8.25) \\ &= 9.87\text{in.}(251\text{mm}) \end{aligned} \tag{53.15}$$

$$R_0 = 0.17(0.67)^{0.7} + 0.28\frac{1.25^{1.6}}{0.35^{0.2}}\left\{1 + 26\left[\frac{9.87}{110 \times 0.2 \times 1.25(7.30 + 1.25)}\right]^{0.8}\right\} = 1.63\text{ hr.} \tag{53.16}$$

Assuming a moisture content of 5 % for lightweight concrete,

$$R = 1.63(1 + 0.03 \times 5) = 1.87\,\text{hours} \tag{53.17}$$

Steel Beams

As in the case of columns, the *W/D* ratio is an important parameter affecting the fire resistance of a beam. Beams with larger *W/D* ratios may be substituted for beams with lesser *W/D* ratios for an equivalent rating with no change in the protection thickness. However, as with columns, designs resulting from the direct substitution of larger beams without reducing the protection thickness may be inefficient.

In 1984, an empirically derived correlation was developed to calculate the required thickness of spray-applied material protection [37]. Correlations of the form for steel columns are not possible, given the deck's role as a heat sink. Thus, the thickness of protection for steel beams is determined based on the following scaling relationship:

$$h_1 = \left(\frac{W_2/D_2 + 0.6}{W_1/D_1 + 0.6}\right)h_2 \tag{53.18}$$

where
h = Thickness of spray-applied fire protection (in.)
W = Weight of steel beam (lb/ft)

D = Heated perimeter of the steel beam (in.) (Fig. 53.11)

and where the subscripts

1 = Substitute beam and required protection thickness

2 = The beam and protection thickness specified in the referenced tested design or tested assembly

Limitations of this equation are noted as follows:

1. $W/D \geq 0.37$ lb/ft-in (0.0217 kg/m^2)
2. $h \geq {}^3/_8$ in. (9.5 mm)
3. The unrestrained beam rating in the referenced tested design or tested assembly = at least 1 h

It should be noted that the above equation pertains only to the determination of the protection thickness for a beam in a floor or roof assembly. All other features of the assembly, including the protection thickness for the deck, must remain unaltered.

Example 3 Calculate the thickness of spray-applied fire protection required to provide a 2-h fire endurance for a W 12 × 16 beam to be substituted for a W 8 × 17 beam requiring 1.44 in. (36.6 mm) of protection for the same rating.

Solution The beam substitution correlation, presented as Equation 53.18, is used.

$$h_1 = \left(\frac{W_2/D_2 + 0.6}{W_1/D_1 + 0.6}\right) h_2 \tag{53.19}$$

Where

W_2/D_2 = 0.54 lb/ft in. (0.070 kg/m^2) for W8X17

W_1/D_1 = 0.45 lb/ft in. (0.058 kg/m^2) for W12X16

h_2 = 1.44 in. (36.6 mm)

$$h_1 = \left(\frac{0.54 + 0.6}{0.45 + 0.6}\right) \times 1.44 = 1.6 in., \tag{53.20}$$

$$h_1 = \left(\frac{0.070 + 0.036}{0.053 + 0.036}\right) 36.6 = 40.6 mm$$

Steel Trusses

There are three types of trusses used in buildings: transfer, staggered, and interstitial trusses. Because of the inherent features of each type of truss, some fire protection systems are more appropriate than others [39].

A load-transfer truss (Fig. 53.12) supports loads from more than one floor. The loads may be suspended from a transfer truss, or the transfer

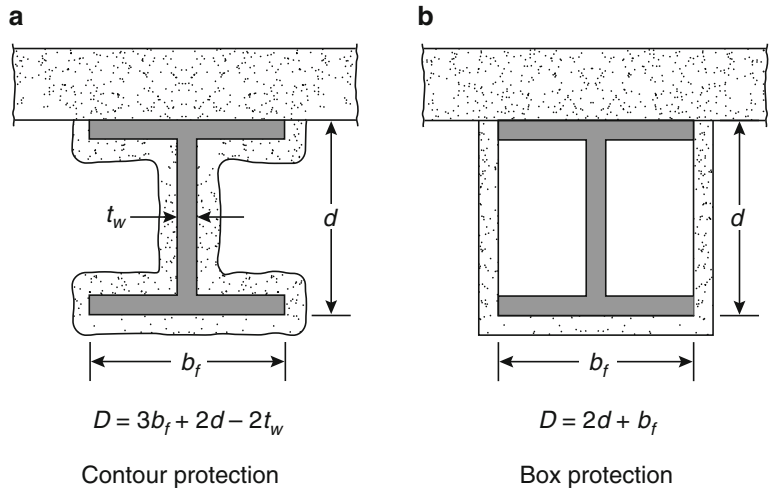

Fig. 53.11 Heated perimeter for steel beams [36]

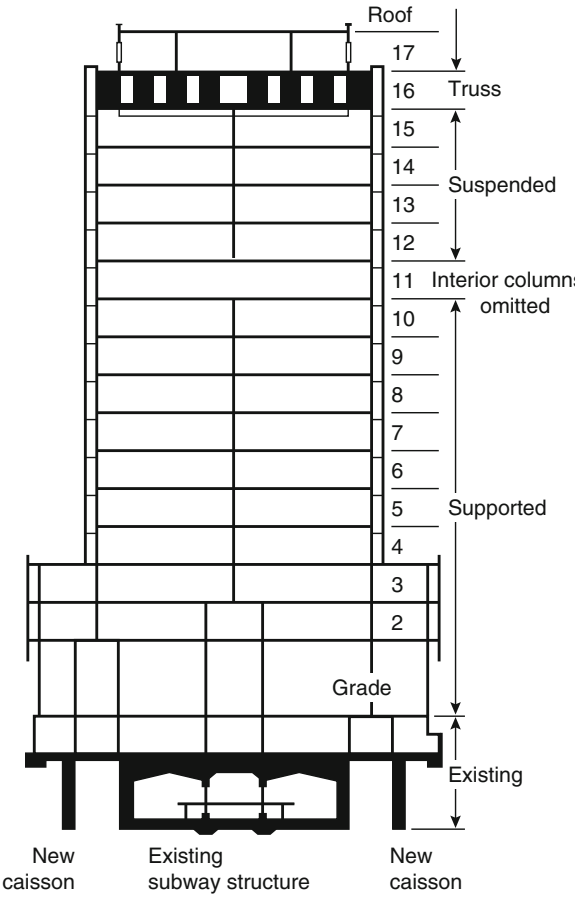

Fig. 53.12 Vierendell truss providing support from above and below [39]

truss can be used to eliminate columns on lower floors.

A staggered truss is illustrated in Fig. 53.13. Generally, staggered trusses are used in residential occupancy buildings. Staggered trusses carry loads from two floors.

Interstitial trusses are used to create deep floor/ceiling concealed spaces containing mechanical and electrical equipment, as shown in Fig. 53.14. Interstitial trusses support only those loads from the equipment enclosure and the floor above. Interstitial trusses are typically used in health care facilities with heavy mechanical equipment needs.

Three methods of fire protection are often used for trusses: membrane, envelope, and individual element protection. Some fire protection methods are more appropriate than others for the specific truss types. The fire protection methods typically used for each truss type are indicated in Table 53.5. Membrane protection is accomplished through the use of a fire-resistant ceiling assembly. Design parameters for such an assembly can be determined from listings of fire-rated designs [3, 39]. No empirical correlations are available to assess the design of membrane protection systems.

The envelope means of protection is illustrated in Fig. 53.15. The truss is enclosed in layers of a board product, with the number of layers determined by the required fire endurance. Some practical rules of thumb based on test results are noted in Table 53.6.

Individual element protection is generally accomplished using a spray-applied material. Because critical truss elements perform structurally as columns, that is, in tension or compression (as opposed to bending), the applicable equations

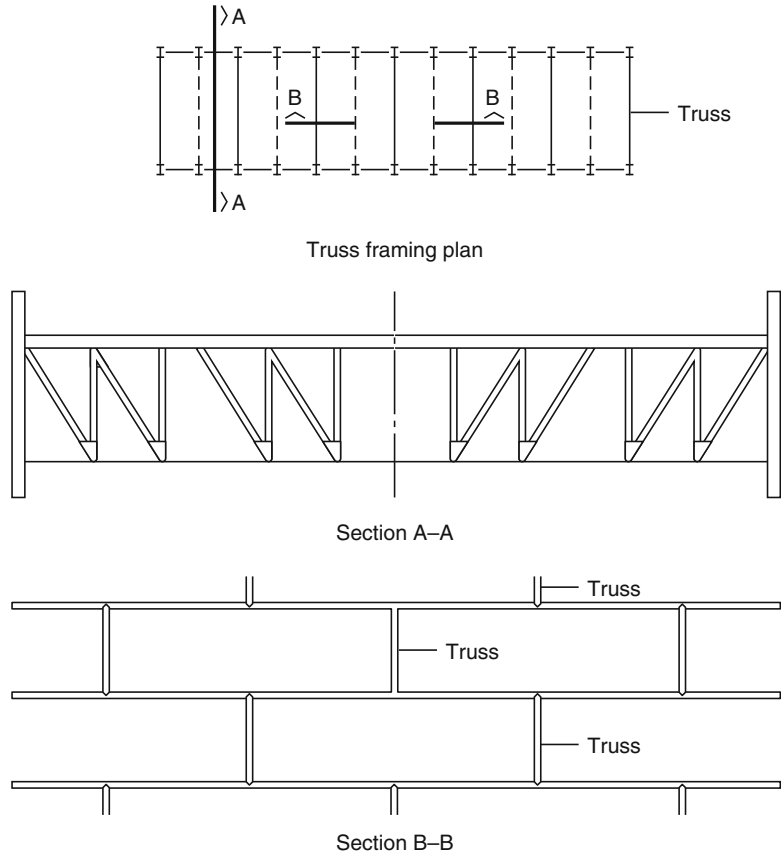

Fig. 53.13 A typical truss and positionings in a staggered truss system [39]

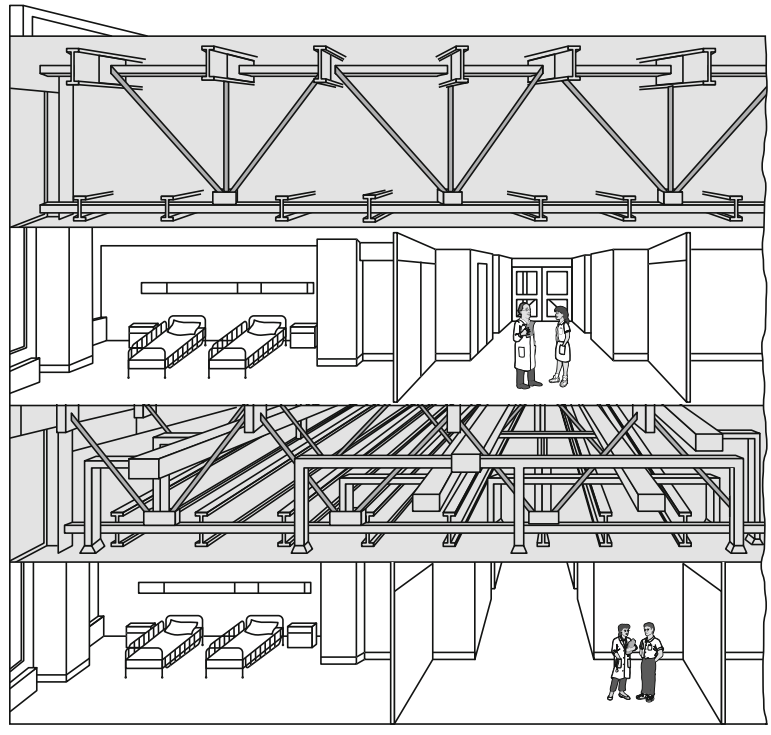

Fig. 53.14 Hospital interstitial truss system [39]

Table 53.5 Typical fire protection methods for steel trusses

	Fire protection method		
Truss type	Membrane	Envelope	Individual element
Transfer	—	X	X
Staggered	—	X	X
Interstitial	X	X	X

Table 53.6 Practical guidelines for thickness of gypsum wallboard for steel truss envelope protection [39]

Fire	Gypsum	Wallboard
Endurance (h)	X	Type
1	$^{5}/_{8}''$ (16 mm)	$^{5}/_{8}''$ (16 mm)
2	$^{11}/_{4}''$ (32 mm)	—
3	—	$1^{1}/_{2}''$ (38 mm)

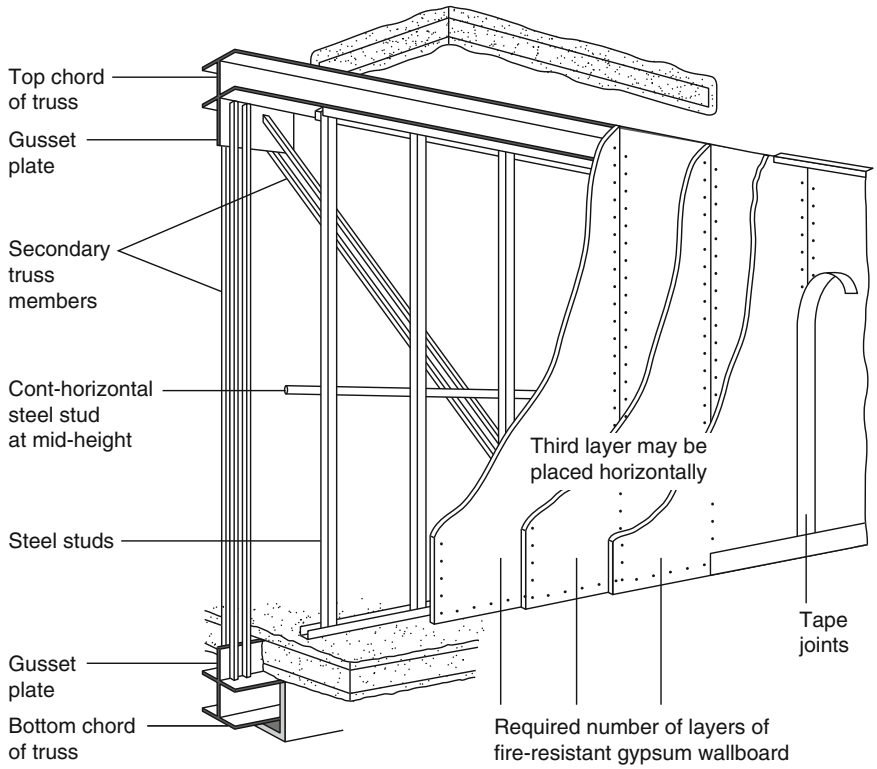

Fig. 53.15 Staggered truss protection with envelope protection [39]

for determining the thickness of spray-applied material for columns is used. In order to use these equations, the *W*/*D* ratio must be calculated for each element. Unlike columns and beams, the ratio may not be readily available. The diagrams in Fig. 53.16 are provided for assistance in calculating the heated perimeter.

Heat Transfer Analyses

Heat transfer analyses are applied to determine the time period required to heat structural members to a specified critical temperature or to provide temperature data as input to the structural analysis of the heated member. The time required to heat the member to a specified critical temperature is often defined as the fire endurance time of the member.

The critical temperature of a structural member can be determined by referring to the temperature endpoint criteria cited in ASTM E119 [1] or by a structural assessment, as is discussed later in this chapter.

The available types of heat transfer analyses can be grouped into the following categories:

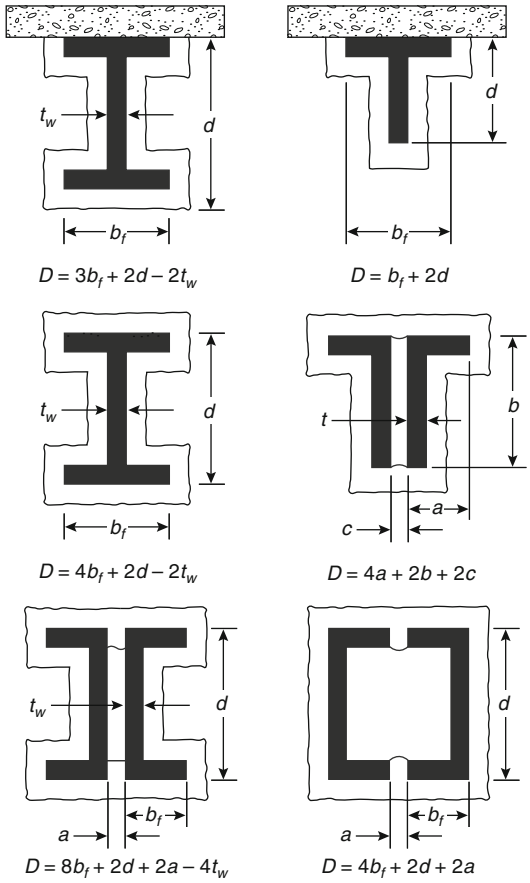

Fig. 53.16 Heated perimeter for steel truss shapes [39]

1. Numerical methods
2. Graphical solutions
3. Computer-based analyses

Numerical Methods

Many numerical methods are available to estimate the temperature rise in steel structural elements. The equations are derived from simplified heat transfer approaches.

Unprotected Steel Members The temperature in an unprotected steel member can be calculated using a quasi-steady-state, lumped heat capacity analysis. This method assumes that the steel member is at a uniform temperature. The equation for temperature rise during a short time period, Δt, is [23]

$$\Delta T_s = \frac{\alpha}{c_s(W/D)}\left(T_f - T_s\right)\Delta t \qquad (53.21)$$

where
ΔT_s = Temperature rise in steel (°F) (°C)
α = Heat transfer coefficient from exposure to steel member (Btu/ft^2·s·R) (W/m^2·K)
D = Heated perimeter (ft) (m) (see Fig. 53.16)
c_s = Steel specific heat (Btu/lb·°F)/(J/kg·°C)
W = Steel weight per lineal foot (lb/ft)/(kg/m)
T_f = Fire temperature (R) (K)
T_s = Steel temperature (R) (K)
Δt = Time step (s)
where
$\alpha = \alpha_r + \alpha_c$
α_r= radiative heat transfer coefficient
$\alpha_r = \frac{c_2 \varepsilon_f}{T_f - T_s}\left(T_f^4 - T_s^4\right)$
α_c= convective heat transfer coefficient
α_c= 9.8 × 10^{-4}–1.2 10^{-3} Btu/ft^2-s-R (20–25 W/m^{2}K)
where $C_1 = 4.76 \times 10^{-13}\text{Btu/s} \cdot \text{ft}^2 \cdot \text{R}^4 (5.67 \times 10^{-8}\,\text{W/m}^2 \cdot \text{K}^4)$ and ε_f, the effective emissivity, can be evaluated from Table 53.7.

The quasi-steady assumption dictates that the time step should be small, that is, on the order of 10 s [41]. Equation 53.21 is successively applied up to the time duration of interest. For the ISO 834 test, T_f at any time, t, can be estimated by the following expression [22]:

$$T_f = C_T \log_{10}(0.133t + 1) + T_0 \qquad (53.22)$$

Where
C_T = 620 with T_f, T_0 in °F
345 with T_f, T_0 in °C
t = time (sec)
T_0 = initial temperature °F, °C

Protected Steel Members For protected members, the thermal resistance provided by the insulating material must be considered. If the thermal capacity of the insulation layer is neglected [23],

Table 53.7 Effective emissivity [40]

Type of construction	Effective Emissivity	
1.	Column exposed to fire on all sides	0.7
2.	Column outside facade	0.3
3.	Floor girder with floor slab of concrete, only the underside of the bottom flange being directly exposed to fire	0.5
4.	Floor girder with floor slab on the top flange	
	Girder of 1 section for which the width-depth ratio is not less than 0.5	0.5
	Girder of 1 section for which the width-depth ratio is less than 0.5	0.7
	Box girder and lattice girder	0.7

$$\Delta T_s = \frac{k_i}{c_s h W/D}\left(T_f - T_s\right)\Delta t \qquad (53.23)$$

where all parameters are as defined in Equation 53.21, and

k_i = Thermal conductivity of insulation material (Btu/ft·s·°F) (W/m·°C)

h = Protection thickness (ft) (m)

Malhotra suggests that the thermal capacity of the insulation material may be neglected if the following inequality is true (see parameter definitions for Equation 53.21 [23]:

$$c_s W/D > 2c_i \rho_i h$$

If the thermal capacity must be accounted for, as in the case of gypsum and concrete insulating materials, then

$$\Delta T_s = \frac{k_i}{h}\left[\frac{T_f - T_s}{c_s(W/D) + 1/2c_i \rho_i h}\right]\Delta t \qquad (53.24)$$

where all parameters are as defined for Equation 53.21, and

c_i = Specific heat of insulating material (Btu/lb·°F) (J/kg·°C)

ρ_i = Density of insulating material (lb/ft^3) (kg/m^3)

An evaluation of the predictive capability of the lumped heat capacity approach using Equation 53.24 for protected steel sections was conducted by Berger for steel columns protected with a spray-applied cementitious material [42]. The analysis consisted of comparing predicted versus measured temperatures for steel columns exposed to the standard fire exposure. A comparison of the predicted versus measured times for the steel column to reach 538 °C is provided in Table 53.8. A comparison of the predicted temperature with that measured for one protected steel column assembly is provided in Fig. 53.17.

Predictions of temperature rise in steel beams by the lumped heat capacity approach are prone to be inherently less accurate than those for steel columns [43]. As noted previously, a steel beam in contact with a slab has only three sides exposed to a fire and also will lose heat to the slab [44]. Consequently, the temperature of a steel beam exposed to fire is likely to vary appreciably from the bottom flange to the top flange, stretching the validity of the uniform temperature assumption. Nonetheless, for many engineering applications, the lumped heat capacity approach can provide a conservative estimate of the average temperature rise of a steel beam [45]. Heat losses to the slab may be compensated for by reducing the effective flame emissivity to 0.5 [40]. However, if the temperature gradient across the beam is important, another analytical approach will need to be applied [43].

Exterior Steel Columns and Steel Spandrel Beams A design guide is available for calculating the exposure of exterior steel columns and steel spandrel beams [46]. The guide is based on research by Law and basic radiation heat transfer principles [47]. A similar calculation procedure is available in the Eurocodes [10].

Table 53.8 Comparison of predicted time from lumped heat capacity analysis and measurements for protected steel column to reach 538 °C

Shape	h (cm)	Test (min)	Calc (min)
W 6 × 16	1.9	58	56
	3.8	112	119
	7.6	210	251
W 8 × 28	3.5	122	121
	8.3	291	298
	9.5	355	352
W 10 × 49	1.9	70	62
	5.6	217	220
W 12 × 106	3.8	200	203
W 14 × 228	1.4	123	140
W 14 × 233	2.9	225	251

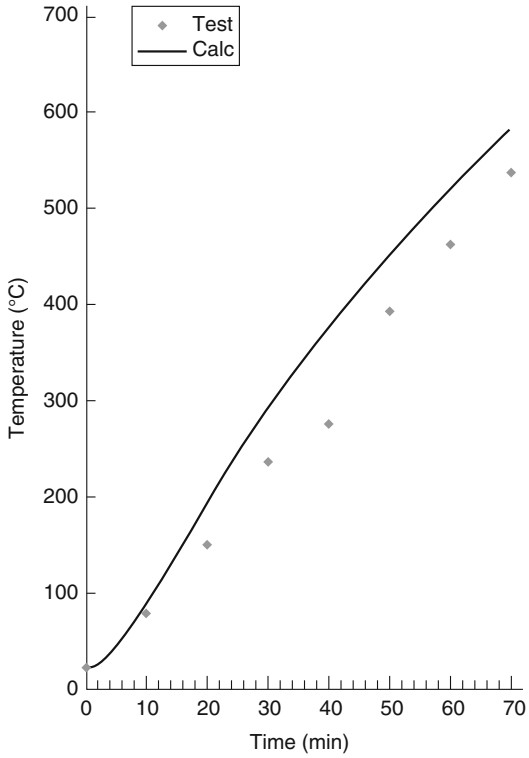

Fig. 53.17 Predicted steel column temperature [42]

The temperature of the steel member is calculated from a steady-state conduction analysis. The exposure boundary conditions consist of radiant heating from a fully developed room fire and flames emitting from windows near the steel member. For this method, a specific design is considered unacceptable if the steel temperature exceeds 1000 °F (538 °C).

Liquid-Filled Columns The design calculations for liquid-filled columns are based on the thermal capacity of the liquid. The design of a liquid-filled column fire protection system consists of three major steps:

1. Heat transfer analysis
2. Determination of volume of liquid required
3. Pipe network design

The heat transfer analysis is used to assess the impact of fire exposure on the liquid-filled column. The heat transfer analysis considers radiation and convection heat transfer from the fire to the column surface, conduction through the column wall, and convection with localized boiling into the liquid. Both temperature of the steel column and total amount of heat transferred to the liquid causing evaporation are determined as a result of this analysis.

The liquid volume calculation is important to ensure the column remains full of liquid for the entire fire exposure period. Because heat transferred to the liquid will cause some evaporation, a supplemental amount of liquid must be provided in a storage tank.

The final step in the design method is a hydraulic analysis of the tubular column and pipe network. This analysis assesses the ability of the liquid to circulate based on friction losses, elevation changes, and buoyancy of the heated liquid.

A comprehensive design aid for liquid-filled columns is available [48]. Because the procedure is rather lengthy, it will not be reviewed here.

Graphical Solutions

Because heat transfer analyses can be very tedious and may involve the use of complex computer programs, graphic solutions have been formulated to simplify the estimation of steel temperature. Graphs of the temperature of protected steel members have been developed by Malhotra [23], Jeanes [13], Lie [16], and others.

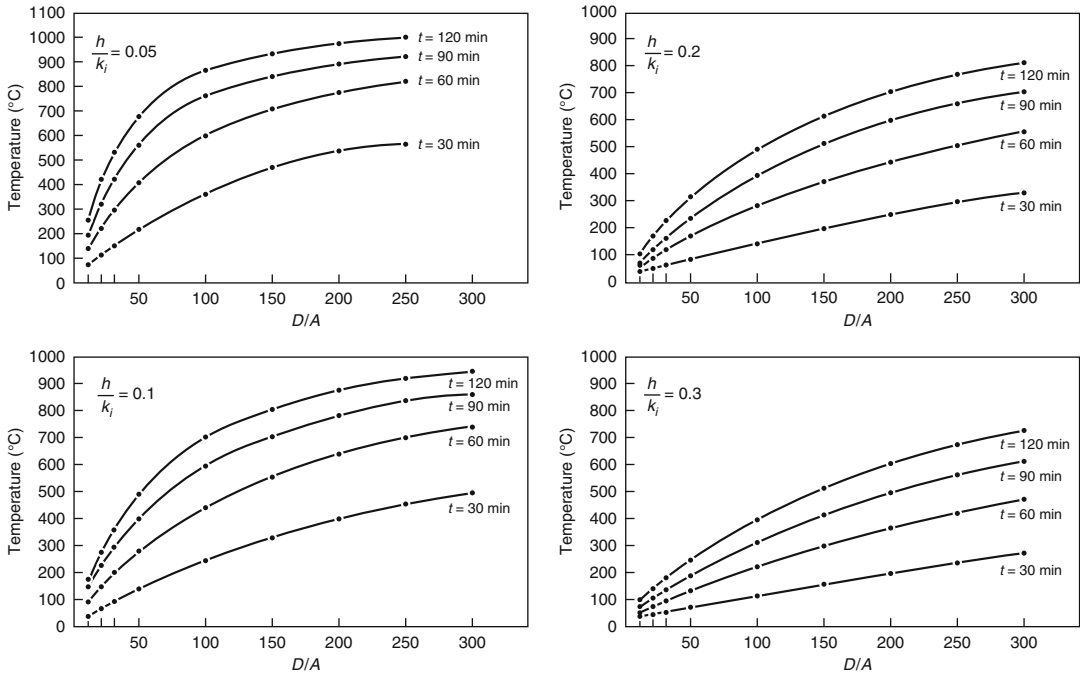

Fig. 53.18 Relationship of heated area to steel weight with temperature [23]

The series of graphs developed by Malhotra [23], presented in Fig. 53.18, for estimating the temperature of steel members exposed to the standard exposure are based on the lumped heat capacity approach described in the previous section. Steel temperatures are plotted versus the *D*/*A* ratio (analogous to the inverse of *W*/*D*) for selected time periods of exposure and thermal resistances of the insulating material. Time periods of 30–120 min are noted in the graphs. The range of thermal resistances of the insulating material covered by these graphs is 0.01–0.30 $(W/m^2 \cdot {}^\circ C)^{-1}$ (0.003–0.10) $(Btu/ft^2 \cdot h \cdot {}^\circ F)^{-1}$.

Based on the application of FIRES-T3, a heat transfer computer program that will be described in the next section, Jeanes formulated a series of time-temperature graphs of protected steel beams [13]. The steel beams are protected by a proprietary specific spray-applied cementitious material with a range of thicknesses of 0.5–1.5 in. (12.7–38.1 mm). Graphs are available for a variety of common wide-flange beam shapes [13]. Examples of these graphs are presented in Fig. 53.19 with graphs addressing the average and single-point steel temperatures relating to the maximum endpoint criteria from ASTM E119 [1]. Average and single-point steel temperatures are represented by the dashed lines. These graphs can be used to determine the thickness of protection material required to provide a desired level of fire resistance. Alternatively, the fire endurance can be estimated for a particular steel beam and insulation thickness design that has not been tested [14].

Information from numerous applications of FIRES-T3 examining the time-temperature response of steel beams protected with a spray-applied cementitious material exposed to the standard fire exposure is summarized in Fig. 53.20. Using this graph, the fire endurance of protected steel beams with a *W*/*D* ratio of 0.4–2.5 lb/ft-in. can be determined for thicknesses of the spray-applied protection between 1.3 and 3.8 cm (0.5 and 1.5 in.).

Example 4 A *W* 24 × 76 steel beam is protected with 0.50 in. (12.7 mm) of spray-applied cementitious material. Based on the temperature endpoint criteria noted in ASTM E119, determine the fire resistance of the beam by two methods:

1. Graphical approach from Jeanes [13]
2. Quasi-steady-state approach by Malhotra [23]

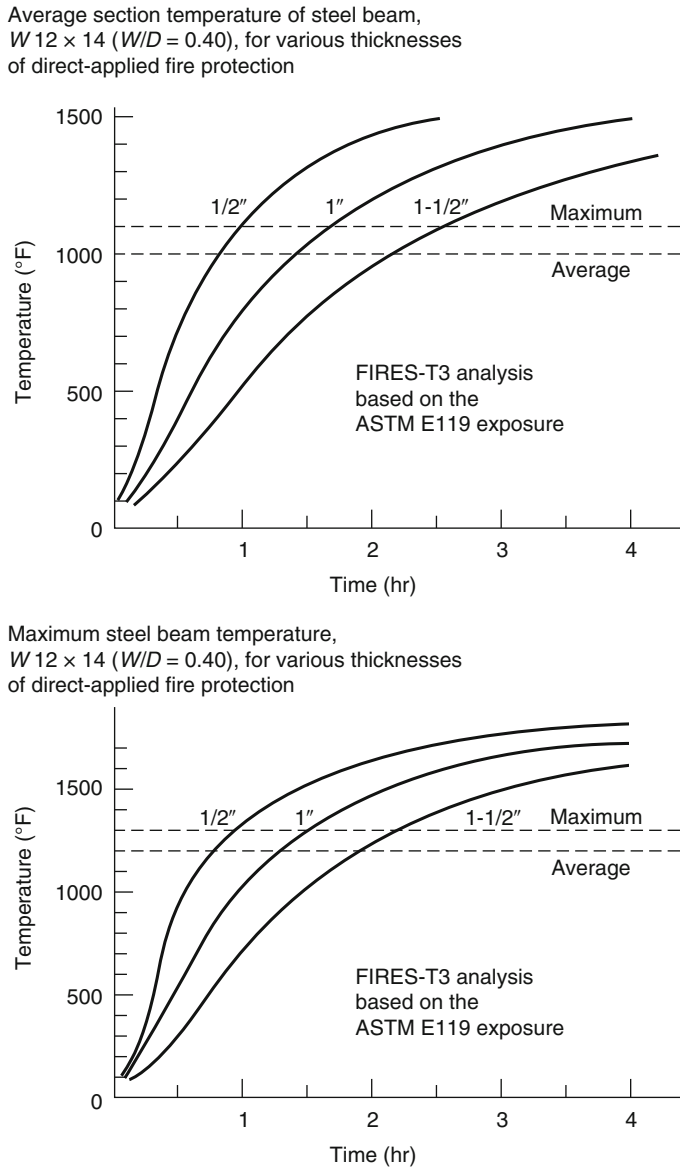

Fig. 53.19 Predicted steel beam temperature by FIRES-T3 [13]

Solution A W 24 × 76 steel beam has a W/D ratio of 1.03 lb/ft·in. or 12.36 lb/ft^2. The material properties are evaluated at mean temperatures expected during the exposure. The fire resistance can be assessed using the temperature endpoint criteria in ASTM E119. Mean temperatures of 500 °F (260 °C) and 750 °F (400 °C) are selected (arbitrarily) for the steel and insulation, respectively, to determine the thermal properties. The following material property values are assumed [13]:

	Steel	Insulation
Thermal conductivity	25.6 Btu/ft·h·°F (44.3 W/m K)	0.067 Btu/ft·h·°F (0.12 W/m K)
Specific heat	0.132 Btu/lb·°F (551 J/kg K)	0.304 Btu/lb·°F (1270 J/kg K)
Density	490 lb/ft^3 (7860 kg/m^3)	15 lb/ft^3 (240 kg/m^3)

Jeanes's Graph Using Fig. 53.21 with a W/D of 1.03 lb/ft·in. (0.060 kg/m^2) and an insulation thickness of 0.50 in. (12.7 mm), the fire endurance is estimated to be 1.33 h or 80 min.

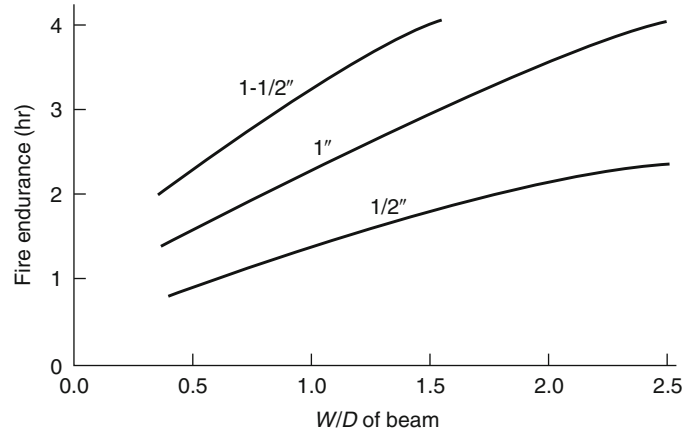

Fig. 53.20 Fire endurance of steel beams versus fire protection thickness for average section temperature of 1000 °F (538 °C) (Based on FIRES-T3 analysis of ASTM E119 fire exposure) [13]

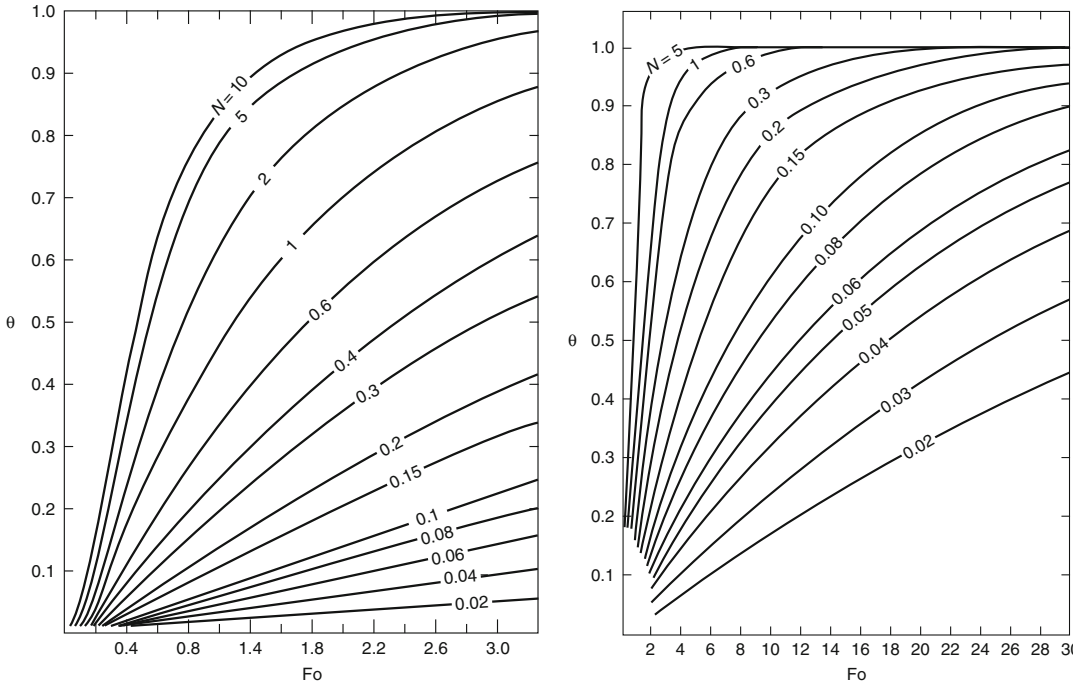

Fig. 53.21 Dimensionless steel temperature versus Fourier numbers [16]

Quasi-Steady-State Approach First, a check is performed to determine whether the thermal capacity of the insulation material must be considered.

$$c_s W/D > 2c_i \rho_i h$$
$$0.132 \times 12.36 > 2 \times 0.304 \times 15 \times 0.50/12$$
$$1.63 > 0.38 \tag{53.25}$$

Disregarding the thermal capacity of the insulation, Equation 53.23 is used to predict the steel temperature rise for each time step.

$$\Delta T_s = \frac{0.067/3600}{0.0132 \times 0.50/12 \times 12.36}\left(T_f - T_s\right)\Delta t$$
$$= 2.74 \times 10^{-4}\left(T_f - T_s\right)\Delta t \tag{53.26}$$

Time	Steel temperature (°C)	Fire temperature (°C)	Fire-steel temperature (°C)	W/m^{2}K k/h	ΔT_s (°C)
10	20.0	46	26	9.13	0.1
20	20.1	72	51	9.13	0.2
30	20.3	96	76	9.13	0.3
40	20.5	120	99	9.13	0.3
50	20.8	143	122	9.13	0.4
3220	534.2	888	353	9.13	1.2
3230	535.3	888	353	9.13	1.2
3240	536.5	888	352	9.13	1.2
3250	537.7	889	351	9.13	1.2
3260	538.9	889	350	9.13	1.2
3270	540.1	890	350	9.13	1.2
3280	541.2	890	349	9.13	1.2

Thus, the fire endurance is 54 min.

The fire endurances calculated by the two methods can be compared as follows:

Jeanes (FIRES-T3)	80 min
Quasi-steady-state	54 min

The significantly reduced fire endurance calculated using the quasi-steady-state approach is attributable to the approximate nature of the lumped heat capacity method assuming an adiabatic surface condition at the beam-slab interface.

Computer-Based Analyses

Several computer-based analyses are available to estimate the temperature rise of steel members. The analyses range from a spreadsheet procedure to perform the iterative calculations for the quasi-steady-state approach to finite element models.

Spreadsheets are one example of providing a framework to perform the iterative, quasi-steady calculations [42, 43, 49]. Typically, the spreadsheet procedures mimic the quasi-steady analysis procedure described previously, including the evaluation of material properties at a mid-range temperature for the exposure of interest. Although temperature-dependent material properties can be included within the spreadsheet framework, the accuracy implied by considering temperature-dependent properties is not consistent with the first-order nature of the quasi-steady approach.

Another framework for conducting computer-based analyses includes the numerous mathematical-equation-solver software packages. This software can be used to conduct the iterations associated with the quasi-steady approach or to solve the partial differential equations exactly.

Harmathy and Lie developed a two-dimensional finite difference model to predict the temperature rise in protected steel columns [50]. The two-dimensional network is formulated over the cross section of the insulation layer, assuming the temperature to be independent of length. The steel is assumed to be a perfect conductor (i.e., the temperature is uniform throughout the steel). Heat transfer via radiation is considered across any air spaces enclosed by the insulation and steel.

The boundary conditions included by Harmathy are those associated with the ASTM E119 test [1]. To simplify the model, convection is disregarded, because convection comprises a minor portion of the heat transfer process in the furnace test.

Pettersson et al. [40] include a finite difference formulation to predict the temperature rise of steel beams protected with a suspended ceiling exposed to a specified fire. The formulation uses a one-dimensional approximation accounting for conduction through the suspended ceiling and floor slab (above the beam), and radiation and convection in the air space between the slab and beam. The temperature of the steel is assumed to be uniform. The assembly is divided into several elements, as depicted in Fig. 53.22.

A system of simultaneous equations is derived for the temperature rise in each of the assembly elements. A numerical integration technique such as Runge-Kutta is used to obtain the solution. A comparison of the calculated versus experimentally observed temperatures for a steel beam is presented in Fig. 53.23.

General heat transfer finite-element programs have been available for many years [51]. FIRES-T3, TASEF-2, SAFIR, SUPER-TEMPCALC, and HEATING 7, among others, have been developed specifically to address the heating of assemblies with steel structural members exposed to fire conditions [52–55].

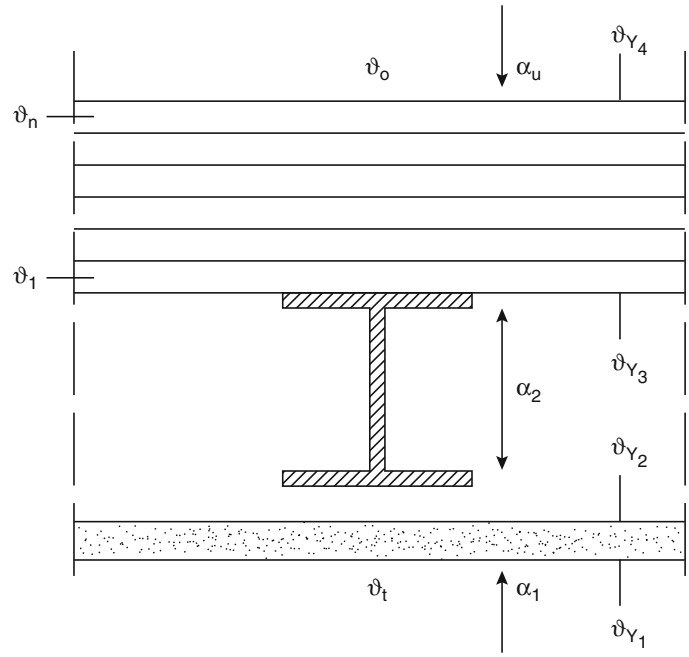

Fig. 53.22 Division of the floor slab into elements [40]

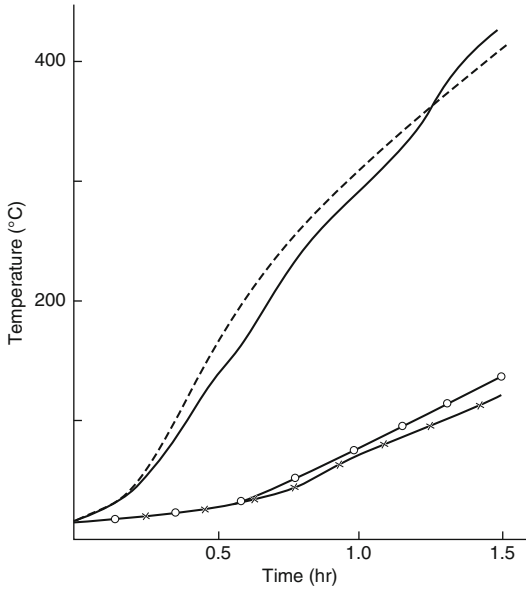

Fig. 53.23 Calculated (- -) and measured (—) steel temperature-time (θ_s – t) curve for a floor girder IPE 140 with insulation in the form of a suspended ceiling of 40-mm-thick mineral wool slabs of density $\gamma = 150$ kg/m^3. The figure also gives the calculated (–°–) and measured (–x–) temperature-time curve for the top of the 50-mm-thick concrete floor slab [40]

TASEF-2 examines the conduction heat transfer through assemblies [52]. Assemblies may include internal voids, in which convection and radiation heat transfer modes are considered. Two time-temperature curves are available: (1) the ISO 834 standard time-temperature curve and (2) a time-temperature curve from a ventilation-controlled fire.

SUPER-TEMPCALC can also be used to analyze the conduction heat transfer through assemblies with air gaps. Numerous fire curves are included within the software.

FIRES-T3 was specifically developed to examine the heating of structural members exposed to fire conditions [53]. FIRES-T3 has been applied successfully to predict the temperature rise in protected steel beams and columns [13, 56]. Almand used a finite-difference heat transfer model to estimate the protection thickness of spray-applied cementitious material required for tubular steel columns [57].

The input data requirements for the heat transfer computer models can be grouped into two categories:

1. A description of the assembly
2. A description of the fire exposure

The information necessary to describe the assembly includes geometric factors (dimensions, shape of member) and material property values (thermal conductivity, specific heat, and density). The fire exposure is characterized in terms of the temperature of the surrounding environment and appropriate heat transfer coefficients. The geometry of the assembly is established by formulating an element mesh for the assembly of interest. Required material property data consists of the density, specific heat, and thermal conductivity of the steel and insulation. Material property data are available for a limited number of insulation materials [13, 58].

For models using an explicit transient solution technique, such as FIRES-T3, caution must be exercised in selecting the time step and mesh size to obtain correct results that are numerically stable. TASEF-2 internally determines a numerically stable time step. Most heat transfer models do not address the effects of phase changes or chemical reactions that may influence the heating process. Phase changes and chemical reactions have been accounted for by altering the value of the material properties. Milke addressed the evaporization of free water in a spray-applied cementitious material by increasing the specific heat in a narrow temperature region around 100 °C (212 °F) [56].

Agreement between the predicted and experimental average steel temperatures is quite good in both applications of FIRES-T3 by Jeanes and Milke. A comparison of the temperature history for a steel column protected with a spray-applied cementitious material subjected to the ASTM E119 test is presented in Fig. 53.24. A similar comparison is presented in Fig. 53.25 for steel beams protected with the same material [13].

FIRES-T3 has also been used to conduct a preliminary analysis of the heating of partially protected steel columns (i.e., where a portion of the spray-applied protection is missing) [59, 60]. The analysis indicated that even a small portion of missing protection significantly decreased the fire resistance of the column, especially for cases involving small columns. Results of the analysis are indicated in Fig. 53.26.

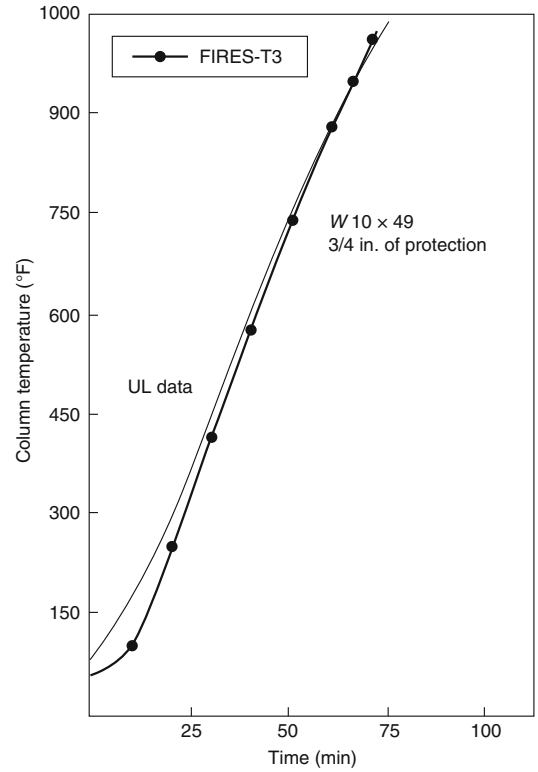

Fig. 53.24 Comparison of predicted and measured average steel column temperature [53]

Structural Analyses

Much of the previous testing and analysis has concentrated on the response of a single isolated member to fire exposure. Recent events, including the Broadgate fire, Cardington tests, and performance of buildings in or near the World Trade Center complex, have indicated that analyses need to account for interactions between structural members for more realistic assessments of behavior in fire. In the fire at the Broadgate construction site, a major fire exposed steel elements that were not yet protected. However, no collapse was observed. In the Cardington tests, no collapses were observed in any of the six tests despite steel temperatures that reached 900 °C in some tests [61].

In the many steel frame buildings involved in the World Trade Center terrorist incident on September 11, 2001, the variety of outcomes

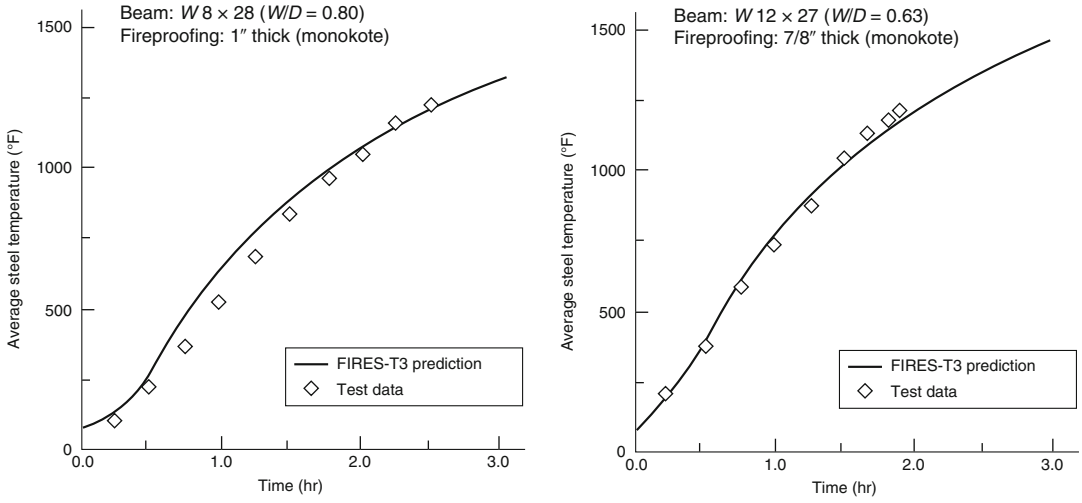

Fig. 53.25 Comparison of experimental data and FIRES-T3 analysis [13]

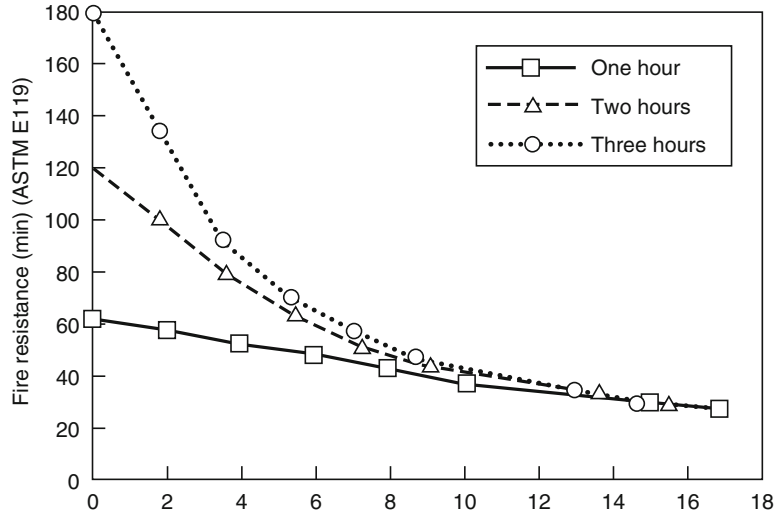

Fig. 53.26 Fire resistance versus percent protection loss for W 10 × 49 column, flange exposure

observed has been attributed to the response of subframes or the interaction of exposed structural members with adjacent structural members [62]. In the North and South Towers, the ability of the towers to remain standing for a period of time after the aircraft impact is attributed to load transfer from the severed exterior columns to core columns. In neighboring buildings, impacts by the debris from the collapsing North and South Towers were withstood because of load transfer. One of the lower buildings in the World Trade Center complex, WTC 5, withstood almost complete burnout of fuels, though beams were significantly deflected.

The interaction of structural components has been an area of increased research in recent years, as will be discussed later in this chapter relative to computer modeling efforts. Part of this interest has concentrated on joints [63]. In WTC 5, a shear plate failed, leading to a partial collapse of the building [61].

The structural analysis methods calculate one of three parameters: deflection, critical temperature, or critical load. In several of the

methods, all three of the parameters may be considered because they are interrelated. Algebraic equations, graphs, and computer programs are available to perform a structural analysis for the purpose of addressing fire resistance.

General Discussion of Three Parameters Addressed in Structural Analysis

Deflection The total deflection and rate of deflection can be calculated for loaded and heated steel beams by considering all sources of strain. The total strain comprises components of the elastic and plastic strains due to the applied loads, thermal strain (due to thermal expansion), and creep strain.

The calculated deflection and rate of deflection can be compared with established maximum limits of each. The Robertson-Ryan criteria have been widely accepted for this purpose [22, 64, 65]. However, calculation of the deflection of unheated beams is difficult except for simple loadings, geometries, and end conditions. Adding the thermal expansion and creep components further complicates the calculation, virtually requiring computer solution.

Critical Temperature As mentioned earlier in the chapter, the material properties of steel change with increasing temperature. The most important material properties for critical-temperature calculations are yield strength, ultimate strength, and modulus of elasticity. The critical temperature is defined as the temperature at which the material properties have decreased to the extent that the steel structural member is no longer capable of carrying a specified load or stress level. In this context, the factor of safety of the member is considered to be reduced if the member reaches unacceptable stress levels, buckling becomes imminent, or deflections exceed maximum limits. The critical temperature can be calculated as long as the dependence of the material properties with temperature is known. There are numerous algebraic equations to calculate the critical temperature of steel structural members [66]. Often, the critical temperature is defined based on temperature limits stated in the standard test. However, in tests steel members experienced temperatures in excess of 800 °C (1470 °F) without collapse [66].

Critical Load The critical load is defined as the minimum applied load that will result in failure if the structural member is heated to a temperature, T. The critical load can be expressed as a point load or distributed load. As with critical temperature, the critical load calculation requires the material properties at elevated temperatures. Critical load calculations can be conducted with algebraic equations or with a computer program.

Algebraic Equations: Critical Temperature

Beams

The critical temperature of Grade 250 steel beams with an allowable stress of 20,000 psi (138 Mpa) can be determined using equations by Lie and Stanzak [35]. The Lie and Stanzak equations account for creep strain and assume the beam is simply supported and thermally unrestrained.

Similar approaches have been developed by Malhotra [23], Vinnakota [65], and Kruppa [67]. Differences in the percent reduction in yield stress or modulus of elasticity are related to design method (elastic or plastic), factor of safety, and end conditions. Equations for the ratio of yield stress at elevated temperature with yield stress at ordinary room temperature are presented in Table 53.9. Typical values of Z_p/Z_e are between 1.13 and 1.15 for I sections [23], and 1.5 for rectangular sections.

Another example of the second approach is the analysis of the critical temperature of beams by European Convention for Constructional Steelwork (ECCS) [41, 68]. The ECCS guide addresses the maximum allowable reduction in yield strength by considering the applied loading, beam geometry, structural end conditions, and whether the applied loading results in stresses

Table 53.9 Critical stress equations [22]

Design basics	Critical yield stress
Elastic design	$\frac{\sigma_{yT}}{\sigma_y} = \frac{1}{F_e} \quad \frac{Z_e}{Z_p}$
Plastic design	$\frac{\sigma_{yT}}{\sigma_y} = \frac{1}{F_p}$

where
σ_{yT} = critical yield stress at elevated temperature, T
σ_y = yield stress at ordinary room temperature
F_e = factor of safety, elastic design
F_p = factor of safety, plastic design
Z_e = elastic section modulus
Z_p = plastic section modulus

in the elastic or plastic range. Critical temperature calculations based on the ECCS analysis are presented in Table 53.10.

Example 5 Determine the critical temperature of a simply supported W 12 × 26 steel beam supporting a 53-in. (1.35-m) thick rectangular slab. The applied moment is 41,750 ft·lb (15,480 N·m). The rectangular slab is 8 ft (2.4 m) wide. The section properties of the beam are

$$Z_e = 33.4\,\text{in.}^3\left(547 \times 10^3\,\text{mm}^3\right)$$
$$l = 204\,\text{in.}^4\left(84.9 \times 10^6\,\text{mm}^4\right)$$

Assume σ_y = 36,000 psi (248 MPa).

Solution Using Lie and Stanzak's equation for a beam,

$$I_d = \frac{3^3 \times 96}{12} = 216\,\text{in.}^4\left(5.19 \times 10^4\text{m}^4\right) \tag{53.27}$$

$$T_{cr} = \frac{70,000}{45.62 - 4.23(I_d/I)} - 460 = \frac{70,000}{45.62 - 4.23(216/204)} - 460 = 1240°\text{F}\ (671°\text{C}) \tag{53.28}$$

Columns

Lie and Stanzak calculated a critical temperature of 941 °F (505 °C) for slender, axially loaded columns [35]. The calculation was based on the temperature for the onset of elastic buckling for columns under maximum permissible applied stress conditions.

The Euler buckling stress at which elastic buckling is imminent is given by

$$\sigma_{cr} = \frac{\pi^2 E_T}{\lambda^2} \tag{53.29}$$

where
σ_{cr} = Euler buckling stress (MPa) (psi)
E_T = Modulus of elasticity at temperature T (MPa) (psi)
λ = Slenderness ratio = Kl/r
r = Radius of gyration (ft) (m)
Kl = Effective length of column (ft) (m)

Included in the ECCS guide [41] are dimensionless buckling curves for steel columns at elevated temperatures. These curves are presented in Fig. 53.27.

Equation 53.29 is valid only for columns that buckle in the elastic range. Generally, slender columns having a slenderness ratio in excess of approximately 90 can be expected to buckle elastically. Buckling stresses for stout columns (slenderness ratio less than 90) are in the plastic range, requiring a more complex analysis. The failure mode for columns with a slenderness ratio between 80 and 100 cannot be reliably predicted [69]. The tangent modulus can be used instead of the modulus of elasticity in Equation 53.29 for stout columns. However, predictions of the critical temperature using Equation 53.29 may not be accurate, due to residual stresses from the steel fabrication process [69]. Thus, for stout columns, a conservative estimate for the critical temperature of steel columns may be obtained by determining the temperature at which the yield stress is equal to the applied stress.

General

Malhotra has observed that critical temperatures determined from the structural analysis algebraic equations will be somewhat low when compared to experimental data [23]. Thus, the following

Table 53.10 Critical temperature of steel beams [43]

			factor $\frac{kq^*}{q_e}$ resp. $\frac{kq^*}{q_p}$				
		Static System	0.3	0.4	0.5	0.6	0.7
Base of structural design at room temperature	Theory of plasticity	Statically determinate Statically indeterminate	585	540	490	430	360
	Theory of elasticity	Statically determinate	605	565	525	475	425
		Statically indeterminate					
		Θ = 1.33 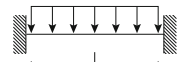	640	605	575	545	510
		Θ = 1.0 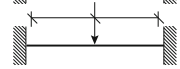	605	565	525	475	425
		Θ = 1.47 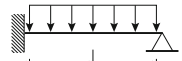	650	615	590	560	535
		Θ = 1.12 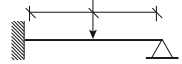	615	580	545	505	465
		Θ = 1.47 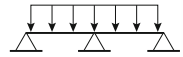	650	615	590	560	535

q_p = Ultimate plastic load
q^* = Applied load
k = Load multiplier
Θ = Factor addressing plastic reserve of beam from redistribution of moments
q_e = elastic load limit

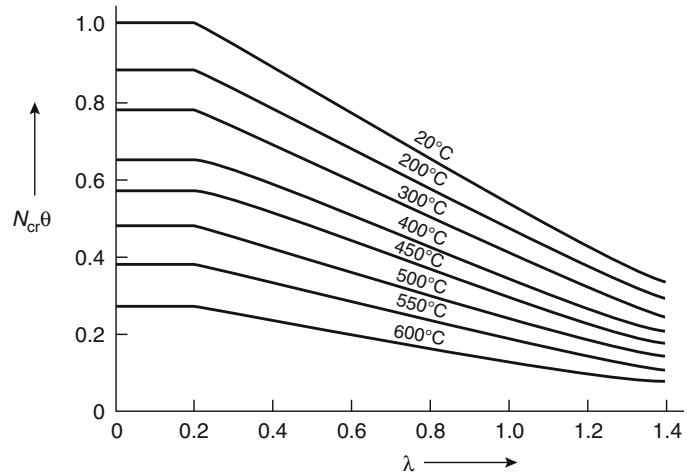

Fig. 53.27 Dimensionless buckling curves for steel columns [41]

correction factors, V, are suggested by Malhotra to improve the prediction capabilities of the approach:

1. Columns: $V = 0.85$
2. Statically determinate beams: $V = 0.77 + 0.15\frac{P_s}{P_u}$
3. Statically indeterminate beams: $V = 0.25 + 0.77\frac{P_s}{P_u}$

where

P_s = Service (applied) load (N or N/m) (lb or lb/ft)

P_u = Load to induce ultimate stress at midspan (N or N/m) (lb or lb/ft)

Example 6 Determine whether the following steel column is expected to buckle if it achieves

an average temperature of 1100 °F (593 °C). The column is simply supported, is 15 ft (4.6 m) long, and has an applied load of 12,000 psi (82.8 MPa). Assume the yield stress is 36,000 psi (248.4 MPa) and the modulus of elasticity is 30,000,000 psi (207 GPa). The characteristics of the column are

$A = 8.23$ in.^{2} (5310 mm^2)
$I = 21.6$ in.^{4} (8.99×10^6 mm^4)
$Kl = 180$ in. (4572 mm)

At 1100 °F (593 °C):

$$E_T = \left(1 + \frac{T}{2000\, ln(T/1100)}\right) E_0 = \left(1 + \frac{593}{2000 \ln(593/1100)}\right) \times 15.6 \times 10^6 = 8.11 \times 10^6 \tag{53.30}$$

Solution Calculate the slenderness ratio to determine the failure mode.

$$\lambda = \frac{Kl}{r} = \frac{180}{\sqrt{21.6/8.23}} = 113 \tag{53.31}$$

Because the slenderness ratio exceeds 90, the column is susceptible to buckling. The buckling stress at 1100 °F (595 °C) is 12,700 psi (87.6 MPa). Thus, the column does not buckle due to the applied load and elevated temperature.

Critical Stress

Columns Simple expressions for determining the critical stress for steel columns [35] are noted below.

$$P_{cr}^2 - P_{cr}\left[\sigma_{yT} + 4.8 \times 10^{-5}\pi^2 E_T + \frac{1}{\lambda^2}\right] + \sigma_{yT} A \frac{\pi^2 E_T}{\lambda^2} = 0 \tag{53.32}$$

where

P_{cr} = Critical point load (N) (lb)
σ_{yT} = Yield stress at temperature T (Pa) (psi)
E_T = Modulus of elasticity at temperature T (Pa) (psi)
$\lambda = Kl/r$

In order to improve the prediction capabilities of the critical stress approach for slender columns, the modulus of elasticity should be replaced by the reduced modulus of elasticity [16]. The reduced modulus is defined as

$$E_r = \frac{4EE_T}{\left(\sqrt{E} + \sqrt{E_t}\right)^2} \tag{53.33}$$

where

E_t = Tangent modulus

In addition, the 0.2 % proof stress may be replaced by the 0.5 % proof stress in the yield stress parameter [70].

Results of a buckling analysis on concrete-filled square hollow sections are provided in Fig. 53.28.

Beams The expressions for the critical loads for beams assume at failure that the beam is in a state of full plasticity at the location of the maximum moment [70]. Obviously, in order to calculate the critical stress, the material property–temperature relationships must be known.

The critical distributed load for a simply supported beam is [66]

$$q_{cr} = \frac{8\sigma_{yT} Z_p}{L^2} \tag{53.34}$$

where

q_{cr} = Critical distributed load (N/m) (lb/ft)
Z_p = Plastic section modulus (m^3) (in.^{3})
L = Span of beam (m) (ft)

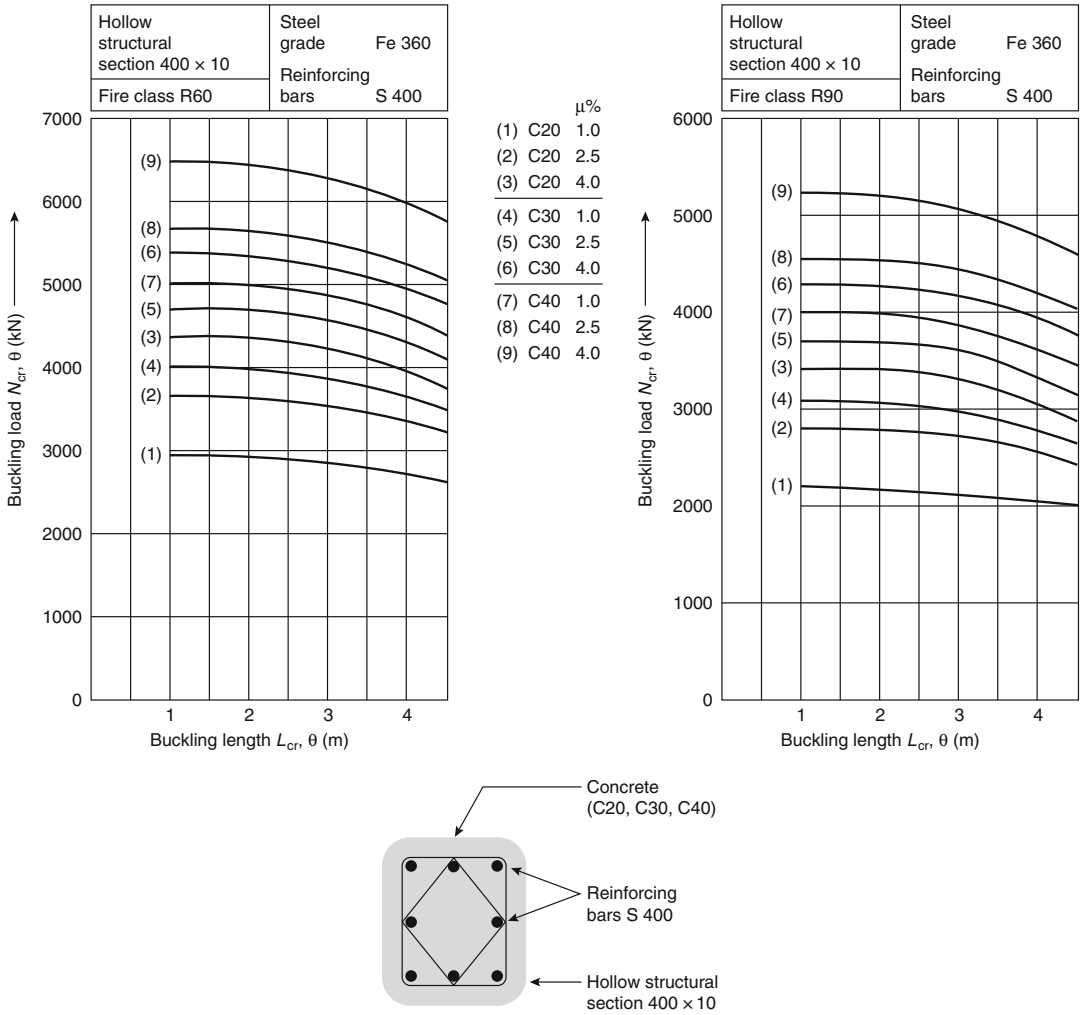

Fig. 53.28 Design graphs for ISO fire resistance requirements R60 and R90. For the concrete-filled square hollow structural section 400 × 10, the axial buckling load is a function of the buckling length, of the concrete quality, and of the percentage m of reinforcement; this design diagram is based on a simple calculation model [9]

σ_{yT} = Yield stress at elevated temperature (MPa) (psi)

Considering a cantilever beam with a point load applied one-third of the span from the fixed end, a plastic hinge can be expected at the fixed end. The critical load can be determined by

$$p_{cr} = \frac{7.5\sigma_{yT}Z}{L} \tag{53.35}$$

The above equations in this section do not account for creep strain. Based on an analysis of the deflection history of heated, loaded beams, Pettersson et al. include a load ratio, β, to determine the critical distributed stress [40].

$$q_{cr} = \beta\frac{8\sigma_z}{L^2} \tag{53.36}$$

where the yield stress is evaluated at ordinary room temperature, relaxing the need to know the yield stress–temperature relationships. β is defined as the ratio of the load causing a maximum allowable deflection under fire conditions to the load inducing stresses equal to the yield stress at ordinary room temperature. Thus, the parameter β takes into account the dependence

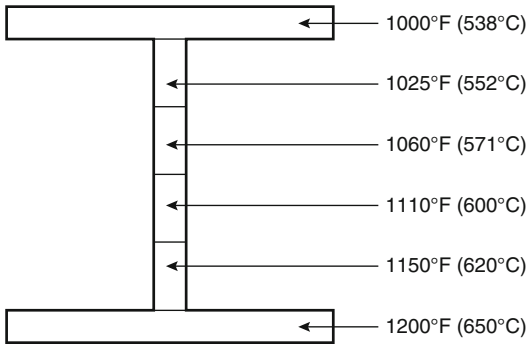

Fig. 53.29 Isothermal sections of beam

of both the yield stress and the creep on temperature. Graphs of β are available for a variety of thermal restraint and structural end conditions.

The Eurocodes include a method of analysis using algebraic equations to consider the moment capacity of steel beams that have a temperature gradient through the depth of the beam [10]. The method involves dividing the beam into small isothermal sections and treating these isothermal sections as a composite beam (Fig. 53.29). In this case, the moment capacity of the beam is given as

$$M_{\text{cap}} = \sum_{i=1}^{n} \sigma_i A_i z_i \qquad (53.37)$$

where

M_{cap} = Moment capacity (N·m) (lb·ft)

σ_i = Applied stress in isothermal element (Pa) (psi)

A_i = Area of isothermal element (m^2) (ft^2)

z_i = Distance from neutral axis to centroid of isothermal element (m) (ft)

Computer Programs

Several finite element computer models are available to assess the structural response of fire-exposed structural members or frames. Sullivan et al. indicate that most of the existing finite element models used for structural fire protection analyses were developed originally for research applications [71].

FASBUS-II is an example of a finite element model developed in the United States to evaluate the structural response of complex building assemblies such as floor assemblies consisting of a two-way concrete slab, steel deck, and steel beam [72]. Sullivan et al. and Franssen et al. provide extensive reviews and comparisons of existing finite element models for structural fire protection applications [72, 74]. At the time of the review, Sullivan et al. noted that all of the models make the following assumptions:

- Plane sections remain plane (Navier-Bernoulli hypothesis).
- Perfect composite action is assumed for steel-concrete assemblies, disregarding any slippage between the steel and concrete.
- Torsion is disregarded.
- Moisture effects are disregarded.
- Large displacements are not accurately modeled.

Traditionally, analysis of the response of the structure exposed to fire has been limited to an analysis of the response of single members. However, in structural frames comprising many members, load transfer or membrane action may occur to permit the steel member to maintain its integrity, despite achieving a temperature in excess of that typically associated with failure [73, 74].

Load transfer allows stronger members to support additional loads not capable of being carried by heated, weak members. In order to capture this phenomenon, a frame analysis is required [49]. Numerous software packages are available to conduct the frame analysis. Results of a frame analysis are presented in Figs. 53.30 and 53.31.

The frame analyses range from algebraic equation–based methods to finite element analyses. Pettersson et al. include a frame analysis via algebraic equations used to determine displacement [40]. The frames consist of beams supported by one or two columns at midspan. The analysis assumes that each beam or column has a uniform temperature (though the temperature of the beam is not required to be that of a column). A pinned connection between the structural members is assumed. The analysis considers the compatibility of the deformation of each member by requiring that the change in length of the column is equal to the beam deflection at the point of contact.

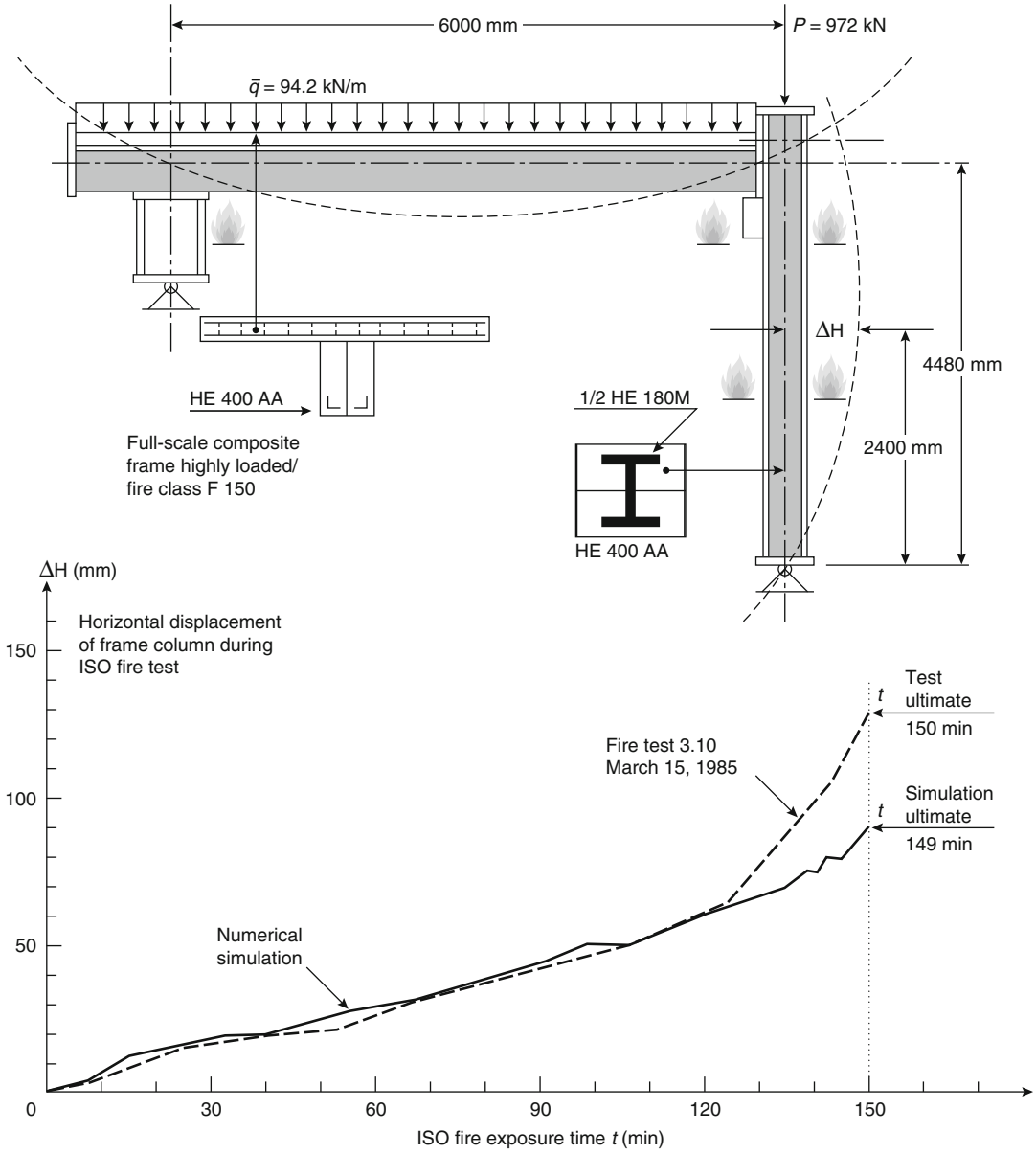

Fig. 53.30 Deformations measured and calculated by a numerical model for a composite frame [9]

Schleich et al. describe the application of CEFICOSS for a frame analysis [75, 76]. The frame consists of a single beam and column, where one end of the column is connected to an end of the beam. Reasonable agreement is indicated between predicted and measured results.

El-Rimavi et al. describe the application of another finite element model, NARR2, for the evaluation of a large building frame involving numerous beams and columns [77]. The large frame is divided into several subframes for computational ease. Good agreement is noted between predictions of deflections and force

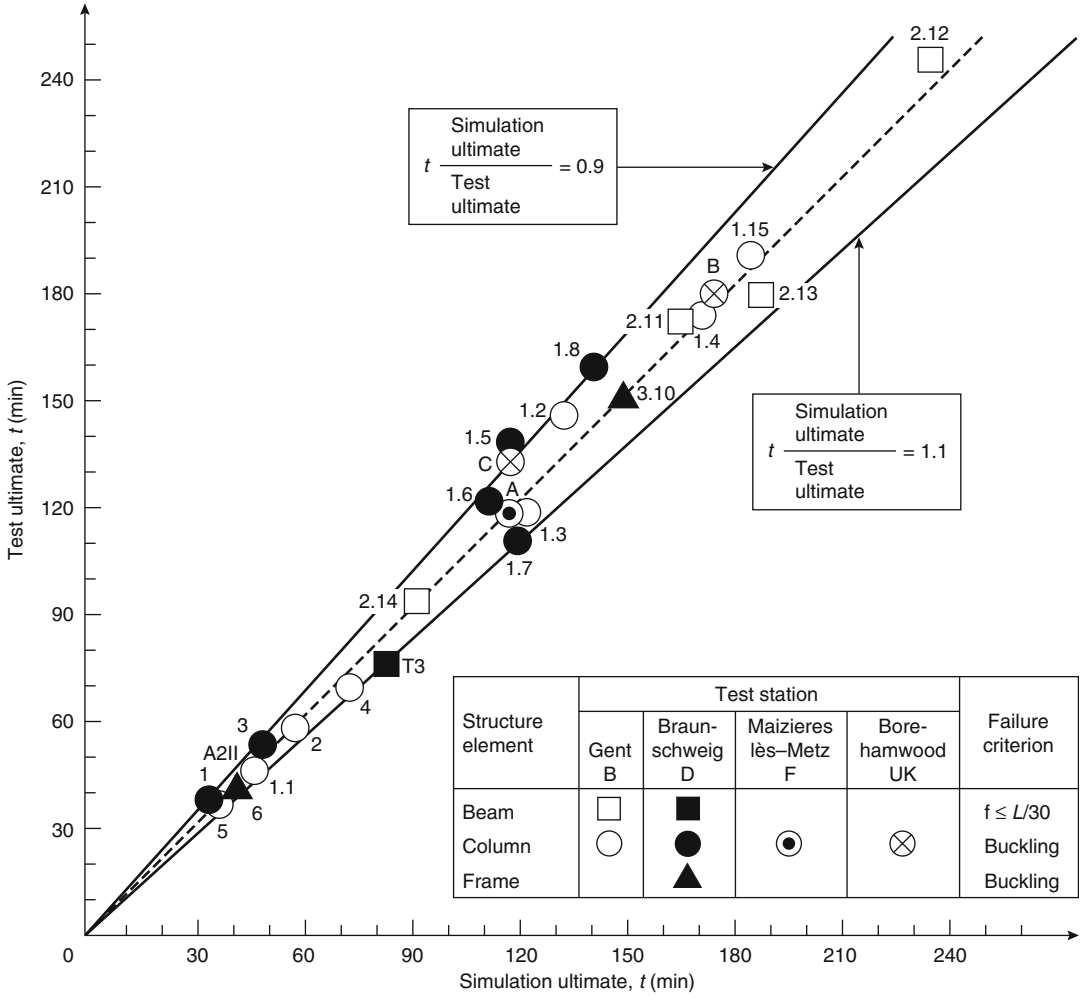

Fig. 53.31 Fire resistance times measured and calculated by a numerical model for columns, beams, or frames of any cross-section types (bare steel, protected steel, composite) [6]

resultants obtained involving simulations of the full building frame and subframes. Slightly greater failure temperatures were determined for semirigid connections as compared to rigid connections. More recently, applications of ABAQUS, SAFIR, and VULCAN to study frame behavior have been described in several references [74, 78, 79]. In contrast to the models reviewed by Sullivan et al., these models have the capability to consider nonlinear effects, large deformations, and torsion. Part of the challenge in conducting frame analyses is to model the response of a joint to fire exposure. This is a current area of research [63, 74].

Nomenclature

a	Characteristic dimension
A	Cross-section area of steel tube, steel column
A_s	Cross-section area of steel column
b	Characteristic dimension
b_f	Width of flange
c	Characteristic dimension
c_c	Specific heat of concrete
c_i	Specific heat of protection material
c_s	Specific heat of steel
C_1	Constant

C_2 Constant
d Outer diameter of steel pipe
d Depth of section
D Heated perimeter of steel section
E_0 Modulus of elasticity at ambient temperature
E_r Reduced modulus
E_t Tangent modulus
E_T Modulus of elasticity at temperature T
F Factor of safety
F_e Factor of safety, elastic design
F_p Factor of safety, plastic design
Fo Fourier number
h Thickness of protection material
H Thermal capacity of steel section at ambient temperature
I Second moment of cross sectional area
k Thermal conductivity of steel
k_c Thermal conductivity of concrete
k_i Thermal conductivity of protection material
K End condition factor
l Unsupported length of column
L Inside dimension of one side of square concrete box protection
L Span of beam
m Moisture content of concrete
M Flexural moment
N Ratio of thermal capacity of protection material to that of steel
P Perimeter of steel tube
P_{cr} Critical point load
P_s Service (applied) load
P_u Ultimate load
q_{cr} Critical distributed load
r Radius of gyration
R Fire resistance
R_0 Fire resistance with zero moisture content of concrete
t Wall thickness of steel pipe
t Time
t_w Width of web
Δt Time step
T Steel temperature
T_f Fire temperature
T_m Mean fire temperature
T_0 Ambient temperature
T_s Steel temperature
ΔT_s Change in steel temperature
V Correction factor
W Weight of steel section per unit length
Z_e Elastic section modulus
Z_p Plastic section modulus

Greek Letters

α Thermal diffusivity (when used with Fourier number)
α Heat transfer coefficient
α_c Convective heat transfer coefficient
α_r Radiative heat transfer coefficient
α_T Coefficient of thermal expansion at temperature T
β Ratio of distributed load causing maximum allowable deflection to distributed load inducing yielding
ε_f Fire emissivity
λ Slenderness ratio
θ Dimensionless temperature
ρ Density
ρ_i Density of insulation material
σ_{cr} Critical stress for buckling
σ_{y0} Yield strength at ambient temperature
σ_{yT} Yield strength at temperature T

References

1. ASTM, ASTM E119, *Standard Test Methods for Fire Tests of Building Construction and Materials,* American Society for Testing and Materials, Philadelphia (2008).
2. L.G. Seigel, "Fire Test of an Exterior Exposed Steel Spandrel," *Materials Research and Standards,* 10, 2, pp. 10–13 (1970).
3. *Fire Resistance Directory,* Underwriters Laboratories, Northbrook, IL (2012).
4. SFPE Engineering Standard on Calculating Fire Exposures to Structural Elements, Society of Fire Protection Engineers, Bethesda, MD 2011.
5. NFPA 251, *Standard Methods of Tests of Fire Resistance of Building Construction and Materials,* National Fire Protection Association, Quincy, MA (2006).
6. UL 263, *Fire Tests of Building Construction and Materials,* Underwriters Laboratories, Northbrook, IL (2003).

7. R.G. Gewain and E.W.J. Troup, "Restrained Fire Resistance Ratings in Structural Steel Buildings," *Engineering Journal,* 2nd Quarter, pp. 78–88 (2001).
8. T.T. Lie (ed.), *Structural Fire Protection,* American Society of Civil Engineers, New York (1992).
9. *International Fire Engineering Design for Steel Structures: State of the Art,* International Iron and Steel Institute, Brussels, Belgium (1993).
10. *Eurocode 3: Design of Steel Structures—Part 1-2: General Rules—Structural Fire Design,* European Committee for Standardization (CEN), Brussels, Belgium (1995).
11. ASCE/SFPE 29, *Standard Calculation Methods for Structural Fire Protection,* American Society of Civil Engineers, New York (2005).
12. D. Boring, J. Spence, and W. Wells, *Fire Protection through Modern Building Codes,* American Iron and Steel Institute, Washington, DC (1981).
13. D.C. Jeanes, *Technical Report 84-1,* Society of Fire Protection Engineers, Boston (1984).
14. T.Z. Harmathy, *NRCC 20956 (DBR Paper No. 1080),* National Research Council of Canada, Ottawa (1983).
15. M.S. Abrams, ASTM STP 685, *Behavior of Inorganic Materials in Fire,* American Society for Testing and Materials, Philadelphia (1979).
16. T.T. Lie, *Fire and Buildings,* Applied Science, London (1972).
17. T.T. Lie and W.W. Stanzak, "Empirical Method for Calculating Fire Resistance of Protected Steel Columns, *Engineering Journal,* 57, 5–6, pp. 73–80 (1974).
18. D.R. Boring, "An Analytical Evaluation of the Structural Response of Simply Supported, Thermally Unrestrained Structural Steel Beams Exposed to the Standard Fire Endurance Test," Master's Thesis, Ohio State University, Columbus, OH (1970).
19. AISC, ANSI/AISC 360-05, *Specification for Structural Steel Buildings,* American Institute of Steel Construction, Chicago (2005).
20. "Structural Use of Steelwork in Building: Part 8: Code of Practice for Fire Resistant Design," *BS 5950-8,* British Standards Institute, London, UK (2003).
21. R.A. Lindberg, *Processes and Materials of Manufacture,* Allyn and Bacon, Boston (1978).
22. D.C. Jeanes, *Methods of Calculating Fire Resistance of Steel Structures,* Engineering Applications of Fire Technology Workshop, SFPE, Boston (1980).
23. H.L. Malhotra, *Design of Fire-Resisting Structures,* Chapman and Hall, New York (1982).
24. T.Z. Harmathy, "A Comprehensive Creep Model," *ASME Journal of Basic Engineering,* 89, pp. 496–502 (1967).
25. T.Z. Harmathy, ASTM STP422, *Deflection and Failure of Steel-Supported Floors and Beams in Fire,* American Society for Testing and Materials, Philadelphia (1967).
26. J.L. Gross and T.P. McAllister, "Structural Fire Response and Probable Collapse Sequence of the World Trade Center Towers," *NIST NCSTAR 1-6,* National Institute of Standards and Technology, Gaithersburg, MD (2005).
27. *Fire Resistant Steel Frame Construction,* American Iron and Steel Institute, Washington, DC (1974).
28. *Designing Fire Protection for Steel Columns,* American Iron and Steel Institute, Washington, DC (1980).
29. W.W. Stanzak and T.T. Lie, *Fire Tests on Protected Steel Columns with Different Cross-Sections,* National Research Council of Canada, Ottawa (1973).
30. PABCO, *Pabco Super Firetemp Fireproofing Board Fire Protection Guide,* Ruston, LA (1984).
31. V.K.R. Kodur and T.T. Lie, "Fire Performance of Concrete-Filled Hollow Steel Columns," *Journal of Fire Protection Engineering,* 7, 3, pp. 89–98 (1995).
32. V.K.R. Kodur and T.T. Lie, "Evaluation of Fire Resistance of Rectangular Steel Columns Filled with Fibre-Reinforced Concrete," *Canadian Journal of Civil Engineering,* 24, pp. 339–349 (1995).
33. L.G. Seigel, "Designing for Fire Safety with Exposed Steel," *Fire Technology,* 6, 4, pp. 269–278 (1970).
34. T.T. Lie and W.W. Stanzak, "Fire Resistance of Protected Steel Columns," *Engineering Journal, American Institute of Steel Construction,* 10, pp. 82–94 (1973).
35. *Designing Fire Protection for Steel Beams,* American Iron and Steel Institute, Washington, DC (1985).
36. *Load and Resistance Factor Design Specification for Structural Steel Buildings,* American Institute of Steel Construction, New York (1993).
37. J.L. Ruddy, S.A. Ioannides, and F. Alfawakhiri, "Fire Resistance of Structural Steel Framing," *Steel Design Guide 19,* American Institute of Steel Construction, Chicago (2003).
38. *Designing Fire Protection for Steel Trusses,* American Iron and Steel Institute, Washington, DC (1980).
39. *Fire Resistance Design Manual,* Gypsum Association, Evanston, IL (1984).
40. O. Pettersson, S. Magnusson, and J. Thor, *Bulletin 52,* Lund Institute of Technology, Lund, Sweden (1976).
41. European Convention for Constructional Steelwork, Technical Committee 3, *European Recommendations for the Fire Safety of Steel Structures,* Elsevier, Amsterdam (1983).
42. G.S. Berger, *Estimating the Temperature Response of Wide Flange Steel Columns in the ASTM E119 Test,* Department of Fire Protection Engineering, University of Maryland, College Park (unpublished) (1987).
43. J.A. Milke, "A Simplified Model for Estimating the Thermal Response of Steel Beam/Concrete Slab Ceiling Assemblies," in *2nd International Conference of Fire Research and Engineering (ICFRE2),* Society of Fire Protection Engineers, Bethesda, MD (1997).
44. W.W. Stanzak and T.Z. Harmathy, "Effect of Deck on Failure Temperature of Steel Beams," *Fire Technology,* 4, 4, pp. 265–270 (1968).
45. I.A. Smith and C. Stirland, "Analytical Methods and Design of Fire Safe Steel Structures," in *International Seminar on Three Decades of Structural Fire Safety,* Fire Research Station, Borehamwood, UK (1983).
46. *Fire-Safe Structural Steel, A Design Guide,* American Iron and Steel Institute, Washington, DC (1979).

47. M. Law, "Prediction of Fire Resistance," *AISC Engineering Journal,* pp. 16–29 (1978).
48. G.V.L. Bond, *Fire and Steel Construction—Water Cooled Hollow Columns,* Constrado, London (1974).
49. W.L. Gamble, "Predicting Protected Steel Member Fire Endurance Using Spreadsheet Programs," *Fire Technology,* 25, 3, pp. 256–273 (1989).
50. T.T. Lie and T.Z. Harmathy, *Fire Study No. 28,* National Research Council of Canada, Ottawa (1972).
51. O.C. Zienkewicz, *The Finite Element Method,* McGraw-Hill, New York (1983).
52. U. Wickström, *TASEF-2 – A Computer Program for Temperature Analysis of Structures Exposed to Fire,* Lund Institute of Technology, Lund, Sweden (1979).
53. R.H. Iding, Z. Nizamuddin, and B. Bresler, *UCB FRD 77-15,* University of California, Berkeley (1977).
54. A. Anderberg, *PC-TEMPCALC,* Institutet for Brandtekniska, Fragor, Sweden (1985).
55. K. Childs, *Heating 7,* Version 7.3, Computer software, Oak Ridge National Laboratory, 486 PC-DOS 4 MB, CD-ROM (1997).
56. J.A. Milke, "Estimating Fire Resistance of Tubular Steel Columns," in *Proceedings of Symposium on Hollow Structural Sections in Building Construction,* American Society of Civil Engineers, Chicago (1985).
57. K. Bardell, ASTM STP826, *Fire Resistive Coatings: The Need for Standards,* American Society for Testing and Materials, Philadelphia (1983).
58. D. Gross, *NBSIR 85-3223,* National Bureau of Standards, Gaithersburg, MD (1985).
59. D.V. Tomecek and J.A. Milke, "A Study of the Effect of Partial Loss of Protection on the Fire Resistance of Steel Columns," *Fire Technology,* 29, 1, pp. 3–21 (1993).
60. N.L. Ryder, S.D. Wolin, and J.A. Milke, "An Investigation of the Reduction in Fire Resistance of Steel Columns Caused by Loss of Spray-Applied Fire Protection," *Journal of Fire Protection Engineering,* 12, 1, pp. 31–44 (2002).
61. C.G. Bailey, T. Lennon, and D.B. Moore, "The Behaviour of Full-Scale Steel Framed Buildings Subjected to Compartment Fires," *Structural Engineer,* 77, 8, pp. 15–21 (1999).
62. World Trade Center Building Performance Study, *FEMA Report 403,* Washington, DC (2002).
63. F.M. Block, I.W. Burgess, and J.B. Davison, "Numerical and Analytical Studies of Joint Component Behaviour in Fire," in *Proceedings of 3rd International Workshop Structures in Fire,* Ottawa, Canada, pp. 383–396 (2004).
64. A.F. Robertson and J.V. Ryan, "Proposed Criteria for Defining Load Failure of Beams, Floors, and Roof Constructions during Fire Tests," *Journal of Research,* 63C, 2, pp. 121–124 (1959).
65. S. Vinnakota, *Calculation of the Fire Resistance of Structural Steel Members,* American Society of Civil Engineers, New York, p. 105 (1979).
66. J. Kruppa, "Collapse Temperature of Steel Structures," *Journal of Structural Division,* 105, pp. 1769–1788 (1979).
67. European Convention for Constructional Steelwork, *Fire Resistance of Steel Structures,* ECCS 89, Brussels, Belgium (1995).
68. B.R. Kirby and D.E. Wainman, *The Behaviour of Structural Steelwork in Natural Fires,* British Steel PLC., Rotherham, UK (1997).
69. A. Chajes, *Principles of Structural Stability Theory,* Prentice-Hall, Englewood Cliffs, NJ (1974).
70. T.T. Lie and W.W. Stanzak, "Structural Steel and Fire: More Realistic Analyses," *AISC Engineering Journal,* 13, 2, pp. 35–42 (1976).
71. P.J.E. Sullivan, M.J. Terro, and W.A. Morris, "Critical Review of Fire Dedicated Thermal and Structural Computer Programs," *Journal of Applied Fire Science,* 3, 2, pp. 113–135 (1994).
72. J.-M. Franssen, J.-B. Schleich, L.-G. Cajot, D. Talamona, B. Zhao, L. Twilt, and K. Both, "A Comparison Between Five Structural Fire Codes Applied to Steel Elements," in *Proceedings of Fourth International Symposium of Fire Safety Science,* International Association of Fire Safety Science, Ottawa, Canada, pp. 1125–1136 (1994).
73. C.G. Bailey and D.B. Moore, "The Structural Behaviour of Steel Frames with Composite Floorslabs Subject to Fire: Part 1: Theory, *Structural Engineer,* 78, 11, pp. 19–27 (2000).
74. D.I. Nwosu and V.K.R. Kodur, "Behaviour of Steel Frames Under Fire Conditions," *Canadian Journal of Civil Engineering,* 26, pp. 156–167 (1999).
75. J.M. Franssen, *Étude du Comportement au Feu des Structures Mixtes Ancier—Béton (CEFICOSS), A Study of the Behaviour of Composite Steel-Concrete Structures in Fire,* Ph.D. Dissertation, Université de Liège, Belgium (1987).
76. J.B. Schleich, J.C. Dotreppe, and J.M. Franssen, "Numerical Simulations of Fire Resistance Tests on Steel and Composite Structural Elements on Frames," in *Proceedings of First International Symposium of Fire Safety Science,* Hemisphere Publishing, Gaithersburg, MD, p. 311 (1986).
77. J.A. El-Rimawi, I.W. Burgess, and R.J. Plank, "Model Studies of Composite Building Frame Behaviour in Fire," in *Proceedings of Fourth International Symposium of Fire Safety Science,* International Association of Fire Safety Science, Ottawa, Canada, pp. 1137–1148 (1994).
78. Z. Huang, I.W. Burgess, and R.J. Plank, "Three-Dimensional Analysis of Composite Steel-Framed Buildings in Fire," *Journal of Structural Engineering,* 126, 3, pp. 389–397 (2000).
79. G.R. Flint and A.S. Usmani, "Investigation into the Impact of Fire on the Twin Towers," in *Proceedings of 3rd International Workshop Structures in Fire,* Ottawa, Canada, pp. 147–155 (2004).

James A. Milke is a professor in the Department of Fire Protection Engineering at the University of Maryland. His research activities have included the impact of fires on the structural response of steel and advanced composite members.

Analytical Methods for Determining Fire Resistance of Concrete Members

54

Charles Fleischmann, Andy Buchanan, and Anthony Abu

Introduction

Concrete structures have a reputation for excellent behavior in fires. Many reinforced concrete buildings that have experienced severe fires have been repaired and put back into use. Concrete is by nature noncombustible and has a low thermal conductivity. Concrete tends to remain in place during a fire, protecting the reinforcing steel, with the cool inner core continuing to carry the load. Catastrophic failures of reinforced concrete structures in fires are rare, but some occasionally occur [1].

Analytical methods developed to predict the fire resistance of structural assemblies can be divided into two groups: (1) standard and (2) nonstandard fire exposure. For the case of the standard fire exposure, a large database exists from referenced standard tests. The analytical methods use empirically based correlations and minimum dimensions to determine fire resistance. For nonstandard fire exposure, the analysis is more complicated, requiring both heat transfer and structural analyses. Analytical methods are an alternative to conventional methods that require destructive testing of exemplar systems in accordance with standard testing procedures, for example, ASTM E119 or ISO 834.

Fire resistance calculations typically use the same acceptance criteria specified in standard test methods, that is, heat transmission and structural integrity. The analysis can be broadly divided into two parts: (1) heat transfer and (2) structural analysis. Heat transfer calculations are used to evaluate the unexposed surface temperature and the temperature distribution throughout the member, in order to evaluate material strength. The structural integrity analysis applies the strength theory [2] used to design reinforced concrete members. The reduced strength of the concrete and steel resulting from elevated temperature is taken into account by using experimental results for the compressive and yield strengths as a function of temperature. This procedure is known as the rational design method.

As the fire protection field advances into performance-based engineering, techniques like the rational design method are more likely to be used. In the rational design approach, a design time-temperature curve, based on the expected fire, is specified. The engineer then performs the heat transfer analysis to determine the temperature profile and unexposed surface temperature. Knowing the temperature distribution of the member, a structural analysis is conducted to determine the fire endurance.

This chapter presents an overview of the analytical methods for calculating the fire resistance of concrete structural members and provides a description of the mechanical properties for concrete and steel at elevated temperatures. A brief discussion of heat transfer for a concrete assembly is given, along with temperature

C. Fleischmann (✉) • A. Buchanan • A. Abu
Department of Civil Engineering, University of Canterbury, in Christchurch, New Zealand

M.J. Hurley (ed.), *SFPE Handbook of Fire Protection Engineering*,
DOI 10.1007/978-1-4939-2565-0_54, © Society of Fire Protection Engineers 2016

profiles from ASTM E119 test results. The structural calculations for simply supported and continuous members are explained. A simple example is shown to further demonstrate the basics of the design concept. Fire resistance for columns and walls is also presented. The methodology in this chapter is based largely on ACI216.1-07—*Code Requirements for Determining Fire resistance of Concrete and Masonry Construction Assemblies* [3], (ACI216) commonly used in North America.

Throughout Europe, the Eurocodes for structural design provide comprehensive chapters on fire design. For reinforced concrete, Eurocode 2: Design of concrete structures—Part 1–2: General rules—Structural fire design [4], (EN1992-1-2) gives minimum dimensions and minimum cover necessary to achieve fire resistance ratings for slabs, walls, tensile members, beams, and columns. It also provides information on thermal and mechanical properties of concrete at high temperatures, with recommended design methods. Other than using the given design solutions, Eurocode 2 allows for two overall types of design: "simplified" calculation methods and "advanced" calculation methods. The simplified calculation method is essentially the same as that described in this chapter. The advanced calculation methods include those that provide a more realistic analysis of concrete structures exposed to fire, based on fundamental physical behavior including high temperature effects. The advanced calculation methods are the only option for design of complex structures regardless of the type of fire exposure, because the interaction between different structural members is critical to the fire resistance. Design of composite steel-concrete slabs in fire conditions is given in: Eurocode 4: Design of Composite Steel and Concrete Structures, EN1994-1-2: General Rules—Structural Fire Design [5].

More comprehensive discussions of the rational design methods for calculating the fire resistance of concrete structural members can be found elsewhere [1–8]. For more detailed overview of the "State-of-Art" for fire design of concrete structures the reader is directed to bulletin 38 [9] and 46 [10] written by Task Group 4.3 of the *fib* (*fédération internationale du béton / The International Federation for Structural Concrete*).

Material Properties of Concrete and Steel

Most of the material properties for concrete and steel change significantly at elevated temperatures. In order to accurately predict the structural fire resistance of concrete members, these changes must be taken into account. Temperature-dependent values of strength and modulus of elasticity are presented in a graphical format to aid in the design process. Values have been taken from both ACI216 and EN1992-1-2. The thermophysical properties that are required for a heat transfer analysis, i.e., thermal conductivity, specific heat, and density are also functions of temperature. These values are not included in ACI216; therefore only the EN1992-1-2 values are given below.

Strength

The strength of the reinforcing steel changes significantly with temperature and must be taken into account in any structural calculation. Figure 54.1 shows the strength–temperature relationship for hot-rolled, cold-drawn, and high-strength alloy steels from both the ACI216 and EN1992-1-2. Yield strength versus temperature relationship is given for hot-rolled steel, used for reinforcing bars. Tensile strength versus temperature relationship is shown for the cold-drawn steel and high-strength alloy steel, used for prestressing bars, wire, or strands. The change from yield strength to tensile strength for the two steel types relates to the design parameters used for reinforced versus prestressed concrete assemblies.

Like steel, the strength of concrete is also diminished at elevated temperatures. Figure 54.2a–c show the strength–temperature relationship for carbonate, siliceous, and sand-lightweight aggregate concretes, respectively. The compressive strength is not only a function of temperature but is also affected by the applied load as shown in ACI216 values given in Fig. 54.2. In Fig. 54.2 the values labeled as (Stressed 0.4f'c) were obtained from specimens initially loaded to 40 % of their

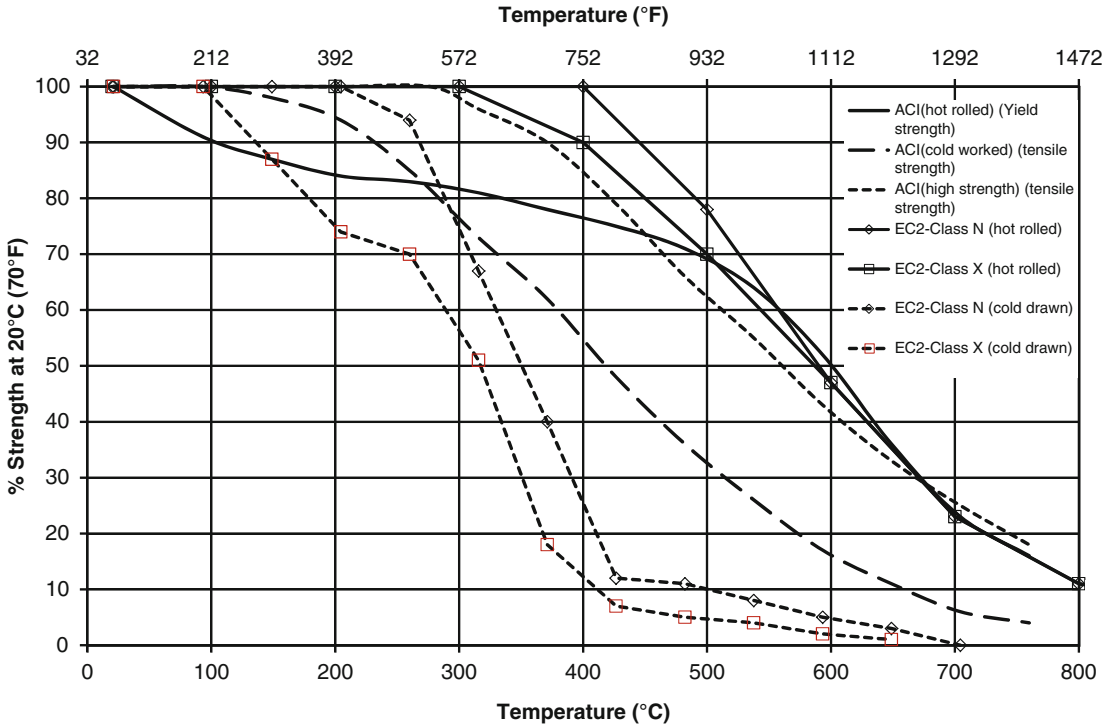

Fig. 54.1 Strength–temperature relationships for hot-rolled, cold-drawn, and high-strength alloy steels [3, 4]

compressive strength during the heating process; when the desired temperature was reached the samples were then loaded to failure. The values labeled (Unstressed) were heated to the desired temperature and then loaded to failure. Those labeled (Unstressed Residual) were heated, allowed to cool back to ambient temperature and then loaded to failure. Figure 54.2b illustrates that for the Stressed 0.4f'c results the compressive strength of concrete remains relatively unchanged up to 500 °C (900 °F). Above 500 °C (900 °F), the compressive strength of the siliceous aggregate concrete starts to decrease rapidly and is considered ineffective at temperatures above 650 °C (1200 °F), where the compressive strength has been reduced by approximately 50 % of the value at normal temperatures. However, for (Stressed 0.4f'c) carbonate and lightweight aggregates, compressive strength remains relatively unchanged up to 650 °C (1200 °F) and is not considered to be ineffective until it reaches a temperature of 760 °C (1400 °F). The experimental method used may influence the reported compressive strength. Specimens heated without compressive loads and then loaded to failure while hot have lower compressive strengths than those heated while loaded [7]. The EN1992-1-2 results are closest to the ACI Unstressed results.

Modulus of Elasticity

The modulus of elasticity for steel decreases as the temperature increases, as shown in Fig. 54.3. Figure 54.4 shows the modulus of elasticity–temperature curve for three different concrete aggregates. In each case, the modulus of elasticity of concrete is greatly reduced at elevated temperatures. This large reduction of the elastic modulus is helpful in reducing induced thermal stresses in concrete members due to fire [7].

Thermophysical Properties

The thermophysical properties required for heat transfer calculations are also strong functions of

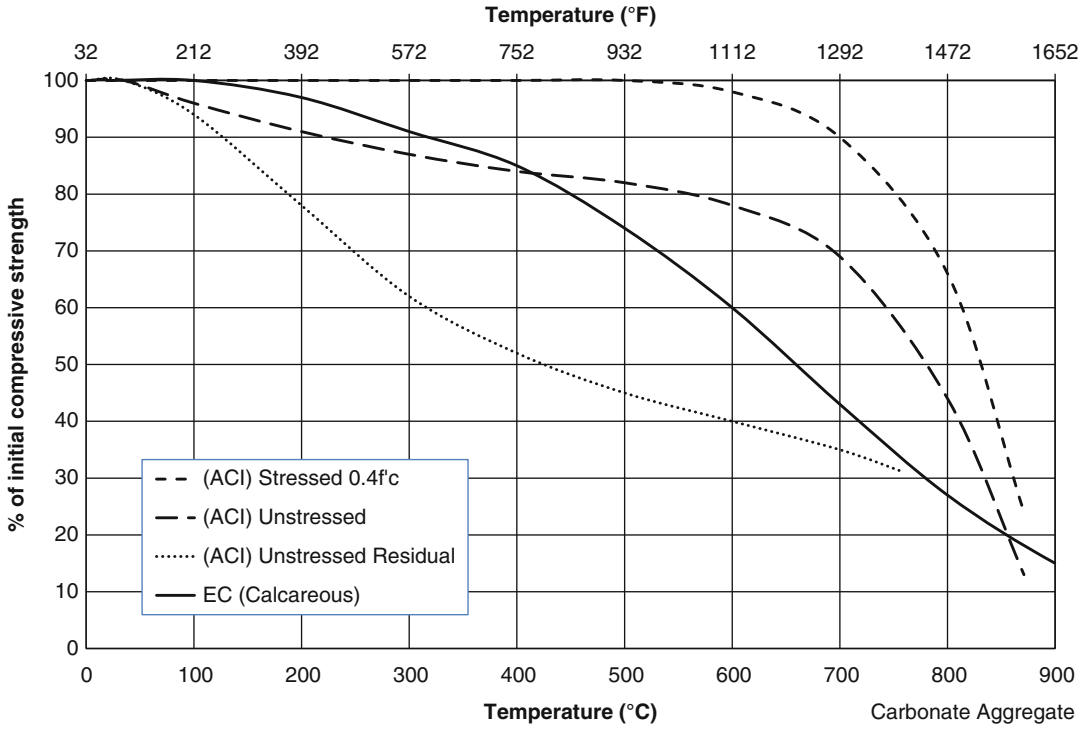

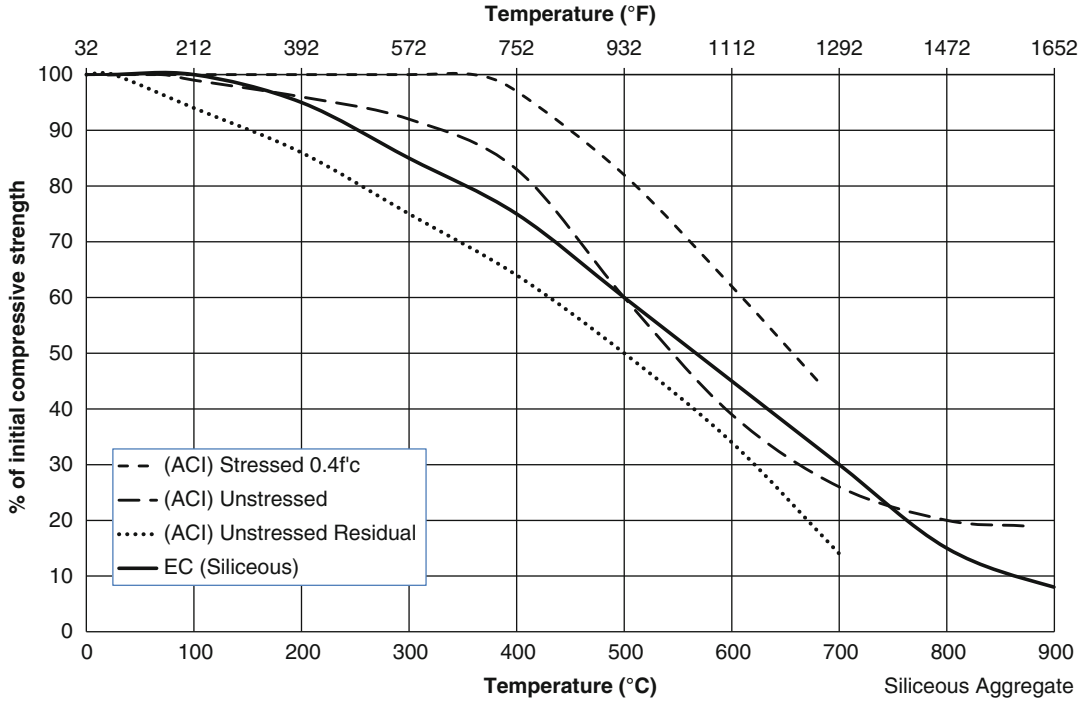

Fig. 54.2 (**a**) Strength–temperature relationship for carbonate aggregate concretes for different loading conditions [3, 4]. (**b**) Strength–temperature relationships for siliceous aggregate concretes for different loading conditions [3, 4]. (**c**) Strength–temperature relationships for sand-lightweight aggregate concretes for different loading conditions [3, 4]

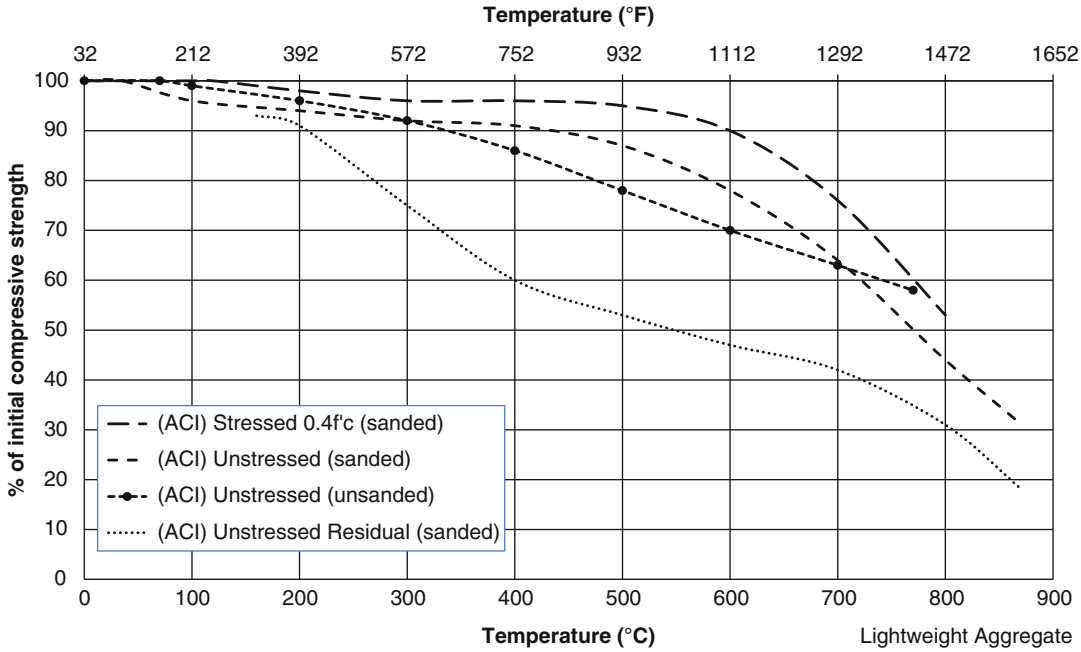

Fig. 54.2 (continued)

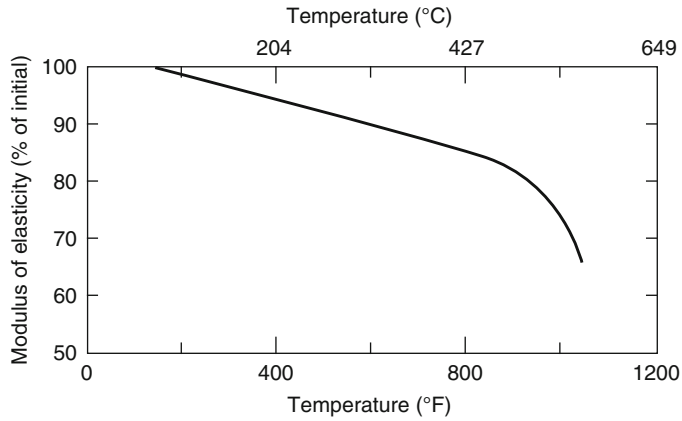

Fig. 54.3 Modulus of elasticity for hot-rolled steel at elevated temperatures [11]

temperature especially for concrete. The evaporation of water as well as changes within the cement and aggregate all play a role in the thermophysical properties.

Density. Figure 54.5 shows the percentage change in concrete density with temperature. From ambient to 1200 °C there is 12 % reduction in the density, with the greatest change occurring between 115 and 200 °C. The following relationship can be found in EC1992-1-2 [4].

$\rho(\theta) = \rho(20\ °C)$	For $20\ °C \leq \theta \leq 115\ °C$
$\rho(\theta) = \rho(20\ °C) \cdot (1-0.02(\theta-115)/85)$	For $115\ °C < \theta \leq 200\ °C$
$\rho(\theta) = \rho(20\ °C) \cdot (0.98-0.03(\theta-200)/200)$	For $200\ °C < \theta \leq 400\ °C$
$\rho(\theta) = \rho(20\ °C) \cdot (0.95-0.07(\theta-400)/800)$	For $400\ °C < \theta \leq 1200\ °C$

Specific Heat. The specific heat, $c_p(\theta)$, for both siliceous and carbonate aggregates is assumed to be identical for dry concrete with zero moisture content. Specific heat varies slightly with

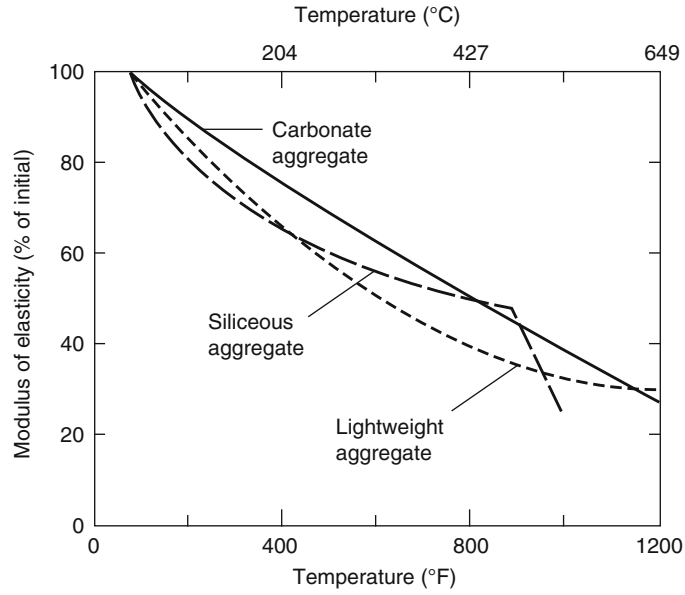

Fig. 54.4 Modulus of elasticity, at elevated temperatures, for carbonate, siliceous, and lightweight concretes [12]

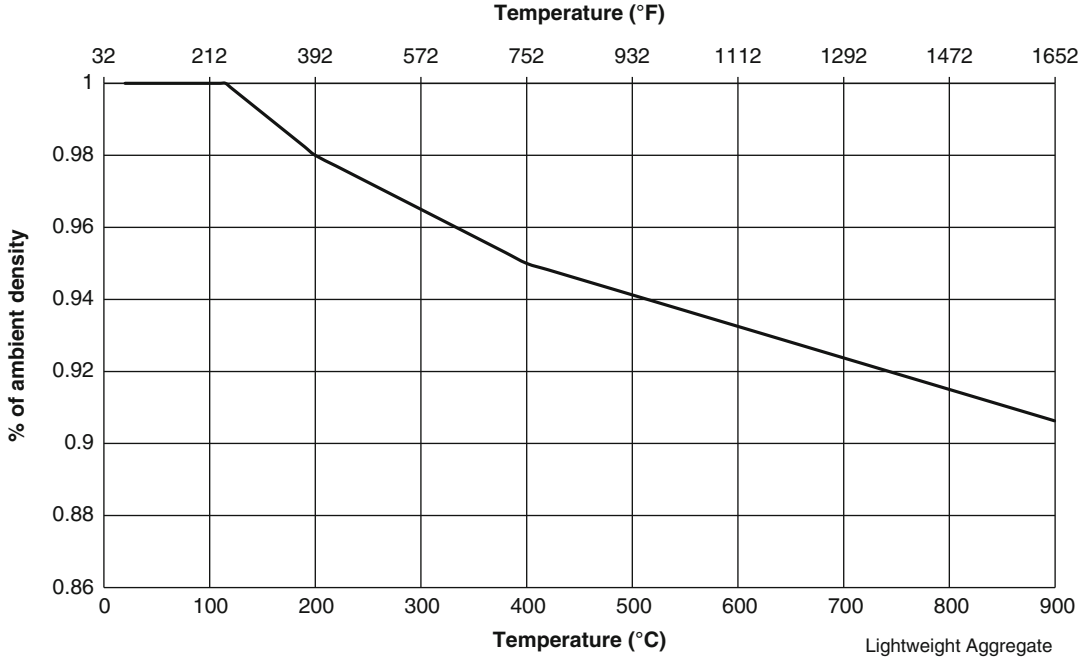

Fig. 54.5 Percentage change in concrete density as a function of temperature based on the ambient density [4]

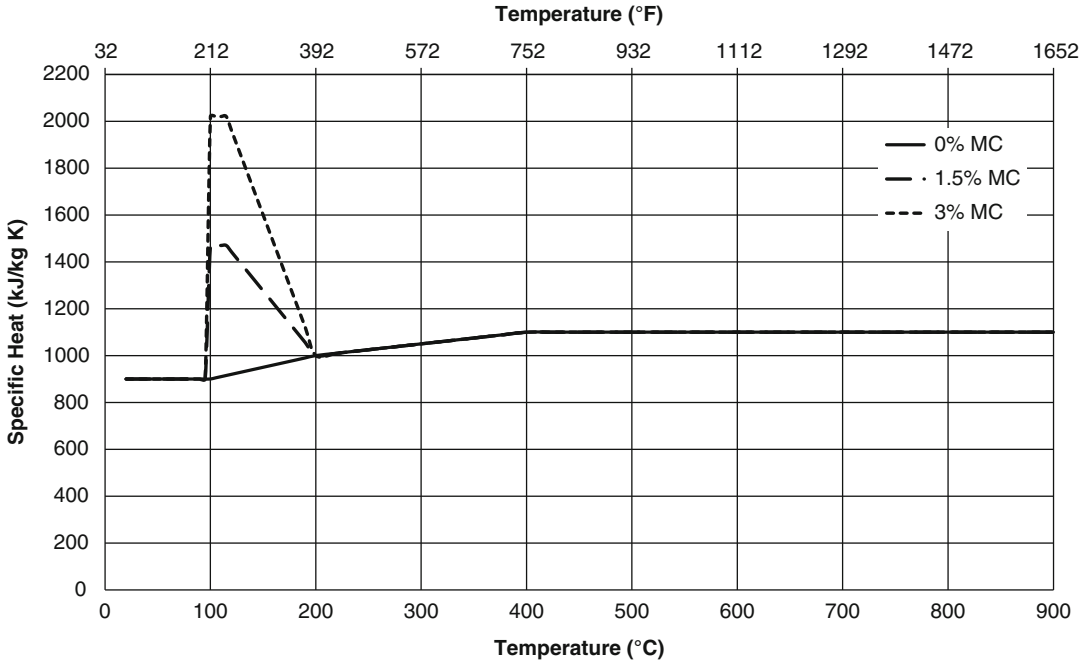

Fig. 54.6 Specific heat for siliceous and carbonate aggregate concrete as a function of temperature incorporating the moisture content [4]

temperature, ranging from 900 J/kg K at ambient to 1100 J/kg K above 400 °C. The following relationship can be found in EC1992-1-2 [4].

$c_p(\theta) = 900$ (J/kg K)	For 20 °C $\leq \theta \leq$ 100 °C
$c_p(\theta) = 900 + (\theta - 100)$ (J/kg K)	For 100 °C $< \theta \leq$ 200 °C
$c_p(\theta) = 1000 + (\theta - 200)/2$ (J/kg K)	For 200 °C $< \theta \leq$ 400 °C
$c_p(\theta) = 1100$ (J/kg K)	For 400 °C $< \theta \leq$ 1200 °C

However, when moisture is not explicitly included in the analysis and is to be included in the c_p value, the specific heat is modelled as a constant value (dependent on the moisture content) from 100 to 115 °C and a linear decline from 115 to 200 °C as shown in Fig. 54.6. The following values are given in EC1992-1-2 [4] for the constant c_p between 100 and 115 °C.

$c_{p(peak)} = 900$ J/kg K	For moisture content of 0 % of concrete weight
$c_{p(peak)} = 1470$ J/kg K	For moisture content of 1.5 % of concrete weight
$c_{p(peak)} = 2020$ J/kg K	For moisture content of 3 % of concrete weight

Conductivity. The conductivity of concrete can be modeled as a quadratic equation of temperature over the range of 20−1200 °C. Due to the variability in concrete a range is recommended for the conductivity in EC1992-1-2 [4]. Figure 54.7 shows the band between the upper and lower limits.

$$\text{Upper limit} \quad k = 2 - 0.2451\,(\theta/100) + 0.0107\,(\theta/100)^2\ \text{W/m K} \quad \text{for} \quad 20°\text{C} \leq \theta \leq 1200°\text{C}$$

$$\text{Lower limit} \quad k = 1.36 - 0136\,(\theta/100) + 0.0057\,(\theta/100)^2\ \text{W/m K} \quad \text{for} \quad 20°\text{C} \leq \theta \leq 1200°\text{C}$$

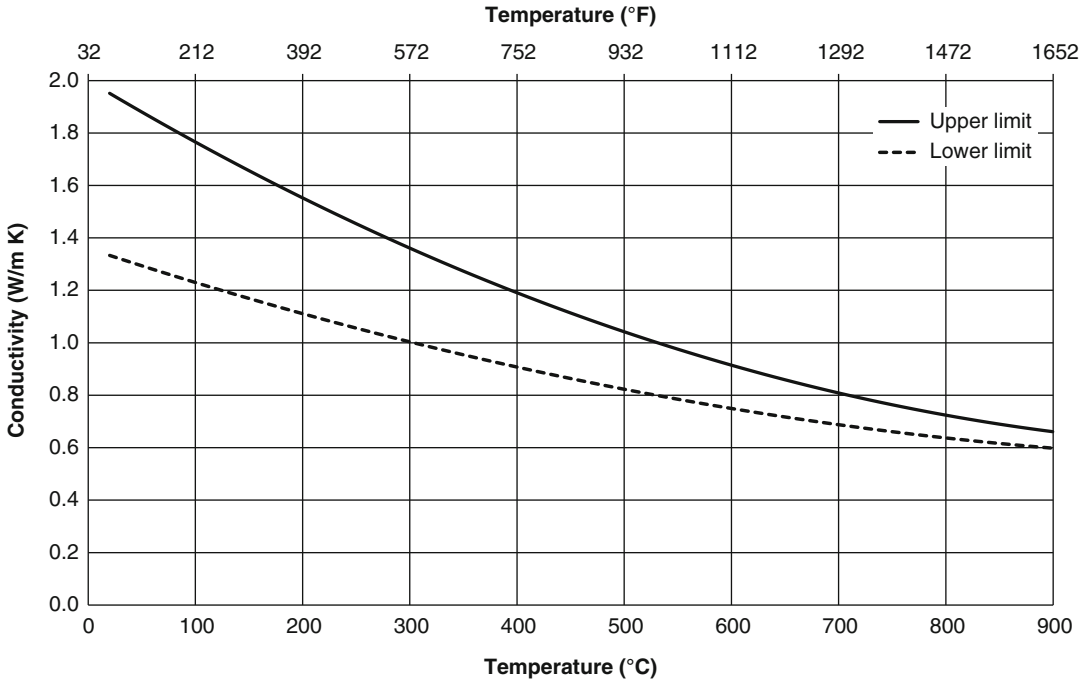

Fig. 54.7 Conductivity for siliceous and carbonate aggregate concrete as a function of temperature showing the upper and lower limit [4]

Heat Transmission

The temperature of the unexposed side of concrete floors, roofs, and walls is usually limited to prevent ignition of combustibles in contact with the unexposed surface. In ASTM E119 the criteria are 121 °C (250 °F) average and 163 °C (325 °F) single-point temperatures. These criteria often govern the fire resistance of the assembly. In addition to the unexposed surface temperature, the temperature distribution throughout the member is required in order to evaluate the material strengths in the structural calculations. Similar criteria are specified in the ISO 834.

Heat is mainly transferred through a solid concrete member by conduction. The temperature of the unexposed side of the slab is a function of the slab thickness and the type of aggregate used. The fire endurance versus slab thickness is presented in Fig. 54.8 for three types of concrete typically used in building construction. The data is based on actual fire tests of concrete slabs [7]. For the normal-weight concretes used in the fire tests, the maximum aggregate size was 20 mm (0.75 in.) and the air content was about 6 %. The maximum aggregate size for the structural lightweight concretes was slightly less than 20 mm (0.75 in.) and the air content was about 7 %. Although the slab thickness and type of aggregate are the main factors that affect heat transmission through the concrete, other factors do have some impact. These factors include moisture content, unit weight, air content, and maximum aggregate size. Within the usual range of values, water-cement ratio, strengths, and age have been shown to have insignificant effects on the heat transfer process [7].

Floor and roof slabs are often composites of materials, for example, a concrete base slab with overlays or undercoatings of either insulating materials or other types of concrete. Research has been conducted on two-course composite assemblies. An example of a composite slab

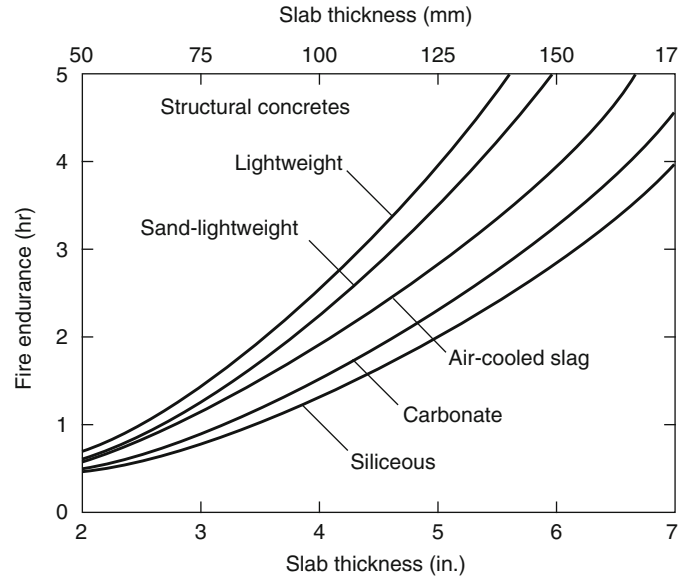

Fig. 54.8 Fire endurance of concrete slabs—effect of thickness and type of aggregate, based on heat transmission [7]

of normal and lightweight concrete is shown in Fig. 54.9. Similar plots for different composite assemblies can be found in Abrams and Gustaferro [13].

The temperature on the unexposed side is not the only temperature of concern. The temperature distribution within the member is used to determine the temperature of the reinforcing or prestressing steel. The temperature of the reinforcing bars is approximately equal to the temperature of the concrete at the level of the center of the bar; [7] that is, the presence of the steel is neglected in the heat transfer analysis. Thus, temperature distribution is primarily affected by the type of concrete, shape of the member, and exposure conditions. During fire tests, slabs and walls are typically heated on one side only; beams are heated from one, two, to three sides; and columns are heated on all four sides. Data on the temperature distribution within concrete members are available from results of fire tests. Figures 54.10, 54.11, and 54.12 show the temperatures within a slab exposed to the standard ASTM E119 time-temperature curve for carbonate, siliceous, and sand-lightweight aggregates, respectively. These data apply to any slab thickness, as long as the slab is at least 25 mm (1 in.) thicker than the point in question.

The temperature distribution within a 250 × 300 mm (10 × 12 in.) rectangular concrete beam exposed to the ASTM E119 standard time-temperature curve is illustrated in Fig. 54.13. Because the temperature distribution is a function of the beam size, it is not practical to present a complete set of figures. A procedure has been developed in which the temperature distribution can be constructed [7]. With the advent of fast, affordable computers, such empirical techniques are rapidly being replaced by complete numerical modeling of the temperature distribution. Computer models such as FIRES T3 [15], TASEF-2 [16], and SAFIR [17] can accurately predict the temperature distribution in various types of concrete members. These models are capable of handling one-, two-, or three-dimensional heat transfer, with time-dependent nonlinear boundary conditions, and temperature-dependent thermal properties. None of these models incorporate mass transfer or moisture migration, and thus require modification to the thermal properties to account for latent heat absorption of the water. All three programs use a finite-element technique to solve the energy

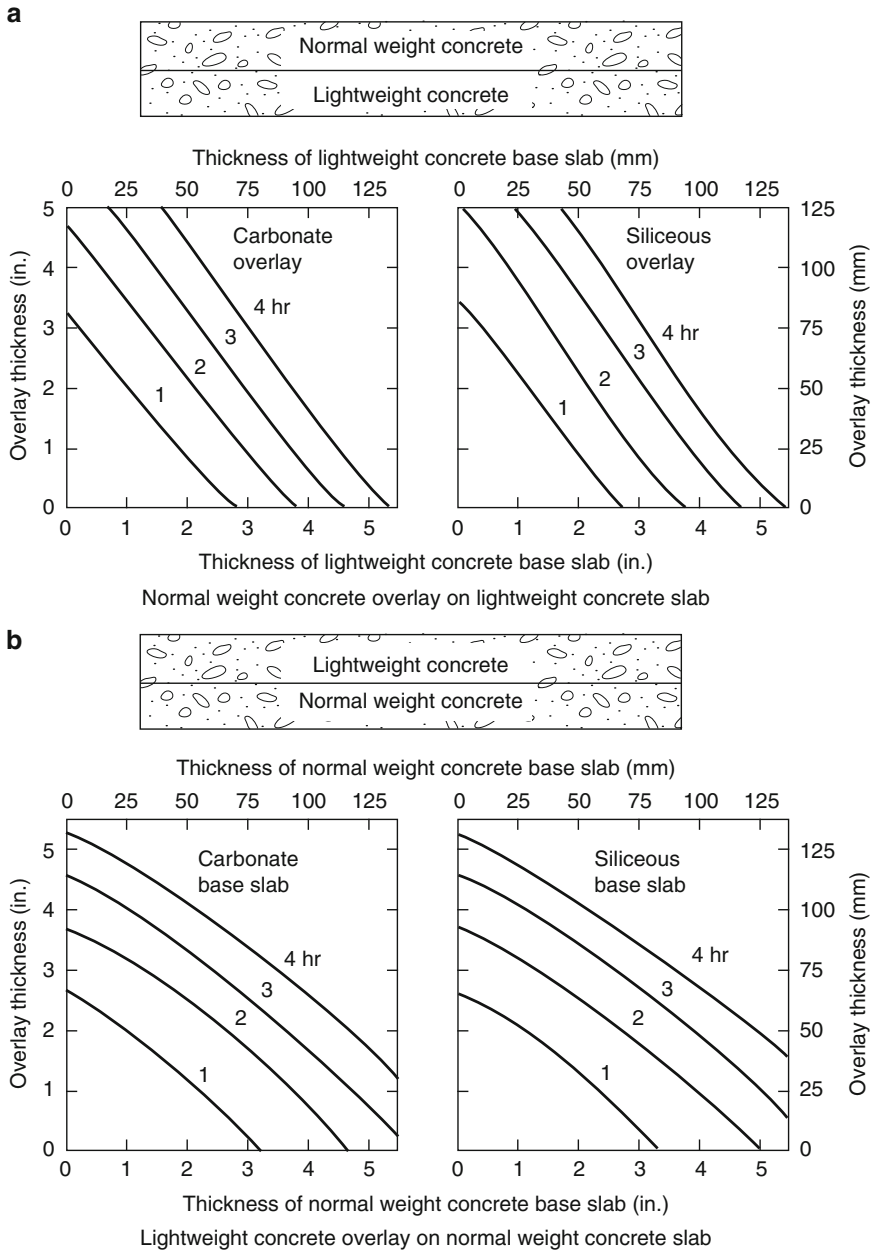

Fig. 54.9 Fire endurance of base slabs and overlays of normal weight or lightweight concretes, based on heat transmission [13]

equation and thus require a skilled operator. Recent improvements to SAFIR include element generation, significantly simplifying the input, and reducing time required. Although these models are not necessary for typical analysis assuming a standard time-temperature curve, with the increased emphasis on performance-based design and more realistic time-temperature curves, the use of such models is likely to increase in the future.

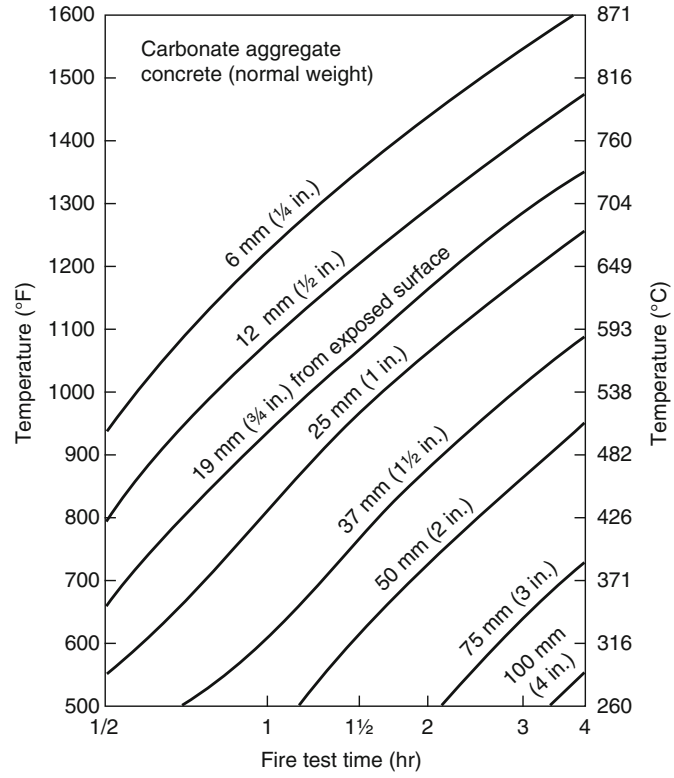

Fig. 54.10 Temperatures within solid or hollow-core concrete slabs during fire tests, carbonate aggregate [14]

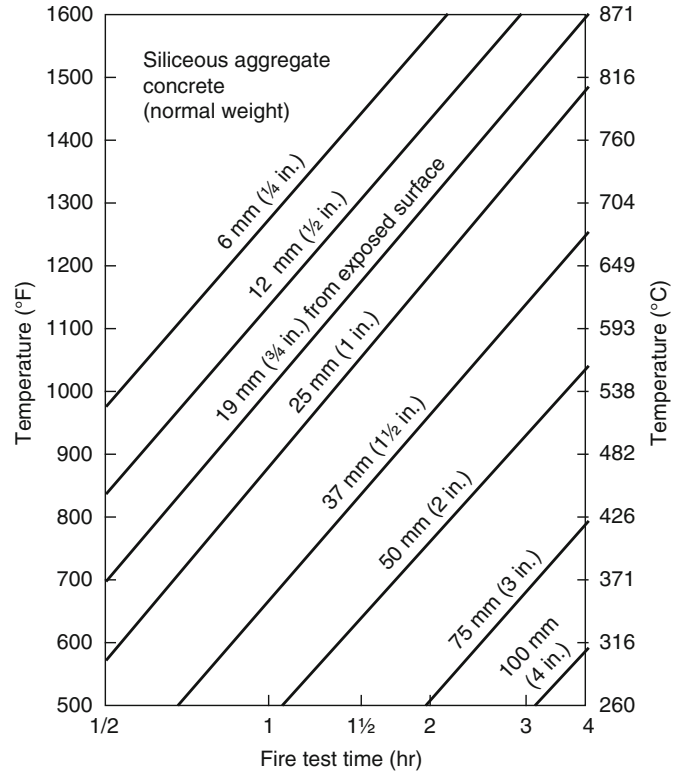

Fig. 54.11 Temperatures within solid or hollow-core concrete slabs during fire tests, siliceous aggregate [14]

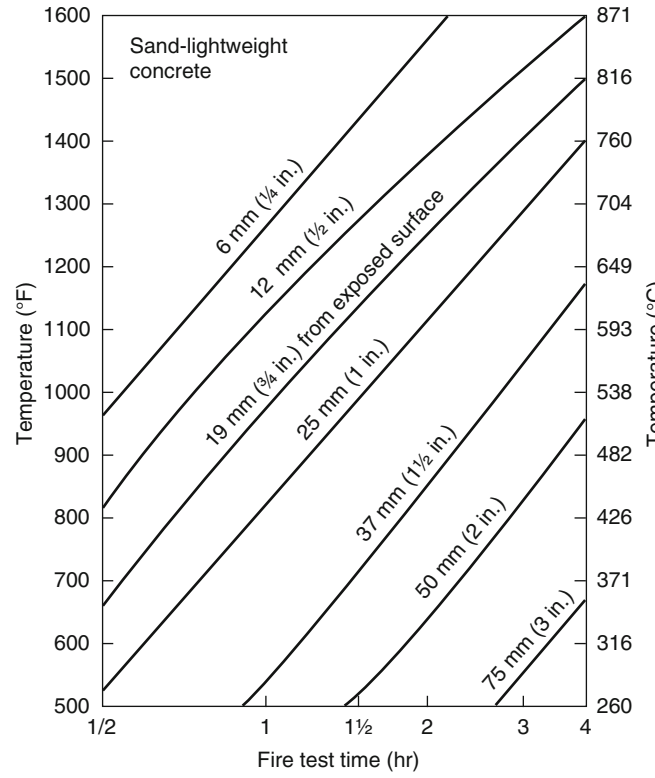

Fig. 54.12 Temperatures within solid or hollow-core slabs during fire tests, sand-lightweight concrete [14]

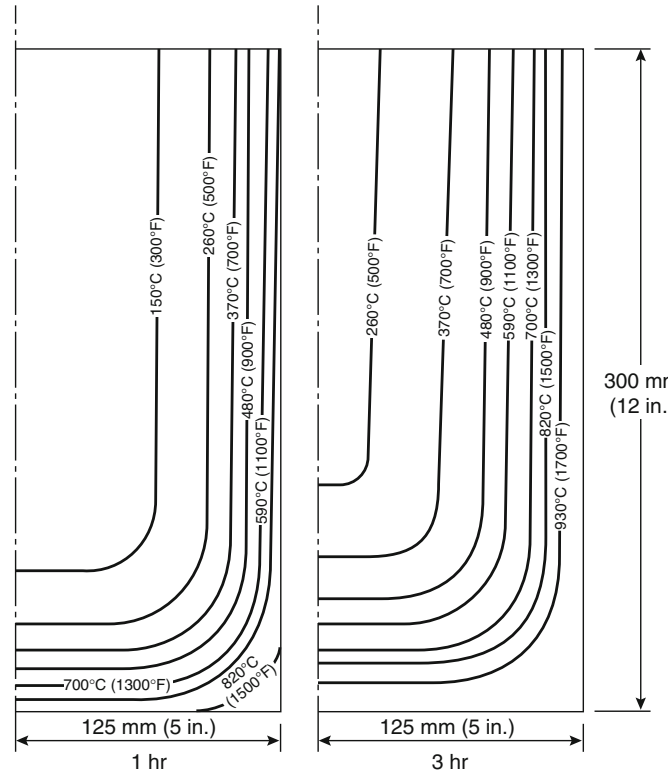

Fig. 54.13 Temperature distribution within a 250 mm × 300 mm (10 in. × 12 in.) lightweight concrete beam, 1- and 3-h exposure time [7]

Simply Supported Slabs and Beams

Simply supported, unrestrained members are not typically cast in place. However, a discussion of simply supported members will make the discussion of continuous members easier to understand. A simply supported, reinforced concrete slab is illustrated in Fig. 54.14.

Note: The calculation methodology closely follows the procedures outlined in ACI216: 2007 [3]. A similar methodology is available in the Eurocode, EN1992-1-2 [4].

The slab is supported by a "frictionless" rollers and a "frictionless" pin, so that the slab is free to expand without resistance but should not deflect at the support. The load, w, is evenly distributed over the surface of the slab, and the reinforcing steel runs the entire length of the slab. Considering these conditions without a fire, the moment diagram for the slab is illustrated in Fig. 54.14b. The moment strength of the slab will be constant along the entire length:

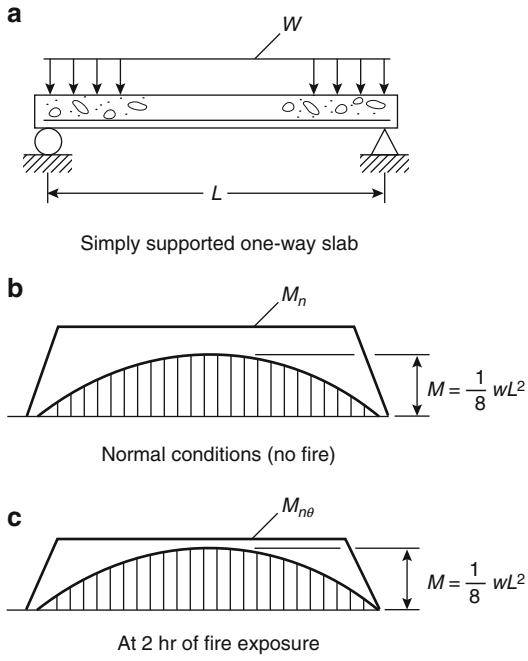

Fig. 54.14 Applied moments and reduced moment strength diagrams for simply supported one-way slab [7]

$$M_n = A_s f_y \left(d - \frac{a}{2}\right) \tag{54.1}$$

where

A_s = Area of the reinforcing steel

f_y = Yield stress of the reinforcing steel

d = Distance from the extreme compression fiber to the centroid of the reinforcing steel

a = Depth of the equivalent rectangular stress block [2]

$$a = \frac{A_s f_y}{0.85 f_c' b} \tag{54.2}$$

f_c' = Compressive strength of the concrete

b = Width of the beam or slab

During exposure to a fire, the temperature of the reinforcing steel will increase. As the temperature of the steel increases, the yield strength decreases (see Fig. 54.14c). This reduction in the steel strength causes a reduction of the moment strength of the slab [7]:

$$M_{n\theta} = A_s f_{y\theta} \left(d - \frac{a_\theta}{2}\right) \tag{54.3}$$

where θ denotes the effects of elevated temperature.

The reduced moment strength diagram is shown in Fig. 54.14c.

With a reduction in the yield stress, $f_{y\theta}$, there is a corresponding reduction in the size of the equivalent stress block, a_θ [7].

$$a_\theta = \frac{A_s f_{y\theta}}{0.85 f_c' b} \tag{54.4}$$

Typically, the temperature at the top of a slab remains relatively unchanged from normal conditions even after 2 h of fire exposure, since the concrete is a good insulating medium (see Figs. 54.10, 54.11, 54.12). Thus, the values for f_c' and d are not affected. However, if the temperatures in the compression zone exceed 480 °C (900 °F) for a siliceous aggregate or 650 °C (1200 °F) for a carbonate aggregate, the concrete compressive strength, f_c', should be reduced (see Fig. 54.2).

As previously noted, the compressive strength of concrete is reduced significantly at a critical temperature, selected here as 650 °C (1200 °F) for a siliceous aggregate or 760 °C (1400 °F) for a carbonate aggregate. To account for this substantial reduction in strength, regions of concrete in the compression zone at temperatures above the critical temperature are neglected in the design process. As a result, the depth and/or width of the compression zone are reduced by subtracting the area of the concrete, which is heated in excess of the critical temperature.

For a simply supported slab it is unlikely that the compression zone would be heated to above the critical temperature without the steel failing first, but it should be noted that, if the section of concrete is reduced, the value of d in Equation 54.3 must be adjusted accordingly.

Flexural failure occurs when the moment strength is reduced to the applied service load moment, M, at the center of the span [7]

$$M = \frac{wL^2}{8} \tag{54.5}$$

where
M = Applied service load moment
L = Length of the span
w = Applied live load plus dead load, with "factor of safety" = 1.0

The factor of safety used in fire endurance calculations is a decision for the authority having jurisdiction. In this section, the fire safety factor has been set equal to 1.0. Load combinations for structural fire design should give lower design loads than those for cold conditions. Guidance on selecting the appropriate safety factors can be found in regulatory documents such as ASCE 7-05 [18]. In North America, guidance is given by ASCE-07 with the recommended load combination for fire conditions being 1.2 dead load + 0.5 live load. Similar load combinations are specified in many other countries.

As indicated in Equation 54.3, the structural fire endurance of a simply supported one-way slab or beam is a function of the load intensity, strength–temperature characteristics of the reinforcing steel, and the depth of protection given to the reinforcement by the concrete cover. There is no benefit of continuity or restraint of thermal expansion with a simply supported slab; the total slab depth, based on heat transmission, h_t, required to obtain the desired fire rating is probably as small or smaller than the total slab thickness, h_s, required for gravity loads [7]. Therefore, there is no advantage of doing a structural fire endurance analysis for unrestrained, simply supported structural members [7].

Continuous Unrestrained Flexural Members

Continuous unrestrained members have a considerably longer fire endurance than simply supported members because of their ability to redistribute the applied moments. Figure 54.15a shows an interior span of a continuous unrestrained slab. The applied moment diagram for a normal condition, with no fire, is shown in Fig. 54.15b. The maximum positive moment occurs near the center of the span, and the maximum negative moments are located over the supports.

When the slab is exposed to fire conditions from below, the moments will be redistributed within the slab. This redistribution may be sufficient to cause the negative moment reinforcement to yield. This yielding generally occurs within the first half hour of the fire, based on observation made during standard fire tests [7]. Figure 54.15c shows the redistribution of moments after 2 h of fire exposure (2 h was selected at random). The American Concrete Institute (ACI) warns that increasing the negative reinforcement will increase the attracted negative moment, possibly leading to a compressive failure. It is important that flexural tension governs the design of concrete members. Thus, to avoid compressive failure in the negative moment region, the negative reinforcement should be small enough so that [6]:

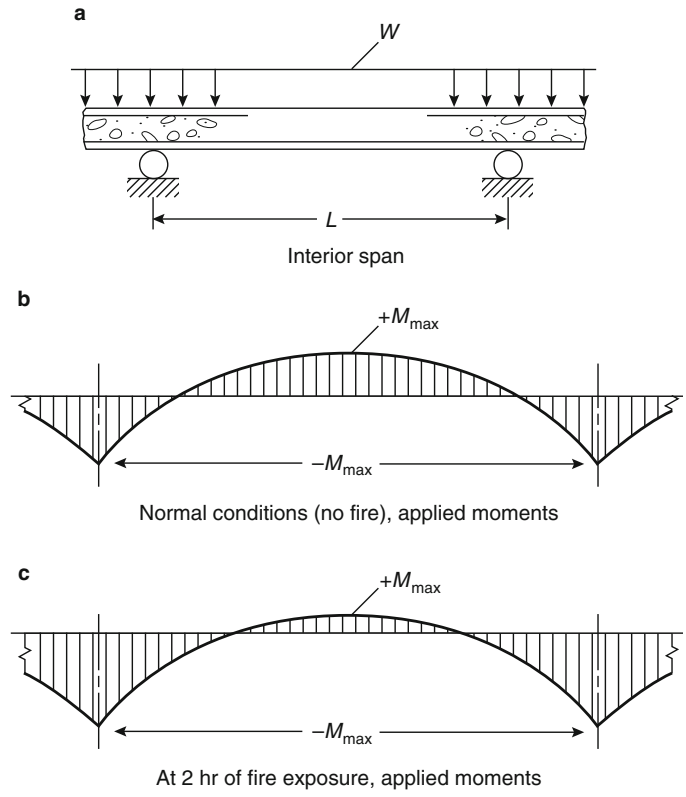

Fig. 54.15 Moment redistribution in interior span of continuous unrestrained one-way slab due to fire exposure [7]

$$\frac{A_s f_{y\theta}}{b_\theta d_\theta f'_{c\theta}} < 0.30 \tag{54.6}$$

Flexural failure of continuous members occurs when three hinges are formed within a span. One of the hinges will form near the midspan and the other two at the adjacent supports. A hinge is formed at the point where the applied moment is equal to the flexural strength at that point.

The flexural strength at any point can be calculated using Equation 54.3 for simply supported members. Figure 54.16 shows the moment diagram for a one-way span with unequal end moments, that is, when the spans are of unequal lengths. This diagram represents the general case and can be used for other conditions, that is, end spans and slabs with equal spans. The member fails when the sum of the flexural strengths is less than the applied moment, $wL^2/8$. The negative moments are calculated at the supports, and the positive flexural strength is calculated at the center of the span. The negative flexural strength is then used in the following equation for the minimum positive flexural strength [7]:

$$\text{Minimum positive flexural strength required} \quad M_{n\theta} = \frac{M^-_{n\theta_1} - M^-_{n\theta_2}}{2wL^2} - \frac{M_{n\theta_1}}{2} - \frac{M_{n\theta_2}}{2} + \frac{wL^2}{8} \tag{54.7}$$

If the minimum positive flexural strength required is less than the positive flexural strength, the member has the calculated fire endurance. The location of the maximum positive moment, X_1, is calculated from

$$X_1 = \frac{L}{2} + \frac{\left(M^-_{n\theta_1} - M^-_{n\theta_2}\right)}{wL} \tag{54.8}$$

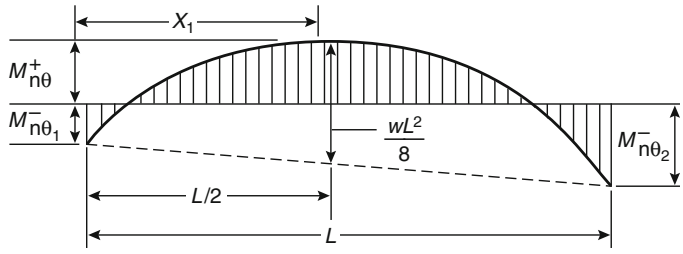

Fig. 54.16 Redistributed applied moment diagram at structural endpoint for span of a uniformly loaded continuous one-way slab or beam with unequal end moments [7]

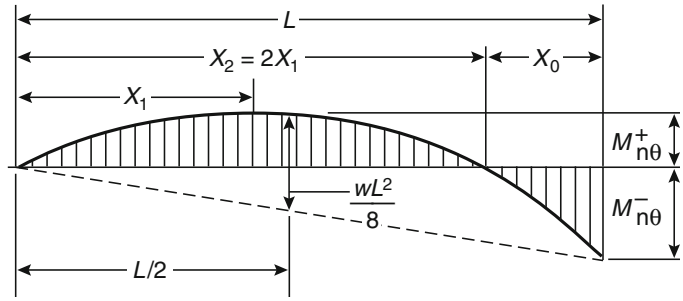

Fig. 54.17 Redistributed applied moment diagram at structural endpoint for end span of a continuous one-way slab or beam [7]

End Span

Equations 54.7 and 54.8 can be modified and used for the end span of a continuous member (Fig. 54.17). For the end span, $M_n = 0$, leaving

$$\text{Minimum required } M^+_{n\theta} = \frac{\left(M^-_{n\theta}\right)^2}{2wL^2} - \frac{M^-_{n\theta}}{2} + \frac{wL^2}{8} \tag{54.9}$$

$$X_1 = \frac{L}{2} - \frac{M^-_{n\theta}}{wL} \tag{54.10}$$

Interior Span with Equal End Moments

Equations 54.7 and 54.8 can also be modified for spans with equal end moments, as indicated in Fig. 54.18. For this case, $M^-_{n\theta_1} = M^-_{n\theta_2}$, changing Equation 54.7 to

$$\text{Minimum required } M^+_{n\theta} = \frac{wL^2}{8} - M^-_{n\theta} \tag{54.11}$$

Equation 54.8 becomes

$$X_1 = \frac{L}{2} \tag{54.12}$$

The location of the points of inflection, X_0, is dependent on the magnitude of the negative flexural strengths and can be calculated using

$$X_0 = \frac{L}{2} - \sqrt{\frac{2M^+_{n\theta}}{w}} \tag{54.13}$$

The negative moment reinforcement must be extended a sufficient distance beyond the point of inflection to allow the bar strength to become fully developed. Design criteria for the development length are outlined in the ACI *Building Code Requirements for Reinforced Concrete* [2]. It is further recommended that at least 20 % of the maximum negative moment reinforcement in the span extends throughout the entire length of the span.

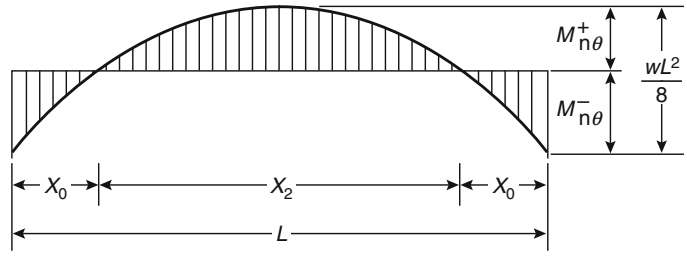

Fig. 54.18 Redistributed applied moment diagram at structural endpoint for symmetrical interior span of a uniformly loaded continuous one-way slab or beam [7]

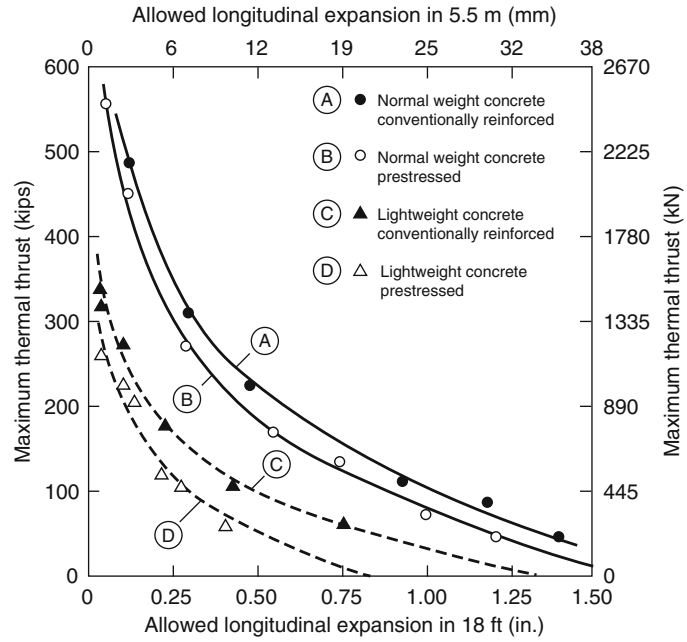

Fig. 54.19 Maximum thrust for allowed expansion of reference specimens [21]

Fire Endurance of Concrete Structural Members Restrained Against Thermal Expansion

When a fire occurs beneath an interior portion of a floor or roof slab, the heated portion of the slab tends to expand. As this portion of the slab expands, the surrounding cooler portions resist the expansion and exert a resistive force on the heated portion of the slab. This resistive force is referred to as the *thermal thrust force*.

Most U.S. fire tests of floor slabs are conducted with the specimen mounted within a restraining frame which restricts the thermal expansion [19]. The amount of restraining force provided by the restraining frame varies from one laboratory to another, based on factors such as frame design, specimen design, and specimen tightness.

Prior to 1960, no research had been conducted to measure the magnitude of the thermal thrust force. In 1960, the Portland Cement Association (PCA) began operation of its floor furnace [20]. This furnace allowed for both variable and monitored restraint during the fire test. Restraining the slab against expansion greatly affects the thermal thrust, as indicated in Fig. 54.19. Notice that with no expansion allowed, the thermal thrust force would be very high, which would cause compression failure of the concrete. However, with only a slight increase in the allowed expansion, there is a significant decrease in the thermal thrust force.

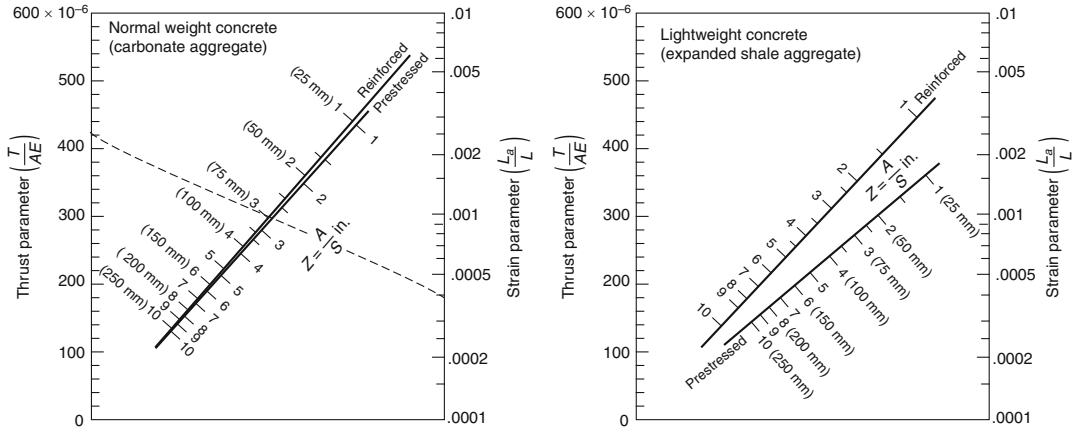

Fig. 54.20 Nomographs relating thrust parameter, strain parameter, and ratio of cross-sectional area to heated perimeter [21]

It should also be noted that the thermal thrust force developed in lightweight concrete is considerably less than is developed within normal-weight concrete. This condition is believed to be due to the lower modulus of elasticity and the lower coefficient of expansion of the lightweight concrete [7].

As a result of the fire research done at PCA, the thermal thrust force was found to vary with the initial modulus of elasticity and the heated perimeter [22]. The heated perimeter, S, is defined as that portion of the perimeter of a section of the specimen, normal to the direction of the thermal thrust, that is exposed to fire. Having assembled a large database of "reference specimens," the thermal thrust from these specimens can be used to predict the thermal thrust within a concrete member [21]:

$$\frac{T_1}{A_1 E_1} = \frac{T_0}{A_0 E_0} \frac{Z_0}{Z_1} \tag{54.14}$$

where

$Z_0 = A_0/S_0$

$Z_1 = A_1/S_1$

S_0 = Heated perimeter of the reference member

S_1 = Heated perimeter of the member in question

T_1 = Maximum thermal thrust of the member in question

T_0 = Maximum thermal thrust of the reference member

A_0 = Cross-sectional area normal to the direction of thermal thrust of the reference member

A_1 = Cross-sectional area normal to the direction of thermal thrust of the member in question

E_1 = Modulus of elasticity of the member in question

E_0 = Modulus of elasticity of the reference member

The parameter $T/(AE)$ is dimensionless, thus the units used for T, A, and E must be consistent.

Nomographs, presented in Fig. 54.20, are used to solve Equation 54.14.

For any given partially restrained expansion of a concrete member exposed to fire, there is a compatible thermal thrust developed in the fire-exposed portion. The effect of the thermal thrust on the structural behavior of a reinforced concrete slab is the same as that of a prestressing force along the line of action of the thrust. In structural fire endurance calculations, the flexural strength is the primary interest, for which case the thermal thrust can be considered a "fictitious reinforcement" along the line of an action of the thrust [23].

The moment due to the thermal thrust, referred to as the thrust moment, is equal to the thrust force multiplied by the distance between the line of action of the thermal thrust and the centroid of the compression block [21]

$$M_T = T\left(d_1 - \Delta - \frac{a_\theta^+}{2}\right) \tag{54.15}$$

where

$$a_\theta{}^+ = \frac{T + A_S^+ f_{y_0}^+}{0.85 f_{c\theta}^{'} b_\theta} \tag{54.16}$$

T = Magnitude of the thermal thrust
d_t = Distance from extreme compression fiber to the line of action of the thermal thrust, T
Δ = Deflection of the slab at the point in question
M_T = Thrust moment strength

The line of action of the thermal thrust must act below the resultant of the equivalent rectangular stress block in order to contribute to the fire endurance of the slab. Results from fire tests have shown that the line of action for the thermal thrust is near the bottom of the member throughout the fire test in most cases, particularly when the thrust is small [21]. Although the line of action acts near the bottom, the actual position changes during the fire test. The exact location of the line of action depends on the shape of the member, type of concrete, amount of reinforcement, stiffness of the restraining frame, and the amount of expansion permitted. Table 54.1 is used to locate the line of action of the thermal thrust for floor systems developing a minimal restraint to thermal expansion. The guidelines presented in Table 54.1 are based on results from standard fire tests [21].

In order to calculate the thrust moment, the deflection must be estimated. Since the deflections at the supports are assumed to be zero, the only other deflection of interest is at the midspan. The midspan deflection can be approximated using the following equation derived from the deflection equation for simply supported members [21]

$$\Delta_1 = \frac{L_1^2 \Delta_0}{3500 y_{b1}} \tag{54.17}$$

where
Δ_1 = Deflection for the member (in.)
Δ_0 = Deflection for the reference member (in.) (Fig. 54.21)
L_1 = Length of the span of the member (in.)
y_{b1} = Distance from the centroidal axis to the extreme fiber (in.)

Table 54.1 Location of thermal thrust line [6]

Type of construction	Fire exposure (h)	Location of thrust line at supports[a]
Solid slab	2	25 mm (1 in.)
	3	32 mm (1.25 in.)
	4	38 mm (1.5 in.)
Slab-and-joist	≤2	0.1 h
	2–4	0.15 h

[a]Distance above bottom of member where h = overall depth of the joist and slab

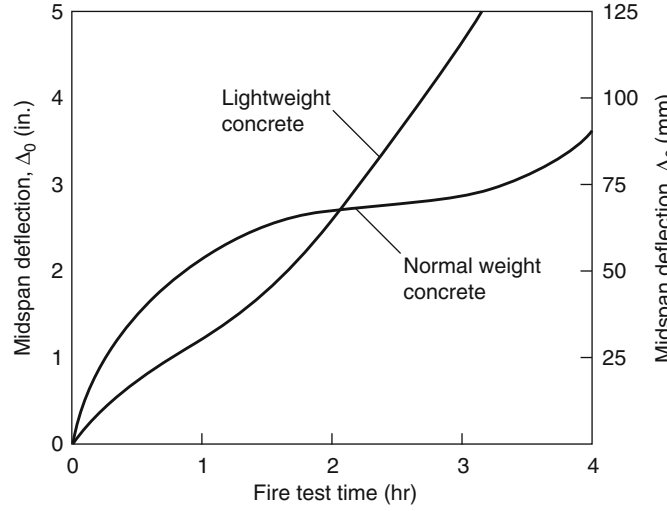

Fig. 54.21 Idealized midspan deflection, Δ_0, of reference specimens with minimal restraint [7]

In SI units, Equation 54.17 becomes

$$\Delta_1 = \frac{L_1 \Delta_0}{88{,}900 y_{b1}}$$

where Δ, L, and y_{b1} are all in mm.

Equation 54.17 is for members with minimal restraint to thermal expansion. Another equation should be used when the thrust is greater than minimal [7].

In order to summarize and illustrate how to apply this information to calculate the structural fire endurance for reinforced concrete members, a step-by-step procedure is presented. This procedure was taken from the Concrete Reinforcing Steel Institute (CRSI), *Reinforced Concrete Fire Resistance* (Table 54.2) [7].

Table 54.2 Step-by-step procedure—structural analysis for fire endurance

Step no.	Description
1	From the building code governing the project (model, municipal, state, etc.), look up the required fire ratings
2	Determine the total depths of slabs, h_t, based on heat transmission to provide the required fire ratings
3	Compare h_t vs. h_s, total slab thickness
4	If $h_t < h_s$, no further fire endurance considerations are necessary
4a	If the governing building code permits a reduced fire rating for heat transmission as long as the required structural fire rating is provided, then proceed to Step 5
5	Only if $h_t > h_s$ (or as in step 4a), compute the structural fire endurance, in hours, based on continuity and/or restraint to thermal expansion
Structural fire endurance for simply supported or continuous slabs with no axial restraint	
6	*Solid slabs*. Compute the reduced nominal positive and negative flexural strengths, $M^+_{n\theta}$ and $M^-_{n\theta}$, available at the required fire rating, for example, 3 h
7	*Interior spans*. If the absolute sum of available nominal flexural strengths is equal to or greater than the applied moment, that is, if $M^+_{n\theta} + M^-_{n\theta} \geq wL^2/8$ the fire endurance is equal to or greater than the required fire rating
7a	*Exterior spans*. Using either the reduced nominal negative or positive flexural strength available at the specified fire endurance, compute the minimum required nominal flexural strength
8	If the nominal flexural strength available is equal to or greater than the minimum required nominal flexural strength, the structural fire endurance is adequate—go to Step 9
8a	If the nominal flexural strength available is less than the required nominal flexural strength, the structural fire endurance based on continuity only is not sufficient—go to Step 10
9	If continuity only is considered in the structural fire endurance calculations, and restraint to thermal expansion is neglected, check the lengths of the top reinforcing bars to make sure the bars are long enough to develop the required nominal negative flexural strength
Note: The procedure for analyzing continuous beams and joist systems is the same as for the solid slab above, except that isothermal diagrams would be required for determining the available nominal flexural strengths	
Structural fire endurance based on restraint to thermal expansion	
10	Estimate the deflection Δ_1, of the heated slab, assuming minimal restraint occurs
11	Locate the line of action of the thermal thrust force at the supports
12	Compute the moment, M_T, that the thermal thrust force has to develop to provide the required additional nominal positive flexural
	Strength for the specified fire endurance
	$M_T = \left(\text{Min. reqd } M^+_{n\theta} - \text{Available } M^-_{n\theta}\right)$
13	Compute the thermal thrust, T_1, required to produce M_T using Equation 54.15
14	Compute the thrust parameter, T_1/A_1E_1
15	Compute the value of $z = A_1/s$
16	With T_1/A_1E_1 and z, determine the strain parameter
17	Compute the expansion ΔL, by multiplying the strain parameter by the heated length, L_h, of the member
18	Determine if the restraining elements, that is, spandrel or effective edge beams, columns, walls, and so forth, can withstand the thermal thrust, T_1, with a displacement no greater than the expansion, ΔL

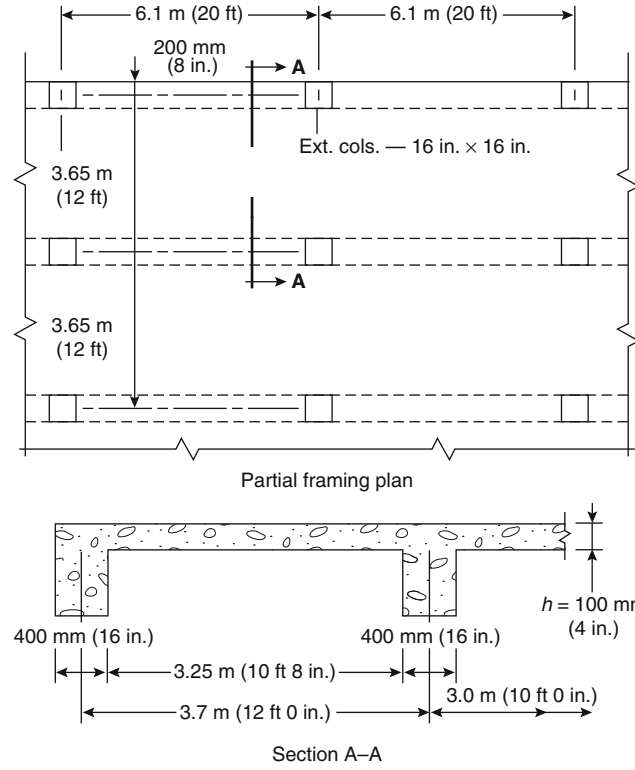

Fig. 54.22 One-way continuous slab, supported on beams [7]

Example of Continuous One-Way Span

The continuous one-way span example has been included to illustrate the step-by-step procedure for structural analysis for fire endurance that is used. The example problem is for a one-way continuous slab with no thermal restraint assumed. The slab is found to have the desired fire endurance, but the development length of the steel bars required for the negative moment strength is significantly longer than is required for standard gravity loading. The development length is then recalculated assuming minimal thermal restraint.

Given. A one-way, multispan continuous slab supported on beams as shown in Fig. 54.22. The slab is 100 mm (4 in.) thick with 3.7 m (12-ft) beam spacing. The concrete for the slab is made from siliceous aggregate with a compressive strength of 20.7 MPa (3000 psi). The slab is subjected to a 3.8 kPa (80 psf) superimposed live load and a 0.25 kPa (5 psf) dead load.

The reinforcement consists of No. 4 bars that meet the requirements of ASTM for A615 Grade 60 (415 MPa). Reinforcing bars are placed in accordance with the 1984 *CRSI Handbook* [24].

Problem: Determine if the slab has a 2 h fire endurance.

Step 1: Determine the required fire rating: 2 h, as stated in the problem.

Step 2: Determine the total depth of the slab, h_t, based on heat transmission: From Fig. 54.8, $h_t = 125$ mm (5 in.).

Step 3: Compare h_t versus h_s:$h_t = 125$ mm (5 in.) > 100 mm (4 in.) $= h_s$.

Step 4: In this example, the authority having jurisdiction has waived the requirements for heat transmission, as long as the required structural fire endurance is provided.

Step 5: Because 125 mm (5 in.) is greater than 100 mm (4 in.), the fire endurance for the end span must be computed based on continuity only.

Structural Fire Endurance Based on Continuity Only

Step 6: Compute the reduced positive and negative moment strengths, $M^{+}_{n\theta}$ and $M^{-}_{n\theta}$, respectively, available after 2 h.

Step 6a: $M^{+}_{n\theta}$ available at 2 h.

U^{+} for bottom bars, $U^{+} = 19 + 6 = 25\,\text{mm}$ (1.0 in.) (Fig. 54.23).

At 2 h, $U^{+} = 25$ mm (1.0 in.), $\theta_s{}^{+} = 360$ °C (1170 °F) (see Fig. 54.17).

$f^{+}_{y\theta} = 0.42(414) = 174\,\text{M pa}\,(25.2\,\text{ksi})$ (see Fig. 54.1).

Reinforcing is 12.5-mm bars at 215 mm (#4 bars at 9 in.)

$$A^{+}_{s} = 570\,\text{mm}^2/\text{m}\left(0.27\,\text{in.}^2/\text{ft}\right)$$

A^{+}_{s} is calculated from the rebar spacing requirements.

$$a^{+}_{\theta} = \frac{A^{+}_{s} f^{+}_{y\theta}}{0.85 f^{'}_{c} b} = \frac{570(174)}{0.85(20.7)(1000)}$$

$$= 5.6\,\text{mm}(0.22\,\text{in})\,[\text{from Equation 54.4}]$$

$$M_{n\theta}{}^{+} = A^{+}_{s} f^{+}_{y\theta}\left(d + \frac{a_{\theta}{}^{+}}{2}\right) = \frac{570(174)(75 - 5.6/2)}{1 \times 10^6}$$

$$= M^{+}_{n\theta} = 7.3\,\text{kN} \cdot \text{m/m}\,(1.64\,\text{ft} \cdot \text{kips/ft})$$

[from Equation 54.3]

Step 6b: $M^{+}_{n\theta}$ available at 2 h

The bottom 25 mm (1 in.) has been neglected, because the concrete temperature is above 650 °C (1200 °F) with a significantly reduced $f^{'}_{c}$.

Top bars, $U^{-} = 100 - (19 + 6) = 75\,\text{mm}\,(3.0\,\text{in.})$ (Fig. 54.24).

At 2 h, $U^{-} = 75\,\text{mm}\,(3.0\,\text{in.}), \theta = 270°\text{C}$ (520 °F). (see Fig. 54.11).

$f^{-}_{y\theta} = 0.83\,(414) = 344\,\text{MPa}\,(49.8\,\text{ksi})$ (see Fig. 54.1).

The $f^{-}_{y\theta}$ stress block, a^{-}_{θ}, is estimated to be about 16 mm (0.625 in.) with a temperature ranging from 650 to 480 °C (1200–900 °F).

Temperature values are estimated from Fig. 54.11. The average temperature is approximately 565 °C (1050 °F). In this example the stressed $f_{c\theta}{}^{'}$ curve was accepted by the AHJ as the appropriate strength for this design.

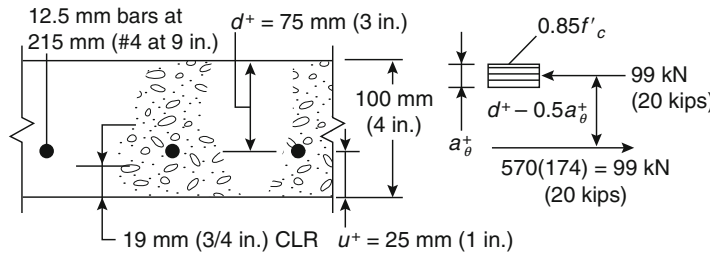

Fig. 54.23 $M^{+}_{n\theta}$ calculation for bottom bars

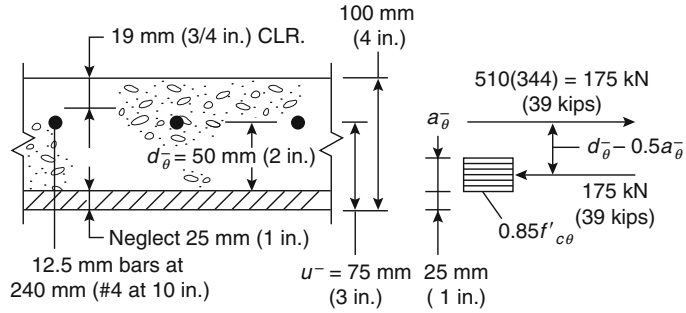

Fig. 54.24 $M^{-}_{n\theta}$ calculation for top bars

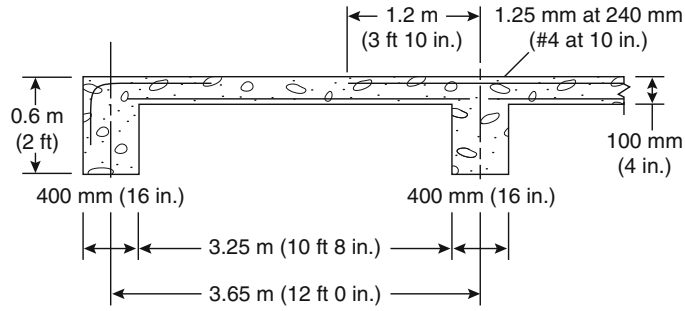

Fig. 54.25 Top bar lengths at 2 h of fire exposure

$f'_{c\theta} = 0.65\,(20.7) = 13.5\,\text{MPa}\,(1.95\,\text{ksi})$ (see Fig. 54.2).

$d^-_\theta = 100 - (19 + 6 + 25) = 50\,\text{mm}\,(2.0\,\text{in.})$.

Reinforcing is 12.5-mm bars at 240 mm (#4 at 10 in.)

$$A_s^- = 510\,\text{mm}^2/\text{m}\,\left(0.24\,\text{in.}^2/\text{ft}\right)$$

$$a_\theta^- = \frac{A_s^- f_{y\theta}^-}{0.85 f'_{c\theta} b} = \frac{510(344)}{0.85(13.5)(1000)}$$
$$= 15\,\text{mm}\,(0.60\,\text{in.})\,[\text{from Equation 54.4}]$$

$$\left\{ M_{n\theta}^- = A_s^- f_{y\theta}^- \left(d_\theta^- - \frac{a_\theta}{2}\right) = \frac{510(344)(50 - 15/2)}{1 \times 10^6} \right.$$
$$= M_{n\theta}^- = 7.5\,\text{kN} \cdot \text{m/m}$$
$$(1.69\,\text{ft} \cdot \text{kips/ft})$$
$$[\text{from Equation 54.3}]$$

Step 7: Calculate the minimum positive moment required at 2 h.

Minimum required

$$M_{n\theta}^+ = \frac{\left(M_{n\theta}^-\right)^2}{2wL^2} - \frac{M_{n\theta}^-}{2} + \frac{wL^2}{8}$$

$$w = 0.1(24) + 0.25 + 3.8$$
$$= 6.45\,\text{kN/m}\,(0.44 \cdot \text{kips/ft})$$

Minimum required

$$M_{n\theta}^+ = \frac{(7.5)^2}{2(6.45)(3.65)^2} - \frac{7.5}{2} + \frac{6.45(3.65)^2}{8}$$

Minimum required

$$M_{n\theta}^+ = 7.3\,\text{kN} \cdot \text{m/m}(1.64\,\text{ft} \cdot \text{kips/ft})$$

Step 8: If the positive moment strength available is greater than the required positive moment strength, structural fire endurance is adequate. Because the moment strength available, 7.3 kN · m/m (1.64 ft · kips/ft), is for practical purposes equal to the required moment strength, 7.3 kN · m/m (1.64 ft · kips/ft), the structural fire endurance for the end span is 2 h.

Step 9: Check the lengths of the top reinforcing bars to make sure the bars are long enough to develop the required negative moment strength. The length of the top bars under normal conditions, considering only gravity loads and no fire, is taken from the *CRSI Handbook* [24] (Fig. 54.25).

Step 9a: Top bar lengths, at first interior support, neglecting restraint to thermal expansion

The distance to the point of inflection at first interior support for structural fire endurance is calculated using

$$X_0 = \frac{2M_{n\theta}^-}{wL}$$

Because the negative reinforcement generally yields early in the fire, as discussed previously, within the first half hour, the value for the negative moment used in Equation 54.13 should be the maximum negative moment that the beam can support.

$$a = \frac{A_s f_y}{0.85 f'_c b} = \frac{510(415)}{0.85(20.7)(1000)} = 12\,\text{mm}\,(0.47\,\text{in.})$$

$$M_n^- = A_s f_y d - \left(\frac{a}{2}\right) - \frac{510(415)(75 - 12/2)}{1 \times 10^6}$$
$$= M_n^- = 14.6\,\text{kN} \cdot \text{m/m}(3.28\,\text{ft} \cdot \text{kips/ft})$$

The value used for w is left to engineering judgment based on the expected loading during a fire.

For this example, the full dead load and one-half the live load is used.

$$w = 0.1(24) + 0.25 + 1.9 = 4.55\,\text{kN/m}(0.31\,\text{kips/ft})$$

$$X_0 = \frac{2(14.6)}{4.55 \times 3.65} = 1.75\,\text{m}\,(5\,\text{ft}\,9\,\text{in.})$$

The distance the top bars have to be embedded beyond the point of inflection is given in the ACI *Building Code* [2]. At least one-third of the bars should be embedded 1/16 of the clear span, d, or $12d_b$, whichever is greater. In this example, the 1/16 of the clear span criterion governs (250 mm or 10 in.). Thus, some of the top bars must extend 2.0 m (6 ft 6 in.) into the end span. The length of the top steel, 2.0 m (6 ft 6 in.), is nearly twice the required length for the gravity load (1.2 m or 3 ft 10 in.). The maximum negative moment strength, M_n, used in Equation 54.13, represents the most severe condition for the development length. However, the assumption of frictionless roller bearing supports used in the above example neglected the restraining force in all calculations. The restraining force, or thermal thrust, T, is developed early in the fire, producing a moment opposite the support moment, which acts to reduce the magnitude of the support moment. The net support moment will then be less than the moment strength, M_n^-, used in the calculation above, thereby overestimating the development length required for the desired fire endurance [7].

The restraint criteria discussed will be used to determine if there is sufficient restraint developed in the longitudinal direction, to reduce the development lengths to that required for the gravity load.

Step 9b: Top bar lengths, at first interior support, including restraint to thermal expansion

Using $X_0 = 1.2$ m (3.83 ft), the length required for gravity loading, we can determine the net moment at the support required.

$$X_0 = \frac{2M_n^-}{wL} \tag{54.18}$$

$$M_n^- = \frac{X_0 wL}{2} = \frac{1.2(4.55)(3.65)}{2} = 10\,\text{kN}\cdot\text{m/m}(2.25\,\text{ft}\cdot\text{kips/ft})$$

The thermal thrust must produce a moment equal to

$$M_T = 14.6 - 10.0 = 4.6\,\text{kN}\cdot\text{m/m}(1.04\,\text{ft}\cdot\text{kips/ft})$$

Early in the fire, T will act at or near the bottom of the slab (see Table 54.1). T is assumed to act 12 mm (1/2 in.) above the bottom of the slab (taking the fire exposure as approximately one-half hour):

$$d_T = 100 - 12 = 88\,\text{mm}(3.5\,\text{in.})$$

$$\Delta = 0 \text{ at the support}$$

The depth of the stress block, a_θ^+, is assumed initially to be zero because the required thrust is small.

$$T = \frac{M_T}{d_T - \Delta - a_\theta^+} = \frac{4.6(1000)}{88 - 0 - 0} = 52.3\,\text{kN/m}(3.6\,\text{kips/ft})$$

Recalculating a_θ^+,

$$a_\theta^+ = \frac{T}{0.85 f_c' b} = \frac{52.2}{0.85(20.7)} = 3\,\text{mm}(0.13\,\text{in.})$$

$$T = \frac{4.6(1000)}{88 - 0 - 3/2} = 53.2\,\text{kN/m}(3.65\,\text{kips/ft})$$

Compute the expansion, L, that corresponds to

$$T = 53.2\,\text{kN/m}(3.65\,\text{kips/ft})$$

$$E_1 = 25{,}000\,\text{MPa}\left(3.6 \times 10^6\,\text{psi}\right)$$

$$A_1 = 1.0(0.1) = 0.1\,\text{m}^2/\text{m}\left(48\,\text{in.}^2/\text{ft}\right)$$

$$\frac{T_1}{A_1 E_1} = \frac{53.2}{0.1(25)} = 21 \times 10^{-6}$$

$$Z = \frac{A_1}{s} = \frac{0.1}{1} = 0.1\,\text{m} = 100\,\text{mm}(4\,\text{in.})$$

$$\frac{\Delta L}{L_h} = 0.006 \text{ (from Fig. 54.18)}$$

$$L = 0.006 \times 3652 = 22(0.86\,\text{in.})$$

In order to maintain equilibrium of the horizontal forces and compatibility of the displacements, the restraining elements must withstand $T = 53.2$ kN/m (3.65 kips/ft) and not deflect more than $\Delta L = 22$ mm (0.86 in.). The next step would be to check the strength and stiffness of the restraining elements, that is, the exterior spandrel beams and columns of the exterior support and the plane floor area of the first interior support. In this example, it is not necessary to check the strength and stiffness toward the interior of the structure, because there is considerable restraint from the large unheated floor area and many columns to provide the thrust moment at the first interior support [7]. However, the spandrel beams and columns at the exterior support should be checked to ensure that there is sufficient strength and stiffness to resist the thrust moment. Determining the strength and stiffness of the spandrel beams and columns requires a long and complex structural analysis and is not shown here. An explanation of the structural analysis of spandrel beams and columns can be found in the literature [7].

Assuming there is sufficient restraint in the spandrel beams and columns to resist the thrust moment, the required length of the top bars over the first interior support at 2 h of fire exposure must be determined. Neglecting restraint to thermal expansion,

$$X_0 = \frac{2M_{n\theta}^{-}}{wL} = \frac{2(7.5)}{(4.55)(3.65)} = 0.90\,\text{m}(2.96\,\text{ft})$$

As previously discussed, at least one-third of the top bars should be embedded 1/16 of the clear span at the point of inflection, X_0, therefore the top steel should extend 1.1 m (3 ft 8 in.) into the end span. This length is less than the top bar length required for gravity loads, so no adjustment in the length of the reinforcement steel is required to obtain the desired fire endurance.

Reinforced Concrete Columns

Throughout the history of concrete construction, reinforced concrete columns have performed well when exposed to fire. The reason for this is threefold:

1. Columns are generally large enough to prevent the center core from losing a significant amount of strength even in prolonged fire exposure.
2. Ties or spirals contain the concrete within the core.
3. The vertical reinforcing bars are generally protected by at least 48 mm (1–7/8 in.) of concrete cover, thereby insulating the steel bars [7].

Most of the building codes in the United States assign 3- and 4-h fire resistance to reinforced concrete columns larger than 300 × 300 mm (12 × 12 in.) for square shapes, or a diameter of at least 300 mm (12 in.) for round columns.

ACI recommends that columns with a specified compressive strength $f'_c \leq 82.7$ MPa (12,000 psi) should have the least dimension of the column sized in accordance with Table 54.3. In addition, minimum concrete cover thickness over the main longitudinal reinforcements should be at least 25 mm (1 in.) times the number to hours of required fire resistance to a maximum of 50 mm (2 in.). The detailing of the ties is also

Table 54.3 Minimum concrete column size

	Minimum column dimension for fire resistance rating, mm (in)				
	1 h	1.5 h	2 h	3 h	4 h
Carbonate	200 (8)	225 (9)	255 (10)	280 (11)	305 (12)
Siliceous	200 (8)	225 (9)	255 (10)	305 (12)	356 (14)
Semi-lightweight	200 (8)	216 (8.5)	225 (9)	270 (10.5)	305 (12)

quite important. ACI216.07 specifies that the ties should be formed with hooks having a six-diameter extension that engage the longitudinal reinforcements and project into the interior of the hoop. Detailed assessments of reinforced concrete columns exposed to fires have been made by Anderberg [25] and Lie and Irwin [26]. EN1992-1-2 uses a more detailed methodology for assessing fire resistance of concrete columns which accounts for the height of the column, slenderness ratio and eccentricity of the loading.

Reinforced Concrete Frames

It is not possible to use simple hand calculation methods for accurate structural design of reinforced concrete frame structures exposed to fires. Individual concrete members can be designed by the methods described above, but for moment-resisting frames, a special purpose computer program is necessary for detailed analysis and design. Available programs include FIRES-RC-II [27], CONFIRE [28], SAFIR [17], and DIANA [29].

Reinforced Concrete Walls

Typically, the fire endurance of concrete and concrete masonry walls is determined by heat transmission criteria as opposed to structural performance [6, 7]. As a result, estimating the fire resistance of walls can be accomplished using a heat transfer analysis only. For this reason, the discussion of thickness requirements presented in the heat transmission section can be used. The required thickness can be determined graphically or by applying a heat transfer computer model.

The distinction between bearing and nonbearing walls is based on building code structural requirements and not fire endurance. For example, some building codes require bearing walls to be thicker than nonbearing walls. Such a requirement has not been justified by results of a fire test. [7] ASTM E119 requires that a superimposed load be applied and maintained at a constant magnitude throughout the test of a bearing wall. When testing nonbearing walls, there is no applied load; however, the edges of the walls may be restrained against thermal expansion, in which case a thermally induced load is applied during the fire test. This thermally induced load is of much greater magnitude than the load applied to bearing walls [7].

Prestressed Concrete Assemblies

Most of this chapter refers to reinforced concrete. The same principles apply to prestressed concrete, which is often more vulnerable in fires for the following reasons: prestressing steels are much more sensitive to elevated temperatures than mild steel reinforcing bars; prestressed concrete is often manufactured in slender components with thin cover concrete; and some failure modes such as debonding, shear, and spalling are more critical in prestressed concrete.

Procedures are also available to calculate the fire resistance of prestressed concrete members. The reader is directed to *Design for Fire Resistance of Precast Prestressed Concrete* [30].

Composite Steel-Concrete Construction

Composite steel-concrete construction refers to concrete slabs cast on permanent steel-deck formwork and steel beams which act compositely with the concrete slab to resist bending moment, as shown in Fig. 54.26.

Composite steel-concrete slabs have excellent integrity in fire conditions because even if cracks occur in the concrete slab, the continuous steel deck will prevent any passage of flames or hot gases through the floor. To meet the insulation criterion, it is simply necessary to provide sufficient thickness of slab. A solid slab of uniform thickness requires the same thickness as a normal reinforced concrete slab, but for other profiles it is necessary to evaluate an effective thickness. Generic listings are given in some codes including Eurocode 4 [5], and manufacturers of steel

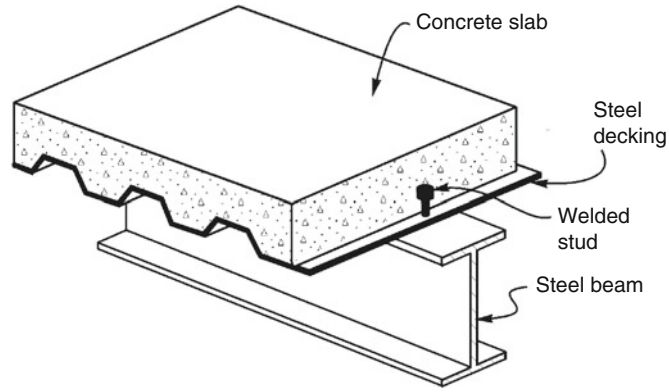

Fig. 54.26 Composite steel-concrete construction

decking have proprietary ratings for their products. It is possible to spray the underside of the steel sheeting with spray-on insulation, but this method is rarely economical.

The strength of composite steel-concrete slabs is severely influenced by fire because the steel sheeting, acting as external reinforcing, loses strength rapidly when exposed to the fire. However, composite slabs can achieve good fire resistance because of three contributing factors: axial restraint, moment redistribution, and fire emergency reinforcement.

Composite slabs often have different fire resistance ratings for restrained and unrestrained conditions [31]. During a fire test, if a composite slab is built into a rigid testing frame which allows almost no axial expansion, the slab can achieve a fire resistance rating with no reinforcing other than the steel sheeting, because of the thermal thrust developed at the supports. Some buildings are sufficiently stiff and strong to provide such restraint to a fire-exposed floor system, but because the amount of restraint is difficult to assess accurately, it is usual to rely on some reinforcing within the slab.

If the nominal reinforcing provided to control shrinkage cracking is placed near the top of the concrete and if the slab is continuous over several supports, it can develop significant negative flexural capacity through moment redistribution and hence retain sufficient load capacity during the fire. If a slab is simply supported, or if moment redistribution is insufficient to resist the applied loads, it is common practice to place *fire emergency reinforcing* in the slab, consisting of steel reinforcing bars in the troughs of the sheeting, with sufficient cover from the bottom surface to control temperatures in the bars. The flexural strength of the slab can be calculated in the usual way using the temperature of the rebars. Further design recommendations are given by ECCS [32], Lawson [33], and Eurocode 4 [5].

Recent Developments

There is continuing international research on fire performance of reinforced concrete. Several recent developments are described below.

Calculation of Temperatures

Recent publications on thermal and mechanical properties of concrete at high temperatures are given by Harmathy [34], Schneider [35], Bazant and Kaplan [36], and Neville [37]. A simple, approximate formula for calculating internal temperatures in reinforced concrete members exposed to the standard fire has been developed by Wickström [38]. Internal temperatures in concrete slabs and beams exposed to realistic fires are given by Wade [39].

Spalling

The design methods in this chapter are based on the assumption that the concrete remains intact for the duration of the fire. This assumption is invalid if the cover concrete spalls off during the fire, exposing reinforcing steel to the fire temperatures. Experiments and real fire experience have shown that most normal weight concrete members can withstand severe fires without spalling, but spalling does occur sometimes. In some cases spalling is related to the type of aggregate, but it is more often linked to the behavior of cement paste. It is generally agreed that spalling most often occurs when water vapor is driven from the cement paste during heating, with high pore pressures creating high tensile stresses in the concrete. Spalling can also occur as result of the presence of high compressive stresses [40]. Susceptibility to spalling results from high free-moisture content (such as in fresh concrete), rapid rates of heating, low water-cement ratio, large aggregate size, low tensile strength of concrete, dense reinforcement, nonuniform thickness of the member, and prestressing. Recent reviews of concrete spalling in normal weight concrete are provided by Hertz [41] and Connolly [42], and in high strength concrete by Ali [43] and Phan [44]. The most promising new development to reduce spalling is the addition of fine polypropylene fibers to the concrete mix so that the polypropylene melts during the fire exposure, leaving cavities through which the water vapor can escape [45].

High-Strength Concrete

There has been considerable recent interest in high-strength concrete as a construction material. High-strength concrete contains additives such as silica fume and water reducing admixtures, which result in compressive strength in the range 60–120 MPa (8400–18,000 psi). An extensive survey of high-strength concrete properties at elevated temperatures by Phan [44] shows that they tend to have a higher rate of strength loss than normal concrete at temperatures up to 400 °C, with explosive spalling being a problem in some cases. High-strength concrete is more susceptible to spalling since it has smaller free-pore volume (higher paste density), so that the pores become filled with high-pressure water vapor more quickly than in normal weight concrete. Fire tests on high-strength columns are reported by Aldea et al. [46] and Kodur [45], and fire tests on high-strength beams are reported by Felicetti and Gambarova [47]. Design recommendations are given by Tomasson [48], who suggests a simple method that ignores concrete above 500 °C (950 °F) for slabs and beams and above 400 °C (750 °F) for columns. A study on residual mechanical properties of high-strength concrete after exposure [49] shows that strength and stiffness of high-strength concrete decrease significantly in fire, and the recovery of strength afterwards is negligible.

Fiber-Reinforced Concrete

Thermal and mechanical properties of steel-fiber reinforced concrete at elevated temperatures are described by Lie and Kodur [50]. They show that the presence of steel fibers increases the ultimate strain and improves the ductility of the concrete during fire exposure. An extensive survey of the mechanical behavior of steel-fiber reinforced concrete at high temperatures has been conducted by Colombo [51], who expresses the flexural behavior as a thermal-mechanical damage model with consideration of irreversible thermal strains.

Hollow-Core Concrete Slabs

With the increasing popularity in recent years of precast prestressed concrete panels in construction, research is being carried out on the behavior of hollow-core concrete slabs in fire, which is more complicated than reinforced concrete because of the effect of prestressing, the small amount of reinforcing, and variable restraint from the surrounding structure. The fire behavior of composite hollow-core concrete units supported on

steel beams is described by Borgogno and Fontana [52]. Several fire tests on hollow-core concrete slabs have been carried out [53–55]. The performance of hollow-core concrete flooring systems in fire has been studied extensively by Fellinger [56] with special focus on the shear and anchorage behavior, and a simulation model of hollow-core concrete flooring systems for design purposes has been proposed by Chang [57].

References

1. A.H. Buchanan, *Structural Design for Fire Safety,* John Wiley and Sons, Chichester, UK (2001).
2. *Building Code Requirements for Reinforced Concrete,* ACI 318-89, American Concrete Institute, Detroit, MI (1989).
3. American Concrete Institute, ACI 216.1-07/TMS-0216-07 – Code Requirements for Determining Fire Resistance of Concrete and Masonry Construction Assemblies, USA, 2007.
4. EN1992-1-2:2004, Eurocode 2: Design of concrete structures – Part 1-2: General rules – Structural fire design, European Committee for Standardisation, Brussels, Belgium (2004).
5. EN1994-1-2:2005, Eurocode 4: Design of Composite Steel and Concrete Structures, EN1994-1-2: General Rules—Structural Fire Design, European Committee for Standardisation, Brussels, Belgium (2005).
6. *Guide for Determining the Fire Endurance of Concrete Elements,* ACI 216-89, American Concrete Institute, Detroit, MI (1989).
7. *Reinforced Concrete Fire Resistance*, Concrete Reinforcing Steel Institute, Chicago (1980).
8. A.H. Gustaferro and T.D. Lin, "Rational Design of Reinforced Concrete Members for Fire Resistance," *Fire Safety Journal,* 11, pp. 85–98 (1986).
9. Fire design of concrete structures – material's, structures, and modelling, state-of-art report, bulletin 38, fib (fédération internationale du béton / the International Federation for Structural Concrete), July 2008.
10. Fire design of concrete structures – structural behaviour and assessment, state-of-art report, bulletin 46, fib (fédération internationale du béton / the International Federation for Structural Concrete), April 2007.
11. R.L. Brockenbrough and B.G. Johnston, *Steel Design Manual,* U.S. Steel Corporation, Pittsburgh, PA (1968).
12. C.R. Cruz, "Elastic Properties of Concrete at High Temperatures," *PCA Research Bulletin,* 191, Portland Cement Association, Skokie, IL (1966).
13. M.S. Abrams and A.H. Gustaferro, "Fire Endurance of Two-Course Floors and Roofs," *Journal of American Concrete Institute,* 66, p. 2 (1969).
14. M.S. Abrams and A.H. Gustaferro, "Fire Endurance of Concrete Slabs as Influenced by Thickness, Aggregate Type, and Moisture," *PCA Research Bulletin,* 223, Portland Cement Association, Skokie, IL (1968).
15. R.H. Iding, Z. Nizamuddin, and B. Bresler, "FIRES T3, A Computer Program for the Fire Response of Structures—Thermal-Three-Dimensional Version," UCB FRG 77-15, University of California, Berkeley (1996).
16. U. Wickström, "TASEF-2—A Computer Program for Temperature Analysis of Structures Exposed to Fire," *Report No. 79-2,* Lund Institute of Technology, Lund, Sweden (1979).
17. J.-M. Franssen, V.K.R. Kodur, and J. Mason, *User's Manual for SAFIR 2002: A Computer Program for Analysis of Structures Subjected to Fire,* University of Liège, Belgium (2002).
18. ASCE 7-05, *Minimum Design Loads for Buildings and Other Structures,* American Society of Civil Engineers, Reston, VA (2006).
19. *Symposium on Fire Resistance of Concrete, ACI Publication SP 5,* American Concrete Institute, Detroit, MI (1962).
20. C.C. Carlson, "Function of New PCA Fire Research Laboratory," PCA Publication RX109, Portland Cement Association, Skokie, IL (1959).
21. L.A. Issen et al., "Fire Tests of Concrete Members: An Improved Method for Estimating Restraint Forces," *Fire Performance,* ASTM STP 464, American Society for Testing and Materials, Philadelphia (1970).
22. S.L. Selvaggio and C.C. Carlson, "Restraint in Fire Tests of Concrete Floors and Roofs," *ASTM STP 422,* American Society for Testing and Materials, Philadelphia; also *PCA Research Department Bulletin 220,* Portland Cement Association, Skokie, IL (1967).
23. E.A.B. Salse and A.H. Gustaferro, "Structural Capacity of Concrete Beams During Fires as Affected by Restraint and Continuity," in *Proceedings,* 5th CIB Congress, Paris (1971).
24. *CRSI Handbook,* Concrete Reinforcing Steel Institute, Chicago (1984).
25. Y. Anderberg, "Computer Simulations and a Design Method for Fire Exposed Concrete Columns," *Report 92-50,* Fire Safety Design, Lund, Sweden (1993).
26. T.T. Lie and R.J. Irwin, "Method to Calculate the Fire Resistance of Reinforced Concrete Columns with Rectangular Cross Section," *ACI Structural Journal,* 90, 1, pp. 52–60 (1993).
27. R. Iding, B. Bresler, and Z. Nizamuddin, "FIRES-RC II, A Computer Program for the Fire Response of Structures—Reinforced Concrete Frames," *Fire Research Group Report No. UCB FRG 77-8,* University of California, Berkeley (1977).
28. N.E. Forsen, "A Theoretical Study of the Fire Resistance of Concrete Structures," *FCB-SINTEF Report STF65 A82062,* SINTEF, Trondheim, Norway (1982).
29. DIANA. *Diana User's Manual, Non-Linear Analysis,* Rel. 6.1, TNO Bouw (1996).

30. *Design for Fire Resistance of Precast Prestressed Concrete,* 2nd ed., Prestressed Concrete Institute, Chicago (1988).
31. UL2007, *Fire Resistance Directory,* Underwriters Laboratories Inc., Northbrook, IL (2007).
32. ECCS, "Calculation of the Fire Resistance of Composite Concrete Slabs with Profiles Steel Sheet Exposed to the Standard Fire," *Publication No. 32,* European Commission for Constructional Steelwork, Brussels (1983).
33. R.M. Lawson, "Fire Resistance of Ribbed Concrete Floors," *CIRIA Report 107,* Construction Industry Research and Information Association, London (1985).
34. T.Z. Harmathy, *Fire Safety Design and Concrete,* Concrete Design and Construction Series, Longman Scientific and Technical, Harlow, UK (1993).
35. U. Schneider, "Concrete at High Temperatures—A General Review," *Fire Safety Journal,* 13, pp. 55–68 (1988).
36. Z.P. Bazant and M.F. Kaplan, *Concrete at High Temperatures—Material Properties and Mathematical Models,* Concrete Design and Construction Series, Longman Group Ltd., Harlow, UK (1996).
37. A.M. Neville, *Properties of Concrete,* 4th ed., John Wiley and Sons, New York (1997).
38. U. Wickström, "A Very Simple Method for Estimating Temperatures in Fire Exposed Structures," *New Technology to Reduce Fire Losses and Costs* (S.J. Grayson and D.A. Smith, eds.), Elsevier Applied Science, London, pp.186–194 (1986).
39. C.A. Wade, "Performance of Concrete Floors Exposed to Real Fires," *Journal of Fire Protection Engineering,* 6, 3, pp. 113–124 (1994).
40. Purkiss J.A, Fire Engineering Design of Structures, Butterworth and Heinemann, 2007
41. K.D. Hertz, "Limits of Spalling of Fire-Exposed Concrete," *Fire Safety Journal,* 38, pp. 103–116 (2003).
42. R. Connolly, "The Spalling of Concrete," *Fire Engineers Journal,* 57, 186, pp. 38–40 (1997).
43. F.A. Ali, D. O'Conner and A. Abu-Tair, "Explosive Spalling of High-Strength Concrete Columns in Fire," *Magazine of Concrete Research,* 53, 3, pp. 197–204 (2001).
44. L.T. Phan, "Fire Performance of High Strength Concrete: A Report of the State-of-the-Art," *NISTIR 5934*, National Institute of Standards and Technology (1996).
45. V.K.R. Kodur, "Studies on the Fire Resistance of High Strength Concrete at the National Research Council of Canada," *Proceedings—International Workshop on Fire Performance of High Strength Concrete, NIST Special Publication 919,* National Institute of Standards and Technology, Gaithersburg, MD, pp. 75–86 (1997).
46. C.-M. Aldea, J.-M. Franssen, and J.-C. Dotreppe, "Fire Test on Normal and High Strength Reinforced Concrete Columns," in *Proceedings—International Workshop on Fire Performance of High Strength Concrete, NIST Special Publication 919,* National Institute of Standards and Technology, Gaithersburg, MD (1997).
47. R. Feticetti, P.G. Gambarova, ASCE Member, and M. Semiglia, "Residual Capacity of HSC Thermally Damaged Deep Beams," *Journal of Structural Engineering,* 125, 3, pp. 319–327 (1999).
48. B. Tomasson, "High Performance Concrete—Design Guidelines," Report, Department of Fire Safety Engineering, Lund University, Sweden (1998).
49. R. Felicetti and P.G. Gambarova, "Effects of High Temperature on the Residual Compressive Strength of High-Strength Siliceous Concretes," *ACI Materials Journal,* 95, 4, pp. 395–406 (1998).
50. T.T. Lie and V.K.R. Kodur, "Thermal and Mechanical Properties of Steel Fibre Reinforced Concrete at Elevated Temperatures," *Canadian Journal of Civil Engineering,* 23, 2, pp. 511–517 (1996).
51. M. Colombo, *FRC Bending Behaviour: A Damage Model for High Temperatures,* PhD Thesis, Politecnico di Milano, Italy (2006).
52. W. Borgogno and M. Fontana, *Versuche zum Tragverhalten von Betonhohlplatten mit flexibler Auflagerung bei Raumtemperatur und Normbrandbedingungen,* IBK ETH Zürich, Zurich, (2006).
53. N.E. Andersen and D.H. Lauridsen, *Danish Institute of Fire Technology Technical Report X 52650 Part 2—Hollow-Core Concrete Slabs,* Danish Institute of Fire Technology, Denmark (1999).
54. FeBe Studiecommissie SSTC, *Résistance au Cisaillement de Dalles Alveolées Précontraintes,* Laboratorium voor Aanwending der Brandstoffen en Warmteoverdracht, Belgium (1998).
55. M. Breccolotti, A.L. Materazzi, and I. Venanzi, "Fire Performance of HPLWC Hollow-Core Slabs," *Proceedings—4th International Workshop on Structures in Fire,* pp. 587–598, Aveiro, Portugal (2006).
56. J.H.H. Fellinger, *Shear and Anchorage Behaviour of Fire Exposed Hollow-Core Slabs,* DUP Science, Netherlands (2004).
57. J. Chang, *Computer Simulation of Hollowcore Concrete Flooring Systems in Fire,* PhD Thesis, University of Canterbury, NZ (2007).

Charles Fleischmann is a professor in the Department of Civil Engineering, University of Canterbury, in Christchurch, New Zealand.

Andy Buchanan is an emeritus professor in the Department of Civil Engineering, University of Canterbury, in Christchurch, New Zealand.

Anthony Abu is a senior lecturer in the Department of Civil Engineering, University of Canterbury, in Christchurch, New Zealand.

Analytical Methods for Determining Fire Resistance of Timber Members

55

Robert H. White†

Introduction

The fire resistance ratings of wood members and assemblies, as with other materials, have traditionally been obtained by testing the assembly in a furnace in accordance with ASTM International (ASTM) Standard E119 "Standard test methods for fire tests of building construction and materials", International Organization for Standardization (ISO) Standard 834 "Fire-resistance tests-Elements of building construction", and similar standards. In the U.S., these ratings are published in listings, such as Underwriters Laboratories *Fire Resistance Directory*, Gypsum Association's *Fire Resistance Design Manual*, American Wood Council's *Design for Code Acceptance* publications, and those in building codes. The ratings listed are limited to the actual assembly tested and normally do not permit modifications such as adding insulation, changing member size, changing interior finish, or increasing the spacing between members. Code interpretation of test results sometimes allows the substitution of larger members, thicker or deeper assemblies, smaller member spacing, and thicker protection layers, without reducing the listed rating.

Two procedures for calculating fire resistance ratings have U.S. building code acceptance: the methodologies for calculating fire resistance ratings of exposed wood members in the American Wood Council's *National Design Specification® for Wood Construction* (NDS®) and the component additive method (CAM) for protected wood-frame walls, floors, and roofs [1]. A third methodology developed by T.T. Lie [2] is expected to be withdrawn from future editions of the U.S. codes in favor of the NDS methodology. The T.T. Lie methodology and the CAM procedures were developed in Canada and currently have both U.S. and Canadian code acceptance [3].

In Europe, the Eurocode 5 of the European Committee for Standardization (EN 1995-1-2:2004 Eurocode 5: Design of timber structures-Part 1–2: General-Structural fire design and its corrigendum EN 1995-1-2:2004/AC:2009) on design of timber structures provides calculation methods for the fire design of timber structures. A review of the development of EN 1995-1-2, improvements from the earlier ENV 1995-1-2 published in 1994, and references for the research results used to support its provisions are provided by König [4, 5]. Provisions of Eurocode 5 and more recent developments in Europe are extensively discussed in "Fire Safety in Timber Buildings—Technical guideline for Europe [6].

When attention is given to all details, the fire resistance of a wood member or assembly depends on three items:

1. Performance of its protective membranes (if any)
2. Extent of charring of the structural wood element

R.H. White (✉)
†Deceased

M.J. Hurley (ed.), *SFPE Handbook of Fire Protection Engineering*,
DOI 10.1007/978-1-4939-2565-0_55, © Society of Fire Protection Engineers 2016

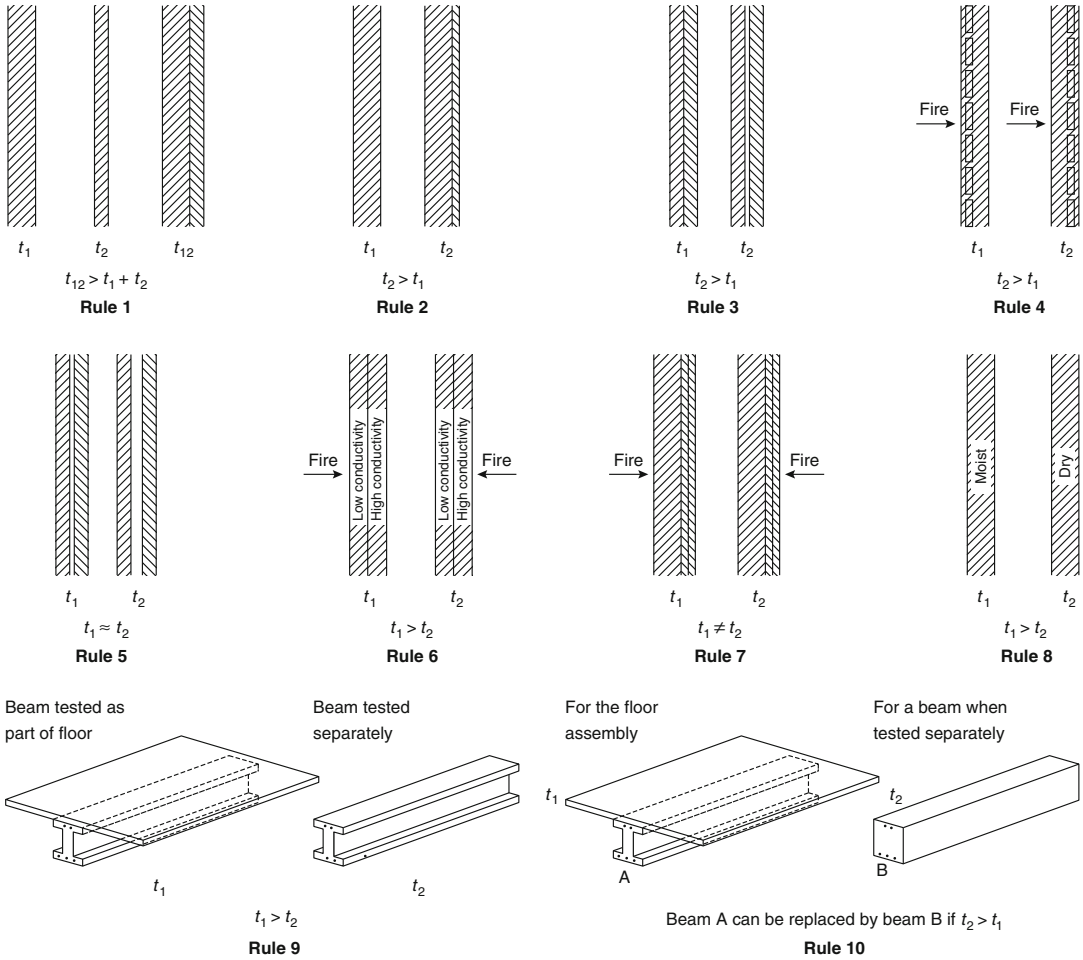

Fig. 55.1 Harmathy's ten rules of fire endurance [7]

3. Ratio of the load-carrying capacity of the remaining uncharred portions of the structural wood elements to the applied load

Contribution of the Protective Membrane

Gypsum wallboard and wood paneling are two common types of protective membrane that provides the first line of resistance to fire in wood construction. The effects of the protective membrane on the thermal performance of an assembly are included in Harmathy's ten rules of fire endurance rating [7]. These ten rules (Fig. 55.1) provide guidelines to evaluate the relative effects of changes in materials on the fire resistance rating of an assembly. However, there are exceptions to some of these general rules. The rules apply primarily to the thermal performance of the assembly.

In the U.S., testing of assemblies often include the reporting of "finish ratings" of the protective membrane. A finish rating of a protective membrane is generally defined as the time to reach either an average temperature rise of 139 °C (250 °F) or a maximum rise of 181 °C (325 °F), as measured on the plane of the wood framing member nearest the fire. Also in the U.S., these same temperature criteria are used in the fire resistance testing of protective membranes (i.e. "thermal barriers") required for the

protection of foam plastic insulation [8]. In Europe, these same temperature increase criteria (140 K average, 180 K maximum) are used for layers in the CAM in the Eurocode 5. The contribution of the protective membrane to the fire resistance rating of a light-frame assembly is clearly illustrated in the CAM.

The North American CAM is initially discussed in the following subsection. In Europe, a new classification system for the abilities of building panels to provide fire protection has been developed [6]. The "K" classes are determined by testing for fire resistance using a temperature rise on the unexposed surface of 250 °C and horizontal orientation of the test panel.

Component Additive Method

The CAM is a calculation procedure to determine fire resistance ratings of light-frame wood floor, roof, and wall assemblies. With this procedure, as with Harmathy's rules 1 and 2, one assumes that a time can be assigned to the type and thickness of the protective membrane and that an assembly with two or more protective membranes has a fire resistance rating at least that of the sum of the times assigned for the individual layers plus the time assigned to the framing. CAM was developed by the National Research Council of Canada (NRCC) and has code approval in both the United States [1] and Canada [3]. Richardson and Batista [9] evaluated the methodology using results from tests of light-frame walls lined with gypsum board.

The times assigned to the protective membranes (Table 55.1), the framing (Table 55.2), and other factors are added together to obtain the fire resistance rating for the assembly. The times are based on empirical correlation with actual ASTM E119 tests of assemblies. The ratings obtained in these tests ranged from 20 to 90 min. The times given in Table 55.1 are based on the membrane's ability to remain in place during fire tests. In this North American CAM, the times assigned to the protective membranes in the component additive method are not the "finish ratings" of the material cited in test reports or listings.

Table 55.1 Time assigned to protective membranes

Description of finish	Time (min)
9.5 mm ($^3/_8$ in.) Douglas fir plywood, phenolic bonded	5
13 mm (½ in.) Douglas fir plywood, phenolic bonded	10
16 mm ($^5/_8$ in.) Douglas fir plywood, phenolic bonded	15
9.5 mm ($^3/_8$ in.) gypsum board	10
13 mm (½ in.) gypsum board	15
16 mm ($^5/_8$ in.) gypsum board	20
13 mm (½ in.) type X gypsum board	25
16 mm ($^5/_8$ in.) type X gypsum board	40
Double 9.5 mm ($^3/_8$ in.) gypsum board	25
13 mm + 9.5 mm (½ in. + $^3/_8$ in.) gypsum board	35
Double 13 mm (½ in.) gypsum board	40

The applicable building code should be checked for acceptance of, modification to, and limitations on the procedure. There are specific requirements for the installation of some of the membranes

Table 55.2 Time assigned for contribution of wood frame

Description of frame	Time (min)
Wood wall studs, 406 mm (16 in.) on center	20
Wood floor and roof joists, 406 mm (16 in.) on center	10
Wood floor and roof truss assemblies, 610 mm (24 in.) on center	5

Minimum size for studs is nominal 51 mm by 102 mm (2 in. by 4 in.). Wood joists must not be less than nominal 51 mm (2 in.) in thickness. The spacing between studs or joists cannot exceed 406 mm (16 in.) on center. The applicable building code should be checked for acceptance of, modification to, and limitations on the procedure

The type of fasteners and their spacing on the protective membrane can be critical factors in the performance of the membrane in a fire resistance test. Reference should be made to similar tested assemblies. The addition of insulation to a wall assembly can increase its fire resistance [10]. Adding rock wool or slag mineral wool insulation batts for additional protection to the wood stud wall generally has an assigned time of 15 min in the CAM procedure, which is added to the sum of the times for the framing and the protective membrane to obtain the rating for the

wall assembly. Assigned times for glass fiber insulation depend on the codes.

The effect of adding insulation to the fire resistance of a floor or roof assembly in a fire test depends on its location within the assembly and the method of attachment. In tests of single layer I-joists systems, the addition of insulation above the unbacked joints in the gypsum board ceiling has been beneficial. In the case of floor assemblies, adding insulation can also decrease the fire resistance of the assembly [10]. Using the results of the series of wall tests conducted in Canada, Sultan and Kodur [11] examined the effects of insulation type, insulation width between studs, resilient channel location, gypsum board thickness, number of gypsum board layers, glass fiber in the gypsum board core, gypsum board mass per unit area, and stud type. For load-bearing wood stud walls, the fire resistance is reduced when resilient channels are used to attach the gypsum boards on the fire-exposed side of the studs [12].

For asymmetrical wall assemblies, the rating in the CAM procedure is based on the side with the lesser fire resistance. For floor/ceiling assemblies, roof/ceiling assemblies, and exterior walls rated only from the interior, there are minimal requirements for the membrane on the face of the assembly not directly exposed to the fire, in order to ensure that the wall or floor/roof assembly does not fail because of fire penetration or heat transfer through the assembly. Specific alternative membranes are identified for the face of wood stud walls not exposed to fire (exterior) and for the flooring or roofing over wood joist framing. The membrane on the side not exposed to fire (the outside or top) may also be any membrane listed in Table 55.1 with an assigned time of 15 min or greater.

The application of the method in the building codes is generally limited to 60 or 90 min. Additional information can be found in publications of the American Wood Council [1] and the Canadian Wood Council [3]. When code acceptance is required, the applicable building code must be checked for acceptance of, modifications to, and limitations of the procedure. There are differences between the codes in what is accepted. CAM gives flexibility, for example, in calculations for plywood and gypsum board combined as an interior finish.

Example 1 The calculated fire resistance rating of a wood stud exterior wall (nominal 2 in. × 4 in. [51 mm × 102 mm] studs, 16 in. [406 mm] on center) with 0.625 in. (16 mm) Douglas fir phenolic-bonded plywood over 0.5-in. (13-mm) type X gypsum wallboard on the side exposed to fire is

From Table 55.1:	
16 mm (0.625 in.) Douglas fir plywood, phenolic bonded	15 min
13 mm (0.5 in.) type X gypsum board	25 min
From Table 55.2:	
Wood stud framing	20 min
Calculated rating (total)	60 min
Mineral wool insulation could be used to increase the fire rating to 75 min	

There is also a CAM in Eurocode 5 based on work in Sweden [13, 14]. In the CAM described in Eurocode 5, the fire separation function of wall and floor assemblies is calculated as the sum of the contribution to fire resistance from each layer of material:

$$t_{ins} = \sum_i t_{ins,0,i} k_{pos,i} k_{j,i} \qquad (55.1)$$

where

$t_{\mathrm{ins},0,i}$ = Basic insulation value of layer i (min)
$k_{\mathrm{pos,i}}$ = Position coefficient of layer i in relation to the fire
$k_{\mathrm{j,i}}$ = Joint coefficient of layer i

The temperature increase criteria of 140 K average or 180 K maximum are used in the determination of the basic insulation value, $t_{ins,0}$, for a single layer. Application of this CAM to address the insulation aspect of fire resistance includes consideration of the different paths for heat transfer through the assembly. The position coefficient adjusts the basic insulation value for the position of the layer within the assembly, and the joint coefficient adjusts for the configuration of any joints in the layer.

Research in Switzerland [15, 16] has resulted in improvements to the methodology. These suggested modifications to the current Eurocode 5 procedure include the impact of the adjacent

layers on the position coefficient and introduce a basic protection value. The position coefficient of Equation 55.1 is modified to be the product of two position coefficients—a position coefficient that takes into account the influence of layers on the fire exposed side of the layer and a position coefficient that takes into account the influence of layers on the non-fire exposed side of the layer. The basic protection value is used instead of the basic insulation value of Equation 55.1 for all layers except the last layer on the unexposed side. The determination of the basic protection value is based on temperature rise criteria of 250 K average or 270 K maximum. Assuming an initial temperature of 20 °C, the 270 K temperature rise corresponds to a temperature of 290 °C which is close to the 300 °C temperature criteria commonly used for the base of the char layer. Östman et al. [6] provide detailed information on this methodology, including design examples. The Eurocode 5 also includes design procedures for fire resistance of load-bearing, insulated, light-frame floors and walls that consider charring of the wood joist or stud. There are separate procedures for wall and floor assemblies with and without cavities filled with rock (mineral wool) or glass fiber insulation.

In New Zealand publications [17], an approach described as the *onset of char* method is used to determine the fire ratings of light-frame assemblies. Because the charring of wood is associated with a temperature of 300 °C (550 °F), another method is to assume that the membrane will protect any wood framing for at least the time of the finish rating of the membrane in a test involving wood framing. As with the onset of char method, the fire rating of the entire assembly with the substituted member is assumed to be at least equal to the finish rating of the protective membrane in the test with the solid-sawn wood framing.

Models for Light-Frame Construction

The protective membrane contributes to fire resistance by providing thermal protection. Numerical heat transfer methodologies are available to evaluate this thermal protection. In most cases, the models were developed for light-frame wall assemblies. An extensive literature review of efforts to model the fire resistance of light-frame construction is provided by Bénichou and Sultan [18]. In early work, Fung [19] developed a one-dimensional finite difference model and computer program for thermal analysis of walls. Gammon [20] developed a two-dimensional finite element heat transfer model for wood-stud wall assemblies. WALL2D, developed by Forintek Canada, is a two-dimensional finite-difference model for predicting heat transfer through wood stud walls exposed to fire [21, 22].

Difficulties in modeling the charring of wood, and the physical deterioration of the panel products complicate these numerical methodologies. Other research on models for light-frame construction includes activities in Canada [23, 24], Sweden [25], New Zealand [26, 27] and Australia [28, 29].

In addition to modeling heat transfer, these efforts have included the modeling of the structural capacity of the light-frame assemblies. WALL2D has been used with a simple structural model to predict structural collapse [30].

In a manner similar to the bilinear char model of Eurocode 5 for initially protected wood, Frangi et al. [31] developed a charring model for timber frame floor assemblies with void cavities. Clancy [32] used his model to examine the effects of various variables on the times for structural collapse.

As part of the development of such models, research has been done on the properties of gypsum board. Cramer et al. [33] examined mass loss and mechanical properties of gypsum board at elevated temperatures. Bénichou and Sultan [34] reported test results for thermal conductivity, specific heat, mass loss, and thermal expansion/contraction for wood, gypsum, and insulation. Craft et al. [35] developed Arrhenius rate constants for the calcinations of the gypsum. Thomas [36] reviewed thermal data for gypsum board and made modifications to obtain apparent values for the properties that were suitable for a heat transfer model.

Direct Protection of Wood Members

The steel industry improves the fire resistance of steel members by directly covering them with fire-resistive panels or coatings. Currently, the marketing of fire-resistive coatings for use on wood is almost nonexistent. The fire-retardant coatings marketed for wood are designed and recognized only for use to reduce the spread of flames over a surface (flame spread).

Depending on its thickness and durability under fire exposure, a coating may merely delay ignition of the wood for a few minutes or may provide an effective insulative layer that reduces the rate of charring. For both fire-retardant coatings and fire-resistive coatings, their performance as a fire-resistant membrane on wood has been evaluated [37–39].

In some full-scale testing of beams, those coated with an intumescent fire retardant produced improvements less than that obtained in earlier tests in a small-scale furnace [40]. Bending of the beams during the fire test resulted in adhesion problems. Tests on coated timber members were also reported in Finland and the U.S.S.R [41].

There are published data on the protection provided by directly covering a wood member with gypsum board or other nonwood panel products. Gardner and Syme [42] found that gypsum board not only delayed the onset of char formation but also reduced the subsequent rate of char formation. In their 2 h tests, 13-mm (0.5-in.) thick gypsum board on wood beams reduced the depth of char by approximately 40 %. Of the 40 %, only 17 % was credited to the initial delay in char formation.

Tsantaridis et al. [43] provided information on the charring of wood protected by gypsum board when exposed to 50 kW/m^2. Richardson and Batista [44] tested wood decks with and without gypsum board protection. A 16-mm (0.625-in.) thick Type X gypsum board increased the times for flame penetration from 4.5 to 44 min.

In a study of engineered wood rim board products, White [45] investigated the charring rates of wood composite rim boards with and without the protection of one or two layers of gypsum board when subjected to ASTM E119 exposure. Based on tests in a cone calorimeter and a series of tension tests, White [46] concluded that a single layer of U.S. 16 mm (0.625-in.) thick type X gypsum board could be used to add 30 min to the rating of an unprotected wood member and two layers could be assigned a time of 60 min. The charring of wood beneath cladding is addressed in the Eurocode 5 by adjusting the charring rate of the wood for the period before and after the failure of the different types of protective panel products [6].

Osborne et al. [47] and Dagenais et al. [48] found that using two layers of directly attached 13 mm (0.5-in.) type X gypsum boards delayed the onset of charring of cross-laminated timber (CLT) assemblies by 40 min; while a single layer of 16 mm (0.625-in.) provides 30 min. In a manner consistent with the design equations in Eurocode 5, Just et al. [49] developed specific design equations for a wide range of different types of gypsum boards.

Fire-Resistive Exposed Wood Members

As the wood member is exposed to fire, charring reduces the cross section of the member. In addition to charring of the member, the residual structural capacity is affected by the elevated temperature gradient within the uncharred wood. The fire-resistive characteristics of exposed wood members are due to the insulative characteristics of the char layer and the sharp temperature gradient beneath the base of the char layer.

As a result, even an unprotected structural wood member retains its structural stability in a fire for a period of time. In an engineering analysis of the fire resistance of an exposed wood member, information is needed on charring rate, ratio of ultimate strength to design values, and reduction in strength due to temperature gradient within the uncharred cross section.

Using such engineering analyses, Lie [2] developed simple formulas for calculating the fire resistance of large wood beams and columns that require the user to know only the dimensions of the structural element and load as a fraction of the full design load. These equations were extensively discussed in previous editions of this chapter. In terms of U.S. code acceptance, the formulas of T. T. Lie [2, 50] for beams and columns are expected to be phased out in favor of the NDS methodology.

In contrast to the more flexible NDS method, the Lie's methodology is applicable only to large wood beams and columns with common loading and bracing conditions. It also does not allow the user to adjust the charring rate. Other procedures such as the NDS method (discussed later in this chapter) and the various methods described in Eurocode 5 allow the user to specify the applicable charring rate.

Charring of Wood

Wood undergoes thermal degradation (pyrolysis) when exposed to fire (Fig. 55.2). The thermal degradation process depends on the temperatures and inorganic impurities such as fire-retardant chemicals [51]. The pyrolysis and combustion of wood have been studied extensively.

Past literature reviews include publications by Browne [52], Schaffer [53, 54], Hall et al. [55], and Hadvig [56]. Babrauskas [57] reviewed literature on wood charring and the use of charring rate of wood as a tool for fire investigations. By converting wood to char and gas, pyrolysis results in a reduction in the wood's density. The pyrolysis gas undergoes flaming combustion as it leaves the charred wood surface. Glowing combustion and mechanical disintegration of the char eventually erode or ablate the outer char layer.

Charring rate generally refers to the linear rate at which wood is converted to char. Under standard fire exposure, charring rates tend to be fairly constant after a higher initial charring rate. Establishing the charring rate is critical to evaluating fire resistance, because char has virtually no load-bearing capacity.

There is a distinct demarcation between char and uncharred wood. A temperature of 300 °C is widely used to define the base of the char layer. Early U.S. research used a temperature of 550 °F, and SI conversion from inch-pound units resulted in 288 °C, 290 °C, and 300 °C being used for 550 °F. To determine charring rate, both empirical models based on experimental data and theoretical models based on chemical and physical principles are used.

Standard ASTM E119 Fire Exposure

Expressions for charring rate in the standard ASTM E119 test are the result of many experimental studies. As given in the Eurocode 5, the normal equation for the char depth at a given time is of the form

$$d_{\text{char}} = \beta t \tag{55.2}$$

where
d_{char} = Char depth
β = Charring rate
t = Time

The design values for charring rate depend on the fire resistance methodology being used. The empirical model that is most generally used assumes a constant transverse-to-grain char rate of 0.6 mm/min. (1.5 in./h) for all woods, when subjected to the standard fire exposure. This is for one-dimensional charring in a semi-infinite slab.

There are differences among species associated with their density, chemical composition, and permeability. In addition, the moisture content of the wood affects the charring rate. Schaffer [58] reported transverse-to-grain charring rates as a function of density and moisture content for Douglas fir, southern pine, and white oak. The regression equations for C (minutes/mm, the reciprocal of charring rate β) were

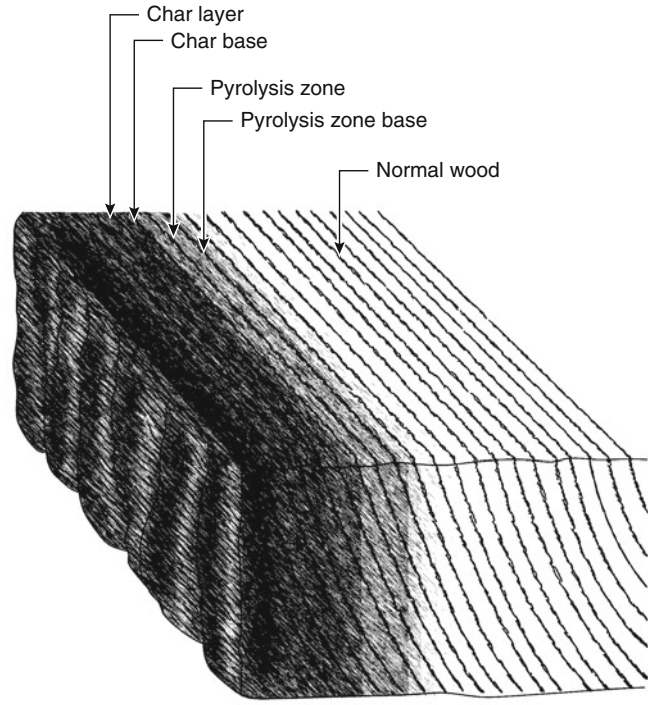

Fig. 55.2 Degradation zones in a wood section

$$C = 1/\beta = (0.002269 + 0.00457u)\rho + 0.331 \quad \text{for Douglas-fir} \tag{55.3}$$

$$C = 1/\beta = (0.000461 + 0.00095u)\rho + 1.016 \quad \text{for southern pine} \tag{55.4}$$

$$C = 1/\beta = (0.001583 + 0.00318u)\rho + 0.594 \quad \text{for white oak} \tag{55.5}$$

where
u = Moisture content (fraction of oven-dry mass)
ρ = Density (dry mass, volume at moisture content u, kg/m^3)

White and Nordheim [59] developed an empirical model based on eight species. The char rate equation was of the form

$$t = mx_c^{1.23} \tag{55.6}$$

where
t = Time (min)
m = Char rate coefficient
x_c = Char depth (mm)

This nonlinear char model is used in the NDS calculation procedure for exposed wood members. The char rate coefficients ranged from 0.42 to 0.84 mm/min$^{1.23}$ for the eight species [59]. Average values for the char rate coefficients were 0.555 for southern pine, 0.554 for western red cedar, 0.598 for redwood, 0.734 for Engelmann spruce, 0.498 for basswood, 0.653 for hard maple, 0.747 for red oak, and 0.607 for yellow poplar.

The char rate coefficient was found to be correlated to density, moisture content, and a char contraction factor, defined as the thickness of the char layer at the end of the fire exposure divided by the original thickness of the wood layer that was charred (char depth).

The application of this nonlinear model to composite wood products is discussed by White [60, 61]. Other researchers have concluded that there is not a correlation between the char rate and density [62]. Results from theoretical charring models have also shown that density has an impact on the charring rate [63]. The equation developed for the influence of density and moisture content was:

$$\beta_{\rho,w} = k_\rho k_w \beta_{450.12} \tag{55.7}$$

with

$$k_p = \sqrt{\frac{450}{\rho_{12}}} \tag{55.8}$$

and

$$k_w = \left(\frac{1.12}{1+w}\right)^{1.5} \tag{55.9}$$

where

$\beta_{450,12}$ = charring rate of wood with density of 450 kg/m^3 and 12 % moisture content, mm/min

ρ_{12} = density of wood at 12 % moisture content, kg/m^3

w = moisture content, kg/m^3

For charring in the longitudinal direction, i.e. along the grain, there is very little available data [63]. The charring rate parallel to the grain of wood has been reported as being approximately twice that transverse to the grain [55]. Based on results from a theoretical model on the impact of variations in thermal conductivity on charring rate, Cachim and Franssen [63] proposed the following relationship between a multiplication factor for thermal conductivity perpendicular to grain, k_λ, and the corresponding charring rates, parallel ($\beta_{||}$) and perpendicular to grain $\beta_\perp$.

$$k_\lambda = \left(\beta_{||}/\beta_\perp\right)^2 \tag{55.10}$$

Consistent with a doubling of charring rate, a value of 4 was suggested for k_λ. Per the Wood Handbook [64], thermal conductivity along the grain has been reported as greater than conductivity across the grain by a factor of 1.5–2.8, with an average of about 1.8. While not generally required for fire design, further work is needed on this question.

In Eurocode 5, the design charring rate, β_o, in Equation 55.2 is the rate observed in one-dimensional experiments. The listed design charring rates for timbers include 0.65 mm/min for solid-sawn or glued-laminated softwood timber (characteristic density of 290 kg/m^3 or greater), solid-sawn or glued-laminated hardwood timbers (characteristic density of 290 kg/m^3), and laminated veneer lumber (LVL) (characteristic density of 480 kg/m^3 or greater); and 0.50 mm/min for solid or glued-laminated hardwood with a characteristic density of 450 kg/m^3 or greater.

The effect of the rounding of the charred member can be taken into account by increasing the values for char rate, as is done in Eurocode 5. Eurocode 5 notional design charring rate, β_n, includes 0.7 mm/min for glued-laminated softwood and beech timbers (characteristic density of 290 kg/m^3 or greater), solid-sawn or glued-laminated hardwood except beech timbers (characteristic density of 290 kg/m^3), and LVL (characteristic density of 480 kg/m^3 or greater); 0.8 for solid softwood and beech timber (characteristic density of 290 kg/m^3 or greater); and 0.55 mm/min for solid-sawn or glued-laminated hardwood except beech (characteristic density of 450 kg/m^3 or greater).

Except for beech, the charring rates for hardwoods with characteristic densities between 290 and 450 kg/m^3 are linear interpolations of charring rates for 290 and 450 kg/m^3. The concept of notional charring rates in the Eurocode 5 is discussed by König [65]. Using results from a conductive/finite element model, Cachim and Franssen [63] suggested modifications to the Eurocode 5 values to address the effects of density, moisture content, and anisotropy on charring rates.

Assumption of a constant charring rate is reasonable when the member or panel product is thick enough to be treated as a semi-infinite slab. For smaller dimensions, the charring rate increases once the temperature has risen above the initial temperature at the center of the member or at the unexposed surface of the panel.

In tests of solid timber beams, Frangi and Fontana [62] observed an increase in the charring rate when the residual cross section was smaller than 40–60 mm. As discussed later, the elevated temperature profile beyond the base of the char layer is estimated to be about 40 mm thick.

In Eurocode 5, design charring rate listed for panels (20 mm thick and characteristic density of

450 kg/m^3) includes 0.9 mm/min for wood paneling and wood-based panels other than plywood and 1.0 mm/min for plywood. Kanury and Holve [66] suggest the model

$$\frac{\ell}{t} \approx \left(\frac{2}{a}\right)\left(1 - \frac{b\ell}{a}\right) \tag{55.11}$$

where
ℓ = Thickness of slab (mm)
t = Fire resistance time (min)
a,b = Constants

They consider the $2/a$ factor an ideal charring rate and the ratio $b\ell/a$ as a correction factor accounting for thickness and thermal diffusion effects. Noren and Östman [67] provided the equation

$$b_m = 1.128x + 0.0088x^2 \tag{55.12}$$

where
b_m = Contribution to fire resistance (min)
x = Panel thickness (mm)

The equation is based on data for various wood-based panel products.

Effect of Adhesives and Treatments

The effect of fire-retardant treatment and adhesives on the char rates depends on the type of adhesive or treatment. The charring rate of wood laminates bonded with phenol adhesives is considered to be consistent with that of solid wood. Early tests of a phenol-resorcinol adhesive and a melamine adhesive showed no delamination at the glueline in the wood beneath the char layer [68]. Delamination beneath the base of the char layer occurred at the gluelines for a polyvinyl adhesive [68].

With the introduction of Cross-Laminated-timber (CLT) construction in Europe and North America, there has been testing of more products with non-resorcinol/phenol adhesives. CLT construction panels are solid wood components built of dimension lumber in manner similar to plywood in which the grain direction of each layer is perpendicular to the adjacent layers. Frangi et al. [69] and Osborne et al. [47] observed the falling off of charred laminates during tests of CLT and the resulting increased charring rate compared with homogeneous specimens. The effect of adhesives on load capacity during a fire is discussed later in this chapter.

Fire-retardant treatments that involve the pressure impregnation of the chemicals are designed to reduce flame spread. However, few fire retardants have been found to improve charring resistance [70].

Nonstandard Fire Exposures

The above equations were stated to apply to the standard ASTM E119 or ISO 834 fire exposure. Data on charring rates for other fire exposures have been limited. Schaffer [58] provided data for constant temperatures of 538 °C (1000 °F), 815 °C (1500 °F), and 927 °C (1700 °F). Lau et al. [71] presented data for constant 500 °C and an empirical model for constant or variable temperatures.

The charring rate is a function of the external flux. For a range of 20–33 kW/m^2, Butler [72] calculated the char rate (mm/min) to be 0.022 times the irradiance (kW/m^2). Because of increased testing with heat release rate calorimeters, such as the cone calorimeter, char rate and temperature profile data as a function of external heat flux are becoming more available [73–80].

In tests of spruce, charring rates obtained were 0.56, 0.80, and 1.02 mm/min for external heat fluxes of 25, 50, and 75 kW/m^2, respectively [78]. In tests of southern pine, the linear charring rate ranged from 0.44 mm/min at 18 kW/m^2 to 0.85 mm/min at 55 kW/m^2 [73, 74]. Charring rate has been found to be proportional to the ratio of external heat flux over density [77, 78]. Eurocode 5 includes equations for parametric fire exposures in which the load-bearing function must be maintained during the complete duration of the decay phase or for a specified period of time.

Hadvig's Equations for Nonstandard Fire Exposure

Hadvig [56] developed equations for nonstandard fire exposure. The charring rate in a real fire depends on the severity of the fire to which

Table 55.3 The transfer coefficient, k [56, 81]

Type of fire compartment[a]	Geometrical opening factor, F′					
	0.02	0.04	0.06	0.08	0.10	0.12
A	1.0	1.0	1.0	1.0	1.0	1.0
B	0.85	0.85	0.85	0.85	0.85	0.85
C	3.0	3.0	3.0	3.0	3.0	2.5
D	1.35	1.35	1.35	1.50	1.55	1.65
E	1.65	1.50	1.35	1.50	1.75	2.00
F[b]	1.0–0.5	1.0–0.5	0.8–0.5	0.7–0.5	0.7–0.5	0.7–0.5
G	1.50	1.45	1.35	1.25	1.15	1.05
H	3.0	3.0	3.0	3.0	3.0	2.5

[a]A = (Standard fire compartment) The average consisting of brick, concrete, and gas concrete
B = Concrete, including concrete on the ground
C = Gas concrete (density 500 kg/m^3)
D = 50 % concrete, 50 % gas concrete (density 500 kg/m3)
E = 50 % gas concrete (density 500 kg/m3), 33 % concrete, and 17 % laminate consisting of (taken from the inside) 13 mm plasterboard (density 500 kg/m^3), 10 cm mineral wool (density 50 kg/m^3), and brick (density 1800 kg/m^3)
F = 80 % steel plate, 20 % concrete. The fire compartment is comparable to a storehouse or other building of a similar kind with an uninsulated roof, walls of steel plate, and floor of concrete
G = 20 % concrete and 80 % laminate consisting of a double plasterboard (2 × 13 mm) (density 790 kg/m^3), 10 cm air space, and another double plasterboard (2 × 13 mm) (density 790 kg/m^3)
H = Steel plate on either side of 100 mm mineral wool (density 50 kg/m^3)
[b]The higher values apply to $q < 60$ MJ/m^2; the lower values apply to $q > 500$ MJ/m^2. Intervening values are found by interpolation

the wood is exposed. The fire severity depends on such factors as available combustible material (fire load) and available air supply (design opening factor) [81]. The design fire load density is

$$q = k \cdot \frac{Q}{A_t} \tag{55.13}$$

where

q = Design fire load density (MJ/m^2)
k = Transfer coefficient (dimensionless)
Q = Sum of the products of mass and lower calorific value of materials to be found in the compartment (MJ)
A_t = Total internal area of the compartment, including floor, walls, ceiling, windows, and doors (m^2)

The transfer coefficients are given in Table 55.3 for different types of compartments and geometrical opening factors. In the case of fire compartments whose bounding structures do not come under any of the types A–H, k is usually determined by a linear interpolation in the table between appropriately chosen types of compartments.

The geometrical opening factor is

$$F' = \frac{A\sqrt{h}}{A_t} \tag{55.14}$$

where

F' = Geometrical opening factor (m^{½})
A = Total area of windows, doors, and other openings in walls (i.e., vertical openings only) (m^2)
h = Weighted mean value of the height of vertical openings, weighted against the area of the individual openings (m)

The design opening factor is

$$F = F' \cdot k \cdot f \tag{55.15}$$

where

F = Design opening factor (m$^{1/2}$)
F' = Geometrical opening factor (m$^{1/2}$)
k = Transfer coefficient of bounding structure (dimensionless)
f = Coefficient (dimensionless) to account for horizontal openings

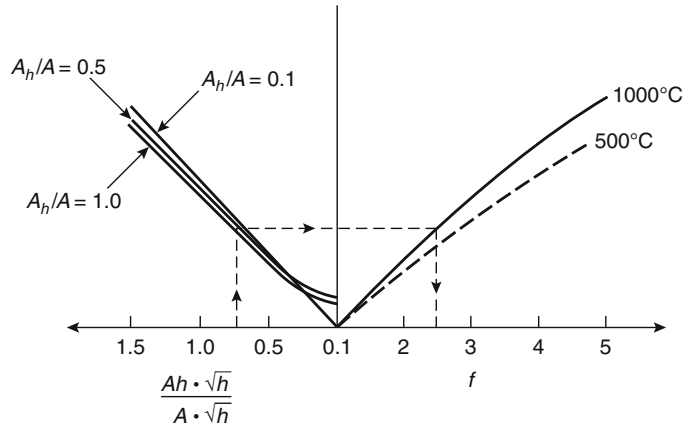

Fig. 55.3 Diagram for the determination of f for fire temperatures of 500 °C and 1000 °C [56]

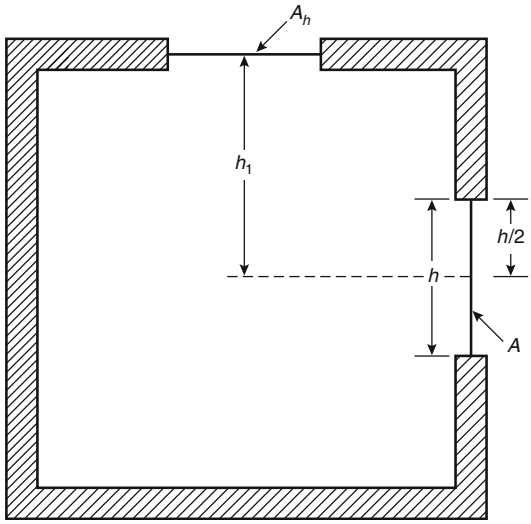

Fig. 55.4 Simplified sketch of vertical cross section of ventilated compartment with notation [56]

The dimensionless coefficient, f (Figs. 55.3 and 55.4), increases the opening factors when there are horizontal openings. For only vertical openings, f is equal to 1.

Hadvig's [56] equations are

$$\theta = 0.0175\frac{q}{F} \tag{55.16}$$

$$\beta_0 = 1.25 - \frac{0.035}{F + 0.021} \quad \text{for } 0.02 \le F \le 0.30 \tag{55.17}$$

$$X = \beta_0 \cdot \tau \quad \text{for } 0 \le \tau \le \frac{\theta}{3} \tag{55.18}$$

$$X = \beta_0 \left(-\frac{1}{12}\theta + \frac{3}{2}\tau - \frac{3}{4}\frac{\tau^2}{\theta} \right) \quad \text{for } \frac{\theta}{3} \le \tau \le \theta \tag{55.19}$$

where

θ = Time at which maximum charring is reached for the values used for F and q (min)
β_0 = Initial value of rate of charring (mm/min)
X = Charring depth (mm)
F = Design opening factor ($m^{1/2}$) (defined in Equation 55.15)
q = Design fire load density (MJ/m^2) (defined in Equation 55.13)
τ = Time (min)

These equations are valid for fire exposures less than 120 min and for a room where the combustible material is wood. Plastic burns more intensely and for a shorter time than wood. When the combustible materials in the room are plastics, Equations 55.16 and 55.17 are therefore modified for faster char rate (β_0 is 50 % higher), shorter time is allowed for maximum charring (θ is cut in half), and Equation 55.18 is applicable for τ less than θ.

Equations 55.16 through 55.19 are for glued-laminated timber with a density of 470 kg/m^3, including a moisture content of 10 % and minimum width of 80 mm or greater or square members of minimum 50 × 50 mm.

Equations 55.18 and 55.19 are valid only for $0 < X < b/4$, where b is the dimension of the narrow face of a rectangular member.

For dimensions of nonsquare cross sections between 30 and 80 mm, the ratio of the original dimensions must be equal to or greater than 1.7, the charring depth perpendicular to the wide face is X, and the charring depth perpendicular to the narrow face is determined by multiplying Equation 55.18 or 55.19 by the dimensionless quantity

$$1.35 - 0.0044(b) \qquad (55.20)$$

where b equals the dimension of the narrow face (mm).

Example 2 The room is a standard fire compartment consisting of brick, concrete, and gas concrete. The floor area is 5 × 10 m, and the height is 3 m. The openings are one window 1.5 m high and 2.0 m wide, three windows 1.5 m high and 1.0 m wide, and one skylight 1.5 × 3.0 m. The skylight is 2 m above the midheight of the windows. The fire load is 6 m^3 of wood.

Assuming a fire temperature of 1000 °C, a wood density of 500 kg/m^3, and a lower calorific value of 17 MJ/kg, describe the charring of a 38 × 250 mm wood beam exposed on three sides after 8 min of the fire. The geometrical opening factor (Equation 55.14) is

$$F' = \frac{A\sqrt{h}}{A_t} = \frac{[1(1.5 \times 2) + 3(1.5 \times 1)]\sqrt{1.5}}{[2(5 \times 10) + 2(3 \times 5) + 2(3 \times 10)]} = \frac{7.5\sqrt{1.5}}{190} = 0.048 \mathrm{m}^{1/2}$$

The design opening factor (Equation 55.15) is

$$F = F' \cdot k \cdot f$$

The k is obtained from Table 55.3 ($k = 1.0$ for type A, $F' = 0.048$). The f is obtained from Figs. 55.3 and 55.4.

$$\frac{A_1\sqrt{h_1}}{A\sqrt{h}} = \frac{(1.5 \times 3)\sqrt{2}}{7.5\sqrt{1.5}} = \frac{4.5\sqrt{2}}{7.5\sqrt{1.5}} = 0.69$$

$$\frac{A_h}{A} = \frac{4.5}{7.5} = 0.6$$

For $A_h\sqrt{h_1}/A\sqrt{h}$ of 0.69 and A_h/A of 0.6, the f from Fig. 55.3 is 2.4.

$$F = (0.048)(1.0)(2.4) = 0.115 m^{1/2}$$

The design fire load density (Equation 55.13) is

$$q = k \cdot \frac{Q}{A_t} = (1.0)\frac{(6 \times 500 \times 17)}{190} = \frac{51,000}{190} = 268 \mathrm{MJ/m}^2$$

Maximum charring rate will be reached at θ min (Equation 55.16):

$$\theta = 0.0175 \frac{268 \mathrm{MJ/m}^2}{0.115 \mathrm{m}^{1/2}} = 41 \mathrm{min}$$

The initial charring rate (Equation 55.17) will be

$$\beta_0 = 1.25 - \frac{0.035}{0.115 + 0.021} = 1 \mathrm{mm/min}$$

At 8 min, the char depth (Equation 55.18) will be

$$X = 1 \times 8 = 8 \mathrm{mm} \text{ for } 0 \le 8 \le \frac{41}{3}$$

The smaller dimension b of the beam is 38 mm. The charring depth criterion $0 < x < b/4$ is $0 < 8 < 9.5$ mm, so Equations 55.18 and 55.19 are valid. The ratio of the original dimensions is 25/3.8, or 6.6. Because 38 mm is less than 80 mm, the multiplying factor (Equation 55.20) is

$$1.35 - 0.0044(38) = 1.18$$

At 8 min, the uncharred area of the beam will be approximately

$$38 \text{ mm} - 2(8 \text{ mm}) = 22 \text{ mm wide}$$

and

$$250 \text{ mm} - (1.18 \times 8 \text{ mm}) = 240 \text{ mm high}$$

As the charring proceeds after (9.5 mm)/(1 mm/min), or 9.5 min, the $b/4$ criterion of the equations no longer holds. This is because the charring rate increases as the temperature at the center of the beam starts to increase.

Using an opening factor method and parametric time-temperature curves, equations for natural fires are provided in Eurocode 5. The approach is a simplification of Hadvig's equations. In the 1994 edition of the Eurocode

5, the equation for the parametric charring rate during the period τ_0 is

$$\beta_{par} = 1.5\beta_0 \frac{5F - 0.04}{4F + 0.08} \quad (55.21)$$

where
$F = F'$ of Equation 55.14
β_0 = Design charring rate of Eurocode 5
The time period τ_0 is

$$\tau_0 = 0.006\frac{q}{F} \quad (55.22)$$

where q is the design fire load density of Equation. 55.13.

At τ_0, the char rate decreases to zero at $3\tau_0$. The maximum charring depth during the fire exposure and the subsequent cooling period is $2\beta_0\tau_0$. Equations are valid for F between 0.02 and 0.30 $m^{1/2}$, τ_0 of 40 min or less, and char depths less than one-quarter of the dimensions.

Buchanan [82] provides a table of char rate, char time, and char depth results from the above equations for a range of opening factors. The equations in the 1994 edition were modified for the 2004 edition of the Eurocode 5. In the 2004 equations, the $5F$ and $4F$ in Equation 55.21 were modified to be a function of the thermal properties of the compartment boundaries.

Oleson and König [83] tested glued-laminated beams and found agreement with Hadvig's equations for the wide vertical side of a member. Oleson and König [83] noted that, compared with conditions at standard exposure, the mechanical behavior at natural fire exposure is different due to the changes of temperature in the residual cross section during the cooling period. The influence of elevated temperature is no longer concentrated to the outer layer of the residual cross section.

Theoretical Models

Considerable efforts have gone into developing theoretical models for wood charring, and work in this area is continuing. Janssens [84] observes that more than 50 wood pyrolysis models have been developed since World War II. Moghtaderi [85] provides a review of pyrolysis models of wood developed over the past 60 years. Theoretical models allow calculation of the charring rate for geometries other than a semi-infinite slab and for nonstandard fire exposures.

Roberts [86] reviewed problems associated with the theoretical analysis of the burning of wood, including structural effects and internal heat transfer, kinetics of the pyrolysis reactions, heat of reaction of the pyrolysis reactions, and variations of thermal properties during pyrolysis. He considered the major problems to be in the formulation of a mathematical model for the complex chemical and physical processes occurring and in the acquisition of reliable data for use in the model.

Many models for wood charring are based on the standard conservation of energy equation. The basic differential equation includes a term for each contribution to the internal energy balance. An early model for wood charring was given by Bamford et al. [87]. The basic differential equation used by Bamford was

$$c\rho\frac{\partial T}{\partial t} = K\frac{\partial^2 T}{\partial X^2} - q\frac{\partial w}{\partial t} \quad (55.23)$$

where
K = Thermal conductivity
T = Temperature
X = Location
w = Weight of volatile products per cubic centimeter of wood
t = Time
q = Heat liberated at constant pressure per gram of volatile material evolved
c = Specific heat
ρ = Density

In Equation 55.23, the term on the left side of the equal sign represents the energy stored at a given location as indicated by the increase or decrease of the temperature with time at that location. The first term on the right side of the equal sign represents the thermal conduction of energy away from or into the given location. The second term on the right side represents the energy absorbed (endothermic reaction) or the energy given off (exothermic reaction) as the wood undergoes pyrolysis or thermal degradation. Numerical solutions using computers are normally used to solve these differential equations.

In Bamford's calculations using Equation 55.23, the rate of decomposition was given by an Arrhenius equation. The heat of decomposition, q, was the difference between the heat of combustion of the wood and that of the products of decomposition. Thermal constants for wood and char were assumed to be the same, and the total thickness of char and wood was assumed to remain constant.

Thomas [88] added a convection term to Bamford's equation to obtain

$$\rho c\frac{\partial T}{\partial t} = K\frac{\partial^2 T}{\partial X^2} + Mc_g\frac{\partial T}{\partial X} - q\frac{\partial w}{\partial t} \qquad (55.24)$$

where
M = Local mass flow of pyrolysis gases
c_g = Specific heat of the gases

The convection term represents the energy transferred in or out of a location due to convection of the pyrolysis gases through a region with a temperature gradient.

The Factory Mutual Research Corporation model (SPYVAP) includes terms for internal convection of volatiles and thermal properties as functions of temperature and density. It was developed by Kung [89] and later revised by Tamanini [90]. Atreya [91] has further revised this model to include moisture absorption. His energy conservation equation is

$$\begin{aligned}\left(\rho_a C_{pa} + \rho_c C_{pc} + \rho_m C_{pm}\right)\frac{\partial T}{\partial t} &= \frac{\partial}{\partial X}\left(K\frac{\partial T}{\partial X}\right) \\ &+ i\left(1 - j\frac{\rho_c}{\rho_f}\right)M_g\frac{\partial H_g}{\partial X} \\ &- \frac{\partial \rho_s}{\partial t}\left[-Q + \left(H_a - H_c\frac{\rho_f}{\rho_w}\right)\Big/\left(1 - \frac{\rho_s}{\rho_w}\right) - H_g\right] \\ &- \frac{\partial \rho_m}{\partial t}\left(-Q_m + H_m - H_g\right)\end{aligned} \qquad (55.25)$$

where
C_p = Specific heat (J/[kgK])
K = Thermal conductivity (W/[m K])
T = Temperature (K)
t = Time (s)
X = Distance (m)
ρ = Density (kg/m^3)
M_g = Outward mass flux of volatile gases (kg/m^{2}s)
H = Thermal-sensible specific enthalpy (J/kg)
Q = Endothermic heat of decomposition of wood for a unit mass of volatiles generated (J/kg at T_x)
i,j = Parameters to simulate cracking, between 0 and 1

Subscripts:
∞ = Ambient
w = Virgin wood
c = Char
g = Volatile gases
a = Unpyrolyzed active material
m = Moisture
f = Final value
s = Solid wood

Equation 55.25 is similar to the previous equations except the material has been broken up into its components (wood, water, and char). The parameter j eliminates the convection term if the pyrolysis gases are escaping through cracks or fissures in the wood. The last term represents the heat absorbed with vaporization of the water. The conservation of mass equation is

$$\frac{\partial M_g}{\partial X} = \frac{\partial \rho_s}{\partial t} + \frac{\partial \rho_m}{\partial t} \qquad (55.26)$$

and ensures that the mass of the gases equals the mass loss due to thermal degradation of the wood and vaporization of the moisture.

As noted before, the decomposition kinetics equation for wood is the Arrhenius equation

$$\frac{\partial \rho_s}{\partial t} = -A\frac{\left(\rho_s - \rho_f\right)}{\left(1 - \rho_f/\rho_w\right)}\exp(-E/RT) \qquad (55.27)$$

where
A = Frequency factor (1/s)
E = Activation energy (J/mol)
R = Gas constant

Atreya [91] uses a moisture desorption kinetics equation for vaporization of the water in the wood, which is

$$\frac{\partial \rho_m}{\partial t} = -A_m\rho_m\exp(-E_m/RT) \qquad (55.28)$$

The CMA model [92] developed for NASA provides good results for oven-dry wood because it includes surface recession. Parker [93, 94] has taken char shrinkage parallel and normal to the surface into account in the model. Parker also includes different Arrhenius equations for each of the three major components of wood: (1) cellulose, (2) hemicelluloses, and (3) lignin.

There may be not only moisture desorption but also an increase in moisture content behind the char front caused by moisture movement away from the surface [95]. A model of Fredlund [96] includes mass transfer as well as heat transfer and provides for surface recession due to char oxidation.

In a model for wood combustion, Bryden et al. [97] modeled the wood pyrolysis kinetics, including tar decomposition, using three competing primary reactions and two secondary reactions. The surface boundary layer includes both char shrinkage and surface recession due to char combustion.

To describe the natural smoldering of logs after a forest fire, Costa and Sandberg [98] modeled the steady one-dimensional propagation of infinitesimally thin fronts of drying, pyrolysis, and char oxidation. Kanury and Holve [66] have presented dimensional, phenomenological, approximate analytical, and exact numerical solutions for wood charring. Other models include those of Havens [99], Knudson and Schniewind [100], Kansa et al. [101], Hadvig and Paulsen [102], Tinney [103], and Janssens [84]. Badders et al. [104] examined the ability of four commercial finite element analysis programs (FIRES-T3, SAFIR, TASEF, COMSOL) to model exposed wood beams.

The option of theoretical models or advanced calculations for the determination of charring rates and temperature profiles is addressed in the Eurocode 5. For purpose of such calculations, the Eurocode 5 provides values for the equivalent conductivity, specific heat capacity and the char/wood density ratio as a function of temperature.

Cachim and Franssen [63] used the finite element program SAFIR and the Eurocode property data to examine the effects of density, moisture content, and anisotropy on charring rates. Janssens [105] used the finite element software package COMSOL Multiphysics and the Eurocode 5 data to model some glued laminated beams in fire resistance test.

A major issue in the use of the more sophisticated models is the adequacy of the available data to use as input. The thermophysical properties for wood pyrolysis models are discussed by Janssens [106, 107]. Wood properties are discussed at the conclusion of this chapter. Most theoretical models for wood charring not only define the charring rate but also provide results for the temperature gradient. This temperature gradient is important in evaluating the load-carrying capacity of the wood remaining uncharred.

Load-Carrying Capacity of Uncharred Wood

In the standard ASTM E119 test of a wood member, structural failure occurs when the member is no longer capable of supporting its design load. The charring of the wood reduces the cross-sectional area of the member such that the ultimate capacity of the residual member is exceeded.

During the charring of the wood member, the temperature gradient is steep in the wood section remaining uncharred. The temperature at the innermost zone of the char layer is assumed to be 300 °C. Because of the low thermal conductivity of wood, the temperature 6 mm inward from the base of the char layer is about 180 °C once a quasi-steady-state charring rate has been obtained. Some loss of strength undoubtedly results from elevated temperatures.

The peak moisture content occurs where the temperature of the wood is about 100 °C, which is about 13 mm from the char base. Schaffer et al. [108] have combined parallel-to-grain strength and stiffness relationships with temperature and moisture content and the gradients of temperature and moisture content within a fire-exposed slab to obtain graphs of relative modulus of elasticity, compressive strength, and tensile strength as a function of distance below the char layer (Fig. 55.5).

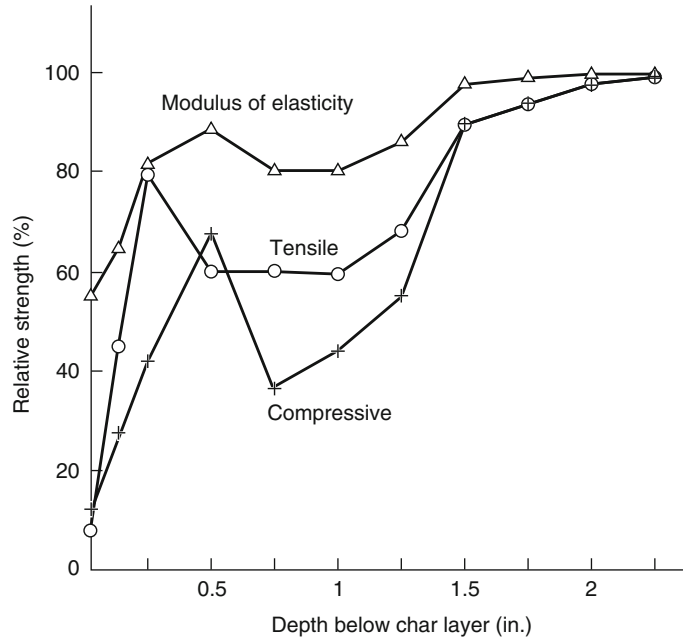

Fig. 55.5 Relative modulus of elasticity and compressive and tensile strength as a function of distance below char layer in softwood section under fire exposures (Expressed in percentage of that at 25 °C and initial moisture content of 12 %.) Duration of fire exposure should be equal to or greater than 20 min to apply results of this figure

Various equations for the temperature gradient within the charred wood slab have been developed [62, 109, 110]. An equation based on a power term is

$$T = T_i + (300 - T_i)\left(1 - \frac{x}{d}\right)^2 \qquad (55.29)$$

where
T = Temperature (°C)
T_i = Initial temperature (°C)
x = Distance from the char front (mm)
d = Thermal penetration depth (mm)

In the tests of White and Nordheim [59], an average value for the thermal penetration depth was 33 mm. Based on European tests, a more conservative value of 40 mm was recommended for the thermal penetration depth [110]. The power term does not provide for the plateau in temperatures that often occurs at 100 °C in moist wood. The power term has also been used to estimate the temperature profile in wood exposed to a constant heat flux [74]. Frangi and Fontana [62] observed that the thermal penetration depth was dependent on time and developed an alternative equation:

$$T(x) = 20 + 180\left(\frac{\beta t}{x}\right)^{\alpha} \qquad (55.30)$$

where
T = Temperature at depth x (°C)
β = Charring rate (mm/min)
t = Time (min)
x = Distance from the surface of the cross section (mm)
and

$$\alpha(t) = 0.025t + 1.75 \qquad (55.31)$$

Equation 55.30 was derived assuming the char front at 200 °C and char rate of 0.7 mm/min. Frangi and Fontana [62] also developed the following equation for a timber beam exposed to fire on three sides:

$$T(x, y) = 20 + 180(\beta t)^{\alpha} \left[\left(\frac{1}{x}\right)^{\alpha} + \left(\frac{1}{b - x}\right)^{\alpha} + \left(\frac{1}{y}\right)^{\alpha}\right] \qquad (55.32)$$

where T, t, α, and β are as defined for Equation. 55.30, and x and y are the depths from the

surfaces of the cross section in millimeters. The theoretical models discussed previously can be used to determine the temperature gradient within the wood remaining uncharred.

There are two approaches to evaluating the load-carrying capacity: to evaluate the remaining section either as a single homogeneous material or as a composite of layers or elements with different properties. In the single homogeneous material approach, one uses either reduced material properties or the room-temperature material properties. A greater reduction in cross-sectional area is calculated if the material properties are not reduced.

Reduced Properties Models

One approach in accounting for the loss in strength in the section remaining uncharred is to assume that the strength and stiffness of the entire uncharred region are fractions α of their room-temperature values. For bending rupture of a beam, an equation of this type would be

$$\frac{M}{S(t)} = \alpha\sigma_0 \tag{55.33}$$

Where
α = fraction of room-temperature values
M = Applied moment (design load)
S = Section modulus of charred member
σ_0 = Modulus of rupture at room temperature
t = Time

Assuming the residual cross section is rectangular in shape before and during fire exposure, the section modulus of charred solid rectangular bending members with the neutral axis perpendicular to depth at center is [109]

$$S(t) = \frac{1}{6}\left[(B - 2C_1 t)(D - jC_2 t)^2\right] \tag{55.34}$$

where
B = Original breadth of beam
D = Original depth of beam (depth>breath)
C_1 = Charring rate in breadth direction
C_2 = Charring rate in depth direction
j = 1 for three-sided fire exposure (top edge covered) or 2 for four-sided fire exposure (Fig. 55.6)

Alternative to Equations 55.33 and 55.34 are the following, Equations 55.35 through 55.36:

$$\left(\frac{k}{\alpha}\right)\frac{\frac{B}{D}}{\left[\frac{d}{D} - \left(1 - \frac{B}{D}\right)\right]} = \left(\frac{d}{D}\right)^2 \tag{55.35}$$

for exposure on all four sides [111], and

$$\frac{k}{\alpha}\frac{B/D}{[B/D - 2(1 - d/D)]} = \left(\frac{d}{D}\right)^2 \tag{55.36}$$

for exposure on three sides [112], [113],
where
k = Load, as fraction of room temperature ultimate load of original member
d = Critical depth of the uncharred beam

The fire resistance is equal to the time to reach the critical depth, or

$$t = (D - d)/jC \tag{55.37}$$

Proposed α values ranged from 0.5 in New Zealand to 0.83 in France [109]. The differences in α values are due to uncertainty, differences in design load, and desired level of safety. The application of the above equations is generally limited to large wood members. In light-frame members, α values would be substantially lower [114]. In Eurocode 5, this approach is called the "reduced properties method." The reduction factors are a function of the perimeter of the fire-exposed residual cross section divided by the area of the cross section.

In addition to bending rupture, the fire resistance of a beam may depend on lateral buckling of the beam [111]. Similar expressions can be developed for columns and tension members [2, 109, 113, 115]. Early reviews of fire resistance design methodologies for large wood members include those of Schaffer [109], Pettersson [116], and Barthelemy and Kruppa [117].

Kirpichenkov and Romanenkov [118] discussed the calculation procedures in the Soviet Union. The fire resistance of wood structures is also briefly discussed by Odeen [119]. In developing a model for fire-exposed

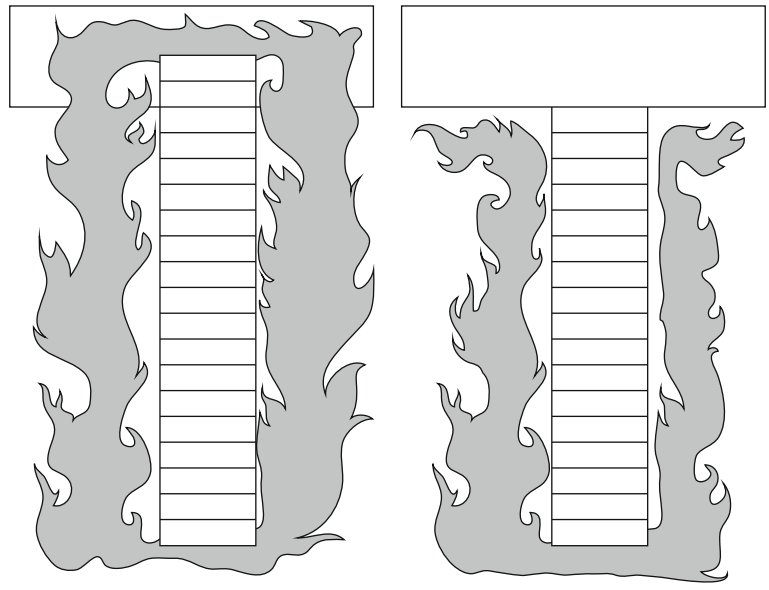

Fig. 55.6 Fire exposure of beams on three or four sides

unprotected wood joist floor assemblies, Woeste and Schaffer [120, 121] evaluated various time-dependent geometric terms that could be used to modify the strength reduction factor. The selected term was

$$\alpha = \frac{1}{1 + \left(\frac{B+2D}{BD}\right)\gamma t_f} \tag{55.38}$$

where

t_f = Failure time

γ = Empirical thermal degrade parameter

The model has been experimentally evaluated [122, 123], extended to floor-truss assemblies [121, 124] and used as part of a first-order second-moment reliability analysis of floor assemblies [120, 121]. Reliability-based design of the fire resistance of light-frame construction is also discussed by Lau and Barrett [114]. In a model for metal plate–connected wood trusses [125], the strength degradation factors for the wood are calculated as a function of the duration of exposure and the temperature profile within the wood component.

The models for load-bearing floor joist and wall studs in Annex C of Eurocode 5 incorporate the notional char depth within the calculation of the modification factor for the strength properties. König and Källsner [126, 127] developed such a modification factor for wood I-joists.

Reduced Cross-Section Area Models

A more common approach is to assume an equivalent zero-strength layer, δ, and then evaluate the rest of the member using room-temperature property values [128]. In the model of Schaffer et al. [108] for beams, the δ was estimated to be 8 mm (0.3 in.) thick. This zero-strength layer, δ, was added to the char depth, βt, to obtain the total zero-strength layer.

This zero-strength layer model was incorporated within a reliability-based model to predict the strength of glued-laminated beams with individual laminates of various grades of lumber [129]. This zero-strength layer approach is called the "reduced cross-section method" in Eurocode 5 [6]. In Eurocode 5, δ is a linear fraction of 7 mm for the initial 20 min and 7 mm after 20 min.

In the NDS method [130, 131], a 20 % increase in the charring rate is used to account for a zero-strength layer. Schmid et al. [128] presented an analysis that indicates that various

factors such as fire exposure, shape, and dimensions of the cross-section may affect the optimum thickness for the zero-strength layer. Further analysis by Klippel et al. [132] also indicated that members in compression would be better modeled using a zero layer thickness greater than the 7 mm currently specified.

For fire-damaged members, Williamson [133] recommended 6 mm (0.25 in.) for designs controlled by compression (16 mm [0.625 in.] if design is controlled by tension) and the use of 100 % of the original basic allowable stresses in calculation of load capacity.

Performance of the structural member in a fire will depend on the ratio of the applied load to the ultimate capacity of the residual member. Calculations of the structural capacity of the remaining cross section are normally made using ultimate strength values. Design or characteristic strength values are used in the Eurocode 5 calculations. In Eurocode 5, the design value of strength is the 20th percentile of the cold strength divided by a partial factor equal to one.

The design stress to member strength adjustment factors in the NDS are discussed in the next section. Design methods account for the various factors affecting performance in different manners. Care must be taken to verify that all the design values and the methodologies are compatible.

The reduced cross-section area approach is being used to predict the fire resistance ratings of walls and floors built of cross-laminated-timber (CLT) construction as described by Dagenais et al. [48]. Frangi et al. [134] developed a reduced cross-section model for calculating fire resistance of timber slabs with hollow core elements. Reduced cross-section methodologies are also used to evaluate the load capacity aspect of fire resistance for both unprotected [130] and protected light-frame assemblies [6].

NDS Method for Exposed Wood Members

The *National Design Specification for Wood Construction* (NDS®) method for the fire design of exposed wood members is a mechanics-based design method that is applicable to all wood structural members covered under the NDS. With explicit equations for the residual fire resistance of the wood members, it is possible to adjust the equations for other member types and loading conditions.

The charring rate can be modified for specific wood products. It is described in a chapter of the NDS and other articles [131]. Full documentation is provided in Technical Report 10 of the American Wood Council [130]. In the United States, code recognition is via adoption of the 2005 or later editions of the NDS. It is limited to ratings of 2 h or less.

This effective cross-section method uses the nonlinear charring model of Equation 55.6 and strength values at ambient temperatures. An increased char rate accounts for reduced strength and stiffness properties and accelerated charring at the corners. The increase in char depth is 20 % over a nominal char rate that is based on 1 h of fire exposure. Thus, the effective char rate is given by

$$\beta_{\text{eff}} = \frac{1.2\beta_n}{t^{0.187}} \tag{55.39}$$

where

β_{eff} = Effective char rate (mm or in. per hour) adjusted for exposure time, t

β_n = Nominal char rate (mm or in. per hour) linear char rate based on 1-h exposure

t = Exposure time

A nominal char rate, β_n, of 38 mm (1.5 in.) per hour is normally assumed for solid-sawn and glued-laminated softwood members. The effective char depth is β_{eff} multiplied by time. Thus, the effective char depth at 1 h is 46 mm (1.8 in.); the actual char depth is 38 mm (1.5 in.) and the equivalent zero-strength layer thickness is 7.6 mm (0.3 in.). The section properties of the members are reduced by the effective char depth for the surfaces that are exposed to the standard fire exposure.

The resisting strength or average ultimate residual strength properties are calculated by multiplying the allowable design stress values

in the NDS by design stress-to-member strength adjustment factors. Values for this adjustment factor are 2.85 for bending and tensile strength, 2.58 for compression strength, and 2.03 for beam-buckling and column-buckling strength.

As appropriate, the allowable design stress values are also multiplied by a size factor, volume factor, flat use factor, beam stability factor, and column stability factor as described in the NDS. For a fire resistance rating of time t, the induced stress of the reduced section of the charred member at time t shall not exceed the resisting strength of the member.

For glued-laminated timber bending members with tension laminations, the NDS has requirements for the substitution of core laminations with tension laminations. The specifics depend on the fire resistance rating and the details of the beam construction.

Decks

The NDS method addresses the structural requirements for fire resistance of timber decks. Decks are specified to have a thickness of at least 51 mm (2 in.). Butt-jointed decking is designed as a series of beams that have reduced charring on the partially protected sides and normal charring on the exposed bottom surface.

The char rate for the sides is one-third of the effective char rate (Equation 55.39). Single and double tongue-and-groove (T&G) decking is assumed to have charring on only the one bottom face. Janssens [135] applied a transformed section analysis of a timber deck and the Eurocode 5 effective cross-section method to develop a simplified design equation (thickness and load factor as variables) for timber decks that was similar to the T.T. Lie equations.

In addition to the requirement of structural stability, the fire resistance rating of a timber deck also depends on requirements for thermal protection. Thermal protection criteria provide for excessive temperature rise on the unexposed surface and flame penetration.

In the United States, there is no recognized procedure for solid wood floors or roofs that include the thermal failure criteria of ASTM E119. The equations for the temperature profile in a wood slab discussed previously can be used to estimate the required thickness to prevent excessive temperature rise [135, 136]. A deck is likely to have joints and gaps between the boards that become the controlling factor in the fire resistance of the deck. Joints can be a critical factor in the fire resistance of a wood barrier. Eurocode 5 provides some guidance for joints in wood-based panel products.

The estimated failure times for such panel products with a butt joint, lap joint, single T&G joint, or double T&G joint are 20, 30, 40, and 60 %, respectively, of the failure times for a solid wood barrier calculated using charring rates for wood.

The application of these adjustments developed for panel products to gaps in decks has been investigated. Based on a series of tests of timber decks, Richardson and Batista [44] concluded that the failure times for simple butt joints, single T&G joints, and double T&G boards were 10, 40, and 40 %, respectively, of the times for a solid wood member estimated using charring rates for wood. In the tests, the specification for the gaps between boards was 2 mm (0.08 in.) or less. These tests also illustrated the effect of increasing the thickness of gaps, particularly with butt joints. For gaps of $\leq$1 mm ($\leq$0.04 in.), the tests suggested that failure times for simple butt joints were 30 % of those for solid-sawn lumber instead of the 10 % for gaps of 2 mm (0.08 in.) or less.

Adding wood flooring or panel products on top of the timber deck improved the failure times in the tests of Richardson and Batista [44]. Paneling on top of the decks provided the most benefits to the fire resistance of decks when the butt joints had 4 mm (0.16 in.) gaps, compared with decks of T&G joints or narrow gaps.

Given the limited ability to control gaps between deck boards over time, the best method to address the joint issue is to provide a

multilayer deck assembly by adding panel products or other floor topping, such as gypsum concrete or lightweight or normal concrete toppings, on top of the heavy timber decks. Frangi and Fontana [62] found that the fissures between nailed-laminated timber planks did not increase the char rate but noted that the nonexposed surface must be sealed airtight to obtain such results.

Connections

Connectors and fasteners relating to support of the member must be protected for equivalent fire-resistive construction. Carling [137] summarizes work done in Europe on the fire resistance of joint details in load-bearing wood construction. Buchanan [82] also reviews the literature on the fire performance of connections. Eurocode 5 provides rules for the fire resistance of connections and protecting connections in fire-rated timber members, and the subject is discussed by König [4, 5, 138] and by Östman et al. [6].

Rules are given for connections made with nails, bolts, dowels, screws, split-ring connectors, shear-plate connectors, and toothed-plate connectors. Moss et al. [139] determined values for embedment strength as a function of temperature and predicted failure times for fire exposed bolted connections with steel and wood splice plates by applying the data to Johansen's yield equations. Racher et al. [140] used a three-dimensional finite element model to examine the thermal and mechanical behavior of dowelled timber connections exposed to fire. Peng et al. [141] reviewed recent studies on fire performance of connections and provided equations for failure times of double shear connections with either bolts or wood dowels.

Configurations for the double sheer connections included wood-wood-wood (W-W-W), wood-steel-wood (W-S-W), and steel-wood-steel (S-W-S). The equations for W-W-W and W-S-W connections incorporated char rate, load ratio, wood side member thickness, and fastener diameter. In the case of S-W-S connections, the equation of Peng et al. [141] included the load ratio and the thickness of the wood component. Peng et al. [141] reported that a single layer of 16 mm (0.625 in.) Type X gypsum board improved the fire resistance of the connections by about 33 min and reviewed results for intumescent paints.

In U.S. procedures with building code recognition, the protection of connections is addressed by prescriptive requirements. Where minimal 1 h fire resistance is required, the International Building Code (U.S.) requires connectors and fasteners must be protected from fire exposure by 38 mm (1.5 in.) of wood or other approved covering or coating for a 1 h rating. Industry publications [130] include diagrams giving typical details of such protection.

Adhesives

There have been a number of recent investigations on the potential impact of new adhesives on the fire resistance of structural wood products. These new adhesives are replacing the traditional resorcinol-formaldehyde and phenol-resorcinol-formaldehyde in structural wood products.

A note in the Eurocode 5 states that the softening temperature is considerably below the charring temperature of the wood for some adhesives. In response to concerns about the fire performance of non-phenol resorcinol adhesives in finger-jointed lumber, there were efforts in the United States to develop qualification tests for the performance of adhesives in fire-rated wood assemblies. An initial effort was a test protocol (ASTM D 7247 "Test method for evaluating the shear strength of adhesive bonds in laminated wood products at elevated temperatures") for evaluating the shear strength of adhesive bonds in laminated wood products at elevated temperatures [142].

Performance criteria based on this test were added to specifications for laminated wood products. To address the specific concerns of finger-jointed lumber, two related ASTM standards (ASTM D7374 "Practice for evaluating elevated temperature performance of

adhesives used in end-jointed lumber and D7470 "Practice for evaluating elevated temperature performance of end-jointed lumber studs" were developed as performance criteria for the "Heat Resistant Adhesives" (HRA) grade stamp on end-jointed lumber. End-jointed lumber with the HRA grade stamp was allowed to continue to be an acceptable substitution in fire-rated assemblies tested with solid-sawn lumber.

In Europe, Frangi et al. [143] tested the shear behavior of five one-component polyurethane (PUR) adhesives as well as a resorcinol-formaldehyde (RF) and an epoxy adhesive as controls at temperatures up to 170 °C. The performance of the five PUR adhesives ranged from the very good high temperature performance of the RF adhesive to the poor high temperature performance of the epoxy.

Finite element calculations using the reduced elevated temperature shear properties were consistent with an unexpected shear failure within a glued laminated beam in a fire resistance test of a timber-concrete composite slab. While generally not used in structural wood products, tests have shown that epoxy-based adhesives can have poor fire performance [82].

Källander and Lind [144] conducted a comparative study of six different adhesives before and after exposure of glulam beams to fire. König et al. [145] tested small-sized glued laminated beams in bending. The fire resistance of the beams made with the two polyurethane adhesives and the melamine urea formaldehyde adhesive were less than that for the beam made with the traditional phenolic resorcinol formaldehyde adhesive.

Frangi et al. [146] reported substantial differences in temperature dependent strength reduction and failure between several different types of adhesives, particularly when tested in tension. It is expected that concerns about the non-phenol adhesives can continued to be successfully addressed either by improvements in the formulations of the adhesives to comply with appropriate performance criteria or modifications to the fire resistance calculation methodologies to accurately reflect the performance of the structural wood composite products.

Composite Models

The most complex approach to evaluating the fire resistance of a wood member is to assume that the uncharred region consists of layers or elements at different temperatures and moisture contents. The strength and stiffness properties depend on the temperature and moisture content profiles. These are referred to as "advanced methods" in Eurocode 5.

In one model with layers, the compressive and tensile strengths and modulus of elasticity of each layer are assumed to be fractions of the room-temperature values. Using one 38 mm (1.5 in.) heated layer with reduced properties, Schaffer et al. [108] analyzed a beam using transformed section analysis. In the similar elastic transformed section model of King and Glowinski [147], the heated zone of the remaining wood section is divided into two layers at elevated temperatures. Transformed section analysis is also used by Lee-Gun Kim and Jun-Jae Lee [148] and by Janssens [135].

Finite difference and finite element methods have been used to solve the governing equations for heat and mass transfer. A finite difference model for wood beams and columns was developed by Tavakkol-Khah and Klingsch [149]. The finite element analysis software COMSOL Multiphysics was used by Janssens [105] to predict failure times of glulam beams tested with load levels of zero, 27 %, 44 % and 91 % of design load. Schnabl at al. [150] examined timber composite beams used the finite element method to solve the Luikov's equations for simultaneous heat and mass transfer. Fragiacomo et al. [151] used the general purpose finite element code Abaqus to conduct 3-D finite modeling of the thermo-structural behavior of laminated veneer lumber (LVL) loaded in tension and exposed to fire.

Do and Springer [152–154] proposed a fire resistance model for wood beams based on mass loss versus strength data. The work included a program to predict the temperatures and mass loss within the wood member. The input data came from small-scale tension,

compression, and shear tests done on specimens that had previously been heated in an oven. Examples of models that use a grid of elements to analyze the residual load capacity of the structural member include ones for wood joists [155], compression members [156], and wood studs [28].

Property Data

Proper input data are critical to the use of any model. For the models discussed in this section, property data include strength and stiffness properties and thermal properties. General property data for clear wood can be found in various chapters of *Wood Handbook*: *Wood as an Engineering Material* [64], which also includes a chapter on fire safety.

Reviews of available data on properties needed to model thermal degradation, charring, and residual load capacity of wood members can be found in the literature [82, 107]. Equations and graphs of the strength and stiffness of wood as functions of temperature and moisture content are available [157–159].

Recent research in the development of fire resistance models has provided additional data specific for application to such models. An extensive study on fire-exposed wood in tension was done by Lau and Barrett [160]. Recent efforts have been on the compression properties of wood [161, 162]. The strength reductions given in Eurocode 5 include the time-dependent effects of creep, moisture, and mechanosorption. Such effects are among the reasons for differences reported in the literature.

Preheating samples in an oven is not the same as exposing samples to simultaneous thermal and structural loads. Other methodology differences, such as rate of loading, affect the experimental results reported.

Thermal properties can also be found in the various references for charring models and Annex B of Eurocode 5 (EN 1995-1-2). As discussed by König [163], the thermal properties of EN 1995-1-2 and other sources are often effective property values that depend on the assumptions of the model and the experiments used to calibrate the input data.

Due to the complexity of wood, thermal degradation, and the heat and mass transfer within the wood element, some aspects of the complexity are accommodated by adjusting the thermal property data. Thus, such thermal property data may be applicable only to the standard fire exposure used in their development and can produce erroneous results when applied to natural fires and parametric fire curves [163]. This is particularly the case for the thermal properties of the char layer. As discussed by Hadvig [56], the "char" of the char layer is complex and its thermal characteristics are not the same as those of charcoal. Lattimer et al. [164] used inverse heat transfer analysis of fire test data for balsa wood to obtain thermal properties, physical properties and decomposition kinetics constants needed for their decomposition model.

Although assuming constant property values is often less complicated, these properties are very often a function of other properties or factors. Most wood properties are functions of density, moisture content, grain orientation, and temperature. Chemical composition may also be a factor.

Because an understanding of these factors is important to the application of property data, the factors are defined in the rest of this section. The oven-dry density of wood can range from 160 kg/m^3 (10 lb/ft^3) to over 1040 kg/m^3 (65 lb/ft^3), but most species are in the 320- to 720-kg/m^3 (20- to 45-lb/ft^3) range [64]. The density of wood relative to the density of water (i.e., specific gravity) is normally based on oven-dry weight and volume at some specified moisture content, but in some cases the oven-dry volume is used.

As the empirical equations for charring rate show, materials with higher density have slower char rate. In the Eurocode 5 discussion of advanced calculations, the suggested char/ dry wood ratios are 1.0, 1.0, 0.93, 0.76, 0.52, 0.38, 0.28, 0.26, and 0 for temperatures of 20, 200, 250, 300, 350, 400, 600, 800, and 1200 °C, respectively.

Wood is a hygroscopic material, which gains or loses moisture depending on the temperature and relative humidity of the surrounding air. Moisture content of wood is defined as the weight of water in wood divided by the weight of oven-dry wood. Green wood can have moisture content in excess of 100 %. However, air-dry wood comes to equilibrium at moisture content less than 30 %. Thirty percent moisture content is also considered the approximate moisture content at which the cell walls are saturated with water, but there is no water in the cell lumens. This condition is known as the *fiber saturation point*. At higher moisture contents, water exists in the cell lumens.

Many physical and mechanical properties of wood change with moisture content only at moisture contents below the fiber saturation point. Under the conditions stated in ASTM E119 (50 % relative humidity), the equilibrium moisture content is about 9 %. Moisture generally reduces the strength of wood but also reduces the charring rate.

Both density and moisture content affect the thermal conductivity of wood. The average thermal conductivity perpendicular to the grain is [64]

$$k = S(0.0001941 + 0.000004064M) + 0.01864 \quad (55.40)$$

where

k = Thermal conductivity (W/mK)

S = Density based on volume at current moisture content and oven-dry mass (kg/m^3)

M = Moisture content (percent)

Equation 55.40 is valid for moisture contents of 25 % or less, densities greater than 300 kg/m^3, and temperature of 24 °C. Conductivity increases about 2–3 % per 10 °C [64]. In the Eurocode 5 discussion of advanced calculations, the suggested values for "apparent thermal conductivity" of the wood/char as a function of temperature are 0.12, 0.15, 0.07, 0.09, 0.35, and 1.50 W/mK for 20. 200. 350, 500, 800, and 1200 °C, respectively.

The fiber (grain) orientation is important because wood is an orthotropic material. The longitudinal axis is parallel to the fiber or grain. The two transverse directions (perpendicular to the grain) are the radial and tangential axes. The radial axis is normal to the growth rings, and the tangential axis is tangent to the growth rings. For example, the longitudinal strength properties are usually about ten times the transverse properties, and the longitudinal thermal conductivity is 1.5–2.8 times the transverse property.

In fire resistance analysis, temperature can have a significant influence on the properties of wood. The preponderance of property data is often limited to temperatures below 100 °C. The effect of temperatures on the strength properties of wood is shown in Figs. 55.7, 55.8, and 55.9. Using data from a variety of sources, Buchanan [82] also provides graphs of the temperature effect on mechanical properties. The heat capacity, c_ρ (kJ/kg K), of dry wood is approximately related to temperature, T (in K), [64] by.

$$c_\rho = 0.1031 + 0.003867T \quad (55.41)$$

In the Eurocode 5, the suggested apparent specific heat capacity values are 1.53, 1.77, 13.60, 13.50, 2.12, 2.00, 1.62, 0.71, 0.85, 1.00, 1.40, 1.65, and 1.65 kJ/kg-K for 20, 99, 99, 120, 120, 200, 250, 300, 350, 400, 600, 800, and 1200 °C, respectively. These values results in a sharp peak between 99 and 120 °C to address water vaporization. These values are tied to the suggested char/wood ratios with the addition of the moisture content to the ratio for temperatures between 20 and 99 °C.

For moist wood below the fiber saturation point, the heat capacity is the sum of the heat capacity of dry wood and that of water and an additional adjustment factor for the wood-water bond [64]. Studies on thermal properties of wood and char continue to be active areas of research.

The major components of wood are cellulose, lignin, hemicelluloses, extractives, and inorganic materials (ash). Softwoods have lignin contents

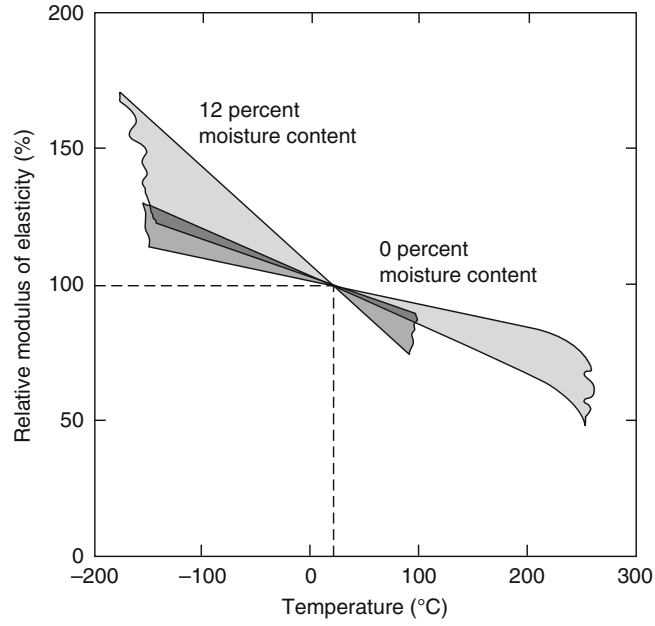

Fig. 55.7 The immediate effect of temperature on modulus of elasticity parallel to the grain at two moisture contents relative to value at 20 °C. The plot is a composite of results from several studies. Variability in reported trends is illustrated by the width of bands [64]

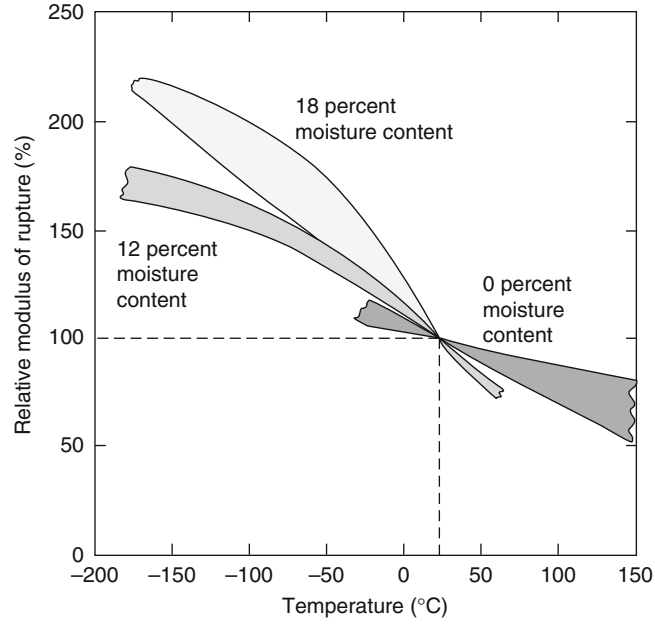

Fig. 55.8 The immediate effect of temperature on modulus of rupture in bending at three moisture contents relative to value at 20 °C [64]

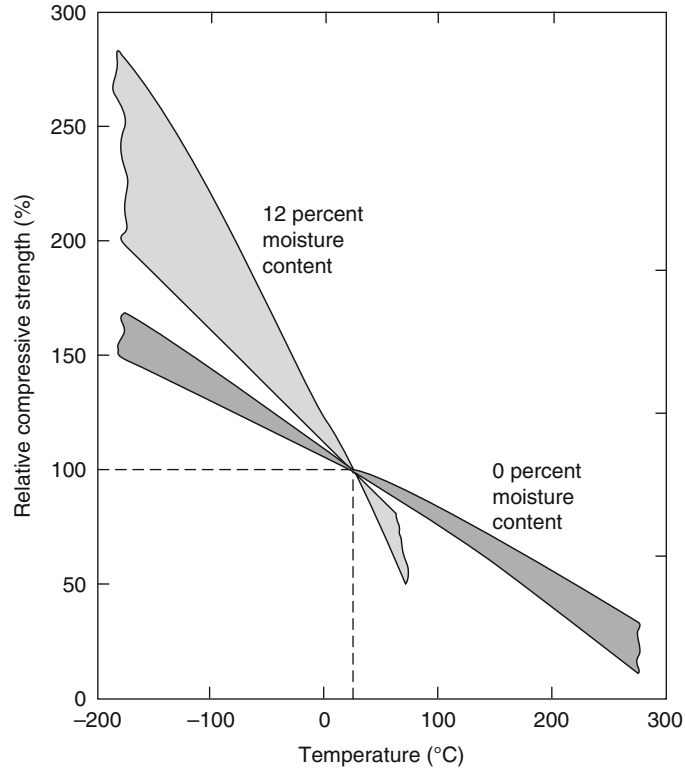

Fig. 55.9 The immediate effect of temperature on compressive strength parallel to the grain at two moisture contents relative to the value at 20 °C [64]

of 23–33 %, whereas hardwoods have only 16–25 %. The types and amounts of extractives vary. Cellulose content is generally around 50 % by weight.

The component sugars of the hemicelluloses are different for the hardwood and softwood species. Chemical composition can affect the kinetics of pyrolysis (Equation 55.27) and the percentage weight of the residual char. In the degradation of wood, higher lignin content results in greater char yield.

References

1. "Component Additive Method (CAM) for Calculating and Demonstrating Assembly Fire Endurance," *Design for Code Acceptance 4,* American Wood Council, Leesburg, VA, 8 p. (2010).
2. T.T. Lie, "A Method for Assessing the Fire Resistance of Laminated Timber Beams and Columns," *Canadian Journal of Civil Engineering,* 4, p. 161 (1977).
3. *Fire Safety Design in Buildings,* Canadian Wood Council, Ottawa (1996).
4. J. König, "Structural Fire Design According to Eurocode 5—Design Rules and Their Background," *Fire and Materials,* 29, p. 147 (2005).
5. J. König, "Structural Fire Design According to Eurocode 5," in *Fire Safety Science—Proceedings of the 8th International Symposium,* International Association for Fire Safety Science, London, UK, p. 303 (2005).
6. B. Östman, E. Mikkola, R. Stein, A. Frangi, J. König, D. Dhima, T. Hakkarainen, and J. Bregulia, "Fire Safety in Timber Buildings – Technical Guidelines," *SP Report 2010:1,* SP Trätek, Stockholm (2010).
7. T.Z. Harmathy, "Ten Rules of Fire Endurance Rating," *Fire Technology,* 1, p. 93 (1965).
8. "Standard Method of Fire Tests for the Evaluation of Thermal Barriers Used Over Foam Plastic Insulation," *NFPA 275*, National Fire Protection Association, Quincy, MA. (2009)
9. L.R. Richardson and M. Batista, "Revisiting the Component Additive Method for Light-Frame Walls Protected by Gypsum Board," *Fire and Materials,* 21, p. 107 (1997).
10. L.R. Richardson, R.A. McPhee, and M. Batista, "Sound-Transmission-Class and Fire Resistance Ratings for Wood-Frame Floors," *Fire and Materials,* 24, p. 17 (2000).

11. M.A. Sultan and V.R. Kodur, "Light-Weight Frame Wall Assemblies: Parameters for Consideration in Fire Resistance Performance-Based Design," *Fire Technology,* 36, p. 75 (2000).
12. V.K.R. Kodur and M. A. Sultan, "Performance of Wood Stud Shear Walls Exposed to Fire," *Fire and Materials,* 24, p. 9 (2000).
13. B. Östman, J. König, and J. Norén, "Contribution to Fire Resistance of Timber Frame Assemblies by Means of Fire Protective Boards," in *Proceedings of Fire and Materials '04 Conference,* Interscience Communication Ltd., London (1994).
14. B. Östman, J. König, and J. Norén, "Fire Behaviour of Timber Frame Structures," *Rapport I 9612091,* Trätek, Stockholm (1996).
15. V. Schleifer, A. Frangi, and M. Fontana, "Separating Function of Light Timber Frame Assemblies," in *Proceedings of the 9th Wood Timber Engineering Conference,* Oregon State University, Corvallis (2006).
16. A. Frangi, V. Schleifer, M. Fontana, and E. Hugi. "Experimental and Numerical Analysis of Gypsum Plasterboards in Fire," *Fire Technology*, 46, p. 149 (2010).
17. P.C.R. Collier, "Design of Loadbearing Light Timber Frame Walls for Fire Resistance: Part 1," *Study Report No. 36,* Building Research Association of New Zealand, Judgeford (1991).
18. N. Bénichou and M.A. Sultan, "Fire Resistance Performance of Lightweight Wood-Framed Assemblies," *Fire Technology,* 36, p. 184 (2000).
19. F.C.W. Fung, "A Computer Program for the Thermal Analysis of the Fire Endurance of Construction Walls," *NBSIR 77-1260,* National Bureau of Standards, Washington, DC (1977).
20. B.W. Gammon, "Reliability Analysis of Wood-Frame Wall Assemblies Exposed to Fire," Ph.D. Dissertation, University of California, Berkeley (1987).
21. J.R. Mehaffey, P. Cuerrier, and G. Carisse, "A Model for Predicting Heat Transfer Through Gypsum-Board/Wood-Stud Walls Exposed to Fire," *Fire and Materials,* 18, p. 297 (1994).
22. H. Takeda and J.R. Mehaffey, "WALL2D: A Model for Predicting Heat Transfer Through Wood-Stud Walls Exposed to Fire," *Fire and Materials,* 22, p. 133 (1998).
23. H. Takeda and S. Kouchleva, "A Model to Predict Fire Resistance of Wood-Framed Floor/Ceiling Assemblies," in *Proceedings of the 7th International Conference on Fire and Materials,* Interscience Communication Ltd., London, p. 507 (2001).
24. H. Takeda, "Model to Predict Fire Resistance of Non-Load Bearing Wood-Stud Walls," *Fire and Materials,* 27, p. 19 (2003).
25. J. König, "Fire Tests of Load-Carrying Timber Frame Assemblies Exposed to Standard and Parametric Fires," in *Proceedings of Fire and Materials '98 Conference,* Interscience Communications Ltd., London (1998).
26. P. Collier, "A Model for Predicting the Fire-Resisting Performance of Small-Scale Cavity Walls in Realistic Fires," *Fire Technology,* 32, 2, p. 120 (1996).
27. A.H. Buchanan and G.C. Thomas, "Predicting the Real Fire Performance of Light Timber Frame Construction," in *Proceedings of the 3rd Wood and Fire Safety Conference,* Technical University of Zvolen, Zvolen, Slovak Republic (1996).
28. P. Clancy, "Advances in Modeling Heat Transfer Through Wood Framed Walls in Fire," *Fire and Materials,* 25, p. 241 (2001).
29. S.A. Young and P. Clancy, "Structural Modelling of Light-Timber Framed Walls in Fire," *Fire Safety Journal,* 36, p. 241 (2001).
30. N. Bénichou, M.A. Sultan, and V.R. Kodur, "Fire Resistance Performance of Lightweight Framed Wall Assemblies: Effects of Various Parameters, Key Design Considerations and Numerical Modeling," in *Proceedings of Fire and Materials 2003 Conference,* Interscience Communications Ltd., London, p. 9 (2003).
31. A. Frangi, C. Erchinger, and M. Fontana, "Charring Model for Timber Frame Floor Assemblies with Void Cavities," *Fire Safety J*., 43, p. 551 (2008).
32. P. Clancy, "A Parametric Study on the Time-to-Failure of Wood Framed Walls in Fire," *Fire Technology,* 38, p. 243 (2002).
33. S.M. Cramer, O.M. Friday, R.H. White, and G. Sriprutkiat, "Mechanical Properties of Gypsum Board at Elevated Temperatures," in *Proceedings of Fire and Materials 2003 Conference,* Interscience Communications Ltd., London, p. 33 (2003).
34. N. Bénichou and M.A. Sultan. "Thermal Properties of Lightweight-Framed Construction Components at Elevated Temperatures," *Fire and Materials,* 29, p. 165 (2005).
35. S. Craft, G. Hadjispphocleous, B. Isgor, and J. Mehaffey, "Predicting the Fire Resistance of Light-Frame Wood Floor Assemblies," in *Proceedings of SiF'06: Fourth International Workshop Structures in Fire,* University of Aveiro, Aveiro, Portugal, p. 939 (2006).
36. G. Thomas, "Thermal Properties of Gypsum Plasterboard at High Temperatures," *Fire and Materials,* 26, p. 37 (2002).
37. R.H. White, "Use of Coatings to Improve Fire Resistance of Wood," in *ASTM STP826,* American Society for Testing and Materials, Philadelphia (1983).
38. R.H. White, "An Empirical Model for Predicting Performance of Fire-Resistive Coatings in Wood Construction," *Journal of Testing and Evaluation,* 14, p. 97 (1986).
39. L.R. Richardson and A.A. Cornelissen, "Fire-Resistant Coatings for Roof/Ceiling Deck Timbers," *Fire and Materials,* 11, p. 191 (1987).

40. Z. Huntierová and G. Wegener, "The Effects of Fire Retardants of the Behaviour of Solid Wood and Glulam Beams Loaded in Bending," in *Proceedings of the 3rd Wood and Fire Safety Conference,* Technical University of Zvolen, Zvolen, Slovak Republic (1996).
41. *Fire Resistance of Wood Structures,* Technical Research Centre of Finland, Helsinki (1980).
42. W.D. Gardner and D.R. Syme, "Charring of Glue-Laminated Australian-Grown Timber Species and the Effect of 13 mm Gypsum Plaster-Board on Their Charring," *Technical Report No. 5,* NSW Timber Advisory Council Ltd., Sydney, Australia (1991).
43. L.D. Tsantaridis, B.A.-L. Östman, and J. König, "Short Communication: Fire Protection of Wood by Different Gypsum Plasterboard," *Fire and Materials,* 23, p. 45 (1999).
44. L.R. Richardson and M. Batista, "Fire Resistance of Timber Decking for Heavy Timber Construction," *Fire and Materials,* 25, p. 21 (2001).
45. R.H. White, "Fire Resistance of Engineered Wood Rim Board Products," *Research Paper FPL-RP-610,* U.S. Department of Agriculture, Forest Service, Forest Products Laboratory, Madison, WI (2003).
46. R.H. White, "Fire Resistance of Wood Members with Directly Applied Protection," In: *Proc. Fire and Materials 2009 Conference*, Interscience Communications Limited, London, p. 535 (2009).
47. L. Osborne, C. Dagenais, and N. Bénichou. *Preliminary CLT Fire Resistance Testing Report, Project No. 301006155*, FPInnovations, Quebec City, Qc. (2012).
48. C. Dagenais, R.H. White, and K. Sumathipala "Chapter 8 – Fire Performance of Cross-Laminated Timber Assemblies," *Cross-Laminated Handbook – U.S. Edition*, FPInnovations, Quebec City, Qc. (2013).
49. A. Just, J. Schmid, and J. König, "Failure Times of Gypsum Boards," in *Proc. 6th International conference Structures in Fire*, DEStech Publications, Inc., Lancaster, PA, p. 593 (2010).
50. "Calculation of Fire Resistance of Glued Laminated Timbers," *Technical Note 7*, American Institute of Timber Construction, Englewood, CO (1996).
51. D. Drysdale, *An Introduction to Fire Dynamics,* 2nd ed., John Wiley and Sons, Chichester, UK (1998).
52. F.L. Browne, "Theories of the Combustion of Wood and Its Control—A Survey of the Literature," *Report No. 2136,* USDA Forest Service, Forest Product Laboratory, Madison, WI (1966).
53. E.L. Schaffer, "Review of Information Related to the Charring Rate of Wood," *Research Note FPL-145,* USDA Forest Service, Forest Product Laboratory, Madison, WI (1966).
54. E.L. Schaffer, "State of Structural Timber Fire Endurance," *Wood and Fiber,* 9, p. 145 (1977).
55. G.S. Hall, R.G. Saunders, R.T. Allcorn, P.E. Jackman, M.W. Hickey, and R. Fitt, *Fire Performance of Timber—A Literature Survey,* Timber Research and Development Association, High Wycombe, UK (1971).
56. S. Hadvig, *Charring of Wood in Building Fires,* Technical University of Denmark, Lyngby (1981).
57. V. Babrauskas, "Charring Rate of Wood as a Tool for Fire Investigations," *Fire Safety Journal,* 40, p. 528 (2005).
58. E.L. Schaffer, "Charring Rate of Selected Woods—Transverse to Grain," *Research Paper FPL 69,* USDA Forest Service, Forest Product Laboratory, Madison, WI (1967).
59. R.H. White and E.V. Nordheim, "Charring Rate of Wood for ASTM E119 Exposure," *Fire Technology,* 28, p. 5 (1992).
60. R.H. White, "Charring Rate of Composite Timber Products," in *Proceedings of the 3rd Wood and Fire Safety Conference,* Technical University of Zvolen, Zvolen, Slovak Republic, p. 353 (2000).
61. R.H. White, "Fire Resistance of Structural Composite Lumber Products," *Research Paper FPL 633,* USDA Forest Service, Forest Products Laboratory, Madison, WI (2006).
62. X.A. Frangi and M. Fontana, "Charring Rates and Temperature Profiles of Wood Sections," *Fire and Materials,* 27, p. 91 (2003).
63. P.B. Cachim and J-M. Franssen, "Comparison Between the Charring Rate Model and the Conductive Model of Eurocode 5," *Fire and Materials,* 33, p. 129 (2009).
64. Forest Products Laboratory, "Wood Handbook: Wood as an Engineering Material," *General Technical Report FPL-GTR-190*, USDA, Forest Service, Madison, WI. 508 p. (2010).
65. J. König, "Notional Versus One-Dimensional Charring Rates of Timber," in *Proceedings of the 8th World Conference on Timber Engineering,* Engineered Wood Products Association, Madison, WI (2004).
66. A.M. Kanury and D.J. Holve, "A Theoretical Analysis of the ASTM E119 Standard Fire Test of Building Construction and Materials," *NBS-GCR 76-50,* National Bureau of Standards, Washington, DC (1975).
67. B.J. Noren and B.A.-L. Ostman, "Contribution to Fire Resistance from Building Panels," in *Fire Safety Science—Proceedings of the First International Symposium,* Hemisphere, New York (1986).
68. E.L. Schaffer, "A Simplified Test for Adhesive Behavior in Wood Sections Exposed to Fire," *Research Note FPL-175,* USDA Forest Service, Forest Product Laboratory, Madison, WI (1968).
69. A. Frangi, M. Fontana, E. Hugi, and R. Jöbstl, "Experimental Analysis of Cross-Laminated Timber Panels in Fire," *Fire Safety J.*, 44, p. 1078 (2009).
70. E.L. Schaffer, "Effect of Fire-Retardant Impregnations on Wood Charring Rate," *Journal of Fire & Flammability,* 1, p. 96 (1974).
71. P.W.C. Lau, I. Van Zeeland, and R. White, "Modelling the Char Behaviour of Structural Timber," in *Proceedings of Fire and Materials '98*

Conference, Interscience Communications Ltd., London (1998).
72. C.P. Butler, "Notes on Charring Rates in Wood," *Fire Research Note No. 896,* Joint Fire Research Organization, Borehamwood, UK (1971).
73. H.C. Tran and R.H. White, "Burning Rate of Solid Wood Measured in a Heat Release Rate Calorimeter," *Fire and Materials,* 16, p. 197 (1992).
74. R.H. White and H.C. Tran, "Charring Rate of Wood Exposed to a Constant Flux," in *Proceedings of the 3rd Wood and Fire Safety Conference,* Technical University of Zvolen, Zvolen, Slovak Republic (1996).
75. T. Harada, "Charring of Wood with Thermal Radiation II," *Mokuzai Gakkaishi,* 42, 2, p. 194 (1996).
76. T. Harada, "Time to Ignition, Heat Release Rate and Fire Endurance Time of Wood in Cone Calorimeter Test," *Fire and Materials,* 25, p. 161 (2001).
77. E. Mikkola, "Charring of Wood Based Materials," in *Fire Safety Science—Proceedings of the Third International Symposium,* Elsevier Applied Science, London (1991).
78. E. Mikkola, "Charring of Wood," *Research Reports 689,* Technical Research Centre of Finland, Espoo (1990).
79. R.M. Nussbaum, "The Effect of Low Concentration Fire Retardant Impregnations on Wood Charring Rate and Char Yield," *Journal of Fire Sciences,* 6, p. 290 (1988).
80. P. Reszka and J.L. Torero, "In-Depth Temperature Measurements in Wood Exposed to Intense Radiant Energy," *Experimental Thermal and Fluid Science,* 32, p. 1405 (2008).
81. O. Pettersson, S.E. Magnusson, and J. Thor, "Fire Engineering Design of Steel Structures," *Publication 50,* Swedish Institute of Steel Construction, Stockholm, Sweden (1976).
82. A.H. Buchanan, *Structural Design for Fire Safety*, John Wiley and Sons, Brisbane, NZ (2001).
83. F.B. Olesen and J. König, "Tests on Glued Laminated Beams in Bending Exposed to Natural Fires," *Report No. I 9210061,* Swedish Institute for Wood Technology Research (Tratek), Stockholm, Sweden (1991).
84. M. Janssens, "Modeling of the Thermal Degradation of Structural Wood Members Exposed to Fire," *Fire and Materials,* 28, p. 199 (2004).
85. B. Moghtaderi, "The State-of-the-Art in Pyrolysis Modelling of Lignocellulosic Solid Fuels," *Fire and Materials,* 30, p. 1 (2006).
86. A.F. Roberts, "Problems Associated with the Theoretical Analysis of the Burning of Wood," in *Thirteenth Symposium (International) on Combustion,* Combustion Institute, Pittsburgh, PA (1971).
87. C.H. Bamford, J. Crank, and D.H. Malan, "The Combustion of Wood, Part I," *Proceedings of Cambridge Philosophical Society,* 46, p. 166 (1946).
88. P.H. Thomas, "On the Rate of Burning of Wood," *Fire Research Note No. 446,* Fire Research Station, Borehamwood, UK (1960).
89. H. Kung, "A Mathematical Model of Wood Pyrolysis," *Combustion and Flame,* 18, p. 185 (1972).
90. F. Tamanini, "A Numerical Model for One-Dimensional Heat Conduction with Pyrolysis in a Slab of Finite Thickness," in *Appendix A of Factory Mutual Research Corporation Report No. 21011.7,* Factory Mutual Research Corporation, Norwood, MA (1976).
91. A. Atreya, "Pyrolysis: Ignition and Fire Spread on Horizontal Surfaces of Wood," Ph.D. Dissertation, Harvard University, Cambridge (1983).
92. R.H. White and E.L. Schaffer, "Application of CMA Program to Wood Charring," *Fire Technology,* 14, p. 279 (1978).
93. W.J. Parker, "Prediction of the Heat Release Rate of Douglas Fir," in *Fire Safety Science—Proceedings of the Second International Symposium,* Hemisphere, New York (1989).
94. W.J. Parker, "Wood Materials (a) Prediction of the Heat Release Rate from Basic Measurements," in *Heat Release in Fires,* Elsevier Applied Science, London, p. 333 (1992).
95. R.H. White and E.L. Schaffer, "Transient Moisture Gradient in Fire-Exposed Wood Slab," *Wood and Fiber,* 13, p. 17 (1981).
96. B. Fredlund, "Modelling of Heat and Mass Transfer in Wood Structures during Fire," *Fire Safety Journal,* 20, p. 39 (1993).
97. K.M. Bryden, K.W. Ragland, and C.J. Rutland, "Modeling Thermally Thick Pyrolysis of Wood," *Biomass and Bioenergy,* 22, p. 41 (2002).
98. F.S. Costa and D. Sandberg, "Mathematical Model of a Smoldering Log," *Combustion and Flame,* 139, p. 227 (2004).
99. J.A. Havens, "Thermal Decomposition of Wood," Ph.D. Dissertation, University of Oklahoma, Norman (1969).
100. R.M. Knudson and A.P. Schniewind, "Performance of Structural Wood Members Exposed to Fire," *Forest Products Journal,* 25, p. 23 (1975).
101. E.J. Kansa, H.E. Perlee, and R.F. Chaiken, "Mathematical Model of Wood Pyrolysis Including Internal Forced Convection," *Combustion and Flame,* 29, p. 311 (1977).
102. S. Hadvig and O.R. Paulsen, "One-Dimensional Charring Rates in Wood," *Journal of Fire & Flammability,* 1, p. 433 (1976).
103. E.R. Tinney, "The Combustion of Wood Dowels in Heated Air," in *Tenth Symposium (International) on Combustion,* Combustion Institute, Pittsburgh, PA (1965).
104. B.L. Badders, J.R. Mehaffey, and L.R. Richardson, "Using Commercial FEA Software Packages to Model the Fire Performance of Exposed Glulam Beams," in *Proceedings of SiF'06: Fourth International Workshop Structures in Fire,* University of Aveiro, Aveiro, Portugal, p. 931 (2006).
105. M. Janssens, "Eurocode 5 Advanced Method Predictions of Glulam Beam Fire Test Performance,"

in *Proceedings of Fire and Materials 2011 Conference*, Interscience Communications Ltd., London, p. 427 (2011).
106. M. Janssens, "Thermo-Physical Properties for Wood Pyrolysis Models," in *Proceedings of Pacific Timber Engineering Conference,* Timber Research and Development Advisory Council, Fortitude Valley MAC, Queensland, Australia (1994).
107. M. Janssens and B. Douglas, Chapter 7, "Wood and Wood Products," in *Handbook of Building Materials for Fire Protection,* McGraw-Hill, New York (2004).
108. E.L. Schaffer, C.M. Marx, D.A. Bender, and F.E. Woeste, "Strength Validation and Fire Endurance of Glued-Laminated Timber Beams," *Research Paper FPL 467,* USDA Forest Service, Forest Product Laboratory, Madison, WI (1986).
109. E.L. Schaffer, "Structural Fire Design: Wood," *Research Paper FPL 450,* USDA Forest Service, Forest Product Laboratory, Madison, WI (1984).
110. M.L. Janssens and R.H. White, "Short Communication: Temperature Profiles in Wood Members Exposed to Fire," *Fire and Materials,* 18, p. 263 (1994).
111. C. Imaizumi, "Stability in Fire of Protected and Unprotected Glued Laminated Beams," *Norsk Skogind,* 16, p. 140 (1962).
112. T.T. Lie (ed.), *Structural Fire Protection,* American Society of Civil Engineers, New York (1992).
113. K. Odeen, "Fire Resistance of Glued Laminated Timber Structures," in *Fire and Structural Use of Timber in Buildings,* Her Majesty's Stationery Office, London (1970).
114. P.W.C. Lau and J.D. Barrett, "Factors Affecting Reliability of Light-Framing Wood Members Exposed to Fire—A Critical Review," *Fire and Materials,* 18, p. 339 (1994).
115. C. Meyer-Ottens, "Junctions in Wood Structures—Total Construction," in *Three Decades of Structural Fire Safety,* Building Research Establishment, Fire Research Station, Borehamwood, UK (1983).
116. O. Pettersson, "Fire Design of Wood Structures," in *Three Decades of Structural Fire Safety,* Building Research Establishment, Borehamwood, UK (1983).
117. B. Barthelemy and J. Kruppa, *Resistance au Leu des Structures,* Editions Eyrolles, Paris (1978).
118. G.M. Kirpichenkov and I.G. Romanenkow, "Basic Principles of Calculating Fire Resistance of Timber Structures," *NBSIR 80-2188,* National Bureau of Standards, Washington, DC, pp. 181–189 (1980).
119. K. Odeen, "Fire Resistance of Wood Structures," *Fire Technology,* 21, p. 34 (1985).
120. F.E. Woeste and E.L. Schaffer, "Second Moment Reliability Analysis of Fire Exposed Wood Joist Floor Assemblies," *Fire and Materials,* 3, p. 126 (1979).
121. F.E. Woeste and E.L. Schaffer, "Reliability Analysis of Fire Exposed Light-Frame Wood Floor Assemblies," *Research Paper FPL 386,* USDA Forest Service, Forest Product Laboratory, Madison, WI (1981).
122. R.H. White, E.L. Schaffer, and F.E. Woeste, "Replicate Fire Endurance Tests of an Unprotected Wood Joist Floor Assembly," *Wood and Fiber,* 16, p. 374 (1984).
123. E.L. Schaffer and R.H. White, "Fire Endurance Model Validation by Unprotected Joist Floor Fire Testing," in *Proceedings of 1988 International Conference on Timber Engineering,* Forest Products Research Society, Madison, WI (1988).
124. E.L. Schaffer and F.E. Woeste, "Reliability Analysis of a Fire-Exposed Unprotected Floor Trusses," in *Proceedings, Metal Plate Wood Truss Conference,* Forest Products Research Society, Madison, WI (1985).
125. R.H. White, S.M. Cramer, and D. Shrestha, "Fire Endurance Model for a Metal-Plate-Connected Wood Truss," *Research Paper FPL 522,* USDA Forest Service, Forest Products Laboratory, Madison, WI (1993).
126. J. König and B. Källsner, "Modeling Resistance of Wooden I-Joists Exposed to Fire," in *Proceedings of SiF'06: Fourth International Workshop Structures in Fire,* University of Aveiro, Aveiro, Portugal, p. 951 (2006).
127. J. König, "Fire Exposed Simply Supported Wooden I-Joists in Floor Assemblies," *SP Report 2006:44,* SP National Testing and Research Institute, Stockholm, Sweden (2006).
128. J. Schmid, J. König, and A. Just, "The Reduced Cross-Section Method for the Design of Timber Structures Exposed to Fire - Background, Limitations, and New Developments," *Structural Engineering International*, 22, 4, p. 514 (2012).
129. D.A. Bender, F.E. Woeste, E.L. Schaffer, and C.M. Marx, "Reliability Formulation for the Strength and Fire Endurance of Glued-Laminated Beams," *Research Paper FPL 460,* USDA Forest Service, Forest Prod. Laboratory, Madison, WI (1985).
130. American Wood Council, "Calculating the Fire Resistance of Exposed Wood Members," *Technical Report 10*, American Forest & Paper Association, Washington, DC (2003).
131. B.K. Douglas, "Calculating the Fire Resistance of Exposed Wood Members," *Wood Design Focus,* 9, 3, p. 15 (1999).
132. M. Klippel, J. Schmid, and A. Frangi, "The Reduced Cross-Section Method for Timber Members Subjected to Compression, Tension and Bending in Fire," in *Proc. CIB-18 Meeting 45*, Paper 45-15-1. Ingenieurholzbau und Baukonstruktionen, Karlsruhe Institute of Technology, Karlsruhe, Germany (2012)
133. T.G. Williamson, "Rehabilitation of Fire-Damaged Timber—The Filene Center," in *Evaluation, Maintenance, and Upgrading of Wood Structures,* American Society of Civil Engineers, New York (1982).

134. A. Frangi, M. Knobloch, and M. Fontana, "Fire Design of Timber Slabs Made of Hollow Core Elements," *Engineering Structures*, 31, p. 150 (2009).
135. M.L. Janssens, "A Method for Calculating the Fire Resistance of Exposed Timber Decks," in *Fire Safety Science—Proceedings of the Fifth International Symposium,* International Association for Fire Safety Science, Boston (1997).
136. R.H. White, "Fire Resistance of Exposed Wood Members," in *Proceedings of the 5th Wood and Fire Safety Conference,* Technical University of Zvolen, Zvolen, Slovak Republic, p. 337 (2004).
137. O. Carling, "Fire Resistance of Joint Details in Loadbearing Timber Construction—A Literature Survey," *Study Report No. 18,* Building Research Association of New Zealand, Judgeford, NZ (1989).
138. J. König and M. Fontana, "The Performance of Timber Connections in Fire-Test Results and Rules of Eurocode 5," in *Proceedings of International Rilem Symposium "Joints in Timber Structures,"* University of Stuttgart, Germany (Sept. 2001).
139. P. Moss, A. Buchanan, M. Fragiacomo, and C. Austruy, "Experimental Testing and Analytical Prediction of the Behavior of Timber Bolted Connections Subjected to Fire," *Fire Technology*, 46, p. 129 (2010).
140. P. Racher, K. Laplanche, D. Dhima, and A. Bouchaïr, "Thermo-Mechanical Analysis of the Fire Performance of Dowelled Timber Connection," *Engineering Structures*, 32, p. 1148 (2010).
141. L. Peng, G. Hadjisophocleous, J. Mehaffey, M. Mohammad, and L. Lu, "Calculating Fire Resistance of Timber Connections," in *Proceedings of Fire and Materials 2011 Conference*, Interscience Communications Ltd., London, p. 455 (2011).
142. B. Yeh and R. Brooks, "Evaluation of Adhesive Performance at Elevated Temperatures for Engineered Wood Products," in *Proceedings of the 9th World Conference on Timber Engineering,* Oregon State University, Corvallis (2006).
143. A. Frangi, M. Fontana, and A. Mischler, "Shear Behavior of Bond Lines in Glued Laminated Timber Beams at High Temperatures," *Wood Sci Technol*., 38, p. 119 (2004).
144. B. Källander and P. Lind, "Strength Properties of Wood Adhesives After Exposure to Fire," in *Proceedings of Wood Adhesives 2005,* Forest Products Society, Madison, WI, p. 211 (2006).
145. J. König, J. Norén, and M. Sterley, "Effect of Adhesives on Finger Joint Performance in Fire," in *Proc. CIB W18 Meeting 41*, Lehrstuhl für Ingenieurholzbzu, University of Karlsruhe, Karlsruhe, Germany (2008).
146. A. Frangi, M. Bertocchi, S. Clauß, and P. Niemz, "Mechanical Behavior of Finger Joints at Elevated Temperatures," *Wood Sci. Technol*., 46, p. 793, (2012).
147. E.G. King and R.W. Glowinski, "A Rationalized Model for Calculating the Fire Endurance of Wood Beams," *Forest Products Journal,* 38, 10, p. 31 (1988).
148. Lee-Gun Kim and Jun-Jae Lee, "Studies on Prediction about Behavior of Wood Beam Under Standard Fire Condition," *Mokchae Konghak,* 23, 4, p. 10 (1995).
149. M. Tavakkol-Khah and W. Klingsch, "Calculation Model for Predicting Fire Resistance Time of Timber Members," in *Fire Safety Science—Proceedings of the Fifth International Symposium,* International Association for Fire Safety Science, Boston (1997).
150. S. Schnabl, I. Planinc, G. Turk, and S. Srpčič, "Fire Analysis of Timber Composite Beams with Interlayer Slip," *Fire Safety Journal*, 44, p. 770 (2009).
151. M. Fragiacomo, A. Menis, P.J. Moss, I. Clemente, A.H. Buchanan, and B. DeNicolo, "Predicting the Fire Resistance of Timber Members Loaded in Tension," *Fire and Materials*, published on-line, DOI: 10.1002/fam.2117, (2012).
152. M.H. Do and G.S. Springer, "Mass Loss of and Temperature Distribution in Southern Pine and Douglas Fir in the Range 100 to 800C," *Journal of Fire Sciences,* 1, p. 271 (1983).
153. M.H. Do and G.S. Springer, "Model for Predicting Changes in the Strengths and Moduli of Timber Exposed to Elevated Temperatures," *Journal of Fire Sciences,* 1, p. 285 (1983).
154. M.H. Do and G.S. Springer, "Failure Time of Loaded Wooden Beams During Fire," *Journal of Fire Sciences,* 1, p. 297 (1983).
155. N. Bénichou. "Predicting the Structural Fire Performance of Solid Wood-Framed Floor Assemblies," in *Proceedings of SiF'06: Fourth International Workshop Structures in Fire,* University of Aveiro, Aveiro, Portugal, p. 909 (2006).
156. I.M. VanZeeland, J.J. Salinas, and J.R. Mehaffey, "Compressive Strength of Lumber at High Temperatures," *Fire and Materials,* 29, p. 71 (2005).
157. C.C. Gerhards, "Effect of Moisture Content and Temperature on Mechanical Properties of Wood: An Analysis of Immediate Effects," *Wood and Fiber Science,* 14, p. 4 (1982).
158. F.C. Beall, "Effect of Temperature on the Structural Uses of Wood and Wood Products," in *Structural Use of Wood in Adverse Environments,* Van Nostrand Reinhold, New York (1982).
159. B.A.-L. Ostman, "Wood Tensile Strength at Temperature and Moisture Contents Simulating Fire Conditions," *Wood Science and Technology,* 19, p. 103 (1985).
160. P.W. Lau and J.D. Barrett, "Modeling Tension Strength Behaviour of Structural Lumber Exposed to Elevated Temperatures," in *Fire Safety Science—Proceedings of the Fifth International Symposium,* International Association for Fire Safety Science, Boston (1997).

161. S.A. Young and P. Clancy, "Compression Mechanical Properties of Wood at Temperatures Simulating Fire Conditions," *Fire and Materials,* 25, p. 83 (2001).
162. F.J. Francisco and P. Clancy, "Compression Properties of Wood as Function of Moisture, Stress and Temperature," *Fire and Materials,* 28, p. 209 (2004).
163. J. König, "Effective Thermal Actions and Thermal Properties of Timber Members in Natural Fires," *Fire and Materials,* 30, p. 51 (2006).
164. B.Y. Lattimer, J. Ouellette, and J. Trelles, "Measuring Properties for Material Decomposition Modeling," *Fire and Materials*, 35, p. 1 (2010).

Robert H. White was a wood scientist at the USDA, Forest Service, Forest Products Laboratory. His research in a wide range of topics pertaining to fire performance of forest products have included studies on wood charring and fire resistance of wood assemblies.

Egress Concepts and Design Approaches

56

Richard W. Bukowski and Jeffrey S. Tubbs

Introduction

Among the most important concepts in fire safety in buildings is to manage those potentially exposed to the fire and its effects, either by protecting them in place or by moving them to a place of safety. Protected spaces and paths of travel needed to accomplish this are the egress components, systems and procedures that are discussed in this chapter. The chapter presents an overview of considerations, concepts, methods, and strategies utilized globally for emergency egress system design. Approaches to full or partial evacuation using stairs or elevators, egress for people with disabilities, protect-in-place strategies, and alternatives to evacuation, are presented. Prescriptive and performance-based approaches are discussed and strategies for selecting specific systems are summarized.

Additional information on performance-based evacuation modeling, occupant movement simulation, human behavior during emergencies, and occupant and scenario factors is detailed in other chapters.

Chapter 57 presents methods for considering occupant factors within designs.

Chapters 61 and 63 present methods for assessing tenability and criteria for use in engineering studies.

Chapter 58 presents human behavior concepts and theory and how data is collected.

Chapter 64 presents studies of flow rate and walking speed applicable for use in engineering studies.

Chapters 59 and 60 present evacuation calculation and simulation methods and techniques.

The purpose of this chapter is to present the historical evolution of emergency egress provisions in public buildings and the varying approaches utilized to facilitate egress along with their scientific basis. By understanding the scientific basis the engineer should understand the intended performance in the context of performance based design and alternate approaches utilized to address the special needs of specific occupants or unique facilities.

The chapter begins with the history of emergency egress systems including the scientific basis for the 44 in. (1100 mm) egress stair width, the concept of exit capacity used in US Codes, flow rate, fire escapes and the 7/11 stair geometry. This should help to understand the goals and objectives of the codes and the levels of performance anticipated from the common prescriptive approaches to egress system arrangements. Next, a discussion of common strategies that address specific objectives and the expanding list of egress system components are discussed in their context of use along with related systems that notify people of the need to

R.W. Bukowski, P.E., FSFPE (✉)
Jensen Hughes, 2001 N Main St #510, Walnut Creek, CA 94597

J.S. Tubbs, P.E., FSFPE
Arup, 955 Massachusetts Avenue, Fourth Floor, Cambridge, MA 02139

M.J. Hurley (ed.), *SFPE Handbook of Fire Protection Engineering*,
DOI 10.1007/978-1-4939-2565-0_56, © Society of Fire Protection Engineers 2016

take action and that provide route guidance during the action. Finally, performance-based design concepts that are frequently used to justify alternative egress system designs in unique or constrained buildings are presented.

Historical Perspective

For many years, buildings were short enough that stairs provided for access were sufficient for safe and rapid egress for most occupants in the event of fire. Until passage of the Americans with Disabilities Act (PL101-336) in 1990, buildings were rarely accessible, and emergency egress of people with disabilities was not a national priority. Even in single stair (mostly residential) buildings, experience indicated that this stair was sufficient for fire egress as long as the fire did not expose or block access to the stair. Fire resistant apartment doors shielded the stair from most fires and exterior fire escapes provided a second egress path beginning early in the Twentieth Century. The 1854 invention of the elevator safety brake enabled the passenger elevator. This system is credited with facilitating increases in building height beyond six floors and the first so-called skyscraper in Chicago in 1885 [1].

Model building regulations in the US started with the National Building Code published by the National Board of Fire Underwriters (NBFU) following the Great Fire of Boston in 1872. Property loss claims from this fire resulted in more than 70 insurance companies being driven into bankruptcy, causing insurance interests to form the NBFU and to develop building fire safety rules aimed at reducing property losses in fires. These rules became the first model building code, called the National Building Code (NBC), first published in 1905. The NBFU was able to tie compliance with their rules to their Municipal Grading Schedule on which insurance rates are based. Cities needed favorable rates to attract investment, so they were motivated to adopt regulations consistent with the National Building Code. The first edition of the NBC required exit stairs to have a minimum width of 20 in. (510 mm) [2].

Origins of the 44 in. Exit Stair in the US

In the 1913 National Fire Protection Association (NFPA) Proceedings, the Committee on Fireproof (later, Fire-Resistive) Construction reported a number of recommendations, including a minimum unobstructed width of 44 in (1100 mm) exit stairs. Handrails were permitted to intrude not more than 3.5 in. (89 mm) on each side. That same year, NFPA formed their Committee on Safety to Life. That committee's first activity was to conduct a comprehensive review of fire safety issues and regulatory approaches found in building codes and local regulations in several, geographically diverse cities. At the meeting [1], they reported that [3],

> . . . existing laws are exceedingly deficient in this very important matter of egress. A number of states report frankly that they have no real legislation upon the subject, many City Ordinances are of the most indefinite character, and in some the matter is simply left to the discretion of the fire department or other officials.

In the 1914 NFPA Proceedings section on egress, the Safety to Life Committee cites the 1913 NFPA Annual Meeting report of the Committee on Fire-Resistive Construction in which they said was presented [1].

> . . . a splendid set of specifications for the construction of a standard building. Egress received detailed attention;—specifications for smokeproof towers, for stairs, for horizontal exits, and for the capacity of vertical and horizontal exits were included.

The committee also cites the 1913 laws of the New York State Department of Labor which, ". . . as regards fundamentals appear to agree entirely with the requirements of our Committee . . .". Extracting from the referenced New York statute, they cite [1],

(a) For buildings erected in the future, a minimum of 22 in. (550 mm) of stair width shall be required for not to exceed 14 persons on any one floor.
(b) On buildings already erected this figure is reduced to 18 in. (450 mm) as a minimum.
(c) A 44-in. (1100 mm) stair in new buildings permits 28 persons to be housed on each floor above the first one.

(d) In arriving at this decision the idea has been that all of the persons on all floors shall be able to remain in the stair tower without any movement, a person requiring about 22 in. (550 mm) in width, and one person to stand on every other stair.

This committee further characterizes the New York laws' stair geometry (7.75 in. riser height by 10 in. tread) as "good", and that they recommend a minimum 44 in. wide stair for new buildings as this width is "sufficient to prevent three persons from forming an arch and blocking traffic" [4].

Exit Capacity

The above explains why the US designs exits for "capacity" and why the capacity is based on the population of a single floor. The exit is sized to "store" people, motionless within the protected exit enclosure, such that the population of one floor will fit entirely within the stair between that floor and the next floor below, with each person in a space 22 in. wide and standing on every other step.

This philosophy was recognized in the 1935 National Bureau of Standards (NBS now NIST) publication, *Design and Construction of Building Exits* [5]. Developed by the Department of Commerce Building Code Committee, this report included survey data on exit sizes and configurations drawn from eight cities chosen, "... with a view to covering places varying in size and sufficiently distributed to give a fair cross section of building construction." The survey included population counts on typical floors and compiled data on movement of people in buildings, as well as railway terminals (particularly at rush hour which was considered to be similar to emergency movement in a fire) and schools. Studies of the flow of occupants in government buildings during fire drills and of the general public exiting railway terminals at rush hour were conducted, and the data resulted in discharge rates for stairs (as a function of width and stair geometry), ramps, and doorways.

The data was used to suggest possible approaches to calculating the minimum width of exits necessary to provide for occupant safety. These included five, proposed methods (text paraphrased from the 1935 NBS report):

1. Capacity Method, which is based on the concept of storing occupants on the stairs within a protected stair enclosure, and allowing for the subsequent safe and orderly evacuation of the building. It recognized that travel down a long series of stairs in high buildings is exhausting even to normal persons. Objections of building owners over the loss of rentable space are noted as well as the comment by some authorities that people may not stand still in stairways, even in relatively taller buildings, preferring instead to proceed to the street.
2. Flow Method, which is based on the concept that people will move down the stairs at a typical flow, assumed to be 45 persons per 22 in. unit of width per minute and 60 persons per minute through doorways. It is stated that this method is usually coupled with an assumed time in which it is safe to exit the building and that this method calls for considerably less stairway width than the capacity method. However, the committee felt that it would be limited to a few occupancies and to buildings of low to moderate height since continuous movement down stairways in relatively taller buildings cannot be expected without serious effects on some occupants.
3. Combined Method suggests the flow method for lower buildings shifting to the capacity method for taller buildings also accounting for type of construction and use. Once again NBS pointed out that taller buildings would require a disproportionate amount of space devoted to stairways as compared with useable floor area.
4. Probability Method considers only the population of the six most densely populated floors since it was considered improbable that simultaneous evacuation of all floors of a large building would be needed. This is the first time that phased evacuation, as currently practiced in tall buildings, was suggested.
5. Floor Area Method relates area to units of exit width needed as a function of construction type and use. As in the probability

method, simultaneous evacuation of all floors is not considered; however, the number of floors that were considered to simultaneously evacuate varied with occupancy.

In the end, the 1935 report suggests that the needs of the vast majority of buildings can be met with the provision of two, two-unit-width (44 in. or 1100 mm) stairs. The capacity method, which includes occupants waiting within the exit enclosure, is appropriate for shorter buildings with a gradual shift to the flow method for taller buildings where people will be less comfortable waiting in the stair. For tall buildings the floor area method has some application as these are of fire resistive construction and only those near the floor of fire origin are initially at risk. NBS suggests half of the floors should be considered with the floor area method.

Early Thoughts on Elevators as a Means of Egress

Both the 1914 NFPA Proceedings [1] and the 1935 NBS report [5] discuss the possible use of elevators for egress from tall buildings. In 1914 the Committee on Safety to Life expressed the opinion that, "... elevator shafts properly enclosed and with openings adequately protected have decided value from an escape standpoint, and are absolutely necessary in high buildings." They cited as "... loss of life possibilities in many modern so-called fireproof buildings ..." the common practice of unenclosed stair and elevator shafts that might permit a fire in lower stories to, "... spread with unexpected speed ..." which "... could result in a loss of life which would stagger the civilized world." The Committee called for enclosing elevator shafts, improving the fire resisting powers of elevator doors, ensuring the integrity of the electric current applied to elevators, and "drilling" elevator operators in emergency procedures, including that persons in the upper stories "shall first be taken to the ground."

The 1935 NBS report discusses a credit for elevators against required aggregate exit width. They discount automatic elevators as unsuitable, as their "...capacity and rate of speed is not great," and "... they are not subject to a single will as in the case of an elevator operator, but to demands from many tenants." While there was a suggestion in the formulae of the flow method that five elevators might be equal to a single unit of exit stair width for some construction types and use, in the end they concluded that the uncertainties were such that no direct credit be given for elevators but to recognize their availability in high buildings.

Early Regulatory Approaches in the US

The 1914 report of the Committee on Safety to Life included detailed recommendations for the design and arrangement of egress stairs and fire escapes with the intent that this material would be incorporated by others into building regulations. No code or standard was produced by the Committee until the 1927 publication of the first edition of the NFPA Building Exits Code (NFPA 101-T) [6] which later became the Life Safety Code.

The 1927 edition of NFPA 101-T defined stairs as Class A, B, or C. Class A stairs were the main stair of a newly-constructed Assembly occupancy, and were 44 in. (1100 mm) wide (handrails could intrude not more than 3.5 in. (89 mm) on each side) with a rise of not more than 7 in. (178 mm) and a tread of not less than 10.5 in. (267 mm). Class B stairs were for new construction of all stairs not required to be Class A, and for existing construction where Class A stairs would be required if new. Class B stairs were the same width as Class A but the rise was permitted to be not more than 7.75 in. (197 mm) with a tread of not less than 9.5 in. (241 mm). Class C stairs covered existing stairs in existing buildings and were at least 36 in. (900 mm) wide (not less than 32 in. or 810 mm between handrails, but stairs less than 44 in. (1100 mm) wide only required a handrail on one side). Occupant load on a floor dictates the capacity (total width of stairs in number of

22 in. (550 mm) units) to be provided in a minimum of two stairs located "as remote as practical."

The 1935 NBS report included recommended code language in an appendix that did not follow any of the five methods for calculating minimum exit widths discussed previously. They explained that tentative requirements were drawn up and compared against the results of the field studies. Eventually a consensus of the Committee was reached and was presented in the recommended code language.

The suggested code requirements largely followed the capacity method for at least two stairs of two 22 in. (550 mm) units of exit width each, with the floor area method used, by means of occupancy load factors consistent with those found in current regulations, to determine aggregate width. No suggestions of maximum egress time, including no references to fire resistance times associated with construction types, building height, and use, that might facilitate the use of the flow method, and no mention of partial evacuation of tall buildings as discussed in the probability and floor area methods was made. These recommendations were consistent with those in the 1927 edition of NFPA 101-T, but this is not surprising since the Committee on Safety to Life was well represented on the NBS Committee. The requirements suggested in the NBS report and NFPA 101 were generally adopted in the model codes and building regulations throughout the US until the mid-1980s when the 22 in. (550 mm) unit of exit width was abandoned for assessing exit capacity in units of people per inch, but retaining the 44 in. (1100 mm) minimum width. This method provides similar results for aggregate exit width but provides more capacity credit for fractions of the 22 in. (550 mm) unit.

Early Scientific Studies of Flow Rate

The 1935 NBS report [5] included field surveys of discharge rates down exit stairs and through doors for various government buildings during drills and for subway and rail terminals at rush hours. The data collected was discussed by the Committee and a consensus reached that there was a clear correlation between width and flow. The committee agreed that "... rates of 45 persons per 22-in. unit per minute for travel down stairways, and 60 persons per 22-in. unit per minute through doorways, which had been in use on the basis of earlier observations, were sufficiently confirmed to warrant their retention in connection with the requirements under development."

Almost from the start there were issues raised with the assumed flow rate on stairs of 45 persons per minute per 22 in. (550 mm) unit of exit width. Togawa [7] in Japan conducted research in the 1940s and 1950s, that showed for densities above one person per square meter (10 ft^2), flow rates decreased significantly. His data suggested a flow rate of 26 persons per minute per (22 in.) unit of exit width.

Pauls [8] has published extensively on this topic and continues to be the scientific conscience of stair design in the US codes. Pauls [8] and Fruin [9] both discussed the concept of effective width of a stair, which is generally 0.3 m (1 ft) narrower than the actual width due to the natural tendency of people to keep a distance from walls and handrails. Fruin further spoke of the personal space (buffer) around people that increases their effective space requirement. Pauls found that for people walking on stairs, their body sways from side to side and they desire sufficient space so that they do not make contact with the person beside them. Pauls work confirmed that of Togawa, finding flow rates in stairs at typical densities to be approximately 27 persons per minute per (22 in.) unit of exit width. Extensive studies in Russia also confirmed the effects of density on flow rates and confirmed the values suggested by Pauls [8] and Togawa [10].

Chapter 64 details flow rate and walking speed studies applicable for use in engineering simulation and studies.

Early Scientific Studies of Exit Width

The current 44 in. (1100 mm) minimum exit stair width is intended to support two, 22 in. (550 mm) queues of occupants either standing still (capacity method) or moving down the stair. This also allows counterflow, which occurs when a single queue of occupants moving down are passed by firefighters or other responders moving up. The 22 in. (550 mm) dimension for the width of a person was offered in 1914, originating from soldiers standing in a line [3].

Challenges to the adequacy of the 22 in. (550 mm) dimension include the need to provide for body sway as people move down the stair [8], and the need to allow for some personal space [9,10]. Recently, the adequacy of the basic 22 in. dimension has been questioned in light of the increasing size and weight of the typical person, especially in the US. The 22 in. dimension refers to the width of a person at the shoulders, which is assumed to be the widest part. Predtechenskii and Milinskii suggest that 4 in. (100 mm) be added to each side to allow for a personal buffer except that for low obstructions (like handrails) the additional space is not needed since one's shoulders are at a higher level and will extend over the obstruction.

From anthropometric data for modern Americans, the width at the hip is approaching the width at the shoulder, and it seems that this exception may no longer be valid. Thus, with the shoulder width of the 97.5th percentile adult male reaching 20 in. (510 mm) [11] and allowing the 4 in. on each side for handrail and personal space, the new unit of exit width should be 28 in. (700 mm) and the minimum stair width 56 in. (1400 mm), see Fig. 56.1.

Arguably the most comprehensive studies of movement on stairs were conducted by Templer [12], beginning with his doctoral research [13] and including work at NBS in the 1980s. Templer observed the movement of many individuals up and down stairs of varying width and tread geometry, tabulating variables ranging from quantitative (speed, number of stumbles) to qualitative (perceived comfort). From this work Templer concluded that the minimum width of an egress stair should be 56 in. (1400 mm).

Scientific Studies of Tread Geometry

One of the earliest studies of stair geometry was conducted by a seventeenth century architect in France named Francois Blondel [14]. Blondel was primarily interested in comfort rather than safety and observed that the main stairs of classic cathedrals were comfortable to use and accommodated large numbers of people attending services. He made measurements and found that the ratio of stair height to tread depth was a constant, and he related this dimension to the length of the human gait. His formula was $2R + G = 24$ in., where R is the rise and G is the going (or run). Templer [15] adjusted Blondel's formula for the use of the old (pre French Revolution) inch and a modern gait more like 28 in. (710 mm) and arrived at the formula, $2R + G = 710\,\text{mm}$. The 7 in. rise, 11 in. run stair geometry commonly required in US codes meets the relation $2R + G = 635\,\text{mm}$.

Templer [15] summarizes a number of research studies of stair geometry and safety. Many such studies were conducted by observing people moving up or down stairs in buildings. Observations in subway or train stations at rush hours provided data for higher population densities. A few studies were conducted in laboratory settings on specially constructed stair sections where the geometries and stair angle could be varied systematically. Templer himself conducted several of these studies, including some at NBS.

Most of the studies reviewed concluded that the measure of Total Energy Cost per Meter Rise [15] is a useful metric for the evaluation of stair design for normal use and comfort; however, stair safety is more closely related to the likelihood of missteps which is a function of how the stair relates to the human gait. In both cases, the effect is different for ascent and descent, with descent being more hazardous.

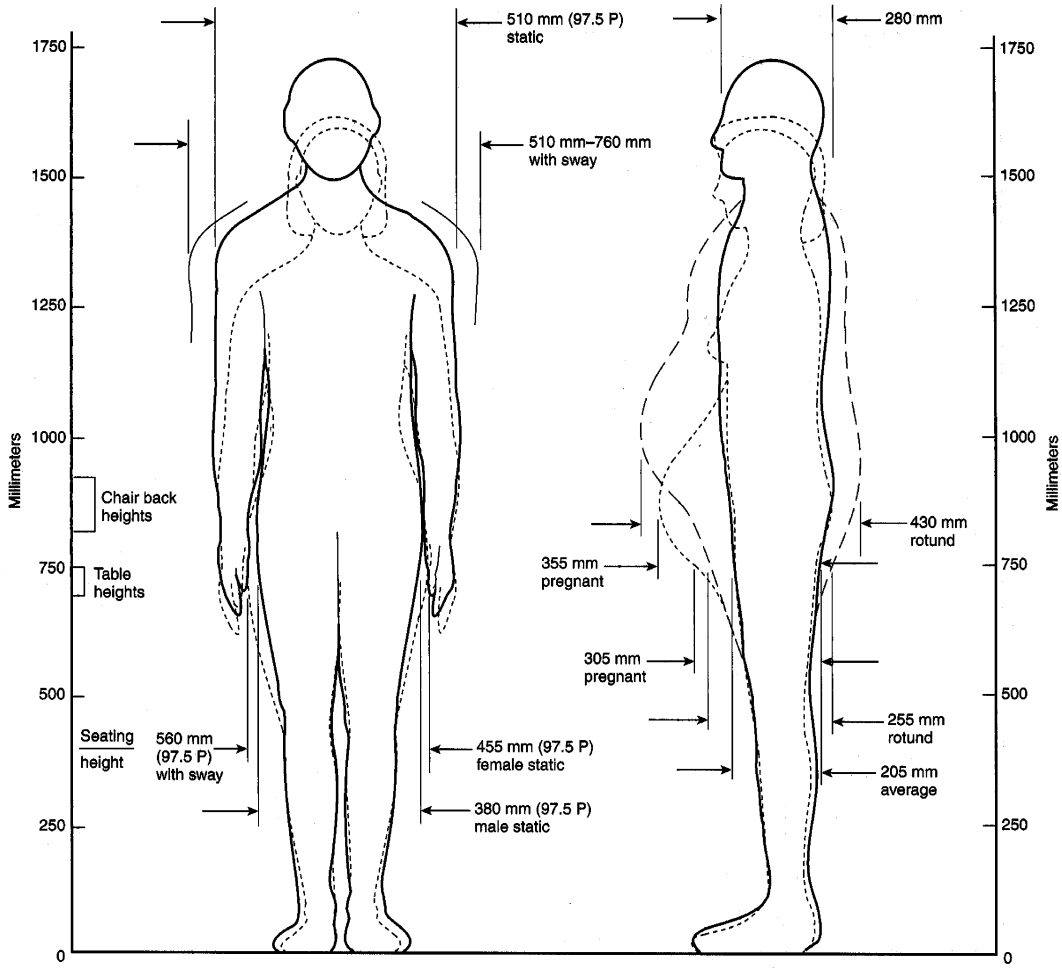

Fig. 56.1 Anthropometric data (in mm.) for adults; males and females of average, 50th percentile, size; some dimensions apply to very large, 97.5 percentile (97.5 P), adults (Reprinted with permission from NFPA 101®-2012, *Life Safety Code*®, Copyright © 2011, National Fire Protection Association, Quincy, MA). This reprinted material is not the complete and official position of the NFPA on the referenced subject, which is represented only by the standard in its entirety

When ascending a stair, a person walks on the ball of the foot with less of the foot placed on the step. Shorter treads (goings) and higher risers produce fewer missteps. When descending a stair, the heel and most of the foot needs to be placed on the tread. Too much of the front of the foot extending over the nosing results in rotation of the foot and a fall, or a distorted gait while trying to place more of the foot on the tread. Tread depths of at least 11 in. (280 mm) are recommended to accommodate the 95th percentile foot, but considering only gait and accident history, treads (goings) of at least 9 in. (230 mm) are required. Riser heights of 6.3–7.2 in. (160–183 mm) had the fewest missteps. Other dimensions apply to curved stairs [16].

Other factors relevant to stair safety include lighting, slip resistance, single steps (most codes prohibit flights of fewer than three steps), handrails, and inability to detect the edge of the tread due to lack of visual contrast.

Fire Escapes

As with so many building code provisions relating to fire safety, requirements for exterior, non-combustible fire escapes began with tragedy. The mid-nineteenth century saw significant numbers of European immigrants settling in New York City, mostly in tenement buildings. The term generally refers to a substandard multi-family dwelling in the urban core, frequently old and occupied by the poor. These wood-frame, six-story buildings (six stories was considered the practical height limit before elevators) were crowded together in ethnic neighborhoods, generally home to several dozen families each crammed into one or two rooms with the only access and egress by a single, narrow stairway. Doors to family living rooms were usually wood panel doors with little fire resistance and the buildings often had commercial space on the ground floor. Fires starting in the commercial space or in a tenant space would quickly burn through the thin door and race up the stair, cutting off egress and trapping occupants who perished in full view of the street crowds attracted by the fire [17].

After a particularly gruesome fire that killed ten women and children in 1860 [18], New York City passed its first egress regulation, Chapter 470, Section 25 of the New York City Acts, entitled,—An Act to Provide Against Unsafe Buildings in the City of New York. This law applied to buildings housing more than eight families and required a 'fire-proof' stair attached to an exterior wall in a fire-proof building with the stair separated from all living spaces by doors. In buildings that were not fire-proof, the law required fire-proof balconies on each story of the exterior of the building connected by fire-proof stairs with all rooms communicating with the balconies and separated by doors. Since fire-proof construction was far too costly for tenement buildings, iron fire escapes became ubiquitous throughout the city.

It is interesting to note that in 1867, the Tenement House Act was enacted that required existing buildings to be furnished with fire escapes; perhaps the first example of a requirement applicable to existing buildings [17]. However, subjective provisions made enforcement difficult and many buildings were exempted or were equipped with fire escapes that collapsed, were not accessible from all rooms, or exited to narrow spaces or enclosed courtyards. Tragic losses continued in buildings without or with inadequate fire escapes, leading to several amendments to the laws, including requirements in 1871 to maintain fire escapes, transfer of responsibility from the health department to the fire department in 1882 and to the building department in 1892. The 1871 legislation extended requirements for fire escapes to hotels and other public buildings including theaters, schools, factories and hospitals.

By the beginning of the twentieth century a New York Tenement Commission surveyed tenement laws in 27 US cities and found that nearly all had some sort of egress regulation requiring fire escapes but often the details were left to the discretion of inspectors. Many disastrous fires with high death counts were attributed to occupants being trapped by the fire on upper floors or fires blocking the single exit. Fires that attracted national attention such as the Brooklyn Theater in 1876 (294 fatalities) and Chicago's Iroquois Theater in 1903 (605 fatalities), Ohio's Lake View school in 1908 (170 fatalities), and the Fifth-Avenue Hotel in St. Louis (100 fatalities) led to fire escape regulations in most major cities and to NFPA's development of the Building Exits Code in 1927. The Triangle Shirtwaist Fire in 1911 (146 fatalities) had a fire escape that collapsed under the weight of too many workers, which contributed to the high death count [19].

Egress Strategies

Egress strategies provide systems and features to allow people to safely exit structures, reach a place of safety, or safely remain in place during emergency conditions. These strategies need to be aligned with and support the overall life safety

goals and objectives, and be developed in concert with the overall fire protection and life safety program. Strategies form the basis of design for egress and other supporting features. Effective egress strategies are appropriate to the facility size and complexity, and reflect the facility, how it is used, characteristics of its occupants, fire protection and life safety systems, security features and arrangements, and hazards within the facility.

Systems are typically designed to allow occupants who are not intimate with the initial fire or emergency to escape the area of immediate hazard in order to reach a place of relative safety. The concept of protecting those "not intimate" with the incident is important. A common example of intimate with the ignition is a person involved with a fire igniting a bed, a chair or a couch while smoking [20].

Egress strategies should be based on the specific hazards expected to occur over the life of the facility. Typical egress strategies include evacuating all occupants to the exterior of the building (simultaneous full evacuation), evacuating a portion of the occupants (partial evacuation), defending occupants in place (defend or shelter in place), or relocating occupants to a safe place within the building (relocation). Partial evacuation relies on protect-in-place strategies for non-evacuating occupants. The process can be phased, initially evacuating only a portion of the occupants, or all occupants can be notified to exit simultaneously. For many structures, a single response for all events is appropriate. For others, a scalable approach that escalates from partial evacuation and protect-in-place to simultaneous full building evacuation may be necessary. Regardless of the strategy, wheelchair users, occupants with mobility impairments, or others with mobility or cognitive conditions that may hinder self-directed egress need to be considered. An overview of these strategies follows [20–23].

Simultaneous Full Building Evacuation

Simultaneous full-building evacuation has been the norm for most buildings up to six stories for many years and tends to be the most common strategy for life safety. This is usually arranged through unprotected paths of travel, with distances appropriate to the building use, to protected stairs that discharge to the public way. For tall buildings, iconic structures, large assembly buildings, or other facilities that require full-building evacuation, a performance-based engineered approach may be necessary to evaluate the impact of evacuating a large number of people simultaneously [20].

Timed egress analysis or computer-based evacuation simulation methods can help to better understand the potential impacts of specific features and strategies on evacuation times. Chapters 59 and 60 provide detail on developing timed egress analysis and computer-based evacuation simulation methods. These tasks can be completed as part of an informal qualitative process or through a formal threat and risk assessment. For tall buildings, evacuation elevators can be used to support simultaneous full-building evacuation and substantially reduce evacuation times while addressing the needs of people with disabilities.

Simultaneous full-building evacuation will require considerably longer times for many occupants to make their way out of a tall building. This leads to questions on messaging strategies and how occupants will react during the evacuation, such as "Are additional features and functionality of the life safety systems necessary to provide an appropriate level of situational awareness?" Special messaging strategies with enhanced voice communication systems and additional zoning to keep occupants informed of the situation in real-time can help to address these issues. Such situational awareness features can provide specific real-time information about an event, allowing occupants to make better decisions regarding whether to stay or leave, or more informed decisions about route choice and adapting route choice to the situation [24–27]. As noted in referenced discussion on these topics, careful planning is necessary to be sure that these systems do not become too complicated, that messages are appropriate, and that increased reliability is built into systems.

Simultaneous full building evacuation messages should be coordinated and directed by the responding local fire authorities or properly trained staff utilizing the voice communication system or the growing range of emergency communication system devices. Messages should follow established procedures defined in the emergency plan developed for the facility [11, 28–30].

When using full building evacuation strategies, attention should be given to notification messages and their effectiveness. Particular concern should be given to assumptions regarding pre-movement time, occupant characteristics, and assumptions regarding mobility and evacuation time, and building features that could restrict or impede occupant flow. Narrow doors or corridors, and other obstructions can impede flow [20].

The time required for evacuation raises concerns related to occupant and staff training. Occupants benefit from training to give people a feeling for the length of time necessary to exit the building. This would be particularly powerful if occupants understood how staff would manage the process and what process and information decision makers use during emergencies.

Consideration should be given to how occupants move and disperse once leaving the structure, particularly for tall buildings or other high occupant load structures in dense urban environments. For these examples, occupants will need a clear path for a safe distance from the structure.

Protect-in-Place

Protect-in-place strategies are also known as defend-in-place or shelter-in-place strategies. These strategies involve providing adequate safety features to allow occupants to remain in place during the event, and they are used in facilities with occupants that have a limited ability to be moved, either because they are incapacitated or they are immobile due to medical or physical restraint. Protect-in-place strategies also are used in highly compartmented structures, such as residential occupancies, where building separations provide protection and allow a portion of the population to safety use phasing strategies [20].

Designs using protect-in-place strategies use a combination of active and passive fire protection features and management procedures to provide an appropriate level of safety for occupants to remain in the initial compartment. Structures using a protect-in-place strategy are typically protected throughout with automatic sprinklers, and include fire-rated compartments to reduce smoke and fire spread.

Typical examples of facilities needing protect-in-place strategies are health care facilities, and detention and correctional occupancies. In hospital surgical suites and intensive care units, it may be difficult—if not impossible—for patients to initiate and complete escape without assistance. Some patients cannot be moved without significantly jeopardizing their safety. For these situations, a protect-in-place may even be used within the compartment of origin.

US building codes have required features for many years in high-rise buildings to allow protect-in-place strategies. In residential buildings, and similar occupancies, tenant and corridor separations compartmentalize floors, which can offer a level of safety that permits protect-in-place strategies. For example, in United Kingdom Approved Document B (Fire Safety), Provision 2.7 a single stair is permitted in sprinkler protected residential buildings regardless of height because general evacuation is not contemplated [31].

For some specific and isolated events, evacuation may not be the most appropriate action because the process of evacuation exposes occupants to higher risk. For example, consider a deadly 1988 fire within a New York City residential high-rise building—four occupants attempting to escape tragically died during this fire, while other occupants that remained in place were not injured [32]. A study of fires in hotel occupancies in the 1980s concluded that guests not in the room of origin may have been safer

sheltering in their rooms because most fatalities occurred during evacuation [33].

Other examples can be drawn from terrorist actions. Terrorists can use the fire alarm system to evacuate occupants to the street, and then detonate a car bomb. DHS [34] provides specific guidance for active shooter situations, which includes sheltering-in-place. Occupants may need to ignore evacuation alarms, as the alarms can be used by the shooter to entice potential victims out of safe locations.

Relocation

Relocating occupants from an area of potential hazard to a protected area of refuge or other safe place within a building can be a safe and effective strategy, and represents a variation on the protect-in-place strategy. The *ICC Performance Code* [35] defines a safe place as "... an interior or exterior area wherein protection from hazards is provided by construction or appropriate separation distance." As with protect-in-place strategies, relocation requires attention to management procedures and may require special detection and notification systems or other appropriate life safety features. Hospitals, nursing homes, detention and correctional facilities, and institutional facilities are examples of facilities that use relocation strategies. These facilities typically use horizontal exits, smoke barriers, protected floor separations, or other appropriate means to protect relocated occupants [22].

Relocation strategies can be used in tall buildings. Here, occupants are directed to relocate to floors below the fire and away from any fire impact. With relocation strategies, the floor and shaft fire ratings and structural fire protection are critical, as the lower floors are relied upon to provide a safe area perhaps for the duration of the incident [22].

Phased or Partial Evacuation

Phased and partial evacuation strategies combine evacuating or relocating a portion of the occupants—those in immediate danger from the incident—with allowing occupants remote from an incident to protect-in-place. In this way, phased evacuation helps to optimize the use of the available egress components. With phased evacuation, occupants remote from the fire initially remain in place, but can be evacuated later if conditions warrant evacuation of the entire building. Partial evacuation strategies require features to protect occupants remote from the incident [20].

In high-rise buildings in the US, typically the event floor and two floors above and below the event floor are evacuated [11, 36]. In theory, this allows occupants on the fire floor unobstructed use of the exit stairs, thus optimizing use of the exit components and reducing the evacuation time for the affected floor or areas. For both phased and partial strategies, occupants remote from the event floor and those in the evacuation floor zones are notified. Occupants not in the affected zone are asked to remain in place to await further instructions [20,22]. Notification of occupants outside of the affected zone is common practice in Canada.

In hospitals, phasing may be necessary for larger incidents if such incidents might compromise adjacent evacuation zones. Large assembly spaces also may allow remote occupants to remain in place, while those closer to and intimate with the incident immediately evacuate. Assembly examples include large convention centers with multiple event halls. Where convention center halls are appropriately separated, it may be possible to phase the evacuation using individual halls as evacuation zones.

Two fundamental assumptions are critical with this strategy: (1) the event will not impact occupants outside of the affected zone during the time necessary to evacuate the affected zone; and (2) occupants in the unaffected areas will remain in place.

This concept works well for 'traditional' events, such as a sprinkler-controlled fire in a high-rise building, because automatic suppression systems in high-rise buildings are designed with a degree of resilience and have proven to be generally effective and reliable in controlling or

suppressing fires. In sprinkler-controlled high-rise fire events, fire-rated floor and shaft separations minimize hazards to occupants on the unaffected floors. If it is deemed that the building will need to address events other than 'traditional' events, additional or more reliable fire safety measures may be necessary.

Changes in risk perception resulting from the September 11, 2001 attacks have impacted public acceptance of phased evacuation. Occupants may become aware of events through communication technologies, such as texting, and social media, rather than the building notification system. In the event of a disaster, occupants might ignore "standby" messages and instead decide to immediately exit the building, particularly where they are afraid that the building might collapse. This has been reported during drills in New York City high rises. Another complicating factor is that today's emergency response procedures are being developed for a broad range of potential threats, not just fires, many of which requiring significantly different actions. To accomplish this, designers need to account for occupant response to non-'traditional' events, such as wide-spread power loss, severe weather events, crowd incidents or civil disturbances, terrorisms, large scale hazardous material incidents, or transportation incidents [23].

Egress Strategies for People with Disabilities

Egress system designs need to accommodate the needs of people with disabilities. The Americans with Disabilities Act (ADA) mandates that expected disabilities be accommodated, and that structures allow for equal access.

The 2010 edition of the ADA references the IBC (2003 Edition) for requirements related to means of egress and areas of refuge. At least one accessible means of egress is required for every accessible space and at least two accessible means of egress are required where more than one means of egress is required. The technical criteria for accessible means of egress allow the use of exit stairways and evacuation elevators when provided in conjunction with horizontal exits or areas of refuge.

While typical elevators are not designed to be used during an emergency evacuation, evacuation elevators are designed with standby power and other features according to the elevator safety standard and can be used for the evacuation of individuals with disabilities. Codes typically require an elevator to serve an accessible floor that is four or more levels above the level of exit discharge [11, 36].

Evacuation elevators provide for occupant self-evacuation through elevators that are intended to be used during fire events [11, 36]. In buildings over 30 m in height, UK standards [37] require a fire service elevator that is also intended to provide egress assistance to people with disabilities.

The IBC provides requirements for areas of refuge, which are fire-rated spaces on levels above or below the exit discharge levels where people unable to use stairs can go to register a call for assistance and wait for evacuation. Individual floors within fully sprinkler protected buildings are considered to meet the requirements for area of refuge [11,20,36].

In general, codes require audible and visible notification appliances throughout public areas of all buildings and structures. Fire alarm systems are required to have capacity to add these devices in other occupancies to address the needs of persons with hearing impairments if hired.

Egress designs that serve those with disabilities need to consider the specific needs of the occupants. Emergency action plans may need to involve the disabled person to ensure that his/her needs are addressed [11,28]. People with service animals will be reluctant to leave those animals behind. Some wheelchairs are equipped with life support equipment and may weigh hundreds of pounds exclusive of the user. Plans may need to allow for these people to evacuate with the wheelchair. Stair descent devices, also known as evacuation chairs, can be provided on floors occupied by a person with a mobility limitation to help when evacuation is required. Traditional "buddy systems" that pair the disabled

with a co-worker to provide assistance are effective; however, this needs the co-worker to be available at the time of the emergency. Guidance on the development of customized plans for occupants of offices was developed after the 1993 WTC bombing [38].

Performance-Based Strategies

Prescriptive codes provide egress design guidance for a broad range of building types, occupancy, and use groups, and allow for many common arrangements. The Life Safety Code Handbook [39] and IBC Commentary [40] include helpful comments and explanations for prescriptive egress design approaches. Prescriptive approaches have been generally successful in providing safe egress from most structures. However, design flexibility is often compromised in order to create a comprehensive set of code provisions that apply to a broad range of uses and occupancies [22].

In contrast, performance-based egress approaches combine first-principles fire engineering analysis with estimates of evacuation times that assess the ability of occupants to safely exit buildings for a range of fire conditions or other events. Performance-based approaches require safety systems to be designed to meet specific life safety goals for a range of hazards and events. This can result in increased design flexibility, as it affords the opportunity to align overall building objectives with fire safety objectives. With this flexibility, however, comes an additional design burden, as analysis is needed to demonstrate that occupants can safely exit under the range of expected design scenarios. Performance-based designs are discussed later in this chapter [22].

Selecting and Evaluating Options

When selecting an appropriate egress strategy, the strategy needs to match the ability, activity and responsiveness of the occupants, the technology used, and the ability and reliability of staff or occupants to assist in the process. The selection of an appropriate egress strategy hinges upon the emergency scenarios considered, and evacuation and emergency response planning. The communication and messaging strategies need to match the evacuation strategy. Other considerations include the number of people who will need to evacuate, whether all occupants within the facility will be exposed to hazardous conditions, and the occupants' familiarity with the exits and egress routes. Egress strategies should be developed to guide the design of egress features, rather than be developed after the building is built [22].

For complex facilities, it is often necessary to develop an overall fire and life safety strategy to coordinate these features. Voice communication, suppression, and detection system zones need to match with the evacuation zones. Emergency lighting is necessary in exit pathways to allow safe movement during power outages. Exiting components will likely require appropriate fire ratings. In some cases, additional voice communication zones, two-way communication, message boards, or other communications systems may be necessary to provide occupants with an appropriate level of situational awareness and a general understanding of the incident. Zones require specific fire separations and structural fire ratings appropriate to the strategy. Other features also may be necessary: elevators may need to be protected and provided with special controls, stair door unlocking may be necessary, and life safety systems will likely need emergency power. All of these features need to coordinate with security systems [22].

A single solution may not be appropriate for complex facilities. These facilities may benefit from adaptive or event-based strategies. With adaptive or event-based evacuation, conditions dictate the specific actions and egress strategy. During an event, the situation is assessed and a strategy is selected based on that assessment. For example, consider a fire event on a single floor, a strategy including relocation through exit stairs and protecting in place those on unaffected floors may be appropriate. For the same building, a building power outage may require full building evacuation.

Adaptive evacuation concepts are particularly useful for facilities that may be exposed to a range of events, this is important when those events can involve threats both inside and outside of the building. Events occurring outside the building may require a very different response than those occurring inside. The presence of an active shooter will likely need a protect-in-place lockdown where spaces can be secured against entry by the shooter. Civil unrest or a hazardous material event outside a building may require occupants to be secured within the building. Release of a biological agent within a building may require potentially contaminated occupants to be secured within the building until it can be determined that they will not contaminate others. This strategy places a large burden on the decision makers and the decision-making process. Decision makers need relevant information and the authority to make critical decisions. While flexibility can be beneficial, simplicity creates increased reliability.

Substantial training is required to minimize confusion, particularly where differing responses are expected for different events. Appropriate systems and methods are needed for decision makers to quickly obtain credible information about the event and to empower decision makers with the appropriate authority to make egress decisions based on that information. Training can help, but the provision of real-time instructions is necessary to increase the likelihood of obtaining the correct response from a wide range of potential responses [20].

Exit Components

In the US codes, a means of egress consists of three parts; the exit access, the exit itself, and the exit discharge. The exit access is any portion of a means of egress that leads to an exit and the exit discharge is any portion of a means of egress between the termination of an exit and a public way. The exit is defined as [11],

> That portion of a means of egress that is separated from all other spaces of a building or structure by construction or equipment as required to provide a protected way of travel to the exit discharge.

Figure 56.2 illustrates the relationship between exit access, exit, and exit discharge.

A means of egress is generally considered to be a protected path of travel to the exit discharge. On floors above grade, this is typically through an exit stair. The exit stair is required to discharge on grade to a path leading to the public way. US codes generally define the public way as a street, alley, or other space open to the air that is dedicated to public use. Exit stairs need to be arranged so that once entered, occupants are not required to leave the stair until reaching the exit discharge. There are exceptions. In some cases, an exit discharge can lead to a space of sufficient

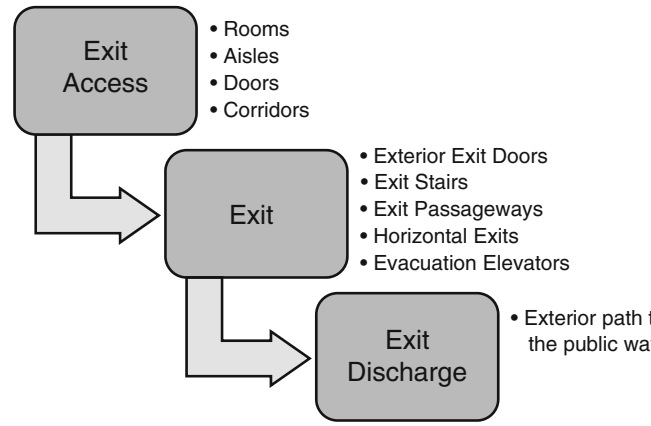

Fig. 56.2 Exit components

size to accommodate all of the occupants expected to use the exit and be located at a safe distance from the building. In other cases, exit stairs are allowed to discharge through an on-grade level floor where a direct and obvious path is provided [11, 36].

Egress systems require that at least two means of egress be provided from any point in a building. One exit can be provided for spaces that meet limits on common paths of travel. Additional exits are required based upon occupant load: three exits for spaces with 500 occupants, and four exits for spaces with 1000 or more occupants. Exits are also required to be located to meet travel distance limits. Stairs enclosed by a fire and smoke rated shaft are the most common exits. Horizontal exits can serve as a means provided that the horizontal exit passes through a rated wall that is continuous from exterior wall to exterior wall and continuous to grade. Occupants are deemed to be in a safe area after exiting through the horizontal exit.

Requirements for exit capacity, which affect the number and width of stairs and doors, are based upon the occupant load of each floor, either estimates of the actual number of occupants including visitors, or an occupant density derived from surveys of actual buildings. The load factors specified for specific occupancies are quite consistent across many international building codes. For example, the occupant load for office occupancies is 100 ft^2 (10 m^2) per person in US, Australia and Spain, 90 ft^2 (9 m^2) per person in Hong Kong and 60 ft^2 (6 m^2) per person in the UK. Some of the traditional load factors are being questioned since most of the surveys on which they are based were taken more than 50 years ago.

Egress stairs are required to be protected from the entry of smoke that could slow evacuation or harm occupants. Besides having a fire rated and smoke resistant shaft enclosure, egress stairs in high-rise buildings are typically pressurized to prevent smoke leakage through construction cracks and doors opened to provide access. Stair pressurization systems are discussed further later in this chapter.

Occupant Evacuation Elevators

Walking down many flights in tall buildings can be a difficult task for many occupants and may be impossible for some. Elderly, disabled, or injured occupants, occupants with other medical issues like heart conditions, or those with or mobility-impairing injuries may have difficulty negotiating stairs or may be incapable of evacuating using stairs. Changes in technology, an aging population, the events of September 11, 2001, and the practicalities of designing for very tall buildings, have converged to make elevators a viable option, and perhaps a necessary alternative, for emergency evacuation in tall buildings. Protected evacuation elevators can provide a safe and effective alternative to walking down many flights of stairs. With appropriate design, it may be possible to allow protected elevators use for a large segment of the building population [20,22].

The use of elevators can speed evacuation within tall buildings. This has been proven in real events. For example, reports indicate that 16 % of World Trade Center Tower Two occupants escaped through the elevators before the second airplane struck the building [41]. Utilizing elevators can result in the total evacuation of any building of any height in less than one hour, without increasing the number, size, or speed of the elevators normally provided for routine use [42].

Fire service access elevators that are also used for assisting disabled or injured occupants have been required in British codes and others following the British system since the mid-1980s [37]. No building regulation has recognized elevators for occupant evacuation in fires until the 2009 editions of the US codes, although some systems (e.g., Stratosphere Tower, Petronas Towers, Taipei 101) were approved as performance-based designs [43].

One strategy is to shuttle occupants from upper levels. Another would be to attempt to restrict elevator usage to those who simply cannot take the stairs due to health or mobility

limitations. If restricted access is planned, training of all occupants, stringent controls enforced by operators or fire wardens, and a management plan would be necessary to prioritize and discern between those that need the elevators versus those that simply choose to use the elevators. Another strategy is to allow occupants to descend stairs from the fire floor to a refuge floor, or a specially designed sky lobby, then to use the elevator from that floor or continue down the stairs [22].

In all cases, strategies need to be well-defined, well-engineered, and coordinated. Special care is necessary to help educate and train occupants in the use of such systems. Elevators must be protected, and appropriate fire and life safety features, appropriate signage and way-finding, and a well-constructed evacuation plan with training are required.

Figures 56.3a and b provide two examples of tall buildings using elevators for evacuation. In Fig. 56.3a, elevators serve the fire floor. In Fig. 56.3b, elevators only serve the sky lobbies.

Taller and taller buildings are be designed and constructed around the world. For these structures protected elevators are an important egress design component. Both the *International Building Code* [36] and the *Life Safety Code* [11] allow elevators to serve as one means of egress. The *Life Safety Code* has allowed emergency evacuation elevators to serve as the second exit within observation, control, operation, and signaling towers since its 1988 edition. These approaches potentially use all public use elevators to minimize evacuation times and to prioritize evacuation of occupants from the most threatened floors.

ASME A17.1/CSA B44 Safety Code for Elevators and Escalators [44] includes specific operational protocol and design features for elevator evacuation—Occupant Evacuation Operation. Requirements include manual elevator recall switches in the elevator lobby and in the fire command, controls to initiate "Elevator Total Building Evacuation" in the fire command center, appropriate fire alarm signs, and variable message signs to indicate elevator status and estimate time duration for the next elevator [44].

Note that in all cases, emergency evacuation elevators only operate prior to Phase I Emergency Recall Operation. This means that elevators only operate in evacuation mode until recalled to the first level by the activation of a smoke detector adjacent to the elevator opening. Phase I recall can be activated manually by the fire department to recall individual elevators while keeping others in service.

Some concerns have broad societal implications—e.g., the overall public reaction to the use of elevators is unknown. Usage of elevators during emergencies is in direct contrast to the message given for years from the life safety community: in case of fire, do not use elevators. Given this message, how will occupants react and what percentage of occupants will use elevators? These questions need to be addressed on a case-by-case basis through planning and training.

Escalators

Escalators are not generally credited to required egress capacity. NFPA 130, *Standard on Fixed Guideway Transit Systems* [45] is an exception. NFPA 130 allows non-combustible escalators to be counted for up to 50 % of required capacity from subway stations, so its acceptance in other occupancies may eventually change. Escalators are present in many buildings, are familiar to occupants through daily use, and there is no prohibition against using them for egress in fires. Thus, evacuation modeling in buildings with escalators performed as part of a performance design or a supporting egress analysis could incorporate the escalators where appropriate and acceptable to the Authority Having Jurisdiction.

NFPA 130 contains specific guidance on escalators used for egress. Escalators moving in the direction of egress travel continue to move, and those moving in the opposite direction are stopped. Note that stopping a moving escalator while people are riding must be done with extreme care to avoid falls—escalators should slow to a stop [45].

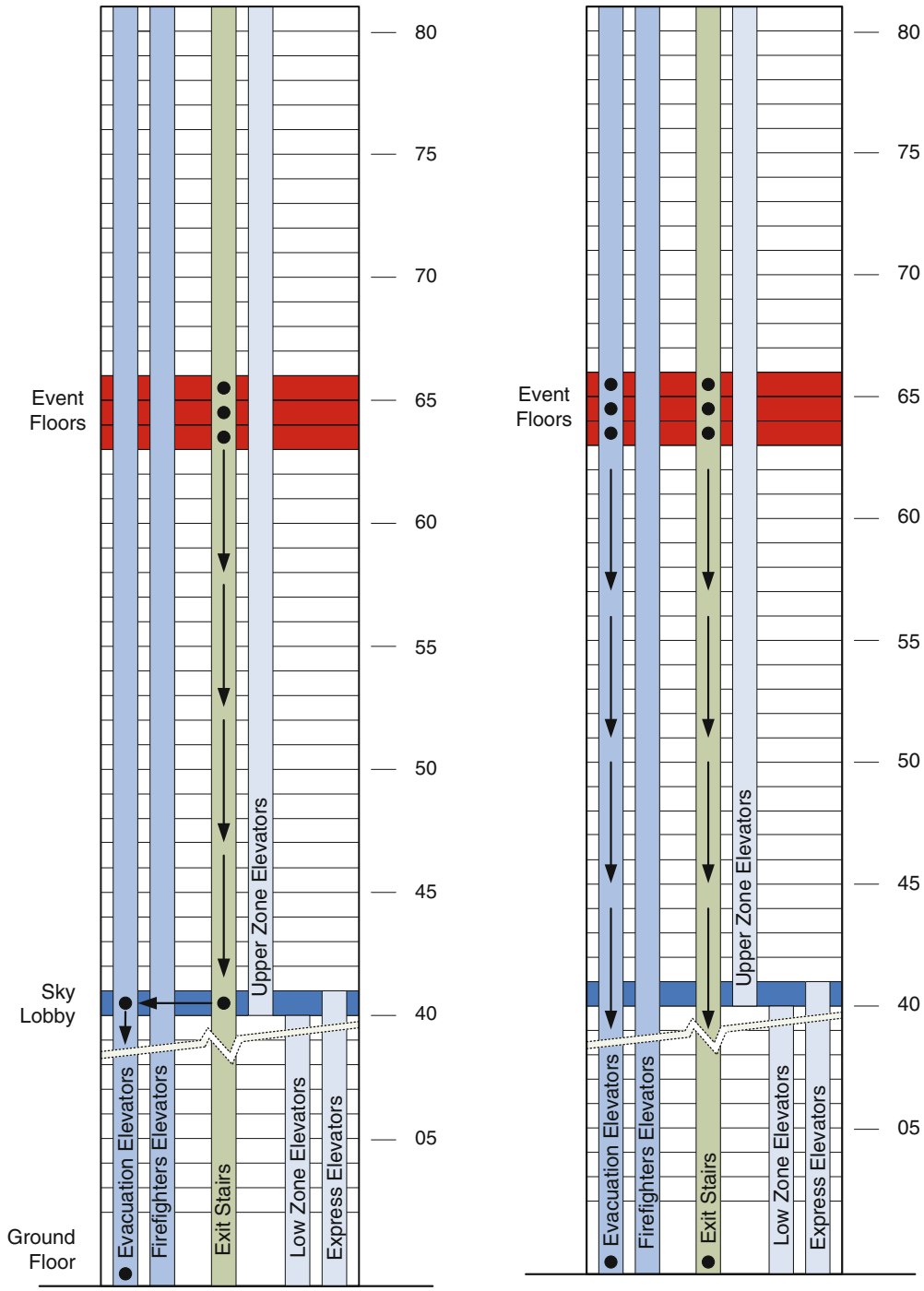

Fig. 56.3 (**a**) Elevators serving the fire floor (left) (**b**) Elevators serving sky lobbies (right) [20]

Capacity of typical escalators is credited the same as egress stairs, defined as 1.41 persons per inch-minute (0.0555 p/mm-min). Escalator speeds have been standardized by ASME A17.1 at 100 ft per minute (33 m/min), although some faster speeds can be found in special applications, especially on very long runs [44]. The egress travel speed on a stopped escalator is defined by NFPA 130 as 48 ft per minute (14.63 m/min) in the down direction and 40 ft per minute (12.19 p/mm-min) in the up direction. NFPA 130 requires that the calculation of egress time must assume at least one escalator out of service.

The main reasons that escalators are not credited as a means of egress component are their lack of a fire rated enclosure and the tread geometry does not comply with typical code requirements. Typical code compliant egress stairs are required to have a 7 in. (178 mm) rise and an 11 in. (280 mm) tread depth. Escalator steps (except at the top and bottom where they are collapsing) have a greater riser height, not more than 8.5 in. (220 mm), and a tread depth of not less than 15.75 in. (400 mm). The increased depth is not an issue since the 11 in. stair depth is a minimum. In a survey of egress stair geometry requirements in a select number of countries, Bukowski [4] found that the maximum riser height permitted for an egress stair is 7.5 in. (190 mm). Escalators do not have intermediate landings, and slopes are not more than 30° where the slope of an egress stair is 32°. In addition, the collapsing riser heights at the top and bottom can interrupt gait which slows movement and pose a potential for tripping.

Refuge Floors

Refuge floors are required in high-rise buildings in Asia and the Middle East to provide an area of temporary refuge and an ability to cross over between stairways. Refuge floors are typically provided every 15–20 floors or more, depending on occupancy, and are frequently co-located on mechanical floors. The refuge space is typically required to be at least 50 % of the floor area and separated from mechanical equipment by fire rated partitions. Exterior walls are required to be at least 50 % open to provide for natural smoke control. Perimeter deluge sprinkler systems are required to reduce the potential for smoke or fire spread into the space.

Some have expressed concerns about the practicality of refuge floors. During drills, it is reported that occupants often evacuate to the nearest refuge floor and await the call to return to their workplace. This can result in overcrowding of the refuge floor with occupants backing up into the stairs and blocking egress flow. It is unclear whether such behavior would be seen in a real emergency. Another concern is storage. Storage is not allowed in refuge areas; however, if items are stored, the area available for occupants to rest would be further reduced. Storage also introduces a fire load into the evacuation path. For these and other reasons, there is controversy over the use of refuge floors.

Pedestrian Walkways and Skybridges

Elevated pedestrian walkways are increasingly popular architectural features of urban buildings that can be found in several US cities connecting downtown buildings, usually at the second floor level. Pedestrian walkways provide a means to access portions of a downtown area protected from the outdoor weather and often connect hotels to shopping and to convention centers. Skybridges connect buildings at higher levels and are less common—the Petronas Towers skybridge is a well-known example.

Pedestrian walkways provide exit paths to adjacent buildings. This can be significant for tall buildings, as this provides an alternative evacuation path. Legal issues regarding responsibility for operating costs, maintenance, and liability must be addressed when Pedestrian walkways connect buildings under different ownership but these clearly can be addressed because such walkways are found in many cities.

Features in Codes Internationally

It is important to understand country specific requirements or cultural norms that may affect the design. The following provides some examples of egress features and design conventions used internationally.

In addition to requirements for refuge floors discussed in previously, Chinese and Korean Codes require vestibules at the entrances to egress stairs and elevators on each floor of a high-rise building. Chinese regulations permit common vestibules but Korean codes require them to be separate and integrated with an area of refuge staging floor. Korean regulations further require that a fire service access elevator be located within 30 m (98 ft) of the building exterior.

In Tokyo where buildings are crowded together and many streets are quite narrow, numerous public parks serve as protected spaces in which people who have evacuated nearby buildings can be sheltered. These parks are surrounded with trees intended to provide shielding from radiant energy from the event. The provision of parks as shelters began after the Great Kanto Earthquake (1923) where the large death toll was mostly from fires and proved its worth in the fire bombing late in WWII.

US codes allow longer travel distances, even for the reduced travel distances required for non-sprinkler protected facilities. In Hong Kong and Macau, travel to an exit must be within 40 m (130 ft). In Australia, the maximum travel distance depends on the type of building, but ranges between 20 (65 ft) and 40 m (130 ft). For comparison, the US is 61–91 m (200–300 ft) depending on the occupancy served.

Some countries utilize scissor stairs to meet code mandates for two egress stairs. In most cases these are required to have the entrance doors separated by at least 9 m (30 ft) and be fully fire separated. Other than in New York City where they are common, scissor stairs are generally not permitted to serve as separate exits due to the perceived difficulties in separating the enclosures and the resulting possibility of simultaneously contaminating both exit enclosures.

In the US, two exits are required for nearly all multi-story buildings. Single exits are common for residential high-rise buildings outside the US. This allowance is typically limited to smaller floor areas so that exits can be reached within 20 m (65 ft).

Design can include merging stairs in the International Building Code, such as basement stairs meeting and combining with tower stairs at the discharge level. In the Middle East, and China, Hong Kong, and other countries [46], designs follow an approach similar to NFPA 5000 and rising and descending flights of stairs need to be separated so that the stairs are separated and there are two independent exit discharges.

Horizontal exits are recognized in the US and Australia as a means of egress. Horizontal exiting concepts are not incorporated within Chinese Codes, but have been used in projects following the *International Building Code* or *Life Safety Code*.

Systems and Features That Support Egress

The egress strategy forms the basis for life safety and needs to be designed as part of a coordinated life safety program that integrates the fire protection and life safety features of the building. Notification, way finding, and fire and smoke protection of egress components are fundamental features that support both prescriptive and performance-based egress concepts because they support the efficient use of the egress system.

Notification

Timely evacuation begins with emergency notification. Most public buildings have a notification system initiated by automatic fire detectors or the detection of water flow in the sprinkler system.

Notification appliances in modern systems are usually voice systems since they provide the flexibility to tailor messages to a range of events. Research has shown that people are more likely to respond to voice messages because many may not understand the meaning of an audible signal or occupants may think it is a false alarm [47]. A significant improvement in voice systems can be attributed to the development of a method to make objective, quantitative measurements of the intelligibility of voice messages coupled with explicit requirements in the Notification Appliances Chapter of the National Fire Alarm Code [30]. Notification systems generally include visible appliances for the hearing impaired and may also include tactile devices. Smaller buildings are not typically required to be provided with voice communication systems.

The effectiveness of messages broadcast over voice systems can vary significantly. Effective messages are more likely to result in the desired response [48]. Attributes of an effective message including being:

- Short but informative
- Easy to understand what is expected
- Authoritative
- Provides information to support effective decisions
- Repeated but not repetitive

In some cases, such as in health care or in detention/correctional occupancies where occupants are restrained or unable to evacuate without assistance, it is unwise to directly notify people of an emergency through public mode alerting systems because of the anxiety that results in those who cannot respond to the call to evacuate. Here, notification appliances can operate in what is called private mode. Private mode signals are presented only to specific parties who then notify and assist others. In contrast, public mode alerts the general population.

Systems need to be audible and intelligible. If occupants can hear the message, it is audible. If occupants can understand the message, it is intelligible. Chapter 40 and the National Fire Alarm Code Handbook [49] describe methods for designing audible and intelligible messages.

Where people may be sleeping, notification appliances need special attention. As required by the National Fire Alarm and Signaling Code [30], audible appliances need to produce sound pressure levels of 75 dBA or more that are at least 15 dBA above the average sound pressure level of any background noises. Visible appliances need to operate at least 177 candela at the pillow to wake occupants. This is significantly higher than the 15 candela minimum at the device for visual notification of alert people. The National Fire Alarm and Signaling Code includes new requirements for low frequency alarm signals in sleeping areas to increase the ability of the waking sleeping occupants. Tactile notification provides an alternative [30].

Wayfinding

Buildings that may contain occupants who are unfamiliar with the egress system are usually required to install some features to guide wayfinding. The traditional wayfinding aid is the exit sign over exit doors and signs that direct people to these exits. Hotels usually have a floorplan map located on the back of the door in every room showing the location of the exit stairways in relation to that room.

In recent years, some regulations have been changed to move signage lower in hotels so that it is not obscured by smoke. In Europe and South America, some countries install lighted chevrons in the baseboards of exit access hallways. For the visually impaired, there are “talking signs” that transmit an audio channel that can be heard on special devices carried by the disabled person and heard as the sign is approached. Another new technology is directional sound transmitted from speakers mounted over exit doors. Even without being able to see, these sounds give the impression of direction, guiding the person to the exit.

Dynamic signage can direct occupants to specific locations, guiding evacuees away from hazards. One example is the use of dynamic signage within stairways to direct occupants to a specific exit or to direct evacuees to cross over

to another stair to avoid hazards. Some have proposed the use of messages transmitted to handheld devices including smart phones to provide way finding guidance in emergencies.

Illumination and Exit Marking

With a few exceptions, the means of egress including the exit discharge is required to be illuminated to at least 1 ft-candle when the building is occupied. Recently, illumination requirements have been supplemented by requirements for luminous egress path markings, including photoluminescent marking. Requirements in the *Life Safety Code* [11] state that, where photoluminescent markings are used, light levels sufficient to charge the material are required to be provided for at least 60 min before the building is occupied. Energy conservation systems that turn off lights when the stairs are not occupied cannot be used. Chapter 7 in Facilities Standards for the Public Buildings Service contains additional information [50].

Fire and Smoke Protection

Egress stairs typically require fire-rated shaft construction and protection from the entry of smoke. Egress stairs in high-rise or tall buildings are typically pressurized to prevent smoke leakage through construction cracks and doors opened to provide access.

Stair pressurization systems typically require pressures of at least 25 pa (0.1 in. of water) to prevent smoke infiltration but not more than 67 pa (0.25 in. of water) which could result in excessive door opening forces. Systems need to meet both limits at every door, and account for pressures resulting from stack effect and the fire itself. Shaft height, high indoor to outdoor temperature differences, and requirements for designing for open stairway doors add complexity to the design. Chapter 50 includes additional information on stair pressurization.

Simple stair pressurization systems can be designed with hand calculations. Complex arrangements such as buildings with adjacent vestibules or corridors pressurized separately from the stairs, buildings with multiple shafts, buildings with shafts taller than 75 ft, or buildings with shafts that connect to spaces that are open to the outside such as parking garages, should be addressed by use of a network model that can account for the multiple flow paths involved [51].

Before pressurization systems there were stair designs called smoke-proof towers that employ stair access through a vestibule that is naturally ventilated to the outside. Smoke-proof towers now combine mechanically vented or purged vestibules with stair pressurizations systems. Smoke-proof towers were found to be reliable and effective as long as the vestibule ventilation is not blocked.

Performance-Based Evacuation Design

The prescriptive egress provisions of the codes have been developed to provide robust evacuation features for a wide range of buildings types, uses and occupancies. While these provisions have worked well for many years, they cannot address all situations. The performance-based evacuation design process is an important tool to address situations that are either not appropriately addressed by prescriptive codes, or to address owner and designer needs that cannot be solved with traditional prescriptive code solutions.

The SFPE Engineering Guide to Performance-Based Fire Protection Analysis and Design in Buildings [52] defines a process to undertake performance-based design, which includes defining scope, developing goals and objectives, developing performance criteria, developing design fire scenarios, developing trial designs, evaluating trial designs and selecting final design, and preparing documentation. Chapters 37 and 57 provide information to help implement this process. Table 56.1 illustrates this process when applied to the evaluation of evacuation designs for fire

Table 56.1 Sample performance-based evacuation design process for fire scenarios

SFPE PBD process	Potential performance-based evacuation assessment tasks
Step 1—Define project scope	Define prescriptive requirements
	Applicable codes
	Define performance–based egress features and strategy
	Chapter 37
Step 2—Identify goals	Identify life safety goals
	Chapter 37
Step 3—Define objectives	Define stakeholder objectives
	Chapter 37
	Define egress design objectives
	Chapter 37
Step 4—Develop performance criteria	Determine tenability criteria
	Chapter 61
	Chapter 63
	Determine fire and smoke detection criteria
	Chapter 40
Step 5—Develop fire scenarios	Determine fire sizes, locations, and simulation parameters
	Chapter 37
	Chapter 26
Step 6—Develop trial designs	Design retained prescriptive–based egress features and requirements
	Applicable codes
	Design performance–based egress features and requirements
	Chapter 59
Step 7—Evaluate trial designs and select final design	Determine occupant scenarios—occupant loads, pre-movement times, and movement parameters
	Chapter 58
	Chapter 57
	SFPE Engineering Guide: *Human Behavior in Fire* [53]
	Determine fire/smoke detection and occupant notification time
	Chapter 40
	Determine Required Safe Evacuation Time (RSET)—Simulate occupant pre-movement (or delay time) and movement time (see
	Chapter 60
	SFPE Engineering Guide: *Human Behavior in Fire* [53]
	Determine Available Safe Evacuation Time (ASET)—Simulate smoke movement, and fire affects, and determine time to untenable conditions
	Chapter 50
	Compare occupant movement and tenability results
	Chapter 37
	SFPE Engineering Guide: *Human Behavior in Fire* [53]
	Review factors of safety
	Chapter 59
Step 8—Prepare documentation	Document analysis, assumptions, results, and limitations
	Chapter 37
	Peer review (if necessary)
	SFPE Guidelines for Peer Review in the Fire Protection [54]
	Design Process

scenarios. The process can be applied to other non-fire emergencies as well as crowd related hazards. The following sections further discuss the process.

Design Considerations

The following list considerations related to evacuation, defend in place, and relocation designs that may be relevant for performance-based evacuation design and analysis [20].

Will occupants investigate alarm signals before deciding to leave?

Will occupants be committed to or be involved in an activity that will slow their reaction to alarm signals?

Will families or other groups attempt to find other group members before beginning to evacuate?

Will all exits be available, or will one or more exits become unusable during specific events?

Will occupants be familiar with or aware of the closest escape route?

Will occupants use the available exits uniformly, or will the main exit be more congested than others?

Will all occupants have similar abilities?

Will some of the population need special assistance?

Define Project Scope (Step 1)

The first step in the process includes gathering information about the structure and the occupants, identifying the stakeholders, and determining the level of application. The project budget and approvals process should also be determined [52].

Stakeholders should agree on the project scope, goals and objectives. The SFPE Guide [52] lists the following example stakeholders: building owner, building manager, design team, authority having jurisdiction, accreditation agencies, construction team, tenants, building operations and maintenance, emergency responders, and peer reviewer. Other stakeholders might include commissioning agents.

The project scope also defines the level of application and clearly identifies systems or components designed using prescriptive code requirements and those designed using performance methods. The scope can include individual fire protection safety components or overall systems, partial buildings, whole buildings, and multiple buildings [52].

Project Scope Examples The following provides typical examples where the performance-based process may be employed to help realize designer, or owner vision.

Performance-based assessments can include developing solutions to safely extend travel distance, extend common paths of travel, or reduce exit widths within large facilities. An integrated strategy including fire detection, smoke management, and carefully planned evacuation features can allow a safe alternative for architectural designs that differ from typical prescriptive code requirements. The process can be used to test the ability of a strategy to meet established goals and objectives, based on the expected hazards.

The process can support evacuation planning and crowd management planning assessments. For example, designs may need to optimize evacuation through the use of elevators in tall and super tall buildings. In these examples, evacuation simulations may be used to facilitate comparison of specific strategies, and elevator operations during emergencies. The process can help inform crowd management planning and can help to understand crowd movement under a range of conditions.

The process also can be used to optimize evacuation for large assembly spaces. Sime [55] notes a strong relationship between normal circulation routes and exit pathways used during emergencies. Exit paths that serve as normal circulation paths will more likely be used than other exits, even if the path of travel is further along the normal circulation route. The

assessment can evaluate strategies to minimize occupant crowding and optimize occupant flow at critical evacuation components, and allow alignment of normal circulation routes with emergency exit paths.

Define Goals and Objectives (Steps 2 and 3)

The next step is for the stakeholder team to agree on fire safety goals and objectives for the project. Chapter 37, the SFPE Engineering Guide to Performance-Based Fire Protection [52], *Life Safety Code*, *NFPA Building and Safety Code*, and the *ICC Performance Code* (ICC 2012), and *Code for Fire Protection of Historic Structures* [56] provide information and guidance on selecting goals and objectives.

Goals and objectives can relate to limiting sources of fire ignition, preventing fire ignition and growth, limiting fire impact, limiting consequences from hazardous materials, protecting people during egress and rescue operations, managing people safely, protecting responders from unreasonable risks, providing notification for emergency responders, providing access and facilities for emergency responders, and providing notification for life safety and property protection [35, 52].

The *Life Safety Code* states in part that "a structure shall be designed, constructed, and maintained to protect occupants not intimate with the initial fire development for the time needed to evacuate, relocate, or defend in place." Section 5.3 of the *Life Safety Code* refers to *Retained Prescriptive Requirements*, which are features that need to follow prescriptive methods or provide an equivalent design. Retained prescriptive requirements within the *Life Safety Code* include design details for: changes in elevation, guards, doors, stairs, ramps, fire escape ladders, alternating tread devices, capacity of means of egress, impediments to egress, illumination of means of egress, emergency lighting, and marking of egress [11].

The *ICC Performance Code* states in part that "the construction, arrangement and number of means of egress, exits, and safe places for buildings shall be appropriate to the travel distance, number of occupants, occupant characteristics, building height, and safety systems and features." The ICC Performance Code requires performance-based egress designs to address the following: exit identification, exit illumination and safety of means of egress, providing unobstructed egress paths, protecting occupants from untenable conditions, provisions to address human biometrics and expectation of consistence, maintenance of means of egress systems, maintenance of clear path, maintaining identification of exits, maintaining ease of use, and maintenance of illumination [35].

Develop Performance Criteria (Step 4)

Performance criteria are "threshold values, bounded ranges of threshold values, or distributions of expected performance," [52] and form the basis for assessment of the design. For fire evacuation events, performance criteria are typically described in terms of occupant tenability. Where performance-based assessments are used for evacuation for events other than fires, such as crowd movement events, performance criteria matching the specific hazards associated with those events is needed.

The *Life Safety Code* [11] lists four methods that provide context to tenability assessments for performance-based egress approaches for fire events. Method One accounts for designs that expose occupants to heat, smoke, or other toxic or damaging products of combustion while evacuating a structure. This method requires a tenability assessment. The Fractional Effective Dose (FED) method can be used to determine if occupants can safety exit through contaminated egress paths. Chapter 63 describes the FED method in detail. Exposures to lower doses of contaminants over a long period of time may be as severe as a higher dose over a shorter exposure. The FED method accounts for low and high exposures.

Method Two compares timed egress and smoke-movement simulation results to determine if occupants are able to evacuate before egress paths become contaminated. Method Three requires the calculated smoke layer to be maintained 6 ft or more above the floor in all egress paths throughout the required egress time. Method Four relies upon passive smoke and fire barriers, or active smoke pressurization systems to maintain pressures across barriers to keep smoke from reaching egress paths. Depending upon geometry and configurations, computer fire models may be necessary to appropriately assess smoke movement. Chapter 50 details smoke pressurization methods. Chapter 51 calculation methods for simulating smoke movement.

Tenability in fires can be quantified in terms of thermal effects, visibility through smoke, smoke toxicity, or limiting impact from falling materials. Some occupants, such those that are ill, young, or elderly can be particularly vulnerable to exposure. Criteria may need to reflect these vulnerabilities. Chapter 63 provides methods for quantifying thermal effects, visibility, and smoke toxicity. Sub-lethal effects may also be important.

Thermal Effects Thermal effects are evaluated based upon occupant exposures to heated gases or flame. Radiant and convective exposures are cumulative. The FED method allows the combined assessment of radiant and convective exposures.

Visibility Visibility estimates the distance occupants can read exit signs or distinguish exit paths through smoke. Visibility is based upon smoke density, illumination, and distance.

Smoke Toxicity Combustion products can be toxic, and can cause reduced decision-making capacity and impaired motor activity. Inhalation of toxic combustion products can lead to incapacitation or death.

Impact Falling objects, airborne building materials, or structural collapse can cause injury or death [57].

Sub-lethal Effects Sub-lethal effects can lead to severe injury and incapacitation. For example, smoke exposure can be irritating to an occupant's eyes and this physiological effect can reduce the ability to see over time. Another example would be an occupant who survives, but sustains permanent damage due to smoke inhalation. Kuligowski [58] details criteria on sub-lethal effects. Chapter 63 includes information on assessing sub-lethal effects.

Events Other Than Fire Historically, fires have been the primary incident of concern for prescriptive building codes. Earthquakes are also considered in seismic design zones. Since the September 11, 2001 attacks on the World Trade Center, there has been more consideration of planning for appropriate response to emergencies other than fire and focus has shifted to address a wider range of events. For example, the Life Safety Code states [11]:

> Life safety in buildings includes more than safety from fire. Although fire safety has been the long-standing focus of NFPA 101, its widely known title, Life Safety Code, and its technical requirements respond to a wider range of concerns, including, for example, crowd safety.

The ICC Performance Code similarly addresses a wide range of events, although the approach is different. In this code, maximum damage or outcome from event scenarios is mandated. Events are categorized as mild, moderate, and severe. For example, a mild event requires: no structural damage, fully operational non-structural systems for both normal and emergency operations, minimal damage to facility or contents, minimal hazardous material released to environment, and only minor occupant injuries with low likelihood of life loss. A moderate event would allow more severe damage. Moderate events are characterized by greater damage

requiring repair prior to reoccupation and an increased likelihood of death and injury. Severe events result in sufficient damage that re-use is unlikely and multiple deaths are likely [35].

Develop Design Scenarios (Step 5)

The next step in the process is to develop design scenarios. The SFPE Guide and Robbins, Gwynne, and Kuligowski [59] detail processes for developing fire safety scenarios, which entails identifying possible fire scenarios, paring the possible scenarios into a sub-set of design scenarios, and quantifying the design scenarios. Design scenarios include the building components and characteristics, occupant scenarios, and fire scenario(s).

There are a range of methods and analysis techniques that can be used to identify possible fire scenarios and rationalize these scenarios into the design scenarios. SFPE [52] describes probabilistic and deterministic approaches and outlines these methods. Robbins et al. [59] further describe this process. Chapter 72 and the SFPE Engineering Guide to Fire Risk Assessment [60] provide detail on fire risk assessment.

Building Characteristics Building characteristics include building height and size, occupancy and uses, architectural features, structural fire protection, egress features, fire protection and life safety systems and features, building services, functions and processes, fire department response features, environmental factors, and expected hazards and threats, criticality, and importance [20, 52, 59].

Occupant Characteristics Occupant characteristics include occupant loads, occupant ages and cognitive and physical abilities, presence of groups, and occupant response characteristics. Chapter 57 overviews occupant scenarios.

Occupant loads are determined through use classification of the spaces. Codes provide prescriptive factors for occupant loads [11,36]. In some cases, occupant loads can be determined through the expected actual use.

Occupant loads will vary based upon the event considered. In many cases, larger occupant loads will increase risk, but this may not always be the case. Consider a convention center used for lecture seating and boat shows. While lecture seating would pose a lower fire hazard, when compared to a boat show, the expected occupant loads would be significantly higher. Other uses may include exhibits with cooking or concerts with pyrotechnics. Each scenario has varying occupant loads, varying occupant conditions, varying hazards, and ultimately varying levels of safety. For these conditions, it may not be intuitive which poses a higher risk, scenarios with higher occupant loads or scenarios with higher fire hazards. The analysis would need to review a representative range of expected scenarios to appropriately characterize the level of safety [57].

Performance-based approaches require a comprehensive understanding of expected reaction times, and occupant movement. Chapter 57 and the SFPE Guide discuss factors that influence pre-movement and movement times. Factors include whether the person is alone or with others, the occupants familiarity with the building's exit paths, emergency procedures, distribution within the space or throughout the building, pre-event activities, occupant alertness, occupant physical and mental ability, social affiliation, role in the evacuation or the organization structure, location, commitment to activities or others, age, culture, occupant condition, and gender. Table 56.2 describes specific characteristics emphasized in the *Life Safety Code* [11] and *ICC Performance Code* [35].

People have a wide range of abilities, and response characteristics. Prescriptive building and safety codes traditionally use occupancy groups to imply the characteristics and typical behavior of occupants in a building. The life safety strategies and egress features required by prescriptive codes are based upon the number and location of occupants, and the building characteristics.

Table 56.2 Code mandated occupant characteristics

Life safety code	ICC performance code
Number of occupants	Number of occupants (LSC)
Length of occupancy	Sleeping characteristics
Response characteristics	Familiarity
Location	Vulnerability
Staff assistance	Relationships
Emergency response personnel	
Post-construction conditions	
Off-site conditions	
Consistency of assumptions	
Special provisions	

Most public buildings classified as Assembly, Business, and Mercantile occupancies by prescriptive building codes are assumed to contain people that are awake and generally capable of unassisted egress. Higher occupant densities associated with large crowds within Assembly buildings pose additional challenges and crowd manager requirements are included to address challenges associated with large crowds. Industrial and Storage occupancies are not typically open to the public and contain people that can be trained in the specific hazards present in the building. Residential occupancies contain occupants of all ages and may require awakening from sleep. Educational, Day Care and Ambulatory Health Care contain children or adults that may need assistance to respond appropriately. Health Care and Detention/Correctional buildings contain occupants that are restrained or incapable of response and may need to be protected in place.

Design Fire Scenarios Fire scenarios include a sequence of events that includes the fire location, source of ignition, and growth rate. If the fire continues to grow the event might reach flashover and full development, and finally decay and extinction. SFPE [52], Chaps. 26, 37, and 38 provide detail on development of design fire scenarios. The *Life Safety Code* [11] mandates use of eight (8) specific design scenarios, where applicable. Other references include the ICC Performance Code [35], NFPA 92, *Standard for Smoke Control Systems* [61], and Babrauskas and Grayson [62].

Develop Trial Designs (Step 6)

After the design scenarios are developed, the team develops trial designs. Trial designs may need to provide features to protect against hazards other than fire. Minimally, the trial design should include the development of clear intuitive egress components and features. Depending upon the level of analysis, a comprehensive and coordinated fire engineering strategy may be necessary to address structural fire protection, fire compartments, fire detection and notification fire suppression, interior finish, smoke control, and emergency power. Fire strategies can also rely upon controlling ignition and controlling the initial spread of fire. SFPE [52] provides additional detail on comprehensive fire strategies. NFPA 550, *Guide to the Fire Safety Concepts Tree* [63] can assist to identify comprehensive conceptual approaches.

Evaluate Trial Designs (Step 7)

The next step includes evaluating the trial design for compliance with the design objectives and performance criteria. For performance-based evacuation designs, this evaluation typically involves a review of Required Safe Evacuation Time (RSET) against Available Safe Evacuation Time (ASET). Required Safe Evacuation Time is the total time between notification of occupants that they need to move to a safe place and the time that the last occupant reaches that place. Available Safe Evacuation Time is the time between notification of the occupants and the onset of untenable conditions or other conditions that might impede egress or cause harm at any location that is occupied or will be traversed by occupants during egress. A timeline can be

developed to compare RSET and ASET for each design scenario.

SFPE [52] outlines a detailed process for evaluating trial designs. ASTM E1355 *Standard Guide for Evaluating the Predictive Capability of Deterministic Fire Models* [64] and "Guidelines for Substantiating a Fire Model for a Given Application," Society of Fire Protection Engineers [31] provide guidance on selecting tools for the analysis. Lord et al. [65] also provides guidance.

Analysis can follow probabilistic and deterministic approaches and outlines these methods. Refer to Chap. 37 and SFPE Engineering Guide to Fire Risk Assessment [60], for details on using fire risk assessment.

Hazard Assessment Fire growth simulation and smoke movement simulation can be used to estimate exposure to smoke, heat and thermal radiation. Other non-fire emergency and crowd related hazards can also be evaluated. Refer to Chap. 62 for information related to assessing and quantifying hazards associated with fire events.

Evacuation Overview Evacuation times consist of detection, notification, pre-movement, and movement times, and represents RSET. Figure 56.4 illustrates the evacuation process.

Detection and Notification The time between ignition of fire and the time for occupants to become aware of the situation is the detection and notification time.

Buildings with egress issues that are of particular concern typically require detection and notification systems. Detection can be through automatic systems, such as air sampling, smoke, heat, linear heat, projected beam, gas, radiant energy, video, multi-criteria, and multi-sensor detectors, sprinkler water flow devices, or through manual alarms. Chapter 40 and the National Fire Alarm Code Handbook [49] describe methods for calculating detection times.

Analysis should include transport lag time and system and detector processing times. Systems using positive alarm sequence and alarm verification should incorporate these inherent delays. The National Fire Alarm Code specifies a maximum time of 10 s for fire alarm systems to actuate alarm notification appliances or voice communication after a detection device activates. Positive alarm sequence allows a delay of up to 180 s for staff to investigate and evaluate conditions to determine if evacuation is necessary. Alarm verification allows a 60 s delay to reconfirm alarm conditions in smoke detectors and reduce unwanted alarms [30].

Audible notification can be through horns, bells, sirens, or speakers. Where a message is necessary to initiate evacuation or other action like shelter-in-place, the message needs to be audible and intelligible. Visual notification is required to alert hearing impaired occupants. Visual notification devices (strobes) are the most common. Textual and tactile appliances are also permitted. Examples of textual devices are private mode LCD devices or public mode messages in areas on large message boards. Examples of tactile appliances are bed shaking devices to wake hearing impaired occupants [30].

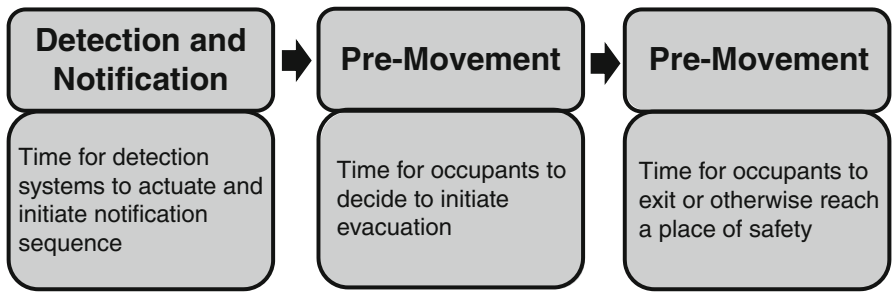

Fig. 56.4 Evacuation time

Pre-movement Time Pre-movement times, or delay times, start when occupants are notified and end when they start to evacuate or take other appropriate action that leads to evacuation. Pre-movement times are impacted by occupant activities prior to notification, method of notification, occupant training, staff assistance, and familiarity with the buildings. For example, a sleeping occupant would need to wake-up and get dressed before exiting. A mother, father, or caregiver would likely locate and assist their children before leaving.

Fahy and Proulx [66] reported actions performed by occupants after the 1993 bombing of the World Trade Center. The most frequent actions included: investigate, seek information, prepare to evacuate, alert others or report incident, assist others, seek refuge, and wait. Fahy [67] lists reasons occupants gave for not voluntarily leaving during this event: occupants "were waiting for information or instructions," occupants felt it was "better to wait or they were told to wait," occupants were not aware of the problem, occupants were "making sure others left," health reasons, "too much smoke," occupants were "waiting for better conditions," or occupants were "waiting for the fire department" as requested. Chapter 58 details pre-movement times.

Movement Time A broad range of engineering calculations are available from algebraic calculations suitable for simple egress systems to detailed models that incorporate behavior sub-models and graphically display results within the building. Regardless of the method employed, the process involves the estimation of the total evacuation time needed for all occupants to get to a safe place and the conditions to which they may be exposed during the evacuation. Models and engineering calculations are discussed in Chaps. 59 and 60; behavioral aspects of evacuation can be found in Chap. 58.

Speed of movement on horizontal egress components and stairs is well documented for non-disabled occupants. Data is available to simulate specific disabilities in Chap. 64. Movement speeds must be reduced to account for higher people densities, occupants exposed to smoke, and queuing at doors and other pinch points. While hand calculations can be used for simple systems, computer models may be necessary to account for higher occupant loads and complex designs.

Evaluate Results and Select Final Design The Required Safe Egress Time is compared with the Available Safe Egress Time to determine if sufficient time is available for occupants to escape, with appropriate safety factors. Results can also be used to determine areas of crowding, to estimate exit usage, and to input into evacuation plans and crowd management plans. When the stakeholders agree that the trial satisfies the objectives, and performance criteria, the final design is selected. To obtain a realistic yet conservative estimate of RSET, common actions and behaviors need to be explicitly included and factors of safety accounting for human variability need to be applied. The factors most often neglected in analyses are pre-movement times (or delay times) and factors of safety sufficient to account for expected variability.

Limitations Analysis of results should consider the limitations inherent with the methodologies. One limitation is that methods typically estimate the optimum egress times rather than simulate a range of expected egress times. Analysis may also need to account for non-simultaneous evacuation start times, uneven use of exits, complications associated with way finding, occupant interaction with smoke, temporary flow stoppages, merging flows, and counter flows. Chapter 64 contains additional information regarding limitations.

Safety Factors and Uncertainties Engineering models and analysis inherently contain limitations, simplifying assumptions, variability, and uncertainty. There may be variability in occupant reactions and behaviors. Models may be based

upon "best fit curves" to represent a set of data. Input data may introduce uncertainties. Assumptions may either increase or decrease the evacuation time or the time to onset of hazards. For example, doubling the fire size may result in predicting more smoke, but it may also decrease the predicted detection time. Using a single walking speed or a single flow through doors may not appropriately represent the range of expected occupant movement. The interaction and influence of these results may not be intuitive.

Safety factors provide one method of accounting for uncertainty and variability associated with limitations and simplifying assumptions inherent to engineering analysis. Safety factors are typically applied to the analysis results, as changes to specific parameters may have a non-linear effect on the results. For a discussion on addressing uncertainty with safety factors, see Frantzich [68].

Probabilistic approaches can be used to account for uncertainty and variability. Chapter 72 outlines risk informed analysis methods. Chapter 76 provides methods for understanding and accounting for uncertainty and variability.

Section 5.5.3.8 of the *Life Safety Code* [11] requires consideration of a design scenario that includes independently rendering each active or passive fire protection system ineffective. Examples include discounting a single stair, or discounting a single exhaust fan. Systematically testing scenarios with less than fully effective systems provides the designers with a better understanding of the consequences of these failures, which helps to understand the robustness and appropriateness of the selected safety factor.

Prepare Documentation (Step 8)

The final step is to document the analysis and design. SFPE [52] states that the following should minimally be included: project scope, designer's capability, goals and objectives, performance criteria, design scenarios, final design, evaluation, critical assumptions, critical design features, and references.

Design and Operational Considerations

The following outlines design and operational considerations for specific buildings and transport infrastructure.

Buildings and Transport Infrastructure

For some complex facilities, such as malls, healthcare facilities, detention and correctional facilities, following the prescriptive code can provide an acceptable and appropriate level of safety. Hospitals are among the most complex and highly regulated buildings due to the condition of most of the occupants. Since some or many patients must remain in their beds, most hospitals depend on horizontal exits to relocate occupants to a safe place on the same floor. For other buildings, a level of assessment beyond typical code compliance is warranted. The following suggests considerations for tall buildings, large assembly spaces, airports, rail stations, and rail and road tunnels. Life Safety Code Handbook [39], IBC Code and Commentary [40], NFPA 5000, Building and Safety Code [46], Appendix A of the ICC Performance Code for Buildings and Facilities [35], and Tubbs and Meacham [20] provide additional insight on a wide range of occupancies.

Systems Coordination and Integration Simple egress strategies provide safe evacuation through simple stair and exit discharge configurations, emergency notification, and emergency lighting. Complex evacuation strategies need to integrate and coordinate with the fire protection and life safety strategy. Comprehensive fire protection and life safety strategies include structural fire protection, fire-resistive compartmentation, fire detection, emergency communication and notification, fire suppression, smoke control, emergency lighting, and emergency power. These systems can have complex interactions. Based on these complexities, egress systems may need to be assessed even when the approach

does not directly relate to the egress systems [57]. Chapter 49 includes additional information on systems coordination and integration.

Tall Buildings Tall and super tall buildings pose particular challenges with respect to egress, as exiting through conventional stairway systems in tall buildings can mean walking down hundreds of flights of stairs. A portion of the population simply may not have the ability to travel down a stair system within a tall building, even with opportunities to rest along the way. Since passing in a crowded stair can be problematic, a person descending slowly due to physical limitations, injury or fatigue may delay everyone behind them.

Before the World Trade Center disaster, typical evacuation schemes for high-rise buildings included partial evacuation of only those occupants thought to be in immediate danger, by evacuating the 'fire' floor, along with one or two floors above and below the 'fire' floor. Code required stair widths have evolved to accommodate three to five floors evacuating simultaneously. If simultaneous full building evacuation from a tall building becomes necessary, it will involve a large number of people—many more than that anticipated by typical building egress designs. This inherent imbalance will result in significant delays and crowding in stairs [23].

The 2009 edition of the International Building Code introduced a requirement for buildings over 420 ft (128 m) in height to be provided with an additional stair to compensate for the high-rise fire-fighting practice of designating one of the stairs as the "attack stair" and fighting the fire from that position. The thought being that once firefighters start operations within the stair, the stair will become impassible at the level of the fire floor due to the presence of charged hose lines. These actions may contaminate the stair with smoke because the fire hoses will hold the door to the fire floor partially open. The IBC requirements further state that the required exit capacity must be met without the additional stair. Occupant additional evacuation elevators can substitute for the stair.

Large Assembly Spaces Large assembly facilities pose a range of competing challenges: airports need to balance security and continuity of operations with safety concerns, sports facilities need to balance sight-lines with providing safe steps for aisles serving seating, arenas and stadia need to provide guardrails to help prevent falls. There are many more examples.

Given the level of risk in large assembly spaces, the *Life Safety Code* [11] requires a Life Safety Evaluation when more than 6000 occupants are present, and when festival seating is used (e.g., when no seating is provided requiring patrons to stand or to provide their own seat). Both the I*nternational Building Code* [36] and *Life Safety Code* (2012a) require a Life Safety Evaluation when the reduced egress widths, increased aisle lengths, and increased travel distances allowed by smoke protected assembly seating are used. Life Safety Evaluations are required to include the following [11]:

- Nature of the events and the participants and attendees
- Access and egress movement, including crowd density problems
- Medical emergencies
- Fire hazards
- Permanent and temporary structural systems
- Severe weather conditions
- Earthquakes
- Civil or other disturbances
- Hazardous materials incidents within and near the facility

Crowd management also can be particularly important in directing the emergency actions of large crowds in assembly spaces. Fruin [69] defines crowd management as "... the systematic planning for, and supervision of, the orderly movement of people..." and provides a comprehensive discussion of crowd management. Information includes crowd communication, crowd motivation, the nature of crowds, crowd management centers, staff training, emergency response, responsibilities of performers, responsibility of staff, ticketing, owner/management duty to warn, appropriate space for occupants, occupant

metering, and ingress/egress pressure points [69]. The International Association of Venue Managers the NFPA Handbook for Fire Protection Engineering, NFPA 101, and Tubbs and Meacham [22] provide additional information on crowd management.

Rail Stations Rail stations are unique structures built to serve large transient occupant loads. In these facilities, customers tend to arrive in groups, based upon train arrival schedules. Stations can be at grade, above grade, or below grade. Underground stations pose greater challenges.

The approach described within NFPA 130, *Standard for Fixed Guideway Transit and Passenger Rail Systems* [45] is a hybrid between prescriptive and performance-based approaches. Specific aspects are prescribed, such as the maximum platform travel distance and maximum egress times, where other aspects are based on performance concepts, such as the occupant loads, egress widths, separations to adjoining spaces, and smoke management systems [20].

Occupant loads are based on ridership, and system surge factors are used to account for variability of arrivals to the station. Egress arrangements need to result in a maximum of four minutes to clear platforms, and a maximum of six minutes to reach a point of safety [45].

Rail and Road Tunnels Rail and road tunnels can be constructed through mountains, underwater, or under urban landscapes. Air-rights structures continue to be constructed over railways and roadways to create a tunnel. NFPA 130 and NFPA 502, *Standard for Road Tunnels, Bridges, and Other Limited Access Highways* address egress in rail and road tunnels. Means of egress include exits to grade at the exit portals, exit stairs discharging at grade, cross passage exit doors to adjacent tunnels, and exits to a protected exit passageway. The exiting strategy needs to be coordinated with the life safety program and specifically with the smoke management concepts [20].

Operational Concerns

Emergency Plans Emergency plans may include a wide range of events, including natural hazards such as hurricanes, tornados, tsunamis, winter storms, floods or flash floods, and earthquakes; technological events, such power outages, vehicle impacts, hazardous material releases, gas releases, and explosions; and deliberate events, such as civil disturbances, bomb threats, and acts of terrorism [70]. Depending on the facility, evacuation strategies may need to address some or all of these hazards. These considerations have led to more complex emergency plans and the need for real-time communication systems to direct occupants in the desired response. Despite this additional complexity, evacuation through protected stairways remains the primary strategy, since they provide safe, protected paths out of a structure.

Emergency planning for appropriate responses to specific threats is an active area that has evolved significantly in the past decade. When planning for events other than fire, risk assessment principles can provide guidance, in identifying and quantifying events [20].

- What threats are possible given the building location and use?
- How likely is each threat?
- What are the potential consequences?
- For each event, what strategies will limit the potential for harm to people?
- What holistic strategy provides an appropriate balance of safety?

In some cases, strategies need to balance the level of safety for differing events, as a strategy optimized for one event may not be appropriate for other events. This is particularly true for iconic buildings and spaces.

Evacuation Drills Evacuation drills are an important means of training occupants on what they are expected to do, especially where there are different responses to different threats. The US General Services Administration (GSA) is responsible for approximately 9600 federally owned or leased properties. The GSA conducts

two drills per year in every federal office building, with one a fire evacuation and the other an evacuation for some non-fire event.

In hotels, drills are important for training staff in their duties since staff are responsible for the safety of guests and it is not feasible to train guests in the procedures of the facility. Most fire codes include a requirement for regular drills, but often owners or operators terminate the drill early for fear of liability for injuring an occupant in a drill. For example, a review of high-rise drill requirements in fire codes conducted by NIST in their investigation of the September 11, 2001 WTC attacks revealed that drills conducted in New York City terminate with occupants meeting at the door to the egress stairs on their floor. In Chicago, occupants are required to enter the stairway and travel down not more than two floors. In Los Angeles occupants are required to follow the entire evacuation plan, traveling down stairs to the street level and gathering at the assembly point. This practice of following the complete plan is particularly important to familiarize the occupants with the entire egress system including any transfer corridors, and the exit discharge including assembly for accountability.

Summary

This chapter first overviewed the evolution of emergency egress provisions to provide a better understanding of current egress requirements and strategies. Next, considerations, concepts, and methods for egress strategies were outlined. Features and components that support and facilitate evacuation and protect in place methods are an essential component of building and transport infrastructure life safety strategies.

In summary, egress strategies need to be appropriate to the building design, safety features, function and use, and occupant characteristics. It is important that evacuation strategies coordinate with the overall fire and life safety strategy and specifically address occupants with disabilities or mobility impairments. Occupant evacuation elevators can be used to help occupants evacuate from tall and very tall buildings quickly and can assist those with mobility impairments. Various methods are available to assess evacuation times and are discussed in other Chapters. Evacuation times and queuing information developed as part of a timed evacuation assessment can be used to better understand the evacuation and crowd management concerns. This information can also be used as part of a performance-based evacuation design. Other chapters provide specific methodologies, data and detail to assess strategies and implement these concepts.

References

1. NFPA. (1914). Proceedings of the 18th Annual Meeting. Quincy, MA: National Fire Protection Association
2. Bukowski, R.W. (1997). "Progress Toward a Performance-Based Codes System for the United States." Applications of Fire Safety Engineering. Symposium for '97 FORUM. Proceedings. Tianjin, China: Tianjin Fire Research Institute and Shanghai Yatai Fire Engineering Co., Ltd.
3. NFPA. (1913). Proceedings of the 17th Annual Meeting. Quincy, MA: National Fire Protection Association
4. Bukowski, R.W. (2009). "NIST Technical Note 1623: Emergency Egress from Buildings." Gaithersburg, MD: National Institute of Standards and Technology
5. NBS (1935). Design and Construction of Building Exits. National Bureau of Standards Miscellaneous Publication M151. Washington. DC: National Bureau of Standards
6. NFPA (1927). *Building Exits Code*. NFPA 101-T. Boston, MA: National Fire Protection Association
7. Togawa, K. (1976). "Study on Fire Escapes Basing on the Observations of Multitude Current, in Building Research Institute of Japan, U.S./Japan Government Cooperative Program on Natural Resources (UJNR)." Panel on Fire Research and Safety. *Human Behavior* 2: 1-13
8. Pauls, J. L. (1997). "Building Evacuation and Other Fire Safety Measures: Some Research Results and their Application to Building Design and Regulation." McLean, VA: Environmental Design Research Association
9. Fruin, J.J. (1987). *Pedestrian Planning and Design*. (rev. ed.). Mobile, AL: Elevator World
10. Predtechenskii, V.M., Milinskii, A.I. (1978). Planning for Foot Traffic Flow in Buildings. New Delhi: Amerind Publishing

11. NFPA (2012). NFPA 101: *Life Safety Code*®. Quincy, MA: National Fire Protection Association
12. Templer, J. (1974). Stair Shape and Human Movement. Ph.D. dissertation. Colombia University
13. Templer, J., Mullet, G.M., Archea, J., Margulis, S.T. (1978). An Analysis of the Behavior of Stair Users. NBSIR 78-1554. Washington, DC: National Bureau of Standards
14. Blondel, F. (1675-1683). Cours d'Architecture Enseigne dans l'Academie Royale d'Architecture, Paris.
15. Templer, J. (1994). *The Staircase, Studies of Hazards, Falls, and Safer Design*. Cambridge, MA: MIT Press:
16. Bukowski, R.W., Kuligowski, E.D. (2004). "The Basis for Egress Provisions in U.S. Building Codes." Edinburgh, UK: InterFlam
17. De Forest, R.W. and Veiller, L. (1903), *The Tenement House Problem* (New York: Arno Press, 1903), 230-1.
18. New York Times (1860), Calamitous Fire, February 3, 1860, Proquest Historical Newspapers, http://proquest.umi.com
19. Hall, J. (2006) Significant Fires Involving Egress, historical data summary provided to ASME Emergency Operations task groups.
20. Tubbs, J., Meacham B.J. (2007). *Egress Design Solutions: A Guide to Evacuation and Crowd Management Planning*. Hoboken, NJ: John Wiley and Sons
21. Tubbs, J., Meacham, B.J. (2008) "Evacuation Design Strategies and Considerations for Tall Buildings: Suggested Best Practices." ASHRAE Transactions. Atlanta, GA: American Society of Heating, Refrigeration and Air Conditioning Engineers
22. Tubbs, J., Meacham, B.J. (2008). "Selecting Appropriate Evacuation Strategies." Consulting-Specifying Engineer, Reed Elsevier Inc., September Vol. 44, No. 3, p 20-28
23. Tubbs, J., Meacham, B.J. (2009) "Selecting Appropriate Evacuation Strategies for Super Tall Buildings: Current Challenges and Needs." Proceedings of the 4th International Symposium on Human Behaviour in Fire. London: Interscience Communications Ltd
24. Bukowski, R.W. (2010). "Addressing the Needs of People using Elevators for Emergency Evacuation", Fire Technology, Special issue containing selected papers from the NIST Pedestrian Dynamics Conference
25. Meacham, B.J. (2009). "Application of Adaptive Management Concepts to Building Evacuation and Emergency Response." Proceedings of the 4th International Symposium on Human Behaviour in Fire. London: Interscience Communications Ltd.
26. Pauls, J., Groner, N., Gwynne, S., Kuligowski, E., Meacham, B., Proulx, G., Ripley, A., Thomas, I. (2009). "Informed Emergency Responses through Improved Situational Awareness, Discussion Panel Paper." Proceedings of the 4th International Symposium on Human Behavior in Fire, London: Interscience Communications Ltd.
27. Kuligowski, E.D., Gwynne, S.M., Butler, K.M., Hoskins, B.L., Sandler, S., (2012). NIST Technical Note 1733: Developing Emergency Communication Strategies for Buildings, Gaithersburg, MD: National Institute of Standards and Technology.
28. ICC (2012) *International Fire Code*. Falls Church, VA: International Code Council
29. NFPA (2010). NFPA 1600: *Standard on Disaster/Emergency Management and Business Continuity Programs*. Quincy, MA: National Fire Protection Association
30. NFPA (2013). NFPA 72: *National Fire Alarm and Signaling Code*. Quincy. MA: National Fire Protection Association
31. SFPE Engineering Guide to Substantiating a Fire Model for a Given Application, Bethesda, MD: Society of Fire Protection Engineers.
32. Proulx, G. 2001. "High-Rise Evacuation: A Questionable Concept?," Human Behaviour in Fire – Understanding Human Behaviour for Better Fire Safety Design, Proceedings of the 2nd International Symposium, London: Interscience Communications, Ltd., pp. 221-230.
33. MacDonald, J.N. (1985) Non-evacuation in compartmented fire resistive buildings can save lives and its makes sense, NBS SP83-1985.
34. DHS (2008) Active Shooter: How to Respond. Washington, DC: US Department of Homeland Security
35. ICC (2012b) *International Code Council Performance Code*. Falls Church, VA: International Code Council
36. ICC (2012a). *International Building Code*. Falls Church, VA: International Code Council
37. HMG (2012) Building Regulations 2012, Approved Document B (Fire Safety), England: HM Government
38. FEMA and USFA. (1993). *Emergency Procedures for Employees with Disabilities in Office Occupancies*. FA-154 and FA-154s, United States Fire Administration Emmitsburg, MD:
39. Coté, R. and Harrington, G. (2012). Life Safety Code Handbook, Quincy, MA: National Fire Protection Association.
40. ICC (2012d). *International Building Code and Commentary (Vol 1 and 2)*. Falls Church, VA: International Code Council
41. Averill, J. (2005). "Occupant Behavior, Egress, and Emergency Communications." Federal Building and Fire Safety Investigation of the World Trade Center Disaster. Gaithersburg, MD: National Institute of Standards and Technology
42. Bukowski, R.W. and Li, F. (2010). "Use of Elevators in Fires." Consulting Specifying Engineer, February 2010
43. Bukowski, R.W. (2010), International Applications of Elevators for Egress in Fires, Proc SFPE Engineering Technology Conference, October 2010 and ASME Workshop on Elevators in Fires.
44. ASME. (2010). ASME A17.1 / CSA B44 Safety Code for Elevators and Escalators. New York, NY: American Society of Mechanical Engineers

45. NFPA (2010). NFPA 130: *Standard for Fixed Guideway Transit and Passenger Rail Systems*. Quincy, MA: National Fire Protection Association
46. NFPA (2012b). NFPA 5000: *Building and Safety Code*. Quincy, MA: National Fire Protection Association
47. Proulx, G. (2000) Strategies for Ensuring Appropriate Occupant Response to Fire Alarm Signals, NRCC Construction Technology Update No. 43.
48. Kuligowski, E.D. (2011) Elevator Messaging Strategies, Fire Protection Research Foundation Report, Quincy, MA: Fife Protection Research Foundation
49. Richardson, L., Roux, R. (2010). National Fire Alarm and Signaling Code Handbook. Quincy, MA: National Fire Protection Association
50. GSA (2010). Facilities Standards for the Public Buildings Service (P100) Washington, DC: US General Services Administration
51. Walton, G., Dols, W. (2010). NISTIR 7251. CONTAM. USER Guide and Program Documentation. Gaithersburg, MD: National Institute of Standards and Technology
52. SFPE (2007). *SFPE Engineering Guide to Performance-Based Fire Protection*. Bethesda, MD: Society of Fire Protection Engineers
53. SFPE (2010). *SFPE Engineering Guide to Human Behavior in Fire*. Bethesda, MD: Society of Fire Protection Engineers
54. SFPE (2009). *SFPE Guidelines for Peer Review in the Fire Protection Design Process*. Bethesda, BD: Society of Fire Protection Engineers
55. Sime, J. D. (2001). "Advancing Human Behavior Theory: Visual Access and Occupancy Research, Modeling and Applications," 2nd International Symposium on Human Behavior in Fire. London: Interscience Communications Ltd.
56. NFPA (2010). NFPA 914: *Code for Fire Protection of Historic Structures*. Quincy, MA: National Fire Protection Association
57. Tubbs, J. (2004). "Pedestrian Movement and Safety," in *Performance-Based Building Design Concepts*, Meacham, B.J. Ed. Falls Church, VA: International Code Council
58. Kuligowski, E. (2009). "NIST Technical Note 1644 – Compilation of Data on the Sublethal Effects of Fire Effluent." Gaithersburg, MD: National Institute of Standards and Technology
59. Robbins, A., Gwynne, S., Kuligowski, E. "NIST Technical Note 1743: Proposed General Approach to Fire-Safety Scenarios." Gaithersburg, MD: National Institute of Standards and Technology
60. SFPE (2006). *SFPE Engineering Guide to Fire Risk Assessment*. Bethesda, MD: Society of Fire Protection Engineers
61. NFPA (2012). NFPA 92: *Standard for Smoke Control Systems*. Quincy, MA: National Fire Protection Association
62. Babrauskas, V.; Grayson, S. (1992) *Heat Release in Fires*. New York, NY: Elsevier Applied Science
63. NFPA (2012). NFPA 550: *Guide to the Fire Safety Concepts Tree*. Quincy, MA: National Fire Protection Association
64. ASTM (2012). ASTM E1355 Standard Guide for Evaluating the Predictive Capability of Deterministic Fire Models. West Conshohocken, PA: ASTM International
65. Lord, J., Meacham, B. J., Moore, A., Fahy, R. F., Proulx, G. (2005). "NIST GCR 06-886 – Guide for Evaluating the Predictive Capabilities of Computer Egress Models." Gaithersburg, MD: National Institute of Standards and Technology
66. Fahy, R.F., Proulx, G. (2009) "Panic and human behavior in fire" Proceedings of the 4th International Symposium on Human Behaviour in Fire. London: Interscience Communications Ltd.
67. Fahy, R.F., Proulx, G. (1995) Collective common sense: a study of human behavior during the World Trade Center evacuation. NFPA J 89(2):59–67
68. Frantzich, H. (1997). "Uncertainty and risk analysis in fire safety engineering." PhD Dissertation, *LUND UNIVERSITY OF TECHNOLOGY, LUND (SWEDEN). 208*: 208.
69. Fruin, J.J. (1993). "The Causes and Prevention of Crowd Disasters." Proceedings of the International Conference on Engineering for Crowd Safety. London: Elsevier Science Publishers
70. FEMA (1993). Emergency Management Guide for Business and Industry. Washington, DC: Federal Emergency Management Agency

Richard W. Bukowski is a Senior Consultant with Rolf Jensen and Associates and has authored numerous publications on elevator egress systems and strategies.

Jeffrey S. Tubbs is a Principal with Arup in Boston and is an author of the text *Egress Design Solutions: A Guide to Evacuation and Crowd Management*.

Selecting Scenarios for Deterministic Fire Safety Engineering Analysis: Life Safety for Occupants

57

Daniel Nilsson and Rita Fahy

Introduction

In many cases, the principle goal of a fire safety engineering (FSE) design is the life safety of the users of a structure. There are, however, other potential fire safety goals to consider, e.g., property protection, continuity of operations, protection of the environment and protection of cultural heritage [1]. Whatever the goal, users of the building, both building managers and occupants, will have a role in its achievement.

The process of evaluating an FSE design involves the development of scenarios that will test the ability of building protection and other design features to meet the fire safety goals of the analysis. The evaluation of the design involves comparing the predicted development of fire and smoke for a selected set of design fire scenarios against the time required to move any occupants to locations of safety. Little attention has been focused in the past on the combinations of occupant characteristics and other factors that would constitute '*design occupant scenarios*' analogous to design fire scenarios.

The selection of fire scenarios for fire safety engineering (FSE) analysis is outlined in Chap. 38 of this handbook. As discussed in that chapter, there are several fundamental fire safety goals for a building, one of which is to provide life safety for building occupants. This chapter will refine the fire scenario selection process for the specific fire safety goal of life safety for the occupants by showing the designer how to consider egress issues through each step. The aim of this chapter is (1) to provide the designer with a systematic method of incorporating occupants in the design fire scenario selection process, and (2) to give guidance on how, in this process, to identify specific occupant characteristics that should be included in the subsequent analysis, i.e., determine the design occupant scenarios that should be analyzed with each design fire scenario.

Chapter Outline

In the initial part of this chapter (section "Use of Deterministic Analysis in FSE Design"), a general description of the use of deterministic analysis in FSE design is given. This is followed by a section which highlights the importance of a clear definition of the context of a FSE analysis before the scenario selection process is initiated (section "Informing the Scenario Selection Process: Establishing the Context"). In this section, an example illustrating the complexity of scenario selection for the goal of providing life safety for building occupants is also presented. In subsequent sections, the scenario selection process is described in detail (section "Scenario Selection Process") and an example of the selection of scenarios for a hypothetical building is presented (section "Example"). The example is

D. Nilsson (✉)
Lund University

R. Fahy
National Fire Protection Association

M.J. Hurley (ed.), *SFPE Handbook of Fire Protection Engineering*,
DOI 10.1007/978-1-4939-2565-0_57, © Society of Fire Protection Engineers 2016

an expanded version of a sub-set of the scenario selection example presented in Chap. 38 of this handbook.

The scenario selection process described in this chapter is based on the procedure outlined in the document ISO/TS 16733—Selection of design fire scenarios and design fires [2]. However, the procedure is only described for the specific fire safety goal of life safety for occupants, and it focuses on the appropriate incorporation of occupants in the scenario selection process.

Use of Deterministic Analysis in FSE Design

In performance-based FSE design, the designer needs to show that the proposed design delivers a sufficient level of safety. This is often done using some form of risk analysis, but these risk analyses can vary in complexity from simple qualitative reasoning to full quantitative risk analyses [3, 4]. In many cases, a deterministic analysis is chosen because it involves a manageable number of scenarios that can be handled with reasonable work effort.

In deterministic analyses, the hazards are mainly described in terms of their consequences [5], which corresponds to level 2 according to the classification by Paté-Cornell [6] of treatment of uncertainty in risk analyses. (Level 2 is defined there as 'quasi-worst case' or 'plausible upper bounds.') The deterministic analysis, sometimes also called scenario analysis, can be compared to putting the building through a severe fire test. If the proposed building design passes the test, it has also been shown that it will survive most other fires according to the deterministic analysis. Because it is imperative that the included scenarios represent the worst credible cases, it is essential that the scenario selection process is both thorough and systematic.

A deterministic analysis hence involves the selection of severe but reasonable scenarios that challenge the proposed fire safety design of the building. The fact that the scenario should challenge the design means that it must be chosen in relation to the goal of the analysis. For example, if the goal is to provide life safety for building occupants, a small and limited trash fire close to the main exit might be highly relevant as it can block the most important means of escape. However, the same fire is probably not particularly relevant, due to its limited size, if the goal is to prevent structural collapse of the building.

When the goal is to provide life safety for building occupants, the building use and users will always influence which fire scenarios are relevant. This is illustrated by the example above involving the small trash fire at the main exit. It is well-recognized that people tend to use the main exit in case of emergencies [7]. Hence, the fact that the building has a main exit (building use) and the fact that people tend to use the main exit in emergencies (behaviour of users) makes the fire scenario suitable for deterministic analysis, i.e., a credible scenario that severely challenges the fire safety design. The selection of this particular fire scenario also implies that the designer has already started to consider possible occupant scenarios. In this particular case, an occupant scenario involving building occupants initially heading towards the main exit is considered highly relevant, and it is the reason that the small trash fire is considered in the analysis.

In FSE analyses, designers often spend a lot of time and effort on the fire problem, e.g., estimating design HRR curves or simulating smoke spread, but occupant aspects may not always be incorporated appropriately in the design. As illustrated by the trash fire example above, there is always an occupant scenario paired with each fire scenario. This means that the selection of fire scenarios and occupant scenarios for deterministic analysis cannot be done independently, but it is instead a process of finding combined scenarios, i.e., coupled fire and occupant scenarios, which challenge the proposed fire safety design.

Informing the Scenario Selection Process: Establishing the Context

Before scenario selection begins, there are three elements that must be specified—the project scope, the Fire Safety Goals (FSG) and the Fire Safety Objectives (FSO)—because they dictate which scenarios are relevant for consideration in the deterministic analysis. These elements are therefore explained below, followed by a case showing that the scenario selection process is not always simple and straightforward.

Because deterministic analysis involves the identification of the worst credible cases, it is of fundamental importance to know (1) what should be protected (FSG), and (2) how this can be achieved (FSO). As previously mentioned, a deterministic analysis can be compared to putting the building through a severe fire test. This test will be different depending on what aspect is evaluated.

Project Scope

Every performance-based design process starts off with the definition of the project scope [8]. The scope is the project context, e.g., if it is an entirely new building or an existing building, if it involves the whole building or just specific components, etc. Proper definition of the project scope is important since it dictates the boundaries of the analysis. The scope is always project specific, and so for the purposes of this chapter, it will be assumed that it has been defined and will not be discussed further.

Fire Safety Goal (FSG)

The FSG, which is defined next in the performance-based design process, is often expressed in quite general terms. It describes the focus of the analysis, i.e., what is worth protecting? Examples of goals can be to protect property, the environment and/or occupants. In this chapter, only the goal to provide life safety for building occupants is treated. This definition of the FSG will inform the scenario selection process.

Fire Safety Objective (FSO)

Based on the FSG, the FSO is then defined. The FSO can be seen as a specification of how the goals will be achieved. Examples of objectives for life safety are that people should not be exposed to specified critical fire conditions, e.g., heat and smoke, or that queuing time should be within defined limits. In this chapter, only the objective to not expose people to critical fire conditions will be treated since this is an often-mentioned objective in rules and regulations [9, 10].

Specific critical fire conditions, i.e., performance criteria, are sometimes given in rules and regulations [9] and often involve limiting values (or doses) for temperature, radiation, toxic gases, visibility and/or smoke layer height [9, 11, 12]. In this chapter, however, critical fire conditions are not specified, but they are assumed to involve limiting values (or doses) related to the effects of fire.

Discussion of Scenario Relevance: A Case Study

Before presenting the steps required for selecting design scenarios, it is important to emphasize that the analysis is an integrated process, where the designer has to consider the fire, building uses and users simultaneously. The choice of scenarios is not necessarily intuitive. It is not sufficient to merely choose the biggest fire, i.e., the fire with the fastest growth rate or the highest peak heat release rate. Such a fire will not necessarily be the fire that presents the greatest challenge when the FSG is life safety for building occupants. For example, it might instead be a smaller fire close to the main entrance, e.g., in the foyer of a hotel, that presents the greatest risk of exposing evacuating occupants to critical fire conditions, i.e., that challenges the achievement of the FSO.

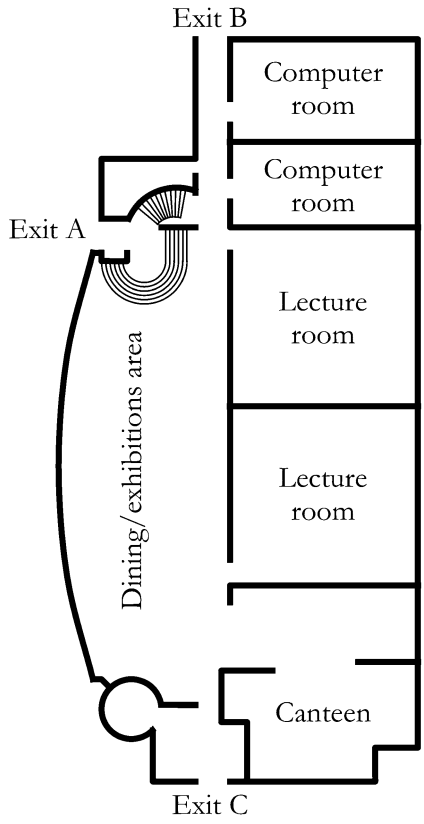

Fig. 57.1 Ground floor of the building

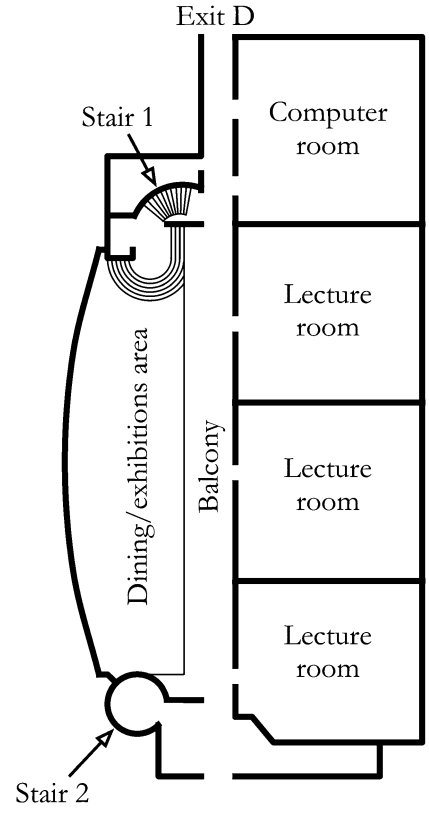

Fig. 57.2 Upper floor of the building

One example that illustrates the complexity of scenario selection is a case study involving cable fires in a university building [13]. The goal of the study was to select the fire scenario that would most severely challenge the FSG, which in this case was life safety for building occupants.

The structure is an existing four-story university building with lecture rooms, computer labs, offices, a small food service area and a combined dining/exhibition area. However, only the combined dining/exhibition area and the adjacent food service area, lecture rooms and computer labs were included in the analysis, see Figs. 57.1 and 57.2. This part of the building covers two floors, referred to as the ground floor and the upper floor. The dining/exhibition area, which has a slanted ceiling, is open from the ground floor to the balcony on the upper floor, see Fig. 57.3.

As the fire under consideration involved burning cables in a vertical cable tray, the heat release rate of the fires was prescribed. Hence, the main variable for the analysis was determining the fire location. Based on an inventory of the fire load in the building, i.e., locations where a significant amount of cable would be expected, it was clear that there were only a limited number of areas where fire could be expected to occur.

A pilot study of people's movement patterns in this building revealed that Exit A is the main exit for most people going to the food service area, lecture rooms and computer labs. People using the lecture rooms on the upper floor most often use Stair 1, which is a spiral staircase in the open area of the dining/exhibition area, near Exit A. This means that the dining/exhibition area is a location that most people pass through every day and therefore also the preferred evacuation route in emergency situations. A key feature in any building is the main exit/entrance of the building, as it is well-established that people tend to move

Fig. 57.3 View of the dining/exhibitions area of the building from the top of Stair 2

towards familiar exits in emergencies [7]. This makes a fire in the dining/exhibition, or the adjacent food service area (no fire separation), most challenging for the achievement of the FSO.

Given that most occupants would move toward Exit A, it might make intuitive sense simply to place the ignition point in the foyer at the exit. In this case study, however, a number of different specific fire locations within the dining/exhibition area and food service area were identified, and the most challenging of these was found with the help of CFD simulations.

The food service area was the first fire location that was tested, see Fire Location I in Fig. 57.4. This location was chosen since it has many possible ignition sources as well as many areas with a considerable amount of cables. CFD simulations showed that smoke spread out through the opening between the food service area and the dining/exhibition area, creating a wide plume at the balcony. Eventually, a relatively well-mixed smoke layer was created at the balcony on the upper floor. Although this smoke layer would engulf people on the balcony, the smoke would not be very dense, according to the simulations.

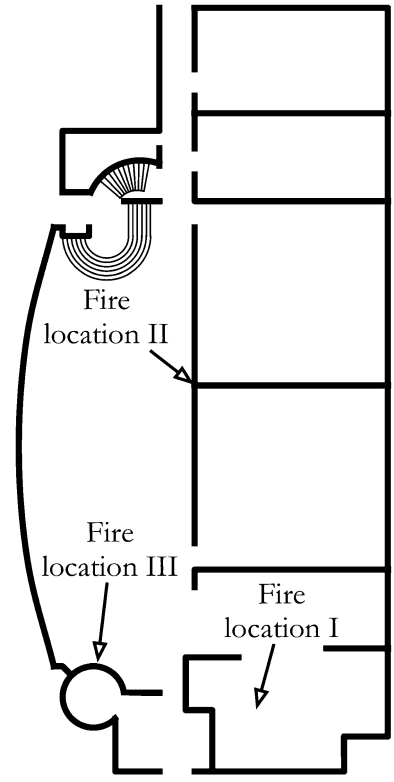

Fig. 57.4 Fire locations in the building (ground floor)

The second fire location was a cable shaft underneath the balcony at the ground floor, see Fire Location II in Fig. 57.4. This location was chosen mainly because of the considerable amount of cables in the cable shaft. CFD simulations of the smoke spread showed that a relatively wide balcony plume was generated, which eventually led to a smoke layer that covered the upper part of the balcony. The conditions in the smoke layer were considerably worse than for the fire in the canteen, which makes it a more challenging scenario in relation to the FSO.

The third and final fire location was close to the food service area but in the part of the dining/exhibition area with the slanted ceiling, see Fire Location III in Fig. 57.4. This location was chosen because cables can be expected during exhibitions and a fire occurring at that time could potentially threaten large numbers of people. CFD simulations of the smoke spread revealed that, once the plume hit the slanted ceiling, the smoke travelled along the ceiling towards the balcony. At the balcony the smoke hit a structural beam, which created a swirl that made the smoke move very rapidly along the ceiling at the balcony towards Stair 1. On hitting the wall, the smoke was pushed down quickly, creating severe conditions at the top of Stair 1.

The third fire location was deemed to be the most severe as it involves a conflict between smoke spread and evacuation. The conditions quickly became severe at the top of Stair 1, which is most likely the preferred evacuation route for people in the lecture rooms on the upper floor. Also, these people could be expected to still be moving through that area. Another important issue is that the fire is located in the far end of the dining/exhibition area, i.e., away from Stair 1, which means that people will move towards Stair 1 if they try to move away from the fire. Also, the rapid deterioration of the conditions at the top of Stair 1 means that people might be caught by the smoke. This conflict between evacuation and smoke spread makes the fire in the dining/exhibition area, under the slanted ceiling, the scenario that most severely challenges the FSO.

In this case study, simulations were used to determine the most challenging fire location, and showed that the most challenging location was not the one that conventional wisdom might have led the designer to choose. Simulations are not always necessary, and the selection process can be based on simpler and more straightforward approaches, e.g., theoretical reasoning. As illustrated by the case study, it is, however, an iterative process that considers both occupant and fire aspects simultaneously. This is necessary for finding the scenarios that challenge the achievement of the FSO. In order for the selection process to be possible, the designer hence needs to know the characteristics of the building users, which depend on the building features and building use.

Scenario Selection Process

After the FSG and FSO are defined, the scenario selection process begins. A key element in appropriate scenario selection for life safety of occupants is to carefully consider the expected *uses* of the building and the type of people who would, as a result, be the expected *users* of the building.

Selection of fire scenarios has often not tied the process as specifically to a particular building design as is necessary for the selection of scenarios for life safety. The focus on a particular design is necessary in order to assist the designer in considering the full range of users, and the variation in the types of users, who might occupy the building and need protection.

Identification of Building Uses

Specifying the building use can be simple (and almost trivial) for a single-use building. It is, however, still important to focus on the function a building is intended to fulfil, in order to fully account for the types of people who will use that building. Most buildings with engineered design will likely have multiple uses, for example, a hotel with sleeping rooms, meeting spaces,

restaurants, pool, etc., or an arena suited for various uses such as sporting events, conventions, entertainment, etc.

One illustrative example of a building with multiple uses is an arena and events centre [14]. This type of building may host a wide range of events, e.g., everything from sporting events to conferences, which in turn will influence the number and composition of occupants. It is therefore imperative for the designer to list all uses that the building is designed for. This is particularly important for structures that are inherently multi-functional, e.g., transit stations, airports, shopping malls, etc. For example, a typical transit station may contain functions such as a bus station, rail station, parking area and shops. Each of these functions or uses of the transit station might be associated with distinctly different users.

The use of a building is not only linked to the abovementioned functions, but also depends on the internal building layout. This layout influences how people move in the building during normal operation, i.e., the circulation paths, and how they usually enter and exit. There might also be specific functions that are important waypoints during everyday use, e.g., a parking garage in a shopping mall or the cash desk in a store. Since everyday physical use also influences the physical use in emergency situations, e.g., the egress paths and choice of exits [7, 15], it is imperative that the designer is familiar with the expected physical use and identifies the:

- *circulation paths*,
- *main exits/entrances*,
- *important waypoints*

Ideally, the emergency egress design of a building should be based on the everyday physical use, but for technical reasons this might not always be possible. When possible, it makes perfect sense to use the everyday exit/entrance of a building as an emergency exit, however, legislation might require a certain maximum length of egress paths, which can result in the installation of several emergency exits between a person's original position and the main exit/entrance. When these emergency exits are not used regularly during everyday building operations, they are likely to be overlooked or ignored during emergency evacuations [15, 16]. They still are an integral part of the emergency egress design, but the designer cannot assume that unfamiliar building features will always be used in an emergency. This is hence an example of why it is essential for the designer to always identify the expected physical use of the building.

Identification of Users and Their Characteristics

The *uses* of the building should provide a strong indication of the expected *users*. Once the uses of the building have been specified, the next step is to consider the types and numbers of people who will make use of the building in those ways.

Inventory of Characteristics

For the purpose of this chapter it is appropriate to divide occupant characteristics into the following categories:

- *permanent/transitory*,
- *trained/untrained*,
- *potential age ranges*,
- *cognitive*, *sensory or mobility issues*,
- *potential vulnerabilities*,
- *awake/asleep/unconscious/intoxicated*,
- *social groupings or not*,
- *role*

The number of people in any category for any characteristic will vary over time. As part of the scenario selection process, the designer must be aware of the distributions of occupant characteristics that may be present.

For example, a hospital would have permanent staff and transitory patients (in some expected proportion); the staff should be trained, the patients would not be; the staff would be working age, the patients' ages would depend on the hospital's specialities; the staff would have an expected distribution of physical disabilities, the patient vulnerabilities would depend on the hospital's speciality; the variability in the composition of the occupant groups would be limited to what would be expected for the hospital's speciality, i.e., the patients would all be sick or injured to some degree.

Similarly, a hotel would have a permanent staff and transitory guests (in some expected proportion); the staff should be trained, the guests would not be; the staff would be working age, the guests could be any age but generally mostly adults; the staff would have an expected distribution of physical disabilities, the guests could have any disabilities and the proportion of guests with disabilities could range from low to high; the hotel guests would be using sleeping rooms as well as function rooms/public spaces and would vary widely—function rooms full of children, drinkers, meetings of people with disabilities need to be considered; sleeping rooms could be filled with guests with special needs attending conferences, possibly.

Shopping centres and offices would have permanent staff and transitory customers and visitors who might have some familiarity with the space (in some expected proportion). The permanent staff may or may not be trained, but the customers and visitors would not. Again, there would be variation in the distribution of occupants with disabilities and of different age groups. All occupants would be awake. The potential for occupants to be intoxicated would have to be considered.

Why These Characteristics Are Issues

Each of the characteristics listed above are important because of the impact they can have on evacuation. These impacts can affect awareness of cues, including alarms, delay times after notification but before movement to exits, travel speeds and vulnerability to toxic exposures, etc. These effects can vary over time and the designer must take this variance into consideration in the scenario selection. A brief description of the eight characteristics is given below:

- *permanent/transitory*—Permanent staff or residents can be expected to be more familiar with a building and its systems than people who are in a building only once or occasionally. This can affect each occupant's ability to recognize alarm signals, identify alternate escape routes, or have any familiarity with a building's emergency management plan. Permanent occupants who are familiar with a building may provide guidance to transitory occupants, either proactively or simply by example, but if they are vastly outnumbered by transitory occupants, that effect may be muted.
- *trained/untrained*—Trained occupants should be familiar with a building's emergency management plan, its alarm signals, procedures and emergency exits. Designers dealing with a building with many untrained people cannot assume that their reactions and actions will be optimal.
- *potential age ranges*—Mobility, sensory and cognitive ability vary with age. Children and those with age-related cognitive issues cannot be assumed to make independent decisions that will lead to self-rescue. Young children will need assistance in evacuating a building, and they and older adults may move more slowly than others. The ages of people present in the building can vary with the current use of a building. For example, an assembly property can be used by an audience of adults or an audience of children or families, with very different ranges of cognitive abilities.
- *cognitive*, *sensory or mobility issues*—Some of the building users may have disabilities not related to age that would affect their ability to perceive or recognize fire cues and/or react to an emergency. These occupants can be either permanent or transitory users of the building.
- *potential vulnerabilities*—The effect of toxic products can vary according to the vulnerability of those exposed, so the designer must recognize that there will be some range of vulnerability among the building users, i.e., one cannot assume that all building occupants will be healthy adults who will be able to tolerate the same level of smoke or other products of combustion.
- *awake/asleep/unconscious/intoxicated*—People who are asleep are likely slow to respond to fire cues [17]. If people sleep through much of a fire incident, the evacuation conditions can be very challenging when they wake up and decide to escape. The fact that people

can be intoxicated might make the problem even worse since studies have shown that even small amounts of alcohol influence the probability of people waking up from a fire alarm [18]. Alcohol has also been shown to impair decision making abilities and increase reaction time [19].

- *social groupings or not*—family groups will assemble before evacuating and will likely move together, at the speed of the slowest member, so the presence of family groups can have an impact on evacuation [7]. This may be true of other groups as well, e.g., friends, colleagues, etc. Social influence has an impact on decision making, so the presence of groups, or of a high proportion of occupants present on their own, can affect how rapidly cues are acted upon [20].
- *role*—It has been observed in real fires that occupants may continue to function in certain roles, particularly those they fill during the normal use of the building; for example, servers in a restaurant assisting the guests at their tables, and the guests looking to the servers for guidance [21]. Similarly, students may look to teachers for guidance, employees may look to managers or supervisors, etc.

The types of people using a building, i.e., the proportion of people in those listed categories, may vary over time. For example, the guests registered in a hotel could be family groups one week and convention attendees another week. Depending on the appeal of special events, the proportion of the occupant population with certain issues or vulnerabilities can vary widely. In places such as specialized hospitals, where the characteristics of the occupants will tend to be the same over time, the number of occupants and the presence of staff might vary.

Determination of Life Safety Challenges

Because the aim of the deterministic analysis is to test the fire safety design using a selection of severe but credible scenarios, it is imperative to identify any issues or conflicts that, in combination with fire, could potentially lead to the failure of the design. These issues and conflicts are referred to here as *life safety challenges*. Such issues are often occupant characteristics that lead to non-optimal response or movement in emergency situations. Conflicts often involve a mismatch between building uses and users or between users and building layout.

An example of an issue that can result in a life safety challenge is intoxication. It has been shown in previous studies that alcohol has an effect on a person's ability to waken and respond to an alarm [18]. Intoxication can therefore pose an important life safety challenge in a hotel where guests can be expected to be asleep. Similarly, a designer will have to consider the effect of large numbers of intoxicated occupants who might be using any place of assembly, either free-standing, e.g., a concert venue, arena or nightclub, or part of a larger complex, e.g., a hotel ballroom.

One example of a life safety challenge involving the conflict between the building layout and building users may occur if people with movement impairments are forced to evacuate via the stairs. If the elevators cannot be used for evacuation, wheelchair users might not be able to leave their floor in case of a fire. Although, it is possible to wait in protected evacuation stairs, this is not an optimal situation for wheelchair users. Similar problems also apply to people who do not use wheelchairs but have other types of movement disabilities.

A typical life safety challenge involving a conflict between building uses and users is people's tendency to use familiar exits [7]. This tendency means that people will try to move towards the main entrance/exit, which is a potential major evacuation bottleneck in case of fire. A fire that quickly renders the main entrance unusable is therefore a scenario that severely challenges the fire safety design.

The case study in section "Discussion of Scenario Relevance: A Case Study" showed that uncovering the life safety challenge of a design is an iterative process that requires consideration of the building layout, fire, building use and users. In that case, the placement of the fire resulted in a choice of exits that itself resulted in a dangerous bottleneck.

Steps in Selecting Scenarios

Once the building uses and users, as well as the relevant life safety challenges, have been identified, the scenario selection process described in Chap. 38 of this handbook can be initiated. This selection is based on the 10-step procedure described in the document ISO/TS 16733. The 10 steps are listed in Table 57.1.

For deterministic analyses, the first five steps involve identification of the fire-related factors/aspects that most severely threatens the achievement of the FSO. The identification of these factors/aspects is always done in relation to the life safety challenges. In steps 6 to 10, the factors/aspects are combined into fire scenarios from which design fire scenarios are then selected.

Table 57.1 Steps in the scenario selection process according to ISO TS 16733

SCENARIO SELECTION PROCESS in ISO TS 16733
A process for selecting design fire scenarios and design fires involves 10 steps:
Step 1—Location of fire Identify the location of the fire
Step 2—Type of fire Specify the type of fire, e.g., initial intensity, rate of growth, items involved, etc.
Step 3—Potential fire hazards Consider potential fire hazards associated with the use of the property or design
Step 4—Systems and features impacting on fire Identify fire safety systems and features that can impact fire growth and smoke spread
Step 5—People response Occupant response following ignition, i.e., responses impacting on fire
Step 6—Event tree Construct an event tree that represents the sequence from ignition to outcome
Step 7—Consideration of probability Consider the probability of each event in the event tree
Step 8—Consideration of consequence Estimate the consequence of each scenario
Step 9—Risk ranking Rank the scenarios in order of risk
Step 10—Final selection and documentation Final selection of design scenarios and documentation of the reasons for selection
Steps 6 to 10 all belong to the **Scenario Selection Process**, i.e., the process in which a set of design scenarios are chosen from the range of identified scenarios

Location of Fire (Step 1)

In keeping with the FSG of life safety for occupants, fire locations most likely to threaten people will be the focus at this step. Locations are chosen in relation to identified life safety challenges. This could be due to the fire's proximity to occupied spaces, escape routes or its potential for spread of fire or toxic products into occupied spaces or escape routes and stairs.

The designer has to be sensitive to potential life safety challenges—bottlenecks in the design, critical route junctions where exit paths converge, and access to the main entrance/exit (favoured route), for example. Occupant characteristics can also impact the selection of ignition location. For example, if intoxication is an expected life safety challenge for the building, then consideration must be given to the ways that intoxication can impact an individual's ability to handle complicated way-finding tasks. Ignition locations that would require occupants to make decisions about a travel path could be a challenge for those cognitively impaired by intoxication.

Fuel packages near sensitive locations might not be involved in ignition but are vulnerable to spread. Fires in remote locations can spread smoke into escape routes. The case study in section "Discussion of Scenario Relevance: A Case Study" illustrated the situation where a fire remote from the main entrance would produce smoke in the locations where occupants would move in their efforts to reach the main entrance.

Fires that will not develop, spread into, or damage areas where occupants are located (originally or during evacuation) can be ignored for this fire safety objective.

Type of Fire (Step 2)

The issues critical to occupant movement and survivability must be considered in this step. The primary issues are visibility (due to either

smoke obscuration or irritants), heat and toxicity. Long-term effects of toxic exposure must also be considered, especially for vulnerable populations.

Visibility will be reduced by fires that generate a lot of soot, due to inefficient combustion or involvement of materials that generate soot. Lack of visibility will slow occupant movement, resulting in longer evacuation times. Exit signs will be obscured, complicating way-finding for occupants, even for those familiar with the building.

Irritants, e.g., hydrogen chloride, formaldehyde, acrolein, isocyanates, etc., can be a factor as a result of pain and discomfort, e.g., people cannot keep their eyes open, and may also be lethal. Toxic levels of irritants and asphyxiants can threaten occupants in under-ventilated fires or fires involving items such as PVC furniture. Plastics and cables, when burning, can generate compounds that are lethal in small quantities. More details on toxicity can be found in Chap. 63 of this handbook.

Slow-growing fires may create more irritants, with potential for long-term consequences in vulnerable people; fast-growing fires can expose people to heat sooner and result in entrapment. In considering the type of fire, the designer should evaluate the potential fire growth and toxicity of the involved materials. For example, for a fire involving a sofa composed of polyurethane foam and some wood, the focus should be on the foam, which will have a higher rate of burning than the wood and a smoke potential that is a factor of 5 or more higher [22] On the other hand, if a small piece of furniture is located close to a large quantity of wood, the greater threat may be presented by the wood.

Potential Fire Hazards (Step 3)

ISO/TS 16733 lists several hazards that should be considered in this step, including earthquakes and terrorist events that can result in multiple fires or disable multiple safety systems simultaneously; non-fire events that can impair structural stability; and the presence of high-hazard materials and operations that can initiate fires or complicate their suppression. Some events might also eliminate the power supply, thus knocking out the building's notification, lighting and communications systems.

Potential fire hazards should be considered in this step as they relate to occupant safety or evacuation. For example, an earthquake or terrorist attack could completely change the evacuation from what is expected. That is, the physical environment is changed and things not included in an ordinary evacuation would have to be considered, such as debris in travel paths, routes eliminated due to broken stairwells, etc. This type of change of physical environment was observed in the explosion test of the METRO project. In this test, a small explosive device not only destroyed the interior of the primary railway car, but also jammed the doors of the adjacent cars [23].

In some areas, a combination of earthquake and fire should be considered. This can be particularly dangerous as an earthquake might damage existing fire safety features or systems. This was the case in the Kobe earthquake where the sprinkler systems in some buildings were damaged by the earthquake [24]. The motion of a building in an earthquake can also distort doorframes and damage locks, affecting the passive resistance of doors and impeding evacuation [25]. This specific potential fire hazard will, however, not be relevant for all parts of the world.

Systems and Features Impacting on Fire (Step 4)

In this step, the designer must consider how the presence and functioning of passive and active protection systems in the building might affect evacuation and life safety. This should also include how the expected occupants might use or misuse the fire safety systems and features of a design, and how that might impact fire development and smoke spread from an evacuation point of view.

Among the passive systems and features that must be considered are doors, windows, structural elements, contents and furnishings and size of compartment. For example, the composition of the occupant population might influence the likelihood that a door will be closed or left open.

If a door is open, fire and smoke can spread into occupied areas and evacuation routes. If a door is closed, the scenario might not be relevant for life safety, as the closed door might afford some protection to occupants on the other side of the door. If occupants will have to move through a closed door, there could be difficulties presented by the latching mechanism or door handle, or by the opening force required by the door.

Active systems include smoke control and suppression systems; detection, warning and communication systems; fire safety management; and firefighting operations. There are various issues to consider as to how life safety can be impacted by the presence and functioning of active systems.

With smoke control systems, for example, occupants in high-rise buildings might regularly prop open the doors into pressurized stairwells. This might influence the functioning of the pressurization in a fire, hence allowing smoke to enter occupied spaces, i.e., the stairwell. A fire management plan or building maintenance program could minimize the likelihood of such a practice.

Without an operating sprinkler system, the smoke layers may be more stratified, with better visibility below the smoke layer. A sprinkler system will be expected to prevent a small fire from becoming an uncontrolled fire, but the increased mixing may result in reduced visibility in travel paths. The designer will have to factor in the effect that that will have on the evacuation or smoke exposure to vulnerable occupants.

Other systems that might influence the consequences of a specific fire scenario, such as notification and egress systems, are important to consider even if they do not directly affect fire or the smoke spread. Notification systems can alert and guide occupants in their evacuation. Determining the effectiveness of the system will have to take into consideration the abilities and disabilities of the expected occupant population. For example, how will people with different sensory impairments, e.g., hearing or vision, be alerted?

Egress systems, such as emergency elevators, will impact the evacuation, as will a fire safety management plan that will establish the likelihood of trained staff present, quality of any training provided, and overall planning and preparation for emergencies.

People Response (Step 5)

For *any* fire safety objective, the designer has to consider how the expected occupants might impact the development and spread of the fire. Under Step 4, the use or misuse of the fire safety systems and features of a design were discussed. In Step 5, consideration is given to the presence of trained occupants, who might begin warning or suppression activities. Occupants might change the conditions in ways that affect the evacuation or exposure to fire and smoke, in positive or negative ways, such as opening a manual smoke hatch (if trained to do this correctly), or inadvertently opening too many doors in a pressurized stairwell, for example. Opening too many doors might influence the functioning of the pressurization system. The mobility of the expected population will affect the likelihood of many doors being open for a long time. A fire management plan, e.g., a phased evacuation, and training could minimize the likelihood of this happening.

Scenario Selection Process (Step 6 to 10)

At this point in the process, the designer has compiled a large number of potential fire scenarios that have factored in issues related to occupant characteristics. The next series of steps (Steps 6 to 10) present a quantitative approach for the selection of design fire scenarios using an event tree. Alternatively, a more qualitative approach for selecting design fire scenarios can be followed, e.g., using a risk matrix.

In either case, at this point, the designer needs to consider the specific descriptions of expected occupants that will complement the design fire scenarios. For example, in order to develop an event tree, the likelihood of occupants attempting fire fighting or interfering in the operation of safety systems will depend on the composition and location of the occupant population.

In Step 6, an event tree is constructed describing the possible chronological sequences of

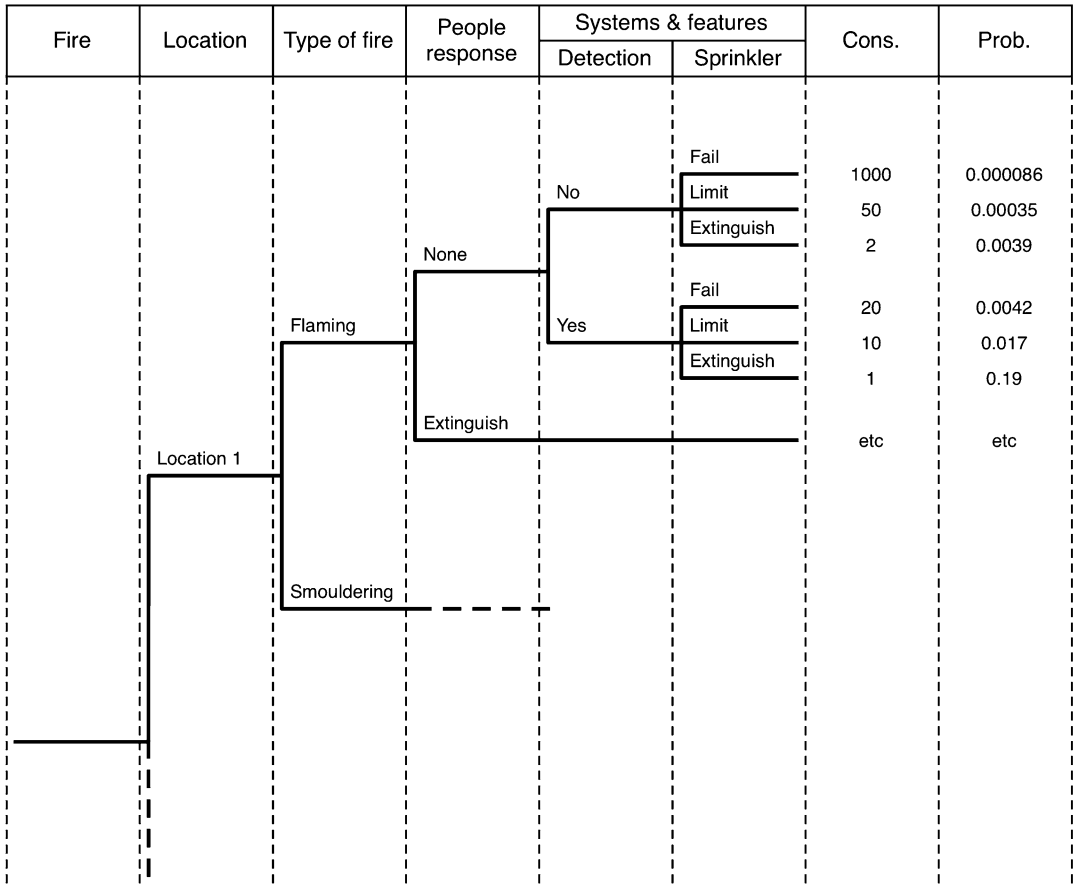

Fig. 57.5 An example of a part of an event tree that combines the aspects/factors identified in Steps 1 to 5 in a chronological order

events from the start of the fire to the final outcome for life safety. This event tree should combine the different factors/aspects identified in Steps 1 to 5, see example in Fig. 57.5. It is not necessary to combine all aspects/factors with each other as some combinations might not even be possible or might not be relevant for life safety. For example, the combination of a fire location with a specific fire safety system may be omitted simply because there is no such system in that part of the building.

In Step 7, the probability of occurrence of each event in the event tree is estimated. These estimates can be based on available statistics or, if no such statistics exist, on engineering judgement. In this step, it is important to consider how the occupant population might influence the probabilities associated with different events. For example, as mentioned in section "Systems and Features Impacting on Fire (Step 4)", the mobility of the expected population might affect the likelihood of failure of any stairwell pressurisation systems. Finally, the probabilities of events are combined to provide the probability of each branch of the event tree, i.e., the probability for each scenario.

In Step 8, the consequences for life safety of each scenario are quantified. If possible, these estimates can be based on available statistics, but in many cases engineering judgement must instead be applied. This step usually involves rough estimates of the consequences in terms of the number of people exposed to critical conditions for each scenario. During this

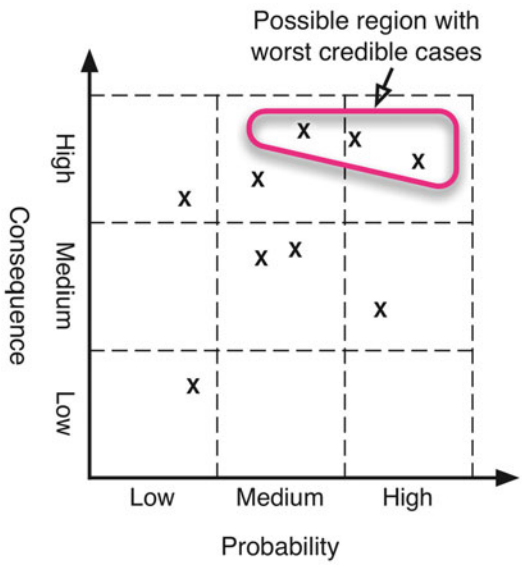

Fig. 57.6 An example of a risk matrix with scenarios (X) and a possible region with worst credible cases

estimation process, it is particularly important to recall the thought process behind the identification of aspects/factors in Steps 1 to 5. For example, a particular system might have been identified in Step 4 due to the potential high impact on life safety if it fails. Therefore, the consequence of scenarios involving failing of that system should most likely be high.

In Step 9, the probabilities and consequences of each scenario are combined into a measure of risk. According to ISO/TS 16733, the relative risk can be estimated by multiplying the probability with the consequence for each scenario. An alternative way to illustrate the risk is to insert the different scenarios in a risk matrix, see Fig. 57.6. Because the axes of the risk matrix are expressed in terms of probability and consequence, the matrix offers a more refined view of the risk associated with each scenario. It is also a useful tool for the deterministic analysis because it can be used to identify worst credible cases, e.g., scenarios with moderate or higher probability and high consequence, see Fig. 57.6.

Finally, the highest ranked scenarios in Step 9 are selected for the deterministic analysis in Step 10. These scenarios constitute the design fire scenarios. Step 10 also includes documentation of the design fire scenarios, as well as documentation of the non-selected scenarios including possible reasons for these not being chosen.

The scenario selection process and the methods/tools that can be applied are not described in great detail in this chapter. The reader is instead referred to the discussion on selection of fire scenarios in Chap. 38 of this handbook. It is, however, important to point out that the selection process for the type of deterministic analysis described in this chapter will focus on finding worst credible cases, i.e., design scenarios that challenge the achievement of the FSO.

Deriving Design Occupant Scenarios

The identification of fire-related factors/aspects that threaten the achievement of the FSO (Steps 1 to 5) and the selection of design fire scenarios (Steps 6 to 10) are linked to the fire safety challenges. Hence, each design fire scenario is linked to occupant-related issues or conflicts that, in combination with fire, could potentially lead to the failure of the design. In fact, every single design fire scenario in the deterministic analysis should have been chosen because of an expected evacuation problem or concern. For example, a fast growing fire in the main entrance of a department store in combination with a failing sprinkler system, i.e., the design fire scenario, might have been chosen because there is a conflict between building uses and users (people's tendency to use familiar exits), i.e., a specific life safety challenge. A severe fire in the main entrance of the department store would result in many people potentially being exposed to critical fire conditions.

Determination of design occupant scenarios is the process of re-examining the basis for the identification of fire-related factors/aspects (Steps 1 to 5) and selection of design fire scenarios (Steps 6 to 10). For the example above involving a severe fire at the main entrance of a department store, the design occupant scenario might involve a large number of untrained

occupants moving towards the everyday exit. Evacuees can be expected to be mainly shoppers, which for a specific combination of time and day might include a significant proportion of elderly, family groups and people with disabilities. Fire experience data can be used to determine the time of day the selected type of fire would most likely occur, and demographic data could help determine the appropriate mix of occupants at that time. In combination, these occupant-related factors/aspects make up the design occupant scenario for the design fire scenario involving the fire at the main entrance of the department store. Together, the design fire and occupant scenarios represent a severe but still credible case, which is the essence of the deterministic analysis.

The design occupant scenario is merely a qualitative description of the relevant occupant factors/aspects to be included in the deterministic analysis. Hence, the scenarios need to be expressed in quantitative terms in order to enable fire safety analysis. This involves the quantification of occupant- and evacuation-related variables for each of the chosen design occupant scenarios. These variables must include, but are not limited to:

- *number of occupants and their location*,
- *exact combination of occupant characteristics*,
- *initial response of occupants*, and
- *initial route choice of occupants*.

These variables are combined to form a qualitative description of the design occupant scenario related to each design fire scenario. The quantification of variables has to produce severe but reasonable conditions. However, much of the work related to the combination has already been considered during the identification of life safety challenges. For data and research that will assist in quantifying the occupant-related variables, the reader is referred to in Chap. 64.

Evacuation Variables for Sensitivity Analysis

Because the deterministic analysis involves a selection of a small subset of all the endless number of possible scenarios, i.e., the worst credible cases, it is important to investigate the effect of reasonable changes of different variables on the end result. If a small change of one variable, e.g., the proportion of people in wheelchairs, leads to the FSO not being achieved, the designer should question the level of safety. A sensitivity analysis, i.e., the process of changing different variables one at a time within reasonable limits [26], is one way to test the robustness of the fire safety design.

A sensitivity analysis should involve both fire- and occupant-related variables. The selection of occupant-related variables for the sensitivity analysis can be based on the occupant- and evacuation-related variables (see section "Deriving Design Occupant Scenarios"). In relation to the combination of occupant characteristics (second bullet in section "Deriving Design Occupant Scenarios"), the previously listed characteristics can be used as a starting point (see section "Inventory of Characteristics").

Example

In the following section, an example that illustrates the incorporation of human behaviour aspects in the scenario selection process is presented. The example is a subset of the example given in the chapter about fire scenarios in Chap. 38 of this handbook, but an expanded explanation of the motives behind the scenario selection is given in this presentation.

The designs used in this example are for a new building complex. This means that the plans are not final and could potentially change depending on the outcome of the analysis. In this example, however, the design is only analysed once, i.e., no modifications are considered. Ideally, the design process should be iterative in order to achieve an acceptable building design at the end of the analysis. However, in this simple example the building design is treated as if it were final.

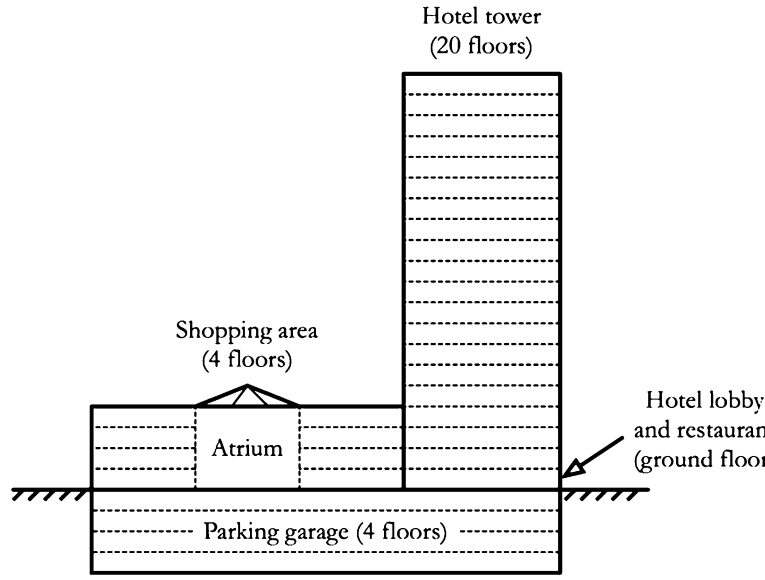

Fig. 57.7 A schematic drawing of the building complex

Description of the Building

The example is a building complex with multiple occupancies, see Fig. 57.7. The four floors underground constitute a parking garage. There is also a shopping area on the first four floors of the building, which are connected through an atrium. At one end of the building there is a 20-story hotel tower. The building is sprinklered and there is a fire alarm system. In case of emergency, people are notified by means of a voice alarm. Also, the atrium is equipped with a smoke exhaust system.

This analysis does not include the entire building complex, but instead focuses on the 20-story hotel tower. The ground floor of the hotel includes a lobby, restaurant, kitchen, three elevators and two independent evacuation stairs, see Fig. 57.8. The ground floor has an open layout, which means that there are no partitions between the lobby and the restaurant. All floors above the ground floor have a similar layout and include hotel rooms, storage rooms, three elevators and two independent evacuation stairs, see Fig. 57.9. One hotel room per floor is designed to be accessible. All accessible rooms are located close to the elevators.

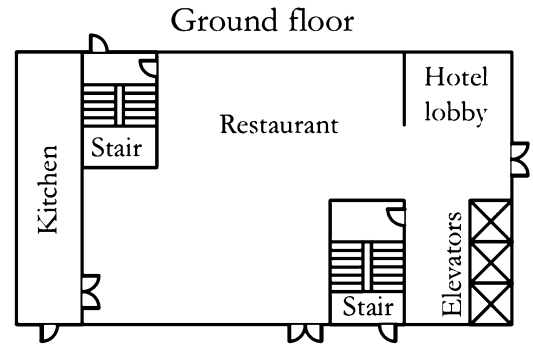

Fig. 57.8 The layout of the ground floor

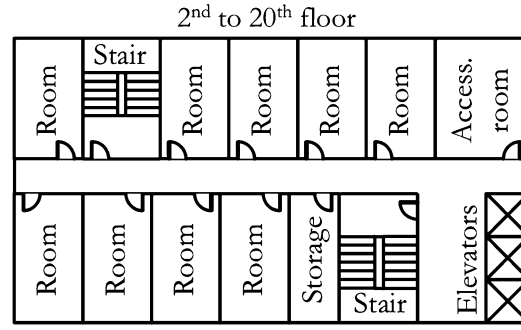

Fig. 57.9 The layout of the 2nd to 20th floor

Fire Safety Goal and Fire Safety Objectives

The only FSG used in this example is the goal to provide life safety for building occupants. This goal is assumed to be reached by achieving the FSO to not expose people to critical fire conditions. The critical conditions are not specified in this example, but include limiting values for species (CO_2, CO, O_2, HCN, etc), temperature, visibility and radiation.

Identification of Building Uses

This building has several uses. It is mainly used as a hotel, i.e., a temporary place of accommodation. As can be seen in Fig. 57.9, there are both regular rooms and accessible rooms on each hotel floor. On the ground floor of the building there is also a restaurant. All types of meals might be served in the restaurant, e.g., breakfast, lunch and dinner, but it might also host other types of events, e.g., private parties or receptions. However, the restaurant is not intended to be used as a nightclub or bar. Finally, the hotel is also the workplace of the hotel/restaurant staff. For example, people will be working in the restaurant, kitchen, hotel lobby, hotel floors, etc.

The most important aspects of physical use of the building are linked to the main exit/entrance and important waypoints. For the 20-story hotel tower, the main exit/entrance of the complex is the entrance door near the hotel lobby. It is expected that this is the main way in and out from the building during everyday use. Two major waypoints for the hotel guests are (1) the hotel lobby, where people can get information or assistance, and (2) the elevator lobby (or elevators), which people usually pass on their way to or from their room. For restaurant guests, one major waypoint is the entrance to the restaurant where the coatroom is also located. As the movement patterns are relatively simple for the 20-story hotel tower, e.g., occupants moving to and from their hotel room or to and from the restaurant, there are no complicated circulation paths.

Identification of Users and Their Characteristics

The uses of the building are each associated with a number of different users. The main users in the example are the hotel guests. Most guests are likely unfamiliar with the building as it is only temporary accommodation (*transitory* and *untrained*). However, other characteristics of the guests may vary widely. It can be expected that the hotel is used by people on, for example, business trips, romantic getaway weekends and family holidays, which implies that the users can be single persons, couples and families (*social groupings*). Both adults and children can be expected (*age range*). It is also expected that people with disabilities will use the hotel, and the types of disabilities can include everything from a hearing impairment to a movement disability (*vulnerabilities*). More specifically, it can be expected that some guests use wheelchairs as the hotel offers accessible rooms (*vulnerabilities*). Another user characteristic that might be relevant for the scenario selection is the level of intoxication (*unconscious/intoxicated*). Finally, guests might be awake or asleep (*awake/asleep*).

The restaurant guests constitute another important group of users in the example. Many of the restaurant guests might also be hotel guests, but others might be people who are just visiting the 20-story hotel tower for a meal (*transitory*). Guests might visit the restaurant in a variety of different combinations, such as families, groups of friends, couples and single individuals (*social groupings*). As the restaurant is not a place that most guests visit frequently, they are expected to be relatively unfamiliar with the environment (*untrained*). Also, a restaurant is a setting in which people's roles and associated rules can be very important, i.e., guest versus server (*role*). This relationship is associated with rules that dictate people's behaviour, and it is, for example, likely that the guests will display more passive behaviour compared to that of servers [27]. Also, since guests have often invested in the situation, e.g., waited for a long time for their food, they might be unwilling to

Table 57.2 Occupant characteristics

Characteristic	Hotel guests	Restaurant patrons	Hotel employees
Familiarity	Transitory	Transitory	Permanent
Training	None	None	Yes
Ages	Adults and children	Adults; children possible	Adults
Disabilities	Wide range possible	Wide range possible	Small range possible
Vulnerabilities	Possible	Possible	Possible
Level of intoxication	Intoxication possible	Intoxication possible	Conscious
Awake	Awake or asleep	Awake	Awake
Social groupings	Individuals, couples, families	Individuals, couples, families, groups	Individuals, co-workers
Role	Guest (expects assistance)	Guest (expects assistance)	Manager/subordinate

evacuate [28]. Level of intoxication is also a very important characteristic to consider as guests might be consuming alcoholic beverages (*intoxicated*). Finally, the restaurant is presumably accessible and different types of disabilities are therefore always relevant (*vulnerabilities*).

Hotel staff are typically familiar with the building since they spend a lot of their time there (*permanent* and *trained*). The staff represent a range of different occupations, and some examples include server, cook, hotel receptionist, hotel manager, housekeeper and security guard. These different occupations are associated with different roles and associated rules, which will govern how they behave in fire emergencies (*role*). For example, the role of *manager* versus the role of *receptionist* may significantly impact how willing the receptionist is to activate a fire alarm without confirmation or permission from his/her boss. As mentioned previously, the different roles of guests and staff may make staff more responsive and staff may also take on more of the responsibility in emergencies. These varying characteristics are shown in Table 57.2.

Determination of Life Safety Challenges

One potential life safety challenge is that guests might be asleep in their hotel rooms, which can lead to slow response in case of a fire emergency. Also, guests with movement disabilities will experience difficulties during evacuation because there are no evacuation elevators.

Another life safety challenge is the fact that the entrance door near the hotel lobby is the everyday main exit for both the people in the hotel rooms and the restaurant. In case of an evacuation, there is hence a risk that people will try to head through the lobby on their way out, which is a severe potential challenge.

Location of Fire (Step 1)

In the example given in Chap. 38 of this handbook, a number of different fire locations were identified, but only the following two are relevant for the 20-story hotel tower:

- *Fire in a hotel room*
- *Fire in the restaurant of the hotel adjacent to the hotel lobby*

These two locations are both identified since they are possible fire locations that severely threaten the achievement of the FSO. As previously mentioned, the fact that hotel guests can be asleep in their room and that some guests can have movement disabilities makes the evacuation situation especially challenging. A fire in close vicinity of hotel rooms is therefore highly relevant.

On the 2nd to 20th floors of the hotel tower there are a number of possible fire locations, but a fire in a hotel room is estimated to be one of the most relevant. The number of fuel packages in the evacuation stairs, hotel corridor, elevators and elevator lobby can be expected to be very limited, and fires at these locations are thus both unlikely and relatively minor. Hotel rooms on the

other hand have a significantly higher fuel load. Also, rooms are occupied by guests who engage in activities that might result in fires, e.g., smoking and ironing, and rooms have electronic equipment that might malfunction, e.g., TVs and refrigerators. This makes a hotel room a credible fire location. Storage rooms are similar to hotel rooms as they contain a large amount of combustible material, but they are typically locked and only accessed by staff. This makes a fire in a storage room much less likely than a fire in a hotel room. Given the reasoning above, a hotel room appears to be a credible location that threatens the achievement of the FSO.

The hotel lobby was identified as a major waypoint, i.e., a potential life safety challenge, and a fire in the adjacent restaurant is therefore considered most relevant. The lobby of the hotel is most likely sparsely furnished and has limited possible ignition sources. A fire in the lobby would therefore be unlikely and relatively minor. However, in the adjacent restaurant there are likely an abundance of possible sources of ignition, e.g., candles on tables or hot surfaces in the kitchen. Also, the restaurant has many fuel sources, e.g., furniture in the dining area or frying oil in the kitchen. Due to the open plan of the ground floor, smoke from a fire in the restaurant can easily spread to the hotel lobby. The restaurant, either the seating area or the kitchen, is therefore a credible location that severely threatens the achievement of the FSO.

Type of Fire (Step 2)

A rapidly growing flaming fire with a high heat release rate is considered the most relevant type of fire for the hotel room since it most severely threatens the achievement of the FSO. Many types of hotel room fires are possible. Firstly, the ignition source might relate to activities that the guests engage in, e.g., smoking or ironing, as well as malfunction of electronic equipment, e.g., TVs and refrigerators. The resulting fire growth characteristics might also vary and include anything from a slowly developing smouldering fire to a rapidly growing flaming fire. For the hotel room example, a rapidly growing flaming fire with a high peak heat release rate is deemed most relevant since it has the potential to make the evacuation situation unacceptable before people have responded to the initial fire cues, which relates to the previously mentioned life safety challenge. This type of fire might be ignited with a cigarette that is thrown in a garbage bin that ignites curtains and subsequently spreads to large fuel items, e.g., a bed and/or a sofa.

For the restaurant location, a rapidly growing flaming fire with a high heat release rate is also considered most relevant since it has the potential to generate a lot of toxic and hot smoke that may quickly fill the hotel lobby, thereby threatening the achievement of the FSO. One example could be a candle that falls over and ignites a tablecloth and then a large fuel item, e.g., a sofa or table/chairs. Alternatively, a fire might start at a deep fryer in the kitchen and subsequently spread to uncleaned and greasy parts of the duct system. Both of these fires have the potential to create and uphold difficult evacuation conditions in the hotel lobby.

Potential Fire Hazards (Step 3)

In this example, one potential fire hazard that could severely threaten the achievement of the FSO is an arson attack. This type of attack may involve combustible liquid, e.g., gasoline, which is carried into the building complex and ignited. Although unlikely, this type of attack has been known to occur, see for example the PUB incident in Stockholm [29]. The liquid might be ignited in the lobby as it is a public area and hence easily accessible. Also, this is a location that relates to one of the previously mentioned fire safety challenges.

In an area susceptible to serious earthquake damage, consideration should be given to the impact of a possible post-quake fire, where occupants might have to deal with damage to components of the egress system, such as doors jammed in distorted doorframes that could result in entrapments.

Systems and Features Impacting on Fire (Step 4)

Some of the systems that are used in the 20-story hotel tower to mitigate the fire effects on people are the automatic sprinkler system, the fire alarm system and the fire barriers. A failing or compromised barrier, i.e., a hotel room door that does not close properly or a stairwell door that is propped open, would make conditions outside the room of origin unacceptable quickly. Similarly, a failing sprinkler system, or a sprinkler system unable to control a shielded fire, could allow a fire to grow bigger more rapidly and a failing fire alarm or voice messaging system would potentially delay people's response. Failure of any of these systems would hence severely threaten the achievement of the FSO for both the fire in a hotel room and a fire in the restaurant.

People Response (Step 5)

The building users may engage in activities that can make conditions either better or worse. In this example, manual suppression is an activity that can improve the chances of achieving the FSO. This occupant response is deemed more likely for the restaurant fire due to the presence of trained staff that is familiar with the building. One activity that threatens the achievement of the FSO is if occupants do not close doors, e.g., a hotel room door, which would make fire barriers ineffective, or if opening too many doors in a pressurized stairwell affects its proper functioning.

Scenario Selection Process (Step 6 to 10)

Steps 6 to 10 of the example, i.e., the compilation of scenarios, the scenario selection process and the documentation, are not described in this chapter and the interested reader is referred to the description in Chap. 38 of this handbook. It should, however, be pointed out that each scenario is evaluated in relation to the achievement of the FSO. The evaluation in the example resulted in the selection of the following design scenario involving a fire in a hotel room in the 20-story hotel tower:

> *Fire started in a garbage container and spread to the curtain and mattress. Nobody was in the room of fire origin. The sprinkler system did not activate because the water supply was turned off for repairs. The fire spread from the room door to the corridor of the hotel. For life safety calculations, assume that occupants were asleep when the fire started.* (Chap. 38)

It is important to note that a number of scenarios believed to challenge the system must be selected in order to adequately test the design. This example will follow only one—a fire in a hotel room.

Deriving Design Occupant Scenarios

No details about the occupants were included in the example in Chap. 38, other than that the occupants outside the room of origin were asleep. In order to do the evaluation of the design, assumptions must be made about the characteristics of the occupants so as to formulate a scenario that will challenge the fire safety design. A suitable design occupant scenario in this example is therefore that all guests are asleep in their rooms and that one accessible room per floor is occupied. All rooms are assumed occupied to their maximum capacity. As hotel guests are transitory occupants, it will also be assumed that they are unfamiliar with the layout of the building and they are not trained in evacuation. As a result, there will be delays in evacuation as they assess the situation after waking, prepare for evacuation and attempt to find the exits. These conditions are believed to represent a worst credible case.

Evacuation Variables for Sensitivity Analysis

In previous sections, a number of occupant characteristics for hotel guests were highlighted in relation to the hotel use of the building. These characteristics are also the evacuation variables that should be the variables included in a

sensitivity analysis. For this example, the evacuation variables for the sensitivity analysis include:

- *transitory*—familiarity with the building
- *social groupings*—alone, couples, families
- *age ranges*—adults, children
- *vulnerabilities*—types of disabilities
- *intoxicated*—level of intoxication

These characteristics are mainly concerned with the ability of building occupants to mitigate or cope with a fire event. All these variables can be varied with regards to their magnitude, e.g., the degree of familiarity with the building, and frequency, e.g., the number of guests who are very unfamiliar with the building. It might also be relevant to vary the initial behaviour and the initial route choice in the sensitivity analysis.

For example, in the baseline scenario, the hotel guests were asleep, but not intoxicated. The sensitivity analysis would assume some percentage of occupants were intoxicated, with the resulting additional delays in waking, and possibly more difficulty in decision making and way-finding. Similarly, the sensitivity analysis can test the effect of varying the ages of the occupants.

The sensitivity analysis will test the robustness of the safety design, which could result in changes to the design or refinements to the fire safety management plan for the building.

Summary

The intent of this chapter has been to extend the discussion on the selection of scenarios for deterministic fire safety engineering analysis according to ISO/TS 16733 when the Fire Safety Goal is life safety. In this case, the fire, building and occupants all play an important role in determining scenario relevance.

Before the scenario selection process can be initiated, the designer must first define the project context by setting the scope, Fire Safety Goal (life safety for building occupants in this chapter), Fire Safety Objectives and critical fire conditions. The subsequent step involves identification of possible building uses, as well as the subsequent users and their characteristics. In this chapter, characteristics are divided into eight categories commonly used in the identification process.

Once the uses and users are known, the designer needs to determine the life safety challenges, which are any issues or conflicts that, in combination with fire, could potentially lead to the failure of the design. These life safety challenges are essential for the scenario selection process because it is in relation to them that the severe but credible scenarios, i.e., the worst credible cases, are chosen in the deterministic analysis.

In the first five steps of the fire scenario selection process of ISO/TS 16733, fire-related factors/aspects, e.g., fire locations and types of fire, that severely threaten the achievement of the FSO are identified. This identification is always done in relation to the life safety challenges as described in this chapter. In Steps 6 to 10 of ISO/TS 16733, design fire scenarios are then chosen for the deterministic analysis from the multitude of possible fire scenarios.

Because the entire fire scenario selection process is linked to the fire safety challenges, each design fire scenario is also linked to occupant-related issues or conflicts. This means that for every design fire scenario there is already a design occupant scenario. The process of determining these design occupant scenarios involves re-examination of the basis for the identification of fire-related factors/aspects (Steps 1 to 5) and selection of design fire scenarios (Steps 6 to 10).

Scenario selection is an iterative process as occupants can impact the fire, the fire can impact the occupants, and the building and its features impact both the fire and the occupants. A failing design might be addressed by changing, for example, the building layout, which in turn might influence both potential fires and occupants. This means that the described process might need to be repeated several times before an acceptable design is found.

The evaluation of the safety of a design involves comparing the expected growth and spread of challenging fires (the design fire scenarios) against the ability of occupants to avoid or survive the effects of those fires. There is a great deal of interaction between the

occupants of a building and the likelihood of fire ignitions and fire spread. While this chapter has focused on life safety, parts of the process could be applied to the consideration of other fire safety objectives, where the number and type of occupants could impact fire ignition, growth, spread and suppression.

References

1. Watts, J.M. (2008). Systems Approach to Fire-Safe Building Design, *NFPA Handbook* (20th ed), 1–159.
2. ISO/TS 16733:2006 – Selection of design fire scenarios and design fires (2006) Geneva: ISO.
3. BBRAD 1 - Boverkets allmänna råd om analytisk dimensionering av byggnaders brandskydd, BFS 2011:26 med ändringar t.o.m. BFS 2012:13 (2011) Karlskrona: Boverket.
4. INSTA/prTS 950 - Fire Safety Engineering - Verification of fire safety design in buildings (2013) Inter Nordic Standardisation Organisation
5. Frantzich, H. (1998). *Uncertainty and Risk Analysis in Fire Safety Engineering*. Report 1016, Lund: Department of Fire Safety Engineering, Lund University.
6. Paté-Cornell, M. E. (1996). Uncertainties in risk analysis: six levels of treatment. *Reliability Engineering and Systems Safety, 54*(2), 95–111.
7. Sime, J.D. (1985). Movement towards the familiar - Person and place affiliation in a fire entrapment setting. *Environment and Behaviour, 17*(6), 697–724.
8. SFPE (2007) *SFPE Engineering Guide to Performance-Based Design* (2nd ed.). Bethesda, MD: Society of Fire Protection Engineers.
9. BBR19 - Regelsamling för byggande, Boverkets byggregler, BFS 2011:6 med ändringar t.o.m. BFS 2011:26 (2011) Karlskrona: Boverket.
10. NFPA 101: Life Safety Code® (2012). Quincy, MA: National Fire Protection Association.
11. NKB (1994). Funktionsbestemte brandkrav og teknisk vejledning for beregningsmeassig eftervisning, NKB Utskotts- och arbetsrapporter 1994:07, Helsinki: NKB.
12. ISO/TS 13571:2002 - Life-threatening components of fire - Guidelines for the estimation of time available for escape using fire data. (2002) Geneva: ISO.
13. van Hees, P., Nilsson, D., & Berggren, E. (2009). *Simulation of critical evacuation conditions for a fire scenario involving cables and comparison of two different cables*. Lund: Department of Fire Safety Engineering and Systems Safety, Lund University.
14. Gwynne, S., Kuligowski, E., & Nilsson, D. (2012). Representing Evacuation Behaviour in Engineering Terms. *Journal of Fire Protection Engineering, 22* (2), 133–150.
15. Nilsson, D. (2009). *Exit choice in fire emergencies - Influencing choice of exit with flashing lights*, Report 1040, Lund: Department of Fire Safety Engineering and Systems Safety, Lund University.
16. McClintock, T., Shields, T.J., Reinhardt-Rutland, A. H., & Leslie, J.C. (2001). A behavioural solution to the learned irrelevance of emergency exit signage. *Proceedings of the 2nd International Symposium on Human Behaviour in Fire*, London, UK, pp. 23–33.
17. Bruck D. & Brennan P. (2001). Recognition of fire cues during sleep. *Proceedings of the 2nd International Symposium on Human Behaviour in Fire*, London, UK, pp. 241–252.
18. Ball, M., & Bruck, D. (2004). The effect of alcohol upon response to different fire alarm signals in sleeping young adults. *Proceedings of the 3rd International Symposium on Human Behaviour in Fire,* Belfast, UK, pp. 291–302.
19. Anderson, B.M., Stevens, M.C, Meda, S.A., Jordan K., Calhoun, V.D., & Pearlson, G.D. (2010). Functional Imaging of Cognitive Control During Acute Alcohol Intoxication, *Alcoholism: Clinical & Experimental Research*; DOI: 10.1111/j.1530-0277.2010.01332.x.
20. Latané, B.,& Darley, J.M. (1968). Group Inhibition of Bystander Intervention in Emergencies, *Journal of Personality and Social Psychology, 10*(3), 215–221.
21. Swartz, J.A. (1979). Human Behavior in the Beverly Hills Fire. *Fire Journal, 73*(3), 73–74, 108.
22. Drysdale, D. (2011). *An Introduction to Fire Dynamics*.(3rd ed.) West Sussex: John Wiley & Sons, Ltd.
23. Ingason, H., Kumm, M., Nilsson, D., Lönnermark, A., Claesson, A., Li, Y.Z., Fridolf, K., Åkerstedt, R., Nyman, H., Dittmer, T., Forsén, R., Janzon, B., Meyer, G., Bryntse, A., Carlberg, T., Newlove-Eriksson. L., Palm, A. (2012). *The METRO project - Final report*. SiST 2012:8, Västerås: School of Sustainable Development of Society and Technology, Mälardalen University.
24. Sekizawa, A., Ebihara, M., & Notake, H. (2003). Development of Seismic-induced Fire Risk Assessment Method for a Building. *Fire Safety Science – Proceedings of the 7th International Symposium, International Association for Fire Safety Science*, pp. 309–320.
25. Kim, J.K., Park, H. & Meacham, B.J. (2013). "Fire Performance of Earthquake-Damaged Buildings: Overview and Preliminary Analysis of Full-Building Earthquake and Fire Tests," *Proceedings, Interflam 2013*, Interscience Communication, Ltd., London, UK, 1407–1418.
26. Hamby, D.M. (1995). A Comparison of Sensitivity Analysis Techniques. *Health Physics, 68*(2), 195–204.
27. Levin, B.M. (1984). *Human Behavior in Fire: What We Know Now*. SFPE Technology Report 84–3, Boston, MA: Society of Fire Protection Engineers.

28. Purser, D.A. and Bensilum, M. (2001). Quantification of behaviour for engineering design standards and escape time calculations, *Safety Science, 38*, 157–182.
29. Harne (1998). Polisen utan spår efter pyromanen [Police without any trace after pyromaniac], *Aftonbladet*, 24th December, 1998.

Daniel Nilsson, PhD is an Associate Professor in the Department of Fire Safety Engineering at Lund University, Sweden, and Chair of ISO TC92/SC4 on Fire Safety Engineering.

Rita F. Fahy, PhD is the manager of fire databases and systems at NFPA and convenes the ISO TC92/SC4 working group on behaviour and movement of people.

Human Behavior in Fire

58

Erica D. Kuligowski

Introduction

Human behavior in fire is at the core of all life safety projects completed by fire safety or fire protection engineers. A better understanding of how people respond to building emergencies can aid in safer building design; improved use or development of calculation tools used to ensure the level of safety afforded by these designs; and more effective emergency procedures, emergency communication systems, and pre-event emergency training for buildings and communities. The purpose of this chapter is to provide a basic understanding of human behavior in fire concepts and theory for use by engineers. The chapter contains the following aspects of human behavior in fire and other emergencies: a definition of human behavior in fire, including a discussion of the types of disciplines employed in the study of people in fires; a presentation on what human behavior in fire is not, including examples of disaster myths; an overview of the disaster-based decision-making process in fires and other emergencies; a discussion relating theory to practice (highlighting studies from fire events that support the decision-making theory); the identification of important factors that influence the decision-making process; and a conclusion highlighting what is missing in the field of human behavior in fire. Each section of this chapter will include an implications section that outlines the reasons why these ideas or theories are important for engineers to understand and incorporate.

Definition of Human Behavior in Fire

Human behavior in fire is the study of human response, including people's awareness, beliefs, attitudes, motivations, decisions, behaviors, and coping strategies in exposure to fire and other similar emergencies in buildings, structures and transportation systems. The study of human behavior in fire is highly multidisciplinary, involving practitioners from the fields of engineering, architecture, computer science, mathematics, law, sociology, psychology, human factors, communications and ergonomics, to mention just a few. The primary focus of human behavior research and its translation into practice is to minimize the risk to people from fire. This is achieved by generating and collecting quantitative and qualitative data on human responses which can be used to develop human fire response theory.[1] A comprehensive theory of human response is key to improve current fire safety engineering design, performance based regulatory systems, egress-

E.D. Kuligowski (✉)
National Institute of Standards and Technology,
100 Bureau Drive, Gaithersburg, MD 20899

[1] This definition of human behavior in fire was first presented in the brochure advertising the 2012 Human Behaviour in Fire Symposium, developed by consensus of program committee members (Interscience Communications).

M.J. Hurley (ed.), *SFPE Handbook of Fire Protection Engineering*,
DOI 10.1007/978-1-4939-2565-0_58, © Society of Fire Protection Engineers 2016

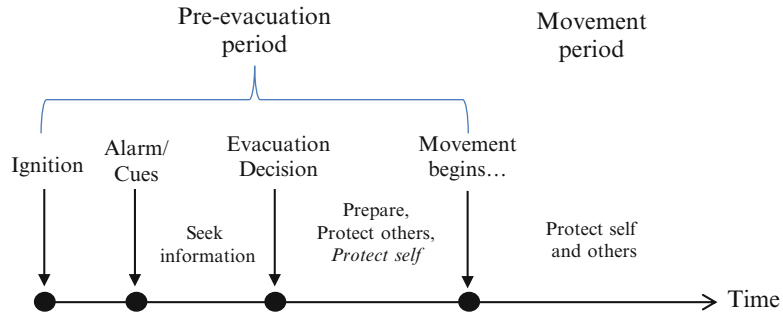

Fig. 58.1 Timeline of a human response to a building fire emergency

related computational models and fire safety management.

The ultimate goal of improving life safety analyses in performance-based design is to develop a comprehensive theory of human fire response. Human behavior is complex and there is more work to be done to achieve this goal. A focus on case studies of specific building fires [1–3], and research on particular aspects of a fire evacuation has left the field of human behavior in fire with a series of partial-theories, rather than a comprehensive theory of human behavior in fire. As a result, human response to fires is often crudely categorized into two main periods: the pre-evacuation period[2] and the movement period, with little understanding of the behavioral processes that take place within each one. The pre-evacuation period estimates the time when ignition begins until the point when an individual or group begins purposive evacuation movement to a place of safety. The time period in which purposive movement to safety occurs is then considered the evacuation or movement period.

As shown in Fig. 58.1, and as will be presented throughout this chapter, the pre-evacuation and movement periods consist of additional sub-phases that the engineer should understand. For example, within the pre-evacuation period, at least three sub-phases can exist:

- The pre-alarm phase, which is the time from the point when fire ignition begins until the point when the building alarm initiates and/or building occupants are exposed to cues from the fire event (i.e., seeing smoke or being told about the fire event by a staff member)
- The evacuation decision-making phase, where building occupants are exposed to or seek out cues/information from the fire event and others in the building, and after processing this information, must decide whether or not it is necessary to protect themselves (e.g., evacuate)
- The protective action phase, whereby individuals engage in certain actions, e.g., gathering personal belongings or assisting others to prepare for evacuation that allows them to protect themselves or others before beginning evacuation.

These phases are important to understand, because in certain types of buildings or emergencies within a building, the pre-evacuation period can be significantly longer than the movement period in a building evacuation.

Additionally, the same types of decisions and actions can take place during the movement period, especially when people are faced with additional environmental cues.

The purpose of this chapter is to aid the engineer in understanding the current state of knowledge regarding the entire process of human behavior in fire emergencies. This process is important to understand because it is often the goal of fire safety or fire protection engineers (as well as fire marshals, authorities having jurisdiction, and other emergency responder personnel) to ensure that a particular structure or transportation system provides the appropriate

[2] Other terms have been used to express the pre-evacuation period, including pre-movement or pre-response.

level of life safety to its users. With this goal in mind, it becomes an almost impossible task to assess life safety (credibly or reliably) without understanding how the structure or transportation system will be used during a fire emergency. In a building, for example, an engineer must understand how the building occupants will respond to a fire in order to assess whether the building and the fire safety features provide an adequate level of safety during a fire emergency event. Therefore, this chapter focuses on communicating current understanding of human behavior in fire, including all phases of the human response, for use in fire safety and life safety analyses of structures and other systems.

Discarded Theories in Human Behavior in Fire

Before we can achieve an understanding of human behavior in fire, we must first discuss what human behavior in fire *is not*. This is critical since our understanding of human behavior in fire has direct implications to the engineering design process. Since behavior in fires has been studied since the 1950s (and for other disasters, earlier than that), certain claims have been made and then subsequently refuted as explanations of human behavior in fires. In this chapter, and elsewhere [4], these claims are labeled as disaster myths. In some cases, these disaster myths are true for a small minority of the population, but have become overgeneralized to hold for the entire population. In other cases, the disaster myth is completely invalid [5]. Three disaster myths will be discussed in this section: panic, disaster shock, and group mind. All three myths have been overgeneralized by society and the media to account for negative situations in some disaster scenarios, but, in reality, are very rare. These are chosen as discussion points in this section, since they have been used in the past to characterize occupant response to building fire disasters. These are not the only disaster myths promulgated by past events, nor the only disaster myths that may be promoted by future events.

Panic Behavior

The concept of panic is often used to explain the occurrence of multiple fatalities in fires. Representatives of the media and public officials often label various types of fire incident behavioral responses as panic [6, 7], often going so far as specifically asking about the presence of the behavior when interviewing disaster survivors [8].

According to most definitions, panic is a flight or fleeing type of behavioral response that also involves extravagant and injudicious effort. Panic is not necessarily limited to a single individual, and may be mimicked and adopted by a body of persons (i.e., mass panic or collective flight). Johnson describes panic as the following: "...selfish competition uncontrolled by social and cultural constraints—i.e., unregulated" and the breakdown of social order [9, 10]. Wenger et al. [11] includes a definition for "panic flight" as "the competitive mass behavior of individuals involved in fleeing from an imminent threat that results in increasing the danger to themselves and others". Quarantelli [7] characterizes panic not only as withdraw (or flight) behavior, but also as a behavior that encompasses a lack of consideration for others (i.e., competition).

Often, however, the concept of self-destructive or animalistic panic-type behavioral responses to fire incident stimuli, such as the presence of flames or smoke, has not been supported by the research on human behavior in fire incidents. As indicated by Sime [12], Quarantelli [13], and others [14–17], panic behavior in which the flight response is characterized by actual physical competition between the participants and personal injuries is rare. For example, Best studied extensive interviews with survivors of the Beverly Hills Supper Club fire (1977) to find that the staff and patrons of the club did not exhibit panic behavior, despite media accounts attributing the large loss of life to the phenomenon [18]. Also, several studies have been conducted on the 2001 World Trade Center Disaster (WTC), allowing researchers to assess the accuracy of the headline of a BBC News Online article, entitled: "Panic on

the stairs" [8, 19]. Studies of both media accounts [20, 21] and survivor interviews [1, 22, 23] of this deadly terrorist attack revealed overall trends of calm and altruism. While there were reported situations of emotion, i.e., crying or being anxious or nervous about the situation, the majority of stories reported rational, orderly, and often times, delayed responses to the disaster event.

Therefore, the use of the concept of panic must be separated from the use of the terms *anxiety* or *fear*. These are natural emotions in emergency situations that do not necessarily lead to competitive, injudicious flight behavior (i.e., panic). Additionally, research has shown that survivors of fire emergencies (or other disasters) may mistakenly categorize their own behavior or the behavior of others as panic, whereas further description of actual actions barely reflect panic behavior [12, 24]. Ramachandran [25], in his review of studies on human behavior in fires in the United Kingdom, has developed the following conclusion relative to nonadaptive behavior:

> In the stress of a fire, people often act inappropriately but rarely panic or behave irrationally. Such behavior, to a large extent, is due to the fact that information initially available to people regarding the possible existence of a fire and its size and location is often ambiguous or inadequate.

In reality, and in stark contrast to panic behavior, engineers should be aware that people's first assumption in many disasters, regardless of the intensity of the information perceived, is that nothing unusual is happening, and thus, no response is required. This phenomenon is known as normalcy bias [26–29]. It is our challenge, as engineers, to ensure that disaster victims (i.e., those who are in danger) become aware that a dangerous situation is taking place, and that they perceive personal risk. If not, they are unlikely to take actions to protect themselves from harm. Even in an event as large and intense at the 2001 WTC disaster, building occupants had to be convinced of the danger to which they were exposed, sometimes taking several minutes, before evacuating the building [30]. Additionally, in reference to the assumption of competition, engineers should acknowledge that altruistic behavior is more likely to occur. Researchers have found that even though disasters can cause shifts in the pre-existing situation, the breakdown of social order is rare [31, 32]. Many of the societal norms and social roles evident before the disaster carry over into the new, evolving situation. Therefore, occupants are likely to engage in pro-social behaviors, including helping others rather than competing with others, as they would do in non-disaster situations. Engineers should also be aware of these types of pro-social behavior, since they could lead to delays in the evacuation process, among other issues. The delays associated with altruist behavior, such as helping, should be accounted for in fire protection and emergency procedural design for buildings in the event of fire emergencies.

Disaster Shock

An additional disaster myth suggests that individuals who do not act irrationally (i.e., panic) are often immobilized by fear in emergency events [4, 33]. This myth creates an image of large numbers of individuals dazed or shocked; i.e., unable to cope with the new disaster-created situation at hand. This myth also extends into the disaster recovery stage, suggesting that the paralyzing shock created by the situation is followed by longer-term personal effects, often labeled as post-traumatic stress disorder, or PTSD. Although this may at first seem irrelevant to fire emergencies, since much of the research on disaster shock is reported in response to the natural or technological disasters, the myth of disaster shock is directly applicable to fire emergencies. In a building fire, the fire ignites and continues to grow as building occupants are made aware of the event and are encouraged to take protection (e.g., evacuate). In fires, different from a tornado event, for example, building occupants are warned about the event after it has already started to cause destruction. Thus, it is possible to assume in building fire events that individuals

will go into shock in response to the fire, and thus rendering themselves incapable of evacuating on their own.

Researchers have found that following disasters, documented reports of disaster shock are rare. Melick [34], after reviewing disaster studies conducted between 1943 and 1983, found the following three conclusions regarding disaster shock: (1) Disaster shock occurs more frequently in sudden onset disaster events that are accompanied by little forewarning and extensive physical and social destruction; (2) Disaster shock affects a relatively small proportion of the population in any one event [7, 35]; and (3) Disaster shock usually occurs within the immediate postimpact period of a disaster, lasting no longer than a few hours or days [5]. Other researchers have shown that this phenomenon is rare and the state is usually short-lived [36].

Disaster researchers attempt to dispel this myth by explaining that disaster response behavior is often performed in an active manner [7]. Instead of waiting for assistance, in a dazed or disoriented manner, disaster victims are more likely to show considerable personal initiative, performing search and rescue activities, casualty care, and restoration of essential services even before emergency responders arrive on scene [11]. This kind of response was observed in the 2001 WTC disaster [30], where survivors were often the first individuals to respond to the needs of their coworkers, assisting them to reach safety before first responders could reach the upper floors. Belief in this assumption could cause engineers to focus more on emergency response officials and their role in evacuation. However, it is important for engineers to understand that building occupants will react in an emergency and proactively engage in their own (and others') safety. In turn, engineers must ensure sufficient and efficient evacuation routes and strategies to ensure safety for all occupants in the building.

One note that should be made here regarding this myth is the inability to interview those who perish from building fires, and the effect that this gap may have on our overall understanding of disaster shock. The fires and disaster fields may not fully understand the role of disaster shock in consequences (i.e., injuries and deaths), and therefore future research should focus on obtaining a better understanding of the circumstances of fatalities from fires (when possible). One way to obtain this type of data is to interview individuals who were physically with (or in contact with) the deceased during the fire emergency.

Group Mind

A third disaster myth is the oversimplification that the group is something other than the sum of individuals responses; i.e., that the group has a "mind" of its own when making decisions in a disaster [37]. Another way of thinking about group mind is the assumption that when a disaster occurs, individuals become a part of a group and the group (as a whole or as one entity) acts in response to the disaster. This assumption can also be characterized as mob behavior or herd behavior.

However, sociologists have stated that thinking that the group acts or thinks in a certain way is "often a serious oversimplification" [37]. Making this assumption can cause the engineer or researcher to be blinded by any diversity associated with the group, including individual characteristics, experiences, decision-making or behavior. If we make this assumption, we may then assign attributes to the group, including a mind, a sense of responsibility, a conscience, or even a lack of self-control (related to mass panic described above).

What is more likely, and what has been seen in actual disaster events, is that groups consist of a variety of different individuals. During disasters, it is more likely that groups engage in what is called "a division of labor" in that certain individuals take on particular roles based upon their experiences and/or relationships with others in the group, which complement each other and allow the group to function [37]. It is therefore important to understand the division of labor within the groups and the characteristics,

experience, decision-making and behavior of the individuals within the group to truly understand human behavior in fire.

It should be noted; however, that there is extensive research in group dynamics and how groups "act" in disasters and building fires. This research will be described later in this chapter. Overall, it is neither the description of the group (only) nor the description of the individual (only) that is sufficient in understanding human behavior in fire. Instead, identifying both his/her attitudes toward the object (or issue at hand, in this case, the fire cue or cues) [38] and attitudes toward the group and others in the building (i.e., the processes of group dynamics) leads to the true understanding of human response in emergencies [37].

Engineering Implications of Disaster Myths or Why Should the Engineer Care?

Unfortunately, these disaster myths can have negative implications on fire safety in our society. Images of human behavior during disasters are often the basis for critical decisions made by engineers and other fire protection designers on building design requirements, emergency communications systems design and guidance, as well as emergency response procedures for fire events. The assumptions of irrationality or human frailty can inappropriately shape the way that engineers and emergency officials plan for response to fires in their buildings, as well as how evacuation models represent evacuation behavior during fires. Instead, it is important for engineers to understand the true needs of building occupants so that engineering and emergency procedural designs and methods more accurately reflect realistic occupant behavior during building fire events.

One example of how a disaster myth has had negative implications on fire safety is the influence of panic on emergency communication during fires [33]. The view that people would panic in response to an incident (and specifically to information describing the incident) has influenced both the notification procedures employed and the language used (by survivors) to report the exhibited behavior [39]. This assumption influenced a difficult and harmful cycle consisting of the following steps: people report that they panicked, emergency officials continue to believe that panic is a normal response, emergency information is withheld in the next disaster so that people do not panic, human response is delayed and inefficient, and the situation becomes more dire. Over the last 25 years, this point of view has been slowly replaced with the recognition that people need detailed and credible information as early as possible in order to initiate and inform their response. The availability of this information encourages people to accept the emergency procedures and to improve their familiarity with the required response, and later informs the decision-making process that determines their response. People need information in order to act. Detailed information by no means guarantees the desired response; however, without this information, an uninformed approach (ignorant of the conditions and the options available) is much more likely. It is now broadly accepted that depriving evacuees of information is more likely to lead to an inefficient and inappropriate response; e.g., misinterpreting the incident and the threat it poses, delaying response, engaging in an inappropriate response, and ignoring safe egress routes. During an incident, people will seek information regarding the nature of the incident and what they should do in response to it. Unfortunately, this information may not always be easy to find, reliable, consistent or accurate. It is critical that an information vacuum is avoided and that accurate, credible information is provided.

The previous section discussed the factors and theories that do not accurately describe human behavior during building fires and other events. Therefore, the following section will focus on describing the theory of human behavior in fires and the foundation upon which this and other related theories were built. This understanding of human behavior focuses on decision-making at the level of the individual, independent of whether the individual is on his/her own, a

member of a group, or a member of a larger crowd during the emergency. Social psychological theories of decision-making during emergencies will be presented in the following section.

Social Psychological Theories of Human Behavior in Emergencies

Everyday, individuals go about their normal lives—attending meetings at work, watching movies at the local cinema, and shopping at the mall or the grocery store for all of their necessities. These are activities in which individuals have engaged so often that they have become routine in nature. When an emergency occurs, these activities may suddenly seem irrelevant. When an alarm is sounding or smoke is billowing into a room from an air conditioning duct, individuals are faced with a potentially new and unique situation where previous actions may no longer apply.

Under these new conditions, individuals are required to make a concerted effort to create meaning out of new and unfamiliar situations, often under time pressure. From this meaning, a set of actions, different from those that have become routine, must be created. Emergent norm theory (ENT), explains the process of meaning-making in the face of uncertain conditions [37], stating that in situations where an event occurs that creates a normative crisis (i.e., an event where the institutionalized norms [e.g., sitting at a desk and working] no longer apply), such as a building fire, individuals interact collectively to create an emergent situationally-specific set of norms to guide their future behavior. In other words, individuals must work together to redefine the situation and propose a new set of actions, which is the product of processes labeled "milling" and "keynoting".

Milling is a communication process whereby individuals come together in an attempt to define the situation, propose and adopt new appropriate norms for behavior, and seek coordinated action to find a solution to the shared problem at hand [40]. The group engages in both physical and verbal communication in order to ask the three following questions: (1) what happened? (2) what should we do? and (3) who should act first? (known as leadership selection) [41, 42]. Leaders emerge as keynoters, or those who advance suggested interpretations of the event or suggestions on what do to next [37, 43]. The consequences of the milling process are that individuals become sensitized to one another, that a common mood develops, and that a collective definition of the situation is decided upon that minimizes initial ambiguity [44]. Overall, in the face of new and uncertain situations, milling and the keynoting processes allow the group to define the situation and to propose next steps for alternative schemes of social action [40, 43, 44].

The new situation and next steps developed do not emerge in a social vacuum, however. Rather, individuals within a group bring with them certain aspects of the "normal" or non-emergency situation that influence decisions made in the new situation. First, individuals bring their "social stock of knowledge" to the situation. The social stock of knowledge consists of an individual's internal set of knowledge about the disaster (or disasters in general), experiences from previous disasters or building evacuations, and his/her relationships and roles within the building, especially those related to building fires and other types of disasters [45]. Second, individuals bring conventional norms, i.e., previous ways of acting within the building and/or society as whole, which are likely to influence the newly developed "next steps for action" during the current disaster situation [31].

Protective Action Decision Model—A Background

A decision-making model has been developed that extends and applies ENT's explanation of the meaning-making process in crises to disaster situations. The Protective Action Decision Model (PADM), which is based on over 50 years of empirical studies of hazards and disasters [28, 38, 46–49], provides a framework that describes the information flow and decision-

making that influences protective actions taken in response to natural and technological disasters [50]. The model posits that cues from the physical environment (e.g., the sight of smoke) as well as information from the social environment (i.e., emergency messages or warnings), if perceived as indicating the existence of a threat, can interrupt normal activities of the recipient. Depending upon the perceived characteristics of the threat (e.g., what is going on and how dangerous is it?), indicative of the milling and keynoting processes described above, individuals will either seek additional information, engage in actions to protect people or property, perform actions to reduce psychological stresses, or resume normal activities [50]. In addition to perceptions of the threat, responses are also determined by the perceived feasibility of protective actions.

Before describing the stages of the PADM in detail, it is necessary to introduce the additional research and social models that it draws upon. Studies of social influence provide insight on the types of cues and information that affect behavior. Research and studies on the decision-making process shed light on the steps in which people engage to make decisions on their next course of action. Additionally, the PADM is based upon other theories and conceptual models that link together cues, cognitive processes and subsequent protection actions.

First, since people perceive information from both the physical and social environment, the PADM incorporates insights from social influence research. Theories of social influence posit that the actions of others and the risk communication process can influence human response in disasters. In ambiguous situations, the presence or actions of others helps to define what behavior is appropriate in a particular situation. If people are seen to be taking protective action, for example, moving to the same stair, others are likely to follow suit [51, 52]. Conversely, if people are not taking emergency action, others are also less likely to engage in emergency actions. Additionally, research has shown the influence of information (for example, warnings provided via emergency communication systems), on a person's beliefs, attitudes, and subsequent behavior [53, 54]. Aspects of the risk communication process, e.g., the source, the message, the channels, and the receiver characteristics (i.e., the receiver's perceptions of the credibility of the message, message comprehension, and channel preferences), can ultimately predict whether or not protective action is taken before or during crisis [38, 50].

As a decision-making model, the PADM also relies on behavioral decision theory. In a perfect world, in which those at risk behave like rational actors, decisions would be made based upon all of the necessary information available to the individual, which would be weighed based on costs and benefits of the various outcomes, leading ultimately to an optimal decision on the best course of action. More often, however, people lack the necessary information needed to make decisions, and they do not always search for additional information. Instead, they make decisions based on their beliefs about the situation, and many times, these beliefs can reflect poor understandings of the situation [55]. For example, in the Beverly Hills Supper Club fire when an employee took the stage and announced the presence of a fire, some of the patrons thought that the announcement was part of the evening's entertainment and in turn, remained in place rather than moving to the exits [18]. Decision scientists argue that people are often poor judges both of the likelihood of a disaster event and of the range and severity of impacts disasters can produce. This is because people use a variety of "quick and dirty" heuristics, which are simple rules or "cognitive short cuts" through which they judge a situation or event [56, 57]. One example of a heuristic that people employ is the availability heuristic, or judging the likelihood of an event based on the ease of recalling similar instances from memory [57, 58]. For example, people often think that deaths due to plane incidents are more frequent than deaths due to car accidents because they can recall more easily dramatic media coverage of large-scale plane crashes [59]. Another short cut, similar to social influence research, is an over-reliance on the actions of others [60]. In cases of procedural uncertainty, where individuals have little

experience dealing with high-stakes decisions, individuals are likely to adopt the decision strategies of others and follow their behavior [60]. Unfortunately, the individuals who are followed may also be using cognitive short-cuts and taking inappropriate action. Heuristics can result in biased understandings of the situation, which may then be used to make sub-optimal decisions during a disaster.

Research in the area of judgment and decision-making under uncertainty also provides insights into the ways in which people make decisions on their next course of action based on their beliefs. "Rational-actor"-based research claims that individuals will optimize decision-making by weighing all options and choosing the best one [61, 62]. In situations of uncertainty or crisis, however, individuals or groups are unlikely to search for a large number of options due to significant time pressures [63–66]; limited mental resources (e.g., when they are under stress) [67–69]; or if they perceive themselves as experienced in or knowledgeable concerning recommended protective procedures [56, 70]. In situations with greater time pressure, dynamic conditions, and ill-defined goals [56], all of which are likely to characterize building emergencies, people are likely to *satisfice*. Satisficing [67, 69, 71] is a method in which an individual chooses what s/he sees as a sufficient rather than optimal option, "not to find the best [option] but to find the first one that works" [56]. For highly trained and experienced individuals, for example, fire fighters, satisficing may in fact lead to quicker, more effective and appropriate decisions for the task at hand. The decision-making technique may be detrimental, however, for occupants who are less experienced in building fires, increasing their delay to safety or even leading to more severe consequences, like injury or death.

Finally, the PADM is based upon theories that link cues, cognitive (internal) processes, and subsequent protective action. Much of that research seeks to establish links between the perception of risk and the performance of protective action. Janis and Mann [72] developed the conflict model to describe the process of emergency decision-making. An individual's response to a warning is based upon his/her perception of the severity and immediacy of the threat, the perceived effectiveness of the possible protective action, and the possibility of gaining more information about the event and possible actions.

Mileti and Sorensen [38] developed a model that describes the influence of cognition on warning response. Whereas the PADM focuses on responses of people to various types of cues before or during a disaster, this model summarizes the determinants and consequences of public responses to disaster warnings. The warning response model outlines a process in which the receiver must hear, understand, believe, and personalize the warning message in order to respond in an appropriate way. The first stage of the process is perceptually receiving the alert or warning; Mileti and Sorensen [38] note that before anyone can respond to a message, they must receive it first. Once the warning is received, it must be understood, and in this instance, "understanding does not refer to correct interpretation of what is heard, but rather to the personal attachment of meaning to the message" [38]. For example, what does a flood warning mean to one person, versus another? The next stage involves whether the person believes the warning or not—involving whether they believe that the warning is authentic and the contents of the message are accurate. Finally, the last stage in the process before response is personalization. This is the stage in which people think of the warning in personal terms, in that they begin to consider the implications of the risk for themselves and others around them. If the individual has heard, understood, believed, and personalized the warning, s/he will then decide what to do about the risk. Mileti and Sorensen [38] do not discuss the decision-making process and subsequent actions in depth, but generally state that people do next what they think is best for them. An important part of this process is confirmation. In threat situations, people are constantly seeking new information to confirm prior information, whether from family, friends, neighbors, and co-workers, or from various media sources and authorities. Confirmation

affects each stage of the warning process, in that it helps people to better understand warnings, believe them, personalize the risk, and make decisions.

Protective Action Decision Model—The Stages of Decision-Making

Although the PADM is similar to the Mileti and Sorensen warning response model, the PADM provides a more general framework that describes information flow and decision-making specifically in response to various types of cues that originate from natural and technological disasters [50, 73]. The PADM asserts that the process of decision-making begins when people witness cues from the disaster event. Individuals can encounter only one type of cue (for example, seeing smoke) or may be presented with a variety of different cues, for example, environmental cues, the behavior of others, and warning messages. Warning messages can consist of both official and unofficial messages; i.e., official messages are those that come from official warning providers (e.g., emergency managers in a building fire) and unofficial messages are those that come from unofficial sources, such as others in the building.

The introduction of these cues initiates a series of pre-decisional processes that must occur in order for the individual to perform protective actions. First, the individual must perceive or receive the cue(s). Then, s/he must pay attention to the cue(s). Finally, the individual must comprehend the cue(s). Comprehension means understanding the information that is being conveyed. If the message uses a different language or highly technical terms, comprehension will be difficult. Comprehension also refers to the development of an accurate understanding of environmental cues. For example, will the individual understand that the smoke s/he smells is coming from a building fire rather than from burnt toast in the kitchen?

People go into any disaster with widely varying pre-event perceptions or beliefs about the elements that go into a disaster—the event itself, the actions that they have taken (or should take) before the disaster occurs, and the individuals involved in the response to a disaster. The differences in these perceptions are important to understand because they often are predictors of the individuals' response behaviors when the disaster occurs. The PADM labels these pre-event perceptions as core perceptions or schemas and highlights as important three main core perceptions: perceptions of threat, perceptions of protective actions, and perceptions of stakeholders [73].

First, perceptions of environmental threats include people's beliefs about the probability and consequences of certain types of disasters as well as their expectations about personal impacts, including death, injury, property damage, and disruption of daily activities (i.e., work, school, shopping, etc.). These can vary from individuals' beliefs that they are very unlikely to be involved in any type of disaster to individuals' severe worry or dread that the next disaster is coming specifically for them. Also associated with perceptions of environmental threats is what Lindell and Perry call "the degree of hazard intrusiveness" [73]. This refers to how often individuals are personally concerned with disaster consequences, the time they spend talking about disasters, and the amount of information they receive (passively) about hazards and disasters.

The second pre-event perception includes people's perceptions of protective actions; i.e., the actions that they can take to prepare for a disaster. Essentially, this perception captures individuals' attitudes about engaging in preparatory actions before a disaster occurs. This can also vary widely, from individuals taking no preparatory action at all and believing that these types of actions are not necessary to individuals taking extensive preparation in their homes and/or work places.

The third pre-event perception consists of individuals' perceptions toward stakeholders in a disaster. Stakeholders in a disaster can be authorities (i.e., federal, state or local government), evaluators (e.g., scientists, universities, medical professionals), watchdogs (e.g., news

media), industry/employers, and individuals themselves (i.e., in their homes or places of work). Here, it is important to understand the ways in which people perceive stakeholders in terms of three factors: their expertise about disasters (in this case, fires), trustworthiness, and responsibility when a disaster or building fire takes place. This pre-event perception is more applicable to community-based disasters, such as hurricanes or tornadoes, but could be applied to fires in instances where, for example, building occupants do not trust warning information provided by a building manager.

All three of these perceptions have been shown in research to vary from individual to individual involved in the disaster situation. More importantly, these factors (among others) have been linked to the decisions that individuals make in disasters, and in turn, their protective actions (discussed below).

After the three pre-decisional processes are completed and the three core perceptions are activated (i.e., it is understood that there are differences among individuals in these three areas), the decision-making model consists of a series of five questions [50]:

- Is there a real threat that I need to pay attention to? [If yes, then the individual believes the threat]
- Do I need to take protective action? [If yes, then the individual decides that s/he needs to take protective action]
- What can be done to achieve protection? [The individual begins searching for possible protective action strategies]
- What is the best method of protection? [The individual chooses one of the action strategies developed in the previous stage and develops a protective action strategy or plan]
- Does protective action need to be taken now? [If yes, the individual follows the plan developed in the previous stage]

Individuals must "answer" each question in order to proceed through the perceptual-behavioral sequence, in which the outcome of the process is the performance of a behavioral action. A graphic of the process is shown in Fig. 58.2.

The first stage of the decision model involves the issue of risk or threat identification. If the individual perceives, pays attention to, and comprehends cues associated with an event, s/he first asks "Is there a real threat that I should pay attention to?" In this stage, according to Lindell and Perry, the individual decides if there is actually something occurring that may require her action, sometimes referred to as warning belief [74], "but this term unnecessarily excludes people's reactions to environmental cues so the term *threat belief* is generally more appropriate" [50]. This stage corresponds to the phase in ENT in which members of a population realize that the norms and behaviors for "stable times" no longer apply [37]. If the individual's answer is yes, then s/he is said to believe the threat, and s/he subsequently moves on to consider the next question in the process.

The second stage of the decision model is referred to as risk assessment. Research has shown that a person's perception of personal risk, or "the individual's expectation of personal exposure to death, injury, or property damage" is highly correlated with disaster response [50]. In this stage, also known as personalizing risk [38], the individual determines the likelihood of personal consequences that could result from the threat and asks oneself the following: "Do I need to take protective action?" At this point, which is also discussed in human factors research as "situation awareness" [75], the individual tries to gain insight on the potential outcomes of the disaster and what those potential outcomes mean for his safety. The internal dialogue that takes place at this stage can be thought of as mental simulation or mental modeling [56], in which the individual develops a mental model of what is going on in his environment, based on perceived cues, and then expands the mental model to predict the personal consequences of the event. The more certain, severe, and immediate the risk is perceived to be, the more likely the individual is to perform protective actions [76].

In the third and fourth stages, the individual engages in a decision-making process to identify (1) what can be done to achieve protection; and (2) the best available method of achieving this

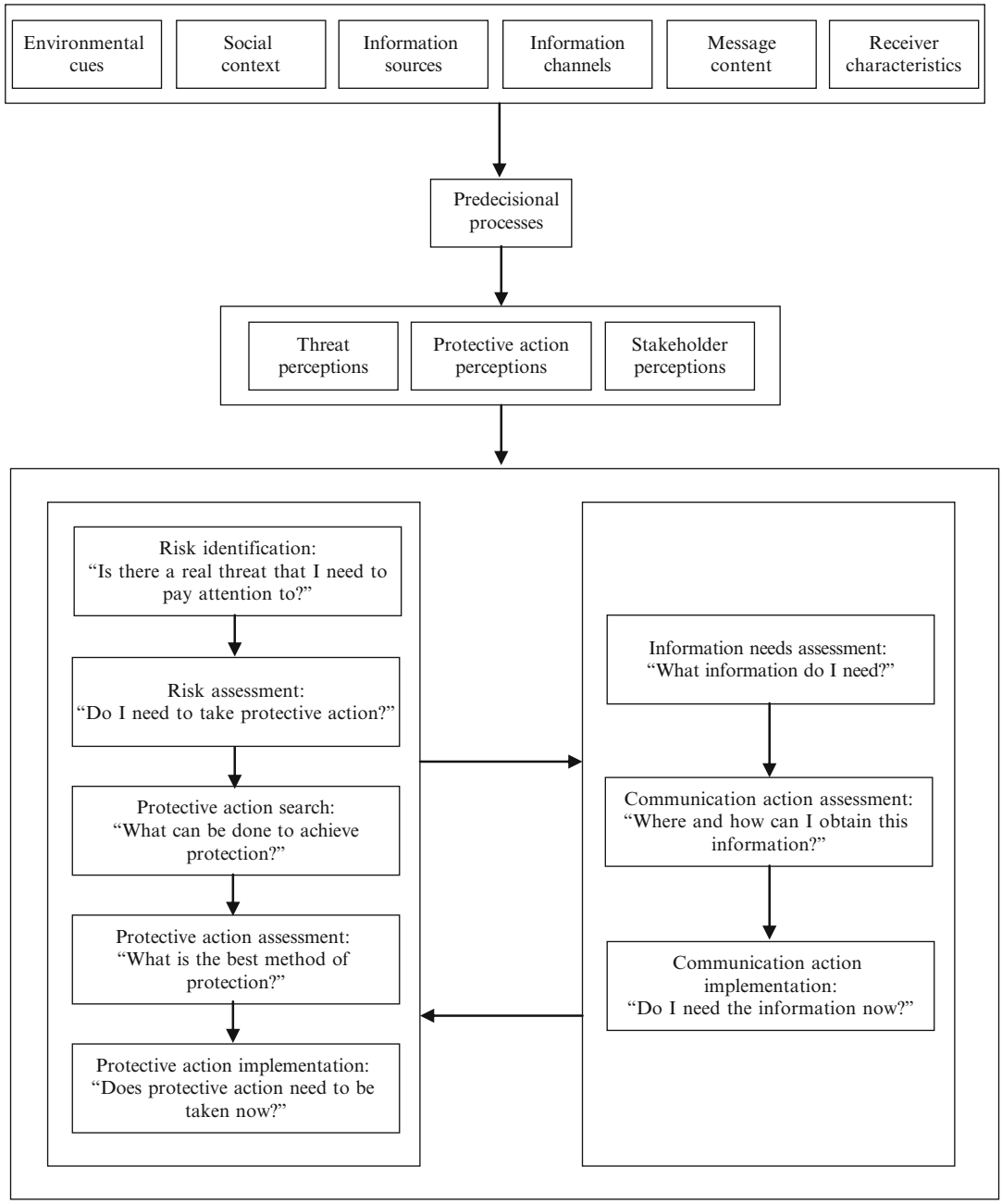

Fig. 58.2 The protective action decision model [73]

protection. The outcome of the third stage is a set of possible protective actions from which to choose. After establishing at least one protective action option, individuals engage in the fourth stage of the PADM: protective action assessment. This stage involves assessment of the potential option(s), evaluating the option(s) in comparison with taking no action and continuing with normal activities, and then selecting the best method of protective action (e.g., evacuating, sheltering in place). Once an action is chosen, the end result of stage 4 is an adaptive plan,

which can vary in its specificity. For example, for households under threat conditions,

> [a]t a minimum, a specific evacuation plan includes a destination, a route of travel, and a means of transportation. More detailed plans include a procedure for reuniting families if members are separated, advance contact to confirm that the destination is available, consideration of alternative routes if the primary route is unsafe or too crowded, and alternative methods of transportation is [sic] the primary one is not available [50].

After a protective action is chosen and the adaptive plan is developed, the final step in the decision process involves the implementation of the protective action plan or strategy. Here, the individual asks whether the protective action needs to be taken now. If the answer is yes, then s/he engages in that action. However, Lindell and Perry [50] note and other studies confirm [18, 77, 78] that individuals are still likely to delay the performance of protective action, even when the threat is perceived as imminent.

Passage through these stages is often problematic. If at any stage the individual is uncertain about the answer to a question, s/he engages in additional information-seeking actions. Information seeking is especially likely to occur when individuals think that time is available to gain additional insight on the question at hand. If information seeking is successful, in that the person at risk judges s/he has obtained enough information to answer the question, then the individual moves on to the next stage or question in the decision-making process. However, if the information-seeking action is unsuccessful, there will be additional searching for information as long as s/he is optimistic that other sources or channels can help [50]. If s/he is pessimistic regarding future information seeking success, s/he is likely to attempt to decide on a protective action based solely on whatever information is available.

This description is not meant to imply that decision processes are linear and straightforward. For example, information feedback loops allow for the receipt of new environmental and social cues after initial engagement in information-seeking actions. An individual who gains additional information is likely to carry on with the decision-making process until s/he is ready to implement a protective action. Additionally, individuals do not have to go through each stage or question in the decision flow chart [50]. For example, if an individual is presented with information about the event from a credible source or if s/he is ordered to evacuate, s/he may move on to later stages in the decision process rather than going through each one in succession.

This decision-making framework describes the process of how individuals respond to disasters. Even though the focus of the models discussed so far is on community-wide disasters, it is clear that the models also apply to decision-making during more localized types of events, such as building fires.

Engineering Implications of the Protective Action Decision Model

Engineers must understand that response to fires and other disasters is the result of a process. Individuals or groups of individuals engage in a decision-making process (i.e., a series of steps) before they respond, based upon the cues presented from their environment (including information), the social context, personal characteristics, past experience [23, 76, 79–81] and hazard knowledge [82]. With this understanding, the engineer should recognize that occupants of a building are unlikely to evacuate immediately, and simultaneously, and instead, recognize that occupants are required to receive and process information on an individual- (or -group-) basis. Also important is that if, at any time in the process, the answer to a decision-making question is unclear (See Fig. 58.2), then the individual will engage in information-seeking actions. Information-seeking actions take time to complete and delay the occupant from reaching safety.

Additionally, just because cues or information are provided to building occupants does not necessarily mean that they will act appropriately.

The cues or information must be perceived (e.g., heard or seen), paid attention to, and then comprehended first before any actions take place. Therefore, engineers must ensure that any information meant for building occupants must be provided in such a way to ensure that these three processes take place. One example of this is to ensure that the public address announcements disseminated in a building fire are set to an appropriate volume level such that all occupants in the buildings can hear them; and if not and in order to reach occupants with hearing disabilities, other means of disseminating the information are used (e.g., visual signage) [83].

Engineers should also acknowledge that occupants must perceive a credible threat and personalize the risk before taking action. Research has shown that individuals are more likely to identify and personalize the risk if they perceive a larger number of cues [43, 84, 85] that are intense or extreme in nature [86, 87]. In building fires, for example, occupants who witness heavy, thick, black smoke that decreases visibility and irritates the eyes are more likely than those noting less intense cues to realize that a serious event has taken place that puts them in danger [88]. However, it is always the responsibility of the engineer to protect building occupants, which includes limiting their exposure to fire effluent.

The main way to prompt safe, effective, and appropriate action from building occupants is to disseminate warning messages during fire emergencies that will positively influence risk identification and assessment. Research has shown that a ***successful warning message*** contains the following factors or qualities:

- Specific about the threat and the risk involved [89–91],
- Repetitive [50],
- Consistent [92],
- Disseminated via multiple channels [93],
- Provided by a credible source [49, 76, 81, 94].

Source credibility is defined in terms of the source's expertise, including access to special skills or information, and trustworthiness, or the perceived ability to communicate information about the disaster without bias [50, 54]. Source credibility can differ depending upon a number of factors, including the type of disaster, characteristics of the source, such as social role and believability, and characteristics of the warning receiver, such as past experience in disasters and social location [95–100]. For some warning receivers, credible sources may be friends and relatives, and for others, credible sources may be disaster authorities, such as government officials [101, 102] or fire fighters [38].

As far as content, a warning message should contain five important topics to ensure that building occupants have sufficient information to respond with little or no additional delay and information seeking [38, 103]. These five topics, labeled here as the five W's of any effective warning message, are as follows:

1. Who is providing the message? (i.e., the source of the message, which should be perceived as credible by the building occupants)
2. What should people do? (i.e., what actions occupants should take in response to the emergency and if necessary, how to take these actions)
3. When do people need to act? (i.e., in rapid-onset events, the "when" is likely to be "immediately")
4. Where is the emergency taking place? (i.e., who needs to act and who does not)
5. Why do people need to act? (including a description of the hazard and its dangers/consequences).

Another way to prompt safe, effective, and appropriate action from building occupants is through training. An individual's past experiences in emergencies, specifically the actions that s/he has performed previously, can influence the actions that s/he considers as options during the current emergency [50, 56, 104]. The individual uses memories of the protective actions s/he performed in the past as options for actions to perform in the current emergency. Similarly, an individual's emergency-based training and knowledge, for example, knowledge about evacuation procedures, can influence the options that s/he develops during an emergency [78, 105–108].

Relating Theory to Practice—Protective Actions in Fires

As shown in the earlier section, research has established the theoretical process through which community residents or building occupants make decisions in response to fires and other disasters [50]. However, these theories do not provide sufficient information on the specifics or the *types* of protective actions in which occupants engage and why they engage in these types of actions during fire emergencies.

Research has been performed that identifies the types of actions that people perform during a building fire evacuation, with a focus on the pre-evacuation period. Both summary research [77, 87, 109] and research on specific incidents [1, 3, 18] highlight certain actions in which occupants are likely to engage. These actions, depending upon the situation, can include seeking information, waiting, investigating the incident, alerting others, preparing for evacuation (or deciding not to evacuate), assisting others, fighting the fire, and searching for or rescuing others. One factor that has been used to differentiate one set of actions from another set of actions is the type of building in which the emergency occurs. For example, individuals who are at home (especially at night) may engage in a different set of preparatory actions than individuals who are awake in their offices when the alarm sounds, for example. Therefore, in this section, studies that have been performed on different types of structures will be presented to identify the actions in which individuals most frequently engaged.

U.S. and UK Residential Studies

One of the first studies of behaviors performed during residential fire evacuations was by Wood [15]. The study involved 2193 fire-department conducted interviews with residents from 952 residential fire incidents in Great Britain. Within the same decade, Bryan [14] also studied residential fire incidents by analyzing on-scene interviews conducted by fire service personnel with 584 participants from 335 fire incidents in the United States.

Both researchers found that behavioral responses to fires could be categorized into the following actions: notifying others, searching for the fire, fighting the fire, calling the fire department, getting dressed, getting the family, asking others to call the fire department, gathering personal property, closing the door to the fire area, turning off appliances, doing nothing, attempting to evacuate, and evacuating; among other more specific actions. The most frequent behavioral responses to fire in both the UK and US studies were identified as evacuating the building, fighting or containing the fire, and notifying other individuals or the fire brigade.

Bryan and Wood also organized these actions into first, second, and third actions in an attempt to begin to order the actions taken during the residential evacuation process. In both studies, it was found that investigation actions, such as searching for the fire; notification actions, such as notifying others, pulling the fire alarm or getting family; and preparation actions, such as fighting the fire, turning off appliances, and getting dressed; were performed. In the U.S. study, Bryan [14] indicated that the action of "investigate" was very common as a first action by 45 % of occupants in the sample and as a second action by 23 %. These authors also report that actions such as "mitigate the fire," "help others," and "call for help" were in the middle of the actions sequence, and "escape" or "go for help" were at the end of the usual sequence of four to five actions. "Call the fire brigade" was generally a fourth action, and "fight the fire" usually occurred between the second and sixth actions.

Bryan [14] and Wood [15] also identified actions that were specifically linked to engagement with the fire and/or subsequent toxic products produced by the fire during these residential evacuations. Some percentage of occupants in both studies engaged in fire-fighting behavior, re-entry behavior (i.e., they returned to the structure after leaving), moved some distance through smoke, and/or turned back (i.e., stopped their movement to or into smoke and redirected

based on environmental conditions) [77]. These results show that individuals were likely to engage in potentially risky behavior, such as fire-fighting or re-entry behavior, during the fire incident.

For more information on the psychophysical effects of smoke on individual movement and actions, including the visibility distances in which people moved through smoke or turned back, please see Chaps. 61, 63, and 64.

MGM Grand Hotel Fire

Analysis was also performed on the behaviors engaged in during the MGM Grand Hotel fire in Clark County, Nevada, on November 21, 1980 [110]. This hotel fire involved both injuries and fatalities among the guests. The management of the MGM Grand Hotel, and the Clark County Fire Department, in cooperation with the National Fire Protection Association (NFPA) [111], conducted an intensive study of the guests registered in the hotel for the evening of November 20 to 21, 1980, to determine how the occupants became aware of the fire incident and their behavioral responses.

The MGM Grand Hotel fire was discovered by an employee of the hotel who entered the deli-restaurant located on the casino level of the hotel at approximately 7:10 a.m. on November 21, 1980. The fire reached a flashover condition in the deli area, immediately spread from east to west through the main casino area, and extended out the west portico doors on the casino level immediately following the arrival of the initial fire department personnel. The heat and smoke extended from the casino area through seismic joints, elevator shafts, and stairways throughout the 21 residence floors of the hotel. The heat was intense enough on the 26th (top) floor to activate automatic sprinkler heads located in the lobby area adjacent to the elevator shafts.

Due to the rapid early evacuation of the telephone staff, guests in their rooms were not alerted by the hotel public address system nor the local fire alarm system. Guests who were alerted early in the fire incident, or guests already awake and dressed, were able to escape prior to the smoke conditions becoming untenable on the residential floors. Guests alerted later in the progression of the fire incident remained in their rooms or moved to other rooms, often with other occupants. The flame propagation did not extend above the casino level, with the exception of very minor extension into two guests' rooms on the 5th floor. The fire resulted in 85 fatalities to guests and hotel employees in the following areas of the hotel [110]: 14 persons were found on the casino level, 29 persons were found in guest rooms, 21 persons were found in corridors and lobbies, 9 persons were found in the stairways, and 5 persons were found in elevators. The victims were located on the casino level, and the 16th through 25th floors, with the majority of fatalities found between the 20th and the 25th floors. Various estimates have been provided of the number of guests and fire department personnel that suffered injuries at the MGM Grand Hotel fire. Morris [112] indicated that 619 persons were transported to hospitals from the fire scene, and another 150 guests were treated at the Las Vegas Convention Center, where the survivors had been transported.

Behavioral responses from survivors of this fire were elicited from 554 returned mail-surveys. Similar to the residential studies, one topic of interest was to collect information on the types of behaviors in which survivors engaged. The initial five behavioral responses of the 554 guests as elicited from the NFPA questionnaire study are presented in Table 58.1. The five most frequent first behavioral responses were "dressed," "opened door," "notified roommates," "dressed partially," and "looked out window." The guests involved in the first responses were predominantly engaged in attempting to define and structure the fire cues relative to the severity of the threat to themselves. Only a small percentage, approximately 8 % of the study population, initiated or attempted to initiate their evacuation behavior as the first response.

Examination of Table 58.1 indicates the five most frequent behavioral responses reported by guests as second actions were "opened door,"

Table 58.1 Compilation of the initial five actions of guests in the MGM grand hotel fire incident [111]

	Percent of population				
Actions	First	Second	Third	Fourth	Fifth
Dressed	16.8	11.6	6.5	–	–
Opened door	15.9	11.7	6.7	3.4	–
Notified roommates	11.6	3.0	–	–	–
Dressed partially	10.1	7.5	4.5	–	–
Looked out window	9.7	5.7	–	–	–
Got out of bed	4.5	–	–	–	–
Left room	4.3	5.4	8.1	2.4	2.0
Attempted to phone	3.4	3.6	–	2.8	–
Went to exit	2.5	10.3	9.5	16.1	6.7
Put towels around door	1.6	2.5	3.0	6.8	7.7
Felt door for heat	1.3	2.3	–	–	–
Wet towels for face	1.3	3.7	6.3	4.6	7.9
Got out of bath	1.1	–	–	–	–
Attempted to exit	1.1	3.0	5.8	4.3	–
Secured valuables	–	6.8	4.3	–	–
Notified other room	–	3.4	2.2	–	–
Returned to room	–	–	3.9	8.4	4.1
Went down stairs	–	–	3.9	5.4	21.3
Left hotel	–	–	3.4	2.6	2.0
Notified occupants	–	–	3.0	–	–
Went to another exit	–	–	–	3.6	4.8
Went to other room	–	–	–	3.6	3.6
Went to other room/others	–	–	–	3.4	8.7
Looked for exit	–	–	–	2.4	–
Broke window	–	–	–	–	4.3
Offered refuge in room	–	–	–	–	1.8
Went upstairs to roof	–	–	–	–	2.9
Went to balcony	–	–	–	–	1.8
Other	14.8	19.5	28.9	30.2	20.4
Total (percent)	100.0	99.1	96.9	90.4	79.6
Number of guests	554	549	537	501	441

"dressed," "went to exit," "dressed partially," and "secured valuables." Whereas approximately 40 % of the population was engaged in evacuation or sheltering actions by the second act, others were engaged in protective actions. Approximately 19 % of the study population reported they were involved in the dressing actions, 10 % were involved in notification activities, and 7 % were gathering valuables prior to initiating evacuation or seeking refuge.

Examination of the third behavioral responses of the 537 guests in the study population indicated the responses of the guests generally progressed to evacuation, attempted evacuation, and notification responses. Thus, approximately 25 % of the MGM Grand Hotel fire incident study population was involved in evacuation-related behavioral responses, and approximately 10 % of the guests were involved in attempted evacuations as identified by their third responses of "attempted to exit" and "returned to room." The alerting and notification actions of the guests were involved with the third behavioral responses of "notified occupants" and "notified other room."

The fourth behavioral responses of the guests in the study population indicated a progression of the guests to evacuation, attempted evacuation,

Table 58.2 Activities prior to evacuation reported in telephone survey by survivors of WTC 1 and WTC 2 [1]

Activities before evacuation	Percent reporting the activity (n = 440 in WTC 1) (%)	Percent reporting the activity (n = 363 in WTC 2) (%)
Talked to others	70	75
Gathered personal items	46	57
Helped others	30	34
Searched for others	23	32
Talked on telephone	16	16
Moved between floors	8	8
Shut down computers	6	7
Continued working	3	6
Fought fire or smoke	6	1
Other activities	25	20

Source: NIST WTC Telephone Survey Data
Note: Total does not add up to 100 % because respondents may have taken multiple actions

and self-protection or room refuge procedural responses. Additionally, the fifth behavioral responses of the guests were primarily for self-protection, including the improvement of the room as an area of refuge, and evacuation behavior.

Overall, in this hotel fire, hotel guests were more likely to take initial actions investigating, notifying others, and preparing for evacuation, which in this case involved getting dressed. This is similar to the residential studies, likely because a hotel and a residence involve similar living circumstances. In both cases, individuals may be alerted to a fire when they are sleeping—meaning that they will require additional time to prepare for evacuation; i.e., getting dressed themselves or getting other family members dressed. Then, after initial investigation, preparation and warning activities ended, and hotel guests engaged in protective actions and evacuation.

2001 World Trade Center Disaster (Office Buildings)

Different from a residential or hotel fire, studies were performed on the 2001 World Trade Center (WTC) evacuation of the two office towers [1, 22, 30]. On September 11, 2001, two commercial airplanes flew into World Trade Center (WTC) Towers 1 and 2 and initiated full building evacuations from both 110-story office buildings. At 8:46 am, Flight 11 slammed into the north face of WTC 1, disconnecting the entire population above the 91st floor from any way out of the building. It was at this moment that the largest full-scale building evacuation in history began for occupants who had the opportunity to evacuate from both WTC 1 and 2. None of them knew, however, that another commercial jet was on its way—one that was heading straight for WTC 2. Sixteen minutes after WTC 1 was struck and after one-third of WTC occupants had already evacuated,[3] Flight 175 sliced into floors 78 to 84 of WTC 2 leaving only one of the three stairs available for evacuees above the 78th floor. Occupants who could evacuate continued to pour from the structures until the towers eventually succumbed to structural collapse (WTC 2 collapsed at 9:58:59 am and WTC 1 collapsed at 10:28:22 am).

The frequency of actions performed in the 2001 WTC disaster by occupants evacuating Towers 1 and 2 was reported by Averill et al. [1] and Day, Hulse and Galea [113], shown in Tables 58.2, 58.3 and 58.4 below. The focus here is an understanding of the actions taken before evacuation movement in the stairs began. As part of the NIST WTC study [1],

[3] 21 % from WTC 1 and 41 % from WTC 2.

803 interviews were conducted via telephone using a computer program that allowed the interviewers to collect data electronically, also known as computer-assisted telephone interviewing (CATI). Quantitative data was captured via an interview schedule designed to measure the following five primary areas: preparedness and training, initial September 11 experience, interim September 11 experience, evacuation experience on September 11, and respondent demographics. The two populations selected for study were all of the people who worked in WTC Tower 1 and WTC 2 who were in the buildings between 8:46 am and the time at which their respective Tower collapsed on September 11, 2001. In the UK, the WTC evacuation was also studied as part of an in-depth research project carried out by the Project High-rise Evacuation Evaluation Database (HEED) research team [22]. Project HEED was a 3-year project to explore human behavior associated with the evacuation of high-rise buildings. The basis for this project was an analysis of the 2001 WTC disaster through both face-to-face interviews with survivors and computer simulation of the evacuation. The project resulted in over 250 face-to-face or telephone interviews with survivors from the 2001 WTC disaster, collected to both inform the development of future building regulations and evacuation computer models and to make data available to bona fide building safety researchers in countries around the world. In both cases, the studies' presentation of actions taken was not ordered in any way (i.e., first, second, and third actions); however, both studies provide an understanding of the actions that were most frequently performed from one tower to another.

Averill et al. [1] presented a list of the "general" pre-evacuation actions performed in both towers, shown in Table 58.2, below, acknowledging that not all actions were covered by these categories by including the "other" category at the end of the list. The majority of individuals in both towers engaged in actions that involved talking to others (70 % in WTC 1 and 75 % in WTC 2) and gathering personal items (46 % in WTC 1 and 57 % in WTC 2). Additionally, about a third of occupants in both towers engaged in helping others and searching for others.

Day, Hulse and Galea [113], on the other hand, grouped pre-evacuation actions into two different categories: information tasks and actions tasks (shown in Tables 58.3 and 58.4). Information tasks, which involved action taken to obtain or receive information, were further divided into three different areas: seeking

Table 58.3 Comparisons of information tasks by tower [113]

	WTC1		WTC2	
Information tasks	% PPTs	Freq	% PPTs	Freq
Seek information tasks				
Environmental (e.g., window)	53	66	83	142
WTC colleagues/friends	36	44	27	46
Waited for further info	13	17	8	11
People outside WTC (e.g., called family, friends)	8	17	3	4
TV/internet/radio	2	2	6	7
Professional bodies (e.g., port authority, security, police, fire)	2	2	5	6
Communication tasks				
Instruct others to evacuate	34	51	40	89
Inform others of my situation	17	25	30	63
Debate/challenge	3	5	11	15
Receive information tasks				
Non-professionals (e.g., managers, family)	12	16	23	35
Professionals (e.g., PA announcements, security, police, fire)	8	9	19	31

WTC1: N = 119, WTC2: N = 121, PPTs participants

Table 58.4 Comparisons of action tasks by tower [113]

	WTC1		WTC2	
Action tasks	% PPTs	Freq	% PPTs	Freq
Personal tasks				
Collected personal items (e.g., wallet)	60	141	63	145
Went to toilet/comfort break	3	3	2	2
Changed footwear/glasses	3	3	1	1
Emergency tasks				
Evacuation facilitation (e.g., searched office/floor, forced exit open)	19	25	26	47
Waited for others so evacuate together	7	8	14	17
Gave others physical assistance (e.g., carried/gave first aid)	6	7	3	4
Protective action (e.g., took refuge, blocked/sealed cracks, got under smoke, made masks)	7	8	3	4
Distributed useful items (e.g., mobiles, masks, bottled water)	0	0	1	1
Work tasks				
Secured items/areas (e.g., locked files, bank vaults)	7	10	3	4
Tidied desk	3	5	8	14
Latent tasks				
Denial/Froze/continued working	2	2	13	17
Travelled to another area/floor/stairwell (reason unknown)	4	5	3	4

WTC1: N = 119, WTC2: N = 121, PPTs participants

information, communicating with others, and receiving information. The action tasks, a term which was not specifically described by the authors, was subdivided into additional categories: personal, emergency, work and latent actions. According to this study, and similar to Averill et al. [1], the majority of tasks undertaken by the participants were "Information tasks" (54 % in WTC 1 and 63 % in WTC 2)—specifically the action termed as "seeking information". Additionally, the most common "Action Tasks" performed by occupants in each tower were "Personal Tasks"—accounting for 68 % of the "Action Tasks" in WTC 1 and 57 % in WTC 2. Personal tasks involved occupants collecting or packing up their personal possessions before evacuating the building. Day, Hulse and Galea [113] also tracked the number of tasks completed by each participant in the study. The range of tasks completed was between 0 and 13 in WTC 1 and 2 and 21 in WTC 2; with an average number of tasks completed in WTC 1 of 3.96 and an average number of tasks completed in WTC 2 of 5.86.

Table 58.5 Range of times associated with WTC pre-evacuation actions [30]

Action	Range of timing (minutes)
Preparation (Action task, personal)	0.5–5
Communicating with others (Information task)	3
Looking out the window (Information task)	1–5
Helping, by authorities (Action task, emergency)	4–10

While most empirical studies of actual incidents [114–116] and evacuation drills [117–119] provide overall timing estimates for activities in the pre-evacuation period, very few researchers discuss times associated with specific pre-evacuation actions. From analysis performed by this author on the Project HEED database [30], pre-evacuation action times were reported by some WTC occupants and are presented in Table 58.5 as a range of times (minutes) for each action type.

University Library Building in the Czech Republic

From a study of an unannounced evacuation drill in a university library in the Czech Republic, Galea et al. [120] collected data on the number, type and duration of pre-evacuation actions. To begin the evacuation, the alarm system, consisting of a combination of tones, recorded voice and live voice messages, was activated. The recorded voice message began by stating the word "attention" multiple times, followed by a declaration that an emergency situation was taking place. The message also instructed people to prepare for evacuation and wait for further instruction. Two live messages were also disseminated during the drill. The message made it clear that the evacuation instruction was directed at occupants in the library building only and then gave instructions on the routes to take, depending upon where the individual was located within the library building. The live messages also warned individuals not to use the elevators, and to only use the stairs to evacuate. On the day of the trial, the alarm system failed to operate in certain parts of the library building. Some individuals heard the alarm tone and announcements and some did not. In the places where the alarm failed to function, the evacuation was initiated by staff intervention.

Video observation and analysis of the evacuation drill allowed for the collection of pre-evacuation action (or task) type and duration. In this study, similar to the WTC study presented above, pre-evacuation actions were categorized in two different ways: information tasks (or actions that involve the occupant seeking, providing or exchanging information regarding the incident) and action tasks (or all other types of pre-evacuation actions, e.g., preparation, fighting the fire, helping others, etc.). Throughout the evacuation, 235 information tasks and 268 action tasks were completed; the average number of information tasks (per person) was 3.7 and the average number of action tasks (per person) was 4.3. On average, an evacuee in this study engaged in a total of 8.0 tasks prior to beginning evacuation movement (e.g., into the stairs).

There were differences in task numbers between evacuees who received staff intervention and those who were alerted by the alarm system. For those who were alerted via staff intervention, the average number of information tasks was 2.0 and the average number of action tasks was 3.6; for an average number of total tasks performed prior to beginning evacuation movement of 5.6. For those alerted via the alarm system, the average number of information tasks was 7.4 and the average number of action tasks was 5.7; for an average number of total tasks of 13.1. The authors of this study noted that individuals alerted by the alarm engaged in twice as many tasks during pre-evacuation than individuals notified by a member of staff.

Work was also performed to measure the time to undertake each individual task from the video footage [120]. The analysis showed that the average duration of a single action task was 6.4 s and the average duration of an information task was 9.7 s (independent of how an evacuee was alerted to the incident). The authors concluded that, in this study, an information task took 1.5 times as long as an action task. Analysis of task timing was also performed by comparing the two groups alerted to the drill via different means. For the population alerted by staff intervention, the average time for an action task was 6.5 s and for an information task was 6.7 s. On the other hand, for the population alerted by the alarm system, the average time for an action task was 6.4 s and for an information task was 9.9 s. The authors of this research noted that there was a considerable difference in the average time to complete information tasks among the two populations—showing that the population alerted by the alarm system took a longer time (on average) to complete information tasks in comparison to the population alerted by staff intervention. This highlights the greater influence of in-person, official communication/instruction on a faster response time when compared with an alarm system.

University of Greenwich Dreadnought Building (Educational and Library Services Building)

A study was performed on an evacuation of a university building known as the Dreadnought building, located on the University of Greenwich campus in London, UK [121]. The Dreadnought building is a three-story structure used for a variety of purposes, including library services, student computing facilities, and a small cafeteria. Data were collected by research staff located at 15 key locations throughout the building via handheld video and manual observations. Additionally, questionnaires were handed out to all evacuees to collect information about their experience during evacuation. Last, 62 closed-circuit cameras were used to gather data on the starting locations of evacuees, their behaviors/actions, and response times. Because of camera locations, initial responses and times could only be captured for 247 evacuees of this building: 228 students and 19 members of staff. In this building, once the alarm sounded, nominated members of staff swept each room, "forcing students to leave their work and belongings, and informing them of the routes they should adopt" [121].

During analysis, a dictionary of potential actions was created based upon examination of the video evidence from the evacuation. The list of actions comprised of the following:

- Evacuate immediately
- Perform a computer shutdown
- Disengage socially
- Collect items, including bags, coats, paperwork, etc.
- Investigate the incident.

Additionally, it was found that 27 % of the participants of this study completed one or no actions prior to beginning evacuation, 55 % completed two actions, and 18 % completed three or more.

Engineering Implications of Actions Taken During Evacuation

Engineers should understand that actions, both information-related actions and protective actions, are performed during fire evacuation. Depending upon the circumstances, these actions can take a considerably long time to complete and will contribute to the time to reach safety. First, engineers must account for these actions in some way when calculating evacuation timing in a proposed design building fire. Actions and delay times associated with these actions can be especially important in certain types of buildings, where individuals are likely to engage in certain types of lengthy actions; i.e., those in which people may be asleep or located on upper floors of uniquely tall buildings. Many times, when performing an evacuation calculation, engineers are asked to provide a specific pre-evacuation time period or distribution as input. Engineers should choose a time that is based upon specific scenarios and resulting occupant actions (and action timing). Additionally, to improve occupant response, engineers should account for evacuation actions when developing fire evacuation plans for buildings. As stated earlier, research has shown that providing specific warning information in certain ways or providing leadership to prompt evacuation response could reduce the need for information seeking, and even the performance of certain protective actions. If engineers understand which evacuation actions they should anticipate in a specific building or fire scenario, they can formulate plans that are successful in decreasing delays caused by evacuation actions. Therefore, it is important to first understand that types of actions that individuals have engaged in previous fires and how these actions can vary from building to building, and from fire event to fire event.

Relating Theory to Practice—The Sequence of Protective Actions in Fires

Beyond identifying the types and percentages of actions, including the percentage of actions that were performed first, second, and third, research has been performed to identify the sequence of actions taken in different types of fires. Canter, Breaux, and Sime [78] developed decomposition diagrams for various types of fire events that

identify the sequence of actions. The study was conducted in the United Kingdom on domestic fires (14 domestic fires and the acts of 41 persons), multiple-occupancy fires (eight multiple-occupancy fires and the acts of 96 persons), and hospital fires (6 hospital fires and the acts of 61 persons). All persons in this study were interviewed about their experiences in the fire; first asking them to give a detailed account of everything that happened starting from the time at which they considered that something out of the ordinary might be occurring. Once individuals had given full accounts, interviewers questioned respondents on certain issues, including recognition of the fire event, location of the occupant, ongoing behavior, sequence of actions, perception of the situation, past experiences, and background information.

The results of this analysis were the development of decomposition diagrams. These diagrams are provided here, as Figures 58.3, 58.4, and 58.5. Dashed circles indicate the acts which occurred with a lower frequency. The relationships between acts are indicated by arrows; and if actions are repeated, the circle (representing the action) would have a looped arrow coming back on itself. The numbers next to an arrow refer to the strength of the association. The higher the association number, the greater the association is; i.e., the more likely it is that given the performance of one act, the next action (specified) will follow.

The decomposition diagram for domestic fires is shown in Fig. 58.3. The domestic diagram summarizes 1189 acts which occurred in 14 domestic fires. It outlines departure from pre-event activities, such as sleeping, to a range of other investigative, notification, and preparation activities. In these domestic fires, individuals tended to perform actions related to investigating which involved encountering or engaging with the fire in some way, and then evacuating; or discuss the situation, notify or warn others, preparing to evacuate, and then leaving the house.

The decomposition diagram for multiple occupancy fires is shown in Fig. 58.4. The multiple occupancy diagram summarizes 1714 acts which occurred in all eight multiple-occupancy fires [78]. All fires occurred in the United Kingdom in hotel occupancies. Similar to the domestic fires, occupants went to investigate the receipt of strange noises, which led to them encountering the fire environment and/or warnings about the emergency. If direct contact with the fire environment ensued, the characteristic sequence that followed involved the occupant going to the window, shouting for help, and then being rescued. Also similar to domestic fires, occupants engaged in activities such as warning others, gathering personal items, and closing or opening windows.

The decomposition diagram for hospital fires is shown in Fig. 58.5. The hospital diagram summarizes 1104 acts which occurred in all six multiple-occupancy fires [78]. The case studies covered a variety of hospital types, i.e., geriatric, psychiatric and general medicine; however, patterns were still revealed among the entire population, as a whole. Detection and investigation actions are performed relatively early in these fires, possibly because the higher spread of people in the building. Also, the sequence of actions is different in this diagram, when compared with others, due to the nature of the organizational hierarchy of the hospital. Senior nursing staff, whose job it was to investigate the fire, relay information to junior colleagues, who then had a series of actions that they performed in response.

The reader should note the inclusion of process-related factors (first described in the PADM) into these action-based diagrams. For example, Figures 58.3, 58.4, and 58.5 contain circles for the receipt of cues, i.e., “hear strange noises” or “encounter difficulties in smoke”, which are not actions. Instead, these are processes in which individuals engage in order to act in a building fire. Also, all three diagrams contains circles for the interpretation of cues, i.e., “misinterpret (ignore)”. The domestic diagram even contains an entry for “feel concern”. These entries also are not actions, but interpretations about the situation and personal risk (first described in the PADM) as direct

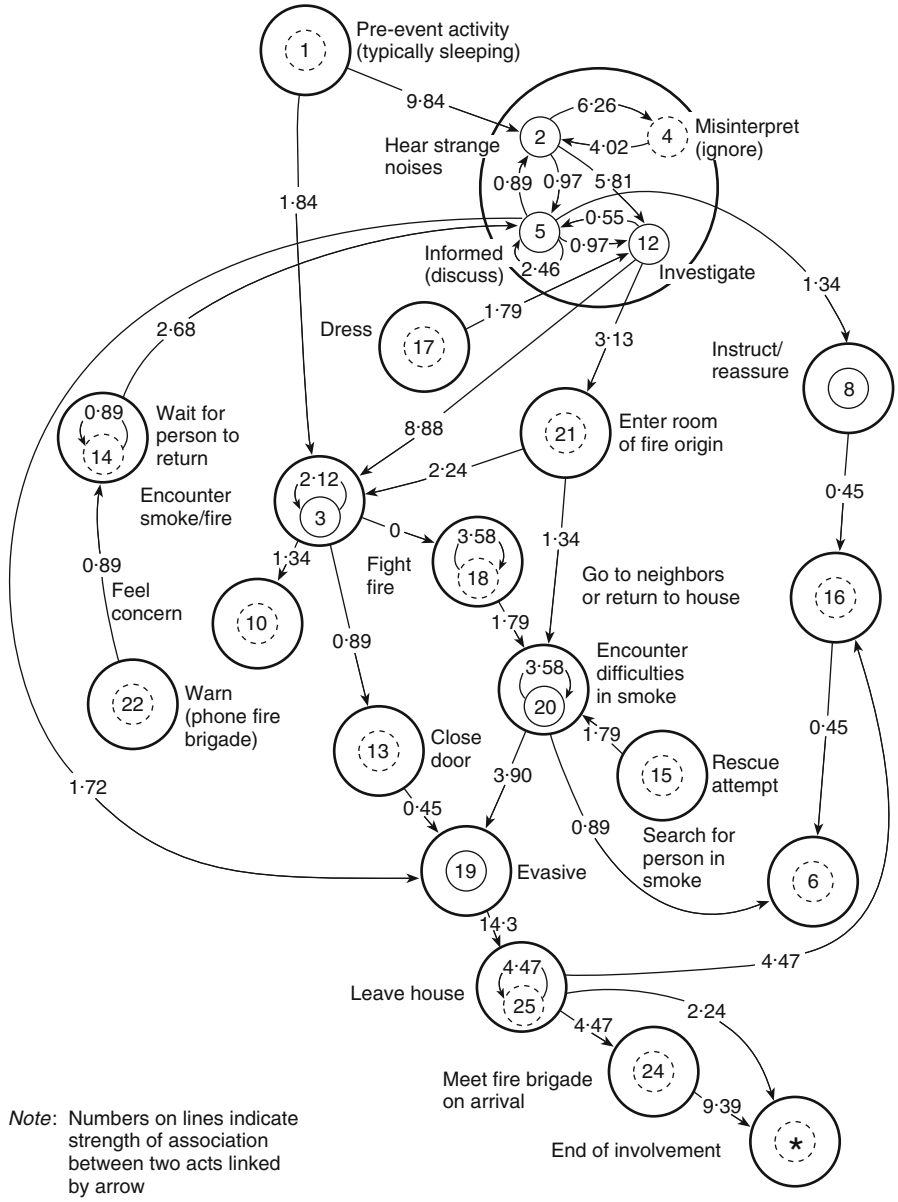

Fig. 58.3 Decomposition diagram—domestic fires [78]

influences of actions. These diagrams truly represent the first attempt at developing an inclusive conceptual model of evacuation actions—that identify not only the action, but also the processes of receiving cues and processing information in order to act in an emergency.

Patterns of behavior exist across all three diagrams (of varying occupancy type). What is important to note here is that certain actions take place in specific locations within the evacuation sequence. First, immediately after the receipt of initial cues, individuals were more likely to

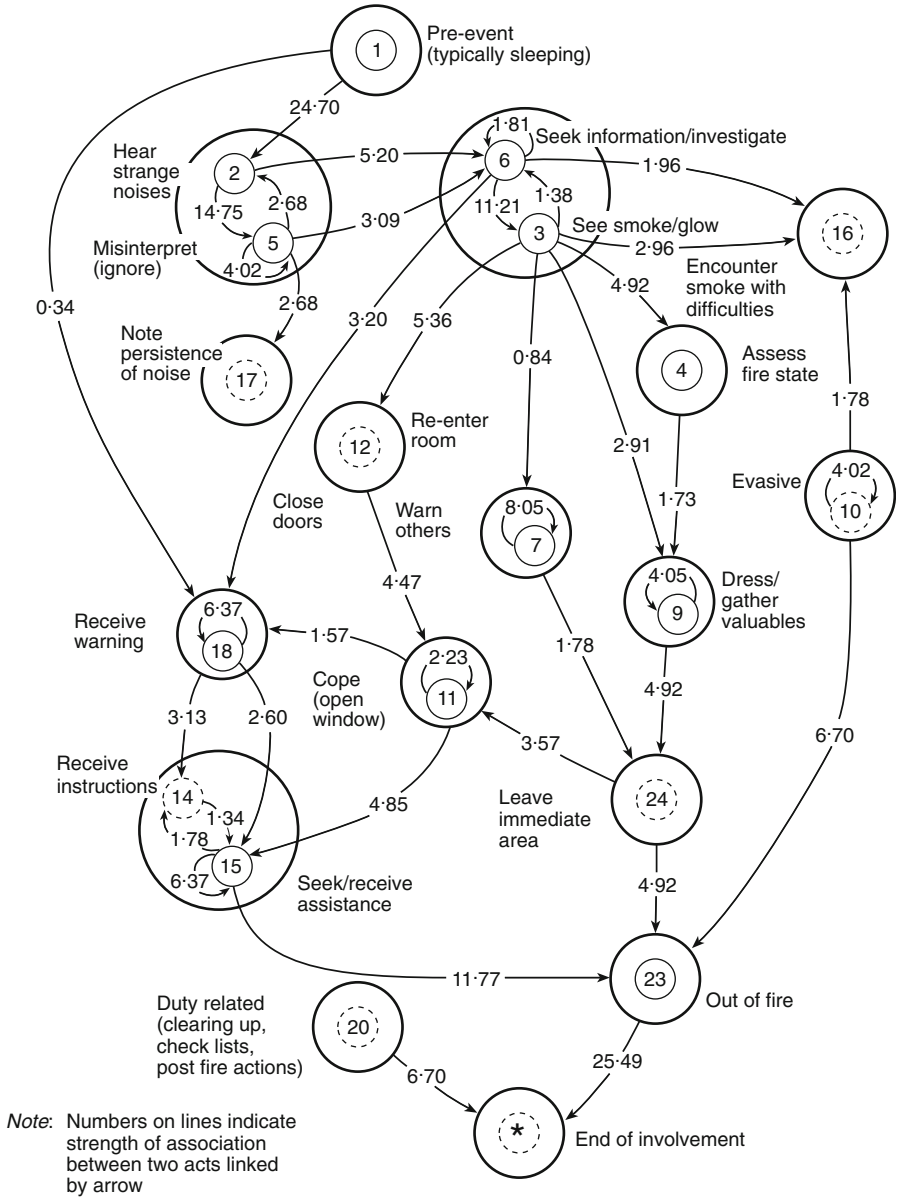

Fig. 58.4 Decomposition diagram—multiple-occupancy fires [78]

'investigate' the situation and/or 'misinterpret' (or ignore) cues that they received early on in the event. Then, after seeing smoke, one of three 'prepare' sequences were more likely to be performed, including 'instruct', 'explore', or 'withdraw'. Finally, depending upon the particular preparation action chosen, occupants were more likely to engage in the following actions: 'wait', 'warn', 'fight' or 'evacuate'.

Engineering Implications of the Linkage of Actions Taken During Evacuation

Actions follow a specific pattern across all types of building fires, and an understanding of the patterns of behavior is important when attempting to accurately model an evacuation scenario (i.e., the methods outlined in Chap. 57). Take for example, an office building

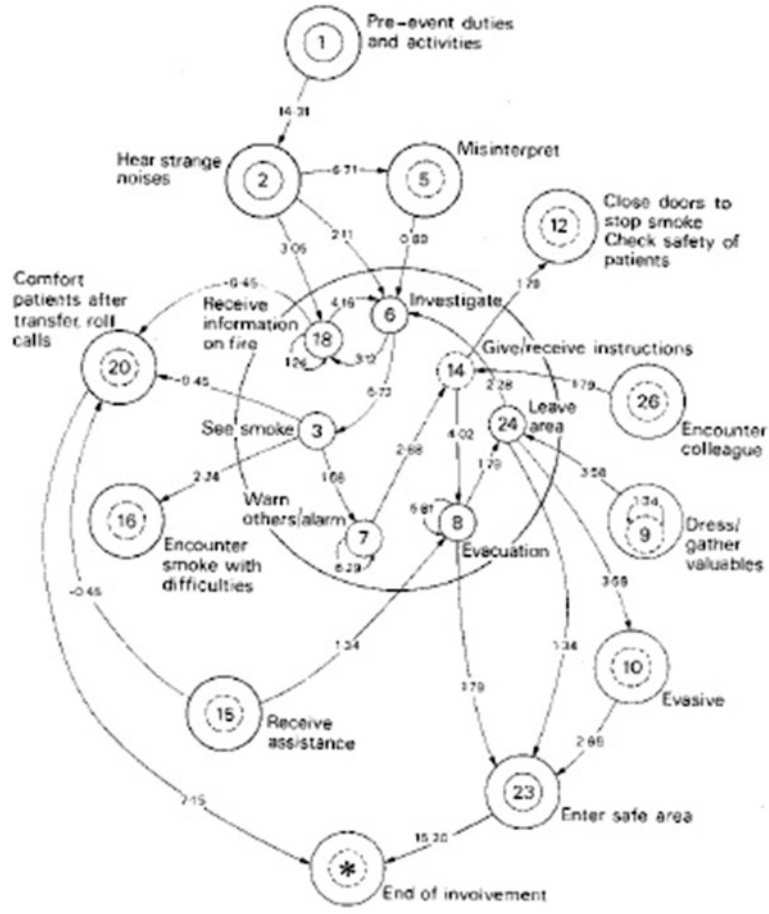

Fig. 58.5 Decomposition diagram—hospital fires [78]

that houses a child daycare for its employees on the 10th floor of a 20-story building. It will be important for engineers to understand that occupants will spend some period of time on their floors investigating the situation and making decisions as to what needs to be done; i.e., if evacuation is necessary or not. Therefore, a determination of the fire and smoke conditions on any occupied floor is important immediately after the fire begins. Next, the engineer should understand that some proportion of occupants may travel to the 10th floor to rescue their children from the daycare center, requiring an assessment of the environmental conditions on that floor for some time period after investigation is complete (i.e., the protective action phase).

An understanding of the behavioral process is important also for the design of evacuation procedures for a building. For example, the presence of staff as well as a building alarm for alerting the population of a building fire may decrease time spent investigating and deciding to evacuate. If staff members instruct building occupants to evacuate, especially if they represent a credible source to the population, then building occupants may be more likely to begin evacuation sooner than if left to their own decisions [30].

Relating Theory to Practice—Group Behavior

Research also exists to explain observations from numerous fire studies that people tend to travel or converge into groups during emergencies. There are theories that support the idea that individuals come together and form a group before evacuating, and then continue their evacuation together until they reach safety. This behavior, labeled as affiliative behavior [107], is described first in this section. Individuals also come together in groups to help one another. Helping behavior is found in almost every disaster, and an overview of this behavior will also be provided in this section. Finally, individuals have been found to converge together in groups during emergencies in order to take refuge from the fire conditions. Convergence groups, or clusters as termed by Bryan [77], were found in situations whereby individuals attempted evacuation and decided that is was not possible at the time.

Affiliative Behavior

According to Sime, who developed the Affiliative model, there is a relationship between people and their physical settings [107]. This model assumes that individuals with close psychological ties will attempt to escape with other group members during an emergency evacuation. Through his study of the Summerland fire, he found that nucleus family members were more likely than others to maintain group ties during travel to and through exits. Mixed groups, on the other hand, including friends and/or relations, did appear to have been less concerned with maintaining group ties during evacuation than they might have under normal circumstances.

Proulx also found this trend in group behavior while studying evacuation timing in apartment building evacuations [122]. Through the analysis of video tapes, it became apparent that people traveled in groups during evacuation: families with children would typically evacuate in a close group with an adult carrying the smallest child. However, family groups would split slightly when traveling with children who were a bit older in age. Additionally, seniors also traveled in groups of two or three; noting that they would exit their apartment and gather to discuss the drill, finally proceeding to evacuate together. Overall, Proulx found that 62 % of the occupants (in the four buildings studied) evacuated in groups. One important aspect to note is that Proulx also monitored the speed of movement of building occupants and found that groups tended to assume the speed of the slowest person, which in many cases in the apartment buildings studied were young children or older adults. Also, people tended to stop to converse during evacuation, rather than maintain the same speed throughout the entire evacuation.

Helping Others

Occupants also help one another during building emergencies, bringing people together in groups at one time or another. Analysis of building fires [77, 78, 108] and community-wide disasters, such as tornadoes [123, 124] and hurricanes [125, 126], provide many examples of instances where evacuees are often the first responders in any emergency. For example, Johnson, Feinberg and Johnston's study [127] of the Beverly Hills Supper club event (where a fire broke out in a nightclub in Kentucky in 1977, causing 165 deaths and over 200 injuries) showed that people put themselves in what they categorized as "grave danger" while assisting others in their group—"at times, returning to the burning building to search for loved ones; staff performing heroic acts while trying to save their clients". Aguirre et al. [128] through their study of another nightclub fire (i.e., The Station Nightclub Fire), which occurred at approximately 11:09 p.m., on February 20, 2003, in West Warwick, Rhode Island [129], found evidence that people cooperated and took care of one another in their group during and after the evacuation, which was a key aspect of their survival.

Drury, Cocking, and Reicher [32] discuss the reasons why helping behavior occurs in

emergencies. They claim that people help others in moments of crisis not only because they know and care about each other, but also because individuals have "internal cognitive categories" that allow identifications with others in certain contexts. In other words, an emergency requires individuals to redefine the situation collectively (as discussed in an earlier section of this chapter), and through this redefinition, individuals can form a sense of 'we-ness'. In emergencies, the redefinition of most situations, especially building fires, can be one where the evacuees are 'all in this together' or 'all in the same boat'—i.e., in need of protection or in search of survival. This redefinition of 'we-ness' then lends itself to the associated behavior of helping others.

Convergence Clusters (for Refuge)

The phenomenon of occupant convergence cluster formation in a fire incident was initially noticed in a study of occupant behavior in a 1979 high-rise apartment building fire [130]. Convergence clusters appear to involve the convergence of the occupants of the building in specific rooms selected as being areas of refuge, when evacuation was perceived as not possible. In the MGM Grand Hotel fire, for example, guests tended to select rooms on the north side of the east and west wings, and rooms on the east side of the south wing, due to the prevailing atmospheric conditions and the external smoke migration. In addition, guests reported that people had converged in rooms that had balconies and doors leading to the balconies because of the ease of ventilation, the reduced smoke exposure, improved visibility, and the communication advantages the balconies offered. The guests who reported their participation in convergence behavior in rooms provided either numerical estimates of the persons occupying the room or suite, or indicated only that "others" or "other persons" were present. Bryan also recorded the numbers of individuals in each convergence cluster, noting that the smallest number of people identified as a single cluster involved three persons and the largest was 35 persons.

Convergence clusters may serve as an anxiety and tension-reducing mechanism for individuals confronted with a fire incident perceived as life threatening. In addition to the detailed human behavior study of the MGM Grand Hotel fire [131], the NFPA conducted a similar questionnaire study of the guests' behavior in the Westchase Hilton Hotel fire [132] and also found the presence of convergence clusters.

Implications of Describing Behavior in Terms of the Group

The main reason for understanding group behavior, especially these three examples provided above, is because groups take time to form and move together as a unit, with decisions made according to the attributes of the group and movement speeds converging to the slowest member of the group to ensure group cohesion. People have been found to delay their own safety in order to help others. Depending upon where others are located in the building, these actions can take a significant amount of time, delaying movement to safety.

However, the previous sections on actions taken during an evacuation, action sequences, or a description of group processes do not yet tell the entire story of human behavior in fire. Not included are the *causes* of the decisions made and actions performed during fires. The studies of convergence clusters did begin to show that individuals reduce stress and anxiety in emergencies when they meet with members of their social circles; more insight is needed here. Therefore, the following section focuses specifically on the factors that affect decisions made or actions taken during a fire evacuation.

Factors that Influence Behavior in Fire

People in fires very rarely act in similar manners throughout the fire event. Instead, based on various environmental and individual factors, they internalize and process the information, and then act in kind.

Research into community disasters and building fires identifies individual and process-related factors that influence behavior [133]. There are some research that identifies the factors that influence various stages of the emergency decision-making process and others that identify factors that they claim directly influences behavior (however, it is more likely that these factors influence some stage in the decision-making process, that then influences behavior). These factors include social influence (or the influence of others in the building), stress, the built environment, leadership, and demographics (notably gender). Each factor will be described in further detail below and supported by appropriate research studies. It is important to identify these factors so that engineers can identify circumstances within fire scenarios in which certain types of behaviors (resulting in times delays) are likely to occur.

Factor 1: The Influence of Other Occupants on Behavior (Social Influence)

Research has been performed on the influence of others in the building on an individual's response to fire cues. This phenomenon is labeled here as social influence. This section will begin by describing psychological experiments performed by Latane and Darley [52] to test the influence of others on behaviors. Then, the section will describe research findings on the effect of groups (i.e., others who have formed a group tie) on the timing of actions during evacuation.

Latane and Darley [52] created an experimental situation involving college students. While the students were completing a written questionnaire, the experimenters would introduce smoke into the room through a small vent in the wall. If the subject left the room and reported the smoke, the experiment was terminated. If the subject had not reported the presence of the smoke within a 6-min interval from the time the smoke was first noticed, the experiment was considered completed. In some cases, subjects were alone in the room. In other cases, subjects were accompanied by "actors" that were told to remain in the room for as long as the subject did, no matter what. Finally, there were cases where subjects were accompanied by other subjects (or participants) who were unaware of the purpose of the experiment.

Subjects alone in the room reported the smoke in 75 % of the cases. When two "actors" were introduced in the room with each subject, only 10 % of the groups reported the smoke. When the total experimental group consisted of three unknowing subjects, one of the individuals reported the smoke in only 38 % of the groups. Of the 24 persons involved in the eight unknowing subject groups, only 1 person reported the smoke within the first 4 min of the experiment. In the situations involving subjects alone in a room, 55% of the subjects had reported the smoke within 2 min and 75 % reported smoke in 4 min.

Latane and Darley reported that noticing the smoke was apparently delayed by the presence of other persons, with the median delay of 5 s for single subjects and 20 s for both of the group conditions. These results would appear to indicate the inhibiting influences that may be imposed on individuals in public places. Latane and Darley reported the behavioral response of nine of the unknowing subjects in the ten passive research situations as follows [52]:

> The other nine stayed in the waiting room as it filled up with smoke, doggedly working on their questionnaire, and waving the fumes away from their faces. They coughed, rubbed their eyes, and opened the window but did not report the smoke.

Latane and Darley suggest that, while trying to interpret ambiguous threat cues as to whether a situation requires a unique response, the individual is influenced by the behavioral response of others who are exposed to identical cues. If these other individuals remain passive and appear to interpret the situation as a nonemergency, this inhibiting social influence may reinforce this nonemergency interpretation for an individual. This behavioral experiment may help explain the reported tendency of persons (1) to disregard initial ambiguous fire incident cues or (2) to interpret the cues as a nonemergency condition when the fire incident occurs with a social

audience of other persons, as in a restaurant, theater, or department store. This experimental study may also be helpful in understanding the incidents reported to fire departments that have been delayed by occupants for periods of minutes or even hours. In the report of the Arundel Park fire [32], several of the residents indicated that when they re-entered the hall after observing the fire from outside the building, they warned other residents and suggested they leave, but they were laughed at and the warning was disregarded.

Latane and Darley indicated that social inhibition, diffusion of responsibility, and mimicking appear to be primarily responsible for the inhibition of adaptive and assistance behavior responses by participants in emergency situations. It would appear that the inhibition of behavioral responses in the early stages of a fire incident (when the fire incident cues are relatively ambiguous) may predispose participants to a nonadaptive type of flight behavior, since the available evacuation time has been expended. In some fire incidents it appears to be difficult to get occupants of a building to evacuate because of the variables of social inhibition and diffused responsibility. The tendency to mimic the interpretation of cues and the behavior responses of others (as established by Latane and Darley) appears to be a frequent occurrence in fire incidents in restaurants, hotels, and other places of public assembly.

Similar to the studies that showed occupants were less likely to react if others were not reacting, studies have found that individuals are likely to follow others (i.e., begin their evacuation) if they witness others acting/reacting in emergencies. Occupants in the 2001 WTC disaster were likely to begin evacuation if they saw others evacuating as well, and this was especially the case if they viewed this individual (or individuals) as a credible decision-maker [30]. Even more interesting is the choice between stairs and elevators in WTC 2. As discussed earlier in this chapter, there were 16 min between the time that WTC 1 was hit and when WTC 2 was subsequently struck by the second plane. Therefore, occupants of WTC 2 who decided to evacuate before their own building was hit had access to both stairs and elevators. There were individuals in WTC 2 who decided to use the elevators for evacuation. One of the factors that influenced their decision was the presence of other individuals also using elevators for evacuation that day. In addition, similar to elevators, a stair route was not considered an option if no one was using it or if people encountered barriers, such as toxic conditions, that inhibited use.

Research has also been performed on the effect of groups on evacuation timing, or the timing to initiate evacuation behavior. First, Aguirre, Wenger and Vigo [40] performed a quantitative study of the 1993 bombing of the World Trade Center Tower 1 (the north tower). After the bombing occurred, researchers sent 690 mail surveys to management representatives to distribute to the 776 occupants selected using a stratified random sampling technique. Overall, the total sample included 415 respondents (161 from WTC 1 and 254 from WTC 2), for an overall response rate of 53.4 %. In this analysis, the dependent variable was the length of time (in minutes) that respondents took to join the evacuation, with the independent variables of interest being group size (large group of 20 or more people [1] or not [0]) and social interaction (a scale starting with: the respondent did not know anyone in group [0] and ending with the respondent knew everyone very well [11]). Results of this analysis showed that the more people whom respondents knew in their evacuating group, and the better that they knew each one, the longer it took them to initiate their evacuation. Further, respondents in large groups took 6.7 min longer to initiate their evacuation than others. Also of interest was the influence of perceived risk on time to evacuate. The study showed that people who perceived more danger tended to initiate evacuation earlier; however, the opposite was true if they were people in large groups who knew people more thoroughly. In other words, people who perceived risk, but were in larger groups of people whom they knew well, took longer to initiate evacuation. According to the researchers, this finding is

likely due to the importance of interacting within the group pro-socially; i.e., spending time trying to help friends or known others to decide to evacuate or prepare themselves before beginning evacuation movement.

Much of the focus of this chapter has been on the behavioral actions taken during evacuation, since other chapters in the handbook focus primarily on movement (e.g., Chap. 59). However, research on social influence has also found that group formation can delay the speed at which the group moves throughout the building during an emergency [122]. This finding is a direct result of the members of the group moving at the speed of the slowest member, so as to keep together during the emergency. Other movement aspects of an evacuation are outside of the scope of this chapter and more information on these can be found in Chap. 59.

Engineering Implications of Social Influence on Behavior

It is important to understand the effects of others on evacuees, especially in highly occupied buildings. In many buildings, occupants are surrounded by others, some of whom they find credible and others they may not. Social influence is especially important to remember when using current evacuation modeling or simulation tools to assess life safety of a structure. Many times, evacuation models simulate each individual (or agent) as if they are not behaviorally influenced by anyone else around them. For example, some models will randomly distribute pre-evacuation times throughout the simulated population, and, when one simulated agent in a room leaves, all other agents remain in place until their assigned pre-evacuation time has expired. This example does not represent a realistic scenario and engineers should be aware of social influence when running simulation tools.

Additionally, a proper understanding of social influence can aid engineers in developing new and more effective evacuation procedures. For example, if a building manager or engineer is aware that designated fire wardens are more likely than anyone else in the building to respond quickly during a fire evacuation, one potential evacuation scenario might be to strategically place these "quick responders" throughout the building (rather than all in one place) to promote faster response from other building occupants. This is simply one example of many for how an understanding of social influence can also help improve occupant response through smarter emergency procedure development.

Factor 2: The Influence of Stress on Behavior (Perception)

Research has also been performed to understand the effect of stress on emergency or evacuation behavior. Stress can be brought on in an emergency via several different complex conditions or states. Other than the obvious threat from physical harm due to the fire, fires can cause other conditions or states, including uncertainty/ambiguity, information overload, and time pressure. *Uncertainty* for building occupants [56, 134] can occur due to missing information, unreliable information (actual or perceived), ambiguous or conflicting information (more than one way to interpret the information) [87, 135], and/or overly complex information. *Information overload* occurs when the individual or group perceives that there is too much information to filter though in the time available, and it is posited that time pressure is necessary to produce the perception of information overload [136]. Last, with *time pressure*, occupants may perceive their situation as urgent and that they only have a limited amount of time to perform certain actions [137]. All of these conditions mentioned above can be considered as stressors for the building occupant [56, 134, 138, 139], leading the occupant to experience a physical state of stress and/or anxiety. In order for the individual to experience acute stress, some of the stressors must be present and the individual must be aware of the presence of stress, motivated to resolve the situation and uncertain of the outcome [138].

One of the main ways in which stress affects evacuation decision-making is through the narrowing of an individual's perceptive field. In this instance, stress makes it more difficult to perceive cues from the event [56, 137], and in turn, individuals may only pay attention to a select number of cues from their physical environment. Because of this, they could very well miss important pieces of information about the event which they would need to make safer or more effective decisions. Additionally, the ability to process information is skewed in three major ways under stress [140]:

- They process information at a faster rate, without carefully connecting the appropriate pieces of information together into an coherent story
- They can engage in the avoidance of optimal decision-making, i.e., making random choices
- Subjectively, the important data are chosen for consideration in the decisions

Another effect of stress on behavior and decision-making is that individuals are more likely to make choices that are less risky, thus, for example, providing additional support for the use of more familiar exits rather than unknown exits during evacuation [66].

Engineering Implications of Stress on Behavior

It is important for engineers to understand the implications of stress because this understanding can help improve the way we design buildings as well as emergency communications systems for fire safety. If individuals are more likely, in stressful situations, to pay attention to a lower number of cues, for example, engineers should design more noticeable signage or warning cues that easily grab people's attention. One example of this is providing information via luminous materials, like visual signage, that are central to people's perception field. Signage should be designed to capture people's attention and keep their attention during a building fire in as many ways as they can (see Kuligowski and Omori [83] for further information on better communication of emergency information during building emergencies).

Factor 3: The Influence of the Built Environment on Behavior

Research has also been performed on the influence of the built environment, i.e., the building, on evacuation behavior. Much of this work has been performed by Jonathan Sime, and refers back to the Affiliative Model [107] presented in an earlier section of this chapter. Similar to how individuals are likely to move toward individuals who are familiar to them before (or during) evacuation movement, people will attempt to use (or evacuate by) the exits or exits routes that are most familiar to them [107]. In general, in the Summerland fire that took place on the Isle of Man in Great Britain in 1973, Sime found that people attempted to leave via the exit route with which they were familiar; often, that was the exit that they had used to gain entry into the building. The Affiliative model also predicts that because a fire route (or exit) is not in regular use, and thus likely unfamiliar to the population, it is less likely to be used in a fire evacuation. People will prefer to use the most familiar exits, and this is exacerbated in emergencies [107].

Nilsson, building upon Sime's findings on familiarity, performed several studies on the features of exits that could increase the attractiveness of one exit over another [141]. He based his analysis of exit design on the theory of affordances [142], which states that people perceive objects in terms of what they can offer or afford. Based upon Gibson's work, Hartson [143] introduces four types of affordances and the types of activities they support:

- Sensory affordance—sensing or seeing
- Cognitive affordance—understanding
- Physical affordance—physically activity (doing or using)
- Functional affordance—fulfillment of an individual's goals

Nilsson [141] provides examples of how the theory of affordances can be used to analyze the design of an emergency exit. The first, or sensory affordance, suggests that the exit must be designed such that it is easy to sense. Nilsson provides specific examples of how to increase an

exit's sensory affordance in the following ways: clearly distinguish the door from other elements in the space (e.g., by using color or pattern) and equipping them with flashing lights, as long as sufficient contrast is provided by the environment. Cognitive affordance suggests that people understand that the exit should be used in emergencies and that it can lead them to a safer place. Examples of increasing cognitive affordance include providing an emergency exit sign above the door, placing flashing lights next to the exit sign (which would cover both sensory and cognitive affordances), and providing green flashing lights that is associative with safety or emergency exits (especially in countries where the exit signs are green). Physical affordance suggests that the user should be easily able to open and operate the door in an emergency. An example of increasing physical affordance is providing a door that is easy to open (i.e., no large force is required to open the door). Finally functional affordance suggests that the exit aids the user in obtaining their goal—to escape as quickly as possible. The difficulty, according to Nilsson, with functional affordance is that individuals during a building evacuation may have a multitude of goals; i.e., to not be the only one using an exit (for fear of looking foolish) or to avoid unpleasant environments in the building. Therefore, it is difficult to identify specific examples of increasing functional affordance in a building evacuation.

Finally, studies have shown that the individual's definition (or perception) of their environment can influence behavior during a fire evacuation. Donald and Canter's study of the King's Cross Disaster [144], where a fire began in the escalators of London, UK's King's Cross underground metro station, showed instances of the influence of place. Individuals located in the underground station were told by police officials to evacuate the underground station; however, the location to which they actually traveled depended upon their definition of the underground station. Some were unsure whether "the station" included the ticket hall area or the concourse or both, causing confusion about where they should actually travel to reach a safer location.

Engineering Implications of the Built Environment on Behavior

In all three studies, individuals' perceptions of the built environment, including familiarity, exit affordances, and the location of safety, influenced their decisions on and actions toward exit routes during the emergency event. It is important for engineers to understand the factors that influence exit choice for two reasons. First, buildings or emergency procedures can be designed to account for this type of behavior—e.g., increasing the size of the main exit for certain type of buildings. Similarly, evacuation procedures can institute a plan whereby staff members direct individuals to exits that are less familiar or are unknown to many of the population. Second, an understanding of exit choice can aid the engineer in designing more efficient emergency communication systems. This may include specifically telling certain individuals which exits to use in the building or equipping potentially unfamiliar exits with flashing lights (see Kuligowski [83] for further information on better communication of emergency information during building emergencies).

Factor 4: The Influence of Leadership (or Role) on Behavior

This section focuses on the influence of leadership (or role) on evacuation behavior. Depending upon the building, leadership may already be in place before an emergency event begins. For example, in office buildings, there usually exist individuals in management positions throughout the building. Similarly, mercantile buildings often consist of customers and employees, some of whom are in management roles. However, in emergencies, leadership has been known to emerge as well [31]. In emergent cases, the individual (or individuals) did not hold a pre-emergency leadership role, but engaged in actions (i.e., helping behavior or the provision

of instructions) that reflect a certain level of responsibility for others.

Jones and Hewitt, for example, studied group formation and leadership during the evacuation of a high-rise office building due to a fire [145]. Overall, a person's role in the organized hierarchy (pre-event leaders) had an influence on the group actions; i.e., in some cases, the leader's group listened, relinquished decision-making to this individual, and followed directions. The same type of scenarios were found in Kuligowski's study of the 2001 WTC evacuation [30] where individuals, more times than not, followed the instructions provided by their management of when and how to evacuate the towers. Jones and Hewitt did find exceptions to this trend, however, noting that when leadership failed to retain influence, new leadership emerged (i.e., even from those who were not previously in leadership roles).

Individuals also followed leadership in the King's Cross Disaster (discussed in the previous section) [144]. Individuals modified their action when they received instructions from people who appeared to hold official authoritative roles, i.e., police officers. In this disaster, even though the police did not have any additional official information and actually gave out incorrect information at times, they felt some responsibility for dealing with the situation and the public looked to them for instructions and guidance. In this particular instance, the reactions of the public to transportation staff was to ignore them, unless their instructions were backed by the police or fire department; showing that the people's confidence in the transportation staff was fairly low.

Engineering Implications of Leadership on Behavior

Leadership studies show the engineer that there are certain people in the building who are more likely than others to assume a leadership position during a fire emergency. These individuals are likely to provide suggestions on what to do, and in turn, influence others' actions. The more credible these individuals are, the more influence they will have on the rest of the population. For example, if the engineer is aware that managers are already more likely to respond and take leadership roles, another possibility is to assign fire safety leadership roles to people who are not already predisposed to help; i.e., empowering other types of occupants, in addition to managers, to enroll in key fire safety roles. Based on previous research, people with previous experiences in disasters or individuals with emergency-related occupations may already hold credibility as emergency experts with the larger population, and as an extension of this research, may be more likely to take interest in fire safety roles. Additionally, if the engineer understands that managers, for example, are already more likely to take leadership roles during a fire event, then managers should receive special fire safety training to ensure that they are providing accurate information and performing appropriate actions during building fires.

Factor 5: The Influence of Demographics (Gender) on Behavior

Demographics refer to the characteristics of a population, notably those characteristics that are genetic to the individual. Examples of genetic-based demographics are provided here: gender, age, physical fitness, physical abilities or disabilities, race, and culture. However, demographics can also include other social factors that can define or label an individual in some way, including socio-economic status, location (i.e., where s/he lives), marital status, occupation, etc. In this section, studies are presented that have been performed on one type of demographic (i.e., gender), and its effects on evacuation or emergency decision-making.

Bryan [14] and Wood [15] studied the influence of gender on certain residential evacuation behaviors. These researchers tested their respective datasets to see if gender had an influence on the first action taken, the action of fire fighting, and the act of notifying others in the building before evacuating.

First, with respect to initial actions taken, Bryan [14] studied the impact of gender. He found statistically significant differences

between males and females in the categories of "searched for fire," "called fire department," "got family," and "got extinguishers." Male participants were predominant in fire-fighting activities: 14.9 % of the males participated in the behavioral response of "searched for fire" as opposed to 6.3 % of the females, and 6.9 % of the males were involved in the action of "got extinguishers" as opposed to 2.8 % of the females. In the U.S. population, females differed significantly from the males in the warning and evacuation activities—11.4 % of the females "called fire department" as their initial behavioral response action as opposed to 6.1 % of the males. In relation to the evacuation behavior, 10.4 % of the females "left building" as the first behavioral response action, contrasted with 4.2 % of the males.

Bryan [77] stated that the cultural influence of gender on female participants is probably explicitly indicated in the concern for other family members, with the finding that 11 % of the females "got the family" as the first behavioral response, whereas only 3.4 % of the males engaged in this behavioral response. It should be noted that the male actions of "searched for fire" or "fought fire" were matched by the female actions of "called fire department" and "got family." This identical pattern of behavioral responses has also been observed in fire incidents in health care and educational occupancies. However, considering the fact that these studies took place in the late 1970s and early 1980s, additional and updated research should be performed on these gender roles to test their current applicability.

In contrast, studies have been performed on building fires where gender was not identified as a predictor of behavior. For example, Proulx et al. [146] studied the 2 Forest Laneway fire in 1995, a high-rise apartment fire that killed 6 people in Canada. Researchers inquired about behaviors by distributing behavioral surveys to survivors, and found no significant differences between the actions taken by males and females.

Horasen and Bruck performed studies of response behavior of students in secondary (junior and senior high) schools [147]. Behavioral intention questionnaires; i.e., questionnaires that ask individuals what they would do if a particular situation were to occur, were completed by 170 students across grades 7 to 12. The first section of the questionnaire contained questions on student demographics, the second section presented students with six scenarios to collect information on the most probable actions taken under the given conditions, and the third section asked about students' previous experiences with evacuation drills and actual fire incidents. Overall, the study found no significant differences in likely behavioral responses of males versus females. However, when asked about scenarios in which they would be alone and with smoke cues, females were more likely to 'leave the building immediately', whereas males were more likely to 'find an extinguisher'. Saunders [148] studied an office building fire, also using behavioral intention questionnaires and found support for gender differences with respect to evacuation actions. Females were more likely than males to report that they would investigate, warn, and evacuate in response to various types of cues. However, neither males nor females wanted to fire fight. These studies may support research showing that women have a higher perception of risk in emergencies, and therefore, are more likely to respond in emergencies.

However, there are limitations associated with the use of behavioral intention questionnaires as a means to understand future behavior. In both studies described above, participants were asked to provide insight on what they would do in a series of hypothetical situations. Here, the participant is asked to mentally picture the scenario without physically being a part of the situation. If the scenario is not described in sufficient detail to the participant of the study, he/she will likely be unable to mentally picture the scenario accurately and make estimates of potential response behavior. Also, even if extensive detail is provided on the scenario description, behavioral intention questionnaires deprive participants from experiencing, first-hand, the cues from the physical (i.e., the fire) and social environments. The inability to experience the environment in the hypothetical scenario can cause difficulty in

determining behaviors that would be performed, since it is the physical and social environments that prompt internal cognitions, decision-making and action in a fire emergency. Additionally, a participant's prediction of future behavior in a particular scenario may be influenced by previous experiences in building fires or other disasters. Thus, participants who have not experienced an actual building fire emergency may be less inclined to accurately predict response behaviors in future fire emergencies.

Engineering Implications of the Influence of Demographics (Gender) on Behavior

As mentioned earlier in this section, there are several demographic factors that could be considered as influential to behavioral actions during emergencies. Gender is simply one demographic factor that is highlighted here in this chapter. While it is important for engineers to understand that demographics can play a role in behavioral response during building fires, engineers must also understand that the relationship between demographics and behavior is complex [133]. Engineers should be aware that individual factors are more likely to be predictors of internal cognitions (such as risk perception), which then influence action, rather than direct influences of action. Rather than stating that all women warn others during fire emergencies, what is more likely to be the case is that situational or emergency-related variables, such as environmental cues and demographics, lead to risk identification and assessment, which then leads to action. Therefore, engineers should inquire how gender and other individual-based factors influence perceptions of the threat and risk, which then directly influence actions performed in response to a fire.

Summary—Behavioral Facts

A great deal of information has been provided on human behavior in fire in this chapter. Following each section, engineering implications were discussed, providing the "so what?" to readers. The engineering implications were provided after each section so that a reader might be able to see the application of these findings to actual engineering projects. In addition, examples of "behavioral facts," first introduced by Kuligowski and Gwynne [149] and extended by Gwynne [150], are listed below to summarize the major findings captured by this chapter, which link to the section in which each fact is discussed. A total of 11 behavioral facts are listed here:

Behavioral fact #1: *Rather than panic, people's first instinct is to feel (sometimes inappropriately) safe in their environment* (*Sections "Discarded Theories of Human Behavior in Fire" and "Panic Behavior"*).

Behavioral fact #2: *Just because information is provided in a fire emergency does not mean that appropriate occupant response will take place. Perception of, attention to, and comprehension of information (in a fire event) is a critical part of occupant response* (*Section "Social Psychological Theories of Human Behavior in Emergencies"*).

Behavioral fact #3: *Occupants must perceive a credible threat and personalize the risk before protective action is taken* (*Section "Social Psychological Theories of Human Behavior in Emergencies"*).

Behavioral fact #4: *People will engage in information seeking actions, especially when cues are ambiguous and/or inconsistent* (*Sections "Social Psychological Theories of Human Behavior in Emergencies"* and *"Relating Theory to Practice—Protective Actions in Fires"*).

Behavioral fact #5: *People are likely to engage in preparation activities before beginning evacuation response. Preparation activities will likely delay their response* (*Section "Relating Theory to Practice—Protective Actions in Fires"*).

Behavioral fact #6: *Generally, people act rationally and altruistically during building fires* (*Section "Relating Theory to Practice—Group Behavior"*).

Behavioral fact #7: *The surrounding population will influence the individual's decision-making process* (*Section "Factor 1: The Influence of Other Occupants on Behavior [Social Influence]"*).

Behavioral fact#8: *Stress can narrow a person's field of perception, causing individuals to miss or ignore certain cues or information* (*Section "Factor 2: The Influence of Stress on Behavior [Perception]*)".

Behavioral fact #9: *People move to the familiar. The relationships with the structure and people that existed prior to the incident influence response during the incident* (*Sections "Relating Theory to Practice—Group Behavior"* and *"Factor 3: The Influence of the Built Environment on Behavior"*).

Behavioral fact #10: *People do not instantaneously switch to a different set of roles in a building fire event. The rules and roles prior to the event form the basis of those employed during the event* (*Section "Factor 4: The Influence of Leadership [or Role] on Behavior"*).

Behavioral fact#11: *People are heterogeneous and these individual differences in characteristics* (*or demographics*) *can influence behavior* (*Section "Factor 5: The Influence of Demographics [Gender] on Behavior"*).

What Is Missing in Human Behavior in Fires?

This chapter first presented an overarching theory of human behavior in disasters; i.e., the period of time in which individuals make decisions on whether protective action is necessary and then which actions they will take in response to the threat (the PADM). However, this theory is more general in nature and does not actually identify the factors that would predict the performance of particular actions, such as helping others or taking a particular route in the building. Next, this chapter presented studies from the field of human behavior in fire to support the larger, general theory. These studies identified the actions that people take in response to fires, the approximate timing of action types, as well as began to identify the factors that influenced these types of actions. Most studies focused on the pre-evacuation period of a building fire.

What is missing in the field of human behavior in fires is a comprehensive theory that brings all of the theory and data from studies together to predict, rather than to simply determine based upon user input, human behavior during evacuations. With a larger comprehensive theory, engineers could perform more accurate calculations for performance-based design (i.e., see Chaps. 57, 59, and 60) and model developers could create more accurate evacuation models that rely less on user input and more on fundamental theory (see Gwynne [150]).

One step in the process of reaching this comprehensive theory is to develop models that can predict *the actions that people take in response to fires*—both before they decide to evacuate (pre-evacuation) and during the evacuation (or movement) time period. Canter, Breaux and Sime's [78] decomposition diagrams begin to tie various sub-theories together, but focus primarily on the linking of evacuation actions together, and often neglect to identify the interpretations and levels of risk perception that are influential to occupant's actions.

One example is provided here of a qualitative model that predicts the pre-evacuation actions of survivors of the 2001 World Trade Center (WTC) Disaster [30, 151]. Through analyses of transcripts from 245 face-to-face interviews with survivors from both WTC towers, collected by Project HEED [22], this model is the first inductively-developed, individually- (or -evacuee-) based model explaining the actions taken during the pre-evacuation period of a building fire/evacuation event. The goal of this research was to describe evacuation decision processes in greater detail than either research on building fires or studies on community-wide evacuation, focusing on how people perceive and interpret environmental cues and warnings, how they seek confirmation during sensemaking and milling processes, and what they do before moving to safety.

There are five main findings that can be highlighted from this research. The findings are as follows:

- The WTC pre-evacuation period was divided into two main phases: the milling/sensemaking phase and the protective action phase. In the milling/sensemaking phase, WTC occupants engaged in two different actions—continuing to work or seeking additional information. In the protective actions phase, on the other hand, occupants engaged in actions that were focused specifically on protecting themselves or others (i.e., helping others, preparing to evacuate, or defending in place). Both phases took place before moving to the stairs or elevators.
- Risk perception, or the feeling of personal danger, was the main predictor of when individuals decided to evacuate—i.e., the transition from the milling/sensemaking phase to the protective action phase. Both individual and environmental factors were identified as influential of risk perception development.
- Some individuals made their decisions to evacuate before others on their floor. These "early responders", as labeled by Kuligowski [30], were primarily higher-level managers, fire wardens, military personnel, or individuals with experiences or occupations in emergency situations. These individuals still required the receipt of information that increased their level of perceived risk, but were also more inclined to act first (before others) because they felt responsibility for others and/or had previously experienced/witnessed negative consequences associated with fire or building evacuations.
- Certain factors, such as personal responsibility, social connections, and the actions of others, influenced which protective actions people engaged.

See Kuligowski [30] for further explanation on the conceptual model.

Kuligowski's model is not without limitations, however. The model focuses specifically on the pre-evacuation period of one building event. Additionally, the model does not incorporate any decisions or actions of the decedents. While the findings in the model were verified with theory from other events, the factors that influenced each action performed were specific to an office building fire and subsequent evacuation, thus making it difficult to generalize the findings. This is a first start to developing a model to predict actions taken during building fires; however, this effort should be expanded upon to include findings from analysis of other building fires, including fires in different types of structures and with different populations, as well as from analysis of other types of disasters, not limited to building fires.

An additional step in the process of reaching this comprehensive theory is to develop models that can predict *the timing associated with the performance of certain actions*—both before they decide to take protection (e.g., evacuate) and during the evacuation (or movement) time period. First, there are a few studies that attempt to predict how long people delay before evacuating [1, 40, 84, 152] as well as the time it takes individuals to evacuate via stairs [1]. For example, NIST's federal investigation of the 2001 WTC disaster performed multiple regression analysis to predict pre-evacuation delay and normalized stairwell evacuation time—identifying factors such as action type, floor number, the number of environmental cues and level of perceived risk as predictors of pre-evacuation delay time and factors such as the presence of counterflow, the presence of crowding, the number of environmental cues, floor number, pre-evacuation delay, and evacuation interruption as predictors of normalized stairwell evacuation time [1].

Other research efforts have attempted to quantify human behavior in the form of an empirical model. One such model was developed by NIST [153] based upon the WTC conceptual model [30], presented earlier in this section. A first-order quantitative model, labeled as the Evacuation Decision Model (EDM), was developed to predict the time when a simulated occupant, or agent, decides to evacuate (i.e., the decision that protective action is necessary). In the EDM, the prediction of the evacuation decision is based upon the agent's perceptions of risk during the

pre-evacuation period. In its simplicity, the EDM model attempts only to simulate the evacuation decision, without additional simulation of protective action behaviors.

At present, these qualitative and quantitative models scratch only the surface of the development of a larger, comprehensive model of human behavior in fire. These models provide a path forward on the methods that could be used in its eventual development. However, there is much work still to be done to improve our understanding of human behavior in fire, and without this understanding, a comprehensive model is near impossible. Listed here are just a few examples of areas in the field that require further study:

- The influence of fire's toxic products and heat on decision-making and behavior (before incapacitation or death occur) in a building fire
- An identification of all of the factors that influence risk perception and how they interact to increase or decrease risk perception levels.
- The types of protective actions that are performed in building fire evacuations
- The factors that influence the various types of protective actions performed in building fire evacuations
- The factors that influence the receipt of cues, the ways in which people pay attention to cues, and the comprehension of cues
- The ways in which individual factors, such as gender, disability, age, body size, culture, marital status, past experiences, training and social role, influence decision-making during building fires
- The timing associated with the performance of behavior during building fires, and the factors that influence this timing
- The influence of urgency or other types of dissemination techniques on the response of building occupants during fires
- The influence of group dynamics on individual decision-making and group decision-making during fires
- The role of place (including building type or building characteristics) on decision-making during fires
- The role of psychological states, including stress or anxiety, on decision-making during building fires.

For the field to reach its goal and develop a larger understanding of human behavior in fire, accurate, rigorous, and comprehensive research must continue. There is still much left to understand, but the ultimate goal of a comprehensive model is in our future.

Chapter Summary

Human behavior in fire is a key aspect of understanding and designing for life safety in building fires. However, the treatment of human behavior in performance-based design analyses often times falls short by ignoring, oversimplifying, or inaccurately accounting for it. Relationships in human response are complex; though, these relationships are not impossible to describe or even predict. The chapter began with a description of three disaster myths, which, if accurate, would make it easier for the field to surrender and admit defeat against the task of predicting human behavior in fire. However, the occurrence of panic, disaster shock, and group mind are rare in fire emergencies; and with this realization, comes an understanding that real patterns of behavior should be identified when studying human response to fires. These patterns are clearly displayed in the PADM, also introduced in this chapter, which describes the process by which individuals make decisions and respond to disaster situations. Patterns are also identified by the studies weaved throughout this chapter—identifying the role of group dynamics, social influence, stress, the built environment, leadership/status, and demographics on behaviors performed by occupants in response to a fire emergency.

Following each section, the author presented the "so what?" or the "who cares?" to the reader. The purpose here was to make clear why this information is important and what influence these various aspects of human behavior in fire have on life safety and building design. All of the information presented in this chapter should be

considered by an engineer performing a life safety analysis and/or developing evacuation procedures for building occupants in fire emergencies. In some cases, data are available that makes this consideration easier, and in other cases, the engineer must use appropriate and technically-sound judgment and decision-making.

The fire field recognizes the need for a comprehensive theory of human behavior in fire, and researchers around the world are working on various aspects of the problem to make this a reality. This theory would then be incorporated into standard engineering tools, so that human behavior in fire can no longer be ignored or discounted in performance-based analyses. Until this occurs, the onus is placed upon engineers and review authorities to ensure that building occupants are accounted for and protected. It is the hope that the results of performance-based analyses are significantly enhanced by the information included in this chapter as well as the suite of egress-related chapters available in this edition of the handbook: design strategies (Chap. 61), egress data (Chap. 64), the design of egress scenarios (Chap. 57), hydraulic modeling (Chap. 59), evacuation modeling (Chap. 60), toxicity (Chaps. 63 and 62), and smoke effects (Chap. 61).

Acknowledgements This chapter is dedicated to the late Dr. John L. Bryan (Prof), who authored this chapter in the previous four editions of the handbook. Dr. Bryan provided mentorship and guidance to so many in the field, including the author of this chapter. He is deeply missed. Dr. Kuligowski would like to thank all of the reviewers of this handbook chapter, including Paul Reneke, Jason Averill, Thomas Cleary, Anthony Hamins, Howard Harary, and Steven Gwynne, all of whom provided insightful comments. Also, special thanks to Elizabeth Landry for help with chapter editing and formatting.

References

1. Averill, Jason D., Dennis S. Mileti, Richard D. Peacock, Erica D. Kuligowski, Norman Groner, Guylene Proulx, Paul A. Reneke and Harold E. Nelson. 2005. Federal Building and Fire Safety Investigation of the World Trade Center Disaster: Occupant behavior, egress, and emergency communications. Report NCSTAR 1–7. Gaithersburg, MD: National Institute of Standards and Technology. (Also available at http://wtc.nist.gov/NISTNCSTAR1–7.pdf).
2. Grosshandler, William, Nelson Bryner, Daniel Madrzykowski, and Kenneth Kuntz. 2005. Report of the Technical Investigation of The Station Nightclub Fire. Report NCSTAR 2: Vol. 1. Gaithersburg, MD: National Institute of Standards and Technology.
3. Isner, Michael S. and Thomas J. Klem. 1993. World Trade Center Explosion and Fire, New York, New York, February 26, 1993. Fire Investigation Report. Quincy, MA: National Fire Protection Association.
4. Fischer, H.W. III. 2008. Response to Disaster: Fact vs. fiction and its perpetuation, 3rd edition. Lanham, MD: University Press of America, Inc.
5. Lindell, Michael K., Carla S. Prater, and Ronald W. Perry. 2006. Introduction to Emergency Management. Wiley.
6. Tierney, Kathleen J. 2003. "Disaster Beliefs and Institutional Interests: Recycling disaster myths in the aftermath of 9–11." Pp. 33–51 in Terrorism and Disaster: New Threats, New Ideas (Research in Social Problems and Public Policy, Volume 11), edited by Ted I. K. Youn. Bingley, UK: Emerald Group Publishing Limited.
7. Quarantelli, Enrico L. and Russell R. Dynes. 1972. "When Disaster Strikes (It Isn't Much Like What You've Heard and Read About)" Psychology Today 5(February): 67–70.
8. Fahy, Rita F., G. Proulx, and L. Aiman. 2012. "Panic or not in fire: Clarifying the misconception." Fire and Materials 36: 328–338.
9. Johnson, Norris R. 1987. "Panic at 'The Who Concert Stampede': An Empirical Assessment." Social Problems 34(4): 362–373.
10. Johnson, Norris R. 1987. "Panic and the Breakdown of Social Order: Popular Myth, Social Theory, Empirical Evidence." Sociological Focus 20(3).
11. Wenger, Dennis E. James D. Dykes, Thomas D. Sebok, and Joan L. Neff. 1975. "It's a Matter of Myths: An empirical examination of individual insight into disaster response." Mass Emergencies 1:33–46.
12. J.D. Sime, in Fire and Human Behavior, John Wiley and Sons, New York (1980).
13. E.L. Quanrantelli, Panic Behavior in Fire Situations: Findings and a Model from the English Language Research Literature, Ohio State University, Columbus (1979).
14. J.L. Bryan, Smoke as a Determinant of Human Behavior in Fire Situations, University of Maryland, College Park (1977).
15. P.G. Wood, Fire Research Note 953, Building Research Establishment, Borehamwood, UK (1972).
16. J.P. Keating and E.F. Loftus, "The Logic of Fire Escape," Psychology Today, 15 (1981).

17. J.P. Keating, "The Myth of Panic," Fire Journal, 76, pp. 57–61 (1982).
18. Best, RL. 1977. Reconstruction of the Tragedy: The Beverly Hills Supper Club Fire. National Fire Protection Association: Boston, MA.
19. BBC News. Panic on the Stairs. September 12, 2001.
20. Proulx, G., Fahy, RF, and Walker, A. 2004. "Analysis of first-person accounts from survivors of the World Trade Center evacuation on September 11, 2001." Research Report #178, National Research Council Canada, Ottawa, Canada.
21. S.J. Blake, E.R. Galea, H. Westeng, and A.J.P. Dixon, "An Analysis of Human Behaviour During the WTC Disaster of 11 September 2001 Based on Published Survivor Accounts," in 3rd International Symposium on Human Behaviour in Fire 2004, Interscience Communications and Ulster University, Belfast, pp. 181–192 (2004).
22. Galea, E.R., J. Shields, D. Canter, K. Boyce, R. Day, L. Hulse, A. Siddiqui, L. Summerfield, M. Marselle, P. Greenall. 2006. "Methodologies Employed in the Collection, Retrieval and Storage of Human Factors Information Derived from First Hand Accounts of Survivors of the WTC Disaster of 11 September 2001." Journal of Applied Fire Science 15(4): 253–276 (published in Nov 2008).
23. Gershon, Robyn R.M., Marcie S. Rubin, Kristine A. Qureshi, Allison N. Canton, Frederick J. Matzner. 2008. "Participatory Action Research Methodology in Disaster Research: Results from the World Trade Center evacuation study." Disaster Medicine and Public Health Preparedness 2(3): 142–149.
24. Brennan, P. "Victims and survivors in fatal residential building fires." Proceedings of the First International Symposium—Human Behaviour in Fires, University of Ulster. Fire Safety Engineering Research and Technology Centre, 1998.
25. G. Ramachandran, "Human Behavior in Fires—A Review of Research in the United Kingdom," Fire Technology, 26, 2, pp. 149–155 (1990).
26. Omer, Haim and Nahman Alon. 1994. "The Continuity Principle: A unified approach to disaster and trauma." American Journal of Community Psychology 22(2): 273–287.
27. Tierney, Kathleen J. 1993. Disaster Preparedness and Response: Research findings and guidance from the social science literature. Preliminary Paper #193. Newark, DE: Disaster Research Center.
28. Drabek, Thomas E. 1986. Human System Responses to Disaster: An inventory of sociological findings. New York, NY: Springer-Verlag.
29. Okabe, Keizo, and Shunji Mikami. 1982. "A Study on the Socio-Psychological Effect of a False Warning of the Tokai Earthquake in Japan." A Paper presented at the Tenth World Congress of Sociology, Mexico City, Mexico.
30. Kuligowski, E. D. (2011). Terror Defeated: Occupant sensemaking, decision-making and protective action in the 2001 World Trade Center disaster. Ph. D. Dissertation. Boulder, CO: University of Colorado at Boulder.
31. Weller, Jack M. and Enrico L. Quarantelli. 1973. "Neglected Characteristics of Collective Behavior." The American Journal of Sociology 79(3): 665–685.
32. Drury, J., Cocking, C. & Reicher, S. (2006). Every man for himself—or for the group? How crowd solidarity can arise in an emergency: An interview study of disaster survivors. Group and Intergroup Relations pre-conference, Society for Personality and Social Psychology 7th Annual Meeting, Palm Springs, California, January.
33. Quarantelli, E.L. and R.R. Dynes. 1971. "Working Paper #37, Disaster Behavior: Myths and Consequences." Columbus, OH; Disaster Research Center.
34. Melick, M. (1985), 'The Health of Postdisaster Populations,' in Laube, J. and Murphy, S. (Eds.), Perspectives on Disaster Recovery, Appleton-Century-Crofts, New York, pp. 179–209.
35. Fritz, C.E. and E.S. Marks. 1954. "The NORC Studies of Human Behavior in Disaster." Journal of Social Issues 10(3):25–41.
36. Barton, A. H. 1970. Communities in Disaster. New York: Anchor.
37. Turner, Ralph H. and Lewis M. Killian. 1987. Collective Behavior. Englewood Cliffs, NJ: Prentice Hall, Inc.
38. Mileti, Dennis S. and John H. Sorensen. 1990. Communication of Emergency Public Warnings: A social science perspective and state-of-the-art assessment. ORNL-6609. Oak Ridge, TN: Oak Ridge National Laboratory, U.S. Department of Energy.
39. Kuligowski, E.D., S.M.V. Gwynne, K.M. Butler, B.L. Hoskins, and C.R. Sandler. (2012) Developing Emergency Communication Strategies for Buildings. Technical Note 1733, National Institute of Standards and Technology: Gaithersburg, MD.
40. Aguirre, Benigno E., Dennis Wenger, and Gabriela Vigo. 1998. "A Test of the Emergent Norm Theory of Collective Behavior." Sociological Forum 13(2): 301–320.
41. McPhail, Clark. 1991. The Myth of the Madding Crowd. New York, NY: Walter de Gruyter, Inc.
42. Turner, Ralph H. and Lewis M. Killian. 1972. Collective Behavior. Englewood Cliffs, NJ: Prentice Hall, Inc.
43. Connell, Rory. 2001. Collective Behavior in the September 11, 2001 Evacuation of the World Trade Center. Preliminary Paper #313. Newark, DE: University of Delaware Disaster Research Center.
44. Turner, Ralph H. and Lewis M. Killian. 1957. Collective Behavior. Englewood Cliffs, NJ: Prentice Hall, Inc.
45. Berger, Peter L. and Thomas Luckmann. 1966. The Social Construction of Reality: A treatise in the sociology of knowledge. Garden City, New York: Anchor Books.

46. Sorensen, John H. and Barbara Vogt-Sorenson. 2006. "Community Processes: Warning and evacuation." Pp. 183–199 in Handbook of Disaster Research, edited by H. Rodriguez, E. L. Quarantelli, and R. R. Dynes. New York, NY: Springer.
47. Mileti, Dennis S. and Lori Peek. 2001. "Hazards and Sustainable Development in the United States." Risk Management: An International Journal 3(1): 61–70.
48. Tierney, Kathleen J., Michael K. Lindell, and Ronald W. Perry. 2001. Facing the Unexpected: Disaster preparedness and response in the United States. Washington, DC: Joseph Henry Press.
49. Mileti, Dennis S., Thomas E. Drabek, and J. Eugene Haas. 1975. Human Systems in Extreme Environments: A sociological perspective. Boulder, CO: Institute of Behavioral Science, University of Colorado.
50. Lindell, Michael K., and Ronald W. Perry. 2004. Communicating Environmental Risk in Multiethnic Communities. Thousand Oaks, CA: Sage Publications.
51. Turner, John C. 1991. Social Influence. Pacific Grove, CA: Brooks/Cole.
52. B. Latane and J.M. Darley, "Group Inhibition of Bystanders Intervention in Emergencies," Journal of Personality and Social Psychology, 10, pp. 215–221 (1968).
53. McGuire, William J. 1985. "The Nature of Attitudes and Attitude Change." Pp. 233–256 in Handbook of Social Psychology, edited by G. Lindzey and F. Arsonson. New York, NY: Random House.
54. Hovland, Carl I., Irving L. Janis, and Harold H. Kelley. 1953. Communication and Persuasion: Psychological studies in opinion change. New Haven, CT: Yale University Press.
55. Tversky, Amos and Daniel Kahneman. 1974. "Judgment Under Uncertainty: Heuristics and biases." Science 185: 1124–1131.
56. Klein, Gary. 1999. Sources of Power: How People Make Decisions. Cambridge, MA: The MIT Press.
57. Kahneman, Daniel, Paul Slovic, and Amos Tversky. 1982. Judgment Under Uncertainty: Heuristics and Biases. New York, NY: Cambridge University Press.
58. Kunreuther, Howard. 2002. "Risk Analysis and Risk Management in an Uncertain World." Risk Analysis 22(4): 655–664.
59. Lichtenstein, S., Slovic, P., Fischhoff, B., Layman, M. and Combs, B. (1978). Judged frequency of lethal events. Journal of Experimental Psychology: Human Learning and Memory, 4, 551–578.
60. Kunreuther, Howard, Robert Meyer, Richard Zeckhauser, Paul Slovic, Barry Schwartz, Christian Schade, Mary Frances Luce, Steven Lippman, David Krantz, Barbara Kahn, Robin Hogarth. 2002. "High Stakes Decision Making: Normative, descriptive and prescriptive considerations." Marketing Letters 13 (3): 259–268.
61. Slovic, Paul, Baruch Fischhoff and Sarah Lichtenstein. 1977. "Behavioral Decision Theory." Annual Review of Psychology 28: 1–39.
62. Peterson, Camerson R. and Lee R. Beach. 1967. "Man as an Intuitive Statistician." Psychological Bulletin 68(1): 29–46.
63. Zakay, Dan. 1993. "The Impact of Time Perception Processes on Decision Making Under Time Stress." Pp. 59–72 in Time Pressure and Stress in Human Judgment and Decision Making, edited by Ola Svenson and A. John Maule. New York, NY: Plenum Press.
64. Karau, Steven J. and Janice R. Kelly. 1992. "The Effects of Time Scarcity and Time Abundance on Group Performance Quality and Interaction Process." Journal of Experimental Social Psychology 28:542–571.
65. Janis, I. L. 1982. "Decision Making Under Stress." Pp. 69–87 in Handbook of Stress: Theoretical and clinical aspects, edited by L. Goldberger and S. Breznitz. New York, NY: The Free Press.
66. Ben Zur, H. and S. J. Breznitz. 1981. "The Effect of Time Pressure on Risky Choice Behavior." Acta Psychologica 47:89–104.
67. Gigerenzer, G. and R. Selten. 2001. Bounded Rationality: The Adaptive Toolbox. Cambridge, MA: The MIT Press.
68. Vaughan, Diane. 1999. "The Dark Side of Organizations: Mistake, Misconduct, and Disaster." Annual Review of Sociology 25:271–305.
69. Simon, H. A. 1956. "Rational Choice and the Structure of Environments." Psych. Rev. 63:129–138.
70. Thompson, Catherine M., John A. Forester, Susan E. Cooper, Dennis C. Bley, and John Wreathall. 1997. Pp. 9–13–9–17 in Proceedings of the IEEE Sixth Annual Human Factors Meeting.
71. Slovic, Paul, Howard Kunreuther and Gilbert F. White. 1974. "Decision Processes, Rationality, and Adjustments to Natural Hazards." Pp. 187–205 in Natural Hazards, edited by Gilbert F. White. New York, NY: Oxford University Press.
72. Janis, Irving L. and Leon Mann. 1977. Decision Making: A psychological analysis of conflict, choice, and commitment. New York, NY: Free Press.
73. Lindell, Michael K. and Ronald W. Perry. 2012. "The Protective Action Decision Model: Theoretical modifications and additional evidence" Risk Analysis 32(4):616–632.
74. Mileti, Dennis S. 1974. A Normative Causal Model Analysis of Disaster Warning Response. Boulder, CO: University of Colorado Department of Sociology.
75. Groner, Norman. 2009. "A Situation Awareness Analysis for the Use of Elevators During Fire Emergencies." Pp. 61–72 in 4th International Symposium on Human Behavior in Fire: Conference

Proceedings. London, UK: Interscience Communications.
76. Perry, Ronald W., Michael K. Lindell, and Marjorie R. Greene. 1981. Evacuation Planning in Emergency Management. Lexington, MA: Lexington Books.
77. Bryan, John L. 2002. "Behavioral Response to Fire and Smoke." Pp. 3–315–3–341 in The SFPE Handbook of Fire Protection Engineering Third Edition, edited by P.J. DiNenno. Quincy, MA: National Fire Protection Association.
78. Canter, David, John Breaux and Jonathan Sime. 1980. "Domestic, Multiple Occupancy and Hospital Fires." Pp. 117–136 in Fires and Human Behaviour, edited by David Canter. New York, NY: John Wiley & Sons.
79. Nigg, Joanne M. 1987. "Communication and Behavior: Organizational and individual response to warnings." Pp. 103–117 in Sociology of Disasters, edited by R. R. Dynes, B. DeMarchi, and C. Pelanda. Milan, Italy: Franco Angeli Libri.
80. Perry, Ronald W. 1979. "Evacuation Decision-Making in Natural Disasters." Mass Emergencies 4 (March): 25–38.
81. Perry, Ronald W. and Marjorie R. Greene. 1982. "The Role of Ethnicity in the Emergency Decision-Making Process." Sociological Inquiry 52(4): 306–334.
82. Perry, Ronald W. and Michael K. Lindell. 1986. Twentieth-Century Volcanicity at Mt. St. Helens: The routinization of life near an active volcano. Tempe, AZ: School of Public Affairs, Arizona State University.
83. Kuligowski, Erica D. and Omori, H. 2014. General Guidance on Emergency Communication Strategies for Buildings, 2nd Edition. NIST Technical Note 1827, National Institute of Standards and Technology: Gaithersburg, MD.
84. Kuligowski, Erica D. and Dennis S. Mileti. 2009. "Modeling Pre-evacuation Delay by Occupants in World Trade Center Towers 1 and 2 on September 11, 2001." Fire Safety Journal 44(4): 487–496.
85. Aguirre, Benigno E. 1991. "Evacuation in Cancun During Hurricane Gilbert." International Journal of Mass Emergencies and Disasters 9(1): 31–45.
86. Mileti, Dennis S. and Colleen Fitzpatrick. 1993. Great Earthquake Experiment: Risk communication and public action. Boulder, CO: Westview Press.
87. Tong, David and David Canter. 1985. "The Decision to Evacuate: A study of the motivations which contribute to evacuation in the event of fire." Fire Safety Journal 9(3): 257–265.
88. Brennan, Patricia. 1995. "Smoke Gets in Your Eyes: The effect of cue perception on behaviour in smoke." Pp. 187–197 in ASIAFLAM'95. International Conference on Fire Science and Engineering 1st Proceedings, edited by W. K. Chow. London, UK: Interscience Communications Ltd.
89. Mileti, Dennis S. and Joanne DeRouen Darlington. 1997. "The Role of Searching in Shaping Reactions to Earthquake Risk Information." Social Problems 44(1): 89–103.
90. Drabek, Thomas and John S. Stephenson, III. 1971. "When Disaster Strikes." Journal of Applied Social Psychology 1(2): 187–203.
91. Fritz, Charles E. and Eli Marks. 1954. "The NORC Studies of Human Behavior in Disaster." Journal of Social Issues 10(3): 26–41.
92. Mileti, Dennis S. and Colleen Fitzpatrick. 1992. "Causal Sequence of Risk Communication in the Parkfield Earthquake Prediction Experiment." Risk Analysis 12(3): 393–400.
93. Mileti, Dennis S. 1975. Natural Hazard Warning Systems in the United States: A research assessment. Program on Technology, Environment and Man. Boulder, CO: Institute of Behavioral Sciences, University of Colorado.
94. Lindell, Michael K., Ronald W. Perry, and Marjorie R. Greene. 1983. "Individual Response to Emergency Preparedness Planning near Mt. St. Helens." Disaster Management 3(Jan/March): 5–11.
95. Peguero, Anthony A. 2006. "Latino Disaster Vulnerability: The dissemination of hurricane mitigation information among Florida's homeowners." Hispanic Journal of Behavioral Sciences 28(1): 5–22.
96. Trumbo, Craig W. and Katherine A. McComas. 2003. "The Function of Credibility in Information Processing for Risk Perception." Risk Analysis 23 (2): 343–353.
97. Flynn, James, Paul Slovic, and C.K. Mertz. 1993. "The Nevada Initiative: A risk communication fiasco." Risk Analysis 13(5): 497–508.
98. Burkhart, Ford N. 1991. Media, Emergency Warnings, and Citizen Response. Boulder, CO: Westview Press.
99. Perry, Ronald W. and Lisa S. Nelson. 1991. "Ethnicity and Hazard Information Dissemination." Environmental Management 15(4): 581–587.
100. Drabek, Thomas E. and Keith Boggs. 1968. "Families in Disaster: Reactions and relatives." Journal of Marriage and the Family 30: 443–451.
101. Mileti, Dennis S. and John H. Sorensen. 1988. "Planning and Implementing Warning Systems." Pp. 321–345 in Mental Health Response to Mass Emergencies, edited by M. Lystad. New York, NY: Bunner/Mazel.
102. Greene, Marjorie R., Ronald W. Perry, and Michael K. Lindell. 1981. "The March 1980 eruptions of Mt. St. Helens: Citizen perceptions of volcano hazard." Disasters 5(1): 49–66.
103. Chandler, R. (2010). Emergency Notification. Santa Barbara: Praeger.
104. Gioia, Dennis A. and Peter P. Poole. 1984. "Scripts in Organizational Behavior." Academy of Management Review 9(3): 449–459.
105. Brennan, Patricia. 1996. "Impact of Social Interaction on Time to Begin Evacuation in Office Building Fires: Implications for modelling behaviour." Pp. 701–710 in Interflam '96. International Interflam Conference, 7th

Proceedings, edited by C. A. Franks and S. Grayson. London, UK: Interscience Communications Ltd.
106. Levin, B. M. 1984. Human Behavior in Fire: What we know now. Report No. SFPE TR 84–03. Gaithersburg, MD: National Bureau of Standards.
107. Sime, Jonathan D. 1983. "Affiliative Behaviour During Escape to Building Exits." Journal of Environmental Psychology 3(1): 21–41.
108. Fahy, Rita F. and Guylene Proulx. 1997. "Human Behavior in the World Trade Center Evacuation." Pp. 713–724 in Fire Safety Science -- Proceedings of the Fifth International Symposium, edited by Y. Hasemi. London, UK: Interscience Communications Ltd.
109. Proulx, Guylene. 2002. "Movement of People: The evacuation timing." Pp. 3–342–3–365 in The SFPE Handbook of Fire Protection Engineering Third Edition, edited by P.J. DiNenno. Quincy, MA: National Fire Protection Association.
110. R.L. Best and D.P. Demers, "Investigation Report on the MGM Grand Hotel Fire—Las Vegas, Nevada, November 21, 1980," Fire Journal, 76, pp. 19–37 (1982).
111. J.L. Bryan, "Human Behavior in the MGM Grand Hotel Fire," Fire Journal, 76, pp. 37–48 (1982).
112. G.P. Morris, "Preplan Was the Key to MGM Rescue Response as EMS Helped Thousands of Hotel Fire Victims," Fire Command, 68, p. 20 (1981).
113. Day, Rachel C., Lynn M. Hulse, and Edwin R. Galea.. "Response Phase Behaviours and Response Time Predictors of the 9/11 World Trade Center Evacuation." Fire Technology 49, 3, 2013.
114. Proulx, Guylene, Irene M. A. Reid and Neil R. Cavan. 2004. Human Behavior Study, Cook County Administration Building Fire, October 17, 2003—Chicago, IL. Ottawa, Canada: National Research Council of Canada.
115. Fahy, Rita F. and Guylene Proulx. 2001. "Toward Creating a Database on Delay Times to Start Evacuation and Walking Speeds for Use in Evacuation Modeling." Pp. 175–183 in 2nd International Symposium on Human Behaviour in Fire. London, UK: Interscience Communications Ltd.
116. Brennan, Patricia. 1997. "Timing Response in Real Fires." Pp. 807–818 in Fire Safety Science—Proceedings of the Fifth International Symposium, edited by Y Hasemi. London, England: Interscience Communications Ltd.
117. Purser, David A. and Marion E. Kuipers. 2004. "Interactions Between Buildings, Fires and Occupant Behavior Using a Relational Database Created From Incident Investigations and Interviews." Pp. 443–456 in Human Behaviour in Fire: Proceedings of the Third International Symposium. London, UK: Interscience Communications Ltd.
118. Shields, T.J. and K.E. Boyce. 2000. "A Study of Evacuation from Large Retail Stores." Fire Safety Journal 35(1): 25–49.
119. Purser, David A. 1998. "Quantification of Behavior for Engineering Design Standards and Escape Time Calculations." Pp. 497–506 in Human Behaviour in Fire: Proceedings of The First International Symposium. London, UK: Interscience Communications Ltd.
120. Galea, Edwin, S. Deere, G. Sharp, L. Filippidis, L. Hulse. 2010. "Investigating the impact of culture on evacuation behavior." Interflam 2010, pp. 879–892.
121. Gwynne, S., E.R. Galea, J. Parke, and J. Hickson. 2003. "The Collection and Analysis of Pre-evacuation Times Derived from Evacuation Trials and Their Application to Evacuation Modeling." Fire Technology 39:173–195.
122. Proulx, G. 1995. "Evacuation Times and Movement Times in Apartment Buildings," Fire Safety Journal 24:229:246.
123. Nelson, L. D. 1973. "Proximity to Emergency and Helping Behavior: Data from the Lubbock Tornado Disaster." Nonprofit and Voluntary Sector Quarterly 2(4): 194–199.
124. Marks, Eli S. and Charles E. Fritz. 1954. Human Reactions in Disaster Situations. Unpublished Manuscript, Volume 3. Chicago, IL: National Opinion Research Center, University of Chicago.
125. Michel, Lacie M. 2007. "Personal Responsibility and Volunteering after a Natural Disaster: The case of Hurricane Katrina." Sociological Spectrum 27(6): 633–652.
126. Rodriguez, Havidan, Joseph Trainor and Enrico L. Quarantelli. 2006. "Rising to the Challenges of a Catastrophe: The emergent and pro-social behavior following Hurricane Katrina." The ANNALS of the American Academy of Political and Social Science 604(1): 82–101.
127. Johnson, Norris R., William E. Feinberg, Drue M. Johnston. 1994. "Microstructure and Panic: The impact of social bonds on individual action in collective flight from The Beverly Hills Supper Club Fire." Pp. 168–189 in Disaster, Collective Behavior And Social Organization, edited by R. Dynes and K. Tierney. Newark, NJ: University of Delaware Press.
128. Aguirre, B.E., M.R. Torres, K.B. Gill, and H.L. Hotchkiss. 2011. "Normative Collective Behavior in The Station Building Fire." Social Science Quarterly, 92(1):100–118.
129. W.L. Grosshandler, N. Bryner, D. Madrzykowski, and K. Kuntz, Report of the Technical Investigation of the Station Nightclub Fire, National Institute of Standards and Technology, NIST NCSTAR 2, Volume 1. Gaithersburg, MD (2005).
130. J.L. Bryan and P.J. DiNenno, Human Behavior in the Fire Incident at the Georgia Towers on January 9, 1979, NBS-GCR-79-187, National Bureau of Standards, Gaithersburg, MD (1979).
131. J.L. Bryan, An Examination and Analysis of the Dynamics of the Human Behavior in the MGM

Grand Hotel Fire, National Fire Protection Association, Quincy, MA (1983).
132. J.L. Bryan, An Examination and Analysis of the Dynamics of the Human Behavior in the Westchase Hilton Hotel Fire, National Fire Protection Association, Quincy, MA (1983).
133. Gwynne, S., E.R. Galea, M. Owen, P.J. Lawrence. 1998–99. "An Investigation of the Aspects of Occupant Behavior Required for Evacuation Modeling" J. Applied Fire Science 8(1):19–59.
134. Proulx, Guylene. 1993. "Housing Evacuation of Mixed Abilities Occupants: A Case Study." CIB Seminar/Workshop, University of Ulster, Northern Ireland.
135. Weick, Karl E. 1995. Sensemaking in Organizations. Thousand Oaks, CA: Sage Publications.
136. Mayer, Michael E., Kevin T. Sonoda, and William B. Gudykunst. 1997. "The Effect of Time Pressure and Type of Information on Decision Quality." The Southern Communication Journal 62: 280–292.
137. Ozel, Filiz. 1998. "The Role of Time Pressure and Stress on the Decision Process During Fire Emergencies" Pp. 191–200 in Proceedings of the First International Symposium Human Behaviour in Fire. London, UK: Interscience Communications.
138. Baumann, Michael R., Janet A. Sniezek, and Clayton A. Buerkle. 2001. "Self-Evaluation, Stress, and Performance: A Model of Decision Making Under Acute Stress." Pp. 139–158 in Linking Expertise and Naturalistic Decision Making, edited by E. Salas and G. Klein. Mahwah, NJ: Lawrence Erlbaum Associates, Inc.
139. Brown, Thomas M. and Charles E. Miller. 2000. "Communication Networks in Task-Performing Groups: Effects of Task Complexity, Time Pressure, and Interpersonal Dominance." Small Group Research 31:131–157.
140. Miller, J.G. 1960. "Information Input Overload and Psychopathology." American Journal of Psychiatry 116(695–704).
141. Nilsson, Daniel. 2009. "Exit choice in fire emergencies—Influencing choice of exit with flashing lights." Doctoral Thesis in the Department of Fire Safety Engineering and Systems Safety, Lund University, Sweden.
142. Gibson, J.J. 1978. The ecological approach to visual perception. Boston: Houghton Mifflin Company.
143. Hartson, H.R. 2003. "Cognitive, physical, sensory, and functional affordances in interaction design. Behavior & Information Technology, 22(5):315–338.
144. Donald, I., and D. Canter. 1990. "Behavioural Aspects of the King's Cross Disaster", in Fires and Human Behaviour (2nd Edition), D. Canter (ed.), Fulton, London, UK, pp. 15–30.
145. Jones, B.K. and J.A. Hewitt. DATE. "Leadership and Group Formation in High-rise Building Evacuations." Pp. 513–522 in Fire Safety Science—Proceedings of the First International Symposium, IAFSS.
146. Proulx, G., J. Pineau, J.C. Latour, and L. Stewart. 1995. "Study of occupants' behavior during the 2 Forest Laneway fire in North York, Ontario, January 6, 1995." Internal Report No 705, National Research Council, Ottawa, Ontario, National Fire Laboratory.
147. Horasen, M. and O. Bruck. 1994. "Investigation of a Behavioural Response Model for Fire Emergency Situations in Secondary Schools." Proceedings of Fourth International Symposium on Fire Safety Science, T.L. Kashiwagi (ed.), pp. 715–726.
148. Saunders, Wendy. 2001. "Gender Differences in Response to Fires" 2nd International Symposium of HB in Fire
149. Kuligowski, E.D. and S.M.V. Gwynne. 2008. "The Need for Behavioral Theory in Evacuation Modeling" Pp. 721–732 in Proceedings of Pedestrian and Evacuation Dynamics, Heidelberg, Germany: Springer.
150. Gwynne, S.M.V. 2012. "Translating Behavioral Theory of Human Response into Modeling Practice." NIST GCR 12–972, National Institute of Standards and Technology, Gaithersburg, MD.
151. Kuligowski, Erica. 2012. "Theory Building: An Examination of the Pre-evacuation Period of the 2001 WTC Disaster." Pp. 24–36 in Proceedings of the 5th International Symposium Human Behaviour in Fire 2012. London, UK: Interscience Communications.
152. Sorensen, John H. 1991. "When Shall We Leave? Factors Affecting the Timing of Evacuation Departures." International Journal of Mass Emergencies and Disasters 9(2): 153–165.
153. Reneke, Paul A. 2013. Evacuation Decision Model. NIST IR 7914, National Institute of Standards and Technology, Gaithersburg MD.http://dx.doi.org/10.6028/NIST.IR.7914

Erica D. Kuligowski is a Fire Protection Engineer and Sociologist in the Engineering Laboratory at the National Institute of Standards and Technology. Her major research interest is human behavior in fires and other emergencies, including preparedness, response and recovery decision-making and behavior. The chapter represents research performed by Dr. Kuligowski both as part of her official duties at the National Institute of Standards and Technology and as part of her doctoral research at the University of Colorado at Boulder, under Dr. Kathleen Tierney.

Employing the Hydraulic Model in Assessing Emergency Movement

59

Steven M.V. Gwynne and Eric R. Rosenbaum

Introduction

This chapter provides the engineer with a model to quantify egress performance. This model is formed from a set of numerical tools that vary in their scope and sophistication. Guidance is provided on the capabilities of these tools and on when they should be employed, making reference to the data on which these tools are based. Detailed examples are presented to clarify the application of these tools, along with a description of how the use of these tools fits in with other fire engineering calculations. This chapter will, therefore, allow the engineer to assess egress performance in a responsible and informed manner.

Prediction of evacuee movement is an essential component of performance-based fire safety analysis. Safe egress from fire is assumed to be achieved if the required safe egress time (RSET) is sufficiently shorter than the available safe egress time (ASET), where ASET is defined as the time until fire-induced conditions within a building become untenable. Methods to evaluate the development of fire-induced conditions and tenability criteria are addressed elsewhere in this handbook.

The model discussed in this chapter provides the engineer with a means to establish RSET (i.e., the time taken to reach safety) and therefore complete this component of a performance-based assessment. This model, albeit imperfect, quantifies the egress performance of a design and, importantly, enables comparisons to be made between different design variants to be made.

The hydraulic model is presented as a means of quantifying egress performance that can support an engineering approach and expert analysis. Hydraulic models are based on a simplification of egress behavior where the evacuating population is described by a set of equations. This population moves from egress component to egress component (e.g., from a corridor to a stairwell), with the speed of their movement dictated by the equations that form the model. Guidance is provided on how best to employ these equations, on the scenarios to which this model can be applied, and on the limitations of the approach.

The inherent structure of the hydraulic model described in this chapter tends to an optimistic estimate of evacuation time. It assumes that the exit paths will be continually used at maximum capacity from the moment of alarm to total evacuation. The model should be considered as a baseline calculation to be extended as appropriate to account for delays caused by human decisions, notifications, and other factors (see Chaps. 58 and 64).

For each evacuee the RSET can be subdivided into a number of discrete time intervals, the sum of which constitute the total RSET:

S.M.V. Gwynne (✉)
National Research Council Canada

E.R. Rosenbaum
Jensen Hughes, Inc.

M.J. Hurley (ed.), *SFPE Handbook of Fire Protection Engineering*,
DOI 10.1007/978-1-4939-2565-0_59, © Society of Fire Protection Engineers 2016

$$\text{RSET} = t_d + t_n + t_{p-e} + t_e \quad (59.1)$$

where

t_d = Time from fire ignition to detection; that is, the detection phase

t_n = Time from detection to notification of occupants of a fire emergency; that is, the notification phase

t_{p-e} = Time from notification (or cue reception) until evacuation commences; that is, the pre-evacuation phase

t_e = Time from the start of purposive evacuation movement until safety is reached; that is, the evacuation phase

The components described are considered the core elements of egress analysis (see Chap. 64 for further discussion), although it is recognized that other components will certainly contribute to evacuee performance (e.g. the Pre-Warning delay incurred through staff actions and their decision-making which may prolong notification of the general population).

The RSET elements t_d and t_n typically involve a technical solution and human interaction, including fire detection devices and fire alarm equipment, and also human intervention, such as the discovery of a fire by a staff member and notification of the population. The theory and design of detection systems are covered elsewhere in this handbook (see Chap. 40).

The element t_{p-e} relates to the individual and collective responses of the occupants; that is, the time between them being notified of the incident and the time to commence their evacuation. This can be prolonged by a number of complex activities (see Chaps. 58 and 64). These include receiving a cue; interpreting the cue; validating the cue; performing pre-evacuation activities; and determining an appropriate response (see Chap. 58). All of these contribute to the time spent in the pre-evacuation phase, prior to commencing purposive evacuation movement to a place of safety.

The element t_e is the time from when an individual initiates evacuation movement up to the point that he or she reaches safety. For an individual evacuee, t_{p-e} and t_e are basically sequential. Crudely speaking, it is typically assumed that for an individual evacuee, t_{p-e} and t_e are basically sequential. There is a period before the individual has determined that an evacuation response is required (through the perception of sufficient risk levels and the subsequent completion of preparatory actions) and a period where this response is conducted (i.e. where protective actions are taken). That is not to say that the individual need be static in either time period or that the performance of actions are not iterative or cyclical—only that at a certain point in time, the individual decides that the situation requires them to take protective actions and their subsequent actions broadly reflect an attempt to disengage from the current actions and take protective actions.

However, across a population, t_{p-e} and t_e are neither independent of each other nor mutually exclusive [1]. There may be significant overlap between these components given the varying conditions evident at different locations within the structure, the different levels of information available, and the differences in the abilities of the population [2].

RSET can be reduced into two sets of components: the phase prior to evacuee involvement, made up of t_d and t_n, and the escape phase (t_{esc}) where

$$t_{\text{esc}} = t_{p-e} + t_e \quad (59.2)$$

It should be noted that, in reality, the evacuation phase can be interrupted through behavioral actions and developments in the incident scenario [3].

This chapter describes the basic hydraulic model enabling t_e to be calculated. It also describes the extension of the hydraulic model to also include t_{p-e} in the calculation and therefore allow an estimation of t_{esc} to be produced. A methodology is presented to enable the engineer to determine the RSET value as part of a performance-based assessment. It provides sufficient information for the engineer to calculate RSET under a number of different incident scenarios, while also making the engineer aware of the limitations and assumptions of the hydraulic model (Fig. 59.1).

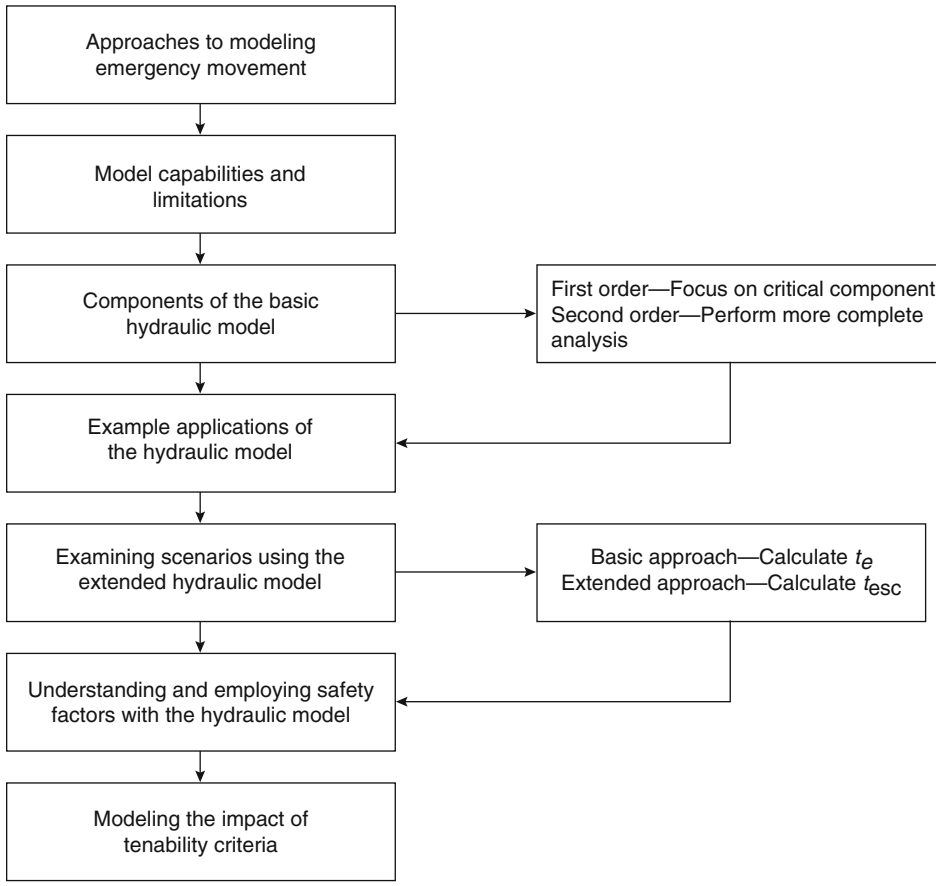

Fig. 59.1 Structure of this chapter

Establishing Egress Performance

Over the last few decades an increasing effort has been made into investigating human behavior in response to fire. This research has provided a clearer understanding of egress behavior and the factors that influence egress performance. As a consequence, human behavior can be taken into consideration when designing emergency procedures and modeling human performance. Prior to this time, human behavior was disregarded altogether, seen as immeasurable, and/or drastically simplified according to a few basic assumptions. The former understanding of human behavior was based on a number of assumptions: people's behavior would likely be panic based [4]; it would likely be selfish and competitive; and it would involve immediate and direct movement once the incident was discovered. Although some of these assumptions are contradictory, they have had a direct impact on the engineering calculations made for a long period of time and continue to exert some degree of influence on egress design decisions to this day [3].

In recent times, a more detailed and comprehensive understanding of human behavior in fire has been established (see Chaps. 58 and 64). This understanding has been derived from the examination of actual incidents, the collection of empirical evidence, and the development of behavioral theories. All of this has, to a large degree, refuted the assumptions that had previously dominated. This realization has allowed engineers (as well as behavioral researchers,

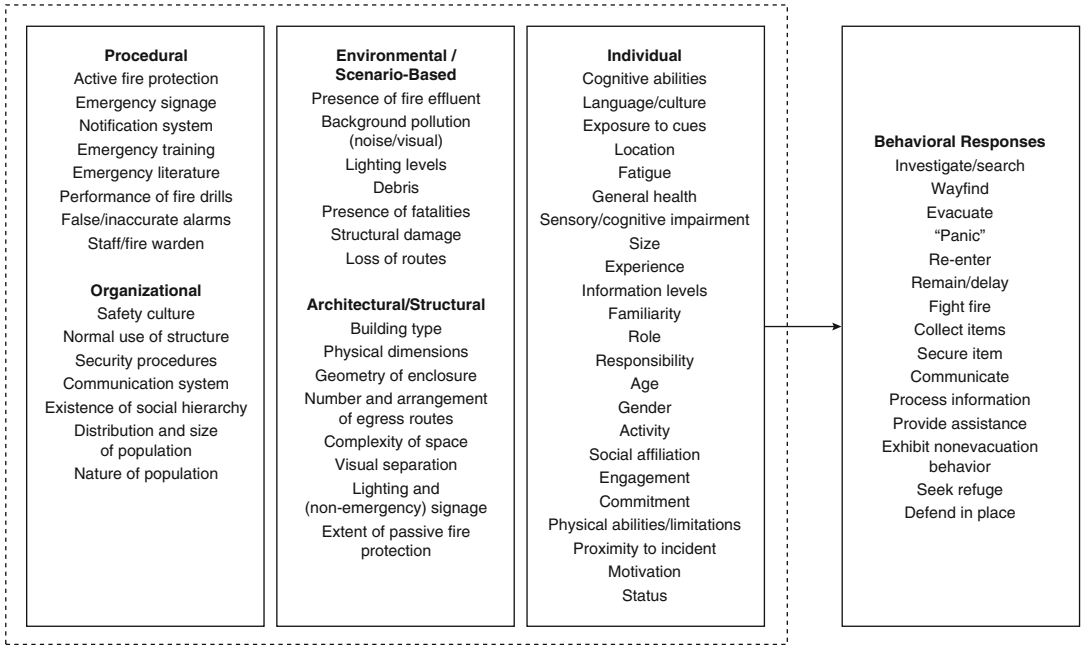

Fig. 59.2 Factors that can influence egress performance

procedural designers, and evacuation modelers) to take human behavior into account, albeit imperfectly, when trying to establish evacuation performance.

It is now felt that the evacuation process is not simply a matter of initiating an evacuation and then controlling the ensuing hysterical crowd response; instead, it is now viewed as a more multifaceted event in which people's responses are sensitive to the incident scenario, the information available, and the local conditions (among other things). The problem of understanding human behavior in fire is not the simple process previously assumed. Instead, it relies on a number of factors that can interact and can influence the outcome in different ways (Fig. 59.2). These factors also influence the engineering methods required to assess performance. Ideally these factors should be considered in any assessment of egress performance; however, the methods employed in this assessment are limited and, to different degrees, exclude many of the key factors influencing egress performance. It is critical that these limitations are understood by an engineer prior to the application of such methods.

Models

Several approaches are available to the engineer to establish egress performance; that is, estimate t_{esc}. Each of these approaches requires the application of a model: a simplified version of reality used as an indicator of actual egress performance. All of these approaches are limited. One or more of the following four model approaches are usually applied:

- *Model Approach A*: *The application of prescriptive codes*. The expertise embedded within the regulations is assumed to satisfactorily represent (or at least account for) the performance of the evacuating population. Generally, these codes focus on the physical constraints imposed by the structure and exclude behavioral and procedural factors.
- *Model Approach B*: *The performance of an egress trial*. An (un)announced trial is

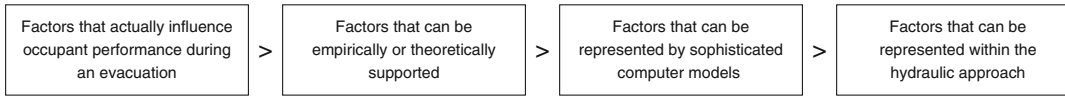

Fig. 59.3 Difference between the actual and modeled evacuation

conducted in order to assess the outcome of a simulated incident using the population of interest. This approach has a number of limitations: it is expensive; there are ethical issues in achieving realism in such an event; the trial produces only a single data point; and the structure has to be in place already [5].

- *Model Approach C*: *The application of a* (*computer-based*) *simulation model*. An attempt is made to incorporate our understanding of human behavior in fire within a computer-based model. This is then applied to a representative set of scenarios in order to establish egress performance. The quality of the results is highly dependent on a number of factors: the sophistication and validity of the model used, the expertise of the user, and the scenarios examined and their appropriateness [6].
- *Model Approach D*: *The application of an engineering calculation*. Here, empirical data are distilled into a representative set of equations. These equations are deemed to represent a simplified version of evacuation movement (instead of behavior), where the results are largely determined by the physical attributes of the components involved; for example, the people, the structure, and so on. As such, they largely overlook many of the complexities apparent in the human response to fire. These calculations can be applied at the level of the structure (see Chap. 64) or the level of the structural component. For instance, details of the structure can be included in an equation that generates an overall egress time; for example, the number of floors, the population size, and the egress width available.

  Alternatively, the attributes of a particular structural component (e.g., staircase, section of corridor, etc.) can be used. These describe the performance of the population when traversing the component in question. These results are then pieced together to form a network representation of a structure to describe the performance of the population when traversing an egress route.

In reality, none of these approaches include all of the factors that influence the outcome of an evacuation; that is, they represent only a subset of those factors mentioned in Fig. 59.2. Indeed, given the relatively immature state of the study of human behavior in fire, it would be not be possible for the models to include all of the factors affecting egress. It is vital to understand the limitations of these models in order to more reliably interpret and assess the results produced. There is a difference between the number of factors that actually affect an evacuation and the number that can be modeled. The gap between this prediction and reality is outlined in Fig. 59.3. The hydraulic model discussed here is an engineering calculation, that is, model approach D.

Model Limitations

Many factors influence the outcome of an evacuation; models have the potential to incorporate a subset of these factors. This potential influence is based on the assumption that (1) sufficient theoretical support exists (i.e., that the factors have been identified and formalized); (2) there are data that can be incorporated into the model (i.e., that the factors can be quantified in some way); and (3) there are no limitations in the technology used to apply the model (e.g., hardware or software).

The hydraulic model is limited in the factors it can represent. Several aspects of the model should be noted:

- Behaviors that detract from movement are not explicitly considered.
- The numbers of people in a structural component are considered rather than their identity and their individual attributes.
- Movement between egress components is considered (e.g., from room to room), rather than within them.
- The results are deterministic and will therefore remain the same unless changes are made to the scenario or the assumptions employed.

The expert user can, to some degree, compensate for these limitations, but these limitations are inherent in the hydraulic model. Therefore, given the nature of the hydraulic model, it is able to represent only a small subset of behavioral factors (primarily related to those that influence movement).

Some time has been spent outlining the limitations of the hydraulic model along with the other modeling approaches available. As with any model, it is critical that the engineer is aware of these limitations prior to its use. When the hydraulic (or any other) model is employed, a brief description of these limitations should be presented along with the results produced and the conclusions drawn. However, despite these limitations, it is possible to employ the hydraulic model to establish egress performance in a consistent and informative manner. A hydraulic model can assess t_e by quantifying egress performance, and therefore provide insight into the effectiveness of a design. In a similar manner, the extended version of the model, described later in this chapter, is able to estimate t_{esc}.

In many cases, the hydraulic model is an acceptable method to model egress. Examples include where only a general estimate of egress time is required and where the hydraulic model is the most sophisticated model available to the engineer: the prescriptive codes may be too restrictive and not allow dedicated data to be incorporated; the resources available may not extend to the use of a complex simulation model; and egress trials may be precluded as the structure may not yet have been built. Where these other models are available, the engineer may want to apply several simultaneously (e.g., the hydraulic model and a computer simulation model) in order to have a stronger basis for the results [1]. Care should be shown in the application of the hydraulic model and the presentation of the results produced. With responsible use, it is able to produce reasonable results in many situations. In some situations a more sophisticated model should, ideally, be employed; for example, where complicated procedures are in place, where complex flows are expected, and where the population is heterogeneous (see Chap. 60).

In the next sections the use of the basic hydraulic model to estimate t_e (the evacuation time) is discussed. The empirical evidence supporting the hydraulic model is outlined, and the calculations involved are described. Two different versions of the basic hydraulic model are described: a simplified approach (first order) and the full approach (second order). Both act at the level of the structural component but do so to different degrees of computational rigor. The engineer must select one of these versions based on the project, his or her expertise, and the time available. Several examples are provided demonstrating how the hydraulic model can be applied. Finally, guidance is provided on how these calculations can be employed and, by extending the model, the types of scenarios that should be examined. An engineer should consider all of these issues when determining t_e (and then eventually t_{esc}).

Estimating t_e Using the Basic Hydraulic Model

This section describes the fundamental components of egress movement that form the basic elements of the hydraulic model; that is, the equations used in calculating the t_e component in Equation 59.1.

Research-based engineering calculations for predicting emergency population flow have emerged over the past few decades. The major contributors include Predtechenskii and

Milinskii [7], Fruin [8], and Pauls [9, 10]. A number of other contributions have been made to the field in recent years; [11–25] however, the methods presented here (originally developed by Nelson and MacLennan [26]) were based primarily on the major contributors highlighted above. A more complete list of the research performed relating to human behavior and movement is presented in Chaps. 58 and 64, as well as elsewhere [4, 27–37].

It should be noted that at the time of writing there is some discussion regarding the validity of several of the data-sets on which these models are based. This has led to data-sets being withdrawn from the SFPE handbook and from other publications (see Chap. 64). However, their contribution to the model described here is not removed given that the data-sets are broadly comparable, that they form a core component to the original model derived by Nelson et al. [26], that they have not yet been proven invalid (in an available, peer-reviewed publication), and that, perhaps more importantly, there is a lack of other equivalently comprehensive data-sets available.

As mentioned, the sources included here are, in most cases, compatible and supportive of each other. All are based on the relationship between the speed of movement and population density of the evacuating population stream. The equations derived from these sources are based on the following assumptions:

1. All persons start to evacuate at the same time.
2. Occupant flow does not involve interruptions caused by evacuee decisions.
3. The evacuees are free of impairments/disabilities that impede their movement.

Given the discussion presented in Chaps. 58 and 64 and from Fig. 59.2, these assumptions exclude a number of factors and behaviors that might detract from egress performance. These assumptions also have the effect of separating the egress components (presented in Equation 59.1) into distinct activities that are then treated separately during the calculations; in reality, these components would be coupled.

When representing an actual event, Equation 59.1 can be rewritten as

$$\mathrm{RSET} = t_d + t_n + t_{p-e} + (t_{\mathrm{trav}} + t_{\mathrm{flow}} + t_{n-e}) \tag{59.3}$$

where t_e is broken down in three constituent parts: t_{trav} is the time spent moving toward a place of safety, t_{flow} is the time spent in congestion controlled by flow characteristics, and t_{n-e} is the time spent in nonevacuation activities that do not directly contribute to the population moving to a place of safety. Even this equation is a simplification, although it does demonstrate that in the evacuation phase there is likely to be an amount of time spent in activities other than moving directly to an exit. Given the assumptions associated with hydraulic models, the RSET calculation using the basic hydraulic model produces the following equation:

$$\mathrm{RSET} = t_d + t_n + t_{p-e} + (t_{\mathrm{trav}} + t_{\mathrm{flow}}) \tag{59.4}$$

The behaviors that do not directly contribute to the evacuation are not modeled (t_{n-e}). Calculations based on these assumptions require compensatory actions in order to account for the factors not included. These actions are discussed later in this chapter.

Fundamental Movement Calculations

The modeled evacuation time (i.e., the time predicted by the hydraulic model) utilizes a series of expressions that relate data acquired from tests and observations to a hydraulic model of human flow. These primarily relate to the following considerations: effective width, population density, speed, flow characteristics, time for passage through a component, and transitions between components. Each of these considerations is discussed in detail by Proulx [38]. By taking these considerations into account, egress movement can be quantified using the hydraulic model. Figure 59.4, shows a typical relationship between the source data and the derived equation. Although the expressions indicate absolute relationships, there is considerable

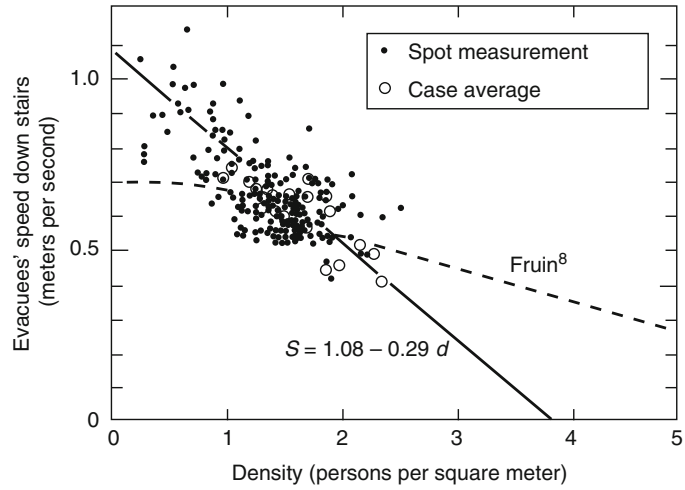

Fig. 59.4 Relation between speed and density on stairs in uncontrolled total evacuations (Dashed line from Fruin [8])

variability in the data. The engineer may wish to take this into account during the calculation process.

The equations and relationships presented in the following paragraphs can be used independently or collected together to solve more complex egress problems. Several examples outlining the use of these equations are presented later in this chapter.

Effective width, W_e The effective width is the usable width of the component, or W_e. Persons moving through the exit routes of a building maintain a boundary layer clearance (i.e., maintain a distance between themselves and the object in question) from walls and other stationary obstacles they pass (see Fruin [8], Pauls [9, 10], and Habicht and Braaksma [39]). This clearance is needed to accommodate lateral body sway and assure balance. Personal preference dictates that people attempt to maintain space around themselves assuming that the population density is sufficiently low.

Discussion of this crowd movement phenomenon is found in the works of Pauls [9, 10], Fruin [8], and Habicht and Braaksma [39]. The useful (effective) width of an exit path is the clear width of the path less the width of the boundary layers. Figures 59.5 and 59.6 depict effective width and boundary layers. Table 59.1 is a listing of boundary layer widths. The effective width of any portion of an exit route is the clear width of that portion of an exit route less the sum of the boundary layers. Clear width is measured

1. From wall to wall in corridors or hallways
2. As the width of the treads in stairways
3. As the actual passage width of a door in its open position
4. As the space between the seats along the aisles of assembly arrangement
5. As the space between the most intruding portions of the seats (when unoccupied) in a row of seats in an assembly arrangement

The intrusion of handrails is considered by comparing the effective width without the handrails and the effective width using a clear width from the centerline of the handrail. The smaller of the two effective widths then applies. Using the values in Table 59.1, only handrails that protrude more than 2.5 in. need be considered; that is, if the handrail protrudes less than 2.5 in. into the stair width, then the overall calculated width will still be less than the 6 in. reduction produced by the stairwell. Minor midbody height or lower intrusions such as panic hardware are treated in the same manner as handrails.

Population Density, D Population density, D, is the measurement of the degree of crowdedness in an evacuation route. The calculations in this

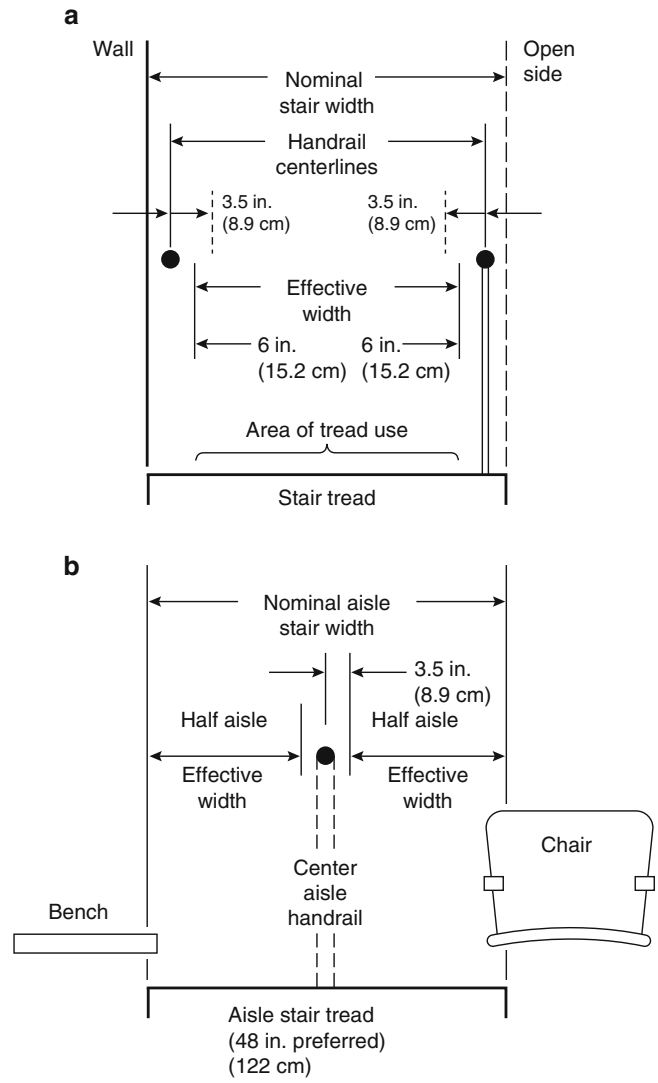

Fig. 59.5 Measurements of effective width of stairs in relation to walls, handrails, and seating

chapter are based on population density expressed in persons per square foot (or persons per square meter). It should be noted that researchers employ several different units when describing population density. These units include the number of people per unit of space, the space available per person, and the proportion of floor space occupied [7]. In reality, the population density will be dependent on the size of the individuals present. These sizes may vary greatly. Here, the sizes are assumed to be uniform or averaged across the population.

Unless specifically stated, the entire population of the first egress component (i.e., the component from which the egress movement starts) is included in any flow calculation. This will demonstrate the capacity limits of the route element. If the evacuating population is widely dispersed within an egress component (i.e., it would take them significantly different times to reach connected egress components), the calculation is based on an appropriate time step that reflects the time of their arrival. At each time increment, the population density of the exit route is based on

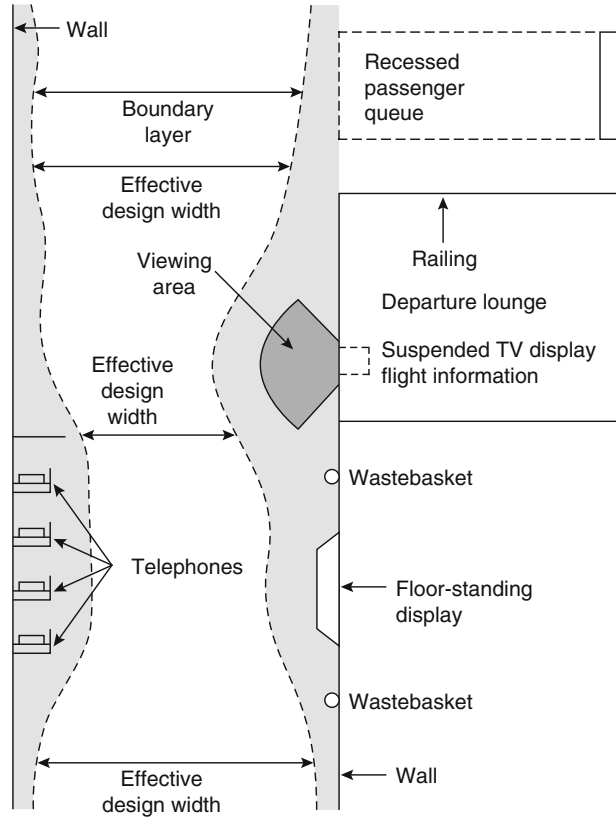

Fig. 59.6 Public corridor effective width

Table 59.1 Boundary layer widths

Exit route element	Boundary layer (in.)	(cm)
Stairways—wall or side of tread	6	15
Railings, handrails[a]	3.5	9
Theater chairs, stadium benches	0	0
Corridor, ramp walls	8	20
Obstacles	4	10
Wide concourses, passageways	<18	46
Door, archways	6	15

[a]Where handrails are present, use the value if it results in a lesser effective width

those that have entered the route minus those that have passed from it. In such situations the engineer may wish to separate the components into subcomponents; for example, a corridor could be broken into several components reflecting the different performances of the population. In this case, the density calculations would then be based on the entire population of each of the new components.

The population density factors in subsequent portions of the egress system are determined by calculation. The calculation methods involved are contained in the section of this chapter titled "Transitions."

Speed, *S* Speed is defined as the movement velocity of exiting individuals, or *S*. Observations and experiments have shown that the speed of a group or an individual in a group is a function of the population density. The relationships presented in this chapter have been derived from the work of Fruin [8], Pauls [9, 10], and Predtechenskii and Milinskii [7]. If the population density is less than approximately 0.05 persons/ft^2 (0.54 persons/m^2) of exit route, individuals will move at their own pace, independent of the speed of others. If the population density exceeds about 0.35 persons/ft^2 (3.8 persons/m^2), it is assumed that no movement will take place until enough of the crowd has passed from the crowded area to reduce the

population density. Between the population density limits of 0.05 and 0.35 persons/ft^2 (0.54 and 3.8 persons/m^2), the relationship between speed and population density is assumed to be represented by a linear function. The equation of this function is

$$S = \mathrm{k} - \mathrm{ak}D \tag{59.5}$$

where
S = Speed along the line of travel
D = Population density in persons per unit area
k = Constant, as shown in Table 59.2
= k_1; and a = 2.86 for speed in ft/min and density in persons/ft^2
= k_2; and a = 0.266 for speed in m/s and density in persons/m^2

Table 59.2 Constants for Equation 59.5, evacuation speed

Exit route element		k_1	k_2
Corridor, aisle, ramp, doorway		275	1.40
Stairs			
Riser (in.)	Tread (in.)		
7.5	10	196	1.00
7.0	11	212	1.08
6.5	12	229	1.16
6.5	13	242	1.23

1 in. = 25.4 mm

Figure 59.7 is a graphic representation of the relationship between speed and population density. The speeds determined from Equation 59.5 are along the line of movement; that is, for stairs the speeds are along the line of the treads. Table 59.3 provides convenient multipliers for converting vertical rise of a stairway to a distance along the line of movement. The travel on landings must be added to the values derived from Table 59.3. To be conservative, it should be assumed that the population does not increase velocity when traversing a landing between stairs but continues on at the same reduced rate associated with stair movement.

Although, in reality, population densities of greater than 0.175 persons/ft^2 (1.9 persons/m^2) can be achieved, it is suggested that these densities should not be assumed in an engineering design [3]. This density produces the maximum achievable flow rate; beyond this density, the flow rate falls rapidly. If the population density increases significantly beyond 0.37 persons/ft^2 (4 persons/m^2), then crush conditions might develop [9, 10, 40]. This suggested maximum compares to the occupancy levels suggested in NFPA *101®*, *Life Safety Code®*, of 0.142 persons/ft^2 (1.54 persons/m^2) to 0.003 persons/ft^2 (0.022 persons/m^2) depending on the type of occupancy [41]. The suggested maximum

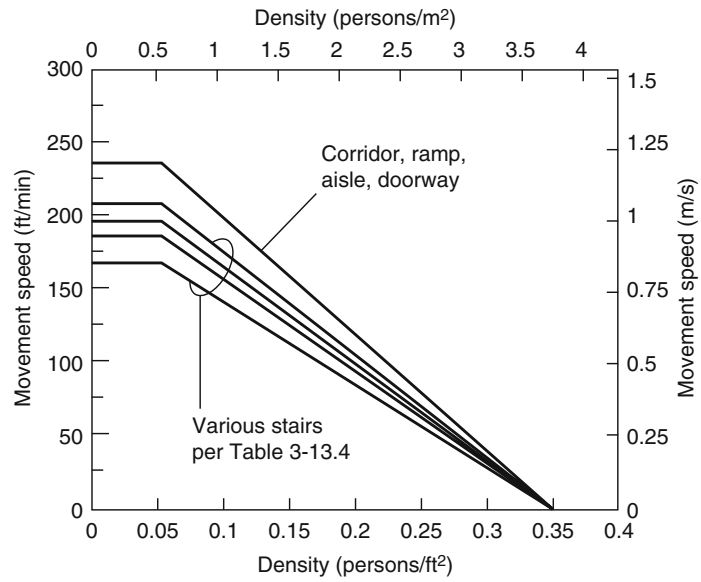

Fig. 59.7 Evacuation speed as a function of density. S = k − akD, where D = density in persons/ft^2 and k is given in Table 59.2. Note that speed is along line of travel

Table 59.3 Conversion factors for relating line of travel distance to vertical travel for various stair configurations

Stairs riser (in.)	Tread (in.)	Conversion factor
7.5	10.0	1.66
7.0	11.0	1.85
6.5	12.0	2.08
6.5	13.0	2.22

1 in. = 25.4 mm

density is therefore beyond the heaviest occupant load suggestion in the *Life Safety Code* and should therefore be adequate for all occupancy types.

A conservative approach is therefore adopted regarding the population densities that might be achieved during the movement of the population. As can be seen in Fig. 59.7, a maximum population density of 3.76 persons/m^2 is assumed. This limit constrains the movement of the population. The relationship between speed/flow and density is similarly affected by this constraint, with achievable population densities below those that might be expected in reality and curtailed earlier than might be expected.

The maximum speed is possible, but not inevitable, when the density is less than 0.05 persons/ft^2 (0.54 persons/m^2). These maximum speeds are listed in Table 59.4.

Within the range of dimensions listed in Tables 59.2, 59.3, and 59.4, the evacuation speed on stairs varies approximately as the square root of the ratio of tread width to tread height. There is not sufficient data to appraise the likelihood that this relationship holds outside this range.

Specific flow, F_s Specific flow, F_s, is the flow of evacuating persons past a point in the exit route per unit of time per unit of effective width, W_e, of the route involved. Specific flow is expressed in persons/min/ft of effective width (if the value of $k = k_1$ from Table 59.2), or persons/s/m of effective width (if the value of $k = k_2$ from Table 59.2). The equation for specific flow is

$$F_s = SD \tag{59.6}$$

Table 59.4 Maximum (unimpeded) exit flow speeds

Exit route element		Speed (along line of travel) (ft/min)	(m/s)
Corridor, aisle, ramp, doorway		235	1.19
Stairs			
Riser	Tread (in.)		
7.5	10	167	0.85
7.0	11	187	0.95
6.5	12	196	1.00
6.5	13	207	1.05

1 in. = 25.4 mm

where
F_s = Specific flow
D = Population density
S = Speed of movement

The flow rate unit is often referred to in persons/ft/minute or persons/m/second. This change in units will have no impact on the results.

F_s is in persons/min/ft when density is in persons/ft^2 and speed in ft/min; F_s is in persons/s/m when density is in persons/m^2 and speed in m/s.

Combining Equations 59.5 and 59.6 produces

$$F_s = (1 - aD)kD \tag{59.7}$$

where k is as listed in Table 59.2.

The relationship of specific flow to population density is shown in Fig. 59.8. In each case the maximum specific flow occurs when the density is 0.175 persons/ft^2 (1.9 persons/m^2) of exit route space. It is possible to establish F_s from Equation 59.7 and solve for D. There is a maximum specific flow associated with each type of exit route element; these are listed in Table 59.5.

Special Consideration for Door Mechanism In Table 59.5 and Fig. 59.8 the maximum achievable specific flow rates for corridors and doorways are considered equivalent. This is based on the original calculations made by Nelson and MacLennan [26]. However, this is based on the assumption that the entire effective width

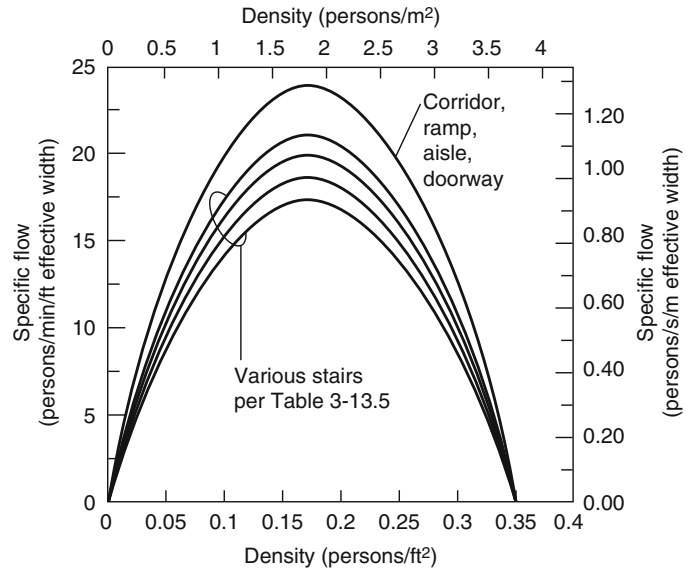

Fig. 59.8 Specific flow as a function of population density

Table 59.5 Maximum specific flow, Fsm

Exit route element		Maximum specific flow	
		Persons/min/ft of effective width	Persons/s/m of effective width
Corridor, aisle, ramp, doorway		24.0	1.3
Stairs			
Riser	Tread		
(in.)	(in.)		
7.5	10	17.1	0.94
7.0	11	18.5	1.01
6.5	12	20.0	1.09
6.5	13	21.2	1.16

of the doorway is available and that the passage of the population through the doorway is not influenced by the door mechanism itself. If the door leaf is not mechanically held open, then the traversing population may be forced to hold it open, delaying their passage. These actions have the potential for slowing the evacuees' movement through the opening, producing a reduced flow rate. It may also reduce the width available to the width of a single person (i.e., the width required for the person holding the door and passing through the exit), rather than the full available width of the exit leaf. In this case, the exit width available may be dynamic and reduced even from the calculated effective width.

These factors may act to limit the flow through the doorway. When doors on an egress route are not mechanically held open, these factors should be considered. In such circumstances, where the interaction with the door leaf influences performance, it may be more conservative to assume a maximum achievable flow rate based on the number of door leaves available rather than the actual width (effective or otherwise) of each door leaf; that is, increasing the door leaf size may not produce a linear increase in the achievable flow, given the need to hold the leaf open and the reduction in the available door width due to the position of the closing leaf. A *maximum* flow rate of 50 persons/min/door leaf is suggested for doors that are not mechanically held open [3, 8]. Fruin originally noted flow rates between 40 and 60 persons/min through exits with door leaves; however, the lower flow rate of 40 persons/min was produced during observations involving slow-moving occupants and so is discounted [3].

The data used to support the flow rate through doors are several decades old and may not accurately reflect the movement and shape characteristics of current populations; for example, the impact that the increasing levels of obesity in some parts of the world might have on the capacity of egress routes and on movement rates

[42]. In addition, the data from which these relationships were derived were collected from nonemergency pedestrian movement and/or egress drills. The functions described should not be assumed to necessarily provide conservative predictions; the engineer should therefore factor this into the design recommendations made.

Calculated flow, F_c The calculated flow, F_c, is the predicted flow rate of persons passing a particular point in an exit route. The equation for calculated flow is

$$F_c = F_s W_e \tag{59.8}$$

where
F_c = Calculated flow
F_s = Specific flow
W_e = Effective width of the component being traversed

Equation 59.8 is based on the assumption that the achievable flow rate through a component is directly proportional to its width.

Combining Equations 59.7 and 59.8 produces

$$F_c = (1 - \mathrm{a}D)\mathrm{k}DW_e \tag{59.9}$$

F_c is in persons/min when k = k_1 (from Table 59.2), D is in persons/ft^2, and W_e is in ft. F_c is in persons/s when k = k_2 (from Table 59.2), D is persons/m^2, and W_e is m.

Time for passage, t_p The time for passage, t_p, is the time for a group of persons to pass a point in an exit route and is expressed as

$$t_p = P/F_c \tag{59.10}$$

where t_p is time for passage (t_p is in minutes where F_c is in persons/min; t_p is in seconds where F_c is persons/s). P is the population size in persons.

Combining Equations 59.9 and 59.10 yields

$$t_p = P/[(1 - \mathrm{a}D)\mathrm{k}DW_e] \tag{59.11}$$

There are several transition configurations that may arise during an engineering calculation that involve the interaction between flows of people. These transitions need to be identified, as they require a different approach and have an impact on the overall calculation produced. The transitions can be categorized into merging or branching flows.

Transitions Transitions are any points in the exit system where the character or dimension of a route changes or where routes merge or branch. Typical examples of points of transition include the following:

1. Any point where an exit route becomes wider or narrower. For example, a corridor may be narrowed for a short distance by a structural change, an intruding service counter, or a similar element. The calculated density, D, and specific flow, F_s, differ before reaching, while passing, and after passing the intrusion.
2. A point where the terrain changes; that is, the point where a corridor enters a stairway. There are actually two transitions: one occurs as the egress flow passes through the doorway, the other as the flow leaves the doorway and proceeds onto the stairs.
3. The point where two or more exit flows merge; for example, the meeting of the flow from a cross aisle into a main aisle that serves other sources of exiting population. It is also the point of entrance into a stairway serving other floors.
4. Where a flow branches into several other flows. A decision has to be made regarding the proportion of the incoming flow that uses each of the outgoing flows, that is, into several other egress components. The proportion of the flows will be influenced by a number of different behavioral and procedural issues (refer to Chaps. 58 and 64, and also to Predtechenskii and Milinskii [7]). The proportion of flow using each of the egress components may be apportioned evenly, according to the capacity of the components, or according to behavioral/procedural issues, such as familiarity. Once this apportionment has been established, then each of the flow calculations proceed as before and can be conducted independently of each other.

The following rules apply when determining the densities and flow rates following the passage of a transition point:

1. The flow after a transition point is a function, within limits, of the flow(s) entering the transition point.
2. During the transition between two components, it will be necessary to establish the density in the new component; that is, it is assumed that sufficient information is available on the previous component to enable this calculation to be made. The density in the new component will be calculated by solving for D in Equation 59.9; this will produce a quadratic in D. In order to do this, the flow rate into the component will need to be known. Unless the maximum value is achieved, there will normally be two solutions of D produced: one above and one below $D_{\max}$ (where $D_{\max}$ is the density value that produces the maximum flow). Nelson and MacLennan [26], and Predtechenskii and Milinskii [7], and Milke [40] state that the smaller of the D values should be employed; that is, less than or equal to $D_{\max}$. If the larger D value (greater than $D_{\max}$) is used, it implies that the flow rate between the two components both rises and falls during a single transition. This is not considered to be reasonable.
3. The calculated flow, F_c, following a transition point cannot exceed the maximum specific flow, F_{sm}, for the route element involved multiplied by the effective width, W_e, of that element.
4. Within the limits of rule 2, the specific flow, F_s, of the route departing from a transition point is determined by the following equations:
   (a) For cases involving one flow into and one flow out of a transition point,

$$F_{s(\text{out})} = \frac{F_{s(\text{in})} W_{e(\text{in})}}{W_{e(\text{out})}} \tag{59.12}$$

   where
   $F_{s(\text{out})}$ = Specific flow departing from transition point
   $F_{s(\text{in})}$ = Specific flow arriving at transition point
   $W_{e(\text{in})}$ = Effective width prior to transition point
   $W_{e(\text{out})}$ = Effective width after passing transition point

   (b) For cases involving two incoming flows and one outflow from a transition point, such as that which occurs with the merger of a flow down a stair and the entering flow at a floor,

$$F_{s(\text{out})} = \frac{F_{s(\text{in}-1)} W_{e(\text{in}-1)} + F_{s(\text{in}-2)} W_{e(\text{in}-2)}}{W_{e(\text{out})}} \tag{59.13}$$

   where the subscripts (in-1) and (in-2) indicate the values for the two incoming flows.

   (c) For cases involving other geometry formations merging together, the following general relationship applies:

$$\left(F_{s(\text{in}-1)} W_{e(\text{in}-1)}\right) + \cdots + \left(F_{s(\text{in}-n)} W_{e(\text{in}-n)}\right) = \left(F_{s(\text{out}-1)} W_{e(\text{out}-1)}\right) + \cdots + \left(F_{s(\text{out}-n)} W_{e(\text{out}-n)}\right) \tag{59.14}$$

   where the letter n in the subscripts (in-n) and (out-n) is a number equal to the total number of routes entering (in-n) or leaving (out-n) the transition point.
5. Where the calculated specific flow, F_s, for the route(s) leaving a transition point, as derived from the equations in rule 4, exceeds the maximum specific flow, F_{sm}, a queue will form at the incoming side of the transition point. The number of persons in the queue will grow at a rate equal to the calculated flow, F_c, in the arriving route minus the calculated flow leaving the route through the transition point.
6. Where the calculated outgoing specific flow, $F_{s(\text{out})}$, is less than the maximum specific flow, F_{sm}, for that route(s), there is no way to predetermine how the incoming routes will merge. The routes may share access through the transition point equally, or there may be total dominance of one route over the other. For conservative calculations, assume that the

route of interest is dominated by the other route(s).

A simple example is presented in order to clarify the required calculations [40]. This simple example is followed by a more comprehensive example illustrating the two different hydraulic models: first- and second-order hydraulic models.

Example 1 A 1.8 m (approximately 6 ft) wide (descending) 7/11 stair has 10 risers and leads to a 10 m long (approximately 33 ft), 1.8 m wide corridor (approximately 6 ft). At the end of the corridor, there is a 1.3 m (approximately 4 ft 3 in.) wide door (Fig. 59.9). This door is mechanically held open. How long does it take for 50 people starting at the top of the stairs with an initial density of 1.5 p/m^2 (p = persons) to exit from the door at the end of the corridor?

Solution The velocity can be calculated according to Equation 59.5:

$$S = \mathrm{k} - \mathrm{ak}D$$

For 7/11 stair, k = 1.08:

$$1.08 - (0.266)(1.08)(1.5)$$
$$\therefore S = 0.65 \text{ m/s} (128 \text{ ft/min})$$

The time to traverse the stair can then be calculated. The distance to be covered is

$$10 \text{ risers} = 70 \text{ in.} = 1.78 \text{ m}; 10 \text{ treads} = 110 \text{ in.} = 2.79 \text{ m}$$
$$\text{diagonal length} = 3.31 \text{ m} (\text{approximately } 10 \text{ ft } 10 \text{ in.})$$

Therefore, the time to cover the stairs is 3.31/0.65 = 5.1 s.

The width of the stair can be calculated using Table 59.1 (1.8–0.3 m). Given that the density (1.5 p/m^2) and the velocity (0.65 m/s) are known, the flow rate on the stair using Equation 59.9 can now be determined:

$$F_c = F_s W_e = (\mathrm{k} - \mathrm{ak}D) D W_e$$
$$F_c = 1.46 \text{ p/s}$$

This value produces a specific flow rate less than the maximum value and so it can therefore be used during the calculation.

Fig. 59.9 Geometry used in Example [1]

The time delay for the last person to start on the stair can be calculated as follows. With a flow rate of 1.46 p/s on the stair (and thus of the queue entering the stair), the time for the queue to dissipate is calculated using Equation 59.10:

$$t_p = P/F_c$$

The time for the population at the top of the stairs to enter the stairs is then

$$50/1.46 = 34.2 \text{ s}$$

The time for the entire population to enter the staircase and the time to traverse the staircase are now known. Given this, the time taken for the last person to enter and traverse the staircase can be determined. The time to traverse the corridor now needs to be calculated.

The flow rate into the corridor is 1.46 p/s; that is, that produced on the staircase. Equation 59.9 states that

$$F_c = F_s W_e = (\mathrm{k} - \mathrm{ak}D) D W_e$$

where F_c can be set to 1.46; this equation can now be solved for D.

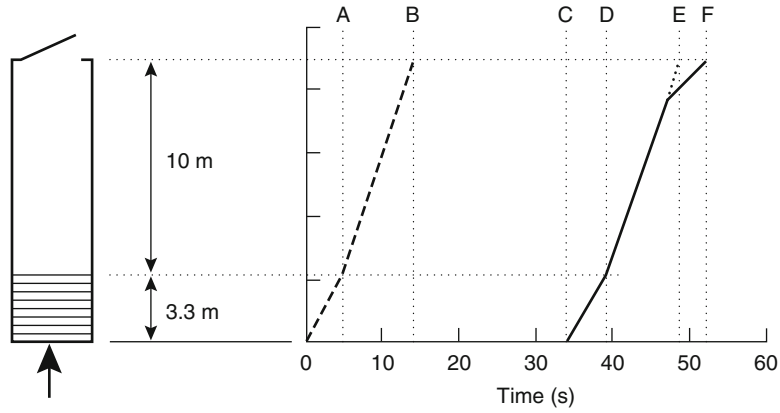

Fig. 59.10 Movement of people through the components

For a corridor, k is set to 1.40. Given the corridor is 1.8 m in width, the effective width is $W_e = 1.4$ m (4 ft 7 in).

Therefore, solving for D

$$0.266D^2 - D + (1.46/1.4 \times 1.4) = 0$$
$$0.266D^2 - D + 0.744 = 0$$

Solving for D, it is therefore either 1.03 or 2.72 p/m^2.

$$\therefore D = 1.03 \text{ or } 2.72 \text{ p/m}^2 \left(0.1 \text{ or } 0.25 \text{ p/ft}^2\right)$$

From the previous discussion regarding selecting D values, a value of 1.03 p/m^2 (0.1 p/ft^2) should be chosen.

Given that the density is known and the relationship between density and velocity is expressed in Equation 59.5:

$$S = \mathrm{k} - \mathrm{ak}D$$

the velocity, S, can be calculated as being 1.02 m/s (201 ft/min). The time to traverse the corridor is therefore 10/1.02 = 9.8 s. The flow through the doorway at the end of the series of components can now be determined. Given the narrowing at the door, the formation of the queue should be examined. The specific flow rate at the door is calculated using Equation 59.8:

$$F_s = F_c/W_e = 1.46/1.0$$

$F_s = 1.46$ p/s/m (27 p/min/ft) $> F_{sm}$, where the value of F_{sm} is 1.3 p/s/m (24 p/min/ft). The time for the population to flow through the doorway is then calculated using Equation 59.10:

$$t_p = N/F_sW_e = 50/(1.3/1.0) = 38.5 \text{ s}$$

The final solution is not simply formed from adding these values together, as some of them occur simultaneously. The final result is better explained by referring to Fig. 59.10.

The dashed line indicates the movement of the first person. This person is not influenced by queuing at any point and is therefore constrained only by the velocity values derived from the densities calculated on the different components. This person therefore spends 5.1 s traversing the stairs and 9.8 s traversing the corridor, reaching the final exit after 14.9 s (marked A and B in Fig. 59.10). The entire population entered the staircase after 34.2 s (marked C in Fig. 59.10) and has reached the end of the stairs after 34.2 + 5.1 = 39.3 s (marked D in Fig. 59.10). The last person from this group will have reached the exit at 49.1 s, assuming that person did not encounter any congestion approaching the door (marked E in Fig. 59.10). Given that the first person has reached the exit after 14.9 s and that the congestion at the final exit lasted for 38.5 s, this congestion is not clear until 53.4 s (marked F in Fig. 59.10, indicating the end of the solid curve). Therefore, the last person to arrive interacts with the congestion at some point prior to reaching the door; that is, the congestion still exists when that person arrives. The evacuation

time is then determined by the time taken for the congestion to clear at the final exit (e.g., 53.4 s).

First- and Second-Order Hydraulic Models

The various calculations discussed in the previous section can be combined in order to assess the movement component of the evacuation process; that is, to calculate t_e. By applying these calculations, the necessary movement components (e.g., flow rates, velocities, population densities, and travel speeds) can be established enabling the overall movement time to be found.

First-Order Hydraulic Model

There are several ways in which these movement calculations can be used; two are described here. The first-order hydraulic model represents a simplified approach: instead of calculating the flow of people between individual components, this method focuses on the component that places the most severe constraint on the flow of people around the structure and then uses this constraint to determine the movement time. The engineer is required to establish the time to reach the controlling component; the time for the population to traverse this component; the time for the last person to leave the controlling component; and the time for the last person to reach safety from the controlling component [43]. This process is outlined in Fig. 59.11a. This approach makes greater use of the maximum flow rates and densities allowed, given the reduced level of calculation required. The controlling component will depend on the nature of the structure; for example, the controlling component could be a stair, an exit from the stair, an exit from a room, and so on.

Second-Order Hydraulic Model

The second-order hydraulic model requires that the flow of people between each of the structural components (i.e., between areas where the physical constraints affecting egress performance change) is calculated. This is more labor intensive than the first-order approach, requiring a larger number of calculations to be made; however, it does require fewer assumptions and provides information on the movement between each of the structural components in the egress route rather than a subset of them. A second-order analysis is by no means a trivial task and requires judgment based on the structure examined and the incident scenario. This process is outlined in Fig. 59.11b.

Example Applications

The first- and second-order hydraulic models can be better understood through the description of two example applications. (More examples can be found elsewhere [43].) A relatively simple example is presented, although even in this case the difference between the effort required in applying the two versions of the model is apparent.

Example 2 Consider an office building (Fig. 59.12) with the following features:

1. There are nine floors, 300 ft by 80 ft (91 m by 24 m).
2. Floor-to-floor height is 12 ft (3.7 m).
3. Two stairways are located at the ends of the building (there are no dead ends).
4. Each stair is 44 in. (1.12 m) wide (tread width) with handrails protruding 2.5 in. (0.063 m).
5. Stair risers are 7 in. (0.178 m) wide and treads are 11 in. (0.279 m) high.
6. There are two 4 ft by 8 ft (1.2 m by 2.4 m) landings per floor of stairway travel.
7. There is one 36-in. (0.91-m) clear width door at each stairway entrance and exit. These are assumed not to be mechanically held open.
8. The first floor does not exit through stairways.
9. Each floor has a single 8-ft (2.4-m) wide corridor extending the full length of each floor. Corridors terminate at stairway entrance doors.

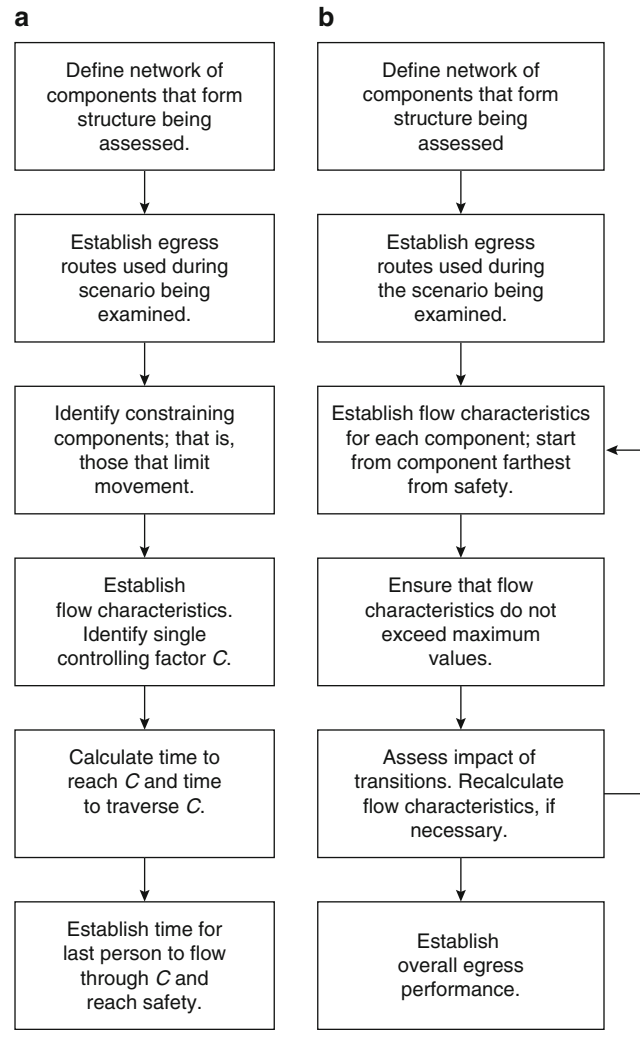

Fig. 59.11 (**a**) First-order hydraulic model; (**b**) second-order hydraulic model

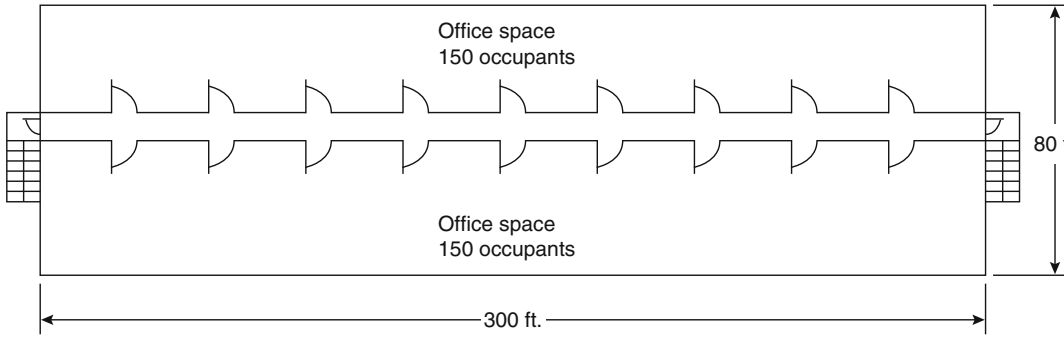

Fig. 59.12 Floor plan for example

10. There is a population of 300 persons/floor.

Solution A First-Order Approximation.

1. Assumptions.

   The prime controlling factor will be either the stairways or the door discharging from them. Queuing will occur; therefore, the specific flow, F_s, will be set to the maximum specific flow, F_{sm}. All occupants start evacuating at the same time. The population will use all facilities in the optimum balance.
2. Estimate flow capability of a stairway.

   From Table 59.1, the effective width, W_e, of each stairway is $44 - 12 = 32$ in. (2.66 ft) (813 mm [0.81 m]). The maximum specific flow, F_{sm}, for the stairway (from Table 59.5) is 18.5 persons/min/ft (1.01 persons/s/m) of effective width. Specific flow, F_s, equals maximum specific flow, F_{sm}. Therefore, using Equation 59.6, the flow from each stairway is limited to $18.5 \times 2.66 = 49.2$ persons/min.
3. Estimate flow capacity through a door.

   Again from Table 59.5, the maximum specific flow through a 36-in. (0.9 m) door is 24 persons/min/ft (1.31 persons/s/m) of effective width. Also, the effective width, W_e, of each door is $36 - 12 = 24$ in. (2 ft) (609 mm [0.61 m]). Therefore, using Equation 59.8, the flow through the door is limited to $24 \times 2 = 48$ persons/min. This is less than the maximum flow rate through an exit that is not mechanically held open (50 p/min). Because the flow capacity of the doors is less than the flow capacity of the stairway served, the flow is controlled by the stairway exit doors (48 persons/stairway exit door/min).
4. Estimate the speed of movement for estimated stairway flow.

   From Equation 59.5 the speed of movement down the stairs is $212 - (2.86 \times 212 \times 0.175) = 105$ ft/min(0.53 m/s). The travel distance between floors (using the conversion factor from Table 59.3) is $12 \times 1.85 = 22.2$ ft (6.8 m) on the stair slope plus 8 ft (2.4 m) travel on each of the two landings, for a total floor-to-floor travel distance of $22.2 + (2 \times 8) = 38.2$ ft(11.6 m). The travel time for a person moving with the flow is $38.2/105 = 0.36$ min/floor.
5. Estimate building evacuation time.

   If all of the occupants in the building start evacuation at the same time, each stairway can discharge 48 persons/min. The population of 2400 persons above the first floor will require approximately 25 min to pass through both exits. An additional 0.36-min travel time is required for the movement from the second floor to the exit. (A more conservative estimate of the travel time might also include the time for the first person to move from within the second floor to the stair.) The total minimum evacuation time for the 2400 persons located on floors 2 through 9 is estimated at 25.4 min.

Solution B Second-Order Approximation.

1. Assumptions.

   The population will use all exit facilities optimally; all occupants start egress at the same time. All persons are assumed to start to evacuate at time zero.
2. Estimate flow density (D), speed (S), specific flow (F_s), effective width (W_e), and initial calculated flow (F_c) typical for each floor.
3. Divide each floor in half to produce two exit calculation zones, each 150 ft (45.7 m) long. To determine the density, D, and speed, S, if all occupants try to move through the corridor at the same time, that is, 150 persons moving through 150 ft of an 8-ft (2.4-m) wide corridor:

$$D = 150 \text{ persons}/1200 \text{ ft}^2\text{corridor area} = 0.125 \text{ persons/ft}^2$$

From Equation 59.5, $S = \mathrm{k} - \mathrm{ak}D$.
From Table 59.2, $\mathrm{k} = 275$.

$$S = 275 - (2.86 \times 275 \times 0.125) = 177 \text{ ft/min } (54 \text{ m/min})$$

From Equation 59.7, $Fs = (1 - \mathrm{a}D)\mathrm{k}D$.
$\mathrm{F_s} = [1 - (2.86 \times 0.125)] \times 275 \times 0.125 = 22$ persons/min/ft(1.2 persons/s/m) effective width

From Table 59.5, F_s is less than the maximum specific flow, F_{sm}; therefore, F_s is used for the calculation of calculated flow.
From Table 59.1, the effective width of the corridor is

$$8 - (2 \times 0.5) = 7 \text{ ft}(2.13 \text{ m})$$

From Equation 59.9, calculated flow, $F_c = (1 - aD)kDW_e$.

$$F_c = [1 - (2.86 \times 0.125)] \times 275 \times 0.125 \times 7$$
$$= 154 \text{ persons/min}$$

At this stage in the calculation, calculated flow, F_c, is termed initial calculated flow for the exit route element (i.e., corridors) being evaluated. This term is used because the calculated flow rate can be sustained only if the discharge (transition point) from the route can also accommodate the indicated flow rate.

4. Estimate impact of stairway entry doors on exit flow.
Each door has a 36-in. (0.91-m) clear width. From Table 59.1, effective width is

$$W_e = 36 - 12 = 24 \text{ in. } (2 \text{ ft})(0.61 \text{ m})$$

From Table 59.5, the maximum specific flow, F_{sm}, is 24 persons/min/ft effective width.
From Equation 59.12,

$$F_{s(\text{door})} = \left(F_{s(\text{corridor})}W_{s(\text{corridor})}\right)/W_{e(\text{door})}$$
$$= (22 \times 7)/2 = 77 \text{ persons/min/ft}$$
$$(4.2 \text{ persons/s/m}) \text{ effective width}$$

Since F_{sm} is less than the calculated F_s, the value of F_{sm} is used. Therefore, the effective value for specific flow is 24 p/min/ft.
From Equation 59.8, the initial calculated flow,

$$F_c = F_s W_e = 24 \times 2 = 48 \text{ persons/min}$$

through a 36-in. (0.91-m) door. Since F_c for the corridor is 154 p/min while F_c for the single exit door is 48 p/min, queuing is expected. The calculated rate of queue buildup will be

$$154 - 48 = 106 \text{ persons/min}$$

5. Estimate impact of stairway on exit flow.
From Table 59.1, effective width, W_e, of the stairway is

$$44 - 12 = 32 \text{ in.}(2.66 \text{ ft}) \quad (0.81 \text{ m})$$

From Table 59.5, the maximum specific flow, F_{sm}, is 18.5 persons/min/ft (1.01 persons/s/m) effective width. From Equation 59.12, the specific flow for the stairway,

$$F_{s(\text{stairway})} = 24 \times 2/2.66 = 18.0 \text{ persons/min/ft}$$
$$(0.98 \text{ persons/s/m}) \text{effective width}$$

In this case, F_s is less than F_{sm} and F_s is used.

The value of 18.0 p/min/ft for F_s applies until the flow down the stairway merges with the flow entering from another floor.

Using Fig. 59.8 or Equation 59.7 and Table 59.2, the density of the initial stairway flow is approximately 0.146 persons/ft^2 (1.6 person/m^2) of stairway exit route. From Equation 59.5 the speed of movement during the initial stairway travel is

$$212 - (2.86 \times 212 \times 0.146)$$
$$= 123 \text{ ft/min}(0.628 \text{ m/s})$$

This value differs from that produced in the first-order, which is based on the maximum achievable density rather than a calculated density.

From the first-order solution, the floor-to-floor travel distance is 38.2 ft (11.6 m). The time required for the flow to travel one floor level is

$$38.2/123 = 0.31 \text{ min}(19 \text{ s})$$

Using Equation 59.8, the calculated flow is

$$F_c = 18.0 \times 2.66 = 48 \text{ persons/min}$$

After 0.31 min, 15 (i.e., 48 × 0.31) persons will be in the stairway from each floor feeding to it. If floors 2 through 9 exit all at once, there will be

$15 \times 8 = 120$ persons in the stairway

After this time the merging of flows between the flow in the stairway and the incoming flows at stairway entrances will control the rate of movement.

6. Estimate impact of merging of stairway flow and stairway entry flow on exit flow.
From Equation 59.13,

$$\begin{aligned} F_{s(\text{out-stairway})} &= \left[\left(F_{s(\text{door})} \times W_{e(\text{door})}\right) + \left(F_{s(\text{in-stairway})} \times W_{e(\text{in-stairway})}\right)\right] / W_{e(\text{in-stairway})} \\ &= [(24 \times 2) + (18 \times 2.66)]/2.66 \\ &= 36 \text{ persons/min/ft}(1.97 \text{ prsons/s/m}) \\ &\quad \text{effective width} \end{aligned}$$

From Table 59.5, F_{sm} for the stairway is 18.5 persons/min/ft (1.01 persons/m/s) effective width. Since F_{sm} is less than the calculated F_s, the value of F_{sm} is used.

7. Track egress flow.

Assume all persons start to evacuate at time zero. Initial flow speed is 177 ft/min (0.9 m/s). Assume that congested flow will reach the stairway in approximately 0.5 min. This conservative assumption is based on the population having to travel a distance of between 50 ft and 150 ft (15.2 m and 45.7 m) to the exit traveling at 177 ft/min (0.9 m/s); that is, the derived travel speed in the corridor. At 0.5 min, flow starts through stairway doors. F_c through doors is 48 persons/min for the next 19 s (0.31 min). At 49 s, 120 persons are in each stairway and 135 are waiting in a queue at each stairway entrance.

How the evacuation progresses from this point on depends on which of the floors take precedence in entering the stairways. Any sequence of entry may occur [1]. To set a boundary, this example estimates the result of a situation where dominance proceeds from the highest to the lowest floor.

The remaining 135 persons waiting at each stairway entrance on the ninth floor enter through the door at the rate of 48 persons/min. The rate of flow through the stairway is regulated by the 48 persons/min rate of flow of the discharge exit doors. The descent rate of the flow is 19 s/floor.

Therefore, referring to Equations 59.8, 59.10, and 59.11, at

$$(135/48) \times 60 + 49 = 218 \text{ s}(3.6 \text{ min})$$

all persons have evacuated the ninth floor.

At

$$[(135/48) \times 60 + 49] + 19 = 237 \text{ s } (4.0 \text{ min})$$

the end of the flow reaches the eighth floor.

At

$$237 + \{[(135/(2.66 \times 18.5)] \times 60\} = 401 \text{ s}(6.7 \text{ min})$$

all persons have evacuated the eighth floor.

At

$$(401 + 19) = 420 \text{ s } (7.0 \text{ min})$$

the end of the flow reaches the seventh floor.

At

$$420 + \{[135/(2.66 \times 18.5)] \times 60\} = 584 \text{ s}(9.7 \text{ min})$$

all persons have evacuated the seventh floor.

At 603 s (10.1 min)	The end of the flow reaches the 6th floor
At 767 s (12.8 min)	All persons have evacuated the 6th floor
At 786 s (13.1 min)	The end of the flow reaches the 5th floor
At 950 s (15.8 min)	All persons have evacuated the 5th floor
At 969 s (16.2 min)	The end of the flow reaches the 4th floor

(continued)

At 1133 s (18.9 min)	All persons have evacuated the 4th floor
At 1152 s (19.2 min)	The end of the flow reaches the 3rd floor
At 1316 s (21.9 min)	All persons have evacuated the 3rd floor
At 1335 s (22.3 min)	The end of the flow reaches the 2nd floor
At 1499 s (25.0 min)	All persons have evacuated the 2nd floor
At 1518 s (25.3 min)	All persons have evacuated the building

From this example it is clear that in some situations little difference exists in the results produced by the use of the two basic hydraulic models (first and second order). This may be expected in simple geometries and simple movement scenarios. However, as the scenarios and geometries become more complex, the results produced by the two versions of the model may differ significantly, especially if there are difficulties in establishing the controlling element in the first-order approximation.

The second-order hydraulic model produces a larger set of information (e.g., the time to clear components, the time to clear floors, the movement conditions between all structural components, etc.). However, it is sensitive to which of the components have precedence (e.g., in merging flows) and in the proportion of the population using particular routes. This may require several calculations to establish the most conservative result. The first-order hydraulic model produces only the overall evacuation time and the results relating to the constraining component. It should also be noted that in complex geometries identifying the constraining component is not a trivial task, and it can be extremely time consuming.

Given that an assessment of a structure is necessary, it is important to identify the scenarios involved in this assessment. It may not be possible to definitively establish the worst-case scenario prior to the calculation. It is therefore essential to examine several representative scenarios that form a set of predictions. This will offer insight into the scenarios examined and more reliably provide an estimate of the longest RSET value to be expected, as compared with the assessment of a single scenario.

Employing Extended Hydraulic Model to Calculate t_{esc}

Factors Influencing an Evacuation

The extended hydraulic model provides a foundation to evaluate evacuation performance, that is, escape time (t_{esc}) as opposed to evacuation movement time (t_e). Figure 59.3 indicates that there are more factors that actually influence an evacuation than can currently be modeled. The factors that can be included are dependent on our understanding of real-life phenomena, on the data available, and on the limitations of the model adopted. As has already been stated, the hydraulic model outlined here can be employed in the examination of different egress scenarios. This is critical in generating a robust and representative solution.

A number of behaviors can influence the performance of the population. It is possible to *implicitly* represent some of these behaviors (i.e., the consequences of these behaviors) by manipulating parameters associated with the hydraulic model and then examining a range of scenarios.

In order to increase the information obtained in any egress analysis and the confidence in this information, a representative set of egress scenarios could be examined. Producing one "definitive" result is insufficient, given the many scenarios that can actually develop and also given the limitations of the modeling approach. Presenting a single answer may produce overconfidence in the accuracy and validity of the result.

Basic Variables

Given the scope of the extended hydraulic approach, the scenarios that can be examined

are limited and require the manipulation of a few basic variables:

- The routes available during the evacuation
- The evacuee's use of the routes available during the evacuation
- The movement attributes of the evacuating population and the presence of impairments and disabilities
- The time taken to respond to the call to evacuate—the pre-evacuation time (t_{p-e})

When using the extended hydraulic model, these variables can be manipulated to produce a number of different scenarios and therefore an envelope of results. By manipulating these variables, at least a small subset of the behaviors that might detract from egress performance can be accounted for, albeit in an implicit way. The manner in which this is performed will be dependent on the nature of the occupancy being examined and the scenarios that are considered as realistic. The scenarios examined (and omitted) by the engineer should be justified through a detailed explanation accompanying the reported results. In addition, the scope of the results can be extended to represent t_{esc} rather than just t_e.

Routes Available During the Evacuation In some scenarios it is possible that routes will be lost due to the nature of the incident or given the use of the space available; for example, a route might not be protected. This loss can be considered.

Some existing codes require such forms of analysis. For instance, in the British Standard BS5588 [44], the largest exit is discounted, assumed blocked by the incident. In NFPA *101* one scenario requires the evaluation of the impact of a fire located in the primary means of egress [41].

The hydraulic model can be manipulated to represent the loss of available egress routes. In the example shown in Fig. 59.12, an entire staircase could be presumed lost due to the nature of the incident. This would have a profound impact on the results produced. Instead of an overall evacuation time of 25.4 min, it instead required 50.4 min, when applying the first-order approximation. The calculation may also involve the loss of individual components, rather than the entire egress route.

Evacuee's Use of the Routes Available During the Evacuation In reality, egress routes are rarely used according to their design capacity (i.e., efficiently). Instead, routes are used according to occupant familiarity, visual access, the procedure in place, and the evolution of the incident itself. [4, 45] This reality can be represented within the hydraulic model by modifying the proportion of the population using a particular route. Although it might be difficult to gather accurate data on the use of the routes available, engineering judgment could still be used to assess the potential impact of the unbalanced use of the egress routes available. For instance, in the example shown in Fig. 59.12 it was assumed that the population used the egress routes in an optimal manner; that is, that they split evenly between the staircases. It may be the case that one route is more familiar to the population than another (through normal use, proximity to elevators, connectivity to nearby car park, etc.). This inefficient use can then be reflected in the calculations by more people using one of the routes available. If it is assumed that 75 % of the population make use of one of the staircases, then applying the first-order model produces an overall egress time of approximately 37.9 min (1800/48 + 0.36). As a consequence, the other staircase would clear more quickly.

Movement Attributes of the Evacuating Population The makeup of the population can vary over time. Variations in the population's capabilities can be represented through the modification of the maximum velocities that can be attained. The range of the population's capabilities can be extended to include the presence of the mobility impaired. Although the reduction of velocities represents only one aspect of impairment (e.g., it does not represent behavioral issues, pre-evacuation issues, the impact that the presence of the mobility impaired might have on population densities, etc.), it is still an important consideration. This may be of

particular importance where the egress performance is not dominated by congestion and flow constraints, but by travel distances. Looking at the example presented above, in the first-order model, the presence of the impaired may increase the 0.36 min to travel between the floors on stairs. In the second-order model, it may have a more complex effect. It could also be taken into consideration when determining the t_{p-e} component, with a population with impairments extending the preparation required.

Time Taken to Respond Part of the RSET calculation (see Equation 59.1) requires the assessment of a pre-evacuation phase, t_{p-e}; this phase is the time between notification and the time for the population to evacuate. It can be varied given the scenario being represented, the notification system in place, the procedures employed, and so on. This time may then allow limited comparisons to be made between different procedural measures, notification systems, and the like. Pre-evacuation time may be particularly important where scenarios are not dominated by flow and the egress route capacities [1]. However, it should be recognized that the potential benefits of distributing the response of the population cannot be represented in the hydraulic approach given its fundamental assumptions.

In reality, the relationship between the pre-evacuation phase and the evacuation phase is complex. It is not simply a case of adding the times of the two phases together. Given the scenario, the extent of the pre-evacuation time distribution may increase or reduce the level of congestion produced. This complex relationship is difficult to represent unless the evacuees are simulated on an individual basis (see Chap. 60).

Data are required in order to include these factors in the calculation. These data, particularly regarding the pre-evacuation phase, are scarce and not always reliable (see Chap. 64). Although this limitation should be acknowledged, it does not preclude further engineering analysis. Even where engineering judgment is required, it is still critical to assess the robustness of the results by trying to account for these factors. Where it is not relevant or possible, then it should be clearly stated allowing the exclusion of the factors from the assessment to be judged.

Developing Escape Scenarios

As mentioned previously, when assessing the egress performance of a structure, it is vital to produce results that cover a range of scenarios. This process adds to the robustness of the results and the credibility; that is, it is not credible that the use of a hydraulic model (or any other model) would produce a definitive, single result. This is discussed in more detail in Chap. 57 and has been discussed and developed elsewhere (e.g. in PD 7975-6:2004) [46]. Ideally, a number of scenarios should be examined. A viable set of scenarios can be produced by varying factors within the hydraulic model (including those identified in the previous section) in a logical manner. Given that several factors are represented (e.g., speed, flow, route availability/usage, pre-evacuation times), each of these factors can be modified to implicitly represent different scenarios. Using this approach, a range of viable scenarios can be examined that produce different RSET values. Once complete, the longest RSET value generated would then be used for comparison against the ASET value produced.

Purser identified two base scenarios that can then be modified through the manipulation of model variables in order to produce sets of scenarios for analysis (Fig. 59.13) [1]. This is just one suggested approach at gaining a broader insight into the evacuation performance of a structure and establishing RSET using an engineering calculation; however, it is indicative of the different scenarios that can be examined.

Purser identified that in sparsely populated spaces, the overall egress time produced (t_{esc}) is more sensitive to the time taken to traverse the distance to a place of safety and the time taken to respond, than to the time for congestion to evaporate. In such situations, it is unlikely that egress

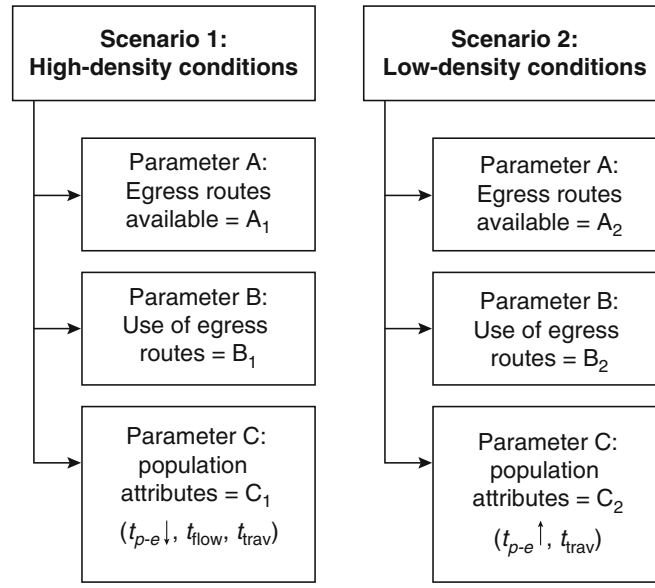

Fig. 59.13 Generation of scenarios by manipulating parameters

components will be overloaded and generate queues that dominate the egress performance.

In densely populated spaces, Purser identified that it is more likely that congestion will be produced. In such situations, the response of individuals may be influenced by observing the activities of other evacuees [45, 47]. This is likely to reduce the distribution of pre-evacuation times produced. This implies that the population will arrive at structural components within a smaller range of times. Therefore, the time to reach a point of safety is likely to be highly sensitive to the clearance of congestion along the egress routes.

When applying a sophisticated simulation model, the factors that determine the outcome of a scenario (e.g., whether it is determined by flow, travel, etc.) will be a *result* of the analysis (see Chap. 60). Given the limitations of the hydraulic model, the engineer has to *impose* these conditions prior to the calculation being conducted (e.g., whether congestion or travel distance determines the time to reach safety) and then assess their impact; the critical behavioral/movement components are determined prior to the calculations being made. The Purser approach can be applied in order to establish what underlying factors determine the overall evacuation time, by examining scenarios where the results are determined by different factors; for example, flow and/or travel and response. For a single structure the impact of these different scenarios can be assessed to establish which of them produces the most prolonged egress time.

When using the Purser approach to establish the evacuation time from a particular structure, it is assumed that the engineer cannot be sure which of these scenarios will produce the longer escape time, prior to the calculation being conducted. Both scenarios are therefore examined. Each of the scenarios includes an assessment of the population movement (i.e., t_e) and the pre-evacuation phase (i.e., t_{p-e}). The combined result of these two phases is termed t_{esc} (see Equation 59.2). Where other new terms are used below, they are described.

Purser identified two situations (labeled Scenarios 1 and 2 in Fig. 59.13). In Scenario 1 it is assumed that congestion dominates the results produced (t_{flow}). In such situations the time required for the evacuation of an enclosure depends on the pre-evacuation time and unrestricted walking time of the first few occupants to start to leave; these determine the time for congestion to develop. Once queues have formed at the "constraining" component, the time to

clear the building becomes a function of the number of occupants and the evacuation flow rate capacity of these components. The evacuation time for an enclosure is estimated to be

$$t_{esc} = t_{p-e1} + t_{trav} + t_{flow} \quad (59.15)$$

where t_{p-e1} is the pre-evacuation time associated with the first people to respond. Purser uses the first percentile of a representative pre-evacuation distribution to estimate this value [1]. If this is not available, then the average pre-evacuation time associated with the occupancy (which is more likely to be available; see Chap. 64) should be used as a conservative estimate. t_{flow} is the time of total occupant population to flow through the most restrictive components. t_{trav} is the time taken to traverse the average distance to a place of safety. (The maximum distance should be employed in this calculation for a more conservative approach.)

It is apparent that either the first- or second-order hydraulic model can be used to generate t_{flow} and t_{trav}; indeed the combination of these two parameters approximates the t_e term previously described (see Equation 59.4).

In Scenario 2 it is assumed that congestion does not dominate the results; the results are primarily influenced by the time taken to reach safety (t_{trav}) and the time to respond (t_{p-e}). This scenario is not necessarily based on the assumption that congestion does not develop; only that the impact of the congestion is dominated by the extensive pre-evacuation phase and the distances that need to be traversed, and is not a factor in the calculation. The egress time for an enclosure is given by

$$t_{esc} = t_{p-e1} + t_{p-e99} + t_{trav} \quad (59.16)$$

where t_{p-e99} is the pre-evacuation time for the last few occupants to respond (i.e. the 99th percentile). Purser uses the 99th percentile of a representative pre-evacuation distribution to estimate this value [1]. If this is not available, then a multiple of the mean pre-evacuation time should be employed; it is not appropriate to use the average pre-evacuation time. The pre-evacuation times usually form a log-normal distribution [1, 47]. Given the limited data currently available it appears that the 99th percentile can be reasonably approximated by a value of four to five times the mean pre-evacuation time [25, 30, 47–50].

Again the example shown in Fig. 59.12 can be used to illustrate the two different scenarios. Let us assume that the structure represents an office space as indicated. In the first analysis, it is assumed that the evacuation is dependent on flow characteristics (i.e., Purser's Scenario 1) and will therefore make use of the flow calculations already made. In addition, pre-evacuation times will be extracted from the work conducted by Fahy and Proulx to support these calculations [25]. Given that it is an office space, pre-evacuation times ranging from 1 to 6 min will be assumed. These times are employed as conservative estimates of the 1st and 99th percentiles.

Given the results already produced, the evacuation time for Scenario 1 can be estimated as being

$$t_{esc} = 1 + 25.3 = 26.3 \text{ min}$$

This time is based on the assumption that t_{trav} and t_{flow} is approximated by the results produced in the second-order model.

If instead it is assumed that, for some reason, this scenario was not determined by flow (i.e., Purser's Scenario 2), then the following calculation can be made:

$$t_{esc} = 1 + 6 + (0.5) + (8 \times 38.2)/187 = 9.2 \text{ min}$$

Here, t_{p-e1} is again assumed to be 1 min, while t_{p-e99} is assumed to be 6 min, with both values being derived from Fahy and Proulx [25]. The distance calculations generated by the first-order model are used here. In this case Scenario 1 produces the most prolonged evacuation times and would therefore be used in the estimation of the RSET value.

If it is now assumed that the space is instead a mid-rise apartment building, rather than an office space, then different pre-evacuation times are suggested by the data [25]. In this case,

pre-evacuation values of 1–24 min are used (again derived from Fahy and Proulx [25]). In this case the calculations become

$$\text{Scenario } 1 : t_{\text{esc}} = 1 + 25.3 = 26.3 \text{ min}$$

and

$$\text{Scenario } 2 : t_{\text{esc}} = 1 + 24 + (0.5) + (8 \times 38.2)/187 = 27.1 \text{ min}$$

Once the set of scenarios have been examined, the longest t_{esc} value produced should then be employed to generate the RSET calculation. In this case Scenario 2 produces the most extended evacuation time and would therefore be used in any RSET calculations.

This is certainly not the only approach for producing a range of scenarios (or at understanding what factors should be taken into consideration [51]). However, it does demonstrate how several different scenarios can be considered using the hydraulic approach allowing comparisons to be made between the results produced. This approach can be taken further by incorporating the other parameters deemed to be amenable to the hydraulic approach; for example, manipulating the routes available, familiarity, mobility impairments, and so on.

The results will always be limited by the sophistication and fidelity of the model employed. However, the examination of different scenarios is critical in providing a reasonable understanding of the conditions that might arise. Inevitably, there may be cases where data are not available to support these calculations. These situations will require engineering judgment. These cases should be documented and based on the most reliable and appropriate information available.

Addressing Modeling Error

The hydraulic model, whether it is the standard or extended version, produces only *modeled* predictions. The actual egress time will exceed the modeled time by an unknown amount. This is due to the exclusion from the model of many of the factors that might inhibit evacuation performance (e.g., t_{n-e}) and also to limitations in the data available (see Chap. 60). The difference between modeled evacuation movement time and actual evacuation movement time can be expressed in the following terms:

$$t_e^{\text{act}} = t_e^{\text{mod}} e \tag{59.17}$$

where

t_e^{act} = Actual time from when purposive evacuation movement commenced to when safety was reached

t_e^{mod} = Modeled estimate from when purposive evacuation movement commenced to when safety was reached

e = Modeling error

It is assumed here that the relationship is multiplicative; however, the relationship could also be additive.

The modeling error, e, is a function of elements that interfere with the model prediction. In the case of a hydraulic model, this includes

- Delays caused by the egress management activities of wardens or others directing the evacuation
- Time delays involved in the stopping and restarting of flows at merging points and conflicting flows
- Evacuee behaviors that detract from their movement to safety

Similar inaccuracies exist in the modeled pre-evacuation phase.

From Fig. 59.2 there are many factors that can interfere with an evacuation, but that cannot be explicitly represented by a hydraulic model. It should be noted that many of these factors are also beyond the most sophisticated simulation models currently available (see Chap. 60).

All of these factors can increase the discrepancy between the modeled and actual results. The first step in appraising emergency movement is usually to calculate the modeled evacuation time, t_e^{mod}. The use of model calculations provides a reproducible base of reference in appraising the impact of overall systems, individual components, or changes in systems. If, however, the results of the modeled evacuation time

are to represent a realistic evacuation time (or are to be compared against expected fire development), then the engineer should understand that the modeled movement time is seldom achieved in reality; that is, that e is greater than 1 in Equation 59.17. A conservative estimate of the movement time requires the modeled time and an appraisal of modeling error (see Equation 59.17). This will allow t_e^{act} to be approximated (or at least surpassed) by the modeled time, which is achieved through the application of a safety factor. The employment of a safety factor is a recognition that the hydraulic model omits some factors that may prolong the time to reach safety and/or represents other factors in a simplistic manner.

For the design of a structure to be acceptable, a sufficient margin of safety is required between ASET and RSET. In order for the engineer to have confidence in the RSET calculations, a safety factor, e', is employed that approximates e (i.e., the discrepancy between the modeled and actual movement time):

$$\text{Safety margin} = \text{ASET} - \left[t_d + t_a + t_{p-e} + e'\left(t_e^{\text{mod}}\right)\right] \tag{59.18}$$

The application of the safety factor described in Equation 59.18 is based on the assumption that the inaccuracies are found in the evacuation movement component and that these inaccuracies need to be addressed (see Chap. 64 and the SFPE Task Group document [43]). In this case, the engineer would need to be confident in the accuracy of the other components in the calculation. A more conservative estimate would be to apply the safety factor, e', to all of the behavioral components (i.e., both the pre-evacuation and evacuation phases):

$$\text{Safety margin} = \text{ASET} - \left[t_d + t_a + e'\left(t_{p-e} + t_e^{\text{mod}}\right)\right] \tag{59.19}$$

Although this is more conservative, it does require the assumption that the error levels in the pre-evacuation and evacuation movement components are comparable and can be addressed by the same safety factor.

The most conservative approach requires the application of the safety factor to the entire RSET calculation:

$$\text{Safety margin} = \text{ASET} - \left[e'\left(t_d + t_a + t_{p-e} + t_e^{\text{mod}}\right)\right] \tag{59.20}$$

This is the approach adopted by Tubbs and Meacham [29]. If the same values are assumed throughout, this approach will generate the largest RSET value of the three methods (shown in Equations 59.18 through 59.20). This approach does assume that the errors that exist are comparable between the behavioral and technical components. Alternatively, separate error factors might be applied to these components, such that

$$\text{Safety margin} = \text{ASET} - \left[e_1'(t_d + t_a) + e_2'\left(t_{p-e} + t_e^{\text{mod}}\right)\right] \tag{59.21}$$

where e_1' may be based on information provided by the manufacturer of the technology involved; and e_2' is based on the research literature available. Given the method adopted, the safety margin needs to be acceptable, even after the RSET value has had a safety factor applied. Guidance on the values to employ in order to estimate the modeling error (particularly relating to the behavioral components) can be established (see Chap. 64). The basis for the safety factors employed should be clearly stated and supported.

Using the Hydraulic Model in Conjunction with Other Models

The hydraulic model can be used in a number of different ways, depending on the resources and expertise available. Currently the expertise in the use of hydraulic models far outweighs the expertise in applying simulation models, that is, computer-based models that attempt to represent the evacuation by simulating the activities of individual agents. However, it is anticipated that this will change in the coming years especially as larger and more complex spaces are examined. Indeed, the hydraulic model is often calculated using a computer. It should also be

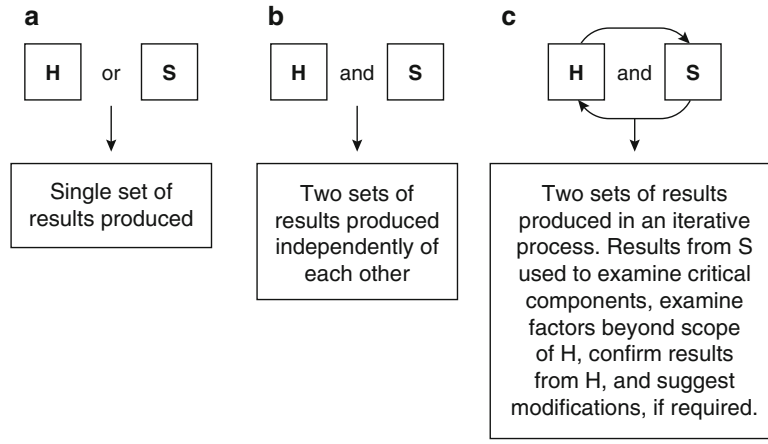

Fig. 59.14 The three uses of the hydraulic and simulation models (**a**) Used on their own; (**b**) used in parallel; (**c**) used in conjunction with each other [1]

recognized that several current computer models are little more than the hydraulic model coded into computer software (see Chap. 60). Therefore, as engineers become more familiar with the computer models available and the results that they can produce, the following points will become increasingly apparent:

- Engineers will gain expertise in a number of modeling approaches.
- Engineers will become more familiar with the capabilities of a number of different modeling approaches.
- Several models will be applied to the same problem.

These points will have an impact not only on how hydraulic models are used but also on the nature of the hydraulic analysis and the expectations of the results produced. Any discrepancy between the results produced by simulation and hydraulic models (in their format and their content) will therefore become more apparent to the engineer. Therefore, when the hydraulic model is applied:

- A number of scenarios should be examined.
- The assumptions and limitations should be identified.
- A detailed set of results should be presented.

The difference between the typical results produced when employing simulation and hydraulic models becomes all the more evident if these models are used together on the same project. It is suggested that the hydraulic model can be employed in three distinct ways (Fig. 59.14) [1]. The manner in which it is employed will be dependent on a number of factors including the expertise and the resources available.

The hydraulic model (identified as H in Fig. 59.14a) is commonly used on its own to determine the evacuation time. Computer simulation models (indicated as S in Fig. 59.14a) are also now routinely employed on their own. Alternatively, more than one model can be employed (Fig. 59.14b). The hydraulic and simulation models may be employed independently of each other and then the final results compared. This would allow comparisons to be made between the results, the strengths of the different models to be exploited, and the level of confidence in the findings to be increased.

The application of more than one model provides benefit but also results in additional efforts since results have to be calculated more than once requiring additional time, expertise and analysis. However, using multiple models may provide some engineering benefits (see Table 59.6). A typical analysis may include both a simple, computationally inexpensive model (e.g., hydraulic approach) and a more refined representation of evacuee response (e.g., simulation tool). This then allows some additional confidence in the overall results produced.

Table 59.6 Engineering benefits of the use of multiple models

Benefit	Description
Triangulation	Given that there is no absolute confidence in any one model being employed, the results of several models may be compared to determine whether the conclusions reached are consistent between different approaches.
Refinement	The scenario may require examination of elements of the evacuation process not represented in the underlying model employed.
Scope	The project may be of such a scale (e.g. WTC) that the most refined models cannot be employed to the whole task. In such projects it may pay for the engineer to employ the most refined models in critical areas, which have the greatest influence over the conclusions drawn. These would then be used in conjunction with the underlying model to assess performance at key spatial or temporal locations.

This would allow comparisons to be made between the results, the strengths of the different models to be exploited, and the level of confidence in the findings to be increased based on the assumption that consistent model results improve confidence.

Finally, models can be run in an iterative manner (or even in a coupled manner), with the results of one influencing the scenarios examined by another. For instance, in a project involving extremely large structures, the hydraulic model can be employed to provide an overview of the results produced, possibly suggesting areas for further analysis (Fig. 59.14c). A more "sophisticated" simulation model could then be used to confirm the key assumptions and findings produced by the hydraulic model (e.g., areas of congestion) and suggest remedies. The simulation tool can confirm the results by examining sections of the structure or events of particular interest to provide detailed analysis. By using the simulation model in a more focused way, fewer computational resources will be required and the results produced by the hydraulic model, especially in critical locations, can be validated (Fig. 59.15). A hybrid approach of hydraulic and simulation analysis may allow for detailed analysis to be conducted, where previously the cost of a full-scale computational analysis was prohibitive. This hybrid approach may also be useful when resources are scarce or the scale of the project is beyond the capabilities of a sophisticated model; for instance, where an evacuation involves a business district or complex, rather than a single building.

Some simulation tools are currently under development that would allow such coupling of simple and more complex tools within the same environment. In this instance, the computational resources available could be targeted at the areas deemed to be most critical within the same computational environment [52]. Currently, users need to define in advance which areas of the geometry are represented in a refined manner, while others are represented in a cruder manner. This distinction requires an understanding of the importance of particular routes, the computational impact of design decisions and the impact that these decisions might have on the results produced. In the future, these decisions may be conducted dynamically, where the models allocate locations to one or other of the various levels of representation, precluding the need for the user to make this judgment in advance.

Impact of Tenability on ASET and RSET

As part of a performance-based assessment, a decision has to be made regarding tenability; that is, the point at which the conditions preclude the evacuation to "safely" continue [3]. The tenability limits will then be used to determine the ASET value: calculations are made to determine when the environmental conditions reach the tenability criteria stated. The ASET value produced will then be the benchmark against which the RSET results will be compared.

In reality, environmental conditions can have a behavioral and a physical (physiological)

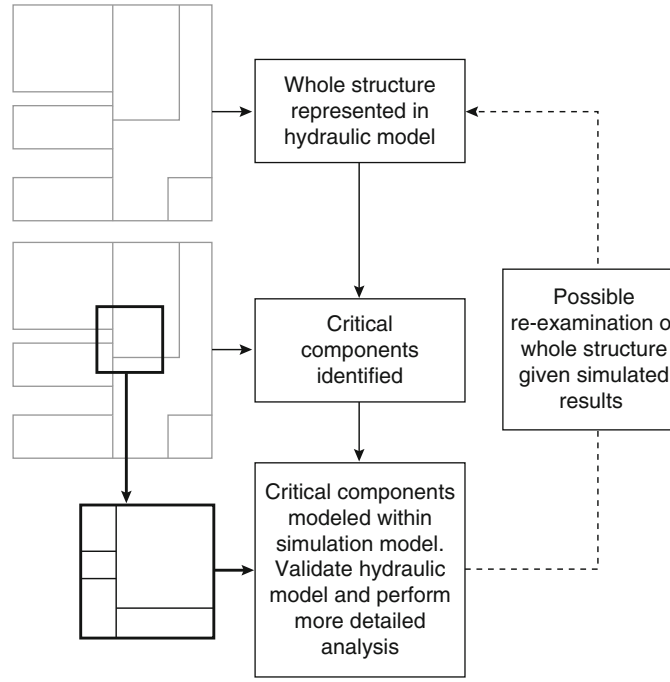

Fig. 59.15 Example application of both hydraulic and simulation models

impact on the performance of the evacuating population (see Chaps. 58, 61, and 63). Ideally, the impact of the tenability criteria should be reflected in the model scenarios employed; that is, if the environmental conditions reach a point at which they are expected to influence physical or behavioral performance, then this should be reflected in the model employed. The assumed occupant performance will have an impact on the validity of tenability criteria selected and on the credibility of the results produced.

There may be a temptation for engineers to select tenability criteria that artificially prolong the ASET time; that is, that the environmental conditions are allowed to develop to a relatively severe level before the tenability limits are reached, allowing a longer RSET calculation to be acceptable. This situation might include severely reduced visibility, elevated temperatures, and smoke layers descending close to the floor. By coupling the assumed tenability limits with the movement calculations made, there will at least be some counterbalance to these assumptions (Fig. 59.16), possibly encouraging a more conservative approach to be adopted throughout. *The adoption of tenability criteria that represent severe environmental conditions will then have a direct impact on the modeled performance of the evacuees.*

Suggested values are available for tenability limits (refer to Chaps. 61 and 63). These values, or similarly derived empirical values, should be used to inform the selection of reasonable and informed tenability criteria. This critical component in the performance-based assessment should be clearly supported in any results reported; effectively these values determine the amount of time available to complete the evacuation.

Given that these tenability criteria are established, their impact can be reflected within the hydraulic model. Some data (albeit, in some instances, supported by engineering judgment) are available to reflect the impact that a deteriorating environment can have upon egress performance (see Chaps. 58, 61, and 63). Data relating to physical performance are provided by Jin, who indicates the possible effect that deteriorating visibility has on travel speeds (see Chap. 61), specifically in relation to smoke. Other physical and behavioral data are also available (see Chaps. 58 and 63). Data on the impact of smoke are particularly important given that in

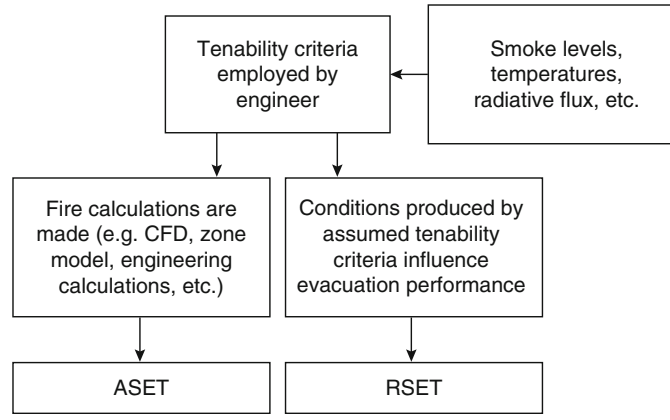

Fig. 59.16 Coupling tenability criteria to egress performance

many instances evacuees will be more likely to interact with smoke than with the fire itself.

Although there may be many ways in which the environment influences evacuee performance, it can be simplified especially given that the evacuating population is typically moving to minimize their exposure. This will produce several scenarios to be considered (in addition to those mentioned in the previous sections) when the hydraulic model is employed. These scenarios relate to the attainable travel speeds and the routes available.

The conditions produced (e.g., specific smoke visibility levels are reached, see Chap. 63) might block off certain routes. For instance, it could be assumed that when smoke reaches a certain level, a proportion of the population might not proceed through the smoke. The tenability criteria reached (e.g., smoke level) could also be deemed to influence attainable travel speeds in the affected areas. This can be modeled by reducing the maximum achievable travel speed; for instance, in Chap. 61 data are provided relating smoke level to visibility and travel speed. A conservative approach might be to assume the impact at the level of the tenability criteria in the affected spaces (i.e., where the environment is deteriorating) throughout the entire evacuation; that is, that whenever tenability criteria are reached the related impact on travel speed is assumed to be present throughout the evacuation. An example of the way in which the two effects of smoke can be included into the hydraulic model is shown in Fig. 59.17.

In Fig. 59.17a, route selection is not influenced by the presence of smoke. Within the hydraulic model the maximum travel speed within this component can be reduced to simulate the impact on the evacuees traveling through this component when filled with smoke (e.g. at or below the tenability threshold). In Fig. 59.17b, it is assumed that the smoke-filled corridor is not used; this is reflected in the hydraulic model by assuming that a larger population uses the East corridor. The potential impact of the two different behavioral scenarios can then be compared.

Attempting to match the development of the fire with the progress of the population in the hydraulic approach is cumbersome and would require numerous additional assumptions. To assess the maximum impact, a scenario could be examined where the entire population refused to pass through the smoke; similarly a scenario could be examined where the entire population is assumed to pass through the affected area at reduced speeds.

It may be impractical to employ these factors within all egress calculations. There is certainly a lack of supporting data. However, even if these additional scenarios are not considered, the impact that the deteriorating environment can have on egress performance should at least be acknowledged and explained in the presentation of any results. Otherwise, it is assumed that the

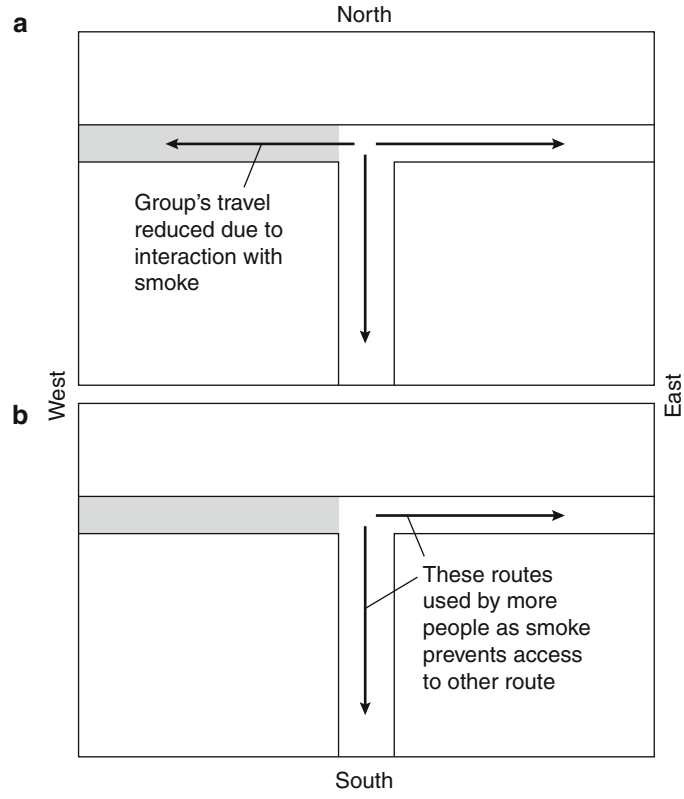

Fig. 59.17 Example of the impact of smoke on the hydraulic model

environmental conditions have no impact upon the performance of the evacuating population prior to tenability conditions being reached. This may be credible; however, it should be acknowledged.

In most designs, there would ideally be no physical interaction at all between the evacuating population and the deteriorating environmental conditions. That does not preclude the population seeing the developing conditions, which might influence their behavior. Even here the untenable conditions could be modeled in the hydraulic model through the loss of available egress routes.

Summary

This chapter described the application of the hydraulic model and its capabilities in assessing emergency movement. The model is able to provide a reliable means of assessing RSET and therefore in conducting performance-based analyses. When employing the model, it should be remembered that the results produced will be optimistic, and therefore remedial measures should be employed to compensate for this.

The limitations associated with the model do not prevent its being used to examine different egress scenarios; neither do they excuse the oversimplistic use of this model or presentation of the results. Those employing this model need to provide sufficient information on the approach adopted, the assumptions made, the scenarios examined, and the results produced.

When using the hydraulic model, it is still possible to examine a number of evacuation scenarios and incorporate the effect of various factors on the performance achieved. Given the potential for hydraulic and simulation models to be employed together, it becomes even more important to provide comparable levels of detail and confidence in the results produced.

Acknowledgment The authors acknowledge that this work includes substantial sections from the original chapter written by Harold "Bud" Nelson in partnership with Hamish MacLennan and then Fred Mowrer.

Nomenclature

ASET	Available safe egress time
RSET	Required safe egress time
t_d	Time from fire ignition to detection
t_n	Time from detection to notification of occupants of a fire emergency
t_{p-e}	Time from notification (or receipt of cues) until evacuation commences
t_e	Time from start of purposive evacuation movement until safety is reached
t_{esc}	Escape phase, being the sum of the pre-evacuation ($t_{p\text{-}e}$) and evacuation (t_e) phases
t_{trav}	Time spent moving toward a place of safety
t_{flow}	Time spent in congestion controlled by flow characteristics
t_{n-e}	Time spent in nonevacuation activities that do not directly contribute to the population moving to a place of safety
W_e	Effective width
D	Population density
S	Travel speed
k	Constant used to calculate travel speed
a	Constant used to calculate travel speed
F_s	Specific flow
F_{sm}	Maximum specific flow
F_c	Calculation flow through a component
t_p	Time for a group of persons to pass a point in an exit route
P	Population size in persons
$F_{s()}$	Specific flow and associated direction of movement
$W_{e()}$	Effective width of a particular component given its location
t_{p-e1}	Pre-evacuation time of the first people to respond
$t_{\text{p-e99}}$	Pre-evacuation time of the last people to respond
t_e^{act}	Actual time from when purposive evacuation movement commenced to when safety was reached
t_e^{mod}	Modeled estimate from when purposive evacuation movement to when safety was reached
e	Modeling error
e'	Approximation of e employed within calculation

References

1. D.A. Purser and S.M.V. Gwynne, "Identifying Critical Evacuation Factors and the Application of Egress Models," *Interflam 2007,* Interscience Communications, London, UK (2007).
2. D. Boswell and S.M.V. Gwynne, "Air, Fire and ICE: Fire & Security Challenges Unique to Airports," *Fire and Security Today* (Aug. 2007).
3. H. Nelson, personal communication (2007).
4. J.D. Sime, "Escape from Building Fires: Panic or Affiliation?" Ph.D. Dissertation, University of Surrey, UK (1984).
5. E.R. Galea, *Validation of Evacuation Models,* CMS Press Paper No. 97/IM/22, CMS Press, London, UK (1997).
6. E.D. Kuligowski and S.M.V. Gwynne, "What a User Should Know About Selecting an Evacuation Model," *Fire Protection Engineering, Human Behaviour in Fire Issue* (Fall 2005).
7. V.M. Predtechenskii and A.I. Milinskii, *Planning for Foot Traffic in Buildings* (translated from the Russian), Stroizdat Publishers, Moscow (1969). English translation published for the National Bureau of Standards and the National Science Foundation, Amerind Publishing Co., New Delhi, India (1978).
8. J.J. Fruin, *Pedestrian Planning Design,* Metropolitan Association of Urban Designers and Environmental Planners, Inc., New York (1971).
9. J.L. Pauls, "Effective-Width Model for Evacuation Flow in Buildings," in *Proceedings, Engineering Applications Workshop,* Society of Fire Protection Engineers, Boston (1980).
10. J.L. Pauls, "Calculating Evacuation Time for Tall Buildings," in *SFPE Symposium: Quantitative Methods for Life Safety Analysis,* Society of Fire Protection Engineers, Boston (1986).
11. R.J.C. Stanton and G.K. Wanless, "Pedestrian Movement, Engineering for Crowd Safety," in *Engineering for Crowd Safety* (R.A. Smith and J.F. Dickie, eds.), pp. 71–79, Elsevier, Amsterdam (1993).
12. K. Ando, H. Ota, and T. Oki, "Forecasting the Flow of People," *Railway Research Review,* 45, pp. 8–14 (1988).

13. B.D. Hankin and R.A. Wright, "Passenger Flow in Subways," *Operational Research Quarterly,* 9, pp. 81–88 (1958).
14. G. Proulx, "Lessons Learned on Occupants' Movement Times and Behaviour During Evacuation Drills," *Interflam 96,* Interscience Communications, London, UK, pp. 1007–1011 (1996).
15. J.-P. Stapelfeldt, *Angst- Und Paknikstande Aus Der Sicht Des Brandschutzes (Conditions of Anxiety and Panic from the Viewpoint of Fire Protection),* vfdb-Zeitschrift 2, 41 (1986).
16. S.J. Melinek and S. Booth, "An Analysis of Evacuation Times and Movement of Crowds in Buildings," *BRE Current Paper CP 96/75,* Borehamwood, UK (1975).
17. R.A. Smith, "Volume Flow Rates of Densely Packed Crowds," in *Engineering for Crowd Safety* (R.A. Smith and J.F. Dickie, eds.), pp. 313–319, Elsevier, Amsterdam (1993).
18. A. Polus, J.L. Schofer, and A. Ushpiz, "Pedestrian Flow and Level of Service," *Journal of Transportation Engineering,* Proceedings ASCE, 109, pp. 46–57 (1983).
19. S.J. Older, *Pedestrians,* Dept. Scientific and Industrial Research, Road Research Laboratory, Ln 275/SJO, Crowthorne, England (1964).
20. I.A.S.Z. Peschl, "Passage Capacity of Door Openings in Panic Situations," *BAUN,* 26, pp. 62–67 (1971).
21. L.F. Henderson, "The Statistics of Crowd Fluid," *Nature,* 229, pp. 381–383 (1971).
22. S.P. Hoogendoorn and W. Daamen, "Pedestrian Behavior at Bottlenecks," *Transportation Science,* 39, 2, pp. 147–159 (2005).
23. A. Seyfried, T. Rupprecht, A. Winkens, O. Passon, B. Steffen, W. Klingsch, and M. Boltes, "Capacity Estimation for Emergency Exits and Bottlenecks," in *Interflam 2007,* Interscience Communications, London, UK (2007).
24. J.D. Averill and W. Song, "Accounting for Emergency Response in Building Evacuation: Modeling Differential Egress Capacity Solutions," *NISTIR 7425,* National Institute for Standards and Technology, Gaithersburg, MD (2005).
25. R.F. Fahy and G. Proulx, "Toward Creating a Database on Delay Times to Start Evacuation and Walking Speeds for Use in Evacuation Modelling," in *2nd International Symposium on Human Behaviour in Fire,* Interscience Communications, London, UK, pp. 175–183 (2001).
26. H.E. Nelson and H.A. MacLennan, "Emergency Movement," in *The SFPE Handbook of Fire Protection Engineering,* 2nd ed., (P.J. DiNenno et al., eds.), National Fire Protection Association, Quincy, MA, pp. 3-286–3-295 (1996).
27. J. Bryan, "A Selected Historical View of Human Behavior in Fire," *Fire Protection Engineering,* pp. 4–16 (Fall 2002).
28. S. Gwynne, E.R. Galea, M. Owen, and P.J. Lawrence, *Escape As a Social Response,* Society of Fire Protection Engineers, Bethesda, MD (1999).
29. J.S. Tubbs and B.J. Meacham, *Egress Design Solutions: A Guide to Evacuation and Crowd Management Planning,* John Wiley and Sons, New York (2007).
30. S.M.V. Gwynne, *Optimizing Fire Alarm Notification for High Risk Groups,* Report Prepared for the Fire Protection Research Foundation, National Fire Protection Association, Quincy, MA (June 2007).
31. D. Canter, *Fires and Human Behaviour,* 2nd ed., Fulton, London, UK (1990).
32. T.J. Shields, K.E. Dunlop, and G.W.H. Silcock, "Escape of Disabled People from Fire; A Measurement and Classification of Capability for Assessing Escape Risk," *BRE Report 301* (1996).
33. H. Muir, C. Marrison, and A. Evans, "Aircraft Evacuation: The Effect of Passenger Motivation and Cabin Configuration Adjacent to the Exit," *CAA Paper 89019,* Civil Aviation Authority, London, UK (1989).
34. P.G. Wood, "The Behavior of People in Fires," *Fire Research Note 953,* Building Research Establishment, Fire Research Station, Borehamwood, UK (1972).
35. J.L. Bryan, *Smoke as a Determinant of Human Behavior in Fire Situations,* University of Maryland, College Park (1977).
36. J.P. Keating and E.F. Loftus, "Post Fire Interviews: Development and Field Validation of the Behavioral Sequence Interview Technique," *Report GCR-84–477,* National Bureau of Standards, Gaithersburg, MD (1984).
37. B. Latane and J.M. Darley, "Group Inhibition of Bystander Intervention in Emergencies," *Journal of Personality Psychology,* 10, 3, pp. 215–221 (1968).
38. G. Proulx, "Movement of People: The Evacuation Timing," in *SFPE Handbook of Fire Protection Engineering,* 3rd ed. (P.J. DiNenno et al., eds.), National Fire Protection Association, Quincy, MA, pp. 3-342–3-366 (2002).
39. A.T. Habicht and J.P. Braaksma, "Effective Width of Pedestrian Corridors," *Journal of Transportation Engineering,* 110, 1 (1984).
40. J. Milke, personal communication (2005).
41. NFPA *101®, Life Safety Code®,* National Fire Protection Association, Quincy, MA (2006).
42. J. Fruin and J. Pauls, *Human Factors of Means of Egress History, Current Problems and Implications for the Future,* World Safety Conference and Exposition, Session SU47, National Fire Protection Association, Boston (2007).
43. SFPE Task Group on Human Behavior, *Engineering Guide to Human Behavior in Fire* (June 2003)
44. BS5588, *Fire Precautions in the Design, Construction and Use of Buildings,* BSI British Standards, London, UK (2004).
45. J.D. Sime, "Visual Access Configurations: Spatial Analysis and Occupant Response Inputs to Architectural Design and Fire Engineering," in *IAPS Conference,* Eindhoven, The Netherlands (Aug. 1997).
46. BSi PD-7974-6:2004, The Application of Fire Safety Engineering Principles of Fire Safety

Design of Buildings, Part 6: Human factors: Life safety strategies—Occupant evacuation, behaviour and condition (Sub-system 6), British Standards, (2004)
47. D.A. Purser, personal communication (2007).
48. D.A. Purser, "People and Fire," *Inaugural Lecture Series,* University of Greenwich, London, UK (1999).
49. S. Gwynne, E.R. Galea, J. Parke, and J. Hickson, "The Collection and Analysis of Pre-Evacuation Times from Evacuation Trials and Their Application to Evacuation Modelling, *Fire Technology,* 39, 2, pp. 173–195 (2003).
50. J. Parke, S. Gwynne, E.R. Galea, and P. Lawrence, "Validating the building EXODUS Evacuation Model Using Data from an Unannounced Trial Evacuation," in *Proceedings of the 2nd International Conference on Pedestrian and Evacuation Dynamics (PED 2003),* CMS Press, University of Greenwich, London, UK, pp. 295–306 (2003).
51. J.D. Sime, "Perceived Time Available: The Margin of Safety in Fires," in *Fire Safety Science—Proceedings of the First International Symposium,* Hemisphere Publishing Corp., Newport, Australia, pp. 561–570 (1986).
52. N. Chooramun, P.J. Lawrence, E.R. Galea, An agent based evacuation model utilising hybrid space discretisation, Safety Science, Vol 50, pp 1685–1694, 2012.

Steven M.V. Gwynne, PhD is a senior research officer at the National Research Council Canada. He specializes in pedestrian and evacuation dynamics. His work includes the collection of data, the development of behavioral theories, and the application of models to assess people movement under emergency and nonemergency scenarios.

Eric R. Rosenbaum, P.E., is Vice-President of Jensen Hughes, Inc. a fire protection engineering, code consulting, and research and development firm. He has been actively involved in the evaluation of egress facilities for structures throughout the world.

Computer Evacuation Models for Buildings

60

Erica D. Kuligowski

Introduction

With the rapid increase in computer capability and the increase in egress model development, there is a need for guidance on evacuation modeling, specifically the process involved and the models available. This chapter provides general guidance to users on the first three steps of the evacuation modeling process, namely, (1) identifying project requirements, (2) selecting the appropriate model (including a review of 26 current building evacuation models), and (3) configuring the model scenarios. In addition, an example of evacuation modeling configuration is provided to identify the factors to consider when configuring the building, the population, and the procedures. The chapter briefly reviews the final three steps of the evacuation modeling process, which are applying the model, obtaining output, and analyzing results. These final steps are important but only briefly mentioned due to the fact that these are often specific to the evacuation model chosen and the goals of the project. Overall, this chapter aims to provide necessary guidance that is general enough to be model independent and specific enough to be valuable to the model user.

Overview of Computer Evacuation Models

The rapid increase in computer capability and decrease in cost have expanded the use of computer models in all fields of engineering, particularly for evacuation models. This chapter introduces a framework for deciding which model or models are appropriate for a particular life safety analysis, presents a review of 26 current evacuation models, and provides an example of an evacuation model configuration that identifies important factors to consider involving the building, population, and procedures.

An engineer performing a life safety analysis on a structure is presented with a number of alternative tools from which to choose to complete this task. Depending on the type of building and the time allotted for the analysis, the engineer may choose to employ a variety of techniques, including empirical calculations [1], manual engineering calculations [2], and/or evacuation modeling.

The empirical engineering approach compares the structure in question to data collected from a comparable structure. The user can then extrapolate from those data in order to make a

E.D. Kuligowski (✉)
National Institute of Standards and Technology,
100 Bureau Drive, Gaithersburg, MD 20899

M.J. Hurley (ed.), *SFPE Handbook of Fire Protection Engineering*,
DOI 10.1007/978-1-4939-2565-0_60, © Society of Fire Protection Engineers 2016

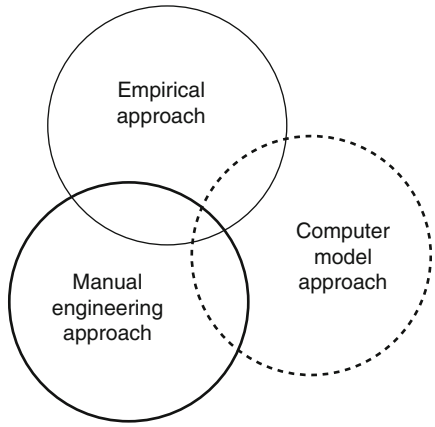

Fig. 60.1 Overlap between computational, empirical, and manual approaches to modeling

prediction of the egress performance of the structure [1]. The manual engineering approach applies empirical data at the component level (doorways, stairs, etc.) in order to ascertain the egress performance across the structure. This is done by predicting the performance of the evacuees on the components in question along predefined routes within the structure [2]. Finally, computer evacuation models represent a diverse set of methods and sophistication, ranging from a relatively crude account of homogeneous occupant flow to autonomous agents moving throughout three-dimensional space. The diversity of this sophistication is such that some models simply incorporate the methods of the empirical and manual engineering approaches (Fig. 60.1), effectively automating the process. Since the *SFPE Handbook of Fire Protection Engineering* [1, 2] describes a life safety analysis using both empirical and manual engineering approaches, this chapter will focus on the use of evacuation models.

In the recent past, both computer evacuation model development and use have expanded due to technological developments as well as the demand for flexible techniques that can cope with complex designs. In addition, the needs of the fire protection community to address problems other than building fires have been apparent. Computer evacuation models can evaluate evacuation results from a variety of structures, such as marine vessels, aircraft, buildings, and cities. In addition to diversity in structure, evacuation models can be used to simulate different types of scenarios, such as evacuation from fires, bomb threats, terrorist events, weather, riots, and even relocation (instead of evacuation) within the building. Acknowledging the different types of computer models and emergency events, this chapter will focus on computer evacuation modeling of fire emergencies in buildings, specifically the process of evacuation modeling.

Figure 60.2 displays a simplified version of the egress modeling process. The steps of the process are the following: [3]

1. Project requirements are provided to the user.
2. The user selects a model based on the project and other requirements.
3. The user constructs detailed model scenarios, which involves obtaining data and configuring the model.
4. The user applies the model.
5. The user obtains outputs from the application.
6. The user analyzes results and formats these results for the client.

The rest of this chapter focuses on providing guidance for Steps 1–3 of the modeling process displayed in Fig. 60.2: obtaining project requirements, selecting a model, and constructing model scenarios. The chapter begins by describing the project requirements that help guide model selection. Next, the features of evacuation models will be described to aid the user in model selection. The features of 26 evacuation models will be presented for comparison. Finally, the chapter will focus on model scenarios and provide an example to illustrate the issues that may arise in model configuration. Although Steps 4–6 are also important to the modeling process, these are often specific to the evacuation model chosen for the project (see Kuligowski and Milke [4] as an example).

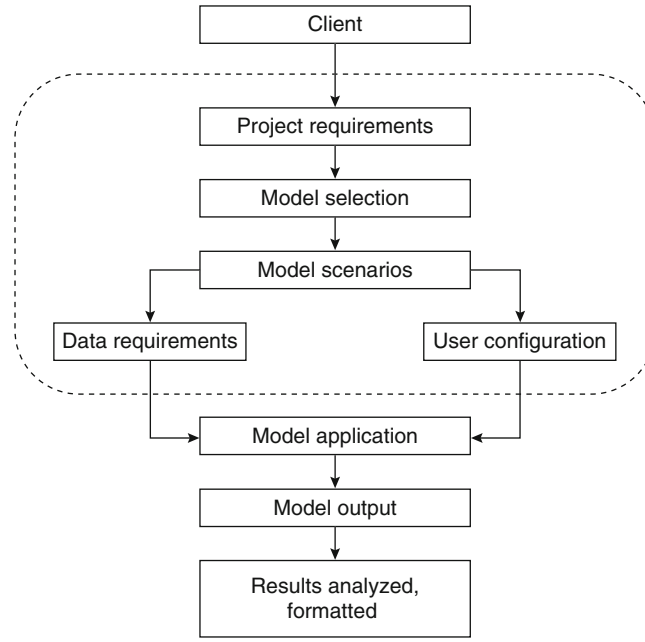

Fig. 60.2 The computer modeling process

Step 1: Project Requirements

Before selecting a model, the user should consider the following key questions relating the suitability of the model to the specific project [3]:

- What information is needed within the project to frame the egress analysis and configure the computer model?
  - What information is available?
- How much time and funding are available to complete the project?
  - What effort is required to configure and execute the model?
- What is the nature and scope of the project?
  - What are the technical resources required?
  - What additional human resources (training, expertise, etc.) are required?
  - What are the conditions that need to be represented?
- What are the deliverables of the project?
  - What output needs to be produced by the model?

This list is not an exhaustive list of the questions that need to be asked, nor are the questions necessarily mutually exclusive; however, by answering these four questions, the user should be able to ascertain whether the model is able to support the project requirements and whether it is appropriate to be used for the project at all.

Project Information Availability

The amount of project information available to the user may influence the model selection. The model may require a number of inputs in order to take advantage of its functionality or to function at all. However, the information that the user has during the project may be limited (e.g., a vague description of the building floor plan rather than a detailed architectural diagram, limited information on the population distribution, etc.). In some instances, this information may be collected/acquired during the life-time of the project. However, typically this will not be the case. If the required information is not available, the user may select a less sophisticated model with a limited number of inputs; i.e., the functionality of a sophisticated model cannot be employed given gaps in the data available.

Nature and Scope of the Project

It is important to examine the nature and scope of the project in order to determine whether the model is able to cope with the requirements of that particular application area. The user may need to establish whether certain factors are represented at all or, if they are, whether they are represented in a sufficiently refined way. For instance, if modeling a building evacuation, the user may need to represent stair movement. However, given the procedure, the user may also require stair counter-flow to be represented—i.e., people simultaneously moving up and down a stairway. The user should then ask whether stair movement is represented, and, if so, whether this representation is sophisticated enough to answer the counter-flow questions being posed within the project.

Deliverables of the Project

Typically, model output can be produced in a number of forms (e.g., numerical, tabular, plot, 2D, 3D, animated, or descriptive) and may represent different levels of refinement (e.g., individual object/agent, a specified set of objects/agents, or the entire collection of objects/agents). Depending on the combination of form and refinement, the user will be able to deduce different information from the results generated— ranging from understanding possible causal factors to examining the conditions that were produced.

The completion of any project involving modeling will require the production of a set of deliverables that will support the desired outcomes. The user should be aware of both the model output that can be produced and whether it provides sufficient detail to satisfy the project deliverables. It may not be feasible to make use of a model when, for instance, a detailed understanding of the experiences of the simulated evacuees is required but only the final arrival time can be produced by the model. In addition, the techniques used within the model (e.g., artificial intelligence techniques, flow calculations, cognitive models, etc.) may not be capable of producing the output required by the project. For instance, a cognitive model may provide information on the decision-making process; however, it might not be able to provide a quantitative assessment of the overall evacuation time.

Project Timing and Funding

Finally, it is important for the user to understand the amount of time and funding allocated to the egress analysis of the project that may influence the selection of the model, potentially precluding those models from selection that are financially and/or computationally expensive and that then cannot be employed given the resources available.

Step 2: Model Selection

The next step in the modeling process, as identified in Fig. 60.2, is model selection. This section will highlight the key factors involved in choosing an appropriate computer evacuation model [3]. This task is often governed by matters of availability, expediency, and economics rather than based on selecting the model best suited for the task at hand. Of primary importance in the selection process is an understanding of the background of the models and their current characteristics (capabilities and limitations). By understanding these aspects of the model, the user can differentiate among the models available and make a more educated choice.

Background Research on Origin of Model

Understanding the background of the model is important in the selection process because it establishes the model development and model validation criteria.

Model Development The user should be aware of the group or individual who developed the model. For many models, information can

be found on the developer/developing institution from the model users' guide. The background of the development team may affect the abilities of the model to capture some of the more complex behaviors or actions of the occupants during an evacuation.

Model Validation An important aspect of model selection is determining the level to which the model has been subjected to validation. It is vital that the user obtain documentation from the developer and other agencies that have performed any type of validation to make his or her own judgments on the validity of the results produced and whether the validation is sufficiently detailed, reliable, and in an area comparable to that involved in the project. For instance, if the model has been validated using scenarios and/or data extracted from a small-scale building, would the validation performed be sufficient to warrant the use of the model in a tall building application? Validation studies help to identify the capabilities of the model as well as its limitations. These validation studies can investigate a number of different aspects of the model: quantitative performance, qualitative performance, functional performance, component-based performance, efficiency, speed, and scope [5]. The availability of the supporting data required to perform such comparisons can limit these vital evaluations. The user should develop his/her own suite of tests to provide a level of confidence in the validation process and an understanding of the use of the model.

Current computer evacuation models are validated using a variety of techniques including validation against code requirements, validation against fire drills or other people movement experiments/trials, validation against literature on past evacuation experiments (flow rates, etc.), validation against other models (see Weckman et al. [6] and Lord et al. [7]), and third-party validation. However, some current computer evacuation models provide no indication of validation of the model in the references available. It should also be recognized that validation is a challenging process constrained by the data available, and the complexity of the processes represented. It is critically important for users that validation efforts are documented in detail allowing them to make an informed choice; understanding (amongst other things),

- What validation activities have been undertaken?
- How these activities have been conducted?
- What aspects of the model have been validated?
- How relevant the validation is to the project at hand?

Model Characteristics

In addition to assessing the project requirements and model's developmental background, it is important to understand the current modeling capabilities and characteristics, thus enabling a comparison between the models currently available. By identifying and understanding the key capabilities and characteristics of the current evacuation models, the user will be able to make a more informed choice of the most appropriate model for the specific project. The key characteristics deemed to define the current evacuation models are displayed in Fig. 60.3.

Modeling Method The modeling method [8] is a feature of computer evacuation models that describes the level of sophistication used to calculate evacuation times for buildings. The modeling method can be broadly categorized as one of the following:

- *Movement models*. Those models that concentrate on the simulation of occupant movement and that do not have a behavioral component. These models demonstrate congestion areas, queuing, or bottlenecks within the simulated building. Also, within the movement category, there are some models that are specifically optimization models, meaning that they aim to optimize time in an evacuation through the exclusion of nonoptimal behaviors.
- *Partial behavior models*. Those models that primarily calculate occupant movement but also simulate evacuee behavior to some degree. Possible behaviors could be implicitly

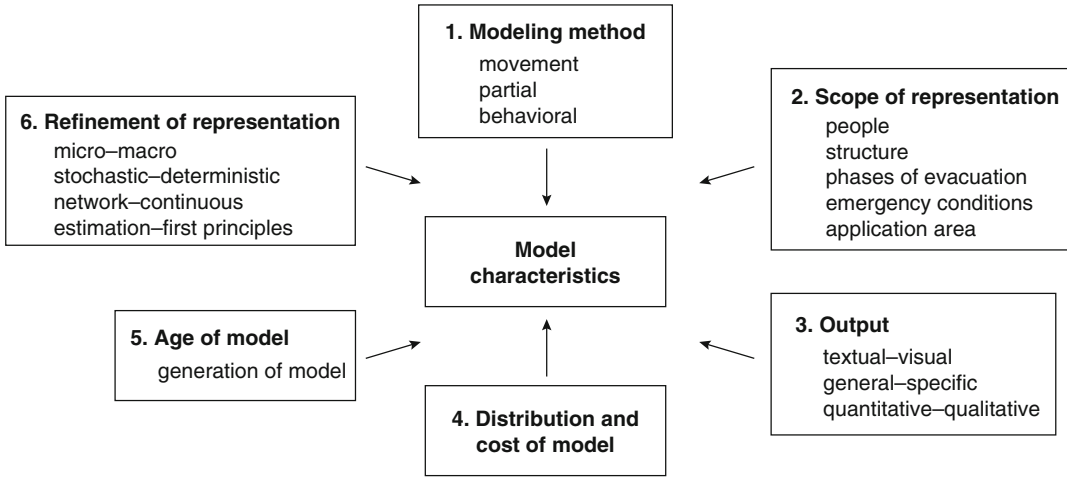

Fig. 60.3 Current characteristics of evacuation models [3]

represented by pre-evacuation time distributions among the occupants, unique occupant characteristics, overtaking behavior, and the introduction of smoke and its effects on the occupants.

- *Behavioral models*. Those models that incorporate occupants performing actions in addition to movement toward a specified goal (exit). These models can also incorporate decision making by occupants and/or actions that are performed due to conditions in the building. The behaviors simulated may detract from the evacuation performance of the individual or the population as a whole. Within this category, there are some models that have the capability of performing a risk assessment of the evacuation.

Scope of Representation Users should also be familiar with the differences in the scope or flexibility of how the models represent aspects of the evacuation, including the occupants, the structure, emergency conditions, the expected evacuee behavior, the procedures present (e.g., whether there are safety, operational and security procedures in place that may affect each other), and so on. Examples of the scope of representation include the simulation of the impact of occupants with disabilities, the inclusion of certain aspects of the structure (e.g., doorways, signage) via engineering plans, the number of phases of the event simulated (e.g., whether ingress, circulation and egress need to be considered), the procedural elements included (e.g., security, operational, safety, etc.) and the simulation of fire conditions and their impact on evacuees against their performance under non-emergency conditions. It is important to understand how a particular model represents/simulates certain aspects of an evacuation, especially if they are a key component of the scenarios required for the project in question. For example, if the project requires the simulation of a population that includes people with differences in age, gender, mobility impairments, and size, the user should ensure that the model has this capability.

Output The output is an important characteristic to consider when selecting a model. Many times, the interested parties will require more information from the simulation than simply the total evacuation time. Current models can provide a variety of output, including textual output (qualitative and quantitative), two-dimensional graphical output, and three dimensional/virtual reality interface. In addition, several models are able to have the nature of their output modified in order to fit the project requirements. Data formats are briefly discussed in Chap. 64.

Distribution and Cost of Model Model availability and cost are considered to be of primary importance, as the initial concern of the users will be to gain access to the model. Some models are distributed for local application, whereas other models are employed by their developers centrally with the results then distributed. In the former case, the model user is actually developing the input, running the simulations, and then analyzing the output; and in the latter, the user is working with the developing company and will have access to the output only. In reality, the model may be distributed in a number of different ways: the software is free of charge; available on a consultative basis; available via a flat rate fee; available under license control, or some combination of these methods.

Age and Generation of the Model In addition to availability, it is important for the model user to be aware of the age of the model and the developments/advancements since its release. In some cases, older models become dated, cease to advance in accordance with technology progress, and therefore become obsolete. Conversely, if it is seen that the developing organization of an older model continually updates and maintains the software, the user may be interested in using a more established model that has been continuously developed and has been involved in a variety of projects over the years. In the case of newly developed models, the user should be cognizant of its validation efforts, specifically if the model has been used for practical purposes and projects since its release.

Level of Refinement The level of refinement of an evacuation model describes to what level of detail the aspects of an evacuation, such as the population and structure, are simulated. The refinement of a structure reflects the method employed to represent the configuration of the building within the model and will also have an impact on how the movement of the occupant is represented. The user should be aware that an increase in refinement may require an increase in the effort needed of the user and an increase in the computer time needed to run the simulation. Computer evacuation models can differ regarding the refinement of the structure, the population, and the behavior of the occupants (if behavior is simulated at all).

The refinement of a structure can be categorized in the following way: a coarse network, a fine network, and a continuous network. A defining attribute of a coarse network is that the nodes do not need to be uniform, representing the actual shapes and sizes of rooms in a building. A coarse network divides the floor plan into rooms, corridors, stair sections, and so on, and the occupants move from one structural component to another (e.g., room to corridor). The fine network, on the other hand, produces a series of small, uniform nodes (in both shape and size). Each can be occupied typically by one person at a time. A fine network divides a floor plan into a number of small grid cells between which the occupants move. The defining attribute of a continuous network is that, instead of nodes, the structure is overlaid with x-y coordinate points, allowing occupants to travel through all possible space in a building. The continuous network applies a two-dimensional (continuous) space to the floor plans of the structure, allowing the occupants to walk from one coordinate to another throughout the building. Fine and continuous networks have the ability to simulate the presence of obstacles and barriers in building spaces that influence individual path route choice, whereas the coarse networks "move" occupants only from one portion of a building to another.

The refinement of a population refers to the method employed by the model to represent the population as either individuals (a microscopic level) or a homogeneous population (a macroscopic level). The refinement of behaviors refers to the method employed by the model to simulate behaviors of the occupants during an evacuation. These behaviors can be defined by the user or model (deterministic) or based on probabilities specified by the user (stochastic).

Given the rapid development of current computer evacuation models, any review attempting to categorize the models currently available may present data that are out-of-date. The categorization presented in the next section attempts to avoid this problem by limiting itself to the fundamental aspects of the models.

Review of Current Computer Evacuation Models

Currently, several evacuation model reviews exist [8–21] that attempt to explain and categorize the computer evacuation models. This section briefly reviews each computer evacuation model,[1] identifying fundamental characteristics of the models currently available. For a more detailed analysis of the models, the reader should refer to the reviews referenced above.

This section covers a total of 26 computer models that simulate emergency egress within the built environment, categorized by the model features outlined in the previous section [16]. Many of the models reviewed can also simulate evacuation from other types of structures; however, evacuation from buildings is the main focus of this review. The model features that will be highlighted involve the model's background and characteristics including the following categories:

- Developer information
- Validation
- Availability
- Modeling method
- Refinement of the population
- Refinement of the structure
- Refinement of the behavior (where behavior is simulated)
- Output

Specific information on each of the 26 models is provided in Table **60.1**. Accompanying references and links for each model can be found in the following references: Kuligowski and Peacock 2010 [16] and the Evacmod.net website [22]. To clarify the abbreviations provided in Table **60.1**, a key is provided.

[1] Certain commercial entities, equipment, or materials may be identified in this document in order to describe an experimental procedure or concept adequately. Such identification is not intended to imply recommendation or endorsement by the National Institute of Standards and Technology, nor is it intended to imply that the entities, materials, or equipment are necessarily the best available for the purpose.

Once a computer evacuation model is chosen, it is often the case that the user has little guidance on possible model scenarios. Even the referenced material may omit information on how the model was configured and simply discuss in detail the results of the particular study. The next section is written from a user's perspective in order to present the key considerations in the creation of model scenarios, specifically focusing on the building, the population, and the procedures during an evacuation [9].

Step 3: Model Scenarios

Once the user is familiar with the project specifications, model features, and specifics on current models, the user should begin developing possible scenarios for model configuration. The purpose of this section is to outline the choices a user will have to consider and offer guidance on how to make the decisions that will eventually lead to application of the model.

In the following sections, the four aspects of scenario configuration will be introduced: the building, the population, the procedures, and environmental conditions. Within each category, the model user will be provided with descriptions of different methods of configuration within the scenario(s) for a project. Following this section on scenarios, the methods within each category will be displayed in an example.

Building Configuration

When using a computer evacuation model, it is up to the user to describe the building characteristics in a manner consistent with the method used by the model to represent the geometry of the building. This description includes the location of open spaces and walls, information on the stairs, and the location of the final destination of safety. The user may be required to provide these data in a number of different ways, according to the model features available. As described previously, the modeling method being employed to represent the structure will

Table 60.1 Model features

	Background of model		Model characteristics					
Model	Developer/institution	Validation	Availability	Modeling method	Refinement of population	Refinement of structure	Refinement of behavior	Output
EVACNET4	Kisko, Francis, and Nobel/Univ. of FL, U.S.	FD	Y	M-O	Ma	C	N/A	T
WAYOUT	Shestopal/Fire Modelling & Computing, AU	FD	Y	M	Ma	C	N/A	V
STEPS	Mott MacDonald, U.K.	C, FD, PE	Y	M/PB	Mi	F	D	V
PedGo	TraffGo, Germany	FD, PE, OM, 3P	Y	PB/B	Mi	F	S	V
PEDROUTE	Halcrow Fox Associates, U.K.	N	Y/N3	PB	Ma	C	D	V
Simulex	Thompson/IES, U.K.	FD, PE, OM, 3P	Y	PB	Mi	Co	D	V
GridFlow	Purser and Bensilum/BRE, U.K.	FD, PE	Y	PB	Mi	Co	D	V
ASERI	Schneider/I.S.T. GmbH, Germany	FD, PE	Y	B-RA	Mi	Co	S	V
BldEXODUS	Galea and FSEG/University of Greenwich, U.K.	FD, PE, OM, 3P	Y	B	Mi	F	S	V
Legion	Legion International, Ltd., U.K.	C, FD, PE, 3P	Y	B	Mi	Co	S	V
FDS + Evac	VTT, NIST, Helsinki Univ of Tech	FD, PE, OM	Y	PB	Mi	Co	S	V
PathFinder 2009	Thunderhead Engineering	C, FD, PE, OM	Y	PB	Mi	Co	D	V
SimWalk	Savannah Simulations AG	FD, PE, 3P	Y	PB	Mi	Co	S	V
PEDFLOW	Edinburgh Napier University, Transport Research Institute	PE	Y	B	Mi	Co	S	V
SpaceSensor	Sun/de Vries	FD, OM	Y	B	Mi	Co	S	V
EPT	Regal Decision Systems, Inc.	FD	Y, N1	B	Mi	C, F, Co	AI	V
MassMotion	Arup	C, FD, PE, OM	Y, N1	B	Mi	Co	AI, S	V
Myriad II	Keith Still	PE, 3P	Y, N1	B	Mi	C, F, Co	AI	V
Pathfinder	Rolf Jensen and Associates, Inc.	N	N1	M	Mi	F	N/A	V
ALLSAFE	InterConsult Group ASA, Norway	OM	N1	PB	Ma	C	D	V
CRISP	Fraser-Mitchell/BRE, U.K.	FD	N1	B-RA	Mi	F	S	V
EGRESS 2002	Ketchell/AEA Technology, U.K.	FD	N1	B	Mi	F	S	V
SGEM	Lo/University in Hong Kong	FD, OM	N1	PB	Mi	Co	D	V
EXIT89	Fahy/NFPA, U.S.	FD, OM	N2	PB	Mi	C	D	T
MASSEgress	Stanford University (Civil and Env Engineering)	PE, OM	N2	B	Mi	Co	S	V
EvacuatioNZ	Spearpoint/Univ of Canterbury, NZ	FD, PE, OM	N2	B	Mi	C	S	V

Key to reading the table:

Validation:
- *C* Validation against codes
- *FD* Validation against fire drills or other people movement experiments/trials
- *PE* Validation against literature on past experiments (flow rates, etc.)
- *OM* Validation against other models
- *3P* Third-party validation
- *N* No validation work could be found on the model

Availability to the Public:
- *Y* The model is available to the public for free or a fee
- *N1* The company uses the model for the client on a consultancy basis
- *N2* The model has not yet been released
- *N3* The model is no longer in use
- *U* Unknown

Modeling Method:
- *M* Movement model
- *M-O* Movement/optimization models
- *PB* Partial behavioral model
- *B* Behavioral model
- *B-RA* Behavioral model with risk assessment capabilities
- *B-AI* Behavioral model with artificial intelligence capabilities

Refinement of the Population:
- *Ma* Macroscopic
- *Mi* Microscopic

Refinement of Structure:
- *C* Coarse network
- *F* Fine network
- *Co* Continuous

Refinement of the Behavior:
- *D* Deterministic
- *S* Stochastic

Output:
- *T* Textual output
- *V* Visual output

directly influence the results produced; therefore, the user should seek information within the user's guide and additional model reviews relating to the specific method being applied. The following sections describe the methods used in current models to configure the building:

- Structure generation
- Structure representation
- Additional building information

Structure Generation The first stage in this process is for the user to determine the format for incorporating the building geometry (known as grid or structure) into the model, which is dependent on the assumptions of the model. Broadly speaking there are three means by which a user can generate the structure and three means by which the models represent the geometry of the building.

There are three main ways that the user can generate the structure within the model. These ways are through computer-aided design (CAD) drawings, manual drawings, and text files. Although these methods can produce an accurate depiction of the structure, it is by no means a trivial activity; indeed the preparation of the engineering diagram can represent a significant proportion of the modeling process when dealing with complex structures. In addition, methods are now becoming available that reflect additional aspects of the building (e.g., BIM), the building as a three dimensional structure (e.g., Google Sketch-Up) and/or other aspects of the structure that might influence evacuee performance.

Alternatively, if an engineering diagram cannot be directly imported, the user is required to manually specify the building geometry, either by drawing it within the model or importing a text file that links building segmented areas to other areas on a floor plan. Several models provide users with the ability to select exactly how they wish to re-create the geometry of the structure within the model.

Structure Representation Irrespective of the means by which the user generates the structure within the model, there are methods by which the model represents the structure. If a coarse network is employed within the model, the model represents the floor plans of the structure as a segmented version of the building. This will normally relate to the connectedness and capacity of each of the structural components (i.e., rooms, corridors, hallways, and stairs) without specifying a detailed geometrical representation of the structure. This segmented version of the building would usually be in the form of a text file, manually or automatically produced from the architectural diagrams. This file identifies certain areas of the building and describes how they are linked together within the building. Many models that use a coarse grid structure do not accept CAD drawings and do not have a visual representation of the structure. This is an important consideration as it usually implies that the user will be expected to manually reproduce the geometry of the structure in some form without making reference to a visual representation of the geometry. Given the sensitivity of the results to this structure, the level of work required here and the likelihood of error in this process should be recognized.

When employing a fine grid structure, the model (via the user) overlays a mesh of small nodes throughout the occupiable space within the entire floor area. These nodes connect to each other to form the paths that occupants might use to travel between and within the structural components. The fine nodes are usually given a uniform default area that corresponds to the space normally occupied by one individual, unlike the coarse representation where the area of the nodes is governed by the configuration and by the user. Many of these models allow the importation of CAD drawings to make this procedure easier. The majority of the models that employ a fine node network are then based on the assumption that a node will only be occupied by one person at a time. Nodes are then generated automatically or manually to cover the occupiable space within the plan. These nodes are generally square, although other shapes have been used (e.g., hexagons). The choice of node size may affect the final evacuation time significantly, especially in the cases where an occupant can occupy only one node at a time. The user needs to understand how varying the node size impacts the results from a particular model [7].

Finally, there are several models that are categorized as continuous models. These incorporate the engineering (e.g., CAD) diagrams of the building and produce a continuous plane to represent both the occupiable space and the potential movement of the simulated occupants using a coordinate-based system. Consequently, simulated occupants move from coordinate to coordinate within the continuous space. Theoretically, this method should involve the least amount of user judgment and adaptation of the building representation.

Additional Building Information In addition to providing network linkages throughout the building, the user is sometimes required to enter additional building information into the model for each scenario. This information consists of areas, lengths, and widths of certain spaces (specifically with the coarse network models) and information about the stairs connecting floors. The stair information is not usually imported with the CAD drawing, since stairs are not strictly part of one floor plan, but rather a linkage between floors. Depending on the sophistication of the building representation, the model user may have to supply the following information: stair width, diagonal length between stories (discussed later in the chapter), riser and tread dimensions, and handrail information.

Summary of User Configuration of the Building When using a computer evacuation model, it is up to the user to describe the building characteristics in a manner consistent with the scenario and the methods used by the model to represent the building. This includes the location of open spaces and walls, information about the stairs, and the location of the final destination of safety. Each provides a different level of time and effort from the user, and the decisions made by the user affect the results produced by the model. Irrespective of the approach adopted, great care has to be shown to ensure that any simplifications made relating to the spatial representation are justified (and justifiable) and that the geometry modeled actually reflects these simplifications as stated.

Population Configuration

Once the structure has been produced, it needs to be populated before the simulation can proceed. In order to do this, the following information from the scenario needs to be supplied to the model:

- The number of occupants and their distribution throughout the building
- Occupant characteristics (e.g., age, gender, knowledge level, impairment, etc.)
- Movement data (e.g. achievable speeds, flow/density relationship, etc.)
- Pre-evacuation delays
- Specified behaviors and associated delays

It should be noted that within the model, the impact of these factors might not be completely independent of each other. For instance, occupant characteristics and pre-evacuation time might influence the time for an evacuee to commence movement; movement data and specified behaviors might influence the time to reach safety, etc.

As the model's sophistication increases, so the number of behavioral variables considered may also increase, potentially increasing the number of possible input parameters. It is then up to the user to select input parameters that specify the entire population, subpopulations, or individuals throughout the building. Often the models provide default values; however, the user should be informed about these defaults and make decisions about whether they pertain to the population involved in the project at hand. Default data sets are not necessarily appropriate for a particular scenario and it is not safe to assume that they necessarily are so.

As discussed earlier in the chapter, there are two fundamental methods to represent the evacuating population within the structure during the simulation. The simulated population can be represented at the micro level as individuals (shown by multiple arrows in Fig. 60.4) or at the macro level, as a homogeneous group given population-wide characteristics (as shown by one large arrow in Fig. 60.5). The method used by the model affects the decisions made by the user when implementing a specific scenario. For

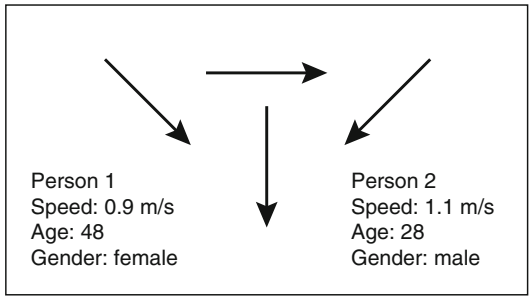

Fig. 60.4 The population represented at the micro level

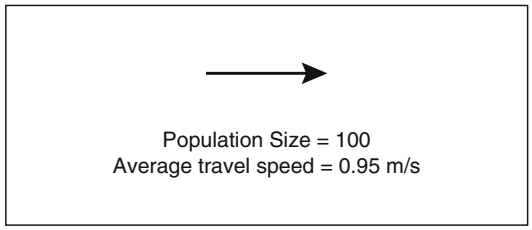

Fig. 60.5 The population represented at the macro level

instance, when the individual evacuee is modeled, there is the potential to simulate a range of personal characteristics for that individual. At the population level, the same attributes may also be included; however, these are assigned to the entire population as a whole.

Number of Occupants in the Building The first thing that a user will have to specify about the population inside the building is the number of occupants and their distribution throughout the structure. This calculation can depend on a variety of factors within a scenario, such as the building type, the locations of facilities/services located inside and outside of the structure, the floor space within the structure devoted to occupants, the date, and the time of day. Depending on the building type and simulation scenario, a particular season of the year and especially a particular day and time of day may warrant more occupants than another season, day, or time of day. For example, if a university building is being simulated, the number of people in the building increases during the months when school is in session and typically peaks between 9:00 a.m. and 3:00 p.m. on school days. The number of occupants influences the interaction between occupants, which therefore directly influences the following performance elements.

Occupant Characteristics Many factors need to be considered when choosing movement data because, in much of the existing evidence available, unimpeded speeds are influenced by gender, age, ability, and other occupant characteristics. If the model represented the population as homogeneous (on a macro level), the user would then need to provide the model with a higher-level representation of data (e.g., an average initial unimpeded movement speed for the occupants of the building) rather than including the details. Resources for movement data can be found in Chap. 64.

It should be noted that there is no correlation between increased sophistication in the refinement of the representation and accuracy. A high modeling sophistication does not necessarily indicate that the evacuation model uses and/or provides the appropriate data to model such behaviors. The user should be aware of the validation methods and associated limitations of each model used.

In addition to physical characteristics, some models allow for the knowledge levels of evacuees and other non-physical factors to be set; e.g., exit awareness, level of motivation, etc. These may influence the actions performed and the manner in which they are performed, depending on the model in question.

Pre-evacuation Times In addition to movement data, the user is confronted with the decision of selecting and applying a pre-evacuation time (i.e., the time between ignition and purposive response safety) for either the entire population or subpopulation (macro level) or for individual occupants throughout the building (micro level). The user will be faced with the following choices:

- No pre-evacuation times (i.e., no delay), where the pre-evacuation component is not

modeled or the response is assumed to be instantaneous (i.e., a best-case scenario)
- A specific time delay that is applied to the entire population
- A specific time delay for particular individuals throughout the building (for instance, with a particular trait or at a specific location)
- A distribution over the population of pre-evacuation times

Enormous care should be taken when importing pre-evacuation times into the model. The results produced and conditions within the scenario are likely to be sensitive to the extent and range of the pre-evacuation times provided. The pre-evacuation phase is often the most extensive phase of the evacuation and is always critical [1].

The nature of the pre-evacuation times employed will depend on a number of factors including the time of day of the event (e.g., was it nighttime when the evacuees initially would be asleep?), the type of alarm system in the building (e.g., was there a traditional bell alarm system or were more advanced techniques employed?), the expected exposure of the individuals to external social/physical cues, the activities of the occupants in the building (e.g., were they committed to an activity?), and the presence of staff. Although these factors should be considered, it is not suggested that the models currently available could explicitly simulate these factors. These factors may need to be implicitly simulated through the provision of suitable data to the model, placing a greater onus on the user.

Movement of Occupants Depending on the level of refinement utilized by the model, the user will need to make certain decisions regarding the movement data supplied for the simulated occupants. For the majority of evacuation models, the user is tasked with providing initial unimpeded movement speeds for the entire population. This may be a single value or be selected from a distribution of values.

The initial travel speed attribute is usually then modified according to the density of the surrounding population. The effect of speed versus density is usually either derived directly from the available density correlations (see Gwynne and Rosenbaum [2], Fruin [23], and Predtechenskii and Milinskii [24]) or calculated according to the position, route choices, trajectory, and/or separation distances of those around the individual in question. However, in some models, the user must provide the model with speed, flow, and density values for each space within the building. Again, whether the evacuees are represented as individuals or as a uniform entity will influence the detail in which the user may have to provide the data. At the individual level, movement speeds might take into consideration the range of abilities and mobility within a population and how these may interact, whereas at the population level, this effect would be averaged out across the population in question.

Behavioral Actions of Occupants In most real situations, there is a diverse set of actions that would be expected of the occupants in response to the incident. Similarly, there is a range of methods employed to simulate these actions—in terms of their nature, their impact and any associated delays that might be incurred when they are performed. In turn, the number of assumptions and the amount of data required by the models will vary greatly.

In order to represent the specific behavioral response of a population, the user may have to select and apply an expected behavioral response for a section of the population. In doing so, the user needs to understand the expected behavior of the population in the scenario, when and where this behavior occurs, and the expected consequences. An example might be that the user is aware of a daycare center in the middle of an office building. Given that this facility is provided to cater for the children of staff, the user might wish to simulate some office workers first traveling to the daycare before evacuating the building. (Refer to the case of the Summerland incident, where just such behavior was evident [25, 26].) As with the previous considerations, the level of refinement of the behavior is dependent on the representation of the population

(e.g., can the performance of individuals be tracked?) and the detail to which their movement is simulated (e.g., can the model assign itineraries?). This is just one example of a possible decision that the user may want to simulate involving behavior.

Models simulate behavior in different ways, including the following methods:

- Neglect to simulate behavior at all (response is then imposed and constant through the population)
- Simulate only occupant characteristics that affect movement
- Simulate behavior conditionally (individuals are affected by conditions within the building)
- Allow behavior to emerge adaptively such that behaviors are constructed according the conditions faced, the internal information available and some analysis of the situational picture available (attempting to simulate the decision-making process)

It is relatively common within those models that include a conditional representation that the user can specify certain behavioral actions for individuals or sometimes distribute certain probabilities of behaviors over a segment of the population. In such circumstances, the user is directly determining the actions performed by the evacuees. Therefore, the conditions under which the actions are performed, the likelihood of their performance (potentially 100 %) and the consequences of their performance (e.g., a delay of between 20 and 60 s or a change in the state of an object or person) should be based on empirical data and guidance wherever possible. Unfortunately, there is not a great deal of information or data on occupant behaviors during evacuations that can then be categorized according to the nature of the structure.

Summary of User Configuration of Resident Population Once the structure has been configured, information needs to be supplied to the model by the user including the number of occupants in the building, movement data, personal characteristics (e.g., age), pre-evacuation delays, and even specified behaviors. The level of detail and sophistication of the resident population simulated depends on the type of evacuation model chosen. See Chap. 57 for additional information on the design of occupant scenarios.

Procedural Configuration

The third area of the evacuation simulation that would need to be addressed is the procedures that are expected to be applied during an evacuation. These relate to credible situations within the scope of the project at hand to be simulated within the model. These may have been defined and presented to the user or arrived at by the user alone.

As the scenarios vary for the building, the user has to make a variety of choices on whether to include certain evacuation procedures and situations (assuming that the model is capable of representing the scenario in question). Considerations involving the configuration of the procedures include the following:

- The route choice of the occupants
- The existence of counterflow (i.e., the occupants and/or fire fighters)
- The inclusion and activity of human and technological resources

Many of these features are only included in the more sophisticated models. Also, since many of these features are specific to the evacuation models themselves, the user should consult model references and/or evacuation model reviews to find out the current information on the procedural capabilities.

Route Choice When simulating fire evacuation scenarios, a user should be cognizant of the occupant route choice. Several evacuation models offer choices as to the route that the population or portion of the population would adopt when evacuating the building. These choices might include the evacuees adopting the shortest route, optimally using exits according to their familiarity and experience, being assigned a predefined route, or configuring a conditional route. Many times, the default choice for the model will be the shortest route available; however, the user should be aware that this choice may not always represent the paths that

occupants will *actually* choose in a fire evacuation. A few models also provide the option of evacuating occupants via elevators and stairs. The route selection of the individual evacuees (if they are simulated individually within the model) will not only directly influence the outcome for the individual but will also influence the overall outcome for the structure. As such, this is a key component of the configuration process.

Representing Emergency Responders Another consideration for alternative evacuation scenarios is the presence of emergency responders in the building. This is primarily of interest in the interaction that they might have with the evacuees and the changes that they may bring to the availability of routes and the environmental conditions. Some of these aspects would be beyond the models currently available and would, therefore, require implicit modeling.

If the user is interested in simulating this type of counterflow situation, then there are several models that have this capability, which is achieved in a variety of different ways. For instance, it might require the provision of the percentage of stair space taken up by the counterflow at certain times, providing a general delay caused by counterflow (i.e., implicitly representing the counterflow) or assigning an itinerary to a group of occupants (e.g., the fire department), so that the group travels to a designated area of the building that causes them to interact with the evacuees (i.e., explicitly modeling the counterflow generated). This would depend on having a relatively detailed understanding of the procedures employed by the fire department and might be sensitive to a range of issues including the body size of this emergency group.

Representing Human and Technological Resources The simulation of a scenario with the explicit inclusion of a human or technological procedural measure that directly affects evacuee performance (e.g., the impact of alarm type or the presence of staff on pre-evacuation time) is a relatively rare capability in the existing set of evacuation models. Most of the models currently available do not have the capability of explicitly simulating this effect. Instead, the impact is more typically represented indirectly or implicitly with numerical values (i.e., timing) assigned to represent the impact [9].

Summary of User Configuration of Procedural Actions The third area of the evacuation simulation involves the procedures that are expected to develop during an evacuation. These relate to credible situations within the structure that need to be addressed within the scope of the project and simulated within the model. These may have been defined and presented to the user or arrived at by the user alone. Specific examples of the decisions made by the user include the route choice of the occupants, the provision of countermeasures (i.e., the counterflow of occupants and/or fire fighters), and the inclusion and activity of staff.

Incident information

When modeling a fire event, the user has to consider the initial location(s) of the fire, depending upon the number of different scenarios simulated. Along with this decision, the user should decide how to coordinate any information about the fire event with the simulation of the occupants in the building (i.e., how closely coupled is the simulation process with the development of the fire?). Depending on the nature of the model, the effect of the fire might be supplied by the user or represented within the simulated environment.

Evacuation models have different means of incorporating fire information with the evacuation process, including no fire representation, input of fire information manually, importation of calculated fire information, and coupling with a fire model. Several models have no representation of the fire conditions. Within these models, the user would have to manually determine when the conditions reached a level that would influence the behavior and well-being of the

evacuees. This would require assumptions to be made on behalf of the user that would directly influence the results produced. Some models allow the user to input fire information manually, requiring the user to either derive a description of a fire suitable for the scenario in question or apply empirical data. Other evacuation models allow fire model results to be imported in order to inform the calculations of how the environmental conditions change during the simulation. In this case, the user would need to be able to configure the fire model appropriately and ensure that the conditions produced within the fire model reflected the same scenario conditions that were being represented within the evacuation model (e.g., position and status of doors). A few of the evacuation models have a fire model built into the program. It is up to the user to decide which method is best to use for the specific project.

Summary of User Configuration of Incident Information The fourth area of the evacuation simulation involves the location and impact of the incident. Examples include the location of the fire and the inclusion of toxicity or fire data.

Summary of Model Scenarios

The examples presented in this section are meant to provide users with guidance when examining and designing scenarios for a project. This section has been designed to provide guidance on the factors that should be considered when using an evacuation model.

Grid size, as well as other user inputs that are occupant-focused (e.g., occupant numbers, occupant size, and occupant speed) may affect the results of the evacuation model. For more information on how inputs can affect evacuation model results, see Lord et al. [7].

Example of Evacuation Model Scenario Configuration

The total evacuation from a high-rise building will illustrate the types of concerns relating to the use and configuration of an evacuation model. This will provide the user with an example of the configuration process to use as a reference. (See Chap. 57 for additional information on the design of occupant scenario's for life safety analyses.) The following paragraphs will describe the building and the scenario.

Although this example does not incorporate results from any specific model, research has been done to highlight differences in results when multiple models are used on the same building [4, 6, 7, 27–29].

Scenario Information

Only one scenario will be discussed in this section to provide an example of the kinds of decisions that users will make when configuring an evacuation model. In this scenario, a fire initiates in a guest room on the 5th floor at 2 a.m. The reason for choosing a fire initiating at 2 a.m. is to provide an example of a worst-case scenario for a hotel building due to the fact that most guests will be in their rooms sleeping. In this scenario, the fire event will trigger a full-building evacuation.

As mentioned previously, the user is faced with decisions on how to configure the building, the population, and the environment. The following discussion provides examples of decisions made for this specific scenario in each category of configuration.

The building used for the example is a hypothetical office/hotel building. The office/hotel building has 20 stories, with each floor occupying an area of approximately 1200 m^2. The distance measured between floors (floor height) is approximately 3 m. The first 10 floors (floors 1–10) consist of a segmented floor plan typical of hotel rooms and the top portion of the building (floors 11–20) consists of an open floor plan used for office space. There are two 1.11 m (44 in.) stairs located on either side of the floor plan that serve all floors in the office/hotel building. It is assumed that the user has been given this design to evaluate for life safety purposes. In reality, the design may be far more complex. However, this design should be sufficient to illustrate the processes at hand.

The following additional information is provided to the user for this scenario:

- The hotel portion of the building is occupied by people on business and leisure travel.
- The hotel has a limited 24-h staff.
- The fire department is located across the street from the hotel.
- Once an alarm sounds in an area of the building, a staff member will investigate. The staff member then decides whether to sound the main building alarm.

The plans for the hotel space on each of the 10 floors (floors 1–10) are identical and the floor plans for the office spaces (floors 11–20) are assumed to also be identical. The floor plans for floors 1–10 and 11–20 are displayed in Figs. 60.6 and 60.7, respectively. In this example, the ground floor is not considered. Therefore, in order to reach an area of safety as part of this life safety analysis, all occupants in the building will move past floor 1, down two flights of steps, and out the final exit.

Building Configuration

The model user is faced with a variety of decisions when configuring the building. Depending on the type of grid/structure method employed by the model, the user will have to construct a coarse network, fine network, or continuous network within the floor plan of the building. Examples are provided here for each type of network. In addition, the user must also make decisions about adding extraneous building information, such as stairs and exits.

Coarse Network When using a coarse network, the network does not explicitly represent all of the occupiable space. Therefore, the user is required to artificially segment the structure in order to produce components that will appear in the network. It is not always apparent how best to segregate the structure and, therefore, represent the structure within a coarse network model.

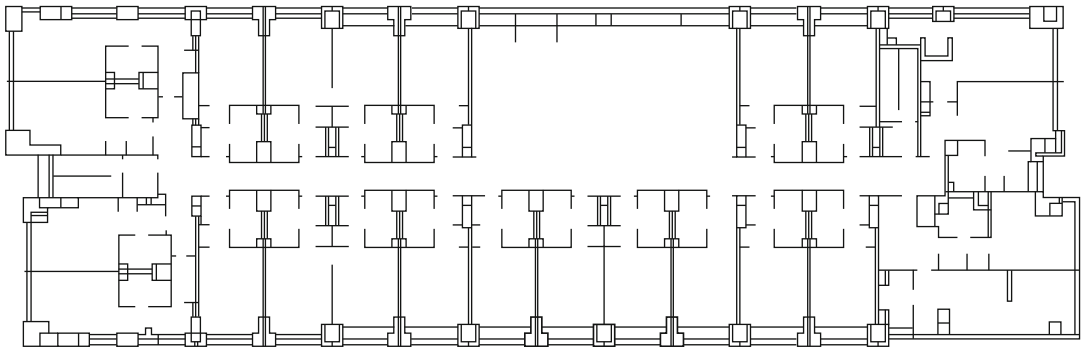

Fig. 60.6 Floor plan of floors 1–10 (the hotel space)

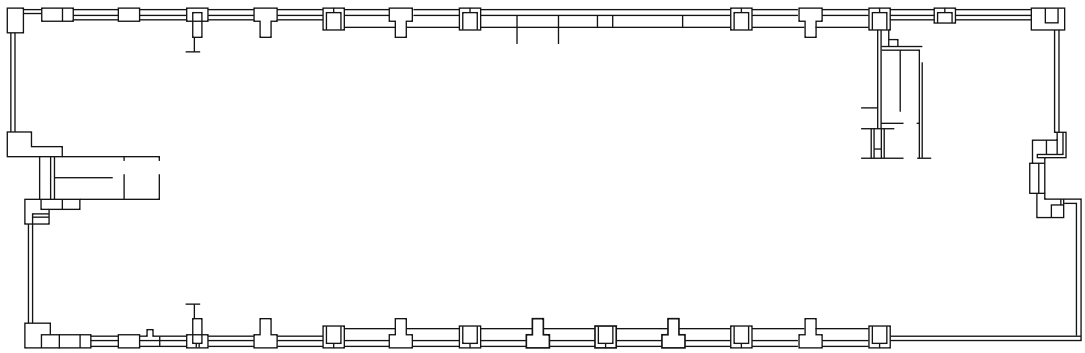

Fig. 60.7 Floor plan of floors 11–20 (the office space)

As mentioned previously, this segmentation will have a direct impact on the results produced. Figures 60.8 and 60.9 are used to demonstrate the different (and equally viable) ways to segment the building for a coarse network. Figure 60.8 shows the open office floor plan that is divided into 12 "user-derived" sections (derived in that they are not immediately apparent from the architectural description of the structure) with each connecting arc. This derived design leaves a longer rectangular box for the hallways and finally two sections for the stairs on either side of the floor plan. In a coarse network, the model simulates that the occupants will move from the middle of one segmented area to the middle of another (with which it is linked). The segmentation of the structure will, therefore, directly influence the movement of the occupants and the routes that may be adopted. Often open floor plans are difficult to segment because users are not privy to the eventual segmentation that each company will employ when the building is in use. Therefore, it is up to the user to provide segmented areas that are representative of how occupants might move throughout this space to safety as shown in Fig. 60.8.

In contrast, Fig. 60.9 provides a different example of larger segmented spaces of the same structure. This space is segmented into fewer office sections than in Fig. 60.8 (eight in total) and two staircase sections. Although this example requires less time to produce, it might not accurately represent occupant movement through this space. When segmenting out any space in a building, the user might want to run sample simulations of each floor plan to analyze the simulated occupant movement to determine whether the movement path and times are representative.

Figure 60.10 shows a segmentation of one of the hotel floors of the example building. The majority of the segmented areas relate to the hotel guest rooms. Therefore, there is less scope for flexibility in the association of nodes

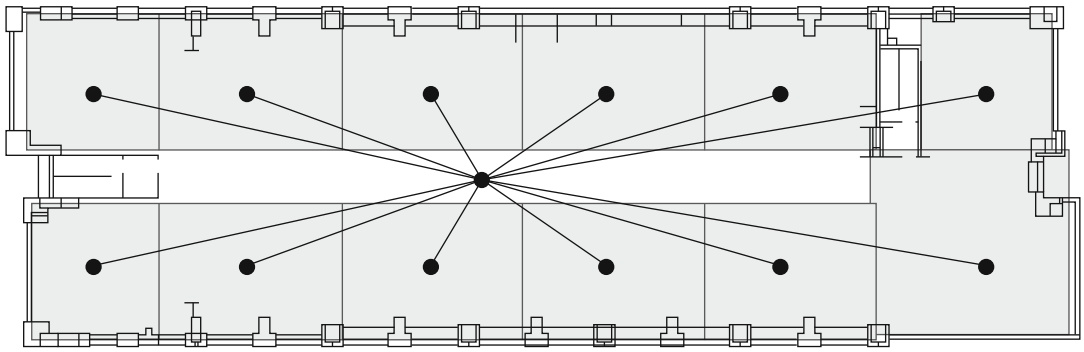

Fig. 60.8 First example of the segmented office floor plan

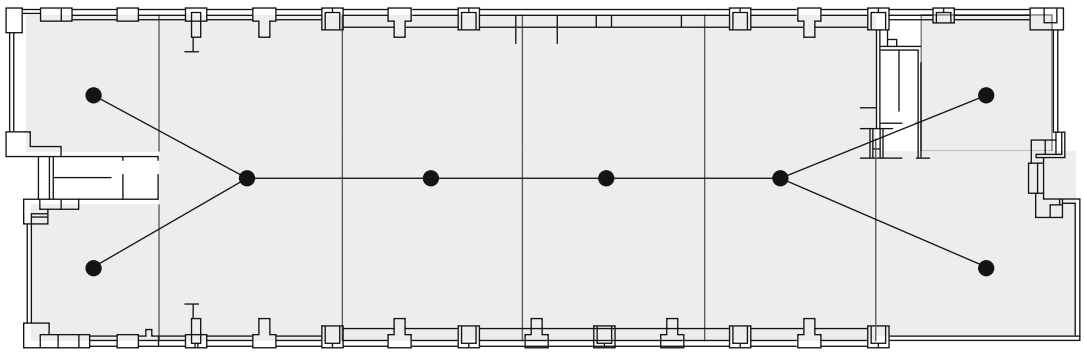

Fig. 60.9 Second example of the segmented office floor plan

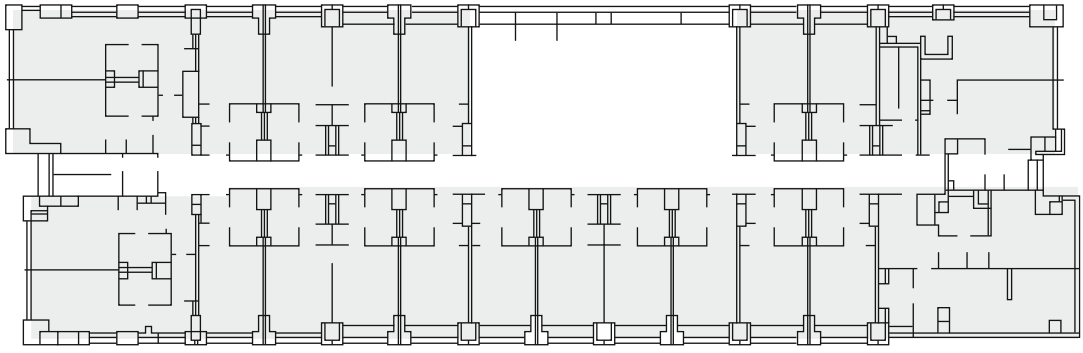

Fig. 60.10 Physical segmentation of hotel design providing a more apparent coarse node network

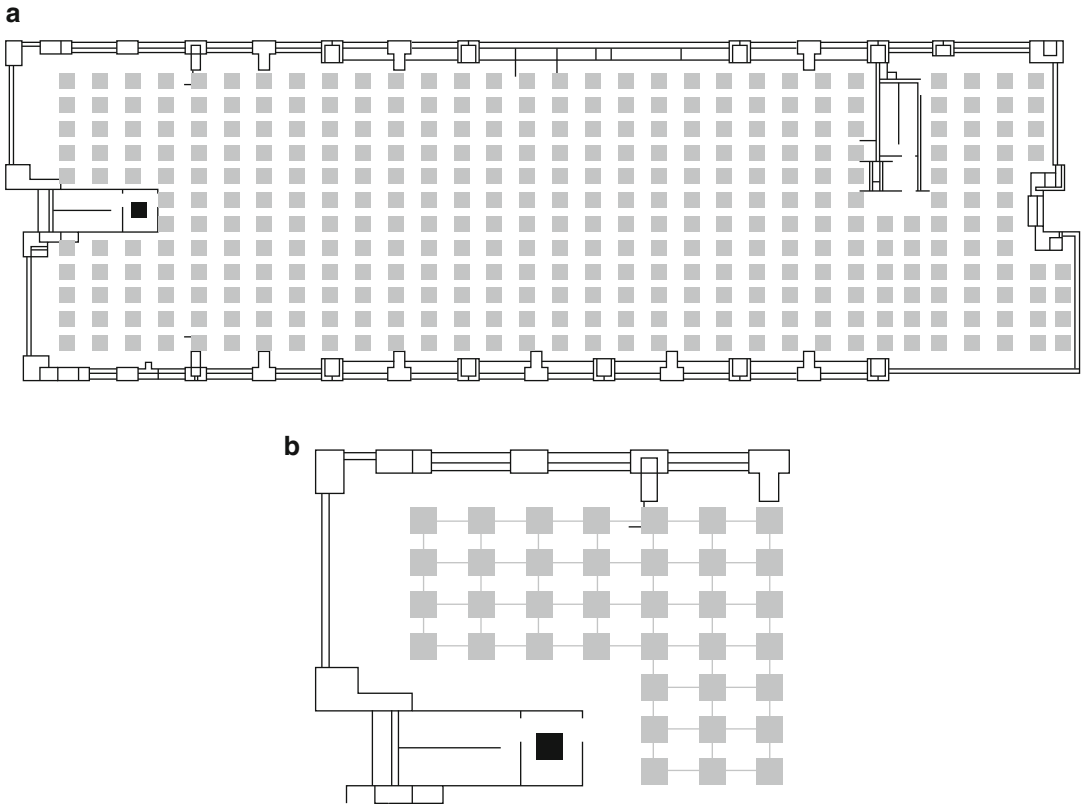

Fig. 60.11 (**a**) Fine nodal mesh; (**b**) horizontal and vertical connections between nodes

with compartments. In this floor plan, the physical structure adequately defines the separate spaces required. The main area of flexibility in the association of the design to a coarse network is the large hallway. Depending on the length of the hallway, the space might require multiple segmented areas rather than representing it as a single node.

Fine Network Grid Figure 60.11a shows a meshed open floor plan for a fine network grid. In comparison to the coarse network, the fine network requires a larger number of small nodes to mesh the geometry. Also the fine network grid is performed at a different level of refinement with the mesh relating directly to occupiable space rather than compartments.

Instead of describing the passage of individuals between components, the nodes are describing the movement of evacuees at a much higher resolution. In Fig. 60.11b the initial steps in this process are shown where the nodes displayed are connected horizontally and vertically. Normally this process would continue to also include diagonal connections to provide the occupants with a greater degree of freedom in their movement.

Figure 60.12a shows the hotel floor plan partially meshed with a fine nodal grid. This is a time-consuming and error-prone procedure if performed manually, given the number of nodes that need to be produced and the precision with which they would need to be positioned. Normally this process would be automatic or semi-automatic, with the mesh being calculated and imposed by the model. Even so, the user would need to check and modify the mesh to determine whether the algorithm in question had represented the occupied space with sufficient accuracy. Figure 60.12b is color coded (shown in different shades of gray here) to show that the connectivity of the rooms should reflect the ability of the simulated occupants to move from space (or component) to space. In other words, the simulated occupant would not be able to pass through a physical barrier (e.g., a wall) that might be present in the actual structure.

Continuous Network Figure 60.13 shows the occupied space within the hotel structure as depicted by a continuous network. As previously described, a continuous network model represents the building floor plan as a continuous plane that simulates the occupants' movement on a coordinate-based system over all occupiable space. Instead of occupants occupying blocks of

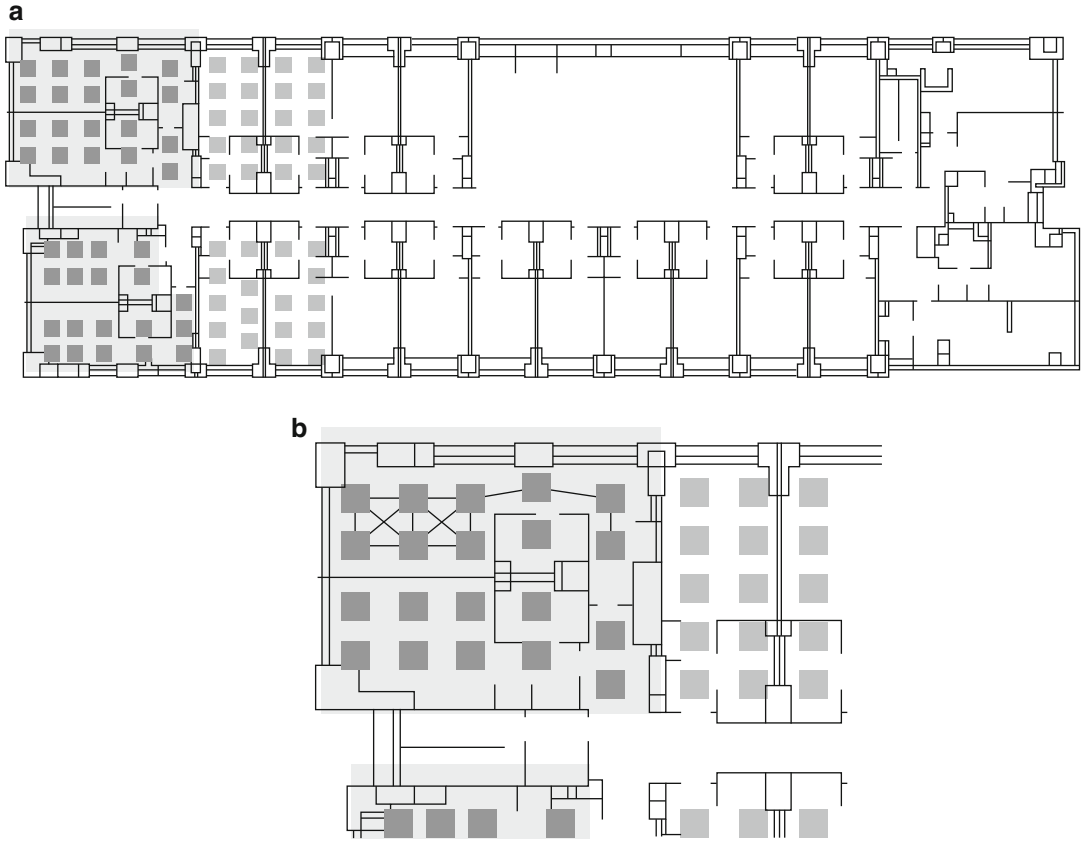

Fig. 60.12 (**a**) Example of fine mesh applied to hotel geometry; (**b**) connectivity of a section of this geometry

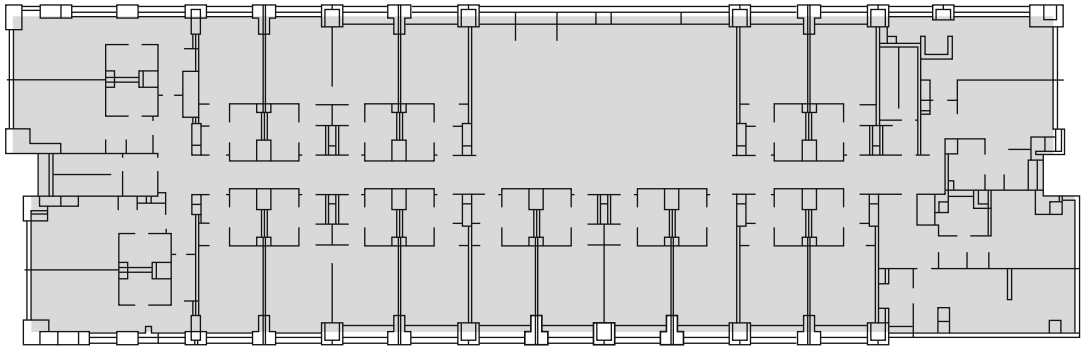

Fig. 60.13 Occupiable space within the hotel structure, represented by a continuous plane

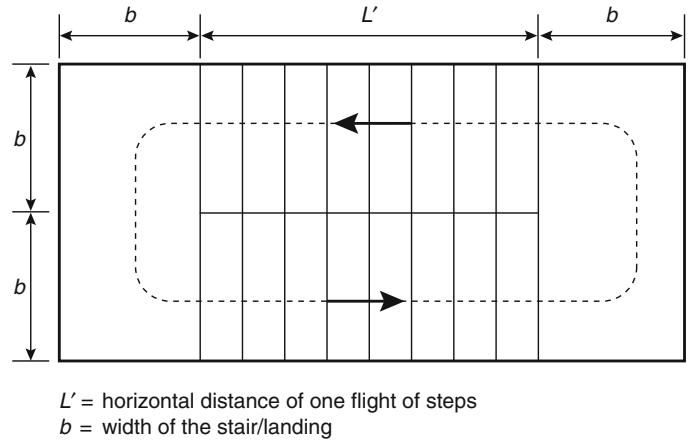

Fig. 60.14 Graphic drawn to explain the stair calculation (Predtechenskii and Milinskii [24], p. 28)

space (coarse network) or square nodes (fine grid), a continuous model simulates occupant movement on a flowing *x*-*y* (and *z* for multiple stories) coordinate system. In most instances, this provides a more accurate representation of the floor plan of a building.

Additional Building Information

In addition to the method with which sections of the building are represented and connected, the model also requires the user to identify information about the stairs and exits (location, width, etc.). In this example, there are two 1.1 m (3.6 ft) wide staircases, one at each end of every floor in the building. Depending on the model, the user may be required to provide the distance along the staircase between floors, either the diagonal distance or the horizontal distance. In both cases, the distance along the landings should be taken into account within the distance calculation. In addition, some models allow the user to incorporate certain distances that the simulated agents will remain away from the walls of the stairwell (e.g., to represent a handrail inside the staircase).

An example of a method used to calculate the diagonal distance along a two-flight staircase measuring 1.1 m (3.6 ft) in width, wall to wall, is provided here. For this example, a staircase flight is the portion of the stair that extends half the distance between floors (Fig. 60.14). Following the development of Predtechenskii and Milinskii [24], Equation 60.1 is used to calculate the diagonal distance of one of the stairs located in the hotel/office building.

$$L = \left[2L^{'} / \cos\ (\theta)\right] + 4b \qquad (60.1)$$

where
L = the total diagonal distance of two flights
L' = the horizontal distance of one flight of steps
θ = the inclination of the stair at each flight
b = the width of the stair/landing

In the case of the example, b is equal to 1.1 m (3.6 ft), L' is equal to 2.0 m (6.56 ft), and the angle of the stairs is 37°, which corresponds to 3 m (10 ft) between floors with 8 steps at 19 cm by 25 cm (7.5 in. by 10 in.) riser and tread for each flight. With these values inserted into Equation 60.1, the diagonal distance of the stairs is calculated to be 9.5 m (31 ft).

Evacuation models also require the user to identify the location of the exits within the building. In this example, the exits are placed at the bottom of the staircase directly below floor 1. The occupants reach the exit once they have traveled down the final staircase and out of the 0.9 m (36 in.) door present.

Population Configuration

All evacuation models require the user to specify characteristics about the population in the building. These characteristics, depending on model sophistication, can include the number of people in the building, movement speeds/flows, pre-evacuation times, and specific behaviors. Macroscopic models, for example, require the user to provide only the number of occupants located in the building and/or in specific sections throughout the building and characteristics representative of the entire population instead of individuals. Therefore, the user need not identify specific information about the occupants other than the number and a representative speed and flow for the population. Identifying the number of occupants in the building, which is required by all models, will be described in the following paragraphs.

Number of People Most building evacuation computer models require the user to specify the number of people in the simulated building evacuation. If the project does not specify the number of people, the user can use information on the building type and available floor space to calculate the number of people using occupant load factors [30]. The occupant load factors provided by NFPA *101*®, *Life Safety Code*®, are estimations of the maximum probable number of occupants present in the building type at any time. (Studies have been done [31] showing that the design loads in NFPA *101* may grossly overestimate the number of people expected to be in particular types of buildings.) For a day-time scenario, the NFPA occupant load factors would be used to estimate a conservative number of occupants on each floor of the office space. The maximum occupancy of the hotel rooms will be used as an example to estimate the occupancy of the hotel floor plans.

For a fire initiating at 2 a.m. on the fifth floor of the office/hotel building, it is expected that there will be more people located in the hotel portion of the building compared with the office floors. Using the maximum occupancy figures for each hotel room, 100 occupants per floor are estimated for the hotel room floors. However, due to the time of the scenario (2 a.m.), only 10 people per floor are assumed for the office floors. These people are included to simulate cleaning staff and the possibility of overnight workers.

Overall, the population of the building is estimated to be 1100 people in the entire 20-story building. This number includes 100 people per floor on the hotel floors and 10 people per floor on the office floors.

Movement Another occupant characteristic provided by the user is unimpeded movement speeds of the population and/or individual occupants in the simulated building. For macroscopic models, the user is required to provide an average or overall speed (unimpeded) for the entire population. On the other hand, microscopic models require the user to provide specific information on characteristics of groups within the simulation in addition to the number of occupants in the building. These can include individual speeds (unimpeded), body sizes, and disabilities.

For the hotel/office building example, there are certain factors that can affect the movement speed of individuals in a building. The following list includes factors to consider when choosing unimpeded movement speeds for members of the population:

- The distribution of men/women within the structure
- The age of the occupants simulated
- The body size of the occupants simulated
- The presence of occupants with disabilities

In the case of the 2 a.m. fire scenario, it is of particular interest that the user understands the characteristics of the hotel population expected in the building at the time of the fire. As discussed earlier, some evacuation models require the user to supply only movement speeds for the entire population. For this type of information, please see Chap. 64. However, there are evacuation models that require the user to specify information about the individuals in the simulated building. Since the majority of the people in the building at the time of the fire will be located in the hotel floors, the majority of the research on individual characteristics for this scenario will be made on the hotel population.

Occupant Characteristics Although difficult, the user can obtain information about the gender and the age of the occupants expected to be in the hotel portion of the building at the time of the fire. The scenario information provided in this example specifies that the hotel is expected to house individuals on both leisure and business travel at any time throughout the year. References such as D.K. Shifflet's DIRECTIONS Travel Information System [32] and the American Hotel and Lodging Association [33] contain a wide variety of information from U.S. hotels such as the percentages of male and female guests, a distribution of the ages staying at hotels for all types of stays (e.g., business or leisure stay), and the additional percentage of children present during leisure trips.

With this type of information, the user can identify the type of occupants in the building, according to the requirement of the evacuation model used. Once an occupant population is determined, information on movement speeds of individuals or groups of individuals based on occupant characteristics can be found in Chap. 64. An example of how hotel distribution information has been used to identify the probability of certain occupant sets has been completed by Stiefel et al. [34].

In addition, if the user and/or the project require the simulation of occupants with disabilities, it is important to understand the number of occupants with disabilities expected to frequent this hotel or, in general, hotels within the United States. With that number in mind, there are sources that provide information on unimpeded speeds of occupants with disabilities [35–37].

Pre-evacuation Time Depending on the model, the user may have the opportunity to provide information on pre-evacuation time for the overall population or individual/groups within the building. In the case of the hotel/office building, the literature provides some guidance on data that could be used to represent the pre-evacuation times for an office building and for a hotel building, depending on the factors just mentioned (see Chap. 64).

If the model allows for the assignment of pre-evacuation times to individuals, the office occupants should be assigned a separate distribution from the hotel guests, thereby implicitly simulating the different responses that may be expected given the role and activity of those involved. However, if the model views the population from a macro level, as with the movement data, an average can be assigned to the entire population, being less sensitive to the differences within the populations in question.

When simulating pre-evacuation times, the hotel population should be assigned a pre-evacuation time that takes into account the time of day that the fire will occur. Since the fire in this example occurs at 2 a.m., it is very likely that the hotel population will be sleeping. Before evacuating their room, the occupants will likely need time to wake up to the sound of the alarm,

dress, retrieve needed items (i.e., glasses, wallet, purse, etc.), and wake any other occupants sleeping in their room or in other rooms nearby. When assigning pre-evacuation times to hotel buildings, because there isn't a large amount of recent information [35], it might be more useful to research pre-evacuation times for apartment buildings as well [38].

Behavior/Actions Finally, the user may wish to assign behavior itineraries or actions to certain individuals during the simulated fire evacuation. Many of the evacuation models available do not provide this option to the user; however, for those models that do, the user should be aware of the lack of data in this area. There have been studies done on behaviors performed by occupants in certain building fire evacuations (e.g., see Chap. 58), which can be used to simulate specific behaviors during an evacuation.

For the example with the hotel/office building evacuation, the user can specify that certain hotel occupants, before evacuating, "visit" other hotel rooms to awaken occupants for evacuation. Or, if there are sufficient data available on turn-back behavior in smoke, the user can simulate that certain occupants turn back when/if the smoke becomes too hazardous to travel through. These are only examples of behaviors that can be simulated. Any behaviors that users do simulate, however, should be accompanied by the appropriate data to support such simulations.

Procedural Configuration

Route Choice In the case of the hotel/office building, even though the choice of exits might appear obvious, it would be beneficial to run several different scenarios where the routes adopted by the occupants differ to determine the sensitivity of the results to the choice of route and the robustness of the structural and procedural design. If alternative scenarios are run such as simulating a predefined route as well as a shortest-route option, the user can compare the results and then make suggestions for improvement. If the user is interested in simulating occupants traveling first to a daycare center or other points located in the building and then evacuating, the user would have to make sure that the model had the capability of a predefined route choice.

Representation of Emergency Responders Another procedural choice of the user is to decide whether it is necessary to include the simulation of emergency responders during the evacuation. In the case of the hotel/office building example, the local fire station is located directly across the street from the simulated building. Since the response time of the fire department is expected to be less than 2 min, it is important to consider the simulation of counterflow of the fire department in the stairs, as long as the evacuation model is capable of simulating such activity. Because the response time of the fire department is expected to be short and the response time of the occupants to evacuate is expected to be higher (greater than 10 min), the simulation of the interaction of fire fighters and occupants in the stairways should be considered.

Representation of Technological and Human Resources Last, although many evacuation models do not have the capability of simulating the presence of staff or alarms, the user should consider whether this is an important part of the evacuation to simulate. With the hotel/office building example, staff is available 24 h per day; however, the nighttime staff is limited. Similarly, the same hotel may have a voice alarm system that is present in each of the guest rooms. The user might consider whether these factors will have an effect on the pre-evacuation time of the occupants if they are active during the incident. There are limited data on this feature of an evacuation scenario, but they should be

kept in mind when running scenarios of a fire evacuation and should certainly be discussed when presenting the assumptions on which the simulated scenarios are based.

Incident information

When performing a life safety analysis of a building, the user should simulate a number of different scenarios. In each fire scenario, the user has to decide the location of the fire source. In the hotel/office building example, there are many different locations where a fire could be assumed to begin. Statistics on fires in offices and/or hotels can be consulted to obtain probable places of origin [39]. These statistics depend on the type of building, the time of day, the type of facilities in the building (e.g., hotel kitchen, laundry area, office space, main lobby, etc.), and the possible activities of the occupants (e.g., can occupants smoke in their hotel rooms?). Information can be obtained from NFPA statistics, including the top causes of civilian deaths, causes of injuries, causes of property damage, and frequent areas of origin. The guest room was chosen as the area of origin for this example because even though only 12 % of hotel and motel fires began in bedrooms, these fires caused a majority of the deaths and injuries [39]. Potential causes of this scenario's fire, based on NFPA data, could be intentional, cooking equipment (in the room), and even heating equipment [39]. Scenarios should be run with guestroom doors held open and closed along with fires beginning in other areas/rooms throughout the building.

User Checklist

The discussion in the previous section outlines the types of factors that need to be examined when configuring and applying computational tools. In many cases, it may not be possible to represent all of the factors in the detail desired. This might be due to issues of time, cost, data available and/or modeling limitations. However, irrespective of whether these factors are addressed, the engineer should be mindful of them when configuring the tool, describing what is (and what is not) addressed in the scenarios examined, and in presenting the results.

Figure 60.15 provides a brief checklist of the types of factors and issues that the user should address when selecting and configuring an evacuation model ready for application within a project specification. This list is by no means exhaustive but should at least prompt the user to address the issues that have been discussed in this chapter. Reference should also be made to Chap. 57, where matters of scenario design are discussed in more detail.

Summary

This chapter has provided an overview of 26 current egress models and developed a checklist to be applied when using a new model. Guidance for applying many of the features found in these egress models has been provided. It is not suggested that the guidance provided in this chapter is sufficient for the user to perform the analysis required. However, it is contended that for many, especially those who are relatively inexperienced in egress modeling techniques, the guidance provided is necessary. This chapter could then act as a companion chapter to those provided within this volume to outline the process of egress analysis from the initial identification to the delivery of the end product.

All modeling is a result of compromise and represents a simplification. The guidance provided in this chapter should highlight the decisions that need to be made, the information that is required to make these decisions, and the tools needed to complete the simulation and analytical process. In effect, it acknowledges that compromises have to made, but such compromises must be informed so that they can be defended.

- ❑ Project specifications
  - ❑ What is the nature and scope of the project?
  - ❑ What are the deliverables of the project?
  - ❑ What information is available within the project to frame the egress analysis?
  - ❑ How much time and funding are available to complete the project?
- ❑ Model selection
  - ❑ Background of the model
    - ❑ Who is the model developer or developing institution?
    - ❑ Is the model validated for this type of application? How?
  - ❑ Model characteristics
    - ❑ What is the modeling method inherent in the model?
    - ❑ What is the scope of the model regarding the building, individuals, and the scenarios?
    - ❑ What kind of output does the model produce?
    - ❑ How is the model available for use?
    - ❑ How old is the model and what advancements has it made since its release? Is the model still supported?
    - ❑ What refinement is used in the model for the building and individuals?
- ❑ Model scenarios
  - ❑ What is involved in building configuration?
    - ❑ How does the model allow for structure generation?
    - ❑ How does the model allow for structure representation?
    - ❑ What other kinds of information are needed to supplement the building grid?
  - ❑ What is involved in occupant configuration?
    - ❑ How many occupants are in the building?
    - ❑ What movement data are required by the model?
    - ❑ What occupant characteristics are required by the model?
    - ❑ What pre-evacuation data are required by the model?
    - ❑ What kinds of behavioral inputs are of interest for the population and is there information available to provide as input?
  - ❑ What is involved in scenario configuration?
    - ❑ What fire information, if any, can be provided to the model?
    - ❑ What options for exit route choice are available in the model?
    - ❑ Can the model simulate the influence of counterflow?
    - ❑ Can the model simulate the influence of building staff?
- ❑ What are the computer requirements to run the model?
- ❑ What is the format of the output?
- ❑ How can the output be organized in a manner required by the client?

Fig. 60.15 Factors and issues in selecting and configuring an evacuation model

Acknowledgments My thanks to Steve Gwynne from Natural Research Council Canada for providing guidance and overall direction for the chapter. My appreciation also to those model developers who provided guidance and detailed information on the characteristics of their model, as well as to Jason Averill, Anthony Hamins, and James Milke for providing detailed and insightful suggestions.

References

1. Gwynne, S. and Boyce, K., "Engineering Data," SFPE Handbook of Fire Protection Engineering, Springer, 2015.
2. S.M.V. Gwynne and E.R. Rosenbaum, "Employing the Hydraulic Model in Assessing Emergency Movement," in *SFPE Handbook of Fire Protection Engineering,* 4th ed. (P.J. DiNenno et al., eds.), National Fire Protection Association, Quincy, MA, pp. 3-373–3-396 (2015).
3. E.D. Kuligowski and S.M.V. Gwynne, "What a User Should Know About Selecting an Evacuation Model," *Fire Protection Engineering Magazine,* Human Behavior in Fire Issue (2005).
4. E.D. Kuligowski and J.A. Milke, "A Performance-Based Design of a Hotel Building Using Two Egress Models: A Comparison of the Results," in *3rd International Symposium on Human Behavior in Fire,* Interscience Communications Limited, London, UK, pp. 399–410 (2004).
5. S. Gwynne, E.R. Galea, M. Owen, and P. Lawrence, *Validation of the building EXODUS Evacuation Model* (Rep. No. 98/IM/29), University of Greenwich, London (1998).
6. H. Weckman, S. Lehtimaki, S. Oy, and S. Mannikko, "Evacuation of a Theatre: Exercise vs. Calculations," *1st International Symposium on Human Behaviour in Fire* (T.J. Shield, ed.), University of Ulster, Fire Safety Engineering Research and Technology Centre, Belfast, pp. 479–488 (1998).
7. J. Lord, B. Meacham, A. Moore, R.F. Fahy, and G. Proulx, *Guide for Evaluating the Predictive Capabilities of Computer Egress Models* (Rep. No. NIST GCR 07-886), National Institute of Standards and Technology, Gaithersburg, MD (2005).
8. H.E. Nelson and F.W. Mowrer, "Emergency Movement," in *SFPE Handbook of Fire Protection Engineering,* 3rd ed. (P.J. DiNenno et al., eds.), National Fire Protection Association, Quincy, MA, pp. 3-367–3-380 (2002).
9. S. Gwynne, E.R. Galea, P.J. Lawrence, M. Owen, and L. Filippidis, "A Review of the Methodologies Used in the Computer Simulation of Evacuation from the Built Environment," *Building and Environment,* 34, pp. 741–749 (1999).
10. H.E. Nelson, "Emergency Evacuation Flow Models," in *U.S./Japan Government Cooperative Program on Natural Resources, Fire Research and Safety, 6th Joint Panel Meeting of the UJNR,* Building Research Institute, Ibaraki, Japan, pp. 282–354 (1982).
11. J.M. Watts, "Computer Models for Evacuation Analysis," *Fire Safety Journal,* 12, pp. 237–245 (1987).
12. S.M. Olenick and D.J. Carpenter, "Updated International Survey of Computer Models for Fire and Smoke," *Journal of Fire Protection Engineering,* 13, pp. 87–110 (2003).
13. R.L. Paulsen, *Human Behavior and Fire Emergencies: An Annotated Bibliography* (Rep. No. NBSIR 81-2438). National Bureau of Standards, Gaithersburg, MD (1981).
14. P.A. Thompson, "Developing New Techniques for Modelling Crowd Movement," Ph.D. Dissertation, Department of Building and Environmental Engineering, University of Edinburgh, Scotland (1995).
15. Davis Associates, L. "Managing Large Events and Perturbations at Stations," Passenger Flow Modeling Technical Review RS021/R.03. Rail Safety and Standards Board, London, UK (2003).
16. E.D. Kuligowski, R.D. Peacock, and B.L. Hoskins, A *Review of Building Evacuation Models, 2nd Edition* (Rep. No. NIST TN 1680) National Institute of Standards and Technology, Gaithersburg, MD (2010).
17. H.W. Hamacher and S.A. Tjandra, "Mathematical Modelling of Evacuation Problems: A State of the Art," in *Proceedings of Pedestrian and Evacuation Dynamics* (M. Schreckenberg and S.D. Sharma, eds.), Springer-Verlag, Duisburg, Germany (2000).
18. G. Sharp, S. Gwynne, and E.R. Galea, *The Effects of Ship Motion on the Evacuation Process, Subsection 3.1, Critical Review on Model of Evacuation Analysis* (Rep. No. RESEARCH PROJECT 490). Report for the MCA by the Fire Safety Engineering Group, University of Greenwich, London (2003).
19. H. Klupfel and T. Meyer-Konig, "Characteristics of the PedGo Software for Crowd Movement and Egress Simulation," in *2nd International Conference in Pedestrian and Evacuation Dynamics (PED),* University of Greenwich, London, UK, pp. 331–340 (2003).
20. E.D. Kuligowski, *The Evaluation of a Performance-Based Design Process for a Hotel Building: The Comparison of Two Egress Models; Chapter 2,* M.S. paper, University of Maryland, College Park (2003).
21. G. Santos and B.E. Aguirre, "Critical Review of Emergency Evacuation Simulation Models," in *Workshop on Building Occupant Movement During Fire Emergencies* (R.D. Peacock and E.D. Kuligowski, eds.), National Institute of Standards and Technology, Gaithersburg, MD, pp. 27–52 (2005).
22. Evacmod.net, Accessed June 17, 2013.
23. J.J. Fruin, *Pedestrian Planning and Design* (rev. ed.), Elevator World, Inc., Mobile, AL (1987).
24. V.M. Predtechenskii and A.I. Milinskii, *Planning for Foot Traffic in Buildings,* Amerind Publishing Co. Pvt. Ltd., New Delhi (1978),

25. Summerland Fire Commission, *Summerland Fire Commission Report,* Isle of Man Government Office, Douglas, Isle of Man (1974).
26. J.D. Sime, "The Outcome of Escape Behaviour in the Summerland Fire: Panic or Affiliation," in *Proceedings of the International Conference on Building Use and Safety Technology,* National Institute of Building Sciences (1985).
27. J. Li and W.K. Chow, "Numerical Studies on Evacuation Pattern in a Lecture Hall," *Journal of Applied Fire Science,* 10, pp. 265–276 (2000).
28. J.D. Averill, D.S. Mileti, R.D. Peacock, E.D. Kuligowski, N.E. Groner, G. Proulx, et al. *Occupant Behavior, Egress, and Emergency Communications* (Rep. No. NIST NCSTAR 1-7), National Institute of Standards and Technology, Gaithersburg, MD (2005).
29. W. Grosshandler, N. Bryner, D. Madrzykowski, and K. Kuntz, *Report of the Technical Investigation of the Station Nightclub Fire* (Rep. No. NIST NCSTAR 2: Vol. 1), National Institute of Standards and Technology, Gaithersburg, MD (2005)
30. NFPA *101®, Life Safety Code®,* 101-65-101-66. National Fire Protection Association, Quincy, MA (2006).
31. J.A. Milke and A.C. Caro, "Survey of Occupant Load Factors in Contemporary Office Buildings," *Journal of Fire Protection Engineering,* 8, pp. 169–182 (1997).
32. DKS&A, Distribution of Hotel Stays, Internet communication (2003).
33. American Hotels and Lodging Association (AHLA), Distribution of Hotel Stays, Internet communication (2003).
34. S.W. Stiefel, R.W. Bukowski, J.R. Hall, and F.B. Clarke, *Fire Risk Assessment Method: Case Study 3, Concealed Combustibles in Hotels* (Rep. No. NISTIR 90-4245). National Institute of Standards and Technology, Gaithersburg, MD (1990).
35. R.F. Fahy and G. Proulx, "Toward Creating a Database on Delay Times to Start Evacuation and Walking Speeds for Use in Evacuation Modeling," in *2nd International Symposium on Human Behaviour in Fire,* Interscience Communications, London, pp. 175–183 (2001).
36. K.E. Boyce, T.J. Shields, and G.W.H. Silcock, "Toward the Characterization of Building Occupancies for Fire Safety Engineering: Capability of Disabled People Moving Horizontally and On an Incline," *Fire Technology,* 35, pp. 51–67 (1999).
37. J.L. Bryan, "Behavioral Response to Fire and Smoke," in *SFPE Handbook of Fire Protection Engineering,* 4th ed. (P.J. DiNenno et al., eds.), National Fire Protection Association, Quincy, MA, pp. 3-320–3-354 (2008).
38. P. Brennan, "Modelling Cue Recognition and Pre-Evacuation Response," in *6th International Symposium,* International Association for Fire Safety Science, Boston, MA, pp. 1029–1040 (1999).
39. M. Ahrens, *U.S. Hotel and Motel Structure Fires,* National Fire Protection Association, Quincy, MA (Feb. 2008).

Erica D. Kuligowski is a fire protection engineer and sociologist in the Engineering Laboratory at the National Institute of Standards and Technology (NIST). Her research interests include human behavior in fires, and other emergencies, including preparedness, responses, and recovery behaviors, behavioral modeling of response and recovery; and emergency communications.

Visibility and Human Behavior in Fire Smoke

61

Tokiyoshi Yamada and Yuki Akizuki

Introduction

This chapter presents the scientific basis for establishing effective safety evacuation countermeasures, that is, evacuation plans, escape signs, and so forth in case of fire. The data were obtained in Japan, but should provide more general guidance internationally. In particular, issues of physical and physiological effects of fire smoke on evacuees are addressed. The chapter consists of three sections: (1) visibility, (2) characteristics of human behavior, and (3) development of an intensive system for escape guidance in fire smoke.

In Japan, since the 1960s, an increasing number of people have been killed by smoke in fire-resistant buildings. Toxic gases and/or depletion of oxygen in fire smoke are the final causes of death of those victims. However, many evacuees are trapped in an early stage of fire by relatively thin smoke, and loss of visibility is an indirect but fatal cause of death. For this reason, the relations between the visibility and optical density of fire smoke were examined experimentally, and practical equations were proposed.

For further understanding of inability of human behavior in fire smoke, many investigations were conducted by interviewing evacuees and analyzing questionnaires. Also, experimental research was carried out with subjects under limited fire smoke conditions and the threshold of fire smoke density for safe evacuation was examined.

Through many field investigations of fires, it is found that an effective guidance sign system is required for safe evacuation in fire smoke. Improvements of conspicuous exit signs have been conducted under various conditions i.e., size, shape, luminance and/or adding flashing light sources. Also, special types of escape guidance instruments were developed. One involves a continuously traveling flashing light source system, the effectiveness of which was examined in a smoke-filled corridor with reduced visibility. The other is a directional sound escape guidance system; its effectiveness was also examined in a smoke-free corridor. These innovative technologies for safe evacuation are now in practical use in Japan in a large underground shopping mall and in facilities used by people with impaired sight and hearing. The former technique is already found in floor lighting of passenger aircraft cabins.

Visibility

Introduction

Generally speaking, three factors are closely related to visibility: environmental conditions, object's conditions and human visual ability. The former two factors define visual stimulus,

T. Yamada (✉)
National Research Institute of Fire and Disaster, Jindaijihigashi-machi 4-35-3, Chofu, Tokyo 182-8508, JAPAN

Y. Akizuki
University of Toyama, Gofuku 3190, Toyama, Toyama 930-8555, JAPAN

M.J. Hurley (ed.), *SFPE Handbook of Fire Protection Engineering*,
DOI 10.1007/978-1-4939-2565-0_61, © Society of Fire Protection Engineers 2016

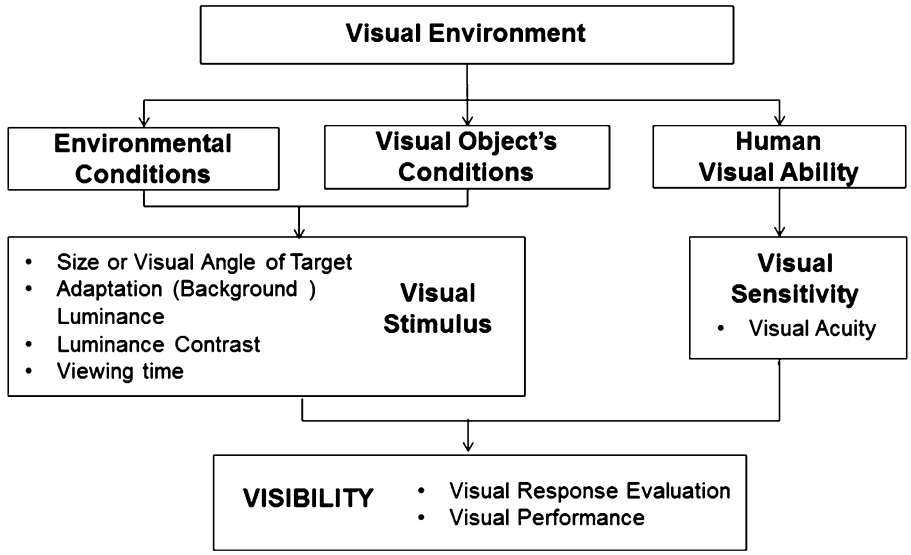

Fig. 61.1 Evaluation system for visibility

and the latter one defines visual sensitivity. Visual response evaluation, namely visibility depends on both visual stimulus and visual sensitivity. Visual stimulus is represented by four elements, namely size [m] or visual angle [minutes] of a visual target, adaptation (background) luminance L_b [cd/m^2], luminance contrast between the visual target luminance and background luminance, and viewing time. If the viewing time is more than 100 ms, the visibility becomes stable regardless of time [1]. The evaluation system of visibility is shown in Fig. 61.1. We can treat visual response evaluation and visual performance, like visible distance or threshold value, as the visibility. Human visual ability consists of many functions like field of view and color sensitivity and so on, but usually the most important is visual acuity (VA).

Visual Acuity

Visual acuity (VA) shows clearness of vision, which is dependent on the sharpness of the retinal focus within the eye. VA can be defined the spatial resolution of the visual processing system, and measured by identifying the direction of characters like letters and numbers on a test chart from a set distance. Normally VA refers to the ability to resolve two separated points or lines, but there are other measures of the ability of the visual system to discern spatial differences. The chart characters are represented as black symbols against a white background for maximum contrast more than 0.9. The distance between the observer's eyes and the test chart is set at a sufficient distance to approximate infinity in the way the lens attempts to focus.

Visual acuity is often measured according to the size of letters viewed on a Landolt ring chart or the size of other symbols, such as Snellen chart or Tumbling E.

The Landolt C (see Fig. 61.2) consists of a ring that has a gap, thus looking similar to the letter C. This is identical to the letter C from a Snellen chart. It was developed by the French ophthalmologist Edmund Landolt, and this optotypes was adopted in 1909 at the 11th International congress of Ophthalmology. The Landolt C is the standard optotypes for visual acuity measurement in most European countries and Japan. It was standardized, together with measurement procedures, by ISO 8596–2009; ophthalmic optics -visual acuity testing—standard optotypes and its presentation [2]. The ISO specifies a range of Landolt C optotypes and describes a method for measuring distance visual acuity under daylight conditions for the purposes

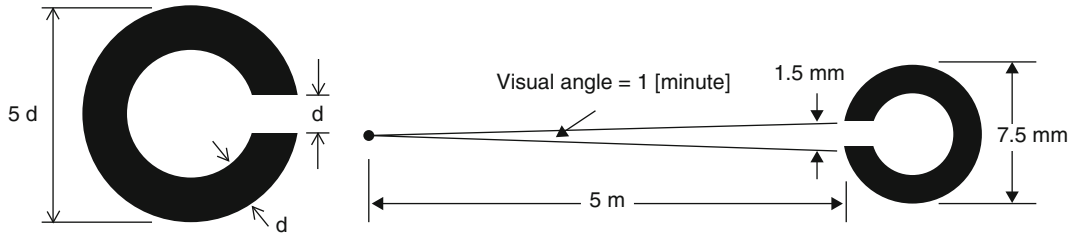

Fig. 61.2 Landolt C as the standard optotypes for visual acuity test

of certification or licensing. The stroke width is one-fifth of the diameter, and the gap width is the same. The height and width of the optotypes (letter) is five times the thickness of the line. The gap can be at various positions (usually left, right, bottom, top and the 45° positions in between) and the task of the tested person is to decide on which side the gap is. The size of the C and its gap are reduced until the subject makes a specified rate of errors. The minimum perceivable angle of the gap is taken as measure of the visual acuity. In the decimal system, the visual acuity is defined as the reciprocal value of the size of the gap (measured in arc minutes) of the smallest Landolt ring that can be reliably identified. Normal visual acuity is frequently considered to be what was defined by Landolt C as the ability to recognize an optotypes when it subtended 1 min of arc (1.00 decimal) or Snellen's chart 20/20 ft (6/6 m). For example a person who can correctly identify Landolt C on the 1.45 mm gap from 5 m distance, i.e. he can discern the gap that are separated by a visual angle of 1 arc minute, his visual acuity is described as 1.0. There is no unit of visual acuity value by Landolt C.

The charts usually display several rows of optotypes (test symbols), each row in a different size (see Fig. 61.3).

A Snellen chart (see Fig. 61.4) is an eye chart used by eye care professionals and others to measure visual acuity. Snellen charts are named after the Dutch ophthalmologist Herman Snellen who developed the chart in 1862. The traditional Snellen chart is printed with 11 lines of block letters. The first line consists of one very large letter, which may be one of several letters, for example E. When printed out at this size, the E on line one will be 88.7 mm (3.5 in.) tall and

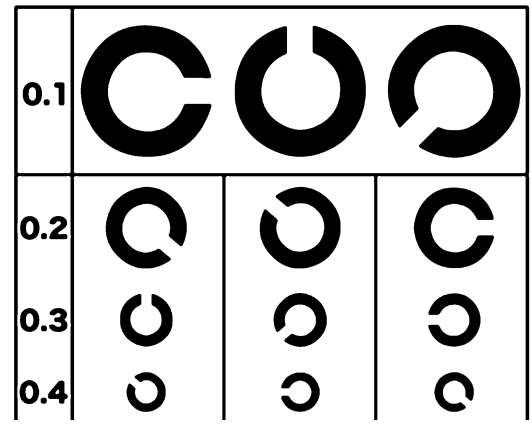

Fig. 61.3 Landolt C optotypes

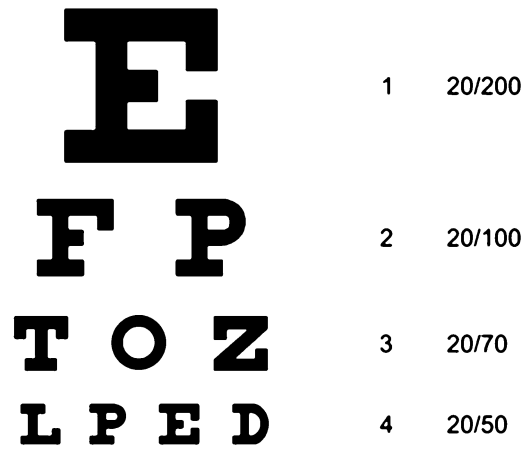

Fig. 61.4 Snellen optotypes

when viewed at a distance of 20 ft, you can estimate your eyesight based on the smallest line you can read. At 20 ft, the letters on the 20/20 line should subtend 5 min of arc. Outside of the US, the standard chart distance is 6 m,

normal acuity is designated 6/6, and other acuities are expressed as ratios with a numerator of 6. If the room don't have 6 m available, and either a half-size chart subtending the same angles at 3 m, or a reversed chart projected and viewed by a mirror is used. By Snellen's normal visual acuity is commonly referred to as 20/20 vision, the metric equivalent of which is 6/6 vision. At 20 ft or 6 m, a human eye with nominal performance is able to separate lines that are 1 arc minute apart a value of 1.0 is equal to 20/20.

Effect of Age on Visual Acuity

There is a significant difference of visual acuity not only among age groups (young/aged) but also among individuals [3]. Figure 61.5 shows the relationship between age and visual acuity by Landolt C chart at near point.

Visual acuity is much better in bright light than dim light. Figure 61.6 shows the relationship between visual acuity and background luminance of Landolt C Chart (the contrast is 0.94) for different age groups [4]. Visual acuity was enhanced with higher luminance. In Fig. 61.6, there are large variations among individual results, but positive correlations were confirmed between visual acuity and background luminance. Equation 61.1 shows the relationship between luminance and visual acuity in the two age groups.

$$VA = \gamma \times (\log_{10} L_b + 1.85)$$
$$\because \gamma_{\text{aged}} = 0.17, \gamma_{young} = 0.34 \quad (61.1)$$

where visual acuity is VA[-], the background luminance of Landolt C chart is L_b [cd/m^2], and age-related constant number is γ[-]. Equation 61.1 shows that the visual acuity of the aged group consistently was about one half of that of the young group under any luminance levels. Therefore, representing visibility under light conditions meant considering age differences by visual acuity.

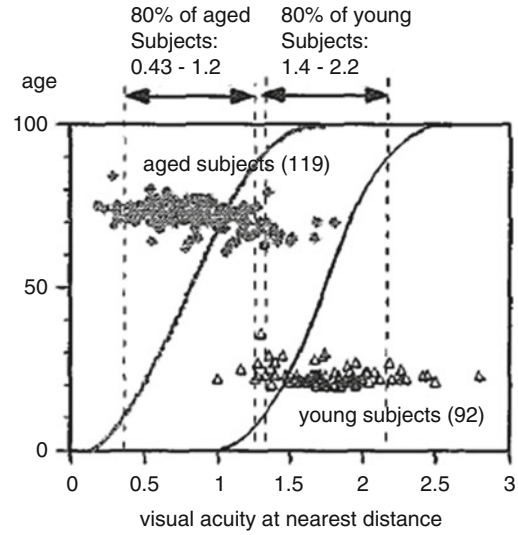

Fig. 61.5 Relationship between age and visual acuity at near point by Landolt C chart [3]

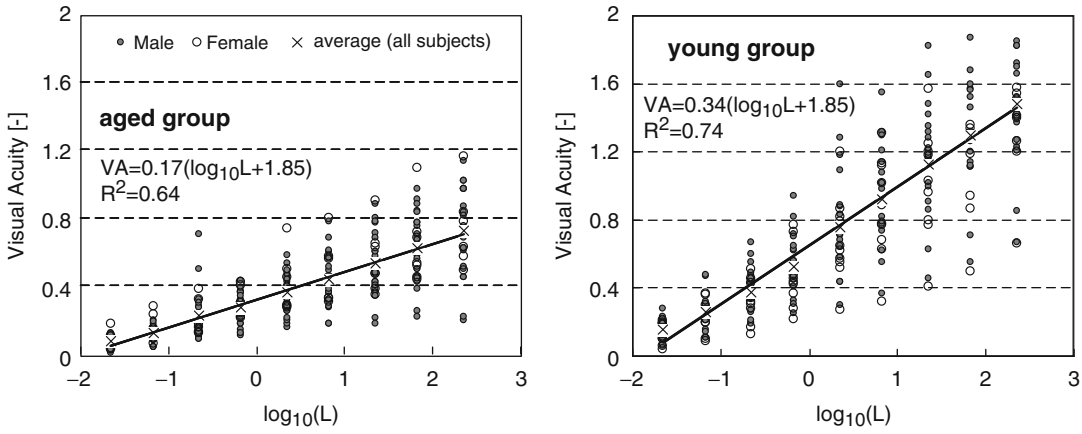

Fig. 61.6 Relationship between background luminance and visual acuity [4]

Visibility in Fire Smoke

Introduction

There has been much research on visibility in fog in the past, whereas relatively little research has been carried out on visibility in fire smoke. This difference is due mainly to the physical characteristics of these composite particles. Fog is composed of water mist and the individual particles are spherical. The particle size is also relatively stable in time and space. These simple characteristics enable a visibility model in fog to be developed. On the other hand, the characteristics of fire smoke, that is, composition, shape, and size of the particles, depend on the combustible materials involved and the conditions of combustion. These characteristics are also highly dependent on surrounding flow and temperature fields and vary with time.

Figure 61.7 shows the result of measuring the relationship between visibility and smoke density on the extinction coefficient obtained from experiments performed in Japan [5]. Data vary under different smoke conditions although the correlation is roughly linear. There are two reasons for the decrease in visibility through smoke: (1) luminous fluxes from a sign and its background are interrupted by smoke particles and reduce its intensity when reaching the eyes of a subject, and (2) luminous flux scattered from the general lighting of corridors or rooms by smoke particles in the direction of a subject's eyes is superimposed on the reduced flux mentioned in (1).

The human eye can distinguish a sign from the background in smoke only when the difference between the luminance of the sign and the background luminance is larger than some threshold value of luminance contrast, that is, when the following Equation 61.2 can be established between the sign's luminance L_t[cd/m^2], the background luminance L_b[cd/m^2], and the threshold value of luminance contrast, δ_c:

$$\left|\frac{L_t - L_b}{L_b}\right| \geq \delta_c \qquad (61.2)$$

The value (the threshold contrast of signs) varies depending on the intensity of luminous flux from the background and the properties of smoke, but particularly when discussing the visibility in a meteorological fog, a constant value $\delta_c = 0.02$ is normally employed for both day and night.

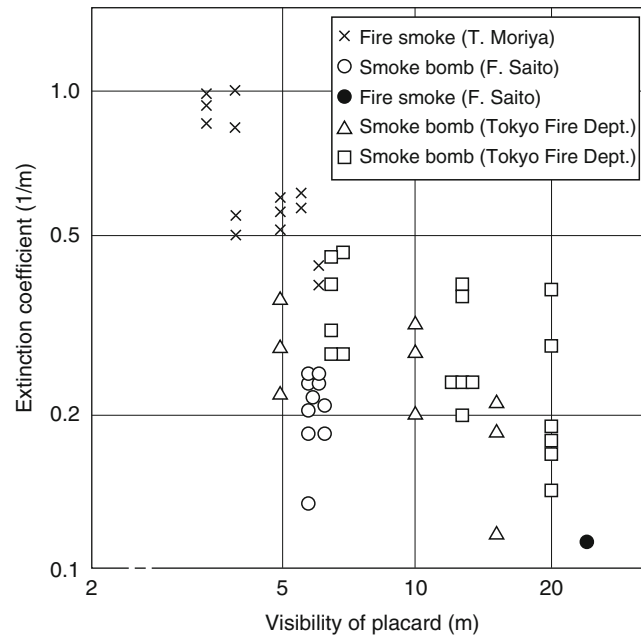

Fig. 61.7 Relation between visibility of the placard-type signs and extinction coefficient by the experiments performed in Japan [5]

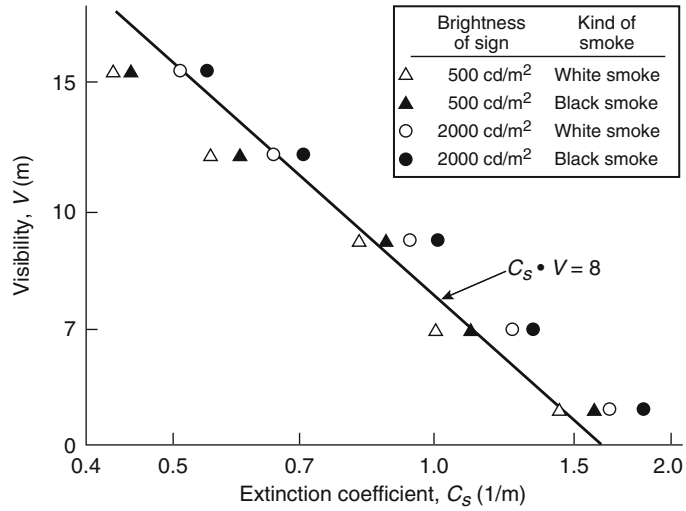

Fig. 61.8 Relation between the visibility of self-illuminated signs at the obscurity threshold and smoke density (extinction coefficient)

Smoke Density and Visibility

Development of a mathematical visibility model based on physical parameters has attracted some researchers, but it is very complicated and tends to be of little practical use. A simple visibility model for signs seen through fire smoke is proposed by Jin as Equation 61.3 [6]:

$$V = \frac{1}{C_s}\log_e\left(\frac{L_t}{\delta_c \alpha E/\pi}\right) \qquad (61.3)$$

where

V = Visibility of signs at the obscuration threshold [m]

C_s = Smoke density expressed by the extinction coefficient [1/m] (hereafter, smoke density will be expressed by the extinction coefficient in 1/m[1])

L_t = Brightness of signs [cd/m^2]

δ_c = Contrast threshold of signs in smoke at the obscuration threshold (0.01 ~ 0.05)

$a = \sigma_s/C_s (0.4 \sim 1.0)$ and $C_s = \sigma_s + \sigma_{ab}$ (σ_s: scattering coefficient; σ_{ab}: absorption coefficient)

E = mean illuminance of illuminating light from all directions in smoke [lm/m^2] or [lx]

The signs in a smoke-filled chamber were observed from outside through a glass window. The results are shown in Fig. 61.8. This shows the relation between the visibility of self-illuminated signs at the obscuration threshold and the density of smoldering smoke (white) or flaming smoke (black). In the range of the visibility of 5–15 m, the product, k, of the visibility, V, at the obscuration threshold and the smoke density, C_s, is almost constant as expressed in Equation 61.4.

$$V = k\frac{1}{C_s} \qquad (61.4)$$

The visibility in black smoke is somewhat better than in white smoke of the same density; this remarkable difference in visibility is not recognized among smokes from various materials. For reflecting signs, the product of the visibility and smoke density is almost constant as well. The product depends mainly on the reflectance of the sign and the brightness of illuminating light. The visibility, V, at the obscuration threshold of signs is found to be

[1] Note that the extinction coefficient C_s can be obtained by the following equation:

$$C_s = -\frac{1}{D}\log_e\left(\frac{I}{I_o}\right)$$

where

I_o = The intensity of the incident light [cd]

I = The intensity of light through smoke [cd]

D = Light path length [m]

$$V = \frac{5}{C_s} \sim V = \frac{10}{C_s} \quad \text{for a light-emitting sign} \tag{61.5}$$

and

$$V = \frac{2}{C_s} \sim V = \frac{4}{C_s} \quad \text{for a reflecting sign} \tag{61.6}$$

The visibility of other objects such as walls, floors, doors, stairways, and so forth in an underground shopping mall or a long corridor varies depending on the interior and its contrast condition; however, the minimum value for reflecting signs may be applicable.

Visibility of Signs Through Smoke

Visibility of exit signs: Additional experiments on visibility of various signs in nonirritant white smoke have been conducted [7] under similar conditions to obtain empirical formulae. There are two types of exit sign currently used in Japan. One is rectangular and the other is square type. The technical standard of the latter was newly prescribed in 2000 by the Fire and Disaster Management Agency [8]. The ordinary type has a light box with an internal light source and a pictograph is lit from behind. As for the new type exit sign, a pictograph is lit from the side section at the top of the pictogram plate by using an inner scattering effect. There are three sizes, i.e. "Small" or "C-class", "Medium" or "B-class" and "Large" or "A-class" with different light sources respectively. The visibility of three exit signs as listed in Table 61.1 was examined.

The data describe above [6] were somewhat scattered, however the correlation expressed by Equation 61.4 in additional experiments [7] is more precise and suitable to the data as shown in Fig. 61.9.

The obscurity threshold is about 10 m for ordinary light-emitting exit sign and 13 m for new small exit sign under 1.0 [1/m] smoke density condition respectively, whereas the B-class exit sign is twice as visible as others due to size effect.

It should be noted that the constant k in Equation 61.4 tends to be larger than the previous data indicated by Jin [6, 9]. Therefore these experimental data were obtained under nonirritant white smoke without background light source condition.

Collins showed other results of visibility of exit signs through smoke [10]. Twelve exit signs of different design were evaluated. Results indicated the importance of sign luminance in determining the visibility through smoke. Signs with mean luminance above 70 [cd/m^2] required substantially greater optical density value for obscuration and longer time to disappearance. The optical density required to obscure these signs was between 0.07 and 0.16 [1/m], in line with the densities

Table 61.1 List of test exit signs and visibility in smoke

No.	Type	Appearance	Size (cm) height × width	Light source	Average luminance (cd/m^2)
1	Ordinary type exit sign (small)		12.5 × 36.0	One fluorescent light tube of 10 W	700
2	New type exit sign (B class)		22.5 × 22.5	One CCFL (cold cathode fluorescent lamp) of 3 W	800
3	New type exit sign (C class)		14.0 × 14.0	One CCFL of 2 W	250

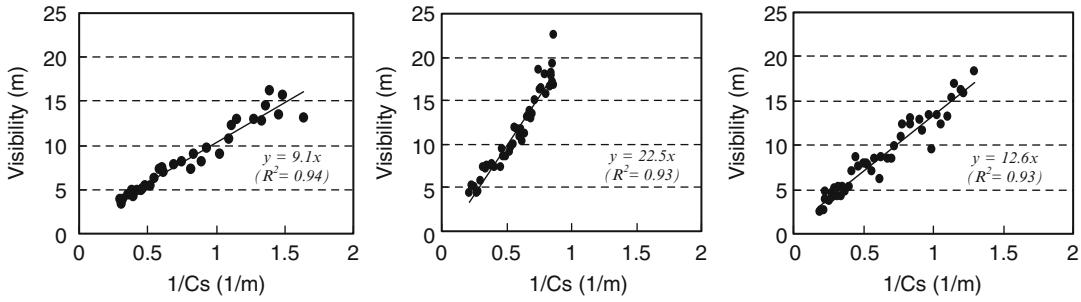

Fig. 61.9 Relation between the visibility of ordinary exit sign at the obscurity threshold and inverse of smoke density through nonirritant white smoke (*left*: Small, *middle*: B-class, *right*: C-class)

observed by Rea [11]. Also Jin [9] determined that exit signs with higher luminance were more visible through smoke.

Visibility of Emergency Lights

There are various types of emergency lights in different installation locations such as buildings and ships The main purpose of the lights is to preserve light in case of power failure. And it is also expected to work for aiding evacuation where no exit signs are equipped such as stairwells in buildings or engine rooms in ships etc. The configuration of the emergency light, i.e. size, color and luminance etc., is different from those of the exit sign as above, and the visibility and the conspicuousness through smoke is different as shown in Table 61.2. Visibility of such emergency lights depends on luminance intensity and distribution of light. General types of emergency lights can be seen at about 10 m under 1.0 [1/m] smoke density condition as mentioned above. In general, narrow light distribution giving high luminance intensity like halogen lamp #1 type improves visibility, however it should be noted that the narrow light beam is too directive to recognize it as a light source from outside of luminous area under thick smoke condition. It is not conspicuous once evacuees stay away from the light axis.

Visibility of Colored Signs

Figure 61.10 shows the change of the relative spectral extinction coefficient (ratio of spectral extinction coefficient to that at a wavelength of 700 nm) with time for smoldering wood smoke. It indicated that reduction of the longer wavelength (red light) is small compared with the shorter wavelength (blue light) in fire smoke. And the reduction (gradients of the curve in the figure) changes with time due to change in the size of smoke particles. In practical aspect, the result supports common knowledge, i.e. "red colored signs are more visible and stable compared with blue colored signs in fire smoke".

The figure shows that the visibilities of red-lighted signs are 20–40 % larger for smoldering smoke. This fact indicates that visibility varies by only a few tens of percent at the most by changing the color while keeping the brightness constant. If we need to double the visibility of a conventional sign, there is no other way but to increase the brightness by a significant factor (see Equation 61.3).

Decrease of Visibility in Irritant Smoke

A 20-m-long corridor was filled with smoke corresponding to an early stage of fire; a highly irritant white smoke was produced by burning wood cribs with narrow spacing between the sticks,

Table 61.2 Lists of test emergency lights and visibility in smoke

No.	Type	Purpose of utilization	Light source area		Max-luminance (cd/m^2)[a]	Illuminance (tx)[b]	Regression linear function	
			Appearance	Size (cm)			Slope (k_1_)	Intercept (k_2_)
1.	Ordinary emergency light	Emergency light and exit sign used for ship		9.5	10,000	7	4.5	3.4
2.	Hanging lamp	Emergency light		13.0	1000	3	9.2	2.1
3.	Halogen lamp #1	General purpose, (unidirectional)		5.5	10,000	690	47.6	−6.3
4.	Halogen lamp #2	General purpose (wide-directional)		5.5	60,000	34	32.9	−3.9
5.	MIL standard emergency lamp	Emergency light based on US military specification		10.0	16,230	103	8.9	2.0

[a]"Max luminance" was the highest luminance of light source surface
[b]"Illuminance" was the vertical illuminance from 1m against the light source center

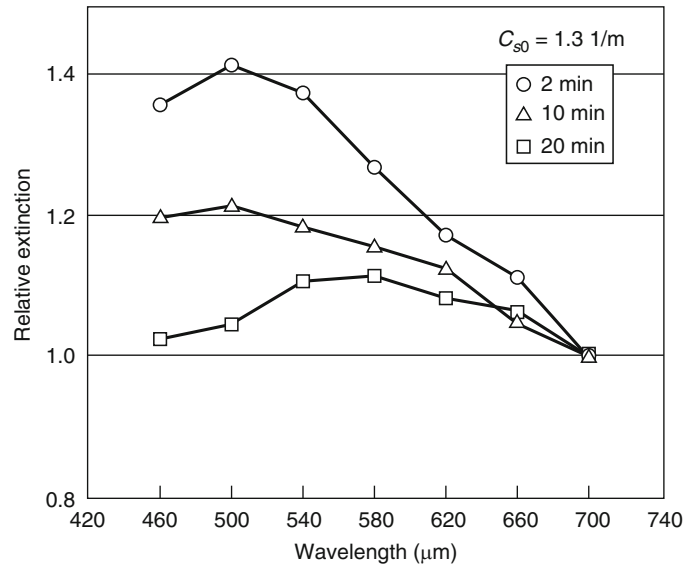

Fig. 61.10 The change of the relative spectral extinction coefficient with time for smoldering smoke from wood. C_{s0} = Initial smoke density

and a less irritant black smoke was produced by burning kerosene. The subjects were instructed to walk into the corridor from one end, or to record the places where they saw a lighted FIRE EXIT sign (signs of the type used before 1982) at another end, or to read the words on the signs [6, 9].

For the obscuration threshold of the sign, the following relation can be found: $C_sV \cong$ constant.

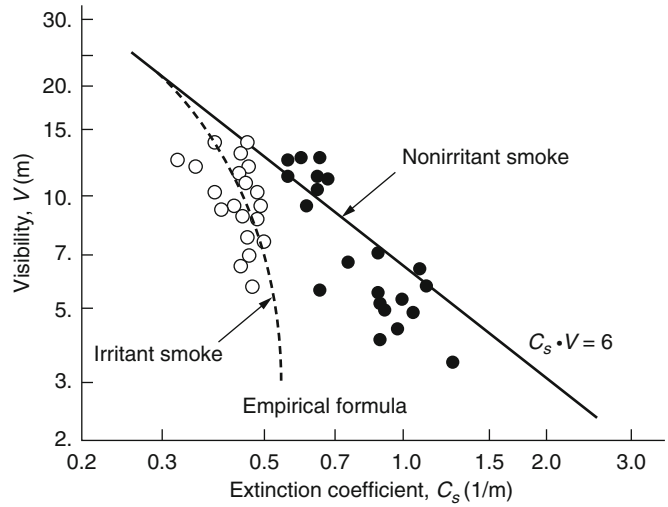

Fig. 61.11 Visibility of the FIRE EXIT sign (signs of the type used before 1982) at the legible threshold of the words in irritant and nonirritant smoke

However, for visibility at the legible threshold of words, this relation can only apply to nonirritant smoke, as shown in Fig. 61.11.

The visibility in irritant smoke decreases sharply at a smoke density exceeding a certain level. In thick irritant smoke under 0.5 [1/m], the subjects could only keep their eyes open for a short time and tears ran so heavily that they could not see the words on the signs. However, in this case when the exit signs are very simple or sufficiently familiar to the occupants to be recognized at a glance, this irritant effect of smoke may not cause so much trouble in locating the exits. Whereas evacuees cannot keep their eyes open in thicker irritant smoke over 0.5 [1/m]. The smoke irritation reduces the visibility and gives physical annoyance such as sneezing for evacuees and consequently there will be a possibility of needless unrest or lose countenance [12, 13]. The smoke hazards of concern are found not only in such psychological reactions, but also in evacuees' actions, especially walking speed as mentioned in the following section.

Decrease of Visibility Due to Smoke Adhesion on Signs

Under a fire, we have to treat the effects of absorption and scattering of smoke on luminous stimuli: the background luminance, target luminance and luminance contrast. Another factor to

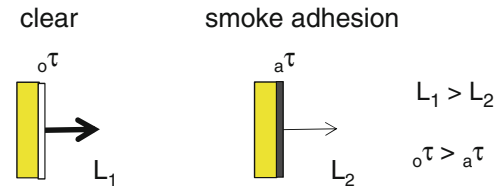

Fig. 61.12 Concept of effect of smoke adhesion on sign's luminance

be considered is that smoke emitted by the fire adheres to the sign surface, light sources, and surrounding walls, causing deterioration of transmission ratio and insufficient light. Therefore, all of them need to be incorporated into the calculation of sign's visibility (see Fig. 61.12). This section proposes a calculation model of target luminance in fire-smoke taking into account of smoke adhesion [14]. The luminance reduction rate due to smoke adhesion ζ is obtained as Equation 61.7 respectively,

$$\zeta = \frac{L_1 - L_2}{L_1} = 1 - \frac{L_2}{L_1} = 1 - \frac{a^\tau}{0^\tau} \qquad (61.7)$$

where L_0 is the initial luminance [cd/m^2], and L_1 and L_2 are the transmitting luminance through glass/acrylic panels [cd/m^2]. $_a\tau$ ($_a\tau \leq {}_0\tau$) is the smoke-adhered transmittance of smoke-adhered glass/acrylic panels, and the initial transmittance of glass/acrylic panels is $_0\tau$ ($0 < {}_0\tau \leq 1$).

Considering the emergency signs, we examined two materials, i.e.: glass (for light sources)

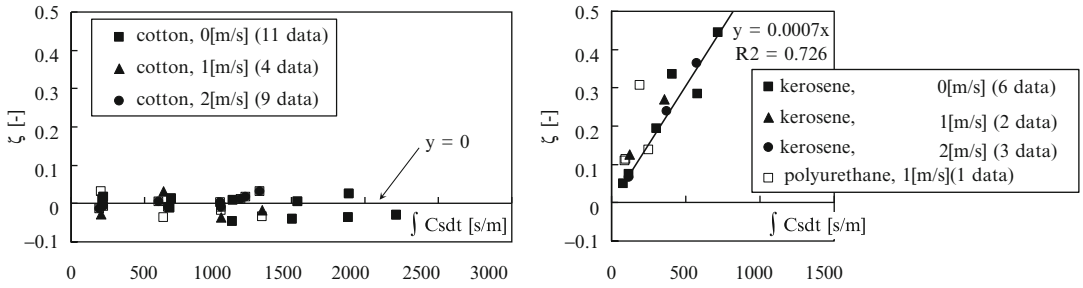

Fig. 61.13 Relationship between e and C_s [14]

and acrylic plate (for emergency signs). It can be concluded that it is not necessary to concern about the effects of the material on smoke adhesion. Rather, fire source affects much more the value of ζ.

As ζ obtained from ${}_a\tau$ is a cumulative result after the transient exposure to smoke in the experiment, we perform the integration of C_s for total exposure time ($\int C_s dt$). In Fig. 61.13, the values of ζ of two kind of smoke (smoldering and flaming smoke) are plotted to versus $\int C_s dt$ for each ventilation velocity. Both kerosene and soft-polyurethane of flaming smoke show linear correlation between ζ and $\int C_s dt$ with similar values of regression coefficient, while in the case of cotton ζ remains around 0 irrespective of $\int C_s dt$. The ventilation velocity may affect the relationship but the difference among the ventilation velocity is not so significant, as long as the present experiments are concerned. We obtained a common regression line for kerosene and soft-polyurethane because they tend to show similar correlations.

Therefore, the relation between ζ and $\int C_s dt$ is represented by

$$\zeta = \eta \int C_s dt \tag{61.8}$$

where the regression coefficient η [m/s] is adhesion coefficient. Adhesion coefficients of three fire sources are obtained from the above data irrespective of ventilation velocity as follows:

$$\eta = const. = \begin{cases} 0.0007 & (Flaming\ Kerosene\ and\ Polyurethane) \\ 0 & (Smoldering\ Cotton) \end{cases} \tag{61.9}$$

The adhered transmittance ${}_a\tau_e$ can be interpreted as the ratio of the non-adhered area to the total area of the object panel. It is considered that area with no smoke adhesion maintains the initial transmittance τ_e. Subscript "a" at the left of transmittance and reflectance means smoke adhesion. ${}_a\tau_e$ can be estimated by

$${}_a\tau_e = \tau_e(1-\zeta) = \tau_e\left(1 - \int \eta C_s dt\right) \tag{61.10}$$

Letting the initial reflectance ρ_e be the reflectance of adhered smoke (virtually no reflection), reflectance decreased by smoke adhesion ${}_a\rho_e$ can be estimated by

$$\begin{aligned} {}_a\rho_e &= \rho_{smoke}\zeta + \rho_e(1-\zeta) \\ &= \rho_e - \int \eta C_s dt(\rho_e - \rho_{smoke}) \end{aligned} \tag{61.11}$$

Light Attenuation by Destructive Hot Smoke

Emergency lights are designed only for an electric blackout, which is caused by damage due to high temperature smoke or flames as shown in Fig. 61.14. Evacuation sign and light are not

Fig. 61.14 Damaged emergency light in Daegu subway fire

Fig. 61.15 Smoke temperature

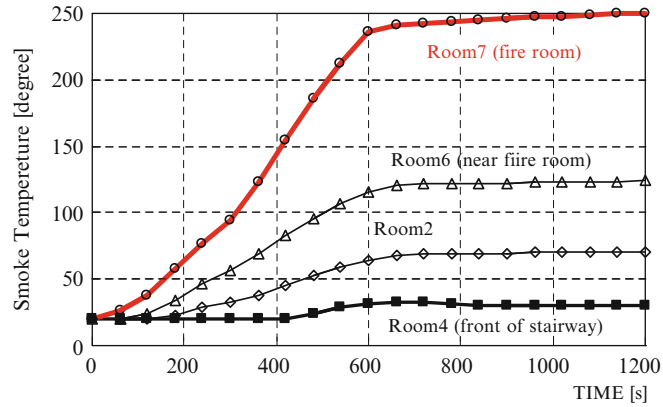

always secured to work, especially in fire smoke, but this tends to be forgotten. Therefore emergency lighting (or illuminating signage) cannot ensure the sufficient light intensity for evacuation visibility against fire smoke.

In JIL55017 [15] (a standard of Japan Luminaries Association), the emergency light is required to work for 30 min in the ambient temperature of 413 [K]. Figures 61.15 and 61.16 show an example of prediction results [16]. The luminous flux in the hot smoke layer was set to 0 [lm] due to its damage when the smoke temperature is over 413 [K]. Smoke temperature was shown in Fig. 61.15, and it related damage of emergency lights. In Fig. 61.16, the floor illuminance of fire room changed drastically, as lighting equipments were broken and the floor illuminance was reduced to almost zero at 420 s after fire ignition. Needless to say smoke height and optical smoke density affected luminous flux attenuation with smoke adhesion. By fire smoke, engineers should consider that the visibility of escape routes decrease due to broken lightings by high temperature, attenuation of initial luminous intensity by smoke adhesion on the surface of lightings (and light sources), and attenuation of ambient light intensity by smoke adhesion on the surface of escape routes and reduction in surface reflectance of the escape routes.

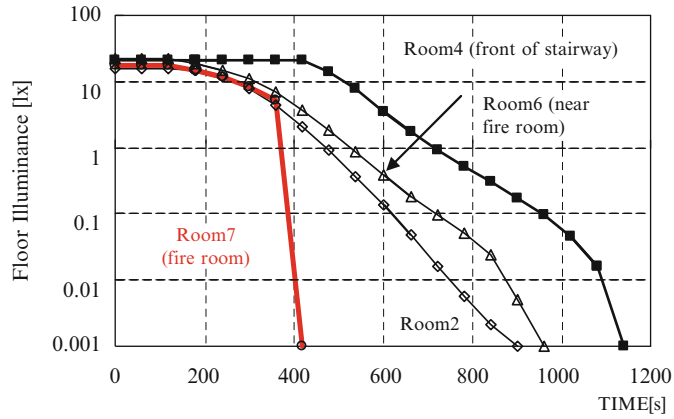

Fig. 61.16 Floor illuminance

Human Behavior in Fire Smoke and Related Environment

Travel Speed in Escape Routes Considering Luminous Condition, Smoke Density and Evacuee's Visual Acuity

There are some important previous studies on evacuation performance. Simmons [17] studied the relationship between illuminance and travel speed of evacuees. The result was referenced by CIE/ISO standards of Emergency lighting [18], which set the standard value 1.0 [lx] of floor illuminance for 1.0 [m/s] of travel speed. Jaschinski [19] compared the travel speed of young and elderly subjects. In his results, the elderly group walked slower than the young group. Webber [20] converted these results from travel time to travel speed versus floor illuminance as shown in Fig. 61.17.

In this section, we dealt with floor luminance of the walking space as the visual stimulus of the space under various lighting/smoke conditions, and elucidate the age-related difference of travel speed in previous studies using subjects' visual acuities [4]. Figure 61.18 shows the relationship between travel speed and floor illuminance for the two age groups. At 1.0 [lx] of floor illuminance and lower, the average speed of the young group was higher than the aged group, which supports the findings of the previous study [19]. If the floor illuminance was higher than 3.0 [lx], the travel speed was similar for both age groups. The relationship between visual acuity and travel speed by age groups is shown in Fig. 61.19. By converting the floor illuminance of the travel space into luminance by using Equation 61.12, it predicted levels of visual acuity under any experimental condition. ρ is reflectance of the floor. E is the horizontal illuminance of the walking space.

$$L = \frac{E\rho}{\pi} \tag{61.12}$$

The age difference is not seen, which implied that travel speed was does not vary by visual acuity regardless of age.

From the relationship shown in Fig. 61.19, the travel speed v_o [m/s] of an observer who adapts completely to the luminous intensity of the walking space (i.e. under complete adaptation) could be correlated with visual acuity VA as expressed by Equation 61.13 ($R^2 = 0.80$ and 0.86). If we can predict visual acuity under a disaster situation's light conditions, we can further predict performance, i.e. travel speed of evacuees by this equation.

$$v_o = \begin{cases} 1.56 \times VA^{0.12} & (VA < 0.25) \\ 1.32 & (VA \geq 0.25) \end{cases} \tag{61.13}$$

Figure 61.20 shows the comparisons between the results in smoke and the results without smoke (Cs = 0.68[1/m]). The result showed the large degradation of travel speed in smoke. Under the

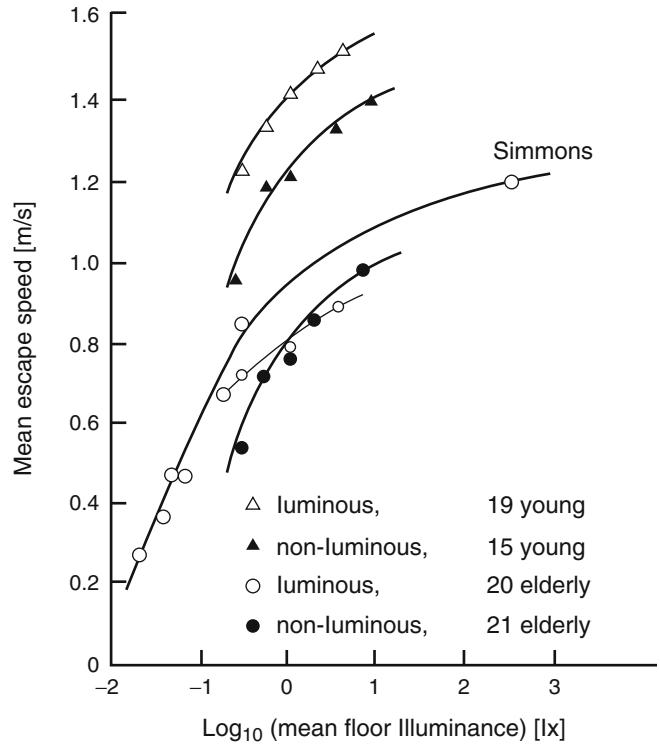

Fig. 61.17 Relationship between ζ and C_s [20]

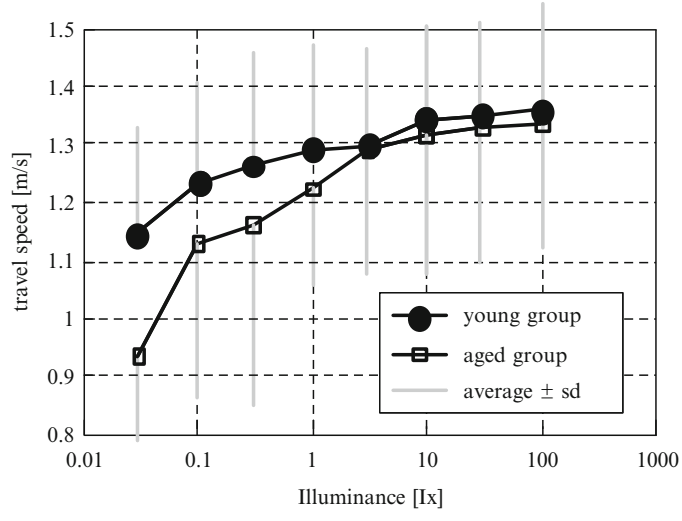

Fig. 61.18 Illuminance and travel speed [4]

same illuminance conditions, subjects walked more slowly in smoke than without smoke. In the above-mentioned Fig. 61.18, there was little difference between travel speed of the young and aged groups, and both travel speeds were constant under the illuminance condition 3.0 [lx] or more. However, under the conditions more than 3.0[lx] in smoke as shown in Fig. 61.20, the travel speeds of both groups increased as illuminance increased. The travel

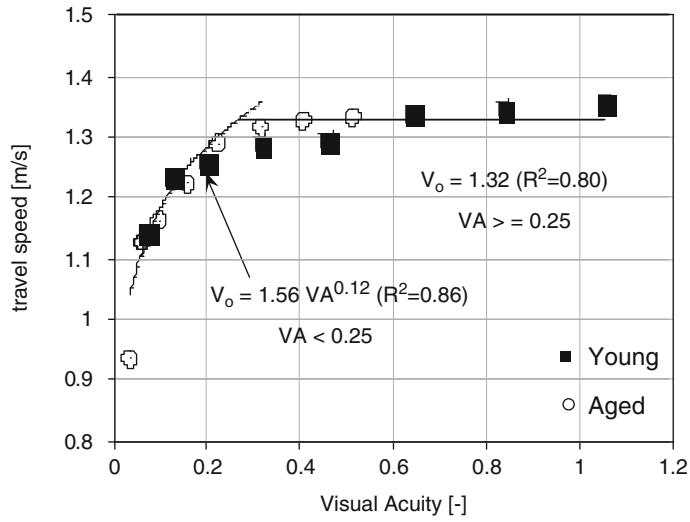

Fig. 61.19 Travel speed and visual acuity [4]

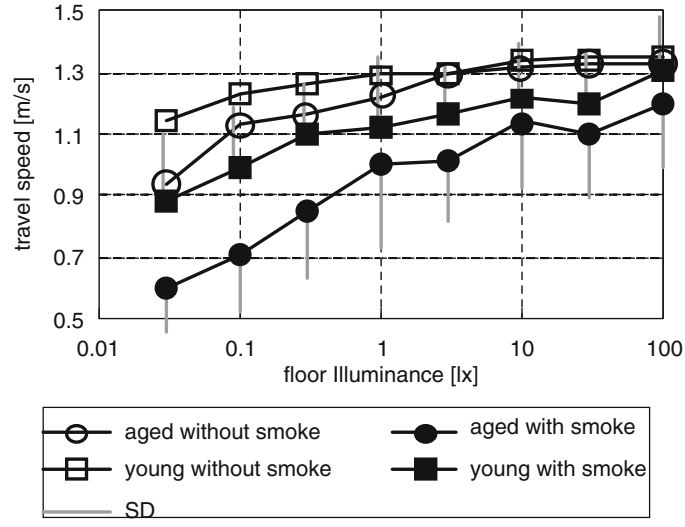

Fig. 61.20 Illuminance and travel speed in smoke

speed of the young group was consistently higher than that of the aged group.

Even under the same illuminance conditions, subjects walked more slowly with smoke than without. Therefore the ratio of travel speed in smoke (Rv_{smoke}) regarding the effect of smoke was defined by Equation 61.14.

$$Rv_{smoke} = \frac{v_{smoke}}{v_o} \tag{61.14}$$

where v_o [m/s] is the travel speed under complete adaptation without smoke, and v_{smoke} [m/s] is the travel speed under complete adaptation in smoke.

The relationship between Rv_{smoke} and visual acuity by age groups are shown in Fig. 61.21. The mean value of Rv_{smoke} is based on each subject's result. The age difference was not seen in Fig. 61.21, which implied that the effect of smoke on travel speed could be explained by visual acuity regardless of age. Equation 61.13 showed convergence with VA ≧ 0.25, but the results in Fig. 61.21 suggested smoke affects travel speed at higher levels of visibility.

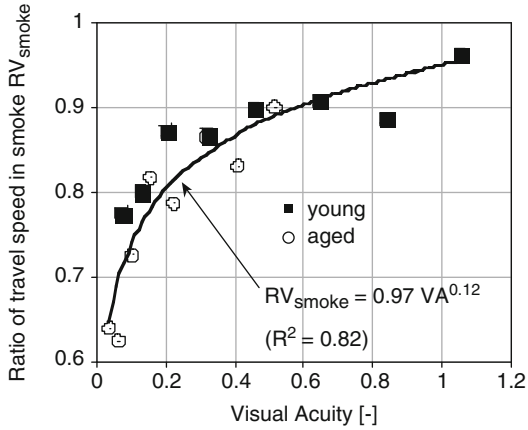

Fig. 61.21 Relative travel speed and visual acuity [4]

Finally the relationship between the travel speeds under complete adaptations with smoke v_{smoke} [m/s] and visual acuity are shown in Equation 61.15.

$$v_{smoke} = \begin{cases} 1.51 \times VA^{0.24} & (VA < 0.25) \\ 1.28 \times VA^{0.12} & (VA \geq 0.25) \end{cases} \quad (61.15)$$

At a fire situation, the power often fails in escape routes, and the light intensity rapidly decreases. Due to the rapidly change of the adaptation state of evacuees, the visibility will decrease too. When the illuminance in the adaptation space E_a [lx] and in the travel space E_t [lx] was significantly different, the travel speed increased to the level of complete adaptation's speed as subjects travel farther. The relationship between the ratio of adapting illuminance change $RE_{adaptation}$ ($=E_a/E_t$) and the ratio of travel speed $RV_{adaptation}$ were examined. Large value of $RE_{adaptation}$ raises deterioration of visibility by adaptation transition and physiological load. Under the condition that $RE_{adaptation}$ value was 10 (i.e., the illuminance of the adapting space is ten times that of the travel space), $RV_{adaptation}$ was nearly 1. Regression equations were established when $RE_{adaptation}$ was more than 100. The regression relationship between visual acuity and v_i [m/s] of the travel speed under incomplete adaptation were given by Equation 61.16.

$$v_i = \begin{cases} 1.56 \times 1.12^{f\left(RE_{adaptation}\right)} \times VA^{\left\{0.08 f\left(RE_{adaptation}\right)+0.12\right\}} & \left(RE_{adaptation} \geq 100, VA < 0.25\right) \\ 1.56 \times VA^{0.12} & \left(RE_{adaptation} < 100, VA < 0.25\right) \\ 1.32 & \left(VA \geq 0.25\right) \end{cases} \quad (61.16)$$

Effect of Irritant Smoke on Travel Speed

Along with the experiment of effect of irritant smoke on visibility, walking speed in the smoke was examined as shown in Fig. 61.22. Both smoke density and irritation appear to affect the walking speed. This figure shows that the walking speed in nonirritant smoke decreases gradually as the smoke density increases. However, in the irritant smoke, the speed decreases very rapidly in the same range of smoke density levels. From this observation, the sharp drop in walking speed is explained by the subjects' movements: they could not keep their eyes open and they inevitably walked zigzag or step by step along the side wall.

Emotional State in Fire Smoke

An attempt was made to monitor the subjects' emotional state of mind when exposed to fire smoke (white smoke by wood chips) using a steadiness tester that is often employed in psychological studies [5]. The subject's task is to hold a metal-tipped stylus in various progressively smaller hole sizes without touching the sides of the steadiness tester under limited time. Figure 61.23 is the result of an attempt to determine the subjects' emotional variations on the basis of the number of stylus contacts on the steadiness tester. Curves with two peaks as shown were obtained for both groups of subjects. These peaks seem to attest to the following facts:

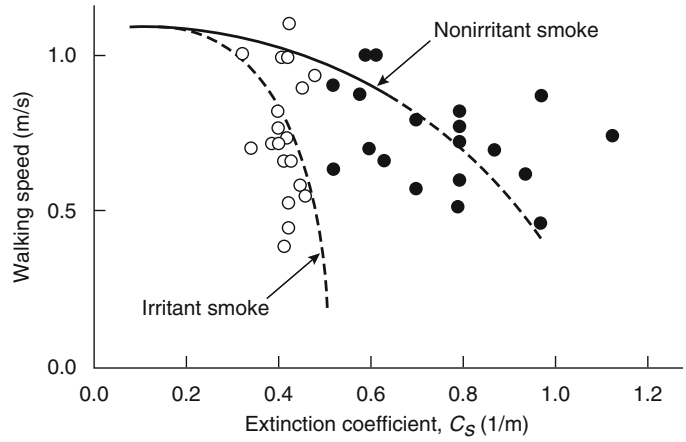

Fig. 61.22 Walking speed in fire smoke

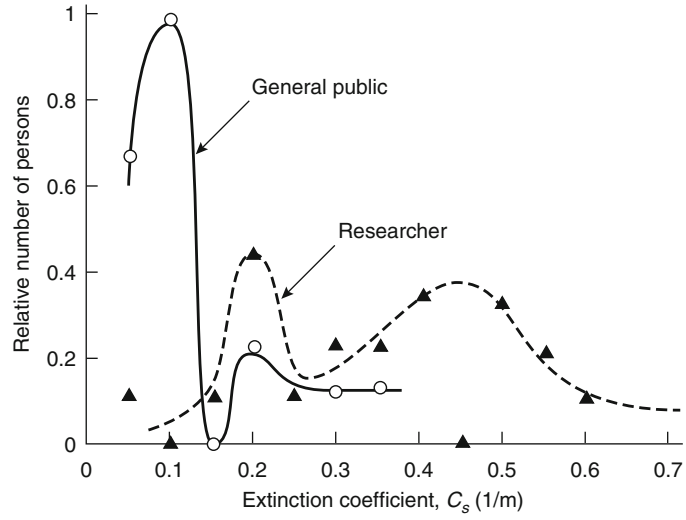

Fig. 61.23 Number of emotionally affected subjects versus smoke density at the point of rapid increase in the number of contacts in the steadiness tester

other than the Institute researchers, most subjects began to be emotionally affected when the smoke density reached 0.1 [1/m], but in a few others, emotional fluctuations did not begin to be pronounced until the smoke reached an extinction coefficient of 0.2–0.4 [1/m]. In contrast, most researchers began to show emotional fluctuations only when the smoke density reached 0.35–0.55 [1/m] although a small number of them responded at the lower smoke density of 0.2 [1/m].

Interviews with some subjects were held after the experiment. Comments by many of the subjects representing the general public could be generalized like this: "Smoke itself didn't scare me much when it was thin, but irritation to my eyes and throat made me nervous. When I thought of the smoke still getting thicker and thicker, I was suddenly scared of what was going to happen next." In other words, these subjects were more afraid of what was going to happen next than they were physiologically unable to withstand the smoke. They were not well informed about the geometry of the test room and smoke in the pre-test briefing not like for the Institute researches as mentioned below.

Hence, the author believes that the data obtained from these subjects could reasonably be treated as equivalent to those that would be

obtained from a group of unselected people who are unfamiliar with the internal geometry of a building on fire. The smoke density of 0.15 [1/m], at which most of the subjects analyzed in Fig. 61.23 began to feel uneasy, could be determined as the maximum smoke density for safe evacuation of a building to which the public have access.

In contrast, the Institute researchers who served as subjects said in the interview, "Irritation to my eyes was rather acute but the smoke didn't scare me because I had heard in the pretest briefing that it was harmless. But as the smoke grew denser, I began to feel more acute irritation in my eyes and throat, and when I got the signal to end the test (smoke extinction coefficient 0.5–0.7 [1/m]), irritation and suffocation were near the limit I could physiologically withstand. Toward the end of the test, visibility in the test room was so limited that I saw only a small floor area around my feet, and this made me a little nervous when I walked through the smoke."

Even though these researchers had some knowledge of smoke from the pretest briefing and were well informed of the geometry of the test room, most of them began to be emotionally affected when the smoke density exceeded 0.5 [1/m]. It could be reasoned that emotional instability of these subjects during the test resulted from physiological rather than psychological reasons.

These facts led the author to believe that the results of this experiment using Institute researchers as the subjects can be treated as data relevant to people who are well informed of the inside geometry of a building on fire. This means that the smoke density of 0.5 [1/m], at which Fig. 61.23 indicates most of the researchers began to lose steadiness, can be determined as the threshold where escape becomes difficult even for persons who are well familiar with the escape route in the building.

Visibility at these smoke densities is listed in Table 61.3, which indicates that those who know the inside geometry of the building on fire need a visibility of 4 m for safe escape while those who do not need a visibility of 13 m.

In Table 61.4, a comparison is made between some of the values of acceptable visibility or allowable smoke density proposed by researchers who have conducted many experiments on escape through fire smoke [2]. Wide variations in the proposed values are probably due to differences in the geometry of the places and the composition of the group escaping from fire.

Table 61.3 Allowable smoke densities and visibility that permits safe escape

Degree of familiarity with inside of building	Smoke density (extinction coefficient)	Visibility
Unfamiliar	0.15 1/m	13 m
Familiar	0.5 1/m	4 m

Table 61.4 Visibility and/or allowable smoke density for fire safe escape proposed by fire researchers

Proposer	Visibility	Smoke density (extinction coefficient)
Kawagoe [21]	20 m	0.1 1/m
Togawa [22]	–	0.4 1/m
Kingman [23]	4 ft (1.2 m)	–
Rasbash [24]	15 ft (4.5 m)	–
Los Angeles Fire Department [25]	45 ft (13.5 m)	–
Shern [26]	–	0.2 1/m
Rasbash [27]	10 m	0.2 1/m

Intensive System for Escape Guidance

Improvement of Conspicuousness of Exit Sign by Flashing Light Source

An emergency exit sign, which indicates a location and/or direction of emergency exit and leads evacuees to a safe place swiftly, is important in case of fire or other emergencies. In Japan, three sizes of emergency exit sign were ordinarily used (h[cm] × w[cm] are 40 × 1200, 20 × 60, and 12 × 36). However, the conspicuousness of an exit sign in a location where there are many other light sources was not known. In the first experiments, the conspicuousness of an "ordinary" exit sign in an underground shopping mall was measured during business hours. The

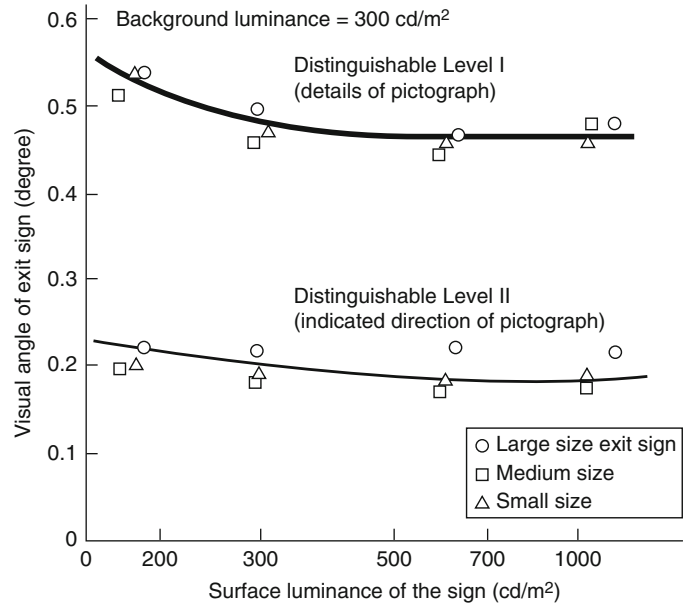

Fig. 61.24 Relation between surface luminance of exit sign and visual angle associated with visibility

experimental variables were the observation distance, size, and luminance of the sign. In the second series of experiments, the conspicuousness of a self-flashing type exit sign (flashing the lamp in the sign) was compared with that of an ordinary exit sign [28].

Visibility and Conspicuousness of Exit Source

Prior to this study, another experimental study on visibility of exit signs had been carried out. In that experiment, the original type of exit sign was observed in a background without other light sources. Figure 61.24 shows one of the results concerned with the relation between visibility expressed by visual angle (defined by the height of the pictograph) and surface luminance. In this figure, visibility is represented on two discrimination levels; one is the level at which a person can distinguish the details of the pictograph and the other is the level at which only the direction of the running person in the pictograph is distinguishable. This result indicates that visibility is almost constant when the luminance of the white part of the exit sign is more than 300 [cd/m^2]. This observation is true for every size of the exit sign. It is independent of the size of the sign when visibility is expressed in terms of the visual angle.

Figure 61.25 shows the relation between conspicuousness of ordinary exit signs and the visual angle according to the evaluation categories given in Table 61.5 [29]. The conspicuousness increases with visual angle. However the same visual angle doesn't give same conspicuousness level especially when the visual angle is larger. The larger-size exit sign is more conspicuous than the smaller one when the visual angle is the same. As above indicated, surface luminance doesn't give much effects on the distinguish level when the visual angle is similar. And lower surface luminance sign needs large visual angle to keep the same distinguishable level. This indicates that conspicuousness depends on the relative scale and brightness of exit sign against those of surrounding light sources.

Improvement of Conspicuousness by Flashing the Light Sources

Figure 61.26 shows the relation between conspicuousness of an ordinary exit sign and that of the self-flashing type exit sign using the

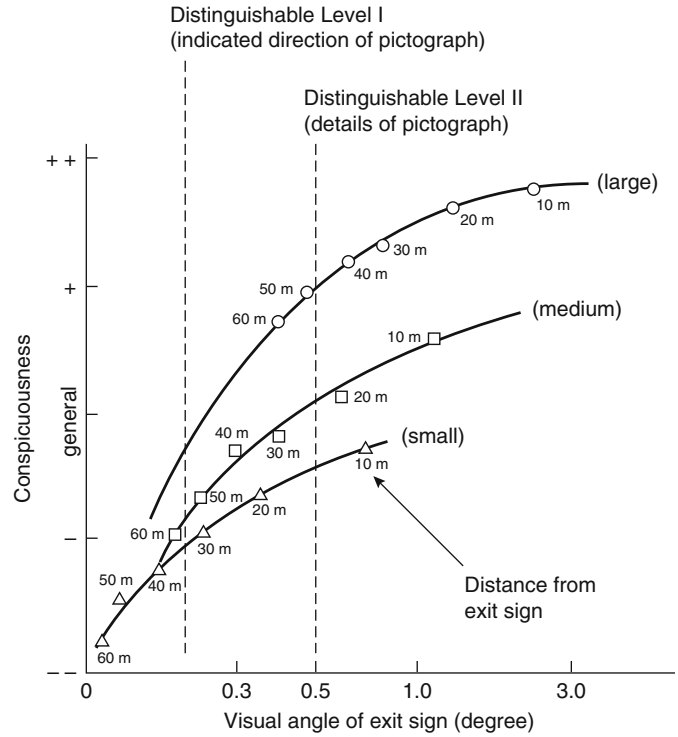

Fig. 61.25 Relation between conspicuousness of ordinary type exit sign and visual angle

Table 61.5 Categories for evaluating conspicuousness of ordinary-type exit sign

Evaluation categories	(Marks in Fig. 61.25)
1. The exit sign is fairly conspicuous	(+ +)
2. The exit sign is slightly conspicuous	(+)
3. The exit sign is similar to the general level	(General)
4. The exit sign is less conspicuous	(−)
5. The exit sign is not conspicuous at all	(− −)

categories for evaluation given in Table 61.6. In this figure the vertical interval between the dash-dotted line and the curves corresponds to the improvement of conspicuousness by the flashing light in the sign. For the medium-size exit sign, a self-flashing type sign is more effective to improve conspicuousness. However, the small-size exit sign of the self-flashing type is not conspicuous enough when observed from a distance more than 20 m in the background with many other lights, because the exit sign is too small to be recognized as an exit sign, even though the flashing was expected to be much more conspicuous. The large exit sign is big enough to have sufficient conspicuousness without flashing even in the background with many competing light sources. Conspicuousness of the sign could also be improved by adding a flashing light source the same as a flashing-type sign.

In addition to the improvement achieved by adding a flashing light, the author has suggested the development of an acoustic guiding exit sign. Adding a speaker and voice recorded IC chip to the flashing exit sign can provide an announcement such as “Here is an emergency exit” when fire is detected by, for example, smoke detectors [30].

Development of Intensive Escape Guidance System

Escape guidance system by traveling flashing light sources: An escape guidance system has been developed for safe evacuation. This system indicates the appropriate escape directions by

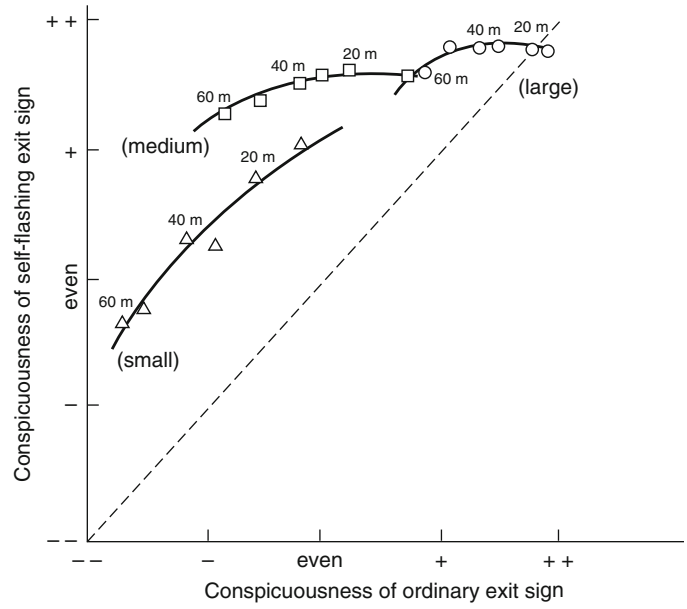

Fig. 61.26 Relation between the conspicuousness of a self-flashing exit sign and that of an ordinary one

Table 61.6 Categories for evaluating conspicuousness of self-flashing exit signs

Evaluation categories (as compared with the ordinary-type exit sign)	(Marks in Fig. 61.26)
1. The flashing exit sign is fairly conspicuous	(++)
2. The flashing exit sign is slightly conspicuous	(+)
3. The flashing exit sign has similar conspicuousness	(General)
4. The flashing exit sign is less conspicuous	(−)
5. The flashing exit sign is not conspicuous	(− −)

creating a row of flashing lights leading away from a hazardous area such as a fire in a building (see Fig. 61.27). A form of this is already found in the floor lighting of passenger aircraft cabins.

An experiment was carried out to evaluate this system using a portion of passageway (1.4 m width, 6.3 m length, and 2.5 m height) filled with smoke. As lighting for the passageway, fluorescent lamps are provided under the ceiling, giving about 200 [lx] at the center of the passage in the absence of smoke. The flashing light unit boxes are set on the floor along the side of the right-hand wall at intervals of 0.5 m, 1.0 m, and 2.0 m as a test guidance system [31].

Table 61.7 Categories for effectiveness of the escape guidance

Score	Effectiveness
7 points	Very effective for escape guiding
5 points	Fairly effective
3 points	A little effective
1 point	Not effective

The effectiveness of the escape guidance was evaluated by 12 subjects under various conditions that is, changing the spacing and the traveling speed of flashing lights and smoke concentration. Under each condition, subjects walk along the system successively with free walking speed.

The degree of effectiveness of escape guidance is classified into seven steps as follows, and the evaluations are made by filling one score from 7 points into an observation sheet directly after each test run by subjects respectively. These categories are adopted as a semantic differential scale and the relative evaluation for escape guidance effectiveness is determined as subjective grading in each test run. (Points 2, 4, and 6 correspond to the middle point between 1 and 3, 3 and 5, and 5 and 7 respectively.) In general, the effectiveness decreases with increasing smoke.

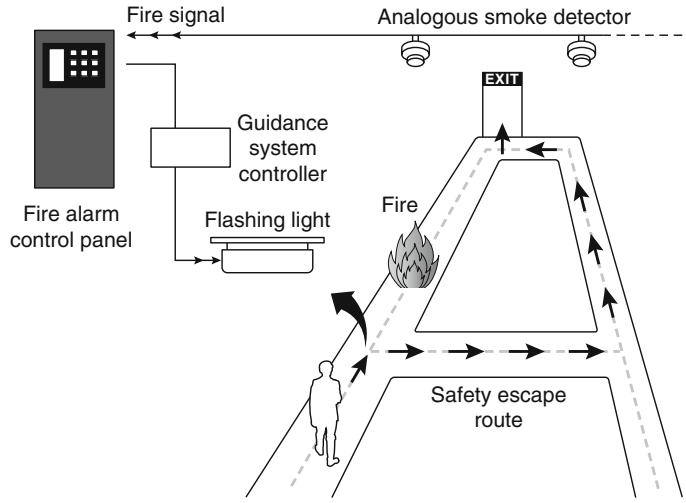

Fig. 61.27 Illustration of the traveling flashing light sources system

The evaluation value of 4 points stands for less effective than fairly effective and more effective than a little effective, so we consider the value a threshold where practical effectiveness of escape guidance is secured.

The correlation between smoke concentration and the effect of escape guidance is shown in Fig. 61.28. This indicates that this system is useful for evacuees to escape in thick smoke (up to an extinction coefficient of 1.0 [1/m]er) when the spacing length is 0.5 m and the flashing speed is 4 [m/s]. When the spacing length is set to be 1.0 m, the effectiveness decreases but it is still useful in smoke under 0.8 [1/m]. However, when the spacing is greater than 2.0 m, less effectiveness is expected even under a no-smoke condition. The evaluation values in the meshed area to the left in Fig. 61.28 were obtained under no smoke conditions.

The effectiveness of flashing traveling signs in an ambient atmosphere is maintained up to smoke density of 0.4 [1/m]. This result is very important for evaluating the escape guidance system from the viewpoint of safe evacuation. Visibility (observable distance) of normal exit signs drops rapidly from more than 10–5 m as shown in Fig. 61.8, and the guidance effectiveness is also lost over the same range of smoke densities [6].

However compared with the decrease in visibility of ordinary exit signs, the decrease in the effectiveness of the guidance system with increasing obscuration seems to be small, so that the new system is expected to maintain high and stable effectiveness of guidance escape, even in relatively dense smoke. Clearly, the spacing between flashing light sources is a very important factor to maintain effectiveness. High effectiveness is expected, especially, when the spacing is less than 1.0 m. The relation between effectiveness and flashing light conditions in the presence of smoke is found to be almost the same as the relation under non-smoke conditions.

Effectiveness of a Directional Sound Escape Guidance System Using the Haas Effect

Directional sound escape guidance systems are expected under smoke filled conditions where visibility is lost. One of methods to create directive sound is to utilize the Haas effect, which is used in a large hall so that a voice can be heard from each speaker where many speakers are installed on the sidewalls with respect to the direction of the lecturer.

In Japan, the system is used in combination with the traveling flashing light sources and it has

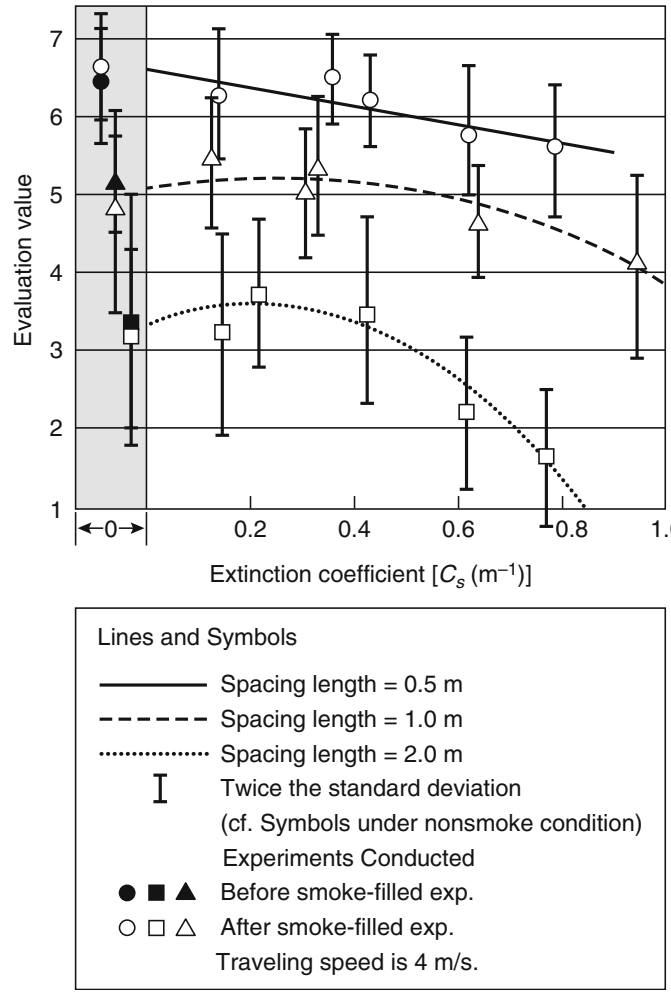

Fig. 61.28 Relation between smoke density and the effect of escape guidance with variation of flashing light sources under a smoke condition

been installed for a large-scale underground shopping mall and in facilities used by people with impaired vision and hearing. The directional sound escape guidance system using the Haas effect has two separate speakers that are located on the ceiling above the emergency exit within a distance of 10 m in a corridor. They are next to each other, but there is a time delay between them. When a fire occurs, a warning message (a chime sound plus an announcement: "Here is the emergency exit") is given from each speaker. The message is heard only from that emergency exit as a result of the Haas effect (also called precedence effect) [32, 33]. Its effectiveness was also examined in a smoke-free corridor.

Table 61.8 Categories for confidential of the escape direction

7	They were very confident that the sound came 968 from the right direction.
5	They were quite confident that the sound came 970 from the right direction.
3	They could identify a direction but were not 972 confident that it was the correct one.

A guidance effect experiment was carried out in the passageway of an assembly area approximately 130 m length, 4.8 m width, and 2.5 m height. Subjects moved strait forward to the end exit with a distance of 2 m between them, and they evaluated their perception of the direction of

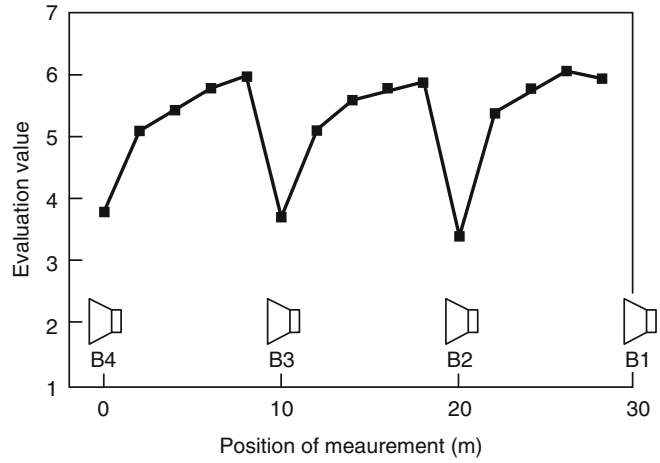

Fig. 61.29 Evaluation of the sound escape guidance system

the sound in relation to the direction in which they were walking. The evaluation was based on the following subjective ranking:

The example shown in Fig. 61.29 is the result of such an evaluation experiment of the direction from various positions. A ranking value above five indicates that the individual has a good feeling of the direction for various locations, although when directly under the speaker it falls to 3.5. As for the distance between speakers, it is desirable to install them less than 10 m apart because the evaluation value close to the speakers is difficult if the separation of the speakers is wide.

As for the direction in which the speaker is pointing, it is better to have it pointing horizontally along the length of the passageway. The worst situation is to have the speaker pointing vertically downwards (90° to the horizontal). The limiting case for a good response is 45° downwards from the horizontal.

The delay time T_d [s] between the speakers is given by

$$T_d = D/v_{sound} + (35 \pm 10) \times 10^{-3} \quad (61.17)$$

Where

D = Distance between the speakers [m]

v_{sound} = Speed of sound in air [m/s]

$(35 \pm 10) \times 10^{-3}$ = A constant that must be adjusted for the building structure

Summary

The following are the major conclusions derived from these research activities:

1. The relationship between smoke density and visibility in fire smoke was examined under various kinds of smoke, and simple equations were proposed for practical use.
2. The visibility in fire smoke depends on its irritating nature as well as the optical density of the smoke. Increasing irritating effect causes a rapid drop of visual acuity. A modification due to irritating effect was made for the visibility versus smoke density equation.
3. There are various indirect effects of smoke on visibility, i.e. light attenuation due to smoke adhesion and/or destructive hot smoke. Empirical equations to evaluate such effects are introduced. Also effects of luminous conditions on travel speed in smoke are examined and correlated with visual acuity depletion.
4. Evacuees' performance could be predicted by visual conditions such as the luminous environment and evacuee's visual acuity. Travel speed was determined by visual acuity regardless of age, whether with or without smoke.

Under complete adaptation or incomplete adaptation, travel speed decreased if the evacuee's visual acuity was less than 0.25. Smoke caused the degradation of travel speed even with sufficient illumination.

5. Evacuees begin to feel emotional instability in relatively thin smoke; however the threshold of smoke density varies with the subject. Ability of evacuees to think clearly when exposed to fire smoke decreases with increasing smoke density. Generally, this is caused by both psychological and physiological effects on evacuees.
6. Conspicuousness of the ordinary exit sign was improved by a flashing light source sign or by adding a flashing light source in conditions where there were many other light noises.
7. Two new types of escape guidance systems have been tested. One is the continuously traveling flashing light source system, the effectiveness of which has been examined in a smoke-filled corridor with reduced visibility. The other is a directional sound escape guidance system that makes use of the Haas effect. Its effectiveness has also been examined in a smoke-free corridor. These innovative technologies for safe evacuation are now in practical use in Japan in a large underground shopping mall and in facilities used by people with impaired vision and hearing.

References

1. ROUFS, J.A.: Dynamic properties of vision-I. Experimental relationships between flicker and flash thresholds, Vision Res. Vol. 12, p. 261 (1972)
2. ISO 8596; Ophthalmic optics -Visual acuity testing – Standard optotype and its presentation (2009)
3. INOUE, Y. and AKIZUKI, Y.: The optimal illuminance for reading, Effects of age and visual acuity on legibility and brightness, Journal of Light & Visual Environment, The Illuminating Engineering Institute of Japan, Vol. 22, No. 1, pp. 23–33, 1998.
4. Y. Akizuki, T. Tanaka and K. Yamao, "Calculation Model for Travel Speed and psychological State in Escape Routes considering Luminous Condition, Smoke Density, and Evacuee's Visual Acuity", *Proceedings of the 9th International Symposium of Fire Safety Science,* International Association of Fire Safety Science, pp. 365–376 (2008).
5. T. Jin, "Visibility through Fire Smoke," *Bulletin of Japanese Association of Fire Science & Engineering,* 19, 2, pp. 1–8 (1970).
6. T. Jin, "Visibility through Fire Smoke," *Journal of Fire & Flammability,* 9, pp. 135–157 (1978).
7. T. Yamada, K. Kubota, N. Abe and A, Iida, "Visibility of Emergency Exit Signs and Emergency Lights through Smoke" *Proceedings of the 6th Asia-Oceania Symposium of Fire Safety Science and Technology,* International Association for Fire Safety Science, Daegu, pp. 227–238 (2004)
8. Fire Disaster Management Agency, "Standard of emergency exit light and sign," Notification No. 2 of the Fire and Disaster Management Agency, March 17 (2000)
9. T. Jin and T. Yamada, "Irritating Effects of Fire Smoke on Visibility," *Fire Science & Technology,* 5, 1, pp. 79–89 (1985).
10. B. L. Collins, M. S. Dahir, and D. Madrqykowski, "Visibility of Exit Signs in Clear and Smoky Conditions", Journal of the Illuminating Engineering Society, Winter, pp. 69–84 (1992).
11. M. S. Rea, R. R. S. Clark, and M. J. Ouellette, "Photometric and Psychophysical Measurements of Exit Signs Through Smoke", National Research Council Canada, Division of Building Research, DBR-1291, NRCC 24627 (1985).
12. T. Jin, "Studies of Emotional Instability in Smoke from Fires," *Journal of Fire & Flammability,* 12, pp. 130–142 (1981).
13. T. Jin, "Studies on Decrease of Thinking Power and Memory in Fire Smoke," *Bulletin of Japanese Association of Fire Science & Engineering,* 32, 2, pp. 43–47 (1982).
14. Y. Akizuki, T. Tanaka, H. Suzuki and T. Tsuchihashi," Calculation Method for Visibility of Emergency Sign in Fire Taking into Account of Smoke Adhesion", *Proceedings of the 8th International Symposium of Fire Safety Science*, International Association of Fire Safety Science, pp. 1093–1105 (2005).
15. Japanese standard of emergency light (JIL5501) : Japan Luminaries Association (2001.6.13 revised).
16. Y. Akizuki, N. Hara and T. Tanaka," Calculating Method of Evacuee's Behavior based on the Floor Illuminance in Fire Smoke Estimated by Two Layer Zone Model", *Proceedings of 4th International Symposium on Human Behaviour in Fire*, pp. 301–311 (2009).
17. R.C. Simmons, "Illuminance, diversity and disability glare in emergency lighting", *Lighting Research and Technology*, Vol. 7, No. 2, pp. 121–132. (1975).
18. CIE Standards 014-4/E, Emergency lighting (2007).
19. Jaschinski Wolfgang,"Conditions of emergency lighting", *Ergonomics*, Vol. 25, pp. 363–372 (1982).

20. G.M.B. Webber," Emergency lighting recommendations", *National Lighting Conference*. (1984).
21. K. Kawagoe and F. Saito, *Journal of Japanese Society for Safety Engineering,* 6, 2, p. 108 (1967).
22. K. Togawa, unpublished manuscript.
23. F.E.T. Kingman, "The Products of Combustion in Burning Buildings," *Journal of Applied Chemistry,* 3, pp. 463–468 (1953).
24. D.J. Rasbash, "Smoke and Toxic Gas," *Fire,* 59, 735, pp. 175–179 (1966).
25. Los Angeles Fire Department, Operation School Burning (1961).
26. J.H. Shern, *Sixty-Ninth Annual Meeting of the ASTM* (1966).
27. D.J. Rasbash, *International Seminar on Automatic Fire Detection,* Aachen, Germany (1975).
28. T. Jin, T. Yamada, S. Kawai, and S. Takahashi, "Evaluation of the Conspicuousness of Emergency Exit Signs," *Proceedings of the Third International Symposium of Fire Safety Science,* International Association for Fire Safety Science, Boston, pp. 835–841 (1991).
29. Illumination Engineering Institute of Japan, *The Report of Basic Research on Visibility of Exit Sign,* 1 (1984).
30. T. Jin and K. Ogushi, "Acoustic Evacuation Guidance," *Bulletin of Japanese Association of Fire Science & Engineering,* 36, 1, pp. 24–29 (1986).
31. T. Jin and T. Yamada, "Experimental Study on Effect of Escape Guidance in Fire Smoke by Travelling of Light Source," *Proceedings of the Fourth International Symposium of Fire Safety Science,* International Association of Fire Safety Science, Boston, pp. 705–714 (1994).
32. Y. Ito, H. Ishii, and T. Jin, "Study on Refuge Leading with the Voice," *The Acoustical Society of Japan,* pp. 463–464 (1992).
33. Y. Ito and H. Ishii, "Study on Refuge Leading with the Voice Haas Effect," *The Acoustical Society of Japan,* pp. 859–860 (1993).

Tokiyoshi Yamada was born in 1954 in Japan. He received his doctor of engineering degree from Tokyo University in 1983. He joined the Fire Research Institute in 1983 and has worked in the field of visibility and human behavior in fire smoke with Dr. Jin. Major research background is fire physics. In 2011, he joined the University of Tokyo as a project professor.

Yuki Akizuki was born in 1970 in Japan. After spending 5 years in the lighting research and development laboratory of Matsushita Electric Works (now Panasonic), she received her Ph.D. degree from Nara Women's University in 2003. She joined Disaster Prevention Research Institute of Kyoto University in 2003 and studied with Prof. T. Tanaka. She got the second doctoral degree of engineering from Kyoto University in 2012. She has been an associate professor at University of Toyama since 2007.

Combustion Toxicity

62

David A. Purser

Introduction

The purpose of this chapter is to review experimental studies, especially those involving combustion chemistry and toxicity test methods, in order to establish the basis and validation for material toxicity and toxic hazard calculations and to obtain yield data for input to fire dynamics and toxicity calculations. The review covers several major topics, including the following:

- How combinations of fire investigation studies, experimental studies of the composition of fire effluent mixtures and studies of their effects on exposed human and animal subjects, have been used to identify the variety of toxic substances produced during combustion of a wide range of materials, and the extent to which these toxic effects can be attributed to a small number of key toxic chemical substances.
- Another related topic, is the extent to which unusual or "super-toxic" substances or effects have been identified from certain materials, which cannot be explained in terms of common toxic combustion products.
- A third topic describes how the yields of key toxic effluents vary with different combustion conditions in fires and how specially designed bench-scale combustion tests have been used to replicate these combustion conditions and measure toxic product yields from a range of materials for application to fire dynamics calculations, toxic potency estimations and environmental contamination assessments.
- Also discussed are the limitations of some simplistic bench-scale "combustion toxicity" tests sometimes used for product specification purposes.

The toxicity of combustion products from materials involved in fires was subject of considerable interest in the 1970s and 1980s. This was stimulated by findings at the time of a fourfold increase in deaths and from exposure to toxic smoke in fires (as opposed to burns) in the UK during the post-war period and a high incidence of smoke deaths in fires in the United States and other countries. During this period there were marked changes in the materials used in construction and contents of buildings and transport vehicles, with the widespread introduction and use of a range of modern synthetic polymeric materials which differed chemically from the traditional (mostly natural) materials used previously. The high incidence of smoke-related injuries and deaths gave rise to concerns that, when they were burned, some of these materials might be producing unknown "supertoxic" substances with a high toxic potency (so that exposure to small amounts could produce severe incapacitation or death) and unusual specific toxicity (so that the nature of the toxic effects might be different from those caused by effluents from traditional materials). Another possibility was that the range of important toxic chemical

D.A. Purser (✉)
Hartford Environmental Research Hatfield,
United Kingdom

M.J. Hurley (ed.), *SFPE Handbook of Fire Protection Engineering*,
DOI 10.1007/978-1-4939-2565-0_62, © Society of Fire Protection Engineers 2016

substances produced by modern materials was similar to those from traditional materials such as wood and that the increased toxic hazards in fires were more related to the burning behavior of modern materials and products. According to this hypothesis, fires at that time involving modern materials (especially fires in domestic dwellings involving upholstered furniture and bedding), were easier to ignite and produced more rapidly growing fires. The yields of common toxic products including smoke, irritants and asphyxiant were also higher, so that the mass production rates of toxic effluents were greater than previously.

During this period a variety of bench-scale combustion devices were used to generate thermal decomposition product atmospheres. These were used with animal exposures to measure toxic effects and potencies, combined with efforts to measure the detailed chemical composition of effluent mixtures from a wide range of materials. There was also a concept that some form of bench-scale "toxicity test" method might be developed which might be used to screen novel materials for the production of super toxicants and also to measure and to rank the toxic potencies of the effluent mixtures from different materials or products.

The findings from this work were the combustion chemistry of materials was indeed very complex so that combustion products from all materials contain many hundreds of toxic compounds with a range of toxic effects and toxic potencies. The chemical composition and in particular the yields of different components of the effluent mixtures vary considerably for any individual material depending on the combustion conditions. Also, when different materials are decomposed there tends to be a set of basic organic and inorganic substances produced that are common to most materials, plus an additional set of substances related to the specific chemistry of the material and sometimes unique to that material or class of materials. In addition to the chemical identity of effluents, the physical form varies in ways that are of toxicological importance. Fire effluents contain a mixture of gases, liquid droplets and solid smoke particles. The aqueous solubility of the gases and the size-range of the droplets and particles determine where they are deposited in the respiratory tract during inhalation, which in turn partly determines their toxic effects.

Despite these detailed complexities only two specific examples have been found of unusual toxic effects. One was for a particular caged biphosphorus ester (TMPP) formed during thermal decomposition of trimethylol polyols in the presence of phosphate additives. The other was a highly toxic nanoparticle mist formed from per-fluorinated materials under specific non-flaming thermal decomposition conditions. Apart from these two cases it was found that in terms of effects on escape and survival during and immediately after fires, the incapacitating physiological effects on fire victims were relatively simple, consisting of irritancy and asphyxia, which could be explained in terms of a small set of toxic gases and smoke particulates common in effluents from most burning fuels.

Combining the results from these studies with detailed studies of full-scale fire experiments and fire incident investigations, it has also become evident that "toxicity" or more correctly "toxic hazard" in fires is a system property of full-scale fires. This involves a series of different physiological effects occurring at different timescales during a fire and caused by different effluent components. The effluent composition also varies during fire development depending upon the combustion conditions, resulting in the varying time-concentration curves for the smoke, irritants and asphyxiant gases. It also became evident that the different forms of bench-scale decomposition apparatus had been chosen mainly for convenience of use rather than in an attempt to replicate any specific combustion conditions occurring in full-scale compartment fires. In practice most studies involved oxidative pyrolysis in a furnace rather than flaming combustion, and for the few cases where flaming conditions were established no consideration was given to the considerable effect that the fuel-air equivalence ratio has on the yields of toxic products at different stages of compartment fires.

Table 62.1 ASET parameters

The time-concentration (or time-intensity) curves for the major toxic products, smoke and heat in the fire at the breathing zone of the occupants, which in turn depend upon
Fire growth curve (mass loss rate of the burning fuel [kg/s] and its dispersal volume [kg/m^3] with time)
The yields of the major toxic products (kg/kg) and heat (kj/kg) (for example kg CO per kg of material burned)
These terms can be measured directly in full-scale tests or calculated using appropriate fire dynamics computations with appropriate input data including reaction-to-fire properties and data on product yields under a range of fire conditions. Guidance on calculation methods for these terms is given in other chapters of this handbook. Some information is provided in this chapter on toxic product yields under a range of fire conditions and also in Chap. 16, [1] and Chap. 36, [2]. Data on toxic product yields can be be obtained using the ISO TS19700 tube furnace or the ASTM E2058 flammability apparatus. A guide to the general characteristics of fires and examples of full-scale fire profiles are presented in Chap. 63 [3]
The concentration/time/physiological effect relationships of these products in terms of the physiological/toxic potency of the products and heat (the exposure concentration [kg/m^3]), or exposure dose (kg·m^{-3}·min or ppm·min) causing toxic effects (and the equivalent effects for heat and smoke obscuration). The important endpoints are:
Concentrations, doses (or heat intensity) likely to impair escape efficiency due to behavioural and/or physiological effects
Exposure concentrations or doses likely to cause incapacitation or prevent escape due to behavioural and/or physiological effects
Lethal exposure concentrations or doses
These terms can be calculated by the application of appropriate physiological methods (Fractional Effective Dose methods [FED equations]) presented in Chap. 63 [3] and in ISO 13571 [4]

Since it is not possible in any bench-scale test to re-create the sequence of fuel combustion and decomposition conditions occurring in a full-scale fire, and since "toxicity" is a sequence of different physiological effects that cannot be represented by a single quantity, it is considered that bench-scale toxicity tests are of limited value for direct application to either toxic hazard assessment or product specification. Toxic hazard in fires is best evaluated using the approach shown in Table 62.1 and described in detail in Chap. 63 [3]. For this method the time-concentration curves for the small range of key toxic products known to be important are measured in full-scale tests or calculated using computer models with appropriate input data on parameters including fuel-composition, heat release rate and toxic product yields as a function of fire type and fuel-air equivalence ratio. These data are then used with the human FED expressions detailed in Chap. 63 to calculate time to impairment of escape capability from smoke and irritants, and time to incapacitation from asphyxiant gases, This is then used to estimate ASET for any specific fire scenario.

Despite the limitations of bench-scale toxicity tests for toxic hazard assessment or product specification a set of published data exists from the animal exposure and chemical analysis studies, and several bench scale test methods are still used for different purposes, with new methods under development. This chapter consists of a review of useful information obtained by past and current test methods in the following areas:

- **Key products and effects**: Where fire effluent mixtures have been generated for animal exposures and chemical analysis it has been possible to measure the toxic effects and establish the extent to which these can be explained in terms of the measured effects of individual toxic substances and interactions between known mixtures of individual substances. Although concentrations and ratios of different substances in the effluent mixtures generated in these bench scale tests may differ somewhat from those occurring in compartment fires, tests carried out under non-flaming decomposition conditions are rich in a wide range of toxic substances so are useful for estimating the extent of toxic

interactions between different atmosphere components and the extent to which key products are responsible. Flaming decomposition tends to produce simpler mixtures containing a few irritant and asphyxiant gases which and have been useful for evaluating the effects of these components and their interactions. The results of these studies form the basis for the development of the human FED calculation methods described in Chap. 63 [3].

- **Measurement of toxic substance yields from materials under different fire conditions**: As set out in Table 62.1, if time-concentration curves for toxic substances in full-scale fire scenarios are to be calculated using computer fire dynamics models, essential inputs are the yields of each key toxic product from each burning fuel as a function of the combustion conditions. Although bench-scale tests cannot produce the dynamics of full-scale fires, it is possible to use some test bench-scale methods to reproduce the chemical decomposition conditions to which fuel pyrolysis products are exposed in terms of flaming/non-flaming behavior, decomposition temperatures and fuel/air ratios, in order to measure smoke particulate and toxic substance yields. Data from a number of test methods are presented in this chapter.
- **Identification of super-toxicants**: Bench-scale animal and chemical measurement tests have been useful to confirm that the majority of polymers have not produced unusual or "super-toxic" substances relevant to acute fire hazards, and in identifying the two cases where such substances have been produced. These are described
- **Measurement and calculation of lethal toxic potency ranges for materials**: Bench-scale chemical measurement tests are also useful in combination with rat lethality FED calculations to establish the range of toxic potencies of effluent mixtures from different materials, and how these vary with combustion conditions. Examples for a range of polymers decomposed under different defined conditions are presented.
- **Simple toxic hazard calculations using material toxic potency data**: Material toxic potency data cannot be used directly to rank toxic hazard, but they can be used as input to a simple form of toxic hazard analysis as an alternative to the human FED methods in Chap. 63 For this simple hazard analysis the calculated toxic potency for a material decomposed in a bench-scale test is combined with fuel mass loss rate and dispersal calculations for a compartment fire. This can then be used to generate a time-FED curve to calculate the time at which a lethal exposure is predicted. Some data and examples of this method are presented.
- **Limitations of bench-scale test methods**: As stated, a number of bench-scale methods have been used to produce toxic yield and potency data, and for product specification purposes, but have severe limitations in terms of the test conditions, form of data and applications to which they are put. A number of test methods are discussed.
- **Generation and yield measurements for environmental toxins**: Bench-scale tests can be used for the generation and detailed measurement of the yields of the wide range of environmental toxins from different materials. This can be very valuable in relation to workplace health and safety and environmental contamination evaluation. For these applications a wide range of systemically toxic and carcinogenic substances, such as halogenated dioxins, furans, volatile organic chemicals and polycyclic aromatic hydrocarbons may be important. When materials are decomposed under defined non-flaming and flaming combustion conditions relevant to different full-scale fire conditions the yields of these substances can be measured. This area is beyond the scope of this chapter on acute fire hazards.

Material-Based and System-Based Approaches to Toxic Hazard Assessment

Materials-Based and Combustion Product–Based Approaches to Toxicity Assessment

There have been two main views as to why smoke toxicity appears to be an increasing problem, which in turn have led to two rather different approaches to the evaluation of toxicity.

1. One view held that smoke from modern synthetic materials contained new toxic products that were not present previously, and that in some cases these products (the so-called "supertoxicants") might be very potent, exerting novel toxic effects at very low doses. Such effects could therefore be detected by means of simple, small-scale toxicity tests that could be used for regulatory purposes [5–7]. To some extent this approach followed the discovery that two materials, a flexible polyurethane foam containing a phosphorus-based fire retardant and polytetrafluoroethylene (PTFE), could under certain laboratory conditions evolve products with a very high toxic potency [5, 6]. This led to the use of rather simplistic materials-based toxicity tests, where the toxicity of materials is ranked in terms of the rodent LC_{50} (the concentration of combustion products expressed in terms of mg of material per liter of air causing the deaths of 50 % of animals exposed) [7, 8]. This approach implies that the engineer should design by using those materials with the better performance in toxicity tests and that are consistent with good performance in other types of small-scale fire tests.
2. The other main view was that the basic toxic products of fires were much the same as always, but that in many modern fires the rate of fire growth and the rate of evolution of the common toxic products were much greater than they had been previously. Therefore, the best way to mitigate toxic hazard in fires was to control such factors as ignition, flame spread, and rate of smoke evolution rather than the qualitative nature of toxic products. For this approach, which is favored in the United Kingdom, there is more interest in estimating toxic hazard by measuring or modeling the yields and time-concentration curves for the main toxic products given off by materials during fires. This can be achieved by carrying out large-scale fire tests. Alternatively, data on the yields of the main toxic products can be obtained from suitable small-scale tests described in this chapter and used as input to calculation of full-scale fire behavior using engineering calculation models such as those described in Chap. 16 [1] and Chap. 36 [2]. These data are then used to estimate time to incapacitation and death. In this context the main function of small-scale toxic potency tests (other than to provide data on yields of the main toxic gases) would be to confirm that the toxicity associated with particular burning materials was indeed due to the common toxic fire products via chemical atmosphere analysis in conjunction with animal exposures and to identify those cases where unusual toxic effects occurred. This approach enables a fire safety engineer to design to a set of fire scenarios in a system (for example, a hotel bedroom or an aircraft cabin) and, by a simple chemical analysis of atmospheres produced during appropriate small- and large-scale fire tests, predict likely toxic hazard. This is the basis of the FED hazard assessment methods presented in Chap. 63. Of course the quality of such assessments is only as good as that of that of the input data and calculation methods.

Another approach, based upon the view that toxicity results from a small number of common toxic products, make use of simple bench-scale "toxicity" tests in which a small sample of a material or product is exposed to a heating regime and the concentrations of a defined set of evolved decomposition products are measured using chemical analysis. The data are then input into a calculation

method to obtain a "toxicity index" for the product, which is then used as the basis for a prescriptive product classification. This approach not considered realistic, because, as described, it is considered that toxic hazard is a time-related emergent property of the full-scale fire scenario, and cannot be measured directly by any bench-scale test. Also, such tests do not replicate the decomposition conditions occurring in full-scale fires, so that the concentrations and yields of toxic gases are very different from those occurring in compartment fires.

In practice there is a need for both appropriate small-scale materials-based toxicity tests and for fire profile modeling based on a few major toxic fire products. Existing information is often inadequate and misleading, and a better standard of research and testing is needed if data are to be produced for practical use. This chapter will give the reader an understanding of what is known about combustion product toxicity, the extent to which effects can be predicted from knowledge of common fire products, and how small-scale tests should be performed and the results interpreted and used.

Use of Small-Scale Tests to Represent Toxicity and Toxic Product Yields

Historically bench-scale tests have been used to measure the "toxicity" of materials or products in terms of single numbers for ranking and specification purposes. A test specimen is decomposed, usually in an enclosed chamber, and either animals (usually rats or mice) are exposed to the effluent atmosphere produced to measure toxicity directly, or measurements of toxic gas concentrations are made and used to calculate the predicted toxicity of the effluent mixture. Results are expressed in terms of lethal concentration for 30-min exposures (LC_{50} concentration) expressed in terms of the mass charge or mass loss of the material tested (for example lethal toxicity of wood g/m^3). Alternatively the results may be expressed in terms of an index value based on 30-min IDLH values (Immediately dangerous to life or health after 30-min exposure).

These methods are considered to be of limited value for hazard assessments because:

- Toxic hazard is a property of a full-scale system depending upon the time-varying dynamics of fire growth and effluent spread in specific fire scenarios
- Yields of toxic species and hence toxicity from any material or products are variables which depend upon the changing combustion conditions during fires. The decomposition conditions in existing toxicity test methods are uncharacterized and give a poor representation of any specific stage of any full-scale compartment fire, let alone a representation of the changing combustion conditions
- Toxicity involves a time varying set of different physiological effects

One area where bench-scale animal exposure tests combined with chemical effluent analysis have been valuable is in establishing that the toxic effects can be understood in terms of a small number of key gases and the interactions between them, despite the fact that fire effluents are known to contain many hundreds of toxic substances [9, 10]. This has enabled validation of the Fractional Effective Dose models based on this small number of key toxic products, with essentially additive effects among the different components.

Another important use of specific bench-scale tests is for measurement of the yields of key toxic products under the different combustion conditions occurring in compartment fires. Two test methods capable of providing these data are the ASTM E2058 flammability apparatus [2] and the ISO TS19700 steady state tube furnace [11–13], which has been developed specifically for this purpose (see this Chapter "The Use of Small-Scale Combustion Product Toxicity Tests for Estimating Toxic Potency and Toxic Hazard in Fires"). The steady state tube furnace has been designed to reproduce the decomposition conditions in all six stages of fires defined in ISO 19706 [14] (including pyrolysis under nitrogen, non-flaming and smoldering oxidative

decomposition, well ventilated flaming, under-ventilated pre- and post-flashover flaming).

The Significance of Toxicity as Part of Total Fire Hazard

For scenarios involving the escape of occupants from a fire, survival depends on the outcome of two parallel processes.

1. *The developing hazard from the fire*. This process incorporates ignition, fire growth, and the spread of fire and fire effluent. These depend on a range of variables, such as the nature and disposition of the fire load, potential ignition sources, the reaction to fire properties of the lining materials and contents, the height and ventilation of the compartment, and the nature of the fire effluent. The actions of occupants and the provision of passive containment and active smoke extraction or suppression systems also affect the rate of development and extent of the hazard from a fire.

   Assessment of these processes for any particular scenario is aimed at calculating the time from ignition to the time when occupants would receive an incapacitating exposure to fire effluent (sufficient to seriously impair their ability to escape). This represents the available safe escape time (ASET).
2. *The process by which occupants escape*. This depends on detection, the provision of warnings, response to warnings (pre-movement time), occupant profile (such as age and physical and mental ability, sleeping or waking, and population density), subsequent pre-egress behavior (such as seeking information, collecting belongings, choosing an exit, and other activities), egress (including way finding, movement toward an exit, crowd flow, and other factors), design of escape routes, exit numbers and widths, and the psychological and physiological influence of exposure to heat and smoke on escape behavior.

   Assessment of these processes for any particular fire scenario is aimed at calculating the time from ignition to the time when occupants have evacuated or reached a place of safety. This represents the required safe escape time (RSET).

Toxic smoke products and heat affect calculations of time available for escape in that they determine the ASET tenability endpoint. They may also affect RSET calculations by effects on exit choice and speed of movement through smoke-filled escape routes.

Once a fire has started, the outcome of the situation depends on the outcome of these two processes. If the occupants have escaped before the fire becomes hazardous, with a reasonable margin of safety, then the design can be considered to have succeeded, but if the fire growth processes result in the fire becoming hazardous before the occupants have escaped, or within a narrow margin of safety, the design may be considered to have failed.

It is evident from this list of parameters that when all the needs of building occupants are considered, there is no single answer to fire safety or fire hazard and that any practical system involves some compromise between all of these parameters. Fire safety can be improved or compromised in a number of different ways, while the occupants are involved in a number of ways, both in terms of their physiology and their behavior.

It is possible to consider the effects of fires on occupants in three phases.

1. The first phase consists of the period when the fire is growing but before occupants are affected by heat or smoke. During this phase the important factors influencing escape and ultimate survival are largely psycho behavioral or logistical factors, such as how occupants are alerted to the fire and react to that knowledge, whether they respond to alarms, attempt to leave or stay to fight the fire, how they interact with other individuals, and how they respond to the geography of the fire environment in effecting an escape.
2. The middle phase is the period when occupants are exposed to smoke, heat, and toxic products, and where physiological factors such as irritancy and asphyxiation affect their escape capability. During this

phase such factors as the toxic nature of fire products and the dynamics of their production become critically important to escape.
3. The third phase is death in the fire, which may be caused by the major factors of toxicity and burns or a number of other factors.

The toxic effects of fire products are, therefore, most important during the second and third phases of fire growth. Most studies of fire toxicity have been confined to aspects of lethality. The ultimate causes of death in fires have been studied through pathological investigations of fire fatalities such as the Strathclyde study in the United Kingdom [15]. Also, the majority of combustion toxicity studies on laboratory animals have been used to measure lethality, principally in terms of the LC_{50} for individual fire products such as carbon monoxide (CO) or hydrogen chloride (HCl), or mixtures of thermal decomposition products from individual materials [16].

The middle phase of incapacitation in fires can be studied either by animal experimentation or by investigations of the circumstances surrounding real fire casualties, particularly survivors of serious smoke exposure. However, this crucial area of toxicity has been largely neglected.

One particular series of studies has been carried out on the sublethal effects of combustion atmospheres on animals, mainly primates, to examine the mechanisms whereby people become incapacitated in fires [17]. Incapacitation rather than death has been studied because most fires are potentially lethal due to heat or CO if occupants are exposed to these for sufficient time. The two major determinants of whether a potential victim escapes are (1) the point at which incapacitation by toxic products is reached, and (2) how these products affect escape capability during the window of time available for escape between ignition and the development of lethal conditions.

In addition to direct physiological effects, behavioral effects can inhibit escape. The effects of seeing smoke or flames or the exposure to irritant smoke may result in some occupants being unwilling to use a particular escape route or turning back. These effects of smoke are discussed later.

The behavioral and physiological effects of exposure to toxic smoke and heat in fires result in varying degrees of incapacitation, which also may lead to death or permanent injury. These incapacitating effects include the following:
1. Behavior-modifying effect of smoke and irritants on willingness to use escape routes
2. Impaired vision resulting from the optical opacity of smoke and from the painful effects of irritant smoke products and heat on the eyes
3. Respiratory tract pain and breathing difficulties or even respiratory tract injury resulting from the inhalation of irritant smoke, which may be very hot. In extreme cases this effect can lead to collapse within a few minutes from asphyxia due to laryngeal spasm and/or bronchoconstriction. Lung inflammation may also occur, usually after some hours, which can also lead to varying degrees of respiratory distress
4. Asphyxia from the inhalation of toxic gases, resulting in confusion and loss of consciousness
5. Pain to exposed skin and the upper respiratory tract followed by burns, or hyperthermia, due to the effects of heat preventing escape, which can lead to collapse

All of these effects can lead to permanent injury, and all except the first two effects can be fatal if the degree of exposure is sufficient.

With regard to hazard assessment the major considerations are the following:
1. The time when partially incapacitating effects are likely to occur that might delay escape
2. The time when incapacitating effects are likely to occur that might prevent escape, compared with the time required for escape
3. Whether exposure is likely to result in permanent injury or death

Up to a certain level of severity, the hazards listed in items 1 through 5 under incapacitating effects cause a partial incapacitation by reducing the efficiency and speed of escape. These effects lie on a continuum from little or no effect at low levels to relatively severe incapacitation at high levels with a variable response from different individuals. It is important to make some estimate of effects that are likely to delay escape, which may result in fewer occupants being able to escape during the short time before conditions

become so bad that escape is no longer possible. Most important in this context is exposure to optically dense and irritant smoke, which tends to be the first hazard confronting fire victims. For more severe exposures a moment may be reached when incapacitation is predicted to be sufficiently bad as to prevent escape. For some forms of incapacitation, such as when asphyxia leads to a rapid change from near normality to loss of consciousness, this moment is relatively easy to define. For other effects a defining moment is less easily characterized; for example, when smoke becomes so irritant that pain and breathing difficulties lead to the cessation of effective escape attempts, or when pain and burns prevent movement. Nevertheless it is considered important to attempt some estimate of the moment when conditions become so severe in terms of these hazards that effective escape attempts are likely to cease and when occupants are likely to suffer severe incapacitation or injuries. In the following text the mechanisms whereby these various factors cause incapacitation and death, and how they are likely to produce partial incapacitation and affect escape capability, are examined in detail. Toxicological and physiological data and models are presented are presented here and in Chap. 63 to enable calculations (or exposure dose) to incapacitation and death.

Basic Toxicity Patterns of Fire Products

As a result of chemical studies of large- and small-scale experimental fires [18] and animal exposures to the thermal decomposition products from a wide range of materials [16, 17], two important basic points have emerged concerning the nature of fire product toxicity.

1. Atmospheres of thermal decomposition products, even from single materials, contained large numbers of potentially toxic products. The chemical composition of the products could vary considerably depending on the different conditions of temperature and oxygen supply under which they were decomposed [17]. When animals were exposed to these atmospheres, similar variations in toxicity were observed. In many cases, however, similar basic ranges of products were evolved from quite different materials [18].
2. Despite the great complexity in chemical composition of smoke atmospheres, the basic toxic effects were relatively simple. For each individual smoke atmosphere the toxicity was dominated either by an asphyxiant gas (CO or HCN) or by irritants. Also, interactions between individual asphyxiant gases or between asphyxiants and irritants were found to be approximately additive, so that a reasonably good predictive model for incapacitation could be developed by summing the effects of each individual toxic component [17].

This work and that done using rodents [16] seem to indicate that the theory that smoke casualties have increased because new, highly toxic products are formed from modern materials is unlikely to be correct. Also, the finding that a small number of basic products are particularly important leads to the possibility of predicting toxic effects from a relatively simple chemical analysis of fire products. (This is not to say that unusual, highly toxic products cannot occur, as at least two examples have been discovered in the laboratory [5, 6, 8, 9], which is one important reason that the toxicity of thermal decomposition products from materials should be submitted to an animal screen.)

Environmental and Health Issues with Regard to Fire Retardants and Combustion Products

Although escape and survival from fires have been found to involve a small number of key toxic gases, combustion product mixtures contain a very large number of systemically toxic and carcinogenic organic compounds produced at low yields. Although not acutely life-threatening, exposure to such compounds in the workplace, home or outside environment can present potential health hazards, especially following repeated exposures over time-scales of

years. In addition, some fire retardant chemicals used as additives to materials can be released into the environment during use and, where these are bioaccumulative, they may present potential environmental and health issues. Some of these fire-retardant treatments, especially those containing halogens, lead to the production of environmental toxicants including polychlorinated biphenyls and halogenated dioxins and dibenzofurans. Concerns regarding potential adverse health implications from environmental release of such compounds have resulted in a recent increase in interest in both releases of pedigree compounds from treated materials and in the release of toxic compounds in combustion products. Ultimately the use of any flame-retardant treatment needs to be justified on the basis of the societal benefits in terms of reduced fire incidence, improved survivability during fires that do occur, and reduced fire effluent releases from fewer fires, compared with any potential environmental hazards from the fire-retardant systems or their combustion products.

Another issue of recent concern has been exposures to the atmospheric release of mineral dusts and fibers during fires such as the World Trade Center fire and aircraft fires, and the subsequent adverse health effects of these releases, especially to fire fighters.

These environmental toxicity aspects are considered beyond the scope of this chapter, which is restricted to consideration of fire-safety design.

Dose/Response Relationships in Relation to Material Toxic Potency

In order to determine the toxic effects of individual toxic fire products and effluent mixtures it is necessary to determine the basic parameters required to quantify exposure. These are described in detail in Chap. 63. For application to bench-scale toxicity tests the main criteria measured are the exposure concentration and exposure dose. For smoke obscuration and sensory irritancy, effects occur immediately or almost immediately on exposure, with the severity proportional to the exposure concentration. For evaluating the effects of animal exposures during a test the important parameters is the concentration (expressed as a volume ratio in ppm or mass concentration (g. m^{-3}). The effects of asphyxiant gases and lung irritants depend upon a dose accumulated over a period of time so that the main parameter is the exposure dose (expressed as ppm·minutes or g·min·m^{-3}). This is a simplification often used by toxicologists assuming toxic effects obey Haber's rule, which states that the toxicity depends on the dose accumulated, and that the product of time and concentration is a constant [19], so that

$$W = C \times t \tag{62.1}$$

where W is a constant dose, specific for any given effect. In practice, dose in inhalation toxicology is often expressed in terms of Ct product. In the case of the LC_{50}, the effect is death of 50 % of the animals and

$$W = LC \cdot t_{50} \tag{62.2}$$

In practice there can be significant deviations from this ideal behavior. The standard exposure period for most bench-scale toxicity tests is usually 30 min.

The Nominal Atmosphere Concentration

There are occasions in combustion toxicology when it may be desirable to relate the toxic effects of an exposure to the material being decomposed rather than to its individual toxic products. This applies particularly to small-scale test results, where, for example, the LC_{50} of wood when decomposed in a particular way might be considered. This is a somewhat unsatisfactory approach, since any material evolves different products at differing yields in compartment fires as the combustion conditions change, so that the toxicity also changes. However, this parameter does have some value when the small-scale test decomposition conditions have been validated against the full-scale fire conditions of

interest, and also when calculated in conjunction with measurements of the actual toxic products. This approach is related to another concept used in inhalation toxicology, that of the nominal atmosphere concentration (NAC). This theoretical concentration of test material in the test atmosphere is calculated from the amount of material produced from the atmosphere generation system each minute, divided by the diluent airflow rate. This concept is not strictly applicable in combustion toxicology since the test material is decomposed in the fire or furnace system, but two analogous concepts are useful with regard to small-scale test methods since they enable some relationship to be established between the test material and the degree of toxicity. These are the nominal atmosphere concentration in terms of mass charged into the furnace and the nominal atmosphere concentration in terms of mass decomposed, as follows:

1. Nominal atmosphere concentration (mass charge) equals mass of material placed in the furnace system divided by volume of air into into which the combustion products are.
2. Nominal atmosphere concentration (mass loss) equals mass lost by material during decomposition divided by volume of air into into which the combustion products are.

In practice the calculation of these parameters depends on the particular decomposition system used (see the section of this chapter "Examples of Small-Scale Test Methods") and a shortcoming of some systems is that these parameters cannot easily be estimated.

If predictions of toxicity are to be made from large-scale fire test atmospheres, or if toxicity data from animals are to be interpreted, the following data should be available:

1. The nominal atmosphere concentration(s) of the test material(s) mass charge ($g \cdot m^{-3}$) (NAC mass charge)
2. The nominal atmosphere concentration of the test material mass loss ($g \cdot m^{-3}$) (NAC mass loss)
3. The concentration of each major toxic product in the atmosphere and the anticipated duration of exposure, that is, the concentration/time profile
4. The rate of uptake of the atmosphere, or V_E
5. Measurement of the blood concentration of certain toxicants
6. Particle size range. This is also important in determining the respirability and site of deposition of atmospheric products. However, smoke from nonflaming decomposition in small-scale tests is usually highly respirable
7. The nature of the effects of toxic products and the time/concentration relationships of these effects

Basis and Validation of Human FED Hazard Models from Human and Animal Exposure Studies

In order to evaluate toxic, smoke and heat hazards to people in fires, it is necessary to determine the main physiological and pathological effects of exposure to toxic fire effluents and the mechanisms whereby they impair escape, cause incapacitation and death. It is, then, necessary to identify the main toxic species responsible for these effects amongst the hundreds of chemical species known to occur in fire effluents and the relationships between exposure concentration (or heat intensity), dose, and severity for each toxic species individually, and in the combinations occurring in fire effluents. One source of relevant information is from fire incidents, associated fire tests and pathology studies. These data are obtained directly for exposed human subjects, survivors and deceased, from real fire scenarios, but there is often limited information regarding the exact fire conditions, the fuel materials involved and the composition of the fire effluent atmospheres. Detailed incident investigation can supply some of these data, especially if large or full-scale incident recreation tests are performed, or by using computer fire modeling to determine the fire conditions. Since fire victims are exposed to the full fire effluent mixtures, it is possible to determine the importance and effects of different symptoms such as irritancy and asphyxiation, and the extent to which these can be understood in terms of the known effluent composition (see Chap. 63).

Another approach has been to expose animals (rodents or primates) to combustion atmospheres generated by thermal decomposition of different materials in bench-scale tests (and in a few cases exposure of rodents to effluents from large-scale fire experiments). A limitation in most cases has been a limited correspondence between the combustion conditions in the test apparatus and those in different stages of full-scale compartment fires, but the test conditions used have generated a general mix of the effluent species occurring in fires. Another limitation has been that most of the experiments were directed at measuring lethality, while the key aspect of fire exposures is the extent to which they are incapacitating and prevent escape—since most fires are eventually lethal due to carbon monoxide or burns. Where such experiments combined detailed chemical analysis of the effluent atmosphere with measurements of toxicity endpoints, this provided an opportunity to determine a number of important aspects:

- The extent to which the overall toxic effects can be understood in terms of a small number of key toxic species.
- The extent to which there were interactions between the toxic effects of different individual toxic species in providing the overall toxicity (whether individual toxic species were acting independently, were additive or synergistic [i.e. multiplicative or more than additive—all variations commonly encountered in toxicology].
- Whether any unexpected or high potency "supertoxic" effects on exposed animals occurred that could not be predicted from the known effects of the chemical effluent components (especially from the range of novel polymeric materials coming into use at around this time).
- The extent to which smoke particulates and organic components contributed to toxicity.
- Where detailed physiological measurements were made, mostly using primates, it was possible to measure incapacitating effects and the toxic species responsible

In addition to these animal studies of mixed effluents from different polymeric materials, experimental studies were carried out on individual fire gases and interactions between specific gas mixtures. Some of these measurements (for example uptake and effects of carbon monoxide, carbon dioxide and low oxygen) and exposure to optically dense smoke, convected and radiant heat, have been carried out directly in human subjects, but mostly at sub-incapacitating levels. For ethical reasons, it is not possible to expose humans to incapacitating levels of toxicants; so non-human primates have been used to supplement the human data at these levels. Additional human data are also available from sources such as industrial exposures and accidents involving individual chemical species, but these are often limited by a lack of data on the exact exposure concentrations.

Rodent data are useful for understanding toxicity mechanisms and effects for different chemicals, but while these have the advantage that comprehensive data sets can be generated, with means and statistical distributions of endpoints, there always remains the difficulty and uncertainties of extrapolating from animal data to predicted effects in humans. The most important difference between animals and humans, which is often ignored, is the scaling effect of body side. In general terms, respiration in mammals (liters of air inhaled each minute/kg body mass) is proportional to the body surface area/volume ratio. The result is that the rate of uptake of a toxic gas such as CO by a mouse is much more rapid than in a human, so that for exposure to a given CO concentration, the time to reach an incapacitating or lethal dose is much shorter. This is illustrated in Fig. 62.1 comparing rate of uptake of CO in terms of increasing blood %COHb in resting rats, macaque monkeys, and humans at inhaled CO concentrations of 1200 ppm and 3000 ppm. For rats, uptake is rapid, reaching high equilibrium levels within 15–20 min, while for humans uptake is much slower, equilibrium being approached only after 100 min or more. Humans and monkeys are incapacitated at 40 %COHb, while the rats were more resistant to the toxic effects and were unaffected until %COHb levels of 66–75 % had been achieved [20].

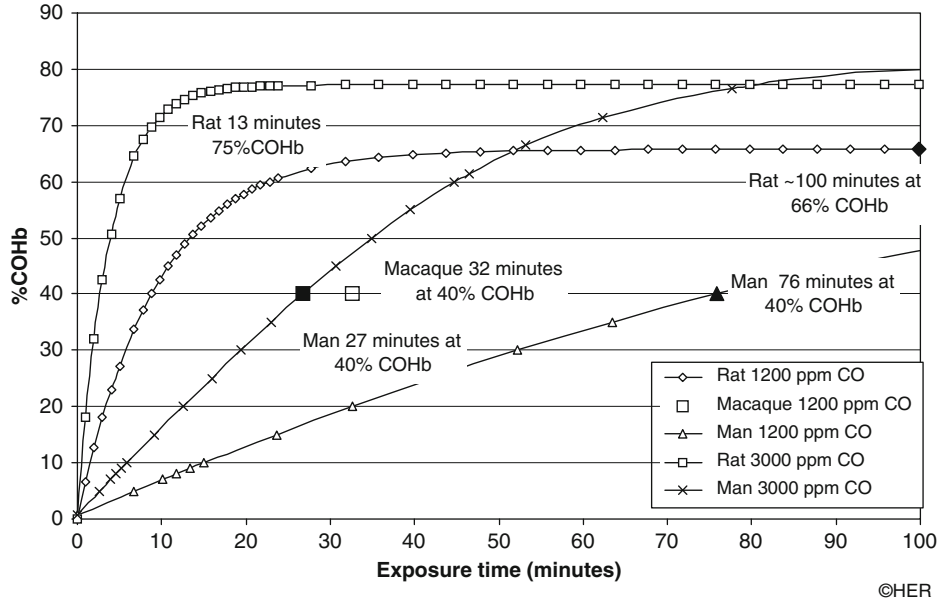

Fig. 62.1 Rate of uptake of CO as %COHb, time to and %COHb at incapacitation for rats, humans and macaque monkey at 1200 and 3000 ppm CO exposure concentrations

Other important differences between rodent and humans are basically allometric. Rodents have very large nasal cavities with a large surface area relative to their body size compared with humans. They are also unable to breathe through their mouths as primates often do. These aspects and other scaling factors result in differences in the uptake, deposition and effects of irritant acid gases and particulates. Rodents also appear to be somewhat more resistant to asphyxia than primates. Although the basic physiological and toxicological effects are very similar in rodents and humans, it is important to understand and take into account the differences when predicting effects in humans. For humans it is also important to take into consideration variations in susceptibility and the effects of aspects such as body size, activity level, age and health status.

The overall position is that since it is not possible to expose human subjects directly to fire effluent atmospheres to measure the effects, it is not possible to produce precise calculation expressions to predict effects of exposure, or to quantify probability distributions for different endpoints. But by taking account of the full set of data available from all the sources described, it has been possible to derive a set of predictive expressions for calculating times to different toxicity, smoke, and heat endpoints during fires with a reasonable level of confidence. Some aspects can be predicted with more confidence than others, and attempts have been made to reflect this as they are discussed.

Recently, it has become possible to validate the predictions of FED and FEC calculations against the conditions occurring in specific incidents, where these have been re-created in some detail using experiments and fire computer simulations (see Chap. 63).

Fire Incident Investigations, Associated Tests and Pathology Studies

Smoke Irritants

An important source of information on toxicity and toxic hazards in fires has been fire incident investigation combined with clinical and pathological studies of fire survivors and fatalities. With regard to conditions during fire incidents, survivors surveyed in a number of studies have reported difficulty or unwillingness to enter and

move through smoke, and that both smoke obscuration and irritancy are factors. Smoke from electrical fires (likely to be high in HCl) is reported as being particularly irritating, and very low smoke levels in minor incidents have resulted in buildings being evacuated due to eye and respiratory tract irritation.

The presence of a significant content of irritants in fire effluent smoke, and its tendency to penetrate deep into the lungs, is also confirmed by the occurrence of chemical pneumonitis in some fire survivors. A typical pattern in a proportion of fire survivors is a transient hypoxic crisis with low arterial blood oxygen concentrations developing several hours after rescue due to pulmonary edema and inflammation. This can be fatal, or can resolve after around 24 h. It may, then, progress to bronchopneumonia, which can also be fatal. If infection is avoided recovery can be rapid, so that while most people report a slight hoarseness and productive cough for a few days after the incident, after 3 months, they are generally free of respiratory symptoms [21].

Irritants are therefore known to be present, and both sensory irritation and lung inflammation are know to occur as result of exposures to fire effluents, but fire incidents do not really enable the identification of important irritant species or provide a method for predicting the severity of effects.

Asphyxiant Gases

CO is always present, often at high concentrations (0.5–1 %CO), in fires and remains in the blood during and after exposure as carboxyhemoglobin. The presence of high %COHb levels in the blood of fire survivors and fatalities is therefore strong evidence that they have inhaled significant quantities of a toxic smoke mixture during a fire, since all fire gases tend to be present simultaneously. Also, studies of fire fatalities and human victims of accidental and deliberate CO poisoning show similar %COHb distributions (See Chap. 63, Fig. 63.15), leading to the suggestion that CO is likely to be the major ultimate cause of death in most fires where serious burns are not present. In fact the %COHb levels in many fire victims are somewhat lower than those from CO deaths, indicating the presence of other asphyxiants [22]. Post-mortem studies also show elevated blood cyanide concentrations in a proportion of fire victims, but elevated blood cyanide levels are always accompanied by elevated %COHb levels [23]. Because cyanide is much less stable in blood than CO [24], and due to the dynamics of uptake and dispersal of cyanide in the blood, it is difficult to determine its importance in producing incapacitation at the fire scenes from post-mortem studies [20, 25, 26]. However, measurements taken during experimental house fires involving typical domestic furnishings showed HCN concentrations exceeding 1000 ppm which is likely to be a major factor in causing incapacitation (loss of consciousness) and thereby limiting time available for escape in many fire incidents [27, 28]. This is supported by a study in which fresh blood samples were taken from fire survivors at the time of rescue from the fire scene, in which high blood cyanide concentrations were measured [29], and also in samples taken from the Manchester Airtours fire victims [30].

Carbon dioxide and low oxygen hypoxia do not leave any obvious traces in fire survivors or fatalities once removed from the fire scene. Carbon dioxide is always present at high concentrations during fire experiments, and in fire victims its main effect is to cause hyperventilation, thereby increasing the rate of uptake of other fire gases. With regard to low oxygen hypoxia the effects are more difficult to predict. During enclosure fire experiments (such as that shown in Chap. 63 Fig. 63.8) it is generally found that oxygen depletion at head height is relatively minor by the time victims are predicted to be severely affected by CO and HCN [27]. However, oxygen concentration in upper layer fire effluent plumes can be as low as 1 %O_2 as well as being at temperatures of several hundred degrees centigrade. If a fire victim were to be exposed to, and inhale, an atmosphere such as this (for example when opening a door on a fire enclosure), they would be expected to collapse unconscious within seconds. A small number of reports do

exist of observations that could be consistent with this effect, in which victims in fire incidents have been observed to collapse or almost collapse following inhalation of a single breath of smoke.

Other potential asphyxiant gases present in fire effluents are oxides of nitrogen (NOx), but concentrations measured have not been high enough to make a significant contribution to asphyxia, except in specific incidents such as fires involving nitrate film [31].

The general indications from fire incident studies and full-scale fire experiments are that a short list of asphyxiant gases is important in most fires, including CO, HCN, CO_2 and low O_2. Of these, CO is present in all fires and almost always found at high concentrations in the blood of fire survivors and fatalities that have received serious smoke exposure in fires. CO is also likely to be the major ultimate cause of deaths during fires, but it is likely that both HCN and CO are important as causes of incapacitation, while their uptake is enhanced by the presence of CO_2. Irritants and simple hypoxia may be important in some fires as additional causes of hypoxia, and all may be additive with CO as ultimate causes of deaths from asphyxia during fires. Based upon the %COHb levels in fire fatalities it is possible to estimate the fatal exposure doses of CO for human fire victims. By comparing clinical status with measured %COHb concentrations in fires survivors it is possible to make some estimates of CO exposure doses and %COHb concentrations causing incapacitation during fires, however wide variations are reported in practice, as described in the section on CO in Chap. 63.

Findings from Primate Exposure Studies

Experiments involving sub-lethal exposures of macaque monkeys to individual asphyxiant fire gases (CO, CO_2, HCN and low oxygen hypoxia) and a set of mixed fire effluent atmospheres generated from a range of polymeric materials [17, 32–35] were used to investigate the physiological mechanisms by which fire effluents impede escape and cause incapacitation. Detailed physiological parameters were measured before, during and after 30-min exposures under dynamic steady-state exposure conditions. Effluent atmospheres were generated using an early version of the ISO19700 tube furnace [11], whereby strips of material were introduced at a constant rate into a tube furnace under a stream of air, and the effluents expelled into a mixing chamber where they were diluted with secondary air, forming an effluent atmosphere to which the animals were exposed (via a face mask or in a whole-body shuttle box chamber). Continuous measurements were made of physiological parameters indicating respiratory, cardiovascular and neurophysiological status, including respiratory flow, tidal volume and frequency, heart rate and electrocardiogram, electrocorticogram, nerve-conduction velocity and auditory-evoked potentials. Clinical signs and status of body reflexes were also monitored, and blood samples were taken at intervals for measurement of carboxyhemoglobin and blood cyanide concentrations. Observations were continued for 14 days post- exposure and some lung pathology investigations were also carried out.

For fire effluent exposures different materials were decomposed in two sets of experiments. For the first set wood (*Pinus sylvestris*), polyacrylonitrile and flexible polyurethane foam were pyrolysed under nitrogen at 300 °C, 600 °C and 900 °C. For the second set of experiments a rigid polyurethane foam, nylon 6, polystyrene and polypropylene were decomposed under non-flaming oxidative decomposition conditions at 440–500 °C. Polypropylene was also decomposed under flaming and pyrolytic decomposition conditions and polystyrene under pyrolysis. The fire effluent atmospheres were monitored continuously for CO, HCN, CO_2, O_2 smoke optical density and total particulates. Based upon these and more detailed investigations of decomposition chemistry by Woolley and Fardell [18], the different effluent atmospheres were found to contain significant concentrations of asphyxiant gases (CO and HCN), and varying concentrations of smoke particulates. GC-MS investigations showed a rich mix of aliphatic and aromatic hydrocarbons generated under pyrolysis, with an additional significant content of partially oxidized species (acrolein, formaldehyde,

crotonaldehyde, acetaldehyde, phenol, aliphatic acids etc.) being formed under non-flaming oxidative decomposition conditions. Under flaming combustion conditions the organic content was mostly consumed in the combustion process. Flexible polyurethane foam decomposed into isocyanate derived "yellow smoke". In addition to these experiments on resting primates two sets of experiments involved animals conditioned to carry out a behavioral task in a chamber. For these experiments the animals were conditioned to press a lever when an audible signal was sounded, after which they had a few seconds to reach the other end of the chamber where a food reward was presented for a brief period. The task was repeated at 3–5 min intervals throughout a 30-min exposure and post-exposure period [33]. The purpose was to test the animal's performance abilities during exposure and to maintain them in an active state. These behavioral experiments were carried out with exposure to different concentrations of carbon monoxide and also to fire effluent atmospheres generated from polypropylene under pyrolytic and non-flaming oxidative thermal decomposition conditions.

Kaplan et al. [36] used a condition escape paradigm to examine effects of 5-min exposures of baboons to different concentrations of acrolein or HCl gas. After 5 min exposure, the animals were conditioned to press a lever to release the door catch and escape from the exposure chamber.

The findings from the individual gas exposure experiments are summarized as follows:

- During exposure to carbon monoxide, no physiological or behavioral effects occurred until the blood carboxyhemoglobin concentration reached approximately 30 %COHb (for active animals) or 40 %COHb (for animals at rest). Free moving animals were unaffected until they suddenly became lethargic and over a period of seconds passed through a brief episode of apparent intoxication to collapse and loss of consciousness. Resting animals were unaffected until a time when their consciousness became suddenly impaired. At this point, there was a decrease in heart rate with occasional arrhythmias, a large increase in slow-wave brain activity, a decrease in respiration and failure of withdrawal reflexes as the animals became unconscious. Loss of consciousness from CO occurred at a threshold exposure dose of around 27,000 ppm·minutes for free moving animals and 36,000 ppm·minutes for resting animals. Inactive baboons became incapacitated at 35,000 ppm·minutes.
- During exposure to hydrogen cyanide there were also no immediate effects, but after a period of a few minutes (depending upon the exposure concentration) the animals started to hyperventilate. This induced a positive feedback in that the increased ventilation increased the rate of uptake of HCN, which further stimulated respiration until the animals lost consciousness, showing similar signs to those exposed to CO. At this point, there was a large decrease in respiration, so that the rate of HCN uptake decreased and the blood cyanide concentration leveled off. Some animals showed signs of recovery during this period, then passed slowly deeper into unconsciousness. Recovery was rapid within a few minutes of the end of the exposure, although whole blood cyanide concentrations showed little decrease over periods of up to an hour [25, 26]. Short exposures to high HCN concentrations (150–200 ppm) produced incapacitation within a few minutes (C·t exposure dose 270 ppm·minutes) while lower concentration of 80–100 ppm required approximately 30 min to cause incapacitation (C·t exposure dose 2610 ppm·minutes).
- Exposure to 10 % oxygen also resulted in signs of cerebral depression and lethargy throughout most of a 30-min exposure, but signs were short of loss of consciousness.
- Exposure to 5 % carbon dioxide produced some minor cerebral effects, but mainly an approximate threefold increase in V_E.
- The findings from the baboon studies were that the animals were able to perform the escape behavior efficiently up to very high concentrations of 15,000 ppm HCl and 2780 ppm acrolein, although post exposure signs or severe irritancy were observed at HCl concentrations above 1000 ppm.

The findings from the studies involving exposure to fire effluent atmospheres were as follows:

- The physiological effects measured were the same as those of the dominant toxic gases present in the effluent atmosphere and where either:
- Dominated by and identical with the effects of CO alone (e.g. wood pyrolysed at 900 °C, flaming polypropylene)
- Dominated by and identical with the effects of HCN (e.g. pyrolysed polyacrylonitrile, 900 °C, rigid polyurethane foam non-flaming oxidative decomposition)
- Dominated by signs of sensory irritancy during exposure and lung inflammation after exposure (polyurethane foam pyrolysed at 300 °C and 600 °C, wood pyrolysed at 300 °C
- In one case where significant concentrations of both CO and HCN were present, the effects were consistent with the toxicity of the two gases being additive.
- Where both CO and irritants were present, although there was some hyperventilation resulting from stimulation of lung irritancy receptors, the uptake of CO was not increased. It was considered that although V_E was increased, it was likely that ventilation-perfusion ratio changes prevented increased CO uptake.
- When polypropylene was pyrolysed, the resultant atmosphere contained a hydrocarbon mist and a wide range of aliphatic and aromatic pyrolysis products, but the atmosphere was innocuous, producing no signs of irritancy or other toxic effects in the animals, and no disruption of the behavioural task performance. When polypropylene was decomposed under non-flaming oxidative conditions, the resultant atmosphere also contained a smoke, and was highly irritant to the animals, producing a distinctive respiratory pattern with hyperventilation, and signs of lung edema and inflammation some hours after exposure. Behavioral task performance was inhibited at 1.85 mg/L mass loss concentration.
- When flexible polyurethane foam was pyrolized the particulate isocyanate-derived "yellow smoke" was highly irritant, producing respiratory changes during exposure and lung inflammation and edema some hours later.

The overall results of these primate studies basically confirmed and quantified the effects reported in fire fatalities and survivors, that the only important effects of exposure to fire effluents from common polymeric materials were asphyxia from the mixed asphyxiant gases present (CO, HCN, CO_2 and low oxygen hypoxia) and irritant effects consisting mainly of sensory irritancy at the time of exposure and lung inflammation and edema after exposure. The effects of CO and HCN were found to be additive as later confirmed in experiments with rats.

The irritant effects were as predicted in general terms from the chemical composition of the effluents, in that atmospheres rich in partially oxidized organic species such as unsaturated aldehydes of isocyanate-derived compounds were found to be highly irritant, while atmospheres low in organic content, or lacking partially oxidized organic species were relatively non-irritant. Polypropylene provides a good example of this finding. When polypropylene was decomposed under nitrogen, the atmosphere formed was rich in organics, but contained no organic species containing oxygen and was non-irritant. Under non-flaming oxidative decomposition condition in air there was a high organic content to the atmosphere produced, consisting of a mixture of products, including both oxygen-containing and non-oxygen containing species. The resultant atmosphere was highly irritant. When the furnace temperature was increased to 700 °C so that flaming combustion occurred, a "cleaner" atmosphere was formed with a lower smoke and organic content and most of the fuel carbon released as oxides of carbon. The resulting atmosphere was of low irritancy but caused asphyxia due to the carbon monoxide content. Irritant atmospheres were produced by both wood and flexible polyurethane foam when decomposed under nitrogen, since both materials contained sufficient molecular oxygen to release significant yields of irritant compounds.

These results confirm that for all materials, the highest irritancy atmospheres, rich in a wide range of organic species at relatively high yields, are obtained under non-flaming oxidative decomposition conditions. For non flame-retarded materials, well-ventilated flaming results in efficient combustion, so that organic species are oxidized to form carbon oxides and irritants are absent or present at low yields. Under vitiated (under-ventilated) combustion conditions the organic content increases, so that atmospheres produced are predicted to be somewhat irritant, but almost certainly less irritant than atmospheres produced under non-flaming conditions, since both the number of species present and the yields are lower than under non-flaming oxidative decomposition conditions [18, 37]. Also, if any exotic acute toxic effects are likely to occur from organic chemical species in fire effluents, they are almost certain to be found in the organic-rich effluents from non-flaming oxidative decomposition, while under flaming combustion conditions, the main toxic effects can be predicted to be those of the major asphyxiant gases, plus a degree of irritancy especially from products of vitiated combustion, or from acid gases. Although none of the materials used in the primate studies were flame-retardant, increased irritancy is to be predicted from flame-retardant materials, mainly from the acid gases released (halogen halides, sulfur oxides and phosphoric acid) under all decomposition conditions, and also because flame retardants acting in the gas phase (especially halogen flame retardants) reduce the efficiency of combustion under flaming conditions, thereby also increasing the content of potential organic irritants [38, 39].

The work involving sublethal exposures of primates to individual fire gases and fire effluent mixtures has therefore provided useful information on the mechanisms of incapacitation of human fire victims. It has also provided important quantitative information on the uptake and effects of toxic fire gases, which have been used to develop predictive methods for calculating time to incapacitation in human fire victims. However, the range of materials studied was limited to a small number typically used in domestic furnishings. In order to study the toxic effects of fire effluents from a wide of variety materials it has been necessary to use rodent animal models.

Sensory Irritancy

Sensory irritancy occurs in all mammals when irritant chemicals are deposited in the eyes and upper respiratory tract, especially the nose and throat. The symptoms occur immediately upon exposure (at least at painfully irritant concentrations), consisting of a burning pain, followed by a characteristic breathing pattern consisting of a pause at the end of each inspiration resulting in reduction in breathing rate. This reflex decrease in breathing rate is well developed and stable in mice, the extent of the rate decrease being proportional to the logarithm of the inhaled concentration of the irritant substance. The mouse respiratory rate depression (RD_{50}) test is used to measure the concentration of an inhaled irritant causing a 50 % decrease in breathing rate and has been used to measure the irritant potencies of a wide range of individual irritant compounds and combustion product mixtures from different materials generated in small-scale combustion toxicity tests. The use of data such as these is discussed in more detail in the irritancy section of this chapter, but an important issue is the interaction of individual irritants in mixtures. Few data are available on this issue but the following points are relevant:

- Certain irritants are chemically similar and stimulate irritant nerve receptors in the same way, so they can be predicted to be additive in their effects. An example would be a mixture of hydrogen chloride and hydrogen bromide.
- Chemically different irritants, such as aldehydes and inorganic acid gases, stimulate irritant nerve receptors by a variety of different mechanisms, but below the saturation level (maximum response level), the effects are considered likely to be additive.
- In experiments in which mice have been exposed to mixed combustion product atmospheres, the observed irritant potency of the mixture was always considerably higher

than that of the individual or summed irritant potencies of the measured known chemical components. This indicates not only that additive effects are likely to be present, but that unknown irritant chemical species of high irritant potency are present in combustion product mixtures.
- The default (conservative) assumption used for assessing the hazards from mixtures for industrial hygiene applications is that they are likely to be additive.

For these reasons, in predicting the effects of mixed irritants in combustion product mixtures it is assumed both in this chapter and in ISO 13571[4] that the effects of individual irritants are additive.

Estimates of Lethal Toxic Potency for Natural and Synthetic Polymers Under Different Fire Conditions Using Rodents, and Contribution to Overall Toxic Potency from Major Toxic Gases

Multi-gas FED Models for Lethality (LC_{50} Concentrations) in Rats Following a 30-min Exposure

There is an extensive database of the lethal toxic potencies to rats (30-min LC_{50} concentrations) for a range of individual common fire gases, and some data on the effects of combinations, which have been used as inputs to rodent lethality FED calculation models. The main concepts in these models are similar, but they differ somewhat in terms of which factors are considered and in the ways the various interactions are handled. The models estimate the FED for lethality for rats in terms of the concentration of each toxic gas present, expressed as a fraction of the LC_{50} concentration for a 30-min exposure period. The basic concept is that fractions of lethal doses of almost all gases are directly additive. Thus, if half the lethal 30-min concentration of CO is present with half the 30-min lethal concentration of HCN, then exposure of rats to this mixture for 30-min will, on average, result in the deaths of half the animals. Deaths are considered both during exposure and over a post-exposure observation period of up to 14 days, which is important for gases causing lung inflammation. It is considered that in terms of overall lethality, the effects of all gases, including asphyxiants and irritants are additive, but it is recognized that CO_2 modifies the toxicity of other gases and this is treated differently in different models. It is also recognized that NO_2 has some protective effect against HCN toxicity due to methemoglobin formation.

The FED calculation models can be used to calculate predicted LC_{50} concentrations for mixed combustion product atmospheres in which these gases have been measured, and the results compared to the measured LC_{50} concentration in exposed rats in the same tests [10].

A number of different combustion toxicity test methods have been used with rats, mostly in the 1970s and 1980s to estimate the lethal toxic potency of the effluents from a range of different natural and synthetic polymeric materials. Unfortunately, few of these have involved LC_{50} concentration measurements in combination with comprehensive measurement of the chemical composition of the atmospheres or the mass loss concentrations of the materials tested. Also, few have been conducted under conditions that can be readily correlated with those in full-scale fires, and for most methods the composition of the test atmosphere and the decomposition conditions change continuously during a test run, so that it is difficult to determine the relationship between the test atmosphere composition and effects. Three methods used have provided some data that can be used to determine LC_{50} concentrations under reasonably constant and well-defined combustion conditions coupled with measurements of the concentrations of at least a few of the major toxic gases.

The most useful data sets are the results obtained by Levin et al. [6] using the then National Bureau of Standards cup furnace method. This method involved decomposing samples of different mass in a crucible furnace under non-flaming oxidative thermal decomposition conditions at a temperature 25 °C below the autoignition temperature of the specimen and

also under flaming conditions at 25 °C above the autoignition temperature. The effluent generated from the crucible passed directly into an enclosed 200-l volume chamber to which groups of six rats were exposed nose-only. Exposure began as the sample was dropped into the crucible furnace, so in practice the composition of the test atmosphere to which the rats were exposed was not constant but increased in concentration for a period as the specimen was decomposed. For flaming exposures there was also a period during which products of non-flaming decomposition were generated before ignition occurred, but this was usually quite short. Exposure concentrations of the major asphyxiant gases (CO, CO_2, O_2 and HCN) were measured and the stated exposure concentrations were averaged over the 30-min exposure period. Animal deaths were scored during the exposure period plus a 30-min post-exposure period (scored as within exposure deaths) and also for the exposure period plus a 14-day post exposure period. The test material exposure concentrations are reported on a mass charge basis.

For a more recent set of experiments, the crucible furnace was replaced by a radiant furnace, which is the basis for the current NIST toxicity test method [40]. For this method the specimen, in the form of a flat strip, is irradiated from above by two angled radiant heaters. The effluent rises through a slit between the heaters into the enclosed 200 l chamber, while replacement air circulates back into the air space between the sample and the heater via two slits at each end of the heated area. The main decomposition mode is flaming combustion, and as with the crucible furnace method the initial decomposition is under non-flaming conditions until the specimen ignites, followed by a period of flaming until the specimen is extinguished, and a subsequent period during which off-gassing may occur from any residue. The basic exposure procedure is the same as for the cup furnace method, involving a total 30-min exposure period over which the gas concentrations are averaged. The mass loss rate of the specimen is also measured and the exposure concentrations are reported on both a mass charge and mass loss basis.

Another method for which some useful rat lethality data have been generated is the DIN 53436 tube furnace method [41, 42]. This method represents an early version of the concept used for the ISO19700 test method, in which the sample in the form of a strip is decomposed continuously in a stream of air, producing a dynamic steady state decomposition condition with a constant atmosphere composition to which the rats are exposed nose-only over a 30-min period (plus 14-day post-exposure observation period). This method has mostly been used for non-flaming decomposition, although some flaming decomposition experiments have been performed [43]. Unfortunately, the test atmosphere composition measurements made were somewhat limited. Table 62.2 shows a compilation of these data to which a rat LC_{50} FED calculation model has been applied. The rat lethality model [10, 44, 45] makes use of the rat LC_{50} data for individual gases and gas interactions obtained by mainly by Levin et al. [46] and Hartzell et al. [47].

The key precepts of the model are:

- Fractions of lethal doses of all gases except CO_2 are directly additive.
- The main effect of CO_2 is considered to be a multiplicative effect on the rate of uptake of other gases depending upon the extent of CO_2 driven hyperventilation. In addition it is considered that once animals are incapacitated, CO_2 induced respiratory acidosis enhances the metabolic acidosis already present, providing an additive toxicity factor.
- Low oxygen hypoxia is usually a minor factor in small-scale rodent toxicity experiments and can be ignored unless oxygen concentrations are allowed to decrease below 12 %. At low levels, a non-linear additive term can be used. An exponential function has been developed to allow for the effects of oxygen at low concentrations.
- A correction for the protective effect of NO and NO_2 on HCN toxicity due to methemoglobin formation can be made if necessary and for the additive effect of other nitriles present.

Table 62.2 LC_{50} concentrations (exposure plus 14-days, mass charge) for materials tested in the NBS cup furnace, NIST radiant furnace and DIN53436 tube furnace apparatus

Test material and abbreviation	Mass Conc. g/m^3	CO_2 %	CO ppm	O2 % dep[a]	HCN ppm	HCl ppm	NOx	Org[b] % term
NBS cup furnace non-flaming								
Acrylonitrile butadiene styrene ABS	30.9	0.53	680	0.63	164	–	–	0.35
Douglas fir DFIR nf	22.8	0.69	2700	1.00	–	–	–	0.347
Flexible polyurethane foam FPU	35.0	0.40	1126	1.00	11	–	–	0.869
Modacrylic MOD	5.3	0.53	435	1.75	249	–	–	0.35
Polyphenylsulfone PPS	9.5	0.51	4465	0.91	–	–	–	0.35
Polyvinylchloride PVC	30.3	0.46	640	0.98	–	2308	–	0.18
Polyvinylchloride/zincferrocyanide	11.3	0.53	1141	0.98	–	–	–	0.108
Red oak REDO	30.3	0.73	2515	0.98	–	–	–	0.35
Wool	25.1	0.70	979	1.19	301	–	–	0.35
NBS cup furnace flaming								
Acrylonitrile butadiene styrene ABS	19.3	1.06	1448	1.13	124	–	–	0.035
Douglas fir DFIR	39.8	3.71	3400	4.70	–	–	–	0.000
Flexible polyurethane foam FPU	20.3	2.10	1040	2.20	86	–	–	0.035
Modacrylic MOD	4.4	0.40	339	1.75	180	–	–	0.035
Polystyrene PS	38.9	1.95	1323	1.81	–	–	–	0.79
Red oak REDO	56.8	4.43	2102	4.22	–	–	–	0.134
Rigid polyurethane foam RPU	13.3	1.20	1689	1.03	126	–	–	0.035
Wool	28.2	2.50	705	1.19	116	–	–	0.035
NIST radiant furnace flaming								
Douglas fire rad DFIRrad	56.0	3.71	3233	4.11	–	–	–	0.007
Rigid polyurethane foam RPUrad	22.4	2.10	1800	2.55	133	–	–	0.000
Flexible polyurethane foam FPUrad	52.0	5.31	1392	6.74	53	–	–	0.035
PVC PVCrad	26.8	1.36	2000	1.90	–	2400	–	0.063
Vinyl fabric VFrad	32.0	1.81	3020	2.42	8	647	12.8	0.035
Melamine Melrad	12.5	0.99	401	1.24	111	–	47.0	0.035
DIN tube furnace 850 °C vitiated fl.								
Scot's pine (Pinus sylvestris) SP	29.2	1.70	5515	2.00	–	–	–	0.090

[a]Depletion

[b]Calculated as mass loss concentration of organic polymer material × fraction of mass loss carbon as organic carbon/35. If data unavailable: non-flaming 0.35, flaming 0.035, vitiated flaming 0.105

- It is considered important to make allowance for the effect of all inorganic acid gases present and for organic irritants.

The estimated FED for lethality in rats for a 30-min exposure and a defined set of toxic gas concentrations is calculated as follows:

$$FED = \left(\frac{[CO]}{LC_{50}CO} + \frac{[CN] - [NOx]}{LC_{50}CN} + \sum_{i=1}^{n} \frac{[I_A]_i}{LC_{50}I_{Ai}} + \sum_{i=1}^{n} \frac{[I_O]_i}{LC_{50}I_{Oi}} \right) \times VCO_2 + A + \frac{1}{H} \qquad (62.3)$$

where:

I_{Ai} represents each irritant acid gas present (summed for 0 to n acid gases)

I_{0i} represents each irritant organic substance present (summed for 0 to n organics)

VCO_2 is a multiplication factor for CO_2 driven hyperventilation $= 1 + (exp\,(0.14 \times [CO_2]) - 1)/2$

A is an acidosis factor $= ([CO_2] \times 0.05) - 0.02$

H is a hypoxia function $= exp\,(8.13 - 0.54 \times [21 - O_2])$. This can be omitted if $[O_2]$ is not less than 12 %.

$[CN]$ represents the concentration of cyanide

$[NOx]$ represents the summed concentration of NO and NO_2

Where data on organic irritant concentrations are absent, it is recommended that a contribution to the overall FED should be derived from an estimate of the total yield of organic products. The FED component for organic irritants (FED_{org}) is then estimated as:

FED_{org} = mass loss concentration of organic material x fraction of mass loss carbon present as organic carbon, divided by 35. FED_{org} is then substituted for the organic irritant term in Equation 3. This term is empirically derived from the contribution to overall lethal toxicity attributable to the organic fraction during rat exposure to non-flaming wood and non-flaming flexible polyurethane foam.

If these data are unavailable, an FED_{org} of 0.35 is used for non-flaming decomposition, 0.105 for vitiated or inefficient combustion, and 0.035 for well ventilated, flaming combustion at the LC_{50} mass loss concentration.

If the concentrations of the irritants present and their lethal exposure doses are known, then the equation can be solved fully. Where unknown irritants are present the equation enables the maximum LC_{50} to be predicted based upon the asphyxiant gases and a generic expression for overall irritants.

The LC_{50} concentration values used for the Purser LC_{50} FED model are (Equation 3) shown in Table 62.3.

The VCO_2 exponential function is derived from the measured increase in the rate of uptake of CO and other inhaled toxic gases in humans and rats to increased CO_2. This is an exponential function of the inhaled CO_2 concentration, as shown from experiments in humans. In rats, inhalation of 5.25 % CO_2 produced a 1.54 times increase in the rate of CO uptake, so an exponential function has been derived intersecting this point. In situations where a 30-min exposure is lethal, animals become comatose after approximately 15 min so that hyperventilation ceases. For this reason the increased rate of uptake is applied for half the exposure time. In addition to the hyperventilation effects, CO_2 is known to cause acidosis and this respiratory acidosis, combined with hypoxia-induced metabolic acidosis, results in an additive toxic component which has been estimated according to the function shown. The data on which the deviation of these functions was based were obtained from references [46, 48].

Table 62.3 LC_{50} concentrations for gases used in the Purser LC_{50} FED—model

Gas	LC_{50} concentrations for 30 min exposures plus 14 day post-exposure period (ppm)
CO	5705
HCN	165
HCl	3800
HF	2900
HBr	3000
SO_2	400
NO_2	170
NO	1000
Acrolein	150
Formaldehyde	750
Hypoxia (using function)	21−5.4 = 15.6 % depletion

The hypoxia function is also based upon experimental data from humans and rats. From human data, it is known that there is an exponential function between percentage oxygen depletion and time to and severity of effects, with minimal effects down to 12 % O_2. In rats, the measured LC_{50} concentration for a 30-min exposure is 5.4 % oxygen (15.6 % oxygen depletion) [46, 49]. For the hypoxia term an exponential function has therefore been derived providing a

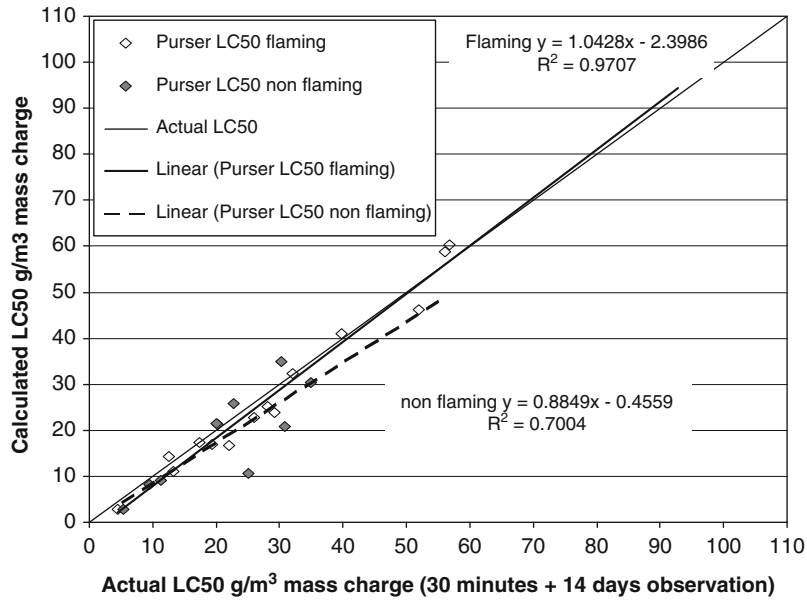

Fig. 62.2 LC_{50} concentrations calculated using the Purser rat LC_{50} model compared with measured rat LC_{50} concentrations for different materials decomposed under non-flaming and flaming combustion conditions

minimal FED at concentrations above 12 % O_2, an FED of 1 at 5.4 % O_2, and increasing FED values at lower concentrations.

The derivation of these terms for the lethal FED contribution effects of mixed organics, carbon dioxide, and low oxygen hypoxia are of necessity estimations, intended to provide a toxicologically and physiologically based approach to the calculation of lethal toxic potency for complex fire effluent mixtures. The extent to which the modified equation including these terms may provide an improved model for the calculation of lethal toxic potency from polymer effluent mixtures is tested here by application to the experimentally derived rat lethal toxicity database.

Figure 62.2 shows the measured rat LC_{50} concentrations plotted against those calculated using the LC_{50} calculation method. Linear regression lines have been fitted for the non-flaming and for the flaming data. The extent to which the regression lines overlay the 45° actual LC_{50} line gives an indication of the predictive power of the FED calculation method. Where the calculated line lies to the left of the 45° line this indicates that the calculation method underestimates the toxic potency of the combustion products mixtures, while a line laying to the right indicates that the calculation method overestimates the toxic potency.

The results show a good fit for the flaming data ($R^2 = 0.9707$) and a reasonably good fit for the non-flaming data ($R^2 = 0.7004$). The models are intended to be general, and therefore applicable to all forms of combustion atmosphere (both flaming and non-flaming). Pooling the non-flaming and flaming data gives the following linear fit equation:

$$\text{Calculated } LC_{50} = 1.026 \times \text{Measured } LC_{50} - 2.498 \qquad R^2 = 0.919 \tag{62.4}$$

The overall findings from the application of the model is that it provides good predictions of actual rat LC_{50} concentrations using measured concentrations of a small number of key toxic gases for a range of common polymeric materials, with a variety of chemical compositions. This is especially true for flaming decomposition, for which the composition of the

atmospheres is much less complex than under non-flaming conditions, consisting mainly of the common asphyxiant gases (for polymers containing C, H, O and N), with the addition of some irritant acid gases (for polymers containing N, F, Cl, Br, P or S), but low concentrations of organic species. Since the model is based primarily on an additive fractional effective dose concept, it also demonstrates that the toxic effects of these gases can legitimately be considered as primarily additive, and in particular that the lethal effects of the asphyxiant gases during exposure can be considered approximately additive with the lethal effects of irritants on the lung, to some extent during exposure, and particularly during the post exposure period up to 14 days (but mainly during the first 48 h after exposure). This is consistent with the findings of Pauluhn of a reasonable agreement between LC_{50} N-gas calculations and experimental data obtained using the DIN43536 apparatus [50].

This is important, because it demonstrates that for a range of common of materials (with the exception of per-fluorinated polymers and particular phosphorus-containing polymers), the toxic effects of fire effluent mixtures can be predicted from this small set of gases using relatively simple additive models, and that (especially for flaming combustion conditions) there is no evidence for any major unknown acute toxic effects other than the asphyxiant and irritant effects predicted from these few mixed gases.

The application of the model also shows the importance of CO_2 as a multiplicative term increasing the uptake of other toxic gases. In practice in these small-scale tests the highest chamber CO_2 in these experiments was only 4.4 % while levels of up to or exceeding 10 % have been measured in full-scale compartment fires. The model also demonstrates the importance of organic irritants. Based upon both observed effects in humans and primates, and the results in the rats and mice (particularly the post-exposure deaths) it is evident that the mixed organic irritants produced, particularly under non-flaming oxidative thermal decomposition conditions, (but also to some extent under vitiated flaming combustion conditions), make an important contribution to overall lethal toxicity. This is particularly the case where the organic atmosphere component is high in relation to that of the asphyxiant gases. Unfortunately, it is difficult to obtain fully quantitative measurements of the concentrations of all the potentially irritant organic compounds in fire effluent mixtures, Such GC-MS studies as have been performed have shown that the mix of compounds formed under specific decomposition conditions are often relatively similar for different materials, containing a range of species common to most materials, with the addition of a number of species more specifically related to the molecular structure of the material [37, 39]. On this basis, the approach taken for the LC_{50} FED model is to use a generic term for the total organic content of the atmosphere, calculated from the organic fuel mass loss multiplied by the fraction of fuel carbon present in the form of organic carbon in the fire effluent.

Fractional Effective Dose Hazard Assessments and Toxic Potency

In the context of fire safety, toxicity information is useful only to the extent that it can be used to assess toxic hazard in a full-scale fire scenario. There are a number of reasons for carrying out such an assessment. It may be needed in order to carry out a fire safety engineering assessment of a building design. In this context a particular set of fire scenarios may be run in order to assess probable outcomes in terms of the relationship between time available for escape compared to time required for escape. Time available for escape depends on the fire dynamics and time to incapacitation for building occupants exposed to toxic smoke. Time required for escape may also depend partly on the effect of toxic smoke on escape behavior. Another reason for modeling time to incapacitation may be the investigation of fire incidents in order to evaluate effects on fire

victims. Another reason may be for a manufacturer to evaluate and compare potential toxic fire hazards from different materials of products or for specifiers to determine the applicability of particular materials or products to particular design applications. In this situation a range of full-scale fire scenarios can be considered in order to evaluate product performance.

A difficulty with carrying out toxic-hazard assessments is that toxic substances exert a range of different effects on building occupants, and toxicity information may be presented in a number of different forms. Confusion also often arises in relation to toxic potency data and their application to toxic-hazard assessment.

The toxic potency of a substance depends on how much is required for a given toxic effect. The smaller the amount needed, the more potent the toxic substance. For example, in fires, hydrogen cyanide is about 20–40 times more potent than carbon monoxide because the amount needed to be inhaled to cause collapse is a much smaller exposure dose for hydrogen cyanide than for carbon monoxide.

Toxic hazard in a fire depends on the extent to which toxic products in that fire scenario present a danger to building occupants. Put simply it depends on how quickly and how much toxic products are produced and how potent the products are.

Toxic Potency

Toxic potency can be considered in terms of

- An individual toxic gas such as carbon monoxide or hydrogen chloride
- A mixture of toxic substances occurring in a fire (for example, the asphyxiant toxic potency of a CO and HCN mixture, or the irritant potency of a mixture of acid gases)
- The mixture of toxic substances evolved from the thermal decomposition under defined conditions of a particular material or product (such as wood, polyethylene, or a length of electrical cable)

The Toxic Potency of Individual Fire Gases and Gas Mixtures

In fires three major toxic effects are important.

1. The concentrations of irritant gases likely to impair escape efficiency or cause incapacitation (sensory irritation)
2. The exposure doses (Ct product doses) of asphyxiant gases likely to cause incapacitation through confusion and loss of consciousness (or to cause death)
3. The exposure doses of irritants likely to cause death through lung edema and inflammation after the fire

For sensory irritants the main criteria are the time during the course of a fire when the concentrations of irritants are sufficient to impair escape efficiency and the time when they are likely to cause incapacitation through pain and respiratory distress. This is evaluated using the concept of fractional irritant concentration (FIC), by which the fractions of an irritant concentration for each irritant present are summed. When FIC = 1, a tenability endpoint (escape impairment) is predicted. Incapacitation is predicted at higher concentrations (FIC ~ 3–5). The sensory irritant potencies of different individual irritants occurring in fire atmospheres cover an enormous range spanning six orders of magnitude. More than 20 irritant compounds are considered to contribute to the overall sensory irritancy of fire atmospheres. The most important irritants identified are acid gases (hydrogen fluoride, hydrogen chloride, hydrogen bromide, nitrogen oxides, phosphoric acid, and sulfur dioxide) and organic irritants (such as acrolein, formaldehyde, and crotonaldehyde). Evaluation of the effects of individual irritant substances and irritant fire effluent mixtures from different materials depends heavily upon data obtained from animal exposure studies together with limited human exposure data. The derivation of methods for the assessment of the effects of irritants and the derivation of tenability limits for human exposures is described in this Chapter in the section "Irritant Fire Products." Detailed

guidance on the assessment of sensory irritancy of fire effluents is presented, and used for the deviation of the Fractional Incapacitating Concentration (FIC). The application to human hazard assessments is then described in Chap. 63 in the section on smoke and irritants.

For asphyxiant gases the main criterion is the time during the course of a fire when a sufficient exposure dose (*Ct* product dose) of asphyxiants has been inhaled to cause incapacitation through confusion and loss of consciousness. This is evaluated using the FED concept, incapacitation being predicted at FED = 1. The gases important in causing asphyxiation are carbon monoxide, hydrogen cyanide, and reduced oxygen concentration. Carbon dioxide is important mainly because it increases the rate of uptake of CO and HCN. The toxic potencies of asphyxiant gases are less simple to define because for cyanide (and reduced oxygen concentration) the incapacitating exposure dose is not a constant. However, the exposure doses lethal to rats over a 30-min exposure period are approximately 5700 ppm for CO and 164 ppm for HCN. For asphyxiant gases, although the results descried in this chapter which have been obtained form primate and rodent experiments provide important information, considerable detailed physiological data are available from human experimental exposures. The evaluation of asphyxiants and derivation of hazard calculation methods has therefore been described in detail in the section "Asphyxiant Fire Products" In Chap. 63.

Another important aspect of irritants that needs to be considered is the time during the course of a fire when a sufficient exposure dose of mixed irritants had been inhaled to cause potentially lethal lung inflammation. The toxic potencies of different lung irritants occurring in fire effluent cover a very wide range of approximately 5 orders of magnitude (Table 62.4). For hazard assessments lung irritancy is calculated in terms of the Fractional Lethal Dose (FLD_{irr}), the exposure dose calculated to cause death after exposure of half an exposed population. Detailed guidance on the evaluation of lethal lung irritation is also given in the section "Irritant Fire Products." Application of the method to human fire hazard calculations is presented in Chap. 63 in the section on smoke and irritants.

Toxic Potencies of Individual Materials

When individual materials are decomposed in full-scale fires or small-scale combustion toxicity tests, they produce a range of individual irritant and asphyxiant toxic products. The overall toxic potency of the resultant effluent mixture will depend on the yields of individual toxic products and their toxic potencies. For any particular material the yields of individual toxic products depend on the thermal decomposition conditions (nonflaming oxidative, well-ventilated flaming, or vitiated flaming). In general, materials produce high yields of toxic products under nonflaming oxidative and vitiated flaming conditions, and lower yields under well-ventilated flaming conditions. This result is described in detail in Chap. 63 [3] in the section "Chemical Composition and Toxicity of Combustion Product Atmospheres" and the section "Fire Scenarios and Victim Incapacitation."

For any individual material decomposed under a particular decomposition condition in a small-scale test, it is possible to evaluate the toxic potency of the effluent mixture in terms of sensory irritation, asphyxiation, or potential for lung inflammation. The toxic potency is then expressed in terms of the nominal concentration of the decomposed material rather than in terms of individual toxic products. Table 62.5 shows examples of the sensory irritant potency of fire effluent from materials, expressed in terms of the mouse RD_{50} concentration of the material decomposed (expressed as the mass loss concentration). The RD_{50} is the concentration causing a 50 % decrease in respiration rate in mice during a short exposure, which is a measure of sensory irritant potency. A reasonably good relationship has been found between the mouse RD_{50} concentrations for a range of irritant vapors and the concentrations reported as being painfully irritant to humans [33] (see section on "Irritant Fire Products"). Table 62.5 shows the mouse RD_{50} for a number of materials, some of which

Table 62.4 Sensory and pulmonary irritancy of combustion products

Irritant	RD_{50} (ppm) mouse[b]	Severe sensory irritancy in humans (ppm)	30-Min LC_{50} (ppm) mammal[c]	LC_{50}/RD_{50}
	0.1–1.0			
Toluene diisocyanate	0.20	1.0 [51]	100 [51]	500
O-chlorobenzylidene-malonitrile (CS)[a]	0.52	0.5 [52]	150–400 [53, 54]	529
α-chloroacetophenone (CN)[a]	0.96	6–50 [52]	300–400 [3, 55, 56]	365
	1.0–10			
Acrolein	1.7	1–5.5 [51, 56]	140–170 [55–57]	91
Formaldehyde	3.1	5–10 [51, 56]	700–800 [55, 58]	242
Chlorine [1]	9.3	9–20 [56]	10,058	11
	10–100			
Crotonaldehyde		4–45 [51]	200–1500 [51, 55, 59]	
Acrylonitrile		>20 [51]	4000–4600 [55]	
Penteneone			1000 [55]	
Phenol		>50 [51]	400–700 [55]	
	100–1000			
SO_2	117	50–100 [51, 56]	300–500 [55, 58]	3
NH_3	303	700–1700 [60]	1400–8000 [55, 58]	16
HF		120 [51]	900–3600 [55]	
HCl	309	100 [51, 56]	1600–6000 [55, 57, 58]	12
HBr		100 [51]	1600–6000 [55]	
NO_2	349	80 [51, 56]	60–250 [55, 58]	0.4
Styrene	980	>700 [51]	10,000–80,000 [55]	46
	1000–10,000			
Acetaldehyde	4946	>1500 [51]	20,000–128,000 [55]	15
	10,000–100,000			
Ethanol	27,314	>5000 [51]	400,000 [55]	15
Acetone	77,516	>12,000 [51]	128,000–250,000 [51, 55]	2

Note: The potential for causing sensory irritation spans 6 orders of magnitude, whereas that for causing death spans approximately 3 orders of magnitude. For substances down to NO_2 death is likely to be due to lung irritation, whereas for the remainder from styrene to acetone death is likely to be due to asphyxiation

[a]Substances not detected in combustion atmospheres

[b]RD_{50} from Alarie [61] where no data exist substances have been ranked according to their reported irritancy in humans

[c]LC_{50} concentrations have been normalized to a 30-min exposure time according to Haber's rule

occur in aircraft, when decomposed under the thermal decomposition conditions indicated, using the BRE tube furnace method [62]. The majority of experiments were conducted under nonflaming oxidative decomposition conditions, but a small number of experiments were conducted under flaming decomposition conditions. The results show that the majority of materials have RD_{50} values lying between 0.05 and 0.5 g/m^3 under nonflaming oxidative decomposition conditions, which means that if the products of decomposition of between 0.05 and 0.5 g of material are dispersed into each cubic meter of air, then the resultant atmosphere is predicted to be painfully irritant to the eyes and respiratory tract. However, under flaming decomposition conditions the smoke irritancy decreases by a factor of 10 or more. For use in a hazard analysis for humans the RD_{50} mass loss concentration should be regarded as producing a total FIC_{irr} of approximately 1 for the effluent from the material in question.

Although it is, therefore, possible to measure or calculate the sensory irritant toxic potency of

Table 62.5 Mass loss concentrations of thermal decomposition products predicted to be painfully irritant (mouse RD_{50} g/m^3) [62]

Material	Temp. (°C)	NF/F[a]	RD_{50} g/m^3 mass loss	95 % confidence limits
General materials				
Acrylonitrile butadiene styrene	500	NF	0.11	0.07–0.17
As above	600	F	~1	
Low density polyethylene	500	NF	0.05	0.03–0.07
Nylon-6	480	NF	0.47	0.29–1.10
As above	600	F	~20	
Polyvinylchloride (PVC) (rigid)	400	NF	0.17	0.12–0.25
Polyvinylchloride (plasticized)	380	NF	0.19	0.09–0.28
As above	600	NF	0.17	0.12–0.22
As above	650	F	~2.6	
Thermoplastic polyurethane	425	NF	0.20	0.14–0.96
As above	600	F	~3	
Cable materials				
PVC insulation (plasticized)	550	NF	0.56	0.39–1.00
PVC jacket (plasticized)	550	NF	0.34	0.27–0.47
Cross-linked polyethylene (insul.)	550	NF	0.12	0.09–0.17
As above XLPE (jacket)	550	NF	0.32	0.20–0.32
Aircraft materials				
Phenolic fiberglass	600	NF	>9.1	
PVC decorative laminate	600	NF	0.10	
Polycarbonate	600	NF	0.25	
Phenolic oil fiberglass insulation	600	NF	0.05	
Aluminized PVF/paper covering	600	NF	0.37	
Redux adhesive	600	NF	0.10	0.06–0.16
Silicone rubber	600	NF	0.06	0.01–0.29
Jointing compound JC5V	600	NF	0.18	0.07–0.32
Viton sealant	600	NF	0.21	0.15–0.27
Berger elastomer	600	NF	1.38	1.12–1.80

[a]*NF* nonflaming, *F* flaming

the fire effluent from materials decomposed under specific decomposition conditions, traditionally, toxic potencies for materials have been expressed in terms of overall lethal toxic potency to rats. This information was originally obtained by exposing groups of rats to thermal decomposition atmospheres from materials in small-scale tests and establishing the exposure concentrations causing the deaths of half the exposed animals (LC_{50} concentrations) during or within 14 days after a 30-min exposure period. These data can also be expressed in terms of an exposure dose (Ct product dose) by multiplying the LC_{50} concentration by 30 to give an LCt_{50} exposure dose. Animal experiments of this kind have now largely been replaced by chemical measurements used in conjunction with appropriate calculation models as a method for estimating the rat LC_{50}. For this method the same small-scale tests may be used and the composition of the fire effluent is measured in terms of the major toxic fire gases. The data are then used as input to the special type of FED calculation designed to predict lethal toxic potency in rats as described. (This should not be confused with the FED calculation methods used to predict incapacitation and death of humans exposed to full-scale fire atmospheres.) Details of these FED calculations for rat lethality are presented in the section on "Multi-gas FED Models for Lethality (LC_{50} Concentrations) in Rats Following a 30-min Exposure". This calculation method

[10, 44] has been published as a Standard method in British [63] and International [45] standards.

The lethal exposure concentrations or exposure doses expressed in this way represent the overall lethal toxic potency of the effluent from both asphyxia and lung irritation. Sensory irritation is not considered. The lethal toxic potency to rats is considered to be similar to that expected to occur in humans. It can therefore be used to represent an exposure dose of effluent from a material under defined fire conditions predicted to be lethal to humans. Incapacitation would be predicted at around a third of this exposure dose. In this context the toxic potency is expressed in terms of the nominal atmosphere concentration of the material (e.g., $g \cdot m^{-3} \cdot min$ mass loss of wood). This obviously provides a very crude estimate of the toxic potency of effluent to humans, since it does not take into account different toxic endpoints such as sensory irritancy and asphyxiation, it does not allow for deviations from Haber's rule known to be important with asphyxiant gases, it does not differentiate between effects occurring at different times during exposure and afterwards, and it does not allow for differences between rodents and humans or the range of different sensitivities occurring within the human population.

The lethal toxic potencies of materials tend to be dominated by toxic gases evolved at high yields such as carbon monoxide, hydrogen cyanide, and acid gases when the relevant anions are present as a significant part of the elemental composition of the material. Under some conditions organic irritants or other compounds, including irritant ultrafine particulates, can be important. Figure 62.3 illustrates the range of lethal toxic potencies from individual compounds occurring in fire atmospheres and for individual materials decomposed under different combustion conditions [64, 65]. The acute lethal toxic potencies of individual toxic products occurring in fire atmospheres range over more than 5 orders of magnitude. The most acutely toxic substance so far identified in the thermal decomposition product atmosphere is the ultrafine fluoropolymer particulate evolved when perfluorinated polymers such as polytetrafluoroethylene (PTFE) are decomposed under nonflaming conditions at temperatures of 400–350 °C [65]. The LC_{50} of this particulate is <0.017 $g \cdot m^{-3}$. This toxic particulate has a short half-life and is unlikely to present a hazard in most fire scenarios. It is not formed at high temperatures or when the fluoropolymer is flaming. Other compounds with a high acute lethal toxic potency evolved during fires are perfluoroisobutylene, carbonyl fluoride, and carbonyl chloride. Hydrogen cyanide and nitrogen dioxide and some low molecular weight carbonyl compounds are also highly toxic in the 0.1– ~1 g/m^3 range. Carbon monoxide and common acid gases such as hydrogen chloride lie in the 1.0–10 g/m^3 range, whereas a range of organic products with varying toxic potencies occupies higher ranges up to some with very low acute toxic potencies such as methane and other aliphatic compounds.

When the range of toxic potencies of these individual toxic products is compared with the acute lethal toxic potencies of effluent mixtures from particular materials or classes of materials expressed in terms of NAC mass loss (g/m^3), then a similar range of approximately 4–5 orders of magnitude occurs, ranging from fluoropolymers decomposed in such a way as to evolve ultrafine particulate (~0.017 g/m^3) to cellulosic materials decomposed under well-ventilated conditions in such a way that very low yields of toxic products are formed (>100 g/m^3). In practice, the lethal toxic potency of perfluorinated polymers covers a very wide range from approximately 0.017 to 8.6 g/m^3, depending on the decomposition conditions [65]. For most materials, the worst-case conditions for producing high toxic potencies are nonflaming or vitiated (under-ventilated) flaming conditions, particularly for materials containing nitrogen or halogens. Many materials show toxic potencies in the range 1–10 g/m^3 under these conditions. Well-ventilated flaming tends to destroy toxic products such as CO, HCN, and organic irritants, so that for polymers containing carbon, hydrogen, and oxygen the toxic potencies are low, with LC_{50} in the 10–100 g/m^3 range (Tables 62.6 and 62.7).

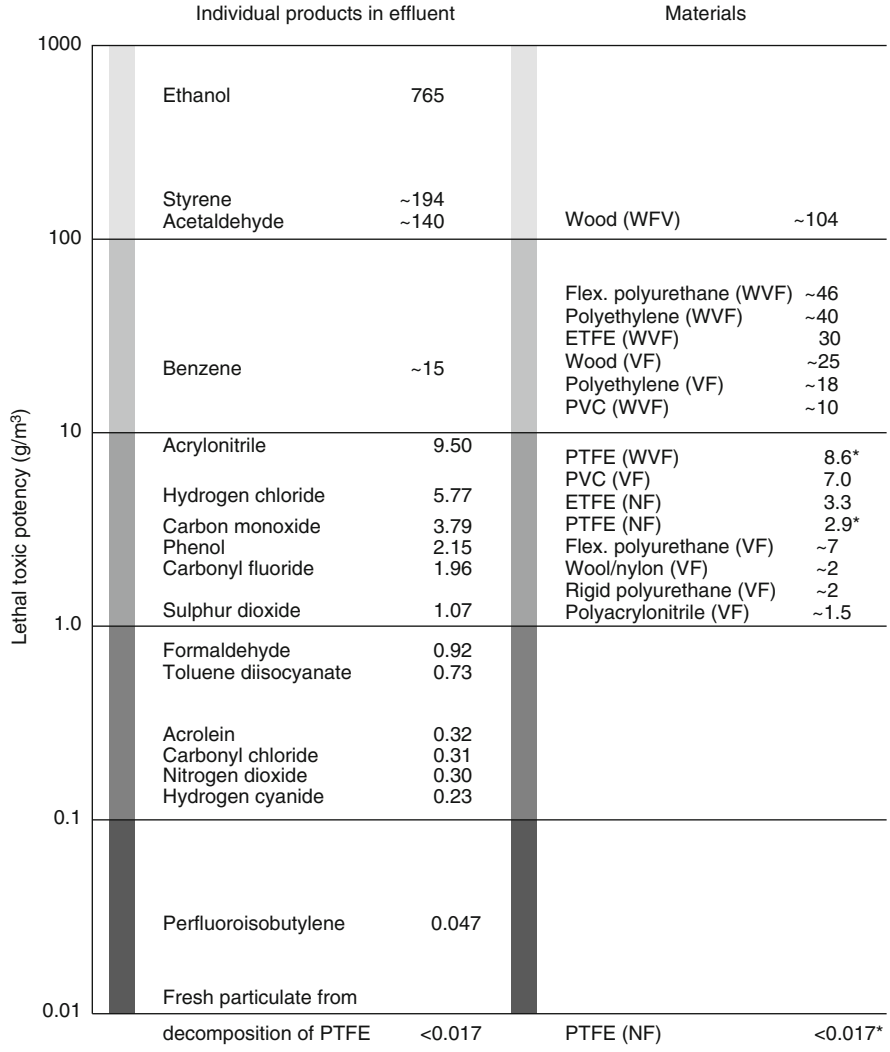

Fig. 62.3 Lethal toxic potencies (g/m^3) of individual compounds and the combustion products from various materials. *NF* Nonflaming, *WVF* well-ventilated flaming, *VF* vitiated flaming. *The toxic potency of particulates evolved from fluoropolymers (and therefore the toxic potency of fluoropolymers themselves) varies considerably with the decomposition conditions and the age of the particulates. Extreme toxic potencies have not been observed for fluoropolymers under full-scale fire conditions

Table 62.6 Lethal toxicity data for combustion products from a range of materials

				30-min LC50 (mg/L mass loss)			L(Ct50) (mg·min/L mass loss)	
Author	*n*	Test	Method	Mean	Range	Wood	Mean	Range
Levin		NBS	(NF)	24	5–40	25	720	150–1200
	11		(F)	27	4–57	49	810	120–1710
Kimmerle and Prager	18	DIN	(NF)	23	6–60	20–50	690	180–1500
Alexeev and Packham	46	UPIT	(Mixed)	19	4–88	68	580	117–2648
Average				23	5–61	42	700	142–1765

NF nonflaming, *F* flaming

Table 62.7 Approximate lethal LC_{50} concentrations ($g \cdot m^{-3}$) and lethal exposure doses (LCt_{50} $g \cdot m^{-3} \cdot min$), for common material classes under different fire conditions

	Non-flaming		Well-ventilated flaming		Under-ventilated flaming		Post-flashover under-ventilated flaming	
Material	LC_{50}	LED	LC_{50}	LED	LC_{50}	LED	LC_{50}	LED
Fluoropolymers	0.017	0.51	~8	240	~8	240	5.4	162
Polyamide,	17	510	17	510	1.4	54	1.8	54
Modacrylic, polyacarylonitrile	5	150	12	240	4.4	132	1.0	60
Wool	25	750	28	840	4	120	4	120
Rigid polyurethane foam	40	1200	15	450	7	210	7	210
Flexible polyurethane foam	27	810	13	390	7	210	7	210
PVC	7	240	7	240	7	240	8	270
C,H,O polymers	17	510	70	2100	20	600	12	360
Cellulosics	24	720	119	3570	25	750	15	450

Approximate rat LC_{50} concentrations and LEDs (Lethal Exposure Doses) for 30 min exposure plus 14 days observation

For most materials under most fire conditions (including fluoropolymers) the lethal toxic potencies (30-min LC_{50}) fall within a range of approximately 2 orders of magnitude. These aspects are discussed in more detail in later sections.

Contribution of Different Toxic Gases to Overall Lethal Toxic Potency from Different Materials

Figures 62.4, 62.5, 62.6, and 62.7 illustrate the extent to which different toxic species contribute to the overall toxic potency of different materials for the main different fire types described in ISO 19706 [14]. The contributions from different chemical species are calculated using the Purser LC_{50} FED model. The chemical atmosphere composition data are from the NBS cup furnace, NIST radiant and mainly from ISO19700 tube furnace [31, 66]. Figure 62.4 shows the results for non-flaming oxidative thermal decomposition (mostly NBS cup furnace data). The data are plotted as toxic potency ($1/LC_{50}$), so that the higher the bar the greater the toxicity. The shading then illustrates the contribution to the overall toxic potency from each atmosphere component.

Under non-flaming oxidative thermal decomposition conditions (Fig. 62.4) toxic potencies are relatively high, ranging from 0.029 to 0.37 (LC_{50} 34.8–3.8 g/m^3). The main toxic components are HCN, with a small contribution from NO_2 (for nitrogen-containing polymers), CO, organic irritants for most materials, and HCl (for PVC).

For well-ventilated flaming (Fig. 62.5) the yields of toxic products are low, so that toxic potencies are generally low. The results are therefore plotted at a scale five times expanded than that for non-flaming decomposition. The overall potencies range from around 0.008 to 0.13 (LC_{50} 118–7.9 g/m^3). A variety of different components contribute to the overall potencies, but for well-ventilated combustion CO_2 is always important as a cause of hyperventilation. In this sense, it is not directly toxic itself, but magnifies the toxicity of the other components by increasing their rate of uptake. It also makes a direct toxic effect at high concentrations due to acidosis. For nitrogen-containing materials HCN is important, but NO_2 also makes a contribution, since the yields of nitrogen oxides are highest under well-ventilated combustion conditions. CO is also important for some materials, and for materials containing chlorine; both CO and HCl are significant components of the overall toxicity (due to inefficient combustion resulting from the gas phase effect of chlorine). Hypoxia and organic irritants also make a contribution at high mass loss concentrations.

As fires in buildings grow and become under-ventilated (Fig. 62.6), the yields of toxic gases and overall toxic potencies are considerably

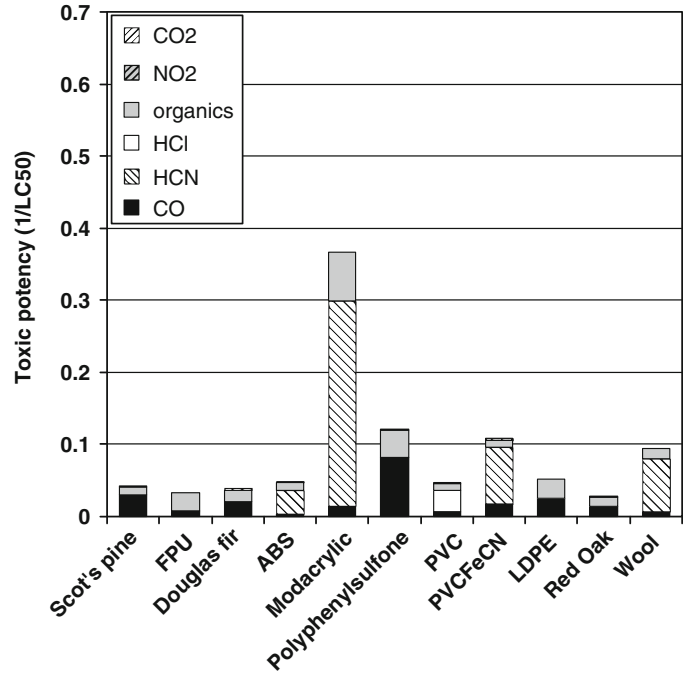

Fig. 62.4 Toxic potencies ($1/LC_{50}$) for non-flaming oxidative decomposition conditions

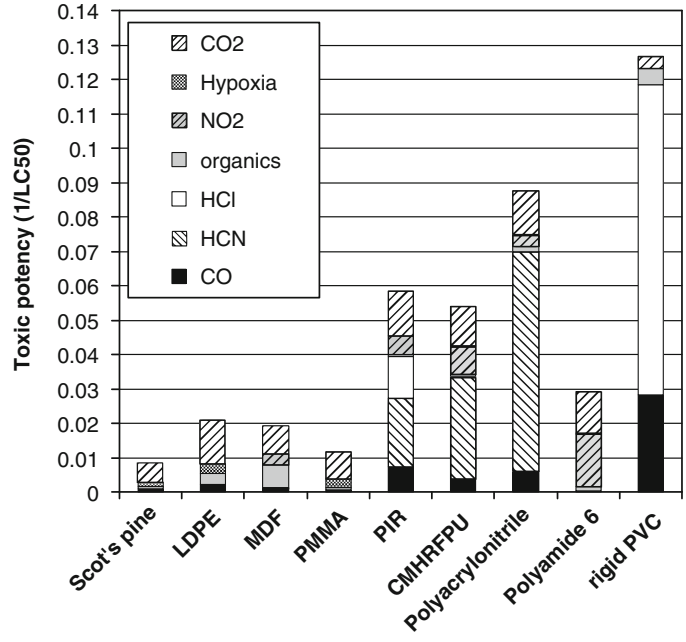

Fig. 62.5 Toxic potencies ($1/LC_{50}$) for well-ventilated flaming conditions

higher than for well-ventilated combustion conditions (0.03–0.09), (LC_{50} 30.8–3.1). Carbon monoxide is a significant toxic component in all cases, with a contribution from CO_2 and organic irritants. For nitrogen-containing materials the toxicity is dominated by HCN, with a small contribution from NO_2, and for PVC, HCl and CO are the main toxic components with a small contribution

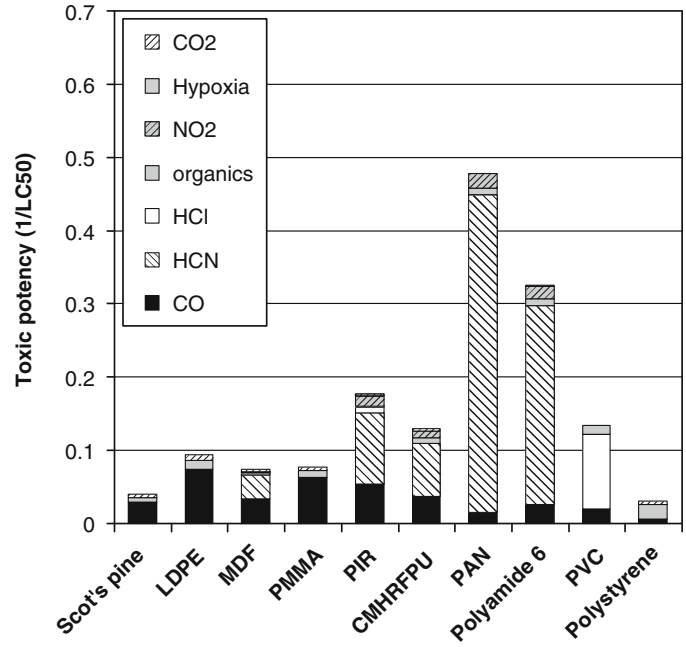

Fig. 62.6 Toxic potencies ($1/LC_{50}$) for under-ventilated flaming conditions

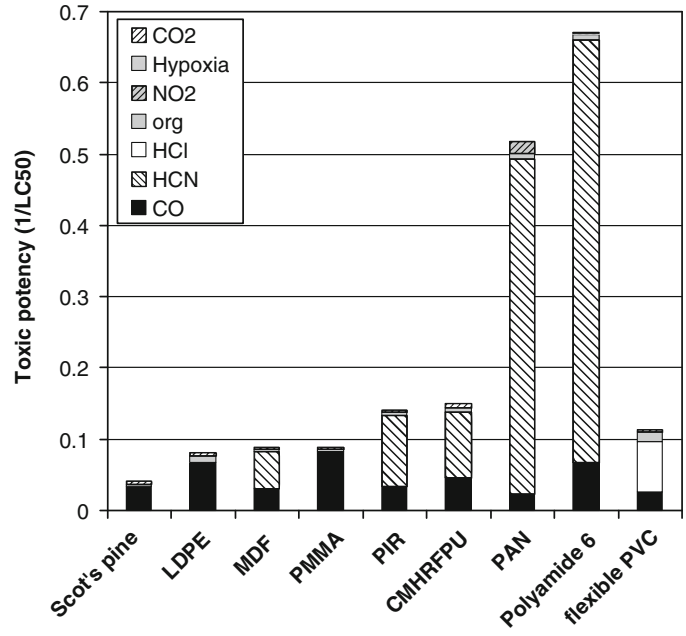

Fig. 62.7 Toxic potencies ($1/LC_{50}$) for post-flashover under-ventilated flaming conditions

from organic irritants. Polystyrene toxicity is heavily influenced by irritant organic particulates.

At higher temperatures representing post-flashover, under-ventilated combustion conditions (Fig. 62.7), the toxic potencies and patterns are similar to those under pre-flashover, under-ventilated combustion conditions, but yields of CO and HCN can be somewhat higher, so that toxic potencies for this set of materials range from 0.04 to 0.67 (LC_{50} 23.9–2 g/m^3).

In this set of materials only one (the fluoropolymer polytetrafluoroethylene), showed toxic effects under certain specific non-flaming conditions not accounted for in terms of simple asphyxiant gases and organic irritants.

Excluding fluoropolymers, the lethal toxic potency (mass loss LC_{50} concentrations of fire effluent mixtures from different materials) ranges from polyamide 6 decomposed under post-flashover, vitiated flaming conditions (LC_{50} 1.51 g/m^3), to Scot's pine and similar cellulosic materials decomposed under well-ventilated, flaming conditions at low equivalence ratios (0.5–0.8), giving an LC_{50} concentration of 119 g/m^3. In practice the lowest possible mass loss toxic potency (highest possible LC_{50} concentration) for any flammable material is limited to somewhere in the 120–150 g/m^3 range, because at these loadings CO_2 and oxygen depletion are in the lethal range, giving a total toxic potency range of approximately 2 orders of magnitude (factor of 79) between the most toxic and least toxic effluent atmospheres for common materials. In general, the toxic potencies are lower under well-ventilated combustion conditions, and higher under non-flaming, and under-ventilated conditions as illustrated in Figs. 62.4, 62.5, 62.6, and 62.7. Table 62.6 shows some historical rodent lethality from three bench-scale test methods while Table 62.7 shows approximate LC_{50} concentrations and approximate lethal exposure doses (calculated as lethal mass loss exposure concentration multiplied by exposure time) for common classes of materials under the four main fire conditions from a wider data set including animal data and LC_{50} estimates calculated using the FED equation applied to ISO TS19700 tube furnace data. Note that strictly speaking an LCt_{50} g·m^{-3}·min represents a value for a lethal dose calculated statistically from a set of animal exposure data. An "LED" represents an estimate of the lethal dose derived from a mixed set of data. For the purposes of the application described here "LCt_{50}" and "LED" both expressed in g·m^{-3}·min may be regarded as the same.

Flaming combustion conditions in compartment fires begin by being well-ventilated and then gradually become more vitiated as the fire grows and the ventilation becomes limiting. Individual materials in fires are therefore first decomposed in well-ventilated conditions at low equivalence ratios, and the equivalence ratio increases as combustion becomes under-ventilated. The effect of this on lethal toxic potency is illustrated in Fig. 62.8, which shows plots of calculated LC_{50} against equivalence ratios for a set of materials combusted in the ISO TS19700 tube furnace (the lower the LC_{50} the greater the toxicity). Most materials show a considerable increase in toxic product yields and overall toxic potency as the equivalence ratio increases. Thermal decomposition and combustion products from fluoropolymers show a great range of toxic potencies, depending upon the precise thermal decomposition or combustion conditions. A detailed account is given in Purser [65, 67].

Despite the limitations of lethal toxic potency data for individual materials, they can be used for simple estimations of toxic hazard in full-scale fires. This method represents one of a number of different approaches that can be used for the assessment of toxic hazard in full-scale fires, with varying degrees of sophistication and validity. The different methods are summarized in the next section.

Basic Requirements for Toxic Hazard Assessments of Full-Scale Fires

A key step in the process of toxic hazard assessment is to describe the growth of the fire, the production of toxic effluent, and its spread. A number of methods can be used to achieve this, but the main elements are as follows:

1. Obtain the mass loss curve for the fire and the dispersal volume of the effluent, either by conducting a simple large-scale test (measuring mass loss or heat release), by using a design fire, or by modeling
2. Determine the time-concentration curves for the main toxic fire gases, smoke optical density, and temperature of the fire either by
   (a) Direct measurement in a full-scale fire test

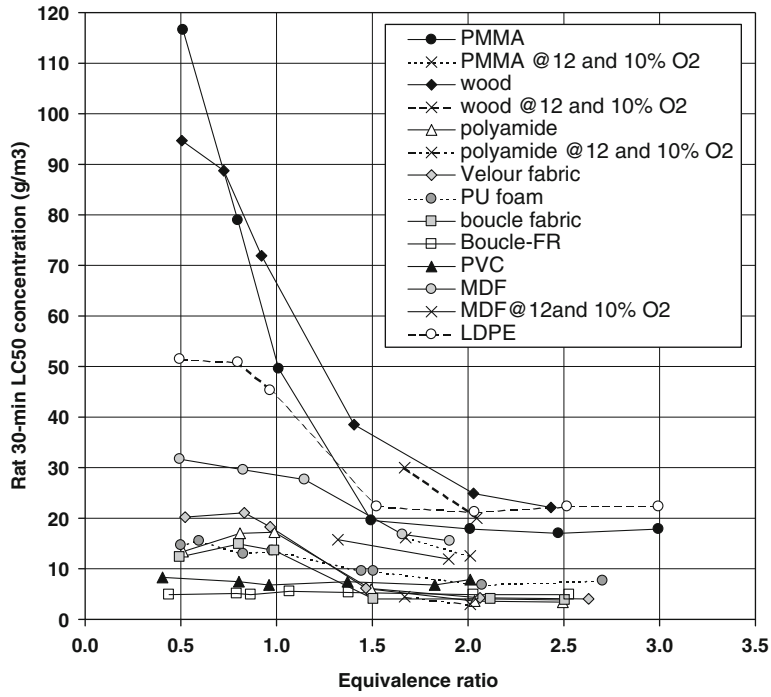

Fig. 62.8 Variations in lethal toxicity (LC_{50}) concentrations with combustion conditions (ISO TS19700 tube furnace)

(b) Calculation from the yields of toxic products, smoke and heat from the materials involved in item (1), measured in small-scale tests performed under appropriate fire conditions
(c) Calculation from a knowledge of the composition of the materials involved in item (1) and fire decomposition chemistry

3. As an alternative to item (2), calculate the mass loss concentrations and mass loss exposure doses for materials involved in the fire

Once the growth of the fire and the spread of the fire and effluent have been described it is possible to proceed to quantify hazardous effects and estimate time to incapacitation and death. This estimate can be done in two main ways.

1. Time to incapacitation and death can be estimated using physiological FIC and FED calculation models for smoke, irritant, and asphyxiant fire gases in conjunction with time-concentration curves for toxic fire gases as input data. This method is described in detail in Chap. 63 and calculates the following:
   (a) Time at which concentrations of smoke and sensory irritants are likely to impair or reduce the efficiency of egress due to psychological or physiological effects
   (b) Time at which exposure concentrations or doses are likely to cause incapacitation or prevent egress due to psychological or physiological effects
   (c) Time at which a lethal exposure dose has been inhaled
2. Alternatively, lethal toxic potency data for the materials involved in the fire can be obtained from small-scale combustion toxicity test atmospheres using animal exposures or using chemical analysis of the key toxic gases measured in such tests in conjunction with rat lethality FED calculations. These data can then be used with mass loss exposure dose curves from method (3) to estimate time to death (i.e. time to inhale a lethal exposure dose). An incapacitating dose can be estimated as approximately 0.3× the lethal dose,

The Application of Small-Scale Tests for the Determination of Toxic Product Yields, and Time-Concentration Curves, to Toxic Hazard Assessment

Where time-concentration curve data are obtained from full-scale fire tests it is possible to proceed directly to an assessment of time to incapacitation using the physiological FED algorithms. The main calculation expressions and a worked example are presented in Chap. 63 Appendix 3. Where full-scale fire data are unavailable, it is necessary to use modeling and small-scale test data obtained from performance-based tests to estimate the full-scale fire and the time-concentration curves of the main fire gases. In order to do this, it is necessary to use some form of fire growth curves (such as a t^2 fire growth curve or curves derived from heat release rate data) and a zone or computational fluid dynamics model to calculate the distribution and concentration of fire effluent (expressed in terms of fuel mass loss concentration) with time within the building enclosures. It is then necessary to obtain data for the yields of toxic fire products per unit mass of fuel decomposed, from which the concentrations of smoke and toxic gases in the fire can be calculated. As described in Chap. 16 and Chap. 36, and as presented in this chapter, for particular fuels, the yields of CO and other toxic gases are dependent on the equivalence ratio (ϕ) and particular characteristics of the fuels (such as the organic structure and the presence of oxygen or fire-retardant additives [such as nitrogen, halogens, or phosphorus]).

As with all fire parameters the yields of toxic gases in full-scale fires can be variable and difficult to measure, while the equivalence ratio can be expressed in several different ways on a global or local basis within a fire enclosure. In practice, it is not practical to carry out full-scale tests to evaluate most hazard scenarios, so it is necessary to rely on modeling using reaction to fire data from small-scale tests or standardized fire curves, although these represent a further abstraction from the full-scale scenario, and need to be used with caution. One way of obtaining data on the relationship between ϕ and the yields of toxic products is to decompose the material in a small-scale toxicity test designed to combust materials under defined equivalence ratios. If the mass loss and product dispersal curve for the full-scale fire and the full-scale equivalence ratios are calculated, it is then possible to estimate the concentrations of toxic products by reference to the small-scale data. One example of such a small-scale test is the ASTM E2058 fire propagation apparatus developed by Factory Mutual Research, data from which are shown in Chap. 36 [2]. Another is ISO TS19700 tube furnace method [10–13, 68, 69]. These methods have been used to examine the relationship between ϕ and toxic products yields, and the results obtained are close to those obtained in full-scale tests [1, 70]. The apparatus is described in the section "Second-Generation Test Methods." The following section gives a simple theoretical example of the application of this method. In addition to measurement of chemical product yields as a function of ϕ the ISO TS19700 method also measures the effective heat of combustion. This also varies as a function of ϕ, so that when using a t^2 heat release rate (HRR) curve to calculate fuel mass loss rate the heat of combustion can be entered as a variable term. At a ϕ of 2 the heat of combustion is approximately halved for most fuels, so that the mass loss rate increases more steeply than the HRR. Of course the HRR curve from a given fuel load inside a fire enclosure will depend not only upon the combustion characteristics of the fuel but also upon the boundary conditions for the enclosure in terms of ventilation and heat exchange. Secondary combustion may also occur beyond the fire enclosure where a fuel rich plume entrains secondary air, so that the changing combustion conditions and product yields beyond the fire enclosure may need to be considered if these areas are also occupied.

Using Small-Scale Toxic Product Yield Data in Toxic Hazard Assessments Figure 62.9 shows the relationship between ϕ and CO yield for two fuels comprised of carbon and hydrogen only. Large-scale data using hexane and fuel are reproduced from Gottuk and Lattimer [1, 70].

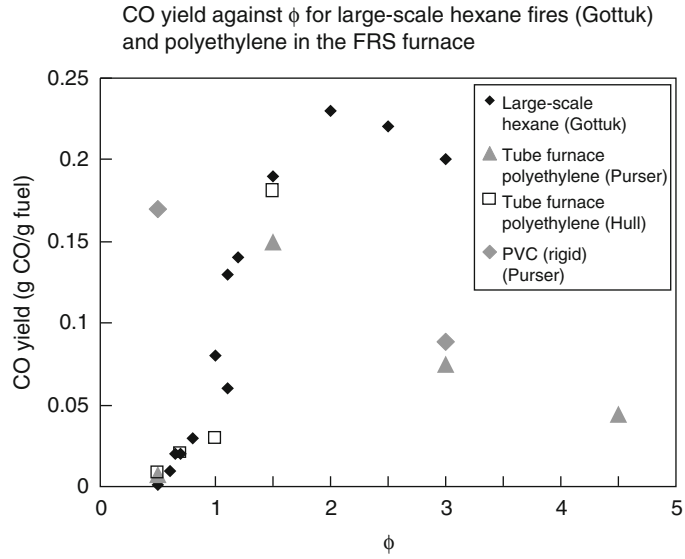

Fig. 62.9 CO yield against ϕ

The small-scale data are taken from Hull et al. [51] and Purser [50] for polyethylene and PVC using the ISO TS19700 tube furnace. As the figure shows, CO yield is very low for these fuels at ϕ values >1 and peaks at ϕ values of around 2 at approximately 0.2 g/g. Similar relationships occur for other toxic products and an inverse relationship for CO_2 (see Tewarson [2]). As a simple example, a full-scale fire is estimated as a medium growth rate t^2 fire, with a theoretical fuel decomposing with the same CO and CO_2 yields as were obtained from the tube furnace tests at ϕ values of 0.5 (well ventilated) and 1.5 (vitiated). The fire is in an enclosed room (2.44 × 3 × 2.44 m) with a 1 × 0.3 m vent at floor level. The fire growth rate, heat release rate, and upper-zone filling rate are modeled using CFAST. The mass loss rate is calculated from the heat release rate. The CO yield and CO_2 yields are taken from the tube furnace experiments as

Well ventilated :	0.007 CO	2.54 CO_2	g/g fuel mass loss
Vitiated :	0.149 CO	1.57 CO_2	g/g fuel mass loss

The FED for human incapacitation from CO and CO_2 is calculated, using Chap.63 Equations 63.15 and 63.35 (Fig. 62.10). Three cases were calculated. For one it was assumed that the CO and CO_2 yields remained fixed at the well-ventilated levels. For the second it was assumed that the yields changed linearly with time from the start to the peak of the fire, and for the third it was assumed that the yields remained constant throughout at those obtained under vitiated conditions. In reality, the yields would be expected to change with ϕ, which could be calculated for the full-scale fire case. The results of the exercise for the variable yields illustrate that the yields of CO and CO_2 during the early, well-ventilated phase of the fire produce only a small increase in FED for asphyxiation. This is partly because the smoke layer is above the occupant's head for some of the time, but mainly because the fire is small and producing only small amounts of effluent. During the later parts of the simulation the fire is larger, producing effluent at a much greater rate. It is also becoming vitiated so that both the mass and yield of CO are increasing. After 200 s the FED is predicted to reach 1 and incapacitation is predicted to occur. If the CO and CO_2 yields are assumed to remain constant at the well-ventilated levels throughout, then the

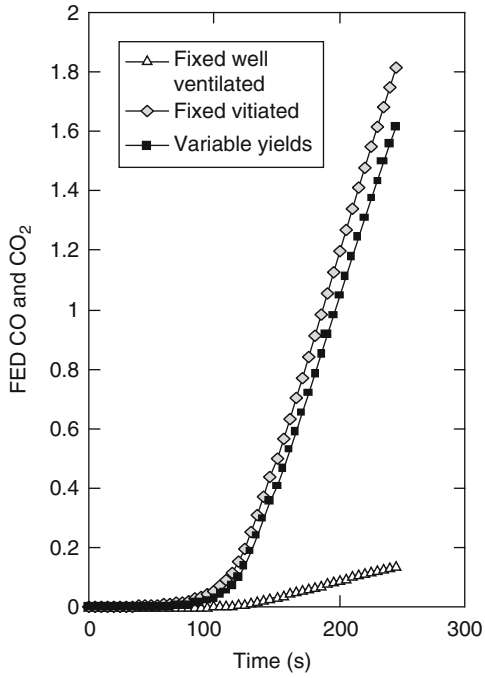

Fig. 62.10 FED for human incapacitation due to CO and CO_2 during a theoretical enclosed room fire involving a polymeric material such as polyethylene. CO and CO_2 yields obtained using the FRS tube furnace, fire modeled using CFAST [68]

increasing toxic hazard is seriously underestimated, reaching an FED value of only 0.1 after 200 s. When the CO and CO_2 yields are assumed to remain constant at the vitiated yield values, then the increasing FED is slightly earlier than, but very similar to, that obtained when continuously varying yields were assumed. This result illustrates the importance of obtaining toxic product yield data under the correct fire conditions and the extent to which the toxic hazard is driven by the later stages when the fire is larger and the CO yields greater. In this example the error obtained by assuming a constant high yield of CO throughout is small.

It is then possible to consider what outcome might have occurred if the polyethylene was substituted by a polymer treated with a fire retardant such as phosphorus or halogen additives. When these materials burn, they tend to produce high yields of CO even under well-ventilated conditions, and so might be considered to present a toxic hazard in some fires. For the example shown here, it is possible to examine the potential toxic hazard from CO and CO_2 if a halogenated polymer such as PVC was burned and the yields were as obtained in the tube furnace. Assuming that initially the fire growth rate of PVC was the same as for polyethylene (while in practice it is likely to be much slower) and the yields of CO were as obtained in the tube furnace, then it is possible to consider the effects on FED development for asphyxiant gases. As Fig. 62.9 shows, the yield of CO from PVC under both well-ventilated and vitiated conditions was very similar to that obtained from polyethylene under vitiated combustion conditions. It can therefore be estimated that the FED for PVC would follow the case calculated for a constant high CO yield. If the toxic potency of PVC (in terms of asphyxiants) under well-ventilated combustion conditions was the only item considered, then it might be estimated that PVC was a much more hazardous material than polyethylene, because the CO yield under these conditions is more than 20 times greater than for polyethylene. However, as the hazard modeling shows, the differences in CO yield during the well-ventilated phase of the fire have very little influence on the hazard development, so that, at least for this example, very little difference in time to incapacitation from asphyxiation would be expected between either fuel. In practice it would be expected that the fire growth curve for the PVC would be much slower than for polyethylene (assuming flaming ignition occurred) with a consequently slower growing FED curve. However, an additional hazard from a PVC fire would be the evolution of hydrogen chloride and other irritants, which would also need to be considered in the model. For all such hazard analysis it must be remembered that it is the concentration of toxic products at the breathing zone of a building occupant that is important. Depending on the positions of the occupants and the time during the fire development, it is likely that concentrations of acid gases in particular will be diluted relative to those near the fire and further reduced by losses to building surfaces.

Using Mass Loss Lethal Toxic Potency Data for a Simple Toxic Hazard Assessment

Another approach to carrying out a simplified toxic hazard assessment is to make use of mass loss lethal toxic potency data. The simplest approach is to use a single generic lethal exposure dose figure for all general mixed fuels under different basic combustion conditions. A slightly more sophisticated method is to take account of generic lethal exposure doses for different categories of fuels. These approaches are described in the following sections and a simple worked example is presented.

Using a Single Generic Lethal Exposure Dose for All Mixed Fuels

A simple hazard assessment can be made using lethal toxic potency data for materials obtained from a small-scale toxicity test. One way of performing a preliminary simple hazard analysis for a fire is to consider what exposure in terms of a single criterion, the mass loss concentration profile of products in a fire, is likely to be lethal to a victim. For such a calculation use can be made of mass loss lethality data from small-scale rodent toxicity test data for the material or materials involved in the fire. The assumption is that the lethal concentration to a human would be similar to that in a rat. This is standard practice in toxicology for making approximate classifications of hazard for the acute effects of industrial chemicals, however it is then usual to apply safety factors to allow for uncertainties relating to the differences between animal species and humans and to allow for variations in sensitivity in the human population. It is also necessary to make the assumption that mass loss lethality data follow Haber's rule. The three items of data needed for such an assessment are the following:

1. The basic fire condition (smoldering, early flaming, pre-flashover underventilated or postflashover)
2. The mass loss/dispersal volume-time curve for the fire
3. The rodent LCt_{50} or LED exposure doses for the materials involved in the fire in terms of the mass loss concentration for a quoted exposure time, determined under the same conditions as those in the fire

As discussed LCt_{50} data for common materials have been derived using a number of small-scale test methods under a variety of decomposition conditions. Most published data relate to nonflaming oxidative decomposition conditions, well-ventilated flaming, or mixed flaming and nonflaming conditions. Very few data are available for underventilated or postflashover fire decomposition conditions. Table 62.6 shows examples of data sets obtained using three well-known test methods. The range of LC_{50} for the references quoted (shown in Table 62.6) was approximately 5–60 $g{\cdot}m^{-3}$ mass loss for a 30-min exposure, which is equivalent to an LCt_{50} dose range of approximately 150–1800 $g{\cdot}m^{-3}{\cdot}min$, with an average value of 23 $g{\cdot}m^{-3}$ (690 $g{\cdot}m^{-3}{\cdot}min$). Allowing for a small margin of safety, it has been suggested within British standards that, for a simple hazard assessment, a single figure of 500 $g{\cdot}m^{-3}{\cdot}min$ might be considered as a single average figure for the approximate toxic potency of the thermal decomposition products from common materials. For the purpose of carrying out hazard calculations, the toxic potency of any individual material can then be expressed in terms of a potency factor relating the actual LCt_{50} to 500, as follows:

$$\text{Toxic potency factor for a material under a defined fire condition} = 500/LCt_{50}\ \ g \cdot m^3 \cdot min$$

Using Toxic Potency Data for Different Common Material Classes Under Four Fire Conditions

Using a wider database than that for Table 62.6, a survey of the toxic potency data for common materials in nonflaming, early well-ventilated flaming, pre-flashover underventilated flaming

and postflashover fire conditions was possible to derive approximate LCt_{50} (LEDs) for common materials [10, 39, 64]. Excluding fluoropolymers, the results for individual materials range over approximately 2 orders of magnitude from 20 to 3750 g·m^{-3}·min; but when the data are reduced to basic types of materials under each decomposition condition, a relatively simple pattern can be described, as presented in Table 62.7. The table shows the approximate average lethal exposure doses (LCt_{50} or LED) for classes of materials, (i.e. the LC_{50} for 30-min exposures). The findings are as follows.

- Under nonflaming oxidative decomposition conditions at >400 °C most materials have a similar potency close to 500 g·m^{-3}·min, due mainly to the effects of carbon monoxide and irritants. The main exceptions are nitrogen-containing materials releasing significant HCN at low temperatures (e.g., polyacrylonitrile, modacrylic, and rigid polyurethane foam).
- Under early well-ventilated flaming conditions most nonfire-retarded materials are substantially less toxic than under nonflaming conditions. Cellulosics (wood and cotton) are the least toxic with an LCt_{50} of >3000 g·m^{-3}·min. Plastics containing carbon, hydrogen, or oxygen are somewhat more toxic (LCt_{50} ~ 1200), and those containing low percentages of nitrogen (e.g., flexible polyurethanes, wool, and nylon) also fall into this area. PVC and fire-retarded materials have a similar toxic potency to that under nonflaming conditions. Rigid polyurethanes and nitrogen-containing acrylics have high potencies similar to those under nonflaming conditions.
- Under postflashover conditions (and preflashover vitiated combustion conditions), the potency of all materials increases due to the increased yields of HCN and CO. More smoke and irritants are also present than under early flaming conditions, which may add somewhat to the potency, particularly of the non-nitrogen-containing materials. For cellulosic materials and hydrocarbon plastics, the potency is similar to that under nonflaming conditions. For all nitrogen-containing materials, the toxic potency is high. PVC has an LED of approximately 270 under these conditions.

It is suggested that the data in Table 62.7 provide a method whereby small-scale toxicity test data, obtained under appropriate decomposition conditions, can be applied in fire engineering calculations. A simple, first estimate could be based on a single lethal toxic potency figure of 500 g·m^{-3}·min for all materials, using total fire load or heat release as the source of the mass term. In order to assess an incapacitating exposure dose (and to allow for possible greater sensitivities between rats and average humans) this should be multiplied by 0.3 to give an incapacitating dose of 150 g·m^{-3}. A further factor of 0.3 could then be applied to allow for the range of sensitivities in the human population, giving a figure of 45 g·m^{-3}·min to allow for escape of the majority of the occupant population. When more detailed information on the nature of the materials likely to be involved in a fire is known, the calculations for particular fire scenarios can be based on the predicted mass loss rate for each material, adjusted by the appropriate toxic potencies. The range of toxic potencies of common materials decomposed under conditions occurring in flaming fires is approximately two orders of magnitude. Difficulties in making estimates of the specific toxicities and toxic potencies of common materials arise from the very poor database of both small- and large-scale tests conducted under appropriate conditions. This is particularly true of the vitiated pre- and post- flashover condition, although ISO TS 19700 data are now available for a range of materials [13].

Theoretical Example of the Application of the Mass Loss Lethal Toxic Potency Data for a Simple Toxic Hazard Assessment [63]

Consideration is being given to replacing the floor covering material in a hotel bedroom. There is a concern that if the material is ignited by a small ignition source the rate of

development of a toxic hazard from the new material (material B) should not be worse than that from the old material (material A). It is considered that the most likely scenario would involve a closed room, so that rapid smoke filling would occur and the effluent can be considered as evenly mixed throughout the room volume (i.e., layering effects can be considered very transient and can be ignored). A problem is that the toxic potency of material B is twice that of material A, although it burns more slowly once ignited.

Information Available The volume of the room is 40 m^3. The floor covering materials are 1 cm thick with an area density of 1 kg/m^2. Horizontal burning tests have shown that both materials burn through rapidly so that a front of complete combustion spreads from the point of ignition. For material A the rate of flame spread is 10 cm/min whereas for material B the rate of flame spread is only 5 cm/min. However, small-scale toxicity tests have shown that, under well-ventilated flaming conditions, the toxic potency of material B (LC_{50} 10 $g{\cdot}m^{-3}$, lethal exposure dose 300 $g{\cdot}m^{-3}{\cdot}min$) is twice that of material A (LC_{50} 20 $g{\cdot}m^{-3}$, lethal exposure dose 600 $g{\cdot}m^{-3}{\cdot}min$).

Hazard Analysis Assuming a small point ignition source, both materials will burn through, and a circle of burned area will spread out from the point of ignition (Fig. 62.11). Since material A burns twice as quickly as material B, the area of material A consumed will be four times that of material B at any time during the early stages of the fire.

Table 62.8 shows how the FED calculations are made using material A as an example. The FED for each point in time is the exposure dose divided by the lethal exposure dose for that material. The FEDs for each time interval are then summed throughout the fire until the FED reaches unity, at which point the toxicological endpoint, in this case lethality, is predicted.

Figure 62.12 shows the results of the FED calculations for materials A and B in the 40-m^3 room. The analysis shows that lethal conditions are attained after approximately 6 min for material A, and approximately 1.5 min later for material B. It can, therefore, be concluded that material B presents less of a toxic hazard than material A in this scenario, despite the fact that material B has twice the toxic potency of material A.

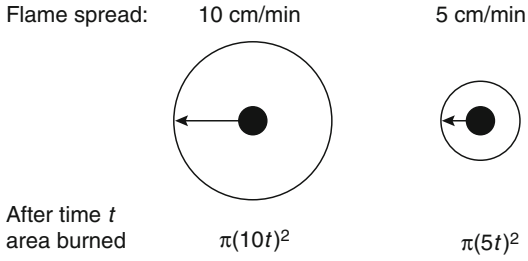

Fig. 62.11 Flame spread rate for two materials

Incapacitation

This rather crude method could be used to give an approximate indication of when conditions in a fire are likely to be lethal, but in practice the effects of fires on exposed victims are not so simple. In many cases death is not due to the immediate toxic effects of exposure but results from the victim being trapped in the fire, either because irritant and optically obscuring smoke prevents escape or because asphyxiant gases cause incapacitation, so that the victim remains in the fire to die either from a fatal dose of toxic products acquired during the prolonged exposure or from burns. One way of taking these factors into account would be to determine the *Ct* product dose at which effects such as incapacitation due to asphyxia occur in small-scale toxicity tests. These could then be applied to the fire hazard analysis to estimate the fractional incapacitating dose rather than the fractional lethal dose. However, because of differences in generating small-scale fire test atmospheres similar to those occurring in large-scale fires, a potentially much more effective way of predicting toxic hazard would be to measure the concentration/time profiles of the important toxic products in the fire and to determine their effects from toxicity data derived from experiments in humans and primates (and to a lesser extent also from rodents) as described in Chap. 63.

Table 62.8 Example FED calculation data for materials A and B

Time (min)	Area burned (cm^2)	Mass consumed (g)	Mass loss concentration (averaged for each time interval) ($g \cdot cm^{-3}$)	Exposure dose ($g \cdot cm^{-3} \cdot min$)	FED
Material A	(LC_{50} 20 $g \cdot m^{-3}$; LCt_{50} 600 $g \cdot m^{-3} \cdot min$)				
0	0	0	0	0	0
0.5	79	79	1.0	0.5	0.001
1.0	314	314	4.9	2.9	0.005
At 5 min	7854	7854	177.7	328.9	0.548
Material B	(LC_{50} 10 $g \cdot m^{-3}$; LCt_{50} 300 $g \cdot m^{-3} \cdot min$)				
0	0	0	0	0	0
0.5	20	20	0.25	0.12	0.000
1.0	79	79	1.2	0.74	0.002
At 5 min	1963	1963	44.4	82.2	0.274

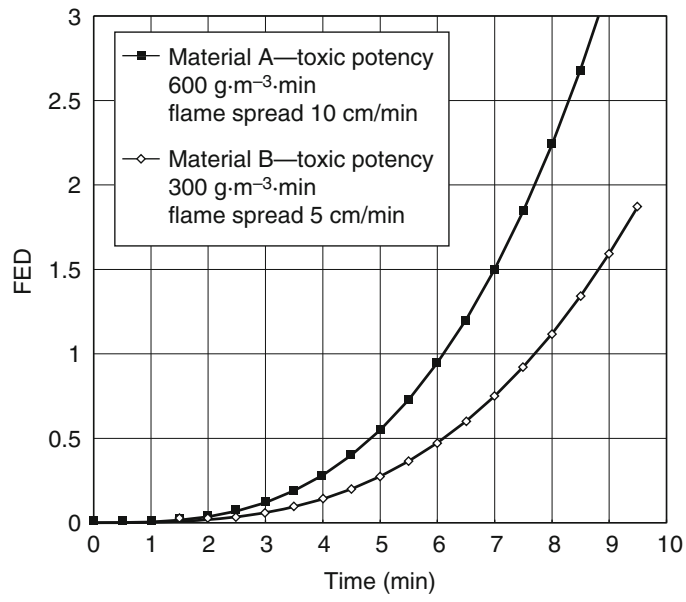

Fig. 62.12 Relative toxic hazard from two materials calculated according to the mass loss lethal exposure dose method (time to lethality when FED = 1) [63]

Assessment of Irritancy and Derivation of Irritancy Calculations for Humans

Chapter 63 shows some data for the effects of exposure to smoke during fire incidents on occupant behavior and willingness to enter and move through smoke. Also presented are data on the experimentally determined relationships between smoke density and walking speed for non-irritant smoke (from kerosene) and somewhat irritant smoke (from smoldering wood chips) or slightly irritant theatrical smoke containing a low concentration of acetic acid. In practice smoke from different burning materials contains a wide range of irritant chemicals the identities and yields of which vary with the materials composition and the combustion conditions. Although data and calculation methods presented for generic "averagely irritant" smoke may be applicable to some design cases, a more complete analysis of the hazards to

escape and survival from exposure to irritants is preferable, especially when the presence of significant yields of the more potent organic irritants and acid gases are considered likely to occur. The following sections consider the nature of irritant fire products and the derivation of method to measure irritancy and derive FEC and FED methods for calculating time to irritancy endpoints in humans, and for estimation of walking speeds in atmospheres of irritant composition. The calculation methods derived from this information for effects of sensory irritant on escape capability and movement speed, and for calculation of lethal lung inflammation are presented in Chap. 63. The basis for the calculation methods is described in the following section.

Irritant Fire Products

Unlike the incapacitating effects of asphyxiants, which are clear-cut and well understood, the incapacitating effects of irritants are much more difficult to determine. Reviews of combustion product irritancy and effects are presented in Purser [71, 72]. Irritant fire products produce incapacitation during and after exposure in two distinct ways. During exposure the most important form of incapacitation is sensory irritation, which causes painful effects to the eyes and upper respiratory tract and to some extent also the lungs. Although exposure may be painful and thus incapacitating, it is unlikely to be directly lethal during exposure unless exceptionally high concentrations of irritants are present. However, the second effect of irritants penetrating into the lungs is an acute pulmonary irritant response, consisting of edema and inflammation, which can cause respiratory difficulties and may lead to death 6–24 h after exposure [32, 73]. The effects do not show the sharp cut-off of asphyxiation but lie on a continuum from mild eye irritation to severe pain, depending on the concentration of the irritant and its potency [52, 56, 74]. For sensory irritation the effects do not depend on an accumulated dose but occur immediately on exposure and usually lessen somewhat if exposure continues [17, 52]. For the later inflammatory reaction the effect does depend on an accumulated dose, approximately following Haber's rule and there seems to be a threshold below which the consequences are minor, but when this dose is exceeded severe respiratory difficulties and often death occur, usually 6–24 h after exposure. However, for most sensory irritants the ratio between the concentration producing severe irritation and the dose causing death is usually large (15–500 times) [57, 58] for 30-min exposure times (see Table 62.4).

The effects of low concentrations of irritants can best be considered as adding to the obscurational effects of smoke by producing mild eye and upper respiratory tract irritation. In this situation irritants may have some effect by impairing the speed of an individual's movement through a building (as would simple visual obscuration), but the combined effects of eye irritation and direct visual obscuration may be more serious, and it has been shown that human volunteers moved more slowly through irritant smoke than through nonirritant smoke [75]. The limitation of escape capability may not be simply restricted to direct physiological effects but also to psychological and behavioral effects such as the willingness of an individual to enter a smoke-filled corridor [76].

At the other end of the scale, when irritants are present at high concentrations, there is some disagreement about the likely degree of incapacitation. Some investigators believe that the painful effects on the eyes and upper respiratory tract would be severely incapacitating, so that, for example, escape from a building would be rendered extremely difficult [77]. Others believe that the effects peak at moderate concentrations, and that although the effects may be very unpleasant they would not significantly impair the ability to escape from a building and would provide a strong stimulus to escape that might almost be beneficial [44].

One of the main difficulties in attempting to predict the consequences of exposure to irritants is the poor quality of data available on humans. Obviously, very few controlled studies have been made of the effects of severe irritancy in humans, so that most data are anecdotal, derived from

accidental industrial exposures, with only a vague knowledge of exposure concentrations. Reports of the severity of the effects also tend to be very subjective, so that the term *severe irritation* could cover a wide range of sensations with varying degrees of actual incapacitation. Another problem is that since sensory irritation covers a continuous range from mild eye and upper respiratory tract irritation to severe pain, there are no simple objective endpoints or thresholds. The most extensive studies of the effects of severe irritancy in humans have been performed on volunteers exposed to riot-control agents such as CS (o-chlorobenzylidene malonitrile) or CN (α-chloroacetophenone). Even these studies do not really show how the ability to escape from a building might be affected, but they do to some extent convey the severity of the effects.

The effects of CS, which are probably similar to those of any severe sensory irritant, have been described by Beswick et al. [52]. They consist of an almost instantaneous severe inflammation of the eyes accompanied by pain, excessive activation (tearing), and blepharospasm (spasm of the eyelids). There is irritation and running of the nose with a burning sensation in the nose, mouth, and throat, and a feeling of intense discomfort during which the subjects cough, often violently. If the exposure continues, the discomfort spreads to the chest and there is difficulty in breathing. Many subjects describe a tightness of the chest or chest pain as the worst symptom of CS exposure. The respiration pattern is irregular and the breath is held for short periods. Attempts to avoid the irritation by breath-holding, followed eventually by fairly deep breaths, are reported as being extremely unpleasant. At this stage most individuals are acutely apprehensive and highly motivated to escape from the smoke. However, if exposure continues there is some remission of signs and symptoms. When subjects were exposed to 0.08 ppm CS, they found the immediate effects very unpleasant but after 4–5 min were able to play cards. Another finding with CS, perhaps related to the development of tolerance, was that subjects could endure a relatively high concentration (~0.8 ppm CS) if it was achieved gradually even over as short a period as 10 min (as is likely to occur in fires) while they were totally unable to bear an immediate exposure to the same concentration [52, 53].

Reports are conflicting among fire victims. Some persons say they went through dense smoke without experiencing any great discomfort, whereas others say that respiratory difficulties prevented them from entering smoke-filled areas [78]. This seems to depend on the type of fire. For example, the smoke from some well-ventilated fires involving primarily cellulosic materials has been reported as irritant but not seriously incapacitating, whereas that from some plastic materials (e.g., the interior of a burning car) was found to cause severe effects when only a small amount of smoke was inhaled. Anyone who has had bonfire smoke in their eyes will know the pain of the experience. However, the effects can be mitigated by blinking or shutting the eyes, and the effects on the nose can be mitigated by mouth breathing and breath-holding. Also, it is known that people in emergency situations are often unaware of painful stimuli [79]. It is, therefore, likely that irritant smoke products do have some severe effects on the escape capability of fire victims, but it is difficult at present to predict accurately the likely degree of incapacitation.

Animal Models for the Assessment of Irritancy and Their Extrapolation to Humans

Having established that irritancy is likely to be a major cause of incapacitation in fires, it is important to find some way of assessing the potential of fire atmospheres for causing irritancy. The basic effects, consisting of an acute inflammatory reaction of the tissues accompanied by stimulation of pain receptors, are common to all mammals, so that animals can realistically be used to assess the potential for irritancy in humans.

The characteristic response to eye irritation is stimulation of trigeminal nerve endings in the cornea leading to pain, blepharospasm (reflex, or more or less involuntary closure of the

eyelids), and lacrimation. Severe damage may also lead to corneal opacity.

The effects of irritants on the upper respiratory tract have been studied in a number of species, including humans, for a wide range of airborne irritants including atmospheres of combustion products [80, 81]. The characteristic physiological response (also due to trigeminal nerve stimulation), is a reflex decrease in respiratory rate accompanied by a prickling or burning sensation in the nose, mouth, and throat, often accompanied by mucus secretion. At very high concentrations rapidly developing inflammatory reactions in the upper respiratory tract and laryngeal spasm may cause death during or soon after exposure, but in humans the lung is likely to be the more seriously affected target organ.

In contrast to these effects, the characteristic response to irritants penetrating into the lung is an increase in respiratory rate, generally accompanied by coughing and a slight decrease in tidal volume. There may also be bronchial constriction and increased pulmonary flow resistance, particularly if the victim is hypersensitive to the irritant [58, 80]. This is accompanied by tissue inflammation and edema, which at very high concentrations can cause death during, or more often after, exposure [15, 32].

The effect (upper respiratory tract or lung irritancy) that predominates depends on a number of factors such as the physical characteristics of the aerosol, the aqueous solubility of the irritant, the animal species, and the duration of the insult. An important difference between mice and rats (which are often used to measure irritancy) and primates, including humans, is that in rodents the nasal passages are complex in structure and have a large surface area, so that soluble gases are readily taken up and particulates are readily deposited. A decrease in respiratory rate in the upper respiratory tract is the major response in rodents, which tends to protect them from exposure. Their great tolerance to hypoxia (and possible circulatory adaptations similar to the diving reflex) also enables them to maintain greatly reduced breathing for long periods. In humans and other primates the nasal passages are simply structured with a relatively small surface area, and in humans particularly, mouth breathing is common. Thus, although upper respiratory tract irritation occurs initially and is accompanied by some respiratory rate decrease, a greater proportion of the inhaled irritant is carried into the lungs, so that lung irritation is generally a more pronounced effect. In primates, including humans, a transient respiratory rate depression is followed rapidly by the increased respiratory rate characteristic of lung irritation [17, 32] (Figs. 62.13 and 62.14).

Rodent Respiratory Rate Depression Test

The method most commonly used to quantify upper respiratory tract irritancy both for pedigree chemicals and combustion products is the mouse respiratory rate depression test [81, 82]. The basic method involves measurement of the percentage decrease in respiratory rate during exposure over a range of different atmosphere concentrations. From this measurement the RD_{50} (the concentration required to produce a 50 % decrease in respiratory rate) is calculated. Since the basic irritant mechanisms are the same in all mammals, it is certainly possible to identify an individual substance, or mixture (such as a combustion atmosphere), that is likely to be irritant to humans; however, it may also be possible to predict the degree of irritation in humans. As a result of comparisons of data from humans with results from mice, Alarie [33, 61], has demonstrated a relationship between the potency of known sensory irritants in humans and a derivative of the mouse RD_{50}. When the log of the TLV (often based on symptoms of irritancy in man) is plotted against the log of 0.03 multiplied by the RD_{50} in ppm, most chemicals known to be sensory irritants in humans fall into a linear relationship with the respiratory effects in mice. Chemicals that are highly irritant in humans such as acrolein or chlorine have low RD_{50} measures in mice whereas mild irritants such as ethanol have a high mouse RD_{50} [33, 61] (see Table 62.4).

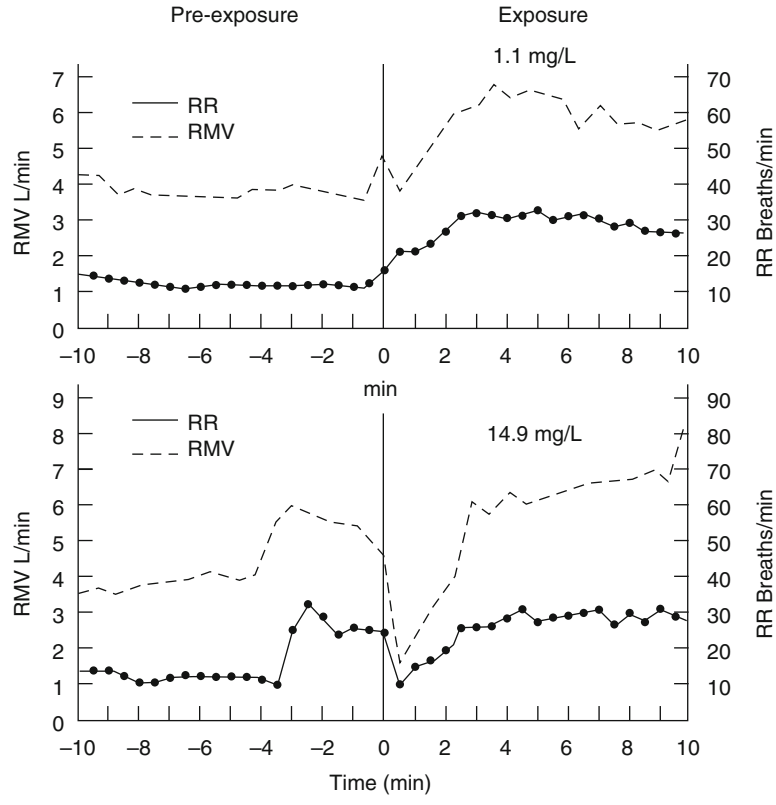

Fig. 62.13 Respiratory effects of polypropylene decomposed under nonflaming oxidative conditions—cynomolgus monkey

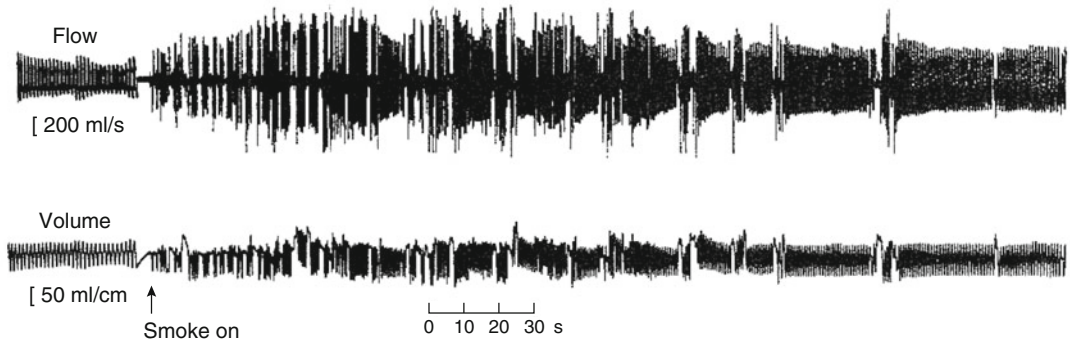

Fig. 62.14 Effects upon respiration of exposure to an irritant smoke atmosphere; wood pyrolyzed at 300 °C. When the smoke reaches the primate there is an initial sensory irritant response consisting of a decrease in respiratory rate with pauses between breaths. This rapidly gives way to a pulmonary irritant response consisting of an increase in respiratory rate and volume, which is maintained for the duration of the exposure [16]

Such methods appear to give good predictions of irritancy at low levels that are suitable for fixing hygiene standards, but for the high concentrations occurring in fires it is necessary to predict which concentrations will produce sufficient incapacitation to cause serious impairment of escape capability and also which concentrations will cause serious lung damage after exposure. As stated previously, such predictions of incapacitation in humans are difficult because of the variable and subjective nature of irritancy. However, Alarie states that a human

exposed at the mouse RD_{50} concentration of any substance would find the atmosphere severely irritating and would be seriously incapacitated within 3 min [61], which certainly seems to be justified in terms of some individual chemicals. For example, the work with CS [52, 53] shows that, although it is very difficult to measure intolerable irritancy in humans, there does seem to be a reasonable agreement between the human and mouse data. Thus the mouse RD_{50} (4 mg/m^3, 0.52 ppm) is very close to the concentration found to be immediately intolerable when humans were exposed for up to 12 min (5 mg/m^3, 0.6 ppm), and the list of RD_{50} levels and concentrations reported as highly irritant in humans [51] given in Table 62.4 shows a reasonable correspondence, particularly for the irritants commonly found in fires.

However, these apparent irritancy correlations between rodents and humans still do not enable the exact prediction of the degree of incapacitation likely in humans, and in some cases there is evidence that the mouse model does not even give a good prediction of the degree of sensory irritation, although it can be used to demonstrate when sensory irritation is likely to occur in humans.

Three experiments, two involving nonhuman primates and the other involving humans, may illustrate the difficulties of extrapolating from the RD_{50} and physiological effects in mice to the degree of irritancy, incapacitation, and physiological effects in primates. In a series of experiments the irritant effects of smoke produced by the nonflaming oxidative decomposition of polypropylene were evaluated in cynomolgus monkeys [17, 32]. The effects of breathing smoke through a face mask were mild at concentrations (NAC mass charge) of up to 4 mg polypropylene/L, consisting of a transient decrease in respiratory rate lasting approximately 30 s (a sensory irritant response), followed by an increased respiratory rate (lung irritant response) with a slight increase in RMV (see Fig. 62.13). The respiratory response pattern is illustrated in Fig. 62.14, where similar effects occurred during exposure to pyrolysis products from wood. For polypropylene the lung irritant response was the most sensitive effect with a threshold of 1 mg polypropylene/L. At concentrations above 6 mg/L the irritant effects were more marked, and although recovery appeared complete immediately after exposure, signs of nasal and pulmonary inflammation occurred some hours later. One animal died following an exposure of 30 min at 8 mg polypropylene/L. When free-moving monkeys trained to perform a behavioral task were exposed, there was evidence of some eye irritation and mild disruption of behavioral performance at a concentration of 1.85 mg polypropylene/L, the effects of exposure at 0.92 mg/L being very slight. However, the mouse RD_{50} for the same polypropylene atmosphere was found to be 0.1 mg/L. According to the model this concentration should have been highly irritant to the monkey, and yet in practice only the mildest of signs occurred at concentrations more than an order of magnitude higher.

Similarly, in another study Potts and Lederer [83] exposed mice and humans simultaneously to smoke from the pyrolysis of red oak (mouse RD_{50} 0.37 mg/L). At this concentration the smoke was barely visible and all human subjects stated that although the smoke was unpleasant and irritating, in no sense were they physically incapacitated, and they were quite capable of performing tasks such as threading nuts and bolts of various sizes.

The third experiment was performed on two pedigree substances, hydrogen chloride and acrolein, often regarded as important irritants in smoke. In these experiments baboons were trained to press a lever in order to escape from a chamber after a 5-min exposure [57]. It was found that the animals could perform this task efficiently even at the incredibly high concentrations of 2780 ppm acrolein or 16,570 ppm HCl, although in both cases the animals died from lung inflammation after exposure. These concentrations compare with mouse RD_{50}s of 1.68 ppm for acrolein and 309 ppm for HCl, and at these concentrations both substances are highly irritant in humans (Table 62.9).

As a result of this work on irritants in rodents, nonhuman primates, and humans, it would seem that the rodent models are good methods for

Table 62.9 Irritancy data

Acrolein[a]
Mouse RD_{50} = 1.68 ppm [77]
Marked irritation of eyes and nose in humans—1 ppm [51]
Severe irritation of eyes and nose in humans—5.5 ppm [51]
Henderson and Haggard [51] state that 10+ ppm is lethal in humans within a short time due to pulmonary irritation. However, 10 ppm for 3.5 h in cats was nonlethal [51]
Kaplan [57] has reported that baboons can escape from a chamber after 5 min exposure at up to 2780 ppm. One animal died due to pulmonary effects following exposure at 1025 ppm, and another following 2780 ppm. No signs of pulmonary effects were observed following exposure at 505 ppm and below
A case has been reported of a man dying following exposure to 153 ppm for 10 min [56]
The 6-h mouse LC_{50} is 66 ppm [55]
The 30-min rat LC_{50} is 135 ppm [55]
Hydrogen chloride[b]
Mouse RD_{50} = 309 ppm [77]
Strongly irritant to humans at 50–100 ppm for 1 h [51]
Brief exposure at 1000–2000 ppm is regarded as dangerous to lethal in humans [56]
Humans LCLO 1300 ppm for 30 min [55]
Kaplan exposed baboons for 5 min to concentrations of up to 16,570 ppm and found that they were able to perform escape maneuvers. One animal suffered permanent lung damage at 11,400 ppm and two died at approximately 17,000 ppm (~2830 ppm for 30 min)

[a]From these rather variable data the concentration lethal to humans following a 20-min exposure would be 80–260 ppm. A severe irritant effect on the upper respiratory tract would be expected at around 5 ppm, but from Kaplan's work [38] this may not be unbearable, even up to several hundred ppm

[b]Therefore, anything over 100 ppm is likely to be highly irritant and over a 20-min period approximately ten times this concentration may cause permanent lung damage or endanger life

identifying smoke atmospheres or individual substances likely to be irritant to humans and even for ranking irritants in order of potency and setting hygiene standards. However, when predicting concentrations of smoke atmospheres that would seriously impair the ability to escape from a fire, there is a need for more work to establish the effects of known irritants in humans and to establish the relationship between the rodent response and human incapacitation.

Lung Inflammatory Reactions

Just as it is difficult to predict the degree of incapacitation from sensory irritation likely to occur in victims during fire exposure, it is also difficult to predict concentrations likely to cause death in humans from lung inflammatory reactions, although experiments in rodents should enable some estimates to be made from postexposure LC_{50} data. When rodents are exposed to smoke atmospheres in small-scale combustion toxicity experiments, death occurs principally either during exposure due to asphyxiant gases (CO, HCN) or some time after exposure, due to lung irritation. In cases where the majority of deaths occur after exposure and are accompanied by signs of lung irritation, measurements of the concentration causing postexposure deaths give some indication of concentrations likely to be hazardous to humans.

Since the effects of asphyxiant gases can be predicted without animal exposure, whereas the potential for causing sensory irritation and lung inflammation cannot, measurements of sensory irritancy by the respiratory depression test (RD_{50}) and measurements of the concentrations causing postexposure deaths (LC_{50}) are important uses for small-scale toxicity tests. It is also important to stress that whereas sensory irritation occurs immediately upon exposure, and is concentration related, the inflammatory reactions resulting from lung irritancy are dose related and depend approximately on the product of exposure concentration and duration (Ct product). When an LC_{50} concentration is quoted, it is also important to quote the exposure duration.

For combustion toxicity experiments exposure times are usually 10 or 30 min, and the 30-min LC_{50} should be approximately one-third of the 10-min LC_{50} when postexposure irritancy is the cause of death. It is also important to know the time over which the deaths were scored. Thus some studies quote LC_{50} levels only in terms of animals dying during exposure (which will be due to asphyxia or very high concentrations of irritants). Other studies include deaths occurring both during or up to 24 h after exposure, whereas other studies use the standard method for inhalation toxicology studies that includes deaths during exposure and for up to 14 days after. For the assessment of toxic hazard in possible fire scenarios, it is important to take all these factors into account when considering different building designs or applications of materials.

Irritant Components of Thermal Decomposition Product Atmospheres

If mathematical models are to be constructed to predict the potential for sensory irritancy and later lung inflammation of exposures in fires, it is important to attempt to identify the main irritant chemical species occurring in fires and to measure their potency individually and in combination. This is an area where knowledge is still inadequate, but large numbers of known irritant chemicals have been found to occur in fire atmospheres [17, 18] (see Table 62.4). The irritant chemicals released in fires are formed during the pyrolysis and partial oxidation of materials, and the combinations of products from different materials are often remarkably similar [18]. Some materials release irritant components simply upon pyrolysis, such as HCL from PVC, isocyanates from flexible polyurethanes, and various substances from natural materials such as wood. However, for all organic materials and particularly for simple hydrocarbon polymers such as polypropylene or polyethylene, the main pyrolysis products, which consist of various hydrocarbon fragments, are innocuous. Thus when polypropylene is pyrolyzed in nitrogen the products listed in Table 62.10 are produced,

Table 62.10 Pyrolytic and oxidative decomposition products of polypropylene at 500 °C showing percentage yields of major irritants as indicated, and Threshold Limit Values (TLVs) where available [51]

MS interpretation	Pyrolysis yield[a] (%) ($\times 10^{-1}$)	Oxidation yield[a] (%) ($\times 10^{-1}$)	TLV (ppm)
Ethylene	10.4	8.1	
Ethane	3.7	2.1	
Propene	18.6	18.4	
Cyclopropane	0.5	0.3	
Formaldehyde[b]	–	33.2	2
Propyne	0.2	–	
Acetaldehyde[b]	–	35.0	100
Butene	9.6	20.1	
Cyclobutene	0.3	0.8	
Methyl vinyl ether[b]	–	10.4	
Acetone[b]	–	38.4	750
Butane	1.2	–	
Methyl propane	0.4	–	
Methyl butane	4.0	–	
Butenone[b]	–	1.3	
Methyl butene	29.7	12.9	
Pentanol[b]	–	12.5	
Cyclopentane	0.5	1.4	
Pentadiene	1.3	–	
Crotonaldehyde[b]	–	7.7	2
Ethylcyclopropane	0.1	–	
Methyl vinyl ketone[b]	–	2.8	
Methyl ethyl ketone[b]	–	4.7	200
Hexane	0.9	1.2	
Cyclohexane	32.2	19.3	
Hexadiene	3.7	2.2	
Hexyne	–	1.3	
Benzene	6.7	5.1	
Methyl propyl ketone[b]	–	1.9	
Pent-2-ene-4-one[b]	–	7.5	
Phenol[b]	–	11.6	5
Toluene	2.4	16.1	
Methyl cyclohexadiene	2.1	0.1	
Xylene	6.1	0.2	
Styrene	5.6	4.0	

[a]Weight percentage conversion of polymer

[b]Oxygen-containing products

and such an atmosphere was found to have no effect on primates [17, 32, 62, 64]. However, when these products are oxidized during nonflaming decomposition in air, some are converted to highly irritant products as shown in the table, and such atmospheres were indeed found to be highly irritant to both mice and primates [16, 42, 84].

These atmospheres produced by the nonflaming oxidative decomposition of materials are always the "worst case" for any material in terms of irritant potency. Both the chemical profile and the irritant potency as determined by the mouse RD_{50} test are often similar for different materials, the majority lying within a range of approximately 1 order of magnitude [62]. However, when materials flame, these organic irritants are destroyed in the flame to produce CO_2 and water, so that the irritancy of the atmosphere depends on how much irritant escapes the actual flame zone and the efficiency of combustion. Thus "clean," smoke-free flames, involving efficient combustion, such as those that occur in a gas burner or well-ventilated fire, are relatively nonirritant, whereas "dirty," smoky flames resulting from inefficient combustion may contain high concentrations of irritants, and produce these irritants at a greater rate than under smoldering or nonflaming conditions. In primates the atmosphere produced by flaming polypropylene was found to retain some irritancy, although considerably less than under nonflaming conditions [17]. In mouse experiments, some fire-retardant materials, which could be induced to flame only intermittently, with considerable smoke production, were found to produce atmospheres up to 300 times more irritant than the same polymer in its non-fire-retardant state, which burned cleanly [85].

The picture is again confused regarding the role of specific chemical products in smoke. Table 62.4 shows some irritants identified in smoke atmospheres in order of their sensory irritancy and includes data on the LC_{50}, due principally to lung inflammation, where these were obtainable from the literature. In some cases there was a considerable range of estimates for both sensory irritancy and lethality, and these are indicated. The lethality data are mostly for rodents, and have been normalized to a 30-min exposure period assuming that lethality is dose related according to Haber's rule. Table 62.9 gives more detailed data for the effects in humans and animals of the best-known fire irritants, hydrogen chloride and acrolein. One point to note from Table 62.4 is that irritants vary enormously in their potency, over 5 orders of magnitude. The most important irritants are probably the ones near the top of the list, including isocyanates (from polyurethanes), the unsaturated aldehydes acrolein and crotonaldehyde, and the first of the saturated aldehyde series—formaldehyde (which is produced by nearly all materials when decomposed). Irritants with a moderate potency, such as phenol and the halogen acid gases HCl, HF, HBr may be important in some fires if they are present in high concentrations, while it is difficult to conceive of any product with an RD_{50} of more than 1000 ppm, such as acetaldehyde, methanol, or any hydrocarbon, being of significance as a smoke irritant.

A difficulty in predicting the irritancy potential of fire atmospheres is that it is not known exactly how the various irritant components of an atmosphere interact, although there are indications that some degree of additive effect occurs. However, a more serious problem is that where comparisons have been made between the mouse RD_{50} of combustion atmospheres and their chemical composition as revealed by GC-MS analysis, the atmospheres in most cases turn out to be much more irritant than can be accounted for by a knowledge of their components. It is possible that small amounts of short-lived reactive chemical species with a very high irritant potency ($RD_{50} < 1$ ppm) are responsible, and more work is needed in this area [86].

Prediction of Incapacitation Due to Sensory and Lung Irritation

In Chap. 63 a model for the prediction of asphyxia in fires has been presented. This model is realistic because it is based on the following facts:

1. Asphyxiation in fires gives two well-defined endpoints, loss of consciousness and death, both of which are likely to occur during the fire exposure.
2. Time and dose to these endpoints can be predicted from established data.
3. Asphyxiation in fires can be shown to depend on a few known toxic gases.
4. The effects of each toxic gas are well known, and so their interactions, so that predictions of asphyxia based on gas profile measurements show a good agreement with observations of animal exposures.

However, it is difficult to develop a predictive model for irritancy for the following reasons:

1. Sensory irritation does not have a clear endpoint but lies instead on a continuum of increasing eye and respiratory tract pain. Although this pain may be considered incapacitating, sensory irritation does not cause obvious incapacitative effects such as loss of consciousness, and it is not lethal, except under extreme conditions. Lung inflammation appears to cause relatively minor effects until near lethal levels of exposure are reached, so the main predictable endpoint is death, although this does not usually occur until several hours after exposure.
2. The identity and number of only a few of the irritant substances important in fires are known. There is also a poor correlation between the composition of experimental fire atmospheres in terms of known irritants and their actual irritant effects on animals, indicating that important unknown irritant remain to be identified.
3. The concentration/time/dose effects of irritants and the degree of interaction between different irritants are also only partly understood
4. The subjective sensation of pain and effects on escape behavior are only partly related to the severity of the irritant stimulus. In emergency situations (for example during military combat situations) individuals may be less affected than at other times.

For these reasons it is currently possible only to develop an approximate mathematical model to predict irritant effects from a knowledge of fire profiles in terms of known irritant products. An alternative is to base a model empirically on the effects on animals of smoke atmospheres produced in small-scale tests (which are described in a later section of this chapter).

To use small-scale test data, it is first necessary to ensure that the test fire model reasonably represents the decomposition conditions in the type of fire of interest (smoldering, early flaming, or postflashover). The concentration of irritants may then be represented in terms of mass charge or mass loss of the test material per liter of diluent air.

Sensory irritation may then be measured in terms of the mouse RD_{50} test. Although this test relates primarily to upper respiratory tract irritation, the results also show some correlation with eye irritation [61]. Sensory irritation may also be assessed directly if required in terms of the severity of eye lesions occurring in the mice (ranging from lacrimation through chromodacryorrhoea to ocular opacity).

Lung edema and inflammation may be measured in terms of the mouse or rat LC_{50} where deaths occur principally after exposure and are accompanied by signs of inflammation such as increased lung weights or histopathological lung lesions.

Attempts may then be made to relate the RD_{50} and LC_{50} to possible effects in humans, but as described there are difficulties with these extrapolations. Fortunately, for most different materials the rodent RD_{50} and LC_{50} levels cover relatively narrow ranges (approximately one order of magnitude) under some given thermal decomposition conditions. For these reasons it is difficult with current knowledge to give guidance on irritancy for hazard modeling. Guideline tenability limits can be presented, based on observations of the sensory and lethal lung irritant effects of exposures of rodents and primates (and humans) to combustion product atmospheres from a range of materials decomposed under a range of conditions. It is, therefore, suggested that irritancy should be treated as follows:

1. Sensory irritation occurs immediately on exposure and is primarily concentration related, not increasing with exposure duration.
2. All fire atmospheres are likely to be highly irritant, and at low concentrations the irritant effects should be regarded as adding to the obscurational effects of smoke through eye irritation, and possibly causing mild behavioral disruption by effects on the respiratory tract. At higher concentrations the disruptive effects of severe sensory irritation on vision and breathing may seriously limit escape capability, and as an approximation non-flaming atmospheres are likely to cause severe sensory irritation at a nominal atmosphere concentration (mass loss) of around 1 mg material/L air. This may occur when the optical density of the smoke is very low (<0.01/m) or even where there is no detectable smoke. It is therefore proposed that an NAC (mass loss) of 1 mg/L should be used as a tenability limit for non-flaming fires, although this may be modified in the light of RD_{50} or other data on the particular material and fire condition of interest.
3. Lung edema and inflammation are most likely to occur some hours after fire exposure, and severity of these is basically dose related, approximately following Haber's rule.
4. Dangerous lung edema and inflammation are likely to occur following a 30-min exposure to an NAC (mass loss) of approximately 10 mg material/L, representing a Ct product of approximately 300 mg/L min. This figure may be replaced by LCt_{50} data on the materials involved in individual fires.
5. These exposure limits for sensory and lung irritation are based largely on exposures to nonflaming atmospheres. Flaming atmospheres may be somewhat less of an irritant, depending on the efficiency of combustion and the severity of the fire. For flaming fires somewhat higher limits such as 5 mg/L might be applied for sensory irritancy and 200 $g{\cdot}m^{-3}{\cdot}min$ for increased risk of lung inflammation.
6. Data for some common fire irritants are shown in Tables 62.4 and 62.9.

Setting Tenability Criteria for Sensory/Upper Respiratory Tract and Lung Irritancy

The work by Jin and others on human behavior in smoke does provide some possibility to determine the effects of smoke obscuration on escape speed and efficiency (see Chap. 63), but a problem remains in determining the likely irritancy of the smoke and the likely severity of the effects of the irritants. It seems from the experience of people exposed in fires that there is a considerable variation in irritant severity between different types of fire effluent. Some fires produce large amounts of sooty smoke that are optically obscuring but relatively nonirritant. Other fires produce smoke that is both optically obscuring and irritant, while in some cases a highly irritant fire atmosphere has been reported when there was little or no visible smoke. From work at BRE Ltd., Fire Research Station (FRS), it has been found that smoke irritants consist of inorganic acid gases (such as hydrogen chloride) and organic compounds, particularly low molecular weight aldehydes (formaldehyde and acrolein). More than 20 irritant substances have been detected in smoke and it is considered that others remain to be identified (see section "Irritant Fire Products"). The yields of inorganic acid gases in fires depend mainly on the elemental composition of the materials being burned, whereas the yields of smoke and organic irritants depend mainly on the decomposition conditions in the fire. In general, smoldering or vitiated flaming fires (fires burning inefficiently) tend to produce irritant smoke whereas well-ventilated flaming fires, if burning efficiently, tend to produce nonirritant smoke.

The first effect of exposure to smoke irritants is sensory irritation, which consists of painful stimulation of the eyes, nose, throat, and lungs. Sensory irritation depends on the immediate concentration of irritants to which the subject is exposed, rather than a dose acquired over a period of time, with the effects lying on a continuum from mild eye irritation to severe eye and respiratory tract pain. Most people are familiar with the effects of smoke with a high-irritant

potency from exposure to bonfire smoke in the garden. The effects can be temporarily incapacitating with severe eye pain, closure of the eyes, and tears. If the smoke is inhaled, coughing and breathing difficulties occur. It is easy to imagine how difficult it must be to find one's way through the escape routes in a building under such conditions. One of the best scientific descriptions of the effects of exposure to a sensory irritant is in a paper on the effects of experimental exposures of human volunteers to a substance designed to cause incapacitation due to sensory irritation, CS riot control gas [52]. The effects described consisted of an almost instantaneous severe inflammation of the eyes, accompanied by pain, excessive lacrimation (tearing), and blepharospasm (involuntary closure of the eyes due to spasm of the eyelids). There is irritation and running of the nose with a burning sensation in the nose, mouth, and throat, and a feeling of intense discomfort during which the subjects cough, often violently. If the exposure continues, the discomfort spreads to the chest and there is difficulty in breathing. Many subjects describe a tightness of the chest or chest pain as the worst symptom. The breathing is irregular and the breath is held for short periods. Attempts to avoid the irritation by breath-holding, followed eventually by fairly deep breaths, are reported as being extremely unpleasant. At this stage most individuals are acutely apprehensive and highly motivated to escape from the smoke.

In evaluating this aspect of irritancy in fires, the aim is to predict what concentration of mixed irritant products is likely to cause such pain and difficulty in breathing that escape attempts would be slowed or rendered less efficient, and what concentration is likely to seriously disrupt or prevent escape (a degree of incapacitation approximately equivalent to that at the point of collapse resulting from exposure to asphyxiant). For example, with regard to hydrogen chloride it is considered that concentrations from approximately 100–500 ppm would be painfully irritant, producing effects similar to those described for the CS experiments, and that the effects may slow escape but probably would not prevent it.

Table 62.11 Example of the effects of exposure to an acid gas irritant—hydrogen chloride

No odor ppm	
<5	Minor nasal irritation can be detected below 5 ppm (the OEL)
10–50	Perceived as irritant, but work is possible at up to approximately 50 ppm
50–100	Strongly irritant, and some people report exposure to 100 ppm as being excruciatingly painful to the eyes and respiratory tract
309	Mouse RD50
1000–2000	Brief exposure regarded as being dangerous to lethal to humans
3800	Lethal exposure dose to rats for a 30-min exposure, representing an exposure dose of 114,000 ppm·min
15,000	5-min lethal exposure concentration in rats and baboons is around 15,000 ppm

However, at approximately 1000 ppm and above it is suggested that the effects might be so severe as to prevent escape [87]. The effects of exposure to different concentrations of an acid gas irritant (HCl), detailed in Table 62.9, are shown in Table 62.11. Figure 62.15 shows the respiratory depression response of mice to exposure to a sensory irritant atmosphere from PVC decomposed under nonflaming oxidative conditions. Figure 62.16 shows the logarithmic concentration—effect relationship. In the absence of detailed information on irritant mixtures it is assumed that all irritants would be additive in their effects, since they are all capable of causing damage to lung tissue. In large-scale fire tests it is possible to measure inorganic irritants directly, but it is difficult to assess the degree of irritancy from organic products, which form a very important component. In general, the effects of organic irritants depend on the concentration of partially oxidized organic species in the smoke. For example, smoke from smoldering wood or polyolefines decomposed under smoldering or vitiated flaming conditions has a high organic content, is highly irritant, and is characterized by low CO_2/CO ratios and high smoke yields. Under well-ventilated flaming conditions, the organic content of the effluent is low, and irritancy is low. In general, it is predicted that smoke from a mixed fuel source with an optical density/meter of 0.5 would be strongly

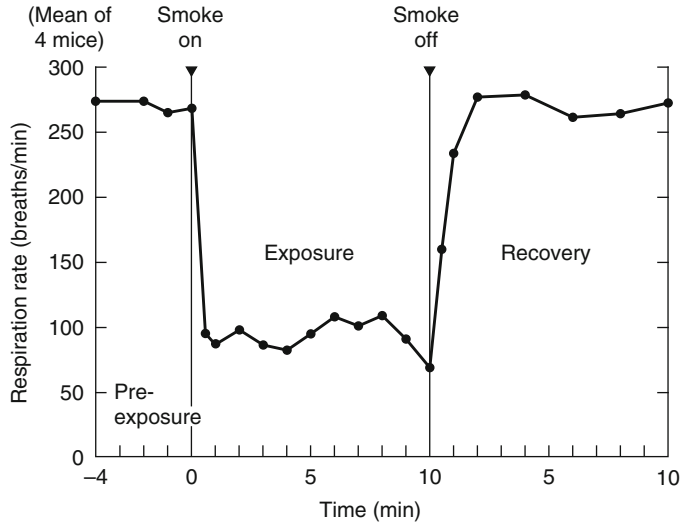

Fig. 62.15 Concentration—effect relationships for sensory irritants: effect of exposure on mouse breathing rate of thermal decomposition products from PVC-J (0.72 g•m^{-3}) [86]

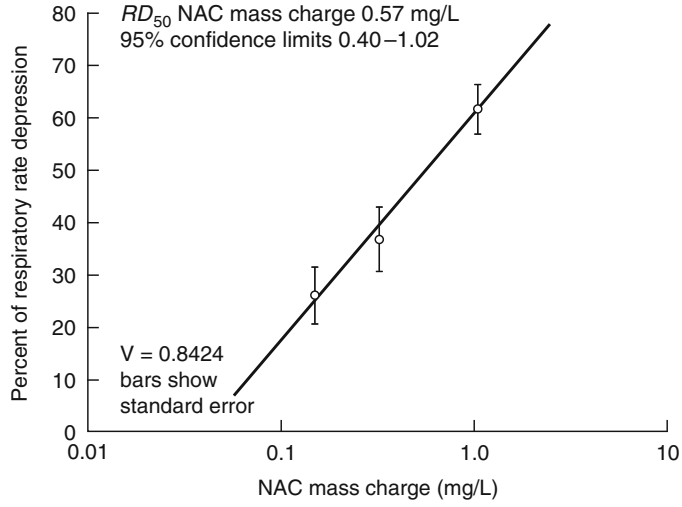

Fig. 62.16 Concentration—effect relationships for sensory irritants percent breathing rate depression in mice is proportional to log concentration [86] RD_{50} PVC-I 0.57 g•m^{-3}

irritant to the eyes and respiratory tract. However, for a given smoke density, there are differences between different types of fires.

It is difficult to quantify these irritant effects exactly because the database on the effects of individual irritants or irritant mixtures on escape behavior in humans is poor, and, because the effects lie on a continuum of severity, there are no precise endpoints. Assessment has to be based on a small number of human experimental exposures, usually at relatively low concentrations, accidental exposures, and the results of bioassay studies. For ethical reasons it is never going to be possible to obtain direct data for effects on humans so that estimates of this important parameter must be based on existing data and the judgment of physiologists. Further details of data from human and animal exposure

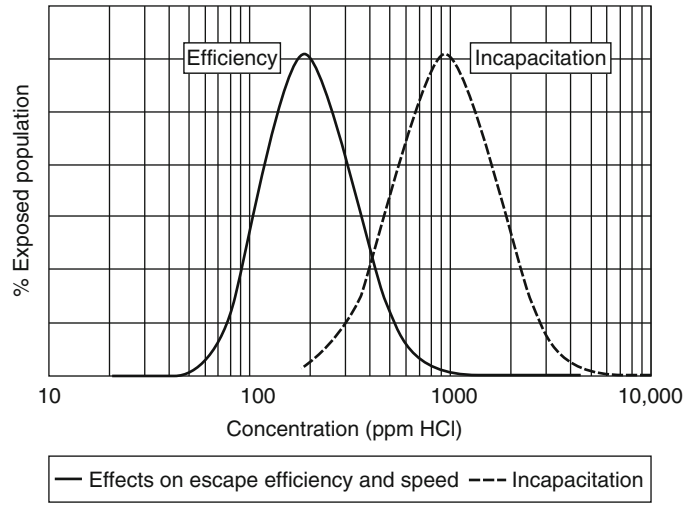

Fig. 62.17 Estimated sensitivity distribution for human population to HCl exposure [27]

to HCl and other irritants are given in Purser [72, 87].

Another concern is the range of susceptibility in the human population. Some individuals, particularly those with respiratory diseases, are likely to be more susceptible than others, whereas particularly fit individuals or those used to working in irritant environments are likely to be more resistant. It is also likely that the subjective irritancy of an exposure is on a log scale of sensitivity for humans, as it is in rodents. Figure 62.17 shows a suggested likely distribution of sensitivity for a human population for HCl, in terms of the proportion of the population likely to suffer severe irritancy, to have impaired escape efficiency at different concentrations and to suffer incapacitation. This is based on existing human and animal data and the judgment of the author. Whereas most individuals are considered likely to be affected at around 200 ppm, some may be affected by low concentrations of around 100 ppm, but some may be able to tolerate exposure to very high concentrations of over 500 ppm without suffering serious effects on escape capability.

In order to assess the combined effects of irritants, a concept of fractional irritant concentration (FIC) has been developed, whereby the concentration of each irritant present is expressed as a fraction of the concentration considered to be severely irritant. The FICs for each irritant are then summed to give a total FIC. If the total FIC reaches unity, then it is predicted that the smoke atmosphere would be highly irritant, sufficient to slow escape attempts. If the total exceeds unity by a factor of approximately four or more, then it is likely that escape would be prevented and possible that collapse might occur due to static hypoxia from bronchoconstriction or laryngeal spasm. On the basis of available data, current estimates of the concentrations of each gas likely to be highly irritant are as shown in Table 62.12.

It is predicted that each gas at the above concentrations is likely to be sufficiently irritant to affect escape efficiency in the majority of subjects and may cause incapacitation in susceptible individuals. A factor of 0.3 FEC for escape impairment should allow for safe escape of nearly all exposed individuals.

On the basis of the somewhat limited evidence that all irritants capable of causing sensory irritancy are additive in their effects, the overall irritant concentration FIC is then given by Equation 62.5:

$$\mathrm{FIC} = \mathrm{FIC}_{\mathrm{HCl}} + \mathrm{FIC}_{\mathrm{HBr}} + \mathrm{FIC}_{\mathrm{HF}} + \mathrm{FIC}_{\mathrm{SO_2}} + \mathrm{FIC}_{\mathrm{NO_2}} + \mathrm{FIC}_{\mathrm{CH_2CHO}} + \mathrm{FIC}_{\mathrm{CH_2O}} + \sum \mathrm{FIC}_x \quad (62.5)$$

where $\sum FIC_x = FICs$ for any other irritants present.

A considerable degree of variability is likely in individual susceptibility within the population and there is a degree of uncertainty as to which tenability thresholds should be recommended. In the recently published international standard for the estimation of time available for escape (ISO 13571[4]) the chosen tenability endpoint has been that of predicted incapacitation (rather than escape impairment), defined as sublethal effects that would render persons of average susceptibility incapable of effecting their own escape. The endpoint and predicted endpoint concentrations are very similar to those in the right-hand column of Table 62.12 with a suggestion that design tenability limits might be set at 0.3 times these concentrations to allow for more sensitive subpopulations. Although these levels may be set rather high, since it is considered that the symptoms of irritancy increase with the logarithm of the concentration, the difference between the levels is not large. The choice of limits also depends on the degree of effect considered acceptable for building occupants attempting to escape. Since the suggested figures for escape impairment in the left-hand column of Table 62.12 represent average susceptibility, the extent of escape impairment might be expected to be greater for sensitive subpopulations, so a factor of 0.3 might also be considered for this endpoint for design applications. The application of this model to fire hazard calculation for human exposure is presented in Chap. 63.

Table 62.12 Irritant concentrations of common fire gases

Gas	Concentration predicted to impair escape in half the population (ppm)	Concentration predicted to cause incapacitation in half the population (ppm)
HCl	200	900
HBr	200	900
HF	200	900
SO_2	24	120
NO_2	70	350
CH_2CHO (acrolein)[a]	4	20
HCHO (formaldehyde)[a]	6	30

[a]Where the concentrations of acrolein and formaldehyde (or other important irritants) are unknown, a term derived from smoke density 0.5 OD/m may be used as an indication of irritancy likely to impair escape efficiency

Current Concerns Regarding Effects of Sensory Irritants

In the preceding sections, the background data and considerations from which guidance on the effects of irritants have been derived have been presented in some detail. The proposed tenability limits can never be precisely verified since the human experiments needed cannot be performed, but by the same token it is not possible to determine accurate lower safety limits. For this reason the best guidance can only be given by toxicologists familiar with the background human and animal data. The figures presented have been derived in this way and are very similar to those proposed by an expert panel of toxicologists in the International Standards Committee (ISO/TC92/SC3), which was responsible for the ISO 13571 standard.

Concerns have been expressed from some quarters that the proposed limits are too low for application to practical fire safety engineering and provide too wide a limit of safety. An important point to consider in this context is that the proposed tenability limits are designed to be applied at the breathing zone of a potential building occupant and not at the fire source. In a fire scenario, it is likely that some time will elapse from ignition to the time these tenability limits are breached in the breathing zone of a building occupant some distance from the fire source. With regard to the actual limits used, these have been chosen in the context of escape and survival in an emergency situation and are considerably in excess of hygiene levels. Even with regard to emergency situations, other expert groups of toxicologists have proposed similar or even lower tenability limits. One set of limits developed for dangerous acute exposures in an industrial context by the American Industrial Hygiene Association is the Emergency Response Planning

Table 62.13 Emergency response planning guidelines for common fire irritants

Definition	HCN	HCl	HF	Acrolein	Formaldehyde
ERPG-3 (ppm)					
The maximum airborne concentration below which it is believed that nearly all individuals could be exposed for up to 1 h without experiencing or developing life-threatening health effects	25	100	50	3	25
ERPG-2 (ppm)					
The maximum airborne concentration below which it is believed that nearly all individuals could be exposed for up to 1 h without experiencing or developing irreversible or other serious health effects or symptoms that could impair an individual's ability to take protective action	10	20	20	0.5	10
ERPG-1 (ppm)					
The maximum airborne concentration below which it is believed that nearly all individuals could be exposed for up to 1 h without experiencing other than mild, transient adverse health effects or without perceiving a clearly defined objectionable odor	na	3	5	0.1	1

Guidelines (ERPG). These are expressed in terms of three limit levels, two of which are relevant to survival in emergencies such as fires:

ERPG-3: maximum levels designed to prevent death

ERPG-2: maximum levels below which nearly all individuals could be exposed for up to 1 h without experiencing or developing irreversible or other serious health effects or symptoms that could impair an individual's ability to take protective action

For irritant gases, there are two issues: concentrations at which individuals are likely to experience serious health effects or symptoms likely to impair escape or ability to take protective action, and exposure doses that might cause life-threatening health effects. For example, with respect to hydrogen chloride:

ERPG-2 set at 20 ppm on the basis that $>20 < 100$ ppm would be expected to cause serious eye and respiratory tract irritation (which might impair an individual's ability to take protective action). This reflects the immediate effect of exposure concentration.

ERPG-3 set at 100 ppm on the basis that exposure exceeding this level for 1 h may be expected to produce severe health effects such as pulmonary edema and possibly death in a heterogeneous human population. This reflects the effect of an exposure dose. The same principle applies to the other irritant gases.

In the context of ability to escape from a fire, the ERPG-2 level would, therefore, represent the appropriate tenability limit. This limit is, in fact, an order of magnitude more stringent than the design tenability limit proposed here for fire engineering design. Although 20 ppm HCl would be sufficiently irritant to adversely affect most people, it is unlikely that such low concentrations would seriously inhibit the ability of most people to perform the actions necessary to escape from a fire. On this basis, the higher concentration of 200 ppm is proposed as a tenability limit for the average person, although it is likely that a proportion of the population might suffer some degree of impairment at lower concentrations as indicated in Fig. 62.17. Table 62.13 shows the ERPG levels for some sensory irritants commonly occurring in fire atmospheres [88].

A more recent set of emergency guidelines has been published between 2004 and 2006 by the U.S. Environmental Protection Agency under the AEGL scheme (Acute Exposure Guideline Levels of Hazardous Substances) [89]. The Acute Exposures Guidelines (AEGL) provide guidance for the assessment of likely acute effects of human exposures a range of individual substances likely to be released during industrial accidents, including a range of irritant gases occurring in combustion product mixtures. These are very useful because the documentation

Table 62.14 Acute Exposure Guideline Levels of hazardous substances (AEGL)

AEGL-1 is the airborne concentration of a substance above which it is predicted that the general population, including susceptible individuals, could experience notable discomfort, irritation, or certain asymptomatic nonsensory effects. However, the effects are not disabling and are transient and reversible upon cessation of exposure
AEGL-2 is the airborne concentration of a substance above which it is predicted that the general population, including susceptible individuals, could experience irreversible or other serious, long-lasting adverse health effects or an impaired ability to escape
AEGL-3 is the airborne concentration of a substance above which it is predicted that the general population, including susceptible individuals, could experience life-threatening adverse health effects or death

Table 62.15 AEGL2 limit concentrations for different exposure periods

Exposure period (hours)/	0.167	0.5	1	4	8
Substance					
HCl	100	43	22	11	11
HBr	100	43	22	11	11
HF	95	34	24	12	12
NO_2	20	15	12	8.2	6.7
SO_2	0.75	0.75	0.75	0.75	0.75
Formaldehyde	14	14	14	14	14
Acrolein	0.44	0.18	0.1	0.1	0.1

includes detailed review of available toxicity data from both human and animal studies, with carefully justified opinion on extrapolation between and within species and application to the choice of guideline ceiling levels for exposure periods from 10 min to 8 h. The AEGL guideline levels (Table 62.14) are for three endpoints in exposed humans as follows:

For application to combustion product exposures all three levels are relevant for different exposure assessment situations For relation to potential lethal levels the AEGL1 values are most relevant, while for effects on escape capability the AEGL2 levels are most applicable. The AEGL 3 values may be relevant to assessment of minor health effects from acute exposures. The AEGL2 levels for some irritant fire gases are shown in Table 62.15.

AEG-1 and AEGL-2 make use of low level human exposure physiological signs and animal toxicity data, especially histopathological changes to the respiratory tract. For sensory irritancy use is made of human experience and mouse RD_{50} data, on the basis that such effects are not dose-related, but concentration-related and maintained. The concentration predicted to cause significant sensory irritancy therefore sets a ceiling on the exposure levels over the entire range of exposure periods from 0 min to 8 h. Where significant pathological effects are reported at lower exposure concentrations (or exposure doses) for different exposure periods these are applied to reduce the ceiling exposure concentrations for longer exposure periods.

For the AEGL-1 levels some form of $C^n t$ relationship is the main basis for setting the ceiling concentrations for the different exposure times. The most reliable animal data are usually obtained using 4-h exposure periods, although this is rather long for most fire incidents, for which the 10 and 30 min exposure periods are most relevant.

The AEGL-2 levels (the level above which irreversible health effects and impaired escape ability are predicted) for irritant gases for an exposure time of up to 10 min (a time period considered more relevant to escape from fires) are somewhat higher than the ERPG-2 levels but are more stringent than the levels proposed in the left-hand column of Table 62.12 (except for formaldehyde).

For smoke atmospheres containing significant concentrations of the acid gases and organic irritants it is also important in the application of egress calculations to consider the effects on the walking speed of escaping occupants at concentrations below those in the right-hand column of Table 62.12. Between zero and the concentration causing incapacitation there will be a relationship between the irritancy of the smoke and walking speed (as demonstrated by Jin [84]). In order to provide some indication of possible effects on walking speed between these limits, an expression has been developed for any irritant based on the concentration estimated to be very painfully irritant [90]. Details of the derivation and application of this expression to walking speed calculations for occupants escaping in irritant smoke is presented in Chap. 63.

The other important effect of irritants is that a proportion of those inhaled penetrate into the deep lung. If a sufficient dose is inhaled over a period of time, a lung inflammatory response can occur, usually some hours after exposure. The deep-lung effects of irritants may be increased by the presence of smoke particulates, which may cause respiratory failure and death or permanent lung damage in survivors. The 30-min exposure doses (30-min exposure LC_{50} concentrations multiplied by 30) likely to be lethal for each irritant gas are as shown in Table 62.16.

The effects depend on the exposure dose, which can be quantified approximately in terms of the product of concentration (c) and exposure time (t) to give the ct product exposure dose (ppm·min). During a fire, when the concentrations of the toxic products vary with time, it is possible to predict when an incapacitating or lethal dose has been received by using the FED method. For this method the ct product doses for small periods of time during the fire are expressed as a fraction of the dose causing a toxic effect, and these FEDs are summed until the fraction reaches unity, when the toxic effect is predicted. The fraction of a lethal dose (FLD) for each irritant is calculated as the ct product exposure dose during a period in the fire (e.g., in ppm·min) expressed as a fraction of the lethal exposure dose. The lethal effects of the different irritants are assumed to be additive on the same basis as the irritant effects, so that the total FLD_{irr} for each time period is given by Equation 62.6:

Table 62.16 Lethal exposure doses of irritants contributing to asphyxia and lung damage [27]

Gas	Exposure doses predicted to be lethal to half the population (ppm·min)
HCl	114,000
HBr	114,000
HF	87,000
SO_2	12,000
NO_2	1900
CH_2CHO (acrolein)[a]	4500
HCHO (formaldehyde)[a]	22,500

[a]Where the concentrations of acrolein and formaldehyde (or other important irritants) are unknown, a term derived from smoke density and time of 90 OD/m·min may be used as an indication of lethal organic irritant exposure dose

$$FLD_{irr} = FLD_{HCl} + FLD_{HBr} + FLD_{HF} + FLD_{SO_2} + FLD_{NO_2} + FLD_{CH_2CHO} + FLD_{HCHO} + \sum FLD_x \quad (62.6)$$

where $\Sigma FLD_x = FLDS$ for any other irritants present.

The FLD_{irr} for short periods of time during the fire are summed until the FLD_{irr} reaches unity, when it is predicted that a lethal dose has been inhaled.

The application of this expression to calculation of lung inflammation hazards to humans for fire hazard analysis is presented in Chap. 63.

Incapacitating and Lethal Effects of Asphyxiant Fire Gases

The effects of asphyxiant fire gases are not instantaneous as with sensory irritant, but develop when a sufficient dose has been inhaled. The main asphyxiant gases in fire effluents are

CO and HCN. The effects of these gases, consisting of tissue hypoxia are additive, and combine to some extent with direct low oxygen hypoxia. Carbon dioxide increases the rate of uptake of CO and HCN, and itself causes narcosis after a few minutes inhalation at concentrations above approximately 7 $\%CO_2$. The combined effect of exposure to these gases is to cause incapacitation (loss of consciousness) during exposure above a critical dose threshold. After a further few minutes as inhalation continues this is followed by death from respiratory and cardiac arrest. The effects of exposure to these gases individually and in fire effluent mixtures on exposed humans and animals has been described earlier in this chapter, with details of the derivation of an FED hazard assessment calculation method for application to humans described in Chap. 63.

The derivation and validation of lethality FED calculation methods for application to small-scale toxicity test data has been described in a previous section of this chapter. These include terms for the lethal toxic exposure doses (30-min exposure period) for CO and HCN, which are added to the lethal exposure doses of the irritant substances present. For lethal mass loss concentrations of fire effluents in small scale tests the asphyxiant gases are found to cause incapacitation and death mostly during or within a hour after the end of an exposure. The irritants mainly cause death by lung inflammation some hours or days after the end of the exposure. As described earlier in this chapter, a lethality expression treating the lethal effects of asphyxiants and irritants as directly additive provides a good prediction of measure rat lethality. This raises the question of the extent to which asphyxiants and irritants are acting independently and sequentially to provide the overall measure lethality, or the extent to which their effects are overall interactive both during and after exposure. Experiments in which deaths are only during and immediately after exposure (as opposed to during exposure and up to 14 days after), show a somewhat reduced effect from the irritants, but still more than would be predicted from the effects of the asphyxiants alone. Further information on rodent lethality interactions and calculation models can be obtained from the following references [6, 10, 40, 44–46, 72].

The Use of Small-Scale Combustion Product Toxicity Tests for Estimating Toxic Potency and Toxic Hazard in Fires

Applications of Small-Scale Toxicity Test Data

Small-scale toxicity tests of different kinds are used for the following main applications:

1. For the development of FED expressions such as those presented in Chap. 63, for application to time to incapacitation (ASET) engineering calculations using full-scale fire data
2. For application to simplified mass loss FED lethal toxicity ASET calculations
3. For measurement of yield data for the main toxic fire gases from burning fuels for application to ASET engineering calculations (for calculating time-concentration curves for each toxic gas during compartment fires)
4. For product specification purposes—particularly for transport applications

Development of FED Expressions Historically, a number of bench-scale combustion furnaces have been used to generate thermal decomposition and combustion product atmospheres from a range of materials and products. Using a combination of chemical measurements of atmosphere composition with animal exposures, it has been possible to establish that the main incapacitating and lethal effects of exposure to fire atmospheres are due to a limited set of toxic gases and to determine their combined effects in fire effluent mixtures [10, 17]. These and other data from human and animal exposures to individual toxic gases and gas mixtures have been used to develop the FED (Fractional Effective Dose) expressions presented in this chapter and in ISO 13571[4] The expressions are used with time-

concentration curve data for full-scale fires (obtained from fire modeling calculations or full-scale fire tests) in order to calculate time to incapacitation (ASET) or time to lethal exposures. The animal experiments have also been useful to identify cases in which unusual toxic effects are present and for the development of methods for handling such effects in performance-based applications. These aspects have been discussed as appropriate throughout this chapter and Chap. 63.

Mass Loss FED A method whereby small-scale toxicity test data can be applied directly to FSE calculations, as an alternative to the use of the individual gas FED expressions, is the mass loss toxicity method. For this method a toxicity endpoint is expressed in terms of a lethal or incapacitating mass loss exposure dose for combustion products from a particular material or product. The mass loss exposure dose with time during a modeled fire or full-scale fire test is then calculated. This method is described here and in ISO 13344,[45] but this approach is rarely used, the individual gas FED method being more widely used for engineering calculations.

Measurement of Toxic Gas Yield Data In order to model the time-concentration curves for toxic gases in full-scale fires it is necessary to establish the yields of the main toxic gases under a range of combustion conditions. Although it is not possible in small-scale tests to reproduce the dynamics of fire growth in full-scale compartment fires or the detailed temporal and spatial variations in fuel exposure and combustion conditions, small-scale methods in combination with large-scale experiments are proving increasingly useful in establishing the relationship between combustion conditions and toxic product yields [13, 38, 39, 66, 69, 90–92]. In particular, it has been established that the yields of key toxic products (especially carbon monoxide, hydrogen cyanide, smoke particulates, and organic irritants) vary considerably with combustion conditions and particularly in the following:

- Flaming or nonflaming decomposition
- For flaming fires the fuel/air equivalence ratio (or mixture fraction)
- Temperature in the combustion zone and upper layer and to some extent oxygen concentration
- Presence of flame-retardant elements active in the gas phase, especially halogenated flame-retardants

Full-scale fires can be classified into four main types or stages in terms of the combustion conditions, which can be replicated in small-scale apparatus. The main types are non-flaming fires, well-ventilated flaming fires, and ventilation-controlled (underventilated) pre-flashover or post-flashover fires with vitiated combustion conditions (see Table 62.23). Two small-scale test methods have been developed that can test materials or products under a range of fuel-air equivalence ratios for the measurement of toxic gas yields. These are the ASTM flammability apparatus, which is described in detail in Tewarson [2], and the BRE tube furnace method [12, 93], which is a British Standard [94] and an ISO Technical Specification [11] and is described later in this section. The tube furnace method has been developed specifically to measure toxic product yield data for application to FSE calculations. It is capable of addressing the combustion conditions in all four fire stages and for flaming fires to generate toxic product yield data as a function of equivalence ratio and temperature. Yield data for a variety of materials over a range of combustion conditions (expressed as a function of equivalence ratio) have shown a good agreement with data from the ASTM flammability apparatus and from large-scale compartment fires [66, 90]. Data obtained using the ASTM flammability apparatus for different materials are presented in Khan Chap. 36 [2] and some tube furnace data are presented later in this section.

Product Specification A number of small-scale toxicity test methods are in use to produce toxicity data for product specification purposes (mainly for transport applications). These test methods generally use small-scale combustion devices for the generation of thermal-decomposition products, with measurement of the concentrations of a specified list of toxic gases. The toxic gas data are input to a specified calculation method in order to generate a toxicity index, usually based on immediately dangerous

to life or health (IDLH) limits for individual toxic gases. The use of materials or products for specific applications is then based on a specified toxicity index score.

The most commonly used methods are the French tube furnace method (NFX 70-100-1) [95] and the E662 smoke box method [96] using the cone heater (in ISO 5659-2) [97] and IMO or Airbus Industries smoke toxicity test procedure [98, 99]. This smoke box is an area-based method designed to generate smoke optical density and toxic gas concentration data for qualification of materials. These methods are considered of limited use for application to FSE calculations because they are generally based on primitive combustion scenarios in which the combustion conditions are undefined and cannot be readily related to those in full-scale fires. Similarly, the toxicity indices consist of simplistic endpoints using additive models that may not be predictive of incapacitation during fires. (See BS 6853 [100] for applications of the NFX and E662 methods to railway passenger trains.)

Essential Criteria for Test Methods

The evolution of toxic products in large-scale fires is determined essentially by two sets of parameters.

One set of parameters relates to the large-scale structure and development of fire scenarios that determine the growth and spread of the fire, the decomposition conditions under which products are formed, and their rate of evolution. It is not possible to replicate ("model") these features in a single physical small-scale test, although they are the most important factors determining the toxic hazard in a fire. This is the main reason why it has not been possible for experts to agree on standard bench or intermediate scale test methods suitable for regulatory control of materials or products in terms of "toxicity" or "toxic hazard". These parameters need to be measured directly in a full-scale compartment fire test with appropriate boundary conditions, or calculated using a computational fire dynamics model using appropriate input data for the necessary combustion properties of the fuel and compartment.

The other set of parameters that contributes to the determination of toxic hazard and that can be replicated using small-scale fire tests (albeit only in a general way) is the set of thermal decomposition conditions encountered by materials at different stages, in different locations or in different types of fires. Basically, the thermal decomposition products given off by any material depend on the temperature and oxygen supply to which it is subjected and whether it is flaming or nonflaming. Although it is possible to identify a number of subsets, there are three basic thermal decomposition conditions, namely:

1. Nonflaming oxidative/smoldering decomposition at midrange temperatures
2. Flaming decomposition in a local environment at midrange temperatures, ranging from well-ventilated flaming (equivalence ratio <1) to vitiated flaming (equivalence ratio >1)
3. High-temperature/low-oxygen vitiated conditions encountered in fully developed or post-flashover fires (equivalence ratio >1)

If it can be demonstrated that a particular small-scale test method can replicate one or more of these conditions, then it has the potential, if used with a suitable bioassay procedure and/or measurements of chemical product yields, to produce toxicity information that can be used as one item in a toxic hazard evaluation. To produce such information, a number of essential test criteria must be fulfilled.

1. The most important criterion for any small-scale fire model is that it should be capable of producing atmospheres with broadly similar compositions to those formed in one or more of the basic stages of a full-scale fire.
2. Following from this, it is essential that measurements should be made of the temperature and/or radiant flux to which the sample is subjected, the air-fuel ratio, the smoke optical density, and whether the sample is flaming or nonflaming. The chemical composition of the atmosphere must also be characterized as fully as possible, the minimum being in terms of CO, CO_2 (with calculation of the CO_2 to CO ratio), O_2, and HCN (if the material

contains nitrogen), or hydrogen halides (if F, Cl, or Br is present) and the effective heat of combustion. These measurements are important for two reasons: first, because they define whether one of the basic fire conditions is being adequately simulated; and second, because they should enable the key products responsible for the animal toxicity to be identified, or at least make it possible to decide if unusual toxic products are present.

The time/concentration profiles of the key toxic products can then be measured in large-scale fire tests, or predicted by mathematical fire modeling. Estimates of likely toxic hazard in realistic fire scenarios can then be attempted.

If possible, a fuller product analysis including GC-MS measurements of the profiles of organic products should be made for more accurate correlations with the observed toxicity. In addition, comprehensive measurements of product composition in small-scale tests enable comparisons to be made with product profiles in large-scale fire tests and a judgment of how well the small-scale decompositions are able to reproduce the chemical "cocktails" present in different large-scale fire conditions [18].

3. The bioassay method must be capable of detecting and measuring the particular types of toxic effects experienced by human fire victims. It must also be possible to make a reasonable extrapolation from the toxic effects in the animal model to those likely to occur in humans. It is, therefore, essential to determine both the qualitative and quantitative aspects of toxicity and the time during or after exposure when they occur. People in fires experience incapacitating effects that may crucially impair their ability to escape, causing them to remain in the fire to be killed later by heat or CO, so a simple body count (LC_{50}) animal test without any description of pre-terminal toxicity is of very limited usefulness for input to toxic hazard models.
4. Some estimate of dose must be made. This estimate should be reported in terms of concentration and duration of exposure as mass charged and mass consumed of material per liter of diluent air and concentrations of basic toxic products as described previously. By carrying out tests at different concentrations, estimates should then be made of dose/time/response relationships.

Practical Methods for Toxic Hazard Assessment

There are essentially two ways in which toxic hazard in fire can be assessed.

1. From large-scale fire tests (or computer fire models) that include measurements (or predictions) of the concentration/time profiles of the major toxic gases and existing knowledge of the toxic effects of these gases
2. From a battery of small-scale tests and mathematical models or simple large-scale tests. The essential components are the following:
   (a) The toxic potency data for materials (lethal mass loss exposure dose [$g \cdot m^{-3} \cdot min$]) obtained from small-scale tests using animal exposures or analytical methods
   (b) The mass loss/concentration curve for the fire

Of these, full-scale simulations and large-scale tests are the most valuable, since they enable the first two major parameters (fire growth and product yield) to be measured directly. For the third parameter (toxicity), an algorithm for calculating times to incapacitation and death for humans from toxic gases, heat, and smoke obscuration from large-scale fire data has been developed and presented in Chap. 63, while simplified versions are presented in ISO/IEC TR 9122-5 [101], 1357 [1, 4] and 13344 [45]. Full-scale tests are already in use for a number of purposes (such as the furniture calorimeter and room calorimeter used for heat release measurements). With the addition of a few simple gas measurements, they can be extended to provide the data for full-scale hazard assessment of compartment fire scenarios with similar boundary conditions. Although the use of full-scale tests for regulating

fire performance has been criticized on grounds of cost, this approach has been used successfully in California.

The other notable method is to make use mainly of small-scale test data. Small-scale tests suffer from the difficulty that they are several steps removed from a full-scale fire, so it is important to determine the validity of the parameters measured with respect to real fire conditions.

It has been claimed that some small-scale tests can be used to give a direct indication of the toxic hazard presented by a material in a full-scale fire, including elements of ignitability, fire growth, and toxic potency. The UPITT test and the NIBS test are claimed to be usable in this way to produce hazard rankings for materials. However, small-scale tests cannot successfully model the complex growth and development of a full-scale fire, so such methods are considered invalid. It may, however, be possible to extract a number of characteristics of the fire behavior of a material from a single test protocol and use these as inputs to mathematical models for making hazard assessments. An example is the use of the cone calorimeter for measurement of both heat release and toxic gas yield from a material in early well-ventilated fire scenarios.

Nevertheless, the main job of small-scale toxicity tests is to provide data on yields and toxic *potency* of the combustion products from materials so that the data can be used as input to toxic hazard analysis in conjunction with fire growth data obtained from other sources.

The lethal toxic potency of combustion products from materials can be measured in small-scale tests in terms of the LCt_{50}, the lethal exposure dose to rodents. This is expressed in terms of the mass loss concentration of products (the mass of material decomposed in the test) divided by the volume of air into which they are dispersed (g/m^3) and multiplied by the time for which the animals were exposed to give the exposure dose ($g \cdot m^{-3} \cdot min$). It is possible to quote the toxic potencies of materials in these terms for most small-scale test protocols, so that the results from different tests can be compared directly and so that the data can be used in conjunction with mass loss data from full-scale fire tests or model calculations to make toxic hazard assessments. The toxic hazard presented by the materials in full-scale fires can then be estimated in terms of the time during a fire when a victim will have received a lethal exposure dose, provided that the decomposition conditions in the small-scale test are the same as those in the full-scale fire. This is done by the fractional effective dose (FED) method, in which the mass loss exposure dose generated each minute during the full-scale fire (either measured or calculated) is expressed as a fraction of the lethal mass loss exposure dose for the material, obtained from the small-scale toxicity tests. When the integrated fractions during the fire reach unity, death is predicted. This method has been developed for use in toxic hazard assessments in British Standards [102] and in ISO/IEC standards [4, 101].

Examples of Small-Scale Test Methods

A variety of different methods have been used to generate combustion product atmospheres and evaluate their toxicity using animal exposures, and it is not possible here to describe these methods or the results obtained from them in detail. There are, however, three test methods that were in relatively wide use in the United States and in Europe during the 1970s and 1980—the NBS test method [6, 83], the DIN test method [41, 42, 103] and the University of Pittsburgh test method [82, 98]. An excellent description of these and other methods, and of the results obtained from them, is given in Kaplan et al. [16]. The value of the published results from these methods is that they provide an animal toxicity database for thermal decomposition and combustion products from a wide range of materials, enabling the main mechanisms of fire effluent toxicity to be established and the toxic potencies of effluents from different materials to be quantified. The main limitations of these and other small-scale test methods have been the extent to which the test decomposition conditions replicate those occurring during different types and stages of full-scale fires. A brief description of the principles of these three

methods and their validity in predicting effects of exposure to large-scale fire environments follows. The methods are illustrated diagrammatically in Fig. 62.18.

National Bureau of Standards (NBS) Test Method

The NBS test method [6, 83] is the simplest of the three. The test apparatus consists of a sealed rectangular polymethylmethacrylate chamber (200-L volume) containing a cup furnace set into the floor at one end. The animals (rats) are exposed nose only and placed in restraining tubes that are plugged into the sides of the chamber. Exposures are carried out under nonflaming conditions 25 °C below the ignition temperature of the sample and under flaming conditions 25 °C above the ignition temperature. The sample is placed into the preheated cup with the animals already in position, and they are exposed to the atmosphere in the chamber for 30 min. For this test there is thus an initial period when the concentration of decomposition products in the box increases as the sample decomposes, followed by a period when the atmospheric composition remains relatively constant for the remainder of the exposure. The concentration of products in the chamber is varied by placing different amounts of sample in the cup. This type of method is referred to as a "static" method, since there is no forced airflow over the sample and no ventilation of the chamber. It is possible to characterize the atmosphere approximately in terms of mass charge per liter of air by assuming a constant composition for the duration of the test. The atmosphere also can be characterized in terms of mass loss by weighing the residue after the test or by placing the cup on a load cell. Measurements are also made of the chemical composition of the atmosphere in terms of the principle products. The animal toxicity is usually quoted in terms of the LC_{50} concentration of mass charge/L, but it is also common to monitor the asphyxiant effects on the animals by means of the leg flexion test. Effects on respiration (such as irritant effects) could be monitored if desired.

The main advantage of this method is its simplicity, but it has the disadvantage that there is little control over the decomposition conditions. Another disadvantage is that the composition of the atmosphere does not remain constant, since there is a variable period during which the sample is decomposing, followed by a period when the smoke is aging and some products may condense onto the chamber walls. In tests where the decomposition product atmosphere has been compared to that produced in large-scale tests [18], it has been found that the method gives a reasonably good simulation of the products from a smoldering or nonflaming fire and also of the conditions during the early stages of a flaming fire. However, it was not possible to model the decomposition conditions of a high-temperature, fully developed fire, since when the cup is heated to high temperatures the pyrolysis products tend to escape from the cup before they are fully decomposed. In general, it should therefore be possible to use data from this method as one item in a toxic hazard assessment for nonflaming or early flaming fires.

University of Pittsburgh Test Method

In this method [98] the sample is also heated statically in a cylindrical furnace (early versions of the test used a tube furnace). However, in this case a flow of air is maintained over the sample and then mixed with diluent air before being passed through the animal (mouse) exposure chamber. In this way fresh products are continually passed to the animals under dynamic airflow conditions as they are generated over a 30-min exposure period. The unique feature of this method is that the sample is not maintained at a constant temperature but is heated by means of a ramped temperature profile, the temperature increasing at 20 °C/min. The animal exposure starts when the sample begins to decompose and lose weight as indicated by a load cell. The mice are exposed in the head-only configuration, as with the NBS method. In the University of Pittsburgh method the composition of the atmosphere changes continuously throughout the

a

University of Pittsburg apparatus

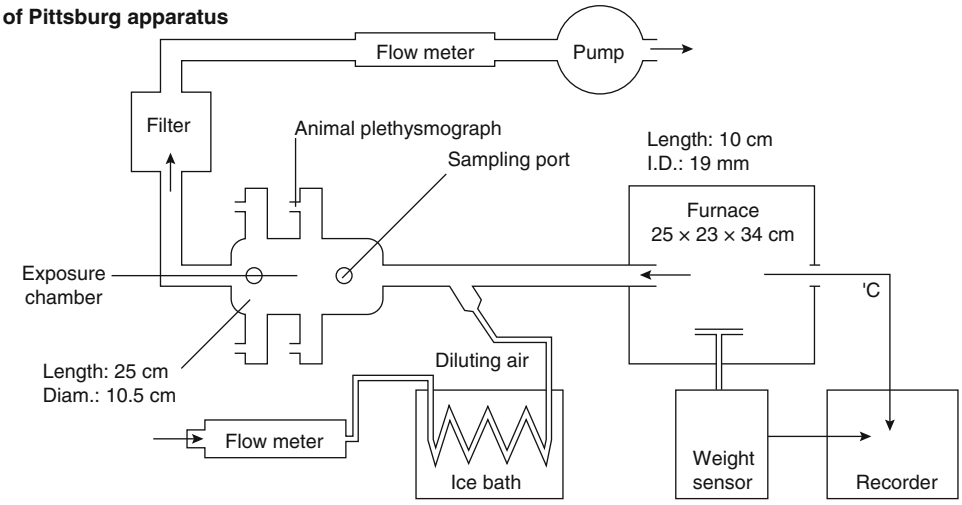

b

National Bureau of Standards (NBS) apparatus.[6]

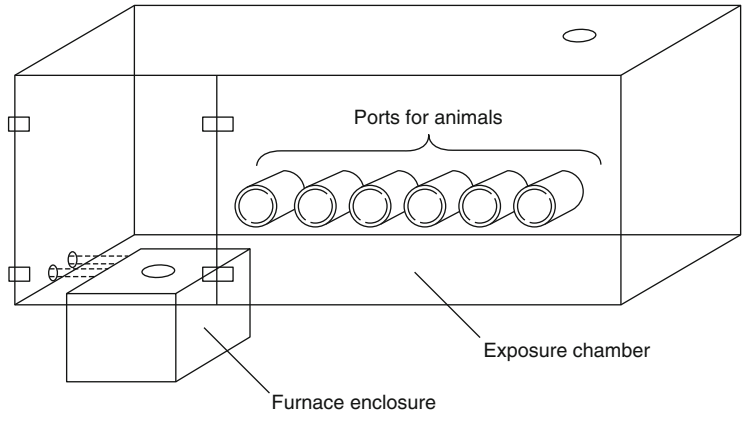

c

DIN53436 apparatus.[166]

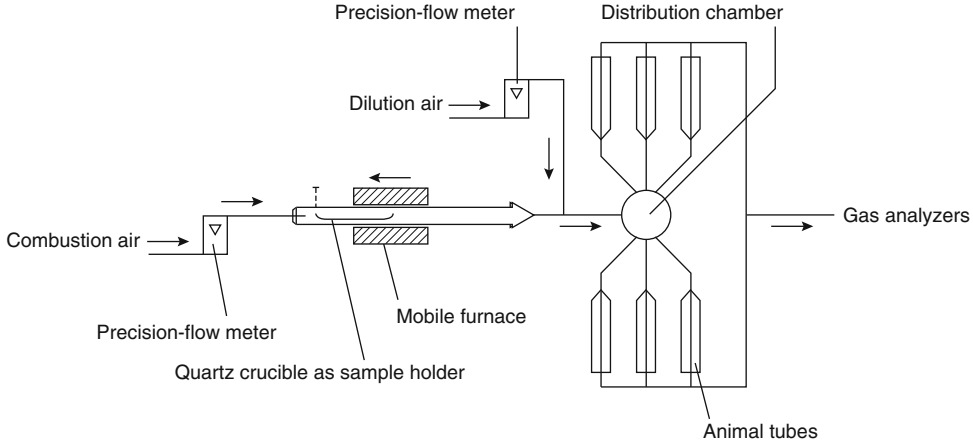

Fig. 62.18 Laboratory-scale combustion toxicity test methods

30-min animal exposure, and the atmosphere usually changes from nonflaming to flaming at some stage. The concentration of the decomposition products can be varied by changing the mass of material placed in the furnace (although presumably this could also be achieved by altering the flow of diluent air). It is possible to measure the changing profile of products to which the animals are exposed throughout the test and also to monitor toxic effects such as asphyxia or irritancy, mainly from recordings of respiratory pattern. However, in its more recent application, the results of the test are usually expressed in terms of the LC_{50} in grams of material charged, which is used to rank different materials.

The main advantage of this method is that it theoretically covers a number of different decomposition conditions within a single test run, ranging from low-temperature nonflaming to high-temperature flaming. It is also said that this situation mimics the conditions in a real fire where materials begin by being cold and are then heated up until they pyrolize and eventually flame. A feature of the test is that the time-temperature increase taken from the start of the decomposition run to the occurrence of the evolution of smoke, toxic effects, and flaming may be used as criteria for judging materials. Thus a material that flames early or produces smoke early may be judged more hazardous than one that does not start to decompose until a high temperature is attained.

Although ramped heating of a sample may provide a useful model for the specific situation where a material is subjected to a slowly rising temperature, it cannot be said to mimic the changing conditions in a fire. In a fire, a material or its immediate pyrolysis products may be subjected to any of a variety of conditions of temperature or oxygen supply under nonflaming or flaming conditions, and the way in which these conditions change is governed by the nature of the large-scale fire scenario. In order to model these various conditions, it is necessary to subject separate samples of test material to a range of different temperatures (or radiant fluxes) and oxygen supplies. The main problem with ramped heating of a sample is that it does not submit the whole material to the necessary range of conditions, since it causes fractional decomposition of the material. Products evolved at relatively low temperatures will not, therefore, be present at a later stage to be involved in flame; neither will they be subjected to high temperatures, since they will have left the furnace before higher temperatures are achieved. This may have a profound effect on the kind of products evolved and, hence, the toxicity.

Another disadvantage of this test method is the difficulty of characterizing dose, since the composition of the atmosphere changes throughout the test. For comparison with other methods, it would be possible to calculate a very approximate nominal atmospheric concentration in terms of mass charged/L if it is assumed that the decomposition averages out over the duration of the test. A better estimate may be made of the atmosphere concentration in terms of mass loss/L if the mass loss as measured by a load cell is integrated over the exposure period. This might give a reasonable measure of dose to enable an LC_{50} to be calculated, but other estimates of toxicity are complicated by the changing nature of the atmosphere. Thus, if death or asphyxia were to occur at 30 min, for example, it is not possible to determine whether this would be due to the delayed effect of a product evolved at 5 min or an immediate effect of a product from 29 min.

There are thus some difficulties with this method, both as a fire model and as a toxicity assay. But, if the method is backed by a full profile of material mass loss and product concentrations, plus qualitative and quantitative estimates of toxic effects throughout and after the exposure, it may be possible to apply the data in certain special situations.

German DIN 53 436 Test Method

This method [41, 42, 103] was used in both the United States and in Europe. It is still in occasional use, although usually in analytical mode only (without animal exposures). It employs a fully dynamic system in that fresh material is decomposed at a constant rate throughout the

test and fresh atmosphere is supplied continuously to the animals. The method has been used with rats, mice, and primates, rats being the principal test animals. The principle of the method is that a strip of test material is placed in a silica tube under a current of air (or nitrogen for studies of pyrolysis) and a traveling annular furnace is moved along the outside of the tube at a constant rate, thereby continuously decomposing the sample. The products are expelled from the silica tube, whereupon they are mixed with diluent air and passed through the animal exposure chamber for 30 min. The rats are exposed in the head-only manner as with the other methods. The sample weight and volume, the primary air supply to the sample, the diluent air, the decomposition temperature, and the concentrations of products in the exposure chamber are measured. The test may be repeated over a range of temperatures under nonflaming or flaming conditions, and the concentration of the products is varied principally by changing the diluent airflow. This has the advantage that the decomposition conditions remain constant as the product concentration is changed, which is not necessarily the case with the other two methods. However, it is also possible to change the product concentration by altering the furnace load, if necessary. The animal toxicity is usually reported in terms of the LC_{50}, which is expressed in terms of mass charged (mass entering the furnace/min)/L diluent air. It is also possible to calculate the concentration in terms of mass loss from the mass of residue remaining after the test run, since the rate of decomposition is constant. Sometimes the results are expressed in terms of the volume of material consumed. In addition, it is possible to monitor the toxic effects on the animals during and after the test as with the other methods.

The great advantage of this method is its versatility, and in theory it the apparatus could be used to model any of the four basic fire conditions: nonflaming, well-ventilated flaming, underventilated-flaming and high temperature post-flashover, as well as variations on them. It is also possible to carry out static ramped temperature decompositions similar to the Pittsburgh method, if required. In practice the method has been found to provide a good correlation with large-scale nonflaming decomposition conditions, and at high temperatures it provides a reasonable model for the conditions of a fully developed flaming or nonflaming fire (high temperature—low oxygen) [18]. However, under standard conditions it does not provide a good model for an early flaming fire (which is reasonably modeled by the NBS method) as the oxygen concentration in the furnace tube tends to be low. Another problem is that the flame tends to travel along the sample more rapidly than the furnace, giving an uneven decomposition. These problems can be overcome by varying the fuel-to-air ratio in the furnace tube and by altering the rate of travel of the furnace.

On balance, the DIN method is reasonably good, and the data obtained could be applied to a number of stages of a fire as one item in a hazard assessment. However, like all small-scale tests it cannot mimic the changing and developing conditions of a large-scale fire; neither can it test materials or objects in their end-use configuration, all of which can have an enormous impact on a developing toxic hazard.

Second-Generation Test Methods

Since these small-scale test methods were developed, there has been considerable progress in understanding of how toxic hazard develops in fires and in particular that hazard depends to a large extent on the general fire properties of materials (in terms of ignitibility, flame spread, rate of fire growth, and smoke evolution), as well as the specific toxicity of the combustion products. Also, critical examination of the fire models used for toxicity test methods (and for small-scale tests for other fire properties such as smoke) has led to the recognition that the models are somewhat inadequate, particularly for the main fire condition of flaming. Another difficulty is that toxicity data are of little value unless they can be related to a range of physical and chemical parameters necessary to characterize the thermal decomposition process, as described in the previous section of this chapter.

There is, therefore, a case for arguing that for many material-based fire properties, a good small-scale test method depends on a decomposition model that can be convincingly related to the essential features of large-scale decomposition conditions. If such a model could be developed, it could be used to measure simultaneously a number of material-based fire performance parameters ranging from ease of ignition, through growth and heat release characteristics, to smoke and toxicity.

A second generation of small-scale fire test methods is being developed, incorporating, hopefully, some of the best features of existing methods and designed to measure a range of parameters.

Cone Calorimeter A second-generation small-scale test method is the NIST cone calorimeter, [104] which has been developed primarily as a heat release apparatus but which also offers the possibility of measuring ignitibility, smoke evolution, and toxicity. This not only enables a range of parameters to be measured simultaneously but also enables the separate parameters to be related, hopefully providing a more comprehensive data set for comparison with, and inputs for modeling of, large-scale fire conditions.

In practice, although useful for measuring reaction-to-fire properties such as ignitability and heat release rate. the cone calorimeter has not proved to be very suitable for measuring toxic potency. It is capable only of reproducing the decomposition conditions in very well-ventilated fires, and the products are subjected to a very large dilution, so that measurement of toxic species is difficult. Attempts are being made to enlarge the range of fire types and stages addressed by modification of the apparatus (vitiated cone), but so far with limited success.

NIST Radiant Method A second-generation version of the NABS cup furnace method has been developed in which the cup furnace was replaced by a radiant panel heater unit. This method has been developed to address the conditions in postflashover fires, but as with the cup furnace version and the cone calorimeter, the combustion process tends to be too well ventilated to reproduce the conditions typical of these fires, which are usually rather vitiated. For further details see Babrauskas et al. [40].

ISO TS19700 Tube Furnace Method [12, 13] The most recently developed method intended to address some of the deficiencies of older methods is a tube furnace method based on the same concept as the DIN tube furnace method. The method employs a strip of sample being advanced through a standard tube furnace under a stream of air (Fig. 62.19). The products are expelled into a

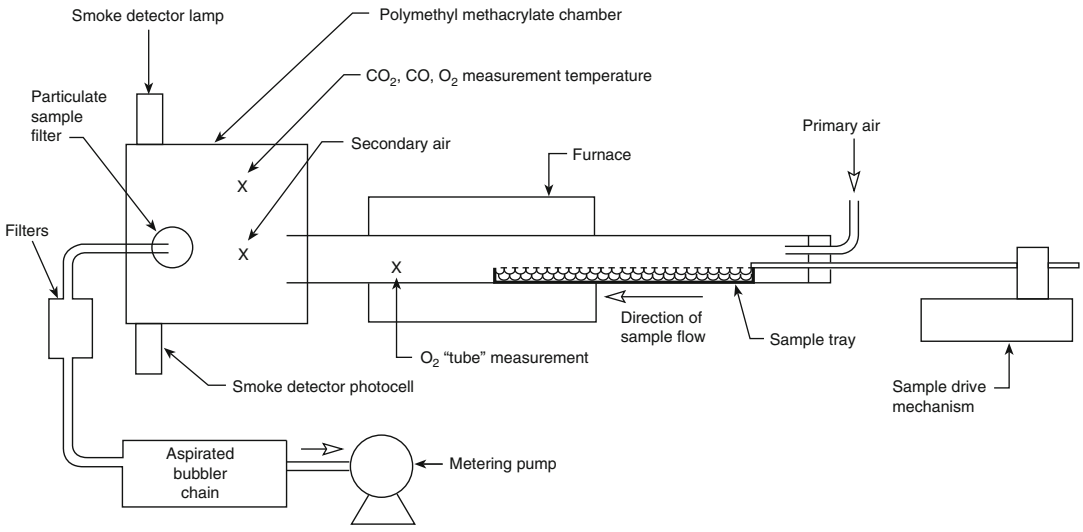

Fig. 62.19 Improved tube test method

Table 62.17 Composition of test materials

Material	Stoich. O_2 demand g/g	Elemental composition (%) C	H	O	N	Cl	Br	P	S	Other
CM flexible polyurethane FR	1.87	56.45	7.67	21.1[a]	8.22	2.53				
Polyisocyanurate foam	1.87	63.5	4.98	21.8[a]	6.15	3.56				
PMMA	1.92	59.98	8.05	31.96						
LDPE granules	3.42	85.63	14.37							
PVC (100 %)	1.28	38.44	4.84			56.73				
Nylon 6	2.33	63.68	9.79	14.14	12.4					
Polystyrene granules	3.07	92.26	7.38							
MDF board	1.29	45.55	6.32	42.44[a]	3.69	0.62	<0.5			
Wood (Pinus sylvestris)	1.36	46.32	5.80	47.56	0.32					
Plywood board	1.24	49.6	6.1	43.98	0.32					
Acrylic/wool/polyester	1.98	61.4	6.3	15	12.89					
38/38/24 boucle fabric									1.5	
Acrylic/wool/polyester FR	1.66	54.16	5.45	21.76	10.83	0.95	6.09			
Acrylic/wool/polyester									0.76	
52/32/17 velour fabric	1.92	61.3	6.0	19.2	13.6					
Acrylic/wool/polyester	1.23	46.30	4.26	34.0	7.28	<0.3	8.16			5.0 Sb_2O_3
FR Polyacrylonitrile >85 % PAN	2.27	68.1	5.79		26.2					

[a]Oxygen calculated by subtraction

chamber where they are diluted with secondary air, and analytical measurements are made or animals can be exposed nose-only. By using a range of different temperatures and airflow rates it is possible to reproduce all the different fire stages and types defined by ISO (and others), including low-temperature nonflaming oxidative decomposition, well-ventilated flaming, under-ventilated flaming high-temperature under-ventilated (postflashover) flaming decomposition conditions. The method also provides stable flaming conditions, solving the problem of mixed, intermittent periods of flaming and nonflaming common with the original DIN method.

The ISO TS19700 tube furnace method [11–13, 66, 90–94] has been developed specifically to measure the yields of toxic products over the full range of non-flaming thermal decomposition and flaming combustion conditions occurring in fires in order to provide data for input to toxic hazard calculations for full-scale fires [11, 13, 66, 90–94]. Detailed data have been obtained for a range of common polymers [66], for which the polymer types and elemental compositions are shown in Table 62.17. The yields of key toxic gases from a number of polymers measured over a range of combustion conditions (defined in terms of equivalence ratio and temperature) have been have been validated against yield data from the same polymers in large-scale compartment fires. The repeatability and reproducibility of the method have been validated in an international "round robin" study including participating laboratories from the United States, Canada, Sweden and the United Kingdom [13].

For these materials the yields of key toxic products such as CO and HCN (kg product/kg material mass loss) depend on the efficiency of conversion of the fuel carbon to CO and fuel nitrogen to HCN (the recovery fraction) and the proportion of these elements in the base material. Table 62.17 shows the mass percentages of each element in materials tested at the UK Building Research Establishment (BRE) [66]. For combustion conditions under which the materials burned with a flame throughout the test the pattern of yields for all toxic products is illustrated by Fig. 62.20. This shows the relationship between equivalence ratio and CO yield (g/g)

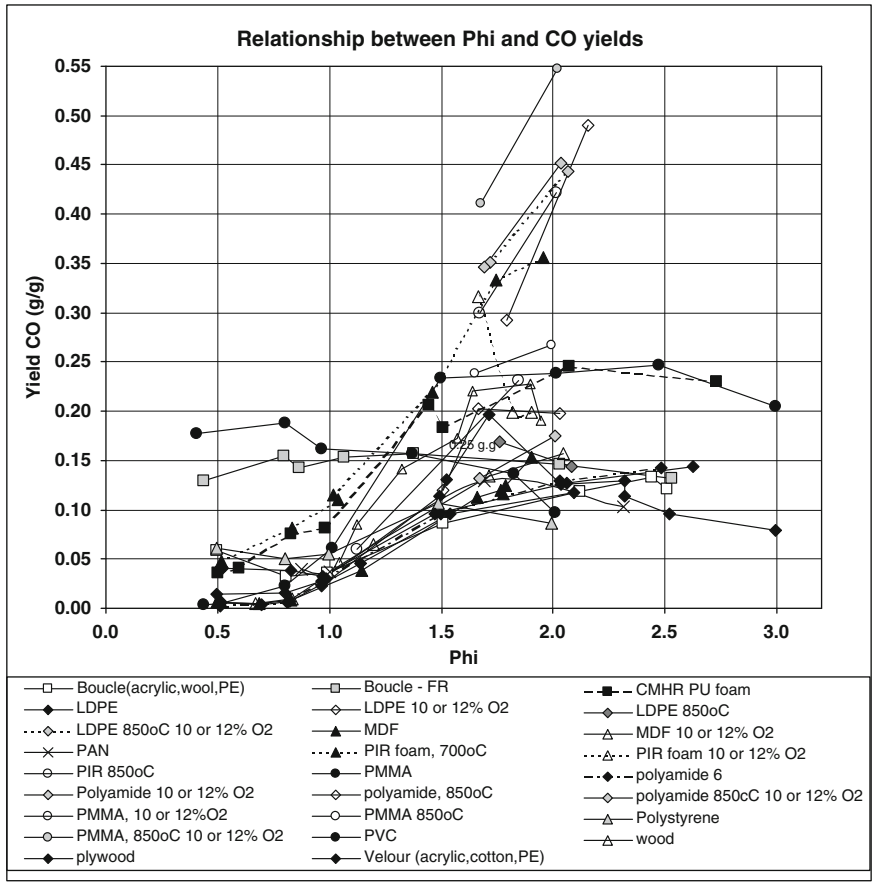

Fig. 62.20 CO yield (g/g) under flaming combustion conditions as a function of equivalence ratio for a range of different polymer types measured using the ISO 19700 tube furnace

for all the materials tested. The basic pattern and yield values are similar to those reported by Khan [2] (See Chap. 36). Under well-ventilated combustion conditions at phi values $< \sim 0.8$ the yields of CO (and other toxic products including particulates, hydrocarbons and HCN) are very low, except for materials containing halogenated fire retardants. There is a sigmoid relationship between equivalence ratio and CO yield in that at around phi values of 1 and above there is a steep increase in CO yield, reaching a plateau at phi values of around 1.5–2.0. Flaming combustion was difficult to sustain at phi levels above approximately 3.0. Most of the results shown in Fig. 62.20 are for a moderate furnace temperature (650 °C) considered to represent the conditions in pre-flashover compartment fires. Under fuel-rich combustion conditions the CO yield depends upon the carbon content of the fuel and the efficiency of conversion of fuel carbon to CO. For aromatic materials (polystyrene) with less efficient combustion, and cellulosic materials (with carbon contents of around 50 %), the yield under fuel rich conditions levels out at around 0.15 g/g, while for aliphatic hydrocarbons and materials such as PMMA somewhat higher yields of around 0.25 g/g fuel mass loss were obtained. For the majority of tests combustion was carried out under a stream of air, but for some tests the same equivalence ratios were obtained at higher flow rates of nitrogen air mixtures (containing 10 % or 12 % oxygen). Under these conditions it was found that some materials produced significantly increased CO

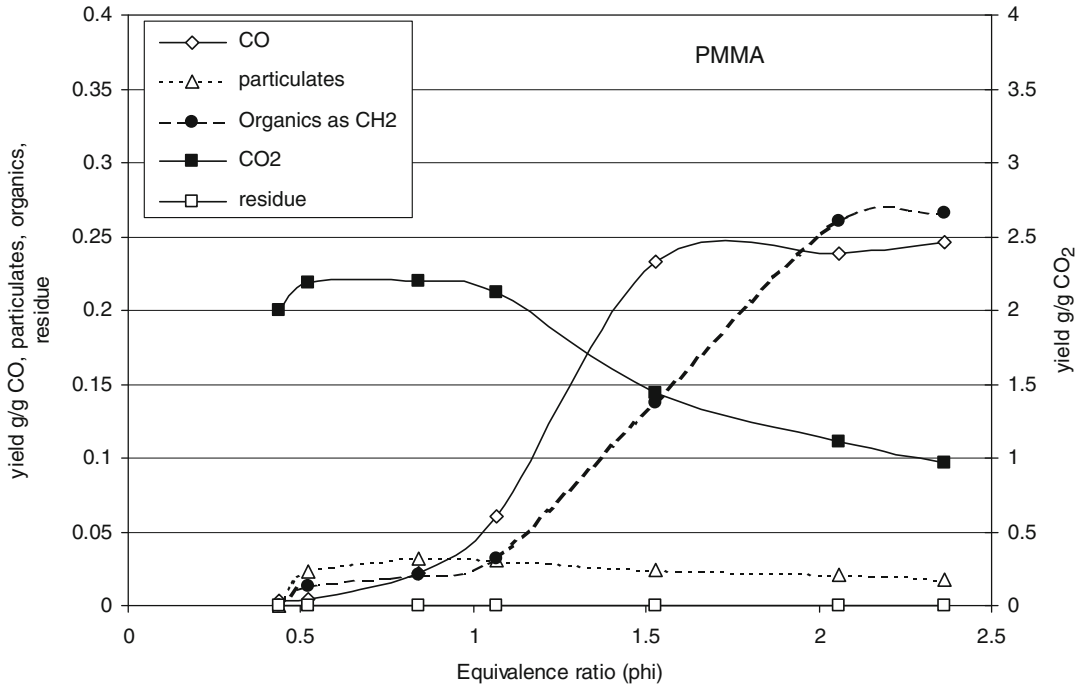

Fig. 62.21 Toxic product yields from a C,H,O polymer (PMMA) under flaming combustion conditions as a function of equivalence ratio (phi) in the ISO TS19700 tube furnace

yields. Higher temperatures (800 °C), also produced somewhat higher CO yields for some materials. Similar variations in CO yields with different oxygen mixtures and temperatures have been observed in compartment fire experiments [1, 27, 31, 70]. For materials with a high halogen content such as PVC, the CO yield remains approximately constant, with inefficient combustion throughout the range of equivalence ratios typical of well-ventilated and under-ventilated fires, and the CO yield tends to be proportional to the halogen content of the fuel [39].

The range of toxic products evolved during flaming combustion fall into three main categories with respect to the relationship between equivalence ratio and yield:

- Products are evolved at approximately constant yields independent of the combustion conditions (mostly halogen acid gases [HF, HCl and HBr]),
- Products for which there is an inverse sigmoid relationship, with yield decreasing as a function of phi are the products of efficient oxidation, comprising mainly CO_2 and water, but also nitrogen oxides (NO and NO_2),
- Products of inefficient combustion with yields increasing as a sigmoid function of equivalence ratio (smoke particulates, partly decomposed organic compounds, CO and HCN)

Figures 62.21, 62.22, and 62.23 illustrate these relationships for thee common polymers: an aliphatic hydrocarbon-based polymer PMMA, a nitrogen-containing polymer polyamide-6 and a polymer with a high halogen content (PVC).

PMMA provides an example of a simple, non-charforming, aliphatic polymer comprised of carbon, hydrogen and oxygen. Under well-ventilated flaming combustion conditions there is no residue and a high yield of CO_2, but at phi values above 1 a large increase in yields of CO, volatile organics and smoke particulates occurs.

For the nitrogen-containing polymer polyamide 6, combustion is also efficient under well-ventilated combustion conditions. A small fraction of the fuel nitrogen is released as NO,

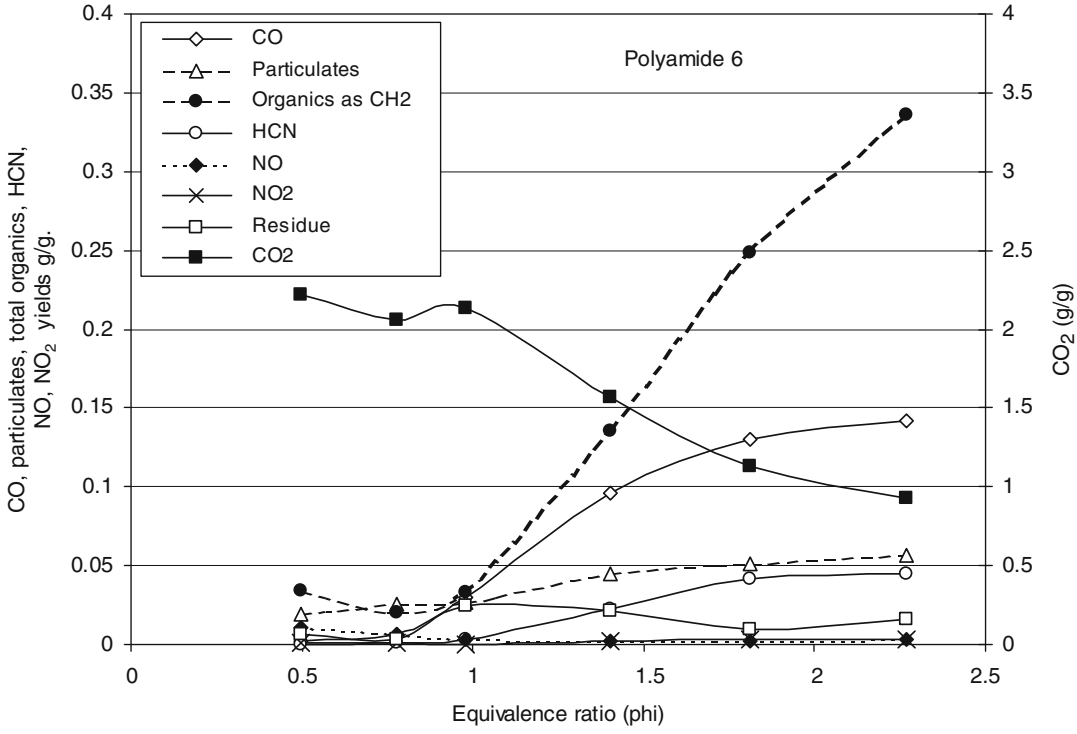

Fig. 62.22 Toxic product yields from a nitrogen-containing polymer (polyamide 6) under flaming combustion conditions as a function of equivalence ratio (phi) in the ISO TS19700 tube furnace

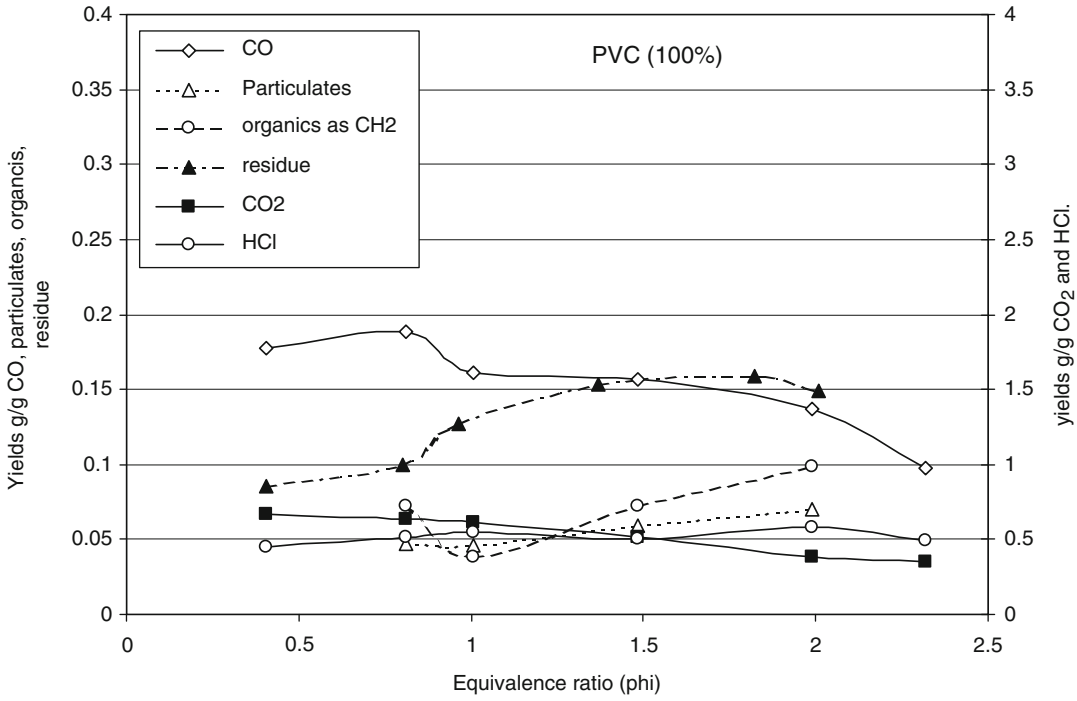

Fig. 62.23 Toxic product yields from a halogen-containing polymer (100 % PVC) under flaming combustion conditions as a function of equivalence ratio (phi) in the ISO TS19700 tube furnace

Table 62.18 Toxic gas yields, effective heats of combustion and oxygen consumption under well-ventilated and under-ventilated combustion conditions for a range of common polymeric materials from the ISO TS19700 tube furnace at 650 °C (PIR 700 °C)

Polymer	phi	Eff Ht KJ/g	CO_2 g/g	CO g/g	HC g/g	O_2 g/g	Soot g/g	SEA m^2/kg	HCN g/g	NO g/g	NO_2 g/g	HCl g/g	HBr g/g	SO_2 g/g
Well ventilated flaming: phi 0.4–0.8														
LDPE	0.49	41.5	2836	15	85	3166	45	268						
Polystyrene	0.49	31.6	2644	61	82	2416	110	621						
Wood	0.51	16.9	1696	6	13	1293	5	12						
Plywood	0.52	17.3	1774	6	11	1324	3	1	0	2	1			
MDF	0.49	16.8	1680	7	24	1283	3	7	0	3	1			
PAN	0.88	30.4	2339	39	54	2320	25	104	8	2	1			
Polyamide 6	0.51	28.4	2216	3	34	2166	19	147	0	11	1			
PIR	0.52	24.6	2340	48	13	1874	33	75	3	2	1	69		
CMHR PU	0.59	25.3	2156	41	48	1928	28	154	4	3	1	9		
Boucle non-FR Acrylic, wool, PE 34/38/24	0.50	24.4	2128	60	19	1861	26	103	1	7	1			12
Boucle FR	0.44	19.3	1486	130	81	1474	90	456	19	8	0	10	30	11
Velour acrylic, cotton, PE 52/31/17	0.52	26.3	2240	41	51	2005	19	84	2	4	0			
PVC	0.40	10.7	667	177	70	815	32	163				447		
Fuel rich (ventilation controlled) flaming phi 1.5–2.0														
LDPE	1.71	29.4	1696	196	334	2242	85	668						
Polystyrene	1.99	21.8	1662	86	299	1664	179	820						
Wood	1.71	9.8	967	134	80	752	19	155						
Plywood	1.54	9.4	986	96	55	714	14	120	0	1	0			
MDF	1.66	8.9	870	113	62	681	19	150	3	1	1			
PAN	1.69	19.1	1271	130	235	1460	60	489	72	2	3			
Polyamide 6	2.03	16.3	1135	130	248	1246	51	413	41	3	3			
PIR	2.08	14.0	937	333	136	1068	72	495	20	1	2	57		
CMHR PU	2.07	14.9	1041	246	197	1134	59	403	14	1	2	5		
Boucle non-FR	2.12	14.2	1138	119	228	1080	104	594	35	1	2			4
Boucle FR	2.03	13.3	920	146	184	1016	100	611	25	2	1	3	28	8
Velour	2.06	14.0	1211	126	239	1071	84	526	34	2	1			
PVC	1.82	7.5	389	137	98	573	70	473				585		

a very small fraction of which is oxidized further to NO_2. At phi levels above 1 the yield of CO_2 and these nitrogen oxides decrease (to very low levels for the nitrogen oxides), while there is a large increase in the yields of CO, HCN, smoke particulates and organics.

The heavily halogenated material PVC shows relatively high yields of all products, both under well-ventilated combustion conditions and throughout the phi range. The HCl yield is constant under all combustion conditions.

Table 62.18 presents the data from all these polymers considered most important for input into fire engineering calculations, which are the toxic product yields under well-ventilated combustion conditions (phi <0.8) and under fuel rich (under-ventilated) combustion conditions (including pre- and post-flashover fires) (phi 1.5–2.0).

Although it is useful to present the yield data directly for each individual polymer, another method is to normalize the data in terms of the

Table 62.19 Generic CO recovery fraction expressions for all materials

CO recovery expression	α	β	k_1	k_2	k_3
Low recovery group minimum	4.7	10.5	0.003	8	12.2
Low recovery group maximum and high recovery group minimum	4.2	17	0.001	12.5	6.3
High recovery group maximum	3.8	19	0.001	12.6	4
PVC	5.0	3.7	0.2	2	8.7
Boucle FR (acrylic, cotton, polyester)	Slope:	0.0019	Intercept:	0.1089	

Table 62.20 Generic HCN recovery fraction expressions for all materials

HCN recovery expression	α	β	k_1	k_2	k_3
Average recovery group (most polymers)	4.5	19	0.01	12.6	6.45
MDF	4.5	16.5	−0.001	12.6	12.5
CMHR polyurethane foam	4	15	0.035	8	16
Boucle FR (acrylic, cotton, polyester)	Slope:	0.017	Intercept:	0.0827	

content of the key element present in the toxic product. The normalized yield then represents the efficiency with which the fuel element is released as the same element in the toxic product (for example the mass fraction of fuel carbon released as carbon in the form of CO or the fraction of fuel nitrogen released in the form of HCN). When expressed in this way the yield curves for different materials collapse into a closer range, so that it becomes more feasible to consider the generic relationship between combustion conditions and toxic product yields for any material (or at least for groups of materials).

For any specific material the yield of any specific toxic product can then be calculated by multiplying the recovery fraction function (or any individual recovery fraction value) by the mass fraction of carbon, nitrogen or other element in the fuel (from the carbon and nitrogen percentages shown in Table 62.17) and a constant representing the mass of the element in the product. For example, the yield of HCN is calculated as:

$$Y_{HCN} = 1.928\, f_{Nfuel} Y_{Nnorm} \tag{62.7}$$

where:

Y_{HCN} = g HCN/g fuel mass loss

f_{Nfuel} = mass fraction of nitrogen in fuel

Y_{Nnorm} = normalized yield: mass of fuel nitrogen recovered as nitrogen in cyanide

1.928 = molar mass HCN/atomic mass N

Table 62.21 Generic organic carbon recovery fraction expressions for all materials

Organic carbon recovery expression	α	β	k_1	k_2	k_3
Low recovery group (cellulosics)	3.5	13	0.015	7	4.7
Medium recovery group (most polymers)	4	34	0.05	18	2.8
High recovery group (LDPE)	4	33	0.05	19	1.9

The sigmoid relationship between the recovery fraction of CO, HCN, organic products, and particulates can be expressed as a Weibull function with the general expression

$$R = k_1 + \left(1 - e^{-(\phi k_2/\beta)^{\alpha}}\right)/k_3 \tag{62.8}$$

where

R = Recovery fraction (e.g., kg carbon in product/kg carbon in fuel mass loss)

ϕ = Equivalence ratio (phi)

α, β, k_1, k_2, and k_3 depend on the specific material (see Tables 62.19, 62.20, 62.21, and 62.22)

Example: yield calculation If R for carbon monoxide for a given fuel at a given ϕ value = 0.1 and proportion of fuel mass as carbon = 0.2, then yield of carbon in the form of carbon monoxide = 0.02. Carbon monoxide mass loss yield

Table 62.22 Generic particulate carbon recovery fraction expressions for all materials

Particulate carbon recovery	α	β	k_1	k_2	k_3
Low recovery group (cellulosics)	3.4	23	0.002	18	27
Medium-low recovery group	8	20	0.037	18	21
Medium-high recovery group	4	33	0.037	19	8
High recovery group	7.6	10.8	0.1	7	10
Fire-retarded group	Slope:	0.0373	Intercept	0.1051	

is then = 0.02 × 28.01/12.01 = 0.047 g CO/g fuel mass loss.

Although the fuel/air equivalence ratio was the main variable affecting the recovery fraction, it was found that for a given ϕ value the conversion efficiency was somewhat higher when materials were decomposed in 10–12 % nitrogen/air mixtures than when decomposed in air. Comparison with large-scale fire tests showed that this condition was likely to be more typical of combustion conditions in more enclosed compartment fires with mixing and recirculation of effluent at low levels, whereas the lower conversion efficiency was more typical of vented fires with fresh air entrainment at low levels in the enclosure but a vitiated upper layer.

Although there were some differences in behavior among individual materials, in terms of the CO recovery fraction, it was possible to classify materials into two main groups:

Low recovery group. Polymers containing only carbon and hydrogen (polystyrene and polyethylene), and some polymers containing some oxygen and nitrogen (boucle and velour fabrics, polyacrylonitrile, and polyamide). These showed low CO recovery fractions under well-ventilated combustion conditions ($\phi < 0.8$) between around 0.01–0.05, increasing to a recovery fraction around 0.08 under vitiated combustion conditions ($\phi > 1.5$). At ϕ values less than 1.5 in 10–12 % oxygen (in air/N_2 mixtures) the recovery fraction increased to 0.15.

High recovery group. Oxygen-containing polymers such as cellulosics, PMMA (polymethylmethacrylate), PU (flexible polyurethane foam), and PIR (polyisocyanurate foam). These also show low CO recovery fractions under well-ventilated combustion conditions ($\phi < 0.8$) between around 0.01–0.05, with the maximum recovery fraction increasing to between 0.16 in air and 0.25 in air/N_2 mixtures.

A third type is the quasi-constant recovery group (materials with a high content of fire-retardant additives acting in the gas phase, such as halogens). Carbon monoxide recoveries from boucle FR, expressed in terms of recovery fraction, were relatively constant at 0.10 across the entire range of ϕ studied. For PVC the recovery fraction was high at low ϕ values and decreased somewhat at higher ϕ values. At low ϕ values (<0.8), for all materials, the CO yield was proportional to the halogen content of the material. For materials containing small amounts of halogen additive the CO recovery increased from less than 0.01 to 0.05 depending on the additive content.

The different expressions for the different recovery behaviors are obtained by using values for the constants shown in Table 62.19 for input to Equation 62.8. For boucle FR a linear expression has been fitted. The slope and intercept are shown in Table 62.19. For PVC the slope is negative, so the plus sign in Equation 49 after k_1 becomes a minus sign.

For nitrogen-containing polymers, the HCN yield depends on the nitrogen content and the recovery fraction of fuel nitrogen as nitrogen in HCN. HCN recovery showed a similar sigmoid relationship with ϕ, being low under well-ventilated conditions. On average the recovery of carbon as CO and nitrogen as HCN was similar at any given ϕ value. In practice some materials gave higher HCN recoveries than others. Table 62.20 gives values for input into Equation 62.8.

Other toxic species produced by combustion of nitrogen-containing materials are oxides of nitrogen. The relationship between ϕ and NO_x

production is the inverse of that for HCN production, in that NO_x yields and recoveries are maximal under well-ventilated conditions and minimal under vitiated conditions. The main component of NO_x recovered in fresh fire effluent was NO and the yields were generally very low at 0.001–0.003 g/g (grams NO/g fuel mass loss) at a ϕ of 0.5, decreasing to 0.005–0.002 g/g at a ϕ of 2. Somewhat higher yields at low ϕ values were obtained for polyamide 6 and the boucle fabric (0.008–0.011 g/g).

For heteroelements such as halogens in fuels, the main combustion product is the equivalent acid gas. Recovery fractions were generally high, so that for PVC and PIR 90–100 % of fuel chlorine was released as HCl. For the boucle fabric 50–70 % of fuel chlorine was released as HCl, and approximately 50 % of fuel bromine and fuel sulfur as bromide and sulfur oxides. Recoveries of chlorine from the PU foam were lower at around 17 %. High fractional releases of these acid gases are, therefore, considered likely to occur into fresh effluent in compartment fires, except where fuels contain additives such as calcium carbonate. Once released into building compartments, acid gases are gradually lost from the effluent over a time scale of some minutes by deposition and reaction with linings and metal surfaces. The recovery of fuel carbon as carbon in the form of organic products followed a sigmoid relationship with equivalence ratio similar to those for CO and HCN ratio. The following groups could be identified:

Low organic recovery group: The cellulosic (wood-based) products and PIR (due to char formation)

Medium organic recovery group: Most synthetic polymers

High organic recovery: LDPE

Table 62.21 gives values for input to Equation 62.8.

The recovery of fuel carbon as carbonaceous particulates also increased with the equivalence ratio. The following groups were identified:

Low particulate recovery fraction: Cellulosic (wood-based) products and PMMA. The maximum recovery fraction was around 0.09.

Medium-low particulate recovery fraction: Polyurethane foam, LDPE, and polyamide. The maximum particulate recovery fraction was around 0.09.

Medium-high particulate recovery fraction: Boucle and velour fabrics, PAN (all three materials containing polyacrylonitrile), and also the PIR foam. The maximum recovery fraction was around 0.16.

High particulate recovery fraction: Polystyrene with a maximum recovery fraction of 0.2, demonstrating the well-known propensity of compounds with a high aromatic content for the formation of soot in flames.

Quasi-constant recovery group (fire-retarded materials): The two fire-retarded materials (PVC and boucle FR) showed high particulate recovery fractions throughout the ϕ range, with a gradual increase to a maximum of 0.2.

Table 62.22 gives values for input to Equation 62.8.

As stated, smoke optical density and smoke yields are proportional to the particulate concentration.

Relationship Between Toxic Potencies of Materials in Small-Scale Tests and Full-Scale Fires

When the toxic potency of the combustion products from a material are expressed empirically in mass loss terms, the data relate to the toxic effects of the total mixed combustion product evolved. This depends on the type of toxic products evolved and their yields. The most difficult problem in estimating the toxic potency of a material in a fire is that the yields of toxic products depend very much on the decomposition conditions, which vary considerably at different stages and between different types of fires [38, 39]. If small-scale test data are to be used as estimates of the likely toxic potency of products evolved in full-scale fires, it is essential that the decomposition conditions in the test be shown to be the same as those in the type or stage of

Table 62.23 Revised classification of fire types [64]

Fire stage or type	Temperature (°C)		Oxygen to fire (%)	Fire effluents	
	Hot	Layer fire		Oxygen from fire (%)	CO_2/CO (v/v)
1. Nonflaming					
(a) Self-sustaining	450–600	RT	21	>20	1–5
(b) Oxidative pyrolysis from externally applied radiation	300–600	<50	21	>20	1–5
(c) Nonoxidative pyrolysis from externally applied radiation	300–600	<50	0	0	<5
2. Well-ventilated flaming where the fire size is small in relation to the size of the compartment, the flames are below the base of the hot layer, and fire size is fuel controlled	>700	RT to 500	>15	5–21	>20[a]
3. Less well-ventilated flaming where the fire size may be large in relation to the size of the compartment, the flames are partly above the base of the hot layer, and fire size is ventilation controlled:					
(a) Small vitiated fires in closed compartments	>700	RT to 500	<15	0–12	2–20
(b) Postflashover fires in large or open compartments	>700	500–1000	<15	0–12	2–20

[a]May be lower if the burning materials contain fire retardants. In order to determine whether flaming decomposition conditions in a particular apparatus fall into category 2 or category 3, it is necessary to use a nonfire-retarded reference material capable of efficient combustion

full-scale fire being modeled; otherwise the small-scale test data are not valid.

The decomposition conditions and yields of toxic products evolved from materials in full-scale fires depend mainly on whether or not the fuel is flaming, the fuel-air ratio (equivalence ratio), and the upper-layer temperature. In ISO/IEC TR 9122-4 [105], and ISO 19706 [14], an attempt has been made to define the major categories of fire in these terms, the type of decomposition for flaming fires being expressed in terms of the CO_2/CO ratio. A revised scheme is shown in Table 62.23. The six fire types shown in the table contain three major categories: (1) nonflaming, (2) well-ventilated flaming, where the fire size is small in relation to the size of the compartment, the flames are below the base of the hot layer, and fire size is fuel controlled, and (3) less well-ventilated flaming ("underventilated" or "vitiated" flaming, where the fire size may be large in relation to the size of the compartment, the flames are partly above the base of the hot layer, and fire size is ventilation controlled. The third case includes small, vitiated fires in enclosed or poorly ventilated compartments and postflashover fires in large or well-ventilated compartments. In ISO/IEC TR 9122-4 small-scale toxicity test protocols are judged by the extent to which the test conditions are relatable to one of these categories in terms of temperature or radiant heat flux, oxygen concentration, and CO_2/CO ratio. If they are to be considered useful to measure the toxic potency of the combustion products from materials, the decomposition conditions must relate to one of these fire stages or types, and the results of any small-scale test are then only valid for the particular category being modeled. Based on the results of full-scale fire tests and fire death statistics, it is suggested here that the most important toxic hazard situations that should be assessed for all materials are the following:

1. Nonflaming oxidative/smoldering decomposition at low/midrange temperatures where the potential hazard relates mainly to victims in the enclosure of fire origin

2. Early/well-ventilated flaming conditions at midrange temperatures, and later small vitiated fires in closed compartments, where the potential hazard relates mainly to victims both in the enclosure of fire origin and remote from the fire
3. postflashover/postflashover, vitiated decomposition at high temperatures, where the potential hazard relates mainly to victims remote from the fire (since occupants of the fire enclosure are likely to have died already during stages 1 and 2)

In the United Kingdom just over half of all fire deaths in buildings occur in the room of fire origin and most result from exposure to toxic smoke evolved from small fires (which may involve periods of nonflaming and both early well-ventilated and later underventilated flaming decomposition). The other major category, particularly related to deaths from smoke exposure, consists of victims in remote locations. These result from pre-flashover underventilated fires and in some cases following fully developed fires. It is this second category that has been identified as the major problem in the United States, particularly in relation to fires in multioccupation buildings.

Unfortunately, many existing small-scale test protocols do not cover the necessary range of decomposition conditions found in full-scale fires, especially pre-flashover underventilated and fully developed, high-temperature, oxygen-vitiated fires. However, a new technique is presented here whereby certain predictions about the toxicity of combustion product atmosphere can be made based entirely on analytical data. This technique enables use of data both from small-scale experiments and full-scale fire tests.

As stated, in the section of this chapter on Multi-gas FED models, it is considered that the major toxic effects of fire effluents can be explained in terms of a small number of well-known fire gases, so that the effects of fire gases on human fire victims can be predicted to a large extent if the concentrations of these gases during a fire are known. In a similar way, it is now possible to a large extent to predict the exposure dose of combustion products generated in small-scale tests that would be lethal to rodents if the concentrations of the major toxic gases are measured. If necessary, it is then possible to verify the prediction by carrying out the animal exposures.

Experiments of this kind, have shown that toxic gases are basically additive in their effects, so that, for example, an exposure to an atmosphere containing half a lethal dose of carbon monoxide mixed with half a lethal dose of hydrogen cyanide constitutes a lethal mixed atmosphere [9, 49, 106].

The toxic effects of combustion products result mainly from asphyxia and irritancy. Asphyxiation is caused by carbon monoxide, hydrogen cyanide, low-oxygen hypoxia, and carbon dioxide, and so can be quite well predicted if the concentrations of these gases are known. Irritancy is somewhat harder to predict because many irritant organic products and inorganic acid gases occur in fire atmospheres. Where acid gases are present the concentrations can be measured and their effects added to those of the asphyxiant gases. In small-scale tests where both chemical analysis and animal exposures are used it is possible to calculate the contribution to the overall toxicity made by the measured asphyxiant gases and acid gas irritants. Any residual lethal toxicity can then be reasonably considered to be due to the effects of organic irritants, except in very rare cases where unusual toxic effects occur. For small-scale tests, or even large-scale fires, where analytical data only are available it is possible to calculate a theoretical LCt_{50} in terms of the main asphyxiant fire gases and acid gases. This calculation then represents the highest estimate of what constitutes a lethal dose for that atmosphere (i.e., the smoke atmosphere must be at least as toxic as this estimate and could be somewhat more toxic if substantial amounts of organic irritants are present or if unusual toxic effects are present). In small-scale tests there is little oxygen vitiation, so low oxygen hypoxia has little effect. On this basis Equation 62.3 was developed to predict the lethal FED to rats of a combustion product atmosphere. Equation 62.3 has been validated by demonstrating a good

agreement between predicted and actual rat LC_{50} results for a wide range of materials as shown in Fig. 62.2 [9, 45].

Currently generally accepted 30-min LC_{50} concentrations for exposure of rats to common fire effluent gases are given in Table 62.3. A difficulty with estimating the toxicity of oxides of nitrogen is that while the main gas generated in fires is NO, with a relatively low lethal toxic potency due to the formation of methemoglobin (30-min LC_{50} approximately 1000 ppm), in fire effluent atmospheres and in animal gas atmosphere exposures some degree of oxidation to the much more toxic lung irritant NO_2 occurs. For more detailed data on the acute toxicity of nitrogen oxides and the other gases listed in Table 62.3 the series of AEGL reports [89] is recommended.

Where data on organic irritant concentrations are unavailable, it is recommended that a contribution to the overall FED should be derived from an estimate of the total yield of organic products. The FED component for organic irritants (FED_{org}) is then estimated as the mass loss concentration of organic fuel material × percent carbon present as organic carbon, divided by 25. FED_{org} is then substituted for the organic irritant term in Equation 62.3 [10, 45].

When the FED for the concentrations of a set of gases entered into this equation equals unity, then death is predicted, and the mass loss exposure dose for the material producing these gas concentrations is then equal to the LCt_{50} for that material decomposed under the conditions of the test. The equation is designed to be applied iteratively. If the calculated FED from a set of gas concentrations is >1 or <1, then it a new set of gas concentrations is calculated for a lower or higher fuel mass loss concentration and the FED is recalculated for different gas concentration set until a set providing FED $= 1$ is found. If the concentrations of the irritants present and their lethal exposure doses are known, then the equation can be solved fully (e.g., the LCt_{50} for HCl is 112,980 ppm·min) [47, 107]. Where unknown irritants are present, the equation enables the maximum LCt_{50} to be predicted based on the asphyxiant gases and any known irritants.

This is a powerful technique because it enables a number of things to be done, as follows:

1. Where a material is tested in a small-scale test using only chemical atmosphere analysis, it enables an estimate to be made of the likely approximate toxic potency of the combustion products from the material, without the use of animal exposures.
2. Where a material is tested in a small-scale test using both chemical atmosphere analysis and animal exposures, then it is possible to determine the extent to which the toxicity of the combustion products can be accounted for in terms of the common toxic gases, or if additional toxicants are present.
3. If the toxic effects are almost entirely accountable in terms of the common toxic gases (as is often the case), then it enables the toxic effects of full-scale test atmospheres to be predicted with confidence, without animal exposures, if these gases are measured.
4. Where the LCt_{50} in a small-scale test is estimated from analytical data, or where it is measured using animals, it enables estimates of toxic potency of full-scale fires to be made simply from the mass loss rate and dispersal of products in the fire, provided the full-scale fire is of the same type (has the same combustion conditions) as the small-scale test decomposition.
5. Where analytical data are available from full-scale tests, they enable some estimates to be made of the toxic potencies of the materials involved.

The following examples show how this technique can be applied, using data from experiments with wood. When samples of Douglas fir were decomposed under flaming conditions in the NBS cup furnace, the LCt_{50} for a 30-min exposure of rats was 1194 $g \cdot m^{-3} \cdot min$. In the test, the CO concentration was 3400 ppm and the CO_2 concentration was 3.71 %, a CO_2/CO ratio of 11/1. According to the FED equation given above, this represents a FED of 1.0. It can therefore be concluded that in this test the observed toxic potency can be fully accounted for in terms of CO and CO_2,

and that there was little or no contribution from irritants or other toxic products on lethality. This result is to be expected, since the NBS cup furnace method generally simulates reasonably well-ventilated early flaming conditions where combustion is usually efficient, so that the yield of organic irritants would be expected to be low. However, in this test it is surprising that the CO_2/CO ratio is so low and more representative of somewhat vitiated burning conditions.

It is now possible to examine some full-scale test data on wood fires of this type, in the knowledge that CO and CO_2 are the main toxic products to consider. Such a test was performed at the U.K. Fire Research Station, where a 5-kg wood crib (Scotch pine) was burned in a closed 26 m^3 room. At 6 min into this fire the CO_2/CO ratio in the smoke was 60/1. Based on a 44 % carbon content for wood, and assuming that all carbon in the mass lost was converted to carbon oxides (CO_2 + CO), it is now possible to calculate what mass loss of wood in a small-scale test would be required for a 50 % rodent lethality at a CO_2/CO ratio of 60/1. It is to be expected that under these conditions the wood smoke would be less toxic than in the reported NBS test, since the major toxicant is the CO, and the CO yield is low at this moment in the fire. This is indeed likely to be the case, since the FED equation predicts an LCt_{50} of 3750 g·m^{-3}·min under these decomposition conditions, approximately three times less toxic than in the small-scale test.

Major Determinants of Toxicity in Fires and Small-Scale Tests

The toxicity of the combustion products from individual materials in fires, in terms of the type and yields of the major asphyxiant, irritant, and other toxic products depends principally on three factors.

1. The elemental composition of the material
2. The organic composition of the material
3. The decomposition conditions

The most important toxic products from fires are usually carbon monoxide and hydrogen cyanide, so that the most important elemental determinants of toxic potency are normally the carbon and nitrogen content of the fuel, with the halogen content being important to a lesser extent in some cases, and organic irritants in others. Figure 62.3 Illustrates the range of toxic potencies of individual compounds and combustion product mixtures, while Figs. 62.4, 62.5, 62.6, and 62.7 illustrate the extent to which different toxic species contribute to the overall toxic potency of different materials for the main different fire types described in ISO 19706 [9, 14].

Nonflaming Oxidative/Smoldering Fires

Nonflaming decomposition is slow, so that a long time is required for the development of hazardous conditions. However, of the small masses of materials decomposed during nonflaming oxidative decomposition, the yield of CO can be quite high, and these conditions generally provide the highest yields or organic products, including irritants, the identity of which is often unknown. In small-scale tests conducted under these conditions, only a small proportion of the observed toxic potency can be accounted for in terms of the common toxic gases [38, 39]. Table 62.24 shows two examples of this type, from experiments using the NBS cup furnace method to decompose Douglas fir and a flexible polyurethane foam under nonflaming oxidative conditions. The results show that at the LCt_{50} of wood to rats of 684 g·m^{-3}·min, only 0.47 of the observed toxicity could be accounted for in terms of common toxic gases, and for the flexible polyurethane foam only 0.29 of the observed toxicity could be accounted for. This result means that for these (and many other) materials decomposed under nonflaming oxidative conditions, a large part of the toxic potency is due to products other than those normally measured, almost certainly organic irritants, so that the FED method tends to underestimate the toxicity, unless allowance is made for irritants (in this case organic irritants) as in the Purser FED equation (Equation 62.3). From experiments such as that shown in Table 62.24 it can be estimated that approximately half of the

Table 62.24 Toxic potency analysis of materials decomposed under nonflaming oxidative conditions in the NBS cup furnace

	Douglas Fir 440 °C		Flexible polyurethane foam 400 °C	
	Concentration	FED	Concentration	FED
Carbon monoxide	2700 ppm	0.47	1261 ppm	0.22
Hydrogen cyanide	0 ppm	0.00	11 ppm	0.07
Carbon dioxide	0.69 %	$\times VCO_2$ 1.0	0.4 %	$\times VCO_2$ 1.0
Total FED asphyxiants		0.47		0.29
FED presumed due to irritants		0.53		0.71
LCt_{50} calculated	1455 g·m^{-3}·min		3621 g·m^{-3}·min	
LCt_{50} observed	684 g·m^{-3}·min		1050 g·m^{-3}·min	

toxic potency is likely to be due to organic irritants for most common materials under these decomposition conditions).

The nonflaming condition is adequately replicated by a number of small-scale test methods, and there is a large toxicity database available for many materials, since by far the greatest amount of published test results are obtained under these conditions.

From reviews of published toxic potency data from common materials and appropriate FED calculations [9, 10, 64] including data from a number of small- and large-scale test methods it is possible to make some general observations regarding the toxic potencies of the decomposition products from materials under a range of fire conditions. For nonflaming oxidative decomposition conditions, the range of LCt_{50} for individual materials covers approximately a factor of 12 from 63 to 767 g·m^{-3}·min (see Table 62.7) and Fig. 62.3.

Early or Well-Ventilated Flaming Fires

In flaming fires, the yields of carbon oxides and nitrogen compounds depend mostly on the decomposition conditions, particularly the air/fuel ratio. With regard to carbon, a key indication is the CO_2/CO ratio, which not only determines the toxic potency of the smoke, since CO is approximately 20 times more toxic than CO_2, but to a large extent defines the fire type. In early, well-ventilated fires combustion is usually efficient, and the CO_2/CO ratio may be as high as 200/1, although in practice somewhat lower ratios around 60/1 are more typical. Under these conditions the yield of organic irritants is usually low, since combustion is efficient, and the yield of CO is so low that the overall toxic potency of materials containing principally hydrogen and carbon can be expected to be low. The exceptions tend to be flame-retardant materials acting in the gas phase, "naturally" fire-retardant materials such as PVC, and some largely aromatic materials such as polystyrene, all of which tend to burn inefficiently and give low CO_2/CO ratios even under well-ventilated conditions. This results in high yields of CO and usually of irritants, and somewhat higher toxic potencies than for more easily and cleanly burning materials.

With nitrogen-containing materials, the situation is somewhat analogous to that with carbon, since in well-ventilated, early flaming fires, most nitrogen in materials is oxidized to nitrogen oxides and N_2. The yield of HCN is generally low (with the exception of acrylic materials, and to some extent rigid polyurethanes). Although NO_2, which is a potent lung irritant, can be expected to be present but at low yields under these conditions, the general effects seems to be that, since the HCN yield is low, toxic potency tends to be low. With materials like PVC, almost all the chloride is released as HCl under almost all decomposition conditions, including flaming conditions.

The general picture then is that the toxic potency of combustion products from most materials is lowest under early, well-ventilated

flaming conditions. Materials that tend to perform comparatively less well under these conditions are FR materials, and materials like PVC, where the halogen acid gases cannot be destroyed by the flames (Fig. 62.5).

Small-Scale Tests Replicating Well-Ventilated Flaming Conditions

To study the toxic potencies of materials under the decomposition conditions similar to those during the early stages of flaming fires it is necessary to use a test method that provides flaming combustion throughout the test until the material is fully decomposed. The test method must also provide good ventilation of non-vitiated air to the specimen and have a general temperature environment of around 400–700 °C (or equivalent radiant flux). Most important, however, it must produce high CO_2/CO ratios (in the range approximately 200/1 to 50/1) from normally combustible (i.e., non-FR) materials.

NBS Cup Furnace Test Of the small-scale test methods commonly used, a number perform well in this area. The one for which the most animal toxicity data are available for well-ventilated flaming is the (now discontinued) NBS cup furnace test. In this test the material specimen is decomposed in a crucible furnace, and the products are evolved into a 200-L box. The key feature of this test is that it is normally used with quite small specimens, so that the oxygen concentration in the box is not significantly lowered during the test, and studies of the combustion process have shown that air circulates rapidly down into the cup furnace during decomposition, so that combustion tends to be reasonably efficient. The CO_2/CO ratios typically produced in tests are in the 40/1 to 60/1 region, so that, although perhaps not representing the most efficient combustion, they are generally a reasonable model for the results obtained in small, well-ventilated, full-scale fire tests.

NIST US. Radiant (NIBS) Test A more recent development of the NBS cup furnace test is the NIBS test or NIST radiant test. The two versions of the test use the same apparatus, but somewhat different test protocols. For this test a radiant heating unit is placed in a cavity under the NBS chamber and connected to it by a slit-shaped chimney. Investigations of the combustion mode of this test [21] have also shown that under flaming combustion conditions the circulation of air is such that the specimen is very well ventilated, so that CO_2/CO ratios are generally reasonably high. Data from this test method suggest that it may best represent the decomposition conditions in a well-ventilated fire. However, in its present form it does not appear to generate the very low CO_2/CO ratios and high CO and HCN yields found in typical underventilated pre- and post-flashover fires in compartments.

A particular issue with all closed-box methods such as these is ageing if the effluents and losses resulting from deposition to the walls of the fraction of the atmosphere consisting of smoke particulates, organic products and acid gases. Also, since the enclosed atmosphere is continuously circulated trough the furnace, changes to the effluent composition can result from secondary decomposition processes.

Cone Calorimeter The cone calorimeter has not been used very successfully with animal exposures, but using the FED model presented in this chapter, it is possible to make some useful estimates of likely toxic potency based on the toxic gas yields and the mass loss of the specimen. The cone calorimeter gives the most efficient combustion conditions of any test method, typically producing CO_2/CO ratios in the 200/1 to 100/1 range for non-FR materials. It can also, therefore, be used as representative of the decomposition conditions during very early and very well-ventilated fires. So far, attempts to modify the combustion process and decrease the combustion efficiency to model other stages of fire have not proved very successful.

DIN 53 436 and ISO19700 Tube Furnace Methods For these methods, decomposition occurs in a tube furnace, the furnace passing over a strip of the sample (DIN) or the sample

passing into the furnace (ISO19700), with decomposition achieved by passing a stream of air through the furnace and over the sample. The products from the tube furnace may then be diluted with secondary air for animal exposures, if required. The atmosphere produced is in a "dynamic steady state," in that the concentrations of decomposition products remain constant because the test material is decomposed at a constant rate throughout the test. The epithet "DIN" has come to represent a number of tube furnace methods based on the same principle, generally accepted as DIN test results, the important point being to demonstrate that the decomposition atmosphere generated is relatable to real fire conditions, rather than that the apparatus design is standard.

The important feature of this design is its versatility, since the decomposition conditions can be varied over a wide range by varying the sample load, air supply, and furnace temperature. This contrasts with the other methods described, which are very restricted in the range of conditions that can be modeled. The improved tube furnace method, originally recently developed at the UK Building Research Establishment, Fire Research Station (FRS) [12], is based on the DIN method concept, and is the only one developed so far that can simulate the decomposition conditions for all fire types, including nonflaming, early flaming, and fully developed fires with restricted ventilation, particularly postflashover fires (see Fig. 62.19). A limitation with the official DIN method, in regard to flaming combustion, is that the decomposition conditions tend to be rather vitiated, giving low CO_2/CO ratios, and flaming is unstable. However, this is remedied in the ISOTS19700, by increasing the air-fuel ratio in the furnace tube and the rate of sample advance, so that it has been possible to increase the ratios to those occurring in early, well-ventilated, full-scale fires, while achieving stable flaming conditions [39].

UPITT Method The University of Pittsburgh method is considered to give a poor representation of actual fire conditions, and it is considered that it is not possible to relate it to any of the fire conditions shown in Table 62.23. For this reason (and others), UPITT data are considered unsuitable for the assessment of toxic potency of materials involved in fires, except in very special cases where the conditions can be shown to be similar to the sequence of events occurring in the UPITT apparatus.

Toxic Potency Data Obtained from Tests Under Early, Well-Ventilated Flaming Conditions

Because well-ventilated flaming conditions tend to destroy compounds such as organic irritants, it is to be expected that the toxic potency will be more completely due to the common toxic gases than for the nonflaming fires shown in Table 62.24. Table 62.25 illustrates this fact with some examples taken from NBS cup furnace test data. The data for Douglas fir show that, unlike the nonflaming situation illustrated in

Table 62.25 Toxic potency analysis of materials decomposed under early, well-ventilated flaming conditions in the NBS cup furnace

	Douglas Fir 485 °C		Flexible polyurethane foam and polyester 525 °C	
	Concentration	FED	Concentration	FED
Carbon monoxide	3400 ppm	0.60	2270 ppm	0.40
Hydrogen cyanide	0 ppm	0.00	63 ppm	0.38
Carbon dioxide	3.71 %	× VCO_2 1.4 + 0.2	3.36 %	× VCO_2 1.25 + 0.1
Total FED asphyxiants		1.04		1.08
FED presumed due to irritants		0		0
LCt_{50} calculated	1148 g·m^{-3}·min		1038 g·m^{-3}·min	
LCt_{50} observed	1194 g·m^{-3}·min		1170 g·m^{-3}·min	

Table 62.26 Toxic potency analysis of materials decomposed less efficiently under early, well-ventilated flaming conditions in the NBS cup furnace

	PVC 625 °C		FR flexible polyurethane foam 425 °C	
	Concentration	FED	Concentration	FED
Carbon monoxide	1100 ppm	0.19	1040 ppm	0.18
HCl or HCN[a]	5000 ppm	1.33	86 ppm	0.52
Carbon dioxide	0.55 %	$\times VCO_2$ 1	2.1 %	$\times VCO_2$ 1
Total FED asphyxiants		0.19		0.70
FED presumed due to irritants		1		0.30
LCt_{50} calculated	341 g·m^{-3}·min		1157 g·m^{-3}·min	
LCt_{50} observed	519 g·m^{-3}·min		810 g·m^{-3}·min	

[a]HCl (hydrogen chloride) for PVC or HCN (hydrogen cyanide) for FR flexible polyurethane foam

Table 62.24, the toxic potency can be fully accounted for in terms of carbon oxides, and an LCt_{50} for wood calculated on this basis would be very close to the observed value. For flexible polyurethane (FPU) foam it was not possible to obtain a lethal concentration in the cup furnace under flaming conditions due to limits on the capacity of the apparatus for the size of sample required, but in other experiments a mixture of polyester and FPU was tested. With this mixture of materials it was possible to obtain lethal exposure conditions, and the data are also shown in Table 62.25. As with the wood, it was possible to account fully for the observed toxic potency on the basis of carbon oxides and hydrogen cyanide.

For materials that burn less efficiently under these conditions or that produce inorganic acid gases, the data analyses indicate contributions to lethality from irritants. For example, Table 62.26 shows data on PVC and an FR polyurethane foam obtained using the NBS cup furnace method. For the PVC test, the contribution to the total FED from carbon oxides was only 0.19, so that the major cause of death had to be some other factor. Unfortunately the HCl concentration was not measured, but from the mass of PVC decomposed, it can be estimated at approximately 5000 ppm. As the analysis shows this would have been more than enough to account for the observed lethality. With regard to the FR FPU, the yield of common toxic gases was significantly greater than that from the untreated foam, so that it was possible to obtain an LCt_{50} using the cup furnace. The concentrations of carbon oxides and hydrogen cyanide were sufficient to account for approximately 0.7 of the observed toxic potency, but it is possible that the remaining 0.3 represents the effects of unidentified irritants evolved due to the less efficient combustion occurring from this foam compared to an untreated foam.

Based on available published small- and large-scale test data, it is possible to make some general observations regarding the early, well-ventilated flaming condition. The basic finding is that the published database involving animal exposures is very poor, there being only a few tests or none on quite common materials. The only materials for which a reasonable number of tests have been performed under flaming conditions are wood, flexible polyurethanes, and PVC. Needless to say, these involve a variety of wood species and polymer formulations. Based on this inadequate database, the pattern that emerges is that the range of toxic potencies of common materials covers approximately a factor of 50, with LCt_{50} exposure doses of from approximately 75–3750 g·m^{-3}·min. As could be predicted, the least toxic materials are the cellulosics and simple hydrocarbon polymers, such as polypropylene. Flexible polyurethanes are of low to intermediate toxic potency within this range. The most toxic materials are the acrylonitriles, which release quite large amounts of HCN even under well-ventilated flaming conditions. PVCs are generally somewhat more toxic than the cellulosic materials under these conditions, due to their relatively low combustion efficiency and high HCl yield.

Small-Scale Tests Replicating Fully Developed Fire Conditions—Especially Postflashover Fires

The decomposition conditions in fully developed fires depend very heavily on the conditions in fire compartments and in particular the ventilation. A general principle would be that in the common situation of a fire in a building, which would typically contain large amounts of combustible fuel, the fire growth will depend on the rate of involvement of the fuel in the early stages with efficient combustion and high CO_2/CO ratios (100/1 to 200/1). Then as the fire grows, combustion becomes increasingly ventilation controlled, so that later and fully developed fires tend to be oxygen vitiated with low CO_2/CO ratios (<10/1). However, it is possible to have fully developed, well-ventilated (fuel controlled) fires with high CO_2/CO ratios (up to 100/1), as indicated in Table 62.23. These conditions can commonly occur during some stages of test fires in large-scale test rigs. Such large-scale tests usually have a relatively small amount of fuel (such as a single chair) and have a rig with an open side or doorway or window openings, which are, in turn, supplied freely with air from outside or from a large test facility building. Another factor that may provide high CO_2/CO ratios in the effluents from a primarily vitiated postflashover fire is secondary combustion outside the fire compartment where the products mix with air and are sufficiently hot to support further combustion. This effect has been observed at the DIN furnace outlet when attempting to simulate postflashover decomposition conditions.

Accidental fires in real occupied buildings often have access to a much larger amount of fuel than test fires and often have access to a more restricted air supply (such as air from inside the building). Thus in the Boston Fire Department study of accidental fires [108], 50 % had CO_2/CO ratios of less than 10/1 and a further 22 % had ratios of approximately 10 to 20/1. Only 17 % fell into the well-ventilated category with ratios above 40/1. When full-scale tests are more closely related to real buildings or contents, then low ratios occur. For example, a simulation of a fire in a fully furnished hotel bedroom, opening on an open corridor with a side room attached, gave CO_2/CO ratios of 2/1 in the burn room and 3/1 in the side room at the fire peak [109].

Once a fire has passed beyond the very early, well-ventilated stage, there are basically two paths for continued development, depending largely on the boundary conditions, especially the dimensions of the fire enclosure, its thermal properties and ventilation.

Where a flaming fire occurs in a domestic room-sized compartment and the room doors and windows are shut, an oxygen depleted upper layer fills down rapidly, so that within a minute or so the combustion becomes vitiated as the flames penetrate the upper layer. Once the upper layer descends to the base of the fire, the fire becomes very small and may self-extinguish. A typical enclosed domestic room will not support complete combustion of more than a few kg of fuel before the oxygen concentration in the room is reduced to approximately 10–15 % and the fire extinguishes or dies down. Fires of this type, involved in many deaths, tend not to develop beyond a small size as long as the compartment is closed, but the CO_2/CO ratio decreases from a very early stage. An example is a burning 5 kg wood crib in a closed room. Table 62.27 shows the gas concentrations in the room during this fire, the atmosphere becoming progressively more vitiated and the CO_2/CO ratio decreasing as the fire progresses. The last column shows the influence this process has on the toxic potency of wood, assuming that carbon oxides are the only important toxic products (and also ignoring any toxic effects of low-oxygen hypoxia). The data show that, if a sample of wood was decomposed in a number of runs of a small-scale test under conditions giving the range of CO_2/CO ratios recorded at different stages of the full-scale fire, then the toxic potency of the wood would increase from very low levels as shown.

A further variant of this situation occurs when exterior doors and windows in a dwelling remain closed, but the fire-room door is open to the hallway. Under situations such as this the

Table 62.27 Toxic gas concentrations and calculated toxic potencies during full-scale wood fires in a room-corridor test rig

1. Fire of 5 kg wood in a closed room—total mass loss 3.5 kg; room temperature approximately 200 °C					
Time (min)	CO ppm	CO_2 ppm	CO_2/CO ratio	O_2%	LCt_{50}[a] for CO_x g·m^{-3}·min
6	750	45,000	60	18	3750
8	1500	75,000	50	13.5	3461
10	2500	88,500	35	11	2857
12	4000	95,000	24	10	2222
20	9000	75,000	8.3	11.5	1034
2. Fires of 44 kg wood in open room with high and low ventilation; room temperature approximately 800 °C					
High vent.	10,000	150,000	15	9	1800
Low vent.	50,000	150,000	3–1.5[b]	4	750

[a]LCt_{50} calculated in terms of mass loss concentration of wood, assuming carbon oxides to be the only toxic products of importance

[b]Second figure shows ratio in corridor, all other figures in room

original enclosure fire also becomes vitiated, and the fire size restricted, at an early stage as the upper layer descends below the flame height. But as the upper layer descends below the doorway soffit, effluent flows out into the hallway and open areas, while fresh air enters new floor level. The resulting fires can then grow somewhat larger than those in a single enclosed room (depending upon the dimensions), and burn in a vitiated manner for longer, filling all open areas with a lethal effluent (see fire scenario descriptions in Chap. 63). After a few minutes such fires die down as the whole system becomes oxygen depleted, and may self extinguish unless exterior windows fail or exterior doors and windows are opened. Pre-flashover underventilated fires such as this are major causes of smoke injuries and deaths for occupants both in and beyond the enclosure of fire origin.

Another other common situation is where a window and door (or door only) is open, or where the compartment has a large area compared to its height, so that there is sufficient ventilation to support a much bigger fire before the air supply becomes the controlling factor. Such fires, also typically a cause of smoke deaths in locations remote from the fire, become both hot and vitiated, and may progress to postflashover. This combustion condition can be simulated in small-scale tests, with a temperature of 800 °C or more, and CO_2/CO ratios of less than 10/1, and as low as 2/1. The lower part of Table 62.27 illustrates this with data from the developed stage of larger (44 kg) wood fires run in the same rig as the 5 kg test. These fires were run with high and low ventilation from the corridor, to simulate well-ventilated and oxygen-vitiated, fully developed (postflashover) fires. The results show that both fires become vitiated when fully developed, the poorly ventilated fire giving very low CO_2/CO ratios of 3/1 in the room and 1.5/1 in the corridor.

If the typical postflashover fire is hot, and oxygen vitiated, with low CO_2/CO ratios, the next consideration is what effects these decomposition conditions have on the toxic potency of the products. The most obvious effect is that the toxic potency is increased compared to well-ventilated fires due to the higher concentrations of CO produced as the CO_2/CO ratio falls. The series of room-corridor fires performed at the Fire Research Station using 44 kg wood cribs provides a good example. When these were burned with restricted ventilation, the CO_2/CO ratio fell to the low values mentioned, of 3/1 in the room and 1.5/1 in the corridor after 3.5 min, with very high concentrations of CO (5 %) in the room. Assuming as before that toxicity would be due solely to carbon oxides, then the theoretical LCt_{50} would be 750 g·m^{-3}·min, which is approximately five times more toxic than that in the well-ventilated, early flaming fire, and is similar to results obtained for pine and sipo wood in the DIN apparatus at 850 °C. Table 62.28 shows the toxic potency analysis for this fire.

Table 62.28 Toxic potency analysis of materials decomposed under high-temperature, vitiated conditions in large-scale fires and in the DIN apparatus

	Scotch Pine 850 °C room corridor low ventilation		Wool 700 °C DIN	
	Concentration	FED	Concentration	FED
Carbon monoxide	5515 ppm	0.97	379 ppm	0.07
Hydrogen cyanide	0 ppm	0	153 ppm	0.93
Carbon dioxide	1.7 %	$\times VCO_2$	0.17 %	$\times VCO_2$
		1		1
Total FED asphyxiants		0.97		1
FED presumed due to irritants		0		0
LCt_{50} calculated	750 g·m^{-3}·min		81 g·m^{-3}·min	
LCt_{50} observed (DIN test under similar conditions)	876 g·m^{-3}·min		No data	

A very important aspect of postflashover fire conditions is the fate of nitrogen in materials. Under hot, vitiated conditions the yield of HCN from all nitrogen-containing materials increases dramatically. Hydrogen cyanide can, therefore, be an important toxic product in postflashover fires where the fuel has a high nitrogen content. Another problem with such fires is the yield of organic irritants. Vitiated postflashover fires produce large quantities of smoke, and experiments with some common materials decomposed under these conditions in a DIN-style tube furnace have shown that the dense smoke is rich in organic products, which are irritant to mice. With regard to inorganic irritants, such as HCl, these are produced at the same high yield as with early flaming fires, except that their effects are less prominent in the fully developed fire in comparison with the high yields of other toxic products.

Results from DIN and Other Tube Furnace Methods and Full-Scale Tests

If the database of small-scale animal toxicity test results on materials tested under early flaming conditions is poor, that on materials tested under postflashover conditions is even smaller. The only small-scale apparatus that can be used to replicate these conditions is the DIN and ISO19700 tube furnace when it is run at high temperatures. A small amount of rodent lethality data is available from tests run using the DIN method at temperatures above 800 °C. Apart from this, other data are from a number of small-scale and large-scale tests where analytical measurements were made. From these which it is possible to make toxic potency assessments, assuming that toxic effects were due only to carbon oxides, HCN, acid gases, and generic organics (such as measured using the ISO19700 tube furnace [11, 13, 66, 69, 91, 92]. In such vitiated postflashover conditions, it is found that carbon monoxide and hydrogen cyanide are dominant toxic species, since carbon monoxide is be present at high yields in all fires and hydrogen cyanide can also be expected at high yields if the materials being burned contain nitrogen. Added to this is a contribution from organic irritants, and a contribution from inorganic irritants if these are present. Although recent work suggests that organic irritants may be more important under these conditions than was thought previously, it is considered likely that they are less important than under nonflaming conditions and are unlikely to be the dominant factor in the toxic potency.

Table 62.28 shows some examples of toxic potency analyses for this fire condition. The table shows analytical data from a large-scale wood fire, compared with animal data from a DIN test on wood for which no analytical data are available, and data from a small-scale (DIN) furnace test on a nitrogen-containing material (i.e., wool). Rats were exposed in the test at an exposure dose of 18 g·m^{-3}·min, and all died. The data shown are projected gas concentrations at the calculated LCt_{50}. For the wood data, the point

illustrated is that, based on the measured carbon oxide concentrations, the toxic potency is likely to be dominated by CO, and on this basis the potency of wood is greater than under well-ventilated flaming conditions. That this projection is reasonable is supported by the results of DIN work on Scotch pine, carried out under nominally similar conditions. This work gave a rat LCt_{50} of 875 $g{\cdot}m^{-3}{\cdot}min$, which is similar to the predicted figure for wood decomposed under these general conditions. Unfortunately, no analytical data were published for the DIN test results. For the wool data, the main point illustrated is that even at 700 °C which is somewhat below what would be considered a postflashover temperature, the toxicity is likely to be dominated by the high HCN yield, and this is also considered to be true for most other nitrogen-containing materials. The other point made strongly by these examples is the paucity of available data for this type of fire.

Based on the available data it is estimated that the toxic potency range for common materials decomposed under vitiated postflashover conditions covers an LCt_{50} range from approximately 21 $g{\cdot}m^{-3}{\cdot}min$ for materials with a high nitrogen content decomposed at temperatures around 1000 °C up to 3000 $g{\cdot}m^{-3}{\cdot}min$ for certain cellulosic or hydrocarbon-based polymers, a range of more than 2 orders of magnitude for the small sample of published data.

Adaptation of Data from Other Small-Scale Tests

It has been recognized that tests other than the DIN, such as the cone calorimeter and the U.S. radiant method, are incapable of simulating postflashover decomposition conditions, producing the wrong yields of CO and the wrong CO_2/CO ratios. However, since it is also considered in the United States that this fire condition is the most important to study, suggestions have been made that a calculation method can be applied to cone and U.S. radiant data toxicity data to allow for the low CO yield in the tests, relative to those in postflashover fires. This is obviously not a realistic suggestion, since even if a calculation factor could be used to correct the CO data, the result would still be wrong if no factor were used to correct for the differences in the yields of HCN and other nitrogen-containing products, and for the yields of the many other organic irritants. Rather, if it is wished to study the behavior of materials under vitiated, high-temperature postflashover conditions, small-scale tests should be used that create such decomposition conditions, so that the chemistry and toxicity of all the decomposition products evolved under these conditions can be studied. Since tube-furnace methods similar to the ISO TS19700 method are cheap and very effective means of simulating this fire condition, it is recommended that this method be used, under appropriate conditions of temperature and airflow, for this purpose. Where calculation methods are to be used, it is better to base them on the elemental composition of the material and knowledge of full-scale fire conditions rather than on small-scale tests conducted under inappropriate conditions.

General Pattern of Toxic Potency for Common Materials Under Three Fire Conditions

The survey of the toxic potency data for common materials under four fire conditions, (1) nonflaming, (2) early flaming, (3) underventilated pre-flashover and (4) underventilated post-flashover, has revealed an inadequate database, but it has been possible to derive approximate LCt_{50} for common materials. The results for individual materials range over approximately 2 orders of magnitude from 20 to 3750 $g{\cdot}m^{-3}{\cdot}min$, but when the data are reduced to basic types of materials under each decomposition condition a relatively simple pattern can be described (Table 62.7). The table shows the approximate average lethal exposure doses (LED $= LCt_{50}$) for classes of materials, the LC_{50} for 30-min exposures. The findings are as follows:

Under nonflaming oxidative decomposition conditions at >400 °C most materials have a

similar potency close to 500 $g \cdot m^{-3} \cdot min$ due mainly to the effects of carbon monoxide and irritants. The main exceptions are nitrogen-containing materials releasing significant HCN at low temperatures (e.g., polyacrylonitrile, modacrylic, and rigid polyurethane foam), which have LED values of 150–1200.

Under early flaming conditions most non-fire-retardant materials are substantially less toxic than under nonflaming conditions. Cellulosics (e.g., wood and cotton) are the least toxic with LCt_{50} of >3000 $g \cdot m^{-3} \cdot min$. Plastics containing carbon, hydrogen, or oxygen are somewhat more toxic with a potency factor of LED ~2100). and those containing nitrogen (e.g., flexible polyurethanes, wool, and nylon) range from 240 to 510. Both PVC and fire-retardant materials have LED values similar to those under nonflaming conditions of approximately 1.

When equivalence ratios in pre-flashover fires exceed 1 the toxicity increases, so that LEDs are similar to or lower than under non-flaming conditions.

Under postflashover conditions the potency of all materials are similar to or slightly greater than for pre-flashover underventilated conditions with high yields of HCN or CO. More smoke and irritants are also present than under early flaming conditions, which may add somewhat to the potency, particularly of the non-nitrogen-containing materials. For cellulosic materials and hydrocarbon plastics, the potency is similar to that under nonflaming conditions or greater. For all nitrogen-containing materials the toxic potency is high, with LED values ranging from approximately 54 for polyamide to 210 for flexible polyurethane foam. It is suggested that rigid PVC would have a potency of approximately 8 under these conditions.

The Conduct and Application of Small-Scale Tests in the Assessment of Toxicity and Toxic Hazard

Small, laboratory-scale toxicity tests are of necessity capable only of investigating materials. Investigation of toxic fire hazard associated with actual items such as furnishings can be investigated only in large-scale tests, although it may be possible to a limited extent to study some composite materials using small-scale tests. The potential usefulness of these tests is then to examine the toxicity of the decomposition products from materials. This information can be used in conjunction with other small-scale test data on such characteristics of materials as ease of ignition, rate of flame spread, heat release, and smoke production to judge the suitability of one material versus another for a particular application, and ideally as a prelude to large-scale fire tests. From these it should be possible to draw some conclusions as to likely fire scenarios as well as the toxic and general fire hazards involved. A sensible approach to the use and application of such toxicity tests should involve the following steps:

1. Decide what kinds of fire scenarios are of interest and likely to involve the material under investigation, and what types of fire conditions it may be subjected to—smoldering/overheat, small flaming fire, or fully developed/postflashover.
2. Choose a small-scale test method or methods capable of simulating these conditions.
3. Run the test without animals and measure as many as possible of the common fire products important with respect to toxicity. A minimum that should be measured include CO, CO_2, O_2, HCN (if nitrogen present in material), HCl (or other appropriate acid gases if likely to be present), smoke optical density, and particulate concentration. All tests should be characterized in terms of NAC mass charge, NAC mass loss, decomposition temperature, and whether the decomposition is flaming or nonflaming. Calculate an approximate LCt_{50} at this point for use in hazard modeling. If there is any reason to suspect from the chemical and physical composition of the material that more exotic toxic chemical products or physical entities such as nanoparticles or fibers may be released into the effluent so that more information is required, proceed to carry out animal experiments.

4. Set up a test atmosphere at a concentration that should be just sublethal for the known toxic atmosphere constituents (in most cases the determining factor will be the CO concentration). Then expose a group of animals and measure the toxic effects in terms of type (asphyxiant or irritant), time of onset, severity, and duration, noting in particular the degree of incapacitation and the occurrence of any deaths. In the first instance this should involve a 30-min exposure followed by a 14-day observation period.
5. Decide from this whether the observed effects are consistent with the toxicity due to common fire products or whether there were any unusual or severe toxic effects. If the toxicity can be interpreted in terms of the common asphyxiant products CO and HCN, then it should be possible to attempt modeling of toxic hazard on a large scale. However, if the products are irritant, as in most cases they will be, or if some unexpected toxic effect should occur, then further investigations are indicated.
6. If some unexpected toxic effect should occur, attempt to identify the toxic product or products responsible, and the conditions under which they are likely to be formed. The minimum necessary is to establish the 30-min exposure LC_{50} concentration to give some indication of the possible toxic potency of the material when decomposed in a fire. However, if the identity of the toxic product and the conditions of its formation are not understood, it is unwise to assume that small-scale tests will adequately predict what might happen in a large-scale fire. A good example is PTFE (Teflon). In one small-scale test method (the NBS method), PTFE decomposes to form a highly toxic lung irritant that causes death at concentrations of 2 to 3 orders of magnitude less than that of other polymeric materials [6]. In the Pittsburgh method the material is approximately 20 % less toxic [110], and in a tube furnace method similar to the DIN method a further three times less toxic [111] although still somewhat more toxic than most other materials. However, when decomposed in a way different from any of these tests, the high toxic potency is lost [112] and it is possible that under real fire conditions the products may not be significantly more toxic than those of other materials, although this is yet to be established.
7. Assess the irritancy potential of a material by measuring the effects of its thermal decomposition and combustion products in animals. With regard to the assessment of irritancy, although many known irritants have been identified in combustion product atmospheres, it is still not possible to predict the irritancy of an atmosphere from an analysis of its composition. The potential for causing upper respiratory tract and eye irritation (sensory irritancy) should be assessed by measuring the mouse RD_{50} concentration of the material. The potential for causing lung irritation with serious or lethal lung inflammation should be assessed by examining postexposure lethality in rats or mice. Thus if carbon monoxide concentrations are relatively low in relation to irritant products, a concentration of decomposition products may occur when the animals die either during, or in most cases after, exposure due to lung inflammation. An LC_{50} concentration for these nonasphyxiant deaths should then be determined to indicate the potency of the material in terms of causing lung inflammation under specific decomposition conditions. If it is not possible to identify the product or products responsible for these irritant effects, it will be necessary to use the material RD_{50} and LC_{50} data in an attempt to predict likely large-scale toxic hazard. Although this measurement is only approximate, there are indications that both the RD_{50} and LC_{50} levels of most materials fall into relatively narrow bands, each effect spanning approximately one order of magnitude, with 1–2 orders of magnitude between the effects, at least under nonflaming conditions. Under nonflaming conditions it is likely that most materials may cause potentially serious lung

inflammation following a 30-min exposure at an NAC mass loss of approximately 10 mg/L, and severe sensory irritation at somewhat lower concentrations, possibly around 1 mg/L, although tenability limits for humans are difficult to estimate. Under flaming conditions the degree of irritancy is likely to be less, sometimes considerably so, depending on the efficiency of combustion.

8. Having evaluated the toxicity of the combustion products from the material in this way, it should be possible to use the data in conjunction with other information from small- and large-scale fire tests, or mathematical models, to assess potential toxic hazard for the material or materials in question in their end use configuration.

Tenability limits for some 5- and 30-min exposures to common toxic fire products in terms of time to incapacitation and death are shown in Appendix 3 of Chap. 63.

Misuse of Toxicity Test Data

Another way of using toxicity test results is to rank materials in order of toxicity and choose the least "toxic" material, as if toxic hazard were an inherent property of the material. This is not a realistic approach, since the toxic hazard is not a single property but a sequence of different toxic effects developing over different time-scales during a fire. The mix of toxic substances in a fire effluent associated with any material is also not an inherent property of a material or product, but a system property of a full-scale fire scenario. The yields and concentrations of toxic substances in fire effluents change continuously during a fire as the fire develops and the combustion conditions change. Indeed, it is very easy to alter the toxic substance yields and "toxicity" of a material in a small-scale fire test simply by altering the test conditions, particularly with respect to CO and HCN yields. Thus, when wood or most other hydrocarbon polymers are decomposed under flaming conditions with restricted oxygen, the CO_2 to CO ratio in the products can be lowered (to around a value of 4) [17, 18] and the toxic potency is high. However, under well-oxygenated efficient combustion conditions, the CO_2 to CO ratios in a fire may be as high as 1000, and under such conditions the toxic potency of the products is very low. Although such anomalies can be overcome to some extent by careful control of the small-scale decomposition conditions and by relating them to conditions known to occur in large-scale fires, it is still difficult to predict the CO concentration-time profile and, hence, the toxic hazard development for a large-scale fire from the small-scale fire model in a toxicity test. For this reason, ranking materials in order of their performance in small-scale toxicity tests does not have much meaning or usefulness.

The best use of small-scale toxicity tests is to identify the products responsible for the major toxic effects and measure their yields under defined combustion conditions validated against full-scale fires. The concentration/time profiles of these products in large-scale fires can then be measured or modeled, and the likely toxic hazard can be assessed.

Appendix

Glossary of Terms

Acidosis: A condition in which the pH of the blood is lowered (i.e., becomes more acidic). Respiratory acidosis in fire exposures results from excess carbon dioxide uptake. Metabolic acidosis results from impaired tissue respiration (due to tissue hypoxia) caused by burns or asphyxia. (See alkalosis.)

Addition: Two or more toxic substances are considered to exert an additive effect when they act in concert, such that the effect in combination is greater than the effect of either substance acting alone but not greater than the sum of the effects of either substance acting alone (when they may be said to be directly additive). (See also synergism.)

Aerodynamic diameter: The aerodynamic diameter of a particle is an expression of particle size, and represents the diameter of a spherical particle of unit density with the

same aerodynamic properties as the particle under consideration.

Aerosol: Solid or liquid particles dispersed in air.

Alkalosis: Respiratory alkalosis occurs when the pH of the blood is increased (i.e., becomes more alkaline). It is caused by excess removal of carbon dioxide from the blood via the lungs during hyperventilation and may cause a loss of consciousness.

Available Safe Escape Time (ASET): ISO Definition: Time available for escape for an individual occupant, the calculated time interval between the time of **ignition** and the time at which conditions become such that the occupant is estimated to be incapacitated, i.e., unable to take effective action to **escape** to a **safe refuge** or **place of safety**

NOTE 1 The time of **ignition** can be known, e.g., in the case of a **fire model** or a **fire test** or it may be assumed, e.g., it may be based upon an estimate working back from the time of detection. The basis on which the time of ignition is determined is always stated.

NOTE 2 This definition equates **incapacitation** with failure to escape. Other criteria for **ASET** are possible. If an alternate criterion is selected, it is necessary that it be stated.

NOTE 3 Each occupant can have a different value of ASET, depending on that occupant's personal characteristics.

Asphyxia: Suffocation; a decrease in the oxygen content, and increase in the carbon dioxide content of the blood that may occur due to laryngeal spasm caused by burns or irritant gases or to impairment of breathing or gas exchange in the lung. The term has been extended to include all causes of tissue hypoxia, including exposure to asphyxiant gases (low oxygen concentration due to the excess of any other gas, or exposure to the asphyxiant gases carbon monoxide and hydrogen cyanide, which produce asphyxia chemically).

Atmosphere (fire atmosphere or test atmosphere): The total airborne medium to which a victim or experimental animal is exposed, consisting of solid and liquid particles and vapors dispersed in air.

Behavioral effects/incapacitation: The extent to which exposure to fire products affects the ability or willingness of a subject or experimental animal to perform coordinated movements or tasks, particularly movements or tasks similar to those required to escape from a fire. (See incapacitation.)

Bioassay: Originally a term reserved for the use of a biological system to detect or measure the amount of a biologically active material. In the fire context, it refers to the use of animal exposures rather than chemical analysis to determine the toxicity of a combustion product atmosphere.

Blepharospasm: Involuntary and sustained closure (spasm) of the eyelids. In fires it is due to the painful stimulation of the cornea by combustion products that are sensory irritants.

Bronchoconstriction: Constriction of the conducting airways in the lung due to the contraction of smooth muscle in the airway walls in response to an agonist or to stimulation of irritant receptors acting through the vagus nerve.

Burn: Tissue lesion caused by heat or chemicals. For description of burn types and degrees, see text.

Carboxyhemoglobin (COHb): Combination of carbon monoxide with hemoglobin in the blood, which limits the combination of hemoglobin with oxygen (oxyhemoglobin), and therefore the carriage of oxygen in the blood.

Cerebral depression: Condition in which the electrical activity of the cerebral cortex as revealed in the electroencephalogram consists mainly of slow wave (or delta wave) activity that is typical of a semiconscious or unconscious state.

Combustion products: Strictly speaking, this term means the products of flaming decomposition and is used in this sense when contrasted with thermal decomposition products. However, in general usage, the term may be taken to include all fire products,

whether produced by flaming or nonflaming thermal decomposition.

Concentration: The amount of a contaminant in the atmosphere per unit volume of the atmosphere, usually quoted as mass/volume (mg/L or mg/m^3) or volume/ volume (ppm or percent). (See nominal atmosphere concentration.)

Dose: The amount of a toxicant to which a fire victim or test animal is exposed. The simplest estimation of dose for inhalation toxicology is to multiply the atmosphere concentration by the duration of exposure (*Ct* product). A lethal dose may be expressed in terms of the LCt_{50}. However, other factors may affect the amount of toxicant actually entering the body, and for fires it may be necessary to express dose in terms of the material in the fire. (See nominal atmosphere concentration.)

Edema: Accumulation of an excessive amount of fluid in cells, tissues, or body cavities. Pulmonary edema occurs when a fluid exudate leaks out of blood vessels as a result of inflammation or circulatory insufficiency, and the lung tissues become swollen and waterlogged. Further development results in a fluid exuded within the alveolar spaces. This fluid accumulation seriously affects gas exchange in the lung and may be fatal.

Electroencephalogram: Waves of electrical activity in the cerebral cortex recorded from the surface of the head, which give an indication of the physiological state of the brain and the degree of alertness of the subject. A preponderance of fast (beta and alpha) activity indicates a conscious and normal state, whereas a preponderance of slow (theta and delta) activity signifies a physiologically depressed or unconscious state.

Erythema: Reddening of the skin in response to heat. This change coincides with pain and just precedes a skin burn.

Fire profile: Record of the changes with time of the concentrations of important fire products and intensities of physical parameters during the course of a fire.

Flaming fire: In the context of this chapter, this term refers to the early stages of fire growth (preflashover), when the fire is still confined to burning items within a well-defined area.

Flashover: Point in growth of a flaming fire where the flames are no longer confined to burning items but also occur within the fire effluent, remote from the seat of the fire.

Fractional incapacitating dose: The dose of a toxic product acquired during a short period of time, expressed as a fraction of the dose required to cause incapacitation at the average exposure concentration during that time interval. The fractional incapacitating doses acquired during each short time period are summed throughout the exposure, incapacitation occurring when the fraction reaches unity.

Fully developed fire: A fire that has reached its maximum extent of growth, usually extending throughout the fire compartment.

Haber's rule: Principle that toxicity in inhalation toxicology depends on the dose available and that the product of concentration and exposure time is a constant.

Hazard: A toxic fire hazard exists when a toxic product is present at a sufficient concentration and over a sufficient period of time to cause a toxic effect. A physical fire hazard exists when a physical fire parameter (heat or smoke) is present at an intensity and over a period sufficient to cause injury or seriously inhibit the ability to escape from a fire.

Hypercapnia: Increased blood carbon dioxide concentration.

Hyperthermia (heat stroke): An increase in body temperature above 37 °C. Hyperthermia is life-threatening if the body core temperature, or temperature of the blood entering the heart, exceeds 42.5 °C.

Hyperventilation: Increased rate and depth of breathing (increased respiratory minute volume, or RMV), in response to increased carbon dioxide, hypoxic hypoxia, hydrogen cyanide, exercise, heat, or stimulation of pulmonary irritant receptors.

Hypoxia: A reduction in the amount of oxygen available for tissue respiration, which can occur in the following four ways:

- **Anemic hypoxia**: The arterial PO_2 is normal, but the amount of hemoglobin available to carry oxygen is reduced and the ability to release oxygen to the tissues is impaired. For fire exposures this results mainly from the formation of carboxyhemoglobin following exposure to CO, but an anemic subject would be at increased risk.
- **Histotoxic hypoxia**: The amount of oxygen delivered to the tissues is adequate, but due to the action of a toxic agent such as HCN, the tissue cells cannot make use of the oxygen supplied to them.
- **Hypoxic hypoxia (low-oxygen hypoxia)**: The PO_2 of the arterial blood is reduced as a result of a low atmospheric oxygen concentration or impairment of gas exchange in the lung, due to bronchoconstriction or respiratory tract damage or disease.
- **Ischemic hypoxia**: Blood flow to a tissue is so low that adequate oxygen is not delivered to it despite a normal PO_2 and hemoglobin concentration. This occurs during shock following burns and in cerebral tissue due to alkalosis or briefly during postural hypotension.

Incapacitation: An inability to perform a task (related to escape from a fire) caused by exposure to a toxic substance or physical agent in a fire. A distinction is sometimes made between severe physiological incapacitation, in which the subject is unable to move normally, such as might occur in an unconscious or badly burned victim, and the more behavioral incapacitation, such as that caused by visual obscuration or eye irritation from smoke, in which the victim is more or less intact, but still unable to escape from the fire.

Inflammation: A complex of reactions occurring in blood vessels and adjacent tissues around the site of an injury. The initial reaction is congestion (engorgement of local blood vessels), exudation of fluid into the tissues (edema), and pain followed by a phase of destruction and removal of injured tissue by inflammatory cells and then a phase of repair.

Intensity: Level of a harmful physical fire parameter (such as radiant heat flux, air temperature, or smoke optical density).

Intoxication: A state in which a subject is adversely affected by a toxic substance. Specifically, the time at which a subject has taken up a sufficient amount of an asphyxiant (narcotic) gas that he or she behaves like someone severely affected by alcohol.

Irritation and irritancy: Irritation is the action of an irritant substance, irritancy is the response. This response takes the following two forms:

- **Pulmonary (lung) irritant**: Response occurs when an irritant penetrates into the lower respiratory tract and may result in breathing discomfort (dyspnea), bronchoconstriction, and an increase in respiratory rate during the fire exposure. In severe cases it is followed after a period (usually of a few hours) by pulmonary inflammation and edema, which may be fatal.
- **Sensory irritant**: Response occurs when an irritant substance comes in contact with the eyes and upper respiratory tract (and sometimes the skin), causing a painful sensation accompanied by inflammation with lacrimation or mucus secretion. At low concentrations, this effect adds to the visual obscuration caused by smoke, but at high concentrations the severe effects may cause behavioral, and to some extent physiological, incapacitation. Sensory irritation causes a decrease in respiratory rate that is transient in humans but continuous in rodents.

Lacrimation: The production of tears in response to sensory irritation of the eyes.

LC_{50}: Lethal concentration—50 %. The concentration statistically calculated to cause the deaths of one-half of the animals exposed to a toxicant for a specified time. It may be

expressed as volume/volume (ppm, percent) or mass/volume (mg/L). Care must be taken in comparing LC_{50}s of both the exposure duration and the postexposure period over which deaths were scored. In combustion toxicology, the LC_{50} may be related to the test material rather than its products and expressed in terms of the nominal atmosphere concentration of material either of mass charge or mass loss. (See nominal atmosphere concentration.)

***LCt*$_{50}$**: The product of exposure concentration and duration causing the deaths of 50 % of animals.

Narcosis: Literally "sleep induction" but used in combustion toxicology to describe central nervous system depression causing reduced awareness, intoxication, and reduced escape capability, leading to loss of consciousness and death in extreme cases. The asphyxiant gases CO, HCN, and CO_2 cause asphyxia, as does lack of oxygen due to the inhalation of an atmosphere low in oxygen, an impairment of breathing, or an impairment of gas exchange in the lung. The terms *narcosis* and *narcotic gases* are used synonymously with the terms *asphxia* and *asphyxiant gases*.

Nominal Atmosphere Concentration (NAC): The theoretical concentration of test substance in a test atmosphere, calculated from the mass of test substance produced from the atmosphere generation system each minute divided by the air volume into which it is generated. This concept is not directly applicable to combustion toxicology since the test material is decomposed in the fire or furnace system, but two derivative concepts are used to relate the test material to the degree of toxicity as follows:

Nominal Atmosphere Concentration mass charge (NAC mass charge): The mass of material placed in the furnace system per volume of air into which it is dispersed (mg material/liter).

Nominal Atmosphere Concentration mass loss (NAC mass loss): The mass loss of material during decomposition per volume of air into which it is dispersed (mg material/liter).

Physiological effects: Effects of chemical fire products or physical fire parameters on the functioning of the body, as opposed to parameters affecting the mind. Thus, a physiological effect of smoke is that it obscures vision, which might have a psychological effect on the willingness of a victim to enter a smoke-filled corridor.

Pneumonia (Pneumonitis): Inflammation of the lungs, in fire victims due to the direct effects of inhaled chemicals or hot gases, or secondarily to skin burns. The initial inflammatory phase may be followed by infection. As it passes through different phases, pneumonia may be life-threatening at any time from 1 h after exposure in a fire to several weeks after exposure.

Potency: The toxic potency is a measure of the amount of a toxic substance required to elicit a specific toxic effect—the smaller the amount required, the greater the potency.

Psychological effects: Psychological effects of exposure to fire scenarios are on the mind of the victim and may result in a variety of behavioral effects. These are distinct from physiological effects on body function (see above). A fire victim is likely to suffer both types of effects at various stages of a fire, and interactions between psychological and physiological effects are likely.

Psychomotor: Psychomotor skills are required to perform behavioral tasks involving a series of coordinated movements of the type required to escape from a fire in a compartment (such as a building).

Pyrolysis: In this chapter, the term *pyrolysis* is restricted to the thermal decomposition of materials without oxidation. In small-scale tests pyrolysis may be achieved by heating the material in a stream of nitrogen.

***RD*$_{50}$**: Respiratory depression 50 %—statistically calculated concentration of a sensory irritant required to reduce the breathing rate of laboratory rodents (usually mice) by 50%.

Respiratory Minute Volume (RMV): Volume of air breathed each minute (liters/minute). RMV = TV × RR.

Respiratory Rate (RR): Respiratory frequency (i.e., number of breaths per minute).

Respiratory tract: The nose, pharynx, larynx, trachea, and large bronchi are termed the upper respiratory tract, and the bronchiole, alveolar ducts, and alveoli are termed the lower respiratory tract.

Required Safe Escape Time (RSET) ISO definition: Time required for escape. Calculated time period required for an individual occupant to travel from their location at the time of **ignition** to a **safe refuge** or **place of safety** cf. **available safe escape time** and **evacuation time**.

Shock: A reduction in the circulating blood volume with a fall in blood pressure.

Smoke: Total fire effluents, consisting of solid and liquid particles and vapors.

Smoldering/nonflaming oxidative decomposition: Thermal decomposition in which there is partial oxidation of the pyrolysis products but no flame. This may result from overheating of materials by means of an external heat source or from self-sustained smoldering.

Specific toxicity: A particular adverse effect caused by a toxicant (e.g., asphyxia, irritancy).

Supertoxicant: A term used to describe a toxicant with an unusual specific toxicity not usually associated with fire effluents, often with a high potency.

Synergism: Situation where the toxic potency of two or more substances acting in concert is greater than the sum of the potencies of each substance acting alone.

Tenability limit: Maximum concentration of a toxic fire product or intensity of a physical fire parameter that can be tolerated without causing incapacitation.

Thermal decomposition: Chemical breakdown of a material induced by the application of heat.

Tidal Volume (TV): Volume of air exhaled in each breath.

Toxicity: The nature and extent of adverse effects of a substance on a living organism.

Ventilation (lung): The volume of air breathed each minute (synonymous with respiratory minute volume).

References

1. D.T. Gottuk and B.Y. Lattimer, "Effect of Combustion Conditions on Species Production." in *SFPE Handbook of Fire Protection Engineering,* 5th ed. (M. J. Hurley et al., eds.), Springer, (2015).
2. Khan, M. et al., "Combustion Characteristics of Materials and Generation of Fire Products," *SFPE Handbook of Fire Protection Engineering,* 5th ed. (M. J. Hurley et al., eds.), Springer, (2015).
3. D.A.Purser and J.L.McAllister. "Assessment of Hazards to Occupants from Smoke, Toxic Gases and Heat" *SFPE Handbook of Fire Protection Engineering,* 5th ed. (M. J. Hurley et al., eds.), Springer, (2015).
4. ISO 13571 Life-threatening components of fire –Guidelines for the estimation of time to compromised tenability in fires. Second edition International Organization for Standardization, Geneva, Switzerland. 2012.
5. J.H. Petajan, K.L. Voorhees, S.C. Packham, R.C. Baldwin, I.N. Einhorn, M.L. Grunnet, B.G. Dinger, and M.M. Birky, "Extreme Toxicity from Combustion Products of a Fire-Retarded Polyurethane Foam," *Science,* 187, pp. 742–744 (1975).
6. B.C. Levin, A.J. Fowell, M.M. Birky, M. Paabo, S. Stolte, and D. Malek, "Further Development of a Test Method for the Acute Inhalation Toxicity of Combustion Products," *NBSIR 82-2532,* National Bureau of Standards, Washington, DC (1982).
7. R.C. Anderson, P.A. Croce, F.G. Feeley, and J.D. Sakura, "Study to Assess the Feasibility of Incorporating Combustion Toxicity Requirements into Building Materials and Furnishing Codes of New York State," *Reference 88712,* Arthur D. Little, Cambridge, MA (1983).
8. C.J. Hilado, "Screening Materials for Relative Toxicity in Fire Situations," *Modern Plastics,* pp. 64–68 (July, 1977).
9. D.A. Purser,. "Application of human and animal exposure studies to human fire safety". in *Fire Toxicity*, A.A. Stec and T.R. Hull (eds) Woodhead, Cambridge, 2010. Chapter 8 pp 283–345.
10. D.A. Purser, Validation of additive models for lethal toxicity of fire effluent mixtures. Polymer Degradation and Stability 97 2552–2561 (2012)
11. Controlled Equivalence Ratio Method for the Determination of Hazardous Components of Fire Effluents," *ISO/TS 19700,* International Organization for Standardization, Geneva (2007).

12. D.A. Purser, P.J. Fardell, J. Rowley, S. Vollam, and B. Bridgeman "An Improved Tube Furnace Method for the Generation and Measurement of Toxic Combustion Products Under a Wide Range of Fire Conditions," in *Proceedings of Flame Retardants 1994 Conference,* Interscience Communications, London, pp. 263–274 (1994).
13. J.A. Purser, D.A. Purser, A.A. Stec, C. Moffatt, T.R. Hull, J.Z. Su, M. Bijloos, P. Blomqvist. Repeatability and reproducibility of the ISO/TS 19700 steady state tube furnace. Fire Safety Journal 55, 22–34 (2013)
14. "Guidelines for Methodology for Assessing the Fire Threat to People," ISO 19706, ISO, Geneva, Switzerland (2007).
15. R.A. Anderson, A.A. Watson, and W.A. Harland, "Fire Deaths in the Glasgow Area: 1. General Conclusions and Pathology," *Medicine, Science and the Law,* 21, pp. 175–183 (1981).
16. H.L. Kaplan, A.F. Grand, and G.E. Hartzell, *Combustion Toxicology: Principles and Test Methods,* Technomic, Lancaster, PA (1983).
17. D.A. Purser and W.D. Woolley, "Biological Studies of Combustion Atmospheres," *Journal of Fire Sciences,* 1, pp. 118–145 (1983).
18. W.D. Woolley and P.J. Fardell, "Basic Aspects of Combustion Toxicology," *Fire Safety Journal,* 5, p. 29 (1982).
19. F. Haber, *Funf Vortrange aus den jaren 1920–1923,* Verlag von Julius Springer, Berlin (1924).
20. D.A. Purser, Chapter 4: Asphyxiant components of fire effluents. In "Fire toxicity" Eds A. Stec and R. Hull. Woodhead, Cambridge UK, 2010 pp 118–198
21. D.A. Purser and M. Kuipers, M. (2004) Interactions between buildings, fire and occupant behaviour using a relational database created from incident investigations and interviews. 3rd International Symposium on Human Behaviour in Fire. Europa Hotel, Belfast, 1–3rd September 2004. Proceedings pp. 443–456 Interscience Communications, London UK.
22. G.L. Nelson, "Carbon Monoxide and Fire Toxicity: A Review and Analysis of Recent Work, "*Fire Technology,* 34, pp. 38–58 (1998).
23. R.A. Anderson, I. Thompson, and W.A. Harland, "The Importance of Cyanide and Organic Nitriles in Fire Fatalities," *Fire and Materials,* 3, pp. 91–99 (1979).
24. J.L. McAllister, R.J. Roby, B. Levine, and D. Purser, Stability of cyanide in cadavers and in postmortem stored tissue specimens: A review. J. Analytical Toxicology. 32, 1–9(2008)
25. D.A. Purser, P. Grimshaw, and K.R. Berrill, "Intoxication by Cyanide in Fires: A Study in Monkeys Using Polyacrylonitrile," *Archives of Environmental Health,* 39, pp. 394–400 (1984).
26. D.A. Purser, "Determination of Blood Cyanide and Its Role in Producing Incapacitation in Fire Victims," *Royal Society of Chemistry Meeting,* Huntingdon (1984).
27. D.A. Purser, "Toxic Product Yield and Hazard Assessment for Fully Enclosed Design Fires Involving Fire Retarded Materials," *Polymer International,* 47, pp. 1232–1255 (2000).
28. D.A. Purser, J.A. Rowley, P.J. Fardell, and M. Bensilum, "Fully Enclosed Design Fires for Hazard Assessment in Relation to Yields of Carbon Monoxide and Hydrogen Cyanide," *Interflam'99. Eighth International Fire Science and Engineering Conference,* Edinburgh, Proceedings pp. 1163–1169, Interscience Communications, London (June–July 1999).
29. F.J. Baud, P. Barriot, V. Toffis, et al., "Elevated Blood Cyanide Concentrations in Victims of Smoke Inhalation," *New England Journal of Medicine,* 325, pp. 1761–1766 (1991).
30. King, D.F. (1988) Aircraft Accident Report 8/88, UK Department if Transport. Air Accidents Investigation Branch. HMSO. London, UK.
31. D.A. Purser and J.A. Purser, HCN yields and fate of fuel nitrogen for materials under different combustion conditions in the ISO 19700 tube furnace. Fire Safety Science – Proceedings of the ninth international symposium. 2008. pp 1117–11128. International Association for Fire Safety Science.
32. D.A. Purser and P. Buckley, "Lung Irritance and Inflammation During and After Exposure to Thermal Decomposition Products from Polymeric Materials," *Medicine Science and the Law,* 23, pp. 142–150 (1983).
33. D.A. Purser and K.R. Berrill, "Effects of Carbon Monoxide on Behaviour in Monkeys in Relation to Human Fire Hazard," *Archives of Environmental Health,* 38, pp. 308–315 (1983).
34. D.A. Purser, "A Bioassay Model for Testing the Incapacitating Effects of Exposure to Combustion Product Atmospheres Using Cynomolgus Monkeys," *Journal of Fire Sciences,* 2, pp. 20–26 (1984).
35. D.A. Purser and P. Grimshaw. (1984) The incapacitative effects of exposure to the thermal decomposition products of polyurethane foams. Fire and Materials. 8, 10–16.
36. Kaplan H. L., Grand, A.F., Switzer, W.G., Mitchell, D.S., Rogers, W.R. and Hartzell, G.E. Effects of Combustion Gases On Escape Performance of the Baboon and the Rat Journal of Fire Sciences, Vol. 3, No. 4, 228–244 (1985) DOI: 10.1177/073490418500300401
37. W.D. Woolley, S.A. Ames, and P.J. Fardell, "Chemical Aspects of Combustion Toxicology of Fires," *Fire Materials,* 3, pp. 110–120 (1979).
38. D.A. Purser, A.A Stec and T.R. Hull, Chapter 2: Fire scenarios and combustion conditions. In "Fire toxicity" Eds A. Stec and R. Hull. Woodhead, Cambridge UK, 2010 pp 26–50

39. D.A. Purser, A.A. Stec and T.R. Hull, Chapter 14: Effects of material and fire conditions on toxic product yields. In "Fire toxicity" Eds A. Stec and R. Hull. Woodhead, Cambridge UK, 2010 pp 515–540.
40. V. Babrauskas, B.C. Levin, R.G. Gann, et al., Toxic Potency Measurement for Fire Hazard Analysis, NIST Special Publication 827 (1991).
41. DIN, "Producing Thermal Decomposition Products from Materials in an Air Stream and Their Toxicological Testing," DIN 53 436, Deutsches Institut für Normung, Berlin, Germany.
42. H. Klimisch, H.W. Hollander, and J. Thyssen, "Comparative Measurements of the Toxicity to Laboratory Animals of Products of Thermal Decomposition Generated by the Method of DIN 53 436," Journal of Combustion Toxicology, 7, pp. 209–230 (1980).
43. Jounay, J.M., Boudene, C. and Truhout, R. The physiogram as a method for the evaluation of combustion products in controlled ventilation experiments. Polymer Conference Salt Lake City, 1976.
44. Purser, D.A. (1992) The evolution of toxic effluents in fires and the assessment of toxic hazard. Toxicology Letters, 64/65, 247–255. doi:10.1016/0378-4274(92)90196-Q
45. Determination of the Lethal Toxic Potency of Fire Effluents," *ISO 13344* (1996).
46. Levin, B.C.(1996) New research avenues in toxicology: 7-gas N-gas model, toxicant suppressants and genetic toxicology. Toxicology, 115: 89–106. doi:10.1016/S0300-483X(96)03497-X
47. Hartzell, G.E., Grand A.F and Switzer, W.G (1987) Modeling of Toxicological Effects of Fire Gases: VI. Further Studies on the Toxicity of Smoke Containing Hydrogen Chloride Journal of Fire Sciences, 5:368–391 DOI: 10.1177/073490418700500602
48. B. Levin, J. Gurman, M. Paabo, L. Baier and T. Holt. Toxicological effects of different time exposures to fire gases: carbon monoxide or hydrogen cyanide or to carbon monoxide combined with hydrogen cyanide or carbon dioxide. Proceedings of the 9th Joint Panel Meeting of the UNJR Panel on Fire Research and Safety, US National Bureau of Standards, Gaithersburg. MD. Report NBSIR 88–3753, p 368, 1988.
49. B.C. Levin, M. Paabo, J.L. Gurman, and S.C. Harris, "Effects of Exposure to Single or Multiple Combinations of the Predominant Toxic Gases and Low-Oxygen Atmospheres Produced in Fires," Fundamental and Applied Toxicology, 9, pp. 236–250 (1987). doi:10.1016/0272-0590(87)90046-7
50. J.A. Pauluhn Retrospective Analysis of Predicted and Observed Smoke Lethal Toxic Potency Values. J. Fire Science 11 109–130 (1993).
51. "Documentation of the Threshold Limit Values for Substances in Workroom Air," *American Conference of Governmental Industrial Hygienists,* Cincinnati (1980).
52. F.W. Beswick, P. Holland, and K.H. Kemp, "Acute Effects of Exposure to Orthochlorobenzylidene Malonitrile (CS) and the Development of Tolerance," *British Journal of Industrial Medicine,* 29, pp. 298–306 (1972).
53. C.L. Punte, J.T. Weimer, T.A. Ballard, and J.L. Wilding, "Toxicologic studies on o-Chlorobenzylidene Malononitrile," *Toxicology and Applied Pharmacology,* 4, pp. 656–662 (1962).
54. B. Ballantyne and S. Calloway, "Inhalation Toxicology and Pathology of Animals Exposed to o-Chlorobenzylidene Malonitrile," *Medicine, Science and the Law,* 12, pp. 43–65 (1972).
55. *Registry of Toxic Effects of Chemical Substances,* National Institute for Occupational Safety and Health, Washington, DC (1982).
56. L. Kane, C.S. Barrow, and Y. Alarie, "A Short-Term Test to Predict Acceptable Levels of Exposure to Airborne Sensory Irritants," *American Industrial Hygiene Association Journal,* 40, pp. 207–209 (1979).
57. H.L. Kaplan, A.F. Grand, W.R. Rogers, W.G. Switzer, and G.C. Hartzell, "Combustion Gases in Postcrash Aircraft Fires," *DOT/FAA/CT-84/16,* Federal Aviation Administration, Washington, DC (1984
58. Y. Alarie, *Proceedings of the Inhalation Toxicology Symposium, Upjohn Company,* Ann Arbor Science (The Butterworth Group), Ann Arbor, MI (1980).
59. H. Salem and H. Cullumbine, "Inhalation Toxicities of Some Aldehydes," *Toxicology and Applied Pharmacology,* 2, pp. 183–187 (1960).
60. T.J. Cole, J.E. Cotes, G.R. Johnson, H. deV. Martin, J.W. Reed, and M.J. Saunders, "Ventilation, Cardiac Frequency and Pattern of Breathing During Exercise in Men Exposed to o-Chlorobenzylidene Malonitrile (CS) and Ammonia Gas in Low Concentrations," *Quarterly Journal of Experimental Physiology,* 62, pp. 341–351 (1977).
61. Y. Alarie, "Bioassay for Evaluating the Potency of Airborne Sensory Irritants and Predicting Acceptable Levels of Exposure in Man," *Food and Cosmetics Toxicology,* 19, pp. 623–626 (1981).
62. D.A. Purser, "Behavioural Impairment in Smoke Environments," *Toxicology,* 115, pp. 25–40 (1996).
63. "British Standard Code of Practice for Assessment of Hazard to Life and Health from Fire. Part 2: Guidance on Methods for the Quantification of Hazards to Life and Health and Estimation of Time to Incapacitation and Death in Fires," *BS 7899-2,* British Standards, London (1999).
64. D.A. Purser, "The Harmonization of Toxic Potency Data for Materials Obtained from Small and Large Scale Tests and Their Use in Calculations for the Prediction of Toxic Hazard in Fire," *Proceedings of First International Fire and Materials Conference,*

Interscience Communications, London, pp. 179–200 (1992).
65. D.A. Purser, "Recent Developments in Understanding the Toxicity of PTFE Thermal Decomposition Products," *Fire and Materials,* 16, pp. 67–75 (1992).
66. Purser, D.A and Purser J.A. The potential for including fire chemistry and toxicity in fire safety engineering. BRE Project Report No. 202804. 26th March 2004. Building Research Establishment. Garston Watford UK.
67. D.A. Purser, Toxicity of fire retardants in relation to life safety and environmental hazards. In: Fire Retardant Materials. Ed. A.R. Horrocks and D. Price. Chapter 3 pp. 69–127.(2001) Woodhead Publishing Ltd, Cambridge UK.
68. D.A. Purser, "Recent Developments in the Use of a Tube Furnace Method for Evaluating Toxic Product Yields under a Range of Fire Conditions," *Fire Protection Research Association 2000 Fire Risk and Hazard Research Application Symposium,* Atlantic City (June 28–30, 2000).
69. T.R. Hull, J.M. Carmen, and D.A. Purser, "Prediction of CO2/CO Ratios of Underventilated Polymer Fires," *Polymer International,* 49, pp. 1259–1265 (2000).
70. W.M. Pitts, "The Global Equivalence Ratio Concept and the Formation Mechanisms of Carbon Monoxide in Enclosure Fires," *Progress in Energy and Combustion Science,* 21, pp. 197–237 (1995).
71. D.A. Purser, The application of exposure concentration and dose to evaluation of the effects of irritants as components of fire hazard. Interflam 2007. 3–5th September 2007 Royal Holloway College, Egham, UK. Proceeding pp. 1033–1041. Interscience Communications, Greenwich, UK.
72. Purser D.A, Chapter 3: Hazards from smoke and irritants. In "Fire toxicity" Eds A. Stec and R. Hull. Woodhead, Cambridge UK, 2010 pp 51–117.
73. D. Campbell, *Respiratory Tract Trauma in Burned Patients,* Colloquium, Borehamwood, UK (1985).
74. C.L. Punte, E.J. Owens, and P.J. Gutentag, "Exposures to ortho-Chlorobenzylidene Malonitrile," *Archives of Environmental Health,* 6, pp. 366–374 (1963).
75. T. Jin, "Studies of Emotional Instability in Smoke from Fires," *Journal of Fire and Flammability,* 12, pp. 130–142 (1981).
76. D.J. Rasbash, *Fire International,* 5, 40, p. 30 (1975).
77. Y. Alarie, "Sensory Irritation by Airborne Chemicals," *CRC Critical Reviews in Toxicology,* 2, p. 299 (1973).
78. D. Canter, Studies of Human Behavior in Fire: Empirical Results and Their Implications for Education and Design, University of Surrey, UK (1983).
79. R. Melzack and P.D. Wall, "Pain Mechanisms: A New Theory," *Science,* 150, pp. 971–979 (1965).
80. D.G. Clark, S. Buch, J.E. Doe, H. Frith, and D.H. Pullinger, "Bronchopulmonary Function: Report of the Main Working Party," *Pharmacology and Therapeutics,* 5, pp. 149–179 (1979).
81. C.S. Barrow, H. Lucia, M.F. Stock, and M.F. and Y. Alarie, "Development of Methodologies to Assess the Relative Hazards from Thermal Decomposition Products of Polymeric Materials," *American Industrial Hygiene Association Journal,* 40, pp. 408–423 (1979).
82. Y. Alarie and R.C. Anderson, "Toxicologic and Acute Lethal Hazard Evaluation of Thermal Decomposition Products of Synthetic and Natural Polymers," *Toxicology and Applied Pharmacology,* 51, pp. 341–362 (1979).
83. W.J. Potts and T.S. Lederer, "A Method for Comparative Testing of Smoke Toxicity," *Journal of Combustion Toxicology,* 4, pp. 114–162 (1977).
84. T. Jin, "Visibility through Fire Smoke—Part 5, Allowable Smoke Density for Escape from Fire." *Report No. 42,* Fire Research Institute of Japan, p. 12 (1976).
85. D.A. Purser, "Interactions Among Carbon Monoxide, Hydrogen Cyanide, Low Oxygen Hypoxia, Carbon Dioxide and Inhaled Irritant Gases," in Carbon Monoxide Toxicity Chapter 7 pp. 157–192. D.G. Penney ed, CRC Press Boca Raton (2000)
86. M.M. Hirschler and D.A. Purser, "Irritancy of the Smoke (Non-Flaming Mode) from Materials Used for Coating Wire and Cable Products, Both in the Presence and Absence of Halogens in their Chemical Composition," *Fire and Materials,* 17, pp. 7–20 (1993).
87. D.A. Purser, "Modeling Time to Incapacitation and Death from Toxic and Physical Hazards in Aircraft Fires," in *Conference Proceedings No. 467, Aircraft Fire Safety, NATO-AGARD,* Sintra, Portugal, pp. 41-1–41-13 (May 22–26, 1989).
88. *Emergency Response Planning Guidelines,* American Industrial Hygiene Association, Akron, OH (1989).
89. NAC/AEGL, "Acute Exposure Guidelines for Selected Airborne Chemicals," National Advisory Committee for Acute Exposure Guideline Levels for Hazardous Substances, Subcommittee on Acute Exposure Guideline Levels, Committee on Toxicology, Board on Environmental Studies and Toxicology, National Research Council of the National Academies, National Academies Press, Washington, DC (2004). Note: Reviews of new substances are being added on a continuing basis.
90. D.A. Purser, "ASET and RSET: Addressing Some Issues in Relation to Occupant Behaviour and Tenability," in *Proceedings of the 7th International Symposium on Fire Safety Science,* International Association for Fire Safety Science, Boston, MA, pp. 91–102 (2003).
91. T.R. Hull, D. Price, J.M. Carman, and D. Purser, "Studies of Carbon/Oxygen Chemistry Under Different Fire Conditions," in *Proceedings of the Interflam'99 Conference,* Vol. 2, pp. 189–199,

Interscience Communications Ltd., London, UK (1999).
92. M. Carman, D.A. Purser, T.R. Hull, D. Price, and G.J. Milnes, "Experimental Parameters Affecting the Performance of the Purser Furnace—A Laboratory Scale Experiment for a Range of Controlled Real Fire Conditions," Fire Retardant Polymers, 7th European Conference, in *Polymer International,* 49, pp. 1256–1258 (2000).
93. P. Blomqvist, "A Small-Scale Controlled Equivalence Ratio Tube Furnace Method—Experience of the Method and the Link to Large-Scale Fires," in *Proceedings of the Interflam 2007 Conference,* London, UK, pp. 391–402 (2007).
94. "Tube Furnace Method for the Determination of Toxic Product Yields in Fire Effluents," BS7900 British Standards Institution, London, UK (2003).
95. NFX 70-100-1, "Methods for Analysing Gases Stemming from Thermal Degradation," AFNOR, Paris, France (2001).
96. NFPA 287, *Standard Test Methods for Measurement of Flammability of Materials in Cleanrooms Using a Fire Propagation Apparatus (FPA),* National Fire Protection Association International, Quincy, MA (2007).
97. "Reaction-to-Fire Tests—Heat Release, Smoke Production, and Mass Loss Rate—Part 1: Heat Release (cone calorimeter method)," ISO 5660-1, ISO, Geneva, Switzerland (2002).
98. ASTM E662, *Standard Test Method for Specific Optical Density of Smoke Generated by Solid Materials,* ASTM International, West Conshohocken, PA.
99. IMO, *FTP Code: International Code for Application of Fire Test Procedures,* Resolution MSC 61(67), International Maritime Organization, London, UK (1998).
100. "Code of Practice for Fire Precautions in the Design and Construction of Passenger Carrying Trains," BS 68553, British Standards Institution, London, UK (1999).
101. "Toxicity Testing of Fire Effluents—Part 5. Prediction of Toxic Effects of Fire Effluents," *ISO/IEC TR 9122-5* (1993).
102. "Code of Practice for Assessment of Hazard to Life and Health from Fire—Part 2. Guidance on Methods for the Quantification of Hazards to Life and Health and Estimation of Time to Incapacitation and Death in Fires, B57899-2 (1999).
103. G. Kimmerle and F.C. Prager, "The Relative Toxicity of Pyrolysis Products. Part II. Polyisocyanate-Based Foam Materials," *Journal of Combustion Toxicology,* 7, pp. 54–69 (1980).
104. V. Babrauskas, "Development of the Cone Calorimeter—A Bench Scale Heat Release Rate Apparatus Based on Oxygen Consumption," *NBSIR 82-2611,* National Bureau of Standards, Washington, DC (1982).
105. "Toxicity Testing of Fire Effluents—Part 4, The Fire Model." *ISO/IEC TR 9122-4,* International Organization for Standardization, Geneva, Switzerland (1993).
106. G.E. Hartzell, W.G. Switzer, and D.N. Priest, "Modeling of Toxicological Effects of Fire Gases: V Mathematical Modelling of Intoxication of Rats by Combined Carbon Monoxide and Hydrogen Cyanide Atmospheres," *Journal of Fire Sciences,* 3, pp. 330–342 (1985).
107. G.E. Hartzell, S.C. Packham, A.F. Grand, and W.G. Switzer, "Modeling of Toxicological Effects of Fire Gases: III. Quantification of Post-Exposure Lethality of Rats from Exposure to HCI Atmospheres," *Journal of Fire Sciences,* 3, pp. 196–207 (1985).
108. W.A. Burgess, R.D. Trietman, and A. Gold, "IR Contaminants in Structural Firefighting," *Final Report to the National Fire Prevention and Control Administration and the Society of Plastics Industry Inc.,* Harvard School of Public Health, Cambridge, MA (1979).
109. D.A. Purser, "The Development of Toxic Hazard in Fires from Polyurethane Foams and the Effects of Fire Retardants," in *Proceedings of Flame Retardants 90, (*British Plastics Federation, ed.), Elsevier, London, pp. 206–221 (1990).
110. R.C. Anderson and Y.C. Alarie, "Screening Procedures to Recognize 'Supertoxic' Decomposition Products from Polymeric Materials Under Thermal Stress," *Journal of Combustion Toxicology,* 5, pp. 54–63 (1978).
111. W.E. Coleman, L.D. Scheel, R.E. Kupel, and R.L. Larkin, "The Identification of Toxic Compounds in the Pyrolysis Products of Polytetrafluoroethylene (PTFE)," *American Industrial Hygiene Association Journal,* 29, pp. 33–40 (1968).
112. S.J. Williams and F.B. Clarke, "Combustion Product Toxicity: Dependence on the Mode of Product Generation," *Fire Materials,* 6, pp. 161–162 (1982).

David A. Purser has a PhD in neurophysiology and a diploma in toxicology from the Royal College of Pathologists. As former director of combustion toxicology research at Huntingdon Research Centre, England, and subsequently as associate director of the Fire Safety Engineering Centre in the Fire and Risk Sciences Division at BRE Ltd., Watford, England, he has worked on fire chemistry, combustion toxicology, fire assessment, fire incident investigation, building code development and human behavior in fires for over 35 years. Since retiring from BRE in 2006, he continues with consultancy and academic work, as adjunct faculty at the University of Maryland (until 2014) and visiting professor at the Universities of Greenwich and Central Lancashire UK. He was a member of the Scientific Advisory Committee of the US National Association of State Fire Marshals (until 2014). He chaired the British Standards Committee on fire hazards until 2011 and serves as an expert on the International Organization for Standardization (ISO) fire hazard and fire safety engineering subcommittees and working groups.

Assessment of Hazards to Occupants from Smoke, Toxic Gases, and Heat

63

David A. Purser and Jamie L. McAllister

Introduction

The aims of this chapter are to provide methods for the assessment of life safety hazards in fires and an understanding of the effects of smoke, heat, and toxic fire effluents on occupants of buildings and other enclosures. Detailed discussions of the physiology and derivation of expressions suitable for a range of applications are presented in the main sections of the chapter. The assessment of toxic products from materials and the findings from studies of the toxicity of fire effluents in humans and animals from fire incident investigations, large and bench-scale fire tests and animal exposures is presented in Chap. 62 [1].

To aid the reader wishing to apply the methods to engineering hazard calculations, a summary of all the principal calculation expressions required for ASET design calculations, is presented in Appendix 1 with an example of an application in Table 63.22 and associated explanations. Full descriptions of the derivation of the different expressions, with more detail variations for specific applications, and further examples are presented in the later sections of this chapter. The summary section expressions are fully cross-referenced to the main text.

D.A. Purser (✉)
Hartford Environmental Research, Hatfield, United Kingdom

J.L. McAllister
National Institute of Standards and Technology

Fire effluents consist of a highly complex mixture of liquid and solid smoke particulates and vapors containing many hundreds of substances many of which are toxic. The range of toxic substances evolved in fires and their yields depends on the composition of the burning fuel and the decomposition conditions. The toxic effects of exposure, the potency of the different toxic substances (concentration or dose required to produce a toxic effect) and the interactions between different components are also complex, ranging from incapacitating effects on escape capability and survival to increased risk of developing cancer after many years of exposure. The toxic hazards considered in this chapter are limited to those considered important in relation to escape and survival during and immediately after exposure in fires. A major simplifying principle is that the main incapacitating effects on fire victims are caused by a small number of key irritant and asphyxiant substances and that the main interactions between the individual substances are essentially additive. The justification for these assumptions, based upon the results of fire incident investigations and experimental studies of the toxicity and physiological effects of individual fire gases and combustion product mixture using animals, is examined in Chap. 62. Chapter 62 also considers the use of small-scale toxicity test data. This includes consideration of methods for the calculation of toxic potency from chemical yield data obtained from small-scale tests and their application to full-scale fire scenario calculations. Toxic hazards in different

M.J. Hurley (ed.), *SFPE Handbook of Fire Protection Engineering*,
DOI 10.1007/978-1-4939-2565-0_63, © Society of Fire Protection Engineers 2016

types of full-scale fire scenarios are discussed here in Chap. 63.

The development of fire hazards is time based, and the endpoint of an ASET (Available Safe Escape Time) design calculation is the time when conditions in each building enclosure are considered untenable. Untenable conditions occur when it is predicted that occupants inside or entering an enclosure are likely to be unable to save themselves due to the effects of exposure to smoke, heat, and/or toxic effluent, or when occupants of refuge areas are exposed to conditions capable of causing injury or death. Exposure to fire effluents also affects escape behavior and travel speeds, thereby influencing the time required for escape (RSET—Required Safe Escape Time).

The effects on occupants of exposure to any particular set of conditions and the probability that they will be able to escape depend on a variety of factors including the fire conditions, the physiological and behavioral susceptibilities of the individuals or groups of occupants exposed, the nature of the occupancy, and the fire scenario. There are also some degrees of uncertainty in the predictability of effects of toxic gases, smoke, and heat on the average person, and also uncertainties related to variations in susceptibility within the population. The margin of safety designated as acceptable for a design therefore needs to be determined by the designer and regulatory authority in the context of any particular application. The different sections in this chapter describe the effects of exposure to different fire hazards and calculation methods that may assist with decisions on acceptable design limits. Information is also presented on lethal and post-exposure health effects, which may also be relevant to these considerations, as well as to probabilistic fire safety engineering design and forensic fire incident investigation.

Fundamental Aspects of Toxicity and Toxic Hazard Assessment

Life Safety Objectives of Design Codes

The main objective of life safety design is to provide building occupants with an acceptable level of safety from fire. What constitutes "acceptable" depends upon the objectives of the local building and life safety codes. In the United States and the United Kingdom, the basic objectives are performance-based. For example, the scope of the NFPA Life Safety code [2] is to prevent danger to life through "construction, protection, and occupancy features" and to provide egress facilities capable of supporting the "prompt escape of occupants" in the event of a fire. The document further states that the goals are to protect occupants not intimate with the fire and improve survivability of those occupants who are intimate with the fire.

For the United Kingdom (England and Wales), the performance-based requirement for means of warning and escape (Requirement of part B1 of the Building Regulations (England and Wales) 2006) [3] states that the design shall provide occupants with" .....early warning of fire, and appropriate means of escape in case of fire from the building to a place of safety outside the building capable of being safely and effectively used at all material times".

Both the U.S. and U.K. requirements can be met by following prescriptive design guidance or by a performance-based design.

On a global level, In the International Organization for Standardization (ISO) publication ISO/TR 13387 Fire safety engineering Part 8: Life Safety—Occupant behaviour, location and condition [4], the life safety objectives of a design are stated as:" Should a fire occur in which occupants are exposed to fire effluent and/or heat, the objective of the fire safety engineering strategy is to ensure that such exposure does not significantly impede or prevent the safe escape (if required) of essentially all occupants, without their experiencing or developing serious health effects".

Hence, the general objective is the same, the design should limit or prevent exposure of most occupants during the majority of envisaged scenarios; This is achieved either by evacuating occupants to the outside of the building (or intermediate area of temporary refuge) via protected escape routes or by using a "defend in place" strategy which relies on the prevention of fire and fire effluent spread into the occupied areas.

Although these design strategies have been effective (e.g., the risk of injuries and death in fire is low compared with other risks), the annual rates of injury and death from fire still remain considerable.

From an engineering design perspective, it is possible to work to a variety of life-safety endpoints depending upon the system being designed and the possible fire scenarios envisaged. For example, the designer may:

- Design for no exposure to heat or smoke for worst-case fire scenarios.
- Accept that for a few envisaged scenarios certain occupants may experience some degree of exposure, but demonstrate that such exposure would be insufficient to significantly impair escape or result in significant injury, long-term health effects, or death.
- Accept that for a few envisaged scenarios there is a risk of deaths but that the risk is acceptable or comparable with those from a code-compliant, prescriptive design (using a probabilistic risk assessment).

The first scenario, where no exposure to occupants occurs, may be possible for some design cases. For example, a shopping mall may be designed with passive or active smoke extraction assuming a worst-case fire scenario. The smoke extraction system may be designed such that the smoke layer never descends lower than a given level above an average walking height and the upper layer temperature never exceeds 200 °C. This would allow occupants to escape without exposure to smoke and without experiencing pain from downward heat radiation.

This strategy relies on all smoke from the fire being sufficiently buoyant such that no smoke that none cools and mixes near the floor. Similarly, evacuation from multi-compartment buildings relies on the passive and active systems completely preventing smoke contamination of escape routes and occupied enclosures. In practice, this ideal situation, often, does not occur and it is not possible to ensure that there is no smoke exposure. When fire occurs within an occupied enclosure, especially small (domestic sized) enclosures and ones with a relatively low ceiling height, then it is difficult to prevent some exposure of occupants, especially those more intimate with the initial fire (as recognized by the NFPA life safety code). Some smoke exposure is also likely in sprinkelered enclosures due to downdrag and loss of smoke buoyancy. Additionally, there is always the potential that a system may be rendered inoperable (e.g., human interaction, mechanical failure, etc.) or fail to operate effectively. For all these situations occupants are likely to suffer some exposure to toxic fire effluents and/or heat.

An example of the second scenario, where some exposures occur but are not expected to be life threatening, might be for an atrium space with high-level balconies near the roof level. For any fire at a lower level, a buoyant smoke plume will rise and mix to form a dilute layer, which may extend down to engulf the upper balconies, or stratify at a certain height. Since the smoke is so dilute, this may be considered a minor hazard to occupants needing to move through it (e.g., to reach protected stairs). In this scenario, it is therefore necessary to determine the highest acceptable concentration of smoke and toxic gases to which occupants may be exposed without significant impairment of escape capability or injury.

The third type of scenario, where there is a risk of death is for serious fires—such as in the Station Nightclub, or domestic dwelling fires. For such fires, conditions are benign for a minute or so after ignition, but then rapidly become life threatening. The rapidly deteriorating conditions result in occupant exposure to hot, dense, irritant smoke impairing escape capability and leading to incapacitation and death. Analysis of such a scenario is aimed at estimating the probability that occupants will be able to escape prior to untenability. It is also aimed at estimating the risk of injury and death throughout the life of the building, either for specific scenarios or for a range of scenarios with varying probabilities. Solutions to preventing or minimizing such outcomes are likely to involve a variety of interventions other than modification of the toxic product yields from the fuels involved, included modifications to the reaction-to-fire properties of fuels, improved warning systems, modified structural

design or installation of active systems. Assessment of the hazards to occupants in different potential fire scenarios can be regarded as the ultimate test of the safety performance of the system. Analysis of hazards during serious fires is also important in relation to incident investigations.

The methods described in this chapter are intended for application to all these kinds of situations

Injuries and Deaths in Fire: Extent to Which Life Safety Objectives Are Achieved

Although exposure to toxic smoke has always been one of the hazards confronting people in fires, there was a considerable increase in concern in this area during the 1970s and 1980s. In the United States, attention was focused on the toxicity of furnishings and building materials and finishes due to a number of large fire disasters where victims died from exposure to toxic smoke products [5]. Although this is also true to some extent for the United Kingdom, the major impetus for work in this area resulted from statistical surveys of fire casualties carried out in the mid-1970s. These surveys of casualties from all fires, and particularly from fires in domestic dwellings, revealed that not only was a large proportion of fatal and non-fatal fire casualties being reported in the category "overcome by smoke and toxic gases" rather than "heat and burns," but also that there was a fourfold increase in the former category between 1955 and 1971 [6] (Figs. 63.1 and 63.2). This increasing trend continued into the 1980s, so that approximately half of all fatal casualties and a third of all non-fatal casualties of dwelling fires (the majority caused by fires in furniture and bedding) were reported as being "overcome by smoke and toxic gases", while burns caused around 40 % of deaths and 20 % of injuries [7]. This increase occurred despite the fact that the total number of fires remained approximately constant.

During the 1990s, there was some reduction in the total annual number of fire deaths in the United Kingdom (and in the United States), but smoke deaths in the United Kingdom were still approximately four times the levels reported in the 1950s. Also, injuries from smoke and toxic

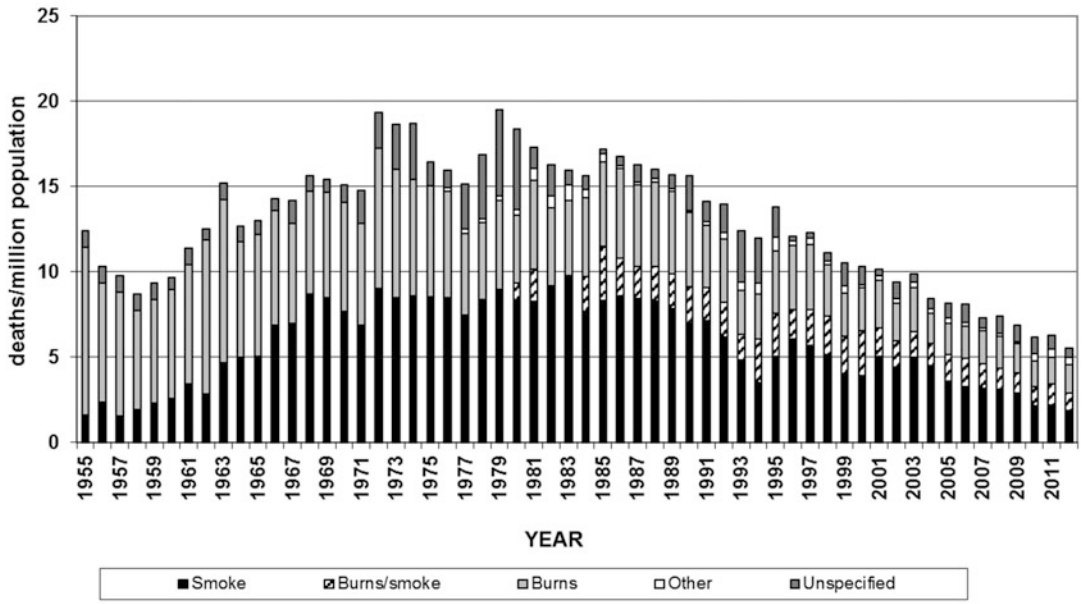

Fig. 63.1 U.K. fire deaths per million population [6, 7]

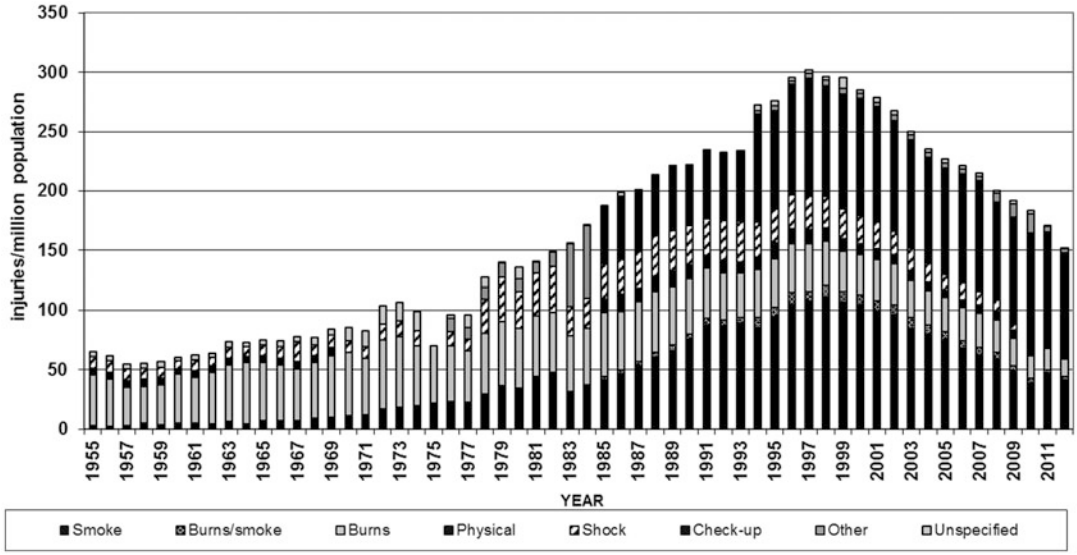

Fig. 63.2 U.K. nonfatal fire injuries per million population [6, 7]

fumes had increased continuously from an annual rate of approximately 170 in the 1950s, to 2600 during the 1980s and more than 6000, during the late 1990s. In the United Kingdom the decrease in fire deaths occurring during the 1990s improved further during the next decade from a total of 613 in 2000 to 388 (7.64/million) in 2010. The total injuries also decreased over this period from 16,183 to 11,134 (219/million of which 74.1/million were due to burns or smoke). Injuries from smoke decreased from 123/million in 2000 to 47/million in 2010.

These improvements may be related to changes in heating and cooking appliances, improved fire performance of upholstered furniture and bedding, reduced tobacco use and/or increased use of smoke detectors.

A number of possible reasons have been suggested for the earlier increase in smoke-related casualties. They have been linked with the increased use of modern synthetic materials in furnishings. Another view is that the increase may not have been directly related to modern materials but to changes in living styles over the period that have led to more furnishing and upholstery material being used in the average British home and, therefore, a greater fire load. Epidemiological data are, often, difficult to interpret, but many of those working in this area are convinced that the earlier increase in smoke-related casualties was real. The situation in the United States is more difficult to interpret, since it contains a larger and more diverse population, and statistics may not have been collected to reveal such a trend.

The U.S. fire death rates were around twice those in the United Kingdom, Western Europe (in general), and Japan 30 years ago but have improved steadily since; they are currently closer to the U.K. and European death rates at approximately 10.5 per million inhabitants [8, 9]. Figure 63.3 compares deaths per million inhabitants in the United Kingdom and United States over the period 1977–2010. The US data are plotted from both the NFPA and NFIRS data sets [10, 11]. The United States data shows a considerable variation between States, ranging from New Hampshire (4.6 deaths per million population) to West Virginia (38.7 deaths per million population [NFIRS 2006]).

In the United States and the United Kingdom, toxic smoke products are recognized as being the major cause of death in fires [12]. A possible difference between the pattern of fire deaths in the United Kingdom and the United States is that in the United Kingdom, the majority of fatalities

occur in the room of fire origin (mainly in domestic dwellings) for fires that have not spread beyond the room of fire origin (65 % of deaths). For 50 % of deaths, the fire spread is restricted to less than one-third of the room area [7] In the United States more than 50 % of deaths are reported to be remote from the room of origin, from fires that have spread beyond the room of origin [13]. Although deaths remote from the room of origin are also common in the United Kingdom, these disparities indicate that cultural differences and variations in building styles can be important. Houses in the United Kingdom are commonly constructed with masonry compared to the combustible timber construction that is more common in the United States. U.S. homes also tend to have open-floor plans, less compartmentation, and larger rooms. As in the UK, in the US by far the greatest numbers of fire deaths (76 % in 2007) and injuries occur in residences (dwellings), with only 9 % in non-residential properties.

For fire deaths, the "dose" of carbon monoxide in the blood expressed as percentage carboxyhemoglobin (%COHb) provides a good indication of the cause of death and how long a victim survived exposure before death. This is for two reasons. Firstly, as carbon monoxide is inhaled in a fire, some minutes are required for the dose to reach fatal levels (>approximately 40–50 %COHb). Secondly, during the early stages of most flaming fires combustion is efficient, so the yields and concentrations of CO in the fire enclosure are low. As compartment fires develop, they become ventilation-controlled and fuel rich, with high yields of CO and other toxic products. Fire deaths with burns and low % COHb levels are therefore indicative that the victim was intimate with the fire and that burns were the most likely cause of death, while high % COHb levels, especially in the absence of burns, are indicative that the victim was remote from the fire and overcome by exposure to toxic smoke after a period of exposure. Figures 63.4 and 63.5 show data from fatal fires in London between 2002 and 2006 [14]. Figure 63.4 is for 109 victims dying in the room of fire origin and shows a wide range of %COHb levels from 0 % to 90 %. The majority of victims have sub-lethal %COHb levels (<~40 %COHb). Almost all of these were recorded as having suffered burns, while "serious burns" indicates that burns were

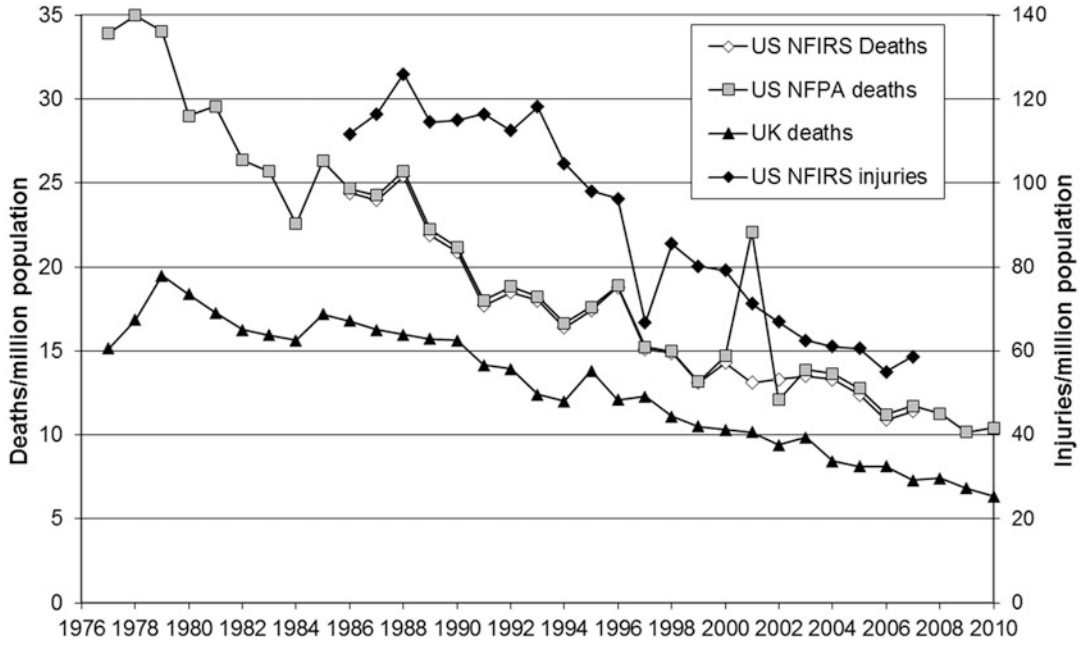

Fig. 63.3 US and UK deaths, US injuries per million population (UK: Communities and Local Government [7], US: National Fire Protection Association and National Fire Incident Reporting System) [10]

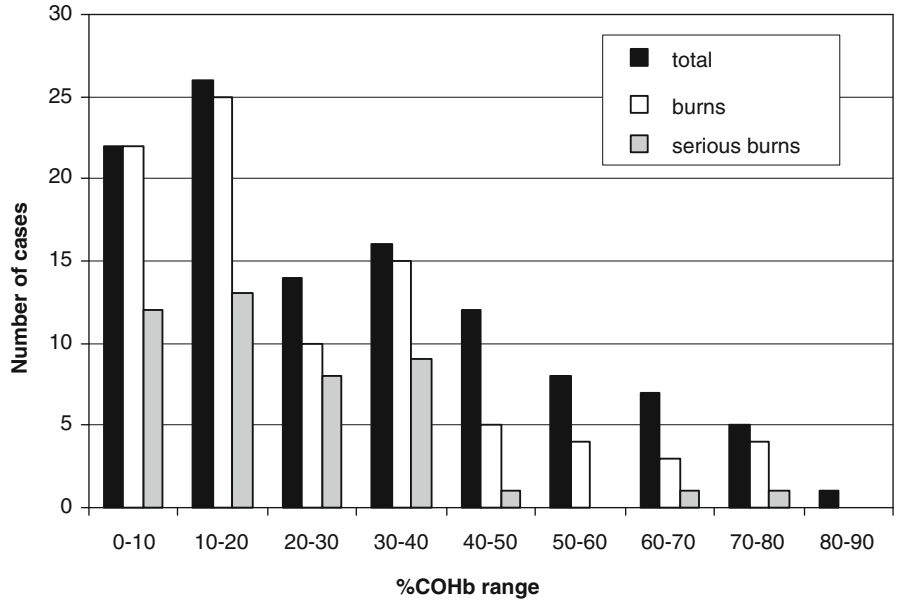

Fig. 63.4 Distributions of %COHb, burns and serious burns in 109 fire fatalities dying in enclosure of fire origin in London 2002–2006 [14]

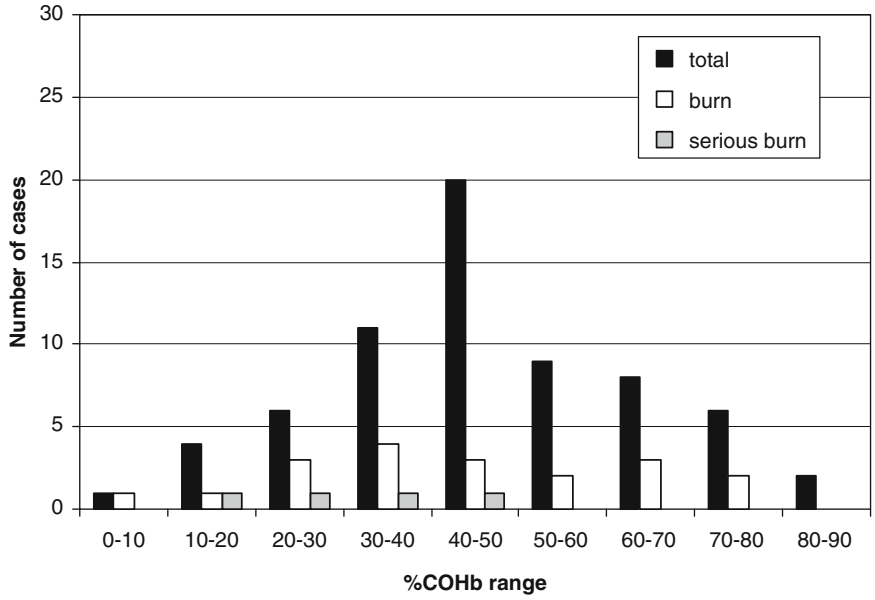

Fig. 63.5 Distributions of %COHb, burns and serious burns in 67 fire fatalities dying in enclosure remote from that of fire origin (Data from London 2002–2006 and a multi-fatality nursing home fire in Scotland) [14]

entered as a contributory cause of death on the death certificate. A smaller subset have lethal % COHb levels and a much lower incidence of burns, and of those recorded as having been more remote from the fire itself the average % COHb was 58 %, indicating that they died from the effects of toxic gases rather than burns, despite being in the same room as the fire.

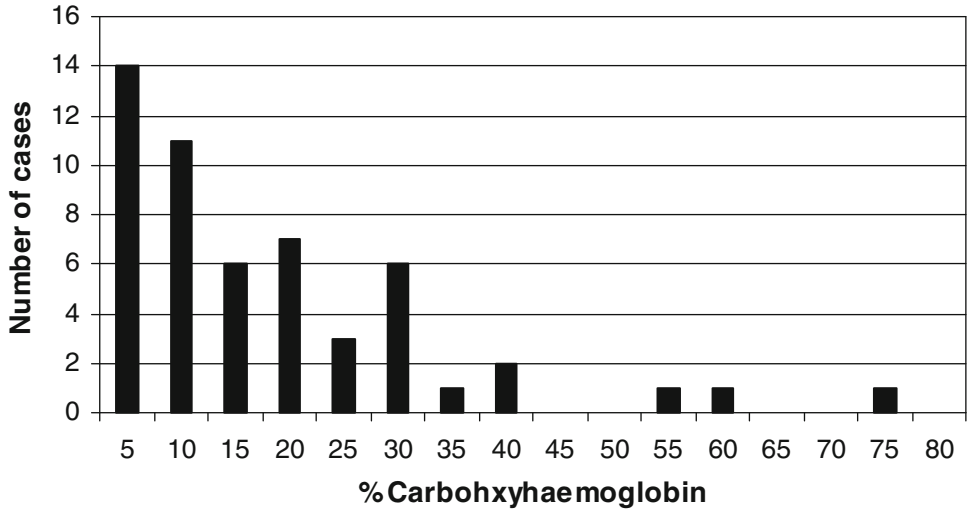

Fig. 63.6 Distributions of %carboxyhemoglobin in 53 fire fatalities in post-crash vehicle fires in Texas for which fire could be identified as contributing to the causes of death [15]

For victims dying beyond the room of fire origin (Fig. 63.5) the incidence of burns is much lower and the majority have %COHb levels in the lethal range, indicating that most people dying beyond the room of fire origin die from toxic smoke rather than from burns.

The distinction is even clearer for post-crash vehicle fires, which often involve rapid conflagrations in the passenger cabin. As Fig. 63.6 for vehicle fire deaths in Texas shows, few victims survive long enough to reach life-threatening %COHb levels [15].

Hazards in fire incidents in general result from an inadequate control of combustible contents leading to rapid fire growth and spread, especially for victims in the fire enclosure, and from failure of construction or design, so that fire or fire effluents penetrate and spread between enclosures and fire compartments. Failure of safe escape by occupants results from failure to understand the extent of fire risk and the needs of occupants, late detection, failure to provide timely and adequate warning and fire safety management, and failure to provide adequate structural containment to protect escape routes or refuge areas.

Life safety hazard from fires in buildings (or other enclosures) depends upon the performance of a dynamic system involving interactions between the building, the fire and the occupants. Since fire hazards are essentially time-based phenomena, the objective is to ensure as far as possible that should a fire occur, the occupants are warned and have time to escape before conditions become untenable. Once a fire occurs in a building the outcome in terms of fire safety and hazard depends on two parallel time-based processes, the growing fire hazard and the escape performance of the occupants.

In fire safety engineering terms it is necessary to ensure that available safe escape time (ASET) is greater than required safe escape time (RSET) by an acceptable margin of safety [16, 17].

- ASET is the time from ignition to that when conditions become untenable to occupants such that they are no longer able to escape without assistance.
- RSET is the time for ignition to that when affected occupants are able to reach a place of safety

In situations designed such that occupants are not expected to escape (defend in place strategy), then conditions in occupied enclosures should not develop so as to threaten safety.

The hazards from toxicity and heat are therefore the main determinants of ASET, but they also affect escape time, mainly in terms of the

Table 63.1 Acute survival hazards during fires

Impaired vision from smoke obscuration
Impaired vision, pain and breathing difficulties from effects of smoke irritants on eyes and respiratory tract.
Asphyxiation from toxic gases leading to confusion and loss consciousness
Pain to exposed skin and respiratory tract followed by burns from exposure to radiant and convected heat leading to collapse

effects of exposure to smoke on occupant behaviour in terms of deciding to enter and continue through smoke or turn back and seek refuge, and on walking speed and wayfinding ability.

Toxicity, or more realistically toxic hazard, in fires is a system property of the full-scale fire scenario. It consists of a sequence of time-varying effects depending upon the changing combustion conditions and the varying rates of development of a sequence of different toxic effects, caused by different toxic fire effluent components. For this reason it is not possible to make meaningful measurements of "toxicity" for any material or product in any small or even large scale fire "toxicity" test. Rather it is necessary to determine toxic hazard in terms of calculated time to incapacitation or death for specified full-scale fire scenarios.

The time required for occupants to escape depends upon a set of parameters related to fire detection and warning times, the behaviour of occupants in response to alarms in terms of starting (pre-movement) times and exit choice, and the time required to travel through escape routes and out of the building. In situations where evacuating occupants see or are exposed to smoke, their exit choice and movement speed (and hence their travel time) can be affected. These effects need to be considered in evacuation calculations, and calculation methods for these parameters are presented in this Chapter in the section on smoke.

The main tenability limits for ASET are conditions that cause incapacitation of occupants such that they are unable to escape.

For the toxic effects of exposure to combustion products in fire effluent, particularly in relation to the survival, injury or death of fire victims, it is mainly the more immediate physiological effects that dominate at the fire scene; This is because physiological effects occur rapidly, often within a few seconds, while pathological changes tend to occur over time scales of hours to years. Physiological effects also occur in response to heat and smoke exposure in fires, interacting to some extent with the effects of toxic products.

Table 63.1 lists the acute physiological fire hazards affecting escape capability. These tend to be encountered more or less in the order shown, with exposure first to smoke, which is likely to be irritant, followed by asphyxia or burns, depending upon the type of fire scenario and the proximity of the person to the fire. Once a victim has become trapped or incapacitated in a fire, then conditions usually become lethal within a further few seconds or minutes. This is because flaming fires grow exponentially, so concentrations of smoke and toxic gases, and the heat intensity, increase rapidly, resulting in death either from asphyxiation or heat exposure. The key determinant of survival is therefore incapacitation so that the lethal potency of fire effluent is of limited relevance.

Figure 63.7 illustrates the sequence and time scales over which physiological and pathological toxic effects occur during and after a fire. A common scenario is for a fire involving room contents such as an upholstered armchair on the lower floor of an enclosed two-story house with the bedroom door closed but the lounge door left open. In experiments re-creating this scenario [18] the fire self-extinguished after approximately 10 min due to oxygen depletion and the effluents then mixed evenly throughout the open volume, giving the maintained toxic gas concentrations and temperature listed in the figure. Consider the sequence of hazards faced by a bedroom occupant if they awoke and opened the

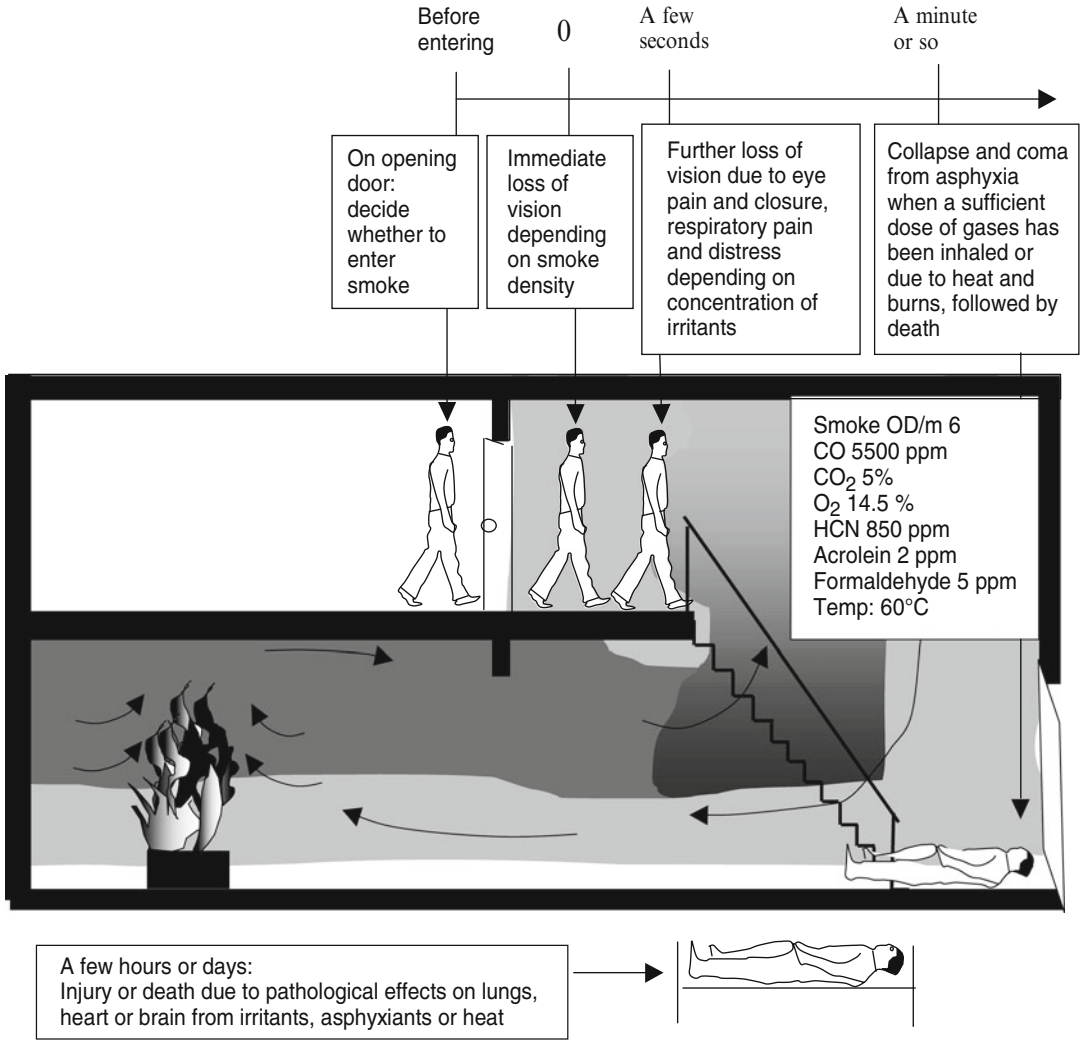

Fig. 63.7 Sequence of hazards affecting a subject escaping from a bedroom of an enclosed two-storey dwelling with a fire on the floor below

bedroom door at this time. On opening the bedroom door an occupant attempting to escape must first decide whether to enter the dense smoke, or close the door and remain in the bedroom. If they step out onto the landing the first physiological effect is immediate loss of vision, which is followed within a few seconds by further visual impairment and eye pain from the effects of smoke irritants, and pain to the nose and chest with breathing difficulties. As the subject inhales asphxyiant gases, especially CO and HCN, a dose builds up in the body. There are no immediate effects but when the inhaled dose reaches a critical level (after a few seconds or minutes) it leads to collapse and coma, followed by death within a further few minutes. In this scenario the smoke is hot (60 °C), but not sufficiently to cause pain or distress within a few minutes. If the victim is rescued alive after collapse, then they may recover, or may suffer a further set of health problems, including brain damage, heart attack or lung inflammation over a period of a few hours to a few days, all of which can be fatal.

Not only do the different physiological effects occur over a time sequence as in this example,

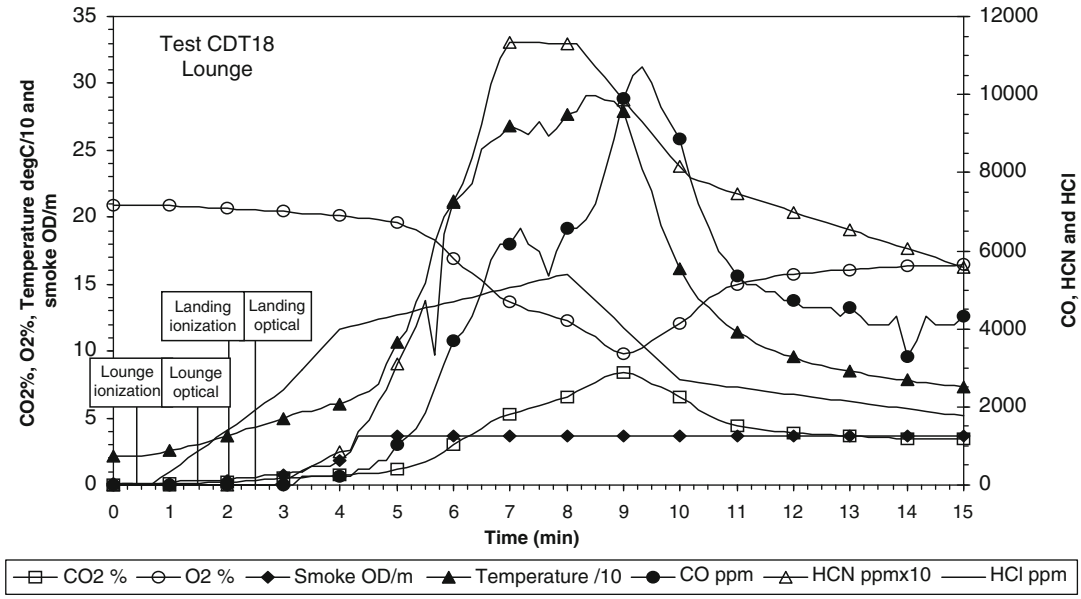

Fig. 63.8 Example of time-concentration curves for smoke, toxic gases and temperature at head height in the domestic lounge of a house during an armchair fire. The doorway to the hall is open but the house is otherwise enclosed. The time for triggering of smoke detectors is shown [18]

but in most cases the fire conditions also change rapidly as the hazards develop. Figure 63.8 shows the time concentration curves of the main fire gases, smoke, and heat in the lower floor fire room during the early stages of the same fire. In order to determine the developing hazard and time to incapacitation, it is therefore necessary to evaluate these time-dependent processes.

Fractional Effective Dose Methods and Application to Fire Hazard Analysis

ASET for any system is determined by the parameters in Table 63.2 [16]:

For application to toxic hazard calculations the concept of Fractional Effective Concentration or Dose (FEC or FED) is used whereby the exposure concentration or dose at any point during a fire is expressed as a fraction of the exposure concentration or dose predicted for a given endpoint. For example, the concentration of smoke present at any time during a fire can be expressed as a fraction of the concentration required to seriously impair escape capability. The accumulated dose of carbon monoxide at any time during a fire can be expressed as a fraction of the dose required to cause collapse and loss of consciousness, or the dose of heat can be expressed as a fraction of the dose of heat required to cause severe pain or burns. Time to loss of tenability from the effects of smoke, or toxic gases of heat is then calculated as the time at which each endpoint reaches a FEC or FED of 1.

The hazard assessment is therefore based on a "step-through" approach whereby the extent of the hazard is calculated for each successive minute (or other appropriate time interval) during the fire until the point is reached where different hazard endpoints are predicted. The behavioral and physiological effects of exposure to toxic smoke and heat in fires combine to cause varying effects on escape capability, which can lead to physical incapacitation and permanent injury or death.

The fire profile should be characterized in terms of the following range of parameters, measured over successive short periods

Table 63.2 ASET parameters

The time-concentration (or time-intensity) curves for the major toxic products, smoke and heat in the fire at the breathing zone of the occupants, which in turn depend upon:
Fire growth curve (mass loss rate of the burning fuel [kg/s] and its dispersal volume [kg/m^3] with time)
The yields of the major toxic products (kg/kg) and heat (kJ/kg) (for example kg CO per kg of material burned).
These terms can be measured directly in full-scale tests or calculated using appropriate fire dynamics computations with appropriate input data including reaction-to-fire properties and data on product yields under a range of fire conditions. Guidance on calculation methods for these terms is given in other chapters in this handbook. Some information is provided in this chapter and Chap. 62 on toxic product on toxic product yields under a range of fire conditions and also in Chaps. 16 [19] and 36 [20]. Data on toxic product yields can be obtained using the ISO TS19700 tube furnace or the ASTM E2058 flammability apparatus. A guide to the general characteristics of fires is shown in Table 63.3 and an example of a fire profile in Fig. 63.8.
The concentration/time/physiological effect relationships of these products in terms of the physiological/toxic potency of the products and heat (the exposure concentration [kg/m^3]), or exposure dose ($kg \cdot m^{-3} \cdot min$ or $ppm \cdot min$) causing toxic effects (and the equivalent effects for heat and smoke obscuration). The important endpoints are:
Concentrations, doses (or heat intensity) likely to impair escape efficiency due to behavioural and/or physiological effects
Exposure concentrations or doses likely to cause incapacitation or prevent escape due to behavioural and/or physiological effects
Lethal exposure concentrations or doses
These terms can be calculated by the application of appropriate physiological methods (Fractional Effective Dose methods [FED equations]) presented in this chapter and in ISO 13571 [21]

(<1 min) at the breathing zone of a potential victim:

1. Mass loss of material decomposed divided by the volume of air into which the material is dispersed in (mass loss concentration)
2. Carbon monoxide concentration
3. Hydrogen cyanide concentration (if materials containing >1 % by mass nitrogen are present)
4. Carbon dioxide concentration
5. Oxygen concentration
6. Incident radiant heat flux to subject
7. Air temperature
8. Smoke optical density (and particulate concentration)
9. Irritant acid gas concentrations (HF, HCl, HBr, SO_2, NO and NO_x)
   Note: If the total content of halogens in the fuel is less than approximately 5 % of the burning fuel mass, the total sulfur content less than 2 %, and the nitrogen content less than 5 %, the contribution to irritancy from acid gases can be considered minor as a first approximation.
10. Concentrations of organic irritant species (especially acrolein, formaldehyde, and crotonaldehyde)
    Note: In practice the relevant yield data for the key irritant organic species are seldom available, and not all the important species have been identified. In general it can be assumed that all smoke from compartment fires involving mixed fuels will contain concentrations of irritant organic species in proportion to the smoke optical density. Overall irritancy can then be expressed in terms of smoke optical density (or particulate concentration) plus the contribution from irritant acid gases if present in significant concentrations (see 9 above).

These data may be obtained from large-scale fire tests or calculated using fire dynamics models with appropriate data on toxic product yields under a variety of fire conditions as in Table 63.3: specifically, smoldering/nonflaming, early (well-ventilated) flaming, developed small vitiated (underventilated) flaming, and fully developed/postflashover underventilated fires.

For a basic fire engineering design there are two main considerations:

1. The time at which the concentration of smoke reaches a level such that safe escape is compromised due to

Table 63.3 Classification of toxic hazards in fires as revealed by large-scale fire simulation tests

Fire	Rate of growth	CO_2/CO	Toxic hazard	Time to incapacitation	Escape time available
1. Smoldering/non-flaming: victim in room of origin or remote	Slow	~1	CO 0–1500 ppm low O_2 15–21 % irritants, smoke	Hours	Ample if alerted
2. Well ventilated Flaming: victim in room of origin	Rapid	1000 decreasing toward 50	CO 0–0.2 % CO_2 0–10 % low O_2 10–21 % irritants, heat, smoke	A few minutes	A few minutes
3. Small vitiated flaming: victim in room of origin or remote	Rapid, then slow	<10	CO 0.2–4 % CO_2 1–10 % O2 < 12 % HCN to 1000 ppm irritants, heat, smoke	A few minutes	A few minutes
4. Fully developed: (postflashover) victim remote	Rapid	<10	O2 0–3 % in upper layer flowing from fire CO 0–3 %[a] HCN 0–1000 ppm some irritants, smoke, and possibly heat	<1 min near fire, elsewhere depends on degree of smoke dilution	Escape may be impossible or time very restricted. More time at remote locations

[a]Concentrations depend on position relative to fire compartment

(a) Behavioral and physiological effects due to exposure to heat and toxic smoke on escape behavior and ability
(b) In the absence of direct exposure, behavioral effects caused by seeing fire effluents

The effects of exposure to smoke result from impaired vision due to the optical opacity of smoke and from the painful effects of irritant smoke products on the eyes and respiratory tract. Occupant movement speed and wayfinding ability is impaired. Behavioral effects of seeing or being immersed in smoke result in a proportion of occupants being unwilling to approach smoke or heat-logged areas or escape routes.

2. The time at which the exposure dose of asphyxiant toxic gases or heat reaches a level at which occupants are likely to become incapacitated, such that they cannot save themselves and are likely to die within a minute or so unless rescued.

In a regulatory or design evaluation context, it is possible to consider several different approaches:

1. *Simple criteria for tenability based on zero exposure*. Where a design fire calculation is based on a descending upper layer of hot smoke filling an enclosure or escape route, engineering tenability criteria are often based on a minimum clear layer height of 2.5 m above the floor and a maximum upper-layer temperature of 200 °C. Occupants are considered to be willing and able to escape in clear air under such a layer and the downward heat radiation is considered tolerable.
2. *Tenability criteria accepting some degree of exposure to smoke, toxic gases and heat in relation to willingness to enter or ability to move through effluent*. In situations where smoke is mixed down to near floor level, some building occupants might move through dense smoke in some situations, but in other situations people might be unwilling to enter smoke logged escape routes, turn back, or be

unable to find an exit. Where heat is not an issue, the immediate effects of smoke depend on the visibility distance and the sensory irritancy of the smoke if people are exposed directly. For such situations, it is necessary to set tenability criteria for design purposes, depending on the level of adverse effects on occupants considered acceptable or unacceptable.

This chapter contains all the different FED and FEC expressions used for calculating time to the different toxicity and heat hazard endpoints and illustrates their use by application to sets of smoke and toxic gas data measured during full-scale experimental fires. Expressions are also presented for the effects of smoke on travel speed and on the probability that exposed subjects will attempt escape through smoke.

An FED Hazard Calculation Model for Time and Dose to Incapacitation and Lethality

From the physiological effects of exposure to the different individual irritant and aspxhyiant gases described, it has been possible to develop a comprehensive set of fractional effective dose calculation models for the assessment of human fire hazards. These models are designed to be applied to time-concentration curves for smoke and toxic gases in full-scale fires for which the data have been obtained either from full-scale fire experiments or from data derived using fire engineering zone or computational fluid dynamics (CFD) models. Complementary models have also been developed for calculating the effect of convected and radiant heat on exposed subjects.

The use of full-scale fire tests is limited by time and expense, leaving fire dynamics modeling as the often-preferred option. Although current models provide good representations of some aspects of full-scale fire scenarios, they are often limited by the extent to which they are able to represent the pyrolysis rates, effective heats of combustion, and yields of major toxic species (such as CO, HCN and acid gases) as they change with changing combustion conditions. The predictability of physiological effects in humans from exposure to toxic gases and mixtures is also affected by variations in susceptibility within the human population and uncertainties related to the need to rely on animal models. Also, while FED models are limited to consideration of a small number of key toxic products, fire effluents are known to contain many hundreds of toxic substances. This is one area where bench-scale animal exposure tests combined with chemical effluent analysis have been valuable in establishing the importance of key gases in complex mixtures and the extent of interactions between them [22, 23], as described in Chap. 62 [1].

Figure 63.8 shows an example of typical data set of fire time-concentration curves to which the FED models can be applied. The models are used to calculate time and dose to incapacitation and lethality for human exposures to fire effluents. Figures 63.9 and 63.10 show examples of FED curves calculated from time-concentration curve data. Figure 63.9 is for the static conditions in the upstairs landing of the fire illustrated in Figs. 63.7 and 63.10 is for the changing fire conditions in the lounge illustrated in Fig. 63.8. The FED models may be used for fire engineering design or product evaluation purposes by calculating ASET. This time may then be compared with an absolute requirement or in a performance-based analysis with RSET. Toxic fire effluents are the main determinants of ASET, but they can also affect RSET in that exposure to fire effluent may affect escape behavior, and movement speed is reduced in smoke, so that methods have also been developed to calculate these effects, which can be applied to evacuation models.

In addition to effects on escape capability, these methods can also be used to evaluate the probability of long-term survival and health consequences in subjects who survive immediate exposure at the fire scene.

In a forensic context, the models are used to establish causes of injury and death in fires in conjunction with full-scale incident re-creation experiments or calculations. In this context, the

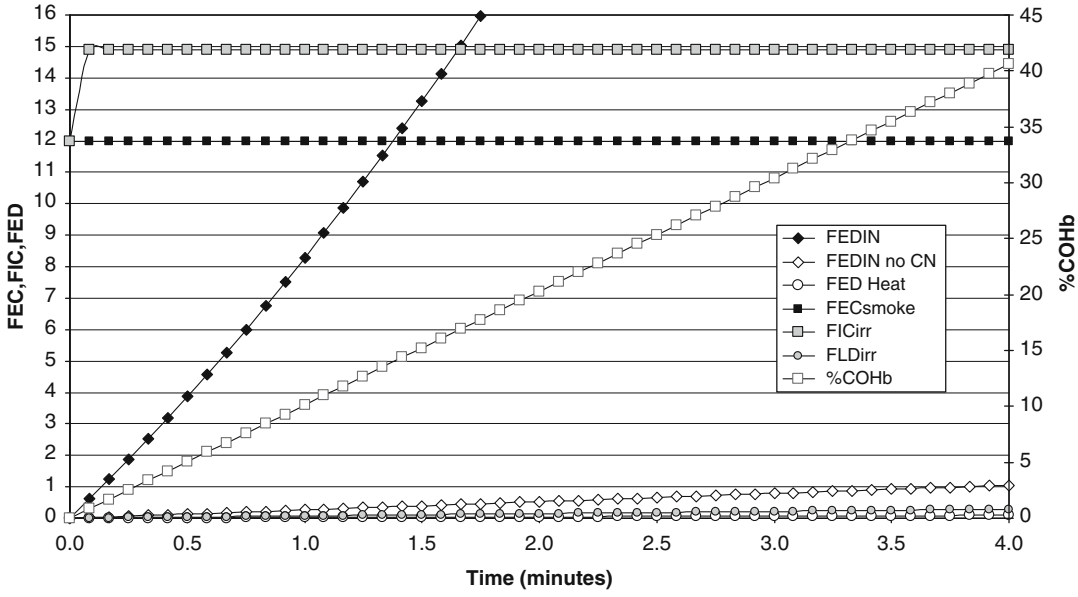

Fig. 63.9 Fractional Effective Dose plots for the static fire hazard condition in Fig. 63.7

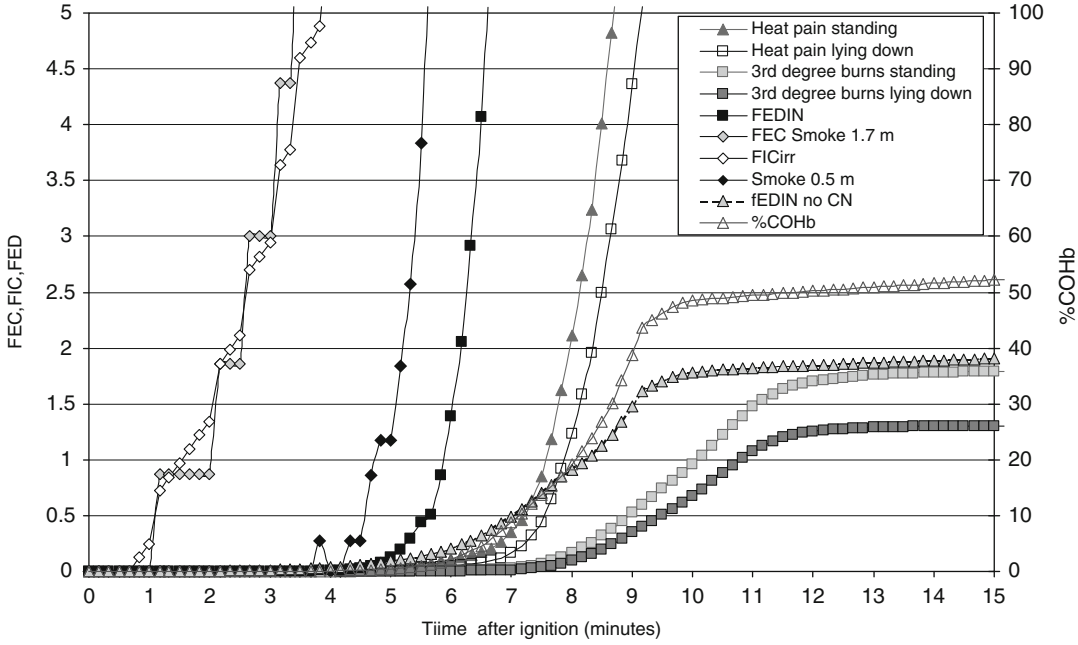

Fig. 63.10 Fractional Effective Dose plots for the changing fire hazard conditions in Fig. 63.8

application of FED modeling can also be valuable as a validation of such re-creation experiments or calculations, in that predicted effects on occupants obtained using the models can be compared to estimates of the conditions to which the actual occupants were exposed, back-calculated from the carboxyhemoglobin and blood cyanide concentrations in decedents and survivors. If the

results of the two approaches agree, this provides good evidence that the actual fire conditions were similar to those in the tests or simulations (see application to the Mont Blanc Tunnel fire [24] and Rosepark Nursing Home fire [25]).

For a hazard analysis of fires such as those shown in Figs. 63.9 and 63.10 it is possible to calculate a number of different, endpoints in relation to ASET as follows:

- Time when optically obscure smoke and irritants are predicted to significantly impair the escape efficiency.
- Time when irritancy is predicted to be so severe as to effectively prevent escape.
- Time to incapacitation (loss of consciousness) from the effects of asphyxiant gases.
- Time to incapacitation due to heat exposure.
- Time at which a lethal exposure dose of asphyxiants has been inhaled.
- Time at which heat exposure and burns are predicted to be lethal.
- Time at which an exposure dose of lung irritant sufficient to cause severe injury or death some hours after exposure has been inhaled.

Each endpoint is predicted when the level of the relevant term exceeds 1 on the y-axis. Thus for Fig. 63.9, the terms of visual smoke density and sensory irritancy (FECsmoke and FICirr) are well in excess of the concentrations predicted to impair escape as soon as the occupant opens the bedroom door, collapse from asphyxia (FED_{IN}) is predicted after 12 s, while the doses of convected heat and lung irritants (FED Heat and FLD_{irr}) are still well below threatening levels after 4 min. Figure 63.10 shows that concentrations of smoke and irritants in the lounge at head height are predicted to impair escape after 2 min, but at 0.5 m height these endpoints are not exceeded until after 5 min, due to the delayed descent of the upper smoke layer to this level. Collapse from asphyxia is predicted after 6 min and pain from heat after 7.5 min (standing) and 8 min (for a subject lying down). Also shown are the calculated times to potentially fatal 3rd degree burns for standing and lying subjects, and the calculated %COHb.

The way the calculations for these different endpoints are applied may depend to some extent on the purpose of the analysis. For a deterministic design application, it may be considered that the design has failed alternatively, if there is any predicted smoke exposure, or exposure to smoke of sufficient density to impair escape efficiency. For a probabilistic design, or for a forensic application, it may be important to consider the further consequences of different exposure scenarios, requiring calculation of time to incapacitation or to a lethal exposure.

For all these calculations, the exposure and effects are calculated for the breathing zone or at the head level of an occupant. For a simple deterministic analysis it is therefore possible to consider the tenability in a specific enclosure during a fire, assuming an occupant is either standing or sitting in the same position throughout. The ASET time then depends on the time-concentration curves for the toxic gases and heat at approximately 1 or 1.5 m height. Depending on the complexity of the fire model, it may be possible to differentiate between effluent concentrations and heat exposure at different locations. For a more sophisticated analysis, using evacuation calculation models in conjunction with a fire model, it is possible to calculate FEDs for a moving subject. ASET for each subject then depends upon their breathing zone exposure throughout the escape process as they move through a building, either walking or crawling. It is therefore possible to perform generic ASET calculations for the conditions inside any specified enclosure, or specific ASET calculations for individuals moving within and through different enclosures.

A summary of all the calculation expressions required for ASET design calculations, is presented in Appendix 1 with an example of an application in Table 63.22 and associated text. Full descriptions of the derivation of the different expressions, with more detailed variations for specific applications, and further examples are presented in the later sections of this chapter. A simplified set of methods is presented in ISO 13571 [21].

Basis of Fractional Effective Dose Methodology

As stated, some toxic or physical effects of exposure to combustion products occur almost immediately on exposure, and the severity of the effect is proportional to the concentration of the substance and its potency. This applies to visual smoke obscuration and to the painful effects of exposure to irritants. For example, irritant smoke in the eyes or nose immediately causes pain (sensory irritation), reflex closure of the eyes, and breathing difficulties.

For other substances, such as asphyxiant gases, the effect depends upon the dose inhaled. The effects therefore take some time to develop and depend upon the concentration inhaled and the time over which it is inhaled. The effects tend to be more persistent that those of sensory irritants, since it takes some time for the toxic material inhaled to be metabolized and excreted (for example carbon monoxide or hydrogen cyanide). An example of a dose-dependent effect is collapse from asphyxia resulting from exposure to carbon monoxide.

In practice, for asphyxiant substances (and to some extent also for heat) a distinct threshold concentration or exposure dose can be identified at which serious effects are predicted, and there is a sudden transition from minor effects to severe effects. Examples include the dose of CO at which a transition from a headache to collapsing unconscious occurs, or the dose of heat to the skin at which a sensation of heat becomes one of severe skin pain. For application to toxic hazard calculations, the concept of Fractional Effective Concentration or Dose is used whereby the exposure concentration or dose at any point during a fire is expressed as a fraction of the exposure concentration or dose predicted to produce a given effect. For example, the concentration of smoke present at any time during a fire can be expressed as a fraction of the concentration required to seriously impair escape capability.

Thus FEC_{smoke} (Fractional Effective Concentration of smoke) = 1 represents a smoke concentration considered capable of seriously limiting escape capability. Where FEC_{smoke} = Concentration (of smoke) present in a fire at any time divided by the concentration considered to significantly affect escape efficiency

A form of Fractional Effective Dose for CO can be expressed as a fraction of the exposure dose predicted to cause incapacitation.

Thus for example F_{Ico} (fraction of an incapacitating dose of carbon monoxide) can be expressed as:

$$F_{Ico} = \frac{\text{conc. gas present} \times \text{time}}{\text{conc.} \times \text{time for incapacitation}} \quad (63.1)$$

$$F_{Ico} = \frac{1000\text{ppm CO} \times 20\,\text{min}}{35,000\,\text{ppm.min}} = 0.57 \quad (63.2)$$

Although the FED calculations for different asphyxiant gases are based upon this simple concept, they are in practice more complex for a variety of physiological reasons, but the user is required to know only the concentration and exposure duration to perform the FED exposure dose calculation.

One reason for expressing the concentration or dose as a fraction of an effective concentration or dose for each toxic product is that fire atmosphere contains a mixture of toxic products of differing potencies. In order to sum the effects of the different effluent components, it is necessary to normalize them in terms of the effective dose. Furthermore, since concentrations of toxic products change with time during a fire, for constituents whose effects are dose-related, it is necessary to calculate the effective doses received, based upon the concentrations averaged over short periods of time, and then integrate these over successive periods. The aim is to calculate the time at which the summed effective doses reach unity, at which point the endpoint (such as incapacitation) is predicted to occur. The general FED equation is therefore:

$$FED = \int_{t1}^{t2} \sum_{i=1}^{n} \frac{C_i}{(Ct)_i} \Delta t \quad (63.3)$$

Where:

C_i is the average concentration, of a dose related toxicant such as an asphyxiant gas "*i*" over the chosen time increment;

Δt is the chosen time increment, expressed in minutes (min)

$(Ct)_i$ is the specific exposure dose expressed as concentration × minutes, that would constitute an effective dose (i.e., an exposure dose producing a defined endpoint such as preventing an occupant's safe escape)

Effective concentrations and exposure doses for defined endpoints for smoke, heat and toxic effluent mixtures are presented in the following sections.

Application of FEC and FED to Full-Scale Compartment Fire Data

In order to carry out and an FEC and FED analysis of compartment fires, such as those depicted in Figs. 63.9 and 63.10, the time-concentration curves for smoke density, toxic gases, temperature and radiation are used to calculate the FEC and FED fractions for the following terms as a function of time during the fire:

- FEC_{smoke}—Fractional effective smoke concentration where FEC = 1 represents a smoke concentration likely to significantly impair escape efficiency.
- FIC_{irr} Fractional irritant concentration: where FIC = 1 represents a concentration of organic irritants and/or acid gases likely to significantly impair escape efficiency. FIC = 5 represents an approximate incapacitating dose predicted to cause collapse.
- F_{IN} Fraction of a dose of asphxyiant gases F_{IN} = 1 represents a dose predicted to cause collapse and loss of consciousness due to asphyxia (F_{IN} = 2 represent an approximate lethal dose).
- FED_{heat} Fraction of an exposure (dose) of radiant and convected heat where FED_{heat} = 1 represents a "dose" sufficient to cause severe pain to unprotected skin (head and hands), (FED_{heat} ~8 represent second degree burns and FED 12 severe third degree burns which may be lethal.
- FLD_{irr} Fraction of a lethal dose of irritants: where FLDirr = 1 represents an inhaled exposure dose of lung irritant sufficient to cause severe injury or death some hours after exposure.

Expressions for the calculation of each of these terms are presented in later sections and summarized in Appendix 1.

Figures 63.9 and 63.10 illustrate the application of this method for the two fire cases in Figs. 63.7 and 63.8. Figure 63.9 shows the effects of exposure to fire effluent on when the upper floor bedroom occupant steps out onto the landing 10 min after ignition of the armchair fire in the open lounge on the floor below. Upon opening the door the occupant is confronted by smoke with an FEC of 12, which means that the smoke density is 12 × the concentration predicted to seriously impair escape attempts. Within a few seconds exposure to this smoke causes severe irritant pain to the eyes, resulting in reflex eye closure (blehparospasm), further impairing and inhibiting escape movement onto the landing. The smoke is also quite hot (60°C), which may further deter escape, but not hot enough to cause distress. The result at this stage is that the occupant is likely to decide that escape is too hazardous, to shut the bedroom door and take refuge in the bedroom. If the subject decides to attempt to descend the stairs, the speed of descent will be slow, and the next occurrence depends on the subjects breathing pattern. If the subject holds their breath before being exposed to the smoke, then there is no intake of toxic gases until they are forced to take a breath. At this point, the inhaled breath will be a deep one, with immediate incapacitation due to the irritancy and asphyxiant gases.

The analysis in Fig. 63.9 assumes the subject is breathing normally throughout, at a rate associated with a moderate level of activity. This results in uptake of asphyxiant gases (HCN, CO. CO_2 and low oxygen) from the time the subject steps onto the landing. Incapacitation (collapse and loss of consciousness) is predicted when the F_{IN} exceeds unity, which occurs after 0.2 min (12 s). This is mainly due to the effects of inhaling hydrogen cyanide, which was present at the high concentration of 850 ppm in this

experiment fire. Also considered in the analysis is the calculated time to incapacitation assuming there was no nitrogen in the burning fuel (armchair), in which case the most important asphyxiant gas is carbon monoxide. Uptake of carbon monoxide (increased by the presence of CO_2) results in accumulation of a dose producing an incapacitating level of carboxyhemoglobin (approximately 40 %COHb) after 4 min exposure, which represents an F_{IN} (no CN) of 1. The accumulating %COHb is calculated as part of the analysis and is shown in Fig. 63.9.

Also shown in Fig. 63.9 are the accumulating doses of heat (FED_{heat}) and of lung irritants, both of which hardly rise above the baseline up to 4 min. Since the smoke temperature is only 60 °C only minor discomfort is predicted over this timescale.

The predicted results from this analysis are then that if a subject attempted to escape through these conditions:

- They would find the effects of the smoke exposure to be painful and distressing and be likely to turn back and take refuge in the bedroom.
- If they were familiar with the building, the distance to the main exit on the lower floor was short, and the door easy to open, they might be able to hold their breath long enough to reach the exit and escape before being overcome.
- If they took a breath at anytime they are likely to collapse more or less immediately from the effects of the high concentrations of asphyxiant gases, especially hydrogen cyanide.
- If they collapsed on the stairs or near the door, they would die within a further few minutes, mainly from the effects of carbon monoxide, with a blood carboxyhemoglobin concentration of around 40–60 %COHb.
- If they were rescued at 4 min and treated with oxygen, they would be likely to make a rapid recovery (depending on their pre-existing health status). They may suffer some eye and throat irritation the next day, and develop a minor productive cough, but would be unlikely to suffer significant lung injury. There would be a possibility of suffering a heart attack or stroke due to the inhalation of fine smoke particles and CO. There would be a possibility of suffering long-term brain damage due to cerebral hypoxia.

During these experiments measurements of smoke and toxic gases were also made in a closed bedroom. It was found that although minor smoke penetration occurred around the bedroom door (no smoke seals), the conditions remained tenable for up to approximately 30–60 min, especially if the bedroom window was opened.

Figure 63.10 shows an FED analysis for an occupant of the lower floor fire room from the data in Fig. 63.8. This differs from the analysis in Fig. 63.9 in that the exposure period starts with ignition of the fire, after which the conditions change rapidly. For a person in the fire room but on the opposite side of the room from the fire, there is no initial exposure to either heat or smoke as the effluent from the early flaming fire collects under the room ceiling. Once the upper layer descends below the soffit of the door to the hall, the smoke starts to flow out into the hall and landing, further reducing the rate of descent of the upper layer in the fire room. For a person standing in the room the first exposure to smoke is predicted from 1 min after ignition, when the upper layer descended to head height (1.7 m). An FEC = 1 for smoke density and FICirr = 1 for the effects of the irritant gases present in the smoke is predicted at 1 min, from which time a subject would be predicted to suffer an impaired escape capability due to the optical obscuration from the smoke and the smoke irritancy, derived from a significant content of both organic irritants and acid gases including HCl, HBr, HF and SO_2, which were measured using ion chromatography. However, if the subject got down to near floor level (0.5 m), then they would be beneath the smoke layer until 4 min. Conditions deteriorated very rapidly from around 4 min, so that at 5.5 min an FED exceeding 1 is calculated simultaneously for both asphyxia and heat. At this time, it is predicted that a standing exposed subject would suffer severe pain to exposed areas

of skin, especially the head and hands, and would collapse unconscious due to the effects of inhaled asphyxiant gases, and in particular hydrogen cyanide. The kink in the F_{IN} curve at this point reflects the reduction in breathing, and thus in the rate of uptake of asphyxiant gases, as a person becomes unconscious. For a person sitting or crouching below the smoke layer up to this time the exposure to hot gases would be somewhat less, so that time to severe pain from heat is predicted at just before 6 min. As the exposure to heat continues an exposed subject would begin to suffer from burns (both to clothed and unclothed areas depending upon the thickness of the clothing), so that for a standing person fatal extensive full thickness (3rd degree) burns are predicted after 8 min and for a sitting person after 9 min. The FED heat curves then level off because by now the fire has self-extinguished and the temperatures in the room are dropping.

The other two curves in Figure 63.10 have been included to consider the situation with regard to asphyxiant gases in the absence of hydrogen cyanide. For these upholstered furniture fires the hydrogen cyanide concentrations increased rapidly to well in excess of those observed to result in loss of consciousness in exposed primates within 2 min. Cyanide is therefore the main driver of collapse from asphyxiation in these fires. If the fuels had not contained nitrogen (or <1 % Nitrogen by mass), then the main asphyxiant gases present would have been carbon monoxide, carbon dioxide and reduced oxygen hypoxia. Another factor would have been the high concentration of irritants smoke gases and particulates. It is considered that these would have made breathing difficult for exposed occupants, thereby adding to some extent to the asphyxiant effects of the inhaled gases. For the full form of the F_{IN} model for asphyxia, the fraction of a lethal dose of irritants (FLD_{irr}) is included as an additive term. When this is done for this fire the main drivers of asphyxia are the inhaled doses of CO and these irritants, increased by the presence of high CO_2 concentrations and with a small contribution for the lowered oxygen concentrations. For this model, the calculated time to FED_{IN} asphyxia (excluding HCN) is 7 min. At this time it is calculated that the overall degree of incapacitation is likely to be sufficient to cause collapse and prevent escape. Since the extent of additive effects from the irritants are somewhat uncertain, the final curve shows the situation with this term removed from the analysis. The result shows loss of consciousness after 8.5 min as the blood CO level reaches 40 % COHb, which happens to coincide with the time by which a person sitting or lying on the floor is likely to receive life threatening burns.

After 10 min the FLD for lung irritants is 0.25, indicating that post-exposure lung inflammation is unlikely if rescued at this time, although elderly subjects in particular have been found to be vulnerable to the development of fatal pneumonia from lung infection.

The predicted results for a subject exposed to these conditions depend very much upon their condition at the time of ignition and their subsequent behavior:

- A subject awake and ambulant at the time of ignition, and aware of the fire from ignition should be able to escape without difficulty, suffering no or minimal exposure.
- A waking subject may get into difficulties if they remain at or enter the scene to carry out activities such as getting dressed, attempting to retrieve belongings or to fight the fire, or if they are unable to escape due to incapacity (for example due to physical or mental disability, alcohol or drugs). Due to the rapid deterioration in conditions after 4 min they may become disorientated and overcome by toxic smoke and heat, collapsing and dying at the fire scene.
- For a sleeping subject the outcome depends upon when they become aware of the fire and their subsequent behavior. Figure 63.8 shows the activation times for smoke detectors placed on the lounge and upper floor landing ceilings for this experiment. The optical detector placed on the landing ceiling activated 2.5 min after ignition, by which time there was already dense smoke at head height in the lounge. Whether or not a subject would escape before being overcome would then depend upon how rapidly they awoke, took in

the situation and when they decided to leave the room. Although escape via the hallway and main exit would be possible following a rapid response, any delay would be likely to result in the occupant being overcome and collapsing, either in the lounge or hall.

- Unlike the bedroom case it is considered that many occupants in this situation would attempt to escape through the smoke even at high density, since they would be motivated by the need to move away from the source of the fire and effluent.
- A similar analysis has been carried out for the conditions faced by an occupant of an open upper floor bedroom during this fire experiment, both for a situation with the fire room door opened and closed. Once smoke from a fires in an open lounge such as these begins to enter an open bedroom on the floor above, the time available for response and escape is very short (around 1–2 min) before incapacitation is predicted.

Case Examples

It is common for occupants of upper floor bedrooms to decide not to attempt escape through landing smoke from a fire involving a single item on the floor below [26]. In some cases victims have closed the bedroom door and escaped through a window or waited for rescue. In other cases they have failed to close the bedroom door, allowing smoke to flow into the open bedroom and either been overcome or survived by hanging out of an open bedroom window until rescued. Others have succeeded in escaping via the stairs past the fire room, especially in cases where the fire room door was closed. As stated in the previous section, most fatalities from such situations are found to have minimal burns but potentially lethal blood %COHb concentrations. In one such case bedroom occupants died half out of bed with high %COHb concentrations before they were able to begin to evacuate. In two other cases, occupants opened the door onto a smoke-logged landing in situations involving an active vitiated fire on the floor below, then failed to close the door and attempted to escape, in one case along a corridor towards an exit and in the other via a window. In the first case, two occupants collapsed and died after traveling approximately 10 m and one was rescued after taking refuge in a closed room. In the other case, one person escaped via the window while the second was overcome and died in the room. In two cases, occupants collapsed unconscious on the floor of a room containing an underventilated fire but survived after rescue. For one case the fire was of a medium size and confined to corner of the open room, providing conditions considered to be similar to those in Fig. 63.10. The occupant collapsed away from the fire area and when rescued after about 15 min had approximately 40 %COHb and potentially lethal 80 % full thickness burns (despite being clothed with the clothes undamaged). This and similar cases are considered to provide some validation of the FED smoke, toxicity and heat models described.

In other cases occupants have taken refuge in closed rooms, but subsequently been overcome over periods of up to an hour or more before they were rescued (but died in hospital) [27]. This kind of incident is important from the perspective of a defend-in-place strategy. The engineering design analysis must be able to demonstrate that conditions in such refuge enclosures remain tenable for as long as necessary.

Fire room occupants commonly become aware of a fire before conditions become life threatening, even in the absence of automatic smoke detection (alerted by noise, heat or smoke), but a significant number remain in the fire room and become incapacitated without escaping. Some are intimate with the fire and suffer severe burns, while others may be away from the immediate fire and be overcome by toxic smoke, either with or without burns.

Despite the fact that in some situations people will take refuge rather than attempting to escape through dense smoke, in other situations people have been shown to travel considerable distances through dense smoke, subsequently escaping or being overcome at the scene. During the Mont Blanc tunnel fire a number of victims escaped from their vehicles and walked several hundred

meters through dense smoke in the tunnel before being overcome. Victims closer to the fire were overcome by a combination of heat and toxic gases, while others 407 m from the fire were overcome by toxic gases having traveled 525 m through smoke[24]. During the Dupont Plaza fire a witness described holding her breath and deliberately entering the lobby, which was filled with dense smoke. There she joined a crowd of people moving some tens of meters along a heavily smoke-filled corridor and escaped from the main entrance. She described walking in the crowd holding her breath, but then being forced to take a breath and immediately almost collapsing, but was able to keep moving and was prevented from falling by contact with the crowd. In a store fire in the UK, a large number of persons were trapped in dense smoke on a sales floor while there was a large queue at the storey exit to the stair. A number of persons subsequently traveled through dense smoke to escape via windows or down the smoke-logged stair. Two deaths resulted from CO intoxication of two persons disorientated and remaining on the floor in a restaurant area [28]. The Station Nightclub provides an example of a situation in which large numbers of persons attempted to escape through dense hot smoke, some of whom succeeded while others were overcome before they could escape [29]. In other cases victims have entered smoke filled corridors and stairwells and been overcome as they attempted to descend.

These descriptions of occupant behaviors and outcomes in different incidents highlight the difficulty of specifying what constitutes an acceptable level of exposure from a design perspective, in situations where some degree of exposure to fire effluent is predicted. The main FEC and FED expressions presented in this chapter are intended to represent exposure conditions likely to seriously impair escape attempts (smoke and irritants) or cause incapacitation (loss of consciousness or severe pain) for asphyxiants or smoke for average adults. Designing to these limits would therefore be predicted to involve failure to escape by a large proportion of an exposed population. Consideration of aspects relating to choice of design limits is discussed in a later section.

Dose/Response Relationships and Dose Estimation in the Evaluation of Toxicity

Before considering the particular effects of individual toxic fire products it is necessary to determine the basic parameters required to quantify exposure. Ultimately, the degree of toxicity is determined by such factors as the concentration of toxic product in the target organ of the body and the time period for which a toxic concentration is maintained. For an asphyxiant product, the most important criterion is the concentration in the cerebral blood supply or inside the brain cells, whereas for an irritant product the most important factor is the concentration in the linings of the nose, throat, or lung. In some cases it is important and feasible to measure such parameters directly. For CO it is not the concentration in the smoke that directly determines how someone will be affected but rather the concentration that has accumulated in the blood in the form of carboxyhemoglobin, which can be determined relatively simply from a drop of blood [30, 31].

In practice, however, it is often not feasible to measure the amount of toxic product directly accumulated in the subject. Also, relating observed toxic effects to measurements of toxic products in the smoke itself is preferable, since it enables predictions of toxicity to be made based on chemical measurements of fire atmospheres without necessarily exposing animals. A series of useful secondary measurements can, therefore, be made that can be related to toxic effects in animals, but it must be remembered that these indirect measurements of exposure always involve some degree of error or uncertainty.

The Relationships Between Concentration Inhaled, Duration of Exposure, and Toxicity

In inhalation toxicology two parameters that are always measured and reported are the actual analyzed concentration of the test material per unit volume of air in the animals' exposure chamber and the duration of exposure. For

droplet aerosols or dusts the particle size range in the atmosphere is also measured so the respirable fraction (the part capable of entering the body) can be calculated. Where toxic effects can occur rapidly, as with the asphyxiant gases, it is also important to measure the rate of uptake of the toxicant. This can be estimated by measuring the volume of air breathed by the animal per minute (the respiratory minute volume (RMV), usually expressed as V_E (the volume of air exhaled per minute), although for accurate calculation of uptake and dose, further measurements, such as of blood levels, must be made. Variations in V_E can have dramatic effects on toxicity as will be described in the following section.

Although such parameters as respiration and particle size of aerosols are important, the most basic parameters reported are the concentration of the toxicant and the duration of exposure, which enables a rudimentary estimation of the dose. Thus, the product of concentration and time (*Ct* product) gives an estimate of the dose available to the animal. In general safety evaluation of novel chemicals for an acute exposure, a standard single 4-h exposure time is used and toxicity is expressed in terms of the concentration of test material causing the death of 50 % of the animals during exposure or within 14 days after exposure. This is known as the 4-h LC_{50} concentration.

In practice, however, it may be necessary to predict what will happen to a subject exposed to a higher concentration for a shorter period of time or a lower concentration for longer time. Although this can be done by carrying out more LC_{50} experiments using different exposure durations, as an approximation toxicologists often resort to Haber's rule, which states that the toxicity depends on the dose accumulated, and that the product of time and concentration is a constant [32], so that

$$W = C \times t \tag{63.4}$$

Where W is a constant dose, specific for any given effect. In practice, dose in inhalation toxicology is often expressed in terms of *Ct* product. In the case of the LC_{50}, the effect is death of 50 % of the animals and

$$W = LC \cdot t_{50} \tag{63.5}$$

expressed in mg · min/L (i.e., the product of the concentration and the duration of exposure causing lethality). This relationship implies a linear uptake of the toxic substance with time (Fig. 63.11). It holds true for some substances where the primary target organ is the lung. In the context of combustion toxicology, this relationship can be applied to estimates of the dose of a lung irritant likely to cause post-exposure fire deaths from lung inflammatory responses. An example of such an irritant is carbonyl fluoride, a highly toxic lung irritant produced during the thermal decomposition of PTFE, which has a 1-h LC_{50} of 0.990 mg/L, which is exactly four times the 4-h LC_{50} of 0.248 mg/L [33].

Unfortunately, this simple principle does not always hold true. In particular, some volatile substances (such as CO) are both taken up and excreted via the lungs. In this case the rate of uptake depends on the difference between the concentration inhaled and that in the body, giving an exponential uptake so that:

$$W = C\left(1 - e^{-tk}\right) \tag{63.6}$$

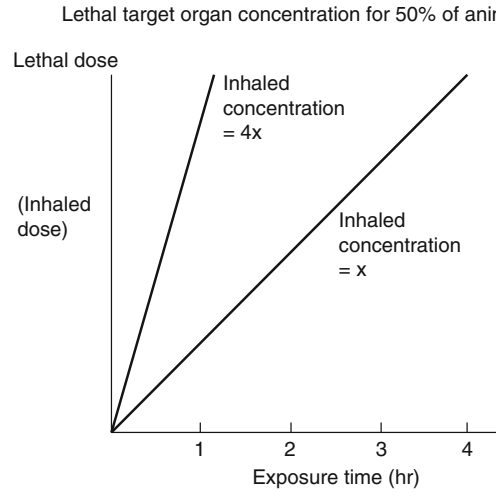

Fig. 63.11 Uptake of a substance obeying Haber's rule (i.e., with a long half-life of detoxification or excretion), where the rate of uptake is directly proportional to the inhaled concentration, so that 1-h LC_{50} is four times the 4-h LC_{50}. The lethal dose represents a lethal target organ concentration for 50 % of the animals

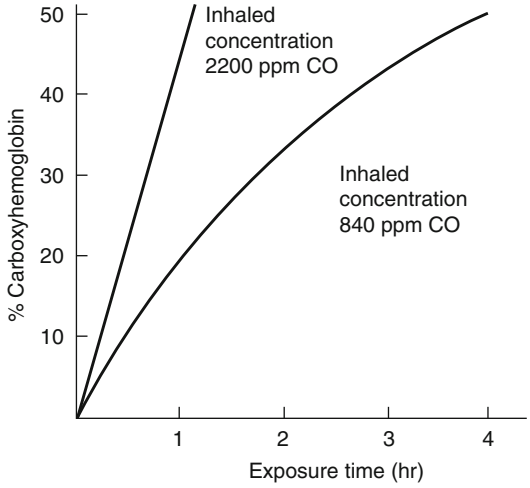

Fig. 63.12 Uptake of a substance (carbon monoxide), which is both absorbed and excreted via the lungs, and where the rate of uptake depends on the difference between the concentration inhaled and that in the body. For short exposures at high concentrations, uptake to a lethal dose is almost linear, obeying Haber's rule. For longer exposure times, uptake follows a curve so that the inhaled concentration necessary to achieve a lethal dose (50 % carboxyhemoglobin) at 4 h (840 ppm) is 0.38 times that required for deaths at 1 h, as opposed to 0.25 times (550 ppm) as predicted by Haber's rule. Uptake was calculated for a 70 kg human at rest (RMV 8.5 L/min) using the CFK equation

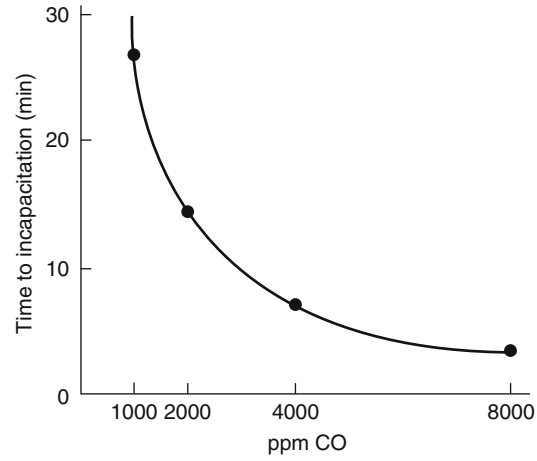

Fig. 63.13 Relationship between time to incapacitation and carbon monoxide concentration in active monkeys. 1000 ppm Ct = 26,600 ppm · min; 2000 ppm Ct = 28,097 ppm · min; 4000 ppm Ct = 26,868 ppm · min; 8000 ppm Ct = 26,086 ppm · min

This is the basis for the Coburn-Forster-Kane (CFK) equation [34, 35] describing the uptake of CO in humans. This relationship approaches the linear Haber's rule (Equation 63.4) when the concentration, C, in the atmosphere is high with respect to the concentration in the body required to cause incapacitation or death (Fig. 63.12), and for short exposures to high CO concentrations, uptake is approximately linear. This effect is illustrated by the results from CO exposure experiments in primates. At a constant level of activity, and thus of respiration, the animals became unconscious when exposed to approximately 27,000 ppm · min of CO at concentrations between 1000 and 8000 ppm (Fig. 63.13). For such situations it is, therefore, possible to use linear models for CO uptake without serious error.

Some toxic effects, however, are not dependent on a dose acquired over a period of time but are concentration related. Thus, the irritant effects of smoke products on the eyes and upper respiratory tract (sensory irritation) occur immediately on exposure with the severity depending on the exposure concentration. In fact, far from increasing as exposure continues, the effects usually lessen, as the subject adapts to the painful stimulus even though the dose is increasing [24, 36].

Other cases where concentration is an important determinant of toxicity as well as duration of exposure are the asphyxiant effects of hypoxic hypoxia (oxygen lack) and hypercapnia (high CO_2 concentrations). If a subject is exposed suddenly to a low oxygen concentration, a finite time is required for the air in the lungs and gases in the blood to equilibrate to the new conditions, so to some extent a "dose" of hypoxia is acquired over a period of time. Once equilibrium is established, usually within a few minutes, the severity of the effects depend on the oxygen concentration and do not then change appreciably with time [37, 38]. This also applies to high CO_2 concentrations. Equilibrium is established within a few minutes and concentration-related effects then determine the pattern of toxicity [25, 37].

For the other main asphyxiant gas in smoke, hydrogen cyanide (HCN), although

accumulation of a dose is one factor, the most important determinant of toxicity appears to be the rate of uptake, which in turn depends on the concentration. Thus, as shown in Fig. 63.14, incapacitation occurs rapidly (after 2 min) at the high concentration of 180 ppm (*Ct* product 400 ppm · min), but at the lower concentration of 100 ppm, incapacitation occurs only after approximately 20 min, requiring a much higher *Ct* product dose (2000 ppm · min). This effect leads to the unusual kinked HCN time/concentration curve shown in Fig. 63.14 compared to the smooth curve for CO.

In attempting to predict what will happen to a subject exposed to a smoke atmosphere containing all these products it is, therefore, important to allow for these different concentration/time/effect relationships.

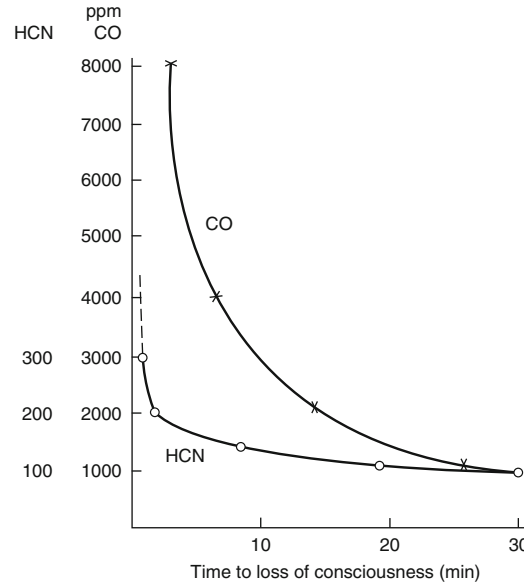

Fig. 63.14 Comparison of the relationship between time to incapacitation and concentration for HCN and CO exposures in primates. Time and concentration are equivalent for CO; for HCN, a small increase in concentration causes a large decrease in time to incapacitation

Ct Product and Fractional Effective Dose

The basic concept established in the previous section is that for the majority of toxic products in a fire atmosphere a given toxic endpoint such as incapacitation or death occurs when the victim has inhaled a particular *Ct* product dose of toxicant. In order to make some estimate of the likely toxic hazard in a particular fire it is, therefore, necessary to determine at what point in time during the course of the fire exposure the victim will have inhaled a toxic dose. This can be achieved by integrating the area under the fire profile curve for the toxicant under consideration. When the integral is equal to the toxic dose, the victim can be assumed to have received a dose capable of producing that toxic effect.

A practical method for making this calculation is the concept of *fractional effective dose* (FED) [39]. The *Ct* product doses for small periods of time during the fire are divided by the *Ct* product dose causing the toxic effect. These fractional effective doses are then summed during the exposure until the fraction reaches unity, when the toxic effect is predicted to occur. Thus, the FED equation can be represented as:

$$\mathrm{FED} = \frac{\text{Dose received at time } t(Ct)}{\text{Effective } Ct \text{ dose to cause incapacitation or death}} \tag{63.7}$$

For substances obeying Haber's rule, the denominator of the equation is a constant for any particular toxic effect. For substances deviating from Haber's rule, the denominator for each time segment during the fire is the *Ct* product dose at which incapacitation or death would occur at the concentration during that time segment. For the hazard model presented in this chapter, the denominator is presented in the form of equations giving the required *Ct* product doses predicted for humans, which have been derived for each toxic gas and are presented in the following sections. Special cases of the fractional effective dose are referred to as the *fractional incapacitating dose* (FID) and the *fractional lethal dose* (FLD).

For sensory irritation—a toxic effect that depends on the immediate concentration of an irritant to which a subject is exposed rather than the dose—a concept of *fractional irritant concentration* (FIC) has been developed, where

$$\mathrm{FIC} = \frac{\text{Concentration of irritant to which subject is exposed at time } (t)}{\text{Concentration of irritant required to cause impairment of escape efficiency}} \tag{63.8}$$

Allowance for Margins of Safety and Variations in Susceptibility of Human Populations

The methods for assessing the effects of toxic gases were originally developed to predict the exposure concentrations or exposure doses that would be expected to cause serious effects such as impairment of escape capability, incapacitation, or death of a building occupant. When they are used for design purposes, the main consideration is not to predict a serious effect level but a maximum safe level. When used in this context, it is necessary to use some degree of conservatism in applying tenability endpoints for two reasons. One reason is to allow for uncertainties in the predictability of the endpoints, which is mainly because the endpoints cannot be fully quantified within narrow limits without performing experimental human exposures to a variety of complex and dangerous toxic effluent mixtures. These tests obviously cannot be done for ethical reasons. Another reason is the wide range of sensitivities to toxic effects in a heterogeneous human population.

The physiological algorithms are based partly on experimental data and reported effects in humans and partly on animal studies. These methods involve either the exposure dose or concentration predicted to produce a given effect on humans exposed to fire effluent. However, the effects are based on data for healthy young adult animals or humans. The exposure dose or concentration, therefore, represents the average in a statistical distribution of subjects' responses surrounding that exposure dose or concentration. This is the mode, or most frequently expected exposure dose for an exposed population. Individual exposure doses or concentrations for the response would, in practice, be statistically distributed around the mode in a probability curve. The overall human population contains a number of subpopulations, which exhibit greater sensitivity to various fire effluent toxicants, principally due to compromised cardiovascular and pulmonary systems.

Two of the largest such subpopulations are the elderly and the approximately 15 % of children and 5 % of adults who are asthmatic [40]. The elderly, and particularly those with impaired cardiac perfusion, are particularly susceptible to asphyxiant gases. Thus the average lethal carboxyhemoglobin (COHb) concentration in adults dying in fires or from accidental CO exposure is lower in the elderly [41]. Figure 63.15 shows the distribution of postmortem carboxyhemoglobin concentrations in human fire and nonfire CO fatalities in the United States [29]. The results show that some individuals died at COHb concentrations below 30 % while others survived long enough to obtain blood concentrations above 90 %COHb. Many fire fatalities occur at lower COHb concentrations than for cases of CO poisoning alone. This may partly reflect the influence of other toxic gases in addition to CO in fire atmospheres. Also it has been shown in experimental studies that as little as 2 %COHb significantly reduces the time to the onset of pain in an exercise test of angina sufferers [42]. This could be very important when attempting to escape from a fire.

A further complication with the CO lethality data illustrated in Fig. 63.15 is that in practice few people survive an exposure of more than 50 %COHb if rescued and treated, even though much higher levels are found in the bodies of decedents. This result is because uptake continues in comatose people until the point where respiration ceases, which is illustrated in data from a study by Pach [43] (Table 63.4). This study shows the proportions of survivors and

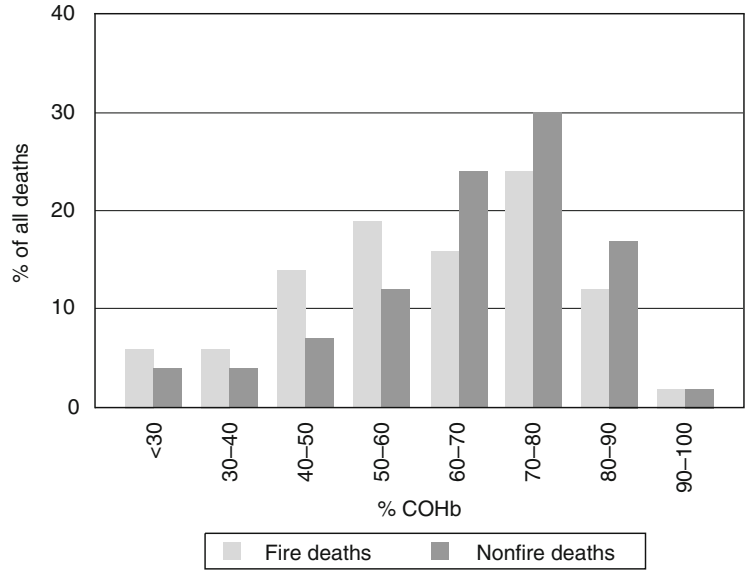

Fig. 63.15 Range of lethal sensitivity to carbon monoxide in humans [41]

Table 63.4 Proportions of survivors and fatalities in different COHb ranges [43]

Percent COHb range	Survival rate	Fatality rate	Number of cases
>30	1.0	0.00	65
30–40	0.9	0.10	29
40–50	0.67	0.33	20
50–60	0.14	0.86	29
60–70	0.02	0.98	43
70–80	0.05	0.95	22
80–90	0.0	1.00	3

fatalities from a sample of 260 CO poisoning cases. The data show that survival is rare above 50 %COHb, that around 67 % of people survive in the 40–50 %COHb range, and that most people survive below 40 %COHb.

Asthmatics and sufferers of other lung conditions, such as chronic bronchitis and reactive airways dysfunction syndrome, are particularly susceptible to bronchoconstriction on even brief exposure to very low concentrations of irritants, with distress, severely reduced aerobic work capacity, collapse, and death resulting, depending on the sensitivity of the individual and the severity of the exposure.

It is the objective of fire safety engineering to ensure that essentially all occupants, including sensitive subpopulations, should be able to escape safely without experiencing or developing serious health effects. Thus, safe levels for exposure of the human population to fire effluent toxicants must be significantly lower than those determined from experiments with uniformly healthy animal or even human surrogates.

The toxicity endpoints from the functions presented in this chapter are all predicted to represent the median of the distribution of exposure doses or concentrations resulting in a given toxicity endpoint. Since individual susceptibility varies in the population, it is considered that approximately 11.3 % of the population is considered likely to be susceptible below an FED of 0.3 (see ISO 13571 [21]). Approximately 90 % of the population is considered to be susceptible below an FED of 1.3. For this reason, it will be necessary for the user to select an FED value to protect an acceptable proportion of vulnerable subpopulations (for example, an FED of 0.3 or some other value). Note: Due to the rapid (t^2) rate of increase of smoke and asphyxiant gas concentrations in most flaming fires, variations in individual susceptibility and uncertainties in prediction of incapacitating doses tend to have relatively minor effects on predicted times to incapacitation.

Application of FED Methodology to Deterministic and Probabilistic Hazard Modeling

The FED endpoints discussed in the previous section may be applied directly to deterministic design in order to set design limits for ASET for a particular design fire scenario. They can also be used for a more probabilistic design by determination of acceptable ASET endpoints for a variety of possible fire scenarios.

Such an application can be to probabilistic scenario modeling cases for one or more specified design fire scenarios. An example could be to estimate the numbers of occupants likely to escape uninjured from a specific fire scenario and the extent of injury and survival rate for other occupants. Gridflow [44] and Exodus [45] are examples of computer evacuation models that can be used in this way. In Gridflow, the time-concentration curves of toxic hazard conditions in any occupied enclosure in a building can be introduced as a smoke-irritancy concentration term and an asphyxiant gas (or heat) dose term. The model is then populated with escaping agents (i.e., people) who are exposed to the concentration term (affecting their walking speed) and also progressively inhaling the exposure dose. When the concentration or dose terms reach critical values, an agent is considered to be incapacitated and ceases to escape. By varying the severity of the levels of the hazard parameters used as endpoints for these terms, it is possible to set conservative criteria: determination of time for safe escape of all occupants, or less conservative criteria: determination of the number of occupants suffering severe incapacitation or full-thickness burns.

In order to reflect the varying sensitivity of individual subjects to a given level of insult, Gridlow has a "FED susceptibility" parameter that can be assigned a mean and standard deviation from which each individual agent can be randomly assigned with a susceptibility level. For a population escaping under identical conditions, this can then result in a proportion escaping while others fail to escape.

A difficulty in carrying out such probabilistic simulations is the limited data available on the behavioral and physiological susceptibility of people in a population to the different hazard parameters. In this Chapter, some data on the variability in susceptibility within the population have been provided. Some guidance has also been given on the proportion of people willing to enter and continue to escape through smoke as a function of smoke density, and a suggested standard distribution for the variations of walking speed around a function relating average walking speed to smoke density. Additionally, in the section on sensory irritation, information is provided on the possible range of susceptibilities of an exposed population as a function of the logarithm of the exposure concentration. This is also complicated by the uncertainty of the available data.

For asphyxiant gas exposures, especially CO, some guidance on variations in susceptibility to collapse has been presented in the previous section. For any exposed individual, it is considered that the degree of impairment is generally minor until a critical dose has been inhaled, at which point severe incapacitation (collapse) occurs after a brief period of intoxication. The variation in sensitivity in the population (variation in the dose required to cause collapse for different individuals) is more difficult to specify. Problems with susceptibility of angina patients at very low CO levels have been described, and cases of syncope (fainting collapse) can occur in mildly hypoxia situations such as aircraft cabins or at moderate altitude in mountains in susceptible individuals. It, therefore, seems likely that some people will succumb to quite low levels of asphyxiant gas exposures during escape from fires. As shown in Figure 63.5, approximately 5 % of fire fatalities exposed to smoke remote from a fire and with no burns had blood CO concentrations <30 %COHb. Based on fire

fatality and experimental data it is considered that, depending upon their activity level, by far the majority of exposed people would not be overcome or seriously affected until they achieved 30–40 %COHb, and few would remain unaffected by 45 %COHb. In terms of overall F_{IN} for asphyxiant gases this would mean that relatively few individuals would be likely to be overcome at F_{IN} levels below 0.5, while few would remain able to function at levels above 1.125.

For heat exposure, individual tolerance endpoints are also difficult to specify. As with smoke, the effects on escape behavior are likely to be affected by the context, in that occupants in or near a place of relative safety may be unwilling to enter hot smoke in an escape route, or turn back if they find the heat intensity painful. For such situations, the relatively conservative endpoints to time to pain may be correct, or in some situations not conservative enough in that an individual may be unwilling to enter areas of significant heat even if the areas are at a level below the pain threshold. In other situations, especially when occupants find themselves immersed in a hot smoke environment, they have been found to continue to move and in some cases succeed in escaping through extreme conditions resulting in serious burns. At some point, a heat exposure results in collapse and death. From case histories, this is considered likely to happen at the point where serious 2nd degree or full-thickness (3rd degree) burns occur. It is considered that although light indoor clothing provides some protection to clothed areas of the body, this is likely to result in only a small increase in tolerance time or time to burns, and of course does not apply to sensitive areas such as the hands and head. For this reason it is considered that the tolerance and time to burns expressions presented in this Chapter are most relevant rather than expressions for clothed subjects, except in situations where protective clothing is in use.

Derivation of a Model for the Prediction of the Effects of Optically Dense, Irritant Smoke on the Eyes and Respiratory Tract

Although it is difficult to make precise predictions of the effects exposure to irritant smoke has on escape behavior, the degree of incapacitation, and the post-exposure effects on lungs, it is important to consider these effects in engineering design, and to be able to make some estimates of the likely effects of exposure. Herein is presented a current "best estimate" model for likely effects.

Smoke presents three hazards affecting escape capability. The first two relate to simple impairment of visibility. Firstly, the presence of smoke in an occupied enclosure obscures illumination from windows and other light sources (especially high level lighting), so that escaping occupants can find themselves in dimly lit conditions, and secondly the smoke directly impairs the ability of the subject to see through it to surrounding objects and signage. The attenuation of general illumination can be modeled to provide an indication of the brightness and contrast of the surroundings of a subject taking the smoke density and distribution into consideration. The effects of smoke obscuration (visibility distance in non-irritant smoke) on escape behavior has been studied (see Chap. 61 [46]), but the sensory irritant effects of smoke, both on the eyes and respiratory tract are also important, affecting both behavior and walking speed. The next section provides a simple method for the evaluation of the effects on escape capability of "averagely irritant" smoke. This represents a default for smoke of an irritant potency likely to occur from flaming fires in most normal occupied enclosures such as domestic dwellings, offices, assembly or sleeping accommodation, in which any combustible fuels are considered to have a low content of elements producing acid gases and organic irritants. The section following this considers in more detail the evaluation of sensory

irritancy for fuels of known composition likely to produce more irritant smoke, such as smoldering fires, flaming fires involving electrical equipment or consumer products (in any building), store fires (e.g., especially supermarkets and DIY stores) and fires involving transport (tunnels, motor vehicles, aircraft and ships).

Evaluation of the Effects of Smoke on Escape Capability

Smoke affects both available safe escape time and the time required for escape. The time available for escape is often limited by the development of smoke conditions that occupants are unwilling to enter or turn back after entering. When occupants do attempt to escape through smoke the time required can be increased by effects on exit choice and wayfinding as well as walking speed through smoke.

Where occupants of a relatively uncontaminated enclosure find their escape route smoke-logged their willingness to enter the smoke and continue through it depends on a range of behavioral parameters related to their individual characteristics, their knowledge of the building and escape routes and their appraisal of the relative risks of seeking refuge or attempting escape. Once exposed to smoke, their willingness and ability to continue also depends upon the optical density, irritancy and temperature of the smoke, the ambient lighting and exit lighting and features of the built environment such as the enclosure size, complexity, presence of obstacles or other hazards.

When occupants are in the fire enclosure and exposed to smoke, or are threatened by rapidly deteriorating fire conditions in their vicinity, then they are more likely to attempt to escape through it than when they have the choice of entering or remaining in a refuge. Studies of occupant behavior during different fire incidents show examples of situations where occupants have turned back or remained in place even when smoke contamination of escape routes is light, and other cases where occupants have successfully or unsuccessfully attempted to escape though conditions of extremely dense hot and irritant smoke. Experimental studies of movement through smoke are useful for measuring movement behavior and speed, but they differ from real incidents in that the participants know they are safe and may therefore move with more confidence than they otherwise would. Even within experimental studies movement behavior and speeds appear to depend to some extent on the nature of the occupants and the physical characteristics of the experimental enclosure. For these reasons it is difficult to provide precise guidance on the relationship between smoke conditions and predicted occupant behavior and walking speeds.

Deciding Whether to Enter a Smoke Contaminated Escape Route, Seek Refuge or Find an Alternative Escape Route

The effects of smoke density on escape behavior during actual fire incidents is reviewed in Chap. 58 [47]. Two studies (in the US and UK) [47–49] report occupant behavior in terms of distance traveled through smoke of different densities (expressed as visibility distance) and numbers turning back or seeking refuge. Although the irritancy and temperature of the smoke is not mentioned it can be assumed that the smoke was in most cases somewhat irritant and hot. Both studies showed remarkably similar results. In the UK study 91 % of those turning back having entered smoke did so when visibility was less than approximately 4 m, representing 62 % of those exposed to smoke at this visibility or lower, while only 11 % of those exposed to smoke with a visibility >4 m turned back (5 % for visibility >9 m). For individual cases the authors have examined or investigated [26] several cases of dwellings fires have been encountered in which occupants on an upper floor have been confronted with dense, hot, smoke from a fire on the floor below when opening a bedroom door. In almost all cases the occupants have decided to close the door and remain in the bedroom or attempt escape via a window rather than to attempt to proceed through the smoke-filled escape route, citing the density,

irritancy and temperature of the smoke as deterrents. In two incidents, five occupants attempted to escape away from a location where they had opened a landing door and enabled a smoke plume to enter from a fire on the floor below. Three were overcome and died while attempting to escape, while one escaped through a window and one was rescued having taken refuge in a closed room.

During the Dupont Plaza hotel incident some witnesses reported occupants being trapped or overcome by smoke, while others successfully traveled a considerable distance and escaped along a long smoke-filled corridor. During the Mont Blanc road tunnel fire most occupants remained (and died) in their vehicles rather than entering the smoke-filled tunnel, while a small number traveled a considerable distance along the tunnel before being overcome by toxic gases or heat [24]. Other cases are described in Chap. 58. The general pattern from these incident investigations is that occupants will generally be unwilling to enter smoke with a visibility of more than approximately 3 m (0.33 OD/m, extinction coefficient 0.76), especially if they have an option of turning back or seeking refuge, and women were more likely to turn back than men. These effects are summarized in Table 63.5. When occupant attempt to move significant distances through dense smoke from enclosed compartment fires, the concentrations of asphxyxiant gases are often sufficient to result in collapse within a few minutes while attempting to escape. On the other hand there have been incidents in which occupants have succeeded in traveling through dense smoke for distances exceeding 10 m and survived. Behavior may also depend on whether layering permits occupants to crouch down to levels where the smoke density is lower and if low-level lighting is used to improve visibility. Behavior also depends on features of the built environment. In corridors or tunnels subjects' behavior changes from walking in the open to feeling their way along a wall at a critical density. Infrared video shows subjects waking slowly forward in a crouching position as if to feel their way with their hands and to minimize trip hazards. Personal experience of attempting to walk along a unfamiliar landing in theatrical smoke was of moving forward slowly, affected by fear of tripping over or walking into unseen objects, or falling down an unknown step or level change. For this reason it is considered that in a setting where obstacles are less likely to occur, such as walking along a tunnel walkway holding a railing, then subjects may progress somewhat more rapidly.

Based on considerations such as those described above for the optical density and irritancy of the smoke it is possible to set tenability limits for smoke density appropriate to particular fire scenarios, in relation to the physiological effects on the ability of occupants to see sufficiently well to escape efficiently, and possible psychological effects on their escape behavior. Appropriate limits will depend on the building and occupant characteristics. For example, for small spaces with short travel distances to exits, it may be possible to set less stringent tenability criteria if occupants are familiar with the building. For large spaces it may be necessary to set more stringent tenability limits, particularly if occupants are likely to be unfamiliar with the building and need to be able to see much farther in order to orient themselves to find exits. With regard to the effects of irritancy on the ability to see, it may be necessary to use more stringent smoke density tenability criteria for scenarios where the smoke evolved is likely to be highly irritant to the eyes. Other factors to be taken into consideration would be the complexity of the space, the lighting, and the visibility of the signage. Suggested tenability limits are presented in Table 63.5. Jin [50] suggests tenability limits of extinction coefficient 0.15/m (OD/m = 0.06) for subjects familiar with an escape route or 0.5/m (OD/m = 0.2) for subjects unfamiliar with the escape route. Rasbash [51] suggested a 10-m visibility limit (equivalent to OD/m = 0.08), whereas Babrauskas [52] suggested a tenability limit of extinction coefficient 1.2/m (OD/m = 0.5) in the context of domestic fires. In order to assess the visual obscuration effects of smoke, a concept of fractional effective concentration (FEC) has been developed, whereby the smoke

Table 63.5 Reported effects of smoke on visibility and behavior

Smoke density and irritancy OD/m (extinction coefficient)		Approximate visibility (diffuse illumination)	Reported effects
None		Unaffected	Walking speed 1.2 m/s
0.5 (1.15)	Nonirritant	2 m	Walking speed 0.3 m/s
0.2 (0.5)	Irritant	Reduced	Walking speed 0.3 m/s
0.33 (0.76)	Mixed	3 m approx.	30 % people turn back rather than enter
Suggested tenability limits for buildings with:			
Small enclosures and travel distances:		OD/m 0.2 (visibility 5 m)	
Large enclosures and travel distances:		OD/m 0.08 (visibility 10 m)	

concentration is expressed as a fraction of the concentration considered to significantly affect escape efficiency. If the total FEC_{smoke} reaches unity, then it is predicted that the level of visual obscuration would be sufficient to seriously affect escape attempts. The default limit levels proposed for design purposes are OD/m 0.2 (α_k 0.5) for small enclosures and OD/m 0..08 α_k 0.5 (α_k 0.18 for large enclosures).

$$FEC_{smoke} = (OD/m)/0.2 \text{ for small enclosures or } (OD/m)/0.08 \text{ for large enclosures} \quad (63.9)$$

Movement Speed in Smoke

Fundamental work on movement speed in smoke was carried out by Professor Jin in Japan (See Chap. 61). In experiments where people were asked to walk down a 20 m smoke-logged corridor, Jin found that for nonirritant black smoke (from burning kerosene), walking speed decreased with smoke density and that at an extinction coefficient of 1.15 (optical density of 0.55/m visibility 2.1 m) walking speed decreased from approximately 1.2 m/s (no smoke) to approximately 0.3 m/s [53]. Under these conditions people behaved as if they were in total darkness, feeling their way along the walls or weaving from side to side rather than walking in a straight line.

When people were exposed to irritant smoke, made by heating wood chippings, movement speed was reduced to that in darkness at a much lower smoke density (extinction coefficient 0.5, optical density 0.2 OD/m), and the experience was found to be more distressing. The visibility in irritant smoke decreased sharply at a smoke density exceeding a certain level. "The subjects could only keep their eyes open of a short time and tears ran so heavily that they could not see the words on the signs". Both density and irritancy were found to affect walking speeds, the speed decreasing very rapidly in the same range of smoke density levels. The subjects could not keep their eyes open and they walked with a zigzag pattern or along the wall.

Figure 63.16 shows plots of Jin's results and those from two tunnel experiments, one from a study by Franzich and Nilsson [54] and another by Fridorf et al. [55]. The Figure shows that although it is possible to suggest a relationship between smoke density and walking speed for both non-irritant and irritant smoke from Jin's data, and walking speed was definitely slower in dense smoke, there is a considerable scatter in the data. Also, although the walking speed in the absence of smoke was stated to be approximately 1.2 m/s, there is no indication of the scatter of individual speeds in clear and low smoke density conditions. The results do appear to show a relationship between smoke density and walking speed for non-irritant smoke over a range of k from 0.2 to 1.13, a linear fit to the data being shown in the Figure. For non-irritant smoke with an average density of $\alpha_k = 0.73$ the average walking speed was 0.74 m/s (standard deviation 0.17). For irritant smoke, although it is possible to obtain a linear fit showing a decrease in speed with smoke density, the data are over a very short density range $\alpha_k = 0.32$–0.5 and there is a large scatter of walking speeds. For example

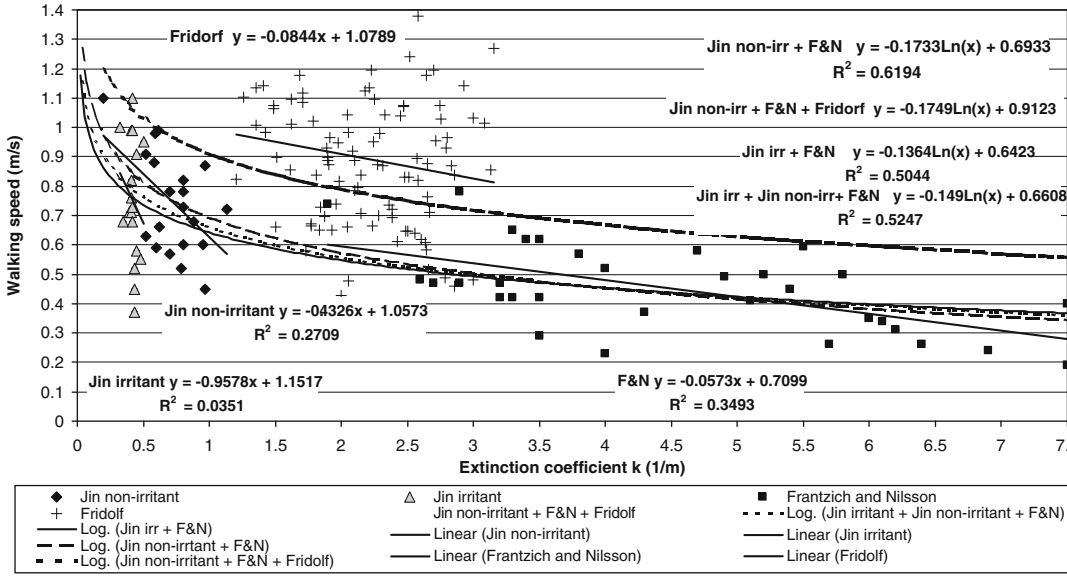

Fig. 63.16 Scatter of data and relationship between smoke density (extinction coefficient α_k (1/m) and walking speed (m/s). Data show Jin (non-irritant smoke), Jin (irritant smoke) in a corridor, Frantzich and Nilsson (mildly irritant smoke) in a tunnel mock up and Fridolf et al. (mildly irritant smoke) in a long tunnel

at $\alpha_k = 0.42$ speeds range between 0.37 and 1.1 m/s. For an average density of $\alpha_k = 0.42$ the average speed is 0.75 m/s (standard deviation 0.21). This is very similar to the average speed in non-irritant smoke, but at a lower density. Taking these data in conjunction with Jin's description of subjects' behavior, it does seem that a person's ability to walk through irritant smoke is more severely impaired than for non-irritant smoke, but it is less obvious that there is a clear relationship between density and speed. Rather it seems that some subjects are severely affects at a low smoke density of around $\alpha_k = 0.42$ (optical density 0.18, visibility approximately 5 m), which is close to the suggested design limit for small enclosure of OD/m 0.2 (See Table 63.5)

The two more recent data set for movement in smoke were those obtained by Frantzich and Nilsson [54] and by Fridolf et al [55]. The scenarios were somewhat different from that of Jin's work in that subjects were asked to walk through a smoke-logged simulated road tunnel. For the Frantzich and Nilsson experiments the "tunnel" contained parked vehicles and had a walkway down the right-hand side from the point at which the subjects were introduced. There was general lighting (on or off in different tests) and an illuminated sign over an exit near the far end on the left side, the subjects being required at some point to cross the tunnel to reach the exit. Smoke was theatrical smoke made slightly irritant by the addition of some acetic acid vapor. The Fridorlf tunnel was a long narrow tunnel without obstacles with wall mounted emergency lighting every 8 m along the sides at waist height at intervals and an illuminated exit sign over an exit 160 m from the start point.

The results for the Frantzich and Nilsson case with general lighting are shown in Fig. 63.16. Apart from differences in the test scenario, a major difference from Jin's experiments are that much higher smoke densities were used varying from α_k 1.9–7.5. The whole data set therefore sits beyond the density at which Jin found that subjects behaved as if in darkness and walked feeling their way along the wall with their hands. A linear fit to Frantzich and Nilsson's results does show a shallow slope of slower speed with increasing smoke density, but another way of looking at the data is to consider it all as constituting dense smoke and consider the average walking speed compared to Jin's figure of a

speed of 0.3 m/s (although the slowest measured speed was 0.37 m/s). For Frantzich and Nilsson's study, the mean walking speed was 0.45 (Standard deviation 0.21), which is quite close to that obtained by Jin in dense smoke. It was also noted in this study that most subjects moved for part of the distance by feeling their way along the walls, and that those subjects doing this for more than 2/3 the total distance had a greater average speed. As with Jin's work, there was a considerable variation in walking speeds between subjects at all smoke densities.

Fridolf et al's data are also shown in Fig. 63.16. These cover a range of smoke densities intermediate between those of Jin and Frantzich and Nilsson. The general pattern from this study again shows a scatter in walking speeds, but the average speeds are rather faster than those from the other two studies. On reason for the relatively rapid walking speeds may be that the tunnel was long and simple, without obstacles. The participants could feel their way along the sides and see the lights every few meters, so that they may have gradually developed a more confident walking pattern as they progressed, in contrast to the short corridor and tunnel used in the other experiments.

In order to derive calculation expressions for the relationship between smoke density and walking speed for non-irritant or irritant smoke, it is possible to perform a variety of fits to these data sets. Figure 63.16 shows logarithmic curves fitted to four data sets: Jin non-irritant plus Frantzich and Nilsson, Jin non-irritant plus Frantzich and Nilsson plus Fridolf, Jin non-irritant plus Jin irritant plus Frantzich and Nilsson, and Jin irritant plus Frantzich and Nilsson. The three fitted curves not including the Fridolf data are quite similar. For a simple deterministic and most conservative calculation an expression fitted to Jin's irritant data and the Frantizich and Nilsson data is suggested as follows:

$$\mathrm{Wsmoke(m/s)} = -0.1364 \times \mathrm{Ln}\,\alpha_k + 0.6423 \qquad (63.10)$$

Where Wsmoke = walking speed in moderately irritant smoke

The standard deviation is 0.157

A logarithmic fit to the "non-irritant" data set (Jin non-irritant, plus Frantzich and Nilsson plus Fridolf) gives a significantly shallower curve. The general impression from these data sets is that, apart from the obvious variation between individual subjects, there do appear to be inverse relationships between smoke density and walking speed, but both individual and average speeds are highly dependent upon the detailed exposure scenario.

For modeling the unrestricted walking speed in smoke of each subject of a population, a speed could be randomly generated from a normal distribution with a mean from Equation 63.12 and standard deviation of 0.125. A difficulty when considering individuals starting to walk in clear air and then entering smoke is that it is not known whether speed in smoke is a fraction of the unrestricted speed (so that fast walkers in clear air walk fast in smoke). A suggested approach is to take the unrestricted starting speed in clear conditions as a mean of 1.2 m/s with a standard deviation of +/- 0.15 m/s then reduce the speed of each person according to Equation 63.12. The Mont Blanc tunnel incident study provides some validation of the predicted effects of smoke density on walking speed [24], and a further study has examined these issues regarding walking speed in smoke and its variability as applied in evacuation models [56].

Composition and Toxic Effects of Smoke

Smoke comprises the total effluents from a fire and consists of two parts: the invisible vapor phase and the visible particulate phase. From a toxicological standpoint, all of the asphyxiant fire products occur in the vapor phase, whereas irritant products may occur in both phases. The particulate phase consists of solid and liquid particles covering a wide range of particle sizes, depending on the nature and age of the smoke. These particles may contain condensed liquid or solid irritant products; or irritant products including gaseous ones may be dissolved in liquid particles (as in acid mists) or be absorbed onto the surface of solid, carbonaceous particles. Particle size is of

great toxicological importance, since it determines how "deeply" particles penetrate into the respiratory tract and the patterns of subsequent deposition. Particles with a mean aerodynamic diameter of less than 5 μm are capable of penetrating deep into the lung, whereas larger particles tend to deposit in the nasal passages and upper airways. Generally speaking, the smoke from smoldering or nonflaming decomposition tends to consist mainly of small particles (less than 1 μm mean aerodynamic diameter, as in cigarette smoke) that are highly respirable. Smoke from flaming fires contains larger particles, particularly as it ages and the particles agglomerate; however, reports on fire victims usually record smoke penetration well into the lung. At very high concentrations, smoke deposits may physically clog the airways. This result could occur even with biologically inert particles at concentrations in excess of 5 mg/L and is more probable with irritant smoke particles that are likely to acutely inflame tissues. Apart from the toxic effects of these particles on the lung, they may also be important in increasing the thermal capacity of the smoke and increasing the likelihood of lung burns.

Tenability Limits and Fractional Irritant Concentrations for Sensory Irritants

The previous section considered assessment of the effects on escape capability and walking speed of exposure to non-irritant and generic "averagely irritant" smoke evolved from typical compartment fires involving mixed fuels. Where the composition of the fire effluents in terms of individual irritant substances is known, and especially when they are know or estimated to contain significantly high concentrations of particularly irritant substances, such as acid gases, then it can be important to assess the effects in terms of the Fractional Irritant Concentration (FIC) for sensory irritants.

$$\mathrm{FIC} = \mathrm{FIC}_{\mathrm{HCl}} + \mathrm{FIC}_{\mathrm{HBr}} + \mathrm{FIC}_{\mathrm{HF}} + \mathrm{FIC}_{\mathrm{SO_2}} + \mathrm{FIC}_{\mathrm{NO_2}} + \mathrm{FIC}_{\mathrm{CH_2CHO}} + \mathrm{FIC}_{\mathrm{CH_2O}} + \sum \mathrm{FIC}_x \quad (63.11)$$

As described in Chap. 62, the immediate effects of exposure to sensory irritants occur over a range of increasing severity from mild eye and respiratory tract irritation to severe pain and breathing difficulties with no obvious threshold levels for different effects. The severity of signs and symptoms is approximately proportional to the logarithm of the exposure concentration. A model relating rate of uptake at the epithelial surface with a concentration-related rate of removal or detoxification has been found to provide a good prediction of the development time and severity of effects on the upper respiratory tract [57]. For humans the eye and upper respiratory tract effects are almost instantaneous and maximal within a few seconds of exposure at painfully irritant exposure concentrations, followed within a short period by lacrimation, mucus secretion and large airway effects including bronchoconstriction and chest pain.

Although there is no specific threshold, for practical application to ASET calculations, two threshold concentration endpoints may be calculated for sensory irritants:

- A concentration capable of seriously impairing escape capability and movement speed.
- A concentration capable of causing incapacitation, such that the subject effectively cannot move.

Table 63.6 shows proposed threshold concentrations for use in ASET calculations (SFPE escape impairment and SFPE incapacitation), compared to threshold concentrations for different endpoints proposed for ISO 13571 and the US EPA Acute Exposure Guidelines. The threshold concentrations proposed here for and in BS7899-2 [58] for design application have been suggested by the authors as concentrations of common fire irritants likely to severely affect escape capability in most humans (escape impairment), while it is proposed that exposure to the higher concentrations shown in the second column is likely to be so painful and cause such severe breathing problems as to effectively incapacitate exposed subjects. As described in Chap. 62, it is difficult to determine threshold levels of human subjects because direct

measurements cannot be made for ethical reasons, and most experimental work has been carried out using animals, mostly rodents. There are, therefore, uncertainties in extrapolating from the existing data to predict the concentrations likely to affect average human subjects. There are also further uncertainties relating to the distribution of sensitivities in the human population. Taking into account the existing data and the fact that effects are on a logarithmic scale of severity, it is considered that a significant proportion of the population are likely to suffer impairment of escape capability at concentrations down to approximately 0.3 × of those affecting the average person, but also that a significant proportion may be able to tolerate twice or even three times that concentration. Thus for HCl, the proposed concentration for escape impairment of the average person (i.e., half the population) is 200 ppm, but some people may be impaired at 60 ppm and others may be able to escape through approximately 400–600 ppm.

For the ISO 13571 guidance documents on assessment of toxic fire hazards [21], a considerably less conservative endpoint of incapacitation for the average person is proposed (which is 1000 ppm for HCl). However, for both here (SFPE) and in ISO13571 more conservative design limits are recommended to allow for sensitive members of the exposed population, such as a design FED of 0.3 for the general population or even 0.1 for particularly sensitive groups (such as for those in health-care premises). For the proposed (SFPE) guidance this would result in a limiting HCl concentration of 60 ppm to avoid escape impairment in the majority of the exposed population. The Acute Exposure Guidelines limits [59] for immediate impaired escape capability and long-lasting adverse health effects (AEGL-2) for exposures of up to 10 min already include provision for sensitive sub-populations, so that for example the proposed limit for HCl of 100 ppm is close to the adjusted SFPE guidance concentration but somewhat more conservative than the ISO 13571 level, which is closer to the AEGL-3 "life threatening concentrations" for 30-min exposures.

Since fire effluents contain a mixture of irritants, it is necessary to consider how they interact in combination. Based on the data reviewed in Chap. 62 and Reference [57], it is currently recommended that they should be considered additive. The overall FIC for an irritant mixture is then as follows:

$$\begin{aligned} \mathrm{FIC} = {} & \mathrm{FIC_{HCl}} + \mathrm{FIC_{HBr}} + \mathrm{FIC_{HF}} \\ & + \mathrm{FIC_{SO2}} + \mathrm{FIC_{NO2}} \\ & + \mathrm{FIC_{CH2CHO}} + \mathrm{FIC_{CH2O}} \\ & + \Sigma \mathrm{FIC_x} \end{aligned} \tag{63.12}$$

Where $\Sigma \mathrm{FIC_X}$ = FICs for any other irritants present.

For each term the numerator is the exposure concentration of an irritant present at any time during an exposure, and the numerator is the concentration predicted to cause impaired escape capability (with use of the SFPE values recommended with an FED factor of × 0.3 to allow for sensitive individuals). Since these are intended to represent immediate sensory effects, they would be expected to ameliorate if the exposure concentrations decreased (for example if, a subject moved out of a contaminated area).

For smoke atmospheres containing significant concentrations of the acid gases and organic irritants, it is also important in the application of egress calculations to consider the effects on the walking speed of escaping occupants at concentrations below those in the SFPE Incapacitation column of Table 63.6. Between zero and the concentration causing incapacitation, there will be a relationship between the irritancy of the smoke and walking speed (as demonstrated by Jin [53]). In order to provide some indication of possible effects on walking speed between these limits, an expression has been developed for any irritant based on the concentration estimated to be very painful [16]. The model is based on a concept that at low concentrations an increase in irritancy will have a relatively minor effect as does smoke (e.g., walking speed in 10 m visibility smoke should be the same as in 100 m visibility smoke). There is, then, a middle range over which an increase in irritancy is likely to have a large effect on walking speed. Then a point occurs where walking is slow and further increases in irritant concentration have less incremental effect. This concept is illustrated in

Table 63.6 SFPE/BS7899-2, ISO13571 and AEGL, guidelines for escape impairment and incapacitation

	SFPE escape impaired	SFPE Incapacitation	ISO 13571 Incapacitation	SFPE 30-min lethal	AEGL-2 10 min escape impairment	AEGL-3 30 min life threatening
HCl	200	900	1000	3800	100	210
HBr	200	900	1000	3800	100	250
HF	200	900	500	2900	95	62
SO_2	24	120	150	400–1400	0.75	30
NO_2	70	350	250	63	20	25
NO	–	>1000	–	~1000	–	–
CH_2CHO (acrolein)[a]	4	20	30	150	0.44	2.5
HCHO (formaldehyde)[a]	6	30	250	750	14	70

[a]where the concentrations of acrolein and formaldehyde (or other important irritants) are unknown, a term derived from smoke density 0.5 OD/m may be used as an indication of irritancy likely to impair escape efficiency

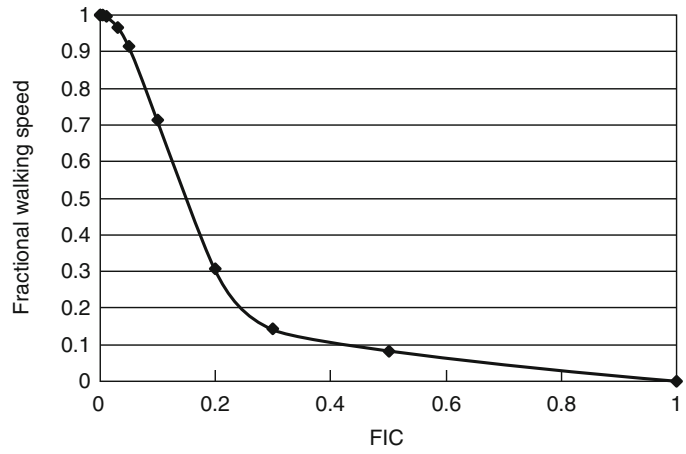

Fig. 63.17 Estimated relationship between fractional walking speed and FIC for a sensory irritant

Fig. 63.17, which shows a general case for the effect of exposure to any irritant gas or mixture of irritant gases on fractional walking speed. The *x*-axis show the fractional irritant concentration (FIC) where FIC = 1 represents incapacitation (e.g., 1000 ppm HCl).

Unlike the situation for nonirritant smoke, the curve reaches a fractional speed of zero when FIC is 1.0 because painful effects on vision and breathing are predicted to be of sufficient severity to cause incapacitation and cessation of effective escape movements. The expression for the curve shown in Fig. 63.17, which can be applied to any individual irritant compound, or to the fractional irritant concentrations for a mixture of compounds, is given by

$$F_{wvirr} = \frac{\left(e^{-(1000x/b)^2}\right) + (-0.2x + 0.2)}{1.2} \quad (63.13)$$

where

F_{wvirr} = Fractional walking speed (1 = normal walking speed of 1.2 m/s)

$b = 160$

x = FIC

The overall effect of exposure to an irritant smoke on walking speed (F_{wv}) would then be given by

$$F_{wv} = 1 - (1 - F_{wvsmoke}) - (1 - F_{wvirr}) \quad (63.14)$$

where

F_{wv} = Overall fractional walking speed (1 = normal walking speed of 1.2 m/s)

$F_{wvsmoke}$ = Fractional walking speed due to smoke effects on visibility

F_{wvirr} = Fractional walking speed due to irritant effects for irritant compounds 1 to n

Post-Exposure Lung Inflammation and Survival

In addition to incapacitating effects of sensory irritation, affecting escape capability, a proportion of inhaled irritant gases and particulates penetrates to the deep lung, and when a sufficient exposure dose is accumulated this can lead to inflammatory processes which can be fatal over periods of several hours to several days after exposure (see Chap. 62 and References [57, 60]). The exposure dose considered likely to cause death in an average exposed human subject is estimated as the rat LCt_{50} exposure for a 30-min exposure and 14-day post-exposure observation period. A guide to exposure doses of common irritant gases likely to cause incapacitation at the scene or death following exposure is given in Table 63.7 (SFPE exposure doses) These are not intended as design limits but for estimates of the extent to which post-exposure deaths from lung edema and inflammation are likely to occur. The 30-min AEGL-3 values shown in Table 63.6 are for concentrations above which it is predicted that the general population, including susceptible individuals, could experience life-threatening adverse health effects or death. When these are expressed as exposure doses and compared with the SFPE levels in Table 63.7 it is evident that the AEGL-3 exposure dose limits for this endpoint are much more conservative. The appropriate choice of limits to use would depend upon the application. Following exposures of primates and rodents to fire effluents, signs of post-exposure inflammatory effects on the lung were minor up an apparent threshold above which effects were severe [60].

Table 63.7 Exposure concentrations and exposure doses for incapacitation and lethal lung damage

Gas	SFPE exposure doses predicted to be lethal to half the population (ppm · min)	AEGL-3 30-min life-threatening exposure doses (ppm · min)
HCl	114,000	6300
HBr	114,000	7500
HF	87,000	1860
SO_2	12,000	900
NO_2	1900	750
NO	~30,000	75
CH_2CHO (acrolein)[a]	4500	2100
HCHO (formaldehyde)[a]	22,500	

[a]where the concentrations of acrolein and formaldehyde (or other important irritants) are unknown, a term derived from smoke density 90 OD/m.min may be used as an indication of lethal organic irritant exposure dose

The fraction of a lethal dose (FLD) for each irritant is calculated as the ct product exposure dose during a period in the fire (e.g., in ppm · min) expressed as a fraction of the lethal exposure dose. The lethal effects of the different irritants are assumed to be additive on the same basis as the irritant effects, so that the total FLD_{irr} for each time period is given by Equation 63.15:

$$FLD_{irr} = FLD_{HCl} + FLD_{HBr} + FLD_{HF} + FLD_{SO_2} + FLD_{NO_2} + FLD_{CH_2CHO} + FLD_{HCHO} + \Sigma FLD_x \quad (63.15)$$

where ΣFLD_x = FLDS for any other irritants present.

The FLD_{irr} for short periods of time during the fire are summed until the FLD_{irr} reaches unity, when it is predicted that a lethal dose has been inhaled.

Asphyxiation by Fire Gases and Prediction of Time to Incapacitation

Asphyxiant gases cause incapacitation mainly by effects on the central nervous system and, to some extent, the cardiovascular system [37].

In general, time to incapacitation and its severity are predictable in that signs are minimal until a critical dose has been inhaled, when a few seconds of intoxication is followed by a sharp decline into loss of consciousness [61, 62]. Most asphyxiant gases produce their effects by causing brain tissue hypoxia [37, 38]. Since the body possesses powerful adaptive mechanisms designed to maximize oxygen delivery to the brain, it is usually possible to maintain normal body function up to a certain dose of asphyxiant, and the victim is often unaware of the impending intoxication. Once a point is reached where normal function can no longer be maintained, deterioration is rapid and severe—beginning with signs similar to the effects of severe alcohol intoxication, consisting of lethargy or euphoria with poor physical coordination, and followed rapidly by unconsciousness and death if exposure continues [38, 62].

Asphyxiant Fire Products

The two major asphyxiant gases in fires are (1) carbon monoxide (CO) and (2) hydrogen cyanide (HCN). Carbon monoxide is always present to some extent in all fires, irrespective of the materials involved or the stage (or type) of fire, so that there is almost always some degree of risk of asphyxia from CO exposure [63]. Hydrogen cyanide is always present to some extent when nitrogen-containing materials are involved in fires. These include materials such as acrylics, polyurethane foams, melamine, polyamide, and wool, which are likely to be involved to some extent in most fires in buildings. Hydrogen cyanide is likely to be present at high concentrations in underventilated (vitiated) fires and especially in large postflashover fires. Unlike carboxyhemoglobin, which is routinely measured in the blood of fire victims, blood cyanide is often not measured. However, it has been detected at high concentrations in the blood of some fire victims, particularly when blood samples have been taken immediately after exposure [64]. In addition, low concentrations of oxygen (less than 15 %) [65] and very high concentrations of carbon dioxide, CO_2 (greater than 5 %), can have asphyxiant effects [66].

Carbon Monoxide

Carbon monoxide combines with hemoglobin in the blood to form carboxyhemoglobin (COHb), which results in a toxic asphyxia because it reduces the amount of oxygen supplied to the tissues of the body, particularly brain tissue. Tissue oxygen supply is reduced because the amount of hemoglobin available for the carriage of oxygen (in the form of oxyhemoglobin) is reduced and also because the ability of the remaining oxyhemoglobin to release oxygen to the tissues is impaired (due to a leftward shift of the oxygen dissociation curve). Carbon monoxide also replaces oxygen in the myoglobin in muscle, and CO entering cells has some inhibitory effect on cellular oxygen metabolism. The effects of CO in fires is reviewed in Purser [67].

The affinity of hemoglobin for CO is extremely high, so that the proportion of hemoglobin in the form of carboxyhemoglobin increases steadily as CO is inhaled. The acute toxicity of CO, therefore, depends mainly on the accumulated dose of carboxyhemoglobin, which is expressed in terms of the percentage of total hemoglobin in the form of carboxyhemoglobin (percent COHb)[31].

There is little doubt that CO is the most important asphyxiant agent formed in fires. In the Strathclyde pathology study [64] lethal levels (>50 %COHb) were found in 54 % of all fatalities, while some 69 % of fatalities had carboxyhemoglobin levels capable of causing incapacitation (>30 %COHb). Incapacitating levels of carboxyhemoglobin are also common in victims surviving immediate fire exposure. Carbon monoxide is, therefore, particularly important because of the following reasons:

1. It is always present in fires, often at high concentrations.
2. It causes confusion and loss of consciousness, thereby impairing or preventing escape.
3. It is the major ultimate cause of death in fires.

To understand the effects of CO exposure on fire victims and to predict the likely consequences of a particular exposure, it is essential to know a number of features of CO intoxication. (To some extent these apply to an evaluation of the toxicity of any fire product.) It is necessary to take the following steps:

1. Determine which types of toxic effects occur at different dose levels.
2. Determine the concentration/time relationships of these toxic effects, whether they occur immediately or some time after exposure, and whether the effects of a short high-concentration exposure are the same as those of a longer, low-concentration exposure.
3. Quantify the parameters that determine the rate of uptake and removal of CO from the body.

Some information on these points is available from accidental exposures and low-level experimental exposures in humans [31], and data are available on the symptoms experienced in humans at various carboxyhemoglobin concentrations at rest [31, 65, 68]. Loss of consciousness is predicted at approximately 40 %COHb, but can occur at lower levels (~30 %COHb) in physically active subjects or more susceptible resting subjects, and lower levels can be dangerous for subjects with compromised cardiac function [31]. Death is predicted at COHb concentrations of 50–70 %COHb, [54, 57, 58, 65, 69]. Survival is rare in subjects with blood levels exceeding 50–60 %COHb (see Table 63.4) and 50 %COHb is usually considered as an average lethal level. It has been suggested that death can occur at lower concentrations in susceptible subjects [31, 70]. The severe incapacitation caused by high-level exposures, such as those encountered in fires, has been studied experimentally in animals [37, 62]. The effects of experimental exposures on cynomolgus monkeys are shown in Fig. 63.18 in terms of physiological parameters (respiration, cardiovascular parameters, and brain electroencephalogram or EEG) monitored in sedentary animals sitting in chairs, and in Fig. 63.13, where free-moving animals were trained to perform a behavioral task designed to simulate some aspects of the escape maneuvers of human fire victims (i.e., tasks involving bodily movements with a certain amount of exercise, requiring the use of coordinated movements and the application of psychomotor skills).

Table 63.8 summarizes findings on the relationship between inhaled CO dose expressed as %COHb and symptoms in humans and primates.

The first important characteristic of CO poisoning illustrated by these experiments is that CO uptake and intoxication are extremely insidious. During the early stages as the carboxyhemoglobin concentration builds up gradually in the blood the effects are minimal. Thus Fig. 63.18 shows no detectible changes in physiological parameters until the end of the exposure when the COHb concentration approached 40 %. In active animals the first minor signs of behavioral performance deficits did not occur until concentrations of 15–20 %COHb were achieved. Similar results have been obtained in humans, where O'Donnel et al. [72] could find no effects on psychomotor performance at levels of up to 12 %COHb, and Stewart et al. [68] reported the first symptoms (consisting of a headache) to occur at 15–20 %COHb, while objective tests at these levels showed only minor deficits in behavioral performance.

Another major characteristic of asphyxia shown clearly by the animal experiments is that when significant effects do occur, their onset is sudden and the degree of incapacitation rapidly becomes severe, so that by the time a victim is aware that he or she is affected effective action is probably not possible. Thus, Fig. 63.18 shows the physiology of a monkey passing from a normal state to unconsciousness within a few minutes after 25 min of exposure, with decreased respiration, a severe decrease in heart rate, and greatly increased slow-wave EEG activity (indicative of cerebral depression). For active animals there was a sudden rapid decline in behavioral task performance accompanied briefly by signs similar to severe alcohol intoxication, which led rapidly to a state of deep coma.

These findings may explain why deaths from CO derived from defective heating appliances are so common. Survivors of such situations often report that they, or other victims who died, experienced headaches or nausea, but had

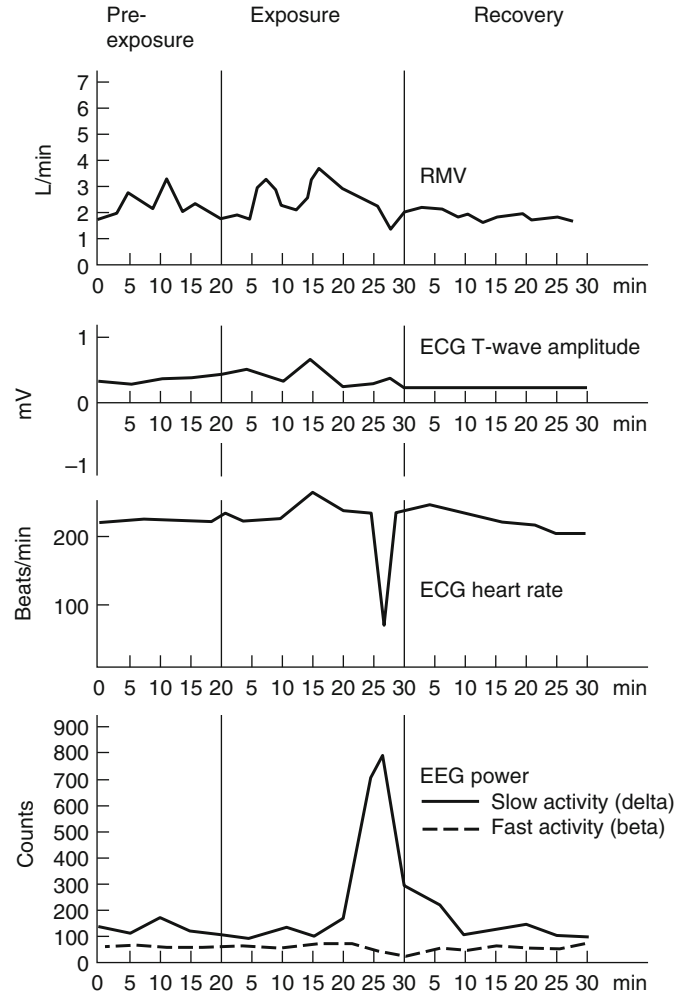

Fig. 63.18 Physiological effects of an atmosphere containing CO (1850 ppm)—wood pyrolyzed at 900 °C [61]

no idea of the cause, so they did not attempt to leave the area until overcome by fumes [73].

During the early stages of incapacitation the main effects appear to be on motivation and psychomotor ability, with a tendency for the victim to sleep if left undisturbed [62]. Under these conditions one might expect a subject, if alerted by a sudden noise such as of breaking glass (often reported by fire survivors), to "sober up" and awake sufficiently to make an escape attempt. However, such a victim is likely to fail for three reasons.

1. This stage is rapidly followed by unconsciousness and coma.
2. Active subjects are seriously affected by carboxyhemoglobin concentrations that have only minor effects on sedentary subjects. Thus, while sedentary primates were often unaffected at carboxyhemoglobin levels of up to 40 %, those engaged in light activity were seriously affected at carboxyhemoglobin levels in the 25–35 % range [62]. Similarly, in one study of humans, although a sedentary subject could perform such tasks as writing, even at the exceptionally high level of 55 % carboxyhemoglobin, the subject collapsed and became unconscious immediately when attempting to rise and walk [74]. Therefore, a victim in a bed or chair attempting to escape not only would be in danger of a rapid collapse due to continued CO uptake, but also even if no further uptake occurred, the ability

Table 63.8 Classical relationship between carboxyhemoglobin concentration and signs exhibited in humans and non-human primates

Blood saturation %COHb	After Stewart [31]	After Sayers and Davenport [71]	After Purser [61, 62, 67] (non-human primates)
0.3–0.7	Normal range due to endogenous production		
1–5	Increase in cardiac output to compensate for reduction in oxygen carrying capacity of blood (heart patient may lack sufficient cardiac reserve		
5–9	Exercise tolerance reduced, visual light threshold increased, less exercise required to induce chest pains in angina patients	Minimal symptoms <10 %	
16–20	Headache, abnormal visual evoked response, may be lethal for patients with compromised cardiac function	Tightness across forehead and headache experienced 10–20 %	
20–30	Throbbing headache; nausea; abnormal fine manual dexterity	Throbbing headache	
30–40	Severe headache; nausea and vomiting; syncope (fainting)	Severe headache; generalized weakness, visual changes; dizziness, nausea, vomiting, and ultimate collapse	30 % caused confusion, collapse and coma in active animals during 30 min exposures with nausea after
40–50		Syncope, tachycardia (rapid heartbeat) and tachypnoea (rapid breathing)	40 % caused coma, bradycardia (slow heartbeat), arrhythmias, EEG changes, in resting animals during 30-min exposures
50+	Coma; convulsions	Coma and convulsions	
60–70	Lethal if not treated	Death from cardiac depression and respiratory failure	

to perform even light work or exercise would be severely impaired. Even the simple act of rising from a horizontal to an upright position may precipitate loss of consciousness.

3. The rate of uptake of CO depends on the respiration (respiratory minute volume) and, hence, the activity of the subject. When the subject becomes active, the blood carboxyhemoglobin is, therefore, likely to increase rapidly to an incapacitating level.

Another issue is the distribution of sensitivities to collapse from CO intoxication in the exposed population during escape from a fire. The range of 30–40 %COHb for collapse in Table 63.8 is for average healthy adults. Some individuals are known to be more sensitive and a proportion of the population may be able to tolerate somewhat higher exposures. Although there are not definitive studies of sensitivity distributions, based upon the information available, the distribution of sensitivity to collapse at different inhaled %COHb ranges is considered likely to resemble that suggested in Fig. 63.19. The shape of the distribution reflects the finding that a small fraction of the population is likely to be at risk from collapse at low %COHb concentrations in the 5–20 %COHb range, while most subjects are likely to collapse at between 30 and 40 %COHb, but very few are likely to even survive exposure above 50 % COHb.

A Model for the Prediction of Time to Incapacitation by CO in Fires

Incapacitation by CO depends on a dose accumulated over a period of time until a

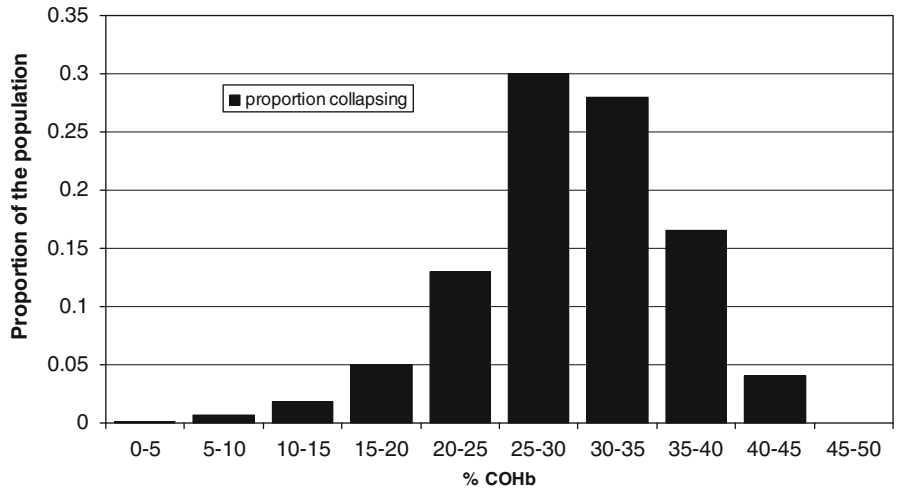

Fig. 63.19 Suggested population distribution of sensitivities to collapse from CO intoxication

carboxyhemoglobin concentration is reached where compensatory mechanisms fail and collapse occurs. To predict time to incapacitation of fire victims due to CO it is necessary to know the carboxyhemoglobin concentrations at which incapacitation is likely to occur and the rate of uptake of CO so that the time to achieve this concentration can be calculated. The carboxyhemoglobin concentrations likely to cause incapacitation depend on the activity of the victim and should be similar to the concentrations causing incapacitation in primates at similar levels of activity [62].

Since CO is both inhaled and excreted via the lungs, the rate of uptake depends on the difference between the CO concentration in the blood, W, and that in the inhaled air, C, and is an exponential function described by the general equation (Equation 63.6):

$$W = C\left(1 - e^{-tk}\right) \qquad (63.6)$$

where t is the time exposed and k is a constant determined by a number of factors, so that uptake is rapid initially but gradually levels off as uptake and removal from the blood reach equilibrium. This relationship is described fully by the Coburn-Forster-Kane (CFK) equation [34, 35], which takes into account a whole range of variables, including respiratory minute volume (V_E), body size, exposure duration, and parameters related to lung and blood physiology (see Appendix 2). When all these various factors are known, this equation enables accurate predictions of CO uptake to be made that agree well with experimental data [35, 75]. The uptake pattern for CO is illustrated in Fig. 63.12, which predicts time to achieve a potentially lethal blood CO concentration (50 %COHb) for a 70 kg human at rest (RMV 8.5 L/min) at two CO concentrations, 2200 and 840 ppm.

When the inhaled concentration is high compared to that in the blood as during short duration, high concentration exposures such as those that occur in flaming fires, the departure from linear uptake is not great as shown in Figs. 63.11 and 63.12 the deviation from Haber's rule ($W = C \times t$) is small. However, over long periods at lower concentrations, as equilibrium is approached, uptake deviates considerably from linearity. This effect is also illustrated in Chap. 62, Fig. 62.1, comparing uptake in rats, monkeys and humans. For the rats, which have a very high respiration rate in relation to their body size, CO uptake reaches non-linear, near saturation levels within a few minutes, whereas for resting humans with a lower respiration rate in

relation to body size, the near-linear phase of uptake is much longer.

Simple C · t Exposure Dose Method

The simplest method for estimating time to incapacitation for an exposure to CO is the C · t product exposure dose method. This method is derived from experimental animal exposure data and then applied to calculation models on the assumption that incapacitation or death occurs at fixed C · t product exposure doses, for any combination of concentration and exposure time. As illustrated in Fig. 63.12, this method works reasonably well for short exposures to high CO concentrations under specific exposure conditions, but makes no allowance for the effects of any physiological variables and especially respiration. For active macaque monkeys (approximately 4 kg bodyweight) the exposure dose for incapacitation was approximately 27,000 CO ppm · min [62]. For sedentary animals of the same body size (but at rest with a lower respiratory minute volume [the volume of air inhaled each minute: V_E]) the exposure dose to incapacitation was higher at approximately 48,000 ppm · min [61]. For moderately active juvenile baboons (approximately 7–10 kg bodyweight), the exposure dose to incapacitation was 34,250 ppm · min and for rats 33,900 ppm · min (both for 5 min exposure periods [76]). The apparent similarity between rats and baboons is coincidental, resulting from a combination of more rapid uptake approaching equilibrium in rats (as illustrated in Chap. 62, Fig. 62.1) and a higher tolerance to hypoxia than in primates. In practice, even over relatively short exposure periods, C · t ≠ K due to the non-linearity of the uptake curve, so that C · t for incapacitation was found to vary experimentally between 37,000 ppm · min at 10,000 ppm CO and 126,750 ppm · min at 1300 ppm CO. The C · t exposure doses for incapacitation and death in different species including humans at different levels of activity are shown in Table 63.9.

Basically, the C · t exposure dose for incapacitation in humans engaged in light-moderate activity (fast waking) while escaping from a building is predicted to be approximately 30,000–35,000 ppm · min, which is similar to that of lightly active baboons and macaques.

This C · t product exposure dose method is proposed for application to fire hazard calculations in ISO 13571 [21], with the proposed C · t exposure dose for incapacitation of 35,000 ppm · min intended to represent humans engaged in moderate physical activity with a V_E of 20 L/min. The advantage of this method is that it is extremely simple to use in a fire hazard modeling context, and it is considered to be valid for moderately active adult humans under the high CO concentrations and short exposure time scales usually occurring during fires (often a few minutes critical exposure period during flaming fires and seldom more than 60 min). A caveat is that for applications outside these limitations (such as application to children, resting adults, long exposure periods at low CO concentrations or other situations involving differences in the variables listed), more complex modeling methods are indicated and a simple default method recommended here, which allows of the important effect of activity level and V_E on CO uptake, is to calculate the actual uptake dose of CO with time as %COHb.

Table 63.9 *C · t* product exposure doses for incapacitation and death by CO for different species at rest and during light activity

	Incapacitation		Fatal	
	CO at rest ppm · min	CO light activity ppm · min	CO at rest ppm · min	CO light activity ppm · min
Human 70 kg	80,000–100,000	30,000–35,000	~110,000–240,000	~60,000–190,000
Baboon ~20 kg		34,000		
Macaque 3–4 kg	38,000–40,000	27,000		
Rat ~ 300 g	30,000–40,000	22,000–36,000	162,000	

Calculation of %COHb Using the Liner Uptake Stewart Model the Exponential Coburn Forster Kane Model

For short exposures at high concentrations when the blood concentration is well below saturation level, an approximate prediction of COHb concentration can be made assuming a linear relationship. Such an equation is derived from experimental human exposures by Stewart et al [69].

$$\%\mathrm{COHb} = \left(3.317 \times 10^{-5}\right)(\mathrm{ppm\,CO})^{1.036}(\mathrm{V_E})(t) \quad (63.16)$$

where
ppm CO = CO concentration (ppm)
V_E = Volume of air breathed per minute (L/min)
t = Exposure time (min)

Thus, for the examples shown in Fig. 63.12, which were calculated using the Coburn-Forster-Kane (CFK) equation [34], a concentration of 50 %COHb is predicted following a 1-h exposure to 2200 ppm CO, while the Stewart equation predicts 49 %COHb. However, for a 4-h exposure the CFK equation predicts 50 % COHb from 840 ppm, while the Stewart equation would predict 50 %COHb from 550 ppm over 4 h, or a concentration of 72 %COHb from 840 ppm.

Justification of the linear uptake relationship under high concentration/short exposure duration circumstances is illustrated by a series of primate exposures carried out over a 1000 to 8000 ppm concentration range. These experiments were performed using an active behavioral model [62], with the endpoint being loss of consciousness, which occurred at approximately 34 % COHb. The results are illustrated in Fig. 63.14 which shows time to incapacitation for different inhaled CO concentrations. At each concentration the inhaled dose (Ct product) required to produce incapacitation in ppm CO · min is constant as predicted by the linear uptake model of Haber's rule.

Accurate predictions of CO uptake can be made for a range of situations by using the CFK equation, provided that a number of variables are taken into account. For a particular individual the most important variable is V_E, which varies considerably depending on the level of activity of the subject. Figures for this variable and others can be obtained from standard reference data [77]. Figure 63.20, generated from these data, shows the calculated time to incapacitation (loss of consciousness) for a 70 kg human exposed to different CO concentrations at three levels of activity. The figure shows that the degree of activity can have a major effect on time to incapacitation. It must also be remembered that V_E

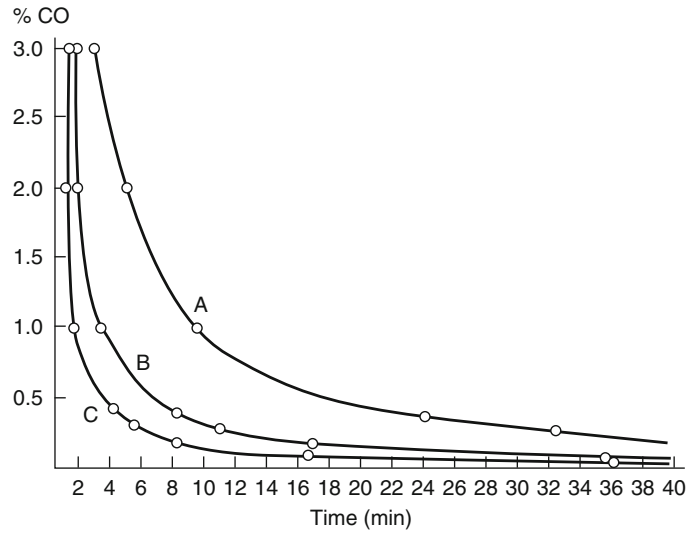

Fig. 63.20 Time to incapacitation by carbon monoxide for a 70 kg human at different levels of activity. *Curve A*—40 % carboxyhemoglobin V_E 8.5 L/min at rest sitting; *Curve B*—30 % carboxyhemoglobin V_E 25 L/min, light work (e.g., walking 6.4 km/h); *Curve C*—20 % carboxyhemoglobin V_E 50 L/min, heavy work (e.g., slow running 8.5 km/h, or for walking 5.6 km/h up a 17 % gradient)

per kilogram of body weight is greater for small subjects, which means that children will take up CO much more rapidly than adults and succumb much earlier, while uptake in small laboratory animals is even more rapid. An assumption made in these calculations is that the level of activity and hence the V_E remain constant during the exposure. In practice there is a tendency for the level of activity and ventilation to vary during the course of an exposure. During the early stages building occupants may be at rest or sleeping with a low V_E. Once alerted by the fire their V_E is likely to increase due to emotional concerns and increased physical activity such as walking to escape. Ventilation may then begin to decrease slightly as the point of incapacitation is approached. It is considered that with a model for predicting time to incapacitation (unconsciousness), errors due to reduced ventilation will be minor, since the primate experiments demonstrate that there is little change in V_E until the point of incapacitation. Once the subject becomes unconscious, the V_E and hence the rate of CO uptake will be considerably reduced, particularly if the subject was previously engaged in heavy work. It is, therefore, possible that for calculating time to death allowance could be made for a low V_E (~6 L/min) once incapacitation has occurred. Not making this allowance does err slightly on the side of safety.

Table 63.10 shows physical work rate, oxygen consumption and minute ventilation (V_E) for average adult humans engaged in different activities [67]. Different data would be needed for children or adults with bodyweights significantly different from 70 kg V_E depends primarily on the body size of the subject and the level of physical activity. Data can be obtained from physiology reference sources and Table 63.10. V_E also depends upon the concentration of inhaled CO_2. This effect is negligible at ambient CO_2 concentrations but is an important factor in fires, where the concentration can be as high as 10 % CO_2.

The rate of CO uptake increases approximately in proportion as V_E increases, however there is an upper limit for the rate of diffusion of CO from the air into the blood in the lungs, which is

Table 63.10 Work rate, oxygen consumption and minute ventilation for different activities (for ~70 kg Bodyweight)

Activity	Speed km/h	Work kcal/min	Work Watts	V_{O2} L/min STPD[a]	V_E l/m ATPS[b]
Sleeping and lying, includes turning over, getting up	0	1.1	77	0.22	4.9
Resting	0	1.26	88	0.252	5.6
Sitting, includes reading, eating, desk work	0	1.5	105	0.3	6.7
Sitting	0	1.9	133	0.38	8.5
Standing	0	1.875	131	0.375	8.4
Standing, includes activities like moving between rooms	0	2.5	174	0.5	11.2
Walking, outdoors, and other activities	3	3	209	0.6	13.4
Walking	4	3.8	265	0.76	17.0
Walking	5	4.45	311	0.89	19.9
Light industry,	5	5	349	1	22.3
Walking	6	5.15	359	1.03	23.0
Walking	6.4	5.6	391	1.12	25.0
Walking	7	5.8	405	1.16	25.9
Manual labor	7.24	8	558	1.6	35.7
Running	5.6	11.2	782	2.24	49.9
Running, climbing stairs, heavy manual work	8.9	11	768	2.2	49.0

[a]STPD = standard temperature (0 °C) and pressure (760 mmHg) dry
[b]ATPS = Ambient temperature and pressure saturated

represented as DL_{CO} expressed in mL/min/unit partial pressure of inhaled CO. This effect is not considered by the Stewart equation but is taken into account in the CFK equation. This means that at very high V_E levels the Stewart equation may somewhat overestimate the rate of CO uptake. Figure 63.21 compares the predictions of the Stewart and CFK equations in young adult males (70 kg bodyweight) for CO uptake expressed as %COHb calculated for CO exposure concentrations of 1000 and 4000 ppm at different V_E levels representing sedentary, light activity and fast walking. The Stewart predictions are linear, as are the CFK predictions for the first 20 min or so, but after this time the CFK predictions become more curved as %COHb begins to approach, equilibrium concentrations. For 1000 ppm CO the rates of uptake are similar for both calculation methods up to around 25 %COHb, but the CFK values then start to deviate from the linear Stewart model as the blood concentration tends to equilibrate, especially at the higher V_E level. For 4000 ppm CO, a concentration more typical of a serious exposure during a fire, the rates of uptake are very similar and almost linear for all three V_E levels up to around 30–40 %COHb at which dose loss of consciousness is predicted. For these calculations a variable expression for DL_{CO} was used :

$$DL_{CO} = (16.147 \times \ln(V_E)) - 16.05 \quad (63.17)$$

Where

DL_{CO} = CO mL/min/mmHg CO partial pressure at STPD

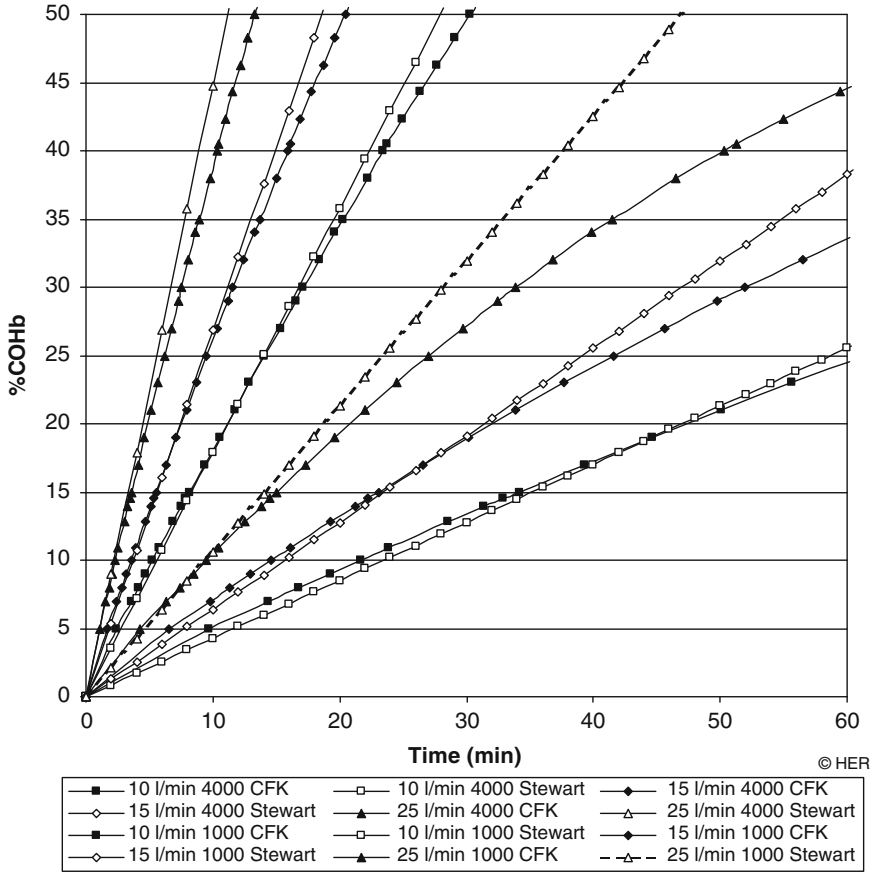

Fig. 63.21 Comparison of calculated CO uptake as % COHb using the Stewart and CFK equations for a 70 kg man (Blood volume 5621 mL, Hb 15.94 g/100 mL, DL_{CO} varies as Equation 63.17 at V_E 10, 15 and 25 L/min, CO 1000 and 4000 ppm)

These deviations illustrate that the rate of CO uptake is not a simple function of V_E. This limitation on the extent of increase in rate of CO uptake with increasing V_E has been allowed for to some extent with the V_{CO2} function, which is intended to be used as multiplier for the rate of CO uptake during exposure to combined CO and CO_2 mixtures in fire, allowing for the increase in V_E caused by the CO_2. As described in the section on CO_2, Equation 63.35 is used instead of Equation 63.33 to allow for these inefficiencies in uptake with increasing V_E.

The Stewart [69] and CFK [34] equations enable reasonably good predictions of time to incapacitation or death for short (less than 1 h) or long (greater than 1 h) exposures, respectively, to constant concentrations of CO in air. In fires, however, victims are exposed to concentrations of CO that change during the course of the fire. For smoldering fires the CO concentration may grow slowly and remain fairly constant over long periods, but for early flaming fires and many fully developed fires where the victim is in a remote location, the CO concentration may increase rapidly over a short period of time as in Fig. 63.22. It is, therefore, necessary to be able to apply the uptake models to situations where the CO concentration is not constant. For most situations, fluctuations in CO concentration do not present a problem since incapacitation depends on the total dose of CO inhaled, in the form of COHb, and is not affected by the immediate CO concentration. The COHb concentration is thus dependent on the average CO concentration over the period of exposure, and significant errors will not occur even if the CO concentration falls somewhat at certain stages of the exposure. Errors in predicting the COHb concentration are possible if the CO concentration drops dramatically toward the end of an exposure, or if it decreases moderately during a prolonged exposure of several hours duration, when COHb concentrations can approach equilibrium with the inhaled CO concentration. In this case a fall in CO may result in a decrease in COHb concentration. The basic rule to apply is that fluctuations are unlikely to cause the COHb concentration to deviate from that predicted by assuming the constant average concentration throughout, providing the CO concentration is on a rising trend, is stable, or is well above the equilibrium concentration with the blood COHb.

Ct Product and Fractional Incapacitating Dose

Although the average CO concentration during a fire exposure can be used to predict COHb

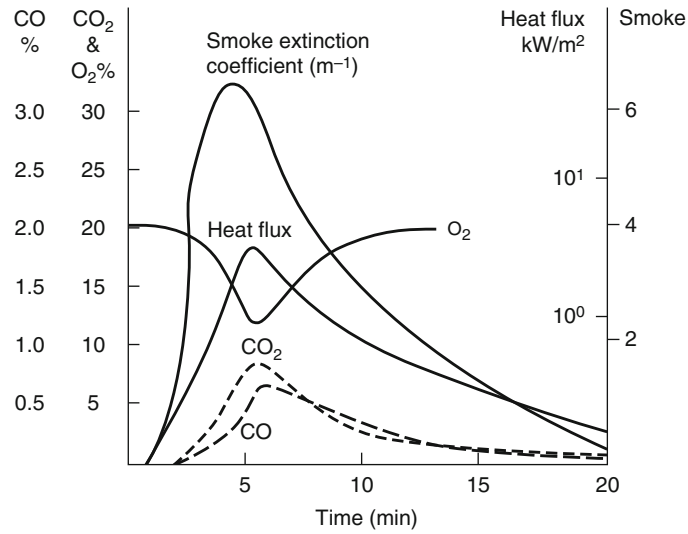

Fig. 63.22 Smoke, heat, and gases during single armchair room burn. Armchair is polystyrene with polyurethane cushions and covers. Room is 39 m^3 with open doorway. Gases measured in doorway at 2.1 m height [52]

concentration and time to incapacitation, another useful concept for predicting incapacitation or death is the relationship with concentration-time (Ct) product, which is a representation of CO "dose." In changing fire conditions the Ct product may be obtained by integrating the CO concentration/time curve. The dose inhaled may then be related to the dose required to cause incapacitation, and the fraction of an incapacitating dose at any time, t, may be calculated, incapacitation occurring when the fractional dose reaches 1.0. Since the Ct "dose" actually represents the COHb concentration, the fractional dose would be better represented by the ratio of the COHb concentration at time, t, with the COHb concentration known to cause incapacitation or death, rather than by simple Ct product ratios. The Stewart equation [69] can be rewritten in the form of COHb ratios, requiring only a knowledge of the CO concentration and the exposure time, as follows:

$$F_{I_{CO}} = 3.317 \times 10^{-5}[\mathrm{CO}]^{1.036}(V)(t)/D \quad (63.18)$$

where

[CO] = Carbon monoxide concentration (ppm v/v 20 °C)

V = Volume of air breathed each minute (L)

t = Exposure time (minutes)

D = Exposure dose (percent COHb) for incapacitation

The following values may be taken for V and D. Other data for V may be taken from Table 63.10.

Activity level of subject	V_E(L/min)	D (percent COHb)
Resting or sleeping	8.5	40
Light work—walking to escape	25	30
Heavy work—slow running, walking up stairs	5	20

The suggested default case for escaping occupants would be that of light work.

This concept of Ct product fractional dose is also useful for predicting incapacitation and death from other fire products and combinations of products, as will be discussed later in this chapter.

CO Washout After Fires

For subjects rescued alive from a fire breathing air or oxygen the CO is gradually excreted via the lungs and the %COHb decreases according to a washout curve. A simple washout model is given by:

$$\%COHb_t = \%COHb_0 e^{-kt} \quad (63.19)$$

Where:

$\%COHb_t$ = %COHb after t minutes

$\%COHb_0$ = %COHb at start time

k = half life constant depending upon treatment and body size

The value of k depends upon the treatment (air, normobaric oxygen or hyperbaric oxygen) and the body size. Although the rate of excretion should be similar for adults, it is much more rapid in small children. The model can be applied to individuals by using a factor related to the ratio of basal metabolic rates in subjects with different body sizes, obtained from published data. The predictions for children from the model have been validated against half-life data obtained from incidents involving children. For different body sizes and treatments k was therefore estimated in terms of the ratio of basal metabolic rates (Table 63.11).

Hydrogen Cyanide

Hydrogen cyanide (HCN) has been measured in the blood of both fatal [78] and nonfatal [79] fire

Table 63.11 Values of half-life constant (k) for different treatments and body sizes

Body size and air mixture inhaled	k	Resting metabolic rate kcal/h/kg
70 kg adult on air	0.0026	1.12
70 kg adult on normobaric oxygen	0.0115	1.12
70 kg adult on 3 bar oxygen	0.0301	1.12
28 kg child	0.0167	1.63
14 kg child	0.0219	2.1

This and other CO washout modeling methods are described in Purser [67]

victims. However, in the Strathclyde fire fatality study high concentrations of hydrogen cyanide in the blood of victims were usually associated with lethal levels of carboxyhemoglobin, so that the role of hydrogen cyanide as a cause of incapacitation was difficult to determine [78]. It is also difficult to relate blood cyanide levels from samples collected after a fire to likely HCN exposure, since the dynamics of HCN uptake and removal from the blood are poorly understood [67, 80–82].

Although the ultimate effects of HCN exposure (consisting of unconsciousness with cerebral depression) are similar to those produced by CO, the pattern of toxicity during the early stages is very different. Whereas the onset of CO intoxication is slow and insidious, HCN intoxication tends to be rapid and dramatic. The physiological signs of incapacitation produced in monkeys by an atmosphere containing HCN are shown in Fig. 63.23 [80] As with CO the immediate effects were relatively minor, consisting of a slightly raised ventilation, but at some time during a 30-min exposure period there was a marked increase in respiration (hyperventilation), the RMV increasing up to four times. Within 1–5 min of the start of this episode of hyperventilation the animals lost consciousness. This was accompanied by EEG signs of severe cerebral depression; loss of muscle tone; and marked

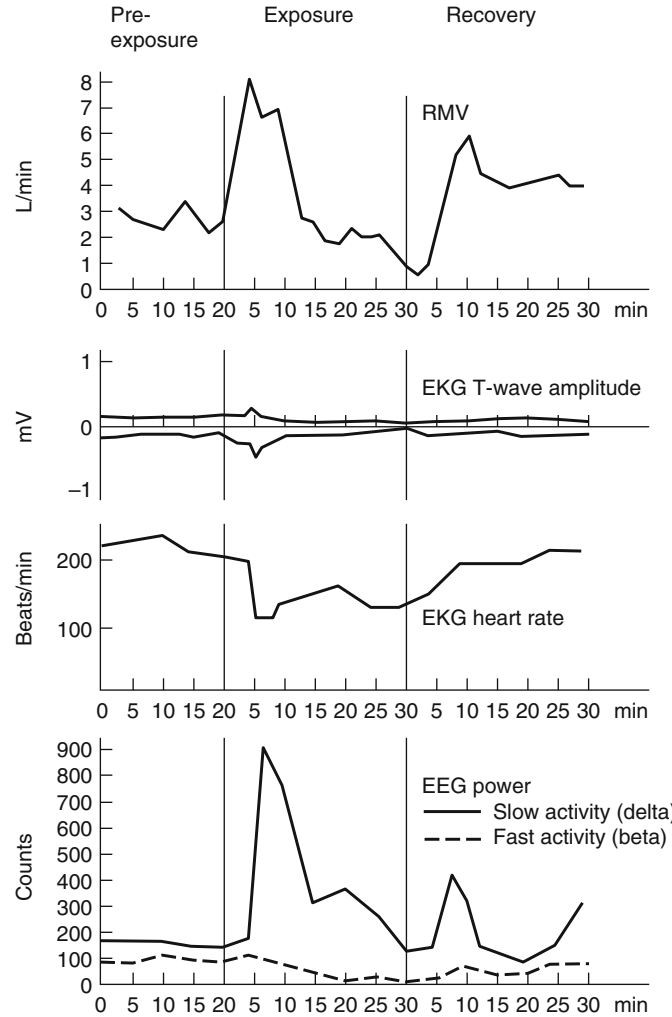

Fig. 63.23 Physiological effects of an atmosphere of HCN gas (147 ppm) on monkeys [80]

effects upon the heart and circulation, including a significant decrease in heart rate, arrhythmias, and changes in the EKG waveform indicative of cardiac hypoxia. This hyperventilatory episode was caused by the stimulatory effects of cyanide on respiration. Since the cyanide was taken in via inhalation, a positive feedback situation resulted, and inhaled cyanide caused hyperventilation that increased the rate of HCN uptake and in turn provided a stronger hyperventilatory stimulus. Once the animals became unconscious the hyperventilation subsided and they went into a slow decline for the remainder of the exposure. This led eventually to a cessation of breathing in some cases, which would have proved fatal if exposure had not been terminated. It was therefore possible for an animal to survive a continuous HCN exposure for some time after the point of incapacitation. Once exposure was terminated the recovery was rapid and almost complete within 5–10 min.

The pattern of incapacitation for HCN is somewhat different from that produced by CO in that the effects occur more rapidly, as unlike CO, HCN is not held almost exclusively in the blood but is carried rapidly to the brain [83]. Although the accumulation of a dose is one factor, the most important determinant of incapacitation with HCN appears to be the rate of uptake, which in turn depends on the HCN concentration in the smoke and the subjects' respiration. Thus in the animal experiments [37, 80], it was found that at HCN concentrations below approximately 80 ppm the effects were minor over periods of up to 1 h, with mild background hyperventilation. At concentrations above 80 ppm up to approximately 180 ppm, an episode of hyperventilation with subsequent unconsciousness occurred at some time during a 30-min period; there was a loose linear relationship between HCN concentration and time to incapacitation. Above 180 ppm the hyperventilatory episode began immediately with unconsciousness occurring within a few minutes.

The exact reason is not known but one factor appears to be related to the relationship between the rate of uptake of HCN and the dynamics of its distribution between different body fluid compartments. This results in a spike in systemic plasma cyanide resulting from the hyperventilatory episode. This may deliver a pulse of cyanide to the heart and brain resulting in collapse before the cyanide fully perfuses other body organs and tissues so that the concentration evens out throughout the body. Another likely contributory cause of loss of consciousness during the hyperventilatory episode is a transient hypocapnia (lower then normal level of carbon dioxide in the blood) and respiratory alkalosis. During this episode ventilation increases by approximately a factor of three, which will result in a temporary respiratory alkalosis with a reduction in blood P_{CO2}. The pH change results in a left shift in the oxygen dissociation curve and the P_{CO2} reduction in a reduced cerebral blood flow, effects known to result in syncope (loss of consciousness) in humans [84]. The effect is likely to be enhanced by the direct effects of cyanide on heart rate and cardiac output, as well as direct effects on cerebral metabolism. The combined result is the reported transient loss of consciousness. The loss of consciousness then results in a decrease in respiration and circulation, enabling P_{CO2} and pH to recover towards normal levels, while the direct effect of cyanide on metabolism results in a metabolic acidosis and increased cerebral blood flow. This may be the reason that animals are seen to make some recovery during this stage of an exposure, followed by a slow decline until exposure is terminated.

Data on human exposures to HCN are limited but Kimmerle [65] does quote some approximate data showing a similar effect in humans, with incapacitation occurring after 20–30 min at 100 ppm HCN and after 2 min at 200 ppm, death occurring rapidly at concentrations exceeding approximately 300 ppm (Table 63.12).

Other data suggest that human victims might be able to survive higher concentrations of HCN for shorter periods. McNamara [87] suggests 539 ppm as the 10-min LC_{50} for humans, and there is a report of a survival from an accidental exposure to 444 ppm [85]. An experimental human exposure to 530 ppm HCN was survived without immediate symptoms for 1.5 min, although a dog exposed at the same time suffered

Table 63.12 Incapacitation by inhaled hydrogen cyanide

HCN (ppm)	Species and effects	Author
100	Loss of consciousness after 23–30 min in primates and humans	Purser [80], Kimmerle [65]
200	Loss of consciousness after approximately 2 min	Purser80, Kimmerle [65]
300+	Death occurs "rapidly"	Kimmerle [65]
444	A man survived an accidental exposure	Bonsall [85]
530	A man, Barcroft, survived a 1.5 min exposure—his dog exposed at the same time died	Barcroft [86]
539	Suggested 10-min LC_{50} in humans	McNamara [87]
1000	One breath may cause loss of consciousness	Purser

respiratory arrest [73]. Dogs are known to be particularly susceptible to cyanide poisoning [87], but it does seem likely that, to some extent, with HCN (as with CO) body size influences time to incapacitation, and that a human would be able to tolerate exposure to a given concentration longer than a cynomolgus monkey. With HCN and CO, physical activity would be likely to cause more rapid uptake in adults, and uptake would be more rapid in children because of their smaller body size. The primate data, therefore, seem to provide a reasonable model for humans, possibly erring slightly on the side of safety.

The differences between CO and HCN in terms of the relationship between inhaled concentration and time to incapacitation are illustrated in Fig. 63.14. Whereas CO gives a smooth curve with incapacitation occurring at a constant *Ct* product of approximately 27,000 ppm · min for all CO concentrations, the almost linear portion of the HCN curve results in a *Ct* product of approximately 2000 ppm · min at 100 ppm HCN and 400 ppm · min at 200 ppm, with very rapid incapacitation at higher HCN concentrations. This deviation from Haber's rule (which predicts a constant *Ct* product) was recognized by Haber himself in 1924, when he stated that the *Ct* product for HCN depended on the exposure concentration [32]. The effect is to render concentrations in the range greater than 150 ppm more toxic than would be predicted from the effects of longer exposures to lower concentrations.

A Model for the Prediction of Time to Incapacitation by HCN in Fires

From these results it is possible to predict that HCN concentrations below a threshold concentration of approximately 80 ppm will have only minor effects over periods of up to 1 h.

From 80 to 180 ppm the time to incapacitation (unconsciousness) t_{ICN} will be between 2 and 30 min. For concentrations above approximately 180 ppm incapacitation will occur very rapidly (within 2 min). In order to derive an expression for calculating time to incapacitation as a function of inhaled HCN concentration a trend line has been fitted to the entire data set for the primate experiments. This includes data for exposures to HCN gas in air, HCN generated from thermal decomposition of polyacrylonitrile, HCN from thermal decomposition of rigid and flexible polyurethane foams, all in resting primates. These data are plotted in Fig. 63.24. The results are very similar for the pure HCN gas exposures and those to the decomposition product atmospheres for which HCN gas was the dominant toxicant although small amounts of other nitriles were also present and some CO from the polyurethane foams. Also shown in Fig. 63.24 are data for time to incapacitation in resting and exercising rats. Times to incapacitation in the resting rats for a given HCN concentration are somewhat longer than in the primates, but those for exercising rats are somewhat shorter, as would be predicted from the increased respiration and hence rate of HCN uptake, and higher metabolic demand, in the exercising animals.

In order to derive an expression for time to incapacitation for humans, it is considered that the monkey data provide the most useful model. Because the monkeys were much smaller animals than humans (approximately 4 kg versus

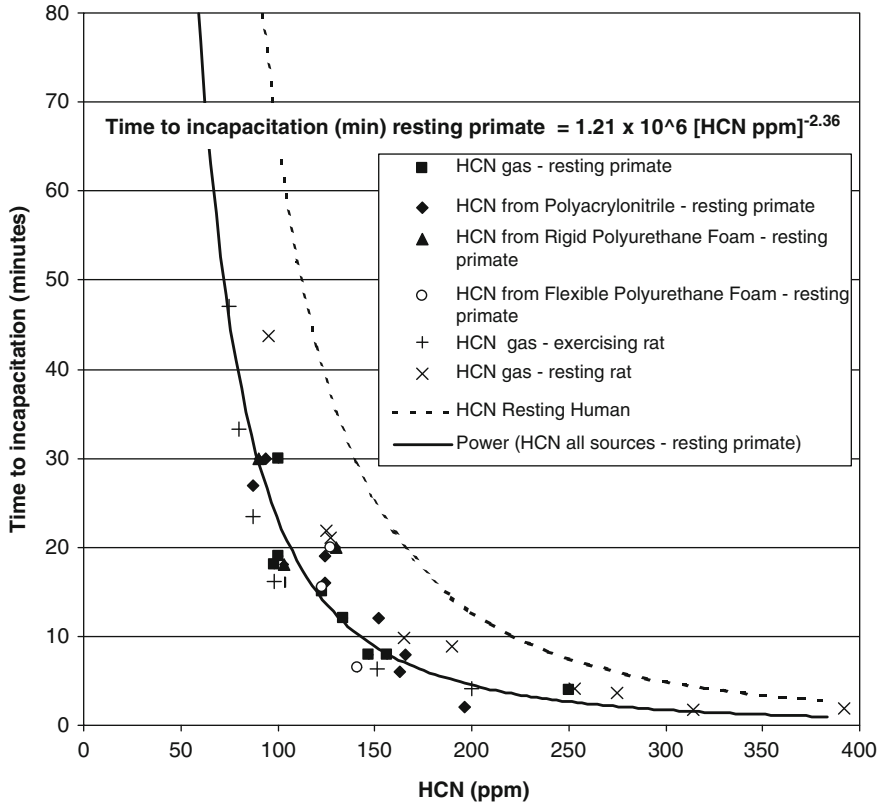

Fig. 63.24 Measured times to incapacitation as a function of HCN concentration in macaque monkeys, resting and exercising rats, and predicted for humans

70 kg for humans) at a given level of physical activity and respiration it is to predicted that the rate of uptake and therefore time to incapacitation would be somewhat shorter than for an adult human. Comparing the resting metabolic rates for monkeys and humans as a function of body size, it is estimated that the time required for a human to inhale the same dose as a monkey would be increased by approximately a factor of 2.83, although for a human infant the relationship would be approximately the same as for the monkey.

In practice, it is considered that time to incapacitation in the average adult human engaged in light physical activity (such walking to escape from a fire), would be similar to that in a resting monkey. On this basis it is proposed that for estimation of time to incapacitation for escaping humans for design purposes, the primate trend line expression should be used directly as follows:

$$t_{ICN} = \frac{1.2 \times 10^6}{[CN]^{2.36}} \tag{63.20}$$

Where:
t_{ICN} = time to incapacitation (minutes)
[CN] = Inhaled HCN concentration (ppm)

This exponential expression gives a reasonably good fit with the data (regression coefficient 0.84).

A more general expression for humans engaged in different levels of physical activity would take into account of the 2.83 metabolism factor and the level of respiration is:

$$t_{ICNg} = \frac{2.43 \times 10^7}{[CN]^{2.36} \times V_E} \tag{63.21}$$

Where:
t_{ICNg} = time to incapacitation (minutes)
[CN] = Inhaled HCN concentration (ppm)
V_E = respiratory ventilation (L/min)
2.43×10^7 is the trend line constant $1.21 \times 10^6 \times 2.83$ (ratio of basal metabolic rate kJ/h/kg bodyweight between monkey and human) $\times$ 7.1 L/min resting human V_E

This expression for humans is consistent with the limited human data available.

HCN could be particularly dangerous in fires due to its rapid "knockdown" effect, and low HCN levels in the 100–200 ppm range could cause fire victims to lose consciousness rapidly and, consequently, to die later as a result of accumulation of CO or some other factor. A small change in HCN concentration could also cause a large decrease in time to incapacitation; for example, doubling the concentration from 100 to 200 ppm could bring the incapacitation time down from approximately 22 min to approximately 4 min [65, 80].

Although this relationship should enable reasonable predictions to be made of time to unconsciousness for subjects exposed continuously to HCN, especially over the critical range between 80 ppm (below which incapacitation is unlikely over periods of up to 1 h) and 180 ppm (above which incapacitation will be rapid), real fires will involve exposures to changing concentrations. One method of predicting time to incapacitation or death would be to take the average concentration over the period of exposure. Although approximate times to incapacitation can be estimated with this method it is prone to error because of the departure from Haber's rule. In practice, since short exposures to high concentrations are more likely to cause incapacitation than longer exposures to lower concentrations, averaging the concentration tends to give longer estimates of time to incapacitation than would be expected. This method also does not include the concept of fractional dose. A better model would include some degree of weighting to allow for the enhanced effect of high concentration exposure and also enable incapacitation to be estimated in terms of *Ct* product fractional dose.

A method for estimating fractional dose to incapacitation has been developed for the rat by Hartzell et al. [39] based on this concept. In that model the *Ct* product over short periods of time is expressed as a fraction of the *Ct* product required to cause incapacitation or death at that concentration. The fractions for each short time interval are summed until the fraction reaches unity, which indicates incapacitation [39]. This approach should enable reasonable predictions of time and dose to incapacitation and death to be made, provided that the HCN concentration is stable or increasing (Hartzell et al. have found a good correspondence between calculated predictions and experimental data in rats). This approach can be used to derive a fractional dose model for humans based on the time to incapacitation equation (Equation 63.22), derived from primate and human data. The default expression recommended for fire engineering design applications uses the expression for resting primates as a predictor of active adult humans.

Dose to incapacitation = (ppm HCN)$(t_{I_{CN}})$

Therefore, for a short exposure time, t, to a given HCN concentration

$$F_{I_{CN}} = \frac{(\text{ppm HCN})(\text{t})}{(\text{ppm HCN})(t_{I_{CN}})} \tag{63.22}$$

where $F_{I_{CN}}$ is the fraction of an incapacitating dose.

Taking $t = 1$ min, this simplifies to

$$F_{I_{CN}} = \frac{1}{t_{I_{CN}}} \tag{63.23}$$

which is given by:

$$\text{Default case}: F_{ICN} = \frac{[CN]^{2.36}}{1.2 \times 10^6} t \tag{63.24}$$

$$\text{General case}: F_{ICNg} = \frac{[CN]^{2.36} \times V_E}{2.43 \times 10^7} \text{t} \tag{63.25}$$

If the fractional doses per minute, $F_{I_{CN}}$ or $F_{I_{CNg}}$ are summed throughout the exposure, the dose and time to incapacitation can be predicted.

Example A subject is exposed to 90 ppm HCN for 15 min, then to 180 ppm HCN for 3 min. Using the default case expression:

HCN concentration (ppm)	F_{ICN} for 1 min		
90	0.034	$0.034 \times 15 =$	0.51
180	0.175	$0.175 \times 3 =$	0.525
		F_{ICN} after 17 min	0.86
		F_{ICN} after 18 min	1.035

Incapacitation is therefore predicted between 17 and 18 min

[CN] represents the concentration of cyanide (ppm). If necessary this can be corrected for the presence of other nitriles besides HCN and for the protective effect on cyanide poisoning of NO and NO_2. [CN] can then be calculated as

$$[CN] = [HCN] + [\text{Total organic nitriles}] - [NO + NO_2] \quad (63.26)$$

For more detailed predictions of time to incapacitation in adult humans for application to evacuation models or incident investigations Equation 63.25 may be used with appropriate values for V_E depending on the activity level of the subject

Cyanide in Blood

The importance of HCN as a cause of incapacitation and death in fires can be underestimated due to poor understanding of the dynamics of cyanide uptake, dispersal and metabolism in the body, and the inadequate database of blood cyanide measurements from both injured and dead fire victims. Carboxyhemoglobin is the only blood toxin routinely measured in fire victims, and when blood cyanide is measured (usually postmortem), the sample and measurements are often taken a day or more after exposure.

Evidence from the primate experiments reported above, and from further experiments where measurements were made of arterial blood cyanide during and after exposure [81], shows that when HCN is inhaled for short periods at air concentrations above approximately 150–200 ppm, loss of consciousness results from a transient high plasma cyanide concentration. HCN uptake rate is then greatly reduced when the subject loses consciousness (or dies) and the cyanide in the plasma disperses throughout the body fluids, leaving a low immediate post-exposure plasma concentration. Also, cyanide decomposes rapidly in cadavers [88], by approximately 50 % in 1–2 days, and may subsequently decrease further or even increase slightly in stored blood. For these reasons, blood cyanide concentrations measured in fire victims are often relatively low, but when blood samples are obtained immediately after exposure [89], higher, toxicologically significant or life-threatening levels are detected. It is suggested that, in freshly obtained whole blood samples, levels of 2.0–2.5 μg CN/mL should be considered capable of causing incapacitation and 3.0 μg CN/mL should be considered lethal, whereas for samples not taken and analyzed immediately after exposure, these concentrations/effect ranges should be at least halved, depending on the time of storage.

From the perspective of establishing the extent of exposure to HCN at the fire scene and the likely contribution of HCN exposure to incapacitation and death during an incident it is necessary to establish the relationship between blood cyanide and tissue cyanide measurements made from samples taken at autopsy and the likely blood cyanide concentrations at the time of exposure. Unlike the relationship between postmortem blood carboxyhemoglobin concentration and carbon monoxide exposure at a fire scene, which can be assessed quantitatively (as described in a previous section), interpretation of blood cyanide data is much more challenging. A particular set of issues relates to changes in cyanide levels in cadavers and in stored blood samples. These have been measured and reviewed in some detail by McAllister et al [82]. Essentially the main issues with respect to interpretation of blood cyanide data are as follows:

- There is low a natural background concentration of cyanide in blood, which is slightly elevated in smokers and following ingestion

of certain foodstuffs (non-smokers 0.075 μg/mL, smokers 0.184 μg/mL) [78].

- As described in the previous section, short exposure to high cyanide concentrations can cause incapacitation at a fire scene within a few minutes in association with transient high blood cyanide concentrations, which can then decrease to much lower levels once incapacitation has occurred, so that blood concentrations at a fire scene at the time of death may be considerably lower than during the critical exposure period when incapacitation occurred.
- Cyanide is unstable in the blood of cadavers and there can be a considerable decrease between death at a fire scene and the time when a blood sample is taken at autopsy. Curry [90] found in a case of death by inhalation of cyanide vapor, that the blood level taken at the moment of death was 3.5 μg/mL while samples taken at autopsy the next day were 1.0 μg/mL (femoral) and 0.5 μg/mL (carotid), a decrease of approximately 79 %. Ballantyne et al. [91] took samples at intervals from 15 rabbits killed by intravenous. KCN (8 mg CN^-/kg bodyweight) stored at a temperature of 10–15 °C. The blood concentrations decreased from 5.41 μg/mL immediately after death, by 30 % after 1 day and 62 % after 3 days, and then to near zero after 14 days.
- Another problem is that cyanide levels continue to decrease in blood stored after removal. Ballantyne [92] studied the effect of storage under three conditions (room temperature 20 °C), refrigerated (4 °C) and frozen (−22 °C). The results were that at room temperature and 4 °C there were considerable decreases of blood level, which fluctuated with time. After 3 months at 4 °C there was an approximate 20 % decrease in concentration.
- Change in cyanide concentration in frozen blood samples: In the above study, small changes occurred in blood samples following freezing and re-thawing. Frozen samples containing significant cyanide concentrations were generally the same after 3 months as when they were first taken. The exception was the control blood, which showed a small increase of approximately 0.1 μg/mL within a few days of freezing, the levels then remaining constant for the remainder of the 3 months. Although this was a small increase it represented a large percentage change in the control value of 0.03 μg/mL. The increase is considered to be due to re-conversion of small amounts of thiocyanate to cyanide. This effect is considered likely to be significant only when examining low concentrations of cyanide such as is found in the blood of smokers, but minor in the context of blood cyanide concentrations relevant to cyanide poisoning during fires.
- In some situations large increases in blood cyanide have been found to occur in stored blood samples. Although not fully understood, this phenomenon is considered to be due to contamination of samples by cyanogenic bacteria. However in several large studies of post-mortem blood samples taken from fire victims [61, 64, 81] such increases have not been reported.

Table 63.13 summarizes reports and opinion on blood cyanide concentrations associated with signs of different severity, although these should be taken as only a very approximate guide for the reasons stated.

Hypoxia

Apart from the tissue hypoxia caused by CO and HCN, hypoxia in fires can also be caused by exposure to low oxygen concentrations. To some extent, a lowered oxygen concentration in the inspired air or a lowered oxygen concentration in the lungs (during exercise for example) is a normal physiological occurrence, and there are compensatory mechanisms that tend to maximize the supply of oxygen to the brain. When a subject is placed in a hypoxic situation, there is a reflex increase in cerebral blood flow and also, up to a point, the unloading of oxygen from the blood is more efficient at lower arterial and venous blood oxygen concentrations [38]. These factors

Table 63.13 Blood cyanide concentrations and signs

Blood cyanide (μg/mL)	Signs
0.2–0.5	No signs (Hall [93])
0.5–1.0	Flushing, tachycardia (Hall)
1.0–2.5	Intoxicated, narcotized (Hall)
1.0–2.0	Lowest level suggested as compatible with death from acute cyanide poisoning (Ballantyne and Marrs [94])
1.7	Human fatality (Ballantyne and Marrs)
2.0	Concentration immediately after death in rabbits (Ballantyne) [83]
2.15	Rapid loss of consciousness in dogs (Ballantyne and Marrs)
2.4	Human fatality (Ballantyne and Marrs)
2.5	Rapid loss of consciousness in primates (Purser et al. [80])
2.5–3.0	Coma (Hall)
3.4	Rapid loss of consciousness in primates (Purser et al.)
3.5	Human case at death −0.75 μg/ul at autopsy next day (Curry [90])
3.6	Rapid death in dogs (Ballantyne and Marrs)
5.0	Human fatality (Ballantyne and Marrs)
In summary:	
~2.0–2.5	Concentration in fresh post-mortem blood consistent with incapacitation due to HCN
~3.0	Concentration in fresh post-mortem blood consistent with death due to HCN
~1.0–1.25	Concentration consistent with incapacitation due to HCN in post-mortem blood not taken and analyzed immediately after exposure
~1.5	Concentration consistent with death due to HCN in post-mortem blood not taken and analyzed immediately after exposure

compensate to a large degree for any decrease in the oxygen concentration of the inspired air. When cynomolgus monkeys were exposed to atmospheres containing 15 % oxygen, no deleterious effects occurred beyond a slight increase in heart rate [37].

However, a time is reached where these compensatory mechanisms fail; a 10 % oxygen atmosphere produced a marked cerebral depression in monkeys [37]. In humans hypoxia due to lack of oxygen (hypoxic hypoxia) has been studied extensively, particularly hypoxia that occurs at high altitudes [38]. As in monkeys there is little effect down to 15 % O_2, beyond a slightly reduced exercise tolerance, but at approximately 10 % O_2 effects suddenly become severe (consisting of lethargy and impaired consciousness), and similar effects have been reported in human volunteers breathing 12 % oxygen for periods of 15 min or more [38, 95]. It is possible, however, to identify a number of degrees of physiological and behavioral decrement, and for low-oxygen hypoxia certain signs can be related to particular exposure concentrations. From experiments in humans the effects have been classified into four phases as follows [26, 38, 54, 65] (Table 63.14), the appropriate altitude ranges and equivalent sea-level oxygen concentrations being given for each phase.

If a subject is suddenly placed into a low-oxygen environment, a finite time elapses before the blood gas concentration equilibrates with the new conditions, and a certain degree of physiological effect then occurs, depending on the equilibrium blood concentration attained. The time-to-effect functions described in the next section have been based on the concept of a certain "dose" of hypoxia being taken up over a period of time to reach equilibrium at the chosen endpoint of severe incapacitation (the catastrophe point). The concept of the catastrophe point relates to observations, mainly during exposures of primates to the asphyxiant gases CO, HCN, and low-oxygen hypoxia [37, 62], that due to physiological compensatory mechanisms there is very little decrement in physiological status or behavioral task performance as the severity of an exposure increases, until a certain point is reached when tissue hypoxia becomes critical and deterioration becomes very marked and very rapid, usually leading to unconsciousness. This endpoint, therefore, marks the sudden change in a potential fire victim from a condition of near normality to a condition in which escape would not be possible.

A Model for the Prediction of Time to Incapacitation by Hypoxia in Fires

Incapacitation due to oxygen lack, consisting of loss of consciousness, occurs when the oxygen

Table 63.14 Effects of low oxygen hypoxia at altitude and equivalent sea level reductions in percent oxygen

Sea level-3000 m equivalent to 20.95–14.4 % O_2 at sea level	**Indifferent phase**
	Minor effects on visual dark adaptation and beginnings of effects on exercise tolerance towards 15 % O_2
3000–4500 m equivalent to 11.8–14.4 % O_2 at sea level:	**Compensated phase**
	Relatively mild effects, Slightly increased ventilation and hear rate, slight loss of efficiency in performance of complex tasks and short-term memory, some effects on judgment. Maximal exercise work capacity reduced
4500–6000 m equivalent to 9.6–11.8 % O_2 at sea level:	**Manifest hypoxia**
	Degradation of higher mental processes and neuromuscular control, loss of critical judgment and volition, with dulling of the senses and a marked increase in cardiovascular and respiratory activity. Emotional behavior may vary from lethargy and indifference to excitation with euphoria and hallucinations. Particularly dangerous during fire exposures, representing the catastrophe point as a victim passes form this stage into the fourth stage at approximately 10 % O_2 (or COHb or blood cyanide concentrations producing an equivalent degree of brain hypoxia)
6000–7600 m equivalent to <7.8–9.6 % O_2 at sea level:	**Critical hypoxia**
	Rapid deterioration in judgment and comprehension leading to unconsciousness followed by cessation of respiration and finally of circulation at death.

supply to cerebral tissue falls below a certain critical value, which in turn occurs when the partial pressure of oxygen in the cerebral venous blood falls below 20 mmHg [38]. Due to the effects of the compensatory mechanisms, to residual oxygen in the lungs, and to oxygen stores available from the blood, a certain period of time elapses before the oxygen tension of venous blood declines to this critical level when a subject is suddenly faced with a reduced oxygen atmosphere after breathing normal air [26]. The time taken for this depletion depends on the level to which the oxygen concentration falls, but also on the activity of the subject (which affects oxygen demand) and the RMV. It is, therefore, possible to plot time to loss of consciousness against oxygen concentration. Studies of this kind have been performed on human subjects, principally for hypoxia caused by exposure to reduced atmospheric pressures simulating the effects of high altitudes, which has similar effects to those of exposure to reduced oxygen concentrations at sea level. Figure 63.25 shows such a plot of time of useful consciousness for humans at rest following sudden decompression (less than 1 s transition time) to a range of simulated altitudes. The data are adapted from Luft [38] and are expressed in terms of altitude. The equivalent sea-level oxygen concentrations have been added to the figure and also the percentage oxygen vitiation (i.e., the equivalent decrease in percentage oxygen concentration at sea level below the normal concentration of 20.9 % oxygen).

From this curve it is possible to derive an equation that should give a reasonable prediction of time to loss of consciousness $\left(t_{I_o}\right)$ for a victim exposed to a hypoxic fire environment, as follows

$$\left(t_{I_o}\right)\text{min} = \exp[8.13 - 0.54(20.9 - \%\text{O}_2)] \tag{63.27}$$

where (20.9—%O_2) is %O_2Vit (percent oxygen vitiation).

As with exposure to HCN, time to incapacitation for exposure to low-oxygen concentrations does not follow Haber's rule, since short exposures to severe hypoxia cause incapacitation very rapidly, and long exposures to modest hypoxia have little effect (e.g., at 17 % O_2Vit, $Ct = 17 \times 0.33 = 5.61$ % · min, while at 11.3 % O_2Vit, $Ct = 11.3 \times 7.73$

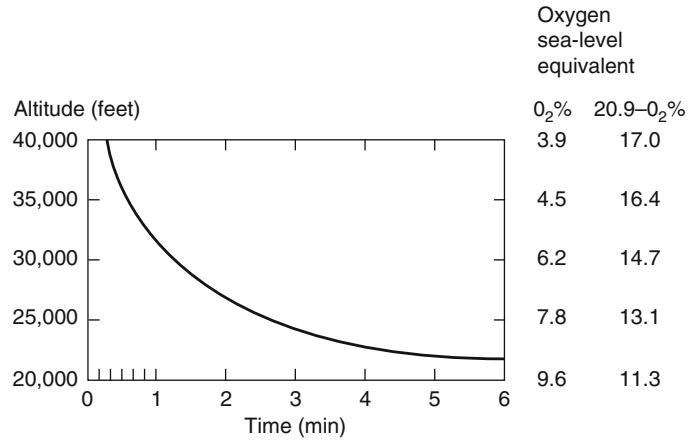

Fig. 63.25 Time of useful consciousness on sudden exposure to high altitudes (less than 1-s transition time). Scales also show equivalent sea-level percent oxygen concentration and percent oxygen vitiation (decrease below 20.9 % O_2) [38]

$= 87.3\ \% \cdot \text{min}$). In attempting to predict time or dose to incapacitation or death for a subject exposed to changing oxygen concentrations, it is therefore necessary to apply a weighting factor to allow for these deviations from ideal behavior. As with HCN this may be achieved by using the fractional effective dose concept as follows:

For a constant level of hypoxia, the time to incapacitation due to oxygen depletion is given by

$$t_{I_o} = \exp[8.13 - 0.54(20.9 - \%O_2)] \quad (63.28)$$

Dose to incapacitation $= (20.9\text{—}\%\ O_2)\ (t_{I_o})$

Therefore, for a short exposure time, t, to a given level of oxygen vitiation

$$F_{I_o} = \frac{(20.9 - \%O_2)(t)}{(20.9 - \%O_2)(t_{I_o})} \quad (63.29)$$

where F_{I_o} = fraction of an incapacitating dose of hypoxia, and where $t = 1$ min. This equation simplifies to

$$F'_{I_o} = 1/t_{I_o} \quad (63.30)$$

If the fractional doses per each minute are summed throughout the exposure, the dose and time to incapacitation can be predicted.

Example A subject is exposed to a concentration of 10 % oxygen for 5 min followed by 7.8 % oxygen for 1.5 min. For 10 % O_2 (10.9 % O_2Vit)

$$t_{I_o} = \exp[8.13 - 0.54(20.9 - 10)]$$
$$1/t_{I_o} = 0.106$$

For 7.8 % O_2 (13.1 % O_2Vit)

$$t_{I_o} = 2.8748$$
$$1/t_{I_o} = 0.3478$$
$$F_{I_o} = 0.106 \times 5 + 0.3478 \times 1.5$$
$$= 0.105$$

Therefore, loss of consciousness is predicted at 6.5 min.

A Model for the Prediction of Hyperventilation and Time to Incapacitation by Carbon Dioxide

Carbon dioxide (CO_2), like carbon monoxide, is universally present in fires. Although carbon dioxide is not toxic at concentrations of up to 5 %, it stimulates breathing, so that at 3 % the RMV is approximately doubled and at 5 % tripled [25]. This hyperventilation, apart from being stressful, can increase the rate at which other toxic fire products (such as CO) are taken up.

For asphyxiant gases such as CO or HCN it is likely that the increased uptake resulting from carbon dioxide induced hyperventilation will significantly reduce time to incapacitation and death. The ventilatory response to carbon dioxide varies among individuals and reported data also

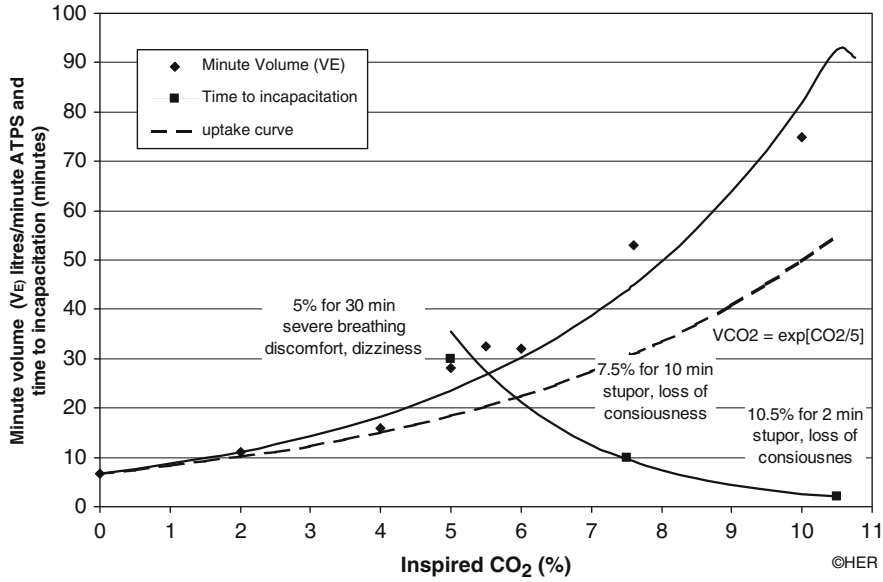

Fig. 63.26 Ventilatory response to carbon dioxide, proposed curve for calculating effects on rate of uptake of CO, HCN and irritants, and incapacitating effects of inhaling 5–10 $\%CO_2$ [96–99]

vary. An average curve has been constructed from data given in three sources [96–98] and is presented in Fig. 63.26, giving the following regression equation

$$\mathrm{RMV(L/min)} = \exp(0.2496 \times \%\mathrm{CO_2} + 1.9086) \tag{63.31}$$

From this expression a multiplication factor ($V\mathrm{CO_2}$) can be calculated for the enhanced uptake of other asphyxiant gases as follows

$$V\mathrm{CO_2} = \frac{\exp(0.2496 \times \%\mathrm{CO_2} + 1.9086)}{6.8} \tag{63.32}$$

where 6.8 L/min is a suggested figure for the resting RMV at the background CO_2 concentration. This equation has been simplified to

$$V\mathrm{CO_2} = \exp\left(\frac{[\mathrm{CO_2}]}{4}\right) \tag{63.33}$$

On further examination of this relationship it is considered that, although it provides a reasonable estimate of the change in $V\mathrm{CO_2}$, it gives an exaggerated value for the increase in uptake rate for other gases, primarily because the efficiency of uptake decreases as ventilation increases. This is particularly the case for CO uptake for which $\mathrm{DL_{CO}}$, the maximum rate of diffusion into the blood and erythrocytes, becomes a limiting factor at high levels of respiratory ventilation. A modified expression has, therefore, been derived based on that used in the CFK equation [34], which gives a somewhat lower prediction for the increase in uptake rate of other gases. A slightly higher figure has also been used for the resting V_E. The modified equation is as follows:

$$V\mathrm{CO_2} = \frac{\exp(0.1903 \times \%\mathrm{CO_2} + 2.0004)}{7.1} \tag{63.34}$$

which has been simplified to

$$V\mathrm{CO_2} = \exp\left(\frac{[\mathrm{CO_2}]}{5}\right) \tag{63.35}$$

At concentrations of approximately 5 % and above carbon dioxide is itself an asphyxiant, but for elevated CO_2 concentrations (hypercapnia) the change in degree of incapacitation with exposure concentration is more gradual than

with hypoxia. From approximately 3 % up to 6 % there is a gradually increasing degree of respiratory distress. This becomes severe at approximately 5–6 %, with clinical comments from subjects such as "breathing fails to satisfy intense longing for air" or "much discomfort, severe symptoms impending," with headache and vomiting also occurring [99]. Although due to the gradual equilibration process these signs tend to worsen during exposure, it seems unlikely that they would proceed as far as loss of consciousness over the course of a 30- or even a 60-min exposure period. However, once the concentration of carbon dioxide is in the 7–10 % plus range, a new set of signs consisting of dizziness, drowsiness, and unconsciousness is superimposed on the severe respiratory effects. A time factor does enter here due to gradual uptake, with loss of consciousness being more certain, and occurring earlier (over a period of a few minutes) as the exposure concentration approaches and exceeds 10 % [65, 66, 99, 100]. Approximate tolerance times for the distressing effects on breathing and the onset of asphyxia for humans are shown in Fig. 63.26. The effects are perceptible to subjects from 3 % as increasingly rapid breathing and at approximately 6 % become intolerable within 20 min. Symptoms of dizziness, headache, and fatigue start to occur at concentrations above 7 %, with danger of unconsciousness occurring within a few minutes increasing from 7 % to 10 %. Loss of consciousness is likely within 2 min at 10 % CO_2 in humans [99].

As with HCN and low-oxygen hypoxia, intoxication by carbon dioxide does not follow Haber's rule (Ct for 10 % CO_2 = 20 % · min, Ct for 5 % CO_2 = 175 % · min). From the approximate data in Fig. 63.26 an expression predicting approximate time to incapacitation $t_{I_{CO_2}}$ has been derived as follows:

$$t_{I_{CO_2}} = \exp(6.1623 - 0.5189 \times \%CO_2) \tag{63.36}$$

Using the fractional-dose concept previously described for HCN and hypoxia, it is possible to predict approximate dose to incapacitation, provided that the CO_2 concentration is stable or increasing, as follows:

For a constant CO_2 concentration

$$t_{I_{CO_2}} = \exp(6.1623 - 0.5189 \times \%CO_2)$$

$$\text{Dose to incapacitation} = (\%CO_2)\left(t_{I_{CO_2}}\right)$$

Therefore, for a short exposure time, t, to a given CO_2 concentration

$$F_{I_{CO_2}} = \frac{(\%CO_2)(t)}{(\%CO_2)\left(t_{I_{CO_2}}\right)}$$

where $F_{I_{CO_2}}$ = fraction of an incapacitating dose, and where t = 1 min. This equation simplifies to

$$F_{I_{CO_2}} = \frac{1}{t_{I_{CO_2}}} \tag{63.37}$$

If the fractional doses per minute are summed throughout the exposure, the dose and time to incapacitation can be predicted.

Example A subject is exposed to a concentration of 5 % CO_2 for 20 min, followed by 9 % CO_2 for 2 min.

$$\text{For } 5\%\,CO_2,\ t_{I_{CO_2}} = 35.44;\ 1/t_{I_{CO_2}} = 0.0282$$
$$\text{For } 9\%\,CO_2,\ t_{I_{CO_2}} = 4.45;\ 1/t_{I_{CO_2}} = 0.2247$$
$$Ft_{I_{CO_2}} = 0.0282 \times 20 + 0.2247 \times 2 = 1.01$$

Severe incapacitation with probable loss of consciousness is, therefore, predicted at approximately 22 min.

Interactions Between Toxic Fire Gases

Although data on the concentration/time/dose relationships of the dangerous and lethal asphyxiant effects in humans of individual fire gases and interactions between them are necessarily limited, they are adequate for the construction of a usable incapacitation model. Estimates of likely degrees of interaction are based on physiological data from individual gases and on such experimental data for gas combinations as do exist.

Effect of Carbon Dioxide on Effects of CO, HCN, and Low-Oxygen Hypoxia

The interaction likely to be most important is that hyperventilation due to carbon dioxide exposure increases the rate of uptake of other toxic gases and thus decrease the time to incapacitation (or the time taken to inhale a lethal dose), in proportion to the increase in ventilation. This interaction is likely to be most important with respect to CO and HCN intoxication. An expression for calculating the increase in V_E resulting from exposure to different carbon dioxide concentrations is given in the section on CO_2, but as an approximation it should be assumed that there would be little effect below 3 % CO_2, while at 3 % CO_2, V_E is doubled, so time to incapacitation by CO and HCN should be halved. At 5 % CO_2, V_E would be approximately tripled and time to incapacitation would be approximately one-third of that in the absence of carbon dioxide. There is a possibility that the effects on time to incapacitation would not be so dramatic, since there is evidence that the presence of carbon dioxide may counteract the leftward shift in the oxygen dissociation curve caused by carbon monoxide, somewhat counteracting its deleterious effects [101]. However, in the absence of experimental data on combination exposures it is best to ignore this possible beneficial effect, since the effect on uptake rate is likely to be dominant. A similar effect on uptake may also occur with HCN. With regard to low oxygen, carbon dioxide has been shown to have a marked beneficial effect on resistance to incapacitation. This result is partly due to the hyperventilatory effect that increases the rate of oxygen uptake and partly due to the rightward shift in the oxygen dissociation curve caused by carbon dioxide. This effect improves the delivery of oxygen to the tissues, counteracting the respiratory alkalosis that otherwise occurs [67, 102, 103]. There is evidence from experiments on the effects of combinations of asphyxiant gases with CO_2 in rodents that, with severe exposures, postexposure lethality is increased by the presence of CO_2. When animals are severely affected and suffering from a hypoxia-induced metabolic acidosis, this appears to be enhanced by the further acidotic effect of CO_2 inhalation, and the animals then fail to recover after exposure under conditions when they would otherwise be expected to do so. The hyperventilation induced by CO_2 will also increase the uptake of substances that irritate the lung, which affects gas exchange in the lung during exposure and also tend to cause toxic effects some time after exposure. Experiments in rodents provide evidence that this is so, with increased deaths possibly caused by postexposure acidosis and increased lung damage. Exercise also causes a CO_2-driven hyperventilation, and there is evidence that this may also cause deaths when rodents are exposed to irritants at normally sublethal concentrations [104].

Interactions Between CO and HCN

Some studies have been made of interactions between CO and HCN with varying results [105]. On theoretical grounds little interaction is to be expected, since CO diminishes the carriage of oxygen in the blood and its delivery to the tissues, while HCN diminishes the ability to use oxygen once delivered to the tissues. It is, therefore, to be expected that either one or the other gas would constitute the rate-limiting step in oxygen supply and utilization. However, the consensus view is that there is at least some additive effect between these two gases. Experiments in primates have shown that time to incapacitation by HCN is slightly reduced by the presence of near-toxic concentrations of CO [86, 105], and the rate of uptake of CO may be increased by the hyperventilatory effect of HCN.

There are several reasons why CO and HCN toxicities may be additive. One reason is the hyperventilation resulting from HCN exposure, which further increases the rate of uptake of cyanide and of any CO present. Another possibility may relate to competition for sites on cytochrome a3 between oxygen and cyanide. Since CO exposure reduces oxygen delivery and arterial $P_{O2,}$ this may alter the balance in favor of cyanide binding to the a3 sites at the mitochondrial level. Certainly

it was found that administration of oxygen was beneficial to cyanide intoxicated primates, improving their clinical condition, and the beneficial effects of oxygen have been reported in a number of other studies. Since oxygen is known to be present in excess during cyanide intoxication, it is difficult to understand why administration of further oxygen would be beneficial, unless it improved the competitive balance with cyanide at the active sites.

Another possible reason derives from a proposed mechanism of CO toxicity. CO has been found to exert a direct effect on tissue toxicity at the mitochondrial level in addition to its effects on the blood [106]. Particularly when the uptake of CO is rapid, it has been suggested that sufficient dissolved CO may reach the tissues to exert direct toxic effects. In vitro, CO has been shown to exert an inhibitory effect on oxygen metabolism. Although the affinity of cytochrome oxidase for CO is considerably less than that of cyanide, it is possible that some degree of additive inhibition of oxygen metabolism may occur at the tissue level. Piantatosi et al. [106] studied cytochrome oxidation-reduction responses to CO and HCN in the intact brains of fluorocarbon-circulated rats (i.e., with all hemoglobin removed) and found that CO and HCN caused inhibition at two different sites in the electron transport chain, whereby b-type cytochromes were sensitive to CO but not cyanide, while cytochrome aa_3 and $c + c_1$ were sensitive to cyanide but not CO. Although the effects of such interaction in intact animals are not fully resolved, it raises the possibility of some form or additive interaction between CO and HCN at the mitochondrial level.

In these circumstances it is probably safest to assume that these gases are additive in terms of time to incapacitation and dose to death and that incapacitation or death will occur when the fraction of the toxic dose of each one adds up to unity.

Interactions Between CO and Low-Oxygen Hypoxia

The most likely interaction between CO and low-oxygen hypoxia would be some degree of addition, since both reduce the percentage oxygen saturation of arterial blood, and CO also impairs the delivery of oxygen to the tissue by causing a leftward shift of the oxygen dissociation curve [101]. It is possible that during the early stages of CO exposure in hypoxic subjects the CO occupies the upper, oxygen-free part of the oxygen dissociation curve, and therefore has little effect. Von Leggenhager [62, 74] reports that subjects at rest at altitude remain symptom free at low levels of CO saturation. However, it is likely that the effect of more severe exposure to CO in a hypoxic subject would be additive to some extent, as reported by Heim [107] and McFarland et al [108].

Interactions Between Irritant Smoke Products and Asphyxiant Gases

An important point is the possible interaction between irritant smoke products and asphyxiant gases. This effect is particularly strong when rats and mice are exposed to smoke, since the rodent response to irritation of the upper respiratory tract is a marked decrease in respiratory rate and V_E. Thus if CO is present in the smoke, the rate of uptake will be considerably reduced if the smoke is irritant. This sometimes leads to misleading results in combustion product toxicity tests, where a material producing irritant smoke will have an apparently low LC_{50}, although high CO concentrations are present in the atmosphere.

This marked, prolonged decrease in respiratory rate does not occur in humans or nonhuman primates; indeed, in primate smoke experiments, irritant products tend to increase rather than decrease ventilation (although not sufficiently to increase CO toxicity) [37, 61].

NO and NO_2 (designated as NO_x in mixtures) also act as asphyxiants, reducing oxygen carriage in the blood due to the conversion of hemoglobin to methemoglobin. To this extent their asphyxiant effects can be considered additive with those of HCN and CO. However, methemoglobin combines with HCN in the blood, thereby reducing its asphyxiant effect. NO_2 is also a potent lung irritant.

Summary of Overall Interactions

In summary, data on interactions between the asphyxiant gases CO, HCN, low oxygen, and CO_2 are limited, but where deleterious interactions are known it would be prudent to include them in the incapacitation model, if only to err on the side of safety. For this reason it is proposed that the interactions should be quantified in the incapacitation model as follows:

1. Assume that CO and HCN are directly additive (1:1) on a fractional dose basis (the evidence suggests that they are additive but that the additive interaction may actually be less than unity).
2. NO and NO_2 (designated as NOx in mixtures) also act as asphyxiants, reducing oxygen carriage in the blood due to the conversion of hemoglobin to methemoglobin. To this extent their asphyxiant effects can be considered additive with those of HCN and CO. However, methemoglobin combines with HCN in the blood, thereby reducing the cyanide asphyxiant effect. NO_2 is also a potent lung irritant
3. The effects of irritants on lung function also cause some hypoxia and so an additive term is included consisting of the FLDirr
4. The rate of uptake of all these asphyxiant gases (CO, HCN, NOx and irritants) depends on the respiratory ventilation (V_E) of the subject in relation to body size, which in turn depends upon their level of physical activity For design purposes it is assumed that the subject is an adult engaged in light work such as walking along an escape route.
5. The main effect of carbon dioxide is to increase the breathing rate and thus the rate of uptake of asphyxiant gases (CO, HCN, NOx and irritants). A multiplicatory term VCO_2 is used to calculate this effect.
6. Low oxygen hypoxia will be additive with the overall hypoxic effects of CO and HCN, but is not increased by VCO_2 (in fact it is improved).
7. The beneficial effects of increased CO_2 on the hypoxic effects of CO and low oxygen hypoxia resulting from right shifting of the oxyhaemoglobin dissociation curve are ignored
8. The direct intoxicating effects of CO_2 are considered unlikely to occur before other effects so are normally ignored but exposure to 7 % CO_2 or higher itself causes incapacitation within a few minutes.

Taking into account these interactions it is possible to derive a general expression for calculating uptake, fractional effective doses and time to incapacitation from asphyxia as described in the next section.

Implications of Interactions for Predicting Time to Incapacitation in Smoke Atmospheres and Derivation of an Overall FED Expression for Asphyxia

In general, although there is evidence for interactions between toxic fire gases, whether these are likely to be important in practice depends on the composition of actual fire atmospheres, which is discussed in a later section of this chapter. For most practical situations, it is considered that HCN is unlikely to be the main driver of time to incapacitation providing the nitrogen content of the burning fuel does not exceed 1 % by mass. The composition of fire atmospheres will then be such that for asphyxiant effects, CO will be the most important toxic product, and the most important interaction will be an increased rate of CO uptake due to hyperventilation caused by CO_2. The additional effects of HCN aphyxia will contribute to the effects of CO-induced asphyxia, and may significantly reduce time to incapacitation when fuels contain more than 1 % nitrogen and the HCN concentration exceeds approximately 50 ppm. Since NOx concentrations in fires are low, their direct contribution hypoxia and effects on HCN toxicity are likely to be small. Low oxygen hypoxia is likely to be a minor term for situations where subjects are exposed to growing compartment fires, but may constitute a major term if subjects

are suddenly exposed a smoke atmosphere containing less than approximately 12 % oxygen, for example when opening a door on a compartment fire. Similarly, sudden exposure to a CO_2 concentration exceeding 7 % CO_2 could itself result in rapid intoxication and collapse. The rate of uptake or all toxic gases and particulates also depends upon the physical activity level and ventilation of the subject.

On this basis the simplified fractional dose equation for asphyxiation for an adult engaged in light work would be[1]

$$\mathrm{F_{IN}} = \left[\left(\mathrm{F_{I_{CO}}} + \mathrm{F_{I_{CN}}} + F_{I_{NOx}} + FLD_{irr}\right) \times VCO_2 + F_{I_O}\right] or\, \mathrm{F_{I_{CO_2}}} \qquad (63.38)$$

where

F_{IN} = Fraction of an incapacitating dose of all asphyxiant gases

$F_{I_{CO}}$ = Fraction of an incapacitating dose of CO

$F_{I_{CN}}$ = Fraction of an incapacitating dose of HCN

Note: If necessary this can be corrected for the presence of other nitriles besides HCN and for the protective effect on cyanide poisoning of NO and NO_2. [CN] can then be calculated as: $[CN] = [HCN] + [\text{Total organic nitriles}] - 0.67[NO + NO_2]$

$F_{I_{NOx}}$ = Fraction of an incapacitating dose of $NO + NO_2 (= [NOxppm \times tmin]/1500)$

FLD_{irr} = Fraction of an irritant dose contributing to hypoxia (This term represents a correction for the effects of irritants on lung function and is developed in the section "Post-Exposure Lung Inflammation and Survival." This term may be omitted if the effects of asphyxiant gases only are under consideration)

VCO_2 = Multiplication factor for CO_2-induced hyper-ventilation

F_{I_O} = Fraction of an incapacitating dose of low-oxygen hypoxia

$F_{I_{CO_2}}$ = Fraction of an incapacitating dose of CO_2

For a simple analysis, the direct asphyxiant effects of NO_x those of NO_x on HCN asphyxia the fraction of an incapacitating dose of CO_2 may be ignored without significant error.

A more general form of the equation incorporating V_E as a user-defined variable is:

$$F_{IN} = \left(F_{ICOg} + F_{ICNg} + F_{INOxg} + FLD_{irrg}\right) \times V_E \times V_{CO2} + F_{I_O} \qquad (63.39)$$

Activity level of subject	V_E (L/min)
Resting or sleeping	8.5
Light work—walking to escape	25
Heavy work—slow running, walking up stairs	50

Both the total volume of air breathed each minute and the efficiency of uptake have upper limits so that a limiting value for $V_E \times V_{CO2}$ of 70 L/min is recommended.

Each individual term in the FED equation is itself the result of the following equations, which give the FED for incapacitation for each gas and the multiplication factor for CO_2, where t is the exposure time at a particular concentration in minutes. The FED acquired over each period of time during the fire are summed until the total FED_{IN} reaches unity, at which point incapacitation (loss of consciousness) is predicted. In order to allow for differences in sensitivity and to protect susceptible human subpopulations a factor of $\times$ 0.3 FED should allow for safe escape of nearly all individuals. For especially vulnerable groups a factor of $\times$ 0.1 FED may be considered. Death is predicted at approximately two to three times the incapacitating dose.

For a 1-min exposure to each gas at a concentration C

$$F_{I_{CO}} = 3.317 \times 10^{-5}[\mathrm{CO}]^{1.036}(V)(t)/D \qquad (63.18)$$

where

[1] The effect of CO_2-induced hyperventilation will be to increase the rate of uptake of inhaled gases as a function of the increase in ventilation. Another approach to the quantification of this effect would be to multiply the concentration of each gas by VCO_2 in the FED expression for that gas rather than in Equation 63.38. This would produce a similar result to Equation 63.38, except for the effect of HCN inhalation, for which a greater value of $F_{I_{CN}}$ corrected for VCO_2 would result. This would represent a more conservative approach, but overall it is considered that this might overemphasize the toxic effects of HCN.

[CO] = Carbon monoxide concentration (ppm v/v 20 °C)
V_E = Volume of air breathed per minute (liters/min)
t = Exposure time in minutes
D = Exposure dose (percent COHb) for incapacitation

For the default case the value of V is 25 L/min and the value of D is 30 %COHb.

For the general case (F_{ICOg}) the V_E term is removed from Equation 63.18.

The default form of the fractional incapacitating dose for HCN (F_{ICN}) is as follows:

$$F_{ICN} = \frac{[CN]^{2.36}}{1.2 \times 10^6} t \tag{63.24}$$

where
CN = HCN concentration (ppm v/v at 20 °C)
t = Exposure time in minutes

For the general case application in Equation 63.39 the term F_{ICNg} is given by:

$$F_{ICNg} = \frac{[CN]^{2.36}}{2.43 \times 10^7} t$$

which is Equation 63.25 with the VE term removed). If necessary this can be corrected for the presence of other nitriles besides HCN and for the protective effect on cyanide poisoning of NO and NO_2. CN can then be calculated as $[CN] = [HCN] + [\text{Total organic nitriles}]\text{-}0.67[NO + NO_2]$

$$VCO_2 = \exp\left(\frac{[CO_2]}{5}\right) \tag{63.35}$$

$$FLD_{irr} = FLD_{HCl} + FLD_{HBr} + FLD_{HF} + FLD_{SO_2} + FLD_{NO_2} + FLD_{CH_2CHO} + FLD_{HCHO} + \Sigma FLD_x \tag{63.15}$$

where ΣFLD_x = FLDs for any other irritants present.

For the general case application in Equation 63.39 the term FLD_{irrg} is given by

$$FLDirrg = FLD/25$$

For the general case application in Equation 63.39 the term N_{INOxg} is given by

$$F_{INOxg} = F_{Inox}/25$$

For the direct effects of low oxygen hypoxia and incapacitation from inhaled carbon dioxide the general case expressions are the same as those for the default case:

$$F_{Io} = \frac{1}{\exp[8.13 - 0.54(20.9 - \%O_2)]} \tag{63.40}$$

$$F_{I_{CO_2}} = \frac{1}{\exp(6.1623 - 0.5189 \times \%CO_2)} \tag{63.41}$$

Figure 63.27 shows an expanded detail of asphyxiant gas profiles during the first 10 min of the single armchair room burn that is presented in more detail in Fig. 63.22. The histograms show the average concentrations of each gas at minute intervals during the first 6 min of the fire, the figures for which are given in Table 63.15. The HCN concentration was not measured in this fire, but it is likely to have been present as a major toxic product. Possible HCN concentrations have, therefore, been suggested for inclusion in the model and are shown in a histogram.

Applying the expressions for the fractional incapacitating dose of each gas to the data in Table 63.15, the total fractional dose of all asphyxiant gases for each minute during the fire (F_{IN}) has been calculated according to Equation 63.21 and summed for each successive minute during the fire, as shown in Table 63.16. Incapacitation (loss of consciousness) is predicted at 5 min when the fractional incapacitating dose exceeds unity ($F_{IN} = 1.2$).

The Exposure of Fire Victims to Heat

There are three basic ways in which exposure of fire victims to heat may lead to incapacitation and death: by (1) heat stroke, (2) body surface burns, and (3) respiratory tract burns.

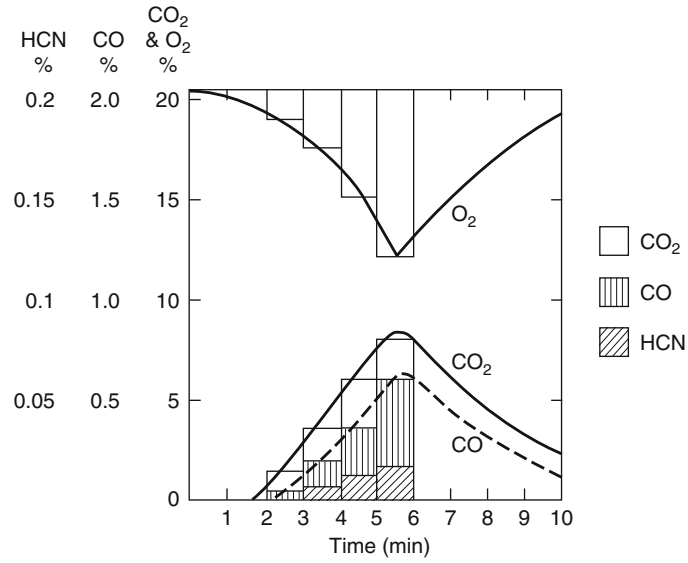

Fig. 63.27 Expanded detail from Fig. 63.22—average concentrations of asphyxiant gases each minute (histograms) from gas profiles (curves) measured during the first 10 min of a single armchair (polystyrene with polyurethane cushions and covers) room burn [52] Since HCN was not measured but was likely to have been present as an important toxic product, possible concentrations have been suggested for inclusion in the model

Table 63.15 Average concentrations of asphyxiant gases each minute during the first 6 min of the single armchair room burn shown in Fig. 63.27

Time (min)	1	2	3	4	5	6
CO ppm	0	0	500	2000	3500	6000
HCN ppm	0	0	0	75	125	174
CO_2%	0	0	1.5	3.5	6	8
O_2%	20.9	20.9	19	17.5	15	12

Table 63.16 Fractions of an incapacitating dose of asphyxiant gases calculated from the data in Table 63.15 According to Equation 63.38 for 1-min intervals during the single armchair room burn Shown in Fig. 63.27 (contributions from NOx and FLD are ignored for simplicity)

Time (min)	1	2	3	4	5
F_{lco}'	0	0	0.017	0.074	0.130
$+F_{lcn}'$	0	0	0.000	0.022	0.074
$\times VCO_2$	0	0	1.442	2.376	4.434
$=$	0	0	0.025	0.228	0.905
$+F_{lo}$	0	0	0.001	0.002	0.007
$=$ Total	0	0	0.026	0.230	0.912
Running total (F_{IN})	0	0	0.026	0.256	1.168
or:					
F_{lco_2}	0	0	0.005	0.013	0.047
Running total (F_{IN})	0	0	0.005	0.018	0.065

$F_{IN} = 1.2$ at 5 min due to the combined effects of CO, HCN, and low-oxygen hypoxia, the uptake of which was increased by CO_2, and incapacitation is predicted at between 4 and 5 min. Although carbon dioxide was present at concentrations sufficient to have caused significant hyperventilation, the fractional incapacitating dose for asphyxiation by carbon dioxide was only 0.065 at 5 min, and this is, therefore, unlikely to have had any effect

Heat Stroke (Hyperthermia)

If a subject is exposed to a hot environment, especially if the humidity is high and the subject is active, there is a danger of incapacitation and death due to hyperthermia. The time to effect and the type of hyperthermia depend principally on the heat flux to which the subject is exposed and are greatly affected by factors such as the amount and type of clothing and degree of work performed. A detailed analysis of the parameters that determine heat transfer to subjects over a range of environmental conditions and levels of activity, and the protective effects of different types of clothing, is given by Berenson and Robertson [109], and Simms and Hinkley [110].

Simple hyperthermia involves prolonged exposure (approximately 15 min or more) to heated environments at ambient temperatures too low to cause burns. Under such conditions, where the air temperature is less than approximately 120 °C for dry air or 80 °C for saturated air, the main effect is a gradual increase in the body core temperature [111]. Increases above the normal core temperature of 37 °C up to

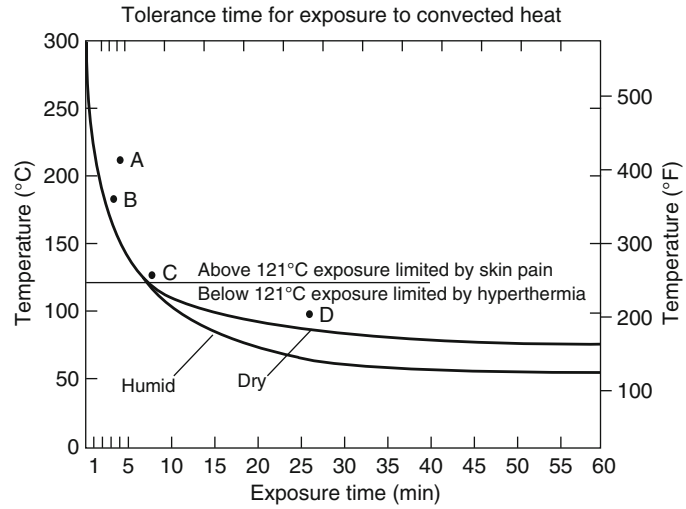

Fig. 63.28 Thermal tolerance for humans at rest, naked skin exposed, with low air movement (less than 30 m/min) (Adapted from Blockley [111]. See text and Table 63.17 for discussion of data points A to D) [110, 113, 114]

Table 63.17 Reported tolerance times for exposures to hot air

Temperature (°C)		Time (min)		Reference	Letter in Fig. 63.28
Dry air					
	110	25		Simms and Hinkley [110]	D
	180	3		Simms and Hinkley [110]	B
	205	4	Bare headed, protected	Veghte [113]	A
	126	7		Elneil [114]	C
Humid air	32 at 100 % RH	32	Men working	Leithead and Lind [115, 116]	

approximately 39 °C are within the physiological range and can occur at normal ambient temperatures during hard exercise, but once 40 °C is reached consciousness becomes blurred and the subject becomes seriously ill. Further increase causes irreversible damage, with temperatures above 42.5 °C being fatal unless treated within minutes [109, 112]. The time taken to reach such a state depends on a number of variables including those mentioned. Figure 63.28, adapted from Blockley [111], shows approximate tolerance times for unclothed subjects at rest, under conditions of low air movement (30 m/min). At temperatures below 120 °C tolerance is limited by hyperthermia, whereas above this temperature pain followed by burns become important. The data points A to D (for clothed subjects) were taken from various authors and are added for comparison. At temperatures below 120 °C evaporative cooling from sweat is important, so that humidity has a considerable influence on tolerance time. Clothing, therefore, offers some immediate protection at temperatures above 120 °C but at lower temperatures may reduce tolerance time by impeding heat loss due to evaporative cooling. Details of the data points and authorship are given in Table 63.17.

Experiments conducted with pigs by Moritz et al. [117] confirm the basic signs of hyperthermia, with death occurring principally due to circulatory collapse associated with severe cardiac irregularities (ventricular tachycardia).

A second situation described by Moritz et al. [117] involves exposure to high temperatures for short periods (less than 15 min), and here hyperthermia is accompanied by cutaneous burns (in pigs at temperatures above 120 °C). When deaths occurred soon after exposure to severe heat (within 30 min)

the cause was considered to be due not to burns but to a rise in blood temperature. In this situation the exposure duration was insufficient to raise the body core temperature greatly, but if the temperature of the blood in the heart reached 42.5 °C, the animal died within a few minutes from circulatory collapse.

It therefore seems that a victim exposed for more than a few minutes to high temperatures and heat fluxes (exceeding 120 °C) in a fire is likely to suffer burns and die either during or immediately after exposure, due principally to hyperthermia. Victims surviving the hyperthermia phase may die later due to burns of the upper respiratory tract, particularly the larynx, or due to the secondary effects of skin burns. A victim or fire fighter exposed to temperatures unlikely to cause burns (less than 120 °C) may also suffer heat stroke after a prolonged exposure (exceeding 15 min), especially if the humidity is high and the person is working hard.

Skin Burns

According to Buettner [118], pain from the application of heat to the skin occurs when the skin temperature at a depth of 0.1 mm reaches 44.8 °C, which agrees with the finding of Lawrence and Bull [119] that discomfort was experienced when the interface between a hot handle and the skin of the hand reached 43 °C. The sensation of pain is followed soon afterward by burns, causing incapacitation, severe injury, or death depending on their severity. The time from the application of heat to the sensation of pain, and from pain to the occurrence of burns of various degrees of severity, depends on the temperature, or more properly, the heat flux to which the skin is exposed. The effects of heating the skin are essentially the same whether the heat is supplied by conduction from a hot body, convection from air contact, or by direct radiation [118, 120]. Curves for the relationship between time and effect have been published for conducted heat from a "hot handle" [120, 121] and radiant heat. The relationship between time and effect is exponential (Fig. 63.29). Thus, for conduction from heated metal at 60 °C, pain occurs after 1 s and a burn after 10 s, while at 80 °C pain occurs at 100 ms and a burn after 1 s contact.

Pain, therefore, occurs when the difference between the rate of supply of heat to the skin surface exceeds the rate at which heat is conducted away by an amount sufficient to raise the skin temperature to 44.8 °C. The thermal inertia of human skin is similar to that of water [118] or wood [120] with a value of $k\rho c$ for the surface (depth 0.1 mm) of 1.05 W/mK. For the skin surface the rate of heat removal is not considered to be affected by blood supply [118] except for the fingertips, where blood flow may

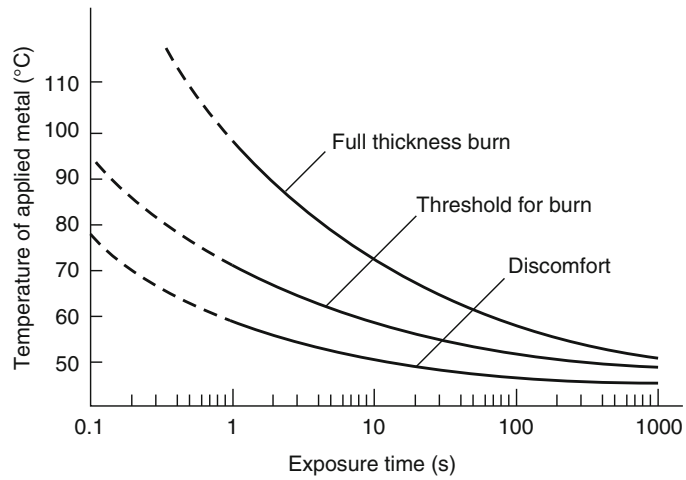

Fig. 63.29 The relation between time and the temperature of metal to cause thermal injury to skin (values below 1 s are extrapolated) [120]

be sufficient to remove a significant amount of heat [118]. However, blood supply may have some effect on the occurrence of burns, especially to the deeper layers of the skin [120]. Obviously, rates of heating and the occurrence of pain and burns are greatly affected by the extent and type of clothing [110, 117, 123, 124], but only effects on naked skin are considered here. The temperature increase of the skin for the situation in which constant radiant heat is absorbed by the upper surface of the skin, or heat from a hot air current is applied to the skin, may be calculated as follows [118]:

$$T - T_0 = \frac{2Q\sqrt{t}}{\sqrt{\pi k\rho c}} \qquad (63.42)$$

where

T = Final temperature of skin at 0.1 mm depth
T_0 = Starting temperature of skin at 0.1 mm depth
Q = Heat supply (W/m^2)
$k\rho c$ = 1.05 W/mk
t = Time (s)

Conducted Heat The effect of conducted heat is related to the temperature of the hot object and its thermal inertia, depending on the interface temperature between the object and the body tissue at the skin surface [120, 124], as illustrated by the examples in Table 63.18.

A skin temperature of 43 °C causes pain and some cellular damage, whereas a temperature of 60 °C coagulates tissue protein. A brass block heated to 60 °C will produce a partial thickness skin burn within 10 s, pain within 1 s and a full thickness burn after approximately 100 s [120]. The time/temperature relationships for these effects of conducted heat are shown in Fig. 63.29.

Table 63.18 Theoretical contact temperatures between skin at 35 °C and a selection of hot bodies at 100 °C [124]

Material of hot body	Contact temperature (°C)
Mild steel	98
Glass	82
Wood	65
Cork	46

Convected Heat For a victim attempting to escape from a fire, the most important sources of heat exposure are radiation from hot areas and convection from hot gases. Pain and the likelihood of skin burns occur at air temperatures above approximately 120 °C. The rate of heat transfer from hot air to the skin depends on the rate of ventilation, humidity, and the protective value of clothing as well as air temperature. The effects of these parameters are described by Berenson and Robertson [109], and Simms and Hinkley [110]. However, for unprotected areas such as the head, data on naked skin are relevant, and the data shown in Fig. 63.28 for temperatures above 120 °C provide limits for tolerance to the painful effects of contact with hot air.

Apart from the problem of hyperthermia, dry air has been tolerated by humans as shown in Table 63.17 Moritz et al. [117] state that dry air at 300 °C injured unprotected skin within 30 s in pigs and dogs. Pigs also suffered burns at 150 °C after 100 s and after 400 s at 100 °C. However, it was considered that humans would be more resistant to burns, especially at temperatures below 120 °C, due to the protective effect of sweating. Air with a high level of humidity not only reduces or prevents heat loss through sweat, but also delivers more heat to the skin. Thus, Moritz et al. [116] found that steam at 100 °C destroyed the epidermis of dogs within a few seconds.

Figure 63.28 shows curves for tolerance time of convected heat for both dry and humid air. A search for the original data used to produce these curves has not been successful, but on careful consideration it seems likely that the humid curve must represent air that was humid (perhaps saturated) at *room* temperature, which was then heated subsequently and was, therefore, nowhere near saturated with water vapor at higher temperatures. This must be the case because the capacity of air for water vapor increases dramatically at temperatures above 60 °C, so that the amount of deliverable latent heat also increases. In practice, 60 °C has been found to be the highest temperature at which 100 % water-vapor saturated air can be breathed. Since all

fires produce a considerable amount of water from combustion, it is possible that the presence of water vapor may be an important neglected hazard in some fires. As an approximate guide, the volume concentration of water vapor derived from fuel combustion in fire effluent is similar to the CO_2 concentration, which can be up to around 10 %. This amount is less than the concentration in saturated air at the breathable limiting temperature of 60 °C (which is 20 % H_2O). For this reason it is considered that the water vapor content of normal fire effluent is not likely to present a serious hazard. However, a serious hazard can occur if water is applied to a large fire but fails to extinguish it.

Radiant Heat For radiant heat, clothing also greatly influences tolerance times, but again, data on naked skin are relevant to exposure of unprotected areas such as the head. Figure 63.30 [109], shows the relationship between time to skin pain and radiant heat flux. Data points A to E, taken from a number of authors (detailed in Table 63.19) have been added for comparison. Points B through E agree with the curve presented by Berenson, but data from one source (Perkins et al.) [122] (points labeled A) deviate somewhat from the rest. From Perkins's data (which were produced by experiments where thermal injury was caused by exposing subjects to radiant heat from a searchlight), the heat fluxes for erythema (reddening of the skin said to coincide with pain [120]) appear rather higher than the heat flux limits for pain supplied by the other authors. This is possibly due to differences in the wavelength and, thus, degree of penetration of the radiation [118]. The searchlight data do, however, show the relationship between time to erythema, time to partial skin burn, and time to full-thickness skin burn. The shape of the radiant heat tolerance curve suggests a fairly obvious tolerance limit for exposure to radiant heat of 0.25 W/cm^2 (2.5 kW/m^2), which is that suggested by Babrauskas [52].

Behavioral and Incapacitating Effects of Skin Pain and Burns Experiments on the effects of radiant heat exposure on behavior of humans have been performed during the development of an "active denial system (ADS)" [121]. This system is designed to incapacitate exposed subjects by inducing skin pain by exposure by heat radiation at a frequency of 95 GHz. This frequency is selected to pass through clothing and heat the

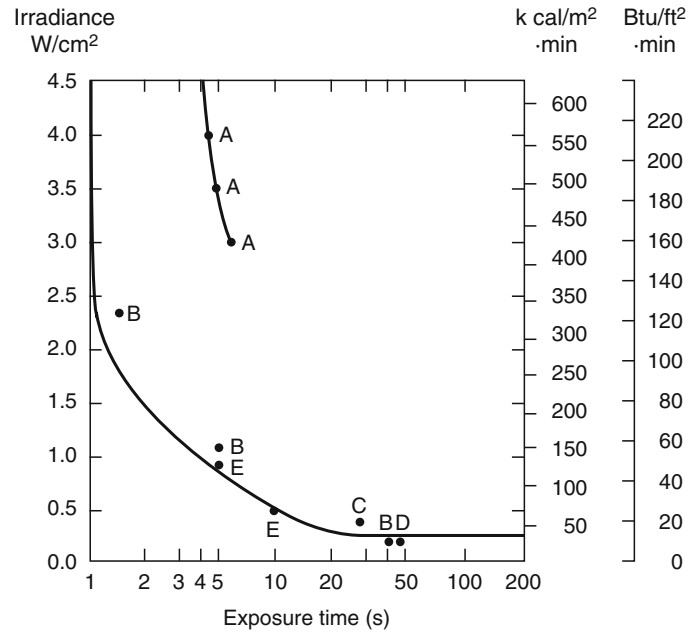

Fig. 63.30 Time to severe skin pain from radiant heat [109]. See text and Table 63.19 for discussion of data points A to E [110, 113, 122, 125, 126]

Table 63.19 Data on the effects of exposure to radiant heat

Reference source	Heat flux W/cm^2	Time to effect(s)			Letter in Fig. 63.30
		Erythema (or pain)	Burn	Full burn	
Perkins et al. [122]	15	1	2.5	4	
	10	2	4	6	
	5	4	7	>15	
	4	4.5	9	>15	A
	3.5	5	9.5	>15	A
	3	6	10	>15	A
Buettner [118]	2.35	1.6			B
	1.05	5			B
	0.25	40			B
Veghte [113]		Blisters			
	0.42	30			C
Simms and Hinkley [109]		Unbearable pain			
	0.126	600			
	0.252	30–60			D
Dinman [125]	0.24	Lower limit for pain after a long period			
	0.82	5			E
	0.48	10			E
Berenson and Robertson [109]	0.34	Limit for blood to carry away heat			
Babrauskas [126]	0.25	Tenability limit			

skin at depth of 0.4 mm without further penetration. The ADS "repellent" effects occur when the skin at this depth is heated just above 43–44 °C, while first degree burns occurred at around 51 °C and second-degree burns at around 58 °C. Exposed subjects reported sensation of intense pain, which they were highly motivated to avoid. One subject stated that it was not so much that he decided to escape from exposure but more that his body took over and forced him to move. This gives some indication of the effects of pain from skin heating in fire victims. In situations where a subject can move away from the heat source they are likely to do so. Where escape involves moving towards or into the heat source, such as entering hot smoke, or under a heat source, such as crossing a room under a hot upper layer, then it is likely that they will be unable or extremely unwilling to do expose themselves for more than a second or so once the heat flux exceeds the pain threshold.

Consequences of Body Surface Burns Apart from the immediate pain caused by exposure to heat and by skin burns, as well as the accompanying psychological shock and fear, incapacitation may result from body surface burns during or after a fire due to physiological shock. In this situation loss of body fluids into the burn results in circulatory failure and a fall in blood pressure, which may lead to collapse and even loss of consciousness [64, 117]. The immediate effect of burns and the later chances of recovery depend on a number of factors such as the site and extent of the burn, the depth of the burn, the age of the victim, and the treatment received [120]. Although victims may continue to function for some time with severe burns, and survivals have occurred with up to 80 % body surface area burns [120], in general, if 35 % or more of the body surface area is burned the chances of survival are low. Young adults generally have the best chance of survival, with a 50 % chance of surviving a 50 % body surface area burn, whereas children and old people are the most vulnerable, with a 50 % chance of surviving a 20 % body surface area burn in the elderly (Fig. 63.31) [64, 120]. The depth of burn is classified on a scale of six degrees. First-, second-, and third-degree burns involve damage to the skin from which it can recover, while fourth-degree burns require skin grafts. Fifth- and sixth-

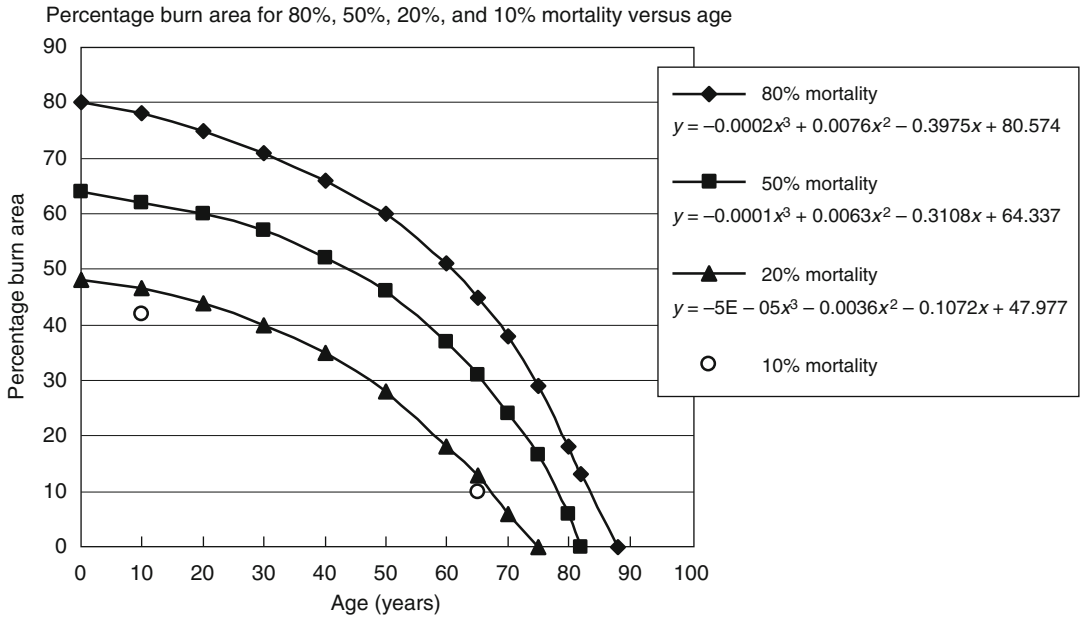

Fig. 63.31 Relationship between burn area, age, and mortality [120]. Equations show polynomial fits to curves

degree burns involve destruction of muscle and/or bones, respectively [64]. Another scheme classifies burns as partial-thickness skin burns, which will heal, or full-thickness burns, which require grafts [120].

If the victim survives the initial period of shock, death may occur over a period of up to a few weeks due to secondary effects on the brain, heart, lungs, liver, and kidneys [64]. The most common secondary effect and cause of death involves the lungs [64, 123, 127, 128], consisting of pulmonary edema resulting from effects on the circulatory system secondary to shock and metabolic acidosis. Postexposure treatment to replace body fluids and control acidosis are important in improving the prognosis for survival. If the victim survives the respiratory distress resulting from edema during the first week after exposure, pneumonia may then develop as a further, possibly fatal, complication [64, 129–131].

This fatal damage to the lungs may occur following body surface burns when there has been no inhalation of heat or toxic gases. In many fire victims, however, damage to the respiratory tract and lungs results from a combination of all three causes [64, 129–131].

Thermal Damage to the Respiratory Tract

Thermal (as opposed to chemical) burns to the respiratory tract never occur in the absence of burns to the skin of the face [131, 132]. Heat damage to the respiratory tract is even more dependent on the humidity of inhaled hot gases than are skin burns. As a result of the low thermal capacity of dry air and the large surface area of the airways, which are lined with a wet surface and good blood supply, thermal burns are not induced by dry air below the top of the trachea. However, steam at around 100 °C is capable of causing severe burns to the entire respiratory tract down to the deep lung, due to its higher thermal capacity and the latent heat released during condensation. These effects of inhaled hot gases are demonstrated by the work of Moritz et al. [117] in which anesthetized dogs and pigs breathed hot air, flame from a burner, or steam, supplied through a cannula to the larynx. Dry air at 350 °C and flame from a blast burner at 500 °C caused damage to the larynx and trachea but had no effect on the lung, whereas steam at 100 °C caused burns at all levels. In these experiments

the most important site of damage was the larynx, and death resulted from obstructive edema of the laryngopharynx within a few hours of exposure. This work was taken further by Zikria [131] using steam burns in dogs, induced by a 15-s application of steam at 100 °C via an endotracheal tube. The animals survived the initial effects and a number of phases of reaction were observed. The first phase consisted of necrosis and edema in the tracheobronchial airway and early lung parenchymal edema within 1 h. This result was followed by increasing parenchymal edema, sloughing of the mucosa, and collapse of lung segments. The next phase after 24 h consisted of bronchopneumonia behind respiratory tract obstructions.

All these effects occur in fire victims, but it is difficult to separate the effects of thermal inhalation burns from edema and inflammation due to burns caused by irritant chemical smoke products, or edema secondary to body surface burns, all of which may be involved [64, 129–131]. Thus, fire victims with facial burns subjected to endoscopy have been found to have burns well into the respiratory tract [132]. If these lesions are caused by heat, it would imply that fire atmospheres resemble steam rather than dry air in terms of their thermal capacity. However, it is possible that such lesions are caused by chemical smoke irritants, which have been shown to produce fatal pulmonary edema and inflammation in the absence of heat [60]. Unfortunately, data on the thermal capacity and latent heat of actual fire atmospheres are not readily available, although it may be possible to calculate probable values from knowledge of fire atmosphere temperature and composition.

The situation is, therefore, complicated but from a fire engineering standpoint a number of basic points may be useful.

1. Thermal burns to the respiratory tract will not occur unless the air temperature and/or humidity are sufficient to cause facial skin burns.
2. Dry air at around 300 °C may cause burns at the larynx after a few minutes. This may result in life-threatening obstructive edema of the larynx within an hour if not treated, although damage to the deeper structures of the lung is unlikely. It is possible that such laryngeal burns may occur at lower temperatures down to approximately 120 °C depending on the duration of exposure, and breathing dry air at these temperatures would be painful. Laryngeal burns followed by obstructive edema are common findings in fire victims and are important causes of incapacitation and death during and immediately after fires [64, 129–131].
3. Humid air, steam, or smoke with a high thermal capacity or latent heat (due to vapor content or suspended liquid or solid particles) may be dangerous at temperatures of around 100 °C causing burns throughout the respiratory tract. It may be possible to predict the likely effects of hot-smoke atmospheres if thermal capacity or latent heat were measured.
4. In practice, fire victims may be affected by the inhalation of chemically irritant smoke, by hot humid gases, and by the secondary effects on the lung of body surface burns, all of which may combine to cause fatal respiratory tract lesions during the hours, days, or weeks following the fire exposure. However, these effects are probably less likely to be fatal during exposure to the fire atmosphere over periods of less than 30 min.
5. Heat flux and temperature tenability limits designed to protect victims from incapacitation by skin burns should be adequate to protect them from burns to the respiratory tract.

Model of the Prediction of Time to Incapacitation by Exposure to Heat in Fires

There are three basic ways in which exposure to heat may lead to incapacitation: through heat stroke (hyperthermia), skin pain and burns, or respiratory tract burns. Thermal burns to the respiratory tract from air containing less than 10 % by volume water vapor do not occur in

the absence of burns to facial skin. Therefore, tenability limits with regard to skin pain and burns are normally lower than for thermal burns to the respiratory tract. Thermal burns to the respiratory tract may occur on inhalation or air above only 60 °C when saturated with water vapor, as may occur when water is used for fire extinguishment.

The tenability limit for exposure of skin to radiant heat is approximately 2.5 kW/m^2, below which exposure can be tolerated for at least several minutes. Radiant heat at this level and above causes skin pain followed by burns within a few seconds, but lower fluxes can be tolerated for more than 5 min. For situations where occupants are required to pass under a hot smoke layer in order to escape, this radiant flux corresponds approximately to a hot layer temperature of 200 °C. Above this threshold, time (minutes) to different endpoints for effects of exposure to radiant heat $t_{I\text{rad}}$, at a given radiant flux of qkW/m^2, is given by Equation 63.41 [133, 134].

$$t_{Irad} = \frac{r}{q^{1.33}} \tag{63.43}$$

where r is the radiant heat exposure dose [(kW · m^{-2})$^{4/3}$·min] required for any given endpoint:

Radiant heat endpoint for exposed skin	r (kW · m^{-2})$^{4/3}$ min
Severe skin pain	1.33–1.67
Second-degree burns	4.0–12.2
Third degree (full-thickness) burns	16.7

The threshold for pain occurs at an r value between approximately 1.33 and 1.67 (kW · m^{-2})$^{4/3}$ min. Second-degree burns occur at 4.0–12.2 (kW · m^{-2})$^{4/3}$·min and third-degree (full-thickness) burns at approximately 16.7 (kW · m^{-2})$^{4/3}$·min. The wide range given for second-degree burns reflects the effects of blistering. If the heating rate is low enough for blisters to form, this presents some degree of protection so that a higher-exposure dose is required. It is proposed that a figure of 1.33 (kW · m^{-2})$^{4/3}$min is used to represent a tolerance threshold and 10 (kW · m^{-2})$^{4/3}$min a threshold for incapacitation and serious injury. For infrared radiation it is also proposed that 10 (kW · m^{-2})$^{4/3}$min represents a fatal level for a vulnerable population (over 65 years of age) or a 1 % fatality level for the average population, whereas 16.7 (kW · m^{-2})$^{4/3}$min represents a 50 % probability lethal level for the average population. Radiant heat tends to be directional in fires, so that the main problem tends to be local heating of particular areas of skin. The air temperature and, hence, that of the air breathed and that in contact with other parts of the body may be relatively low, even when the radiant flux is high. For this reason the main hazard is pain and burns to the skin, rather than hyperthermia. Skin temperature depends on the relationship between the rate of heat supply to the skin surface and the removal of heat from inner layers by the blood. There is, therefore, a threshold radiant flux below which significant heating of the skin is prevented, but above which rapid heating of the skin occurs.

For exposures of up to 2 h to convected heat from air containing less than 10 % by volume of water vapor, the time (minutes) to incapacitation $t_{I\text{conv}}$ at a temperature T (°C) is calculated from Equation 63.44, which is derived from Fig. 63.28.

$$t_{I\text{conv}} = 5 \times 10^7 T^{-3.4} \tag{63.44}$$

This expression tends to follow the worst-case (100 % humidity) line. It also deviates somewhat from Blockley's curve at the high and low ends. It is, therefore, a somewhat nonconservative expression for exposure to higher temperatures and somewhat overconservative at the low-temperature end. The following expressions have been developed for the midhumidity case, giving a better fit to the empirical data.

Tolerance time t_{tol} (minutes) under midhumidity conditions is then given by

$$t_{\text{tol}} = 2 \times 10^{31} \times T^{-16.963} + 4 \times 10^8 \times T^{-3.7561} \tag{63.45}$$

where T is the ambient temperature (°C). This expression is considered suitable for calculating tolerance time as a possible tenability limit for design purposes. For other applications, such as

probabilistic risk assessments or forensic investigations other endpoints may be required. These may include those when serious injury from severe hyperthermia or second-degree burns (considered to represent a point of incapacitation for the average occupant) or the time to a potentially lethal heat exposure (involving prolonged hyperthermia and/or third-degree burns) may occur.

Based on the hyperthermia data and the relationship between heat doses causing pain and those causing serious injury or causing fatal third-degree burns, similar expressions have been derived for predicting time to serious injury and death.

Time (minutes) to serious injury or severe incapacitation

$$t_{\text{injury}} = 5 \times 10^{22} \times T^{-11.783} + 3 \times 10^{7} \times T^{-2.9636} \quad (63.46)$$

Time (minutes) to fatal exposure conditions with extensive third-degree burns is then given by

$$t_{\text{fatal}} = 2 \times 10^{18} \times T^{-9.0403} + 10^{8} \times T^{-3.10898} \quad (63.47)$$

These expressions are related to exposure to heated air with less than 10 % water content by volume.

As with toxic gases, the body of a fire victim may be regarded as acquiring a "dose" of heat over a period of time during exposure, with short exposure to a high radiant flux or temperature being more incapacitating than a longer exposure to a lower temperature or flux. The same fractional incapacitating dose model as with the toxic gases may be applied and, providing that the temperature in the fire is stable or increasing, the fractional dose of heat acquired during exposure can be calculated by summing the radiant and convected fractions using Equation 63.46

$$\text{FED} = \int_{t_1}^{t_2} \left(\frac{1}{t_{I\text{rad}}} + \frac{1}{t_{I\text{conv}}} \right) \Delta t \quad (63.48)$$

Note: $t_{I\text{rad}}$ will tend to zero as q tends to <2.5 kW/m^2.

Table 63.20 Limiting conditions for tenability caused by heat [18]

Mode of heat transfer	Intensity	Tolerance time
Radiation	<2.5 kW · m^{-2}	>5 min
	2.5 kW · m^{-2}	30 s
	10 kW · m^{-2}	4 s
Convection	<60 °C 100 % saturated	>30 min
	100 °C <10 % H_2O[a]	12 min
	120 °C <10 % H_2O	7 min
	140 °C <10 % H_2O	4 min
	160 °C <10 % H_2O	2 min
	180 °C <10 % H_2O	1 min

Copyright BRE Ltd

[a] v/v

Thermal tolerance data for unprotected skin of humans suggest a limit of about 120 °C for convected heat, above which considerable pain is quickly incurred along with the production of burns within a few minutes. Depending on the length of exposure, convective heat below this temperature may still result in incapacitation due to hyperthermia. Examples of tolerance times to different radiant fluxes and air temperatures are shown in Table 63.20. Conducted heat is physiologically important only when skin is in contact with hot surfaces, such as door handles. A 1-s contact with metal at 60 °C can cause burns.

The radiant component from immersion in hot air is negligible, but in situations in which subjects are immersed in hot smoke, there will be a significant radiant component from hot smoke particles in addition to convective heat transfer from contact with hot gases. One way to estimate the effect of such an exposure is to calculate the FED from the radiant heat flux ($1/t_{I\text{rad}}$) and sum it with the FED from the convected component ($1/t_{I\text{conv}}$) as in Equation 63.48. Another method is to calculate the total heat flux from the radiant and convected components of the smoke. On this basis it is proposed that the total incident flux to the skin of a person immersed in hot smoke is given by

$$q = \varepsilon\sigma\left(T_i^4 - T_m^4\right) + h_c(T_i - T_m)/1000 \quad (63.49)$$

where

q = Heat flux (kW/m^2)
T_i = Heat source temperature (°K)
T_m = Material surface temperature (°K)
ε = Emissivity (0.05 for a gas to 1 for a black body, perhaps 0.5 for smoke)
σ = Stefan Bolzmann constant (5.67×10^{-8} Wm^{-2} K^{-4})
h_c = Convective heat transfer factor. For air this depends on the flow rate past the object. It will be approximately 5–8 for slow-moving air.

The first term in the equation represents the radiant component of heat flux and the second term represents the convected component of heat flux. Using this equation it is, therefore, possible to calculate total heat flux from the ambient surroundings at body height. The radiant component is relatively small at low temperatures and is negligible for hot air due to its low emissivity. However, for smoke the emissivity is likely to be much higher (around 0.5) so that at higher temperatures both components should be considered in order to calculate the total heat flux to the skin. In addition to the heat flux from the fire effluent enveloping a subject additional heat radiation is likely from hot upper layers and/or directly from the fire. If the subject is in air (with a low emissivity), below a hot smoke layer, the only significant radiative heat flux sources are likely to be the upper layer, the fire, or hot surfaces.

Time to the different heat effect endpoints for total heat fluxes in excess of 2.5 kW/m^2 is then given by Equation 63.49 using the appropriate exposure dose endpoints as the numerator:

1.33 (kW · m^{-2})$^{4/3}$ min (tolerance limit/pain/first-degree burns)
10 (kW · m^{-2})$^{4/3}$ min (severe incapacitation and second-degree burns)
16.7 (kW · m^{-2})$^{4/3}$ min (fatal exposure with third-degree burns)

For all the expressions in this section estimation of the time to effect is based on measured effects on exposed skin of subjects for given exposures to hot air or different levels of incident radiant heat flux. An alternative approach would be to calculate heat transfer into a subject and the temperature of the skin at different depths with time. The BURNSIM model has been developed using this method for radiant heat [135].

Example of a Calculation of Time to Incapacitation for Physical Fire Parameters and Irritancy

In a previous section the single armchair room burn shown in Fig. 63.22 was used to illustrate how the model for prediction of asphyxiation could be applied to a practical fire scenario. To complete the incapacitation model it is necessary to include calculations for the effects of physical parameters (heat, smoke optical density) and mass loss concentration as an indication of irritancy. The curves for radiant heat, air temperature, smoke extinction coefficient, and mass loss during the first 10 min of the armchair burn are shown in Fig. 63.32.

Of the physical factors likely to affect a victim during the fire exposure, the majority are basically concentration or intensity related rather than dose related, and for these factors tenability limits have been set (radiant heat, smoke optical density, and sensory irritancy). The other two factors, convected heat and lung irritancy, are primarily dose related, but lung irritant effects are likely to be relatively minor until after exposure, which leaves the fractional incapacitating dose of convected heat to be calculated. The average temperatures per minute during the first minutes of the fire are shown as histograms in Fig. 63.32 with Table 63.21 showing the fractional incapacitating dose calculation.

Convected Heat The effects of exposure to convected heat increase dramatically in this type of fire as shown in Fig. 63.32. Incapacitation, mainly due to skin pain and burns, is predicted sometime during the fourth minute, when the air temperature is 220 °C. The situation then rapidly worsens, and it would seem likely that severe and probably fatal burns or fatal hyperthermia would be sustained by any victim remaining in the fire during the fifth minute. Even if the victims were protected to some extent

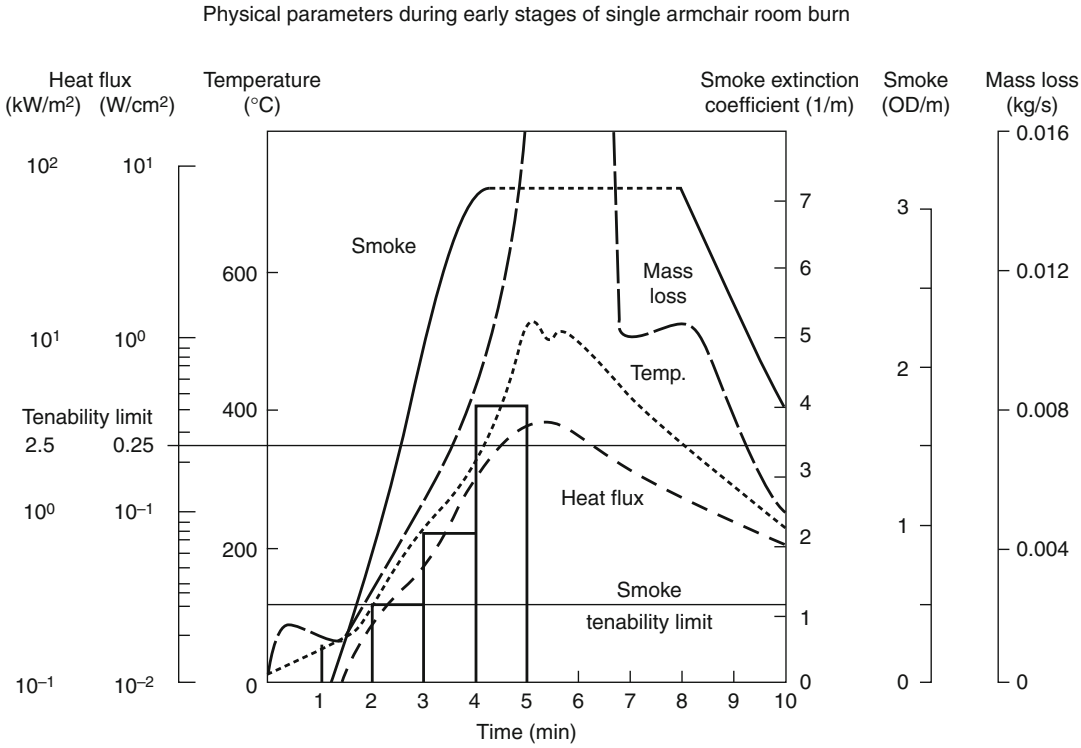

Fig. 63.32 Profiles for heat (radiant flux and temperature), smoke, and mass loss rate during the first 10 min of a single armchair (polystyrene, with polyurethane cushions and covers) room burn [52]. (Expanded detail from Fig. 63.22) Histogram shows average temperature each minute during the first 5 min

Table 63.21 Calculation of fractional incapacitating accumulation of convected heat for the single armchair room burn data shown in Fig. 63.32 (Calculated According to Equation 63.44)

Time (min)	1	2	3	4	5	6
Average temp. (°C)	20	65	125	220	405	405
F_{lh}	0	0.02	0.19	1.57	15.55	15.55
Cumulative F_{lh}			0.21	1.78	17.33	32.88

Incapacitation occurs when $F_{lh} = 1$, and is, therefore, predicted during the fourth minute of exposure

by clothing, they would sustain burns to the face and probably fatal burns to the larynx. The occurrence of lung burns would depend on the thermal capacity (principally the latent heat) of the smoke.

Radiant Heat From Fig. 63.32, it would seem that the effects of radiant heat would be relatively minor in this fire compared to the effects of convected heat. The radiant heat peaks at just above 3 kW/m^2 during the sixth minute and, therefore, just exceeds the tenability limit. Nevertheless, the radiation alone would probably be sufficient to cause some burns and seriously inhibit escape during the sixth minute, and there would almost certainly be some degree of additive effect with convected heat.

Smoke From the point of view of its obscurational effects, incapacitation by smoke is concentration related rather than dose related. For this series of chair burns, Babrauskas sets a tenability limit of extinction coefficient 1.2/m (OD/m 0.52) [52]. This would give approximately 2 m visibility, which should be adequate for escaping from a room and could be used as a tenability limit for input into the model. Incapacitation due to visual obscuration would occur at the end of the second minute. The smoke curve is rising very steeply at this point, with an OD/m of 1 at the beginning of the third

minute. Escape would, therefore, become extremely difficult and certainly slow during the third minute, unless the victim was familiar with the surroundings and able to find the exit in the dark.

Irritancy As stated in the section "Irritant Fire Products" in this chapter there are two factors to consider: the immediate incapacitation due to the painful effects of sensory irritation of the eyes and respiratory tract, adding to the obscurational effects of smoke and disrupting escape behavior, and the later inflammatory effects on the lung that may cause death after exposure.

The first consideration is whether the victim would be able to escape from the fire. In this context, sensory irritation is the most important. This is concentration related, so to predict the irritancy of the smoke, it is necessary to know the RD_{50} concentration of the atmosphere produced by the materials involved under the particular decomposition conditions existing in the fire. Most importantly, it is necessary to know the concentration/time profile of the fire products in terms of mass loss per liter of air (NAC mass loss). Although the mass loss curve for the armchair is shown in Fig. 63.32, there are no data on the volume of air into which this mass was dispersed during the fire; so for the purposes of this example it will be necessary to make an estimate of possible mass loss concentration. Also, since the RD_{50} of the polyurethane and polystyrene components of the chair under flaming conditions are unknown, it will be necessary to use estimated values.

In the discussion of irritancy, a general tenability limit for severe sensory irritation was set at a concentration of 1 mg/L NAC mass loss, and an incapacitating dose for serious postexposure lung inflammation was set at 10 mg/L NAC mass loss for 30 min (a Ct product of 300 mg · min/L). From the general conditions, the smoke curve, and the CO concentration curve, it is estimated that the tenability limit for sensory irritancy would be exceeded during the third minute, greatly adding to the deleterious effects of smoke on vision and escape behavior.

With regard to lung irritation, it is estimated that the average mass loss concentration over the first 5 min of the fire would be approximately 10 mg/L. If so, this would represent a fractional incapacitating dose of 50 mg · min/L, which would probably be insufficient to cause significant lung damage after exposure, compared to the more serious effects of heat exposure. However, if the average mass loss concentration over the first 5 min should reach 60 mg/L, serious effects on the lung would likely occur after and probably during exposure.

Interactions In terms of physiological effects, it is likely that there would be some degree of interaction between asphyxia and several of these physical factors, but it is likely that most would be relatively minor during the fire, except for some possible enhancement of pulmonary irritation due to the hyperventilatory effect of CO_2 during the fourth to sixth minutes of the fire. A reasonable model can be used in which asphyxia, sensory irritancy, and the effects of heat and visual obscuration can be treated separately. Interactions may be more important at the behavioral level. The interaction between sensory irritation and visual obscuration has been mentioned and there is some experimental evidence for such an interaction in humans [50]. After exposure, as mentioned in the section "The Exposure of Fire Victims to Heat," the effects of skin burns, respiratory tract burns, and chemical irritation (and even possibly CO asphyxia) all combine to increase the probability of fatal pulmonary edema and inflammation.

Summary From the analyses performed, the effects on a victim exposed to the conditions in the armchair room burn (see Fig. 63.22) are predicted as follows:

1. Toward the end of the second minute and beginning of the third minute, the smoke optical density and mass loss/liter would sufficiently exceed the tenability limits for visual obscuration and sensory irritancy to severely inhibit escape from the room.
2. During the fourth minute, the average temperature was 220 °C and sufficient heat would be accumulated in the skin surface to cause skin burns resulting in incapacitation.

3. During the fifth minute, a victim is likely to lose consciousness due to the combined effects of the accumulated doses of asphyxiant gases.
4. It is predicted that a victim escaping or rescued after the fourth minute would suffer severe postexposure effects due to skin burns, plus pulmonary edema and inflammation that might well be fatal (due to the combined effects of inhaled hot gases, chemical irritants, and the pulmonary secondary effects of skin burns). After the sixth minute, it is likely that a rescued victim would die at some time between a few minutes and 1 h due to the effects of asphyxia and circulatory shock.

It is unlikely that an otherwise healthy adult would be able to escape from such a fire if he or she remained longer than 3 min after ignition. However, 3 min is a long time in which to leave a room, so that providing the victim is awake and aware of the fire, is not otherwise incapacitated, and does not stay after 2 min in an attempt to fight the fire or rescue belongings, it is likely that he or she would be able to escape without serious injury. In the next section, data on real fire victims are examined in an attempt to relate fire conditions to actual injury and death statistics.

A full worked example of the application of these methods to an FED analysis for smoke, toxic hazards and heat, with accompanying Figures and Table is presented in this chapter in the section "Worked Example of a Simplified Life Threat Analysis".

Worked Example of a Simplified Life Threat Hazard Analysis

In the previous sections, the various elements of a physiological FED model for predicting time to incapacitation of occupants during full-scale fires have been developed. The following section consists of a worked example including tenability calculations for all toxic and physical hazards: time-to-escape efficiency impairment from the effects of optical obscuration by smoke, time-to-escape efficiency impairment from sensory irritation, time to incapacitation by asphyxiant gases, time to incapacitation due to skin pain and burns from radiant and convected heat, and time to inhale a lethal exposure dose of lung irritants. The worked example is for data from the single armchair open room burn involving a rapidly growing fire in an armchair constructed from polystyrene with polyurethane covers and cushions. The fire conditions are illustrated in Fig. 63.22. Figure 63.27 shows expanded details of the asphyxiant gases with the concentrations averaged during each minute. Figure 63.32 shows details of the profiles for radiant heat flux, temperature, smoke concentrations and mass loss rate.

Table 63.22 shows the input data and calculation results for the life threat hazard analysis calculation using the methods described. The results of the analysis are presented in Fig. 63.33. This figure shows plots of the FED for smoke, FIC for sensory irritation, and FED values for each hazard parameter as they increase with time. The endpoints of escape impairment or loss of tolerability (for smoke obscuration and irritants) and incapacitation (for heat and asphyxiant gases) are reached when the line for each parameter crosses 1. Higher FECs and FEDs indicate more severe effects. For irritancy, incapacitation is predicted at FEC_{irr} values of approximately 5–10 and for asphyxiation death is predicted at FED_{in} values of approximately 2–3.

The analysis is designed to predict the severity of each hazard and the time during the fire at which it becomes significant. The toxic gas concentrations, smoke optical density, temperature, and radiant heat flux have been averaged over each of the first 6 min of a theoretical furniture fire but are generally similar to conditions obtained in the smoke layer at head height in some experiments performed in ISO room tests. The analysis shows that the smoke obscuration is the first hazard confronting a room occupant. The level of obscuration exceeds the tenability limit for irritant smoke in a small enclosure after the second minute, with an FEC of 1. The second hazard to confront the occupant

Table 63.22 Illustration of life threat analysis for the first 6 min of a furniture fire based on a single armchair room burn (The armchair is polystyrene with polyurethane cushions and covers. The room is 39 m^3 with open doorway. CO, CO_2, O_2, smoke, temperature, and radiant flux are as measured in doorway at 2.1 m height. Other gases are estimates to illustrate calculation method)

Each minute	1	2	3	4	5	6
Gas concentrations						
Smoke (OD/m)	0.1	0.2	0.5	1.5	3.0	3.5
HCl (ppm)	10	50	150	200	250	200
Acrolein (ppm)	0.4	0.8	2.0	6.0	12.0	14.0
Formaldehyde (ppm)	0.6	1.2	3.0	9.0	18.0	21.0
CO (ppm)	0	0	500	2000	3500	6000
HCN (ppm)	0	0	50	150	250	300
CO_2 (%)	0	0	1.5	3.5	6.0	8.0
O_2 (%)	20.9	20.9	19.0	17.5	15.0	12.0
Temp (°C)	20	65	125	220	405	405
Heat flux (kW/m^2)	0	0.1	0.4	1.0	2.5	2.5
Fractional smoke concentration FEC_{smoke}	0.50	**1.00**	2.50	7.50	15.00	17.50
Fractional irritant concentration						
FIC_{HCl}	0.05	0.25	0.75	1.00	1.25	1.00
$FIC_{acrolein}$	0.10	0.20	0.50	1.50	3.00	3.50
FIC_{form}	0.10	0.20	0.50	1.50	3.00	3.50
Σ FIC	0.25	0.65	**1.75**	4.00	7.25	8.00
Fractional lethal dose (irritants)						
FLD_{HCl}	0.00	0.00	0.00	0.00	0.00	0.00
$FLD_{acrolein}$	0.00	0.00	0.00	0.00	0.00	0.00
FLD_{form}	0.00	0.00	0.00	0.00	0.01	0.01
Σ FLD_{irr}	0.00	0.00	0.00	0.00	0.01	0.02
Fractional asphyxiant dose						
$FED_{I_{CO}}$	0.00	0.00	0.02	0.07	0.13	0.23
$FED_{I_{CN}}$	0.00	0.00	0.01	0.11	0.38	0.58
FLD_{irr}	0.00	0.00	0.00	0.00	0.01	0.02
VCO_2	1.00	1.00	1.35	2.01	3.32	4.95
$FED_{I_{O_2}}$	0.00	0.00	0.00	0.00	0.01	0.04
FED_{IN} (asphyxiants)	0.00	0.00	0.04	0.38	1.72	4.08
Σ FED_{IN}	0.00	0.00	0.04	0.42	**2.14**	6.23
Fractional heat doses						
$FED_{rad\ pain}$	0.00	0.00	0.00	0.00	2.54	2.54
$FED_{conv\ pain}$	0.00	0.02	0.19	1.57	15.55	15.55
$FED_{heat\ pain}$	0.00	0.02	0.19	1.57	18.10	18.10
Σ $FED_{heat\ pain}$	0.00	0.02	0.21	**1.78**	19.88	37.98
$FED_{rad\ burns\ full\ thickness}$	0.00	0.00	0.00	0.00	0.20	0.20
$FED_{conv\ burns\ full\ thickness}$	0.00	0.00	0.03	0.19	1.28	1.28
$FED_{heat\ burns\ full\ thickness}$	0.00	0.00	0.03	0.19	1.48	1.48
Σ $FED_{heat\ burns\ full\ thickness}$	0.00	0.00	0.03	0.22	**1.70**	3.18

The endpoint, escape impairment (for smoke obscuration and irritancy), or incapacitation (for heat and asphyxiant gases) is reached when the FIC or FED value reaches 1

Limiting values are in bold. Lethal values are approximately two to three times incapacitating levels for dose-related parameters, and incapacitation five to ten times the FIC

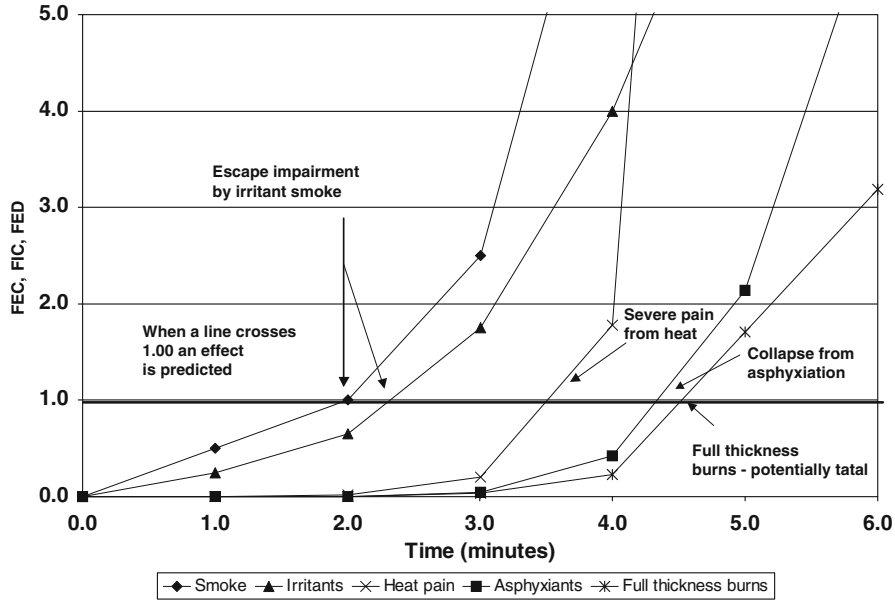

Fig. 63.33 Plots of FED analysis calculated in Table 63.22 (Copyright HER)

is irritancy. This becomes significant during the third minute, exceeding an FIC of 1 at 3 min. The tenability limit designed to protect vulnerable individuals (FIC 0.3) is exceeded approximately 1 min earlier. It is therefore predicted that after the second minute the level of obscuration and the irritancy of the smoke would be sufficient to impair and possibly prevent escape from the room due to difficulty in seeing and increasing pain in the eyes and respiratory tract. The effects of radiant and convected heat then become significant, crossing the tenability limit during the fourth minute and reaching an FED_{heat} value of 1.70, so that it is predicted that a room occupant would suffer severe skin pain and burns due to the effects of convected heat. Extensive, potentially fatal, full-thickness burns are predicted during the fifth minute.

During the fifth minute the radiant flux reaches the tenability limit of 2.5 kW/m^2, so that skin pain would be predicted within seconds due to radiation alone, were it not that the temperature has already exceeded the limiting exposure dose. Also during the fifth minute the FED_{IN} reaches 2.14, predicting that anyone breathing the smoke would lose consciousness due to asphyxia and might die after 6 min. The level for exposure to asphyxiants considered to provide protection for vulnerable sub-populations (FED_{IN} of 0.1) is crossed at approximately 3.5 min, and that to allow for more normal sensitivity variations (FED_{IN} 0f 0.3) a few seconds later, and only half a minute before the FED_{IN} reaches 1. The exposure dose of irritants is very small during the first 6 min of the fire, so that there should be little danger of postexposure lung damage. An important point about all these parameters is that the FIC and FED curves are rising very steeply after the tenability threshold (FIC or FED of 1) is crossed. This means that even if the true exposure concentrations or exposure doses required to cause incapacitation were higher than the tenability limits chosen there would be little effect on predicted time to incapacitation.

The overall prediction is that for this fire, escape would become difficult during the third minute and incapacitation could occur due to the effects of irritant smoke. A person remaining in the room after this time would suffer severe pain and burns after 4 min, which would probably be lethal a minute or so later. The would lose consciousness during the fifth minute. In this analysis it is assumed that the head of a room occupant

would be in the smoke at all times. In practice, if the room doorway was open, the hot, effluent-rich layer would descend from the ceiling to a level probably between 1 and 1.2 m above the floor as the chair reached its peak burning rate. A more sophisticated analysis could allow for the possibility that a room occupant might be at, or move to, a lower level in the room. If the height of the smoke layer with time is measured, then it is possible to allow for this factor in the calculation.

Chemical Composition and Toxicity of Combustion Product Atmospheres

In the preceding sections, the effects of individual asphyxiant gases and irritant chemical products known to occur in fires have been described together with their interactions. As described in the next section on "Fire Scenarios and Victim Incapacitation", the range of toxic substances and their relative concentrations vary considerably in the fire effluent mixtures produced by different fuels under different combustion conditions. An important aspect of combustion toxicity studies has been to examine the chemical composition and toxic effects of such effluent mixtures to determine the range of toxic effects and the extent to which they can be understood in terms of the small number of major substances described.

The effects of decomposition conditions on chemical product formation in different types and stages of fires, and the resultant toxicity, have been shown in a series of experiments involving exposures of primates to combustion products [61]. In these experiments, a number of materials were decomposed under a range of temperatures and oxygen supplies designed to simulate some of the conditions described previously. In one series of experiments, a study was made of the effects of temperature on the pyrolysis of three materials—polyacrylonitrile, flexible polyurethane foam, and wood. These were decomposed at 300, 600, and 900 °C to cover as far as possible the full temperature range known to occur in fires, simulating conditions where oxygen supply might be limited. Another set of experiments was then carried out on a further range of polymers to examine the effects of nonflaming and flaming oxidative decomposition on toxicity over midrange temperatures (440–700 °C). These conditions were chosen to embrace the conditions known to give the greatest complexity of products, particularly with polymers that are known to be sensitive to oxidation in product formation. In this series the test materials were rigid polyurethane foam, polypropylene, polystyrene, and nylon. In all cases, the sublethal toxic effects of exposure were evaluated using primates.

With the series of pyrolysis experiments, it was found that up to midrange temperatures, a rich product mix occurred, whereas at 900 °C clear atmospheres containing high yields of simple, low molecular weight products occurred. Thus for wood, which contains oxygen in its structure, the principal products at lower temperatures were oxidized organics, which caused upper respiratory tract and lung irritancy. There was a relatively low CO yield with wood, causing signs of asphyxia at sufficiently high wood nominal atmosphere concentrations. Polyacrylonitrile produced relatively low yields of HCN and other nitriles, causing signs of cyanide intoxication [16]. With the flexible polyurethane foam, the lower-temperature atmospheres consisted principally of a dense yellow isocyanate smoke, which was a powerful lung irritant capable of causing severe pulmonary inflammation after exposure [60, 61, 136, 137]. Low yields of CO and HCN resulted with this foam.

At 900 °C the isocyanate smoke from flexible polyurethane foam was destroyed, giving a clear atmosphere consisting mainly of HCN and CO, the main signs being of cyanide poisoning. Polyacrylonitrile also produced high yields of HCN, causing cyanide intoxication, and wood produced clear atmospheres consisting principally of CO.

An example of the effects of oxidation on product formation and toxicity is given by the effects of polypropylene decomposition products. Under pyrolytic conditions, polypropylene decomposed to give a nontoxic

atmosphere consisting of hydrocarbon fragments (see Chap. 62, Table 62.10). Under nonflaming oxidative conditions, some of these fragments were oxidized to form a highly irritant atmosphere that caused upper respiratory tract and lung irritation during exposure and severe pulmonary inflammation after exposure [60, 61]. There were also minor signs of CO-induced asphyxia. Under flaming conditions the pyrolysis and oxidation products were partially destroyed, with the most important products being carbon monoxide, carbon dioxide, water, and some irritants. The principal toxic effect of this atmosphere was CO intoxication with some signs of irritancy. With flaming atmospheres, however, the nature and degree of toxicity depend on the efficiency of combustion. By varying the decomposition conditions it is possible to substantially alter the toxicity.

From the animal exposures to these thermal decomposition and combustion product atmospheres, the major findings were that despite the great complexity in chemical composition of the test atmospheres, the basic toxic effects were relatively simple. For each individual atmosphere, the toxicity was always dominated either by an asphyxiant gas (CO or HCN) or by irritants. The toxicity of each atmosphere was, therefore, basically that of the major component that was present at its most toxic concentration. For asphyxia, the effects of individual atmospheres were virtually identical to those of either CO or HCN as individual gases at the same concentrations as they were present in the smoke atmosphere.

The presence of low concentrations of hydrocarbons (which are potentially asphyxiant at high concentrations) and of CO_2 in the 1000–7000 ppm range did not contribute to the asphyxia. The effects of irritant products on respiratory patterns for primates did not affect the pattern of CO or HCN asphyxia. There may have been a marginal additive effect of CO on HCN toxicity, but in these cases the pattern of asphyxia and times to incapacitation were very similar to those produced by equivalent HCN/air mixtures. Irritant effects did, of course, occur in these exposures in conjunction with asphyxia, but there was no interaction between them, in that irritancy did not affect the progress of asphyxia, and asphyxiant gases did not affect the response to irritants.

As a result of this work, and other studies described in Chap. 62 it can be stated with some confidence that the asphyxiant effects of fire atmospheres should be predictable on the basis of the common asphyxiant gases CO, HCN, low O_2, and CO_2, with a contribution from irritants, and that the models derived from the work on individual gases should be valid. It is also possible with current knowledge to predict approximately the potential of a fire atmosphere to cause sensory irritation or lung inflammation from a chemical analysis of the product composition.

Fire Scenarios and Victim Incapacitation

From the point of view of both product composition and toxic hazard, it is possible to distinguish four basic types of fire (see Table 63.3).

1. Non-flaming thermal decomposition and smoldering fires hazardous mainly to victims the room of origin of the fire
2. Early flaming fires hazardous mainly to victims in the room of origin
3. Small oxygen-vitiated fires in poorly ventilated enclosures (pre-flashover underventilated fires) hazardous to victims both in the room of origin or a remote location
4. Fully developed or postflashover fires hazardous to victims remote from the fire

In the United Kingdom, 80 % of fire deaths and injuries occur in domestic dwellings. In just over half of these cases the casualties occur in the compartment or origin of the fire. This class of fire is responsible for the highest incidence of deaths (60 %) and a high incidence of injuries (39 %). These fires occur mostly in living rooms or bedrooms and in upholstery or bedding [7]. In these cases, fire is often confined to the material first ignited. The toxic hazard in such fires depends on whether there is a long period of smoldering or a rapidly growing flaming fire.

As described, injuries and deaths occurring in the room of origin usually involved burns and toxic smoke, while most casualties in enclosures beyond the fire enclosure are from smoke and toxic gases.

Smoldering Fires

The work of Woolley and his colleagues at the U.K. Fire Research Station [63] showed that at midrange temperatures (400–700 °C) such as those found in smoldering fires or in the vicinity but beyond the flame zone of early flaming fires, materials are decomposed into pyrolysis products and oxidation fragments containing a mixture of asphyxiant and irritant gases and particulates. Under these conditions, the highest yields of a variety of potentially toxic products are formed (see Table 63.3 and Chap. 62, Table 62.10), many of which are irritant [61, 63] and since incomplete oxidation is favored, CO yields are high with CO_2:CO ratios approaching unity. CO is therefore likely to be an important toxic component. The formation of high yields of HCN is, however, not normally favored [61]. For many materials the product mix remains fairly constant over this temperature range, although the yields may increase somewhat with temperature.

Although toxic products are formed under these conditions, the rate of evolution is slow, smoke is seldom dense, and room temperatures are relatively low. A potential victim, therefore, has ample time to escape if alerted sufficiently early but may be overcome by fumes after a long period of time if unaware of the danger, particularly if asleep. The main danger here is almost certainly asphyxia by CO, with possibly a small contribution from low oxygen if the victim is in a room with a poor air supply [61, 138–141]. It is not possible from fire statistics to determine how often this type of fire occurs, since in many cases smoldering fires become flaming fires before they are detected. However, it is likely that fires estimated to have burned for 30 min or more before discovery have involved long-term smoldering, and it may be relevant that for victims in the 19–49 age group, deaths are 20 times more likely in this situation than for fires discovered within 5 min of ignition, which are often rapidly growing flaming fires [7].

The ability of smoldering fires to build up concentrations of CO capable of causing incapacitation and death in potential victims has been shown in large-scale fire tests [142]. A good example of such a situation is presented by a FED analyses of a series of tests carried out at NIST [143, 144], where two armchair types made from a standard and a fire-retarded polyurethane foam with cotton covers (combustible mass 5.7 kg) were burned in a simulated small apartment (volume 101 m^3) consisting of a burn room (11.8 m^3), connected via a corridor 12 m long to a target room (volume 12.08 m^3) (Tables 63.23 and 63.24). The armchairs were tested by flaming ignition of the seat back and also by smoldering caused by one or two cigarettes placed in the seat angle for approximately 1 h, followed either by spontaneous flaming or ignition from a flaming source. Under smoldering conditions, approximately 1 kg of foam was decomposed in just over 1 h. The smoke layer had reached the floor after 1 h, but there was a concentration gradient for smoke and toxic gases between the burn room and the target room. The major asphyxiant gas present was CO, which gradually increased in concentration in the burn room from 180 ppm during the first 13 min to 1000 ppm between 67 and 75 min. This was sufficient to have caused incapacitation (i.e., loss of consciousness) in just over 1 h in the burn room but probably not in the target room where the concentration was lower. When flaming ignition occurred, the armchair burned very rapidly and produced high concentrations of asphyxiant gases that would have been almost immediately fatal in the burn room. Within the target room an occupant would have become unconscious within less than 1 min and received a fatal dose within 2 min. The smoke in the system was also very irritant, and it is likely that anyone spending more than 1 h in the burn room would have suffered serious and possibly fatal lung damage, even if that person had been rescued. This example illustrates the dangers of

Table 63.23 Concentrations of toxic gases and FEDs in burn room for smoldering followed by flaming ignition of standard foam armchairs

Fractional effective doses of narcotic gases								
Time (min)	0–13	13–27	27–40	40–53	53–67	67–75	75–76	76–77
Gas concentrations—burn room								
CO ppm	180	300	360	700	700	1000	10,000	
HCN ppm	0	0	0	0	0	0	1320	
CO_2%	0.11	0.16	0.18	0.30	0.30	0.40	15.00	
O_2%	21	21	21	21	21	21	3	
Fractional effective doses for incapacitation								
FEDCO	0.006	0.010	0.012	0.024	0.024	0.035		
FEDHCN	0	0	0	0	0	0	Immed.	
VCO_2	1.019	1.032	1.037	1.069	1.069	1.096	fatal	
FEDO	0	0	0	0	0	0		
FED/min	0.006	0.010	0.013	0.026	0.026	0.039		
Σ FED	0.078	0.218	0.387	0.725	**1.089**	1.401		

By 71 min the mass loss exposure dose of irritants was approximately 600 g · m3 · min, which may cause fatal lung damage

Table 63.24 Concentrations of toxic gases and FEDs in target room for smoldering followed by flaming ignition of standard foam armchairs

Fractional effective doses of narcotic gases								
Time (min)	0–13	13–27	27–40	40–53	53–67	67–75	75–76	76–77
Gas concentrations—target room								
CO ppm	0	0	100	270	550	800	2700	2000
HCN ppm	0	0	0	0	0	0	125	120
CO_2%	0.04	0.04	0.08	0.15	0.20	0.30	9.00	8.50
O_2%	21	21	21	21	21	21	13	14
Fractional effective doses for incapacitation								
FED_{CO}			0.003	0.009	0.019	0.028	0.099	0.073
FED_{HCN}			0	0	0	0	0.080	0.072
VCO_2			1.012	1.030	1.042	1.069	5.772	5.248
FED_O			0	0	0	0	0.021	0.012
FED/min	0	0	0.003	0.009	0.020	0.030	1.054	0.773
Σ FED	0	0	0.039	0.156	0.436	1.676	**1.730**	2.503

Note: By 71 min the mass loss exposure dose of irritants was approximately 300 g · m^3 · min, which may cause some lung damage

smoldering conditions, which can continue for several hours and spread lethal products throughout a building, creating danger for the sleeping, trapped, or otherwise incapacitated occupant. Since such fires often change to flaming before they are discovered, it is difficult to know the true incidence of incapacitation and death occurring during the nonflaming phase of fires. For this example, both the standard and fire-retarded (FR) chairs would have caused incapacitation after 1 h in the burn room, but due to its higher yield of CO and irritants, the FR chair would also cause incapacitation in the target room soon after, and death in the burn room after 1.5 h of smoldering. The standard foam death at both locations would occur within 1 min of the spontaneous transition to flaming after 75 min. These dangers can be overcome by the provision of

detection and warnings, but the silting of detectors can be important for effective operation.

Flaming Fires

For flaming fires where the victim is in the room of origin, the hazard relates to the early stages of fire growth. Such fires often grow quickly, but even the most rapidly growing flaming fires take approximately 3 min to reach levels of heat and gases hazardous to life [52], unless exposed subjects are intimate with the fire. As Fig. 63.22 shows, the hazard in this situation relates to a number of factors, all of which may reach life-threatening levels simultaneously as the fire reaches the rapid phase of exponential growth. In the high temperature, well-oxygenated flames of early flaming fires, much of the thermal decomposition products are consumed to form simple, comparatively innocuous products such as CO_2 and water, the CO_2 to CO volume ratios being high initially even up to the 500–1000 range and then decreasing to the region of 50–100 as the oxygen concentration decreases toward 15 %. Since CO is only approximately 10–50 times as toxic as CO_2, it is conceivable that in this type of fire CO_2 could present more of a toxic hazard than CO. However, as the CO_2 concentration in the fire compartment approaches 5 % and the O_2 concentration decreases toward 15 %, the combustion becomes less efficient and the CO_2 to CO ratios decrease to the region of 50–100, CO becoming a more important toxic factor.

With such flaming fires, the yields of irritant, oxidized fragments and of CO are generally lower than under nonflaming conditions, but the yields and relative rates of production of CO_2, CO, and irritant smoke depend on the rate and efficiency of combustion. As Fig. 63.22 and Table 63.3 show, the atmospheres obtained in a rapidly growing fire can develop asphyxiant concentrations of CO_2 (greater than 5 %), CO (greater than 1000 ppm), and low oxygen (less than 15 % O_2), as well as some dense irritant smoke from products escaping the flame zone. During the early, fuel-controlled, stages of compartment fires both the rates of fire growth and yields of products depend on the physical and chemical properties of the fuel. Initially the toxic hazards are low, because the mass loss rate of the fuel is low, and for most common non-flame retarded natural and synthetic polymers, the yields of toxic products and smoke are low. Also, any products formed are carried into the upper layer under the ceiling and above heat height for the occupants. If the fuels are flame-retarded then the combustion efficiency is reduced, so that higher yields of toxic products are formed, but the rate of initial fire growth, and therefore the rate of upper layer filling and descent, tends to be slower, allowing more time for escape before exposure.

As the fire grows the fuel mass loss rate increases. If fire is in the open, or in a large, high, well-ventilated enclosure such as an atrium, then combustion remains efficient for non-flame retarded fuels and a large, fuel-controlled fire results. If the fire occurs in a single-storey enclosure with a relatively low ceiling, then as the fire grows the upper layer fills down, so that the flames enter the somewhat oxygen-depleted upper layer. The fuel-air equivalence ratio increases and the combustion efficiency decreases so that high yields of smoke and toxic substances are produced by all fuels (as measured in compartment fire and bench-scale experiments involving a wide range of fuels) [138, 145, 146]. This stage therefore represents a transition to pre-flashover ventilation-controlled combustion conditions. This stage is much more hazardous to occupants both within and beyond the fire enclosure because the fire is larger, so that the mass loss rate is greater than during the early, well-ventilated, stage, the yields of toxic species are much greater and the upper layer descends below head height so that room occupants are likely to be exposed. The effects of combustion conditions on toxic product yields is reviewed in Purser et al [140, 141].

Under vitiated flaming combustion conditions and the severe conditions found in high-temperature postflashover fires [16, 138, 140, 141, 147] (upper-layer temperature exceeding

800 °C) where oxygen concentrations are low, there is a major change in decomposition in that the main pyrolysis products break down into low molecular weight fragments and can contain high concentrations of asphyxiant substances such as CO and HCN, with low CO_2 to CO ratios (see Table 63.3).

Conditions in the enclosure of fire origin become fatal to exposed victims from the effects of heat and toxic products before the onset of flashover. For victims beyond the enclosure of origin the toxic effluents from ventilation-controlled pre- and post-flashover fires can spread throughout buildings producing lethal conditions beyond the enclosure of origin. As effluents spread within buildings the temperature decreases as they mix with air beyond the enclosure of origin and as heat is lost to the structure. Toxic effluents are also subject to dilution, but no depletion due to losses for CO and HCN. For smoke particulates and acid gases, some losses to the walls can occur over period of 10s of minutes under static conditions, but are generally minor in fresh effluent plumes from large fires as they flow through buildings.

Victims in the enclosure of origin are therefore likely to be confronted simultaneously by high temperatures and heat radiation, smoke, and high concentrations of CO, HCN, irritants and CO_2 accompanied by low O_2, any one of which could incapacitate and prevent escape. Victims in remote locations are likely to be overcome by toxic smoke rather than by heat.

The inability of victims to escape from such fires seems to depend on a number of factors. Casualties include a higher proportion of young children and the elderly than does the general population. (In 1978, fatalities in bedding fires for those over 65 were seven times those expected from the distribution in the 1978 population [7, 64].) People who are incapacitated by a previous period of smoldering or by some other infirmity (such as a physical disability or alcohol or drug intoxication) are obviously more at risk [64]). However, there seem to be two other factors of importance: (1) the behavior of the victim and (2) the exponential rate of fire development.

In many cases, the victim has a short period in which to carry out the correct actions enabling escape, after which he or she is rapidly trapped. Some victims may be asleep during this critical escape "window," but there are also reports of situations where the victim was aware of the fire from time of ignition but remained in an attempt to extinguish the fire or for some other reason failed to leave before the phase of very rapid fire growth when heat and asphyxiant gases rapidly reach life-threatening levels as combustion becomes inefficient. Another, perhaps surprising, finding is that victims often appear to be unaware of the fire and are discovered in a burned-out chair or bed where they have remained. The insidious nature of CO intoxication has been described; it also seems that irritant smoke products often fail to wake sleeping victims, although a sudden noise such as of breaking glass may do so. It may seem odd that acrid fumes may fail to alert sleeping victims, but a possible explanation may lie in the adaptation to sensory irritation during continuous exposure reported for the experiments with CS gas [36]. In smoldering fires, the concentration buildup of irritants is slow, allowing time for adaptation to occur. There may be no subsequent response to a high concentration that, if presented suddenly (as, for example, with smelling salts), would rouse the subject. Other victims appear to have roused themselves at some stage of the fire but have been overcome, again probably by CO or HCN, before they are able to escape and are found behind a door. There are also cases reported by survivors where a victim has attempted to extinguish a rapidly growing flaming fire but failed to leave in time and is discovered near the fire having been overcome by fumes [139]. Unfortunately, reports of such effects on victims are largely anecdotal, and systematic studies of fire victim experience are few. The apparent anomaly of why so many casualties occur in the room of fire origin when theoretically there should be time to escape would seem to be a particular area that needs further investigation. The following pilot study has, therefore, been made of this problem.

Pilot Study of Room-of-Origin Deaths

As stated, the results of large-scale fire tests suggest that even in a worst-case situation there should be a period of at least 3 min before conditions in a rapidly growing flaming fire become untenable, and in many cases fire growth will take considerably longer. From a knowledge of the toxicity of fire products, it would, therefore, seem that a normal, healthy, waking individual should be able to escape from such situations without much difficulty, while a sleeping or otherwise incapacitated victim may be overcome by a smoldering or slowly growing fire, as well as by a rapidly growing fire. To test this hypothesis, an examination was made of the 1981 U.K. statistics, specifically for textile fires in dwellings for casualties in the 19–49 year age group, a group most likely to be active and able-bodied. The data are summarized in Table 63.25 for fires estimated to have been discovered within 5 min of ignition (most likely to have been rapidly growing flaming fires) and for fires where the time to discovery is estimated to have been 30 min or more (most likely to have involved a period of prolonged smoldering before severe flaming).

The data show that there were 23,082 fires in the first category, but only four fatalities, while for the second category there were fewer fires (5870) but 20 fatalities, a ratio per fire of 1:20. Obviously, a number of interpretations could be put on these data, but it does seem that people in this active age group are often able to escape from rapidly growing fires in domestic-sized compartments. Fatalities are much more likely in fires that have undergone a period of prolonged smoldering, when victims may have been overcome by prolonged, low-level exposure to asphyxiant fumes. If this is the case, perhaps there should be more concern about the ability of materials to continue smoldering, with toxic gas buildup over a long period of time then often followed by transition to flaming, at least in the context of this class of fire.

Table 63.25 Fatal casualties in room of fire origin (textile fires in dwellings for 1981 [7], age group 19–49 years)

Time to discovery (min)	Number of fires	Number of fatalities
<5	23,082	4
>30	5870	20
		Ratio 1:20

Small Restricted-Ventilation Fires in Closed Compartments

Closed-room fires are hazardous situations, wherein a smoldering, or especially a flaming, fire quickly uses up the available oxygen, and as the oxygen concentration falls after a minute or so of burning the combustion becomes inefficient, producing a dense smoke rich in carbon monoxide and other toxic products. These, together with the lowered oxygen concentration in a room, can produce a rapidly lethal atmosphere. An example is a fire case involving an adult and a 4-year-old child. Both were in a small bedroom for a short time during which the adult went to sleep and the child is thought to have ignited a small piece of foam using a cigarette lighter. The fire was discovered after a few minutes, when the door was opened by a family member, who extinguished the very small fire with a bucket of water. Both the adult and child were dead, with blood carboxyhemoglobin concentrations of about half a lethal level. Based on the dimensions of the room, it is calculated that the decomposition of approximately 0.5 kg of material would be sufficient to lower the oxygen concentration to 10 % and give carbon monoxide concentrations of approximately 1 % or more, which together with other toxic products would cause incapacitation and death within a few minutes. With such small fires it would seem that early detection and warning, coupled with materials giving a slow fire growth, would greatly increase the probability of escape and survival.

During the period when most occupants are at risk, the majority of fires in small, enclosed, buildings (such as houses, flats, hotels, boarding houses, cellular offices, and small shops) are likely to be restricted ventilation (vitiated) pre-flashover fires. However, if external

windows or doors are open or (as often happens) are opened at a later stage of the event, then flashover may occur. The characteristics of restricted ventilation fires are that there are three main regions at which combustion reactions occur. One is at the interface between the solid (or liquid) fuel and the base of the flame, where fuel materials are decomposed and partially oxidized by heat to form the gaseous fuel for the fire. The second is in the lower part of the flame zone, where air and fuel gases combine to produce heat and primary products. The third is in the vitiated hot zone in the upper part of the flame and beyond where hot, partially combusted fuel gases react in a restricted oxygen atmosphere to produce high yields of irritant and asphyxiant smoke products. These conditions occur when the upper layer has filled down to a low level above the fire in the fire enclosure and where partially combusted fire effluent may be recycled into the fire from outside the fire enclosure. Such fires are usually relatively small, often being limited to the item first ignited, sometimes involving some decomposition (nonflaming or vitiated flaming) of combustible materials at high levels in the room (such as paint, coving, or objects placed on cupboards or the upper levels of bookcases or racks).

The main hazards from such fires during the critical stages are likely to be from irritant smoke and asphyxiant gases. Inefficient combustion leads to high yields of these toxic smoke products. Apart from the immediate vicinity of the fire, the temperatures in the fire enclosure and beyond are not particularly high, so that heat is usually not the primary hazard.

These descriptions of fire scenarios illustrate that fire hazards, particularly the toxic hazards, vary considerably depending on the combustion conditions. In buildings, the majority of fires hazardous to occupants are likely to involve vitiated flaming combustion conditions to some extent, either pre- or postflashover depending on the scenario. This is likely to be especially true of fires in domestic dwellings, which account for the vast majority of injuries and deaths. Most fire deaths in the United Kingdom (61 % in 1992) [7] result from small fires when the victim is in the room of fire origin. In order to study the development of hazardous conditions in typical domestic fires and to develop a series of realistic design fires for smaller enclosures with restricted ventilation, a series of 23 fires were been carried out at the Fire Research Station over a number of years. These fires were carried out in three experimental rigs (Fig. 63.34), consisting of a room–corridor rig, a room–corridor–room rig, and a typical domestic two-story house. The first rig simulates conditions for a fire in a small enclosure connected via a corridor to a source of ventilation, such as an open door or window, or a much large interior space. The second rig simulates conditions in a small single-story apartment, whereas the third simulates conditions for house fires. For all these experiments the fire was in one room and the developing fire conditions were measured in the fire room and other locations throughout the experimental rigs. The majority of fires involved single items of upholstered furniture (armchairs).

In order to give an example of the developing conditions in a typical fire in a domestic house and the likely hazards faced by occupants, one of these experiments is described. This experiment involved a common situation in which a fire was started in the seat of an armchair. The armchair was typical of modern furniture, upholstered with combustion modified foam and fire retardant back coated acrylic covers. A flaming ignition source was used, consisting of a No. 7 wood crib, which is approximately equivalent to two-three sheets of newspaper. The armchair was placed in the downstairs lounge with the door to the hallway open. Upstairs, the front bedroom door was open and the back bedroom door shut. The kitchen and bathroom doors were also shut. Figures 63.35 and 63.36 show the developing conditions in the lounge and bedroom, with estimates of the developing hazards faced by occupants of the lounge and open bedroom. For each of Figs. 63.35 and 63.36 the upper graphs show the gas and smoke concentrations, whereas the lower graphs show the hazard development at head height for a standing occupant. The hazard development is expressed in terms of the FEC (smoke), FIC

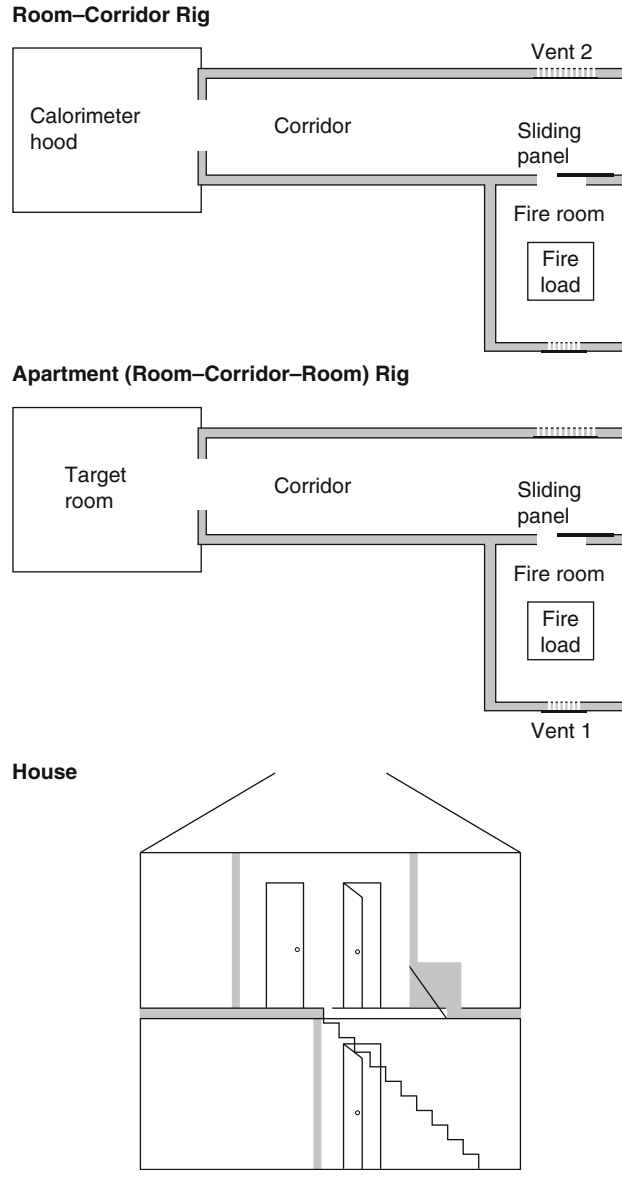

Fig. 63.34 Full-scale fire test rigs [138]

(fractional irritant concentration), or FED (fractional effective dose) for each hazard parameter. This means that for each parameter a tenability limit is reached when the line crosses 1 on the *y*-axis. The graphs for the fire gases show that in the lounge the fire grows slowly at first producing some smoke but then grows more rapidly after about 4 min. From about 5 min the oxygen concentration in the fire room starts to decrease so that at around 9 min the fire self-extinguishes. The peak temperature at the ceiling in the hottest region above the fire was 350 °C. The peak carbon monoxide concentration was 1.1 % and the peak hydrogen cyanide concentration was 1100 ppm. The ionization smoke detector in the lounge was triggered at 0.5 min and the optical detector at 1.5 min. The first hazard confronting an occupant of the lounge would be smoke, and from the smoke analysis it is considered that the smoke would be irritant. The line for irritant smoke crosses the tenability limit at around 1.5 min in the lounge. From this point, a room

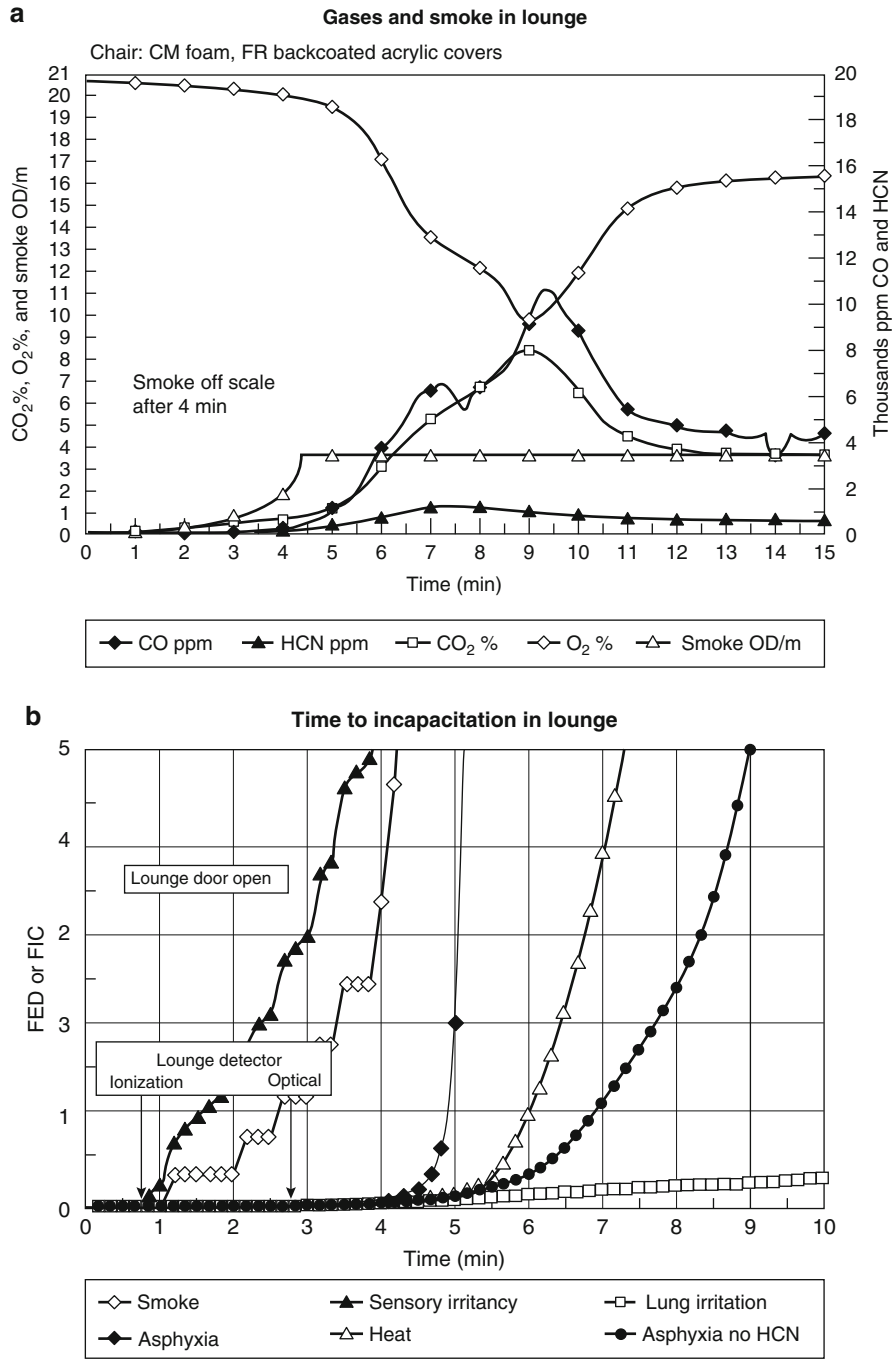

Fig. 63.35 Gases, smoke, and hazard analysis in lounge for armchair fire in house [18]

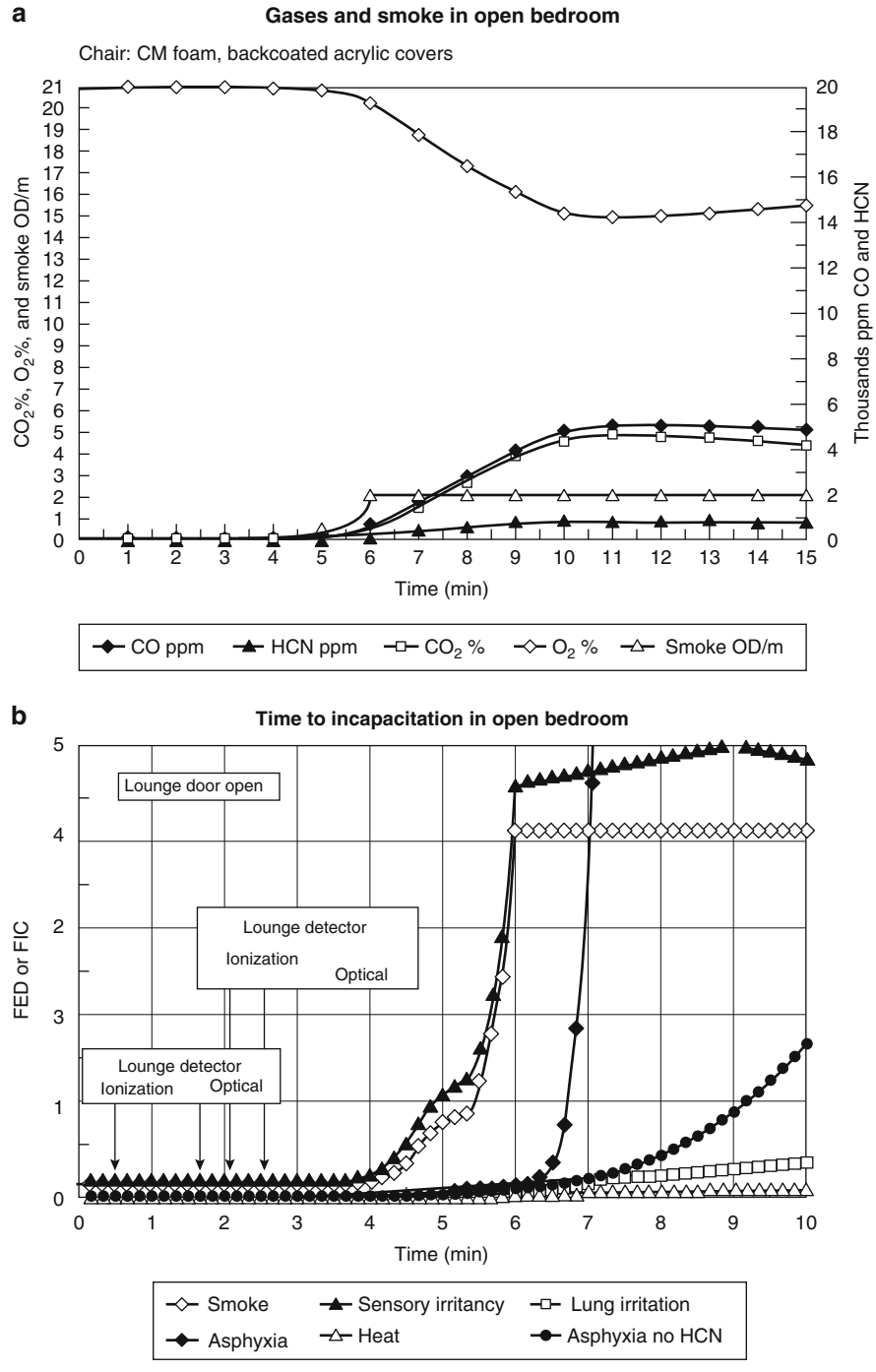

Fig. 63.36 Gases, heat, and hazard analysis in open bedroom for armchair fire in house [18]

occupant would experience difficulties in seeing, due to painful eye irritation and the presence of smoke, and breathing difficulties. It is likely that these effects would hamper, but probably not prevent, room occupants from finding their way out of the room to the front door. One minute later, the purely visual obscuration effects of the smoke (i.e., assuming the smoke was nonirritant) reach the tenability limit of 2 m visibility. If occupants were still in the room at 5 min, it is predicted that they would collapse unconscious due to the effects of asphyxiant gases. This collapse is largely due to the presence of hydrogen cyanide. If there was no cyanide present, it is predicted that collapse would not occur for a further 2 min (at 7 min). At 8 min it is predicted that an occupant would be overcome by heat, suffering burns to unprotected skin.

Figure 63.36 shows the conditions in the open upstairs bedroom. The smoke and gases start to increase significantly from around 4 min, but there was sufficient smoke on the upstairs landing to trigger the ionization smoke detector at around 2 min and the optical detector at around 2.5 min. The gas and smoke concentrations increase more gradually than in the lounge, since they are well mixed by the time they reach the bedroom. From around 11 min the smoke and gas concentrations are similar throughout the house. The temperature in the bedroom peaked at around 60 °C after 9 min. The hazard analysis shows that irritant smoke is predicted to be a problem from around 4.5 min. After this time bedroom occupants might experience some difficulties in finding their way out of the room and down the stairs. They would also have to decide whether it would be better to close the bedroom door and stay in the room until the fire brigade arrived or to attempt to escape via the door or window. Analysis of the conditions in the closed bedroom showed protection for some 20 min or so if the door was closed throughout. If open bedroom occupants were still in the room after approximately 5.5 min, it is predicted that they would collapse unconscious from the effects of asphyxiant gases. As with the lounge, this is predominantly due to the effects of hydrogen cyanide, conditions remaining tenable for around 9.5 min if this gas is absent. The temperature in the bedroom is insufficient to cause incapacitation.

This example shows how typical flaming furniture fires are likely to develop and threaten the occupants of a domestic house. The main hazards, in order, are first irritant smoke and second asphyxiant gases, particularly hydrogen cyanide and carbon monoxide. The fires are often small, being limited to the item first ignited, and self-extinguish when the oxygen concentration decreases. In practice, many domestic fires begin by a variable period of nonflaming/smoldering before flaming ignition occurs. This may last for several hours. Depending on the nature of the smoldering materials, a hazard may develop, primarily from carbon monoxide. The house fills with a slowly thickening and irritant smoke, which may trigger detectors before the situation becomes dangerous. Another possibility is that the fire will grow rapidly, possibly to flashover. This is particularly likely if external doors or windows are open (or if windows break and fall out). Such large fires commonly develop when occupants are roused during the early stages and open external doors or windows during the fire to affect escape or rescue. The conditions rapidly become fatal, due to the large amounts of heat and toxic smoke produced, and there is often considerable damage resulting from fire spread throughout the building. All data from the 23 fire tests have been placed on a CD-ROM database. Further details of the fire loads and results of tests are given in Purser et al [148]. Table 63.26 shows examples of four fires in terms of times to alarm and different tenability limits.

Figures 63.37 and 63.38 illustrate the times between ignition, detection, and the various tenability criteria in the lounge and bedroom for these and other fires [138, 148].

For all fires except Experiment CDT 16, the fire room door was open to the remainder of the apartment or house. Figure 63.37 shows similar results in the apartment rig to those in the two-story house for the same type of chair (Experiments CDT 11, 21, and 23), but when fire-retarded covers were used, the tenability

Table 63.26 Apartment and house fires: times to alarm and tenability limits

Parameter	Times (min:s) to effect							
	CDT11 CM						CDT23 CM	
	Non-FR		CDT16 CM		CDT17 CM FR		Non-FR acrylic	
Test	Acrylic		FR cotton		Cotton		Fully furnished	
Conditions:								
Building/fire	Apartment		2-story house, door shut		2-story house, door 750 mm		2-story house, door 750 mm	
Room door	Door 630 mm							
Alarm lounge								
Ion Optical			1:00	3:00	1:00	3:00	0:50	1:25
Alarm landing								
Ion optical	1:50	1:55	4:30	4:35	2:50	3:35	1:20	1:30
Smoke								
Lounge Bedroom	2:50	3:20	2:35	7:10	3:35	5:50	2:20	3:50
Irritants								
Lounge Bedroom	2:50	3:20	2:35	7:10	3:30	5:50	2:10	3:35
Asphyxia + HCN								
Lounge Bedroom	3:00	4:20	4:40	6:50	4:35	6:50	2:25	3:55
Asphyxia − HCN								
Lounge Bedroom	4:30	5:30	6:00	>10	6:50	8:00	2:35	4:45
Heat								
Lounge Bedroom	3:40	>10	5:30	>10	5:50	>10	3:30	>10
Time available lounge								
Smoke: ion optical	1:00	0:55	−1:55	−2:00	0:40	0:00	1:00	0:50
Asphyxia: ion optical	1:10	1:05	0:10	0:05	1:45	1:00	1:05	0:55
Time available bedroom								
Smoke: ion optical	1:30	1:25	2:40	2:05	3:00	2:15	2:30	2:20
Asphyxia: ion optical	2:30	2:25	>5:30	>5:25	4:00	3:25	2:35	2:25

times for asphyxia are increased by approximately 1.5 min (Experiments CDT 17 and 18). The importance of HCN as a primary cause of incapacitation in these fires is shown by comparing the asphyxia with HCN bar with asphyxia without HCN bar. If no HCN were present, the time to asphyxia is increased by up to 2.5 min. For flaming fires in the fire room, ionization detectors triggered 1–2 min earlier than optical detectors, although optical detectors would be expected to trigger earlier if the fires had been initiated by a nonflaming source. Times in Fig. 63.37 are for optical detectors on the upstairs landing ceiling. For this location there was only a small difference between ionization and optical triggering times as shown in Fig. 63.37. Figure 63.38 shows the situation in the open upstairs bedroom. In this situation the results are similar to those from the fire room, in that times to loss of tenability from asphyxia are several minutes longer for the chairs with fire-retarded covers.

Hazardous situations in fires develop as a result of a complex interaction between the building, the burning contents, and the occupants. When evaluating materials, it is important to consider not just the toxic potency of the combustion products but also the overall fire risk and burning behavior of the item. Although some modern materials and flame-retardant systems may present possible toxic potency and environmental problems, they give rise to considerable overall benefits if they reduce the number of fires occurring. It is also obvious that slow fire development, buying time for occupants to escape, is beneficial, particularly when linked with efficient detection and warning systems. It is likely that a combination of these factors has led to recent reductions in fire deaths

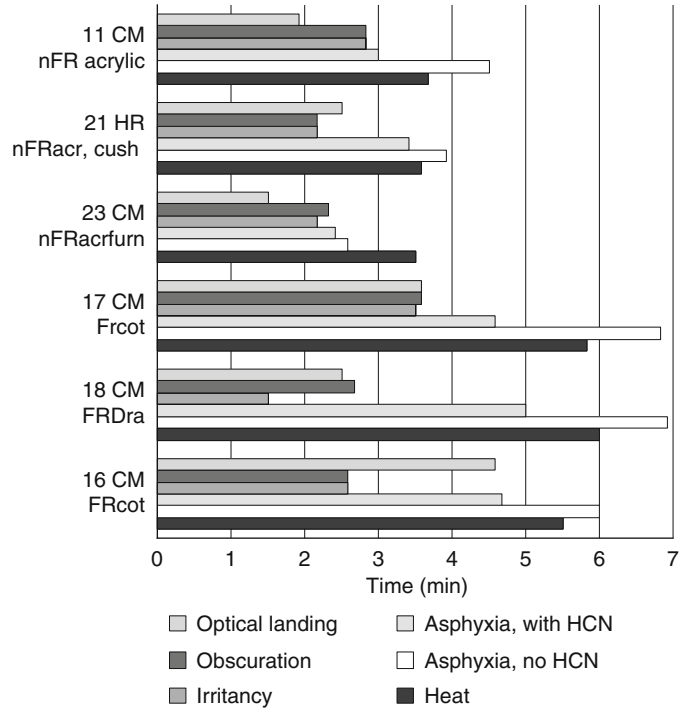

Fig. 63.37 Time to detection and effect for armchair fire in the lounge (fire room). Key: 11 CM nFR acrylic (armchair, non-fire-retarded acrylic covers, combustion modified foam—apartment rig), 21 h nFRacr, cush (nonFR acrylic covers, combustion modified foam, foam scatter cushions—house), 23 CM nFRacrfurn (nonFR acrylic covers, combustion modified foam, fully furnished room—house), 17 CM FRcot (FR back-coated cotton covers, combustion modified foam—house), 18 CM FRDra (FR back-coated acrylic covers, combustion modified foam—house), 16 CM FRcot (same as for 17, but fire room door closed)

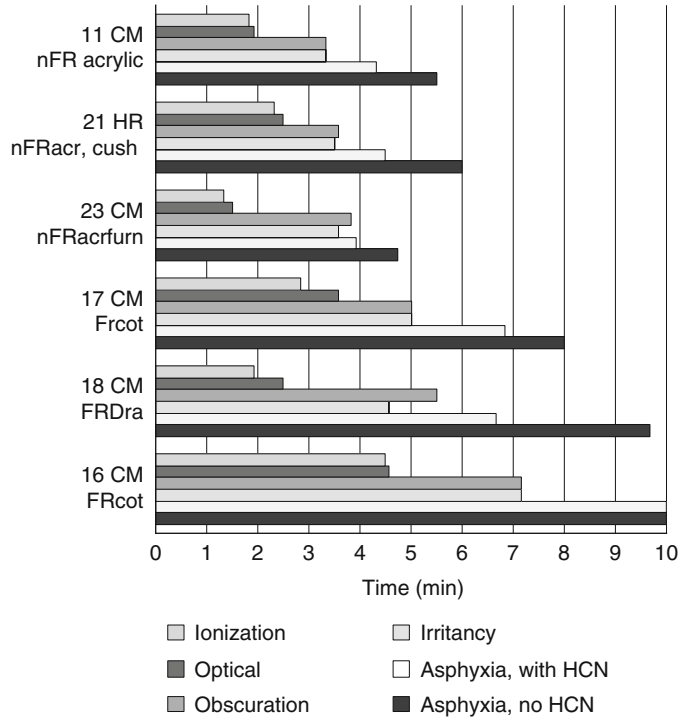

Fig. 63.38 Time to detection and effect for armchair fire in the bedroom (fire in the lounge). Key as for Fig. 63.37

compared with the early 1980s. Although the majority of fires and toxic effluent derive mainly from building contents rather than the structure, it is evident that the building and its systems are very important factors in the development of the fire and its hazards. In the domestic context, the type, maintenance, and placement of smoke alarm systems are likely to be important in the provision of early warnings to occupants. The simple expedient of closing doors and windows on unoccupied rooms is also likely to considerably reduce fire hazards while providing a tenable escape route. The use of sprinklers and smoke venting systems are other important strategies, particularly in nondomestic buildings.

These restricted-ventilation fires in enclosed compartments (compartments varying in size from a single closed room to the entire internal volume of an enclosed apartment or store unit) tend to remain relatively small as long as the boundaries remain enclosed (no open doors or windows), with the fire itself generally restricted to a small area of a room. However, as described in the examples presented, the vitiated fire effluent, which contains high concentrations of toxic products, rapidly contaminates all contiguous open areas remote from the source with a lethal atmosphere, resulting in many casualties occurring in remote locations. An even greater degree of contamination occurs when there is more ventilation so that fires can become fully developed.

Fully Developed Fires

The third scenario involves large, fully developed fires where casualties occur remote from the source of the fire. This type of fire has progressed beyond the stage of local growth and has spread from the material first ignited to others. The fire may still be largely confined to the compartment or area of origin, but large amounts of toxic smoke are formed, which spread throughout buildings, giving rise to lethal atmospheres remote from the actual fire, and often penetrating beyond compartment boundaries. Apart from being a common occurrence in domestic dwellings, such situations often occur in public buildings where there may be major loss of life in a single incident. Materials in such fires are subjected to substantial external heat flux and in some cases to oxygen deficient environments. Under the severe conditions found in such high-temperature, post-flashover fires with low oxygen concentrations, the basic pyrolysis products break down into low molecular weight fragments and can contain high concentrations of asphyxiant substances such as CO and HCN, with CO_2 to CO ratios of less than 10 [63].

Under such conditions, a building can fill rapidly with a lethal smoke capable of causing incapacitation and death within minutes. Fires where the victim is remote from the compartment of origin are responsible for the highest incidence of nonfatal casualties (48 %) and a large proportion of deaths (37 %) in the United Kingdom [7]. Many such fires are likely to be non-flashover fires, but a proportion involve fires progressing to flashover. The victim is still five times more likely to be killed by smoke than by burns and is often unaware of the fire during the crucial early phase, so that the gases may not penetrate to the victim until the fire has reached its rapid growth phase and the victim is already trapped. The major causes of incapacitation and death in this type of fire are almost certainly asphyxiant gases, particularly CO and HCN, which can build rapidly to high concentrations (although the role of irritants in causing incapacitation and impeding escape attempts may be crucial to victim survival).

An example of such a fire is provided by some studies of the effects of the penetration of a large external fuel fire into the cabin of an airplane, as happened in the Manchester Airtours fire [149]. Table 63.27 shows the results obtained inside the cabin of a Boeing 707 containing a few rows of seats opposite an open doorway, outside which was 50 gal of burning aviation fuel [143, 150]. The rapid involvement of the cabin contents gave rise to a dense smoke containing large amounts of carbon monoxide and hydrogen cyanide at a measurement point halfway down the fuselage. Incapacitation is predicted just after 2 min followed rapidly by

Table 63.27 Average concentrations of toxic and physical hazards and fractional incapacitating doses over 30-s periods during aircraft cabin fire

Fractional effective doses of asphyxiant gases							
Time (min)	0.5	1.0	1.5	2.0	2.5	3.0	3.5
Gas concentrations							
CO ppm	8	34	282	1157	3326	8410	19,490
HCN ppm	0	10	38	143	340	740	1380
CO_2%	0.0	0.0	0.4	1.2	2.8	4.1	6.0
O_2%	21	21	21	20	18	16	13
Fractional incapacitating doses							
FED_{CO}	0.00	0.00	0.00	0.02	0.06	0.16	0.38
FED_{HCN}	0.00	0.00	0.01	0.06	5.65	>10	>10
VCO_2	1.00	1.00	1.12	1.31	1.77	2.27	3.26
FED_O	0.00	0.00	0.00	0.00	0.00	0.00	0.01
FED/30s	0.00	0.00	0.00	0.10	10.10	>10	>10
Σ FED	0.00	0.00	0.00	0.11	11.10	>10	>10
Fractional effective doses of convected heat							
Temp °C	12	14	28	81	156	274	408
FED/30s	0.00	0.00	0.01	0.03	0.20	4.96	>10
Σ FED	0.00	0.00	0.01	0.04	0.24	5.20	>10
Radiant heat flux							
W/cm^2	0.10	0.12	0.14	0.18	0.23	0.28	0.57

Time to exceed smoke tenability limit: 1 min 40 s
Time to incapacitation by asphyxiant gases: 2 min 15 s
Time to incapacitation by convected heat: 2 min 45 s
Time to tenability limit for radiant heat: 2 min 45 s
Effects of irritants
Over period between 1 and 4 min: average respirable particulates 6.7 mg/L
Average total particulates 11.6 mg/L
Average HCl concentration 1027 ppm
Average HBr concentration 1228 ppm
It is considered that the oily, be highly irritant and extremely painful to eyes and breathing, causing incapacitation and impairing escape attempts. It is considered likely that these irritants reached high concentrations (approaching 1000 ppm total acid gases) early in the fire at approximately 1–1.5 min, from which time escape capability would be significantly impaired. It is likely that sufficient irritants would be inhaled up to 4 min to cause life-threatening postexposure lung damage

death, mainly from the effects of hydrogen cyanide (high concentrations of which were found in the blood of the Manchester victims). For this experiment there were two large vents, the doorway next to the external fuel fire near the rear of the cabin and a door at the front of the cabin. This flow-through ventilation coupled with the small cross-section area of the fuselage resulted in rapid fire growth once the seats were ignited.

Although in many large fires the original fuel and the major source of heat and toxic products may be the contents, a significant contribution may be made by construction products. Of great importance in some cases are surface coverings or components with a large surface area, such as doors or partitions. Surface coverings may contribute to flashover spread (as in the Dublin Stardust disco fire and the Station Nightclub fire) and may release a bolus of toxic products very quickly, which may have a serious incapacitating effect on victims. An example would be vinyl wall coverings or the vinyl laminates used in aircraft cabins. PVC releases all its hydrogen chloride at a low temperature (approximately

250–300 °C), so that, as a fire develops and the hot layer reaches this temperature, HCl may be suddenly released. In another aircraft fire test conducted by the FAA, high concentrations of HCl and HF occurred in the cabin atmosphere before other gases reached toxic levels [147]. Another problem with surface materials treated with halogenated flame-retardants is that if the fire reaches a sufficient size to cause the retardants to off-gas, the remaining fuel residue is may no longer be protected an so become vulnerable to a sudden flashover.

In general, although in some cases fire and heat may eventually kill victims, this is usually preceded by dense, highly toxic smoke that can spread rapidly throughout a space or a building, which is usually responsible for the initial incapacitation of occupants, as well as being the cause of many deaths.

A common feature in many major fire disasters is a failure in early detection and effective warnings. In many cases the fire was detected at an early stage, and some attempts were made to deal with the fire, but often there was a failure to instruct people to leave while the fire was small and a failure to realize that a small fire grows with exponential speed into a life-threatening one. For example, in Summerland [151] the initial fire was considered non-threatening, and occupants were encouraged to remain seated rather than to leave. At the Manchester Woolworth's fire [152] people continued to eat in the restaurant area while the fire was growing on the other side of the sales floor. At the Bradford stadium fire people watched the early fire development at the end of the stand and did not begin to move until a late stage. At the Dupont Plaza hotel, the fire began in an unoccupied furniture storage area but was discovered and fought at an early stage; however, mass evacuation of the hotel did not occur until after the fire went to flashover and started to spread. At the Beverly Hills Supper Club fire [151], 20 min elapsed between discovery and evacuation instructions. At a number of major incidents in transport situations (road and rail tunnels or stations) the fires were discovered at an early stage, but considerable times elapsed as information passed up management chains before evacuation warnings and other emergency actions were taken. Examples include the Kings Cross fire subway station fire [151] in which the escalator fire was burning for some time before attempts were made to close the station, the Daegu subway train fire, the Mont Blanc road tunnel fire and the Dusseldof airport fire [24, 153]. At the Dublin Stardust disco, the fire grew unnoticed behind a partition. It could be said that when people are able to perceive a fire as a possible threat to their life, it may already be too late to escape. In the majority of these cases, evacuation occurred at a late stage and there were failures in the provision of accurate, authoritative, and informative evacuation instructions.

General Comment

The severe asphyxiant incapacitation and subsequent death of many fire victims are almost certainly due to the common asphyxiant gases. However, the effect of irritants in impeding escape is an important consideration, and it is not obvious from asphyxiant gas profiles why so many fatalities occur in the room of fire origin. Useful information may be obtainable from survivors who have experienced exposure to dense, irritant smokes and from case studies of room of origin fires.

Possible Routes to Mitigation of Toxic Hazard

For smoldering fires it would be advantageous if materials were designed to self-extinguish, and if the formation of products other than CO during decomposition (such as oxidized hydrocarbon fragments or CO_2) could be encouraged. Early audible warning by smoke alarms may be particularly advantageous, as sound often appears to alert victims where the presence of irritant smoke or heat fails.

For early flaming fires where the victim is in the room of origin, any measure that limits the rate of growth once ignition has occurred will give a victim more time to extinguish a small fire or escape from a growing one.

For fully developed fires where the victim is remote from the point of origin, the most important mitigating factors are early warning and containment of the fire and gases within the original fire compartment.

The development of hazardous situations in a fire involves a whole range of factors, including fire development from ignition to the post-flashover spread of fire and smoke, toxicity, and the interaction of the fire with the structure and with passive and active fire protection, as well as escape-related factors, including detection, warnings, the provision of escape routes, wayfinding, physiological and behavioral impairment, and escape movements or rescue. In designing a system to be safe in fire, all these factors should be considered, and the ultimate evaluation of safety depends on whether it is possible to ensure, by performing a life threat hazard and risk assessment, that the occupants can reasonably be expected to have escaped before they are exposed to levels of heat and smoke that may endanger health and threaten life.

The Use of Fractional Effective Dose Methodology in Fire Investigation

The (FED) methods described for calculating exposure doses and times to incapacitation and death from fire data have proved to be a useful tool for investigating fire incidents in which occupants have been injured or died. It has been applied usefully to investigations of several major incidents including the Dupont Plaza fire, the Mont Blanc Tunnel fire [24] and the Rosepark Care home fire [25]. Where data have been obtained on the fire conditions (time-concentration curves for toxic products and heat in these fires), either from full-scale fire reconstruction experiments of from fire modeling computations, it is possible to calculate the predicted effects on occupants and their timing. Beyond this, when forensic data are available from the victims (primarily blood carboxyhemoglobin and cyanide concentrations, extent of smoke deposition in the lungs and extent of burns), it has been possible to use FED calculations to partially validate the fire test or fire modeling calculations.

A difficulty with incident re-creation tests and fire models is that, due to the variability of fires, it can be difficult to establish exactly how close results are to the conditions in the actual incident. From the time-concentration curves of CO in a fire, it is possible to calculate the uptake by exposed subjects and hence the %COHb in the blood at the time of death or rescue (if these times are known). For subjects dying in the fire, the calculated %COHb level can be compared directly with the actual levels measured at post-mortem. For fire survivors, if the post-fire treatment (in terms of air exposure or oxygen therapy) is known and the time at which a blood sample was taken in hospital is known, then it is possible to back-calculate from the CO wash-out curve to find the %COHb at the time of rescue, which can be compared with the forward-calculated value. If there is reasonably good agreement between the forward and back-calculated values, then this provides a good indication that the combustion conditions and history of the test or modeled fire were close to those occurring during the actual incident. The same considerations apply to the blood cyanide concentrations, burns and smoke deposition. In practice, the FED and forensic approaches tend to be complementary with the fire testing and modeling approaches, in that while some uncertainties often apply to both methods, when used together the level of confidence in the findings can be considerably enhanced.

One example of the use of these methods was for the Mont Blanc Tunnel fire inquiry [24]. During this fire, it was possible to establish the time at which some vehicle occupants had stopped in the tunnel, had attempted to walk back towards the French portal and the locations at which they had collapsed and died. From CFD modeling calculations of the vehicle fire, smoke data recorded in the tunnel and FED modeling, it was possible to calculate how long occupants would have been able to walk along the tunnel, how fast they would move in the smoke and when (and especially at what location) they would have been overcome by heat and toxic gases. The results of these calculations showed a good agreement between the actual time and location of collapse and the times and locations

of collapse calculated according to the CFD and FED modeling. The CFD and FED modeling was therefore validated, and the combined approach provided a good understanding of the conditions during the fire and effects on the tunnel occupants.

Another example was application to the Rosepark Nursing Home fire [25, 27]. In this incident a brief intense fire involving mixed fuels and some exploding aerosol cans occurred at night in a cupboard opening onto a corridor. Ten elderly sleeping occupants of open rooms off this corridor died at the scene, while two who had their room doors closed were rescued after approximately an hour, but were overcome by toxic smoke exposure and subsequently died in hospital. During the fire, a fire door between the main fire corridor and the next compartment was blown open by the pressure pulses as the aerosols exploded so that a considerable quantity of smoke passed through, resulting in five occupants of open or partly open rooms off this corridor being overcome so that two died after rescue. A full-scale reconstruction of the affected part of this building and the fire incident was carried out by BRE on behalf of the Scottish Office and the Procurator Fiscal. FED calculations were applied to the fire test data to calculate timing and effects on the occupants, assuming the conditions in the reconstruction were similar to those during the actual incident. Forensic data, principally the %COHb concentrations and extent of burns in the decedents and those rescued from the fire were also examined. Figure 63.39 shows the time-concentration curves of toxic gases and heat in the fire corridor. Figure 63.40 shows the FED hazard analysis for a standing corridor occupant.

The FED calculations show dense smoke from 4 min after ignition, with collapse from the effects of asphyxiant gases predicted after 5.5 min due mainly to the effects of HCN and CO, with a lethal (50 %COHb) level of CO predicted by 6.5 min. Severe pain from convected heat exposure is predicted after 6 min in the corridor. The smoke and toxic gas conditions at bed height in the open rooms were similar to those in the corridor, but temperatures at bed height were much lower. It was therefore predicted that all open room occupants would

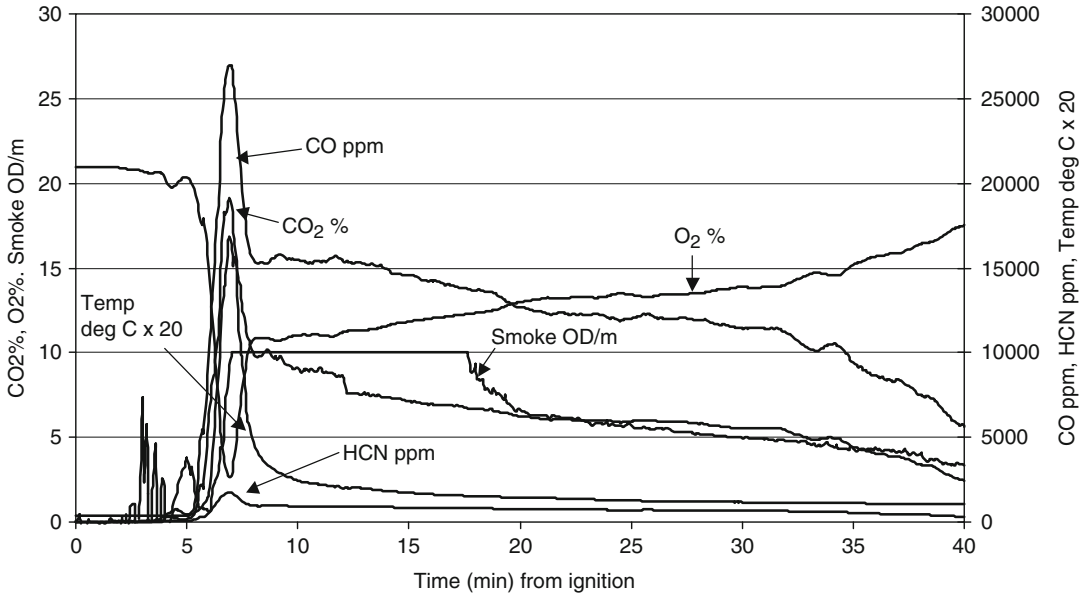

Fig. 63.39 Smoke, toxic gases and temperature profile in the fire corridor during the BRE full-scale recreation of the Rosepark nursing home fire. Conditions in the open bedrooms off this corridor were similar except that temperature at bed height was considerably lower

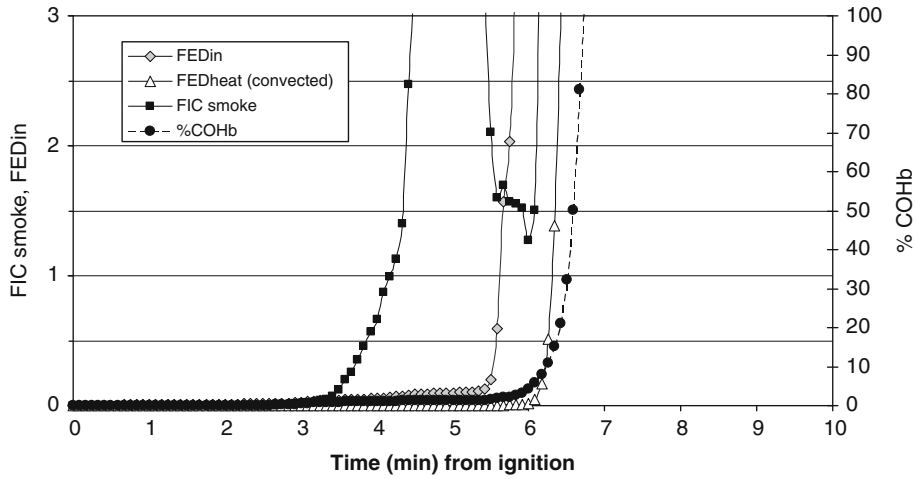

Fig. 63.40 Fractional effective dose hazard analysis for the corridor fire profile shown in Fig. 63.39

have been overcome and died within a few minutes due to the effects of asphyxiant gases, with lethal %COHb blood levels but no burns, and this was the finding from the forensic data, with all room occupants dead at the fire scene when the fire service entered the area. These findings and the pattern of fire damage were supportive that the reconstructed fire conditions were similar to those in the incident, but since the exact times of death for the room occupants were unknown, these findings could not fully validate the fire conditions. Figure 63.41 shows the conditions in one of the closed rooms off the fire corridor from which the uptake of CO (% COHb) could be calculated for the room occupant. The time of rescue for this occupant is known as well as her subsequent treatment and the %COHb concentration in her blood measured soon after her arrival at hospital. Figure 63.42 shows the FED analysis in terms of the forward-calculated %COHb from the fire data and the back-calculated %COHb from the actual blood data.

As the figures shows there are some uncertainties in these calculations. The forward calculated CO uptake depends on the bedroom CO concentration curve, but also on the activity level hence V_E of the subject. From the reported activities of this subject, her average V_E is estimated at between 6 and 8 L/min. Also, although the exact time she arrived at the hospital and the fact that she received oxygen by face-mask after rescue are known, the exact time at which her blood sample was taken was not recorded, so three estimates were made based upon the emergency room records. Despite these uncertainties, there is a good agreement between the range of forward and back-calculated values, which therefore validates the test fire conditions in terms of CO concentrations against those in the actual incident. For the occupants of rooms off the corridor beyond the fire door, a similar set of calculations showed consistently higher actual % COHb blood levels in the rescued occupants than the forward calculated values, from which it was concluded that the penetration of smoke through the fire door (and other leakage paths) in the actual incident was somewhat greater than that in the reconstruction test.

Appendix 1: Summary of Toxicity and Heat Hazard Assessment Model Calculation Equations

The main expressions for applications to the fire safety engineering design calculations are presented in this section. Wider applications and more detailed discussions of the physiology

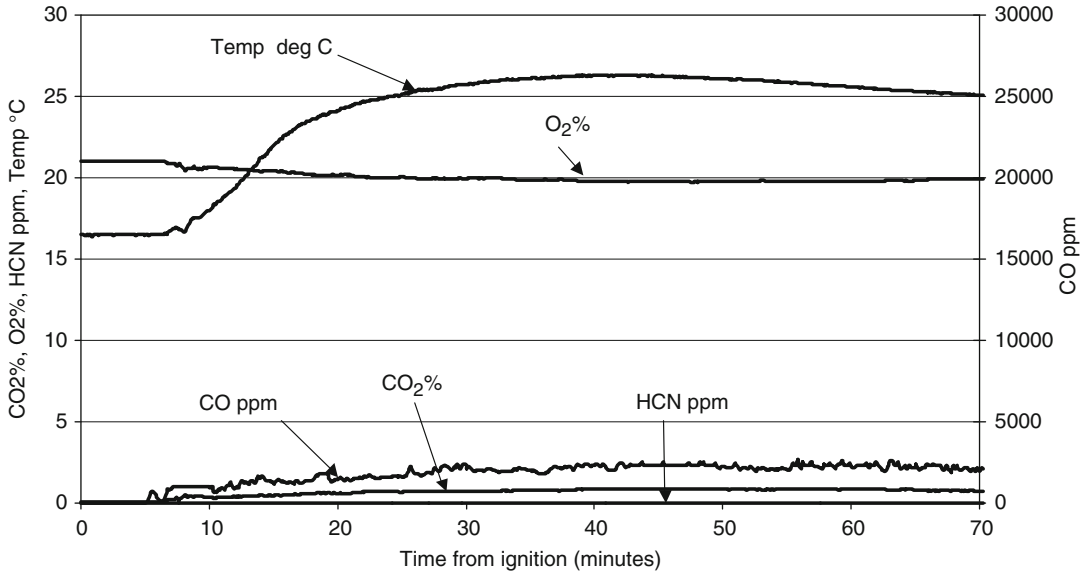

Fig. 63.41 Smoke, toxic gases and temperature profile for a closed room off the fire corridor during the BRE full-scale recreation of the Rosepark nursing home fire

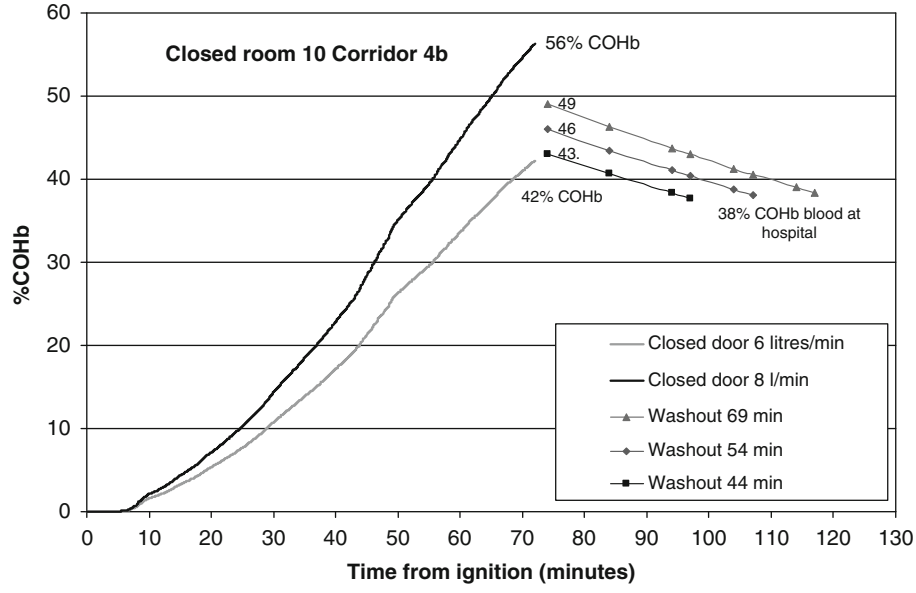

Fig. 63.42 Forward calculated %COHb level for the occupant of closed room 10 from the CO and CO_2 gas profiles in Fig. 63.41, assuming sleeping and standing V_E values of 6 and 8 L/min compared with %COHb levels back-calculated to the time of rescue after 72 minutes when oxygen was started, using three estimates of the time when the blood sample was taken after arrival at hospital

and derivation of the expressions have been presented in the relevant main sections of the chapter.

Effects of Fire Effluent and Heat

Estimates of potential hazards to enclosure occupants in terms of fire effluent or heat can be made by consideration of the following two sets of information:

1. The time-concentration (or time-intensity) profiles for the major toxic products, optically dense smoke and heat in the fire at the breathing zone of the occupants, which in turn depend on
   (a) The fire growth curve in terms of the mass loss rate of the fuel (kg/s) and the volume into which it is dispersed (kg/m^3) with time
   (b) The yields of toxic products, smoke, and heat in the fire (e.g., kg CO per kg of material burned)

   Guidance on calculation methods for these terms is given in other chapters in this handbook. Some information is provided in this chapter and Chap. 62 on toxic product yields under a range of fire conditions and also in Chap. 16 [19] and Chap. 36, [20]. A guide to the general characteristics of fires is shown in Table 63.3 and examples of fire profiles in Figs. 63.8 and 63.22.
2. The concentration/time/toxicity relationships of these products, in terms of the toxic or physiological potency of the heat and effluent (the exposure concentration, kg/m^3), or exposure dose (kg · m^{-3} · min or ppm · min) required to cause toxic effects (and the equivalent effects of heat and smoke obscuration). This term includes consideration of the following three aspects:
   (a) Exposure concentrations or doses likely to impair or reduce the efficiency of egress due to behavioral and/or physiological effects
   (b) Exposure concentrations or doses likely to produce incapacitation or prevent egress due to behavioral and/or physiological effects
   (c) Lethal exposure concentrations or doses

   Guidance on calculation methods for items (a) and (b) are presented in this section, whereas lethality is considered in the main chapter.

The fire profile should be characterized in terms of the following range of parameters, measured over successive short periods (<1 min) at the breathing zone of a potential victim:

1. Mass loss of material decomposed divided by the volume of air into which the material is dispersed in (mass loss concentration)
2. Carbon monoxide concentration
3. Hydrogen cyanide concentration (if materials containing >1 % by mass nitrogen are present)
4. Carbon dioxide concentration
5. Oxygen concentration
6. Incident radiant heat flux to subject
7. Air temperature
8. Smoke optical density (and particulate concentration)
9. Irritant acid gas concentrations (HF, HCl, HBr, SO_2, NO and NO_x)

   Note: If the total content of halogens in the fuel is less than approximately 5 % of the burning fuel mass, the total sulfur content less than 2 %, and the nitrogen content less than 5 %, the contribution to irritancy from acid gases can be considered minor as a first approximation.
10. Concentrations of organic irritant species (especially acrolein, formaldehyde, and crotonaldehyde)

    Note: In practice the relevant yield data for the key irritant organic species are seldom available, and not all the important species have been identified. In general it can be assumed that all smoke from compartment fires involving mixed fuel will contain concentrations of irritant organic species in

proportion to the smoke optical density. Overall irritancy can then be expressed in terms of smoke optical density (or particulate concentration) plus the contribution from irritant acid gases if present in significant concentrations (see 9 above).

These data may be obtained from large-scale fire tests or calculated using fire dynamics models with appropriate data on toxic product yields under a variety of fire conditions: specifically, smoldering/nonflaming, early (well-ventilated) flaming, developed small vitiated (underventilated) flaming, and fully developed/postflashover underventilated fires.

The hazard assessment is based on a "step-through" approach whereby the extent of the hazard is calculated for each successive minute (or other appropriate time interval) during the fire until the point is reached where different hazard endpoints are predicted. The behavioral and physiological effects of exposure to toxic smoke and heat in fires combine to cause varying effects on escape capability, which can lead to physical incapacitation and permanent injury or death.

For a basic fire engineering design there are two main considerations:

- The time at which the concentration of smoke reaches a level such that safe escape is compromised due to
  (a) Behavioral and physiological effects of exposure to heat and toxic smoke on escape behavior and ability
  (b) In the absence of direct exposure, behavioral effects caused by seeing fire effluents on escape behavior

  The effects of exposure to smoke result from impaired vision due to the optical opacity of smoke and from the painful effects of irritant smoke products on the eyes and respiratory tract. Occupant movement speed and wayfinding ability is impaired. Behavioral effects of seeing or being immersed in smoke result in a proportion of occupants being unwilling to approach smoke or heat-logged areas or escape routes.
- The time at which the exposure dose of asphyxiant toxic gases or heat reaches a level at which occupants are likely to become incapacitated, such that they cannot save themselves and are likely to die within a minute or so unless rescued.

In a regulatory or design evaluation context, it is possible to consider several different approaches:

1. *Simple criteria for tenability based on zero exposure*. Where a design fire calculation is based on a descending upper layer of hot smoke filling an enclosure or escape route, engineering tenability criteria are often based on a minimum clear layer height of 2.5 m above the floor and a maximum upper-layer temperature of 200 °C. Occupants are considered to be willing and able to escape in clear air under such a layer and the downward heat radiation is considered tolerable.
2. *Tenability criteria accepting some degree of smoke exposure in relation to willingness to enter or ability to move through smoke*. In situations where smoke is mixed down to near floor level, some building occupants might move through dense smoke in some situations, but in other situations people might be unwilling to enter smoke logged escape routes, turn back, or be unable to find an exit. Where heat is not an issue, the immediate effects of smoke depend on the visibility distance and the sensory irritancy of the smoke if people are exposed directly. For such situations it is necessary to set tenability criteria for design purposes, depending on the level of adverse effects on occupants considered acceptable or unacceptable.

In a number of studies of fires in buildings, a proportion of people (approximately 30 %) were found to turn back rather than continue through smoke-logged areas (see main section on effects of smoke in this chapter and Chap. 58). The average density at which people turned back was at a "visibility" distance of 3 m. This represents an optical density ($OD \cdot m^{-1}$) of 0.33, (extinction coefficient 0.76) with women more likely to turn back than men. A difficulty with this kind of statistic is that, in many fires in buildings, there is a choice between passing

through smoke to an exit or turning back to take refuge in a place of relative safety such as a closed room. In some situations, people have moved through very dense smoke when the fire was behind them, whereas in other cases people have failed to move at all.

Behavior might also depend on whether layering permits occupants to crouch down to levels where the smoke density is lower and whether low-level lighting is used to improve visibility. Based on considerations such as these in relation to parameters such as the size and complexity of the building, it is possible to set design limits for optical density of smoke (see Table 63.5).

As an approximate guide, it might be assumed that occupants will not use an escape route if the visibility in that route is less than 3 m (OD/m = 0.33, extinction coefficient 0.76). However, if they enter an escape route contaminated to this optical density and become exposed to the smoke, then their ability to progress depends on both the optical density and the irritancy of the smoke. Based on the finding that people move as if in darkness at a visibility of 5 m in irritant smoke and that smoke from most fires contains a variety of irritant chemical species, the following generic design tenability limits are proposed on the basis that concentrations exceeding these levels could impair or even prevent occupants' safe escape (for situations where the concentrations of acid gases are considered unlikely to be significant due to the fuel composition):

Small or domestic enclosures: visibility 5 m

$$(\text{OD/m} = 0.2 \text{ or } \alpha_k\ 0.5)$$

Large enclosures: visibility 10 m

$$(\text{OD/m} = 0.08 \text{ or } \alpha_k\ 0.18)$$

where OD/m is $\log_{10}(I_o/I)$, the logarithm of the ratio of the intensities of light transmitted over a path length of 1 m from a light source to a receiver in the absence and presence of smoke, respectively. The light extinction coefficient α_k is $\ln(I_o/I)$.

For situations where smoke is expressed in terms of particulate mass concentration, these equate to approximately 0.7 and 0.3 g particulates/m^3, respectively (where particulates g/m^3 ~ 0.356 × OD/m).

Where concentrations of acid gases are likely to be a significant factor, then the tenability limit for irritant smoke should be calculated according to Equation 63.11.

These effects of smoke on behavior and suggested design limit criteria are summarized in Table 63.5.

Another advantage of using these smoke concentration limits as tenability criteria is that the concentrations of asphyxiant gases present are most unlikely to exceed levels capable of causing incapacitation (loss of consciousness) in exposed occupants within 30–60 min.

These proposed design criteria are intended to represent a low probability that occupants will feel trapped and fail to escape. For a probabilistic design, incident investigation, or evacuation simulation, it may be of interest to estimate the number of individual occupants likely to remain in place. This approach considers the subsequent tenability as the fire develops, and also provides an estimate of the number of occupants likely to attempt to move through smoke, the effects of smoke on their wayfinding ability and walking speed, and their subsequent tenability. At any time during an escape simulation, the key parameters are the smoke density at head height for each occupant (who may be waking erect or stooping) as they move through the escape route and the tenability conditions in terms of toxic gases and heat exposure. For occupants walking through smoke, walking speeds show some variability between individuals, but the average speed has been shown to be approximately proportional to the smoke density down to a minimum of around 0.3 m/s for people walking in darkness. For able-bodied occupants walking through typically irritant fire smoke, a suggested expression for average unrestricted walking speed (Wsmoke [m/s]) as a function of extinction coefficient α_k is

$$\text{Wsmoke}(\text{m/s}) = -0.1364 \times \text{Ln}\,\alpha_k + 0.6423 \quad (63.10)$$

Where Wsmoke = walking speed in moderately irritant smoke

For a population of able-bodied occupants a standard deviation is 0.157 is suggested (see Fig. 63.16 in the main section on smoke).

3. *Tenability criteria accepting some degree of smoke exposure in relation to calculated time of incapacitation*. Although the foregoing smoke density limits may be used as design limits, they do not represent conditions under which escape is necessarily prevented, and do not allow for occupants remaining in place. A design calculation should therefore also evaluate predicted time to incapacitation due to the effects of heat or toxic gases. It might also be important to know the time between the visibility criteria being exceeded and that when incapacitation is predicted, especially for probabilistic design. The methods presented are designed to predict time to incapacitation (loss of consciousness) for an average person, after which a factor should be applied to allow for more susceptible members of the occupant population.

Time to loss of tenability due to smoke, irritants, asphyxiant gases, and heat in fires is calculated using fractional effective dose (FED) methodology as described in the following sections.

For the effects of the density or average irritancy of fire smoke on escape capability, the tenability limits already described are recommended, so that at any time during a fire:

$$\text{FEC}_{\text{smoke}} = (\text{OD/m})/0.2 \text{ for small enclosures or } (\text{OD/m})/0.08 \text{ for large enclosures} \quad (63.9)$$

This equation allows for the predicted irritancy of the smoke from fires involving mixed building contents.

Sensory Irritancy

Where significant concentrations of irritant acid gases are likely to be present the overall irritant concentration (FIC_{irr}) is given by Equation 63.11, on the basis of the assumption that all irritants capable of damaging lung tissue are additive in their effects,

$$\text{FIC} = \text{FIC}_{\text{HCl}} + \text{FIC}_{\text{HBr}} + \text{FIC}_{\text{HF}} + \text{FIC}_{\text{SO}_2} + \text{FIC}_{\text{NO}_2} + \text{FIC}_{\text{CH}_2\text{CHO}} + \text{FIC}_{\text{HCHO}} + \sum \text{FIC}_x \quad (63.11)$$

where $\sum \text{FIC}_x$ = FICs for any other irritants present. Each term in Equation 63.11 consists of a fraction for which the numerator is the concentration of the specific gas present at a particular time during the fire divided by the concentration of that gas predicted to cause a specified endpoint (either escape impairment or incapacitation). The proposed denominator values for each gas are given in Table 63.6 (SFPE escape impairment or SFPE incapacitation recommended)

It is predicted that each gas at the concentration in Table 63.6 is likely to be sufficiently irritating to affect escape efficiency in the majority of subjects and may cause incapacitation in susceptible individuals. A factor of 0.3 FEC for escape impairment should allow for safe escape of nearly all exposed individuals. As with the outcome for smoke, the sensory effects of irritants have been found to occur immediately on exposure at concentrations causing significant impairment [154, 155].

Lethal Effects of Inhaled Irritants

In addition to the immediate concentration-related painful effects on the eyes and respiratory tract, as occupants inhale irritant smoke an increasing dose of irritant gases and particulates is delivered into the deep lung. During exposure this is considered to impair respiratory efficiency (for example as a result of bronchoconstriction), thereby contribution somewhat to the overall asphyxiant effects of inhaled toxic gases. The inhaled irritants also cause inflammation and edema in the deep lung if a sufficient dose is inhaled. This requires a period of several hours

to develop, and can result in severe and sometimes fatal respiratory impairment over a period of approximately 2–36 h after rescue, especially in elderly or otherwise health-impaired subjects. Since lung irritation has relatively little effect on escape capability, it can be omitted from an escape calculation. For design considerations relating to occupant survival and health effects or for incident investigations, however, lung irritation can be an important consideration.

Equation 63.15 is a proposed expression for the accumulating fraction of a lethal exposure dose of lung irritants (FLD_{irr}). The fraction of a lethal dose (FLD) for each irritant is calculated as the *ct* product exposure dose during a period in the fire (e.g., in ppm · min) expressed as a fraction of the lethal exposure dose. The lethal effects of the different irritants are assumed to be additive on the same basis as the irritant effects, so that the total FLD_{irr} for each time period is given by Equation 63.15:

$$FLD_{irr} = FLD_{HCl} + FLD_{HBr} + FLD_{HF} + FLD_{SO_2} + FLD_{NO_2} + FLD_{CH_2CHO} + FLD_{HCHO} + \Sigma FLD_x \quad (63.15)$$

where ΣFLD_x = all the FLDs for any other irritants present.

The FLD_{irr} for short periods of time during the fire are summed until the FLD_{irr} reaches unity, when it is predicted that a lethal dose has been inhaled. The lethal exposure doses for each irritant gas used for the denominators of each term in Equation 63.15 are shown in Table 63.6.

Tenability Limits and Hazard Calculations for Asphyxiant Gases

The main cause of incapacitation and death during and immediately after fires is exposure to asphyxiant gases. Incapacitation results from loss of consciousness due to the combined effects of carbon monoxide, hydrogen cyanide, and carbon dioxide, with some additional effects from low-oxygen hypoxia and inhaled irritants. Loss of consciousness prevents escape and further uptake of asphyxiants while comatose is likely to result in death within a further minute or so. The most useful tenability endpoint to work to is, therefore, considered to be loss of consciousness ($FED_{IN} = 1$), with design limits set to prevent an occurrence. Since individual susceptibility varies in the population, this prediction represents the median of the distribution of exposure doses resulting in collapse. Approximately 11.3 % of the population is considered likely to be susceptible below an FED of 0.3 (see ISO 13571 [21]). For design purposes it will be necessary for the designer or regulatory authority to select an FED level suitable to protect vulnerable subpopulations in the chosen application (e.g., 0.3 or some other value depending on the application). The effects of combinations of asphyxiant gases causing incapacitation in fires are considered to be approximately additive, but the following interactions need to be considered:

- The FEDs for CO and HCN are considered directly additive as has been demonstrated experimentally.
- The effects of irritants on lung function also cause some hypoxia and so an additive term is included consisting of the FLD_{irr} .
- The main effect of carbon dioxide is to increase the breathing rate and, thus, the rate of uptake of CO and HCN. A multiplicatory term, VCO_2, is used to calculate this effect.
- Low-oxygen hypoxia will be additive with the overall effects but is not increased by VCO_2 (in fact oxygen uptake is improved).
- The direct intoxicating effects of CO_2 are considered unlikely to occur before other effects and so are normally ignored.
- The overall rate of uptake of asphyxiant gases depends upon the volume of air breathed each minute (V_E), in relation to body size, which in turn depends mainly upon the level of physical activity. For design purposes, it is assumed that the subject is an adult engaged in light work such as walking along an escape route.

On this basis a simplified version of the overall FED equation (Equation 63.38) for asphyxiants is as follows. (A more comprehensive version is presented in the main section on asphyxiant gases.)

$$\mathrm{F_{IN}} = \left(\left(\mathrm{F_{I_{CO}}} + \mathrm{F_{I_{CN}}} + F_{I_{NOx}} + FLD_{irr}\right) \times VCO_2 + F_{I_O}\right) or\ \mathrm{F_{I_{CO_2}}} \quad (63.38)$$

where

F_{IN} = Fractional effective dose for incapacitation (loss of consciousness) due to asphyxiants

$F_{I_{CO}}$ = Fractional effective dose for incapacitation by CO

$F_{I_{CN}}$ = Fractional effective dose for incapacitation by HCN

$\mathrm{FLD_{irr}}$ = Fractional lethal dose for irritants

Note: Where significant concentrations of acid gases are present this term is calculated according to Equation 63.15. Otherwise it may be expressed in terms of smoke optical density as $\mathrm{OD/m} \times \mathrm{t(min)}/90$.

VCO_2 = Multiplicatory effect of inhaled CO_2

F_{I_O} = Fractional effective dose for incapacitation by low-oxygen hypoxia

$\mathrm{F_{I_{CO_2}}}$ = Fraction of an incapacitating dose of CO_2 (but can be ignored without significant error for most cases)

A more general form of the simplified equation incorporating V_E as a user-defined variable is:

$$F_{IN} = \left(F_{ICOg} + F_{ICNg} + FLD_{irrg}\right) \times V_E \times V_{CO2} + FED_{IO} \quad (63.39)$$

Activity level of subject	V_E (L/min)
Resting or sleeping	8.5
Light work—walking to escape	25
Heavy work—slow running, walking up stairs	50

Both the total volume of air breathed each minute and the efficiency of uptake have upper limits so that a limiting value for V_E x V_{CO2} of 70 L/min is recommended.

For each of these gases it is necessary to obtain an expression for the fraction of a dose required to cause incapacitation. The derivation of these expressions is detailed in the section "Asphyxiation by Fire Gases and Prediction of Time to Incapacitation" in this chapter. Basically, the exposure dose acquired over any period of time during a fire is expressed as a fraction of the dose required to cause incapacitation for each asphyxiant component. These are then summed and corrected for VCO_2 and V_E to provide an overall F_{IN} for each time period.

The expressions used to calculate the FEDs for each individual component are as follows:

For the effects of CO the FED is expressed in terms of percent COHb. This is representative of the dose of CO actually inhaled and presents a more accurate estimate of the CO dose than the Ct product dose of 35,000 ppm · min, which does not allow for physiological variables affecting uptake. The denominator is the percent COHb predicted to cause loss of consciousness in an active (escaping) person, which is 30 %COHb (or 40 %COHb for a resting person). The numerator is the Stewart Equation [69], by which the percent COHb in the subject is calculated from the inhaled CO concentration in the fire, the exposure time, and the volume of air breathed each minute:

$$F_{I_{CO}} = 3.317 \times 10^{-5}[\mathrm{CO}]^{1.036}(V)(t)/D \quad (63.18)$$

where

[CO] = Carbon monoxide concentration (ppm v/v 20 °C)

V_E = Volume of air breathed per minute (liters/min)

t = Exposure time in minutes

D = Exposure dose (percent COHb) for incapacitation

For the default case the value of V is 25 L/min and the value of D is 30 %COHb.

For the general case ($\mathrm{F_{ICOg}}$) the V_E term is removed from Equation 63.18.

Note 1 This expression (the Stewart equation) was obtained from young adult male human volunteers. It is suitable for adults in situations where the CO concentration is high in relation to the blood COHb concentration (as for most flaming fires and short exposure durations). Where long exposures may lead to near equilibrium conditions, the Coburn-Forster-Kane [34] (CFK) equation should be used (see Appendix 2) since significant deviations from the Stewart

equation may then occur. The Stewart equation somewhat underestimates uptake rates for children. Where more precise CO uptake calculations are required, differences in body size (including children) can be accommodated using the CFK equation. For a basic design, use of the Stewart equation is recommended. Differences in body size and other susceptibilities can be considered as allowed for in the overall safety margin chosen to accommodate more susceptible subpopulations (e.g., an FED of 0.3 or other endpoint).

Note 2 As an alternative to using this expression (the Stewart equation) the FED_{Ico} may be expressed as a CO exposure dose ratio. This method is used for ISO 13571 [21] For this method the FED_{Ico} is expressed as CO ppm × t/35,000. This is approximately equivalent to a "light work" case for a subject breathing approximately 20 L air per minute.

For the effects of hydrogen cyanide and low-oxygen hypoxia, the expressions are more complex because the denominators are not constants. Exponential expressions have been developed to fit the time to incapacitation versus exposure concentration curve from experimental exposures in nonhuman primates (HCN) and humans (hypoxia). The default form of the fractional incapacitating dose for HCN (F_{ICN}) is as follows:

$$F_{ICN} = \frac{[CN]^{2.36}}{1.2 \times 10^6} t \qquad (63.24)$$

where
CN = HCN concentration (ppm v/v at 20 °C)
t = Exposure time in minutes

For the general case application in Equation 63.39 the term F_{ICNg} is given by:

$$F_{ICNg} = \frac{[CN]^{2.36}}{2.43 \times 10^7} t$$

which is Equation 63.25 without the VE term. For the general case application in Equation 63.9 the term FLD_{irrg} is given by

$$FLDirrg = FLD/25$$

The expression for low oxygen hypoxia is

$$F_{I_O} = t/\exp[8.13 - 0.54(20.9 - [\%O_2])] \qquad (63.50)$$

where
$[\%O_2]$ = Oxygen concentration (% v/v at 20 °C)
t = Exposure time (minutes)
I = Exposure dose for incapacitation

Similarly, a curve has been fitted to the effect of CO_2 on ventilation (breathing volume per minute) based on human experimental data.

Ventilatory stimulation by CO_2:

$$VCO_2 = \exp([CO_2]/5) \qquad (63.35)$$

where $[CO_2]$ is the carbon dioxide concentration (% v/v at 20 °C).

FEDs are calculated for successive short periods during the fire and then integrated with time in order to calculate the time when incapacitation is predicted (FED = 1).

Since occupants must at least walk in order to escape from a fire, the default case suggested is that for light work. However, this could be varied according to the case. For example, a sleeping person escaping from a basement might start by being at rest, but then awaken, walk to a stair (light work), and then climb the stairs (heavy work).

Note: Due to the rapid (t^2) rate of increase of asphyxiant gas concentrations in most flaming fires, variations in individual susceptibility and uncertainties in prediction of incapacitating doses tend to have relatively minor effects on predicted times to incapacitation.

Tenability and Hazard Calculations for Development of Pain, Incapacitation, Injury, and Death from Exposure to Heat and Burns

There are three basic mechanisms by which heat exposure may lead to incapacitation and death in fires:

1. Heat stroke (hyperthermia)
2. Skin pain followed by body surface burns
3. Respiratory tract burns

The effects of heat are described in detail in the section "The Exposure of Fire Victims to Heat" in this chapter. Hyperthermia involves prolonged exposure (approximately 15 min or more) to heated environments at ambient temperatures too low to cause burns. Under such conditions, where the air temperature is less than approximately 121 °C for dry air or 80 °C for saturated air, the main effect is a gradual increase in body core temperature [111]. Hyperthermia leads to confusion and collapse. Exposure to air temperatures above approximately 121 °C (or to radiant heat fluxes above 2.5 kW/m^2) leads to pain to exposed skin followed by body surface burns and hyperthermia if exposure is prolonged. Respiratory tract burns can also occur if exposure to heated air is sufficient to cause facial burns.

For a basic engineering design it is proposed that a tenability endpoint for exposure to heat should be taken as the limits of heat tolerance due either to the onset of hyperthermia or to severe pain to exposed areas of skin (such as the head and hands). It is proposed that under such conditions exposed building occupants may be unable to escape (if affected by hyperthermia) or unwilling to move through painfully hot environments.

Note: It is known that in some fires people have moved through (and escaped from) scenarios under conditions hot enough to cause severe burns. It is suggested that severe incapacitation is likely to occur under conditions that may cause second-degree burns. It is suggested that death is likely to occur under conditions that may cause third-degree burns. For situations where endpoints such as these are of interest, see the section "The Exposure of Fire Victims to Heat" in this chapter.

There are also three basic heat exposure scenarios for building occupants during a fire:

1. Exposure to convected heat in a hot air environment
2. Exposure to radiant heat direct from a fire or from a hot upper smoke layer
3. Exposure of a subject immersed in hot smoke—subjected to both radiant heat from hot smoke particles and convected heat from contact with hot gases in the hot smoke environment

Experimental human exposure data are available for the first two cases, from which time-tolerance curves have been obtained for exposure to convected or radiant heat. For direct exposure to radiant heat (e.g., from a fire or heater), empirical relationships between exposure time and effect have been measured by a number of authors. For these experiments heat radiation is expressed in terms of received heat flux (kW/m^2). The relationship between heat flux and time to pain is presented in this section, whereas a detailed treatment of time and exposure dose of radiant heat for pain, second and third-degree burns is presented in the section "Radiant Heat" of this chapter and in Hockey and Rew [133]. Survivability issues are also discussed.

The tenability limit for exposure of skin to radiant heat is approximately 2.5 kW/m^2, below which exposure can be tolerated for at least several minutes. Radiant heat at this level and above causes skin pain followed by burns within a few seconds, but lower fluxes can be tolerated for more than 5 min. For situations where occupants are required to pass under a hot smoke layer in order to escape, this radiant flux corresponds approximately to a hot smoke layer temperature of 200 °C. Above this threshold, time (minutes) to incapacitation due to radiant heat $t_{I\mathrm{rad}}$ at a radiant flux of q (kW/m^2) is given by Equation 63.43.

$$t_{I\mathrm{rad}} = \frac{1.33}{q^{1.33}} \tag{63.43}$$

where

$t_{I\mathrm{rad}}$ = Time to endpoint (pain in this case) (minutes)

q = Heat flux (kW/m^2)

Calculating Effects of Exposure to Convected Heat Only

Some experimental data are available for exposure of unclothed or lightly clothed subjects to hot air environments in terms of tolerance time to pain or hyperthermia. The Blockley [111] curve shown in Figure 63.28 is for dry air and humid air (saturated at normal room temperature), which is then heated. This is very different from the effects of air saturated with water at higher

temperatures. Water is a serious potential problem in fires due to its high latent heat. If fire effluent contains water at above 100 °C (i.e., steam), it releases considerable heat if it comes in contact with the skin or is inhaled. Although the hazards of contact with steam are well known, it may be less obvious that air saturated with water vapor at lower temperatures can be dangerous. The highest temperature at which saturated air can be breathed for more than a few minutes is 60 °C. As an approximate guide, the volume concentration of water vapor in fire effluent is similar to the CO_2 concentration, which might reach as much as 10 % and is less than the concentration in saturated air at the breathable limiting temperature of 60 °C. For this reason it is considered that the fuel-derived water vapor content of normal fire effluent is not likely to present a serious hazard except where steam may be generated by the application of water for fire suppression.

An expression has been derived for exposures of up to 2 h to convected heat from air containing less than 10 % by volume of water vapor. The following expression has been developed for the midhumidity case from Blockley [111] and other data. Tolerance time t_{tol} (minutes) is then given by

$$t_{tol} = 2 \times 10^{31} \times T^{16.963} + 4 \times 10^{8} \times T^{3.7561} \quad (63.45)$$

where T is room temperature (°C).

Another expression presented in the section "The Exposure of Fire Victims to Heat" (Equation 63.44) tends to follow the worst-case (100 % humidity) line. It also does not fit the empirical data as well, deviating somewhat from Blockley's curve at the high and low ends. It is, therefore, a somewhat non-conservative expression for exposure to higher temperatures and somewhat over-conservative at the low temperature end.

As with toxic gases, the body of a fire victim may be regarded as acquiring a "dose" of heat over a period of time during exposure, with short exposure to a high radiant flux or temperature being more incapacitating than a longer exposure to a lower temperature or flux. The same fractional incapacitating dose model as with the toxic gases may be applied and, providing that the temperature in the fire is stable or increasing, the fractional dose of heat acquired during exposure can be calculated.

For Equations 63.43 and 63.45, the fractional effective dose of heat received each minute is given by the reciprocal of the expression.

For situations when a subject is exposed to both radiant heat (e.g., from a heated upper layer) and convected heat from exposure to heated air, the overall heat dose received may be estimated by summing the radiant and convected fractions using Equation 63.48:

$$\mathrm{FED} = \int_{t_1}^{t_2} \left(\frac{1}{t_{I\mathrm{rad}}} + \frac{1}{t_{I\mathrm{conv}}} \right) \Delta t \quad (63.48)$$

The doses acquired in each unit of time are then integrated. The tenability limit is predicted when the FED for heat = 1.

An alternative method for estimating tolerance time for exposure to combinations of radiant and convected heat, especially for the case of a subject immersed in hot smoke, is presented in the section "Model of the Prediction of Time to Incapacitation by Exposure to Heat in Fires" in this chapter. Consideration is also given to the estimation of time to second-degree burns (representing incapacitation) and third-degree burns (representing a potentially lethal exposure).

A worked example of a simplified life threat hazard analysis is presented in Table 63.22.

Appendix 2: Coburn-Forster-Kane Equation for the Uptake of Carbon Monoxide in Man

The Coburn-Forster-Kane (CFK) equation [34] provides an accurate method for predicting the blood carboxyhemoglobin concentration in humans (or various animal species) resulting from exposure to a given concentration of carbon monoxide. The theoretical predictions of the equation have been validated for humans by experimental human exposures to carbon monoxide [35, 75]. The strength of the equation is that it is based on numerical values for all the main constants and variables that determine the uptake of CO into the

blood; it is, therefore, not based on a simple empirical fit to observed uptake data in individuals, as are other CO uptake equations [31, 39]. The result is a powerful equation that can be used to predict CO uptake over wide ranges of concentrations and time scales and can accommodate variables such as the degree of activity of the subject, body size (for men, women, or children), blood volume, hemoglobin concentration, and lung function status, all of which can affect CO uptake and, therefore, time to incapacitation or death for a given subject, as well as CO washout after exposure when breathing air or oxygen. The equation should be equally applicable to animals, providing of course that data for the various constants and variables are available. The disadvantage of the CFK equation is its complexity. In particular, several of the variables need to be calculated from other equations, which in turn contain variables that must be calculated from further equations. The data in the text and figures in this chapter are all based on CO uptake for a 70-kg human, either at rest (RMV approximately 8.5 L/min, engaged in light work [e.g., walking 6.4 km/h—RMV approximately 25 L/min]) or engaged in heavy work (e.g., slow running 8.5 km/h or walking 5.6 km/h up a 17 % gradient—RMV (i.e., V_E) approximately 50 L/min) [77]. In this Appendix, data for necessary constants and equations for the derivation of all variables, with their sources, have been provided to enable uptake calculations to be made for any particular situation.

The basic Coburn Forster Kane equation is a differential equation developed initially to calculate %COHb in blood for endogenous production of CO using all the major physiological parameters [34]. The equation is written as follows:

$$\frac{d(HBCO)_t}{dt} = \frac{V_{CO}}{V_B} - \frac{1}{V_B\left(\frac{1}{DLco} + \frac{(PB - P_{H_2O})}{V_A}\right)}\left(\frac{(HbCO)_t \overline{P}c_{O2}}{(HBO_2M} - P_{Ico}\right) \tag{63.51}$$

Peterson and Stewart [35, 156] used the model to calculate CO uptake and %COHb for male students exposed to different inhaled CO concentrations and found a good agreement. They used the following integrated form of the equation, which has been used to calculate the CFK uptake curves presented in this chapter:

$$\frac{A[HbCO]_t - BVco - P_{Ico}}{A[HbCO]_0 - BVco - P_{Ico}} = \exp(-tA/VbB) \tag{63.52}$$

All volumes are STPD (standard temperature and pressure, dry i.e., 1 atm and 0 °C) and the various terms in the two forms of the equation are as follows:

$$A = \overline{P}c_{O_2}/M[HbO_2] \tag{63.53}$$

$$B = 1/DLco + P_L/V_A \tag{63.54}$$

M = ratio of the affinity of blood for CO to that for O_2 (the Haldane constant) = 218

$[HbO_2]$ = mL of O_2 per mL blood. This depends on the extent of saturation, but at 100 % saturation I gram of Hb will hold 1.38 mL of oxygen (or CO) (at STPD).

$$[HbO_2]_{\max} = 1.38[Hb]/100 \tag{63.55}$$

[Hb] = Hb concentration (g/100 mL whole blood). Normal ranges are: Adult males 13.5–18.0, Adult females 11.5–16.4

$[HbCO]_t$ = mL of CO per mL of blood at time t

$[HbCO]_0$ = mL of CO per mL of blood at the beginning of the exposure, taken as 0.8 % COHb = 0.00176 mL CO/mL blood for non-smokers

$\overline{P}c_{O_2}$ = average partial pressure of oxygen in lung capillaries, mmHg

Vco = rate if endogenous CO production mL/min, set at 0.007 mL/min

$DLco$ = diffusivity of the lung for CO, mL/min/mmHg
P_L = barometric pressure minus vapor pressure of water at body temperature (760–47 = 713 mmHg)
Vb = blood volume, mL, 74 mL/kg bodyweight (approximately 5500 mL for a 70 kg human) (or 66.8?)
P_{Ico} = partial pressure of CO in the inhaled air, mmHg
V_A = alveolar ventilation rate, mL/min
t = exposure duration (minutes)
$e = 2.7182$

Expressions for different input terms required are as follows:

$$A_r(m^2) = 11.7(cm^2/g)W(g)^{0.667} \quad (63.56)$$

Where:
A_r = Body surface area (m^2)
W = Bodyweight in grams or kilograms as indicated

$$DLco(ml/\text{min}/mmHg) = \left(\frac{1}{\left(-0.0287\left(\frac{150}{W(kg)}\right)^{0.667}\right) + \frac{0.1188}{A_r(m^2)}}\right) \text{ [Ref. 161]} \quad (63.57)$$

Alternatively Bernard and Duiker [158] treated DL_{co} as a variable related to oxygen consumption (up to 4 L O_2/min)

$$DLco = 35{Vo_2}^{0.33}(ml/\text{min}/mmHg) \quad (63.58)$$

$$Vo_2 = 0.001V_E(ml/\text{min})/22.274 - 0.0309(L/\text{min}STPD) \text{ [Ref. 77]} \quad (63.59)$$

$$V_A = 0.933V_E(ml/\text{min}) - 132f(m/\text{min}) \text{ [Ref. 35]} \quad (63.60)$$

$$f = \exp(0.0165V_E(ml/\text{min}) + 2.3293 \text{ [Ref. 35]} \quad (63.61)$$

where
Vo_2 = rate of oxygen consumption (L/min STPD)
V_E = respiratory minute volume (mL/minSTPD)
f = respiratory frequency (breaths/min)

Alternatively:

$$V_A = V_E(mL/\text{min}) - (W(kg)/V_T)V_D(mL/\text{min}STPD) \quad (63.62)$$

$$V_D = 2.24W(kg)(mLSTPD) \quad (63.63)$$

$$V_T = 7.4W(kg)(mLSTPD) \quad (63.64)$$

where:
V_D = anatomical dead space (mL STDP)
V_T = respiratory tidal volume (mL STDP)

Appendix 3: Tenability Limits

Asphyxiants Concentrations at which there would be danger of incapacitation (loss of consciousness) and death after approximately 5 and 30 min exposure in a person engaged in light activity are shown in Table 63.28.

Irritants The initial painful effects of irritants (sensory irritation) are mainly on the eyes and upper respiratory tract. These effects do not worsen with prolonged exposure and may even lessen. The toxic effects on the lungs increase with prolonged exposure, are often most serious some hours after exposure, and may cause death.

For sensory irritation two levels are presented: level a represents unpleasant and quite severely disturbing eye and upper respiratory tract irritation; level b represents severe eye and upper respiratory tract irritation with severe pain, blepharospasm, copious lacrimation, and mucus secretion accompanied by chest pain. For deaths, the levels represent concentrations at which there

Table 63.28 Tenability limits for incapacitation or death from exposures to common asphyxiant products of combustion

	5 min		30 min	
	Incapacitation	Death	Incapacitation	Death
CO	6000–8000 ppm	12,000–16,000 ppm	1400–1700 ppm	2500–4000 ppm [65, 105]
HCN	150–200 ppm	250–400 ppm	90–120 ppm	170–230 ppm [65, 80]
Low O_2	10–13 %	<5 %	<12 %	6–7 % [33, 37, 65]
CO_2	7–8 %	>10 %	6–7 %	>9 % [33, 37, 65]

Table 63.29 Tenability limits for sensory irritation or death from irritant substances

	Sensory irritation		Death (minutes)		
	a	b	5	10	30
Acrolein (ppm)	1–5 [33, 159]	5–95 [159, 160]	500–1000 [160]	150–690 [39, 160]	50–135 [39, 160]
HCI (ppm)	75–300 [33]	300–11,000 [159, 161]	12,000–16,000 [159, 161]	10,000 [160]	2000–4000 [33]

is danger of death occurring during or immediately after exposure.

In general, smokes are irritating when they contain oxidized organic products [16]. The most irritating of these substances known to occur commonly in smokes from a number of different materials is acrolein. Another well-known irritant is the acid gas hydrogen chloride, which is evolved during the thermal decomposition of polyvinyl chloride (PVC). Data on these two products are presented in Table 63.29 as examples of irritant effects.

References

1. D.A, Purser, "Combustion toxicity." in *SFPE Handbook of Fire Protection Engineering,* 5th ed. (M. J. Hurley et al., eds.), Springer (2015).
2. NFPA, 101 in Life Safety Code. National Fire Protection Association, Quincy, MA (2012)
3. The Building Regulations 2000: Approved Document B 2006 edition Communities and Local Government
4. ISO TR 1338 7 Part 8 Fire Safety Engineering—Life safety: occupant behaviour, location and condition. International Standards Organisation, Geneva, 1999.
5. NFPA, The Reconstruction of a Tragedy, the Beverly Hills Supper Club Fire. National Fire Protection Association, Quincy, MA (1978).
6. P.C. Bowes, "Smoke and Toxicity Hazards of Plastics in Fire," *Annals of Occupational Hygiene,* 17, pp. 143–156 (1974).
7. *Fire Statistics In The United Kingdom 2011, Communities and Local Government*, London (published annually).
8. B.F. Clarke, "Fire and Smoke: Understanding the Hazards," in *Fire Deaths, Causes and Strategies for Control,* Technomic, Lancaster, PA (1984).
9. J.R. Hall and A.E. Cote, "An Overview of the Fire Problem and Fire Protection," in *Fire Protection Handbook,* 20th ed. (A.E. Cote, editor-in-chief), National Fire Protection Association, Quincy, MA, Ch. 3-1 (2008).
10. Fire loss in the United States During 2010. M.J. Karter Jr. National Fire Protection Association September 2011
11. Fire in the United States 2003–2007 Fifteenth Edition. US Fire Administration/National Fire Data Center Federal Emergency Management Agency October 2009.
12. V. Berl and B. Halpin, *NBS Grant Contract Report NBS-GCR 168,* National Bureau of Standards, Washington, DC (1979).
13. J. Hall NFPA, personal communication
14. Fire fatalities data for London 2002–2006 provided by London Fire and Rescue Service.
15. B.T. Davies and L.I Griffin, A Clinical Evaluation of the Death Investigations of 206 Decedents Who Died in Passenger Vehicles that Experienced Post-Crash Fires. NHTSA-1998-3588-170, 1998.
16. D.A. Purser, "ASET and RSET: Addressing Some Issues in Relation to Occupant Behaviour and Tenability," in *Proceedings of the 7th International Symposium on Fire Safety Science,* International

Association for Fire Safety Science, Boston, MA, pp. 91–102 (2003).
17. The application of fire safety engineering principles to fire safety design of buildings. PD7974-6: Human Factors: Life safety strategies—occupant evacuation, behaviour and condition. British Standards Institution 2004.
18. D.A. Purser, "Toxic Product Yield and Hazard Assessment for Fully Enclosed Design Fires Involving Fire Retarded Materials," *Polymer International,* 47, pp. 1232–1255 (2000).
19. D.T. Gottuk and B.Y. Lattimer, "Effect of Combustion Conditions on Species Production." in *SFPE Handbook of Fire Protection Engineering,* in *SFPE Handbook of Fire Protection Engineering,* 5th ed. (M. J. Hurley et al., eds.), Springer (2015).
20. M. Khan et al., "Combustion Characteristics of Materials and Generation of Fire Products," in *SFPE Handbook of Fire Protection Engineering,* 5th ed. (M. J. Hurley et al., eds.), Springer (2015).
21. ISO 13571 Life-threatening components of fire –Guidelines for the estimation of time to compromised tenability in fires. Second edition International Organization for Standardization, Geneva, Switzerland. 2012.
22. D.A. Purser,. "Application of human and animal exposure studies to human fire safety". in *Fire Toxicity*, A.A. Stec and T.R. Hull (eds) Woodhead, Cambridge, 2010. Chapter 8 pp 283–345.
23. D.A. Purser, Validation of additive models for lethal toxicity of fire effluent mixtures. Polymer Degradation and Stability 97 2552–2561 (2012)
24. D.A. Purser, Application of human behaviour and toxic hazard analysis to the validation of CFD modelling for the Mont Blanc Tunnel fire incident. Advanced Research Workshop: Fire Protection and Life Safety in Buildings and Transport systems University of Cantabria, Spain. 17-17 October 2009. Proceedings pp 23–57.
25. Experimental research for Scottish Building Standards Agency following the fire at the Rosepark Care Home, Glasgow, 31st January 2004. BRE Project Report number 219132, October 2004.
26. D.A. Purser. Personal Communication—From experience of detailed investigations of a number of cases involving exposure scenarios similar to those described.
27. D.A. Purser. Fire safety and evacuation behaviours and hazard development in two fatal care home incidents. Fire and Materials 39, pp.430-452 (2015). doi:10.1003/flam.2250
28. D.A. Purser and M. Bensilum. Quantification of behaviour for engineering design standards and escape time calculations. Safety Science, 38, 157–182 (2001)
29. Grosshandler, W., Bryner, N., Madrzkowski, D. and Kuntz, K. Report of the technical investigation of the Station Nightclub fire. NIST NCSTAR 2: Vol. 1. June 2005.
30. B.T. Commins and P.J. Lawther, "A Sensitive Method for the Determination of Carboxyhaemoglobin in a Finger Prick Sample of Blood," *British Journal of Industrial Medicine,* 22, pp. 139–143 (1965).
31. R.D. Stewart, "The Effects of Carbon Monoxide on Man," *Journal of Combustion Toxicology,* 1, pp. 167–176 (1974).
32. F. Haber, *Funf Vortrange aus den jaren 1920–1923,* Verlag von Julius Springer, Berlin (1924).
33. "Documentation of the Threshold Limit Values for Substances in Workroom Air," *American Conference of Governmental Industrial Hygienists,* Cincinnati (1980).
34. R.F. Coburn, R.E. Forster, and P.B. Kane, "Consideration of Physiological Variables That Determine the Blood Carboxyhaemoglobin Concentrations in Man," *Journal of Clinical Investigation,* 44, pp. 1899–1910 (1965).
35. E. Peterson and R.D. Stewart, "Predicting the Caboxyhaemoglobin Levels Resulting from Carbon Monoxide Exposures," *Journal of Applied Physiology,* 39, pp. 633–638 (1975).
36. F.W. Beswick, P. Holland, and K.H. Kemp, "Acute Effects of Exposure to Orthochlorobenzylidene Malonitrile (CS) and the Development of Tolerance," *British Journal of Industrial Medicine,* 29, pp. 298–306 (1972).
37. D.A. Purser, "A Bioassay Model for Testing the Incapacitating Effects of Exposure to Combustion Product Atmospheres Using Cynomolgus Monkeys," *Journal of Fire Sciences,* 2, pp. 20–26 (1984).
38. U.C. Luft, "Aviation Physiology—The Effects of Altitude," in *Handbook of Physiology,* American Physiology Society, Washington, DC, pp. 1099–1145 (1965).
39. G.E. Hartzell, D.N. Priest, and W.G. Switzer, "Modelling of Toxicological Effects of Intoxication of Rats by Carbon Monoxide and Hydrogen Cyanide," *Journal of Fire Sciences,* 3, pp. 115–128 (1985).
40. L. Brodie, National Asthma Audit (Press Release), National Asthma Campaign, London (1996).
41. G.L. Nelson, "Carbon Monoxide and Fire Toxicity: A Review and Analysis of Recent Work, "*Fire Technology,* 34, pp. 38–58 (1998).
42. A.L. Hinderliter, K.F. Adams, C.J. Price, M.C. Hebst, G. Koch, and D.S. Sheps, "Effects of Low-Level Carbon Monoxide Exposure on Resting and Exercise-Induced Ventricular Arrhythmias in Patients with Coronary Artery Disease and No Baseline Ectopy." *Archives of Environmental Health,* 44, pp. 89–93 (1989).
43. J. Pach et al., "Analysis of Predictive Factors in Acute Carbon Monoxide Poisonings," *Folia Medica Cracoviensia,* 20, pp. 159–168 (1978).
44. M. Bensilum M and D.A. Purser .(2002) GridFlow: an object-oriented building evacuation model combining

pre-movement and movement behaviours for performance-based design. 7th International Symposium On Fire Safety Science, Worcester Polytechnic Institute—Worcester Massachusetts, USA 16–21 June 2002 (Proceedings in press). FIRE SAFETY SCIENCE—Proceedings of the seventh international symposium. International Association for Fire Safety Science, 2003 pp. 941–952
45. E.R. Galea, S. Gwynne, M. Owen, P.J. Lawrence, P.J. and L. Filipidis, "A comparison of predictions from the building EXODUS evacuation model with experimental data." Proceedings of the First International Symposium on Human Behaviour in Fire, 1998, pp 711–720.
46. T. Yamada and Y. Akizuki T. "Visibility and Human Behavior in Fire Smoke" in *SFPE Handbook of Fire Protection Engineering,* 5th ed. (M. J. Hurley et al., eds.), Springer (2015).
47. E. Kuligowski, "Human Behavior in Fire". in Fire Smoke in *SFPE Handbook of Fire Protection Engineering,* 5th ed. (M. J. Hurley et al., eds.), Springer (2015).
48. P.G. Wood, "The Behavior of People in Fires," *Fire Research Note 953,* Fire Research Station, Watford, UK (1972).
49. J.L. Bryan, "Smoke As a Determinant of Human Behavior in Fire Situations (Project People)," *NBS-GCR-77-94,* U.S. Department of Commerce, National Bureau of Standards, Washington, DC (1977).
50. T. Jin, "Studies of Emotional Instability in Smoke from Fires," *Journal of Fire and Flammability,* 12, pp. 130–142 (1981).
51. D.J. Rasbash, *Fire International,* 5, 40, p. 30 (1975).
52. V. Babrauskas, "Full Scale Burning Behavior of Upholstered Chairs," *Technical Note 1103,* National Bureau of Standards, Washington, DC (1979).
53. T. Jin, "Visibility through Fire Smoke—Part 5, Allowable Smoke Density for Escape from Fire." *Report No. 42,* Fire Research Institute of Japan, p. 12 (1976).
54. Frantzich, H., Nilsson, D., Evacuation Experiments in a Smoke Filled Tunnel. Human Behaviour in Fire, Proceedings of the 3rd International Symposium, Belfast, UK, p229–p238.
55. Fridolf, K., Andreé, Nilsson, D and Frantzich, H. The impact of smoke on walking speed. Interflam 2013. Royal Holloway College, Wiindsor, U.K. 24–26th June 2013.
56. E.Ronchi, S.M.V. Gwynne and D.A. Purser. and P. Colonna, Representation of the Impact of Smoke on Agent Walking speeds in Evacuation Models. July 2012 Fire Technology DOI 1007/s10694-012-0280-y
57. Purser D.A, Chapter 3: Hazards from smoke and irritants. In "Fire toxicity" Eds A. Stec and R. Hull. Woodhead, Cambridge UK, 2010 pp 51–117.
58. "British Standard Code of Practice for Assessment of Hazard to Life and Health from Fire. Part 2: Guidance on Methods for the Quantification of Hazards to Life and Health and Estimation of Time to Incapacitation and Death in Fires," *BS 7899-2,* British Standards, London (1999).
59. NAC/AEGL, "Acute Exposure Guidelines for Selected Airborne Chemicals," National Advisory Committee for Acute Exposure Guideline Levels for Hazardous Substances, Subcommittee on Acute Exposure Guideline Levels, Committee on Toxicology, Board on Environmental Studies and Toxicology, National Research Council of the National Academies, National Academies Press, Washington, DC (2004). Note: Reviews of new substances are being added on a continuing basis
60. D.A. Purser and P. Buckley, "Lung Irritance and Inflammation During and After Exposure to Thermal Decomposition Products from Polymeric Materials," *Medicine Science and the Law,* 23, pp. 142–150 (1983).
61. D.A. Purser and W.D. Woolley, "Biological Studies of Combustion Atmospheres," *Journal of Fire Sciences,* 1, pp. 118–145 (1983).
62. D.A. Purser and K.R. Berrill, "Effects of Carbon Monoxide on Behaviour in Monkeys in Relation to Human Fire Hazard," *Archives of Environmental Health,* 38, pp. 308–315 (1983).
63. W.D. Woolley and P.J. Fardell, "Basic Aspects of Combustion Toxicology," *Fire Safety Journal,* 5, p. 29 (1982).
64. R.A. Anderson, A.A. Watson, and W.A. Harland, "Fire Deaths in the Glasgow Area: 1. General Conclusions and Pathology," *Medicine, Science and the Law,* 21, pp. 175–183 (1981).
65. G. Kimmerle, "Aspects and Methodology for the Evaluation of Toxicological Parameters During Fire Exposure," *Journal of Combustion Toxicology,* 1, p. 4 (1974).
66. J.S. Haldane, *Respiration,* Yale University, New Haven (1922)
67. D.A. Purser, Chapter 4: Asphyxiant components of fire effluents. In "Fire toxicity" Eds A. Stec and R. Hull. Woodhead, Cambridge UK, 2010 pp 118–198.
68. R.D. Stewart, J.E. Peterson, E.D. Baretta, H.C. Dodd, and A.A. Herrmann, "Experimental Human Exposure to Carbon Monoxide," *Archives of Environmental Health,* 21, pp. 154–164 (1970).
69. R.D. Stewart, J.E. Peterson, T.N. Fisher, M.J. Hosko, E.D. Baretta, H.C. Dodd, and A.A. Herrmann, "Experimental Human Exposure to High Concentrations of Carbon Monoxide," *Archives of Environmental Health,* 26, p. 1 (1973).
70. Consumer Product Safety Commission, *Federal Register,* 45–182, 61925 (1980).
71. Sayers, P.R. and Davenport, S.J. Review of Carbon Monoxide Poisoning. Public Health Bulletin 195.

U.S. Government Printing Office, Washington D.C. 1930
72. R.D. O'Donnel, P. Miluka, P. Heinig, and J. Theodorem, "Low Level Carbon Monoxide Exposure and Human Psychomotor Performance," *Toxicology and Applied Pharmacology,* 18, pp. 593–602 (1971).
73. "Carbon Monoxide Poisoning Due to Faulty Gas Water Heaters in British Holidaymakers on the Algarve," *Sunday Times,* London (1983).
74. K. Von Leggenhager, "New Data on the Mechanisms of Carbon Monoxide Poisoning," *Acta Medica Scandinavica,* 196/suppl. 563, pp. 1–47 (1974).
75. H. Hauck and M. Neuberger, "Carbon Monoxide Uptake and the Resulting Carboxyhaemoglobin in Man," *European Journal of Applied Physiology,* 53, pp. 186–190 (1984).
76. Kaplan H. L., Grand, A.F., Switzer, W.G., Mitchell, D.S., Rogers, W.R. and Hartzell, G.E. Effects of Combustion Gases On Escape Performance of the Baboon and the Rat Journal of Fire Sciences, Vol. 3, No. 4, 228–244 (1985) doi: 10.1177/073490418500300401.
77. *Handbook of Respiration,* Saunders, Philadelphia (1958).
78. R.A. Anderson, I. Thompson, and W.A. Harland, "The Importance of Cyanide and Organic Nitriles in Fire Fatalities," *Fire and Materials,* 3, pp. 91–99 (1979).
79. C.J. Clark, D. Campbell, and W.H. Reid, "Blood Carboxyhaemoglobin and Cyanide Levels in Fire Survivors," *Lancet,* pp. 1332–1335 (June 20, 1981).
80. D.A. Purser, P. Grimshaw, and K.R. Berrill, "Intoxication by Cyanide in Fires: A Study in Monkeys Using Polyacrylonitrile," *Archives of Environmental Health,* 39, pp. 394–400 (1984).
81. D.A. Purser, "Determination of Blood Cyanide and Its Role in Producing Incapacitation in Fire Victims," *Royal Society of Chemistry Meeting,* Huntingdon (1984).
82. J.L. McAllister, R.J. Roby, B. Levine, and D. Purser, Stability of cyanide in cadavers and in postmortem stored tissue specimens: A review. J. Analytical Toxicology. 32, 1–9(2008).
83. B. Ballantyne, "Artefacts in the Definition of Toxicity by Cyanides and Cyanogens," *Fundamental and Applied Toxicology,* 3, pp. 400–408 (1983).
84. Nunn, J.F. Applied Respiratory Physiology Butterworth and Co. London 1969.
85. J.L. Bonsall, "Survival Without Sequelae Following Exposure to 500 mg/m3 of Hydrogen Cyanide," *Human Toxicology,* 3, pp. 57–60 (1984).
86. J. Barcroft, "The Toxicity of Atmospheres Containing Hydrocyanic Acid Gas," *Journal of Hygiene,* 31, pp. 1–34 (1931).
87. B.P. McNamara, "Estimates of the Toxicity of Hydrocyanic Acid Vapors in Man," *EB-TR-76023,* Edgewood Arsenal, Aberdeen Proving Ground, MD (1976).
88. B. Ballantyne, "The Forensic Diagnosis of Acute Cyanide Poisoning," in *Forensic Toxicology,* Wright, Bristol (1974).
89. F.J. Baud, P. Barriot, V. Toffis, et al., "Elevated Blood Cyanide Concentrations in Victims of Smoke Inhalation," *New England Journal of Medicine,* 325, pp. 1761–1766 (1991).
90. Curry, A.S. (1963) Cyanide poisoning. Acta. Pharmacol. Toxicol. 20, 291–294.
91. B. Ballantyne, "The Forensic Diagnosis of Acute Cyanide Poisoning," in *Forensic Toxicology,* Wright, Bristol (1974).
92. Ballantyne, B. (1976) Changes in blood cyanide as a function of storage time and temperature
93. Hall, A., Rumack, B.H., Schaffer, M.I. and Linden, C.H. (1987)Clinical toxicology of cyanide: North American clinical experiences. In: Clinical and experimental toxicology of cyanides Ch. 12. pp. 312–333.
94. Ballantyne, B. and Marrs, T.C. (1987) Post-mortem features and criteria for the diagnosis of acute lethal cyanide poisoning. In: Clinical and experimental toxicology of cyanides Ch. 9. pp. 217–247.
95. Coburn, R.F. The carbon monoxide body stores. Ann N.Y. Acad. Sci. 1970, 174: 11–22.
96. C.J. Lambertson, "Carbon Dioxide and Respiration in Acid-Base Homeostasis," *Anaesthesiology,* 21, pp. 642–651 (1960).
97. J.H. Comroe, R.E. Forster, A.B. Dubois, W.A. Briscoe, and E. Carlsen, "Pulmonary Ventilation," in *The Lung,* Year Book Medical Publishers, Chicago, pp. 52–53 (1962).
98. *Environmental Biology (*P. Altman and D.S. Ditter, eds.), Federation of American Societies for Experimental Biology, Bethesda, MD (1966).
99. B.G. King, "High Concentration–Short Time Exposures and Toxicity," *Journal of Industrial Hygiene and Toxicology,* 31, pp. 365–375 (1949).
100. J.E. Schulte, "Sealed Environments in Health and Disease," *Archives of Environmental Health,* 8, pp. 437–452 (1964).
101. W.S. Root, "Carbon Monoxide," in *Handbook of Physiology,* American Physiology Society, Washington, DC, pp. 1087–1098 (1985).
102. F.A. Gibbs, E.L. Gibbs, W.G. Lennox, and L.F. Nims, "The Value of Carbon Dioxide in Counteracting the Effects of Low Oxygen," *Journal of Aviation Medicine,* 14, pp. 250–261 (1943).
103. A.A. Karl, G.R. McMillan, S.L. Ward, A.T. Kissen, and M.E. Souder, "Effects of Increased Ambient CO_2 on Brain Tissue Oxygenation and Performance in the Hypoxic Rhesus," *Aviation, Space, and Environmental Medicine,* 49, pp. 984–989 (1978).
104. G.E. Hartzell, B.C. Levin, and Y. Alarie, personal communications (1988).

105. D.A. Purser and P. Grimshaw. (1984) The incapacitative effects of exposure to the thermal decomposition products of polyurethane foams. Fire and Materials. 8, 10–16.
106. Piantadosi, C.A., Sylvia, A.L. and Jőbis-Vandervliet, F. Differences in brain cytochrome responses to carbon monoxide and cyanide in vivo. (1987) J. Appl. Physiol. 62, 1277–1284
107. J.W. Heim, "The Toxicity of Carbon Monoxide at High Altitudes," *Journal of Aviation Medicine,* 10, pp. 211–215 (1939).
108. R.A. McFarland, F.J. Roughton, M.H. Halperin, and J.I. Niven, "The Effects of Carbon Monoxide and Altitude on Visual Thresholds," *Journal of Aviation Medicine,* 15, pp. 381–394 (1944).
109. P.J. Berenson and W.G. Robertson, in *Bioastronautics Data Book,* Biotechnology, Virginia, pp. 65–141 (1972).
110. D.L. Simms and P.L. Hinkley, *Fire Research Special Report No. 3,* Her Majesty's Stationary Office, London (1963).
111. W.V. Blockley, "Temperature Tolerance: Man: Part 1. Heat and Cold Tolerance with and Without Protective Clothing," in *Biology Data Book,* Federation of American Societies for Experimental Biology, Bethesda, MD, p. 781 (1973).
112. D.C. Edholm, "On Being Lost on Mountains, in Deserts and at Sea," in *A Companion to Medical Studies,* Blackwell, Oxford, UK, pp. 41.1–41.7 (1968).
113. J.H. Veghte, *Fire Service Today,* 49, p. 16 (1982).
114. H. Elneil, "Man in Hot and Cold Environments," in *A Companion To Medical Studies,* Blackwell, Oxford, UK, pp. 40.1–40.7 (1968).
115. C.S. Leithead and A.R. Lind, in *Heat Stress and Heat Disorders,* Cassel and Co., London (1963).
116. A.R. Moritz, F.C. Henriques, and R. McLean, "The Effects of Inhaled Heat on the Air Passages and Lungs," *American Journal of Pathology,* 21, pp. 311–325 (1945).
117. A.R. Moritz, F.C. Henriques, F.R. Dutra, and J.R. Weisiger, "Studies of thermal injury. IV. Exploration of casualty-producing attributes of conflagrations. The local and systemic effects of generalised cutaneous exposure to excessive circumambient (air) and circumambient heat of varying duration and intensity." *Archives of Pathology,* 43, pp. 466–488 (1947).
118. K. Buettner, "Effects of Extreme Heat and Cold on Human Skin. II. Surface Temperature, Pain and Heat Conductivity in Experiments with Radiant Heat," *Journal of Applied Physiology,* 3, pp. 703–713 (1951).
119. J.P. Lawrence and J.C. Bull, "Thermal Conditions Which Cause Skin Burns," *Journal of Engineering in Medicine,* 5, pp. 61–63 (1976).
120. J.P. Bull and J.C. Lawrence, "Thermal Conditions to Produce Burns," *Fire Materials,* 3, pp. 100–105 (1979).
121. A narrative summary and independent assessment of the Active Denial System. Penn State Applied Research Laboratory Human Effects Advisory Panel. 11th February 11, 2008.
122. J.B. Perkins, H.E. Pearse, and H.D. Kingsley, "Thermal Conditions to Produce Skin Burns," *UR217 Atomic Energy Project,* University of Rochester, New York (1952).
123. Y. Enson, R.M. Harvey, M.L. Lewis, W.B. Greenough, K.M. Ally, and R.A. Panno, "Hemodynamic Effects of Metabolic Acidosis in Cholera: Implications for Fluid Repletion in Severe Burns," *Annals of the New York Academy of Sciences,* 150, pp. 577–583 (1968).
124. BSI, "Medical Information on Human Reaction to Skin Contact with Hot Surfaces," *PD 6504,* British Standards Institution, London (1983).
125. B.D. Dinman, *Journal of the American Medical Association,* 235, p. 2874 (1976).
126. V. Babrauskas, B.C. Levin, R.G. Gann, et al., Toxic Potency Measurement for Fire Hazard Analysis, NIST Special Publication 827 (1991).
127. W.E. Zimmermann, "Acidosis in Severe Burns," *Annals of the New York Academy of Sciences,* 150, pp. 584–603 (1968).
128. S.M. Rosenthal and R.C. Millican, "Fluid and Electrolyte Disturbances in Experimental Burns," *Annals of the New York Academy of Sciences,* 150, pp. 604–610 (1968).
129. B.C. Zawacki, R.C. Jung, J. Joyce, and E. Rincon, "Smoke, Burns and the Natural History of Inhalation Injury in Fire Victims," *Annals of Surgery,* 185, pp. 100–110 (1977).
130. H.N. Harrison, "Respiratory Tract Injury, Pathophysiology and Response to Therapy Among Burned Patients," *Annals of the New York Academy of Sciences,* 150, pp. 627–638 (1968).
131. B.A. Zikria, W.O. Sturner, N.K. Astarjian, C.L. Fox, Jr., and J.M. Ferrer, *Annals of the New York Academy of Sciences,* 150, pp. 627–638 (1968).
132. D. Campbell, *Respiratory Tract Trauma in Burned Patients,* Colloquium, Borehamwood, UK (1985).
133. S.M. Hockey and P.J. Rew, "Human Response to Thermal Radiation," Contract Research Report No. 97/1996, HSE Books, Sudbury Suffolk, UK (1996).
134. D.A. Purser, "Review of Human Response to Thermal Radiation," *Fire Safety Journal,* 28, pp. 290–291 (1997).
135. K.A. Strom, A.J. Harner, and R.J. Karlsson, "Burn Hazard Assessment Model. Software for Characterization of the Hazards Posed by Heat and Exposure to Toxic Agents Associated with Fire," NHTSA-1998-3588-118, National Highway Traffic Safety Administration, Washington, DC (2000).
136. W.D. Woolley,"Nitrogen-Containing Products from the Thermal Decomposition of Flexible Polyurethane Foams," *British Polymer Journal,* 4, pp. 27–43 (1972).
137. W.D. Woolley, S.A. Ames, and P.J. Fardell, "Chemical Aspects of Combustion Toxicology of Fires," *Fire Materials,* 3, pp. 110–120 (1979).

138. D.A. Purser, "Toxic Product Yield and Hazard Assessment for Fully Enclosed Design Fires Involving Fire Retarded Materials," *Polymer International,* 47, pp. 1232–1255 (2000).
139. A. Silcock, D. Robinson, and N.P. Savage, "Fires in Dwellings—An Investigation of Actual Fires," *Current Paper CP80/78,* Building Research Establishment, Borehamwood, UK (1978).
140. D.A. Purser, A.A. Stec and T.R. Hull, Chapter 2: Fire scenarios and combustion conditions. In "Fire toxicity" Eds A. Stec and R. Hull. Woodhead, Cambridge UK, 2010 pp 26–50
141. D.A. Purser, A.A. Stec and T.R. Hull, Chapter 14: Effects of material and fire conditions on toxic product yields. In "Fire toxicity" Eds A. Stec and R. Hull. Woodhead, Cambridge UK, 2010 pp 515–540.
142. J.G. Quintiere, M.M. Birky, F. Macdonald, and B. Smith, "An Analysis of Smoldering Fires in Closed Compartments and Their Hazard Due to Carbon Monoxide," *Fire Materials,* 6, pp. 99–110 (1982).
143. D.A. Purser, "Interactions Between Behaviour Patterns and Physiological Impairment in Escape from Fire," in *Proceedings of Interflam'93,* Interscience Communications, London, pp. 579–593 (1993).
144. D.A. Purser, "The Development of Toxic Hazard in Fires from Polyurethane Foams and the Effects of Fire Retardants," in *Proceedings of Flame Retardants 90, (*British Plastics Federation, ed.), Elsevier, London, pp. 206–221 (1990).
145. J.A. Purser, D.A. Purser, A.A. Stec, C. Moffatt, T.R. Hull, J.Z. Su, M. Bijloos,.P. Blomqvist. Repeatability and reproducibility of the ISO/TS 19700 steady state tube furnace. Fire Safety Journal 55, 22–34(2013).
146. G.V. Alexeev and S.C. Packham, "Evaluation of Smoke Toxicity Using Concentration-Time Products," *Journal of Fire Sciences,* 2, pp. 363–379 (1984).
147. D.A. Purser, "Modeling Time to Incapacitation and Death from Toxic and Physical Hazards in Aircraft Fires," in *Conference Proceedings No. 467, Aircraft Fire Safety, NATO-AGARD,* Sintra, Portugal, pp. 41-1–41-13 (May 22–26, 1989).
148. D.A. Purser, J.A. Rowley, P.J. Fardell, and M. Bensilum, "Fully Enclosed Design Fires for Hazard Assessment in Relation to Yields of Carbon Monoxide and Hydrogen Cyanide," *Interflam'99. Eighth International Fire Science and Engineering Conference,* Edinburgh, Proceedings pp. 1163–1169, Interscience Communications, London (June–July 1999).
149. King, D.F. (1988) Aircraft Accident Report 8/88, UK Department if Transport. Air Accidents Investigation Branch. HMSO. London, UK.
150. D.A. Purser, "Behavioural Impairment in Smoke Environments," *Toxicology,* 115, pp. 25–40 (1996).
151. J. Sime, "Crowd Safety Design, Communications and Management: The Psychology of Escape Behavior," *Easinwold Papers No. 4,* pp. 16–29, Home Office Emergency Planning College, York, UK (1992
152. The Fire at Woolworth's, Piccadily, Manchester, on 8 May 1979, Home Office, London (1980).
153. Purser, D.A. Design behavioural scenarios for escape behaviour modelling in tunnels and underground complexes Advanced Research Workshop, Evacuation and Human Behaviour in Emergency Situations, University of Cantabria, Spain 21st October 2011. Proceedings pp 1–19.
154. D.A. Purser, The application of exposure concentration and dose to evaluation of the effects of irritants as components of fire hazard. Interflam 2007. 3–5th September 2007 Royal Holloway College, Egham, UK. Proceeding pp. 1033–1041. Interscience Communications, Greenwich, UK.
155. Purser D.A, Chapter 3: Hazards from smoke and irritants. In "Fire toxicity" Eds A. Stec and R. Hull. Woodhead, Cambridge UK, 2010 pp 51–117
156. Peterson, J.E. and Stewart, R.D. Absorption and elimination of carbon monoxide by inactive young men. Arch. Environ. Hlth. 21, 165–171. 1970
157. Lambersten, D. J. The atmosphere and gas exchanges with the lungs and blood. In: *Medical Physiology* (12th ed.), edited by Mountcastle, V. B. Saint Louis: The C. V. Mosby Company, 1968, volume 1, chapt. 36, p. 636–650.
158. T.E. Bernard and J. Duker, "Modeling Carbon Monoxide Uptake During Work," *American Industrial Hygiene Association Journal,* 42, pp. 361–364 (1981).
159. Y. Alarie, *Proceedings of the Inhalation Toxicology Symposium, Upjohn Company,* Ann Arbor Science (The Butterworth Group), Ann Arbor, MI (1980).
160. H.L. Kaplan, A.F. Grand, W.R. Rogers, W.G. Switzer, and G.C. Hartzell, "Combustion Gases in Postcrash Aircraft Fires," *DOT/FAA/CT-84/16,* Federal Aviation Administration, Washington, DC (1984
161. H. Salem and H. Cullumbine, "Inhalation Toxicities of Some Aldehydes," *Toxicology and Applied Pharmacology,* 2, pp. 183–187 (1960).

David A. Purser has a Ph.D. in neurophysiology and a diploma in toxicology from the Royal College of Pathologists. As former director of combustion toxicology research at Huntingdon Research Centre, England, and subsequently as associate director of the Fire Safety Engineering Centre in the Fire and Risk Sciences Division at BRE Ltd., Watford, England, he has worked on fire chemistry, combustion toxicology, fire assessment, fire incident investigation, building code development and human behavior in fires for over 35 years. Since retiring from BRE in 2006, he continues with consultancy and academic work, as adjunct faculty at the University of Maryland (until 2014) and visiting professor at the Universities of Greenwich and Central Lancashire UK. He was a member of the Scientific Advisory Committee of the US National Association of State Fire Marshals

(until 2014). He chaired the British Standards Committee on fire hazards until 2011 and serves as an expert on the International Organization for Standardization (ISO) fire hazard and fire safety engineering subcommittees and working groups.

Jamie L. McAllister has a Ph.D. in Toxicology from the University of Maryland, School of Medicine in Baltimore. Her doctoral studies focused on the exposure of fire victims to carbon monoxide and hydrogen cyanide and the development of a physiological-based hydrogen cyanide uptake model. Dr. McAllister is also a licensed Professional Engineer and holds a Bachelor and Master of Science in Fire Protection Engineering from the University of Maryland, College Park. Dr. McAllister currently serves as the Leader of the Fire & Facilities Safety Group at the National Institute of Standards and Technology in Gaithersburg, MD.

Engineering Data

64

S.M.V. Gwynne and K.E. Boyce

Introduction

This chapter is an updated version of the previous chapter "Evacuation Timing" that appeared in the fourth edition of the *SFPE Handbook*. This new version of the chapter represents a significant change to previous versions, moving from a narrative description of important case studies that include data to a tabular representation of a broader range of data-sets. It is hoped that this approach provides a useful reference resource for readers [1, 2].

Evacuation and human behavior in fires is an important consideration in any fire safety engineering design. Research in this area essentially started in the mid-1950s with the work of John Bryan [3] and was continued over the proceeding decades by numerous researchers from within fire safety and those in adjacent areas of research [4]. A renewal of enthusiasm in this work was observed with the arrival of many new researchers into the field in the 1990s and the advent and adoption of performance-based fire safety design (see Chap. 57). The improved understanding that this work generated, and the subsequent modeling capabilities that it both suggested and facilitated, forms the basis of a key element of the fire safety equation; i.e. comparing the time for a population to reach safety with the time for the conditions to become untenable, typically adopted as part of performance-based design (see Chap. 57). This work is enabled and driven by the availability of detailed, comprehensive and appropriate data to support the development of theories and engineering practice alike. This chapter represents an attempt to help the reader locate and select data for use in this work.

It is generally (although not universally) acknowledged that "hard" fire science alone cannot solve the fire problem; knowledge of human behavior is also essential [5]. The vagaries of human performance cannot be eliminated from the design process. There is a degree of skepticism in the field of fire safety engineering as to whether human behavior in fire can be understood and then represented credibly in egress analysis [6]. However, the expansion of this section of the handbook and the increasing reference to human response in regulatory documentation and guides [7, 8] is nothing if not evidence of the broad recognition that, although difficult, it is a 'necessary evil'. This chapter provides a summary of some of the key data (predominantly produced after 1985) that might support those in the fields of fire safety and fire engineering who are attempting to understand and represent human behavior in fire. This chapter should provide a useful introduction to this data and point to key reference sources for the practitioner to employ in their work.

Work on understanding evacuation and human behavior in fire, developing tools to assess it and then producing designs that account

S.M.V. Gwynne (✉) • K.E. Boyce
Built Environment Research Institute, Ulster University, UK

M.J. Hurley (ed.), *SFPE Handbook of Fire Protection Engineering*,
DOI 10.1007/978-1-4939-2565-0_64, © Society of Fire Protection Engineers 2016

for it, is multi-disciplinary in nature and requires expert input from a variety of sources. This input may take the form of ideas, models, theories and data. The variety of this input produces new ideas in the field, disparate opinions and expertise. It also introduces many inconsistencies in the terminology and techniques employed, the assumptions made and the overall objectives. These inconsistencies may influence model development, configuration, application and then the interpretation of the results produced by the model.

It should also be noted at the outset that human behavior in fire is still a relatively immature area of analysis. This is true of our understanding of basic phenomena (see Chap. 58), but particularly true of the numerical data-sets available to describe egress performance. These data originate from different sources, are provided in different formats, are based on different assumptions and described in different ways [9]. This chapter attempts to take these differences into account allowing the reader to select between the data available in as informed a manner as possible.

Given the variety of data sources available and the data formats employed, only a summary of each selected data set is provided in this chapter, providing insight into the data available and aiding the data selection process. As such this chapter provides a resource to inform the reader's selection of data, but it is essential that he/she should further investigate the data from the original source as part of the selection process. The limitations of the data available are acknowledged and therefore the informed selection between these often partial and incomplete data-sets becomes all the more important.

Using this Chapter

This chapter is intended to aid the representation of egress performance within engineering models (see Chaps. 59 and 60). There is an enormous variety in the methods adopted and the assumptions made in these models—and therefore in the data used by them. The model may be embedded within regulatory codes (i.e. the behavioral assumptions made in order to develop the regulatory rules), it may be an empirical model (where the data forms the very basis of the model), an engineering model (where data is used to derive relationships that then represent some aspects of the response), or a simulation model (where data allows the more complex computer-based tools to be configured, calibrated and validated, see Chaps. 59 and 60). This variety is reflected in the impact that the selection of different data-sets will have on the results produced by these models.

This chapter will support the use of these models by presenting data that could be used in the quantification of egress performance as part of regulatory assessment (the primary function), and presenting data that enables the examination of design variants, developing procedures, or further research. The chapter is intended to provide an overview of this data. It will provide, in most cases, a *tabular* summary of a range of data-sets available for the basic behavioral elements required to assess egress performance. These elements, derived from the basic engineering timeline which is typically used to describe expected performance phases [10], will be briefly discussed. The data-sets will be presented in the same format within each of the core behavioral elements identified, thus simplifying comparison between them. These behavioral elements have been deliberately selected as those that are fundamental to the most basic egress analysis (see Chaps. 59 and 60). It is hoped that this approach will allow the reader to compare the appropriateness of the data-sets shown and then follow up on the details of the data-sets once an initial selection has been made. The tables will provide information sufficient for the reader to identify whether the data set is representative of the scenario that they wish to represent. However, it is essential that the reader accesses the original source of the data set (also provided in the table) for further information to enable them to utilize it with confidence. It is acknowledged that this chapter presently excludes some data that might be of value; specifically, data regarding the decision-making process during the evacuation is not included. Although this data is critical,

it is not widely employed within the modeling or the performance based design process (irrespective of how much the authors would like it to be). Given space constraints, this is left to be addressed elsewhere (see Chap. 58).

This chapter is not intended to provide definitive guidance on which of the data-sets should be used in particular scenarios of interest. This decision should be taken through examining this chapter in conjunction with several of the other chapters in this handbook. It would currently be impractical to provide definitive data-sets for the myriad scenarios that may be examined and the many engineering models that might be employed [11, 12]. This chapter is, therefore, intended to provide the reader with sufficient information to identify data-sets of interest and then explore them further; i.e., provide an initial reference for the fire safety engineer to focus their search and guidance to aid in this search. In addition, there are a number of online resources that the reader may consult to find contemporary reviews of the data available [13–16]. Even here, the reader is advised to seek out the original source material to ensure suitability.

The data-sets might be used in a number of ways including:

- Configuring hydraulic calculations for use e.g. augmenting the guidance provided in Chap. 59.
- Developing hydraulic calculations independently from Chap. 59.
- Configuring egress tools for use (see Chaps. 59 and 60). For instance, providing model parameter values to be used in representing a particular scenario (see Chap. 57).
- Developing egress tools (see Chaps. 59 and 60).
- Examining the assumptions of the work of others (see Chap. 57).
- Performing expert analysis i.e. helping to support a particular expert opinion regarding evacuee performance.

The approach outlined has been adopted to ensure that it benefits a range of potential readers, although primarily focused at the fire safety engineer. It is expected that engineers, designers, those assessing designs (e.g. Authorities Having Jurisdiction (AHJ)), model developers and researchers may find value in the data-sets provided. These users will have different requirements of the data-sets presented and needs that might only be completely satisfied through a full and lengthy description of each data-set.

Using the Data Provided

The data described in this chapter should not be employed without an understanding of the subject matter involved; i.e. human behavior in fire. The data-sets provided in this chapter are intended to be used in conjunction with the methods and data provided in a number of the companion chapters in this handbook. It is therefore highly recommended that the reader examines all of the chapters in this section prior to selecting any of the data-sets for further use. This should then at least provide a basic understanding of the key factors and behavioral elements to be taken into consideration during the selection process. When taken as a whole, this set of chapters should provide the reader with sufficient information to understand expected human response, quantify this response, represent this response as part of engineering analysis (within a design scenario) and then interpret and present the results in an informed manner. A schematic of the assumed relationship between the subject areas covered in these chapters is presented in Fig. 64.1, although it is recognized that the exact relationship between these chapters will be somewhat dependent upon the nature of the application.

As noted above, the user will typically require a basic understanding of the subject matter involved. The currently available theories which explain human response in fire are provided in Chap. 58. This chapter should form the basis of any analysis as it describes the subject matter involved and enables the reader to develop a qualitative understanding of the evacuation process with the evacuee as the focus

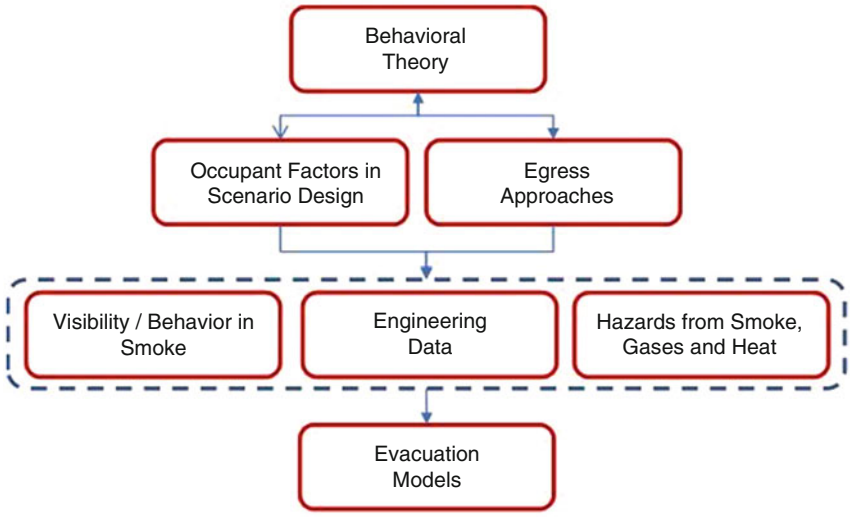

Fig. 64.1 Relationship between subject areas in this section

before attempting to quantify performance. The nature of the engineering design process and the emergency procedures that might appear within that process are described in Chaps. 56 and 57. These chapters formulate the way in which the behavioral theories might be applied; i.e. what aspects of the underlying subject matter should be represented and what impact might they have in a real-world environment. Chapters 61 and 63 provide data to quantify this design process; they provide a numerical underpinning to the qualitative and scenario-based descriptions outlined earlier. These chapters are vital in translating the real-world elements into the simulated environment. Finally, Chaps. 59 and 60 describes the models that might be applied to utilize this data in order to assess performance within the simulated environment.

Quantifying Egress

This section discusses the key factors that influence the quantification of egress. In section "Subject Matter: Human Behavior in Fire", the primary subject matter of egress analysis, i.e. human behavior in fire, is briefly discussed. An understanding of the subject matter directly influences how the models are constructed, the data that is deemed to be required and then use of the data within the quantification process.

Section "Engineering Timeline" describes the engineering timeline. This is important as it defines, at a high-level, the core components that need to be represented during the engineering analysis and therefore that need to be supported by data. As has been noted, in reality, individuals operate at a more refined level and in a more complex manner. It is the discrepancy between the individual and engineering levels that often leads to misinterpretation of the data available. It is anticipated that the following sections will help the reader address some of the issues highlighted.

Subject Matter: Human Behavior in Fire

In contrast to the panic model previously assumed, the response of an individual during an incident can be better characterized as involving a decision-making *process* [17, 18]. This process is influenced by internal and external elements that can interact and change as the incident progresses. If this response is oversimplified or ignored, then the engineer may neglect key elements that they need to represent using the data available. It is therefore important

to understand the key subject matter elements that may be represented or ignored in specific data-sets in order to assess their appropriateness for the application in question. These elements include:

- The procedures in place within the structure as dictated by the resident organization,
- The environmental conditions to which the individual is exposed at any point in time,
- The actions of those around the individual given the relationships that exist between them,
- The physical, cognitive, sensory and experimential attributes of the individual,
- The information available and the sub-set of this information that is noted by the individual (given their current alertness, attention levels and actions),
- The individual's perception of this information, their ability to understand it and to assess the situation and the threat posed to them or significant others,
- The individual's role and position within the current group/organizational/social structure, and the associated norms and responsibilities with this role,
- The viable options available to the individual in any situation,
- The individual's ability to assess and select a response option, given the temporal, physical and social constraints present, and
- The ability of the individual to enact this option [19].

The decision making process is a highly coupled, iterative process where each of the elements are often interchanged and modified in real-time, depending on the scenario faced. Understanding this process and the factors that influence response is critical for model development and model application; i.e. critical to the engineering process in general [20, 21]. Although this process is complex, it is comprehensible and is in contrast to both the panic model (where an almost complete absence of process is assumed) and stimulus-response approach (where the process is reduced to individual responses initiated only by external triggers).

The decision making process is then an important influence upon performance and therefore upon the data that might be collected. Any data collected or used will need to account for the key elements of this process (see Chap. 58). However, these elements may be combined, simplified or deliberately omitted in the data representation (along with other limitations with our understanding of the subject matter). It is therefore important that the manipulation of these elements in the original data analysis needs to be clearly understood and justified this can only be achieved through an understanding of the decision-making process itself.

This description of the decision-making process is very much from the individual's perspective. The combined actions and interactions of individuals produce emergent conditions by which a design might then be judged during an engineering analysis (see section "Engineering Timeline" discussing the engineering timeline). Within the engineering analysis, these emergent conditions may be predicted by the model employed or imposed by the user [22]. The data will need to reflect some aspect of the engineering timeline (see Fig. 64.2). In reality the partitions present in the timeline may not be sufficient to reflect the complexity and variety of the individual decision-making processes or the associated data. It is therefore important for the engineer to understand the compromises being made by selecting certain data-sets.

The individual decision-making process is described in more detail in Chap. 58. This process can also be accounted for within the scenario design; i.e., the outcome of the decision-making process can be reflected in the scenarios to which the egress models are employed. This is described in Chap. 57. In addition, the manner in which the decision-making process and associated behavioral actions are represented within the egress models applied is described in Chaps. 59 and 60. As is apparent, the assumption that the individual goes through a decision-making process during an evacuation is fundamental to many of the chapters in this section. In this chapter, the decision-making process

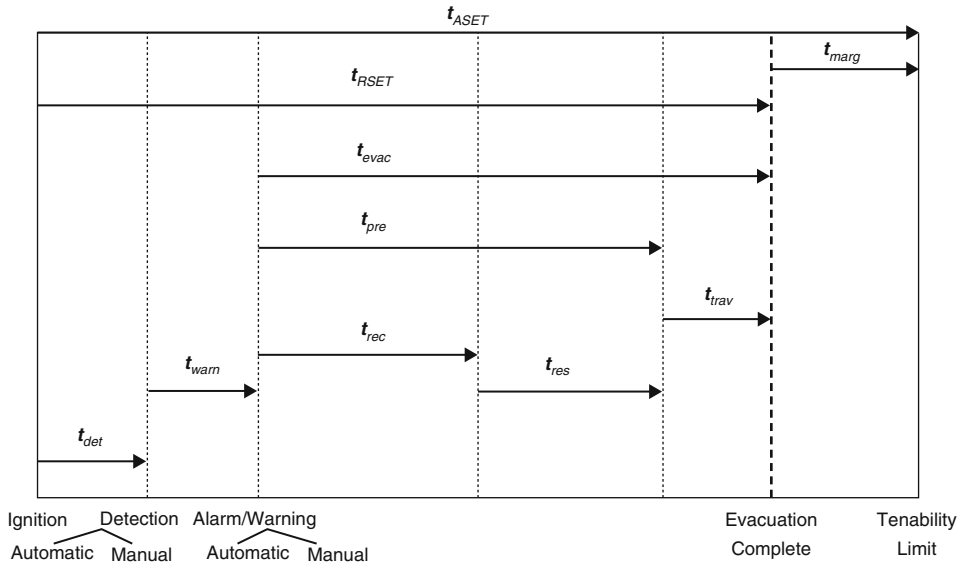

Fig. 64.2 Engineering timeline

influences the categorization of the data-sets and the manner in which the data is presented.

Engineering Timeline

Typically, engineering and computational models are employed to establish an engineering timeline, or some aspect of it. This timeline represents the total evacuation process, which is broken down into several distinct components. This timeline typically operates at the level of the population, rather than the individual and is therefore a simplification of numerous individual actions and responses that take place, the complexity of which has been alluded to above and in Chap. 58. The components within the timeline are therefore aggregates of lower level performance, based on technical or human resources. Different versions of this timeline are available in numerous regulatory and guidance documents [7, 22, 23]. A version of this timeline is shown in Fig. 64.2. This timeline also represents subject areas discussed in other chapters in this Handbook.

The engineering timeline shown in Fig. 64.2 includes the following components:

- *Detection time* (t_{det})—The interval between fire ignition and the first detection of the fire by a device or an individual.
- ***Warning time*** (t_{warn})—The interval between detection of the fire and the time at which an alarm signal is activated or notification of occupants takes place.
- ***Pre-evacuation time*** (t_{pre})—The interval between the time at which a general alarm signal or warning is given and the time at which the first deliberate evacuation movement is made. This consists of two components: recognition time and response time.
- *Recognition time* (t_{rec})—The interval between the time at which the alarm signal is perceived and the time at which the occupant interprets this signal as indicating a fire/emergency event. This time includes investigation and milling, for example, to determine the situation.
- *Response time* (t_{res})—The interval between recognition time and the time at which the first move is made to evacuate the building. This time includes activities such as fire-fighting, warning others, gathering family members and pets, dressing, retrieving

personal belongings, calling the fire department, and so on.

- ***Travel time*** (t_{trav})—The time needed, once movement toward an exit has begun, for all occupants to reach a place of safety.
- *Evacuation time* (t_{evac})—The time from the alarm signal to the time at which the occupants reach a place of safety. This is the sum of the pre-evacuation time (t_{pre}) and the travel time (t_{trav}).
- *Required Safe Escape Time* (t_{RSET})—The calculated time necessary between ignition of a fire and the time at which all occupants can reach an area of safety. This is the sum of the detection time (t_{det}), the warning time (t_{warn}) and the evacuation time (t_{evac}). This is equivalent to the escape time (t_{esc}).
- *Available Safe Egress Time* (t_{ASET})—The calculated time available between ignition of a fire and the time at which tenability criteria are exceeded in the means of egress. t_{ASET} should be longer than t_{RSET} by an acceptable margin of safety.

The terms highlighted in bold are the focus of this chapter. It should be noted that the terms used to describe t_{RSET} can vary. The term Required Safe Escape Time [7] is adopted here, but *Required Safe Egress Time* [23] is also often used. The exact terminology employed to describe the other components also differs based on its origin and intended use. This has been described in detail by Gwynne [9], where a range of different terms is explored. A summary of the various terms employed for two of the key behavioral components, t_{pre} and t_{trav} are provided in Table 64.1.

The engineering timeline extends from the time of ignition to when untenable conditions are reached. The time of ignition is the starting point of the fire event. Following ignition, a time should be calculated for detection to take place. Detection could take anywhere from a few seconds to a few hours depending on the type of fire and the detection devices in place. Detection could be accomplished by staff/occupants who discover the fire or perceive cues of the incident (e.g., smell of smoke) or through the activation of a detection system.

Table 64.1 Range of terminology used to describe behavioral components

Timeline behavioral component	Terminology employed	
t_{pre}	Pre-response time	PIA (perception, interpretation, action) time
	Response time	Time to initial move
	Pre-evacuation time	Pre-egress activity time
	Pre-movement time	Time to start evacuation
	Pre-travel activity time	Pre-evacuation activity time
	Delay time	Time to start
	Start-up time	Dawdle time
t_{trav}	Movement time	Arrival time
	Event time	Clearance time
	Evacuation movement time	Evacuation time
	Travel time	Trans-movement decisions
	Egress time	Time

An elapsed time might need to be calculated between detection and alarm activation. In some cases, these two events are almost simultaneous; for instance, smoke detectors are often linked to a general alarm which issues an immediate warning signal. There could, however, be a delay between detection and alarm, for example, if occupants discover a fire and have to manually activate the fire alarm signal at a pull-station, or where a procedure is in place that requires confirmation of the incident by a member of staff and staff communication to allow the public alarm to be provided [11, 12].

The first two components of the RSET calculation i.e., t_{det} and $t_{warn,}$ can be formed from a combination of technological and/or human resources and the balance of these resources will depend on the scenario and on the procedural measures in place to respond to it. Where automatic detection and alarm is employed, typically, t_{det} and t_{warn} will be determined with reference to manufacturer's guidance on sensor response and often do not take staff activities into account. However, this is not always the

case and in some instances human resources play a more prominent role and therefore need to be accounted for within the engineering timeline.

The selection of the procedural resources employed to detect and alert will be influenced by a number of factors; e.g., the cost, the infrastructure, the nature of the occupancy and the expected incident scenarios. However, it is certainly possible that staff (or other occupants) will be involved in the detection of the original incident and the raising of the alarm and it is important to recognize that this involvement might delay the point at which the pre-evacuation phase begins for the general population; i.e., there is a potential delay as staff interpret the cues available to them and then respond.

Any delay in detection and warning (also previously referred to as Pre-Warning time [11, 12, 24, 25] may be procedural and/or cognitive (i.e. part of the formal procedure) and/or dependent on the decision-making activities of the staff in question. The need for and extent of human involvement in issuing a warning can vary depending on the emergency response procedures of the affected building and the detection and warning systems used.

Typically, the delay in detection and warning is either not accounted for in engineering analysis or is based on the time for the technical system in place to detect the incident, rather than the staff response to it. Just as with the pre-evacuation time for an evacuee, these times i.e. t_{det} and t_{warn} can amount to a significant time period depending on the nature of the event, the technological and human resources available, the nature of the space, the staff involved, the staff hierarchy present and the procedures in place.

There are often legitimate reasons as to why staff involvement prior to the raising of the alarm is deemed necessary in some buildings, especially major public venues: (a) an evacuation can lead to significant disruption to the normal operation of the building; (b) starting an evacuation automatically regardless of the circumstance is not only commercially costly, but also unacceptable to the public, and may prejudice later evacuee interpretation of emergency alarms; (c) evacuation is not without risk and can produce additional (and more significant) hazards than the original incident; (d) the evacuation may need to be carefully managed, requiring staff to be briefed and in position before commencement or (e) depending upon the circumstances a full scale evacuation of a building may not be the most appropriate course of action. Many of these potential procedural influences can be recognized during the design phase and, as such, the engineer may be able to factor these into the design process through the use of an extended warning/delay time.

Often, detection and notification systems have 'failsafe' measures to ensure that once an incident has been detected it is not entirely ignored. For instance, should a detection signal not be acknowledged or acted upon within a certain period of time e.g., 2 min then a general alarm will automatically be signalled. If enabled, these may provide an upper limit as to the warning time in such a procedure. However, where this measure is deliberately overridden, disabled or absent, then the warning delay may not be limited or predicted by the 'failsafe' setting associated with the system. Again, the potential for this may be acknowledged within the design process, albeit that it is difficult to quantify.

The engineer might therefore choose to include a detection and warning delay component to account for the staff decision-making and response activities, especially if they form part of the formal procedure and can therefore be expected to take place. In effect, the warning period could be better represented by including an estimate of the accumulation of individual staff decision-making processes and subsequent activities that go to delay the provision of the warning.

When a cue, a warning by a notification system or an individual has been perceived, then the population has the opportunity to commence evacuation. However, typically there is a delay between initial awareness of the incident and purposive movement towards safety, the pre-evacuation time (t_{pre}) which is due to the population's interpretation of the information available and/or actions that they might need to perform prior to evacuating. Purser (and others)

identified that pre-evacuation time comprises of two subcomponents; i.e. recognition and response [26]. In the recognition phase, the occupant will perceive information such as the fire alarm signal, the sight of smoke, or warning by others. Interpretation of this information may take some time. As information on the unfolding event is perceived, the occupant will start responding by taking different actions such as investigating the situation, attempting to fight the fire, calling for help, and gathering belongings and family members i.e. actions that do not necessary move them closer to a place of safety. Eventually the decision to evacuate the building, to search for a refuge or to protect-in-place will be taken, which will complete the pre-evacuation phase (assuming that the entire population decides to eventually evacuate). In this chapter, the data is typically presented in terms of the overall pre-evacuation time. Where the data is broken down to a lower level (e.g. recognition and response), this is also noted.

The travel time only starts when the occupant has initiated movement towards a place of safety, whatever that might be. In this context, travel relates to the movement performed as part of the evacuation process. It is acknowledged that an individual may also move during the pre-evacuation phase, but it is assumed here that this is addressed in the pre-evacuation delay experienced. In its most basic form, travel time should be calculated from the traversal time to move along the specified egress route and the flow time through various elements of the egress system (as discussed in Chap. 60). In reality, an evacuee may engage in numerous activities during this phase that are not directly involved in moving towards a place of safety (see Chap. 58). However, these are not typically (or explicitly) represented in an egress analysis, except where they involve an evacuee responding to the evacuation movement of others; e.g. being delaying in congestion.

All the times previously discussed together comprise The Required Safe Escape Time (t_{RSET}) is calculated from the time of ignition until the last occupant to evacuate has reached a location of safety. This time should be less than the time for untenable conditions to occur in the egress path (t_{ASET}). The time between the population reaching safety and the conditions becoming untenable should be sufficient to provide an acceptable margin of safety (t_{marg} in Fig. 64.2). The t_{RSET} value can therefore be formulated as follows

$$t_{RSET} = t_{det} + t_{warn} + t_{pre} + t_{trav}$$

Depending on the scenario, each of the t_{RSET} phases can have a significant impact on the time for the target population to reach safety. Although there is some general (primarily qualitative) discussion of the detection time, t_{det} and the warning time t_{warn} in section "Detection and Warning Phases: Human Aspect", of this chapter, the focus here is on the primary behavioral components: t_{pre} and t_{trav}. The data-sets described will relate specifically to the quantitative assessment of these components and the factors that might contribute to this assessment.

In section "Model Approaches and Data Requirements", the approaches adopted within egress models are discussed, specifically relating to the requirements that these approaches place on the data available.

Model Approaches and Data Requirements

Establishing the time for a population to reach safety is relatively complex, and it is considerably more difficult than estimating movement time alone (see Chap. 58 and previous section). The various attempts at representing this process as part of egress analysis are described in Chaps. 59 and 60.

There are a range of different models that are used to explicitly or implicitly establish egress performance; i.e. models that produce a *quantitative* assessment or assume a performance level. These models require a range of data either in their development or their application in support of the behavioral model in situ [22]. The various types of models employ different techniques, cover different areas of the evacuation process

and operate at different levels of sophistication and refinement. As a consequence, models require data in different formats and to address different subject matter. Models can be broadly categorized into six different types, each with their own data needs:

1. Prescriptive Codes: Pre-defined rules based on experience (i.e., expertise and lessons learned from real incidents), that are then codified into a guidance/regulatory framework. Data are used to support the development of these rules, which form an implicit behavioral model. This data is not used to subsequently apply the model (as might the case in other types of models) but rather to support the development of the rules.
2. Full-scale evacuation demonstration: The use of a representative population and scenario (s), e.g. the evacuation of an actual office block to gain insight into performance of a structure under specific conditions. Data may be used to help inform expectations regarding performance and then organize the management and data-collection activities. In this context, the mock evacuation is taken as an indication of how the population may perform during an actual incident; i.e., is a model of reality.
3. Theoretical Model/Expert analysis: Data-sets are used to develop a theory describing some performance component. A set of theories are then employed as part of expert analysis/engineering judgment to assess some issue. This assessment may well use further data to support the analysis and make it more specific. This process is highly dependent on the availability and use of data from the development of the theories to their application.
4. Engineering calculation at the level of the *Structure*, based on empirical correlation/analysis: Empirical data relating to an entire structure are analyzed to produce high-level functions to predict performance assuming similarities (i.e., at the structural level). Data-sets are used directly in the production of the model and in the application to examine the performance of other similar structures. Data-sets may also be used in verification and validation of the model developed.
5. Engineering calculation at the level of the *Component* (Hydraulic models): Data-sets are collected from the evacuation of structures and then analyzed to produce low-level component-based functions to predict performance at the component level (e.g., doorway, corridor, stair, etc.). These are then chained together to represent the egress performance along paths out of the structure based on the flow, speed and density relationships assumed and the structural and occupancy assumptions made. Data-sets are then used directly in the production of the model and in the application. Data-sets may also be used in verification and validation of the model developed.
6. Computational Egress models: These tools include the coding of the previous three bullets. These provide different levels of sophistication and have different data requirements depending on the nature of the model itself. These may require data both to develop and configure the models for use. Data-sets may also be used in verification and validation of the model developed.

Egress models will employ different methods to produce a performance assessment [22]. Each model type also represents the key components (e.g., the structure, the population, behavior, procedural activities, environmental conditions, etc.) in some form using different techniques and to a different degree of refinement (see Chap. 60). More refined models represent individual agents and their movement within a detailed representation of the structural space; i.e. where the internal structure, obstacles, etc., are represented. In this space, the simulated agents may be subject to environment, behavioral and procedural influences present, i.e. they attempt to represent some of the influences and processes described previously in a simplified manner. Conversely, other models employ a less refined representation with the population flowing between more crudely defined architectural spaces. Other models fall somewhere in

between these two extremes [22, 27]. The variety of this representation (and therefore the relationship with the data available) is further complicated through the approach employed to represent evacuee behavior, i.e. whether it focuses on movement alone, has a behavioral model, or somewhere in between (see also Chaps. 59 and 60). *In addition to each model needing data in their development*, *each has their own data needs in their application*; *however*, *they will all need data in order to be applied at all*.

Depending on the sophistication of the model, they could be employed in a number of different application modes, each of which places a different onus on the user and on the data required. For instance, the level of configuration required of the user will be dependent on the sophistication of the model, the predictive capabilities of the model and the application. This will influence the scope and detail required of the data-sets sought out. This is described in more detail in Chap. 60.

Human Behavior Data

The evolution of the field has led to an incomplete, disorganized and disparate understanding of the subject of human behavior in fire. This has been due in part to the diverse background of those contributing to the field (e.g., engineers, social scientists, field researchers and model developers) and the changing opinions in the field as to what constitutes necessary information.

Human behavior in fire is not adequately supported by the data available [9] and this should be understood before interrogating the data-sets presented. This suggests that there may well not be an ideal data 'fit' for the scenario at hand, i.e. compromises are often required. The data-sets that are available are therefore often not sufficient, i.e. not sufficiently comprehensive or detailed for the range of intended applications. This limitation should influence model development, selection and application. This constraint underlies the selection of the approach adopted during this chapter which is to provide a synopsis of a wide variety of data-sets rather than a detailed narrative of a limited number of seminal research or well publicized incidents.

Given the increased use of these egress calculation techniques (through greater adoption of performance based design to accommodate innovation, ethical issues, financial issues), it is essential that the underlying methods employed are appropriate to their respective, often wide ranging applications. These methods require the provision of accessible, detailed and unambiguous data in order for them to be appropriately configured and validated. Empirical data-sets addressing human performance are difficult to locate, not sufficiently detailed, dispersed, and are often employed without sufficient understanding of the context in which they were collected. The application of this data could be improved with better knowledge of:

- The conditions of the event from which the data originated,
- The methods used before and after the event to collect and analyze the data, and
- A detailed representation of the data itself.

Without this context data can be misunderstood and misapplied. The intention here is to provide sufficient information for the user to identify the underlying conditions influencing the data and/or identify where omissions exist regarding our understanding of these conditions. The importance of context is discussed in the following sections.

Data Collection: Context

Data can be obtained using a variety of research methods and data collection techniques. It is important to understand how the data was obtained, since the choice of research method and data collection techniques can influence the validity (internal and external) and reliability of the results. Validity refers to the correctness of the study findings; in other words, the extent to which it measures what it is supposed to measure. Internal validity is the extent to which cause and effect relationships can be accurately identified within the study, whereas external

validity refers to whether the findings of the study are generalizable to a real-life setting. It is often useful to consider the external validity of the research relative to the objective of the study. For example, if a study aims to determine the effectiveness of a particular type of alarm system on pre-evacuation time, then the external validity of an announced evacuation would be lower than that of an unannounced evacuation since it is expected that in the latter case participants' behavior would be more similar to a real emergency than in the former. This may influence the value which is placed on the data that is subsequently produced. Reliability, on the other hand, refers to the repeatability of a study; i.e. whether the study is properly documented such that the conditions can in fact be characterized and described in detail and that the data collection techniques used are sufficiently precise. Although not explicitly considered here in relation to the data sets presented, the validity of any data-set should be established by the reader when examining the appropriateness of the data-sets for use. It is therefore important when considering any data set to determine how representative, detailed, comprehensive, consistent and robust the data is and whether it is appropriate for this data to be used in the application at hand.

Broadly speaking, research methods can be categorized as follows [9].

- Experimental trials:
  - Hypothetical scenarios (e.g. response to video playback, simulated environment, tabletop exercises, large-scale pre-planned field exercises, etc.). Typically, those taking part are aware that they involved in the event given the artificial nature of the surroundings and the obvious preparations required to organize and conduct the scenario. For instance, getting participants to control an avatar within a simulated environment, or asking commanders to respond to simulated feedback within a command room.
  - Controlled experiments (e.g. laboratory trials). Again, typically participants would be aware of the nature of the trials being conducted. These might focus on, for example, a particular act (time to ascend stairs, open a door), a particular influence of a factor on performance (the impact of smoke on decision-making, etc.), or behavior in a specific situation (e.g. being alone, in a group, etc.), The user of data produced by small-scale component tests should be aware of the primary performance factor being examined and how this might be integrated into the analysis being performed. This will allow them to establish the credibility of the claims made—especially regarding other secondary or peripheral factors derived from the data-set.
  - Field investigations (drills, etc.). These may be announced or unannounced. Depending on the nature of the experiment, the population involved may have some forewarning of the event, may not be exposed to deteriorating environmental conditions, and/or may become aware that the event is not real. All of these may influence the external validity of the results produced.
- Case Studies / Formal incident investigations. These are performed in order to understand the events during an actual incident and what factors contributed to it [9]. Such investigations tend to focus on establishing the chain of events and factors that contributed to the outcome, rather than producing quantitative estimates of times or capabilities relative to the time line. The user should therefore be cautious if presented with such from this type of study.

It should be noted that not all of these research methods are represented in the various tables that present the data-sets examined here. However, this does not preclude the reader from encountering them in data-sets not presented here or in the presentation of future data-sets.

In reality, the individual is part of a temporal-spatial environment formed within the structure in which the incident has occurred, the history of the structure's use, and the procedural framework associated with the incident—the physical, historical and procedural environment [22].

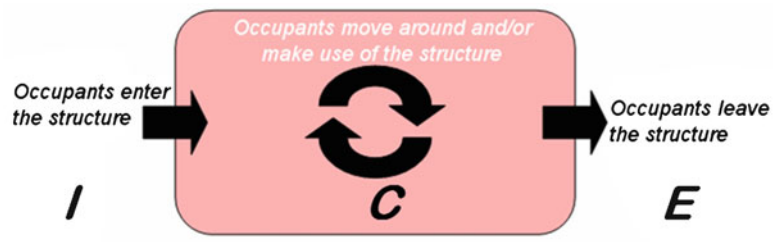

Fig. 64.3 ICE—the three phases of people movement [27]

This is briefly described below in order to further elaborate on the importance of *context* when understanding the data available, its limitations, its applicability to the target scenario and then how it might eventually be employed.

A building can be seen as a people movement system that operates in three phases: ingress (people enter the building), circulation (people use the building) and egress (people leave the building). Therefore, for the building to function people have to arrive and enter the building; during its use, people circulate around the building and, eventually, people leave the building (see Fig. 64.3). Data may relate to any of these phases—it may have been collected when people entered, used or left a building under different situations. This is not reflected in the engineering timeline which (deliberately) partitions the events into distinct separate sections. This is obviously a simplification. In this chapter the description of the data-sets makes reference to these phases where appropriate and where known.

The acronym ICE (ingress, circulation and egress) is used to describe the system of people movement [27–29]. The phases shown in Fig. 64.3 are highly coupled—they co-exist and interact; for instance, people may enter a building while others use and leave the building. Furthermore, the way that a building is entered may influence the way that it is left, which is important during any egress analysis. These phases may also occur at any point during the engineering timeline, or vice versa. This has implications for the understanding and use of movement data; i.e., the phase of movement during which a data-set was produced may not necessarily be the same phase to which it is required to be applied. For instance, escalator data is typically collected during circulation movement, but might conceivably be applied in future analyses where escalators are employed as a component used in an emergency. This does not necessarily preclude its use or prevent there being a significant overlap between the underlying conditions and the expected behavior; however, it is important for the data user to be aware of this in order for them to use the data in an informed manner.

In this chapter data-sets representing general circulation, emergency egress and non-emergency egress are presented. In the description of each data-set, the nature of the event being represented is made clear using abbreviated terms (real incident [I], circulation movement [C], an announced evacuation drill [AE], an unannounced evacuation drill [UE] or an experimental trial [ET]), reflecting the variety of emergency/non-emergency circulation and egress being represented.

Data Collection: Techniques

Data collection techniques are the "measuring instruments" of the research study; i.e., these can be employed during the data collection activities of the various research methods highlighted previously. These instruments can be used individually, but often studies combine them to improve the quality of the research. Triangulation of data using different instruments can be used to corroborate findings and lead to improved validity and reliability of results i.e. data. Data collection techniques commonly used in human behavior in fire research can be broadly categorized as surveys (including interviews and questionnaires), observations, reviews and simulations.

- Surveys—getting information from a sample. Data collected through questionnaires or interviews designed to determine the characteristics, actions, opinions etc., of a particular sample. The user should be aware of the nature of the survey (e.g., whether it was open or closed), the content (e.g., what was actually being asked), the mode (telephone, online, face-face), the sampling approach adopted, and the size and nature of the sample obtained
- Observations—getting information on the sample. Movement/actions are directly observed in some form, without necessarily relying on the verbal communication with those involved. The technique employed to collect the data will influence the format in which the data is collected, the focus of data collection resources, the nature of the data collected, whether the data relates to a time, a space, a person, a condition, etc., and the overall precision and accuracy of the data. There are a number of methods available to collect data:
  - Stationary video camera—providing a fixed stream of information for a particular location/situation, using existing CCTV/security cameras or specially located cameras. This data source has the potential to record behavior in both emergency and non-emergency situations; therefore the user of the data should be aware that there may be discrepancies between the scenario recorded and the scenario of interest,
  - Roving video camera—allows for capturing of progressive conditions experienced by selected individuals or groups,
  - Still photograph—allows a snapshot of a situation to be established at a point(s) in time,
  - Human observer—allows individuals to make manual numerical and/or descriptive observations,
  - Human participant—first person accounts of researcher participation in a situation (either contrived or accidental).
  - Electronic Sensor/Automated Measurement/RFID technology—devices deliberately inserted (often requiring the participants to carry a device) into a location to monitor movement/behavior.
  - Scanner—non-visual methods (e.g. laser techniques) to establish the movement of populations. Often this does not involve identifying those involved.
- Simulated data—generating information on the sample. The use of computational tools to explore egress performance under conditions that could not be explored directly, such as catastrophic fire conditions. The strength of this type of data is highly dependent upon the nature and sophistication of the model used. It may be one of the few options available to investigate performance under extreme conditions; however, the limitations of the model, the process and the data produced should be clearly understood. Simulated or compiled data (e.g. engineering curves) are often confused with direct observations and so great care should be used to identify the source appropriately.

Although not based on new data, the review of existing material/secondary resources such as academic literature, journalistic sources, anecdotal evidence, and material from adjacent fields of research [20, 30–32] i.e. compiling information on/from previous samples, can also provide additional evidence. The value of the source will be dependent on the appropriateness and credibility of the secondary source given the intended application. The ability to assess this appropriateness will largely be influenced by the background information provided by the original authors.

Third-party data users need to be aware of the data collection methods employed to better assess the underlying research, the validity and reliability of the data, and hence the suitability of this data for their needs.

Data Collection: Process

Data does not exist independently of the collection process, i.e. data are not collected in a vacuum. The data collection process requires

decisions to be made at a number of stages, and these directly influence the scope and refinement of the data, and the applicability of this data. Hence, it is important to understand the process by which data are produced in order to apply it appropriately and responsibly.

Initially, a decision has to be made by someone to acquire or seek out data—an omission or weakness in the data available has to be noted and a need established. The data acquisition process is therefore selective. The data collection methods selected may be based on their appropriateness, but also based on less rational reasons, e.g., available expertise, cost, convenience and these choices directly influence the credibility and applicability of the data.

Once the research is conducted, the data are extracted and analyzed and then the data and the derived understanding are described and presented, i.e., the data is distilled into a representative state from a raw form and summarized along with the background information that is available (according to the information collected) and deemed worthy of inclusion by the researchers. When researchers produce a document and present the data, they decide what is relevant and specifically what is relevant to the project at hand. This means that sometimes insufficient information is presented on the data collection methods, context or the results to enable selection to be made in an informed manner by third parties.

The data-sets are then shared with an audience of interested third parties (in academic journals, conferences or readers of this handbook). Having had access to the data, these third parties (engineers, modelers, other researchers) attempt to understand the data according to the presented format and the associated background information and, on this basis, the data are then applied. However, it is important to note that not only is data acquisition selective, but data use is also selective and not necessarily based on the appropriateness of the data itself, i.e. third party users of data may not necessarily source or utilize the most appropriate data for their application, but instead make judgments based on those sources with which they are most familiar or to which they have ready access. This choice is compounded and made difficult by the limited background information associated with the data and the data being provided in a summarized form. In such circumstances the likelihood of data being inappropriately employed for a particular application is increased.

There are a number of opportunities within this process for the data to be misrepresented, misunderstood and misapplied. In most instances, only a sub-set of the data collected is shared, i.e., it is shared in a reduced/distilled format rather than in a complete format. Potentially, and more importantly, in the vast majority of cases only a limited amount of information is provided on the background conditions evident during the original event, i.e., the scenario that produced the data. The reduced data-set and limited context then requires a greater degree of interpretation by the third party. This increases the potential for the underlying causal factors being misunderstood, the results being misinterpreted, and the data-set being inappropriately applied. Although it may be impossible for the third party viewer to understand the content of the information omitted, it may be possible for them to ascertain the type of information omitted and then draw their own conclusions—determining whether or not this omission is critical.

When viewing past data collection, it is important to understand the assumptions made by the data collectors. The collector's 'theoretical' assumptions would have influenced the methods employed, the data collection techniques used and the data actually collected. The format adopted in this chapter represents an attempt to intervene in this process by providing the reader with sufficient background information for them to establish the appropriateness of a data-set (and the data included and excluded), and also to encourage data users to become aware of the importance of understanding the context in which any data set was developed whenever data-sets are to be employed in the future.

Data Selection and Representation

The intention is that the data-sets described in the following sections are presented in sufficient detail such that they might reasonably be employed as part of the engineering process where deemed applicable. Where there is sufficient data to support it, a table is produced. Where there is insufficient data, the data-sets are described in the text, with a detailed description of each data-set provided.

The following paragraphs describe the sources of the data and the structure of the data presentation. *An attempt has been made to ensure consistency between the table designs and content to allow comparison and to improve accessibility*.

Sources of Data

Data has been sought from those sources typically considered as credible outlets within the field. These outlets include:

- Journal publications: Journal of Fire Protection Engineering, Fire Safety Journal, Fire Technology, Fire and Materials, Safety Science, International Journal of Performance-Based Fire Codes, Journal of Applied Fire Sciences, Building and Environment, Journal of Transportation Engineering Transportation Research Record, Physica A, and
- Conference proceedings: International Association Fire Safety Science (IAFSS), Interflam, Pedestrian and Evacuation Dynamics (PED), Human Behavior in Fire, Asia-Oceania Association for Fire and Technology, Mobility and Transport for Elderly and Disabled People.

In addition to these publications, other reports were included, where deemed appropriate; for instance, reports of National Bureau of Standards (NBS), National Institute of Science and Technology (NIST), National Fire Protection Association (NFPA), National Research Council Canada (NRCC), Fire Protection Research Foundation (FPRF), Lund Department of Fire Safety Engineering, Building Research Establishment (BRE, UK), VTT (Finland), Fire Research Institute of Japan.. Occasionally, PhD dissertations which are readily accessible (on-line) are also included, although these were identified and used on a more selective basis.

These sources were identified according to the following criteria:

- Publically available—so that the sources can be followed up by interested readers,
- Written in English (or where translations were available on request)—so that the resources can be understood by those reading this handbook,
- Published after 1985—so that the data sources are fairly contemporary. Note that the authors have taken a decision, in a very select number of cases, to include data pre-1985. The decision to include this data was on the basis that the data represented seminal work with respect to that behavioral component, a data set which is commonly used and cited, or where no other more contemporary data was identified.

For each of the core behavioral components, a table is presented which provides not just the data but background information that allows the reader to understand the context in which the data was collected, the scenarios associated with the data-sets and the data collection methods employed. Thus, the user is armed with information which will facilitate an assessment of the potential validity, utility and applicability of the data and enable an informed selection of the data which is most appropriate to his/her application.

Currently, there is some debate regarding the applicability of egress-related data collected during the 1950s–1970s. This includes the work of Pauls [33], Fruin [34], amongst others. In many instances, this data still forms the basis for much of the current egress analysis (using engineering calculations and/or egress models). A number of these authors have requested that their work not

be included in current handbook chapters as this may be seen as suggesting that the data should still be used in engineering calculations. This data is therefore not presented in detail here. However, if the reader is interested in this data, detailed reference to it can be found elsewhere [33–35].

Structure of Data Presentation

The data-sets are presented according to each of the key behavioral components that comprise the engineering timeline described previously, i.e., detection and warning phases, pre-evacuation phase and travel phase:

- Detection and Warning Phase: This focuses on the delays in the time for the alarm to be raised in the absence (or override) of automatic detection and alarm system; i.e., when detection and general alarm is reliant on the actions of staff only that can lead to significant delays between detection and notification.
- Pre-Evacuation Phase: This focuses on the pre-evacuation times of occupants who are awake in a range of buildings including Transport, Assembly, Health Care, Educational, Industrial, Mercantile, Residential, and Business premises. It also presents data on important components of pre-evacuation time for those who are asleep (i.e., the time to awaken and the probability of awakening), as well as considering the influence of impairment on time to prepare to evacuate which can be considered another component of pre-evacuation time in some circumstances. The data in this section is therefore sub-divided into the following three categories:
  - Pre-Evacuation—Awake
  - Pre-Evacuation—Asleep,
  - Pre-Evacuation—Impaired
- Travel Phase: This focuses on data related to the movement characteristics (i.e. speed and flow of people). These are provided for each of the most common escape route components namely, horizontal, stairs, exits and escalators. Unimpeded movement speeds of the elderly and others with mobility impairments on the horizontal, ramps and stairs are also presented as is data on both upright and crawling speeds in smoke. The data in this section is therefore sub-divided into the following six categories:
  - Horizontal Movement (flow/speed/unassisted/assisted impaired),
  - Stair Movement (flow/speed/impaired/elderly),
  - Exit (flow/traversal speeds),
  - Escalators (flow, speed),
  - Ramps (for unassisted/assisted mobility impaired)
  - Situational Vulnerabilities (Smoke-upright, Smoke-crawling)

Data-sets are presented for each of the behavioral elements above in tabular form. A simple representation of the engineering timeline is provided at the beginning of each behavioral element to signify the phases to which it relates (see Table 64.2).

The tables are presented in as standardized a format as possible—certainly within each of the components presented. The tabular format includes a description of the background conditions under which the data was collected, when and how the data was collected and the key results derived. Other information important to the understanding and interpretation of the key

Table 64.2 Phase from the engineering timeline within which the behavioral components fall

t_{det}	t_{warn}	t_{pre}	t_{trav}	t_{det}	t_{warn}	t_{pre}	t_{trav}	t_{det}	t_{warn}	t_{pre}	t_{trav}
Detection and Warning Phases				Pre-Evacuation Phase				Travel Phase			

results are also presented. This then places the data in context, allowing the reader to better discriminate between the data-sets and select between them. The importance of many of the attributes of the data collection process and event scenario is apparent—primarily as they apply directly to the selection and application of the data. For instance, the building in which the original data collection took place may be a key criterion in the reader's selection process. Similarly, the nature of the population and the procedure employed. However, the reader should also be cognizant of the nature of the original incident (i.e. the source of the material) and the manner in which the data were collected. Although, this may only be considered an indirect impact on the relevance of the data it directly affects the external validity of the data collected and the format/content of this data. Understandably, some of the behavioral components have different attributes—given the nature of the component being represented and the detail in which the data-sets are presented. However, in all instances, the following attributes are described (although not necessarily in exactly the same format depending on the different data represented)

- Source (original reference)
- Observational Conditions represented by:
  - L: Location: the country or city in which the event took place (if known)
  - N: Nature—this can relate to the component being examined in the event (real incident [I], circulation movement [C], an announced evacuation drill [AE], an unannounced evacuation drill [UE] or an experimental trial [ET]) and Location (if known)
  - SC: Spatial Configuration
  - P: Participants or Sample (with A: Age, G: Gender and I: Impairment)
  - E: Environmental conditions are presented where the information is available; otherwise, the 'E:' is removed for brevity
  - V: Variable—specifically, the variable (s) that influence the data collected (i.e., the independent variables)
- Sample/Data Collection Considerations/ Method—data collection techniques are identified as being an [I]nterview, [S]urvey, [V]ideo, [E]xisting or [O]bserver based.
- Results—unless otherwise stated, these are presented in the following format: **average** [**standard deviation**, **minimum—maximum**] and are aligned with the most influential factors presented in the other columns where appropriate. Omissions are denoted with a hyphen (-).
- Additional Information

In order to reduce the space taken up by these tables, several abbreviations are used to ensure that the maximum amount of information is provided. These are outlined next to each of the tables where they are used in order to improve the reading of the data presented along with a description of additional factors described in each type of table (e.g., configuration, performance attributes, etc.). Additionally, in many of the cases, background information is absent, due to limitations in the original description of the data collection process or the event scenario. Where information is missing in the original source material this absence is noted (typically through the presence of a dash '–').

Many of the reference sources provide multiple data-sets that reflect often subtly different conditions. In order to distinguish clearly between these data sets an 'Observational Conditions' column in each table provides background information on the data and, in particular, the Variable (V) entry records factors that distinguish the data sets presented. These conditions are wide ranging and may represent: differences in the samples used (e.g. different age groups, abilities), independent variables that the researchers set out to investigate (e.g. type of alarm), the nature of the event (e.g. announced/ unannounced evacuation), or spatial configuration of the experimental set up (e.g. up/down direction on stairs/escalator). In each case the variables are noted and abbreviations (derived from those outlined earlier in this section) given. These abbreviations are then used elsewhere in the respective tables to distinguish the values of each variable and to clearly identify (in the results column) which results relate to which combination of variables.

Data-Sets

The data-sets are presented in the following sections. These cover three phases of the engineering timeline: *Detection and Warning*, *Pre-Evacuation* and *Travel*.

In each section, an overview is provided regarding the structure of the associated tables, along with a brief discussion of previous attempts to compile equivalent types of data together, where appropriate. These brief discussions are only intended to indicate that previous reviews exist and indicate the format that some of these reviews have taken. It should not be assumed that these reviews are preferred over the many others that may have been performed.

Detection and Warning Phases: Human Aspect

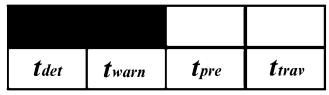

As noted previously, in an engineering design, both human and/or technological resources may be employed to detect an incident and raise the general alarm to initiate the evacuation procedure; i.e., any delay in detection and warning (also previously referred to as Pre-Warning time [11, 12, 24, 25], may be procedural and/or cognitive. Where automatic detection and alarm is employed, typically, t_{det} and t_{warn} will be determined with reference to manufacturer's guidance on sensor response and often do not (and may not need to) take staff activities into account.

However, it is certainly possible that staff (or other occupants) will be involved in the detection of the original incident and the raising of the alarm and it is therefore important to recognize that this involvement might delay the point at which the pre-evacuation phase begins for the general population.

The human element in establishing warning times therefore arises in any situation in which the behavior of an individual intervenes between the detection of a fire and the raising of the general alarm [11, 12, 24, 25]. The need to determine the times required for persons aware of the incident to initiate warnings to affected occupants is recognized in fire safety engineering standards [11, 12, 24, 25]. However, limited guidance is available on the behavioral parameters involved, how the evacuee behavior should be managed and how they can be quantified in a design context.

In reality, the delays associated with these activities may be difficult for the engineer to estimate precisely. However, the engineers may choose to either insert estimates based from previous incidents to provide some representation of this phenomena where deemed relevant or compile an estimate based on expected procedural activities (discussed in detail elsewhere [11, 12, 24, 25]. Examples of such delays from real incidents (both fire and non-fire emergencies) are shown in Table 64.3.

Staff decision-making may occur in a number of situations, e.g., in discovering a fire, interpreting cues first hand (and recognizing them as indicating a real incident), or being notified of an incident (i.e., via the notification system at the fire panel, by other members of staff, by members of the occupant population,

Table 64.3 Estimated staff-related delays from historical incidents [22, 24, 25]

Fire incident	Delay period (minutes)	Number of fatalities
King Cross Subway station	<15	31
Dusseldorf Airport	<27	16
Dupont Plaza Hotel	10	97
Chesterfield Littlewoods Department store	0.5–1	2
Nagasaki Store Fire	6	15
Tokyo security staff training	3.9	–
Ulster Department Stores	0.5–1.0	–

etc.). In these instances, staff members will need to perceive, interpret, determine and then perform the action—in much the same way as other occupants, all of which takes time. Although staff may be better trained and have more experience (both of which will influence the extent of any delay), they would still have to go through this process, delaying their response and, in turn, the response of the general population of the building. The understanding and representation of this component is still relatively immature and, as such, there are relatively few data-sets available to support the representation of this phenomenon within the engineering process.

Pre-evacuation Phase

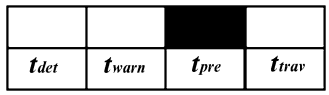

The time that occupants take to initiate their evacuation movement can be difficult to estimate. In the past, this delay was often not included in an engineering analysis at all [36]. Although, this certainly made the calculation easier (i.e. fewer components needed to be assessed), it also potentially underestimated the expected evacuation times in many of the scenarios examined.

In the calculation of an expected total time to evacuate a building, it is now common practice for engineers to include some time to account for a delay to the start of evacuation, the t_{pre}. This may be achieved simplistically, by segregating the pre-evacuation phase from the travel phase, or in a more coupled manner where the nature of the pre-evacuation phase can influence the development of the travel phase. The tables in the following sections should help an engineer identify such pre-evacuation times.

There have been a number of previous efforts to explore the pre-evacuation phase and produce a collection of the data-sets available. Key advances in compiling pre-evacuation data-sets were made by Fahy and Proulx [37], who collected together a range of data-sets while presenting contextual information to aid the reader's assessment (see Table 64.4).

Other pre-evacuation data (referred to as pre-movement) has been compiled by Shi et al. in a similar format, although in this case data was categorized primarily according to the occupancy type [38]. Bruck and colleagues [39–41], Purser and Bensilum [10] and Proulx and McQueen [42] also provide detailed summaries of their own research regarding pre-evacuation responses. Gwynne also examined a range of pre-evacuation data-sets in order to identify how vulnerabilities in the population might be addressed using notification systems and to identify where gaps might exist in our understanding [43, 44].

Peacock et al. performed a detailed analysis of egress trials conducted by NIST [45, 46]. Although, this focused upon stair travel, a number of pre-evacuation data-sets, based on data collected from buildings ranging from 6 to 31 floors in height, were also summarized. These evacuations produced average pre-evacuation times of between 89 and 224 s [45, 46].

Other pre-evacuation times are presented by the type of occupancy involved in the original event and are described in Tables 64.5, 64.6, 64.7, 64.8, 64.9, 64.10, 64.11, and 64.12. In these tables, pre-evacuation times for business, residential, mercantile, industrial, educational, health care, assembly and transport occupancies are provided. Broadly speaking, the same information is provided throughout Tables 64.5, 64.6, 64.7, 64.8, 64.9, 64.10, 64.11, and 64.12: Source Observational Conditions (Location (country where known), Nature, Spatial Configuration, Participants, Environment and Variables), Procedure (Strategy, Staff, Technology), Sample (Collection method and Size), Results (Mean, Standard Deviation, Range in Seconds). Information is only included in the tables if it appeared in the original source or if can readily be derived. If the information is derived by the authors, this is noted in the table. The Additional Information column is used to provide the reader with more

Table 64.4 Delay times (min) derived from actual fires and evacuation exercises reported in the referenced literature [37]

Event description	*N*	Min	1st Q	Median	3rd Q	Max	Mean	Factors
High-rise hotel	536	0	3.3	60.0	130.9	290	NA	MGM Grand Hotel fire, no alarm notification, grouped data from questionnaires
High-rise hotel	47	0	2.0	5.0	17.5	120	NA	Westchase Hilton Hotel fire, no alarm in early stages, grouped data from questionnaires
High-rise office building	85	0	2.0	5.0	10.0	245	11.3	World Trade Center explosion and fire, no alarm notification (building closer to explosion)
High-rise office building	46	0	4.5	10.0	31.5	185	28.4	World Trade Center explosion and fire, no alarm notification (building farther from blast)
High-rise office building	107	1.0	1.0	1.0	1.0	≈6.0	NA	Fire incident, no alarms, data from interviews with occupants of four floors of building (11 interviewees were trapped)
High-rise office building	12	0.5	NA	1.0	NA	2.3	1.2	Unannounced drill on three floors; data for first person to reach each of four stairwell doors to wait for voice instruction; trained staff; data from video recordings
Mid-rise office building	92	0	0.4	0.6	0.8	<4	0.6	Unannounced drill, good alarm performance; fire wardens; warm day
Mid-rise office building	161	0	0.5	0.9	1.4	<5	1.1	Unannounced drill, good alarm performance; fire wardens; cool day
One-story department store	95	1	0.2	0.3	0.5	0.9	0.4	Unannounced drill; trained staff; data here derived from grouped data for 95 participants
Three-story department store	122	0.05	NA	NA	NA	1.6	0.6	Unannounced drill; trained staff; times distilled from analysis of videotapes
One-story department store	122	0.07	NA	NA	NA	1.7	0.5	Unannounced drill; trained staff; times distilled from analysis of videotapes
One-story department store	71	0.03	NA	NA	NA	1.0	0.4	Unannounced drill; trained staff; times distilled from analysis of videotapes
High-rise apartment building	NA	0	NA	NA	NA	NA	10.5	Forest Laneway fire; for occupants who attempted to evacuate in the first hour, based on questionnaire responses
	219	0	NA	187.8	NA	720	190.8	Forest Laneway fire, for all occupants
High-rise apartment building	33	0.3	0.8	1.3	4.4	10.2	2.8	Unannounced drill; good alarm performance
High-rise apartment building	93	0.4	1.5	3.6	6.9	18.6	5.3	Unannounced drill; good alarm performance; heavy snow during drill
High-rise apartment building	27	1.0	2.0	8.0	14.0	>20	NA	Fire incident in early morning, alarm functioned, fewer than half the occupants evacuated
Mid-rise apartment building	42	0.6	1.0	1.4	3.0	>14	2.5	Unannounced drill; good alarm performance
Mid-rise apartment building	55	>0.5	1.6	4.4	13.5	>21	8.4	Unannounced drill; poor alarm performance
Mid-rise apartment building	77	>0.3	1.9	7.7	19.1	>24	9.7	Unannounced drill; poor alarm performance
Mid-rise apartment building	80	>0.3	1.2	2.5	3.7	>12	3.1	Unannounced drill; good alarm performance
Training facility	566	<0.2	0.7	1.1	1.5	>5	NA	Testing sleeping subjects at a training facility

NA not reported

Table 64.5 Pre-evacuation data—business occupancy

Occupancy	Source	Observational conditions (L: location, N: nature, SC: spatial configuration, P: participants, E: environment, V: variable)	Procedure			Sample		Results (sec)	Additional information
			Strategy	Staff (designated)	Technology	Collection method	Size	Mean S.D., range	
Business	Gwynne et al. [47]	L: USA N: UE1–2 SC: 14 floors P: 825 evacuees: 44 % F, 56 % M, 1 % impaired V: impact of procedure (UE1–2)	Phased UE1: local alarm UE2: general alarm	2–4/floor	AL, PV (duration 15–20s) to 3 floors followed by general alarm Tone alert	Video, observer	UE1: 132 UE2: 150	[74.0 –, 23–152][a] [–, 5–173][a]	[a]Times are arrive to stair door Raw data and frequency distributions Categorized by floor and collection method
	Sharma et al. [48]	L: UK N:UE, pre-2009 SC:6 floors P:- E:- V: performance	Full	–	–	Video, survey	19	28 [11, 10–55]	Paper gives raw data (to nearest 5 s)
	Christoffersen and Söderlind [49]	L: Denmark N: UE, pre-2009 SC: 12 floors P: V: performance given pre-recorded voice	Full	–	PV	Video, Observer	70	–[–, 12–105]	
	Proulx and Benichou [51]	L: Canada N: UE, 2006 SC: 3 floors, 6 stairwells (4 observed) P: 350 workers per floor—(18–64) E:PLM installations/reduced V: performance given alarm	Full	Floor emergency officers	AL	Video	1191	329	Bell alert used
	Purser [52]	L: UK N: UE SC: room within office P: 12 V: performance given voice alarm	Full	–	-V	Video	12	46 [–, 32–57]	

Peacock et al. [53]	L: USA N:UE1–2 SC: SC1:6, SC2:11, SC3:18 floors P:SC1:277, SC2: 134, SC3: 727 V: impact of FF entry (UE1–2); spatial configuration (SC1–3)	Full	UE1: No FF entered stairwell UE2: FF entered stairwell	–	Video	SC1: [277] SC2: [134] SC3: [483]	SC1, UE1: 144 [68,–] SC1, UE2: 140 [53,–] SC2, UE1: 89 [54,–] SC3, UE1: 220 [144,–] SC3, UE2: 188 [93,–]	
Gwynne [43, 44]	L: UK N:UE1–2 SC: S1: 11, S2:4 floors P: UE1:229, UE2: 348 E: UE1: snow, UE2: cold V: UE1-2: trials based on different technologies	UE1: Partial UE2: Full	1–2/floor evac 25–30	PV T3	Video, observer, survey	72 348	141 [–. 40–426] 102 [–, 7–330]	
Purser and Bensilium [26]; Purser and Raggio [54]	L: UK N: UE, 1995 SC: 17 floors P: 489 V: performance given alarms used	Full	None	AL, PV (17 s)	Video	7	46.3# [–, 32–56#]	#Calculated from raw data Recognition and Response time given Tone alert used
Fahy and Proulx [55]	L: USA N: I1-2, 1993 SC: I1: 110, I2:110 P: 50,000, mixed pop E: loss of light, smoke V: nature of incident I1–2	Full	1 on each floor + 25 managers	None	Survey	I1:229 I2:163	534 [–, 120–1800] 2394 [–, 600–14,414]	Descriptive statistics Cumulative frequency distribution
Brennan [56]	L: Australia N: I SC: 14 floors P: 250 E: smoke V: impact of incident	Full	–	None note: public address used but after most left	Interview, existing data held by work/fire brigade	36	–[–, 60–300]	By location
Proulx and Fahy [57]; Proulx et al. [58]	L: Canada N: UE1–2, 1995 SC: UE1: 6; UE2: 7 floors P: UE1: 180; UE2: 500 V: different trials (UE1–2)	Full	–	AL	Video	–	UE1: 36 [–,–][a] UE2: 63 [–,–][a]	[a]Time left desk /reach door Paper gives combined frequency distribution

Table 64.6 Pre-evacuation time—residential occupancy

Occupancy	Source	Observational conditions (L: location, N: nature, SC: spatial configuration, P: participants, E: environment, V: variable)	Procedure			Sample		Results (sec)	Additional information
			Strategy	Staff	Technology	Collection method	Size	Mean [S.D., range]	
Residential	Gwynne [43, 44]	L: USA N:UE1–2 SC: university residences P:33 + 40 E: evening/cold V: different trials (UE1–2)	Full	>1	T3	Video, survey	UE1: 33 UE2: 40	61 [–, 28–104] 39 [–, 9–89]	
	Shields et al. [59]	L: UK N:UE, 1997 SC:2 floors P:14–12 residents (mental impairments), 2 staff V: trial involving mental impairments	Full	none	AL	Video	10	43.8[a] [–, 6–157][a]	[a]Times to leave bedroom Median of 17 s Raw data and result presented by gender Bell used
	Brennan [56]	L: Australia N: I SC: 18 floors P: 100 out of 200, residents, 40 % transient, mostly elderly E: smoke V: incident involving elderly	Full	Fire fighters in attendance	AL	Interview, data held by work/ fire brigade	27	–[–, 60–1200+]	By location Bell/siren employed
	Proulx [60, 61]; Proulx and Fahy [57]	L: Canada	S1: two stage, full	Fire fighters in attendance	AE1: AL until 300 s then continuous + V	Video	AE1: 42	S1,AE1:150 [–,–]	Descriptive statistics
		N: AE1–4, UE5–6 SC: AE1–4: 6–7 floors; UE5–6: 12–15 floors	S2 one stage, full		AE 2–4: AL UE5: AL*		AE2:55 AE3:77	S2,AE2:502 [–,–] S2,AE3:582 [–,–]	Frequency distribution During AE1 alert was a bell, while sounder used during AE2–4
		P: AE1–4: 150 each; UE5–6: 180–500+, mixed age/gender, 20 % impaired			UE6: AL*		AE4:80	S2,AE4:188 [–,–]	*Derived from questionnaire response
		E: AE1–4, UE5: good weather; UE6: cold V: nature of event (AE1–4, UE5–6) Evacuation strategy (S1–2)					UE5: 180 UE6:500	UE5: 168 [–,–] UE6: 319 [–,–]	

Table 64.7 Pre-evacuation time—mercantile occupancy

Occupancy	Source	Observational conditions (L: location, N: nature, SC: spatial configuration, P: participants, E: environment, V: variable)	Procedure			Sample		Results (sec)	Additional information
			Strategy	Staff	Technology	Collection method	Size	Mean [S.D., range]	
Mercantile	Nilsson and Frantzich [62]	L: Sweden, 2004, 2005 N: S1–6, six trials examining three voice types (T1–T3) SC: IKEA store P: 51, avg age = 2018–30 years V: nature of trial sample (S1–6); technology (UE1–3)	Full	–	UE1:V (male) UE2: V (synthetic) UE3: V (male)	Video + survey	S1: 9 S2: 5 S3: 8 S4: 16 S5: 9 S6: 4	UE1, S1:55 [9.4,–] UE1, S2: 36 [3.4,–] UE2, S3: 39 [8.4,–] UE2, S4: 51 [16.3,–] UE3, S5: 69 [11.0,–] UE3, S6: 49 [5.9,–]	
	Samochine et al. [63]	L: UK N: UE1–4,1995–2001 SC:UE1:3; UE2: 3; UE3: 1; UE4: 1 floor P: 409–616 customers/staff V: impact of alarm	Full	–	AL	Video	102	18# [12.4, 2–57]#	#Times from alarm for staff to initiate "positive evacuation activities" Siren used
	Frantzich [64]	L: Sweden N: UE1–3, pre-2001 SC: UE1:1;UE2:1; UE3:3 floors. Three areas examined: warehouse (SC1), restaurant (SC2) and cash desk (SC3) P:UE1:210; UE2: 150;UE3: 375, customers/staff V: different events (UE1–3) and areas (SC1–3)	Full	–	AL (5 s) + repeated PV (40s)	Video + observer	Not stated	UE1, SC1: 30 [–, 19–54] UE1, SC2: 50 [–, 35–73] UE1, SC3: 50 [–,51–57] UE2, SC1: 27 [–, 9–46] UE2, SC2: 51 [–,40–67] UE2,SC3: 31 [–,27–38] UE3, SC1:26 [–, 15–50] UE3, SC2: 62 [–,45–100] UE3, SC3: 83 [–,35–130]	Tone used
	Shields and Boyce [65]	L: UK N: UE1–4, 1995–1997 SC:4 shops, 1–3 floors P:UE1:571,UE2: 616, UE3: 477,UE4: 409; mixed age, 70 % + female V: nature of event (UE1–4)	Full	–	AL	Video, survey	UE1: 122 UE2: 122 UE3: 95 UE4: 71	UE1: 37 [19, 3–95] UE2: 31 [18, 4–100] UE3: 25 [14, 1–55] UE4:25 [13, 2–60]	Descriptive statistics provided Results presented by department Siren used
	Purser and Bensilium [10, 26]; Purser and Raggio [54]	L: UK N:UE1–2, 1995 SC: UE1–2:shop V: impact of voice alarm on event (UE1–2)	Full	–	PV	Video	–	UE1: 90 [–,–] UE2: 150 [–,–]	

Table 64.8 Pre-evacuation time—industrial occupancy

Occupancy	Source	Observational conditions (L: location, N: nature, SC: spatial configuration, P: participants, E: environment, V: variable)	Procedure			Sample		Results (sec)	Additional information
			Strategy	Staff	Technology	Collection method	Size	Mean [S.D., range]	
Industrial	Frantzich and Nilsson [66]	L: Sweden N: UE, 2004 SC: nuclear power plant P: 37, mixed age (22–65), 92 % male V: impact of alarm type	Full	1	AL+ PV (Swedish/ English) + Siren (16 s)	Video, observers, survey	[16]	97# [–, 30–217]	#Derived from raw data Tone used
	Gwynne [43, 44]	L: US	Full	>1	UE1: strobe/AL	Observer	–	UE1, SC1:-[–,–75][a]	[a]Only maximum values were provided
		N: UE1–2, 2007 SC: SC1–5: distribution depots V: spatial configuration (SC1–5), procedural technology (UE1–2)			UE2: strobe/T3			UE1, SC2: -[–,–75] UE1, SC3: -[–,–107] UE2,SC4: -[–,–60] UE2,SC5: -[–,–65]	Tone used

Table 64.9 Pre-evacuation time—educational occupancy

Occupancy	Source	Observational conditions (L: location, N: nature, SC: spatial configuration, P: participants, E: environment, V: variable)	Procedure			Sample		Results (sec)	Additional information
			Strategy	Staff	Technology	Collection method	Size	Mean [S.D., range]	
Educational	Kholshevnikov et al. [67]	L: Russia N: UE, 2008–10 SC: 8 × kindergarten P: mixed gender and age (<3–7) in clothing for different seasons S1: spring S2: winter (donning blankets) S3: autumn S4; winter (donning coats) E: spring, autumn, winter V: sample population performance given different weather conditions (S1–4)	Full	2 per 10–15 children	AL	Video	S1: 52 S2: 32 S3: 25 S4: 77	–[–, –30] –[–, –66] –[–, –300] –[–, –450]	Populations compiled across evacuations
	Galea et al. [68]	L: Poland N: UE, 2010 SC: library, 7 floors P: 689 students/staff, 18–60 years, 66 % M, 34 % F (sample: 46 % M, 54 % F) V: voice alarm on performance	Full	None	-V	Video	192	69.9 (4.06[a]) [0.77[a], 0.1–178]	[a]Mean and s.d of logarithm of response times
	Capote et al. [69]	L: Spain N: UE, 2012 SC: School, 3 floors P: 291 children, aged 4–10; 16 adults V: impact of alarm on performance	Phased	16	AL	Video	125	10–38[a] [–,–]	[a]Mean times for children to be ready to leave room, dependent on age range
	Galea et al. [68, 70, 71]	L: Turkey N: UE, 2010 SC: 2 floors P:120 staff/students, (sample 49 % M, 51 % F) V: impact of alarm type on performance	Full	None	AL, PV (7.5 s duration)	Video, survey	51	56.1 [–,11–181]	Results presented by zone Frequency distribution Descriptive statistics Tone used

(continued)

Table 64.9 (continued)

Occupancy	Source	Observational conditions (L: location, N: nature, SC: spatial configuration, P: participants, E: environment, V: variable)	Procedure			Sample		Results (sec)	
			Strategy	Staff	Technology	Collection method	Size	Mean [S.D., range]	Additional information
	Galea et al. [72]	L: Czech Republic, 2009 N: UE1—alerted by staff; UE2—alerted by alarm SC: library, 5 floors P: 70+ students/staff (sample: 78 % M, 22 % F, 18–44 years) V: impact of staff and alarm on response (UE1–2)	Full	None	AL, PV, LV (7 min 46 s total duration)	Video, survey	UE1: 47[a] UE2: 23	43 [–, 20–100] 193.7 [–,50–390]	[a]Issue occurred in sounding of alarm Results presented by nature of notification Tone used Frequency distributions
	Galea et al. [72]	L: UK N:UE,2007–2011 SC: library, 2 floors P: 453 (sample: 51 % M, 48 % F) V: impact of alarm on performance	Full	27	AL	Video, survey	103	98 [–,22–287]	Frequency distribution Description statistics Tone used
	Kholshevnikov et al. [73]	L: Russia N: UE1–2, 2005 SC: UE1: 2 floors;UE2: 3 floors P: UE1: 70; UE2: 220 children, age 3–17 V: nature of event (UE1–2)	Full	–	UE1: staff UE2: staff	Video	70 220	–[–,–260] –[–,–590]	
	Purser [52]	L: UK N: ET1–3 SC: lab P: 59 unfamiliar recruits (15 F, 34 F, 21–50) V: impact of alarm given (ET1–3)	Full	–	ET1: AL ET2: PV long ET3: PV short	Video	17 15 16	41.3 [–, 26–74] 28.5 [–, 17–36] 17.1 [–, 5–33]	Graphical information provided Sounder used
	Gwynne [43, 44]	L: UK N: UE1–2 SC: UE1: 3 floors, UE2: 1 floor P: UE1: 453, UE2: 15 E: UE1: rain, UE2: cold V: nature of event, technology (UE1–2)	Full	UE1:>5 UE2: 0	AL PV	Video, survey	153 15	102 [–, 5–290] 52 [–, 20–89]	Tone used

Tavares et al. [74]	L: Brazil N: UE1–2, 2005 SC: UE1: 3 floors; UE2: 2 floors P: UE1:18; UE2: 39 staff/students V: impact of staff in different events (UE1–2)	Full	UE1: 2 UE2: 1	Staff Staff	Video, survey, observer	18 16	38.7 [–,8–70] 55.8 [–,5–98]	Descriptive statistics Frequency distribution
Gwynne et al. [75], [76]	L: UK, 2000 N: UE SC: library, 3 floors P: 361 S1—evacuee; S2— staff V: (S1–2) different population samples	Full	19	AL	Video, observer, survey	S1: evacuees 228 S2: staff: 19	73.7 [–,37.4, 8–200] 70.8 [–, 60, 0–246][a]	[a]Times to 'purposefully initiate evacuation' Descriptive stats, frequency distribution, scatterplots Results presented by no. of prior actions, level of prompting, employment hierarchy, procedural role
Olsson and Regan [77], [78]	L: NZ N:AE1–3 SC: university AE1: floor 1; AE2 floors 8; AE3: 5 floors P: AE1: 278, AE2: 716, AE3: 494 V: different events and alarms (AE1–3)	Full	–	AE1: AL AE2: PV AE3: LV	Video	–	38, 28[a] [–,–] 19,24[a] [–,–] 20, 27[a][–,–]	[a]Means for different location/areas in each event A siren was used

Table 64.10 Pre-evacuation time—health care occupancy

Occupancy	Source	Observational conditions (L: location, N: nature, SC: spatial configuration, P: participants, E: environment, V: variable)	Procedure			Sample		Results (secs)	Additional information
			Strategy	Staff	Technology	Collection method	Size	Mean [S.D., range]	
Health care	Gwynne et al. [75, 76]	L: UK N: UE, 2000 SC: outpatients hospital P: 19 patients V: S1–2 different population types	Full	14	AL	Video, observer, survey	S1: patients: 19 S2: staff: 14	50.8 [–, 30–66] 44.1 [–, 16–91][a]	[a]Times for staff to react to a call in an area Results presented by area A bell was used
	Purser and Bensilum [10]	L: UK N: UE, 1996 SC: [outpatients hospital, 2 floors; 2 areas examined: SC1, SC2] P: >225 V: different spaces evacuated SC1–2	Full	–	PV English (24 s)/Urdu (29 s)	Video (handheld)	SC1: 14 SC2: 7	–[–, 21–29] –[–, 20–29]	Results presented by area

Table 64.11 Pre-evacuation time—assembly occupancy

Occupancy	Source	Observational conditions (L: location, N: nature, SC: spatial configuration, P: participants, E: environment, V: variable)	Procedure			Sample		Results (sec)	
			Strategy	Staff	Technology	Collection method	Size	[Mean S.D., range]	Additional information
Assembly	Tancogne-Dejean et al. [79]	L: France N: UE1–4 SC: cinema P: 122 (aged 19-63; 25% F, 75% male) V: cinema trials	Full	–	AL + PV + lights on + cessation movie	Video, observer	488 (4 × 122)	10[a] [–, 8–12]	[a]Results represent estimate of when people were on their feet AL—pulse used
	Purser and Bensilum [10, 26]	L: UK N: UE, 1996 SC: theatre, 3 floors P: 311 public/staff V: theatre population	Full	–	LV (from stage) + PV(5 s)	Video	–	[–, 10–36]	Results presented by location
	Purser and Bensilium [10]; Purser and Raggio [54]	L: UK N: UE, 1995 SC:restaurant in shopping centre, 2 floors P: 432, 16 in restaurant V: restaurant population	Full	–	AL (two level-9 s) followed by PV (13 s) repeated	Video	11	48.5 [–, 41–60]	Raw data presented Recognition and response AL-tone used

Table 64.12 Pre-evacuation time—transport

Occupancy	Source	Observational conditions (L: location, N: nature, SC: spatial configuration, P: participants, E: environment, V: variable)	Procedure			Sample		Results (sec)	Additional information
			Strategy	Staff	Technology	Collection method	Size	Mean S.D., range	
Transport	Brown et al. [80]	L: at sea, Scandinavia	Muster at assembly point	Crew	AL	Video	UE1–2: 1003	53 –,0.6–470 (3.516[a]) 0.901[a],–	[a]Mean and standard deviation. of the logarithm of response times (log normal distributions)
		N: UE1–3, 2009–10					UE3 (overall): 1228	–,8–1379 (5.012[a] 0.89[a],–, –)	
		SC: 2 × cruise ships					UE3 (cabin areas): 595	333 –, <1379*	
		P: passengers mixed age and gender					UE3 (public areas): 633	88 –,< approx 440*	
		V: three events (UE1–3)						*Deduced from graphs	
	Proulx and Sime [17, 81]	L: UK	Full	UE 1: 0	AL	Video	66 (concourse) + 45 (platform)	495,540[a]	[a]Median times to start to move according to initial location on concourse and bottom escalator (platform) respectively
		N:UE1–5, 1989–1990		UE 2: 2	AL		30 + 53	135,180[a]	Bell used
		SC: underground station concourse and platform		UE 3: 0	AL +2 × non directive PV		13 + 48	75,460[a]	
		P: commuters mixed age and gender		UE 4: 2	AL + directive PV		20 + 15	75,90[a]	
		V: five events (UE1–5)		UE 5: 0	AL + informative, directive LV		19 + 16	90,60[a]	

detail on other data or analysis provided in the original source.

In this examination, pre-evacuation time data have been collected in several ways, primarily from evacuation exercises and experimental/laboratory trials. This data, at least in part, reflects the decision-making process of those involved. Therefore, the credibility (or at least the applicability) of the data collected is dependent upon the information available to the target population during the event since that impacts the external validity of the research. Of critical importance here is whether the participants were aware that it was a drill/experiment rather than a real incident. Prior knowledge may well have influenced the nature of their response, the participants' ability to prepare for their response and the time they took to respond. It should be noted that in a real incident, the information available to those involved would differ significantly according to the cues available to them and differs from a situation where people definitively know that the incident is not real. *A positive understanding of the negative* (*unambiguous warning of the drill before it commences*), *is not equivalent to the negative understanding of the positive* (*evacuee assessment of a smoke cue that may or may not indicate a threat to the individual*).

It is important to note that the different data-sets represent markedly different pre-evacuation time distributions. A number of characteristics that could have impacted on the pre-evacuation time have been identified and discussed previously [7, 36]. It is presently understood that the pre-evacuation time will vary according to situational, structural, procedural, organizational, behavioral and environmental factors present. Kuligowski provides a detailed description of the factors that influence the pre-evacuation phase [20], some of which are also discussed in Chap. 58 of this handbook. A brief overview of the factors derived from the most recent work on human behavior is presented below.

It should be noted that not all of the factors discussed in the following paragraphs are represented in the data-sets described, often because this information was not available in the original source. It may not therefore be feasible for engineers to account for these factors within the data selected. However, even if it is not possible or feasible for the engineer to account for these factors, it is still important for them to be aware of their impact during an actual incident. *Where the factors can be identified within the data-sets*, *it is noted in the description below*.

Building type, *layout and complexity*. The building type and layout provides the spatial environment within which the event occurs. It may determine the nature of the occupants, the resources employed, the hazards present, and the social/organizational hierarchy present and may influence the types of actions that might be expected within a particular space. As such, it is a primary influence upon the scenario produced in physical, sociological and psychological terms. The way each floor and the whole building are organized has an impact on the familiarity and use of the space by an occupant both before and during an incident; e.g. through visual access to routes and exit points. Occupants are more likely to spend time obtaining information or devising a plan of action in a complex building or in a building where wayfinding is difficult. The way the building is designed may or may not also provide occupants with visual access to the behavior of others, to the original incident or to procedural attempts at notifying them as the target population. *If available*, *the building type and the population are described in the Observational Conditions column* (*under Spatial Configuration and Participants*). *The data-sets are also categorized according to the type of occupancy within which the event occurred. This factor was selected as it is likely to be the first factor that the engineer encounters and is likely to form the base assessment of the scenario represented. Where available*, *the number of floors involved in the structure is also given.*

Procedure—Notification System—the technology employed as part of the procedure to inform the target population that an incident

has occurred. This may include a range of different technologies, each of which carries different types of information, suggests different degrees of urgency and which have different degrees of comprehension and intelligibility. This would typically need to be represented as part of the engineering design process. *If available, the technological resources that are part of the emergency procedure are described in the Procedure column* (*under Technology*). *Typically these are systems that alert that something has happened using sirens*, *bells*, *horns* [*AL*]; *using a T-3 fire alarm system* [*T3*]; *provide information beyond simply an alert using a live voice notification* [*LV*], *a pre-recorded voice notification* [*PV*], *or a voice notification where the nature of the voice was unclear* [*-V*]).

Procedure—Human Resources—Staff form a key component within the procedural response. It is widely recognized that the presence of well-trained, engaged, authoritative and informed staff presents the most effective means to initiate occupant response [28, 63, 82, 83]. *If available the human resources that are part of the emergency procedure are described in the Procedure column* (*see* section "Pre-evacuation Phase") *under Staff. It should be noted that only those staff for whom specific mention of their particular role was made in the original source are included.*

Alertness and limitation. Occupants may have situational or innate characteristics that reduce their alertness. Occupants may be asleep, intoxicated, or impaired all of which might reduce the information available to them. *The impact of alertness is addressed in* section "Pre-evacuation Phase: Asleep" (i.e. *that people may be sleeping when cues are provided*) *while the impact of impairment is addressed in* section "Pre-evacuation Phase: Impaired".

Focus—Commitment and background noise. In situations where occupants focus their attention on a particular point, e.g., at a cinema, attention may be diverted from critical environmental and procedural cues. Similarly, in environments where aural or visual background noise is present, the cues available to the population may be confounded and confused, delaying their response. Occupants may also be committed to their actions, potentially having committed resources to the performance of this action, making them reluctant to interrupt it on the basis of ambiguous cues. *The impact of commitment is not addressed* per se *in* Tables 64.5, 64.6, 64.7, 64.8, 64.9, 64.10, 64.11, and 64.12, *although the building type may give some indication of the range of activities undertaken by the samples involved. The presence of background noise is noted where known in* section "Pre-evacuation Phase: Asleep" *in relation to the response of sleeping persons.*

Training—Training is a characteristic of the organizational structure within a building, since training should be specifically tailored to each building evacuation procedure present. That is not to say that the populations do not bring more general experience to an incident; however, this is more difficult to predict and quantify within the engineering process. The likelihood and nature of occupant training will depend on the occupancy type; for instance, in public buildings, occupants are unlikely to be trained for that specific building, whereas some form of training is likely to be the norm for office spaces (although the sophistication of this training may vary significantly).

False alarms. The number of false alarms in a building is an important determinant of the efficiency of this system to warn occupants. If the number of false alarms is high, the pre-evacuation time will likely be extended since occupants are unlikely to look for information and will be less receptive to other cues.

Familiarity. Occupants who are familiar with a building, who have participated in evacuation drills, and who are aware of the evacuation procedure are more likely to start evacuation rapidly. What is not well understood is the point at which the performance of drills and training exercises starts to make the occupant

population skeptical of the information being provided.

Social Affiliation. The nature of the relationship between the occupant and the surrounding population will influence the manner in which information is perceived and the actions subsequently performed. It will influence the responsibility felt by an occupant for those around them, information exchange, perceived risk and the preparatory actions that might be performed before movement to safety is initiated. *Social affiliation is not presented in the tables*; *however*, *the building type and sample description may give some indication of the types of relationships present among the sample*.

Event Conditions and Proximity to Event. The nature and severity of the incident will influence the type of cues provided to the population. Their proximity to the incident will influence access to these cues, the degree of ambiguity and the perceived sense of risk derived from the cues received.

Surrounding Population and their Actions. The population can be a source of information, with their actions indicating their interpretation of the incident and the options available. However, research has also suggested [84] delayed responses in the presence of others, given their identity and actions. These influences have been referred to as informational and normative social influence [85]. They may also limit viable responses, should routes become overloaded or congestion develops, discouraging the use of certain routes.

The core data-sets relating to the pre-evacuation phase are presented in Tables 64.5, 64.6, 64.7, 64.8, 64.9, 64.10, 64.11, and 64.12. These relate to a range of occupancies and scenarios—cutting across the various factors highlighted above. Further data-sets, exploring the status of the population (i.e. whether they are asleep) and the impairments present in the population (e.g. whether additional preparatory actions are required by the occupants before they initiate egress movement) are presented in more detail in sections "Pre-evacuation Phase: Asleep" and "Pre-evacuation Phase: Impaired" below.

Pre-evacuation Phase: Asleep

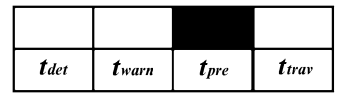

As discussed, an extended pre-evacuation time is often the most significant component of the evacuation process. As shown in Table 64.4, these values can range from seconds to hours. Indeed, it is possible that when occupants are asleep the pre-evacuation times could be especially prolonged. Comprehensive reviews of the research literature on arousal from sleep have previously been conducted by Bruck and colleagues [39, 86, 87]. As noted by Bruck [39] this literature falls into two categories: the first comprises investigations into the characteristics of sleep and in particular the arousal thresholds of persons related to the various stages of sleep across the night to different sound stimuli; the second comprises of more focused investigations by those interested in the response of individuals in fire situations who have investigated the likelihood of wakening to a range of specific fire cues, including smoke detector alarms. Since the context of this chapter is in relation to human behavior data for use in fire safety design, the focus here is on the latter. The main findings are summarized in Table 64.13. Table 64.13 includes the summaries already presented in previous literature reviews [39, 86], but has also been updated to include studies conducted post 2005.

Table 64.13 presents the results of a series of experimental trials [ET] conducted in controlled environments (in household, laboratory or hospital settings). Table 64.13 contains information on the Source of the data, the Observational Conditions under which the study was conducted (Location (country in which conducted), Nature of the study (since these were all experimental trials [ET], this section provides details of the experimental set up including the nature of the alarm presentation, stage of sleep, and the

Table 64.13 Pre-evacuation sleep data

Source	Observational conditions (L: location, N: nature of alarm presentation, stage of sleep, measure of awakening, SC: spatial configuration, V: variable)	Experimental Sample Description A: Age G: Gender I: Impairment	Size	Signal Type	Frequency (Hz)	Intensity pillow (dBA)	Results Mean auditory arousal threshold (dBA) [s.d]	% awakening	Mean time to awaken (secs) [standard deviation]	Additional information
Bruck and Thomas [88]	L: Australia N: [ET] alarm activated by parents 1–3 h after sleep onset Visual determination awakening SC: own home V: impact of residential alarm	A: mean: 8.82, range: 5–15 G: 60 M, 63 F I: none	123	AL (residential) 30 s duration	–	50–80 (82 % cases)	n/a	22#	–	#20 % during alarm, 2 % after; another 17 % Small numbers had impairment (hearing (2), cold (2), medication (2))
Bruck and Thomas [89]	L: Australia N: [ET] modified method of limits (increasing signal volume every 30 s) Signals presented in stage 3 or 4 sleep (EEG) Pressed button to signal awake SC: own home V: impact of different signal type and frequencies (S1–4)	A: 65–83 G: 22 M, 23 F I: none	45	S1:[T3] (mixed)	500–2500	35–95	48.0 [13.3]	100 (at or before 95dBA)	93.3 [77.9]	Participants primed. Each exposed to each signal, two signals each night × 2 nights testing
				S2: [PV] (male, 10 s loop)	200–2500	35–95	55.9 [19.2]	97 (at or before 95dBA)	153.9 [147.7]	Significant differences found between all signals
				S3:[T3] (high)	>3000	35–95	63.7 [15.3]	99 (at or before 95dBA)	192.1 [105.2]	
				S4:[T3]	<500	35–95	52.6 [18.1]	99 (at or before 95dBA)	124.5 [121.8]	
Thomas and Bruck, [89, 90]	L: Australia N: [ET]modified method of limits (increasing signal intensity every 30 s) Signals presented in stage 3 or 4 sleep (EEG) Pressed button to signal awake SC: own home V: impact of signal type and intensity levels (S1–S5)	A: 18–77 G: 16 M, 22 F I: mild-moderate hearing loss	38	S1:T3,Strobe	–	3 levels 177–420 cd	–	58 (at or before 420 cd)	–	Participants primed. Each exposed to each signal; signals presented across two nights, 1 week apart (3 signals/night) Paper presents cumulative frequency graphs of total percentage of each group waking for each signal across intensities
				S2: pillow shaker (T-3 pulse)	–	5 levels 0.086–0533 ms^{-2}	–	97 (at or before highest intensity)	–	
				S3: bed shaker (T-3 pulse)	–	3 levels 1.09–2.41 ms^{-2}	–	89 (at or before highest intensity)	–	
				S4: auditory signal (T-3)	520	55–95	–	100 (at or before 95 dBA)	–	
				S5: auditory signal (T-3 pure tone)	3100	55–95	–	85 (at or before 95dbA)	–	

Thomas and Bruck [87]	L: Australia N: [ET] modified method of limits (increasing signal intensity every 30 s) Signals presented in stage 3 or 4 sleep (EEG) Pressed button to signal awake SC: own home V: signal type, frequency and intensity (S1–5), given blood alcohol level	A: 18–26 G: 15 M, 17 F I: alcohol 0.05 BAC	32	S1: strobe (T-3 pulse)		–	3 levels 177–420 cd	–	68 (at or before 420 cd)	Participants primed. Each exposed to each signal; signals presented across two nights, 1 week apart (3 signals/night) Paper presents cumulative frequency graphs of total percentage of each group waking for each signal across intensities
				S2: pillow shaker (T-3 pulse)		–	5 levels 0.086–0533 ms^{-2}	–n	68 (at or before highest intensity)	
				S3: bed shaker (T-3 pulse)		–	3 levels 1.09–2.41 ms^{-}	–	75 (at or before highest intensity)	
				S4: auditory signal (T-3)		520	55–95	–	100 (at or before 75dBA)	
				S5: auditory signal (pure tone)		3100	55–95	–	75 (at or before 95dBA)	
Smith et al. [91]	L: USA N: [ET] alarm activated in first and second cycle stage 4 sleep (EEG) Repetition of alarm for 60 s, 10 s pause, duration 5 min SC: hospital environment V: impact of different signal types (S1–2)	A: 6–12 G: 11 M, 13 F I: none	24	S1: AL (residential)	–	100	n/a	58	180 s (median)	#Children pre-exposed to message which included child's name
				S2: V (parent)	–	100	n/a	96	20 s (median)	Study also gives cumulative probabilities of awakening, correlation between age and awakening and time to awaken Order of alarm presentation to sample was varied but no statistical association found
Du Bois et al.; Ashley [92, 93]	L: USA N: [ET] subjects exposed to each signal for 2 min; if no arousal then other devices sequentially activated (2 min recovery). Presented in sleep stages 4,2, REM SC: V: experimental sample (ES1–ES3) exposed sequentially to signals of different types, frequency and intensity (S1–S5)	**ES1**: A: adult G:- I: profoundly deaf	ES1: 32	S1: [AL] (residential)	S1: 3100	S1:>75	n/a	S1, ES1:0 S1, ES2: 57 S1, ES3: 92	Within 120 s	Paper also gives breakdown of waking effectiveness for each group for each device and breakdown by sleep stages
		ES 2: A: adult G:- I: hard of hearing	ES2:45	S2: low frequency smoke detector	S2: 450	S2:>75	n/a	S2, ES1: 11 S2, ES2: 92 S2, ES3:100		
		ES 3: A: adult G:- I: no hearing impairment	ES3: 34	S3: strobe light	S3: 1	S3: 110 cd	n/a	S3, ES1: 57 S3, ES2: 34 S3, ES3: 32		
				S4: bed shaker continuous	S4: 0.14–0.19 RSS	S4:n/a	n/a	S4, ES2: 82 S4, ES1: 93 S4, ES3: 92		
				S5: bed shaker inter-mittant	S5: 0.14–0.19 RSS	S5:n/a	n/a	S5: 100 (all)		

(continued)

Table 64.13 (continued)

Source	Observational conditions (L: location, N: nature of alarm presentation, stage of sleep, measure of awakening, SC: spatial configuration, V: variable)	Experimental Sample Description A: Age G: Gender I: Impairment	Size	Signal Type	Frequency (Hz)	Intensity pillow (dBA)	Results Mean auditory arousal threshold (dBA) [s.d]	% awakening	Mean time to awaken (secs) [standard deviation]	Additional information
Ball and Bruck [94]	L: Australia N: [ET] Modified method of limits (increasing signal volume in 5dBA intervals; signals 30 Vasec duration with 30 s interval) Signals presented at stage 4 sleep (EEG) Awakening determined EEG S: own homes (2 in laboratory) V: impact of different signal types (S1–3)	A: 18–25 G: 4 M, 4 F I: deep **sle**epers	8	S1: naturalistic house fire#	–	35–95	50.00 [14.39]	100 (at or before 95)	198.00 [172.84]	# (Sound of glass explosion and fire sounds)
				S2: [LV] female actor's voice (emotional tone)	–	35–95	47.50 [12.82]	100 (at or before 95)	167.00 [147.81]	Participants primed and familiar with sounds/ screened—no sleep disorders
				S3: spliced portions of above	–	35–95	51.25 [17.47]	100 (at or before 95)	203.13 [208.85]	Each participant exposed to each signal
										Differences between each signal found to be significant
Bruck et al. [95]	L: Australia N: [ET] signals presented 3 min periods. Wrist actigraphy to determine wakening (15 or 16 s activity data) SC: own homes V: experimental sample (ES1–2) exposed to two different types of signal and signal frequencies (S1–S4),	A: 6–10 G: 10 M, 10 F I: none	ES1:19	S1: [V] (mother) (30 s)	S1: 315–2500	S1: 89 ± 3	n/a	ES1, S1: 100	78.9 (within 30s) 100 (within 60s)	#Each participant given 2 presentations
			ES2: 14#	S2: [V] (actor) (30 s)	S2: 315–2500	S2: 89 ± 3	n/a	ES1, S2: 94.4	70.6 (within 30s) 100 (within 60s)	
				S3: [T3] (low)	S3: 500–2500	S3: 89 ± 3	n/a	ES2, S3: 96.4	66.7 (within 30 s)	
				S4: [AL] (resident)	S4: 4000	S4: 89 ± 3	n/a	ES2, S4: 57.1	73.4 (within 60s)	
									66.7 (within 30s) 100 (within 60s)	
Ball and Bruck [96]	L: Australia N: [ET1–3] modified method of limits (increasing volume by 5dBA every 30 s) Signal presented in stage 4 sleep (EEG) Three treatments examined: ET1: no alcohol ET2: 0.05 BAC ET3: 0.08 BAC SC: own home V: impact of different signal types (S1–3) given alcohol levels (ET1–3)	A: 18–25 G: 7 M, 5 F I: self-reported deep sleepers varying alcohol:	12	S1:[-V] (female)	315–2500	35–95	59.6 [14.06]	100 (at or before 95)	S1, ET1: 161.75 [80.50]	Each participant exposed to 3 signals × 3 alcohol levels)
								100 (at or before 95)	S1, ET2: 336.00, [199.93]	Background noise 50 dBA
								100 (at or before 95)	S1, ET3: 330.17 [176.52]	
			12	S2: [AL] (residential)	4000–5000	35–95	72.5 [17.77]	100 (at or before 95)	S2, ET1: 252.33 [140.66]	
									S2, ET2: 336.83, [119.59]	
									S2, ET3: 380.67 [153.91]	

			12	S3: T-3	500–2500	35–95	59.2 [15.64]	100 (at or before 95)	S3/ET1: 158.25 [90.63] S3/ET2: 299.92 [146.56] S3/ET3: 351.58 [195.38]	
Bruck and Bliss [97]	L: Australia N: [ET] exposed to constant stimulus between 1 and 4 m on 2 nights Wrist actigraphy (16 s activity data) to signal awake SC: own home V: impact of residential alarms across two experimental sample (ES1–2)	**ES1**: A: 6–10 G: 7 M, 7 F I: none	14	[AL] (residential)	–	89 ± 3	n/a	29 (both nights)	100 % within 3 min	Alarm presented to each participant on 2 nights of a 5 night study, 28 data points each group
		ES2: A: 11–15 G: 7 M, 7 F I: none	14	[AL] (residential)	–	89 ± 3	n/a	71 (both nights)	77 % within 32 s	
Bruck [98]	L: Australia N: [ET1] exposed to constant stimulus between 1 and 4.30 am on 2 nights. Wrist actigraphy (16 s activity data) to signal awake SC: own home V: impact of residential alarm across experimental samples (ES1–2)	**ES1**: A: 6–17 G: 9 M, 11 F I: none	20	AL (residential)	2000–4000	60 ± 3	n/a	15 (both nights) 30 (one night)	Within 64 s	Participants primed
		ES2: A: 30–59 G:8 M, 8 F I: none	16					100 both nights	Within 32 s	Alarm presented to each participant on 2 nights of a 5 night study, 72 data points
Bruck and Horasan [99]	L: Australia N: [ET] exposed to constant stimulus in sleep stages 4, 2 and REM (EEG) SC: laboratory setting V: impact of residential alarm	A: 28–24 G: 12 M, 12 F I: none	24	AL (residential)	2000–4000	60dBA	n/a	75 (stage2 and REM) to 87 (stage 4)	34.19 (overall)	Each participant subjected to 2 presentations (1st unprimed, 2nd primed)
									12.4 (stage 2)	48 presentations (16 each sleep stage)
									78.9 (stage 4)	Paper includes breakdown of results by ‘naïve’,non-naïve presentations and frequency distribution time to awaken
Kahn [100]	L: Belgium N: [ET] exposed to constant stimulus 2, 4 and 6 h after lights out SC: own home V: impact of signal intensity (S1–3)	A: 21.3 (mean) G: - I: none	12	AL (residential)	2000–4000	S1: 44 (44BN) S2: 54 (no BN) S3: 78 (no BN)	n/a	25	Within 20 min	Participants primed and exposed to each signal each time

(continued)

Table 64.13 (continued)

Source	Observational conditions (L: location, N: nature of alarm presentation, stage of sleep, measure of awakening, SC: spatial configuration, V: variable)	Experimental Sample		Signal			Results			
		Description A: Age G: Gender I: Impairment	Size	Type	Frequency (Hz)	Intensity pillow (dBA)	Mean auditory arousal threshold (dBA) [s.d]	% awakening	Mean time to awaken (secs) [standard deviation]	Additional information
Zepelin et al. [101]	L: USA N: [ET]Method of limits (modifying volume, tone presented at 2 min intervals SC: laboratory setting V: impact of alarm on experimental samples based on age (ES1–3)	**ES1**: A: 18–25 G:- I: none	9	[AL] 5 s duration	800	Direct to ear	101 (stage 4) 82 (stage 2) 82 (REM)	–	–	Participants primed and each age group presented with tone in 3 sleep stages; i.e., 81 data points
		ES2: A: 40–48 G: - I: none					87 (stage 4) 71 (stage 2) 81 (REM)	–	–	
		ES3: A: 52–71 G: - I: none					71 (stage 4) 61 (stage 2) 66 (REM)	–	–	
Nober et al. [102]	L: USA N: [ET] 30 students exposed to constant stimulus at varying times of night BN = background noise SC: own home V: impact of signal intensity (S1–S5)	A: 18–29 G: - I: none	10	[AL] (residental)		S1: 55dBA (no BN)	n/a	100	Within 21 s	Each participant primed and exposed to each signal
						S2: 70 dBA (no BN)		100	Within 16 s	
						S3: 85 dBA (no BN)		100	Within 11 s	
						S4: 70 dBA (BN-53)		100	Within 85 s	
						S5: 55 dBA (BN-53)		100	Within 75 s	

measure used to determine awakening), Spatial Configuration (own, home, laboratory), Variables, the Experimental Sample (Nature and Size), the Signal Employed (Type, Frequency and Intensity), Results (Mean Auditory Threshold, percentage of Awakening and Time to Awaken as appropriate). The Additional Information column provides other information that may have influenced the outcome [39] regarding the study, e.g., the presence or absence of background noise (if known) and whether subjects were primed to expect a signal or were naïve in this respect.

The main method adopted in the included studies is that of a *constant stimulus* being presented to the participants. In this case, the frequency of responses is simply measured within the sample to determine the percentage of participants that awoke and the time it took them to awaken. Another common method which is used to determine, not just the response to a particular signal of certain frequency/volume but the waking thresholds (or AAT—Auditory Arousal Thresholds) for the participants, is the *method of limits* [39]. In this approach, a tone of a standard frequency is presented to a sleeping person at a specific intensity and the intensity increased (usually in five dBA intervals) if there is no response within a certain time period. A response or "no response" to each presentation enables the auditory arousal threshold (AAT) for the person to be obtained. This results in a mean AAT rather than a percentage awakening output (since all eventually awake).

Table 64.13 only provides a summary of some of the most significant data in this area. For a more in-depth treatment of this complex subject area the reader is directed to the comprehensive reviews of Bruck and colleagues [39, 86, 87].

Pre-evacuation Phase: Impaired

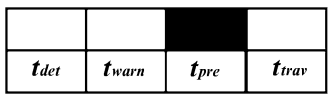

Research has shown that during the pre-evacuation phase, building occupants spend time in various activities prior to evacuation. In public spaces, these activities commonly include gathering belongings, turning off computers, packing belongings away, etc. In some evacuation scenarios, particularly in dwellings or other occupancies with sleeping accommodation, these 'preparation activities' may also include turning on bedside lights and getting dressed. This 'preparation time' can be considered a sub-component of the 'pre-evacuation' time and it is recognized that this time could be considerably longer for some individuals, e.g., people with disabilities.

Two studies have directly compared the 'preparation time' for disabled and able-bodied persons. An early study by Pearson and Joost [103] was designed specifically to determine the preparation times of subjects exposed to a simulated fire emergency in a residential setting. The first study involved 18 healthy able-bodied male undergraduate students, 11 blind persons (4 female and 7 male aged from 21 to 58) and 9 male wheelchair users. The second study involved 20 healthy young adults (3 male and 17 female aged from 30 to 48), 20 elderly persons in good health (4 male and 16 female aged 59–79) and 20 elderly with arthritic impairments (3 male and 17 female aged 55–80). Each subject was required to complete a range of scenarios that involved the completion of various activities such as searching for a personal item, donning clothes, retrieving personal effects, and activating lights. Pearson and Joost's [103] study concluded that the mean time for blind subjects to complete these activities was 2.47 times greater than that of young, able-bodied subjects and the mean time for wheelchair users was 2.36 times greater than that of able-bodied subjects.

A later study by Shields et al. [104] also compared the time to prepare to evacuate as part of three evacuation studies of hotel accommodation involving mixed ability populations, including four wheelchair users. Two of these studies were designed to simulate day-time evacuation of hotel accommodation in which participants were initially located in a chair or in their wheelchair and were asked to retrieve a personal item from a drawer before leaving the

room. In the third study, designed to simulate a night-time scenario, participants were initially lying on the bed, and were required to turn on a bedside light, get into their wheelchair (if applicable) and retrieve a personal belonging from a drawer before leaving the room. The results from the Shields' studies suggest that wheelchair users took 1.6 and 1.9 times longer than able-bodied persons to perform the tasks which comprised the day time scenario and 2.4 times longer than able-bodied to perform the tasks which comprised the night time scenario.

These findings are interesting and suggest that, in situations where those with impairments are present, the expected pre-evacuation times might then be increased given the potential difficulties in responding and the need for preparation. However, it is important to note that in both studies the samples were small and the range and severity of disability rather limited. Therefore they should be treated as indicative only and used with care. For a more detailed understanding of the factors described and the base values collected in each case, the reader is referred to the original source material.

Travel Phase

Egress models (engineering or computational) require a number of basic quantitative and qualitative information in order to configure the initial scenario to be examined, i.e. to reflect the core behavioral elements of the engineering timeline. As mentioned these include the pre-evacuation time (addressed in previous sections), quantitative travel elements (travel speed, flow conditions/constraints and their relationship to population density) and qualitative elements (route availability and choice). This section focuses upon the quantitative travel elements only—Chaps. 57 and 58 should be referred to for the more qualitative factors mentioned.

In an engineering context, crowd movement is quantitatively specified using three key characteristics. These are density, speed, and flow. These underpin the engineering hydraulic model presented in Chap. 59 and are also employed or generated in computational egress models. Within the hydraulic model, relationships are assumed between density and speed, and density and flow that then directly influence the results produced. As such, data is often collected relating the three measures in this manner. It is debatable as to the exact causal relationship between flow/speed and density, with density being both an emergent property of crowd movement and a constraining factor. However, in this instance, the relationship is retained given the format and content of the data-sets provided.

Population density is generally expressed as the number of persons in a unit area of measured space, e.g. 2.0 persons/m^2. Alternatively, this factor can be represented by (i) using the inverse of density, that is, the area per person or pedestrian module (occupancy levels), e.g. 0.5 m^2 (5.4 ft^2) per person, (ii) the distance maintained between occupants, in terms of headway or proximity, or (iii) the perpendicular projected area occupied by the population over a unit area (e.g., m^2/m^2) [105, 106]. Given that the density (persons/unit area) is still most commonly used, it will be adopted here and a more comprehensive discussion of this issue is left for future editions of this chapter. It is acknowledged that there are limitations with all of these methods of representation, including the population density. These limitations include the averaging of the densities over a large area, the inclusion of persons within the variable that are not directly influencing movement, and the variety of body sizes not represented within the analysis [105].

Speed is the distance covered by a moving person in a unit of time, e.g. 1.0 m/s (3.3 ft/s). The term "flow" is often used in a casual, non-technical way when the general term "movement" is implied, or when speed is actually being specified. However, flow is specifically the number of people that pass some reference point in a unit of time, e.g. 2.0 persons/s. Flow can be presented in relation to the unit width, in which case it is termed the specific flow and it is presented in units of persons/unit width/time period or it can be presented across a component of a particular width where it is presented in units

of persons/time period. In the tables which follow the specific flow is typically employed; however, it will be made clear for each of the data-sets where other formats are employed.

Assuming no other constraint is present, people can move at their desired speed (given their innate capabilities) if there is sufficient space available for them to move freely, i.e. if the surrounding population does not constrain their movement. The desired speed may change with motivation, which can be influenced by time constraints, social considerations and perceived risk, amongst other things, e.g., the nature of the scenario. However, as the space available reduces, so the ability of the individual to maintain their desired speed, and act on their intentions, is reduced. There is a relationship between the ability to maintain a speed and the local population density.

Relationships between speed and density for specific terrains are provided in Chap. 59. These are based on the work of Nelson and Maclennan [107], who derived these relationships from the work of Fruin [34], Pauls [33], and Predtechenskii and Milinskii [106] *inter alios*. The relationships derived by Nelson and Maclennan [107] represent engineering approximations of several diverse data-sets. As such, these relationships should not be seen as empirical data but as engineering representations.

Another example of this engineering representation is shown in Fig. 64.4. This is derived by Pretorius [108] from the work of Nelson and Maclennan [107] and Kholshevnikov et al. [109]. Kholshevnikov et al. [109] highlighted the different influences that population density might have upon the physical and psychological factors influencing individual movement. Pretorius transposed this onto the assumed relationship between speed and flow produced by Nelson and Maclennan [107] and presented in the SFPE handbook. Pretorius achieved this by using slightly different body sizes (derived from Still [110]) and assuming an engineering rather than empirical approach.

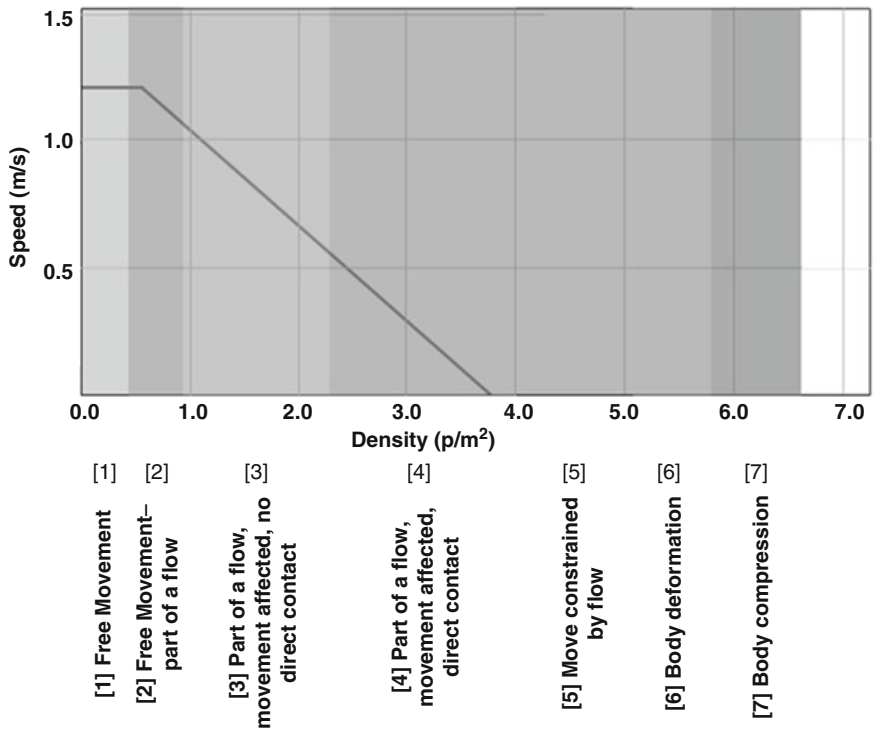

Fig. 64.4 Derived relationship between speed and density [108]

The relationship between flow and density is more complex, given the number of variables involved, i.e., that flow is dependent on the speed of movement and the number of people moving. This relationship tends to be a higher order function than that between speed and density.

The relationship between speed, flow and density becomes more complex as the degrees of freedom in movement increases—the relationship is different on the horizontal from that on the vertical, where movement is more three dimensional in nature. Indeed, some have questioned the direct relationship between speed/flow and population density on stairs, given the impact of the stair configuration upon gait and forward movement [105]. Notwithstanding, the direct relationship is implicitly assumed in much of the data presented, and the nature of this relationship is not investigated here.

A number of reviews of movement data already exist in the literature; they either combine disparate data-sets from a variety of different researchers, or summarize the work of a suite of data collection exercises performed by the same researcher(s). In the following sections, some of these reviews are presented as examples of data-sets collected for a particular behavioral or movement element. However, a number of broader reviews exist that relate to more than one element. These include reviews by Predtechenskii and Milinskii [106], Smith [111], Tubbs and Meacham [112], Thompson [113], Fahy and Proulx [37], Graat et al. [114], Lord et al. [115], Daamen [116], Teknomo [117], Helbing [118], Fruin [34], and Pauls [33]. Many of these broader reviews have been conducted as part of research dissertations and so fall outside of the relatively narrow scope of this chapter.

It is important for the user to understand the nature of the relationship between these variables before applying any of the data presented in this chapter. Some of the models (engineering or egress) assume this relationship [27]. Others can adopt different relationships depending on the data provided to them or the rules embedded, with the relationship occasionally predicted and generated rather than imposed. Either way, it is important for the reader to understand that this relationship is often assumed without due reference to the implications of this assumption.

When employing these quantitative data-sets, a number of qualitative engineering decisions will need to be made. These relate to the use of the space (width) available, the routes available and the routes used, amongst many others. The selection and credible combination of these qualitative decisions are discussed in detail in Chap. 57. The routes available during an incident will be influenced by the environmental conditions present (discussed in Chaps. 61 and 63). The choice and use of the available routes will be influenced by a number of population characteristics (discussed in Chap. 58) and procedural measures (discussed in Chaps. 56 and 58). Guidance should therefore be sought from these other chapters in order to frame the use of the quantitative data-sets presented below.

In the following sections the movement on the horizontal (see section "Travel Phase: Horizontal Movement"), on stairs (see section "Travel Phase: Stair Movement (Up and Down)"), through exits (see section "Travel Phase: Exits and Narrowings"), on escalators (see section "Travel Phase: Escalators (Up and Down)"), in smoke (see sections "Vulnerabilities: Situational: Movement in Smoke" and "Vulnerabilities: Innate: Impaired Movement") and movement involving those with impairment (see section "Vulnerabilities: Innate: Impaired Movement") is discussed. Where there is other important review material or material that does not meet the selection criteria highlighted in section "Sources of Data" then this is briefly discussed as are the table formats employed.

Travel Phase: Horizontal Movement

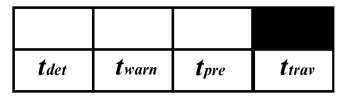

A number of previous reviews have been conducted exploring the relationship between density and speed [37, 38, 109, 113, 116, 119–122]. Irrespective of the material covered, an array of different approaches (i.e. numerical, graphical, descriptive, tabular, etc.), have been adopted to

summarize the data and equations have been derived [9]. The approach adopted by a particular reviewer is likely to have been influenced by their theoretical understanding of the factors involved, the purpose of the summary, e.g. intended application area, and the material included in the review itself. Several examples of the different approaches adopted are presented below. The reader is encouraged to examine some of the reviewed material and analysis available from the original source, as a great deal of it falls outside of the remit of this chapter.

Kholshevnikov et al. presented their own work and that of a number of other Russian/Soviet researchers performed over a period of approximately 30 years [109]. This data was gathered in a number of different building types, population types and in a range of environmental conditions. Of particular note in this work is the extreme population densities included in the reviewed material (see Fig. 64.5).

Brocklehurst [120] and Daamen [116] both reviewed a range of material relating to the speeds produced during general circulation activities but presented the material in different ways. Brocklehurst [120] examined the work of Hankin and Wright, Peschel, Henderson, Helbing, Fruin, Older, Polus, Still and presented the average speeds produced given the background factors present during the original events. These factors included the nature of the event, the location, densities, gender/age of the population and the speeds produced. Daamen [116] produced a graphical representation of the data of Fruin, Weidmann, Virkler, Older, Sarkar, and Tanariboon, a functional representation of speed and flow (including the data of O'Flaherty, Lam, Navin, Pauls, Pushkarev in addition to those represented graphically) and mean speed

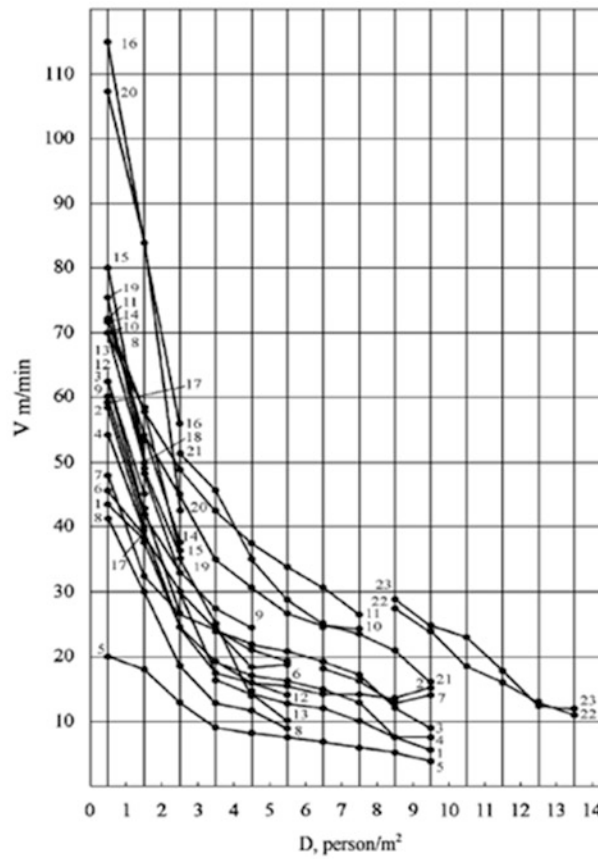

Fig. 64.5 Speed—density relationship for horizontal movement presented by Kholshevnikov et al. [109] (Reproduced from original)

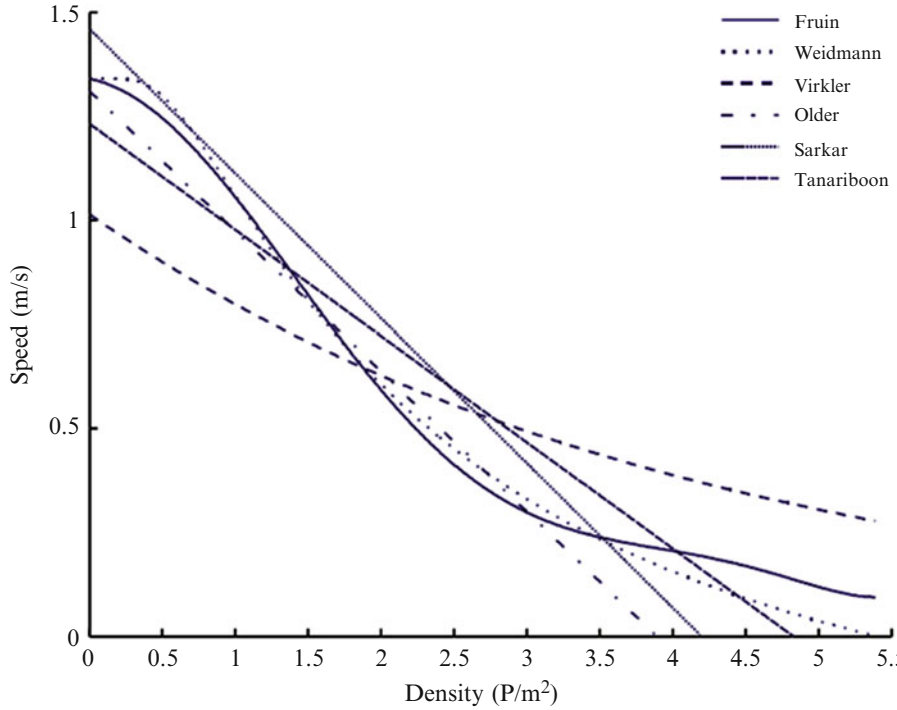

Fig. 64.6 Speed—density relationships summarized by Daamen [116] (Reproduced from the original)

estimates (from data of Daly, Fruin, Hankin and Wright, Henderson, Hoel, Knoflacher, Koushki, Lam, Morrall, Navin, O'Flaherty, Older, Pauls, Roddin, Sarkar, Sleight, Tanariboon, Tregenza, Virkler, and Young). It should be noted that both Brocklehurst [120] and Daamen [116] presented significant reviews of data within their doctoral theses; dissertations such as these are useful sources of data, given the space available for a more detailed review and description of the material available (see Fig. 64.6).

Al-Gadhi [119] also examined a number of pedestrian sources (as well as many collected himself from situations such as the Hajj) that included unidirectional and bidirectional movement, whilst Schadschneider et al. [122] examined several different sources that might be used to support an understanding of evacuation dynamics to facilitate numerical and computational model development. This included a variety of different sources (in terms of the scenario, the geographical origin and the age of the data), including the work of Weidman, Predtechinskii and Milinskii, Older and Helbing [122].

Thompson [113], in his seminal thesis outlining his model development, presented a broad review of core data in order to develop an understanding of the data required to develop a computational egress model and indeed went on to collect his own data in order to develop his model. Thompson [113] summarizes, in some detail, the work of a number of key researchers including Fruin, Predtechenskii and Milinskii, Hankin and Wright, Pauls, Weston and Marshall, Peschl, Ando et al., and Polus, Schofer and Ushpiz.

Finally, in the same vein as the work conducted by Fahy and Proulx [37], Shi et al. [38] attempted to collect together a small number of data-sets in order to develop a database; although in this instance it was conducted to support the development of evacuation modeling tools. Shi et al. [38] produced a table where the data was categorized according to several factors deemed to influence the results produced (see Table 64.14); i.e. free movement or

Table 64.14 Summary of walking speeds produced by Shi et al. [38] (Reproduced from original)

Influencing factors		Speed (m/s)	Range (m/s)	References
Walking type	Free move		1.2–1.8	[120, 219]
	Exit move		0.8–1.5	
Walking conditions for corridors, doorway on ship	Low	1.4		[24, 219]
	Optimum	0.70		
	Moderate	0.39		
	Crush	0.10		
Place type	Public place		0.51–1.27	[56, 220]
	High-rise apartment	1.05	0.57–1.20	
	apartment	0.95	0.56–1.12	
Occupant type[a]	Children	1.08		[131]
	Female elderly	1.04		
	Male elderly	1.05		
	Elderly	1.04		
	Female adult	1.24		
	Male adult	1.30		
	Adult	1.27		

exit movement, density levels (low, optimum, moderate, crush), location type and occupant type. Other comparable reviews have also been conducted [114, 117, 118, 124–126].

Data appears (both within fire engineering and from adjacent areas of analysis) in a number of formats and representing an array of different scenarios. This data broadly reflects the difference performance capabilities of pedestrians under different physical and social conditions.

An examination of the review material available was conducted and the data simplified and compiled into a single figure (see Fig. 64.7). Given the lack of contextual information, the different criteria used to include representative data-points and the different results formats used, this figure should, at very best, be seen as only indicative. However, it is does crudely demonstrate that much of the data collected (and the relationships produced) focus on a relatively narrow band of population densities; i.e. between 0 and 6 persons/m^2. Furthermore, the range of speeds produced within this envelope of densities appears to narrow as the density increases—from a relatively wide range of speeds between 0 and 2 persons/m^2 that narrow beyond 4 persons/m^2. This claim is supported by the work presented by Kholshevnikov [67, 109].

A summary of a range of data relating to travel speeds achievable during horizontal movement are presented in Table 64.15, while the subsequent flow rates produced are described in Table 64.16. It should be noted that there is some overlap between the data described above and the data-sets that appear in Tables 64.15 and 64.16. In Table 64.15, the following information is provided: Source, Observational Conditions (Location, Nature, Spatial Configuration, Participants, Environment, Variable), Sample (Collection method and Size), Results (Density, Speed, Relationship between Speed and Density), and Additional Information. In Table 64.16, the following information is provided: Source, Observational Conditions (Location, Nature, Spatial Configuration, Participants, Environment, Variable), Sample (Collection method and Size), Results (Density, Specific Flow, Relationship between Flow and Density), and Additional Information. In both cases, this information is only provided if it appears in the original source or if can readily be derived. In a limited number of cases, the values provided in the tables, although not given explicitly in the original source, have been derived from other information provided in the original source; e.g., a calculation of a mean

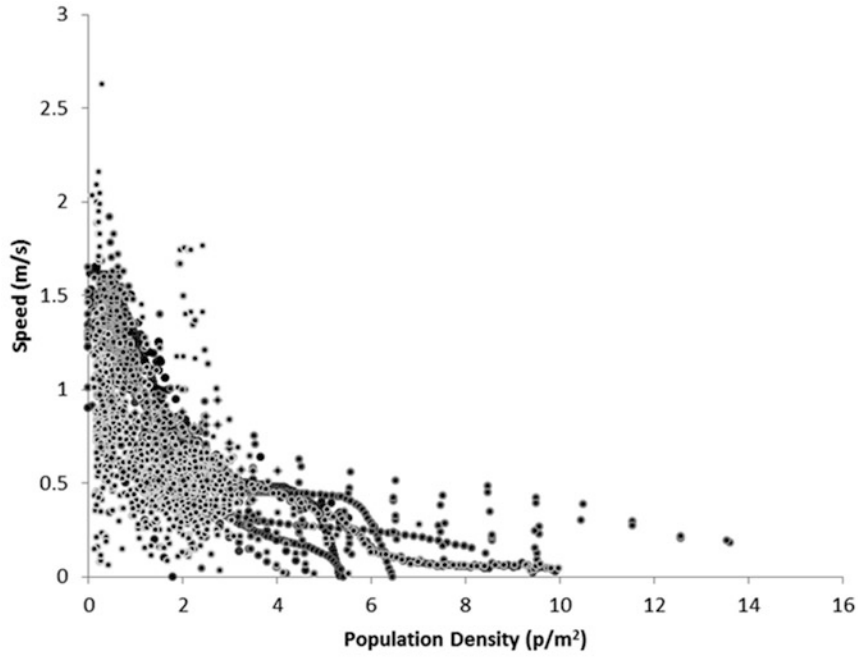

Fig. 64.7 Simplistic compilation of reviewed data on horizontal movement speed derived from the work of Hankin, Helbing, Oeding, Daamen (Weidmann, Virkler, Tanariboon, Sarkar, Polus, Lam), Predtechiniski and Milinskii, K+V, VTT, Weston and Marshall, Navin, V+S, Mori, Averill, Ando, Hoskins, Duives [13–15]

from the source data. If a value has been derived in this way, then that is noted in the table beside that value.

Travel Phase: Stair Movement (Up and Down)

t_{det}	t_{warn}	t_{pre}	t_{trav}

In tall structures, especially those where elevators have not been approved for use in fire emergencies, stair movement may form a considerable part of the overall t_{RSET} calculation. Even in lower rise buildings, stair movement may still be a pivotal, especially for those with difficulties traversing stairs. Indeed, stair movement has determined the outcome of a number of serious incidents [8, 20, 37, 145]—with both the attainable speed, the impact of congestion, fatigue/rest effects, and the direction of required movement all influencing the nature of the outcome.

Movement on stairs presents a different challenge than horizontal movement given the extra degree of freedom available in the movement, the constraints imposed by the stair design and the additional effort required to traverse the stair component. In addition, the relationship between density and speed/flow may be more complex during vertical movement than it is on flat surfaces. For instance, the size and configuration of the treads may have a confounding influence upon this relationship. This issue has recently been examined by Hoskins [105].

Over the last few decades, a number of researchers have examined pedestrian and evacuee performance on stairs. Some [11, 12, 37, 105, 109, 114, 115] have addressed the quantitative aspects of stair movement e.g. speeds and flow rates, while others [33, 146, 147] have focused on the more qualitative aspects of stair movement, e.g. spacing, passing, merging behavior, counter-flow, lane formation, group behavior, gait, falls, handrail use.

Given the importance of stair movement, there are a number of significant reviews available regarding stair data. Some of these, such as

Table 64.15 Travel data—horizontal travel speeds (m/s)

Source	Observational Conditions (L: location, N: nature, SC: spatial configuration, P: participants, E: environment, V: variable)	Sample		Results			Additional information
				Density	Speed		
		Collection method	Size	Mean/range of means (persons/m^2)	Mean/range of means unless otherwise specified (m/s)	Relationship speed and density	
Schultz, Schulz and Fricke [127]	L: Germany	Video analysis over 150 m^2 area	C1: 330		C1, S1: 1.42		
	N:C -airport passenger observations over 8.5 h. C1: business use C2: leisure use				C1, S2: 1.33		
	SC: airport				C1, S3: 1.32		
	P: 595 passengers		C2: 265		C1, S4: 1.27		
	S1: trolley bag				C2, S1: 1.19		
	S2: handbag				C2, S2: 1.07		
	S3: rucksack				C2, C3: 1.07		
	S4: bag cart				C2, C4: 1.04		
	V: movement according to object being carried (S1–4) and type of passenger (C1–C2)						
Ono et al. [128]	L: São Paolo, Brazil	Video	906 (am)	–	0.20–3.75 (range of actual speeds across all drills, varies with age)	–	Drill procedure involved classes being led out in single file with a leader. Data collected over 9 horizontal sections (long corridors)
	N:ET-three drills conducted in each of 2 time periods (morning and afternoon)		706 (pm)				Paper gives evacuation times each drill, frequency distribution speeds for all drills, breakdown of mean speeds by age and drill and max and min speed by age
	SC: school						
	P: aged 5–17; data relates to age range 6–14						
	V: movement across three drills						
Zanlungo et al. [129]	L: Osaka, Japan	–	–	0.02-0.04 (unimpeded)	1.15*–1.3* *Extracted from graph	n/a	Paper considers patterns of movement over route and collision avoidance model described
	N: C						
	SC: two corridors, underground pedestrian area						
	P:						
	V: unimpeded movement along corridors						

(continued)

Table 64.15 (continued)

Source	Observational Conditions (L: location, N: nature, SC: spatial configuration, P: participants, E: environment, V: variable)	Sample		Results			
				Density	Speed		
		Collection method	Size	Mean/range of means (persons/m^2)	Mean/range of means unless otherwise specified (m/s)	Relationship speed and density	Additional information
Kholshevnikov et al. [67]	L: Moscow, Russia	Video	234	<1	0.41–1.61[a]	Paper derives relationships between speed and density for each age group and movement (walking, running)	[a]Dependent on age grouping
	N: ET		261	1–2	0.41–1.31[a]		Paper gives breakdown of walking speeds by density for different age groups as well as standard deviations, confidence intervals. Running speeds by density also given
	SC: 8 kindergartens		159	2–3	0.41–1.09[a]		
	P: children mixed gender and age (<3–7 years)		35	3–4	0.41–0.94[a]		
	V: different age characteristics		6	4–5	0.83 (5–7 years)		
Lárusdóttir and Dederichs [130, 131]	L: Denmark	Video	71 participants	<0.5 (unimpeded)	S1, UE1: 0.6 ± 0.17	n/a	Paper gives frequency distribution of walking/running speeds
	N:UE - UE1:walking, UE2:running				S2, UE1: 0.84 ± 0.25		
	SC: daycare centres				S1, UE2: 1.14 ± 0.30		
	P: mixed gender and age:				S2, UE2: 2.23 ± 0.64		
	S1: 1:½–2 years (young child)						
	S2: 3–6 years (older child)						
	V: impact of different procedure employed (UE1–2) given the different age groups examined (S1–2)						
Winkens and Kingsch [132]	L: Dusseldorf, Germany	Video and specialist image analysis	14–107 participants	0.5–4.5 (depending on corridor width and number of participants)	1.56 (maximum measured)	–	Paper explores influence of chosen measurement areas and method of measurement on values of speed and density and presents speed × density relationship in graphical form for different widths of corridor and measurement methods
	N: ET						
	SC: corridors of different width (0.7 –1.0 m)						
	P: 14–107						
	V: movement rates through corridors of different width						

Yeo and He [133]	L: Singapore	Video	785	C1: <0.43 (unimpeded)	1.04–1.30[a] (depending on age and gender)	–	[a]Individual speeds
	N: C1–2, weekday peak hours in 2005. C1—less than 0.43 p/m^2, unimpeded C2—between 0.1 and 0.8 p/m^2		–	C2: <0.1*–0.8* *Extracted from graph	0.7*–1.7*[a] *Extracted from graph	v = 1.29–0.11ρ	Paper gives breakdown of unimpeded walking speeds of 785 persons by age and gender Also walking speed by density given in graphical form and compares regression line with Fruin
	SC: mass rapid transit (MRT) stations, during morning Walkways 3.5–64 m length and 1.2–4.8 m width						
	P: commuters of mixed age and gender						
	V: movement rates given population densities (C1–2)						
Fang et al. [134]	L: Wuhan City, China	Video	–	0.25*–2.75 *Extracted from graph	0.1–1.54* *Extracted from graph	Given in graphical form only	Author notes high use of luggage during data collection
	N: C						
	SC: exit tunnel of railway station during rush hour in 2003. Observed area, 4 × 5 m						
	P: mixed age and gender						
	V: movement rate across population density range						
Wong and Cheung [135]	L: China	Video	44	ET1: <1–3 ET2: <1–2	ET1:1.1*–1.5* ET2:3*–3.6* *Extracted from graph	Given in graphical form only	Compares findings to other published
	N: ET1–2. 5 trials. ET1-'normal' and ET2-'emergency' (i.e. fast as they could walk) Trials involved 10, 20, 30 and 40 persons						
	S: 17 m section of 27 m corridor (2 m width) leading to 1.4 m exit						
	P: 44 college students aged 20–24, 29 males and 15 females						
	V: movement rates given procedure employed (ET1–2)						
Lee and Lam [136]	L: Hong Kong, China	Video (time-lapse photography)	1232	Uncongested	0.31–1.4* *Extracted from graph for uncongested conditions	–	Paper gives graphical representation of relationship flow and speed and explores relationship between mean walking speed and standard deviation
	N: C –3 × 2 h peak periods over 5 days						
	SC: two underground stations						
	P: commuters mixed age and gender						
	V: movement rates in uncongested conditions						

(continued)

Table 64.15 (continued)

Source	Observational Conditions (L: location, N: nature, SC: spatial configuration, P: participants, E: environment, V: variable)	Sample		Results			
				Density	Speed		
		Collection method	Size	Mean/range of means (persons/m^2)	Mean/range of means unless otherwise specified (m/s)	Relationship speed and density	Additional information
Hoskins and Spearpoint [137]	L: New Zealand and Australia	Video	–	0.1*–3.0* (across different locations)	2.6*–0.4* (across different locations)	–	Gives speed × density from different egress paths in graphical form and compares with previous studies, but doesn't derive relationship
	N: [C] during and following sporting activities			*Extracted from graph	*Extracted from graph		
	SC: 23 egress paths in 11 stadia						
	P:						
	V: movement rates in range of population densities						
Daamen and Hoogendoorn [138]	L: Netherlands	Video		Variable (measured as headway)		Graphical representation only	
	N: [ET1–5] 10						
	ET1: unidirectional (1 m corridor bottleneck)		ET1: 1123		0.93 [0.41,–]		
	ET2: Unidirectional (open)		ET2: 1167		1.49 [0.18,–]		
	ET3: opposite (open)		ET3: 709		1.33 [0.19,–]		
	ET4: crossing (open)		ET4: 532		1.33 [0.24,–]		
	ET5: unidir (2 m corridor bottleneck)		ET5: 1843		1.22 [0.29,–]		
	SC: corridor width 1–2 m						
	Open space						
	View 14 × 12 m						
	P: 75 students + other						
	V: movement rate given procedure employed (ET1–5)						

Berrou et al. [139]	L: USA, UK, Hong Kong, Monaco	Video		Variable, not presented		–
	N: C1–8 2000–2005	(900 h)				
	SC: train and metro stations, sport arenas, evacuation drills, street parties					
	SC1: train station(US)		SC1: 4762		1.5 [0.21]	
	SC2: train station (UK)		SC2: 1043		1.55 [0.23]	
	SC3:train station(HK)		SC3: 588		1.47 [0.21]	
	SC4: train station (HK)		SC4: 485		1.32 [0.22]	
	SC5: train station (HK)		SC5: 1560		1.25 [0.22]	
	SC6: train station (Monaco)		SC6: 2524		1.40 [0.19]	
	SC7: sports (UK)		SC7: 6777		1.43 [0.20]	
	SC8: sidewalk (Singapore)		SC8: 519		1.23 [0.20]	
	P: passengers					
	V: movement rate given structure (SC1–8)					
Klupfel [140]	L: Germany	Video	C1: 95	–	1.38	–
	N: C1–6		C2: 149		1.28	
	SC: world expo 2000		C3: 59		1.24	
	P:		C4: 17		1,24	
	E: mixed		C5:10		1.22	
	V: nature of event (C1–6)		C6:2		1.10	
Seyfried et al. [141]	L: Germany	Video	Unclear	Presented in figure	1.24 [0.15]	
	N: ET Told not to hurry. Single file					
	Free movement					
	SC: track 0.8 m in width, 17.3 m in length					
	P: N = 1, 15, 20, 25, 30, 34					
	V: movement rate given range of conditions					
Seyfried et al. [142]	L: Dusselfdorf, 2006	Video	14–70	0.25–2.75 p/m* [2D calculation]	1.2–0.1 m/s	
	N: ET –99 trials. 2D calculations			*Extracted from graph		
	SC: experimental track, including straights of 4 m. Width modified					
	P: 250 soldiers					
	V: movement rate across range of densities					

(continued)

Table 64.15 (continued)

Source	Observational Conditions (L: location, N: nature, SC: spatial configuration, P: participants, E: environment, V: variable)	Sample		Results			
				Density	Speed		
		Collection method	Size	Mean/range of means (persons/m^2)	Mean/range of means unless otherwise specified (m/s)	Relationship speed and density	Additional information
Tanaboriboon and Guyano [143]	L: Bangkok, Thailand	Video	C1: 542	Low density (unimpeded speeds)	1.22 ± 0.13# (adults)	n/a	#Units changed from m/min in text
	N: C1–3		C2: 596		1.23 ± 0.11# ('young')		Note that 'young' and 'elderly' not defined in paper. Significant differences found between genders. Paper also gives ranges, and compares findings other countries
	SC: three sidewalks and overpass		C3: 94		0.82 ± 0.13# ('elderly')		
	P: mixed gender. Different population types (adults, young, elderly) associated with each event, although few details provided						
	V: movement rates given event examined (C1–3)						

V velocity, ρ density in persons/m^2

Table 64.16 Travel data—horizontal flow

Source	Observational conditions (L: location, N: nature, SC: spatial configuration, P: participants, E: environment, V: variable)	Sample		Results			
				Density	Specific flow		
		Collection method	Size	Mean/range of means (persons/m^2 unless otherwise specified)	Mean/range of means (persons/m/min, unless otherwise specified)	Relationship flow and density	Additional information
Winkens and Kingsch [132]	L: Dusseldorf, 2006 N: 29 trials SC: corridors of different width (SC1: 0.7 m, SC2: 0.85 m, SC3: 1.0 m) P: 250 soldiers V: flow given spatial configuration (SC1–3)	Video and specialist image analysis	14–107 participants in each trial	0.5–4.5 (depending on corridor width and number of participants)	SC1: 0.18–0.68 SC2: 0.35–0.8 SC3: 0.16–0.9	–	Paper explores influence of measurement methods. Results reflect 'mean method'
Irzik [144]	L: Germany (2003) N: 78 × 2 min observations of pedestrian flow SC: 2–6.5 m sidewalks P: 7000 pedestrians V: flow generated given the measured density	Video and specialist image analysis	7000 pedestrians	0–2.5		Flow = 0.261 (density^2) + 1.1738 (density)	
Yeo and He [133]	L: Singapore N:[C] –peak hours in 2005 SC: mass rapid transit (MRT) stations Measurements on walkways 3.5–64 m length and 1.2–4.8 m width P: commuters of mixed age and gender V: flow rate across population densities	Video	–	2–7.5 m^2/person * *Extracted from graph	63–10* *Extracted from graph	$F = -2.4 \times 10^{-4} + 73.85/\gamma$ where: F = specific flow in persons/m/min, γ = space per person in m^2/person	Relationship shown in graphical form
Fang et al. [134]	L: Wuhan City, China N:[C] –peak period 2003 SC: exit tunnel of railway station Observed area, 4 × 5 m P: mixed age and gender V: flow rate across population densities	Video	–	0.25*–2.75 *Extracted from graph	0.42*–0.81 persons/m/s (max at density of 1.48 persons/m^2) *Extracted from graph	Complex relationships derived—see paper	Results given in graphical form only

(continued)

Table 64.16 (continued)

Source	Observational conditions (L: location, N: nature, SC: spatial configuration, P: participants, E: environment, V: variable)	Sample		Results			
				Density	Specific flow		
		Collection method	Size	Mean/range of means (persons/m^2 unless otherwise specified)	Mean/range of means (persons/m/min, unless otherwise specified)	Relationship flow and density	Additional information
Lee and Lam [136]	L: Hong Kong, China	Video (time-lapse photography)	1232	–	C1–3: 31*–120*	–	Paper gives graphical representation of relationship flow and speed and explores relationship between mean walking speed and standard deviation
	N: [C1–3] –3 × 2 h peak periods over 5 days				*Extracted from graph for 'congested' conditions		
	SC: two underground stations						
	P: commuters mixed age and gender						
	V: flow rate given nature of event (C1–3)						
Hoskins and Spearpoint [137]	L: New Zealand and China	Video	–	0.25*–2.75* (for different egress paths)	0.3*–1.55* persons/s/m $_{eff}$ (for different egress paths)	–	Gives specific flow × density from different egress paths in graphical form and compares with previous studies
	N: [C] –during sporting activities			*Extracted from graph	*Extracted from graph		
	SC: 23 egress paths in 11 stadia						
	P: attendees						
	V: flow rate across population densities						
Daamen and Hoogendoorn [138]	L: Netherlands	Video		Variable (measured as headway)		–	
	N: [ET] –10 trials						
	SC: corridor width 1–2 m Open space, view 14 m × 12 m						
	SC1: unidirectional (1 m corridor bottleneck)		SC1: 1123		0.63 (p/s)		
	SC2: unidirectional (open)		SC2: 1167		0.18		
	SC3: opposite (open)		SC3: 709		0.11		
	SC4: crossing (open)		SC4: 532		0.05		
	SC5: unidir (2 m corridor bottleneck)		SC5: 1843		0.45		
	P: 75 participants in each trial						
	V: flow rate given spatial configuration (SC1–5)						

the work of Hoskins [105], have attempted to derive representative functions to describe the relationship between density and speed on stairs, and have provided a detailed review of a range of other speed/flow conditions produced and the maximum densities measured by researchers such as Pauls, Khisty, Kagawa, Proulx, Shields, Kratchman, Hostikka, Peacock, Fruin, Daly, Tanaboriboon, Lee, Ye, Galea, Averill, Melinek, Predtechinskii, Templer, Smith, Frantzich, Boyce, Wright, and Fujiyama [105]. It should be noted that Hoskins [105] then goes on to produce a different formulation to generate stair speeds from that typically employed relating stair flow/movement to the physical conditions present.

Shi et al. [38] also examined stair movement data and categorized it according to dimensions, incline and configuration of the stair. Peacock et al. [45] summarized their own studies involving the evacuation of a series of structures involving stair movement, placed the evacuations in a historical context (see Fig. 64.8) and then compared the speed/density relationships with the SFPE curve derived by Nelson and Maclennan (see Fig. 64.9).

Kholshevnikov et al. [73] presented a summary of movement data relating stair descent speeds to population density within multi-purpose, sports buildings, universities, schools, street areas and experimental rigs in the Soviet Union/Russia over a 30 year period. The results are shown in Fig. 64.10. Once again, the elevated population densities present in the Russian studies, relative to the other studies presented above (e.g. those of Peacock et al. [45]) should be noted. Other reviews include those produced by Fahy and Proulx [37] (that categorize performance according to building type and presence of high densities), Graat et al. [114] (where the speeds are categorized according to direction of movement and location type), and Lord et al. [115] (where speeds are categorized according to direction, demographics, and likelihood).

A compilation of a range of data relating to travel speeds during movement on stairs is presented in Table 64.17, while the subsequent flow rates produced are presented in Table 64.18. In Table 64.17, the following information is provided: Source (Author and Year),

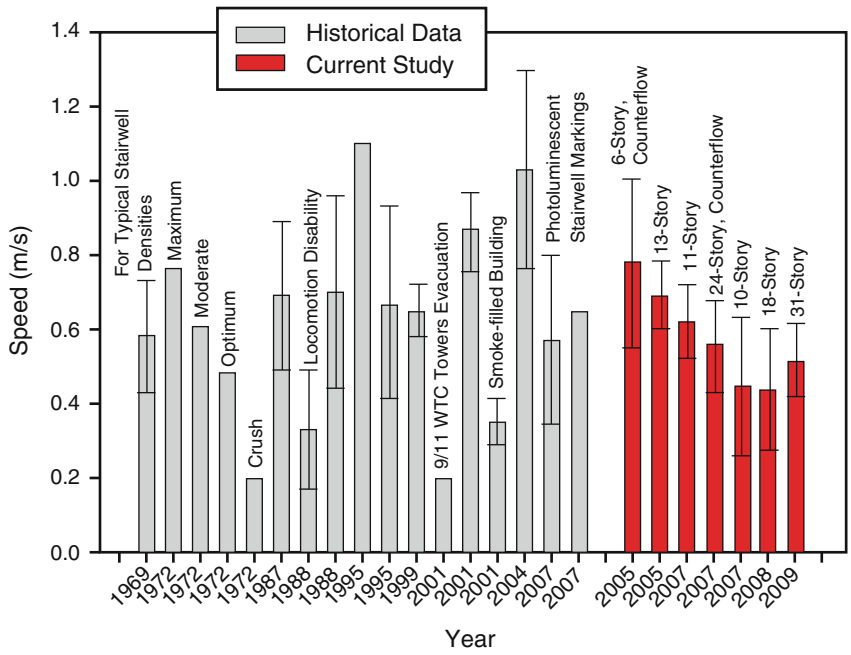

Fig. 64.8 Historical comparison of stair speeds produced by Peacock et al. (Reproduced from original [45])

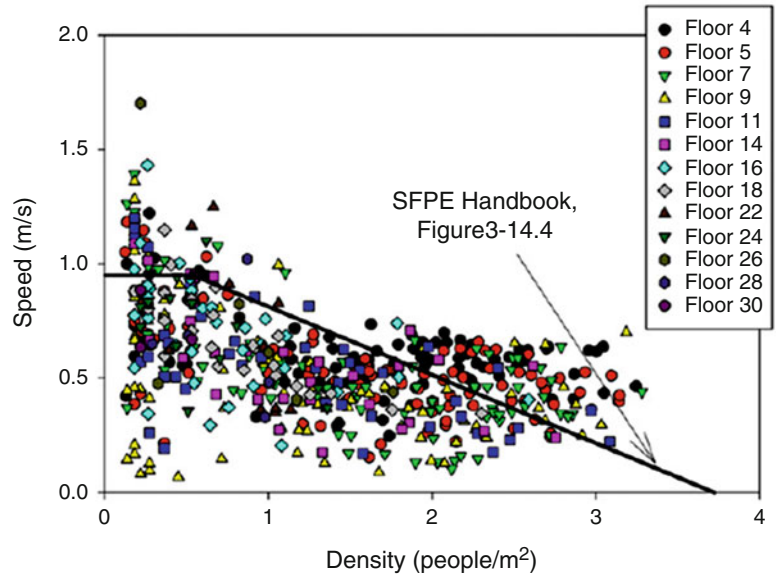

Fig. 64.9 Comparison of speed-density relationships—Peacock et al. and SFPE produced by Peacock et al. (Reproduced from original [45])

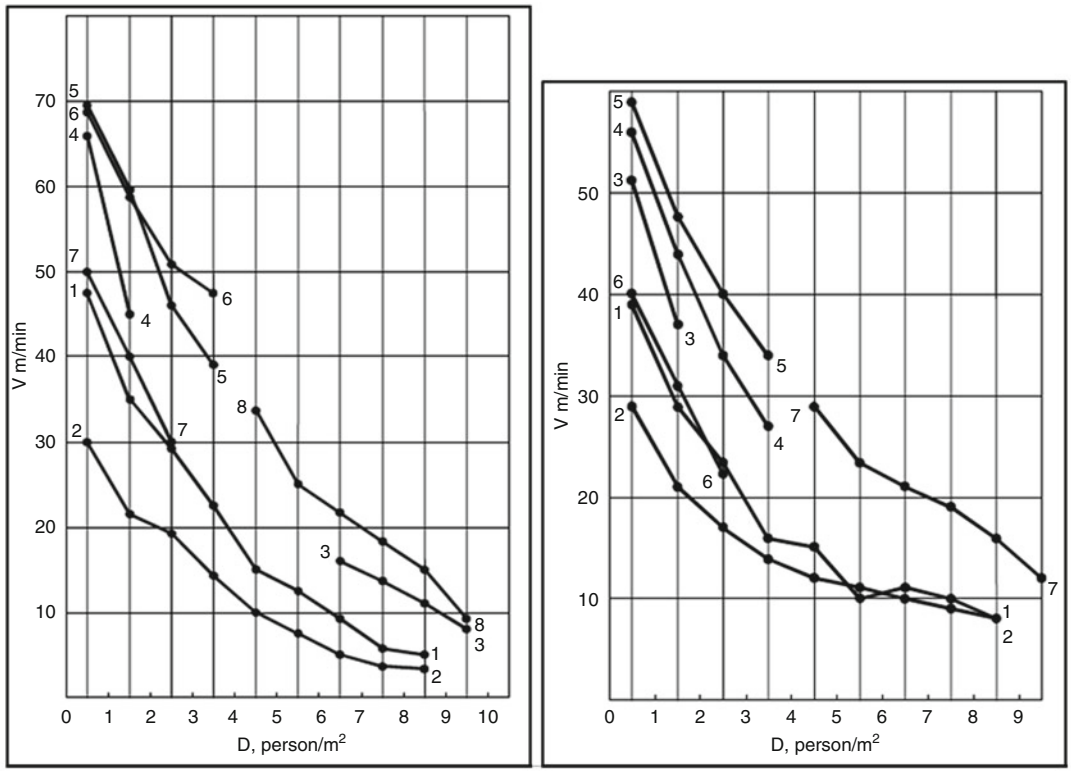

Fig. 64.10 Kholshevnikov et al. review of stair descent data (*left*) and ascent data (*right*) (Reproduced from original [109])

Table 64.17 Travel data—speed of movement (crowds) on stairs

Source	Observational conditions (L: location, N: nature, SC: spatial configuration, P: participants, E: environment, V: variable)	Configuration			Sample		Results			
							Density	Incline Speed		
		Direction (up/down)	Slope	Distance (m/steps/storeys)	Collection method	Size	Mean/range of means (persons/m^2 unless otherwise specified)	Mean/range of means (m/s) ± standard deviation	Relationship speed and density	Additional information
Peacock et al. [45] (updated version of Peacock et al. [46])	L: USA	Down	CS1: 32.5° (2 of)	10 storeys	Video	436/368 evacuees per stair	0.1–3.3 p/m^2 (local density)	0.44 ± 0.19	Graphical representation across four evacuations	Data for 5 buildings 6–62 stories is available on NIST website: http://fire.nist.gov/egress/
	N: [UE]		CS2: 36.9° (4 of)	18 storeys		255/292/340/197		0.44 ± 0.15		Paper gives probability distributions of movement speeds for several evacuations, local movement speeds by floor of origin, graphical representation of speed × density and regression model for local movements speed
	SC: 2–4 stairs in each of 4 office buildings. Four different slopes examined (CS1–4)		CS3: 32.5° (2 of)	24 storeys		249/356		0.56 ± 0.12		
	P: mixed age and gender		CS4: 33.1° (2 of)	31 storeys		704/538		0.52 ± 0.10		
	V: impact of stair slope on movement (CS1–4)							0.48 ± 0.16 (mean across all)		
								0.056–1.7 (range observed across all stairs)		
Capote et al. [69]	L: Spain	Down	CS1: 33.5°	15 steps	Video	(12–16 years):		CS1, UE1:0.48 [0.28–0.77] ± 0.14[a]	–	[a]Vertical speeds
	N: [UE] –two drills (UE1–2), staged evacuations with rooms evacuating in order					UE1:47	<4		–	Paper gives cumulative distributions of speed for each evacuation and gives range for each evacuation and age grouping. Also frequency of different movement patterns on stairs
	SC: day-care centres					UE2: 46	<2.5	CS1, UE2: 0.61 [0.14–1.12] ± 0.21[a]	–	
	P: 3–16 years		CS2: 33.5°	15 steps	Video	(8–12 years):		CS2,UE1:0.87 [0.29–1.39] ± 0.29[a]		
	V: impact of stair slope (CS1–3) given procedure (UE1–2)					UE1:48	–	CS2,UE2:1.06 [0.58–1.22] ± 0.17[a]		
						UE2:102	–			
			CS3: 33.9°	8 steps	Video	(12–16 years):		CS3, UE1:1.00 [0.63–1.46] ± 0.18[a]		
						UE1: 104	–			
						UE2:63	–	CS3, UE2: 0.95 [0.70–1.61] ± 0.25[a]		

(continued)

Table 64.17 (continued)

Source	Observational conditions (L: location, N: nature, SC: spatial configuration, P: participants, E: environment, V: variable)	Configuration: Direction (up/down)	Configuration: Slope	Configuration: Distance (m/steps/storeys)	Sample: Collection method	Sample: Size	Results: Density: Mean/range of means (persons/m^2 unless otherwise specified)	Results: Incline Speed: Mean/range of means (m/s) ± standard deviation	Results: Relationship speed and density	Additional information
Ono et al. [128]	L: São Paolo, Brazil	Down	–	3 storeys	Video	906 (am)	–	0.11–2.07	–	Drill procedure involved classes being led out in single file with a leader. Paper gives evacuation times each drill, frequency distribution speeds for all drills, breakdown of mean speeds and confidence intervals by age and drill and max and min speed by age. Noted that changing densities and contraflows
	N: [AE]– three trials conducted in each of 2 time periods (morning and afternoon)					706 (pm)				
	SC: school									
	P: aged 5-17; data relates to age range 6-14.									
	V: movement rate of young adults across different times									
Kadokura et al. [148]	L: Japan, 2007–11		30.6°	25 storey	Video and 22 observers whose arrival was an indicator of travel speeds	E1: 116	–	E1–3: 0.62* ± 0.15 (speed of observers across all phases)	–	Paper gives graphical representation of speed of observers on each floor
	N: [-E] (phased evacuation strategy) E1: floor 4–6, phase 1 E2: floor 7–12 + Floor 21–25, phase 2) E3: floor 13–20, phase 3)					E2: 304		E2: 0.74 ± 0.12 (speed of observers phase 2, F 7–12)		*Average speed 0.9 m/s when measured individually
	SC: 25 storey office building					E3: 443				
	P: 5516 (2088 participants)									
	V: movement rate given procedure employed (E1–3)									

Kholshhevnikov et al. [67]	L: Moscow, Russia	CD1: down	–	–	Video	S1: 152*	<1	[0.34–1.16][a]	Paper derives relationships between speed and density for each age group	[a]Dependent on age grouping
	N: ET					S2: 249*	1–2	[0.33–0.97][a]		Paper gives breakdown of walking speeds by density for different age groups as well as standard deviations, confidence intervals
	SC: 8 kindergartens					S3: 240*	2–3	[0.34–0.88][a]		
						S4: 133*	3–4	[0.33–0.78][a]		
	P: [S1–12— children mixed gender and age (<3–7 years)]					S5: 42*	4–5	[0.32–0.72][a]		
						S6: 4*	5–6	0.68 (aged 5–7)		
	V: movement given direction (CD1–2) and age of participants—S1–12)	CD2: up	–	–	Video	S7: 172*	<1	[0.34–1.32][a]		
						S8: 202*	1–2	[0.34–1.07][a]		
						S9: 227*	2–3	[0.33–0.89][a]		
						S10: 108*	3–4	[0.34–0.76][a]		
						S11: 24*	4–5	[0.45–0.67][a]		
						S12: 3*	5–6	0.40 (aged 4–5)		
						*Determined from information given in tables				
Hoskins [105]	L: USA	Down	CS1–2: 32.5° (2 of)	24 storeys	Video	258/364 evacuees per stair	1.67 ± 0.55	0.72 ± 0.25	$s = \frac{1}{1.93 + 0.51D}$ (from slowest occupant category)	It should be noted that some of the data quoted here overlaps with the data described by Peacock et al. [45]
	N: [AE]		CS3–4: 32.5° (2 of)	10 storeys		436/371	1.83 ± 0.63	0.59 ± 0.23	$s = \frac{1}{0.30 + 0.35D}$ (upper bound)	
	SC:11 stair configurations, in office buildings		CS5–8: 38.2° (4 of)	62 storeys		113/156/121/217	1.01 ± 0.48	0.61 ± 0.12	$s = \frac{1}{0.93 + 1.67D}$ (lower bound)	
	P: mixed age and gender		CS9: 36.9° (1 of)	18 storeys		312	1.89 ± 0.69	0.48 ± 0.20		
	V: movement rate given component slope (CS1–11)		CS10–11: 33.1°(2 of)			684/519	1.72 ± 0.61	0.44 ± 0.15		
						0.28–3.51 (range of observed densities across all)		[0.07–2.02] (range observed speeds across all)		

(continued)

Table 64.17 (continued)

Source	Observational conditions (L: location, N: nature, SC: spatial configuration, P: participants, E: environment, V: variable)	Configuration			Sample		Results			
							Density	Incline Speed		
		Direction (up/down)	Slope	Distance (m/steps/storeys)	Collection method	Size	Mean/range of means (persons/m^2 unless otherwise specified)	Mean/range of means (m/s) ± standard deviation	Relationship speed and density	Additional information
Lárusdóttir and Dederichs [149]	L: Copenhagen, Denmark N: [AE] SC: seven elementary schools P: children mixed gender and age V: movement down stairs	Down	30–34°	–	Video	667 persons (1943 data points)	1.24–2.21 (range of densities across all data points)	0.69–0.81 (range of average speeds across ages 9–15)	–	Paper gives breakdown of mean speeds for girls and boys different ages. Also evacuation behaviours, eg hand holding, and using handrails
Lárusdóttir and Dederichs [130, 131, 150]	L: Denmark N: [AE] SC: 3 spiral stairs in daycare centres P: mixed gender, 3–6 years V: movement down stairs given component slope (CS1–3)	Down	CS1: 33° CS2: 33° CS3:30°	–	Video	–	<0.5	0.58 ± 0.31 0.38 ± 0.07 0.13 ± 0.06	–	Differences in speeds across stairs attributed to different designs and familiarity of children with stair

Fujiyama and Tyler [151]	L: UK N: [ET] SC: 4 sets of stairs each of 1 flight P: mixed gender (7 M, 8 F), 'young' (average age 34.5 ± 12.7), walking 'normal' and 'fast' V: movement up stairs	Up	24.6–38.8°	1 flight	–	15	Unimpeded moving separately	0.56 ± 0.23–1.49 ± 0.43# (depending on stair type, 'normal' weight or obese and walking 'normal' or 'fast')	–	Incline speeds derived from horizontal speeds given in paper Relationship between stair speeds (ascent and descent) as % of horizontal speeds (y) by stair gradient (x)—also given in graphical form Also gives descriptive stats and graphically ascending walking speed by stair gradient for normal BMI and overweight and 'fast' walking speeds
Proulx and Bénichou [51, 152]	L: Canada, 2006 N: UE 1–4 SC: office, 13 floors, 4 stairwells (4 observed—1.1 m) UE1: stair A (PLM—no light) UE2: stair E (PLM—no light) UE3: stair G (PLM—no light) UE4: stair C (reduced lighting) P: 350 workers per floor (18–65 years) E: PLM installations/ reduced lighting V: movement given procedure (UE1–4)	Down	–	13 storey	Video	UE1:345 UE2:287 UE3:281 UE4:278	1.56* 1.60* 1.58* 1.60*	0.66 ± 0.25 0.40 ± 0.17 0.57 ± 0.21 0.66 ± 0.31	–	*Calculated from the five busiest minutes

(continued)

Table 64.17 (continued)

Source	Observational conditions (L: location, N: nature, SC: spatial configuration, P: participants, E: environment, V: variable)	Configuration			Sample		Results			
							Density	Incline Speed		
		Direction (up/down)	Slope	Distance (m/steps/storeys)	Collection method	Size	Mean/range of means (persons/m^2 unless otherwise specified)	Mean/range of means (m/s) ± standard deviation	Relationship speed and density	Additional information
Proulx et al. [153]; Proulx and Bénichou [152]	L: Canada, 1996–1999	Down	–	13 storey	Video	UE1:82	1.25*	0.70 ± 0.16	–	*Density calculated for busiest 3 min periods
	N: UE					UE2:101	1.30*	0.61 ± 0.10		
	SC: Office, 13 floors, 4 stairwells (4 observed—1.1 m) UE1: stair A (emerg lighting) UE2: stair B (full lighting) UE3: stair C (PLM) UE4: stair D (PLM + emergency lighting)					UE3:144	2.05*	0.57 ± 0.12		
						UE4:65	1.0*	0.72 ± 0.09		
	P: 150 workers per floor									
	E:PLM installations/ reduced lighting									
	V: movement given procedure (UE1–4)									
Yeo and He [133]	L: Singapore	CD1: down	1.8–4.8 m wide, 12–16 steps, 0.15–0.175 m rise		Video	795	C1: <0.72 (unimpeded)	CD1,C1: 0.6–0.42 (depending on age and gender)	–	Paper gives breakdown of unimpeded walking speeds of persons by age and gender
	N: [C] –peak hours in 2005. C1–4 representing different density conditions					?	C2: 0.3–<2*	CD1, C2: 0.23–0.98*	v = 0.57–0.02ρ[a]	Also given in graphical form. [a] $R^2 = 0.06$
							*Extracted from graph	*Extracted from graph		
	SC: 63 mass rapid transit (MRT) stations	CD2: up	1.8–4.8 m wide, 12–16 steps, 0.15–0.175 m rise		Video	643	C3: < 0.72 (unimpeded)	CD2, C3: 0.27–0.32 (depending on age and gender)	–	Paper gives breakdown of unimpeded walking speeds of persons by age and gender
	P: commuters of mixed age and gender						C4: 0.25–2.25	CD2, C4: 0.31–0.86*	v = 0.48–0.02ρ[a]	
	V: movement given population densities (C1–4) and direction (CD1–2)						*Extracted from graph	*Extracted from graph		Also given in graphical form [a] $R^2 = 0.11$

Choi et al. [154]	L: Korea N: ET SC: apartment building, P: in 20s, 225 male and 126 female V: movement down stair	Down	30°	30 storeys	Video	351	–	0.65*– 1.22* *Extracted from graphs	–	Breakdown of escape speeds of persons from various floors depending on starting location provided graphically
Peacock, Averill and Kuligowski, [53]	L: USA N: UE-three evacuations conducted in three buildings, with a total of nine monitored stairs UE1: no fire fighters. UE2: fire fighters entering SC: 3 buildings - SC1: 6 floors, 2 stairs (CS1–2); SC2: 11 floors, 2 stairs (CS3–4) SC3: 18 floors, 12 stairs (five observed-CS5–9)] P: mixed age and gender V: evacuation procedure (UE1–2) and spatial configuration (SC1–3)	Down	CS1–2: 47* CS3–4: 38 CS5–9: 37	SC1: 6 floors SC2: 11 floors SC3: 18 floors	Video	SC1:277 SC2:134 SC3: 483		UE1,SC1: 0.83 ± 0.18 UE2,SC1: 0.73 ± 0.26 UE1, SC2: 0.62 ± 0.1 UE1,SC3: 0.40 ± 0.09 UE2, SC3: 0.54 ± 0.18		Graphical representation provided * derived from stair configuration

(continued)

Table 64.17 (continued)

Source	Observational conditions (L: location, N: nature, SC: spatial configuration, P: participants, E: environment, V: variable)	Configuration			Sample		Results			
							Density	Incline Speed		
		Direction (up/down)	Slope	Distance (m/steps/ storeys)	Collection method	Size	Mean/range of means (persons/m^2 unless otherwise specified)	Mean/range of means (m/s) ± standard deviation	Relationship speed and density	Additional information
Kretz et al. [155]	L: Germany	CD1: Up	CS1: (long stair): 35.1°	35.8* (vertical height)	Video	C1:73	'Unimpeded'	0.52 ± 0.16	–	*Walking speeds measured after 25 m; actual densities not given
	N: C					C2: 390	'Low density'	0.47 ± 0.18		Medians, ranges, standard deviations given for all categories and graphical form
	SC: two stairways: S1: outer stairway at expo (Hannover), and S2: at tennis tournament (Dusseldorf)					C3: 23	'High density'	0.44 ± 0.05		
	P: spectators mixed age and gender	CD1: up	CS2:(short stair): 22° 12 steps 0.15 m rise, 0.367 m tread		Video	C4:10	'Unimpeded'	0.78 [0.13–1.43][a]	–	[a]Note these are horizontal speeds
	V: range of different variables characterised as different cases (C1–C12) representing movement in different directions (CD1–2) on different stair configurations (CS1–2)					C5: 62	'Low density'	0.70 [0.41–1.86][a]		Paper gives maximum and minimum as well as means across categories
						C6: 19	'High density'	0.71 [0.53–1.29][a]		
						C7: 91	All	0.71 [0.13–1.86] [a]		
		CD2: down	CS2: (short stair):22° 12 steps 0.15 m rise, 0.367 m tread		Video	C8: 6	'Unimpeded'	0.83 [0.54–1.33][a]		
						C9: 38	'Low density'	0.63 [0.38–0.96][a]		
						C11: 38	'High density'	0.65 [0.21–1.39][a]		
						C12: 91	All	0.65 [0.21–1.39][a]		
Lee and Lam [136]	L: Hong Kong, China	CD1: down	27.3°	5.58	Video (time lapse)	8642	–	0.48–0.65[a]	–	[a]Bi-directional stair. Figures depend on flow ratios up/down. Paper includes graphical representation of data and relationships between walking speed and flow ratio, standard deviation
	N: C1–3-3 × 2 h peak periods over 5 days									
	SC: two underground stations	CD2: Up	27.3°	5.58	Video (time lapse)	6244	–	0.42–0.56[a]	–	
	P: commuters mixed age and gender									
	V: movement given direction of movement (CD1–2)									

Hoskins and Spearpoint [137]	L: New Zealand and Australia	Down	–	–	Video	–	0.1 *–3.3* (across different egress paths)	1.3*–0.25* (across different egress paths)		Gives speed × density from 2 egress paths in graphical form
	N: C-during and following sporting activities						*Extracted from graph	*Extracted from graph		
	SC: 23 egress paths in 11 stadia									
	P: mixed age and gender									
	V: movement rate down stairs									
Proulx and Bénichou [152]	L: Canada	Down	0.18 m riser	4–6 storey[a]	Video	SC1: 82	SC1: 1.25	SC1: 0.70	–	[a]Measurements made between initial floor (11–9) and floor 5
	N: UE					SC2: 101	SC2: 1.30	SC2: 0.61		Each stair had different lighting/wayguidance system. Stair C had some counter flow fire fighters
	SC: 4 stairs, 3 floors (11–9) in a 13 storey office building,					SC3: 144	SC3: 2.05	SC3: 0.57		
	P: occupants mixed age and gender					SC4: 65	SC4: 1.0	SC4: 0.72		
	V: movement given nature of stairs (SC1–4)									
Tanaboriboon and Guyano [143]	L: Bangkok, Thailand	CD1: down	CS1: 34.0°	5 m	Video	205	Unimpeded	0.58 ± 0.07 [0.39–0.87]	n/a	Paper tests significance between different groups and compares findings other countries
	N: C		CS2: 35.0°	5 m		307		0.60 ± 0.07 [0.44–0.82]		
	SC1:4 stairs		CS3: 28.6°	4.4 m		140		0.61 ± 0.06 [0.46–0.82]		
	P: pedestrians mixed age and gender		CS4: 27.6°	4.5 m		215		0.62 ± 0.06 [0.46–0.89]		
	V: movement given direction (CD1–2) and component slope (CS1–4)	CD2: Up	CS1:34.0°	5 m	Video	222	Unimpeded	0.47 ± 0.04 [0.35–0.76]	n/a	
			CS2: 35.0°	5 m		561		0.50 ± 0.06 [0.34–0.68]		
			CS3: 27.6°	4.4 m		168		0.53 ± 0.05 [0.39–0.70]		
			CS4: 27.6°	4.5 m		202		0.56 ± 0.07 [0.40–0.76]		

(continued)

Table 64.17 (continued)

Source	Observational conditions (L: location, N: nature, SC: spatial configuration, P: participants, E: environment, V: variable)	Configuration			Sample		Results			
							Density	Incline Speed		
		Direction (up/down)	Slope	Distance (m/steps/storeys)	Collection method	Size	Mean/range of means (persons/m^2 unless otherwise specified)	Mean/range of means (m/s) ± standard deviation	Relationship speed and density	Additional information
Daly et al. [156]	L: London, UK	CD1: Down	–	6–9.3 m	Observer	796 data points	–	0.56–0.67[a]	Hoskins [105] derives relationship between speed and density using data in paper	[a]Speeds are proposals for speeds based on this data set and previous data
	N: C	CD2: up	–	6–9.3 m	Observer	496 data points	–	0.36–0.59[a]		
	SC: 8 underground stations,									
	P: commuters mixed age and gender									
	V: movement rate given direction of movement (CD1–2)									
Kagawa et al. [157]	L: Japan	Down	1200 mm wide	Up to 22 storeys, 3.65 m floor height	Video	835 (73 % M, 27 % F)	3.0 (max)	16 s/floor	–	
	N: AE– movement between 28th and 6th storey									
	SC: 53 storey office building,									
	P: approximately 1500 office workers mixed age and gender									
	V: movement down stair									

Khisty [158]	L: Washington, USA	Down	165–190 mm riser, 279–305 mm tread	3–12 storeys	Time-lapse photography and observations	400 data points	UE1: 1.39 (median) [0.79–3.08]#	UE1: 0.25–0.64 #	Paper gives relationship speed (ft/min) and density (persons/sq ft)	*'Normal' and 'emergency' conditions not clearly defined in paper. Graphical representation of speed × density
	N: UE1–2 UE1:'normal' movement; UE':'emergency' movement*						UE2: 1.41 (median) [0.79–3.08]#	UE2: 0.28–0.70#		
	SC: 21 dormitory buildings									
	P: 99 % students aged 18–30						#Converted from sq ft/person	#Converted from ft/min		
	V: movement given procedure (UE1–2)									

Observational Conditions (Location, Nature, Spatial Configuration, Participants, Environment, Variable), Stair Configuration (Direction of Movement (up/down), Slope, Distance), Sample (Collection method and Size), Results (Density, Incline Speed, Relationship between Speed and Density), and Additional Information. In Table 64.18, the following information is provided: Source, Observational Conditions (Location, Nature, Spatial Configuration, Participants, Environment, Variable), Stair Configuration (Direction of Movement (up/down), Slope, Distance), Sample (Collection method and Size), Results (Density, Specific Flow, Relationship between Flow and Density), and Additional Information.

Travel Phase: Exits and Narrowings

As described in Chap. 59, a key element in assessing the movement of sub-populations around a space is the change of widths of the spaces traversed. These typically occur at exit locations, which act as a connector between adjacent spaces. These changes influence the local population densities experienced, along with the potential for operating exit devices (e.g. the ability to get the door open or open to its full extent given the local population density). As such, exits (which include a device for separating two or more spaces that typically also represents a narrowing) and openings (a breach in space separation that typically represents a change in the width of the space) provide an important constraint to the movement of sub-populations within a structure, and certainly one that should be supported by empirical data within any egress analysis.

The representation of exits and openings can be addressed in a number of ways ranging from imposing a flow rate that limits the achievable flow, to allowing the flow conditions to emerge from the predicted conditions produced by the model [9, 22] (see also Chap. 60). Given the variety of attributes that may be required to produce a genuinely predictive model and the manner in which data-sets are typically presented, the following data, in its current form, is likely to be of most value in capping flow rates and validating predictive approaches, This does not preclude its use to configure predictive models; it may, however, mean that the data needs to be manipulated for the specific methods adopted within the predictive model being employed.

Many of the previously reviewed examples of horizontal movement also include reference to flow through exits and openings as a key constraint upon horizontal movement, i.e. a change in the density and flow conditions present. It is also explicitly represented in the original work by Nelson and MacLennan [107] and in Chap. 60. A wide range of previous empirical work in this area is also described in Daamen's thesis [116] and Daamen and Hoogendoorn [121] have published an array of their own empirical results describing exit flows by exit width, lighting levels, population type and door status (see Fig. 64.11). Daamen [116] also provides estimates for flow capacities associated with a range of different exits in rail rolling stock.

A number of other works provide specific examples of flow performance through exits and openings (be they narrowings or bottlenecks). These include Seyfried et al. [160, 161], who examined the flow rates generated at exits and narrowings based on their width and the densities evident, and reviewed the estimations of Nelson and MacLennan, Predtechenskii and Milinskii, Weidmann, Hoogendoorn, and the measurements of Kretz, Nagai and Muller (see Fig. 64.12).

Rinne et al. [125] performed a number of evacuations and monitored the performance of 32 exits to establish the flow rates produced. The exits were categorized according to the 22 evacuations from which the data came, the nature of this evacuation, the type of door involved, the door width, the flow performance produced, the people involved and the status of the door [125]. The data from these evacuations are shown in Fig. 64.13.

Table 64.18 Travel data—stair flows

Source	Observational conditions (L: location, N: nature, S: spatial configuration, P: participants, V: variable)	Configuration: Direction (down/ up)	Configuration: Slope	Configuration: Distance	Sample: Collection method	Sample: Size	Results: Density Mean/ Range of means (person/ m^2 unless otherwise specified)	Results: Specific flow Mean/ range of means (persons/m/min unless otherwise specified)	Results: Relationship flow and density	Additional information
Kadokura et al. [159]	L: Japan N: [-E] phased evacuation strategy E1: floor 4–6, phase 1 E2: floor 7–12 + floor 21–25, phase 2) E3: floor 13–20, phase 3) S: 25 storey office building, (phased evacuation strategy) P: office workers mixed age and gender V: flow given procedure employed (E1–3)	Down	30.6°	25 storey	Video, observer	E1: 116 E2: 304 E3: 443	–	E1: 46.3 (average) 55.8 (max) E2: 41.1 (average) 53.3 (max) E3: 54.4 (average) 60.8 (max)	–	Paper gives flows over time for different sections stair graphical form
Yeo and He [133]	L: Singapore N: C during peak hours in 2005 SC: mass rapid transit (MRT) stations	CD1: down	1.8–4.8 m wide, 12–16 steps, 0.15–0.175 m rise		Video	–	0.5–2.0* m^2/ person *Extracted from graph	63–12* *Extracted from graph	$F = -7.1 \times 10^{-4} + 35.43/\gamma$ F = specific flow in persons/m/min γ = space per person in m^2/ person	Relationships also shown in graphical form
	P: commuters of mixed age and gender V: flow given direction of movement on component (CD1–2)	CD2: up	1.8–4.8 m wide, 12–16 steps, 0.15–0.175 m rise		Video	–	0.5–3.75 m^2/ person* *Extracted from graph	68–6* *Extracted from graph	$F = 1.95 \times 10^{-4} + 28.77/\gamma$ F = specific flow in persons/m/min γ = space per person in m^2/person	Relationships also shown in graphical form

(continued)

Table 64.18 (continued)

Source	Observational conditions (L: location, N: nature, S: spatial configuration, P: participants, V: variable)	Configuration			Sample		Results			
		Direction (down/ up)	Slope	Distance	Collection method	Size	Density Mean/ Range of means (person/ m^2 unless otherwise specified)	Specific flow Mean/ range of means (persons/m/min unless otherwise specified)	Relationship flow and density	Additional information
Lee and Lam [136]	L: Hong Kong, China N: 3 × 2 h peak periods over 5 days	CD1: down	27.3°	5.58	Video (time lapse)	8642	–	12*–79 *Extracted from graph for 'congested conditions'	–	Bi-directional stair. Figures depend on flow ratios up/down. Paper includes graphical representation of data and relationships between walking speed and flow ratio, s.d
	SC: two underground stations P: commuters mixed age and gender V: flow given direction of movement (CD1–2)	CD2: up	27.3°	5.58	Video (time lapse)	6244	–	20*–67* *Extracted from graph for 'congested conditions'	–	
Brocklehurst et al. [123]	L: UK N: C SC: race course. Two stairs P: subjects were mixed age (20–30% 55+) and gender (40–50% female) V: flow down stairs examined	Down	–	–	Video	–	–	45 (average of 30 sampled flows)		
Graat et al. [114]	L: Eindhoven, Netherlands N: C SC: football stadium P: persons leaving football stadium, Mixed gender and age V: flow down stairs examined	Down	30–36°	–	Video	–	–	Mean: 0.4 persons/ m_{eff}/min Range: 0.5–0.93[a] persons/m_{eff}/s	–	[a]0.93 given in text, Table in paper suggests may be 0.98

Graat et al. [114]	L: Eindhoven, Netherlands	Down	CS1:30°	–	Video	–	–	1.09 persons/m_e/s (normal)	Graphical format only	
	N: ET– 'normal' and 'high' motivational conditions							1.14 persons/m_{eff}/s (high)		
	SC: football stadium, two stairs. CS1–2	Down	CS2:38°	–	–	–	–	1.00 persons/m_e/s (normal)	Graphical format only	
	P: students aged 13–16 years							1.10 persons/m_{eff}/s (high)		
	V: flow given slope of stair (CS1–2)									
Daly et al. [156]	L: London, UK	CD1: down	–	6–9.3	Observer	796	–	4100 people/m/h[a]	–	[a]Flows are proposals based on this data set and previous data
	N: C	CD2: up	–	6–9.3	Observer	496	–	3720 people/m/h[a]	–	
	SC: several underground stations									
	P: commuters mixed age and gender									
	V: flow given direction of movement (CD1–2)									
Khisty [158]	L: Washington, USA	Down	165–190 mm riser, 279–305 mm tread	–	Time-lapse photography, observer	400 data points	UE1: 1.39 (mode)#	52.5 (max)#	–	*'Normal' and 'emergency' conditions not clearly defined in paper. Graphical representation of flow × density
	N: UE1–2 -UE1: 'normal' movement; UE2: 'emergency' movement.*						UE2: 1.41 (mode)#	59.9 (max)#		
	S: 21 dormitory buildings,						#Converted from sq ft/person	#Converted from ped/ft/min		
	P: 99 % participants are students aged 18–30									
	V: flow given procedure employed (UE1–2)									

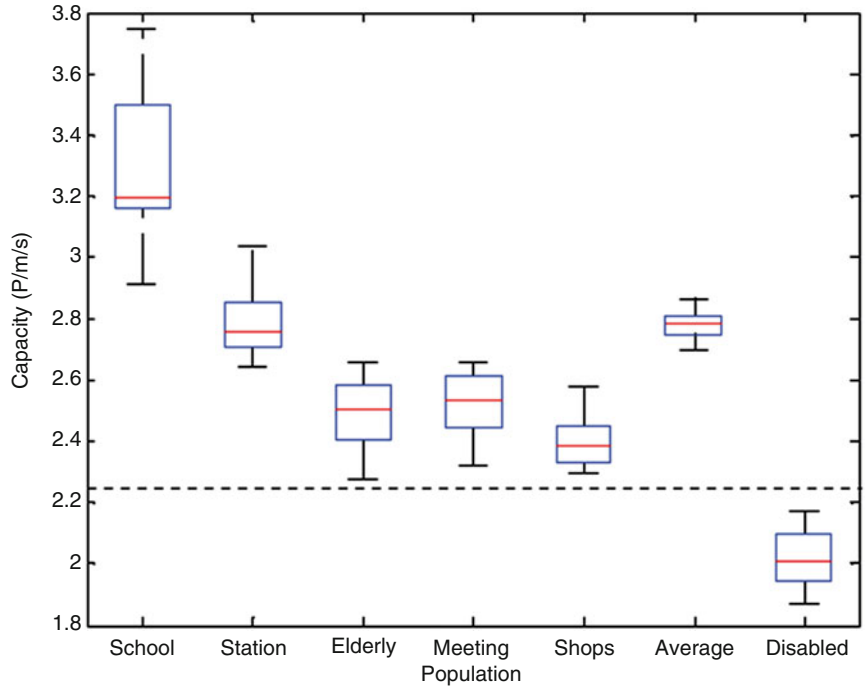

Fig. 64.11 Daamen and Hoogendoorn flow capacity of the exit as a function of population type (Reproduced from original [116, 121])

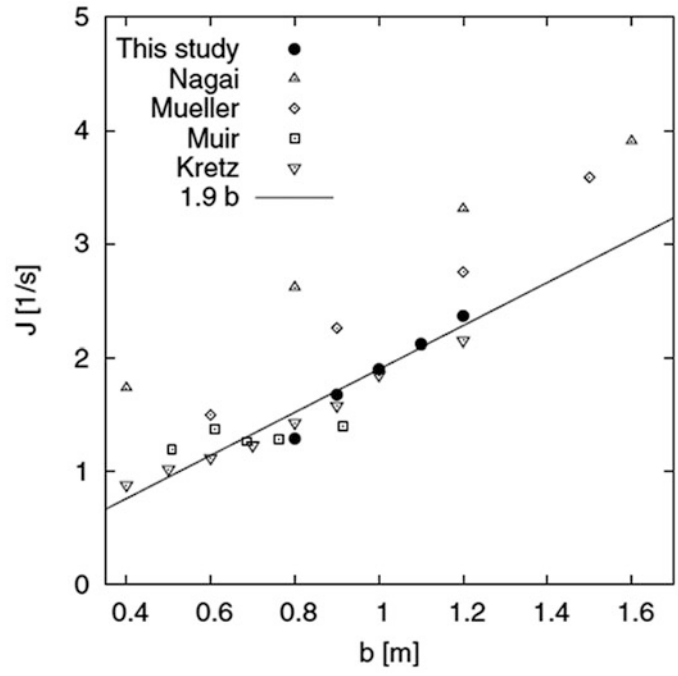

Fig. 64.12 Seyfried et al. comparison of flow performance (/s) through exits with work of others (Reproduced from original [160, 161])

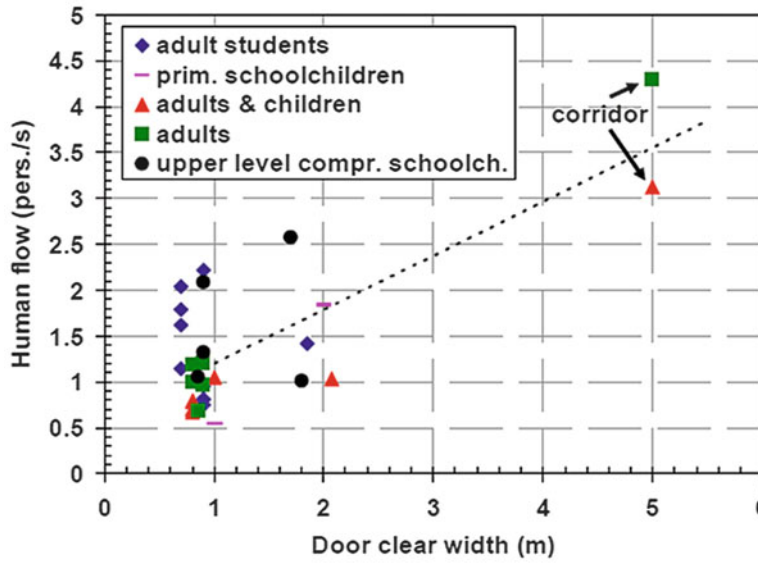

Fig. 64.13 Rinne et al. data relating to exit performance (Reproduced from original [125])

Several researchers have also looked at the travel speeds that can be achieved at and around exit points. This data can be used where flow rates are predicted/simulated by models, as opposed to being imposed by the user. Kholshevnikov et al. [109] presented a vast amount of data collected over 30 years in Russia from a number of data collection activities and combined it with their own efforts to produce the relationships between speed and density at exits, shown in Fig. 64.14. This is categorized according to the population densities recorded (which ranged from 1 to 13.5 persons/m^2) and the occupancies involved (retail, sports structures, train station, and experimental surroundings).

Schadschneider et al. [122] reviewed the experimental work of Kretz, Muir, Muller, Nagai and Seyfried, looking in some detail at the experimental conditions (and the initial distribution of the participants) along with the width of the exit/narrowing and the existence of competition among the participants (see Fig. 64.15).

The above paragraphs give a flavor of the range of studies regarding the performance of exits and narrowings. Others which the reader may wish to refer to include Thompson [113], Kendik [162], Smith [111], Gwynne et al. [47, 163], and Gwynne [164].

A summary of other data on exit flow through openings is given in Table 64.19. Although there is some overlap with the review material discussed, it is presented in a more consistent manner, in context with the scenario conditions and is presented in more detail. In order to achieve this, the following information is provided: Source, Observational Conditions (Location, Nature, Spatial Configuration, Participants, Environment, Variable), Door Configuration (Type—Single/Double/Sliding, Direction of Opening Relative to Movement—Against/ With, Width), Sample (Collection method and Size), Density, Results (Component Flow and Specific Flow), and Additional Information.

Travel Phase: Escalators (Up and Down)

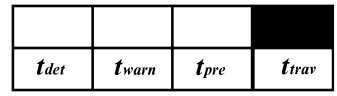

Kinsey [173], in his PhD dissertation, performed a review of data currently available related to movement on escalators, collected and presented more data on escalator usage (speeds and flows) and also considered decision-making in relation to escalator usage.

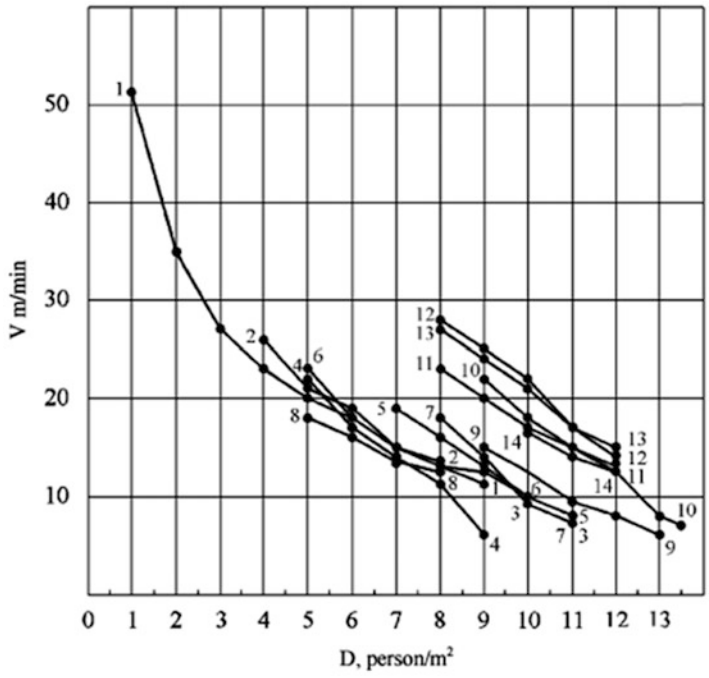

Fig. 64.14 Kholshevnikov et al. relationship between speed and density relating to exit opening (Reproduced from original [109]). Where curve (*1*) represents different buildings, (*2–4*) retail, (*5*) sports structures, (*6–9*) underground stations, (*10–14*) experimental conditions

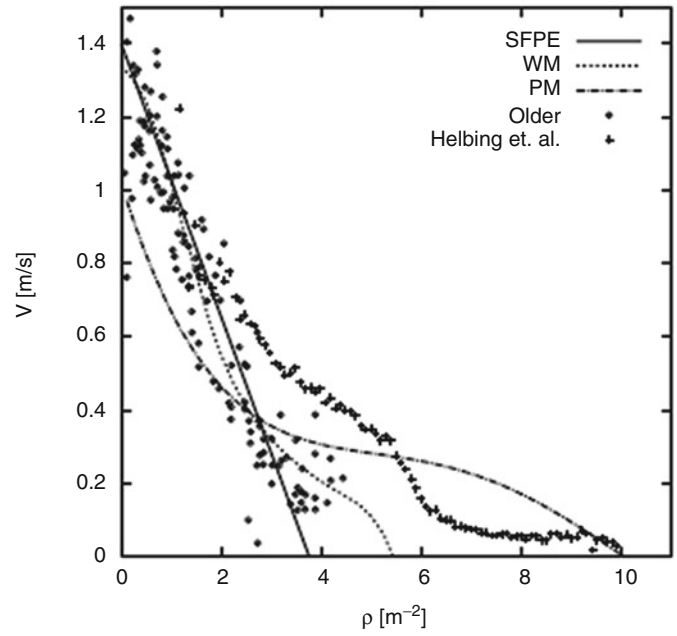

Fig. 64.15 Speed—density relationships summarized by Schadschneider et al. [122] (Reproduced from the original)

Table 64.19 Exit flow

Source	Observational conditions (L: location, N: nature, S: spatial configuration, P: participants, V: variable)	Configuration			Sample		Density (persons/m^2)	Component Flow [min, max] (ped/sec) (unless otherwise specified)	Specific Flow (ped/m/s) (unless otherwise specified)	Additional information
		Type	Direction of opening relative to flow (with/against)	Width (m) [effective width]	Collection method	Size				
Kholshevnikov et al. [67]	L: Russia N: [AE] SC: 8 kindergarten, 2008–2010 P: children aged 4–7, mixed gender V: flow of young through range of exit conditions	Single and double leaf	Against	0.6 and 1.2 m	Video	604 data points	1–2 to 16–17		1.65–3.80 (max@ 10–11 p/m^2)	Paper gives breakdown of specific flows by density interval and derives relationships for approximating flow × density
Sano et al. [165]	L: Japan N: ET SC: full-scale compartment (3 doors of varying width formed from exits of 0.8 m and 1.6 m) P: 56 mixed gender (61%M, 39%F), 21–39 years V: flow rates through exits of various widths	Sliding	–	0.8–2.4 m	Video	56	Approx. 1–3 p/m^2		Approx 3 p/m/s at 1 p/m^2 Approx 2 p/m/s at 3p/m^2	Figures given here relate to final 0.8 m door but paper gives graphical representation of flows for different door/corridor configurations Participants wore coats. Experiments considered different conditions of door width, corridor area
Daamen et al. [121, 166]	L: Netherlands N: ET1–7 SC: different exit widths (0.5–2.75 m) ET1: school, ET2: station, ET3: elderly, ET4: meeting, ET5: shops, ET6: Average, ET7: disabled P: varying ratios of children (75) adults (90), elderly (50) V: flow given nature of event (ET1–7)	Opening only	–	ET1: 0.85 ET2: 0.85 ET3: 1.1 ET4: 0.85 ET5: 0.85 ET6: 0.85–2.75 ET7: 0.85	Video	90–150 persons/exp	–	–	ET1: 3.2 [2.7–3.8]* ET2: 2.7 [2.65–3.05] ET3: 2.5 [2.25–2.65] ET4: 2.55 [2.3–2.65] ET5: 2.4 [2.35–2.6] ET6: 2.8 [2.7–2.85] ET7: 2.0 [1.85–2.2]*	Participants exposed to different stress and illumination levels. *Rough estimates extracted from graph

(continued)

Table 64.19 (continued)

Source	Observational conditions (L: location, N: nature, S: spatial configuration, P: participants, V: variable)	Configuration			Sample		Density (persons/m^2)	Component Flow [min, max] (ped/sec) (unless otherwise specified)	Specific Flow (ped/m/s) (unless otherwise specified)	Additional information
		Type	Direction of opening relative to flow (with/against)	Width (m) [effective width]	Collection method	Size				
Hoogndoorn et al. [167]	L: Holland	Opening only	–	CW1: 75	Video	–	–	–	CW1: 1.75	
	N: ET			CW2: 75					CW2: 1.75	
	SC: 10 × 4 m observable area CW1: no constraint CW2: 2 m CW3: 1 m			CW3: 75					CW3: 1.68	
	P: 75									
	V: width of bottleneck (CW1–3)									
Lárusdóttir and Dederichs [150]	L: Denmark, 2009	–	–	–	Video	805 data points		–		Note that children were accompanied by adults in the ratio of 3–4 children/adult in younger age group (0–2) and 6–10 children/adult in older age group (3–4). Paper provides information on flow by density in graphical form
	N: AE, 14 trials									
	SC: 10 daycare centres									
	P: [S1–2] children and adults aged 0–2 (S1) and 3–6 (S2) years, mixed gender					S1: 0–2 years	1.5*–7.0*	–	0.7*–1.5* (max @ 3.5 p/m^2*)	
						S2: 3–6 years	1*–10*		0.8*–3.25* max@ 5.0 p/m m^2*)	
	V: flow given type of population (S1–2)						*Extracted from graph		*Extracted from graph	
Gwynne et al. [47, 163]	L: USA	Double leaf	With	1.82 [1.52]	Video	–	–	1.4# [1,2.1]#	0.77 (0.92 p/m_{eff}/s)	#Converted from ped/min in paper Paper also considers fluctuations in specific flow with dynamic width (changing available width of doorway over time due to its continual use (subject to opening and closing of door leaves))
	N: C									
	SC: sporting arena, 1989									
	P: mixed age and gender									
	V: flow rate produced across population									

Shimada and Naoi [168]	L: Japan N: ET (270 trials) SC: constructed rig P: students (able-bodied) and wheelchair users in different proportions V: flow rate for population with different movement capabilities	Opening only	–	0.75–2.4	Video	40–92 participants	3.0–6.0	–	–	Paper gives graphical representation of the ratio of the flow coefficient (people/m/s) for different % of wheelchairs among the sample
Kretz et al. [169]	L: Germany N: ET (3–6 trials per opening width) SC: constructed rig of different widths (CW1–10) P: students, 34 % F, 66 % M V: flow given width of opening (CW1–10)	Opening only (depth 0.4 m)	–	CW1: 0.4 CW2: 0.5 CW3: 0.6 CW4: 0.7 CW5: 0.8 CW6: 0.9 CW7: 1.0 CW8: 1.2 CW9: 1.4 CW10: 1.6	Video	80/100	–	CW1: 0.88* CW2: 1.02* CW3: 1.12* CW4: 1.23* CW5: 1.43* CW6: 1.58* CW7: 1.85* CW8: 2.15* CW9: 2.20* CW10: 2.25* *Extracted from graph in paper	2.2 2.05 1.85 1.75 1.8 1.85 1.89 1.8 1.5 1.4	Paper also presents time gaps between participants. Gives regression equation for flow for different widths

(continued)

Table 64.19 (continued)

Source	Observational conditions (L: location, N: nature, S: spatial configuration, P: participants, V: variable)	Configuration			Sample		Density (persons/m^2)	Component Flow [min, max] (ped/sec) (unless otherwise specified)	Specific Flow (ped/m/s) (unless otherwise specified)	Additional information
		Type	Direction of opening relative to flow (with/against)	Width (m) [effective width]	Collection method	Size				
Nagai et al. [170]	L: Japan	Opening only	–	CW1: 0.4	Video	<75 participants (varied across experiments)	<0.8 (varied across experiments)	ET1, CW1: 1.7*	4.25	Experiment varied width of exit and number of students. Asked to walk or crawl at normal speed
								ET2, CW1:0.6*	–	
	N: ET (10 trials each number of participants). Different procedures: ET1— walking; ET2— crawling			CW2: 0.8				ET1, CW2:2.6*	3.25	Paper gives flow rate by density for crawlers and walkers for two widths (0.4 m and 1.2 m) in graphical form
								ET2, CW2:0.7*	–	
	SC: constructed rig of different widths (CW1–4)			CW3: 1.2				ET1, CW3:3.3*	2.75	
								ET2, CW3:1.1*	–	
	P: students—walking and crawling			CW4: 1.6				ET1, CW4:3.9*	2.44	
								ET2,CW4: 1.3*	–	
	V: flow given procedure (ET1–2) and component width (CW1–4)							*Extracted from graph in paper		
Rupprecht et al. [171]	L: Germany	Opening only (depth 0.06–4 m)		CW1: 0.9	Video	50–230 per trial		CW1: 1.7*	CW1: 1.9*	*Extracted from graph in paper
	N:ET			CW2: 1				CW2: 2*	CW2: 2.0*	
	SC: width of bottleneck varied			CW3: 1.1				CW3: 2.2*	CW3: 2.0*	
	CW1: 0.9 m			CW4: 1.2				CW4: 2.3*	CW4: 1.9*	
	CW2: 1 m			CW5: 1.4				CW5: 2.7*	CW5: 1.9*	
	CW3: 1.1 m			CW6: 1.6				CW6: 3*	CW6: 1.9*	
	CW4: 1.2 m			CW7: 1.8				CW7: 3.7*	CW7: 2.1*	
	CW5: 1.4 m			CW8: 2				CW8: 4*	CW8: 2.0*	
	CW6: 1.6 m			CW9: 2.2				CW9: 4.3*	CW9: 2.0*	
	CW7: 1.8 m			CW10: 2.5				CW10: 5.4*	CW10: 2.2*	
	CW8: 2 m CW9: 2.2 m CW10: 2.5 m									
	P: 230 soldiers									
	V: width of bottleneck (CW1–10)									

Wong and Cheung [135]	L: Hong Kong, China	–	–	1.4	Video	44	–	ET1: 2.1#	1.88 p/m_{eff}/s	Participants asked to walk under 'normal' and 'emergency' conditions where 'emergency' means walk (but not run) as fast as they could. Paper gives specific flow v density in graphical form
	N: ET. (ET1:normal. ET2: emergency)							ET2: 3.2#	2.94 p/m_{eff}/s	#Derived from information provided in paper
	SC: university									
	P: 44 students aged 20–24, 66 % M, 34 % F									
	V: flow given procedure (ET1–2)									
Muller [172]	L: Germany	–	–	CW1:0.6	–	150–195		ET1: 1.5*	2.5*	Both data for 'normal' and 'alarm' conditions
	N: ET. (ET1:'normal'. ET2:'alarm')			CW2: 0.9				ET1: 2.26 ET2: 2.92	2.5 3.2	*Derived from graphs
	SC: constructed rig different widths (CW1–5)			CW3: 1.2				ET1: 2.75 ET2:4.79	2.3 3.9	
	P: 150–195 volunteers			CW4: 1.5				ET1: 3.59 ET2: 6.56	2.39 4.37	
	V: flow given width of component (CW1–5) and procedure employed (ET1–2)			CW5: 1.8				ET1: 3.83 ET2: 8.81	2.13 4.89	

Table 64.20 Travel—unimpeded horizontal walking speed on escalators

Source	Observational Conditions (L: location, N: nature, SC: spatial configuration, P: participants, V: variables)	Configuration					Sample		Results	Additional information
		State	Direction (up/down)	Speed (m/s)	Height (m)	Horizontal length (m)	Collection method	Size	Mean [range] (m/s)	
Kinsey [173]	L: Spain N: C– 30 min periods peak /off peak SC: underground station. Escalators connecting a ticket hall level to a train platform below P: commuters mixed gender, aged <12–60+ V: configuration direction (CD1-2) on moving escalator	Moving	CD1: up	0.5	6.3	15.5	Video	34	0.74 [0.50–1.39]	Includes breakdown of speeds by rush/non-rush hour, gender (significant differences); also presents data on side usage and proportion of walkers
		Moving	CD2: down					18	0.86 [0.59–1.51]	
Kinsey [173]	L: China N:C– during 1 h periods in peak/off peak SC: underground station, two identical up escalators P: commuters mixed gender, aged <12–60+ V: travelling upwards on moving escalator	Moving	Up	0.5	4.8	11.5	Video	79	0.83 [0.39–1.3]	Paper includes breakdown of speeds by rush/non-rush hour (significant differences), gender (significant differences); also presents data on side usage and proportion of walkers
Kinsey [173]	L: London, UK N: C– recorded during 20 min two peak/off-peak periods for 2 days SC: underground station P: commuters mixed gender, aged <12–60+ V: Configuration Direction (CD1–2) on moving escalator	Moving	CD1: up	0.5	3.7	8.8	Video	451	0.71 [0.32–1.51]	Paper includes breakdown of speeds by rush-hour and non-rush hour, gender (significant differences); also presents data on side usage and proportion of walkers
			CD2: down			8.8		359	0.82 [0.38–1.67]	
Kadokura et al. [174]	L: Japan N: ET– individual measurements SC: escalator P: university students V: movement on static escalator	Static	Up	–	13.2	27.2	Video	79	0.72#[–]	#Converted from incline speed of 0.8 m/s quoted in paper Paper includes data on crowd horizontal walking speed on escalators (quoted as 0.61 m/s) and compares with crowd walking speed on stairs

Okada et al. [175]	L: Japan	CS1: moving	Up	0.5	CH1: 22	CH1: 49.5	Video	S1: 38 (healthy)	CS1,CH1,S1 0.76 #[–]	#Derived from velocity presented in paper which included escalator velocity
	N: ET, individual measurements								CS1, CH1,S2 0.43#[–]	Paper includes data for subjects walking as part of a group and for subjects walking in two lines with different mixes 'healthy' and 'elderly'
	SC: convention facility. Range of escalators				CH2: 5.7	CH2: 12.3		S2: 12 (elderly)	CS1, CH2, S1 0.71#[–]	
	P: 70 % male; 30 % female, average age 21. 12 subjects (24 %) wore 'instant senior' devices to simulate 75–80 year old ('elderly')	CS2: static	Up	0.0					CS1, CH2,S2 0.43#[–]	
	V: impact of configuration state (CS1–2), height and length, (CH1–2), on sample (S1–2)								CS2, CH1, S1 0.79–#[n]	
									CS2, CH1, S2 0.50#[–]	
									CS2, CH2,S1 0.78#[–]	
									CS2, CH2,S2 0.53#[–]	
Cheung and Lam [176]	L: Hong Kong	Moving	CD1:Up	0.75	Incline 30°		Video	611	0.77#[–]	# Converted from what is assumed to be incline speeds presented in paper (units also converted)
	N: C									
	SC: 5 underground/elevated railway stations		CD2: Down	0.75	Incline 30°		Video	692	1.05#[–]	
	P: commuters mixed age and gender				Incline 30°					
	V: impact of movement direction—configuration (CD1–2)									

Table 64.21 Travel—flow on escalators

Source	Observational conditions (L: location, N: nature, SC: spatial configuration, P: participants, V: variable)	Configuration				Sample			Additional information
		State	Direction	Horizontal speed (m/s)	Width (m)	Collection method	Size	Peak recorded flow (ped/min)	
Kinsey [173]	L: Spain	Moving	Up	0.5	1	Video	S1, C1: 404	41.0	[a]Lower flow rates are reflective of dispersed arrival times rather than maximum achievable
	N: C– recorded 30 min periods in (C1) peak/(C2) off peak						S2, C2: 186	19.0[a]	
	SC: underground station. Connecting a ticket hall level to a train platform						S3, C1: 252	19.0	
	P: commuters mixed gender, aged 12–60+						S4, C2: 114	9.0[a]	
	V: upwards flow given sample (S1–4) and circulation movement examined (C1–2)								
Kinsey [173], Kinsey et al. [177]	L: China	Moving	Up	0.5	1	Video	–	102	Flow rates given in graphical form for each minute, together with proportions of males/females, walkers/riders, side usage
	N: C, recorded during hour periods at peak/off-peak								
	SC: underground station. Two identical escalators								
	P: commuters mixed gender, aged <12–60+								
	V: upwards flow								
Kinsey [173], Kinsey et al. [178]	L: London, UK	Moving	CD1: up	0.5	1	Video	3595	75.0	Paper includes breakdown of flows by rush-hour period and non-rush hour. Flows given in graphical form for each minute, together with proportions of males/females, walkers/riders, side usage
	N: C– 20 min periods in different peak/off peak periods for 2 days								
	SC: underground station		CD2: down	0.5	1	Video	2528	47.0	
	P: commuters mixed gender, aged <12–60+								
	V: impact of movement direction—configuration direction (CD1–2)								
Okada et al. [175], Okada [179]	L: Japan	CS1: moving	Up	0.5	0.99	Video	50	102	Paper compares results with adjacent stairway
	N: ET1-2								
	SC: convention facility, 2 escalators	CS2: static			1.02			66	
	P: participants were 70 % male and 30 % female, average age 21. 12 subjects (24 %) wore ‘instant senior’ devices to simulate athletic capability of 75–80 year old (‘elderly’)								
	V: impact of moving or static escalator—configuration state (CS1–2)								

Davis and Dutta [180]	L: London, UK N: C– peak periods S: 10 underground stations P: commuters mixed age and gender V: upward movement	Moving	Up	0.72	1	Video	–	119.0	
Cheung and Lam [176]	L: Hong Kong N: C S: 5 underground/elevated railway stations P: commuters mixed age and gender V: impact of movement direction -configuration direction (CD1–2)	Moving	CD1: up CD2: down	0.75	1.005	Video	9750 9540	120 120	Also considered stair movement and developed regression equations for travel time
Al-Sharif [181]	L: London, UK N: C– counts made 1 min intervals for 1 day SC: 7 escalators in underground station (4 up, 3 down) P: commuters, mixed gender and age. Escalator use: 12,179–52,622 ped/day in underground V: impact of movement direction -configuration direction (CD1–2)	Moving	CD1: up CD2: down	0.75	1	Observer	90,285# 95,882#	122[a] 140[a]	[a]Across all escalators in particular direction in 1 day Paper gives breakdown by escalators of different heights
Daly et al. [156]	L: London, UK N: C SC: several underground stations P: commuters mixed age and gender V: direction of movement—configuration direction (CD1–2)	Moving	CD1: up CD2: down	0.74	–	Observer	457 402	151 ped/m/min# 159 ped/m/min#	#Converted from different units in paper

Tables 64.20 and 64.21, provide a summary of published data on speeds and flows on escalators, respectively. This includes the data reviewed by Kinsey and Kinsey's own data. The following information is provided in Table 64.20: Source Observational Conditions (Location, Nature, Spatial Configuration, Participants, and Variable), Escalator Configuration (State (Moving/Static), Direction (up/down), Speed, Height, Horizontal Length), Sample (Collection method and Size), Results (Mean and Range) and Additional Information. It should be noted that horizontal speed is utilized in Table 64.20 rather than incline speed presented previously in Table 64.17 relating to stair movement. Horizontal speed is presented here since this is the speed commonly presented in the literature to describe movement on escalators. It should also be noted that in the case of moving escalators that the speed presented is the speed of movement of the individual over and above that of the speed of the moving escalator.

In Table 64.21, the following information is provided: Source, Observational Conditions (Location, Nature, Spatial Configuration, Participants, and Variable), Escalator Configuration (State, Direction, Horizontal Speed, and Width), Sample (Collection method and Size), Peak Recorded Flow, and Additional Information. It should be noted that, unless otherwise specified, the width of the escalator is the step width.

Vulnerabilities - Situational: Movement in Smoke

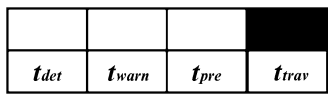

The presence of smoke during an emergency has been shown to have a range of different effects upon evacuee performance. These effects may be psychological (see Chap. 58), physiological and physical (see Chaps. 61 and 63). These impacts may affect the performance in a number of ways in terms of the following:

- Recognition and response to fire (t_{pre})—in that the presence of smoke may act as a cue to indicate the existence of an incident and may then influence the time for an individual to respond to the incident,
- Redirection of movement—in that the perception of the presence and severity of the smoke may discourage the use of a particular route,
- Reduction in the efficiency of movement (t_{trav})—where the presence of smoke can lead to reduced walking speeds [31] and
- Posture change—in some cases the presence of smoke may lead occupants to abandon walking and adopt crawling behaviors, which in turn can influence the travel speeds that can be attained [31].

It is specifically the last two effects (i.e. the impact of smoke on walking speed and crawling speed), that are discussed in this section. Some discussion regarding the first two impacts listed above (i.e. impact of smoke on recognition and response and impact of smoke on exit choice behaviors), is presented in Chaps. 58, 61, and 63. Data relating to these aspects have also been reviewed in some detail by Xie Hui [182], Ronchi et al. [183], Gwynne [164], and Nilsson [184].

It is now widely acknowledged that some people are prepared to move through smoke in order to reach a position of safety [31]. In some circumstances (e.g. tunnels), it is accepted that evacuees will be exposed to smoke for a short duration [185]. However, in most engineering applications, the interaction between the evacuating population and smoke is assumed not to take place, i.e. the separation of the evacuating population and the deteriorating environment is assumed to be successful. Although engineering designs are likely to be developed on the basis that evacuees are *not* exposed to deteriorating environmental conditions, the potential for this interaction should still be considered. There may be situations, for example, where the engineer is testing the robustness of his/her design, making extremely conservative assumptions regarding the performance of the evacuating population, or going beyond the standard performance based scenarios considered as part of engineering design. For that reason, information and data regarding movement in smoke is included in this chapter.

It has been estimated that over 60 % of evacuees in small residential buildings move through smoke to evacuate [36]. A study of the behavior of evacuees from the bomb blast in the World Trade Center in 1993 [36] showed that 94 % of occupants of Tower 1 moved through smoke. Given the location of the incident, and the routes available once the evacuation commenced, movement through smoke was unavoidable; however, this did not prevent people commencing or continuing their evacuation. Detailed study of the evacuation of two high-rise residential buildings [36] has also shown that around 96 % of the occupants located above the fire floor moved through smoke.

Studies by Bryan [30] have shown that the proportion of people turning back rather than entering smoke increases with the smoke density. However, the exact proportion of those willing to move through smoke will be scenario-specific. In a space relatively free of smoke where smoke-free options are available, people may turn back rather than attempting to move through dense smoke, while those escaping the enclosure of fire origin or those with no alternative options will continue to move through often dense smoke, particularly if they know it will lead to an exit in a relatively short period of time. The decision to move through smoke may also depend on the person's motivation, e.g. in dwelling fires, parents are prepared to move through smoke to rescue their children or other precious belongings. In tunnel fires, some have been known to walk for several hundred meters in dense smoke [186].

The examples given in the previous paragraphs have demonstrated that people are willing to move through smoke when required to do so. It is clear, however, that the actual percentage of people that will be willing to move through smoke may be highly dependent upon the scenario faced and the options available. In this section, the actual percentage of people that are willing to move through smoke is not the focus of the discussion; instead, it is the impact that the smoke has on movement performance that is considered in some detail.

Given that people may interact with smoke, it is important to consider the impact that smoke has on walking speed. This section considers the available data sets that describe (1) the correlation between the smoke and occupant speed assuming the individual remains upright, and (2) the travel speeds that can be expected should an individual decide/be forced to crawl. The likelihood of an individual initiating crawling behavior is not addressed.

In section "Upright Movement in Smoke" we present several data-sets related to the travel speeds during the upright movement in smoke on a horizontal place. In section "Crawling Movement in Smoke" we present several data-sets on the travels speeds attained when crawling in smoke. In both cases, only a small number of data-sets are available and, therefore, rather than presenting in tabular form, a more detailed discussion of the data-sets is presented.

In the studies which have considered the impact of smoke on movement, smoke conditions are generally represented through an extinction coefficient (m^{-1}) or optical density (m^{-1}) (see Chaps. 61 and 63). The extinction coefficient unit is adopted here. The smoke has a number of influences upon an individual's ability to move: (1) highly irritant smoke can cause intense pain to the eyes, affecting the individual's ability to keep his/her eyes open; (2) the extinction coefficient of the smoke reduces visibility levels. The toxic and irritant agents can also have physiological effects that further reduce the individual's well-being and then indirectly reduce their walking speed (see Chap. 63).

Before examining or employing the data discussed below, it is important to note that the experimental conditions present in these studies vary considerably in terms of the presence and type of irritant gases, the characteristics of the participants, the structural configuration employed in the trials, and measurement techniques adopted. The variation in experimental conditions is a feature of all of the data discussed in this chapter; however, particular care should be taken with regards to movement

in smoke, given the limited data available. This area of investigation is particularly susceptible to ethical constraints which may limit the conditions to which trial participants might be exposed, and which inevitably impacts on the credibility and utility of the results. Again, it is recommended that readers should refer to the original papers before making decisions as to the most relevant data set to use.

The Ph.D. theses of Xie Hui [182], Nilsson [184], Kady and Davis [187], Ronchi [188] include extensive reviews of the data available relating to different aspects of movement in smoke and the reader is referred to these for further information.

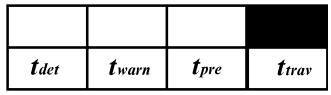

Upright Movement in Smoke

Four data-sets which suggest a correlation between extinction coefficient and attainable speed are presented below: Jin [189], Frantzich and Nilsson [190, 191], Wright et al. [192], and Galea et al. [193]. An overview of these data-sets, derived from the work of Xie Hui [182], is provided in Table 64.22.

The first set of experiments in this area was performed by Jin in 1976 [189, 194–196]. The details of his experiments are discussed at length in Chap. 61 of this handbook; therefore only a brief overview is provided here. Jin tested 38 individual subjects (age range 20–51 years) in a 20-m-long corridor filled with two types of smoke analogous to the early stage of a fire: the first was a highly irritant white smoke produced by burning wood cribs and the second, a less irritant black smoke produced by burning kerosene. From the experimental results Jin derived a correlation between the extinction coefficient and the achievable walking speeds for both the irritant and non-irritant smoke (see Fig. 64.16).

In the experiments involving irritant smoke, the visibility fell away sharply as the extinction coefficient approached 0.5 m^{-1}. The occupant speed of movement, which was initially over 1 m/s reduced rapidly to approximately 0.3 m/s as extinction coefficients reached approximately 0.5 m^{-1}. The sharp drop in walking speed is explained by the fact that the subjects could not keep their eyes open in the irritant smoke, causing a zigzag movement or use of the walls for guidance (see Chap. 61).

A more gradual decrease in walking speeds was evident in non-irritant smoke (see Fig. 64.16). Participants once again moved initially at over 1 m/s and slowed down to approximately 0.5 m/s when the extinction coefficient reached 1.0 m^{-1}. In these trials, participants continued to walk at a reduced speed, behaving as if in darkness and feeling their way along the walls, but without the associated discomfort and clenched eyes that were apparent in the irritant smoke. The Jin data-set, although small, provides a direct comparison between the impact of irritant and non-irritant smoke in comparable conditions.

Frantzich and Nilsson's study [190, 191] (see also Chap. 61) involved a series of

Table 64.22 Overview of smoke travel speeds for upright individuals (Derived from the work of Xie Hui [182])

Research	Corridor length (m)	Smoke properties	Extinction coefficient (m–1)	Data points
Jin [189]	20	Black, burning woods, kerosene, etc.	[I]: 0.32–0.47	38
			[N-I]:0.51–1.13	
Frantzich and Nilsson [191]	27	Mixture of polyglycoles, distilled water and acetic acid.	[N-I]:1.93–7.39	46
Wright et al. [192]	13	Generated from a mineral based fluid, white, and non-toxic.	[N-I]: 2.53	18
Galea et al. ; Xie Hui [182, 193]	11	Glycerin (C3H8O3), Dipropylene Glycol (C6H14O3) and Propylene Glycol (C3H8O2)	[N-I]:0.0–2.30	360

[*I*] indicates irritant smoke, [*N-I*] indicates non-irritant smoke

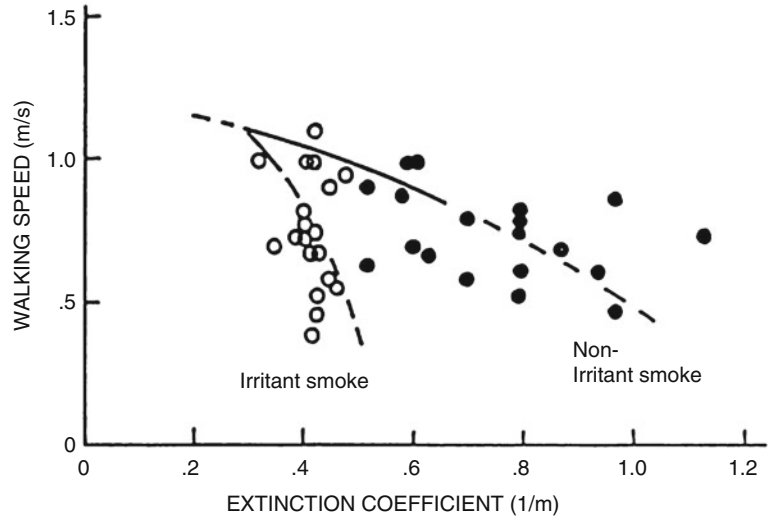

Fig. 64.16 Walking speed in smoke from Jin [189] (Reproduced from original)

experiments conducted in a smoke-filled tunnel. The sample comprised 30 males and 16 females aged 18–29 years (45 valid measurements were made). Participants were asked to walk through a tunnel 37 m long by 5 m wide, with a ceiling height of between 2.5 and 2.7 m in one of two illumination levels (lights on (21 lx) and lights off) and wayguidance systems (flashing lights, rows of flashing lights and floor markings). The route was more complex than that in Jin's experiments in that participants had to negotiate a number of obstacles, namely pillars which supported the ceiling and six cars placed inside the tunnel. The tunnel was filled with artificial smoke, with acetic acid used to provide irritation. The range of extinction coefficients measured was 1.9–7.4 m^{-1}, which was greater than in Jin's experiments. The participants were provided with the scenario that they had entered the tunnel in their car, and they were asked to get out and act as they would in such a situation if it was a real incident. The movement of participants was filmed using thermal imaging infra-red cameras. The calculated walking speeds ranged from 0.2 to 0.8 m/s (speeds included time stopping to rest) and results indicate that the speed decreased across the data-set as the extinction coefficient increased. Subjects also continued walking despite the low visibility and also tended to walk using the tunnel walls for guidance, an observation also noted by Jin (see Chap. 61,).

A comparison of Frantzich and Nilsson [191] and Jin's data [189] is provided in Fig. 64.17.

From Fig. 64.17 it is apparent that there is a wide scattering in the data currently available, which seems to have been due to differences in participants' characteristics, the levels of irritancy produced, the complexity of the spaces (Jin's experiments involved a simple corridor whilst Frantzich and Nilsson's was more complex including obstacles), and potentially the wayguidance systems in place. It should also be noted that the participants were in close proximity to the walls in both the Jin and Frantzich and Nilsson trials; the opportunity for evacuees to use walls as a means of guidance may well be different in an open space which in turn may influence their behavior and performance. It is therefore difficult to determine, with any level of confidence, a representative walking speed for a particular extinction coefficient. Frantzich and Nilsson developed two regression models from their data [191] for situations with no illumination (lights off) and illumination (lights on). The relationship between the smoke extinction coefficient K and walking speed for the illuminated movement ($R^2 = 0.32$) is given below. This is the

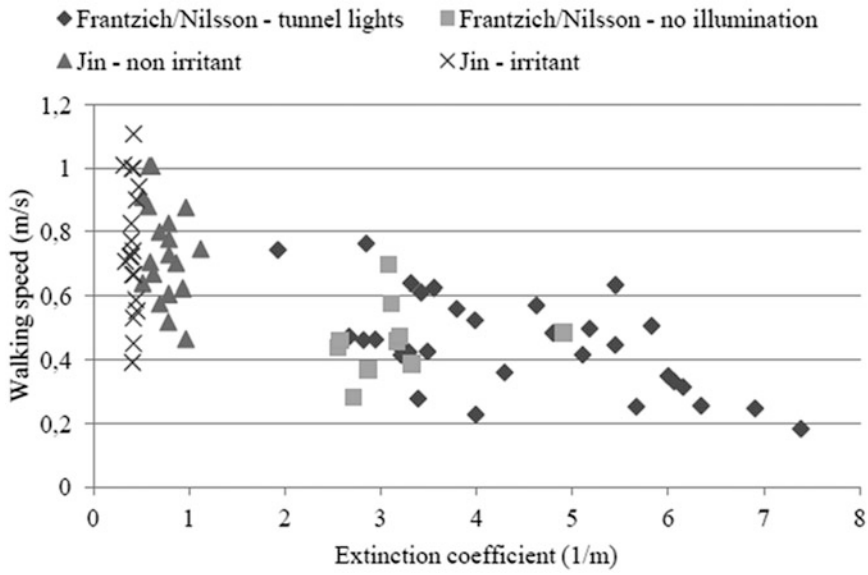

Fig. 64.17 Comparison of Frantzich and Nilsson and Jin's data (Reproduced from Ronchi [188])

relationship that has been adapted by Korhonen and Hostikka [197] for use in the FDSEvac model.

$$Walking\ Speed(m/s) = 0.706 - 0.057K$$

Frantzich and Nilsson [191] also conducted regression analysis to consider the influence of being in proximity to walls and produced the following ($R^2 = 0.454$):

$$Walking\ Speed\ (m/s) = 0.692 - 0.073K + 0.139\ (proportion\ wall\ contact)$$

Wright et al. [192] also conducted experimental trials to examine travel speeds in a smoke-filled environment that employed different lighting and wayguidance systems. The trials were performed in a two-storey test facility that included a 13 m corridor. Non-toxic white smoke was generated from a mineral-based fluid. A single smoke density (extinction coefficient 2.5 m^{-1}, OD 1.1 m^{-1}) was maintained in the corridor during the trials. The trials therefore focused on the performance of different systems at a given extinction coefficient. Eighteen participants (7 men and 11 women, ranging from 23 to 63 years of age, mean 46 years) took part in the trials and experienced the same set of six scenarios; i.e. five way guidance systems separately employed and a separate scenario with normal overhead lighting only. The speeds recorded ranged from 0.61 to 0.71 m/s for normal lighting [192], producing an average speed of 0.5 m/s. A range of other scenario conditions, employing two different LED systems, incandescent lighting, electroluminescent lighting and overhead emergency lighting were also examined. These produced mean speeds of 0.85 m/s (range 0.79–0.91 m/s) for LED1, 0.82 m/s (range 0.76–0.88 m/s) for LED2, 0.84 m/s (range 0.78–0.91 m/s) for Incandescent lighting, 0.75 m/s (range 0.69–0.81 m/s) for electroluminescent lighting and 0.53 m/s (range 0.48–0.58 m/s) for overhead emergency lighting. Other trials were conducted by Wright et al. and are described in detail elsewhere [192].

Galea et al. [193] also conducted a series of experiments to collect data on human movement

and behavior that might occur during a maritime evacuation. The experiments were conducted in a specially designed Ship Evacuation Behaviour Assessment Facility (SHEBA), and involved an assessment of the walking speeds of 360 participants as they traversed an 11 m corridor. Measurements of participant speed were performed in a clear (smoke-free) environment and in a smoke-filled environment with extinction coefficients of 0.0, 0.23, 1.15, and 2.30 m^{-1}. These were conducted at various degrees of heel and trim (i.e. pitching perpendicular to the direction of movement or in the direction of movement), in order to represent various sea states and scenario conditions; however, only the trials conducted on the flat are reported here, given their potential applicability to the built environment.

According to the SHEBA data-set, the participants' average unimpeded walking speed measured in a smoke free environment was approximately 2.2 m/s. This speed is much higher than the unimpeded walking speeds suggested in the Jin [189] and Frantzich [191] data-sets (see Chap. 61 and Frantzich and Nilsson [66, 190, 191]) and has been attributed [193] to a combination of factors, i.e. the participants in the SHEBA data set were highly motivated, familiar with the environment, required to perform relatively straightforward tasks and traverse a shorter route. Notwithstanding, the results indicate a reduction in walking speed with increased smoke density which is consistent with other studies, see Fig. 64.18.

The SHEBA study also defined 'mobility' as the walking speed in smoke as a fraction of the walking speed measured in a smoke free environment (i.e., the speed as a fraction of the speed attained in a clear environment). Figure 64.19, compiled by Hui Xie [182] illustrates how the mobility varied with different smoke densities for the SHEBA data set, and how this compares with the derived 'mobility' from the Jin and Frantzich and Nilsson studies. It is apparent that the relative reduction factor is broadly comparable across the three studies examined.

Xie Hui [182] performed a further analysis on the results from Jin's work (as part of his model development), and reported the relationships between extinction coefficient, K, and the *reduction* in walking speed as being (i.e. relative to performance in smoke-free environment):

$$Reduction\ Factor = -0.16K^2 - 0.488K + 1.105$$

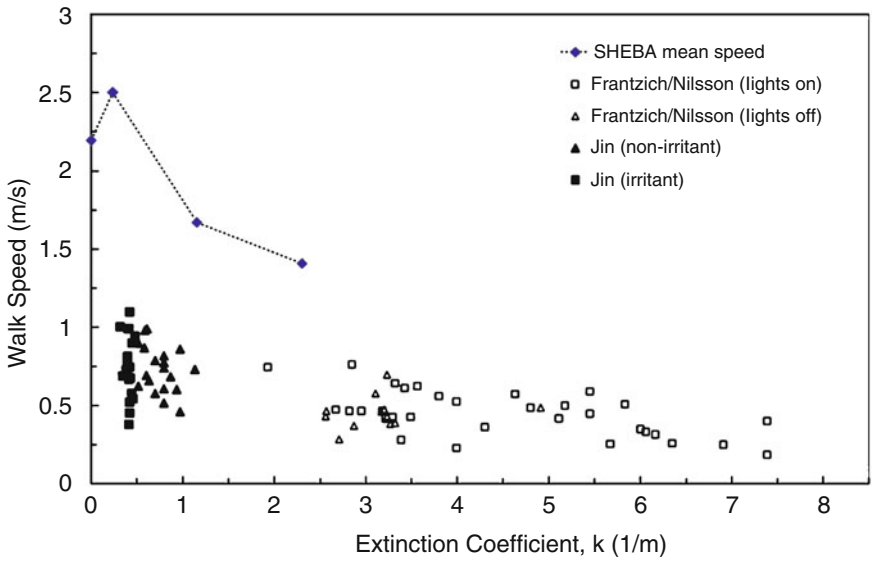

Fig. 64.18 Relationships between walking speed and extinction coefficient from a number of researchers derived by Xie Hiu [182]

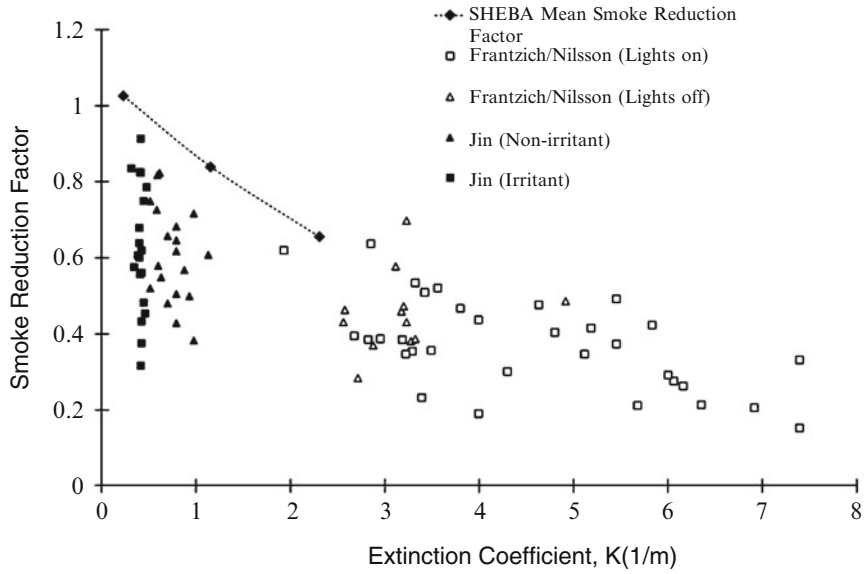

Fig. 64.19 Relationships between speed reduction factor and extinction coefficient derived by Xie Hiu [182]

between extinction coefficients of 0.2 and 1.0 m^{-1} for non-irritant smoke and

$$Reduction\ Factor = -2.08K^2 - 0.38K + 1.06$$

between extinction coefficients of 0.1 and 0.5 m^{-1} for irritant smoke.

These equations might then be applied to an individual's initial travel speed to estimate the impact of the smoke conditions upon performance. This assumes that the effect is *relative* to an individual's initial starting performance rather than producing an *absolute* effect upon all individuals in the same manner and then determining a specific walking speed for a given extinction coefficient; i.e., the impact gets progressively more severe in relation to the individual's initial performance rather than being independent of the individual involved. These two assumptions are discussed in detail by [183].

Crawling Movement in Smoke

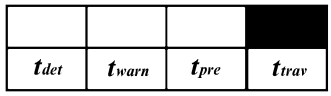

As discussed in Chaps. 61 and 63, the physiological effects of exposure to fire can influence evacuees' decision making and performance. The descending hot smoke layer can also lead occupants to crawl in an attempt to evacuate the building safely—either forcing them to do so in an attempt to avoid the worsening conditions or instigating a planned response to the presence of smoke through some procedural instruction or training. It may therefore be important, depending on the complexity of the engineering analysis being performed, to refer to data on crawling speeds and to understand the interrelationships between crawling speed and density. This is discussed in the paragraphs below.

Compared to the research on the upright walking speeds, there has been relatively little research conducted in this area until recently. The most significant being the work of Muhdi et al., Nagai et al., and Kady [170, 198], Kady et al. [187, 199].[1] The study by Muhdi et al. [200] was designed to measure and compare individual maximum and normal walking and crawling speeds, and concluded that (assuming a comparable level of effort), crawling results in a significant reduction in speed compared to walking. His

[1] It should be noted that Kady and Muhdi in this paragraph refer to the same person.

later study [187] compared the walking speed and crawling speed of persons of different body composition (normal, overweight and obese) and concluded that gender and body composition were major determinants of occupant normal crawling speed, accounting for 80 % of the variance. He again showed that the mean individual normal crawling speed was significantly less than the mean walking speed, with the mean crawling speeds of 0.79 m/s being comparable to that of 0.71 m/s obtained in his earlier study [200]. The study by Nagai et al. [170] also compared speeds of walkers and crawlers through a corridor and exit, and examined the impact of crowd density on crawling and walking speeds. The average individual normal crawling speeds measured in these experiments was 0.73 m/s which is also comparable to that obtained by Kady and Muhdi [187, 200]. Kady [199] further investigated the relationship between speed and density and concluded that the location of crawlers relative to the exit affects the density of crawlers produced and subsequently the speed of the individual crawlers and the population movement speed. The relationship derived between crowd crawling speed and crawling crowd density is shown in Fig. 64.20 and can be expressed by:

$$Crawling\ Speed = 0.7973 + 0.2909D - 0.1503D^2$$

It appears that this quadratic model provides a good fit to the data ($p = 0.004$), whilst the R^2 value indicates that crowd density accounts for 42.7 % of the variability in crowd crawling speed.

A summary of the current data on crawling speeds is given in Table 64.23. In addition to the crawling speed data (means, standard deviation and ranges), Table 64.23 provides information on the Source Observational Conditions (Location, Nature of the experiment, Spatial Configuration (details of the test route), Participants and Variables). An Additional Information column provides other relevant information related to the instructions to the subjects and precision of measurement. In all of the experiments, crawling was considered to be achieved when a subject rested on their knees and flattened palms with arms and thighs perpendicular to the floor and feet comfortably extended and spaced [201]. *It should be noted that in each of the experiments, subjects utilized adjustable knee pads and gloves which would not be expected to be available under normal emergency conditions.*

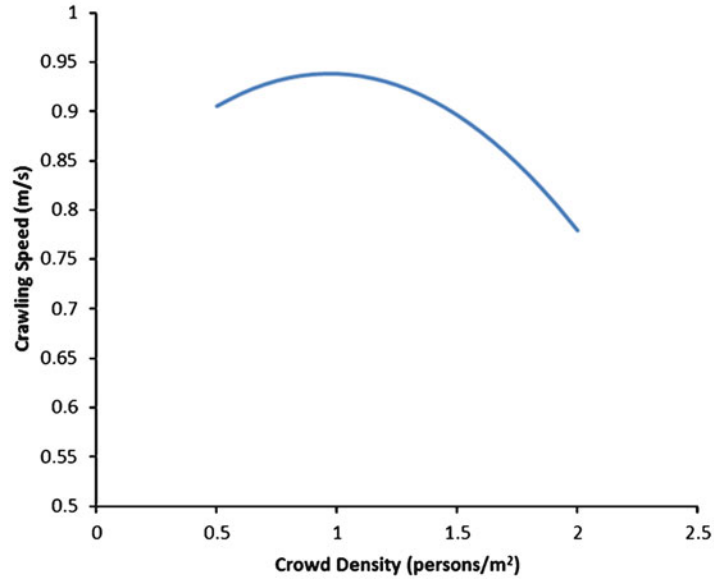

Fig. 64.20 Relation between crawling speed and density on a flat surface (From [199])

Table 64.23 Summary crawling speed data

Source	Observational conditions (L: location, N: nature, S: spatial configuration, P: participants, V: variable)	Type of crawling	Sample		Mean (m/s) [standard deviation, range]	Additional information
			Collection method	Size		
Kady [199]	L: USA	'Normal' pace	Timing by 6 photo sensors at 10 ft. intervals to digital timer	Groups of 2–9	**CW1**: 0.68 [–, 0.63–0.72][a]	[a]Crowd crawling speeds depending on group size— individuals randomly assigned to walking/crawling in different groups (n = 2–9) and track widths (CW1 = 3, CW2 = 4, CW3 = 5 ft) allowing for recovery time
	N: ET- start and finish lines set 10 ft. (3.05 m) from beginning and end respectively to overcome performance acceleration/deceleration				**CW2**: 0.76 [–, 0.70–0.81][a]	Measurements to 0.01 s
	SC: measured over 50 ft. (15.3 m) test track with adjustable widths: **CW1** = 3 ft, **CW2** = 4 ft, **CW3**: 5 ft				**CW3**: 0.66 [–, 0.62–0.69][a]	Subjects directed to crawl at 'normal' pace, with each subject performing 3 crawls
	P: aged 19–29, 10 males (5 normal, 4 overweight, 1 obese); 10 females (7 normal, 2 overweight, 1 obese)					
	V: movement rate given width of component (CW1–3)					
Kady and Davies [187]	L: USA	'Normal' pace	Timing by 6 photo sensors at 20 f. intervals to digital timer	All: 18 (54 data points)	0.77 [0.08, 0.54–0.93]	[#]Derived from data presented in paper
	N: ET 100 ft. (30.5 m) test track					Measurements to 0.01 s
	SC: start and finish lines set 10 ft. (3.05 m) from beginning and end respectively to overcome performance acceleration/deceleration					Crawling speeds measured for each individual on a random schedule allowing for recovery time
	P: aged 19–29 with mixed BMI/gender					Subjects directed to crawl at 'normal' pace
	S1: 18.5 < BMI ≤25.0 (normal), male			S1: 3 (9 data points)	0.87[#] [0.84–0.93]	Each subject performed 3 crawls
	S2:18.5 < BMI ≤25.0 (normal), female			S2: 3 (9 data points)	0.81[#] [0.76–0.88]	
	S3: 25.0 < BMI ≤ 29.9 (overweight), male			S3: 3 (9 data points)	0.78[#] [0.71–0.86]	
	S4: 25.0 < BMI ≤ 29.9 (overweight), female			S4: 3 (9 data points)	0.73[#] [0.68–0.78]	
	S5: BMI > 30 (obese), male			S5: 3 (9 data points)	0.76[#] [0.74–0.78]	
	S6: BMI > 30 (obese), female			S6: 3 (9 data points)	0.65[#] [0.54–0.70]	
	V: movement rate given BMI of sample (S1–6)					
Muhdi et al. [200]	L: USA	ET1	Timing by 6 photo sensors at 20 f. intervals to digital timer	26	0.71	Measurements to 0.01 s
	N: ET- ET1:'normal', ET2:'maximum' pace	ET2			1.47	Crawling speeds measured for each individual on a random schedule allowing for recovery time
	SC: 100 ft. (30.5 m) test track start and finish lines set 10 ft. from beginning and end to overcome performance acceleration/deceleration					Subjects directed to crawl at] 'normal' crawling (ET1) and 'maximum crawling' (ET2) pace
	P: unknown					
	V: movement rate given procedure (ET1–2)					

Nagai et al. [170]	L: Japan	'Normal' speed	Video	S1: 5	S1, CW1: 10s*	Participants directed to move at 'normal' speed. Paper also gives flows by density
	N: ET				S1, CW2: 7.5 s	*Mean speeds not given in the paper. Paper presents escape time (which may have included queuing time) by initial number of crawlers
	SC: 2 m breadth × 6 m length, ending in single exit. Exit width varied from 0.4 to 1.2 m. 10 repetitions of each. CW1: = 0.4 m; CW2:1.2 m			S2: 10	S2, CW1: 18 s	
	P: number of crawlers varied from 5 to 25				S2, CW2: 11.5 s	
	S1 = 5, S2 = 10, S3 = 15, S4 = 20, S5 = 25			S3: 15	S3, CW1: 22.5 s	
	V: escape time* across a number of component widths (CW1–2) given sample size (S1–5)				S3, CW2: 14.5 s	
				S4: 20	S4, CW1: 32 s	
					S4, CW2: 17 s	
				S5: 25	S5, CW1: 37 s	
					S5, CW2: 21 s	

Vulnerabilities: Innate: Impaired Movement

During the last three decades, there has been a growing effort to improve access to buildings for the entire population. It is now reasonably established in the regulation of developed countries that all new or refurbished public buildings should provide access for all and that existing buildings should make 'reasonable' provision. This improved access means that building populations are now more diverse and span a spectrum of movement abilities. The fast-changing anthropometric profile of occupants, as well as the large number of mobility-limiting diseases such as asthma and heart conditions, may have an impact upon issues relating to ingress and egress from a building. Although, the exact nature of this impact is not well understood at the moment, this still needs to be taken into account in fire safety design.

As noted previously, significant percentages of national and international populations have disabilities/impairments that impact on their ability to evacuate buildings [202]. These include those with physical and mental impairments, including the elderly and the obese. Since the prevalence of disability increases with age, and we are an increasingly aging society, it is expected that building populations will become even more diverse in terms of the physical and mental capabilities in the future. One potential impact on the engineering timeline is with respect to the t_{trav} component and it is therefore important to understand the range of capabilities of people with disabilities in terms of movement on both flat and inclined surfaces; i.e. stairs and ramps. It is also important to recognize that the percentage of those with mobility impairments may increase during an incident where injuries may occur leading to immediate limitations that cannot be immediately addressed through the presence of movement aids/devices. Limitations and impairments are certainly not confined to movement; for instance, sensory and cognitive impairments may also influence the performance of an evacuee. Those with visual impairments may experience difficulty in wayfinding, including locating and reading exit signage and indeed also may have reduced movement speeds. Those with hearing impairments may find it difficult to hear alarms, those with mental impairments may experience difficulty in recognizing alarms and understanding the need to evacuate, and those with limited dexterity may experience difficulty using particular types of door furniture to facilitate their escape. Although some [203–207] have researched the latter the body of research is limited and therefore this section focuses upon data specifically related to movement.

Although design and procedural measures are frequently implemented in multi-storey buildings to aid those who are unable or find movement (particularly stair movement) difficult e.g. use of refuges, elevators, assistive evacuation devices, buddy systems, it is clear that many people with disabilities will attempt to use stairs irrespective of their limitations. This was particularly noticeable in the WTC evacuation on 9/11, where the evacuation of mobility impaired occupants within the entire evacuating population was described as "slow and arduous" [145].

It is important to note that those with mobility impairments often use devices such as walking sticks/canes, crutches, rollators, frames or manual or electric wheelchairs to aid their movement and may also be assisted by friends/family. Therefore, in addition to expected lower movement speeds people with such impairments may often require more space (both in a stationary position and in movement) than a person evacuating without such aids. Clearly, if the routes that comprise the means of escape are not of sufficient width to facilitate passing in such cases, this may impact the movement of the entire evacuating population using that particular component. This was evident in the evacuation of WTC where it was reported that 51 % of the occupants of WTC1 and 33 % of the occupants of WTC2 indicated that injured and disabled people in the stairwell were a 'constraint to evacuation' [145], and where the evacuating population often reported having to wait until reaching the landings before being able to overtake slower moving individuals on stairs [208].

Design guidance regarding exit and stair sizing generally makes assumptions of optimum flows derived from data on largely able-bodied

populations. It is therefore essential to understand the capabilities of those with disabilities in the movement component of means of escape, namely their speeds on the horizontal, on ramps and on stairs.

Summaries of the data related to both unassisted and assisted unimpeded speeds on the horizontal, ramps and stairs (ascent and descent) and door traversal speeds are given in Tables 64.24, 64.25, 64.26, 64.27, 64.28, and 64.29. Tables 64.24, 64.25, 64.26, 64.27, 64.28, and 64.29. include, in addition to descriptive statistics (mean, standard deviation and range) for each data set, the Source of the data as well as the conditions under which the measurements were made; i.e., Observational Conditions (Location, Nature of the study, Spatial Configuration of the space in which measurements were made, Participants and the Variables). Separate tables are provided according to whether the subject group was moving with assistance of another person or without assistance, since this may have affected the movement speed. It is important to note, however, that across the studies, the nature and level of assistance varied. In all tables the conditions under which the observations/measurements were made are noted. In most cases the research comprised of an experimental study involving persons moving as individuals within a building or space; however, in some studies the measurements related to individuals moving in a more general evacuation involving others. In the former, the speeds are presented as in the original papers as unimpeded movement speeds, while in the latter, although densities were described as low, there may have been some influence of others on an individual's movement and so additional information is provided. Attention should be paid to the *Additional Information* columns in the tables which describe these conditions.

Where known, the distances over which measurements were made are also noted (under Spatial Configuration); in the case of horizontal movement this is simply a distance covered; in the case of stairs, information is in the form of a distance (if available) or the number of storeys over which the measurements were made. The distance over which movement is measured is particularly important when choosing speed data since individuals with reduced mobility may be expected to experience some reduction in speed as they tire over longer distances, i.e. the development of fatigue. The study by Kuligowski [220] reported in Table 64.27 is the only study to consider the variation in speed achieved over subsequent portions of the escape route and reference should be made to the original source for further information.

It is also important to mention in this respect that the movement speeds presented in the tables do not generally include periods of rest, unless otherwise noted. The exception is the study by Hunt et al. [214] which did include stops in the calculation of movement speed. The study by Boyce et al. [203, 204] noted that 14 % of those with a 'locomotion disability' required at least one rest over the 50 m horizontal route. Analysis of the WTC evacuation on 9/11 [145, 208] also suggested that some individuals with impairments had to stop to rest for short periods of time. The need to rest is likely to be dependent upon the distance travelled and exertion required relative to the severity of one's disability, although no studies have specifically looked at the impact of fatigue on the movement of people with disabilities over longer distances. The behavior of individuals with disabilities evacuating may also be important for evacuation modeling. For example, the Boyce et al. study [203, 204] noted that the majority of persons with disabilities sought support from handrails; this was particularly evident when ascending and descending stairs where 91 % and 94 % respectively of those moving unassisted utilized the hand-rail for support.[2]

The stair incline is also important in relation to stair movement and is described in Table 64.27 if reported in the original source or if it could be

[2] where significant differences are evident in the terminology used in this section, the authors have adopted the terms employed in the source material.

Table 64.24 Travel data—unassisted horizontal movement speeds (m/s) for people with disabilities

Source	Observational conditions (L: location, N: nature, SC: spatial configuration, P: participants, V: variable)	Sample			Results	Additional information
		Collection method	Description	Size	Mean(m/s) [standard deviation, range]	
Unassisted						
Jiang et al. [209]	L: China	Video	S1: disability, no aid	40	1.27 [0.19, 0.84–1.60]	Measurements to 0.04 s precision
	N:ET(unimpeded)		S2: single crutch	20	0.87 [0.18, 0.52–1.11]	Instructed to move 'at the highest speed they could maintain'
	SC: 40 m, subway station		S3: double crutch	40	0.78 [0.22, 0.37–1.24]	Results also presented by gender and by varying passage widths
	P: (S1–3: mix age/gender)					
	V: different movement capabilities (S1–3)					
Sørensen and Dederichs [210]	L: Denmark	Video	Visually impaired	46	0.98 [–, 0.35–1.72]	Paper also explores and presents relationship between speed and density
	N: (ET1–3)					
	SC: (ET1–2:2 floors, ET3:3 floors)					
	P: (mix age (10–69)/gender)					
	V: different trials involving the visually impaired (ET1–3)					
Jiang et al. [211]	L: China	Video	S1: disability, no aid	11	1.24 [0.12, 1.01–1.49]	Measurements to 0.04 s precision
In Chinese, data provided by author	N: ET(unimpeded)		S2: single crutch	6	0.66 [0.08, 0.58–0.81]	Instructed to move 'at the highest speed they could maintain'
	SC: 40 m, subway station		S3: double crutch	12	0.74 [0.20, 0.58–1.07]	
	P: S1–3: mix age/gender two 2-storey buildings and two 3- storey buildings					
	V: different movement capabilities (S1–3)					
Fujiyama and Tyler [212]	L: UK	Observer (stop-watch)	ET1 (normal)	18	1.31 [0.23,–]	Paper also explores correlation between physical characteristics and walking speeds and between speed on horizontal and stairs
	N:ET-ET1: 'normal' movement; ET2: 'fast' movement		ET2 (fast)	18	1.71 [0.29,–]	Instructed to walk at both 'normal' and 'fast' speeds
	SC: 8 m					
	P: mix gender, 60–81 years					
	V: different procedures (ET1–2)					
Brand et al. [213]	L: Sweden	–	S1:'locomotion' disability	9	–[–, 0.6*–1.4*]	Raw data given in graphical form
	N: ET (unimpeded)		S2: manual w.c. user	12	–[–, 0.3*–2.4*]	
	SC:31 m		S3: electric w.c. user	15	–[–, 1.2*–2.5*]	
	P:S1–3:>15 years with different movement capabilities (S1-3)				*Extracted from graph	
	V: different movement capabilities (S1–3)					

Boyce et al. [203]	L: UK N: ET- unimpeded SC: 50 m, various floor coverings P:S1–8: mix age/gender V: different movement capabilities (S1–8)	Observer (stop-watch)	S1: all disabilities	107	1.00 [0.42, 0.10–1.77]	Measurements to 0.1 s precision Instructed to move in 'prompt manner'
			S2:'locomotion disability' (all)	101	0.80 [0.37, 0.10–1.68]	
			S3: 'locomotion disability', no aid	52	0.95 [0.32, 0.24–1.68]	
			S4: crutches	6	0.94 [0.30, 0.63–1.35]	
			S5: walking stick	33	0.81 [0.38, 0.26–1.60]	
			S6: walking frame or rollator	10	0.57 [0.29, 0.10–1.02]	
			S7: electric wheelchair	2	0.89 [–, 0.85–0.93]	
			S8: manual wheelchair	12	0.69 [0.35, 0.13–1.35]	
Shields [104]	L: UK N: UE SC: hotel bedroom, carpeted corridor P: wheelchair users, mix age/gender V: mobility impaired	Video	Manual wheelchair	4	0.72 [–, 0.44–1.22]	

Table 64.25 Travel data—assisted horizontal movement speeds (m/s) for people with disabilities

Source	Observational conditions (L: location, N: nature, SC: spatial configuration, P: participants, V: variables)	Sample			Results	Additional information
		Collection method	Description	Size	Mean(m/s) [standard deviation, range]	
Assisted						
Hunt et al. [214]; Adams and Galea [215]	L: Belgium	Video	ET1: evac + chair (1 trained handler + 1 for doors)	8	1.46	Paper by Hunt et al. [204] also gives preparation time each device and breakdown by gender of handlers
	N:[ET1–4: four different devices with 8 trials per device]		ET2: carry chair (1 trained handler + 1 for doors)	8	1.50	
	SC: [hospital, 50 m corridor, hard vinyl flooring]		ET3: stretcher (4 trained handlers)	8	1.04	
	P: males and female groupings		ET4: drag mattress (2 trained handlers)	8	0.89	
	V: movement devices (ET1–4)					
Boyce et al. [203]	L: UK	Observer, stop-watch	S1: locomotion disability, ambulant	18	0.78 [0.34,0.21–1.40]	Measurements to 0.1 s precision
	N: [ET - unimpeded]		S2: manual wheelchair	16	1.30 [0.34, 0.84–1.98]	Assistors instructed to move in ‘prompt manner’
	SC: [50 m, various floor coverings]					
	P: S1–2: [mixed age and gender]					
	V: different movement capabilities (S1–2)					

Table 64.26 Travel data—unassisted/assisted movement speeds (m/s) for people with disabilities on ramps

		Configuration			Sample			Results	
Source	Observational conditions (L: location, N: nature, P: participants, V: variable)	Direction (down/up)	Slope	Distance (m)	Collection method	Description	Size	Mean(m/s) [standard deviation, range]	Additional information
Unassisted									
Brand et al. [213]	L: Sweden	CD1: up	1:12	6	–	S1: locomotion disability, ambulant	9	CD1, S1: [–, 0.6*−1.2*]	*Raw data given in graphical form., figures extracted from graph
	N: [ET - unimpeded]					S2: manual wheelchair user	12	CD1, S2: [–, 0.0*−1.9*]	
	S1:3 different mobility impairments, >15 years					S3: electric wheelchair user	15	CD1, S3: [–, 1.0*–2.1*]	
	V: impact of direction of use (CD1–2), given mobility impairment (S1–3)								
		CD2: down	1:12	6	–	S1: locomotion disability, ambulant	9	CD2, S1:[–, 0.5*−1.2*]	
						S2: manual wheelchair user	12	CD2,S2:[–, 0.4*−2.1*]	
						S3: electric wheelchair user	15	CD2, S3:[–, 0.4*−2.4*]	
Boyce et al. [203]	L: UK	Up	3–4°	–	Observer, stop watch	S1: locomotion disability (all)	48	0.59 [0.26, 0.21–1.08]	Measurements to 0.1 s precision
	N: [ET - unimpeded]					S2: locomotion disability, no aid	19	0.68 [0.24, 0.30–1.08]	Paper also gives results for all disabilities combined
	SC: ramps of various lengths and floor coverings					S3: crutches	4	0.46 [–, 0.35−0.53]	Instructed to move in ‘prompt manner’
	P:[S1–5: mixed age, gender and impairment]					S4: walking stick	20	0.52 [0.24, 0.21–1.05]	
	V: different mobility capabilities (S1–5)						5	0.35 [–, 0.30–0.42]	

(continued)

Table 64.26 (continued)

Source	Observational conditions (L: location, N: nature, P: participants, V: variable)	Configuration			Sample			Results	Additional information
		Direction (down/up)	Slope	Distance (m)	Collection method	Description	Size	Mean(m/s) [standard deviation, range]	
						S5: walking frame or rollator			
Boyce et al. [203]	L: UK	Down	3–4°	–	Observer, stop watch	S1: locomotion disability (all)	48	0.58 [0.25, 0.10–1.22]	Measurements to 0.1 s precision
	N:[ET - unimpeded]					S2: locomotion disability, no aid	19	0.68 [0.24, 0.28–1.22]	Paper also gives results for all disabilities combined
	SC: [ramps of various lengths and floor coverings]					S3: crutches	4	0.47 [–, 0.42–0.53]	Instructed to move in 'prompt manner'
	P: [S1–5: mixed age, gender and impairment]					S4: walking stick	20	0.51 [0.20, 0.18–1.04]	
	V: different mobility capabilities (S1–5)					S5: walking frame or rollator	5	0.36 [–, 0.10–0.52]	
Assisted									
Boyce et al. [203]	L: UK	CD1: up	3–4°	–	Observer, stop-watch	S1: locomotion disability	8	CD1, S1: 0.53 [0.17, 0.23–0.72]	Measurements to 0.1 s precision
	N: [ET - unimpeded]					S2: manual wheelchair	7	CD1, S2: 0.89 [0.20, 0.53–1.05]	Paper also gives results for all disabilities combined
	SC: ramps of various lengths, floor coverings								Instructed to move in 'prompt manner'
	P:[S1–2: mixed age, gender and impairment]								
	V: direction of movement on ramp (CD1–2), different mobility capabilities (S1–2)								

Table 64.27 Travel data—unassisted movement speeds on stairs (m/s) for people with disabilities/elderly

Source	Observational conditions (N: nature, S: spatial configuration, P: participants, V: variable)	Configuration			Sample			Results	Additional information
		Direction (up/down)	Slope	Distance	Collection method	Description	Size	Mean(m/s) [standard deviation, range]	
Descent									
Jiang et al. [209]	L: China	Down	17.7°#	1 storey	Video	S1: disability, no aid	40	0.85 [0.19, 0.32–1.34]	#Derived from information in paper
	N: ET					S2: single crutch	20	0.43 [0.14, 0.21–0.69]	Measurements to 0.04 s precision. Instructed to move 'at the highest speed could maintain'
	SC: 2 floors, in subway station					S3: double crutch	40	0.33 [0.13, 0.12–0.68]	Results also presented by gender and by varying passage widths
	P: [S1–3: mixed age/gender]								
	V: different mobility capabilities (S1–3)								
Kuligowski et al. [21]	L: USA	Down	25.1°#	13 storey	Video	S1: elderly, no aid	83	0.41 [0.17, 0.11–0.91]	#Derived from information in paper low densities implied, however, speeds presented may not always be unimpeded movement speeds
	N: AE					S2: disability, using cane	14	0.23 [0.08, 0.11–0.33]	Paper also presents localized speeds between various floor groupings
	SC: 13 floors, assisted living residential building								
	P: [S1–2: mixed elderly]								
	V: different mobility capabilities (S1–2)								
Sørensen and Dederichs [210]	L: Denmark	Down	–	–	Video	Visually impaired	46	0.73 [0.09, 0.54–0.92]	Paper also explores and presents relationship between speed and density
	N:[ET1–4]								
	SC:ET1–2:2 floors/ET3–4:3 floors								
	P: mix gender (10–69 years)								
	V:-								
Jiang et al. [211]	L: China	Down	17.7°#	1 storey	Video	S1: disability, no aid	9	0.81 [0.11, 0.68–1.06]	#Derived from information in paper
In Chinese, data provided by author China	N: ET					S2: single crutch	6	0.28 [0.08, 0.18–0.40]	Measurements to 0.04 s precision
	SC: [40 m, subway station]					S3: double crutch	10	0.31 [0.13, 0.12–0.48]	Instructed to move 'at the highest speed could maintain'
	P: [S1–3: mixed age/gender]								
	V: different mobility capabilities (S1–3)								

(continued)

Table 64.27 (continued)

Source	Observational conditions (N: nature, S: spatial configuration, P: participants, V: variable)	Configuration			Sample			Results	Additional information
		Direction (up/down)	Slope	Distance	Collection method	Description	Size	Mean(m/s) [standard deviation, range]	
Fujiyama and Tyler [212]	L: UK	Down	CS1: 38.8.0	3.5 m#	Observer		18	CS1, ET1: 0.60 [0.16,–]	#Incline length derived from horizontal and vertical length given in paper
								CS1, ET2:0.79 [0.22,–]	
	N: [ET1–2] - ET1: normal movement; ET2: fast movement		CS2: 35.0°	3.7 m#			18	CS2, ET1: 0.72 [0.20,–]	Paper also explores correlation between physical characteristics and walking speeds and between speed on horizontal and stairs
								CS2, ET2; 0.86 [0.22,–]	
			CS3: 30.5°	4.6 m#			18	CS3, ET1:0.73 [0.17,–]	
								CS3, ET2: 0.96 [0.21,–]	
	SC: [various geometries]		CS4: 24.6°	3.4 m#			18	CS4, ET1:0.91 [0.26,–]	Asked to walk at both ‘normal’ and ‘fast’ speeds
	P: [S1–8: age 60–81, mixed gender]							CS4, ET2:1.15 [0.30,–]	
	V: impact of component slope (CS1–4), with the procedure employed (ET1–2)								
Boyce et al. [203]	L: UK	Down	37–38°	1 storey	Observer, stop-watch	S1: locomotion disability (all)	30	0.33 [0.16, 0.11–0.70]	Measurements to 0.1 s precision
	N: [ET/ - unimpeded]					S2: locomotion disability, no aid	19	0.36 [0.14, 0.13–0.70]	[a]Rollator user, not used during descent Instructed to move in ‘prompt manner’
	SC: 1 storey					S3: crutches	1	0.22	
	P: [S1–5: mixed age/gender]					S4: walking stick	9	0.32 [0.12, 0.11–0.49]	
	V: different mobility capabilities (S1–5)					S5: rollator[a]	1	0.16	
Proulx et al. [216]	L: Canada	Down	–	6–7 storey	Video	UE1, S1	–	0.88[a]	[a]all speed calculations include time at rest/ stop
	N: [UE1–3]					UE2, S1	–	0.61	Speeds measured during low density but may not necessarily be unimpeded speeds
	S: [mid-rise apartments]					UE3, S1	–	0.57	
	P: [S1-2 - mixed age/gender + disability]. S1 included those with movement disabilities, S2 were over 65 years old					UE2, S2	–	0.57	
	V: different trials (UE1-3) involving populations with different mobility levels and age attribute (S1–2)					UE3, S2	–	0.58	

Ascent									
Jiang et al. [209]	L: China	Up	17.7°#	1 storey	Video	S1: disability, no aid	40	0.76 [0.18, 0.52–1.19]	#Derived from information in paper
	N: ET - unimpeded					S2: single crutch	20	0.39 [0.14, 0.18–0.67]	Measurements to 0.04 s precision. Instructed to move 'at the highest speed could maintain'
	SC: [2 floors in subway station]					S3: double crutch	40	0.27 [0.14, 0.08–0.50]	
	P: [S1–3: mixed age/gender]								
	V: different mobility capabilities (S1–3)								Results also presented by gender and by varying passage widths
Fujiyama and Tyler [212]	L: UK	Up	CS1: 38.8°	3.5#	Observer		18	CS1, ET1: 0.56 [0.15,–] CS2, ET2: 0.77 [0.23,–]	Paper also explores correlation between physical characteristics and walking speeds and between speed on horizontal and stairs
	N: [ET1–2] - ET1: normal movement, ET2: fast movement		CS2: 35.0	3.7#			18	CS2, ET1: 0.64 [0.15,–] CS2, ET2:0.85 [0.25,–]	#Incline length derived from paper Instructed to walk at both 'normal' and 'fast' speeds
	SC: [1 floor, various geometries]		CS3: 30.5°	4.6#			18	CS3, ET1: 0.68 [0.15,–] CS3, ET2: 0.91 [0.23,–]	
	P: [S1–8: age 60–81, mixed gender]		CS4: 24.6°	3.4#			18	CS4, ET1: 0.83 [0.19,–] CS4, ET2:1.14 [0.26,–]	
	V: the impact of the component slope (CS1–4) given the procedure employed (ET1–2)								
Jiang [211]	L: China	Up	17.7°	1 storey	Video	S1: disability, no aid	9	0.77 [0.13, 0.62–1.06]	
In Chinese, data provided by author China	N: ET - unimpeded					S2: single crutch	6	0.32 [0.09, 0.19–0.43]	
	SC: [40 m, subway station]					S3: double crutch	10	0.25 [0.11, 0.10–0.37]	
	P: [S1–3:mixed age/gender]								
	V: different mobility capabilities (S1–3)								
Boyce et al. [203],	L: UK	Up	37–38°	1 storey	Observer, stop-watch	S1: locomotion disability (all)	30	0.38 [0.14, 0.13–0.62]	#Rollator user, not used during descent Instructed to move in 'prompt manner'
	N: ET - unimpeded					S2: locomotion disability, no aid	19	0.43 [0.13, 0.14–0.62]	
	SC: [1 floor]					S3: crutches	1	0.22 [–, 0.13–0.31]	
	P: [S1–5: mixed age/gender]					S4: walking stick	9	0.35 [0.11, 0.18–0.49]	
	V: different mobility capabilities (S1–5)					S5: rollator	1	0.14#	

Table 64.28 Travel data—assisted movement speeds on stairs (m/s) for people with disabilities/elderly

Source	Observational conditions (N: nature, S: spatial configuration, P: participants, V: variable)	Configuration			Sample			Results	Additional information
		Direction (up/down)	Slope	Distance	Collection method	Description	Size	Mean (m/s) [standard deviation, range]	
Descent									
Kuligowski et al. [21]	L: USA	Down	25.1°#	13 storey	Video	S1: disability assisted other occupant	4	0.25 [0.13, 0.16–.42]	#Derived from information in paper
	N: AE					S2: disability assisted by fire fighter*	3	0.18 [0.04, 0.13–0.21]	*Note this was part of a training exercise
	SC: 13 floors, assisted living residential building					S3: assisted using stair descent device	15	0.21 [0.03, 0.15–0.27]	Low densities implied, however, speeds presented may not always be unimpeded movement speeds
	P: 119 persons varying mobility								Paper also presents localized speeds between various floor groupings
	V: different mobility capabilities (S1–3)								
Lavender et al. [217]	L: USA	Down	CS1: 31.4°	2 flights stairs +2 landing	Video	S1: manual carry (wheelchair)	12	CS1, S1 : 0.316* [0.017[a], –]	*Presented in graphical form—figures confirmed by authors
	N: ET - unimpeded					S2: basic stair chair	12	CS1, S2 : 0.336* [0.014[a], –]	[a]Standard error
	SC: stair width 91–132 cm					S3: fabric seated chair	12	CS1, S3 :0.342* [0.014[a], –]	Assistors were professional fire fighters. Focus of study was on ergonomic evaluation of different devices
	P: S1–9: 73 kg person equivalent weight					S4: extended handle stair chair	12	CS1, S4 : 0.754* [0.04[a], –]	
	V: configuration slope (CS1–2), different mobility capabilities (S1–9)	Down	CS2:31.4°	3 flights of stairs + 2 landings	Video	S5: standard friction (4 wheel)	12	CS2, S5 : 0.731* [0.021[a], –]	
						S6: long track	12	CS2, S6 : 0.742* [0.035[a], –]	
						S7: standard friction (2 wheel)	12	CS2, S7: 0.923* [0.030[a], –]	
						S8: narrow standard friction (4 wheel)	12	CS2, S8: 0.839* [0.029[a], –]	
						S9: long track, rear facing occupant	12	CS2, S9: 0.787* [0.030[a], –]	
Hunt et al. [214]; Adams and Galea [215]	L: Belgium N: ET1–4: different devices, with 8 trials per device	Down	34°	11 storey	Video	ET1:evac + chair (1 trained handler)	8	0.83	Assistors were highly trained hospital personnel. Paper by Hunt et al. [204] also gives preparation times each device, breakdown of speeds by gender of handlers, and average speeds by floor for each device. Note that 2010 paper gives slightly different speeds due to differences in the distances over which speeds were calculated
	SC: 11 floors, hospital, hard vinyl flooring					ET2: carry chair (3 male or 4 female trained handlers)	8	0.58	
	P: 75 kg person equivalent weight					ET3: stretcher (4 trained handlers)	8	0.53	
	V: different movement approaches (ET1–4)					ET4: drag mattress (2 trained handlers)	8	0.67	

Sano et al. [218]	L: Japan	Down	–	SC1: 10	Video		9	SC1, ET1:– [–, 0.5–0.75#]	#Converted from m/min in paper
	N: [ET1: trained in using evac chair; ET2: untrained in using evac chair]			SC2: 20			5	SC1, ET2:– [–, 0.42–0.58#]	*Raw data given in graphical form in paper
	SC: 2 buildings - SC1: 10 storey; SC2: 20 storey						4	SC2, ET1:– [–, 0.75–1.00#]	
	P: aged 20–30 assisting 65 kg male						1*	SC2, ET2:– [–, 0.8–1.17#]	
	V: spatial configuration (SC1–2), movement approaches (ET1–4)								
Shields et al. [219]	L: UK	Down	30	2 storey	Video	Manual wheelchair. user, 2 untrained handlers	1	0.32	
	N: [UE]								
	SC: [2 storey, university]								
	P: wheelchair user assisted								
	V:								
Boyce et al. [203]	L: UK	Down	37–38°	1 storey	Observer, stop-watch	S1	3	0.19 [–, 0.11–0.27]	Measured to 0.1 s precision
	N: ET - unimpeded					S2	1	0.90 [–,–]	Instructed to move in ‘prompt manner’
	SC: [1 storey]								
	P: [S1: blind, assisted; S2: seeing, assisted. Mixed age and gender]								
	V: different impairments (S1–2)								
Sime and Gartshore [50]	L: UK	Down	–	6 storey	–	Manual wheelchair user, 2 male handlers	1	0.41	
	N: [ET]								
	SC: 6 storey								
	P: assisted/wheelchair user								
	V: mobility impaired movement								
Ascent									
Shields and Boyce [65]	L: UK	Up	–	1 storey	Video	Manual wheelchair users, 2 untrained handlers	1	0.26	
	N: UE, retail store								
	SC: from single storey basement								
	P: Wheelchair user assisted by staff								
	V: mobility impaired movement								
Boyce et al. [203]	L: UK	Up	37–38°	1 storey	Observer, stop-watch	S1: blind with assistor	3	0.26 [–, 0.17–0.36]	Assistors instructed to move in ‘prompt manner’
	N: ET					S2: seeing with assistor	1	0.37 [–,–]	
	SC: 1 storey								
	P: [S1: blind with assistance; S2: seeing with assistance. Mixed age and gender]								

(continued)

Table 64.29 Travel data—door traversal speeds for people with disabilities/elderly (unassisted and assisted)

Source	Observational conditions (L: location, N: nature, S: spatial configuration, P: participants, V: variables)	Configuration			Sample			Results	Additional information
		Opening (to/away)	Closing force (N)	No. leaves	Collection method	Description	Size	Mean (sec) [standard deviation, range]	
Unassisted									
Boyce et al. [204]	L: UK	CO1: to (pull)	21–70	1	Computer recording of door swing	S1: with disability, no aid	63	CO1, S1: 3.2–4.6[a] [–, 1.4–12.6]	[a]Range of means (21–70 N)
	N: ET					S2: crutch user	5	CO1, S2: 2.8–4.6[a] [–, 2.2–6.3]	Individuals only participated at a higher level if they were successful at the level below—therefore care needs to be taken in interpretation of data
	SC: door operation (lever handle with door closer)					S3: walking stick user	28	CO1, S3: 3.2–4.9[a] [–, 1.4–9.7]	Paper also gives breakdown by closing force and % failures at each level
	P: Mixed abilities - S1: no aids, S2: crutch user, S3: walking stick user, S4: walking frame/rollator user					S4: walking frame, rollator user	8	CO1, S4: 3.2–8.9[a] [–, 1.9–17.0	
	V: opening direction of component (CO1–2), given movement capabilities (S1–4)	CO2: away (push)	21–70	1	Computer recording of door swing	S1: with disability, no aid	63	CO2, S1: 3.0–4.3[a] [–, 1.7–15.0]	
						S2: crutch user	5	CO2, S2: 3.0–3.9[a] [–, 2.5–5.2]	
						S3: walking stick user	28	CO2, S3: 3.7–4.6[a] [–, 1.5–11.1]	
						S4: walking frame, rollator user	8	CO2, S4: 5.2–7.9[a] [–, 1.7–14.3]	
Assisted									
Hunt et al. [204]	L: Belgium	CO1: to	–	2	Video	ET1: stretcher (4 trained handlers)	8	CO1, ET1: 7 [–,–] (male handlers)	[a]Evac + chair measurements conducted University of Greenwich
								CO1, ET1: 7 [–,–] (female handlers)	
	N: ET1–9 different devices					ET2: mattress (2 trained handlers)	8	CO1, ET2: 8 [–,–] (male handlers)	No bolt on door
								CO1, ET2: 12 [–,–] (female handlers)	
	SC: hospital					ET3: evac + chair (1 trained handler)	6	CO1, ET3: 5[a] [–,–] (male handlers)	
	P: trained hospital staff handling movement assistance devices							CO1, ET3: 6[a] [–,–] (female handlers)	
	V: opening direction of component (CO1–3) given movement device being employed (ET1–9)	CO2: away	–	2	Video	ET4: stretcher (4 trained handlers)	8	CO2, ET4: 5 [–,–] (male handlers)	
								CO2,ET4: 4 [–,–] (female handlers)	
						ET5: drag mattress (2 trained handlers)	8	CO2,E T5: 6 [–,–] (male handlers)	
								CO2, ET5: 7 [–,–] (female handlers)	
		CO2: away	–	2	Video	ET6: stretcher (4 trained handlers)	8	CO2, ET6: 12 [–,–] (male handlers)	
								CO2, ET6: 16 [–,–] (female handlers)	
						ET7: drag mattress (2 trained handlers)	8	CO2, ET7: 11 [–,–] (male handlers)	
								CO2, ET7: 20 [–,–] (female handlers)	
		CO3: away	–	1	Video	ET8: stretcher (4 trained handlers)	8	CO3, ET8: 6 [–,–] (male handlers)	
								CO3, ET8: 7 [–,–] (female handlers)	
						ET9: drag mattress (2 trained handlers)	8	CO3, ET9: 6 [–,–] (male handlers)	
								CO3, ET9: 11 [–,–] (female handlers)	

derived. The study by Fujiyama and Tyler [212] is interesting in that it is the only study presented here which compared the movement speeds for the same subject group across different stair geometries. Tables 64.24, 64.25, 64.26, and 64.27 also include a brief description of the floor covering if noted in the original source; different floor coverings may provide different resistances to movement and therefore may have an influence on speeds achieved, particularly for wheelchair users, and this should be taken into account when considering the data relative to the intended application. It should also be noted that different researchers have used different terminology to denote the subject groups, e.g., those who have difficulty walking in some studies are described as 'mobility impaired', in others as having a 'locomotion disability'. The terminology used in the tables is simply that which was adopted in the source material and users should refer to the source for a fuller understanding of the definitions of these terms. Care should also be taken to note the instructions given to participants of the experimental studies as they began their movement. Instructions ranged from moving in a 'prompt manner' to 'normal speed' and 'fast speed'. The nature of the instructions provided is important as it might have influenced the efforts of the participants and subsequently the speeds achieved.

It will be noted that few studies have been designed specifically to consider speeds of movement that can be achieved by those using different assistive techniques/devices (carry chairs, evacuation chairs, stretchers, drag mattress). In this respect the reader is directed to the studies of by Hunt et al. [214], Kuligowski et al. [21], and Lavender et al. [217]; the former study investigated speeds of assistive movement of highly trained personnel in a hospital environment; the latter the speeds which could be achieved by professional fire fighters in assisted escape. Data from these studies is presented in Table 64.18.

It is clear from Tables 64.24, 64.25, 64.26, and 64.27 that the abilities of people with disabilities and the elderly cover a wide spectrum with respect to horizontal and vertical movement. It is important in egress analysis to consider not only the variance in speed but also variation in spatial requirements of different individuals, since this may have a significant impact on flow performance produced. Indeed Boyce et al. [203, 204] has suggested that for analytical purposes, individuals should be categorized according to the mobility aid used and whether or not they require assistance so that potential interactions with the evacuating population can be fully realized.

The ability of individuals with disabilities and those assisting persons with disabilities to negotiate doors has also been studied by a number of researchers. Boyce et al. [203, 204], for example, examined the necessary time for people with disabilities to go through a door by pulling and pushing the door, which was subjected to a range of closing forces. The analysis of this data suggested that the ability of people with disabilities to negotiate doors subjected to a range of closing forces may depend on different factors including: the type of aid used (since it is implies a movement speed and particular technique in maneuvering the technical aid though the door), how old the participant was (since this is inherently related to strength) and the presence and severity of a dexterity or reaching and stretching disability. Hunt et al. [214] also investigated the time for teams of well-trained hospital staff to negotiate doors whilst handling different evacuation devices, i.e., a stretcher, rescue sheet and Evac+chair. They found that female handling teams took longer than male handling teams to maneuver through closed doors and found that generally it was easier to negotiate doors which opened away from the handlers. The data from both studies is presented in Table 64.25.

Identifying Applicable Data-Sets

Egress analysis is frequently presented to a third party for scrutiny as part of the performance-based design process (see Chap. 57). As mentioned previously, egress analysis is used to

provide an estimate of the Required Safe Egress Time (t_{RSET}). This is then compared against the Available Safe Egress Time (t_{ASET}). Egress analysis is typically achieved through the use of engineering calculations or computational tools (see Chaps. 59 and 60), both of which require support from the use of data. In this process, one group of people perform the analysis while another group (e.g. AHJs, code enforcers, etc.) judge the approach adopted, including the relevance and credibility of the data employed. For this judgment to be fair, accurate and credible, a comprehensive and detailed description of the key elements involved is required—including the data employed. Just as this assessment is required in the presentation of any results to a third party, an equivalent description (and understanding) is required on the part of the engineer in initially selecting the data. This is not trivial; indeed, given the immature nature of the field, it can be problematic. Given this, it is important that the engineer poses a series of questions of the data-sets to be used to establish if the background information related to the data is to their satisfaction. The answers to these questions will then determine whether the data is appropriate for the current application and the same answers should also be reflected in the presentation of any results produced. The reader should also examine the material provided in Chap. 57, as the answers to these questions shown below may complement the material presented in that chapter.

Below is a list of questions that the engineer should consider when identifying data sets for use. Although not a definitive list, these questions should assist the engineer in the selection of the most appropriate data-sets. Indeed, these questions formed the basis of the table format used when presenting the various data-sets provided earlier in the chapter. The engineer should consider the answers to these questions whilst choosing, interpreting and using the data and the answers to these questions should also be reflected in the eventual presentation of the results to the third parties, i.e. the background information that places the data (and the egress results) into context.

What is the origin of the data? **For instance**, **is it derived from**:

- Non-emergency movement,
- Evacuation drills or unannounced evacuations
- Experimental work,
- A real incident,
- Survey?

Is this appropriate and valid for the current project?

What is the nature of this data? **For instance**, **is the format**

- Numerical: Raw/Compiled/Composite/Extrapolated,
- Descriptive: reports/anecdotes/journalism,
- Graphical,
- Function/Relationship-based,
- Primary/Secondary, and

Is the sample large/small, **representative/unrepresentative**?

Does the data format support the current application? *If not*, *is the engineer able to derive the necessary data from it*? *Is the data sufficiently representative to be used in the current application*?

Is this source considered appropriate, **valid and reliable**?

- Is it adequately documented?
- Who collected it?
- How was it collected?
- When was it collected?
- What data collection techniques were employed?
- What research methods were employed to collect and analyse the data?
- What was the observed scenario?

Is there enough known about the data and the original event scenario?

Population characteristics/performance issues

- How many people were involved in the event and in the sample?
- Who was involved?
- Were they familiar with the structure?
- Where was the population located?

- What were they doing at the time of the incident?
- Are there sub-populations of particular concern within the space e.g., an impaired population?
- What attributes/issues might influence the results produced?
  - Physical—age/gender/health/fatigue/impairment/weight/encumbrance/children/elderly
  - Psychological/Behavioral—exposure to information/familiarity/cognitive abilities/experience/motivation/status
  - Social—role/hierarchy/relationships (employment/social/familial)/responsibilities/(alone/groups/crowd)/affiliation/culture
  - Situational—activities/engagement/commitment/alertness/location/proximity to incident/intoxication

Procedural (organizational) characteristics

- What was the emergency procedure employed?
- Was the population aware that the incident was going to take place?
- What notification systems were in place?
- How many staff members were actively engaged in the emergency procedure?
- What was the nature of the message/information being provided?
- Were people expected to assemble and, if so, where were the assembly points?
- What non-emergency procedures were in place that might have influenced the effectiveness of the emergency procedure?

Structural characteristics

- What was the structural configuration?
  - Existence of egress routes, doors, etc.,
  - Number of floors,
  - Use of the structure,
  - Dimensions of the space and egress components.

Environmental characteristics

- What was the cause of the incident?
- How did the incident develop?
- Where was the incident located?
- Did it spread beyond the room of origin?
- What cues were present?
- Did this influence the availability of egress routes?
- Did the spaces have environmental pollution/noise (visual/aural) that might have influenced evacuee performance?
- Were the spaces cluttered/confined?
- What were the expected lighting levels?
- What impact did the environmental conditions have on the evacuating population?
  - Physiological,
  - Psychological,
  - Behavioral.
- Were there external conditions (e.g. weather conditions) that influenced the performance of the evacuating population?

It would be impossible in this chapter to provide this level of detailed information for all of the data sets that exist in the public domain. However, the tables are structured such that space is provided for the key elements for each type of data to be included (see section "Structure of Data Presentation"). The tables presented in this chapter should therefore allow the engineer to answer the majority of these questions, or at least establish, with additional reference to the original source material, where insufficient information is provided to answer them; i.e. the omission of information can be established.

Using the Data

It is acknowledged that the presentation and availability of the data is only a small part of the engineering process. Another key step is for the engineer to select an appropriate data-set (or more likely data-sets) for the scenario at hand. Given the nature of this scenario, it may be that the scenario conditions do not exactly match those of the data presented; i.e., that the engineer is required to potentially select and use several data-sets to represent a single real-world scenario. This might occur where the key factors

in the scenario are not adequately addressed by a single data-set, where the data is not considered reliable enough, where the data is not adequately described and/or where the data is considered too old.

In addition, the engineer may also be required to manipulate single/combined data-sets in order to reflect specific aspects of the scenario, even where the original data-set is deemed to be an ideal match. The engineer might therefore be required to combine whole data-sets, splice parts of data-sets together, or manipulate the manner in which a data-set is applied across the area/population/timeline being examined. For this to occur the engineer would need to be able to match the data-sets against the scenario factors being represented and ensure that the manipulation of the data-sets adequately represented the real-world conditions while not undermining the original meaning of the data; i.e., the appropriateness of the original data selection.

As an example, a workflow of such data manipulation is shown in Fig. 64.21. This is intended to outline the process through which an engineer might pass and is but one of many that might occur. Stages (4, 7, 8) outline the initial definition of the quantitative component of the data-sets (i.e., the extent of certain factors), while Stages (5, 6, 9, 10) outline the qualitative aspects that help define the scenario and influence the manipulation of the eventual data-set generated (i.e., the nature of certain factors).

Initially, the engineer describes the scenario, $\boldsymbol{S}$, given the real world situation at hand and the factors and conditions associated with it. For instance, the engineer has to calculate the egress time for a population in a hotel with a fire assumed to start in one of the rooms on an upper floor.

The engineer first outlines the scenario in question in as much detail as possible (Stage (1)). The engineer then (Stage (2)) determines whether specific data and supporting information is available to enable the examination of the scenario described, $\boldsymbol{S}$. For instance, a previous incident may have been documented at that site or a number of evacuation trials may have been recorded from that structure (or similar structures). Given that this data is not available, the engineer consults the available guidance and literature (Stage (3)), to identify data-sets and information, $\boldsymbol{L}$, that may relate to the scenario. For instance, the data presented in Table 64.4. In Stage (4), the quantitative data included in $\boldsymbol{L}$ is collated to produce a number of data-sets, $\boldsymbol{E}$, that are deemed to relate to the scenario. Similarly in Stage (5), given the issues highlighted in $\boldsymbol{L}$, a set of behavioral and procedural issues, $\boldsymbol{I}$, are identified that need to be accounted for in the representation of the scenario—in the 'model' of the scenario.

In Stage (6), these issues, $\boldsymbol{I}$, are coupled together—integrated to establish a schema describing how they might interact to produce effects during the simulated scenario. In other words, how do the issues identified combine to produce the modeled scenario of interest? This schema may take the form of a number of questions that guide the engineer in what might be expected. For instance, how might intoxication affect performance of guests in a hotel given the use of voice alarm? In Stage(7), given the data-sets, $\boldsymbol{E}$, the real-world scenario, $\boldsymbol{S}$ and the schema describing expected performance, $\boldsymbol{F}$, the data-sets are compiled such that the data-sets selected are clearly associated with key elements in the schema in order to represent the scenario, $\boldsymbol{E}^*$. Here, the interaction between key factors is quantified; for instance, the pre-evacuation times of the intoxicated, in a hotel given the use of voice alarm. Whereas $\boldsymbol{E}$ represents data-sets that address factors associated with the scenario, $\boldsymbol{S}$, $\boldsymbol{E}^*$ represents how these may be spliced and combined to specifically address aspects of the behavioral schema produced, $\boldsymbol{F}$.

In Stage (8), the refined data-sets are manipulated such that a final distribution of data is produced for the factors highlighted, $\boldsymbol{Q}$. This reflects the range of values that might represent the key factors and interactions in $\boldsymbol{F}$. For instance, several functions are produced to represent the influence of intoxication and voice alarm in a hotel setting. In Stage (9), the data distribution, $\boldsymbol{Q}$, is compared against the schema, $\boldsymbol{F}$, to identify shortfalls in the quantitative representation of the schema—of the qualitative factors that are expected to influence performance—to

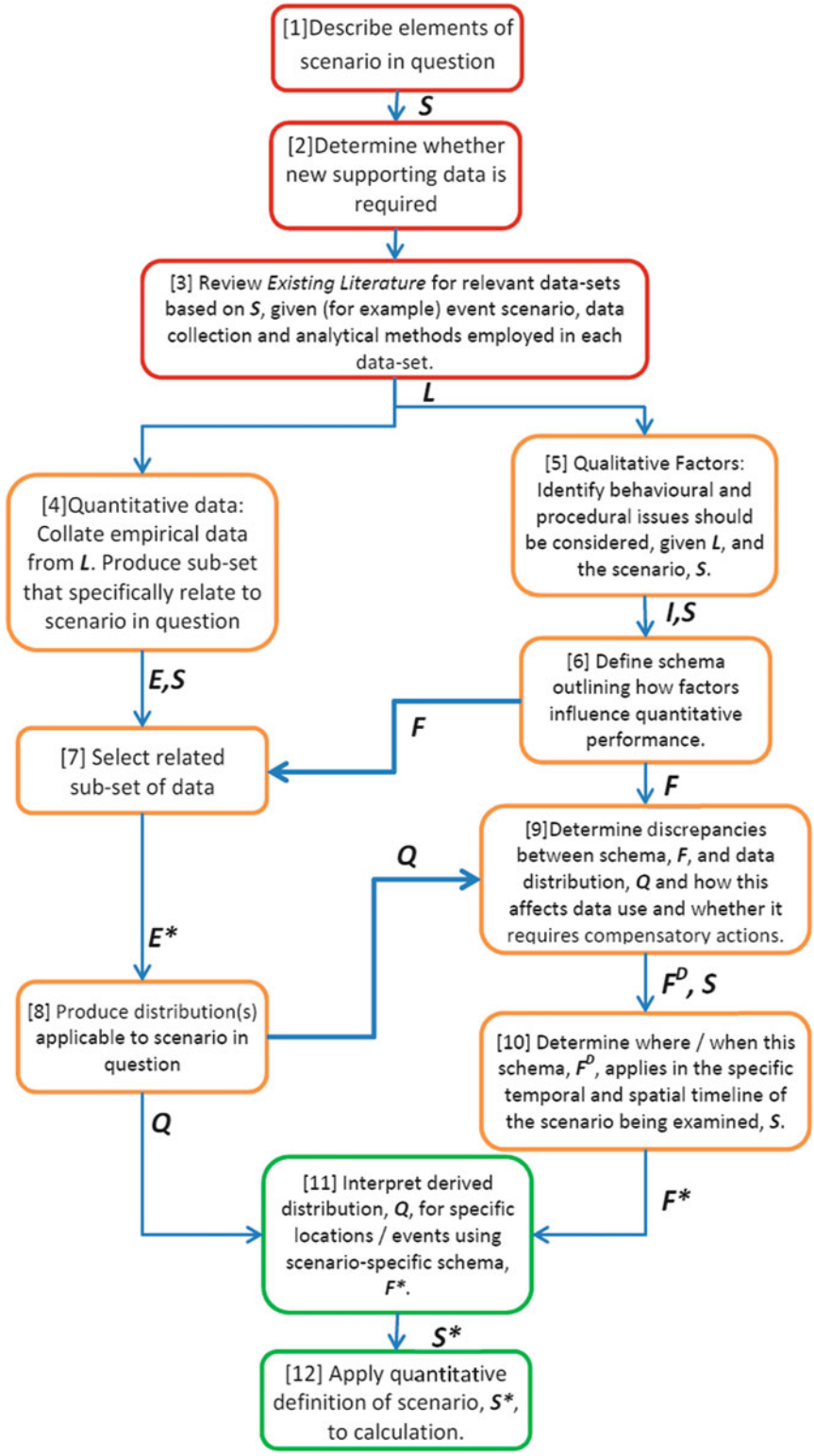

Fig. 64.21 Manipulation of multiple data-sets to fit the scenario

generate a schema that is numerically represented to some degree, $\boldsymbol{F^D}$. This represents the factors that will be depicted in the 'model' scenario. In Stage (10), this schema, $\boldsymbol{F^D}$, is then applied across the space and time being represented in the scenario, $\boldsymbol{S}$, to determine whether modifiers need to be applied, producing $\boldsymbol{F}$*. For instance, whether proximity to the incident, alarm coverage/notification, etc., need to be taken into account when applying the data to different areas/times/populations during the scenario. Will someone in the room of origin respond in the same way as someone with no visual access to the incident given that they are both intoxicated, in a hotel, awake, etc.?

In Stage (11), the refined schema, $\boldsymbol{F}$*, representing both the quantifiable issues and the manner in which is applied across the temporal/spatial environment is then applied to the data distribution, $\boldsymbol{Q}$. This then produces a quantified definition of the scenario, $\boldsymbol{S}$*, that is used to configure the model employed in the egress analysis.

Obviously, the process is over-simplified and presented in a linear manner when in fact it may be a highly iterative process. In reality, the engineer may iterate between these stages, ignore some and/or introduce others. However, the example is presented to demonstrate that the data presented may need significant manipulation both to broadly address the factors present in the scenario being addressed and then to customize the derived data-sets to represent local situations within the scenario. This will require skill and judgment. This process should be documented, not only to identify the data-sets and the steps involved, but also to make the assumptions and actions clear to third party viewers.

Summary

This chapter has presented a range of data-sets relative to the engineering time line commonly used to represent response and evacuation behaviors. Although these may inform a number of research, engineering and regulatory practices, the objective of this chapter has been to facilitate more effective, reliable and informed egress analysis as part of the performance-based design process. This data might be used to therefore to develop, configure, employ and validate computational and engineering egress tools as part of this effort.

Given the range of data types provided, the data have been provided in a number of tables reflecting the different evacuation phases, behavioral elements and influential factors involved. In each case, the data is accompanied by as much relevant background information as possible. Where space was an issue, background information has been abbreviated, and, in all instances by necessity, background information that would ideally have been included has been excluded due to space and time limitations.

The data-sets are not, therefore, provided in sufficient detail for the reader to make a definitive selection. Instead, the data and associated description should provide sufficient information for the reader to narrow down their review and focus on the most relevant data-sets for their particular application. This emphasizes the importance of the user following up on data-sets of interest by reference to the original sources. It is hoped that this approach should save them time and ensure that the most credible data is employed.

Acknowledgements The authors would like to acknowledge the following researchers for their feedback during the development of this chapter: Dr. David Purser, Dr. Brian Hoskins, Dr. Daniel Nilsson. The authors would also like to acknowledge Dave Boswell (Hughes Associates, Inc), for his efforts during the review process, along with Dr. Erica Kuligowski (NIST), section editor. Finally, the authors would like to acknowledge the following researchers for reviewing the data-sets presented to ensure consistency and accuracy: Dr. Michael Kinsey (Arup), Dr. Enrico Ronchi (Lund University), Dr. Anand Veeraswamy, Dr. Xie Hui, Ms. Maria Pretorius and Ms. Aoife Hunt (University of Greenwich).

References

1. Littell, JH, Pillai, VK, Corcoran, J (2008), Systematic reviews and meta-analysis, Oxford University Press.

2. Bailey, KD (1994), Typologies and taxonomies: an introduction to classification techniques, Sage Publications.
3. Bryan JL (1957) A study of the survivors' reports on the panic in the fire at the Arundal Park Hall, Brooklyn, Maryland on January 29, 1956. University of Maryland, College Park, USA.
4. Bryan JL (1998) Human behavior in fire: the development and maturity of a scholarly subject area. In: Proceedings of first international symposium human behaviour in fire, Belfast 31 Aug – 2 September 1998. University of Ulster, ISBN 1 85923 103 9.
5. Shields TJ, Proulx G (1999) The science of human behaviour: past research endeavours, current developments and fashioning a research agenda. In: Curtat M (ed) Fire safety science – proceedings of the 6th international symposium. International Association for Fire Safety Science, pp. 95–114.
6. Gwynne SM, Kuligowski ED (2010) The faults with defaults. In: Proceedings of 12th Interflam conference, University of Nottingham, UK. Interscience communications, pp 1473–1478.
7. British Standards Institution (2004) PD 7974–6:2004, The application of fire safety engineering principles to fire safety design of buildings. Human factors. Life safety strategies. Occupant Evacuation, behaviour and condition (Sub-system 6). British Standards Institution, London, UK.
8. NFPA 101A, Alternative approaches to life safety, 2013 edition. National Fire Protection Association, Quincy, MA, USA. ISBN: 978-145590419-8.
9. Gwynne SMV (2010) Conventions in the collection and use of human performance data. NIST GCR 10-928, National Institute of Standards and Technology, February 2010.
10. Purser DA, Bensilum M (1999) Quantification of escape behavior during experimental evacuations. Building Research Establishment Report CR 30/99. Building Research Establishment Ltd, Garston, Watford, UK.
11. Gwynne S, Kuligowski E, Nilsson D (2012) Representing evacuation behavior in engineering terms. J.Fire Protect. Eng. 22(2): 133–150, Sage.
12. Gwynne SMV, Purser DA, Boswell DL, Sekizawa A (2012) Understanding and representing staff pre-warning delay. J. Fire Prot. Eng. 22(2), 77–99, Sage.
13. EvacMod (2013), < http://evacmod.net/ >
14. FireEvacuation (2013), < http://fireevacuation.ru/english.php >
15. Ped-Net (2013), < http://www.ped-net.org/ >
16. University of Wuppertal Datenbank (2013), <http://www.asim.uni-wuppertal.de/datenbank.html>
17. Sime JD (1995) Crowd psychology and engineering. Saf. Sci. 21 (1):1–14.
18. Sime J (1984) Escape behaviour in fire: 'panic' or affiliation?. PhD Dissertation, Department of Psychology, University of Surrey, UK.
19. Lindell MK, Perry RW (2004) Communicating environmental risk in multiethnic communities. Thousand Oaks, CA: Sage Publications.
20. Kuligowski ED (2011) Terror defeated: occupant sense making, decision-making and protective action in the 2001 World Trade Centre disaster. Phd Dissertation, University of Colorado, Boulder, USA.
21. Kuligowski E, Hoskins B, Peacock R (2012), Evacuation of people with disabilities on stairs. In: Proceedings of the fifth international symposium human behaviour in fire, Cambridge, England, 19–21 September 2012. Interscience Communications, pp 315–327.
22. Gwynne SMV (2012) Translating behavioral theory of human response into modeling Practice. NISTGCR – 12–972, National Institute of Standards and Technology, 2012.
23. SFPE (2003) Engineering Guide on Human Behavior in Fire, Society of Fire Protection Engineers, Bethesda, MD.
24. Au Z, Gwynne SMV, Purser D (2011) Pre-warning delays: staff response in emergency incidents. In: Proceedings of EMEVAC (Emergency Evacuation of People from Buildings), Warsaw, Poland, pp 43–52.
25. Gwynne SMV, Au SYZ, Purser D, Boswell, D (2011) Accounting for staff response in engineering design. Evacuation and human behavior in emergency situations, University of Cantabria, Santander, Spain, 2011.
26. Purser DA, Bensilum M (2001) Quantification of behaviour for engineering design standards and escape time calculations, Safety Science, 38 (2): 157–182.
27. Gwynne SMV, Kuligowski ED, (2009) Simulating a building as a people movement system. J. Fire Sci. (27):343–368.
28. Boswell D, Gwynne SMV (2007) Air, fire and ICE: fire & security challenges unique to airports. Fire and Security Today, August 2007.
29. Gwynne SMV, Boswell DL (2009) Pre-evacuation data collected from a mid-rise evacuation exercise. J. Fire Prot. Eng. 19 (1): 5–29.
30. Bryan J (2002) A Selected Historical Review of Human Behavior in Fire, Fire Protection Engineering, 16, Fall.
31. Bryan J (1996), Behavioral response to fire and smoke. In: DiNenno PJ, Beyer CL, Custer RLP, Walton WD, Watts JMW, Drysdale D, Hall JR (eds), The SFPE, handbook of fire protection engineering (2nd Edition). National Fire Protection Association, Quincy, MA, pp (1-241)-(1-262).
32. Ye J, Chen X, Jian N (2012) Impact analysis of human factors on pedestrian traffic characteristics. Fire Saf. J. 52: 46–34
33. Pauls J (1996) Movement of people. In: DiNenno PJ, Beyer CL, Custer RLP, Walton WD, Watts JMW, Drysdale D, Hall JR (eds) The SFPE, Handbook Of

Fire Protection Engineering (2nd Edition). Society of Fire Protection Engineers, NFPA, pp (3-263)–(3-285).
34. Fruin JJ (1987) Pedestrian planning and design. Revised Edition. Elevator World Educational Services Division, Mobile, AL.
35. Pauls J (1980) Building evacuation research methods and case studies. In: Canter D (ed) Fires and human behaviour, Fulton, pp 227–249.
36. Proulx G. (2002) Movement of people: the evacuation timing In: DiNenno et al. (eds.), SFPE Handbook of Fire Protection Engineering (third ed., pp. 3-341–3-366). Society of Fire Protection Engineers, Bethesda MD
37. Fahy RF, Proulx G (2001) Towards creating a database on delay times to start evacuation and walking speeds for use in evacuation modeling. In: Proceedings of the second international symposium on human behavior in fire, 26/28 March 2001, Massachusetts Institute of Technology, USA. Interscience Communications (London, UK), pp175 – 179.
38. Shi L, Xie Q, Cheng X, Chen L, Zhou Y, Zhang R (2009) Developing a database for emergency evacuation model. Build. Environ. 44:1724–1729.
39. Bruck D (2001) The who, what, where and why of waking to fire alarms: a review. Fire Saf. J. 36 (7): 623–639.
40. Bruck D, Thomas I (2007) Waking effectiveness of alarms (auditory, visual and tactile) for adults who are hard of Hearing. Fire Protection Foundation, National Fire Protection Association, June 2007.
41. Bruck D, Thomas I, Ball M (2007) Waking Effectiveness of alarms (auditory, visual and tactile) for adults who are alcohol impaired. Fire Protection Foundation, National Fire Protection Association, June 2007.
42. Proulx P McQueen C (1994) Evacuation timing in apartment buildings. National Fire Laboratory, Institute for Research in Construction, National Research Council of Canada, Ottawa, Canada.
43. Gwynne SMV (2007) Optimising fire alarm notification for high risk groups: summary report. The Fire Protection Research Foundation, Quincy, MA, USA, pp 127.
44. Gwynne SMV (2007) Optimising fire alarm notification for high risk groups: notification effectiveness for large groups. The Fire Protection Research Foundation, Quincy, MA, USA, pp132.
45. Peacock RD Hoskins BL, Kuligowski ED (2012) Overall and local movement speeds during fire drill evacuations in buildings up to 31 stories. Saf. Sci. 50:1655–1664.
46. Peacock RD, Hoskins BL, Kuligowski ED (2011) Overall and local movement speeds during fire drill evacuations in buildings up to 31 stories. In: Peacock RD et al (eds) Pedestrian and evacuation dynamics. Springer Science and Business Media, DOI 10.1007/978-1-44-19-9725-8+3, pp 25–35.
47. Gwynne SMV, Boswell DL, Proulx G (2009) Understanding the effectiveness of notification technologies in assisting vulnerable populations. J. Fire Prot. Eng. 19 (1): 31–49.
48. Sharma SB, Tabak V, Brocklehurst D, Sagun A, Bouchlaghem D (2009) A comprehensive modern approach to developing evacuation data capture/analysis and simulation tools for real world fire engineering. In: Proceedings of fourth international symposium on human behaviour in fire, Cambridge England, 2009. Interscience Communications, pp 195–206. ISBN 978-0-9556548-3-1.
49. Christoffersen B, Söderlind C (2009) Comparison of two egress models and a full-scale experiment. In: Proceedings of the fourth international symposium on human behaviour in fire, Cambridge, England, 2009. Interscience Communications, pp 573–578, ISBN 978-0-9556548-3-1.
50. Sime JD, Gartshore PJ (1987) Evacuating a wheelchair user down a stairway: a case study of assisted escape. In: Harvey J, Henning D (eds) Proceedings Environmental Design Research Association Conference, Ottawa, Canada, pp 128–133.
51. Proulx G, Bénichou N (2008) Evacuation movement in photoluminescent stairwells. In: Kingsch WWF, Rogsch C, Schadschneider A, Schreckenberg M (eds) Pedestrian and evacuation dynamics. ISBN 978-3-632-04503-5 (print) 978-3-642-04504-2 - (on-line), pp 25–42.
52. Purser D (2008) Comparison of evacuation efficiency and pre-travel activity times in response to a sounder and two different voice alarm messages. In: Kingsch WWF, Rogsch C, Schadschneider A, Schreckenberg M (eds) Pedestrian and evacuation dynamics. ISBN 978-3-632-04503-5 (print) 978-3-642-04504-2 (on-line), pp 121–134.
53. Peacock RD, Averill JD, Kuligowski ED (2008) Stairwell evacuation from buildings: what we know we don't know. In: Kingsch WWF, Rogsch, Schadschneider A, Schreckenberg M (eds) Pedestrian and evacuation dynamics. ISBN 978-3-632-04503-5 (print) 978-3-642-04504-2 (on-line), pp 55–66.
54. Purser DA, Raggio AJT (1995) Behaviour of crowds when subjected to fire intelligence, Building Research Establishment Report CR 143/95. Building Research Establishment Ltd, Garston, Watford, UK.
55. Fahy R, Proulx G (1997) Human behavior in the World Trade Center evacuation. In: Hasemi Y (ed) Fire safety science – proceedings of the fifth international symposium. International Association Fire Safety Science, pp 713–724.
56. Brennan P (1997) Timing human response in real fires. In: Hasemi Y (ed) Fire safety science – proceedings of the fifth international symposium.

International Association Fire Safety Science, pp 807–818.
57. Proulx G, Fahy R (1997) The time delay to start evacuation: review of five case studies. In: Hasemi Y (ed) Fire safety science – proceedings of the fifth international symposium. International Association Fire Safety Science, pp 783–94.
58. Proulx G, Kaufmann A, Pineau J (1996) Evacuation time and movement in office Buildings. Internal Report IRC-IR 711, Institute for Research in Construction, National Research Council Canada, Ottawa, Canada, 74 pp.
59. Shields TJ, Smyth B, Boyce KE, Silcock GWH (1998) Evacuation behaviours of occupants with learning difficulties in residential homes. In: Proceedings of the first international symposium on human behaviour in fire, Belfast 1998. University of Ulster, pp 369–377. ISBN 1 85923 103 9.
60. Proulx G (1995) Evacuation time and movement in apartment buildings, Fire Saf. J. 24(3), pp. 229–246.
61. Proulx, G. (1994a), The Time Delay to Start Evacuating Upon Hearing a Fire Alarm, Proceedings of Human Factors and Ergonomics Society, 38th Annual Meeting.
62. Nilsson D, Frantzich H (2008) Design of voice alarms – the benefit of mentioning fire and the use of a synthetic voice. In: Kingsch WWF, Rogsch C, Schadschneider A, Schreckenberg M (eds) Pedestrian and Evacuation Dynamics. ISBN 978-3-632-04503-5 (print) 978-3-642-04504-2 (on-line), pp 135–144.
63. Samochine DA, Boyce K, Shields J (2005) An investigation into staff behaviour in unannounced evacuations of retail stores – implications for training and fire safety engineering. In: Gottuk DT, Lattimer BY (eds) Fire safety science – proceedings of the eight international symposium. International Association Fire Safety Science, pp 519–530.
64. Frantzich H (2001) Occupant behaviour and response time – results from evacuation experiments. In: Proceedings of the second international symposium on human behaviour in fire, 2001, Massachusettes. Interscience Communications, 2001, pp 159–166. ISBN 0 9 5 3 2312 6 7.
65. Shields TJ, Boyce KE (2000) A study of evacuation from large retail stores. Fire Saf. J. 35 (1): 25–49.
66. Frantzich H, Nilsson D (2009) Evacuation in complex environments – an analysis of evacuation conditions in a nuclear power plant and a tunnel construction site. In: Proceedings of the fourth international symposium on human behaviour in fire, Cambridge England, 2009. Interscience Communications, pp 207–218. ISBN 978-0-9556548-3-1.
67. Kholshevnikov VV, Samoshin DA, Parfyonenko AP, Belosokov IP (2012) Study of children evacuation from pre-school education institutions. Fire Mater. 36: 349–366. DOI: 10.1002/fam.2152, John Wiley and Sons Ltd.
68. Galea, E.R., Filippidis, L.,Sharp, G.,Deere, S.,and Sauter,M. (2012) Investigating the impact of culture on evacuation response phase behaviour – the project BeSeCu evacuation experiments (2nd Edition). CMS Press, 12/IM/160,978-1-904521-78-5.
69. Capote JA, Alvear D, Abreu O, Cuesta A, Hernando J (2012) Children evacuation: empirical data and egress modeling. In: Proceedings of fifth international symposium human behaviour in fire, Downing College Cambridge, 19th – 21st September 2012. Interscience Communications, pp 109–119.
70. Galea ER, Sharp G, Sauter M, Deere S, Filippidis L (2012) Investigating the impact of culture on evacuation behaviour – a Polish data set. In: Proceedings of fifth international symposium human behaviour in fire, Downing College Cambridge 19–21 September 2012. Interscience Communications, pp 62–73.
71. Galea ER, Saute M, Deere SJ, Filippidis L (2011) Investing the impact of culture on evacuation behaviour – A Turkish data set. In: Spearpoint M (ed) Fire science – proceedings of the tenth international symposium, International Association Fire Safety Science, pp 709–722.
72. Galea ER, Deere S, Sharp G, Filippidis L, Hulse L (2010) Investigating the impact of culture on evacuation behavior. In: Proceedings of the twelfth international conference Interflam 2010, Vol 1, pp 879–892. Interscience Communications, ISBN 978-0-9541216-5-5.
73. Kholshevnikov VV, Samoshin DA, Parfenenko A P (2009) Pre-school and school children building evacuation. In: Proceedings of the fourth international symposium on human behaviour in fire, Cambridge England, 2009. Interscience Communications, pp 243–254. ISBN 978-0-9556548-3-1.
74. Tavares RM, Gwynne S, Galea ER (2006) Collection and analysis of pre-evacuation time data collected from evacuation trials conducted in library facilities in Brazil. J App. Fire Sci. 15 (1): 23–40.
75. Gwynne, S, Galea, ER, Parke J, Hickson J (2003) The collection and analysis of pre-evacuation times derived from evacuation trials and their application to evacuation modeling. Fire Tech. 39 (2):173–195.
76. Gwynne S, Galea ER, Parke J, Hickson J (2002) The collection of pre-evacuation times from evacuation trials involving a hospital outpatient facility. In: Evans DD (ed) Proceedings of the seventh international symposium fire safety science. International Association Fire Safety Science, pp 877–888.
77. Olsson PÅ, Regan MA (1998), A comparison between actual and predicated evacuation times. In: Proceedings of the first international symposium on human behaviour in fire. University of Ulster, pp 461–468. ISBN 1 85923 103 9.
78. Olsson PÅ, Regan MA (2001) A comparison between actual and predicted evacuation times Saf. Sci. 38 (2) pp. 139–145.
79. Tancogne-Dejean M, Colina H, Ilsbrock D, Van Niel K (2009) Evacuation drills of a cinema auditorium.

In: Proceedings of the fourth international symposium on human behaviour in fire, Cambridge England, 2009. Interscience Communications, pp 645–657. ISBN 978-0-9556548-3-

80. Brown R, Galea E, Deere S, Filippidis L (2012) Response time data for large passenger ferries and cruise ships. In: Proceedings of fifth international symposium human behaviour in fire, Downing College Cambridge 19–21 September 2012. Interscience Communications, pp 460–471.
81. Proulx G, Sime JD (1991) To Prevent 'Panic' in an Underground Emergency: Why Not Tell People the Truth? In: Cox G, Langford B (eds) Fire safety science – proceedings of the third international symposium. International Association Fire Safety Science, pp 843–852.
82. Gwynne S (2006) Emergency show and tell: the use of audible and visual notification systems. Int. Fire Prot. Mag. November 2006.
83. Gwynne SMV, Boswell D (2007) Integrating fire safety and security into movement management. Fire and Secur. Today, January/February 2007, pp. 38–45.
84. Latane B, Darley J (1970) The unresponsive bystander: why doesn't he help? New York, NY: Appleton-Century Crofts.
85. Deutsch M, Gerard HB (1955) A study of normative and informational social influences upon individual judgment. J. Abnorm. Soc. Psychol. 51(3): 629–636.
86. Bruck D, Ball M (2005) Sleep and fire: who is at risk and can the risk be reduced? In: Gottuk DT, Latimer BY (eds) Fire safety science – proceedings of the eighth international symposium. International Association of Fire Safety Science, pp 37–51.
87. Thomas I, Bruck D (2008a) Strobe lights, pillow shakers and bed shakers as smoke alarm signals. In: Karlsson B (ed) Fire safety science – proceedings of the ninth international symposium fire safety science. International Association for Fire Safety Science, pp 415–424.
88. Bruck D, Thomas IR (2009) Community based research on the effectiveness of the home smoke alarm in waking children. In: Proceedings of the fourth human behavior in fire symposium, Cambridge. Interscience Communications, pp 335–344.
89. Bruck D, Thomas I (2008) Comparison of the effectiveness of different fire notification signals in sleeping older adults. Fire Technol. 44 (1): 15–38.
90. Thomas I, Bruck D (2010) Awakening of sleeping people: a decade of research. Fire Technol. 46 (3): 743–761.
91. Smith G, Splaingard M, Hayes J, Xiang H (2006) Comparison of a personalized parent voice smoke alarm with conventional residential tone smoke alarm for awakening children. Pediatr. 118:1623–1632. Doi:10.1542/peds.2006-0125.
92. Ashley E, Du Bois J, Klassen M, Roby R (2005) Waking effectiveness of audible, visual and vibratory emergency alarms across all hearing levels. In: Gottuk DT, Lattimer BY (eds) Fire safety science – proceedings of the eighth international symposium. International Association for Fire Safety Science, (poster presentation).
93. Du Bois J, Ashley E, Klassen M, Roby R (2005) Waking effectiveness of audible, visual and vibratory emergency alarms on people of all hearing abilities. Paper presented at Accessible Emergency Notification and Communication: State of the Science Conference, Gallaudet University Washington DC, November 2–3 2005. Accessed online 18 September 2012 <http://www.silentcall.com/strobe-vs-shaker.pdf.>
94. Ball M, Bruck D (2004a) The salience of fire alarm signals for sleeping individuals. In: Proceedings of the third human behavior in fire symposium (Belfast), Interscience Communications, London pp 303–314.
95. Bruck D, Reid S, Kouzma J, Ball M (2004) The effectiveness of different alarms in waking sleeping children. In: Proceedings of the third international symposium human behavior in fire (Belfast), Interscience Communications, London pp 279–290.
96. Ball M, Bruck D (2004b) The effect of alcohol upon response to different fire alarm signals. In: Proceedings of the Third Human Behavior in Fire Conference (Belfast), Interscience Communications, London pp 291–302.
97. Bruck D, Bliss RA (2000) Sleeping children and smoke alarms, In: Yamada T (ed) Proceedings of the fourth Asia-Oceania symposium on fire science and technology, Asia-Oceania Association for Fire and Technology, Tokyo, pp 602–613.
98. Bruck D (1999) Non-awakening in children in response to a smoke detector alarm. Fire Saf. J. 32 (4): 369–376.
99. Bruck D, Horasan M (1995) Non-arousal and non-action of normal sleepers in response to a smoke detector alarm, Fire Saf. J. 25(2):125–139.
100. Kahn MJ (1984) Human awakening and subsequent identification of fire-related cues. Fire Technol. 20 (1): 20–26.
101. Zepelin H, McDonald CS, Zammit GK (1984) Effects of age on auditory awakening. J Gerontol. 39(3): 294–300.
102. Nober EH, Peirce H, Well A (1983) Waking effectiveness of household smoke and fire detection devices, Fire J. 75: 86–91.
103. Pearson RG, Joost MG (1983) Egress behaviour response times of handicapped and elderly subjects to simulated residential fire situations. Report No PB83-222695. National Bureau of Standards, Department of Commerce, Washington D.C.
104. Shields TJ (1993) Fire and disabled people in buildings. Building Research Establishment Report BR231, ISBN 0 85125 546 9.
105. Hoskins BL (2011) The effects of interactions and individual characteristics on egress down stairs. PhD

Dissertation, University of Maryland – College Park. Available on-line at http://drum.lib.umd.edu/handle/1903/12515 (accessed 10th October 2012).
106. Predtechenskii VM, Milinskii AI (1978), Planning for foot traffic in buildings, Stroizdat Publishers, Moscow (1969). English translation published for the National Bureau of Standards and the National Science Foundation, Amerind Publishing Co., New Delhi, India.
107. Nelson HE, MacLennan HA (1996) Emergency Movement. In: DiNenno PJ et al (eds) The SFPE Handbook of Fire Protection Engineering, 2nd ed. National Fire Protection Association, Quincy, MA, pp. 3-286–3-295.
108. Pretorius M (2012) Personal Communication.
109. Kholshevnikov VV, Shields TJ, Boyce KE, Samoshin DA (2008) Recent developments in pedestrian flow theory and research in Russia. Fire Saf. J. 43(2):108–118.
110. Still K (2000) Crowd dynamics. PhD Dissertation, University of Warwick, United Kingdom.
111. Smith R A (1993) Volume flow rates of densely packed crowds. In: Smith RA, Dickie JF (eds) Engineering for crowd safety. Elsevier, pp313–319. ISBN 0444899200.
112. Tubbs J, Meacham B (2007) Egress design solutions: a guide to evacuation and crowd management planning. Wiley.
113. Thompson PA (1994) Developing new techniques for modelling crowd movement. Phd Dissertation, University Of Edinburgh, Scotland.
114. Graat E, Midden C, Bockholts P (1999) Complex evacuation: effects of motivation level and slope of stairs on emergency egress time in a sports stadium, Safe.Sci. 31:127–141.
115. Lord J, Meacham B, Moore A, Fahy RF, Proulx G (2005) Guide for evaluating the predictive capabilities of computer egress models. Report No. NIST GCR 07-886. National Institute of Standards and Technology, Gaithersburg, MD.
116. Daamen W (2004) Modelling passenger flows in public transport facilities. Thesis Series, T2004/6, The Netherlands TRAIL Research School, DUP Science.
117. Teknomo K (2002) Microscopic pedestrian flow characteristics: development of an image processing data, collection and simulation model. PhD Dissertation, Tohoku University, Japan.
118. Helbing D, Johansson A (2010) Pedestrian, crowd and evacuation dynamics. Encyclopedia of Complexity and Systems Science 16, 6476–6495.
119. Al-Gadhi SAH (1996) A review study of crowd behavior and movement. j.King Saud University. Eng. Sci. 8(1):77–108 (AH 1416/1996).
120. Brocklehurst D (2005) People flow modeling. Dissertation, Loughborough University, UK.
121. Daamen W, Hoogendoorn SP (2012) Emergency door capacity: influence of door width, population composition and stress level. Fire Technol. 48: p 55–71.
122. Schadschneider A, Klingsch W, Klupfel H, Kretz T, Rogsch C, Seyfried A (2008) Evacuation dynamics: empirical results, modeling and applications. Encyclopedia of complexity and system science. Springer, Berlin, 2008.
123. Brocklehurst D, Green MG, Bouchlaghem D, Pitfield DE, Still K (2004) Capacity flows on stadia stairs; potential for low flow rate systems. In: Proceedings of third international symposium human behaviour in Fire, Belfast, UK, 1–-3 September 2004. Interscience Communications, pp 489–494.
124. Hostikka S, Paloposki T, Rinne T, Saari J, Korhonen T, Heliövaara S (2007) Evacuation experiments in offices and public buildings. VTT, Working Papers 85.
125. Rinne T, Tillander K, Grönberg P (2010) Data collection and analysis of evacuation situations, VTT Tiedotteita Research Notes 2562, VTT, Finland. ISBN 978-951-38-7673-9.
126. Helbing D, Johansson A, Al-Abideen H Z (2007) The dynamics of crowd disasters: An empirical study. Phys. Rev. E 75, 046109.
127. Schultz M, Schulz C, Fricke H (2008) Passenger dynamics at airport environment. In: Kingsch WWF, Rogsch C, Schadschneider A, Schreckenberg M (eds) Pedestrian and evacuation dynamics. ISBN 978-3-632-04503-5 (print) 978-3-642-04504-2 - (on-line), pp 381–396.
128. Ono R, Valentin M, Vittorino F (2012) Walking speed data of fire drills at an elementary school. In: Proceedings of fifth international symposium human behaviour in fire, Downing College Cambridge, 19th–21st September 2012. Interscience Communications, pp 98–108.
129. Zanlungo F, Chigodo, Y. Ikeda, T. and Kanda, T. (2012) Experimental study and modelling of pedestrian space occupation and motion pattern in a real world environment, Paper presented at 6th Pedestrian and Evacuation Dynamics Symposium, 6th–8th June 2012, Zurich.
130. Lárusdóttir AR, Dederichs A (2011) A step towards including children's evacuation parameters and behaviour in fire safe building design. In: Spearpoint M (ed) Proceedings of the tenth international symposium fire safety science. International Association for Fire Safety Science, ISBN 1817-4299, pp 187–185.
131. Lárusdóttir AR, Dederichs A (2011) Evacuation dynamics of children – walking speeds, flows through doors in day-care centres. In: Peacock et al (eds) Pedestrian and Evacuation Dynamics, Springer Science and Business Media, DOI 10. 1007/978-1-44-19-9725-8+3, pp 139–147.
132. Winkens A, Kingsch W (2011) New data for human performance in planar corridors. In: Peacock RD

et al (eds) Pedestrian and evacuation dynamics. Springer Science and Business Media, DOI 10.1007/978-1-44-19-9725-8+3, pp 61–70.
133. Yeo SK, He Y (2009) Commuter characteristics in mass rapid transit stations in Singapore. Fire Saf. J. 44: 183–191.
134. Fang Z, Yuan JP, Wang YC, Lo SM (2008) Survey of pedestrian movement and development of a crowd dynamics model. Fire Saf. J. 43: 459–465.
135. Wong LT, Cheung TF (2006) Evaluating probable risk of evacuees in institutional buildings. Saf. Sci. 44:169–181.
136. Lee JYS, Lam WHK (2006) Variation of walking speeds on a unidirectional walkway and on a bidirectional stairway. Transp. Res. Rec. 1982: 122–131.
137. Hoskin KJ, Spearpoint M (2004) Crowd characteristics and egress at stadia. In: Proceedings of third international symposium human behaviour in fire, Belfast, UK, 1–3 September 2004. Interscience Communications, pp 367–376.
138. Daamen W, Hoogendoorn SP (2005) Free speed distributions – based on empirical data in different traffic conditions. In: Waldau N et al (eds) Pedestrian and evacuation Dynamics 2005. Springer Science and Business Media, pp 167–181.
139. Berrou JL, Beecham P, Kagarlis MA, Gerodimos A (2005) Calibration and validation of the Legion simulation model using empirical data. In: Waldau N et al (ed) Pedestrian and evacuation dynamics. Springer Science and Business Media, pp 167–181.
140. Klüpfel H (2005) The simulation of crowd dynamics at very large events – calibration, empirical data, and validation. In Gattermann P, Waldau N, Schreckenberg M (eds) Proceedings of the 3rd international conference on pedestrian and evacuation dynamics -2005, Berlin. Springer, pp 285–296.
141. Armin Seyfried, Bernhard Steffen, Wolfram Klingsch and Maik Boltes The fundamental diagram of pedestrian movement revisited J. Stat. Mech. (2005) P10002 doi:10.1088/1742-5468/2005/10/P10002
142. Seyfried A, Boltes M, Kahler J, Klingsch W, Portz A, Rupprecht T, Steffen B Winkens A (2010) Enhanced empirical data for the fundamental diagram and the flow through bottlenecks. In Klingsch et al (eds), Pedestrian and evacuation dynamics 2008, Springer, pp145–156.
143. Tanaboriboon Y, Guyano JA (1991) Analysis of pedestrian movements in Bangkok. Transp. Res. Rec. 1294:52–56.
144. Irzik M, (2003) Design of pedestrian facilities. In: Proceedings of the 2nd International Conference of Pedestrian Evacuation Dynamics, pp111–119.
145. Averill JD, Milleti DS, Peacock RD, Kuligowski ED, Groner N, Proulx G, Reneke AP, Nelson HE (2005) Final report on the collapse of the World Trade Center towers, NIST NCSTAR 1–7 Federal Building and Fire Safety Investigation of the World Trade Center Disaster, Occupant Behavior, Egress and Emergency Communications. National Institute of Standards and Technology.
146. Templer J (1995) The staircase: studies of hazards, falls, and safer design. Massachusettes Institute of Technology Press.
147. Boyce KE, Purser D, Shields TJ (2012) Experimental studies to investigate merging behaviour in a staircase. Fire Mater. 36 (5–6):383–398.
148. Kadokura H, Sekisawa A, Sano T, Yajima M, Masuda S (2012) Study of Congestion in Stairs During Phased Evacuation in a High-Rise Building – Analysis based on the Observational Data of a Real Total Evacuation Drill, in Proceeedings 5th International Human Behaviour in Fire Symposium, Cambridge, England, pp 171-181.
149. Lárusdóttir AR, Dederichs A (2012a) Behavioural aspects of movement down stairs during elementary school fire drills. In: Proceedings of fifth international symposium human behaviour in fire, Downing College Cambridge, 19th – 21st September 2012. Interscience Communications, pp 120–127.
150. Lárusdóttir AR, Dederichs A (2012b) Evacuation of children – movement on stairs and on horizontal plane. Fire Technol. 48 (1):43–53.
151. Fujiyama T, Tyler T (2011) Free walking speeds on stairs: effects of stair gradients and obesity of pedestrians. In: Peacock et al (eds) Pedestrian and evacuation dynamics. Springer Science and Business Media, DOI 10.1007/978-1-44-19-9725-8+3, pp 95–105.
152. Proulx G, Bénichou N (2010) Photoluminescent stairway installation for evacuation in office buildings. Fire Technol. 46: 471–495.
153. Proulx G, Bénichou N, Hum JK, Restivo KN (2007) Evaluation of the effectiveness of different photoluminescent stairwell installations for the evacuation of office building occupants. Research Report 232. National Research Council of Canada, Ottawa, Canada.
154. Choi J, Hwang H, Hong W, Choi Y (2009) Analysis of occupants' escape speed and reason of bottleneck occurrence through the trial evacuation experiment at a high rise apartment housing. In: Proceedings of fourth international symposium human behaviour in fire, Cambridge, UK, 13–15 July 2009. Interscience Communications, pp 123–134.
155. Kretz T, Grünebohm A, Kessel A, Klüpfel H, Meyer-König T, Schreckenberg M (2008) Upstairs walking speed distributions on a long stairway. Saf. Sci. 46:72–78.
156. Daly PN, McGrath F, Annesley TJ (1991) Pedestrian speed/flow relationships for underground stations. Traffic Eng. Control, 32 (2): 75–78.
157. Kagawa M, Kose S, Morishita Y (1985) Movement of people on stairs during fire evacuation drill-Japanese experience in a high-rise office building. In: Grant CC, Pagni PJ (eds) Fire safety science: proceedings of the first international symposium,

Gaithersburg, Maryland. International Association Fire Safety Science, pp. 533–540.
158. Khisty CJ (1985) Pedestrian flow characteristics on stairways during disaster evacuation. Transp. Res. Rec. 1047: 97–102.
159. Kadokura H, Sekisawa A, Sano T, Yajima M, Masuda S (2012) Study of Congestion in Stairs During Phased Evacuation in a High-Rise Building – Analysis based on the Observational Data of a Real Total Evacuation Drill, in Proceeedings 5th International Human Behaviour in Fire Symposium, Cambridge, England, pp 171–181.
160. Seyfried A, Steffen B, Klingsch W, Boltes M (2007) Steps towards the fundamental diagram – empirical results and modeling In: Waldau N et al (eds), Pedestrian and evacuation dynamics – 2005. Springer, pp 377–390.
161. Seyfried A, Rupprecht T, Winkens A, Passon O, Steffen B, Klingsch W, Boltes M (2007) Capacity estimation for emergency exits and bottlenecks. In: Proceedings 11th Interflam. Interscience Communications, pp 247–258.
162. Kendik E (1985) Assessment of escape routes in buildings and a design method for calculating pedestrian movement. SFPE Technology Report 85-4. Society of Fire Protection Engineers, Boston, Massachusetts, 1985.
163. Gwynne SMV, Kuligowski ED, Kratchman J, Milke JA (2009) Questioning the linear relationship between doorway width and achievable flow rate. Fire Saf.. J. 44: 80–87.
164. Gwynne S (2000) Mathematical modelling of egress behaviour. Phd Dissertation, University of Greenwich
165. Sano T, Jo A, Ikehata Y (2012) Experimental study on crowd flow through an opening connected to a crowded corridor: a comparison of experiment and multi-agent simulation. In: Proceedings of fifth international symposium human behaviour in fire. Interscience Communications, pp 206–217.
166. Daamen W, Hoogendoorn SP (2011), Emergency door capacity: influence of population composition and stress level. In: Peacock RD et al. (eds), Pedestrian and Evacuation Dynamics, Springer, pp15–24.
167. Hoogendoorn, SP, Daamen W, Bovy P (2003) Microscopic pedestrian traffic data collection and analysis by walking experiments. In: Proceedings of the 2nd international conference, Pedestrian and Evacuation Dynamics 2003, pp89–100.
168. Shimada T, Naoi H (2009) An experimental study on the evacuation flow of crowd including wheelchair users. In: Proceedings of fourth international symposium human behaviour in fire, Cambridge, UK, 13–15 July 2009. Interscience Communications, pp 579–584.
169. Kretz T, Grunebohm A, Schreckenberg M (2006) Experimental study of pedestrian flow through a bottleneck. J. Stat. Mech.: 100–104.
170. Nagai R, Fukamachi M, Nagatani T (2006) Evacuation of crawlers and walkers from corridor through an exit. Physica A 367: 449–460.
171. Rupprecht T, Klingsch W, Seyfried A (2011) Influence of geometry parameters on pedestrian flow through bottleneck. In: Peacock R et al. (eds.), Pedestrian and evacuation dynamics, pp71–80.
172. Müller K (1981) Zur Gestaltung und Bemessung von Fluchtwegen für die Evakuierung von Personen aus Bauwerken auf der Grundlage von Modellversuchen. Dissertation, Technische Hochschule Otto von Guericke Magdeburg, Germany.
173. Kinsey MJ (2011) Vertical transport evacuation modeling. PhD Dissertation, University of Greenwich, UK.
174. Kadokura H, Sekizawa A, Takahashi W (2011) Study on availability and issues of evacuation using stopped escalators in a subway station. Fire Mater. Published on-line in Wiley On-line Library, DOI: 10.1002/fam.1097.
175. Okada N, Hasemi Y, Moriyama S, Hirakawa K, Takemori K, Hebiishi T, Lu Y (2009) Feasibility of upward evacuation by escalator – an experimental study. In: Proceedings of fourth international symposium human behaviour in fire. Interscience Communications, pp161–172.
176. Cheung C, Lam W (1998) Pedestrian route choices between escalator and stairway in MTR Stations. J. Transp. Eng. 124 (3): 227–285.
177. Kinsey MJ, Galea ER, Lawrence PJ (2009) Extended model of pedestrian escalator behaviour based on data collected within a Chinese underground station. In: Proceedings of the fourth international symposium human behaviour in fire Robinson College, University of Cambridge, UK. Interscience Communications, pp173–182.
178. Kinsey MJ, Galea ER, Lawrence PJ (2012) Modelling evacuation using escalators: a London underground dataset. In: Proceedings of Pedestrian and Evacuation Dynamics Conference, ETH Zurich, Switzerland, 2012.
179. Okada N, Hasemi Y, Moriyama S, Hirakawa K, Takemori K, Hebiishi T, Lu Y (2012) Feasibility of upward evacuation by escalator – an experimental study. Fire Mater. 36:429–440. DOI: 10.1002/fam.2152, John Wiley and Sons Ltd.
180. Davis P, Dutta G (2002) Estimation of capacity of escalators in London Underground, No 2002-11-01. IIMA Working Papers from Indian Institute of Management Ahmedabad, Research and Publication Department.
181. Al-Sharif L (1996) Escalator handling capacity: standards versus practice, Elevator World.
182. Xie Hui (2011) Investigation into the interaction of people with signage systems and its implementation within evacuation Models. Phd Dissertation, University of Greenwich, UK.
183. Ronchi E, Gwynne SMV, Purser DA, Colonna P (2012) Representation of the impact of smoke on

agent movement speeds in evacuation models. Fire Technol. 49(2): 411–431.
184. Nilsson D (2009) Exit choice in fire emergencies – influencing choice of exit with flashing lights. Doctoral Thesis, Lund University, Sweden.
185. Karlsson M, Eklund B, Lundman P (2011) TVRK Tunnel 11 Trafickverkets tecniska krav Tunnel (In Swedish). TRV publ nr 2011:087, Trafikverket, Sweden.
186. Purser DA (2009) Assessment of hazards to occupants from smoke, toxic gases and heat. In: DiNenno PJ (ed) SFPE Handbook of Fire Protection Engineering, 4th Edition. National Fire Protection Association, Quincy, MA, pp 2-96–2-193.
187. Kady RA, Davis J (2009) The effect of occupant characteristics on crawling speed in evacuation. Fire Saf. J. 44 (4): 451–457.
188. Ronchi E (2012) Evacuation modelling in road tunnel fires. PhD Dissertation, University of Bari, Italy.
189. Jin T (1976) Visibility through fire smoke. Report of Fire Research Institute of Japan2, Fire Research Institute of Japan 33:12–18.
190. Frantzich H, Nilsson D (2004) Evacuation experiments in a smoke filled tunnel. In: Proceedings of the third international symposium on human behaviour in fire. Interscience Communications, pp 229–238.
191. Frantzich H, Nilsson D (2003) Utrymning genom tät rök: beteende och förflyttning [Evacuation in dense smoke: behaviour and movement] (No. 3126). Lund: Department of Fire Safety Engineering and Systems Safety.
192. Wright MS, Cook GK, Webber GMB (2001) The effects of smoke on people's walking speeds using overhead lighting and way-guidance provision. In: Proceedings of the second international symposium on human behaviour in fire 2011, MIT, Boston, USA. Interscience Communications Ltd, London, pp.275–284.
193. Galea ER, Gwynne SMV, Blackshields D, Lawrence PJ, Filippidis L (2001) Predicting the evacuation performance of passenger ships using computer simulation. In: Proceedings of the 9th international fire science and engineering conference Interflam 2001, Edinburgh, Scotland. Interscience Communications Ltd: London, Vol. 2, pp.853–864.
194. Jin T (1997) Studies on human behavior and tenability in fire smoke. Howard W Emmons invited plenary lecture. In: Hasemi Y (ed) Fire safety science, proceedings of the fifth international symposium. International Association Fire Safety Science, pp 3–21.
195. Jin T (1978) Visibility through fire smoke. J. Fire Flammabl. 9:135–157.
196. Jin T, Yamada T (1985) Experimental study of human behaviour in smoke filled corridors. In: Grant CE, Pagni PJ (eds) Fire safety science – proceedings of the first international symposium. International Association Fire Safety Science, NIST, USA, pp 511–519.
197. Korhonen T, Hostikka S (2009) Fire Dynamics Simulator with Evacuation: FDS+Evac, Technical Reference and User's Guide, (FDS 5.5.0, Evac 2.2.1), VTT, Finland.
198. Muhdi R (2008) The development and representation of occupant performance in building evacuation modeling. Phd Thesis, Auburn University, USA.
199. Kady RA (2012) The development of a movement–density relationship for people going on four in evacuation. Saf. Sci. Vol. 50, no. 2, pp. 253–258.
200. Muhdi R, Davies J, Blackburn T (2006) Improving occupant characteristics in performance based evacuation modeling. In: Proceedings of the HFES 50th Annual meeting, San Francisco, CA pp 1199–2202.
201. Cott HPV, Kinkade RG (1972) Human engineering guide to equipment design. Rev Ed McGraw Hill, American Institute for Research, Washington D.C.
202. World Health Organisation (2011) World Report on Disability, World Health Organisation and World Bank. ISBN 978 92 4 156418 2.
203. Boyce KE, Shields TJ, Silcock GWH (1999a), Toward the characterization of building occupancies for fire safety engineering: capabilities of disabled people moving horizontally and on an incline. Fire Technol. 35 (1): 51–67.
204. Boyce KE, Shields TJ, Silcock GWH (1999b) Toward the characterization of building occupancies for fire safety engineering: capability of disabled people to Negotiate Doors. Fire Technol. 35 (1): 68–78.
205. Covington SA (1982) Ergonomic Requirements for Building Components and Associated Operating Devices. Building Research Establishment, UK, CP1/82.
206. Johnson BM (1981) Door use study. National Research Council Canada, Division of Building Research.
207. Steinfield E, Schroeder S, Bishop M (1979) Accessible buildings for people with walking and reaching limitations. US Department of Housing and Urban Development, Washington DC, USA.
208. Shields T J, Boyce KE (2009) The behavior and evacuation experiences of WTC 9/11 evacuees with self-designated mobility impairments. Fire Saf. J. 44 (6): 881–893.
209. Jiang CS, Zheng SZ, Yuan F, Jia HJ, Zhan ZN and Wang JJ (2012) Experimental assessment on the moving capabilities of mobility-impaired disabled. Saf. Sci. 50(4): 974–985, ISSN: 0925-7535 DOI: 10.1016/j.ssci.2011.12.023.
210. Sørensen JG, Dederichs AS (2012) Evacuation characteristics of blind and visually impaired people: walking speeds on horizontal planes and descending stairs. In: Proceedings of fifth international symposium on human behaviour in fire, Cambridge, England, 19–21 September 2012. Interscience Communications, pp 304–314.

211. Jiang CS (2009) Study on self-evacuation capability of the disabled as well as its impact on evacuation capability of healthy population. Final Report on Projects Supported by National Natural Science Foundation of China.
212. Fujiyama T, Tyler N (2004) An explicit study on walking speeds of pedestrians on stairs. In: Proceedings 10th international conference on mobility and transport for elderly and disabled people, 23–26 May 2004, Hamamatsu, Japan.
213. Brand A, Sörqvist M, Håkansson P, Johansson JE (2001) Evacuation safety for locomotion disabled people. In: Proceedings of the second international symposium human behaviour in fire, Massachusettes Institute of Technology, USA, 26–28 March 2001. Interscience Communications, pp 445–450.
214. Hunt A, Galea E, Lawrence P (2012) An analysis of the performance of trained staff using movement assist devices to evacuate the non-ambulant. In: Proceedings fifth international symposium human behaviour in fire, 19–21 September 2012, Cambridge. Interscience Communications, pp 328–339.
215. Adams APM, Galea ER (2011) An experimental evaluation of movement devices used to assist people with reduced mobility in high-rise building evacuations. In: Peacock et al (ed) Proceedings 5th international conference pedestrian and evacuation dynamics, March 8–10 2010. Springer, New York, pp 129–138.
216. Proulx G, Latour JC, McLaurin JW, Pineau J, Hoffman LE, Laroche C (1995) Housing evacuation of mixed abilities occupants in highrise buildings. Internal Report No. 706, National Research Council of Canada, Ottawa, Canada.
217. Lavender S, Hedman GE, Reichelt PA, Mehta J, Conrad KM, Park S (2012) Ergonomic evaluation of manually carried and track-type stair descent devices used for the evacuation of high rise buildings. In: Proceedings of fifth international symposium human behaviour in fire, Cambridge, England, 19–21 September 2012. Interscience Communications, pp 340–345.
218. Sano T, Omiya Y, Hagiwara I (2004) Evacuation from high-rise buildings by using an evacuation chair. In: Proceedings 6th Asia Oceania symposium on fire science and technology, 17–20 March 2004. International Association Fire Safety Science.
219. Shields TJ, Boyce KE, Silcock GWH, Dunne B (1997) The impact of a wheelchair bound evacuee on the speed and flow of evacuees in a stairway during an uncontrolled unannounced evacuation. J. App. Fire Sci. Vol 7 (1).
220. Kuligowski E (2012) Theory building: an examination of the pre-evacuation period of the 2001 WTC disaster. In: Proceedings of the fifth international symposium human behaviour in fire, Cambridge, England, 19–21 September 2012. Interscience Communications, pp 24–36.

S.M.V. Gwynne is a Senior Research Officer at the National Research Centre Canada, a Senior Research Fellow at the University of Greenwich and part of the Adjunct Faculty at the University of Maryland. He holds a Ph.D. in the Mathematical Modeling of Egress Behavior.

K.E. Boyce is a Senior Lecturer at Ulster University, UK. She holds a Ph.D. in the Egress Capability of People with Disabilities.

Liquid Fuel Fires

65

D.T. Gottuk and D.A. White

Introduction

Liquid fuel spill and pool fires represent potential hazards in many applications ranging from accidents at industrial plants using combustible liquids to arson fires with flammable fuels. A pool is characterized as a confined body of fuel that typically has a depth greater than 5 mm. A pool can result due to a liquid fuel release that collects in a low spot, such as a trench, or can exist as a result of normal storage of fuels in tanks and containers. A fuel spill is generally associated with thin fuel layers resulting from an unconfined release of fuel. The nature of a spill fire is highly variable, depending on the source of the release, surface features of the substrate (e.g., concrete, ground, water) on which the fuel is released, and the point and time of ignition. The ability to characterize fuel spills and the resulting fires in a consistent and conservative manner is required for many engineering analyses. This chapter provides an overview of the most relevant factors and methodology for evaluating a liquid fuel spill or pool fire in terms of fire growth and size.

The chapter is organized in three major sections corresponding to the three primary steps of evaluating the development of a liquid fuel spill or pool fire: (1) "Spill or Pool Size," (2) "Fire Growth," and (3) "Fire Size." The first section deals with the process of estimating the physical size of any given fuel release or pool of fuel. Both static (fixed quantity of liquid) and continuously flowing spill fires have been considered. Once a liquid fuel spill or pool has occurred, ignition of the fuel will lead to a transient fire growth period. This transient period of a liquid fuel fire is dictated by the flame spread rate across the surface of the liquid. The second section of the chapter addresses the assessment of fire growth rate by providing an overview of flame spread on liquid fuels. The third section discusses the available data and correlations that can be used to evaluate the size of the fire in terms of heat release rate and flame height.

The heat release rate of a fire is the primary parameter used in determining the impact of a fire on its surroundings. The impact of a fire is dealt with in other chapters of this handbook. The heat transfer from liquid fuel spill or pool fires is addressed by Beyler [1].

Spill or Pool Size

The first step in analyzing a liquid fuel fire is to characterize the physical dimensions of the fuel spill or pool. The area of the initial body of fuel will correlate to the size of the resulting fire. A confined fuel release or existing open container of fuel will result in a pool fire of a known area. A pool fire represents a body of fuel that is confined by physical boundaries. In other words, the walls of a room or obstructions on a floor will limit a fuel release to a smaller area than the potential

D.T. Gottuk (✉) • D.A. White
Jensen Hughes, 3610 Commerce Drive, Suite 817
Baltimore, MD 21227, USA

M.J. Hurley (ed.), *SFPE Handbook of Fire Protection Engineering*,
DOI 10.1007/978-1-4939-2565-0_65, © Society of Fire Protection Engineers 2016

unconfined spill area. In almost all cases, a confined fuel release will create a pool that has a greater depth than the depth of an unconfined spill. When fuel is released onto a surface, it will spread laterally based on several factors, including the initial momentum of the fluid, the fluid surface tension, and the features of the substrate onto which it spilled. Some substrate features that need to be considered are porosity of material and surface roughness. Porous materials, such as sand or even some floor coverings like carpet, can result in different spill sizes and different fuel burning rates. Surface structure can have similar effects, either by impeding liquid spread due to roughness, non-uniformity pooling, or by exaggerating liquid spread via slopes.

In general, fuel spills can be characterized as either continuously flowing or instantaneous (static). These characterizations are considered with respect to when the spill is ignited. In the case of a continuously flowing spill, ignition has occurred while the fuel is moving away from the source. For a static spill, the fuel nominally spreads to a maximum area and then is ignited, such that the flame spreads across the fuel surface. For a continuously flowing spill fire, the flame may spread across the fuel surface initially, but the flame front is ultimately controlled by the spread of the fuel over the substrate until steady-state burning conditions occur.

The area of a continuously flowing spill that is not burning will continue to increase until a physical boundary is reached or the source of the release is exhausted. A continuous spill that is burning will have a steady-state spill size based on a balance between the volumetric flow rate and the volumetric burning rate of the fuel. This concept is developed later in the section "Fire Size."

For a confined pool, the area, A, is dictated by the boundaries, and the pool depth, δ, can be simply calculated based on the volume, V, of liquid:

$$\delta = \frac{V}{A} \tag{65.1}$$

For an unconfined spill, the area has typically been determined via Equation 65.1 with an estimate of the fuel depth. In the past, engineers have conservatively estimated spill depths based on the minimum depth required to support flame spread (see "Fire Growth Rate" section). The use of a minimum depth will result in the largest possible spill area that can support a flame, therefore, the largest possible fire.

Literature results provide a basis for estimating spill depths. Table 65.1 summarizes spill depths for both noncombustible liquids and combustible fuel spill fires on unconfined surfaces. Although the table shows a range of fluid depths, the data can be simplified when considering only a range of typical hydrocarbon fuels that are commonly associated with fire scenarios, as discussed below.

The most recent work of Benfer [7] and Mealy et al. [8], systematically evaluated spill depths for a range of liquids and substrates. The average spill depth for all liquid/substrate combinations evaluated by Mealy et al. [8] was 0.72 mm, which is consistent the previously cited data and the general rule proposed in the last edition of this handbook for estimating an unknown spill fire scenario. However, it should be noted that the range of spill depths measured by Mealy et al. and Benfer was from 0.12 up to 2.9 mm depending upon the specific liquid/substrate scenario. This relatively wide range of empirical depths demonstrates the importance of understanding key variables governing fluid spread such that an appropriate spill depth is used when performing an engineering analysis. The primary two factors governing the spread of a liquid and the spill depth are the surface tension of the liquid and the surface characteristics of the substrate.

Fundamental fluid dynamics and empirical data have clearly established that spill depth is a function of the surface tension of the liquid. Figure 65.1 shows this relationship based on the experimental results for a range of liquids. As can be seen in Fig. 65.2, the surface tension of different fuels from 10 °C to 50 °C ranges from 16 to 27 dyn/cm. Water based liquids will bound most fuels of interest, as can be seen in Table 65.1 and Fig. 65.1. The surface tensions of water

Table 65.1 Summary of fixed-quantity, unconfined liquid spill data

Reference	Fuel	Quantity of fuel	Spill depth	Spill area	Surface
Chambers [2]	JP-4	4–189 L (1–50 gal)	1.1–2.9 mm	3–65 m^2	Concrete runway
Gottuk et al. [3]	Water	3.8–30 L (1–8 gal)	1.1–3.4 mm	1–11 m^2	Smooth, unfinished concrete and tile floor
Gottuk et al. [3]	6 % AFFF	3.8–19 L (1–5 gal)	0.6–1.1 mm		Smooth, unfinished concrete
Gottuk et al. [4]	JP-8	2–3 L (0.5–0.8 gal)	0.7–1.1 mm	2.1–3.1 m^2	Smooth concrete with polyuethane coating
Purtorti et al. [5]	Gasoline	0.25–1 L (0.07–0.26 gal)	0.5–0.7 mm	0.4–1.8 m^2	Wood parquet and vinyl tile
Modak [6]	#2 fuel oil	0.005–0.030 L	0.22 mm	0.0075–0.04 m^2	Both epoxy-coated concrete and steel (spill depths were the same for both surfaces and were independent of the volume of liquid spilled.)
	Lubricating oil		0.34 mm		
	Motor oil		0.75 mm		
	Hydraulic oil		0.84 mm		
Benfer [7]	3 % AFFF	0.2–450 mL	0.17–0.65 mm	0.01–1 m^2	Smooth, unfinished concrete
	6 % AFFF		0.22–0.67 mm		
	Water		0.95–2.9 mm		
	Gasoline		0.22–0.64 mm		
	Denatured alcohol		0.12–0.77 mm		
Mealy et al. [8]	All	0.25–20 L (0.07–5.2 gal)	0.72 + 0.34[a]	0.2–30 m^2	Smooth, unfinished concrete/ smooth concrete with polyurethane coating/brushed concrete/plywood/oriented strand board/vinyl tile
	3 % AFFF		0.43 + 0.15[a]		
	3 % FP Foam		0.97 + 0.53[a]		
	Lubricating Oil		1.54 + 0.55[a]		
	Gasoline		0.71 + 0.15[a]		
	Kerosene		1.01 + 0.10[a]		
	Denatured Alcohol		0.79 + 0.17[a]		
	All[b]		0.66 + 0.18[a]		Coated concrete
			0.53 + 0.08[a]		Smooth concrete (sample 1)
			0.53 + 0.20[a]		Smooth concrete (sample 2)
			0.76 + 0.26[a]		Brushed concrete
			0.63 + 0.26[a]		Vinyl flooring
			1.02 + 0.41[a]		Plywood
			1.04 + 0.51[a]		Oriented strand Board

[a]Values presented are average spill depths measured during multiple tests with one standard deviation
[b]All fuels noted for Mealy et al. reference, excluding lube oil

is 73 dyn/cm and AFFF has a value of approximately 15–16 dyn/cm at temperatures of 15–32 °C [9]. Figure 65.1 shows results for 3 % aqueous film forming foam (3 % AFFF) concentrate and a 3 % fluoro-protein foam concentrate (3 % FP) with surface tension of 17 and 27 dyn/cm, respectively.

Given that the surface tension of most fuels is relatively similar (i.e., 20–27 dyn/cm); this parameter is generally not as influential when

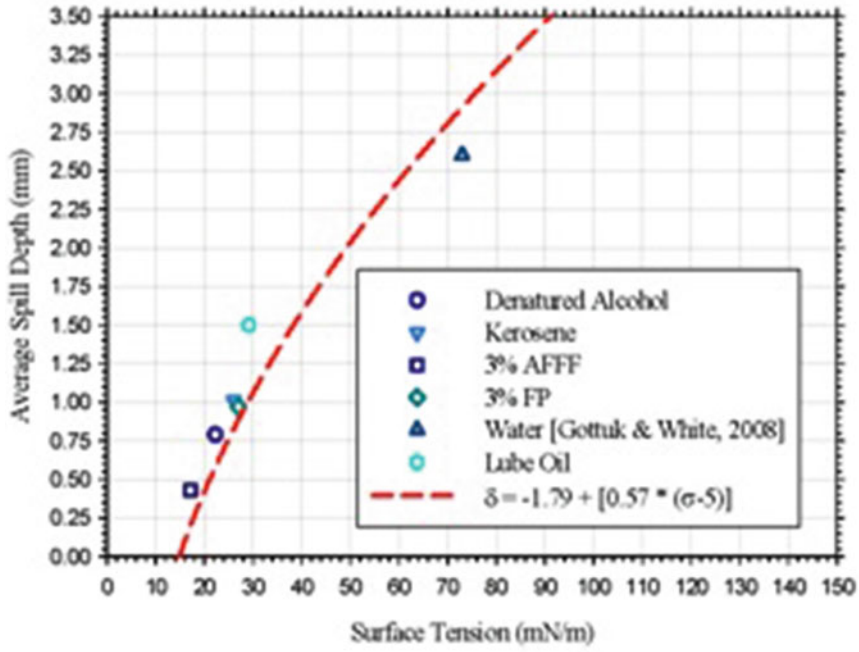

Fig. 65.1 Relationship between average spill depth and liquid surface tension [8]

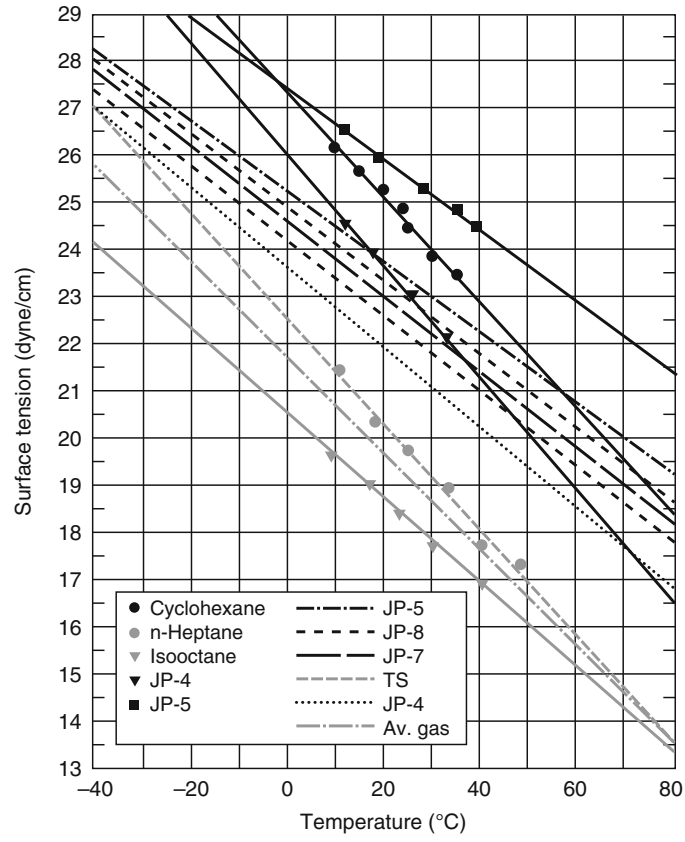

Fig. 65.2 The effect of temperature on surface tension of hydrocarbon liquids (Data taken from Moran et al. [9] and CRC [10])

considering the characteristics of a fuel spill (i.e., average depth variation of 0.71–1.01 for fuels excluding lube oil, which has a surface tension above 27) (see Fig. 65.1). The more dominant variable is the surface topography which can play a larger role in the extent of spread and the spill depth. The impact of substrate on spill depth is shown in Table 65.1. The roughness and uniformity of a substrate will dictate the speed and extent to which a liquid spreads and, thus, the equilibrium spill depth. For rougher, non-uniform surfaces, deeper equilibrium spill depths will be achieved due to the fuel being unable to spread to its full potential. Deeper spill depths result in longer burning durations with higher peak mass burning rates (i.e., larger fires). It is for this reason, from a spill dynamics standpoint, that an understanding of the surface on which a spill occurs is typically more important than understanding the fuel that was spilled.

Although from an ideal fluid dynamics point of view [8], there should be no dependence of spill depth on spill quantity, empirical data as well as transient spill models (Raj et al., 1974 and Grimaz et al., 2007) indicate that some dependence exists. These inconsistencies are an artifact of the variability in the surface characteristics that are not accounted for in the theoretical solution using ideal smooth, flat surfaces. Figure 65.3 shows the spill areas per unit volume and spill depths from spilling 0.5, 5.0, and 20 L of 3 % AFFF and 3 % FP on smooth concrete [8]. The measured area per unit volume for these scenarios consistently decreased with increasing fuel spill quantity, which is indicative of an increasing trend in spill depth. The JP-4 fuel spill data of Chambers [2] (Table 65.1) shows a similar trend for spills on a concrete runway, but with higher depths; the area per volume of fuel spilled decreased from 0.88 to 0.34 m^2/L for spills ranging from 4 to 190 L with a corresponding increase in spill depth from 1.1 to 2.9 mm. Due to limited experimental data, this data by Chambers provides the best estimate of upper limit fuel depths for large quantity spills at a time of 120 s. Spill depths of upwards of 3.4 mm were also noted for spills of water up to 30 L (where water has a surface tension of 73 dyn/cm compared to most fuels, which are below 27).

Total spill area will also be dictated by time until the liquid spread reaches the maximum area. Various spread models can be used for estimating this transient period; however, the use of idealized substrates will impact the results [8]. Based on the results from extended duration spill tests [8] with liquids (3 % AFFF, 3 % FP and gasoline) of 0.25–0.5 L spilled on smooth, impermeable surfaces (i.e., coated concrete and vinyl), the spill area was at least 90 % of the maximum spill area by 300 s. At 30 s, the spill area was approximately 50 % of the maximum steady-state area. This transient development period can have an impact on the resulting fire size

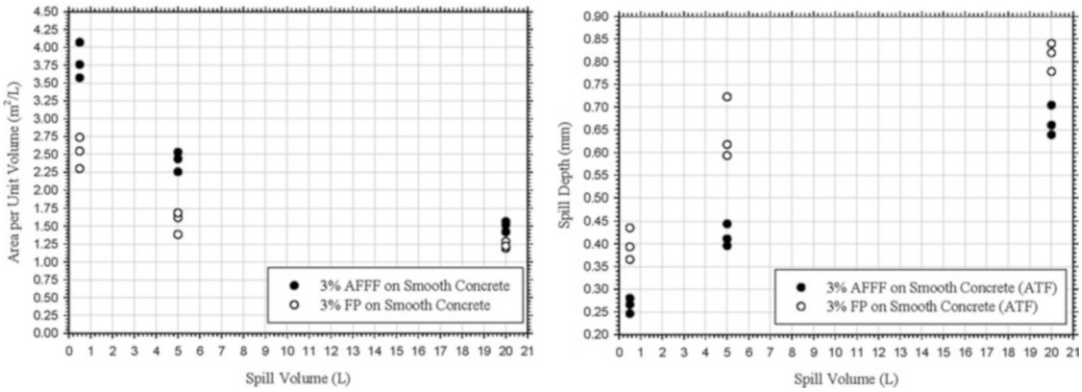

Fig. 65.3 Comparison of area per unit volume (*left*) and spill depth (*right*) to various quantity spills of 3 % AFFF and 3 % FP on smooth concrete (surface tension of 17 and 27 (dynes/cm, respectively))

based the time of ignition compared to the time to reach the maximum spill area [8].

For similar test on coated concrete, vinyl, and smooth concrete, lube oil exhibited a slightly different trend then the other liquids, reaching 75–90 % of the total spill area in the initial 30-s. This larger fraction is attributed to the high viscosity of the liquid relative to all other liquids. The high viscosity of the lube oil inhibits the spread of the liquid beyond the initial spill area.

Spills on rough/absorbent surfaces or spills involving fluids with high viscosities, generally achieve a large fraction of their spill area potential soon after being spilled. The lack of fluid spread after the initial spill can be attributed to several different factors including; the physical characteristics of the substrate impeding the movement of the fluid, the absorbency of the substrate removing liquid from the bulk flow of fluid thus reducing the spill area potential, or the internal forces within the liquid (i.e., viscosity) inhibiting the spread of the spilled volume.

As can be noted in Table 65.1, there is quite a bit of variability in spill depths for smaller quantities of fluid. The larger variability of depths for smaller spill quantities is attributed to the greater dependency on multiple variables, such as the initial spill height, surface features, and fluid properties. An example of the variability in spill depths is shown in Fig. 65.4, which presents the 6 % AFFF solution and water data of Fig. 65.1. For the water, depths varied for releases at different heights and different quantities. However, this effect was not observed for releases of the 6 % AFFF solution. Figure 65.4 also shows that similar water spills on vinyl tile floor produced the same spill depths as released on smooth concrete. Modak [6] reported that for very small spills of various oils (see Table 65.1) on steel and epoxy-coated concrete, the spill areas (and depths) were the same for both substrate materials. However, spill areas were smaller for untreated concrete due to fuel absorption into the substrate surface. This is similar to the trends observed by Mealy et al.

In summary, spill depths for liquids can vary significantly based on a number of factors ranging from the type of liquid and substrate, the volume spilled, the time frame and other spill parameters. However, as a general rule for common fuels, a spill depth of 0.7 mm can be used with reasonable confidence. Based on the work of Mealy et al. [8], the differences in calculated mass burning rates resulting from the use of an average spill depth of 0.7 mm as opposed to a substrate specific mass burning rate value were generally small and highly dependent upon the

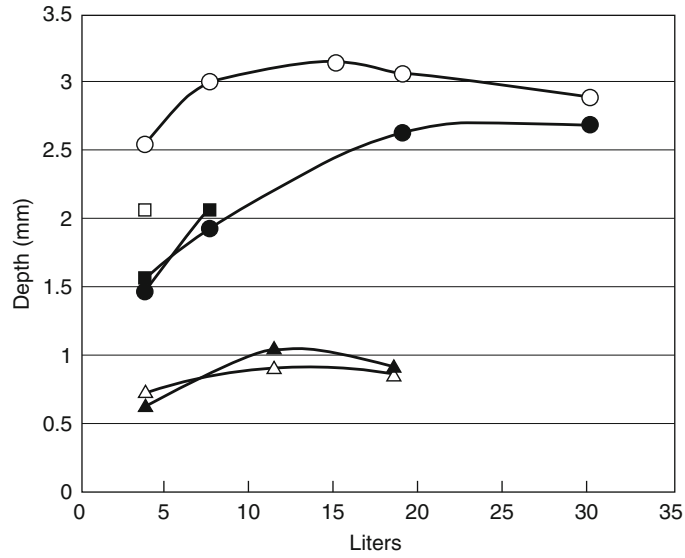

Fig. 65.4 Spill depths for 6 % AFFF solution and water releases on smooth concrete and tile floors for various fuel volumes and release heights: [3] AFFF on concrete from 0.6 m (△), AFFF on concrete from 1.0 m (▲), water on concrete from 0.6 m (○), water on concrete from 1.0 m (●), water on tile floor from 0.15 m (□), and water on tile floor from 0.9 m (■)

quantity of fuel spilled. The use of the 0.7 mm spill depth approximation as opposed to a substrate specific spill depth for spills greater than 1 L (0.26 gal), will provide baseline mass burning data that is accurate to within 10 %.

Based only on the few tests by Chambers [2] for JP-4 fuel spilled on a concrete runway, large quantities of fuel (~38 L (10 gal) and more) may result in deeper spill depths of upwards of 3 mm. This greater depth can be used as a bounding value in a fuel spill fire analysis when a longer lasting but smaller fire is worth evaluating compared to using a depth of 0.7 mm. Equation 65.4 summarize the rule of thumb for fuel depths, $\boldsymbol{\delta}$:

$$\boldsymbol{\delta = 0.7 \text{ mm for most fuels and conditions}} \tag{65.2a}$$

$$\boldsymbol{\delta = 2.9 \text{ mm for quantities of 38 L(10 gal) where analysis warrants longer duration fires}} \tag{65.2b}$$

If a more accurate estimate is needed, then Table 65.1 and reference [4] should be used to provide guidance.

It is also interesting to note that Chambers [2], Gottuk et al. [3], and Putorti et al. [5] observed increases in burning fuel spill areas after the liquid spill was ignited. Fires increased the initial fuel spill area by 22–89 % for fuel releases ranging from 2 to 190 L. The practical implication of this increase in spill area is that the fires may be substantially larger than would be predicted per the initial fuel spill areas. However, the larger area would also result in much shorter burning times before the fuel is consumed. Since the last edition of this chapter, additional work by Mealy et al. [8] showed that there was no measurable increase in burn area compared to initial spill area on non-combustible surfaces for spills up to 20 L.

Fire Growth Rate

The temperature of the spilled liquid relative to its flashpoint is the single most important factor in identifying the flame spread rate over the surface of the liquid. The flame spread rate, in turn, determines the heat release rate history of the growing fire. Other factors also affect the flame spread rate, including the depth of the spilled liquid, size of the spill, type of liquid, and the substrate.

Generally, hazard assessments involving flammable, liquid pool fires require a conservative characterization of the fire growth rate history, peak burning rate, and fire duration. The purpose of the hazard assessment often defines that only a subset of these parameters are required. Peak burning rate and maximum burning duration at the peak burning rate are typically relevant to fire effects such as fire exposure to building elements, ignition of other fuel targets, or general environmental conditions that result from the fire.

The characterization of the spill or pool fire heat release rate history from ignition to peak burning rate (full involvement of pool fuel surface area) is important when dealing with time-related concerns or events. Examples of time-dependent concerns include egress or life safety conditions, activation of detection or suppression systems, spread of fire to other fuel packages, or failure of building elements. Presuming that one is interested in the pool fire heat release rate growth history, this can be defined as the integration of the flame spread rate for the particular geometry in question (e.g., circular for unconfined pools, rectangular for trenches) multiplied by the burning rate per unit surface area for the given liquid. Estimating the flame spread rate over the surface of the flammable/combustible liquid spill becomes critical in characterizing the fire growth history.

Most ignitions of flammable liquid fuels result in flame spread that can be characterized by one of two major flame spread mechanisms for liquid fuels: liquid phase-controlled flame spread or gas phase-controlled flame spread. Flame spread rates for these two regimes can be grossly benchmarked: 1–12 cm/s for liquid phase-controlled flame spread and 130–220 cm/s for gas phase-controlled flame spread. A third regime for flammable liquid spills on porous surfaces can be defined where flame spread rates are measured in terms of cm/min. For some hazard analyses, identifying the appropriate flame spread region may sufficiently characterize the flame spread rate in a conservative fashion. The primary driver of the flame spread regime is the temperature of the spilled liquid relative to its flashpoint.

Basic Theory of Flame Spread on Liquids

Flame spread on liquid fuels has been widely studied in small-scale experiments and theoretical studies [11–29]. The flame spread rates are known to be dependent on fuel temperature and fuel flashpoint. Below the flashpoint temperature, the flame spreads by way of surface tension-induced flow of hot fuel ahead of the advancing flame. Above the flashpoint, the flame spread is by way of gas phase spread, which can be as rapid as 2 m/s. The majority of liquid flame spread studies have been limited to pure fuels, and most of the studies have used alcohol fuels in trays less than 10 cm wide. The majority of liquid flame spread studies have been focused on pure fuels with heavy emphasis on alcohol fuels in trays less than 10 cm wide. This chapter includes empirical data from nonpure hydrocarbon fuels [30] as well as data from large-scale studies [8, 31].

Flame Spread Regimes Several flame spread regimes have been identified in the literature. These flame spread regimes are most notably a function of the liquid temperature. The dependence of flame spread rates on liquid temperature has been studied by a number of investigators [11–27]. The most extensive work has been done with narrow pans of alcohol fuels with fuel depths of 2–5 mm. These investigations indicate that the flame spread velocity is a strong function of fuel temperature, even when the fuel temperature is well below the flashpoint. Figure 65.5 shows the extensive work that Akita [14] conducted using methanol in a 2.6-cm-wide pan. Akita observed a number of different flame spread regimes. Above the flashpoint, spread was via the gas phase. Below the flashpoint, he

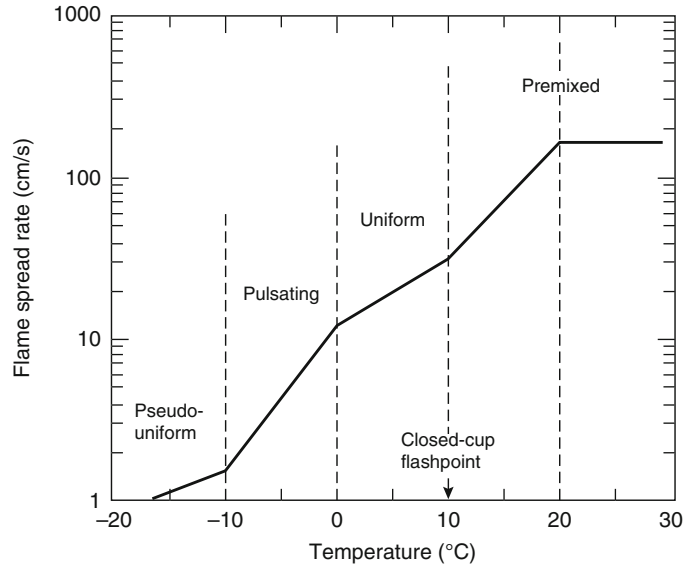

Fig. 65.5 Flame spread rate on 1-cm-deep methanol as a function of fuel temperature in a 2.6-cm-wide pan [14]

observed regions of uniform, pulsating, and pseudo-uniform spread. The mechanistic explanations for these phenomena below the flashpoint are not widely agreed upon. A more detailed discussion of flame spread regimes and their mechanisms can be found in the review article by Ross [32].

Semilog plots of flame spread rate as a function of liquid temperature have a characteristic shape with three regions: the liquid-controlled region, the gas phase–controlled region, and the asymptotic gas phase-controlled region. The slopes of the curve are different in each of these regions, and these differing slopes serve to define the regions. The transition from liquid to gas phase–controlled burning occurs at a temperature T_{go}; the transition from gas phase control to asymptotic gas phase spread occurs at a temperature T_{gm}. Figure 65.6 graphically portrays these temperatures with respect to flame spread rates. Figure 65.6 is intended as a conceptual depiction and the omission of units on the axes is intentional.

Figure 65.6 is conceptually the same as a figure first described by Glassman and Hansel [33]. In their paper, they identified the temperature at which gas phase-controlled flame spread begins as the firepoint of the liquid; they also identified the temperature at which the maximum flame spread rate occurs as the stoichiometric temperature (the liquid temperature at which the vapor concentration at the surface is stoichiometric). While this interpretation is consistent with the interpretation of data for multicomponent fuels, in light of Glassman and Dryer [19], it is not practical to define a firepoint temperature for a multicomponent fuel. The difficulties are due to the need to model evaporation of many high-volatility components in a multicomponent fuel during the open heating that is required in the determination of a firepoint. Determination of the firepoint of a multicomponent fuel would require closed-cup heating of a fuel to a test temperature, exposing the liquid surface, and applying an ignition source. If the fire does not continue, the test temperature is below the firepoint. Additional temperature tests would be required until the firepoint temperature is bracketed to the desired accuracy. This process is not practical. Similarly, for a multicomponent fuel it is not always practical to define the stoichiometric temperature, since determination of the vapor pressure of each component is, at the least, tedious and often impossible. Thus, while Glassman and Hansel's definitions are not easily generalized to multicomponent fuels, their pure fuel concepts can still provide guidance and

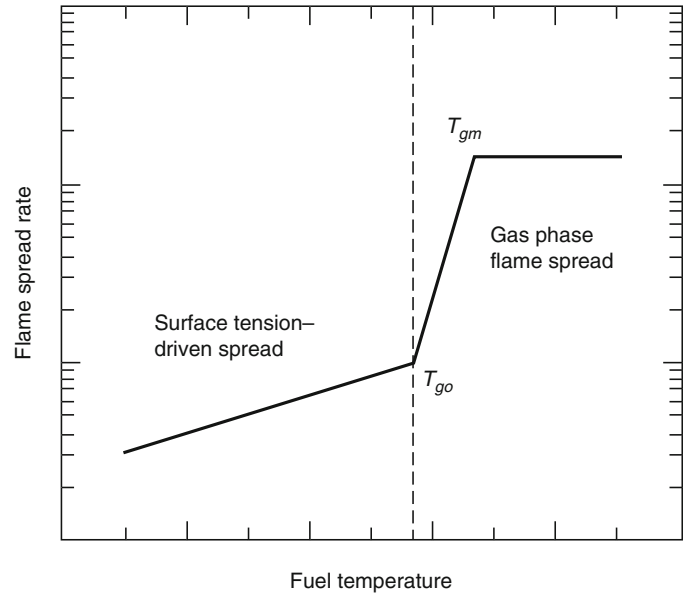

Fig. 65.6 Graphic representation of the definitions of T_{go} and T_{gm}

motivation for the interpretation of multicomponent liquid fuel flame spread results.

Pool Dimensions The physical dimensions of a liquid fuel spill or pool influence the flame spread rate, assuming an ignition source is present. The primary factors of importance are pool depth and characteristic width of the pool, as discussed below.

Pool dimensions, including fuel depth, have no effect on the flame spread rate for situations where the flame spread mechanism is considered gas phase-controlled. However, the depth of a flammable liquid does have a significant impact on the flame spread rate for liquid phase-controlled burning. In general, the average flame spread velocity for liquid phase-controlled spread increases with fuel depth, which is primarily governed by whether the fuel release is confined or unconfined.

Scientific study of liquid flame spread can be traced back as far as the 1930s [11]. Most of the early work was done on relatively small-scale test setups, much using pans only 1–6 cm wide with alcohol fuels at depths of 2–5 mm [12–14]. Work by Mackinven, Hansel, and Glassman [15] at Princeton is especially relevant here because it involved extensive experiments with decane, a pure fuel with similar characteristics to aviation fuels and other low-flashpoint multicomponent hydrocarbon fuels that are common to fire hazard assessments. The Princeton research documented the effects of pan width and fuel thickness on observed flame spread rates [15].

Several investigators have performed experiments to characterize the impact of fuel depth on liquid-controlled flame spread. Mackinven et al. [15] demonstrated the systematic variation of flame spread rates with fuel depth. They investigated decane fuel depths from 1 mm to 2 cm and found the flame spread rate to increase with fuel depth as shown in Fig. 65.7. This increase can be attributed to the retarding effect of small fuel depths on liquid recirculation flows that cause flame spread. Calculations by Torrance [16, 17] are in excellent agreement with Mackinven et al.'s experimental data shown in Fig. 65.7. These calculations indicate that decane flame spread rates increase with pool depth up to 3 cm, with greater fuel depths beyond this no longer increasing the flame spread rate. Of course, fuel depths for unconfined fuel spills will always be far less than 3 cm. Investigations by Mackinven et al. [15] as well as Burgoyne and Roberts

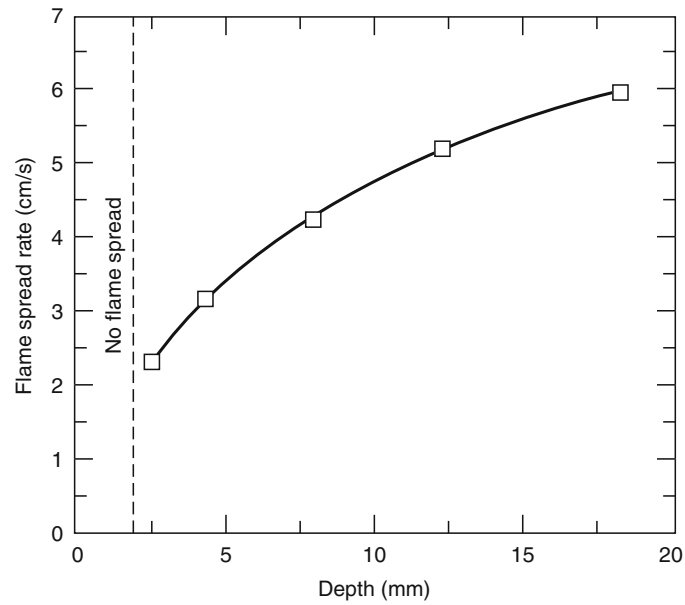

Fig. 65.7 Flame spread rate on decane as a function of fuel depth [15]

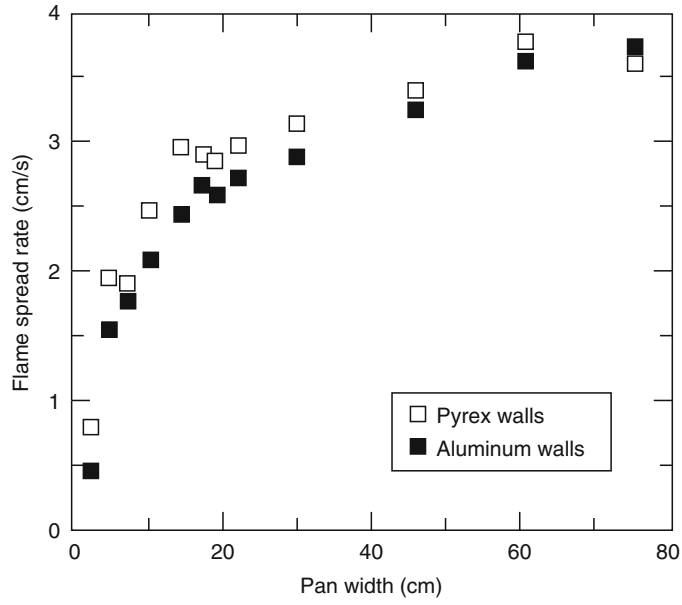

Fig. 65.8 Flame spread rate on decane as a function of pan width [15]

[12, 13] indicate that flames do not spread away from the ignition source in liquid pools at or less than 1.5 mm deep. More recent work by Burelbach, Epstein, and Plys [34] demonstrated that the limiting fuel thickness for flame spread was 2.0 mm for decane and 2.3 mm for dodecane. Minimum fuel depths for flame spread are for the liquid-controlled spread regime. There is no evidence for fuel depth or pan width effects on gas phase flame spread [12, 14, 18, 20, 23, 25].

Mackinven et al. [15] found that for pan widths up to 20 cm the flame spread rates on decane are a strong function of pan width. At pan widths from 20 to 80 cm, the maximum width they studied, they observed only slight increases in flame spread rate. Their results are shown in Fig. 65.8. Both aluminum and glass pan walls were used. The small differences between these two wall materials may be attributed to heat conduction effects; however, the major influence at pan widths less than 20 cm is independent of wall material and has been attributed to a momentum reduction associated with viscous drag on the walls. The relative independence of pan width above 20 cm indicates that flame radiation is not a pivotal mechanism in determining liquid phase-controlled flame spread. The results were confirmed by Mackinven et al. by shielding the liquid ahead of the flame from flame radiation during flame spread experiments (20- to 80-cm-wide pans). They observed modest changes in flame spread rates between the shielded and unshielded experiments.

Temperature Effects The work of Burgoyne and Roberts [12] showed that at small pan widths the temperature dependence of the flame spread rate is a function of the pan width as shown in Fig. 65.9. Unfortunately, their work extends only from 2.5 to 6.3 cm widths. The dependence on pan width disappears above 41 °C, the flashpoint of isopentanol. The work of Mackinven et al. [15] using varying pan widths (see Fig. 65.8) with decane 21 °C below the closed-cup flashpoint (44 °C) as well as work by Burgoyne and Roberts [12] indicates that pan width ceases to have an impact on the temperature dependence of the flame spread rate at pan widths greater than 20 cm.

Flame spread experiments above the flashpoint indicate that flame spread is via the gas phase. The flame spread rate increases rapidly from the flashpoint to the liquid temperature at which a stoichiometric fuel-air mixture exists above the liquid surface. Above this temperature, the flame spread rate is no longer temperature

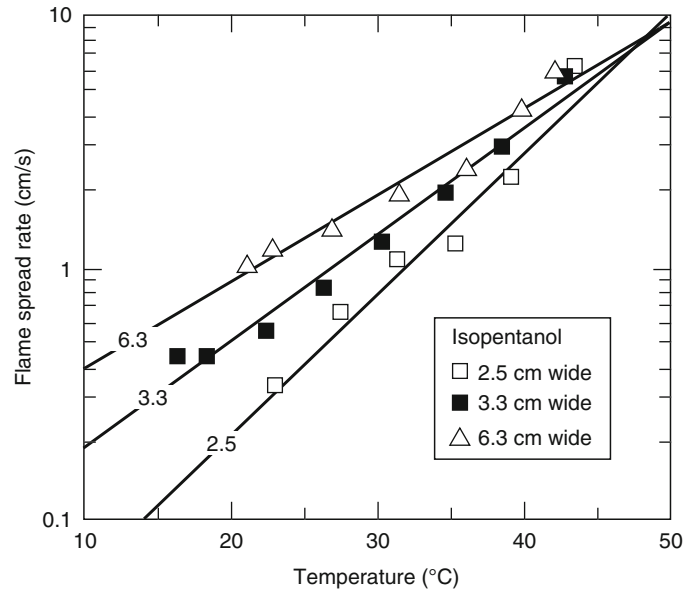

Fig. 65.9 Effect of pan width on the temperature dependence of flame spread rate on isopentanol [12]

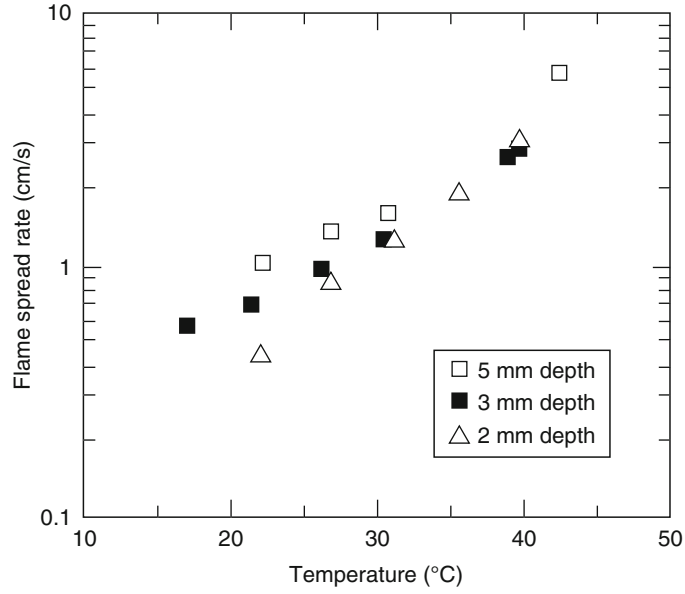

Fig. 65.10 Effect of fuel depth on the temperature dependence of flame spread rate on isopentanol [12]

dependent. The flame spread velocities measured by Burgoyne and Roberts [12], Akita [14], Nakakuki [20], and Hirano et al. [25] in this temperature region are from 1.3 to 2.2 m/s depending on the fuel. These velocities are similar to flame spread rates measured in stratified fuel-air mixtures found near ceilings of mine tunnels [35–37].

The work of Burgoyne and Roberts also indicates that the temperature dependence of the flame spread rate is a function of the fuel depth [12]. They investigated isopentanol at fuel depths of 2–5 mm and their results, shown in Fig. 65.10, indicate that variations in flame spread rate with fuel temperature below the flashpoint (41 °C) are lessened by increasing fuel depth.

Empirical Data

An overview of the experimental results for flame spread velocities follows, including alcohol fuels, multicomponent hydrocarbon fuels, and blends of multicomponent hydrocarbon fuels. Although the bulk of the data is for laboratory-scale pools, there is limited data for large-scale pools of hydrocarbon fuels as well as some data for large-scale spills of jet fuel (hydrocarbon).

White, Beyler, Fulper, and Leonard [30] measured flame spread rates for aviation fuels, mixtures of these multicomponent hydrocarbon fuels, as well as 1-pentanol (alcohol). These measurements were made over a range of fuel temperatures in a pan 20 cm wide by 163 cm long. The results for pure JP-5 and JP-8 are shown in Figs. 65.11 and 65.12. The flame spread rates range from 3 to 140 cm/s over a temperature range of 10–90 °C. The solid symbols indicate liquid-controlled flame spread and the open symbols indicate gas phase flame spread. JP-5 is a high-flashpoint kerosene used by the U.S. Navy that has a specified minimum flashpoint of 60 °C [38]. JP-8 is a newer U.S. Air Force fuel, very similar to commercial Jet A-1, that is a kerosene with a lower specified minimum flashpoint of 38 °C [39]. The flame spread rates in the liquid-controlled regime for JP-8 are 0.5–2 cm/s greater than for JP-5. At temperatures approximately 12–20 °C above the closed-cup flashpoint, flame spread rates increase very rapidly to over 100 cm/s. The major difference in flame spread characteristics of JP-5 and JP-8 is the temperature at which the flame spread rate rapidly increases: 68 °C for JP-5 and 58 °C for JP-8.

Figure 65.12 shows several data points where the application of the ignition source was systematically varied from 3 to 460 s in the most sensitive temperature region (the transition between liquid-controlled and gas phase–controlled flame spread). At higher and lower temperatures such ignition delays have little or no effect on the observed flame spread rate. Assuming that the flame spread rate is a function of the liquid temperature relative to the flashpoint temperature, the results are consistent with an increase in the flashpoint of approximately 10 °C during the 3–460 s between fuel discharge and ignition. No systematic study of flashpoint variations with time for multicomponent fuels appears elsewhere in the literature.

The flame spread results for JP-5 and JP-8 indicate that the single most important determinant of flame spread is the initial temperature of the liquid prior to ignition relative to the fuel's

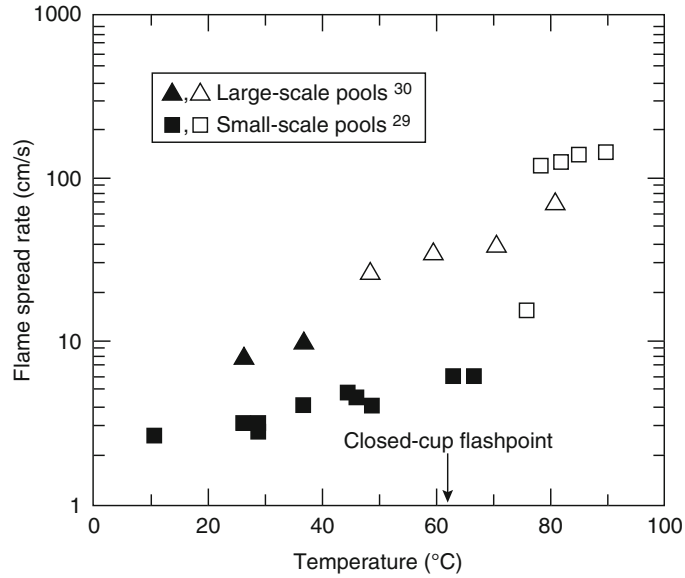

Fig. 65.11 Flame spread rate for JP-5 as a function of temperature. *Solid symbols* denote liquid-controlled flame spread and *open symbols* denote gas phase flame spread for small-scale data only

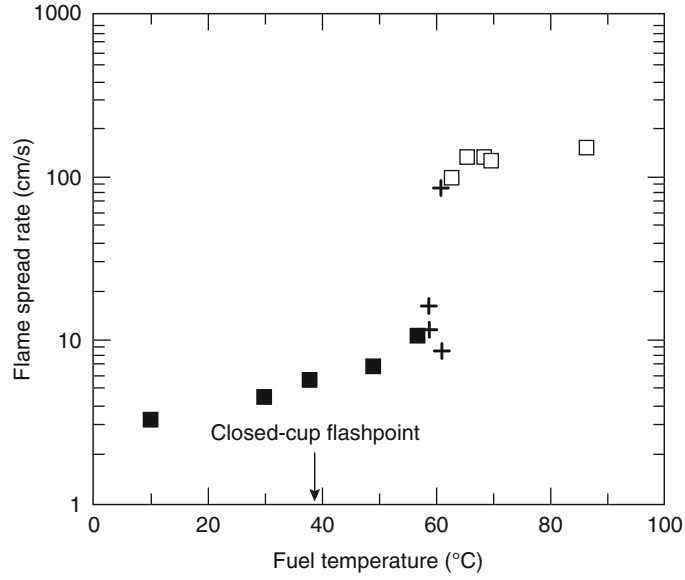

Fig. 65.12 Flame spread rate for JP-8 as a function of temperature. *Solid symbols* denote liquid-controlled flame spread and *open symbols* denote gas phase flame spread; + indicates variable times to ignition of 3, 160, 240, and 460 s. The normal time to ignition is 35 s. Longer ignition times reduce the flame spread rate [30]

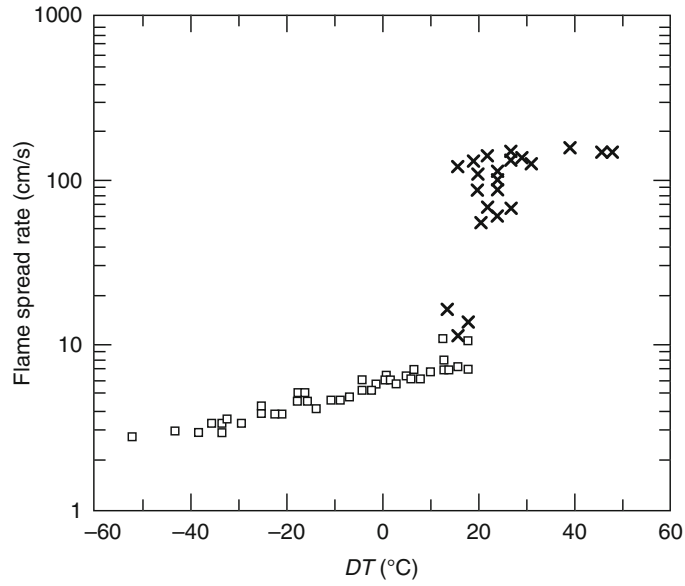

Fig. 65.13 Flame spread rate for all JP fuels as a function of $DT(T_{fl} - T_l)$ [30]

flashpoint. Hillstrom [18] also observed this correlation and found that plotting the flame spread rate as a function of the temperature difference between the closed-cup flashpoint, T_{fl}, and the liquid fuel temperature, T_l, correlated data for a number of hydrocarbon fuels. Figure 65.13 shows flame spread rate data for pure JP-5, pure JP-8, and mixtures of the two fuels plotted as a function of $DT(T_{fl} - T_l)$. In Fig. 65.13 square symbols represent liquid-controlled flame spread and the *X* symbols indicate gas phase flame spread. The treatment of the data effectively correlates all of the jet fuel data over a range of *DT* from −50 °C to +50 °C. This representation of the data clearly shows the importance of *DT* $(T_{fl} - T_l)$ in determining flame spread rate.

Figure 65.13 also shows excellent consistency in the transition from liquid-controlled flame spread to gas phase spread at $DT = 18$ °C.

Leonard et al. [31] performed large-scale flame spread experiments as part of an effort to evaluate the fire hazards of mixed jet fuels on aircraft carrier flight decks. The experiments, which evaluated pure JP-5, pure JP-8, and mixtures of these two jet fuels, were carried out in a large-scale pan 1.52 m in width by 12.2 m in length. The Leonard et al. experiments are the largest pool fire flame spread experiments reported in the literature. The jet fuels were evaluated over a range of temperatures by introducing heated fuel into the large pan, which was also temperature controlled by circulation of water through chambers on the underside of the pan bottom. The results for JP-5 are presented in Fig. 65.11. The results for JP-8 are illustrated in Fig. 65.14.

The large-scale results can easily be compared with small-scale results in both Figs. 65.11 and 65.14. This comparison yields identical qualitative results. The flame spread rates for the large-scale tests are notably higher for both the JP-5 and JP-8 liquid-controlled flame spread tests. Data for the JP-8 tests indicate that the liquid-controlled flame spread rate is 10–11.6 cm/s whereas the JP-5 tests show 8.2–10 cm/s in this regime. As with the small-scale tests, there is approximately 1.5–1.8 cm/s difference between the two jet fuels, with the JP-8 fuel slightly faster. The transition to gas phase flame spread appears to occur at a lower temperature for both fuels. Similar gas phase flame spread velocities are obtained between small- and large-scale tests. The disparity between the small- and large-scale tests for these two fuels cannot be attributed to a single factor. It is speculated that the difference in flame spread behavior of the two experimental data sets may be due, in part, to width effects and flame radiation effects. Further work is necessary to identify the specific mechanisms responsible for this observed difference.

A recent set of experiments evaluating aircraft hangar fire detection technologies [8] included large-scale jet fuel spill fires. The work of Hill, Scheffey, Walker, and Williams [8] evaluating alternative fire protection methods for U.S. Air Force aircraft hangars represents the largest spill fires evaluated in the literature for flame spread. A volume of 114 L (30 gal) of JP-8 was spilled on a concrete pad. The main focus of this research was fire suppression systems, and an important aspect evaluated was the impact of various suppression systems on the flame spread rate after system activation. Experiments measured the flame spread rate over the large

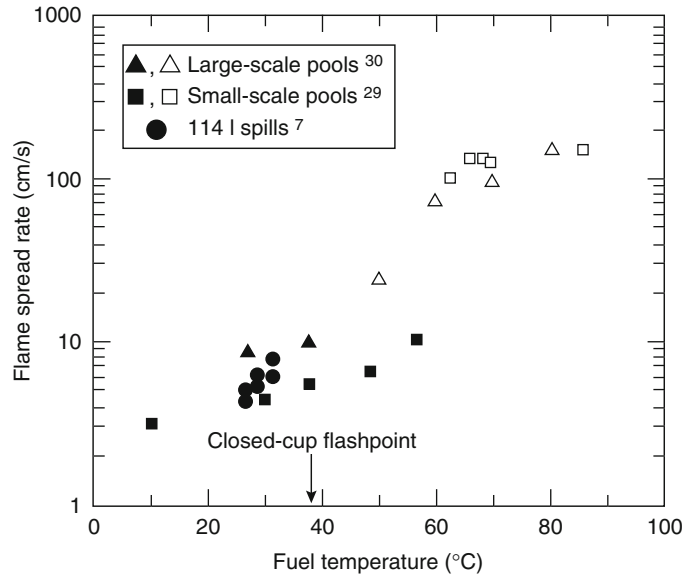

Fig. 65.14 Flame spread rate for JP-8 as a function of temperature. *Solid symbols* denote liquid-controlled flame spread and *open symbols* denote gas phase flame spread

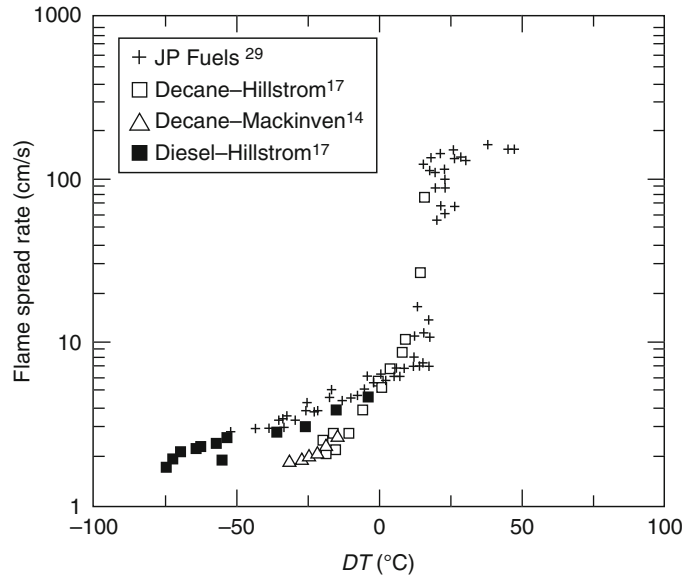

Fig. 65.15 Comparison of JP fuel data with other hydrocarbon flame spread data from the literature

spill area, which covered approximately 30 m^2 at the time of ignition, both before and after operation of the suppression system. The full free-burn spill size was on the order of 37 m^2 with time for complete burnout at roughly 2 min. Measured flame spread rates for the JP-8 spills prior to suppression system activation have been identified in Fig. 65.14. The temperature of the JP-8 fuel was approximately 25 °C ± 2 °C. These flame spread rates fall close to the data points from the small-scale tests. The Hill et al. data points show a 1.5–3.5 cm/s increase over the small-scale data for the liquid-controlled flame spread results. The large-scale spill data show higher flame spread rates in comparison to the small-scale pool experiment data.

Although there are depth issues associated with the comparison of pool experiments to spill experiments, the trend appears to be that larger-scale flame spread experiments yield higher flame spread rates for the liquid-controlled flame spread regime with a transition to gas phase spread occurring at a lower temperature than observed in the small-scale pool experiments. While these differences may not be fully explainable, it is important to note that irrespective of the experiment scale, peak flame spread rates for the liquid-controlled flame spread regime are approximately 10 cm/s for JP-5 and 12 cm/s for JP-8. Furthermore, although the transition to gas phase spread seems to occur at a lower temperature, the maximum gas phase flame spread rates are maintained in the 120–200 cm/s range for both JP-5 and JP-8. Support for using a maximum flame spread velocity of 10 cm/s for liquid-controlled flame spread over hydrocarbon fuels can be drawn from Fig. 65.15, which shows a comparison of the jet fuel data from White et al. [30] and other hydrocarbon data from the literature. The results of the jet fuels were consistent with those of Hillstrom [18] and Mackinven et al., [15], which show a very modest variation in flame spread rate below the flashpoint temperature. Figure 65.15 shows a comparison between the jet fuel data of White et al., [30], the decane data from Hillstrom [18], the diesel fuel data from Hillstrom [18], and the decane data from Mackinven et al. [15]. The decane results show a rise in the flame spread rate at a smaller value of *DT* than for the JP fuels. Also, below the closed-cup flashpoint, the decane shows lower flame spread rates. This variation may be due to the effect of using a water substrate in the decane tests rather than steel as used in the jet fuel work. All the data in Fig. 65.15 were collected in 20-cm-wide pans.

Empirical data for flame spread over alcohol pools consist of small-scale test data. White et al. [30] performed the largest experiments, utilizing a 20-cm-wide pan evaluating 1-pentanol as part of their study. Results from these 1-pentanol flame spread tests, illustrated in Fig. 65.16, were performed to assess the effect of fuel type on flame spread for an alcohol fuel that had a similar flashpoint to the jet fuels primarily under study in this specific piece of work. Pentanol was chosen, in part, due to the previous pentanol flame spread work performed by Burgoyne and Roberts [12].

Liquid-controlled flows were observed at temperatures less than 52 °C. The change from liquid-controlled flame spread to gas phase flame spread occurred at approximately 4 °C above the closed-cup flashpoint. Figure 65.16 illustrates a comparison of the 1-pentanol results from White et al. [30] with the alcohol data from Burgoyne and Roberts [12]. The 1-pentanol results take on the same characteristic dependence on *DT*, with the Burgoyne and Roberts data showing rapid rise in the flame spread rate at somewhat lower values of *DT* than the 1-pentanol data. The slope difference between the Burgoyne and Roberts data and the 1-pentanol data for the liquid-controlled flame spread regime can be attributed to the effect of pan width on the temperature dependence of flame spread rate in this regime. It is very interesting to note that in Fig. 65.16 the data for alcohol flame spread are similar to the hydrocarbon data with respect to the maximum of 10 cm/s liquid-controlled for flame spread rates with the gas phase flame spread rates falling between 150 and 200 cm/s.

Table 65.2, reproduced from White et al. [30] shows the closed-cup flashpoint, T_{fl}, the transition from liquid to gas phase-controlled burning, T_{go}, and the transition from gas phase control to asymptotic gas phase spread, T_{gm}, for the small-scale jet fuel data, the 1-pentanol data, and the decane data from Hillstrom [18]. The difference $T_{go} - T_{fl}$ averages 15 °C for the hydrocarbon fuels. The difference $T_{gm} - T_{go}$ averages 6 °C and the overall difference $T_{gm} - T_{fl}$ averages 21 °C. These results may be expected to represent general properties for small hydrocarbon pools but should not be used for alcohol fuels.

Glassman and Dryer [19] have pointed out some discrepancies in the measurement of flashpoints and firepoints of alcohols versus hydrocarbons and the relevance of flashpoints to the hazards of liquid fuels. Although each of the standard flashpoint/firepoint testing methods has its own difficulties, it is clear from the work

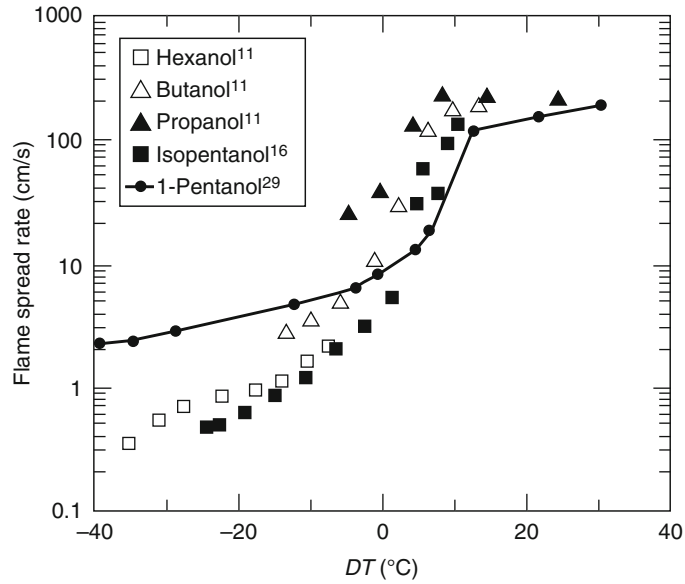

Fig. 65.16 Comparison of the 1-pentanol data with the alcohol (Data of Burgoyne and Roberts [12])

Table 65.2 Critical temperatures (°C) for flame spread [30]

Fuel	T_{fl}	T_{go}	$(T_{go} - T_{fl})$	T_{gm}	$(T_{gm} - T_{go})$	$(T_{gm} - T_{fl})$
JP-8	39	57	18	62	5	23
25/75 JP-8/5	42	60	18	66	6	24
50/50 JP-8/5	48	65	17	72	7	24
75/25 JP-8/5	54	68	14	74	6	20
JP-5	63	76	13	79	3	16
Decane [5]	44	56	12	62	6	18
Average 1–6	—	—	15	—	6	21
1-Pentanol	48	52	4	62	10	14

of Glassman and Dryer that none of the standard flashpoint testing methods correlate with the onset of gas phase flame spread for all fuels. Glassman and Dryer point out major differences between alcohol and hydrocarbon flashpoints and point to the large quenching diameter for these two classes of fuels. Based on Glassman and Dryer's observations, transition to gas phase flame spread would be expected at temperatures near the closed-cup flashpoint for alcohol fuels, as observed for the 1-pentanol test results.

However, there are differences in $T_{go} - T_{fl}$ between jet fuels and decane. The more volatile aviation fuels are characterized by $T_{go} - T_{fl} \sim 18\ ^\circ\text{C}$ while decane and JP-5 are characterized by $T_{go} - T_{fl} \sim 12\ ^\circ\text{C}$. This 6 °C difference may be due to the loss of light ends from the more volatile hydrocarbon mixtures and is consistent with the variations in flame spread rate with ignition time delay represented in Fig. 65.12. White et al. point out that it appears that the actual flashpoint of the JP-8 may have increased by approximately 6 °C during the discharge and ignition delay period. While this deduction seems reasonable, a more systematic study of this issue is warranted. The important consideration for hazard analyses is that multicomponent hydrocarbon fuels can incur a reduction in effective flashpoint depending on the volatility of the fuel and the time period between the fuel release and ignition. The conservative approach would be to assume instantaneous ignition of the released fuel.

Fuel-soaked beds of porous media (e.g., small beads of glass or metal) have been used in flame spread experiments to simulate a fuel spill onto a porous surface. Flame spread over porous media generally occurs at rates on the order of 1–8 cm/min, which is similar to measures of flame spread over the surface of relatively thick solids. Takeno and Hirano [40] have experimentally evaluated several parameters important to characterizing the flame spread rate over porous media soaked with fuel. Figure 65.17 represents the results from their study. Table 65.3 identifies the conditions of each experiment portrayed in Fig. 65.17.

These tests used a steel tray 3.5 cm wide and 60 cm long that was filled with either glass or lead beads. Four observations can be made from these data: (1) the flame spread velocity increases slightly as the diameter of the beads, d, increases and there appears to be little dependence on the liquid viscocity (see Fig. 65.17, conditions A, B, C) for 90 % by volume of decane and 10 % hexane; (2) the flame spread for pure decane is a function of the bead diameter and the viscosity (conditions E, F, G, H) with the flame spread velocity decreasing as d increases for smaller values of d, reaching a minimum flame spread rate at approximately $d = 0.25$ cm, from which point the flame spread velocity increases with d, and fuel viscosity effects are more pronounced with flame spread rate decreasing as the viscosity of the fuel increases; (3) for situations where the liquid level is below the top surface of the bead bed (conditions J, K), flame spread velocities are reduced and depend little on bead diameter or fuel viscosity; (4) when the glass beads are replaced with lead beads (conditions D, I, L), similar variations are observed as with the glass beads; however, the flame spread rates are reduced by approximately 10 %. In general,

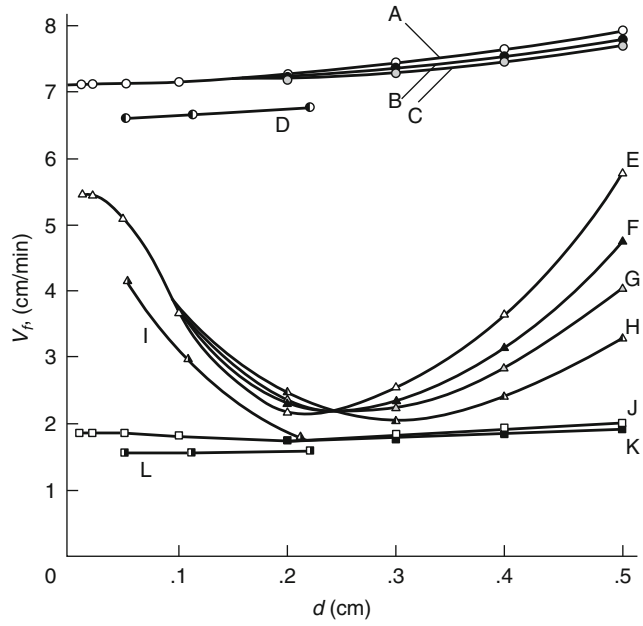

Fig. 65.17 Variations of flame spread rate with bead diameter [40]. Table 65.3 lists conditions

the flame spread rates for pure decane ranged from 2 to 6 cm/min whereas the mixtures of 90 % decane/10 % hexane spanned 7–8 cm/min.

Ishida [41] has also investigated fire growth on fuel-soaked ground with a rectangular pan using central ignition. The shallow square steel tray measured 50 · 50 · 2 cm deep. The tray was filled with glass beads. Radial flame spread rates were measured for decane fuel over varying bead diameters. Figure 65.18, which reproduces Ishida's results, demonstrates that the average flame spread velocity decreases as the bead diameter increases. It is also interesting to note that the flame spread rate accelerates as the fire size increases. The average flame spread rate over the duration from a 2 cm flame diameter to a 30 cm diameter ranges from 6 to 10 cm/min for the bead diameters investigated.

Using Flame Spread Velocities to Characterize the Rate of Involvement of a Pool or Spill

Characterizing the fire growth rate history of a fuel release fire is dependent on describing the time-dependent history of the area involved with fire. The flame spread rate must be placed in the context of the fuel release geometry as well as the location of the ignition point. Thus, the geometry of the released fuel and the relative location of the ignition source define the framework for characterizing the area of involvement.

An example for a circular pool of fuel follows. A circular pool with the ignition source in the center yields the most rapid involvement of the entire fuel release. Assuming that uniform spread occurs, a circular fire will develop and the area of the pool involved will be a function of the fire radius:

$$A_{\text{fire}} = \pi r^2 \tag{65.3}$$

where A_{fire} is the area of the fire in m^2 and r is the radius of the fire in m at any given time, t (s). Assuming a constant flame spread velocity, the radius of the burning area can be defined as

$$r = vt \tag{65.4}$$

where v is the flame spread velocity in m/s. Substituting Equation 65.4 into Equation 65.3:

$$A = \pi v^2 t^2 \tag{65.5}$$

Table 65.3 Experimental conditions of fuel-soaked beds presented in Fig. 65.17

	Combustible liquid	Viscosity μ (cp)	Material of beads	Initial liquid level y_s (cm)	Symbol
A	90 % decane + 10 % hexane	0.846 (normal)	Glass	0.0	○
B	90 % decane + 10 % hexane	2.617	Glass	0.0	●
C	90 % decane + 10 % hexane	4.552	Glass	0.0	○
D	90 % decane + 10 % hexane	0.846	Lead	0.0	◐
E	Pure decane	0.846	Glass	0.0	△
F	Pure decane	2.617	Glass	0.0	▲
G	Pure decane	4.552	Glass	0.0	△
H	Pure decane	6.872	Glass	0.0	△
I	Pure decane	0.846	Lead	0.0	▲
J	Pure decane	0.846	Glass	–0.5	□
K	Pure decane	4.552	Glass	–0.5	■
L	Pure decane	0.846	Lead	–0.5	◨

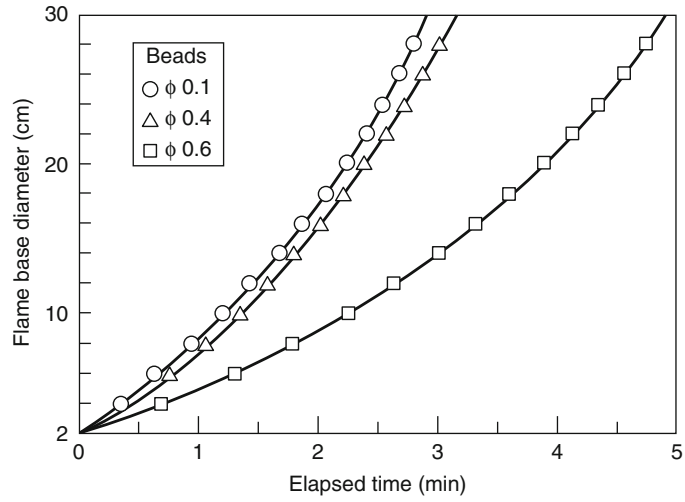

Fig. 65.18 Diameter of flame pillar base as a function of elapsed time [41]

In this manner, Equation 65.5 can be used to identify the area of the spill involved at any time subsequent to the ignition. Assuming that the mass burning rate per unit area is at a constant value $\dot{m}'' = \dot{m}''_{\max}$ and does not change as a function of time, a t^2 fire develops. Of course the time limit is defined when the fire involves the maximum area of the spill and this limit can be defined as follows:

$$t_{A,\max} = \frac{r_{A,\max}}{v} \tag{65.6}$$

where $t_{A,\max}$ is the time the entire pool surface becomes involved with fire, and $r_{A,\max}$ is the maximum radius of the fuel release.

A similar approach can be applied to a rectangular trench. Assuming an ignition source at one end of the trench, an alternative example can be developed. The trench geometry area is defined as

$$A = wl \tag{65.7}$$

where w is the width of the trench in m and l is the length of the trench involved with fire in m. Assuming w is small compared to l and that the ignition source at one end of the trench spans the width of the trench and that the flame spread rate is constant, the length of trench involved is

$$l = vt \tag{65.8}$$

Substituting Equation 65.8 into Equation 65.7 yields the time-dependent area of the trench involved:

$$A = wvt \tag{65.9}$$

In this manner, Equation 65.9 can be used to identify the area of the trench involved at any time subsequent to the ignition at one end. Assuming that the mass burning rate per unit area is at a constant value $\left(\dot{m}'' = \dot{m}''_{\max}\right)$ and does not change as a function of time, a t^1 fire develops. Of course the time limit is defined when the fire involves the maximum area of the trench and this limit can be defined as follows:

$$t_{A,\max} = \frac{l_{\max}}{v} \tag{65.10}$$

where $l_{\max}$ is the maximum length of the trench.

This type of approach can be used for other fuel release configurations and ignition source locations. The heat release rate is then the area of the fuel release involved multiplied by the burning rate per unit area as well as the heat of combustion. This relationship is explained in more detail in the following section.

Fire Size

The fire size is primarily characterized by the heat release rate and the flame height. The heat release rate, $\dot{Q}$, is calculated as

$$\dot{Q} = \dot{m} \cdot \Delta h_c \tag{65.11}$$

where $\dot{m}$ is the mass burning rate of the fuel and Δh_c is the fuel heat of combustion. The fuel mass burning rate can be calculated via Equation 65.12 or 65.13 as follows:

$$\dot{m} = A \cdot \dot{m}'' \tag{65.12}$$

where A is the spill fire area and $\dot{m}$ is the mass burning rate per unit area (kg/m^{2}s),

$$\dot{m} = A \cdot \dot{y} \cdot \rho \tag{65.13}$$

where $\dot{y}$ is the fuel burning regression rate (m/s) and ρ is the density of the fuel. The regression rate is the rate at which the fuel surface descends in a vertical direction as it burns; values are often reported in units of mm/min and therefore must be converted to m/s for the above calculations. Both, $\dot{m}''$ and $\dot{y}$ are empirically based values that are related per Equation 65.14:

$$\dot{m}'' = \dot{y} \cdot \rho \tag{65.14}$$

The literature has presented data for both parameters and both are presented below. The most commonly referenced database was developed by Blinov and Khudiakov [42] for pool fires and presented by Hottel [43] as shown in Fig. 65.19, which shows the regression rate and flame height results for various fuels burning in a broad range of pan sizes, 0.004–23 m in diameter. The data indicate that the fuel regression rate is approximately constant at 4 mm/min for all fuels tested burning as confined pool fires with diameters greater than 1 m. For smaller diameter fires, there is considerable difference in regression rates for the fuels presented. Hottel [43] discusses the trends in the burning rate data based on the balance of heat transfer to the fuel.

For fire sizes greater than about 1 m in diameter, the dominant mode of heat transfer to the liquid is via radiation from the plume. For smaller sizes, heat conduction from the pan (walls) or the substrate and convective heat transfer will constitute a larger fraction of the heat transferred to the liquid, thus having a larger effect on the burning rate of the fuel. Hottel [43], Burgess, Strasser, and Grumer [44], and Burgess, Grumer, and Wolfhard [45] present detailed discussions on these heat-transfer effects. At larger diameters (typically 1–2 m), the burning fuel regression rate tends to level out at a constant maximum value, $\dot{y}_{\max}$. For these pools in the radiation dominant region, Burgess et al. [44] with the U.S. Bureau of Mines correlated the maximum regression rates of various single-component burning fuels (pan fires) based on the thermochemistry of the liquids as follows:

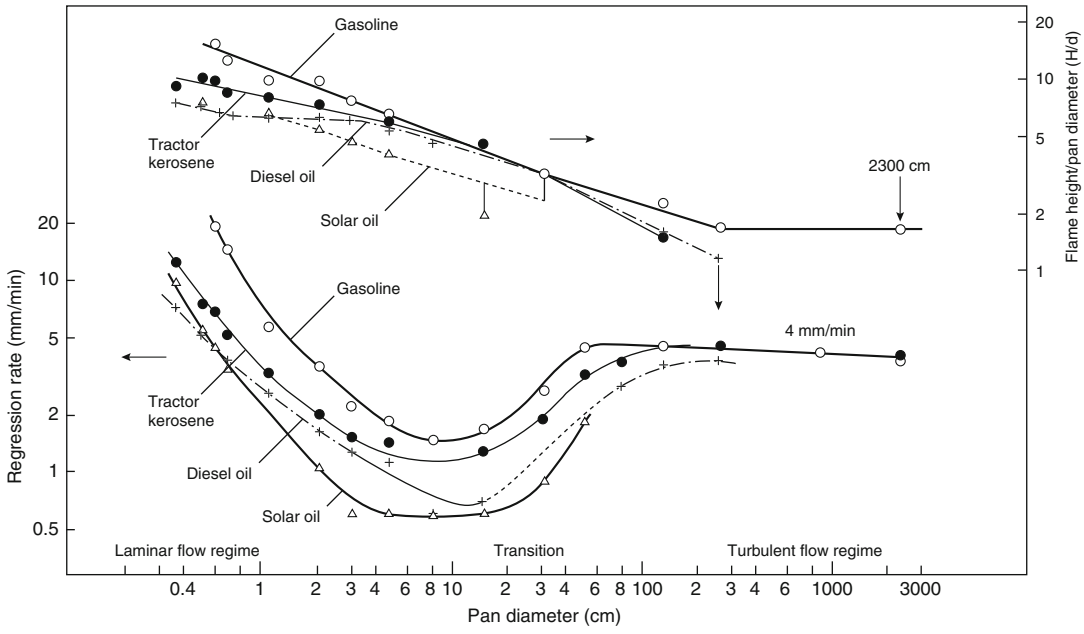

Fig. 65.19 Regression rate and flame height data for liquid pools (From Blinov and Khudiakov [42])

$$\dot{y}_{\max} = 1.27 \times 10^{-6} \frac{\Delta h_c}{\Delta h_{v,\text{sen}}} (\text{m/s}) \qquad (65.15)$$

where Δh_c is the heat of combustion and $\Delta h_{v,\text{sen}}$ is the sensible heat of vaporization, calculated as

$$\Delta h_{v,\text{sen}} = \Delta h_v + \int_{T_0}^{T_b} C_p dt \qquad (65.16)$$

where

Δh_v = Heat of vaporization at the boiling point, T_b

C_p = Specific heat of the liquid fuel

T_o = Initial temperature of the liquid

The use of the sensible heat of vaporization accounts for the temperature dependence of the regression rate, which will vary appreciably (up to tens of percent) from the value calculated using only Δh_v. As the correlation expressed by Equation 65.15 suggests, the fuel regression rate is not constant for all fuels at larger diameters as indicated for the limited fuels in Fig. 65.19. Based on a broad range of hydrocarbon pan fires, Zabetakis and Burgess [46] fit Equation 65.15 to the data shown in Fig. 65.20. The fit is quite good except for the cryogenic fuels, liquefied natural gas and liquefied propane gas. It is noted that the data apply to single-component fuel fires burning in unvitiated air under calm conditions (e.g., no wind).

Further work by the Bureau of Mines researchers, Grumer et al., [48], suggested that the regression rate for blended fuels can be represented by the same correlation (Equation 65.15) when the heats of combustion and vaporization are presented as shown in Equation 65.17 for each component of the fuel.

$$\dot{y}_{\max} = 1.27 \times 10^{-6} \left[\frac{\sum_{i=1}^{N} n_i \Delta h_q}{\sum_{i=1}^{N} n_i \Delta h_{vi} + \sum_{i=1}^{N} m_i \int_{T_0}^{T_b} C_p(T) dt} \right] \qquad (65.17)$$

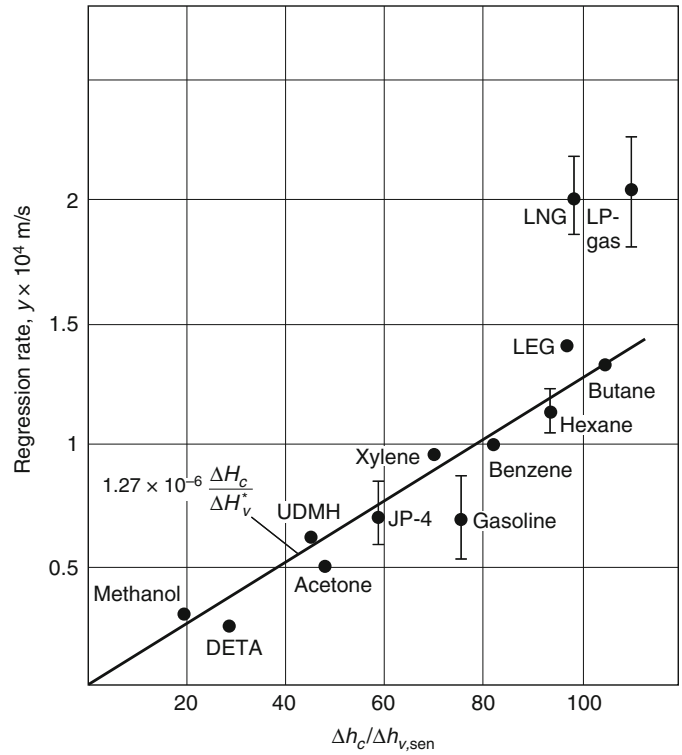

Fig. 65.20 Burning fuel regression rate plotted versus thermochemical properties of fuels burning as pan fires (Taken from Mudan [47])

where n_i and m_i are the mole fraction composition in the vapor and liquid phases, respectively.

A blended fuel with components of widely varying volatility will not burn at a uniform rate. Initially, the high volatile components will burn, and as time proceeds the burning will become more characteristic of the remaining lower volatile components. For blends such as gasoline that have components with similar heats of combustion and heats of vaporization and $n_i \approx m_i$ Equation 65.17 can be represented by

$$\dot{y}_{\max} = n_1 \dot{y}_1 + n_2 \dot{y}_2 + \ldots \qquad (65.18)$$

Equation 65.18 has been reported to yield good estimates of the regression rate for multicomponent fuel blends [48]. Even for blends with widely varying boiling points, Equation 65.18 provides rough estimates except for the initial and final stages of the fire.

Converting the regression rate data of Fig. 65.20 via Equation 65.14 allows the corresponding maximum mass burning rate per unit area, $\dot{m}''_{\max}$, to be plotted against the ratio of the heat of combustion to the heat of vaporization (Fig. 65.21). The fit to the data is represented by

$$\dot{m}''_{\max} = 1 \times 10^{-3} \frac{\Delta h_c}{\Delta h_{v,\,\text{sec}}} = \text{kg/m}^2\text{s} \qquad (65.19)$$

The fit of Equation 65.19 to the burning rate data is not as good as Equation 65.15 to the regression rate data. However, Equation 65.19 does cover a wider range of fuels, including the liquefied gases.

The regression rate is particularly useful for confined pool fires of significant depth. For many spills, particularly continuously flowing fuels, the more useful quantity is the mass burning rate per unit area. As noted in the previous discussion, the burning rate of pool fires with diameters greater than 0.2 m (see Fig. 65.19) increases with increasing diameter. Zabetakis and Burgess [46] developed the following relationship to represent the burning rate per unit area as a function of pool diameter, D:

$$\dot{m}'' = \dot{m}''_{\max}[1 - \exp(-k\beta D)] \qquad (65.20)$$

where the product $k\beta$ is represented as a single value. k is the extinction coefficient (m^{-1}) and ® is the mean-beam-length correction. The maximum steady-state burning rate per unit area, $\dot{m}''_{max}$, is also referred to in the literature by Babrauskas [49] as $\dot{m}''_{\infty}$, the mass burning rate for an infinite-diameter pool. If a confined pool is not circular, D is equal to the effective diameter, expressed as

$$D = \left(\frac{4A}{\pi}\right)^{1/2} \tag{65.21}$$

where A is the area of the pool.

Other than the data presented in Fig. 65.21, the most comprehensive collection of burning rate data has been compiled by Babrauskas [49] and is presented in Table 26.13 in Chap. 26, "Heat Release Rates." The correlation presented by Equation 65.20 agrees extremely well with the experimental data of some fuels, such as gasoline. The greatest disagreement occurs for alcohol fuels for which Babrauskas proposes a set of constant values for different diameter ranges (see Chap. 26) [50]. Due to difficulties in experimentally evaluating the cryogenic fuels, there tends to be more scatter in the data, and thus not as good a correlation with Equation 65.20 as seen for other hydrocarbon fuels.

The use of Equation 65.20 applies to confined pool fires burning in the open, under still-air conditions and in a vessel (e.g., pan or tank) without an excessive lip height [49]. The burning rate correlations presented have been developed from confined pool fire experiments. There generally has been limited data available for burning rates of unconfined fuel spill fires.

Gottuk et al. [4] conducted a series of JP-8 and JP-5 fuel spill fires on a smooth polyurethane-coated concrete slab, as used in Navy aircraft hangars. The spill fires consisted of both continuously flowing fuel releases (~0.4, 0.8, and 1.7 L/min) and 1–3 L of fixed quantities of fuel that were poured onto the concrete, allowed to spread

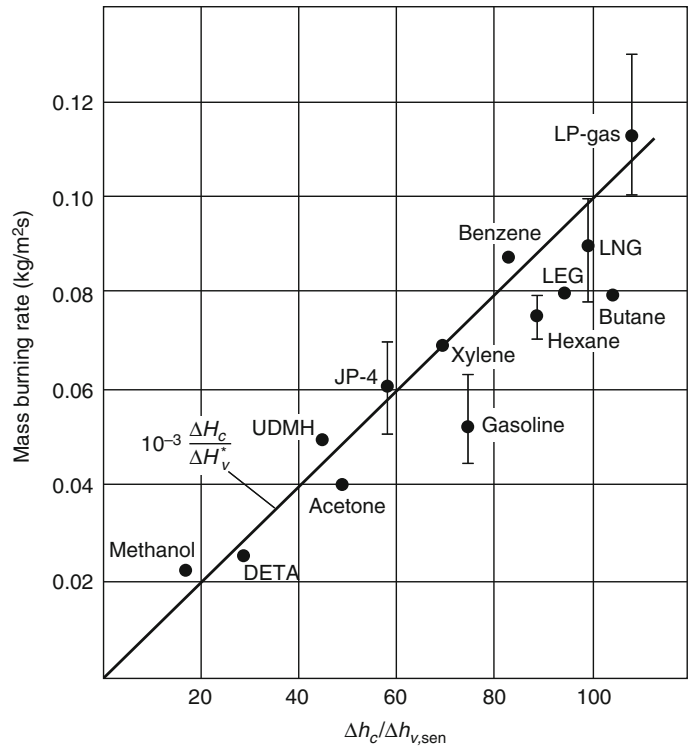

Fig. 65.21 Mass burning rate per unit area versus the thermochemical property of fuels burning as pan fires (Taken from Mudan [47])

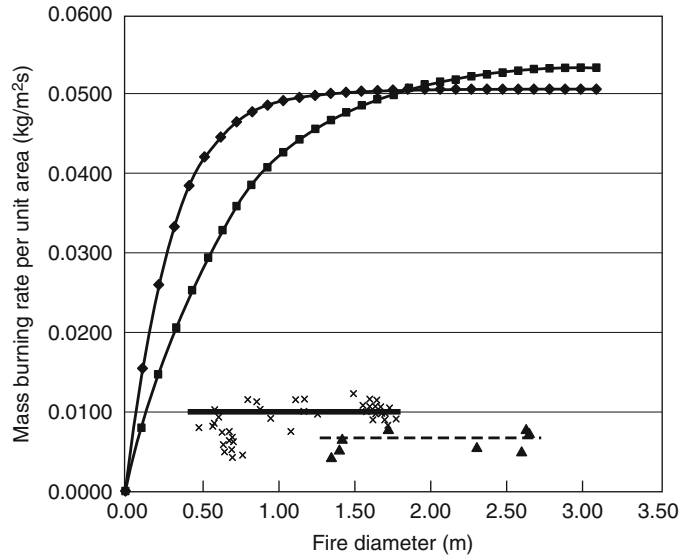

Fig. 65.22 Mass burning rates for unconfined JP-8 spill fires on concrete: [4] (x) denote 0.4–1.7 L/min continuous spill fires with an average value (—) for diameters >1.5 m; (▲) denote 1–3 L fixed-quantity spills with an average value (– – –) for diameters >1.5 m; the calculated pool fire burning rates per Equation 65.20 are shown for JP-4 (—◆—) and JP-5 (—■—)

to nearly a maximum size, and then ignited at the edge of the spill. The burning rate per unit area data for the unconfined spill fires are presented in Figs. 65.22 and 65.23 for both JP-8 and JP-5, respectively. Figures 65.22 and 65.23 show the experimentally measured $\dot{m}''$ for each test versus the measured diameter of the spill fires. Also included for comparison are the curves for burning rate for pool fires as calculated per Equation 65.20, using the data of Table 26.13. A curve for JP-8 does not appear in Fig. 65.22, due to a lack of experimental pool fire data. However, it is expected, based on fuel property data, that the burning rate curve for JP-8 is bounded by the curves for JP-4 and JP-5.

Putorti et al. [5] investigated gasoline spill fires on parquet and vinyl flooring substrates and various carpets. These fires consisted of fixed quantity (0.25–1.0 L) spills that were ignited approximately 60 s after release. Consistent with the results for the JP-8 and JP-5 spill fire data noted above [4], the burning rates for gasoline on the nonabsorbing materials were found to be one-fifth that of the maximum rate for pool fires (i.e., ~80 % reduction). Based on these limited fuel spill fire data, the previous edition of this chapter suggested that burning rates for unconfined liquid fuel spills be estimated as one-fifth of the maximum pool burning rate. At the time, the actual mechanism for this large difference was not known, but had been hypothesized to be primarily due to differences in heat transfer between the fuel and substrate for spills compared to deeper pools. Since the last edition of this chapter, work has shown this hypothesis to be incorrect [8].

A more recent test program conducted by Mealy, Benfer and Gottuk [8] has provided additional insight regarding the burning dynamics of unconfined fuel spills compared to pool fires. A series of tests evaluated the burning dynamics of multiple fuels (gasoline, kerosene, denatured alcohol), at various depths (0.5–20 mm), on multiple substrates (concrete, wood, vinyl, steel, water). Several different fuel supply scenarios were also considered: fixed quantity pool fires, continuously flowing spill fires, and fixed quantity spill fires. Based upon the testing conducted, the burning rate of a liquid fuel spill/pool fire was determined to be primarily dependent upon several factors, including, fuel depth, fuel supply duration and substrate.

Fuel depth was identified as a factor because it is directly related to the fuel supply duration for fixed quantity/fixed area fires (i.e., a pool fire). For these scenarios, a depth of 5 mm represents the minimum depth for which a peak, steady-state mass burning rate comparable to the

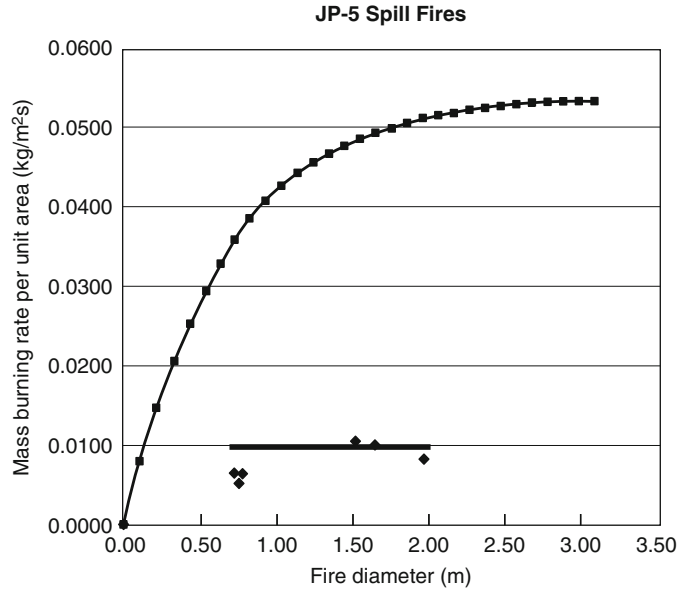

Fig. 65.23 Mass burning rates for 0.4–1.7 L/min unconfined JP-5 spill fires on concrete (◆) [4]. The average value for diameters >1.5 m is shown as (—); the calculated pool fire burning rate per Equation 65.20 is shown as (—■—)

diameter dependent maximum mass burning rate (see Equation 65.20) has sufficient time to be achieved. This was true for steel, water, concrete, and vinyl substrates. At depths less than 5 mm, the peak burning rates were consistently less than the diameter dependent maximum burning rate. This reduction in peak burning rate (also presented as heat release rate per unit area, HRRPUA, of fuel surface) can be seen in Fig. 65.24, which shows burning rates for six pan fires of gasoline with increasing fuel depths from 1 to 18 mm. As can be seen, until the depth reached 5 mm, the fire did not burn long enough to achieve the steady-state peak burning rate as achieved at the 18 mm depth, which burned for over 6 min. At the shallower depths approaching unconfined spill fires (~1 mm), the fires burned for less than a minute, which is typical for a spill fire.

The reduction in mass burning rate associated with a 1 mm fuel depth was on the order of 70–80 %, equivalent to the trends observed by the previous studies [4, 5] noted above. The results of spill fire tests are summarized in Table 65.4. Based upon the data collected, correlations were developed for both gasoline and kerosene that can be used to predict the reduction in peak mass burning rate as a function of fuel depth and fuel area:

$$C_\delta = 0.95^*\left(1 - e^{-0.71\delta}\right) \quad \text{for gasoline} \tag{65.22a}$$

$$C_\delta = 0.91^*\left(1 - e^{-0.58\delta}\right) \quad \text{for kerosene} \tag{65.22b}$$

where C_δ is the depth coefficient and δ is the calculated fuel depth (mm). However, to date, depth coefficient correlations have only been developed for gasoline and kerosene fuels. If depth coefficients for other fuels are required it is recommended that either Eq. 22a or 22b be used based on similar properties or an average coefficient of 0.69 be used for spill depths ≤5 mm and a coefficient of 1.0 be used for spill depths >5 mm.

The product of these depth correlations with the diameter dependent mass burning rate correlation (Equation 65.22) provides a more accurate prediction of mass burning rates for thin fuel layer fire scenarios:

$$\dot{m}''(D,\delta) = C_\delta^*\left(\dot{m}''_\infty\left(1 - e^{-k\beta D}\right)\right) \tag{65.23}$$

Although the 5 mm depth criterion is appropriate for all fixed quantity scenarios, the same is not true for continuously-fed fire scenarios. For continuous-fed spills, Mealy et al. maintained

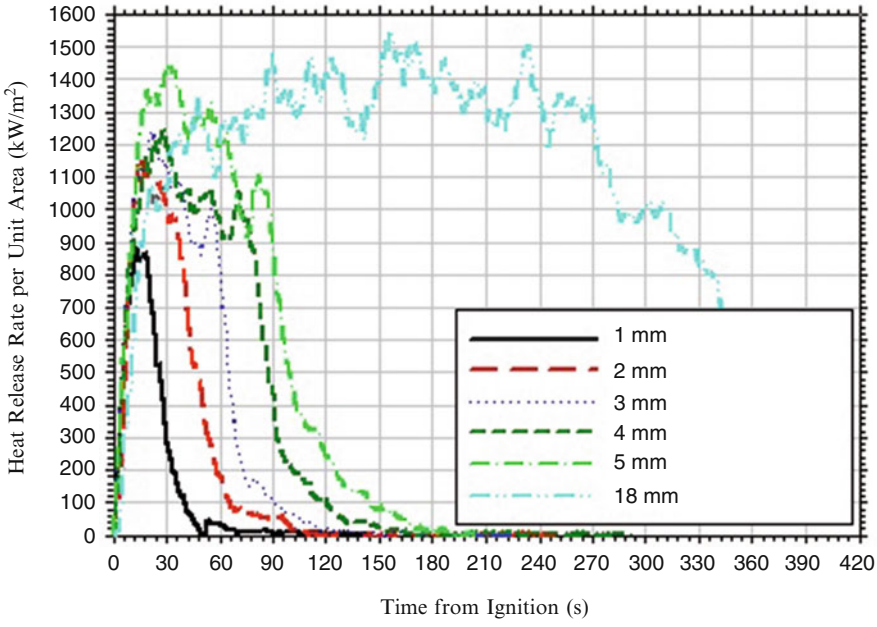

Fig. 65.24 Summary of HRRPUA data measured for gasoline on water in 1.5 m^2 (16 ft^2) pan fire tests with fuel depths of 1, 2, 3, 4, 5 and 18 mm

Table 65.4 Peak burning rates for unconfined fuel spill fires

Description	Peak mass burning rate per area (kg/m^2s)	Standard deviation	Reference
JP-8			
1–3 L spills	0.007[a]	0.0014	Gottuk et al. [4]
0.4–1.7 L/min spills	0.010[a]	0.0009	Gottuk et al. [4]
JP-5			
0.4–1.7 L/min spills	0.010[a]	0.0008	Gottuk et al. [4]
Gasoline	0.011	–	Putorti et al. [5]
Gasoline	0.016[b]	–	Mealy et al. [8]
Kerosene	0.010[c]	–	Mealy et al. [8]
Denatured alcohol	0.014[d]		Mealy et al. [8]

[a]Represents average for fires with diameters greater than 1.5 m burning for a maximum of 3 min
[b]Represents average for fires with diameters between 0.75 and 1.45 m
[c]Represents average for fires with diameters less than 0.75 m
[d]Represents average for fires with diameters less than 0.6–3.0 m

fuel depths on the order of 1 mm while still achieving peak mass burning rates that were comparable to the diameter dependent maximum mass burning rates. These results further demonstrate that it is not the depth of fuel that impacts the peak mass burning rate, but that it is the duration of fuel supply. If the fuel supply is sufficient to allow enough time to reach a steady-state, than the maximum mass burning rate is achievable. In addition to the impact of fuel supply duration on the burning rate of combustible fuels, specifically kerosene and diesel, the ignitability and flame spread potential of the fuel at thin depths is very small, making the fuel very challenging to ignite and burn in a thin depth spill scenario without a large external heat exposure.

An additional parameter identified as having an impact on the mass burning rate of a fuel was

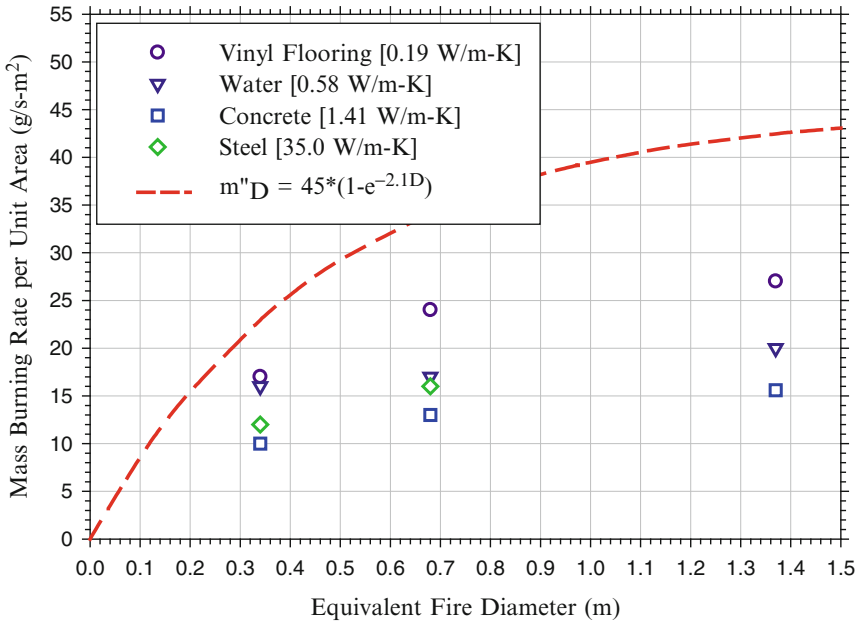

Fig. 65.25 Comparison of peak mass burning rates per unit area for 1 mm (0.04 in.) gasoline fires on substrates with various thermal conductivities (shown in *brackets*) [8]

the substrate on which the fuel is burning. However, the influence of the substrate was only found to be significant for fuel depths less than 5 mm. The data collected by Mealy et al. [8] showed differences in the mass burning rates of 1 mm depth liquid fuels burning on surfaces with differing thermal properties (Fig. 65.25). The rank order of the mass burning rates for each fire size were consistent with the highest burning rates occurring on vinyl flooring and the lowest on concrete. For the scenarios evaluated, no specific thermal property of the substrates (i.e., thermal conductivity, thermal inertia, thermal effusivity, and thermal diffusivity) could be directly correlated to the rank order of burning rates. In general, less thermally conductive materials (i.e., vinyl and water) produced mass burning rates higher than those achieved in tests with more thermally conductive substrates (i.e., steel and concrete). However, the ranking of mass burning rates with respect to the thermal conductivity of the substrates was not appropriate when evaluating the case of the concrete and steel. In this case, the mass burning rates measured on the concrete were consistently lower than those measured on the steel despite the fact that the thermal conductivity of steel is an order of magnitude larger than that of concrete. This discrepancy may be attributed to the reflectivity of the steel and the resulting re-radiation from the steel substrate to the fuel layer. This reflected heat would then be transferred into the fuel layer thus raising the mass burning rate of the fuel.

Empirical data has also shown that a delay in ignition time of a fixed quantity fuel spill can have a significant effect on the peak fire size obtained. Changing the ignition delay (i.e., the time between the spill and the ignition of the fuel) from 30 to 300 s produced an average reduction in fire size (burning rate) of approximately 50 % for 0.5 and 1 L gasoline and denatured alcohol spill fires [8]. The primary impact of longer ignition delay times is the result of shallower fuel depths due to a combination of larger spill areas and prolonged periods of evaporation. Given that most fuel spill fires nominally burn out in less than 1–2 min, longer ignition

delay times can lead to both lower peak heat release rates and shorter duration fire exposures that are quite fast events.

Based on Equations 65.11 and 65.12, the heat release rate of an unconfined spill or confined pool fire can be calculated per Equation 65.24 once the area of the fire is determined and an appropriate mass burning rate per area is identified.

$$\dot{Q} = \dot{m}'' \cdot A \cdot \Delta h_c \tag{65.24}$$

However, in the case of an unconfined, continuously flowing spill fire, the area is neither known a priori nor can it be calculated per any fuel depth correlations as with a fixed quantity spill. As fuel flows from a continuous source, the size of the resulting spill will continue to increase indefinitely until a physical boundary is reached or the fuel is ignited and burns. The transient nature of a continuous spill fire is very dependent on the timing of the fuel ignition and the flame spread rate relative to the fuel flow rate and size of the spill at the time of ignition. For example, if a continuously flowing spill is immediately ignited at the source, the fire size will be equal to the spill size if the flame spread rate is faster than the fuel spill spread rate. However, if the fuel spill spread rate is faster than the flame spread rate, the spill will continue to spread out ahead of the flame front.

As discussed below, a continuously flowing spill fire will reach a steady-state burning size, characterized by the equivalent steady-state diameter, D_{ss}. It is possible for a fuel spill to reach a diameter that is larger than D_{ss} before it is ignited. In this case, the flame will spread across the fuel surface to the larger diameter and then the spill fire will reduce in size until D_{ss} is reached. These examples are only several of multiple scenarios that can occur. Currently, complete and accurate models of burning fuel spills do not exist. In order to estimate the transient nature of a continuous fuel spill fire, the engineer must consider the fuel spill rate, the relative time of ignition, and the steady-state burning spill area.

The steady-state burning spill area, A_{ss}, results due to a balance between the volumetric flow rate of the liquid release, $\dot{V}_L$ (m^3/s), and the volumetric burning rate of the fire as described by

$$\dot{V}_L = A_{ss} \cdot \dot{y} = \frac{\pi {D_{ss}}^2}{4} \dot{y} \tag{65.25a}$$

or, alternatively in terms of the mass burning rate as

$$\dot{V}_L = A_{ss} \frac{\dot{m}''}{\rho} = \frac{\pi {D_{ss}}^2 \dot{m}''}{4\rho} \tag{65.25b}$$

The steady-state size of the spill can be explicitly solved by rearranging Equations 65.25a and 65.25b in terms of D_{ss} (m):

$$D_{ss} = \left(\frac{4\dot{V}_L}{\pi \dot{y}}\right)^{1/2} \tag{65.26a}$$

$$D_{ss} = \left(\frac{4\dot{V}_L \rho}{\pi \cdot \dot{m}''}\right)^{1/2} \tag{65.26b}$$

The calculation of the spill size per Equation 65.26 assumes that all fuel is burned from the spill; that is, there are no other losses of fuel from the spill, such as into a porous substrate. As noted by the examples above, D_{ss} does not necessarily correspond to the maximum fire size but equals the size of the fire once the burning rate becomes constant and equilibrium conditions are reached.

Empirical correlations can also be used to calculate the equivalent diameter of a continuous spill fire. Mansfield and Linley [51] developed a correlation for the burning spill diameter as a function of fuel flow rate for large release rate fires on concrete. The following correlation was developed for 568–2271 L/min (150–600 gpm) continuous spill fires of JP-5 ranging in size from 15 to 24 m in diameter:

$$D_{ss} = 134\left(\dot{V}_L\right)^{1/2} : D_{ss}\,(\mathrm{m}) \text{ and } \dot{V}_L\left(\mathrm{m}^{3/5}\right) \tag{65.27a}$$

$$D_{ss} = 3.5\left(\dot{V}_L\right)^{1/2} : D_{ss}\,(\mathrm{ft}) \text{ and } \dot{V}_L(\mathrm{g\,pm}) \tag{65.27b}$$

where 1 m^3/s = 15,850 gpm.

The tests of Mansfield and Linley [51] were conducted outside with 2.2–12.5 m/s (5–28 mph)

winds and ambient temperatures ranging from 7 °C to 32 °C. Using Equation 65.25b with the diameter and spill rate data of Mansfield and Linley [51], the mass burning rate per unit area of the large JP-5 continuous spill fires is calculated to be in the range of 0.055 kg/m^{2}s, which agrees with the pool fire burning rate data reported by Babrauskas [50] in Table 26.21 of this handbook. As noted above, despite typical spill depths of about 1 mm and less, continuous flowing spill fires will reach the peak (steady-state) mass burning rate if allowed to burn long enough.

In order to assess the thermal threat associated with a fuel spill/pool fire scenario, the peak fire size must be coupled with exposure duration. Estimating exposure duration can be accomplished using one of two techniques. The first technique assumes that the peak fire size is reached instantly and is maintained so long as fuel is present. Using this technique, the burning duration for a given fire scenario can be calculated using Equation 65.28.

$$t_b = \frac{4m}{\pi D^2 \dot{m}''_\infty} \tag{65.28}$$

where t_b is the burning duration for a given scenario (s), m is the mass of fuel available to burn (kg [lbs.]), D is the effective spill diameter (m [ft]), and $\dot{m}''_\infty$ is the peak mass burning rate per unit area for the given fuel (g/s-m^2 [lbs./s-ft^2]). Traditionally, many have assumed that the peak heat release rate of a liquid fuel fire is reached instantaneously and maintained for the duration of the fire as calculated via Equation 65.28. Consequently, the exposure times associated with this assumption are most likely underestimated as shown in Fig. 65.26 as the "predicted" curve. In general, this approach tends to over-predict the peak thermal exposure resulting from a fuel spill/pool scenario.

The second technique that can be used to approximate the transient behavior of a fire resulting from the ignition of a liquid fuel spill/pool is to characterize the development, peak, and decay of the fire. This is accomplished by approximating the spread velocity on the hydrocarbon pool surface from the point of ignition, the time to develop maximum burning conditions, and the time to consume all fuel at a

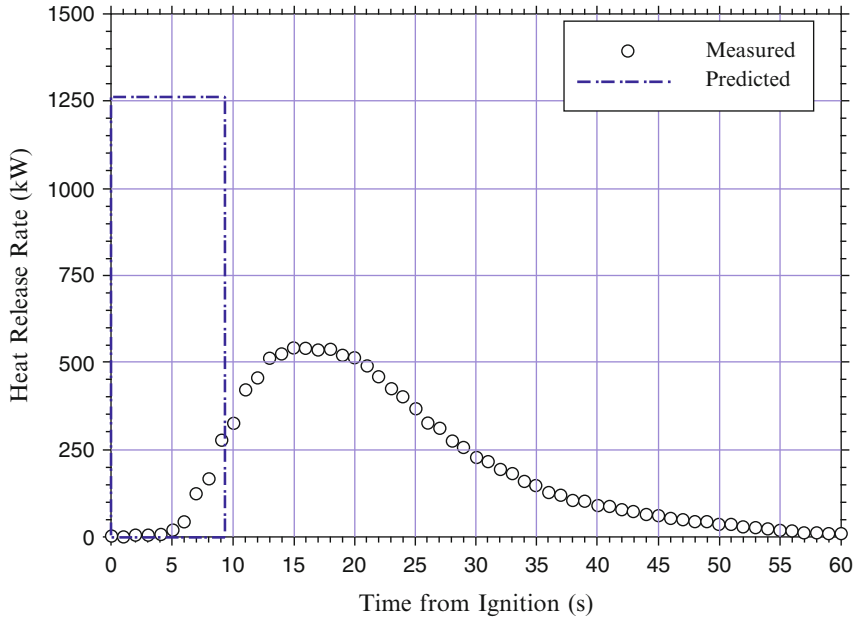

Fig. 65.26 Comparison of measured and predicted spill fire heat release rates using assumption that peak heat release rate is achieved instantly [8]

given location. Mealy et al. provide a methodology for estimating the fire growth and decay [8].

For liquid pool fires (depths ≥0.5 mm), although the entire fuel surface may be fully involved, the burning rate per area (or regression rate) will increase over time until the maximum steady-state value is reached [46]. The transient time period may be tens of seconds to minutes, depending on the type of fuel, the fuel depth, and the bounding materials (e.g., building walls or metal tank). During this transient period, the temperature gradient in the fuel is being established. Once the fuel surface reaches the boiling temperature, the burning rate approaches the steady-state value. If a transient analysis of a fire is required, further consideration must be given to the mass burning rate (or regression rate) that is selected. The use of the maximum value may not be appropriate for the entire burning duration.

Other Factors and Limitations

The spill areas and burning rates of liquid spill or pool fires presented in this chapter have been developed from experimental data of fires on level surfaces. In many applications, fuel spills will occur on inclined and/or cluttered surfaces. Under these conditions, fuel spread will ultimately be dependent on the geometry of the surface, which may lead to pooling of the fuel, channeling, and/or larger wetted areas than would occur on a level surface. Fuel flowing on an inclined surface can result in faster and wider spread of fire. No published studies have evaluated the impact of three-dimensional fuel flow on spill fire burning rates.

This chapter has primarily addressed the burning of liquid fuel fires that occur in the open. Liquid fuel fires in enclosures were studied by Mealy et al. [52] and showed that spill fire scenarios are unaffected by the enclosure (assuming sufficient air supply) since the duration of a spill fire is quite short. However, pool fires in an enclosure have been shown to have enhanced burning (~60 %) relative to open burning when a radiating upper layer is created in the compartment fire [52]. This increase can be moderated by restricted ventilation to the compartment, which can decrease the mass burning rate of a pool fire.

Babrauskas [49] and Zabetakis and Burgess [46] have reported that burning rates of pool and spill fires both increase and decrease under increased wind speeds. Burgess and Hertzberg [53] reported that wind speeds increased the burning rate for small-diameter fires; however, burning rates never exceeded the maximum burning rate in still air corresponding to larger diameter fires. High wind speeds can cause fuel to spill out of contained areas or cause unconfined spill fires to move in the direction of the wind. At higher wind speeds, flames can also be blown off.

For pool fires in pans or tanks, the lip height can impact the burning rate of the fuel. There is limited data on this topic and experimental results show both an increase and decrease in the burning rate with larger lip heights [49]. Much of the experimental data have been for small pan diameters (<1 m) (e.g., Emmons [54]).

Flame Height

The flame height of a liquid spill or pool fire can be calculated based on a number of experimental correlations [55]. The following correlation developed by Heskestad [55] has been shown to be quite robust for different fuels over a wide range of pool fire sizes:

$$L_f = 0.23\dot{Q}^{2/5} - 1.02D \qquad (65.29)$$

where

L_f = The 50 percentile intermittent flame height (m)

$\dot{Q}Z$ = The heat release rate (kW)

D = The diameter of the fire (m)

The use of Equation 65.29 to characterize unconfined spill fire heights was evaluated by Gottuk [4] for JP-8 and JP-5 spill fires on concrete. The results of the comparison are shown in Figs. 65.27 and 65.28, which present measured intermittent flame heights (50 percentile) and

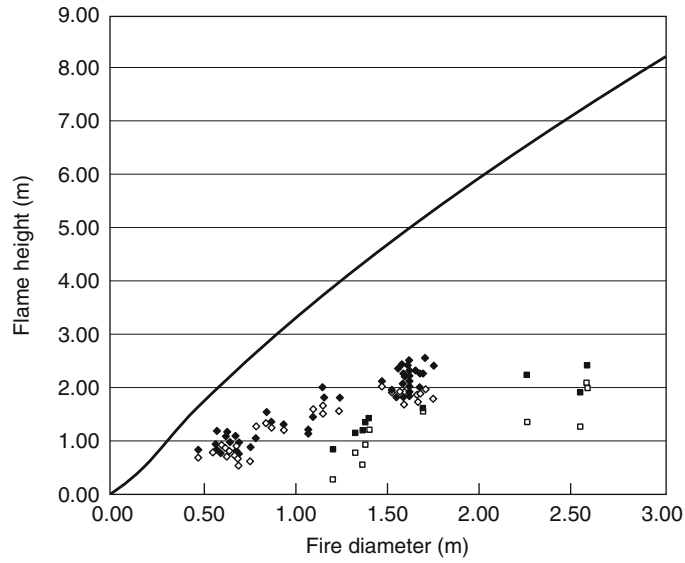

Fig. 65.27 Comparison of measured and predicted flame heights for unconfined JP-8 spill fires: [4] measured (◆) and predicted (◇) 0.4–1.7 L/min continuously flowing spill fires; measured (■) and predicted (□) 1–3 L fixed-quantity spill fires; and predicted pool fires (——)

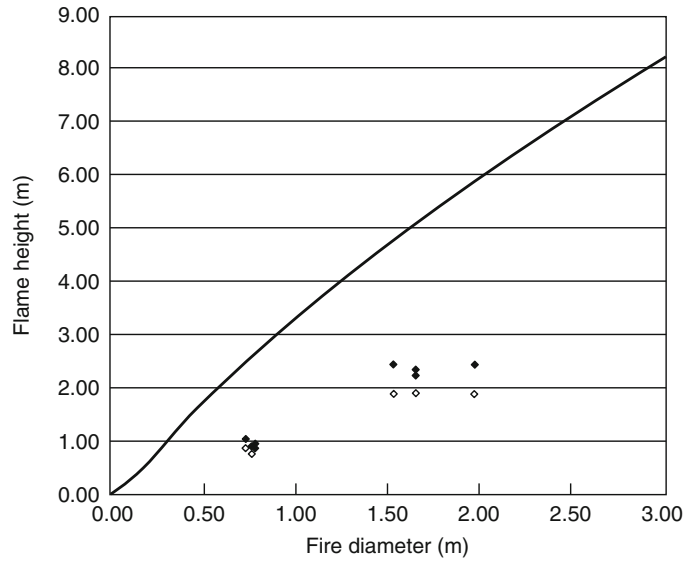

Fig. 65.28 Comparison of measured and predicted flame heights for unconfined JP-5 spill fires: [4] measured (◆) and predicted (◇) 0.4–1.7 L/min continuously flowing spill fires; and predicted pool fires (——)

predicted flame height values plotted versus the spill diameter. For comparison, the predicted flame heights of pool fires are also plotted as a curve in each figure. The predicted pool fire heights are based on Equation 65.29 and pool burning rate data of Table 26.13. Consistent with the difference in the mass burning rates between spill and pool fires, the spill flame heights are considerably shorter than those for pool fires of the same diameter. Using the Heskestad flame height correlation (Equation 65.29) with the spill fire data yields predicted heights that are approximately 17 % lower compared to the measured spill fire flame heights. For most engineering applications, the Heskestad flame height correlation (Equation 65.29) provides satisfactory predictions for both liquid pool and spill fires.

Fire Hazard Analysis Framework

When conducting fire hazard analyses, fuel type and spill/pool configuration parameters are often user selected and/or varied to assess a wide range of fire scenarios. In this case, the user would identify the fuels of interest and obtain the relevant fire property data. Four different scenarios are identified for fire hazard analyses based upon the identification of confined and unconfined spill scenarios and fixed quantity and continuously-fed fuel supplies. These four paths generally encompass the vast majority of potential liquid fuel scenarios and require different analytical approaches to understand the resulting fire threat. The approach presented will lead to the calculation of the largest possible fire size. It is important to note that in some analyses, a smaller fire size that lasts longer may actually be a worst-case of more challenging fire hazard. The discussion above can be used to assess such scenarios (Fig. 65.29).

The first spill/pool scenario considered was a fixed quantity of fuel in a confined area. For the purposes of this discussion, it is assumed that the quantity of fuel is such that it covers the entire area of confinement otherwise it is considered as a fixed quantity, unconfined scenario. Based upon this assumption, an equilibrium spill depth can be calculated using the known volume of

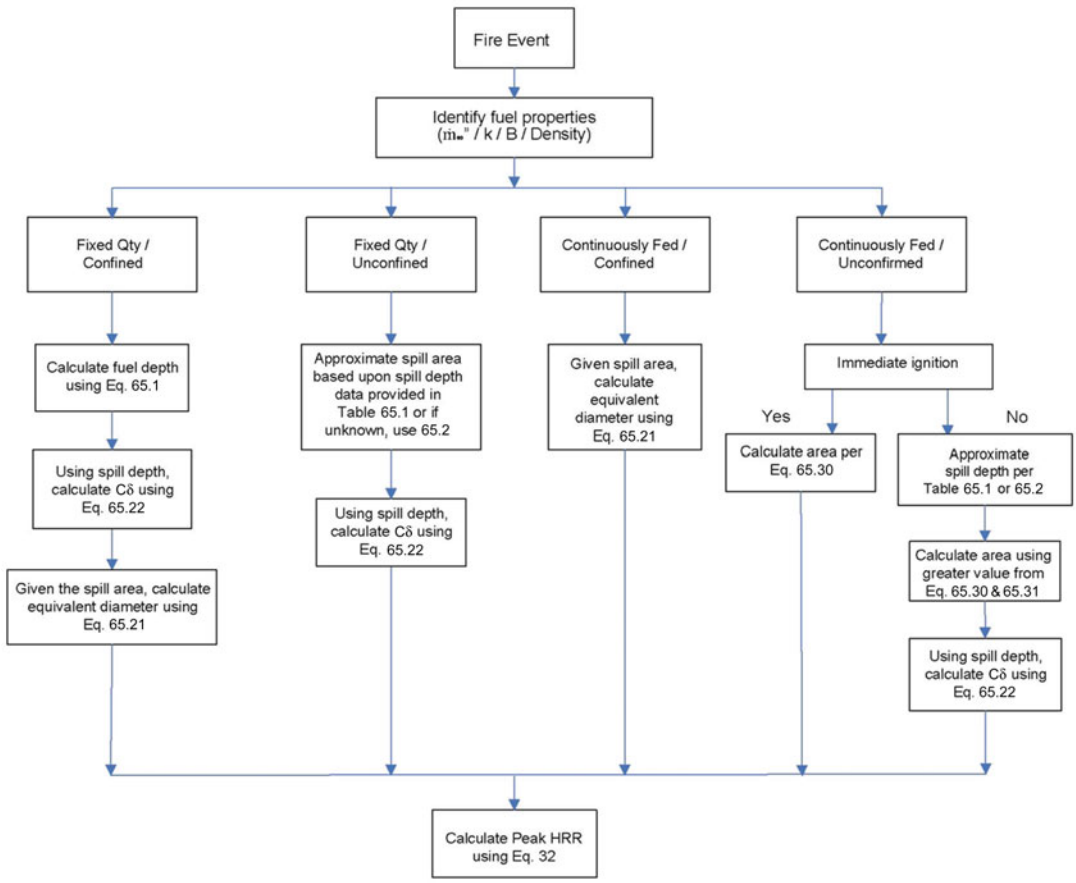

Fig. 65.29 Analytical framework for characterizing fuel spill/pool fire scenarios from a fire hazard viewpoint

liquid spilled and the area of confinement as shown in Equation 65.1.

$$\delta = \frac{V_o}{A_o} \tag{65.1}$$

where δ is the fuel depth (mm [ft]), Vo is the volume of liquid (L [gal.]), and the A_o is the area of confinement (m^2 [ft^2]).

The second scenario considered is a fixed quantity spill that is unconfined. In this scenario, the bulk flow of the liquid as well as the length of time between the spill and the ignition of the liquid dictates the area covered as opposed to bounding obstacles inhibiting the flow. For a specific spill scenario in which the substrate and/or ignition delay times are known, more representative spill depths can be approximated using the data provided in Table 65.1 (and Table 7.1 of Ref. [4]). Otherwise Equation 65.2 recommended for guidance:

$$\delta = 0.7 \text{ mm for most fuels and conditions} \tag{65.2a}$$

$$\delta = 2.9 \text{ mm for quantities of 38 L (10 gal) where analysis warrants longer duration fires} \tag{65.2b}$$

Once an appropriate spill depth has been determined, the area of coverage for a given quantity spill can be calculated using Equation 65.1. Similarly, if the area of coverage is known and a fuel depth is assumed, one can approximate the quantity of liquid spilled using Equation 65.1.

The next scenario considered is a continuously-fed, fixed area (i.e., confined) fuel supply. In this scenario, it is assumed that the fuel supply rate is equal to or greater than the mass burning rate, such that a fixed area of some depth is maintained for an extended period of time. It is also assumed that the fuel does not overflow the confined area. In this scenario, the area is known and the depth of fuel is not important given that fuel is continuously supplied, and thus burn-out does not occur (i.e., steady-state burning is allowed to develop).

The final scenario identified is a continuously-fed, unconfined spill scenario. For this scenario, it necessary to identify the time of ignition given that this time will dictate the initial spill area. To address this parameter, two paths are possible. The first path assumes ignition immediately upon release of the liquid. Once ignited, the burning area of fuel will grow in size until an equilibrium spill area is achieved, which will occur when the fuel burning rate equals the fuel supply rate. Equation 65.32 represents the balance between these rates (based on Equation 65.25).

$$A_{ss} = \frac{\rho \dot{V}_L}{\dot{m}''} \tag{65.30}$$

where A_{ss} is the equilibrium spill fire burning area (m^2 [ft^2]), $\dot{V}_L$ is the volumetric fuel supply rate (m^3/s [ft^3/s]), ρ is the fuel density (kg/m^3 [lbs./ft^3]), and $\dot{m}''$ is the mass burning rate per unit area (kg/s-m^2 [lbs./s-ft^2]). Once this equilibrium solution is obtained, the maximum area of the spill is known, and the depth of fuel is not important given that fuel is continuously supplied and burning will reach a steady-state.

The other path identified for the continuously-fed, unconfined scenario is a delayed ignition (i.e., liquid is permitted to spill and spread for some period of time prior to ignition). As shown in Equation 65.31, in this scenario, the area of coverage of the spilled liquid prior to ignition can be determined based upon the product of the volumetric flow rate, $\dot{V}_L$, the ignition delay time, and an assumed spill depth.

$$A_t = \frac{\dot{V}_L t}{\delta} \tag{65.31}$$

where A_t is the spill area (m^2 [ft^2]) at a given point in time, $\dot{V}_L$ is the volumetric fuel supply rate (kg/s [lbs/s]), t, is the time in seconds after the spill occurs prior to ignition, and δ is the calculated fuel depth (m [ft]). Using a spill depth from Table 65.1 or the average spill depth of 0.72 mm, an initial spill area can be approximated by Equation 65.33. Once ignited,

the initial spill area will grow or regress to the equilibrium spill area, as calculated for the immediate ignition scenario with Equation 65.32. Consequently, the initial area calculated may provide the maximum fire size, but it will only last for a brief period of time as the fire regresses to the equilibrium area.

Once the spill areas and corresponding spill depths have been calculated, it is necessary in some spill scenarios to calculate the depth coefficient, a parameter developed to modify the maximum fuel burning rate based on small depths causing early burn out before steady-state burning can be achieved. The correlations developed for gasoline and kerosene are provided in Equations 65.22a and 65.22b.

$$C_\delta = 0.95^*\left(1 - e^{-0.71\delta}\right) \quad \text{for gasoline} \tag{65.22a}$$

$$C_\delta = 0.91^*\left(1 - e^{-0.58\delta}\right) \quad \text{for kerosene} \tag{65.22b}$$

where C_δ is the depth coefficient and δ is the calculated fuel depth (mm). If depth coefficients for other fuels are required it is recommended that either Eq. 22a or 22b be used based on similar properties or an average coefficient of 0.69 be used for spill depths ≤5 mm and a coefficient of 1.0 be used for spill depths >5 mm.

Once the fuel depth, fuel coverage area, and depth coefficient are determined using the methods described above, the final step in the analysis is the prediction of the heat release rate of the fire. Calculating the peak and/or transient heat release rates requires knowledge of a fuel's maximum mass burning rate per unit area ($\dot{m}''_\infty$, also seen as $\dot{m}''_{max}$), optical properties of the fire plume (kβ), and the heat of combustion of the fuel (ΔH_c). Using this fuel data, combined with the spill parameters described above, a transient heat release rate for the given scenario can be calculated. The general form for this calculation is presented in Equation 65.26 and expanded below as Equation 65.32, which calculates the peak heat release rate for a given fuel:

$$\begin{aligned}\dot{Q}_p &= C_\delta \dot{m}''_\infty \left(1 - e^{-k\beta D}\right) A \Delta H_C \\ &= C_\delta \dot{m}''_\infty \left(1 - e^{-k\beta D}\right) \frac{\pi D^2}{4} \Delta H_C\end{aligned} \tag{65.32}$$

where $\dot{Q}_p$ is the peak fire size (kW [Btu/s]), C_δ is the depth coefficient, $\dot{m}''_\infty$ is the peak mass burning rate per unit area for the given fuel (g/s-m^2 [lbs./s-ft^2]), kβ is an empirical constant specific to the fuel, A is the spill area (m^2 [ft^2]), ΔH_c is the heat of combustion of the fuel (MJ/kg [BTU/lbs.]), and D is the effective spill diameter (m [ft]). The effective diameter of non-circular spills can be calculated using Equation 65.21.

$$D = \sqrt{\frac{4A}{\pi}} \tag{65.21}$$

Equations 65.32 and 65.21 provide a means of calculating a peak heat release that is both fuel depth and fire diameter dependent. This prediction provides the largest potential fire that a given liquid fuel fire can produce.

Example 1 A 208 L (55 gal) drum of gasoline is suddenly ruptured during a warehouse accident. The fuel is released quickly across the floor of the warehouse and is ignited when it comes in contact with a piece of faulty equipment. Determine the maximum size of the resulting fire.

Solution First, the size of the spill is calculate by estimating the spill depth. Since gasoline is spilled on an unknown floor material, a depth value of 0.71 mm is selected from Table 65.1. Using Equation 65.1 and assuming that the release occurs instantaneously (i.e., the spill is nearly at its maximum diameter at the time of ignition) and is allowed to spread freely, the spill area is calculated as

$$A = V/\delta = 208\ \text{L}/0.71\ \text{mm} = 293\ \text{m}^2$$

Per Equation 65.21, the corresponding diameter of the burning spill is 19.3 m. To account for the short duration of the spill fire due to the shallow spill depth, δ, the depth coefficient is

calculated per Equation 65.22a to modify the peak mass burning rate:

$$C_\delta = 0.95^*\left(1 - e^{-0.71\delta}\right) = 0.38$$

The heat release rate for the fire is then calculated per Equation 65.32 as

$$\dot{Q}_p = C_\delta \dot{m}''_\infty \left(1 - e^{-k\beta D}\right) A \Delta H_C = C_\delta \dot{m}''_\infty \left(1 - e^{-k\beta D}\right) \frac{\pi D^2}{4} \Delta H_C$$
$$= 0.38 \cdot 0.055 \cdot (1 - \mathrm{e}\text{^}(-2.1\ \ 19.3))\,\pi\,(19.3\mathrm{m})^2/4 \cdot 43.7 = 267\,\mathrm{MW}$$

From Table 26.21, the heat of combustion of gasoline is 43,700 kJ/kg, the density is 740 kg/m^3, and the maximum mass burning rate per unit area of gasoline, $\dot{m}''_{\max}$, is 0.055 kg/m^{2}s.

The intermittent flame height is calculated per Equation 65.29 as

$$L_f = 0.23\dot{Q}^{2/5} - 1.02D$$
$$= 0.23(26.700\,kW)^{2/5} - 1.02(12.2\,m) = 5.8\,m$$

If it is assumed that the fuel spill burns at the maximum rate for the duration of the fire, the burn time, t_b, for the fuel spill fire will be only 2 min:

$$t_b = \frac{m_f}{\dot{m}''A} = \frac{V \cdot \rho}{\dot{m}''A} = \frac{0.208\,m^3 \cdot 740\mathrm{kg}/m^3}{0.021\mathrm{kg}/m^2 s \cdot 293\,m^2}$$
$$= 25\,s$$

Where the mass burning rate, $\dot{m}''$, is calculated per Equation 65.23 as

$$\dot{m}''(D,\delta) = C_\delta * \left(\dot{m}''_\infty \left(1 - e^{-k\beta D}\right)\right)$$
$$= 0.38\left(0.055\left(1 - \left(1 - e^{-21*193}\right)\right)\right)$$
$$= 0.0209\frac{kg}{m2s}$$

As illustrated in Example *2*, the predicted burn time of 25 s is most likely too short. In reality, the fire will last longer due to the fact that the flame takes time to spread across the spill.

Example 2 Consider the situation in Example *1*. What is the time required for the entire spill to become involved in the fire? The temperature in the warehouse is 20 °C.

Solution The most critical step in determining the time for the entire spill to become involved in the fire is to identify both the temperature of the liquid fuel spill and the flashpoint of the fuel. The flashpoint of gasoline is indicated to be −45 °C as documented in the third edition of the *SFPE Handbook* in Kanury's [56] table, "Selected Ignition, Flammability, and Autoignition Properties of Some Fuels in Air." Assuming that the gasoline is at the same temperature as the warehouse, 20 °C, the spill temperature is well above the closed-cup flashpoint. The elevated temperature indicates that gas phase flame spread will occur if the spill is ignited. A reasonable and generally conservative approximation of the upper gas phase flame spread velocity is 200 cm/s.

The problem statement does not specify the location of the ignition source relative to the spill. The most conservative posture for fastest involvement would be to assume that the ignition source is in the center of a circular spill. Using Equation 65.8 for circular spills will define the time for full involvement:

$$t_{A,\max} = \frac{r_{A,\max}}{v}$$

where $r_{A,\max}$ is 6.1 m and v is 2.0 m/s. The time for full involvement becomes

$$t_{A,max} = \frac{9.65}{2.0\,m/s}$$

$$t_{A,max} = 4.8\,s$$

If the ignition source was located at the perimeter of the gasoline spill, it would take approximately

10 s to travel the full 19.3 m diameter of the pool to involve the spill completely. Irrespective of the ignition location, the time to involve the entire spill is small in the context of most hazard analyses time scales. Therefore, when gas phase flame spread is governing the involvement of a spill or pool of flammable liquid, it is often acceptable to assume instantaneous ignition of the entire fuel surface. This assumption may not be valid for extremely large spills (e.g., tanker spills) or when there are short time-scale concerns.

The difference between gas phase flame spread and liquid-controlled flame spread can be illustrated by assuming that the drum of gasoline in the foregoing example contained diesel fuel. The flashpoint of diesel fuel ranges from 52 °C to 96 °C according to the 1994 edition of NFPA 325 [57]. Since the warehouse is at 20 °C, substantially below the flashpoint of diesel fuel, flame spread would be governed by liquid-controlled mechanisms. A conservative upper bound of the liquid-controlled flame spread in this case would be 10 cm/s. Assuming that the area of the diesel spill was identical to the gasoline spill and that there was a strong enough ignition source present to ignite the spill, a time to full ignition of the spill can be estimated. Assuming that the ignition source was in the center of the spill, Equation 65.8 would be used again, where the maximum radius of the spill is 6.1 m and the flame spread velocity is 0.1 m/s. The time for full involvement becomes

$$t_{A,max} = \frac{9.65}{0.1\,m/s}$$

$$t_{A,max} = 67\,s$$

The conservative estimation of the time for full involvement of the diesel fuel is significantly greater than for the gas phase spread over gasoline.

Nomenclature

A	Area (m^2)
A_s	Area of spill (m^2)
A_{ss}	Steady-state area of continuously flowing burning fuel spill (m^2)
C_p	Specific heat of liquid fuel
D	Diameter (m)
D_{ss}	Steady-state area of diameter of burning fuel spill (m)
DT	$T_{fl} - T_l$
Δh_c	Heat of combustion (kJ/kg)
$\Delta h_{v,sen}$	Sensible heat of vaporization (kJ/kg)
k	Extinction coefficient (m^{-1})
l	Length of a trench involved with fire (m)
l_{max}	Maximum length of trench (m)
L_f	Flame height (m)
$\dot{m}''$	Fuel-mass burning rate per unit area (kg/m^2s)
$\dot{m}''_\infty$	Fuel-mass burning rate per unit area for infinite size pools (kg/m^2s)
$\dot{m}''_{max}$	Maximum fuel-mass burning rate per unit area (kg/m^2s)
m_i	Mole fraction of fuel in liquid phase
n_i	Mole fraction of fuel in vapor phase
$\dot{Q}$	Heat release rate (kW)
r	Radius of the fire
$r_{A,max}$	Maximum radius of the fire for complete involvement of fuel release
t	Time
$t_{A,max}$	Time at which fuel release becomes completely involved
T_b	Boiling point temperature of liquid fuel
T_{fl}	Closed-cup flashpoint temperature of fuel
T_{gm}	Minimum liquid temperature at which asymptotic gas phase spread occurs
T_{go}	Liquid temperature at the transition from liquid to gas phase–controlled burning
T_l	Liquid fuel temperature
T_o	Initial temperature of liquid fuel
v	Flame spread velocity (cm/s)
V	Volume (m^3)
$\dot{V}_L$	Volumetric flow rate of liquid fuel (m^3/s)
w	Width of a trench (m)
$\dot{y}$	Regression rate (m/s)
$\dot{y}_{max}$	Maximum regression rate (m/s)

Greek Letters

β Mean-beam-length correction
ρ Density (kg/m^3)
δ Pool or spill depth (m)

References

1. C. Beyler, "Fire Hazard Calculations for Large Open Hydrocarbon Fires," *The SFPE Handbook of Fire Protection Engineering,* 4th ed., Springer (2015).
2. G.D. Chambers, "Flight Line Extinguisher Evaluation," U.S. Air Force Report DOD-AGFSRS-76-9 (1977).
3. D.T. Gottuk et al., Hughes Associates Inc., Internal Research, 2000.
4. D.T. Gottuk, J.L. Scheffey, F.W. Williams, J.E. Gott, and R.J. Tabet, "Optical Fire Detection (OFD) for Military Aircraft Hangars: Final Report on OFD Performance to Fuel Spill Fires and Optical Stresses," *NRL/MR/6180-00-8457,* Naval Research Laboratory, Washington, DC (2000).
5. A.D. Putorti, Jr., J.A. McElroy, and D. Madrzykowski, "Flammable and Combustible Liquid Spill/Burn Patterns," *NIJ Report 604-00,* National Institute of Justice, Washington, DC (2001).
6. A.T. Modak, "Ignitability of High-Fire-Point Liquid Spills," *EPRI NP-1731,* Factory Mutual Research Corporation, Norwood, MA (1981).
7. Benfer, M., "Spill and Burning Behavior of Flammable Liquids," Master's Thesis, University of Maryland, 2010.
8. Mealy, C.L., Benfer, M., and Gottuk, D.T., "Fire Dynamics and Forensic Analysis of Liquid Fuel Fires," Grant No. 2008-DN-BX-K168, Office of Justice Programs, National Institute of Justice, Department of Justice, February 18, 2011. https://www.ncjrs.gov/pdffiles1/nij/grants/238704.pdf
9. H.E. Moran, J.C. Burnett, and J.T. Leonard, "Suppression of Fuel Evaporation by Aqueous Films of Fluorochemical Surfactant Solutions," *NRL Report 7247,* Naval Research Laboratory, Washington, DC (1971).
10. Coordinating Research Council, *Handbook of Aviation Fuel Properties,* Alpharetta, GA (1983).
11. T. Kinbara, *Bulletin of the Institute of Physics and Chemical Research (Japan),* 9, p. 561 (1932).
12. J.H. Burgoyne and A.F. Roberts, "The Spread of Flame across a Liquid Surface, II. Steady-State Conditions," *Proceedings of the Royal Society A,* 308, pp. 55–68 (1968).
13. A.F. Roberts, Ph.D. Thesis, University of London (1959).
14. K. Akita, "Some Problems of Flame Spread along a Liquid Surface," in *Proceedings of the 14th International Symposium on Combustion,* Combustion Institute, Pittsburgh, PA, pp. 1075–1081 (1973).
15. R. Mackinven, J.G. Hansel, and I. Glassman, "Influence of Laboratory Parameters on Flame Spread across Liquid Fuels," *Combustion Science and Technology,* 1, pp. 293–306 (1970).
16. K.E. Torrance, "Subsurface Flows Preceding Flame Spread over a Liquid Fuel," *Combustion Science and Technology,* 3, pp. 133–143 (1971).
17. K.E. Torrance and R.L. Mahajan, "Fire Spread over Liquid Fuels: Liquid Phase Parameters," in *Proceedings of the 15th International Symposium on Combustion,* Combustion Institute, Pittsburgh, PA, pp. 281–287 (1975).
18. W.W. Hillstrom, "Temperature Effects on Flame Spreading over Fuels," *Paper to Eastern Section,* Combustion Institute, Pittsburgh, PA (1975).
19. I. Glassman and F.L. Dryer, "Flame Spreading across Liquid Fuels," *Fire Safety Journal,* 3, pp. 123–128 (1980).
20. A. Nakakuki, "Flame Spread over Solid and Liquid Fuels," *Journal of Fire & Flammability,* 7, pp. 19–40 (1976).
21. K. Akita and O. Fujiwara, "Pulsating Flame Spread along the Surface of Liquid Fuels," *Combustion and Flame,* 17, pp. 268–269 (1971).
22. H. Ishida, "Flame Spread over Fuel-Soaked Ground," *Fire Safety Journal,* 10, pp. 163–171 (1986).
23. H. Ishida, "Flame Spread over Ground Soaked with Highly Volatile Liquid Fuel," *Fire Safety Journal,* 13, pp. 115–123 (1988).
24. W.A. Sirignano and I. Glassman, "Flame Spreading above Liquid Fuels: Surface-Tension-Driven Flows," *Combustion Science and Technology,* 1, pp. 307–312 (1970).
25. T. Hirano, T. Suzuki, I. Mashiko, and N. Tanabe, "Gas Movements in Front of Flames Propagating Across Methanol," *Combustion Science and Technology,* 22, pp. 83–91 (1980).
26. A. Ito, D. Masuda, and K. Saito, "A Study of Flame Spread over Alcohols Using Holographic Interferometry," *Combustion and Flame,* 83, pp. 375–389 (1991).
27. F. Miller and H. Ross, "Further Observations of Flame Spread over Laboratory-Scale Alcohol Pools," *Proceedings of the 24th International Symposium on Combustion,* Combustion Institute, Pittsburgh, PA, pp. 1703–1711 (1992).
28. W.A. Sirignano, "A Critical Discussion of Theories of Flame Spread across Solid and Liquid Fuels," *Combustion Science and Technology,* 6, pp. 95–105 (1972).
29. D.D. Cline and L.N. Koenig, "The Transient Growth of an Unconfined Pool Fire," *Fire Technology,* 19, 3, pp. 149–162 (1983).
30. D. White, C.L. Beyler, C. Fulper, and J. Leonard, "Flame Spread on Aviation Fuels," *Fire Safety Journal,* 28, pp. 1–31 (1997).

31. J.T. Leonard, C.R. Fulper, R. Darwin, G.G. Back, R.E. Burns, and R. Ouelette, "Fire Hazards of Mixed Fuels on the Flight Deck," *Naval Research Laboratory Memorandum Report 6975* (1992).
32. H.D. Ross, "Ignition of and Flame Spread Over Laboratory-Scale Pools of Pure Liquid Fuels," *Progress in Energy and Combustion Science,* 20, pp. 17–63 (1994).
33. I. Glassman and J. Hansel, "Some Thoughts and Experiments on Liquid Fuel Spreading, Steady Burning, and Ignitability in Quiescent Atmospheres," *Fire Research Abstracts and Reviews,* 10, 3, pp. 297–322 (1948).
34. J.P. Burelbach, M. Epstein, and M.G. Plys, "Brief Communication—Initiation of Flame Spreading on Shallow Subflash Fuel Layers," *Combustion and Flame,* 114, 1/2, pp. 280–282 (1998).
35. I. Liebmann, J. Corry, and H.E. Perlee, "Flame Propagation in Layered Methane-Air Systems," *Combustion Science and Technology,* 1, pp. 257–267 (1970).
36. C.C. Feng, S.H. Lam, and I. Glassman, "Flame Propagation through Layered Fuel-Air Mixtures," *Combustion Science and Technology,* 10, pp. 59–71 (1975).
37. H. Phillips, "Flame in a Buoyant Methane Layer," *Proceedings of the 10th International Symposium on Combustion,* Combustion Institute, Pittsburgh, PA, pp. 1277–1283 (1965).
38. Military Specification, "Turbine Fuel, Aviation, Grades JP-4, JP-5, and JP-5/JP-8 ST," *MIL-T-5624N* (1989).
39. Military Specification, "Turbine Fuel, Aviation, Grades JP-8," *MIL-T-83133B* (1988).
40. K. Takeno and T. Hirano, "Behavior of Combustible Liquid Soaked in Porous Beds During Flame Spread," in *Proceedings of the 22nd International Symposium on Combustion,* Combustion Institute, Pittsburgh, PA, pp. 1223–1230 (1988).
41. H. Ishida, "Initiation of Fire Growth on Fuel-Soaked Ground," *Fire Safety Journal,* 18, pp. 213–230 (1992).
42. V.I. Blinov and G.N. Khudiakov, "Diffusion Burning of Liquids," U.S. Army Translation, *NTIS No. AD296762* (1961).
43. H.C. Hottel, "Certain Laws Governing Diffusive Burning of Liquids," *Fire Research Abstracts and Reviews,* 1, p. 41 (1959).
44. D.S. Burgess, A. Strasser, and J. Grumer, "Diffusive Burning of Liquid Fuels in Open Trays," *Fire Research Abstracts and Reviews,* 3, p. 177, (1961).
45. D.S. Burgess, J. Grumer, and H.G. Wolfhard, "Burning Rates of Liquid Fuels in Large and Small Open Trays," *International Symposium on the Use of Models in Fire Research, Publication 786,* National Academy of Sciences—National Research Council, Washington, DC, pp. 68–75 (1961).
46. M.G. Zabetakis and D.S. Burgess, "Research on Hazards Associated with the Production of and Handling of Liquid Hydrogen," *RI 5705,* U.S. Bureau of Mines (1961).
47. K.S. Mudan, "Thermal Radiation Hazards from Hydrocarbon Pool Fires," *Progress in Energy Combustion Science,* 10, pp. 59–80 (1984).
48. J. Grumer, A. Strasser, T.A. Kubala, and D.S. Burgess, "Uncontrolled Diffusive Burning of Some New Liquid Propellants," *Fire Research Abstracts and Reviews,* 3, p. 159 (1961).
49. V. Babrauskas, "Estimating Large Pool Fire Burning Rates," *Fire Technology,* 19, p. 251 (1983).
50. V. Babrauskas, "Heat Release Rates," in *The SFPE Handbook of Fire Protection Engineering,* 5th ed., Springer (2015).
51. J.A. Mansfield and L.J. Linley, "Measurement and Statistical Analysis of Flame Temperatures from Large Fuel Spill Fires," *NWC TP 7061,* Naval Weapons Center, China Lake, CA (1991).
52. Mealy, C.L. and Gottuk, D.T., "Ignitable Liquid Fuel Fires in Buildings – A Study of Fire Dynamics," Grant No. 2009-DN-BX-K232, Office of Justice Programs, National Institute of Justice, Department of Justice, January 31, 2013.
53. D.S. Burgess and M. Hertzberg, "Radiation from Pool Flames," *Heat Transfer in Flames,* Chapter 27 (N.H. Afgan and J.M. Beer, eds.), Scripta Book Co., Washington, DC (1974).
54. H.W. Emmons, "Some Observations on Pool Burning," *The Use of Models in Fire Research,* Publication 786 NAS-NRC, Washington, DC, pp. 50–67 (1961).
55. G. Heskestad, "Luminous Heights and Turbulent Diffusion Flames," *Fire Safety Journal,* 5, pp. 103–108 (1983).
56. A.M. Kanury, "Ignition of Liquid Fuels," *SFPE Handbook of Fire Protection Engineering,* National Fire Protection Association, Quincy, MA, pp. 2-188–2-199 (2002).
57. NFPA 325, *Guide to Fire Hazard Properties of Flammable Liquids, Gases, and Volatile Solids,* National Fire Protection Association, Quincy, MA (1994).

D.T. Gottuk is VP of Specialty Services and the Technical Director of Jensen Hughes. He is actively involved in fire hazard analyses, fire research and testing, and forensic engineering relative to fire dynamics and fire detection.

D.A. White is a Vice President at Jensen Hughes. His technical expertise is primarily focused in industrial fire protection, litigation services, and special hazards.

Fire Hazard Calculations for Large, Open Hydrocarbon Fires

66

Craig L. Beyler

Introduction

A major challenge in industrial fire protection is controlling the impact from large, open hydrocarbon fires. The primary mechanism for injury of damage from such fires is thermal radiation. Depending on the circumstances and conditions leading to such an event, a different type of open fire may result. For example, ignited releases can produce pool fires, jet flames, vapor cloud fires, or fireballs, all of which behave differently and exhibit markedly different radiation characteristics. This chapter presents detailed techniques for calculating impacts from large, open hydrocarbon fires. Examples are included throughout this chapter to illustrate the application of these expressions.

The first section of this chapter discusses hydrocarbon pool fires, an area in which considerable work has been done, including various important geometric parameters (e.g., flame height), thermal radiation models, and atmospheric absorption of radiation. The second section deals with turbulent jet flames and flares, first presenting significant geometric effects and thermal radiation models, then discussing aerodynamic effects on radiant energy and flame stability.

Whereas the above cases involve primarily steady-state thermal radiation, the third section considers two very important cases that involve unsteady radiant effects—burning vapor clouds and fireballs. Although developmental work in both of these areas is still ongoing, limited data are available to lend some confidence to the use of these models.

The following part of this introduction presents an event tree for the release of a flammable material to guide the user's selection of appropriate potential impacts and model application. It cannot be overstressed that prudent judgment should be exercised in the application of any of these calculation schemes to yield a safe and fair evaluation of scenarios of interest.

Event Tree for Flammable Material Release

Figure 66.1 depicts a typical event tree for the release of a flammable material, showing the pathways that lead to the various types of open fires. For this purpose, assume the release occurs from a pressurized container because all types of open fires may be realized from a pressurized release. In this example, the pressurized container may be either a large vessel (for storage, reaction, batching, etc.) or a pipeline (for transfer, fittings, instruments, etc.). The pressure may be the result of either normal operations or abnormal external events. For example, a tank may be pressurized because it contains a compressed liquid or because it has been exposed to an external fire; a pipeline may be pressurized because of a pumping operation or because of

C.L. Beyler (✉)

M.J. Hurley (ed.), *SFPE Handbook of Fire Protection Engineering*,
DOI 10.1007/978-1-4939-2565-0_66, © Society of Fire Protection Engineers 2016

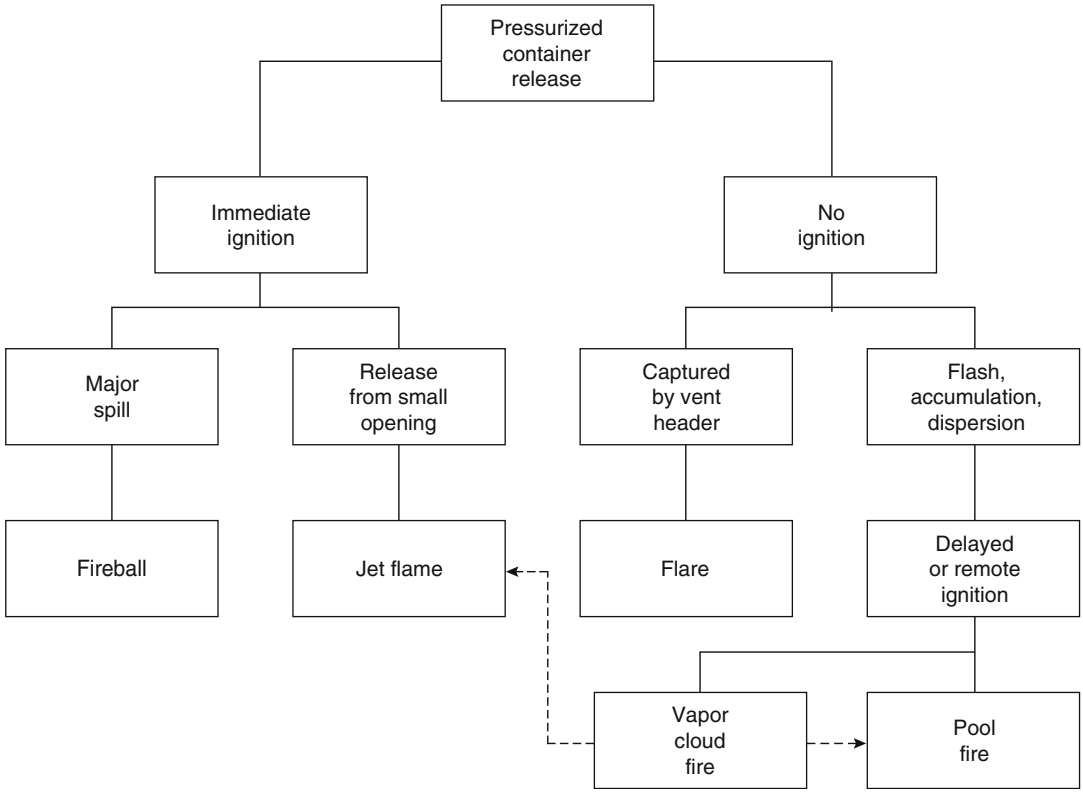

Fig. 66.1 Example event tree for release of flammable material

steam tracing on a blocked-in segment. Finally, the release may be due to a major failure (e.g., spontaneous tank failure) or a minor accident (e.g., breakage of a fitting).

While tracing the pathways in the event tree, note that a release may or may not be accompanied by immediate ignition. With immediate ignition, that is, following the left branch of the tree, a jet flame will result if the release is from a relatively small opening. Such a release could be either vapor or liquid and, if liquid, could also involve flashing of liquid into vapor and/or accumulation of liquid. If the release is the result of a major spill and there is immediate ignition, the result is usually a fireball, the size of which is strongly affected by the amount of flash vaporization and liquid entrainment that occurs on release.

If ignition does not occur immediately upon release, the right branch of the event tree is followed. Releases through relief valves, either accidental or intentional, may be captured by a vent header system and directed to a flare. Flares must accordingly be designed for expected accident or operational flow capacities, and the design should include consideration of resulting hazard zones.

If the unignited release is to the atmosphere, the spill will be accompanied by flash vaporization, liquid entrainment, accumulation, and/or vapor dispersion. A delayed local ignition following accumulation results in a pool fire whose characteristics are strongly influenced by the geometry of containment (or lack thereof).

Absence of a local ignition source, either immediate or delayed, allows a vapor cloud to form as the vapors disperse downwind. A portion of this vapor cloud will be flammable, and, depending on the size of the release, the flammable region could extend significantly downwind. A remote ignition source can ignite the cloud, resulting in a vapor cloud fire that burns from the

point of ignition back toward the source of the cloud, that is, the release point. Note also that the event tree shows dashed pathways from the vapor cloud fire to a pool fire or a jet flame. This is intended to show that the transient burning of the vapor cloud fire back to the release point can initiate a subsequent steady burning jet flame or pool fire, and consideration must be given to potential impacts from both types of fire.

Finally, this event tree represents an example of potential pathways leading to hazardous open fires. Scenarios will be encountered that will be similar to the event tree depicted in Fig. 66.1 or to parts thereof, but it is important to recognize that in all cases, the event tree must be structured to reflect the actual scenario under consideration.

Hydrocarbon Pool Fires

The thermal radiation hazards from hydrocarbon pool fires depend on a number of parameters, including the composition of the hydrocarbon, the size and shape of the pool, the duration of the fire, its proximity to the object at risk, and the thermal characteristics of the object exposed to the fire. The objectives of this section of the chapter are to review available techniques for determining the thermal radiation hazards from liquid hydrocarbon pool fires under various credible spill conditions.

The state of the art of predicting the thermal environment of hydrocarbon pool fires consists essentially of semiempirical methods, some of which are based on experimental data. Needless to say, such semiempirical methods are always subject to uncertainties.

Estimating the thermal radiation field surrounding a fire involves the following three major steps:

1. Geometric characterization of the pool fire; that is, the determination of burning rate and the physical dimensions of the fire. In calculating thermal radiation, the size of the fire implies the time-averaged size of the visible envelope.
2. Characterization of the radiative properties of the fire; that is, the determination of the average emissive power of the flames. The intensity of thermal radiation emitted by pool fires depends on a number of parameters, including fuel type, fire size, flame temperature, and composition. The major sources of emission in large hydrocarbon fires are the water vapor, carbon dioxide, and soot.
3. Calculation of radiant flux at a given location. This can be accomplished once the geometry of the fire, its radiation characteristics, and the location, geometry, and orientation of the receiver are known. For large distances (hundreds of meters), the absorption of thermal radiation in the intervening atmosphere becomes appreciable. This is dependent on the pathlength, flame temperature, and the relative humidity in the atmosphere.

Certain references [1–7] provide general information concerning radiation heat transfer relevant to pool fires, and others [8–37] are specific studies of pool fire radiation heat transfer underpinning the methods of analysis.

Pool Fire Geometry

The flame geometry for the solid flame model is generally determined by assuming that the flame is a solid, gray emitter having a regular well-defined shape such as a circular or a tilted cylinder. The dimension of the flame area is characterized by the flame base diameter, the visible flame height, and the flame tilt. The flame diameter is dependent on the pool size (spill volume and/or spill rate). The flame height appears to depend on the flame diameter and the burning rate. These factors, which influence the flame geometry, are discussed in this chapter.

The pool fire geometry is determined by the manner and location of the fuel release. Chapter 17 provides detailed means for predictions of the extent of the spill or pool, the spread of flame over the fuel surface, and the resulting burning rate. This information will

be required for determination of the flame height and the radiation analyses that follow.

The height or length of a flame is a significant indicator of hazard because it directly relates to flame heat transfer and the propensity to impact surrounding objects. A plume of hot gases rises above a flame; the temperature, velocity, and width of this plume change as it rises due to the mixing of the plume with the surroundings. The height and temperature of the flame are important in estimating the ignition of adjacent combustibles. Above the fuel source, the flaming region is characterized by high temperature and is generally luminous. Flame from the pool fires fluctuate periodically so that the tip of the flame will be significantly different from the length of the continuous combustion (or luminous) region. Consequently, flame height has been defined by various criteria in order to correlate data. Investigators have used the degree of luminous flame intermittency, flame temperature, or visible estimations. Hence, correlations for flame height could have inherent variation with the instantaneous flame length due to factors involving flame fluctuation and flame definition. For additional information, see Chap. 13.

Flame Length Many investigators have developed correlations for turbulent flame lengths in a quiescent air environment. Most are based on the dimensional analysis of experimental data using Froude modeling principles; some are based on approximate theoretical models involving some empirical factors (see Chap. 13 for additional general information on flame heights).

These correlations are generally cast in terms of a nondimensional burning rate and a nondimensional velocity that arise out of Froude modeling as follows:

$$m^* = \frac{\dot{m}''}{\rho_a \sqrt{gD}} \tag{66.1}$$

$$u^* = \frac{u_w}{u_c} = \frac{u_w}{\left(g\dot{m}''D/\rho_a\right)^{1/3}} \tag{66.2}$$

An alternative to m^* is the nondimensional heat release rate, Q^*, which is proportional to m^*:

$$Q^* = \frac{\dot{Q}}{\rho_a c_p T_a D^2 \sqrt{gD}} \tag{66.3}$$

Most flame length correlations take the form of

$$\frac{H}{D} = a\left(m^*\right)^b \left(u^*\right)^c \tag{66.4}$$

Correlations of this form for mean flame length are summarized in Table 66.1. Mean flame length is generally defined as the height where the flame is present above this height 50 % of the time.

Mudan [14] and Munoz et al. [41] have compared correlations with pool fire data. Figure 66.2 shows the comparison of data compiled by Mudan [14] with the various correlations. The correlations based on smaller-scale data tend to overestimate the flame heights. Munoz et al.'s comparisons with their 1- to 6 m-diameter pool fires show the same general trend. Munoz's data are both the most modern data and the smallest flame heights observed overall. Considerable variations are apparent among the correlations and considerable scatter exists in the data.

Table 66.1 Correlations for nondimensional mean flame lengths, L/D

Investigator	A	B	C	Notes
Thomas [38]	42	0.61	[a]	Wood cribs
Moorhouse [16]	6.2	0.254	−0.044	LNG pools (~15 m)
Mangialavori and Rubino [39]	31.6	0.58	[a]	HC pools (1–6 m)
Prichard and Binding [40]	10.615	0.305	−0.03	HC (mostly LNG) pools (6–22 m)
Munoz et al. [41]	7.74	0.375	−0.096	HC pools (1–6 m)
Heskestad [42, 43]	$3.7Q^{*0.4} - 1.02$		[a]	Wide range (mostly laboratory)

When u^* is less than 1, $u^* = 1$ is used
[a]Wind effects not considered

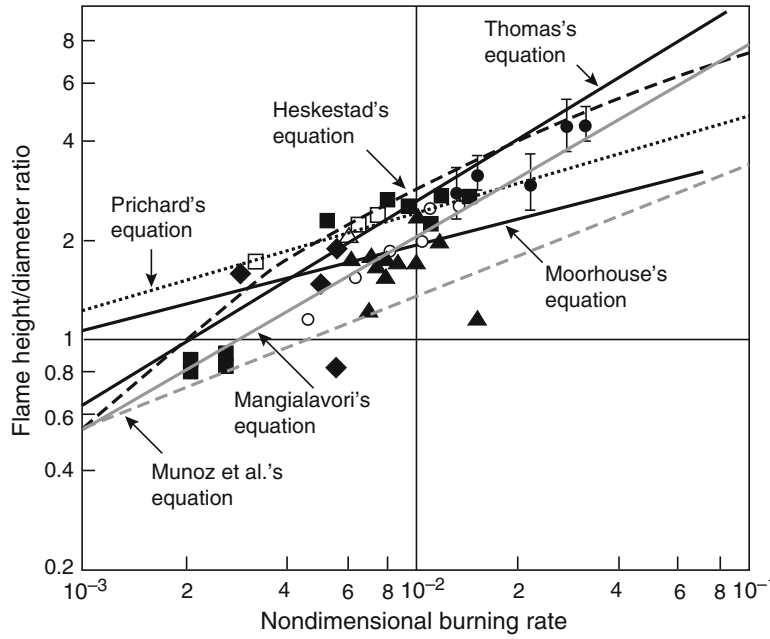

Fig. 66.2 Flame heights for various hydrocarbon pool fires on land and water (As modified [14])

Figure 66.2 shows the flame height to diameter ratio, H/D, as a function of the nondimensional burning rate, m^*, for a range of pool fire data assembled by Mudan [14] with the correlations shown in Table 66.1 for comparison.

Flame Tilt Angle Flame length under wind conditions has been studied by several investigators. Figure 66.3 illustrates a general schematic for the windblown flame. The pool fire flame follows a curved trajectory, and the angle, θ, approximates the trajectory. The vertical and horizontal components of the flame length measured along the angle are also shown in the figure.

Welker and Sliepcevich [44] and Emori and Saito [45] derived correlations from small-scale experiments. They correlated the angle of inclination as a function of crosswind velocity, $v_{\tilde{a}}$, but the results do not compare well with larger-scale data. Flame tilt angle correlations in the literature take the form of

$$\cos\theta = \begin{matrix} du^{*e} \\ 1 \end{matrix} \quad \text{for} \quad \begin{matrix} u^* \geq 1 \\ u^* < 1 \end{matrix} \qquad (66.5)$$

Table 66.2 summarizes the available correlations.

In Fig. 66.4, a comparison of observed flame tilt angle is shown for hydrocarbons pool fire data

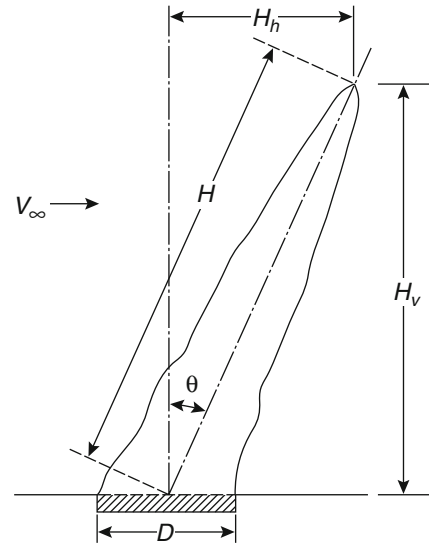

Fig. 66.3 Flame inclinations due to wind

Table 66.2 Correlations for nondimensional mean flame tilt angle, θ^*

Investigator	d	e	Notes
Thomas [46]	0.7	−0.49	Wood cribs
AGA [37]	1	−0.5	LNG pools
Moorhouse [16]	0.86	−0.25	LNG pools
Munoz et al. [41]	0.96	−0.26	HC pools (1–6 m)

Note: For all correlations when u* is less than one, use value calculated for u* = 1

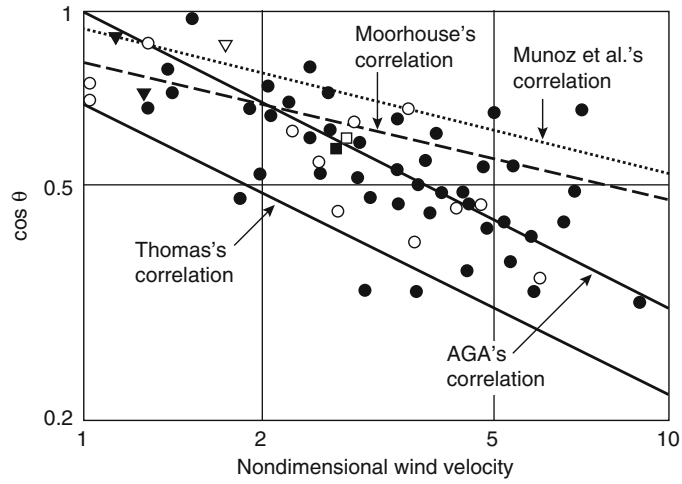

Fig. 66.4 Relationship between nondimensional wind velocity and flame tilt angle (As modified [14])

compiled by Mudan [14] with correlations summarized in Table 66.2. Although there is considerable scatter in the measured flame tilt, the correlation given by AGA represents the flame tilt most accurately. Defaveri et al. [47] have studied the effects of wind on high-momentum flames.

Geometry of Trench or Line Fires Moorhouse [16] conducted limited large-scale LNG trench fires with aspect ratios ranging from 1.5 to 2.5. Mudan and Croce [17] reported on large-scale tests with LNG trenches having aspect ratios of up to 30.0. All the data seem to indicate that flame geometry of trench fires is more sensitive to wind conditions than is flame geometry of conventional pool fires. Flame height is a strong function of trench width and relatively independent of the trench length. Indeed, for large aspect ratios, the trench fires break up into small flamelets having a typical base dimension of the trench width, W.

Based on an extensive analysis of the motion picture data of LNG trench fires, Mudan and Croce [17] suggested that the trench fire geometry can be represented by a Froude number or dimensionless wind velocity, u_t*:

$$u_t^* = \frac{u_w}{2\sqrt{gW}} \tag{66.6}$$

The measured flame length as a function of the modified Froude number is shown in Fig. 66.5. The flame length correlation is

$$\frac{H}{W} = \begin{cases} 2.2 & u_t^* \geq 0.25 \\ 0.88 u_t^{*-0.65} & \text{for} \quad 0.25 < u_t^* \leq 0.1 \\ 4.0 & u_t^* \leq 0.1 \end{cases} \tag{66.7}$$

The flame drag distance along the ground, W', is given by the following expression:

$$\frac{W'}{W} = \begin{cases} 3.5 & u_t^* \geq 0.25 \\ 23.3 u_t^{*1.37} & \text{for} \quad 0.25 < u_t^* \leq 0.1 \\ 1 & u_t^* \leq 0.1 \end{cases} \tag{66.8}$$

The flame tilt, θ, is given by the following expression:

$$\frac{\theta}{\theta} = \begin{cases} 3.5 & u_t^* \geq 0.25 \\ 23.3 u_t^{*1.37} & \text{for} \quad 0.25 \leq u_t^* \leq 0.042 \\ 1 & u_t^* \leq 0.042 \end{cases} \tag{66.9}$$

Caution must be exercised in using the correlations given by Equations 66.7, 66.8, and 66.9 because they are based only on LNG fire data.

Thermal Radiation Hazards from Liquid Hydrocarbon Pool Fires

The structure of hydrocarbon pool fire flames generally follows the description of flames and plumes in Chap. 13. Figures 66.6, 66.7, and 66.8 show velocities and temperatures in heptane pool fires up to 6 m in diameter. Figure 66.6 shows velocities rising as the square root of height and maximizing near the top of the flame before declining. These general trends mirror that of smaller flames. Figure 66.7 shows the centerline temperatures of heptane pool fires. Although most of the results are similar to trends in smaller flames, the centerline temperatures for the 6 m pool are larger than is seen in smaller flames. This has been observed by others in large pool fires [32, 41]. Figure 66.8 shows the thermal structure of the lower portion of a 6 m heptane pool fire, which is remarkably similar to the trends in smaller flames.

Although the general thermal and flow structure of large hydrocarbon pool fires is similar to smaller flames, the radiative behavior of large

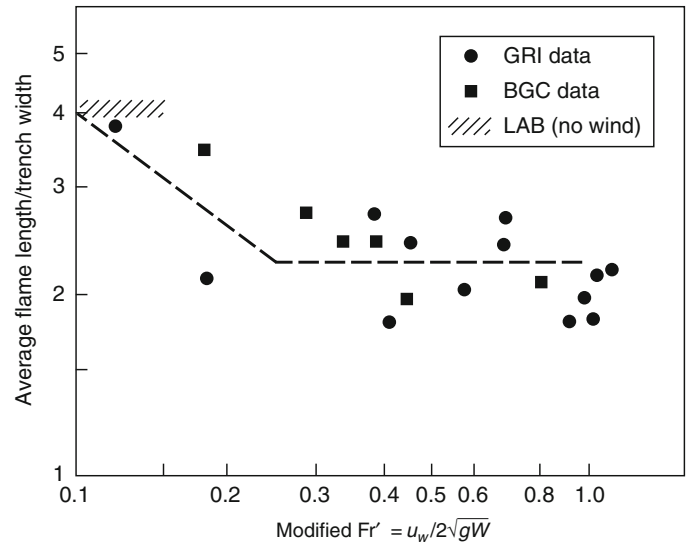

Fig. 66.5 Nondimensional flame height as a function of the Froude number [17]

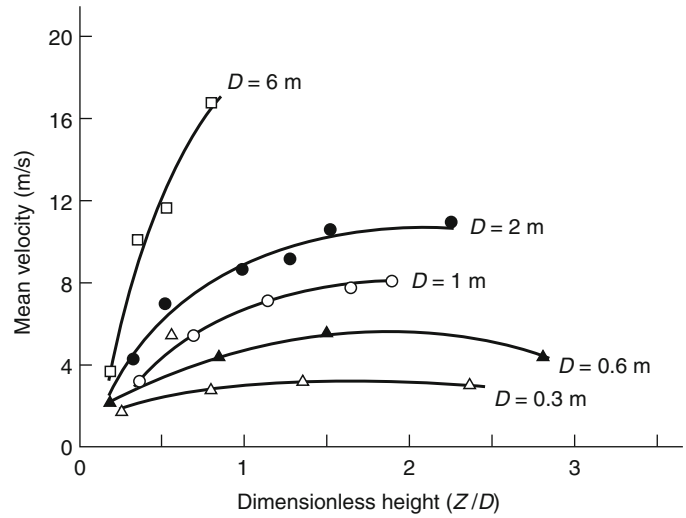

Fig. 66.6 Centerline upward velocities measured in heptane pool fires from 0.3 to 6.0 m diameters. Z is the height above the pool surface and D is the pool diameter [26]

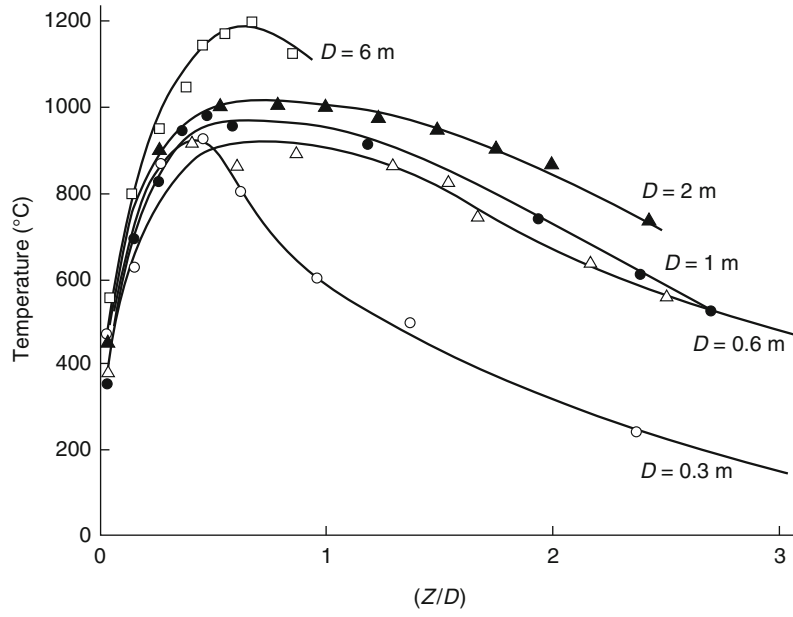

Fig. 66.7 Centerline temperatures measured in heptane pool fires from 0.3 to 6.0 m diameters. Z is the height above the pool surface and D is the pool diameter [26]

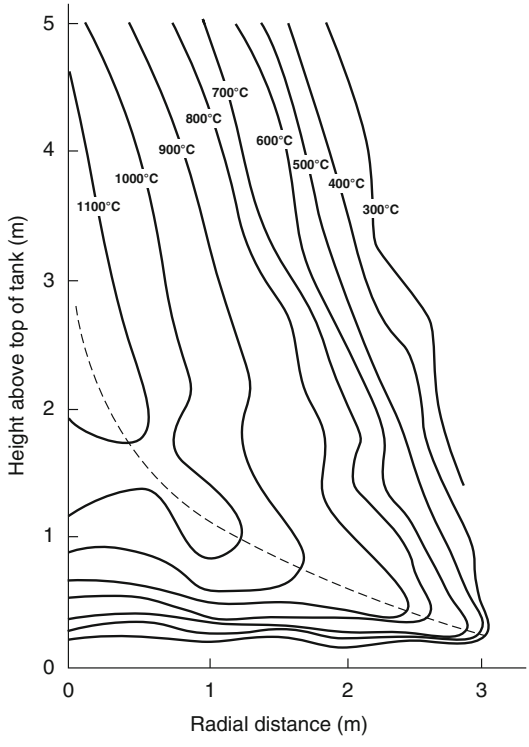

Fig. 66.8 Thermal structure of the near pool region of a 6-m-diameter heptane pool fire. The origin is the center of the pool surface [26]

pool fires is significantly different than smaller flames. Figure 66.9 shows the radiative fraction, the fraction of the heat release rate emitted as radiation, as a function of the pool diameter. The radiative fractions for diameters up to 1 m are in the region of 0.3–0.4, typical of sooty fuels in smaller fires. As the diameter of the pool fire increases beyond 1 m, the radiative fraction begins to decrease as smoke begins to obscure the flame from view and blocks radiation from the luminous flame regions. This effect becomes quite pronounced with radiative fractions as low as 0.05 for a 50-m-diameter kerosene pool fire.

Models and calculation procedures for radiation from hydrocarbon pool fires make use of simplifications and idealizations. Before delving into these methods, it is worthwhile to examine the actual radiative structure of pool fire flames as determined from detailed measurements [41]. In contrast to calculation methods, the radiant output of a pool fire is not uniform over a supposed flame surface area defined by the visible flame height and the pool diameter. Figure 66.10 shows the contours of mean emissive power from a 3-m-diameter gasoline pool fire and a 6-m-diameter diesel fuel pool fire.

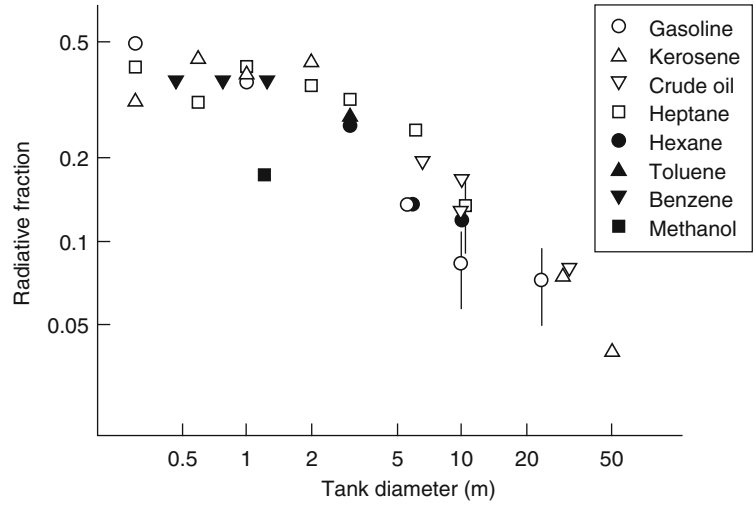

Fig. 66.9 Radiative fractions measured for pool fires from 0.3 to 50.0 m diameters [49]

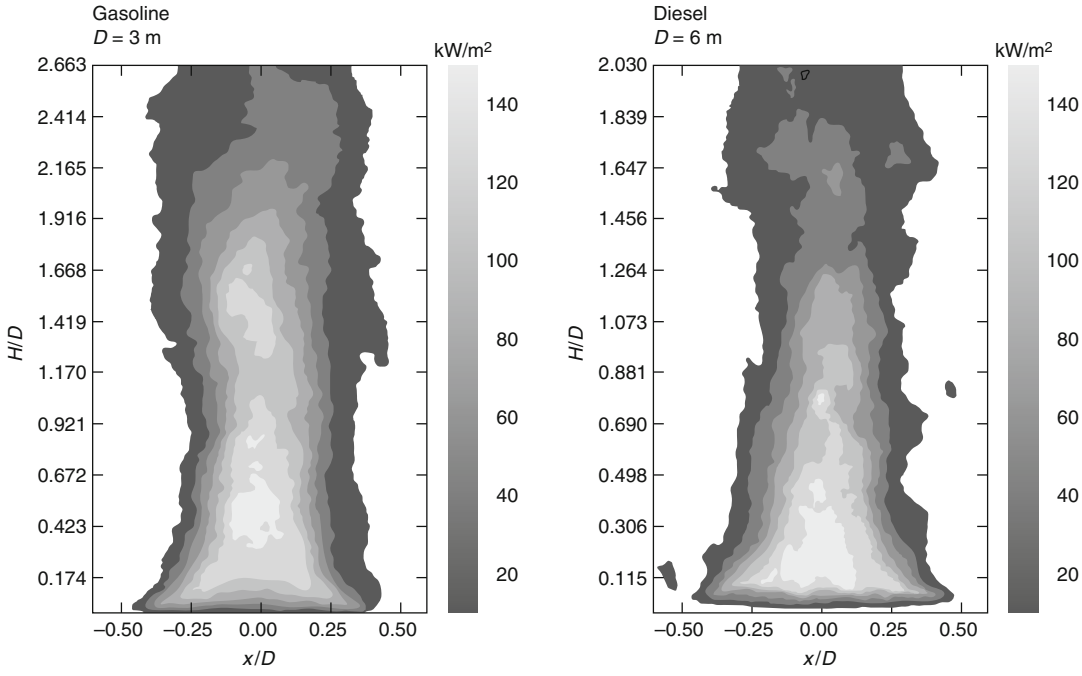

Fig. 66.10 Measured mean emissive power contours for a 3-m-diameter gasoline pool fire (*left*) and a 6-m-diameter diesel fuel pool fire (*right*) [41]

These contours were determined from quantitative infrared camera data. Clearly, the emissive power is a strong function of space, ranging from over 140 kW/m^2 to near zero within the cylindrical space that would normally be regarded as the flame in most pool fire radiation models. Figure 66.11 shows the emissive power averaged over the width of the radiation profile as a function of height above the pool surface normalized by the pool diameter. Note that the averaging occurs over a radial distance less than the pool diameter due to the necking of the flame as seen in Figs. 66.8 and 66.10. This look at actual pool fire emissive power distributions should tend to

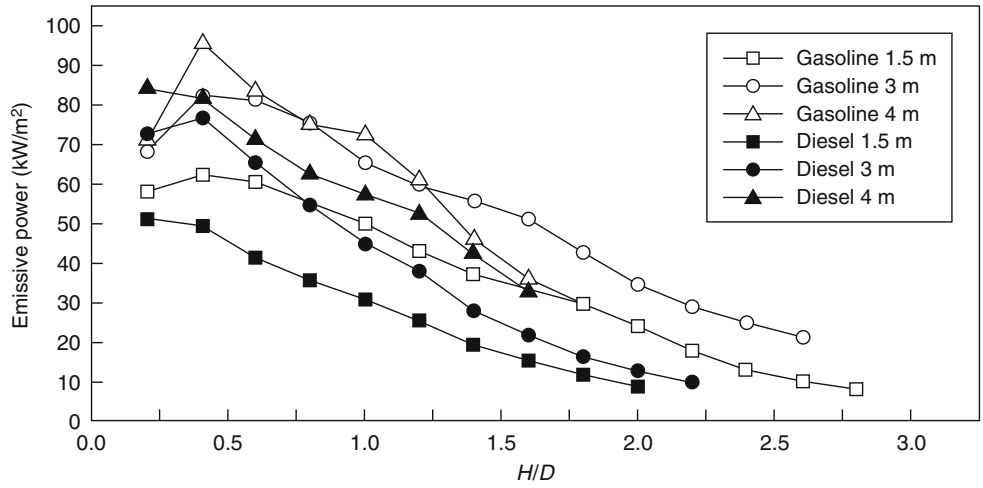

Fig. 66.11 Emissive power averaged over the measured flame width as a function of the nondimensional height above the pool surface [41]

remind us of the approximations made in defining a flame shape, height, and average emissive power over that shape. Although it is a useful formalism, the emissive power found and used in these methods should be regarded as an empirical fitting parameter that results in suitable agreement with radiant flux measurements at a distance. Also, it should tend to reinforce that methods described in the following sections should be used as a complete package without mixing methods or sources of data.

Calculation Procedure: Flame Radiation to External Target

This section provides methods for assessing the impact of radiation from pool fires to potential targets. The goal is to provide methods for calculating safe separation distances between fire sources and potential targets that would be damaged or adversely affected by radiation from the fire. The methods in this section include a range of levels of detail and rigor. Some methods are most appropriate for very crude initial hazard assessments, whereas the more detailed methods are capable of better predictions though requiring more engineering effort. Where separations exist and a simple method demonstrates that the separation is far more than required for safety, it may not be necessary to perform a more rigorous analysis. In other more critical applications, the highest accuracy methods available are required.

The methods presented in this section have been evaluated and included by the Society of Fire Protection Engineers (SFPE) in *Engineering Guide on Pool Fire Radiation* [50]. In that reference, the methods are described fully, the assumptions inherent in the methods are identified, limits of applicability are assessed, and available input data and data sources are identified. The accuracy of the methods are examined through comparisons of the methods with available experimental data.

Calculation Methods

Estimating the thermal radiation incident on an object involves the following three major steps:

1. Determine the geometric characteristics of the pool fire, that is, determine the burning rate and physical dimensions of the fire.
2. Determine thermal radiation characteristics of the fire.
3. Calculate the incident radiant flux at the target location.

It is extremely important that a single methodology be used for all three steps of this process. The available methods include empirical elements that, if indiscriminately used, can lead to unpredictable results. Because of this fact, each method is described fully and independently from other methods, even when some elements of the analysis appear similar.

Four methods for estimating radiation from pool fires were identified and evaluated [50]. Two methods are generally classifiable as simple screening methods and two are more detailed procedures. The screening methods include a very simple correlation developed by Shokri and Beyler [48], and the classical point source model. The more detailed procedures are those developed by Shokri and Beyler [48] and by Mudan [14].

Screening Methods

Shokri and Beyler Correlation Based on experimental data from large-scale pool fire experiments, Shokri and Beyler [48] developed a simple correlation of radiant heat flux at ground level as a function of the radial position of a vertical target. The incident heat-flux correlation (in kW/m^2) is given by

$$\dot{q}'' = 15.4\left(\frac{L}{D}\right)^{-1.59} \tag{66.10}$$

where D is the diameter of the pool fire and L is the distance from the center of the pool fire to the target edge. Note that the edge of the circular pool has a value of L/D of 0.5. Although this correlation was determined from circular pool fires, an equivalent-area circular source can be used for noncircular pools with an aspect ratio of approximately one. The equivalent diameter is given by

$$D = \sqrt{\frac{4A}{\pi}} \tag{66.11}$$

where A is the surface area of the noncircular pool.

This method assumes that the pool is circular or nearly circular. It assumes that the target is vertical and located at ground level. It is known that the radiant heat flux is maximized near the midheight of the radiating source and that a target facing the center of radiation will give the maximum heat flux at a given location. As such, at heights above ground level the radiant flux is expected to exceed that given by Equation 66.10.

Figure 66.12 shows a semilogarithmic plot of the data from Hägglund and Persson [18], Yamaguchi and Wakasa [19], Seeger [20], Yumoto [21], Dayan and Tien [22], and May and McQueen [23] with the correlation given by Equation 66.10. Figure 66.13 shows a comparison of the measured and predicted heat fluxes for the original data included in Fig. 66.12, as well as additional data from the literature that were not used to develop the correlation.

A safety factor of 2 is recommended for use with Equation 66.10 [50]. Figure 66.14 shows a comparison of all the available data to the predictions using Equation 66.10 with a safety factor of 2. Figure 66.14 clearly shows that essentially all the data is overpredicted by Equation 66.10 with a safety factor of 2 applied. The safety factor of 2 is a recommendation for use in design applications. Where a realistic result is required, no safety factor should be applied.

Point Source Model To predict the thermal radiation field of flames, it is customary to model the flame by a point source located at the center of real flame. The point source model is the simplest configurational model of a radiant source. Whereas more realistic radiator shapes give rise to very complex configuration factor equations, the point source model provides a simple relationship that varies with the inverse square of the distance, R. For an actual point source of radiation or a spherical source of radiation, the distance R is just the distance from the point or from the center of the sphere to the target. See Fig. 66.15 for a graphic representation of relevant nomenclature.

The point source model is widely used (see Drysdale [51], for example), though it has really never been developed as a rigorous methodology. The method as presented and evaluated here follows the development as given by Drysdale [51].

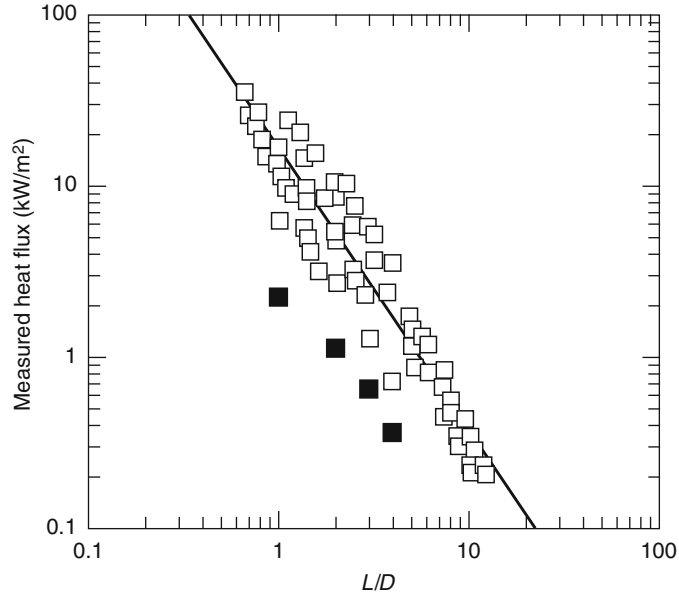

Fig. 66.12 Measured incident radiant heat flux at ground level to a vertical target as a function of the distance from the pool center to the target normalized by the pool diameter. Solid symbols are 50-m-diameter kerosene data. The *solid line* is Equation 66.10 [48]

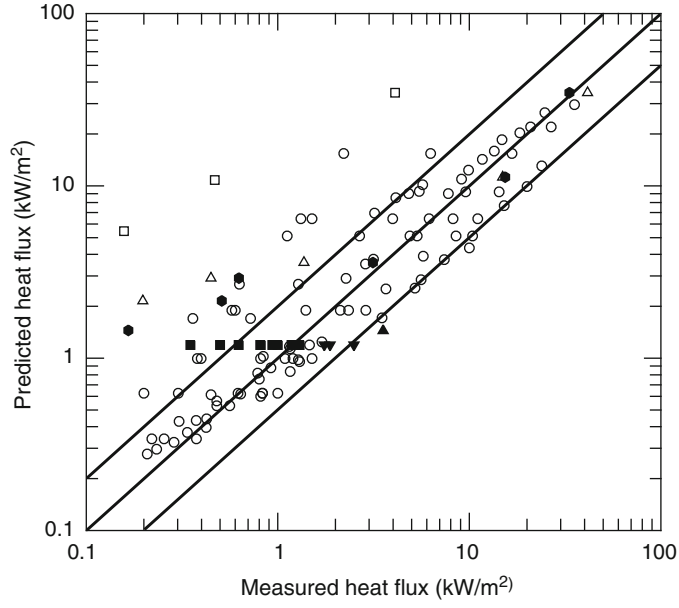

Fig. 66.13 Comparison of measured and calculated radiative heat flux from large pool fires using the Shokri and Beyler correlation (Equation 66.10). *Solid lines* indicate equality of measured and predicted heat fluxes based on the correlation developed by Shokri and Beyler [48]

The incident radiative heat flux is given by

$$\dot{q}'' = \frac{\dot{Q}_r \cos\theta}{4\pi R^2} \tag{66.12}$$

where

$\dot{Q}_r$ = Total radiative energy output of the fire

θ = Angle between the normal to the target and the line of sight from the target to the point source location

R = Distance from the point source to the target

The location of the equivalent point source, P, is at the center of the pool fire and at the midheight of the flame. The flame height in

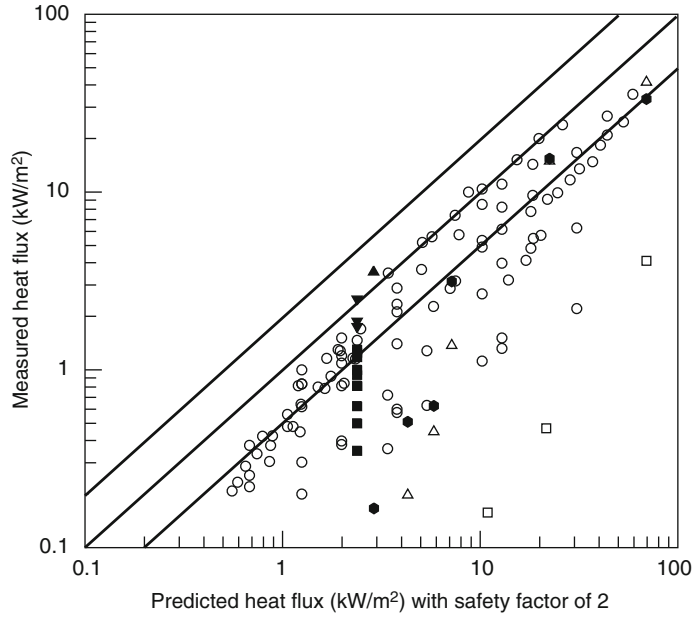

Fig. 66.14 Comparison of measured and calculated radiative heat flux from large pool fires using the Shokri and Beyler correlation (Equation 66.10) and a safety factor of 2. *Solid lines* indicate equality of measure and predicted heat fluxes based on the correlation developed by Shokri and Beyler [48] with a safety factor of 2

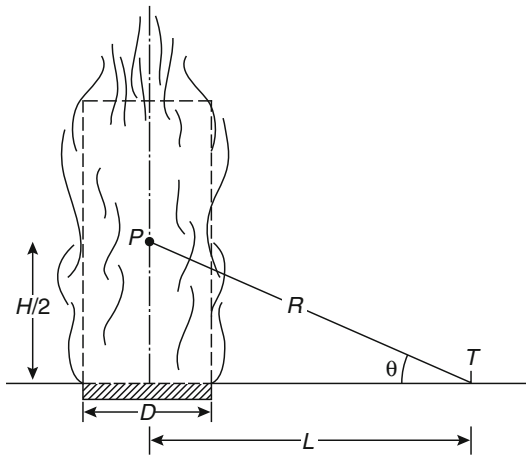

Fig. 66.15 Nomenclature for use with the point source model

meters is given by the Heskestad [42] correlation, Equation 66.13:

$$H = 0.235\dot{Q}^{2/5} - 1.02D \tag{66.13}$$

where $\dot{Q}$ is the heat release of the pool fire in kW and D is the diameter of the pool fire in meters.

If the pool has a length-to-width ratio near one, an equivalent diameter can be used for noncircular pools in the determination of the flame height. The equivalent diameter is given by Equation 66.11:

$$D = \sqrt{\frac{4A}{\pi}} \tag{66.11}$$

where A is the surface area of the noncircular pool.

The distance from the point source location to the target location is given by the Pythagorean theorem:

$$R = \sqrt{L^2 + {H_T}^2} \tag{66.14}$$

where H_T is the height of the target relative to the height of the equivalent point source at $H/2$, and L is the horizontal distance from the center of the pool to the target.

For a target on the ground, $H_T = H/2$. For a target at the midheight of the flame, $H_T = 0$.

The radiative energy output is given by the radiative fraction, χ_r, multiplied by the total heat release rate:

$$\dot{Q}_r = \chi_r \dot{Q} = (0.21 - 0.0034D)\dot{Q} \tag{66.15}$$

where the radiative fraction is a function of both the fuel and the pool area and D is the pool diameter in meters.

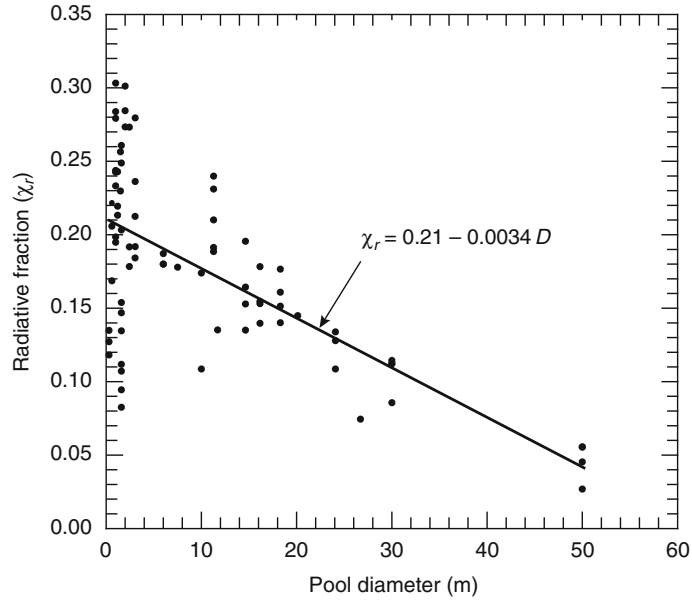

Fig. 66.16 Radiative fraction (χ_r) as a function of pool diameter. The *solid line* is a curve fit to the data [50]

The radiative fraction deduced from the experiments [50] is plotted in Fig. 66.16 as a function of pool diameter, D. The radiative fractions were determined using the point source method for the most remote data point for each experiment. The curve fit used in Equation 66.15 above is also shown in Fig. 66.16. At pool diameters above 50 m, the radiative fraction for 50 m should be used.

Estimating the thermal radiation from a pool fire to a target involves the following steps based on the point source model:

1. Determine the heat release rate, $\dot{Q}_r$.
2. Determine the diameter of the pool fire, or use Equation 66.11 for noncircular pools.
3. Determine the location of the equivalent point source, P. The equivalent point source is on the centerline of the pool at a height equal to one-half the flame height given by Equation 66.13.
4. Calculate the distance, R, from the equivalent point source location to the target location using Equation 66.14.
5. Determine the radiative output of the flame from Equation 66.15.
6. Calculate the radiative heat flux to the target using Equation 66.12.

Figure 66.17 shows a comparison of all the available data with the prediction of the point source model [52]. The lines shown on the plot reflect predictions that are one-half and twice those of the measured data. At heat fluxes above about 5 kW/m^2, there are systematic, non-conservative results.

The point source configuration factor is known to be a very simplistic representation of a pool fire. It is a correct assumption at large distances from the fire. A theoretical analysis of radiation from a small pool fire by Modak [52] indicated that the point source model is within 5 % of the correct incident heat flux when L/D is greater than 2.5. This result is, however, dependent on the specific flame modeled and was not derived from experimental data. The method is known to underpredict incident heat fluxes at closer locations (e.g., see Drysdale [51]). The poor performance at heat fluxes above 5 kW/m^2 indicates that the point source model is not a good choice under conditions where ignition of combustibles is to be considered.

A safety factor of 2 is recommended for use with the point source model at heat fluxes less than 5 kW/m^2. Figure 66.18 is a comparison of predicted and measured heat fluxes with the

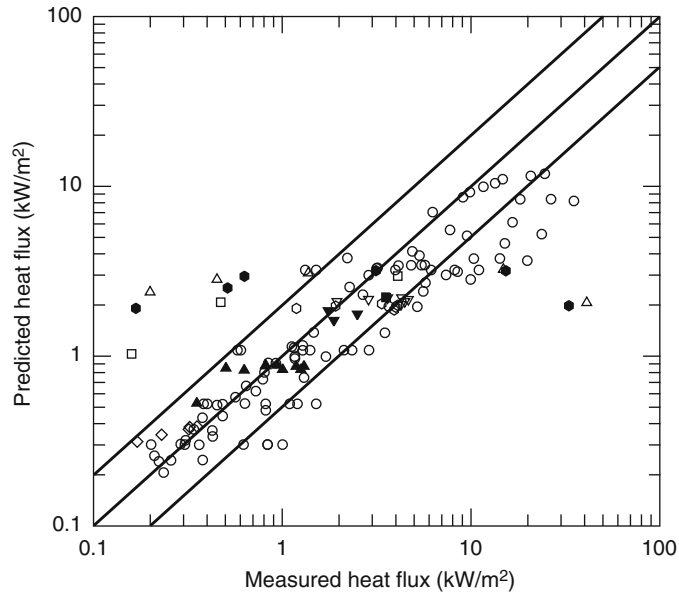

Fig. 66.17 Comparison of measured and calculated radiative heat flux from large pool fires using the point source model. *Solid lines* indicate equality of measured and predicted heat fluxes based on the point source model

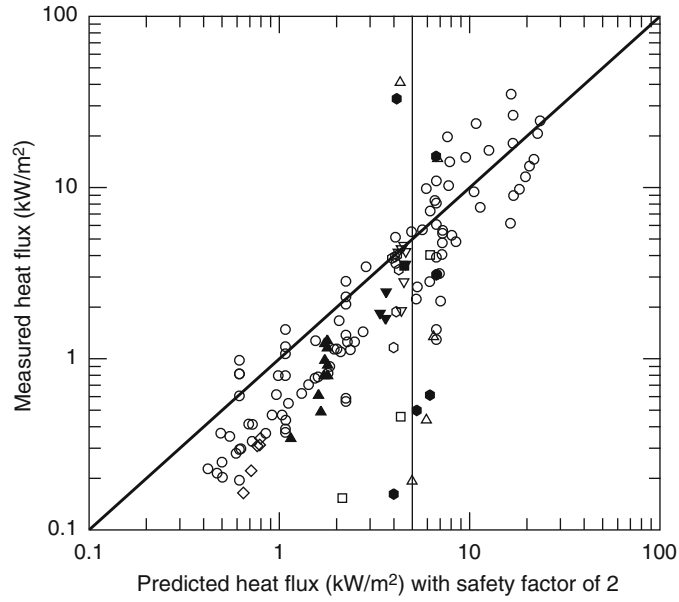

Fig. 66.18 Comparison of measured and calculated radiative heat flux from large pool fires using the point source model and a safety factor of 2. *Solid lines* indicate equality of measured and predicted heat fluxes based on the point source model

inclusion of the recommended factor of safety. The vertical line is located at the maximum heat flux for which the point source model is recommended for use. Figure 66.18 clearly shows that essentially all the data are overpredicted by the point source model with a safety factor of 2 applied for heat fluxes less than 5 kW/m^2. The safety factor of 2 is a recommendation for use in design applications. Where a realistic result is required, no safety factor should be applied.

Detailed Methods

Shokri and Beyler Shokri and Beyler [48] have described a method for prediction of radiation from pool fires based on the pool fire radiation

data available in the open literature. They correlated experimental data of flame radiation to external targets in terms of an average effective emissive power of the flame. The flame is assumed to be a cylindrical, blackbody, homogeneous radiator with an average emissive power. Shokri and Beyler [48] have treated radiant heat transfer from a source to a target based on the concept of the angle factor, also variously known as the shape, geometrical, configuration, or view factors, including those given by many authors [1, 3, 53–60] and the incident radiative flux (in kW/m^2) to a target outside the flame, $\dot{q}''$ is given by

$$\dot{q}'' = EF_{12} \tag{66.16}$$

where E is the emissive power of the pool fire flame, kW/m^2, and F_{12} is the view or configuration factor between the target and the flame.

The configuration factor is a function of the target location, the flame height, and the diameter, and lies between zero and one. When a target is very close to a flame, the configuration factor approaches one because everything viewed by the target is the flame. The flame is idealized as a cylinder with a diameter equal to the pool diameter, D, and a height equal to the flame height, H_f. If the pool has a length-to-width ratio near one, an equivalent-area circular source can be used for noncircular pools in the determination of flame height. For noncircular pools, the effective diameter will be defined as the diameter of a circular pool with an area equal to the actual pool area given by Equation 66.11:

$$D = \sqrt{\frac{4A}{\pi}} \tag{66.11}$$

where A is the surface area of the noncircular pool.

Flame height of the pool fire flame is determined using the Heskestad [42] correlation given by Equation 66.13:

$$H = 0.235\dot{Q}^{2.5} - 1.02D \tag{66.13}$$

where

H = Flame height, m
$\dot{Q}$ = Heat release of the pool fire, kW
D = Diameter of the pool fire, m

Given the diameter and height of the flame, the view factor, F_{12}, is determined using Equation 66.17 applicable to cylindrical radiation sources. For horizontal and vertical target orientations, expressions for estimating the configuration factor are found in Equations 66.17a and 66.17b, respectively.

$$F_{12,H} = \frac{(B - 1/S)}{\pi\sqrt{B^2 - 1}} \tan^{-1}\sqrt{\frac{(B+1)(S-1)}{(B-1)(S+1)}} - \frac{(A - 1/S)}{\pi\sqrt{A^2 - 1}} \tan^{-1}\sqrt{\frac{(A+1)(S-1)}{(A-1)(S+1)}} \tag{66.17a}$$

$$F_{12,V} = \frac{1}{\pi S}\tan^{-1}\left(\frac{h}{\sqrt{S^2-1}}\right) - \frac{h}{\pi S}\tan^{-1}\sqrt{\frac{(S-1)}{(S+1)}} + \frac{Ah}{\pi S\sqrt{A^2-1}}\tan^{-1}\sqrt{\frac{(A+1)(S-1)}{(A-1)(S+1)}} \tag{66.17b}$$

where

$$A = \frac{h^2 + S^2 + 1}{2S}, \qquad B = \frac{1 + S^2}{2S}$$
$$S = \frac{2L}{D}, \quad h = \frac{2H}{D}$$

and

L = Distance between the center of the cylinder to the target
H = Height of the cylinder
D = Cylinder diameter

See Figs. 66.19 and 66.20 for an illustration of the nomenclature.

The maximum configuration or shape factor at a point is given by the vectorial sum of the horizontal and vertical view factors:

$$F_{12,\max} = \sqrt{F_{12,H}^2 + F_{12,V}^2} \tag{66.18}$$

Precalculated maximum view factors are shown in Figs. 66.21, 66.22, 66.23, 66.24, and 66.25.

Fig. 66.19 Cylindrical flame-shape configuration factor geometry for vertical and horizontal targets at ground level

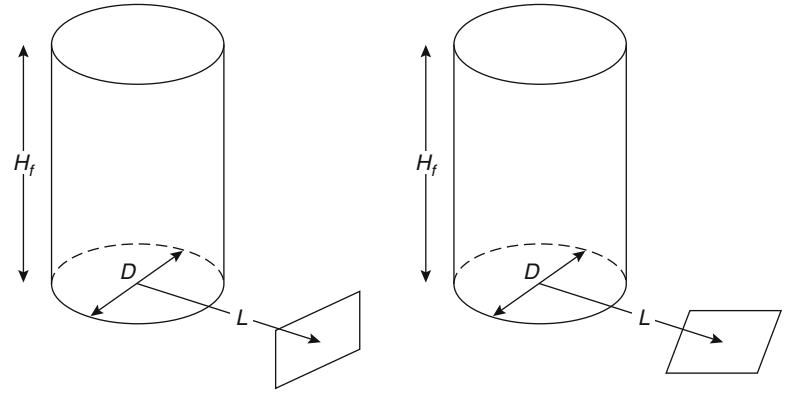

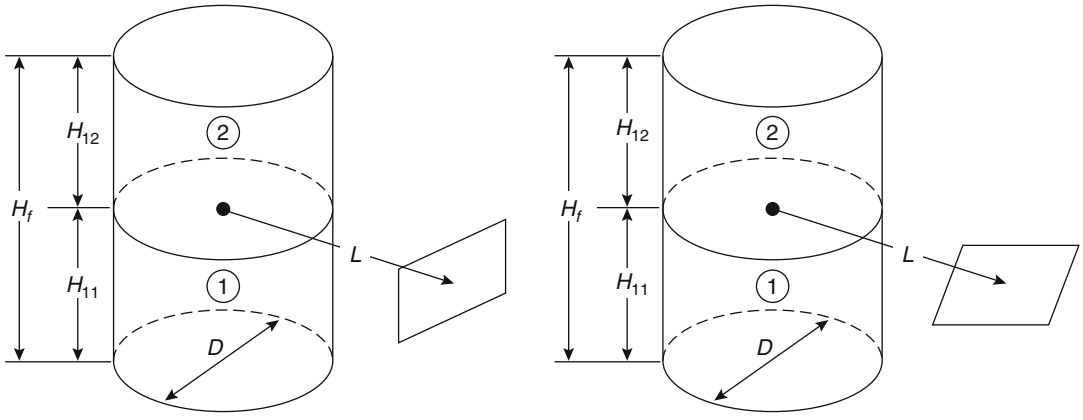

Fig. 66.20 Two-cylinder representations of the configuration factor for target above ground level

Fig. 66.21 Maximum configuration factor for a flame height to pool fire radius ratio $H/R_p = 2$

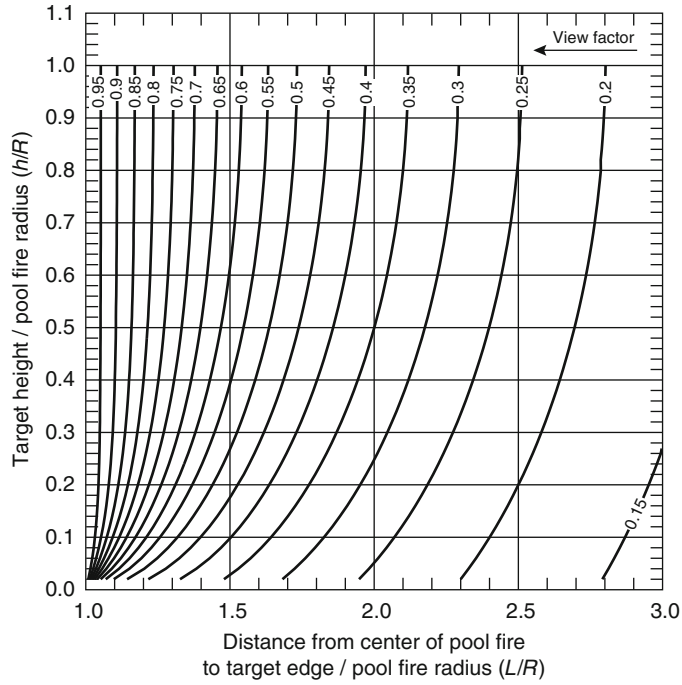

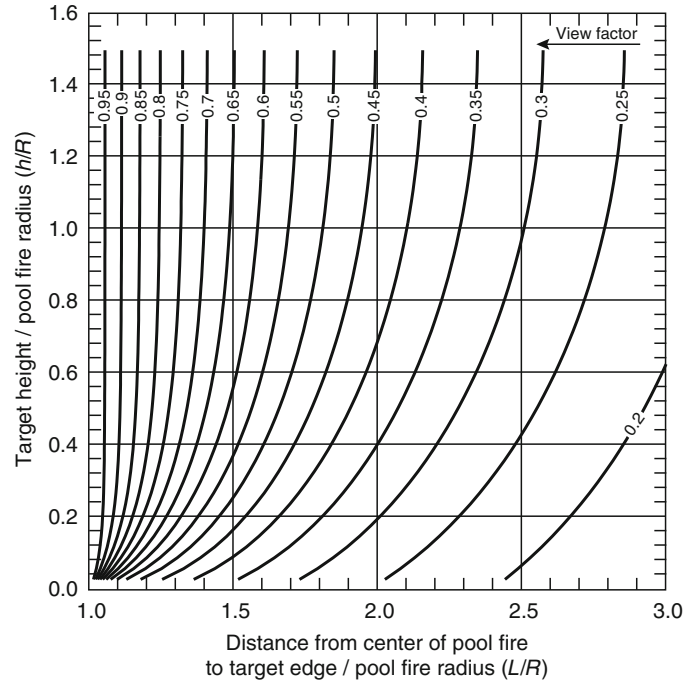

Fig. 66.22 Maximum configuration factor for flame height to pool fire radius of ratio $H/R_p = 3$

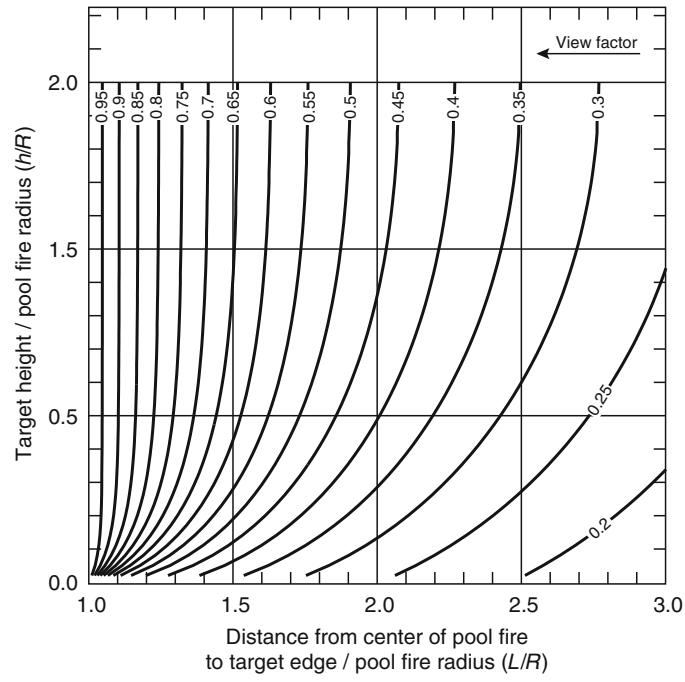

Fig. 66.23 Maximum view factor for a flame height to pool fire radius ratio $H_f/R = 4$

Each figure gives the maximum view factor for a flame of a particular flame height to pool radius ratio (H/R_p): 2, 3, 4, 5, and 6, respectively. The target location is defined in each figure by the ratio of the target height to the pool radius, and the ratio of the distance of the target from the pool center to the pool radius. The view factors are represented as contours. The figures

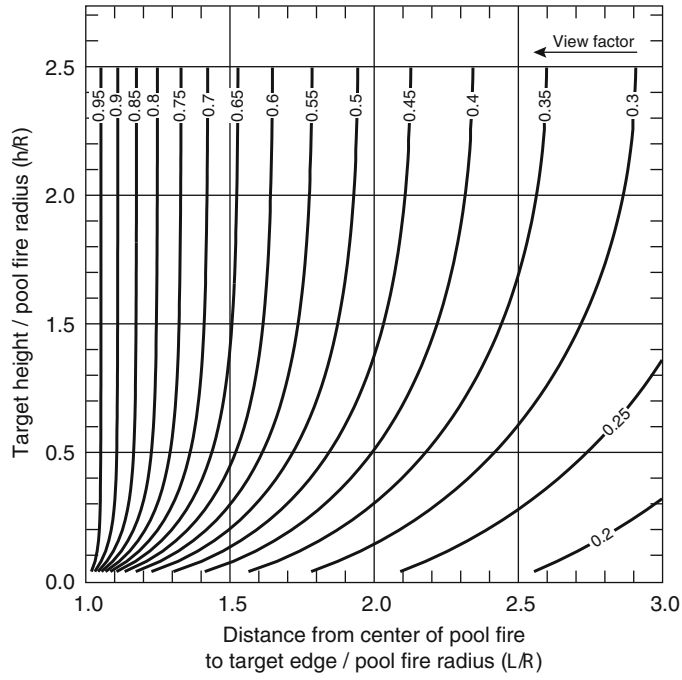

Fig. 66.24 Maximum configuration factor for a flame height to pool fire radius ratio $H/R_p = 5$

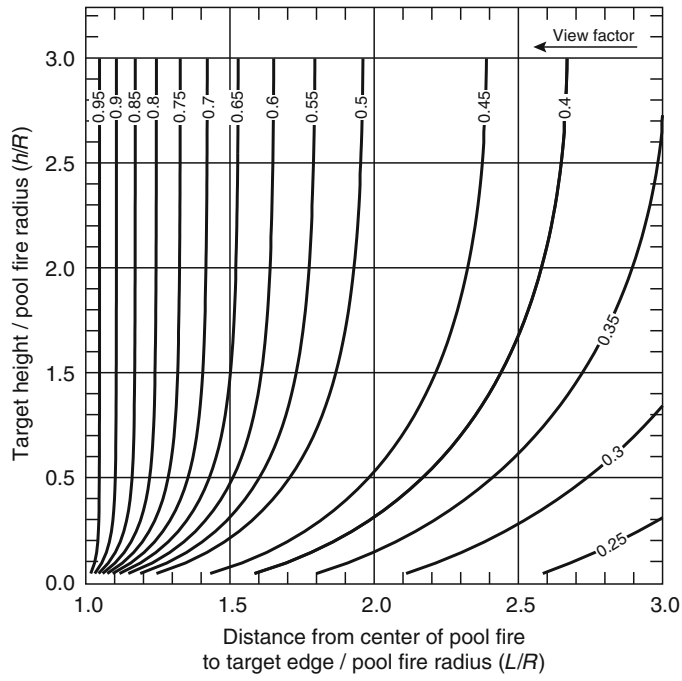

Fig. 66.25 Maximum configuration factor for a flame height to pool fire radius ratio $H/R_p = 6$

include only target locations up to one-half the flame height. The curves for target heights above one-half the flame height are symmetric about the half-height and as such need not be included. For example, the view factor for a target at one-fourth of the flame height and three-fourths of the flame height are identical.

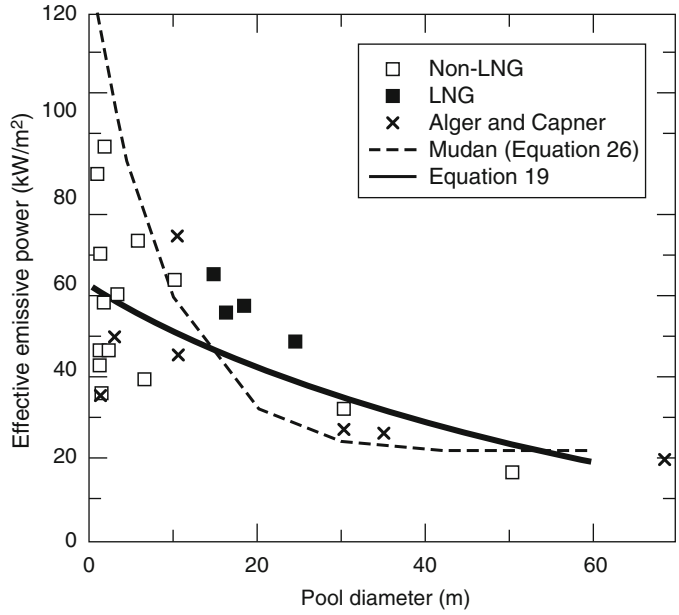

Fig. 66.26 Effective emissive power as a function of the pool diameter determined by Shokri and Beyler [48]. The *solid line* is Equation 66.19 and the *dashed line* is Equation 66.26

Shokri and Beyler [48] determined the effective emissive power of the flame by fitting experimental measurements of radiant heat flux from pool fires to external targets. The effective emissive power of the pool fire in terms of effective pool diameter is given by the following correlation:

$$E = 58\left(10^{-0.00823D}\right) \tag{66.19}$$

This represents the average emissive power over the whole of the flame and is significantly less than the emissive powers that can be attained locally. The emissive power is reduced with increasing pool diameter due to the increasing prominence of black smoke outside the flame that obscures the radiation from the luminous flame. Figure 66.26 is a comparison of Equation 66.19 with the data used by Shokri and Beyler [48] to develop Equation 66.19.

Figure 66.27 shows a comparison of the predicted and measured heat fluxes, using the best fit emissive power for each experiment (the value plotted in Fig. 66.26). Figure 66.27 shows that the cylindrical model is an excellent representation of the view factor over a wide range of conditions. Figures 66.26 and 66.27 together illustrate that the major uncertainty is in the definition of the emissive power and not in the view factor model. Figure 66.28 shows the overall performance of the model.

Summary of the Procedure for the Shokri and Beyler Pool Fire Radiation Method Estimating the thermal radiation field surrounding a fire involves the following steps based on the method developed by Shokri and Beyler [48]:

1. Determine the heat release rate, $\dot{Q}$.
2. Determine the height of the pool fire flame from Equation 66.14.
3. Calculate the view factor from Equation 66.17 (and Equation 66.18, if needed). If the target is above ground level, then a two cylinder representation is required. Alternatively, the precalculated view factors in Figs. 66.21, 66.22, 66.23, 66.24, and 66.25 may be used.
4. Determine the effective emissive power of the flame from Equation 66.19.
5. Calculate the radiative heat flux to the target using Equation 66.16.

Factor of Safety A safety factor of 2 is recommended for use with the Shokri and Beyler method [50]. Since this method is most applicable at heat fluxes greater than 5 kW/m^2, the

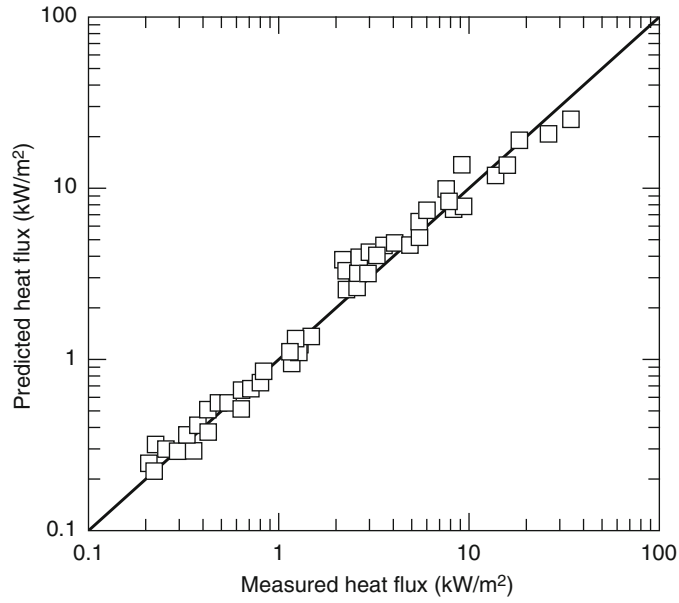

Fig. 66.27 Comparison of measured and calculated incident radiant heat flux using effective emissive powers. The *solid line* indicates equality of the measured and predicted heat fluxes based on the method developed by Shokri and Beyler [48]

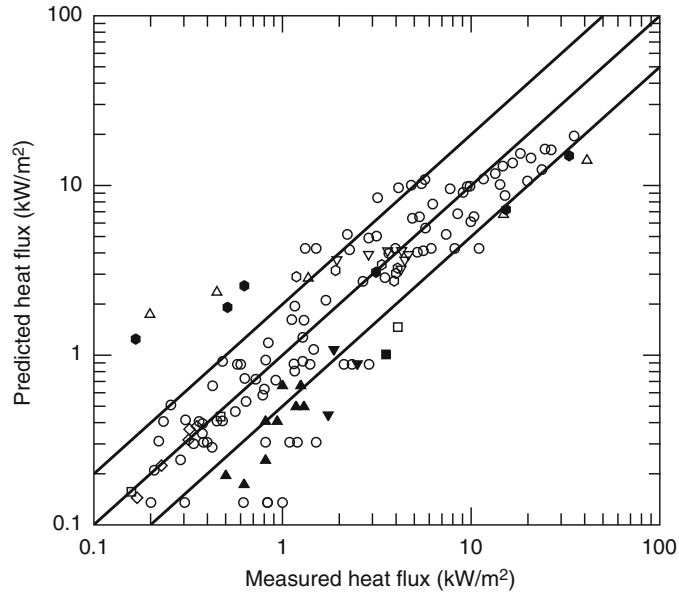

Fig. 66.28 Comparison of measured and calculated radiative heat flux from large pool fires using the detailed method developed by Shokri and Beyler [48]. *Solid lines* indicate equality of measured and predicted heat fluxes based on the method developed by Shokri and Beyler [48]

recommended factor of safety is applicable only for heat fluxes above this level. Figure 66.29 is a comparison of predicted and measured heat fluxes with the inclusion of the recommended factor of safety. The vertical line is located at the minimum heat flux for which the Shokri and Beyler model is recommended for use. Figure 66.24 clearly shows that essentially all of the data are overpredicted by the Shokri and Beyler model with a safety factor of 2 applied for heat fluxes greater than 5 kW/m^2. The safety factor of 2 is a recommendation for use in design applications. Where a realistic result is required, no safety factor should be applied.

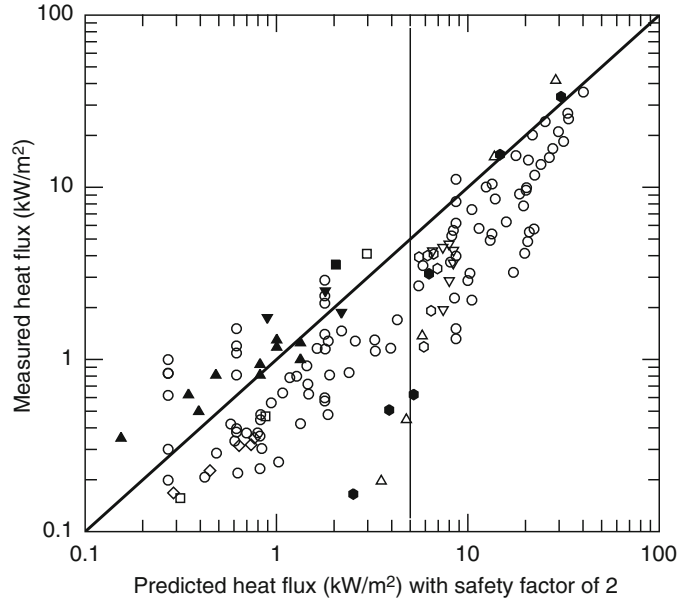

Fig. 66.29 Comparison of measured and calculated radiative heat flux from large pool fires using the detailed method developed by Shokri and Beyler and a safety factor of 2. *Solid lines* indicate equality of measured and predicted heat fluxes based on the detailed method developed by Shokri and Beyler [48] with a safety factor of 2

Mudan Method Mudan [14] has presented a method for estimating thermal radiation from pool fires for no-wind conditions and for wind-blown flames. The thermal radiation intensity to an element outside the flame envelope is given by the following equation:

$$\dot{q}'' = EF_{12}\tau \tag{66.20}$$

where

E = Average emissive power at flame surface, kW/m^2

F_{12} = View factor

τ = Atmospheric transmissivity

Equation 66.20 is used with the assumption that the flame is a vertical or tilted cylinder. This requires the flame diameter and height to be determined. The flame diameter is taken to be the pool diameter, D. See Fig. 66.30 for general nomenclature.

The flame height correlation used in this method is based on the correlation of mean visible height, H_f, of turbulent diffusion flames (in absence of wind) developed by Thomas [38]. The correlation for a circular fire is given by Equation 66.21:

$$\frac{H}{D} = 42\left(\frac{\dot{m}''_\infty}{\rho_a\sqrt{gD}}\right)^{0.61} \tag{66.21}$$

where

D = Pool diameter

$\dot{m}''_\infty$ = Mass burning rate per unit pool area, kg/m^{2}s

ρ_a = Ambient air density, kg/m^3

g = Gravitational acceleration, 9.8 m/s^2

If the pool has a length-to-width ratio near one, an equivalent-area circular source can be used for noncircular pools in the determination of the flame height. For noncircular pools, the effective diameter will be defined as the diameter of a circular pool with an area equal to the actual pool area, given by Equation 66.11 as

$$D = \sqrt{\frac{4A}{\pi}} \tag{66.11}$$

In the presence of wind, the flame length is given by the following correlation developed by Thomas [38] (Equation 66.22):

$$\frac{H}{D} = 55\left(\frac{\dot{m}''_\infty}{\rho_a\sqrt{gD}}\right)^{0.67} \left(u^*\right)^{-0.21} \tag{66.22}$$

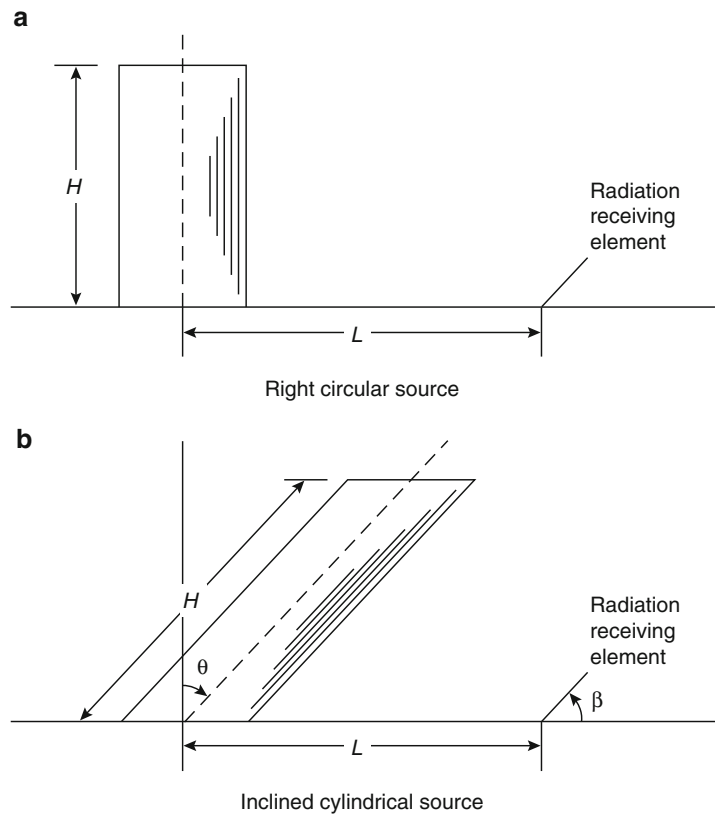

Fig. 66.30 Configuration factor calculation geometries for right and inclined cylinders

where u^* is the nondimensional wind velocity given by Equation 66.22:

$$u^* = \frac{u_w}{\left(g\dot{m}''_\infty D/\rho_a\right)^{1/3}} \tag{66.2}$$

where u_w is the wind speed, m/s, and ρ_a is the ambient density, kg/m^3.

In the presence of a significant wind, the flame may not remain vertical, and a flame tilt angle due to the wind is relevant to the assessment of radiation. The American Gas Association (AGA) [37] proposed the following correlation to determine the flame tilt (Equation 66.23):

$$\cos\theta = \begin{cases} 1 & \text{for } u^* \le 1 \\ 1/\sqrt{u^*} & \text{for } u^* \ge 1 \end{cases} \tag{66.23}$$

where u* is the nondimensional wind velocity given by Equation 66.19 with the wind velocity measured at a height of 1.6 m above the ground.

The turbulent flame is approximated by a cylinder. Under wind-free conditions, the cylinder is vertical (Fig. 66.30a). Under the influence of wind, the cylinder is assumed to be tilted (Fig. 66.30b). View factors for horizontal and vertical targets of a vertical cylinder for no-wind conditions are as follows:

$$F_{12,V} = \frac{1}{\pi S}\tan^{-1}\left(\frac{h}{\sqrt{S^2-1}}\right) - \frac{h}{\pi S}\tan^{-1}\sqrt{\frac{(S-1)}{(S+1)}} + \frac{Ah}{\pi S\sqrt{A^2-1}}\tan^{-1}\sqrt{\frac{(A+1)(S-1)}{(A-1)(S+1)}} \tag{66.24a}$$

$$F_{12,H} = \frac{(B-1/S)}{\pi\sqrt{B^2-1}}\tan^{-1}\sqrt{\frac{(B+1)(S-1)}{(B-1)(S+1)}} - \frac{(A-1/S)}{\pi\sqrt{A^2-1}}\tan^{-1}\sqrt{\frac{(A+1)(S-1)}{(A-1)(S+1)}} \tag{66.24b}$$

where

$$S = \frac{2L}{D} \quad h = \frac{2H}{D}$$
$$A = \frac{h^2 + S^2 + 1}{2S} \quad B = \frac{1 + S^2}{2S}$$

and

L = Distance between the center of the pool fire and the target
H = Height of the pool fire
D = Pool fire diameter

If the target is either at ground level or at the flame height, then a single cylinder can represent the flame. If the target is above the ground, then two cylinders must be used to represent the flame. One cylinder represents the flame below the height of the target, and the other represents the flame above the height of the target. See Fig. 66.20 for an illustration of the nomenclature.

The overall view factor is the sum of the two component view factors.

The maximum configuration factor at a point is given by the vectorial sum of the horizontal and vertical target configuration factors given by Equation 66.18:

$$F_{12,\max} = \sqrt{F_{12,H}^2 + F_{12,V}^2} \tag{66.18}$$

The configuration exchange factor for windblown flame has been given by Mudan [57], who employed a contour integral approach developed by Sparrow [58] to determine closed-form equations for view factors from a tilted cylinder.

The view factor for a tilted cylindrical flame with a circular base is as follows:

$$\begin{aligned}\pi F_V = {} & \frac{a\cos\theta}{b - a\sin\theta}\frac{a^2 + (b+1)^2 - 2b(1 + a\sin\theta)}{\sqrt{AB}}\tan^{-1}\sqrt{\frac{A}{B}\left(\frac{b-1}{b+1}\right)}^{1/2} \\ & + \frac{\cos\theta}{\sqrt{C}} \times \left[\tan^{-1}\frac{ab - \left(b^2 - 1\right)\sin\theta}{\sqrt{b^2 - 1}\sqrt{C}} + \tan^{-1}\frac{\left(b^2 - 1\right)\sin\theta}{\sqrt{b^2 - 1}\sqrt{C}}\right] \\ & - \frac{a\cos\theta}{(b - a\sin\theta)}\tan^{-1}\sqrt{\frac{b-1}{b+1}}\end{aligned} \tag{66.25a}$$

$$\begin{aligned}\pi F_H = {} & \tan^{-1}\sqrt{\frac{b+1}{b-1}} \\ & - \frac{a^2 + (b+1)^2 - 2(b + 1 + ab\sin\theta)}{\sqrt{AB}} \times \tan^{-1}\sqrt{\frac{A}{B}\left(\frac{b-1}{b+1}\right)}^{1/2} \\ & + \frac{\sin\theta}{\sqrt{C}} \times \left[\tan^{-1}\frac{ab - \left(b^2 - 1\right)\sin\theta}{\sqrt{b^2 - 1}\sqrt{C}} + \tan^{-1}\frac{\left(b^2 - 1\right)^{1/2}\sin\theta}{\sqrt{C}}\right]\end{aligned} \tag{66.25b}$$

where

$a = H/R$
$b = L/R$
$A = a^2 + (b+1)^2 - 2a(b+1)\sin\ \theta$
$B = a^2 + (b-1)^2 - 2a(b-1)\sin\ \theta$
$C = 1 + \left(\mathrm{b}^2 - 1\right)\cos^2\theta$

When the angle of tilt is zero, Equations 66.25a and 66.25b reduce to Equations 66.24a and 66.24b, respectively. The maximum configuration factors at the target location are determined using Equation 66.18. Figures 66.31 and 66.32 show the calculated configuration factor for no-wind conditions and underwind conditions for a target at ground level. For the no-wind condition, Fig. 66.20 can also be used to determine the view factor for a more general set of target locations.

The emissive power, E, of the flame is given by the following correlation:

$$E = E_{\max}\mathrm{e}^{-sD} + E_s\left[1 - \mathrm{e}^{-sD}\right] \tag{66.26}$$

where

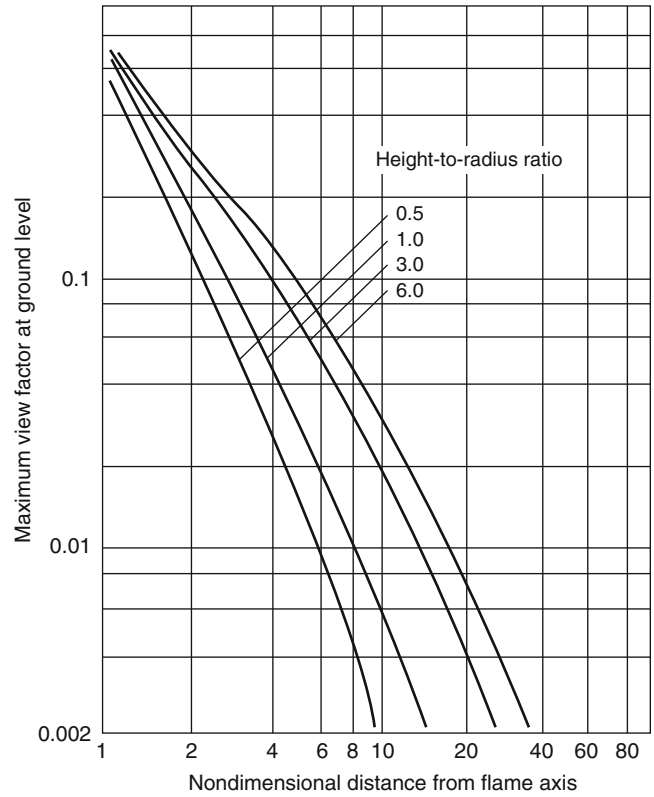

Fig. 66.31 Maximum configuration factors for a ground-level object from a right circular cylinder. The nondimensional distance from the flame is L/R

E = Equivalent blackbody emissive power, 140 kW/m^2
s = Extinction coefficient, 0.12 m^{-1}
D = Equivalent pool diameter, m
E_s = Emissive power of smoke, 20 kW/m^2

Atmospheric Absorption

The radiation from the fire to surrounding objects will be partially attenuated by absorption and scattering along the intervening path. The principal constituents of the atmosphere that absorb thermal radiation are water vapor (H_2O) and carbon dioxide (CO_2). Table 66.3 indicates the composition of various gases in the atmosphere. The CO_2 content in the atmosphere is generally constant at about 330 ppm by volume. The water vapor content varies strongly with temperature and humidity. Figure 66.33 indicates the relationship between atmospheric temperature, relative humidity, and the amount of precipitable water vapor in a given pathlength.

The principal absorption bands for water vapor are at 1.8, 2.7, and 6.27 μm. Minor absorption bands also exist at 0.94, 1.1, 1.38, and 3.2 μm. Strong absorption by CO_2 exists in the 2.7 μm region, the 4.3 μm region, and the region between 11.4 and 20 μm. Weaker absorption bands are present at 1.4, 1.6, 2.0, 4.8, 5.2, 9.4, and 10.4 μm. As the temperature of the emitting or absorbing species increases, the bands tend to broaden.

A useful concept for the quick estimation of atmospheric absorption of continuum radiation is the "equivalent bandwidth of complete absorption." One calculates the integral of absorption over an absorption band and interprets the result as the width of a "rectangular," *complete* absorption band equivalent to the real band profile. For a continuum source, the effect of such opaque bands is then easy to estimate. Three absorption

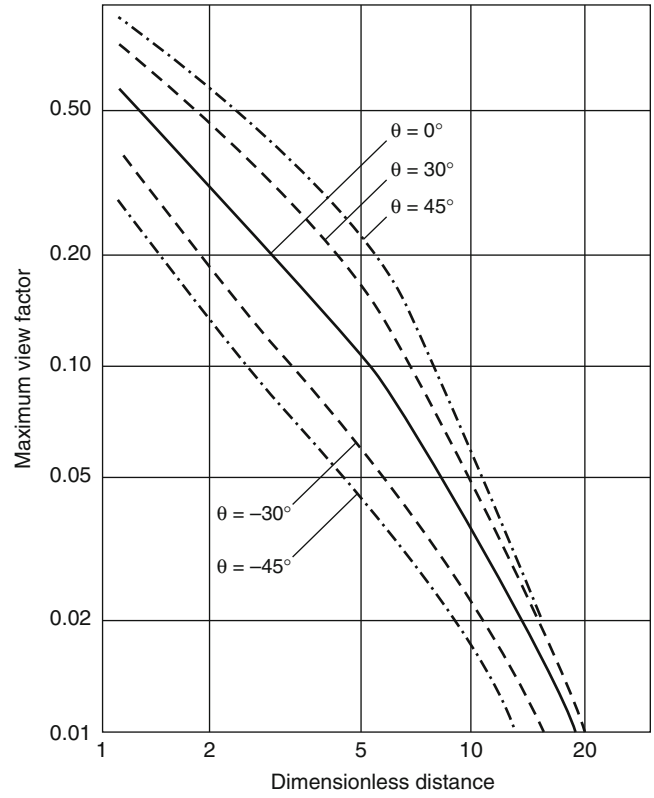

Fig. 66.32 Maximum configuration factors for tilted circular cylinders with targets at ground level. The dimensionless distance is L/R

bands in the range of interest (5.5 m → 5.5 μm) can be described in this way. These are the water vapor bands at 1.87 and 2.7 μm and the 4.3 μm, CO_2 band. The water absorption beyond about 4.7 μm is not as readily dealt with, because the band structure is not narrow compared to the range of interest. However, the fraction of total energy from a 1300 K blackbody that lies beyond 4.7 μm is about 25 % and that beyond 5.5 μm is only 19%. The results of total absorption bandwidth calculations for the above three bands of interest are given in Tables 66.4 and 66.5. These calculations are based on the data available in the *Infrared Handbook* [59]. Also given in the tables are the fractions of a 1300 K blackbody energy that will be absorbed in each of these bands.

The absorption by the water vapor and carbon dioxide in a certain length of the atmosphere of blackbody radiation from a source can also be

Table 66.3 Composition of constituent gases in the atmosphere and their concentrations

Constituent gas	Concentration in atmosphere (% by volume)
Nitrogen	78.088
Oxygen	20.949
Argon	0.93
Carbon dioxide	0.033
Neon	1.8 × 10−3
Helium	5.24 × 10−4
Methane	1.4 × 10−4
Krypton	1.14 × 10−4
Nitrous oxide	5.0 × 10−5
Carbon monoxide	2.0 × 10−5
Xenon	8.6 × 10−6
Hydrogen	5.0 × 10−6
Ozone	Variable
Water vapor	Variable (depends on temperature and relative humidity)

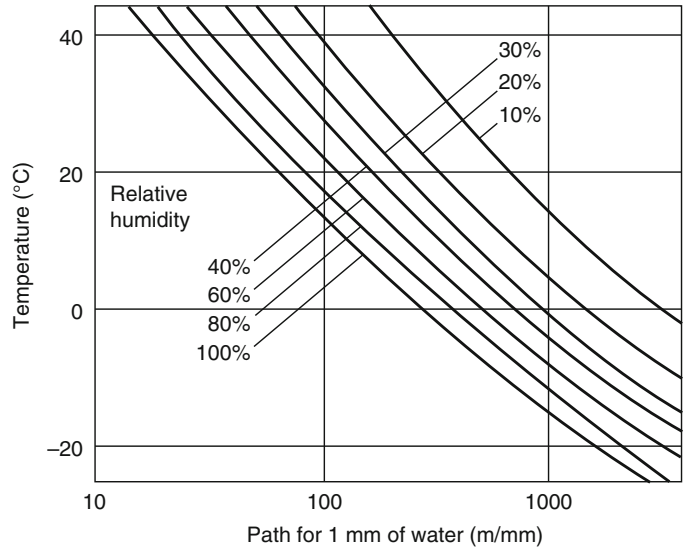

Fig. 66.33 Variation of precipitable water content of the atmosphere with temperature, humidity, and pathlength

Table 66.4 Total absorption bandwidth for 1.87-and 2.7-mm bands at 300 K

	1.87 μm Band		2.7 μm Band	
Precipitable Water (mm)	Total absorption Bandwidth, Δλ (μm)	Fraction of 1300 K Blackbody energy absorbed	Total absorption Bandwidth, Δλ (μm)	Fraction of 1300 K Blackbody energy absorbed
5	0.16	0.04	0.58	0.16
2	0.12	0.03	0.51	0.14
1	0.1	0.03	0.45	0.12
0.1	0.033	0.01	0.22	0.06
0.01	0.01	0.003	0.07	0.02

Table 66.5 Total absorption bandwidth for 4.3 μm CO_2 band at 300 K

Pathlength through the atmosphere (m)	Total absorption bandwidth Δλ (μm)	Fraction of 1300 K blackbody energy absorbed
1000	0.28	0.04
100	0.22	0.03
10	0.17	0.02
1	0.065	0.01
0.3	0.033	0.004

calculated using the emissivity charts published by Hottel and Sarofim [60]. The procedure to calculate the absorption in the water vapor band is as follows:

1. Determine the partial pressure of water vapor, in atmospheres, based on

$$p_w' = \frac{RH}{100}\exp\left(14.4114 - \frac{5328}{T_a}\right) \qquad (66.27)$$

where RH is the relative humidity and T_a is the ambient temperature in Kelvin.

2. Define a pathlength, L (in m), from the flame surface to observer. Determine the partial pressure-pathlength parameter:

$$p_w L = p_w' L(T_s/T_s) \qquad (66.28)$$

where
T_s = Source surface temperature (K)
T_a = Ambient temperature (K)

3. For the source temperature, and $p_w L$, determine the water vapor emissivity, ε_w, using emissivity plots given in Fig. 66.34.
4. Calculate the water vapor absorption coefficient.

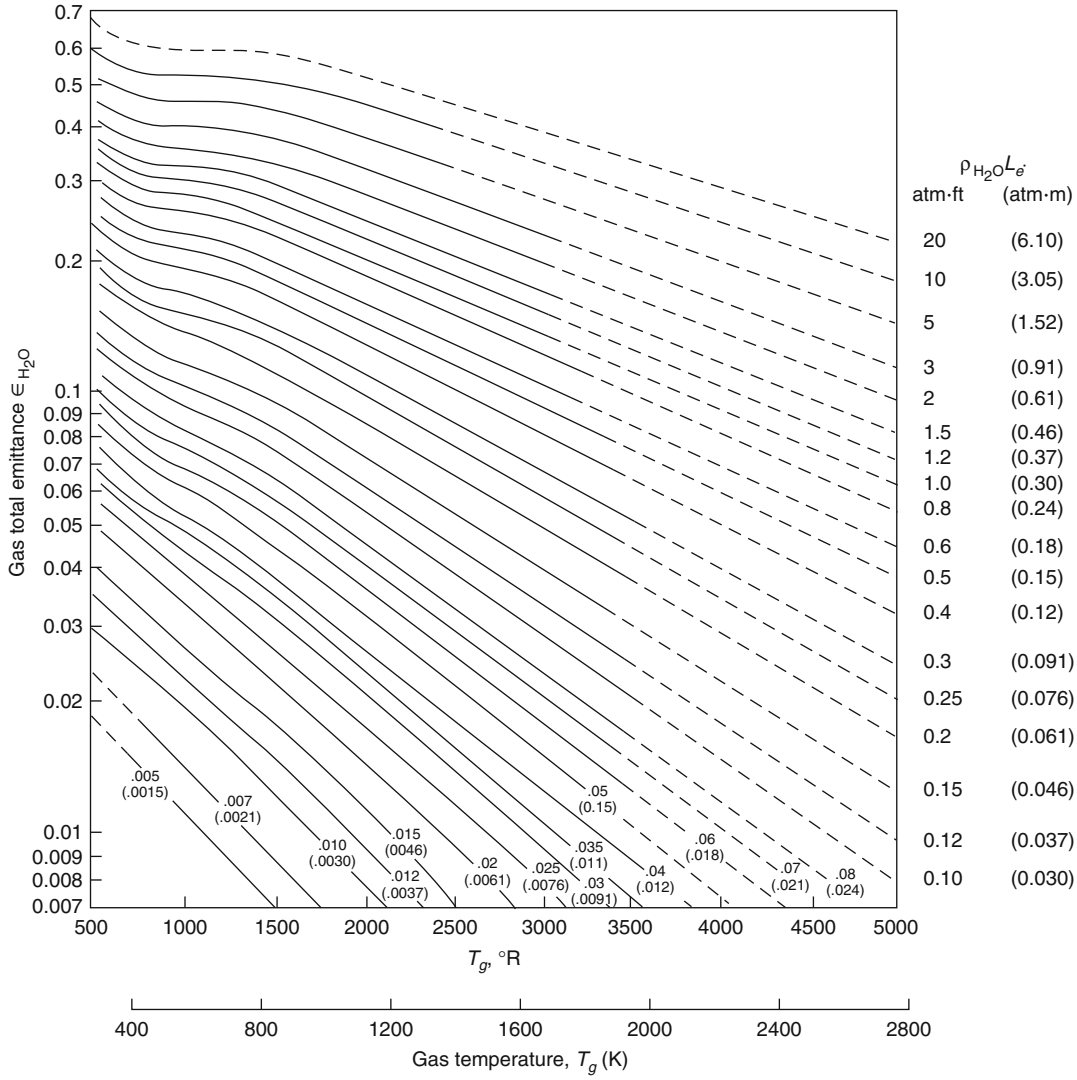

Fig. 66.34 Total emissivity of water vapor in a mixture of total pressure of 1 atm [60]

$$\alpha_w = \varepsilon_w (T_a/T_s)^{0.45} \tag{66.29}$$

The procedure to determine the absorption by carbon dioxide is very similar. The partial pressure of CO_2 remains relatively constant at about 3×10^{-4} atm. The absorption coefficient is given by

$$\alpha_c = \varepsilon_c (T_a/T_s)^{0.65} \tag{66.30}$$

The emissivity of the carbon dioxide band is shown in Fig. 66.35. There is also a correction factor due to spectral overlap for the calculation of emissivity of a CO_2-H_2O mixture. This effect, however, accounts for a change in emissivity of about 5 % at 1200 K and even less at higher temperatures [60].

The transmissivity is given by

$$\tau = 1 - \alpha_w - \alpha_c \tag{66.31}$$

and is used in determining the thermal radiation hazard. The procedure outlined in this section may be simplified further if it is assumed that the flame temperature and the ambient temperature remain constant. For most hydrogen fuels,

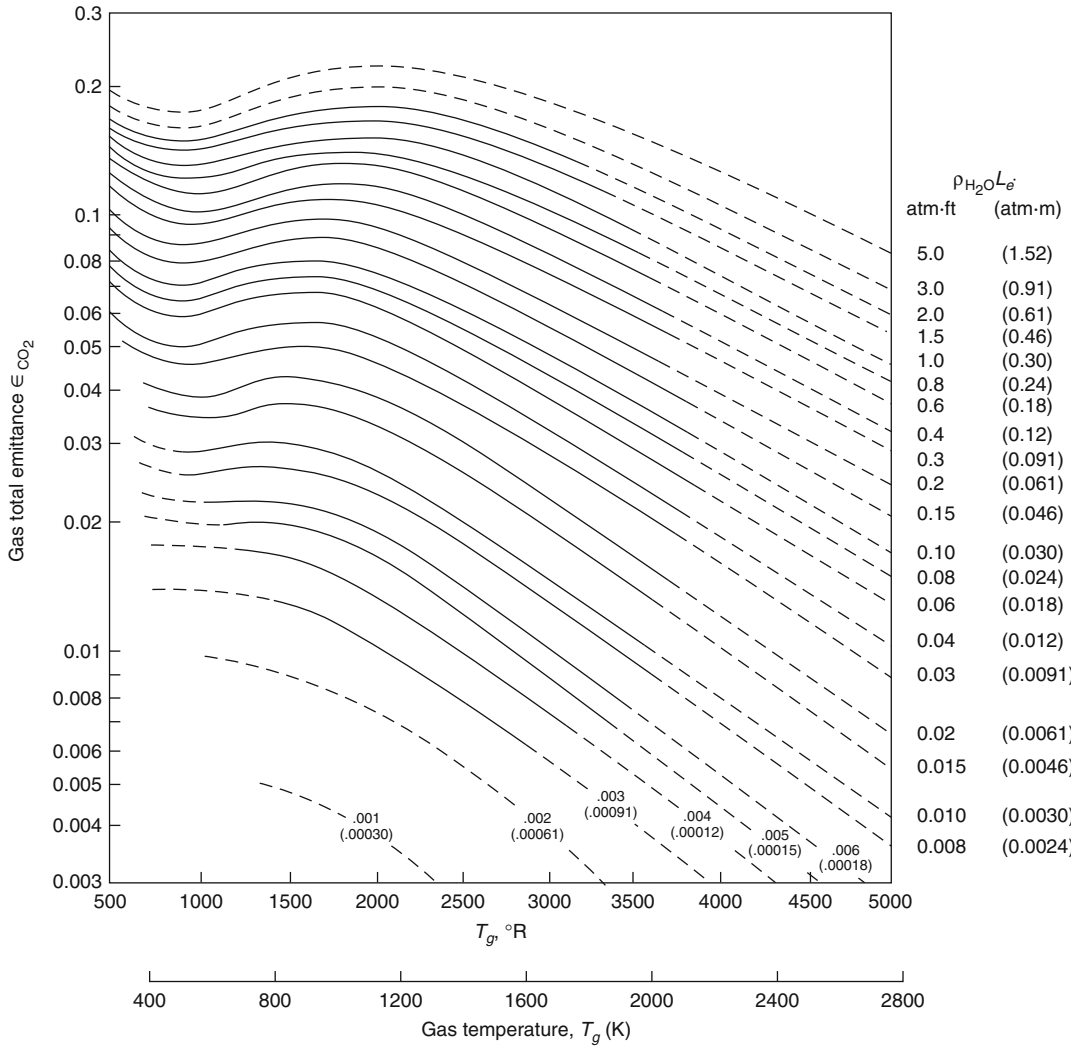

Fig. 66.35 Total emissivity of carbon dioxide in a mixture of total pressure of 1 atm [60] where p_{CO_2} is the partial pressure of carbon dioxide and L_e is the equivalent pathlength

the flame temperature is approximately 1400 K. If it is assumed that the typical ambient temperature is 293 K (20 °C) the transmissivity may be plotted as a function of pathlength. In Fig. 66.36 the transmissivity is shown as a function of pathlength for various relative humidities. Figure 66.36 provides a quick estimate of atmospheric absorption of thermal radiation.

Summary of the Procedure for the Mudan Pool Fire Radiation Method Estimating the thermal radiation field surrounding a fire involves the following steps based on the method developed by Mudan [14]:

1. Determine the height of the pool fire flame and tilt angle from Equations 66.2, 66.21, 66.22, and 66.23.
2. Calculate the configuration factor from Equations 66.18, 66.24, and 66.19. Figures 66.21, 66.22, 66.23, 66.24, and 66.25, 66.31, or 66.32 may be used where appropriate.
3. Determine the effective emissive power of the flame from Equation 66.26.

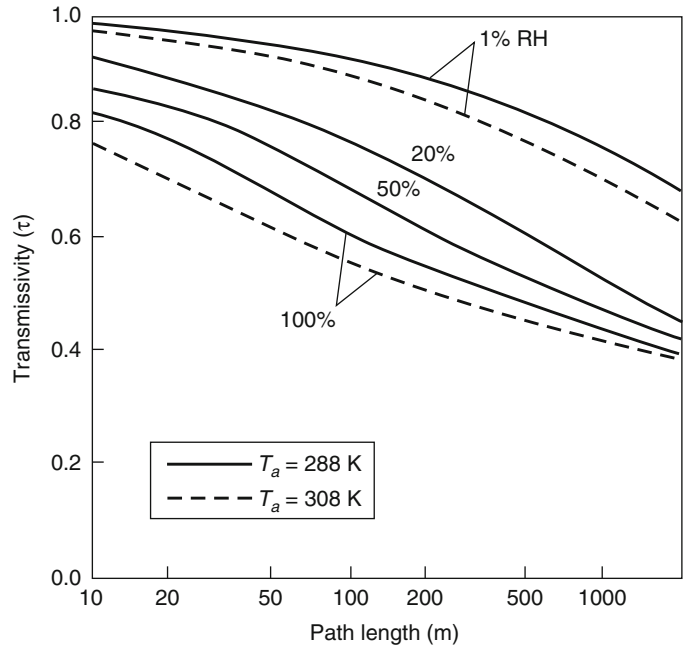

Fig. 66.36 Transmissivity as a function of pathlengths; source temperature 1400 K

4. Calculate the radiative heat flux to target using Equation 66.20.

Figure 66.37 shows a comparison of data with the predictions of this method [50]. The predictions tend to be conservative, and the differences between measured and predicted values are relatively uniform over the full range of heat fluxes. No validation data are available for wind-tilted conditions.

A safety factor of 2 is recommended for use with the Mudan method [50]. Figure 66.38 is a comparison of predicted and measured heat fluxes with the inclusion of the recommended factor of safety. Figure 66.33 clearly shows that essentially all the data are overpredicted by the Mudan model with a safety factor of 2. The safety factor of 2 is a recommendation for use in design applications. Where a realistic result is required, no safety factor should be applied.

Summary and General Recommendations

Table 66.6 summarizes the methods included in this section and their ranges of applicability. All the methods used with the indicated safety factors provide conservative results. However, the variations in the predicted versus measured heat fluxes (i.e., the goodness of fit) vary considerably between methods. Methods that minimize these variations are inherently more reliable in that the method better explains the experimental data. The methods that minimize the variation are the point source model and the Shokri and Beyler method, when used in their applicable ranges. Table 66.7 shows the correlation coefficient of each method over the indicated ranges of application. The methods with the greatest correlation coefficient better explain the variations observed in the database. Although at less than 5 kW/m^2 there is little difference between the performance of the point source model and the Mudan [14] model, the simplicity of the point source model argues for its use.

The point source model and the Shokri and Beyler model are the preferred models based on both the conservative nature of these methods and the minimization of the variations between the data and the experiments.

Because heat fluxes below 5 kW/m^2 cannot lead to ignition of combustibles, any analysis involving a combustible target should be performed using the Shokri and Beyler model.

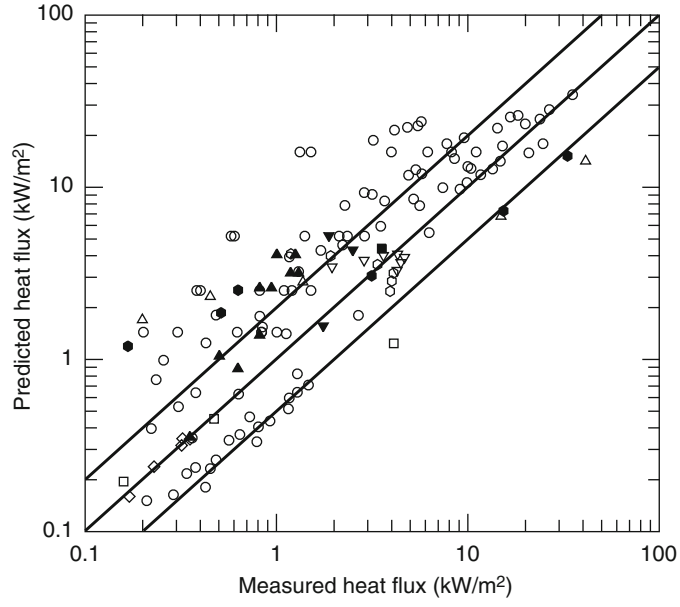

Fig. 66.37 Comparison of measured and calculated radiative heat flux from large pool fires using the detailed method developed by Mudan [14]. *Solid lines* indicate equality of measured and predicted heat fluxes based on the detailed method developed by Mudan [14]

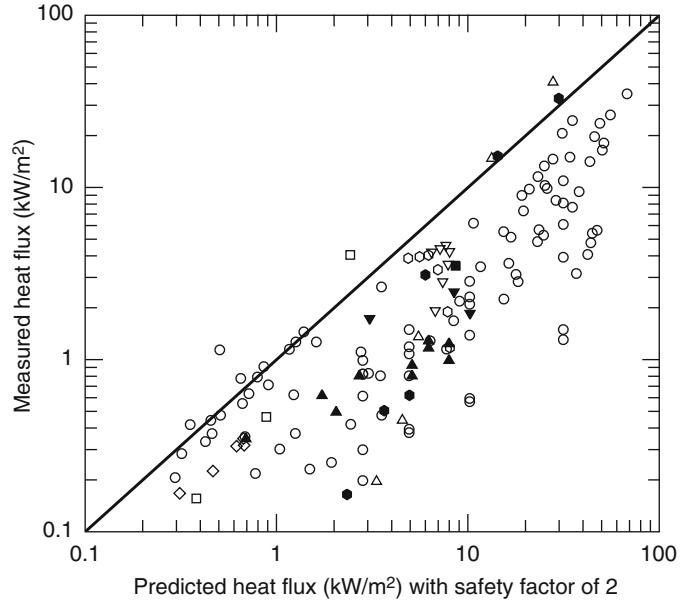

Fig. 66.38 Comparison of measured and calculated radiative heat flux from large pool fires using the detailed method developed by Mudan with a safety factor of 2. *Solid lines* indicate equality of measured and predicted heat fluxes based on the detailed method developed by Mudan with a safety factor of 2 [14]

Table 66.6 Summary of the methods

Method	Range of use (kW/m^2)	Recommended safety factor	Preferred methods
Shokri and Beyler correlation	All heat fluxes, ground level only	2	–
Point source model	0–5 kW/m^2	2	$\leq$5 kW/m^2
Shokri and Beyler model	$\geq$5 kW/m^2	2	$\geq$5 kW/m^2
Mudan model	All heat fluxes	2	–

Table 66.7 Correlation coefficients for the methods

Heat-flux calculation method	Correlation coefficient	Correlation coefficient with safety factor
Point source model (below 5 kW/m^2)	0.51	0.38
Mudan model (below 5 kW/m^2)	0.53	0.34
Shokri and Beyler model (above 5 kW/m^2)	0.52	0.66
Mudan model (above 5 kW/m^2)	0.35	0.57

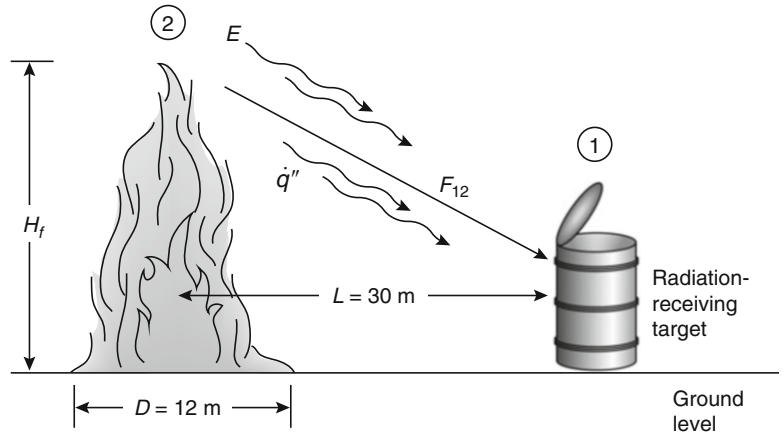

Fig. 66.39 Toluene pool fire with target at ground level

Because pain and second-degree burns can occur at 5 kW/m^2, many analyses involving human exposure can be performed using the simple point source model. If exposure is less than 1 min, it may be necessary to use the more complex Shokri and Beyler model for human exposure.

Illustration of the calculation procedure: In this section two sample calculations are presented to illustrate the calculation procedure for the thermal radiation from pool fires.

Example 1 Toluene from a tank is assumed to spill to form a pool in a diked area of 12 m diameter. The distance from the center of the pool fire to the target edge is assumed to be 30 m.

Calculate flame radiative heat flux to the target at ground level with no wind (Fig. 66.39) using:

(a) Shokri and Beyler correlation
(b) Point source model
(c) Shokri and Beyler detailed method using shape factor algebra
(d) Mudan detailed method using shape factor algebra

CALCULATION PROCEDURE

Properties of toluene (Chap. 26):

Heat of combustion, $\Delta H_c = 40{,}550$ kJ/kg

Mass burning rate, $\dot{m}''_\infty = 0.1126$ °kg/m$^2 \cdot$ s

Properties of air at 20 °C, $\rho_a = 1.2$ kg/m^3

(a) Heat flux from the Shokri and Beyler correlation, Equation 66.10:

$$\dot{q}'' = 15.4\left(\frac{L}{D}\right)^{-1.59}$$

where $L = 30$ m and $D = 12$ m. Therefore, heat flux to the target is

$$\dot{q}'' = 15.4\left(\frac{30}{12}\right)^{-1.59} = 3.6 \text{ kW/m}^2$$

(b) Heat flux from point source model, Equation 66.12:

$$\dot{q}'' = \frac{\dot{Q}_r \cos\theta}{4\pi R^2}$$

The radiative energy output, $\dot{Q}_r$, is given by the

radiative fraction, χ_r, multiplied by the total heat release rate, $\dot{Q}$, from Equation 66.15:

$$\dot{Q}_r = \chi_r \dot{Q}$$

Figure 66.18 can be used to determine χ_r from curve fit to the experimental data as

$$\chi_r = 0.21 - 0.0034D$$

and $\dot{Q}$, total heat release rate, is given by

$$\dot{Q} = \dot{m}''_\infty \Delta H_c A$$

and A, area of the pool, can be expressed from Equation 66.11:

$$A = \frac{\pi}{4} D^2$$

Combining the above equations yields

$$\dot{Q}_r = (0.21 - 0.0034D)\left(\dot{m}''_\infty \Delta H_c \frac{\pi}{d} D^2\right)$$
$$= 87,371 \text{ kW}$$

The distance, R, from the point source location to the target location is given by the Pythagorean theorem, Equation 66.14:

$$R = \sqrt{L^2 + H_T{}^2}$$

where $L = 30$ m and H_T is given by

$$H_T = \frac{H}{2}$$

H is the height of the flame from Equation 66.13:

$$H = 0.23\dot{Q}^{2/5} - 1.02D = 32.11 \text{ m}$$

$$\mathrm{H}_T = \frac{0.23\left(\dot{m}''_\infty \Delta H_c (\pi/4) D^2\right)^{2/5} - 1.02D}{2} = 16 \text{ m}$$

$$R = \sqrt{30^2 + 16^2} = 34 \text{ m}$$

The angle, θ, between the normal to the target and the line of sight from the point source location can be estimated as

$$\theta = \tan^{-1}\left(\frac{1H}{2L}\right) = 0.49 \text{ rad}$$

The heat flux from the point source model is

$$\dot{q}'' = \frac{\dot{Q}_r \cos\theta}{4\pi R^2} = \frac{87,371 \times \cos(0.49)}{4 \times \pi \times 34^2}$$
$$= 5.3 \text{ kW/m}^2$$

(c) Heat flux from the Shokri and Beyler detailed method using shape factor algebra with target at ground level and no wind, Equation 66.16:

$$\dot{q}'' = EF_{12}$$

The emissive power of the flame, E, is given by Equation 66.19:

$$E = 58\left(10^{-0.00823D}\right)$$
$$E = 58\left(10^{-0.00823 \times 12}\right) = 46.2 \text{ kW/m}^2$$

Equation 66.17a can be used to determine the shape factor in the horizontal direction:

$$F_{12,H} = \frac{[B - (1/S)]}{\pi\sqrt{B^2 - 1}} \tan^{-1}\sqrt{\frac{(B+1)(S-1)}{(B-1)(S+1)}}$$
$$- \frac{[A - (1/S)]}{\pi\sqrt{A^2 - 1}} \tan^{-1}\sqrt{\frac{(A+1)(S-1)}{(A-1)(S+1)}}$$

Equation 66.17b can be used to determine the shape factor in the vertical direction:

$$F_{12,V} = \frac{1}{\pi S}\tan^{-1}\left(\frac{h}{\sqrt{S^2 - 1}}\right) - \frac{h}{\pi S}\tan^{-1}\sqrt{\frac{(S-1)}{(S+1)}}$$
$$+ \frac{Ah}{\pi S\sqrt{A^2 - 1}}\tan^{-1}\sqrt{\frac{(A+1)(S-1)}{(A-1)(S+1)}}$$

where

$$S = \frac{2L}{D} = \frac{2 \times 30}{12} = 5$$
$$H_f = 0.23\dot{Q}^{2/5} - 1.02D = 32.11 \text{ m}$$
$$h = \frac{2H_f}{D} = \frac{2 \times 32.11}{12} = 5.35$$
$$A = \frac{h^2 + S^2 + 1}{2S} = \frac{5.35^2 + 5^2 + 1}{2 \times 5} = 5.46$$
$$B = \frac{(1 + S^2)}{2S} = 2.6$$

Substituting values of A, B, S, and h in the shape factor equation to determine $F_{12,H}$ and $F_{12,V}$, the $F_{12,H}$ is equal to 0.039, and $F_{12,V}$ is equal to 0.088.

The maximum shape factor at a point is given by the vectorial sum of the horizontal and vertical shape factors:

$$F_{12,\max} = \sqrt{F_{12,H}^2 + F_{12,V}^2}$$

Therefore, the maximum shape factor at a point is equal to 0.097. Therefore, heat flux to the target is

$$\dot{q}'' = EF_{12,\max} = 48 \times 0.097 = 4.5 \text{ kW/m}^2$$

(d) Heat flux from the Mudan detailed method using shape factor algebra with target at ground level and no wind, Equation 66.20:

$$\dot{q}'' = EF_{12}\tau$$

The emissive power of the flame, E, is given by Equation 66.26:

$$E = E_{\max} e^{-sD} + E_s(1 - e^{-sD})$$
$$E = 140e^{-0.12 \times 12} + 20(1 - e^{-0.21 \times 12}) = 48.43 \text{ kW/m}^2$$

Equation 66.24a can be used to determine the shape factor in the horizontal direction:

$$F_{12,H} = \frac{[B - (1/S)]}{\pi\sqrt{B^2 - 1}} \tan^{-1}\sqrt{\frac{(B+1)(S-1)}{(B-1)(S+1)}} - \frac{[A - (1/S)]}{\pi\sqrt{A^2 - 1}} \tan^{-1}\sqrt{\frac{(A+1)(S-1)}{(A-1)(S+1)}}$$

and Equation 66.24b can be used to determine the shape factor in the vertical direction:

$$F_{12,V} = \frac{1}{\pi S}\tan^{-1}\left(\frac{h}{\sqrt{S^2-1}}\right) - \frac{h}{\pi S}\tan^{-1}\sqrt{\frac{(S-1)}{(S+1)}} + \frac{Ah}{\pi S\sqrt{A^2-1}}\tan^{-1}\sqrt{\frac{(A+1)(S-1)}{(A-1)(S+1)}}$$
$$H_f = 42D\left(\frac{\dot{m}''_\infty}{\rho_a\sqrt{gD}}\right)^{0.61} = 27.79 \text{ m}$$
$$h = \frac{2H_f}{D} = \frac{2 \times 27.79}{12} = 4.63$$
$$S = \frac{2L}{D} = \frac{2 \times 30}{12} = 5$$
$$A = \frac{h^2 + S^2 + 1}{2S} = \frac{4.63^2 + 5^2 + 1}{2 \times 5} = 4.74$$
$$B = \frac{(1 + S^2)}{2S} = 2.6$$

Substituting values of A, B, S, and h in the shape factor equation to determine $F_{12,H}$ and $F_{12,V}$, $F_{12,H}$ is equal to 0.035, and $F_{12,V}$ is equal to 0.084.

The maximum shape factor at a point is given by the vectorial sum of the horizontal and vertical shape factors:

$$F_{12,\max} = \sqrt{F_{12,H}^2 + F_{12,V}^2}$$

Therefore, the maximum shape factor at a point is equal to 0.091.

Therefore, heat flux to the target is

$$\dot{q}'' = EF_{12,V}\tau = 48.43 \times 0.091 \times 1 = 4.45 \text{ kW/m}^2$$

Table 66.8 summarizes the results for each of the methods.

EXAMPLE 2 Calculate flame radiative heat flux from a 10-m-diameter toluene pool fire to a vertical target 2 m above the ground at 12 m from the center of the pool (Fig. 66.40) with no wind, using:

(a) Shokri and Beyler method using shape factor algebra
(b) Mudan method using shape factor algebra

CALCULATION PROCEDURE

(a) Heat flux from the Shokri and Beyler detailed method using shape factor algebra with target height 2 m above ground level and no wind

Properties of toluene (Chap. 26)

Heat of combustion, $\Delta H_c = 40{,}550$ kJ/kg

Mass burning rate, $\dot{m}''_{\infty} = 0.1126°\text{kJ/kg}$

Properties of air at 20 °C $\rho_a = 1.2$ kg/m^3

Heat flux is given by Equation 66.16:

$$\dot{q}'' = EF_{12}$$

The emissive power of the flame, E, is given by Equation 66.19:

$$E = 58\left(10^{-0.00823D}\right)$$
$$E = 58\left(10^{-0.00823\times 10}\right) = 48 \text{ kW/m}^2$$

The flame height, H, is given by Equation 66.13:

$$H = 0.23\dot{Q}^{2/5} - 1.02D$$

where

$$\dot{Q} = \dot{m}''_{\infty}\ \Delta H_c A \text{ kW}$$

$$\dot{Q} = 360{,}000 \text{ kW}$$

$$H = 28 \text{ m}$$

Because the target is above the ground, but it is not at the flame height, two cylinders must be used to represent the flame. Because the target is strictly vertical, it is not necessary to calculate the horizontal shape factor.

The shape factor for the target located above ground level can be calculated from Figs. 66.21, 66.22, 66.23, 66.24, and 66.25 or by the following method. For the vertical target, Equation 66.17b can be used to determine the shape factor at location H_{f1}:

Table 66.8 Summary of the heat flux from 12-m-diameter toluene pool fire to 30 m target at ground level with no wind

Heat flux calculation method	Heat flux (kW/m^2)
(a) Shokri and Beyler correlation	3.6
(b) Point source model	5.3
(c) Shokri and Beyler method using shape factor algebra	4.5
(d) Mudan method using shape factor algebra	4.45

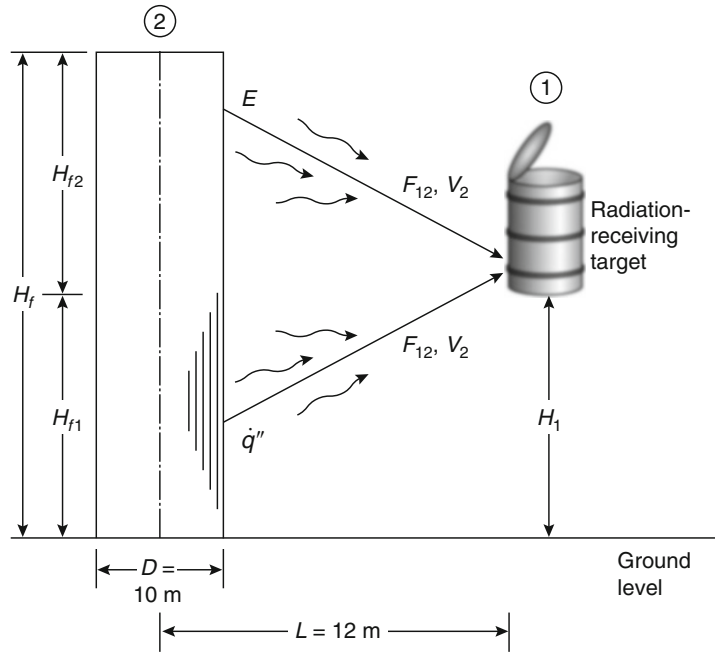

Fig. 66.40 Toluene pool fire with target above ground level

$$F_{12,V1} = \frac{1}{\pi S}\tan^{-1}\left(\frac{h}{\sqrt{S^2-1}}\right) - \frac{h_1}{\pi S}\tan^{-1}\sqrt{\frac{(S-1)}{(S+1)}} + \frac{A_1 h_1}{\pi S\sqrt{A_1^2-1}}\tan^{-1}\sqrt{\frac{(A_1+1)(S-1)}{(A_1-1)(S+1)}}$$

$$S = \frac{2L}{D} = \frac{2\times 12}{10} = 2.4$$

$$H_{f1} = \frac{2H_{f1}}{D} = \frac{2\times 2}{10} = 0.4$$

$$A_1 = \frac{H_{f1}^2 + S^2 + 1}{2S} = \frac{0.4^2 + 2.4^2 + 1}{2\times 2.4} = 1.44$$

Substituting values of A_1, S, and H_{f1} in the shape factor equation to determine $F_{12,V1}$, the $F_{12,V1}$ is equal to 0.066. Shape factor at location $H_{f\,2}$ is given by

$$F_{12,V2} = \frac{1}{\pi S}\tan^{-1}\left(\frac{H_{f2}}{\sqrt{S^2-1}}\right) - \frac{H_{f2}}{\pi S}\tan^{-1}\sqrt{\frac{(S-1)}{(S+1)}} + \frac{A_2 H_{f2}}{\pi S\sqrt{A_2^2-1}}\tan^{-1}\sqrt{\frac{(A_2+1)(S-1)}{(A_2-1)(S+1)}}$$

$$S = \frac{2L}{D} = \frac{2\times 12}{10} = 2.4$$

$$H_{f2} = \frac{2H_{f2}}{D} = \frac{2\left(H_f - H_{f1}\right)}{D} = \frac{2(28-2)}{10} = 5.2$$

$$A_2 = \frac{H_{f2}^2 + S^2 + 1}{2S} = \frac{5.2^2 + 2.4^2 + 1}{2\times 2.4} = 7.04$$

Substituting values of A_2, S, and $H_{f\,2}$ in the shape factor equation to determine $F_{12,V2}$, $F_{12,V2}$ is equal to 0.206. Therefore, total shape factor is given by

$$F_{12,V} = F_{12,V1} + F_{12,V2} = 0.066 + 0.206 = 0.27$$

Therefore, heat flux to the target at 2 m above ground is

$$\dot{q}'' = EF_{12,V} = 48\times 0.27 = 13.0\ \text{kW/m}^2$$

(b) Heat flux from Mudan [14] method using shape factor algebra with target height 2 m above ground level and no wind

Heat flux is given by Equation 66.20:

$$\dot{q}'' = EF_{12}\tau$$

The emissive power of the flame, E, is given by Equation 66.20:

$$E = E_{\max}\mathrm{e}^{-sD} + E_s\left(1-\mathrm{e}^{-sD}\right)$$

$$E = 140\mathrm{e}^{-0.12\times 10} + 20\left(1-\mathrm{e}^{-0.21\times 10}\right) = 56.14\ \text{kW/m}^2$$

The flame height, H, is given by Equation 66.21:

$$H_f = 42D\left(\frac{\dot{m}''_\infty}{\rho_a\sqrt{gD}}\right)^{0.61} = 25.4 \text{ m}$$

Because the target is above the ground, but it is not at the flame height, two cylinders must be used to represent the flame. Because the target is strictly vertical, it is not necessary to calculate the horizontal shape factor.

The shape factor for the target located above ground level can be calculated from Figs. 66.21, 66.22, 66.23, 66.24, and 66.25 or by the following method. For the vertical target, Equation 66.24a can be used to determine the shape factor at location H_1:

$$F_{12,V1} = \frac{1}{\pi S}\tan^{-1}\left(\frac{H_1}{\sqrt{S^2-1}}\right) - \frac{H_1}{\pi S}\tan^{-1}\sqrt{\frac{(S-1)}{(S+1)}} + \frac{A_1H_1}{\pi S\sqrt{A_1^2-1}}\tan^{-1}\sqrt{\frac{(A_1+1)(S-1)}{(A_1-1)(S+1)}}$$

$$S = \frac{2L}{D} = \frac{2\times 12}{10} = 2.4$$

$$H_1 = \frac{2L}{D} = \frac{2\times 2}{10} = 0.4$$

$$A_1 = \frac{H_1^2+S^2+1}{2S} = \frac{0.4^2+2.4^2+1}{2\times 2.4} = 1.44$$

Substituting values of A_1, S, and h_1 in the shape factor equation to determine $F_{12,V1}$, $F_{12,V1}$, is equal to 0.066.

Shape factor at location H_2 is given by

$$F_{12,V2} = \frac{1}{\pi S}\tan^{-1}\left(\frac{H_2}{\sqrt{S^2-1}}\right) - \frac{H_2}{\pi S}\tan^{-1}\sqrt{\frac{(S-1)}{(S+1)}} + \frac{A_2H_2}{\pi S\sqrt{A_2^2-1}}\tan^{-1}\sqrt{\frac{(A_2+1)(S-1)}{(A_2-1)(S+1)}}$$

$$S = \frac{2L}{D} = \frac{2\times 12}{10} = 2.4$$

$$h_2 = \frac{2H_{f2}}{D} = \frac{2\left(H_f - \mathbf{H}_{f1}\right)}{10} = \frac{2(24.5-2)}{10} = 4.5$$

$$A_2 = \frac{H_2^2+S^2+1}{2S} = \frac{4.5^2+2.4^2+1}{2\times 2.4} = 5.62$$

Table 66.9 Summary of the heat flux from 10-m-diameter toluene pool fire to 12 m target at 2 m high above ground level with no wind

Heat flux calculation method	Heat flux (kW/m^2)
(a) Shokri and Beyler method using shape factor algebra	13.0
(b) Mudan method using shape factor algebra	15.2

Substituting values of A_2, S, and h_2 in the shape factor equation to determine $F_{12,V1}$, $F_{12,V2}$ is equal to 0.206. Therefore, total shape factor is given by

$$F_{12,V} = F_{12,V1} + F_{12,V2} = 0.066 + 0.188 = 0.27$$

Therefore, heat flux to the target at 2 m above ground is

$$\dot{q}'' = EF_{12,V} = 56.14 \times 0.25 = 15.2 \text{ kW/m}^2$$

Table 66.9 summarizes the results for each of these methods.

Heat Transfer to Targets Within Pool Fires

Temperatures within pool fires have been widely measured and reported [61]. Over a very wide range of pool sizes (0.1–50 m diameter), the maximum time-averaged flame temperatures are generally observed to be approximately 900–1100 °C. Table 66.10 shows measured maximum average temperatures reported in the literature. This maximum has been found to be remarkably independent of the fuel. The maximum time-averaged temperature is observed on the pool centerline over approximately the lower 40 % of the flame height.

Effective radiation temperatures can be measured with optical pyrometers, narrow angle radiometers, or scanning spectrometers. These measurements tend to yield maximum, average, effective radiation temperatures somewhat larger than the actual maximum temperatures, up to 1200 °C (see Wayne and Kinsella [69], Hägglund and Persson [18]), which is a reflection of the fourth-power dependence of radiation on temperature. The radiation is affected by the maximum temperature excursions rather than simply the average. Effective radiation temperatures measured outside the flame can be significantly lower than this due to obscuration by smoke outside the flame.

Table 66.10 Maximum time-averaged temperatures of pool fires

Investigator	°C
Cox and Chitty [62]	1000
McCaffrey [63]	820
Terai and Nitta [72]	770
Kung and Stavrianidis [65]	920
Hägglund and Persson [18]	1000
Russell and Canfield [66]	1100
Gregory et al. [72]	1000
Johnson et al. [32]	1200
Anderson et al. [68]	1000

Average fluxes to objects immersed in flames have been widely measured. Most of the work that has been reported was performed to assess the energy input to liquid tanks for the purpose of determining venting requirements while the remainder of the work has been performed to assess the heating of weapons and nuclear fuel containers. Most of this work has focused on objects located in the lower portions of the flame where the maximum temperatures and fluxes are expected. Table 66.11 summarizes the results of a number of investigations and assessments of existing data. Based on the available data, a maximum time-averaged heat flux of 120 kW/m^2 is a reasonable, conservative representation of the available data. These investigations include data in which the size of the object was small relative to the size of the flame, but the objects were sized to represent tanks and/or weapons. The object was fully immersed in optically thick flames on all sides.

Measurements made with objects comparable inside to the pool fire are far less common (Taylor et al. [70], McLain [71]). Heat fluxes in this situation are less than those observed when the object is much smaller than the pool fire. This

Table 66.11 Large-scale pool fire maximum average heat-flux measurements

Large calorimeters	kW/m^2
Gregory et al. [72]	120
Wachtell and Langhaar [73]	85
Anderson et al. [68]	100
National Academy of Science [74] (average of data in the literature pre-1970)	110
Moodie [75]	100
Tunc and Venart [76]	105
McLain [71]	85[a]
Taylor et al. [70]	75[a]
Small calorimeters	kW/m^2
Russell and Cansfield [66]	170
Gregory et al. [72]	160

[a]Object site comparable to pool fire

results from the reduced flame pathlengths observed. The flames are not uniformly optically thick as seen by the object. Measurements of heating rates to objects on the order of 1–3 m in size heated by comparably sized pool fires result in average heat fluxes in the range of 75–85 kW/m^2 (see Table 66.11). These heat fluxes were deduced from measured rates of the temperature of tank contents.

The extinction coefficient, k, of pool fires has been measured by several investigators. Typically, pool fires are found to have average extinction coefficients of about 2 1/m. An extinction coefficient of 2 1/m is consistent with the observation that pool fires reach their asymptotic, radiatively dominated burning rate at pool diameters of 1 m.

The effect of the object size on flame heat fluxes has not been systematically studied. However, it has been observed that larger objects, even if significantly smaller than the flame, do yield smaller heat fluxes than smaller objects. Gregory et al. [72] have observed this effect in 9 × 18 m pool fires with objects up to 1.4 m in diameter. They found fluxes to 1.4-m-diameter calorimeters were 30–40 % less than for 0.1–0.2-m-diameter calorimeters. Similarly, measurements using conventional heat-flux transducers (Gardon or Schmidt/Boelter) tend to yield higher fluxes than observed with calorimeters, which are sized to represent normal tanks or weapons. Table 66.11 summarizes available heat-flux data as measured with small calorimeters. It is thought that these effects result from two phenomena. First, the larger calorimeters effectively average the fluxes over the size of the calorimeter. This spacial averaging process tends to reduce the measured fluxes. Second, the larger calorimeters can significantly perturb the flame in the region surrounding the calorimeter, yielding reduced temperatures surrounding the calorimeter. The size of the region affected scales with the diameter of the calorimeter. With small calorimeters, this length is small compared to 1/k so that the radiant fluxes are not much affected. For large calorimeters, the reduction in local flame temperature may be significant over radiative length scales, and radiant fluxes are reduced.

Most measurements that have been performed have been made in the center of the flame where the highest fluxes are expected. Relatively few measurements have been made within the flame near the flame edge. Temperature profiles have been measured by Russell and Canfield [66] and Johnson et al. [32]. Their temperature results indicate that temperatures are reduced to about half the centerline value at one-half the pool radius. Russell and Canfield [66] made small-scale calorimeter measurements about 0.3 m from the visible flame edge. Measurements made facing the flame edge were less than 20 kW/m^2 while measurements made facing the body of the flame were about 135 kW/m^2. This value should be compared to fluxes measured on the centerline of the fire of 160 kW/m^2 made with Gardon gauges. This indicates that fluxes within the flame are relatively constant until and unless the radiative pathlengths are small enough to reduce the flame emissivity as discussed previously.

Thermal Radiation from Jet Flames

Large turbulent diffusion flames are encountered in a processing environment as a result of an accidental release of hydrocarbon vapors or the intentional disposal of unwanted gases in a flare. Flaring is the combustion process that has been the traditional method for safe disposal of large

quantities of unwanted flammable gases and vapors in the petroleum industry. With the advent of air quality standards, flaring has also taken on an added importance as a method of industrial environmental control, because most gases that could previously be vented to the atmosphere must now be burned in a flare. The flaring of gases in the petroleum industry occurs in three ways:

1. *Production flaring*. In a production oil field where no provision exists for collecting and processing of gas, there is a requirement for safe disposal of flammable gases. There was a time when almost all gas released was flared, but the great value now placed on natural gas has made gas recovery economical for some fields. Nevertheless, if gas occurs in small quantities that are uneconomical to process or if the gas is so sour that processing is expensive, it can still be flared.
2. *Process flaring*. Flaring also takes place in petrochemical plants, oil refineries, and gas processing plants where the flare system is one of the off-site facilities. In process flaring, the gas that leaks past safety valves protecting various process units is brought to the flare and burned. This gas feeds the small flames that burn almost continuously on refinery stacks. Process flaring can occur at much greater rates when process units are evacuated during a shutdown or when off-specification products are produced during start-up.
3. *Emergency flaring*. This occurs when large volumes of volatile liquids or flammable gases have to be disposed of safely in an emergency such as fire, power failure, or overpressure in a process vessel.

The flaring process involves the release of a tremendous amount of energy. Because a portion of this energy release is in the form of thermal radiation, it represents a substantial hazard to personnel, equipment, and the environment. The sizing of flare system, both in diameter and height, is of major importance to ensure personnel safety during flaring operations. The ability to predict the thermal radiation field from flares is essential in the design of a reasonably sized, safe operating flare. Experimental data on thermal radiation from full-scale flares are rare, and when available at all, the flow rate and composition of the flared gases are usually unknown. However, several scale-model studies have been conducted to examine the geometric and radiative characteristics of flares.

The geometric characteristics of hydrocarbon flares are similar to turbulent jet flames. In fact, many of the geometric descriptions of flares are based on small-scale turbulent jet flame experiments. The base diameter of a flare stack, height of the stack, and composition of the burning substance are often known to the user. In modeling accidental releases of hydrocarbon gases, these relevant data may have to be estimated.

The analytical models describing the geometric characteristics of turbulent jet diffusion flames are described in the following section. The models describe parameters such as the flame height, flame width, and flame tilt. Thermal radiation models, the aerodynamic effects on radiation heat transfer, and blowout stability of jet flames, as well as calculation procedures, are also described in this section.

Geometry of Turbulent Jet Flames

Combustion in a flare or jet fire occurring in the form of a strong turbulent flame may be buoyancy or momentum dominated. Such a flame presents a number of challenging phenomena for study, including the effect of crosswind on flame shape and size; radiation and formation; and dispersion of smoke and other gaseous pollutants. While applying these models to industrial flares, it is also important to recognize the effects of steam in suppressing smoke formation and thermal radiation. The fundamentals of combustion in flares have been studied by Brzustowski [77–79], Brzustowski and Sommer [80], and Brzustowski et al. [81, 82]

Turbulent Jet Flame Height in Stagnant Surroundings

A reasonable measure of progress of burning of a diffusion flame is its height or length. At low velocities the flame is generally attached to the

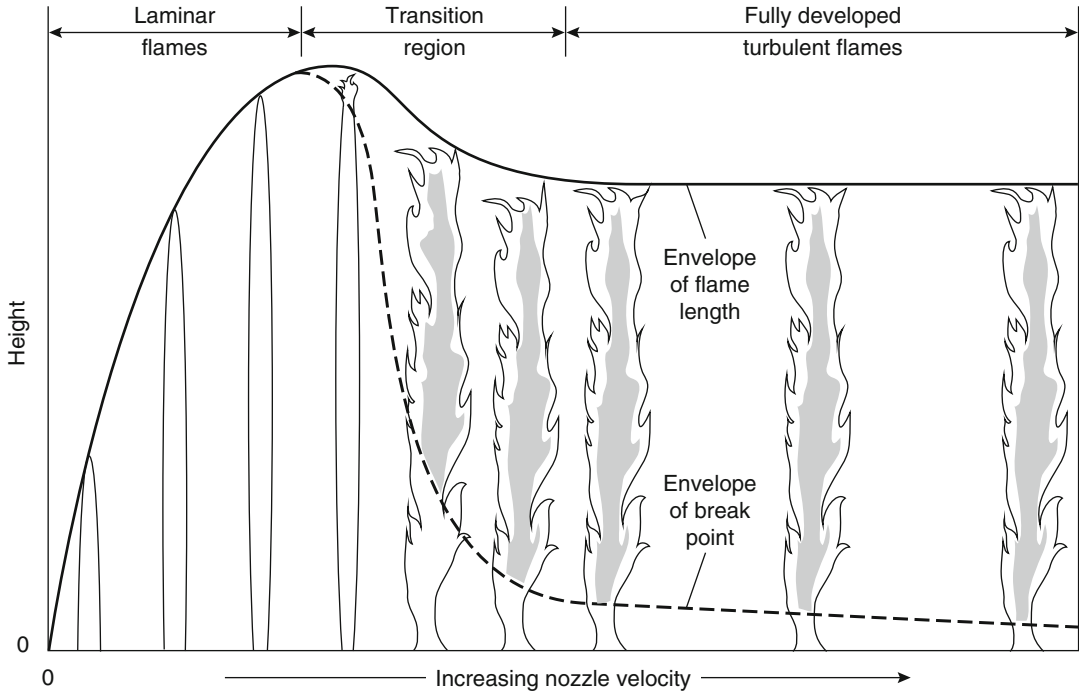

Fig. 66.41 Progressive change in flame type with increasing jet velocity

point of release, but at higher velocities it becomes detached, may become unstable, and extinguish. If, however, the flame impinges on an obstruction, this may serve to stabilize it. Predicting the height or length of the diffusion flame of gas jet burning in still air has long been considered one of the classical solved problems in combustion science. State-of-the-art papers on this subject were published by Hottel and Hawthorne [83], and Hawthorne et al. [84]. Hottel and Hawthorne [83] considered the case of a primary fuel jet of higher velocity issuing into an infinite atmosphere of air with allowance for primary air in the fuel jet. They observed the progressive change in the flame shape and size as the nozzle velocity was increased. This is illustrated in Fig. 66.41, which is based on the work of Hottel and Hawthorne [83] and further interpretation by Gugan [85]. In the laminar regime the flame length is approximately proportional to the velocity, while in the turbulent regime it is independent of velocity. Turbulence spreads from the flame tip downward. As velocity increases there are, successively, a region where the flame may be on the port or lifted, a region where only a lifted flame occurs, and a point beyond which there is blow-off.

Hawthorne et al. [84], in the earliest attempts, have developed a set of experimental data and a theoretical model for flame length for turbulent flame jets. They envisage the flame as an inverted cone with the apex on the orifice. The equation for the length of the flame was shown to be expressible, largely from momentum consideration, in the form

$$L = \frac{5.3 d_j}{C_T} \left\{ \frac{T_F}{\alpha_T T_j} \left[C_T + (1 - C_T) \frac{M_a}{M_f} \right] \right\}^{1/2} \tag{66.32}$$

where

L = Length of visible turbulent flame measured from the break point, m

d_j = jet diameter, m

C_T = Fuel concentration in stoichiometric fuel-air mixture

Table 66.12 Constant for Equation 66.32

Hydrocarbon fuel	CT	αT	T_F/T_j
Methane	0.091	1.0	7.4
Ethane	0.074	1.04	9.0
Propane	0.038	0.96	7.6

α_T = Mole of reactant per mole of product for stoichiometric fuel-air mixture
M_a, M_f = Molecular weight of air and fuel
T_F, T_j = Adiabatic flame temperature and temperature of jet fluid (absolute)

The factor 5.3 appearing in Equation 66.32 is the ratio of visible length to the width of the flame at the point where stoichiometric air has been entrained. This factor was determined from experimental data.

Equation 66.32, for determining the flame length, reduces to a much simpler expression for most hydrocarbon gases. The value of parameters C_T, α_T, and T_F/T_j for various hydrocarbons are given in Table 66.12.

Because C_T is typically much less than unity, α_T is approximately unity, and T_F/T_j varies between 7 and 9. Equation 66.32 may be approximated by the following equation:

$$L = \frac{15 d_j}{C_T}\left(\frac{M_a}{M_f}\right)^{1/2} \tag{66.33}$$

Momentum-controlled flame lengths as discussed above are generally 200–300 times the jet nozzle diameter. Although these are the tallest possible jet flames, over a wide range of conditions, jet flames are buoyancy controlled.

A number of investigators have measured jet flame lengths [77, 80, 86–89]. All their flame height results are in the form of a power law of the Froude number, u^2/gD, where u is the nozzle velocity and d is the nozzle diameter. Flame heights, L, are correlated as

$$\frac{L}{D} \approx (\mathrm{Fr})^{1/5} \sim \left(\frac{u^2}{gD}\right)^{1/5} \sim \frac{\dot{Q}^{2.5}}{D} \tag{66.34}$$

where $\dot{Q}$ is the heat release rate. All the available results can satisfactorily be described by

$$L = 0.2\dot{Q}^{2/5}$$

Figure 66.42 from McCaffrey [89] shows L/D as a function of $u/\sqrt{gD}, \sqrt{\mathrm{Fr}}$. The correlation is seen to hold over a range of about five decades in $\sqrt{\mathrm{Fr}}$. The low end of the correlation corresponds to pool fires and the high end corresponds to momentum-dominated flames.

Kalghatgi [90] and McCaffrey and Evans [91] have studied the stability and liftoff characteristics of momentum jet flames. These phenomena have a profound effect on flame radiation as indicated in Fig. 66.42.

Brzustowski [77] and Brzustowski and Sommer [80] proposed that the end of a turbulent diffusion flame at very high Reynolds number occurs at that point on the axis of maximum fuel concentrations where the fuel concentration equals the lean limit. In theory, this criterion can be applied to any flow configuration for which cold-flow concentration data at sufficiently high Reynolds number are available. Brzustowski [77] has also used some full-scale flare test data to support the lean limit criterion. With this criterion, the flame length for momentum-dominated jets is given by the following equation:

$$\frac{L}{d_j} = \frac{Y_{fj}}{0.32}\left(\frac{\rho_j}{\rho_a}\right)^{1/2}\left[1 + \frac{M_a}{M_f}\left(\frac{1}{0.297\ C_L} - 1\right)\right] \tag{66.35}$$

For a flame where buoyancy is the dominating force, the flame length is given by

$$\frac{L}{d_j} = 2.96\left(\frac{\rho_j}{\rho_a}\right)^{1/2} \mathrm{Fr}^{1/5} Y_{fj}^{3/5} \times \left[1 + \frac{M_a}{M_f}\left(\frac{1}{0.297 C_L} - 1\right)\right]^{3/5} \tag{66.36}$$

where C_L is fuel concentration at the lean flammability limit, by volume, and Fr is the Froude number. Because C_L is about 5 % or less for most hydrocarbons and M_a/M_f is approximately unity, Equations 66.35 and 66.36 may be simplified to the following two equations for momentum- and buoyancy-dominated flames, respectively.

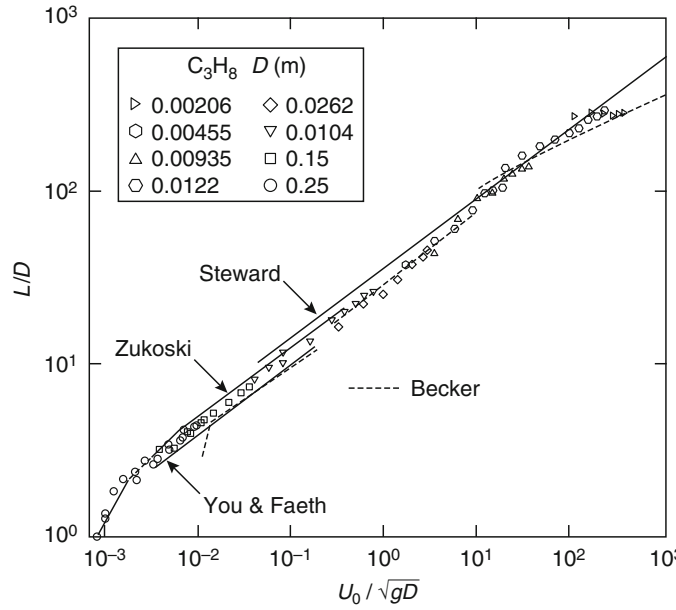

Fig. 66.42 Flame height per nozzle diameter as a function of $u\sqrt{gD}$ [89]

$$\frac{L}{d_j} = \frac{10.5}{C_L}\left(\frac{M_a}{M_f}\right)^{1/2} \tag{66.37}$$

$$\frac{L}{d_j} = 6.1\left(\frac{u_j^2}{d_j g}\right)^{1/5}\left(\frac{1}{C_L}\right)^{3/5}\left(\frac{\widetilde{C}_a T_a}{\Delta\widetilde{H}}\right)^{1/5} \tag{66.38}$$

where $\widetilde{C}_a$ = molar heat capacity of air and $\Delta\widetilde{H}$ = molar heat of combustion.

Equations 66.37 and 66.38 are functionally very similar to the expressions obtained by Hawthorne et al. [84] and Putnam and Speich [87]. These expressions indicate the similarity in three independent experiments.

Turbulent Jet Flame Length in Crosswind Conditions

A series of controlled experiments have been conducted by Brzustowski et al. [81] and Gollahalli et al. [92] in wind tunnels involving hydrogen and propane flames in the presence of wind. The work indicates that in such fires the initial effect of cross flow was to shorten the flame, after which increases in a cross-flow velocity caused increases in the flame length. Shortly before blow-off conditions were reached, flame length was observed to decrease with an increase in crosswind.

The results obtained by Brzustowski et al. [81] and Gollahalli et al. [92] with zero-wind condition are consistent with the model equations given in the previous section. Based on wind tunnel data and limited comparison with full-scale data, Brzustowski [79] has proposed the following procedure to determine the flame shape in the presence of crosswind for a jet flame.

1. Calculate the dimensionless lean limit concentration:

$$\overline{C}_L = C_L\left(\frac{u_j}{u_w}\right)\left(\frac{M_f}{M_a}\right) \tag{66.39}$$

2. If $\overline{C}_L \le 0.5$, then $\overline{S}_L = 2.04\left(\overline{C}_L\right)^{-1.03}$
   If $\overline{C}_L > 0.5$, then $\overline{S}_L = 2.71\left(\overline{C}_L\right)^{-0.625}$
3. If $\overline{S}_L > 2.35$, then $\overline{X}_L = \overline{S}_L - 1.65$.
   If $\overline{S}_L \le 2.35$, then determine $\overline{X}_L$ by following the equation

$$\overline{S}_L = 1.04\overline{X}_L^2 + 2.05\overline{X}_L^{0.28} \tag{66.40}$$

4. Determine the dimensionless rise, $\overline{Z}_L$, of the flame tip above flame tip:

$$\overline{Z}_L = 2.04\overline{X}_L^{0.28} \tag{66.41}$$

5. Calculate dimensional coordinates of the flame tip using the following equation:

$$X = \overline{X}_L d_j \left(\frac{\rho_j}{\rho_a}\right)^{1/2} \left(\frac{u_j}{u_w}\right)$$
$$Z = \overline{Z}_L d_j \left(\frac{\rho_j}{\rho_a}\right)^{1/2} \left(\frac{u_j}{u_w}\right) \tag{66.42}$$

Kalghatki [93] conducted a series of 103 small-scale wind tunnel experiments to determine the size and shape of turbulent hydrocarbon jet diffusion flames in the presence of crosswind. The tests were conducted with methane, propane, ethylene, and commercial butane. The burner diameter ranged from 6 to 22 mm, and the range of velocities was between 13 and 200 m/s. The crosswind velocities were varied from 2.6 to 8.1 m/s. Based on these tests, Kalghatki [93] concluded that the turbulent jet flame can be described by a frustum of a cone and the geometry of a jet flame under influence of wind can be represented by five geometric parameters:

1. Angle α_B, subtended by the burner tip and the tip of the flame with respect to vertical
2. Angle α, subtended by the flame with respect to vertical
3. Vertical length, L_{BV}, of the flame tip from the plane of the burner
4. The flame base width, W_1
5. The flame tip width, W_2

These parameters are expressed in terms of a dimensional variable called *effective source diameter* and a nondimensional velocity, R. The definitions of these two parameters are

$$D_s = D\left(\frac{\rho_j}{\rho_a}\right) \tag{66.43}$$

where
D = Source diameter, m
ρ_j = Density of jet fuel, kg/m^3
ρ_a = Density of ambient air, kg/m^3

$$R = \frac{U}{U_j} \tag{66.44}$$

where
U = Crosswind speed, m/s
U_j = Jet velocity, m/s

In Fig. 66.43 the variation of the vertical flame length parameter is shown as a function of the nondimensional velocity, R. Also shown in Fig. 66.43 are the correlations suggested by Brzustowski for propane, methane, and ethylene. In order to predict the actual flame length, the flame tilt with respect to the burner axis must be known. Figure 66.44 shows the data on flame tilt and the comparison with Brzustowski's calculation procedure. It is seen that the calculation procedure underestimates the flame tilt. Therefore, the measured flame lengths are slightly larger than the ones predicted using Brzustowski's model. Based on these results, Kalghatki [93] suggests the following correlations to determine the flame length and flame tilt parameters.

$$\alpha_B = 94 - \frac{1.6}{R} - 35R \tag{66.45}$$

$$\alpha = 94 - \frac{1.1}{R} - 30R \tag{66.46}$$

$$\frac{L_{BV}}{D_s} = 6 + \frac{2.35}{R} + 20R \tag{66.47}$$

Here the angles α are in degrees. The range of validity of these correlations are for the values of R greater than 0.02 and less than 0.25. The upper limit for R is not a serious limitation to the applicability of the model. For values of R less than 0.02, the wind-free data may be used to determine the flame lengths and the tilt may be assumed to be zero. It should be noted that the flame length given by Equation 66.47 determines only the vertical component. Actual inclined flame height is given by dividing Equation 66.47 by the cosine of the angle of tilt given by Equation 66.45. It is worth noting that the actual inclined flame length ratio is independent of the velocity ratio and is relatively constant at a value of about 120. This indicates that the majority of the tests conducted in this program were momentum-dominated turbulent jets. Sonju and

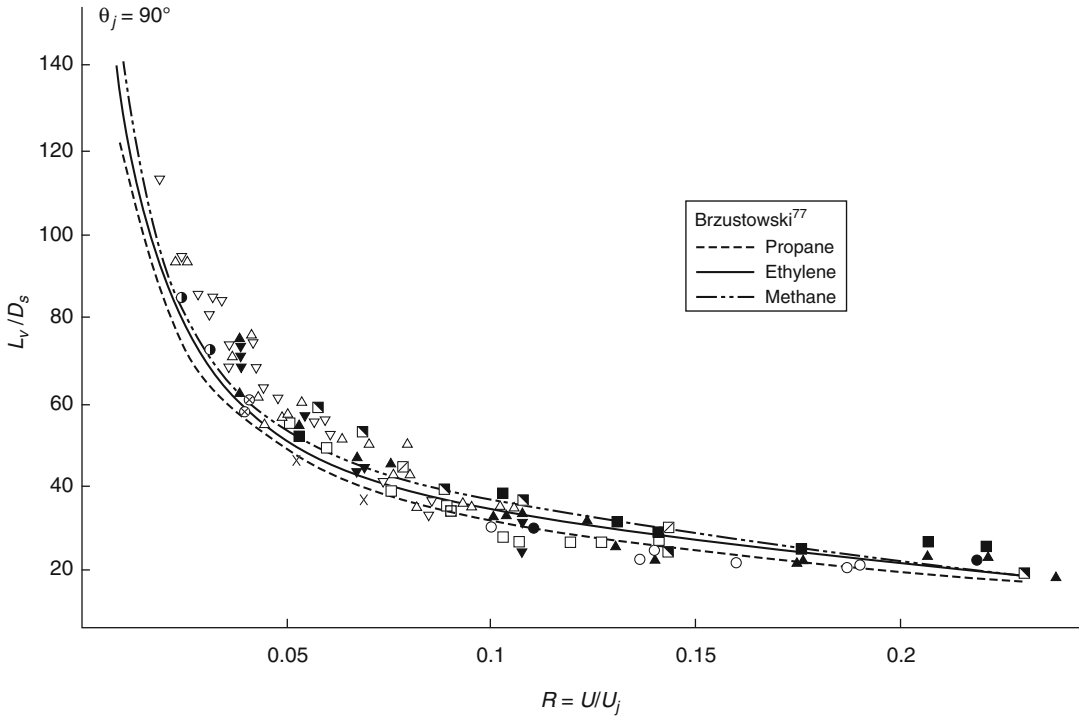

Fig. 66.43 Variation of the flame length above burner tip with velocity ratio, R [93]

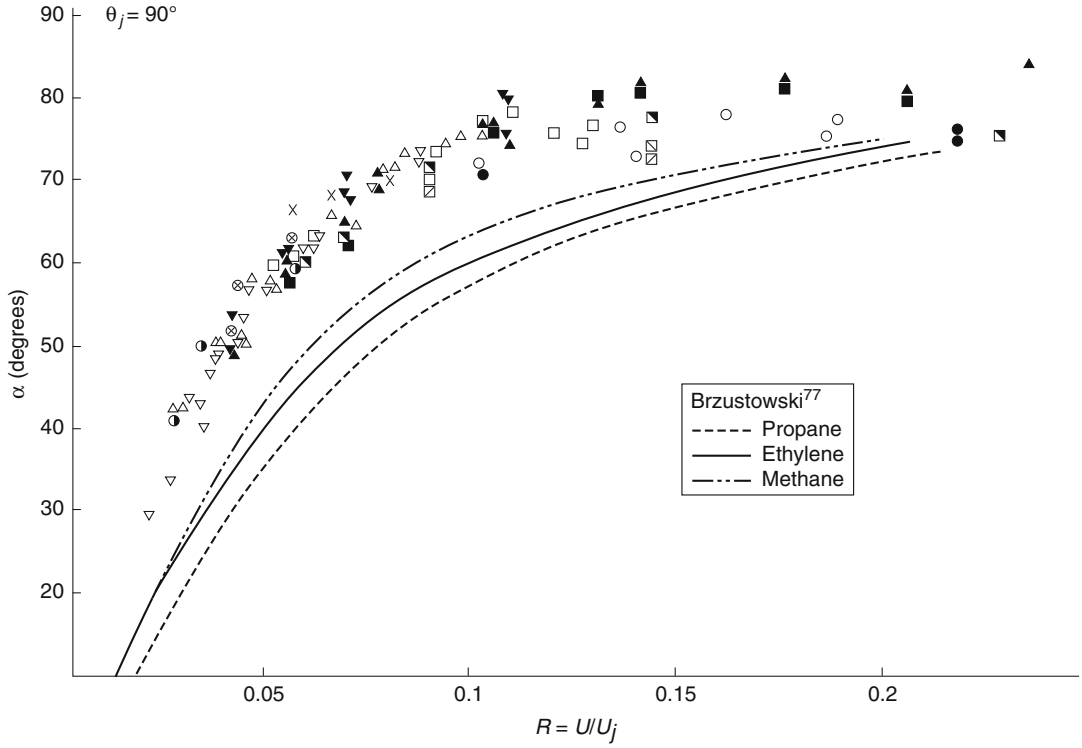

Fig. 66.44 Variation of angle of tilt with velocity ratio, R [93]

Hustad [94] conducted an experimental study on turbulent diffusion flames. The flare diameters ranged from 2.3 to 80 mm and the velocities ranged from 5 to 250 m/s. Their data indicate that the flame length is proportional to the one-fifth power of the Froude number. For Froude numbers greater than 100,000, the flame lengths appear to be independent of the Froude number. These results are consistent with the data of Putnam and Speich [87].

Turbulent Jet Flame Diameter in Crosswind Conditions

The work of Hawthorne et al. [84] described above also includes jet flame diameter calculation. They observed that the jet diameter increases as a function of distance. The measured spreading angles were in the range of 3–8° (one-half angle). The equivalent diameter for thermal radiation calculations can be calculated from the following equation:

$$\frac{D_c}{d_j} = \sec\theta + \frac{L}{d_j}\sin\theta\sec^2\theta \qquad (66.48)$$

The data of Kalghatki [93] for the base and tip widths of the flames indicate the spreading angle is a function of the nondimensional velocity ratio, R. For a jet flame in windblown surroundings, Kalghatki [93] gives the following correlation of jet diameter:

$$\frac{W_2}{D_s} = 80 - \frac{0.57}{R} - 570R + 1470R^2 \qquad (66.49)$$

$$\frac{W_1}{D_s} = 49 - \frac{0.22}{R} - 380R + 950R^2 \qquad (66.50)$$

From these calculations, it can also be deduced that the cone half-angle for the frustum decreases from a value of about 5° at $R = 0.025$ to a value of about 2.8° at $R = 0.2$. Therefore, at large, relative wind speeds, a diffusion flame takes an almost cylindrical shape. The data of Sonju and Hustad [94] indicate that the flame diameter increases as one-fifth power of the flame Froude number. The suggested constants, proportionally, for methane and propane flames are 2.5 and 4.0, respectively.

Kalghatki [93] also conducted some limited tests with nonorthogonal jet flames and concluded that the flame lengths are dependent on wind direction. These tests were conducted with relative wind angles varying from 45 to 135° (with 90° representing orthogonal cross flow). The value of the nondimensional velocity was greater than 0.025. The data indicate that for a given angle of tilt, the flame length remains relatively constant; however, the flame length decreases with increasing angle of tilt. The data of flame length and wind direction over the entire velocity ratios are shown in Fig. 66.45. As can be seen from Fig. 66.45, there appears to be a linear relationship between flame length and wind direction. The correlation suggested by Kalghatki [93] is

$$\frac{L_B}{D_s} = 163 - 0.64\theta_j \qquad (66.51)$$

where θ_j is the angle between wind and jet (degrees).

Aerodynamic Effects on Flame Stability

A jet diffusion flame in still air will lift off the tip of the burner and form a stable lifted flame when the flow velocity through the burner is increased beyond a limiting value known as the liftoff stability limit. If the flow velocity is increased further, the flame is extinguished at some limiting rate known as the *blowout stability* limit.

At the base of a lifted diffusion flame, the local turbulent burning velocity will be equal to the local flow velocity. If the flow rate through the burner is increased, the flow velocity will also increase and the base of the flame will be blown downstream to a new position where the turbulent burning velocity equals local flow velocity. The flame will blow out when the change in the burning velocity cannot keep up with the flow velocity anywhere in the jet as one moves downstream from the base of the jet flame.

The distance along the burner axis where the mean concentration equals the stoichiometric

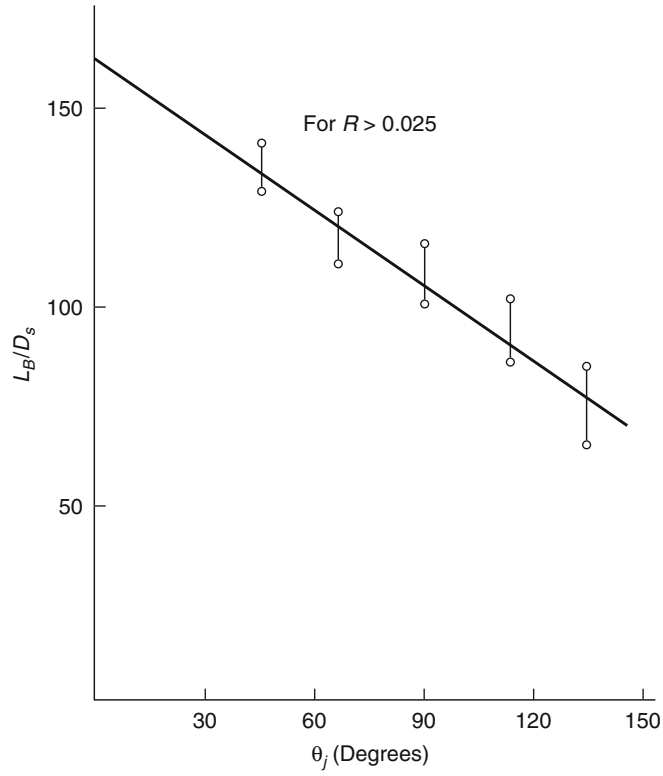

Fig. 66.45 Variation of flame length with jet axis orientation [93]

level is independent of the flow velocity and is given by the following equation:

$$\frac{H}{d_e} = 4\frac{\widetilde{\theta}_e}{\widetilde{\theta}_s}\left(\frac{\rho_e}{\rho_a}\right)^{1/2} + 5.8 \qquad (66.52)$$

where
H = Height along the jet axis, m
d_e = Effective jet diameter, m
$\widetilde{\theta}_e$ = Fuel mass fraction at jet exit
$\widetilde{\theta}_s$ = Stoichiometric fuel mass fraction
ρ_e = Jet mixture density, kg/m^3
ρ_a = Ambient air density, kg/m^3

The effective jet diameter is defined as follows. For subsonic jets:

$$d_e = d_j \text{ for } \mathrm{M} < 1$$

For choked flow:

$$d_e = d_j\left[\frac{2+(\gamma-1)\mathrm{M}^2}{\gamma+1}\right]^{(\gamma+1)(\gamma-1)}\frac{1}{\sqrt{M}} \qquad (66.53)$$

where
d_j = Jet diameter, m
M = Mach number after expansion to ambient pressure
γ = Ratio of specific heats

All things being equal, the larger of the value of H, the more scope there will be for the base of the flame to seek a new stable position as the flow velocity is increased, and therefore it will be more difficult to blow out the flame. Similarly, larger values of burning velocity will lead to larger flow velocities to blow out the flame. The critical velocity at the burner exit for blowout will depend on the burning velocity, the density ratio, and the Reynolds number based on H.

$$\frac{U_e}{S_u} = f\left(R_H, \frac{\rho_e}{\rho_a}\right) \qquad (66.54)$$

where
U_e = Critical velocity at jet exit, m/s
S_u = Maximum burning velocity, m/s
R_H = Reynolds number given by

Table 66.13 Relevant properties of hydrocarbon gases to determine blowout stability

Gas	Molecular weight	Dynamic viscosity at 0 °C (micropoises)	Maximum burning rate S_u (m/s)	Ratio of specific heats	Stoichiometric air-fuel ratio
Methane	16	102.7	0.39	1.31	17.2
Propane	44	74	0.45	1.13	15.7
Ethylene	28	91	0.75	1.255	14.9
Acetylene	26	93.5	1.63	1.25	13.3
Butane	54	80	0.44	1.1	15.7
Hydrogen	2	84	3.06	1.33	34.7

$$R_H = HS_u \frac{\mu_e}{\mu_e} \tag{66.55}$$

where μ_e = dynamic viscosity.

The typical values of the relevant parameters for typical fuels are given in Table 66.13.

Kalghatki [90] conducted a systematic study of the blowout stability of jet diffusion flames in still air. The fuel gases used were methane, propane, ethylene, acetylene, and commercial butane. The burner diameters ranged from 0.2 to 12 mm. The universal stability limit is given by the following equation:

$$\overline{U}_e = 0.017 R_H \left(1 - 3.5 \times 10^{-6} R_H\right) \tag{66.56}$$

where

$$U_e = \frac{U_e}{S_u} \left(\frac{\rho_e}{\rho_a}\right)^{1.5} \tag{66.57}$$

The validity of Equation 66.56 is shown in Fig. 66.46. It should be noted that Equation 66.56 is valid only up to a Reynolds number of 100,000.

Thermal Radiation Hazards from Hydrocarbon Jet Flames

Point Source Model for Jet Flame Radiation

For incident heat flux from a jet flame to a target outside the flame, it is customary to model the flame by a point located at the center of the real flame, as mentioned earlier in the pool fire section. The radiant heat flux per unit area and per unit time received by a target at a distance R from the point source is given by

$$\dot{q}'' = \frac{\dot{Q}_r \cos\theta}{4\pi R^2} \tag{66.58}$$

where $\dot{Q}_r$ is the radiative output given by the radiation fraction, χ_r, multiplied by the total heat release rate:

$$\dot{Q}_r = \chi_r Q$$

The geometrical aspects of the representation of thermal radiation field given by the point source model are surprisingly accurate for flare stacks, even in the case of long windblown flames. Many of the early experimental investigations relevant to jet flames were concerned with flares. The work covers a variety of jet flames, including flames of natural gas and of liquified petroleum gas (LP-gas). Representative accounts of work using natural gas are those by Chamberlain [95], Johnson et al. [96] at Shell, and by Cook et al. [97] at British Gas. Accounts of work on jet flames of LP-gas at Shell and British Gas have been given by Hirst [98] and Tam and Cowley [99]. The work on flames formed part of a study of emission and gas dispersion of jets as well as of combustion.

Hirst [98] describes experiments using liquefied propane. Tests were carried out using orifices ranging from 9 to 52 mm in diameter and pressures from about 6 to 20 bar. Both horizontal and vertical releases were studied. A series of tests were done with vertical releases. The liquid rose in a strongly divergent cone bending with the wind. The cone angle was typically 30° for the plume but up to 90° in the flash region. The

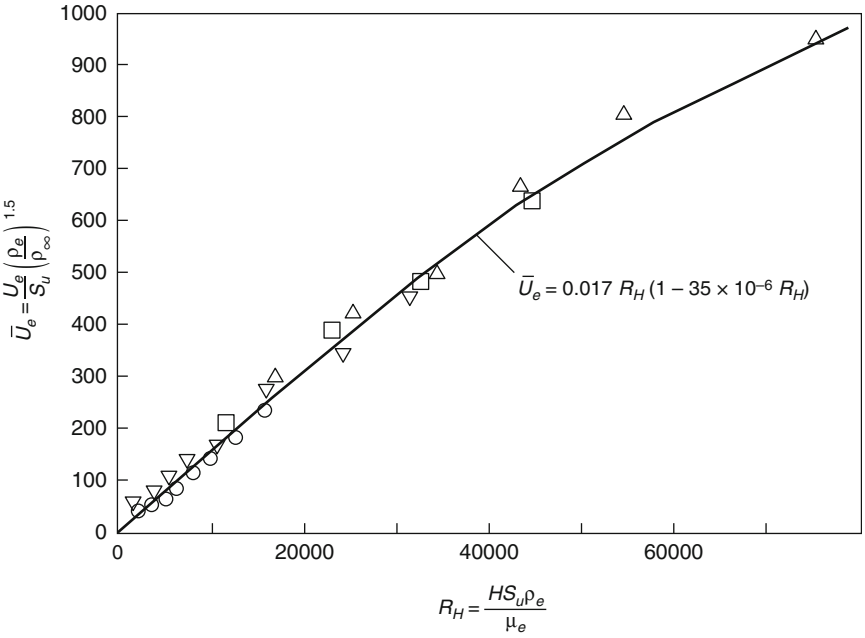

Fig. 66.46 Universal blowout stability curve for diffusion flames [90]

releases usually reached a steady state before ignition. The visible clouds at ignition were large, extending up to 45 m vertically and 70 m downwind. In most cases fireballs formed and in several tests rose to 100 m; the most fully developed fireballs occurred at low wind speeds. The overpressure generated by the flames were also measured. The maximum observed fell from some 3 bar at 20 m from the release point to about 0.8 bar at 100 m.

Other tests were done with horizontal releases. One of the features measured in these trials was the distance reached by the flame. Figure 66.47 gives the relation between the mass flow and the impingement distance of the flame for a 50-mm-diameter pipe. In one of the trials in which a 35-m-long jet flame from a full bore release of 7.9 kg/s from a 50 mm pipe at pressure of 13 bar. The combustion energy was 365 MW. The maximum surface emissive power was 250 kW/m^2 and occurred 25 m from the release point and just before the flame underwent transition from the momentum-dominated to the buoyancy-dominated condition. However, for such full-scale bore discharges the heat radiation within the flame was complex, and steady heat fluxes were mainly in the range of 50–220 kW/m^2 and depended on the discharge conditions and the target distance. The maximum temperature occurred at a distance of 4 m and had a value of 1570 K.

Brzustowski [100] considered a flare (in the presence of high crosswind) as a uniformly radiating cylinder. He observed that the thermal radiation flux given by the point source model is similar to those predicted using a cylindrical source model except at distances very close to the source. Brzustowski [100] also computed radiation heat flux for vertical elements parallel and perpendicular to the wind direction and has concluded that the corrected point source model and the uniform cylinder radiation model essentially yield very similar results.

Brzustowski et al. [81] carried out small- and pilot-scale experiments to study the radiative characteristics of turbulent flares using commercial-grade methane and propane. Small-scale test data were taken at jet velocities from 6.8 to 70 m/s with jet Reynolds numbers from 7500 to 94,000, and ratios of crosswind velocity to jet velocity from 0 to 0.113. Pilot-scale experiments were conducted on an outdoor site

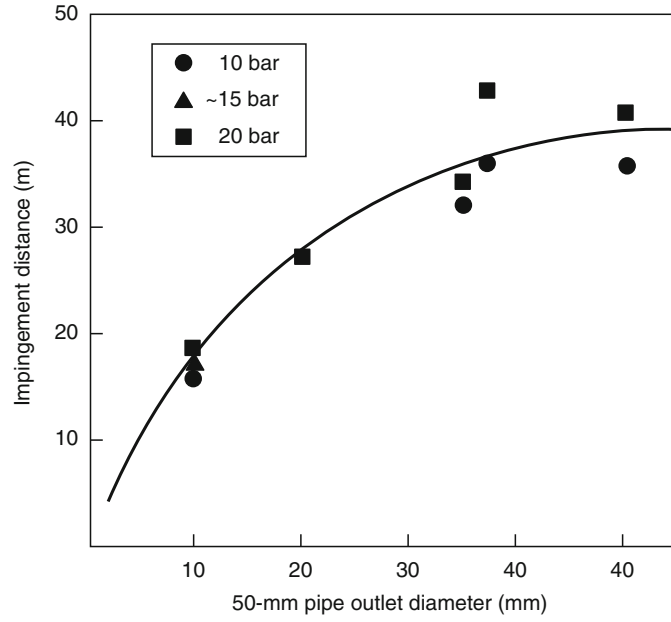

Fig. 66.47 Jet flames: flame impingement distance versus mass flow for propane [60]

with the flare modeled by a vertical 25 mm inner-diameter pipe 1.5 m high. In these tests, provisions were made for injecting steam into the gas below the tip of the flare. The incident heat flux at various distances was measured with and without steam.

Oenbring and Sifferman [101] compared the point source model predictions with full-scale measurements. The full-scale data consisted of radiation measurements in the Oenbring and Sifferman [101] studies that were conducted at the oil refinery facility in Conoco's Ponca City, Oklahoma, and in the Gillis gas plant facility in Los Angeles, California. The Gillis flare stack was 40 cm (16 in.) in diameter and 23 m high. The gas velocity ranged from a Mach number of 0.2 to 0.49. All test data indicate that the inverse square law predicts the thermal radiation accurately.

Radiative Fraction for Jet Flames

In order to predict the incident heat flux accurately, it is necessary to determine the fraction of total combustion energy resulting in thermal radiation. In general, the fraction of heat radiated depends on the efficiency of combustion and soot formation and on the heat lost by convection to the entrained air.

Most thermal radiation prediction models tends to ignore the details of the combustion process and concentrate on the overall combustion efficiency, or fraction of the energy that is radiated to the environment. Markstein [7] conducted a series of radiation measurements on propane turbulent diffusion flames. The total radiative powers of the flames were determined using wide-angle radiometer. The flow rates varied from 44 to 412 cm^3/s. A collimated beam radiometer was used to measure the radiation characteristics of different parts of the flames. Based on these measurements, Markstein [7] concluded that the thermal radiation from diffusion flames is at a maximum at approximately the center of the flame and tapers off on either side, forming a Gaussian distribution. The total radiative power of the flame was observed to be directly proportional to the total heat release rate. Figure 66.48 shows that the fraction of combustion energy released in the form of radiation is approximately 20 % for the propane diffusion flames. Burgess and Hertzberg [36] measured the fraction of combustion energy radiated to

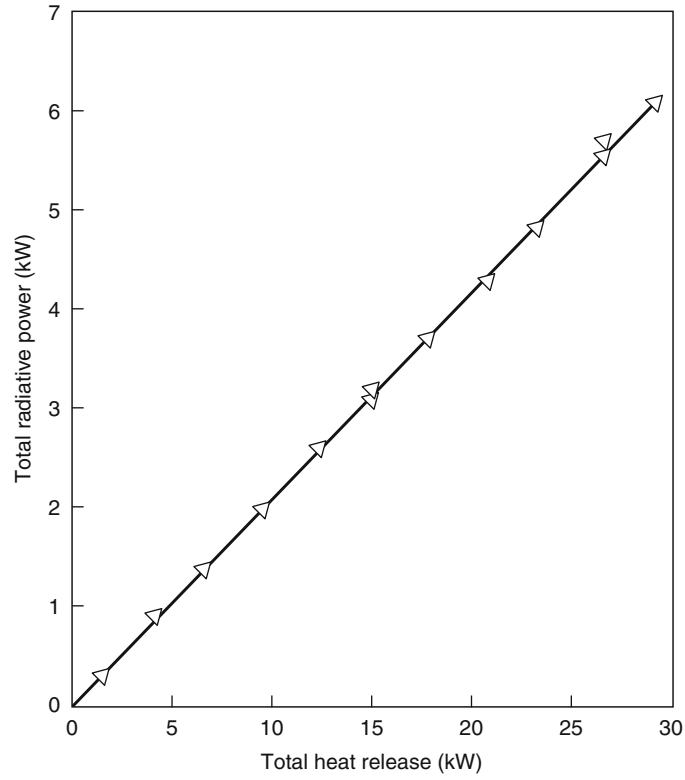

Fig. 66.48 Radiative power for propane diffusion flames [7]

Table 66.14 Comparison of radiative fraction, χr of various fuels

Fuel	f_s	χ_r Brzustowski [100]	χ_r Burgess and Hertzberg [36]	χ_r Tan [102]	χ_r Kent [103]	χ_r McCaffrey [89]
Hydrogen	1.0	0.2	0.17	–	–	–
Methane (C_1)	0.189	0.2	0.23	0.20	0.19	0.22
Ethylene (C_2)	0.170	0.25	0.36	0.26	0.25	0.38
Propane (C_3)	0.176	0.30	–	0.32	0.32	0.302
Butane (C_4)	0.175	0.30	0.30	0.37	0.37	–
C_5 and higher	–	0.40	–	–	–	–

the surroundings for several gaseous fuels. Tan [102] and Kent [103] have also suggested values for the radiated energy for a variety of fuels.

Table 66.14 compares the values of radiative fraction, χ_r, suggested by various investigators. The parameter f_s in Table 66.14 represents the fuel mass fraction at which carbon particles begin to form. For any hydrocarbon fuel, C_nH_m burning in air, the fraction f_s is given by

$$f_s = \frac{12n + m}{12n + m + [n/2(137.3)]} \tag{66.59}$$

For the same entrainment/mixing history, a gas with a higher value of f_s has less tendency to form solid carbon particles than a gas with a lower value of f_s. Higher values of f_s, therefore, correspond to lower radiation levels.

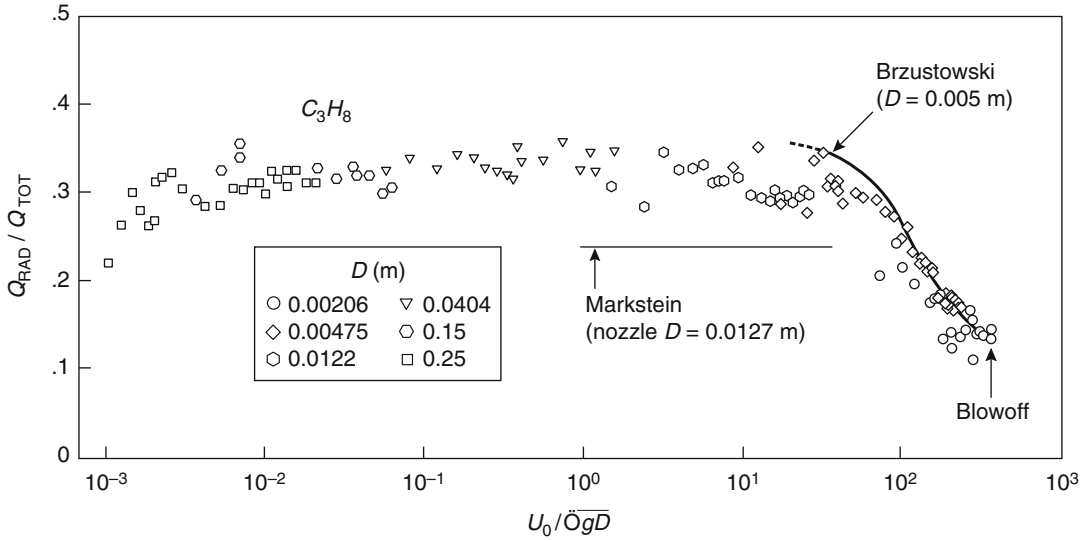

Fig. 66.49 Radiative fraction measured by McCaffrey [89]

Examination of Table 66.14 shows good qualitative agreement. Propane and butane have similar values of f_s, and their χ_r values are comparable. Methane and hydrogen have lower values of χ_r and higher f_s values. But ethylene has a lower value of f_s and, except in one study by Burgess and Hertzberg [36], the χ_r values are also lower. This may be partially due to straight molecular weight corrections applied by Tan [102] and Kent [103].

The intensity of flame radiation may be affected by the medium through which it passes. An appreciable attenuation may occur when radiation is transmitted from a source to a target through the atmosphere. The values of radiative fraction χ_r in Table 66.14 are properties of the fuel only. They do not take into account the variation of the operating parameters such as stack exit velocity, crosswind velocity, and the presence of air steam. However, these parameters have a profound influence on the temperature profiles and affect the fraction of combustion energy radiated, χ_r.

Figure 66.49 shows the radiative fraction measured by McCaffrey over six decades: $u/\sqrt{gDs}$. Comparing this figure with Fig. 66.42 shows that the radiative fraction is constant in the buoyancy-controlled regime, but for momentum-controlled jet flames, the radiative fraction decreases until blow-off occurs.

Evans and Pfenning [104] and McCaffrey [105, 106] have studied jet flame extinction via water spray. They also document significant reductions in flame radiation at subsuppression water spray addition rates of up to 50 %.

Brzustowski et al. [82] conducted a series of laboratory-scale tests on the effects of jet velocity and free stream velocity on the fraction of energy radiated, χ_r, from the turbulent flames. Figure 66.50 shows the effect of jet velocity on radiation in the absence of crosswind for methane and propane flames. Also drawn in Fig. 66.50 are the suggested values of radiative fraction χ_r from Tan [102] and Kent [103]. As can be seen from Fig. 66.50 the fraction of energy radiated, χ_r, is strongly dependent on jet velocity and decreases with increasing jet velocity. Figure 66.51 shows the effects of crosswind velocity on the radiant energy. In general, increasing crosswind velocity appears to increase the fraction of energy radiated, χ_r.

The significant departures of measured values of χ_r from the values previously published (which do not take into account the aerodynamic effects) can be understood in relation to variation of the

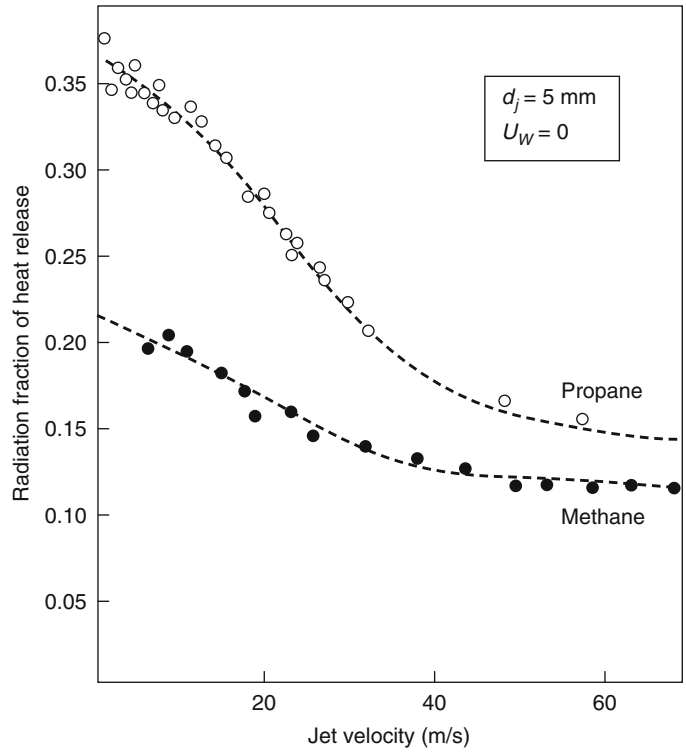

Fig. 66.50 Effect of jet velocity on radiated fraction of combustion energy [82]

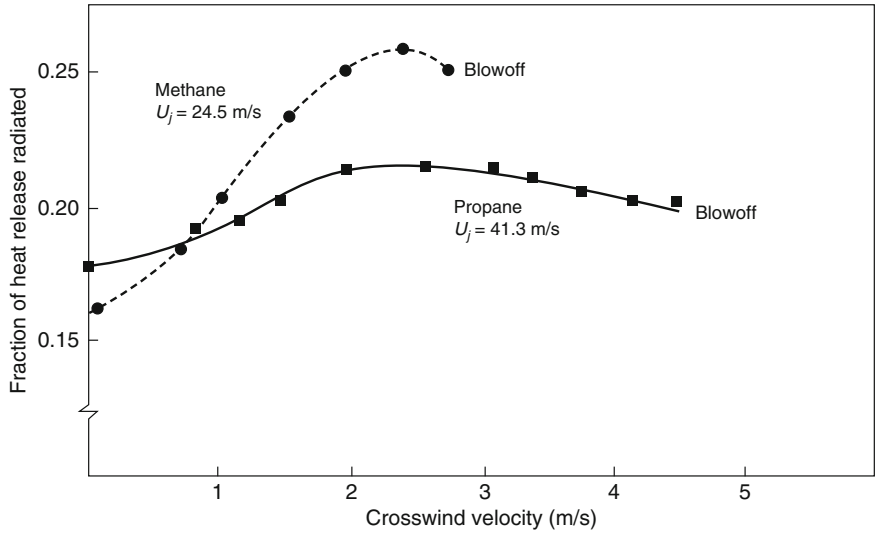

Fig. 66.51 Effect of crosswind velocity on radiated fraction of combustion energy [82]

detailed temperature profiles in the flames. The underlying explanation deals with the competing processes by which the products of hydrocarbon pyrolysis near the flare stack oxidize directly or form soot that burns in the downstream portion of the flames. Quite obviously, predictions based on the traditional values of χ_r would have overestimated the thermal radiation in all

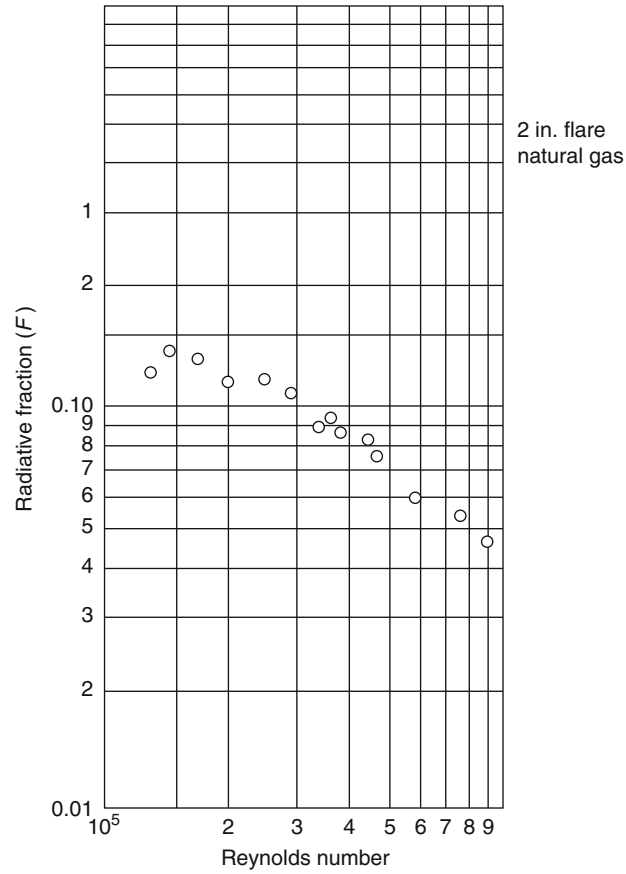

Fig. 66.52 Radiative fraction for natural gas flames full-scale tests [107]

these laboratory-scale experiments. Brzustowski et al. [82] also measured thermal radiation from a full-scale flare. The 0.406-m-diameter flare was operating at about 25 % of the design flaring rate. The best estimates of jet velocity and wind velocity were 28 and 4 m/s, respectively. The flame length was measured to be 25 m and flame tip was about 10 m above the flare tip level. The value of χ_r calculated from the radiation measurements at two ground sections 0.223 was about 30 % lower than the values predicted using the Tan [102] and Kent [103] approaches.

Figure 66.52 shows the fraction of net heat release radiated as a function of the flare Reynolds number for a 5 cm (2 in.) natural gas flare from Straiz et al. [107]. The Reynolds numbers in these tests are comparable to full-scale Reynolds numbers (of the order of 10^5–10^6). The fraction of energy radiated, χ_r, shows a significant departure at higher Reynolds numbers from its traditionally assumed value of 0.2.

It is quite evident that the aerodynamics of the flow have a significant effect on the radiation from a large turbulent diffusion flame. However, the radiation data described above were obtained on the laboratory-scale experiments, and their validity for large flames encountered in an offshore environment cannot be taken for granted.

Line and Cylinder Models for Jet Flame Radiation

As mentioned in the previous section, a point source model is a simple representation of a jet flame and applies only at large distance from the fire. The point source model can be inaccurate for target positions close to the fire. This is

particularly important when one is evaluating safe separation distances for storage of hydrocarbon fuels.

The tilted cylinder model discussed in the pool fire section can be used to overcome the inaccuracy of the point source model to determine the thermal radiation from large diffusion flames. This model assumes that the fire can be represented by a solid body of a simple geometrical shape, and all thermal radiation is emitted from its surface.

The incident radiation per unit area per unit time is given by

$$\dot{q}'' = FE\tau \tag{66.60}$$

where

E = Surface emissive power of flame, kW/m^2

F = Configuration factor

τ = Atmospheric attenuation factor (transmissivity)

The configuration factor is the fraction of the radiation falling directly on the receiving target. The shape or configuration factor depends on the shapes of the fire and receiving target, and on the distance between them.

The surface emissive power is the total radiative power leaving the surface of the fire approximated by the following equation [108]:

$$E = E_{bb}\left(1 - e^{-\kappa L}\right) \tag{66.61}$$

where

E_{bb} = Equivalent blackbody emissive power, kW/m^2

κ = Extinction coefficient, m^{-1}

L = Effective pathlength, m

The blackbody emissive power, E_{bb}, can be calculated by

$$E_{bb} = \sigma T_f^4 \tag{66.62}$$

where σ is the Stefan-Boltzmann constant (5.67×10^{-11} kW/m^2·K^4) and T_f is the flame temperature (K).

Fumarola et al. [109] suggested a line source model to compute radiation from jet flames. An elemental length of the flame is assumed to radiate similar to a point source model. The total incident heat flux at any observer location is computed by integrating the heat flux due to an elemental source over the flame length. They compared their results with Brzustowski [100] and the Oenbring and Sifferman model [110] and observed that their model predicted lower-incident heat fluxes at ground level.

Galant et al. [111] proposed a three-dimensional numerical model to estimate the flame geometry and thermal radiation from large diffusion flames. The model considers the variation in flow conditions based on a pseudo-stream-function formulation and includes effects of turbulence, combustion, and soot concentration. The model has been validated with field experiments of up to 254-mm (10-in.) diameter methane jets and agreement between predicted and measured heat flux is within 15 %.

Jet Fire Impingement Exposure

The severity of the thermal exposure from impinging jet flames far exceeds that observed for pool fire exposures. Heat fluxes of up to 250 and 300 kW/m^2 for two phase LP-gas and sonic natural gas jets, respectively, have been measured in large-scale jet flame tests (e.g., Cowley and Prichard [112]). In these tests where the flame fully engulfed a cylindrical target, heat fluxes averaged over the impingement area were 200 kW/m^2 for sonic natural gas jets and were 150 kW/m^2 for two phase LP-gas jets.

The severity of jet flame impingement exposures results from highly radiative, optically thick flames with high convective heat fluxes. The radiative and convective components of the total heat flux tend to be roughly equal in the high heat flux regions of the target (Parker [113]). Wighus and Dransgsholt [114] report temperatures as high as 1200 °C and impingement velocities of up to 80 m/s in gaseous propane jet flames. They also found that the temperatures observed at the location of peak velocity were lower for higher gas velocities. For instance, they measured 1150 °C at 30 m/s and 650 °C at 80 m/s. They measured heat fluxes as high as 340 kW/m^2 in some tests, and

the radiative fraction of the total heat flux tended to be about 2/3. Their results would indicate that differences found by Cowley and Prichard [112] for natural gas and two phase LP-gas flames were primarily the result of the two phase nature of the LP-gas release rather than differences between natural gas and propane gaseous flame properties.

Unsteady Thermal Radiation Analysis

Liquefied fuel gases having boiling points below normal ambient temperatures have come to be stored and transported in large quantities. Liquefied natural gas (LNG) is stored for peak demand use. It is also transported by sea in bulk carriers designed for cryogenic cargos. Liquefied petroleum gas (LP-gas) is stored under pressure and is transported by trucks, railroad tank cars, and by sea in bulk carriers. Although liquefied hydrogen has been used in limited quantities as a rocket fuel, serious consideration is being given to its use as a fuel for aircraft and possibly highway vehicles. Because volatile fuels are being transported in rapidly increasing volumes, speculation is being devoted to the kinds of accidents that could result from the release of these fuels.

The failure of a container carrying a pressurized cargo will result in the flash evaporation of a portion of the released liquid and the sudden formation of a vapor cloud from the evolved vapors. Upon contact with an ignition source, one of two situations may occur: the generation of a propagating plume flame, or the formation of a fireball. If the vapor puff is ignited immediately after its formation, it may burn as a rising sphere, usually referred to as a *fireball*. The rapid combustion of vapor clouds in the form of fireballs has been observed in several accidents involving vehicles carrying liquid propane. Here some of the accidents where a fireball has been reported to be observed are reviewed.

In the General Accounting Office report to the U.S. Congress regarding liquefied energy gases safety, an accident is cited involving a tractor-semitrailer carrying 34 m^3 (9000 gal) of LP-gas. About 2 min after the accident, a fireball of about 123 m (135 yd) in diameter was observed. The radiant heat from the fireball burned several people, a house, several other buildings, and some 12 acres of woods.

The National Fire Protection Association has maintained descriptions of several accidents involving LP-gas where a rising fireball was observed. One such accident happened in Oneonta, New York, where a freight train derailed involving 27 cars, 7 of which contained 120 m^3 (33,000 gal) of liquid propane. Seconds after the derailment, a huge fireball erupted from the area where the tank cars were piled up. It is believed that this fireball was the result of ignition of LP-gas when one of the tank cars split open. The fireball heated other tanks carrying LP-gas, which resulted in several BLEVEs (boiling liquid expanding vapor explosions).

One of the most cited fireballs occurred in Crescent City, Illinois, when a freight train carrying 15 cars derailed, 10 of them containing 130 m^3 (34,000 gal) of LP-gas each. One of the derailed tank cars rode up and over the pile and tore a hole in another tank car containing propane, causing the release of gas that produced the first fireball. There were several subsequent explosions that lasted for hours and destroyed 24 individual living quarters and 18 businesses.

The fireballs resulting from such accidents are large—usually of the order of about 100 m in diameter. The duration of the fireball is on the order of a few seconds because of rapid mixing with the surrounding air. During this brief period, a fraction of the combustion energy present in the initial mass of vapor is radiated as thermal energy to the surroundings. The adverse effect of this thermal radiation to population and property depends on the intensity and the duration of the radiation.

If, however, the vapor cloud is allowed to travel with the wind and is ignited at a location away from the source, the resulting vapor fire assumes the form of a propagating plume flame. In both cases, an unsteady diffusion flame is produced. However, the flame geometry is defined by the particular mode of burning. Accordingly, the levels of resulting thermal radiation differ significantly for each

mechanism. The unique behavior of these vapor cloud fires is discussed in this chapter. The following sections present an analysis of burning vapor clouds that define a plume fire; a discussion of the formation and burning of a hydrocarbon fireball; and a sample calculation procedure for burning of a vapor cloud in the form of a fireball.

Thermal Radiation from Burning Vapor Clouds

Estimating the thermal radiation field surrounding a burning vapor cloud involves geometric characterization of the cloud, that is, the time-averaged size of the visible envelope. It also requires estimation of the radiative properties of the fire, that is, the average emissive power, and so forth. Finally, the radiant intensity at a given location must be determined. Because the burning behavior of a moving vapor cloud can be best described as unsteady, the standard equations for pool fires do not apply. In the discussion that follows, the flame geometry and effective thermal radiation parameters that characterize a burning vapor cloud are identified.

Given a spill of a volatile, flammable chemical, initially a pool is formed. As the pool vaporizes due to heat transfer from the medium surface (land or water), a vapor cloud is formed above the pool. These vapors are entrained by the ambient wind and are dispersed in the downwind direction. Two conditions must be met for a burning cloud to be produced; first, there must be an ignition source located away from the spill point; second, the concentration within the vapor cloud must be within the flammability limit range for that material. Assuming these conditions exist, the fire that results is in the form of a propagating plume flame.

Based on experiments with spills of LNG on water, Mudan [115] and Raj et al. [33] identified three stages of vapor fire development. First, a transient turbulent flame spreads through the cloud. The flame propagates in both upwind and downwind directions. The second stage in the development of a vapor fire is the steady-state propagation toward the liquid pool. At this location, there appears to be a stationary diffusion flame. The third and final stage of burning results in a small pool fire at the source location. Based on limited experimental data on vapor cloud fires, the burning behavior and resultant flame geometry can be analyzed.

Flame Propagation Velocity Within a few seconds after ignition, flames tend to spread quickly both upwind and downwind of the ignition source. Flame travel in both directions is consistent if the ignition occurs after the flammable vapor cloud travels over it. The flames are initially contained within the cloud, but subsequently extend in the form of a flame plume above the cloud. This is consistent with premixed burning of the regions in the cloud that are within flammable limits prior to flame arrival, followed by diffusive burning of the richer regions in the cloud. After consuming the flammable vapors downwind of the ignition source, the downwind edge of the flame starts moving toward the spill point. Generally, the flame zone is normal to the wind direction.

During this transient flame growth, an *average* flame propagation velocity with respect to the ground can be determined by noting the location of the upwind edge of the flame at various time intervals. The flame speed with respect to gases may be obtained by adding the wind speed to the flame speed with respect to the ground. The initial, rapid propagation of the flame in the premixed vapor cloud can also be measured by the same technique.

Wind speed plays a significant role in the vapor cloud propagation. The flame velocity tends to increase with wind speed. Also, an increase in wind velocity increases the dispersion process. The ignition delay is also affected by the wind speed. Clearly, for a fuel-rich vapor cloud, an increase in mixedness will increase the flame propagation velocity. However, if the fuel concentration is well below stoichiometry, a further increase in ignition delay may, in fact, cause a decrease in flame propagation speed.

Mizner and Eyre [35] conducted vapor fire tests with propane spilled on water. The spill

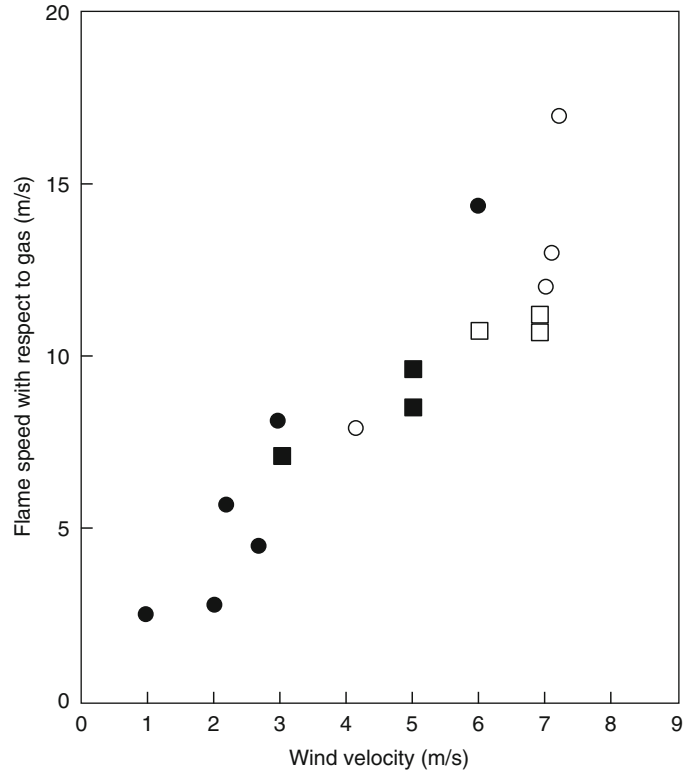

Fig. 66.53 Flame propagation velocities for LP-gas and LNG vapor fires [115]

rates of propane varied from 2.1 to 5.6 m^3/min and the ignition source was located approximately 130 m from the spill point. The wind speeds varied between 6 and 7 m/s. The flame propagation velocities were measured by locating the upwind edge of the flame as a function of time. Their analysis indicates that the flame propagation velocity (with respect to the ground) varies between 3.75 and 4.8 m/s.

In Fig. 66.53 the measured flame propagation velocities (with respect to unburnt gases) are shown for various wind speeds. The data indicate that there is no significant variation in the flame propagation velocities for methane (LNG) and propane (LP-gas). The maximum laminar burning velocity for methane is 0.45 m/s; laminar flame speed is 3.5 m/s; and the typical expansion ratio is 7.4. The corresponding properties for propane are 0.52, 4.0, and 7.6 m/s, respectively. Because these properties are somewhat similar for methane and propane, it is reasonable to expect the turbulent flame propagation velocities to be similar.

Flame Geometry Model Fay and Lewis [116] proposed a model for unsteady burning of unconfined fuel vapor clouds. Based on small-scale experiments with methane, ethane, and propane, and a simple entrainment model, they gave expressions to compute the maximum diameter, height, and duration for complete combustion. The model suggested by Fay and Lewis [116] assumes that the unsteady, turbulent diffusion flame is in the form of a fireball. The correlations given by the authors are validated over a range of small-scale experimental data (up to 200 cm^3) with methane, ethane, and propane gases at room temperature. However, experiments conducted with cold propane vapors ignited in an open environment do not show evidence of a fireball. In fact, the experiments performed by Shell [35] with LNG and LP-gas, and earlier tests involving LNG vapor fires, fail to confirm Fay and Lewis's [116] proposition that diffusive burning in unconfined vapor clouds takes place only in the form of a fireball.

Raj and Emmons [117] presented a theoretical analysis to estimate the ground level width of a large combustible vapor cloud. The model is based on the principle that the plume above a heat source is characterized by the strength of the heat source. In the case of a burning vapor plume, the rate of burning controls the plume characteristics, and the rate of burning itself is a function of the gas velocity within the plume.

The essential features of the Raj and Emmons [117] model are illustrated in Fig. 66.54. The assumptions made in the model development are as follows:

1. The geometry of the burning vapor cloud is two dimensional.
2. The burning is controlled by natural convection (buoyancy).
3. The flame propagation velocity with respect to unburnt gases is relatively constant.
4. The depth of the vapor cloud is uniform and is not affected by the flame.
5. The variation of the depth of vapor in the preburning zone is linear.
6. The steady-state turbulent flame correlation for the ratio of visible flame height to base width is valid.

Using experimentally derived values for flame height-to-width ratio and flame propagation velocity, Raj and Emmons [117] gave the following equation to determine the flame width as a function of time:

$$\tau = \left(\frac{\mathrm{Fr}_f}{\mathrm{Fr}}\right)^{1/3}\left\{\frac{\pi}{3\sqrt{3}} + \frac{2}{3}\ln\left[\frac{\sqrt{\chi^2+\chi+1}}{(1-\chi)}\right] - \frac{2}{\sqrt{3}}\tan^{-1}\left[\frac{2}{\sqrt{3}}\left(\chi+\frac{1}{2}\right)\right]\right\} \tag{66.63}$$

and

$$\chi = \left[\left(\frac{\mathrm{Fr}}{\mathrm{Fr}_f}\right)^{1/3}\xi\right]^{1/2}$$

where

$\xi = W/\delta$

$\tau = 2\ St/\delta$

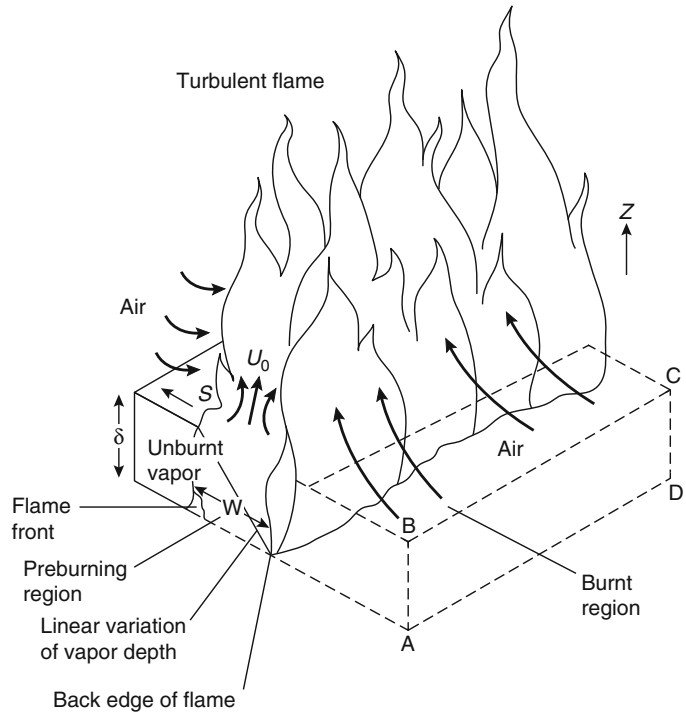

Fig. 66.54 Schematic diagram showing the unconfined burning of a pure flammable vapor cloud

$\mathrm{Fr}_f = S^2/g\delta$ = Flame Froude number
Fr = Froude number = U_0^2/gW
S = Flame propagation velocity, m/s
g = Acceleration due to gravity, m/s^2
δ = Unburnt vapor cloud thickness, m
U_0 = Upward velocity at flame base, m/s
W = Flame width, m

Raj and Emmons [117] estimated the Froude number based on Steward's [88] data on flame heights for hydrocarbon diffusion flames. The analysis indicates the following relationship for the flame height in a linear heat source.

$$\left(\frac{H}{W}\right)_{\text{stoichiometric}} = 4.98 N_{\text{CO}}^{1/3} \tag{66.64}$$

where N_{CO} is the combustion number defined as follows:

$$N_{\text{CO}} = \mathrm{Fr}\frac{\rho_0' 2\omega\left[r + \omega/\rho_o'\right]^2}{(1-\omega)^3} \tag{66.65}$$

where
ρ_0' = Density ratio = Density of vapor at flame base/density of air.
R = Stoichiometic air-fuel mass ratio
ω = Inverse volumetric expansion ratio and is defined as follows:

$$\omega = \frac{1}{\left(1 + Q_c/rC_pT_a\right)} \tag{66.66}$$

where
Q_c = Heat of combustion, J/kg
C_p = Specific heat, J/kg·K
T_a = Ambient temperature, K

The maximum width of the vapor fire is given by the following equation:

$$\xi_\infty = \frac{W_\infty}{\delta} = \left(\frac{\mathrm{Fr}}{\mathrm{Fr}_f}\right)^{-1.3} \tag{66.67}$$

Steward's [88] data indicate that nearly 400 % excess air is entrained in the fire plume. The typical height-to-width ratios measured in Steward's [88] data range between 5 and 50. Raj and Emmons assumed a height-to-width ratio of 2 for LNG vapor fires and demonstrated that Equation 66.67 predicts the observed behavior of flame width.

Experimental data on methane and propane vapor fires indicate that the flame width varies as the cloud propagates back to the spill point. Typically, it has been observed that the flame width increases as a function of time until all the flammable vapor is consumed. The width of the fire reduces to the dimension of the pool. That rate of increase in flame width appears to be slightly less than the flame propagation velocity (with respect to the ground).

The flame length variation can also be estimated as a function of flame width. It is interesting to note that flame length also increases slightly with time, but the ratio of the flame length to flame width is relatively constant. A plot of flame length-to-width ratios for propane vapor flames is shown in Fig. 66.55 [115]. In general, flame length is about 40 % of the flame width. The data of Mizner and Eyre [36] show that the typical flame length-to-width ratio varies between 20 % and 40 %. It is worth noting that vapor fire flame length-to-width ratios are significantly less than flame height-to-diameter ratios for pool fires.

The time-dependent flame width may be calculated using Equation 66.67. Figure 66.56 compares the computed flame width to measured flame widths as a function of time. Although there is considerable scatter in the data, the overall agreement between predicted and observed growth rates is good.

Thermal Radiation The incident flux received by a stationary observer from a propagating vapor is a complex function of several factors. First, the emissive power, which defines the radiative properties of the fire, should be determined. Because the duration of a vapor fire is short, and the steady burning period is even shorter, it is difficult to assign an averaging time for determining emissive powers and average incident fluxes. There is, however, a short period over which the thermal radiation appears to have less fluctuation. This duration can be used in determining average incident fluxes and corresponding emissive powers.

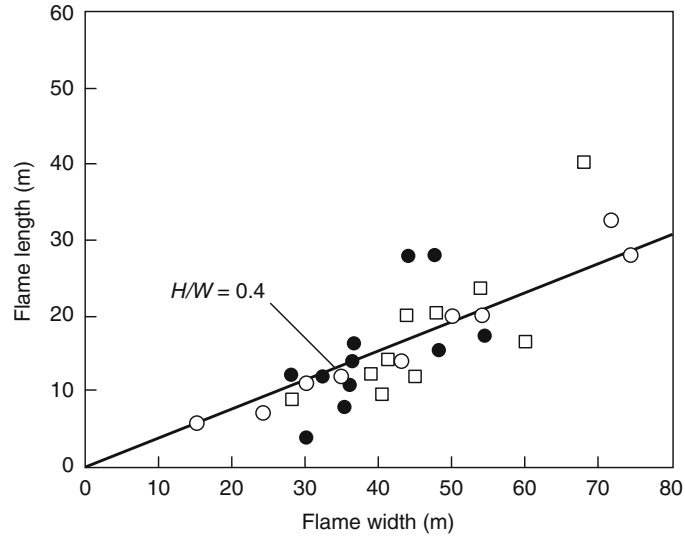

Fig. 66.55 Flame length as a function of flame width [118]

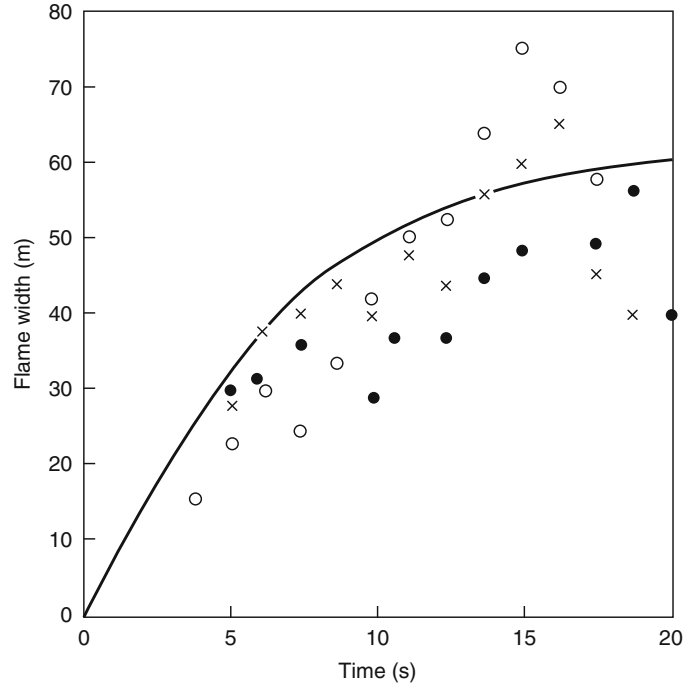

Fig. 66.56 Comparison of predicted and measured flame widths for LP-gas vapor fires [115]

Another important geometrical parameter influencing the thermal radiation from vapor fires is the area of the visible flame. If the flame is optically thick, the thermal radiation increases with an increase in the flame surface area. The area increases rapidly immediately following ignition because both the flame width and flame height increase with time. Therefore, the flame area increases approximately like the square of time. Once the flammable vapors are consumed, the flame area decreases rapidly. The incident flux also increases rapidly due to increasing flame area and drops off as the burnout process begins. The distance to the flame surface is also a

key parameter. Because the flame is in motion, the distance varies continuously until the cloud approaches the spill points where a pool fire is formed. Coupled with the variation in distance is the changing effect of absorption by the water vapor and carbon dioxide in the atmosphere. And finally, the geometry of the flame relative to the observer influences the view factor, that is, that portion of flame "seen" by the observer. Therefore, it is evident that the transient nature of the burning process, affected by the changing geometry, severely limits a detailed characterization of thermal radiation from a vapor cloud fire.

For a simple rectangular flame geometry, the centerline horizontal and vertical view factors can be determined using the following equations [2]:

$$F_h = \frac{1}{2\pi}\left(\tan^{-1}\gamma + \frac{X}{\sqrt{1+X^2}}\tan^{-1}\frac{Y}{\sqrt{1+X^2}}\right) \tag{66.68}$$

$$F_v = \frac{1}{2\pi}\left(\frac{X}{\sqrt{1+X^2}}\tan^{-1}\frac{Y}{\sqrt{1+X^2}} + \frac{Y}{\sqrt{1+Y^2}}\tan^{-1}\frac{X}{\sqrt{1+Y^2}}\right) \tag{66.69}$$

where X = flame length divided by observer distance, and Y = flame width divided by observer distance.

For asymmetric configurations, trigonometic variations of Equations 66.68 and 66.69 can be used to determine the appropriate view factors. The leading edge of the flame (with respect to the observer) may be calculated using the ignition location and the flame propagation velocity. The time-dependent flame width may be calculated using Equation 66.67. Because flame height is related to flame width, the crosswind radiation may be calculated using appropriate view factors. The incident thermal flux is given by the following equation:

$$\dot{q}''_{\text{crosswind}} = EF_{V,H}\tau \tag{66.70}$$

where τ represents the atmospheric transmissivity.

A similar procedure may be adopted to calculate incident thermal radiation in the downwind direction. Here the flame is moving away from the observer at flame propagation speed. Therefore, the downwind incident flux will be at its maximum at the time of ignition (assuming ignition occurs at the downwind edge of the cloud) and will decrease rapidly.

Because of the complex phenomena of a vapor fire, a simple calculation procedure cannot be developed to determine the incident thermal flux. A numerical program based on equations described in this section may be used to determine the time-dependent thermal flux.

Thermal Radiation from Hydrocarbon Fireballs

Fireball combustion occurs when volatile hydrocarbons are released and rapidly ignited. In order to characterize the radiation from fireballs, it is necessary to define the size and dynamics of the fireball and then to assess the radiation based on these results.

Fireball Size and Dynamics

The maximum size of a fireball is governed primarily by the mass of the fuel released and vaporized. Although the fireballs are rarely spherical, an equivalent spherical volume is widely used to characterize the size of a fireball. The maximum diameter of the equivalent spherical fireball is given by

$$D = 5.8\ \text{m}^{1/3} \tag{66.71}$$

where D is the maximum diameter in meters and m is the mass of fuel in kilograms. This expression was synthesized by Roberts [119] from prior work and has been adopted by others since that time (see CCPS [118]). The maximum fireball diameter is independent of the initial pressure of the fuel so long as the pressure and temperature are sufficient to vaporize the fuel. Hasegawa and

Sato [120, 121] suggest that for propane at or above normal ambient temperature (20 °C) complete vaporization will occur.

Although the maximum size of the fireball is independent of the release pressure, the dynamics of the fireball are dependent on the momentum of the release, which results from the flash evaporation of the fuel. For momentum-dominated fireballs, the burning duration is given by

$$t_d = 0.45m^{1/3} \tag{66.72}$$

(see CCPS [118]), where t_d is in seconds and m is in kilograms. For buoyancy-dominated fireballs, such as would be expected for atmospheric pressure releases, the burning duration is given by

$$t_d = 2.6m^{1/6} \tag{66.73}$$

(see CCPS [118]) where t_d is in seconds and m is in kilograms. Not only do burning durations differ for momentum-dominated and buoyancy-dominated fireballs, but the growth histories of the fireballs over their lifetime also differ. For momentum-dominated fireballs, the maximum fireball diameter is reached quickly with the fireball diameter growing initially as the one-fourth power of time (see Fig. 66.57). The fireball diameter remains approximately constant over its lifetime. Conversely, the size of a buoyancy-dominated fireball initially grows as the square of time, controlled by buoyant entrainment processes (Fay and Lewis [116]).

Comparing the above fireball duration equations, it becomes clear that for large fuel masses, the momentum-dominated duration exceeds the buoyancy-dominated duration. Because buoyancy is ever present, the duration should never exceed the buoyancy-dominated duration. As such, even pressurized releases will be dominated by buoyancy for very large masses (greater than about 30,000 kg), and the buoyancy-dominated expression should be used.

For buoyancy-dominated fireballs, not only is the entrainment rate lower, but the fireball rises during its lifetime. As such, during its lifetime the fireball lifts off from the ground. Roberts [119] adopts the correlation of Hardee and Lee [122] for the time to fireball liftoff:

$$t_e = 1.1m^{1/6} \tag{66.74}$$

where t_e is in seconds and m is in kilograms. As one would expect, the liftoff time scales in the same manner as the buoyant fireball duration,

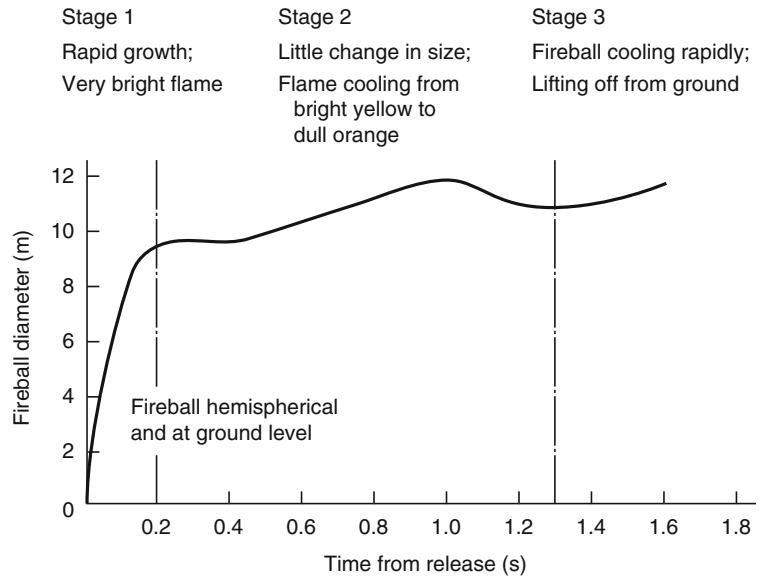

Fig. 66.57 Fireball development as a function of time; 7.5 kg LP-gas released from cylinder bursting [119]

with the liftoff time being about 40 % of the burning duration. Based on the work of Fay and Lewis [116], the maximum rise height of a buoyancy-dominated fireball is approximately five-thirds of the maximum fireball diameter. As such, the maximum rise heights range from one- to five-thirds of the maximum fireball diameter for both momentum- and buoyancy-dominated fireballs.

Fireball Radiation

Radiation models for fireballs use either the point source or spherical source model. The expressions are essentially equivalent under the simplest conditions but vary with geometric conditions where the target cannot view the entire fireball.

Point Source Fireball Model

For the point source model, the incident radiant flux, q, is given by

$$q = \tau \chi_R \cdot \frac{\dot{Q}}{4\pi L^2} \cos\theta \tag{66.75}$$

where
τ = Atmospheric transmissivity
χ_R = Radiative fraction
$\dot{Q}$ = Heat release rate
L = Distance from the target to the point source location
θ = Angle of the target relative to the line of sight connecting the source and target

The heat release rate is normally estimated by assuming that the total heat content of the fireball, Q, is released uniformly over the fireball duration.

$$\dot{Q} = \frac{Q}{t_d} \tag{66.76}$$

The radiative fraction is generally in the range 0.1–0.4. Roberts [119] correlated the data of Hawegawa and Sato [120, 121] to obtain the following correlation for the radiative fraction as a function of the fuel vapor pressure:

$$\chi_R = 0.27P^{0.32} \tag{66.77}$$

where P is the storage pressure (in MPa), and the original data included vapor pressures from 0.2 to 1.4 MPa.

The distance from the point source to the target is given by simple geometry as

$$L = \sqrt{R_T{}^2 + \left(Z_p - H_T\right)^2} \tag{66.78}$$

where
R_T = Horizontal distance from the release to the target
H_T = Target height
Z_p = Height of the point source

The appropriate selection of Z_p is the average height of the center of the fireball. This can range from $D/2$ for high-momentum releases with no buoyancy effects to 5/6 D for buoyancy-dominated releases.

Spherical Fireball Model

The spherical fireball model assumes that the fireball can be characterized as having an average fireball surface emissive power, E, and a diameter, D. The incident radiant flux to a target outside the fireball is given by

$$q = \tau E F \tag{66.79}$$

where τ is the transmissivity of the atmosphere between the fireball and the target and F is the configuration factor.

The configuration factor is strictly a geometric factor. Figure 66.58 shows the relevant geometric details required for the determination of the configuration factor where ϕ is the half-angle subtended by the fireball; θ is the angle of the normal to the target relative to the axis to the fireball; L is the separation of the target from the fireball center; and r is the fireball radius ($r = D/2$) [118]. When $\theta < \pi/2 - \phi$ the configuration factor is simply

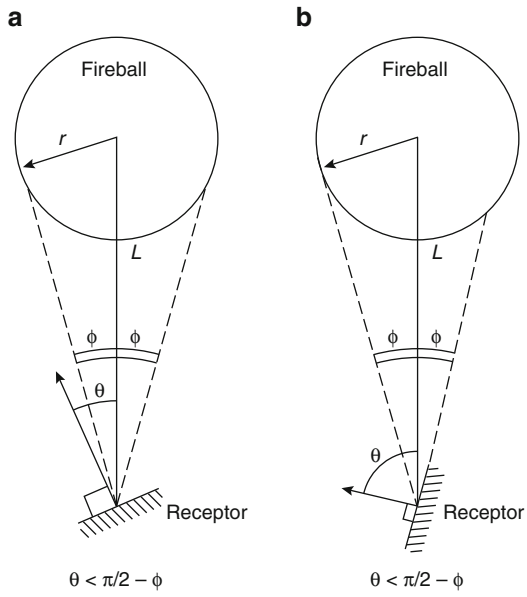

Fig. 66.58 Geometry of a radiative sphere (fireball). (**a**) Receptor "sees" the whole fireball. (**b**) Receptor "sees" part of the fireball

$$F = \left(\frac{r^2}{L^2}\right)(\cos\theta) \quad \text{for } \theta < \frac{\pi}{2} - \phi \tag{66.80}$$

When $\theta > \pi/2$—ϕ, portions of the fireball are not visible to the target and the configuration factor is more complex.

$$F = \frac{1}{2} - \frac{1}{\pi}\sin^{-1}\left[\frac{\left(L^2 - r^2\right)^{1/2}}{L\sin\Theta}\right] + \frac{r^2}{\pi L^2}\cos\Theta\cos^{-1}\left[\frac{\left(L^2 - r^2\right)^{1/2}}{r}\cos\Theta\right] - \frac{1}{\pi L^2}\left(L^2 - r^2\right)^{1/2}\left(r^2 - L^2\cos^2\Theta\right)^{1/2} \quad \text{for } \Theta > \frac{\pi}{2} - \Phi \tag{66.81}$$

where

r = Radius of fireball ($r = D/2$), m
D = Diameter of fireball, m
L = Distance to center of sphere, m
Θ = Angle between normal to surface and connection of point to center of sphere, rad
2Φ = View angle, rad

The appropriate selection of Z_p is the average height of the center of the fireball. This can range from $D/2$ for high-momentum releases with no buoyancy effects to $5/6D$ for buoyancy-dominated releases.

The emissive power of the fireball surfaces have been measured by several investigators and have been found to be in the range of 100–450 kW/m^2. Pape et al. [123] have correlated the data of Hasegawa and Sato in a form similar to the radiative fraction correlation by Roberts [119].

$$E = 235P^{0.39} \tag{66.82}$$

where E is the emissive power in kW/m^2 and P is the vapor pressure in MPa. Measurements by Johnson et al. [124] for 1000 and 2000 kg butane and propane releases at 0.75 and 1.6 MPa yielded surface emissive powers in the range of 320–370 kW/m^2. An emissive power for large-scale releases of 350 kW/m^2 is widely used.

Thermal Radiation Hazards to Personnel

Thermal radiation from hydrocarbon fires may pose significant hazards to both personnel and property. Hazards to personnel result from exposure to intense thermal radiation, causing severe burn injury. In the following subsection the criteria for thermal radiation hazard assessment for determining safe separation distances for personnel are discussed. Discussions of the effects on combustibles and structures can be found elsewhere in the handbook (see Chap. 21).

A comprehensive treatment of skin burn injury calculations is provided by the SFPE [125] and additional information is available in the Institution of Chemical Engineers monograph [126]. The thermal radiation from a fire may cause skin burns if the intensity of radiation and duration of exposure are sufficiently high. Skin burns occur over a continuous range of severity, starting from a burn so minor that the skin is barely damaged and extending

through complete destruction of all skin layers to the underlying tissues or bone. Several classifications of skin burn severity have been proposed, each depending on the degree of skin damage. The most familiar classification is to divide skin burns into three degrees. Even with these three degrees, there are several recognized sublevels. For present purposes, the following levels of burn severity can be used, with the attached simple descriptions:

1. *First degree*. The mildest level of skin burn, characterized by erythema (reddening), but no formation of blisters. The mildest of first-degree burns are not particularly painful and commonly present no medical problem. They may, in fact, not even cause symptoms other than a mild impression of warmth. More severe first-degree burns will produce some pain, but no permanent damage. Flaking or scaling of the skin will occur several days after exposure because of damage to the outer skin layer.
2. *Second degree*. An intermediate level of skin burn, characterized by formation of blisters. Blister depth may be shallow, with only the surface layers of the skin damaged, resulting in a moderate second-degree burn, or with nearly the full depth of the skin destroyed, that is, a severe second-degree burn.
3. *Third degree*. Deep burns, characterized by destruction of all skin layers. The underlying tissue may also be destroyed.

The medical problems of burns covering large areas of the body include the severe loss of fluid and the extreme potential for infection following the loss of a large portion of the protective layers of the skin. Survivability among burn patients has improved over recent decades due to improvements in treatment methods. Survivability of first-degree burns is excellent. Survival of individuals experiencing second-/third-degree burns varies with age, percent of body burned, and preexisting conditions [126–129]. For exposures to radiation from hydrocarbon fires at a distance, it is unlikely that the area of exposure will be below 20 % so that second-degree burns should be regarded as producing significant injury and likely death. Little credit can be taken for reduction of burn hazards by ordinary clothing not designed as thermal protection gear.

Pain and tissue damage are both related to heating of the skin. The skin consists of two main layers: the epidermis, which is a thin (0.05–0.1 mm) outer layer, and the dermis, which is an inner layer (1–2 mm thick). Although the skin is a complex system, models can be used as an aid in predicting skin response to heating. The simplest analysis begins with the assumptions that the skin and underlying tissue behave as a one-dimensional medium with constant thermal properties and heat transfer is due to conduction only.

The data of Buettner [130] and Hardy [131] obtained by having volunteers expose their forearms to varying degrees of thermal radiation, indicate that the threshold pain is felt by human beings when the average temperature of 0.1 mm depth of skin is increased to about 45 °C. They found the critical heat flux for initiation of pain was 1.4–1.7 kW/m^2 (the solar constant is about 1 kW/m^2 on a clear summer day). Hardy artificially varied the initial skin temperature and found that the temperature threshold for pain remained the same and the critical radiant flux for pain was reduced by increased initial skin temperature. Examining the data available in the literature, it was found that the time required for pain at normal initial skin temperatures (~32.5 °C) can be correlated with the intensity of radiation by the following equation [125, 130–133]:

$$t_p = \left(\frac{35}{\dot{q}''_r}\right)^{1.33} \tag{66.83}$$

where t_p is the time to produce pain in seconds, and $\dot{q}''_r$ is the incident radiant flux in kW/m^2. Equation 66.83 applies only at heat fluxes above the critical heat flux for pain of 1.4–1.7 kW/m^2 and normal skin temperature (32.5 °C).

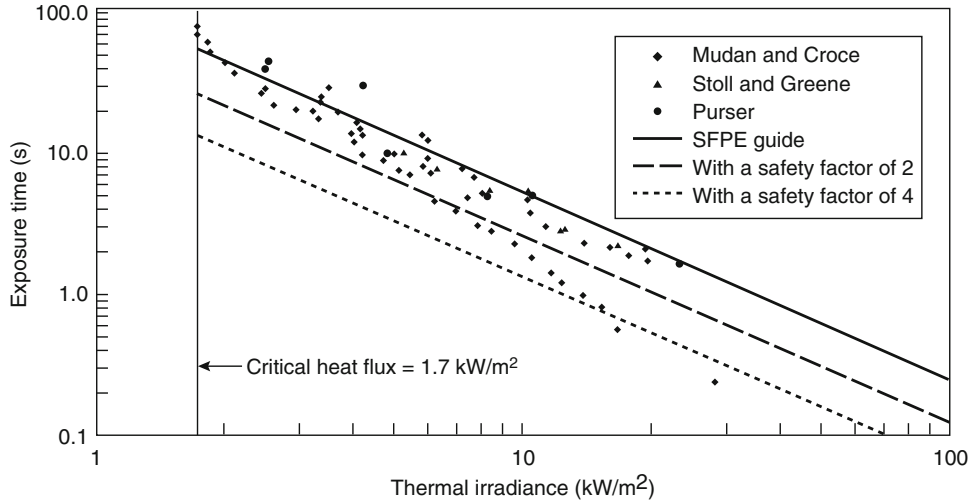

Fig. 66.59 Time for pain on a plot of exposure time versus thermal irradiance [125]. Individual data are shown as points and curve fits to data are shown as *thin lines*

In Fig. 66.59 the time required to cause pain is shown as a function of the incident thermal flux. The figure includes Equation 66.83 as well as curves reflecting factors of safety of 2 and 4 [125]. The sources of data used in Fig. 66.59 include Buettner [130], Hardy [131], Bigelow et al. [132], and Stoll and Greene [133]. The SFPE guide recommends a safety factor of 2 below 6 kW/m^2 and 4 above 6 kW/m^2.

Correlations of the onset of second-degree burns due to radiant heating have also been developed. The SFPE guide [125] recommends the following for second-degree burns:

$$t_B = \left(\frac{300}{\dot{q}_r''}\right)^{-1.46} \tag{66.84}$$

where t_B is the time in seconds to second-degree burns, and q_r'' is the radiant flux in kW/m^2. In Fig. 66.60 the time required to cause second-degree burns is shown as a function of the incident thermal flux. The SFPE guide recommends a safety factor of 1.5. Wieczorek and Dembsey [134] have examined the variability of the exposure required to produce burns based on conditions of exposure.

Correlations of this type are useful for scoping calculations, but because they assume a constant radiant flux, they are not applicable to more realistic time-dependent problems. More detailed methods have been developed, which include different thermal properties for each skin layer, blood profusion, and metabolic heat generation. In addition to more detailed treatment of heat transfer effects, these models also include burn damage to the skin via simple Arrhenius chemical kinetics, denoted the *damage integral*. This approach was developed by Henriques in the late 1940s. This damage integral reaches a value of one at the indicated burn level at the depth within the skin for which the damage has been determined. Mehta et al. [135], Dillon et al. [136], Torvi and Dale [137], Diller and Hayes [138], and Bamford and Boydell [139] are examples of such models. The SFPE guide includes discussion of the damage integral approach.

The *United States Federal Safety Standards for Liquefied Natural Gas Facilities* (49 *CFR*, Part 193, 1980) suggest an acceptable level of 5 kW/m^2 for direct exposure of human beings. At this incident flux, exposure time on bare skin

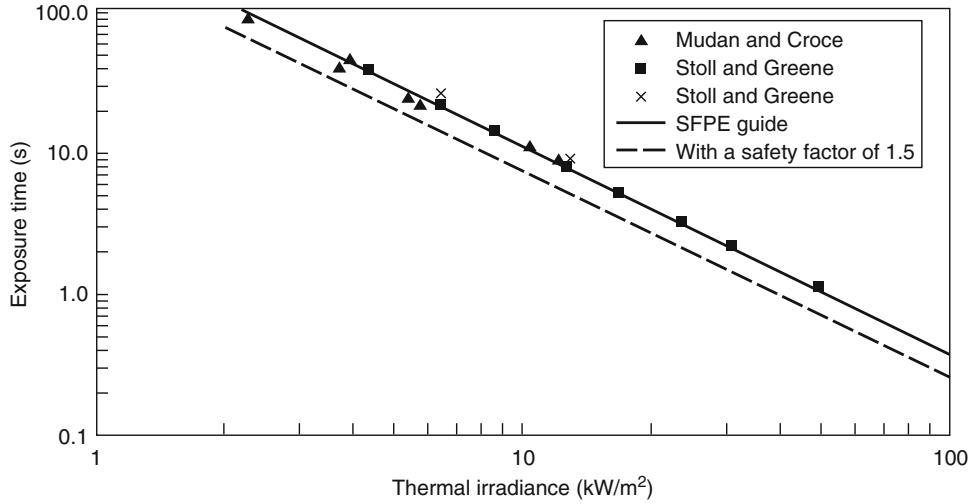

Fig. 66.60 Time for superficial second-degree burn on a plot of exposure time versus thermal irradiance [125]. Individual data are shown as points and curve fits to data are shown as *dashed lines*

before unbearable pain is about 13 s and second-degree burns may occur in about 40 s. This level can, therefore, be used as a criterion for injury for short-duration fireball exposures. Lower radiant flux criteria would be expected for pool or jet fires where the exposure durations can be significantly longer (as low as 1.4–1.7 kW/m^2, the threshold for pain and injury).

Summary

In the previous sections, we have given detailed techniques for computing impacts of large, open hydrocarbon fires. In particular, we have addressed steady-state thermal radiation from pool fires and flame jets and unsteady-state thermal radiation from vapor fires and fireballs. Particular emphasis has been placed on supporting the assessment methodology with available experimental data. These models can be used to appropriate impact criteria to evaluate the fire and flammability hazards associated with hydrocarbon releases.

References

1. E.M. Sparrow and R.D. Cess, *Radiation Heat Transfer,* Brooks Publication Company, Belmont, CA (1966).
2. E.M. Sparrow and R.D. Cess, *Radiation Heat Transfer,* rev. ed., McGraw-Hill, New York (1978).
3. R. Siegel and J.R. Howell, *Thermal Radiation Heat Transfer,* 3rd ed., Hemisphere Publishing Corporation, Washington, DC (1992).
4. M.F. Modest, *Radiation Heat Transfer,* McGraw-Hill, New York (1993).
5. W.H. McAdams, *Heat Transmission,* 3rd ed., McGraw-Hill, New York (1954).
6. D.Q. Kern, *Process Heat Transfer,* McGraw-Hill, New York (1950).
7. G.H. Markstein, "Radiative Energy Transfer from Turbulent Diffusion Flames," *Combustion and Flame,* 27, pp. 51–53 (1976).
8. V.I. Blinov and G.N. Khudiakov, "Certain Laws Governing Diffusive Burning of Liquids," *SSSR Doklady,* Academiia Nauk, pp. 1094–1098 (1957).
9. H.C. Hottel, "Certain Laws Governing Diffusive Burning of Liquids," *Fire Research Abstract and Revision,* 1, p. 41 (1959).
10. J. DeRis and L. Orloff, "A Dimensionless Correlation of Pool Burning Data," *Combustion and Flame,* 10, pp. 381–388 (1972).

11. D.S. Burgess, A. Strasser, and J. Grumer, "Diffusive Burning of Liquid Fuels in Open Trays," *Fire Research Abstract and Revision,* 3, p. 177 (1961).
12. J. Grumer, A. Strasser, T.A. Kubala, and D.S. Burgess, "Uncontrolled Diffusive Burning of Some New Liquid Propellants," *Fire Research Abstract and Revision,* 3, p. 159 (1961).
13. M.G. Zabetakis and D.S. Burgess, "Research in Hazards Associated with the Production and Handling of Liquid Hydrogen," *U.S. Bureau of Mines Report, RI 5707,* Pittsburgh, PA (1961).
14. K.S. Mudan, "Thermal Radiation Hazards from Hydrocarbon Pool Fires," *Progress Energy Combustion Science,* 10, pp. 59–80 (1984).
15. S.R. Gollahalli and H.F. Sullivan, "Liquid Pool Fires—A Review," *Research Report #23,* University of Waterloo, Canada (1973).
16. J. Moorhouse, "Scaling Criteria for Pool Fires Derived from Large-Scale Experiments," *Institution of Chemical Engineers Symposium,* 71, pp. 165–179 (1982).
17. K.S. Mudan and P.A. Croce, "Thermal Radiation Model for LNG Trench Fires," *ASME Winter Annual Meeting,* New Orleans (1984).
18. B. Hagglund and L. Persson, "The Heat Radiation from Petroleum Fires," *FOA Report C 20126-D6 (A3),* Stockholm, Sweden (1976).
19. T. Yamaguchi and K. Wakasa, "Oil Pool Fire Experiments," *Fire Safety Science*, 1, pp. 911–918 (1986).
20. P.G. Seeger, "On the Combustion and Heat Transfer in Fires of Liquid Fuels in Tanks," in *Heat Transfer in Fires* (P.L. Blackshear, ed.), Scripta Book Company, Washington, DC, pp. 95–126 (1974).
21. T. Yumoto, "Fire Spread Between Two Oil Tanks," *Journal of Fire and Flammability,* 8, p. 494 (1977).
22. T. Dayan and V.L. Tien, "Radiant Heating from a Cylindrical Column," *Combustion Science and Technology,* 9, pp. 51–56 (1974).
23. W.G. May and W. McQueen, "Radiation from Large Liquefied Natural Gas Fires," *Combustion Science and Technology,* 7, pp. 51–56 (1973).
24. M. Klassen and J.P. Gore, "Structure and Radiation Properties of Pool Fires," *NIST-GCR-94-651,* U.S. Department of Commerce, Building and Fire Research Laboratory, National Institute of Standards and Technology, Gaithersburg, MD (1994).
25. H. Koseki and G.W. Mulholland, "The Effect of Diameter on the Burning of Crude Oil Pool Fire," *Fire Technology,* 27, 1, pp. 54–65 (1991).
26. H. Koseki and T. Yumoto, "Air Entrainment and Thermal Radiation from Heptane Pool Fires," *Fire Technology,* 24, 1, pp. 33–47 (1988).
27. H. Koseki and T. Yumoto, "Burning Characteristics of Heptane in 2.7-m Square Dike Fires," *Fire Safety Science*, 2, pp. 231–240 (1989).
28. T. Yumoto, "An Experimental Study on Heat Radiation from Oil Tank Fire," *Fire Research Institute, Report No. 33—Report of Oil Tank Fire,* Fire Research Institute, Tokyo, p. 23 (1971).
29. "Report of Oil Tank Fire Experiment," Japan Society of Safety Engineering (1979).
30. "Report of Oil Tank Fire Extinguishment," *Technical Report No. 8,* Fire Research Institute (FRI), Tokyo (1976).
31. T.T. Fu, "Heat Radiation from Fires of Aviation Fuels," *Fire Technology,* 10, 1, pp. 54–67 (1973).
32. H.T. Johnson, L.J. Linley, and J.A. Mansfield, "Measurement of the Spatial Dependence of Temperature and Gas and Soot Concentrations within Large Open Hydrocarbon Fuel Fires," *NASA Technical Memorandum 58230,* Lyndon B. Johnson Space Center, Houston (1982).
33. P.K. Raj, K.S. Mudan, and A.N. Moussa, "Experiments Involving Pool and Vapour Fires from Spills of LNG on Water," *Report No. CG-D-55-79, NTIS AD77073,* U.S. Coast Guard, Washington, DC (1979).
34. R.S. Alger, R.C. Corlett, A.S. Gordon, and F.A. Williams, "Some Aspects of Turbulent Pool Fires," *Fire Technology,* 15, 2, pp. 142–156 (1979).
35. G.A. Mizner and J.A. Eyre, "Radiation from Liquefied Gas Fire on Water," *Combustion Science and Technology,* 35, pp. 33–57 (1983).
36. D.S. Burgess and M. Hertzberg, "Radiation from Pool Fires," in *Heat Transfer in Fire* (N.H. Afgan and J.R. Beer, eds.), Scripta Book Company, Washington, DC, pp. 413–430 (1974).
37. "LNG Safety Research Program," *Report IS 3-1,* American Gas Association (1974).
38. P.H. Thomas, "The Size of Flames from Natural Fires," *Ninth Symposium (International) on Combustion,* Combustion Institute, Pittsburgh, pp. 844–859 (1962).
39. G. Mangialavori and F. Rubino, *Seventh International Symposium on Loss Prevention and Safety Promotion in Process Industry,* Taorina, Italy (May 1992).
40. M. Prichard and T. Binding, *Symposium on Major Hazards Onshore and Offshore,* Institution of Chemical Engineers, London, UK, pp. 491–505 (1992).
41. M. Munoz, J. Arnaldos, and C. Planas, "Analysis of the Geometric and Radiative Characteristics of Hydrocarbon Pool Fires," *Combustion and Flame,* 139, pp. 263–277 (2004).
42. G. Heskestad, "Luminous Height of Turbulent Diffusion Flames," *Fire Safety Journal,* 5, 2, pp. 103–108 (1983).
43. G. Heskestad, "Peak Gas Velocities and Flame Heights of Buoyancy-Controlled Turbulent Diffusion Flames," *Eighteenth Symposium (International) on Combustion,* Combustion Institute, Pittsburgh, pp. 951–960 (1981).

44. J.R. Welker and C.M. Sliepcevich, "Bending of Wind-Blown Flames from Liquid Pools," *Fire Technology,* 2, 2, pp. 127–135 (1966).
45. I. Emori and K. Saito, "Scaling Correlation and Smoke Observations of Oil Tank Fires Under Wind-Blown Conditions," *Chemical and Physical Process in Combustion, Fall Technical Meeting, Combustion Institute/Eastern States Section,* Providence, RI, Vol. 67, pp. 1–4 November (1983).
46. P. Thomas, "Fire Spread in Wooden Cribs, Part III, The Effect of Wind," *Fire Research Note 600,* Fire Research Station, Borehamwood, UK (1965).
47. D.M. Defaveri, A. Vidili, R. Pastorino, and G. Ferraiolo, "Wind Effects on Diffusion Flames of Fires of High Source Momentum," *Journal of Hazardous Materials,* 22, pp. 86–100 (1989).
48. M. Shokri and C.L. Beyler, "Radiation from Larger Pool Fires," *SFPE Journal of Fire Protection Engineering,* 4, 1, pp. 141–150 (1989).
49. H. Koseki, "Combustion Properties of Large Liquid Pool Fires," *Fire Technology,* 25, 3, pp. 241–255 (1989).
50. "Assessing Flame Radiation to External Targets from Pool Fires," *SFPE Engineering Guide,* Society of Fire Protection Engineers (SFPE), Bethesda, MD (1999).
51. D. Drysdale, *An Introduction to Fire Dynamics,* 3nd ed., John Wiley and Sons, New York, p. 148 (2011).
52. A. Modak, "Thermal Radiation from Pool Fires," *Combustion and Flame,* 29, pp. 177–192 (1977).
53. J.R. Howell, *A Catalog of Radiation Configuration Factors,* McGraw-Hill, New York (1982).
54. H.C. Hottel, "Radiant Heat Transmission," in *Heat Transmission,* 3rd ed. (W.H. McAdams), McGraw-Hill, New York (1954).
55. J.H. McGurie, "Heat Transfer by Radiation," *Fire Research Special Report 2,* HM Stationary Office, London (1953).
56. D.C. Hamilton and W.R. Morgan, "Radiant-Interchange Configuration Factors," *National Advisory Committee for Aeronautic (NACA), Technical Note 2836,* Washington, DC (1952).
57. K.S. Mudan, "Geometric View Factors for Thermal Radiation Hazard Assessment," *Fire Safety Journal,* 12, 2, pp. 89–96 (1987).
58. E.M. Sparrow, "A New Simpler Formulation for Radiative Angler Factors," *Journal of Heat Transfer,* ASME, 85, pp. 81–88 (1963).
59. *Handbook of Military Infrared Technology* (W.L. Wolfe, ed.), Office of National Research, Washington, DC (1965).
60. H.C. Hottel and A.F. Sarofim, *Radiative Transfer,* McGraw-Hill, New York (1967).
61. C.L. Beyler, "Fire Plumes and Ceiling Jets," *Fire Safety Journal,* 11, pp. 53–75 (1986).
62. G. Cox and R. Chitty, *Combustion and Flame,* 60, p. 219 (1985).
63. B. McCaffrey, *NBSIR 79-1910,* National Bureau of Standards, Washington, DC (1979).
64. T. Terai and K. Nitta, *Symposium of Architectural Institute of Japan,* Nagoya (1976).
65. H.C. Kung and P. Stavrianidis, *Nineteenth International Symposium on Combustion,* Combustion Institute, Pittsburgh, p. 905 (1982).
66. L.H. Russell and J.A. Canfield, "Experimental Measurement of Heat Transfer to a Cylinder Immersed in a Large Aviation Fuel Fire," *Journal of Heat Transfer,* 95, pp. 397–404 (1973).
67. J.J. Gregory, N.R. Keltner, and R. Mata, Jr., "Thermal Measurements in Large Pool Fires," *Journal of Heat Transfer,* 111, (1989).
68. C. Anderson et al., "Effects of a Fire Environment on a Rail Tank Car Filled with LPG," *Report No. FRA-OR&D 75-31,* U.S. Department of Transportation, Federal Railroad Administration, Washington, DC (1974).
69. F.D. Wayne and K. Kinsella, "Spectral Emission Characteristics of Large Hydrocarbon Pool Fires," *84-WA/HT-74,* The American Society of Mechanical Engineers, New York (1984).
70. A.J. Taylor et al., "Engulfment Fire Tests on Road Tanker Sections," *Rarde Technical Report 7/75,* Controller HMSO, London (1975).
71. W.H. McLain, "Investigation of the Fire Safety Characteristics of Portable Tanks Polyethylene Tanks Containing Flammable Liquids," *Report No. CG-M-1-88,* U.S. Coast Guard, Washington, DC (1988).
72. J.J. Gregory, N.R. Keltner, and R. Mata, Jr., "Thermal Measurements in Large Pool Fires," *SAND-87-0094C,* Sandia National Laboratories, Albuquerque (1987).
73. G.P. Wachtell and J.W. Langhaar, "Fire Test and Thermal Behavior of 150-Ton Lead-Shielded Cask," *DP 1070, Engineering and Equipment, TID-4500,* E.I. DuPont De Nemours and Co., Wilmington, DE (1966).
74. National Academy of Science Committee on Hazardous Materials, Division of Chemistry and Chemical Technology (National Research Council, ed.), *Pressure-Relieving Systems for Marine Cargo Bulk Liquid Containers,* National Academy of Sciences, Washington, DC (1973).
75. K. Moodie et al., "Total Pool Fire Engulfment Trials on a 5-Tonne LPG Tank," *HSE Internal Report No. IR/L/FR/87/27,* London (1987).
76. M. Tunc and J.E.S. Venart, "Incident Radiation from an Engulfing Pool Fire to a Horizontal Cylinder, Part I & II," *Fire Safety Journal,* 8, pp. 81–95 (1984/1985).
77. T.A. Brzustowski, "A New Criterion for the Length of a Gaseous Turbulent Diffusion Flame," *Combustion Science and Technology,* 6, pp. 313–319 (1973).

78. T.A. Brzustowski, "Flaring in the Energy Industry," *Progress Energy Combustion Science,* 2, pp. 129–141 (1976).
79. T.A. Brzustowski, "Flaring: State of the Art," *Loss Prevention,* 11, p. 15 (1977).
80. T.A. Brzustowski and E.C. Sommer, "Predicting Radiant Heating from Flares," *Proceedings of the API Division of Refining,* 53, p. 865 (1973).
81. T.A. Brzustowski, S.R. Gollahalli, and H.F. Sullivan, "The Turbulent Hydrogen Diffusion Flame in a Cross-Wind," *Combustion Science and Technology,* 11, pp. 29–33 (1975).
82. T.A. Brzustowski, S.R. Gollahalli, M.P. Gupta, M. Kaptein, and H.F. Sullivan, "Radiant Heating from Flares," *ASME Paper 75-HT-4,* American Society of Mechanical Engineers (ASME), New York (1975).
83. H.C. Hottel and W.R. Hawthorne, "Diffusion in Laminar Flame Jets," *Third Symposium (International) on Combustion,* Combustion Institute, Pittsburgh, pp. 254–266 (1949).
84. W.R. Hawthorne, D.S. Weddell, and H.C. Hottell, "Mixing and Combustion on Turbulent Gas Jet," *Third Symposium (International) on Combustion,* Combustion Institute, Pittsburgh, pp. 266–288 (1949).
85. K. Gugan, "Flixborough—A Combustion Specialist's Viewpoint," *Chemical Engineering,* 309, London (1976).
86. F.P. Ricou and D.B. Spalding, "Measurements of Entrainment by Axisymmetrical Turbulent Jets," *Journal of Fluid Mechanics,* II, p. 21 (1961).
87. A.A. Putnam and C.F. Speich, "A Model Study of the Interaction of Multiple Turbulent Diffusion Flames," *Ninth Symposium (International) on Combustion,* Combustion Institute, Pittsburgh, pp. 867–877 (1963).
88. F.R. Steward, "Prediction of the Height of Turbulent Diffusion Buoyant Flames," *Combustion Science and Technology,* 2, pp. 203–212 (1970).
89. B. McCaffrey, "Some Measurements of the Radiative Power Output of Diffusion Flames," *WSS/CI 81-15, Western States Section,* Combustion Institute, Pittsburgh (1981).
90. B. Kalghatgi, "Blow-Out Stability of Gaseous Jet Diffusion Flames, Parts I and II," *Combustion Science and Technology,* 26, pp. 233–250 (1981).
91. B. McCaffrey and D. Evans, "Very Large Methane Jet Diffusion Flames," *Twenty-First Symposium (International) on Combustion,* Combustion Institute, Pittsburgh, pp. 25–31 (1986).
92. S.R. Gollahalli, T.A. Brzustowski, and H.F. Sullivan, "Characteristics of a Turbulent Propane Diffusion Flame in a Cross-Wind," *Transactions of CSMC,* 3, pp. 205–214 (1975).
93. G.T. Kalghatki, "The Visible Shape and Size of a Turbulent Jet Diffusion Flame in a Crosswind," *Combustion and Flame,* 52, pp. 91–106 (1983).
94. O.K. Sonju and J. Hustad, "An Experimental Study of Turbulent Jet Diffusion Flame in a Crosswind," *Norwegian Maritime Research,* pp. 2–11 (1984).
95. G.A. Chamberlain, "Developments in Design Methods for Predicting Thermal Radiation from Flares," *Chemical Engineering Research and Design,* 65, p. 299 (1987).
96. A.D. Johnson, H.M. Brightwell, and A.J. Carsley, "A Model for Predicting the Thermal Radiation Hazards from Large-Scale Horizontally Released Nature Gas Jet Fires," *Hazards,* XII, p. 123 (1994).
97. D.K. Cook, M. Fairweather, J. Hammonds, and D.J. Hughes, "Size and Radiative Characteristics of Natural Gas Flares," *Chemical Engineering Research and Design,* 65, pp. 310, 318 (1987).
98. W.J.S. Hirst, "Combustion of Large Scale Jet-Releases of Pressurised Liquid Propane," *Comm.* 1241 (London: Institution of Gas Engineers) (1984).
99. V.H.Y. Tam and L.T. Cowley, "Consequence of Pressurised LPG Release—A Full-Scale Experiment," *Gastech 88, Paper 4.3* (1989).
100. T.A. Brzustowski, "Predicting Radiant Heating from Flares," *Esso Engineering Research and Development Report, EE 15ER.71* (1971).
101. P.R. Oenbring and T.R. Sifferman, "Flare Design—Are Current Methods Too Conservative?" *Hydrocarbon Processing,* pp. 124–129 (1980).
102. S.H. Tan, "Flare System Design Simplified," *Hydrocarbon Processing,* 46, pp. 172–176 (1967).
103. G.R. Kent, "Practical Design of Flare Stacks," *Hydrocarbon Processing,* 43, pp. 121–125 (1964).
104. D. Evans and D. Pfenning, "Water Sprays Suppress Gas-Well Blowout Fires," *Oil and Gas Journal,* 83, pp. 80–86 (1985).
105. B. McCaffrey, "Jet Diffusion Flame Suppression Using Water Sprays, An Interim Report," *Combustion Science and Technology,* 40, pp. 107–136 (1984).
106. B. McCaffrey, "Momentum Diffusion Flame Characteristics and the Effects of Water Spray," *Combustion Science and Technology,* 63, pp. 315–335 (1989).
107. J.F. Straitz III, J.A. O'Leary, J.E. Brennan, and C.J. Kardan, "Flare Testing and Safety," *Loss Prevention,* II, pp. 23–30 (1977).
108. W.W. Yuen and C.L. Tien, "Simple Calculation Scheme for the Luminous Flame Emissivity," *Sixteenth Symposium (International) on Combustion,* Combustion Institute, Pittsburgh, pp. 1481–1487 (1976).
109. G. Fumarola, D.M. de Faveri, R. Pastorino, and G. Ferraiolo, "Determining Safety Zones for Exposure to Flare Radiation," *Institute of Chemical*

Engineering Symposium, Series 82, Loss Prevention and Safety Promotion, pp. G23–G30 (1983).
110. P.R. Oenbring and T.R. Sifferman, "Flare Design Based on Full-Scale Plant Data," *Forty-Fifth Midyear Meeting, API Refining Department Proceedings,* 59, Houston (1980).
111. S. Galant, D. Grouset, G. Martinez, P. Micheau, and J.B. Allemand, "Three-Dimensional Steady Parabolic Calculations of Large Scale Methane Turbulent Diffusion Flames to Predict Flare Radiation Under Cross-Wind Conditions," *Twentieth Symposium (International) on Combustion,* Combustion Institute, Pittsburgh, pp. 531–540 (1984).
112. L. Cowley and M. Prichard, "Large-Scale Natural Gas and LPG Jet Fires and Thermal Impact on Structures," *GASTECH 90 Conference,* Amsterdam (1990).
113. A. Parker, "Evaluating High-Temperature Intumescent Insulation Materials Under Fire and Blast Conditions," *Insulation Materials: Testing and Applications: Third Volume, ASTM STP 1320* (Graves and Zarr, eds.), American Society for Testing and Materials, Philadelphia (1997).
114. R. Wighus and G. Dransgsholt, "Impinging Jet Fire Experiments—Propane 14 MW Laboratory Tests," *Report STF25 A92026, SINTEF NB,* Norwegian Fire Research Laboratory (1993).
115. K.S. Mudan, "Hydrocarbon Pool and Vapor Fire Data Analysis," *U.S. DOT Report DE-AC01-83EP16008,* U.S. Department of Transportation, Washington, DC (1984).
116. J.A. Fay and D.H. Lewis, "Unsteady Burning of Unconfined Fuel Vapor Clouds," *Sixteenth Symposium (International) on Combustion,* Combustion Institute, Pittsburgh pp. 1397–1405 (1976).
117. P.K. Raj and H.W. Emmons, "On the Burning of a Large Flammable Vapor Cloud," *Combustion Institute/Central and Western States Sections (Joint Meeting): Flammability and Burning Characteristics of Materials and Fuels,* San Antonio, Combustion Institute, Pittsburgh, pp. 1–23 (1975).
118. Center for Chemical Process Safety, *Guidelines for Evaluating the Characteristics of Vapor Cloud Explosions, Flash Fires, and BLEVE's,* American Institute for Chemical Engineers, New York, pp. 157–180 (1994).
119. A.F. Roberts, "Thermal Radiation Hazards from Releases of LPG from Pressurized Storage," *Fire Safety Journal,* 4, pp. 197–212 (1982).
120. K. Hasegawa and K. Sato, "Study on the Fireball Following Steam Explosion of *n*-Pentane," *Loss Prevention and Safety Promotion,* 2, p. 297 (1977).
121. K. Hasegawa and K. Sato, "Experimental Investigation of the Unconfined Vapor Cloud Explosions of Hydrocarbons," *Technical Memorandum 12,* Fire Research Institute, Tokyo (1978).
122. H.C. Hardee and D.O. Lee, "Thermal Hazard from Propane Fireballs," *Transportation Planning and Technology,* 2, pp. 121–128 (1973).
123. R.P. Pape et al., "Calculation of the Intensity of Thermal Radiation from Large Fires," *Loss Prevention Bulletin, 82,* pp. 1–11 (1988).
124. D.M. Johnson, M.J. Pritchard, and M.J. Wickens, "Large Scale Catastrophic Releases of Flammable Liquids," *Commission of the European Communities Report,* Contract No. EV4T.0014.UK(H), Brussels, Belgium (1990).
125. SFPE, *Predicting 1st and 2nd Degree Skin Burns from Thermal Radiation,* Society of Fire Protection Engineers, Bethesda, MD (2000).
126. I. Hymes, W. Boydell, and B. Prescott, *Thermal Radiation: Physiological and Pathological Effects*, Institution of Chemical Engineers, Rugby, UK (1996).
127. J. Bull and J. Lawrence, "Thermal Conditions to Produce Skin Burns," *Fire and Materials,* 3, 2, pp. 100–105 (1979).
128. S. Meshulam-Serazon, S. Nachumovsky, D. Ad-El, J. Sulke, and D. Hauben, "Prediction of Morbidity and Mortality on Admission to a Burn Unit," *Plastic and Reconstructive Surgery,* 118, 1, pp. 116–120 (2006).
129. J. Saffle, B. Davis, and P. Williams et al., "Recent Outcomes in the Treatment of Burn Injury in the United States, a Report from the American Burn Injury Association Patient Registry," *Journal of Burn Care and Rehabilitation,* 16, pp. 219–232 (1995).
130. K. Buettner, "Effects of Extreme Heat and Cold on Human Skin, II. Surface Temperature, Pain and Heat Conductivity in Experiments with Radiant Heat," *Journal of Applied Physics,* 3, p. 703 (1951).
131. J. Hardy, "The Nature of Pain," *Journal of Chronic Diseases,* 4, 1, pp. 22–51 (1956).
132. N. Bigelow, I. Harrison, H. Goodell, and H.G. Wolf, "Studies on Pain: Quantitative Measurements of Two Pain Sensations of the Skin, with Reference to the Nature of Hyperalgesia of Peripheral Neuritis," *Journal of Clinical Investigation,* 24, pp. 503-512 (1945).
133. A.M. Stoll and L.C. Greene, "Relationship Between Pain and Tissue Damage Due to Thermal Radiation," *Journal of Applied Physics,* 14, pp. 373-382 (1959)
134. C. Wieczorek and N. Dembsey, "Human Variability Correlations Factor for Use with Simplified Engineering Tools for Predicting Pain and Second Degree Skin Burns," *Journal of Fire Protection Engineering,* 2, 2, pp. 88–111 (2001).
135. A.K. Mehta, F. Wong, and G.C. Williams, "Measurement of Flammability and Burn Potential of Fabrics," *Summary Report to NSF—Grant #GI-31881,* Fuels Research Laboratory, Massachusetts Institute of Technology, Cambridge, MA (1973).
136. K. Dillon, L. Hayes, and G. Blake, "Analysis of Alternative Models for Simulating Thermal Burns," *Journal of Burn Care and Rehabilitation,* 12, 2, pp. 177–189 (1991).

137. D. Torvi and J. Dale, "A Finite Element Model of Skin Subjected to a Flash Fire," *Transactions of the ASME,* 111, pp. 250–255 (1994).
138. K. Diller and L. Hayes, "A Finite Element Model for Burn Injury in Blood-Perfused Skin," *Transactions of the ASME,* 105, pp. 300–307 (1983).
139. G. Bamford and W. Boydell, "ICARUS: A Code for Evaluating Burn Injuries," *Fire Technology,* 31, 4, pp. 307–335 (1995).

Craig L. Beyler is the technical director Emeeritus of Jensen Hughes. He was the founding editor of the *Journal of Fire Protection Engineering* and serves on a wide range of committees in the fire safety community. This chapter is based on the chapter written by Krishna Mudan and Paul Croce for the first and second editions of the *SFPE Handbook of Fire Protection Engineering*.

Vapor Clouds

67

Nicolas F. Ponchaut, Francesco Colella, and Kevin C. Marr

Introduction

Vapor cloud explosions can be devastating events that result in significant damage to property and loss of life. Although vapor cloud explosion hazards are more common for oil and gas facilities, vapor cloud explosion incidents have occurred at other industrial facilities, such as chemical waste and water treatment plants [1, 2]. Analysis of vapor cloud explosions presents many challenges to engineers and investigators and requires an understanding of several issues. Some of these issues include the potential phase change of the source via condensation or flashing, dispersion characteristics of the vapor due to atmospheric conditions, and effects of buildings and structures on cloud dispersion and flame front propagation. The scope of this chapter is to discuss several of these key issues and present practical tools that can be used in vapor cloud explosion investigations or hazard analyses. Owing to the potentially large scale of vapor clouds, representative experimental testing is limited and often impractical. Therefore, this chapter focuses on analytical and computation methodologies that have been validated using experimental tests, and notes several standardized tests that can be used to quantify specific vapor cloud hazards. It is important to note that these methodologies only provide order of magnitude estimates and analysis, and therefore careful interpretation is required. Engineering experience often serves as the most important element to a successful vapor cloud explosion analysis.

In general, four main criteria are required for a vapor cloud explosion—a vapor source, or leak, must occur, the vapor must disperse and form a flammable vapor cloud, the vapor cloud must be ignited by a competent source, and an overpressure must be large enough to produce a pressure wave. This chapter is divided into three main sections—*Vapor Cloud Source*, *Vapor Dispersion*, and *Vapor Ignition*. The *Vapor Cloud Source* section discusses various types of vapor sources and methods to estimate the amount of source fuel. The *Vapor Dispersion* section provides an overview of the fundamentals of vapor dispersion that are useful in determining the size of the vapor cloud. Both sections introduce practical analytical methods and computational models. The *Vapor Ignition* section discusses analytical methods to determine the flammable portion of the vapor cloud, ignition sources, and estimates of the strength of resultant pressure or blast waves. Analyses of hazard scenarios where one or more of these criteria is not met, i.e. BLEVEs (boiling liquid expanding vapor explosions), flash fires and fireballs, are discussed in Chap. 71.

The general procedure for a vapor cloud explosion analysis is to estimate the vapor source, determine the size of the flammable cloud, determine the ignition scenario, and estimate the characteristics of the resultant blast wave. Conceptually, this procedure is straightforward.

N.F. Ponchaut Ph.D., PE (✉) • F. Colella Ph.D.
K.C. Marr Ph.D., PE
Exponent, Inc., I Strathmore RD., Natick, MA 01760, USA

M.J. Hurley (ed.), *SFPE Handbook of Fire Protection Engineering*,
DOI 10.1007/978-1-4939-2565-0_67, © Society of Fire Protection Engineers 2016

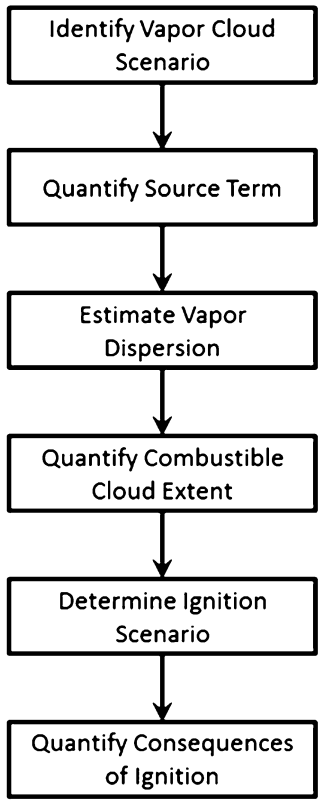

Fig. 67.1 Steps required for a vapor cloud explosion analysis

However, in practice, vapor cloud explosions are complicated events where each scenario consists of several linked events that are influenced by a variety of factors. Depending on these factors, different methods may be required. For example, a gasoline spill may require pool evaporation calculations, whereas a pipe leak may require an orifice flow calculation. Furthermore, variations in atmospheric conditions can affect estimates of cloud size, which in turn affect the magnitude of the resulting blast wave. Figure 67.1 shows a flow chart that organizes the various steps required in performing a vapor cloud explosion analysis. The individual elements of the flow chart are discussed in the subsequent sections in this chapter.

Vapor Cloud Source

Before estimating the extent and the hazard of a vapor cloud, it is first required to evaluate its source. The source of vapor clouds can be sorted in four categories depending on the properties of the involved substance:

- **Gas source:** when the substance is in vapor form both at ambient conditions and inside the leaking system (e.g. natural gas leak);
- **Liquid source:** when the substance is in liquid form, both at ambient conditions and inside the leaking system (e.g. leak of gasoline);
- **Liquefied gas source:** when the substance is in vapor form at ambient conditions but is in liquid form inside the leaking system (e.g. leak of Liquefied Natural Gas or of pressure liquefied propane)
- **Condensing vapor source:** when the substance is in liquid form at ambient conditions (boiling point is above ambient temperate) but is in vapor form inside the leaking system (e.g. in some industrial processes)

A summary of the different types of vapor sources is given in Fig. 67.2.

Gas Source

In the case of a Gas Source, the vapor is released through an orifice and the mass flow rate can be estimated using orifice flow equations. For a compressed vapor at pressure P_1, and density ρ_1, discharging to an ambient pressure P_a, through an orifice opening of area A (see Fig. 67.3), the vapor source mass flow rate can be estimated as

$$\dot{m} = CA\sqrt{2P_1\rho_1\frac{\gamma}{\gamma-1}\left(\frac{P_a}{P_1}\right)^{\frac{2}{\gamma}}\left[1-\left(\frac{P_a}{P_1}\right)^{\frac{\gamma-1}{\gamma}}\right]} \quad \text{if } \frac{P_a}{P_1} > \left(\frac{2}{\gamma+1}\right)^{\frac{\gamma}{\gamma-1}}$$

$$\dot{m} = CA\sqrt{\gamma P_1\rho_1\left(\frac{2}{\gamma+1}\right)^{\frac{\gamma+1}{\gamma-1}}} \quad \text{if } \frac{P_a}{P_1} < \left(\frac{2}{\gamma+1}\right)^{\frac{\gamma}{\gamma-1}} \text{ (choked flow)}$$

where C is a discharge coefficient that is typically assumed to be lower than but close to 1 (typically around 0.98) [3]. The constant γ is

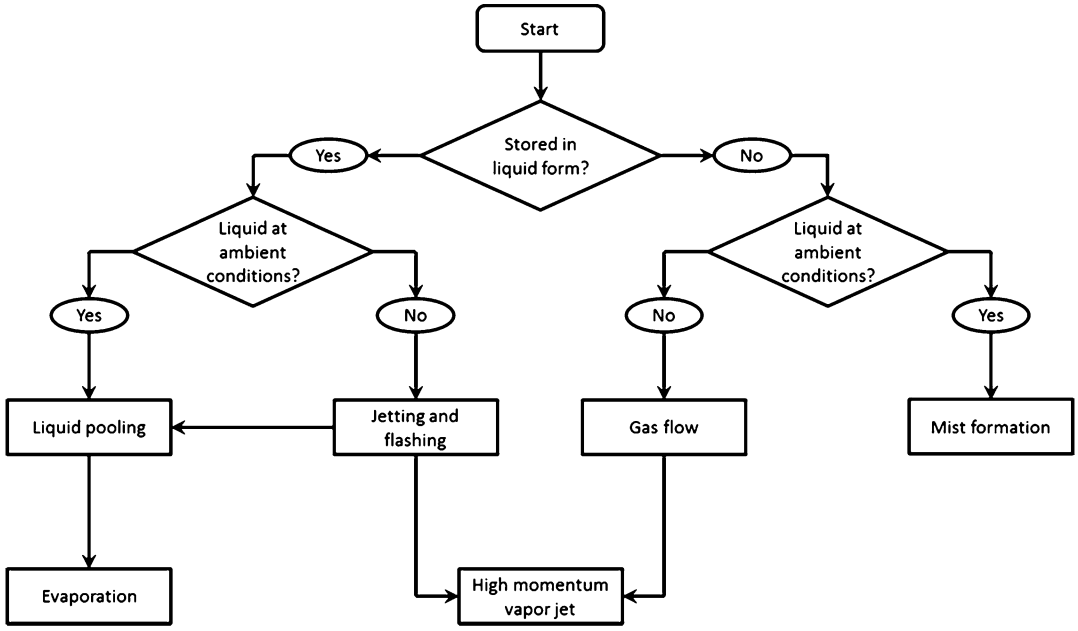

Fig. 67.2 Flowchart of vapor source scenarios

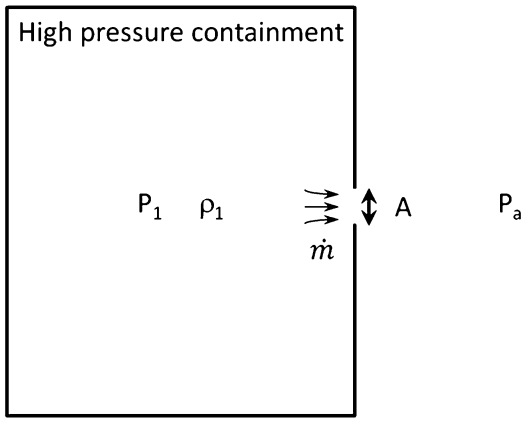

Fig. 67.3 Nomenclature for high pressure gas source

the ratio of specific heats (c_p/c_v), which depends on the gas properties. Values of γ range from 1.00 to 1.67, with more complex molecules leading to lower values. Example values of the ratio of specific heats are given in Table 67.1. Combustible vapors have γ ranging from 1.00 to 1.40. Also included in Table 67.1 is the critical pressure ratio, Above which the flow is choked.

Note that absolute pressures are used in the orifice formula. The vapor leaking through the orifice forms the vapor cloud immediately starting at the orifice.

Liquid Source

When the source is in liquid form and remains liquid when spilled on the ground, a three-step procedure is required to estimate the Vapor Cloud Source. The first step is to determine the spill rate of the substance on the ground or in the containment structure. The second step is to determine how fast the liquid pool is growing, while the third step is to calculate how quickly the pool vaporizes.

Although the evaporation of the pool can influence its growth, for most practical applications the effect of the vaporization rate on pool growth is small. Considering that the pool grows as if it were not evaporating leads to a slight overestimate of its size and therefore produces slightly overestimated evaporation rates.

Table 67.1 Specific heat ratio (γ) for various gases at ambient conditions [4]

Gas	Ratio of specific heat (γ)	Critical pressure ratio $\left(\frac{2}{\gamma+1}\right)^{\frac{\gamma}{\gamma-1}}$
Monoatomic gas (Ar, He, Ne, Xe)	1.67	0.4867
Diatomic gas (Air, H_2, O_2, N_2, CO)	1.40	0.5283
Carbon dioxide (CO_2)	1.29	0.5475
Ammonia (NH_3)	1.31	0.5439
Methane (CH_4)	1.32	0.5421
Ethane (C_2H_6)	1.19	0.5664
Ethylene/ethene (C_2H_4)	1.24	0.5568
Acetylene (C_2H_2)	1.25	0.5549
Propane (C_3H_8)	1.13	0.5785
Propylene/propene (C_3H_6)	1.15	0.5744
Butane (C_4H_{10})	1.10	0.5847

Spill Rate Estimate

The spill rate can be estimated in various manners, depending on the situation. Some examples of spill scenarios are provided in the following list:

- A valve remaining unintentionally open would spill liquid on the ground at a rate determined by a pump or by the pipe system upstream of the valve (e.g. for a gasoline spill from a dispenser in a gas station, the flow is typically <10 gpm);
- For a pressurized liquid spilling through a breach, the orifice flow equation for liquid can be used to determine the spill rate. For a liquid of density ρ, pressurized to a pressure P_1, at an elevation h above the orifice and spilling into an ambient pressure P_a through an orifice opening of area A (see Fig. 67.4), the vapor source mass flow rate can be estimated as

$$\dot{m} = CA\sqrt{2\rho(P_1 - P_a + \rho g h)}$$

where C is a discharge coefficient that is typically assumed to be around 0.60 [4–6], and g is the acceleration due to gravity (9.81 m/s^2).

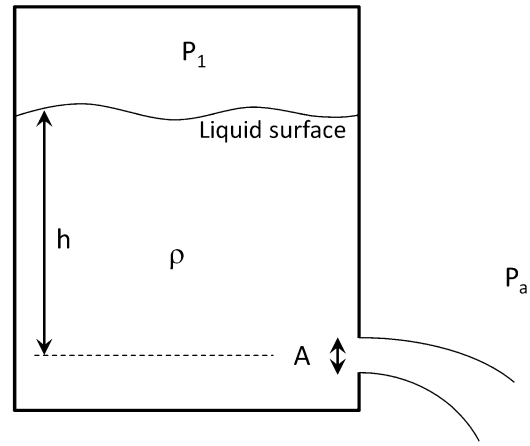

Fig. 67.4 Nomenclature for a pressurized liquid source

- For a liquid container spilling through a pipe system, the leak rate can be estimated using methods such as the K-factor, the equivalent L/D, the Crane or the 3-K (Darby) methods (for example, see [5–8], as well as Chap. 41).

Liquid Pool Growth

Once the spill rate has been identified, the growth of the liquid pool can be estimated. Various methodologies can be used depending on the ground layout and the properties of the fluid. Generally, a conservative assumption is to assume that the liquid spreads instantaneously either to cover the entire containment area or, when the spill is uncontained, to reach a minimum pool thickness. In other words, the area of the pool is:

$$A = \min\left(\frac{V_{\text{Spill}}}{h_{\min}}, A_c\right)$$

where V_{spill} is the spill volume, A_c the containment area, and $h_{\min}$ is the minimum pool thickness that depends on both the liquid and substrate properties: [9]

$$h_{\min} = \max\left(\sqrt{\frac{2\,\sigma\,(1-\cos\theta)}{g\,\rho}}, \varepsilon\right)$$

where σ is the surface tension at the air/liquid interface, θ is the contact angle (i.e. the angle of

the air/liquid interface where it meets the ground), and ε is the roughness of the substrate. The first term in the parentheses represents the thickness of a pool on a flat surface due to its surface tension, while the second represents the effect of surface roughness. In most practical applications, spills occur on concrete or on soil, and the surface roughness dominates any surface tension effects ($h_{\min} = \varepsilon$). A few examples of minimum pool thicknesses are given in Table 67.2.

Assuming that the pool spreads instantaneously leads to an upper bound on the vapor source rates. When a more refined analysis is required, such as a finite pool growth analysis, numerical models should be used. A non-exhaustive list of available model types is presented below in order of increasing complexity and accuracy:

- **Integral models**: In these models, the pool is assumed to spread axisymmetrically and its size and thickness are stretched according to energy and mass balance equations. The axis of symmetry of the pool coincides with spill location. The pool depth is usually either uniform or has a quadratic profile. This quadratic profile is based on a theoretical solution of the spread of a pool profile on *liquid* substrate as obtained by Hoult [11]. The edge of the pool has a typical thickness $h(t)$ and moves at a velocity $U(t)$ such that

$$U(t) = \sqrt{K\, g \max(0, h(t) - h_{\min})}$$

for spills on solid substrates;

$$\sqrt{K\, g \left(1 - \frac{\rho_{\text{Spill}}}{\rho_{\text{Substrate}}}\right) \max(0, h(t) - h_{\min})}$$

for spills on liquid substrates.

In this equation, K is a constant with a value between 1.16 and 2.0, depending on the software that is used [12]. Because of the assumptions used in integral models, features such as hydraulic jumps that are clearly observed for example when a garden hose is pointed at a wall are not considered. An anomaly of these models is that changes of leak rate affect the entire pool instantaneously. These models can only be used in axisymmetric geometries with flat ground and no obstacles. Integral models are used in GASP (Gas Accumulation over Spreading Pools), SuperChems, Breeze and PHAST [10, 11, 13–16].

- **One-dimensional—"shallow water equations"**: These models are best suited for pools that spread in a single direction such as round pools with radial spread or flow in long trenches. The effect of a sloped ground is included in some models. The models do not assume that the pool is of predefined thickness and can therefore capture most of the details of the pool. [17] These models cannot model the flow through trench branches or elbows (that slow down the liquid spread). Packages such as LSMS (Liquid Spill Modeling System) and ESM (Exponent Spill Model) use this type of model. [17, 18]
- **Two-dimensional—"shallow water equations"**: These models are suited for most pool scenarios and ground configurations. They can represent most of the flow features. The only drawback is their inability to model three dimensional effects such as step changes in ground height or vortices behind obstacles and trench corners. This type of model is used in the Computational Fluid Dynamics (CFD) software FLACS [19, 20].
- **Full three-dimensional models**: Modern CFD (Computational Fluid Dynamics) models can represent virtually any geometries and obstacles. They solve the full three-dimensional flow and are therefore the most accurate method to predict pool growth, but can be computationally intensive. The

Table 67.2 Value of minimum pool height for different substrates. [10]

Substrate	$h_{\min}$
Dry soil	2 cm (0.8 in.)
Wet soil	1 cm (0.4 in.)
Concrete	0.5 cm (0.2 in.)

Table 67.3 Properties of different liquid hydrocarbons at 20 °C. See Chap. 18 and Appendix 3. Refer to [23] for a more exhaustive list of substances

		Molecular mass MW	Vapor p ressure P_v	Liquid heat capacity c	Latent heat of vaporization ΔH_v
n-Pentane	C_5H_{12}	72	50.0 kPa	2.33 kJ/kg-K	357 kJ/kg
n-Hexane	C_6H_{14}	86	14.3 kPa	2.24 kJ/kg-K	335 kJ/kg
n-Heptane	C_7H_{16}	100	5.35 kPa	2.20 kJ/kg-K	316 kJ/kg
iso-Octane	C_8H_{18}	114	4.88 kPa	2.15 kJ/kg-K	272 kJ/kg

Volume Of Fluid (VOF) model is typically used to track the interface between the pool and the ambient air. Both the spilled substance and the ambient air flows are solved in the simulations. Commercially available software such as Fluent [21] and Star-CCM+ [22] are examples of Computational Fluid Dynamics models that can be used for such simulations.

Pool Evaporation

Once the evolution of the pool size has been estimated, the evaporation can be modeled. Since the substance is in liquid form at ambient conditions, the vaporization is heavily dictated by the vapor pressure of the spilled substance, P_v (see Table 67.3 for typical vapor pressures). The higher the saturation pressure, the faster the evaporation. While the vapor is at saturation conditions right above the surface of the pool, the surroundings are not. This leads to diffusion of the vapor from the pool surface to the atmosphere.

The vapor pressure is highly dependent on temperature and can be easily estimated using the Clapeyron-Clausius equation

$$P_v = 133.3 \times 10^{-0.2185\frac{E}{T}+F}$$

where P_v is the vapor pressure in Pa, T is the temperature in K, and E and F are constants. Example values of the constants E and F are provided in Table 67.4 along with the temperature range in which the equation is applicable.

The evaporation rate of a liquid pool in ambient air, $\dot{m}$ (in kg/s), can be estimated by the Mackey and Matsugu model:

Table 67.4 Clapeyron-Clausius equation constants for common organic compounds. [24]

		E	F	Temperature range
n-Pentane	C_5H_{12}	6595.1	7.4897	−77 °C to 191 °C
n-Hexane	C_6H_{14}	7627.2	7.7171	−54 °C to 209 °C
n-Heptane	C_7H_{16}	8928.8	8.2585	
iso-Octane	C_8H_{18}	8548.0	7.9349	−36 °C to 99 °C

$$\dot{m} = 0.00482\, A_p\, Sc^{-0.67} u_{10}^{0.78}\, l^{-0.11} \frac{P_v\, MW}{\overline{R}\, T}$$

where A_p is the pool area in m^2, u_{10} is the wind speed measured 10 m above the ground in m/s, P_v and MW are the vapor pressure in Pa and the molecular mass of the spilled substance (in kg/kmol), and T is the pool temperature in K [25, 3, 26]. l is the characteristic length of the pool in m (i.e. the diameter in the case of a circular pool and the length along the wind direction for a rectangular pool). Finally, $\overline{R}_r$ is the universal gas constant (8314 Pa-m^3/kmol-K) and Sc is the Schmidt number of the substance. The Schmidt number for gases and vapors is typically around 0.8, which simplifies the Mackey and Matsugu model to [15].

$$\dot{m} = 6.73 \text{ x } 10^{-7}\, A_p\, u_{10}^{0.78}\, l^{-0.11} \frac{P_v\, MW}{T}$$

Note that at vapor pressures above 0.2 atm, the air over the pool starts to contain a significant amount of vapors affecting the thermodynamic properties of the surrounding air. For this reason, for vapor pressures above 0.2 atm, several authors recommend that the vapor pressure P_v be replaced by [16]

$$P_a \ln\left(\frac{P_a}{P_a - P_v}\right)$$

Since vapor pressures are heavily dependent on temperature, it is often required to evaluate the evolution of the pool temperature as it evaporates. The temperature of the pool is primarily influenced by an energy balance accounting for:

- Heat transfer with the ground that can supply or remove heat depending on temperature;
- Heat transfer due to the wind blowing over the pool and, when applicable, due to sun radiation;
- Heat sink due to the vaporization itself that removes energy directly from the pool.

For a pool of evolving mass m, the average pool temperature changes according to:

$$\frac{dT}{dt} = \frac{1}{m\, c_l}\left(\dot{Q}_c + \dot{Q}_g - \dot{Q}_v + \dot{Q}_r\right)$$

where c_l is the heat capacity of the liquid (see Table 67.3). In this equation, the different heat contributions, $\dot{Q}_c$ are the following:

– $\dot{Q}_c$ is the heat transferred from the atmosphere to the pool due to convection

$$\dot{Q}_c = \frac{A_p\, k_a}{l}\,(T_a - T)\left(0.037\left(\frac{\rho_a\, u_{10}\, l}{\mu_a}\right)^{0.8} - 871\right) Pr_a^{1/3}$$

where the values of the thermal conductivity and the viscosity of air are given in Table 67.5. More detailed convection correlations are provided in Chap. 3.

– $\dot{Q}_g$ is the heat transferred from or to the ground. Since the ground temperature evolves over time, the time from when the liquid first wet the ground is an important parameter. This time parameter differs for different parts of the pool due to the finite growth of the pool. At the center of the pool the ground is wetted earlier than near its leading edge. The following equation should be used [25, 28]

$$\dot{Q}_g(t) = \frac{k_g}{\sqrt{\alpha_g\, \pi}}\,(T_g - T)\int_0^{A_p(t)} \frac{dA_p}{\sqrt{t - \tau(A_p)}}$$

where $A_p(t)$ is the area of the pool at time t, $\tau(A_p)$ is the time at which the pool has grown to an area A_p, k_g is the ground thermal conductivity, and α_g is the ground thermal diffusivity. Typical values for ground thermal properties are provided in Table 67.6.

Table 67.5 Thermal properties of air at ambient temperatures. [27]

Air properties at 10 °C		
Density	ρ_a	1.293 kg/m^3
Thermal conductivity	k_a	0.02492 W/m-K
Dynamic viscosity	μ_a	1.71×10^{-5} kg/m-s
Prandtl number	Pr_a	0.71

Table 67.6 Thermal properties of various ground substrates at ambient temperature. [25, 27, 17]

Substrate material	Thermal conductivity k_g	Thermal diffusivity α_g
Concrete	1.35 W/m-K	5.2×10^{-7} m^2/s
Aerated concrete	0.28 W/m-K	2.6×10^{-7} m^2/s
Soil (average)	0.96 W/m-K	4.6×10^{-7} m^2/s
Soil (sandy, dry)	0.26 W/m-K	2.0×10^{-7} m^2/s
Soil (sandy, 8 % moist)	0.59 W/m-K	3.3×10^{-7} m^2/s
Carbon steel (1 %)	45.8 W/m-K	1.27×10^{-5} m^2/s

This formula can be simplified in the case where the pool wets the entire area instantaneously at time $t = 0$, leading to:

$$\dot{Q}_g = \frac{A_p\, k_g}{\sqrt{\alpha_g\, \pi\, t}}\,(T_g - T)$$

Note that that the two equations above assume that the temperature difference between the pool and the ground remains much larger than the temperature variation of the pool; a more accurate analysis should be performed when this approximation is invalid.

– $\dot{Q}_v$ is the heat taken away from the pool due to vaporization:

$$\dot{Q}_v = \dot{m}\, \Delta H_v$$

Where ΔH_v is the heat of vaporization of the substance being evaporated (see Table 67.3).

– $\dot{Q}_r$ is the heat exchanged by radiation. This includes direct radiation from the sun (which typically involves consideration for solar angle and cloud coverage), radiation between the pool and the atmosphere and, if applicable, radiation from the flames if the pool is involved in a fire.

It is important to realize that in the case of liquid spills, the vapor cloud source can last for much longer than the spill itself. For clouds forming outside of buildings or in well ventilated locations, vapors will continue to form for as long as there is liquid on the ground.

Liquefied Gas Source

The liquefied gas source refers to substances stored in liquid form that vaporize at ambient conditions. The gas can be liquefied in two different ways. In the pressure liquefied gas case, the substance is pressurized in the system to stay in liquid form at a temperature above its boiling point at ambient conditions (e.g. propane or butane bottles). In the subcooled gas case (refrigerated liquid), the gases are kept sufficiently cold to be in liquid form (e.g. cryogenic liquids, LNG—Liquefied Natural Gas).

When contained under pressures above ambient, the liquefied gas source leak creates a two phase jet that is commonly referred to as "jetting and flashing." A portion of the liquid ejected through the breach flashes immediately and becomes vapor, while the remainder remains liquid and forms small droplets that can either remain suspended and evaporate before reaching the ground or rain-out and pool on the ground (see Fig. 67.5). The speed of the jet and the amount of flashing depends on the pressure at which the liquid is stored and on the size of the breach.

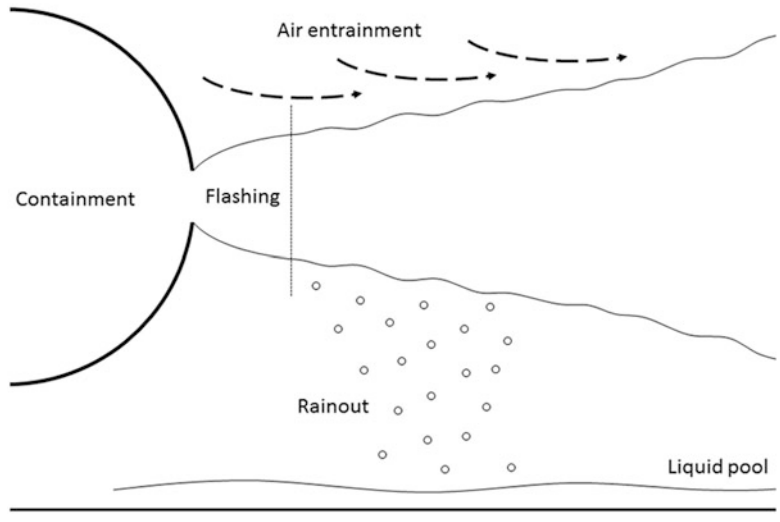

Fig. 67.5 Schematic of a jetting and flashing event

Pressure Liquefied Gas

In the case of a pressure liquefied gas source, a portion will vaporize as the pressure drops across the breach. The liquid will start vaporizing within the breach, and as a result, the orifice flow equations need to be adjusted. In particular, Leung [25] found that for a substance stored at an absolute temperature, T_0, and pressure, P_0, expanding through an orifice to an ambient pressure, P_a, a correlating parameter ω can be defined as

$$\omega = c_l \, T_0 \, P_0 \, \rho_l \left(\frac{\frac{1}{\rho_v} - \frac{1}{\rho_l}}{h_v - h_l} \right)^2$$

where all the properties are taken at T_0 and P_0. The subscripts l and v refer to saturated liquid and vapor properties, respectively; c, ρ and h are the specific heat, the density and the enthalpy of the substance. Using the parameter ω the critical pressure ratio P_c/P_0 can be obtained using Fig. 67.6.

If the critical pressure P_c is above the ambient pressure P_a, the flow through the breach is choked. In this case, the substance does not expand completely in the breach, but continues to flash away from the orifice until the substance reaches the ambient pressure. The choked flow rate can be estimated as

$$\dot{m} = A \, P_c \sqrt{\frac{\rho_l}{P_0 \, \omega}}$$

If the flow is not choked, i.e. if the critical pressure is below ambient, the flow is estimated by

$$\dot{m} = A \, P_a \sqrt{\frac{\rho_l}{P_0 \, \omega}}$$

As a result of this change of phase, the jet cools down. If the jet does not cool sufficiently to reach the boiling temperature at ambient pressure, all the substance turns into vapor immediately (i.e. there is no pooling on the ground). However, if the jet cools down sufficiently to reach its boiling temperature, the vaporization stops and a portion of the substance remains in liquid droplet form inside the cloud or forms a cold pool on the ground. Note that the jet entrains surrounding air which provides additional heat to the jet, resulting in additional vapor formation.

Refrigerated Liquid

In the case of a refrigerated liquid source, most of the phase change process is a result of temperature differences rather than of a pressure change. The flow through the breach can therefore be estimated using the orifice flow for liquid sources. Once the liquid has gone through the

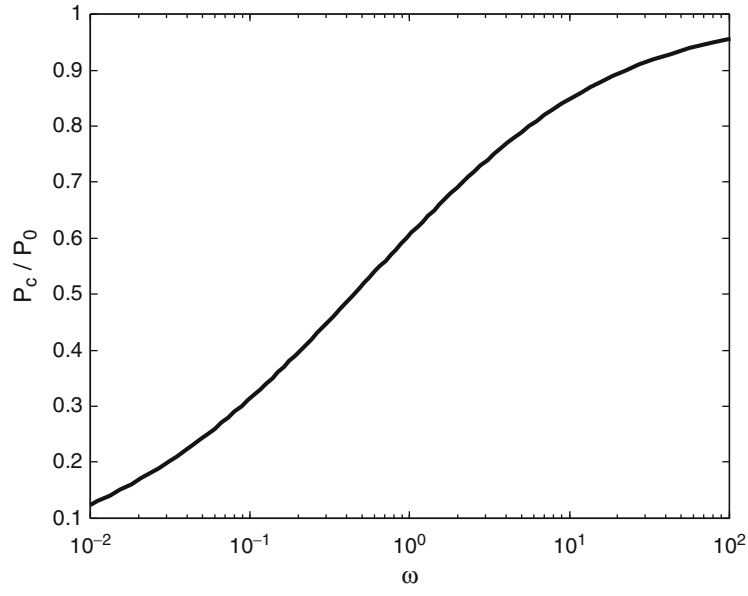

Fig. 67.6 Pressure ratio at critical flow

breach, it mixes with the surrounding air due to turbulence. The ambient air provides the heat required to vaporize the substance. If the mixing is sufficiently strong compared to the leak rate, the gas vaporizes completely. If it does not, a portion of the jet will remain in liquid form (i.e. droplets or pool on the ground).

Vaporization

Both pressure liquefied gas and refrigerated liquid leaks can lead to pooling of the substance at its boiling temperature. Once the leak rate through the breach has been obtained, the expansion of the jet due to flashing can be estimated. Software such as PHAST and FLASH (sub routine of the FLACS software) can be used to estimate the proportion of the substance that vaporizes immediately and the amount of liquid that pools on the ground. Such software relies on conservation of mass, momentum and energy, but also includes empirical correlations to estimate the amount of air entrained into the jet, the jet cone angle and the droplet size.

In addition to the portion of the jet that vaporizes immediately, the resulting droplets will continue to vaporize as the cloud mixes with warm ambient air. As for the liquid portion pooling on the ground, since it is at its boiling temperature, the vaporization rate is only limited by the amount of heat that the pool can extract from its surrounding. As a result, the following vaporization rate can be used

$$\dot{m} = \frac{\dot{Q}_c + \dot{Q}_g + \dot{Q}_r}{\Delta H_v}$$

Where $\dot{Q}_c$, $\dot{Q}_g$, and $\dot{Q}_r$ are the heat fluxes due to wind convection, ground conduction and radiation, respectively. The temperature of the pool stays constant at its boiling point.

Note that when pool is much colder than ambient temperature (i.e. in the case of a spill of a refrigerated liquid such as a cryogenic liquid), the conduction from the ground is by far the dominant heat source term. In such cases, convection and radiation can be ignored [18].

Condensing Vapor Source

When the substance has a boiling point that is above ambient temperature and is stored and/or utilized as a vapor, any release will cause it to condense when it comes in contact with ambient air. Under these conditions, the vapor source flow rate can be estimated as a gas source. However, once the vapors mix with air, they condense to form small droplets that may either pool on the ground or stay in suspension and evaporate particularly if the vapor pressure of the substance is high.

The proportion of droplets that would be light enough to stay in suspension depend on the pressure of the source and the velocity at the point of release and also require empirical correlations and the knowledge of the ambient conditions (i.e. wind). Condensing vapor sources are not common but can occur in industrial settings under very specific conditions. Detailed analysis of the behavior of condensing vapor source clouds is beyond the scope of this chapter.

Vapor Dispersion

The accidental release and ignition of flammable gases can result in hazards associated with heat exposure (i.e. in case of flash fires) or structural damage due to overpressure (i.e. in case of a vapor cloud explosion). The dispersion process of vapor or gas clouds is a complex phenomenon that is controlled by several variables including geometry and nature of the leak (see Chap. 71), atmospheric conditions, terrain features and the presence of obstacles and obstructions. The atmospheric variables that affect the cloud dispersion process include atmospheric stability, wind velocity and direction as well as humidity and temperature.

Determination of the Atmospheric Stability

Atmospheric stability is a measure of the tendency of the atmosphere to enhance or to decrease the vertical displacement of air parcels

and can be interpreted as a measure of atmospheric vertical mixing. A detailed description of the physical aspects of atmospheric stability is beyond the scope of this chapter and can be found in Hanna [29].

Atmospheric stability is usually classified according to the Pasquill and Gifford scheme. Stability classes A through C refer to unstable conditions and are characterized by significant vertical mixing. These conditions are generally encountered during the daytime hours where strong movements of upward convected air are generated due to ground heating from strong solar radiation. Stability classes E and F refer to stable conditions and generally occur during night time hours. In these conditions, the ground cools due to radiant heat transfer to the atmosphere, and atmospheric turbulence is suppressed due to the formation of stable density stratification. Stability class D represents neutral stability conditions and can be assumed for overcast conditions during day or night regardless of the wind speed.

Several methods have been developed for the determination of the atmospheric stability conditions. They are based on detailed temperature profiles or vertical wind speed measurements. A review of the different classification schemes is given by Woodward [30]. The simplest method for the evaluation of the atmospheric stability based on simple observable quantities (wind speed and sun radiation) has been developed by Gifford [31] and is summarized in Table 67.7.

According to Turner [32], night refers to the period from 1 hour before sunset to 1 hour after sunrise. Turner specifies that the neutral class D can be used for overcast conditions during day or night regardless of the wind speed. The categories of "strong" and "slight" solar radiation are typically associated with clear skies and solar altitude above the horizon greater than 60° and between 15° and 35°, respectively. Daytime cloudiness will reduce "strong" solar radiation to "moderate" with broken middle clouds (5/8 to 7/8 cloud cover) and to "slight" with broken low clouds.

It should be noted that the above methodology applies to open flat terrain and rural areas and is less accurate for urban areas due to the increased surface roughness and non-uniform temperature distribution. In these conditions, alternative methods would provide more accurate estimations [30].

Determination of the Wind Conditions

Wind direction information can be obtained by wind rose diagrams. These are polar diagrams in which the length of the sections is proportional to the frequency of particular wind directions and speeds. The shape of the vertical wind profile is dictated by the presence of an atmospheric boundary layer that reflects the gradual rise in wind velocity above the ground. There are two common approaches used for the definition of the wind profile in the lowest 1000 m of the atmosphere: the logarithmic and the power law profiles [30].

Table 67.7 Determination of the atmospheric stability as function of wind speed and solar radiation according to Gifford [31]

	Day			Night	
	Incoming solar radiation				
Surface wind speed (at 10 m) [m/s]	Strong	Moderate	Slight	Thinly overcast or ≥4/8 low cloud	≤3/8 cloud cover
<2	A	A–B	B	E	F
2–3	A–B	B	C	E	F
3–5	B	B–C	C	D	E
5–6	C	C–D	D	D	D
6	C	D	D	D	D

According to the power-law profile, the wind speed at different heights from the ground can be correlated as:

$$u = u_{10}\left(\frac{z}{z_{10}}\right)^{\alpha}$$

where u is the wind velocity at the height z, u_{10} is the wind velocity at the height of 10 m and α is a coefficient that depends on the atmospheric stability class and the terrain roughness. Some variability has been observed in the literature on the value of the power-law exponent α [33]. Table 67.8 contains some typical power law exponents as a function of the atmospheric stability class and the type of environment.

The alternative form for the wind profile is based on the logarithmic law

$$u = \frac{u_*}{\kappa}\left[ln\left(\frac{z}{z_0}\right) - \Psi\left(\frac{z}{L}\right)\right]$$

where u_* is the friction velocity, κ is the Von Karman constant (equal to 0.40), z_0 is the surface roughness length, L is the Monin-Obukov length scale, and Ψ is a function of the height z, the Monin-Obukov length scale L and the atmospheric stability class. The friction velocity u^* is determined from substituting a reference height and the actual wind velocity at the reference height for z and u in Equation X. Typical a reference height of 10 m is chosen.

Table 67.8 Power law exponent dependence on stability atmospheric stability class and the type of environment [33]

	Stability class	α Urban environment	α Rural environment
Very unstable	A	0.15	0.07
Unstable	B	0.15	0.07
Slightly unstable	C	0.20	0.10
Neutral	D	0.25	0.15
Stable	E	0.40	0.35
Very stable	F	0.60	0.55

The Monin-Obukov length scale represents the approximate height at which the production of turbulent kinetic energy due to buoyancy and shear forces are comparable [34]. The atmospheric stability conditions and the Monin-Obukov length scale are correlated as follow:

- $L > 0$ stable
- $L < 0$ unstable
- $L = \infty$ (practically $>10^5$) neutral

An estimation of the typical roughness length for various types of environments is provided in Table 67.9.

The most immediate calculation of L is based on a set of interpolation functions that have been proposed by Spicer and Havens (see [36]) in order to fit meteorological data from Pasquill [37]. The interpolation functions relate L to roughness height z_0 using the following power law equation:

$$L = cz_0{}^b$$

The curve fitting coefficients, c and b, for each atmospheric stability class are summarized in Table 67.10.

An alternative method proposed by Golder [38] relates the atmospheric stability class and the local surface roughness length to the Monin-Obukov length scale. Golder's results were presented in graphical form (see Fig. 67.7). Ana-

Table 67.9 Roughness length of various types of environments [35]

Terrain	z_0 [m]
Open water (at least 5 km)	0.0002
Mud, snow (no vegetation and n obstacles)	0.005
Open flat terrain; grass (few isolated obstacles)	0.03
Low crops (occasional large obstacles x/h >20)[a]	0.10
High crops (scattered obstacles 15 < x/h <20)[a]	0.25
Parkland; bushes; numerous obstacles (x/h <15)[a]	0.5
Regular large obstacle coverage (suburb, forest)	1
City center with high-rise and low-rise buildings	3

[a]x/h represents the ratio between the typical upwind distance and the height of the major obstacles.

Table 67.10 Monin-Obukov length scale curve fitting coefficients [36]

	Stability class	c	b
Very unstable	A	−11.4	0.10
Unstable	B	−26.0	0.17
Slightly unstable	C	−123	0.30
Neutral	D	n.a.	n.a.[a]
Stable	E	123	0.30
Very stable	F	26.0	0.17

[a]Note: the Monin-Obukov length scale is infinite for Neutral stability

lytical expressions have been derived and can be found in [35].

According to Spicer and Havens the term $\Psi\left(\frac{z}{L}\right)$ can be evaluated as follows [36]:

$\Psi = 2\ln\left(\frac{1+a}{2}\right) + \ln\left(\frac{1+a^2}{2}\right) - 2tan^{-1}(a) + \frac{\pi}{2}$ Where $a = \left(1 - 15\left(\frac{z}{L}\right)\right)^{1/4}$	For stability A, B and C
$\Psi = 0$	For stability D
$\Psi = -4.7\left(\frac{z}{L}\right)$	For stability E and F

The interested reader can refer to [34] for a complete description of the procedure or for the calculation of the temperature profile in all stability classes.

Types of Vapor Clouds

The cloud dispersion behavior strongly depends on the characteristics of the leak—material released, nature of the release (low momentum release or high speed jet)—and on the atmospheric condition. Several research papers and reports on the atmospheric dispersion of vapor clouds have been published in the last few decades. The interested reader should refer to Hanna et al. (1982) [29], Britter and McQuaid (1988) [39], Britter (1989) [40], Spicer and Havens (1989) [36], Luketa-Hanlin (2006) [41], and Koopman and Ermak (2007) [42] for a complete review of the subject.

Classification

All the above mentioned references propose a classification of vapor clouds based on some sort of release Richardson number. One of the most comprehensive vapor cloud classification procedures has been proposed by Spicer and Havens [43]. The authors defined the release Richardson number as

$$Ri_c = \frac{g}{u_*^2}\left(\frac{\rho_i - \rho_a}{\rho_a}\right)\frac{\dot{m}}{\rho_i u_{10} D}$$

where $\dot{m}$ is the release rate, ρ_i is the initial density of the flammable gas, D is the diameter of the source, u_{10} is the wind velocity at 10 m elevation, u_* is the friction velocity, ρ_a is the ambient density and g is the acceleration due to gravity. Depending on the Richardson number, the release, and the wind velocity, four different regimes can be identified [36]:

- **Negative buoyancy dominated flows**: In this regime, typical dense gas features such as gravity induced slumping and lateral spreading of the cloud can be observed. This regime is typically observed when $Ri_c > 30$ and $\left(\frac{u_0}{u_*}\right)^2 < 10\,Ri_c$, where u_0 is the estimated release velocity at the leak location.
- **Stably stratified shear flows**: In this regime, the cloud is embedded in the mean wind flow and the density stratification tends to damp turbulence and reduce vertical mixing. This regime is typically observed when $1 < Ri_c < 30$ and $\left(\frac{u_0}{u_{10}}\right) < 16/(19 + Ri_c)$
- **Passive dispersion regime**: This regime is typically observed when $Ri_c < 1$ and $\left(\frac{u_0}{u_{10}}\right) < 0.8$. In the passive dispersion regime the dense gas effects are negligible and can be ignored.
- **High momentum release (jets)**: Any release not falling in one of the three categories above should be classified as high momentum release. In these cases the vapor dispersion process is strongly influenced by the jet induced turbulence. In comparison to the other cases, high momentum jets entrain

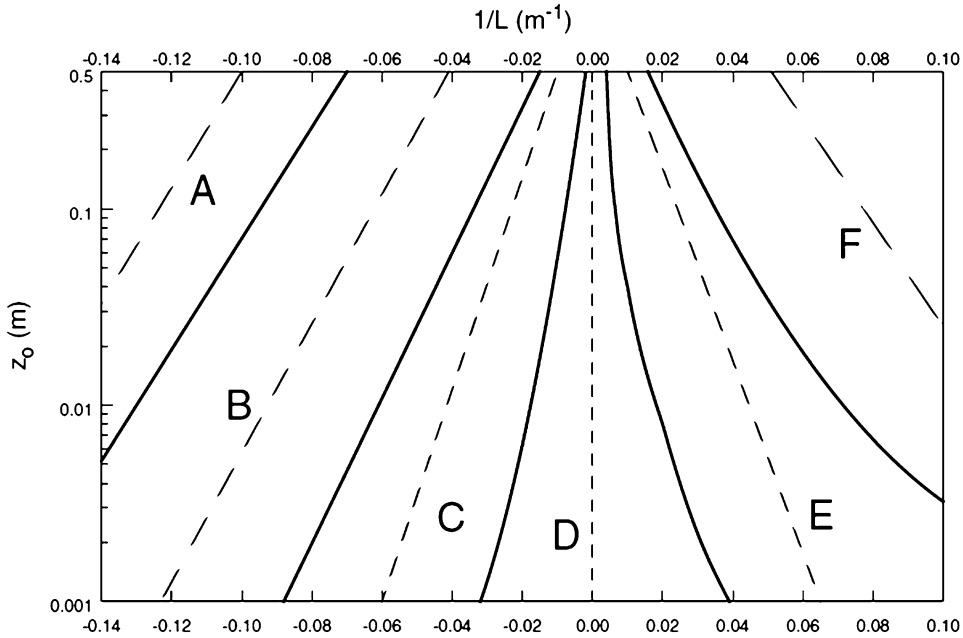

Fig. 67.7 Graph proposed by Goldner [38] for the evaluation of the Monin-Obukov length scale as function of the stability class and local surface roughness

more air and typically lead to a rapid reduction of the vapor concentration very close to the leak. High momentum releases will gradually transition to low momentum releases (one of the three other cases) as the distance from the source increases.

Release types can also be classified according to the duration in continuous and instantaneous releases. In general, the following classification can be adopted:

- A release is instantaneous when the release time is shorter than the time required by the vapor cloud to reach a given location.
- A release is continuous when the release time is longer than the time required by the vapor cloud to reach a given location.

Therefore, a given release will be classified as continuous or instantaneous depending on the relative position of the observer. According to the criteria proposed by Britter and McQuaid [39] and described by Casal [33], a release is considered continuous at a downstream location x, when

$$\left(\frac{u\,t_r}{x}\right) \geq 2.5$$

where t_r is the duration of the release, and u is the wind speed. A release will be classified as instantaneous when

$$\left(\frac{u\,t_r}{x}\right) \leq 0.6$$

Releases with intermediate duration should be analyzed as both instantaneous and continuous where the smaller resulting concentration should be taken as upper bound [33].

Characteristics of Vapor Clouds

This section provides an overview of the different release types: (1) dense gas clouds, (2) jets, and (3) neutral clouds.

Negative Buoyancy Dominated and Stably Stratified Shear Flows

Dense gas clouds are generated by the release of vapor or gas characterized by a density sufficiently larger than the ambient density. The

density of the cloud will be determined by both the molecular properties of the cloud chemical compounds and its temperature. According to Britter [40], dense gas clouds can be classified in the following categories:

- Clouds containing high molecular weight compounds (e.g. chlorine clouds)
- Clouds containing low molecular weight compounds at low temperature (e.g. LNG cloud generated by the evaporation of an liquid LNG pool onto a warm surface)
- Clouds containing low molecular weight compounds whose vapor at the boiling temperature is less dense than the environment but includes liquid droplets. The presence of the liquid droplets as well as their evaporation result in an increased cloud density (e.g. ammonia).
- Clouds containing chemical compounds that react with the ambient water vapor resulting in high density clouds (e.g. nitrogen Tetroxide (N_2O_4) and hydrogen fluoride (HF)).

Dense vapor clouds are characterized by phenomena that are radically different from those observed for positively buoyant or momentum driven clouds:

- Reduction of the vertical turbulent mixing due to the generation of a stable stratified environment;
- Generation of horizontal spreading currents controlled by the density difference between the cloud and the environment.

Due to the above effects, negatively buoyant clouds are characterized by a lower average cloud height and larger width compared to neutral clouds. The low-level dispersion process is therefore particularly sensitive to artificial and natural obstacles, which has driven the effort of the international community to study the interaction between dense vapor clouds and a variety of obstacles [40].

Several field experiments have shown a de-coupling between the dense gas dispersion process and the actual ambient atmospheric conditions [42]. In this scenario, the dense vapor cloud displaces the wind field resulting in a stably stratified density distribution that can reduce or entirely inhibit turbulent mixing. As a result, dense-gas clouds can manifest significant lateral and upwind spread. In addition, dense clouds tend to follow down-hill slopes almost independently of the atmospheric conditions and stagnate in valleys or in lower altitude regions.

The horizontal spreading of the cloud is determined by the hydrostatic pressure difference between the leading edge of the vapor cloud and the ambient. The movement of the dense cloud edge results in an intense mixing between the ambient air and the dense cloud localized at the cloud leading edge. The mixing mechanism, similar to that observed in Kelvin-Helmholtz instability problems, is induced by light fluid ingested underneath the leading edge that rises due to buoyant forces and is carried forward by the motion of the cloud. The resulting leading edge is characterized by a lobe and cleft structure. Additional mixing induced by shear layer instability at the leading edge interface enhances growth of finite amplitude billows [44].

De-stratification within the cloud results from heat transferred from the ground, which leads to a decreasing density and enhanced turbulent mixing across the interface. However, it has been observed for LNG clouds that the increased gas temperature is not sufficient for the cloud to transition to a buoyant regime within a short distance from the release point [42].

Jets and Pluncs

Vapor dispersion from high momentum jet releases is mainly controlled by the property of the jet itself. The momentum transfer between the ambient and the high speed release results in entrainment of ambient air into the jet, which reduces the jet velocity and concentration. Purely buoyant jets (or plumes) are generated from sources with low or negligible initial momentum (i.e. heat diffuser, chimneys, pool fires). Positively buoyant jets are characterized by a lower than ambient density (i.e. hot flue gases from a stack). Negatively buoyant jets are characterized by a higher than ambient density (i.e. high speed release of dense gases).

Chen and Rodi showed that both buoyant and non-buoyant jets have the tendency to become self-similar in the flow regions where either the

inertial forces or the buoyancy forces dominate the fluid-dynamic behavior [45]. Note that self-similarity does not exist in intermediate regions where the plume transitions from inertia to buoyancy domination. In particular, it has been shown that in self-similar regions, the spanwise profiles (i.e. velocity, concentration, jet width) at any distance along the axis of the jet become self-similar if scaled with an appropriate similarity variable. An overall review of similarity and scaling laws for jet releases is beyond the scope of this work. The interested reader should refer to [45] for a comprehensive monographic review that includes a wide review of experimental data as well as scaling constants, and range of validity of each scaling law.

Passive Dispersion Regime

Passive clouds are observed for releases of chemical compounds with molecular weight similar to that of the air, or of dense vapor clouds that have been sufficiently diluted due to ambient air entrainment. This is also the case with releases of air that contain low concentrations of a specific species. The dispersion of neutral clouds is mainly controlled by the atmospheric turbulence which in turn will be a strong function of the atmospheric stability class.

Modeling

Accurate and reliable predictions of vapor cloud dispersion are an important part of fire safety engineering for the design of new infrastructure. Current international standards are trending toward performance-based design, which allows engineers and hazard analysts to deal with innovative industrial design solutions.

Historically, the analysis of vapor cloud dispersion has made use of both experiments and computational modeling. For example, vapor dispersion experiments have been conducted since the 1970s at both small scale and field scale [42]. Typically, field experiments require measurements of weather conditions including wind speed and direction, turbulence, humidity, solar radiation, as well as vapor dispersion parameters such as concentration and temperature in various downwind locations and at different elevations. Although, full scale experiments and high fidelity diagnostics require large financial investments, they provide unique and valuable data that is useful for developing a phenomenological understanding of the dispersion mechanisms and are required for benchmarking computational models.

With recent developments in computation models, analyses of vapor dispersion scenarios can be performed on a single workstation. Computational modeling is more economical and time efficient, and can be used as a predictive tool. Different modeling approaches can be used depending on the accuracy required and the resources available. Typically, hazard calculations require quantitative knowledge of the evolution of the vapor cloud, in terms of variables such as:

- Distance to a given concentration (e.g. lower flammability limits *LFL* or *1/2 LFL*);
- Size, composition and shape of the cloud, which are required to predict thermal radiation estimates in case of combustion or for vapor cloud explosion modeling.
- Mass of vapor within the upper and lower flammability limits, which are used in the TNT Equivalency Method or the TNO multi-energy method.
- The time-dependent concentration in a specific location for the evaluation of toxicity effects.

Rather than presenting a comprehensive review of individual models for vapor dispersion, a review of the main model types is presented. Vapor dispersion modeling can be generally classified into categories of increasing complexity: simplified empirical models, one-dimensional integral models, shallow layer models, Lagrangian models and Navier-Stokes based models. This section will describe the main features of each of the categories including typical assumptions, limitations and accuracy achieved. This section also provides examples of models in each category.

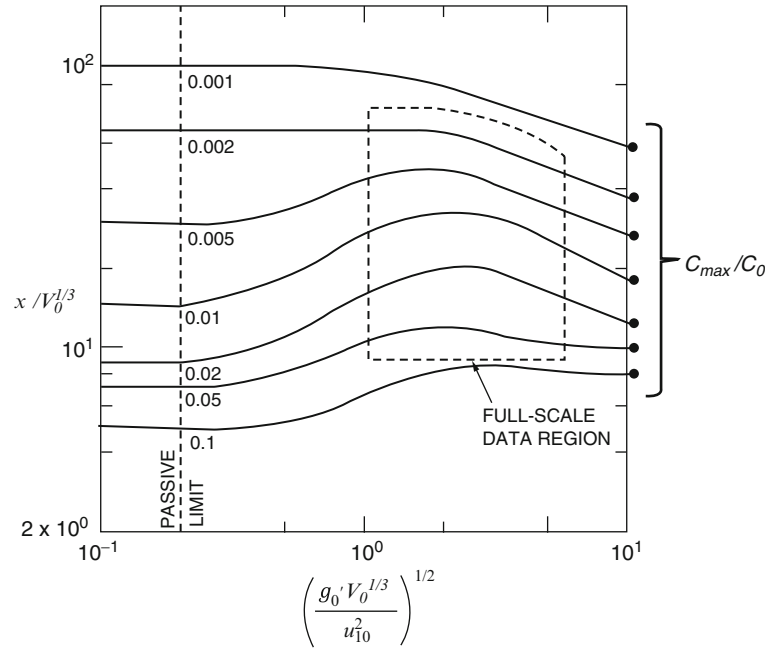

Fig. 67.8 Nomogram for instantaneous releases according to [39] (Note: the *curves* correspond to the indicated value of c_{max}/c_0)

Simplified Semi-empirical Models

Britter and McQuaid Model for Dense Clouds

The Britter and McQuaid model is based on a series of empirical correlations describing the main properties of a dense gas cloud generated at ground level and dispersing over a flat terrain. The model allows for the estimation of average concentration along the plume axis for a continuous release and the maximum concentration along the downwind direction for an instantaneous release. The model does not account for atmospheric stability class nor for terrain roughness. The model relies heavily on nomograms derived from large scale test data and from wind tunnel data [39].

Instantaneous Releases

For instantaneous releases, the model uses a set of curves or nomograms for downwind maximum concentration (expressed as c_{max}/c_0) representing the correlation between two functional groups $x/{V_0}^{1/3}$ and ${u_{10}}^2/({g_0}'V_0)^{1/3}$ where x is the downwind distance, V_0 is the initial volume of the release, u_{10} is the mean wind velocity at 10 m height, and ${g_0}'$ is the effective gravitational constant at the source. The effective gravitational constant can be estimated as

$$g_0' = \frac{g(\rho_0 - \rho_a)}{\rho_a}$$

where ρ_a and ρ_0 are the ambient and release source densities, respectively.

The determination of the iso-concentration contours for instantaneous releases is based on the following 3 steps:

1. Determine the downwind distance x to a given concentration for a particular iso-contour (e.g. LFL) using the nomograms from Fig. 67.8.
2. Calculate the cloud arrival time t at the downwind position x from the correlation

$$x = 0.4u_{10}t + b(t)$$

where $b(t)$ is the cloud radius at the time t to be estimated as

$$b(t) = \sqrt{b_0^2 + 1.2t\sqrt{{g_0}'V_0}}$$

where b_0 is the cloud radius at the source. The mean height of the cloud at a given time can be estimated as

$$h(t) = \frac{c_0 V_0}{\pi b(t)^2 c_{max}(t)}$$

Continuous Releases

For continuous releases, the model uses a set of curves or nomograms for downwind mean concentration (expressed as c_{mean}/c_0) representing the correlation between two functional groups

$$x\sqrt{\frac{u_{10}}{\dot{V}_0}} \text{ and } \left(\frac{g_0^{'2}\dot{V}_0}{u_{10}^5}\right)^{1/5}$$

where x is the downwind distance, $\dot{V}_0$ is the volume flow rate, u_{10} is the mean wind velocity at 10 m height, and $g_0^{'}$ is the effective gravitational constant at the source. The mean concentrations refer to long time average (calculated over 10 min). Greater concentrations can be observed for short durations due to turbulent fluctuations. According to [39] short term concentrations can be as high as 1.6 times the long term average values.

The determination of the iso-concentration contours for continuous releases is based on the following three steps:

1. Determination of the downwind distance x to a given concentration for a particular iso-contour (e.g. LFL) using the nomograms from Fig. 67.9.
2. Determination of the plume upwind extension x_u (see Fig. 67.10) as

$$x_u = b_0 + 2L_b$$

where b_0 is the source radius and L_b is given by

$$L_b = \frac{\dot{V}_0 g_0^{'}}{u^3}$$

3. The downwind half width b (see Fig. 67.10) of the plume can be estimated as

$$b(x) = 2b_0 + 8L_b + 2.5{L_b}^{1/3}x^{2/3}$$

The height of the plume at a downwind distance x can be obtained as

$$h(x) = \frac{\dot{V}_0}{2\,u\,b(x)}$$

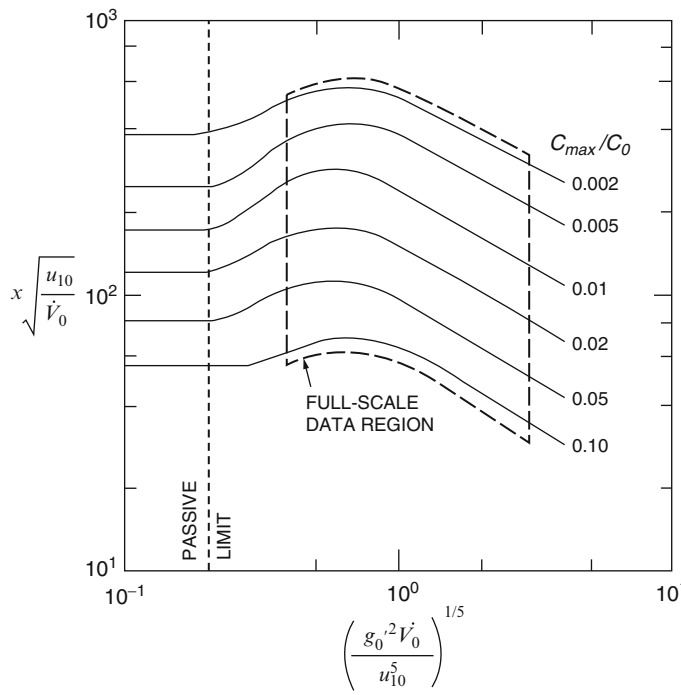

Fig. 67.9 Nomogram for continuous releases according to [39] (Note: the *curves* correspond to the indicated value of c_{mean}/c_0)

Intermediate Releases

According to [39], releases that cannot be classified as instantaneous or continuous should be studied using both approaches. The smaller of the concentration estimates should provide the upper bound for an intermediate duration release. The same authors recommend using the release duration as a time scale for converting the total leak volume V_0 into volume flow rate $\dot{V}_0$

Gaussian Plume for Passive Clouds

Under homogeneous turbulence and wind speed, the dispersion of passive clouds can be reasonably well described by Gaussian dispersion models. Gaussian dispersion models are based on the assumption that the cloud is essentially neutral (i.e. no gravitational effects are present), the meteorological conditions are constant during the release, the ground is flat, the surface roughness is constant and there are no obstacles near the release [33].

Depending on the release type (i.e. continuous or instantaneous) the concentration of a released compound (in kg/m^3) can be described using the following Gaussian plume models:

- $c(x,y,z) = \frac{\dot{m}}{2\pi u \sigma_y \sigma_z} exp\left(\frac{-y^2}{2{\sigma_y}^2}\right) exp\left(\frac{-(z-H)^2}{2{\sigma_z}^2}\right)$ for continuous release
- $c(x,y,z,t) = \frac{\dot{m}}{(2\pi)^{3/2}\sigma_x \sigma_y \sigma_z} exp\left(\frac{-y^2}{2{\sigma_y}^2}\right) exp\left(\frac{-(z-H)^2}{2{\sigma_z}^2}\right) exp\left(\frac{-(x-ut)^2}{2{\sigma_x}^2}\right)$ for instantaneous release

where $c(x, y, z)$ is the concentration at the x, y, z location defined according to Fig. 67.11, q and Q are the release rate and the total mass released (in kg/s and kg), u is the wind velocity (at the height of the plume centerline) at which the cloud is convected and H is the effective height of the plume centerline. The constants σ_x, σ_y, and σ_z represent the Gaussian plume dispersion parameters in the cross wind directions (σ_y, and σ_z) and along the wind direction (σ_x). They are functions of the downwind distance from the release and the ground roughness (i.e. release in rural or urban areas). At a certain distance downwind from the source, the plume may have spread enough to interact with the ground. In this condition, the vertical spread on the bottom side of the plume is inhibited resulting in what is known as ground reflection. In order to account for ground reflection additional terms have to be included (see [33]).

The effective height of the plume centerline H should be calculated accounting for the geometric height of the release source h (i.e. stack

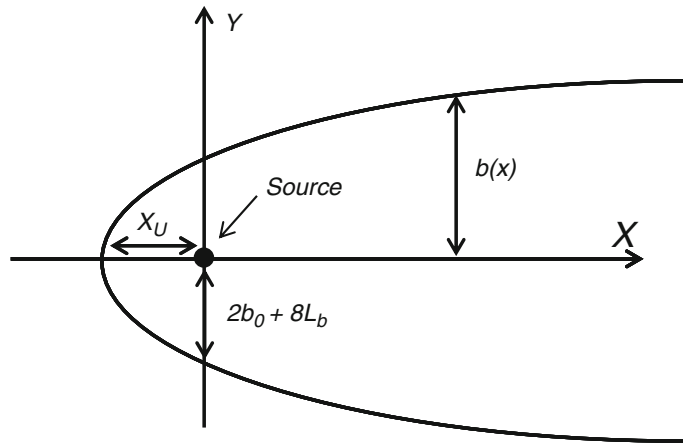

Fig. 67.10 Approximations of iso-concentration contours for a continuous release according to [39] (plan view). Wind blows in the positive x direction

height) and for the initial rise of the release due to the inertial and buoyancy forces ΔH. The latter can be computed according to the Holland equation [46]

$$\Delta H = \frac{u_0}{u} b_0 \left[1.5 + 2.68 P_a b_0 \left(\frac{T_0 - T_a}{T_0} \right) \right]$$

where u_0 is the vertical discharge velocity (in m/s), u is the wind velocity at the stack height (in m/s), b_0 is the internal diameter of the stack or leak (in m), P_a is the atmospheric pressure (in bar) and T_0 and T_a are the source and atmospheric temperatures (in K). Other methods for the calculation of the initial plume rise are summarized.

The Gaussian dispersion parameters can either be calculated by using parametric plots (see [32] or [33]) or by using the following correlations for continuous sources proposed in [35]:

- $\sigma_y = e\, x^m$ (in m)
- $\sigma_z = f\, x^n$ valid for distances from the release between 100 m and 10,000 m (in meters)

where the constants e, m, f and n are defined in accordance with Table 67.11. For distances smaller than 100 m, a linear interpolation between 0 and the σ values at 100 m should be performed. Additional corrections of σ_z as a function of the surface roughness can be included and are given in [35].

For instantaneous releases, the dispersion parameters can be evaluated as

- $\sigma_x = 0.13\, x$ (in meters)
- $\sigma_y = \frac{e}{2} x^m$ (in meters)
- $\sigma_z = f\, x$ (in meters)

where, coefficients e, f and m are the same as those previously defined in Table 67.11. The flammable mass between the LFL and the UFL for passive releases can be easily calculated using numerical integration procedures. Approximate analytical solutions for the estimation of the flammable mass and ground distance to LFL can be obtained following the procedures that

Table 67.11 Curve fitting constant for the evaluation of Gaussian dispersion parameters σ_y and σ_z [35]

	Stability class	e	m	f	n
Very unstable	A	0.527	0.865	0.28	0.90
Unstable	B	0.371	0.866	0.23	0.85
Slightly unstable	C	0.209	0.897	0.22	0.80
Neutral	D	0.128	0.905	0.20	0.76
Stable	E	0.098	0.902	0.15	0.73
Very stable	F	0.065	0.902	0.12	0.67

Note: Valid for $z_0 = 0.1$ and h <20 m; σ_y to be considered as a 10-min average

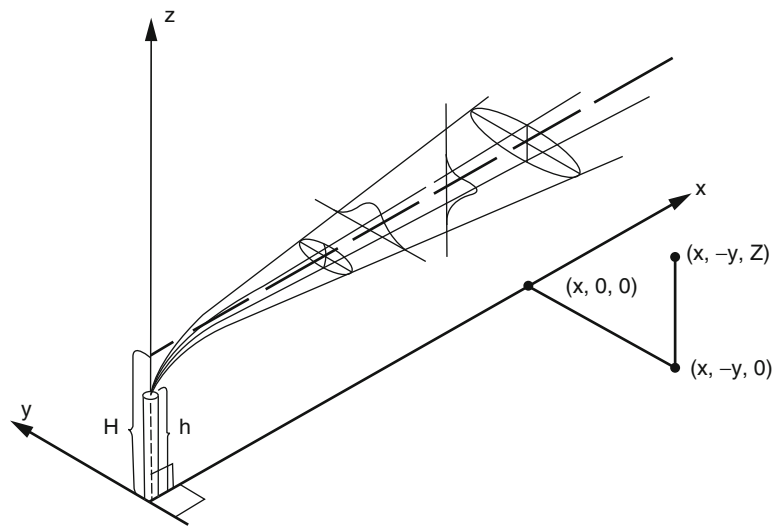

Fig. 67.11 Coordinate system used for the definition of the Gaussian plume model [32]

are described in [35] and [30]. However, the solutions are complicated and not practical for general use. In most cases, numerical integration or dedicated dispersion models are preferred.

TNO Method for Turbulent Jets

The flammable mass contained in free turbulent jets can be calculated using the TNO method for turbulent incompressible jets in a quiescent environment. The TNO method applies to axisymmetric, continuous releases with radius b_0, uniform concentration c_0 and uniform velocity u_0 in a quiescent environment [35]. The model is applicable for all cases where inertial forces are dominant compared to buoyant forces.[1] The last constraint limits the applicability of the model to the region characterized by an axial distance from the source x

$$x \leq 0.5\, b_0 \sqrt{Fr}\left({}^{\rho_0}/_{\rho_a}\right)^{1/4}$$

where Fr is the densimetric Froude number, defined as

$$Fr = \frac{\rho_0}{|\rho_a - \rho_0|}\frac{u_0^2}{2b_0 g}$$

ρ_a and ρ_0 are the ambient air density and the source density and g is the gravitational constant. The quiescent environment assumption can be relaxed by assuming that the jet velocity is atleast one order of magnitude larger than the ambient wind condition at the height of the release. If any of the above mentioned assumptions are not valid or in the presence of obstacles or complex terrain features, the TNO method is likely to provide incorrect results. More refined calculation techniques based on integral models or three-dimensional CFD models should be adopted.

The TNO model is based on the experimental observation that, after the potential core of the jet has disappeared at a distance x_s from the source, the velocity and concentration profiles assume the following Gaussian distributions:

[1] This method is limited to incompressible jets where u_0 is lower than 1/3 of the speed of the sound at ambient pressure.

Table 67.12 Empirical constants for the non-buoyant jet model defined in accordance with [47]

Non-buoyant empirical parameters	Value
C_u	6.2
C_c	5
C_{yu}	94
C_{yc}	57

$$\frac{u(y/x)}{u_c(x)} = e^{\left(-C_{yu}(y/x)^2\right)}$$

$$\frac{c(y/x)}{c_c(x)} = e^{\left(-C_{yc}(y/x)^2\right)}$$

where y is a radial coordinate, x is the axial coordinate, $u_c(x)$ and $c_c(x)$ are the jet centerline velocity and concentration values (function of the axial distance from the source) and C_{yu} and C_{yc} are empirical constants determined according to [47] (Table 67.12). It should be noted that the concentrations are expressed in parts per unit volume. The potential core represents the core region of the jet located immediately downstream of the release point where the fluid is not affected by the shear with the quiescent air and maintains the initial velocity u_0. An estimation of the extension of the potential core for non-buoyant plumes can be approximated by $25b_0$. A schematic showing the main features of a turbulent jet along with the main parameters is shown in Fig. 67.12.

For non-buoyant and buoyant jets, it has been observed that the origin of the axial coordinate x should be taken at a distance $-x_0$ from the real source (i.e. see discussion on the virtual point source Chap. 13). As a first order approximation it can be assumed that the virtual point source and the real source coincide (i.e. x_0 equal to zero).

For non-buoyant and buoyant jets, the centerline properties can be calculated as

$$\frac{u_c(x)}{u_0} = \sqrt{\frac{\rho_0}{\rho_a}}\frac{C_u b_0}{x}$$

$$\frac{c_c(x)}{c_0} = \sqrt{\frac{\rho_a}{\rho_0}}\frac{C_c b_0}{x}$$

where C_u and C_c are empirical constants determined by [47].

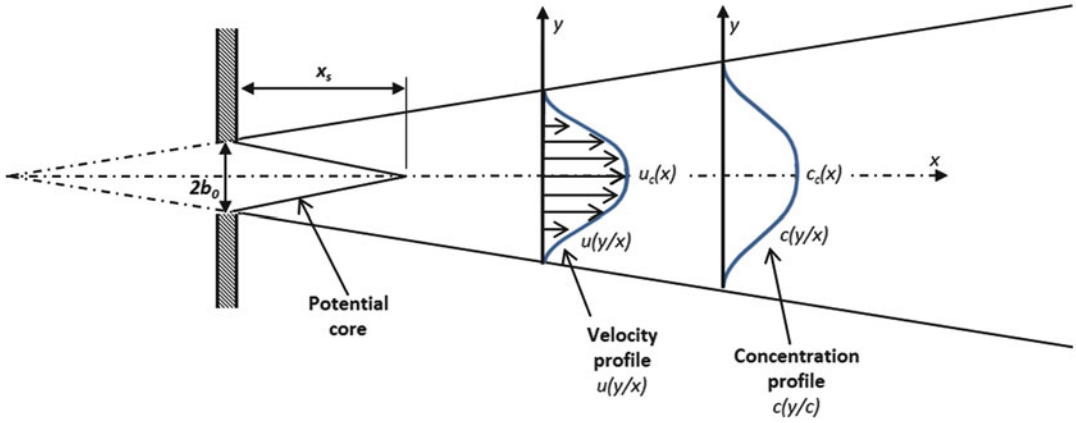

Fig. 67.12 Development of a turbulent jet in a quiescent environment (not to scale)

For negatively buoyant jets the above correlations are valid as long as x is lower than x_h, the maximum height reached by the jet before it falls back. An estimation of x_h can be obtained from

$$x_h = 4.11\sqrt{Fr}b_0$$

The maximum axial distance to the LFL concentration (expressed in parts per unit volume) can be conservatively assumed to be equal to

$$x_{LFL} = min\left(\sqrt{\frac{\rho_a}{\rho_0}}\frac{C_c b_0 c_0}{c_{LFL}}; x_h\right)$$

At axial distances larger than the length of the jet potential core, the radial position of the LFL concentration contours is given by

$$y_{LFL}(x) = \frac{x}{\sqrt{C_{yc}}}\sqrt{ln\left(\frac{b_0}{x}\sqrt{\frac{\rho_a}{\rho_0}}C_c\frac{c_0}{c_{LFL}}\right)}$$

The mass content of the chemical compound between the UFL and the LFL can be obtained by integrating the concentration profiles over the volume. The flammable mass can be estimated as

$$M = \frac{\pi\rho_0 {b_0}^3 c_0}{6C_{yc}}\frac{{\rho_a}^{3/2}}{\rho_0}{C_c}^3\left[\left(\frac{c_0}{c_{LFL}}\right)^2 - \left(\frac{c_0}{c_{UFL}}\right)^2\right]$$

A calculation method for under-expanded fuel-gas and volatile liquid-fuel jets with positive or negative buoyancy has been proposed by Epstein and Fauske [48]. These methodologies will not be presented here, but interested readers should refer to Epstein and Fauske for a complete overview.

Integral Models

Integral models are based on a limited number of equations that describe the overall properties (integral properties) of a flow. The literature over the last few decades contains many examples of integral models for vapor dispersion. Some of these examples include SLAB [49], HEGADAS [50], DEGADIS [36] and DRIFT [51], GASTAR [52].

Integral models are based on the solution of ordinary differential equations representing the evolution of the cloud average properties. Once the average properties are calculated, pre-determined profiles are used to obtain a three-dimensional distribution. For example, the DEGADIS and the HEGADAS models use a modified Gaussian profile with a flat middle portion in the cross-wind direction, and a power law concentration distribution in the vertical direction [53]. Integral models describe the horizontal cloud spread using common formulations for gravity currents. The ambient air entrainment into the cloud is quantified by entrainment velocities calculated as functions of the Richardson number. Integral models also account for different atmospheric conditions (wind speed and stability class) as well as surface roughness. They are formulated to simulate

continuous buoyancy-dominated, dense, or neutral gas releases. Dispersion of momentum driven releases (jets) is also accounted for.

Integral models are not suitable for modeling releases on terrains with sloping ground, complex topography or in the presence of buildings. Despite the effort to extend the applicability of integral models to non-idealized release scenarios (i.e. in the presence of variable terrain roughness, solid and porous obstacles, i.e. in GASTAR) accurate experimental validation is required to verify the model accuracy.

Shallow Layer Models

Shallow layer models have been applied to heavy gas dispersion modeling and represent a compromise between the simplicity of integral models and the computational complexity associated with full three-dimensional CFD models [54]. The TWODEE model [55], the SLAM model [56], and the DISPLAY-2 model [57] are examples of shallow layer models.

The use of shallow layer approximations to model heavy gas dispersion is appropriate because dense gas clouds typically have a low aspect ratio, *i.e*. the height of the cloud is typically much smaller than the horizontal spread of the cloud. In these models, the low aspect ratio allows for the fundamental conservation equations that describe the flow behavior to be simplified in a depth-averaged fashion. However, empirical correlations are still required to include the ambient air entrainment into the dense cloud.

In comparison to integral models, shallow layer models can accommodate the effects of complex or sloping terrains. The locally enhanced entrainment is included by adding an obstacle characteristic velocity to the base entrainment velocity [59]. Despite many advantages associated with shallow layer models, they are predominately used as a research tool and have not been extensively used for industrial hazard analyses.

Lagrangian Puff/Plume Models

Historically, Gaussian puff models have been used for buoyant or neutral cloud dispersion [58–60]. These models are generally based on the Gaussian formulation and describe the concentration field as the sum of a collection of discrete vapor/gas parcels or puffs. Each puff is allowed to be convected by the ambient wind and to evolve in size. The final concentration in a given position will be generated by the superposition of independent Lagrangian puffs.

The application of Lagrangian puff models to strongly buoyancy driven flows (i.e. dense vapor cloud dispersion) requires extreme care because in reality, the dynamics of one puff can be strongly coupled to other puffs. Dense cloud effects are taken into account in the SCIPUFF model where the puffs are convected and distorted in agreement with buoyancy driven dynamics [61]. The model has been developed to capture the flow patterns associated with the interaction between the dense cloud and the terrain that generates reduction of the vertical turbulent mixing and horizontal gravity spreading currents.

Given the low computation time associated with Lagrangian puff models, they are well suited for situations in which a wide range of atmospheric conditions have to be investigated as is the case in preliminary screening studies or emergency response applications.

Full Three-Dimensional CFD Models

Three dimensional computational fluid-dynamics (CFD) models are the most robust tools for the analysis of vapor cloud dispersion. The vapor dispersion dynamics are simulated by solving three-dimensional conservation equations for mass, momentum, energy and chemical species both in transient or steady state fashions.

Given the inherently turbulent nature of vapor cloud dispersion processes, the fundamental transport equations are averaged and complemented with the transport equations of several turbulent quantities (i.e. mainly turbulent

kinetic energy k and dissipation rate ε). The turbulence models implemented in CFD tools are optimized to account for the suppression of the turbulent mixing due to stable vertical density gradients as observed in dense vapor clouds. The entire set of transport equations is discretized on a grid of cells (mesh) and solved using highly sophisticated numerical algorithms.

The most advanced CFD codes are able to deal with very complex geometry which allows for the representation of arbitrary geometries, obstacles or complex terrain features.

There are several CFD codes that are specifically developed for vapor dispersion simulations. The two most well-known CFD dispersion tools are FEM3C developed at the Lawrence Livermore National Laboratory [62] and FLACS developed by GEXCON [20]. General purpose CFD software packages can also be used for vapor dispersion simulations. FLUENT developed by ANSYS [21] and Star-CCM+ developed by CD-Adapco are two examples of such general purpose CFD software. The application of general purpose CFD codes requires additional efforts to implement specific features that are built-in in dedicated vapor dispersion software. These include the implementation of specific atmospheric boundary layer models that account for the atmospheric stability class as well as appropriate routines to simulate two-phase flashing, droplet transport and evaporation, and pool evaporation [34, 63, 64].

CFD models have been remarkably successful given their flexibility and the wide range of possible scenarios that can be analyzed. Given the computational complexity associated with CFD models, they are better suited for design verification of specific scenarios or for post-incident analysis. Despite the wide range of applicability of CFD models for comprehensive hazard calculations, they are still limited by the inherently long run time, even when run on modern workstations (2013).

Vapor Ignition

For a vapor cloud explosion to occur, a competent ignition scenario must exist. However, to determine the likelihood of competent ignition, it is not sufficient to simply identify an ignition source. Other factors, including ignition source energy and presence of inert species, must also be considered to adequately determine not only the likelihood of ignition but also the hazards associated with the resultant ignited vapor cloud explosion. The following sections give a brief overview of some of the main contributing factors associated with vapor ignition and practical methodologies to quantify and access potential vapor ignition hazards.

Flammable Limits

For a vapor cloud to ignite, a portion of the vapor cloud must be within the flammable limits of the particular vapor/air mixture. For vapor clouds consisting of single common fuel species, the flammability limits are well defined in literature. A list of upper and lower flammable limits for several common fuel species can be found in Chap. 17. These limits are for mixtures of single fuel species and air. The presence of multiple fuel species or inert gases in the vapor cloud will affect the flammable regime.

Flammability Diagram

Flammability diagrams are often used to show the flammable regime of a particular fuel. A more detailed discussion of flammability diagrams can be found in Chap. 17. Here, a brief overview is given. Figure 67.13 shows an example of a flammability diagram. The upper and lower flammable limits are defined by the upper and lower portions of the thumb curve, respectively, where the regime inside the thumb curve is flammable. The flammability limits listed in Chap. 17 are represented by the points on the air line. As the oxygen concentration decreases, the two flammable limits approach one another. The point where the two portions of the curve meet is defined as the limiting oxygen concentration (LOC)—mixtures with oxygen concentrations lower than the LOC are not flammable. For most vapor cloud scenarios, vapor is released into atmospheric air. In these cases, there is always sufficient air available to

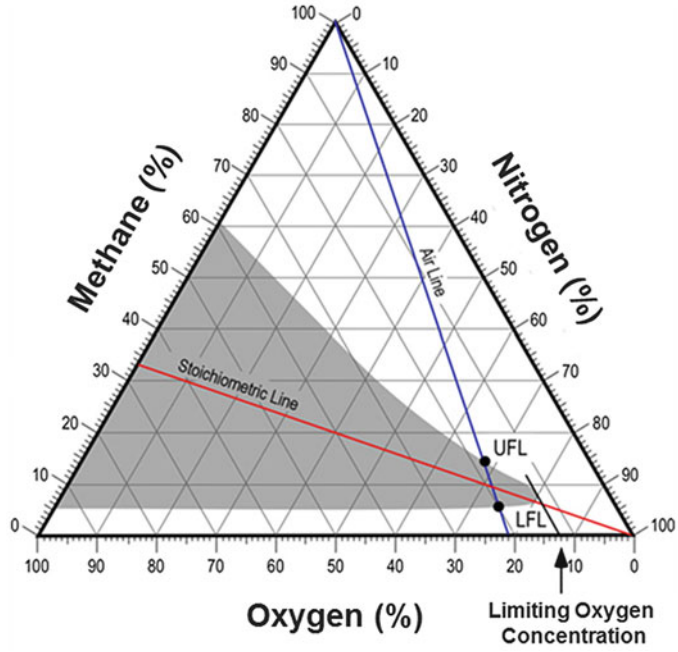

Fig. 67.13 Flammability diagram for methane

mix with the fuel vapor, and the lower flammable limit is more relevant in determining the flammable region. In general, elevated or reduced oxygen conditions are limited to enclosed chambers or buildings, such as hyperbaric chambers, and at high elevations. For example, the oxygen level in mountainous areas can be 15–20 % lower than the oxygen level at sea level.

Analytical Methods for Estimating Flammable Limits for Mixtures

Although vapor clouds often consist of single fuel species, there are scenarios, such as leaks from petroleum refineries, which may involve a complex mixture of combustible and inert species. Although flammable limits have been measured for some mixtures of common fuels [65, 66], flammable limits for a particular multi-species mixture of interest may not be readily available in literature. The presence of inert species, most commonly water vapor, carbon dioxide, nitrogen or argon, will also affect the flammable limits. Figure 67.14 shows the effect of several inert species on methane flammability. In general, the lower flammable limit is less

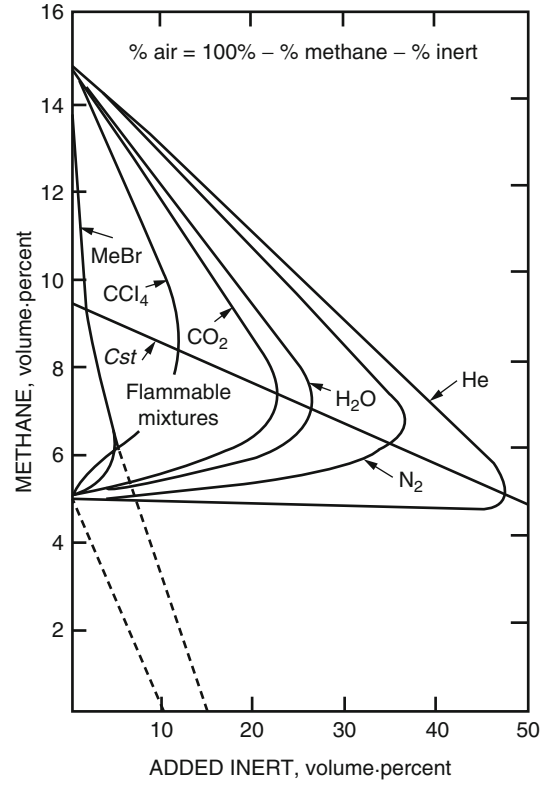

Fig. 67.14 Effect of various inert species on flammability limits of methane [66]

affected by inert species than the upper flammable limit. The sources of accidental vapor releases do not commonly contain inert species. However, even for releases of purely combustible vapors, mitigation techniques such as sprinklers and water hoses can introduce water vapor into the vapor cloud.

In practice, the most reliable method is to experimentally determine flammable limits for a particular fuel mixture. However experimental determination of flammable limits for mixtures with many species may not be practical. Several analytical correlations have been proposed to determine flammable limits. Although the accuracy of analytical methods may vary depending upon the mixture, these methods can be useful in obtaining engineering estimates of the flammable limits.

Le Chatelier's Principle

As discussed in Chap. 17, one common method to estimate upper and lower flammable limits is to apply Le Chatelier's principle, which is often used in determining physical properties of gas mixtures. Expressions for the lower flammable limit are reproduced below. Similar expressions for the upper flammable limit can be obtained by replacing the lower flammable limit with the upper flammable limit in the following equations. Applying Le Chatelier's principle, the lower flammable limit of the mixture in percent volume, LFL_{mix}, is determined by the following equation:

$$LFL_{mix} = \frac{1}{\sum_{j=1}\left(\frac{\chi_j}{LFL_j}\right)} \tag{67.1}$$

where χ_j and LFL_j are the respective molar concentration and lower flammable limit of each individual species, j. Although Le Chatelier's principle was originally intended for binary mixtures of combustible species, Equation 67.1 can be generalized to mixtures of multiple combustible species mixtures.

Le Chatelier's principle can be further generalized to include inert species. The simplest method is to artificially impose that the lower flammable limit of any inert gas approaches infinity [67]. In this limit, summation terms in the denominator of Equation 67.1 associated with inert species are zero. There is some evidence that this method provides a reasonable prediction for fuel mixtures with nitrogen. However, as seen in Fig. 67.14, the effect of inert species on flammable limits depends on the specific species. To address the behavior of various inert species, a nitrogen equivalency factor can be defined for non-nitrogen inert species. This method is described in detail by Molnarne et al. [68]. Applying nitrogen equivalency factors to Equation 67.1, the lower flammable limit of the mixture with any inert can be calculated by the following equation:

$$LFL_{mix} = \frac{1}{\sum_{j=1}\left(\frac{\chi_j}{LFL_j}\right) - \sum_{k=1}(N_{e,k} - 1)\chi_k} \tag{67.2}$$

where χ_k and $N_{e,k}$ are the respective molar concentrations and coefficients of nitrogen equivalency for inert species, k. Recommended coefficients of nitrogen equivalency for mixtures of water and carbon dioxide with a single fuel species are listed in Table 67.13. For multi-species fuel mixtures, an effective coefficient of nitrogen equivalency, $N_{e,k,eff}$, for each inert species can be determined by molar averaging the individual coefficients listed in Table 67.13 as follows:

$$N_{e,k,eff} = \sum_{i=1}(\chi_i N_{e,k,i}) \tag{67.3}$$

where the subscript k indicates the specific inert species and the summation subscript i indicates the single fuel species.

Table 67.13 Nitrogen equivalency coefficients for water and carbon dioxide [68]

Combustible species	$N_{e,H2O}$	$N_{e,CO2}$
Methane	1.87	2.23
Ethane	1.40	1.87
Propane	1.51	1.93
Ethylene	1.68	1.84
Propylene	1.36	1.92
Hydrogen	1.35	1.51
Other combustibles	1.50	1.87

Thermal Balance Method

A more rigorous method to estimate flammable limits for complex mixtures was proposed by Ma [69]. In this approach, the flammability of a mixture is derived from a balance between heating and quenching potentials. The upper and lower flammable limits for a single fuel species can be represented by the heating, H_F, and quenching, Q_F, potentials as follows:

$$LFL = \frac{1}{1 + H_F - Q_F} \tag{67.4}$$

$$UFL = \frac{0.2095H_0 - 1}{0.2095H_0 - 1 + Q_F} \tag{67.5}$$

where the constant 0.2095 is the mole fraction of oxygen in air. For elevated or limited oxygen scenarios, the appropriate mole fraction of oxygen would be used. The heating and quenching potentials are defined as follows:

$$H_F = C_0 H_0 \tag{67.6}$$

$$Q_F = 1 - \frac{1}{LFL} + C_0 H_0 \tag{67.7}$$

where C_0 is the number of moles of oxygen required for stoichiometric combustion of one mole of fuel, and H_0 is the heating potential of oxygen based on air, which is defined as

$$H_0 = \frac{UFL - LFL}{C_0(UFL)(LFL) - 0.2095(1 - UFL)LFL} \tag{67.8}$$

Equations 67.4, 67.5, 67.6, 67.7, and 67.8 are for single species fuels. To generalize the equations to multi-species fuel mixtures, the input parameters, H_F, H_0, Q_F, Q_0, and C_0 can be determined by mole averaging in a similar manner to Equation 67.3, where the effective parameter for the mixture is determined by summing the product of the molar concentration and the input parameter for the individual species.

The advantage of the thermal balance method is that the effect of inert species can be incorporated directly. The general forms of Equations 67.4 and 67.5 become

$$LFL_{mix} = \frac{1}{1 + \left(\frac{1}{1+R}\right)H_{F,mix} - \left(\frac{1}{1+R}\right)Q_{F,mix} - \left(\frac{R}{1+R}\right)Q_{D,mix}} \tag{67.9}$$

$$UFL_{mix} = \frac{0.2095H_{0,mix} - 1}{0.2095H_{0,mix} - 1 + \left(\frac{1}{1+R}\right)Q_{F,mix} + \left(\frac{R}{1+R}\right)Q_{D,mix}} \tag{67.10}$$

where the $H_{0,mix}$, $H_{F,mix}$, $Q_{F,mix}$ are the respective heating potential of oxygen, heating potential of the fuel, and quenching potential of the mixture. The ratio R is defined as the ratio between the molar concentrations of the inert and the fuel species. The effect of inert species is accounted by incorporating the quenching potential, $Q_{D,mix}$, of inert species. Similar to Equation 67.3, the quenching potential for multiple inert species can be determined by molar averaging to obtain an effective quenching potential for the inert mixture as follows:

$$Q_{D,mix} = \frac{\sum_{k=1}\left(\chi_{D,k}\, Q_{D,k}\right)}{\sum_{k=1}\chi_{D,k}} \tag{67.11}$$

where $\chi_{D,k}$ and $Q_{D,k}$ are the molar concentration and quenching potential for inert species k.

Quenching potentials depend on the adiabatic flame temperature. For most hydrocarbons, the flame temperature is approximately 1600 K. Quenching potentials for common inert species are listed in Table 67.14. Figure 67.15 shows a comparison of the predicted and measured flammable limits with dilution of carbon dioxide and argon for methane and ethane. The concentration of inert species at which the curves predicted by Equations 67.9 and 67.10 cross is often referred to as the inertion or inertization point. The error observed in the inertion point region arises due to several factors including incomplete reaction and decreased flame temperature. Corrective scaling for better prediction of the nose region of the flammability plot is discussed in Ma [69].

Testing Methodologies

When practical, flammable limits of a flammable vapor are best determined through testing. In certain cases where the composition of the vapor may be unknown, testing may be the only viable method. Relevant standardized tests for gas or vapor flammability are listed below:

- *ASTM E681 Standard Test Method for Concentration Limits of Flammability of Chemicals* (*Vapors and Gases*).
- *ASTM E918 Standard Practice for Determining Limits of Flammability of Chemicals at Elevated Temperature and Pressure*
- *ASTM E2079 Standard Test Methods for Limiting Oxygen* (*Oxidant*) *Concentration in Gases and Vapors*

Table 67.14 Quenching potentials for common inert species at an adiabatic flame temperature of 1600 K [69]

Inert species	Q_D
Helium	0.642
Argon	0.642
Nitrogen	0.992
Oxygen	1.046
Carbon dioxide	1.603
Air	1.000

Ignition Sources

Determining potential ignition sources is a crucial element in both fire and explosion investigation and hazard analysis of vapor cloud explosions. Because the minimum ignition energy required to ignite gases or vapors is on the order of tenths of millijoules, many potential competent ignition sources may exist in nearly all vapor cloud scenarios. In addition to the obvious sources such as open flames or fire in furnaces or heaters, sparks from electrical equipment, static discharges, or even friction from a cutting wheel can provide sufficient energy to ignite vapors.

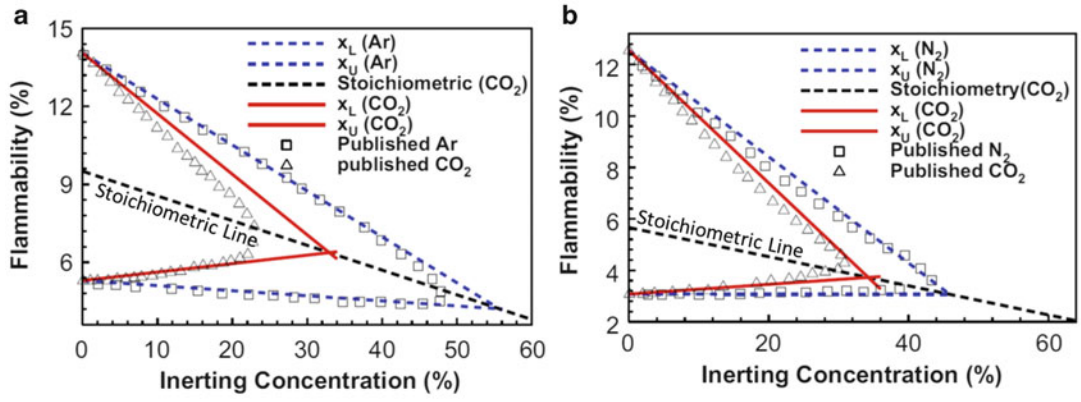

Fig. 67.15 Measured and predicted flammability diagrams for (**a**) methane and (**b**) ethane [69]. Reprinted from Fire Safety Journal, Vol. 46, T. MA, "A thermal theory for estimating the flammability limits of a mixture," pp. 558–567, Copyright (2011), with permission from Elsevier.

Table 67.15 Minimum ignition energy for common hydrocarbon-air mixtures [70]

	Minimum ignition energy (mJ)	
Gas mixture	Deflagration	Detonation
Acetylene-air	0.01	1.8×10^5
Propane-air	0.25	4.1×10^8
Methane-air	0.21	9.9×10^{10}
Hydrogen-air	0.016	5.2×10^6

Minimum Ignition Energy

The minimum ignition energy (MIE) for vapors is low and even weak sparks from static discharges may be strong enough to ignite a vapor cloud. The type of combustion mode ignited by a source can be either a deflagration a detonation, or both further discussion on the characteristics of deflagrations and detonations is discussed in later sections. However, the difference in minimum ignition energy for deflagrations compared to direct detonation is worth mentioning here. Table 67.15 lists the minimum ignition energy for select fuel-air mixtures for deflagration and detonation. The MIE required for a deflagration is on the order of 10^{-4} J, whereas the MIE required for a direct detonation is at least on the order of 10^2 J. Owing to the large amount of energy required to directly initiate a detonation, the vast majority of vapor cloud explosions begin as deflagrations.

Mechanical Sparks and Static Discharges

Mechanical sparks from process equipment and static discharges are common ignition sources for vapor cloud explosion. For example, the use of sparking tools in areas with flammable vapors can lead to a vapor cloud ignition. Other common ignition sources are static discharges, which can be classified as follows:

Spark Discharge. Spark discharges occur as a result of charge accumulation on a conductive object. When the potential between two conductive objects exceeds the dielectric strength of the gas between the conductive objects, a spark discharge will occur. Spark discharges transfer up to 10 J, which is large enough to ignite vapors and dusts. Spark discharges commonly arise as a result of improper grounding of ducts or pipes.

Brush Discharge. Brush discharges can occur between a conductive object and a charged non-conductive object. For example, a brush discharge can occur when a conductive sampling probe is lowered into a tank with a charged liquid. The energy transferred by brush discharges can be up to 4 mJ.

Propagating Brush Discharge. When an insulating layer with high resistance and dielectric strength is placed between two conductive surfaces, a propagating brush discharge can occur if the potential difference between the conductive surfaces is sufficiently large. Most often, only one conductor is in contact with the insulating layer. It is possible for propagating brush discharges to occur when filling epoxy-coated tanks or pipes. The energy transferred by propagating brush discharges can be up to 2 J.

Cone Discharge. Cone discharges can occur when a large vessel is rapidly filled with a high resistivity bulk product. A static discharge results from charge accumulation in the bulk product. The energy transferred by a cone discharge can be up to 1 J.

Corona Discharge. A corona discharge is the result of ionization of fluid surrounding an electrically energized conductor. Corona discharges are highly diffuse. A common example is dissipation of charge from fine wires or conductive threads. The energy transfer from a corona discharge is typically less than 0.1 mJ, which is less than the MIE of most flammable gases with the exception of lower MIE gases such as hydrogen or acetylene.

In fire and explosion investigation, static discharges and sparks often do not leave behind conclusive evidence. Evidence such as arcing on wires or improper grounding of electrical equipment is often used to support the possibility of static ignition. However, these types of evidence do not provide irrefutable proof that that the ignition was the result of a static discharge, since arcing can often occur post ignition. On the other hand, the lack of observed arcing on wires or surfaces and other circumstantial evidence is useful to eliminate the possibility of

spark ignition. A more detailed discussion of ignition hazards due to static discharges can be found in [71].

Autoignition Temperature and Hot Surface Ignition

Flammable mixtures can also be ignited if the gas temperature is sufficiently high. Although most common hydrocarbon fuels and hydrogen have autoignition temperatures greater than 400 °C, the autoignition temperature for some gases can be as low as 150 °C. The autoignition temperatures for many single species have been determined experimentally. Chapter 17 gives a table of autoignition temperatures for various gas species. For mixtures of gases, it is common to use the lowest autoignition temperature of the individual species in any vapor cloud ignition analysis to provide a conservative estimate. In cases where the autoignition temperature of a vapor cloud of unknown composition or of a vapor cloud with suspended dust particles, the autoignition temperature may be determined experimentally. Typically, testing standards for determining autoignition temperatures are related to dusts and liquid chemicals. Although these standards are not specific to vapors, they can be used as guidelines for developing specialized testing protocols. The testing standards for determining autoignition temperature include:

- *ASTM E659 Standard Test Method for Autoignition Temperature of Liquid Chemicals*
- *ASTM E1491 Standard Test Method for Minimum Autoignition Temperature of Dust Clouds*

Ignition of flammable mixtures can also result from sufficient heat transfer from hot surfaces. Unlike autoignition, the ignition of a gas by a hot surface depends on the temperature of the surface and on several additional parameters. The ignition of a flammable gas mixture that comes in contact with a heated surface depends on the energy that is transferred from the surface to the gas mixture, which depends on the fluid dynamics of the gas as it comes in contact with the surface. In practice, the autoignition temperature of the gas can be used as a conservative lower bound to assess explosion hazards from hot surfaces. Note that the ignition of flammable gases due to hot surfaces is different than the hot surface ignition of flammable liquids. The scope of this section is to address vapor cloud explosions. Hot surface ignition of flammable liquids is discussed in Chap. 18.

Deflagrations and Detonation

Vapor cloud explosions are characterized by a rapid increase in pressure. The rapid pressure rise is the result of rapid heating due to a deflagration or detonation. In this section, a brief overview of the fundamentals of deflagrations and detonations is given. The primary focus of this section is to discuss the application of these fundamental principles to vapor cloud explosions. For hazard assessment and mitigation related to deflagrations and detonations see Chap. 69.

Deflagrations

As discussed previously, the majority of vapor cloud explosions can be characterized as deflagrations. Nearly all vapor cloud explosions begin as a deflagration. A deflagration is characterized by subsonic propagation of the flame away from the ignition source. The flame propagation is the result of heat produced by the chemical reaction in the flame being transported into the unburned fuel-air mixture. As a result, the fuel-air mixture just ahead of the flame is preheated, which enables the flame to propagate into the unburned fuel-air mixture. This propagation will terminate once the flame reaches a fuel-air mixture that is not within the flammable limits or as a result of the reaction being quenched by turbulence generated by obstructions or by the expansion of the flame front itself, or some other heat loss mechanism.

In general, immediately after a vapor cloud ignites, the initial flame propagation is dominated by molecular diffusion and radiation, which results in laminar flame propagation. In most practical scenarios, flame propagation will increase in speed due to interaction with a turbulent flow field. In general, the source of turbulence is a combination of the following phenomena:

Table 67.16 Maximum laminar flame speed for common fuel-air mixtures at 25 °C [72]

Fuel	Flame speed (cm/s)
Methane	44.8
Ethane	47.6
Propane	46.4
n-Butane	44.9
Acetylene	155
Ethylene	73.5
Hydrogen	325

- Flow field turbulence of the unburned mixture;
- Turbulence generated from flow past obstacles;
- Turbulence generated from the expanding flame front itself.

The turbulence interacts with the flame front by wrinkling the flame. The wrinkling effectively enhances the combustion rate, and thus increases the flame propagation speed. The acceleration of the flame front results in a positive feedback mechanism where the turbulence generated by the flame front increases as the flame speed increases.

Historically, flame speeds have been measured experimentally. Several methods have been used including Bunsen burners and flat flame burners. Descriptions of these methods can be found in several combustion reference texts [72–74]. Table 67.16 shows laminar flame speeds for several common fuels. Flame speeds can also be computed numerically using commercially available combustion kinetics software such as Chemkin and DARS, which can account for parameters such as turbulence intensity, fuel mixtures, inert species, and elevated or reduced temperature and pressure. However, numerical computation of flame speed is limited to the accuracy of the assumed kinetics for the specific fuel of interest. Chemical kinetics are reasonably well defined for several common fuels including methane, propane, butane and some jet fuels.

Detonations

If the flame propagation accelerates to supersonic speeds, the propagation is referred to as a detonation and results in a shock wave. The detonation velocity can be derived from Chapman-Jouget (C-J) theory. Details of the derivation can be found in Glassman [72]. The detonation velocity, u_{det}, is as follows:

$$u_{det} = \frac{\gamma_b + 1}{\gamma_b}\sqrt{\frac{\gamma_b \overline{R} T_b}{MW_b}} \tag{67.12}$$

where $\overline{R}$ is the universal GAS constant, and where γ_b, T_b, and MW_b are the respective ratio of specific heats, temperature and molecular weight of the burned gases.

As discussed previously, significant energy is required to immediately initiate a detonation, and therefore immediate detonations are uncommon. The more common detonation scenario occurs when a deflagration continues to accelerate and abruptly transitions to a detonation. As discussed previously, a deflagration will accelerate due to turbulence interactions. Because these interactions result from many possible mechanisms, it is not feasible to generalize a theory for the acceleration phase of a deflagration-to-detonation transition (DDT) event. It is the combination of turbulent mechanisms—flow-field turbulence in the unburned mixture, turbulence generated from obstacles, and induced turbulence from the flame front itself—that augment the flame propagation speed and can result in a transition to detonation. Experimental data shows that in practice, augmentation of the flame speed to levels approaching detonations requires spaced obstacles and partial confinement of the vapor cloud [70]. Examples of such scenarios include obstacles such as process equipment, railcars, and industrial structures as well as tunnels, bridges or crowded parking lots. For vapor cloud explosions, detonations are not commonly observed, and it has been suggested that the inhomogeneity of the fuel-air mixture in a vapor cloud is the dominant limiting condition for self-sustaining detonations [70].

In theory, an analysis of a possible DDT event in a vapor cloud explosion can be performed using computational simulations. Several of the commercial software packages discussed in this chapter—Fluent, Star-CCM+, etc.—include combustion models that can be used to predict

DDT for simple geometries. In practice, current computing power is not sufficient to spatially resolve the flame front in a vapor cloud explosion, while having a sufficiently large computational domain to include an entire cloud, which can be up to several kilometers in size. In the future, as computing power increases, simulating full scale vapor clouds with complex geometries may become more feasible. Irrespective of computational resources, computational predictions are limited to the fidelity of the combustion model and must be used with caution. To extract the most value from a computational simulation of DDT, careful interpretation is required.

Blast Waves

The rapid heat released from a deflagration or a detonation results in the expansion of high temperature combustion products. Through this thermal expansion mechanism, a portion of the chemical energy generated by the fuel-air reaction is converted into mechanical energy in the form of a blast wave. The blast wave is characterized by a rapid increase in pressure, density and local fluid velocity followed by a less rapid decay to sub-atmospheric pressure conditions and an even slower recovery to atmospheric conditions. The shape of the blast wave is unique and dependent on the conditions of the explosion. Figure 67.16 shows examples of blast wave shapes. As discussed previously, a detonation of a vapor cloud is highly unlikely. However, overpressure due to a confined or partially confined deflagration can result in blast waves that approach detonation levels.

Analytical Methods

Although vapor cloud explosions are typically deflagrations rather than detonations, analyzing the detonation scenario is important because it provides the worst-case scenario. Also, pressure waves produced by an accelerating deflagration can potentially coalesce to form a shock. Determining worst-case scenario conditions is not only important in back-of-the-envelope analysis, but can also serve as an upper bound when interpreting results from computational simulations. The two most common analytical methods for predicting vapor cloud explosions are the TNT equivalency method and the TNO multi-energy method.

TNT Equivalency Method

The TNT-equivalency method is the simplest analytical procedure to analyze vapor cloud explosions. Physically, the TNT-equivalency method represents the efficiency of the conversion of chemical energy into mechanical energy. The conversion of available energy for the mass of a particular fuel, W_f, to an equivalent charge weight of TNT, W_{TNT}, is defined as follows:

$$W_{TNT} = \alpha_e \frac{W_f H_f}{H_{TNT}} = \alpha_m W_f \qquad (67.13)$$

where the TNT equivalency coefficients α_e and α_m are based on energy and mass, respectively. The energy and mass based TNT equivalency coefficients are related by the ratio of heat of

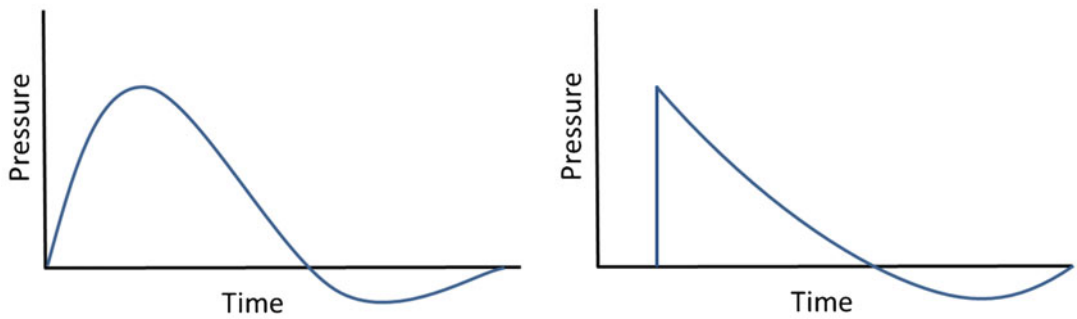

Fig. 67.16 Blast wave shapes for a deflagration (*left*) and a detonation (*right*)

combustion of the fuel, H_f, and the TNT blast energy, H_{TNT}. Once the equivalent charge weight of TNT is determined, blast parameters as a function of distance from the explosion can be determined based on empirical data and are commonly represented graphically. Common blast parameters of interest include the peak side-on overpressure, and the arrival time and duration of the blast wave.

Several TNT-equivalency methods have been proposed by various studies [75–80]. Although the details for each particular method differ slightly, the basis for these TNT-equivalency methods is similar. The TNT equivalency and blast energy are determined from statistical descriptions of historical vapor cloud explosions. The value of TNT equivalency energy coefficients proposed by various sources may range from 1 % up to 20 % and are shown in Table 67.17. In general, the TNT blast energy is assumed to be between 1800 and 2000 Btu/lb (4.19–4.65 MJ/kg) [70]. Because TNT-equivalency methods are reliant on a wide range of previous incidents—the graphical representations of the relationship between fuel and equivalent charge weight of TNT are effectively an average of historically significant vapor cloud explosion events—the accuracy of the TNT-equivalency predictions is limited to the scatter in the historical data. In fact, the scatter in the data contradicts the proportionality assumption between the fuel and equivalent charge weight of TNT, and thereby inherently limits the predictive accuracy of TNT-equivalency methods. TNT-equivalency methods tend to over predict the blast overpressure and under predict the duration. However, the advantage of TNT-equivalency methods is that they provide a simple, direct empirical relationship between a charge weight of TNT and the resulting structural damage. For hazard analyses, TNT-equivalency methods can be useful in determining potential structural damage and can give reasonable estimates of far-field blast effects as long as the actual explosion conditions are similar to an "average" historical event.

Table 67.17 TNT equivalency proposed by various studies

Studies	α_e
Brasie and Simpson [75], Brasie [76]	0.02–0.05
HSE [77, 78]	0.01–0.03
[a]FM Research [79]	0.05 (Class I)
	0.10 (Class II)
	0.15 (Class II)
British Gas [80]	0.2

[a]Class I—low reactivity materials (e.g. propane, butane, other ordinary flammable liquids)
Class II—moderately reactive materials (e.g. ethylene, diethyl ether, acrolein)
Class III—highly reactive materials (e.g. acetylene)

A commonly used TNT-equivalency method was proposed by U.K. Health & Safety Executive (HSE). In the HSE method, the fuel source is assumed to be liquid fuel that flashes to form a vapor cloud. The flash fraction of fuel, F, is estimated based on thermodynamic data as follows:

$$F = 1 - exp\left(\frac{-C_p \Delta T}{\Delta h_v}\right) \tag{67.14}$$

where the mean specific heat, C_p, and latent heat of vaporization, Δh_v, are defined for the specific fuel, and ΔT is defined as the temperature between the liquid fuel temperature in the storage vessel and the boiling temperature of the fuel at ambient pressure. The mass of the fuel is determined from the flash fraction and the mass of fuel released, m_f, as follows:

$$W_f = 2Fm_f \tag{67.15}$$

The multiplicative coefficient of two is included to account for spray and aerosol formation. Note that the maximum possible W_f is the amount of fuel released. The mass of fuel determined in Equation 67.15 is then used in Equation 67.13 to determine W_{TNT}. The values for α_e and H_{TNT} are assumed to be 0.03 and 4.68 MJ/kg, respectively. Once W_{TNT} is determined, the blast parameters can be determined directly from Fig. 67.17, where the x-axis is a scaled distance, z, that is defined as the real distance from the explosion, r, divided by the cubic root of W_{TNT}. The y-axis parameters, are also scaled by the cubic root of W_{TNT}.

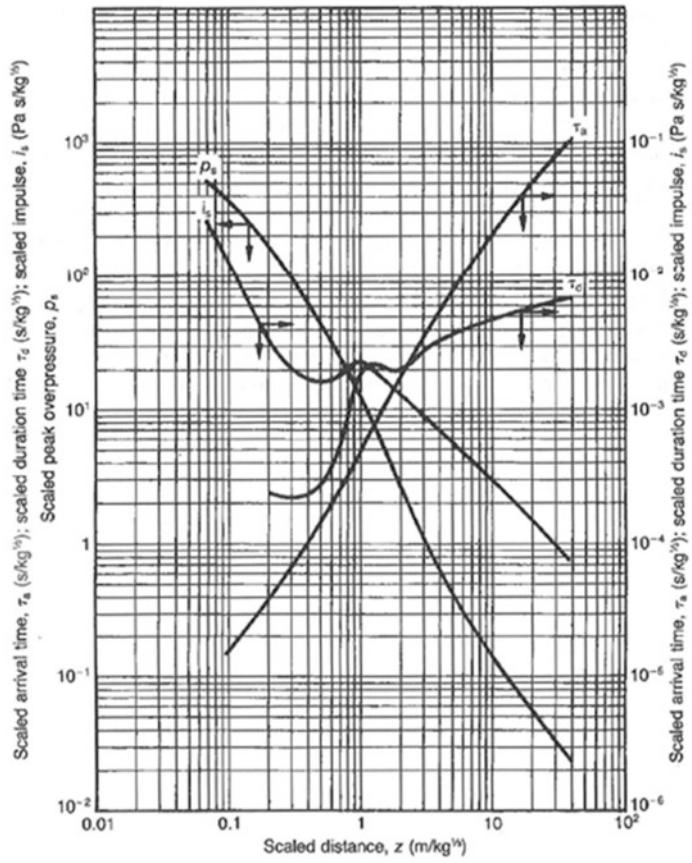

Fig. 67.17 Side-on blast parameters for a TNT hemispherical surface burst [70]

TNO Multi-energy Method

The multi-energy method is based on experimental observation that only a portion of the vapor cloud contributes to the blast [81, 82]. In the multi-energy approach, the blast wave is assumed to be produced by the portion of the vapor cloud that is partially confined or obstructed. Several experimental studies have shown that the unconfined or non-obstructed portion of the vapor cloud does not contribute to the blast [83]. In other parts of the vapor cloud where turbulence may have been generated at the time of ignition, blast generating conditions may also exist. An example of such a source is a highly turbulent jet resulting from a high pressure fuel release. The vapor cloud explosion is then viewed as an aggregate of sub-explosions from various sources in the cloud.

The multi-energy method is similar to TNT-equivalency methods in that the blast parameters are directly read off a blast chart. Figures 67.18 and 67.19 show multi-energy blast charts for side-on blast overpressure and duration curves. The method includes 10 blast classes (see Table 67.18), each one represented by separate curves in the figures. The axes variables are non-dimensional parameters. The combustion energy-scaled distance, $\overline{r}$, on the x-axes, the normalized side on overpressure, $\overline{\Delta P_s}$, and the normalized duration, $\overline{\tau}$, are defined as follows:

$$\overline{r} = \frac{r}{(E/P_a)^{1/3}} \tag{67.16}$$

$$\overline{\Delta P_s} = \frac{\Delta P_s}{P_a} \tag{67.17}$$

$$\overline{\tau} = \frac{\tau C_0}{(E/P_a)^{1/3}} \tag{67.18}$$

where the dimensional distance from the charge, r, and duration, τ, are normalized by the cube root of the available combustion energy, E,

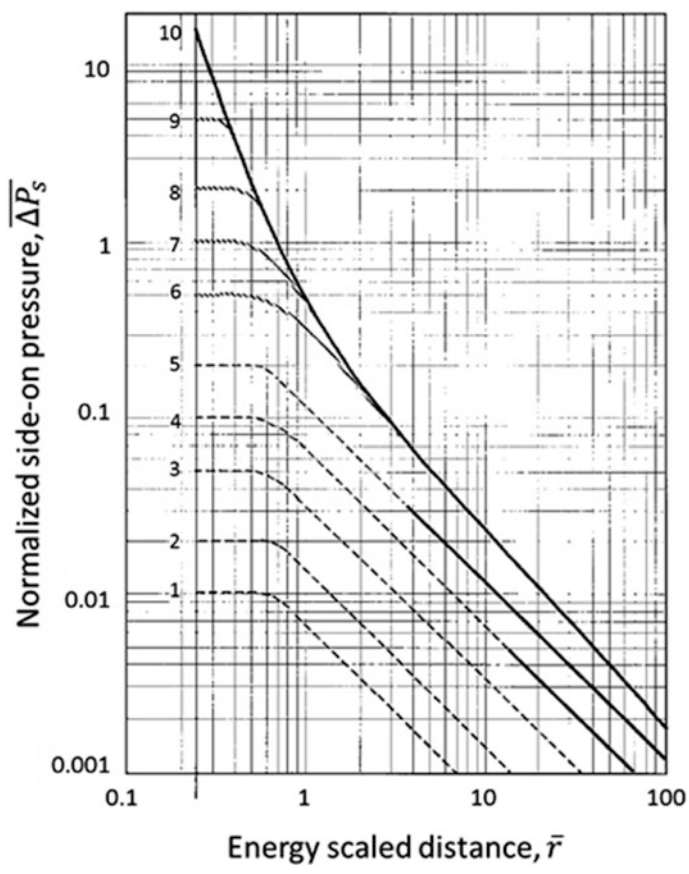

Fig. 67.18 Multi energy method side-on blast overpressure curves [86]

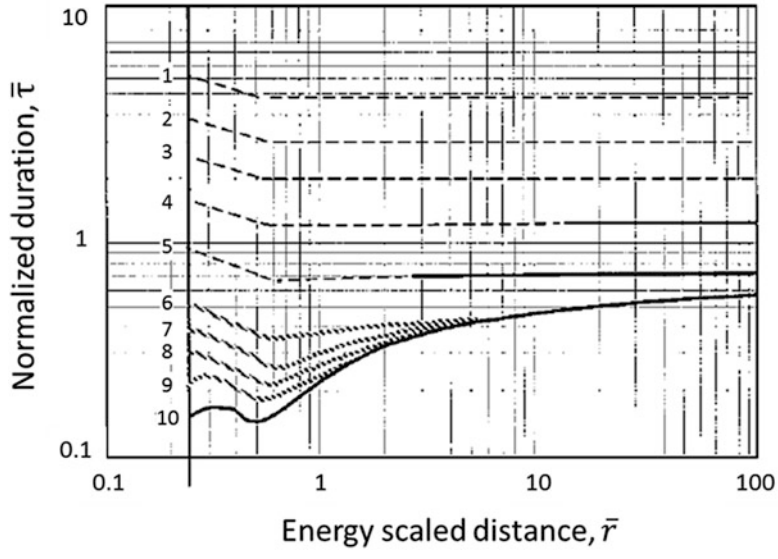

Fig. 67.19 Multi energy method blast duration curves [86]

Table 67.18 Initial blast strength index [87]

Blast strength	Ignition energy	Obstruction	Confinement	Class
1	High	High	Parallel plane	7–10
2	High	High	Unconfined	7–10
3	Low	High	Parallel plane	5–7
4	High	Low	Parallel plane	5–7
5	High	Low	Unconfined	4–6
6	High	None	Parallel plane	4–6
7	Low	High	Unconfined	4–5
8	High	None	Unconfined	4–5
9	Low	Low	Parallel plane	3–5
10	Low	Low	Unconfined	2–3
11	Low	None	Parallel plane	1–2
12	Low	None	Unconfined	1

divided by the atmospheric pressure, P_a. The side on overpressure, ΔP_s, is normalized by the atmospheric pressure. The symbol C_0, is the speed of sound of atmospheric air. The numbered curves indicate the class of blasts with strengths rated from 1 (weak) to 10 (detonation strength). For blast with strengths above 6, the curves approach the detonation limit as $\bar{r}$ increases.

The multi-energy method is not nearly as simple and direct as the TNT-equivalency method. A more detailed step-by-step discussion of the multi-energy method is given in Mercx and van den Berg [83]. An overview of the steps of the multi-energy method is given below.

1. ***Understand the applicability of the method***. The multi-energy method is applicable to unconfined vapor cloud explosions and is a conservative approach. It does not take into consideration directional effects due to non-uniform distribution of obstacles or confinement.
2. ***Determine the size of the cloud***. The multi-energy method requires an estimate of the size of the flammable cloud. For simple geometries or back-of-the-envelope estimates, the flammable region of the cloud can be determined from scaling laws [84] for plumes or jets and flammable limits for the fuel as discussed earlier in this chapter. For more accurate analyses, dispersion models as discussed previously may be employed.
3. ***Identify potential blast sources***. Engineering judgment must be used to properly determine the potential source of the blast. Some examples of common locations where blast sources can initiate include process equipment at chemical plants or refineries, space between extended parallel walls or barriers, spaces in tunnels, corridors or covered conveyor belts, and intense turbulent fuel-air mixture due to high pressure releases.
4. ***Define obstructed regions***. In addition to the blast source, the multi-energy method also incorporates sub-blasts due to obstructions. Below is a procedure given by Mercx and van den Berg to determine obstructed regions [83].
   (a) Approximate the structures as basic geometrical shapes.
   (b) Determine the obstacle orientation by taking the smallest dimension, D_1, oriented perpendicular to the assumed flame propagation direction. The dimension parallel to the flame propagation is identified as D_2.
   (c) Define an obstructed region as a group of obstacles that are located within a $10D_1$ or $1.5D_2$ radius from the center of the region. Note that D_1 and D_2 are dimensions for any obstacle in the region. Exclude any obstacle that has an outer boundary 25 m or further from the outer boundary of the obstructed region.
   (d) Determine the free volume of the obstructed region by subtracting the volume of the obstacles from the volume of the box. Note that the obstructed region can also be defined by multiple boxes to get a more accurate estimate of the free volume.
5. ***Determine the unobstructed volume***. Subtract the free volume of obstructed regions that are within the cloud from the total cloud volume.

6. ***Calculate the available combustion energy for the obstructed and unobstructed regions***. The combustion energy, E, can be determined by multiplying the volume of a region by the heat of combustion (volume basis) for the particular fuel. Conversely, the calculation can also be determined from the heat of combustion (mass basis) and the mass of the region.
7. ***Estimate the blast strength of each region***. A conservative approach would be to assign a blast class of 10 to any obstructed region and a class of 1 for unobstructed regions. In the case of turbulence in an unobstructed region due to, for example, the momentum of a fuel release, a blast class of 3 is recommended. Alternatively, blast class can be determined from Table 67.18 [84]. Definitions of the selection criteria are given below.
   (a) ***Ignition Energy***. An example of a *high* ignition energy source is a confined vented explosion. An example of *low* energy sources are sparks, flames, hot surfaces, etc.
   (b) ***Obstruction***. Obstructions are considered *high* if the ratio of total volume of the obstructions to the total volume of the obstructed area is greater than 0.3 and the spacing between obstacles is less than 3 m. If the obstacles in an area do not meet these criteria, the obstructions are considered *low*. *None* refers to the absence of any obstructions.
   (c) ***Confinement***. Confinement is considered a *parallel plane* confinement if a part of the vapor cloud is confined by barriers or walls on two or three sides. Confinement is considered *unconfined* if the gas vapor is only confined by the ground.
8. ***Multiple obstructed regions***. For cases where there is more than one obstructed region, define a single equivalent blast source by combining the combustion energy for all the regions and defining the center of the blast source as the energy weight-averaged location.
9. ***Blast source location of the unobstructed region***. If there are separate unobstructed regions, the source location of the unobstructed region of the cloud can also be determined by an energy weighted average of the separate unobstructed regions.
10. ***Calculate blast parameters***. For each source, use the estimated combustion energy to determine blast parameters from Figs. 67.18 and 67.19 and Equations 67.16, 67.17, and 67.18. If the distance between blast sources is small, the far-field blast parameters can be determined by assuming the blast sources are initiated simultaneously and the combustion energy for the sources can be summed.

Although, the multi-energy method will provide more accurate predictions than TNT-equivalency methods, it still has limitations and constraints. The multi-energy method assumes blast strengths of the blast sources, uses generalized criteria for defining obstructed regions, and assumes that the blast sources do not interact. Understanding how these assumptions affect the accuracy of the predicted results is essential in any vapor cloud explosion investigation or hazard analysis. In light of recent increases in computational power, computational codes are beginning to replace the tedious analytical approach of the multi-energy methods. Although computational codes such as FLACS provide higher fidelity analysis, analytical methods can still provide valuable insight when interpreting the results of computational simulations. Analytical methods can also be a more cost effective options when conducting a process hazard analysis where safety precautions are based on worst-case scenario conditions and the higher fidelity of computational codes are not required.

Computational Methods

Although analytical methods are useful tools for evaluating vapor cloud explosions, their limitations often require the use of computational tools. Several of the commercial software packages discussed in this chapter—FLACS, PHAST, Fluent, Star-CCM+, etc.—can be used

to analyze vapor cloud explosions. FLACS was developed specifically for vapor cloud explosion applications. FLACS simulations can predict several parameters, including overpressure due to blast waves and flame propagation, and can account for complex geometries. Several studies have been performed to validate FLACS with experimental results from medium to large scale tests [85–87].

Vapor cloud explosion scenarios may include complicating factors that analytical methods are unable to address. One such example is the explosion that occurred at the Buncefield Oil Storage Depot in Hertfordshire, England in 2005 that resulted from a gasoline leak from an overfilled tank [88]. Approximately 10 % of the oil turned into vapor and mixed with the ambient air to form a vapor cloud that appeared to have ignited and initiated a blast wave near a parking garage located west of the site. The Buncefield explosion was unique because the observed damaged due to the blast wave suggested that the overpressure was much higher than that expected for the low congestion levels dictated by the physical structures and equipment located at the site. Analyses showed that to predict an overpressure consistent with the observed damage, the computations needed to include the foliage of the surrounding trees [89]. Testing used to validate the simulations demonstrated the acceleration of a flame front as it passed along a row of dense tree foliage. Although computational methods can give insightful results, care must be taken when interpreting any computational simulation. In practice, careful validation with experimental results, physical observations, or analytical methods is essential in developing confidence in simulation results.

References

1. U.S. Chemical Safety and Hazard Investigation Board, "Case Study: Explosion and Fire in West Carrollton, Ohio," U.S. Chemical Safety and Hazard Investigation Board, West Carollton, Ohio, 2010.
2. U.S. Chemical Safety and Hazard Investigation Board, "Investigation Report: Methanol Tank Explosion and Fire-Bethune Point Wastewater Treatment Plant," U.S. Chemical Safety and Hazard Investigation Board, 2006.
3. S. R. Hanna and P. J. Drivas, Guidelines for Use of Vapor Cloud Dispersion Models, Center for Chemical Process Safety, 1987.
4. E. A. Avallone, T. Baumeister III and A. M. Sadegh, Marks' Standard Handbook for Mechanical Engineers. 11th Edition, New York: McGraw Hill, 2007.
5. R. D. Blevins, Applied Fluid Dynamics Handbook, Malabar: Krieger Publishing Company, 2003.
6. Crane, Flow of Fluids Through Valves, Fittings and Pipe. Technical Paper No. 410M. Metric Version., Crane, 2010.
7. R. Darby, Chemical Engineering Fluid Mechanics, 2nd Edition, Boca Raton: CRC Press, 2001.
8. I. E. Idelchik, Handbook of Hydraulic Resistance. 3rd edition., Jaico Publishing House, 2005.
9. G. K. Batchelor, An Introduction to Fluid Dynamics, Cambridge University Press, 2002.
10. Det Norske Veritas, "PVAP Theory Document," DNV Software, 2006.
11. D. P. Hoult, "Oil Spreading on the Sea," *Annual Reviews of Fluid Mechanics,* vol. 4, pp. 341–368, 1972.
12. N. F. Ponchaut and H. K. Kytömaa, "Transient Spreading of LNG on Water," in *Mary Kay O'Connor Safety Center*, College Station, TX, 2009.
13. S. R. Saraf and G. A. Melhem, "Modeling LNG Pool Spreading and Vaporization," in *AIChE Spring Meeting*, Atlanta, GA, 2005.
14. D. M. Webber and S. J. Jones, "A Model of Spreading Vaporising Pools," in *International Conference on Vapor Cloud Modeling*, 1990.
15. C. J. H. van den Bosch, "Chapter 3: Pool Evaporation," in *Methods for the Calculation of Physical Effects due to Releases of Hazardous Materials (Liquids and Gases)- CPR 14E*, The Hague, 2005.
16. I. G. Opschoor, "Ch. 5," in *Methods for the Calculation of the Physical Effects of the Escape of Dangerous Material*, TNO Yellow Book, 1978.
17. N. F. Ponchaut, H. K. Kytömaa, D. R. Morrison and M. K. Chernovsky, "Modeling the Vapor Source Term Associated with the Spill of LNG into a Sump or Impoundment Area," *JLPP,* vol. 24, no. 6, pp. 870–878, 2011.
18. D. M. Webber, S. E. Gant, M. J. Ivings and S. F. Jagger, "LNG Source Term Models for Hazard Analysis: a Review of the State-of-the-Art and Approach to Model Assessment," The Fire Protection Research Foundation, 2009.
19. J. Melheim and M. Ichard, "Pool and Fire in FLACS v9.0," in *FLUG Meeting*, Bergen, May 6, 2008.
20. GexCon, "FLACS v9.0 User's Manual," 2009.
21. F. Inc., FLUENT 6.3 User's Guide, 2006.
22. CD-Adapco, User Guide Star-CCM+ Version 8.02, 2013.
23. W. M. Chase, NIST JANAF Thermochemical Tables, 4th Edition. (Part I and Part II), 1998.
24. D. Drysdale, An Introduction to Fire Dynamics. 2nd Edition, John Wiley & Sons, 2002.

25. F. P. Lees, Loss Prevention in the Process Industries. Hazard Identification, Assessment and Control. 2nd Edition, Butterworth Heinemann, 1996.
26. D. Mackay and R. S. Matsugu, "Evaporation Rates of Liquid Hydrocarbon Spills on Land and Water," *Canadian J. of Chem Eng.,* vol. 51, pp. 434–439, 1973.
27. M. R. Lindeburg, Mechanical Engineering Reference Manual for the PE Exam, 12th Edition, Professional Publications, Inc. (PPI), 2006.
28. F. P. Incropera, D. P. Dewitt, T. L. Bergman and A. S. Lavine, Introduction to Heat Transfer, 5th edition, John Wiley & Sons, 2007.
29. S. B. G. H. R. Hanna, "Handbook of atmospheric diffusion," Technical information center, U.S. department of Energy, 1982.
30. J. Woodward, Estimating the flammable mass of a vapor cloud, American Institute of Chemical Engineers, 1999.
31. F. Gifford, "Turbulent diffusion typing schemes: a review," *Nuclear Safety,* pp. 68–86, 1976.
32. D. Turner, "Workbook of atmospheric dispersion estimates," Environmental Protection Agency, 1970.
33. J. Casal, Evaluation of the Effects and Consequences of Major Accidents in industrial Plants, Elsevier, 2008.
34. C. Alinot and C. Masson, "k-ε Model for the atmospheric boundary layer under various thermal stratifications," *Journal of solar energy engineering – Transaction of the ASME,* pp. 127: 438–443, 2005.
35. TNO, "Methods for the calculation of physical effects (Yellow book)," Directorate General of labor, The Hague, 1997.
36. T. Spicer and J. Havens, "User's guide for DEGADIS 2.1 dense gas dispersion model environmental protection agency, EPA-450/4-89-019," 1989.
37. F. Pasquill, Atmospheric diffusion, 2nd ed., Halstead Press, 1974.
38. D. Golder, "Relations among stability parameters in the surface layer," *Boundary-Layer Met.,* pp. 3: 47–58, 1972.
39. R. E. Britter and J. McQuaid, "Workbook on the dispersion of dense gases," Health and Safety Executive, Sheffield, 1988.
40. R. Britter, "Atmospheric dispersion of dense gases," *Annual review of Fluid mechanics,* pp. 21: 317–344, 1989.
41. L.-H. Anay, "A review of large-scale LNG spills: Experiments and modeling," *Journal of Hazardous materials,* vol. A132, pp. 119–140, 2006.
42. R. Koopman and D. Ermak, "Lesson learned from LNG safety research," *Journal of Hazardous Materials,* pp. 140: 412–428, 2007.
43. T. Spicer and J. Havens, "Application of dispersion models to flammable cloud analyses," *Journal of Hazardous materials,* pp. 49: 115–124, 1996.
44. J. E. Simpson and R. E. Britter, "The dynamics of the head of a gravity current advancing over a horizontal surface," *Journal of Fluid Mechanics,* pp. 94: 477–495, 1979.
45. C. Chen and W. Rodi, "A review of experimental Data of vertical turbulent jets," Iowa Institute of Hydraulic Research, 1976.
46. J. Holland, "A meteorological survey of the Oak ridge area: final report covering the period 1858-1952.," Atomic Energy Comm, Report ORO-99, Washington DC, 1953.
47. C. Chen and W. Rodi, Vertical Turbulent buoyant jets, Oxford: Pergamon Press, 1980.
48. M. Epstein and H. Fauske, "Total Flammable mass and volume within a vapor cloud produced by a continuous fuel-gas or volatile liquid-fuel release," *Journal of Hazardous Materials,* pp. 147: 1037–1050, 2007.
49. D. Ermak, "Users Manual for SLAB: An atmospheric dispersion model fo denser-than-air releases, ACRL-MA-105607," Lawrence Livermore National Laboratory, 1980.
50. HGSYSTEM, "THE HEAVY GAS DISPERSION MODEL HEGADAS – Technical Reference Manual".
51. D. Webber, S. Jones, G. Tickle and T. Wren, "A model for a dispersing dense gas cloud and the computer implementation DRIFT I: Near instantaneous Release.","SRD Report SRD/HSE R586, 1982.
52. C. E. R. Consultants, "GASTAR Version 3," Cambridge, UK, 2002.
53. T. Spicer and J. Havens, "Field test validation of the DEGADIS model," *Journal of hazardous materials,* vol. 16, pp. 231–245, 1987.
54. R. Hankin, "Heavy Gas dispersion: integral models and shallow layer models," *Journal of hazardous materials,* pp. 203: 1–10, 2003.
55. R. Hankin and R. Britter, "TWODEE: the Health and Safety laboratory's Shallow layer model for heavy gas dispersion. Part 1. Mathematical Basis and Physical Assumptions," *Journal of hazardous Materials,* pp. 66: 211–226, 1999.
56. S. Ott and M. Nielsen, "Shallow layer modeling of dense clouds – Risoe-R-901," Risoe National Laboratory, Roskilde,, 1996.
57. A. Venetsanos, J. Bartzis, J. Wuertz and D. Papailiou, "DISPLAY-2: a two-dimensional shallow layer model for dense gas dispersion including complex features," *Journal of hazardous Materials,* pp. A99: 111–144, 2003.
58. J. S. Scire, D. G. Strimaitis and R. J. Yamartino, "A User's Guide for the CALPUFF Dispersion Model, V.5," Earth Tech. Inc., 2000.
59. N. van Egmond and H. Kesseboom, "Mesoscale air pollution dispersion modes – II Lagrangian Puff model and comparison with Eulerial grid model," *Atmospheric Environment,* pp. 17: 267–274, 1983.
60. F. Ludwig, L. Gasiorek and R. Ruff, "Simplification of a Gaussian puff model for real-time minicomputer use," *Atmospheric Environment,* pp. 11: 431–436, 1977.

61. R. Sykes, C. Cerasoli and D. Henn, "The representation of dynamic flow effects in a Lagrangian Puff dispersion model," *Journal of Hazardous Materials,* pp. A64: 223–247, 1999.
62. S. Chan, "FEM3C: An improved three-dimensional heavy-gas dispersion model: user's manual, UCRL-MA-116567 Rev.1," Lawrence Livermore National Laboratory, 1994.
63. M. Pontiggia, M. Derudi, V. Busini, and R. Rota, "Hazardous gas dispersion: A CFD model for atmospheric stability," *Journal of Hazardous Materials classes,* pp. 171: 739–747, 2009.
64. R. K. Calay, A. E. Holdo, "Modelling the dispersion of flashing jets using CFD," *Journal of Hazardous Materials,* pp. 154: 1198–1209, 2008.
65. H. Coward and G. Jones, "Limits of flammability of gases and vapors," U.S. Bureau of Mines, Bulletin 503, 1952.
66. M. Zabetakis, "Flammability characteristics of combustible gasses and vapors," U.S. Bureau of Mines, Bulletin 627, 1965.
67. G. Karim, I. Wierzba and S. Boon, "Some considerations of the lean flammability limits of mixtures involving hydrogen," *International Journal of Hydrogen Energy,* vol. 10, no. 1, pp. 117–123, 1985.
68. M. Molnarne, P. Mizsey and V. Schröder, "Flammability of gas mixtures. Part 2: influence of inert gases," *Journal of Hazardous Materials,* vol. 121, no. 1–3, pp. 45–49, 2005.
69. T. Ma, "A thermal theory for estimating the flammability limits of a mixture," *Fire Safety Journal,* vol. 46, pp. 558–567, 2011.
70. Center for Chemical Process Safety, Guidelines for vapor cloud explosion, pressure vessel burst, BLEVE and flash fire hazards, 2nd Ed., Hoboken, NJ: John Wiley & Sons, 2010.
71. M. Glor, "Ignition hazard due to static electricity in particulate processes," *Powder Technology,* Vols. 135–136, pp. 223–233, 2003.
72. I. Glassman, Combustion, 3rd Ed., San Diego, CA: Academic Press, 1996.
73. S. Turns, An introduction to combustion: concepts and applications, 3rd Ed., McGraw-Hill, 2012.
74. C. Law, Combustion Physics, Cambridge University Press, 2006.
75. W. Brasie and D. Simpson, "Guidelines for estimating damage explosion," in *63rd National AIChE Meeting*, New York, 1968.
76. W. Brasie, "The hazard potential of chemicals," *AIChE Loss Prevention,* vol. 10, pp. 135–140, 1976.
77. Health and Safety Executive, "Second report: advisory committee major hazards," U.K. Health and Safety Commission, 1979.
78. Health and Safety Executive, "The effect of explosions in the process industries," *Loss Prevention bulletin,* vol. 68, pp. 37–47, 1986.
79. Factory Mutual Research Corporation, "Guidelines for the estimation of property damage from outdoor vapor cloud explosions in chemical processing facilities," Technical Report, 1990.
80. R. Harris and M. Wickens, "Understanding vapor cloud explosions-an experimental study," in *55th Autumn meeting of the Institution of Gas Engineers*, Kensington, UK, 1989.
81. A. Van den Berg, "The multi-energy method-a framework for vapor cloud explosion blast prediction," *Journal of Hazardous Materials,* vol. 12, pp. 1–10, 1985.
82. A. Van den Berg, J. van Wingerden, J. Zeeuwen and H. Pasman, "Current research at TNO on vapor cloud explosion modeling," in *International Conference on Vapor Cloud Modeling*, Cambridge, MA, 1987.
83. W. Mercx and A. van den Berg, "Chapter 5. Vapour cloud explosions," in *Methods for the Calculation of Physical Effects due to Releases of Hazardous Materials (Liquids and Gases)- CPR 14E*, The Hague, 2005.
84. K. Kinsella, "A rapid assessment methodology for the prediction of vapour cloud explosion overpressure," in *International conference and exhibition on safety, health and loss prevention in the oil, chemical and process industries*, Singapore, 1993.
85. N. R. Popat, C. A. Catlin, B. J. Antzen, R. P. Lindstedt, G. H. Hjertager, T. Solberg, O. Saeter and A. C. van der Berg, "Investigations to improve and assess the accuracy of computational fluid dynamic based explosion models," *Journal of Hazardous Materials,* vol. 45, pp. 1–25, 1996.
86. C. Savvides, V. Tam, J. E. Os, H. O. R., K. van Wingerden and J. Renoult, "Dispersion of fuel in offshore modules: Comparison of prediction using FLACS and full-scale experiments," in *Major Hazards Offshore: Conference proceedings*, London, 2001.
87. S. Dharmavaram, S. R. Hanna and O. R. Hansen, "Consequence analysis-using a CFD model for industrial sites," *Process Safety Progress,* vol. 24, no. 4, pp. 316–327, 2005.
88. Buncefield Major Incident Investigation Board, "The Buncefield Incident 11 December 2005: The final report of the Major Incident Investigation Board," 2008.
89. S. G. Davis, P. Hinze, H. O. R. and K. van Wingerden, "Investigation techniques used to determine the massive vapor cloud explosion at the Buncefield fuel depot," in *International Symposium of Fire Investigation Science and Technology*, 2010.

Nicolas F. Ponchaut performs hazard and process safety analyses related to fires, explosions, chemical releases, and equipment failures. He has been involved in numerous analyses including hazard quantification of LNG spills, the dispersion of flammable vapor clouds, and of pollutants resulting from flaring operations, and the thermal behavior and failure of large battery packs.

Francesco Colella specializes in the area computational fluid-dynamics, heat transfer, and computational fire

modeling. His professional expertise encompasses fire safety evaluations for industrial plants and LNG terminals, as well as failure analysis of industrial equipment, consumer products, and battery packs. Dr. Colella is principal member of the NFPA 502 committee on tunnel fire protection and his expertise includes life safety evaluations for underground structures such as car parks and tunnels.

Kevin C. Marr specializes in engineering analysis of physical phenomena related to heat transfer, fluid mechanics, multi-phase flow, combustion, and fire science. Dr. Marr has conducted several origin and cause investigations of fires and explosions at residential, commercial and industrial facilities and has conducted process hazard analyses for combustible dust and chemical releases from industrial facilities.

Effects of Thermal Radiation on People: Predicting 1st and 2nd Degree Skin Burns

68

Christopher J. Wieczorek and Nicholas A. Dembsey

Introduction

The human body can not tolerate elevated temperatures for any long duration of time. Pain and damage to the skin, i.e., skin burns, begins to occur when the temperature at the basal layer exceeds 44 °C [1]. The amount of damage is a function of both the skin temperature and duration of time for which the temperature is elevated above 44 °C. Previous studies on the effects of thermal radiation on the skin have led to empirical models, graphical techniques, and simple algorithms to predict the temperature-time histories of the skin and the degree of damage due to a constant radiative exposure. All of the methods discussed in this chapter are limited to predicting ONLY 1st and superficial 2nd degree burns. For more severe burns engineering guidance is not currently possible due to the lack of reliable data. Although this chapter provides guidance on calculating the onset of pain from empirical studies it does not include any prediction of humane response to pain as it relates to fire safety decision.

C.J. Wieczorek (✉)
FM Global, Johnston, RI, USA

N.A. Dembsey
Fire Protection Engineering, Worcester Polytechnic Institute, Worcester, MA, USA

The Skin

The largest human organ is the skin. Skin represents approximately 15 % of the total weight of an average adult and has a surface area of 1.7 m^2 [2]. The skin serves in many different capacities that are essential to life. These include "(1) protection of underlying tissues from physical, chemical, and thermal trauma; (2) thermal regulation by sweating, heat conduction (insulation), and control of blood flow to a profuse plexus of minute surface vessels; (3) impermeability to both tissue fluids and environmental chemicals; and (4) sensory perception of touch, pain, and temperature."[2] As with the many functions which it serves the physiology of the skin is equally as complex.

For the purpose of this chapter it is not necessary to provide a full clinical definition of the skin. Understanding the complexity of the structure and functions of the skin is not required in order to predict and evaluate the severity of skin burns. It should be noted however that due to the complexity of the skin, simplified models and algorithms only provide an estimation of the skin damage.

A glossary of medical definitions can be found at the end of this chapter. An attempt has been made to define key terms within the body of the text to maintain a continuity of flow when reading.

The skin is composed of three primary layers: the epidermis, dermis (or corium), and hypodermis

M.J. Hurley (ed.), *SFPE Handbook of Fire Protection Engineering*,
DOI 10.1007/978-1-4939-2565-0_68, © Society of Fire Protection Engineers 2016

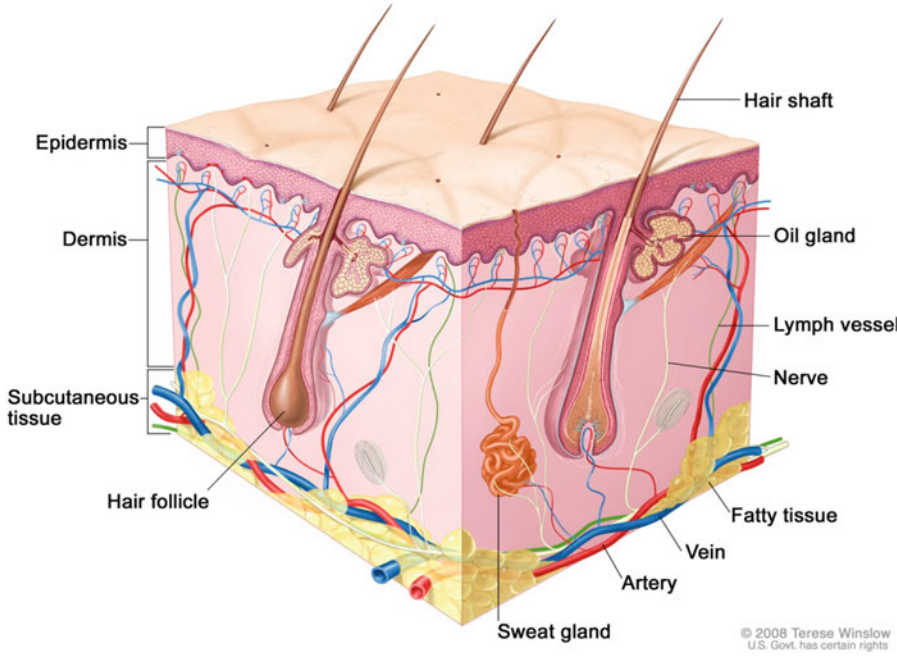

Fig. 68.1 The human skin. The skin is composed of three primary layers: the epidermis, the dermis, and hypodermis (subcutaneous fatty tissue)

stratum corneum stratum lucidum	stratum corneum
stratum granulosum	stratum granulosum
stratum germinativum	prickle layer
	basal layer

Fig. 68.2 Subdivisions of the epidermis

(or subcutaneous fatty tissue), Fig. 68.1 [3]. Each of these primary layers are further subdivided into other layers, all of which serve a different function.

The epidermis is divided into four layers. These layers are from top to bottom, the stratum corneum, stratum lucidum, stratum granulosum, and stratum germinativum [4, 5]. Other authors have defined the four primary layers as the stratum corneum, stratum granulosum, prickle layer, and basal layer [2]. Based on these definitions Fig. 68.2 was developed to illustrate the divisions of the epidermis from top to bottom.

Of these layers the stratum corneum is the only non-living layer of cells, the cells are considered dead or horny. The stratum lucidum and stratum granulosum are layers of cells "in transition between dead or dying squamous cells and the basal cells."[4] Also depending on the location either one or both of these layers may be absent [5].

The stratum germinativum or prickle layer is a "three-dimensional network of irregular interpapillary convolutions that afford a large surface area between the" epidermis and the dermis [2]. The basal cells form the lower layer of the stratum germinativum and are "arranged in a palisade-like manner over the dermis." [4] "Cells are generated in this layer and gradually extend toward the skin surface" forming the various layers of the epidermis as they begin and proceed to die [2].

The epidermis varies in thickness between 75 and 150 μm, except in the palms and soles where it varies between 0.4 and 0.6 mm [4]. It contains no blood vessels, lymphatic or connective tissue, and obtains all of its nourishment from the dermis[2]. The outermost layer, stratum corneum, of the epidermis contains approximately 10–20 % water, this percentage varies depending on whether or not the skin was dried, at which point it cracks,

or if it was soaked in water, resulting in wrinkling. The stratum germinativum contains approximately 70 % water and aids in the body's heat regulation [2, 5].

The dermis or corium is divided into two layers, the subepithelial or papillary layer and the reticular layer. The important feature of the dermis is the presence of the mastocyte cell. This type of cell contains large quantities of histamine and heparin. Histamine is defined as "a substance in the body found wherever tissues are damaged. Red flush of a burn is due to the local production of histamine; product of histidine catabolism." [6]

The dermis is approximately 1–4 mm thick. It contains the vascular, nervous, lymphatic and supporting structures of the skin. The dermis is approximately 10–30 % fibrous protein, most of which is collagen fibers. The remainder of the dermis is a complex of polysaccharide existing in the form of a viscoelastic gel. Along with enclosing the fibers in the dermis, it also contains proteins, electrolytes, tissue fluid and a mucinous material, which are all essential to the existence of the dermis [4].

> The papillary layer is a superficial layer of the corium, lying adjacent to the epidermis. It consists of numerous small, vascularized, and highly sensitive protuberances called papillae, which rise perpendicularly from its surface. The papillae are minute conical eminences with rounded or blunted extremities that are received into corresponding pits of the undersurface of the epidermis. Each papilla has many very small and closely interlaced bundles of finely fibrillated tissue, with a few elastic fibers and a single blood capillary loop.
>
> The blood supply to the skin accounts for nutritional supply, cellular and humoral defenses, and a major portion of the thermal regulatory function. The vasculature is highlighted by the presence of a rich network of branching arterial and venous arcades that are interconnected in a regular pattern. Small arteries entering the subcutaneous tissue form a system of long arterioles about 50 μm in diameter as the subdermal plexus. Adjacent links of the arteriolar system branch off to form the dermal plexus, which in turn forms a mesh of much finer arcuate capillaries, the subpapillary plexus. The capillaries combine into an even more complex venular mesh.
>
> An important and unique aspect of the skin circulation is the presence of a large number of direct shunts from arteries to veins, called arteriovenous (AV) anastomoses. Activation of these AV shunts enables nearly all blood flow to be diverted past the capillaries to increase the effective thermal insulation between the subcutaneous tissue and the environment. On the other hand, this complex and vast vascular bed can accept up to 20 % of the total cardiac output when the subpapillary plexus becomes engorged with blood. The small blood vessels of the skin have extensive sympathetic innervation and are highly responsive to neurogenic constrictor and dilator influences arising from various forms of local and systemic stress. This responsiveness is known to play an important role in the human thermoregulatory mechanism [2].

The dermis also contains hair follicles, located approximately 2 mm below the skin surface [7]. "Hair follicles play an important role in the re-growth of skin after severe burns because they are lined with epithelial cells which act as growth points. If the skin burn depth is greater than the follicle depth then re-growth is slow or even impossible." [7]

"The subcutaneous tissue below the skin consists of fat followed by muscle. Bundles of fat are bound together by collagen fibrils. It is not necessary to have muscle below the fat in all skin sites. Only in special parts of the body does subcutaneous muscle exist, e.g., in face and neck etc. The thickness of subcutaneous fat is of great importance in maintaining body temperature. Although this fat is not part of the skin proper, it exerts a great influence on the conductance of the body surface. The thickness of fat varies from virtually zero in some areas to 1.5–2.0 cm in others, the thigh being the fattest." [4] "Individual and anatomical differences in this fat deposition are very large and can play a major role in determining the degree of injury for a severe thermal insult." [2]

Human Variability

Sensation of Pain

The sensation of pain is believed to be a function of pain receptors, which are free nerve endings located throughout the body [8]. The number of pain receptors varies from one location to

Table 68.1 Number of pain receptors per square centimeter at various locations on the human body [8]

Location	Number of skin receptors for pain per cm^2
Tip of nose	44
Sole of foot	48
Ball of thumb	60
Scalp	144
Eyelid	172
Buttocks	180
Forehead	184
Back of hand	188
Inside forearm	203
Shoulder blade	212
Bend of elbow	224
Neck region	228
Back of knee	232

another. The number of receptors per centimeter squared, listed in Table 68.1, causes different parts of the body to be more or less sensitive to pain.

From Table 68.1 it can be seen that the least sensitive locations are the tip of the nose and the sole of the foot; while the back of the knee, neck region, and bend of the elbow, all contain more than 220 pain receptors per centimeter squared making them the more sensitive areas. The inside of the forearm contains 203 pain receptors per centimeter squared. Many of the initial studies performed to determine pain from thermal radiation consisted of exposing the forearm to the thermal source [9]. Therefore, the experimental time to pain values can be considered conservative when compared to most other locations on the body.

Along with the physical aspect of pain, the sensation of pain is also psychological. "...much depends on a person's attitudes, previous experiences, and culture. For example, athletes often report not feeling the pain of an injury until after the competition has ended. Some cultures are more stoical about pain and teach individuals to endure individual suffering; in Western cultures, there is the widespread illusion that pain and suffering are ennobling. Also, boys and girls within Western cultures are often taught to respond differently to pain."[8]

Table 68.2 Skin temperature at various locations on the body

Region	Surface area m^2 [10]	Temperature °C [11]	Temperature °C [10]
Head/ forehead	0.20	34.7	33.4
Chest/ thorax	0.17	34.7	32.8
Abdomen	0.12	34.7	34.2
Back	0.23	34.7	–
Buttocks	0.18	34.7	–
Thighs/ clavicle	0.33	33.0	33.6
Calves	0.20	30.8	33.2
Feet	0.12	28.6	–
Arms	0.10	33.0	32.8
Forearms	0.08	30.8	–
Hands	0.07	28.6	–
Sole of feet	–	–	30.2
Palm	–	–	32.8
Lumbar area	–	–	33.3
Knee	–	–	32.5
Toe	–	–	31.0

Information was not provided within the reference

Initial Skin Temperature

The initial skin temperature of individuals varies significantly. Factors affecting the skin temperature include age, sex, personal habits, i.e., smoking versus non-smoking, occupation, physical activity, and even pregnancy. In addition to variations between individuals, the skin temperature at different locations on the body varies as well. Millington and Wilkinson state "measurement of skin temperature reveals significant differences between one part of the body surface and another." [10]

The skin temperatures for various locations on the body are shown in Table 68.2 [10, 11]. The skin temperature across the body varies between 28.6 °C and 34.7 °C. The data from both sources were taken with subjects at rest. The ambient temperature for one study[10] was provided as 23 °C, no ambient temperature was given for the other study.

The ambient temperature has two different effects on the skin temperature. First, "At ambient temperatures between 10 °C and 20 °C the range and distribution of skin temperatures are

Table 68.3 Seasonal effects including the ambient temperature (T_{amb}) and relative humidity (R.H.) on the skin temperature (T_{skin}) [12, 13]

Gender	N	Age	T_{amb} (°C)	R.H. (%)	Month	Number of sites	T_{skin} (°C)	Ref.
Male/female	18	19–55	21.6	57.4	October	1	31.8 ± 1.7	[12]
Male/female	23	–	15.1	35.1	January	1	29.1 ± 2.8	[12]
Male/female	23	–	19.9	65.4	April	1	31.8 ± 1.5	[12]
Male/female	23	–	27.5	70.5	July	1	33.0 ± 1.3	[12]
Male	6	10–12	45.0	20	–	10	36.8 ± 0.2	[13]
Male	5	10–12	45.0	20	–	10	37.0 ± 0.3	[13]

n = number of test subjects

Information was not provided within the reference

Table 68.4 Skin temperature, T_{skin}, taken at the volar and dorsal side of the index finger of employees in seven different occupations [14]

Gender	n	Age	T_{amb}[a] (°C)	R.H.[a] (%)	Occupation	Location	T_{skin} (°C)
Male	16	18–57	20	50	Fish processing	Volar	17.3 ± 2.4
Female	127					Dorsal	16.7 ± 2.1
Male	1	21–67	23	34	Cleaners	Volar	28.6 ± 3.7
Female	29					Dorsal	29.0 ± 3.7
Male	36	20–58	23	26	Metal workers	Volar	32.6 ± 2.2
Female	16					Dorsal	32.7 ± 1.9
Male	2	21–41	22	48	Gut cleaners	Volar	29.8 ± 2.4
Female	23					Dorsal	30.0 ± 2.1
Male	0	24–58	23	34	Nurses	Volar	25.6 ± 2.9
Female	16					Dorsal	27.4 ± 2.3
Male	14	19–55	23	26	Office workers	Volar	32.7 ± 1.9
Female	6					Dorsal	32.9 ± 1.4
Male	7	20–55	23	34	Controls	Volar	29.5 ± 3.2
Female	22					Dorsal	30.6 ± 2.7

n = number of test subjects

[a]T_{amb} and R.H. are the ambient temperature and relative humidity respectively during the test

more variable (±10 °C) than they are in a warmer environment. At about 32 °C, a thermally neutral condition, both adults and infants have an overall temperature range of only 4 °C."[10] In addition to affecting the range of skin temperatures, the ambient temperature also affects the mean skin temperature as well. Studies have been performed to determine the effect of seasonal temperature changes and elevated ambient temperatures on the skin temperature for subjects during rest. The results from these studies are shown in Table 68.3 [12, 13].

Another study indicated that an individual's occupation also affects the skin temperature. A study of employees in seven different occupations was performed; skin temperature measurements were made at two locations, the volar and dorsal side, of the index finger [14]. The results from the study are shown in Table 68.4.

Employees in the fish processing industry had the lowest skin temperatures, on average 17 °C, while office workers and metal workers had the highest skin temperatures of approximately 32.7 °C. The temperature measurements in the study were performed on the index finger of the test subjects, this was shown previously, Table 68.2, to be the location at which the lowest skin temperatures on the body were measured. Also, a skin temperature of 17 °C is on the verge of the threshold of pain, which is listed as 16 °C in;

Table 68.9 therefore, it is believed that the skin temperatures at other locations of the body were higher than those reported for the tip of the finger.

A person's personal habits and health also affect the initial skin temperature. Studies have shown that a person who smokes or chews nicotine gum will have an increase in skin temperature of 0.62 °C [15]. Also, women who are pregnant have an increase in skin temperature of 2 °C above their normal skin temperature.

Skin Thickness

Determining skin thickness accurately is difficult since it is difficult to define clear boundaries between the different layers. Various techniques have been developed in an attempt to provide the best values. "While there are no great changes in skin thickness demonstrated by these methods, it is possible to show that the thickness of male and female skin, when young, is significantly different, but because the natural scatter of the data increases with age, it is doubtful whether the differences above the age of 65 years are real. Indeed, large variability in the measurement of skin thickness has been a feature in older people."[10] Differences in the forearm skin thickness among males and females of various ages are shown in Table 68.5.

As can be seen from Table 68.5 there is a significant difference between the skin thickness of males and females between the ages of 24 and 37, the male forearm skin is approximately 25 % thicker than the female's. The variation for all individuals below the age of 65 decreases to a difference of only 3 %, while the difference between males and females above the age of 65 is approximately 10 %.

The depth of the basal layer, which is the lowest layer of the epidermis, is critical in determining superficial 2nd degree burns. The reference state of the skin assumes that the basal layer is located at a depth of 80 μm. Millington and Wilkinson state however: "The measurement of epidermal thickness presents further difficulties, since the dermal papillae and rete ridges give an undulating lower surface."[10] They further state that: "It is now well established, however, that epidermal thickness varies considerably over the whole body surface and variation at comparable sites between individuals is also high."[10] The mean values for full epidermal thickness at 13 different sites of the body are shown in Table 68.6.[10]

As can be seen in Table 68.6, only three sites, the palm, fingertip, and back of hand have an epidermal thickness greater than 80 μm. The surface area encompassed by these three locations is only 3.5 % of the total skin surface area.

Table 68.5 Forearm skin thickness for four different age groups measured using different measurement techniques

Sex of subjects	Age group	Type of measure	Range (mm)	Average thickness (mm)	Mean value (mm)
Male	Under 65	X-ray	1.0–1.7	1.3	1.3
	Under 65	X-ray	1.1–1.8	1.43	
	24–37	X-ray	0.9–1.19	1.1	
	24–37	Ultrasound	1.0–1.16	1.12	
Female	Under 65	X-ray	0.9–1.4	1.1	1.26
	Under 65	X-ray	1.0–1.7	1.34	
	28–37	X-ray	0.82–0.95	0.88	
	28–37	Ultrasound	0.75–0.92	0.83	
Male	Over 65	X-ray	0.7–1.2	0.9	1.1
		X-ray		1.19	
Female	Over 65	X-ray	0.6–1.2	0.9	1.0
		X-ray		1.06	

The range of skin thickness and average for each study are listed along with the mean value of all studies in each group [10]

Table 68.6 Mean values for full epidermal thickness at thirteen different locations on the body [10]

Body site	Mean thickness (μm)
Palm	429.0
Fingertip	369.0
Back of hand	84.5
Forearm	60.9
Upper arm	43.9
Thoracic region	37.6
Abdomen	46.6
Upper back	43.4
Lower back	43.2
Thigh	54.3
Calf	74.9
Forehead	50.3
Cheek	38.8

The remaining 96.5 % of the body has a mean epidermal thickness of less than 80 μm. The values listed in Table 68.6 are mean values; at some locations the variations among different individuals can be significant. For example the epidermal thickness of the abdomen and thorax have been published to vary between 16 and 50 μm.[10]

Skin Burns

Thermal damage to the skin has been evaluated over the years in a number of ways. The most common scheme for evaluating thermal injury is ranking the burns as 1st, 2nd, or 3rd degree. Other methods include classifying the burns as partial or full thickness burns or using the University of Rochester's grading system.

The traditional ranking system of 1st, 2nd, or 3rd degree burns is dependent on the level of necrosis and the depth of damage. First-degree burns are superficial burns. Only the epidermis is affected. The skin is typically red and painful and does not blister. The epidermis often flakes off in the subsequent days or weeks [16]. Severe sunburns are the most common form of 1st degree burns [16].

A second-degree burn is indicative of complete necrosis of the epidermis. If no damage to the dermis occurs it is considered a superficial 2nd degree burn. Visually the skin is blistered, a moist bright pink-red mottled coloration and very painful [4]. If minor damage to the dermis has occurred it is considered a deep 2nd degree burn. The skin is blistered and is a very pale white or mottled color under the blisters [16].

A third-degree burn is complete necrosis of the dermis, extending and possibly including the subcutaneous fat. ASTM C 1055 defines complete or significant necrosis of the dermis as 75 % destruction of the dermis [17]. Other considerations include cell destruction below the depth of the hair follicles, approximately 2 mm [7]. With third-degree burns the skin rarely blisters [16]. The skin is dry, gray and charred and may feel leathery [7, 18]. Usually there is no feeling and no possibility for natural skin regeneration.

Additional levels of burns include 4th, 5th, and 6th degree burns. "Fourth-degree burns require skin grafts. Fifth- and sixth-degree burns involve destruction of muscle and/or bones, respectively." [19]

The criticism behind the traditional ranking system includes the lack of correlation between the initial surface appearance and the depth of injury. The depth of injury is the most reliable measure of burn severity [18]. "Short duration contact with a very hot object can cause immediate necrosis in the outer layers of the epidermis, giving the appearance of a third-degree burn without the injury penetrating to the underlying dermis. In contrast, longer-duration exposures to lower temperatures can cause a burn through the dermis without any immediate apparent surface necrosis."[18]

Based on this information a second classification of burns was developed and originally described by Zawacki [18] This method uses two categories of burns, partial thickness and full thickness. "A partial-thickness burn occurs when cell necrosis has proceeded part way through the dermis. A full-thickness burn occurs when the cells have been destroyed through the depth of the dermis. Under this categorization, a first degree burn is considered below the burn threshold, while a minimum severity partial-thickness burn occurs when the heat transfer is sufficient to

destroy cells at the base of the epidermis."[18] Other authors use the terms deep dermal and full thickness burns interchangeably [7].

The University of Rochester developed a classification system in which burns were evaluated as 0, 1°, 2°, 3°, 4° and 5° [20]. These grades corresponded to the following visual appearances:

0. No burn visible
1. Erythematous burn
2. Patchy white burn
3. Uniform white burn
4. Blebbed white burn
5. Carbonized burn

"Each of the five major categories of burn severity was divided into mild, moderate, and severe, giving 16° of damage."[20]

Knox [21] later modified the grading system developed at the University of Rochester. This method not only uses burn depth, but also cellular change with or without acidophilism present to classify burn damage. Table 68.7 provides the grade, description and approximate depth of burn.

"A grade of zero was given to all tissue sections showing no thermal damage. Burned tissue was categorized into epidermal, transepidermal, dermal, and adipose. Epidermal burns were subclassified as to whether cellular change without acidophilism was present (grade 1), whether acidophilism was present involving only partial depth of the epidermis (grade 2), or all the epidermal depth (grade 3). Transepidermal burns (those showing separation between the epidermis and the dermis) were subcategorized as to whether the separation was focal (grade 4) or complete (grade 5). Dermal burns were classified as to whether the damage was superficial, mid, deep, or complete (grades 6, 7, 8, and 9 respectively). Grade 10 was assigned to burns extending beyond the dermis into the adipose tissue."[21]

Table 68.8 compares the various burn classifications. No one method has been shown

Table 68.7 University of Rochester burn depth grading system [21]

Grade	Description	Depth (μ)
0	No thermal damage	0
1	Cell damage without acidophilism	1–20
2	Partial epidermal acidophilism	20–50
3	Complete epidermal acidophilism	50–100
4	Partial dermal–epidermal separation	100–150
5	Complete dermal–epidermal separation	150–250
6	Superficial dermal	250–500
7	Mid dermal	500–1000
8	Deep dermal	1000–1500
9	Complete dermal to adipose border	1500–2000
10	Adipose	>2000

Table 68.8 Comparison of skin burn classifications

General	Reed [18]	Lawton [7]	Knox [21]
1st degree	Below threshold	Superficial	1 – Cell damage without acidophilism
			2 – Partial epidermal acidophilism
			3 – Complete epidermal acidophilism
2nd degree	Partial thickness	Partial thickness	4 – Partial dermal–epidermal separation
			5 – Complete dermal–epidermal separation
3rd degree	Full thickness	Deep dermal	6 – Superficial dermal
			7 – Mid dermal
			8 – Deep dermal
			9 – Complete dermal to adipose border
			10 – Adipose

to be substantially better than the others. For the purpose of this chapter the traditional classification of 1st, 2nd, and 3rd degree burns, as defined above, will be used.

Burn Statistics and Clinical Treatment Time

There is an estimated 1.25 million burn injuries per year (1992) in the United States alone [22]. These injuries are due to a number of sources including fire and flame, motor vehicle accidents, electricity, lightning, aircraft crashes and other fire and burn injuries [22]. The percentage of burns caused by radiation hazards is not known. A recent study of 6417 burn injuries between 1991 and 1993 indicated that only 10 were directly attributed to radiation; other sources included flames, scalding, contact, chemical, electrical, and other [23]. Treatment is largely a function of burn depth, while patient survivability is primarily a function of the location and amount of skin area damaged and age; secondary effects such as preexisting health conditions (cardiac, liver, or lung disease), obesity, alcohol abuse, and any number of burn effects such as shock, pulmonary edema, and infection are also important variables which effect a patients survivability [16, 23, 19, 24]. It has been shown [24] that withholding any secondary effects, the survivability of a patient is only a function of age and percent of the body area burned, younger individuals can survive a much larger burn area than older individuals. A study on the probability of survival indicated that for individuals between the ages of 0 and 19 there was a 90 % probability of surviving burns covering up to 42 % of their body, while for the same burn area the probability of individuals older than 65 surviving was only 10 % and there was no chance of survival for individuals older than 70 [24].

Treatment of patients is dependent on the degree of thermal injury. First-degree may not even require medical treatment. Medical treatment for superficial 2nd degree burns will be minimal, while severe 2nd degree burns and 3rd degree burns will require extended hospital time and autograft surgery [9].

Other very important considerations include the emotional and psychological impacts from burn injuries. 'The impact of a severe facial burn, especially with noticeable scarring, is hard to overestimate. The majority of patients report anxiety, depression, and withdrawal that may be life-long. Patients with severe facial burns are rarely noticed in public, because many avoid all outside contact except with family members. Even the arts and literature portray persons with facial burns as emotionally scarred or sinister (c.f. *Phantom of the Opera*, *Nightmare on Elm Street*, *Darkman*, *Man Without a Face*.) Few of us can comprehend the difficulty of re-integrating into society with cosmetically unacceptable facial scars.' [25]

Prediction of Skin Burns

The essential elements for injury are "exposure to heat, and elevation of the skin temperature to an injurious level for a sufficient time to produce damage."[5] Over the years a large database of irradiance verses exposure time for varying degrees of injury has been compiled. These data are essential in evaluating the risk of human injury due to radiation hazards. In conjunction with these data empirical equations, graphical methods, simple algorithms, and finite element models have been developed to predict the degree of human injury. Of these the latter is the only method which will not be discussed in detail, as it is beyond the scope of this chapter.

The normal human skin temperature is 32.5 °C [1, 26]. Damage to the skin increases logarithmically with a linear increase in skin temperature [1]. As the temperature of the skin is elevated, an individual begins to experience different sensations and physical damage to the skin occurs. Skin injury begins when the skin temperature is greater than 44 °C. The amount of damage is a function of the skin temperature and the period of time for which the temperature is greater than 44 °C, at a tissue temperature of approximately 72 °C the skin is

Table 68.9 Thermal sensations and other effects at various temperatures [5]

Sensation	Skin color	Tissue temperature °C	Tissue temperature °F	Process	Injury
Numbness	White			Protein coagulation	Irreversible
	Mottled red and white	72	162	Thermal inactivation of tissue constituents	Possibly reversible
		68			
		64			Reversible
Maximum pain Severe pain Threshold pain	Bright red Light red	60	140		
		56			
		52			
		48			
Hot	Flushed	44	111	Normal metabolism	None
		40			
Warm		36			
Neutral	Flesh	32			
		28	82		
Cool Cold	Blanched red	24			
		20			
Threshold Pain	Bluish red	16		Physicochemical inactivation of tissue constituents	Reversible
Severe Pain	Reddish purple	12			Possibly reversible
	Bright pink	8			
		4			
Numbness	White	0	32	Protein coagulation	Irreversible
		−4	25		

destroyed virtually instantaneously [1]. The initial skin temperature is also a factor; even a 1 °C difference can produce significantly different results [26]. Table 68.9 indicates the various stages of thermal sensations and associated effects at different skin temperatures [5].

The recommended property values define the reference state for the skin and are shown in Table 68.10. The effects of changes in initial skin temperature, T_0, epidermal thickness, x_b, and pain receptor depth, x_p, due to human variation will be discussed below. Methods used to predict pain and superficial 2nd degree burns are presented here and are calibrated for a constant incident thermal radiative exposure against experimental data using a set of recommended properties for the skin.

Thermal damage to the skin can occur via conduction, convection or radiation. Only skin damage due to radiation will be addressed within this chapter. Unless otherwise noted all of the methods discussed assume the following parameters for the skin and source of thermal radiation. The thermal insult is a *constant infrared* source over the exposure time. The skin is opaque to infrared radiation and has an initial skin temperature of 32.5 °C.

As indicated in Table 68.9, the first substantial sensation experienced, as the skin temperature is elevated, is pain. Pain receptors are located at an approximate skin depth of 0.1 mm [26]. Threshold pain is felt by human beings when the average temperature at the pain receptor depth is increased to about 45 °C [27].

Prediction of Skin Burns: Simple Algorithms

Two models for predicting the thermal damage to the skin due to radiation have been developed. They are the damage integral model and the "critical energy model." For both of these models it is required to know the temperature-time history of the skin. Four algorithms have been

Table 68.10 Reference state properties for the skin

Property	Symbol	Value	Units
Thermal conductivity (heating)	k_h	0.5878	W/m-K
Thermal conductivity (cooling)	k_c	0.4518	W/m-K
Volumetric heat capacity	ρc	4,186,800	J/m^3-K
Activation energy (44 °C ≤ T ≤ 50 °C)	ΔE	7.78×10^8	J/kmol
Activation energy (T > 50 °C)	ΔE	3.27×10^8	J/kmol
Pre-exponential (44 °C ≤ T ≤ 50 °C)	P	2.185×10^{124}	1/s
Pre-exponential (T > 50 °C)	P	1.823×10^{51}	1/s
Epidermal thickness (Bayer layer depth)	x_b	80	μm
Pain receptor depth	x_p	100	μm
Initial skin temperature	T_0	32.5	°C

developed to model skin temperature over time, based on a square-wave pulse of radiant energy.

Each of these models assumes that the skin is a single layer, opaque semi-infinite solid. The complexities of the skin, i.e., its layered non-homogenous structure, blood perfusion, sweating, etc. are all ignored. The incident radiant flux to the skin surface is assumed equal to the net flux absorbed by the skin. This is a reasonable assumption considering the simplified view of the skin, the skin absorptivity, and the skin surface cooling. The skin absorptivity can be taken to be between 0.94 [28] and 0.99 [11] for infrared incident radiation. Based on a skin temperature of 72 °C and a convection heat transfer coefficient of 0.025 kW/m^2 K, the convective and radiative cooling at the skin surface is at maximum 1.3 and 0.80 kW/m^2 respectively. The skin is assumed to be exposed to a constant heat flux for an exposure time τ, after which the flux is removed.

Equation 68.1 is used to predict the temperature profile at depth x below the skin surface [27]. Equation 68.1 can only be used to predict the time to pain. Only the heating period of the skin is considered, the cooling period is not taken into account.

$$T = T_0 + \frac{\dot{q}''}{k}\left[\frac{2\sqrt{\alpha t}}{\sqrt{\pi}}\exp\left(-\frac{x^2}{2\alpha t}\right) - x\,erfc\left(\frac{x}{2\sqrt{\alpha t}}\right)\right] \tag{68.1}$$

At the surface of the skin Equation 68.1 reduces to:[27]

$$T_s = T_0 + \frac{2\dot{q}''\sqrt{t}}{\sqrt{\pi k \rho c}} \tag{68.2}$$

Where:

$\dot{q}''$ = incident thermal radiation (W/m^2)
t = time (sec)
x = depth below the surface of the skin (m)
T = temperature at time t, and distance x below the skin surface (K)
T_0 = initial skin temperature (K)
T_S = temperature of the skin surface (K)
α = k/ρc = thermal diffusivity (m^2/s)
c = specific heat (J/kg-K)
k = thermal conductivity (W/m-K)
ρ = density (kg/m^3)

Damage to skin occurs whenever the skin temperature is above 44 °C, therefore it is important to include the relaxation or cooling period. At low irradiances as much as 10 % of the thermal damage occurs during the cooling period, at higher irradiances the damage during cooling can be as much as 35 % [29]. "This accounts for the well-known prevention of a blister by prompt application of ice to an exposed area. If this is done soon enough, a third of the injury can be eliminated. "[29] Three algorithms were developed which include relaxation or cooling of the skin. The first is shown as Equation 68.3 [30].

$$T = T_0 + \frac{2\dot{q}''}{\sqrt{k\rho c}}\left[\sqrt{\tau}\ ierfc\left(\frac{x}{2\sqrt{\alpha t}}\right) - \sqrt{t-\tau}\ ierfc\left(\frac{x}{2\sqrt{\alpha(t-\tau)}}\right) S(t)\right] \quad (68.3)$$

Where:
$\dot{q}''$ = incident thermal radiation (W/m^2)
t = time (sec)
x = depth below the surface of the skin (m)
S(t) = step function where S(t) = 0 if t < τ and S(t) = 1 if t ≥ τ
T = temperature at time t, and distance x below the skin surface (K)
T_0 = initial temperature (K)
α = k/ρc = thermal diffusivity (m^2/s)
k = thermal conductivity (W/m-K)
ρc = volumetric heat capacity (J/m^3-K)
τ = exposure time (sec)

The second is shown as Equation 68.4 [28].

$$T = T_0 + \frac{\dot{q}''}{k}\left[\frac{2\sqrt{\alpha t}}{\sqrt{\pi}}\exp\left(-\frac{x^2}{4\alpha t}\right) - x\left(1 - erf\left(\frac{x}{2\sqrt{\alpha t}}\right)\right)\right] - \frac{\dot{q}''}{k}\left[\frac{2\sqrt{\alpha(t-\tau)}}{\sqrt{\pi}}\exp\left(-\frac{x^2}{4\alpha(t-\tau)}\right) - x\left(1 - erf\left(\frac{x}{2\sqrt{\alpha(t-\tau)}}\right)\right)\right] \quad (68.4)$$

Where:
$\dot{q}''$ = incident thermal radiation (W/m^2)
t = time (sec)
x = depth below surface (m)
T = temperature at time t, and distance x below the skin surface (K)
T_o = initial skin temperature (K)
α = k/ρc = thermal diffusivity (m^2/s)
c = specific heat (J/kg-K)
k = thermal conductivity (W/m-K)
ρ = density (kg/m^3)
τ = exposure time (sec)

"Assuming constant heat flow and initial isothermal conditions, Equation 68.4 has two parts: First during the heating phase t ≤ τ the first two terms are real and the third term is imaginary. Second during the cooling phase t > τ all three terms are real. As time approaches infinity T approaches T_o. The third term is a Laplace solution for a negative $\dot{q}''$ input in the interval τ < t ≤ infinity so that the effective heat input is zero." [28]

Equations 68.3 and 68.4 are equivalent. Using the following relationships between the error function (erf), complimentary error function (erfc) and the integral of the complimentary error function (ierfc), Equation 68.3 can be transformed into Equation 68.4. Similarly, Equation 68.1 is equivalent to the first two terms of Equation 68.4 if similar substitutions are made.

$$\begin{aligned} &\text{erfc}\ \beta = 1 - \text{erf}\ \beta \\ &\text{and} \\ &\text{ierfc}\ \beta = \frac{1}{\sqrt{\pi}}e^{-\beta^2} - \beta\ \text{erfc}\ \beta \end{aligned} \quad (68.5)$$

The final algorithm, Equation 68.6, developed to model the temperature-time history of the skin assumes that the temperature profile in the semi-infinite slab is linear with a slope equal to the slope of the actual temperature profile at the surface [27]. Also, the model only predicts the temperature at the skin surface and not at a depth below the surface.

$$T(t_2) = T_0 + [T(t_1) - T_0]\sqrt{\frac{t_1}{t_2}} + \frac{\left[\dot{q}''(t_2) + \dot{q}''(t_1)\right](t_2 - t_1)}{2\sqrt{k\rho c\, t_2/\pi}} \quad (68.6)$$

Where:
$\dot{q}''(t_2)$ = incident thermal radiation at the current time step (W/m^2)
$\dot{q}''(t_1)$ = incident thermal radiation at the previous time step (kW/m^2)
t_1 = previous time (sec)

t_2 = current time (sec)
$T(t_1)$ = surface temperature at previous time step (K)
$T(t_2)$ = surface temperature at current time step (K)
T_o = initial skin temperature (K)
α = thermal diffusivity (m^2/s)
c = specific heat of skin (J/kg-K)
k = thermal conductivity of the skin (W/m-K)
ρ = density of skin (kg/m^3)

Thermal properties for the skin are required to solve the algorithms. Values for skin properties, although similar, vary from source to source. Table 68.10 contains the recommended values for the required properties.

The thermal conductivity was found to vary with temperature and whether or not the skin is being heated or cooled. It was determined that a constant value for the thermal conductivity during heating provided satisfactory results as compared to experimental data. During the cooling period however, the same constant value did not provide a satisfactory representation. To achieve a good fit to the experimental data, the thermal conductivity during cooling was stepped down by increments of -4.186×10^{-6} W/m-K at each time step [28]. For the purpose of this chapter it was determined that taking an average of these values provided an acceptable fit to the data. Figure 68.3 shows the experimental temperature-time history at a skin depth of 80 μm, the basal layer, for a heat flux of 15.7 kW/m^2 and an exposure time of 5.55 s. Superficial second-degree burns are obtained under these conditions. Also included in Fig. 68.3 are the histories predicted by Equations 68.4 and 68.6. The values indicated in Table 68.10 were used for the thermal properties of the skin, constant values for the thermal conductivity of 0.5878 and 0.4518 W/m-K were used for the heating and cooling phases respectively (Fig. 68.3).

An excellent correlation, for the basal layer temperature, between the experimental and theoretical values predicted by Equation 68.4 can be seen. Due to the level of agreement between Equation 68.4 and the experimental data at the basal layer, Equation 68.4 was used to predict the temperature of the skin at the skin surface.

The values predicted by Equation 68.6 are at a maximum 40 % greater than the surface temperatures predicted using Equation 68.4. The peak surface temperature is 74.4 °C. Instantaneous death to the skin occurs at a basal layer

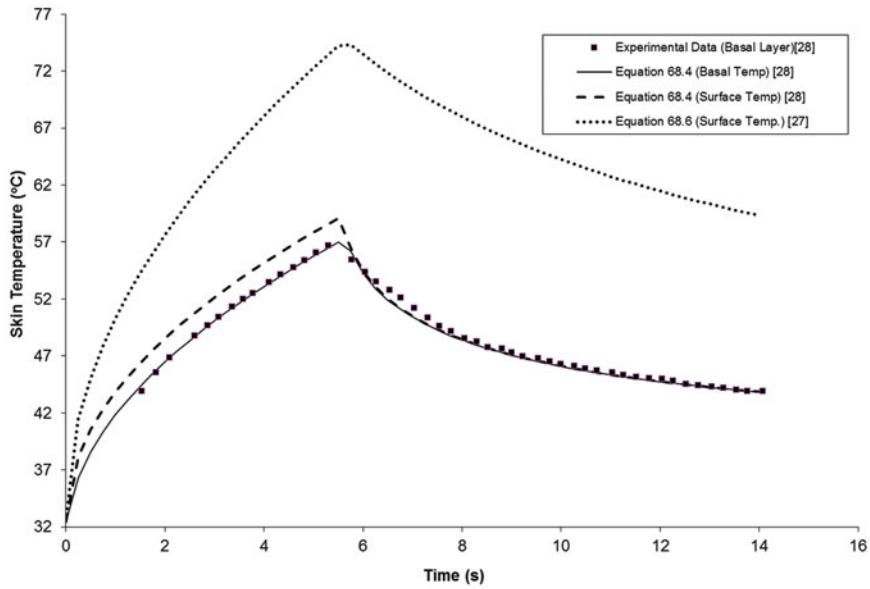

Fig. 68.3 Temperature-time history for the skin at the surface and basal layer caused by a thermal irradiance of 15.7 kW/m^2 for a duration of 5.55 s

temperature of 72 °C [1]. A surface temperature peak of 74.4 °C will produce burns significantly greater than superficial second-degree. It is not recommended that Equation 68.6 be used to model the skin temperature.

The rate at which epidermal injury occurs can be "modeled as a rate process governed by an activation energy and pre-exponential constant:", [31, 32]

$$\frac{d\Omega}{dt} = P \exp\left(\frac{-\Delta E}{RT}\right) \tag{68.7}$$

Where:

dΩ/dt = rate at which Ω, an arbitrary function of the epidermal injury as determined by histologic examination, is produced

T = basal epidermal layer temperature (K)

R = universal gas constant (8314 J/kmol-K)

P = pre-exponential term determined from experimental data (1/s)

ΔE = activation energy determined from experimental data (J/kmol)

By integrating Equation 68.7,

$$\Omega = \int_0^t P \exp\left(\frac{-\Delta E}{RT}\right) dt \tag{68.8}$$

the cumulative damage to the skin is determined. The severity of the burn injury is determined based on the quantitative values of the injury parameter Ω shown in Table 68.11.

The pre-exponential term and activation energy were originally determined to be 3.1×10^{98} 1/s and 6.28×10^{8} J/kmol respectively [32]. Later, application of the damage integral to include the cooling period lead to new values for these terms [28, 31]. Also, new numerical methods and techniques lead to more accurate curve fits to the original data providing even further revision to the terms [31]. Table 68.12 contains the various values for the pre-exponential and activation energy and the temperature range for which each is appropriate.

Table 68.11 Injury parameter values [31]

Injury parameter (Ω) value	Level of injury
0.53	First degree burn
1.0	Superficial second-degree burn

The values listed in Table 68.12 for the activation energy and the pre-exponential constant vary by several orders of magnitude between the different models. These variations are attributed to the numerical methods used to determine the values from the original experimental data. A recent study indicated that the values determined by Henriques could not be duplicated [31]. It was also indicated that use of these models "outside of the range of times and temperatures for which the model coefficients are verified by correlation with experimental data are likely to issue in injury values of questionable value."[31]

Table 68.13 lists the values predicted by each set of parameters for first (Ω = 0.53) and superficial second-degree (Ω = 1) burns. For each of the thermal irradiances indicated the temperature-time histories at the basal layer were determined using Equation 68.4. The exposure time was varied until the desired values for Ω were achieved.

It can be seen that at the lower fluxes, less than 20 kW/m^2, predictions by Weaver and Stoll are lower than those by the other models for both 1st and superficial 2nd degree burns. At the higher fluxes all of the models predict approximately the same time to injury. These predictions are compared to the pain and superficial 2nd degree burn data which will be presented later, see Figs. 68.4 and 68.5. Although a first-degree burn is not equivalent to pain, as a consistency check, the predictions are included with the pain data, see Fig. 68.4. As can be seen, all of the model's predicted times to 1st degree injury are above that of time to pain. The time to pain (time at which the basal layer temperature reaches 44 °C) based on Equation 68.1 is also included in Fig. 68.4; the Equation 68.1 predictions fall between Equation 68.9 values and the Equation 68.11 (safety factor of 4) values. Finally, the predicted time to superficial 2nd degree injury lies in good agreement with the experimental data shown in Fig. 68.5.

Safety factors need to be incorporated into Equations 68.1, 68.4 and 68.8, for predicting

Table 68.12 Activation energy and frequency factors for different models [4, 31, 35]

Model	Temperature range °C	Activation energy, ΔE J/kmol	Pre-exponential, P 1/s
Weaver & Stoll	$44 \leq T \leq 50$	7.72×10^8	2.185×10^{124}
	$T > 50$	3.25×10^8	1.823×10^{51}
Fugitt	$44 \leq T \leq 55$	6.27×10^8	3.1×10^{98}
	$T > 55$	2.96×10^8	5.0×10^{45}
Takata	$44 \leq T \leq 50$	4.18×10^8	4.322×10^{64}
	$T > 50$	6.69×10^8	9.389×10^{104}
Wu	$44 \leq T \leq 53$	6.27×10^8	3.1×10^{98}
	$T > 53$	6.27×10^8–5.10×10^5 (T-53)	3.1×10^{98}
Henriques	All T	6.27×10^8	3.1×10^{98}
Diller and Klutke	$44 \leq T \leq 52$	6.04×10^8	1.3×10^{95}
Mehta and Wong	All T	4.61×10^8	1.43×10^{72}
Torvi & Dale	$44 \leq T \leq 50$	7.82×10^8	2.185×10^{124}
	$T > 50$	3.27×10^8	1.823×10^{51}

Table 68.13 Predicted time to first and superficial second-degree burns

Irradiance ($KW/m^{2)}$	Weaver & Stoll (sec)	Fugitt (sec)	Takata (sec)	Wu (sec)	Henriques (sec)	Diller & Klutke (sec)	Mehta & Wong (sec)
$\Omega = 0.53$							
4	42.5	65.1	68.1	61.6	62.8	59.2	58.3
7	17.3	25.8	24.8	23.5	23.8	22.6	22.8
10	9.7	14.7	13.7	12.6	12.8	12.5	12.7
15	5.4	7.8	6.8	6.5	6.7	6.5	6.7
20	3.4	5.1	4.14	3.82	4.1	3.7	3.9
30	1.9	2.65	2.14	1.9	2.12	2.01	2.0
40	1.18	1.69	1.38	1.18	1.21	1.19	1.64
50	0.89	1.2	0.93	0.89	0.92	.91	0.9
$\Omega = 1.0$							
4	47.1	72	72.3	66.1	69.2	64.1	64.3
7	19.3	29.3	27.4	24.3	26.3	24.5	25.4
10	11.1	16.6	14.6	13.2	13.75	13.4	14.2
15	5.9	8.7	7.2	6.2	6.7	6.6	7.4
20	3.8	5.62	4.4	3.9	4.32	4.2	4.7
30	2.1	3	2.2	2.1	2.2	2.2	2.6
40	1.4	1.9	1.5	1.2	1.4	1.4	1.5
50	0.94	1.4	0.95	0.91	0.94	0.93	1.1

time to pain, time to superficial 2nd degree burns, and the degree of thermal injury. The recommended safety factor to be used with Equation 68.1, for predicting time to pain, is 2. By dividing the time to pain values from Equation 68.1, by the safety factor of 2, the predicted values will be consistent with those of Equation 68.11. No safety factor can be recommended for the prediction of 1st degree burns due to the lack of data for comparison. Superficial 2nd degree burns predicted using Equations 68.4 and 68.8 should be done using the pre-exponential and activation energy constants given by Weaver and Stoll. The recommended safety factor to be used, with these equations, is 1.6. Dividing the predicted times by 1.6 is consistent with the values predicted by Equation 68.14. (See Fig. 68.5.)

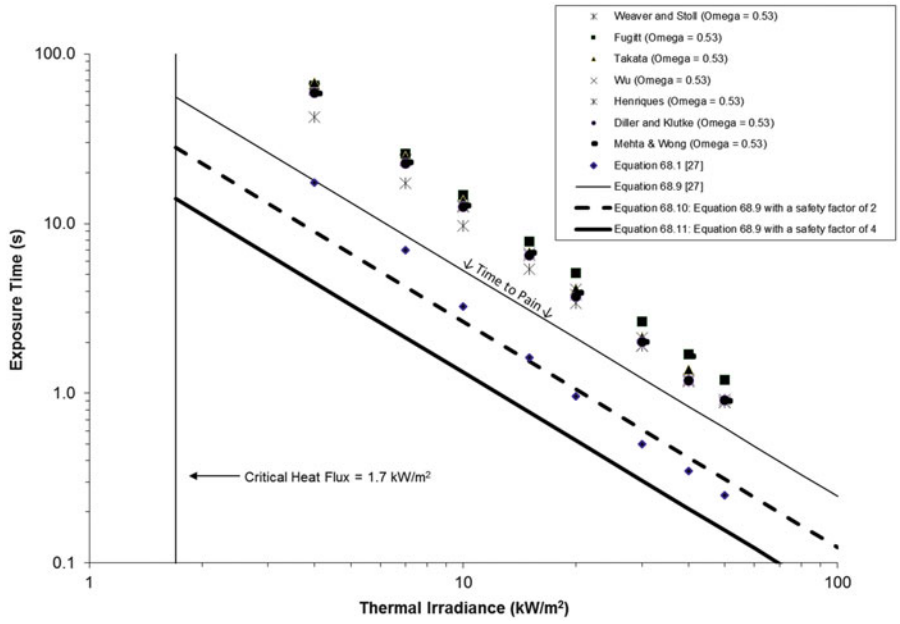

Fig. 68.4 Calculated exposure times to first-degree burns and pain on a plot of exposure time versus thermal irradiance

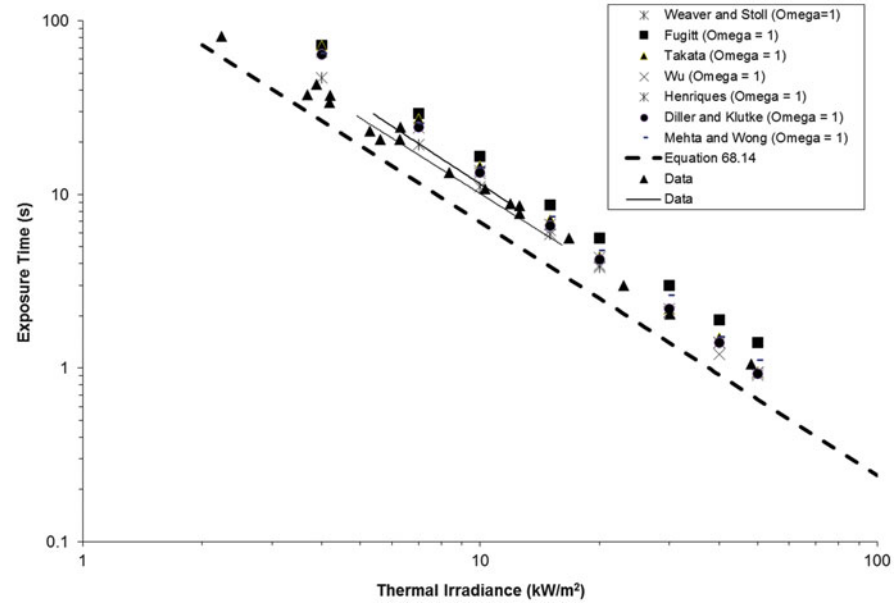

Fig. 68.5 Calculated exposure times to superficial second-degree burns on a plot of exposure time versus thermal irradiance. Values determined using the Henriques damage integral are compared to the data

The recommended safety factors need to be used in the proper manner depending on what calculation is being performed. Calculations in which the thermal irradiance is used to determine the time to injury, the resulting time is DIVIDED by the recommended safety factor. When calculating the degree of thermal injury (Ω value) using a thermal irradiance and an exposure time, the exposure time is MULTIPLIED by the recommended safety factor.

Using the damage integral to predict burn levels beyond superficial 2nd degree burns ($\Omega = 1$) should NOT be done. A recent paper stated "little difference in times to second-degree burn resulted from changing the values of the pre-exponential factor and activation energy for this range of heat fluxes [24–166.4 kW/m^2]."[30] Similar results were discussed above. "The effect of changing the values on third-degree burn predictions was much larger than with the second-degree burn times. As the times to third-degree burn are much longer, this would be expected. It is often difficult to distinguish between deep second degree, and third-degree burns. Therefore, it would be difficult to get accurate values for the pre-exponential factor and activation energy in third-degree burn experiments than in first and second-degree burn experiments."[30]

Another method developed for determining the amount of thermal damage to the skin is the "critical energy model." "The critical energy model states that the severity of the burn depends upon the amount of energy that is absorbed by the skin after the surface temperature reaches 55 °C. If the amount of excess energy is 41.9 kJ/m^2, pain or mild second-degree burns will be experienced. For an additional exposure of more than 83.8 kJ/m^2, a blister or severe second-degree burn will become evident. Finally, for an exposure of greater than 162.5 kJ/m^2, severe third-degree burns will result in permanent injury."[27] This model "was based on no physical reasoning whatsoever, and as such was completely empirical; moreover, only one burn level, namely, 2° mild burn was correlated."[4] Due to the limited applications and verification, this method is NOT recommended.

Comparison to More Complex Models

A brief discussion on the validity and prediction accuracy of the single layer model of the skin as compared with more complicated models needs to be included. Several large assumptions are made in the above equations and therefore incorporated into the later simplified equations. As stated previously the skin is a complicated structure. Both single layer, constant property models, such as Equations 68.1, 68.4 and 68.8, and more complex multiple layer, variable property finite element models have been developed. A sensitivity study using a finite element model indicated that variations in skin properties had minimal effects on the time to superficial 2nd degree burns [30]. Comparisons between the single layer and the multiple layer models for predicting times to 2nd degree burns for low intensity continuous exposures and high intensity short duration exposures (3 s) were also made. For continuous low intensity exposures the single layer model predicted times slightly higher than the multiple layer model, better agreement between the two was seen at higher irradiance levels, about 42 kW/m^2 [30]. Results between the models for predicting superficial 2nd degree burns from flash fires, i.e., high intensity short duration exposures showed that both the single layer model and the multiple layer model predicted the same times to 2nd degree burns [30]. Agreement between the predicted times to second degree burns between the single layer model and multiple layer model is expected since superficial 2nd degree burns only involve a single layer of the skin, the epidermis. Blood perfusion can be ignored since the epidermis contains no blood vessels; in addition it has been shown that it takes about 20 s for the skin to react by increasing the blood flow [30]. Most damage to the skin occurs before the increase in blood flow occurs [30].

Prediction of Skin Burns: Empirical Equations and Graphical Methods

Equation 68.9 is a correlation between the incident thermal radiation and the time to pain [27].

$$t_p = \left(\frac{35{,}000}{\dot{q}''}\right)^{1.33} \tag{68.9}$$

Where:
t_p = time required for pain (sec)
$\dot{q}''$ = incident thermal radiation (W/m^2)

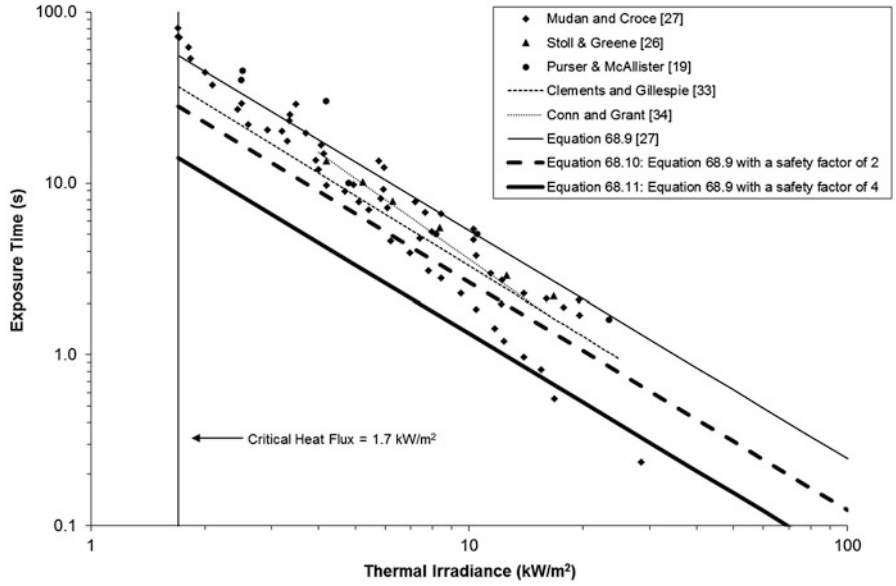

Fig. 68.6 Time for pain on a plot of exposure time versus Thermal irradiance. Individual data are shown as points and curve fits to data are thin lines

Figure 68.6 shows the time to pain on a plot of exposure time verses thermal irradiation [19, 26, 27, 33, 34]. The data were compiled from a variety of sources and includes both "prickling" and "threshold" pain [27]. The data are shown as individual data points in addition to exposure time verses irradiance curves, indicated as thin lines.

In one study, no pain was experienced by any test subject below an incident heat flux of 1.7 kW/m^2, no matter what the time duration [27]. This is considered the critical heat flux required to cause pain. From Fig. 68.6 it is also seen that Equation 68.9 predicts the time to pain well at the lower fluxes and over predicts the time at higher heat fluxes. A conservative approach would be to use a safety factor of 2; i.e., divide the predicted time by 2. As can be seen a larger percentage of data is encompassed with the second curve. The equation still over predicts the time to pain for some data at heat fluxes greater than 6000 W/m^2. A larger factor of safety, factor of 4, should be used for heat fluxes greater than 6000 W/m^2. The final recommended equations are,

$$t_p = \frac{1}{2}\left(\frac{35{,}000}{\dot{q}''}\right)^{1.33} \qquad \dot{q}'' \le 6{,}000 \text{ W/m}^2 \tag{68.10}$$

and

$$t_p = \frac{1}{4}\left(\frac{35{,}000}{\dot{q}''}\right)^{1.33} \qquad \dot{q}'' > 6{,}000 \text{ W/m}^2 \tag{68.11}$$

If the initial skin temperature is not between 32.5 °C and 33 °C then the exposure time for pain can be "corrected" for the initial temperature variation using [26].

$$t_{P2} = t_{P1}\left(\frac{44 - T_{02}}{44 - T_{01}}\right)^2 \tag{68.12}$$

Where:

t_{P1} = exposure time to pain at initial skin temperature T_{01}

t_{P2} = exposure time to pain at initial skin temperature of the given case T_{02}

T_{01} = initial skin temperature as given for chart (32.5 °C or 33 °C)

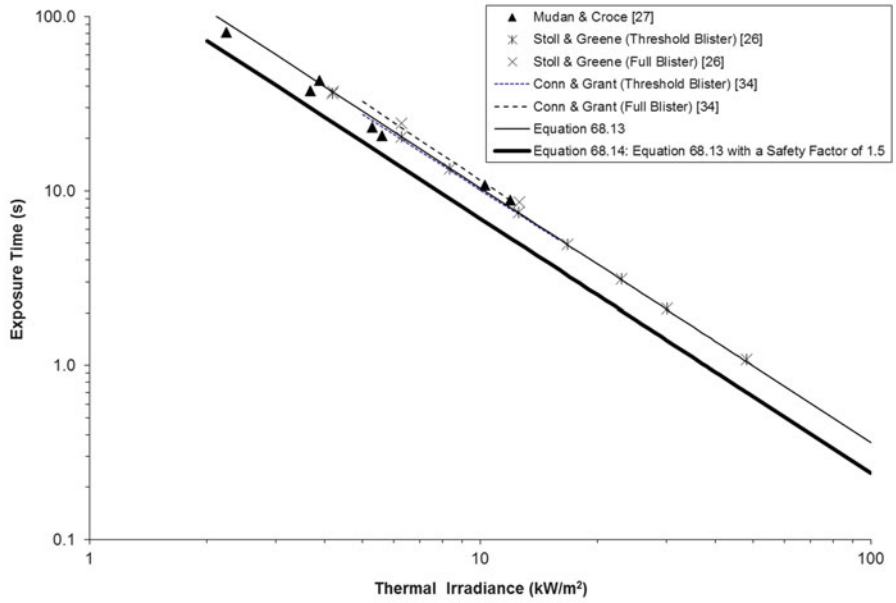

Fig. 68.7 Time for superficial second-degree burn on a plot of exposure time versus thermal irradiance. Individual data are shown as points and curve fits to data are thin lines

T_{02} = initial skin temperature for the given case (°C)

A blister is the separation of the epidermis from the dermis. The base of a blister forms at the basal layer, approximately 80 μm below the surface of the skin.[5] Figure 68.7 shows the time to blister (superficial 2nd degree burn) on a plot of exposure time verses thermal irradiance [26, 27, 34]. The experimental data are shown as provided in literature, either as individual data points or as exposure time versus thermal irradiance curves indicated as thin lines. All of the data are in excellent agreement. "Threshold" blister data and "Full" blister data are both included in the figure, as can be seen there is an insignificant difference between the two.

Equation 68.13 is a curve fit to the data.

$$t_B = 300\left(\frac{\dot{q}''}{1{,}000}\right)^{-1.46} \tag{68.13}$$

Where:

t_B = time to blister (sec)

$\dot{q}''$ = incident thermal radiation (W/m^2)

Equation 68.13 provides a good estimation of all the data shown. Using a safety factor of 1.5, which encompass all of the experimental data, Equation 68.13 becomes:

$$t_B = 200\left(\frac{\dot{q}''}{1{,}000}\right)^{-1.46} \tag{68.14}$$

It is recommended that Equation 68.14 be used to predict the time to blister.

Data beyond full blisters is almost nonexistent. Figure 68.8 was developed based on "the relation between thermal radiation intensity and burn injury for nuclear explosions at different yields."[27] The figure includes the significant injury, 1 %, 50 %, and 100 % fatality curves. Also, included in the figure are data by Mixter [36]. Mixter's data are for second-degree burns caused by a carbon arc source. Data of this nature was not included in the other figures since the carbon arc source is of a shorter wavelength than the radiation hazards addressed in this chapter. In all instances however, the carbon arc searchlights produced time to pain and time to blister results that exceeded the values obtained with the infrared radiation.

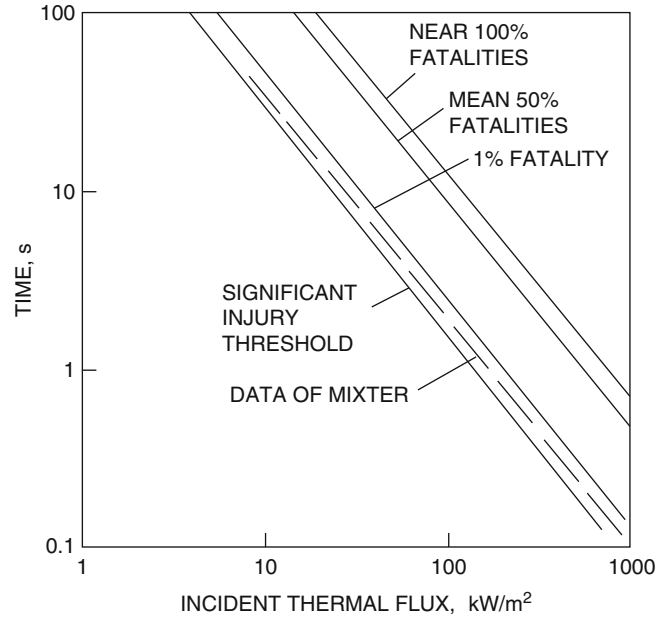

Fig. 68.8 Time required for 1 %, 50 %, and 100 % fatalities due to exposure to thermal radiation

New Simplified Methods

The use of either Equation 68.1 for determining the time to pain; or the use of Equation 68.4 and Equation 68.8 for determining the time to superficial 2nd degree burns although not difficult requires the use of a simple computer code or spreadsheet to do the calculations in an efficient manner. In an effort to simplify the calculations, two correlations, one for time to pain, Equation 68.15, and another for time to superficial 2nd degree burns, Equation 68.16, were developed. The units for time to pain, t_p, and time to superficial 2nd degree burns, t_{2b}, are seconds. The units for the incident thermal radiant heat flux, $\dot{q}''$, are kW/m^2.

$$t_p = 125\ (\dot{q}'')^{-1.9} \tag{68.15}$$

$$t_{2b} = 260(\dot{q}'')^{-1.56} \tag{68.16}$$

Equation 68.15 was developed by calculating the time to pain at the reference state properties of the skin, Table 68.10, using Equation 68.1 for incident thermal radiation levels between 1.7 kW/m^2 and 20 kW/m^2. The form of Equation 68.15 shown was specifically developed for levels of 1.7 kW/m^2 to 10 kW/m^2 and confirmed for levels of 10 kW/m^2 to 20 kW/m^2. This range of irradiances corresponds to the levels Equation 68.1 was calibrated for within this chapter. The lower thermal irradiance of 1.7 kW/m^2 is the critical heat flux, below which no pain is experienced no matter how long the duration of the exposure [9]. Equation 68.16 was developed by solving Equations 68.4 and 68.8 at the reference state properties of the skin, Table 68.10, to calculate the time to superficial 2nd degree burns for incident thermal radiation levels between 2 kW/m^2 and 50 kW/m^2. The range of values chosen in developing Equation 68.16 was selected based on the range of irradiance levels for which Equations 68.4 and 68.8 were calibrated for within this chapter.

Equations 68.15 and 68.16 are based on the reference state properties for the skin listed in Table 68.10 and are only functions of the incident thermal radiation. Neither equation takes into account any human variation in skin temperature or skin thickness. The reference state values may provide erroneous results depending on the target population for which the

calculations are being performed. Variations in these properties among different individuals and at different sites of the body exist. These variations can be accounted for by use of appropriate correction factors with Equations 68.15 and 68.16.

Equations similar to the new simplified equations presented here have been developed in the United Kingdom based on dose-response criteria [24]. The thermal dose is defined as $\dot{q}''^{4/3}t$, where the units of $\dot{q}''$ are kW/m^2 and the units of t are seconds. Pain results when the dose reaches 92 (kW/m^2)$^{4/3}$ s and a superficial 2nd degree burn results when the dose reaches the range of 210–700 (kW/m^2)$^{4/3}$ s. The thermal dose equations can be arranged to take the form $t = A(\dot{q}'')^{-4/3}$ where A is a constant. For pain the constant is 92 while for superficial 2nd degree burns the constant ranges between 210 and 700. Mudan and Croce have also used the above form of the thermal dose equation to predict time to pain; their recommended value for the constant A is 113 (kW/m^2)$^{4/3}$ s [27]. None of the equations incorporate safety factors. Therefore for comparative purposes if the safety factors are removed from Equations 68.15 and 68.16, they become:

$$t_p = 250\ (\dot{q}'')^{-1.9}. \tag{68.15a}$$

$$t_{2b} = 416\ (\dot{q}'')^{-1.56}. \tag{68.16a}$$

For a heat flux range of 4–18 kW/m^2 (which is the range used to develop the thermal dose equation), Equation 68.15a and $t_p = 92\ (\dot{q}'')^{-4/3}$ differ in magnitude on average by 1.2 s, while the deviation in magnitude in predicted times of 1.4 s is seen if the coefficient is 113, as recommended by Modan and Croce [27] Equation 68.16a and $t_{2b} = 210\,(\dot{q}'')^{-4/3}$ over the heat flux range of 14–50 kW/m^2 differ in magnitude by less than 1 s. For heat fluxes between 2 and 14 kW/m^2 Equation 68.16a gives times to superficial 2nd degree burns greater than $t_{2b} = 210\,(\dot{q}'')^{-4/3}$ but well less than $t_{2b} = 700(\dot{q}'')^{-4/3}$. Equations 68.15a and 68.16a then are very consistent with the thermal dose equations. Based on the discussion within this chapter it is believed that safety factors should be incorporated into the calculated times to pain and superficial 2nd degree burns, therefore further discussion within this chapter will be based on Equations 68.15 and 68.16 which incorporate the necessary safety factors.

Human Variability Correction Factors

The data presented in the previous sections clearly indicates that the reference state values for the initial skin temperature and epidermal thickness may not be valid in every situation. To use the simplified methods of Equations 68.15 and 68.16 correction factors are needed to account for variations in properties of human skin. The data presented previously allows a range of values for the initial skin temperature and epidermal thickness to be defined for a diverse population, see Table 68.14. The temperature values were selected based on typical values listed in the tables above. Although cooler skin temperatures are listed in the tables a minimum value of 27 °C was selected since the cooler temperatures are for very limited cases. The typical values for the epidermal thickness were taken as the minimum and maximum values listed in the literature. The minimum value is the published value for the abdomen and thorax, and the maximum value is that for the palm.

There are no data, known to the authors, that define the variation of pain receptor depth with age or body site location, therefore the pain receptor depth will be assumed to be fixed as defined by the reference state.

The effect of the initial skin temperature on the time to pain was studied using Equation 68.1 and varying the initial skin temperature between the values listed in Table 68.14. The results from the parametric study are shown in Fig. 68.9.

Table 68.14 Range of values for skin temperature and epidermal thickness for a diverse population

Property	Minimum value	Maximum value
Skin temperature	27 °C	38 °C
Epidermal thickness	16 μm	430 μm

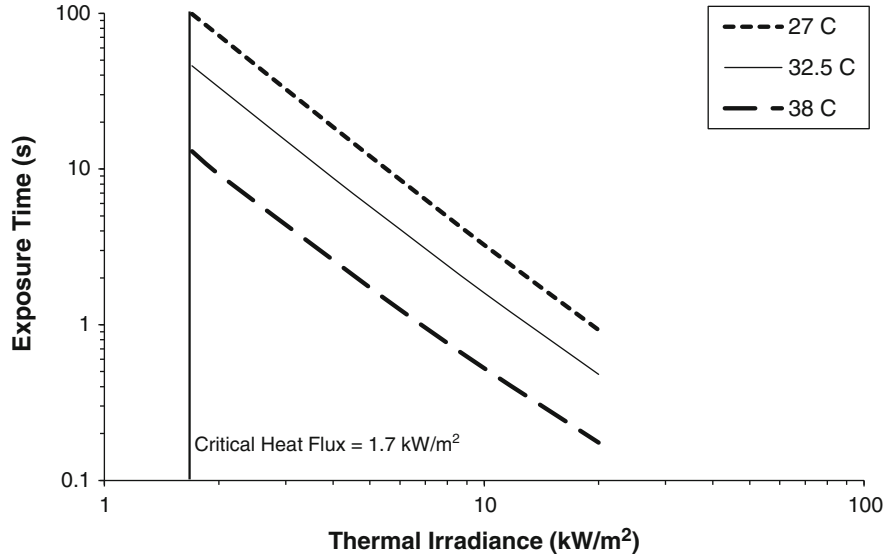

Fig. 68.9 Time to pain (exposure time) versus incident thermal radiation for the reference state initial skin temperature (32.5 °C) in comparison to initial skin temperatures of 27 °C and 38 °C. The temperature range represents a diverse population, see Table 68.14

The initial skin temperature has a significant effect on the time to pain. As the initial skin temperature is decreased there is an increase in the time to pain, while for elevated initial skin temperatures the time to pain decreases. For example, for irradiance levels of 1.7, 10, and 20 kW/m^2 the times to pain at the reference state are 46, 1.6, and 0.48 s respectively. At an elevated skin temperature of 38 °C the times to pain for the three irradiance levels respectively decreases to 13, 0.52, and 0.18 s, while at a lower skin temperature of 27 °C the times increase to 99, 3.3, and 0.18 s.

A correction factor, CF_p, for use with Equation 68.15 to account for the variation in initial skin temperature based on the results shown in Fig. 68.9 is,

$$CF_p = 3.7\ \beta^2 - 12.2\ \beta + 9.5 \qquad (68.17)$$

Where β is $T_{act}/32.5$, T_{act} is the actual initial skin temperature in °C and $0.83 < \beta < 1.17$. The time to pain calculated from Equation 68.15 is multiplied by the correction factor to account for variation in initial skin temperature from the reference state.

Equation 68.17 is similar to a correction factor that can be developed based on the work of Stoll and Greene [26]: $CF_{Stoll} = (3.8 - 2.8\beta)^2$. For initial skin temperatures above 32.5 °C Equation 68.17 is on average 6.4 % higher. For skin temperatures lower than 32.5 °C Equation 68.17 is 7.8 % lower on average.

For determining superficial 2nd degree burns variation in two skin properties, initial temperature and epidermal thickness, must be examined. Examining the effect of initial skin temperature using Equations 68.4 and 68.8 it is seen that the variation in the initial skin temperature has a similar effect on the time to 2nd degree burns as previously discussed for pain, see Fig. 68.10. The times to superficial 2nd degree burns for irradiance levels of 2, 10, and 50 kW/m^2 are 95, 6.9, and 0.6 s respectively for the reference state. If the initial skin temperature is decreased to 27 °C then the times to 2nd degree burns for the same irradiance levels increase to 158, 10, and 0.8 s respectively. Conversely, as the skin temperature is increased to 38 °C the times to 2nd degree burns decrease to 48, 4.3, and 0.42 s for irradiance levels of 2, 10, and 50 kW/m^2 respectively.

The time to superficial 2nd degree burns based on the reference state, calculated using

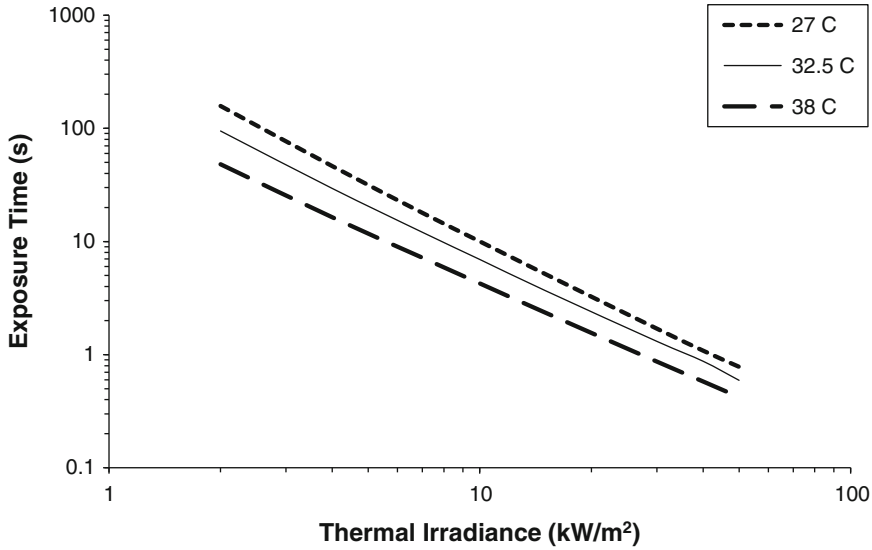

Fig. 68.10 Time to superficial 2nd degree burn (exposure time) versus incident thermal radiation for the reference state initial skin temperature (32.5 °C) in comparison to initial skin temperatures of 27 °C and 38 °C. The temperature range represents a diverse population, see Table 68.14

Equation 68.16, can be adjusted for variation in initial skin temperatures by multiplying the calculated time by the correction factor, CF_T, determined using Equation 68.18, where $0.83 < \beta < 1.17$,

$$CF_T = -4.4\ \beta^2 + 6.6\beta - 1.2 \qquad (68.18)$$

The second parameter that affects the time to superficial 2nd degree burns is the epidermal thickness (basal layer depth). The effect as calculated from Equations 68.4 and 68.8 of variation in thickness between the minimum and maximum values listed in Table 68.14 and the reference state depth is shown in Fig. 68.11. The time to superficial 2nd degree burns for the reference state were listed above as 95, 6.9, and 0.6 s for irradiance levels of 2, 10, and 50 kW/m^2 respectively. If the only variable to change is the basal layer depth the times to 2nd degree burns increase to 103, 9.0, and 1.2 s for a basal layer depth of 430 μm and decrease to 93, 6.4, and 0.48 s for a basal layer thickness of 16 μm. As can be seen, at lower incident radiation levels the epidermal thickness does not have as large effect on the time to superficial 2nd degree burns, as the radiation levels increase the effect of the basal layer depth increases.

The time to 2nd degree burns based on the reference state, calculated using Equation 68.16, can be adjusted for variation in epidermal thickness by multiply the calculated time by the correction factor, CF_d, determined using Equation 68.19,

$$CF_d = 0.000020\ (\dot{q}'')^2\ (1-\gamma) + 0.0060\ \dot{q}''\ (\gamma - 1) + 0.013\gamma + 0.99 \qquad (68.19)$$

Where γ is $x_{act}/80$, x_{act} is the actual epidermal thickness in μm and $0.20 < \gamma < 5.38$. The incident thermal radiation, $\dot{q}''$, in Equation 68.19 has units of kW/m^2. For time to superficial 2nd degree burn calculation using Equation 68.16, if both the initial skin temperature and epidermal thickness are different from the reference state then both correction factors need to be calculated, using Equations 68.18 and 68.19, and multiplied by the time from Equation 68.16.

A comparison between the predicted times to pain and superficial 2nd degree burns using Equations 68.1, 68.4, and 68.8, and the corresponding simplified equations with the correction factors was undertaken. The comparison for time to pain was conducted at heat fluxes of 1.7 kW/m^2, 10 kW/m^2 and 20 kW/m^2 for three

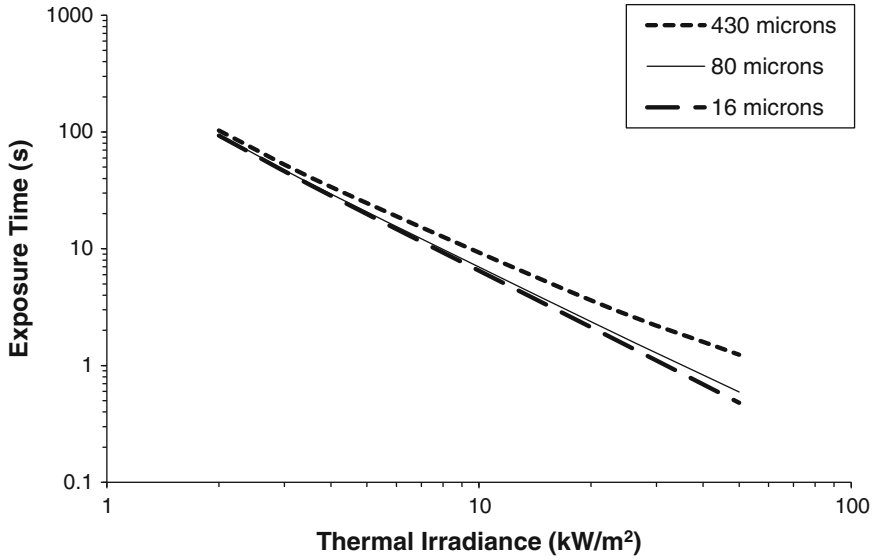

Fig. 68.11 Time to superficial 2nd degree burn (exposure time) versus incident thermal radiation for the reference state epidermal thickness (80 μm) in comparison to epidermal thickness of 16 to 430 μm. The thickness range represents a diverse population, see Table 68.14

values of $\beta = 0.83, 1, 1.17$ resulting in 9 points of comparison. For superficial 2nd degree burns the comparison was conducted at heat fluxes of 2 kW/m^2, 10 kW/m^2 and 50 kW/m^2 for three values of $\beta = 0.83$, 1, 1.17, and for three values of $\gamma = 0.20, 1, 5.38$ resulting in 27 points of comparison. The ranges of values for $0.83 < \beta < 1.17$ and $0.20 < \gamma < 5.38$ are based on the limit values for the skin temperature and epidermal thickness, Table 68.14, used to develop the correction factors CF_p, CF_T and CF_d. The range of heat fluxes covers the range used to develop the simplified equations.

The magnitude of the difference between Equation 68.1 and the simplified equations for the times to pain at 20 kW/m^2 is on average 0.08 s with a standard deviation (SD) of 0.04 s. At 10 kW/m^2 the average is 0.1 s with a SD of 0.1 s. At 1.7 kW/m^2 the difference for $\beta = 1$ and 1.17 is less than 0.5 s, and for $\beta = 0.83$ it is 11.8 s or 12 %. The magnitude of the difference between Equations 68.4 and 68.8 and the simplified equations for the times to superficial 2nd degree burns at 50 kW/m^2 is on average 0.1 s with a SD of 0.1 s. At 10 kW/m^2 the average is 0.7 s with a SD of 0.3 s. At 2 kW/m^2 the difference for $\beta = 1$ and 1.17 (all γ) is on average 5 s with a SD of 2 s, and for $\beta = 0.83$ (all γ) is on average 46 s or 29 %. For all the 1.7 kW/m^2 and 2 kW/m^2 cases the simplified equations for pain and superficial 2nd degree burns predict shorter times than do Equations 68.1, 68.4 and 68.8, respectively.

The range of values for the skin temperature and epidermal thickness listed in Table 68.14, $0.83 < \beta < 1.17$ and $0.20 < \gamma < 5.38$ respectively were then used to determine the minimum and maximum values for the correction factors shown in Table 68.15. Since the correction factor for skin thickness is a function of non-dimensional depth and the irradiance level, three irradiance values are shown.

The non-dimensional temperature coefficient, β, represents a variation from the reference state temperature of 32.5 °C. For the minimum and maximum temperatures listed in Table 68.14 there is a ±17 % deviation from the reference state, see Table 68.15. The equal negative and positive change in temperature does not produce an equal effect on the time to pain and superficial 2nd degree burns. A 17 % decrease in the initial skin temperature produces a 92 % increase in the time to pain and a 25 % increase in the time to superficial 2nd degree burns, and a 17 % increase in skin temperature

Table 68.15 Range of values for correction factors for pain and superficial 2nd degree burns based on initial skin temperature and epidermal thickness ranges shown in Table 68.14

Correction factor	$\beta = 0.83$	$\beta = 1.17$	$\gamma = 0.20$	$\gamma = 5.38$
Pain				
CF_p	1.92	0.29	–	–
2nd degree burns				
CF_T	1.25	0.50	–	–
CF_d ($\dot{q}'' = 2$ kW/m^2)	–	–	0.98	1.11
CF_d ($\dot{q}'' = 10$ kW/m^2)	–	–	0.95	1.31
CF_d ($\dot{q}'' = 50$ kW/m^2)	–	–	0.76	2.35

Initial skin temperature and epidermal thickness are represented via the non-dimensional parameters β and γ respectively

produces a 71 % decrease in the time pain and a 50 % decrease in the time to superficial 2nd degree burns, see Table 68.15.

The effect of a 1 °C change in the initial skin temperature on the time to pain and superficial 2nd degree burns can be examined as well. For a 1 °C (3 %) decrease in the skin temperature there is a 15 % and 6.4 % increase in the time to pain and superficial 2nd degree burns respectively. A 1 °C (3 %) increase in skin temperature produces a 14 % decrease in the time to pain and 7 % decrease in the time to 2nd degree burns.

The deviation in the basal layer depth from the reference state is represented by γ. The minimum epidermal thickness of 16 μm is an 80 % decrease from the reference state thickness of 80 μm and the maximum skin thickness of 430 μm is a 438 % increase, see Table 68.14 and Table 68.15. These large changes in epidermal thickness have a smaller effect on the time to superficial 2nd degree burns for low irradiance levels. For example an irradiance level of 2 kW/m^2 results in a 2 % difference between the calculated reference state burn time and the 16 μm burn time, and a 11 % difference between the reference state and the 430 μm burn time. As the irradiance level increases to 10 kW/m^2 a 5 % difference results between the calculated reference state burn time and the 16 μm burn time, and a 31 % difference results between the reference state and the 430 μm burn time. As the irradiance level increases further, up to 50 kW/m^2, the deviation from the time calculated at the reference state changes by 24 % and 135 % for the 16 μm and 430 μm states respectively, see Table 68.15.

Examples

Sample problems for three thermal irradiances will be shown and solved using the discussed methods. Values of 4 kW/m^2, 10 kW/m^2 and 20 kW/m^2 are assumed to have been determined based on previous methods [37]. The values were chosen to represent the lower limit for pain and skin damage, 4 kW/m^2, a typical value for wood based ignition, 10 kW/m^2, and a typical value for flashover, 20 kW/m^2.

Example 1 An individual is exposed to an incident heat flux of 4 kW/m^2 for a duration of 30 s. At what time will pain be experienced assuming an initial skin temperature of 1.) 32.5 °C 2.) 30 °C and 3.) 34 °C? What degree of damage will occur?

Since the thermal irradiation is less than 6 kW/m^2, Equation 68.10 is used to predict the time to pain. For case 1, an initial skin temperature of 32.5 °C, the time to pain is:

$$t_p = \frac{1}{2}\left(\frac{35{,}000}{\dot{q}''}\right)^{1.33}$$

$$t_p = \frac{1}{2}\left(\frac{35{,}000}{4{,}000}\right)^{1.33}$$

$$t_p = 9.0 \text{ sec}$$

For case 2 and 3, Equation 68.12 is used to "correct" the time for the variation in initial skin temperature. The time to pain for case 2 then becomes:

$$t_{P2} = t_{P1}\left(\frac{44 - T_{02}}{44 - T_{01}}\right)^2$$
$$t_{P2} = 9.0 \cdot \left(\frac{44 - 30}{44 - 32.5}\right)^2$$
$$t_{P2} = 13.3 \text{ sec}$$

and for case 3, the time to pain is,

$$t_{P2} = t_{P1}\left(\frac{44 - T_{02}}{44 - T_{01}}\right)^2$$
$$t_{P2} = 9.0 \cdot \left(\frac{44 - 34}{44 - 32.5}\right)^2$$
$$t_{P2} = 6.8 \text{ sec}.$$

Equation 68.1 is also be used to determine the time to pain.

$$T = T_0 + \frac{\dot{q}''}{k_h}\left[\frac{2\sqrt{\alpha_h t}}{\sqrt{\pi}}\exp\left(-\frac{x^2}{2\alpha_h t}\right) - x\,erfc\left(\frac{x}{2\sqrt{\alpha_h t}}\right)\right]$$

The values for the skin properties found in Table 68.10 are used. Since Equation 68.1 only takes into account the heating phase the thermal conductivity for heating is used. Equation 68.1 is solved by using a spreadsheet or simple computer code to calculate the skin temperature over time.

Case 1: Initial skin temperature of 32.5 °C

Step 1: Set the initial parameters.

Initial skin temperature, T_0:	305.5 K
Depth below surface, x:	8.00E-05 m
Effective radiation, $\dot{q}''$:	4000 W/m^2
Volumetric heat capacity, ρc:	4,186,800 J/m^3-K
Thermal conductivity during heating, k_h:	0.5878 W/m-K
Thermal diffusivity during heating, α_h:	1.40 E-7 m^2/s

Step 2: Set time interval for the calculations.

To obtain an appropriate resolution it is recommended that 0.1-s be used.

Step 3: Solve Equation 68.1 at each time interval until the skin temperature is 44 °C.

Step 4: Incorporate the recommended safety factor of 2. Since an irradiance is used to determine a time, the time is DIVIDED by the safety factor.

$$t_p = \frac{t}{Safety\ factor}$$
$$t_p = \frac{17.50}{2}$$
$$t_p = 8.8 \text{ sec}.$$

For case 2 and 3 the same procedure is used with the appropriate values for the initial skin temperature.

For case 2 the calculated time to pain is:

$$t_p = \frac{t}{Safety\ factor} = \frac{25.6}{2} = 12.8 \text{ sec},$$

and for case 3:

$$t_p = \frac{t}{Safety\ factor} = \frac{13.4}{2} = 6.7 \text{ sec}.$$

All of the methods for predicting the time to pain produce similar values.

Based on Equation 68.14 the time to blister is determined to be,

$$t_B = 200\left(\frac{\dot{q}''}{1{,}000}\right)^{-1.46}$$
$$t_B = 200 \cdot \left(\frac{4{,}000}{1{,}000}\right)^{-1.46}$$
$$t_B = 26.4 \text{ sec}.$$

Therefore, from the 30-s exposure a superficial 2nd degree burn is expected.

An alternative method for determining the degree of damage is to determine the temperature-time history of the skin and calculate the Henriques' damage function. This solution will require the use of a spreadsheet or simple computer program.

Step 1: Set the initial parameters. Use the values listed in Table 68.10 for skin properties.

Initial skin temperature, T_0:	305.5 K
Exposure time, τ:	30 s
Exposure time with safety factor of 1.6, τ:	$30 \cdot 1.6 = 48$ s
Depth below surface, x:	8.00E-05 m
Effective radiation, $\dot{q}''$:	4000 W/m^2
Volumetric heat capacity, ρc:	4,186,800 J/m^3-K
Thermal conductivity during heating, k_h:	0.5878 W/m-K
Thermal conductivity during cooling, k_c:	0.4518 W/m-K
Thermal diffusivity during heating, α_h:	1.40 E-7 m^2/s
Thermal diffusivity during cooling, α_c:	1.08 E-7 m^2/s

The recommended safety factor is MULTIPLIED by the exposure time, because the thermal irradiance and exposure time are used to determine the degree of thermal injury.

Step 2: Set time interval for the calculations.

To obtain an appropriate resolution it is recommended that for low thermal irradiances, $\dot{q}'' \leq 10$ kW/m^2, a 1-s time interval be used, and for thermal irradiances greater than 10 kW/m^2 a time interval of 0.25-s or less be used.

Since $\dot{q}'' = 4000$ W/m^2, 1-s time steps will be used.

Step 3: Calculate the skin temperature, T.

For the heating period, $t \leq \tau$, the first two terms of Equation 68.4 are used.

$$T = T_0 + \frac{\dot{q}''}{k_h}\left[\frac{2\sqrt{\alpha_h t}}{\sqrt{\pi}}\exp\left(-\frac{x^2}{4\alpha_h t}\right) - x\left(1 - erf\left(\frac{x}{2\sqrt{\alpha_h t}}\right)\right)\right]$$

During the cooling period, $t > \tau$, all three terms are used.

$$T = T_0 + \frac{\dot{q}''}{k_c}\left[\frac{2\sqrt{\alpha_c t}}{\sqrt{\pi}}\exp\left(-\frac{x^2}{4\alpha_c t}\right) - x\left(1 - erf\left(\frac{x}{2\sqrt{\alpha_c t}}\right)\right)\right] - \frac{\dot{q}''}{k_c}\left[\frac{2\sqrt{\alpha_c (t-\tau)}}{\sqrt{\pi}}\exp\left(-\frac{x^2}{4\alpha_c (t-\tau)}\right) - x\left(1 - erf\left(\frac{x}{2\sqrt{\alpha_c (t-\tau)}}\right)\right)\right]$$

It is important that the proper values for the thermal conductivity and thermal diffusivity be used during the heating and cooling periods.

Step 4: Set the pre-exponential constant and activation energy according to the skin temperature at each time interval, using the values of Weaver and Stoll.

If 44 °C $\leq$ T $\leq$ 50 °C,

$\Delta E = 7.78 \times 10^8$ J/kmol

$P = 2.185 \times 10^{124}$ 1/s

and if T > 50 °C,

$\Delta E = 3.25 \times 10^8$ J/kmol

$P = 1.823 \times 10^{51}$ 1/s.

Step 5: Since Equation 68.8 can not be solved directly, numerical techniques are required to solve for the damage function, Ω. First Equation 68.7,

$$\frac{d\Omega}{dt} = P\exp\left(\frac{-\Delta E}{RT}\right),$$

needs to be solved at each time interval. Then a numerical integration technique such as the trapezoidal rule needs to be used to integrate the function over time. The trapezoidal rule for this application is:

$$I_1 = \sum_{i=1}^{n-1} \frac{\left(\left(\frac{d\Omega}{dt}\right)_i + \left(\frac{d\Omega}{dt}\right)_{i+1}\right)}{2} (t_{i+1} - t_i) \tag{68.20}$$

Applying Equation 68.20 to all times for which T is greater than 44 °C, the value for the damage function is determined to be 1.13. Comparing the calculated result to the values for the damage function listed in Table 68.11 it is seen that a superficial 2nd degree burn will occur.

Example 2 An individual is exposed to an incident heat flux of 10 kW/m^2 for a duration of 10 s. If the initial skin temperature is 32.5 °C, at what time will pain be experienced and what degree of damage will occur?

Since the thermal irradiation is greater than 6 kW/m^2, Equation 68.11 is used to predict the time to pain.

$$\begin{aligned} t_p &= \frac{1}{4}\left(\frac{35{,}000}{\dot{q}''}\right)^{1.33} \\ t_p &= \frac{1}{4}\left(\frac{35{,}000}{10{,}000}\right)^{1.33} \\ t_p &= 1.3 \text{ sec} \end{aligned}$$

Applying the method discussed above for solving Equation 68.1, the time to pain is determined to be:

$$t_p = \frac{t}{Safety\ factor} = \frac{3.2}{2} = 1.6 \text{ sec}.$$

Both Equations 68.11 and 68.1 predict similar results.

Based on Equation 68.14 the time to blister is determined to be,

$$\begin{aligned} t_B &= 200\left(\frac{\dot{q}''}{1{,}000}\right)^{-1.46} \\ t_B &= 200 \cdot \left(\frac{10{,}000}{1{,}000}\right)^{-1.46} \\ t_B &= 6.9 \text{ sec}. \end{aligned}$$

The 10-s exposure will produce AT LEAST a superficial 2nd degree burn.

Following the same procedure described in the previous example, the damage integral is determined to be 7.7. This also indicates that AT LEAST a superficial 2nd degree burn will occur. It is important to understand that once Ω exceeds 1, the function has NO meaning relative to additional burn injury.

Example 3 An individual is exposed to an incident heat flux of 20 kW/m^2 for a duration of 5 s. At what time will pain be experienced and what degree of damage will occur, for an initial skin temperature of 32.5 °C?

Since the thermal irradiation is greater than 6 kW/m^2, Equation 68.11 is used to predict the time to pain.

$$\begin{aligned} t_p &= \frac{1}{4}\left(\frac{35{,}000}{\dot{q}''}\right)^{1.33} \\ t_p &= \frac{1}{4}\left(\frac{35{,}000}{20{,}000}\right)^{1.33} \\ t_p &= 0.5 \text{ sec}. \end{aligned}$$

Solving Equation 68.1 using the methodology discussed above, the time to pain is determined to be:

$$t_p = \frac{t}{Safety\ factor} = \frac{1.0}{2} = 0.5 \text{ sec}.$$

Again, the values determined using Equations 68.11 and 68.1 are comparable.

Based on Equation 68.14 the time to blister is determined to be,

$$\begin{aligned} t_B &= 200\left(\frac{\dot{q}''}{1{,}000}\right)^{-1.46} \\ t_B &= 200 \cdot \left(\frac{20{,}000}{1{,}000}\right)^{-1.46} \\ t_B &= 2.5 \text{ sec}. \end{aligned}$$

The 5-s exposure will produce AT LEAST a superficial 2nd degree burn.

Following the same procedure described in Example 1, the damage integral is determined to be 124.1 indicating AT LEAST a superficial 2nd degree burn. It is important to understand that once Ω exceeds 1, the function has NO meaning relative to additional burn injury.

Conclusions

Thermal damage to the skin is a function of skin temperature and the time duration for which the basal layer temperature is greater than 44 °C. Various models and techniques have been developed to predict the time and degree of damage due to a constant thermal irradiance. Methods for determining the time to pain, 1st degree burns and superficial 2nd degree burns have been evaluated and discussed with regards to appropriate applications and limitations.

A summary of the recommended techniques and equations for determining each condition follows:

Simple Algorithms

Simple algorithms which can be used to predict the degree of thermal damage, time to pain and superficial 2nd degree burns, exist but require the use of a spreadsheet or simple computer code to perform the calculations efficiently.

The time to pain is determined using Equation 68.1. The recommended safety factor of 2 is included in the calculation by DIVIDING the calculated time to pain.

The degree of damage produced by a thermal irradiance of a given duration is determined using the Henriques damage integral (Equation 68.8). Calculation of the damage function, Ω, requires that the temperature-time history of the skin be known. It is recommended that Equation 68.4 be used to determine the temperature-time history since it incorporates both the heating and cooling phases of the skin. When solving Equation 68.4 it is important to use the proper properties for the heating and cooling periods. The recommended skin properties are listed in Table 68.10.

The Henriques' damage integral, Equation 68.8, needs to be solved using numerical integration techniques; the trapezoidal rule provides a reasonable solution to the integral and can easily be programmed in a spreadsheet. The pre-exponential and activation energy constants provided by Weaver and Stoll should be used. The safety factor of 1.6 is used by MULTIPLYING the exposure time.

Proper use of the safety factors is required to obtain accurate results. Calculations in which the thermal irradiance is used to determine the time to injury, the resulting time is DIVIDED by the recommended safety factor. When calculating the degree of thermal injury (Ω value) using a thermal irradiance and an exposure time, the exposure time is MULTIPLIED by the recommended safety factor.

In an effort to simplify the calculation procedure, the algorithms were solved for a large number of incident thermal radiation levels and a reference state condition of the skin. Based on the results two simplified equations, Equations 68.15 and 68.16, were developed which predict the time to pain and superficial 2nd degree burns which are only a function of the incident thermal radiation. The simplified equations were compared to thermal dose equations recommended in the United Kingdom [24] for predicting pain and superficial 2nd degree burns, and an equation recommended by Mudan and Croce[27] for pain. When the safety factors which were incorporated into the Equations 68.15 and 68.16 are removed, they predict times that are consistent with those predicted using the thermal dose equations.

Graphical Methods

Figures 68.6 and 68.7 can be used to determine the time to pain and superficial 2nd degree burns respectively.

Empirical Equations

The time to pain is calculated for thermal irradiances less than or equal to 6 kW/m^2 using Equation 68.10 and for higher irradiances using Equation 68.11. If the initial skin temperature is not within the range of 32.5 °C and 33 °C, the

time to pain needs to be corrected for the temperature variation using Equation 68.12. Equation 68.12 can only be used to correct for time to pain and NOT time to blister.

It is recommended that Equation 68.14 be used to determine the time to superficial second-degree burns.

The simplified equations neglect any variation in the physical parameters of the skin among different individuals. Three important skin properties are the pain receptor depth, the initial skin temperature, and the epidermal thickness (basal layer depth). Little information is available in literature on pain receptor depth and therefore the effect of variation in the depth could not be studied. A literature study of how the initial skin temperature and basal layer depth vary, among individuals and at different sites of the body, was performed. The effect of age, sex, occupation, and personal habits on these parameters was examined. Based on a parametric study involving Equations 68.1, 68.4, and 68.8, correction factors were developed to adjust the times to injury calculated using the simplified equations. The correction factors, Equation 68.17, 68.18, and 68.19, are a function of non-dimensional temperature (β) and depth (γ) coefficients and the irradiance level. The difference in the times to pain and superficial 2nd degree burns between the simplified equations with correction factors and Equations 68.1, 68.4, and 68.8 was found to be negligible for heat fluxes greater than 10 kW/m^2. At low heat fluxes (1.7 kW/m^2 and 2 kW/m^2), the difference was found to be up to 30 % with the simplified equations predicting shorter times.

It was found that the initial skin temperature typically varies between 27 °C and 38 °C; this is a deviation of ±5.5 °C (±17 %) from the reference state temperature of 32.5 °C. The deviation in initial skin temperature can have effects as high as 92 % on the time to pain, and as high as 50 % on the time to superficial 2nd degree burns, this can mean the difference between no sensation and a 2nd degree burn for the same exposure.

The variation in basal layer depth (epidermal thickness) was found to be between 16 and 430 μm depending on an individual's age and sex, and depending on the body site. The reference state defines the basal layer depth as 80 μm. Examination of how the skin thickness affects the calculations showed that the variation was not simply a function of the skin thickness but the irradiance level as well. At lower irradiance levels the skin thickness has a smaller effect on the calculated times, in most instances less than 31 %; however, at higher irradiance levels (greater than 10 kW/m^2) there is a significant difference, in as much as 135 %, in the calculated times to superficial 2nd degree burns.

The simplified equations, along with the correction factors, allow the practicing fire protection engineer to evaluate the degree of thermal injury that can be expected by individuals in a hazardous situation. These tools can be incorporated into life safety models and risk assessment analyses without any difficulty in the calculation procedure.

Nomenclature

$\dot{q}''$	Incident thermal radiation (W/m^2)
t	Time (sec)
x	Depth below the surface of the skin (m)
ΔE	Activation energy deGlossaryTermined from experimental data (J/kmol)
P	Pre-exponential GlossaryTerm deGlossaryTermined from experimental data (1/s)
R	Universal gas constant (8314 J/kmol-K)
S(t)	Step function
T	Temperature at time t and distance x below the skin surface (K)
α	k/ρc = thermal diffusivity (m^2/s)
c	Specific heat (J/kg-K)
k	Thermal conductivity (W/m-K)
ρ	Density (kg/m^3)
ρc	Volumetric heat capacity (J/m^3-K)
τ	Exposure time (sec)
Ω	Henriques' damage function

Subscripts

c	Cooling
h	Heating
o	Initial
p	Pain
s	Surface
2b,B	Blister
1	Previous time
2	Current time

Definitions[1]

Acidophilism	Capable of being stained by acid stains such as eosin.
Acidosis	A disturbance in the acid-base balance of the body in which is an accumulation of acids or an excessive loss of bicarbonate.
Adipose	Fatty; pertaining to fat.
Basal	Pertaining to the base of anything; the base.
Bullae	A large blister or skin vesicle filled with fluid.
Collagen	A substance existing in the various tissues of the body, as in the white fibers of connective tissue.
Cutaneous	Pertaining to the skin.
Edema	A condition in which the body tissues contain an excessive amount of tissue fluid. It may be local or general.
Erythema	A form of macule showing diffused redness over the skin. Caused by capillary congestion, usually due to dilation of the superficial capillaries as a result of some external influence, such as heat, sunburn, etc.
Fibril	A small fiber. A very small filamentous structure, oftentimes the component of a cell or a fiber.
Heparin	A complex organic acid found especially in lung and liver tissue and having the ability in certain circumstances to prevent the clotting of blood.
Histamine	A substance in the body found wherever tissues are damaged. Red flush of a burn is due to the local production of histamine; product of histidine catabolism.
Histidine	An amino acid, $C_6H_9N_3O_2$, obtained by hydrolysis from tissue proteins and necessary for tissue repair and growth.
Horny	A cutaneous outgrowth composed chiefly of keratin. A horn-like projection.
Macule	Discolored spot or patch on the skin neither elevated nor depressed, of various colors, sizes and shapes.
Matrix	The intercellular substance of a tissue.
Melanin	The pigment which gives color to hair, skin and the choroid of the eye, and it is present in some cancers, as in melanoma.
Melanocyte	A phagocyte which has ingested melanin.
Necrosis	Death of areas of tissue or bone surrounded by healthy parts; death in mass as distinguished from necrobiosis, a general degeneration.
Papillary layer	The layer of the corium which adjoins the epidermis.
Petrolatum	

[1] (All definitions are taken from reference 6 unless otherwise noted.)

	A purified semi-solid mixture of hydrocarbons obtained from petroleum.
Phagocyte	A cell which has the ability to ingest and destroy particulate substances such as bacteria, protozoa, cells and cell debris, dust particles, and colloids.
Pulmonary	Concerning or involving the lungs.
Skin temperature	Surface temperature of the skin [26].
Squamous cells	Flat, scaly, epithelial cell.
Stratum	A layer.
Subcutaneous	Beneath or to be introduced beneath the skin.
Tissue temperature	Temperature at a depth approximately 80 μm below the skin surface [26].

References

1. Stoll, A.M., and Chianta, M.A., "A Method and Rating System for Evaluation of Thermal Protection", Naval Air Development Center Report No. NADC-MR-6809, Johnsville, PA (1968).
2. Diller, K.R. "Analysis of Skin Burns", in *Heat Transfer in Medicine and Biology: Analysis and Applications*. Vol. 2, Shitzer A., and Eberhart, R.C., eds., Plenum Publishing Co., New York, NY (1985).
3. Larson, D. E., *Mayo Clinic Family Health Book,* William Morrow and Company, Inc., New York, 1990.
4. Mehta, A., and Wong, F., "Measurement of Flammability and Burn Potential of Fabrics" (Summary Report December 1971 – January 1973.), Fuels Research Laboratory, Project DSR 73884, Massachusetts Institute of Technology, Cambridge, MA (1973).
5. Stoll, A.M., "The Role of Skin in Heat Transfer", in *Advances in Heat Transfer*, Vol. 4, Academic Press, New York (1967).
6. Taber's Cyclopedic Medical Dictionary, 11th ed., F. A. Davis Company, Philadelphia, PA, 1968.
7. Lawton, B., "Heat Dose to Produce Skin Burns in Humans", in *Proceedings of the 1994 International Mechanical Engineering Congress and Exposition,* Fundamentals of Biomedical Heat Transfer, HTD V 295, American Society of Mechanical Engineers, New York, NY (1994).
8. Lefton, L.A., *Psychology*, Allyn and Bacon, Needham Heights, MA (1997) 106–107.
9. *Engineering Guide for Predicting 1st and 2nd Degree Skin Burns from Thermal Radiation*, Society of Fire Protection Engineers, Bethesda, MD, (2000).
10. Millington, P.F., and Wilkinson, R., *Skin*, Cambridge University Press, New York, NY (1983) 23–25, 50–52.
11. Berenson, P.J., and Robertson, W.G., "Temperature", in *Bioastronautics Data Book*, NASA SP-3006, National Aeronautics and Space Administration, Washington, D.C. (1973) 65–87.
12. Abe, T., Mayuzumi, J., Kikuchi, N., and Arai, S., "Seasonal Variations in Skin Temperature, Skin pH, Evaporative Water Loss and Skin Surface Lipid Values on Human Skin", *Chem. Pharm. Bull.,* **28** (1980) 387–392.
13. Delamarche, P., Bittel, J., Lacour, J.R., and Flandrois, R., "Thermoregulation at Rest and During Exercise in Prepubertal Boys", *European Journal of Applied Physiology*, **60** (1990) 436–440.
14. Halkier-Soreensen, L., and Therstrup-Pedersen, K., "The Relationship Between Skin Surface Temperature, Transepidermal Water Loss and Electrical Capacitance Among Workers in the Fish Processing Industry: Comparison with Other Occupations. A field Study", *Contact Dermatitis*, **24** (1991) 345–355.
15. Usuki, K., Kanekura, T., Aradono, K., and Kanzaki, T., "Effects of Nicotine on Peripheral Cutaneous Blood Flow and Skin Temperature", *Journal of Dermatological Science*, **16** (1998) 173–181.
16. Ahrenholz, D.H., Clayton, M.C., and Solem, L.D., "Burns and Wound Management", *Otolaryngologic Clinics of North America*, **28**:5 (1995).
17. ASTM, "Standard Guide for Heated System Surface Conditions That Produce Contact Burn Injuries", *Annual Book of ASTM Standards*, American Society for Testing and Materials, Philadelphia, PA (1986) C 1055–86.
18. Reed, M.P., Schneider, L.W., and Burney, R.E., "Laboratory Investigations and Mathematical Modeling of Airbag-Induced Skin Burns", in *Proceedings of the 38th Stapp Car Crash Conference*, Society of Automotive Engineers, Warrendale, PA (1994).
19. Purser, D.A. & McAllister, J., "Assessment of Hazards to Occupants from Smoke, Toxic Gases, and Heat", in *The SFPE Handbook of Fire Protection Engineering, 5th ed*., Springer (2015).
20. Lyon, J.L., Davis, T.P., and Pearse, H.E., "Studies of Flash Burns: The Relation of Thermal Energy Applied and Exposure Time to Burn Severity", Atomic Energy Report 394, University of Rochester, Rochester, NY (1955).
21. Knox, F.S., III, Wachtel, T.L., Trevethan, W.P., McCahan, G.R., Jr., and Brown, R.J., "A Porcine Bioassay Method for Analysis of Thermally Protective Fabrics: A Histological and Burn Depth Grading System", USAARL Report No. 78–11, U.S. Army Aeromedical Research Laboratory, Fort Rucker, AL (1978).

22. Brigham, P. A., and McLoughlin, E., "Burn Incidence and Medical Care Use in the United States: Estimates, Trends, and Data Sources", *Journal of Burn Care Rehabilitation*, **17** (1996) 95–107.
23. Saffle, J. R., Davis, B., Williams, P., et al., "Recent Outcomes in the Treatment of Burn Injury in the United States: A Report From the American Burn Association Patient Registry", *Journal of Burn Care Rehabilitation*, **16** (1995) 219–232.
24. Hymes, I., Boydell, W., and Prescott, B, "Thermal Radiation: Physiological and Pathological Effects", Institution of Chemical Engineers, Rugby, Warwickshire, UK (1996) Chapters 5, 6 and 7.
25. Ahrenholz, D.H., Clayton, M.C., and Solem, L.D., "Burns and Wound Management", *Otolaryngologic Clinics of North America*, **28**:5 (1995) 1039–1055.
26. Stoll, A., and Greene, L.C., "Relationship between Pain and Tissue Damage due to Thermal Radiation", *Journal of Applied Physiology*, **14** (1959) 373–383.
27. Mudan, K.S., and Croce, P.A., "Fire Hazard Calculations for Large Open Hydrocarbon Fires", in *The SFPE Handbook of Fire Protection Engineering, 2nd ed*., National Fire Protection Association, Quincy, MA (1995) Chap. 3–11.
28. Weaver, J.A., and Stoll, A.M., "Mathematical Model of Skin Exposed to Thermal Radiation", *Aerospace Medicine*, **40** (1969) 24–30.
29. Stoll, A.M., and Chianta, M.A., "Heat Transfer through Fabrics as Related to Thermal Injury", *Transactions-New York Academy of Sciences*, **33**:7 (1971) 649–670.
30. Torvi, D.A., and Dale, J.D., "A Finite Element Model of Skin Subjected to a Flash Fire", *Transactions of the ASME -- Journal of Biomechanical Engineering*, **116** (1994) 250-255.
31. Diller, K.R., and Klutke, G.A., "Accuracy Analysis of the Henriques Model for Predicting Thermal Burn Injury", *Advances in Bioheat and Mass Transfer: Microscale Analysis of Thermal Injury Processes, Instrumentation, Modeling, and Clinical Applications*, ASME HTD-Vol. 268 (1993) 117–123.
32. Henriques, F.C., "Studies of Thermal Injury. V. The Predictability and the Significance of Thermally Induced Rate Processes Leading to Irreversible Epidermal Injury", *Archives of Pathology*, **43** (1947) 489–502.
33. Clements, P.A., and Gillespie, D., "Egress Constraints on Occupants When Subjected to Radiant Energy", in *Proceedings International Conference on Fire Research and Engineering*, Society of Fire Protection Engineers, Boston, MA (1995) 209–214.
34. Conn, J.J., and Grant, G.A., "Review of Test Methods for Material Flammability", Defensce Research Establishment Ottawa, Contractor Report DREO/PSD/CPS-02/91, Contract No. W7714-9-5932/01-ST (1991).
35. Diller, K.R., Hayes, L.J., and Blake, G.K., "Analysis of Alternate Models for Simulating Thermal Burns", *Journal of Burn Care Rehabilitation*, **12**:2 (1991) 177–189.
36. Mixter, G., "The Emperical Relation Between Time and Intensity of applied Thermal Energy in Production of 2+ Burns in Pigs," University of Rochester Report No. UR-316, Contract W-7041-eng-49 (1954).
37. Beyler, C., "Assessing Flame Radiation to External Targets from Pool Fires," The SFPE Task Group on Engineering Practices, SFPE, June 1999.

Christopher J. Wieczorek, Ph.D. is the Group Manager for Fire & Explosion Protection at FM Global.

Nicholas A. Dembsey, Ph.D., P.E. is a professor of Fire Protection Engineering at Worcester Polytechnic Institute.

Flammable Gas and Vapor Explosions 69

Robert Zalosh

Pertinent Gas and Vapor Flammability Properties

Flammable gases and vapors can produce an explosion when they are ignited while at a concentration between their lower and upper flammable limits, usually in a confined volume. Values of the lower and upper flammable limits for a particular flammable gas or vapor depend on the oxidant and inert gas in the mixture, as well as the mixture temperature. Flammable limits for gas-air mixtures are listed in Chap. 17 and Appendix 3. A more extensive compilation is available in the Zabetakis Bureau of Mines Report [1].

Ignition of the flammable mixture results in flame propagation away from the ignition site, and the expansion of the burned gases behind the propagating flame front. Confinement creates a restraint of this expansion and a resulting increase in pressure within the enclosure. When this pressure increase becomes large enough to create a structural damage potential, the result is an explosion. In the case of the NFPA standards, the term explosion is defined as the bursting or rupture of an enclosure or container due to the development of internal pressure. However, in this chapters an explosion will be regarded as a rapid potentially damaging pressure rise, whether the enclosure remains intact or breaches. In fact, some gas explosions can occur outside an enclosure if the flame speed becomes sufficiently rapid to produce compression waves and potentially damaging pressures with little or no confinement, as discussed at the end of this chapter.

When the flame propagates through the gas-air (or gas-oxidant) mixture at a speed lower than the speed of sound in the unburned gas mixture, the explosion is a deflagration. On the other hand, if and when the flame speed increases so that it is faster than sound speed in the unburned gas mixture, the explosion is called a detonation. The pressures produced in a detonation are substantially higher than those in a deflagration, and the detonation pressure increase occurs as a shock wave whereas the pressure rise in a deflagration occurs more gradually.

The flame speed, v_f, measured in a fixed reference frame, is given by the following equation:

$$v_f = S_u + v_u \tag{69.1}$$

where S_u is the burning velocity of the fuel-oxidant mixture, and v_u is the unburned gas velocity ahead of the propagating flame front. In the absence of turbulence, S_u is called the fundamental or laminar burning velocity of the mixture, and depends on the fuel/oxygen ratio as well and the oxygen/diluent ratio. As described in Chap. 12, the value of the laminar burning velocity is related to the mixture combustion kinetics and flame temperature, and varies inversely as the characteristic combustion reaction time. Tabulated values of S_u, such as those in Table 69.1, refer to the highest measured value of

R. Zalosh (✉)
Firexplo, Wellesley Hills, MA, USA

M.J. Hurley (ed.), *SFPE Handbook of Fire Protection Engineering*,
DOI 10.1007/978-1-4939-2565-0_69, © Society of Fire Protection Engineers 2016

Table 69.1 Deflagration parameters for flammable gases and vapors in air

Gas or vapor	P_{max} (bar g)	Laminar burning velocity (cm/s)
Acetylene	10.6	166
Ammonia	5.4	13[a]
n-Butane	8.0	45
Diethyl ether	8.1	47
Ethane	7.8	47
Ethanol	7.0	41[b]
Ethylene	8.0	80
Hydrogen	6.8	312
Isopropyl alcohol	7.8	41
Methane	7.1	40
Methyl alcohol	7.5	56
n-Pentane	7.8	46
Propane	7.9	46
Toluene	7.8	41

Values taken from Annex D and E of NFPA 68-2007 [2] except for ammonia and ethanol
[a]Value from C. Duynslaegher [3]
[b]Value from Takashi and Kimitoshi [4]

S_u for a particular fuel, oxidant, and diluent, over the entire range of flammable concentrations. This maximum mixture burning velocity often occurs at a concentration slightly richer than the stoichiometric concentration. Representative values for the alkanes and several other hydrocarbons are 40–47 cm/s. Double and triple bond hydrocarbons have significantly higher burning velocities due to their much faster combustion reaction rates.

Most combustion and fire dynamics textbooks, e.g. Drysdale [5], contain theoretical derivations of equations for the laminar burning velocity in terms of gas mixture thermochemical properties. These equations show that S_u is proportional to the mixture thermal diffusivity because it depends on the conduction of heat from the combustion products to the reactants. Since turbulence augments the thermal diffusivity by enhanced mixing of combustion products and reactants, turbulent burning velocities are usually significantly greater than laminar burning velocities, as discussed later in the section on explosions in elongated and obstructed enclosures.

Britton [6] has offered the following empirical equation for estimating laminar burning velocities from the gas-air mixture heat of combustion and the stoichiometric oxygen/fuel ratio.

$$S_u = 1666.1 - 34.228(-\Delta H_c/X_{OF}) + 0.18039(-\Delta H_c/X_{OF})^2 \quad (69.2)$$

where S_u is in cm/s, and
ΔH_C = Heat of combustion of the fuel, kcal/mole
X_{OF} = Stoichiometric ratio of oxygen to fuel.

For example, in the case of methane, $-\Delta H_C = 192$ kcal/mol, and $\chi_{OF} = 2$. In this case, Equation 69.2 yields $S_u = 42.7$ cm/s. This is about 7 % higher than the measured value of 40 cm/s listed for methane in Table 69.1.

The unburned gas velocity in Equation 69.1 depends on the gas mixture geometry and ignition location. For example in the case of a pipe with one closed end, ignition towards the closed end of the pipe will produce a much higher unburned gas velocity than ignition at the open end because the closed end restrains unburned gas motion induced by hot gas expansion. In unrestrained flame propagation, the unburned gas velocity causes the flame speed to be larger than the burning velocity by a factor equal to the ratio of the flame temperature to the unburned gas temperature.

Closed Vessel Deflagration Pressures and Pressure Rise Times

Ignition of a gas-air mixture in an unvented compact enclosure will usually result in a deflagration that produces a pressure increase because of hot gas and unburned gas confinement. The pressure developed in the enclosure is dependent on the extent of flame propagation and the temperature and composition of the burned gas. If the flame has propagated throughout the enclosure, the ratio of the deflagration pressure to the initial pressure in the enclosure can be obtained from the ideal gas equation as it applies to the post-deflagration and pre-deflagration gas-air mixtures, both of which occupy the same enclosure volume. Thus

$$\frac{P_m}{P_0} = \frac{n_b T_b}{n_0 T_0} \quad (69.3)$$

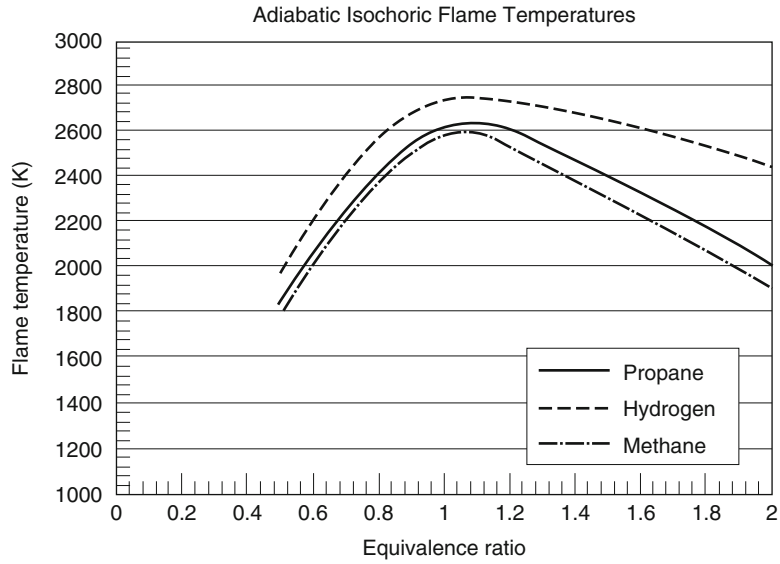

Fig. 69.1 Calculated adiabatic, constant volume flame temperatures as a function of equivalence ratio

where

P_m = Pressure developed at the completion of a closed vessel deflagration

P_0 = Initial pressure in the enclosure

n_b = Number of moles of burned gas at the completion of the deflagration

n_0 = Number of moles of gas-air mixture initially in the enclosure

T_b = Temperature of the burned gas at the completion of the deflagration

T_0 = Initial temperature of the gas-air mixture

Conservative estimates of burned gas temperature and composition can be obtained using the assumption that combustion occurs adiabatically at constant volume. Thus, the calculation of deflagration pressures becomes an exercise in thermochemical equilibrium in which the initial fuel-oxidant mixture is specified to react adiabatically at constant volume. Chemical equilibrium calculation principles and examples are described in Chap. 6. Various computer codes can be used to do these calculations as described below.

Calculated results obtained with the STANJAN code (written and distributed by Professor William Reynolds of Stanford University) are shown in Fig. 69.1 for the adiabatic constant-volume flame temperature, for methane-air, propane-air, and hydrogen-air mixtures of varying concentrations. The fuel concentration used in Fig. 69.1 is the equivalence ratio, defined as the fuel-to-air ratio divided by the stoichiometric fuel-to-air ratio. In terms of fuel volume fraction, x, the equivalence ratio is equal to $[x(1–x_{st})]/[x_{st}(1–x)]$, where x_{st} is the stoichiometric volume fraction of fuel. The stoichiometric fuel volume fraction for methane-air is 0.095, for propane-air, 0.040, and for hydrogen-air, 0.296. The calculated adiabatic constant-volume flame temperatures shown in Fig. 69.1 are generally 200–400 °C higher than the corresponding adiabatic, isobaric flame temperatures for the same fuel-air concentrations.

Although STANJAN is no longer easily available, similar calculations of adiabatic flame temperatures and pressures and combustion products can now be conducted using the GASEQ computer program available for downloading from http://www.arcl02.dsl.pipe.com. Output from GASEQ can also be used for the shock wave and detonation calculations described later in this chapter.

Calculated adiabatic constant-volume deflagration pressures for the same fuel-air mixtures are shown in Fig. 69.2. The maximum pressures for each flammable gas occur at fuel equivalence ratios in the range 1.1–1.2 (i.e., at slightly richer than stoichiometric concentrations). These worst-case deflagration pressures are in the

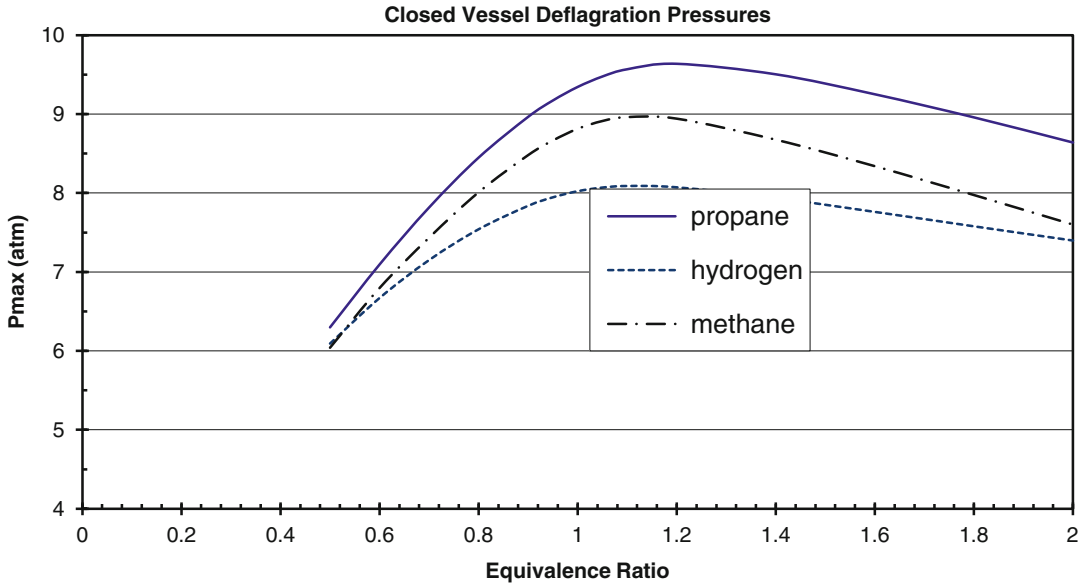

Fig. 69.2 Flammable gas-air deflagration pressures as a function of fuel equivalence ratio

range 8–9.6 atm abs. Theoretical values of P_m at an equivalence ratio of 0.5, which corresponds to the lower flammable limit for methane and propane, are in the range 6–6.5 atm abs. Experimental measurements of closed vessel deflagration pressures agree well with the theoretical values of P_m at near-stoichiometric concentrations but are significantly less than the theoretical values at concentrations near the lower and upper flammable limits. The reasons for the deviation at near-limit concentrations are (1) incomplete combustion due to flame propagation through only a portion of the enclosure and (2) slow flame propagation allowing time for heat losses from the burned gas mixture to the enclosure walls. As an example of the incomplete combustion, extensive deflagration testing of lean hydrogen-air mixtures has shown that the fraction of hydrogen burned ranges from zero to one as the hydrogen concentration increases from its lower limit of 4–8 vol.%, and remains equal to approximately one (complete combustion) as the hydrogen concentration ranges from 8 vol.% to about 40 vol.% (equivalence ratio of 1.6).

Measured values of $P_{\max}$ (worst-case P_m) are shown in Table 69.1 for 14 flammable gases and vapors. All but two values are in the range 6.8 bar–8.1 bar g. The two exceptions are acetylene ($P_{\max} = 10.6$ bar g) and ammonia ($P_{\max} = 5.4$ bar g).

The rate of pressure rise during a deflagration is primarily dependent on the rate of flame propagation and the vessel size, as well as the flame temperature. Theoretical calculations are usually based on the following assumptions. First, it is assumed that the flame speed is small in comparison to sound speed so that the pressures in the enclosure are spatially uniform at any given time during the deflagration. The rate of flame propagation relative to the unburned gas ahead of the flame front is the same burning velocity, S_u, *discussed above*. The mass burning rate is

$$\frac{dm_b}{dt} = -\frac{dm_u}{dt} = \rho_u \chi S_u A_f \qquad (69.4)$$

where

m_b = Mass of burned gas in enclosure at time t
m_u = Mass of unburned gas in enclosure at time t
ρ_u = Density of unburned gas at time t
A_f = Surface area of flame front at time t
χ = Ratio of turbulent burning velocity to laminar burning velocity

Flame propagation into a near-stoichiometric gas-air mixture will occur as an expanding

spherical flame until the flame approaches the walls of the enclosure. Expansion of the burned gas, and the corresponding motion of the unburned gas away from the ignition site as the flame propagates, causes the actual flame velocity relative to a fixed observer (i.e., the flame speed) to be significantly larger than the burning velocity. Before any compression occurs, the flame speed is $(T_b/T_0)S_u$, which is equal to 350–440 cm/s for many hydrocarbons at near-stoichiometric concentrations. Turbulent motion of the unburned gas can further increase the burning velocity and flame speed, as represented either by the augmentation factor χ, or by generating wrinkled or distorted flames with corresponding larger flame surface areas, A_f.

A second key assumption invoked in most theoretical models of closed vessel deflagrations is that the fractional pressure rise at any time during the deflagration is equal to the fraction of the total mass burned, that is,

$$\frac{P - P_0}{P_m - P_0} = \frac{m_b}{m_0} \tag{69.5}$$

where
P = Deflagration pressure at time t
m_0 = Total mass in the enclosure

The justification for Equation 69.5 is that it has been verified by more complicated models, such as the Complete Computer Solution described by Bradley and Mitcheson [7] as well as by experimental data reported in that paper and in Lewis and von Elbe [8]. Equation 69.5 can also be used to calculate the maximum pressure developed in enclosures that are partially filled with fuel-air mixtures (i.e., partial volume deflagrations), as described below in Example 3. Other analytical equations for partial volume deflagrations have been reported by Ogle [9] for a homogeneous pocket of gas and by Jo and Park [10] for a Gaussian gas concentration distribution within the enclosure.

The third assumption needed for a closed vessel deflagration model is the type of thermodynamic process undergone by the unburned gas as it is compressed. The most common assumption is that the unburned gas is compressed isentropically, that is, $P/P0 = (\rho/\rho_u)^{\gamma}$, where γ is the ratio of specific heats of the unburned gas (1.4 for most flammable hydrocarbon-air mixtures). Although it is not necessary, it is also common to assume the flame continues to propagate spherically such that its radius at any time t is r_b in a vessel of radius a. The resulting equations for $P(t)$ and $r_b(t)$ are

$$\frac{dP}{dt} = \frac{3\chi S_u}{a}\left(\frac{P}{P_0}\right)^{1/\gamma}(P_m - P_0)\left(\frac{r_b}{a}\right)^2 \tag{69.6}$$

$$\left(\frac{r_b}{a}\right)^2 = \left\{1 - \left(\frac{P_0}{P}\right)^{1/\gamma}\left[\frac{P_m - P}{P_m - P_0}\right]\right\}^{2/3} \tag{69.7}$$

Equations 69.6 and 69.7 can be solved simultaneously starting from the initial condition that $r_b/a = \varepsilon$ at $t = 0$, where ε is some small number $<<1$ representing the kernel of flame at ignition. An example solution for P(t) and $r_b/a(t)$ for the case $S_u = 45.5$ cm/s, $\chi = 1$, $P_m = 640$ kPa g, $a = 7.15$ m, is shown in Figs. 69.3 and 69.4. The curve in Fig. 69.3 labeled "numerical solution" refers to the numerical integration of Equation 69.6. The curve labeled "analytical approximation" refers to the following simplified solution for P(t) early in the deflagration when $\frac{P-P_0}{P_0} << 1$.

$$\frac{P - P_0}{P_0} = \left[\frac{1}{\gamma} + \frac{P_0}{P_m - P_0}\right]^2\left(\frac{P_m - P_0}{P_0}\right)^3 \times \left(\frac{\chi S_u t}{a}\right)^3 << 1 \tag{69.8}$$

The analytical approximation in Fig. 69.3 is virtually identical to the numerical solution when $P < 2$ psig, and only differs by about 20 % up to $P = 8$ psig. The flame radius at the time $P = 2$ psig is equal to half the enclosure vessel radius, and it is equal to 80 % of the vessel radius when $P = 16$ psig. Since the pressure ultimately increases to 93 psig in this particular deflagration, it is clear that most of the pressure increase occurs when the flame has propagated very close to the enclosure wall, such that the entire enclosure is almost filled with flame.

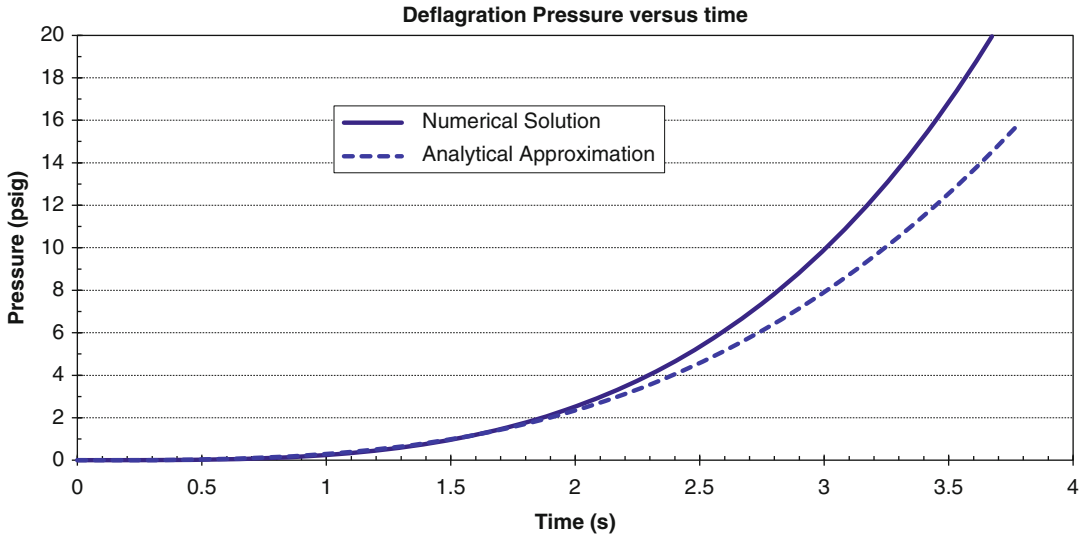

Fig. 69.3 Pressure versus time for a closed vessel deflagration with $S_u = 45.5$ cm/s, a = 7.15 m, and $P_m = 640$ kPa g

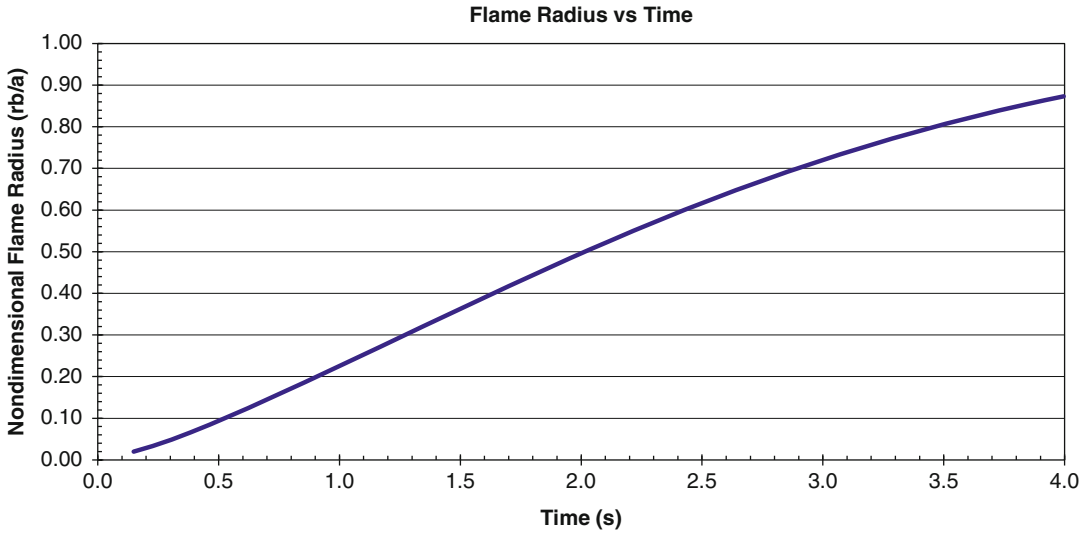

Fig. 69.4 Calculated nondimensional flame radius during deflagration

The continued integration of Equation 69.6 up to $P = P_m$ would require an empirical correlation to account for the variation of S_u with increased pressure and temperature of the unburned gas as it is compressed. Bradley and Mitcheson [7] have carried out non-dimensionalized solutions using such correlations. Their results indicate that the time, t_m, at which P reaches P_m, can be approximated as $t_m = \frac{a}{0.3 S_u}$, where the burning velocity is the mean value of the burning velocities at the beginning and end of the deflagration, i.e., when $P = P_0$ and $P = P_m$. In other words, the mean flame speed, a/t_m, during the deflagration is equal to 3.3 times the mean burning velocity.

Experimental measurements of the rate-of-pressure-rise in a closed vessel explosion are often characterized in terms of the parameter, K_G, defined as

$$K_G = \left(\frac{dP}{dt}\right)_{\max} V^{1/3} \qquad (69.9)$$

where V is the vessel volume, and the maximum rate of pressure rise is measured at the inflection point in the P versus time curve. Theoretically, there is no inflection point (because there is no heat loss or other mechanism to decelerate the flame), and $(dP/dt)_{max}$ occurs when $P = P_m$. Based on Equation 69.5, the theoretical relationship between K_G and S_u is

$$K_G = 4.84\chi S_u \left(\frac{P_m}{P_0}\right)^{1/\gamma} (P_m - P_0) \qquad (69.10)$$

Experimentally determined K_G values have been used in some gas explosion venting guidelines, such as the high strength enclosure method in NFPA 68-2007 [2, 11]. However, the experimental determination of K_G is scale dependent (as described in NFPA 68-2007 Annex D) because the turbulence parameter χ is scale dependent as well as dependent on the possible effects of various flame instabilities.

Partial Volume Deflagrations: Minimum Amount of Flammable Gas to Produce Possible Explosion Hazard

A partial volume deflagration is a deflagration in an enclosure that is only partially filled with a flammable mixture. This is much more likely than having a uniform mixture in flammable gas or vapor release incidents, particularly in large enclosures. A frequent question in these partial volume deflagration scenarios is how much pressure to expect from the burning of the flammable mixture associated with a limited amount of flammable vapor in the enclosure. The following example illustrates a worst-case answer to this question.

Example 1 Approximately 200 g of n-butane are released into an aerosol can-filling room due to a valve misalignment on one large deodorant can. A butane-air mixture forms around the filler as shown in Fig. 69.5. Suppose the butane mixes in stoichiometric proportions with air in this flammable region, and there is no butane in the rest of the 4 × 4 × 3 m room. If the stoichiometric n-butane-air mixture is subsequently ignited, what will the peak pressure be in the absence of any explosion venting?

Solution Equation 69.5 can be used to solve this problem if we first calculate the mass of butane needed to fill the entire room with a stoichiometric butane-air mixture. We can do this calculation in terms of the mixture density, ρ_0, and the butane mass fraction as follows.

$$m_0 = \left(\frac{x_{but} M_{but}}{M_{mix}}\right) \rho_0 V$$

where the mixture molecular weight, M_{mix}, is calculated based on the stoichiometric concentration of butane (3.1 v%).

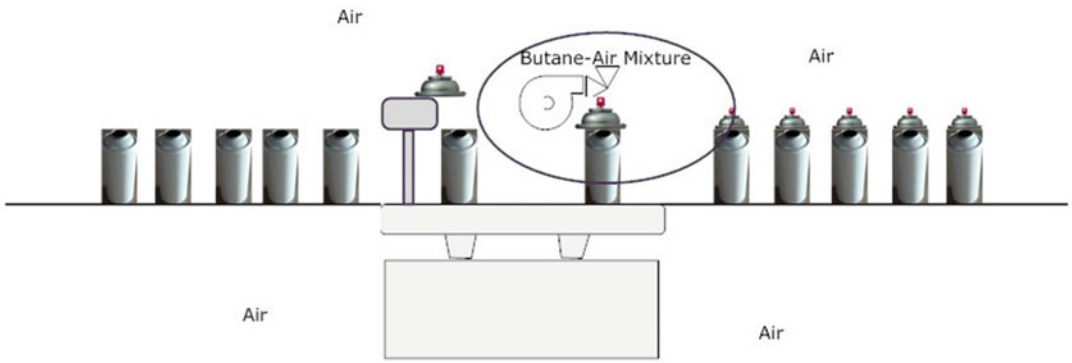

Fig. 69.5 Butane-air mixture formation around aerosol can filler

$$M_{mix} = x_{but}\,M_{but} + (1 - x_{but})M_{air}$$
$$= (0.031)(58) + (1 - 0.031)(28.8) = 29.7$$

The mixture density (which is not much different than air density) is calculated from the ideal gas equation:

$$\rho_0 = \frac{M_{mix}\,P_0}{R\,T_0} = \frac{(29.7\,kg/kmol)\left(101\,x\,10^3\,Pa\right)}{(8314 J/kmol - {}^\circ K)(298\,{}^\circ K)}$$
$$= 1.21\,kg/m^3$$

Therefore,

$m_0 = \left(\frac{(0.031)(58)}{29.7}\right)(1.21\,kg/m^3)(48\,m^3) = 3.52\,kg$

and $m_b/m_0 = (0.20\text{ kg})/(3.52\text{ kg}) = 0.057$.

Using the value for $P_m - P_0$ for n-butane in Table 69.4, $P - P_0 = (8.0\ bar\,g)(0.057) = 0.456\,bar\,g = 6.6\,psig$

We note that since this pressure is greater than the strength of rooms in industrial facilities, some form of explosion venting or explosion suppression would be needed. We also note that this scenario is entirely possible even though the 200 g of n-butane released would be too small to form a flammable mixture if it was dispersed uniformly throughout the 48 m^3 enclosure.

More general partial volume deflagrations calculations have been reported by Ogle [9] for stoichiometric mixture partial volumes and by Jo and Park [10] for Gaussian distribution flammable mixtures. The Ogle result is equivalent to Equation 69.5. Assuming the flammable mixture and air densities are equal, Equation 69.5 can be rewritten as

$$\frac{V_f}{V} = \chi_{st}\frac{P_{dam} - P_0}{P_m - P_0} \tag{69.11}$$

where V_f is the volume of fuel gas or vapor that creates a flammable mixture at stoichiometric concentration, x_{st}, in the enclosure volume V, and P_{dam} is the enclosure structural damage threshold pressure. Jo and Park [10] present the following more alternative equation for V_f/V assuming constant volume combustion to pressure P_m followed by isentropic expansion to pressure P_{dam}.

$$\frac{V_f}{V} = \frac{\chi_{st}}{\omega}\left[\frac{1 - \left(\frac{P_m}{P_0}\right)^{1/\gamma}}{1 - \left(\frac{P_{dam}}{P_0}\right)^{1/\gamma}}\right] \tag{69.12}$$

The parameter ω in Equation 69.12 is the fraction of flammable gas at concentrations between the lower and upper flammable limit. Jo and Park state that the maximum value of ω for their assumed Gaussian concentration distribution is

$$\omega_{max} = \text{erf}\sqrt{\left[\left(ln\left(x_{ufl}/x_{lfl}\right)\right]\right.} \tag{69.13}$$

where erf [ ] denotes the error function, and x_{ufl} and x_{lfl} denote the upper and lower flammable limit volume fraction concentrations, respectively. The value of ω_{max} for most flammable gases is in the range 0.9–1.0, implying that almost all the released gas is in the flammable range in the Jo and Park gas release scenario.

Damage threshold values pertinent to room and building construction and relatively slow pressure rise times (compared to structure characteristic deformation or vibration times) are listed in Table 69.2. The values show that a pressure of 7 kPa (0.07 bar, 1 psig) corresponds to shattering of all windows and the threshold for wood and aluminum panels to start failing. A pressure of about 23 kPa (0.23 bar, 3.3 psig) corresponds to major damage or destruction of typical steel panel industrial buildings.

Table 69.3 shows the values of V_f/V, i.e. flammable gas partial volume fraction,

Table 69.2 Pressure damage thresholds for buildings

Pressure (kPa)	Damage description[a]
3.5–7	Small and large windows usually shattered
7–15	Wood and aluminum panels fasteners fail; panels buckle or blow out
15–20	Unreinforced concrete and cinderblock walls shattered
20	Steel frame buildings distorted and pulled away from foundations
20–28	Self-framing steel panel building demolished
35–50	Nearly complete destruction of houses

[a]From Table B-2 of the CCPS Guidelines for Evaluating the Characteristics of Vapor Cloud Explosions, Flash Fires, and BLEVEs, AIChE 1994

Table 69.3 Partial volumes to produce minor and moderate building damage

Gas or vapor	X_{lfl} (v%)	V_f/V (v%) for $P_{dam} = 7$ kPa	V_f/V (v%) for $P_{dam} = 23$ kPa
Acetylene	2.5	0.051	0.168
n-Butane	1.8	0.027	0.090
Ethanol	3.3	0.048	0.158
Ethylene	2.7	0.057	0.188
n-Hexane	1.2	0.017	0.057
Hydrogen	4.0	0.304	0.998
Methane	5.0	0.083	0.273
Propane	2.1	0.036	0.117
Propylene	2.4	0.036	0.118

calculated from Equation 69.11 to produce the two aforementioned structural damage levels for an assortment of flammable gases and vapors. In the case of the 7 kPa damage level, the fuel partial volume fraction ranges from 0.017 to 0.304 v%. These values are one-to-two orders-of-magnitude lower than the lower flammable limits for the corresponding flammable gases. The V_f/V values reported by Jo and Park [10] are even lower than those in Table 69.3. Thus the common practice of alarming at a flammable gas concentration of one-fourth of the LFL does not necessarily prevent a deflagration if the vapor disperses so as to produce a near stoichiometric concentration in a small portion of the enclosure volume away from the gas sensor location.

Accident scenarios involving flammable liquid spills or heavy flammable vapor releases near floor level produce layered flammable mixtures above the floor. DeHaan et al. [13] conducted experiments with liquid hexane spills, and Tamanini and Chaffee [14] reported on experiments with propane floor layers. The hexane spills in the unventilated enclosure were ignited with an ignition source at an elevation of 5 cm above the floor when the ambient temperature was in the range 11–26 °C, and 20 cm above the floor when the ambient temperature was 33–34 °C. Ignition sources at higher elevations did not produce any ignitions in the 2.4 m high enclosure. Pressure increased as a quadratic function of time rather than the cubic variation indicated in Equation 69.8 because the thin floor layer only allowed cylindrical flame propagation rather than the more spherical flame propagation that occurs with larger or deeper flammable mixtures. Explosion pressures caused explosion vents to open at a pressure of 5–6 kPa.

Some of the propane floor layer ignition tests were conducted in an unvented 64 m^3 enclosure. Flammable mixture volumes occupied from 1.5 % to 7.15 % of the enclosure volume. In some tests ignition occurred while a significant portion of the floor layer had propane concentrations above the upper flammable limit, and flame expansion induced some of the fuel rich propane to mix with air and also contribute to the peak pressure rise. Calculated pressures based on Equation 69.11 (including an attempt to account for the rich mixture fill fraction contribution) agreed to within 9 % of the measured peak pressures in four of the six tests, and were 15–31 % higher than the measured pressures in the other two tests. Thus, Equation 69.11 can be used to obtain reasonably conservative estimates of partial volume deflagration pressures as long as there is some way to estimate the contribution of the fuel rich vapors. Examples of calculation methods for flammable liquid evaporation and stratified layer formation are described by [15] and in the CCPS Guidelines for Use of Vapor Cloud Dispersion Models [16].

Buoyant flammable gas releases form ceiling layers that also produce partial volume deflagrations when and if they are ignited. The partial volume equations are applicable providing the flame propagates through the buoyant ceiling layer, and providing flame accelerations do not produce shock waves. In the case of hydrogen ceiling layers, several test series have been conducted by Kuznetsov et al. [17] to delineate the conditions required for flame propagation with and without shock wave formation. Their results for a 60 cm deep uniform hydrogen ceiling layers in an unobstructed channel showed that hydrogen concentrations of about 15 v% and larger would produce propagation and flame acceleration along the length of the channel. This concentration corresponds to a laminar burning velocity of about 40 cm/s. The magnitude of the acceleration

was even greater when there was a concentration gradient even though the maximum hydrogen concentration at the top of the ceiling layer was no greater than that for a uniform layer. When there were obstructions simulating ceiling beams in a 24 cm deep layer, accelerating flame propagation was observed by Grune et al. [18] with hydrogen concentrations as low as 11 or 12 v%, corresponding to a laminar burning velocity of about 20 cm/s. The flame accelerations produced shock waves at hydrogen concentrations greater than 16–20 v% depending on the layer depth and type of obstructions.

Gas Explosions in Elongated and Obstructed Enclosures

Flame accelerations and corresponding high deflagration pressures are more likely in elongated enclosures, including pipes, and in highly obstructed areas. In both cases the flame accelerations are primarily due to flame stretch and turbulence effects. These effects are more pronounced in reactive mixtures with high burning velocities and flame temperatures (which produce larger burned gas to unburned gas expansion ratios).

Flame acceleration and flame stretch in a pipe are illustrated conceptually in Fig. 69.6. Ignition in the pipe interior produces a near spherical initial flame shape as represented at time t1 in the diagram. At time t2 the flame surface appears like a parabola with the leading edge at the center of the tube where the highest unburned gas velocities are located due to the induced flow ahead of the flame. At time t3 a turbulent boundary layer adjacent to the pipe wall has increased the rate of mixing and heat transfer between burned and unburned gas such that flame acceleration in the region near the wall has caused the flame to stretch in that region to propagate ahead of the flame on the centerline of the pipe. At time t4 the flame is more stretched and fully turbulent and is thicker than the laminar flames. At time t5 the turbulent boundary layer at the wall has caused a significant flame stretch with the leading edge at the wall. Compression waves ahead of the propagating flame have steepened to form a shock at time t5. The advancing compression waves and shock waves can cause the deflagration pressure to be greater than the constant volume deflagration pressures shown in Table 69.1 and Fig. 69.2. Propagating flame and shock wave images corresponding to the diagram in Fig. 69.6 can be found in the textbooks by Strehlow ([19], p. 435) and Lewis and von Elbe ([8], p. 299).

The magnitude of the flame acceleration depends on the pipe/tube dimensions and ignition location and the gas mixture reactivity. For example, Bartknecht [20] obtained the flame acceleration data shown in Fig. 69.7 illustrating the effects of ignition location and pipe end conditions for methane-air flames in a 40 m long pipe. When ignition occurred at the open end, there was virtually no flame acceleration at all because the burned gas expanded out of the pipe rather than inducing a flow toward the opposite end. When ignition occurred in the pipe with both ends closed, the flame accelerated to a maximum speed less than 100 m/s before decelerating and being quenched at the end wall. When ignition was at the closed end and the other end was open, the flame continued to accelerate to a speed of about 250 m/s at the open end of the pipe. Andrews et al. [21] did similar closed pipe experiments on a smaller scale with a range of methane-air concentrations. The highest flame speeds were obtained with near-stoichiometric concentrations, but the maximum flame speed reached in the 7.6 cm diameter pipe closed at both ends (about 37 m/s) was less than Bartknecht observed in the larger pipe. This demonstrates that the turbulence induced flame acceleration is scale dependent such that higher

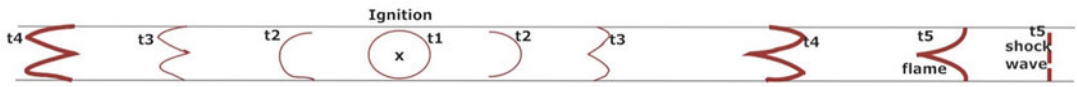

Fig. 69.6 Flame propagation in a tube or pipe

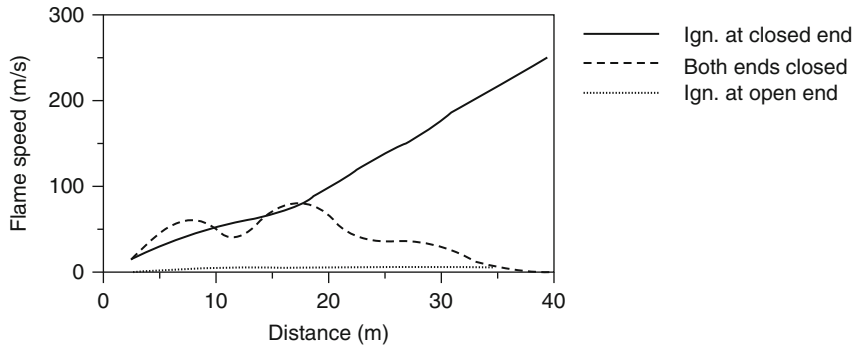

Fig. 69.7 Methane-air mixture flame acceleration in a 1.4 m diameter pipe (From Bartknecht [20])

flame speeds are observed in larger scale pipes and elongated enclosures.

The following linear acoustic relationship between flame speed and deflagration pressure has been shown by Richmond and Liebman [22] and Sapko et al. [23] to be a good approximation for planar flame propagation in pipes and mine galleries.

$$\Delta P = \rho_0 a_0 v_f \tag{69.14}$$

where ΔP is pressure at the flame front, ρ_0 the unburned gas density, a_0 is sound speed in the unburned gas, and v_f is the flame speed. The value of c_0 can be calculated from the following equation

$$a_0 = \sqrt{\frac{\gamma R T_0}{M_0}} \tag{69.15}$$

where γ is the ratio of specific heats, R is the universal gas constant, T_0 is the unburned gas mixture absolute temperature, and M_0 is the unburned gas molecular weight. The acoustic approximation implies that flame speeds are much less than sound speed for Equation 69.14 to be applicable. Equation 69.14 is not applicable when high vent flow velocities near an open pipe or gallery induce high flame speeds at lower pressures than those given by Equation 69.14.

Flame accelerations in elongated enclosures are enhanced by the presence of repeated obstacles in the enclosure because the obstacles stretch the flame and create turbulent wakes as the unburned gas mixture flows around them ahead of the flame. Extensive testing has been conducted with different shaped obstacles that produce various blockage ratios defined as the obstacle area divided by the pipe or channel cross-sectional area. As an example, the circular shaped obstacle blockage ratio effect on the maximum ethylene-air mixture flame speed for propagation in an 11 m long channel and the same length wedge shaped test sector is shown in Fig. 69.8. In the case of the wedge sector, the flame speed increases by an order-of-magnitude as the obstacle blockage ratio increases from zero to about 0.50 and higher.

Figure 69.9 shows the maximum explosion pressures measured in two hydrogen deflagration test programs in obstructed elongated enclosures. The tests in a 5 cm diameter tube with repeated orifice rings were reported by Lee et al. the data obtained with the 0.44 blockage ratio rings are shown in Fig. 69.9. The measured peak pressures were much lower than the constant volume deflagration pressures (Equation 69.3) when the hydrogen concentration was less than 13 vol.%, but were larger than the constant volume deflagration pressure at hydrogen concentrations of 13 vol.% and greater. This clearly demonstrates that the repeated obstacles are particularly important for reactive mixtures with relatively high laminar burning velocities. The laminar burning velocity for a 15 % H_2 in air mixture is about 40 cm/s, and for a 30 % (near-stoichiometric) hydrogen concentration the mixture burning velocity is about 210 cm/s ([24], p 44).

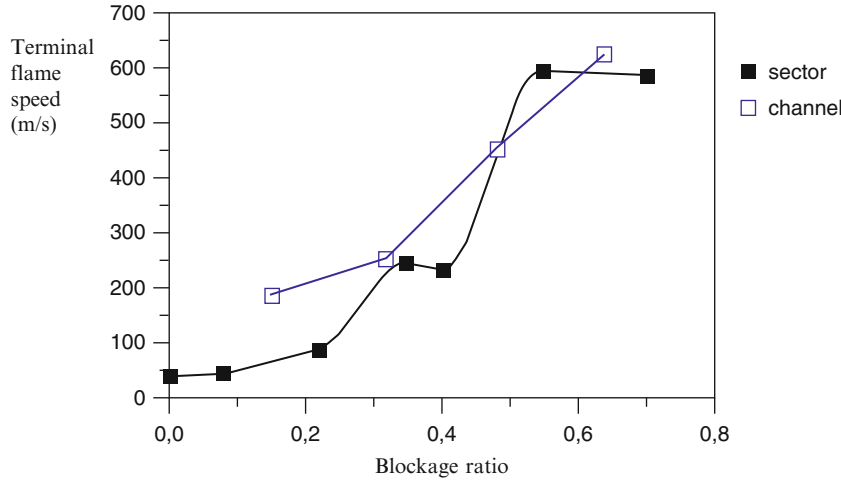

Fig. 69.8 Obstacle blockage ratio effects on ethylene-air mixture flame speeds in a channel and wedge sector (From GexCon Online Gas Explosion Handbook)

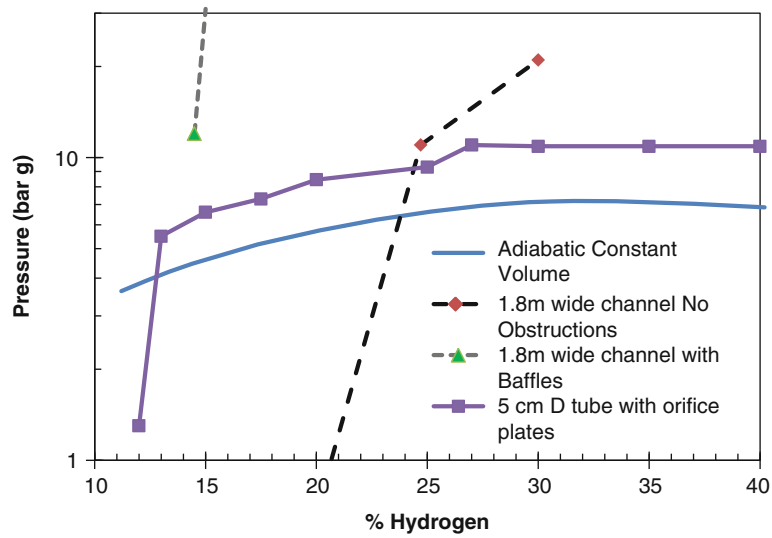

Fig. 69.9 Pressures measured during hydrogen flame propagation in tubes and channels

Qualitatively similar results on a much larger scale were obtained by Sandia National Laboratories [25] in hydrogen-air mixture tests in their FLAME test structure which is a 30.5 m long channel with a 1.83 × 2.4 m cross-section. As shown in Fig. 69.9, without any obstacles in the channel, the pressures were much less than the adiabatic constant volume pressure for hydrogen concentrations less than about 25 %, but exceeded the constant volume pressures at 25 % and above. When equally spaced vertical obstructions with a 0.33 blockage ratio were installed in the channel, the measured peak pressures were much larger than the adiabatic, constant volume pressures in both tests with hydrogen concentrations of about 15 %. Additional data not shown in Fig. 69.9 were obtained with higher concentrations, but with part of the obstructed channel roof removed to allow for venting. Most, but not all of those tests resulted in pressures well below the constant volume pressures.

Repeated obstacles can also induce large flame accelerations and potentially damaging deflagration pressures in large open and partially confined applications. However, for a given flame speed and gas mixture, the pressures developed are lower as the degree of confinement decreases. As in the completely confined situation, the magnitude of the flame acceleration is scale dependent, and also dependent on the characteristics of the turbulent flow ahead of the propagating flame. The two independent characteristics of this turbulence are the integral length scale, $\underline{L}$, and the root-mean-square (rms) turbulent velocity fluctuation, u'. In the case of repeated obstacles, the turbulence length scale is some fraction of the obstacle characteristic dimension, and the rms turbulence velocity is some fraction of the unburned gas velocity ahead of the propagating flame. In the case of fan induced turbulence, the integral length scale is some fraction of the fan blade length, and the rms turbulent velocity is some fraction of the blade tip speed.

In principle, the effects of turbulence on flame propagation speed can be expressed in the following functional form.

$$\frac{S_t}{S_u} = f\left(\frac{u'}{S_u}, Re_{\underline{L}}, Le\right) \tag{69.16}$$

where S_t is the gas mixture turbulent burning velocity, S_u is the previously discussed mixture laminar burning velocity, and $Re_{\underline{L}} = \frac{u'\underline{L}}{\nu}$, $Le = \frac{k}{\varrho_u c_p \mathcal{D}}$. The unburned gas property values in $Re_{\underline{L}}$ and Le are ν, the kinematic viscosity, k, the thermal conductivity, c_p, the specific heat, and $\mathcal{D}$ is the diffusion coefficient of the reactant (oxygen or flammable gas) whose concentration is less than stoichiometric. Abdel-Gayed et al. [26] have developed graphical correlations representing Equation 69.16 for laboratory data on fan stirred closed vessel explosions and turbulent burner flames. Their correlations show S_t/S_u increases with increasing values of u'/S_u and also increasing values of $Re_{\underline{L}}$. For example, a maximum value for S_t/S_u of about four occurs when u'/S_u is in the range 5–8 and $Re_{\underline{L}}$ is 100, but S_t/S_u can be as large as 10 when $Re_{\underline{L}}$ is equal to 1000. Thus, accounting for the turbulent burning velocity is a key factor in any realistic estimate of enhanced flame speeds due to repeated obstacles and other sources of turbulence. This is also one of the primary considerations governing the accuracy and reliability of current Computational Fluid Dynamics computer code calculations for explosions entailing turbulent flame propagation.

Two other considerations pertinent to understanding and assessing explosions in obstructed and complex geometries are flame instabilities and flame quenching. Flame instabilities generate increases in the flame surface area due to wrinkling and distortions caused by various hydrodynamic and thermo-diffusive mechanisms. The increased flame surface area causes increases in the burning rate, as indicated by Equation 69.4, and associated rates of pressure rise. Flame quenching can occur due to heat losses from the reacting gases, and also when the turbulence becomes so great that the gases pass through the reacting region before the combustion reaction is complete. In turbulence parlance, the chemical reaction time becomes larger than the turbulent eddy (where mixing of burned and unburned gases occurs) time scale. Abdel-Gayed and Bradley [27] have developed criteria for flame quenching due to excessive turbulence.

Detonations

A detonation is an explosion in which the combustion wave (i.e., flame) propagates at supersonic speeds through the unburned fuel. Detonations are fundamentally different than the closed vessel deflagrations described in the previous section of this chapter. Since flames in a deflagration propagate at speeds well below the speed of sound (which is about 340 m/s in room temperature air), the pressure increase during a deflagration occurs virtually uniformly throughout the enclosure as the explosion evolves. In contrast, the pressure rise during a detonation is highly non-uniform and occurs virtually instantaneously as the shock wave propagates through the gas-air mixture. If the flame speed is slightly

less than the speed of sound, such that the pressure rise is non-uniform but shock waves do not occur, the explosion is called a quasi-detonation.

The practical significance of this fundamental difference between detonations and deflagrations is that they require different approaches to explosion protection. The sudden, spatially non-uniform pressure rise during a detonation or quasi-detonation precludes the use of explosion venting or explosion suppression systems. Furthermore, the high-peak, short-duration detonative pressure loads warrant special considerations in the evaluation of structural resistance.

The peak pressure during a detonation can be calculated from the classical Chapman-Jouguet theory, which is a combination of thermochemical equilibrium and gas dynamic conservation equations across the detonation front [8, 19]. Figure 69.10 shows calculated detonation pressures as a function of fuel concentration for seven different flammable gases. Chapman-Jouguet calculations for these and other mixtures can be conducted with both the GASEQ and CET89 computer codes mentioned previously for deflagration calculations. Burgess et al. [28] and others have suggested that a good approximation to the Chapman-Jouguet detonation pressure, P_{CJ}, P_{CJ} is $= 2P_m$ (i.e., twice the closed vessel deflagration pressure). This approximation represents a much simpler alternative to the Chapman-Jouguet theory of calculating detonation pressures. As indicated in Fig. 69.10, P_{CJ} for a near-stoichiometric gas-air mixture initially at atmospheric pressure is in the range 16–20 atm.

The pressure distribution behind the C-J detonation front is shown in Fig. 69.11 for the case of a detonation wave propagating in both directions away from the initiation site in a tube. Behind the propagating detonation front the pressure decreases to a plateau value equal to about 0.35 P_{CJ}. The speed of propagation is equal to the C-J Mach number times the speed of sound in the unburned gas-air mixture. If the tube has one or more closed ends, the detonation wave will be reflected and propagate in the reverse direction with increased amplitude. If the end wall is rigid, the reflected shock wave for many gas-air mixtures is equal to 2.76 P_{CJ}. If the end wall is open, the detonation wave will be reflected as a rarefaction wave propagating back toward the detonation initiation site.

The structural load associated with a detonation wave depends on the impulse, I_D, per unit area, where

$$I_D(x,t) = \int_{t_a}^{t} [p(x,t) - p_a]\,dt$$

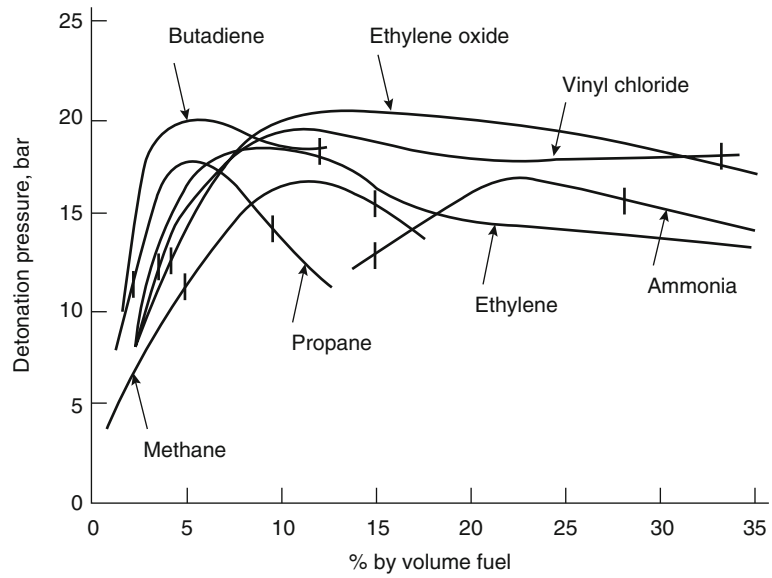

Fig. 69.10 Chapman-Jouget detonation pressures

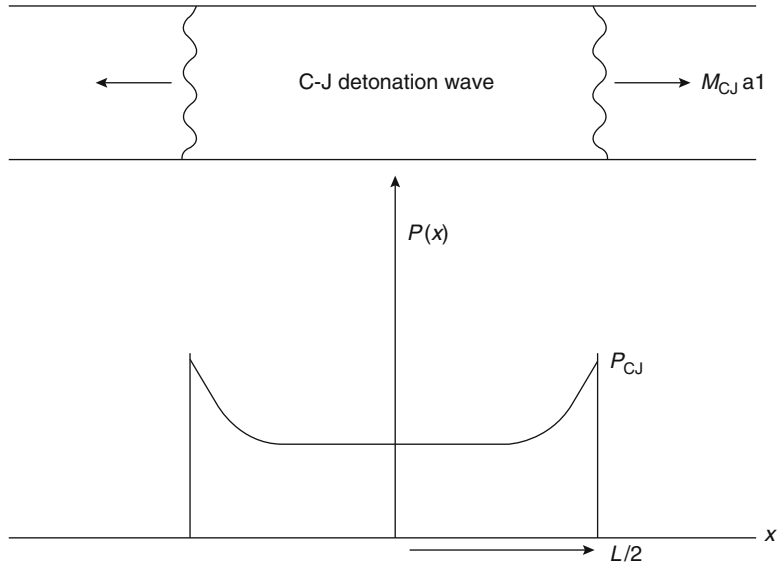

Fig. 69.11 Detonation wave propagation and pressure distribution in a pipe

The detonation front arrival time, t_a, is equal to $\frac{x}{M_D a_1}$, where x is the distance from the detonation initiation site, M_D is the detonation Mach number, and a1 is the speed of sound in the unburned gas-air mixture.

Neglecting any reflected waves, Sichel [29] has shown that a good approximation for I_D is

$$I_D = \frac{0.35 \rho_1 a_1 M_D x}{(\gamma_2 + 1)} \qquad (69.17)$$

where γ_2 is the ratio of specific heats in the burned gas; in many cases γ_2 is equal to 1.2. The C-J detonation Mach numbers for several stoichiometric gas-air mixtures are listed in Table 69.4. They are in the relatively narrow range 4.9–5.5. The unburned gas sound speed for most stoichiometric hydrocarbon-air gas mixtures is in the narrow range 330–350 m/s, while for hydrogen it is 403 m/s.

An interesting aspect of Equation 69.17 is that the specific impulse is linearly proportional to the distance from detonation initiation site. Burgess et al. [28], note that pipeline detonations often cause periodic ruptures along the pipeline length, with each break serving as a pressure relief expansion, requiring the pressure duration/impulse to rebuild to the structural failure threshold again by propagating over another length of pipe. Methods to assess the structural damage potential from these impulsive loads generated during detonations are described by Baker et al. [30]. One after-the-fact indication of structural failure due to detonative loads is the occurrence of fragmented structural debris associated with brittle failure, as opposed to the bulging and more ductile failure of structural steel subjected to deflagration pressures beyond the yield point.

In view of the drastically different explosion protection considerations for detonations, it is important to assess the potential for a detonation

Table 69.4 Detonation Mach numbers and cell sizes for stoichiometric gas-air mixtures

Gas	C-J Mach number[a]	Cell width (cm)[b]
Acetylene	5.46	0.98
n-Butane	–	5.0–6.2
Ethane	–	5.4–6.2
Ethylene	–	2.8
Hydrogen	4.89	1.5
Hydrogen sulfide	–	10
Methane	5.17	28
Propane	5.38	6.9
Propylene	–	5.4

[a]C-J Mach numbers were calculated with the STANJAN computer code
[b]Detonation cell width data is from Sulmistras et al. [12]

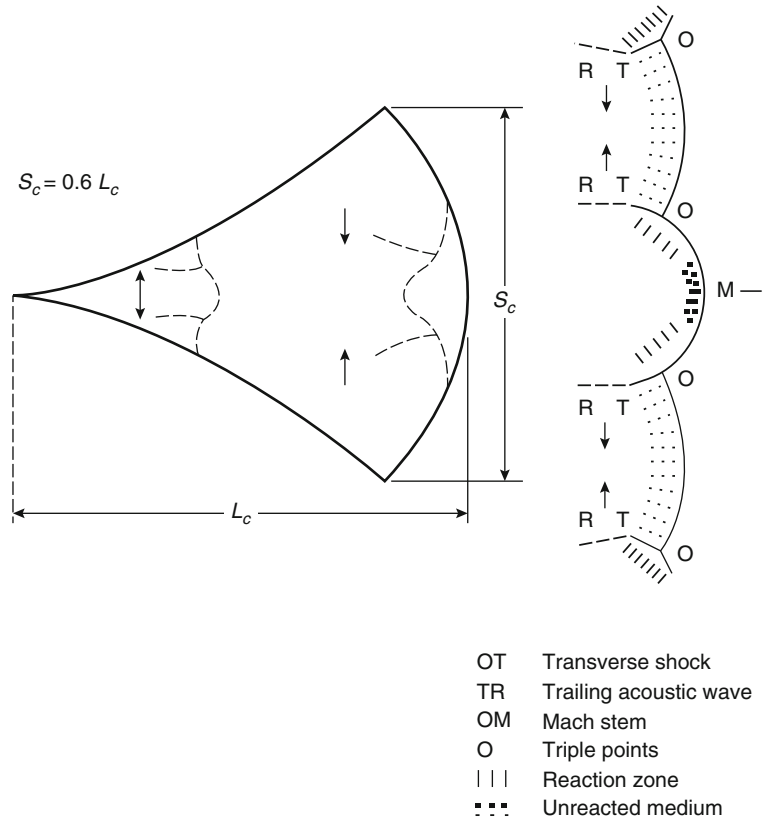

Fig. 69.12 Detonation cell structure

to occur as opposed to a deflagration. Some guidance, as described below, can be offered for this assessment, but there are no exact criteria to provide an unequivocal answer.

The detonability length scale is the detonation cell width, S_c, shown in Fig. 69.12. As indicated in Fig. 69.12, the detonation front consists of a complicated network of curved shock segments that propagate transversely to the detonation propagation direction. The transverse wave structure includes curvilinear triangles with a width S_c. If a smoke foil is inserted on the inner wall of a detonation tube, the detonation cells create a diamond or fish-scale shaped pattern on the smoke foil. Detonation cell widths are measured from the traces deposited on these smoke foils as described, for example, by Gelfand et al. [31].

Detonation cell widths can also be correlated with the detonation reaction zone length in a one-dimensional representation of the shock wave initiated chemically reacting flow behind the leading edge of a detonation. This model, which is called a ZND model (the initials stand for three original model developers), requires some chemical kinetics data as well as an assumption about heat losses and drag associated with the tube wall. The calculations and their relationship to cell size are described by Gelfand et al. [31], by Shepherd [32], and by Stamps et al. [33].

Detonation cell widths measured/calculated for nine different stoichiometric gas-air mixtures are listed in Table 69.4. Values range from about 1 cm for acetylene to about 28 cm for methane. These values were obtained at atmospheric pressure and room temperature. Higher initial pressures and temperatures would result in smaller cell widths. Furthermore, some of the gases listed in Table 69.4 have smaller cell widths at some fuel-rich concentrations, with minimum values for a given fuel being as

much as 40 % smaller than the values shown in the table.

A sustained detonation can only occur if the characteristic length scale of the gas-air mixture is greater than some multiple of the detonation cell width. The value of the multiplication factor depends on the geometry. In the case of a pipe, the detonation will not propagate down the pipe if the pipe diameter is less than about $S_c/3$. The detonation will not propagate from open end of the pipe into the surrounding gas mixture if the pipe diameter is less than 13 S_c.

What is the likelihood of a detonation occurring in an enclosure or cloud larger than the critical size indicated by the detonation cell size? The answer depends on the strength of the ignition source and the presence of either a highly elongated enclosure geometry or an exceptionally high level of turbulence for promoting flame acceleration. The minimum ignition source energy required for the direct initiation of a detonation ranges from a low of about **5** kJ for acetylene and hydrogen in air to a high estimated to be 93,000 kJ for methane. Since these initiation energies are many orders-of-magnitude larger than the energies associated with accidental ignition sources, direct initiation can be precluded from almost all accident initiation scenarios.

In the case of an accidental ignition source in a pipe or some other elongated enclosure, the deflagration-to-detonation transition (DDT) distance depends upon the following parameters.

Mixture Reactivity: The more reactive the mixture, the more rapid is the flame acceleration to DDT.

Enclosure or pipe wall roughness and the possible presence of obstruction: The rougher the pipe interior surface or the more obstructions present, the shorter is the transition length to DDT.

Enclosure or pipe diameter: The larger the pipe or enclosure diameter, the shorter is the transition to DDT.

Initial pressure and temperature: The higher the initial temperature and pressure, the shorter is the transition length to DDT.

Initial turbulence level: The more turbulence or initial gas velocity in the enclosure, the shorter is the DDT transition length.

Figure 69.13 illustrates how mixture reactivity influences the DDT length/diameter ratio for the case of a smooth walled 2-in. (5-cm) diameter pipe [34]. The ratio of DDT transition length to pipe diameter is plotted as a function of the ratio of nitrogen/oxygen concentration for methane, for ethane, and for propane at near-worst-case

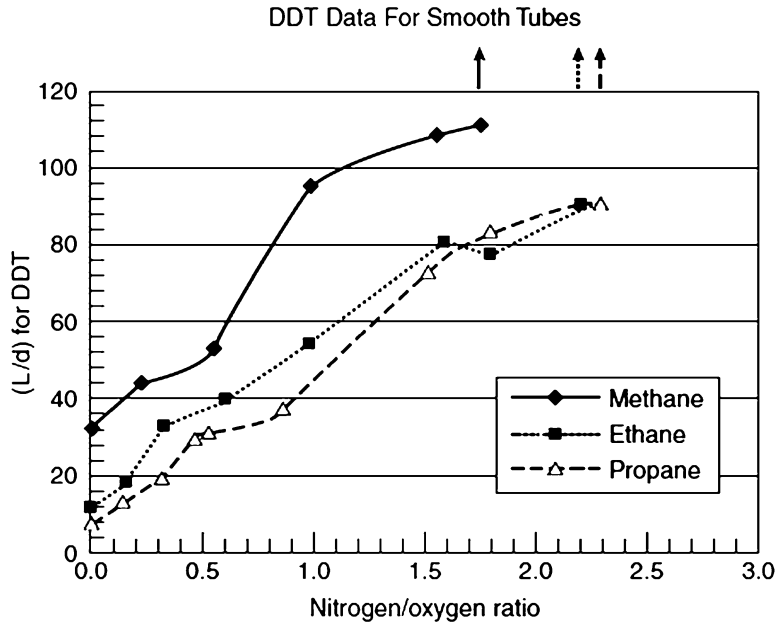

Fig. 69.13 Detonation run up L/D in smooth tubes

fuel/oxygen ratios that produce stoichiometric combustion with CO formation instead of CO_2. The L_{DDT}/diameter ratio increases rapidly as the nitrogen/oxygen ratio increases for all three alkanes, with the transition length being shortest for propane and longest for methane. In these experiments, the largest N_2/O_2 ratio at which transition occurred (last data point on each curve) was less than the 3.76 ratio corresponding to air. In other words, the L_{DDT}/diameter ratio for these alkanes in air (at a 2-in. pipe diameter) is larger than the largest ratio (120) measurable in these experiments. The three arrows in the graph represent the absence of transition at the indicated N_2/O_2 ratio. This data is consistent with the experimental observations of Flessner and Bjorklund [35], who did not see DDT with gasoline-air mixtures in a 15 cm-diameter, 16 m long smooth wall pipe, but saw DDT at a distance of 74 pipe diameters when they inserted an expanded metal liner in the pipe entrance to simulate a rough wall section.

Hydrogen-air mixtures are susceptible to DDT in both smooth and obstructed pipes and channels providing the hydrogen concentration is sufficiently high. The data in Fig. 69.9 provide a good indication of the minimum hydrogen concentration for DDT in the presence of obstructions in small diameter (5 cm) piping, and for smooth and baffled large width (1.8 m) channels. The flame speeds measured in the 1.8 m wide channel confirm DDT at hydrogen concentrations that produced peak pressures well above the adiabatic constant volume deflagration pressures. In the case of highly obstructed channels and piping, the critical hydrogen concentration for DDT seems to be 13–14 %. In case of large unobstructed channels, the critical concentration appears to be about 25 %.

Near stoichiometric concentration hydrogen-air mixture smooth pipe Length-to-diameter ratios needed for DDT were measured by Blanchard et al. [36] in a 16 cm diameter pipe. The DDT run up distance depended on the igniter location relative to the pipe end wall. The shortest measured DDT length was 8 m, corresponding to a L_{DDT}/diameter ratio of 50.

Sherman and Berman [37] have developed a semi-quantitative methodology to categorize the probability of detonations occurring in specific industrial accident scenarios by subjectively extrapolating the experimental data on the various effects mentioned above. They categorize gas mixture reactivities on the basis of detonation cell size, and they categorize enclosure geometries on the basis of size, confinement, level of obstructions, amount of venting, etc. They have applied their methodology to the case of a possible hydrogen detonation during hypothesized severe accident scenarios in one particular nuclear plant containment building.

Although most accidental explosions are deflagrations, there are some occasional well-documented accounts of detonation incidents. One excellent example is the Jacobs et al. [38] description of a particularly destructive detonation in a section of a petroleum refinery in which a gas mixture of 3 % naptha, 19 % oxygen, and 78 % inert gas at 105 psig was accidentally allowed to enter several large pieces of process equipment connected by over 1000 ft of piping. Their account of the incident includes a description of the flame propagation path and associated pressures (3000–4000 psi in some locations) developed.

Example 2 A large process oven is heated with a burner utilizing a 1-cm-diameter, 5-m-long fuel line containing a stoichiometric propane-air mixture. What is the likelihood of a detonation occurring in the oven and the fuel line as a result of a delayed ignition after the oven has been inadvertently filled with a fuel-air mixture? How would the situation change if a stoichiometric hydrogen-air mixture replaced the propane-air mixture in the fuel line?

Solution From Table 69.4 $Sc = 6.9$ cm for a stoichiometric propane-air mixture. Thus, the minimum pipe diameter for detonation propagation in this case is $Sc/3 = 2.3$ cm. Therefore, a sustained propane-air detonation will not propagate through the 1 cm fuel line. If the propane is replaced by hydrogen, $Sc/3 = 0.50$ cm, and a fuel line detonation would be possible,

particularly in view of the 500:1 length to diameter ratio.

In order for the detonation to be transmitted into the oven, the fuel line would have to be larger than 13 $Sc = 20$ cm for hydrogen. Thus, the oven should not experience a detonation. Explosion venting could be a viable form of explosion protection for the oven.

Example 3 If a detonation did propagate through a stoichiometric hydrogen-air mixture in the fuel line, what would the specific impulse be on the pipe wall. Neglect any reflected shock wave effects, and use a sound speed of 400 m/s for the unburned stoichiometric hydrogen-air mixture.

Solution Before using Equation 69.11 to evaluate the specific impulse, we need to calculate the molecular weight and density of the stoichiometric hydrogen-air mixture.

$$\rho_{mix} = \frac{M_{mix}}{M_{air}}\rho_{air} = \frac{[(0.295)(2) + (1 - 0.295)(28.8)}{28.8}\left(1.2\,kg/m^3\right) = 0.87\,kg/m^3$$

Using the C-J detonation Mach number for stoichiometric hydrogen-air listed in Table 69.4,

$$I = \frac{0.35(0.87\,kg/m^3)(400\,m/s)(4.89)(5\,m)}{(1.2+1)}$$
$$= 1354\,Pa - s$$

If we assume the pressure is effectively relieved when the detonation reaches the open end of the tube, the detonation duration in the 5 m long pipe is $\frac{5m}{4.89\,(400\,m/s)} = 2.56\,m\,\mathrm{sec}$. The average pressure exerted on the pipe wall is $I/t_{dur} = 530$ kPa = 77 psig. This value is about one-third of the C-J detonation pressure. Structural analysts familiar with dynamic loadings can use these values and the pipe wall properties to determine whether the fuel line should survive the detonation.

Blast Waves and Vapor Cloud Explosions

Blast waves are the explosion pressure disturbances that propagate away from the energy source. In the case of flammable gases and vapors, the energy source is usually the combustion energy. However, in the case of pressure vessel bursts, the blast energy is due to the compressed gas expansion energy released upon vessel rupture. The blast wave will propagate into the surrounding atmosphere and will decay with distance from the enclosure. A common question with regard to explosion protection is whether the blast wave at a particular location will be sufficiently strong to cause damage or injury. Simplified methodology to address this question is presented here along with reference citations for more thorough and extensive analyses.

If we confine our attention to distances that are large in comparison to the characteristic diameter of the breached enclosure or the energy deposition spatial scale, we can often deal with relatively simple far-field blast wave scaling correlations. The characteristic shape of the far-field blast wave is shown in Fig. 69.14. It consists of a shock wave with a pressure rise, P_S, followed immediately by a rarefaction wave in which the pressure decays to some value below atmospheric pressure, and then a gradual recovery to atmospheric pressure, P_0. Sometimes the final pressure recovery occurs in the form of a second shock, and the shape takes the form of a slightly deformed letter N, thus leading to the term *N wave*.

Blast wave correlations are often in the form of a non-dimensional pressure $(Ps - P_0)/P_0$ and a non-dimensional distance from the blast source. The non-dimensional distance, $\overline{R}$, is defined as:

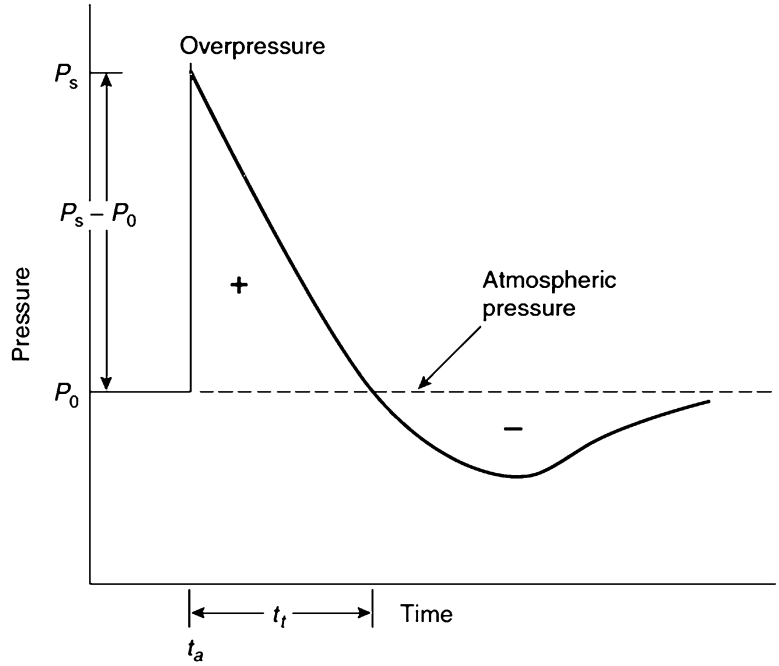

Fig. 69.14 Blast N-wave pressure vs time

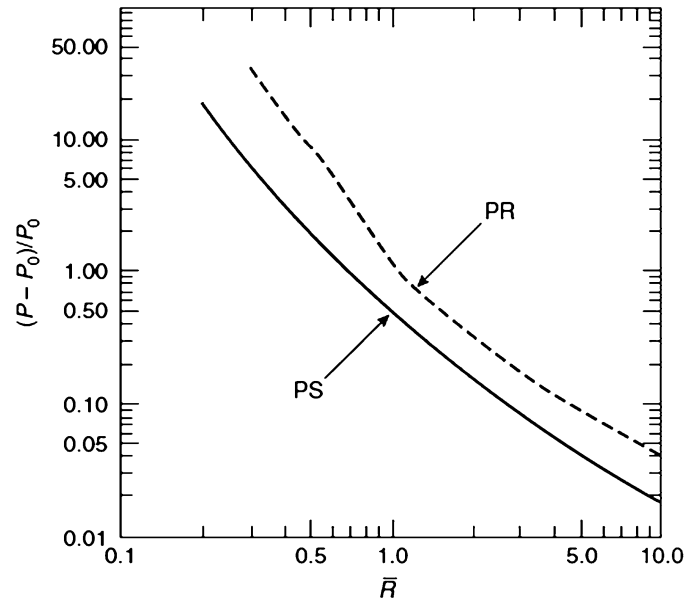

Fig. 69.15 TNT equivalent blast wave pressure versus energy scaled distance

$$\overline{R} = R\left(\frac{P_0}{E}\right)^{1/3} \tag{69.18}$$

where R is the actual distance from the blast source (m), E is the blast wave energy (J), and P_0 is in Pa.

The correlation for non-dimensional pressure versus $\overline{R}$ is shown in Fig. 69.15. The curve labeled PS in Fig. 69.15 refers to the incident overpressure, and the curve labeled PR refers to the reflected blast wave pressure resulting from a blast wave being reflected head-on from a rigid

wall. Neither curve in Fig. 69.15 accounts for the reflection of the shock wave off the ground surface. The usual procedure for including ground surface reflection is to use twice the calculated blast wave energy when using the correlations in Fig. 69.15.

The implication in this type of blast wave scaling correlation is that the blast wave is characterized by only one parameter, the blast energy, E. In the early theoretical models of blast wave pressure, the energy is assumed to be released instantaneously, at a single point. This approach is called ideal blast wave theory. The correlations for ideal blast waves are based on a combination of theory and test data from condensed phase, compact explosives. Baker et al. [30] describe the development of these correlations, which include non-dimensional blast wave impulses, positive-phase durations, and many other parameters. The impulse is particularly important for doing dynamic structural response analyses, such as those described by Kinney and Graham [39].

Can the blast waves from various accidental explosions be predicted from these ideal blast wave correlations? In some cases the answer is unequivocally yes. A good example is the blast wave from a ruptured pressure vessel containing a gas that is not ignited upon release.

The energy associated from this type of physical explosion is the energy of expansion of the gas as it goes from an initial pressure, P_1, to atmospheric pressure. Perfect gas isentropic expansion representations of this energy is

$$E = \frac{(P_1 - P_0)V}{\gamma - 1} \qquad (69.19)$$

where V is the vessel volume and γ is the gas ratio of specific heats. Other approaches to this problem including the assessment of vessel fragment shrapnel effects are described in the AIChE Consequence Analysis Guidelines [40].

If the breached vessel fails as a result of an internal combustion explosion, of if the vessel is vented per explosion venting guidelines, the blast wave analysis is considerably more complicated because there is a combustion energy contribution to the total blast wave energy. Correlations to predict blast waves from vented explosions are contained in NFPA 68 [2]. More detailed equations, including two-dimensional considerations, are described by Forcier and Zalosh [41].

Another special consideration in breached vessel blast waves is the blast wave and fragment shrapnel released when a liquefied gas undergoes a Boiling Liquid Expanding Vapor Explosion (BLEVE) as a result of severe fire exposure. Correlations for BLEVEs, and some of the research leading to these correlations, is described in the AIChE Center for Chemical Process Safety *Guidelines for Evaluating the Characteristics of Vapor Cloud Explosions, Flash Fires, and BLEVEs* [42].

Another very important special consideration is the blast wave associated with vapor cloud explosions. These explosions occur when a very large cloud of flammable gas or vapor is ignited in a highly obstructed environment such as a chemical or petrochemical plant with a high density of process/storage equipment and piping. The strength of the blast wave that occurs in a vapor cloud explosion is dependent on the flame speed that develops and the degree of confinement in and around the vapor cloud.

In some extreme cases of repeated obstructions, vapor cloud detonations can occur with blast wave pressure transients similar to the ideal blast wave shape shown in Fig. 69.14. More often, the flame speed is subsonic and the blast wave pressure transient appears as shown in Fig. 69.16, i.e. without a leading edge shock wave. The pressure rise time in these vapor cloud deflagrations depends on the flame speed and distance from the flammable cloud, with high subsonic flame speeds producing relatively steep compression waves ahead of the flame front.

There are separate impulses, I_+ and I_- associated the areas under the portions of the curve with positive pressures relative to atmospheric pressure, and with sub-atmospheric pressures. The blast wave scaling of these impulses is given by the following equation.

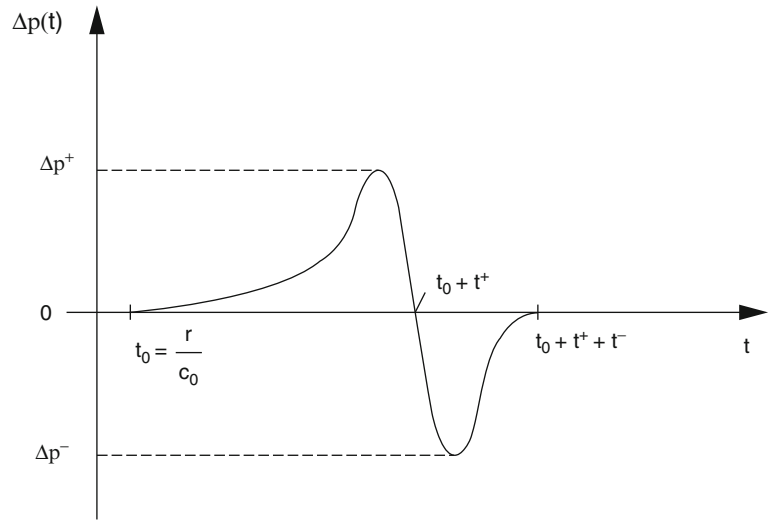

Fig. 69.16 Blast wave pressure transient for subsonic flame propagation in vapor cloud (From Souchet [43])

$$\bar{I}_+ = \frac{I_+ a_0}{p_0^{4/3} E^{1/3}} \tag{69.20}$$

where $\bar{I}_+$ is the non-dimensional impulse, and a_0 is sound speed in air.

The vapor cloud explosion blast wave energy is usually calculated from the volume of flammable gas in the obstructed or partially confined region of a facility. If we denote this volume as V_{vc}, and conservatively assume that the gas concentration in the cloud is the stoichiometric concentration, x_{st}, the vapor cloud explosion energy is

$$E = \rho_g V_{vc} x_{st} \Delta H_c \tag{69.21}$$

where the heat of combustion, ΔH_c, is now on a per unit fuel mass basis. If a vapor dispersion analysis is conducted, the resulting average flammable gas concentration in the obstructed region can be used instead of x_{st}.

Early assessments of vapor cloud explosion blast waves were conducted using the idealized blast wave type correlations described here, along with some rough guess at the energy yield (i.e., the fraction of the available combustion energy actually contributing to the blast wave). However, these early efforts were not very successful because (1) most of the interest is in the near field rather than the far field, and (2) even the far-field assessments were not accurate because the vapor cloud explosion blast wave strength and impulse decay much less rapidly than that of an ideal blast wave. Therefore, three other types of blast wave models are utilized now for vapor cloud explosions.

The mostly used approach is the use of numerical solutions to the full set of compressible gas conservation equations assuming one-dimensional (usually spherical) flame propagation at some assumed constant flame speed through a size vapor cloud of specified radius. The flame speed is usually expressed as a Mach number, $M_f = v_f/a_0$, (where a_0 is ambient air sound speed) and the computational results are presented in non-dimensional form using blast wave scaling. Figures 69.17 and 69.18 are the plots developed by Baker et al. [44, 45] for non-dimensional pressure and impulse versus energy scaled distance from the center of the vapor cloud. The maximum pressures in Fig. 69.17, corresponding to small values of $R\left(\frac{P_0}{E}\right)^{1/3}$, are the pressures developed within the cloud itself. They can be estimated with the following equation from Tang and Baker [46].

$$\frac{P_{max} - P_0}{P_0} = 2.4 \frac{M_f^2}{1 + M_f} \tag{69.22}$$

After comparing calculated pressures with pressures measured in medium scale vapor

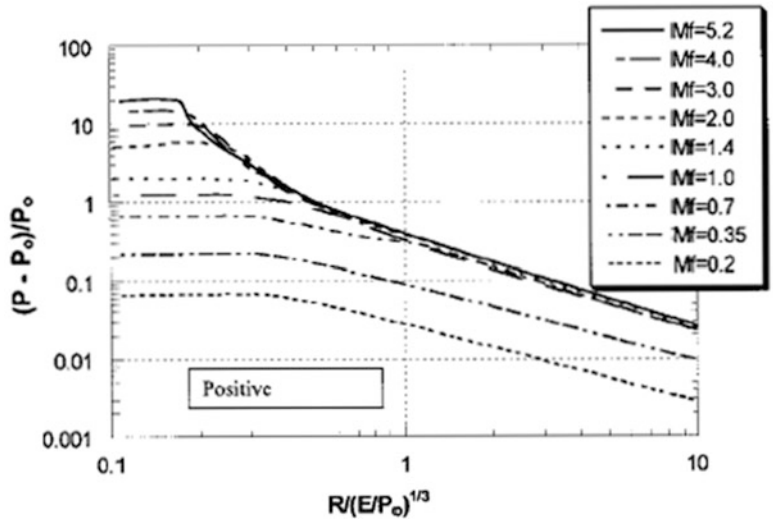

Fig. 69.17 Baker-Strehlow-Tang vapor cloud explosion pressure versus distance (From Pierorazio et al. [44])

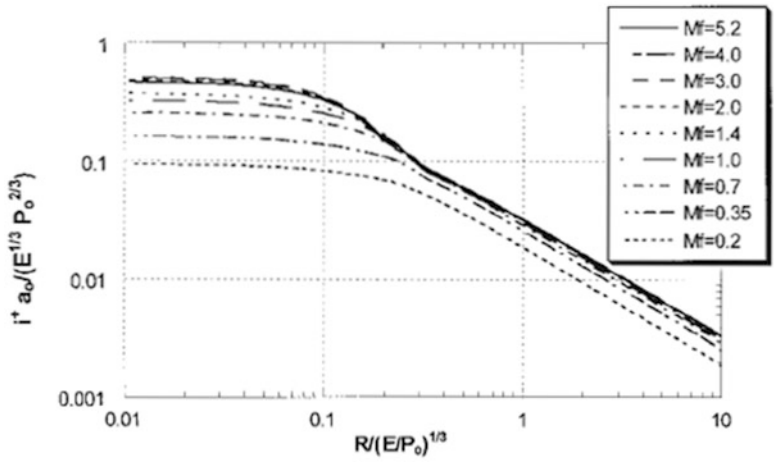

Fig. 69.18 Positive phase blast wave impulse versus energy-scaled distance (From Pierorazio et al. [44])

cloud explosion tests, Perorazio et al. [44] offer Table 69.5 as guidance in selecting the appropriate flame Mach number. The gas reactivity categories of Low, Medium, and High are designated based on the flammable gas laminar burning velocity as follows.

- Low reactivity refers to gases and vapors with S_u <40 cm/s
- Medium reactivity refers to gases and vapors with 40 cm/s < S_u <75 cm/s
- High reactivity refers to gases and vapors with S_u >75 cm/s.

Table 69.5 Flame speed Mach number selection table

		Congestion		
Confinement	Reactivity	Low	Medium	High
2-D	High	0.59	DDT	DDT
	Medium	**0.47**	0.66	**1.6**
	Low	0.079	0.47	0.66
2.5D	High	**0.47**	**DDT**	**DDT**
	Medium	**0.29**	0.55	1.0
	Low	0.053	0.35	**0.50**
3-D	High	**0.36**	**DDT**	DDT
	Medium	**0.11**	**0.44**	**0.50**
	Low	0.026	**0.23**	**0.34**

The 2-D confinement category was based on cylindrical flame propagation numerical calculations, and corresponds to flame propagation between the ground and a ceiling, in the absence of any confining wall. The 3-D confinement category corresponds to spherically symmetric flame propagation calculations with the premise that twice the energy should be used for hemi-spherical flame propagation associated with unconfined clouds on the ground. The 2.5-D confinement category was developed by averaging the results from 2-D and 3-D numerical calculations. According to Pierorazio et al. [44] the 2.5-D confinement category is "to be used in cases where the confinement is made of either a frangible panel or by a nearly solid confining plane (e.g., pipe rack where the pipes are almost touching)."

The Low, Medium, and High equipment Congestion categories can be selected by comparison of an application with the following table characterizing the level of pipe-like blockages used in the testing described by Pierorazio et al. Figure 69.19 shows a plan view representation of these three prototypical obstruction configurations.

The European approach that is equivalent to the Baker-Strehlow-Tang method and results in Figs. 69.17 and 69.18 is the so-called Multi-Energy method. It is described by van den Berg and Lannoy [47]. Taveau [48] has described the application of both the Baker-Strehlow-Tang method and the Multi-Energy method to the Buncefield tank farm vapor cloud explosion.

The second approach to Vapor Cloud Explosion blast pressure estimation is to use either empirical equations or analytical equations based on idealized geometries and assumed flame speeds. Dorofeev [49] offered the following empirical equation as a fit to many of the numerical calculations and experimental measurements of blast pressures.

$$\frac{P - P_0}{P_0} = \frac{0.34}{\overline{R}^{4/3}} + \frac{0.062}{\overline{R}^2} + \frac{0.033}{\overline{R}^2} \quad \text{for } 0.21 < \overline{R} < 3.77 \tag{69.23}$$

Two of the analytical solutions to the spherical flame or piston propagation conservation equations have been described by Souchet [43]. In the thin region near the propagating flame front ($R \approx R_f$) the following solution to the incompressible gas flow equations is applicable.

$$P - P_0 = 2\rho_a v_f^2 \left[1 - \frac{\rho_b}{\rho_a}\right] \left(\frac{R_f}{R}\right) \left[1 - \frac{1 - \frac{\rho_b}{\rho_a}}{4} \left(\frac{R_f}{R}\right)^3\right] \tag{69.24}$$

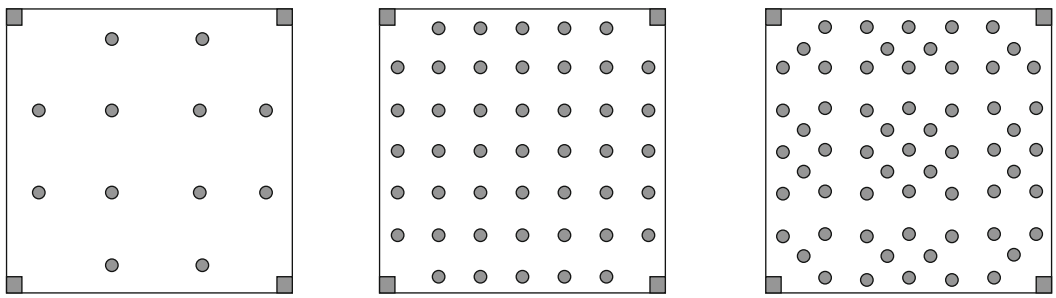

Fig. 69.19 Plan view of obstructions in vapor cloud explosion tests reported by Piezoranio et al. [44]

where the density ratio is approximately equal to the temperature ratio T_a/T_f for most flammable gases with stoichiometric concentrations less than 0.10.

In the far field where $P\text{-}P_0 << P_0$, the following acoustic flow solution is applicable.

$$P - P_0 = 2\rho_a v_f^2 \left[1 - \frac{\rho_b}{\rho_a}\right] \left(\frac{R_f}{R}\right) \left[1 - \frac{R}{a_0 t}\right] \text{ for } R < a_0 t \text{ and } R >> R_f \tag{69.25}$$

The third current approach for vapor cloud explosion calculations is to utilize CFD models of the actual two-dimensional or three-dimensional flame propagation, in which the flame speed and acceleration are calculated as part of the solution. The models used for this approach are also capable, in principle, of doing the vapor cloud dispersion calculations to determine the mass of flammable gas in and beyond the obstructed region. Although full CFD simulations of potential vapor cloud explosions are few and far between, their use may increase with increasing availability of faster and more powerful computers, along with the education of potential users of these sophisticated models. In a sense, this issue is only a microcosm of the more general question of what level of modeling will be utilized for performance based explosion hazard assessments.

Example 4 Figure 69.20 is an aerial view of a natural gas fueled power generation facility that was in the final stages of construction when it suffered an explosion when a flammable gas

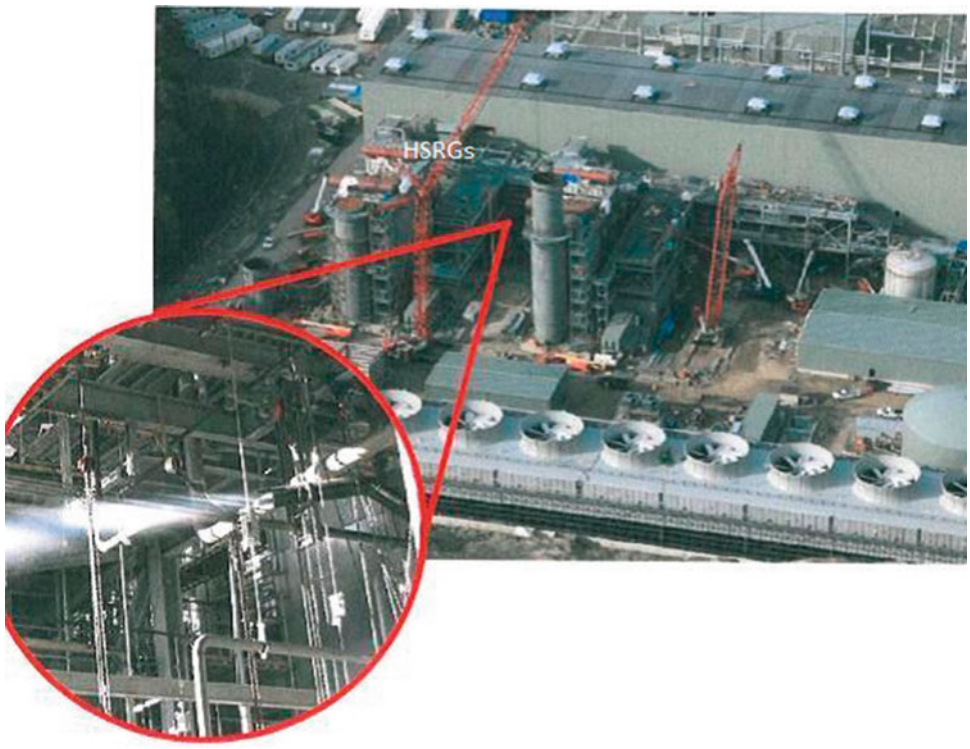

Fig. 69.20 Natural gas release sites in Kleen Energy explosion incident (From Chemical Safety Board Presentation)

cloud was ignited in the area of the Heat Recovery Steam Generators (HSRGs). The insert photo shows a similar gas release in the obstructed, semi-confined area between the two HSRGs. Assuming that the gas cloud volume within the area of the HSRGs is 7700 m^3, use the Baker-Strehlow-Tang method to estimate the vapor cloud explosion pressures that would be generated within the obstructed HSRGs. If the blast wave pressure at which about 10 % of windows are broken is 0.3 psig (0.021 barg), estimate the distance corresponding to this pressure for a vapor cloud explosion of the natural gas that accumulated in the HSRG area.

Solution Natural gas is composed primarily of methane, which is the prototype upper end of the Low Reactivity gas in the B-S-T method. The Confinement Level in this example is either 2-D or 2.5-D depending on whether there is some type of wall or barrier around the HSRGs at the time of the explosion. If we assume there was some type of soft or frangible wall, then this is a 2-D application. The Congestion Level can be estimated by making a rough estimate of the area blockage ratio of the structures and piping shown in the insert. This estimate is probably in the range 10–20 %, corresponding to either a Low or Medium Congestion level by comparison to the values in Table 69.6. A similar categorization would result from comparison of the insert photo to the diagrams in Fig. 69.19.

Looking at the Table 69.5 Mach Numbers for 2-D confinement and a Low Reactivity gas, we would specify 0.079 for Low Congestion and 0.47 for Medium Congestion. In view of the large difference in Mach numbers and the uncertainty in Congestion Categorization, the prudent approach would be to choose the Mach number of 0.47 to avoid a significant underestimate of blast wave pressures. Using this value of M_f in Equation 69.22, results in a calculated $(P_{max}–P_0)/P_0$ of 0.36. This corresponds to a $P_{max}–P_0$ of 5.3 psig, which is above the threshold for significant damage to steel panel industrial buildings. Indeed, the large power generation building behind the HSRGs in the photograph did suffer significant damage, as apparently did steel panels within the HSRGs.

Table 69.6 Congestion categories used in vapor cloud explosion tests

Congestion level	Obstruction pitch to diameter ratio	Obstruction area blockage ratio (%)	Volume blockage ratio (%)
Low	7.6	13	1.5
Medium	4.3	23	4.3
High	3.1	23	5.7

To determine the distance corresponding to a far-field blast wave pressure of 0.3 psig, we first calculate $(P–P_0)/P_0 = 0.3/14.7 = 0.020$. The corresponding value of $\bar{R}$ in Fig. 69.16 is found by interpolating between the $M_f = 0.35$ and $M_f = 0.7$ curves, i.e. between 5 and 10. The approximate result is $\overline{R} = 5 + (0.47 - 0.35) \times 5/(0.7 - 0.35) = 6.7$. The conversion from $\bar{R}$ to the actual distance R requires calculating the blast wave energy, $E = (7700\,m^3)\,(0.10\,m^3\,\text{methane}/m^3)*(0.71\,\text{kg–methane}/m^3\text{–methane})\,(50\,\text{MJ/kg} - \text{methane}) = 27.3\times 10^3\text{MJ}$. The methane density of 0.71 kg/m^3 is based on an assumed gas temperature of 0 °C (273 K) since there is substantial cooling of the gas blown down from a much higher pressure. The resulting R value is

$$R = 6.7\left(27.3 \times 10^9 J/1.01 \times 10^5 N/m^2\right)^{1/3} = 433\,m.$$

A value of R for $(P - P_0)/P_0 = 0.02$ can also be obtained from the acoustic approximation represented by Equation 69.25 at time $t >> R/a_0$. Using a value of $v_f = 0.47*340 = 160\,m/s$, and $R_f = (3*7700)/(4\pi)^{1/3} = 12.2\,m$, the calculated R is 332 m. Since the volume surrounding the HSRGs is shaped more like a box than a sphere, the choice of R_f would be different in the three directions, such that the largest R_f is about 33 m, and the corresponding value of R is about 930 m. This value is in better agreement with news media accounts of isolated window breakage in some homes away from the explosion site.

References

1. Zabetakis, M. (1965) "Flammability Characteristics of Combustible Gases and Vapors," U.S. *Bureau of Mines Bulletin 627*.
2. NFPA 68, "Standard for Explosion Protection by Deflagration Venting," NFPA 2007.
3. C. Duynslaegher, (2010) "Experimental and numerical study of ammonia laminar burning velocity," Université Catholique de Louvain, Belgium, www.academia.edu/889459/
4. Takashi, H. and Kimitoshi, T., (2006) "Laminar Flame Speeds Of Ethanol, N-Heptane, Isooctane Air Mixtures," F2006SC40, http://www.fisita.com/education/congress/sc06papers/f2006sc40.pdf
5. D. Drysdale, *Fire Dynamics*, 2nd Edition, John Wiley & Sons, 1998.
6. Britton, L.G. (2002) "Using Heats of Oxidation to Evaluate Flammability Hazards," Process Safety Progress, 21(1): 1–24.
7. D. Bradley and A. Mitcheson, "Mathematical Solutions for Explosions in Spherical Vessels," *Combustion and Flame,* 26, pp. 201–217 (1976).
8. B. Lewis and G. von Elbe (1961), *Combustion, Flames, and Explosions of Gases,* Academic Press, New York.
9. R. Ogle, "Explosion Hazard Analysis for an Enclosure Partially Filled with a Flammable Gas," *Process Safety Progress,* 18, p. 170 (1999).
10. Y.-D. Jo and K.-S. Park, "Minimum Amount of ? Flammable Gas for Explosion Within a Confined Space," *Process Safety Progress,* 23, pp. 321–329 (2004)
11. NFPA 69, Standard on Explosion Prevention Systems," NFPA 2008.
12. A. Sulmistras, I.O. Moen, and A.J. Saber, "Detonations in Hydrogen Sulphide-Air Clouds," *Report No. 11,* Defense Research Establishment Suffield, Ralston, Alberta (1985).
13. J. DeHaan, D. Crowhurst, D. Hoare, M. Bensilum, and M.P. Shipp (2001), "Deflagrations involving stratified heavier-than-air vapor/air mixtures," Fire Safety Journal, v 36, pp 693-710.
14. F. Tamanini and J. Chaffee, (2000) "Mixture Reactivity in Explosions of Stratified Fue/Air Layers," Process Safety Progress, v 19, pp 219-227.
15. F. Tamanini, (2002) "Development of an Engineering Tool to Quantify the Explosion Hazard of Flamble Liquid Spills," Process Safety Progress, v 21, pp 246-253.
16. CCPS (1996) "Guidelines for Use of Vapor Cloud Dispersion Models," 2nd Edition, AIChE.
17. M. Kuznetsov, J. Grune, W. Rudy, A. Teodorczyk (2012) "Detonation initiation and propagation in a semiconfined layer of hydrogen-air mixture," Proceedings 8th International Symposium on Hazards,, Prevention, and Mitigation of Industrial Explosions, Krakow.
18. J. Grune, K. Sempert, H. Haberstroh, M. Kuznetsov, T. Jordan (2011) "Experimental investigation of hydrogeneair deflagrations and detonations in semi-confined flat layers," J. Loss Prevention in the Process Industries, doi:10.1016/j.jlp.2011.09.008.
19. R. Strehlow (1984) *Combustion Fundamentals,* McGraw Hill.
20. Bartknecht, W. (1971) Explosion, Course, ...
21. G.E. Andrews, P. Herath1, H.N. Phylaktou, "The influence of flow blockage on the rate of pressure rise in Large L/D cylindrical closed vessel explosions," J. Loss Prevention in the Process Industries, 3, 291-302 (1990).
22. Richmond, J. and Liebman, L, (1975) "A Physical Description of Coal Mine Explosions," Fifteenth (Intl) Comb Symp. Pp 115–126.
23. Sapko, M., Weiss, E., Cashdollar, K., and Zlochower, I. (2000) "Experimental mine and laboratory dust explosion research at NIOSH," J. Loss Prevention, v 13, pp 229 – 242.
24. Molkov, V. (2012) *Fundamentals of Hydrogen Safety Engineering 1, bookboon.com,* ISBN: 978-87-403-0226-4.
25. Sherman, M., Tieszen, S. and Benedick, W., FLAME Facility, The Effect of Obstacles and Transverse Venting on Flame Acceleration and DDT at Large Scale," NUREG/CR-5275, 1989.
26. Abdel-Gayed, R., Bradley, D., and Lawes, M., (1987) "Turbulent burning velocities: a general correlation in terms of straining rates," Proc. R. Soc. A414, pp 389-424.
27. Abdel-Gayed R. and Bradley, D., (1985) "Criteria for Turbulent Propagation Limits of Premixed Flames," Combustion and Flame, v 62, pp 61-68.
28. D.S. Burgess, J.N. Murphy, N.E. Hanna, and R.W. Van Dolah, "Large-Scale Studies of Gas Detonations," U.S. Bureau of Mines RI 7196, Washington (1971).
29. Sichel, M., "Simplified Calculation of Detonation Induced Impulse," Proceedings of the Second International Conference on the Impact of Hydrogen on Water Reactor Safety, October 1982
30. W.E. Baker, P.A. Cox, P.S. Westine, J.J. Kulesz, and R.A. Strehlow, *Explosion Hazards and Evaluation,* Elsevier, New York (1983).
31. B.E. Gelfand, S.M. Frolov, and M.A. Nettleton, "Gaseous Detonations," *Progress in Energy and Combustion Science,* 17, pp. 327–371 (1991).
32. J.E. Shepherd, "Chemical Kinetics of Hydrogen-Air-Diluent Detonations," *Dynamics of Explosions: ? Progress in Astronautics and Aeronautics,* 106, pp.? 263–293 (1986).
33. D.W. Stamps, W.B. Benedick, and S.R. Tieszen, "Hydrogen-Air Diluent Detonation Study for Nuclear Reactor Safety Analysis," *Sandia Report* NU*REG/CR-5525,* Sandia National Laboratories, Albuquerque, NM (1991).
34. R.P. Lindstedt and H.J. Michels, "Deflagration to Detonation Transition in Mixtures of Alkane

LNG/LPG Constituents with O2/N2," *Combustion and Flame,* 72, pp. 63–72 (1988).
35. Flessner and Bjorklund, *Coast Guard Report* (1980).
36. R. Blanchard, D. Arndt, R. Gratz, and S. Scheider, "Effect of ignition position on run-up distance to DDT for hydrogen-air explosions," J. Loss Prevention in the Process Industries, v 24, pp 194-199, 2011.
37. M.P. Sherman and M. Berman, "The Possibility of Local Detonations during Degraded-Core Accidents in the Bellefonte Nuclear Power Plant," *Nuclear Technology,* 81, pp. 63–77 (1988).
38. R.B. Jacobs, W.L. Bulkley, J.C. Rhodes, and T.L. Speer, "Gaseous Detonation," *Chemical Engineering Progress,* 53, pp. 565–573 (1957).
39. G. Kinney and K. Graham, *Explosive Shocks in Air,* 2nd ed., Springer-Verlag, New York (1985).
40. CCPS "*Guidelines for Consequence Analysis of Chemical Releases,*" AIChE Center for Chemical Process Safety, New York (1999).
41. T. Forcier and R. Zalosh, "External Pressures Generated by Vented Gas and Dust Explosions," *Journal of Loss Prevention in the Process Industries,* 13, pp. 411–417 (2000).
42. CCPS, *Guidelines for Evaluating the Characteristics of Vapor Cloud Explosions, Flash Fires, and BLEVEs,* AIChE Center for Chemical Process Safety, New York (1994).
43. I. Sochet, "Blast Effects of External Explosions," Eighth International Symposium on Hazards, Prevention, and Mitigation of Industrial Explosions, Yokohama, 2010.
44. Pierorazio JA, Thomas JK, Baker QA, Ketchum DE. An Update to the Baker-Strelhow-Tang Vapor Cloud Explosion Prediction Methodology Flame Speed Table, Process Safety Progress 2005,24(1):59–65.
45. QA Baker, CM Doolittle, GA Fitzgerald, and Tang, Recent Developments in the Baker-Strehlow VCE Analysis, Process Safety Progress, 17, pp 297-301 (1998)
46. M.J. Tang and Q.A. Baker, "Comparison of blast curves from vapor cloud explosions," J. of Loss Prevention in the Process Industries, v 13, pp 433-438, 2000.
47. A.C. Van den Berg and A. Lannoy, "Methods for vapour cloud explosion blast modelling," J Hazard Mater 34 (1993), 151–171.
48. J. Taveau, "The Buncefield Explosion: "Were the Resulting Overpressures Really Unforeseeable?," Process Safety Progress, v 31, 2012.
49. Dorofeev, S. B. Blast effects of confined and unconfined explosions. In *Proceedings of the 20th International Symposium on Shock Waves* (1995).

Robert Zalosh, is a Fire Protection Engineering Professor Emeritus at Worcester Polytechnic Institute (WPI) and has a consulting practice called Firexplo in which he advises clients on how to deal with special industrial fire and explosion hazards and investigates major industrial fire and explosion incidents. He formerly was a FPE Professor at WPI and the Applied Research Department Manager and Assistant Vice President at Factory Mutual Research Corporation.

Dust Explosions

70

Robert Zalosh

Introduction: Dust Explosibility

Fine particulates of combustible materials can pose a dust flash fire hazard when dispersed as a cloud and ignited. If the suspended dust concentration is sufficiently high, a flame will propagate through the dust cloud. The dust flash fire hazard can escalate into a dust explosion hazard when there is confinement that restrains the dust laden air flow induced ahead of the propagating flame front such that potentially damaging pressures are developed.

For many materials, there is no doubt about whether the powder or dust form of the material is explosible. If a material is combustible in the sense that it poses a fire hazard, that material will also pose a dust explosion hazard if the characteristic particle size is less than roughly 500 micrometers (μm). However, the inverse is not necessarily true, i.e. some materials that do not normally pose a fire hazard can pose a dust explosion hazard. For examples, many metal dusts and powders can be oxidized rapidly enough when suspended in air to be explosible. Of course materials that are either already fully oxidized or inherently inert are neither combustible nor explosible.

Although 420–500 μm has been a traditional rule of thumb for the limiting particle size for a combustible material to also be explosible, the actual value depends on the material reactivity and the particle morphology. Weakly combustible materials such as polyvinyl chloride and iron need to be much smaller than 420 μm to be explosible, whereas test data for reactive materials such as stearic acid show they explosible at a median particle size greater than 1,000 μm ([1], p. 620). Elongated particles such as wood, paper fibers, and flock are also explosible even though their longest dimension is significantly larger than 1,000 μm.

Laboratory screening tests have been developed to determine whether a particular dust sample is explosible. The screening test described in ASTM E1226 [2] is now used by most commercial laboratories in the U.S. doing combustible dust testing. Figure 70.1 is a diagram of the test apparatus used in ASTM E1226 testing. The explosion test vessel has an internal volume of at least 20 L, and is either spherical or cylindrical with a length to diameter ratio of approximately 1. The vessel is equipped with electrically triggered pyrotechnic ignitors and pressure sensors to measure the explosion pressure development. Figure 70.2 is a photograph of a 20 l sphere in a commercial testing laboratory.

A pre-weighed dust sample is loaded into the dust container prior to the test. The explosion chamber is pre-evacuated so that the injection of the dust sample using compressed air will bring the test vessel pressure back to approximately 1 atm at the time of ignition. The dust is injected through the rebound nozzle shown at the bottom of the vessel in order to produce a near uniform distribution of dust at a concentration

R. Zalosh (✉)
Firexplo, Wellesley, MA, USA

M.J. Hurley (ed.), *SFPE Handbook of Fire Protection Engineering*,
DOI 10.1007/978-1-4939-2565-0_70, © Society of Fire Protection Engineers 2016

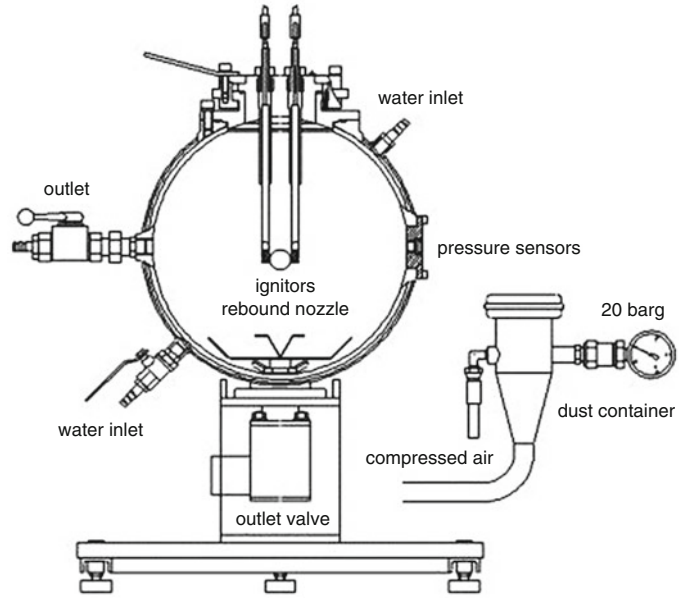

Fig. 70.1 20-l sphere test apparatus used in dust explosibility tests

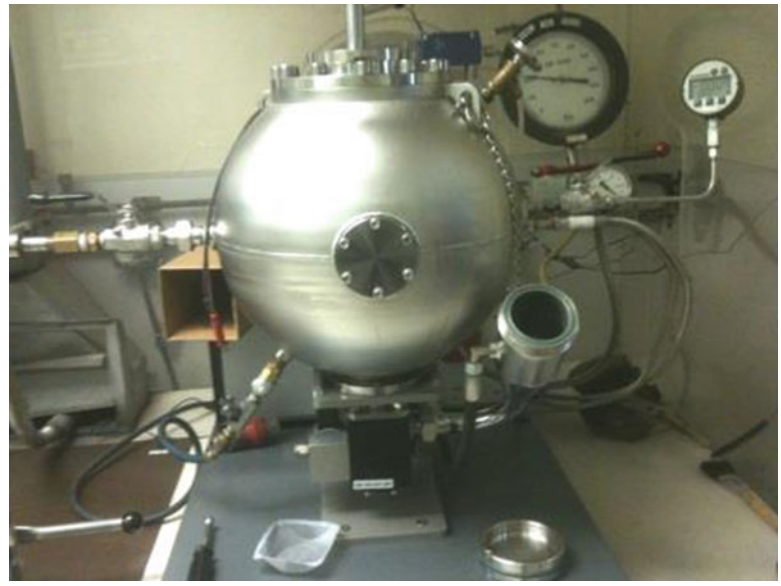

Fig. 70.2 20-l sphere test vessel

equal to the mass of the dust sample divided by the 20-l vessel volume. The time delay between the beginning of injection and ignition is an important parameter that is controlled by an automated timing circuit. The value of the time delay is selected by calibrating the test apparatus against benchmark data obtained for two particular dusts used in round robin tests.

Section 13 of ASTM E1226-10 specifies that screening tests be conducted using a 5 kJ or greater energy igniter and dust concentrations of 1,000 and 2,000 g/m^3. The dust samples are to have a moisture content no greater than 5 wt%, and usually have a particle size distribution corresponding to at least 95 wt% smaller than 75 μm. The test results are classified as combustible if either of the

two tested concentrations results in a pressure ratio, PR, greater than 2, where PR is defined as follows.

$$PR = \frac{P_{ex} - \Delta P_{ign}}{P_{ign}} \qquad (70.1)$$

where P_{ex} is the absolute explosion pressure measured for each concentration, P_{ign} is the absolute pressure in the vessel at the time the igniters are fired, and ΔP_{ign} is the pressure increase in the vessel due only to the firing of the igniter.

There are several variations of the ASTM E1226 screening tests. The Occupational Safety and Health Administration (OSHA) Salt Lake Tech Center's tests to determine if a dust sample is explosible are conducted with an igniter energy of 2.5 kJ, and a longer time delay than the ASTM testing. Comparison tests conducted in a 20-l sphere and a 1-m^3 test vessel have shown that ignition energies of 5 and 10 kJ in the 20-l sphere can sometimes cause over-driven explosions in the sense that the large ignition energies heat all the dust particles to the point that they start burning because of the igniter rather than because of flame propagation through the dust cloud [3]. The OSHA laboratory use of a 2.5 kJ igniter and the European standard (EN 14034-3) use of 2 1-kJ igniters avoid this problem. The European standard uses a minimum explosion pressure of 0.5 barg as the explosibility criterion, which corresponds to a pressure ratio of 1.3 in their tests [4]. After analyzing the effects of various ignition energies on the pressure ratios obtained for three different dust materials at various concentrations, Kua et al. [4] have concluded that there is an optimum ignition energy that produces neither over-driven explosions nor under-driven explosions in which too small a fraction of the dust is heated to produce flame propagation [4]. Their results indicate that the optimum ignition energy is 5–7 kJ for carbonaceous dusts that devolatilize before burning, and 2–5 kJ for metals that burn without vaporization.

Besides the choice of ignition energy used in testing, dust explosibility determinations can also depend on the selection and conditioning of the dust test sample. Dust composition may depend on the possible presence of contaminants in the sample or upon normal variations in composition due to variable process and feedstock conditions. Likewise the particle size distribution can be sensitive to the sample location, e.g. finer particles of fugitive dust usually settle upon surfaces at higher elevations than larger dust particles. In the case of metals, significant delays between sample acquisition and testing can result in particulate surface oxidation that can cause misleading negative results. Therefore, the choice of sample location and sample conditioning prior to testing are important considerations that can influence the results of explosibility determinations, as well as the deflagration parameter values described in the next section of this chapter.

Closed Vessel Deflagration and Ignition Parameters

The potential consequences of a dust explosion involving a particular material with a particular particle size distribution are best represented by the maximum explosion pressure, P_{max}, and the maximum rate-of-pressure-rise, $(dP/dt)_{max}$. The ISO 6184-1 [5] and ASTM E1226-10 test methods, which are virtually identical, are often used for such determinations. These methods have been developed on the premise that standardized testing and appropriate scaling laws can produce laboratory data that can be scaled up to much larger applications. Specifically, the value of P_{max} should be independent of test vessel size providing a minimum test volume of 20 l is used in a near spherical geometry. The value of $(dP/dt)_{max}$ is presumably inversely proportional to the characteristic vessel length scale, such that a material constant, K_{st}, is defined as:

$$K_{st} = (dp/dt)_{\max} V^{1/3} \qquad (70.2)$$

where $(dP/dt)_{max}$ is the maximum slope of the measured pressure versus time curve in tests in a vessel of volume V.

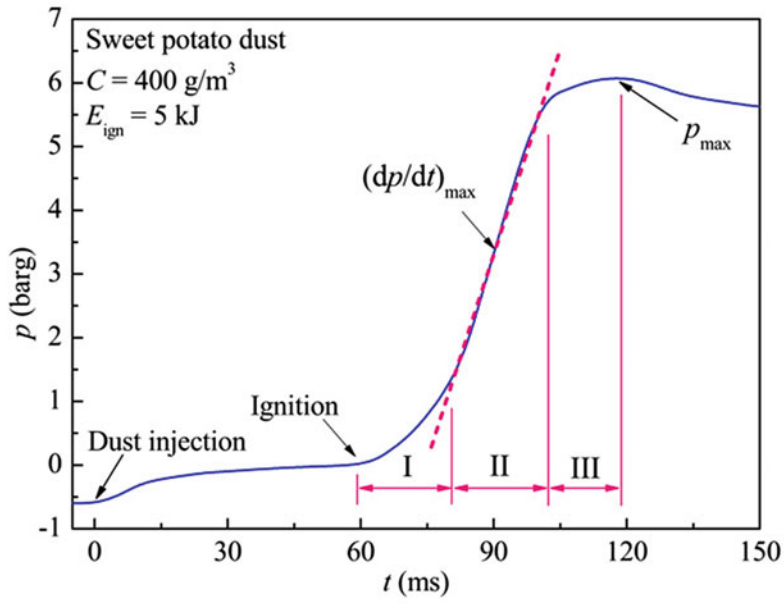

Fig. 70.3 Typical ISO 6184 test pressure transient (From Kuai et al. [4])

A typical ISO 6184-1 [5] transient pressure measurement is shown in Fig. 70.3. The vessel pressure gradually increases from about −0.6 to 0 barg as the dust sample is injected with the compressed air in the sample load chamber. After a 60 msec delay from the start of dust injection, the 5 kJ igniter is fired to start the beginning of the first period of the dust combustion process. During this first period, also called the induction period, the igniter is causing the burning of a sufficient number of dust particles to initiate flame propagation. The second period, also caused the period of steady state flame propagation, has a characteristic linear increase of pressure with time. This is the period in which $(dp/dt)_{max}$ is measured at the test concentration. The third period, which begins at the inflection point where the slope starts to decrease and ends at the time the maximum pressure occurs, might also be called the burnout period because the flame front has already reached the vessel wall and the dust behind the flame front is burning [4].

The ASTM E1226 and ISO 6184-1 test methods entail running three series of tests at varying dust concentrations, with measurements of the p_{max} and $(dp/dt)_{max}$ at each concentration. A typical set of results is shown in Fig. 70.4. In this set, the maximum pressure occurred at a concentration of 1,500 g/m^3 and the maximum rate-of-pressure rise occurred at a concentration of 1,000 g/m^3.

ASTM E1226 specifies that the value of P_{max} for the tested dust sample is calculated as the average of the three measured values for the three dust series after subtracting the pressure at ignition. The value indicated by the asterisk for the data in Fig. 70.4 is 6.6 barg. Similarly, the average of the three highest $(dP/dt)_{max}$ values shown in Fig. 70.4 is 480 bar/s. The corresponding value of K_{st} calculated using the 0.020 m^3 vessel volume is 130 bar-m/s.

Values of P_{max} and K_{st} for an assortment of combustible dust samples are shown in the last two columns of Table 70.1. The median dust particle size is listed along with the generic material.

Aluminum powder has the highest K_{st} value (515 bar-m/s) of the materials listed in Table 70.1, whereas aluminum shavings with a median particle size of 240 μm, are not even explosible. This illustrates the importance of particle size and morphology on dust explosion test parameter values. Most of the materials listed in Table 70.1 have a K_{st} value well below 200 bar-m/s. This is also true for the larger assortment of dust materials listed in Eckhoff's book [1].

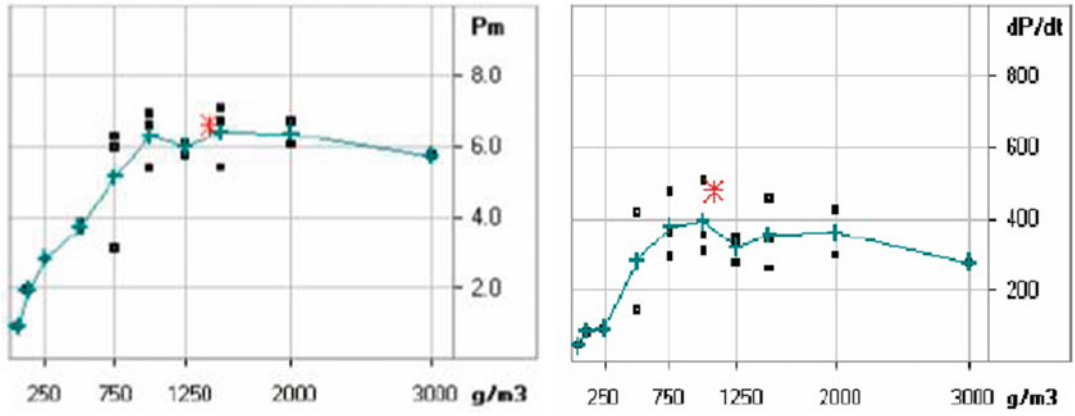

Fig. 70.4 Maximum pressure and maximum rate-of-pressure-rise versus dust concentration

Table 70.1 Explasibility data for representative powders and dusts[a]

Material	Median particle size (μm)	Minimum explosive concentration (g/m^3)	Min cloud ignition temp (°C)	Min layer ignition temp (°C)	Min ign energy (mJ)	P_{max} (bar g)	K_{ST} (bar-m/s)
Activated carbon	18	60	790	>450	–	8.8	44
Aluminum powder	<10	60	560	430	–	11.2	515
Aluminum shavings	240	No ignition					
Ascorbic acid	39	60	460	Melts	–	9.0	111
Calcium stearate	<10	30	580	>450	16	9.2	99
Coal, bituminous (high volatility)	4	60	510	260	–	9.1	59
Corn starch	<10	–	520	>450	300	10.2	128
Epoxy resin	26	30	510	Melts	–	7.9	129
Fructose	200	60	440	440	180	7.0	28
Iron from filter	12	500	580	>450	–	5.2	50
Magnesium	28	30	–	–	–	17.5	508
Methyl cellulose	37	30	410	450	29	10.1	209
Milk powder	165	60	460	330	75	8.1	90
Napthalene	95	15	660	>450	<1	8.5	178
Paper tissue dust	54	30	540	300	–	8.6	52
Phenolic resin	<10	15	610	>450	–	9.3	129
Polyethylene, l.d.	<10	30[b]	420	Melts	–	8.0	156
Polyethylene, l.d.	150	125	480	Melts	–	7.4	54
Polyvinylchloride	25	125	750	>450	>2,000	8.2	42
Rubber	80	30	500	230	13	8.5	138
Silicon	<10	125	>850	>450	54	10.2	126
Sugar	10	60	440	Melts	14	8.3	75
Sulfur	20	30	280	–	6.8	151	
Toner	23	60	530	Melts	8	8.8	145
Wood from chip board	43	60	490	320	–	9.2	102
Zinc	<10	250	570	440	–	6.7	125

[a]Data from R. Eckhoff, *Dust Explosions in the Process Industries*, Butterworth-Heinemann

[b]This MEC for polyethylene was determined in a 1.2 l cylinder

The Minimum Explosible Concentration (MEC) values listed in Table 70.1 are based on the same 20-l sphere standard test methodology described above. The ASME E1515 [6] determination of MEC entails conducting tests with lower and lower dust concentrations until the pressure ratio, PR, falls below 2, i.e. the same criterion as for dust explosibility. Preceding comments about the effects of the igniter energy and the turbulence level at ignition, as controlled by the time delay between dust injection initiation and igniter firing are also applicable to the MEC determination [4]. MEC values listed in Table 70.1 range from 15 g/m^3 for phenolic resin to 500 g/m^3 for iron dust.

When the dust concentration is significantly higher than the MEC, the P_{max} value is not sensitive to the characteristic particle size, but the K_{st} value does increase significantly with decreasing particle size. Since the particle size effect is due to the variation of particle surface area, the more general effect of particle size on rate-of-pressure-rise can be presented in terms of the particle surface area per unit mass. This effect is shown in Fig. 70.5 for aluminum particles, which often have flat or flake-like shapes.

Table 70.1 lists data for three dust ignitability parameters. The minimum dust cloud ignition temperature is determined by injecting dust samples into an oven, and repeating this test at various oven air temperatures [7]. The dust layer hot surface ignition temperature [8] is determined by placing a 1.27 cm deep layer of dust on an electrical hot plate, and slowly increasing the hot plate surface temperature until there is an indication of ignition either visually or from a thermocouple embedded in the dust layer. The dust cloud Minimum Ignition Energy (MIE) is determined in a 1.2 l cylindrical test apparatus equipped with spark electrodes energized by a circuit with adjustable voltage and/or capacitance, so as to produce adjustable spark discharge energies [9] generated upon injecting dust at varying concentrations into the test cylinder.

Dust cloud minimum ignition temperatures listed in Table 70.1 range from a low of 280 °C for sulfur to a high of 790 °C for activated carbon. Most values are in the much narrower range from 420 to 580 °C The value for a given material increases slightly with increasing dust characteristic particle size.

Most of the dust layer hot surface ignition temperatures listed in Table 70.1 are at least 100C lower than the corresponding dust cloud minimum ignition temperature. This is primarily due to the increased time available for the dust material to be heated to be heated to its ignition temperature. The dust layer ignition temperature test has a duration of 30 min, while the dust cloud ignition temperature test duration is effectively equal to the dust cloud settling time in the test chamber, which is usually on the order of a few seconds. The dust layer surface ignition temperature test is not applicable to thermoplastics since they melt and flow prior to ignition. One other pertinent ignition temperature test is the heated

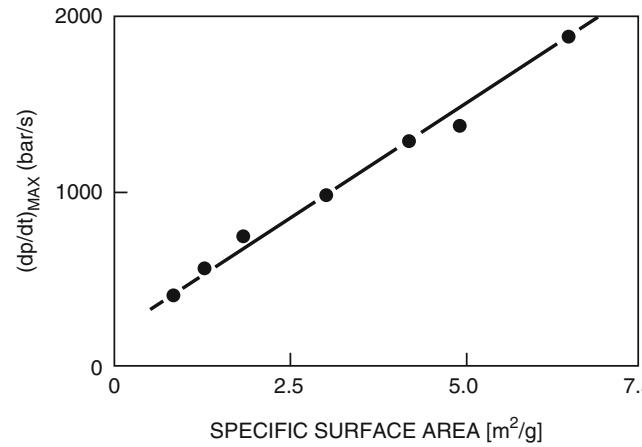

Fig. 70.5 Effect of specific surface area on $(dP/dt)_{max}$ (From Eckhoff [1])

air over dust layer. This test, which does not have an ASTM standard, usually produces ignition temperatures even lower than the dust layer surface ignition temperature because dust ignition usually occurs near the layer top surface (where there is ample oxygen to support ignition) and heating from below causes a decrease in layer temperature with elevation above the heated surface. The dust layer hot surface ignition temperature deceases with increasing layer thickness so that a safety margin is needed in establishing safe surface temperatures for equipment subject to layer accumulations deeper than the 12.7 mm thickness in ASTM E 2021, or the 5.0 mm thickness in IEC 61241-2-1 test method.

MIE data for the dust samples in Table 70.1 range from less than 1 mJ to more than 2,000 mJ. For a given material, the MIE is known to be influenced by the following parameters:

- The MIE decreases as the spark duration increases due to the presence of either inductance or resistance in the capacitive discharge circuit. For example, adding a series inductance in the range 0.1–1.0 H, or a series resistance in the range 10^4–10^5 Ω, decreases the MIE by an order-of-magnitude. The practical significance of this is that it takes more spark energy for an electrostatic (capacitive) discharge to ignite a dust cloud than for a spark in electrical equipment due perhaps to actuation of an electromechanical switch. The MIE data in Table 70.1 were obtained with long duration inductive discharges.
- The MIE decreases as the dust median particle size increases; Siwek and Cesana [11] show that the variation is to the −2.5 power of particle diameter.
- The MIE varies with dust concentration, but the most sensitive concentration depends on the particular material. The data in Table 70.1 are for the most sensitive concentration.
- The MIE decreases with increasing air-dust temperature.
- The MIE and the MIT increase with increasing velocity of the dust-air mixture such as might occur in a pneumatic transport piping or dust collection ducting.

The theoretical spark energy can be calculated for simple electrical discharges. For example, the energy (J) in a purely capacitive discharge is $½CV^2$, where C is the capacitance (farads), and V is the stored voltage prior to discharge. In the case of a purely inductive circuit, the theoretical spark energy is $½Li^2$, where L is the circuit inductance, and i is the current (A). The inductance spark energy can be compared directly to the MIE for a particular dust to assess the likelihood of ignition; the capacitive spark energy comparison should account for the higher ignition energies associated with short duration capacitive discharges. The energy associated with mechanical friction and impact sparks is much more difficult to determine.

Partial Volume Deflagrations in Equipment and Rooms

Since a suspended dust cloud is needed at a concentration above the measured MEC in order to have a dust deflagration, hazard assessments often entail estimating the average dust concentration in operating equipment. Although this type of estimate is applicable to powder and dust transport piping and ducts because there usually is a continuous near-uniform dust concentration in the pipe or duct, it is not applicable to equipment in which there is an inherently non-uniform suspended dust/powder concentration. One example of such equipment is the spray dryer shown schematically in Fig. 70.6.

The typical spray dryer consists of a large cylindrical upper chamber and a smaller conical lower chamber. Wet product sprayed through nozzles at the top of the dryer encounters a swirling heated air flow and gradually dries as it falls into the conical lower chamber. Dried product is removed at the bottom of the drier. The outlet air flow often contains fine particulates which are often removed in a dust collector. If the product is a combustible powder, dust explosion hazards exist in both the drying chamber and the dust collector.

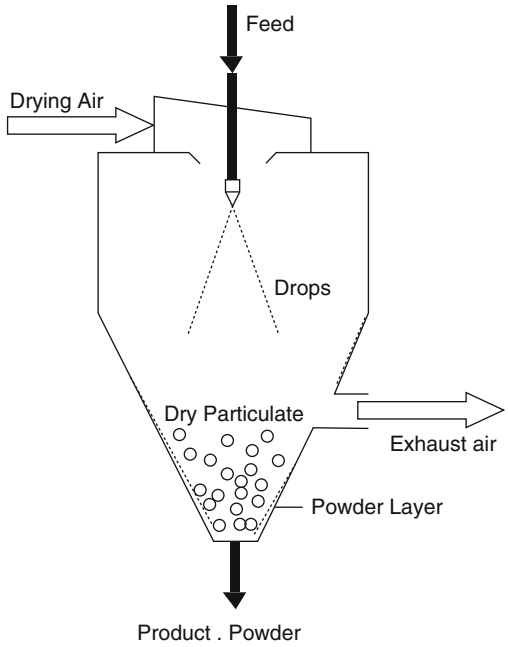

Fig. 70.6 Simplified spray dryer diagram

Siwek et al. [12] have conducted powder concentration measurements in various operating spray dryers. Their results for three different products show that the concentration decreases with distance above the dryer outlet such that concentrations above the MEC only exist in the lower section of the dryer. The average concentration in that region is reported to be less than 100 g/m^3. Similarly, the dust concentration in baghouses is highly non-uniform with the maximum concentrations occurring near the bags when they are pulsed. However, in both the spray dryer and the baghouse, there are often substantial layers of dust/powder on the walls and, in the case of the baghouse, on the filter bags. Tests conducted by Siwek et al. [12] in a vented spray dryer with and without dust layers showed that the dust layer can cause the pressure in the vented explosion to be 3–4 times as high as the same explosion in a dryer without any dust layer.

In view of the highly non-uniform nature of the dust in process equipment and the common occurrence of dust layers on the equipment surfaces, the NFPA 654-2013 standard [13] has the following criteria to determine if a dust explosion hazard exists in process equipment. According to paragraph 6.1.7 of NFPA 654-2013, an explosion hazard exists if there is a sufficient quantity of combustible dust to cause equipment rupture if the dust is suspended and ignited, and if there is a means of suspending the dust within the equipment. These conditions do in fact exist in most spray dryers, baghouses, and many other process equipment.

The pressure developed in a partial volume closed vessel dust explosion can be estimated by assuming that the dust concentration in the partial volume is equal to the worst case concentration, c_w, corresponding to the measured P_{max} value for the dust material, and that the flame propagates through the dust cloud until it reaches the perimeter of the dust cloud. This hypothesis leads to the following equation for the unvented enclosure partial volume pressure, P_{pv}.

$$P_{pv} = P_{\max}\frac{m_{dust}}{V\ c_w} \tag{70.3}$$

where V is the equipment total volume, and m_{dust} is the mass of suspended dust and suspendable layered dust, i.e.

$$m_{dust} = m_{susp} + \eta\ m_{layer} \tag{70.4}$$

The nomenclature for Equation 70.4 is m_{susp} is the mass of dust normally in suspension in the equipment, m_{layer} is the mass of accumulated dust in layers within the equipment, and η is the fraction of layered dust that can be lifted either due to some disturbance or to the initial flame propagation following ignition of the suspended dust.

The partial volume calculation approach represented by Equations 70.3 and 70.4 has been incorporated into NFPA 654 [13] for the determination of the maximum allowable amount of accumulated dust in a room or building such that a partial volume deflagration will not produce a pressure than can damage or blow out a portion of the room/building walls or ceiling. Section 6.1 of NFPA 654-2013 requires that a facility dust

explosion hazard area assessment be conducted with one of four alternative methods for calculating the maximum allowable accumulation. The most general of the four methods has the following equation for the maximum allowable amount of dust, M_{exp}, in a room or single dust hazard area based on pressure produced from a partial volume explosion not exceeding the enclosure strength.

$$M_{\exp} = \left[\frac{P_{es}}{DLF}\right] \cdot \left[\frac{C_w}{P_{\max}}\right] \cdot \frac{A_{floor} \cdot H}{\eta_D} \qquad (70.5)$$

M_{exp} = threshold dust mass kg based on building damage criterion

P_{es} = enclosure strength evaluated based on static pressure for the weakest building structural elements not intended to vent ot fail (bar g) per NFPA 68

DLF = dynamic load factor, the ratio of maximum dynamic deflection to static deflection per NFPA 68

C_w = Worst-case dust concentration (Kg/m3) at which the maximum rate-of-pressure-rise results in tests conducted per ASTM E 1226

P_{max} = maximum pressure (bar g) developed in ASTM E 1226 tests with the accumulated dust sample

A_{floor} = enclosure floor area (m2)

H = enclosure ceiling height (m)

ν_D = entrainment fraction = 0.25

A conservatively high value of 1.5 for the Dynamic Load Factor can be used in lieu of structure dynamic response analysis. When and if the accumulated mass of combustible dust in the room or area exceeds M_{exp}, NFPA 654-2013 section 6.1 requires that the dust be cleaned or that building deflagration venting be implemented to prevent the deflagration pressure from reaching the enclosure strength. There is also a flash fire hazard evaluation equation to determine when and if a flash fire hazard exists due to the potential lifting and ignition of a fraction, η_D, of the accumulated combustible dust.

EXAMPLE 1 Calculate the partial volume deflagration pressure in a powdered milk spray dryer with a suspended powder concentration of twice the powder MEC in the conical section of the dryer and a 3 mm layer of powder on the cone interior surface. The dryer cylindrical section is 6 m in diameter and 5 m high, and the conical section is 4 m high. The bulk density of the powder milk layer is 300 kg/m^3, the worst case dust concentration is 750 g/m^3 and a layer entrainment coefficient of 0.25 can be assumed.

SOLUTION The dryer volume is equal to $\pi\,(6)^2(5)/4 + \pi\,(6)^2\,(4)/12 = 141\ \text{m}^3 + 37.7\ \text{m}^3 = 179\ \text{m}^3$. The cone surface area is equal to $\pi\,(6/2)\quad (4^2 + 3^2)^{1/2} = 15\pi = 47.1\quad \text{m}^2$. From Table 70.1, the MEC for powdered milk is 60 g/m^3, so the concentration of suspended powder ignited in the conical section of the dryer is 120 g/m^2. From Equation 70.4,

$$m_{dust} = (0.120\ \text{kg/m}^3)(37.7\ \text{m}^3) + 0.25(300\ \text{kg/m}^3)(0.003\ \text{m})(47.1\ \text{m}^2) = 15.1\ \text{kg}$$

P_{max} for milk powder (from Table 70.1) = 8.1 barg. The volume fraction of milk powder in the dryer is

$m_{dust}/(c_w V) = 15.1\ \text{kg}/[(0.75\ \text{kg/m}^3)\,47.1\ \text{m}^3] = 0.113$. From Equation 70.3, $P_{pv} = 8.1(0.113) = 0.92$ barg.

This value of P_{pv} is comparable or higher than the strength of many spray dryers. A still higher value would have resulted from use of a higher layer entrainment coefficient or consideration of accumulations higher in the dryer. Therefore, explosion protection is probably needed.

EXAMPLE 2 A wood cabinet manufacturing plant has a 60 m by 40 m room for cutting chipboard panels. The room, has a 7 m ceiling supported by steel beams which will fail at an internal pressure on the roof panels of 75 lb/ft^2 = 0.036 bar. Chipboard dust samples have undergone ASTM E 1226 explosibility tests that resulted in a P_{max} of 9.2 bar and a worst-case suspended dust concentration of 600 g/m^2. What is the maximum allowable mass accumulation of sawdust in the room? Assuming that this accumulation occurs over 10 % of the floor area, and the sawdust bulk density is 218 kg/m^3, what is the maximum allowable accumulated dust layer thickness.

SOLUTION Substitution of the given parameter values into Equation 70.5,

$$M_{\exp} = \frac{(0.036\ bar)\left(0.60\frac{kg}{m^3}\right)(60m)(40m)(7m)}{1.5(9.2\ bar)(0.25)}$$
$$= 105\ kg$$

The corresponding maximum allowable dust layer thickness is equal to $M_{exp}/(\rho_b A_{dust})$ = 105 kg/[(218 kg/m^3) (0.10) (2400 m^2)] = 0.002 m = 2 mm. An alternative maximum dust layer thickness criterion in NFPA 654-2013 paragraph 6.1.3.1 for this material is 0.8 mm (1200 kg/m^3)/(218 kg/m^3) = 4.4 mm. However this layer thickness is only allowed over a maximum of 93 m^2 of floor area. Since the dust in the room accumulates over a 240 m^2, the allowable thickness must be scaled down to 4.4 mm (93 m^2)/(240 m^2) = 1.7 mm, which is very close to the 2 mm maximum allowable layer thickness calculated above from the value of M_{exp}.

Dust Explosion Propagation Phenomena

The dust explosion propagation process through a cloud of particles at a concentration above the MEC has some similarities and important differences from the corresponding process for a flammable gas mixture. As with flammable gas flame propagation, the flame heats the unburned fuel ahead of it to its ignition temperature, and the rate of flame propagation is governed by the rate of heat transfer and the fuel combustion reaction time. Similarly, the expansion of the burned gases due to its flame temperature induces a flow of the fuel-air mixture ahead of it.

One important difference between dust and gas flame propagation is that the dust combustion zone or flame thickness is significantly larger, being at least 10–100 mm [1] because the time scale for the dust particle to burn completely is usually significantly larger than the gas combustion reaction time. The dust combustion time scale depends on the dust particle combustion mechanism. Many dust materials undergo pyrolysis and devolatilization prior to combustion. Other materials, such as most combustible metals, undergo a combustion reaction at their surface. The rate of the combustible metal surface reaction depends on the rate of gaseous oxygen diffusion through the surface oxide layer.

Another difference between dust and gas flame propagation is that the dust flame is almost always turbulent with an irregular apparent flame surface that can be a collection of mini flames associated with the burning of individual particles or groups of particles. Figure 70.7 is a schematic representation of the turbulent dust flame propagation process showing the relative velocities of the flame, and the dust particles and air ahead of the propagating flame.

The flame heat transfer to the unburned dust particles is predominantly by flame radiation, as opposed to the convection and conduction associated with flammable gas flame propagation. Flame radiation is enhanced in the case of combustible metals with high flame temperatures reported by Cashdollar and Zlochower [14].

The air velocity induced ahead of a propagating dust explosion will lift at least some of any settled dust on the floor ahead of the flame. This phenomenon is illustrated in Fig. 70.8, which also shows a non-uniform cloud of lifted dust particles in front of the propagating flame.

In the case of dust explosion propagation down a gallery or duct, several test programs have been conducted to determine the minimum

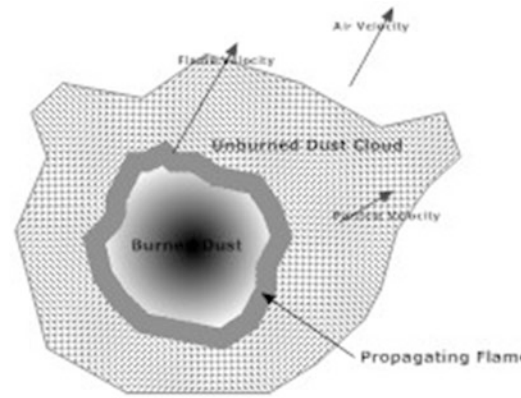

Fig. 70.7 Dust flame propagation schematic

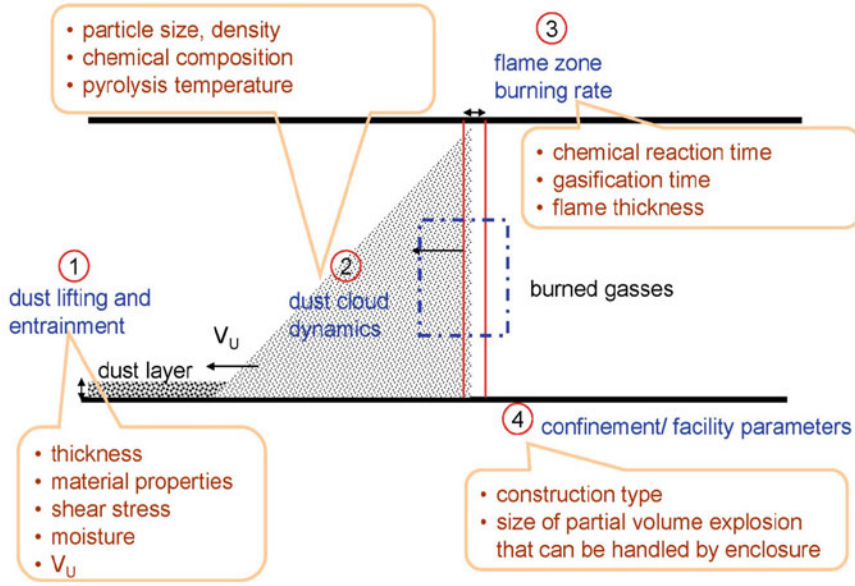

Fig. 70.8 Lifted dust forms cloud ahead of propagating flame (From A. Rangwala 2011)

dust layer equivalent concentration (dust loading per unit gallery length divided by gallery cross-sectional area) that will support the continuing propagation of a dust explosion initiated at one end of the gallery/duct. This question is critical to assessing the amount of accumulated dust needed for dust explosion propagation in coal mines and grain elevator conveyor galleries. Lebecki et al. report [15] that the minimum corn starch concentration required for explosion propagation in a 100 m long, 2 m diameter, gallery is 75 g/m^3 when a methane explosion initiates propagation, and 50 g/m^3 when the initial methane explosion is enhanced with an extra load of grain dust near the initiation site. When the equivalent accumulated corn starch concentration is 150 g/m^3 or greater, the flame accelerates and the peak pressure increases with distance away from the explosion initiation site. Flame speeds for the 150 g/m^3 dust loading reached 330 m/s at the far end of the gallery, and peak pressures reached 4 barg. Significantly higher flame speeds and pressures were measured for tests with a dust loading of 200 g/m^3. Dust-free gallery segments 20 m in length did not prevent flame propagation to the downstream dust laden remainder of the gallery.

Tamanini reported [16] on corn starch explosion propagation tests in 6 m length and 24.4 m length galleries with a larger cross-section primary explosion chamber attached to one end and open to the atmosphere at the other end. Flame propagation down the length of the galleries was observed in all tests with floor dust loadings as low as 50–77 g/m^3, but the flame only occupied the lower one third of the gallery cross-section, and there was no increase in explosion pressure with distance along the gallery. When baffles (flow obstructions) were installed in the gallery, the entrained dust cloud and flame extended to the gallery ceiling.

Another type of dust explosion propagation application is the propagation from one enclosure to another via a connecting pipe or duct. This is a common configuration both in powder production facilities and in facilities with dust collectors connected to dust generating equipment. An explosion in one vessel produces a pressure and temperature increase in the second vessel, such that an explosion in the second vessel will be initiated at a higher temperature and pressure than the initial explosion. This is sometimes called pressure piling. The resulting pressure of the second explosion

can be significantly higher than the P_{max} values measured in single vessel standard tests such as the ASTM E1226 tests, particularly when the second vessel is smaller than the first vessel.

Lunn et al. [17] presented test results and theoretical calculations demonstrating the increase in pressure in the second vessel when the ratio of the second vessel volume to the first vessel volume is less than 4. When the ratio is less than 0.5, the second vessel explosion pressure could be greater than twice the P_{max} value measure in standard 20-l sphere tests. Lunn et al. found that the diameter and length of the interconnecting pipe did have a significant effect on whether the flame from the first vessel would propagate into the second vessel to ignite the suspended dust cloud there. Explosion propagation was not observed in small pipe diameters (15 cm and less) with lengths of at least 5. CFD simulations conducted by Kosinski and Hoffman [18] showed that the percentage of still burning dust particles entering the second vessel was less than 20 % for a duct height of 15 cm, but was at least 75 % for a 50 cm high duct. Thus, explosion propagation between enclosures is more likely when the explosion is initiated in the larger enclosure, and when the interconnecting pipe or duct is greater than approximately 15 cm. Additional observations are presented in the section on explosion isolation.

Secondary Dust Explosion Hazards

Most of the serious injuries and fatalities resulting from dust explosions occur when a primary explosion in some type of process equipment produces a blast wave and burning dust cloud in an area occupied by personnel. The casualties can be great if fugitive dust near the primary explosion is lifted and ignited so as to produce either a large flash fire or a secondary dust explosion. Examples of combustible dust incidents where this has occurred are listed in Table 70.2. The incidents listed in Table 70.2 are described in the Chemical Safety Board's 2006 combustible dust incidents survey report [19] and Imperial Sugar incident report [20]. In many of these incidents victims were situated far away from the primary explosion, but there were extensive fugitive dust accumulations that extended far beyond the area of origin.

The initiating explosion blast wave causes an air velocity that decreases with distance from primary explosion site. Fugitive dust will be lifted if the air velocity exceeds a threshold value, U_t, that Ural [21] has approximated with the following simple equation.

$$U_t = 0.46\ \rho_p^{1/3} \tag{70.6}$$

where ρ_p is the dust particle density (kg/m^3) and U_t is in m/s. The mass flux of dust entrained

Table 70.2 Examples of dust explosion incidents with secondary dust explosions or flash fires

Type of plant	Primary explosion location	Combustible dust for secondary explosion or flash fire	Injuries	Fatalities
Textile mill	Flocking machinery	Nylon fibers	37	0
Power plant	Boiler	Pulverized coal	36	6
Iron foundry	Gas-fired oven	Phenolic resin	9	3
Rubber recycling	Dryer & bagging bin	Rubber	7	5
Rubber compounding	Space above suspended ceiling	Polyethylene	38	6
Acoustic insulation	Curing oven	Phenolic resin	37	7
Sugar refinery	Belt conveyor	Sugar	36	14

locally into the air flowing at velocity U is given by the following equation in the Research Foundation report [21].

$$m'' = 2\rho_a U \left(U^{\frac{1}{2}} - \frac{U_t^2}{U^{\frac{3}{2}}} \right) \qquad (70.7)$$

where m'' is in g/m^2-s, ρ_a is ambient air density (1.2 kg/m^3), and U and U_t are in m/s. These equations can be used for a scenario specific calculation of the local dust layer mass fraction entrained, as an alternative to using the NFPA 654 default value of 0.25 described previously.

Since many combustible metals have large bulk densities and high flame temperatures and P_{max} values, the allowable accumulation thicknesses based on Equation 70.5 and the NFPA 654-2013 equivalent for flash hazards are very thin. The NFPA Combustible Metals standard [22] does not allow any dust accumulation for certain extremely explosible metals such as magnesium. This implies immediate cleanup of any visible dust. NFPA 484 and NFPA 654 and the other NFPA combustible dust standards describe recommended cleanup methods to minimize the chances of creating a dust cloud and/or introducing an ignition source during cleanup. These measures include the use of portable vacuum cleaners certified for use in Class II (combustible dust) hazardous locations, which implies that they have been tested to verify that they are dust-ignition-proof for the particular combustible dust category (Group E, F, or G) for which they are listed. Of course, hand shoveling and sweeping are also viable cleaning methods. The NFPA Guide to Combustible Dusts [23] has descriptions and examples of the various recommended combustible dust cleaning equipment and tools.

Other important aspects of reducing the secondary dust explosion/fire hazard are training of personnel and development of documented cleaning schedules and reports. FM Loss Prevention Data Sheet 7-76 [24] states that a rule of thumb is to use a dust thickness of 1.6 mm (1/16th inch or the thickness of a quarter coin) is cause for cleanup of many dusts with bulk densities similar to that of wood. It also provides guidance on estimating the amount of surface area that may have accumulations of at least this depth, so that a dusty area in excess of 5 % of the room floor area would be a cleanup trigger. The NFPA Guide [23] includes examples of housekeeping data collection sheets to be completed and signed by plant personnel or contractors. It also has an example of a tabulated fugitive dust collection report showing the amounts of dust cleaned in various plant areas.

Dust Explosion Scenario Examples

Various categorized tabulations of dust explosion incidents, such as those in FM Data Sheet 7-76 [24] and the CCPS Guidelines for Powders and Bulk Solids [25], show that the equipment involved in many incidents include dust collectors, hammermills and similar size reduction equipment, storage silos and attached product conveying equipment, and ovens and dryers. Examples of dust cloud formation and ignition scenarios in this equipment are presented here.

In the case of the spray dryer shown schematically in Fig. 70.6, the hottest areas are the nozzles and walls in the upper section of the dryer. The hot air surrounding the nozzles often enters the dryer at a temperature above the powder hot surface ignition temperature or the hot air over layer ignition temperature so that product accumulations on the spray nozzles and the upper wall area are heated sufficiently to initiate burning of the accumulated product. If the burning product in the upper section of the dryer is lodged, it will fall toward the conical region where there may be a sufficient suspended dust cloud concentration to support a partial volume deflagration. The deflagration can then propagate to downstream process and dust collection equipment and cause other fires and explosions in that equipment.

Rotating drum dryers have also been the site of dust explosions and flash fires. Some of these incidents have occurred because of the inadvertent recycling of already dried product. This is particularly hazardous in direct fired dryers where the internal temperature can be above the

dust cloud auto-ignition temperature. In the case of steam tube dryers, the tubes can be dried product accumulation sites with hot surface temperatures above the dust layer hot surface ignition temperature.

Grinders, hammermills, and other size reduction equipment inherently dissipate large energy inputs required to break up the particles. This energy dissipation inevitably causes heating of the particles and metal surfaces. One scenario that produces particularly high temperatures is the inadvertent entrance of tramp metal into the mill. High concentration powder/dust clouds are an inherent result of hammermill operation, and they can be readily ignited by the hot hammer surface.

Figure 70.9 shows evidence of the frictional or impact heating of hammers in a hammermill used to produce powdered sugar. The heating of sugar and metal in that vicinity of the mill ignited a sugar dust explosion that burned the hammermill operator who was responding to the sound of severe vibration due to tramp metal or a broken hammer in the mill.

Recommendations in the CCPS Guidelines book [25] for preventing grinder/pulverizer dust explosions include monitoring the mill motor current and having an interlock shutdown upon high current draw, use of magnetic separators to find and remove tramp metal before it enters the mill, and use of special enclosed mills to allow inerting of powders with extremely low MIE and AIT values.

Possible reasons for the high occurrence of dust collector explosions are (1) they are almost always in particulate handling facilities, (2) they inherently concentrate the smaller particles which are easier to ignite than the mostly larger particles in other equipment, and (3) by being downstream of other process equipment they

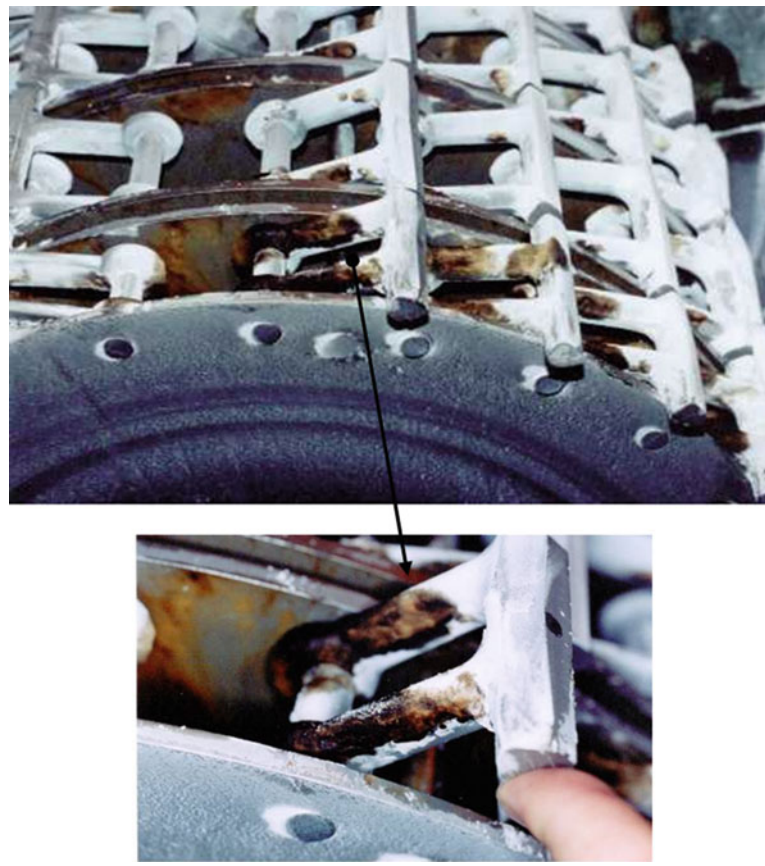

Fig. 70.9 Evidence of scorch marks in a sugar hammermill

often receive transported ignition sources as well as dust. Data from a German compilation of dust explosions cited by Eckhoff [1] indicate that the most frequent ignition sources have been mechanical sparks (41 %), burning embers and particle agglomerations (11 %), electrostatic discharges (10 %), and mechanical heating via friction (7 %).

Zalosh et al. [26] describe a dust explosion that occurred when some steel bolts accidentally entered and became trapped in a hammermill such that they became sufficiently hot to ignite the pharmaceutical powder in the mill. When the burning powder was conveyed to the dust collector, it ignited an explosion when the bags were pulsed. Other dust collector explosions described by Zalosh et al. [26] involved electrostatic discharge ignitions due to electrostatic charging of powder (tantalum) in one case and an ungrounded drum under the collector hopper in another case.

Figure 70.10 shows the burned and ruptured ducting attached to a roof mounted cyclone dust collector that was the site of an explosion due to burning fine particulate resulting from a fire in a rotating drum dryer upstream of the cyclone. The return air duct from the cyclone allowed the explosion to propagate back into the process building where it caused a secondary dust explosion.

Several dust collector explosions occur during maintenance and repair operations. One example is the double fatality explosion that occurred when a pipefitter was attempting to clear a clogged rotary valve at the outlet of a cyclone collector at an aluminum powder production facility [26]. Another example is the aluminum cuttings fire in abandoned dust collection ducting that had not been cleaned and checked before starting hot work to cut down the ducting. The discharge of a Halon fire extinguisher onto the burning aluminum cuttings caused an explosive reaction that resulted in a fatality.

A coal dust explosion occurred in a dust collector that was shut down to replace broken dry pipe sprinkler piping in which water inadvertently entered during a period of extremely cold weather. Scaffolding had to be erected in the dust collector hopper to reach the broken piping above the hopper. Vibrations caused by the

Fig. 70.10 Evidence of dust explosion and fire in cyclone collector and ducting

Fig. 70.11 Dust collector hopper in which coal dust explosion occurred

erection of the scaffolding caused dust to be dislodged from the many bags above the hopper, and the descending dust cloud was ignited by a halogen light bulb. Figure 70.11 shows the 28-in. (71 cm) diameter access opening in the hopper through which the injured scaffolding crew had to escape. Portions of some dust collector bag cages and some scaffold piping, as well as a pile of burned coal dust, are visible inside the hopper.

Other examples of dust explosion scenarios can be found in various Chemical Safety Board reports [19, 20] and British Health and Safety Executive reports.

Dust Explosion Venting and Suppression

The two most common forms of dust explosion protection for equipment are deflagration venting and suppression systems. The actions associated with both protection measures are initiated after the dust cloud starts burning in the enclosure and are intended to prevent the explosion pressure from reaching the enclosure damage threshold pressure. In the case of explosion venting, the protection action is the sudden opening of a vent closure to allow burning and unburned dust and combustion products to be vented at a rate sufficient to prevent damaging pressures from developing. In the case of explosion suppression systems, an extinguishing agent is rapidly injected into the enclosure so as to prevent additional burning of the dust cloud.

NFPA explosion venting design, installation, and maintenance requirements are described in NFPA 68 [27]. The NFPA 68 minimum required vent area, A_v in units of square meters, is calculated from the following basic equation.

$$A_v = 1 \times 10^{-4} \left(1 + 1.54 {P_{stat}}^{4/3}\right) K_{ST} V^{3/4} \sqrt{\frac{P_{max}}{P_{red}} - 1} \tag{70.8}$$

where

P_{stat} is the vent deployment pressure (bar g) in response to a slowly increasing (static) pressure,

V is the enclosure volume in m^3,

P_{red} is the reduced pressure (less than P_{max}) in the enclosure because of venting. NFPA 68 specifies that the value of P_{red} shall be no greater than 2/3rd the enclosure strength based either on incipient permanent deformation or actual enclosure (structural member) rupture, at the discretion of the facility owner.

In the limit of P_{red} approaching P_{max}, the vent area calculated from Equation 70.8 approaches zero because no venting is needed to prevent enclosure damage. In the other limit of $P_{red} << P_{max}$, the vent area varies as $1/\sqrt{P_{red}}$, which is the limit corresponding to incompressible gas flow through the vent.

Equation 70.8, which is applicable to compact enclosure with $L/D \leq 2$, and lightweight vent disks/panels, was developed by the NFPA Explosion Protection Technical Committee as a modification of a similar analytical approach to dust explosion venting derived by Tamanini and Valiulis [28] for FM Global applications.

The original development of the 2002 version of Equation 70.8 is described by Ural [29]. The coefficients and exponents in Equation 70.8 are empirical values selected to obtain agreement with large-scale dust explosion venting test data.

The test data used to refine and validate Equation 70.8 come from several European test programs in a variety of test vessels with a variety of combustible dusts. Since the dust concentration and turbulence level in the enclosure at the time of ignition significantly affect the rate of burning and associated rate-of-pressure-rise, the dust cloud generation and ignition in almost all these tests were set up to match the corresponding dust K_{ST} values measured in 1-m^3 and 20-l standardized closed vessel laboratory tests. The level of agreement between calculated values of A_v to obtain the P_{red} value measured in the tests with a given A_v is shown in Fig. 70.12. Test series 1 indicated in Fig. 70.12 was conducted in a 18.5 m^3 vessel with dusts having a range of K_{ST} values from 144 to 630 bar-m/s. Test series 2 was conducted with several different test vessels ranging in volume from 2.4 to 250 m^3, and with dusts having K_{ST} values in the range 206 to 322 bar-m/s. Test series 3 was conducted in a 10 m^3 test vessel using dusts with K_{ST} values between 130 and 280 bar-m/s. Thus, Equation 70.8 calculated results have been checked against dust with moderate to high K_{ST} values, but not yet with low K_{ST} dusts.

Vent areas calculated using Equation 70.8 are increased per NFPA 68 prescriptions for the following conditions: (1) large enclosure length-to-diameter ratios, (2) heavy vent panels, and (3) vent ducts used to direct the burning dust out of the building in which the equipment is located. The prescriptions for the first two factors are based on empirical correlations, whereas the vent duct vent area increase is based primarily on the pressure drop due to the vent flow in the vent duct.

NFPA 68-2013 has a provision for using less explosion vent area when the worst-case explosion scenario involves a dust cloud in only part of the enclosure volume. The ratio of the partial volume vent area to the full volume vent area is calculated from the following equation.

$$\frac{A_{pv}}{A_v} = X_f^{-1/3}\sqrt{\frac{X_f - \Pi}{1 - \Pi}} \quad \text{for} \quad X_f > \Pi\,, \tag{70.9}$$

where A_{pv} is the vent area required for a partial volume deflagration,

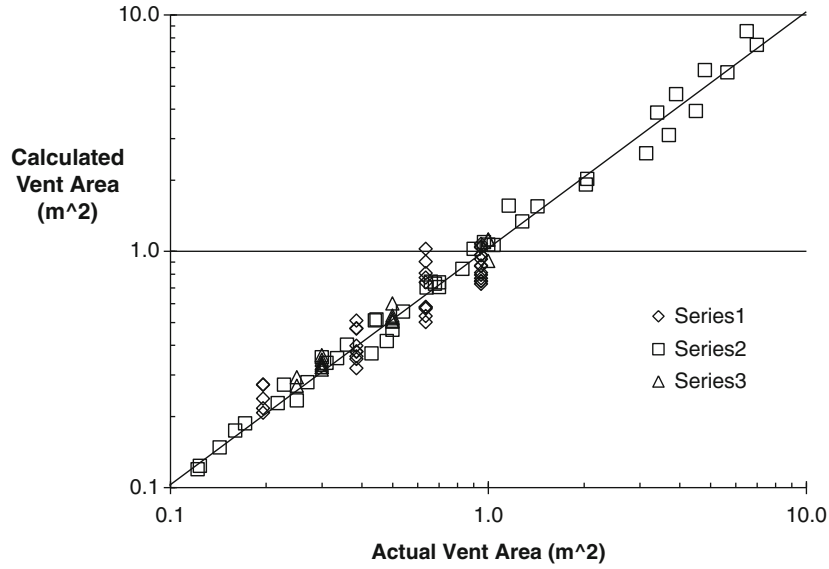

Fig. 70.12 Comparison of calculated and actual dust explosion test vent areas

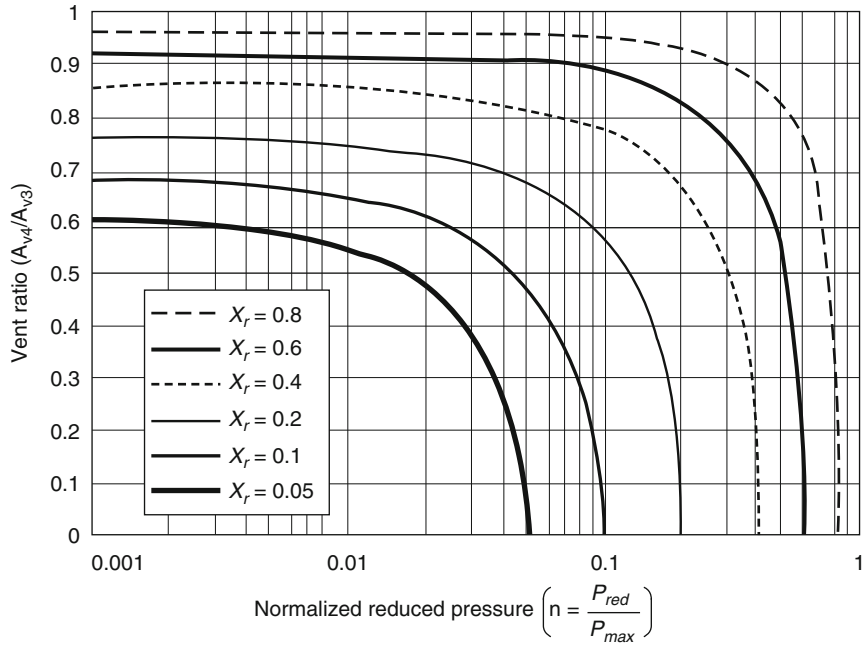

Fig. 70.13 Partial volume explosion vent area ratio versus P_{red}/P_{max} (From NFPA 68)

A_v is the vent area calculated from Equation 70.8 and any increase for enclosure L/D and vent panel mass,

X_f is the partial volume fill fraction in the enclosure,

$\Pi = P_{red}/P_{max}$.

As in Equation 70.3, the partial volume to be used in Equation 70.9, is m_{dust}/c_w, where m_{dust} is determined by Equation 70.4. Figure 70.13 shows the ratio A_{pv}/A_v, as a function of the pressure ratio, P_{red}/P_{max}, for various values of the partial volume fill fraction, X_f. The ratio is greater than 0.90 for pressure ratios less than about 0.1 combined with X_f values greater than 0.5. As the fill fraction tends toward Π, the required vent area decreases sharply toward zero since no venting is needed when $X_v \leq \Pi$. Some of the applications in which the partial volume approach is explicitly permitted per NFPA 68 are spray dryers (where the partial volume is based on measurements) and building dust explosions. The use of partial volume explosion venting is particularly advantageous for buildings because NFPA 68-2013 requires a 70 % increase in the vent area calculated from Equation 70.8 to account for potential secondary dust explosion scenarios with flame jet ignition of dust clouds generated from the primary explosion.

Although flameless explosion vents are now available for dust explosion protection, an explosion suppression system often becomes more pragmatic when explosion protection is required for equipment located far from an external wall or for materials that cannot be vented outside. The conceptual design of an active explosion suppression system is illustrated in Fig. 70.14. The three primary components of the system are (1) a pressure detector, (2) a control panel, and (3) one or more suppressant agent discharge containers. An incipient explosion is detector by the pressure sensor and the control cabinet actuates the high-speed discharge of suppression agent from the agent container(s). The component actuation times shown in Figure are just examples since the actual actuation times depend on the application, particularly the rate of explosion pressure rise.

One of the primary suppression system design considerations is the choice and quantity of

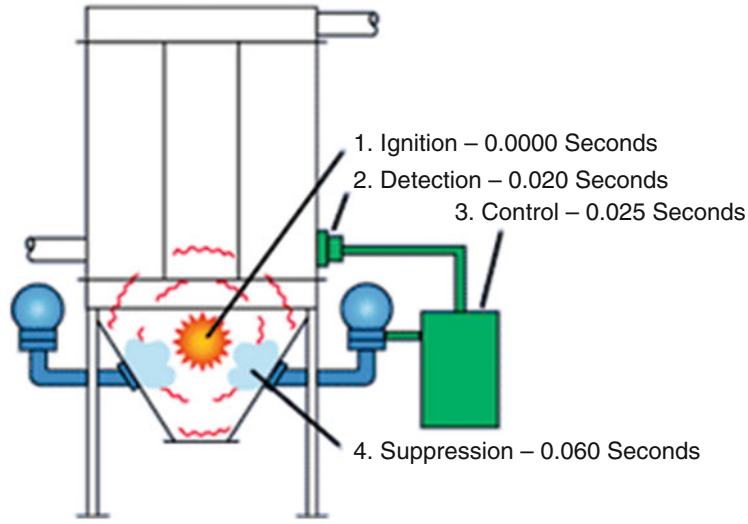

Fig. 70.14 Conceptual layout of an explosion suppression system (From Fenwal/IEP)

suppression agent. The most commonly used agent by U.S. suppression system designers is sodium bicarbonate with additives to prevent clumping and promote rapid discharge. Sodium bicarbonate (SBC) absorbs heat from the developing explosion as it starts to decompose via the following reaction.

$$2\,NaHCO_3 \rightarrow Na_2CO_3 + H_2O + CO_2$$

European suppression systems often use monoammonium phosphate (MAP), which also decomposes upon heating. The amount of SBC or MAP needed to achieve suppression depends on the combustible dust properties, e.g. flame temperature, ignition temperature, and K_{ST}, as well as the enclosure size and configuration. Experiments reported by Chatrathi and Going [30] determined the pre-ignition concentrations of SBC and MAP needed to provide inerting for explosions of various dusts in a 1-m^3 chamber using the ASTM E1226 standard igniter and ignition delay. Their results are listed in Table 70.3. The minimum required inerting concentrations generally increase with dust K_{ST}, but the relative increase is different for the two agents. Aluminum, which required the highest agent concentrations, has the highest flame temperature and probably the highest K_{ST} of the five dusts tested.

Since the suppression agents are supplied in pressurized containers, the amount of agent needed for a suppression system depends on the container size, pressure, and discharge characteristics, as well as the agent discharge actuation pressure. Suppression test data reported by Chatrathi and Going for sodium bicarbonate and potassium bicarbonate agents show that the Total Suppressed Pressure (TSP, maximum pressure developed in a test with a suppression system) was sensitive to the system actuation pressure, particularly when trying to suppress dusts with K_{ST} values of 300 bar-m/s and greater.

Explosion suppression test data reported by Bartknecht [10] indicate that the number of suppression agent filled containers required for suppression of a given dust in different size enclosure volumes varies as $V^{2/3}$ rather than being linearly proportional to V, which would be the case if there was just a required agent concentration in the enclosure. This implies that suppression is not just due to inerting of the dust, but to a dynamic balance proportional to the total surface area of the injected agent. This also suggests that agent particle size and rate of mixing with the burning particulate play significant roles in determining suppression system effectiveness.

Each suppression system provider has developed its own proprietary software tool to guide

Table 70.3 Minimum agent concentrations for inerting dust explosions

Combustible dust	K_{ST} (bar-m/s)	Min SBC concentration (g/m^3)	Min MAP concentration (g/m^3)
Pittsburgh seam coal	116[a]	550	125
Cornstarch	220	625	875
Polyethylene	240–280[a]	1,000	NA
Anthraquinone	Not reported[a]	1,750	>1,500
Aluminum	300	>2,750	>2,750

From Chatrathi and Going [30]

[a]K_{ST} values for these dust samples were not reported by Chatrathi and Going but can be estimated based on published data. Data for anthraquinone in Eckhoff [1] are in the range 94–364 bar-m/s

the design of system parameters for various customer applications. Going [31] has suggested that one of the equations in the Fike software tool to account for the parameters besides the required amount of agent is of the following form.

$$TSP = f\left(K_{ST}^{a} V^{b} Throw^{c} P_{act}^{d}\right) \qquad (70.10)$$

where Throw is the agent throw distance and P_{act} is the system actuation pressure as triggered by the pressure detector. This inclusion of throw distance in this functional form demonstrates that the location of the agent containers, so as to achieve complete coverage of the entire enclosure, is another important suppression system design consideration. Since the TSP value calculated from equations functionally similar to Equation 70.10 has to be less than the pressure resistance of the enclosure, the effectiveness and viability of explosion suppression systems are dependent on the margin between P_{act} and the enclosure strength.

Chapter 10 of NFPA 69 [32] describes the NFPA requirements for explosion suppression systems. One requirement is that the system design basis and range of applicability have been supported by testing and verified by an independent third party acceptable to the Authority Having Jurisdiction. One such independent third party is FM Global, which approves explosion suppression systems per Approval Standard 5700 [33]. FM Approval is contingent upon FM review of the system design software and the conducting of both unsuppressed and suppressed explosion tests in a vessel with a minimum volume of 1 m^3. The tests are conducted with a dust having the highest K_{ST} value for which the suppression system provider wants the FM Approval to be applicable. Other independent third parties doing certification testing are the various European notifying bodies that conduct examinations per the European ATEX Directive 1999/92/EU. Their examination and certification is presumably in accord with the CEN standard for explosion suppression systems [34]. This standard requires that at least 95 % of all suppression test pressures, i.e. measured TSP values, be less than the corresponding values calculated by the system designer's software.

Dust Explosion Isolation Devices and Combined Protection Systems

Dust explosion isolation devices are intended to prevent or interrupt the propagation of a deflagration through a duct or pipe connected to an enclosure in which a dust explosion originates. These devices can be divided into two categories: passive isolation devices and active isolation devices. Passive devices, described in Chap. 12 of NFPA 69-2008, function without the need for any separate deflagration sensor, control hardware, or actuation device. Active isolation devices use auxiliary sensors and controls and are electrically actuated upon deflagration detection.

Two examples of passive isolation devices are known generically as float valves and flap valves. Diagrams for these devices are shown in Figs. 70.15 and 70.16.

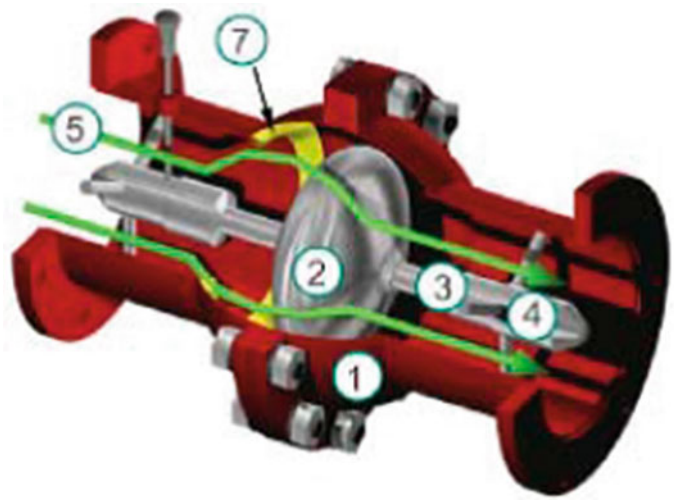

Fig. 70.15 Float isolation valve schematic (From Fike data sheet)

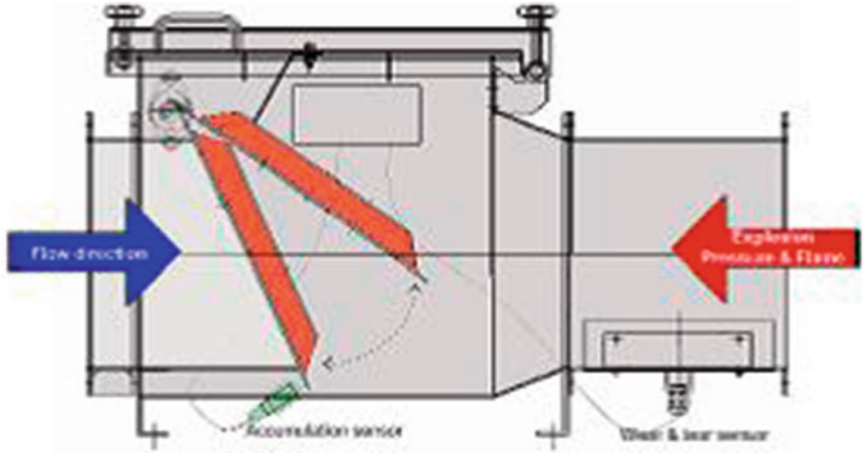

Fig. 70.16 Flap isolation valve schematic (From Fenwal/IEP)

The float component (# 2 in Fig. 70.15) in the float isolation valve slides within guide vanes (# 3 in Fig. 70.15) in the valve body such that a spring (# 5 in Fig. 70.15) holds the float in the open position during normal air flow through the valve. The back pressure wave caused by a propagating deflagration overcomes the spring force and causes the float to side shut against the valve seat (# 7 in Fig. 70.15). One manufacturer's valve requires a minimum deflagration pressure of 0.05 bar to close the valve. This valve comes in a double acting version in order to provide protection for a deflagration propagating in either direction.

The flap isolation valve shown in Fig. 70.16 relies on the normal air flow (typically a minimum air velocity of 15 m/s) to push open the hinged flap and allow powder/dust transport through the valve. A back pressure caused by a propagating deflagration overcomes the normal air flow pressure and forces the flap to slam shut. Since powder/dust accumulations on the valve bottom can prevent complete closure of the flap, there is often a dust accumulation sensor to provide a notification alarm when the accumulation reaches a level that might compromise isolation effectiveness.

In order to be effective, both the float valve and the flap valve must be fully closed before the deflagration flame front reaches them. Therefore the valves have to be located some minimum distance, l_{min}, from the pipe/duct connection to the enclosure in which the primary explosion occurs. The value of l_{min} depends on the flame velocity and the valve closing time. On the other hand, if the valves are located too far from the pipe/duct connection the propagating deflagration can accelerate and develop pressures that exceed the strength of the pipe/duct and valve. Therefore, as Fig. 70.17 indicates, there is also a maximum distance of the valve from the pipe/duct entrance. Siwek [35] has provided empirical prescriptions for l_{min} and l_{max} as a function of pipe diameter and maximum pressure in the protected equipment. Later proprietary guidelines by system designers also account for dust K_{ST} value.

Another type of passive explosion isolation device is the diverter valve shown in Fig. 70.18. It is configured to direct the normal air/product flow up and then back down into the horizontal pipe or duct. A hinged closure cap at the top of the diverter valve rapidly opens in response to an abnormal pressure caused by the propagating dust explosion. The suddenly opened valve then channels the burning dust and flame up out of the pipe or duct. This type of valve is suitable for

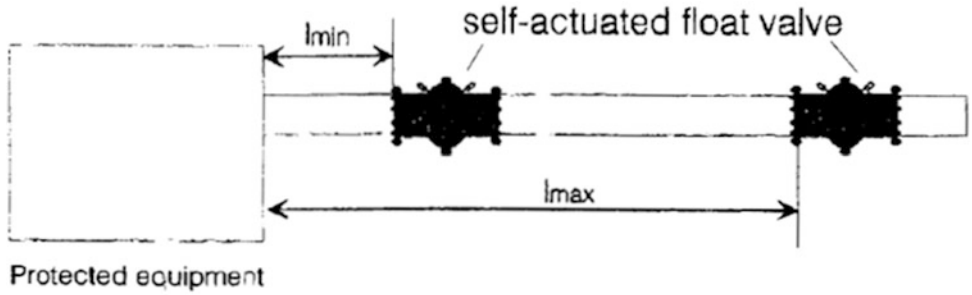

Fig. 70.17 Minimum and maximum distances for isolation device location (From Siwek [35])

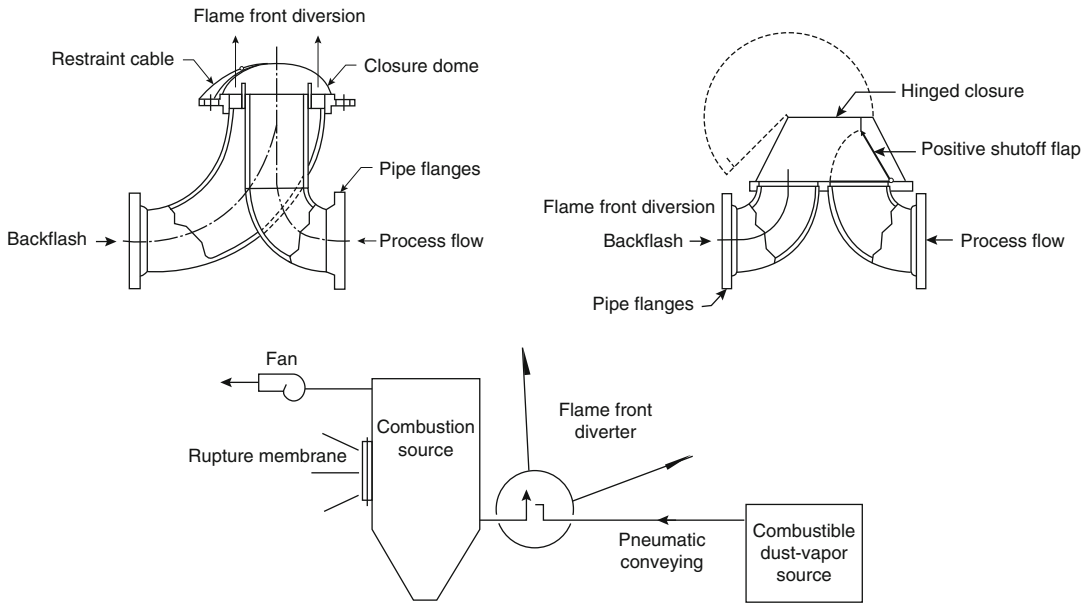

Fig. 70.18 Diverter explosion valve (From NFPA 69)

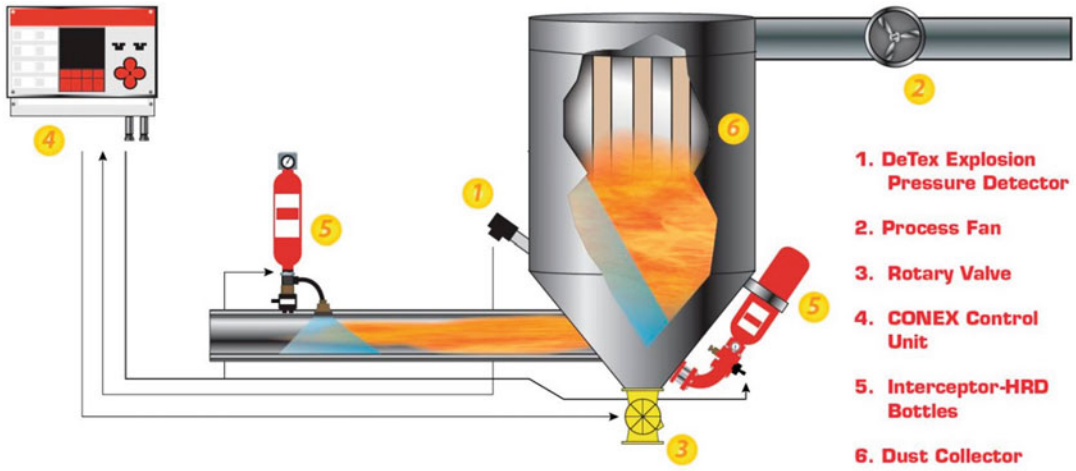

Fig. 70.19 Combined chemical isolation and suppression system (From CV Technology)

outdoor ducts and pipes where the burning dust discharge does not endanger personnel.

The most common active isolation device entails the triggered injection of a suppression agent into the pipe/duct before the propagating flame reaches that location. Since the agent is often triggered by a pressure sensor installed in the connected equipment, chemical isolation systems are commonly coupled with explosion suppression systems. Figure 70.19 is a conceptual layout of this combined system for the protection of a dust collector and the attached inlet duct. The suppression and isolation agent bottles (items # 5 in figure) are fired simultaneously by the control unit (item # 4).

Another type of active isolation device is a fast acting mechanical gate valve such as illustrated in Fig. 70.20. The electric initiator on the valve is actuated by a control panel wired to some type of deflagration detector located between the isolation valve and the enclosure in which an explosion is anticipated.

The float valve described above as a passive isolation device is also made as an externally actuated valve in which the float closure is driven by gas jets actuated by a separate deflagration detector. The advantage of this active isolation version of the float valve, shown in Fig. 70.21, is that it can be closed at a lower pressure than the passive, self-actuated version.

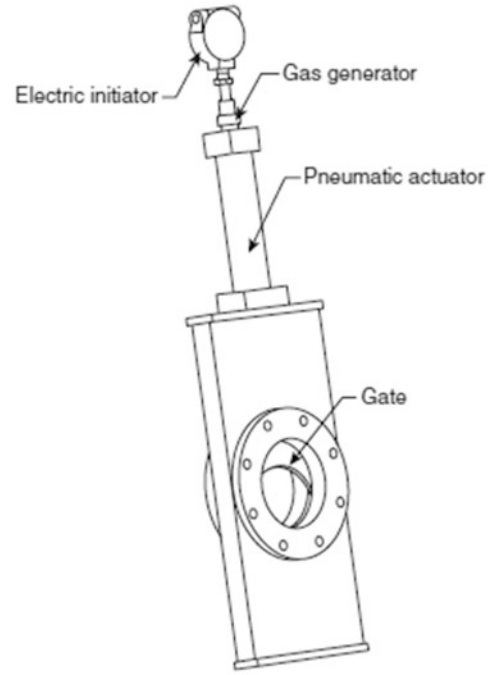

Fig. 70.20 Fast-acting, pneumatically actuated mechanical isolation valve (From NFPA 69)

Still another type of active isolation valve is the externally actuated pinch valve. As the cutaway diagram in Fig. 70.22 indicates, the valve interior has an elastomeric pinch that is normally open but can be closed by rapid compression via

an air line connected to the valve air chamber. The attached pressurized air source and actuation component are not shown in the figure.

NFPA 69 requires that both active and passive explosion isolation devices be tested and be certified by an independent organization. The European Community standard for such certifications is EN 15089 [36]. The standard has three types of testing requirements; explosion resistance testing, flame transmission testing, and functional testing. There are also requirements for optical and pressure detectors and control and indicating equipment used in active isolation devices. Certification documentation includes minimum and maximum isolation device installation distances, l_{min} and l_{max}, pressures developed on both sides of the isolation device, and commissioning and maintenance requirements. NFPA 69 requires quarterly inspections of isolation and suppression systems.

Fig. 70.21 Externally actuated float isolation valve (From NFPA 69)

The complexity of dust explosion suppression and isolation systems, and their potential deterioration in harsh powder/dust processing environments, has generated concern about their long term reliability. In order to address these reliability issues, Date et al. [37] have developed a mathematical reliability analysis for applications of these explosion protection systems. They describe the application of their analysis to an exemplar spray drying system shown in Fig. 70.23. The dryers are protected by explosion suppression systems and the cyclones are protected by explosion vents. There are also chemical and mechanical explosion isolation valves on the piping to and from the fluidized bed dryers. Actuation of the various devices is controlled by three control panels, one for each zone indicated in the diagram.

Date et al. [37] assigned nominal mean-times-to-failure for each of the explosion protection devices and control panel zones indicated in Fig. 70.23. Their lowest mean-times-between-

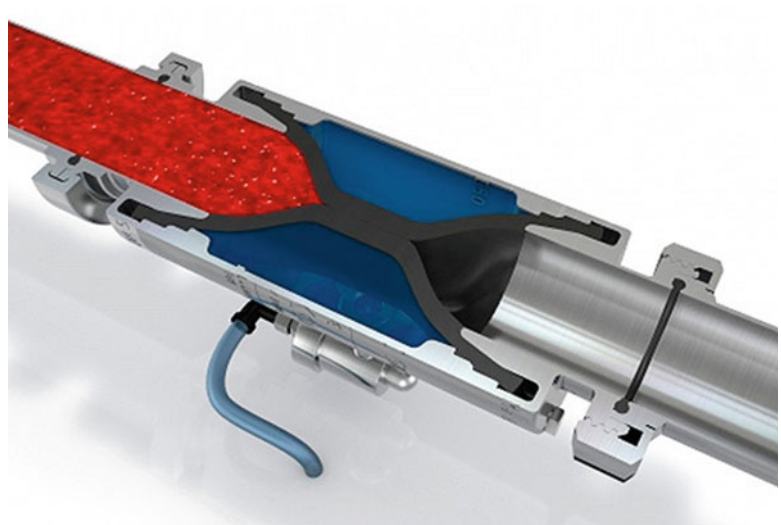

Fig. 70.22 Pinch isolation valve (From solidsonline.com AKO Web page)

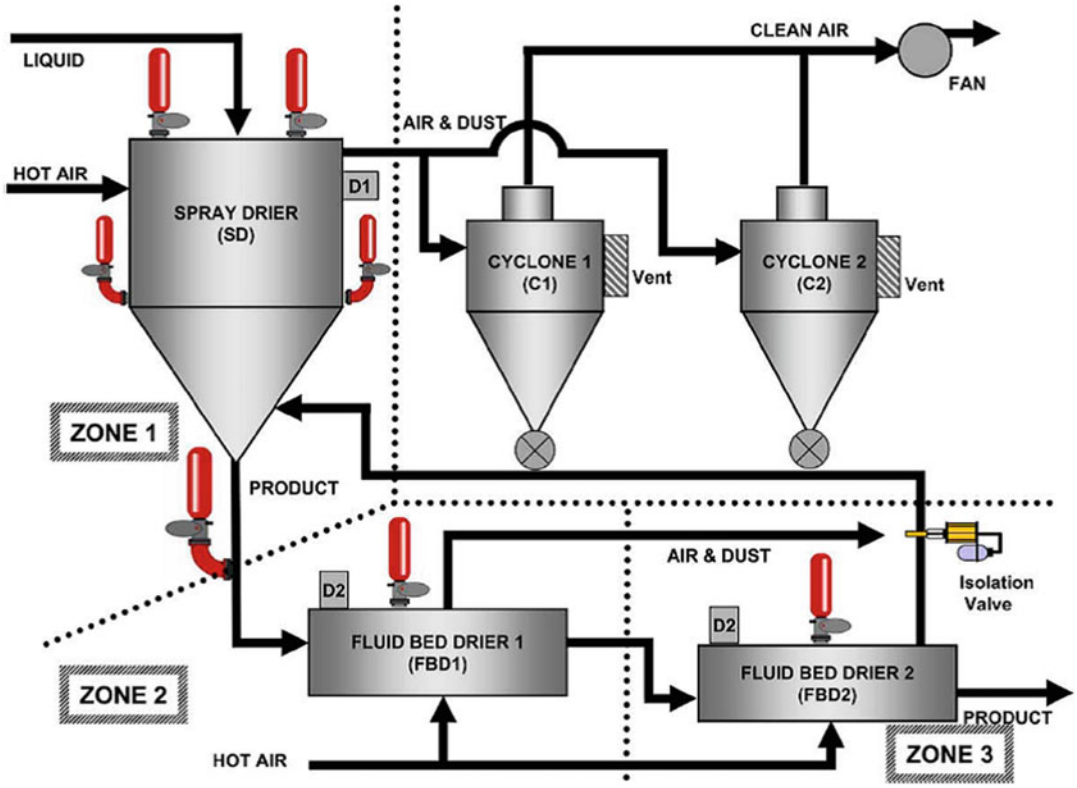

Fig. 70.23 Spray drying system used in Date et al. reliability analysis example (from Date et al.)

failures (MTBFs) were for the detectors (4,000 h) and the isolation devices (2,000 h). They converted the component MTBFs to corresponding component failure rates (without explicitly accounting for effects of maintenance and inspection intervals), and combined these with probabilities of flame propagation and vessel explosion pressures exceeding the vessel strengths. Date et al. used probability equations to calculate the probability of vessel failures and the overall system residual risk, i.e. the annual probability of explosion protection system failure. They also showed how the residual risk could be significantly reduced by combining Zones 2 and 3 so that an explosion in either fluidized bed dryer would trigger the simultaneous discharge of the suppression systems and isolation devices in both dryers, and thereby reduce the probability of late system actuation or the systems being overpowered by flame jet ignition associated with propagation between the two dryers.

Although quantitative evaluations of explosion protection reliability are not commonly conducted, there is growing concern for protection system reliability as well as system cost and installation priorities. These concerns can best be addressed by informed evaluations of dust explosion risks and the effectiveness and limitations of the various options for explosion protection.

References

1. R. Eckhoff, Dust Explosions in the Process Industries, 2nd Edition, Butterworth Heinemann, 1997.
2. ASTM E1226, *Standard Test Method for Explosibility of Dust Clouds*, 2010.
3. J. Going, C. Chatrathi and K. Cashdollar, "Flammability Limit Measurements for Dusts in 20-L and 1-m3

vessels," *Journal of Loss Prevention in the Process Industries, v 13,,* pp. 209–219, 2000.
4. N. Kuai, W. Huang, B. Du, J Yuan, Z. Li, "Experiment-based investigations on the effect of ignition energy on dust explosion behaviors," *Journal of Loss Prevention in the Process Industries, v 26,,* pp. 869–877, 2013.
5. ISO 6184-1, *Explosion protection systems – Part 1: Determination of explosion indices of combustible dusts in air.,* 1985.
6. ASTM E1515, *Standard Test Method for Minimum Explosible Concentration of Combustible Dust,* 2007.
7. ASTM E1491, *Standard Test Method for Minimum Autoignition Temperature of Dust Clouds,* 2006.
8. ASTM E2021, *Standard Test Method for Hot Surface Ignition TEmperature of Dust Layers,* 2000.
9. ASTM E2019, *Standard Test Method for Minimum Ignition Energy of a Dust Cloud in Air,* 2007.
10. W. Bartknecht, Dust Explosions, Course, Prevention and Control, 1978.
11. R. Siwek and C. Cesana, "Ignition behavior of dusts: meaning and interpretation," *Process Safety Progress,* vol. 4, pp. 107–119, 1995.
12. R. Siwek, van Wingerden, K., Hansen, O.R., Sutter, G., Kubiansky, Chr., Schwartzbach, Chr., Giger, G., and Meili, R.,, "Dust Explosion Venting and Suppression of Conventional Spray Dryers," in *11th International Symposium on Loss Prevention and Safety Promotion in the Process Industries*, Prague, 2004.
13. NFPA 654, *Standard for the Prevention of Fire and Dust Explosions from the Manufacturing, Processing, and Handling of Combustible Particulate Solids,* 2013.
14. K. Cashdollar and I. Zlochower, "Explosion temperatures and pressures of metals and other elemental dust clouds," *Journal of Loss Prevention in the Process Industries,* vol. 20, pp. 337–348, 2007.
15. K. Lebecki, Cybulski, K., Sliz J, Dyduch Z., Wolanski P "Large scale grain dust explosions – research in Poland," *Shock Waves,* vol. 5, pp. 109–114, 1995.
16. F. Tamanini, "Dust Explosion Propagation in Simulated Grain Conveyor Galleries," National Grain and Feed Association Fire and Explosion Research Report, 1983.
17. J. A. Lunn, "Dust explosions in interconnected vessels," *Journal of Loss Prevention in the Process Industries,* 1998.
18. P. Kosinski and A. Hoffman, "An Investigation of the Consequences of Primary Dust Explosions in Interconnected Vessels," *Journal of Hazardous Materials, A137, pp 752–761,* 2006.
19. Chemical Safety Board, "Combustible Dust Hazard Study," 2006.
20. Chemical Safety Board, "Sugar Dust Explosion and Fire," 2009.
21. E. Ural, "Towards Estimating Entrainment Fraction for Dust Layers," National Fire Protection Research Foundation, 2011.
22. NFPA 484, *Standard on Fire and Explosion Protection for Combustible Metals,* 2012.
23. W. Frank and S. Rodgers, Guide to Combustible Dusts, NFPA, 2012.
24. FM Data Sheet 7-76, "Combustible Dust Fire and Explosion Protection," FM Global, 2013.
25. AIChE Center for Chemical Process Safety, Guidelines for Safe Handling of Powders and Bulk Solids, 2002.
26. R. Zalosh, S. Grossel, R. Kahn, and D. Sliva, "Safely Handle Powdered Solids," *Chemical Engineering Progress,* pp. 23–30, 2005.
27. NFPA, *Standard on Explosion Protection by Deflagration Venting,* 2013.
28. F. Tamanini and J. Valiulis, "Improved guidelines for sizing of vents in dust explosions," *Journal of Loss Prevention in the Process Industries,* vol. 9, pp. 105–118, 1996.
29. E. Ural, "A simplified development of a unified dust explosion vent size formula," *Process Safety Progress,* vol. 20, pp. 136–144, 2001.
30. K. Chatrathi and J. Going, "Dust Deflagration Extinction," *Process Safety Progress,* vol. 19, 2000.
31. J. Going, "Practical Aspects of Explosion Suppression," in *NFPA Symposium on Dust Explosions*, 2011.
32. NFPA 69, *Standard on Explosion Prevention Systems,* 2008.
33. FM Global, *Approval Standard for Explosion Suppression Systems, Class Number 5700,* 1999.
34. CEN, *EN 14373: Explosion Suppression Systems,* 2005.
35. R. Siwek, "Review of Explosion Isolation Techniques," in *World Seminar on the Explosion Phenomenon and the Application of Explosion Protection Techniques in Practice*, 1996.
36. CEN, *Explosion Isolation Systems, EN 15089,* 2009.
37. P. Date, R. Lade, G. Mitra, and P. Moore, "Modelling the reliability of explosion protection systems," *Journal of Loss Prevention in the Process Industries,* vol. 22, pp. 492–498, 2009.

Robert Zalosh is a Fire Protection Engineering Professor Emeritus at Worcester Polytechnic Institute (WPI) and has a consulting practice called Firexplo in which he advises clients on how to deal with special industrial fire and explosion hazards and investigates major industrial fire and explosion incidents. He formerly was a FPE Professor at WPI and the Applied Research Department Manager and Assistant Vice President at Factory Mutual Research Corporation.

BLEVES and Fireballs

71

Alfonso Ibarreta, Hubert Biteau, and Jason Sutula

The storage of flammable liquids and vapors in closed vessels can lead to a catastrophic failure of the vessel during a fire. When a vessel explosion involves a flammable substance, it is usually followed by a fireball [1]. If the flammable material is stored as a pressure liquefied gas, a sudden failure of the storage vessel may result in a **B**oiling **L**iquid **E**xpanding **V**apor **E**xplosion (BLEVE). A BLEVE event will result in a sudden conversion of stored thermal energy into mechanical energy in the form of a pressure wave. Additionally, the rupture of a compressed gas storage vessel may also result in a pressure wave.

A sudden energy release from a compressed vessel failure will result in damage associated with the pressure wave and the impact of missiles displaced by the explosion. In the case of a vessel filled with a flammable gas or liquid, the sudden ignition of the material can result in a fireball that travels upward while burning. This fireball may cause additional damage due to the associated flame radiation.

The following chapter discusses these types of events, the potential mitigation strategies, and the calculation of total energy released.

A. Ibarreta
Exponent

H. Biteau (✉)
Exponent

J. Sutula
Jensen Hughes

BLEVEs

A BLEVE is one of the major container and gas storage hazards within the chemical process industry and industry in general. In brief, a BLEVE consists of the rupture of a pressurized vessel containing a liquid that is above its atmospheric boiling point [2]. The consequences of a BLEVE can be substantial, even if the stored liquid is non-flammable. If the liquid is flammable, the hazards can be the fragmentation of the vessel, a pressure wave, and a secondary fireball. If the liquid is non-flammable, the main hazard will be associated with an overpressure event [2].

One of the most frequently cited BLEVE events took place in Crescent City, Illinois in 1970. A freight train with 15 cars derailed. Ten of the rail cars were tank storage cars carrying liquefied propane gas. At the start of the derailment, one of the liquefied propane gas cars collided with another, tearing a large rupture into one of the other tanks. The result was a large initial fireball and subsequent sustained fire. Five of the liquefied propane gas cars achieved a BLEVE in the first 4 h [2]. Nearby structures sustained severe damage and 66 injuries were reported as a result [2].

The BLEVE acronym was coined in 1957 by researchers from Factory Mutual Research Corporation [2]. J. B. Smith, W.S. Marsh, and W.L. Walls proposed the acronym after an in-house incident involving the rupture of a phenol reservoir that had become superheated [3]. Walls followed up the initial use of the

M.J. Hurley (ed.), *SFPE Handbook of Fire Protection Engineering*,
DOI 10.1007/978-1-4939-2565-0_71, © Society of Fire Protection Engineers 2016

acronym by defining a BLEVE as "a failure of a major container into two or more pieces, occurring at a moment in time when the contained liquid is at a temperature well above its boiling point at normal atmospheric pressure" [4, 5].

Birk and Cunningham redefined the BLEVE in a 1994 study as "the explosive release of expanding vapor and boiling liquid when a container holding a pressure liquefied gas fails catastrophically" [6]. More recently, the current definition that is in the greatest use stems from the Center for Chemical Process Safety and is given as "an explosion resulting from the failure of a vessel containing a liquid at a temperature significantly above its boiling point at normal atmospheric pressure" [2].

Description of a BLEVE Event

A BLEVE event begins when a pressurized container that is filled with a liquid at a temperature above its boiling point at normal atmospheric pressure undergoes an impairment that results in the rupture of the container. The rupture can be caused either thermally or mechanically. In the thermal case, the heating of the container is responsible for the mode of failure. In the mechanical case, the container rupture is due to an impact or other event that causes a portion of the container to be breached. When the container is breached, the vapor of the liquid expands while the liquid becomes superheated. The superheating of the liquid results in flashing of the liquid. Additionally, a pressure wave is generated at the time of rupture and release, which can lead to the fragmentation of the container and the production of missiles. If the liquid in the container is flammable, a premixed system of fuel and air will develop which may result in a fireball [7].

Abbasi and Abbasi [7] provided a summary of the steps observed in a typical BLEVE event by collating the works of McDevitt et al. [8], Prugh [9, 10], Leslie and Birk [11], Lees [12], Birk and Cunningham [6, 13], Casal et al. [14], Venart [15], Reid [16], Shebeko et al. [17], and Birk et al. [18]:

(A) **A container holding a pressurized liquefied gas receives a heat load or mechanically fails due to the impact of a missile, fatigue, or corrosion.** Heating from an exterior source to a container holding a pressurized liquefied gas will be problematic. As the heat loading increases, the pressure inside the container will begin to rise. Eventually, the pressure will increase to the point that a pressure relief valve will activate. If the container is not completely filled with liquid, the open pressure relief valve will allow for vapor to escape. Over time, the liquid level within the container will fall. As the liquid level falls, the cooling effect of the liquid on the metal walls of the container will be reduced. The heat exposure on the uncooled metal will lead to weakening and, eventually, a rupture of the container. This failure mode can occur even when the pressure relief valve has operated normally [7].

Missiles from the violent failure of other containers can result in the weakening or damage to nearby containers. Additionally, aging of a particular container can result in metal fatigue or corrosion, which can also lead to a more rapid failure when the container is exposed to exterior heat sources [7].

(B) **The container fails.** Containers that are designed to hold pressurized liquids can withstand pressures up to the set pressure for the relief valve. The expectation is that this set pressure would be achieved at room temperature. Heating of the container due to an exterior heat source (e.g., a nearby fire) immediately exposes the container to an environment that it was not designed to handle. If the temperature of the metal walls of the container increases sufficiently, the metal will lose strength and eventually rupture. Steel is commonly used in the construction of liquefied propane containers. These vessels will typically fail when the metal walls achieve a temperature of approximately 650 °C and a pressure of approximately 15 atm [7].

(C) There **is an instantaneous depressurization of the container and an explosive event.** Once a container has ruptured, the pressure within the container drops nearly instantaneously from a high pressure to atmospheric pressure. The temperature of

the pressurized liquefied gas remains well elevated above the liquid's boiling point. This is commonly referred to as a superheated liquid. Every liquid will have a unique superheat limit temperature, which is a property of the liquid. This temperature is a measure of how much superheating a particular liquid can withstand. When a liquid is stored at pressure, is above its superheat limit temperature, and a failure of the container occurs, the liquid will undergo an instantaneous and homogenous nucleation. The result is a rapid flashing of the liquid into a vapor, which can produce the BLEVE effect [7].

It is possible to produce the BLEVE effect if the liquid is below its superheat limit temperature, but still in a significant superheat condition. Several other conditions must be present for this to occur, which have been researched by Yu and Venart [19].

(D) **The container sustains pressure wave damage resulting in fragmentation of the container.** The near instantaneous transition of the liquid to a vapor produces an expansion on the order of several hundred to over a thousand times the original volume of the liquid. Additionally, the pressurized vapor within the container also expands rapidly. This rapid change produces a powerful overpressure blast wave that can fragment the container into various sized pieces that are propelled outward from the area of origin.

Fragments from the shattered container become missiles as they move away from the initiation point and move at high velocities in all directions. It is very common for these missiles to collide with other nearby containers, damaging or weakening them enough to allow for additional cascading BLEVE events to occur [7].

(E) **A resulting fireball or toxic dispersion is produced.** The final marker of a BLEVE event is the production of a fireball or the dispersion of a toxic substance. If the liquid in the container is non-toxic, such as water in a boiler, the only hazards will be the resulting pressure wave and missiles from the fragmentation of the container. If the liquid is flammable, the release of the flammable vapor will result in the mixing of the vapor with air into a flammable range that may ignite and produce a fireball. A fireball produced in this manner can be substantial in size and produce large amounts of thermal radiation.

BLEVEs that occur with toxic chemicals that are not flammable can create hazardous conditions through the rapid dispersion of the chemical. Chlorine has been involved in a number of historical BLEVE events where the dispersion has resulted in fatalities due to exposure from a toxic cloud [7].

Theory of BLEVE Precipitation

The main theory behind the precipitation of a BLEVE event was first put forth in 1979 by Reid [16]. This theory was centered around the idea of the superheat limit temperature. In this case, the superheat limit temperature was defined as the maximum temperature that could be achieved before a liquid must transition to a gaseous state. The superheat limit temperature is a unique property of a fluid and is pressure dependent.

The Superheat Limit Theory

The superheat limit theory for the initiation of a BLEVE event is described by the following chronology. First, a vessel that contains a pressure liquefied gas ruptures. Second, the vapor, which was previously in equilibrium with its liquid, begins to blow off. Third, the resulting liquid pressure drops rapidly and the liquid becomes superheated as the temperature of the liquid is now far above its boiling point at the reduced pressure [16].

The superheat limit for a given liquid can be reached by one of two means. First, at a constant pressure, the temperature of a liquid can be increased until a threshold value is achieved. This threshold value is the minimum temperature at

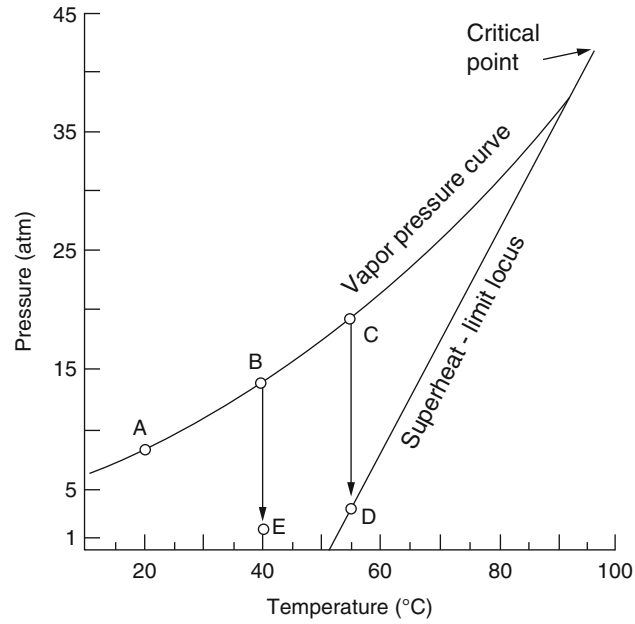

Fig. 71.1 Propane saturated vapor pressure and superheat limit [16]

which the liquid becomes homogenously nucleated in the absence of nucleation sites [7]. Second, at a constant temperature, the superheat limit is achieved if a container with a pressure-liquefied gas is rapidly depressurized [7].

In both of these pathways, there exists an instantaneous liquid to gas phase change of a portion of the liquid, resulting in a superheated liquid vapor explosion. The timing of these transitions is on the order of a few milliseconds, which allows for an extremely large increase in the volume of the system over a very small time scale. The combination of the newly created vapor with the expansion of the compressed vapor results in a strong pressure wave. An explosion produced in this fashion will be of high order and can shatter the storage container in multiple pieces, which will be thrown outward from the origin location [7].

The BLEVE pathways can be visually expressed in terms of the pressure and temperature evolution of the system. Figure 71.1 shows an example of how the superheat limit changes as a function of pressure and temperature for propane.

In examining Fig. 71.1, point A represents a system under a pressure of 9 atm and at ambient temperature. Once a thermal loading is applied on the container, both the pressure and temperature inside the container will increase following the saturation vapor pressure curve to maintain equilibrium of the liquid-vapor system. This is represented by points B and C. Upon containment failure (e.g., rupture of the vessel), the pressure drops rapidly as seen in the transition lines from B to E and C to D. The rapid depressurization transition allows for superheated liquid conditions as now the liquid is well above its boiling point (point D) [3].

Abbasi and Abbasi [7] illustrated the superheat limit theory by also presenting superheat temperature data on ammonia, chlorine, and butane, which is reproduced in Fig. 71.2. All three gases demonstrate typical superheat behavior, with the variation of the vapor pressure curve and the superheat limit a function of the type of fluid.

Determination of the Superheat Limit Temperature

Both experimental and theoretical approaches have been followed to determine the superheat limit temperature for a given fluid. While the complete knowledge of a particular superheat

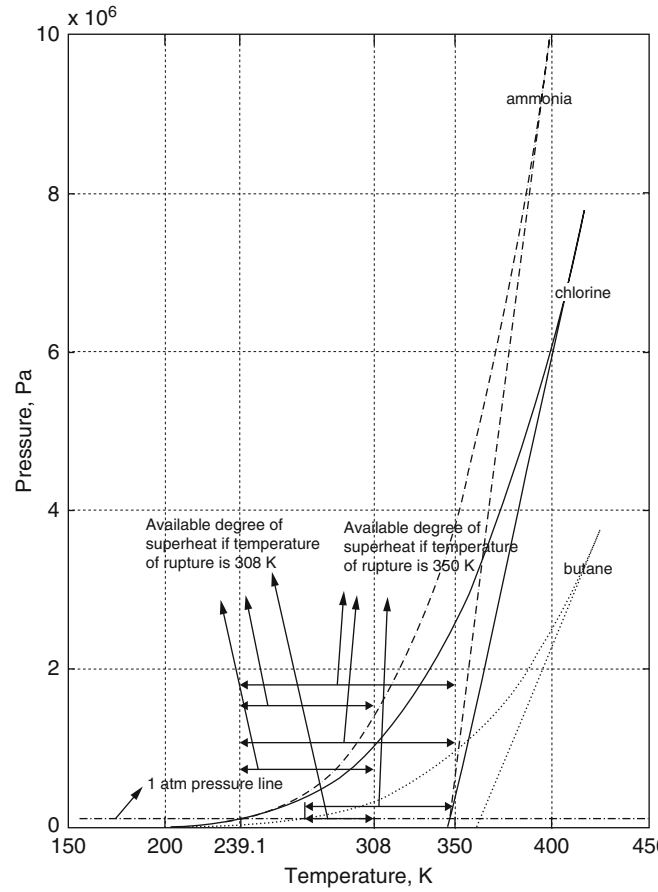

Fig. 71.2 Pressure-temperature curves and superheat limit loci for ammonia, chlorine, and butane, showing degrees of superheat at different stages of container rupture [7]

limit temperature would be a boon to industrial fire safety design, no approach to date has been performed that does not have some limitations.

The most widely used experimental approach for the determination of the superheat limit temperature is a droplet explosion technique first proposed by both Moore [20] and Wekeshima and Takata [21]. The experimental approach is conducted by injecting small droplets of the test liquid in a column filled with a different liquid that is less volatile relative to the test liquid. A temperature gradient is produced throughout the column with cooler temperatures at the base of the column and higher temperatures toward the top. As the droplet rises through its host liquid, it undergoes heating until the liquid droplet transitions to the gas phase. The temperature within the column where this rapid phase change occurs is recorded as the superheat limit temperature [7].

There are several limitations that must be considered when using this approach to determining a superheat limit temperature. First, at a molecular level, unstable bubble nuclei can reach sizes near the molecular level. At these scales, small fluctuations can initiate the formation of a nucleus bubble at temperatures below the actual superheat limit temperature. Errors using this method can also be compounded by the heat transfer dynamics to the droplet. Droplet size, the velocity of the droplet as it rises through the column, column temperature, and heat diffusivity of the droplet liquid can all influence the results of the testing method [7].

A second experimental approach utilizes a hot wire method. In this case, the test liquid sample

surrounds a very thin wire. The wire is rapidly heated, allowing for a temperature measurement of the liquid as it gasifies around the wire. The accuracy of this method is highly dependent on the rapidity of the temperature measuring device as well as the geometry of the wire surface, which can influence the nucleation of the liquid. Of the two experimental methodologies, the column method is considered to be the most accurate [7].

From the theoretical side, the superheat limit temperature can be explained utilizing the "homogeneous nucleation theory" by Gibbs [22]. Gibbs explored the factors that precipitate homogeneous nucleation in a superheated liquid and described the minimum amount of work required for the formation of vapor voids in a given liquid. Historically, this is now referred to as the classical theory, and it can be used to explain the fundamental mechanisms of explosive boiling in liquids. The theory can also be used to predict the steady-state rate of nucleation within the liquid and the expected size of bubble formation [22].

The theoretical approach for the superheat limit temperature varies from the data obtained through the experimental approaches. When accounting for the errors generated in the experimental approaches and additional research expanding on the homogeneous nucleation theory [23–28], the difference between the experimental data and theory suggests that the underlying fundamental mechanisms for the prediction of a superheat limit temperature are not yet completely understood.

Alternative Theory

Birk et al. [29] demonstrated that BLEVEs can occur at temperatures lower than the superheat limit temperature. In their study, they sub-divided a BLEVE into two types: a "hot BLEVE" and a "cold BLEVE". A cold BLEVE was defined as a BLEVE that occurs prior to a liquid reaching its superheat limit temperature. A hot BLEVE was defined similarly to the common BLEVE definition. Figure 71.3 depicts a flow diagram of the BLEVE process as defined by Birk et al. [29].

In describing the process in Fig. 71.3, Birk et al. [29] observed that cold BLEVEs typically occur in weaker containers, which fail at lower pressures. The consequences of these types of BLEVE events are correspondingly not as severe. Hot BLEVEs, then, occur with stronger containers. The delayed failure allows for a much larger pressure increase in the container and a correspondingly more severe event at the moment of failure.

Venart [30] also presented a modified theory to the work of Reid [16]. Venart introduced a new acronym called a BLCBE or Boiling Liquid Compressed/Collapsed Bubble Explosion. The BLCBE begins with a small failure in the vapor space of the container. The energy created by the failure is not sufficient to propagate the failure crack along the entire length of the container vessel. A vapor jet develops at the small breach, which allows for a pressure drop in the container. As the pressure drops, the liquid starts to boil, creating a two-phase flow within the vessel. As the liquid continues to boil, the pressure begins to increase once again within the container. The pressure increase leads to a bubble collapse, which results in a power amplified shock wave. Rapid destruction of the container ensues, with an explosive dispersal of the remaining liquid as fine droplets. Figure 71.4 shows a schematic of the BLCBE process. Figure 71.5 depicts a graph of the pressure change at the top of a container during a BLCBE event.

Time to BLEVE

Estimating the time to achieve a BLEVE for a given system is of great interest to industry and safety professionals. Unfortunately, a general methodology for predicting the time at which a particular vessel that is filled with a pressure liquefied gas will produce a BLEVE has not been currently developed. This is due to the complexity of the problem when examining the variables that effect whether or not a BLEVE will occur.

Birk and VanderSteen [32] conducted BLEVE experimentation with nine 1.8 m^3 propane tanks. Each tank was filled to 80 % capacity at approximately 10–20 °C. The results of the

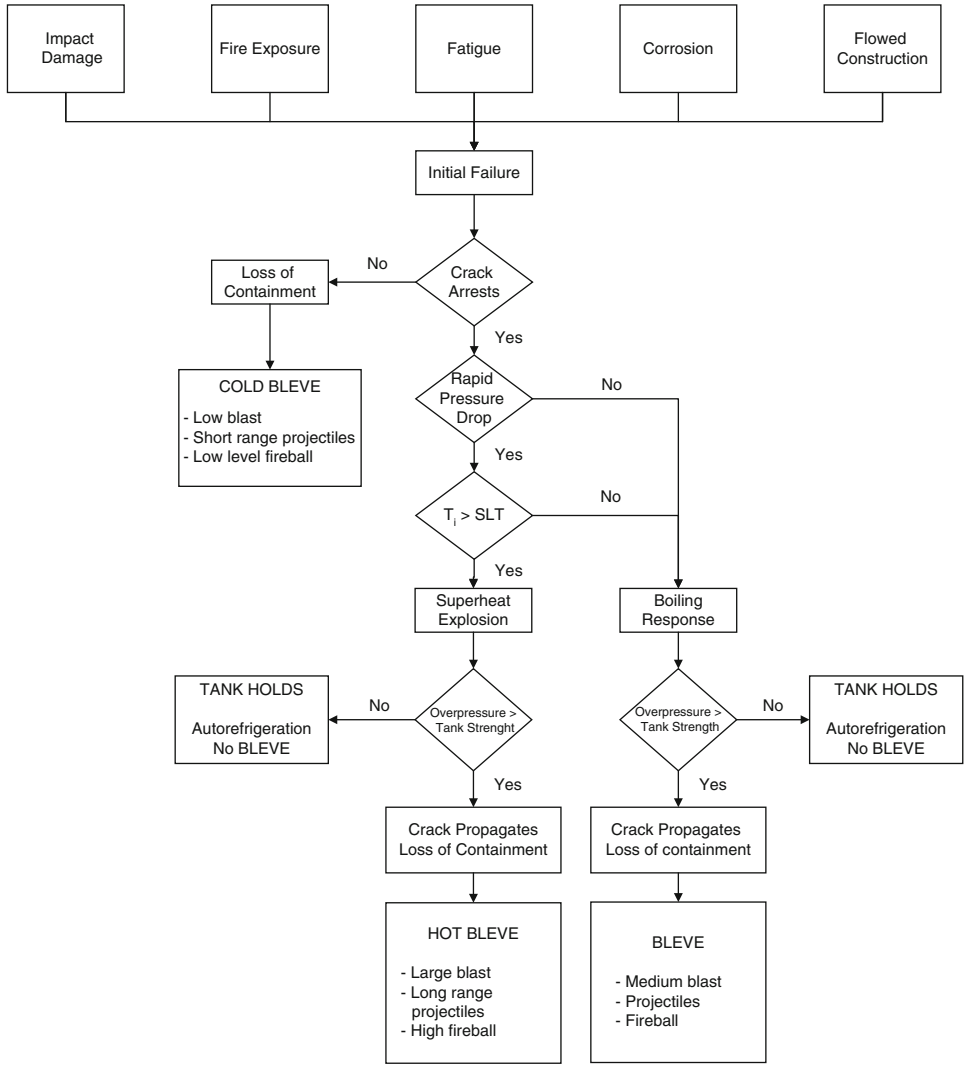

Fig. 71.3 Flow diagram of the BLEVE process by Birk et al. [29]

testing helped to provide some general insight into determining the time necessary for the initiation of a BLEVE event. The findings can be summarized as:

(A) The time needed to achieve an initial rupture of a particular container filled with a pressure liquefied gas is dependent on the type of pressure liquefied gas, overall geometry of the vessel, type of vessel material, manufacturing of the vessel, and pressure relief system of the vessel.

(B) If a failure of containment occurs in a vessel that is near or at its superheat limit temperature, it may not always precipitate a BLEVE. For a BLEVE to occur, the container must be weakened enough to open completely.

(C) When the vapor space of a particular vessel is severely heated, a critical length of that vapor space can be determined where the probability of a BLEVE event becomes highly likely over a large range of fill conditions.

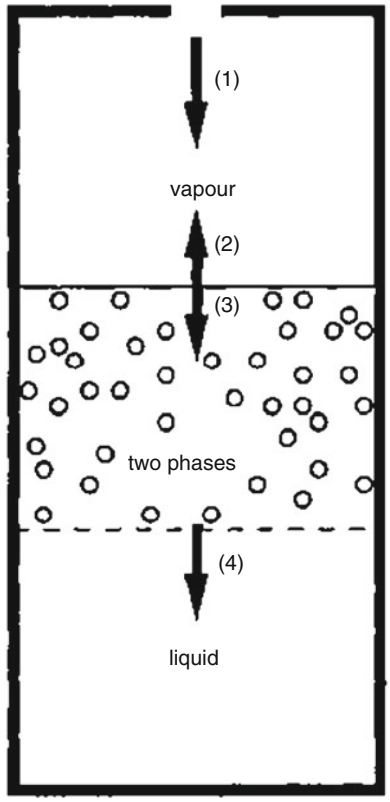

Fig. 71.4 Schematic diagram of BLEVE/BLCBE process in a vessel [19]

These generalities can be expanded to most pressure liquefied gases and vessels of all sizes.

Vessel-specific experimental studies have been conducted by numerous authors [33–35]. Blything and Reeves [33] examined horizontal cylinders filled 75 % with butane that were exposed to jet flame impingement and partial fire engulfment. The observed time to a BLEVE event ranged from 4 to 48 min.

Selway [34] examined 1000 t LPG storage spheres when exposed to full fire engulfment, partial fire engulfment, and jet flame impingement. For full fire engulfment, the time to BLEVE ranged from 7 to 11 min. For partial fire engulfment, Selway observed a range of 25–38 min. For jet flame impingement, times ranging from 5.5 to 7 min were recorded.

Roberts et al. [35] tested four 2-t propane vessels by exposure to a jet fire. Each of the vessels was fitted with a pressure relief value set at 17.24 barg. After 1–2 min of direct flame impingement, the pressure relief valves opened. Within an additional 3 min, a BLEVE event ensued.

Fig. 71.5 Pressure change at the top of a container during rupture [31]

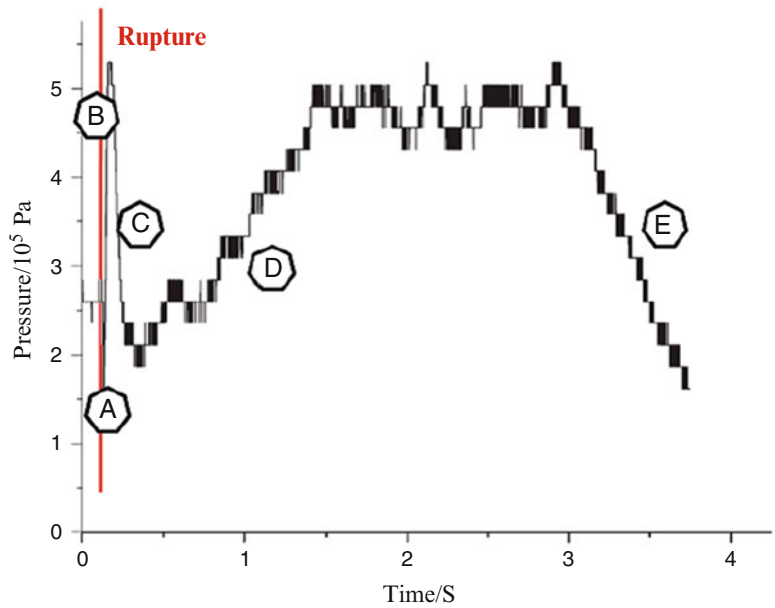

Calculating the Energy Release

Failure of a vessel containing a pressure liquefied gas will induce one of the two scenarios [36]:

- Partial failure of the container with a finite rupture and single or two phase jet release;
- Complete failure with total loss of containment and BLEVE;

The evolution to one scenario or the other depends on the fluid storage conditions, the conditions the vessel is exposed to, as well as its ability to withstand external and internal mechanical or thermal aggressions. The outcome of a pressurized vessel failure is strongly related to the vessel properties as well as the amount of potential energy stored in the container.

Birk et al. conducted several series of testing on propane fuel tanks [6] exposed to various fire conditions. The failure process began with the formation of a crack in the vapor space. Once the crack appeared, propane vapor vented from the vessel. Three different types of development followed the original crack:

i. The crack stopped and a jet release was observed;
ii. The crack did not stop and a transition to BLEVE was observed;
iii. The crack stopped; a jet release was observed. Shortly after, the crack further expanded and a transition to BLEVE occurred.

Birk et al. [6] stated that a BLEVE takes place if the vessel undergoes a total loss of containment. A total loss of containment is witnessed when the stresses in the vessel exceed the level required to propagate a crack along its entire length. There is a coupling between the vessel failure and the fluid properties. The expanding fracture acts as a relief valve and creates a pressure drop in the tank. The liquid in the vessel undergoes flashing [36]. Vapor is suddenly released and produces a shock wave. The sudden expulsion of the vapor space causes the liquid phase to transition to a superheated state. It undergoes flashing and generates a BLEVE.

The energy necessary to generate a BLEVE is provided by the vapor and liquid phases of the tank. Energy from the vapor phase is available as soon as the failure process initiates. However, the liquid energy becomes only available after a phase change (i.e., flashing or boiling). Under rapid depressurization, large superheats can occur, resulting in very energetic boiling. According to Birk et al. [36], BLEVEs of weak vessels are of short duration and are driven by energy stored in the vapor phase. Longer duration BLEVEs of stronger vessels have been observed. Energy stored in the vapor phase plays a key role in the formation of the initial failure. However, Birk et al. observed that if the energy stored in the vapor phase was insufficient to obtain a total loss of containment through the initial failure, the crack could stop. Depressurization through the latter could stimulate a boiling response to the liquid. The pressure gradient may be large enough to expand the initial crack and cause a total loss of containment and a BLEVE.

Prior to failure and venting, the pressure in the vessel equals the vapor pressure at the liquid temperature. The energy release during a BLEVE is produced in the transformation of internal energy into mechanical energy. The intensity of the blast overpressure is correlated to the available internal energy. An expression of the total expansion energy E_{av} [kJ] is given in the 'Yellow Book' [37] as:

$$E_{av} = M_{liq}\left(u_{liq,1} - u_{liq,2}\right) + M_{gas}\left(u_{gas,1} - u_{gas,2}\right) \tag{71.1}$$

Where M_{liq} and $u_{liq,i}$ are, respectively, the mass of liquid (kg) and the internal energy of the liquid phase at state i (kJ.kg^{-1}) and M_{gas} and $u_{gas,i}$ are, respectively, the mass of gas (kg) and the internal energy of the gas phase at state i (kJ.kg^{-1}).

Roberts [35] corrected the previous formula to account for the fraction of liquid that flashed to vapor:

$$E_{av} = M_{liq,1}\,u_{liq,1} + M_{gas,1}\,u_{gas,1} - M_{liq,2}\,u_{liq,2} - M_{gas,2}\,u_{gas,2} \tag{71.2}$$

With

$$M_{liq,2} = (1-\chi_f)M_{liq,1} + \left(1-\chi_g\right)M_{gas,1} \tag{71.3}$$

$$M_{gas,2} = \chi_f M_{liq,1} + \chi_g M_{gas,1} \tag{71.4}$$

And,

$$\chi_f = \frac{s_{liq,1} - s_{liq,2}}{s_{gas,2} - s_{liq,2}} \tag{71.5}$$

$$\chi_g = \frac{s_{gas,1} - s_{liq,2}}{s_{gas,2} - s_{liq,2}} \tag{71.6}$$

Where X_f is the fraction of the initial liquid mass that flashes to vapor, $s_{liq,i}$ the specific entropy of the liquid phase at state i (kJ.kg^{-1}.K^{-1}) and $s_{gas,i}$ the specific entropy of the gas phase at state i (kJ.kg^{-1}.K^{-1}), while X_g is the fraction of the initial vapor mass that does not condense during the expansion.

Prugh [9] proposed a different expression for the expansion of the vapor in the vessel. The vapor is assimilated as an ideal gas and the expansion is assumed adiabatic and reversible (isentropic process). The expansion energy is given by:

$$E_{av} = \int PdV \tag{71.7}$$

Considering an isentropic process, the following relationships can be assumed for two given states 1 (initial) and 2 (final):

$$P_1V_1^{\gamma} = P_2V_2^{\gamma} = constant \tag{71.8}$$

$$\frac{V_1}{V_2} = \left(\frac{P_2}{P_1}\right)^{\frac{1}{\gamma}} = \left(\frac{T_2}{T_1}\right)^{\frac{1}{\gamma-1}} \tag{71.9}$$

Where γ is the ratio of specific heats $\left(\gamma = \frac{C_p}{C_V}\right)$.

By integrating Equation 71.7 and introducing the relationships (71.8) and (71.9), the energy release can be expressed as,

$$E_{av} = \frac{PV}{\gamma-1}\left(1-\left(\frac{P_{atm}}{P}\right)^{\frac{\gamma-1}{\gamma}}\right)\cdot 10^{-3} \tag{71.10}$$

Where, P is the pressure in the vessel just before the expansion (in Pa), P_{atm} is the atmospheric pressure (101,325 Pa), V is the initial volume of vapor (in m^3).

The energy can also be expressed as TNT equivalent. The conversion factor is given as 4680 J/g of TNT by Planas-Cuchi et al. [38],

$$W_{TNT} = \frac{PV}{\gamma-1}\left(1-\left(\frac{P_{atm}}{P}\right)^{\frac{\gamma-1}{\gamma}}\right)\cdot\frac{1}{4.68} \tag{71.11}$$

Where W_{TNT} is in equivalent mass of TNT (kg).

Equations 71.10 and 71.11 are relevant for gas filled vessels. If the vessel contains a pressurized liquid, the energy release can be approximated using the same method. The fraction of liquid that will flash must be accounted for in the calculation. The volume of liquid vaporized must also be added to the volume of vapor considered in (71.10) and (71.11).

$$V^* = V + fV_{liq}\left(\frac{\rho_{liq}}{\rho_{gas}}\right) \tag{71.12}$$

Where, V_{liq} is the volume of liquid in the vessel before the expansion (in m^3), f is the fraction of liquid that vaporized and ρ_{liq} (ρ_{gas}) the density of the liquid (gas) phase (in kg.m^{-3}). Prugh [9] and Van den Berg et al. [39] derived an expression of the vaporized fraction from the following heat balance:

$$M_{liq}C_{p,liq}dT = LdM_{liq} \tag{71.13}$$

Where M_{liq} is the liquid mass (kg), $C_{p,liq}$ is the specific heat of the liquid phase (kJ/kg.K^{-1}), and L is the latent heat of vaporization (in kJ.kg^{-1}).

The vaporized fraction is obtained by integrating Equation 71.13:

$$f = 1 - e^{-\frac{C_{p,liq}(T_o - T_B)}{L}} \tag{71.14}$$

With T_o, the temperature of the liquid phase at the time of the expansion (K); T_B is the boiling temperature of the liquid at the atmospheric pressure (K).

Equation 71.14 becomes inapplicable for a temperature T_o close to the critical temperature or above it. At the critical temperature, the latent

heat of vaporization is equal to zero while the specific heat tends toward infinity. Prugh [9] corrected the latter equation by introducing pertinent approximations of $C_{p,liq}$ and L:

$$f = 1 - e^{-2.63\left(C_{p,liq}/L\right)(T_c - T_b)\left(1-((T_c-T_0)/(T_c-T_b))^{0.38}\right)} \tag{71.15}$$

Where T_c is the critical temperature of the liquid (K). Finally, a corrected expression of the energy release equation is provided by Plans-Cuchi et al. [38],

$$W_{TNT} = \frac{PV^*}{\gamma - 1}\left(1 - \left(\frac{P_{atm}}{P}\right)^{\frac{\gamma-1}{\gamma}}\right) \cdot \frac{1}{4.68} \tag{71.16}$$

In 2004, Planas-Cuchi et al. [38] stressed that the assumption of an isentropic expansion was an ideal case. The release energy models based on this assumption overestimate the expansion. Planas-Cuchi et al. proposed that the real expansion energy ranges between two extreme values: the expansion energy based on the isentropic assumption and the expansion energy based on an adiabatic and irreversible expansion where the only expansion work is given by $-P_{atm}\Delta V$, where ΔV is the variation in volume of the whole content of the vessel when it changes from the explosion state to the assumed final state.

For an adiabatic process, the expansion work is equal to the variation of internal energy. Consequently,

$$-P_{atm}\Delta V = \Delta U \tag{71.17}$$

(71.17) is solved graphically by plotting on the same figure, the variation in work $-P_{atm}\Delta V$ and the variation in internal energy ΔU for different liquid-vapor equilibrium conditions corresponding to different vapor fraction values [38]. Equation 71.17 can also be solved analytically by using mass and energy balances:

$$\begin{aligned} -\Delta U = {} & x\ M_{total}\left(u_{liq} - u_{gas}\right) \\ & - M_{total}\ u_{liq} + U_i \end{aligned} \tag{71.18}$$

$$-P_{atm}\Delta V = P_0\left(x\left(v_{liq} - v_{gas}\right)M_{total} + M_{total}\, v_{liq} - V_i\right) \tag{71.19}$$

Where x is given by,

$$x = \frac{P_{atm}\ v_{liq}\ M_{total} - V_i\ P_{atm} + + M_{total}\ u_{liq} - U_i}{\left[\left(u_{liq} - u_{gas}\right) - \left(v_{gas} - v_{liq}\right)P_{atm}\right]M_{total}} \tag{71.20}$$

With u_{liq} and u_{gas}, respectively, the internal energy of the liquid and the vapor at the final state of the irreversible process (kJ/kg); v_{liq} and v_{gas}, respectively, the specific volume of the liquid and the vapor at the final state of the irreversible process ($m^3.kg^{-1}$); M_{total} the overall mass in the vessel (kg); U_i the overall internal energy of the system just before the expansion (kJ); V_i the volume of the vessel (m^3).

Equations 71.19 and 71.20 are used to estimate the change in internal energy, ΔU. The TNT equivalent mass is given by:

$$W_{TNT} = \beta\frac{1}{4.68}\Delta U \tag{71.21}$$

Where W_{TNT} is in kg and β is the fraction of the energy released converted into the blast wave.

In 2008, Genova et al. [40] proposed a different model to estimate the amount of energy release during a blast-wave overpressure. The authors assumed that flashing of the liquid generated most of the expansion work. They considered that the excess of heat stored in the liquid allowed the initiation and propagation of flashing. The heat stored in the liquid was expressed as follows:

$$Q = M_{liq}\ C_{p,liq}(T - T_B) \tag{71.22}$$

Where T is the temperature of the overheated liquid (K) and T_B is the boiling temperature of the liquid at atmospheric pressure (K). Changes in the heat capacity with temperature are assumed negligible. The authors assumed a high level of vessel filling and thus neglected the contribution of the vapor to expansion. The energy release is then modeled as follow:

$$E_{av} = \alpha\ Q = \alpha\ M_{liq}\ C_{p,liq}(T - T_B) \tag{71.23}$$

Where α is the fraction of excess heat stored in the liquid and converted into expansion work. Genova et al. [40] estimated α to be equal to 0.07 based on the analysis of experimental results.

Percent of Stored Energy Transferred to Blast Wave

Another critical parameter of the BLEVE intensity is the percentage of released energy that is transferred to the blast wave. When a vessel bursts, several phenomena take place. Each of them dissipates fractions of the energy release through:

- The energy of the blast wave;
- The kinetic energy of the different fragments;
- The potential energy absorbed by the fragments;
- The heat released in the surrounding atmosphere.

The exact distribution between the different phenomena depends on the incidental conditions of the BLEVE. Casal et al. [14] indicated that a critical condition is the type of failure (fragile or ductile). According to the authors, in the case of a fragile failure of a vessel, 80 % of the energy released contributes to the pressure wave. In comparison, they state that in the case of a ductile failure, only 40 % of the energy released is transferred to the pressure wave. Identical results are provided by Genova et al. [40].

Calculation of Blast Overpressures

The form of a blast wave is not simple to predict. One needs to account for the non-spherical shape of the vessel as well as reflecting phenomena from the ground and other objects. For instance, in the case of a vessel located slightly above ground, the ground will reduce the expansion volume by half which doubles the energy release. The ground also reflects the incident wave. The reflected wave can be two times stronger than the incident one. If the vessel is cylindrical, the blast has a stronger intensity on its sides than on the ends [36].

The blast overpressure is calculated based on the energy release estimation. Birk et al. [36] as well as the 'Yellow Book' [37] proposed a procedure to determine the blast overpressure.

i. Effective Blast Wave Energy

As mentioned previously, the energy release should be corrected to only account for the energy converted into expansion work. Additional corrections such as the presence of a reflecting ground surface need to be accounted for.

The effective blast wave energy is given by the following formula,

$$E_{ex} = \varepsilon \; E_{av} \tag{71.24}$$

Where ε takes into account the presence of a reflecting ground surface. If the vessel is high in the air, then $\varepsilon = 1$. $\varepsilon = 2$ when the vessel is less than 15 degrees above the horizon, as seen from the target [37].

ii. Estimation of the scaled distance

Explosive scaling is used to relate physical variables between different masses of an explosive material. For two explosive charges of a material, exploded in atmospheres with pressure P_1 and P_2, the Sachs scaling for distance is given by the following formula [41]:

$$\frac{R_1}{R_2} = \left(\frac{E_1}{E_2}\right)^{1/3} \left(\frac{P_2}{P_1}\right)^{1/3} \tag{71.25}$$

The Sachs scaled distance, $\overline{R}$, is derived from the previous expression:

$$\overline{R} = r\left(\frac{P_{atm}}{E_{ex}}\right)^{1/3} \tag{71.26}$$

With r the distance from the explosion source (m).

iii. Estimation of the overpressure of the blast wave

According to the value of $\overline{R}$, the peak overpressure P_S is evaluated differently.

- For $\overline{R} \geq 2$ the distance from the source is long enough to be considered in the far-field. Empirical relations are available to predict far-field pressure wave. Once

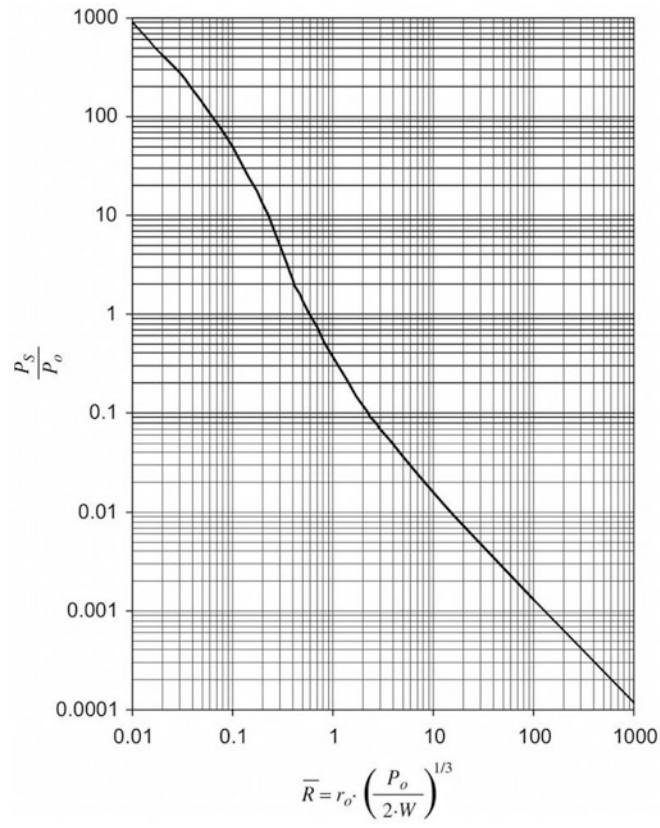

Fig. 71.6 Scaled-overpressure vs. scaled-distance curve [37]

the scaled-distance has been estimated, the peak overpressure P_S can be evaluated using scaled-overpressure vs. scaled-distance curves [37] as the one shown in Fig. 71.6.

- For $\overline{R} < 2$, the distance from the source is small enough to consider a near-field explosion. The same procedure as above would provide overly conservative approximations of the overpressure. In the near-field, high explosives generate higher overpressures than bursting vessels. A refined method is necessary to predict the blast overpressure [37].

This method assumes that the blast wave is symmetrical. The burst of a hemispherical vessel just above ground would create such a blast. Consequently, a hemispherical vessel is used calculation purposes. The hemispherical vessel's radius, r_0, is given by the following expression:

$$r_0 = \left(\frac{3V_g}{2\pi}\right)^{1/3} \tag{71.27}$$

With V_g, the volume of gas-filled part in the vessel (m^3). The non-dimensional starting distance is estimated using $r = r_0$ in Equation 71.26:

$$\overline{R_o} = r_0 \left(\frac{P_{atm}}{E_{ex}}\right)^{1/3} \tag{71.28}$$

For the near-field explosion, the initial shock overpressure at the vessel wall is given by,

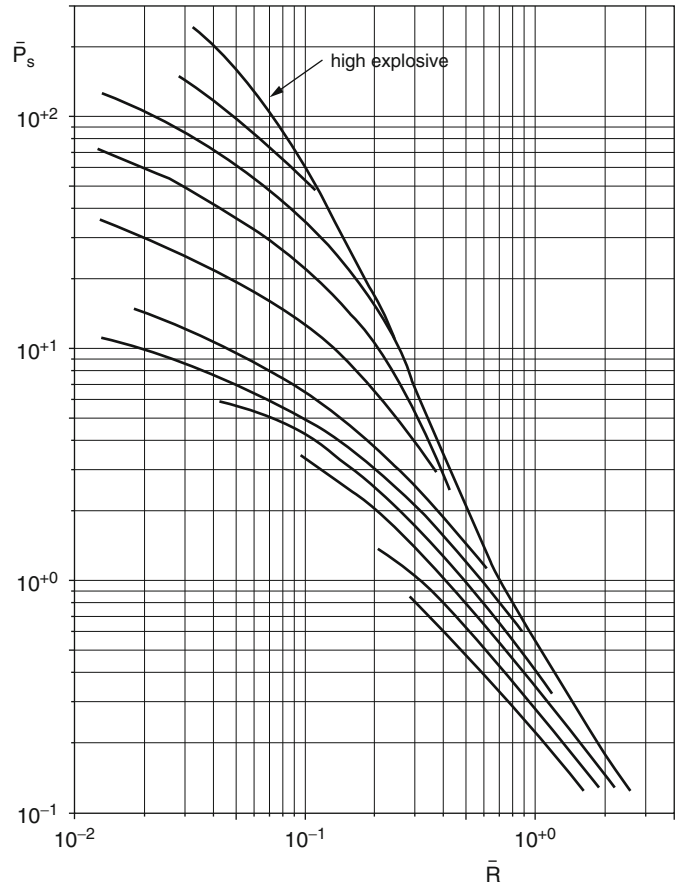

Fig. 71.7 Scaled-overpressure vs. scaled-distance curve [37]

$$\frac{P_1}{P_{atm}} = \frac{P_{so}}{P_{atm}}\left(1 - \frac{(\gamma_1 - 1)\left(\frac{a_0}{a_1}\right)\left(\frac{P_{so}}{P_{atm}} - 1\right)}{\sqrt{2\gamma_0\left(2\gamma_0 + \left((\gamma_0 + 1)\left(\frac{P_{so}}{P_{atm}} - 1\right)\right)\right)}}\right)^{\frac{-2\gamma_1}{\gamma_1 - 1}} \tag{71.29}$$

With, P_1, the pressure in the vessel (Pa), P_{so} the air shock overpressure (Pa), γ_1 the ratio of specific heats of compressed gas, γ_0 the ratio of specific heats of ambient air, a_0 the speed of sound in ambient air (m.s^{-1}) and a_1 the speed of sound in compressed gas (m.s^{-1}).

The ratio $\frac{a_0}{a_1}$ is calculated using the following expression:

$$\frac{a_0}{a_1} = \frac{\gamma_1 T_1 M_1}{\gamma_0 T_0 M_0} \tag{71.30}$$

Where, T_1 and M_1 are respectively the temperature (K) and the molar mass (g.mol^{-1}) of the compressed gas; T_o and M_0 are respectively the temperature (K) and the molar mass of ambient air (g.mol^{-1}).

Equation 71.29 is solved using an iteration procedure. The pressure of the blast wave decreases as it spreads further from its source. Estimations of $\overline{R_o}$ and P_{so} provide the initial conditions for the blast wave. Using Fig. 71.7 and given that $\overline{P_{so}} = \frac{P_{so}}{P_{atm}} - 1$, the pressure

curve of interest is the one containing the point with coordinates $\left(\overline{R_o}, \overline{P_{SO}}\right)$. Once the correct curve is identified, the blast overpressure P_s is found by reading the ordinate $\overline{P}_S$ of the point taken from the curve with abscissa $\overline{R}$ (estimated using Equation 71.26) and by using the following expression:

$$P_S = P_{atm}\left(\overline{P}_S + 1\right) \tag{71.31}$$

iv. Adjustment of the overpressure value
The previous methods presented for the estimation of P_S are based on the assumption of a perfectly symmetrical blast wave that would result from the burst of a hemispherical vessel above ground or a spherical vessel in the air. Since vessels are often cylindrical or spherical and slightly above ground, adjustments are necessary to the methods introduced previously. Adjustment factors are given in Table 71.1.

Table 71.1 Adjustment factors for the non-dimensional blast overpressure $\overline{P}_S$ [37].

	$\overline{R}$	Multiply $\overline{P}_S$ by
Cylindrical vessel	$\overline{R} < 0.3$	4
	$\overline{R} \in [0.3 - 1.6]$	1.6
	$\overline{R} \in [1.6 - 3.5]$	1.6
	$\overline{R} > 3.5$	1.4
Vessel slightly elevated above ground	$\overline{R} < 1$	2
	$\overline{R} \geq 1$	1.1

Consequence of Overpressures

Damages resulting from blast waves have been historically associated with the peak overpressure. Overpressure-damage criteria can be found in the literature [42–44]. Table 71.2 summarizes the information found in the previous references.

It is critical to stress that the values associated with the correlations peak overpressure—Damage indicated in Table 71.2 correctly approximate the magnitude of large explosions with long blast wave duration times. These criteria ignore the blast wave duration and the blast impulse. Consequently, they should not be used for blast waves with relatively small yields and/or short duration times. In these cases, use of Table 71.3 is advised.

Table 71.2 Blast damage—overpressure correlation

Type of damage	Pressure (kPa)
Minimum damage to glass panel [42]	0.1–0.3
Typical window glass breakage [42]	1–1.5
Windows shattered, plaster cracked, minor damage to buildings [42]	3.5–7.5
Person knocked down [42]	7–10
Panel of sheet metal buckled [42]	7.5–12.5
Failure of wooden siding in conventional homes [42]	7.5–15
Failure of walls constructed of concrete blocks or cinder blocks [42]	12.5–20
Oil storage tanks ruptured [42]	20–30
Utility poles broken off [42]	30–50
Serious damage to buildings with structural steel framework [42]	30–50
Reinforced concrete structures severely damaged [42]	40–60
Railroad cars overturned [42]	40–60
Probable total destruction of most buildings [42]	200–500
Wood roof joist, 13 ft. span [43]	3
Brick wall—minor damage [43]	5
Brick wall—major damage [43]	14
Wood frame building collapse [44]	20–31
Cladding of light industrial buildings ruptured [44]	27
Steel towers blown down [44]	205
Crater damage [44]	606

Table 71.3 Blast damage—impulse correlation [43]

Type of damage	Impulse (kPa–msec)
Brick wall—minor damage	110
Brick wall—major damage	295
Wood frame building collapse	248
Overturning of 10 ft. high truck	758

Sample Cases

Water Tank BLEVE

In January 1982, at the Star Elementary School of Spencer, OK, shortly after 12:00 p.m. as the students were eating lunch, a water heater exploded. Six children and 1 teacher were killed and 33 people were injured. The explosion blew up the concrete wall that separated the lunch room from the kitchen. The 300 l (0.3 m^3, 10.6 ft^3) water tank was propelled 41 m (135 ft.) away from its original location [45, 46].

The Fire Marshall's investigation revealed that some time before the explosion occurred, the temperature gauge indicated that the water temperature was 104 °C (220 °F) instead of 82 °C (180 °F) under normal operation. It also stressed that the pressure relief valve supposed to open at 8.6 bar (125 psig) was faulty. Later testing revealed that the valve did not open below 9.2 bar (133 psig) [45].

Based on the previous information, an estimation of the explosion overpressure can be obtained using expressions (71.10) from Prugh [9] and 71.23 from Genova et al. [40].

Prugh's Method

The calculation assumptions are the following:

- The pressure of the water inside the tank: $P_{water} = 917$ kPa;
- The temperature of the water inside the tank: $T_{water} = 377$ K;
- The density of liquid water: $\rho_{liq} = 1000\,kg/m^3$;
- The density of water vapor: $\rho_{vap} = 0.804\,kg/m^3$;
- The heat capacity of liquid water: $C_p = 4.2\ kJ.kg^{-1}.K^{-1}$;
- The heat capacity ratio of water: $\gamma = 1.329$;
- The latent heat of vaporization of water: $H_v = 2257\ kJ.kg^{-1}$;
- The critical temperature of water: $T_{crit} = 647$ K;
- The boiling temperature of water at atmospheric pressure: $T_{boil} = 373$ K;
- The total volume of the tank: $V = 0.3\ m^3$;
- The percentage of filling level of the tank was assumed to be 80 %;

The vaporization fraction f was calculated using Equation 71.15 and was found to be approximately, $f \sim 0.0074$. Expressions (71.10) and (71.12) are used to estimate the energy release:

$$E_{av} = \frac{PV^*}{\gamma - 1}\left(1 - \left(\frac{P_{atm}}{P}\right)^{\frac{\gamma-1}{\gamma}}\right) \cdot 10^{-3} \sim 2.67\,MJ$$

Assuming a ductile fracture, the energy in the pressure wave was taken as 40 % of E_{av}, approximately 1.07 MJ.

The scaled distance $\overline{R}$ was then calculated based on Equation 71.26, assuming the boiler was about 4 m away from the collapsed concrete wall,

$$\overline{R} \sim 1.45$$

Using the chart of Fig. 71.6, for scaled overpressure, gives a ratio $\frac{P_s}{P_{atm}} \sim 0.18$, hence a peak side on overpressure $P_s \sim 18$ kPa (2.6 psig).

Genova's Method

Based on the same assumptions as provided above, Equation 71.23 can be rewritten for water as,

$$E_{av} = 294\,M_{water}(T_{water} - T_{Boil}) \qquad (71.32)$$

$$E_{av} \sim 0.3\,MJ$$

And

$$\overline{R} \sim 2.17$$

Using the chart of Fig. 71.6, for scaled overpressure, gives a ratio $\frac{P_s}{P_{atm}} \sim 0.11$, hence a peak side on overpressure $P_s \sim 11$ kPa (1.6 psig).

Although a discrepancy is observed between the two methods, their order of magnitude is the same. While Prugh bases his calculation on the

assumption on the pressure, Genova's calculation uses the liquid temperature.

Testing of the relief valve stressed that it would not open below 920 kPa but it is possible that the burst pressure was under this value. Similarly, the last witnessed water temperature on the tank temperature gauge was 104 °C but the temperature might have continued to rise.

Despite the discrepancy between the two overpressure values, based on Table 71.2, their estimated magnitude could generate failure of a concrete wall.

Propane Railcar BLEVE

It would be of interest to have an estimation of the pressure inside a vessel prior to its transition to a BLEVE. In the case of road or rail car tanks, it is unlikely that the pressure gets recorded and in-vehicle pressure gauges might not be found after the explosion. Nevertheless, an approximation of the energy release can be obtained from the damages observed.

Assume a cylindrical rail car tank with a diameter of 2.5 m (8.2 ft) and a length of 20 m (65.6 ft) with a volume of 100 m^3 (3,531 ft^3). This tank is filled with LPG at 80 % of its total capacity. The temperature of the LPG is 22 °C (72 °F) and the pressure 8.7805 bar.

Due to excessive speeding, the train violently came off the track, tipped over and finally came to a halt. Immediately, flames appeared under the car. A few minutes after, a large explosion occurred. The glass windows of a house located approximately 250 m (820 ft) away did not break. Based on this information and using Table 71.2, one can determine that the peak overpressure was below 1.5 kPa (0.22 psig). By using Fig. 71.6, the scaled distance $\overline{R}$ is estimated to be:

$$\overline{R} \sim 10.3$$

Assuming a ductile fracture, the energy release can be estimated from Equation 71.26,

$$E_{av} = \left(\frac{r}{\overline{R}}\right)^3 \frac{P_{atm}}{0.8} \sim 1811.10^3 \text{ kJ}$$

By using an inverse approach on Equation 71.10, and with the following assumptions,

- The density of liquid propane: $\rho_{liq} = 582 \text{ kg/m}^3$;
- The density of gaseous propane: $\rho_{vap} = 2.423 \text{ kg/m}^3$;
- The heat capacity of liquid propane: $C_p = 2.72 \text{ kJ.kg}^{-1}.\text{K}^{-1}$;
- The heat capacity ratio of water: $\gamma = 1.1344$;
- The latent heat of vaporization of propane: $H_v = 425.31 \text{ kJ.kg}^{-1}$;
- The critical temperature of propane: $T_{crit} = 367 \text{ K}$;
- The boiling temperature of propane at atmospheric pressure: $T_{boil} = 231 \text{ K}$;

the pressure P prior to explosion can be estimated to be approximately 67 bars (972 psig).

Fireballs

The 'Yellow Book' [37] defines fireball as 'a fire, burning sufficiently rapidly for the burning mass to rise into the air as a cloud or ball.' A fireball takes place when a flammable liquid, gas or dust cloud is suddenly released and has limited mixing with air prior to ignition. This event differs from a flash fire or vapor cloud explosion in that the flammable release ignites prior to mixing with the outside air. The fireball combustion event therefore involves entrainment and mixing with the surrounding air as it burns. Burning occurs primarily in the outer layer of the fireball, where the fuel-rich cloud mixes with the surrounding air. As the gases inside the fireball are heated, buoyancy increases, and the fireball rises as it expands [47].

There are a number of scenarios that can lead to a fireball, including [48]:

- The ignition of a flammable release during a BLEVE event.
- The ignition of a fuel-rich vapor cloud.
- The ignition of a release of a liquefied gas pipeline, where the jet flame is preceded by a fireball.
- An ignition of a sudden flammable release following a boilover event.
- A release of flammable vapors into a building and subsequent ignition.
- Ignition of explosives or propellants.
- Venting of a deflagration inside an enclosure.

This type of combustion is relatively slow, since the speed of combustion is limited by the air entrainment and mixing time. There is, therefore, no associated blast wave. The fireball, however, poses a radiation hazard, as the thermal energy release during combustion is emitted radially.

Description of a Fireball Originating from a BLEVE

About 80 % of all BLEVEs involve flammable materials [7]. When a BLEVE is the result of an external fire, the ignition of the flammable release is an inevitable consequence, and will result in the formation of a fireball. If a tank containing a pressurized flammable gas or liquid is heated due to an external fire, two things will happen: (1) the pressure inside the vessel will increase due to either heating of the gas or an increase in the saturation pressure of the liquid and (2) the vessel walls will weaken as the temperature increases. If the heating continues and the vessel is not able to vent adequately, the walls of the vessel will fail at some point, resulting in a sudden release of the flammable material which will likely be ignited. The fireball event will initiate at the level of the release. After ignition, the volume of burning gas will increase and it will rise, producing a wake [1].

The fireball size and duration will directly depend on the amount of fuel that is burned within the fireball. A simple and conservative approach is to assume that the entire vessel's flammable contents are consumed in the fireball. In a realistic BLEVE scenario, however, a portion of the vessel contents will instantly flash due to the temperature of the liquid at the time of vessel failure (isentropic flash fraction), a portion of the liquid will form fine droplets that will vaporize as they fall and during the formation of the fireball, and a portion will rainout and form a pool on the ground that will be consumed as a pool fire. Hasegawa and Sato [49] showed that once the isentropic flash fraction equals 36 % or more, all of the fuel in the vessel is consumed in the fireball. Therefore, the assumption can be made that during a BLEVE event, the amount of fuel that will contribute to the subsequent fireball is three times the isentropic flash fraction, up to a maximum of 100 % of the liquid contained in the vessel [2].

There are physical models that can be used to calculate the motion, air entrainment and temperature of a fireball [50]. Alternatively, a number of experiments have been performed and analyzed over the years to come up with empirical relations of the fireball size and duration as a function of fuel mass consumed. These models are exponential relationships based on the flammable mass consumed. The variability on the empirical models is relatively small, and is related to the range in the scale of the experiments considered. As described in Chap. 66, the maximum diameter, D, of a spherical fireball originating from a BLEVE can be calculated as:

$$D = 5.8\,m^{1/3}$$

Similarly the duration of the fireball can be estimated from the flammable mass as [2]:

$$t_d = 0.45\,m^{1/3} \quad \text{for} \quad m < 30{,}000\,kg$$

$$t_d = 2.6\,m^{1/6} \quad \text{for} \quad m > 30{,}000\,kg$$

The duration of the fireball as a function of flammable mass is shown in Fig. 71.8. The figure shows how the fireball is a transient event lasting only seconds. The total radiation reaching nearby objects during such an event is less than that associated with a longer-lasting flammable liquid pool fire, limiting its potential hazard [50].

The fireball will quickly expand to its maximum diameter, D, as it rises. The fireball normally ascends at a constant rate from a height of $D/2$ to approximately $3D/2$. The maximum height of the fireball is reached in the last two-thirds of its duration [1]. Figure 71.9 shows the fireball height as a function of time. If an average fireball height is used, it can be estimated as 0.75 D.

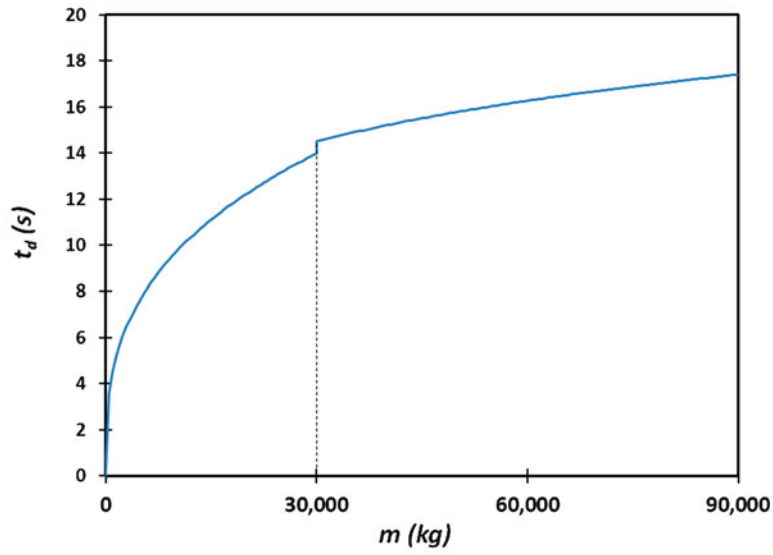

Fig. 71.8 Fireball duration as a function of flammable mass

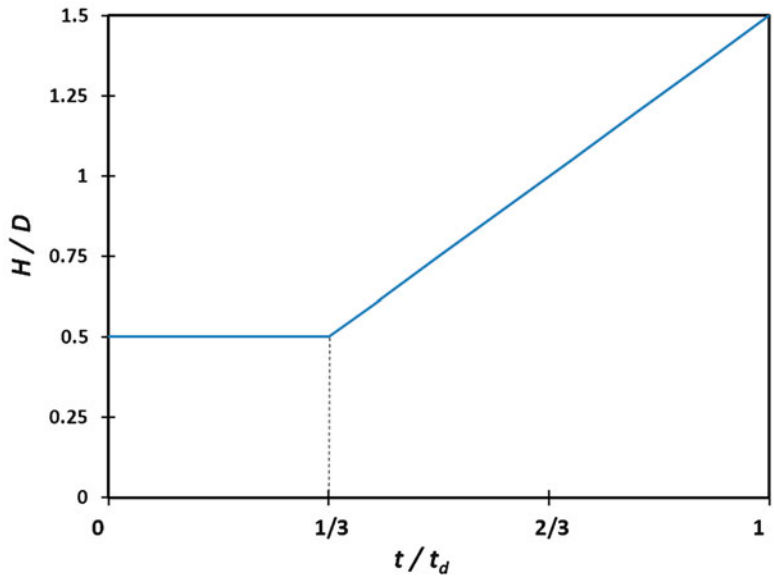

Fig. 71.9 Fireball height as a function of time

Fireball Radiation

The damage caused by the fireball comes from either flame impingement or radiant heat. The structural damage caused by a BLEVE blast wave and impact of missiles is limited to the near-field. In comparison, the radiation effects of the resulting fireball can often extend over much greater distances [2]. About one fourth of the energy released during the combustion of the fireball is transferred as radiant energy [7]. The burning rate is equal to the total amount of flammable material divided by the duration of the fireball [37].

There are three basic methods of calculation the radiation emitted by a fireball [48]:

1. Calculating the heat release rate of the fireball and the fraction of heat radiated.

2. Calculating the fireball flame surface temperature and emissivity.
3. Estimating the fireball surface emissive power.

The first method, which calculates the fraction of the heat release that is radiated, is used in conjunction with a point-source radiation model. The fraction of the energy released that goes into the radiant heat transfer varies, and it is one of the largest uncertainties in the fireball radiation models. The radiant energy fraction varies from 0.13 to 0.4, depending on the study [14].

The second and third methods, which determine the fireball surface emissive power, are used in conjunction with the solid flame radiation model. The third method, using empirically determined surface emissivity values or correlations, is discussed herein and detailed in Chap. 66. Using this method, a solid flame model can be used in order to calculate the radiation received by an object or surface located a certain distance away. This requires knowledge of the flame emissive power, view factor, the atmospheric transmissivity and the distance between the flame and the target [1]. The view factor can be calculated from the geometry of the fireball, the emissive power is dependent on the vapor pressure of the fuel involved, and the transmissivity can be estimated from the atmospheric conditions. The amount of radiation absorbed by a target is therefore dependent on the fireball duration, diameter and height [1]. The shape of the fireball can vary according to the type of tank failure. Rapid failures produce nearly-spherical fireballs, while slower releases tend to produce cylindrical releases with high lift-offs [1]. Most fireball radiation models assume the fireball is shaped as a perfect sphere.

Methods used to calculate the radiation exposure from a fireball formed during ignition of a hydrocarbon are detailed in Chap. 66, using both a point source and solid flame model. Experimental measurements of full-scale butane and propane fireballs have estimated their emissive power as 320–370 kW/m^2 [51]. An emissive power of 350 kW/m^2 is often used as a reasonable estimate for hydrocarbon fireballs involving a flammable mass of 1000 kg or more [2]. Most models assume that the fireball radiation is constant during the event. This simplification tends to over-estimate the amount of radiation observed by a target, and therefore over-estimates the extents of the radiation hazard zone. New techniques have been developed to account for variations in radiation levels during the duration of the fireball [1, 52].

Potential fire damage to buildings can be minimized using the following mitigation strategies [47]:

- Increasing the separation distance between the building and potential release locations of flammable storage vessels.
- Applying fireproofing to the exterior of buildings.
- Using water sprays or a water deluge system to cool exposed surfaces.

Fireballs Resulting from Deflagration Venting (NFPA 68)

Fireballs can be formed during explosion venting of a deflagration inside an enclosure. Explosion vents are commonly used to protect equipment and enclosures containing combustible gases and dusts. The NFPA 68 Standard for Explosion Protection by Deflagration Venting describes in detail how explosion vent systems should be designed and operated [53]. The vents are designed to open at relatively low pressures and allow the expanding gas to exit the enclosure during the deflagration. This reduces the maximum overpressure observed during a deflagration inside the protected vessel or enclosure.

During a deflagration in a vessel or enclosure protected by explosion vents, the unburned gases first exit the volume, followed by the flame. The combustible material is ejected some distance away from the protected vessel and combusts outside of the enclosure. The venting of the explosion produces both a pressure wave and a radiating fireball.

Explosion venting can be used to protect buildings and equipment, but can lead to a number of hazards that need to be addressed [54]:

- The ejection of flames and burning material, in the form of a fireball, from the vent opening.
- Emission of blast waves from the vent opening.
- Reaction forces on the enclosure.
- Emission of missiles (vent panels or other objects)
- Emission of toxic combustion products.

According to NFPA 68 (2013) §A.7.7 and §A.6.6 [53]:

> The fireball from a vented gas or dust deflagration presents a hazard to personnel in the vicinity. People caught in the flame itself will be at obvious risk from burns, but those who are outside the flame area can be at risk from thermal radiation effects. The heat flux produced by the fireball, the exposure time, and the distance from the fireball are important variables to determine the hazard.
>
> Flames and pressure waves that emerge from an enclosure during the venting process can injure personnel, ignite other combustibles in the vicinity, result in ensuing fires or secondary explosions, and result in pressure damage to adjacent buildings or equipment. The amount of a given quantity of combustible mixture that is expelled from the vent, and the thermal and pressure damage that occurs outside of the enclosure, depends on the volume of the enclosure, the vent opening pressure, and the magnitude of the vented overpressure, P_{red}. In the case of a given enclosure and a given quantity of combustible mixture, a lower vent opening pressure results in the discharge of more unburned material through the vent, resulting in a larger fireball outside the enclosure. A higher vent opening pressure results in more combustion taking place inside the enclosure prior to the vent opening and higher velocity through the vent. (See 6.2.3.) The fireball from vented dust deflagrations is potentially more hazardous than from vented gas deflagrations, because large quantities of unburned dust can be expelled and burned during the venting process.
>
> Deflagration venting generates pressure outside the vented enclosure. The pressure is caused by venting the primary deflagration inside the enclosure and by venting the secondary deflagration outside the enclosure.

The NFPA 68 standard provides an empirical correlation to predict the maximum size of a fireball produced during venting of a deflagration. According to §7.71 of NFPA 68, for venting of gas explosions, the axial extent of the hazard area from the vent location can be calculated as:

$$D = 3.1 \cdot \left(\frac{V}{n}\right)^{0.402}$$

Where V is the volume of the vented enclosure (m^3), and n is the number of evenly distributed vents. In the case of venting of dust explosions, the fireball hazard area distance can be calculated as (see §8.9.2 of NFPA 68):

$$D = K \cdot \left(\frac{V}{n}\right)^{1/3}$$

Where K is equal to 10 for metal dusts and 8 for chemical and agricultural dusts, D is the axial distance from the vent (m), V the volume of vented enclosure (m^3) and is the number of evenly distributed vents. The maximum distance, D (m), is limited for venting of combustible dusts to 60 m. The width and height of the projected fireball is taken as D. The fireball hazard area is described as a cone, as described in Fig. 71.10.

Personnel should be prevented from entering this hazard area during normal operation [55]. In addition, a separate hazard area associated with overpressures experienced during venting is defined in NFPA 68. The maximum overpressure immediately outside the vented enclosure is:

$$P_{max,a} = 0.2 \cdot P_{red} \cdot A_v^{0.1} \cdot V^{0.18}$$

Where P_{red} is the maximum overpressure inside the protected enclosure during venting (bar), Av is the vent area (m^2), and V is the volume of the protected enclosure (m^3). The maximum pressure as a function of radial distance from the vent, r (m), is shown graphically in Fig. 71.11 and is defined in NFPA 68 as:

$$P_{max,r} = P_{\max,a} \cdot \frac{(\alpha \cdot D)}{r}$$

Where α is 0.20 for horizontal vents and 0.25 for vertical vents. The external overpressure near the vent, up to a distance of $\alpha \cdot D$ (m), is constant and equal to $P_{max,a}$ (bar).

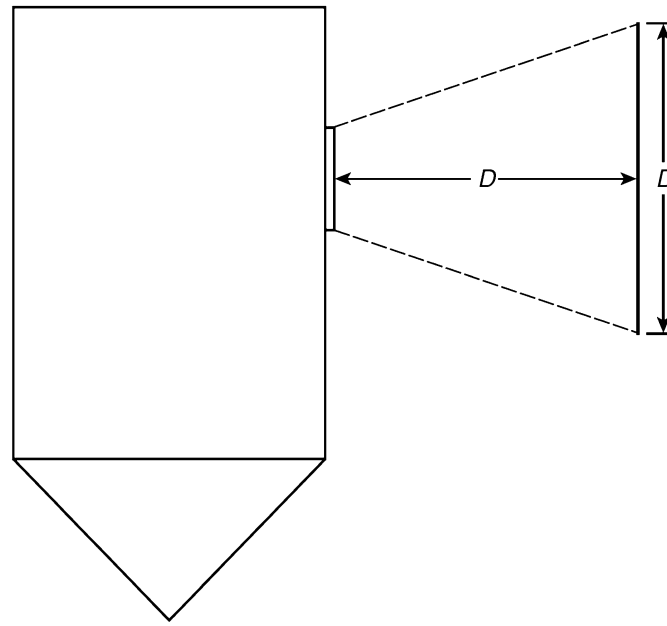

Fig. 71.10 Fireball dimensions for a vented deflagration (Figure from NFPA 68 (2013) Fig. 8.9.2.2) [53]

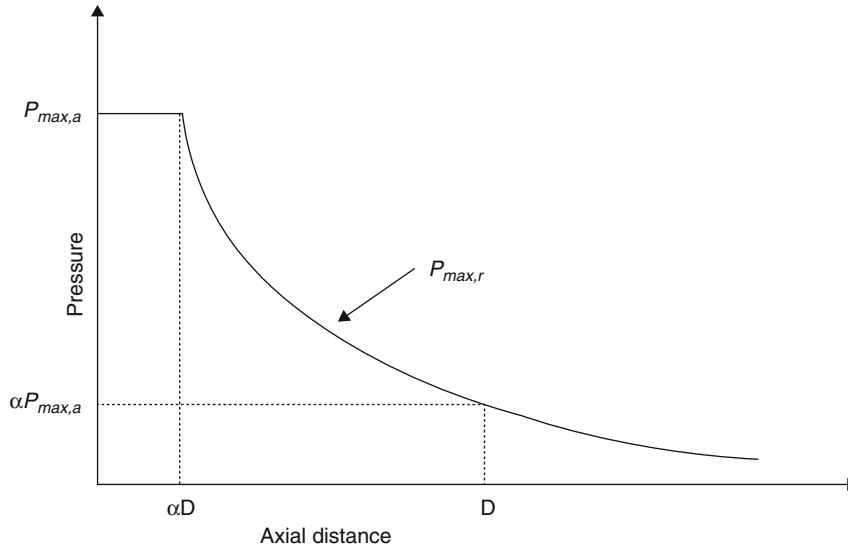

Fig. 71.11 Maximum overpressure during deflagration venting as a function of radial distance from the vent (Figure from Frank et al. (2012) [55])

Sample Cases

LPG Release in Italy

During the transfer of LPG at an unloading facility from a 13 m^3 (459 ft^3) tanker truck to an underground tank, a release of LPG occurred from the back of the truck [56]. The tanker at the time was carrying approximately 4200 kg (9259 lb) of liquid LPG. The leak of LPG ignited, forming a pool fire under the tanker, while the tanker continued to leak fuel. After 25 min of continued burning, the tanker ruptured and

underwent a BLEVE. Witnesses described a fireball that was 20–25 m (65–82 ft) from the ground. No one was injured up to a distance of 100 m (328 ft) from the fireball. Calculations demonstrated that at the time of the BLEVE, the tanker held 250–600 kg (551–1323 lb) of fuel which was consumed during the fireball.

LNG Release in Spain

On 22 June 2002, a tanker truck carrying approximately 20 t of LNG overturned [57]. A fire ensued, enveloping the tank. The tank burst 20 min after the start of the incident. The driver was killed and two people were burned approximately 200 m (656 ft) from the truck. Calculations showed that the resulting fireball would have had a diameter of 150 m (492 ft), located 113 m (371 ft) above ground, and lasted 12 s [58]. The authors estimated a surface emitted flux of 260 kW/m^2.

Nomenclature

A_v	Vent area (m^2)
C_p	Specific heat at constant pressure (kJ·kg^{-1}· K^{-1})
C_v	Specific heat at constant volume (kJ·kg^{-1}· K^{-1})
D	Fireball diameter (m)
E_{av}	Total expansion energy (kJ)
L	Latent heat of vaporization (kJ · kg^{-1})
m	Flammable mass (kg)
M_{liq}	Liquid mass (kg)
P	Pressure (Pa)
R	Distance from explosive material (m)
S	Specific entropy (kJ·kg^{-1} · K^{-1})
T	Temperature (K)
t_d	Duration of the fireball (s)
u	Internal energy (kJ.kg-1)
V	Vessel volume (m3)
W_{TNT}	Equivalent mass of TNT (kg)
X_f	Mass fraction of the initial liquid mass that flashes to vapor
X_g	Mass fraction of the initial vapor mass that does not condense during expansion

Greek Letters

β	Fraction of energy released converted into the blast wave
γ	Ratio of specific heats $\left(\gamma = \frac{C_p}{C_v}\right)$
ν	Specific volume (m3 · kg^{-1})
ρ	Density (kg · m^{-3})

Subscripts

atm	atmospheric
gas	Gas
liq	Liquid

References

1. J. Casal, Evaluation of the Effects and Consequences of Major Accidents in Industrial Plants, Oxford, UK: Elsevier, 2008, pp. 104–117.
2. Center for Chemical Process Safety (CCPS), Vapor Cloud Explosion, Pressure Vessel Burst, BLEVE and Flash Fire Hazards, 2nd ed., Hoboken, NJ: John Wiley and Sons, 2010, pp. 336–342.
3. D. Laboureur, Experimental characterization and modeling of hazards: BLEVE and Boilover, ULB, Ecole Polytechnique de Bruxelles, 2012.
4. W. L. Walls, "What is a BLEVE?," *Fire Journal,* vol. 31, p. 46–47, 1978.
5. W. L. Walls, "The BLEVE — Part 1," *Fire Command,* vol. 17, p. 35–37, 1979.
6. A. M. Birk and M. H. Cunningham, "The boiling liquid expanding vapor explosion," *J. Loss Prev. Process Ind.,* vol. 7, p. 474–480, 1994.
7. T. Abbasi and S. Abbasi, "The boiling liquid expanding vapour explosion (BLEVE): Mechanism, consequence assessment, management," *Journal of Hazardous Materials,* no. 141, pp. 489–519, 2007.
8. C. A. McDevitt, C. K. Chan and K. N. Tennankore, "Initiation step of boiling liquid expanding vapor explosions," *J. Hazard. Mater.,* vol. 25, p. 169–180, 1990.
9. R. W. Prugh, "Quantitative evaluation of "BLEVE" hazards," *J. Fire Protect. Eng.,* vol. 3, p. 9–24, 1991.
10. R. W. Prugh, "Quantify BLEVE hazards," *Chem. Eng. Prog.,* vol. 87, p. 66–72, 1991.
11. I. R. Leslie and A. M. Birk, "State of the art review of pressure liquefied gas container failure modes and associated projectile hazards," *J. Hazard. Mater.,* vol. 28, p. 329–365, 1991.
12. F. P. Lees, Loss Prevention in the Process Industries-Hazard Identification, Assessment, and Control, vols. 1–3, Oxford: Butterworth-Heinemann, 1996.

13. A. M. Birk and M. H. Cunningham, "Liquid temperature stratification and its effect on BLEVEs and their hazards," *J. Hazard. Mater.,* vol. 48, p. 219–237, 1996.
14. J. Casal, J. Arnaldos, H. Montiel, E. Planas-Cuch and J. A. Vílchez, "Chapter 22 – Modelling and Understanding BLEVEs," in *The Handbook of Hazardous Materials Spills Technology*, New Tork, NY, McGraw Hilll, 2001, pp.22.1–22.27.
15. J. E. S. Venart, "Boiling liquid expanding vapor explosions (BLEVE); two phase aspects of failure," in *Proceedings of the 39th European Two-phase Flow Group Meeting*, Aveiro, 2001.
16. R. C. Reid, "Possible mechanism for pressurized-liquid tank explosions or BLEVEs," *Science,* vol. 203, p. 1263–1265, 1979.
17. Y. N. Shebeko, A. P. Shevchuck and I. M. Smolin, "BLEVE prevention using vent devices," *J. Hazard. Mater.,* vol. 50, p. 227–238., 1996.
18. A. M. Birk, J. D. VanderSteen, M. H. Cunningham, C. R. Davison and I. Mirzazadeh, "Fire tests to study the effect of pressure relief valve blowdown on the survivability of propane tanks in fires," *Process Saf. Prog.,* vol. 21, p. 227–236, 2002.
19. C. M. Yu and J. E. Venart, "The boiling liquid collapsed bubble explosion (BLCBE): a preliminary model," *J. Hazard. Mater.,* vol. 46, p. 197–213., 1996.
20. G. R. Moore, "Vaporization of superheated drops in liquids," *AIChE Journal,* vol. 5, p. 458–466, 1959.
21. H. Wekeshima and K. Takata, "On the limit of superheat," *J. Phys. Soc. Jpn.,* vol. 13, p. 1398–1403, 1958.
22. W. Gibbs, The Scientific Papers, vol. 1, New York: Dover Publications, 1961.
23. M. Volmer and A. Weber, "Keimbildung in Ubersattigten Gebilden," *Z. Phus. Chem.,* vol. 119, p. 277–301, 1926.
24. L. Farkas, "The velocity of nucleus formation in supersaturated vapors," *J. Phys. Chem.,* vol. 125, p. 236, 1927.
25. R. Becker and W. Doring, "The kinetic treatment of nuclear formation in supersaturated vapors," *Ann. Phys.,* vol. 24, p. 719–752, 1935.
26. M. Blander and J. L. Katz, "Bubble nucleation in liquids, AIChE J. 21 (1975) 883.," *AIChE Journal,* vol. 21, p. 883, 1975.
27. C. E. Brennen, Phase change, nucleation, and cavitation, in: Cavitation and Bubble Dynamies, London: Oxford University Press, 1995.
28. J. Li, G. P. Peterson and P. Cheng, "Mechanical nonequilibrium considerations in homogeneous bubble nucleation for unsteady-state boiling," *Int. J. Heat Mass Transf.,* vol. 2005, p. 3081–3096, 2005.
29. A. M. Birk, Z. Ye, J. Maillette and M. H. Cunningham, "Hot and cold BLEVEs : observation and discussion of two different kinds of BLEVEs," in *AIChE Symposium Series*, 1993.
30. J. E. Venart, A. Rutledge, K. Sumathipala and K. Sollows, "To BLEVE or not to BLEVE: anatomy of a boiling liquid expanding vapour explosion," *Process Safety Progress,* vol. 12(2), pp. 67–70, 1993.
31. S. N. Chen, J. H. Sun and W. Wan, "Boiling liquid expanding vapor explosion: explosion research in the evolution of the two-phase flow and over-pressure," *Journal of Hazardous Materials,* Vols. 156(1-3), pp. 530–537, 2008.
32. A. M. Birk and J. D. VanderSteen, "On the transition from non-BLEVE to BLEVE failure for a 1.8 m3 propane tank," *Am. Soc. Mech. Eng. Pressure Vessels Piping Div. PVP 446,* p. 143–152, 2002.
33. K. W. Blything and A. B. Reeves, "An initial prediction of the BLEVE frequency of a 100 tonnes butane storage vessel, Report SRD/R488," UK Atomic Energy Authority, Safety and Reliability Directorate, 1988.
34. M. Selway, "The predicted BLEVE frequency of a selected 2000m3 butane sphere on a refinery site, Report SRD/R492," UK Atomic Energy Authority, Safety and Reliability Directorate, 1988.
35. M. W. Roberts, "Analysis of boiling liquid expanding vapour explosions events at DOE sites," Proceedings of the EFCOG Safety Analysis Workshop, 2000.
36. A. M. Birk, C. Davison and M. Cunningham, "Blast overpressures from medium scale BLEVE tests," *Journal of Loss Prevention in the Process Industries,* vol. 20, p. 194–206, 2007.
37. C. v. d. Bosch and R. Weterings, "CPR 14E Yellow Book – Methods for the Calculation of Physical Effects," Committee for the Prevention of Disasters, The Hague, 2005.
38. E. Planas-Cuchi, J. Salla and J. Casal, "Calculation overpressure from BLEVE explosions," *Journal of Loss Prevention in the Process Industries,* vol. 17, p. 431–436, 2004.
39. A. C. Van den Berg, M. M. Van der Voort, J. Weerheijm and N. H. Versloot, "Expansion-controlled evaporation: a safe approach to BLEVE blast," *Journal of Loss Prevention in the Process Industries,* vol. 17, p. 397–405, 2004.
40. B. Genova, M. Silvestrini and F. J. Lean-Trujillo, "Evaluation of the blast-wave overpressure and fragments initial velocity for a BLEVE event via empirical correlations derived by a simplified model of released energy," *Journal of Loss Prevention in the Process Industries,* vol. 21, pp. 110–117, 2008.
41. R. G. Sachs, "Dependence of blast on ambient pressure and temperature, Technical Report BRL-466," Army Ballistic Research Lab, Aberdeen Proving Ground, 1944.
42. G. F. Kinney and K. J. Graham, Explosive Shocks in Air, 2nd Edition, New York: Springer-Verlag, 1985.
43. R. G. Zalosh, Industrial Fire Protection Engineering, Chichester: Wiley, 2003.
44. NFPA 921: Guide for Fire and Explosion Investigations, Quincy, MA: National Fire Protection Association, 2011.
45. *Manora v. Watts Regulator Co., 784 P. 2d 1056, Oklahoma Supreme Court,* 1989.
46. "Hot Water Heater Explodes in Elementary School, Lessons Learned the Hard Way," Combustion Safety, Inc Communication, [Online]. Available: http://www.

combustionsafety.com/secured/pdf/safetyalerts/star_spencer_lesson.pdf.
47. Center for Chemical Process Safety (CCPS), Guidelines for Evaluating Process Plant Buildings for External Explosions, Fires and Toxic Releases, 2nd ed., Hoboken, NJ: John Wiley and Sons, 2012, p. 94.
48. F. P. Lees, "Volume 2: Chapter 16," in *Loss Prevention in the Process Industries*, Oxford, Reed Educational and Professional Publishing, 1996, pp. 16/182–16/197.
49. K. Hasegawa and K. Sato, "Study on the Fireball Following Steam Explosion of n-Pentane," in *Proceedings of the Second International Symposium on Loss Prevention and Safety Promotion in the Process Industries*, Heidelberg, Germany, 1977.
50. R. M. Woodward and R. M. Pitblado, LNG Risk Based Safety, Hoboken, NJ: John Wiley & Sons, Inc., 2010, pp. 291–302.
51. D. M. Johnson, M. J. Pritchard and M. J. Wickens, "Large Scale Catastrophic Releases of Flammable Liquids, Report EV4T.0014.UK(H)," Commission of the European Communities, 1990.
52. W. E. Martinsen and J. D. Marx, "An Improved Model for the Prediction of Radiant Heat from Fireballs," in *International Conference and Workshop on Modeling Consequences of Accidental Releases of Hazardous Materials*, San Francisco, CA, 1999.
53. NFPA 68 Standard on Explosion Protection by Deflagration Venting, Quincy, MA: National Fire Protection Association, 2013.
54. R. K. Eckhoff, Explosion Hazards in the Process Industries, Houston, TX: Gulf Publishing Company, 2005, pp. 138–140, 299–304.
55. W. L. Frank, S. A. Rodgers and G. R. Colonna, NFPA Guide to Combustible Dusts, Quincy, MA: National Fire Protection Association (NFPA), 2012, pp. 214–217.
56. R. Bubbico and M. Marchini, "Assessment of an explosive LPG release accident: A case study," *Journal of Hazardous Materials,* no. 155, p. 558–565, 2008.
57. R. Pitblado, "Potential for BLEVE associated with marine LNG vessel fires," *Journal of Hazardous Materials,* no. 140, p. 527–534, 2007.
58. E. Planas-Cuchi, N. Gasulla, A. Ventosa and J. Casal, "Explosion of a Road Tanker Containing Liquefied Natural Gas," *J. Loss Prev. Process Ind.,* no. 17, pp. 315–321, 2004.
59. J. Casal, J. Arnaldos, H. Montiel, E. Planas-Cuch and J. A. Vílchez, Handbook of Hazardous Spills, New Tork, NY: McGraw Hilll, 2001.

Dr. Alfonso Ibarreta is a Managing Engineer at Exponent, Inc. He specializes explosion protection systems.

Dr. Hubert Biteau is a Senior Associate at Exponent, Inc. He specializes in fire dynamics, explosions and heat transfer.

Dr. Jason Sutula is a Senior Fire Protection Engineer at Jensen Hughes. His main focus is the forensic analysis of fire and explosion losses.

Introduction to Fire Risk Analysis

72

John M. Watts Jr. and John R. Hall Jr.

Introduction

The risk assessment chapters in this section describe concepts and methods to be used in answering the three questions: What could happen? How bad would it be? How likely is it? This chapter in particular is intended to provide an overview of fire risk analysis as a whole, indicating how the subsequent chapters fit together and how a completed fire risk analysis connects to other evaluative and management activities. The purpose of this introductory chapter is threefold:

1. Introduce some generic terminology and fundamental concepts (building on the three questions raised above)
2. Provide an overview of the other chapters in this section
3. List some broad resources for conducting fire risk analysis (FRA)

What Is Risk?

Risk has always been a part of human endeavor, and for much of human history, the notion that risk could be actively controlled or prevented would have been considered mad or even blasphemous. Even today, when we increasingly expect protection against risk and use codes, regulations, insurance provisions, built-in and planned response mechanisms, and incentives, all to control or reduce risk, very few of our risk reduction and risk management actions proceed from a formal or quantitative risk analysis.

This aspect, too, is changing. Governments around the world are mandating risk analyses in areas of health and safety. Computations of the odds of harm are becoming a powerful force in decisions about activities involving risk.

Every decision related to fire safety is a fire risk decision, whether it is treated as such or not. And so, as our scientific understanding and our suite of quantitative engineering tools have rapidly expanded, we have discovered that we cannot make our fire safety decision-making process more scientific and quantitative unless we first place our new engineering tools into an appropriate fire risk analysis context. To do otherwise is to make many implicit assumptions about patterns of danger and preferences for certainty and for safety versus other human wants and needs.

Basing decisions on fire risk not only requires the challenging technical steps of fire risk estimation but also requires the identification of an acceptable level of risk, which is more a philosophical task than a technical one. Consider, for example, the recent fire loss experience of any country. Does this experience represent a level of fire risk acceptable to the citizens of that country? If the answer is no, then why is there so little attention paid to the problem? If the answer is

J.M. Watts Jr. (✉)
Director of the Fire Safety Institute

J.R. Hall Jr.
Division director for fire analysis and research of the National Fire protection Association

M.J. Hurley (ed.), *SFPE Handbook of Fire Protection Engineering*,
DOI 10.1007/978-1-4939-2565-0_72, © Society of Fire Protection Engineers 2016

yes, meaning we accept certain losses, then why is there a great clamor for change following every serious fire?

Accepting a level of risk requires a value judgment, and people have different value judgments. Consider four perspectives on the value of residential sprinklers: technical, societal, enforcer, and managerial.

Technical value judgments are made by experts based on the available technical information and their acquired expertise. Experts pretty much agree that residential sprinklers can significantly reduce the calculated fire risk. The experts most aware of the risk reduction potential of sprinklers are also most likely to evaluate the attractiveness of sprinklers based on that potential, more than on other bases. They may embrace residential sprinklers with great enthusiasm on that basis.

Societal value judgments are the judgments of ordinary people balancing benefits, costs, and risks of the full range of activities and events that affect their daily lives. Their estimation of the benefits and the negative side effects of sprinklers may be based on folklore more than the best thinking of the experts, and they are likely to attach more importance to costs and to other hazards and needs than the experts—having a specific focus—do. Currently, it appears that the reduced fire risk produced by a residential sprinkler system is not valued as highly by the average citizen as is the increased benefit of a new car.

Enforcer value judgments are the judgments of a few professionals who are asked by society to protect their interests in a specific area. Enforcers are a special group within the larger group of individuals who provide *fire risk management*. An engineer performing a fire risk analysis will usually be working on behalf of a client with fire risk management responsibility, but the engineer cannot base his or her analysis on the values of the client alone. Instead, the fire risk analysis will need to address the client's values and also societal values. Enforcers are often seen as the interpreters and guardians of societal values, but at the same time, their technical expertise and focused mission of providing fire safety give them a distinctive set of values. Their estimation of benefits and side effects are likely closer to those of the experts, but their evaluation of those benefits and side effects are likely closer to those of the general public, embodied in societal value judgments. And because they directly incur neither the costs nor the benefits of their decisions, they must factor in some other considerations having to do with when it is acceptable to dictate safety choices to people. Is it equitable to require automatic sprinklers in *all* residences? How can cost be fairly distributed? Who is responsible for system reliability? Should production, installation, and maintenance of sprinklers be regulated?

Managerial value judgments are the judgments of all the other professionals with special responsibilities relevant to fire risk management, which for residential fire sprinklers would include such groups as architects, builders, managers of hardware retail chains, and so forth. Their estimation of the benefits and side effects of sprinklers may be similar to the general public's, their estimation of the costs is probably more accurate than that of any other group, and, most important, they themselves are likely to be directly affected by those costs more than by the benefits or side effects. Different information and different goals and values are likely to lead to a different assessment—though still risk based like all the others—of the attractiveness of residential sprinklers.

The chapters of this section are designed to provide the practicing engineer with the contextual tools and supplementary information that will permit him or her to use the knowledge and tools embedded in all the earlier sections and to produce a sound evaluation of alternative choices.

Fire risk estimation is the scientific process of answering three questions: (1) What could happen? (2) How bad would it be if it did happen? (3) How likely is it to happen? Or, to put it another way, risk has two essential components: exposure and undesired consequences. Exposure is a potential risk that becomes real with uncertainty, and so exposure refers to the likelihood or probability of experiencing a destructive event, for example, fire. Undesirable consequences,

ranging from deaths or dollars of property damage, to significant intangible losses such as business interruption, mission failure, environmental degradation, and destruction of cultural artifacts, are also potential risks. They become real if exposure occurs. Thus when we speak of fire risk, we are referring to the uncertainty of loss.

Let's return to the three questions that opened this chapter.

What could happen? can refer to a sequence of events ending in a fire loss, the sequence as a whole being called a *scenario,* or to an object or other entity having the potential for a sequence of events ending in a fire loss. A *hazard* is such an object, and *hazard* itself is the potential for loss. *Fire hazard analysis* is a term often used to refer to analyses of what could happen and how bad it would be, without analysis of likelihood.

How bad would it be if it did happen? is often called *consequence* and sometimes called *hazard,* in the sense of a specific measure of potential for loss. The measure of consequence can be direct (e.g., property is damaged) or indirect (e.g., the company is out of business for several days). It can be objective (e.g., replacement cost in monetary units) or subjective (e.g., pain and suffering effects of injury, utility measures of damage).

How likely is it to happen? is usually called *probability*. Probability can be relative (e.g., likelihood of this loss is how much greater or smaller than likelihood of that loss) or absolute (e.g., how many times a year, given a population of people or property). Probability can be regarded as objective and measured objectively (e.g., how many occurrences per year in a recent period of time). It can be regarded as objective but measured subjectively (e.g., how many occurrences do we estimate will occur next year, given data on the number of occurrences last year and impressions on what has changed since last year). It can be regarded as and measured subjectively.

Both consequence and probability can be either explicit in a formal fire risk analysis or implicit and unquantified in a more simplified fire risk analysis (e.g., *fire risk index*).

For purposes of use by fire protection engineers, we assume that fire risk analysis is a scientific process, closely linked to calculations based on proven relationships and the collection and analysis of valid and appropriate data, to describe the form, dimension, and characteristics of the fire risk. Fire risk analysis can take different approaches depending on the purpose and scope of the analysis or assessment. Some assessments look back to try to infer probabilities and other risk-related measures based on practices and fire loss experience after an event such as the introduction of home smoke alarms. Other assessments look ahead and try to predict what the practices and fire loss experience would be after an event such as legislating residential sprinklers in homes.

The approach taken to fire risk analysis can also differ based on the availability—quantity, quality, and detail—of data for the purpose. Assessing the fire risk for U.S. residences, for example, one is able to draw on a very large number of documented fire events but with limited detail. Assessing the fire risk for U.S. nuclear power plants, by contrast, has far fewer fire events to draw upon but much more detail on each such event. And assessing the fire risk in any specific existing building will involve very few events in that building and questions of relevance for data from any other building or group of buildings.

In fire safety engineering, risk analysis is most generally used to evaluate fire protection strategies for a particular application or for a class of facility or operation. In other words, there are a sizeable number of buildings and some considerable relevant fire loss history to draw upon.

Terminology and Concepts

The terminology of fire risk analysis is not consistent. For example, a committee of the Society for Risk Analysis identified 17 different definitions of *risk* [1]. If one considers risk to be the full probability distribution of hazardous events and loss consequences associated with a

building, product, or other entity to be studied, then all 17 definitions can be seen as alternative summary measures taken from that common distribution. The important point, however, is that for many people, a summary measure is not just a summary measure related to risk, useful for analysis; it *is* the risk. As another example, the terms *analysis* and *assessment* are often used interchangeably, yet some sources make sharp distinctions. We will provide distinct definitions.

The rest of the chapters in this section also show some inconsistencies in definitions and concepts. These are largely a function of differences in the authors' backgrounds, topics, resources, and intents. In general, the definitions and concepts used are similar, even when they are not identical.

An overview of terms is best presented in the form of a glossary, but the list below is presented in what is meant to be a logical sequence, rather than alphabetically. More extensive glossaries can be found in Grose [2] and Rowe [3].

Hazard A hazard is a chemical or physical condition that has the potential for causing damage to people, property, or the environment [4]. Hazard is any situation that has the potential for causing injury to life or damage to property and the environment [5].

Risk Risk is the potential for realization of unwanted, adverse consequences to human life, health, property, or the environment. Estimation of risk (for an event) is usually based on the expected value of the conditional probability of the event occurring times the consequence of the event given that it has occurred [6]. It follows that risk for a building, a product, or some other entity would be the probability distribution of events and associated consequences relevant to that building, product, or entity.

Probability According to the frequency interpretation, probability is the proportion of the time an event will occur in the long run. According to the subjective interpretation of probability, it is a measure of the strength of a person's belief concerning the occurrence or nonoccurrence of an event [7]. Probabilistic analysis is not well established in fire protection engineering, where empiricism, heuristics, and, more recently, physics-based modeling are principally used to make decisions. Probabilistic analysis is more established in fields such as decision analysis, management science, operations research, industrial and systems engineering, and systems safety. The mathematics of probability allow us to formulate engineering models which recognize uncertainty and deal with it quantitatively and consistently. Probability and statistics are covered in Chap. 73.

Consequence Consequence is a measure of the expected effects of an incident outcome case [4].

Perceived Risk Any measure of risk preferences in which the scale is not fully explainable by some objective measure of loss, direct or indirect, may be a measure of perceived risk. Studies of risk perception have identified a number of factors that consistently cause objectively equal risks to be perceived differently, including preferences for more certainty over less certainty (i.e., *risk aversion*), familiar over unfamiliar risks, voluntary over involuntary risks, readily detectable risks over undetectable or hidden risks, and common or ordinary risks over dramatic or memorable risks. The field of *risk communication* is devoted, in part, to finding ways for individuals and groups with differing ways of perceiving risks to communicate effectively, understand one another, and collaborate on mutually acceptable analyses and decisions.

Risk Analysis Risk analysis is the detailed examination, including risk assessment, risk evaluation, and risk management alternatives, performed to understand the nature of unwanted, negative consequences to human life, health, property, or the environment. Risk analysis is an analytical process to provide information regarding undesirable events, and it is the process of quantification of the probabilities and expected consequences for identified risks [6].

Risk Assessment Risk assessment is the process of establishing information regarding acceptable levels of a risk and/or levels of risk for an individual, group, society, or the environment [6].

Risk Estimation Risk estimation is the scientific determination of the characteristics of risks, usually in as quantitative a way as possible. These characteristics include the magnitude, spatial scale, duration, and intensity of adverse consequences and their associated probabilities as well as a description of the cause and effect links [6]. One complication is that a totally objective or scientific way to measure fire risk does not exist. Problem identification, data collection and reduction, and integration of information are all replete with subjective evaluations.

Risk Evaluation Risk evaluation is a component of risk assessment in which judgments are made about the significance and acceptability of risk [6].

Risk Identification Recognizing that a hazard exists and trying to define its characteristics is called risk identification. Often risks exist and are even measured for some time before their adverse consequences are recognized. In other cases, risk identification is a deliberate procedure to review, and, it is hoped, to anticipate possible hazards [6].

Acceptable Risk A value judgment applied to a particular scale for the measurement of risk yields a definition of acceptable risk. It therefore requires a prior decision on the scale and method used to estimate or measure risk and a second decision on the person or group whose views on acceptability are to be used. For a practicing engineer, acceptable risk is likely to be risk acceptable to the client. For an authority having jurisdiction (AHJ) or anyone answerable to an AHJ, acceptable risk is meant to be acceptable to society in general or to a particular community.

It is an axiom of fire risk analysis that zero risk is not an achievable goal. There are no risk-free alternatives available to individuals or organizations. No technology is 100 % reliable or totally immune to misuse, and even if technological risk could be eliminated, natural catastrophes such as lightning strikes, wildland fires, earthquakes, and wind storms include the potential for fire loss. An important corollary is that reducing fire risk may increase other forms of risk. An obvious case is the potential damage to the ozone layer from use of halon.

The goal that comes closest to being practical and yet striving for zero risk is to require that risk be as low as is technically possible. For fire protection engineering, this goal may take the form of accepting the residual risk after all identified risk reduction strategies and choices have been adopted. Or, for individuals with special preferences for particular fire protection strategies (e.g., active systems over product or material requirements, or vice versa, and either over education and training), acceptable risk may be the residual risk after favored choices are in place. One complication is that the residual risk in these cases may be perceived as zero, implying no prior acceptance of the nonzero risk that actually remains.

A Universally Acceptable Level of Fire Risk Does Not Exist No matter how one defines the term *acceptable level of fire risk,* it will be dependent on the problem context and on the individual judging acceptability, that is, on the alternatives and objectives. Individuals and organizations are inconsistent in their risk aversion. Surveys show wide variations with respect to factors such as voluntary versus involuntary risk and perceived versus calculated risk.

One contention is that the present public fire risk situation must be acceptable since otherwise there would be greater concern and call for action. This view is not a fully reliable generalization. People may have "accepted" the current risk because they believed it to be lower than it really is, believed no technically feasible alternative existed (which can change because technology changes or because perceptions of technology change), or saw no politically effective way to make their lack of acceptance known. Moreover, the current situation is a compromise among the greatly differing preferences of many

individuals and groups, whose relative influence on the process of choice may also change. More elaborate discussion of the issues associated with acceptable risk can be found in Lowrance [8] and Fischoff et al. [9].

Vulnerability The susceptibility of life, property, and the environment to injury or damage if a hazard manifests its potential is vulnerability [5].

Methods of Fire Risk Analysis

Fire risk analysis is basically a structured approach to decision making under uncertainty. Within this general structure, there are many techniques or approaches to both qualitative and quantitative fire risk analysis. For each application, consider the level of mathematical sophistication appropriate to meet objectives.

A generalized concept of fire risk analysis has these steps:

1. Identify fire hazards.
2. Quantify the consequences and probabilities of the fire hazards.
3. Identify hazard control options.
4. Quantify the effects of the options on the risks of the hazards.
5. Select the appropriate protection.

At each of the two stages of quantification, there is a wide range of possibilities of depth and detail, and the actual quantification can take place anywhere on a spectrum from a principal basis in hard data and established science to a principal basis in expert judgment.

Fire risk analysis begins—and for some applications may end—with the identification of fire hazards. A preliminary assessment of areas of potential concern in facility design and operational concepts may be organized by location (e.g., area of a plant) or by activity (e.g., manufacturing versus office functions, wherever they occur). This identification provides a structure for subsequent estimates of the probability of occurrence of the events in each possible accident sequence and thereby of each possible deleterious consequence.

Formal fire risk assessment evolved with the insurance industry in the nineteenth century. Methods of fire risk analysis may be classified into four categories: (1) checklists, (2) narratives, (3) indexing, and (4) probabilistic methods [10]. Checklists and narratives are nonquantitative approaches that may address steps 1, 3, and 5 above while bypassing steps 2 and 4. Indexing is a thorough quantification method that is heuristic rather than fundamentally based. Probabilistic methods have grown in use over the last third of a century but remain rare even today.

Checklists are a common accessory of fire safety consisting of a listing of hazards, usually with recommended practices. A checklist is usually less generic than a model code or standard. It may even be so specific that it is intended to apply to a single class of buildings under management of a single owner, reflecting the special concerns of that owner.

A checklist is a practical tool to support analysis of a building relative to a code or standard that forms the basis for the checklist. It is very seldom that all criteria in a code or standard apply to a single building. The fire protection engineer must focus on only those requirements that are applicable to a specific project. A checklist can aid in this process. It also makes requirements easier to read, understand, and track to compliance.

Checklists face a trade-off between practicality and ease of interpretation. A long checklist might list 50 fire safety factors, with each item described in a manner that is readily visible or measurable, but those 50 items are not all likely to be comparably important. A short checklist, on the other hand, is usually composed of conceptual features of fire safety, which may all be very important but may all require interpretation to be made measurable.

Moreover, checklists do not capture the interaction of fire risk factors, including the manner in which the importance of one fire risk factor will change as a function of performance on another factor. For example, the relative value of hydrants, sprinklers, and extinguishers is not constant but a function of other features of a structure's form and utility.

Narratives consist of a series of recommendations—things to do and not do—related to fire risk and safety. They are probably the earliest approach to fire risk assessment, stemming from the observation that fire is capable of destroying certain materials, such as wood, fur, and flesh. This realization would have led to a communication from parent to child on the avoidance of these fire dangers. In this earliest form, narratives were much simpler and less finished than checklists. They were not comprehensive with regard to hazards, and so they did not support a thorough review.

As the piecemeal parent's advice format evolved over the years, the narrative approach developed into the present multivolume set of the NFPA *National Fire Codes*® 2000 edition [11]. These contain the bulk of our present-day wisdom on fire safety. The information is presented in the form of descriptions of various hazardous conditions and ways to reduce or eliminate them. In this modern form, narratives are often more finished than checklists, which may be developed as simplified, practical tools to serve the more basic narratives.

Like checklists, narratives do not attempt to evaluate the fire risk quantitatively. A risk is judged acceptable if it is addressed in accordance with published recommendations. The criterion is one of pass or fail, and the residual risk remaining if you pass is never quantified or evaluated. Also like checklists, narratives cannot hope to cover the myriad conditions of human activity. While there is much common ground among different fire hazard situations, there is considerable variation in detail.

Indexing is representative of the quantitative fire risk assessment that originated with the insurance rating schedule. The approach has broadened to include a wide variety of applications. In general, fire risk indexing assigns values to selected variables based on professional judgment and past experience. The selected variables represent both positive and negative fire safety features and the assigned values are then operated on by some combination of arithmetic functions to arrive at a single value. This single value can be compared to other similar assessments or to a standard to rank the fire risk. Chapter 82 covers this subject.

Some measures used in fire risk analysis, such as *probable maximum loss* (PML), sound more fundamentally grounded than fire risk indexes but may actually be less so. There is no established consensus on how improbable a loss must be to be ineligible as the probable maximum loss, and the designation is sometimes given without benefit of any explicit or formal analysis. The resulting subjectivity of such a determination suggests that this value is more of an ordinal label than a quantitative measure of risk (which is not to say that it does not have usefulness).

Matrices and *contours* are methods that can fall between indexes and full-fledged probabilistic methods. A risk matrix typically provides a discrete partitioning of relative consequences along one dimension and relative likelihood along the other. The entry in each matrix cell may include a description of hazards known or believed to have that combination of consequence severity and likelihood, and may also be used to record judgments on the acceptability of such risks and/or recommendations on steps to take to reduce such risks. A risk contour is a continuous analogue to a risk matrix. Curves are drawn on a two-dimensional graph with one axis for consequence and one for probability, with a curve representing types of hazards or technically achievable states.

Probabilistic methods are the most informative approaches to fire risk assessment in that they produce quantitative values, typically produced by methods that can be traced back through explicit assumptions, data, and mathematical relationships to the underlying risk distribution that all methods are presumably seeking to address. Most of the chapters in this section of the handbook are devoted to engineering methods of use in executing a formal probabilistic analysis of fire risk. Some common, generic methods of fire risk analysis follow.

Event Tree An event tree is a graphical logic model that identifies and quantifies possible outcomes following an initiating event [4]. The

tree structure is organized by temporal sequence. Probabilities can be calculated from the tree, and consequences are typically assigned to the end states but may cumulate along the tree.

Fault Tree A fault tree is a method for representing the logical combinations of various system states that lead to a particular outcome [4]. The tree structure is organized by logical dependency. Probabilities can be calculated from the tree. Consequences are typically defined in an either/or form (success or failure) so that the probabilities suffice to calculate the risk, as defined.

Decision Tree A decision tree is a method for representing the possible outcomes following a succession of events, combining points where the ensuing path is subject to choice and points where it is not. The analysis operates similarly to an event or fault tree, and the simplest decision trees consist of a set of initial choices and an event or fault tree associated with each.

Influence Diagram An influence diagram is a graphical representation of the relationship of the decisions and uncertainties in a decision problem [12, 13]. The diagram is more flexible and less unidirectional than any type of tree diagram. It is designed to focus more on the elements of decision making and less on relevant underlying physical phenomena.

Overview of the Section

This section of the handbook is organized into three broad areas that progress from the general to the specific. There are some basic tools that most approaches to fire risk analysis should consider if not incorporate. There are some examples of generic models applied to fire safety problems, and there are detailed descriptions of fire risk analysis procedures that have been adopted in several areas of application.

The most common use of fire risk analysis is as a basis from which to make choices. The choice may be between two alternative designs for a building or two alternative formulations for a model code or standard. The choice may be whether to tighten requirements on product type A or product type B. Chapter 77 describes *decision analysis,* a generic field on forms of analysis that support this kind of decision making. *Cost-benefit analysis* is a specific type of decision analysis, in which a fire risk analysis provides estimates for some of the benefits, and other analysis quantifies corresponding costs.

Chapter 74 addresses *reliability*. Fire risk analysis depends upon many types of probabilities. One is fire scenario probability, the estimation of likelihood for the initial conditions and ensuring major events in fire development. Another group of probabilities might be transitory conditions related to people, such as the locations and capabilities of occupants when a fire begins. A critically important set of probabilities have to do with status and capabilities of fire protection equipment, features, and arrangements. Is the battery working in the smoke alarm? Is the sprinkler valve open or closed? Is the fire door working or blocked open? These are all questions of reliability addressed in Chap. 74.

Chapter 76 addresses *uncertainty*. Early on, the comment was made that the term *fire risk* refers to the uncertainty of loss. The concept of safety itself is one of uncertainty. There is no such thing as absolute safety; human activity will always and unavoidably involve risks. Chapter 76 addresses a narrower definition of uncertainty—not the uncertainty of the potential victim regarding the fact of fire loss but the uncertainty of the engineer or decision maker regarding estimates of the magnitude of fire risk.

Uncertainty may be caused by imprecision or bias in our techniques of observation or calculation, a lack of clarity in our goals, uncontrollable technological variation, or variations of natural phenomena, to name only the major components. The concept of fire is also uncertain. Unwanted combustion is perhaps the least predictable common physical phenomenon. Uncertainty analysis is the scientific calculation procedure that should underpin choices of *safety factors* and *safety*

margins. It is central to the valid use of fire risk analysis—or any other form of engineering analysis—for code equivalency, design approval, or any other important decision in the real world.

Chapter 78 addresses *data sources* for engineering analysis, particularly data useful for calculating scenario probabilities, reliability probabilities, or any other probabilities needed for fire risk analysis.

Chapter 79 addresses the *measurement of consequences in economic terms*. This measurement includes indirect losses, economic measures of the value of a lost life or of an injury, and the use of utility measures to capture people's desire to avoid uncertainty about loss, as well as loss itself, the implications for people's risk aversion for the basic mathematics of insurance, and so on. The common theme is treating consequences comprehensively and in a form that captures people's real preferences and can be readily compared to the costs of alternative choices. Chapter 81 addresses *other economic topics* that arise in the practice of engineering analysis, with particular emphasis on monetary valuations over time (e.g., rate of return, interest, discounting).

Chapter 80 describes techniques and available models using *computer simulation,* with special emphasis on those having a fire risk analysis basis, such as state-transition models. Chapter 82 describes less-quantified methods of fire risk analysis, involving *fire risk indexing*. Fire scenarios play an important role in many aspects of fire safety engineering. Significant among these is fire risk analysis, hence Chap. 38 describes methods of scenario development and quantification. This is a task that applies to all applications of fire risk analysis, though it tends to take a different form specific to each application, but is not required in this form or detail in other types of fire protection engineering analysis.

Chapters 75 and 83, respectively, describe general techniques and available methods for fire risk analysis of buildings and processes. Chapter 89 describes the specific methods tailored to application where the use of fire risk analysis is far more common than in others, namely, nuclear power plants. Chapter 90 describes applications for transportation vehicles. Chapter 84 presents the means to use fire risk analysis in the evaluation of the safety of consumer products. Chapter 85 shows applications to *health care facilities*.

Activities and Resources

Every major group involved in guidance related to fire safety now has a committee or a publication devoted to fire risk analysis, and the emphasis on risk-based or risk-informed approaches to decision making is growing rapidly. Thus, in addition to the many sources of specific models and methods mentioned in the subsequent chapters, there are a growing number of sources for generic work and guidance. Among the more important activities are the following:

- SFPE has added the *SFPE Engineering Guide to Fire Risk Assessment* to its growing collection of practice guides. In addition, fire risk analysis is addressed in context in a more limited form in the SFPE publication on an overview of performance-based design, the *SFPE Engineering Guide to Performance-Based Fire Protection.*
- NFPA's Technical Committee on Fire Risk Analysis, whose purpose is to provide assistance and guidance to other committees on methods and concepts in fire risk analysis, published NFPA 551, *Guide for the Evaluation of Fire Risk Assessments,* in 2004. The same committee now maintains NFPA 550, *Guide to the Fire Safety Concepts Tree,* 2002 edition, one of the most widely cited and used fault tree formats in fire risk analysis. Development of fire risk analysis methods for general and specific purposes has been a recurring emphasis of projects organized by NFPA's Fire Protection Research Foundation.
- ASTM maintains Standard E 1776, *Standard Guide for the Development of Fire-Risk-Assessment Standards,* to guide the writing of fire risk assessment standards for burnable products.

- The International Organization for Standardization (ISO) TC 92/SC 4 has published Technical Specification 16732, *Guidance on Fire Risk Assessment*. This international document is compatible with but much less detailed than the SFPE guide, which was published later.
- The Society for Risk Analysis is the principal worldwide professional organization devoted to risk analysis. It devotes comparatively little emphasis to engineering applications and to acute outcomes, instead focusing more on long-term chronic illness consequences.
- The Institute for Operations Research and the Management Sciences (InFORMS) has areas of emphasis in decision analysis and applies and develops risk analysis concepts and methods through that activity.

References

1. *RISK Newsletter,* September, Society for Risk Analysis, McLean, VA, p. 5 (1987).
2. V.L. Grose, *Managing Risk,* Prentice Hall, Englewood Cliffs, NJ (1987).
3. W.D. Rowe, *An Anatomy of Risk,* John Wiley and Sons, New York (1977).
4. *Guidelines for Chemical Process Quantitative Risk Analysis,* Center for Chemical Process Safety, American Institute of Chemical Engineers, New York (1989).
5. *Hazardous Materials Emergency Planning Guide,* National Response Team, Washington, DC (1987).
6. *Glossary of Risk Analysis Terms,* McLean, VA, Society for Risk Analysis, http://www.sra.org/glossary.htm (2000).
7. J.E. Freund and F.J. Williams, *Dictionary/Outline of Basic Statistics,* McGraw-Hill Book Company, New York (1966).
8. W.W. Lowrance, *Of Acceptable Risk,* William Kaufman, Los Altos, CA (1976).
9. B. Fischoff, S. Lichtenstein, P. Slovic, S.L. Derby, and R.L. Keeney, *Acceptable Risk,* Cambridge University Press, Cambridge, UK (1981).
10. J. Watts, "Systematic Methods of Evaluating Fire Safety: A Review," *Hazard Prevention,* 18, 2, pp. 24–27 (1981).
11. NFPA, *National Fire Codes®,* National Fire Protection Association, Quincy, MA (2000).
12. R.A. Howard and J.E. Matheson, "Influence Diagrams," in *Readings on the Principles and Applications of Decisions Analysis* (R.A. Howard and J.E. Matheson, eds.), 2, Strategic Decisions Group, Menlo Park, CA, pp. 719–762 (1983).
13. R.A. Howard, "From Influence to Relevance to Knowledge," in *Influence Diagrams, Belief Nets and Decision Analysis* (R.M. Oliver and J.Q. Smith, eds.), John Wiley and Sons, New York, pp. 3–24 (1990).

John M. Watts Jr. holds degrees in fire protection engineering, industrial engineering, and operations research. He is director of the Fire Safety Institute, a not-for-profit information, research, and educational corporation located in Middlebury, Vermont. Dr. Watts also serves as editor of NFPA's *Fire Technology*.

John R. Hall Jr. is assistant vice president for fire analysis and research at the National Fire Protection Association. He has been involved in studies of fire experience patterns and trends, models of fire risk, and studies of fire department management experiences since 1974 at NFPA, the National Bureau of Standards, the U.S. Fire Administration, and the Urban Institute.

Probability and Statistics

73

John R. Hall Jr. and Francisco Joglar

Introduction

This chapter introduces the basic definitions and methods of probability and statistical analysis, which are the foundation for the reliability, and fire risk analysis, and other topics presented in this section. With increased availability of sizeable quantities of reliable data on a whole range of topics related to fire protection engineering, it is essential that the analysis of this data be based on sound mathematical principles from probability and statistical theory. The chapter is divided into two main sections: probability theory, and statistics.

Basic Concepts of Probability Theory

Probability Theory

Probability theory is the branch of mathematics dealing with the modeling of uncertainty through measures of the relative likelihood of alternative occurrences, whether specifically or generally defined. The term "set" is often introduced when describing probability theory from a classical perspective.

J.R. Hall Jr.
National Fire Protection Association

F. Joglar (✉)
Jensen Hughes

Set

A set is a collection of elements. For a set to be well-defined, it must be possible to identify with certainty whether any object is or is not an element or part of the set.

Set Theory

The theory of sets is the most fundamental branch of mathematics and is relevant to probability theory, because all probabilities are built up from sets.

Subsets

A set, A, that consists entirely of elements that are also contained in set B is called a subset of B. Each element in a set may also be considered a subset of that set.

Set Operators

There are three basic operators essential to the algebraic manipulation of sets:

Complement (~): The complement operator applies to a single set A and produces the set of all elements that are *not* in A. Such an operator is always applied relative to some specification of the set of all elements,

M.J. Hurley (ed.), *SFPE Handbook of Fire Protection Engineering*,
DOI 10.1007/978-1-4939-2565-0_73, © Society of Fire Protection Engineers 2016

which is called the *universal set* (∪). The complement of the universal set is the *null set* (Ø) or *empty set,* the set with no elements.

Union (∪): The union operator is applied to two sets, as in $A \cup B$. It produces the set consisting of all elements that are members of *either* A or B or both.

Intersection (∩): The intersection operator is applied to two sets, as in $A \cap B$. It produces the set consisting of all elements that are members of *both* A and B.

Relationships Among the Operators

$$\sim (A \cup B) = \sim A \cap \sim B$$
$$\sim (A \cap B) = \sim A \cup \sim B$$
$$(A \cup B) \cap C = (A \cap C) \cup (B \cap C)$$
$$(A \cap B) \cup C = (A \cup C) \cap (B \cup C)$$
$$(A \cup B) \cup C = A \cup (B \cup C)$$
$$(A \cap B) \cap C = A \cap (B \cap C)$$

Venn Diagrams Venn diagrams are a graphical technique for displaying relationships among sets (represented by circles) and operators, within a rectangle that represents the universal set, ∪ (Figs. 73.1, 73.2, and 73.3).

Sample Space

Sample space is a set of mutually exclusive elements, each representing a possible outcome or occurrence and collectively representing all possible outcomes or occurrences for the experiment or problem under consideration. Mutually exclusive elements refer to those elements with no common outcomes (i.e., no intersection between them). A sample space must also have the property that the set operators defined previously, if applied to the subsets of the sample space in any combination, will always produce subsets of the sample space. Subsets of a sample space are called *events*.

Probability Measure

A probability measure is a mathematical function, P, defined on the subsets (events) of a sample space, U, and satisfying the following rules:

1. $P(A) \geq 0$ for any A, where A is an event subset of U.
2. $P(\text{Ø}) = 0$.
3. $P(U) = 1$.
4. If $A \cap B = \text{Ø}$, then $P(A \cup B) = P(A) + P(B)$.

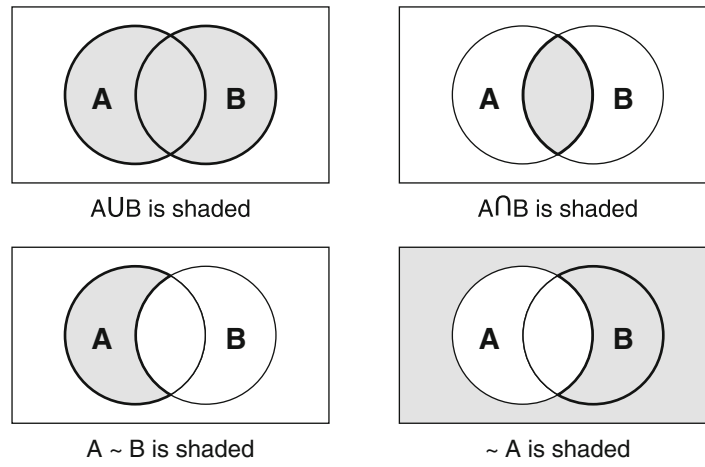

Fig. 73.1 Examples of set operators using shading for display

In the classical theory of probability, it was assumed that all probability measures must be based on experiments (actual or at least imaginable) which could be run repeatedly, so that for each outcome e (an element of the sample space of possible outcomes), $P(e)$ would be given asymptotically as the ratio between the number of times outcome e occurs and the number of times the experiment is performed. This interpretation is called the *frequency interpretation of probability*. More recently, theorists associated with the Bayesian school of statistical inference have argued for the interpretation of probability only as a measure of the individual's strength of belief in the likelihood of an outcome. This interpretation is called *subjective probability*. Each of these two schools represents both an underlying conceptual model and an approach that makes practical sense in some but not all situations. In assigning probabilities to the outcomes of heads and tails for a single coin, for example, a relatively brief frequency experiment is easy to conduct. In assigning probabilities to the possible values of the annual inflation rate for next year, the requisite experiment cannot be performed repeatedly. The mathematics of probability theory applies regardless of the source of the probability measure.

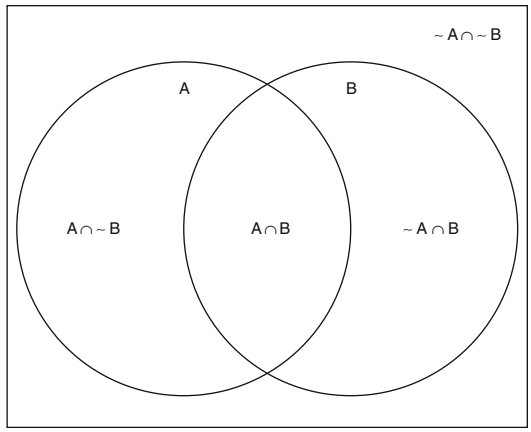

Fig. 73.2 Example of set operators applied to two sets

Probability Formulas Related to Set Operators

1. $P(A \cup B) = P(A) + P(B) - P(A \cap B)$
2. $P(\sim A) = 1 - P(A)$

These two formulas state, respectively, that (1) the probability that either (inclusive version) of two events will occur is equal to the sum of the probabilities that each event will occur minus the

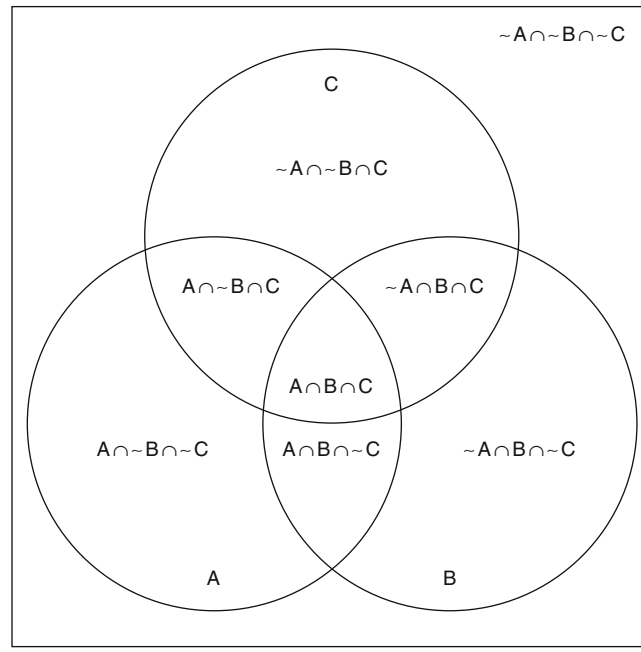

Fig. 73.3 Example of set operators applied to three sets

probability that both will occur; and (2) the probability that an event will not occur is equal to one minus the probability that it will occur.

Independence and Conditionality

The two events, A and B, are called *independent* if $P(A \cap B) = P(A) \times P(B)$. Two events that are not independent are called *dependent*.

The *conditional probability of A given B*, $P(A|B)$, is defined as $P(A \cap B)/P(B)$. It is normally interpreted to mean the probability that A will occur, given that B has occurred or will occur. If A and B are independent, then $P(A|B) = P(A)$ and $P(B|A) = P(B)$; in other words, the occurrence of A does not affect the likelihood of B, and vice versa.

It is important to note that two events may be dependent without either being the cause of the other and without any apparent logical connection. A common phenomenon involves two apparently unrelated variables (e.g., annual fire department expenditures on gasoline, annual sales revenue from plastics and petrochemicals) that are dependent because each is related in an understandable way to a third variable (e.g., price per barrel of oil).

Bayes's law (also called *Bayes's theorem* and *Bayes's formula*) states that

1. If B_i, $i = 1, \ldots, N$, are sets (events), and
2. If $B_1 \cup B_2 \cup \ldots \cup B_N = U$, and
3. If $B_i \cap B_j = \emptyset$ for all $i \neq j$ between 1 and N, and
4. If $P(B_i) \neq 0$, $i = 1, 2, \ldots, N$

then

$$P(B_i|A) = \frac{P(B_i) \times P(A|B_i)}{\left[P(B_1) \times P(A|B_1) + P(B_2) \times P(A|B_2) + \cdots + P(B_N) \times P(A|B_N)\right]}$$

Bayes's law is a particularly powerful consequence of the laws of conditional probability and is the foundation for modern statistical decision theory. What makes it so powerful is this application. Suppose $P(B_1), \ldots, P(B_N)$ represent the current best estimates of the probabilities of various events of interest prior to the performance of an experiment (or the collection of some data on experience). These are called *prior probabilities*. Suppose A is a possible outcome of that experiment whose probability of occurrence, given each of the events $B_1, \ldots, B_N$, can be derived. Then Bayes's law can be used to develop a new set of probabilities, $P(B_1 \mid A), \ldots, P(B_N \mid A)$ that incorporate the information provided by the experiment. These are called *posterior probabilities* because they are probabilities calculated *after* the gathering of information (e.g., through an experiment).

Example Suppose you have ten coins, nine of which are fair (0.5 probability of heads) and one of which is fixed (1.0 probability of heads). Choose one coin. With no other information, the probability that you have a fair coin (B_1) is 0.9 and the probability that you have the fixed coin (B_2) is 0.1. Suppose you flip the coin once.

If it comes up tails, you know it is a fair coin and Bayes's law confirms this. Let A be the event of getting tails on the one coin flip. Then

$$P(A|B_1) = 0.5 \quad \text{and} \quad P(A|B_2) = 0$$

Therefore,

$$P(B_1|A) = \frac{(0.5)(0.9)}{(0.5)(0.9) + (0)(0.1)} = 1$$

If the coin comes up heads, you still do not know whether it is the fixed or a fair coin. Since

heads is more likely with the fixed coin, the evidence points slightly in that direction. Let A' be the event of getting heads on the single coin flip. Then

$$P\left(A^{'}\middle|B_1\right) = 0.5 \quad \text{and} \quad P\left(A^{'}\middle|B_2\right) = 1$$

Therefore,

$$P\left(B_1\middle|A^{'}\right) = \frac{(0.5)(0.9)}{(0.5)(0.9) + (1.0)(0.1)} = 0.82$$

Thus the result of flipping the coin once and obtaining heads has lowered the estimate of the probability that you hold a fair coin from 0.9 to 0.82; correspondingly, your estimate that you hold the fixed coin has risen from 0.1 to 0.18.

Random Variables and Probability Distributions

A *random variable* is a real-number-valued function defined on the elements of a sample space. In some cases, the elements of a sample space may lend themselves to association with a particular random variable (e.g., the sample space consists of outcomes of tossing a die; the random variable is the number of spots on the exposed face). In other cases, the random variable may be only one of many that could easily have been associated with the sample space (e.g., the sample space consists of all citizens of the United States; the random variable is the weight to the nearest pound).

Each value of a random variable corresponds to an event subset of the sample space consisting of all elements for which the random variable takes on that value. The *probability of a value of the random variable,* then, is the probability of that event subset.

A *discrete probability distribution* is one for which the random variable has a finite or countably infinite number of possible values (e.g., values can be any integer from 0 to 10; values can be any integer).

A *continuous probability distribution* is one for which the random variable can take on an uncountably infinite number of possible values (e.g., values can be any real number from 0 to 10; values can be any real number).

A *probability distribution function* (also called *probability density, probability density function,* and *probability distribution*) is a mathematical function that integrates to 1.0, *f,* that gives the probability associated with each value of a random variable, $f(y) = P(x = y)$. The term *density* is usually reserved for random variables that can take on an uncountably infinite range of values, so that the probability of a range of values of the variable must be computed through integral calculus.

Because each value, *y,* of a random variable, *x,* is associated with a subset of the sample space, $f(y) \geq 0$ for all y.

Because no element of a sample space can take on two or more values of a random variable and each element must take on some value, the values of the random variable collectively correspond to a set of mutually exclusive subsets that exhaust all elements of the sample space, and so

$$\sum_{\text{all } x} f(x) = 1$$

for discrete probability distributions, and

$$\int_{\text{all } x} f(x)dx = 1$$

for continuous probability distributions.

A *cumulative distribution* is a mathematical function that, for each value of a random variable, gives the probability that the random variable will take on that value or any lesser value

$$F(y) = P(x \leq y) = \sum_{x \leq y} f(x)$$

for discrete probability distributions, and

$$F(y) = \int_{x \leq y} f(x)dx$$

for continuous probability distributions.

Note that some references use the term "probability distribution" to refer to the cumulative distribution function, *F,* of a continuous probability distribution, while referring to the

probability density function, *f,* only as a probability density function.

A *survival function* is a mathematical function that, for each value of a random variable, gives the probability that the random variable will exceed that value

$$S(y) = P(x > y) = \sum_{x>y} f(x)$$

for discrete probability distributions, and

$$S(y) = \int_{x>y} f(x)dx$$

for continuous probability distributions.

Therefore, for any probability distribution function $P(x)$ and any value y, the cumulative distribution and the survival function based on sum to one for all values of y.

$$F(y) + S(y) = 1$$

A *multivariate probability distribution* gives the probability for all combinations of values of two or more random values, for example, $f(u, v) = P(x = u \text{ and } y = v)$.

Key Parameters of Probability Distributions

Certain key parameters of probability distributions are of use because (1) they help to provide essential summary information about the random variable and its probability distributions and (2) they are included in the functional forms of certain probability distributions that are of use in many practical situations.

The mean, μ, of a random variable (also called its *expected value* or *average*) is defined as

$$\mu = \sum_{\text{all } x} xf(x)$$

for discrete probability distributions, and

$$\mu = \int_{\text{all } x} xf(x)dx$$

for continuous probability distributions. Notice that the mean is the center of mass of a probability distribution. Recall that the center of mass of a two-dimensional shape single rigid body (in this case the probability distribution function) is the point in the x axis where the distribution "balances" itself (i.e. the weighted relative position of the distributed mass sums to zero) and the average of the weighted position coordinates of the distributed mass defines its value. It is also written as $E(x)$, which stands for *expected value of x*. This is the most commonly used of several parameters that relate to some concept of the most typical or average value of a random variable.

The expected value can also be calculated for a function of the random variable, as follows:

$$E[g(x)] = \sum_{\text{all } x} g(x)f(x)$$

for discrete probability distributions, and

$$E[g(x)] = \int_{\text{all } x} g(x)f(x)dx$$

for continuous probability distributions. In Microsoft Excel, the expected value of a given sample size can be calculated using the "=AVERAGE(Sample_Range)" function, where the Sample_Range input is the group of cells containing the sample data.

The *variance,* σ^2, of a random variable is a measure of the likelihood that a random variable will take on values far from its mean value. It is a parameter used in the functional form of some commonly occurring probability distributions.

$$\sigma^2 = \sum_{\text{all } x} (x - \mu)^2 f(x)$$

for discrete probability distributions, and

$$\sigma^2 = \int_{\text{all } x} (x - \mu)^2 f(x)dx$$

for continuous probability distributions. In Microsoft Excel, the variance of a given sample size can be calculated using the "=VAR (Sample_Range)" function, where the

Sample_Range input is the group of cells containing the sample data. The function "=VARP(Sample_Range)" can be used for calculating the variance of an entire population.

The variance can also be expressed as the expected value of a function of the random variable, as follows:

$$\sigma^2 = E\left[(x-\mu)^2\right] = E\left(x^2\right) - \mu^2$$
$$= E\left(x^2\right) - [E(x)]^2$$

The variance is expressed as σ^2 because most calculations use the square root of the variance, which is called the *standard deviation,* σ. In practical terms, the standard deviation is the average of the distances of the different observations in sample to the sample mean. In Microsoft Excel, the standard deviation of a given sample size can be calculated using the "=STDEV(Sample_Range)" function, where the Sample_Range input is the group of cells containing the sample data. The function "=STDEVP(Sample_Range)" can be used for calculating the standard deviation of an entire population.

Example Suppose that ten experiments are conducted to evaluate the heat release rate of new product. Table 73.1 lists that resulting heat release rate values. The average, variance and standard deviation functions in Microsoft Excel are used to evaluate the statistics from the experimental results. Table 73.1 also indicates the Excel functions used for calculating the values. Notice that the function argument E5:E14 is the range of cells where the data is stored in the Excel worksheet.

The *moments* of a probability distribution are defined as the expected values of powers of the random variable. The *n*th moment is $E(x^n)$. Thus, the mean is the first moment, and the variance is the second moment minus the square of the first moment. The value given by $E[(x - \mu)^n]$ is defined as the *n*th moment about the mean.

The function defined by $E[e^{\theta x}]$ is called the moment generating function because it is equivalent to an infinite series whose terms consist of, for all *k,* the *k*th moment of *x* times $(\theta^k/k!)$.

Table 73.1 Heat release values from repeated experiments

Iteration	Sample (kW)	
1	652	
2	649	
3	671	
4	535	
5	583	
6	710	
7	652	
8	649	
9	683	
10	659	
Average (kW)	645	=AVERAGE(E5:E14)
Variance	2250	=VAR(E5:E15)
Standard deviation (kW)	50	=STDEV(E5:E14)

Percentiles refer to the value of the random variable where a specific amount of probability is accumulated. For example, the 5th percentile is the value of the random variable where 5 % of the area under the probability distribution curve is located. In mathematical form, the ith percentile P_i of a distribution can be found solving the integral of the distribution for its upper limit of integration. That is, the equation:

$$P_i = \int_{-\infty}^{x} f(x)dx$$

is solved for x. Recall that x represents the value of the random variable where the area under the distribution curve from $-\infty$ is equal to i. For continuous probability distributions, the median is that value, *y,* for which the cumulative distribution, $F(y)$, is equal to 0.5. For discrete probability distributions, the median is that value, *y,* for which $f(x < y) = f(x > y)$. If the random variable can take on only a finite number of values, the median may not be uniquely defined. The median is less sensitive than the mean to extreme values of the random variable and is the "average" of choice for certain kinds of analyses.

From a discrete perspective, the function "=PERCENTILE(Sample_Range, k)" in

Microsoft Excel can be used for determining the k^{th} percentile of a value in a data sample.

Skewness refers to the symmetry of a probability distribution function around its mean. The median is not equal to the mean in a skewed distribution. An age distribution of fire department uniformed personnel will be skewed, for example, because the small number of personnel in their 50s and 60s will raise the average (mean) age well above the typical age (middle to late 20s). The term is used more frequently than is any specific measure of it. A symmetric distribution has a skewness of zero, no matter how skewness is measured.

Kurtosis is a rarely used term for the relative flatness of a distribution.

Degrees of freedom is the term given to certain parameters in many commonly used distributions (e.g., Student's t, chi-square, F). The distributions that use these parameters are used in tests of the variance of samples. In those tests the parameters always correspond to positive integer values based on the size of the sample (e.g., n, $n-1$, $n-2$). Since increasing sample size gives the sample more freedom to vary, it is natural to call those parameters measures of the "degrees of freedom" to vary in the sample.

Conditional Distributions

From the general definition of conditional probability, the probability of random variable is larger than a conditional value x_o is given by:

$$F(x|x > x_o) = \frac{\Pr(x \le X/x > x_o)}{P(x > x_o)} = \frac{F(x) - F(x_o)}{1 - F(x_o)}$$

where x is the random variable. Figure 73.4 provides a conceptual representation of this formulation. The numerator represents the area under the curve between the variables x_o and x (shaded). The denominator is the area under the curve after the variable x_o (Fig. 73.4).

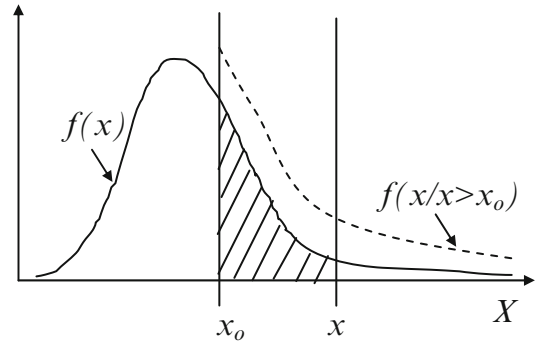

Fig. 73.4 Conceptual representation of the conditional probability of failure

Differentiating with respect to x, the conditional density function is obtained (see Papoulis, "Probability, Random Variables, and Stochastic Processes", 1991).

$$f(x|x > x_o) = \frac{f(x)}{1 - F(x_o)}$$

This conditional density, which is a function of x_o and x will be applied later in the chapter in the analysis of repairable systems. The denominator is by definition a number between 0 and 1, which forces the integral of the function from x_o to infinity to be 1.0. As illustrated by the dashed line in Fig. 73.4, the normalizing factor shifts the function upwards after x_o, but the shape of the distribution remains the same after that point. Again, the area under the curve of the conditional distribution after x_o is 1.0.

Commonly Used Probability Distributions

Uniform and Rectangular Distributions

These distributions give equal probability to all values. The term *rectangular distribution* is reserved for the continuous probability distribution case. It is used to characterize random variables with identical probabilities throughout its range. As a simple example of its discrete form, consider the outcome of rolling a fair dice. Clearly, the outcome is one of six numbers,

each with identical probability of one sixth. Notice that the uniform distribution is "uninformative" over its range. That is, it only suggests a finite range of possible values with equal probability.

1. $f(x) = 1/N$, for $x1, \ldots, x_N$, if $f(x)$ is a discrete probability distribution over N values of a random variable.
2. $f(x) = 1/(b-a)$, for $a \le x \le b$, if $f(x)$ is a continuous probability distribution over a finite range.

Multivariate versions of the uniform distribution can be readily constructed for both the discrete and the continuous cases.

The uniform and rectangular distributions are used when every outcome is equally likely. As such, they tend to be useful, for example, as a first estimate of the probability distribution if nothing is known; that is, if nothing is known, treat every possibility the same. In

Example 1 One of the 30 fire protection engineers in a firm is to be selected at random to accompany the local fire department on a fire code inspection. Each engineer is assigned a playing card, the reduced deck of 30 cards is shuffled and cut several times, and the top card is selected. Here, N is 30, so $f(x) = 1/30$ for each engineer.

Example 2 When the winning engineer arrives at the fire department, a random procedure is used to select one point on the city map. Whatever point is selected, they will inspect the buildings on the property of which that point is part.

Suppose A is the total area of the city. Then $f(x) = 1/A$, for every point in the city. For a given occupancy B, whose lot has area a, the probability of the event of choosing B (which corresponds to choosing any point on B's property) is equal to

$$\int_{\text{all points in } B} \left(\frac{1}{A}\right) dx = \frac{a}{A}$$

Note that although this is a uniform (rectangular) distribution over all *area* in the city, it is not a uniform distribution over all occupancies of the city, because an occupancy's probability of being chosen will be proportional to the size of its lot. In any analysis, there may be several different, incompatible ways of treating all possibilities "equally."

Normal Distribution (Also Called Gaussian Distribution)

The normal distribution, the familiar bell-shaped curve, is the most commonly used continuous probability density function in statistics; its density is a function of its mean, μ, and standard deviation, σ, as follows:

$$f(x) = \frac{1}{\sigma\sqrt{2\pi}} \exp\left[-\frac{1}{2}\left(\frac{x-\mu}{\sigma}\right)^2\right] \text{ for } -\infty < x < +\infty$$

The *Central Limit Theorem* establishes that for *any* probability density function, the distribution of the sample mean, $\bar{x}$ of a sample from that density asymptotically approaches a normal distribution as the size of the sample increases. This means that the normal distribution can be used validly to test hypotheses about the means of any population, even if nothing is known or can be assumed about the population's underlying distribution. Also, the *Law of Large Numbers* establishes that the standard deviation of the distribution of the sample mean is inversely proportional to the square root of the sample size, which means that larger samples always produce more precise estimates of the sample mean. These two results are the cornerstones of sample-based statistical inference.

In addition to proving a valid distribution for sample *means* in all situations, the normal distribution also directly characterizes many *populations* of interest, including experimental measurement errors and quality control variations in materials properties.

A sample size of at least 30 should be used to obtain an acceptable fit of the sample mean distribution to the normal distribution.

The standard tables of the normal distribution are for a random variable with mean 0 and variance 1. They can be used for values from any normal distribution by subtracting the mean, then dividing the result by the standard deviation. The standardization equation is:

$$z = \frac{x - \mu}{\sigma}$$

Where z is the random variable from the standard normal distribution, and x, μ and σ are the random variable mean and standard deviation of the normal distribution.

The multivariate form of the normal distribution is also commonly used. Its parameters are given by a vector of the means of all the variables and a matrix with both the variances of all the variables and the covariances of pairs of variables (which are functions of the variances and the correlation coefficients).

In Microsoft Excel, the functions "=NORMDIST(x, μ, σ, cumulative)", "=NORMINV(p,μ, σ)", and "=STANDARDIZE(x, μ, σ)", are commonly used to plot and solve the normal distribution. The function NORMDIST solves for the function f(x) described earlier in this section, where x is the random variable, μ and σ are the mean and standard deviation of the normal distribution and the "cumulative" input (which is a Boolean input) is set to FALSE. Setting the "cumulative" input to TRUE returns the value of the cumulative distribution function F(x) instead of f(x). The NORMINV function returns the value of the random variable x that follows a normal distribution that is associated with a probability p. That is, the function solves for the integral equation for percentiles described earlier in this chapter. Finally, the STANDARDIZE function returns the standardized value of the random variable x, which is often characterized with the letter "z". The value of z follows a standard normal distribution.

Example As an example, consider the normal distribution with mean 650 and standard deviation 100 plotted in Microsoft Excel using the function NORMDIST described earlier (See Fig. 73.5). The profile with the square markers is the cumulative function and is obtained setting the cumulative argument to TRUE. The values for this function are read in the rightmost y axis (secondary axis). Notice that the distribution reaches the value of 1.0 when the full range of the distribution is covered. The profile with the diamond markers is the probability density function. Most distribution functions in Microsoft excel are plotted the same way.

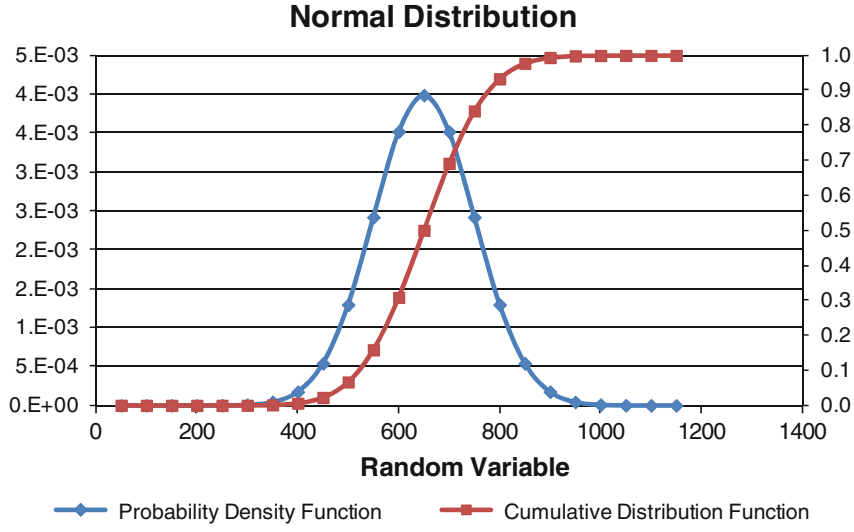

Fig. 73.5 Normal distribution

Example 1 The promotional examination for lieutenant is taken by 100 fire fighters, whose test scores, shown in Table 73.2, fit a normal distribution with mean score of 50 and standard deviation of 15. The fit is not exact because strictly speaking, the 100 scores comprise a discrete distribution, not a continuous distribution, and the possible scores are bounded by 0 and 100. Also, with only 100 scores, the fit to a normal distribution can be seen in this grouped data but might not be apparent if every score had its own frequency entered separately (Fig. 73.6).

Example 2 Suppose the widths of U.S. adults, fully clothed (including overcoats), at their widest points are normally distributed with mean 0.5 m and standard deviation of 0.053 m. Then, a door width equal to the mean (0.5 m) would accommodate 50.0 % of the population $[F(x \leq \mu) = 0.50]$. A door width equal to the mean plus one standard deviation (0.553 m) would accommodate 84.1 % of the population $[F(x \leq \mu + \sigma) = 0.841]$. A door width equal to the mean plus two standard deviations (0.606 m) would accommodate 97.7 % of the population $[F(x \leq \mu + 2\sigma) = 0.977]$.

But some buildings hold 10,000 persons, so suppose it is desired to construct a door width that will be too narrow for only one of every 20,000 persons. Then the value of a is desired, such that $F(x \leq \mu + a\sigma) = 0.99995$. That value of a is 3.87, which translates to a door width of 0.705 m, or more than 40 % wider than the door width that sufficed for one-half the population.

All basic statistics texts contain tables of the cumulative distribution function for the normal distribution.

In engineering practice, the primary use of the normal distribution will be in estimation of parameters. For example, an estimate of a burning characteristic of a product or material can be derived from a series of experiments or tests by calculating the mean value from the test, then

Table 73.2 Normal distribution sample test scores

Score	Number of fire fighters receiving that score
0–9	1
10–19	2
20–29	7
30–39	15
40–49	25
50–59	25
60–69	15
70–79	7
80–89	2
90–100	1

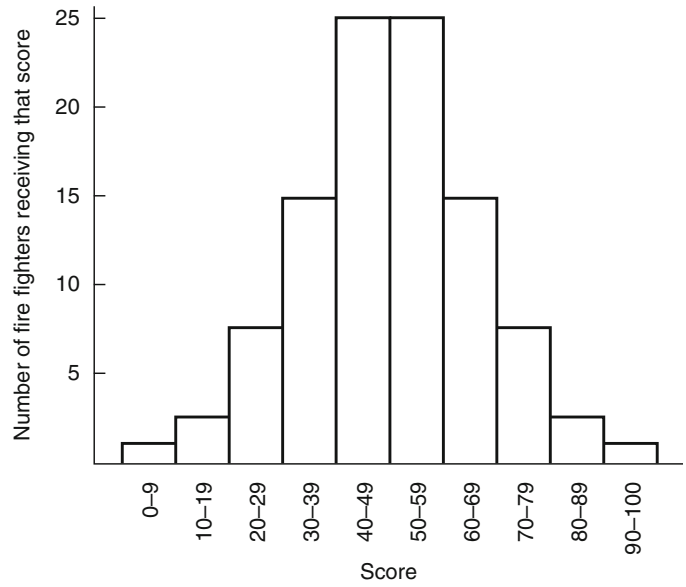

Fig. 73.6 Illustrative frequency bar chart

confirming that the test measurements reasonably fit a normal distribution around the mean. This latter step confirms that the errors are normally distributed, which means the sample mean is an unbiased best estimate of the underlying characteristics.

Example 3 The critical temperature for a steel beam is assumed to be normally distributed with mean = 550 °C and standard deviation of 40 °C. A fire protection engineer is evaluating the potential hazard of a fire below the beam, which will subject it to fire plume temperatures. Based on the heat release rates generated by the type and configuration of combustibles in the location, calculated fire plume temperatures range from 250 to 475 °C. Considering that the evaluation may not have included the lowest and highest heat release rates, the analysts assumes a normal distribution for the plume temperature with a 5th percentile = 250 °C and a 95th percentile = 475 °C. Since the normal distribution is symmetrical, the percentile values can be used for determining the mean of the distribution as follows: 250 + (475–250)/2 = 362.5 °C. Using the = NORMINV(0.05, 0, 1) = −1.64 function in excel for the standard normal distribution returns the random variable value for a probability of 0.05. We can now solve for the standard deviation of the normal distribution for temperature using the standardization formula as follows:

$$-1.64 = \frac{250 - 362.5}{\sigma}$$

The resulting normal distribution has a mean of 362.5 °C and a standard deviation of 68.6 °C.

Log-Normal Distribution

It is not unusual to deal with random variables whose logarithms (to any base) are normally distributed. In such cases, the original variables are said to be log-normally distributed. The log-normal distribution is defined for positive values only. The distribution is particularly appropriate for random variables constrained by zero that can assume few very large values. Equipment down time and failure times, fire load density (i.e., mass of combustibles per unit floor area) among others. The log-normal distribution results from the transformation x = ln (t) where the random variable x is normally distributed with mean μ and standard deviation σ. The mathematical form of the distribution is:

$$f(t) = \begin{cases} \frac{1}{\sqrt{2\pi}\sigma t} e^{\frac{-1}{2}\left(\frac{\ln(t)-\mu}{\sigma}\right)^2} & t \geq 0 \\ 0 & otherwise \end{cases}$$

where μ and σ are the mean and standard deviation of the normally distributed random variable x. The cumulative distribution function F(t) is obtained by a numerical integration of f(t).

The expected value and the variance of t can be obtained with the following equations:

$$E(t) = e^{\mu + \frac{\sigma^2}{2}}$$

$$V(t) = e^{2\mu + 2\sigma^2} - e^{2\mu + \sigma^2}$$

If E(t) and V(t) are known instead, μ and σ can be calculated using the equations above.

In risk analysis and reliability studies we often use the term "error factor" to characterize log-normal distributions. The error factor, EF, is defined as the ratio between the 95th and 50th percentiles of the distribution. Equivalently, it can be also defined as the ratio between the 50th and 5th percentiles of the distribution. It is also useful to note that the μ and σ parameters of the normal distribution can be obtained using the following relationships:

$$\sigma = \log(EF)/1.645$$

$$\mu = \log(mean) - \frac{\sigma^2}{2}$$

where the variable "mean" is the mean of the lognormal distribution.

The log-normal distribution has also been confirmed as a good fit for the distribution of magnitude of monetary loss, [1] which makes it a good choice for estimating extreme-event probabilities. In particular, this permits estimation of the probability or magnitude of the

maximum probable loss, an essential measure in insurance analysis, even if no such large losses have ever been documented.

The log-normal and Weibull distributions are popular choices to represent any skewed dataset when there is no fundamental or established basis for selecting a particular distribution. These distributions are both used, for example, to model occupant premovement times.

In Microsoft Excel, the functions "=LOGNORMDIST(t, μ, σ)", and "=LOGINV (p, μ, σ)", are commonly used to plot and solve the lognormal distribution. The function LOGNORMDIST solves for the function F(t) described earlier in this section, where ln(t) is the random variable, and μ and σ are the mean and standard deviation of the normally distributed ln(t). The LOGINV function returns the value of the random variable t that follows a lognormal distribution that is associated with a probability p. That is, the function solves for the integral equation for percentiles described earlier in this chapter.

Distributions for Significance Tests

The Student's *t,* chi-square, and *F* distributions are the workhorses for statistical hypothesis testing. They are used to determine that two or more objects are or are not clearly different from each other.

Student's *t* Distribution

For small samples, the distribution of the sample mean is not well approximated by the normal distribution. Even for somewhat larger samples, the population variance is typically not known, and the sample variance must be used instead. The Student's *t* distribution may be used instead of the normal distribution, but it does assume that the population is normally distributed. Its distribution is a function of its degrees of freedom, *m*.

$$f(t) = \frac{[\Gamma(m+1/2)]\left[(1+t^2/m)^{-(m+1)/2}\right]}{\sqrt{\pi m}[\Gamma(m/2)]} \quad \text{for} \quad -\infty < t < +\infty$$

where

$$\Gamma(u) = \int_0^\infty y^{u-1}e^{-y}dy$$

Expressed in this standard form, the *t* distribution has a mean of zero and a variance of $m/(m-2)$. Since the Student's *t* distribution is used primarily in statistical testing, an example of its use is included in Chap. 42, "Automatic Sprinkler System Calculations."

In Microsoft Excel, the functions "=TDIST(t, deg_freedom, tails)", and "=TINV(p, deg_freedom)", are commonly used to plot and solve the student's t distribution. The function TDIST solves for the function f(t) described earlier in this section, where t is the random variable, the "deg_freedom" input refers to the number of degrees of freedom characterizing the distribution and the input "tails" is a value of 1 or 2 specifying if the results are for one-tailed or two-tailed distribution. The TINV function returns the value of the random variable t that follows a student's t that is associated with a probability p. That is, the function solves for the integral equation for percentiles described earlier in this chapter.

Chi-Square Distribution

Whereas the normal and *t* distributions may be used to test hypotheses about means, the chi-square distribution may be used to test hypotheses about variances or entire distributions. Its density is a function of its degrees of freedom, *m*.

$$f(x) = \frac{x^{(m-2)/2} e^{-x/2}}{2^{m/2}\Gamma(m/2)} \quad \text{for } x \geq 0$$

where

$$\Gamma(u) = \int_0^\infty y^{u-1} e^{-y} dy$$

Expressed in this standard form, the chi-square distribution has its mean equal to m, the number of degrees of freedom, and its variance equal to $2m$.

In Microsoft Excel, the functions "=CHIDIST(x, deg_freedom)", and "=CHIINV (p, deg_freedom)", are commonly used to plot and solve the chi-square distribution. The function CHIDIST solves for the function f(x) described earlier in this section, where x is the random variable, and the "deg_freedom" input refers to the number of degrees of freedom characterizing the distribution. The CHIINV function returns the value of the random variable x that follows chi-square distribution that is associated with a probability p. That is, the function solves for the integral equation for percentiles described earlier in this chapter.

F Distribution

Whereas the normal distribution may be used to test hypotheses about the means of samples of a single random variable, the F distribution permits simultaneous testing of hypotheses about the means of samples reflecting several random variables, each with its own variance, and each pair of variables correlated to some unknown degree. Its density is a function of two non interchangeable degrees-of-freedom parameters, m_1 and m_2 .

$$f(x) = \frac{(m_1/m_2)^{m_1/2} x^{(m_1-2)/2} \{\Gamma[(m_1+m_2)/2]\}}{[\Gamma(m_1/2)][\Gamma(m_2/2)]\left[(1+m_1 x/m_2)^{(m_1+m_2)/2}\right]}$$

where

$$\Gamma(u) = \int_0^\infty y^{u-1} e^{-y} dy$$

The mean of the F distribution is $m_2/(m_2 - 2)$, and the variance is given by

$$\sigma^2 = \frac{2m_2^2(m_1+m_2-2)}{m_1(m_2-2)^2(m_2-4)} \quad \text{if } m_2 > 4$$

In Microsoft Excel, the function "=FDIST(x, deg_freedom1, deg_freedom2)", is commonly used to plot and solve the F distribution. The function FDIST solves for the function f(x) described earlier in this section, where x is the random variable, and the "deg_freedom" inputs refer to the two values of degrees of freedom characterizing the distribution.

Distributions for Reliability Analysis

Exponential Distribution

The exponential distribution is the simplest distribution for use in reliability analysis, where it can be used to model the time to failure. Its density is a function of a parameter, θ, that is equal to its mean and its standard deviation.

$$f(x) = \left(\frac{1}{\theta}\right) e^{-x/\theta} \quad \text{for } x \geq 0$$

Its hazard rate is a constant, 1/θ, so the exponential distribution is the one to use if the expected time to failure is the same, regardless of how much time has already elapsed. This distribution also is commonly used to represent the time required to serve customers waiting in a queue.

The exponential distribution is useful as a starting point in any attempt to model the length of a time interval in a sequence of time intervals. For example, the exponential distribution has been used to model the time between successive evacuating occupants leaving a building [2]. The exponential distribution also has been used to model the probability that a fire is still burning, as a function of time after ignition. In most cases, the exponential distribution will be abandoned in favor of more complex distributions once there is sufficient fundamental understanding, or sufficient data, to point to a specific better-fitting distribution.

In Microsoft Excel, the function "=EXPONDIST(x, Lambda, cumulative)" is commonly used to plot and solve the exponential distribution. The function EXPONDIST solves for the function f(x) described earlier in this section, where x is the random variable, and Lambda is the distribution parameter. Readers should notice that the parameter Lambda in excel equals 1/θ in the function above. The "cumulative" input to the function is a Boolean term used to specify if the function solves the density (set to FALSE) or the cumulative (set to TRUE) distribution function.

Example A smoke alarm is installed in a private home and is powered by a battery from a lot with average life of 6 months. Suppose the time until the battery dies can be represented by an exponential distribution. (In practice, retailed batteries have a more complex failure rate function.) Then the time until failure might look like that shown in Table 73.3.

Table 73.3 Example of exponential distribution (smoke alarm batteries)

Months old	Probability of failure by this age (i.e., this soon or sooner)
0–1	0.154
1–2	0.283
2–3	0.393
3–4	0.487
4–5	0.565
5–6	0.632
6–7	0.689
7–8	0.736
8–9	0.777
9–10	0.811
10–11	0.840
11–12	0.865
Over 12	1.000

Note that there is a high probability of failure in the first month and a high probability of survival past 1 year

Example A review of impairment data on smoke detectors in a specific facility indicates that a smoke detector device fails on average once every 5 years for various reasons. Upon failure, the detectors are replaced with a new device. Determine the probability that a smoke detector will last: (1) at least 10 years, (2) at most 10 years, and (3) between 5 and 10 years.

Solution From the available data, the parameter λ is estimated as $\lambda = 1/5 = 0.2$ years^{-1}. The probabilities are calculated integrating the exponential distribution as follows:

Probability of the detector lasting at least 10 years:

$$\Pr(t \geq 10) = \int_{10}^{\infty} \lambda e^{-\lambda t} dt = 1 - \int_{0}^{10} \lambda e^{-\lambda t} dt = e^{-0.2(10)} = 0.135$$

This can easily be solved in Microsoft Excel using the function "=1-EXPONDIST(10,0.2, TRUE) = 0.135

Probability of the detector lasting at most 10 years:

$$\Pr(t \leq 10) = \int_{0}^{10} \lambda e^{-\lambda t} dt = 1 - 0.135 = 0.865$$

This can easily be solved in Microsoft Excel using the function "=EXPONDIST(10,0.2, TRUE) = 0.865

Probability of the detector lasting between 5 and 10 years:

$$\Pr(5 \leq t \leq 10) = \int_{5}^{10} \lambda e^{-\lambda t} dt = 0.23$$

This can easily be solved in Microsoft Excel using the function "=EXPONDIST(10,0.2, TRUE)—EXPONDIST(5,0.2,TRUE) = 0.23

The process for computing probabilities would be identical if a different probability distribution is selected provided that the distribution parameters are known.

Poisson Distribution

If a system has exponentially distributed time to failure with mean time θ, then the distribution of the total number of failures, *n,* in time, *t,* has a Poisson distribution. Its distribution is given by a parameter, λ, that is equal to both its mean and its variance.

$$f(n) = \frac{\lambda^n e^{-\lambda}}{n!}$$

for

$$n = 0, 1, 2, \ldots, + \infty$$

where

$$\lambda = \frac{t}{\theta} \quad \text{and} \quad n! = n(n-1)(n-2)\cdots(3)(2)(1)$$

This distribution also is commonly used to represent the number of customers entering a queue for service in a unit of time. It assumes that the expected number of arriving customers in any short interval of time is proportional to the length of time. As a further example of the linkage between exponential and Poisson distributions, if the exponential distribution is used to model the time between evacuating occupants leaving a building, then the Poisson distribution can be used as the distribution for the total number of occupants who have left the building [2].

In Microsoft Excel, the function "=POISSON (x, mean, cumulative)" is commonly used to plot and solve the poisson distribution. The function POISSON solves for the function f(n) described earlier in this section, where x is the random variable, and "mean" is the mean of the poisson distribution. The "cumulative" input to the function is a Boolean term used to specify if the function solves the density (set to FALSE) or the cumulative (set to TRUE) distribution function.

Example Using the smoke alarm scenario in the previous example, suppose each time the battery fails, it is detected immediately and immediately replaced with a new battery of similar expected life. Then the number of times the batteries will fail in the first year is given by a Poisson distribution (Table 73.3). Here t is 12 months and θ is 6 months, so λ is 2. With this information, lets calculate the probability that no more than 1 failures are observed in 10 months using the function in Microsoft Excel. The function "=POISSON(1, 2, TRUE)" will add the probabilities of observing zero and one failure respectively. The numerical results is "=POISSON(1, 2, TRUE) = 0.406" with is equivalent to adding the first two probabilities listed in Table 73.3.

Gamma Distribution (Also Called Erlang Distribution)

The gamma distribution is also commonly used to represent time to failure for a system, particularly in a situation where m independent faults, all with identical exponential distributions of time to occur, are required before the system fails. Its density is a function of two parameters, m and θ, which must both be greater than zero; m need not be an integer.

$$f(x) = \frac{x^{m-1} e^{-x/\theta}}{[\theta^m \Gamma(m)]} \quad \text{for } x \geq 0$$

where

$$\Gamma(m) = \int_0^\infty y^{m-1} e^{-y} dy$$

The mean is $m\theta$ and the variance is $m\theta^2$, which makes it convenient to calculate the values by matching moments with the mean and variance from a sample or population.

In Microsoft Excel, the functions "=GAMMADIST(x, alpha, beta, cumulative)", and "=GAMMAINV(p, alpha, beta) are commonly used to plot and solve the normal distribution. The function GAMMADIST solves for the function f(x) described earlier in this section, where x is the random variable, alpha and beta are the parameters of the gamma distribution and the "cumulative" input (which is a Boolean input) is set to FALSE. Setting the "cumulative"

input to TRUE returns the value of the cumulative distribution function F(x) instead of f(x). Notice that the input alpha is the same as the m parameter used in the equation above and the input beta is equivalent to the θ parameter used in the equation. The GAMMAINV function returns the value of the random variable x that follows a normal distribution that is associated with a probability p. That is, the function solves for the integral equation for percentiles described earlier in this chapter.

Example A set of fire tests for peak heat release rates suggest a sample mean of 1100 kW with a standard deviation of 300 kW. Since the normal distribution has tails extending into the negative range, it may not be a good selection for representing this sample. Lets try to fit a gamma distribution to the data. By matching moments, we can set $1100 = m\theta$ and $300^2 = m\theta^2$ and solve the system of two equations for m and θ, which are the parameter of the gamma distribution. The resulting values are m = 82 (the beta value), and θ = 13 (the alpha value). Using these values, the gamma distribution can be plotted for a range of heat release rate values as inputs to x and the following function "=GAMMADIST(x,13,82, FALSE)", where x are the values listed under the column HRR (kW) in Fig. 73.7.

Weibull Distribution

The most popular complex distribution used in reliability studies to represent time to failure, the Weibull distribution is flexible enough to permit failure rates that increase or decrease with system age. Its density is a function of two parameters, a and b, which must both be greater than zero.

$$f(x) = abx^{b-1}e^{-ax^b} \quad \text{for } x \geq 0$$

$$\mu = a^{-(1/b)}\Gamma\left(\frac{b+1}{b}\right)$$

$$\sigma^2 = a^{-(2/b)}\left\{\left[\Gamma\left(\frac{b+2}{b}\right)\right] - \left[\Gamma\left(\tfrac{b+1}{b}\right)\right]^2\right\}$$

where

$$\Gamma(u) = \int_0^\infty y^{u-1}e^{-y}dy$$

The cumulative distribution can be expressed in closed form, as follows:

$$F(x) = 1 - e^{-ax^b}$$

Therefore, the failure rate has a simple form

$$h(x) = abx^{b-1}$$

The failure rate increases with x (e.g., system age) if $b > 1$ and decreases if $b < 1$. If $b = 1$,

HRR (kW)	PDF
0	0.0E+00
200	9.8E-08
400	3.5E-05
600	4.0E-04
800	1.1E-03
1000	1.4E-03
1200	1.1E-03
1400	6.0E-04
1600	2.6E-04
1800	9.3E-05
2000	2.9E-05
2200	7.9E-06
2400	2.0E-06
2600	4.5E-07
2800	9.5E-08

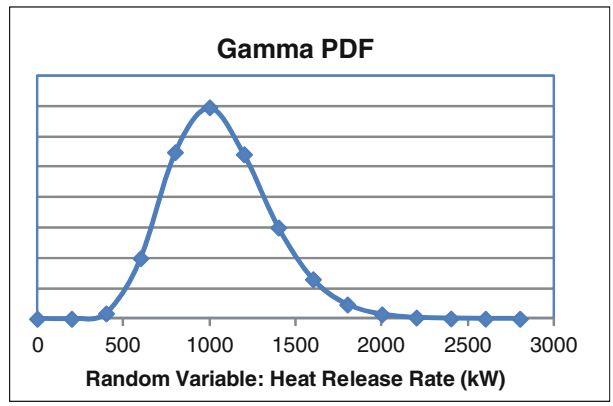

Fig. 73.7 Gamma distribution

the Weibull distribution becomes an exponential distribution, with $\theta = 1/a$.

The Weibull distribution, like the log-normal distribution, is popular to represent skewed datasets about which little is known. For example, the Weibull distribution has been used to represent premovement times of occupants [2].

The Weibull distribution will often provide good results for any phenomenon that resembles a reliability problem. For example, glass breaking in fire may be considered the end result of a number of micro-failures or changes. The Weibull distribution has been shown to work well as the distribution for breaking stress required to break windows [3].

In Microsoft Excel, the function "=WEIBULL (x, Alpha, Beta, cumulative)" is commonly used to plot and solve the weibull distribution. The function WEIBULL solves for the function f (x) described earlier in this section, where x is the random variable, and alpha (variable b used in the equation) and beta (which is represented as 1/a in the equation above) are the distribution parameters. The "cumulative" input to the function is a Boolean term used to specify if the function solves the density (set to FALSE) or the cumulative (set to TRUE) distribution function.

Example Suppose the example in Table 73.2 is modified to show the time to failure for the smoke alarm batteries as having a Weibull distribution. Suppose $\alpha = 1/6$. Then if $b = 1$, the Weibull distribution will be the same exponential distribution shown in Table 73.2. If $b < 1$, early failures are less likely, and if $b > 1$, early failures are more likely. Some examples are shown in Table 73.4. Note that it is not necessary to reduce b in order to make early failures unlikely. An exponential distribution with a higher θ (or Weibull distribution with a lower α) will also make early failures unlikely (Table 73.5).

Table 73.4 Poisson distribution

Number of times smoke alarm will have dead batteries in 1 year	Probability
0	0.135
1	0.271
2	0.271
3	0.181
4	0.090
5	0.036
6 or more	0.016

Table 73.5 Weibull distribution (smoke alarm batteries)

Probability of failure by this age (i.e., this soon or sooner)				
Months old	$b = 1$	$b = 2$	$b = 0.5$	$b = 0.1$
0–1	0.154	0.154	0.154	0.154
1–2	0.283	0.487	0.210	0.164
2–3	0.393	0.777	0.251	0.170
3–4	0.487	0.931	0.283	0.174
4–5	0.565	0.984	0.311	0.178
5–6	0.632	0.998	0.335	0.181
6–7	0.689	1.000	0.357	0.183
7–8	0.736	1.000	0.376	0.186
8–9	0.777	1.000	0.393	0.187
9–10	0.811	1.000	0.410	0.189
10–11	0.840	1.000	0.425	0.191
11–12	0.865	1.000	0.439	0.192
Over 12	1.000	1.000	1.000	1.000

Extreme Value Distributions

Extreme value distributions are used primarily to develop appropriate probabilistic models for rare events. In other words, extreme value distributions are probabilistic functions for the largest, or smallest, observation in a sample. As a conceptual example, consider a probability distribution f(x). Now let's generate N samples from that distribution. Each of these samples will have a maximum and a minimum value. If we group the maximum and minimum values from the N samples respectively, the resulting data sets can be described by extreme value distributions. Fire protection is an area of application of extreme value distributions where these functions can be use for predicting the behavior and statistics of the tails of for example fire losses.

Specifically, the largest member of a sample (i.e., the maximum) of size n has what is known as Type I largest extreme value distribution. This is also called the Gumbel, distribution, regardless of the probability distribution for the parent population. Two conditions however must be

met: The parent probability distribution needs to have a decreasing unbounded tail, and the distribution needs to have finite moments. A normal distribution for example would meet these criteria, where the right tail is decreasing and the mean and standard deviation are known. The mathematical structure for the largest extreme value distribution (LEV) is:

$$f(x|\theta_1,\theta_2) = \frac{1}{\theta_2}\exp(-z-\exp(-z))$$

where $z = \dfrac{x-\theta_1}{\theta_2}$ and θ_1, θ_2 are the location and scale* parameters, respectively, and $\theta_2 > 0$.

In the case of the minimum values from a parent distribution, the *smallest* member of each of the N samples can be modeled with the smallest extreme value distribution (SEV), also referred as Type I smallest extreme value distribution, with density

$$f(x|\theta_1,\theta_2) = \frac{1}{\theta_2}\exp(z-\exp(z))$$

as n increases. The parameters are similar to those described for the largest extreme value function.

In practice, the extreme value distributions "alter" the parent distribution to model the corresponding left or right tails (i.e. smallest or largest values of the random variables). As a conceptual example, let's assume the parent distribution is normal with mean and standard deviation 2000 and 400 respectively. In this case, the values of θ_1 and θ_2 are the mean and standard deviation of the normal distribution- which are the scale and shape parameters for the parent (i.e. normal) distribution. Plotting the parent normal distribution, and the smallest and largest extreme value distribution we can understand the behavior of these functions. Notice that the largest extreme distribution has higher cumulative probabilities in the right tail compared to the parent one. Similarly, the smallest extreme distribution has higher cumulative probabilities in the left tail compared to the parent one (Fig. 73.8).

A similar example is developed assuming the parent distribution is an exponential probability density function. In this case of the exponential distribution, the scale and shape parameters θ_1 and θ_2 are the same value. Notice that the same behavior observed for the normal distribution is also observed for the exponential density (Fig. 73.9).

There are cases however, where not all distribution moments are know. Two other extreme value distributions are available. The Type II or Frechet distribution can be used to model the largest observation. Mathematical the Frechet extreme value distribution is defined as:

$$f(x) = \frac{\alpha}{\beta}\left(\frac{\beta}{x}\right)^{\alpha+1}\exp\left(-\left(\frac{\beta}{x}\right)^{\alpha}\right)$$

where α is the shape parameter $(\alpha > 0)$, and β is the scale parameter $(\beta > 0)$. This distribution is bounded on the lower side $(x > 0)$ and has a

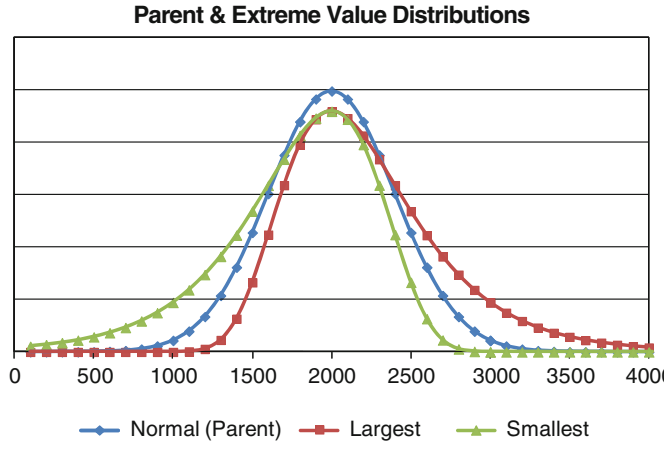

Fig. 73.8 Parent and extreme value distributions

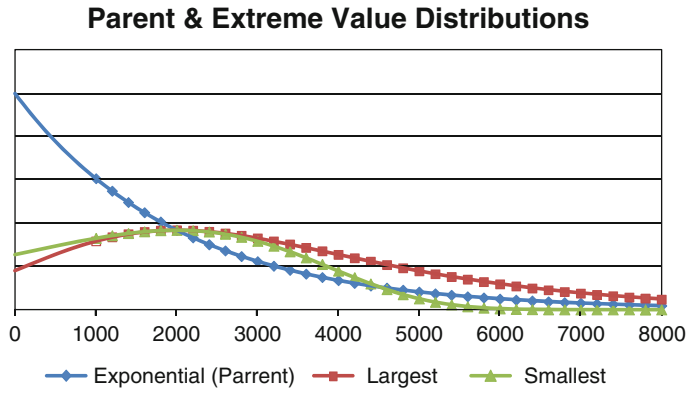

Fig. 73.9 Exponential parent and extreme value distributions

heavy upper tail. Finally, if the parent distribution function has a bounded tail, the smallest observation in a sample of size n, can be modeled with a Type III, or Weibull (described earlier in this chapter) distribution for the minimum. This distribution is routinely used in reliability engineering. It should be noted that the largest value distributions are seldom used for reliability analysis

Pareto Distribution

The Pareto distribution is not as commonly used but does provide a simple form for a distribution whose failure rate decreases with system age. Its density is a function of two parameters, a and b, which must both be greater than zero.

$$f(x) = ab^a x^{-(a+1)} \quad \text{for } x > b$$

$$\mu = ab/(a-1)$$

$$\sigma^2 = ab^2/\left[(a-1)^2(a-2)\right]$$

$$F(x) = 1 - b^a x^{-a}$$

$$h(x) = a/x$$

The parameter a must be greater than 2 for the mean and variance to converge to the values shown above. In general, a must be greater than k for the kth moment to converge.

Note that the formula for probabilities in a Pareto distribution includes only power-law relationships (i.e., the random variable x appears only *with* an exponent, never *in* an exponent or an additive term). This distinguishes the Pareto distribution from other major distributions, such as the Weibull distribution.

Tillander and Keski-Rahkonnen have refined traditional power law formulas for estimating ignition probability as a function of floor area [4]. Their proposed distribution uses both Pareto and log-normal distributions. Under special conditions, this formulation reduces to a simpler power law or sum of power laws formulation, which is the form previous analysts had developed.

Discrete Probability Distributions

A family of distributions exists to address calculations of the probability that a certain number of trails will have a common characteristic. Very few fire protection engineering calculations or models use these distributions. More commonly, individual probability values are chained together in fault trees, event trees, network models, or Markov processes, each of which connects states of the model by using probabilities to determine which of two or more alternative paths from one state will be followed.

Bernoulli Distribution

The Bernoulli distribution is the most basic of the discrete probability distributions and it represents a single trial or experiment in which there are only two possible outcomes—success

(with probability p) and failure. The random variable is the number of successes.

$$f(x) = px(1-p)(1-x) \quad \text{for } x = 0, 1$$

Therefore $f(x) = p$ if $x = 1$ and $f(x) = (1-p)$ if $x = 0$. The mean is p and the variance is $p(1-p)$.

Example Suppose there are 100 fire fighters in a department, 15 of whom are minorities. If all fire fighters are equally qualified, the probability that a minority fire fighter will be chosen as the next lieutenant is give by a Bernoulli distribution, with $p = 15/100 = 0.15$.

Binomial Distribution

The binomial distribution is the probability distribution for the number of successes in n independent Bernoulli trials, all having the same probability of success.

$$f(x) = \binom{n}{x} p^x (1-p)^{(n-x)} \text{ for } x = 0, 1, \ldots, n$$

where

$$\binom{n}{x} = \frac{n!}{x!(n-x)!}$$

and

$$x! = x(x-1)(x-2)\ldots(3)(2)(1)$$

The mean is np and the variance is $np(1-p)$.

The use of *factorials* (e.g., $x!$) can lead to time consuming calculations. It is possible for large values of n to approximate the binomial distribution by a normal distribution [with $\mu = np$ and $\sigma^2 = np(1-p)$]. This approximation will work acceptably if $np \geq 5$ and $n(1-p) \geq 5$. For small values of p, μ and σ^2 become very close, and one can approximate the binomial distribution by a Poisson distribution (with $\lambda = np$). This works acceptably if $n > 100$ and $p < 0.05$.

In Microsoft Excel, the function "=BINOMDIST(number_s, trials, probability_s, cumulative)" is commonly used to plot and solve the binomial distribution. The function BINOMDIST solves for the function f(x) described earlier in this section, where x is the random variable, number_s is the number of successes in the trails, trails is the number of trials, and probability_s is the success probability. The "cumulative" input to the function is a Boolean term used to specify if the function solves the density (set to FALSE) or the cumulative (set to TRUE) distribution function.

Example Suppose in the fire fighter promotion example just used, five lieutenants have been selected sequentially. Also suppose that each time a fire fighter is promoted to lieutenant, that slot is filled with another fire fighter of the same race before the next lieutenant is selected. Under these conditions, the five promotions represent five Bernoulli trials, all having the same probability that a minority fire fighter will be promoted. The number of minority fire fighters promoted will then be governed by a binomial distribution, as shown in Table 73.6.

Example How many fires in 1 year raise suspicion of arson?

Periodically, insurance companies or prosecutors will be tempted to infer a likelihood of arson from no more evidence than a history of multiple fires attached to a particular party in a limited period of time. The probability question underlying this line of reasoning is a binomial distribution question, specifically, the probability that one household will have n or more fires in a period when there were N total fires. Each fire is a "trial," as the term is used here, and each fire involving the one household of interest may be called a "success."

Table 73.6 Example of binomial distribution

Number of minority fire fighters promoted	Probability
0	0.444
1	0.392
2	0.138
3	0.024
4	0.002
5	0.000

Suppose the allegation is that no one could have three unintentional home structure fires in 2 years. In very rough terms for easy calculation, there are about 100 million U.S. housing units (occupied year-round) and 400,000 home structure fires per year, of which roughly 40,000 are intentional. Therefore, $n = 720{,}000$ (each fire is a trial and the annual fire toll is counted over 2 years) and $p = 1/100$ million (each fire could occur in any household). Using the Poisson approximation for ease of calculation, $np = 7.2/1000$.

$$P(k \text{ Successes}) = (7.2/1000)^k \left(e^{-7.2/1000}\right)/k!$$

The probability of three fires exactly will then be 6.2/100,000,000, and the probability of three or more fires will be slightly higher but will round to the same value. This is a very low probability, but applied to 100 million occupied housing units, it translates into an expectation of six housing units somewhere in the United States that will have three or more reported unintentional structure fires in a 2 year period.

Sometimes, allegations like these are buttressed by reference to brush fires, outdoor trash fires, car fires, or even public building fires that are linked to the same individual or household. However, such an allegation brings more fires into the mix, and the probability for a given number of fires in a given period of time will go up.

Geometric Distribution

In the case of a potentially unlimited number of independent Bernoulli trials with identical probabilities of success, the geometric distribution gives the distribution of the trial on which the first success will occur.

$$f(x) = p(1-p)^{(x-1)} \text{ for } x = 1, 2, 3, \ldots, +\infty$$

The mean is $(1/p)$ and the variance is $(1-p)/p^2$.

Example Continuing the example of serial promotions in which each open slot is filled by a new fire fighter of the same race, the geometric distribution would give the probability of which of the promotions will be the first to involve a minority fire fighter (Table 73.7).

Table 73.7 Geometric distribution with serial promotion example

First promotion to involve a minority fire fighter	Probability
First	0.150
Second	0.128
Third	0.108
Fourth	0.092
Fifth	0.078
Sixth	0.067
Seventh	0.057
Eighth	0.048
Ninth	0.041
Tenth	0.035
Later than tenth	0.196

Note the high probability that chance alone will delay the first minority promotion past the tenth promotion

Negative Binomial Distribution (Also Called Pascal Distribution)

This generalization of the geometric distribution gives the probability distribution for the trial on which the kth success will occur.

$$f(x) = \binom{x-1}{k-1} p^k (1-p)^{-(x-1)}$$

$$\text{for } x = k, k+1, k+2, \ldots, +\infty$$

where

$$\binom{x-1}{k-1} = \frac{(x-1)!}{(k-1)!(x-k)!}$$

and

$$x! = x(x-1)(x-2)\ldots(3)(2)(1)$$

Hypergeometric Distribution

The hypergeometric distribution is a variation on the binominal distribution that applies to cases where the initial probability of success, p, reflects

a fixed number of total successes and failures, N, available for selection so that each trial reduces either the number of successes remaining or the number of failures remaining. (For example, imagine an urn filled with balls of two different colors. If each trial consists of removing a ball, then replacing it in the urn, the binomial distribution applies. If each trial consists of removing a ball and keeping it out, the hypergeometric distribution applies.)

$$f(x) = \frac{\binom{Np}{x}\binom{N(1-p)}{n-x}}{\binom{N}{n}} \quad \text{for } x = 0, 1, 2, \ldots, n$$

where

N is the total number of successes and failures possible, $n \leq N$. Np and $N(1 - p)$ are integers

$$\binom{m}{y} = \frac{m!}{y!(m-y)!}$$

and

$$y! = y(y-1)(y-2)\ldots(3)(2)(1)$$

The mean is np and the variance is $np(1–p)[(N–n)/(N–1)]$. For very large values of N (relative to n), the hypergeometric distribution asymptotically approaches the binomial distribution.

In Microsoft Excel, the function "=HYPGEOMDIST(sample_s, number_sample, population_s, number_pop)" is commonly used to plot and solve the hypergeometric distribution. The function HYPGEOMDIST solves for the function f(x) described earlier in this section, where x is the random variable, sample_s is the number of successes in the sample, number_sample is the size of the sample, population_s is the number of successes in the population and number_pop is the population size.

Example Continuing the fire fighter promotion example, suppose five promotions are carried out all at once (Table 73.8). The hypergeometric distribution then gives the probability distribution for the number of minorities promoted; note how its probabilities differ from those generated by the binomial distribution.

Table 73.8 Example of hypergeometric distribution

Number of minority fire fighters promoted	Probability
0	0.436
1	0.403
2	0.138
3	0.022
4	0.001
5	0.000

For example,

$$0.436 = \frac{\binom{15}{0}\binom{85}{5}}{\binom{100}{5}} = \frac{[15!/(15!0!)][85!/(80!5!)]}{[100!/(95!5!)]} = \frac{(85)(84)(83)(82)(81)}{(100)(99)(98)(97)(96)}$$

Multinomial Distribution

The multinomial distribution is a generalization of the binomial distribution that addresses the case where there are more than two possible outcomes. Given k possible outcomes, such that the probability of the ith outcome is always p_i and the p_i collectively sum to unity, then for a series of n independent trials

$$f(x_1, \ldots, x_k) = \frac{n!}{x_1!x_2!\ldots x_k!} p_1^{x_1} p_2^{x_2} \cdots p_k^{x_k}$$

for all cases of $x_1 = 0, 1, 2, \ldots, n$, for $i = 1, 2, \ldots, k$, subject to

$$\sum_{i=1}^{k} x_i = n$$

$$\mu_i = n p_i$$

$$\sigma_i^2 = n p_i (1 - p_i)$$

Example Continuing the fire department example, suppose that the department's 100 fire fighters include 15 black fire fighters and 5 female fire fighters, none of whom is black. Suppose two

Table 73.9 Example of multinomial distribution

Number of fire fighters promoted			
Minority males	Female	White males	Probability
0	0	2	0.640
0	1	1	0.080
0	2	0	0.002
1	0	1	0.240
1	1	0	0.015
2	0	0	0.023

promotions are made, and the slot vacated for the first promotion is filled by a fire fighter of the same race and sex before the second promotion is made. Then the multinomial distribution (Table 73.9) describes the possible outcomes of interest.

For example, this is the probability that the promotions will go to one white male and one white female:

$$0.080 = \frac{2!}{0!1!1!}(0.15)^0(0.50)^1(0.80)^1$$
$$= 2 \times 0.05 \times 0.80$$

Beta Distribution

In Bayesian statistical inference, if the phenomenon of interest is governed by a Bernoulli distribution, then one needs a probability distribution for the parameter, p, of that Bernoulli distribution, and a Beta distribution is typically used.

$$f(p) = \frac{\Gamma(a+b)}{[\Gamma(a)][\Gamma(b)]} p^{a-1} 1 - p^{(b-1)}$$

where

$$\Gamma(u) = \int_0^\infty y^{u-1} e^{-y} dy$$

The mean is $a/(a + b)$ and the variance is given by

$$\Gamma_2 = \frac{ab}{(a+b)^2(a+b+1)}$$

If $a = b = 1$, this becomes a *uniform distribution*. Larger values of b correspond to smaller variances, hence tighter confidence bands around the mean estimate of the parameter.

In Microsoft Excel, the functions "=BETADIST(x, alpha, beta, a, b)", and "=BETAINV(p, alpha, beta, a, b) are commonly used to plot and solve the beta distribution. The function BETADIST solves for the function f(x) described earlier in this section, where x is the random variable, and alpha and beta are the parameters of the gamma distribution (represented with the variables a and b in the function above). Notice that the next two parameters in the Excel function, a and b, are not included in the equation above. These parameters are the minimum and maximum range value for the random variable. Consequently, the equation above has a range between zero and one. In practice these two parameters shift and expands the distribution between the values a and b.

Frequency Histograms

It is practical and convenient to discuss frequency histograms before describing applications of probability theory. A frequency histogram is a bar chart depicting the number of occurrence of events in different intervals. A *histogram* is a technique of exploratory data analysis for displaying the frequency of occurrence of a finite set of data. The data values are arrayed along the x-axis of a graph, and the y-axis is used to plot the frequency, usually as number of occurrences or percentage of total occurrences.

As suggested in this section, frequency histogram are a useful tool for providing a general idea of how the probability distribution may look like, and serve as the first step for determining which distribution represents the random variable. Consider as an example the duration of fire events of a specific type recorded in sample of similar industrial facilities listed in Table 73.10. There are a total of 49 events.

Treating the duration of the fire as a random variable, we are interested in identifying an appropriate probability distribution for the fire

duration. As a first step, let's develop a frequency histogram. Microsoft Excel provides a relatively easy way of building frequency histograms by using the = FREQUENCY(data array, bins array) array function. The data array input is an array of data from which the histogram will be developed. The bins array is an array of intervals in which the data will be classified. Notice that FREQUENCY is an array function. An array function in excel provides an output in more than one cell. Therefore, the range of cells in which the output is desired needs to be highlighted before the function is typed/assigned to the top-left cell in the output array. The analyst will then need to press CTRL-SHIFT-ENTER for the function to calculate the output values. In the case of the FREQUENCY array function, the array output is always a one column table with the same number or rows as the bin array.

Table 73.10 Recorded fire durations

ID	Duration (min)	ID	Duration (min)	ID	Duration (min)
1	120	18	0	35	2
2	25	19	1	36	10
3	25	20	0	37	76
4	20	21	7	38	2
5	25	22	15	39	10
6	10	23	2	40	2
7	5	24	6	41	2
8	10	25	59	42	10
9	39	26	2	43	10
10	5	27	5	44	2
11	11	28	7	45	10
12	15	29	24	46	2
13	10	30	5	47	2
14	10	31	5	48	10
15	1	32	3	49	17
16	10	33	7		
17	50	34	2		

In this particular example, the data array is the duration of the events. The bin array is a user defined column of time intervals. Figure 73.10 illustrates two sample histograms for the fire duration data listed above. The left most histogram groups the data in 10 min bins. Consequently, the FREQUENCY function calculates 35 fire events with durations between zero and 10 min. The right most histogram classifies the data in 10 min intervals. Consequently, there are 14 events with durations between zero and 2 min.

It was mentioned earlier that frequency histograms are a good first step in determining an appropriate probability distribution. By inspecting the histograms depicted in Fig. 73.10, the following preliminary observations can be made:

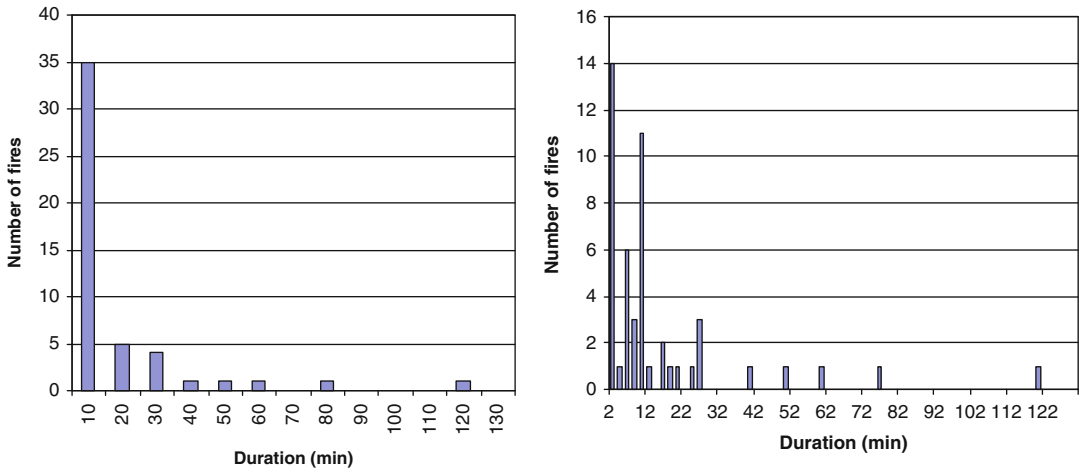

Fig. 73.10 Frequency histograms for the recorded fire durations

1. The probability distribution for fire events duration in the collected sample is not symmetric. It appears to be skewed to the left as most of the events lasted less than 30 min.
2. The fire durations are within the same order of magnitude. That is, the events lasted with 10–100 min. There are no events lasting high hundreds, or thousands of minutes.
3. There are no negative values in the fire durations.

These observations help us narrow the parametric probability distributions that may govern the data.

1. Two arguments may dismiss the use of the normal distribution. First, it does not appear this would be a symmetric distribution. Second, since most of the events are near the origin, the normal distribution is likely to have tails expanding to negative values, which are not "physical".
2. Since the fire duration data is within the same order of magnitude, the use of the lognormal distribution is not appropriate.
3. The histogram suggests the shape of an exponential distribution.

Random Number Generation

It is often necessary in applications of probability theory to generate random numbers from specific probability distributions. Uncertainty propagation is an example of these applications. Algorithms for generating random numbers from different probability distributions are described in numerous simulation and probability text books. Furthermore, these algorithms are readily available for use in most spreadsheet and mathematical computer packages. Since a detail explanation of most of these algorithms is out of the scope of this chapter, only a conceptual description of the process of generating random numbers based on the inversion method. This method can be used for generating numbers by analytically solving the probability distribution for its random variable or using the predefined inverted functions in Excel. Readers are encourage and expected to become familiar with random number generator functions a computer package of their choice since they are necessary for solving some of the exercises in this and future modules.

Inversion Method

Let's say we are interested in generating a random vector of size n for the uncertain variable t. In this example, t has units of time and follows an exponential distribution $f(t) = \lambda\exp(-\lambda t)$ where λ is known.

First, the cumulative distribution function for the exponential distribution is determined.

This example is relatively simple because the cumulative distribution function for the exponential distribution can be solved analytically and solved for the variable t. That is, the cumulative distribution function for the exponential distribution is

$$\int \lambda e^{-\lambda t} dt = e^{-\lambda t}$$

Then a random number from the uniform distribution U(0,1) is generated and set equal to the cumulative distribution, which represents an area under the curve of f(t) to the left of the value t.

$$u = e^{-\lambda t}$$

The random number is finally obtained solving for t as follows:

$$t = -\frac{\ln(u)}{\lambda}$$

This process is repeated for as many random numbers are necessary. Let's assume $\lambda = 0.2$ and 10 random numbers are necessary. Table 73.11 lists the uniform random numbers and the corresponding values for the variable t.

This process is conceptually represented in Fig. 73.11.

In most cases however the distributions do not have closed form integrals that can be inverted, requiring additional numerical methods and/or techniques for generating the random vectors. Another alternative is to use the inverted

probability distribution functions in Microsoft Excel. Some of these functions are listed in Table 73.12.

Basic Concepts of Statistical Analysis

Having discussed the basic principles of probability theory, this chapter now focuses on statistical analysis. Statistical analysis is basic to all aspects of fire protection engineering that involve abstracting results from experiments or real experience. Statistical analysis is the applied side of the mathematics of probability theory. Let's start first with some basic definitions.

Table 73.11 Random numbers for the exponential distribution

	λ	0.2
Iteration	U(0,1)	t
1	0.9	0.6
2	0.2	7.3
3	0.2	8.8
4	0.2	8.8
5	0.8	1.4
6	0.7	1.9
7	0.1	10.9
8	0.7	1.5
9	0.5	3.1
10	0.4	4.2

Perhaps the best way to visualize the "t" column in Table 73.1 is using a histogram. This can be done in Excel using the = Frequency() function. Notice that this is an "array" function, i.e., the output of the function is not a single cell

Statistic

A statistic is (a) any item of numerical data, or (b) a quantity (e.g., mean) computed as a function on a body of numerical data, or the function itself.

Statistical Analysis

Statistical analysis is the use of mathematical methods to condense sizable bodies of numerical data into a small number of summary statistics from which useful conclusions may be drawn.

Statistical Inference

Statistical inference is statistical analysis that consists of using methods based on the mathematics of probability theory to reason from properties of a body of numerical data, regarded as a sample from a larger population, to properties of that larger population.

In *classical statistical inference,* a single best estimate of each statistic of interest is developed from available data, the uncertainty of that statistic is estimated, and hypotheses are tested and conclusions drawn from those bases. Notice that

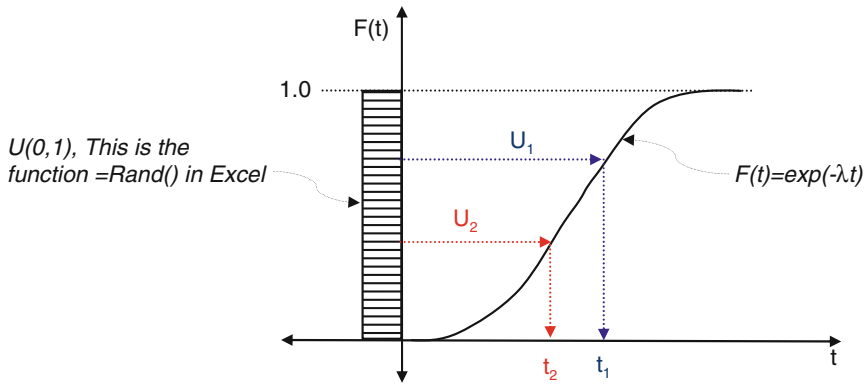

Fig. 73.11 Conceptual representation of the process of generating random numbers

Table 73.12 Microsoft excel functions

Distribution	Parameters	Random number generator	In microsoft excel
Uniform	A, B	Mathematical, statistical and spreadsheet software packages include pre-programmed functions for generating random numbers form a u(0,1) distribution	=Rand() for u(0,1) random numbers =A + Rand()*(B-A) for u(A,B) random numbers
Normal	μ, σ	Box Muller method for generating a pair of random variables from the standard normal distribution: 1. Generate 2 random numbers form the u (0,1), u_1, and u_2 2. Set $x = 2u_1 - 1$ and $y = 2u_2 - 1$ 3. If $q = \sqrt{x^2 + y^2} < 1$, set $z = \frac{x}{q}\sqrt{-4\ \ln(q)}$ and $w = \frac{y}{q}\sqrt{-4\ \ln(q)}$ Where z and w are standard normal random variables 4. Reject x and y and start over if the condition is not met	=Norminv(p,μ,σ) Where p is the cumulative probability, μ is the mean and σ is the standard deviation of the normal distribution
Lognormal*	μ, σ	The random number $z = \exp(\mu + \sigma \cdot r)$ follows a lognormal distribution where r is a standard normal random variate and μ and σ are the parameters of the lognormal distribution	=Loginv(p,μ,σ) Where p is the cumulative probability, μ is the mean of ln(x) and σ is the standard deviation of ln(x)
Exponential	λ	The random variable $z = -\frac{\ln(u)}{\lambda}$ follows an exponential distribution where u is a random number from the u(0,1) and λ is the parameter of the exponential distribution	N/A, but can be easily programmed in the spreadsheet
Chi-Square	ν	The random variable $z = \sum_{i=1}^{\nu} n(0,1)_i^2$ follows a Chi-Square distribution where n(0,1) is a random number from the standard normal distribution and ν is the parameter of the Chi-Square distribution Perhaps a prefered alternative is to use the Wilson-Hilferty transformation: $z = \nu\left[n\sqrt{2/9\nu} + 2/9\nu + 1\right]^3$ Where n is a random n(0,1,) variable and ν is the parameter of the Chi-Square distribution	=Chiinv(p,ν) Where p is the cumulative probability and ν is the parameter of the Chi-Square distribution
Gamma	α, β	The random variable $z = \sum_{i=1}^{\alpha} -\beta\ \ln(u)$ follows a gamma distribution where u is a random number from the u(0,1) and α and β are the parameters of the gamma distribution. The parameter alpha must be an integer	=Gammainv(p,α,β) Where p is the cumulative probability and α and β are the parameters of the gamma distribution
Beta	A, B, α, β	See rejection algorithm in this section	=Betainv(p,α,β,A,B) Where p is the cumulative probability and α, β, A, and B are the parameters of the Beta distribution
Weibull	α, β	The random variable $x = \alpha[-\ln(u)]^{1/\beta}$ follows a weibull distribution where u is a random number from the u(0,1), and α and β are the parameters of the Weibull distribution	N/A, but can be easily programmed in the spreadsheet

this is consistent with the classical or frequentist definition of probability provided earlier in this chapter.

In *Bayesian statistical inference,* a probability distribution for each statistic of interest is developed, using a form that permits new information, when it is acquired, to be used to adjust that distribution. Bayes's law, which was described in earlier in this chapter is used to adjust the distribution in light of the new information. Notice that this is consistent with the Bayesian or subjective definition of probability.

Conceptual Example: Suppose an engineer needs to develop a probability distribution for fuel load likely to be encountered in a new high-rise office building, to support estimation of fire growth and intensity in a full-floor burnout scenario. Fuel load would be measured in energy per unit area, such as BTUs per square meter. Suppose a field survey has been conducted that provides fuel load energy and areas for 400 rooms or areas in existing similar office properties.

Obviously, the most difficult task in this analysis would be to conduct such a field survey and convert its results to the indicated form. This will probably involve (1) estimating the mass of each item of contents and furnishings in each office or area assessed, (2) converting those estimates to estimates of total mass by category of material for each office or area assessed, (3) using existing or new test results to convert estimates' mass by material into estimates of energy content by material, and (4) summing the energy estimates into combined estimates for the room. With so many estimates required, it is likely that the data for each room will be in the form of a minimum, a maximum, and a best estimate and not just a point estimate.

Development of the probability distribution will then need to reflect the variation in fuel load from room to room, as reflected in part by the variation in best estimates across rooms, and the uncertainty in room fuel load estimates, as reflected by the minimums and maximums. A good situation would be data supporting the proposition that the variation in fuel load across rooms and the error in fuel load estimates for individual rooms both fit normal distributions. Other distributions (such as a lognormal distribution for the variation and a normal distribution for error) would still be mathematically tractable, though any such calculations go well beyond the guidance provided in this chapter.

Exploratory Data Analysis

Exploratory data analysis is the development of *descriptive statistics,* that is, statistical analysis that does not make inferences to a population.

Key Parameters of Descriptive Statistics

The *mean, median, variance,* and *standard deviation,* as described earlier in this section, can all be applied here, using the relative frequency of occurrence of each value in the body of data to define a discrete probability distribution.

The *mode* is the value that occurs most frequently, that is, the value of x for which $f(x) > f(y)$ for all $y \neq x$.

A body of data is called *unimodal* if $f(z) < f(y)$ in all cases where $|z - x| > |y - x|$, that is, if the probability distribution function steadily decreases as one moves away from the mode.

A body of data is called *multimodal* if it is not unimodal. In such cases there will be two or more values of x for which $f(x) > f(y)$ for all $y \neq x$ and $|y - x| < \varepsilon$, where ε is some small value. Although there may be only one mode in the sense of a most frequently occurring value, the existence of local maximums in the probability distribution function is sufficient to make the distribution multimodal. Multimodal data usually occur when data are combined from two or more populations, each having an underlying unimodal distribution. For example, if data were collected on the lengths of fire department vehicles, it probably would be multimodal, having one peak each for automobiles, ambulances/vans, engines, and ladders.

A *geometric mean* is another type of average:

$$\text{G.M.} = (x1x2x3 \ldots xn)^{1/n}$$

The geometric mean is useful in averaging index numbers reflecting rates of change. For example, suppose a, b, and c are annual rates of increase in the fire department budget for three successive years. Then $A = 1 + a$, $B = 1 + b$, and $C = 1 + c$ would be index numbers reflecting those three rates. The index number, D, reflecting the cumulative increase over all 3 years, would be given by $D = ABC$, and so an index number yielding an "average" rate of inflation for the 3-year period would be given by $(ABC)^{1/3}$, or the geometric mean of the index numbers. This geometric mean is the index number that could be compounded over the 3 years to obtain the actual cumulative increase. Note that the geometric mean is equivalent to computing the arithmetic mean of the logarithms of the data values, then exponentiating the result, that is, using the result as an exponential power to be applied to the base used in computing the logarithms. In Microsoft Excel, the function "=GEOMEAN(range)" calculates the geometric mean, where in the parameter "range" is the cells containing the relevant data.

Example In a fire risk analysis, the frequency of fires (i.e., the ignition frequency) is often considered a random variable that is characterized with a probability distribution. In a specific application, relevant fire events data is collected for determining the ignition frequency of specific equipment in a facility. The results of the collection process suggest that there is no data for some of the potential sources of ignition identified in the facility. For those sources of ignition, the analysis team decides to characterize their frequency with a lognormal distribution. The analysis team considers that the 5th and 95th percentile of the distribution are 1 event every 25 years and 1 every 5 years respectively. The mean for this lognormal distribution is then calculated using the geometric mean as follows: "=GEOMEAN(1/25, 1/5) = 0.089" events per year.

The *harmonic mean* is a less commonly used average that consists of the reciprocal of the arithmetic mean of the reciprocals of the data values. For example, suppose $V1, \ldots, Vn$ are a set of n values of the speed achieved by an engine company on a set of test runs from the firehouse to a single location. Then these speeds can also be represented as $d/t1, d/t2, \ldots, d/tn$, where d is the constant distance and $t1, \ldots, tn$ are the times of the n runs. The average speed would be given by $nd/(t1 + t2 + \cdots + tn)$, or total distance divided by total time. That value will also be given by the harmonic mean of the speed values. This example also helps illustrate why the harmonic mean is rarely used. It is likely that anyone who had access to the speed values would also have access to time values, $t1, \ldots, tn$, and could compute the average more quickly by using them directly.

The *range* is the difference between the highest and lowest values, or the term may be used to refer to those two values and the interval between them. In Microsoft Excel, the "=MIN (range)" and "=MAX(range)" functions can be used for determining the minimum and maximum value of a sample respectively.

Quartiles, deciles, and *percentiles* are useful measures of the dispersion of the data. If the data are arranged in ascending or descending order, the three quartiles, $Q1$, $Q2$, and $Q3$, are the values that mark off 25 %, 50 %, and 75 %, respectively, of the data set. In other words,

$Q1$ is chosen so that $F(Q1) = 0.25$

$Q2$ is chosen so that $F(Q2) = 0.50$; $Q2$ is also the median

$Q3$ is chosen so that $F(Q3) = 0.75$

In Microsoft Excel, the functions "=PERCENTILE(array, k)" and "=QUARTILE (array, quart)" can be used for determining the percentile o quartile of a range of data respectively. The parameter k is the percentile value expressed in a number from 0 to 1. The parameter quart refers to the first, second, third or fourth quartile.

Deciles and percentiles are defined analogously so as to divide the data set into tenths or hundredths, respectively, rather than fourths. Like the second quartile, the fifth decile equals the median. The *interquartile range,* or $Q3 - Q1$, is an alternative to the full range that is less sensitive to extreme values.

A *scatter plot* or *scatter diagram* is a technique of exploratory data analysis for displaying the patterns of a finite set of bivariate data. Each pair of data values is plotted on an (x,y) graph. This technique works best if both dimensions of the data are continuous so that the same pair of values does not occur more than once.

The *coefficient of variation* is given by the standard deviation divided by the mean. When the result is multiplied by 100, it gives the scatter about the mean in percentage terms relative to the mean.

Correlation, Regression, and Analysis of Variance

Correlation analysis and (linear) regression analysis are the two most basic and most common forms of analysis of variance, a collection of statistical analysis techniques that also includes experimental design and discriminant analysis.

Correlation

In qualitative terms, correlation refers to the degree of association between two or more random variables. Random variables with discrete and continuous probability distributions were defined earlier in this chapter.

The most common quantitative measure of correlation specifically addresses the extent to which two random variables are linearly related.

Correlation Coefficient (Also Called the Pearson Product-Moment Correlation Coefficient)

Let two discrete random variables, X and Y, have a joint probability distribution given by f (xi, yj) = probability ($X = x$i and $Y = y$j).

Then the correlation coefficient of X and Y is given by

$$\rho_{XY} = \frac{\left[\sum_{i=1}^{\infty}\sum_{j=1}^{\infty}(x_i-\mu_X)(y_i-\mu_Y)f\left(x_i,y_j\right)\right]}{\sqrt{\sum_{i=1}^{\infty}\sum_{j=1}^{\infty}\left[(x_i-\mu_X)^2 f\left(x_i,y_j\right)\right]}\sqrt{\sum_{i=1}^{\infty}\sum_{j=1}^{\infty}\left[y_i-\mu_Y)^2 f(x_i,y_i)\right]}}$$

where

$$\mu_X = \sum_{i=1}^{\infty}\sum_{j=1}^{\infty} x_i f\left(x_i,y_j\right)$$

and

$$\mu_Y = \sum_{i=1}^{\infty}\sum_{j=1}^{\infty} y_i f\left(x_i,y_j\right)$$

Let two continuous random variables, X and Y, have a joint probability density function given by $f(x,y)$ such that

$$\int_{-\infty}^{y}\int_{-\infty}^{x} f(u,v)du\,dv = \text{probability}(X \le x \text{ and } Y \le y)$$

Then the correlation coefficient of X and Y is given by

$$\rho_{XY} = \frac{\left[\int_{-\infty}^{\infty}\int_{-\infty}^{\infty}(x-\mu_X)(y-\mu_Y)f(x,y)dxdy\right]}{\sqrt{\int_{-\infty}^{\infty}\int_{-\infty}^{\infty}(x-\mu_X)^2 f(x,y)dxdy}\sqrt{\int_{-\infty}^{\infty}\int_{-\infty}^{\infty}(y-\mu_Y)^2 f(x,y)dxdy}}$$

where

$$\mu_X \int_{-\infty}^{\infty} \int_{-\infty}^{\infty} xf(x,y)dxdy$$

and

$$\mu_X \int_{-\infty}^{\infty} \int_{-\infty}^{\infty} yf(x,y)dxdy$$

If $y = ax + b$, then $\rho = 1$ if $a > 0$ and $\rho = -1$ if $a < 0$.

It is possible for one variable to be a function of another, yet have zero correlation with it (e.g., $y = x$ for $x \geq 0$ and $y = -x$ for $x < 0$).

If two random variables are independent, they will have zero correlation. However, zero correlation can occur without independence.

Even if two variables are highly correlated, it is not necessary for either to be the cause of the other. Many so-called spurious correlations occur. An example is a case of two variables (e.g., sales of fire extinguishers, sales of chewing gum) that are both strongly influenced by a third variable (e.g., disposable income) and so will be highly correlated with each other because each is correlated with the third variable.

In the case of a multimodal joint probability distribution, the correlation may be quite different at a macro- and a microlevel. Consider the variables of fire rate per household and average income per household with regard to census tracts in a city. A small number of tracts typically will have high fire rates and low incomes; the rest will have low fire rates and high incomes. The two variables will be highly correlated if all census tracts are considered together, but if the two relatively homogeneous areas are analyzed separately, there may be little correlation.

If a sample of size n consists of pairs of values (xi, yi), then the sample correlation coefficient is

$$r_{XY} = \frac{\sum_{i=1}^{\infty} (x_i - \overline{x})(y_i - \overline{y})}{\sqrt{\sum_{i=1}^{n} (x_i - \overline{x})^2} \sqrt{\sum_{i=1}^{n} (y_i - \overline{y})^2}}$$

Example Suppose the scores of ten fire fighters on a promotional exam are compared to their numbers of years with the fire service, with results shown in Table 73.13 and in Fig. 73.12.

Table 73.13 Distribution of test scores

Age	Score
18	54
20	85
20	62
20	60
22	66
25	70
25	75
28	88
29	70
30	90

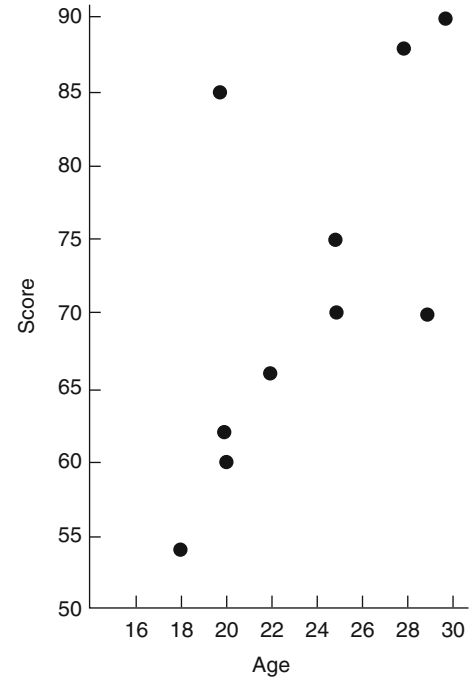

Fig. 73.12 Distribution of test scores

Using Microsoft Excel, then the mean age is "=AVERAGE(Age range)" = 23.7 and the mean score is "=SCORE(Score range)" =72, where the parameters age range and score range are the corresponding data sets listed in Table 73.1. The correlation coefficient can be also calculated using Microsoft Excel as follows: "=CORREL(Age range, Score range)" =0.67, indicating moderate correlation. If the second individual's score, which is the farthest from the group pattern, were changed from 85 to

60, the correlation coefficient would rise to 0.89, indicating high correlation.

The *coefficient of determination* (also called the *percentage of variation explained*) is given by the square of the correlation coefficient.

Regression

Regression analysis consists of fitting a relationship, usually but not limited to a linear relationship ($Y = aX + b$), to two random variables, X and Y. The term *regression* is left over from one of the findings in one of the earliest applications of the theory, where it was discovered that heights of parents are good predictors of heights of children but that heights of children tend to "regress" toward the mean. (In other words, for this problem, the best fit was $Y = a(X - \mu_x) + \mu_y$, where $a < 1$.)

Method of Least Squares

The method of least squares assumes that the best fit is obtained by minimizing the weighted sum of the squared differences between predicted and observed values of Y. In other words:

For two discrete random variables, X and Y, with joint probability distribution $f(xi, yj)$, choose a and b to minimize

$$\sum_{i=1}^{\infty}\sum_{j=1}^{\infty}(y_i - ax_i - b)^2 f\left(x_i, y_j\right)$$

For two continuous random variables, X and Y, with joint density function $f(x, y)$, choose a and b to minimize

$$\int_{-\infty}^{\infty}\int_{-\infty}^{\infty}(y - ax - b)^2 f(x, y)dx\ dy$$

For a sample of size n of pairs of values (xi, yi), choose a and b to minimize

$$\sum_{i=1}^{n}(y_i - ax_i - b)^2$$

The method of least squares is the best method if the deviations between observed and expected values of Y are themselves normally distributed, independent random variables. This condition would be satisfied, for example, in most experiments if the only source of deviation were error in reading a measuring device. The deviations are also called *residuals*.

Analysis of patterns in residuals can be done to confirm the normality assumptions cited above. Also, data points may be selected with extremely large residuals and studied for common characteristics as a means of trying to identify other factors that may be correlated to the outcomes, y. These results, in turn, may lead to a more sophisticated, multivariate regression analysis.

Regression Coefficients

The least-squares fit of a relationship of the form $Y = aX + B$ will be given by

$$a = \frac{\rho_{xy}\sigma_y}{\sigma_x}$$
$$b = \mu_y - a\mu_x$$

For a sample of size n of pairs (xi, yi), the formulas are

$$a = \frac{\left(n\sum_{i=1}^{n}x_i y_i\right) - \left[\left(\sum_{i=1}^{n}x_i\right)\left(\sum_{i=1}^{n}y_i\right)\right]}{\left(n\sum_{i=1}^{n}x_i^2\right) - \left[\left(\sum_{i=1}^{n}x_i\right)^2\right]}$$

$$b = \frac{\left[\left(\sum_{i=1}^{n}x_i^2\right)\left(\sum_{i=1}^{n}y_i\right)\right] - \left[\left(\sum_{i=1}^{n}x_i\right)\left(\sum_{i=1}^{n}x_i y_i\right)\right]}{\left(n\sum_{i=1}^{n}x_i^2\right) - \left[\left(\sum_{i=1}^{n}x_i\right)^2\right]}$$

Example Reexamine the case of age versus test score examined earlier under the discussion of correlation. In that case, as noted, the correlation coefficient was 0.67, the mean age was 23.7, and the mean score was 72. The ratio of standard deviations can be calculated as 2.87. Therefore, $a = 1.92$ and $b = 26.5$. This means that the predicted score for age 20 would be 64.9, compared to the 60, 62, and 85 scored by persons of that age, whereas the predicted score for age 30 would be 84.1, compared to the 90 scored by the person of that age. The values of a and be can be calculated using the array function in Microsoft Excel "=LINEST(known_y's, known_x's, const, stats). The known_y's and known_x's parameters are the array of data for the y values (dependent variable), and the x values (independent variable) respectively. The parameters const and stats are optional and not used in this example. As an array function, LINEST must be specified selecting first two adjacent cells in excel and using CTRL-SHIFT-ENTER to solve it. Readers are encourage to review all the technical description and examples of this function in the corresponding Microsoft Excel help file.

Continuing with the example, this regression line tends to overpredict scores for younger persons because the line is tipped as it tries to accommodate the 85 score achieved by one 20-year-old. If that score had been a 60, then as noted the correlation coefficient would be 0.89; also, the mean score would be 69.5 and the ratio of standard deviations would be 2.78. Therefore, a would be 2.47 and b would be 11.0. The predicted score for age 20 would change from 64.9 to 60.4, and the predicted score for age 18 would change from 61.1 to 55.5, much closer to the score actually achieved by the 18-year-old.

Although it is theoretically (i.e. mathematically) possible to fit any relationship, not just a linear one, between X and Y, it is rarely possible to develop least-square formulas for a and b if the relationship is not linear. A simple scatter plot would suggest if the relationship with the data is linear. If it's not linear, the analyst will usually want to try to transform problems into linear regression problems. For example, if the true relationship is believed to be of the form $y = c^{(x+d)}$, one would set up a linear regression of $\log y$ versus x. Then $d \log c = b$ and $\log c = a$.

Example 5: Developing Empirical Correlations One of the most widely used empirical correlations is the McCaffrey-Quintiere-Harkleroad (MQH) correlation of temperature rise (dT) with heat release rate (Q) and height above heat source (z):

$$dT \propto Q_{2/3} z_{5/3}^{-}$$

Although this relationship was developed from energy balance fundamentals and other established theory, such a correlation could emerge as an empirical finding from experiments. In fact, the three authors for whom the correlation is named took such an approach in a 1981 paper [1]. One analysis of data from 112 experiments produced an inferred exponent of 0.624 for Q (compared to the 0.667, or 2/3, in the correlation as it is best known) and an associated r-squared value (percentage of variation explained) of 92 %. A second analysis of the same data cited in the same paper used a slightly different setup for the modeling parameters and derived a best-estimate exponent of 0.650 for Q with an r-squared value of 90 %.

The procedure for such an analysis begins with conversion of the hypothesized relationship to a general linear model:

$$\begin{aligned} \log\ dT &= \log\left[(\text{Proportionality constant}) Q^{\mathrm{A}} z^{\mathrm{B}}\right] \\ &= A\ \log\ Q + B\ \log\ z + C \end{aligned}$$

where C is the logarithm of the proportionality constant (not shown) in the MQH correlation.

The method of least squares calls for the analyst to produce values of A, B, and C that minimize the sum of squares of differences between the terms to left and right of the equal sign. By taking the partial derivatives with respect to A, B, and C of the sum of squared differences and setting those derivatives equal to zero (in order to solve for the minimum), one obtains three linear equations in three unknowns and can solve for A, B, and C:

$$U = \sum_i (\log\ dT_i - A\ \log\ Q_i - B\ \log\ z_i - C)_2$$
$$\partial/\partial A\ \ U = \sum_i (-2 \log\ Q_i)(\log\ dT_i - A\ \log\ Q_i - B\ \log\ z_i - C) = 0$$
$$\partial/\partial B\ \ U = \sum_i (-2 \log\ z_i)(\log\ dT_i - A\ \log\ Q_i - B\ \log\ z_i - C) = 0$$
$$\partial/\partial C\ \ U = \sum_i (-2)(\log\ dT_i - A\ \log\ Q_i - B\ \log\ z_i - C) = 0$$

where *i* refers to the *i*th experiment in the series of 112 experiments.

It is possible to produce not only best (maximum likelihood) estimates—which is what 0.624 and 0.650 presumably are—for the exponent for *Q* but also confidence ranges for the values, which would probably be very tight given the *r*-squared values of 92 % and 90 % and the fact that the data set contained more than 100 experiments. Of greater interest would be an analysis of the MQH correlation, with its 0.667 exponent, as given. One can conduct a goodness-of-fit chi-square analysis using the same experimental data set. The authors did not take their analysis in that direction, at least for their article.

Regression analysis assumes that an error in one observation (temperature change vs. heat and height) is independent of an error in any other observation. It is important to take steps to make sure this assumption is reasonably true of the data set. For example, the assumption will not be true of observations over time, where a phenomenon called "autocorrelation" is of concern. Any deviation or error in temperature at time *t* can be expected to influence temperatures at later times.

Hypothesis Testing in Classical Statistical Inference

Hypothesis and Test

A statistical *hypothesis* is a well-defined statement about a probability distribution or, more frequently, one of its parameters. A classical *test* of a statistical hypothesis is based on the use of several concepts to organize the uncertainty inherent in any probabilistic situation.

The hypothesis being considered is called the *null hypothesis* and implies a probability distribution. Classical statistical inference asks whether the probability of having obtained the statistics actually collected, given the null hypothesis, is so low that the null hypothesis must be rejected.

The test works on the basis of a statistic computed from a sample. That statistic is compared to a reference value. If the statistic falls to one side of the reference value, then the null hypothesis is rejected; if the statistic falls to the other side, then the null hypothesis is not rejected.

For the reasons given above, a statistical test resolves doubts in favor of the null hypothesis. Therefore, an analyst may choose to say that the null hypothesis was "not rejected" rather than say it was "accepted." The analogy is to a criminal trial, which may find a defendant "not guilty" but does not make findings of "innocent."

A *Type I error* occurs when the null hypothesis is really true, but the test says that it should be rejected. A *Type II error* occurs when the null hypothesis is really false, but the test says it should not be rejected. (Informally, many analysts use the term *Type III error* to refer to analyses that set up the initial problem incorrectly, thereby producing results that, however precise, are irrelevant to the real issue.)

A *confidence coefficient,* or measure of the *degree of confidence,* is used to indicate the maximum acceptable probability of Type I error. In most cases, the null hypothesis corresponds to a single, well-defined probability distribution. Therefore, the probability of the sample statistic falling on the reject side of the reference value can be calculated precisely, and the reference value can be selected so as to set that probability equal to the confidence coefficient.

One way of using the confidence coefficient is to set *confidence limits* or define a confidence

interval. These limits or internal boundaries are set so that if the null hypothesis is true, then the probability of obtaining a sample whose test statistic is outside the limits (or interval) is equal to the confidence coefficient. These confidence limits indicate to the user how precisely the probability distribution or its parameter can be defined, given the size of the sample and its variability.

The value of the confidence coefficient can be set at any of certain standard levels (90 %, 95 %, and 99 % are often used), or it can be derived from an analysis that seeks to balance Type I and Type II errors. The latter approach is more comprehensive, but it is much more difficult because the alternative(s) to the null hypothesis rarely correspond(s) to a single probability distribution. In a typical case, the null hypothesis states a single value for a population parameter ($\mu = a$) and the alternative corresponds to all other values ($\mu \neq a$). Each specific alternative defines a specific probability distribution with a specific probability of Type II error. The *power function of the test* is that function that gives the probability of *not* committing a Type II error for each parameter value covered by the alternative(s) to the null hypothesis.

As the parameter value approaches the value in the null hypothesis (e.g., $\mu \rightarrow a$), the power of the test drops toward the confidence coefficient.

Test of Mean: *z* Test

If a sample has been collected from a population with known standard deviation σ, the central limit theorem indicates that the sample mean has an approximately normal distribution about the true population mean μ_0.

Let

$$z = \left(\sqrt{n}\right)(\overline{x} - \mu_0)\sigma$$

where
n = Sample size
μ_0 = Hypothesized true value of μ
$\overline{x}$ = Sample mean

Let z_α be the value for which $F(z_\alpha) = 1 - \alpha$, where F is the cumulative distribution function of a normal distribution with mean zero and variance one (Note that $z_{1-\alpha} = -z_\alpha$.).

A *two-sided test* presumes that, if the true population mean is not μ_0, then it is equally likely to be greater than or less than μ_0. In that case, positive and negative values of z are treated the same and the confidence coefficient must be divided between the two sides of the confidence interval. Then if α is the confidence coefficient, the two-sided test says accept the null hypothesis if

$$-z_\alpha/2 \leq z \leq z_{\alpha/2}$$

A *one-sided test* presumes that if the true population mean is not μ_0, then it must be greater than (or less than) μ_0. If α is the confidence coefficient, then the one-sided test says accept the null hypothesis if

$$z \geq -z_\alpha \text{if the alternative to } \mu = \mu_0 \text{is } \mu < \mu_0$$

or

$$z \leq z_\alpha \text{if the alternative to } \mu = m_0 \text{is } \mu > \mu_0$$

The value

$$\frac{\sigma}{\sqrt{n}}$$

is called the *standard error of the mean*. In Microsoft Excel, the function "=ZTEST(Array, x, sigma)" can be used for calculating the one tail p value of a z test. In statistical hypothesis testing, the p-value is the probability of obtaining a test statistic at least as extreme as the one that was actually observed, assuming that the null hypothesis is true [1]. One often "rejects the null hypothesis" when the p-value is less than the significance level α, which is often 0.05 or 0.01. When the null hypothesis is rejected, the result is said to be statistically significant. The parameter Array is the sample data. The parameter x is the tested value. Finally, the parameter sigma is optional- it's the standard deviation for the population if the value is known. If left blank, the function will use the sample standard deviation.

Test of Difference Between Two Means: *z* Test

If two samples from populations with known standard deviations, σ_1 and σ_2, have been collected, a null hypothesis might be that they are from the same population, which means their means would be the same ($\mu_1 = \mu_2$). Then a two-sided test is applied, using the following statistic:

$$z = \frac{(\overline{x}_1 - \overline{x}_2)}{\sqrt{\sigma_1^2/n_1 + \sigma_2^2/n_2}}$$

where $\overline{x}$, σ_{i2}, and n_i are the sample mean, population variance, and sample size, respectively, of the *i*th sample. In Microsoft Excel, this statistical test is available in the Data Analysis tools under Data/Data Analysis. Readers are referred to the help file for information about how to install the Data Analysis as it is not usually installed by default. It should be also noted that the Data Analysis tools are not typical Excel functions like the ones that have been discussed earlier in this chapter. These functions provide solutions only "once", and these solutions are not live in the spreadsheet. That is, the solutions are not updated with inputs parameters change unless the functions are run again through the Data Analysis dialog box.

For this specific test, the Data Analysis dialog box requires the following input

- Variable 1: Range Enter the cell reference for the first range of data that you want to analyze. The range must consist of a single column or row of data.
- Variable 2: Range Enter the cell reference for the second range of data that you want to analyze. The range must consist of a single column or row of data.
- Hypothesized Mean Difference: Enter the number that you want for the shift in sample means. A value of 0 (zero) indicates that the sample means are hypothesized to be equal.
- Variable 1: Variance (known) Enter the known population variance for the Variable 1 input range.
- Variable 2: Variance (known) Enter the known population variance for the Variable 2 input range.
- Labels: Select if the first row or column of your input ranges contains labels. Clear this check box if your input ranges have no labels. Microsoft Office Excel generates the appropriate data labels for the output table.
- Alpha: Enter the confidence level for the test. This value must be in the range 0...1. The alpha level is a significance level that is related to the probability of having a type I error (rejecting a true hypothesis).
- Output Range: Enter the reference for the upper-left cell of the output table. Excel automatically determines the size of the output area and displays a message if the output table will replace existing data.
- New Worksheet Ply: Click to insert a new worksheet in the current workbook and paste the results starting at cell A1 of the new worksheet. To name the new worksheet, type a name in the box.
- New Workbook: Click to create a new workbook in which results are added to a new worksheet.

Test of Proportion: *z* Test

If a sample has been drawn from a population governed by a binominal distribution, then the normal approximation gives the following statistic, to be used in one- or two-sided tests

$$z = \frac{n(\overline{p} - p_0)}{\sqrt{p_0(1 - p_0)}}$$

where p_0 is the hypothesized true proportion and p is the sample proportion.

Test of Difference Between Two Proportions: *z* Test

Again the normal approximation to the binomial distribution gives the test statistic

$$z = \frac{(\overline{p}_1 - \overline{p}_2)}{\sqrt{[\overline{p}_1(1 - \overline{p}_1)/n_1] + [\overline{p}_2(1 - \overline{p}_2)/n_2]}}$$

Test of Mean: *t* Test

The z tests assume known variance(s), so if variances are not known, a test based on Student's t distribution must be used. Let $t_{\alpha,\mathrm{m}}$ be defined such that $F(T_{\alpha,\mathrm{m}}) = 1 - \alpha$, where F is the cumulative distribution function for a Student's t distribution with m degrees of freedom. Note that $t_{(1-\alpha),\mathrm{m}} = -t_{\alpha,\mathrm{m}}$. Then

$$t = \frac{\sqrt{n}(\bar{x} - \mu_0)}{s}$$

where
n = Sample size
μ_0 = Hypothesized population mean
s = Sample standard deviation

A two-sided test says accept the null hypothesis if

$$-t_{(\alpha/2),(n-1)} \leq t \leq t_{(\alpha/2),(n-1)}$$

Note that the number of degrees of freedom is one less than the sample size. An informal method of remembering this is that 1 degree of freedom is used to estimate the standard deviation.

A one-sided test says accept the null hypothesis if

$t \geq -t_{\alpha,(\mathrm{n}-1)}$ if the alternative to $\mu = \mu_0$ is

$\mu < \mu_0$ or

$t \leq -t_{\alpha,(\mathrm{n}-1)}$ if the alternative to $\mu = \mu_0$ is

$\mu < \mu_0$ A test of differences between two means is constructed analogously.

In Microsoft Excel, the function "=TTEST (Array1, Array2, Tails, Type)" can be used for solving the t test. The Arrays input parameters are the first and second data sets respectively. The Tails input parameter specifies the number of distribution tails to return: a value of 1 can be use for the one-tailed distribution, the value of 2 can be used for the two tailed distribution. The Type parameter refers to the type of tests. A value of one is used if the test is paired. (Paired samples t-tests typically consist of a sample of matched pairs of similar units, or one group of units that has been tested twice -a "repeated measures" t-test. A typical example of the repeated measures t-test would be where subjects are tested prior to a treatment, say for high blood pressure, and the same subjects are tested again after treatment with a blood-pressure lowering medication.) A value of three is used two samples with unequal variances. A value of three is used for two samples with unequal variances.

The Data Analysis tools (see the discussion of Data Analysis tools under the z-test provided earlier in this chapter) also have functions to solve the following t – tests: (1) paired two-sample for means, (2) two-sample assuming equal variances, and (3) two-sample assuming unequal variances.

Example This example will illustrate all the tests described thus far. Suppose there are two fire departments, each of which has given promotional tests to 100 fire fighters. Scores can range from 0 to 100, and the passing score is 70. The actual distributions of scores are shown in Table 73.14 and Figs. 73.2 and 73.13.

Suppose that nationwide the standard deviation for this test is 17.45, the mean score is 50, and the proportion who pass is 0.17. Is

Table 73.14 Distribution of test scores

	Number of fire fighters with that score in	
Score	Department A	Department B
10	0	5
20	6	5
30	5	10
40	20	20
50	29	25
60	20	20
70	9	10
80	5	3
90	3	2
100	3	0
Total	100	100
Sample mean	53.2	48.2
Sample standard deviation	17.54	17.34
Proportion of sample passing	0.20	0.15

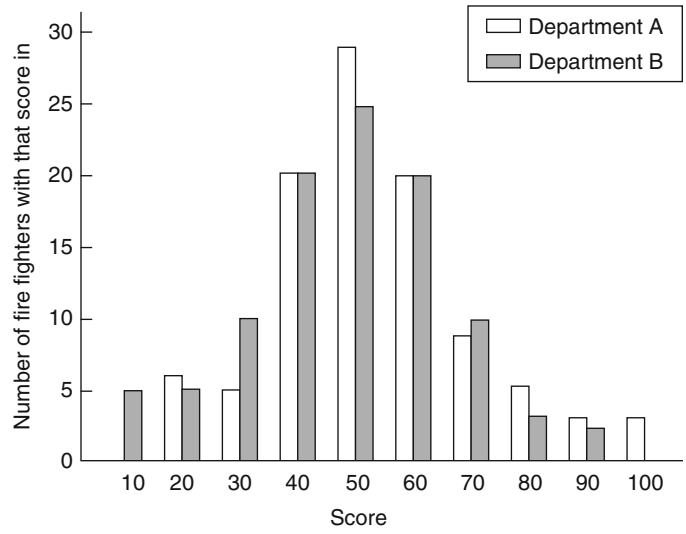

Fig. 73.13 Distribution of test scores in two fire departments

Department A an average department? This suggests a two-sided test of the mean score, using the z test because the standard deviation is known. Let α be 0.05, so $z_{\alpha/2} = 1.96$. The z statistic for the test is

$$\frac{\left(\sqrt{100}\right)(53.2 - 50)}{17.60} = 1.83$$

which is between −1.96 and +1.96 so the null hypothesis is accepted. Department A is average.

Suppose it is asked instead whether Department A is a better-than-average department. This formulation suggests a one-sided test of the mean score, again using the z test because the standard deviation is known. Again, let $\alpha = 0.05$, so $Z_{\alpha/2} = 1.64$. The z statistic for the test is again 1.83, which is greater than 1.64, so we reject the null hypothesis and conclude that Department A is above average.

The results for these two tests seem contradictory because one concludes that Department A is average and the other concludes that Department A is above average. Such discrepancies are inherent to statistical tests. They can be sensitive to the choice of α. (If α were 0.10, both null hypotheses would be rejected, whereas if α were 0.01, both null hypotheses would be accepted. In either case, the two tests would give consistent results.) They can be sensitive to how the alternatives were posed, as was true here.

Suppose it is asked whether Departments A and B have significantly different mean scores. This formulation suggests a z test of the difference between two means. In this case the standard deviations are the same and the sample sizes are the same, so the z statistic reduces to

$$\frac{53.2 - 48.2}{\sqrt{2 \times 17.45/100}} = 8.46$$

The two-sided test reference value of 1.96, calculated earlier, is easily exceeded, and we conclude that the two departments do have statistically significant differences in their mean scores.

Suppose it is asked whether Department A's proportion of students passing (0.20) is statistically significantly greater than the overall average of 0.17. This formulation calls for a z test of a proportion, and the z statistic is

$$\frac{\left(\sqrt{100}\right)(0.20) - 0.17}{\sqrt{(0.17)(0.83)}} = 0.80$$

This result is not statistically significant under either a one-sided or a two-sided test.

Are the proportions passing in Departments A and B different? This formulation suggests a z test of the difference between two proportions, and the z statistic is

$$\frac{0.20 - 0.15}{\sqrt{[(0.20)(0.80)/100] + [(0.15)(0.80)/100]}} = 0.93$$

Even though the average scores for Departments A and B were found to be different by a statistically significant margin, their percentage of test takers passing were not found to be significantly different.

Suppose the value of the overall standard deviation for the test was not known, or it was not known whether it applied to these departments, but it was known that the overall average score was 50. Is Department A's score significantly better? This formulation suggests a one-sided t test. The t statistic is

$$\frac{\sqrt{100}(53.2 - 50.0)}{17.54} = 1.82$$

For a one-sided t test with a 0.05 confidence level and 99 degrees of freedom, the reference value is the same as for a one-sided z test with a 0.05 confidence level, namely 1.64. Because the sample standard deviation is also nearly equal to the overall standard deviation used earlier, the test results are virtually the same, and the null hypothesis is rejected. This would not have been the case if the sample size had been considerably smaller, leading to a larger reference value. The smaller the difference you are examining, the larger the sample size required to be sure that difference is real and not just the result of random variation.

Test of Variance: Chi-Square Test

Assuming a normal population, one can test the hypothesis $\sigma = \sigma_0$ with the following:

$$\psi_2 = \frac{(n-1)s^2}{\sigma_0^2}$$

where n is the sample size and s_2 is the sample variance.

A two-sided test accepts the null hypothesis if

$$\psi^2_{(1-\alpha/2),(n-1)} \leq \psi^2 \leq \psi^2_{(\alpha/2),(n-1)}$$

where ${\psi_{\alpha,m}}^2$ is the value such that $F\left(\psi^2_{\alpha,m}\right) = 1 - \alpha$, where F is the cumulative distribution function of a chi-square distribution with m degrees of freedom. Note that the degrees of freedom used in the test are one less than the sample size. One-sided tests can be constructed analogously.

Test of Goodness of Fit to a Distribution: Chi-Square Test

The Chi-Square (χ^2) is the distribution of the sum of squares of a number of normal random variables. If for example a theoretical model is compared with experimental data, the difference (i.e., the error) between the model output and the data is assumed normal. This "error" is often squared to eliminate any negative sign. Therefore, the χ^2 distribution can be used to test the goodness of fit between the observed data points and the values predicted by the model, subject to the difference been normally distributed.

The Chi-Square test is often used to test distributions when a relatively large sample size is available (i.e., sample sizes $\geq$30). The test can be summarized as follows: the expected number of events per bin in a histogram is compared to the number of events resulting from the probability distribution that is been tested. If both frequencies are relatively similar throughout the range of the random variable, then the distribution may be a good fit.

A special use of the test of variance is to test how well a set of experimental data fit a presumed theoretical probability distribution. Suppose the distribution in question is represented as a set of k values or ranges of values for the random variable. Let p_{i} , . . . , p_{k} be the hypothesized probabilities for those k values or ranges; let p_{i} , . . . , p_{k} be the sample estimates of those probabilities; and let n be the sample size. Then the statistic is

$$\psi^2 = \sum_{i=1}^{k} \left\{ \frac{[u(p_i, \overline{p}_i, n)]^2}{n p_i} \right\}$$

where

$$u(p_i, \overline{p}_i, n) = \begin{cases} 0 & \text{if } -\frac{1}{2} \le n p_i - n\overline{p}_i \le \frac{1}{2} \\ n p_i - n\overline{p}_i - \frac{1}{2} & \text{if } n p_i - n\overline{p}_i > \frac{1}{2} \\ n\overline{p}_i - n p_i - \frac{1}{2} & \text{if } n\overline{p}_i - n p_i > \frac{1}{2} \end{cases}$$

This process of reducing the gap between np_i and $n\overline{p}_i$ by ½ is called the *Yates continuity correction,* and it compensates for the fact that the chi-square distribution, a continuous function, is being used to approximate a discrete probability distribution. Also, to apply this test validly, one must make sure that the k classes are grouped sufficiently that $np_i \ge 5$ for all $i = 1, \ldots, k$.

The null hypothesis says this sample came from the distribution represented by $p_1, \ldots, p_k$. That hypothesis is accepted if

$$\psi^2 \le \psi^2_{\alpha, j}$$

where j is at most $k - 1$ and may be less if the p_i are based in part on the sample.

For example, suppose an analyst wishes to test goodness of fit to a binomial distribution but has no prior estimate of which binomial distribution should be used. The analyst would select the particular binomial distribution that has p equal to the sample proportion. In that case one parameter has been estimated from the sample, and j would be reduced by one to $(k - 2)$. If the analyst were testing goodness of fit to a normal distribution and estimated both mean and variance from the sample, then j would drop by two to $(k - 3)$.

Example In the frequency histogram example described earlier in the Frequency Histogram section, each bin had a size of 10 min. There were 35 fires in the first bin, 5 fires in the second, etc. Each of this values would be compared with the events predicted by the probability distribution been tested to determine the "goodness of fit". This statistical test can best described in seven steps. The seven steps are best described using the example above as follows:

Step 1: Given a sample data of size n, determine the number of intervals

The number of intervals is equivalent to the bins in a frequency histogram. Consequently, this step consists of determining the bins in which the classified data will be compared with the value suggested by the probability distribution. For best results, it is recommended that the number of data points in each bin be equal or larger than five.

Let's consider the left most histogram in Fig. 73.10, which was developed with a bin size of 10 min. The first bin has 35 fires. The second bin has 5 fires. All other bins have less than 5 fires. Therefore, these bins can be combined for the purposes of the test. See Table 73.15:

In summary, the chi-square test will have three intervals for this example.

Table 73.15 Number of intervals for Chi-Square goodness of fit test example

Bin interval	Number of fires
0–10	35
10–20	5
20–120	9[a]

[a]This interval groups durations from 20 to 120 min to capture the remaining fire events so that the number of fires is equal or larger than 5

Step 2: Choose a distribution for testing

The second step is to determine which distribution will be tested. The distribution parameters should be also identified.

Following our histogram example above, it was preliminarily concluded that the gamma distribution was a good candidate for testing. Recall that the parameters of the gamma distribution are α and β.

Step 3: Estimate the distribution parameters

Using the data available (e.g., the data use for developing the histogram), the distribution parameters should be estimated. For some distributions, parameters can be estimated using closed form algebraic equations. In some other distributions however, numerical methods are necessary for solving a system of simultaneous equations to calculate the corresponding parameters.

We know that $E(x) = \mu = \alpha \cdot \beta$, and $V(x) = \sigma^2 = \alpha \cdot \beta^2$. Therefore, the expected value (e.g., using the average( ) function in Excel) and variance (e.g., using the Var( )) function in Excel) can be directly obtained from the available data in order to obtain α and β from solving the system of simultaneous equations. The resulting system of equations is:

$$E(x) = \mu = \alpha \cdot \beta = 14.44$$
$$V(x) = \sigma^2 = \alpha \cdot \beta^2 = 471.2$$

Solving the above system, the α and β parameters are 0.44 and 32.6 respectively. Let's super-impose the gamma distribution in the histogram to start assessing if our preliminary judgment of the gamma distribution is appropriate. This comparison is depicted in Fig. 73.14. By visual examination, the gamma distribution approximates to the frequency histogram, which suggests that it is a good candidate for quantitative testing.

Step 4: Calculate the expected frequency

This step consists of calculating the expected number of events in each bin.

The following is a description of the columns in Table 73.16.

1. The first column is the bin interval as described earlier. Notice that in this example there is a total of three bins.
2. The second column, observed frequency, lists the counted number of fire events per bin. For example, there are 35 fire events with durations between zero and 10 min.
3. The third column is the probability associated with each bin. This probability

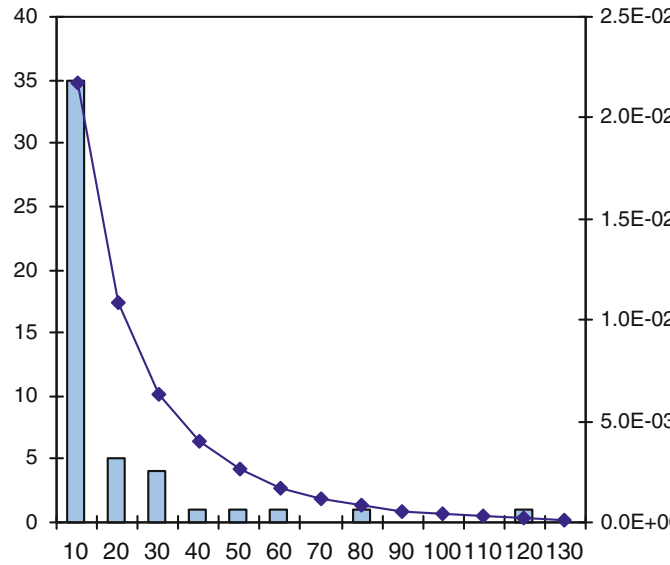

Fig. 73.14 Comparison of frequency histogram (*bars*) and gamma distribution function (*line*)

Table 73.16 Observed and expected frequency for χ^2 goodness of fit analysis

Bin interval	Observed frequency	Probability	Expected frequency
0–10	35	0.61	30.07
11–20	5	0.15	7.51
20–120	9	0.23	11.17

Table 73.17 Observed and expected frequency for χ^2 goodness of fit analysis

Bin interval	Observed frequency	Probability	Expected frequency	Calculated χ^2
0–10	35	0.61	30.07	0.81
11–20	5	0.15	7.51	0.84
20–120	9	0.23	11.17	0.42
			Total	**2.07**

is calculated using the distribution that is been tested, in this case, the gamma distribution. The probability is the area under the distribution curve within the bin interval.

4. The expected frequency column lists the expected frequency within the bin. This frequency is calculated by multiplying the probability by the total number of observations. In this example, there are a total of 49 observations. See Table 73.16. Therefore, the expected frequency for the first interval is $0.61 \times 49 = 30.07$.

Step 5: Calculate the χ^2 value

The calculated χ^2 value is obtained from:

$$\chi^2 = \sum_{i=1}^{k} \frac{(F_e - F_o)^2}{F_e}$$

where k is the number of intervals evaluated, F_e is the expected frequency for each bin, and F_o is the observed frequency for each bin. Notice that the equation consists of a sum of the square of the differences between the theoretical value and the observed values. The calculated values in our example are listed in Table 73.17 under the calculated χ^2 column. The shaded cell is the sum of the calculated χ^2 values for the individual bins.

Step 6: Identify the critical χ^2 value

The critical χ^2 value is compared with the calculated one to determine if the null hypothesis can be accepted or rejected. The determination of the critical value requires: (1) the determination of the degrees of freedom (which is the parameter of the chi-square distribution), and (2) a confidence level α. For the goodness of fit test, the degrees of freedom ν is simply k-1, where k is the number of bins used in the test. The confidence level α suggests that the random variable of the χ^2 will be within (1-α) range of the distribution.

The critical χ^2 value can be obtained from χ^2 tables in the back of probability and statistics books, or preferably, calculated using the = CHIINV( ) (i.e., inverse of the chi-square) function in Excel. In this particular example, the Excel function is = CHIINV (0.05,2), where 0.05 is the confidence level $\alpha = 5.99$ and 2 are the degrees of freedom.

Step 7: Final Decision

The null hypothesis is not rejected if the calculated χ^2 value is less than the critical one. Finalizing our example, it is then concluded that the gamma distribution is a good fit for the experimental data. Properly stated, there is no evidence to reject the gamma distribution as a good fit for the data.

Contingency Test of Independence: Chi-Square Test

A special case of the goodness of fit test is a test of the hypothesis that two random variables are independent, in which case the goodness of fit

test is displayed in a *contingency table,* as follows:

Let $X_1, \ldots, X_m$ be the m values or subranges of a random variable, X; and let $Y_1, \ldots, Y_k$ be the k values or subranges of a random variable, Y.

Let p_i be the estimated probability of X_i, for $i = 1, \ldots, m$; and let q_i be the estimated probability of y_j, for $j = 1, \ldots, k$.

Let n be the size of a sample such that, for each sample entry, a value of X and a value of Y are provided. (Be sure $np_iq_j \geq 5$ for all i and j.)

Let r_{ij} be the number of sample entries for which $X = X_i$ and $Y = Y_j$.

Therefore

$$\sum_{i=1}^{m}\sum_{j=1}^{k} r_{ij} = n$$

Then the sample will provide estimated values of p_i and q_j as follows

$$p_i = \frac{\left(\sum_{j=i}^{k} r_{ij}\right)}{n}$$

and

$$q_i = \frac{\left(\sum_{i=j}^{m} r_{ij}\right)}{n}$$

If the two random variables are independent, then the expected values for r_{ij} are given by np_iq_j.

The test statistic, therefore, is given by

$$\psi^2 = \sum_{i=1}^{m}\sum_{j=1}^{k}\left\{\frac{\left[u\left(r_{ij}, p_i, q_j, n\right)\right]^2}{np_iq_j}\right\}$$

where

$$u\left(r_{ij}, p_i, q_j, n\right) = \begin{cases} 0 & \text{if } -\frac{1}{2} \leq r_{ij} - np_iq_j \leq \frac{1}{2} \\ r_{ij} - np_iq_j - \frac{1}{2} & \text{if } r_{ij} - np_iq_j > \frac{1}{2} \\ np_iq_j - r_{ij} - \frac{1}{2} & \text{if } np_iq_j - r_{ij} > \frac{1}{2} \end{cases}$$

The null hypothesis of independence is accepted if

$$\psi^2 \leq \psi^2_{\alpha,[(m-1)(k-1)]}$$

The number of degrees of freedom comes from the formula given for goodness of fit tests. One begins with $mk - 1$ degrees of freedom. There are m values of p_i, but they sum to one, so only $m - 1$ need be estimated from the sample, and similarly $(k - 1)$ values of q_j must be estimated. Therefore the degrees of freedom for the test equal $(mk - 1) - (m - 1) - (k - 1) = (m - 1)(k - 1)$.

Nonparametric Tests

There are a large number of nonparametric tests, so called because they use no sample or population parameters and make no assumptions about the type of probability distribution that produced the sample.

Sampling Theory

A *random sample* is a sample chosen in accordance with a well-defined procedure that assures (a) each equal item (e.g., each person) has an equal chance of being selected; or (b) each value of a random variable (e.g., height) has a likelihood of being selected that is the same as its probability of occurrence in the full population. A sample that is selected with no conscious biases still may not be truly random; the burden of proof is on the procedure that claims to produce a random sample. A random sample may not be as representative as a sample that is chosen

to be representative, but a sample chosen to be representative on a few characteristics may not be random and may not be representative with respect to other important characteristics.

In addition to requiring that each item have an equal chance of being selected, a random sample must assure that every combination of items also has an equal chance of being selected. For example, a random sample of currently married couples would not be a random sample of currently married persons, because spouses would be either selected or not selected together in the former but not necessarily in the latter.

A *sampling frame* is a basis for reaching any member of a population for sampling in a way that preserves the randomness of selection. An example would be a mailing list, although if it had missing names or duplicate names it would be deficient as a sampling frame, because each equally likely name would not have an equal chance at selection. A *sample design* is a procedure for drawing a sample from a sampling frame so that the desired randomness properties are achieved.

A *simple random sample* is a sample that is drawn by a procedure assuming complete randomness from a population all of whose elements are equally likely. If they are not all equally likely, a procedure that assures complete randomness is called a *probability sample*.

A *stratified random sample* is a sample that achieves greater precision than a simple random sample by taking advantage of existing knowledge about the variance structure of subpopulations. By concentrating a disproportionate share of the sample in subpopulations that account for disproportionate shares of the total variance, a stratified random sample produces lower total variance for a given sample size. The annual National Fire Protection Association survey of fire departments that produces the annual estimates of total U.S. fire loss is a stratified random sample.

A *cluster sample* is a sample that randomly selects certain subpopulations, then samples only them. This approach often involves subpopulations that consist of geographical areas, in which case it is also called an *area sample*. The purpose of cluster sampling is to hold down the cost of sampling. It is not as statistically acceptable as a simple or stratified random sample.

A *systematic sample* begins with a listing of the population, then random selection of the first sample member, and finally selection of the remaining members at fixed intervals (e.g., every *k*th name on the list). This approach is simpler than true random sampling but not as acceptable.

A *representative sample* is one chosen to guarantee representation from each of several groups. If properly designed, it is a special case of stratified random sampling, but often the term is used for samples where the need for representation is the only part of the procedure specified. If the size of the representation is also specified, it is called a *quota sample*. The statistical properties of a sample constructed in this way cannot be determined, and nothing useful can be said about its accuracy or precision. That is also true of a *judgment sample,* in which the only rules governing sample selection are the statistician's judgments.

Characterization of Data from Experimentation or Modeling

Data Variability

Any data source is subject to variability for reasons other than those with substantive importance. Results of a test of burning behavior of a material may vary because of the ambient temperature or humidity. Such variation can be virtually eliminated through careful experimental controls. Results may vary because of naturally occurring variations in the composition of the material or human variability in the production process. Such variation can be reduced through careful controls, and it may be possible to measure the variation that cannot be eliminated. Test results may vary because of moment-to-moment variations in airflow or in the heat output of the heating apparatus or in many other physical conditions and characteristics. Such variation

can be reduced through careful controls, but residual variation may be difficult or impossible to measure. And because test results may vary as a result of standardization and care, or the lack thereof, it is also true that test results may vary with the laboratories, organizations, and people conducting the tests.

Interpretation of test results—or of modeling results based on input test data—must take account of data variability from causes other than those of interest. Such variability is often called "error" in statistical terminology, where the term *error* is used to refer to all deviations between predicted and actual results, not just to deviations involving improper human behavior. Standards for test methods typically have sections for what is called *precision* and *bias* information. Precision refers to the magnitude of error. Bias refers to the symmetry of error. Precision asks, "Are large differences possible even if there is no difference in the characteristics we intended to test for?" Bias asks, "Are we more likely to err in one direction than in another?"

Precision and bias sections are often lacking in test method documentation—or at least lacking in detail. For laboratory testing the principal source of precision and bias information is interlaboratory studies. Through reported experiments at each of several laboratories under what are intended to be identical testing conditions, one can quantify the magnitude of variation from one run to the next in a single laboratory (called *repeatability*) and of variation between laboratories (called *reproduceability*).

There are standard statistical methods for assessing such variation, but the work is expensive, which accounts for the scarcity of such data. Also, the results, when published, are attached to a test method but may show more precision than a user will obtain in another application (e.g., different material) or in a laboratory without the heightened attention to precise controls that one expects in an interlaboratory evaluation. (No laboratory wishes to be found less precise, or less capable generally, than its competitors, but in most day-to-day work, there is no expectation of such calibration of performance, and people may relax.)

One might think that inherently statistical databases—such as fire incident databases—would be easier to assess, and it is true that precision can be readily calculated based on sample size. However, bias depends on the adequacy of the sampling—is the sample truly random and so representative of its universe?—and most statistical databases are not truly random. The National Fire Incident Reporting System (NFIRS) captures nearly a million fire incidents a year, typically close to half the total fires reported to fire departments. The precision of NFIRS is outstanding, on that basis. However, national estimates of specific fire problems project and calibrate NFIRS using a smaller database, the NFPA annual fire experience survey, and so reflect that smaller database's lesser (though still excellent) precision. More importantly, NFIRS is not a true random sample (although the NFPA survey is), and so its bias cannot be calculated from any standard statistical methods. Instead, NFIRS users note the large share of total fires it represents and the absence of any obvious sources of significant bias. (For example, NFIRS is believed to be less represented in rural or large urban areas but is well represented in both.)

In the end, engineering analysis must consider and address data variability issues but typically cannot hope to fully quantify or resolve them.

Testing Models for Goodness of Fit

Earlier in this chapter, the use of the chi-square test to assess goodness of fit was described for a statistical distribution. The same method can be used to assess goodness of fit between any set of model predictions and laboratory data. In essence, this statistical test assumes that each laboratory data point is equally likely. If there are n data points, then the test is based on

$$\psi^2 = \sum_{i=1}^{n} \frac{\left(x_{i,\text{measured}} - x_{i,\text{predicted}}\right)^2}{x_{i,\text{predicted}}}$$

This method is a one-sided test using $n - 1 - k$ degrees of freedom, where k is equal to the number of model parameters estimated from the data. (The more the data are used indirectly to predict themselves, the less variation one would expect to see.)

The more common practice in assessing goodness of fit is to "eyeball" the two curves, that is, be guided by an impression of proximity. This can be highly misleading. The eye tends to measure distances between two curves as the shortest distance between the curves, whereas accuracy of prediction is based on differences in predicted versus actual y-axis values for given x-axis values. These differences can be very large between two curves with steep slopes that look close together, and steep slopes are commonplace in curves for variables that describe fire development and related environmental conditions.

On the other hand, sometimes the most relevant and appropriate measures of the correspondence between two curves lie in the correspondence between key summary measures and not in the exactness of the correspondence between the full curves. For example, the timing of the transition from smoldering to free burning is not well described by any model and is subject to enormous variability. However, this should not be allowed to obscure the agreement of model with empirical data during the free-burning stage.

One way to adjust the comparison so that it excludes the smoldering phase is through recalibration of the curve. Set the timing and fire conditions at the onset of free burning for the model equal to the timing and fire conditions from the lab data. Then, use formal statistical methods to assess how well the model predicts the data from that point on. Note, however, that the steepness of the curves makes it quite possible that calculated agreement will be poor even with this adjustment.

Another way to adjust the comparison is to compare the timing of transition points (also called *inflection points* in calculus), such as time from the onset of free burning to flashover; and appropriate maximums (e.g., peak heat release rate) and minimums (e.g., oxygen concentration). The problem with this approach is that there may not be simple statistical tests, such as the chi-square test for goodness of fit of whole curves, that will indicate how much difference in timing of transition points or in other summary measures can be expected statistically due to measurement error or other normal variability and how much difference is significant. There needs to be an extended dialogue between fire protection engineers and statisticians to determine which statistical bases for evaluating goodness of fit of models to empirical data are both executable as statistical tests and meaningful to the modelers.

Example The first example in this chapter discussed statistical inference of a best probability distribution to describe fuel load (as energy per unit area). However, that example assumed that the form of the distribution was already known, possibly from fundamentals, possibly from past empirical studies. Only the parameters needed to be estimated. Suppose that is not the case.

One way to select a best form for the distribution is to identify candidate distributions (e.g., normal, log normal, exponential, Weibull, uniform) and then conduct a chi-square goodness of fit assessment of each, using comparable setups. Use the techniques discussed to develop best sample-based estimates of the parameters for each distribution (e.g., the two parameters of normal, lognormal, and Weibull distributions; the one parameter of exponential, Poisson, or uniform distributions). Then convert each distribution into a histogram-style discrete probability distribution for a set of intervals. For example, set up 20 intervals, where the first interval begins at zero (the lowest value fuel load can take) and the last interval includes all the highest fuel load values that may occur.

Use these same intervals in evaluating each distribution. Convert the empirical data (which in the earlier example came from analysis of 400 rooms or areas) to a set of measured probability values, which will be the same for every distribution. Then convert the candidate distribution with its sample-based parameters to a set of predicted probability values for each interval. Also, take account of differences in degrees of freedom. A distribution with two inferred parameters (e.g., lognormal) will have one less degree of freedom than a distribution with one inferred parameter (e.g., exponential), which means the same chi-square statistic will be more significant in the latter case as compared to the former case.

Reference

1. B.J. McCaffrey, J.G. Quintiere, and M.F. Harkleroad, "Estimating Room Temperatures and the Likelihood of Flashover Using Fire Test Data Correlations," Fire Technology, 17, pp. 98–119(1981).
2. Y. He, M. Horasan, P. Taylor, and C. Ramsay, "Stochastic Modelling for Risk Assessment," *Proceedings of the Seventh International Fire Safety Science Symposium,* International Association for Fire Safety Science, London, pp. 336–337 (2002).
3. P.J. Pagni, "Thermal Glass Breaking," *Proceedings of the Seventh International Fire Safety Science Symposium,* International Association for Fire Safety Science, London, pp. 12–13 (2002).
4. K. Tillander and O. Keski-Rahkonnen, "The Ignition Frequency of Structural Fires in Finland, 1996–99," *Proceedings of the Seventh International Fire Safety Science Symposium,* International Association for Fire Safety Science, London, pp. 1051–1062 (2002).

John R. Hall is assistant vice president for fire analysis and research at the National Fire Protection Association. He has been involved in studies of fire experience patterns and trends, models of fire risk, and studies of fire department management experiences since 1974 at NFPA, the National Bureau of Standards, the U.S. Fire Administration, and the Urban Institute.

Francisco Joglar is a senior consultant for Hughes Associates Inc.

Reliability, Availability, and Maintainability

74

Francisco Joglar

Introduction

Many engineering fields can benefit from reliability, availability, and maintainability, concepts and techniques. Fire protection engineering is not an exception. For example, fire protection engineers may be interested in estimating the number of failures of fire pumps under their watch. Other practical applications may include increasing the reliability and/or availability of a fire protection system, optimizing inspection, testing and maintenance intervals and calculating probabilistic values for a fire risk assessment. As the use of risk-informed, performance based methods increases, fire protection researchers and engineers continue to improve and apply reliability, availability, and maintainability methods and techniques in the field.

The primary objective of a reliability analysis is the prediction of failures by monitoring equipment condition as a function of time. Consequently, the fundamentals of reliability analysis can be found primarily in probability and statistical theory and in the physical characterization of the failure mechanisms. In principle, failures can be predicted either by statistical analysis of reliability data or by physical models simulating corresponding failure mechanisms. In some applications however, it is necessary to use both approaches simultaneously given the specific characteristics and complexity of the system or components under analysis. Because the physical modeling of each possible failure mechanism (e.g., simulating corrosion inside a sprinkler system pipe) can be a field of study by itself, this chapter concentrates on the statistical methods for analyzing reliability data in which time is considered an aggregate agent of failure.

This chapter provides an overview of basic concepts and analytical methods associated with reliability, availability, and maintainability. Such concepts are necessary since reliability analysis not only applies to simple replaceable components but also to repairable items that may undergo routine inspections, testing, and maintenance and complex systems including hardware, software, and human interaction. The material includes treatment of repairable and replaceable components, system reliability analysis, and a general description of human and software reliability. The chapter includes enough theoretical background and practical examples so that fire protection engineers can perform the suggested calculations with a good understanding of the advantages and limitations of the selected analysis. The solution of some practical problems requires the use of numerical methods for solving them and the use of mathematical software packages is recommended.

F. Joglar (✉)
Jensen Hughes

M.J. Hurley (ed.), *SFPE Handbook of Fire Protection Engineering*,
DOI 10.1007/978-1-4939-2565-0_74, © Society of Fire Protection Engineers 2016

Basic Concepts

This section provides a qualitative overview of reliability, availability, and maintainability analysis with a process for conducting such analyses.

Reliability, Availability, and Maintainability

Reliability, represented by the letter R, is the probability of an item functioning after a predefined time, T. This definition introduces the concept of probability in reliability analysis. As such, the time to failure of a system or component is considered a random variable characterized by a probability distribution. The curve in Fig. 74.1 represents the probability distribution characterizing the time to failure. The reliability of the system is the area under the probability distribution to the right of time T. The unreliability of a system or component, represented by the letter F, is simply $F = 1 - R$. That is, the unreliability will be the area under the curve to the left of time T. Figure 74.1 illustrates this concept.

Maintainability refers to the analysis of downtime, that is, the times that a system or component may not be operational due to an inspection, testing, or preventive or corrective maintenance activities. Consequently, maintainability analysis includes the statistical techniques necessary to characterize inspection, testing, and preventive and corrective maintenance times. As in the case of times to failure in reliability analysis, the times to repair are assumed random in maintainability analysis.

The concept of availability is somewhat different. Availability is the probability that an item will be operational at a predefined time, T. It is important to stress the difference between reliability and availability. Recall that reliability is the probability of an item functioning *after* time, T. Availability refers to the probability of the item being operational *at* time, T. Availability analysis is important because it incorporates the concepts of uptime and downtime of systems and components, which for the most part are associated with repairable items or items that undergo inspections, testing, and maintenance activities. Fire protection systems are good examples of such items.

Individual Components

In the context of this chapter, components are those items that are analyzed as individual units with no direct consideration to interaction between different subcomponents, including software and human actions. Components can be broadly classified as repairable and nonrepairable (i.e., replaceable).

Nonrepairable components are those that are replaced after a failure (e.g., a sprinkler head). Consequently, the concepts of availability and maintainability are not relevant in the analysis of individual nonrepairable components. Once an item is determined to be (or assumed to be) nonrepairable for the purpose of a particular analysis, the problem reduces to determining failure modes, collecting reliability data, and performing reliability modeling.

The reliability modeling can be approached from two different perspectives: (1) assuming

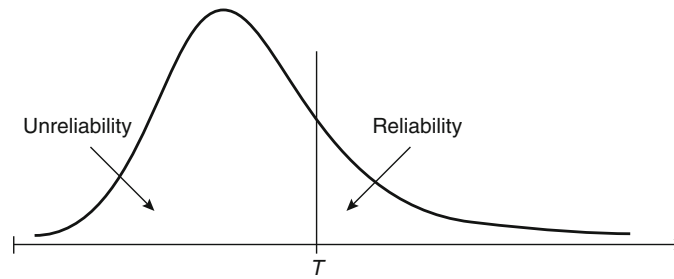

Fig. 74.1 Conceptual representation for the definition of reliability and unreliability

time is an aggregate agent of failure, which requires the collection of time to failure data; or (2) a probabilistic modeling of the physical stress and strength associated with the component. In the former, the reliability modeling usually includes the determination of an appropriate probability distribution for the time to failure and the calculation of the mean time to failure (MTTF) or other relevant probability metric. In the latter, reliability modeling requires the characterization of the physical stress affecting the component as a probability distribution. The capacity of the component to withstand the stress, referred to as the strength, is also characterized as a probability distribution.

Repairable items are those that are returned to operation after a failure. Depending on the analysis objectives, and the duration of repair times relative to operational times, the concepts of maintainability and availability may be fully applicable since repairable items can be routinely inspected, tested, and subjected to preventive or corrective maintenance activities. Consequently, the reliability, maintainability, or availability analysis becomes relatively complex, often requiring numerical methods for the solution. Typical reliability studies for repairable items involve the analysis of mean time between failures (MTBF), trend analysis, mean time to repair (MTTR), the prediction of failures in a predefined period of time, and the determination of optimum inspection and maintenance intervals.

Systems

Many professionals in the fire protection engineering field have the responsibility of maintaining in optimal condition fire protection systems such as detection systems, halon and CO_2 systems, and so on. Fire protection features can be either in standby mode or in continuous operation. Most of these systems consist of electronic, electrical, and mechanical devices working together. Although an entire system can be treated as an individual component lumping together all failure modes, it is often necessary to characterize individual subcomponents in order to analyze their effect on the overall system.

Systems are classified in this chapter as hardware systems or complex systems. Hardware systems are those consisting only of electronic, electrical, or mechanical components. Complex systems are those operating based on interactions between hardware, software, and human actions. Today, more and more systems are complex. The need for modeling the reliability/availability of such systems has generated considerable research in the area of software and human reliability. Readers should appreciate that fire, as a common cause failure mode, can impact the operation of complex systems such as the space shuttle or a commercial nuclear power plant.

In general, system analysis requires the individual treatment of subcomponents and a logic model connecting such subcomponents. Once the reliability or availability of each individual subcomponent is properly characterized, the overall system reliability or availability can be calculated.

Finally, system models are usually top-bottom models in which the events leading to the failure of interest are logically deduced from the failure itself. The most common modeling approach is the fault tree. Currently, fault trees are developed to include hardware, software, and human action, as well as considerations for common cause failures.

Conducting a Reliability, Availability, or Maintainability Analysis

The process of conducting a reliability, availability, or maintainability analysis consists of the following general steps:

1. Definition of system boundaries
2. Failure mode analysis
3. Collection of reliability data
4. Selection of appropriate modeling method or technique
5. Quantification
6. Documentation

In some cases, steps 3 and 4 may switch in order or be conducted in parallel since the required inputs to the selected model are usually generated from data. A qualitative discussion of each step follows.

Step 1: Definition of System Boundaries The first step, definition of system boundaries, refers to the identification of which subcomponents will be included and the resolution of each component or system. This may be a trivial step in the case of a simple replaceable component. At the same time, it can also require careful consideration in the case of complex systems such as the space shuttle, a nuclear reactor, and so on. In practice, the definition of system boundaries involves evaluating each component of the system and determining if it should be part of the analysis or not. There are usually good economical and technical reasons whether or not to include the component. Notice also that this evaluation may include software and human elements in the system. Some general characteristics to consider may include the following:

- Is the item repairable or nonrepairable?
- For repairable systems:
  - Is the item subjected to routine inspections?
  - Is the item subjected to preventive maintenance?
  - What is the typical duration of inspection and maintenance activities?
- Should the item be treated as an individual component or a system?
- Does the item involve only hardware component(s) or a combination of hardware, software, and human elements?
- What is the main objective of the system and which subsystems are critical to accomplishing such objectives?

Another important consideration is the level of resolution that can be supported with reliability data. For example, a fire pump may be modeled as an individual component or as a system of interconnected subcomponents. In the latter case, reliability data describing each of the subcomponents and a logic model integrating all of the subcomponents will be necessary.

Step 2: Failure Mode Analysis At this point, the concept of failure mode must be introduced. A *failure mode* is the way in which a particular system or component can fail. The term failure mode should be distinguished from the term *failure mechanism*, which refers to the fundamental chemical or physical effect responsible for a particular failure mode.

Once the system or component has been defined, it is important to understand the different failure mechanisms that will eventually suggest the different failure modes for which reliability data will be collected. Depending on the complexity of the system or component, the identification of failure modes of a system often requires input from experts involved in its design, operation, inspection, testing, and maintenance. As in step 1, the ability to collect reliability data also influences the level of resolution at which the failure modes are identified or quantified.

A tool that is regularly used for analyzing failure modes is the Failure Modes and Effects Analysis or FMEA [1]. The FMEA is a bottom-up (inductive) analysis that identifies failure modes in the system. The term *bottom-up* refers to identifying failure modes starting from the component level of a system. As such, FMEA is a very methodical tool that looks at every component in the system and then identifies the failure modes. As the failure modes are identified, the effects of such failure modes in the system are also assessed. The information resulting from a FMEA analysis is tabulated using a relatively rigorous table structure. The table includes the component or system name, failure mode, effects, and so on. Another alternative is the use of top-bottom (deductive) methods for identifying relevant failure modes (e.g., fault trees).

Step 3: Collection of Reliability Data Reliability or availability calculations using statistical methods will ultimately depend on the collection of reliability data. Reliability data are collected once the failure modes are identified. In most cases, reliability data will suggest the rate of

occurrence of the different failure modes. The data typically required for reliability studies include times to failure, inspection and test durations, duration of preventive or corrective maintenance, and so on.

Among others, Ebeling [2] (p. 284) suggests the following classification of reliability data:

1. Operational versus test-generated data
2. Complete versus censored data

Operational data are collected in the field by monitoring the operation of the system or component. In contrast, test-generated data are collected from controlled experiments designed to imitate the operational condition of an item. This step is usually necessary during the design stage before the release of new products. In some cases, accelerated testing techniques are necessary when failures of the system and components may take long times. As stated by Nelson [3], accelerated testing consists of a variety of test methods for shortening the life of products or hastening the degradation of their performance.

The concept of complete and censored data is best explained with an example. Consider a simple experiment consisting of ten lightbulbs in operation with the objective of recording the time to failure. A complete data set would include the times to failure of each of the ten lightbulbs (failure-terminated test). In a censored data set, the test would have been stopped some time before the failure of all the lightbulbs (a time-terminated test). Therefore, the censored data set will include some number of bulbs lasting longer than the duration of the test.

Finally, data collection may be a continuous effort if reliability, availability, and maintainability techniques are used for a continuous monitoring of equipment conditions. In this case Bayesian methods can be used to update previously recorded data with new information.

Step 4: Selection of Appropriate Modeling Method or Technique The selection of an appropriate modeling method or technique largely depends on the type of system and the supporting reliability data. The analysts should carefully consider the assumptions governing the different modeling tools to determine applicability to the system or component being analyzed.

A number of these methods or techniques are currently included in software packages in which the user inputs the data and selects the type of analysis. At the same time, the use of these software packages requires understanding of the fundamental assumptions governing the analysis and expertise in the interpretation of the results.

In some cases, however, preprogrammed software packages may not offer the modeling capabilities required by the system or component under analysis. In that case, analysts may need to develop their own models or combine capabilities from different software packages in order to obtain the desired solution. For example, different tools may be used for the statistical analysis of reliability data and for prediction of failures in a specified period of time.

Step 5: Quantification Quantification refers to exercising the selected modeling tool or technique in order to obtain quantitative results. As in the case of the collection of reliability data, the quantification process may be a one-time exercise or may consist of a continuous process of monitoring equipment condition.

Step 6: Documentation The final step is documentation. The documentation of a reliability, availability, or maintainability analysis should include detailed descriptions of the five steps documented earlier.

The remaining sections in this chapter describe selected quantitative techniques in support of the steps listed previously.

Reliability Analysis of Nonrepairable Items

Recall that nonrepairable items are those that are replaced upon failure. As such, this section describes analytical techniques for evaluating the reliability and predicting the time to first failure of components. The most common approach for quantifying the reliability of

nonrepairable items is treating the time to failure, t, as a random variable governed by a probability distribution $f(t)$. Consistent with the definition of reliability provided earlier, the reliability can be expressed as

$$R(t) = \int_{T}^{\infty} f(t)dt = 1 - \int_{0}^{T} f(t)dt \qquad (74.1)$$

The MTTF is, therefore, the expected value of t, which is represented as

$$\text{MTTF} = E(t) = \int_{0}^{T} t \cdot f(t)dt \qquad (74.2)$$

As shown in Papoulis [4] (p. 166), it can be proven that

$$\text{MTTF} = E(t) = \int_{0}^{\infty} R(t)dt \qquad (74.3)$$

since $R(t)$, which is the reliability of the system, tends to zero as time goes to infinity. It can be proven also that

$$R(t) = \exp\left[-\int_{0}^{t} h(x)dx\right] \qquad (74.4)$$

where $h(x)$ is the conditional failure rate or hazard rate of the system. The concept of hazard rate is described later in this chapter.

Probability Distributions

A probability distribution, or probability density function (PDF), is a mathematical function governing the probability of a random variable over its physical range. Any equation whose area under the curve is exactly 1.0 is a probability distribution. A number of distributions have been identified as practical for different engineering applications. That is also the case for reliability engineering.

Consider the failure history illustrated in Fig. 74.2. The round markers indicate the failure times of equipment measured from time 0. Given this failure history, one or more probability distributions representing the data could be identified, as represented by the different curves in Fig. 74.2. The shape and scale of the selected distribution are important factors to consider in the analysis.

This section describes the most common distributions used in reliability applications for representing the random nature of times to failure. These distributions are the exponential, Weibull, log-normal, and empirical distributions. Depending on the specific application, other distributions not covered in this chapter may be also selected.

Exponential Distribution The exponential distribution is routinely used in reliability analysis for nonrepairable items. The distribution is used as a model for determining the probability of times between successive events. In fire protection engineering applications, times between successive events can be (but are not limited to) the times between failures of a fire protection system, times between fires in a facility, or times between 9-1-1 calls to a fire department.

The exponential PDF is a one-parameter distribution, which is usually represented by the symbol λ and should be interpreted as the constant rate (units of 1/time) at which a given event

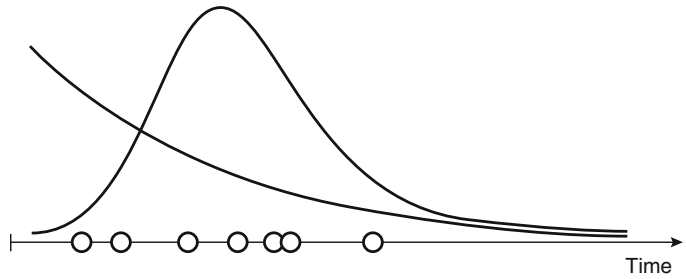

Fig. 74.2 Conceptual representation of a failure history represented by probability distributions

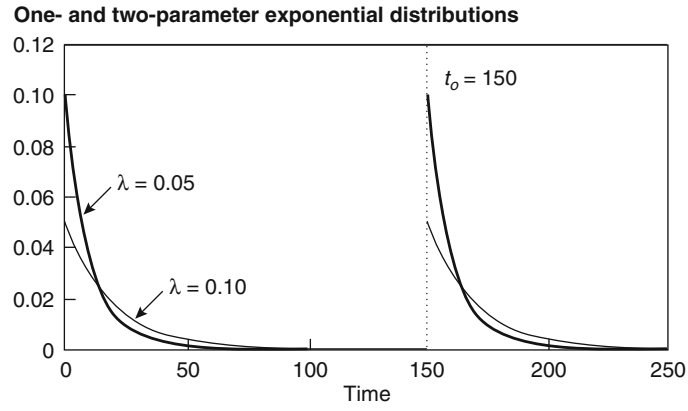

Fig. 74.3 Example representations of the exponential distribution

occurs. The mathematical form of the distribution is

$$f(t) = \begin{cases} \lambda e^{-\lambda t} & t \geq 0 \\ 0 & \text{otherwise} \end{cases} \tag{74.5}$$

where t is the random variable, usually time, and λ is the parameter characterizing the distribution. The mean and standard deviation of the exponential distribution is $1/\lambda$.

The exponential distribution can be easily integrated to obtain the following cumulative distribution function (cdf):

$$F(t) = \begin{cases} 0 & t < 0 \\ 1 - e^{-\lambda t} & \text{otherwise} \end{cases} \tag{74.6}$$

And from Equation 74.1, $R(t) = e^{-\lambda t}$. The exponential distribution always starts at $t = 0$. This origin can be shifted using the two-parameter exponential distribution

$$f(t) = \begin{cases} \lambda e^{-\lambda(t-t_0)} & t \geq t_0 \\ 0 & \text{otherwise} \end{cases} \tag{74.7}$$

where t_o represents the minimum life of the component.

Figure 74.3 illustrates examples of shapes and locations the exponential distribution can assume. Notice two identical groups of distributions. The only difference between the two groups is the use of the one- or two-parameter exponential distribution. The λ value is the same for both groups.

Weibull Distribution Another distribution that is widely used for representing the time to failure of a component is the Weibull distribution. The mathematical form of the distribution is

$$f(t) = \begin{cases} \dfrac{\beta t^{\beta-1}}{\alpha^{\beta}} e^{-\left(\frac{t}{\alpha}\right)^{\beta}} & t \geq 0 \\ 0 & \text{otherwise} \end{cases} \tag{74.8}$$

where β is the shape parameter and α is the scale parameter. The Weibull distribution reduces to the exponential distribution if $\beta = 1$ and $\lambda = 1/\alpha$. The cdf for the Weibull distribution is

$$F(t) = \begin{cases} 1 - e^{-\left(\frac{t}{\alpha}\right)^{\beta}} & t \geq 0 \\ 0 & \text{otherwise} \end{cases} \tag{74.9}$$

From Equation 74.1, $R(t) = e^{-\left(\frac{t}{\alpha}\right)^{\beta}}$. The mean and variance of the distributions are given by the following expressions:

$$E(t) = \alpha \cdot \Gamma\left[\frac{\beta+1}{\beta}\right] \tag{74.10}$$

$$V(t) = a^2\left(\Gamma[(b\ +\ 2)/\beta]\ -\ \{\Gamma[(\beta +\ 1\ )/\beta]\}^2\right) \tag{74.11}$$

where $\Gamma(\cdot)$ is the gamma function.

In every Weibull distribution, 63.2 % of all the probability under the curve will occur at $t = \alpha$. In other words $Pr(t < \alpha) = 0.632$.

For values of $\beta < 1$, the shape of the distribution is similar to an exponential distribution. For values of β between 1 and 3, the distribution is skewed to the left. Finally, with β values larger than 3 the distribution will start to approach a bell shape.

The origin of the two-parameter Weibull distribution is always 0. In cases where it is necessary to shift the origin to $t_o > 0$, the three-parameter Weibull distribution can be used. In this distribution, the parameter t_o would represent the minimum life of a component. That is, no failures are expected before t_o.

$$f(t) = \begin{cases} \dfrac{\beta(t-t_o)^{\beta-1}}{\alpha^{\beta}} e^{\left(\frac{t-t_o}{\alpha}\right)^{\beta}} & t \geq t_o \\ 0 & \text{otherwise} \end{cases} \tag{74.12}$$

Figure 74.4 illustrates examples of shapes and locations the Weibull distribution can assume. Notice two groups of distributions. The only difference between the two groups is the use of the two- or three-parameter Weibull distribution. The α and β values are the same for both groups.

Log-Normal Distribution Similar to the Weibull, the log-normal distribution is defined for positive values only. This characteristic makes it a suitable selection for probabilistic distribution of failures. The distribution is particularly appropriate for random variables constrained by zero that can assume few very large values. Equipment downtime may be a good example. The log-normal distribution results from the transformation $x = \ln(t)$ where the random variable x is normally distributed with mean μ and standard deviation σ. The mathematical form of the distribution is

$$f(t) = \begin{cases} \dfrac{1}{2\pi\sigma t} e^{\frac{-1}{2}\left(\frac{\ln(t)-\mu}{\sigma}\right)^2} & t \geq 0 \\ 0 & \text{otherwise} \end{cases} \tag{74.13}$$

where μ and σ are the mean and standard deviation of the normally distributed random variable x. Figure 74.5 provides an example of the log-normal distribution. The cumulative distribution function $F(t)$ as well as the reliability function $R(t)$ are obtained by a numerical integration of $f(t)$.

The expected value and the variance of t can be obtained with the following equations:

$$E(t) = e^{\mu+\frac{\sigma^2}{2}} \tag{74.14}$$

$$V(t) = e^{2\mu+2\sigma^2} - e^{2\mu+\sigma^2} \tag{74.15}$$

If $E(t)$ and $V(t)$ are known instead, μ and σ can be calculated using Equations 74.14 and 74.15.

Empirical Distribution Sometimes the use of an empirical distribution is necessary since the collected data may not follow any known parametric probability distribution. According to Modarres [5] (p. 286), for a complete set of data (see definition of complete data in the reliability data section) and a small sample size

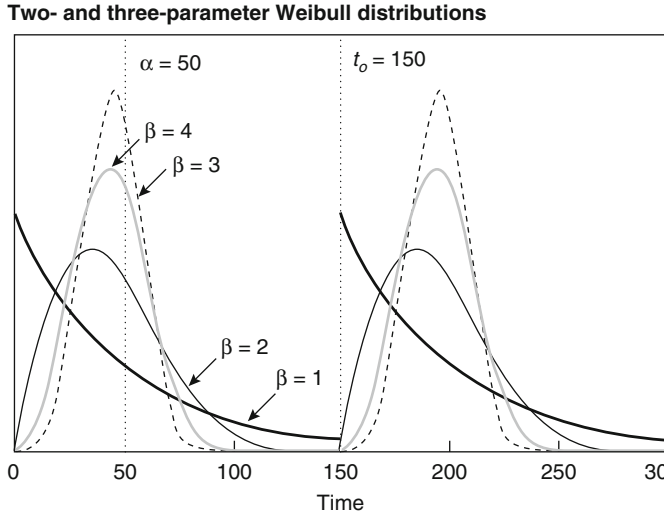

Fig. 74.4 Example representations of the Weibull distribution

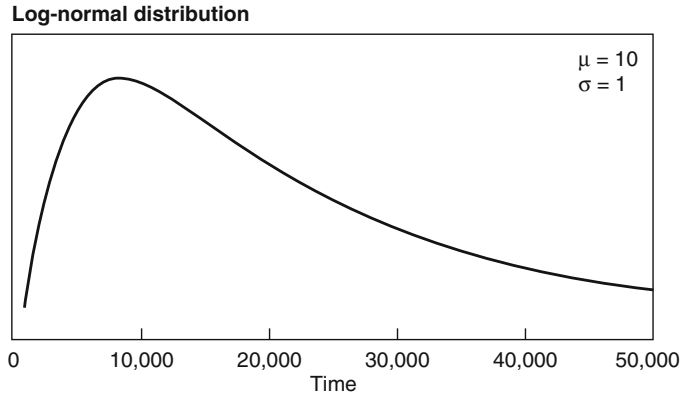

Fig. 74.5 Example of the log-normal distribution

($n < 15$), the empirical distribution function for times to failures t_i, t_{i+1},,. . ., t_n has the following mathematical form:

$$\hat{f}(t_i) = \frac{1}{(n+0.25)(t_{i+1} - t_i)}, \quad i = 1, 2, \ldots, n-1 \tag{74.16}$$

The symbol "^" indicates that the estimate is obtained from sample data. The reliability function is, therefore,

$$\hat{R}(t_i) = 1 - \hat{F}(t_i) = \frac{n + 0.625 - i}{n + 0.25}, \quad i = 1, 2, \ldots, n \tag{74.17}$$

This empirical formulation implies that the same number of failures is expected between two failure times (t_i, t_{i+1}). Finally, the sample expected value and variance of the failure data can be calculated using

$$\hat{E}(t) = \sum_{i=1}^{n} \frac{t_i}{n} \tag{74.18}$$

$$\hat{V}(t) = \frac{\sum_{i=1}^{n} t_i^2 - n\hat{E}(t_i)^2}{n-1} \tag{74.19}$$

Example 1 A review of impairment data on smoke detectors in a given facility indicates that a smoke detector device fails on average once every 5 years for various reasons. Upon failure, the detectors are replaced with a new device. Determine the probability that a smoke detector will last (1) at least 10 years, (2) at most 10 years, and (3) between 5 and 10 years.

Solution From the available data, the parameter λ is estimated as $\lambda = 1/5 = 0.2$ years^{-1}. The probabilities are calculated integrating the exponential distribution (Equation 74.5) as follows:

Probability of the detector lasting at least 10 years:

$$Pr(t \geq 10) = \int_{10}^{\infty} \lambda e^{-\lambda t} dt = 1 - \int_{0}^{10} \lambda e^{-\lambda t} dt = e^{-0.2(10)} = 0.135$$

Probability of the detector lasting at most 10 years:

$$Pr(t \leq 10) = 1 - \int_{10}^{\infty} \lambda e^{-\lambda t} dt = 1 - 0.135 = 0.865$$

Probability of the detector lasting between 5 and 10 years:

$$Pr(5 \leq t \leq 10) = \int_{5}^{10} \lambda e^{-\lambda t} dt = 0.23$$

The process for computing probabilities would be identical if a different probability distribution is selected. Readers are referred to the section on parameter estimation later in this chapter for methods for calculating parameters for the probability distributions described earlier.

Failure No.	Time to Failure (Days)	$\hat{R}(t_i) = \frac{n + 0.625 - i}{n + 0.25}$
1	42	$\frac{4 + 0.625 - 1}{4 + 0.25} = 0.85$
2	296	$\frac{4 + 0.625 - 2}{4 + 0.25} = 0.62$
3	467	$\frac{4 + 0.625 - 3}{4 + 0.25} = 0.38$
4	596	$\frac{4 + 0.625 - 4}{4 + 0.25} = 0.15$

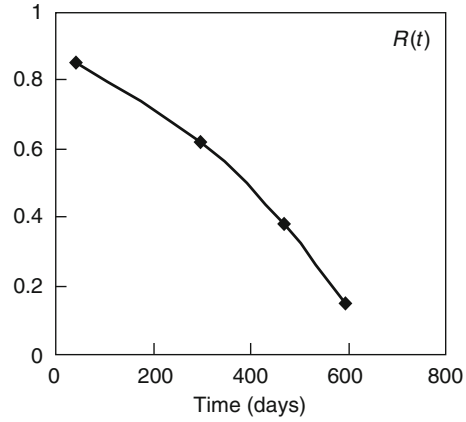

Fig. 74.6 Numerical solution for Example 2

Example 2 Plot the reliability curve for the following times to failure (in units of days) using the empirical distribution 42, 296, 467, 596.

Solution Before Equation 74.17 is used to calculate the reliability, the failure times must be in ascending order. In this case $n = 4$. Results are presented in Fig. 74.6.

Conditional Distributions and Hazard Rate

From the definition of conditional probability, the probability of a system functioning at time t_o fails before time $t > t_o$ is expressed as

$$F(t|t>t_o) = \frac{Pr(t \le T/t>t_0)}{P(t > t_0)} = \frac{F(t) - F(t_o)}{1 - F(t_o)} \qquad (74.20)$$

where t is the random variable for time. Figure 74.7 provides a conceptual representation of this formulation. The numerator represents the area under the curve between the variables t_o and t (shaded). The denominator is the area under the curve after the variable t_o, which is also the reliability of the system.

Differentiating with respect to x, the conditional density function is obtained [4].

$$f(t|t>t_o) = \frac{f(t)}{1 - F(t_0)} \qquad (74.21)$$

This conditional density, which is a function of t_o and t, will be applied later in the chapter in the analysis of repairable systems. The denominator is by definition a number between 0 and 1, which forces the integral of the function from t_o to infinity to be 1.0. As illustrated by the dashed line in Fig. 74.4, the normalizing factor shifts the function upwards after t_o, but the shape of the distribution remains the same after that point. Again, the area under the curve of the conditional distribution after t_o is 1.0.

The value of the conditional density function at $t_o = t$ is a function only of t. This function, which is usually denoted as $h(t)$, is called the conditional failure rate or hazard rate of a component. The hazard rate is found by dividing the PDF of the component by its reliability at time t. From Equation 74.21,

$$h(t) = \frac{f(t)}{1 - F(t)} = \frac{f(t)}{R(t)} \qquad (74.22)$$

Accordingly, the product $h(t) \cdot dt$ represents the conditional probability that a component surviving at time t, will fail between time t and $(t + \Delta t)$ for the first and only time. The component will then be replaced. Although $h(t)$ equals the value of the conditional density for times $t_o = t$, it is not a probability distribution because the area is not

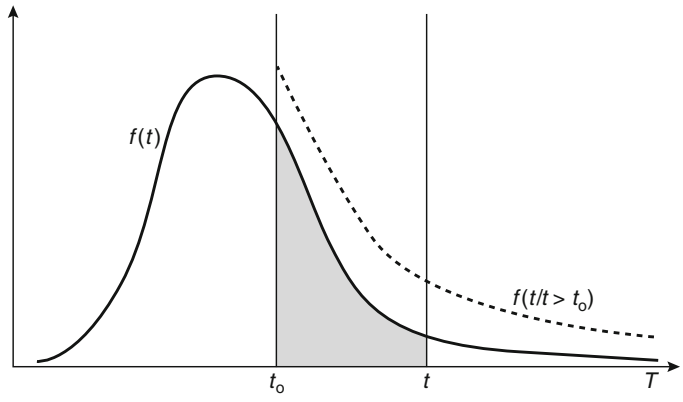

Fig. 74.7 Conceptual representation of the conditional probability of failure

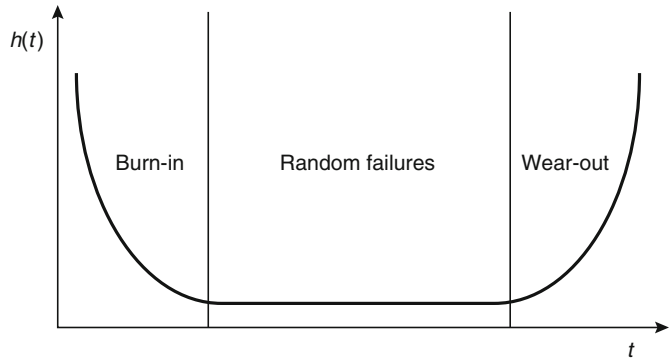

Fig. 74.8 Typical bathtub curve

1.0. However, the hazard rate is an important function in reliability analysis since it shows changes in the probability of failure over the lifetime of a component.

A representative shape of $h(t)$ is the *bathtub* curve for replaceable items. A typical bathtub curve is shown in Fig. 74.8. This bathtub curve is divided in three regions: burn-in, random failures, and wear-out. The *burn-in* region is characterized by a decreasing failure rate due to improvements in early failures attributable to defects in design, manufacturing, or construction. The *random failure* region is characterized by a constant failure rate. As the system or component ages, it starts to exhibit an increasing failure rate. This increasing failure rate characterizes the *wear-out* region.

Exponential Distribution The failure rate of an exponential distribution is independent of time (constant failure rate). It empirically fits the experience of many systems and components over the random failure region of the bathtub curve. The inherent characteristic of a constant failure rate limits the application of the exponential distribution as will be described later in the chapter. From Equation 74.22, the conditional probability distribution $f(t/t > t_o)$ and hazard function $h(t)$ for the exponential distribution are

$$f(t|t>t_o) = \frac{f(t)}{1-F(t_o)} = \frac{\lambda e^{-\lambda(t+t_o)}}{e^{-\lambda t_o}} = \lambda e^{-\lambda(t)}$$

and

$$h(t) = \frac{f(t)}{1-F(t)} = \frac{\lambda e^{-\lambda t}}{e^{-\lambda t}} = \lambda$$

Notice that the latter is independent of time. This result demonstrates one very important characteristic of the exponential distribution for reliability applications: its memory-less property. In other words, the distribution of the remaining lifetime (the conditional distribution) of a component is independent of the current age or what is equivalent, identical to the exponential PDF. At

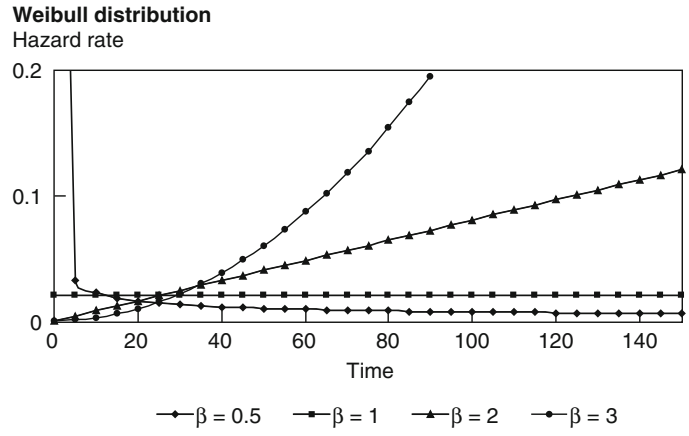

Fig. 74.9 Examples of Weibull distribution hazard rates

each point in time, a given component shows no effect of wear.

Weibull Distribution A more general distribution for representing probability of failures in increasing (wear-out region), decreasing (burn-in region), and constant failure rate conditions is the Weibull distribution. The conditional probability distribution and hazard rates are

$$f(t|t>t_o) = \frac{f(t+t_o)}{1-F(t_o)} = \frac{\frac{\beta t^{\beta-1}}{\alpha^{\beta}} e^{-\left(\frac{t+t_o}{\alpha}\right)^{\beta}}}{e^{-\left(\frac{t_o}{\alpha}\right)^{\beta}}} = \frac{\beta t^{\beta-1}}{\alpha^{\beta}} e^{\left(\frac{t_o}{\alpha}\right)^{\beta}-\left(\frac{t+t_o}{\alpha}\right)^{\beta}} \tag{74.23}$$

$$h(t) = \frac{f(t)}{1-F(t)} = \frac{\frac{\beta t^{\beta-1}}{\alpha^{\beta}} e^{-\left(\frac{t}{\alpha}\right)^{\beta}}}{e^{-\left(\frac{t}{\alpha}\right)^{\beta}}} = \frac{\beta t^{\beta-1}}{\alpha^{\beta}} \tag{74.24}$$

Clearly $h(t)$ is a function of time. Figure 74.9 illustrates various examples of $h(t)$. Notice that the function is decreasing for β values less than 1, constant for β values approximately equal to 1, and increasing for β values greater than 1. Therefore, β values other than 1.0 are an indication of increasing or decreasing hazard rates as a function of time. As mentioned earlier, a β value of 1.0 results in the exponential distribution, which has been demonstrated to have a constant hazard rate.

Log-Normal Distribution The hazard rate of the log-normal distribution does not have a close-form mathematical expression and, therefore, has to be evaluated numerically. In general it is an increasing function followed by a decreasing one. Ebeling [2] suggests that this is an uncommon hazard rate behavior for most components. The conditional distribution and the hazard rate can be expressed as

$$f(t|t_o) = \frac{\frac{1}{\sqrt{2\pi}\sigma t} e^{\frac{-1}{2}\left[\frac{\ln(t+t_o)-\mu}{\sigma}\right]^2}}{1-\int_0^{t_0} \frac{1}{\sqrt{2\pi}\sigma t} e^{\frac{-1}{2}\left[\frac{\ln(t)-\mu}{\sigma}\right]^2} dt} \tag{74.25}$$

And

$$h(t) = \frac{\frac{1}{\sqrt{2\pi}\sigma t} e^{\frac{-1}{2}\left[\frac{\ln(t)-\mu}{\sigma}\right]^2}}{1-\int_0^{t} \frac{1}{\sqrt{2\pi}\sigma t} e^{\frac{-1}{2}\left[\frac{\ln(t)-\mu}{\sigma}\right]^2} dt}$$

where the integral in the denominator needs to be evaluated numerically. Figure 74.10 illustrates an example of the log-normal hazard rate.

Empirical Distribution The hazard rate for the empirical distribution, which assumes a complete data set, can be found using Equations 74.16 and 74.17 [5]. That is,

$$\hat{h}(t) = \frac{\hat{f}(t)}{\hat{R}(t)} = \frac{1}{(t_{i+1}-t_i)(n+0.624-i)}, \quad i = 1, 2, \ldots, n-1 \tag{74.26}$$

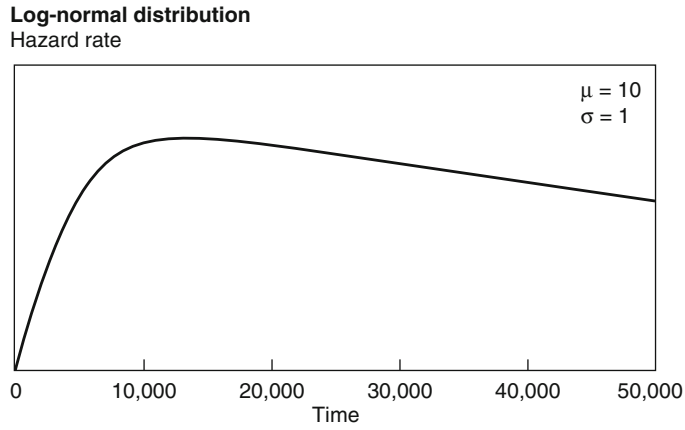

Fig. 74.10 Sample hazard rate of the log-normal distribution

Stress and Strength Interference Model

As suggested by Wulpi [6], "All fractures are caused by stresses, and a version of the 'weakest link' theory applies: fracture will originate wherever the local stress first exceeds the local strength." Expanding this concept from fractures to failures in general, the stress and strength interference model can be formulated for calculating probabilities of failure. In this context, Ebeling [2] (p. 12a) defines *stress* as any load that produces a failure. The *strength* is the capacity of a system or component to withstand the stress. A failure will occur if the stress exceeds the strength of a system or component. The stress-strength interference model can be considered a static reliability model. That is, the probability of failure is based on the comparison of instantaneous loads placed on the system or component with its ability to withstand that load rather than based on past failure profiles.

It is important to clearly identify the stress and strength that will be evaluated since there may be many different types of stresses and strengths in any given system. Some stresses may not be obvious as, for example, residual stresses in metals. Ebeling [2] lists four major categories of stress: electrical, thermal, mechanical, and chemical. Mechanical failures may include fractures or distortions. Corrosion is an example of a chemical failure. These stresses may occur as the system interacts with environmental conditions (fire or corrosion) or may be due to operating conditions (vibration). To predict the reliability of a system or component, the nature of both the stress and the strength must be known. In most situations, physical models describing both the stress and the strength are necessary.

As a conceptual example, consider the case of a steel beam heated by fire plume conditions. Assuming steady-state conditions, the stress-strength interference model can be formulated in terms of temperature. The plume temperature at the location of the steel element would represent the thermal load on the steel element. The ability to withstand the thermal load would be represented by the damage temperature of the steel.

The following general stress-strength combinations can be analyzed: (1) random stress–fixed strength, (2) fixed stress–random strength, and (3) random stress–random strength. A random stress or strength refers specifically to a probability distribution describing, respectively, the load or the capacity to withstand that load. In contrast, a fixed stress or strength refers to a deterministic magnitude of the load or capacity to withstand it, respectively.

The reliability in Case 1 is the area under the curve of the stress distribution $f(s)$ to the left of the strength limit S_o. In Case 2, the reliability is the area under the curve of the strength distribution $f(s_o)$ exceeding the stress limit S. In these cases, the probabilities of failure are calculated by integrating the probability distribution for stress or strength with the corresponding limits

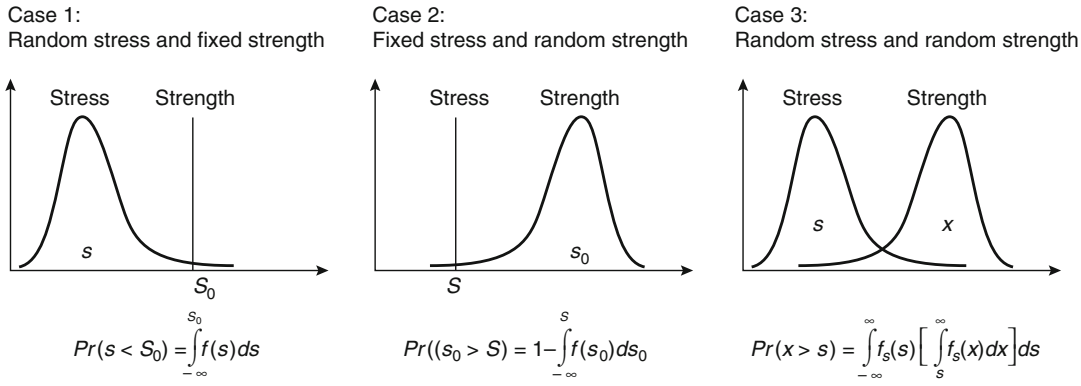

Fig. 74.11 Summary of stress-strength interference models

of integration. The integral equations are shown in Fig. 74.11.

In Case 3, where both stress (s) and strength (x) are random variables represented by probability distributions, the overlap area between the two curves is an indicator of the probability of failure. Notice that in this case the probability of failure is not the overlap area as illustrated in a two-dimensional graphical representation. The reliability calculation must consider the combinations of all the values assumed by the random variables s and x. The probability of the strength being larger than a given value of s, say S, is given by

$$R = Pr(x>S) = \int_{S}^{\infty} f_x(x)dx \qquad (74.27)$$

where $f_x(X)$ is the probability distribution for the strength. This probability corresponds to one and only one possible value of the random variable S. By definition, the probability of observing the value S is $f_s\,(S) \cdot ds$, where $f_s\,(s)$ is the probability distribution for the stress. Therefore, the probability of the stress assuming the value s and the strength exceeding it is the multiplication

$$f_s(s)ds \cdot \int_{S}^{\infty} f_x(x)dx \qquad (74.28)$$

assuming both stress and strength are independent random variables. Finally, since the reliability estimate must consider all possible values of s,

$$R = \int_{-\infty}^{\infty} f_s(s) \cdot \left[\int_{s}^{\infty} f_x(x)dx\right] ds \qquad (74.29)$$

Again, Fig. 74.11 provides a summary of the stress-strength interference cases.

Applications in Fire Risk Analysis A recent fire risk assessment methodology [7] defines the concept of severity factor as the probability of a fire with the duration and heat release rate necessary to generate target damage. In this application, a target is any item selected for evaluation in a postulated fire scenario that can be subjected to fire damage.

The severity factor is calculated as described in Case 1 in Fig. 74.11. That is, the stress is the probability distribution for the heat release rate and the fixed strength is the heat release rate necessary for generating target damage. Therefore, the probability is the severity factor, which represents the fractions of fire intensities capable of generating target damage.

Additional Applications: Probabilistic Safety Factors and Safety Margins The safety factor, sf, is defined as $sf = x/s$, where both x and s are random variables. Propagating the uncertainty from x and s, the probability distribution for sf, as shown in Papoulis [4] (p. 138, footnote 4), is given by

$$f_{SF}(sf) = \int_{-\infty}^{\infty} |s| f(sf \cdot s, s) ds \qquad (74.30)$$

Notice that $f(sf \cdot s, s)$ is the joint probability distribution of x and s where $x = sf \cdot s$.

The safety margin, sm, is defined as $sm = x - s$. Again, both x and s are random variables. The probability distribution for sm is given by the following expression:

$$f_{sm}(sm) = \int_{-\infty}^{\infty} f(sm + s, s) ds \qquad (74.31)$$

In this case, $f(sm + s, s)$ is the joint probability distribution of x and s where $x = sm + s$. In this context, the probability of failure is $Pr(sm < 0)$ or

$$1 - \int_{0}^{\infty} f_{sm}(sm) dsm \qquad (74.32)$$

Example 3 The critical temperature[1] for a steel beam is assumed to be normally distributed with mean = 550 °C and standard deviation of 40 °C. A fire protection engineer is evaluating the potential hazard of a fire below the beam, which will subject it to fire-plume temperatures. Based on the heat release rates generated by the type and configuration of combustibles in the location, calculated fire-plume temperatures range from 250 to 475 °C. Since the evaluation may not have considered the lowest and highest heat release rates, the fire protection engineer assumes a normal distribution for the plume temperature with a 5th percentile = 250 °C and a 95th percentile = 475 °C. The resulting normal distribution has a mean of 362.5 °C and a standard deviation of 68.6 °C. Based on this hazard analysis, calculate the probabilistic safety factor and safety margin.

[1] The critical temperature for a steel member is defined as the temperature at which the material properties have decreased to the extent that the steel structural member is no longer capable of carrying a specified load or stress level (*SFPE Handbook of Fire Protection Engineering*, 3rd ed., p. 4–230).

Solution The first step in solving this problem consists in identifying the stress and the strength. The stress is generated by the fire plume, which subjects the beam to elevated temperatures. Such stress is characterized by a normal distribution with a mean of 362.5 °C and a standard deviation of 68.6 °C. The strength is the damage temperature of the beam. It is characterized by another normal distribution with a mean of 550 °C and standard deviation of 40 °C. The two normal distributions are illustrated in Fig. 74.12a. Notice some overlap between the two curves. This overlap indicates that there is some probability of the fire damaging the beam. Solving Equation 74.29 numerically (Case 3 in Fig. 74.11), the reliability of the beam is $Pr(x > s) = 0.991$.

The distribution for the safety factor, calculated with Equation 74.30, is illustrated in Fig. 74.12b. The mean safety factor is 1.6. Finally, the safety margin can be obtained using Equation 74.31. The safety margin is plotted in Fig. 74.12c. The mean of the safety margin is 187 °C. The probability of failure using the safety margin is $Pr(sm < 0) = 0.009$.

Generic Reliability Values for Fire Protection Systems

Various studies have been conducted for assessing generic reliability values for fire protection features. This section provides a summary of the scope and findings of some of these studies.

Bukowski et al. [8] documented a detailed study for assessing the operational reliability of automatic sprinklers and smoke detectors. A large literature review was conducted as part of this study, including national fire incident database reports, U.S. Department of Defense safety records, industry and occupancy specific studies, insurance industry historical records, inspection reports documented in the open literature, and experimental data.

The reliability values for automatic sprinklers (mean and 95 % confidence intervals) resulting from this study are listed in Table 74.1 for

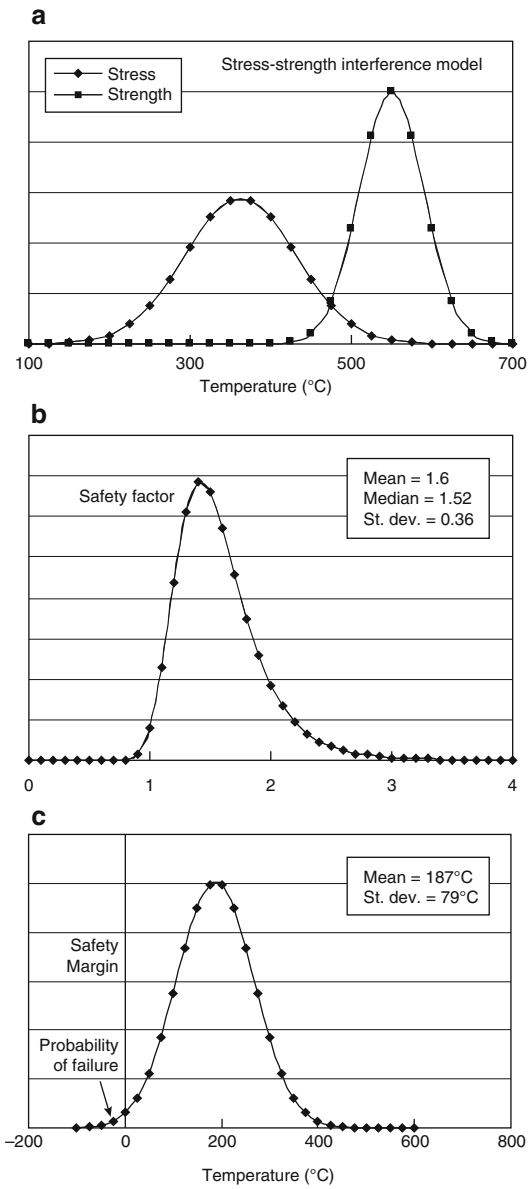

Fig. 74.12 Stress-strength interference model, safety factor, and safety margin for Example 3

different occupancies. These reliability values are unconditional of a fire event and represent the probability that the sprinklers will not fail dangerous (fail at the time of a fire). In the discussion, the authors provide a careful description of the type and biases of the reliability data, which included different reporting periods, types of occupancies, level of detail regarding types of fires, and sprinkler system design. In addition, the inspection, testing, and maintenance activities varied among the different sets of data collected. It should be noted that most of the sprinkler systems involved in the documented incidents included standard spray systems. Finally, the authors stress that the use of these reliability values should consider the confidence interval instead of a point estimate.

In the case of smoke detectors (Table 74.2), the available data had larger sample sizes and were collected in a period of 10 years. The data analysis suggested significantly different reliability values for different occupancies. The authors indicate that the resulting reliabilities should be used only after examining the referenced studies and determining their applicability to the particular safety strategy employing the analyzed system.

Another set of generic reliability values for fire protection systems is reported in Appendix P, NUREG/CR-6850 [7]. These values are based on an earlier study conducted by EPRI [9]. for determining suppression reliability values for nuclear power plant fire risk analyses. The values, as reported, are the following [7]:

- Carbon dioxide = 0.96
- Halon systems = 0.95
- Wet pipe sprinkler systems = 0.98
- Deluge or preaction sprinkler systems = 0.95

These estimates do not include maintenance contributions to unavailability, credit for manual actuation of the system, dependent failures, and plant specific data. It should be noted that fire protection systems in commercial nuclear power plants are subjected to an aggressive inspection and testing program [10].

Although generic reliability values such as the ones listed in this section are available, they usually do not capture important factors affecting individual fire protection systems. These factors include specific environmental conditions, inspection, testing and maintenance procedures, and system design features. Therefore, collection of operational data and analysis for specific systems should provide better insights than the use of generic reliability values. At the same time, if the use of generic values is necessary, the use of confidence intervals, as recommended in Bukowski et al. [8], is important in order to capture differences in the data selected for the

Table 74.1 Generic reliability values for automatic sprinklers [8]

Residential	Institutional	Commercial	General	Combined
96.6	96.6	88.1 < 93.1 < 98.1	93.9 < 96 < 98.1	92.2 < 94.6 < 97.1

Table 74.2 Generic reliability values for smoke detectors

Residential	Institutional	Commercial
75.1 < 77.8 < 80.6	82.3 < 83.5 < 84.6	70.2 < 72.0 < 73.7

estimation of the generic values. In addition, it is recommended that the reliability analysts provides technical justification that any generic value used provides good representation of the systems or components under analysis.

Reliability Analysis of Repairable Items

Recall that a repairable system is one that is brought back to operation after a repair. A repairable system or component may be brought back to operation in any of the following states [11]:

1. As good as new (also referred to as "as new" or "same as new")
2. As bad as old (also referred to as "same as old")
3. Better than old but worse than new
4. Better than new
5. Worse than old

Current probabilistic models used in the analysis of repairable items can account for these five after-repair states. The two most common assumed states are "as good as new" and "as bad as old." Under the "as good as new" assumption, the repair is considered perfect and the item is restored to as new condition. In contrast, the "as bad as old" assumption refers to a minimal repair. In this state, the item is brought back to the condition it had just before the failure.

Perhaps the most important concept in predicting failures in repairable systems is the concept of trend. The term *trend* refers to the behavior of the failure rate as a function of time. A constant failure rate, which results in identical MTBF, shows no trend. This is the "as good as new" after-repair state. In contrast, equipment in which the failure rate is either increasing or decreasing as a function of time does show trend. Once a trend is identified, the appropriate statistical model for predicting failures of repairable systems can be selected.

This section describes models for predicting failures and calculating the reliability of repairable systems under the assumption of the first two after-repair states listed previously: "as good as new" and/or "as bad as old." The probabilistic analysis of the remaining three after-repair states provides failure predictions similar to those obtained under the "as good as new" and "as bad as old" assumptions at least for the immediate future (next few failures) [12]. Given that conclusion and the additional technical complexities associated with those after-repair states, models supporting the last three after-repair states are out of the scope of this chapter.

Probabilistic Models for Failure Predictions

Ascher and Feingold [13] suggest a general strategy for analyzing repairable systems. This strategy is simplified to account for the techniques within the scope of this section only. The strategy is summarized in Fig. 74.13.

The first step in the flowchart consists of ordering the data in chronological order. This is necessary for conducting the trend analysis. Once the failure behavior of the component in terms of trend has been established, the analysis can proceed using the renewal process (RP) or nonhomogenous (NHPP) Poisson process accordingly.

In general, the RP and NHPP are stochastic processes. The term *stochastic process* refers to a random variable as a function of time, or $f(T, t)$, where T is the random variable for time to next

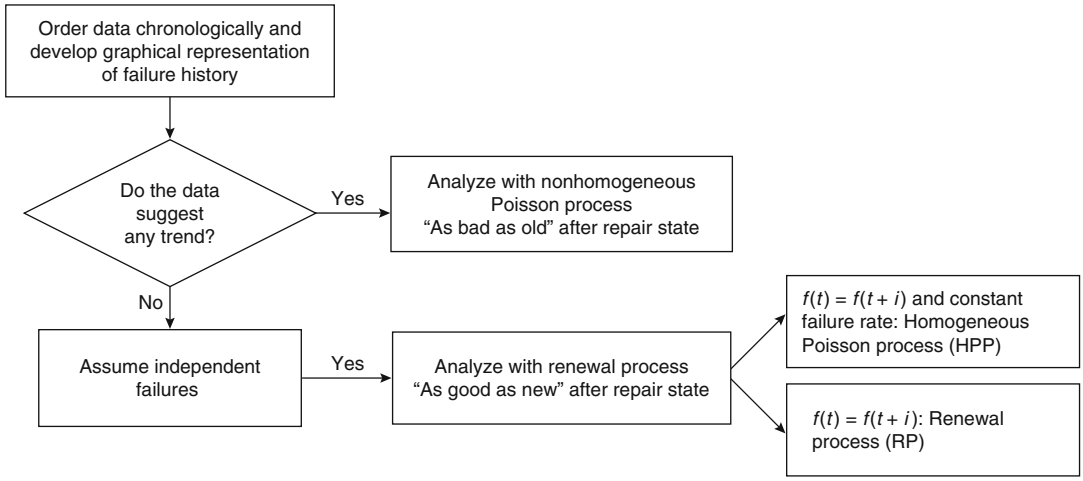

Fig. 74.13 Simplified strategy for analyzing repairable systems

failure. Notice that at a given time t, $f(T)$ is a probability distribution for the time to next failure. Cox and Lewis [14] describe a Poisson process as ". . . a mathematical concept and no real phenomena can be expected to be exactly in accord with it. Whether or not a particular series is in reasonable agreement with a Poisson process is ultimately an empirical matter, even though the key assumptions have varying degrees of plausibility in different applications" (p. 18). The RP assumes failures are independent of each other. This assumption is captured in the analysis by setting $f(T_i) = f(T_{i+1}) = \ldots = f(T_n)$. That is, the probability distributions for the times between failures are identical. In the special case of a constant failure rate, the RP becomes the homogeneous Poisson process (HPP). That is, the HPP is a renewal process where the number of events in a time interval is a random variable following a Poisson probability distribution (the times between failure are exponentially distributed).

In the case of the NHPP, failures are dependent. As a result, the NHPP is characterized by each failure having a different $f(T)$. In practice, each $f(T)$ is modeled using a conditional distribution of the form $f(t_i / t_i > t_{i-1})$ where t_i is the time to next failure and t_{i-1} is the time of the last failure. Clearly, the failure rate changes as a function of time.

The numerical techniques for estimating the number of failures of a repairable item discussed in this chapter assume that the repair time is significantly smaller than the operating time. Under that assumption, repair times are not considered in the analysis. The following subsections describe the flowchart in Fig. 74.13 in detail.

Order Data Chronologically with Graphical Representation of Failure History The first step in the flowchart is to organize the data in chronological order. This exercise, although simple, results in a very useful visual tool for identifying failure trends when plotted in a failure number versus cumulative operating time format in linear paper. Depending on the resulting shape of the plot, the three distinct trends illustrated in Fig. 74.14 can be identified.

A straight line, labeled Case A in Fig. 74.14, is an indication of constant times between failures. Case B, which has a concave down shape, represents increasing times between failures. Case C has a concave up shape, indicating that the times between failures are decreasing.

The Laplace or Centroid Test The Laplace or centroid test can also be used for determining trends in the data by comparing the centroid of the observed times with the midpoint of the period of observation. This test is described in detail in Cox and Lewis [14]. The test consists of calculating the value of u using the following equation for a "failure-terminated" analysis:

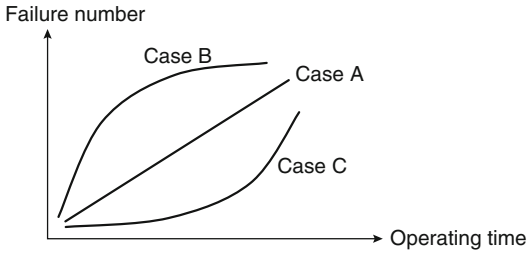

Fig. 74.14 Summary of general trends observed in repairable systems

$$u = \frac{\dfrac{\sum_{i=1}^{n-1} t_i}{n-1} - \dfrac{t_o}{2}}{t_o\sqrt{1/(12/n-1)}} \qquad (74.33)$$

where t_o is the time of the last failure, t_i are the failure times (i.e., $t_i - t_{i-1}$ is a time between failures), and n is the total number of failures. In the case of a "time-terminated" analysis, in which the observation is terminated sometime after the last failure, t_o is the time when the observations were terminated and the $n - 1$ terms in the numerator and denominator should be replaced by n. In commenting on the use of the Laplace test, Modarres [5] indicates that if u is close to 0, there is no evidence of trend in the data. If $u < 0$, the trend is decreasing. Finally, $u > 0$ suggests an increasing trend. Since u follows a standard normal distribution, the following statistical test can be formulated:

H_o: The data show no trend

H_a: The data show trend

Arbitrarily choosing a confidence level α of 0.9, the 5th and 95th percentiles of the standard normal distribution are, respectively, –1.64 and 1.64. Therefore, if u is outside those percentiles, there is evidence to reject the null hypothesis of no trend in the data (i.e., there is a trend).

Example 4 An industrial facility has recorded the following data (Table 74.3) for electrical cabinets of the same type over a period of 10 years (from 1/1/1990 to 12/31/1999). A fire protection engineer is interested in determining if specific changes implemented in the second half of the 1990s in the cabinet maintenance activities performed to the cabinets have made a difference in the number of fires. Do the failure data suggest any trend?

Solution The problem states that the trend analysis should be performed over a period of 10 years. Therefore, this is a time-terminated analysis. In this case, $t_o = 10$ years, $n = 7$ failures, and $\sum t_i = 33.63$ years. With these input values, u is calculated as

$$u = \frac{\dfrac{\sum_{i=1}^{n-1} t_o}{n} - \dfrac{t_o}{2}}{t_o\sqrt{1/(12/n)}} = \frac{\frac{33.63}{7} - \frac{10}{2}}{10\sqrt{1/(12/7)}} = \frac{-0.2}{7.63} = -0.026$$

Since $u \approx 0$, it can be concluded that the data present an almost negligible decreasing trend. The engineer should conclude that the implemented maintenance activities are still not producing the expected effects. Furthermore, −0.026 is inside the 10 % (two-side test) confidence range for the standard normal distribution, which suggests that there is no evidence to reject the hypothesis of no trend in the data.

The Renewal Process (RP) In an RP, the different times to failure are considered independent and identically distributed random variables (a stationary stochastic process), which is consistent with the primary underlying notion of this process that assumes that the system is restored to its original ("as new") condition following a relatively short repair action. The mathematical formulation follows from the failure history depicted in Fig. 74.15.

Consider a new repairable item starting its operating life at $t = 0$. The probability distribution for the first failure, occurring at time T_1, is $f(T_1)$. Assuming a short repair action between failures, the age of the equipment after n failures can be generalized as

Table 74.3 Electrical cabinet failures due to ignition of internal components

Date	Days between failures	Years between failures
1/1/1990		
4/30/1990	119	0.33
11/2/1990	186	0.51
10/12/1992	710	1.95
7/25/1993	286	0.78
10/15/1996	1178	3.23
8/16/1999	1035	2.84
8/24/1999	8	0.02
		0.34[a]

[a]0.34 years since last failure in 10-year period of analysis

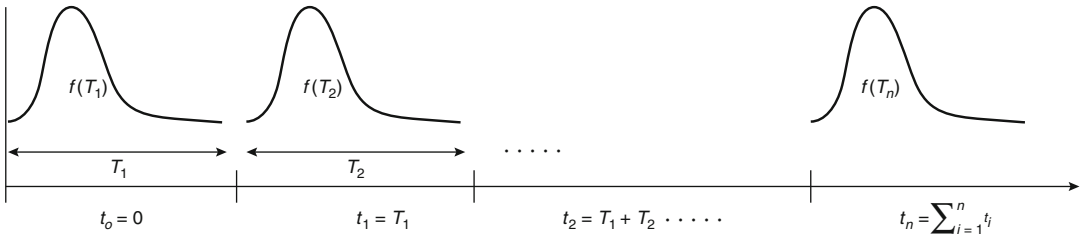

Fig. 74.15 Conceptual representation of the renewal process

$$t_n = \sum_{i=1}^{n} T_i$$

where n is the total number of failures. Notice that T_i is the time between the $i-1$ and the ith failure and t_i represents the age of the item after the ith failure. Both of these variables are random. Since t is a linear combination of random variables, its probability distribution after the ith failure, $f^{(i)}(t)$ is the convolution of $f^{(i-1)}(t)$ and $f(t)$. Recall that the $f(t)$'s in the renewal process are identical. The convolution integral is

$$f^{(i)}(t) = \int_0^t f^{(i-1)}(t-s) \cdot f(s)ds \qquad (74.34)$$

Integrating Equation 74.34 over t, the following cumulative distribution function is obtained:

$$F^{(i)}(t) = \int_0^t F^{(i-1)}(t-s) \cdot f(s)ds$$

Clearly, $F^{(i)}(t) = P[T_1 + T_2 + \ \ldots \ + T_n \leq t]$. From this formulation and the fundamental definition as found in Nelson [3] (p. 186)

$$P[N(t) = n] = F^{(n)}(t) - F^{(n+1)}(t)$$

where $N(t)$ is the number of failures at time t. The following expressions for the expected number of failures (or renewals) can be formulated as

$$W(t) = F^{(1)}(t) + \int_0^t W(t-s)f(s)ds \qquad (74.35)$$

$$\frac{dW}{dt} = w(t)$$

$$= f^{(1)}(t) + \int_0^t w(t-s)f(s)ds \qquad (74.36)$$

The terms of these equations can be explained as follows: $w(t)\Delta t$ is the probability that a failure (and, therefore, a renewal) occurs in the interval $(t, t + \Delta t)$. This event can occur in either of two mutually exclusive ways: (1) the first item that was placed in operation fails in $(t, t + \Delta t)$, or (2) a renewal took place at $(t - s)$, $0 < s < t$, and the unit placed in operation fails in $(t, t + \Delta t)$. These two events have probabilities equal to the first and second term of the right side of the renewal equation, respectively.

Equation 74.36 has a closed-form solution if $f(T)$ is exponential. Specifically, if $f(T) = \lambda e^{-\lambda \cdot T}$, the convolution integral is solvable through the Laplace transform and yields $W(t) = \lambda \cdot t$. This is the HPP described earlier, which is a sequence of independent and identically distributed random failures *with a constant failure rate*, λ. Furthermore, a number of numerical solutions exist for the Weibull, truncated normal, gamma, and log-normal distributions [11].

The applications of the RP model are limited. Krivtsov [11] and Ascher and Feingold [13] suggest that the RP is a poor model for a repairable system, unless the system consists of one nonrepairable component in a socket. Furthermore, Ascher and Feingold [13] (p. 59) argue that the RP is "not necessarily the appropriate model even for a socket." The reasons provided by Ascher and Feingold in support of this statement include (1) externally induced stress on the socket may change over time, (2) stress on the part in the socket at time t may have been affected by damage to other parts caused by failures in that socket before time t, and (3) in the real world, the replacement components may not come from the same population.

The Superimposed Renewal Process In a superimposed renewal process (SRP), it is assumed that n renewal processes are operating independently. The SRP is then formed collecting the failures (or renewals) from each independent process in a single history. Figure 74.16 illustrates this process. The failures in each of the three renewal processes illustrated in Fig. 74.16 are depicted with different markers. The failure history labeled SRP is the collection of the three RP failure histories.

The SRP is in general not a renewal process since the distributions for failure times are not identical. However, the superimposed failure history can be analyzed assuming an NHPP as described in the following section.

The Nonhomogeneous Poisson Process (NHPP) The NHPP relaxes the necessary assumption characterizing the RP, which states that the probability distributions for the time to next failure are identical. As a result, the probability distributions governing the time to next failure can be different to the one governing the previous failure (a nonstationary stochastic process). This flexibility offered by the NHPP is particularly appropriate for the analysis of repairable components since it is expected that, on average, the times to next failure will decrease as the equipment ages. Notice, however, that the NHPP is not only applicable to the analysis of components with increasing failure rates. The process applies to components characterized with constant or decreasing failure rates as well.

The Weibull is perhaps the most common probability distribution selected for the NHPP. Recall that the Weibull distribution has the flexibility of characterizing times to failure for components with constant, increasing, or decreasing failure rates.

A common formulation of the NHPP for reliability applications can be conceptually described as the following:

- The time to first failure, T_1, follows the probability distribution $f(t)$.
- The times for subsequent failures, $T_{2,\,3,\ldots n}$, is governed by the conditional probability distribution $f(t_i / t_i > t_{i-1})$.

Recall from Fig. 74.15 that T_i is the time between failures, and t_i is the equipment age at the time of failure i. This formulation is governed by the following assumption: the equipment condition is assumed "as bad as old" after each

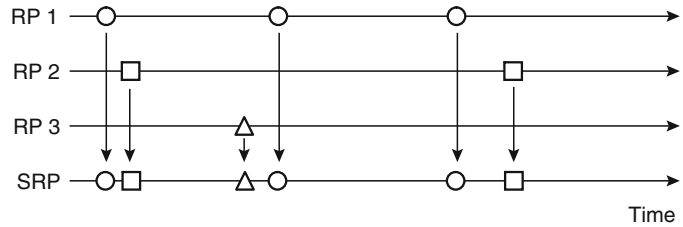

Fig. 74.16 Conceptual representation of the superimposed renewal process

failure. The use of the conditional distribution after the first failure not only suggests that the equipment is modeled as having survived up to failure time $t_i (i > 1)$ but also that the equipment was subjected to a "minimal repair." A minimal repair is one that restores the equipment to the condition it had just before the last failure.[2]

Assuming that the times to failure follow a Weibull distribution, the distribution for the first failure is (Equation 74.8)

$$f(s) = \frac{\beta t_1^{\beta-1}}{\alpha^{\beta}} e^{-\left(\frac{t_1}{\alpha}\right)\beta}$$

For the subsequent failures, the probability distribution function is conditional as follows (see Equation 74.23):

$$f(t_i|t_i > t_{i-1}) = \frac{\beta t_i^{\beta-1}}{\alpha^{\beta}} e^{\left(\frac{t_{i-1}}{\alpha}\right)^{\beta}\left(\frac{t_i}{\alpha}\right)^{\beta}}$$

Numerical Algorithm for Predicting Failures of Repairable Systems Krivtsov [11] describes a very useful algorithm for determining the expected number of failures of a repairable system by solving the process described previously. It can be used for the RP or the NHPP. Figure 74.17 depicts the flowchart for the algorithm. The algorithm calculates the expected number of failures using a Monte Carlo simulation. The formulation consists of generating n number of failure histories for a given repairable item. A failure history refers to the number of failures experienced by the repairable item in a period of analysis t_f.

For each failure history H, the time accumulator is set to 0 and failure times are generated using a random number generator from a corresponding probability distribution. Notice that any applicable distribution can be used and the parameters of the distribution are provided as inputs to the algorithm (see section on "Data Analysis and Parameter Estimation" later in this chapter for details). For any failure history, the algorithm determines if the failure j is the first in the history. If $j = 0$, then the distribution $f(T)$ is used to generate the time for this first failure. The time for the second failure ($j \geq 1$) is generated using the conditional distribution $f(T_i/T_i > T_{i-1})$ for the nonhomogeneous Poisson process or $f(t)$ for the renewal process. The process continues by generating additional failures with their corresponding times. The failure times are accumulated until $t > t_f$. At this point, the number of failures in the history is stored for future use, and the generation of the next failure history begins. Once the n failure histories have been generated, there are n calculated number of failures. Finally, the number of failures in each history are averaged and reported as the expected number of failures for the repairable item.

An important assumption in this algorithm is that the times to repair are neglected. That is, they are considered short when compared with the times to failure. The algorithm, however, can account for repair times by adding them to the time accumulator. Repair times can be generated from a probability distribution, as described in the "Maintainability" section later in this chapter, after each failure. The impact of the repair time in the algorithm can be twofold depending on the governing assumptions. First, it will increase the amount of time the item is not operating. Second, it can affect the condition at which the item is returned to service. The "as good as new" and "as bad as old" assumptions are still applicable as long as the repair time is not included in the conditional distributions for time to failure.

Example 5 Continuing with Example 4, how many failures are expected by 12/31/2003? Let us apply the algorithm in Fig. 74.17 assuming the times between failures follow a Weibull distribution. For illustrative purposes, failure predictions are made assuming an NHPP and an RP. Recall that this is a time-terminated analysis. Therefore, Equations 74.59 and 74.60 are used for calculating the parameters of the Weibull distribution.

[2] This assumption can be relaxed implementing the concept of virtual age [15]. The virtual age is calculated as $A = q \cdot \sum_{i=1}^{n} t_i$. A q value of 0 indicates that the equipment is new. A q value of 1 indicates that the equipment is as old as the last failure, which is the assumption of the NHPP. A q value between 0 and 1 indicates that the equipment is worse than new but better than old. An NHPP developed using the concept of virtual age is described in Krivtsov [11], Hurtado et al. [12], and Yanez et al. [16].

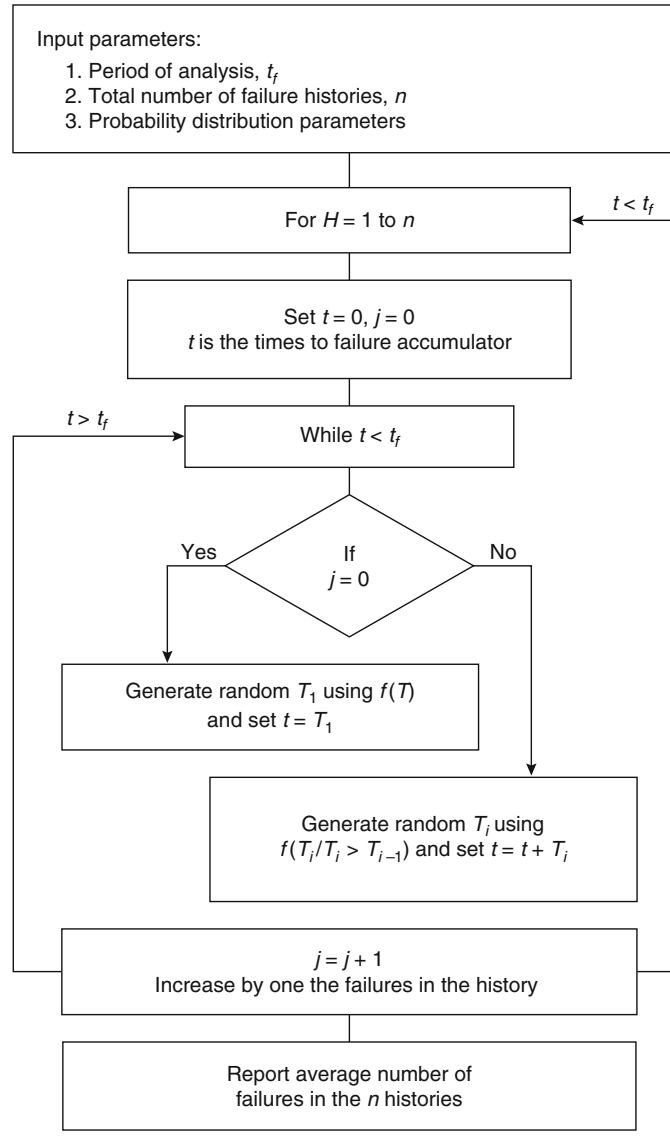

Fig. 74.17 Flowchart describing the algorithm for calculating the expected number of failures of a repairable system

The following values are obtained: $\alpha = 288.8$, and $\beta = 0.75$ for the NHPP. Notice a β value lower than 1.0, suggesting a decreasing failure rate. This is consistent with the results of Example 4. In the case of the RP, Equations 74.56 and 74.57 suggest $\alpha = 282.3$, and $\beta = 0.9$. A β value close to 1 suggests an almost constant failure rate.

Solution Solving the algorithm for a period of 13 years, the solution plotted in Fig. 74.18 is obtained. Figure 74.18 illustrates both the failure data and the predictions up to approximately 13 years. The NHPP model is predicting a total of eight failures by the 13th year. That is only one additional failure from the ones recorded so far. In contrast, the RP predicts ten failures; an additional three failures to the ones recorded so far.

Finally, the shapes of the RP and NHPP predictions are consistent with Cases A and B, respectively, in Fig. 74.14. This example illustrates the effects trend has on failure

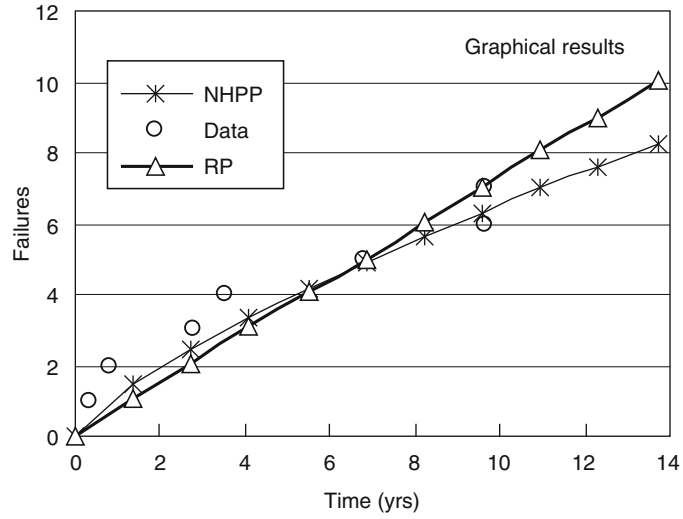

Fig. 74.18 Graphical solution for the prediction of failures using the algorithm in Fig. 74.17 assuming Weibull distribution

predictions and, therefore, the importance of model selection.

Maintainability

In repairable or replaceable systems, particularly in those where the repair or replace time is not negligible (i.e., long relative to the operational time) downtimes should be properly characterized. Maintainability refers to the probabilistic characterization of such downtimes. As described later in this chapter, downtimes can be an important factor in availability calculations.

For the purpose of this chapter, maintainability includes the inspections, testing, and maintenance activities to which an item is subjected. As indicated in SAND 95-1361, "It is clear that most fire protection system failures are discovered during testing and maintenance activities and not when the fire protection systems are required to actuate [10]." NFPA 25, *Standard for the Inspection, Testing and Maintenance of Water-Based Fire Protection Systems*, defines inspections as "visual examinations of a system or portions thereof to verify that it appears to be in operating condition and is free of physical damage [17]." NFPA 25 also defines testing as "a procedure used to determine the status of a system as intended by conducting periodic physical checks." In fire protection systems, testing may include water flow tests, fire pump tests, alarm tests, and so on. Testing is particularly important in standby systems such as those required to operate in emergency situations. Finally, NFPA 25 defines maintenance as a work performed to keep equipment operable or to make repairs [17].

Maintenance activities can be preventive or corrective. Preventive maintenance refers to the actions taken to retain an item at a specified level of performance. It has the potential of reducing failure rate. Corrective maintenance represents actions taken to restore a machine to an operational state after it is disabled due to a part of system failure.

Most fire protection engineering systems are subjected to scheduled inspections, testing, and maintenance activities. NFPA standards, devoted to specific suppression systems, include specific inspection, testing, and maintenance recommendations. Some examples are the following:

- NFPA 25 [17] provides specific recommendations for inspection, testing, and maintenance schedules and procedures for sprinkler systems, standpipe and hose systems, private fire service mains, fire pumps, water storage tanks, and valves,

among others. The scope of the standard also includes impairment handling and reporting.
- *NFPA 72®, National Fire Alarm Code®* [18], provides specific recommendations for inspection, testing, and maintenance activities for the different elements of fire detection systems including control equipment, generators, uninterrupted and standby power supplies, batteries, annunciators, initiating devices, communication equipment, and so on.
- NFPA 2001, *Standard on Clean Agent Fire Extinguishing Systems*," [19] provides specific recommendations for inspection, testing, and maintenance of clean agent fire suppression systems.

Additional examples include NFPA 12, *Standard on Carbon Dioxide Extinguishing Systems*, for CO_2 systems; NFPA 12A, *Standard on Halon 1301 Fire Extinguishing Systems*, for Halon systems; and NFPA 17, *Standard for Dry Chemical Extinguishing Systems*, for dry chemical systems. Ultimately, the selection of inspection, testing, and maintenance strategies will depend on existing regulations, adopted standards, cost, and the type of system. Most of these inspection, testing, and maintenance strategies can be quantified and included in maintainability and availability studies.

Maintainability Quantification

As suggested earlier, maintainability refers to the probabilistic characterization of downtimes. Factors affecting downtime include activities before and after failure.

Before a failure occurs, consider the following:

1. *Inspection time*. Although inspections are usually quick, some systems may require relatively longer inspection times. Usually, inspections do not require the system to be down and, consequently, this time is not considered in maintainability studies.
2. *Testing time*. The time required for system testing. This time is only considered in maintainability studies if the system is down during the test.
3. *Preventive maintenance time*. The time required for preventive maintenance activities. As in the case of testing time, this time is only considered in maintainability studies if the system is down during the maintenance.

After the failure occurs, the following corrective maintenance-related activities are usually conducted [20]:

1. Realization time—the time to detect a failure. In some systems or components, this time can be minimized with relevant alarms.
2. Access time—the time to isolate the system before any diagnosis or repair activities can begin. Some mechanical design considerations can reduce the access time. For example, access time can be reduced if the system components with the highest failure rates are accessible.
3. Diagnosis time—the time required for identifying the specific components that should be replaced or repaired in the system.
4. Logistic time—refers to the time taken to develop a repair strategy and assemble required parts/components, equipment, and personnel.
5. Repair/replacement time—the time required to repair the failure. As in the case of the access time, it can be minimized with a good mechanical and human factors design.
6. Checkout time—refers to the time taken to verify that the failure no longer exists.

The preceding classification suggests two general downtime characterizations: (1) before failure occurs, which is dominated by testing and preventive maintenance activities; and (2) after the failure occurs, which can be influenced by many factors depending on the type of system and the availability of parts and personnel to perform the repair. These two downtime classifications can be considered random

and, therefore, represented with probability distributions.

In practice, downtimes are often characterized using the exponential distribution. By using the exponential distribution, downtimes can be readily included in availability analyses using Markov models (as discussed later in the chapter).

The most common parameter used to characterize repair times is the mean time to repair (MTTR). Assuming that the distribution for the repair time is $g(t)$, the MTTR is defined as

$$\text{MTTR} = \int_0^\infty t \cdot g(t)dt \tag{74.37}$$

Availability

The analysis for repairable systems described so far assumes relatively short repair actions. In practice, this assumption simplifies the analysis by not considering the inspection, testing, and/or the repair time. In some applications, however, the quantification of equipment downtime is necessary. Accordingly, the scope of the analysis is not about calculating the probability of the equipment successfully operating after time t, but the probability that the system is available over a specified period of time. The latter is referred to as an availability analysis. As an example, consider a room protected with a CO_2 system. For life safety reasons, the system may be taken out of service some periods of time. As a result, the probability of the system being available is affected by the time it is out of service.

The term *availability* is defined as the probability that an item, when used under stated conditions, will be operational at a given time. Notice the difference between the concept of reliability and availability. Recall that the former refers to the probability of a continuous operation over a time interval. The complement of the availability is termed *unavailability* or $U = 1 - A$. A very simple mathematical expression capturing this definition is

$$\text{A} = \frac{u}{u+d} \tag{74.38}$$

$$U = \frac{d}{u+d} = 1 - A \tag{74.39}$$

where u is the uptime, and d is the downtime during a predefined period of time T.

The concept of availability can be extended further considering the terms *instantaneous* and *average availability*. The instantaneous availability is the probability that the system is operational at a specific time t. The average availability, on the other hand, is defined for a fixed period of time T as

$$\overline{A} = \frac{1}{T}\int_0^T a(t)dt \tag{74.40}$$

where $a(t)$ is the availability as a function of time.

Both of these terms are important. That is, two systems may have the same average availabilities, but the instantaneous values may suggest periods of time when the unavailability is high. Consider as a conceptual example Fig. 74.19, which illustrates the behavior of the unavailability of a system as a function of time. Notice how the unavailability grows to the limit where the system is fully unavailable and needs repair. The repair returns the unavailability to low levels and the cycle starts again.

Reliability engineers have developed computer programs that follow and quantify the cycle described in Fig. 74.19 (see, for example, NUREG/CR-1924 [21]). Also relatively simple mathematical expressions for calculating availability in systems with different inspection and repair schedules are available. Modarres [5] (p. 205) lists the equations in Table 74.4.

The equations listed in Table 74.4 assume a constant failure rate λ (1/h). T_m is the mission length (hour), τ is the average downtime MTTR (hour), T is the test interval (hour), T_R is the average repair time (hour), T_t is the average test duration (hour), f_r is the frequency of repair per test interval, and T_o is the operating time (uptime) $= T - T_R - T_t$. Notice that these simple

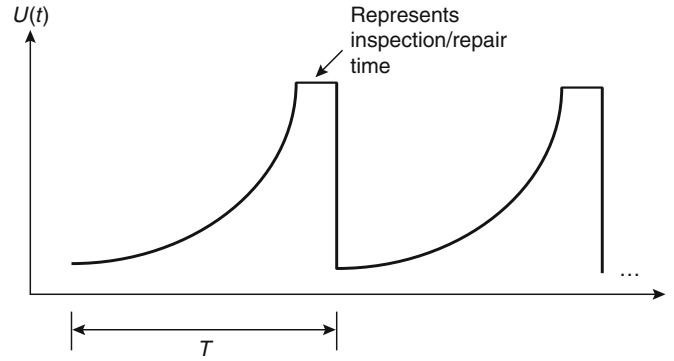

Fig. 74.19 Conceptual representation of system unavailability as a function of time

Table 74.4 Summary of equations for availability calculations

Type	Average availability
Time independent (constant)	A
Nonrepairable	$\overline{A} = \frac{1}{T}\int_0^T a(t)dt = \frac{1}{T}\int_0^T (1-\lambda t)dt = 1 - \frac{1}{2}\lambda T_m$*
Repairable (failures immediately detected)	$\frac{1}{T+\lambda t}$ (from solution to Markov model, Case 2 with $\mu = 1/\tau$)
Repairable (periodically tested)	$1 - \frac{1}{2}\lambda T_o - f_r\frac{T_R}{T} - \frac{T_t}{T}$

*$a(t) \approx 1 - \lambda t$ (for $\lambda t < 0.1$). This is an approximate form of the availability as a function of time, which assumes perfect repair and very short repair and test durations (their contribution is neglected in the unavailability calculation)

equations are for very specific applications. Another alternative for calculating availability is using Markov modeling.

Use of Markov Modeling for Determining System Availabilities

Markov modeling refers to a simulation based on the different *states* a system may be in time. As such, it is particularly appropriate for solving availability problems in which the main interest is to calculate the probability of an item being operational at a given time t.

There are three general classes of Markov processes: [4] (1) discrete time–discrete state, (2) continuous time–discrete state, and (3) continuous time–continuous state. In most reliability engineering applications, states are discrete. Therefore, this section focuses on the first two classes only. These two classes apply nicely to the failure/repair process because combinations of failure create discrete system states. Furthermore, the failure/repair process moves between discrete states only as a result of current state and current failure [19].

The following characteristics of Markov models are important:

- Markov models are stochastic processes developed and solved based on the assumption that the probability of being in state i depends only on the state $i - 1$ (i.e., the previous state). In other words, the future state of the system is determined by the present state but is independent of previous states. This is consistent with the memory-less property of the exponential distribution previously described in this chapter.
- Identified states should be mutually exclusive. That is, the system can be in only one state at a given time. States are usually represented graphically as circles.
- Once the states have been determined, transitions between states must be established.

Each transition is characterized by a probability in the case of discrete time models or a constant rate of transition in the case of continuous time models. A transition is represented graphically with an arrow starting at the current state and pointing to the state to which the system might change. The exponential distribution characterizes the transition times between states since the rates of transitions are constant.

- A state can transition to itself. This is represented with an arrow leaving the state and pointing to the same state.
- Absorbing states are those from which there is no transition out. If the system reaches an absorbing state, it will remain in that state.

Developing the Markov Model The first step in developing a Markov model of a system is determining the system states over time. Typical states in reliability engineering may include the following:

- Operational, which refers to a system operating in normal conditions
- Failure, which refers to a system that has failed and is not operating
- Degraded, which refers to an item that can achieve its operational goals without being in optimal operational conditions
- Repair, which refers to a system that is undergoing repair activities
- Inspection, which refers to a system that is undergoing inspection
- Testing, which refers to a system that is undergoing testing activities
- Standby, which refers to a system operating in standby mode

Consider as examples the Markov models summarized in Fig. 74.20. The simplest (and also trivial) example is the case of a nonrepairable item, which is characterized by two states: operational and failed. Obviously, the item will change from an operational state to a failed state as represented in Case 1 of Fig. 74.20. In this example, the transition can be defined by a probability of failure (discrete model) or a failure rate (continuous model). Notice that the failure state is absorbing.

The simplest Markov model for a repairable system is depicted in Case 2 of Fig. 74.20. Notice that in this case an additional transition is included from the repair state to the operational one. This transition is defined by the repair probability or a repair rate.

Case 3 of Fig. 74.20 consists of a repairable system subjected to scheduled testing. The system is represented with three states: operational, test, and repair. The system may transition from the operational state to the repair state with a probability of failure P_f or a failure rate λ. It can also transition from the repair state to the operational state with a probability of repair P_r or a repair rate μ. Due to the scheduled tests, the system will move to the test state with a probability P_i or a test rate τ. Once in the test state, it may return to operation if no degraded condition requiring repair is found. That transition is represented with the probability P_s or the rate ψ. Finally, if a degraded condition requiring repair is found during the inspection, the system transitions to the repair state with probability P_r or a rate γ.

Case 4 of Fig. 74.20 represents a standby system. That is, one component of the system is operational and an identical component serves as a backup. The system is designed so that if the operating component fails, the backup component automatically starts. In this example, the system is considered operational if one of the two components is operating. The Markov model of this system consists of four states, labeled for clarity States 1, 2, 3, and 4, respectively. State 1 represents both the primary and backup components operating. In this state, the backup components will operate if the primary fails. Transitions from this state may occur to State 2, 3, or 4. In State 2 the backup has failed, leaving the system with no redundancy. In State 3, the primary component has failed and the system is operating with the backup one. The transition from State 1 to State 4, where both the primary and the backup have failed, can occur, for example, due to a common cause failure (see discussion on common cause failure later in the chapter) or failure to the switching device. If repairs in State 2 or 3 have not been

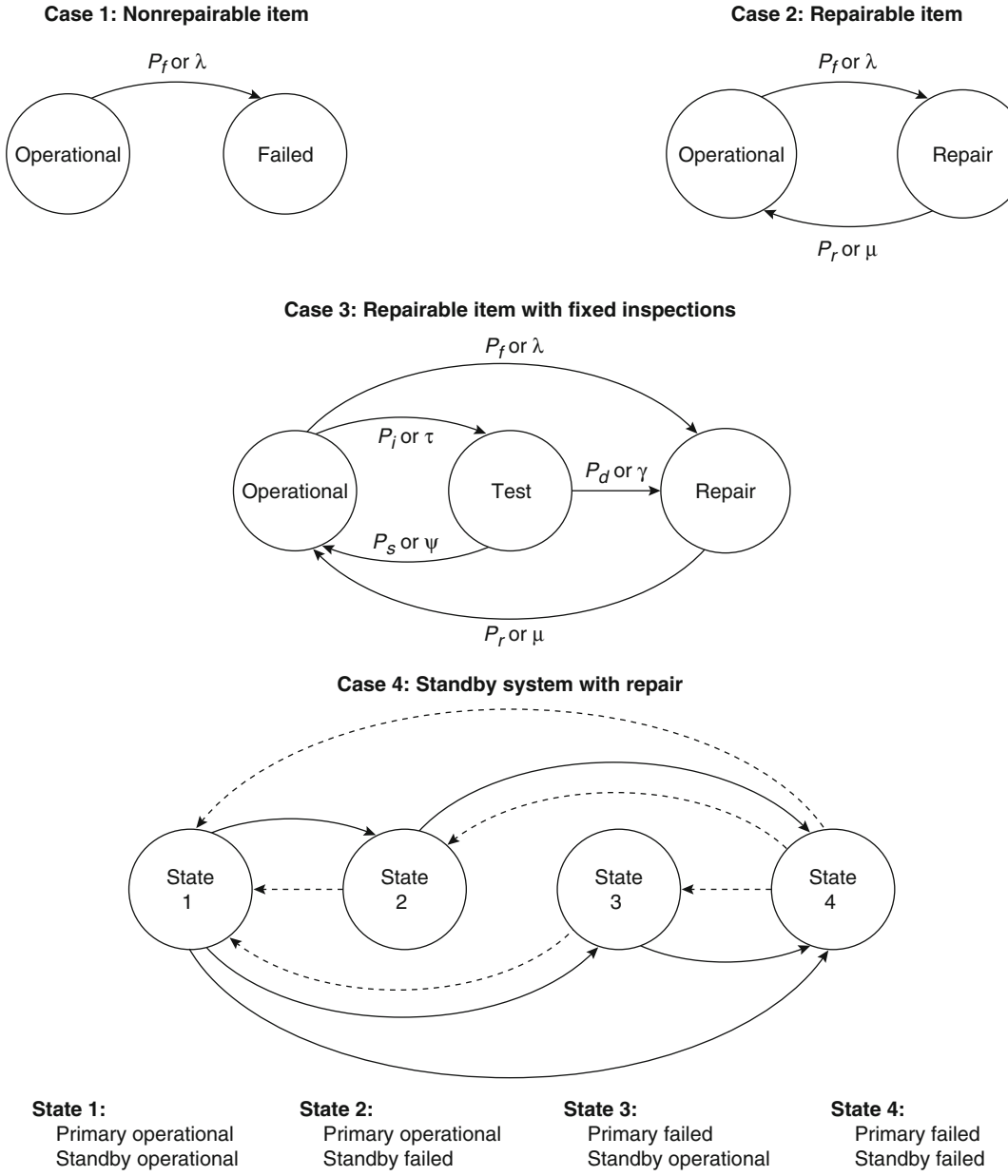

Fig. 74.20 Four Markov models for selected systems or components

made on time, a failure of the only operating component will force a transition to State 4 also. Notice that if no repairs are considered, State 4 becomes an absorbing state. On the other hand, if repair transitions are included, as illustrated with dashed lines in Case 4 of Fig. 74.20, the system will eventually return to State 1, 2, or 3 when the corresponding repairs are completed. Notice also that repair transitions have been included from States 2 and 3 to State 1.

The transition matrices and availability solutions for the systems described in Fig. 74.20 are discussed in the following sections.

Transition Matrix The transition matrix, T, summarizes all transition probabilities or rates

in a Markov model. It is a square matrix with n rows and columns where n is the number of states in the model. For clarity purposes, the matrices in the section have an additional row and column for identifying the corresponding state.

In a discrete time Markov model analysis, the transition matrix will include probability values representing the transition from one state to the other. In the case of a continuous time analysis, the transition matrix will include rates of transitions from one state to the other. To add the probabilities or rates in the matrix, start from the first state in the first column. From that state, add transition probabilities or rates to the state in the first row of the different columns. Continue this process until all the states in the different rows have been completed. In the case of discrete time Markov models, the values in each row must add to 1.0. No transitions are characterized by a 0 numeric value. Tables 74.5 and 74.8 are the transition matrices that correspond to the four Markov models listed in Fig. 74.20.

Case 1, shown in Table 74.5, consists of only one transition from operational to failure. The failure state is absorbing. As such, the transition matrix includes only the failure probability or rate from operational to failure, P_f or λ. In Case 2, however, there are no absorbing states. Notice that the transition matrix in Table 74.6 includes both the failure rate or probability characterizing the change of state from operational to repair (P_f or λ) and the repair probability or rate characterizing the change of state from repair to operational (P_r or μ).

As shown in Table 74.7, Case 3 consists of a larger matrix since it has three states. The transition from operational to test states is characterized by the inspection probability or rate, P_i or τ, respectively. Similarly, the transition from operational to repair states is characterized by the failure probability or rate, P_f or λ. Those two transitions complete the first row of the matrix, since there are only two arrows moving out of the operational state. The test state is evaluated next. From this state, there are transitions to the operational and repair states.

Table 74.5 Transition matrix for Case 1 of Fig. 74.20

	Operational	Failure
Operational		P_f or λ
Repair		

Table 74.6 Transition matrix for Case 2 of Fig. 74.20

	Operational	Repair
Operational		P_f or λ
Repair	P_r or μ	

These two transitions are characterized by the variables (P_s or ψ) or (P_d or γ), respectively. Finally, there is only one transition out of the repair state. This transition is characterized by P_r or μ, which is the probability or rate of moving from repair to operational states.

The transition matrix for Case 4 is illustrated in Table 74.8. Recall that this case consists of four states, labeled State 1, State 2, State 3, and State 4. The process to complete this matrix is identical to the one described for the earlier matrices. As such, the transition from State 1 to State 2 is characterized by the failure of the standby system. A transition from State 1 to State 3 is characterized by the failure of the primary system. The transition from State 1 to State 4, which would include the failure of both components at the same time, is characterized by a common cause failure probability or rate. Notice that there are transitions from States 2 and 3 to State 4, which represent failures of the primary and standby components when the other has already failed. In contrast, the transitions from States 2 and 3 to State 1 represent the repair of the primary or standby component, respectively, when the other is operating. Finally, transitions out of State 4 represent repairs. These repairs can move the system to any of the first three states.

Solving the Discrete Time Markov Model Recall that in a discrete time Markov model there is a state transition at every time step according to the transition matrix. At this point in the analysis, the Markov model and the transition matrix are developed. From this

Table 74.7 Transition matrix for Case 3 of Fig. 74.20

	Operational	Test	Repair
Operational		P_i or τ	P_f or λ
Test	P_s or ψ		P_d or γ
Repair	P_r or μ		

Table 74.8 Transition matrix for Case 4 of Fig. 74.20

	State 1	State 2	State 3	State 4
State 1		P_{sb} *or* λ_{sb}	P_p or λ_p	P_{cc} or λ_{cc}
State 2	P_r or μ			P_p or λ_p
State 3	P_r or μ			P_{sb} *or* λ_{sb}
State 4	P_s or μ_s	P_r or μ	P_r or μ	

information, the steady-state probabilities of being in each of the states can be calculated.

When a discrete time Markov model starts at time 0 in a particular state, the probabilities of being in state i will vary with time. Since the transition matrix shows probabilities for moving from any one state to another in one time interval, the matrix can be multiplied by itself to obtain transition probabilities for multiple time intervals. For example, when the transition matrix is squared, the result is another $n \times n$ matrix that gives probabilities of going between states in one time step [22]. Mathematically, these transition probabilities as a function of time are represented as

$$T^{t+1} = T\tilde{n}T^t \tag{74.41}$$

where $\boldsymbol{T}$ is the transition matrix and t is the time step. After some number of matrix multiplications, these resulting transition probabilities will reach steady state or $T^{t+1} \approx T^t$.

Let us also define a vector of initial conditions, that is, the state of the system at time 0. This vector is a $1 \times n$ matrix (recall that n is the number of states in the system) and is identified with the letter L. In most practical applications, it has a value of 1.0 in the initial state and 0 in the others. The value of 1.0 for state i is the probability of the system in state i at time 0. The probability of a system in state i after t number of transitions can be calculated multiplying $\mathbf{L}$ by the corresponding T matrix. Mathematically this is expressed as

$$\mathrm{L}^t = \mathrm{L}^{t=0}\,\tilde{n}\,T^t$$

In the long run, as $t - \infty$, $\mathbf{L}^{t+1} = \mathbf{L}^t \cdot \boldsymbol{T} = \mathbf{L}^t$. In other words, the state probabilities captured in the vector $\mathbf{L}$ will not change. Although the process of matrix multiplication is relatively easy, there is a straightforward technique for calculating the steady-state probabilities. The technique consists of determining the normalized eigenvector for the eigenvalue 1.0 of the transposed transition matrix [23] (pp. 393–394). In practice, this technique reduces to solving for the vector $\mathbf{X}$ in the following equation:

$$\left(T^T - \mathrm{I}\right)\tilde{n}\,\mathbf{X} = 0 \tag{74.42}$$

where $\boldsymbol{T}^T$ is the transposition of $\boldsymbol{T}$, and $\mathbf{I}$ is the unit vector. Again, vector $\mathbf{X}$ is the steady-state probabilities. As an example, consider the following transition probabilities for the Markov models presented in Fig. 74.20.

CASE 1 Since there is only one transition, and the failed state is absorbing, the steady-state probabilities for the system being operational and failed are 0 and 1.0, respectively.

CASE 2 Let us assume the following values for the transition matrix:

$$T = \begin{vmatrix} 0.99 & 0.01 \\ 0.75 & 0.25 \end{vmatrix}$$

The values should be interpreted as follows:

- 0.01 is the transition probability from the operational to the repair state. Consequently, $1-0.01 = 0.99$ is the probability of not transitioning to the repair state.
- 0.75 is the transition probability from the repair state to the operational state. Consequently, $1-0.75 = 0.25$ is the probability of not transitioning from the repair state to the operational state.

The steady-state probabilities of state are the nontrivial solution ($\mathbf{X} \neq 0$) of Equation 74.42, which is a normalized eigenvector of $\boldsymbol{T}^T$ for the eigenvalue 1. The system of equations from Equation 74.42 is

$$(0.99\ \ 1)x_i + (0.75\ \ 0)x_2 = 0$$
$$(0.01\ \ 0)x_1 + (0.25\ \ 1)x_2 = 0$$

where

$$T^t = \begin{vmatrix} 0.99 & 0.75 \\ 0.01 & 0.25 \end{vmatrix}$$

and

$$\mathrm{I} = \begin{vmatrix} 1 & 0 \\ 0 & 1 \end{vmatrix}$$

The foregoing system must be solved with the restriction that $x_1 + x_2 = 1$. The solution can be also found directly from the normalized eigenvector for the eigenvalue 1.0 of the transposed transition matrix. The resulting steady-state probabilities are 0.987 and 0.013 of being in the operational and repair states, respectively. Notice that the availability of the system is 0.987.

CASE 3 In Case 3, the following transition probabilities are assumed.

$$T = \begin{vmatrix} 0.1 & 0.5 & 0.4 \\ 0.9 & 0 & 0.1 \\ 0.75 & 0 & 0.25 \end{vmatrix}$$

The transition probabilities should be interpreted as follows:

- The probability for transitioning from the operational state to the test state is 0.5. The transition probability from the operational state to the repair state is 0.4. Consequently, the probability of not transitioning from the operational state is 0.1.
- The probability of transitioning from the test state to the repair state is 0.1. This value represents cases where a degraded condition in the fire pump has been identified. The transition probability from the test to the operational state is 0.9. This value represents the case in which the inspection found the fire pump in good operational condition and, therefore, it is returned to service. At the same time, there is no probability of staying in the inspection state. The pump will eventually return to service or will be sent to repair.
- The probability of transitioning from the repair state to the operational state is 0.75. There is no probability of transitioning from the repair state to the test state. Consequently, there is a 0.25 probability of not transitioning from the repair state.

The normalized eigenvector for the eigenvalue 1.0 of the transposed transition matrix suggests steady-state probabilities 0.476, 0.238, and 0.286 of being in the operational, inspection, and repair states, respectively. Notice that the availability of the system is 0.476. The unavailability of the system is the sum of the probabilities of being in the test and repair states or 0.238 + 0.286 = 0.524.

CASE 4 The transition probabilities for Case 4 are summarized in the following matrix.

$$T = \begin{vmatrix} 0.6 & 0.2 & 0.15 & 0.05 \\ 0.4 & 0.4 & 0 & 0.2 \\ 0.4 & 0 & 0.4 & 0.2 \\ 0.3 & 0.3 & 0.3 & 0.1 \end{vmatrix}$$

The following interpretation should be given to the transition probabilities:

- From State 1, in which both batteries are operable, there are transition probabilities to States 2, 3, and 4. As such, the probability of not transitioning from State 1 is 0.6.
- From State 2, there are transition probabilities to State 1, when the backup battery is replaced, to State 4, if the primary battery also fails before the backup is replaced. There is no probability of transitioning to State 3, since the backup battery would need to be replaced first. Consequently, there is a probability of 0.4 of staying in State 2 (1−(0.4 + 0.2 = 0.4)).
- The transition probabilities from State 3 are similar to those in State 2. The only difference, of course, is that transitions start from State 3. As such, there is no probability of transitioning to State 2, since the primary battery would need to be replaced first.
- There are equal probabilities of 0.3 of transitioning from State 4 to any of the first three states. That is, the probability of replacing one or two batteries is 0.3. Consequently, the probability of not transitioning from State 4 is 0.1.

The normalized eigenvector for the eigenvalue 1.0 of the transposed transition matrix suggests steady-state probabilities 0.486, 0.22, 0.179, and 0.115 of being in States 1, 2, 3, and 4, respectively. Notice that the availability of the system is 0.486 + 0.22 + 0.179 = 0.885. The unavailability of the system is 0.115.

Solving Continuous Time Markov Modeling Solving continuous time Markov models requires the development of a system of ordinary differential equations. Depending on the number of states and different transitions, the system may have an analytical solution. However, it is often practical to input the system of equations in a differential equation solver available in most mathematical software packages, which provides numerical answers in seconds. These systems can be also solved using Monte Carlo simulation.

As mentioned earlier, in the case of continuous time Markov models the transition probabilities are substituted by a constant rate of transition. This is because the rate of the exponential distribution equals the instantaneous probability as in the time interval $(t, t + \Delta t)$ as Δt goes to 0. The development of the system of differential equations is best described using the four cases listed in Fig. 74.20.

CASE 1 Recall that this is a trivial case included for explanatory purposes. In this case, there is only one differential equation. The probability of being in the operational state, L_O,, at time $t + \Delta t$ is

$$L_O(t + \Delta t) = L_O(t)\ \tilde{n}\ (1 - \lambda \Delta t)$$

where the term on the right-hand side is the probability of being in the operational state at time t times the instantaneous probability of no failure in time interval $(t, t + \Delta t)$. Rearranging, dividing by ΔT, and taking the limit as $\Delta t \to 0$, the equation can be written as

$$\frac{dL_O(t)}{dt} = -\lambda \tilde{n} L_O(t)$$

and as expected, solving the differential equation, $L_O\ (t) = \mathrm{e}^{-\lambda t}$. Notice that this is the reliability of a nonrepairable component.

CASE 2 This is the simplest model for a repairable item. One ordinary differential equation should be written for each of the two states. For the operational state

$$L_O(t + \Delta t)\ = L_O(t)\ \tilde{n}\ (1\ - \lambda \Delta t)\ + L_R(t)\ \tilde{n} \mu \Delta t$$

The first term on the right-hand side represents the probability of being in the operational state at time t and a failure doesn't occur. The second term in the right-hand side is the probability of being in the repair state at time t and a repair occurs. For the repair state

$$L_R(t + \Delta t) = L_R(t) \tilde{n} (1 - \ \mu \Delta t) + L_O(t) \tilde{n} \lambda \Delta t$$

Rearranging, dividing by ΔT and taking the limit as $\Delta t \to 0$ in both equations, the resulting system is

$$\frac{dL_O(t)}{dt} = -\lambda \cdot L_O(t) + \mu\ \tilde{n}\ L_R(t)$$

$$\frac{dL_R(t)}{dt} = -\lambda \cdot L_O(t) - \mu\ \tilde{n}\ L_R(t)$$

Solving the foregoing system of equations results in the probability of being in the operational and repair states as a function of time. These are the availability and unavailability values, respectively. The analytical solutions are

$$a(t) = \frac{\mu}{\lambda + \mu} + \frac{\lambda}{\lambda + \mu} \mathrm{e}^{-(\lambda + \mu)t} \qquad (74.43)$$

$$u(t) = \frac{\lambda}{\lambda + \mu} - \frac{\lambda}{\lambda + \mu} \mathrm{e}^{-(\lambda + \mu)t} \qquad (74.44)$$

These equations can be reduced to the first term on the right-hand side, respectively, since the exponential term approximates to 0 for large values of t. The step-by-step analytical result of this system is documented in a number of reliability engineering textbooks [5] (p. 208) and is not reproduced here.

CASE 3 A system of three differential equations must be developed for Case 3, one equation for each of the three states: operational, test, and

repair. For the operational state, the probability of being in state L_O at time $t + \Delta t$ is

$$L_O(t+\Delta t) = L_O(t) - \lambda \Delta L_O(t) - \tau \Delta t L_O(t) + \psi \Delta t L_I(t) + \mu \Delta t L_R(t)$$

The terms on the right-hand side in the preceding equation are

- The probability of being in L_O at time t (first term)
- Minus the probability of transition to the repair state (second term)
- Minus the probability of transition to the test state (third term)
- Plus the probability of being in the test state and transition to operational state (fourth term)
- Plus the probability of being in the repair state and transition to the operational state (fifth term)

Rearranging, dividing by ΔT, and taking the limit as $\Delta t \to 0$, the resulting equation is

$$\frac{dL_O(t)}{dt} = \psi L_I(t) + \mu L_R(t) - \lambda L_O(t) - \tau L_O(t)$$

The process is similar for developing the differential equation for the test state:

$$L_T(t+\Delta t) = L_T(t) + \tau \Delta t L_O(t)\ \psi \Delta t L_T(t) + \gamma \Delta t L_T(t)$$

Rearranging, dividing by ΔT, and taking the limit as $\Delta t \to 0$, the resulting equation is

$$\frac{dL_T(t)}{dt} = \tau L_O(t) - \psi L_T(t) - \gamma L_T(t)$$

Finally, for the repair state:

$$L_R(t+\Delta t) = L_R(t) + \lambda \Delta t L_O(t) + \gamma \Delta t L_I(t) - \mu \Delta t L_R(t)$$

Rearranging, dividing by ΔT and taking the limit as $\Delta t \to 0$, the resulting equation is

$$\frac{dL_R(t)}{dt} = \lambda L_O(t) + \gamma L_I(t) - \mu L_R(t)$$

Example 6 Consider the case of a fire pump subjected to weekly testing as recommended in NFPA 25. The duration of the test is approximated to 1 day. In addition, reliability data for the pump suggest an MTBF of 36 months, and a 5 % chance that the inspection and testing activities will find pump problems requiring repair. Finally, the pump's MTTR is 1 week. What is the availability of the pump?

Solution The problem statement suggest the following rates: (1) the failure rate λ is 1/36 months^{-1}, (2) the repair rate μ is 1/0.25 months^{-1} (approximating 1 week as 0.25 months), (3) the inspection rate τ is also 1/0.25 months^{-1}, (4) the rate at which the pumps return to service after inspection and testing is 1/0.033 months^{-1}, approximating 1 day as 1/30 months, and (5) rate at which pump problems requiring repair are detected during inspection and testing is $0.05 \cdot \tau$. These values are summarized in the transition matrix shown in Table 74.9.

Solving the foregoing system of differential equations numerically with the values in Table 74.9, the state probabilities plotted in Fig. 74.21 are obtained. The steady-state probability of being in the operational state is 0.873. This example was solved assuming the system starts at time 0 in the operational state.

CASE 4 In Case 4, the system consists of four differential equations, one of each of the four states in the Markov model. For State 1,

$$L_1(t+\Delta t) = L_1(t) - \lambda_{sb}\Delta t L_1(t) - \lambda_{cc}\Delta t L_1(t) - \lambda_p \Delta t L_1(t) + \mu \Delta t L_2(t) + \mu \Delta t L_3(t) + \mu_s \Delta t L_4(t)$$

Rearranging, dividing by ΔT, and taking the limit as $\Delta t \to 0$, the resulting equation is

$$\frac{dL_1(t)}{dt} = \mu \cdot L_3(t) + \mu \cdot L_2(t) + \mu_s L_4(t) - \lambda_{sb} L_1(t) - \lambda_{cc} L_1(t) - \lambda_p L_1(t)$$

For State 2,

Table 74.9 Transition matrix for Example 6 (all units in months^{-1})

	Operational	Test	Repair
Operational		$\tau = 1/0.25$	$\lambda = 1/36$
Test	$\psi = 1/0.033$		$\gamma = 0.05 \cdot \tau$
Repair	$\mu = 1/0.25$		

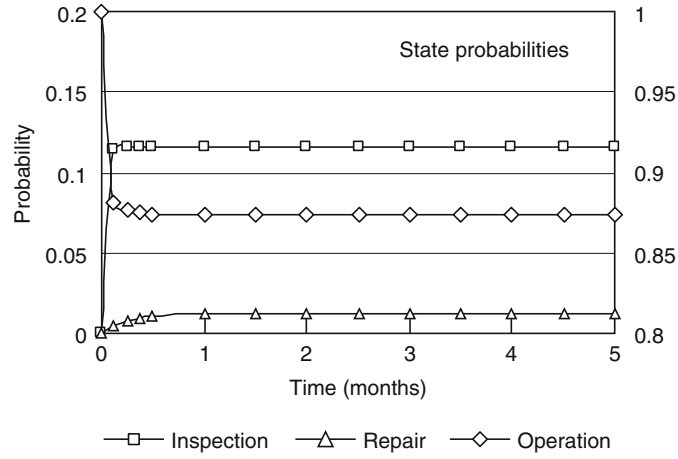

Fig. 74.21 Graphical solution for Example 6. Steady-state probabilities: operational = 0.873 (read in the right y-axis), inspection = 0.116, repair = 0.012

$$L_2(t+\Delta t) = L_2(t) + \lambda_{sb}\Delta t L_1(t) + \mu\Delta t L_4(t) - \mu\Delta t L_2(t) - \lambda_p \Delta t L_2(t)$$

Rearranging, dividing by ΔT, and taking the limit as $\Delta t \to 0$, the resulting equation is

$$\frac{dL_2(t)}{dt} = \lambda_{sb} \cdot L_1(t) + \mu \cdot L_4(t) - \mu L_2(t) - \lambda_p L_2(t)$$

For State 3,

$$L_3(t+\Delta t) = L_3(t) + \mu\Delta t L_4(t) + \lambda_p \Delta t L_1(t) - \lambda_{sb}\Delta t L_3(t) - \mu\Delta t L_3(t)$$

Rearranging, dividing by ΔT, and taking the limit as $\Delta t \to 0$, the resulting equation is

$$\frac{dL_3(t)}{dt} = \mu \cdot L_4(t) + \lambda_p \cdot L_1(t) - \lambda_{sb} L_3(t) - \mu L_3(t)$$

For State 4,

$$L_4(t+\Delta t) = L_4(t) + \lambda_{cc}\Delta t L_1(t) + \lambda_{sb}\Delta t L_3(t) + \lambda_p \Delta t L_2(t) - \mu\Delta t L_4(t) - \mu\Delta t L_4(t) - \mu_s \Delta t L_4(t)$$

Rearranging, dividing by ΔT, and taking the limit as $\Delta t \to 0$, the resulting equation is

$$\frac{dL_1(t)}{dt} = \lambda_{cc} \cdot L_1(t) + \lambda_{sb} \cdot L_3(t) + \lambda_p L_2(t) - \mu L_4(t) - \mu L_4(t) - \mu_s L_4(t)$$

Example 7 Consider a water-based fire protection system designed with redundant pumps. Based on reliability and maintainability data collected over a period of time, the following rates have been calculated:

- The MTBF of the primary pump is 24 months. Therefore, the failure rate, λ_p, is 1/24 months^{-1}.
- The MTBF of the standby pump is 36 months. Therefore, the failure rate, λ_{sb}, is 1/36 months^{-1}.
- The MTTR of either the primary or the standby pump is 2 weeks. Therefore, the repair rate, μ, is 1/0.5 months^{-1}.
- The mean time to common cause failure is 60 months. Therefore, the failure rate, λ_{cc}, is 1/60 months^{-1}.
- The MTTR of both pumps is 3 weeks. Therefore, the repair rate, $\mu_{s,,}$ is 1/0.75 months^{-1}.

Solution The information provided in the problem statement is summarized in the transition matrix in Table 74.10.

Solving the foregoing system of differential equations numerically with the values in Table 74.7, the state probabilities plotted in Fig. 74.22 are obtained. The steady-state probability of being in the operational state is 0.958 + 0.016 + 0.023 = 997. This example was solved assuming the system starts at time 0 in the operational state.

Inspection, Testing and Maintenance Schedules for Achieving Target Availability

Availability is interpreted as the probability of success on demand (i.e., the system is available at the time of the fire). As discussed earlier, fire protection systems are required to be subjected to inspection, testing, maintenance activities with the purpose of increasing the system's availability. Given the requirements for inspection, testing and maintenance, it can be qualitatively argued that such activities will have a positive impact on systems availability. However, a qualitative argument is often not enough to provide fire protection professionals with flexibility to manage inspection, testing and maintenance activities on a performance based/risk informed regulatory framework. The ability to explicitly incorporate these activities into a quantitative model taking advantage of the existing data infrastructure based on current requirements on documenting impairment, provides can quantitative approach for managing fire protection systems.

Table 74.10 Transition matrix for Example 7 (all units in months^{-1})

	State 1	State 2	State 3	State 4
State 1		$\lambda_{sb} = 1/36$	$\lambda_p = 1/24$	$\lambda_{cc} = 1/60$
State 2	$\mu = 1/0.5$			$\lambda_p = 1/24$
State 3	$\mu = 1/0.5$		$\mu = 1/0.5$	$\lambda_{sb} = 1/36$
State 4	$\mu_s = 1/0.75$	$\mu = 1/0.5$		

In practical applications, quantitative availability models are based on performance data generated over time from maintenance, inspection and testing activities. Once explicitly modeled, decision can be made based managing maintenance activities with the goal of maintaining or improving target availability values. Examples include:

- Performance data may suggest key system failure modes that could be identified in time with increased inspections (or completely corrected by design changes) preventing system failures or unnecessary testing.
- Time between inspections, testing and maintenance activities may be able to be increased without affecting the system unavailability

The examples above stress the need for an availability model based on performance data. Consider as an example the Markov models Cases 3 and 4 discussed in examples 6 and 7 earlier in this chapter. The model includes three states: operational, testing and repair. Performance data on the system can be used for determining if random system failures generate to increase or decreased schedule inspections and maintenance activities without affecting the availability values. For a number of systems, the availability models are relatively easy to develop and solved. At the same time, the model inputs are based on the ability to obtain and maintain quality reliability and availability data for characterizing the system.

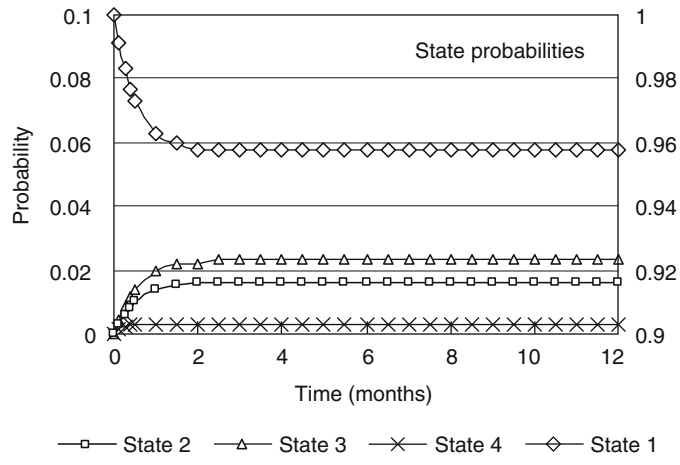

Fig. 74.22 Graphical solution for Example 7. State probabilities: State 1 = 0.958 (read in the right y-axis), State 2 = 0.016, State 3 = 0.023, State 4 = 0.0032

Data Analysis and Parameter Estimation

Statistical data form the basis for most reliability, availability, and maintainability analyses. The collected data are used for estimating the parameters of the appropriate statistical model. This section describes the process of collecting and classifying reliability data and selected statistical techniques for parameter estimation.

Collection of Reliability Data

Reliability data can be obtained from laboratory tests or field observations. Other sources may include generic handbook data or expert judgment. One of the defining attributes of the method of observation is the way the beginning and the end of observation are defined. Ebeling [2], (p. 284) suggests the following classification of reliability data:

1. Operational versus test-generated data
2. Complete versus censored data

Operational versus test-generated data refers to the source of the data. Operational data are usually less expensive and reflect actual operation conditions. On the other hand, test-generated data may be expensive and are usually generated in controlled environments. There are situations, however, where the use of test-generated data is unavoidable. A typical example of this situation is in the testing of a new product where no operational experience is available. Once the data are gathered, it is usually necessary to structure the data such that the data provide the maximum amount of information and are usable in the maximum number of applications for the minimum amount of cost in time and expense.

Complete versus censored data refers to how the data were recorded. A complete data set is one in which all the tested items failed. That is, the time to failure of all tested items is known. Much life data, however, are incomplete [3] (p. 13). In contrast, a censored data set is one in which not all the tested items failed. Specifically, Nelson [3] offers the following classification of censored data:

1. Singly censored data: All units have identical test time, and the test is terminated before all units fail.
   (a) Censored on the left: The failure time is known to be before a specific time.
   (b) Censored on the right: Not all items failed at the end of the test. Consequently, the time to failure of the resulting operating items is known only to be beyond the end of the test. Resulting operating items are usually referred to as survivors or suspensions.
      i. Type I censoring (or time terminated): The data collection process has a predefined duration.
      ii. Type II censoring (or failure terminated): The data collection process ends after a fixed number of failures has occurred.
2. Multiply censored data: Test times or operating times differ among the censored units.

Parameter Estimation: The Maximum Likelihood Estimator

The maximum likelihood (ML) is a method that is often used for estimating probability distribution parameters in most applications. It is most efficient if used with relatively large data samples. To obtain estimates of the distribution parameters, the following likelihood function is developed:

$$L(t,\theta) = \prod_{i=1}^{n} f(t_i,\theta) \tag{74.45}$$

where t_i is the data sample of size n, and θ is the parameter(s) of the probability distribution $f(t)$. The log-likelihood function is a convenient way of representing Equation 74.45.

$$L(t,\theta) = \ln f(t,\theta) = \sum_{i=1}^{n} ln[f(t_i,\theta)] \quad (74.46)$$

For singly censored data, the likelihood function can be modified as follows:

$$L(t,\theta) = \prod_{i=1}^{r} f(t_i,\theta)^{\delta_i} \cdot [1 - F(t_i,\theta)]^{1-\delta_i} \quad (74.47)$$

where δ is 1 for exact failure times and 0 for right-censored data, and $1 - F(t)$ is the probability that the censored units do not fail before the termination of the test. Assuming identical components, the second term in Equation 74.47 can be simplified as follows:

$$[1 - F(t_i,\theta)]^{1-\delta_i} = [R(T_e)]^{n-r} \quad (74.48)$$

where $n - r$ are the censored units and T_e is the test duration for either Type I or Type II data.

Notice that the likelihood function represents the probability distribution $f(x)$ expressed as a function of θ. Therefore, the value of θ that maximizes the function $L(x, \theta)$ can be obtained differentiating Equation 74.46 with respect to θ, setting it to zero, and solving for θ. In the case that $f(x)$ has more than one parameter (let us assume m parameters), a system of m equations resulting from the partial derivative of $L(x, \theta)$ with respect to each of the parameters will need to be solved simultaneously (in most cases using numerical methods).

In the following subsections, the ML method is used for estimating the parameters of the probability distributions discussed previously in the chapter.

Estimating Parameters of the Exponential Distribution Recall that the exponential distribution has only one parameter, λ. Assuming n exact failure time observations (complete data),

$$L(t,\lambda) = \prod_{i=1}^{r} \lambda e^{-\lambda t_i} \quad or \quad \ln[L(t,\lambda)] = \sum_{i=1}^{n} \ln\left[\lambda e^{-\lambda t_i}\right]$$
$$= \sum_{i=1}^{n} [\ln(\lambda) - \lambda t_i] = n\ln(\lambda) - \sum_{i=1}^{n} \lambda t_i$$

From differentiating and setting the resulting function to zero, the following estimate for λ is obtained:

$$\frac{\partial}{\partial \lambda} = \frac{n}{\lambda} - \sum_{i=1}^{n} t_i - 0$$
$$\hat{\lambda} = \frac{n}{\sum_{i=1}^{n} t_i} \quad (74.49)$$

In the case of singly censored data,

$$L(t,\lambda) = \left\{ \prod_{i=1}^{n} \lambda e^{-\lambda t_i} \right\} \left(e^{-\lambda T_e}\right)^{n-r} \quad (74.50)$$

Expressing Equation 74.50 in logarithmic terms, differentiating with respect to λ, and setting the differential to 0 results in (see derivation in Ebeling [2])

$$\hat{\lambda} = \frac{r}{\sum_{i=1}^{r} t_i + (n-r)T_e} \quad (74.51)$$

Estimating Parameters of the Weibull Distribution If the times between failures follow a Weibull distribution, the ML is

$$L(t,\alpha,\beta) = \prod_{i=1}^{n} \frac{\beta t_1^{\beta-1}}{\alpha^{\beta}} e^{-\left(\frac{t_i}{\alpha}\right)^{\beta}} \quad (74.52)$$

Expressing Equation 74.52 in logarithmic terms, differentiating with respect to α and β, setting the two differential equations to 0, and solving the system of equations produces the following estimates [24]:

$$\alpha = \left[\frac{\sum_{i=1}^{n} t_i^{\beta}}{n} \right]^{1/\beta} \quad (74.53)$$

$$\beta = \frac{n}{(1/\alpha)\sum_{i=1}^{n} \left[t_i^{\beta} \ln(t_i)\right] - \sum_{i=1}^{n} \ln(t_i)} \quad (74.54)$$

Notice that this system of equations must be solved simultaneously. In the case of singly censored data

$$L(t,\alpha,\beta)=\left\{\prod_{i=1}^{n}\frac{\beta t_1^{\beta-1}}{\alpha^{\beta}}e^{-\left(\frac{t_i}{\alpha}\right)^{\beta}}\right\}\left(e^{-(T_s/\alpha)^{\beta}}\right)^{n-r} \tag{74.55}$$

Expressing Equation 74.55 in logarithmic terms, differentiating with respect to α and β, setting the two differential equations to 0, and solving the system of equations produces the following estimates (see derivation in Ebeling [2]):

$$\alpha=\left[\frac{(n-r)\cdot t_s^{\beta}\sum_{i=1}^{r}t_i^{\beta}}{r}\right]^{1/\beta} \tag{74.56}$$

$$\frac{1}{r}\sum_{i=1}^{r}\ln(t_i)+\frac{1}{\beta}=\frac{(n-r)t_s^{\beta}\ln(t_s)+\sum_{i=1}^{r}\left[t_i^{\beta}\ln(t_i)\right]}{(n-r)t_s^{\beta}+\sum_{i=1}^{r}\ln(t_i)} \tag{74.57}$$

where t_s is $\sum_{i=1}^{r}t_i+(n-r)T_e$.

Estimating Parameters of the Log-Normal Distribution From the transformation of the normal distribution, the parameters of the log-normal distribution μ and σ are

$$\mu=\frac{1}{n}\sum_{i=1}^{n}\ln(t_i),\ \text{and}\ \sigma^2=\left(\frac{1}{n-1}\right)\sum_{i=1}^{n}[\ln(x_i-\mu)]^2$$

Ebeling [2] describes a numerical algorithm for the estimators for singly censored data of the normal and log-normal distribution.

Estimating Parameters of the Renewal Process In the renewal process, the times between failures are identically distributed. If these times are exponentially or Weibull distributed, the distribution parameters can be obtained using the ML method as described earlier in this section. Specifically, the parameter for the exponential distribution is obtained from Equations 74.49 or 74.50. The parameters for the Weibull distribution can be obtained from Equations 74.53 and 74.54 or 74.56 and 74.57. A similar procedure would need to be followed if failure times are characterized by a different distribution.

Estimating Parameters of the Nonhomogeneous Poisson Process Recall that in the nonhomogenous Poisson process, the first failure is represented with a probability distribution $f(t)$. Subsequent failures are then represented by the conditional distribution $f(t_i/t_i > t_{i-1})$. As an example, the parameters for the nonhomogeneous Poisson process are estimated assuming the failure times follow a Weibull distribution. A similar procedure would need to be followed if failure times are characterized by a different distribution.

For a time-terminated evaluation (e.g., predicting the next failure considering that the item has been operating for some time after the last failure)

$$L(t,\alpha,\beta)=\frac{\beta t_1^{\beta-1}}{\alpha^{\beta}}e^{-\left(\frac{t_1}{\alpha}\right)^{\beta}}\cdot\left\{\prod_{i=2}^{n}\frac{\beta t_i^{\beta-1}}{\alpha^{\beta}}e^{\left(\frac{t_{i-1}}{\alpha}\right)^{\beta}-\left(\frac{t_i}{\alpha}\right)^{\beta}}\right\}\cdot R(T_e/t_n) \tag{74.58}$$

The first term in the right-hand side is the Weibull distribution for the first failure. The second term in the right-hand side, which is inside the product, is the conditional Weibull distribution for failures 2 to n. Finally, the third term in the right-hand side is the probability that the item will not fail before the test is terminated. This last probability is calculated using the conditional Weibull from the time of the last failure until time T_e.

Expressing Equation 74.58 in logarithmic terms, differentiating with respect to α and β, setting the two differential equations to 0, and solving the system of equations produces the following estimates:

$$\alpha=\frac{t_n}{n^{1/\beta}} \tag{74.59}$$

$$\beta = \frac{n}{\sum_{i=1}^{n} \ln\left(\frac{t_n}{t_i}\right)} \tag{74.60}$$

Failure-terminated evaluation:

$$L(t, \alpha, \beta) = \frac{\beta t_1^{\beta-1}}{\alpha^{\beta}} e^{-\left(\frac{t_1}{\alpha}\right)^{\beta}} \cdot \prod_{i=2}^{n} \frac{\beta t_i^{\beta-1}}{\alpha^{\beta}} e^{\left(\frac{t_{i-1}}{\alpha}\right)^{\beta} - \left(\frac{t_i}{\alpha}\right)^{\beta}} \tag{74.61}$$

The first term in the right-hand side is the Weibull distribution for the first failure. The second term in the right-hand side, which is inside the product, is the conditional Weibull distribution for failures 2 to n.

Expressing Equation 74.61 in logarithmic terms, differentiating with respect to α and β, setting the two differential equations to 0, and solving the system of equations produces the following estimates:

$$\alpha = \frac{t_n}{n^{1/\beta}} \tag{74.62}$$

$$\beta = \frac{n-1}{\sum_{i=1}^{n} \ln\left(\frac{t_n}{t_i}\right)} \tag{74.63}$$

Parameter Estimation: Bayesian Analysis

Bayes theorem provides a very useful tool for estimating and updating probability distribution parameters. It should be mentioned that reliability-engineering applications represent a small sample of the universe of applications of Bayes theorem. In general terms, Bayes theorem is expressed as

$$\pi(\lambda/E) = \frac{L(E/\lambda)\pi_o(\lambda)}{k} \tag{74.64}$$

where

$\pi(\lambda/E)$ is the posterior probability of λ given the evidence E, $L(E/\lambda)$ is likelihood function, $\pi_o(\lambda)$ is the prior distribution, and k is a normalizing factor so that the function $\pi(\lambda/E)$ integrates to 1.0 over the appropriate range. Mathematically,

$$k = \int_{-\infty}^{\infty} L(E/\lambda)\pi_o(\lambda)d\lambda$$

The posterior distribution includes two sources of information: (1) the prior distribution, which captures any prior knowledge on the parameter λ; and (2) the likelihood function, which captures the available evidence. The ability to estimate parameters updating prior knowledge as evidence becomes available is a key advantage of using Bayes theorem.

The prior distribution captures any prior knowledge on the parameter λ. In the cases where there is no prior knowledge about λ, the prior distribution can be represented with a uniform probability distribution. Depending on the application, the prior distribution can be developed based on expert judgment.

The likelihood function usually captures the available evidence. It is the probability of the evidence E assuming the value of the unknown quantity is λ.

The posterior distribution $\pi(\lambda/E)$ is a probability distribution for the parameter λ itself. Notice that λ is treated as a random variable. Calculating the mean or median of the posterior distribution would provide a point estimate of λ.

Example 8: Applications to Updating Failure Rates Generic industry data suggest that a diesel generator in an industrial facility can experience three small fires over a period of 5 years due to leaking oil in contact with a hot surface. The same type of diesel generator was installed in a facility 3 years ago. In 3 years of operation, no fire associated with the diesel generator has been recorded. Calculate an updated failure frequency of diesel generator failures due to ignition of oil due to contact with a hot surface.

Solution The posterior distribution represents the updated failure rate. In order to obtain the posterior distribution, the prior distribution and the likelihood function must be identified first. In the case of the prior distribution, a very useful

option for representing the failure rate as a distribution is described in this example in addition to the Bayesian approach.

The prior information consists of a failure rate of $\lambda = 3/5 = 0.6$ failure per year. This value needs to be represented as a probability distribution. Epstein [25] suggests that the random variable $x = 2\lambda T$ follows a chi-square distribution with $\nu = 2r$ degrees of freedom if λ is assumed constant. The variable r is the number of failures and T is the time in which the failures were observed. By transformation $\lambda = x/2T$ (see Papoulis [4], p. 93), a probability distribution for λ can be found from the chi-square distribution for x. In general, the distribution for λ, which is the prior distribution, is

$$\pi_o(\lambda) = \frac{x^{\nu/2-1}\mathrm{e}^{-x/2}}{2^{\nu/2}\Gamma(\nu/2)} \cdot 2T \qquad (74.65)$$

where x is $2\lambda T$, ν is $2r$, and the term $2T$ results from the transformation from x to λ.

The likelihood function incorporates the new evidence into the analysis. In this case, the new evidence is no fires in 3 years. The Poisson distribution as stated in Papoulis [4] (p. 57) is a likely choice to capture evidence in this form. Accordingly,

$$L(\lambda) = \mathrm{e}^{-\lambda T_a}\frac{(\lambda T_a)^k}{k!} \qquad (74.66)$$

where k is the number of failures observed in period T_a. In this example, $k = 0$ and $T_a = 3$. Solving Equation 74.64 numerically as a function of λ using Equations 74.65 and 74.66 as inputs, the mean and median for the posterior are 0.38 and 0.33 fires per year, respectively. These values are lower than the 0.6 and 0.54 fires per year for the mean and median of the prior distribution. The reduction in the mean and median is consistent with the evidence of no fire in the subsequent 3 years. The prior and posterior distributions are plotted in Fig. 74.23.

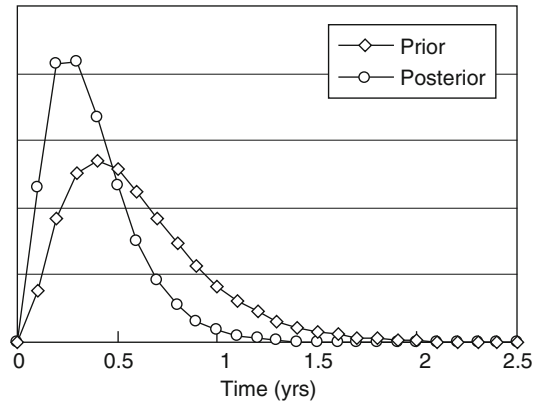

Fig. 74.23 Prior and posterior distribution in Example 8

Accelerated Testing

As stated by Nelson [3], "Accelerated testing consists in a variety of test methods for shortening the life of products or hastening the degradation of their performance. The aim of such testing is to quickly obtain data which, if properly modeled and analyzed, yields desired information on product life and performance under normal use."

Accelerated tests can be broadly classified in two groups: accelerated degradation tests and accelerated life tests. Both of them shorten the time to degradation or failure, respectively, of the tested element. These two broad categories of accelerated tests are further classified in different types of testing methods (see, for example, Nelson [3]). The accelerated life or degradation tests are used to estimate reliability by conducting tests at increased levels of stress. That is, the tested element is evaluated at different stress levels, which at the same time fit a stress life distribution (life-stress relationship model). In the case of accelerated life tests, the main goal is to accelerate the failure of a product. In the case of accelerated degradation tests, the interest is in evaluating predetermined performance measures in the product. Examples of degradation processes may include crack grow/propagation, corrosion, and so on.

Perhaps the most important aspect of accelerated testing is the identification and characterization of the stresses affecting the operating environment of the component. A component can be stressed by increasing its usage rate, increasing the aging rate, or increasing the level of stress affecting any of its failure

mechanisms. Stresses may vary in type and in time. Examples of stresses are temperature, usage rate, loading, and so on. Furthermore, stresses can be constant, progressive, cyclic, and so on. It is important to choose accelerating variables that correspond to the failure mechanism. Once the stress has been identified, a life-stress relationship model can be developed.

Life-stress relationship models can be physical or empirical. Physical models are used for well-understood failure mechanisms. These models are based on physical/chemical theory that describes the failure-causing process. The advantage of physical models is that they may be used for extrapolation. Empirical models are used when there is little understanding of the chemical and physical processes describing the failure mechanisms. Empirical models may often provide an excellent fit to available data but may not be used for extrapolations. Figure 74.24 illustrates a conceptual representation of a life-stress relationship model. A physical or empirical model defines the life expectancy of an item subjected to a given stress level. There is a probability that the item will fail given a stress level. This probability is represented by a distribution reflected on the *y*-axis.

Some Popular Models

The following subsections briefly describe two popular life-stress models and the process of characterizing probability distributions for different stress levels.

The Arrhenius life-temperature relationship: Perhaps the most common model for predicting an item's life as a function of temperature is the Arrhenius life-temperature relationship. This relationship is used to describe products that fail as a result of degradation due to chemical reactions or metal diffusion. According to this relationship, the rate of reaction is given by

$$\text{Rate} = A' e^{-E/kT} \tag{74.67}$$

where E is the activation energy (usually in electron volts), k is the Stefan Boltzmann constant ($8.6171 \cdot 10^{-5}$), T is the absolute temperature, and A' is a constant usually obtained from data. Considering that the reaction rate is inversely proportional to the item's life, the Arrhenius life-temperature relationship is

$$t = Ae^{-E/kT} \tag{74.68}$$

Example: Application in Fire Testing NUREG/CR-5546 [26] describes an investigation of thermal aging on the fire damageability of electric cables. The investigation consisted in subjecting energized cables to high-temperature environments in a chamber. Previous to the experiments in the chamber, the Arrhenius model was utilized to account for the thermal aging of cables. A thermal oven was used to provide a constant elevated aging temperature for a period of 28 days. It was determined that the 1-month aging temperature was equivalent to a 40-year life. The aging temperature was calculated as follows:

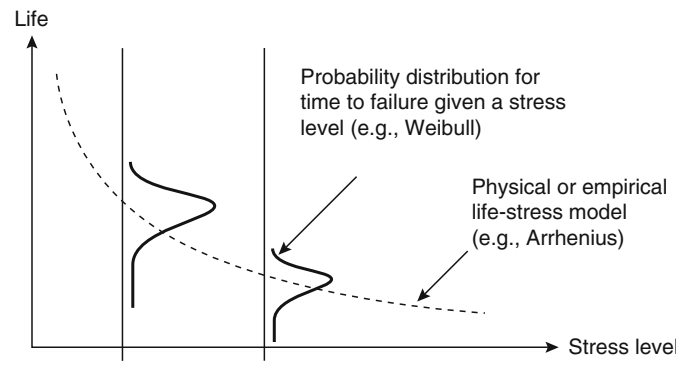

Fig. 74.24 Conceptual representation of a life-stress relationship model

$$\frac{t_o}{t_a} = \frac{A\mathrm{e}^{-E/kT_{\mathrm{amb}}}}{A^{-E}\mathrm{e}^{kT_{\mathrm{oven}}}}$$

where T_{amb} is the "real" temperature at which the cables are usually exposed, T_{oven} is the aging temperature at which the oven is going to be set, t_o is 40 years, and t_a is 28 days. Assuming $E = 0.83$ eV, and $T_{\mathrm{amb}} = 59$ °C, A cancels resulting in $T_{\mathrm{oven}} = 150$ °C. That is, according to the Arrehnius life-temperature relationship model, having cables in a 150 °C thermal environment for 28 days is equivalent to having cables in a 59 °C thermal environment for 40 years.

The Inverse Power Relationship In the case of the inverse power relationship (or inverse power law), the item's life is associated with an accelerated stress. This relationship has been found to be empirically adequate for many products including ball and roller bearings, flash lamps, and so on.

For an accelerated stress variable S, the item's life t is approximated with the inverse power relationship as

$$t(S) = \frac{A}{S^{\gamma}} \qquad (74.69)$$

where A and g are constant parameters obtained from the data.

Probabilistic life-stress relationships: As suggested earlier in this section, the probabilistic life-stress relationship, such as the one depicted in Fig. 74.24, requires two general elements: (1) a physical or empirical model, and (2) a probability distribution. In addition to those two elements, experimental data are usually required to find the correlating constants in both the model and the distribution.

Example: Application: The Arrhenius-Weibull Model. Let us assume that after careful evaluation, temperature has been identified as an important factor affecting a product's life and the Arrhenius relationship has been selected as the model for associating operating temperature and life. Let us further assume that under a given operating temperature, the item's life follows a Weibull distribution:

$$f(t) = \begin{cases} \dfrac{\beta(t-t_o)^{\beta-1}}{\alpha^{\beta}}\mathrm{e}^{-\left(\frac{t-t_o}{\alpha}\right)^{\beta}} & t \geq t_o \\ 0 & \text{otherwise} \end{cases}$$

Since α is the location parameter, it is set equal to the Arrhenius life-temperature model.

$$\alpha = A\mathrm{e}^{-E/kT}$$

Substituting in the Weibull distribution,

$$f(t,T) = \begin{cases} \dfrac{\beta(t-t_o)^{\beta-1}}{\left(A\mathrm{e}^{-E/kT}\right)^{\beta}}\mathrm{e}^{-\left(\frac{t-t_o}{A\mathrm{e}^{-E/kT}}\right)^{\beta}} & t \geq t_o \\ 0 & \text{otherwise} \end{cases}$$

Assuming a known activation energy, the parameters t_o, β, and A can be obtained from experimental data using methods such as the maximum likelihood estimator. As constants, these parameters are independent of temperature.

Other Probabilistic Life-Stress Relationships The Arrhenius-Weibull relationship is only one in many relationships that have been and can be developed. In general, this combination of physical or empirical models governing the behavior of an item under stress and probability distribution can be a useful tool for considering uncertainty in failure predictions.

Examples of other combinations available in the accelerated testing literature are Arrhenius–log-normal, inverse power–Weilbull, and inverse power–log-normal.

Cautionary Remarks

Three general assumptions govern the foregoing accelerated testing discussion:

1. Only a transformation of time will be observed due to elevated stresses.
2. Failure or degradation times are accelerated.
3. No new failure modes are introduced.

These assumptions, however, may not be applicable to all products. The following cautionary remarks are important to consider:

1. It may be argued that accelerated tests do not reflect actual use conditions of the product in

the field. As an example, consider the case of some levels of an accelerating factor increasing (instead of shortening) the life of a product. Such an argument stresses the importance of careful selection and evaluation of accelerating factors.
2. High levels of stresses may introduce new failure modes not observed under "normal" operating conditions. Also, high stress levels may change the life-stress relationship model.
3. Some products are characterized by multiple and relatively equally likely failure modes. In those cases, life-stress relationships should capture both failure modes so that life predictions result from a contribution of the modeled failure modes.

Software Reliability

Software reliability is a relatively young field. At the same time, the need for estimating software reliability is growing, as longer and more complex software is available for different applications. Treatment of software failures may be critical in some applications where computer programs perform important tasks. At the same time, software reliability applications in fire protection engineering are limited. Some applications may include the development process of computer fire models, treatment of fire protection system failures due to software errors, and treatment of software failures in fire risk assessments.

The following definitions are important in the field of software reliability:

- *Software reliability*. The probability that the software will be operational during a predefined period of time
- *Software maintainability*. The probability that the software will be restored to working condition in a given period of time
- *Software availability*. The probability that the software is operational (not failed) at a given time t
- *Bug*. A software design flaw that will result in symptoms exhibited during testing or normal operation
- *Software error*. An error made by the programmer (e.g., typographical error, omission, or incorrect numerical value [constant])
- *Software fault*. Software defect that causes a failure
- *Software failure*. A software failure occurs when the user perceives that the output of the program is incorrect, that is, an unacceptable departure of a program operation from program requirements

Notice that most of these definitions are consistent with the reliability, availability, and maintainability analysis of hardware items. In fact, some of the modeling techniques are similar, including (but not limited to) the failure data collection during tests, the determination of software failure rates, and the failure prediction using the nonhomogenous Poisson process. Pham [27](p. 4) indicates that there are more than 50 models for quantifying software reliability. Currently, the field has matured to the point that models can be applied in practical situations providing meaningful results. At the same time, there is no one model that is best for all situations.

From a reliability point of view, software is different from hardware in the sense that it does not degrade or wear out because of time. The failure mechanisms are different. The majority of hardware faults are physical faults due to inherent material defects or the interaction of materials with the environment. In the case of software, most of the faults are design faults, which are introduced by humans during the development process. Software deterioration may also occur in the process of upgrading it due to the introduction of new programming errors. This characteristic is conceptually captured in Fig. 74.25, which presents a conceptual hazard rate curve for software.

Another important difference between hardware and software failures is that the latter often do not provide any warnings.

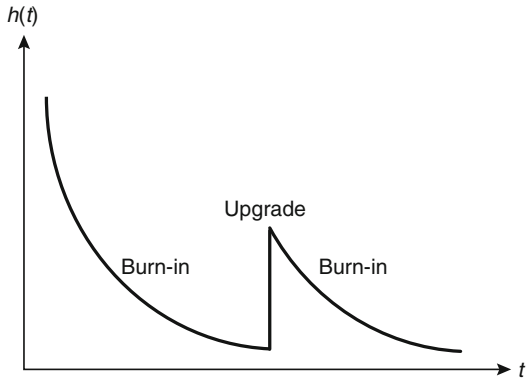

Fig. 74.25 Conceptual hazard rate curve for software

Software Reliability and Fire Risk Assessment

Currently, even detailed fire probabilistic risk assessment methodologies [7] do not include specific qualitative or quantitative treatment of software failures. Instead, software-related failure modes are assumed to be part of a broader hardware system failure or initiating event. That is, the system model is not developed to a resolution in which software failure modes are explicitly modeled. However, the explicit treatment of software failures may eventually be incorporated in fire risk assessments as the interest in detailed fire risk analysis grows.

Software Verification and Validation

The subject of software verification and validation (V&V) of fire models is closely related to the software reliability field. The main difference between software reliability and software V&V is that the former is intended for the evaluation of the probability of software failures and the latter can be considered a rigorous software quality check.

In the case of a computer fire model, software verification refers to a detailed evaluation of the computer implementation. Verification includes activities such as verifying that the selected algorithm for solving a system of equations is correctly programmed. In general terms, a software verification process is intended to check that the software product meets the designed specifications.

On the other hand, software validation refers to an assessment of the predictive capabilities of the model. In the case of a computer fire model, a validation process includes activities such as comparing model results to experimental data. In general terms, a software validation process is intended to check that the software can be used for its intended applications.

ASTM E1355-05, *Standard Guide for Evaluating the Predictive Capability of Deterministic Fire Models* [28], documents guidelines for performing a fire model V&V analysis. It recommends the following steps for conducting a software V&V:

- Define the model and scenarios for which the evaluation is to be conducted.
- Assess the appropriateness of the theoretical basis and assumptions used in the model.
- Assess the mathematical and numerical robustness of the model.
- Validate the model by quantifying its accuracy in predicting the course of events for intended fire scenarios.

It should be stressed that ASTM E1355-05 recommends a quantitative assessment of the predictive capabilities of the model under evaluation.

Human Reliability

Human reliability analysis (HRA) is a structured approach used to identify potential human error events and to systematically estimate the probability of those errors using data, models, or expert judgment [7]. *Notice that this definition is perhaps more appropriate to the term "Human Unreliability Analysis" as it refers to calculating human error probabilities*. Nevertheless, this structured approach enables analysts to incorporate the impact of human actions on the quantitative reliability analysis of complex systems that may support a risk assessment.

Human behavior in fire has always been an important aspect of fire protection engineering. Traditionally, fire protection engineers have

considered human behavior and human factors in fire department or fire brigade activities, life safety, egress, and fire protection system designs. However, the current knowledge in human behavior in fire and human response to fire events has not been formalized as a quantitative model for identifying and evaluating human errors. Although a specific model for fire HRA may not be available, the current HRA technology can be very helpful in the following areas:

- *Quantitative fire risk analysis*. Human error probabilities may be explicitly included in the basic events of logic models such as fault trees. Consequently, a logic model quantification process will require a numerical representation of the human error events.
- *Risk reduction potential*. In contrast with a quantitative risk assessment, which may be used for supporting regulatory decisions, human reliability analysis can be used for determining risk reduction potential. In this case, human error events expressed in relative terms as the resulting risk values are only compared with each other and not against regulatory criteria.
- *Prevention of industrial accidents*. This is mostly a qualitative assessment generally intended for identifying and protecting against consequences generated by human errors. In the case of fire protection engineering, this may include (1) preparing inspection and maintenance procedures such that human errors are minimized, (2) identifying human errors that may generate a fire event, and/or (3) identifying human errors that may affect (delay or prevent) the timely response to a fire

Qualitatively, identifying conditions that can lead to erroneous actions (human error events) in work operations requires a systematic evaluation of the system under analysis. The process of identifying human error events requires a team with expertise in cognitive science, psychology, human factors, and the operations under evaluation. In some cases, particularly during the design stage, such conditions can be corrected or improved with relatively small amount of resources.

The quantitative aspect of HRA builds on the qualitative analysis of work operations where human errors are identified. In practice, probabilities are calculated for the identified human error events. The actual process of calculating probabilities may have different levels of complexity depending on the selected model, the nature of the human error events, and the conditions leading to those errors. Available HRA models (discussed briefly later in this section) usually provide relative indicators or error likeliness, which are very useful in determining areas where improvements to tasks or procedures can be made.

Some Relevant Definitions

Let's start our brief discussion of human reliability by considering some useful definitions. It should be noted that recent HRA literature suggests that there is still disagreement within the community in the use of some key terms and definitions [29]. Considering any disagreement still present in the field, the following definitions can be helpful in understanding different HRA methods (the definitions were compiled from a number of sources):

Human factors	The study of how humans behave physically and psychologically in relation to particular environments, products, or services.
Human action	The motion(s), decision(s), or thinking of one or more people required to complete a postulated mission defined in a scenario.
Human error	Failure of a postulated human action in a given scenario.
Human error probability (HEP)	The probability of a human error.

Error of commission	Manifestation of an unintended or unplanned action; in other words, an incorrect action was performed.
Error of omission	Failure to perform an action; an omission is registered if the appropriate action was not carried out when required.
Extraneous error	Refers to a wrong (or unrequired) action performed.
Latent error	Those errors committed pre-event initiation and whose effects are not realized until the event occurs. Latent conditions influencing an accident event can be present for long periods of time before combining with other workplace factors including active errors to produce the accident.
Active error	Those errors resulting in accident initiations, or those that occur in response to an accident.
Cognition	Refers to the conscious process to obtain knowledge, think, decide, and learn, considering aspects such as situation awareness, perception, reasoning, and judgment.
Cognitive error	The cause for the manifestation of either errors of omission or commission. The potential for cognitive errors may increase if, for example, an operator needs to rely on theory or abstract knowledge to make a decision.
Human failure event (HFE)	In risk analysis, a human failure event is a basic event in a logic model (see the discussion on fault trees later in this chapter).
Performance shaping factor	A factor influencing the probability of human error. Typical performance shaping factors include: available time to complete the task, stress (e.g., mental stress, excessive workload, physical stress), environmental conditions (e.g., noise, toxicity), task complexity, experience and/or training conducting the task, available procedures for completing the task, ergonomics and/or human-machine interactions, and fitness for duty.
Error-forcing context	The situation that arises when particular combinations of performance shaping factors and situation conditions create an environment in which unsafe actions are more likely to occur.
Action	An activity, typically observable and usually involving the manipulation of equipment, that is carried out by an operator(s) to achieve a certain outcome. The required diagnosis of the need to perform the activity; the subsequent decision to perform the activity; obtaining any necessary equipment, procedures, or other aids or devices necessary to perform the activity; traveling to the location to perform the activity; implementing the activity; and checking that the activity has had its desired effect are all

	implied and encompassed by the term *action*.
Available time (or time available)	The time period from a presentation of a cue for an action to the time of adverse consequences if the action is not taken.
Diagnosis time	The time required for an operator(s) to examine and evaluate data to determine the need for, and to make the decision to implement, an action.
Implementation time	The time required by the operator(s) to successfully perform the manipulative aspects of an action (i.e., not the diagnosis aspects themselves, but typically as a result of the diagnosis aspects), including obtaining any necessary equipment, procedures, or other aids or devices; traveling to the necessary location; implementing the action; and checking that the action has had its desired effect.
Mental model	From a system operations perspective, a mental representation that integrates a person's understanding of how systems and plants work. A mental model enables a person to mentally simulate plant and system performance in order to predict or anticipate plant and equipment behavior.
Situation assessment	Situation assessment involves developing and updating a mental representation of the factors known or thought to be affecting the current set of conditions at a given point in time.
Situation model	A mental representation of the current set of conditions, and the factors thought to be affecting these conditions, resulting from the operator's situation assessment. The situation model is created by an interpretation of operational data in light of the operator's mental model. An operator's situation model is usually updated constantly as new information is received.

Some Human Error Examples

NUREG/CR-6738, "Risk Methods Insights Gained from Fire Incidents" [30] summarizes the following examples of human errors associated with fire events in commercial nuclear power plants (see NUREG/CR-6738 for additional details on the events). The following human errors occurred after the fire ignition:

- Waterford (1985): A main feedwater pump caught fire. The plant operator at the scene called the control room with the wrong pump tag number. This error resulted in the undamaged pump being shut down from the control room.
- Robinson (1989): During an outage a maintenance crew connected a hydrogen source to the plant compressed air system in error. The compressed air system was operating at a lower pressure than the hydrogen source. Hydrogen entered the compressed air system, was distributed to pipes throughout the plant, and exited the system at several locations (wherever the compressed air system was being used within the plant). The escaping

hydrogen caught fire at various points where ignition sources were present.
- Waterford (1995): During a switchgear fire, operators failed to promptly declare the event. The plant procedures apparently did call for operators to verify the presence of flames before declaring a fire emergency. However, the failure to declare a fire given the reports of "heavy smoke" issuing from the switchgear room is considered a human error event in the context of a fire probabilistic risk assessment. This error led to a substantial delay in activating the fire brigade.

The following examples, also listed in NUREG/CR-6738, suggest errors that led to a fire or compromised the response to the fire:
- At Browns Ferry (1975), the fire was ignited by a technician who allowed the lit candle he was carrying near penetration seals to touch unprotected seal material. Several fires involving the same ignition scenario, albeit all of no significant consequence, had occurred prior to the incident on March 22, 1975. Plant management and operators failed to take note of the earlier events and to disallow further usage.
- At Armenia (1982), the fixed suppression system for the cable gallery where the fire started was switched to the manual actuation mode (disabling automatic initiation) prior to the event. Fire damage to associated system cables rendered the system inoperable relatively early in the incident. Repeated attempts to manually actuate the system failed.
- At South Ukraine (1984), the fixed fire suppression system for the containment had been switched to the manual actuation mode (disabling automatic initiation) sometime before the fire occurred. Plant personnel apparently also failed to switch the system back to its automatic mode or to manually actuate the system after the existence of the fire was verified.

It is interesting to note that some of the human error scenarios described above (Robinson, 1989, and Waterford, 1985) can be categorized as errors of commission. That is, the operators took an action that further complicated the situation or created a new undesired condition for the plant. The remaining case examples involved errors of omission. That is, operators failed to take an action that would have contributed to mitigation of the incident.

The HRA Process

This section describes in very general terms a process for conducting human reliability analysis. Not all the steps may be necessary in a given application. At the same time, it should be noted that a comprehensive HRA may require expertise in more than one HRA method or a team of experts in relevant technical areas.

Problem Definition Kirwan [31] suggests the following two questions should be answered in defining the HRA problem:
1. Should the HRA be qualitative or quantitative?
2. How far should the scope of the HRA analysis extend?

The latter question refers to which specific tasks or events within the process or accident under analysis will require quantification of human error probabilities. In answering these two questions, analysts often compromise between the ideal outcome of the analysis and any availability constraints (e.g., available data, available resources, analytical capabilities, etc.).

Notice that the process or accident under analysis may consist of relatively complex interactions between operators and hardware and software systems associated with multiple human error events. In such cases, it may not be feasible or desirable to analyze all possible tasks that may be undertaken. Consequently, the HRA analyst must set the scope of the analysis in a way that offers an appropriate and reasonable level of investigation, assessment of the system vulnerability to human errors, and human error quantification.

Qualitative Analysis The qualitative analysis consists primarily of (1) identifying human error events in the scenarios or tasks under analysis, (2) determining the appropriate performance shaping factors affecting the human error probabilities, and (3) determining how the human errors will be represented in the quantitative risk assessment.

Identifying human errors (*task analysis*). Generally, the process of identifying human error events consists of

- Developing a description (or reviewing existing procedures) of typical expected steps to be followed in the tasks under analysis, for example, in response to a fire event
- Understanding the impact of specific trainings offered for conducting the tasks under analysis

The process of identifying human errors may need to incorporate (1) operators or personnel with expertise performing the tasks under analysis; (2) experts in cognitive science, psychology, and human factors; and (3) interviews and simulations of the corresponding tasks. Such activities should be focused on understanding the human thought process before and after conducting an action. Particular attention should be given to the interaction between the human(s), the procedures being followed, the system response to operator actions, and the environmental conditions. Specifically, errors could be identified by postulating what operators are likely to think and do, what types of actions they may take in a given situation, and how the system or sequence of events may be affected by such actions.

As an example, consider a procedure requiring an operator to read information from an interface [32]. Some considerations that should be evaluated in determining if such an activity may result in an erroneous action include (but may not be limited to):

1. Can the display be read with sufficient accuracy from different viewing positions?
2. Is the information in the display presented in an appropriate form for an operator to use it effectively?
3. Can the display be located easily?
4. Can the display be confused with other nearby information?
5. Does the information processing impose an unacceptable memory load?
6. Does the information require interpretation from the operators?

The answers to these questions may suggest different types of errors that may need to be included in a logic model and quantified. Kirwan [31] offers the following classification of basic error modes:

- Errors of omission
  - Omits an entire task or omits steps in a task
- Errors of commission
  - Time errors: errors too early or too late
  - Latent error prevents execution
  - Qualitative errors: too much of an action, too little from an action, action repeated
  - Selection errors: right action on wrong object, wrong action on right object, wrong action on wrong object
  - Wrong information or communication error
  - Sequence errors: incorrect sequence
- Extraneous errors
  - Rule violations

Performance Shaping Factors Many, if not most, HRA methods use performance shaping factors (PSF) information in the estimation of human error probabilities. In general, performance shaping factors may enhance the degree of realism present in HRA analysis. It is important to understand which performance shaping factors are within the capabilities of the selected quantitative model and how they should be specified. The following list provides examples of performance shaping factors [33].

- *Available time*. Refers to the amount of time available for an operator or a crew to diagnose and act upon an abnormal event. A shortage of time can affect the operator's ability to think clearly and consider alternatives. It may also affect the operator's ability to perform.

- *Stress/stressors*. Stress has been broadly defined and used to describe negative as well as positive motivating forces of human performance. Stress can include mental stress, excessive workload, or physical stress (such as that imposed by difficult environmental factors). Environmental factors often referred to as stressors, such as excessive heat, noise, poor ventilation, or radiation, can induce stress in a person and affect the operator's mental or physical performance.
- *Complexity*. Refers to how difficult the task is to perform in the given context. Complexity considers both the task and the environment in which it is to be performed. The more difficult the task is to perform, the greater the chance for human error. Similarly, the more ambiguous the task is, the greater the chance for human error. Complexity also considers the mental effort required, such as when performing mental calculations; the memory requirements; the process of understanding the underlying model of how the system works; and the reliance on knowledge instead of training or practice. Complexity can also refer to physical efforts required, such as physical actions that are difficult because of complicated patterns of movements.
- *Experience and training*. Refer to the experience and training of the operator(s) involved in the task. Included in this consideration are the years of experience of the individual or crew and whether or not the operator or crew have been trained on the type of accident, the amount of time that has passed since training, and the systems involved in the task and scenario. Another consideration is whether the scenario is novel or unique (i.e., whether the crew or individual has been involved in a similar scenario, in either a training or an operational setting).
- *Procedures*. Refers to the existence and use of formal operating procedures for the tasks under consideration. Common problems seen in event investigations for procedures include situations where procedures give wrong or inadequate information regarding a particular control sequence. Another common problem is the ambiguity of steps.
- *Ergonomics and HMI*. Ergonomics refers to the equipment, displays and controls, layout, quality and quantity of information available from instrumentation, and the interaction of the operator or crew with the equipment to carry out tasks. Aspects of human-machine interaction (HMI) are included in this category. The adequacy or inadequacy of computer software is also included in this PSF.
- *Fitness for duty*. Fitness for duty refers to whether the individual performing the task is physically and mentally fit to perform the task at the time. Factors that may affect fitness include fatigue, sickness, drug use (legal or illegal), overconfidence, personal problems, and distractions. Fitness for duty includes factors associated with individuals but not related to training, experience, or stress.
- *Work processes*. Refer to aspects of doing work, including interorganizational, safety culture, work planning, communication, and management support and policies. How work is planned, communicated, and executed can affect individual and crew performance. If planning and communication are poor, then individuals may not fully understand the work requirements. Work processes include consideration of coordination, command, and control. Work processes also include any management, organizational, or supervisory factors that may affect performance.

In the specific case of fire risk analysis, research is still needed for further developing some of the performance shaping factors listed above to account for fire-generated conditions. Notice that performance shaping factors for fire risk analysis applications should include those (1) associated with humans in direct contact with fire-generated conditions (e.g., a control room operator performing a task with smoke migrating into the control room) or (2) those associated with humans making decisions and performing actions in response to the fire but away from

the fire-generated conditions. NUREG/CR-6850 [7] lists various performance shaping factors associated with fire events. These performance shaping factors are developed for commercial nuclear power plant applications where operators must monitor and control the plant while keeping track of fire suppression activities. Furthermore, the shaping factors for fire applications have not been numerically characterized yet and are not included in any quantitative HRA method.

- *Available staffing resources*. Fire can introduce additional demands for staffing resources beyond what is typically assumed for handling accidents not involving fire. These demands can take the form of needing to use and coordinate with more personnel such as the fire brigade and/or local fire department personnel.
- *Applicability and suitability of training and experience*. The familiarity and level of training (e.g., types of scenarios, frequency of training, or classroom discussions or simulations) for addressing the range of possible fires and potential actions.
- *Suitability of relevant procedures and administrative controls*. Depending on the fire, the operators may need to use other procedures or controls than those typically used in response to accidents not involving fires. This could lead to less familiarity or even confusion with regard to implementing different or multiple procedures simultaneously.
- *Availability and clarity of instrumentation* (*cues to take actions as well as confirm expected plant response*). Fires can introduce multiple spurious events and indications unlike that expected in other accidents not involving fires. This can add confusion with regard to the true plant status and the subsequent actions for operators to take as they sort out what is false from what is actually happening, as well as the need to address unwanted spurious events (e.g., spurious closing of an injection valve). This sorting-out process can, at best, add to the time to perform necessary actions and, at worst, cause the operators to not take appropriate actions at all or perform procedure-directed actions under the wrong circumstances or at the wrong time (e.g., by procedure, shut down an otherwise operable pump because of a spurious high-temperature alarm).
- *Time available and time needed to complete the act*, *including the effect of concurrent and competing activities*. Many of the other PSFs may influence the overall estimate of the time available and needed to complete desirable actions. For example, spurious closure of a valve used in the suction path of many injection paths may need quick detection and response by the crew. Use of less familiar or otherwise different procedure steps and sequencing could change the anticipated timing of actions in response to a fire. Interfacing with the fire brigade may delay performing some actions. The desired actions may be more complex and necessitate an increased workload than for internal events response (e.g., disable an equipment item before repositioning it, as opposed to simply repositioning it during an internal event). Accessibility issues, harsher environments, the need for other special tools, and so on, may also impact the overall timeline of how quickly actions normally addressed in response to internal events can be performed under fire conditions. Furthermore, potential fire growth and suppression could alter equipment failure considerations from those considered for internal events. The timing of important actions needs to be reconsidered with the fire and its effects.
- *Environment in which the act needs to be performed*. Fires can introduce new environmental considerations not normally experienced in the response to internal events. These include heat, smoke, the use of water or other fire-suppression agents or chemicals, toxic gases, and different radiation exposure or contamination levels. Any or all of these may affect the accomplishment of the desired action.

- *Accessibility and operability of equipment to be manipulated*. Fires and their effects (e.g., environment) could eliminate or at least delay the ability to take actions otherwise credited in other types of accidents because the location is inaccessible. Additionally, fires can cause failure of equipment used in the desirable action (e.g., irreversible damage) so that it should be considered inoperable, even manually.
- *The need for special tools* (*keys*, *ladders*, *hoses*, *clothing to enter a radiation area*, etc.). Fires may cause the need for special tools or clothing (e.g., breathing gear, protective clothing) not otherwise considered in response to internal events. The accessibility of these tools or clothing needs to be checked so that the desired actions can indeed be performed in a fire situation. Furthermore, the level of familiarity and training on using these special tools need to be assessed.
- *Communications*. Necessary communications to carry out the desired actions may or may not be available in some fires. This needs to be checked, as does the level of familiarity and training to use any special communication devices.
- *Special fitness needs*. Should the fire and its effects cause the need to consider actions not previously considered under accidents not involving fires, or changes to how previously considered actions are performed, checks should be made to ensure unique fitness needs are not introduced.

Depending on the HRA model selected, performance shaping factors such as the ones listed above are numerically characterized in one form or another in the quantification process.

Representation of Human Error Events in a Quantitative Risk Assessment Finally, human error events usually need to be included in a system model as part of a quantitative risk assessment. To do so, it is necessary to incorporate them in the logic model so that the operation of the system is accurately represented. In very general terms, the human events can be modeled using fault trees and event trees considering the capabilities of each tool. For example, an event tree is probably more appropriate to capture the sequential order of human actions. At the same time, the event tree will only capture dependencies between events by probability point values in the branch lines.

Quantitative Analysis A comparison between the nature of the human actions under analysis and the capabilities of specific HRA methods will ultimately suggest an appropriate method to use. Quantitative HRA methods can be generally classified as simulation models, expert judgment methods, and analytical methods. Simulation models are those that primarily rely on computer methods to mimic human behavior under certain conditions. Expert judgment methods may be necessary where there is little or no useful human error data for supporting a quantitative analysis. Finally, analytical methods generally use a model based on a number of parameters to provide an estimate of human reliability. It should be noted that analytical methods are often used in quantitative risk assessments in the commercial nuclear industry.

Documentation Documentation is particularly important in HRA since a number of technical aspects in the analysis may be on the analysis team judgment. The following aspects of the analysis should be carefully documented: (1) the analysis team, (2) the task analysis including the identified human errors, (3) specification of performance shaping factors, (4) quantification of human error probabilities, (5) representation of human errors in a quantitative risk assessment, and (6) data sources.

HRA Models

HRA methods have evolved over the past 30 years in response to the need to improve the understanding of human performance in the behavioral sciences and to improve human error probability estimates in a quantitative risk assessment. Simple

modeling and quantitative techniques developed more than 25 years ago continue to be used today. At the same time, newer methods try to better incorporate the conditions under which human actions could be performed.

Specifically, there are a number of HRA models available. Swain [34] (p. 306), for example, lists 15 of them. In discussing the limitations of HRA, Swain indicates that there is a "wide disparity in the use of HRA methods." Swain's paper [34] also lists references for the 15 models. Hollnagel [29], for example, describes and discusses some of these methods. Furthermore, NUREG-1842, "Evaluation of Human Reliability Methods Against Good Practices" [35] presents a comparison among some of the available methods and models. Given the status of the technology, describing each model is out of the scope of this section. Instead, this section briefly describes general trends, strengths, and limitations of some of these models.

HRA models can be classified as first or second generation. This classification is not based on the chronological order in which they were developed but in the explicit consideration of the human decision-making process. The first generation of HRA methods consider a safety-related human action to be similar to a component or system that either succeeds or fails in its intended function. In the second generation, methods explicitly incorporate some kind of a model of human cognitive behavior that takes into account advances in behavioral sciences. This is intended to provide a much richer description of the human-system interactions, which considers, among other issues, the context in which the human makes decisions.

Another practical classification is in terms of the model capabilities for qualitative and quantitative analysis. That is, some methods and models have capabilities for identifying human error events and searching for the most relevant human performance factors, and others only address the quantification aspects of the analysis.

There are strengths and limitations in every HRA model. Perhaps the most important limitation is the lack of validation data. Curiously, this is a limitation present in the first generation models that the second generation models did not address. To the contrary, second generation models may need even more data for validation. Nevertheless, HRA practitioners are continuously trying to collect relevant data and improve available methods models to expand the application of human reliability analysis to different fields (such as fire risk assessment) and to generate probabilities that best represent the identified human errors.

System Modeling and Analysis

A system is a collection of items (e.g., subsystems, components, etc.) whose proper coordinated function leads to the proper functioning of the system itself. As mentioned by Vesely [36], the primary objective of system analysis is not to develop a system model but to gain information about it. In system analysis, it is important to model the proper relationship between subsystems and components as well as the reliability or availability of the individual items to determine the reliability or availability of the system as a whole.

Perhaps the first step in developing a system model is to determine its boundaries. System boundaries refer to the number of subsystems to include and the resolution of each subsystem (i.e., which component to include). The determination of system boundaries usually considers economic resources and the level of sophistication the model needs to have in order to support practical applications.

Subsystems or components are not limited to hardware items. They may include software or human actions necessary for the successful operation of the system. Ultimately, the hardware and software elements of the system, as well as the human actions, are represented as probabilities in the overall system model.

There are several system modeling schemes for reliability or availability analysis. Two of the most common ones are the reliability block diagrams and the fault tree. The use of reliability block diagrams is usually appropriate for relatively simple systems. For complex systems,

such as those including numerous interactions between components, those including the role of humans, and common causes failures, the use of fault trees (or other logic models) is usually more appropriate.

Block Diagrams

Reliability block diagrams are frequently used to model the effects of items failing (or functioning) on system performance. The diagrams often correspond to the physical arrangement of the components in the system. Block diagrams can be classified as series, parallel, standby, share loads, or other.

Series Systems In a system consisting of individual components in series, the failure of one component results in the failure of the system. Accordingly, all components in a series system must work for the intended mission of the system in order for it to be operational. Figure 74.26 illustrates a system with two components in series.

The reliability function for a system of n units in series is the multiplication of the reliability of the individual units. This is expressed as

$$R_s(t) = \prod_{i=1}^{n} R_i(t) \qquad (74.70)$$

where R_i is the reliability of the ith unit. The hazard rate of the system is

$$h_s(t) = \sum_{i=1}^{n} h_i(t)$$

or in the case of a constant failure rate $\lambda_s = \sum_{i=1}^{n} \lambda_i$

Consequently, for the case of the exponential distribution,

$$R_s(t) = \exp\left(-\sum_{i=1}^{n} \lambda_i\right) \cdot t, \text{ and the}$$

$$\text{MTTF}_s(t) = \frac{1}{\lambda_s}$$

Parallel Systems A reliability block diagram is in parallel configuration (Fig. 74.27) if the failure of one of all units in the system results in the system failure. Accordingly, success of only one unit would be sufficient to guarantee the success of the system.

According to the definition of a parallel system, failure of all units results in the failure of the system. Therefore, for a set of n items in parallel,

$$R_s(t) = 1 - \prod_{i=1}^{n} [1 - R_i(t)] \qquad (74.71)$$

Analytical expressions for the hazard rate and MTTF of the systems are rather complex. However, these values can be found numerically from Equations 74.3 and 74.22 presented earlier in the chapter. In general, the design of an active parallel system results in an MTTF exceeding that of an individual unit. However, the contribution from the second unit, the third unit, and so on would have a diminishing return as the number of units in parallel increases. Notice that there would be an optimum number of units in the system for which the designer would balance cost and reliability in its life cycle.

A more general form of a series and parallel system is the so-called k-out-of-N system. In this type of system, if any combination of k-out-of-N independently working units are operational, it guarantees the success of the system. Assuming that all units are identical, the reliability of the

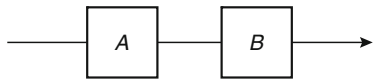

Fig. 74.26 Reliability block diagram for two components in series

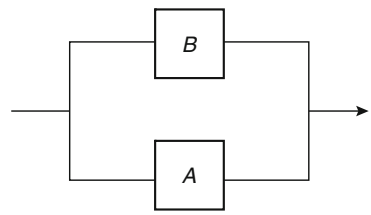

Fig. 74.27 Reliability block diagram for two components in parallel

k-out-of-N system can be represented using the binomial distribution as follows:

$$R(t) = \sum_{r=K}^{n} \binom{n}{r} [R(t)]^r [-R(t)]^{n-r}$$
$$= 1 - \sum_{r=0}^{k-1} \binom{n}{r} [R(t)]^r [-R(t)]^{n-r}$$

Standby Systems In a standby system, some of its units remain idle until they are called for service by a sensing and switching device. The idle unit operates when the failure of the primary unit is detected. Clearly, the reliability of the system should include considerations for the primary and standby units, as well as for the sensing and switching device.

According to the foregoing definition, the mathematical function for the reliability of the standby system shown in Fig. 74.28 can be expressed as

$$R_s(t) = R_A(t) + R_{ss}(t_1) \cdot R'_B(t_1) \cdot R_B(t - t_1) \cdot \int_0^t f_A(t_1) dt_1 \qquad (74.72)$$

where $f_A(t)$ is the probability distribution function for the time to failure of unit A, $R_{ss}(t_1)$ is the reliability of the sensing and switching device, $R'_B(t_1)$ is the reliability of unit B in the standby mode, and $R_B(t - t_1)$ is the reliability of unit B after it started to operate at time t_1. As for the case of the parallel system, the hazard rate and MTTF values can be found numerically from Equations 74.3 and 74.22 presented earlier in the chapter.

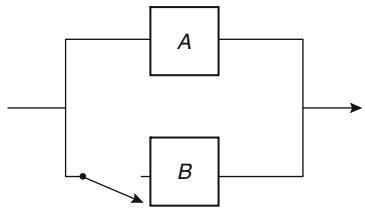

Fig. 74.28 Reliability block diagram for two-component standby system

Share Load Systems A share load system refers to a parallel system whose units equally share the system function. Consider as an example the case of a set of two parallel pumps delivering x gpm of water to a fire protection system. Each pump delivers $x/2$ gpm. If one of the pumps fails, then the second pump must provide the total amount of water. For a share load system to work, both units have to supply $x/2$ gpm, or in the case either unit fails, the operating unit must supply x gpm. Accordingly, the mathematical expression is

$$R_s(t) = [R_h(t)]^2 + 2 \cdot \int_0^t f_h(t_1) R_h(t_1) R_h(t - t_1) dt_1 \qquad (74.73)$$

The first term in the right-hand side represents the contribution of both units working successfully with each carrying a half load. The second term represents the two equal probabilities that unit 1 fails first and unit 2 takes the full load at time t_1, or vice versa. If there are switching mechanisms involved in the shift from a half to a full load, its reliability should also be incorporated in the equation. As for the case of the parallel system, the hazard rate and MTTF values can be found numerically from Equations 74.3 and 74.22 presented earlier in the chapter.

Other Systems There are systems that are not in series or parallel. In fact, most practical systems are not in parallel or series but exhibit some hybrid combination of the two. For those systems with combinations of series and parallel subsystems (series-parallel systems), each subsystem can be reduced to an equivalent component with R_s given by the equations listed previously for series or parallel systems, respectively. Eventually, the reliability function for the entire system can be developed by a systematic combination of the reliability functions for series or parallel subsystems. A conceptual example of such a system is presented in Fig. 74.29. Notice that there is a group of three units in series and another group of three units in parallel. Representing the reliability of the parallel group

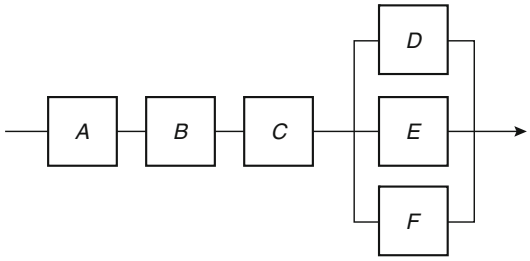

Fig. 74.29 Reliability block diagram for system with series parallel groups

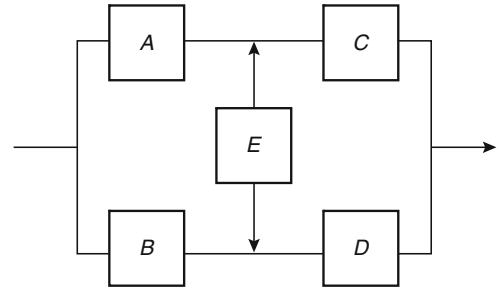

Fig. 74.30 Reliability block diagram for system not having units in series or in parallel

with an equivalent reliability function using Equation 74.71 results in a system of four units in series.

In the case of systems with units that are not in series or parallel, other analytical methods must be used for developing the reliability function. A conceptual example of such a system is presented in Fig. 74.30. Notice that the individual units are not in series or in parallel.

Depending on the number of units in the system, methods for calculating reliability can become computationally intensive, often requiring the use of a computer and software with capabilities for developing and analyzing system models.

Cut Sets and Path Sets Cut sets and path sets are computationally intensive methods of determining the reliability of systems. As suggested in the previous section, the method can be applied by hand if the number of units in the system is relatively small. At the same time, as the number of units in the system increases, the use of a computer becomes necessary. Path sets are a group of units that connect the input and output of a system when traversed in the direction of the arrows in the reliability block diagram. Therefore, a path set is actually a path through the diagram. A minimal path set is a path set that would not provide a connection between input and output if any of the units fail or were removed. For example, the minimal path sets in Fig. 74.30 are (*A*-*C*), (*B*-*D*), (*A*-*E*-*D*), and (*A*-*E*-*B*). If at least one of the items in each path set is removed, there would be no path from input to output.

If a system has n minimal path sets, denoted as $P_1, P_2 \ldots P_n$, the reliability can be expressed as follows:

$$R_s(t) = Pr(P_1 \cup P_2 \cup \ldots \cup P_n) \qquad (74.74)$$

where each path set P_i represents the event that units in path set i work. That is, the system will be operational as long as at least one of the path sets is operational. Notice, however, that in many cases, the P_i's are not mutually exclusive, which complicates the calculation of the system reliability. Assuming mutually exclusive path sets, Equation 74.74 offers an upper bound of the system reliability:

$$R_s(t) \leq Pr(P_1) + Pr(P_2) + \ldots + Pr(P_n) \qquad (74.75)$$

It should be stressed that the assumption of mutually exclusive path sets is a limitation in the use of the equation. The equation may provide useful answers when used with small reliability values and is usually not a good bound for practical applications.

A cut set is a set of units that interrupts all possible connections between input and output points. A minimal cut set is the smallest set of units needed to guarantee an interruption of the flow. In the case of Fig. 74.30, the cut sets are (*A*-*B*), (*C*-*D*), (*C*-*E*-*D*), (*A*-*E*-*B*), (*B*-*E*-*C*), and (*A*-*E*-*D*). The system reliability can be also calculated using the cut sets as follows:

$$R_s(t) = 1 - Pr(C_1 \cup C_2 \cup \ldots \cup C_n) \quad (74.76)$$

where C_n represents the event that units in the cut set fail sometime before the mission time. The probability term on the right-hand side represents the probability that at least one of the minimal cut sets exists before time t. Thus, the reliability is obtained by subtracting this term from 1.0. Since the cut sets are not usually mutually exclusive, Equation 74.76 provides the following lower bound for reliability:

$$R_s(t) \geq 1 - [Pr(C_1) + pr(C_2) + \ldots + Pr(C_n)] \quad (74.77)$$

This bounding technique yields a much better representation of the reliability because most engineering units have reliabilities much greater than 0.9 over the mission time, making the use of Equation 74.77 appropriate.

Fault Trees

The most popular logic model is the fault tree. A fault tree is a graphic model of the various parallel and sequential combinations of faults that will result in the occurrence of the predefined, undesired event. The faults can be events that are associated with component hardware failures, human errors, or any other pertinent event, which can lead to an undesired event [36]. Fault trees are very powerful as a qualitative analysis tool but can be quantified. In reliability engineering, this quantification results in the calculation of the probability of failure of the system captured in the fault tree logic.

A fault tree is not a model of all possible system failures or all possible causes for system failures. Instead, a fault tree is developed based on a top event and, thus, includes those failures contributing to the top event only. The events are connected with gates that provide the logic interactions between the events. Tables 74.11 and 74.12 list the most common event and gate symbols used in fault trees and the corresponding description [36].

It is important to stress also that fault trees do not capture the dynamic interactions of the different events. Dynamic interactions are changes in the system as a function of time or other physical parameters such as temperature, humidity, and so on.

Example 9 An automatic CO_2 fire suppression system (total flooding) provides protection to a relatively small cable room in a commercial power plant. The CO_2 system includes the following components:

- A detection system consisting of a panel, two heat detection devices, and an alarm
- One CO_2 storage tank that has an actuator valve connected to the panel and a cylinder valve
- One discharge nozzle
- One manual pull station

The detection system is connected to a power supply and has a backup battery. Upon a detection signal, the alarm sounds and after a 60-s delay, the actuator valve operates releasing the CO_2 into the room. The manual pull station can be used to release the CO_2 any time. The manual actuation will also trigger the alarm and the 60-s delay time. It is assumed that the system will suppress the fire if the CO_2 is released at the proper concentration and that the concentration is maintained for a predefined period of time.

Develop a fault tree for the top event "CO_2 suppression system fails to suppress fire in the cable room before damage occurs." In this case, damage refers to any postulated scenario consequence.

Solution The event tree is depicted in Figs. 74.31 and 74.32. Notice that Fig. 74.32 is a continuation of the main fault tree in Fig. 74.31. The continuation node is represented by a triangle. The top event is "CO_2 suppression system fails to suppress the fire before damage occurs," assuming a fire in the cable room, failure of the CO_2 system if the fire is not detected, or the fire is not suppressed. These two events are connected with an OR gate to the top event.

The event "failure to detect the fire" is further developed in the events "failure of the automatic

Table 74.11 Summary of typical events in fault trees

Events	Symbol	Description
Basic event		A basic initiating fault requiring no further development
Conditioning event		Specific conditions or restrictions that apply to any logic gate (used for priority AND and INHIBIT)
Undeveloped event		An event that is not further developed either because it is of insufficient consequences or because information is unavailable
External event		An event that is normally expected to occur
Intermediate event		A fault event that occurs because of one or more antecedent causes acting through logic gates

Table 74.12 Summary of typical gates used in fault trees

Events	Symbol	Description
AND		Output fault occurs if all the input faults occur
OR		Output fault occurs if at least one of the input faults occurs
Exclusive OR		Output fault occurs if exactly one of the input faults occurs
Priority AND		Output fault occurs if all the input faults occur in a specific sequence (as described by the conditioning event)
INHIBIT		Output fault occurs if the single input fault occurs in the presence of an enabling condition (as described in the conditioning event)

detection system" and "failures of any other means of detection." The latter event is intended to account for detection means such as personnel detecting the fire. The failure of the automatic heat detection system is also further developed to consider failure of the detection devices or the panel. Failure of the detection devices can occur due to failures of the detectors, or a fire not large enough to be detected before damage. Notice that there is an element of time, "before damage," that is not explicitly captured in the fault tree. Failure of the panel can occur due to failures in the primary and backup systems or other panel failure.

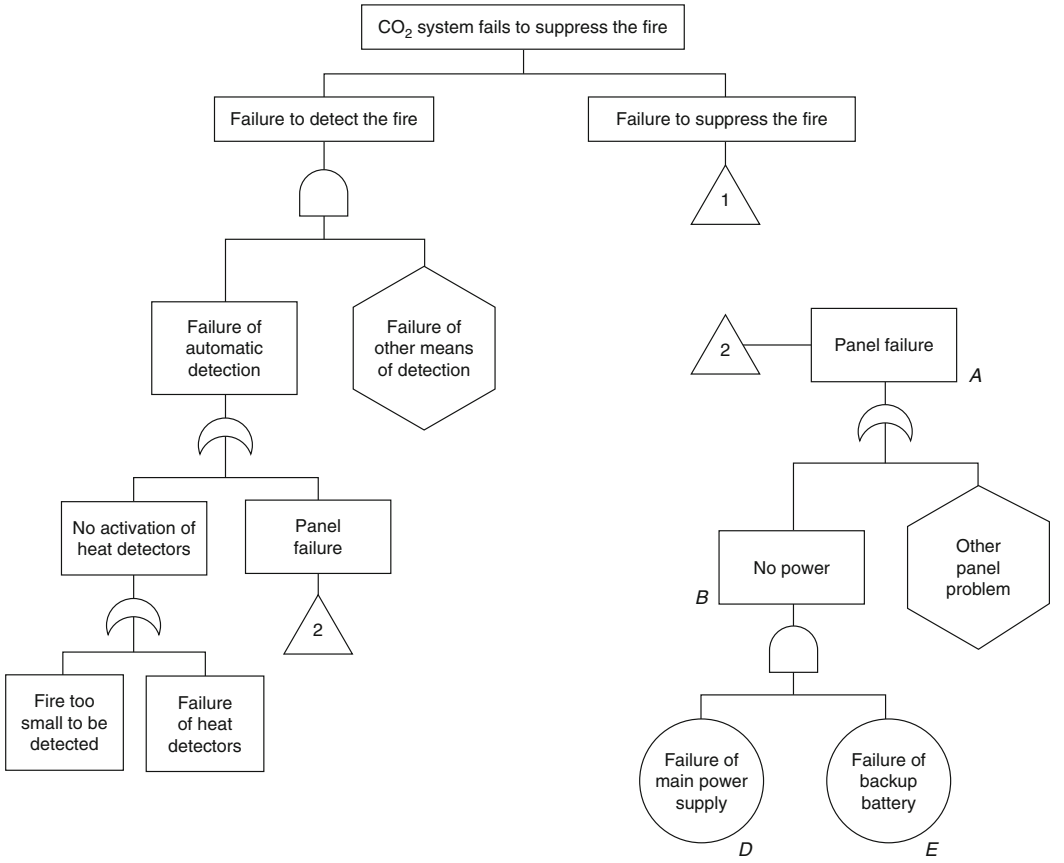

Fig. 74.31 Fault tree for Example 9

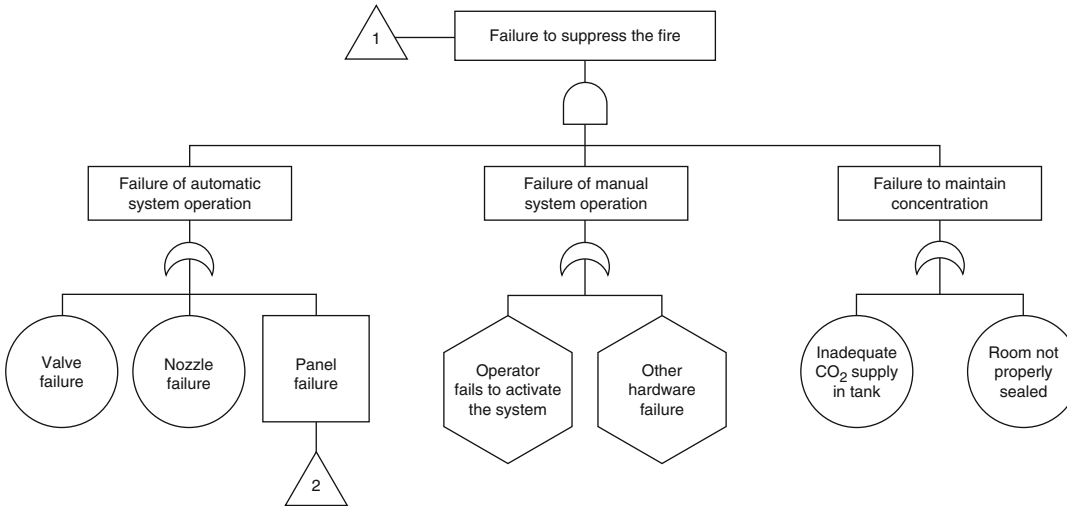

Fig. 74.32 Fault tree for Example 9

In terms of failure of the suppression system, the event tree considers failures of the automatic system, failure of a manual activation of the system, or failure to maintain CO_2 concentration in the room. Notice again the element of time that is not explicitly captured in the fault tree. That is, failure to automatically or manually activate the system can include cases in which the activation worked, but it was activated too late to prevent any fire damage. These three events are further developed to consider hardware failures, room leakages, and manual actions.

Fault Tree Quantification

The quantification of fault trees, which refers to the probability of the top event, given the logic relationships and the probabilities of the basic events, can be solved by hand or using computer programs. In practice, a solution by hand is usually time consuming and limited only to relatively small trees. Fault trees for most complex systems would need to be quantified using a computer.

In solving fault trees by hand, the use of the rare event approximation and Boolean algebra are necessary. In the rare event approximation, the term $Pr(A \cap B)$ in $Pr(A \cup B) = Pr(A) + Pr(B) - Pr(A \cap B)$is assumed to be a very small contributor and, therefore, is neglected. For example, if $Pr(A) = Pr(B) = 0.1$, then $Pr(A)Pr(B) = 0.01$, which is an order of magnitude less. The rare event approximation provides an upper bound that is reasonable if the probabilities of the individual events are small. Once the fault tree has been developed, the quantification process consists of the following steps:

1. Determine the probability or frequency of the basic events. These probabilities or frequencies are the input parameters for the analysis.
2. Starting from the top, write the Boolean expression for each level of the fault tree.
3. Combine the Boolean expressions for the different levels.
4. The resulting cut set combination can be used for determining the probability or frequency of the top event using Equation 74.77.

Example 10 Using the subtree 2 in Example 2, determine the reliability of the panel. For simplicity, the events in the fault tree have been labeled with letters A to E.

Solution Let us follow the four steps listed previously in order to solve this example. The first step is to determine probabilities of the basic events. In this case, the fault tree has two basic events and one undeveloped event at the lowest level. Let us assume the probabilities for the basic events are $D = P_1$ and $E = P_2$ and for the undeveloped event is $C = P_3$.

The second step is to write a Boolean expression for each fault tree level. Starting from the top,

$A = B + C$, notice the use of the rare event approximation

$B = D \cdot E$

The third step is to combine the Boolean expressions. Accordingly,

$$A = D \text{ñ} E + C$$

Finally, the foregoing expression suggests the cut sets of the tree. There are two cut sets, C and DE. These cut sets are easy to identify even by visual inspection of the fault tree. From Equation 74.77, the reliability of the panel is

$$\begin{aligned} R &\approx 1 - [Pr(C_1) + Pr(C_2) + \ldots + Pr(C_n)] \\ &\approx 1 - [Pr(D) \cdot Pr(E) + Pr(C)] \\ R &\approx 1 - [P_D \cdot P_E + P_C] \end{aligned}$$

Dependent and Common Cause Failures

Dependent failures are events in which the probability of each failure is dependent on the occurrence of other failures. For simplicity, let us assume that the failures of items A and B are dependent. The probability of failure of the two items can be expressed as

$$P(AB) \neq P(A) \text{ñ} P(B)$$

where in general $P(AB)$ is greater than $P(A)P(B)$. That is, the probability of failure of the two items is usually, but not always, greater than the failure of the two items assuming independence. Mosleh

et al. [37] classifies dependencies as intrinsic and extrinsic. Intrinsic dependencies are those in which the functional status of a component is affected by the functional status of another. These dependencies are usually due to the physical configuration of the component. Some examples may include dependencies such as "B is not needed when *A* works." Extrinsic dependencies are those in which the dependency is due to external factors not considered in the designed functional characteristics of the system. Examples of extrinsic dependencies may include environmental factors and human interactions (maintenance activities, etc.). Notice that fire-generated conditions can be considered an extrinsic dependency.

Intrinsic dependencies are usually explicitly captured in logic system models such as fault trees. At the same time, extrinsic dependencies are often not included in such models. The term *common cause failures* (CCF) is intended to capture those dependencies, for the most part extrinsic, that are not known or are difficult to explicitly include in a system model. Mosleh et al. [33] defines CCF as ". . . a subset of dependent events in which two or more component fault states exist at the same time, or in a short time interval, and are direct results of a shared cause." According to Modarres [5], CCFs have been shown by many reliability studies to contribute significantly to the overall unavailability or unreliability of complex systems.

Mosleh et al. [37] suggest that CCFs are due to a particular root cause and a coupling factor. The coupling factor makes the root cause of the failure common to all the dependent components. Coupling factors are classified as hardware based, operation based, and environment based [37]. Examples of hardware-based coupling factors include the same component internal parts and the same maintenance/test/calibration characteristics. In terms of operation-based coupling factors, examples include the same operating staff, procedures, or schedules. Finally, environment-based coupling factors refer to similar location.

As a conceptual example, consider a scenario involving a fire damaging control cables for two motor-operated valves. In a particular room, the cables are routed in different cable trays in the same stack. The root cause of the valve control system failure is the actual failure of the control cables. The coupling factor is location. Since the cables are in the same room and cable tray stack, fire conditions affect both cables at the same time.

Modeling Common Cause Failures

Modeling common cause failures in fault trees have the potential of increasing the size of the tree considerably. Typically, the process involves screening steps for determining which common cause groups impact the overall reliability of the system. Mosleh et al. [37] describes both qualitative and quantitative screening steps.

The actual modification of a fault tree to include common cause failure is best described considering the basic events of a fault tree as illustrated in Fig. 74.33a. In this example, the system fails if any of the three basic components fails. Figure 74.33b depicts an expanded fault tree considering common cause failures. Each basic event in Fig. 74.33a is further developed in four basic events in Fig. 74.33b (the only development of event *B* fails is presented). The four basic events are (1) "*B* fails," which refers to the independent failure of component *B*, (2) components *A* and *B* fail due to common cause, (3) components *B* and *C* fail due to common cause, and (4) components *A*, *B*, and *C* fail due to common cause.

The Boolean representation of the total failure of the components is $F(B) = F(B) + F(AB) + F(BC) + F(ABC)$. Similar expressions can be written for components *A* and *C*. The cut sets for the tree are $(A_i \cdot B_i \cdot C_i)$, $(A_i \cdot BC)$, $(B_i \cdot AC)$, $(C_i \cdot AB)$, and (ABC). The subscript *i* refers to the independent failure of the component. That is, the first cut set is the independent failure of the three components. The second cut set is the independent failure of component *A* and failure of components *B* and *C* due to common cause. The

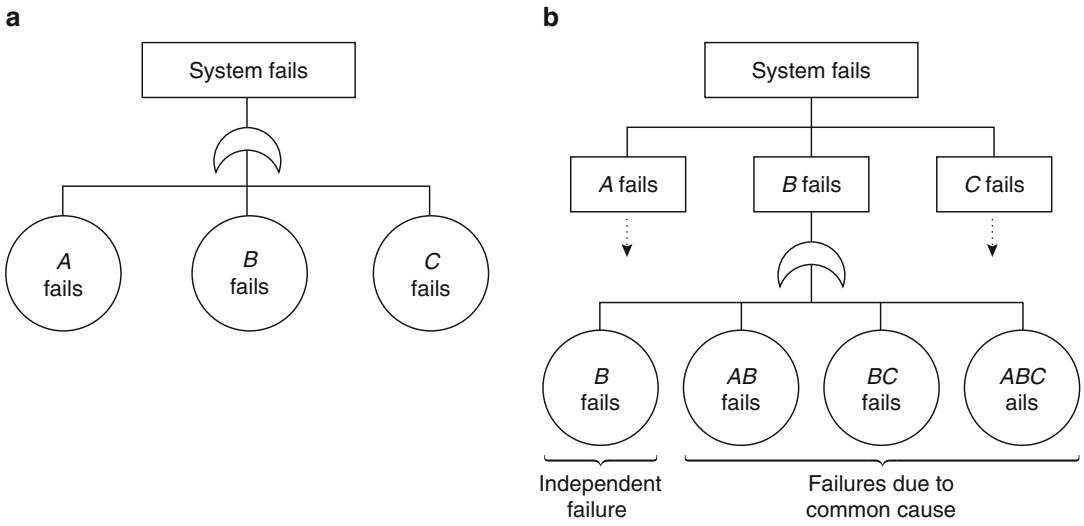

Fig. 74.33 Pictorial representation of a fault tree considering common cause failures

last cut set is the failure of the three components due to common cause. At this point, readers should appreciate how considerations for common cause failures can significantly increase the size of the logic models. If common cause failures are not considered, only the first cut set would be necessary. Applying the rare event approximation,

$$Q_s = Pr(A_i) \cdot Pr(B_i) \cdot Pr(C_i) + Pr(A_i) \cdot Pr(BC) + Pr(B_i) \cdot Pr(AC) + Pr(C_i) \cdot Pr(AB) + Pr(ABC)$$

Assuming components A, B, and C are identical,

$$Q_1 = Pr(A_i) = Pr(B_i) = Pr(C_i)$$
$$Q_2 = Pr(BC) = Pr(AC) = Pr(AB)$$
$$Q_3 = Pr(ABC), \text{ and}$$
$$Q_s = Q_1^3 + 3 \cdot Q_1 \cdot Q_2 + Q_3$$

Mosleh et al. [37] recommend the representation of the Q_k values with quantifiable parameters for practical purposes. One of the most common models is the alpha factor (α-factor) model. The α-factor model develops common cause frequencies from a set of failure ratios and the total component failure rate Q_T . In very general terms, $Q_k = \alpha Q_T$,, where Q_T represents total frequency including independent and common cause events, and α is the fraction of the total frequency involving the failure of k events. The description of the specific details of this model (or other parametric models for CCF) is out of the scope of this chapter.

Summary

This chapter summarizes reliability engineering topics relevant to fire protection engineers. In most cases, reliability engineering offers statistical models that can be used by fire protection practitioners in support of their day-to-day activities. Examples of such activities may include improving maintenance practices for fire protection systems, developing fire risk assessments, identifying failure modes of a fire protection system, improving the reliability and availability of a particular fire protection system design, improving operator procedures, and so on.

Most of the statistical models require the collection of data for calculating relevant parameters. In some applications, the data

collection process can be a challenging task. However, even with limited data or values based on expert judgment assessments, the statistical models described in this chapter can be used for obtaining a better understanding of failure modes and failure likelihoods of systems and components through time. Such an understanding usually provides insights on how to better manage or improve the reliability and availability of fire protection systems, components, and procedures.

Nomenclature

A	Availability
A	Empirical variable (in Arrhenius life-time relationship)
C_i	Cut set i
d	Downtime in availability analysis
E	Activation energy (in Arrhenius life-time relationship)
$E(t)$	Expected value of variable t
$f(t)$	Probability distribution function for random variable t
$F(t)$	Cumulative distribution function for random variable t
fr	Frequency of repair per test interval (in availability analysis)
$g(t)$	Probability distribution for the repair time
$h(t)$	Hazard rate of variable t
I	Unit vector (in Markov analysis)
k	Normalizing factor in Bayesian analysis
k	Number of events in Poisson probability distribution
k	Stefan Boltzman constant (in Arrhenius life-time relationship)
L	Vector of initial state conditions (in Markov analysis)
$L(t,\theta)$	Likelihood function for parameters t and θ.
L_i	State i (in Markov analysis)
MTTF	Mean time to failure
MTTR	Mean time to repair
N, n	Counter variable usually for number of failures
P_i	Path set i
$R(t)$	Reliability as a function of time
$R(t)$	Reliability function
S	Stress variable (in inverse power law relationship)
S, s	Stress variable or random variable for stress (stress and strength analysis)
sf	Probabilistic safety factor
s_m	Probabilistic safety margin
T	Test interval (in availability analysis)
T	Transition matrix (in Markov analysis)
T	Absolute temperature (in Arrhenius life-time relationship)
T, t	Time variable or random variable for time
T_m	Mission time length (in availability analysis)
To	Uptime (in availability analysis)
T_R	Average repair time (in availability analysis)
T_t	Average test duration (in availability analysis)
u	Laplace or centroid trend indicator (for Laplace or centroid test)
U	Uptime in availability analysis
U	Unavailability
$V(t)$	Variance of variable t
$W(t)$	Expected number of failures as a function of time
X	Vector to be solved for (in Markov analysis)
X, x	Strength variable or random variable for strength (stress and strength analysis)

Greek Letters

α	Weibull distribution location parameter
$\alpha(t)$	Availability as a function of time
β	Weibull distribution shape parameter
λ	Constant failure rate and exponential distribution parameter

μ	Normal distribution mean
ν	Degrees of freedom in chi square distribution
$\pi(\lambda)$	Posterior distribution in Bayesian analysis
$\pi_o(\lambda)$	Prior distribution of variable l in Bayesian analysis
σ	Normal distribution standard deviation

References

1. N. Bahr, *System Safety Engineering and Risk Assessment: A Practical Approach,* London, UK Taylor & Francis (1997).
2. C. Ebeling, *An Introduction to Reliability and Maintainability Engineering,* McGraw Hill, New York (1997).
3. W. Nelson, *Accelerated Testing,* John Wiley & Sons, Hoboken, NJ (1990).
4. A. Papoulis, *Probability, Random Variables, and Stochastic Processes,* 3rd ed., McGraw Hill, New York (1991).
5. M. Modarres, *What Every Engineer Should Know About Reliability Engineering,* Marcel Dekker Inc., New York (1993).
6. D. Wulpi, *Understanding How Components Fail,* American Society for Metals, Materials Park, OH (1985).
7. NUREG/CR-6850 or EPRI 1011989, *EPRI/NRC-RES Fire PRA Methodology for Nuclear Power Facilities,* 2 (Sept. 2005).
8. R. Bukowski, E. Budnick, and C. Schemel, *Estimates of the Operational Reliability of Fire Protection Systems,* in *Proceedings for the Third International Conference on Fire Research and Engineering,* Society of Fire Protection Engineers, Bethesda, MD (1999).
9. W. Parkinson et al., "Automatic and Manual Suppression Reliability Data for Nuclear Power Plant Fire Risk Analyses," NSAC-179L (February 1994).
10. SAND 95-1361, "Aging Assessment for Active Fire Protection Systems" (June 1995).
11. V.V. Krivtsov, "Monte Carlo Approach to Modeling and Estimation of the Generalized Renewal Process in Repairable System Reliability Analysis," Ph.D. dissertation, University of Maryland (2000).
12. J. Hurtado, M. Modarres, and F. Joglar, "Generalized Renewal Process: Models, Parameter Estimation and Applications to Maintenance Problems," *International Journal of Performability Engineering,* 1, 1 (2005).
13. H. Ascher, and H. Feingold, *Repairable System Reliability—Modeling, Inference, Misconceptions and Their Causes.* Marcel Dekker, Inc., New York (1984).
14. D.R. Cox, and P.A.W. Lewis, *The Statistical Analysis of Series of Events,* Methuen & Co Ltd, London (1978).
15. M. Kijima, H. Morimura, and Y. Suzuki, "Periodical Replacement Problem Without Assuming Minimal Repair," *European Journal of Operational Research,* 37, pp. 194–203 (1988).
16. M. Yanez, F. Joglar, and M. Modarres, "Generalized Renewal Process for Analysis of Repairable Systems with Limited Failure Experience," *Reliability Engineering & System Safety,* 77, pp. 167–180 (2002).
17. NFPA 25, *Standard for the Inspection, Testing, and Maintenance of Water-Based Fire Protection Systems,* National Fire Protection Association, Quincy, MA (2002).
18. *NFPA 72®, National Fire Alarm Code®,* National Fire Protection Association, Quincy, MA (2007).
19. NFPA 2001, *Standard on Clean Agent Fire Extinguishing Systems,* National Fire Protection Association, Quincy, MA (2004).
20. J.P. Bentley, *Introduction to Reliability and Quality Engineering,* 2nd ed., Prentice Hall, Englewood Cliffs, NJ, p. 144 (1999).
21. NUREG/CR-1924, "FRANTIC II—A Computer Code for Time Dependent Unavailability Analysis," U.S. Nuclear Regulatory Commission, Washington, DC (April 1981).
22. W. Goble, "Evaluating Control Systems Reliability, Techniques and Applications," *Technometrics,* 37, 3, pp. 344–345 (1995).
23. E. Kreyszig, *Advanced Engineering Mathematics,* 7th ed., John Wiley & Sons, Hoboken, NJ (1993).
24. M. Evans, N. Hastings, and B. Peacock, *Statistical Distributions*, 3rd ed., John Wiley & Sons, Hoboken, NJ (2000).
25. B. Epstein, "Estimation from Life Test Data," *Technometrics,* 2, 447 (1960).
26. NUREG/CR-5546 *An Investigation of the Effects of Thermal Aging on Fire Damageability of Electric Cables,* U.S. Nuclear Regulatory Commission, Washington, DC (May 1991).
27. H. Pham, *Software Reliability,* Springer, Singapore (2000).
28. *Standard Guide for Evaluating Predictive Capability of Deterministic Fire Models,* ASTM E1355-05, American Society for Testing and Materials, West Conshohoken, PA (2004).
29. E. Hollnagel, *Cognitive Reliability and Error Analysis Method, CREAM,* Elsevier, New York (1998).
30. NUREG/CR-6738, "Risk Methods Insights Gained from Fire Incidents," U.S. Nuclear Regulatory Commission, Washington, DC (Sept. 2001).
31. B. Kirwan,, *A Guide to Practical Human Reliability Assessment,* CRC Press, Boca Raton, FL (1994).
32. J. Noyes and M. Bransby, *People in Control: Human Factors in Control Room Design,* IET, Stevenage, UK (2002).

33. NUREG/CR-6883 "The SPAR-H Human Reliability Analysis Method," U.S. Nuclear Regulatory Commission, Washington, DC (Aug. 2005).
34. A. Swain, "Human Reliability Analysis: Need, Status, Trends, and Limitations," *Reliability Engineering and System Safety,* 29, pp. 301–313 (1990).
35. NUREG-1842, "Evaluation of Human Reliability Analysis Methods Against Good Practices," U.S. Nuclear Regulatory Commission, Washington, DC (Sept. 2006).
36. NUREG-0492, "Fault Tree Handbook," U.S. Nuclear Regulatory Commission, Washington, DC (January 1981).
37. NUREG/CR-5485, *Guidelines on Modeling Common–Cause Failures in Probabilistic Risk Assessment,* U.S. Nuclear Regulatory Commission, Washington, DC (November 1998).

Francisco Joglar is a fire and risk analyst at Hughes Associates Inc.

Building Fire Risk Analysis

75

Brian J. Meacham, David Charters, Peter Johnson, and Matthew Salisbury

Introduction

The aim of building fire risk analysis is to gain insight into and characterize fire-related risks to better inform the wide range of decisions that must be made as part of building design, construction, and operation. As used in this chapter, risk is defined as the possibility of an unwanted outcome in an uncertain situation, where the possibility of the unwanted outcome is a function of three factors: loss of or harm to something that is valued, the event or hazard that may occasion the loss or harm, and a judgment about the likelihood that the loss or harm will occur [1]. Specifically, fire risk is the possibility of an unwanted outcome in an uncertain situation, where fire is the hazard that may induce the loss or harm to that which is valued (e.g., life, property, business continuity, heritage, the environment, or some combination of these). Building fire risk analysis, then, is the process of understanding and characterizing the fire hazard(s) in a building, the unwanted outcomes (relevant losses or harm) that may result from a fire, and the likelihood of fire and unwanted outcomes occurring.

Building fire risk analysis must consider several factors. Some of these factors are familiar to fire protection engineers and some perhaps are not. For example, building fire risk analysis should consider (1) what the fire hazards are and how fires might occur; (2) how the unwanted outcomes (consequences) are valued and by whom (including offsetting benefits); (3) what differences in risk perception and valuation exist and how they should be treated (i.e., should high-consequence events be disregarded if the probability of occurrence is very low); (4) if there are any social or cultural issues that may be relevant; (5) if there are different stakeholder views on the likelihood of fire occurrence and of the resulting consequences; and (6) whether uncertainty, variability, and unknowns have been identified and appropriately addressed.

Evaluation of fire hazards is something that many (or generally) fire protection engineers do well, and for which numerous tools and methods exist (e.g., this handbook). The valuation of consequences, however, requires data, tools, and methods that differ from those used for fire hazard assessment. Valuation of consequences requires consideration of physical, economic, health, environmental, social, cultural, and psychological factors. In valuing life safety consequences, for example, many engineers consider only injury and loss of life to an individual. However, there are also such factors as reduced quality of life, the inability to continue to work, and the impact on family relationships. On property protection, factors such as smoke and water damage should be considered, in addition to thermal damage. On business continuity, there are long-term issues, such as loss of image and market share, in addition to the short-term monetary losses associated with downtime.

B.J. Meacham (✉) • D. Charters • P. Johnson
M. Salisbury

M.J. Hurley (ed.), *SFPE Handbook of Fire Protection Engineering*,
DOI 10.1007/978-1-4939-2565-0_75, © Society of Fire Protection Engineers 2016

Much like the valuation of consequences, the issue of determining the likelihood of fire occurrence and of resulting consequences requires data, tools, and methods not typically used by fire protection engineers. In addition, there are two approaches to the concept of probability (likelihood): the frequentist approach and the subjectivist approach [1, 2]. In brief, the frequentist approach comes from classical statistics, which considers probability to be a property of a process that is ideally determined from an infinite population of data. It considers probability to be a measured value and that information needed to estimate it can come mainly from observing the process. (For example, one can determine the probability of a coin landing with "heads" up or "tails" up only by flipping the coin an "infinite" number of times.) The subjectivist view, however, holds that probability has a value at any time that represents the total available knowledge about the process at that particular time. (For example, one can look at a coin having a "head" and a "tail," assess whether it is well balanced, observe a single coin toss, and estimate the probability of getting a "head" or a "tail" if one flips the coin again.) In practice, the main difference in approach is often one of how nonstatistical information is treated in the risk analysis. The frequentist approach attempts to keep the statistical values unaltered in the analysis, while commenting on limitations and bias so that they can be considered in the overall evaluation of the risk at the end of the process. The subjective approach attempts to generate numerical values using nonstatistical information and integrate them directly into the risk calculation.

Regardless of the difference in approach, the availability of information to determine probabilities is critical, as is the applicability of the probability information to the problem at hand. For example, (1) what data are available (e.g., how many fire ignitions have there been in office buildings in the past 10 years that did not result in significant fire damage?); (2) how applicable are historical data as an indicator of future events (e.g., were fire loss data from cellulosic materials prior to 1960 an appropriate indicator of fire losses involving synthetic materials after 1960?); and (3) how might changes to the building or its contents in the future impact the likelihood of fire occurrence and/or magnitude and type of consequences?

It is difficult to provide comprehensive guidance on what obstacles one should look out for when using fire safety data for fire risk analysis. However, some simple questions can be used to assess the suitability of data for fire risk analysis. Suggested key points for reviewing data include

- What is the set of cases that the data are drawn from?
- What scenarios are the data measuring?
- How similar is the building being analyzed to the cases being considered?
- Especially if the data are from another country, how do definitions, thresholds, and other design and collection rules and practices affect the relevance to the building being analyzed?

Other considerations include

- How old are the data (are they still applicable, given changes that may have occurred since the data were obtained)?
- Are corroborative data available?
- Are the data from statistical studies or based on engineering judgment?

When reviewing the results of the analysis, consideration should include

- Do the answers look realistic when compared to historical data for similar events?
- How sensitive are the results to data?

The above points to a critical factor in building fire risk analysis: there will be uncertainty, variability, and unknowns in any risk problem. How these factors are identified and addressed will be critical to the risk analysis, especially with respect to the stakeholders involved in passing judgment on the "acceptability" of the risk. Should point values be used or are distributions preferable? How is the variability in parameters such as building occupant health and ability addressed in the analysis? These are just a few items that must be addressed.

Building fire risk analysis is one of the main ways of assessing uncertainty, sensitivity, and variability in unknowns in fire protection engineering; for example, will a particular system

operate in a fire, and what are the potential consequences and risk implications of system failure? Building fire risk analysis requires evaluation of the likelihood of fires occurring and the consequences that may result. Developing these evaluations requires significant information from numerous sources, including objective data (e.g., historical fire loss data), subjective judgment, and input from interested and affected stakeholders. To help the diverse stakeholders involved in building fire risk analysis better understand how each views each building fire risk problem, and to address the preceding issues, an understanding of risk characterization is needed.

Building Fire Risk Characterization

Risk characterization requires a well-defined problem that those involved agree with, a sound scientific base, the proper use of analytical techniques with proper consideration of uncertainties and unknowns, and sufficient discussion and deliberation so that everyone understands all of the issues [3]. The risk characterization process will likely require several iterations as new information and data become available and as participants gain better understanding and raise more issues. It should be an inclusive, informed, consensus-building process, and not one where one person or group dominates the deliberations and/or analysis and forces a solution.

To help characterize building fire risks, a number of questions need to be asked: [1, 3–6]

1. Who or what is exposed?
2. If it is people, what groups are exposed?
3. What is posing the risk?
4. What is the nature of the harm or loss?
5. What qualities of the hazard might affect judgments about the risk (e.g., voluntary/involuntary, known/unknown, etc.)?
6. Where is the hazard experience?
7. Where and how do hazards overlap?
8. How adequate are the databases on the risks?
9. How much scientific consensus exists about how to analyze the risks?
10. How much scientific consensus is there likely to be about risk estimates? How much consensus is there among the affected parties about the nature of the risk?
11. Are there omissions from the analysis that are important for decisions?

Various tools and methods exist to help obtain needed information for building fire risk characterization. Several of these are outlined in the following section. Detailed discussion on the above questions can be found in the literature [1, 4–6].

Methods for Gathering Building Fire Risk Information

To help obtain the necessary information regarding what is valued and how, the likely impacts of fire and fire effects, how particular fire hazard conditions may occur, and the likelihood of losses occurring, several tools, methods, and approaches are available. This section provides a brief overview of various tools, methods, and approaches available to fire protection engineers for the purpose of gathering needed information. This section does not constitute a comprehensive review, and readers are urged to consult the fire and risk literature for more tools, methods, and approaches and for more details on the approaches discussed herein.

As part of a risk analysis, one should identify what is of value, assess the hazards that may result in harm or loss to that which is valued, and make an estimate regarding the likelihood of the loss occurring. In building fire risk analysis, life safety, property protection, business continuity, the environment, and/or heritage are the value foci. To determine how they are valued and the associated levels of unacceptable impact (damage, injury, or failure), consequence analysis is used. To determine the extent of exposure from potential hazard situations, fire hazard assessments are undertaken. To complete the risk analysis, evaluation of the likelihood of hazard events occurring and their levels of impact that result in unacceptable or intolerable levels of risk is required.

Consequence Analysis

To determine how a hazard may occasion loss or harm to that which is valued, some form of consequence analysis is required. Consequence analysis, a key component of risk characterization, is concerned with determining the potential impacts of a hazard event without consideration of the likelihood of the consequences occurring. Consequence analysis is more difficult than hazard assessment, in that it may not always be clear in what ways and to what extent something is valued and how the loss should be characterized. For life safety, the line may be drawn simply between life and death, or may be extended to cover quality of life, pain and suffering, and/or rehabilitation after a fire-induced injury. For property protection, it may not always be clear to the interested and affected parties where, how, and how much damage may occur. Some may not realize that code compliance, for example, can be significantly different than protecting their building, process, contents, or other assets of value. The issues can get even more complex for assessing potential business continuity impacts and damage to historically important buildings or contents. Nonetheless, such differences are important for characterizing risks, determining tolerable impacts, and selecting acceptance (damage, failure) criteria, and are why interested and affected parties must be involved in the process.

The nature of consequence analysis will vary based on the risk problem, with the issues of what is valued and how it is valued being two central foci. Determination of what is valued and how it is valued may require facility surveys, research into the impact of fire effects on that which is valued, an understanding of the state of knowledge for assessing impacts on that which is valued, and discussions with a wide variety of interested and affected parties. Uncertainty, variability, and unknowns will be key factors in many consequence analyses, especially as related to such factors as available data, randomness in affected populations, selection of acceptance criteria, selection of methods for assessing the impacts, and values of the affected and interested parties. (See Chap. 76 for discussion on uncertainty, variability, and unknowns.)

In the taxonomy of performance-based fire safety design, consequence analysis is often described in terms of establishing fire safety goals, objectives, and criteria; and tools, methods, and approaches to determining fire safety performance can be found in pertinent references [7–10]. Although such documents contain some guidance on selecting acceptance (performance) criteria, there is often a need to refer to more specific resources for details on particular physiological thresholds, material failure points, and related impact-related criteria (e.g., see pertinent chapters in this handbook). For monetary valuation equivalents, guidance can be found elsewhere in this handbook (see Chap. 79 by Ramachandran and Hall) as well as in the general risk literature [11–13]. It is worth noting, however, that valuation in terms of monetary worth can be difficult to achieve. This is especially true for life safety, where identifying a value for human life can be difficult (if not impossible) and sometimes controversial [14–21]. Discussions on monetary valuation for the purpose of insurance/no-insurance trade-offs can also be found in the literature [22, 23].

One way of potentially addressing this controversy is to try to quantify the risk/cost effectiveness of alternative life safety solutions in terms of "cost per life saved," "cost of premature death averted," or similar approach. By using such approaches, risk/cost effectiveness can be compared without placing a value on human life. See Chap. 81 for discussion on benefit-cost analysis and related monetary valuation issues.

Hazard Assessment

The purpose of a fire hazard assessment is to identify possible sources of fire ignition and various conditions that may result from the fire without consideration of the likelihood of occurrence. Fire hazard assessments typically involve surveys of facilities or processes to obtain such information as potential ignition sources, potential fuel sources, arrangement of fuel packages,

building and compartment configurations, and presence of fire safety features. Armed with this information, one either assumes ignition or established burning and estimates or predicts the fire growth, spread, and impact under a variety of fuel, compartment, and fire protection systems configurations. Identification of ignition sources requires knowledge of how ignition can occur (see Chap. 18 in this handbook) and often involves simply a visual survey. However, visual inspections may be supplemented by general or facility-specific loss data, material hazard data sheets, and other sources of information as appropriate. This latter point is important, as a review of historical loss data can help minimize the chance of focusing too closely on unique hazards, while overlooking more common, but equally important, hazards.

There are a number of tools and methods available to the fire protection engineer for the purpose of fire hazard assessment. Checklists are often used as a quick method to verify compliance with codes, standards, or recommended practices. They can be as simple or as detailed as needed, and can provide a good foundation for inexperienced persons to gain an understanding of potential hazards by making them focus on areas of concern. They can be used during design, as part of an approval process, and/or as part of an inspection and maintenance program. A potential downside is that too much focus on the checklist can lead to other hazards or potentially hazardous conditions being ignored. In addition, the user, if inexperienced, may not understand the relative importance of one item on the checklist over another, or how the hazard condition could manifest itself.

Safety reviews are typically performed for existing facilities and involve regularly scheduled visual inspections [24]. The primary purpose is to identify conditions or procedures that could lead to accidents (initiating events), illness, injury, or damage (consequences). As with a checklist, the scope of the review can be as simple or complex as deemed necessary. It may be simply a walk-through or may require review of material safety data sheets (MSDSs), testing of systems, or other safety-related functions. Checklists and a routine schedule are often helpful components of a safety review.

A "what if" analysis is primarily a conceptual divergent thinking process used to help identify areas of concern for use in checklists, safety reviews, and the following tools and methods [24]. It involves people asking "what if" about potential situations or scenarios that could arise, such as "what if the pump fails?" or "what if the operator mistakenly activates switch A instead of switch B?" "What if" analysis is typically informal and is used as a basis for initiating more detailed analyses.

Checklists and "what if" analyses can be combined as part of hazard and operability (HazOp) studies [24]. A HazOp study primarily involves taking a checklist, an MSDS, a system flow or operation chart, or other document about a process or system and systematically asking questions aimed at determining outcomes for specific actions. For example, if a valve on a drawing is labeled "flow," the question might be asked, what happens when there is "no flow"? Where the answer is unknown or unsatisfactory, additional analysis is undertaken. HazOps tend to be quite formal.

More formal approaches include failure modes and effects analysis (FMEA) and failure modes and effects and criticality analysis (FMECA) [24]. FMEA and FMECA require a tabulation of equipment, components and systems, their failure modes, the effect of the failure, and the criticality of the failure (in a FMECA). These analyses typically focus on single-mode failures and usually do not include human failure analysis.

If, after application of one of the above methods, a potential failure mode or hazard condition is deemed to require more detailed analysis, fault tree analysis (FTA) or event tree analysis (ETA) is often used [24]. FTA is essentially a "reverse thinking" or "top down" deductive technique that focuses on one particular event that could (or did) occur (typically an accident) and provides a structure for evaluating the potential causes of the event (e.g., given failure X, what could have been the cause). It does this by providing a structure, in the form of a graphic representation of a logic model, that

an analyst uses to display various events, conditions, actions, and outcomes. The output of an FTA is a set of combinations of root or initiating events that could lead to (or could have lead to) a failure and may include component, equipment, system, operating and/or human actions, failures, or errors. Although FTA may be a qualitative tool as used in hazard assessment, it can be used as a quantitative risk assessment tool if probabilities or frequencies are assigned to the various initiating or root causes.

Fault tree analysis (FTA) can be used to predict the probability or frequency of an event's outcome by combining the probabilities or frequencies of initiating events using logic gates (primarily AND gates and OR gates), as illustrated in Fig. 75.1. Use of an AND gate implies that all branches leading into the upper event must happen for the event to occur. In Fig. 75.1, using a hospital as an example, "failure to detect a fire on a ward within 5 min of ignition" is expected to occur only if "failure to detect by automatic fire detection system" AND "failure by staff to observe (detect) fire" conditions are met. Use of an OR gate implies that only one of the connected branch events must occur. For example, "failure to detect by automatic fire detection system" could result if either "no automatic fire detector present" OR if "failure of automatic detector to detect fire" occurs. By assigning a probability or frequency associated with each event in the tree, and combining the probabilities or frequencies according to the AND and OR gates, the probability or frequency of the top event can be estimated [25].

Whereas FTA begins with a failure and provides a structure to look for potential causes, event tree analysis (ETA) provides a structure for postulating an initiating event and analyzing the potential outcomes. The principal tool is a decision tree (as used in decision analysis) with branches for success or failure (yes or no, or other binomial output). The basic approach is to identify an initiating event, identify systems or strategies intended to mitigate the event, and ask the "success or failure" question for each system or strategy, building the tree in the process. As with FTA, ETA is primarily a qualitative tool as used in hazard assessment but is often used as a quantitative risk assessment tool by assigning probabilities, much the way probabilities are used in a decision tree (see also Chap. 83 and other sources [26–28]).

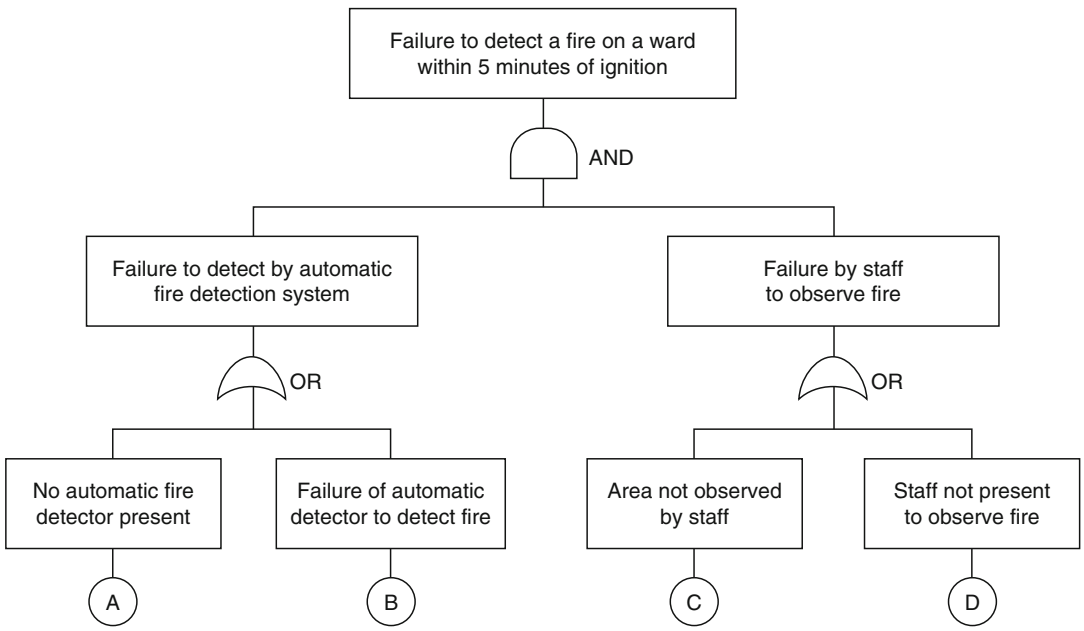

Fig. 75.1 Simple fault tree—fire detection in a hospital ward

For example, consider the simple event tree in Fig. 75.2. The initiating event is "ignition inside hospital ward" and the aim is to assess the probability or frequency of that ignition resulting in a "small fire" or a "fully developed fire" (more developed trees could include other options, such as "self-termination"). For each question (statement, or intervention), either a probability of occurrence or frequency can be assigned (e.g., the probability of fire growth is *X*, or fire growth has been observed to occur *Y* times per year for similar occupancies). If taking a probability approach, conditional probabilities for each factor can be estimated using a combination of historical data and expert judgment, as appropriate, resulting in a probability estimate for a specific outcome (scenario). By assessing the likelihood of the initial event in conjunction with the probabilities of the various factors, the frequency of the outcomes (scenarios) can likewise be estimated [25].

The data for event trees can be taken from fire statistics and other observations and measurements [29]. The effectiveness of an event tree in representing real fire events can be undertaken by quantifying the conditional probabilities for all fires in a type of building and then comparing the predicted outcome frequencies with the frequencies of deaths and injury in real events in that data set [30].

Cause-consequence analysis combines the forward thinking concept of ETA with the reverse thinking concepts of FTA to provide a more broadly encompassing picture of possible sequences of events [24]. Although primarily a qualitative tool as used in hazard assessment, it can be overlaid with frequencies or probabilities where used as a quantitative risk assessment tool.

Human error analysis describes a group of task-analysis-based qualitative techniques used to better understand the types of errors people might make and under what circumstances. Although helpful in better understanding potential sources of error, it has been noted that some such analyses treat human error and reliability in much the same way as mechanical systems, and it is argued that "desirable systems states" may be a more appropriate model [31]. In essence, "desirable systems states" focus on the goals that systems are aiming to achieve; and with why, what, and how questions, focus in on the potential for errors in various states of the system. Where people are part of the system, this approach highlights areas of concern and uncertainty related to human reliability and error.

In addition to the above methods, a variety of analytic tools, such as models, are used to assist in the hazard assessment. As Britter [32] points out, models are useful for a variety of tasks, including

- A means of summarizing extensive analytical and experimental results in order to assist in the transfer of that knowledge and to focus attention on deficiencies in the knowledge base

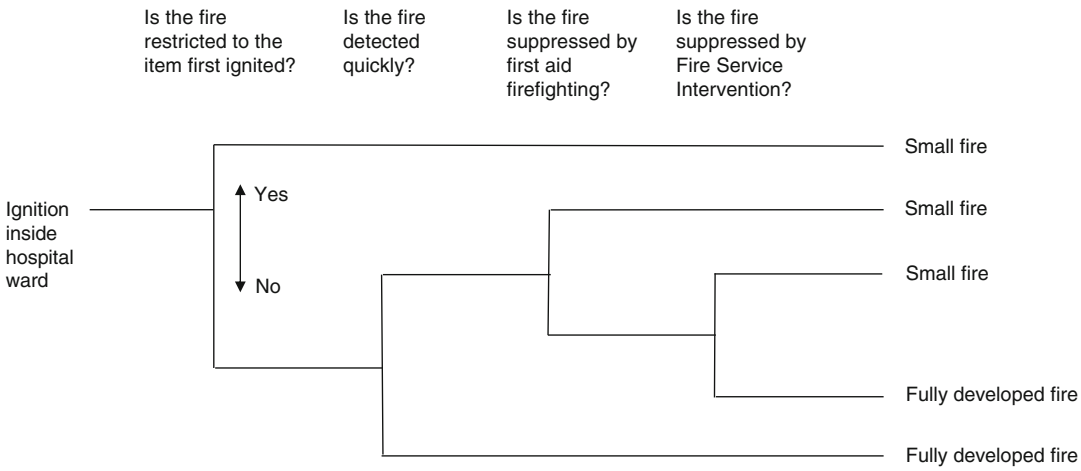

Fig. 75.2 Simple event tree—fire extinguishment in a hospital ward

- A means to provide knowledge in a form accessible to users with varying levels of expertise in the subject area
- A means to highlight the sensitivity of the output to the various input parameters
- Predictive tools for various scenarios of interest that have not, themselves, been tested

As used here, models can be mathematical or physical. Mathematical models include empirical models (based on correlation), models based on fundamental equations, analytical models (exact or approximate solutions to a set of equations in closed form), and numerical models (computational models). Physical models (simulations) rely on actual physical representations, often at a reduced scale (e.g., a wind tunnel), and sometimes with the actual material of concern (e.g., air movement in a wind tunnel), and sometimes with different materials with similar properties. Models are widely used to support fire hazard assessment. Details on fire effects modeling are provided elsewhere in this handbook and can be found throughout the fire literature. It is worth noting here that, regardless of the model one uses for fire hazard assessment or risk analysis, one must understand its uses, applications, and limitations; and appropriately account for the sources of uncertainty and variability that matter (see Chap. 76 for more details).

Causal Relationship of Initiating Events, Hazards, and Consequences

In addition to being viewed as separate components, consequence analysis and hazard assessment can be thought of as two parts of a process for identifying and evaluating the potential for unwanted consequences (loss or harm of something that is valued) given some initiating event. This definition implies that an event without unwanted consequences does not constitute a hazard and that there is a causal relationship between initiating events and unwanted consequences. One way to assess the potential for some initiating event to result in unwanted consequences is to view the situation in terms of a causal sequence, which looks at the situation as starting with some basic human need and ending in some consequence(s) [33]. The basic causal structure is illustrated in Fig. 75.3.

In brief, there are a variety of basic human needs, such as shelter, companionship, and love, which in turn lead to wants or desires. These wants or desires often result in the application of some technology to address the want. Unfortunately, the choice of technology can result in an outcome that exposes someone or something to loss or harm, resulting in some potential for unwanted consequences. To change the potential for unwanted consequences, one can modify the causal sequence by initiating one of six alternatives: modify wants, alter technology, block events, block outcomes, block the exposure, or block the consequence. This can be illustrated by example.

One basic human need is protection from the elements. To address this need, humans want shelters that provide protection from things such as rain, snow, and cold temperatures. To address this want, they may choose to live in structures that provide protection from rain and snow and can be heated to a comfortable temperature. Furthermore, they may choose to build

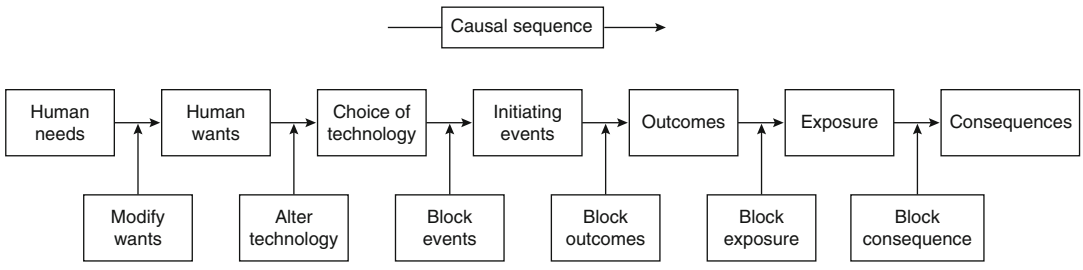

Fig. 75.3 Causal sequence [33]

these structures out of wood and to use an open fire as a source of heat. Under "normal" circumstances, everything could work fine, and the choice of technologies would provide the desired benefits. However, there could be some event, such as the blocking of a ventilation opening or too much fuel being put on the fire, that could lead to potentially unwanted outcomes. These outcomes, such as the presence of smoke, CO, or excessive temperatures in the structure, could then lead to exposures to people and property and ultimately result in unwanted consequences. Such a sequence can be illustrated diagrammatically, as shown in Fig. 75.4.

By applying an assessment methodology such as the causal sequence, one is able to visualize events, outcomes, exposures, and consequences in a systematic manner. The application can be as simple or as complex as needed, with the addition of multiple events, outcomes, exposures, and consequences and the addition of feedback loops providing further detail. Furthermore, the approach is compatible with various other hazard assessment techniques, as outlined previously, that may be more focused on specific parts of an overall assessment problem. This is illustrated in Fig. 75.5.

As can be seen in Fig. 75.5, numerous methods and approaches can be used for specific hazard assessments. Although some are applicable to a variety of problems, many are intimately associated with specific characteristics of the hazard, the type of risk problem, the current state of knowledge, and the available technology. For example, most health hazard and risk assessments (toxicological, physiological, cancer, disease) rely heavily on epidemiological studies and dose-response relationships and models [34–38]. In these cases, a causal relationship is often sought between exposure to a substance and unwanted outcomes (e.g., exposure to asbestos and the causation of cancer). Such approaches may be considered if an incapacitation assessment is being undertaken. For technology-related hazard and risk assessments, the focal point is typically the relationship between initiating events and outcomes (through to consequences). For these analyses, methods such as those outlined previously, like failure mode and effects analyses, fault tree analyses, and event tree analyses, are often used [2, 24, 39–43].

Fire Safety Concepts Tree

A useful tool for fire hazard and consequence analysis is the *fire safety concepts tree* [44]. The fire safety concepts tree is a graphical

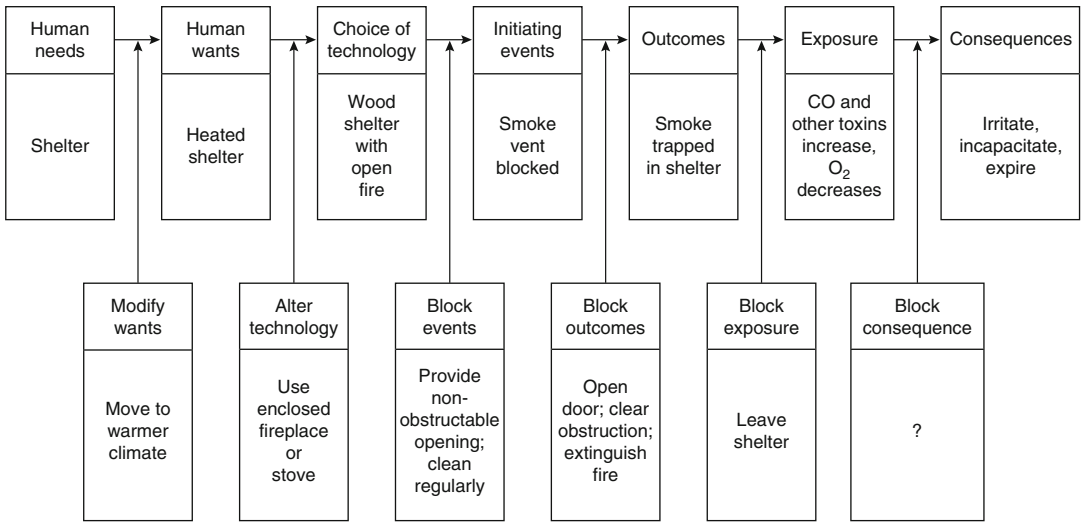

Fig. 75.4 Illustration of potential unwanted fire-related consequences

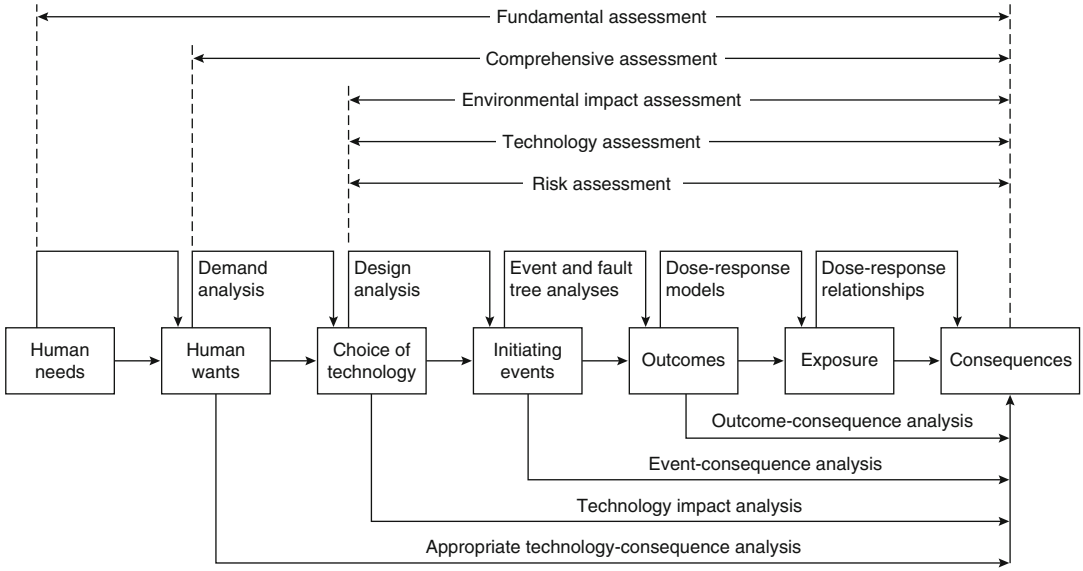

Fig. 75.5 Modes of analysis compatible with the causal structure [33]

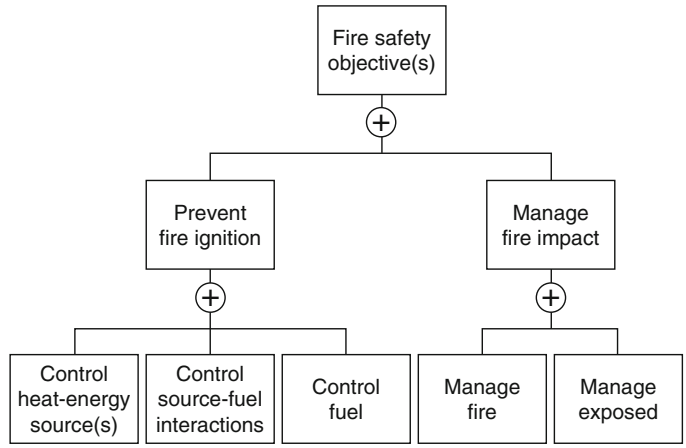

Fig. 75.6 Top branch of the fire concepts tree [44]

representation of the deliberations and professional judgments of the NFPA Technical Committee on Systems Concepts for Fire Protection in Structures, and represents one way in which building fire safety can be viewed [45]. It is divided into two primary branches, "prevent fire ignition" and "manage fire impact," with the concept being that one or the other must be accomplished in order to meet one's fire safety objectives. One can use the tree as a guide to evaluate potential fire impacts in those cases where a building fails to meet the criteria of one or more branches (e.g., if ignition is not prevented, one can evaluate the ability of the building's systems to manage the fire impact). One can also modify the fire safety concepts tree into the form of an event tree or a decision tree for risk analysis.

A portion of the fire concepts tree is provided in Fig. 75.6, which shows the top-level choices, "prevent fire ignition" or "manage fire impact." A complete version of the event tree can be found in NFPA 550, *Guide to the Fire Safety Concepts Tree* [44].

Assessing the Likelihood of Occurrence

Thus far, the risk analysis components of determining what is valued and assessing the hazard conditions that may occasion the loss or harm have been discussed. The final component is concerned with obtaining a judgment on the likelihood of specific losses occurring to what is valued. The concepts of frequency, probability, and the differing views of probability are important to this discussion.

One dictionary defines probability as the likelihood of an occurrence expressed as the ratio of the number of actual occurrences to that of possible occurrences, and frequency as the rate of occurrence [46]. Inherent in the latter definition is the concept of events per unit time. Thus, a frequency of fire ignitions during a specific period of time, on its own, is not an indication of the probability of fire ignition. To obtain a probability of fire ignition, an estimate of the number of possible occurrences is required as well. For example, a hypothetical statistic of 20 fires per year occurring in toasters as they are switched on is a *frequency*. To estimate the *probability* of a fire in a toaster when it is switched on, one would also need data on the total number of times toasters are switched on per year. If one had data that indicated that toasters are switched on 20 million times per year, one could then estimate the probability of fires in toasters as they are switched on as 20 fires per 20 million toaster starts per year, or one in a million per year.

Probability theory is a branch of mathematics that deals with the modeling of uncertainty through measures of relative likelihood of alternative occurrences [47].

This is one place where the differing approaches of objectivism and subjectivism come into play: the estimation of the likelihood of occurrence. As noted earlier in this chapter, some approaches tend to give more weight in the analysis to data from observed events with a narrative to address the effects of current state of knowledge to inform a judgment, whereas other approaches tend to utilize the current state of knowledge coupled with judgment to modify data from observed events as part of the analysis. This distinction is important to remember when certain high-consequence fire events are relatively rare and thus data are somewhat limited. In addition, people can change the nature of the fire hazard over time (e.g., by reconfiguring buildings, changing contents); and the material composition of building products and contents will likely change, making the ability to predict future hazards or risks challenging at best.

Such conditions provide an argument for the use of subjective probability measures over objective measures for building fire risk analysis. Because data are often scarce, and actual occurrences and possible occurrences may not be precisely known, it is often necessary to make estimates. At issue is how one chooses to make the required estimates [48]. For example, whereas one may have frequency data on fire ignitions in a particular class of buildings, a subjective judgment relative to the number of possible future occurrences may be more appropriate than a judgment based on statistical treatment of limited and potentially highly uncertain data.

Regardless of the differences in philosophy between objectivism and subjectivism, data are needed. Sources of fire loss data, including fire frequency data, can be found in Chap. 78 by Hall and Ahrens, as well as in various other publications, including annual [49] and periodic [50, 51] journal articles, NFPA reports [52], government reports [53], and handbook appendices [10, 54, 55]. Likewise, approaches which illustrate how data are used in different ways for evaluating and characterizing risk can be found in the literature [56–60]. In addition, it should be clear that the concepts of uncertainty, variability, and unknowns, by the nature of the problem, are critical concerns in risk analysis and must be appropriately addressed (see the following section as well as Chap. 76).

FN Curves

In managing building fire risks, it is important to differentiate between high-frequency/low-consequence events and high-consequence/

low-frequency events. This is important because society tends to be less tolerant of high-consequence events (consequence aversion), and the means for managing risks may be affected by the nature of their frequency and consequence.

FN curves were developed in the nuclear industry in the 1960s [61] as a means of analyzing and communicating the different levels and natures of risks, particularly those with the potential for high consequences but with low frequencies.

Figure 75.7 [62] shows an FN curve for multifatality accident rates. It is possible to see that road fatalities are the highest level of risk, but are at the high-frequency/low-consequence end of the graph; whereas aircraft crashes risks are higher at the high-consequence/low-frequency end of the graph, where society tends to show greater concern.

Figure 75.8 shows how FN curves can be used to compare levels of fire risk in different parts of a building or indeed in different buildings [63].

As Low as Reasonably Practicable (ALARP)

One way of testing risks that are neither negligible nor intolerable is the principle of as low as reasonably practicable (ALARP). That is, if the cost of risk reduction or the benefits of the activity grossly outweigh the risks, then the level of risk can be said to be ALARP [64]. The degree to which a risk is ALARP is usually calculated using cost-benefit analysis.

EXAMPLE: Financial Risk Assessment Using Cost-Benefit Analysis

Concern was expressed by a major bus operator with respect to the risk to business from fires in bus garages. In particular, the operator was interested in whether or not it should install sprinkler systems in its existing bus garages or take some action. Obviously, the cost of this would be considerable, and so the bus operator commissioned

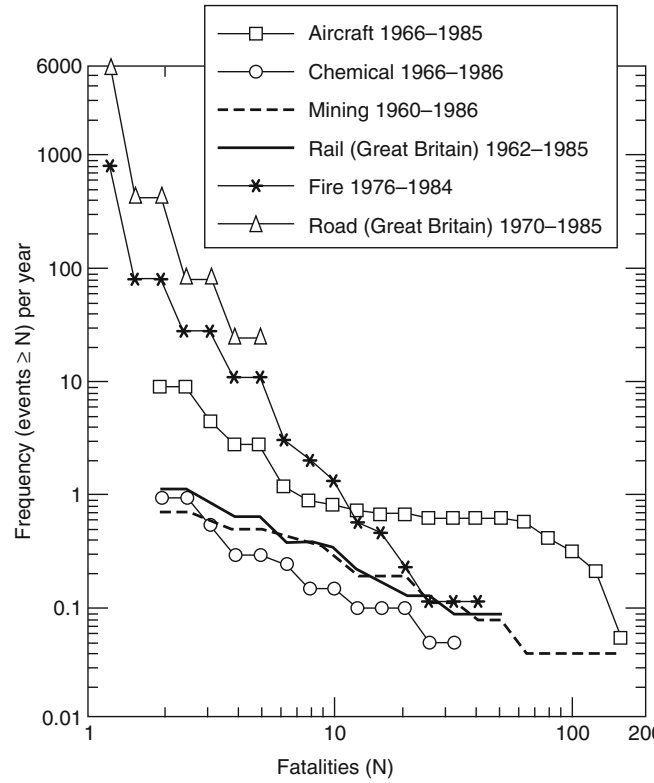

Fig. 75.7 Frequency of multiple fatality accidents in the United Kingdom [62]

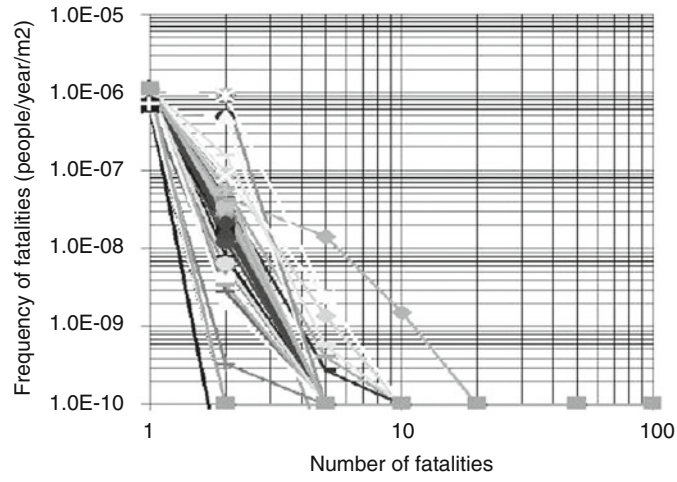

Fig. 75.8 Example of FN curves for fire risk/occupant year in a building [63]

a study to quantify the benefits in terms of property protection [65].

This risk assessment involves

1. Identifying events that could give rise to the outcome of concern
2. Estimating how often the events happen
3. Estimating what the severity of the outcome of those events would/will be
4. Assessing the implications of the level of risk

Identifying Events

The events of concern are fires causing significant damage to vehicles and property in bus garages. From operating experience, fire safety judgment, and full-scale fire tests, these events were narrowed down to one "reasonable worst case" event:

A seat fire at three points on a double-deck bus parked among others.

The risk parameter chosen for the study was the cost of fires per calendar year. This could allow the bus operator to put these risks in context with historical data on other risks.

Estimating the Frequency of Events

To estimate how often the fire event happens, historical data were collected on how often fires occur on buses in garages. Because large fires on buses are relatively infrequent, there was insufficient information to directly estimate how often these severe events occur. Therefore, an event tree was constructed to help generate the missing information.

An event tree was constructed to predict the possible outcomes from an initial event (Fig. 75.9). For example, an initial event of "Seat fire in the lower saloon of a double-deck bus" may have outcomes of "Damage less than £200,000" and "Damage greater than £500,000." The likelihood of each outcome depends on other factors such as "Is the fire noticed at an early stage of development?" "Does the fire spread to neighboring buses?" or "Is the fire extinguished using fire extinguishers?"

The conditional probability of each of these other factors is estimated using historical data and informed judgment. Therefore, using the likelihood of an initial event and the probabilities of the other factors, an estimate can be made of how often an event occurs.

Estimating the Severity of the Outcome

There are several ways to estimate the severity of the outcome: using historical information, using simple analytical methods, using computer models, and/or using full-scale tests. Each approach has its advantages and disadvantages. Historical data describe what the outcomes have been in the past but may not be complete or relevant. Simple analytical methods can predict

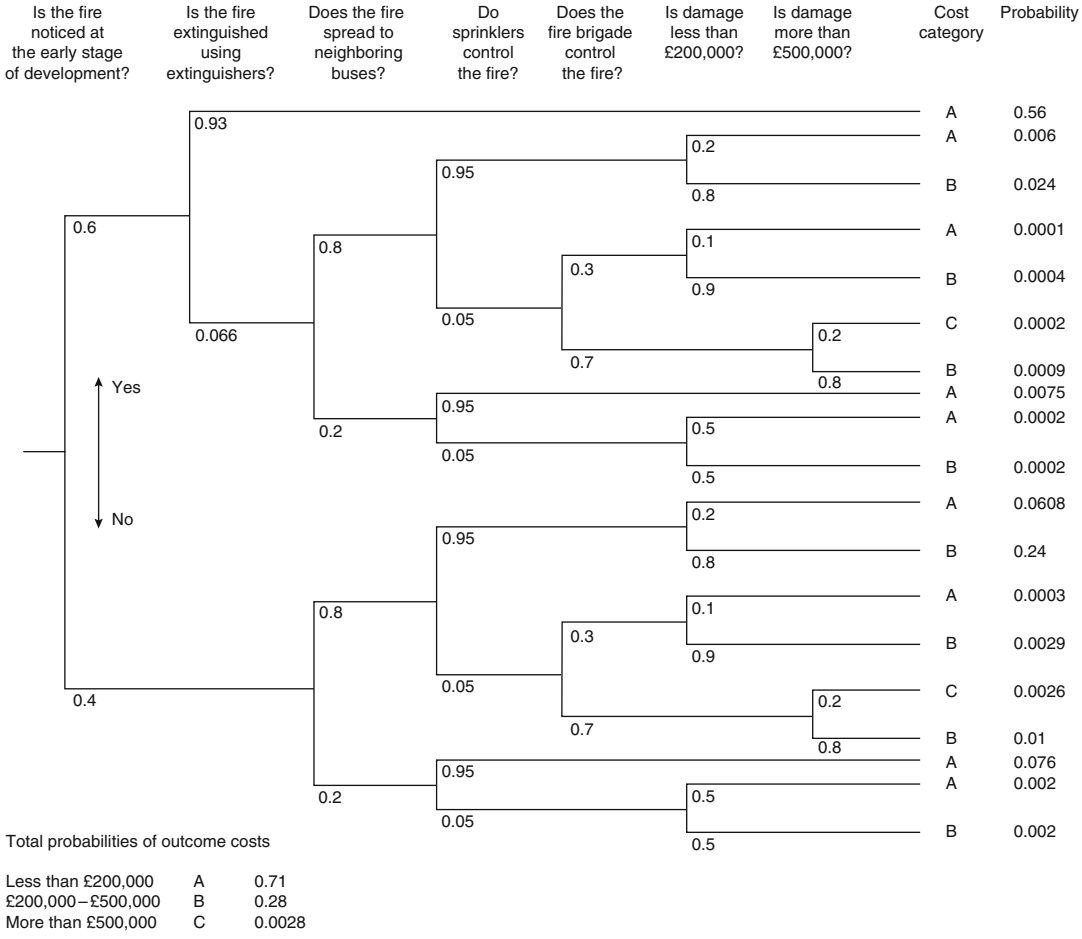

Fig. 75.9 Simplified event tree for bus garage fires with sprinklers installed [65]

the severity of outcomes cost effectively, but the answer is only as good as the assumptions made. Computer models can predict the severity of outcomes more closely but can be expensive and time consuming. Full-scale testing probably gives the most accurate assessment of the severity of outcomes, but it is usually even more costly and time consuming.

In this case the severity of the outcome (i.e., losses due to damaged buses/garage) depended heavily on the spread of fire from bus to bus and the effective spray density of different sprinkler systems. Therefore, a combination of full-scale testing and computer modeling was used to predict fire growth, fire spread, and the effectiveness of sprinklers.

Results

The risk assessment indicated that, for the event identified, a higher than ordinary level of sprinkler spray density was necessary to prevent fire spread from bus to bus. The frequencies of fires in bus garages was about 0.1 per garage year. The fire risk was then calculated for the bus garages with and without sprinklers. The difference between the two figures is the benefit rate from reduced property losses by fitting sprinkler systems, and this was of the order of £2000 per year (but this varied with the size of garage).

Historical accident data indicate that the predicted risk of damage is pessimistic; very few records of such fire damage could be found. Having quantified the benefits of sprinklers in

reducing risks in bus garages, cost-benefit analysis was used to assess whether they would represent a good investment in fire safety.

Cost-Benefit Analysis

The first step was to determine the total costs of the sprinkler installation. This not only included the initial installation costs but also covered the annual running costs. The following list, although not meant to be exhaustive, covers the main costs included in this case:

- Design fees
- Installation/construction
- Commissioning/training of staff
- Maintenance/running and so forth

The capital cost for the sprinkler system was £25,000 with an annual maintenance cost of £100. The benefits of the new installation are then listed, including

- Reduced property loss
- Reduced consequential losses
- Reduced insurance premiums
- Improved life safety and so forth

The benefit rates from the quantified fire risk assessment were added to the difference in insurance premiums to give the total benefit rate of £2500 per garage year.

This is the figure used in the investment appraisal. Table 75.1 shows the discounted cash flow over a 30 year period. The discount factor used is 10 %; this is the norm for commercial premises and is spread over a 30 year life span (because of the life of the sprinkler system). The financial data in Table 75.1 do not represent those of any particular garage or operator but may be typical of some circumstances.

The cost-benefit analysis showed a small positive net present value at the end of 30 years. The positive figure indicated that, strictly speaking, the installation of bus garage sprinkler systems did not represent a good investment. However, the smallness of the value indicated that this was a marginal case. In the light of the risk assessment, the bus operator decided that it had sufficient redundancy and diversity of bus supply through ownership (in several garages), leasing and buying, and insurance not to require bus garage sprinklers. However, the risk assessment had highlighted several other risk management issues, such as fire safety management and the separation of the information technology (IT) center, where risk reduction was much more cost effective.

Study Conclusions

A study to assess the benefits of installing sprinkler systems in bus garages [65] indicated that there were business continuity and property protection benefits to the operator. However, the cost-benefit analysis and the operator's contingency plans meant that there was no cost-benefit or consequence case for installing sprinklers in bus garages. As a result of the risk assessment,

Table 75.1 Discounted cash flow for Bus garage sprinkler system [60]

Year	Capital cost (£)	Annual cost (£/year)	Total cost (£/year)	Savings (£/year)	Net costs/ savings (£/year)	Discount factor (9 %)	NPV of costs/ savings (£)	Cumulative NPV
0	25,000	–	25,000	0	25,000	1	25,000	25,000
1		100	100	–2,500	–2,400	0.9091	–2,182	22,818
2		100	100	–2,500	–2,400	0.8265	–1,983	20,835
3		100	100	–2,500	–2,400	0.7513	–1,803	19,032
4		100	100	–2,500	–2,400	0.6830	–1,639	17,392
5		100	100	–2,500	–2,400	0.6209	–1,490	15,902
26		100	100	–2,500	–2,400	0.0839	–201	3,014
27		100	100	–2,500	–2,400	0.0763	–183	2,831
28		100	100	–2,500	–2,400	0.0693	–166	2,664
29		100	100	–2,500	–2,400	0.0630	–151	2,513
30		100	100	–2,500	–2,400	0.0573	–138	2,375
		Total	28,000	–75,000	–47,000	–	2,375	–

the operator did implement other safeguards and fire precaution measures.

Uncertainty, Variability, and Unknowns

The extent of literature on the topics of uncertainty, variability, and unknowns indicates that identifying, understanding, and addressing these are clearly critical issues. For example, these issues pervade discussions of acceptable risk [66–69], risk characterization [3], risk assessment [42, 70–74], and decision analysis [11, 13, 75–78]. However, as one can see from a review of the various reference sources, there seems to be little consensus regarding how to treat these factors. There are several reasons for this, many of which impact building fire risk analysis and even drive the need for risk analysis, including

- The risk problem may not be clearly understood or sufficiently well defined [3, 68]. Any uncertainty in the problem definition will be propagated throughout the risk assessment and management process. If this uncertainty is large (i.e., if the stakeholders do not agree on key issues or parameters of the problem), the uncertainty in any proposed solution will be some factor greater.
- There are many types of uncertainties that go unrecognized or ignored [3, 68, 71, 73]. These include uncertainties in variables that are built into analytical tools and methods; uncertainties associated with criteria selected for assessing acceptability; and uncertainties in human behavior, attitudes, and values.
- There may be variability that is treated as uncertainty [36, 73, 74]. If the risk problem relates to the human population, for example, it should be recognized that both uncertainty and variability exist, and that they need to be addressed differently. It may not be known how many people may be exposed (uncertainty), and for any population postulated to be exposed, there will be differences among the individuals (variability). Uncertainty and variability become important when discussing issues such as using the entire population or some subset of sensitive or vulnerable persons, and if the latter is selected, what defines the subset.
- There may be unknowns that are treated as uncertainties [3, 79–81]. In some cases, it is impossible to accurately predict some event that may happen far into the future, or to control the circumstances on which certain assumptions are based. If these indeterminate events are treated as events that can be accurately predicted, the uncertainties in any solution could be significant (see Stern and Fineburg [3]).
- There may be disagreement regarding how to address uncertainties of different types. First, the differences between uncertainty, variability, and indeterminacy need to be identified [74]. Then one needs to identify appropriate mechanisms to address the uncertainty, variability, or indeterminacy. For example, Morgan and Henrion [71] argue that the only type of quantities whose uncertainty may be appropriately represented in probabilistic terms are empirical quantities. However, there are other types of quantities, such as model domain parameters, decision variables, and value parameters. For these, parametric or switchover analysis (or other) may be needed.
- There may be disagreement on a quantitative methodology (or set of quantitative methodologies) for treating uncertainty. Even if it is decided to perform a probabilistic analysis on an empirical quantity, there may be disagreement as to an appropriate approach to apply. For example, probabilistic approaches range from classical, statistical-based analyses to subjective, Bayesian analyses, with other types of quantitative or qualitative analyses scattered in between [3, 48, 82, 83]. To complicate the issue, frequentists often reject the Bayesian approach, and vice versa.
- There is concern that the data, mathematical rigor, and expertise needed to conduct a quantitative uncertainty analysis would render such an analysis impracticable in many situations, and as a result, the analysis would

not be undertaken or would be performed incorrectly [84].

To help people better understand the complex issues surrounding uncertainty, variability, and unknowns (hereafter lumped as uncertainty for convenience), various taxonomies and treatments have been suggested [3, 7, 68, 72, 85, 86]. Regardless of specific differences, much of the literature identifies the following areas as requiring consideration: scientific uncertainty; human factors uncertainty; uncertainty in risk perceptions, attitudes, and values; and decision-making uncertainty.

Scientific uncertainties result from lack of knowledge (either obtainable through further study or due to random chance and variations) and from necessary approximations. They are often among the most readily recognizable and quantifiable uncertainties and can be grouped into five subcategories: theory and model uncertainties, data and input uncertainties, calculation limitations, level of detail of the model, and representativeness [7, 32, 85, 86].

Theory and model uncertainties may arise when physical processes are not modeled due to a lack of knowledge about them or about how to include them, when processes are modeled based on empirically derived correlation, and/or when simplifying assumptions are made. Data and input uncertainties arise from inaccuracies in data collection and reporting, incomplete knowledge of specific input values and variations in those values as a function of confounding factors, and input errors made by the modeler. Calculation limitations encompass such factors as the control volume selected for modeling, the level of detail of the model, and the model-domain parameters specified. Representativeness relates to how well the modeled situation reflects reality.

In considering human factors, uncertainty and variability are present in several modes. There is uncertainty regarding who might be affected and how. That is, it is not always known who will be impacted (uncertainty or indeterminacy), and within the population affected, there will be physiological uncertainties and variability. There are also uncertainties and unknowns related to how people will react in different situations, especially under stress.

As discussed earlier, there can be significant differences in the ways people perceive and value risk, as well as in their attitudes about risk. Differing perceptions give rise to both variability and uncertainty, and capturing these differences is important. There will be situations in which age, family, infirmity, or other factors or conditions will impact perceptions of risk. There may be social, economic, philosophical, religious, or cultural differences in people's values systems. In addition, some people are risk tolerant, whereas others are risk averse. It is important to recognize these differences exist, and thus reduce uncertainty and unknowns, and better understand and address variability where it exists. Also important are the perceptions and issues of equity, efficacy, and fairness—issues of importance in risk characterization and management [78]. Here again, social, economic, or cultural differences of the interested and affected parties may play a major role.

There is also uncertainty in the decision-making process, including uncertainty about how to best define the decision problem, difficulties in assessing the facts of the matter, difficulties in assessing relevant values, uncertainties about the human element in the decision-making process, and difficulties in assessing the quality of the decisions that are produced [68].

All of these factors should be considered and appropriately accounted for when undertaking a building fire risk analysis. For more details on uncertainty and its treatment, see Chap. 76.

Building Fire Risk Analysis Approaches, Methods, and Models

This section provides a brief overview of various qualitative and quantitative risk analysis approaches, tools, and methods available to fire protection engineers. This section does not constitute a comprehensive review, and readers are urged to consult the fire and risk literature for more approaches to risk analysis and for more details on the approaches discussed herein.

Magnusson [27] suggests that there are two primary approaches to risk analysis: the single

scenario, analytic safety index ß approach, and the multiscenario, event tree approach. In the single scenario, analytic safety index ß approach, there is a single-limit state described by an analytical expression developed from physically derived correlation (e.g., mass flow in plumes, smoke-filling times, radiation from flames) or from response surface equations describing output from a computer program. The design problem is formulated in terms of the limit state function, G, as $G(X_1, X_2, \ldots, X_n) = 0$. The parameters X_i are stochastic parameters describing the system, such as fire growth rate and response time of occupants. The goal is to find a solution given the constraint that $P(G < 0) < P_{\text{target}}$.

Challenges and limitations to the use of this approach include difficulty in developing appropriate analytical expressions, difficulty in developing uncertainty factors, and the limitation of being a single scenario application. Nonetheless, this approach is useful for some applications, and details can be found in the literature [26–28]. Although not developed, it has been suggested that this basic approach can be applied more broadly to the building fire problem as well [87, 88].

A response surface approach to probabilistic assessment of risk to life from fire as presented by Albrecht [89, 90] is similar to the probabilistic scenario and event tree risk assessment methodology outlined by Magnusson et al. [27] in which the probability (P), and a safety index (β), respectively, of a limit state violation is calculated as

$$P(\Omega_f) = \Phi(-\beta),$$

where Ω_f is the failure domain of the limit state function, for example

$$\Omega_f = \mathrm{G(X)} \leq 0,$$

and $\Phi(\cdot)$ is the function of the standardized normal distribution.

Since probabilistic calculations usually require a high number of evaluations of the underlying limit state it is usually not feasible to use numerically expensive models. Hence, so far only plume formulations or zone models have been utilized within those uncertainty calculations [27, 86, 91]. Yet, for performance-based life safety risk analysis it is nowadays inevitable to use state-of-the-art simulation models, such as computational fluid dynamics (CFD) or microscopic evacuation models for each scenario within a system of various possible scenarios.

In order to bypass the high numerical cost and to allow for probabilistic calculations using advanced and complex numerical models, an adaptive response surface algorithm was developed that uses so-called moving least squares (MLS) [92] with an interpolating weighting function [93] instead of the traditional global linear or quadratic regression functions [94]. These response surface formulations provide a good surrogate model with a comparably low number of required evaluations of the numerically expensive models and thus allow for a fast and accurate overall computation. The calculation of the failure probabilities is performed by exploiting the surrogate with an optimized adaptive importance sampling Monte Carlo algorithm (AIS) [95] which additionally allows to compute sensitivities to identify the highest contributors to the overall variance, i.e. the most relevant input parameters. The complete algorithm flowchart is shown in Fig. 75.10 and is described in detail in reference 89, Chap. 6.

The derived failure probabilities were then be compiled into event trees [26–28, 94, 96, 97] to perform a holistic system failure analysis. The advantage of the event tree analysis can be the identification of the most influential scenario by looking at the highest product of each scenario probability and the expected outcome if the scenario occurs. This constitutes the classic approach to quantitative risk analysis [94, 96, 97].

Another area of application of event tree analysis is the possibility to quantify the effect of fire protection systems on the safety level considering their potential failure. This can be achieved by comparing the two scenarios with and without the chosen fire protection system being functional while incorporating its probability of malfunction. Values for these failure probabilities can be found, for example, in the British

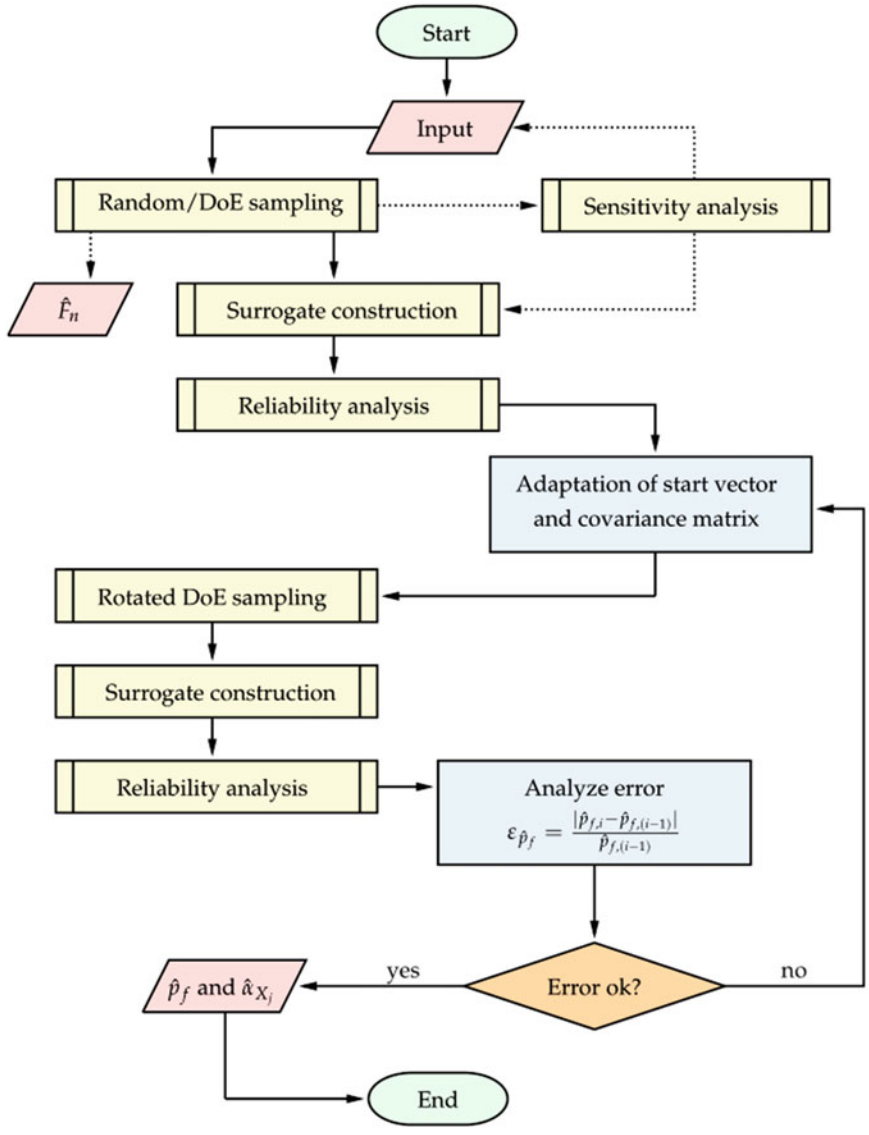

Fig. 75.10 Flowchart of the IMLS response surface Algorithm [89]

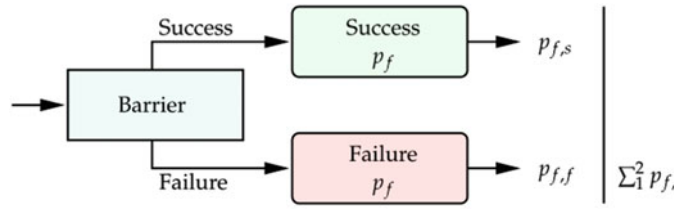

Fig. 75.11 Modeling of fire protection barriers within an event tree considering their possible failure to assess the overall impact on the safety level [89]

Standard 7974 [98]. The sub-event tree for this analysis is shown in Fig. 75.11. Further branches can be added to analyze, for example, interaction effects between various fire protection systems, such as sprinklers and ventilation systems. A comprehensive application with various scenarios and different fire protection systems can be found in reference 89, Chap. 7.

The combination of full probabilistic, performance-based scenario analysis and system analysis with state-of-the-art numerical simulation tools in fire protection engineering yields valuable quantitative information which can be used to identify the most critical scenarios and to quantify the effect of fire protection systems and thus provide a risk-optimized as well as cost-benefit optimized solutions.

To simplify this rather mathematical approach for practical application, it is possible to derive semi-probabilistic safety concepts as has been proposed [99] for the Eurocode structural fire protection where safety factors for one or multiple input parameters are derived that implicitly fulfill the required target reliability when applied. In order to develop such a safety concept for life safety analysis, for example a semi-probabilistic safety factor γ for ASET $\geq \gamma$(RSET), those target reliabilities would have to be agreed upon first.

Event tree analysis (ETA) is often used to analyze complex situations with several possible scenarios, where several fire or life safety systems are in place or are being considered. In brief, event trees are developed for a scenario, and probabilities and frequencies for components are applied (see previous discussion on ETA). In the *SFPE Engineering Guide to Performance-Based Fire Protection Analysis and Design of Buildings* [10], the method for quantifying fire risk from multiple fire scenarios is given as

$$\sum \text{Risk}_i = \sum (\text{Loss}_i \cdot F_i)$$

where

Risk_i = Risk associated with scenario i
Loss_i = Loss associated with scenario i
F_i = Frequency of scenario i occurring

This relationship is similar to the earlier general discussion on engineering risk analysis; but in this case, the term *loss* is used instead of *consequence*, and the summation indicates "total" risk from multiple scenarios. This type of risk analysis, commonly referred to as probabilistic risk assessment (PRA), is widely used in the chemical process industry (see Chap. 83) and for fire safety assessments of nuclear facilities [41], and is beginning to see broader application in fire protection engineering applications [10, 26–28, 43].

Although ETA-based risk analyses methods are applicable to multiscenario situations, it does not mean such approaches are necessarily simple. This can be illustrated using a three-room example. Figure 75.12 shows an event tree for a three-room building that is compartmented as shown. For this example, the fire scenario frequency, F_i, is assumed to be uniformly distributed across the three rooms, and the consequence of a single room loss is $C/3$ (i.e., the consequence of losing all three rooms to a fire would be C) [10].

If the probability that the fire will be contained in one room is P_c, and that it is prevented from propagating to the third is P_f, then the overall risk as shown in Fig. 75.10 can be estimated as

$$\begin{aligned} R = {} & \frac{C}{3}(F_i P_1 P_c) + \frac{2C}{3}\left[F_i P_1 (1-P_c) P_f\right] \\ & + C\left[F_i P_1 (1-P_c)(1-P_f)\right] + \frac{C}{3}(F_i P_2 P_c) \\ & + \frac{2C}{3}\left[F_i P_2 (1-P_c) P_f\right] + C\left[F_i P_2 (1-P_c)(1-P_f)\right] \\ & + \frac{C}{3}(F_i P_3 P_c) + \frac{2C}{3}\left[F_i P_3 (1-P_c) P_f\right] \\ & + C\left[F_i P_3 (1-P_c)(1-P_f)\right] \end{aligned}$$

where P_1, P_2, and P_3 are the probabilities that a fire will start in room 1, 2, or 3, respectively.

With some mathematical manipulation, the above equation simplifies to the following:

$$R = \frac{CF_i}{3}\left(3 - 2P_c - P_f + P_c P_f\right)$$

For this example, P_c and P_f can be interpreted as the success probabilities of the fire barriers. To place these results in context, numeric values will be added. If P_c and P_f are both equal to 0.1 (i.e., fire propagates 9 in 10 times), then the *risk* is

$$R = \frac{CF_i}{3}[3 - 2(0.1) - (0.1) + (0.1)(0.1)] = 0.90CF_i$$

If P_c and P_f are both equal to 0.9 (i.e., fire propagates 1 in 10 times), then the *risk* is

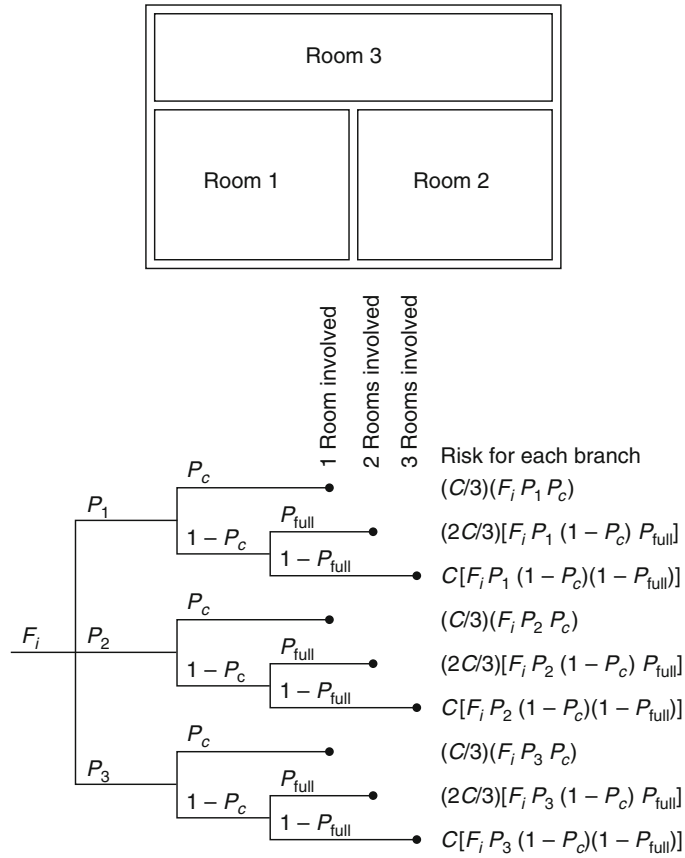

Fig. 75.12 Event tree for three-room fire risk analysis [10]

$$R = \frac{CF_i}{3}[3 - 2(0.9) - (0.9) + (0.9)(0.9)]$$
$$= 0.37CF_i$$

If P_c and P_f are set to unity (i.e., fire barriers never fail), then the *risk* is

$$R = \frac{CF_i}{3}[3 - 2(1) - (1) + (1)(1)] = \frac{CF_i}{3}$$
$$\simeq 0.33CF_i$$

Although this example is very simplified, it suggests how complicated a classical ETA-based engineering risk analysis can be. For each fire protection feature considered, the number of branches (i.e., potential outcomes) in the event tree will increase. Given that this increase is usually geometric, the analysis can become quite complex.

The above example also illustrates an important concept in risk-based calculations. The bounding risk for this problem would be CF_i (i.e., complete facility loss). This is the risk if all fire protection features are assumed to always fail. The risk when the fire protection features are always assumed to work (i.e., the fire barriers never fail, thus P_c and P_f are set to unity) is the lower bound risk. Thus, the potential range for the calculated risk is bounded between $0.33CF_i$ and CF_i. The better the protection, the closer the risk will approach $0.33CF_i$.

The above example can also be used to illustrate the difference between fire scenarios (all possible scenarios that could occur) and design fire scenarios (that subset of fire scenarios selected for design purposes) [10]. For example, the total range of fire scenarios for the above example could consider various room-to-room sequences (e.g., starts in room 1, then goes to

room 2 and finally to room 3). If this is done, one finds that there are a total of 15 possible paths of fire propagation:

1. Starts in room 1 and is contained in room 1
2. Starts in room 1 and propagates to room 2, but not to room 3
3. Starts in room 1 and propagates to room 3, but not to room 2
4. Starts in room 1 and propagates to room 2 and then to room 3
5. Starts in room 1 and propagates to room 3 and then to room 2
6. Starts in room 2 and is contained in room 2
7. Starts in room 2 and propagates to room 1, but not to room 3
8. Starts in room 2 and propagates to room 3, but not to room 1
9. Starts in room 2 and propagates to room 1 and then to room 3
10. Starts in room 2 and propagates to room 3 and then to room 1
11. Starts in room 3 and is contained in room 3
12. Starts in room 3 and propagates to room 1, but not to room 2
13. Starts in room 3 and propagates to room 2, but not to room 1
14. Starts in room 3 and propagates to room 1 and then to room 2
15. Starts in room 3 and propagates to room 2 and then to room 1

If simultaneous propagation to the second and third rooms were considered a significant threat, there would be three additional scenarios. This brings the total scenarios to 18 before considering details such as doors being open or closed, whether people of various characteristics are in the rooms, and whether they are sleeping.

It is also important to address the fact that fire protection systems may not always be operational. As such, the concepts of availability and reliability should be addressed. A system is considered available when it is ready and able to perform its intended function (e.g., a smoke detection system is installed and working). If a system is taken out of service, even temporarily (e.g., it is undergoing maintenance), it is unavailable. A risk-based approach should consider some probability that a system will be unavailable if it is a possibility. A system that is available but not functional is considered unreliable (e.g., the smoke detection system is installed but the smoke detector opening is blocked with duct tape). Probabilities can be developed for evaluation of system availability and reliability. Availability and reliability are reported or derived as a composite value. (When the latter is the case, it should be made explicit.)

Risk-Cost Assessment Model

Because of the complexity of ETA-based risk analysis, computers are often used to enable multiple scenarios to be evaluated in relatively short time frames. Two such models, FIRE-RISK (formerly known as CESARE-Risk) and FiRECAM, are based on a fire risk and cost assessment model developed by Beck [100–102] and expanded collaboratively by Beck and Yung [102, 103].

A brief description of the current risk-cost assessment model and its submodels is given in this section [104]. More detailed descriptions are given for the design fire submodel, the fire growth submodel, and the smoke movement submodel. As for the other submodels, more details can be found in other publications [101, 103, 105–107].

The risk-cost assessment model employs an event-based modeling approach in which events are characterized by discrete times and probability of occurrence. The event-based approach is used to define the outcomes of fire growth and spread scenarios in terms of the times of occurrence of untenable conditions. The consequence of these outcomes is in terms of the number of people exposed to untenable conditions.

The risk-cost assessment model for office and apartment buildings assesses the fire safety performance of a fire protection design in terms of two decision-making parameters: (1) the expected risk to life (ERL) and (2) the fire-cost expectation (FCE). The ERL is the expected number of deaths over the lifetime of the building divided by the total population of the

building and the design life of the building. The FCE is the total fire cost, which includes the capital cost for the passive and active fire protection systems, the maintenance cost for the active fire protection systems, and the expected losses resulting from fires in the building. The ERL is a quantitative measure of the risk to life from all probable fires in the building, whereas the FCE quantifies the fire cost associated with the particular fire safety system design.

To calculate the ERL and FCE values, the risk-cost assessment model considers the dynamic interaction between fire growth, fire spread, smoke movement, human behavior, and the response of fire brigades. These calculations are performed by a number of submodels interacting with each other, as shown in the flowchart in Fig. 75.13. In Fig. 75.13, the term *submodel* has been abbreviated as *model*.

The FIRE-RISK model, like FiRECAM and other more complex risk-cost models, is at present suited only to fire research or for use in assessment of building code requirements by researchers. These models are not currently well suited to use by fire protection engineers for individual building design, although that could be the ultimate aim.

FIRE-RISK has been used to assess building code requirements in Australia for Class 2 apartment buildings [108]. In particular, the current prescriptive requirements in the Building Code of Australia (BCA) have been evaluated in terms of the risks to life safety due to fire using this risk-cost model. Fatality rates per 1000 fires have been estimated for occupants in the apartment of fire origin (AFO) and in the apartments of nonfire origin (ANFO). Results of this research are shown in Table 75.2.

The lower rates for high-rise apartment buildings are likely to reflect the more stringent fire protection provisions required for buildings over 25 m under the BCA. It is suggested by Thomas et al. [108] that these results reflect the fatality rates from fire statistics for this class

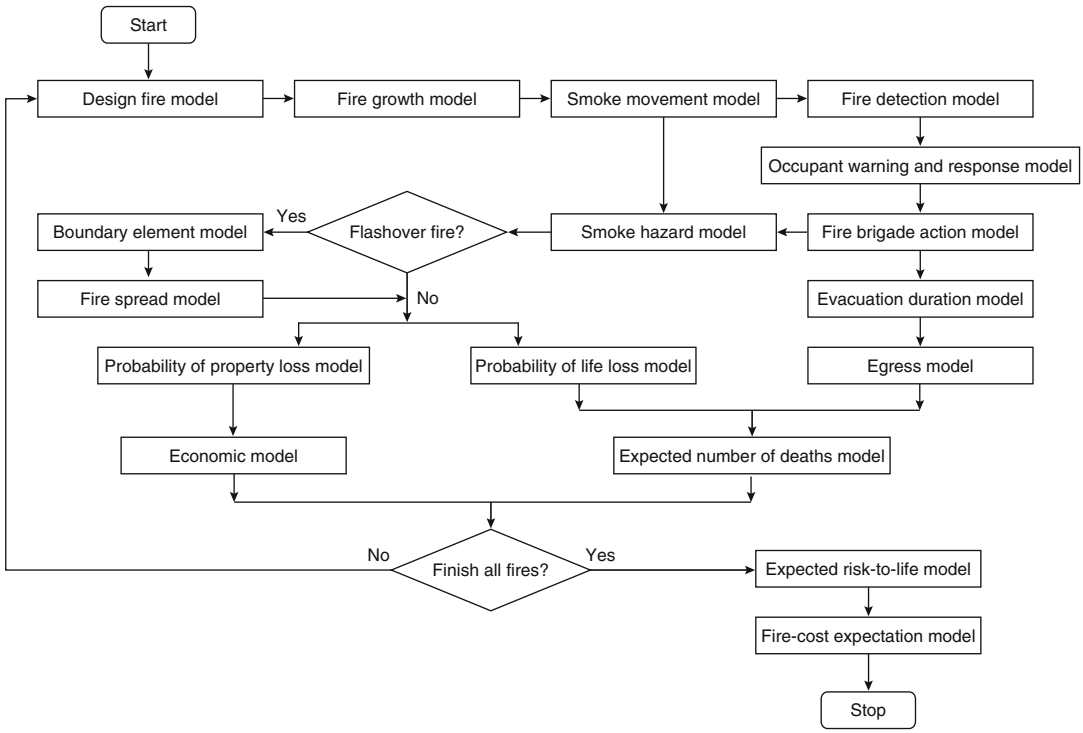

Fig. 75.13 Risk-cost assessment model

Table 75.2 Average ANFO fatality rates using CESARE-risk [92]

Building height	Fatality rate	
Low rise (<4 stories)	<0.2	ANFO fatalities/1000 fires
Medium rise (<25 m, >4 stories)	3.3–3.4	ANFO fatalities/1000 fires
High rise (>25 m)	1.7–2.1	ANFO fatalities/1000 fires

of buildings, which lends credibility to this approach.

The next step in the Australian process is to evaluate alternative fire safety solutions from those currently prescribed as deemed-to-satisfy solutions within the BCA. This would allow other prescriptive solutions to be developed and included in the BCA, which could provide building owners and designers with more flexibility to choose from a wider set of agreed prescriptive design solutions.

The risk-cost assessment model uses six design fires in the room of fire origin, and the subsequent fire and smoke spread, to evaluate life risks and protection costs in office and apartment buildings. The six design fires, representing the wide spectrum of possible fire types, are

1. Smoldering fire with room entrance door open
2. Smoldering fire with room entrance door closed
3. Flaming nonflashover fire with room entrance door open
4. Flaming nonflashover fire with room entrance door closed
5. Flashover fire with room entrance door open
6. Flashover fire with room entrance door closed

The probability of occurrence of each design fire, given that a fire has occurred, is based on statistical data. For example, in Canada, statistics show that 18 % of all apartment fires reach flashover and become fully developed fires, 63 % are flaming fires that do not reach flashover, and the remaining 19 % are smoldering fires that do not reach the flaming stage [109]. If sprinklers are installed, the model assumes that some of the flashover and nonflashover fires, depending on the reliability and effectiveness of the sprinkler system, are rendered nonlethal.

The risk-cost assessment model evaluates the effects of various fire scenarios that may occur in the building during its life. For example, in an apartment building, one fire scenario is the fire and smoke spread resulting from one design fire in any one of the apartment units in the building and during a time when the occupants are either awake or asleep. The number of fire scenarios, therefore, is the product of the number of design fires, the number of apartment units, and whether the occupants are awake or asleep.

The fire growth submodel [110] predicts the development of the six design fires in the room of fire origin. The submodel calculates the burning rate, the room temperature, and the production and concentration of toxic gases as a function of time. With these calculations, the model determines the time of occurrence of five important events: (1) time of fire cue, (2) time of smoke detector activation, (3) time of sprinkler activation, (4) time of flashover, and (5) time of fire burnout. The first three detection times are used by the evacuation duration submodel to estimate the time available for evacuation; the flashover time is used by the fire brigade action submodel, in combination with the arrival time of the fire brigade, to evaluate the effectiveness of fire fighting; and the burnout time is used by the smoke hazard submodel as part of the calculation for the maximum smoke hazard. The submodel also predicts the mass flow rate, the temperature, and the concentrations of CO and CO_2 in the hot gases leaving the fire room. This latter information is used by the smoke movement submodel to calculate the spread of smoke to different parts of the building as a function of time.

The smoke movement submodel [111] calculates the spread of smoke and toxic gases to different parts of the building as a function of time. The submodel also calculates the critical time when the stairs become untenable, which is considered to be the time when the occupants are

trapped in the building. This critical time is used later by the evacuation duration submodel to calculate the time available for evacuation.

The fire detection submodel calculates the probabilities of detection at the first three detection times mentioned under the fire growth submodel, based on the probabilities of detection by smoke detectors, sprinklers, and occupants. This information is used by the occupant warning and response submodel to calculate the probabilities of response of the occupants.

The occupant warning and response submodel calculates the probabilities of warning and response at the first three detection times mentioned under the fire growth submodel. This information is used by the fire brigade action submodel to calculate the probability of response of the fire brigade, and by the egress submodel to model the evacuation of the occupants.

The fire brigade action submodel calculates the probability and time of arrival of the fire brigade. This submodel also evaluates the effectiveness of fire fighting, based on the flashover time from the fire growth submodel and the arrival time of the fire brigade. The information on arrival and effectiveness of the fire brigade is used by the smoke hazard submodel to calculate the maximum smoke hazard to the occupants, and by the fire spread submodel to calculate the probabilities of fire spread.

The smoke hazard submodel calculates the maximum smoke hazard to the occupants based on the burnout time from the fire growth submodel and the arrival time and effectiveness of the fire brigade from the fire brigade action submodel. This information is used by the life loss submodel to calculate the probabilities of life loss.

The evacuation duration submodel uses the three fire detection times from the fire growth submodel and the critical time in the stairs from the smoke movement submodel to calculate three durations available for evacuation. This information is used by the egress submodel to model the evacuation of the occupants.

Based on the evacuation time available and the probability of response of the occupants, this submodel calculates the number of occupants who have evacuated the building and the number trapped in the building. This information is used by the expected number of deaths submodel to calculate the expected number of deaths.

The boundary element submodel calculates the probabilities of failure of the boundary elements (walls, floors, doors, etc.) when they are subjected to fully developed, realistic fires. The submodel comprises the following probabilistic models: fire severity, temperature distribution, thermomechanical material properties, failure performance for each limit state, and overall probability of failure.

Based on the probabilities of failure of the boundary elements, this submodel calculates the probabilities of fire spread to each part of the building given a fully developed fire in any enclosure. A probabilistic network of the building is developed where nodes represent building volumes, links represent boundary elements between volumes, and probabilities of failure of the boundary elements are assigned to links. Allowance is made for the effectiveness of the fire brigade. The probability of fire spread information is used by both the property loss submodel and the life loss submodel to estimate fire losses and life loss.

Based on the probabilities of smoke hazard from the smoke hazard submodel and fire spread from the fire spread submodel, this submodel calculates the probabilities of life loss.

Based on the probabilities of life loss from the life loss submodel and the number of occupants trapped in the building from the egress submodel, this submodel calculates the expected number of deaths in the building.

Based on the probabilities of fire spread from the fire spread submodel, this submodel calculates the expected property loss.

Based on the expected property loss and the capital and maintenance costs of the fire protection systems, this submodel calculates the expected fire costs.

The expected risk-to-life submodel calculates the overall expected risk to life (ERL) by summing the expected number of deaths in the

building for each fire scenario and the probability of each fire scenario.

The fire-cost expectation submodel calculates the fire-cost expectation (FCE) using the capital and maintenance costs of the fire protection systems, the expected fire loss for each fire scenario, and the probability of each fire scenario.

In the risk-cost assessment model, due to the complexity and the lack of sufficient understanding of fire phenomena and human behavior, certain conservative assumptions and approximations were made in the mathematical modeling. In addition, not all aspects of the risk-cost assessment model have been fully verified by full-scale fire experiments or actual fire experience. Only some of the submodels have been verified by experiments or statistical data.

As a result, the predictions made by the model can be considered as only approximate. The model, therefore, should not be used for absolute assessments of life risks and protection costs. For comparative assessments of life risks and protection costs, and for the selection of a cost-effective fire safety system design solution, the model is considered to be reliable.

As in many computer models, the model uses certain input parameters to describe the characteristics of various fire safety designs. These include the fire resistance rating of boundary elements, the reliability of smoke alarms and sprinklers, the probability of doors open or closed, and the response time of fire brigades. The sensitivity of these parameters on the predicted risks has been checked and found to be reasonable [112].

FRAMEworks

Another computer-based risk assessment model, *FRAMEworks*, was developed through a collaborative effort between the National Institute of Standards and Technology (NIST), the NFPA Fire Analysis & Research Division, and the private consulting firm of Benjamin/Clarke Associates [113, 114]. The goal of this effort was to develop an objective, comprehensive, generally applicable, and widely recognized fire risk assessment methodology for products that go into buildings. The result was a method for quantifying the fire risk associated with a specific class of products in a specified occupancy.

FRAMEworks is similar in many respects to the fire risk and cost assessment model of Beck described above. It combines a quantitative (fire effects modeling) method to evaluate specific products in specific fire scenarios with a statistical method of relating fire deaths to the specific scenarios in order to establish a death rate baseline for the scenarios. The impact of new or replacement products can then be evaluated against the baseline scenarios to determine if the risk is comparatively higher or lower with a change of product(s).

The modeling sequence to compute fire risk in *FRAMEworks* is illustrated in Fig. 75.14. A more detailed description of the model can be found in the NFPA *Fire Protection Handbook*® [114].

CRISP

A computer-based fire risk assessment model is also under development in the United Kingdom by the Building Research Establishment, Fire Research Station. This model, called CRISP (Computation of Risk Indices by Simulation Procedures), is similar to the Beck model in that it provides a Monte Carlo simulation of entire fire scenarios but is an object-oriented model as opposed to a state transition model [115, 116]. The basic concept of the CRISP approach is that the building-contents-people system is treated as a collection of objects, represented by a section of the program that defines the objects' behavior in response to stimuli (input data). The objects may interact in a number of ways, depending on the information exchanged between them, but data associated with an object cannot be changed by another object (only by changing that object's code). Thus, for any given scenario, the objects will interact with each other but not change each

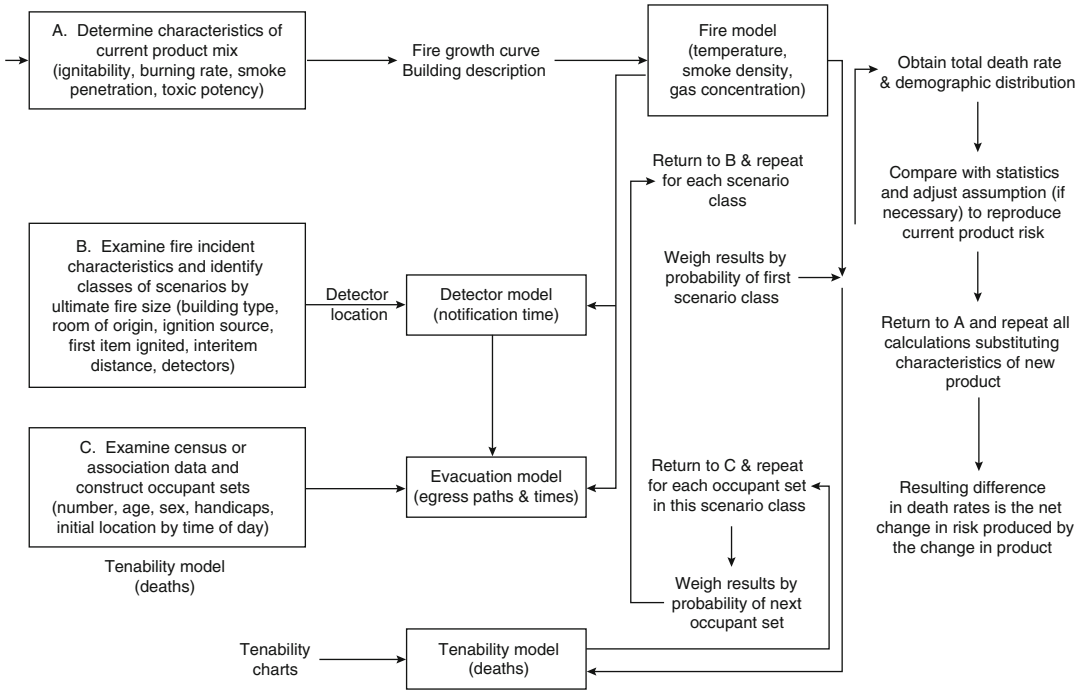

Fig. 75.14 Modeling sequence to compute fire risk in FRAMEworks [113]

other, based on the associated object definition and input parameters.

The types of objects modeled include furniture, hot and cold gas layers, vents, walls, rooms, alarms, occupants, and fire fighters [115]. The actions of the objects are governed by physical relationships (e.g., fire growth) and tables of rules (e.g., for people). For each run, various conditions, contents, and occupant characteristics are randomly selected and probabilities are assigned. Once the conditions have been defined, the simulation predicts how a scenario develops with time until the fire is out or the occupants are dead or have escaped.

Thus far, the scope of CRISP runs has been limited to two-story residential occupancies, and has been used to evaluate such trade-offs as fire detection installation versus the need for additional passive fire protection, and caution has been urged relative to the model's use in more complex buildings [105].

FRIM-MAB

A fire risk index method has been developed for multistory apartment buildings (FRIM-MAB) [117]. The approach uses a semiquantitative approach to characterize the fire risk associated with timber-frame buildings common within the Nordic countries of northern Europe.

Specific fire-related parameters such as apartment linings, smoke detection, escape routes, and the like are defined, with supporting decision tables to allow consistent evaluation of each parameter. The parameters are indexed based, for example, on the type of suppression system provided. The whole building is then assessed using a semiquantitative method. A comparative risk value is then determined for each building. This approach provides a consistent method for categorizing the risk within buildings. The approach has been supported by more complex modeling using quantified risk assessment

(QRA) techniques. The risk index provided has been shown to be consistent with the calculated expected risk from using QRA; however, it is noted the risk determined is not quantitative but provides valuable comparison between buildings assessed with the same method.

Of particular interest is the ability to provide repeatable and consistent evaluations of risk. The approach has been validated via assessment of separate buildings by independent engineers, evaluating the buildings with identical information. The results show, for the sample buildings assessed, that a consistent answer can be provided.

BuildingQRA

BuildingQRA [141] is a software package developed to help assess safety and financial risks associated with fires in buildings. An event tree structure is used. Scenarios are solved probabilistically for the event tree using Monte Carlo analysis. The software includes options assessment and cost-benefit prioritization. Multiple scenarios assessments are based either on discrete hazard (smoke) and egress analysis using zone models or user defined values. Specific event trees can be developed. Distributions are used for input parameters. Other user defined functions, including fault trees, are available as well.

B-RISK

B-RISK is a fire simulation model and software program comprising a fire risk simulator for generating probability distributions for relevant model outputs, given that the statistical distributions to key input parameters are assigned [142]. Central to B-RISK is an underlying deterministic fire zone model, BRANZFIRE [143], for which the physics have been expanded, and a new tools for users has been implemented which allows for a better understanding and description of the uncertainty and risk associated with fires in building enclosures. The B-RISK model may be used for both single deterministic runs as well as for multiple iterations of a scenario for the purpose of sensitivity analysis or for producing probabilistic descriptors of fire risk under defined conditions.

CUrisk

A quantified risk assessment (QRA) program is being developed at Carlton University, CUrisk [118], to evaluate the fire safety designs, predominantly for timber-framed commercial buildings. Risk, in this instance, is determined with the use of an overriding system model, providing an event tree, with supporting submodels used to determine fire growth and smoke movement, boundary failure and fire spread, occupant response and evacuation, and building cost and economic loss.

The model uses deterministic analysis of separate fire scenarios to calculate, for example, smoke temperatures and toxic smoke concentrations within the fire compartment and neighboring compartments. The approach uses an advanced occupant evacuation model to determine the time taken for occupants to evacuate including a "rule-based" behavior system and random procedures within the decision-making process.

The results provide the expected risk to life (ERL) and the expected risk injury (ERI), based on the tenability criteria to yield both death and also incapacitation. The expected annual financial cost of fire within the building can also be determined.

Structured Technical Analysis of Risks from Fire (STAR-Fire) and Simplified Approach to Fire Risk Assessment (SAFiRE) Methods

Structured Technical Analysis of Risks from Fire (STAR-Fire) [119] and Simplified Approach to Fire Risk Assessment (SAFiRE) methods [120] were first developed following analysis of the King's Cross Underground Station fire. The approaches are based on the risk assessment

methods first developed in the nuclear industry and further developed in the offshore and transport industries, modified to provide quantified fire risk assessment for the design of buildings. These methods can address life safety, property protection, and business continuity fire safety objectives, with selection dependent on user needs, and can be used for both new and existing buildings. To date, a large cross section of building types has been assessed using these methods, including retail, public, transport, education, and industrial facilities [58, 120, 121].

Generic fault and event trees, and balanced modeling of frequency and consequence, are used in each approach [121, 122]. Individual and societal risk to life can be assessed, and average or distributional representations of financial loss measures can be used, with results presented in either tables or FN curves. The outcomes can then be used for absolute risk assessment, using risk criteria agreed on by stakeholders, or, comparatively, benchmarking to the risk levels associated with a code compliant design or other agreed benchmark (the latter being the preferred approach).

In these methods, individual fire events are defined by their frequency and their consequences. Scenarios are defined by fault and event tree analysis, with Monte Carlo analysis of highly variable parameters (e.g., number of people in the building at the time of ignition). Input data include geometry of spaces and escape routes, fire growth, detection, occupant number, premovement time and velocity/flow, frequency of ignition, and probabilities of failure of fire protection systems, with probability distributions being calculated for the most variable parameters; and evacuation time, tenability time, and statistical analysis of some scenarios being generated. Simulation of one million fire scenarios requires on the order of 1–2 h. Uncertainty, safety factors, sensitivity, precision, and bias are addressed through a qualitative narrative.

Hazard and Risk Matrices

In addition to the more complicated single-scenario and ETA-based engineering approaches and computer-based risk modeling, various risk analysis alternatives exist that combine hazard analysis, consequence analysis, and judgments about likelihood of events in less quantitatively rigorous manners. This does not imply the methods are less rigorous, or less appropriate, but that they are simply easier to apply. In many cases, such simplified approaches will be more widely accepted by interested and affected parties, as the concepts may be familiar.

One such approach is the hazard matrix [123], or risk matrix approach [10, 124]. This approach is simpler to apply than a classical engineering risk analysis approach, as the importance of identifying all possible outcomes is less critical. In essence, it works by quantifying the consequences of the most severe events anticipated and coupling these with approximate event frequencies. The result is a quantified approximate risk estimate. In this approach, a maximum consequence for each type of loss is identified (life safety, property, business interruption, environmental damage, etc.) that represents the largest realistic event of each type. Each maximum consequence is then ranked. Table 75.3 provides an example of possible consequence ranking thresholds (i.e., negligible, low, medium, and high) that may be selected. For these estimates, the consequence predictions should bound all possible event outcomes at the 95th percentile or better [10]. The 95th percentile value is suggested because it has gained ready acceptance in other engineering fields, and by using such a standard value, it may be possible to compare different analyses. If it is desired to use a different bounding level, all stakeholders must agree. An extensive analysis can often be avoided when selecting the maximum consequence if the total replacement costs are assumed to be the maximum consequence.

The frequencies must also be ranked in this type of analysis. Here, the frequencies should be for exceeding a specific loss (i.e., consequence) rather than for a specific scenario, as frequencies based solely on a specific scenario can be misleading. For example, a scenario may have a frequency of 10^{-7} per year, leading one to the conclusion that fire is not a concern. However, the reported fire risk should actually represent

Table 75.3 Possible consequence ranking criteria [10]

Consequence level	Impact on populace	Impact on property/operations
High (H)	Immediate fatalities, acute injuries—immediately life threatening or permanently disabling	Damage > $XX million—building destroyed and surrounding property damaged
Moderate (M)	Serious injuries, permanent disabilities, hospitalization required	$YY < damage < $XX million—major equipment destroyed, minor impact on surroundings
Low (L)	Minor injuries, no permanent disabilities, no hospitalization	Damage < $YY—reparable damage to building, significant operational downtime, no impact on surroundings
Negligible (N)	Negligible injuries	Minor repairs to building required, minimal operational downtime

Table 75.4 Example frequency criteria used for probability ranking [10]

Acronym	Description	Frequency level (median time to event)	Description
A	Anticipated, expected	$>10^{-2}$/year (<100 years)	Common incidents that may occur several times during the lifetime of the building
U	Unlikely	$10^{-4} < f < 10^{-2}$/year (100–1,0000 years)	Events that are not anticipated to occur during the lifetime of the facility. Natural phenomena of this probability class include UBC-level earthquake, 100-year flood, maximum wind gust, etc.
EU	Extremely unlikely	$10^{-6} < f < 10^{-4}$/year (1,0000–1 million years)	Events that will probably not occur during the life cycle of the building
BEU	Beyond extremely unlikely	$<10^{-6}$/year (>1 million years)	All other accidents

the frequency of multiple fire scenarios, so if 30 specific scenarios are developed, each at 10^{-7} fires per year, the net effect is 3×10^{-6} fires per year. Table 75.4 provides a specific example for frequency ranking [10, 122]. As with consequence ranking, alternate frequency rankings (bins) from those presented in Table 75.4 can be developed provided that all interested and affected parties agree. It is also possible to add additional layers of ranking where desirable.

Once the bounding consequences and their respective frequencies have been estimated, they must be converted to an estimate of risk. An estimation is accomplished by plotting the consequence-frequency combination in a matrix, as shown in Fig. 75.15 (the numbers in boxes are for identification purposes and do not imply a ranking). The stakeholders assign each consequence-frequency combination, and the resultant risks are considered bounding risks. After this analysis, events that meet a certain risk criterion may be considered "acceptable" based on the objectives and input from the interested and affected parties (e.g., the interested and affected parties may consider moderate, low, and negligible risk events acceptable).

Performance Matrix

A concept similar to that of the hazard and risk matrices approach described above has been developed for use in building and fire safety regulations [1, 4, 5, 125–128]. This approach establishes a performance matrix that compares performance groups (building types grouped by like performance expectations) by magnitude of design events (probabilistic or deterministic descriptions of hazard event). Within the

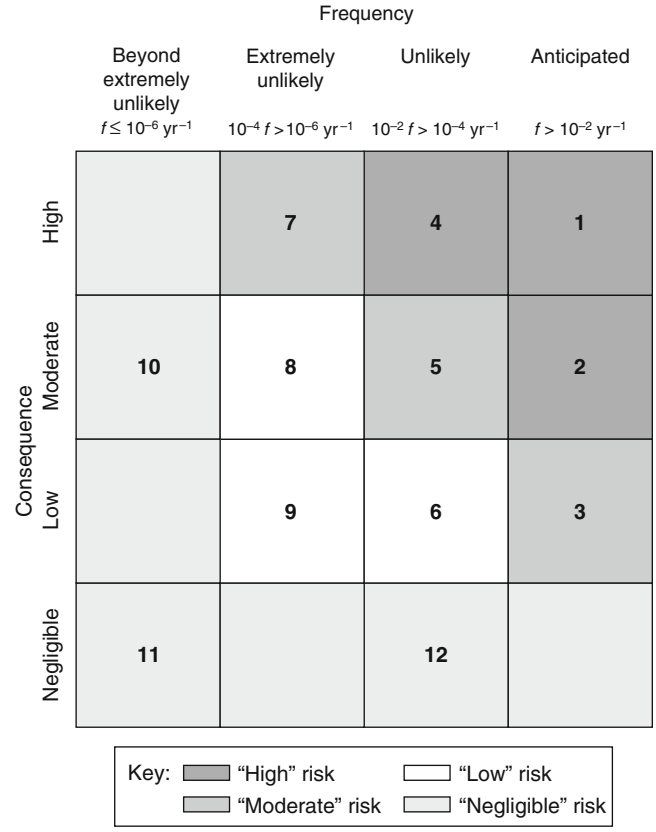

Fig. 75.15 Example risk ranking matrix [10]

performance matrix, instead of having risk bins (groups), there are tolerable levels of impact (reflecting the amount of damage expected for buildings within different performance groups given specific magnitudes of design events). As the performance group increases from Group I to Group IV, the level of required performance increases, as do the corresponding levels of tolerable impact. This is illustrated in Fig. 75.15.

Within the performance matrix, tolerable levels of impacts reflect various limit states of damage, injury, or loss that can be estimated, measured, and/or calculated when subjected to design loads of various magnitudes. As the impacts get larger, it is expected that more damage will occur, unless a higher level of performance is desired. In this manner, the levels of impact are inversely proportional to building performance: less impact means better performance. Establishment of these levels of tolerable impact requires a balance of technical knowledge and ability and societal values. The term *tolerable* is used to reflect the fact that absolute protection is not possible, and that some damage, injury, or loss is currently tolerated in structures, especially after a hazard event. The term *impact* is used as a broad descriptor of loss.

If one so chooses, one can overlay probabilities and consequences on the performance matrix in a manner similar to the hazard and risk matrices discussed previously. In the performance matrix (Fig. 75.16), the magnitudes of design event can be overlaid with probabilities (or frequencies) of event occurrence, from high at the bottom to low at the top. For all high-probability events, the allowable magnitude of impact (consequences) is either mild or moderate depending on the performance group. For low-probability events, the allowable magnitude of impact can be moderate, high, or severe depending on the performance group. This approach allows for decisions to be made on the

required level of building performance for low-probability, high-consequence events, based on the performance group to which a building is designated.

Performance groups are simply consolidations of use groups with common performance requirements. They are developed as part of the risk characterization process, considering such issues as numbers of people in a building, sensitive or vulnerable populations, the hazards posed by the building, its contents or processes, and essential facilities and services [126]. The number of performance groups that is required should be based on an analytical-deliberative risk characterization process as described previously. The following definitions of performance groups represent one example, as used in the *International Performance Code for Buildings and Facilities* [125].

Performance Group I is intended to cover those buildings or facilities, such as utility sheds, where the failure of such buildings poses a low risk to human life. Performance Group II is intended to be the minimum for most typical buildings, such as business, mercantile, or storage uses. Performance Group III includes building and facilities with an increased level of societal benefit or importance. These structures and classes of structures require increased levels of performance as they house large numbers of people, vulnerable populations, or occupants with other risk factors; or they fulfill some role of increased importance to the local community or to society in general. Examples include post-disaster command control centers, acute-care hospitals, or a school used as an emergency shelter. Performance Group IV contains building uses or facilities that have an unusually high risk. Such facilities may include nuclear facilities or explosives storage facilities. For specific facilities, for specific jurisdictions, or in countries outside of the United States, other definitions for the performance groups may be appropriate.

Fig. 75.16 Performance matrix [1, 125]

Magnitude of design event Increasing magnitude of event	**Increasing level of building performance** Performance groups			
	Performance group I	Performance group II	Performance group III	Performance group IV
Very large (very rare)	**Severe**	**Severe**	**High**	**Moderate**
Large (rare)	**Severe**	**High**	**Moderate**	**Mild**
Medium (less frequent)	**High**	**Moderate**	**Mild**	**Mild**
Small (frequent)	**Moderate**	**Mild**	**Mild**	**Mild**

Likewise, the number of tolerable levels of impact can be selected based on the level of detail deemed appropriate by interested and affected parties. One possibility is the use of four levels: mild, moderate, high, and severe [128]. The definition of each level would reflect the tolerability limits as developed by a risk characterization effort. For example, a moderate level of impact may be defined as follows (remember that levels of impact are inversely proportional to levels of performance, and that these are design goals):

- There is moderate structural damage that is repairable; some delay in reoccupancy can be expected due to structural rehabilitation.
- Nonstructural systems needed for normal building use are fully operational, although some cleanup and repair may be needed. Emergency systems remain fully operational.
- Injuries to building occupants may be locally significant, but generally moderate in numbers and in nature. There is a low likelihood of single life loss and a very low likelihood of multiple life loss.
- Damage to building contents may be locally significant but is generally moderate in extent and cost.
- Some hazardous materials are released to the environment, but the risk to the community is minimal. No emergency relocation is necessary.

Associated with the tolerable levels of impact is the actual hazard event. One way to look at the hazard event is in terms of its size, or magnitude. The magnitude of a hazard event can be represented deterministically or as a frequency of occurrence. When characterizing the magnitude of hazard events, it is important to remember that (1) they are on a continuum and are compartmentalized for ease of analysis and design; and (2) they should be considered "design loads" and not as a reflection of the actual magnitude of event that could impact a building.

As with tolerable levels of impact, the number of magnitude of event levels can be established by the interested and affected parties. For example, four categories of event magnitude (design loads) can be selected: small (frequent), medium (occasional), large (rare), and very large (very rare). To understand how the magnitudes can be described, consider earthquake loads and fire loads, where earthquake loads are shown in terms of their mean return period, and fire loads are shown deterministically in terms of extent of flame spread.

Earthquake loads (mean return period)	
Frequent	72 years
Occasional	225 years
Rare	474 years
Very rare	2475 years
Fire loads (deterministic)	
Small	Contained to object of origin
Medium	Contained to room
Large	Contained to floor
Very large	Contained to building

There is often correlation between frequent, occasional, rare, and very rare; and small, medium, large, and very large; in that frequent events tend to be small, whereas very large events tend to be very rare. Also, it is often the very large or very rare events that are of particular concern, as it is these events for which providing high levels of protection against is costly and may not be considered reasonable or cost-effective for all buildings.

The Building Fire Safety Evaluation Method (BFSEM)

Another approach to identifying hazards and consequences, for obtaining judgments on the likelihood of events occurring, and for characterizing risk, is the *Building Fire Safety Evaluation Method* (BFSEM) [129–133]. The BFSEM can be used to analyze an existing building or a proposed new building. A primary goal is to understand how the building will perform for credible diagnostic fire scenarios. Describing expected risk characterizations are another part of a complete BFSEM analysis. One can perform either a holistic analysis or an individual component analysis.

Figure 75.17 illustrates the scope of fire performance and risk characterizations [132]. After one understands the building's performance and can characterize the associated risks, an integrated design or risk management program can be developed.

The system of building-fire behavior is dynamic. Therefore, time links all parts of the system. The method's organization provides a way to coordinate dynamic fire changes and fire defense operations. An analysis incorporates time-based changes in component performance by adapting conventional event trees of risk analysis. Performance evaluations for any instant of time adapt conventional fault tree analysis. Component interactions are incorporated into evaluations.

The method is based on deterministic analyses of the fire defense components. An analysis uses modules that are obtained by decomposing the complete functional system of fire and buildings and repackaging the components into analytical networks. Adapting techniques of failure analysis to additional decompositions provides a basis for evaluating events that are critical to performance.

Time-based relationships can be captured in an *Interactive Performance Information* (IPI) chart, which orders and records important information for performance evaluations and risk characterizations. It allows one to observe changes in any component over time as well as to examine the status of any or all components at any instant of time. An IPI chart is illustrated in Fig. 75.18 [132]. In Fig. 75.18, the diagnostic fire scenario and each of the major fire defense parts are shown by the horizontal rows. Each of these rows describes an event tree adapted from conventional risk analysis. The status of the events

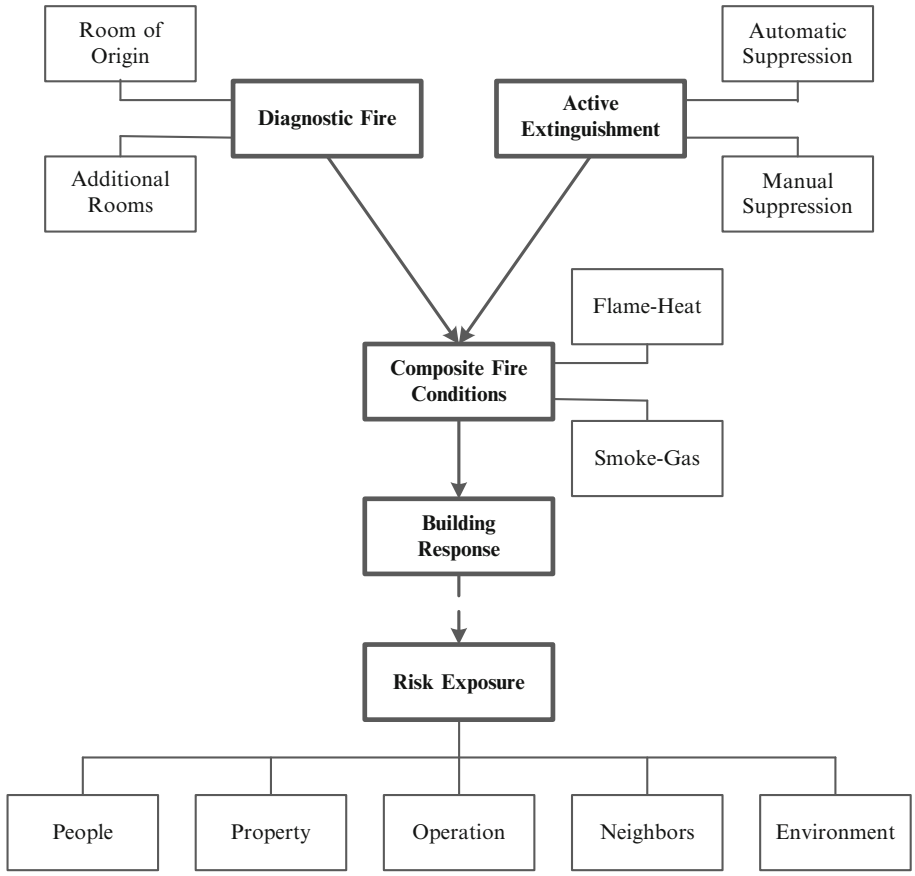

Fig. 75.17 Fire risk characterization in the BFSEM [132]

changes over the duration of the fire. The vertical columns identify time steps from ignition to extinguishment. The component events in a column are based on fault tree analysis.

The horizontal rows (event trees) are analogous to a continuous video of the operation of the major fire defenses and their major components. If we were to "stop the world" at an instant of time (i.e. examine the events in a single vertical column), the status of each component could be described and their interactions with other parts of the dynamic building-fire system would be recognized. This is analogous to examining a group of still photographs all taken at that time. For any fire scenario, each cell of the IPI chart is effectively a cell of a spreadsheet. A broad range of attributes, including a description of performance, can be shown for each instant of time.

A relatively narrow window of functional operation exists for each component of Fig. 75.18. One part of a performance analysis coordinates the time durations to understand the impact of functional operation sequencing for the building fire scenario. Each building has unique features that distinguish its fire performance from that of others. Thus, IPI charts provide a means to compare risks and the effectiveness of design improvements.

Performance quantification is deterministic. However, today's state of the art of fire technology is inadequate to quantify the performance of all components and their interactions. Consequently, evaluations incorporate Bayesian techniques to describe expected performance. This enables the contributions of other components at that instant of time to be incorporated into an evaluation. The process enriches performance understanding and communication by expressing results in terms of a probabilistic degree of success. This use of probability should not create the impression that the method is probabilistic. To the contrary, the method is deterministic, but uses Bayesian theory to bridge the gap between "benchmarks" of known behavior.

Application of the BFSEM provides a comprehensive method for identifying factors that affect the fire safety performance of a building. The method has been widely used, including being adapted by the U.S. Coast Guard to become its ship fire safety engineering methodology (SFSEM) [133].

Guidance Documents for Fire Risk Assessment

Given the growing interest in the use of risk assessment techniques for building fire safety evaluation, a number of organizations have prepared guidance documents that are useful to designers and approval authorities (i.e., AHJs) in relation to buildings.

These guides are not risk assessment methodologies or risk analysis techniques. Rather they are directed at assisting practitioners in selecting the appropriate methodology for any given building and ensuring that the process of risk assessment and approval is undertaken in a proper engineering manner.

SFPE Engineering Guide—Fire Risk Assessment

The *SFPE Engineering Guide*: *Fire Risk Assessment* [134] is aimed at those qualified practitioners undertaking design and evaluation of buildings and/or process fire safety. The document provides guidance on the selection and use of risk assessment techniques and provides a recommended process to follow.

The *SFPE Guide* does not specify particular risk assessment methods or techniques. However, it highlights

- A recommended process for fire risk assessment (Fig. 75.19)
- Tools that may be used for hazard identification
- Sources of data for risk assessment
- Approaches to consequence modeling
- Methods for calculating fire risk
- Documentation of fire risk assessment

The *SFPE Guide* is structured to follow the flowchart represented in Fig. 75.19, providing guidance and information association with each

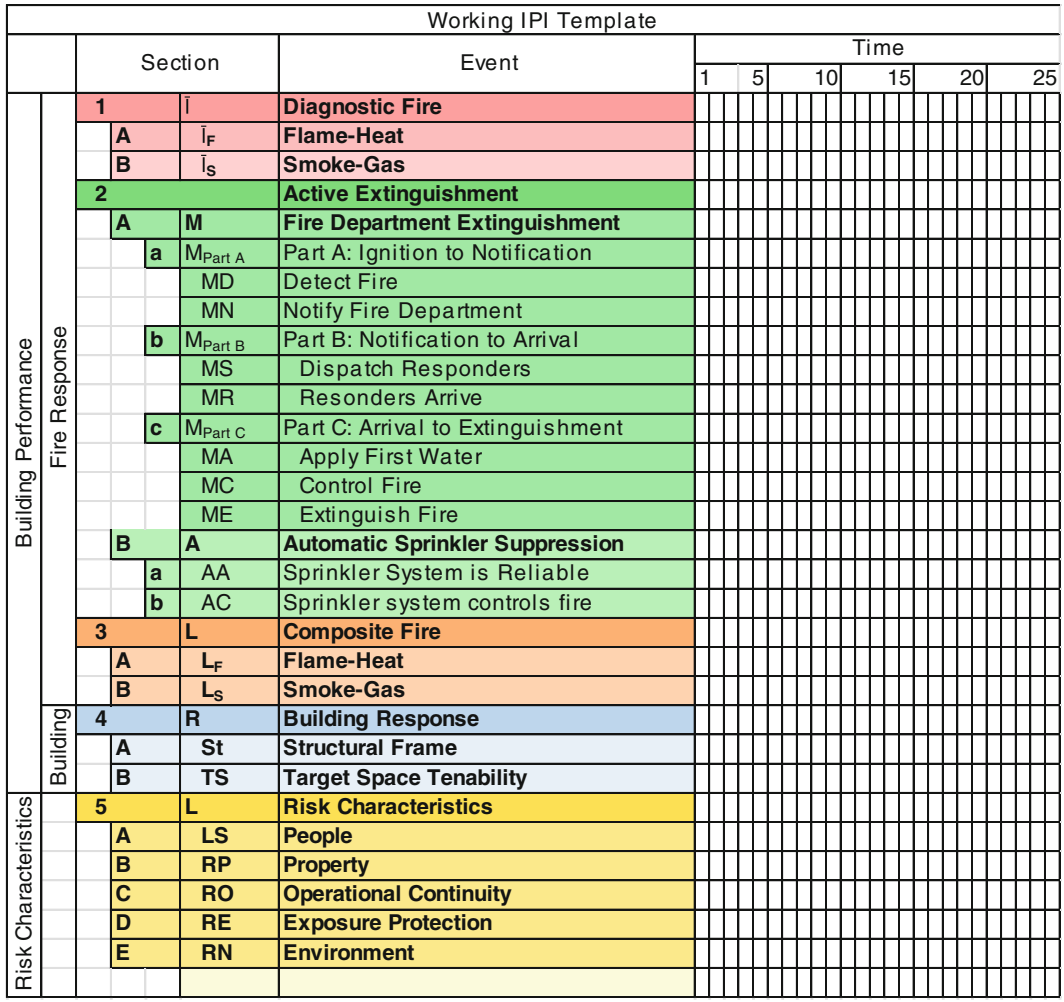

Fig. 75.18 Interactive Performance Information (IPI) chart representation of BFSEM [132]

step in the process. This information is supported with many references and a comprehensive list of information sources for further reading for each step of the risk assessment process. An overview of the SFPE process can be found in reference [135].

NFPA 551, *Guide for the Evaluation of Fire Risk Assessments*

NFPA 551, *Guide for the Evaluation of Fire Risk Assessments* [136], was developed in the United States in recognition of the fact that fire risk assessment methods are increasingly being used in developing fire and life safety solutions for buildings and other facilities.

This guidance document is directed at those responsible for approving or evaluating fire and life safety solutions based on a fire risk assessment. It provides a framework that describes the properties of a fire risk assessment, particularly where it is being used in a performance-based regulatory framework. As a result, this guide is suited to a building or fire official or other authority having jurisdiction required to evaluate or approve a building design where the design is being supported by a fire risk assessment.

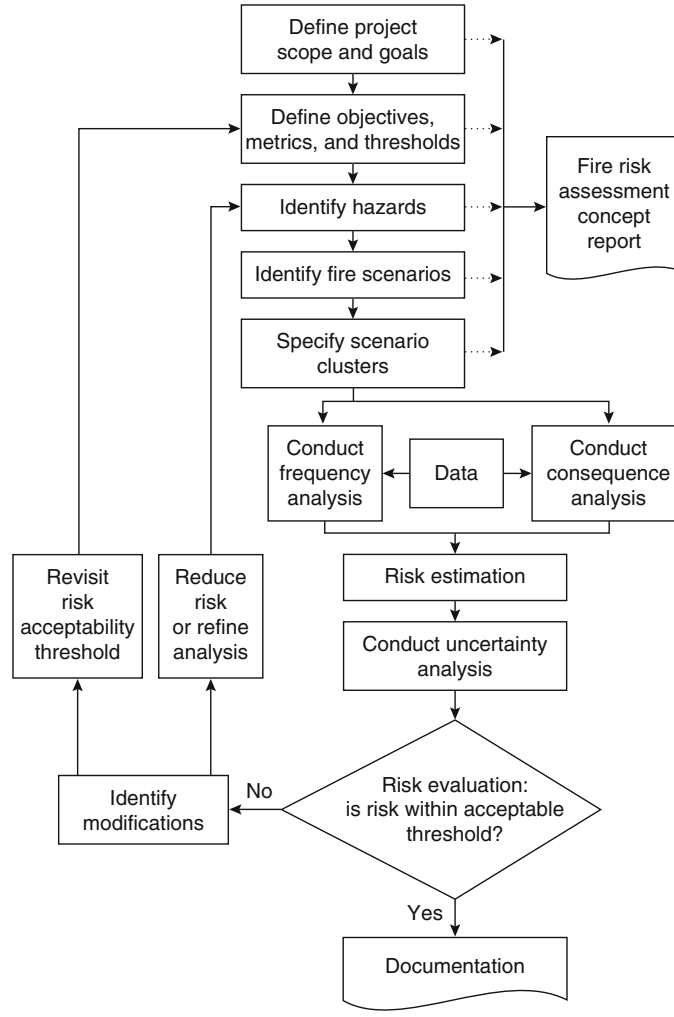

Fig. 75.19 Fire risk assessment flowchart [134]

Like the *SFPE Guide* referenced above, NFPA 551 neither specifies particular fire risk assessment methods nor attempts to set acceptance criteria. Rather it sets out the technical review process and documentation that should be used by those evaluating or approving. The review process is illustrated in Fig. 75.20.

NFPA 551 defines five categories of fire risk assessment methods in order of increasing complexity, namely

- Qualitative methods
- Semiqualitative criteria-based methods
- Semiqualitative consequence methods
- Quantitative methods
- Cost-benefit risk methods

It highlights the importance of identifying the objectives of any fire risk assessment and other factors that should be considered by those undertaking fire risk assessments. For each of the five categories of methods, the characteristics of each approach are identified, and issues of inputs and outputs, assumptions and limitations, selection of fire scenarios, and uncertainty are discussed.

BS 7974-7, *Probabilistic Risk Assessment*

The British Standards Institute (BSI), the National Standards Body of the United Kingdom (U.K.), provides a number of fire-related design

standards. A framework for the application of fire safety engineering principles for the design of buildings is provided within BS 7974. This document is supported by the Published Document series PD 7974 Parts 0 to 7. The final document, Part 7, provides guidance for the probabilistic risk assessment of buildings [137].

The document provides a framework for risk assessment commensurate with a number of approaches within this handbook. Specifically, the document provides guidance with regard to acceptance criteria for life safety and financial assessments, which may use either comparative or absolute methodologies. The absolute criteria for individual risks and societal risk are provided. The logic tree is illustrated using both event trees and fault trees. An assessment methodology using *complex* analysis techniques is also provided, whereby risk is evaluated understanding the reliability of systems, use of stochastic models to evaluate the spread of fire within a building, Monte Carlo analysis used to evaluate a random distribution of variables addressing low-probability scenarios, and safety factors.

The annex to this document provides very useful guidance about the probability of fire starting dependent on the type and use of the building. Further, the average area damaged and the distribution of damage are provided. There are also valuable statistics on the frequency distribution of the numbers of deaths attributed to fire, the probability of flashover, and reliability data concerning active and passive fire safety systems.

These data are principally based on U.K. fire statistics recorded over a representative sample period and as such are considered a valuable

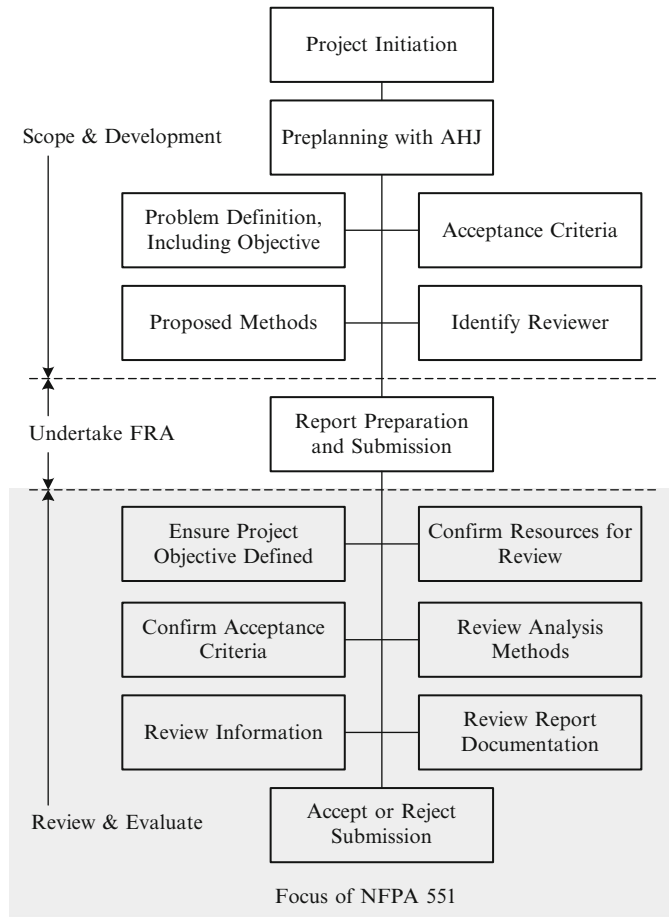

Fig. 75.20 NFPA 551 review process [136]

source of information, although generally applicable to U.K. projects. The data, for example, illustrate fire damage for an 8000-square-meter textile industry building is twice as large for a nonsprinkled building when compared to a sprinkler protected building.

ISO 16732-1:2012 *Fire Safety Engineering—Fire Risk Assessment*

ISO 16732-1:2012 provides the conceptual basis for fire risk assessment by stating the principles underlying the quantification and interpretation of fire-related risk [138]. The principles and concepts outlined in the standard can be applied to any fire safety objectives, including safety life, conservation of property, business continuity, preservation of heritage and protection of the environment. The fire risk principles discussed in the standard apply to all fire-related phenomena and user applications, which means that the principles can be applied to all types of fire scenarios.

In ISO 16732-1:2012, principles underlying the quantification of risk are presented in terms of the steps to be taken in conducting a fire risk assessment. These quantification steps are initially placed in the context of the overall management of fire risk and then explained within the context of fire safety engineering. The use of scenarios and the characterization of probability (or the closely related measure of frequency) and consequence are then described as steps in fire risk estimation, leading to the quantification of combined fire risk. Guidance is also provided on the use of the information generated, i.e., on the interpretation of fire risk. Finally, there is guidance on methods of uncertainty analysis, in which the uncertainty associated with the fire risk estimates is estimated and the implications of that uncertainty are interpreted and assessed.

As described by ISO 16732-1:2012, risk management includes risk assessment, but also typically includes risk treatment, risk acceptance, and risk communication (see Fig. 75.21).

In this approach, fire risk assessment is part of a larger process, which starts with setting fire risk goals and objectives, and where risk acceptance marks the conclusion of the assessment. If risk is not accepted, another risk assessment is necessary, and risk treatment is an option after each risk assessment. Risk communication is conducted after risk acceptance.

The component of fire risk assessment is defined as a procedure for estimation of fire risk for a built environment and evaluation of estimated fire risk in terms of well-defined acceptance criteria [138]. Fire risk assessment is can be used to quantify the risk associated with specific scenarios, but can also be used to assess alternative designs, prior to selecting a specific design or making changes to that design to achieve compliance with the acceptance criteria.

Fire risk assessment begins with the fire risk goals and objectives and a proposed design specification for the structure or other part of the built environment to be assessed. The risk associated with the design specification is estimated and then evaluated. Risk evaluation consists of comparison of the estimated risk for the design to the acceptance criteria.

Fire risk estimation begins with the establishment of a context. The context provides a number of quantitative assumptions, which are required with the objectives and the design specifications to perform the estimation calculations. Figure 75.22 describes the sequence of steps involved in fire risk estimation as it is conducted when the scenario structure is explicit and when frequencies and consequences are explicitly calculated in quantitative form (other sections of the standard describe the use of risk curves, risk matrices and other techniques for which the flow chart is not fully applicable in detail).

The standard goes on to describe in some detail the components in the fire risk estimation, as well as the role of uncertainty in the fire risk assessment process. Examples of application of fire risk assessment are also included.

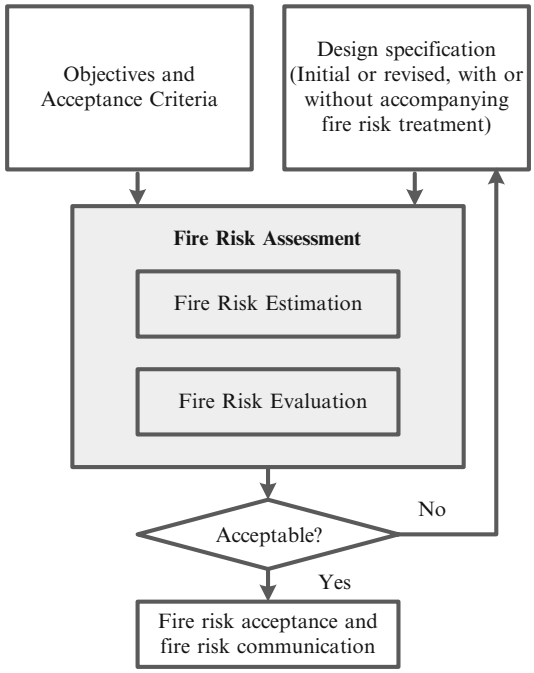

Fig. 75.21 Fire risk management concept [138]

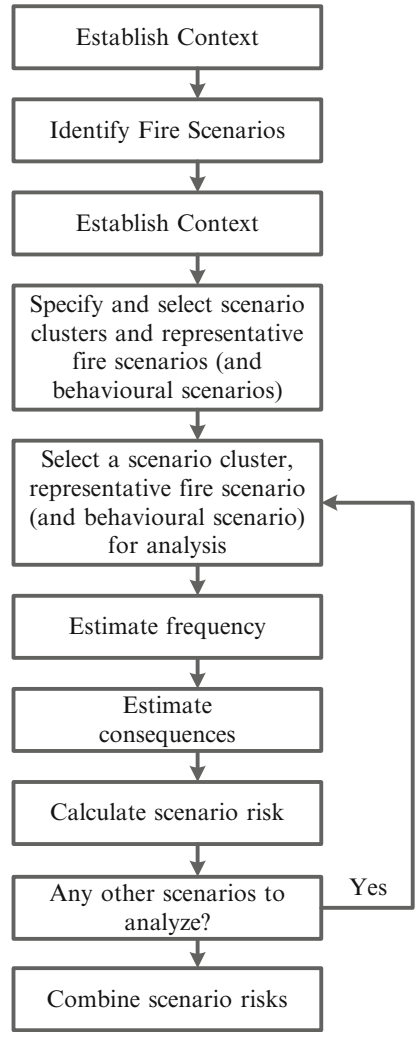

Fig. 75.22 Risk estimation [138]

Textbooks

As noted in the previous section, there has been a growing interest in fire risk assessment over the last two decades, which has prompted the development of several guidance documents and standards on fire risk assessment. In addition, there have been new chapters added to the SFPE Handbook on various aspects of fire risk assessment, e.g. by industry, occupancy type and sector (built environment, transportation), with each new edition. As another indicator of the growing interest in fire risk assessment, and the desire for information relative to tools and techniques for fire risk assessment, there have been a number of textbooks published in the last decade, with others in development. It is worth noting these as additional resource for fire protection engineers, with the hope that this section continues to expand in future editions.

Published in 2004, *Evaluation of Fire Safety* [139], while not strictly a text on fire risk assessment, includes many aspects of fire risk assessment throughout. Written by a collection of five leading authorities in fire safety engineering, the text includes chapters on sources of statistical fire loss data, measurements of fire risk, various fire risk evaluation methods (e.g., point systems, logic tress, stochastic fire risk modeling and the fire safety concepts tree and derivative approaches). It provides a comprehensive suite of information for anyone embarking on fire safety evaluation of the built environment.

Following the tragic events of September 11, 2001, the text *Extreme Event Mitigation in Buildings*: *Analysis and Design* [140] was published to provide a resource for understanding and assessing building performance under

extreme events. While not focused solely on fire, the text provides information on assessing likelihood of occurrence, potential impacts, and strategies for mitigation for a wide range of extreme events—natural, technological and deliberate, while aiming to achieve a balance of acceptable levels of risk, performance and cost. The text outlines how risk-informed performance-based analyses can be used to help make important risk mitigation decisions.

In 2007, a trio of risk experts from Australia published the book, *Risk Analysis in Building Fire Safety Engineering* [94]. As the title implies, this text is focused on tools and techniques that are fundamental to applying risk concepts in fire safety engineering. It starts with elements of probability theory required for the understanding of risk analysis, then transitions into various tools for risk analysis, including the beta reliability index, Monte Carlo Analysis, Event Tree and Fault Tree analysis, and cost-benefit analysis. Several chapters are then provide relative to modeling the probabilistic and stochastic aspects of fire safety systems. Case studies are provided to illustrate the application of these concepts in performance-based fire safety design.

2008 saw the publication of a text focused on building fire risk assessment, *Principles of Fire Risk Assessment in Buildings* [96]. This text is presented in two parts: Part I overviews simple approaches to fire risk assessment, and Part II outlines a fundamental approach to fire risk assessment, considering fire growth, smoke spread, occupant response and other factors using fire risk assessment concepts. Like the text above, this was authored by an expert in the field who has developed models for fire risk assessment described earlier in this chapter.

Most recently, two renowned fire risk experts from the UK collaborated on the 2011 text, *Quantitative Risk Assessment in Fire Safety* [97]. This text presents a broad ranging discussion of qualitative, semi-quantitative and quantitative risk assessment techniques, discussing sources of data, structuring of the assessment technique, assessment and evaluation. Probabilistic and stochastic analysis of fire development and spread and response of fire safety systems is also provided. Reliability of fire safety systems, performance of people and effectiveness of the fire services is also presented.

These texts, as well as others written for specific industries, hazards and risks, provide fire protection engineers with additional resources for tackling the challenges of building fire risk analysis.

Summary

Building fire risk analysis is a complex subject. This chapter has provided a brief overview of key issues in the subject area, including discussions on difficulties in defining risk, on risk characterization, on tools and methods to help identify hazards and consequences, and on building fire risk analysis methods. Given the complexities involved in building fire risk analysis, it is intended that this chapter provide a starting point rather than an end point. With this in mind, extensive references and sources for further reading are provided for additional information. A review of other risk-related chapters in this handbook, such as those by Hall; Notarianni and Parry; Ramachandran and Hall; Watts; Barry; and Siu, Hyslop, and Nowlen is a good place to start. In addition, in the post-9/11 environment, building fire risk analysis should consider extreme fire and other events and be part of the overall risk assessment for the building [140]. Finally, it is important to remember that when embarking on a building fire risk analysis effort, one should take care to identify and involve the interested and affected stakeholders, carefully consider the range of risk issues involved, and seek the most appropriate approaches, tools, methods, and data for the problem.

References

1. B.J. Meacham, "A Process for Identifying, Characterizing, and Incorporating Risk Concepts into Performance-Based Building and Fire Regulations Development," Ph.D. Dissertation, Clark University, Worcester, MA (2000).

2. N.C. Rassmussen, "The Application of Probabilistic Risk Assessment Techniques to Energy Technologies," in *Readings in Risk* (Glickman and Gough, eds.), Resources for the Future, Washington, DC, pp. 195–206 (1990).
3. P.C. Stern and H.V. Fineburg (eds.), *Understanding Risk: Informing Decisions in a Democratic Society,* National Academy Press, Washington, DC (1996).
4. B.J. Meacham, "Understanding Risk: Quantification, Perceptions and Characterization," *Journal of Fire Protection Engineering*, 14, 3, pp. 199–227 (2004).
5. B.J. Meacham, "Incorporating Risk Concepts into Performance-Based Building and Fire Regulation Development," in *Safety Engineering and Risk Analysis,* SERA Volume 9 (J.L. Boccio, ed.), American Society of Mechanical Engineers, New York, pp. 63–70 (1999).
6. B.J. Meacham, "Application of a Decision-Support Tool for Comparing and Ranking Risk Factors for Incorporation into Performance-Based Building Regulations," in *Proceedings of the Third International Conference on Performance-Based Codes and Fire Safety Design Methods,* SFPE, Bethesda, MD (2000).
7. B.J. Meacham and R.L.P. Custer, "Performance-Based Fire Safety Engineering: An Introduction of Basic Concepts," *Journal of Fire Protection Engineering,* 7, 2, pp. 35–54 (1995).
8. R.L.P. Custer and B.J. Meacham, *Introduction to Performance-Based Fire Safety,* NFPA, Quincy, MA (1997).
9. B.J. Meacham, "Assessment of the Technological Requirements for Realization of Performance-Based Fire Safety Design in the United States: Final Report," *NIST GCR 98-763,* NIST, Gaithersburg, MD (1998).
10. Society of Fire Protection Engineers, *SFPE Engineering Guide to Performance-Based Fire Protection Analysis and Design of Buildings,* SFPE and NFPA, Quincy, MA (2000).
11. R.L. Keeney and H. Raiffa, *Decisions with Multiple Objectives: Preferences and Value Tradeoffs,* John Wiley and Sons, New York (1976).
12. R.L. Keeney, "Formal Analysis Including Value Judgments and Public Risk," *Toxic Substances Journal,* 3, 1, pp. 8–22 (1981).
13. R.T. Clemen, *Making Hard Decisions: An Introduction to Decision Analysis,* Duxbury Press, Pacific Grove, CA (1996).
14. R. Schwing and W. Albers (eds.), *Societal Risk Assessment: How Safe Is Safe Enough?,* Plenum, New York (1980).
15. E. Crouch and R. Wilson, *Risk/Benefit Analysis,* Ballinger Publishing Company, Cambridge, MA (1982).
16. R. Wilson, "Commentary: Risks and Their Acceptability," *Science, Technology and Human Values,* 9, 2, pp. 11–22 (1984).
17. D.J. Alesch and W.J. Petak, *The Politics and Economics of Earthquake Hazard Mitigation: Unreinforced Masonry Buildings in Southern California,* Institute on Environment and Behavior, University of Colorado, Boulder (1986).
18. S. Kelman, "Cost-Benefit Analysis: An Ethical Critique," in *Readings in Risk* (Glickman and Gough, eds.), Resources for the Future, Washington, DC, pp. 129–137 (1990).
19. S. Breyer, *Breaking the Vicious Circle: Toward Effective Risk Regulation,* Harvard University Press, Cambridge, MA (1993).
20. T. O. Tengs et al., "Five Hundred Life-Saving Interventions and Their Cost-Effectiveness," *Risk Analysis,* 15, 3, pp. 369–390 (1995).
21. W.K. Viscusi and J.E. Aldy, "The Value of a Statistical Life: A Critical Review of Market Estimates Throughout the World," *Related Publication 03-2,* AEI-Brookings Joint Center for Regulatory Studies (Jan. 2003).
22. H. Kunreuther and R.J. Roth, Sr., *Paying the Price: The Status and Role of Insurance Against Natural Disasters in the United States,* Joseph Henry Press, Washington, DC (1998).
23. P.R. Kleindorfer and H.C. Kunreuther, "The Complementary Roles of Mitigation and Insurance in Managing Catastrophic Risks," *Risk Analysis,* 19, 4, pp. 727–738 (1999).
24. *Guidelines for Chemical Process Quantitative Risk Analysis,* American Institute of Chemical Engineers, Center for Chemical Process Safety, New York (1985).
25. Health Facilities Note, HFN 09, "Fire Safety—Cost or Benefit?" Her Majesty's Stationery Office, London, UK (1995).
26. S.E. Magnusson, H. Franzich, and K. Harada, "Fire Safety Design Based on Calculations: Uncertainty Analysis and Safety Verification," *Report 3078,* Lund University, Lund, Sweden (1995).
27. S.E. Magnusson, H. Frantzich, K. Harada. "Fire Safety Design Based on Calculations: Uncertainty Analysis and Safety Verification," *Fire Safety Journal*, 27: 305–334, 1996.
28. H. Frantzich, "Uncertainty and Risk Analysis in Fire Safety Engineering," *Report LUTVDG/(TVBB-1016),* Lund University, Lund, Sweden (1998).
29. D.A. Charters et al., "Assessment of the Probabilities That Staff and/or Patients Will Detect Fires in Hospitals," *Proceedings of the Fifth International Symposium of Fire Safety Science,* Melbourne, Australia (1997).
30. D.A. Charters, "Quantified Assessment of Hospital Fire Risks," *Proceedings of Interflam'96,* InterScience Communications, Cambridge, UK (1996).
31. N. Groner, "A Critique of Event Modeling as Applied to Human Reliability and a Suggested Alternative," in *Proceedings of the SFPE Symposium on Risk, Uncertainty and Reliability in Fire Protection*

Engineering, SFPE, Bethesda, MD, pp. 190–199 (1999).
32. R.E. Britter, "The Evaluation of Technical Models Used for Major-Accident Hazard Installations," *EUR 14774EN,* Commission of the European Communities, Brussels, Belgium (1993).
33. C. Hohenemser, R. Kasperson, and R.W. Kates, "Causal Structure," in *Perilous Progress: Managing the Hazards of Technology (*Kates, Hohenemser, and Kasperson, eds.), Westview Press, Boulder, CO, pp. 25–42 (1985).
34. M.C. White et al., "A Quantitative Estimate of Leukemia Mortality Associated with Occupational Exposure to Benzene," in *Readings in Risk* (Glickman and Gough, eds.), Resources for the Future, Washington, DC, pp. 165–180 (1990).
35. B.N. Ames, R. Magow, and L.S. Gold, "Ranking Possible Carcinogenic Hazards," in *Readings in Risk* (Glickman and Gough, eds.), Resources for the Future, Washington, DC, pp. 76–99 (1990).
36. D. Hattis and D. Kennedy, "Assessing Risks from Health Hazards: An Imperfect Science," in *Readings in Risk* (Glickman and Gough, eds.), Resources for the Future, Washington, DC, pp. 156–163 (1990).
37. B.D. Goldstein, *Issues in Risk Assessment,* National Research Council, National Academy Press, Washington, DC (1993).
38. C.T. Petito and B.D. Beck, "Evaluation of Evidence of Nonlinearities in the Dose-Response Curve for Arsenic Carcinogenesis," *Trace Substances in Environmental Health,* 24, pp. 143–176 (1990).
39. F.P. Lees, *Loss Prevention in the Process Industries,* Butterworths, London (1980).
40. R.L. Keeney et al., "Assessing the Risk of an LNG Terminal," in *Readings in Risk* (Glickman and Gough, eds.), Resources for the Future, Washington, DC, pp. 207–217 (1990).
41. G. Apostolakis, "Fire Risk Assessment and Management in Nuclear Power Plants," *Fire Science and Technology,* 13, Supplement, pp. 12–39 (1993).
42. Y.Y. Haimes, *Risk Modeling, Assessment, and Management,* John Wiley and Sons, New York (1998).
43. Proceedings of the SFPE Symposium on Risk, Uncertainty and Reliability in Fire Protection Engineering and Joint SFPE/UMD/Clark University Workshop on Encouraging the Use of Risk Concepts in Performance-Based Building and Fire Regulation Development, SFPE, Bethesda, MD (1999).
44. NFPA 550, *Guide to the Fire Safety Concepts Tree,* National Fire Protection Association, Quincy, MA, 2002 edition.
45. J.M. Watts, Jr., "Systems Approach to Fire-Safe Building Design," in *Fire Protection Handbook,* 20th ed. (A.E. Cote et al., eds.), National Fire Protection Association, Quincy, MA, pp. 1-157–1-170 (2008).
46. Random House, *The Random House College Dictionary,* Random House, Inc., New York (1980).
47. J.R. Hall, Jr., "Probability Concepts," in *SFPE Handbook of Fire Protection Engineering,* 3rd ed. (P.J. DiNenno et al., eds.), National Fire Protection Association, Quincy, MA, pp. 1-182–1-192 (2002).
48. G. Apostolakis, "Probability and Risk Assessment: The Subjectivistic Viewpoint and Some Suggestions," *Nuclear Safety,* 19, 3, pp. 305–315 (1978).
49. M.J. Karter, Jr., "1996 U.S. Fire Loss," *NFPA Journal,* 91, 5, pp. 77–83 (1997).
50. M. Fontana, J.P. Favre, and C. Fetz, "A Survey of 40,000 Building Fires in Switzerland," *Fire Safety Journal,* 32, 2, pp. 137–159 (1999).
51. J. Rahikainen and O. Keski-Rahkonen, "Determination of Ignition Frequency of Fire in Different Premises in Finland," *Fire Engineers Journal,* 58, 197, pp. 33–37 (1998).
52. J.R. Hall, Jr., *The U.S. Fire Problem Overview Report—Leading Causes and Other Patterns and Trends,* National Fire Protection Association, Quincy, MA (1998).
53. *Fire in the United States, 10th Edition, 1986–1995,* National Fire Center, United States Fire Administration, Federal Emergency Management Agency, Emmitsburg, MD (1998).
54. *Fire Safety Engineering in Buildings,* British Standards Institute, DD 240: Parts 1 and 2 (1997).
55. Fire Code Reform Centre, *Fire Engineering Guidelines,* Sydney, Australia (1996).
56. D. Charters, C. Sherwood and E. Warren, (2012), "A Study of the nature of fire risks in tall buildings," Proceedings, 9th International Conference on Performance-Based Codes and fire Safety Design Methods. SFPE, Bethesda, MD.
57. Y. Kobayashi and H. Nozaki, (2005), "A Statistical Method to Evaluate Fire Risks in Non-Residential Buildings in Japan," Fire Safety Science: Proceedings of the Eight International Symposium, China, International Association for Fire Safety Science, pp. 341-352
58. J. Taveau (2010), "Risk assessment and land-use planning regulations in France following the AZF disaster," Journal of Loss Prevention in the Process Industries, Volume 23, issue 6, November 2010, pp. 813–823
59. K. Tillander (2004). *Utilisation of statistics to assess fire risk in buildings*, VTT Publications 537, VTT, Espoo, Finland.
60. M. Tsujimoto (2006), "Death risk by building fires in Japan and its usage," Fire Science and Technology, vol. 25, no. 2, pp. 63–68
61. F.R. Farmer, "Siting Criteria—A New Approach," *IAEA Symposium on the Containment and Siting of Nuclear Power Reactors, IAEA SM-89/34,* Vienna, Austria (Apr. 3–7, 1967).
62. D.P. Fernandes-Russell, "Societal Risk Estimates from Historical Data for UK and Worldwide Events," *Research Report No. 3,* Environmental

Risk Assessment Unit, University of East Anglia, UK (1987).
63. D. Charters, M. Salisbury, and S. Wu, "The Development of Risk-Informed Performance-Based Codes," *Proceedings of the 5th International Conference on Performance-Based Codes and Fire Safety Design Methods,* Society of Fire Protection Engineers, Luxembourg (2004).
64. F.R. Allen, A.R. Garlick, M.R. Hayns, and A.R. Taig, *The Management of Risk to Society from Potential Accidents,* Elsevier Applied Science, London (1992).
65. D.A. Charters, *Fire Safety Assessment of Bus Transportation,* AEA Technology, Warrington, UK, C437/037 (1992).
66. D. Kahneman and A. Tversky, "Judgment Under Uncertainty: Heuristics and Biases," *Science,* 185, pp. 1124–1131 (1974).
67. W.W. Lowrance, *Of Acceptable Risk,* William Kaufmann, Inc., Los Altos, CA (1976).
68. B. Fischhoff et al., *Acceptable Risk,* Cambridge University Press, New York (1981).
69. P. Slovic, "Perception of Risk," *Science,* 236, pp. 280–285 (1987).
70. V.T. Covello et al. (eds.), *Uncertainty in Risk Assessment, Risk Management, and Decision Making,* Plenum Press, New York (1987).
71. M.G. Morgan and M. Henrion, *Uncertainty: A Guide to Dealing with Uncertainty in Quantitative Risk and Policy Analysis,* Cambridge Press, Cambridge, UK (1990).
72. S.O. Funtowicz and J.R. Ravetz, "Three Types of Risk Assessment and the Emergence of Post-Normal Science," in *Social Theories of Risk* (Krimsky and Golding, eds.), Praeger, Westport, CT, pp. 251–274 (1992).
73. D. Hattis and D.E. Burmaster, "Assessment of Variability and Uncertainty Distributions for Practical Risk Analysis," *Risk Analysis,* 14, 5, pp. 713–730 (1994).
74. F.O. Hoffman and J.S. Hammonds, "Propagation of Uncertainty in Risk Assessment: The Need to Distinguish Between Uncertainty Due to Lack of Knowledge and Uncertainty Due to Variability," *Risk Analysis,* 14, 5, pp. 707–712 (1994).
75. M.W. Merkhofer, A Comparative Evaluation of Quantitative Decision-Making Approaches, SRI International, Menlo Park, CA (1983).
76. M.W. Merkhofer, "Comparative Analysis of Formal Decision-Making Approaches," in *Risk Evaluation and Management* (V.T. Covello et al., eds.), Plenum Press, New York, pp. 183–220 (1986).
77. D.E. Bell, H. Raiffa, and A. Tversky (eds.), *Decision Making: Descriptive, Normative, and Prescriptive Interactions,* Cambridge University Press, Cambridge, UK (1988).
78. D. Hattis and E. Anderson, "What Should Be the Implications of Uncertainty, Variability, and Inherent Biases/Conservatism for Risk Management Decision Making?" Paper presented at *Second Workshop on When and How Can You Specify a Probability Distribution if You Don't Know Much,* University of Virginia, Charlottesville (1997).
79. J.L. Casti, *Searching for Certainty: What Scientists Can Know About the Future,* William Morrow and Company, New York (1990).
80. V. Brannigan et al., "Risk Models Involving Human Decisions: Intentional Uncertainty and the Need for Regulation," *Proceedings of the Second International Conference on Fire Research and Engineering,* SFPE, Bethesda, MD, pp. 252–262 (1998).
81. V.M. Brannigan and C. Smidts, "Performance-Based Fire Safety Regulation Under Intentional Uncertainty," in *Proceedings of the 1st International Symposium on Human Behavior in Fire,* University of Ulster, Jordanstown, Northern Ireland, pp. 411–420 (1998).
82. J.R. Benjamin and C.A. Cornell, *Probabilities, Statistics, and Decision for Civil Engineers,* McGraw-Hill, New York (1970).
83. D. Von Winterfeldt and W. Edwards, *Decision Analysis and Behavioral Research,* Cambridge University Press, Cambridge, UK (1986).
84. G.S. Omenn et al., *Risk Assessment and Risk Management in Regulatory Decision-Making,* Presidential/Congressional Commission on Risk Assessment and Risk Management, Final Report, Volume 2, Washington, DC (1997).
85. K.A. Notarianni and P. Fischbeck, "Dealing with Uncertainty to Improve Regulations," in *Proceedings of the 1999 Conference on Fire Design in the 21st Century,* SFPE and WPI, Worcester, MA (1999).
86. K.A. Notarianni, "The Role of Uncertainty in Improving Fire Protection Regulations," Ph.D. Dissertation, Carnegie Mellon University, Pittsburgh, PA (2000).
87. D.A. Lucht, "Public Policy and Performance-Based Engineering," in *Proceedings of the International Conference on Performance-Based Codes and Fire Safety Design Methods,* SFPE, Bethesda, MD (1997).
88. B.J. Meacham, "Identifying and Addressing Uncertainty in Fire Protection Engineering," in *Proceedings of the 2nd International Conference on Fire Research and Engineering,* SFPE, Bethesda, MD, pp. 238–251 (1998).
89. Albrecht, C. *A risk-informed and performance-based life safety concept in case of fire,* PhD thesis, TU Braunschweig, ISBN 978-3-89288-202-2, 2012.
90. Albrecht, C., Hosser, D., "A Response Surface Methodology for Probabilistic Life Safety Analysis using Advanced Fire Engineering Tools." *Fire Safety Science* 10: 1059–1072, 2011.
91. M. Siemon, C. Albrecht and D. Hosser, "Considerations for the development of a quantitative life safety design concept using performance based fire engineering methods'," *Proceedings of the 9th International SFPE-Conference on Performance- Based Codes and Fire Safety Design Methods*, SFPE, Bethesda, MD, USA, 2012.

92. P. Lancaster and K. Salkauskas, "Surfaces generated by moving least squares methods," *Mathematics of Computation*, 37(155):141–158, 1981.
93. T. Most and C. Bucher, "New concepts for Moving least squares: An interpolating non-singular weighting function and weighted nodal least squares," *Engineering Analysis with Boundary Elements*, 32:461–470, 2008.
94. A.M. Hasofer, V.R. Beck, and I.D. Bennetts, *Risk Analysis in Building Fire Safety Engineering*, Butterworth-Heinemann, Oxford, England, 2007, p 87.
95. C. Bucher, "Adaptive sampling-an iterative fast Monte Carlo procedure," *Structural Safety*, 5 (2):119–126, 1988.
96. D. Yung, Principles of Fire Risk Assessment in Buildings, John Wiley & Sons Ltd, Chichester, England, 2008.
97. G. Ramachandran and D. Charters, *Quantitative Risk Assessment in Fire Safety*, Spon Press, London, England (2011)
98. BS7974, Application of fire safety engineering principles to the design of buildings. Code of practice. Technical report, British Standards Institution (BSI), 2001.
99. C. Albrecht and D. Hosser, "A risk-informed framework for performance-based structural fire protection according to the Eurocode fire parts," Proceedings, *Interflam 9*, Interscience Communications, Ltd, UK, 2010.
100. V.R. Beck, "Cost-Effective Fire Safety and Protection Design Requirements for Buildings," Ph.D. Dissertation, University of New South Wales, Australia (1986).
101. V.R. Beck, "A Cost-Effective Decision-Making Model for Building Fire Safety and Protection," *Fire Safety Journal,* 12, pp. 121–138 (1987).
102. V.R. Beck, "Performance-Based Fire Engineering Design and Its Application in Australia," in *Fire Safety Science—Proceedings of the Fifth International Symposium,* IAFSS, Bethesda, MD, pp. 23–40 (1997).
103. V.R. Beck and D. Yung, "A Cost-Effective Risk Assessment Model for Evaluating Fire Safety and Protection in Canadian Apartment Buildings," *Journal of Fire Protection Engineering,* 2, 3, pp. 65–74 (1990).
104. D. Yung, G.V. Hadjisophocleous, and H. Takeda, "Comparative Risk Assessments of 3-Storey Wood-Frame and Masonry Construction Office Buildings," in *Proceedings of Interflam'93,* Interscience Communications Ltd., London, pp. 499–508 (1993).
105. V.R. Beck and S.L. Poon, "Results from a Cost-Effective Decision-Making Model for Building Fire Safety and Protection," *Fire Safety Journal,* 13, pp. 197–210 (1988).
106. V.R. Beck and D. Yung, "A Cost-Effective Risk Assessment Model for Evaluating Fire Safety and Protection in Canadian Apartment Buildings," *International Fire Protection Engineering Institute, 5th Conference,* Ottawa, Canada (1989).
107. V.R. Beck and D. Yung, "A Risk-Cost Assessment Model for Evaluating Fire Risks and Protection in Apartment Buildings," in *Proceedings of the International Symposium on Fire Engineering for Buildings and Structures,* The Institution of Engineers, Melbourne, Australia (1989).
108. I. Thomas, D.W. Weinert, and B. Ashe, "Quantified Levels of Risk to Life Safety in Deemed-to-Satisfy Apartment Buildings," in *8th International Symposium on Fire Safety Science,* IAFSS, Beijing, China (Sept. 2005).
109. J. Gaskin and D. Yung, "Canadian and U.S.A. Fire Statistics for Use in the Risk-Cost Assessment Model," *IRC Internal Report No. 637,* National Research Council, Ottawa, Canada (1993).
110. H. Takeda and D. Yung, "Simplified Fire Growth Models for Risk-Cost Assessment in Apartment Buildings," *Journal of Fire Protection Engineering,* 4, 2, pp. 53–66 (1992).
111. G.V. Hadjisophocleous and D. Yung, "A Model for Calculating the Probabilities of Smoke Hazard from Fires in Multi-Storey Buildings," *Journal of Fire Protection Engineering,* 4, 2, pp. 67–80 (1992).
112. G.V. Hadjisophocleous and D. Yung, "Parametric Study of the NRCC Fire Risk-Cost Assessment Model for Apartment and Office Buildings," *Proceedings of the 4th International Symposium on Fire Safety Science,* IAFSS, Bethesda, MD, pp. 829–840 (1994).
113. R.W. Bukowski, F.B. Clarke, J.R. Hall, Jr., and S.W. Stiefel, *Fire Risk Assessment Method: Description of Methodology,* National Fire Protection Research Foundation, Quincy, MA (1990).
114. J.R. Hall, Jr., "Product Fire Risk," in *SFPE Handbook of Fire Protection Engineering,* 3rd ed. (P.J. DiNenno et al., eds.), National Fire Protection Association, Quincy, MA, pp. 5-143–5-152 (2002).
115. J. Fraser-Mitchell, "An Object-Oriented Simulation (CRISP II) for Fire Risk Assessment," in *Fire Safety Science: Proceedings of the Fourth International Symposium,* IAFSS, Bethesda, MD, pp. 793–803 (1994).
116. J. Fraser-Mitchell, "Risk Assessment of Factors Related to Fire Protection in Dwellings," in *Fire Safety Science: Proceedings of the Fifth International Symposium,* IAFSS, Bethesda, MD, pp. 631–642 (1997).
117. Bjorn Karlsson, Iceland Fire Authority, Reykjavik, Iceland; Bodvar Tomasson, Linuhonnun Consulting Engineers, Reykjavik, Iceland. B. Karlsson, and B. Tomasson, "Repeatability Tests of a Fire Risk Index Method for Multi-Storey Apartment Buildings," *8th International Symposium on Fire Safety Science,* IAFSS, Beijing, China (Sept. 2005).
118. G. Hadjisophocleous and Z. Fu, "Development and Case Study of a Risk Assessment Model CUrisk for

Building Fires," *8th International Symposium on Fire Safety Science,* IAFSS, Beijing, China (Sept. 2005).
119. D.A. Charters and D. Berry, "Application of Quantified Fire Risk Assessment in the Design of Buildings," *Proceedings of Interflam '99,* Interscience Communications Ltd., London (1999).
120. D. Charters and S. Wu, "The Application of 'Simplified' Quantitative Fire Risk Assessment to Major Transport Infrastructure," SFPE Symposium on Risk, New Orleans (2002).
121. D. Charters, J. Paveley, and F.B. Steffensen, "Quantified Fire Risk Assessment in the Design of a Major Multi-Occupancy Building," in *Proceedings of Interflam 2001,* Interscience Communications Ltd, Edinburgh, UK (2001).
122. D. Charters, "What Does Quantified Fire Risk Assessment Need to do to Become an Integral Part of Design Decision-Making," SFPE International Conference on Performance Based Codes, San Francisco (2000).
123. System Safety Program Requirements, Military Standard 882C, U.S. Department of Defense, Washington, DC (1993).
124. *Preparation Guide for U.S. Department of Energy Nonreactor Nuclear Facility Safety Analysis Reports, DOE-STD-3009-94,* U.S. Department of Energy, Washington, DC (1994).
125. *International Code Council Performance Code for Buildings and Facilities,* International Code Council, Falls Church, VA (2012).
126. B.J. Meacham, "Application of a Decision-Support Tool for Comparing and Ranking Risk Factors for Incorporation into Performance-Based Building Regulations," *Proceedings, 3rd International Conference on Performance-Based Codes and Fire Safety Design Methods*, SFPE, Bethesda, MD, 2000, pp. 59–70.
127. B.J. Meacham, "Identifying and Regulating for Multiple Levels of Performance," in *Proceedings of the International Council for Building Research and Innovation, World Congress—Wellington, NZ,* CIB, the Netherlands (Apr. 2001).
128. B.J. Meacham, "Performance-Based Building Regulatory Systems: Structure, Hierarchy and Linkages," *Journal of the Structural Engineering Society of New Zealand*, Vol. 17, No. 1, pp. 37–51, 2004.
129. R.W. Fitzgerald, "An Engineering Method for Building Fire Safety Analysis," *Fire Safety Journal,* 9, 2, pp. 233–243 (1985).
130. R.W. Fitzgerald, "An Engineering Method for Translating Fire Science into Building Design," in *Proceedings of the CIB W14 International Symposium and Workshops, Engineering Fire Safety in the Process of Design: Demonstrating Equivalency,* University of Ulster, Jordanstown, Northern Ireland (1993b).
131. R.W. Fitzgerald, *Building Fire Performance Analysis,* John Wiley & Sons, Chichester, UK, 2004.
132. Fitzgerald, R.W. and Meacham, B.J., *Fire Performance Analysis of Buildings,* John Wiley & Sons, Chichester, UK, in development, target publication May 2016.
133. R.W. Fitzgerald, R.C. Richards, and C.L. Beyler, "Fire Analysis of the Polar Icebreaker Replacement Design," *Journal of Fire Protection Engineering,* 3, 4, pp. 137–150 (1991).
134. Society of Fire Protection Engineers, *SFPE Engineering Guide: Fire Risk Assessment,* Society of Fire Protection Engineers, Bethesda, MD (Nov. 2006).
135. John Hall Jr. and A. Sekizawa, "Revisiting Our 1991 Paper on Fire Risk Assessment," *Fire Technology*, 46, pp 789–901, (2010).
136. NFPA 551, *Guide for the Evaluation of Fire Risk Assessments,* National Fire Protection Association, Quincy, MA, 2004 edition.
137. BS 7974-7, "Part 7—Probabilistic Risk Assessment," *Code on the Application of Fire Safety Engineering Principles to the Design of Buildings,* British Standards Institute, London, UK (2003).
138. ISO/PDTS 16732, *Fire Safety Engineering—Guidance on Fire Risk Assessment,* International Organization for Standardization (ISO), Geneva, Switzerland (2004).
139. D. Rasbash, G. Ramachandran, B. Kandola, J. Watts and M. Law, *Evaluation of Fire Safety*, John Wiley & Sons Ltd, Chichester, England, 2004.
140. B.J. Meacham, "Extreme Event Mitigation Through Risk-Informed Performance-Based Analysis and Design," in *Extreme Event Mitigation in Buildings: Analysis and Design* (B.J. Meacham and M.A. Johann, eds.), National Fire Protection Association, Quincy, MA, Chapter 2 (Apr. 2006).
141. *BuildingQRA*, Quantified Fire Risk Assessment Software for the Built Environment, Salisbury Fire Engineering Software, (www.fire-engineering-software.com), 2015.
142. C. Wade, G. Baker, K. Frank, A. Robbins, R. Harrison, M. Spearpoint, and C. Fleischmann. *B-RISK User Guide and Technical Manual*, BRANZ Study Report 282, BRANZ Ltd, Porirua, New Zealand (2013).
143. C.A. Wade. *BRANZFIRE Technical Reference Guide (revised)*, BRANZ Ltd, Porirua, New Zealand (2004).

Further Readings

C. Albrecht, "Quantifying life safety: Part I: Scenario-based quantification," *Fire Safety Journal*, doi:10.1016/j.firesaf.2014.01.003, Volume 64, Pages 87–94 (2014).
C. Albrecht, "Quantifying life safety: Part II: Quantification of fire protection systems," *Fire Safety Journal*, doi:10.1016/j.firesaf.2014.01.002, Volume 64, Pages 81–86 (2014).

V. Babrauskas, "Ensuring the Public's Right to Adequate Fire Safety Under Performance-Based Building Codes," in Proceedings of the 1998 Pacific Rim Conference and Second International Conference on Performance-Based Codes and Fire Safety Design Methods, ICBO and SFPE, Whittier, CA, pp. 239–247 (1998).

M.S. Baram, *Alternatives to Regulation: Managing Risks to Health, Safety and the Environment,* Lexington Books, Lexington, MA (1982).

V. Beck et al., *Fire Safety and Engineering Project Report,* The Warren Center for Advanced Engineering, Sydney, Australia (1989).

V.R. Beck et al., "Microeconomic Reform: Fire Regulation," *National Building Fire Safety Systems Code,* in Building Regulation Review Task Force, Department of Industry Technology and Commerce, Canberra, Australia, p. 165 (1991).

M. Belsham, "Probable Cause," *Fire Risk Management*, p. 41–46, February 2009.

V.M. Brannigan and A. Kilpatrick, "Performance-Based Codes: Reengineering the Regulatory System," in *Proceedings of the International Conference on Performance-Based Codes and Fire Safety Design Methods,* SFPE, Bethesda, MD, pp. 139–149 (1997).

H.S. Brown and R.L. Goble, "The Role of Scientists in Risk Assessment," *Risk: Issues in Health and Safety,* 1, 4, pp. 283–311 (1990).

D. Canter (ed.), *Fires and Human Behavior,* 2nd ed., Fulton Publishers, Ltd., London (1990).

R.E. Cheit, *Setting Safety Standards: Regulation in the Public and Private Sectors,* University of California Press, Berkeley, CA (1990).

G.Q. Chu, T. Chen, Z.H Sun, and J.H. Sun, "Probabilistic Risk Assessment for Evacuees in Building Fires," *Building and Environment*, 42:1283–1290, 2007.

G. Chu and J. Sun, "Quantitative Assessment of Building Fire Risk to Life Safety," *Risk Analysis*, DOI: 10.1111/j.1539-6924.2008.01048.x, Volume 28, Issue 3, pages 615–625 (2008).

G. Chu, J. Sun, "Decision analysis on fire safety design based on evaluating building fire risk to life," *Safety Science*, doi:10.1016/j.ssci.2007.06.011, Volume 46, Issue 7, Pages 1125–1136 (2008).

V.T. Covello et al. (eds.), *The Analysis of Actual versus Perceived Risks,* Plenum Press, New York (1983).

V.T. Covello et al. (eds.), *Risk Evaluation and Management,* Plenum Press, New York (1986).

V.T. Covello and M.W. Merkhofer, *Risk Assessment Methods: Approaches for Assessing Health & Environmental Risks,* Plenum Press, New York (1993).

V.T. Covello and J. Mumpower, "Risk Analysis and Risk Management: A Historical Perspective," in *Risk Evaluation and Management* (V.T. Covello et al., eds.), Plenum Press, New York, pp. 519–540 (1986).

R.E. Donnelly, "Implications of De Minimis Risk Concepts for OSHA," in *De Minimis Risk* (C. Whipple, ed.), Plenum Press, New York, pp. 95–99 (1987).

R.F. Fahy, "Building Fire Simulation Model. An Overview," *Fire Safety Journal,* 9, pp. 189–203 (1985).

A. Finkel, "Comparing Risks Thoughtfully," *Risk: Health, Safety & Environment,* 7, 4, pp. 325–359 (1996).

B. Fischhoff, "Acceptable Risk: A Conceptual Proposal," *Risk: Health, Safety & Environment,* 5, 1, pp. 1–28 (1994).

B. Fischhoff, "Public Values in Risk Research," *The Annals of the American Academy of Political and Social Science,* 545, pp. 75–84 (1996).

B. Fischhoff, "Ranking Risks," *Risk: Health, Safety & Environment,* 6, 3, pp. 191–202 (1996).

B. Fischhoff, P. Slovic, and S. Lichtenstein, "Lay Foibles and Expert Fables in Judgements About Risk," *The American Statistician,* 36, 3, pp. 240–255 (1982).

R.W. Fitzgerald, "Thoughts on Building Codes, Design Standards, and Performance Evaluations for Fire," Proceedings of the First International Conference on Performance-Based Codes and Fire Safety Design Methods, SFPE, Bethesda, MD, pp. 127–137 (1997).

H. Frantzich. *Uncertainty and Risk Analysis in Fire Safety Engineering*. PhD thesis, Lund University Sweden, Department of Fire Safety Engineering, 1998.

W. Freudenburg, "Perceived Risk, Real Risk: Social Science and the Art of PRA," *Science,* 242, pp. 44–49 (1988).

S.O. Funtowicz and J.R. Ravetz, "Three Types of Risk Assessment," in *Risk Analysis in the Private Sector* (Whipple and Covello, eds.), Plenum Press, New York (1985).

B.J. Garrick and W.C. Gekler (eds.), *The Analysis, Communication and Perception of Risk,* Plenum Press, New York (1991).

T.S. Glickman and M. Gough (eds.), *Readings in Risk,* Resources for the Future, Washington, DC (1990).

J.D. Graham et al. "Science and Analysis: Roles in Risk and Decision Making," in *Risk Evaluation and Management* (V.T. Covello et al., eds.), Plenum Press, New York, pp. 503–518 (1986).

J.R. Hall, Jr., "Societal Issues in Performance-Based Fire Safety Design," in *Proceedings of the Workshop on Performance-Based Fire Safety Design, the Society of Fire Protection Engineers and the Centre for Environmental and Risk Engineering,* Victoria University of Technology, Melbourne, Australia (1997).

J.R. Hall, Jr., "Using Data for Public Education Planning and Decision Making," in *Fire Protection Handbook,* 20th ed. (A.E. Cote et al., eds.), National Fire Protection Association, Quincy, MA, pp. 5-103–5-118 (2008).

J.R. Hall, Jr., and A.E. Cote, "An Overview of the Fire Problem and Fire Protection," in *Fire Protection Handbook,* 20th ed. (A.E. Cote et al., eds.), National Fire Protection Association, Quincy, MA, pp. 3-3–3-30 (2008).

J. R. Hall Jr. and A. Sekizawa, "Fire risk analysis: General conceptual framework for describing models," *Fire Technology*, Volume 27, Issue 1, pp 33–53 (1991).

Y. Hasemi, "Wooden 3-Storey Apartment Building Shake and Burn Test Report," Building Research Institute, Tsukuba, Japan (1992).

Health and Safety Executive, *The Tolerability of Risk from Nuclear Power Stations,* HMSO, London (1988).

S. Hostikka and O. Keski-Rahkonen, "Probabilistic Simulation of Fire Scenarios," *Nuclear Engineering and Design*, 224:301–311, 2003.

S. Hostikka, *Development of fire simulation models for radiative heat transfer and probabilistic risk assessment*. PhD thesis, VTT Technical Research Centre of Finland, 2008.

House Committee on Science, *Unlocking Our Future: Toward A New National Science Policy,* Washington, DC (1998).

D.W. Hubbard, *The Failure of Risk Management: Why It's Broken and How to fix It*, John Wiley & Sons Inc., Hoboken, NJ, 2009.

C.R. Jennings, "Socioeconomic Characteristics and Their Relationship to Fire Incidence: A Review of the Literature," *Fire Technology,* 35, 1, pp. 7–34 (1999).

X. Jing and H. Chongfu, "Fire risk analysis of residential buildings based on scenario clusters and its application in fire risk management," *Fire Safety Journal*, Special Issue on Spatial Analytical Approaches in Urban Fire Management, doi:10.1016/j.firesaf.2013.09.022, Volume 62, Part A, Pages 72–78 (2013)

S.N. Jonkman, P.H.A.J.M. van Gelder, and J.K. Vrijling, "An Overview of Quantitative Risk Measures for Loss of Life and Economic Damage," *Journal of Hazardous Materials,* 99, 1, pp. 1–30 (2003).

D. Kahneman and A. Tversky, "The Psychology of Preferences," *Scientific American,* 246, 1, pp. 162–173 (1982).

R.E. Kasperson, "Acceptability of Human Risk," *Environmental Health Perspectives,* 52, pp. 15–20 (1983).

R.E. Kasperson, "Six Propositions for Public Participation and Their Relevance for Risk Communication," *Risk Analysis,* 6, 3, pp. 275–281 (1986).

R.E. Kasperson, "The Social Amplification of Risk: Progress in Developing an Integrative Framework," *Social Theories of Risk* (Krimsky and Golding, eds.), Praeger, Westport, CT, pp. 153–178 (1992).

R. Kasperson, D. Golding, and S. Tuler, "Social Distrust as a Factor in Siting Hazardous Facilities and Communicating Risks," *Journal of Social Issues,* 48, 4, pp. 167–187 (1992).

R.E. Kasperson and J.X. Kasperson, "Determining the Acceptability of Risk: Ethical and Policy Issues," in *Proceedings of Risk: A Symposium on the Assessment and Perception of Risk to Human Health in Canada* (J.T. Rogers and D.V. Bates, eds.), Royal Society of Canada (1982).

R.E. Kasperson and J.X. Kasperson, "Hidden Hazards," in *Acceptable Evidence: Science and Values in Hazard Management* (D.C. Mayo and R. Hollander, eds.), Oxford University Press, New York, pp. 9–28 (1990).

R. Kasperson et al., "The Social Amplification of Risk: A Conceptual Framework," *Risk Analysis,* 8, pp. 177–187 (1988).

R.E. Kasperson et al., *Corporate Management of Health & Safety Hazards: A Comparison of Current Practice,* Westview Press, Boulder, CO (1988a).

R.E. Kasperson and I. Palmlund, "Evaluating Risk Communication," in *Effective Risk Communication* (V.T. Covello et al., eds.), Plenum Press, New York, pp. 143–158 (1989).

R.E. Kasperson and P.J.M. Stallen (eds.), *Communicating Risk to the Public,* Kluwer Academic Publishers, Dordrecht, Netherlands (1991).

R. Kates et al., *Perilous Progress: Managing the Hazards of Technology,* Westview Press, Boulder, CO (1985).

R.L. Keeney, *Value Focused Thinking: A Path to Creative Decision Making,* Harvard University Press, Cambridge, MA (1992).

R.L. Keeney, "The Role of Values in Risk Management," *The Annals of the American Academy of Political and Social Science,* 545, pp. 126–134 (1996).

P.R. Kleindorfer, H.C. Kunreuther, and P.J.H. Schoemaker, *Decision Sciences: An Integrative Perspective,* Cambridge University Press, New York (1993).

M. Kobayashi, "A Methodology for Evaluating Fire/Life Safety Planning of Tall Buildings," in "Evaluation of Fire Safety in Buildings," *Occasional Report of Japanese Association of Fire Science and Engineering* (Nihon Kasaigakka, ed.), 3, pp. 204–214 (1979).

S. Krimsky and D. Golding (eds.), *Social Theories of Risk,* Praeger, Westport, CT (1992).

H. Kunreuther and P. Slovic, "Science, Values, and Risk," in special edition of *The Annals of the American Academy of Political and Social Science* (Kunreuther and Slovic, eds.), 545, pp. 116–125 (1996a).

H. Kunreuther and P. Slovic (eds.), "Challenges in Risk Assessment and Risk Management," in special edition of *The Annals of The American Academy of Political and Social Science,* 545 (1996b).

T.T. Lie, "Safety Factors for Fire Loads," *Canadian Journal of Civil Engineering,* 6, pp. 617–628 (1979).

W-C.T. Ling and R.B. Williamson, "Using Fire Tests for Quantitative Risk Analysis," in *ASTM Special Publication STP 762* (G.T. Castino and T.Z. Harmathy, eds.), American Society for Testing and Materials, Philadelphia (1982).

D. Litai, *A Risk Comparison Methodology for the Assessment of Acceptable Risk,* Ph.D. Dissertation, MIT, Cambridge, MA (1980).

D. Litai, D.D. Lanning, and N. Rasmussen, "The Public Perception of Risk," in *The Analysis of Actual Versus Perceived Risks* (V.T. Covello et al., eds.), Plenum Press, New York, pp. 213–224 (1983).

D.A. Lucht (ed.), *Proceedings of the Conference on Fire Safety Design in the 21st Century,* Worcester, MA (1991).

B.D. McDowell and A.C. Lemer, *Uses of Risk Analysis to Achieve Balanced Safety in Building Design and Operations,* National Academy Press, Washington, DC (1991).

B.J. Meacham, "Risk-Informed Decision-Making in Performance-Based Building and Fire Code Development," in *Proceedings of the NFPRF Fire Risk and*

Hazard Assessment Research Application Symposium, NFPRF, Quincy, MA, pp. 62–77 (1998).

B.J. Meacham, "Concepts of a Performance-Based Building Regulatory System for the United States," *NIST GCR 98-762,* NIST, Gaithersburg, MD (1998b).

B.J. Meacham, "The Evolution of Performance-Based Codes and Fire Safety Design Methods," *NIST GCR 98-763,* NIST, Gaithersburg, MD (1998c).

B.J. Meacham, "Integrating Human Factors Issues into Engineered Fire Safety Design," in *Proceedings of the 1st International Symposium on Human Behavior in Fire,* University of Ulster, Northern Ireland, pp. 47–58 (1998d).

B.J. Meacham, "Incorporating Risk Concepts into Performance-Based Building and Fire Code Development," in *Proceedings of the Second Conference on Fire Design in the 21st Century,* Worcester, MA (1999a).

B.J. Meacham, "Integrating Human Behavior and Response Issues into Fire Safety Management of Facilities," *Facilities,* 17, 9/10, pp. 303–312 (1999b).

B.J. Meacham, "Integrating Human Factors Issues into Engineered Fire Safety Design," *Fire and Materials,* 23, pp. 273–279 (1999c).

B.J. Meacham, "Challenges in Decision-Making for Fire Risk Problems," *Journal of Fire Protection Engineering,* 14, 2, pp. 149–168 (2004).

B.J. Meacham and M. Johann (eds.), *Extreme Event Mitigation in Buildings: Analysis and Design,* National Fire Protection Association, Quincy, MA (Apr. 2006).

B.J. Meacham, "Using Risk as a Basis for Establishing Tolerable Performance: An Approach for Performance-Based Building Regulation," in *Proceedings of the 7th International Conference on Performance-Based Codes and Fire Safety Design Methods,* Society of Fire Protection Engineers, Bethesda, MD (Apr. 2008).

B.J. Meacham and C. Galioto, "Protecting Against Extreme Events," in *Fire Protection Handbook,* 20th ed. (A.E. Cote et al., eds.), National Fire Protection Association, Quincy, MA, pp. 1-109–1-136 (2008).

M. Modarres and F. Joglar-Billoch, "Reliability," in *SFPE Handbook of Fire Protection Engineering,* 3rd ed. (P.J. DiNenno et al., eds.), National Fire Protection Association, Quincy, MA, pp. 5-24–5-39 (2002).

M.G. Morgan, "Choosing and Managing Technology-Induced Risk," in *Readings in Risk* (Glickman and Gough, eds.), Resources for the Future, Washington, DC, pp. 17–28 (1990).

NFPA, *Fire Protection Handbook,* 20th ed., Quincy, MA (2008).

NFPA 101A, *Guide on Alternative Approaches to Life Safety,* National Fire Protection Association, Quincy, MA (2007).

NIST "1994 Northridge Earthquake: Performance of Structures, Lifelines and Fire Protection Systems," *NIST Special Publication 862* (ICSSC TR14), NIST, Gaithersburg, MD (1994).

NKB "Performance Requirements for Fire Safety and Technical Guide for Verification by Calculation," *NKB Committee and Work Reports, 1994:07 E,* Nordic Committee on Building Regulations (NKB), Fire Safety Committee, Helsinki, Finland (1995).

K.A. Notarianni and P. Fischbeck, "A Methodology for the Quantitative Treatment of Variability and Uncertainty in Performance-Based Engineering Analysis and/or Decision Analysis with a Case Study in Residential Fire Sprinklers," in *Proceedings of the Second International Conference on Performance-Based Codes and Fire Safety Design Methods,* ICBO and SFPE, Whittier, CA, pp. 297–311 (1998).

NRC *Risk Assessment in the Federal Government: Managing the Process,* National Research Council, National Academy Press, Washington, DC (1983).

NRC *Improving Risk Communication,* (J.F. Ahearne et al., eds.), National Research Council, National Academy Press, Washington, DC (1989).

NRC *Science and Judgment in Risk Assessment,* National Academy Press, Washington, DC (1994).

T. O'Riordan, "Approaches to Regulation," in *Regulating Industrial Risks—Science, Hazards and Public Protection* (H. Otway and M. Peltu, eds.), Butterworths, London, pp. 20–39 (1985).

H. Otway "Regulation and Risk Analysis," in *Regulating Industrial Risks—Science, Hazards and Public Protection* (H. Otway and M. Peltu, eds.), Butterworths, London, pp. 1–19 (1985).

H. Otway and M. Peltu (eds.), *Regulating Industrial Risks—Science, Hazards and Public Protection,* Butterworths, London (1985).

H. Otway and D. Von Winterfeldt, "Beyond Acceptable Risk: On Social Acceptability of Technologies," *Policy Sciences,* 14, pp. 247–256 (1982).

H. Otway and B. Wynne, "Risk Communication: Paradigm and Paradox," *Risk Analysis,* 9, 2, pp. 141–145 (1989).

M.E. Pate, "Acceptable Decision Processes and Acceptable Risks in Public Sector Regulations," *IEEE Transactions on Systems, Man, and Cybernetics,* SMC-13, 3, pp. 113–124 (1983).

C. Perrow, *Normal Accidents,* Basic Books, New York (1984).

N. Pidgeon et al., "Risk Perception," *Risk: Analysis, Perception and Management,* Report of the Royal Society, London, pp. 89–134 (1992).

A. Plough and S. Krimsky, "The Emergence of Risk Communication Studies: Social and Political Context," in *Readings in Risk* (Glickman and Gough, eds.), Resources for the Future, Washington, DC, pp. 223–232 (1990).

M. Pollak, "Public Participation," in *Regulating Industrial Risks—Science, Hazards and Public Protection* (H. Otway and M. Peltu, eds.), Butterworths, London, pp. 76–93 (1985).

R.A. Pollak, "Government Risk Regulation," *The Annals of the American Academy of Political and Social Science,* 545, pp. 25–34 (1996).

D. Proske, *Catalogue of Risks: Natural, Technical, Social and Health Risks*, Springer Berlin Heidelberg, ISBN 978-3540795544, 2008

D.J. Rasbash, "Criteria for Acceptability for Use with Quantitative Approaches to Fire Safety," *Fire Safety Journal,* 8, pp. 141–158 (1984).

N.C. Rassmussen, *Reactor Safety Study: WASH-1400,* U.S. Nuclear Regulatory Commission, Washington, DC (1975).

O. Renn, "Concepts of Risk: A Classification," in *Social Theories of Risk* (Krimsky and Golding, eds.), Praeger, Westport, CT, pp. 54–79 (1992).

O. Renn and D. Levine, "Credibility and Trust in Risk Communication," in *Communicating Risks to the Public* (R.E. Kasperson and P.M. Stallon, eds.), Kluwer, Dordrecht, Netherlands, pp. 175–218 (1991).

W.D. Rowe, *Anatomy of Risk,* John Wiley and Sons, New York (1977).

W.D. Rowe, "Understanding Uncertainty," *Risk Analysis,* 14, 5, pp. 743–750 (1994).

A. Sekizawa, "Fire Risk Analysis: Its Validity And Potential For Application In Fire Safety," *Fire Safety Science,* 8: 85–100. doi:10.3801/IAFSS.FSS.8-85 (2005).

SFPE *Proceedings of the 1998 International Conference on Performance-Based Codes and Fire Safety Design Methods,* SFPE and ICBO, Bethesda, MD (1998).

T.J. Shields, *A Fire Safety Evaluation Points Scheme for Dwellings,* Ph.D. Dissertation, University of Ulster, Jordanstown, Northern Ireland (1990).

T.J. Shields (ed.), *Proceedings of the 1st International Symposium on Human Behaviour in Fire,* University of Ulster, Antrim, Northern Ireland (1998).

N. Siu and G. Apostolakis, "Uncertain Data and Expert Opinions in the Assessment of the Unavailability of Fire Suppression Systems," *Fire Technology,* 24, pp. 138–162 (1988).

P. Slovic, "Perception of Risk: Reflections on the Psychometric Paradigm," in *Social Theories of Risk* (Krimsky and Golding, eds.), Praeger, Westport, CT (1992).

M.B. Spangler, "A Summary Perspective on NRC's Implicit and Explicit Use of De Minimis Risk Concepts in Regulating for Radiological Protection in the Nuclear Fuel Cycle," in *DeMinimis Risk* (C. Whipple, ed.), Plenum Press, New York, pp. 111–143 (1988).

C. Starr, "Societal Benefit vs. Technological Risk," *Science,* 165, pp. 1232–1238 (1969).

C. Starr, "Risk Management, Assessment, and Acceptability," in *Uncertainty in Risk Assessment, Risk Management, and Decision Making* (V.T. Covello et al., eds.), Plenum Press, New York, pp. 63–70 (1986).

T. Tanaka, D. Nii, J. Yamaguchi, H. Notake, and Y. Ikehata, "A Study on Risk-Based Evacuation Safety Design Method in Fire for Office Buildings," *Proceedings, Interflam 9*, Interscience Communications, Ltd, UK, p. 849–860, 2010.

T. Tanaka, "Risk-Based Selection of Design Fires to Ensure an Acceptable Level of Evacuation Safety." *Fire Safety Science – Proceedings of the Ninth International Symposium*, IAFSS, pp 49–62, 2008.

I.R. Thomas, I.D. Bennetts, P. Dayawansa, D.J. Proe, and R.R. Lewis, *Fire Tests of the 140 William Street Office Building*, Report No. BHPR/ENG/R/92/043/SG2C, BHP Research—Melbourne Laboratories, Australia, Feb. 1992.

W.K. Viscusi, *Regulating Consumer Product Safety,* American Enterprise Institute for Public Policy, Washington, DC (1984).

Warren Centre "Project Report" and "Technical Papers, Books 1 and 2," Fire Safety and Engineering Project, The Warren Centre for Advanced Engineering, the University of Sydney, Australia (1989).

J.M. Watts, Jr., "Dealing with Uncertainty: Some Applications in Fire Protection Engineering," *Fire Safety Journal,* 11, pp. 127–134 (1986).

C. Whipple (ed.), *De Minimis Risk,* Plenum Press, New York (1987).

C.A. Williams and R.M. Heins, *Risk Management and Insurance,* 4th ed., McGraw-Hill, New York (1981).

R. Wilson, "Analyzing the Daily Risks of Life," in *Readings in Risk* (Glickman and Gough, eds.), Resources for the Future, Washington, DC, pp. 55–61 (1990).

A. Wolski, *Addressing Building Fire Safety as an Acceptable Risk Problem: A Guide for Developing Performance-Based Fire Safety Regulations,* Masters Thesis, Worcester Polytechnic Institute, Worcester, MA (1999).

A. Wolski, N. Dembsey, and B. Meacham, "Application of Acceptable Risk Principles to Performance-Based Building and Fire Safety Code Development," in *Proceedings of the 2nd International Conference on Performance-Based Codes and Fire Safety Design Methods,* ICBO and SFPE, Whittier, CA (1998).

A. Wolski, N. Dembsey, and B. Meacham, "Accommodating Perceptions of Risk in Performance-Based Building Fire Safety Code Development," *Fire Safety Journal,* 34, 3, pp. 297–310 (2000).

B. Wynne, "Risk and Social Learning: Reification to Engagement," in *Social Theories of Risk* (Krimsky and Golding, eds.), Praeger, Westport, CT, pp. 275–300 (1992).

D. Yung and G.V. Hadjisophocleous, "The Use of the NRCC Risk-Cost Assessment Model to Apply for Code Changes for 3-Storey Apartment Buildings in Australia," in *Proceedings of the Symposium on Computer Applications in Fire Protection Engineering,* Worcester, MA, pp. 57–62 (1993).

R.J. Zeckhauser and W.K. Viscusi, "The Risk Management Dilemma," in special edition of *The Annals of the American Academy of Political and Social Science* (Kunreuther and Slovic, eds.), 545, pp. 144–154 (1996).

Brian J. Meacham is an Associate Professor at Worcester Polytechnic Institute (WPI) in the United States. He has more than 30 years of professional experience as a consultant, researcher and educator in the areas of risk-informed and performance-based fire engineering and regulation. He is a licensed Professional Engineer (US), a Chartered Engineer (U.K.), a Fellow of the Society of

Fire Protection Engineers, and a Fellow of the Institution of Fire Engineers.

David Charters is with the specialist risk management consulting and training company Risktec Solutions in the U.K. He has more than 25 years of professional experience as a consultant, research and educator in fire risk analysis and engineering. He is a Chartered Engineer (U.K.), a Professional Member of the Society of Fire Protection Engineers, and a Fellow of the Institution of Fire Engineers.

Peter Johnson is a Principal and Fellow with the global engineering consultancy and design firm Arup and is based in Melbourne, Australia. He has had 40 years of professional fire engineering experience involving fire testing, education, and design of buildings and transport infrastructure. He is an Arup Fellow and a Fellow of the Society of Fire Protection Engineers.

Matthew Salisbury is a practicing Fire Engineer with Michael Slattery Associates. He has 15 years of fire engineering experience, is a Chartered Engineer (U.K.), a Member of the Society of Fire Protection Engineers and a Member of the Institution of Fire Engineers. He has developed a number of fire engineering software packages, including BuildingQRA.

Uncertainty

76

Kathy A. Notarianni and Gareth W. Parry

Introduction

To provide fire protection engineering decisions that are meaningful and defendable, the practitioner must understand and be able to characterize the impact of uncertainty on fire safety engineering calculations. This requirement is true for all fire safety engineering calculations, whether conducted to meet a performance-based code, to aid in the establishment of a prescriptive requirement; to compare a performance option to its prescriptive counterpart; or as part of a fire risk analysis used in managing a complex facility, such as a nuclear power plant. At present, however, there is no clear guidance for the treatment of uncertainty in the use of fire safety engineering calculations to support decision making. Development of such guidance will assist engineers and architects in the design process; assist code officials by increasing confidence in the acceptance of a performance calculation; aid researchers in prioritizing enhancements to both the physics and structure of fire models; and aid policy makers by incorporating scientific knowledge and technical predictive abilities in policy decisions. It is essential for the application of risk analysis in the regulation and management of complex facilities.

The overarching objective of this chapter is to provide guidance on, and examples of, addressing uncertainty in the use of fire safety engineering calculations and to document the latest research relating to uncertainty. The chapter consists of ten sections. The first part of the chapter, sections "Understanding and Identifying Uncertainty", "Uncertainties in the Design Process: Problem of Switchover", "Treatment of Uncertainty with Safety Factors", and "Techniques for the Quantitative Treatment of Uncertainty" focus on increasing awareness of uncertainties and providing methods by which to treat uncertainty. Section "Understanding and Identifying Uncertainty" covers basic concepts of uncertainty and variability in order to develop a common language for discussion among fire safety professionals. It includes identification of various sources of uncertainty in Fire Protection Engineering. Section "Uncertainties in the Design Process: Problem of Switchover" provides a motivating example that shows the importance of dealing with uncertainty in the application of our scientific tools. The example shows how variations in analysis parameters, assumptions, or model inputs can lead to changes in the acceptability of a fire safety design, which is termed *switchover* [1]. The treatment of uncertainty with both implied and explicit safety factors, the use of safety factors in both prescriptive and performance-based codes, and guidance on selecting an appropriate factor of safety and on combining safety factors is given in section "Treatment of Uncertainty with Safety Factors." Section "Techniques for the Quantitative Treatment of Uncertainty" introduces many

K.A. Notarianni (✉) • G.W. Parry

M.J. Hurley (ed.), *SFPE Handbook of Fire Protection Engineering*,
DOI 10.1007/978-1-4939-2565-0_76, © Society of Fire Protection Engineers 2016

techniques and methods for treating uncertainties in measurement; in analysis parameters, assumptions, and values; and in complex fire models.

The middle part of the chapter, sections "Application of Uncertainty Analysis to Fire Safety Engineering Calculations", "Application of Uncertainty to Cost-Benefit Models, Improving Regulation, and Overall Decision Making", and "Uncertainty in Probabilistic Risk Assessment", tackles the important applications of uncertainty analysis. Section "Application of Uncertainty Analysis to Fire Safety Engineering Calculations" outlines a procedure for applying uncertainty analysis to a fire safety engineering calculation. It shows how results of this type of analysis are used to create distributions of time to untenability, to demonstrate the effect of selecting various sets of performance criteria, to compare two designs, and to provide insight to model development. Section "Application of Uncertainty to Cost-Benefit Models, Improving Regulation, and Overall Decision Making" uses a case study to look at the application of Uncertainty to Cost-Benefit Models and Decision Analysis Models and Section "Uncertainty in Probabilistic Risk Assessment" covers "Uncertainty in Probabilistic Risk Assessment." Probabilistic risk assessment (PRA) is an analytical tool that provides for the analysis of uncertainty in a comprehensive manner. This is illustrated by an example of the way in which uncertainty is addressed in the context of risk-informed regulatory decision making for nuclear power plants, with an emphasis on the fire-related aspects. This example, although specific to nuclear power plants, serves to illustrate many of the principals involved in the analysis of uncertainty. The third and final part of the chapter documents recent research that explores uncertainty as it applies to fire modeling and egress modeling (section "Uncertainties in Fire Modeling and Egress Modeling"), Measurements and Test Standards (section "Uncertainties in FPE Measurements and Test Standards"), and Determining Effectiveness (section "Use of Uncertainty to Determine Effectiveness"). In summary, a lot of good work on uncertainty has been done recently.

Understanding and Identifying Uncertainty

Uncertainty is a broad and general term used to describe a variety of concepts including but not limited to lack of knowledge, variability, randomness, indeterminacy, judgment, approximation, linguistic imprecision, error, and significance. These and many other facets of uncertainty are discussed in more detail in Chapter 4 of the book *Uncertainty* [1]. Examples of sources of uncertainty are discussed below.

Sources of Uncertainty

Uncertainty is often discussed as though it were synonymous with measurement uncertainty, that is, doubt about the validity of the result of a measurement. Measurement uncertainties are characterized both from a statistical analysis of a series of observations (to determine the random error) and from systematic effects associated with corrections and reference standards (to determine the systematic error). The total error is defined as a combination of random and systematic errors. Much work has been done to reach an international consensus on the evaluation and expression of measurement uncertainty. General rules for evaluating and expressing uncertainty in measurement are provided in a guide published by the American National Standards Institute and the National Conference of Standards Laboratories [2]. An example of dealing with measurement uncertainty in fire protection engineering can be found in a study of the uncertainty surrounding the use of thermocouples to measure temperature [3].

Uncertainty can arise because of disagreement among information sources. Rates of generation of products of combustion per gram of fuel burned vary from study to study and even from test to test in the same study using the same instruments.

Uncertainty can arise from a lack of complete knowledge. For example, what is the heat release rate or radiative fraction of a mixed-fuel

package? We have not measured and cannot reliably predict the value of these quantities for all potential fuel packages. Furthermore, the heat release rate and radiative fraction vary with parameters such as geometry, source and strength of ignition, and ventilation conditions. Uncertainty may also arise from *randomness*, such as where and how the fire will start.

Uncertainty in predictability results from *variability*; for example, the ambient temperature and the total number of deaths from fire. These quantities vary in time by season, month, and day. They also vary in space by regional location and community size. Even if we have complete information, we may be uncertain because of simplifications and approximations introduced due to computational limitations.

Uncertainty may arise from *indeterminacy*, defined as the inability to know what will happen in the future. For example, building occupancy and furnishings may differ 10 or 20 years after they were first constructed. Or uncertainty may arise due to the unpredictability of human behavior. It is unknown what actions each occupant will take when discovering a fire or hearing an alarm.

Other sources of uncertainty are related directly to the determination of the acceptance criteria for any decision made using the results of the analysis. Uncertainty may arise from difficulties in defining the problem. For example, a goal may be established to provide an equivalent level of fire safety. However, equivalency may be defined as providing the same time available for egress, providing the same level of property protection, providing the same level of fire safety for fire fighters entering the building, or all of the above.

Uncertainty in defining the problem may also arise from *linguistic imprecision*. For example, a goal stated as "flame spread should be limited" is not well defined. There are also important questions related to understanding uncertainties in perceptions, attitudes, and values toward risk. "In addition to being uncertain about what exists in the external world, we may be uncertain about individual preferences, uncertain about decisions relating to potential solutions, and even uncertain about the level and significance of our uncertainty" [1].

Uncertainties inherent in the performance-based analysis and design process are discussed in *Introduction to Performance-Based Fire Safety* [4].

Uncertainty and Variability

Understanding the level and significance of our uncertainty is crucial to making good fire safety design decisions. The variety of different uses of the term *uncertainty*, along with the absence of agreed-upon terminology, can generate considerable confusion in the fire protection engineering world. However, in the context of the performance and use of fire safety engineering calculations in decision making, it has become increasingly common practice to classify uncertainty into two major categories, namely aleatory and epistemic uncertainty [5, 6].

- *Aleatory uncertainty* is uncertainty associated with randomness. It is manifested, for example, in the unpredictability of the time at which a particular event will occur, whether that event is the failure of an operating component or the occurrence of a fire, or whether a particular component will operate as required when demanded. As discussed in more detail below, fire models of complex facilities are built up from events that are random and unpredictable. Randomness is, therefore, an essential element of a fire model of the system under analysis.
- *Epistemic uncertainty* is uncertainty associated with incompleteness of the analyst's state of knowledge. For example, as with any model, a fire safety engineering model is an approximation of reality. Because the analyst's state of knowledge is incomplete, there will be uncertainty about how best to model the system and its behavior. Furthermore, it is usually necessary to make simplifications or approximations so that the model can be solved in an efficient and timely manner. Therefore, the results of the model are subject to epistemic uncertainty.

In addition, as discussed earlier, there is uncertainty related to the choice of acceptance criteria associated with a decision.

Both types of uncertainty are addressed mathematically using probability theory, but it is important to maintain the distinction between them. An essential difference between aleatory and epistemic uncertainties is that the latter are, in principle, reducible through the collection of more knowledge, whereas the former are not: they represent a property of the system being analyzed in the following sense. The probabilities of events generated by probability models essentially represent the relative fractions with which various outcomes would be expected given that populations of identical replications of the system of concern were hypothetically to be observed a large number of times [7].

What these fractions represent is not necessarily an "inherent" randomness in the system behavior, but the fact that, at the level at which the events are defined, there is hidden variability that is accommodated in the model as if the events were random processes. There is variability in underlying conditions that has an impact on the behavior of individuals in the population who are not being explicitly accounted for. Instead the impact of the variability is implicit in the use of the probability models used for the events. Thus, the relative fractions are parameters of a model of the world [5] in which groups of components are regarded as being members of the same population.

A different model of the world can lead to different sets of variables being suppressed, different definitions of basic events, and different probability models. Because the models of concern are models of complex systems or complex phenomena, of necessity they involve approximations. In making these approximations, the distinction between the aleatory and epistemic uncertainties can become confused, particularly since the mathematics of probability is used to address both types. However, it is important to maintain the distinction because the interpretation of the results of the analysis and their use in decision making are a function of the nature of the uncertainty [8].

In summary, aleatory uncertainty is embedded in the structure of the model, whereas epistemic uncertainty is associated with the confidence that can be associated with the results of that model. The principal focus of this chapter is the treatment of epistemic uncertainty.

Identifying Sources of Uncertainty in Fire Protection Engineering

Scientific Uncertainties Scientific uncertainties are due both to lack of knowledge (e.g., in the underlying physics, chemistry, fluid mechanics, and/or heat transfer of the fire process) and to necessary approximations required for operational practicality of a model or calculation. Of the many types of uncertainty found in performance-based fire safety design calculations, scientific uncertainties are typically the most easily recognizable and quantifiable. The many types of scientific uncertainties can be roughly divided into five subcategories: (1) theory and model uncertainties, (2) data and input uncertainties, (3) calculation limitations, (4) level of detail of the model, and (5) representativeness of the design fire scenarios.

Theory and model uncertainties arise when physical processes are not modeled due to lack of knowledge of how to include them, processes are modeled based on empirically derived correlations, and/or simplifying assumptions are made. These types of uncertainties are present in most compartment fire models, where each of these factors leads to uncertainties in the results. Most compartment fire models are zone models, which make the simplifying assumption that each room can be divided into two volumes or layers, each of which is assumed to be internally uniform, and that changes in energy or state are implemented immediately throughout the layers. Current zone models do not contain a combustion model to predict fire growth, forcing the model user to account for any interactions between the fire and the pyrolysis rate. Many compartment fire models also use an empirical correlation to determine the amount of mass moved between the layers.

Data and input uncertainties arise from both lack of knowledge of specific input values and variations in input values as a function of many factors, such as time, temperature, or regional location. For example, the rate of heat release of a three-cushion upholstered sofa may be uncertain due to lack of available data for sofas with the same dimensions, stuffing, and cover materials. It may also be uncertain because the test method by which the heat release rate was measured could not specify all combinations of ignition source and strength and because there are inaccuracies inherent in the instrumentation used in the test. Other inputs, such as concentrations of toxic gases produced, vary with time as the fire develops and are uncertain. The species production rates used to predict concentrations are a function of the material or combination of materials actually burned. This is unknown a priori at the design stage.

For most fire models and calculation procedures, very different answers can result depending on the calculation limitations, control volume selected for modeling, the level of detail of the model, and the model-domain parameters specified. Model-domain parameters set the scope of the system being modeled and define the model's level of detail and/or baseline properties. Though these parameters or quantities are often ignored during uncertainty analysis, they have the potential for considerable impact [1]. This has been shown for fires in high bay spaces. Differences in the outcome criteria, such as maximum temperature and time to activation of fire detectors and sprinklers, are found when a large space is modeled with a simple zone fire model versus a more detailed computational fluid-dynamics model [9]. Differences in the outcome criteria are also found when a large space, which is typically subdivided by draft curtains,[1] is modeled. If a control volume is drawn around a single draft-curtained area (as opposed to drawing the control volume around multiple draft-curtained areas or around the entire building), higher temperatures and faster activation times of installed fire protection devices will be predicted. Also significant to the uncertainty in the outcome parameters are the index variables of the model. Index variables are used to identify a location in the domain of a model or to make calculations specific to a population, geographic region, and so forth.

Uncertainty arises in both the number and type of design-fire scenarios that need to be modeled for a given design/building. There may be significant differences between reality and the design-fire scenarios that were used to judge the adequacy of the performance-based design. Variations in the ignition source, rate of growth, and/or the materials burned affect confidence in the results. It is unclear whether all statistically significant fire scenarios must be modeled or whether worst-case or reasonable-worst-case scenarios are adequate. Furthermore, a worst-case scenario may be defined in terms of many different variables. A scenario may be the worst case because it is most likely to cause death, because it has potential for large property loss, or for other reasons.

Uncertainties and Variability in Behavior Human behavior can affect the likelihood of ignition, the choice of actions when confronted with a fire, and the effectiveness or ineffectiveness of both those actions and the passive and active features and systems installed to provide protection for occupants. Human behavioral uncertainties can apply to any of these factors and may affect different steps in the design process (e.g., definition of project goals, selection of performance criteria, and development and evaluation of trial designs). Human behaviors can range from predictable with low uncertainty to predictable with high uncertainty. Behavioral scientists tell us that actions are likely to be more effective and predictable with less uncertainty when choices are limited, procedures are practiced, the situation is not novel, and little chaos is present. Unfortunately, during a fire, few if any of these conditions occur. Any modeling that assumes these conditions are present when

[1] A draft curtain is a barrier that extends a certain vertical distance down from the roof or ceiling. Draft curtains are installed to subdivide a large area with the intent of corralling the heat and smoke.

they are not is likely not only to understate the uncertainty but also to over-estimate the likely effectiveness of the actions. Brannigan discusses what he calls *intentional uncertainty* in relationship to human behavior [10]. Brannigan states, "Human decision making does not follow the same kind of well understood rules that control the physical science variables used in models. Human decisions represent intentional uncertainty."

Human behavior in response to a fire alarm must be modeled in terms of time to respond to the alarm and type of response. Does the person immediately begin evacuating the building? Does he or she take the stairs or the elevator? What factors into that choice? Does the person try to fight the fire? Does the person stop to gather personal possessions or call a neighbor? Another area of human behavior relevant to performance-based calculations is behavior during egress. Do people use the best exit or the most familiar one? How long do people take to start to exit?

Human factors also affect the analysis needed for identifying goals and objectives and developing performance criteria. Fire safety goals typically include levels of protection for people, with performance criteria being a further refinement of these objectives. Performance criteria are numerical values to which the expected performance of trial designs can be compared. What range of occupant characteristics, such as age or disability, should be considered? How do human behaviors, for example, during egress influence the numerical values chosen for performance criteria?

When developing and evaluating trial designs, the efficacy of the proposed fire safety measures mitigating all likely fire scenarios should be determined. This determination involves varying human behavioral elements. For instance, two very different fire scenarios could develop from the same cooking-initiated design fire: (1) a grease fire from cooking sets off a smoke alarm, which alerts the occupant, who reacts quickly and then properly extinguishes the fire while it is still small; or (2) the same grease fire sets off the same smoke alarm, but the occupant has left the cooking unattended and taken a sleep aid so that he is not awakened by the smoke alarm and the fire is able to spread to adjacent items. The First International Symposium on Human Behaviour in Fire was held in 1998. Proceedings from this conference are illustrative of a body of literature, course curricula, and standards that should be considered when delving into this topic [11].

Uncertainties and Variability in Risk Perceptions and Values People perceive and value risk with both variability and uncertainty. Capturing differences that people have in their perceptions of risk and values related to risk is a necessary step in the design process. Research has shown that, although people typically view consequences from voluntary risks less severely than equal consequences resulting from an unknown and/or involuntary risk, variability exists [12]. For example, although some people would agree that an increase in risk to fire fighters (people who accept risk as part of their job) is justifiable if a corresponding decrease in risk to the public could be achieved, others would not. Few studies have been conducted that clearly demonstrate how society values fire safety risks at the level needed to support performance-based trade-offs. Work on incorporating risk concepts and identifying levels of acceptable risk is discussed in Chap. 75. It is important to identify where value judgments enter into a performance-based calculation and to make any assumptions explicit regarding values and the impact of different values on the final design.

Another important factor is the concept of *equivalency*. Equivalency can mean different things to different stakeholders. For example, one person may determine that noncombustible construction is equivalent to an installed sprinkler system if they are both shown to provide time to fully egress the building. Another may argue that they are not equivalent—that the sprinkler system is less reliable. Designs may be equivalent in terms of life safety, property protection, business interruption, injuries, and/or prevention of structural collapse, but they are most likely not equivalent in all regards.

It is, therefore, important to make explicit the assumptions on which equivalency depends.

Uncertainties Related to the Life-Cycle Use and safety of Buildings Many factors change over the lifetime of a building. The uncertainties surrounding future use, occupancy, and other factors contribute to the difficulty in conducting a structured, performance-based design. Even daily fluctuations in these design parameters can affect the safety of a building. For example, a building or area of a building that is normally occupied 24 h per day may become unoccupied (or occupied by very different people) for extended periods of time due to extraneous factors (e.g., business closing, maintenance, renovation). The characteristics of the different occupants can lead to very different design considerations. Other changes that may affect the life-cycle safety of the building are fire service characteristics such as location, expected response time, and operating procedures and capabilities.

Uncertainties Related to Providing for Equity and Incorporation of Societal Values Providing for equity and incorporating societal values involves determining what is important to the stakeholders and to what degree protection should be provided. A mechanism should be provided to ensure equal outcomes for subgroups. Since most projects have many stakeholders, such as building owner, design engineer, architect, code official, and the public (users of the building), it is difficult to assign worth to the usefulness or importance of something and apply it across all individual and societal issues. The key here is that decisions that change when a value, attitude, or risk perception varies must be made explicit in the design. Agreement on these key decisions by all stakeholders is critical to the success of a performance-based design.

Relation to Steps in the Design Process Several types of uncertainty will be encountered at each step in a performance-based design process or during the process of setting a new prescriptive requirement. For example, when developing performance criteria, one will have to deal with scientific uncertainty, such as determining what level of carbon monoxide will cause unacceptable consequences and how to account scientifically for interactions among products of combustion. One will also have to deal with issues of equity and societal values. At present, performance criteria are not established or agreed on. Changes to the set of performance criteria selected could cause the same design for the same building to be deemed acceptable in one jurisdiction and unacceptable in another. Uncertainties related to life-cycle use and safety of buildings also arises when selecting performance criteria. Over the life cycle of the building, many factors, such as use and occupant characteristics, change.

Uncertainties in the Design Process: Problem of Switchover

Of practical significance is the fact that direct measurement of the fire safety performance of a building or building system is not usually possible; therefore, we must rely on the technical predictive ability of scientific tools, such as existing fire models. The problem is this: the numerous uncertainties in the application of these fire safety design tools often go unrecognized or ignored. Many of these uncertainties are inherent in the design process itself. Variations in analysis parameters, assumptions, or model inputs may cause output criteria to change. *Switchover* occurs when outcome criteria change enough so as to cause a change in the design decision (e.g., the acceptability of a final design). It is critical to know if different sets of reasonable inputs, scenarios, or parameters used in a fire safety engineering design have potential to cause switchover and lead to different acceptable designs.

The Society of Fire Protection Engineers *SFPE Engineering Guide to Performance-Based Fire Protection* details several steps in the design process [13]. These are shown in Fig. 76.1, adapted from the SFPE engineering guide. The stated intent of the guide is to

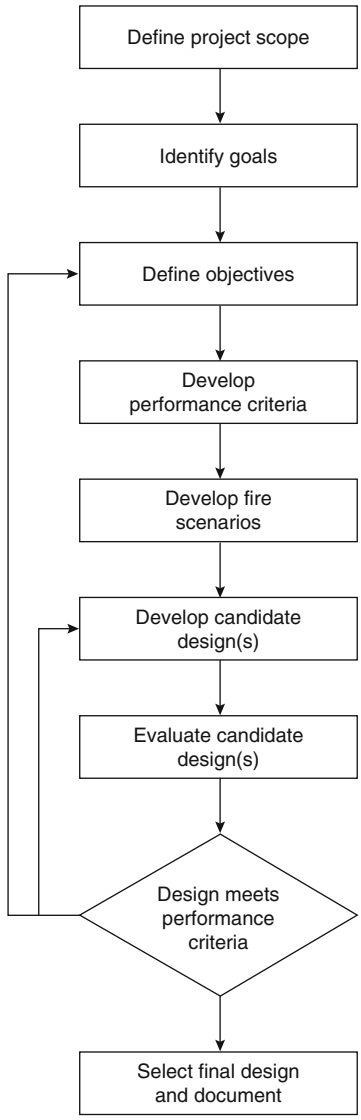

Fig. 76.1 Overview of the performance-based design process

"provide guidance that can be used by both design engineers and approving authorities as a means to determine and *document achievement of agreed upon levels of fire safety* for a particular project."

A review and analysis were conducted of the performance-based design process for fire safety engineering outlined in the guide along with a review of several case studies of performance-based, fire safety engineering designs for actual buildings [14]. This review uncovered seven major barriers to determining and documenting achievement of agreed-upon levels of fire safety for a particular project. All seven barriers involve various types of uncertainty. Thus there is a well-defined and strong role for uncertainty analysis in improving the ability to document achievement of agreed-upon levels of fire safety. The seven barriers identified are presented here along with a discussion of how they might lead to switchover of a design from acceptable to unacceptable.

1. **Performance criteria are not established or no agreement exists:** There is uncertainty in the selection of performance criteria. In fact, performance criteria have not been established or agreed upon by the fire safety community, and current policy allows the stakeholders themselves to select the criteria to be used for each design. Discussions occur around questions such as the following: Is the set of performance criteria sufficient? What do the numerical values actually represent? Should different criteria be used for different subpopulations, such as for people who are sick, elderly, or have disabilities? At one recent international conference, two engineers presented their performance-based case studies conducted for real clients on actual buildings. They had each followed the current design guidelines; however, they had selected very different performance criteria [15, 16]. Differences existed on three levels: (1) the parameters included in the set of performance criteria, (2) numerical values selected as the critical or cutoff values for these parameters, and (3) the presence or absence of a time element for reaching the cutoff values. Since predictions of fire models are compared to selected performance/life-safety criteria in order to determine if a design is acceptable, variations in criteria can cause the same design to pass or fail.
2. **The design fire selection process is unspecified:** Design fires are descriptions of fire events (e.g., a grease fire on the stove, a smoldering cigarette fire on the sofa). Along with design fires, several fire scenarios, or descriptions of possible fires that could occur, are developed. For each design fire

evaluated, the goal is to provide a fire safety design that would prevent unwanted fires from developing.

Because it is impossible to evaluate physically the performance of building systems in response to all design fires that might occur, the design fires and the resulting fire scenarios chosen may not adequately represent the range of fires that might occur in the building. Usually a designer will try to select worst-case or reasonable worst-case scenarios.[2] However, it is not always intuitive which scenarios present a worst-case situation or how likely (or unlikely) a particular scenario is. It is debatable whether we should be designing for the one-in-a-million fire and how many design fires and fire scenarios are sufficient. A methodology is needed that would incorporate the likelihood of a design fire and/or associated design fire scenario. It is easy to see how the same design may be deemed acceptable if based on a limited number and type of design fires or deemed unacceptable if based on an expanded set of scenarios or a different set of scenarios.

3. **Assumptions are made about human behaviors during fire:** During several critical steps in the design process, assumptions are made about human behaviors during fire. For example, some egress models used by fire protection engineers to predict the time required for safely evacuating a building (or part of a building) make many assumptions about how humans behave. Two assumptions are stated in one internationally used egress model: (1) 100 % of the occupants are readily mobile, and (2) occupants begin leaving the building immediately on hearing an alarm [17]. Experience demonstrates that these assumptions often are not the case [18, 19].

   Other behavior assumptions may not be explicitly stated but can be inferred from an analysis of model outputs. For example, results from a recently published study of a performance calculation using the egress model in FASTlite reveal that assumptions are made about human behavior during fires [17]. A decrease in the number of exits by one-third increases the egress time by exactly one-third, which suggests an implied assumption that an equal number of people egress through each available exit. More typically, the different exits will not be used equally. Some may be more familiar because they are used for normal entering and exiting, and some may be better marked or more visible or easier to get to. As a result, significant differences in exit use are not only possible but likely. Existing egress calculations and models need to be evaluated so that unrecognized and/or unstated uncertainties resulting from assumptions regarding human behavior can be identified. Once revealed, the implications of these assumptions need to be explored quantitatively.

4. **Predictive fire models have limitations that are not well documented or widely understood:** Fire models and other calculation methodologies are often inappropriately used to develop and evaluate trial designs for buildings and/or scenarios outside the predictive capabilities of the models. This occurs because limitations of fire models are not well documented or widely understood. For example, computer fire models do not model fire directly and only predict fire effects based on user-selected input data. Because many existing fire model and calculation methodologies were originally developed as research tools, model conditions, defined as "fundamental requirements for the model's validity," [10] are often unknown or unstated. Estimates provided by a model are technically credible only when model conditions have not been violated.

5. **Outputs of fire models are point values that do not directly incorporate uncertainty:** Even when the model is used within its intended limitations, fire model outputs are point values that do not reflect inherent input uncertainties (e.g., fire growth rates, initial

[2] The term *worst-case scenario* is used in this chapter to represent both worst-case and reasonable worst-case scenarios as understood in the fire protection design field.

conditions). Without knowledge of the uncertainty surrounding a prediction, it is impossible to be certain of a design's acceptability. One example is modeling the response of fire protection equipment such as sprinklers, heat detectors, and smoke detectors. Predictions of the time to activation of such devices would specify, for example, 121 s. However, the actual time to activation may be higher or lower depending on uncertain inputs or on any number of factors not modeled, such as individual detector characteristics and distance below the ceiling.

6. **The design process often requires engineers to work beyond their areas of expertise:** Problems can also occur when fire protection engineers are required to work in domains outside their expertise. Conservative assumptions made by well-intentioned engineers may not be as conservative as intended. For example, a design engineer intending to be conservative may assume that tenability would be violated if, out of a set of criteria, any one particular criterion, such as temperature or carbon monoxide, exceeded its minimum value. However, toxicity experts might argue that temperature and gas interactions cause tenability to be violated even when every individual species is in acceptable ranges. Likewise, a design engineer may assume that the time needed for a resident to react to an alarm be conservatively set equal to the travel time needed to go from one remote corner of the unit to the other most remote corner of the same unit. However, this may not be that conservative, since even a fully ambulatory occupant may stop to gather belongings, rescue a pet, call a neighbor, and so forth.
7. **No standardized methods exist to incorporate reliability of systems:** The last barrier identified is the uncertainty surrounding both the reliability of a given fire protection device, system, or characteristic and the lack of a standardized method to incorporate reliability into performance-based engineering calculations and decisions based on these calculations. We may be uncertain about the reliability of a given fire suppression system. Sometimes a fire suppression system is proposed as an alternative to passive fire protection, such as compartmentalization. However, these two alternatives have different reliabilities. There is uncertainty (e.g., no agreement) on how to account for these differences.

These seven barriers to determining and documenting achievement of agreed-upon levels of fire safety for a particular project must be addressed fully in order for all stakeholders to have a known level of confidence in the science-based predictions and the resulting final design. All seven barriers involve various types of uncertainty. Thus there is a well-defined and important role for uncertainty analysis in fire safety engineering calculations. Although this clear role for uncertainty in improving the development and implementation of performance-based fire safety regulations exists, uncertainty analysis is clearly an uncomfortable topic for many of the stakeholders in the process.

Difficulties with Uncertainty Analysis and Complexity

Discussion of the proper treatment of uncertainty in a fire safety engineering calculation is difficult for several reasons:

1. *Magnitude of the problem.* It is widely assumed that a mixture of conservative assumptions and factors of safety can be used to explain away uncertainties. However, the magnitude of the problem is not clearly understood. Factors of safety that are applied at various stages of the analysis are not necessarily linearly related to the critical output parameters, potentially resulting in a reduced (or nonexistent) factor of safety in the results.
2. *Uncertainties that go unrecognized or ignored.* These types of uncertainties include those in variables hardwired in scientific tools, those in tenability/performance criteria, those surrounding the selection of design fires, and those in human behaviors and values.
3. *Effect on the implementation of performance regulations.* It is feared that identification and

treatment of uncertainty would show that our current ability to predict the buildup of heat and toxic products of combustion is not accurate enough to judge the acceptability of a proposed design with a high enough confidence level. This would delay implementation of the entire performance process until predictions of critical outcome criteria can be more certain.

4. *Quantitative methodology*. No quantitative methodology exists for treating uncertainty in performance-based designs. A methodology is needed that is both rigorous and user-friendly.
5. *Impracticality*. It is feared that the mathematical rigor needed to conduct such an analysis would render the process impractical.
6. *Paucity of data*. To quantify uncertainty adequately, a large quantity of data would be needed to determine ranges of values for input parameters, such as heats of combustion, rates of production of various gaseous species, and other important inputs. A large quantity of data would also be needed to validate predicted values with empirical data from real burn scenarios.

It should be pointed out that these are real and valid concerns due to the combination of poorly defined and unstructured problems, and the lack of a user-friendly methodology. Current common practice for conducting uncertainty analyses involves completing a series of single-variable sensitivity studies. Application of these techniques to a complete performance-based design containing hundreds of variables is impractical. Later sections focus on practical ways to identify and account for uncertainties in fire protection engineering design.

In conclusion, *uncertainty* is a broad and general term used to describe a variety of concepts, including, but not limited to, lack of knowledge, variability, randomness, indeterminacy, judgment, approximation, linguistic imprecision, error, and significance. Many of these uncertainties are inherent in the design process itself. Variations in analysis parameters, assumptions, or model inputs may cause output criteria to change. Switchover occurs when outcome criteria change enough so as to cause a change in the design decision (e.g., the acceptability of a final design). It is critical to know whether different sets of reasonable inputs, scenarios, or parameters used in a fire safety engineering design have potential to cause switchover and to lead to different acceptable designs. This section on identifying sources of uncertainty provided an overview of terminology used to describe uncertainty, described aspects of the design process that introduce uncertainty, and presented a taxonomy useful as an aid in identifying uncertainties.

Treatment of Uncertainty with Safety Factors

When considering uncertainty in a fire protection engineering calculation, fire protection engineers typically consider first the uncertainties associated with the calculation inputs, usually empirically measured quantities, such as heat release rate. However, there are many other types of uncertainty integral to fire safety engineering design.

In a complete uncertainty analysis, not all uncertain parameters are treated quantitatively, only parameters or combinations of parameters with the potential to cause switchover in the final decision on the acceptability of a design. Others are negligible and best-guess values of these parameters can be used in the calculations. Still others, such as societal values, become policy or regulatory issues, not engineering issues. The intelligent use of safety factors can often cover more than one type of uncertainty. Still, it is useful to first identify sources and types of uncertainty from a broad perspective. Without first adequately identifying the sources of uncertainty, we cannot understand how best to handle them.

Safety factor and *margin of safety* are two commonly used terms in the field of engineering. The dictionary defines *factor of safety* in terms of stress: "The ratio of the maximum stress that a structural part or other piece of material can withstand to the maximum stress estimated for it in the use for which it is designed." Safety factors do not apply only to stress, however.

The idea of a safety factor is that the design values are multiplied by the factor of safety, and the design is checked to ensure that the design is safe at the larger value (i.e., the product of the design value and the safety factor). Safety margin is a slightly different concept. A safety margin is additive and not multiplicative. A *safety margin* is defined as the difference between the design value and the value that would no longer be safe.

Implied Versus Explicit Safety Factors

Safety factors are used with both prescriptive and performance codes. These factors of safety can be implied or explicit. Implied safety factors generally are found at various sub stages or components of a design. Implied safety factors provide for an extra margin of safety simply attributable to the choice of a component of a system. Implied safety factors may also take the form of conservative assumptions or worst-case scenarios. Explicit safety factors are multipliers applied to critical analysis parameters, often (and preferably) the final outcome criteria used to judge the acceptability of a design. Both types of safety factors are used to increase safety by lowering the probability that critical values of analysis parameters will be reached or exceeded.

Use of Safety Factors in Prescriptive and Performance Codes

An example of an implied safety factor in a prescriptive code is use of a pipe material or thickness that exceeds the strength and durability needed to meet the requirements of a sprinkler system. Pipe schedules have implied safety factors. An example of an explicit safety factor incorporated into a prescriptive code provision is a requirement to use a sprinkler flow density of 1.5 or some other multiple higher than the minimum shown experimentally to control a given type of fire. In this example, the safety factor is used to cover for uncertainties in the measurement of the needed flow density, variations in the actual fuel package versus the fuel package tested, and uncertainties and variations in geometry, building characteristics, and so forth. An example of an implied safety factor in a performance code is an assumption that the rate of production of carbon monoxide for a given fuel package is equal to the rate of production of the component fuel with the highest production. An example of an explicit factor of safety incorporated into a performance-based design is to directly multiply the time necessary for egress by a factor of 2.

Selecting an Appropriate Factor of Safety

The first step in the use of safety factors is to determine which analysis parameters would be appropriate for the application of a safety factor. When a factor of safety is applied to measures of the final outcome criteria, it is most clear what margin of safety has actually been achieved; however, it is least clear how to alter the design specifications when a higher factor of safety is desired.

Safety factors may also be applied to different analysis parameters at various stages of the analysis. Careful judgment must be used, however, when applying these intermediate safety factors, because the quantity to which they are applied may not be linearly related to the final outcome criteria. Even if the quantity is linearly related to the final outcome criteria, it may not possess a relationship. Specifically, a relationship exists when a unit change in the analysis parameter causes a proportional unit change in the outcome criteria. In fire protection engineering calculations, input variables and analysis parameters are not often linearly related to outcome criteria, such as upper-layer temperature. Also, they usually do not share common units of measure. In fire protection engineering calculations, time is the only common measure. It is likely that a safety factor of 2 applied to an intermediate quantity will not carry through the calculation and allow for a safety factor of 2 in the final design. In some cases, a safety factor of

2 applied to an intermediate quantity may not allow for *any* factor of safety design.

This lack of carry-through of the factor of safety is particularly true for implied factors of safety often found in the form of conservative assumptions. For example, an assumption that a fast growth rate fire is a worst-case scenario is not true in all cases. A fast-flaming fire may not pose the greatest danger if it activates the sprinkler more quickly. A more slowly developing fire may be more able to overpower the sprinkler in some circumstances, and a fire originating in an unprotected or shielded space, even though slower growing may also be more deadly. Therefore, if we wish to provide a safety factor of 2 to the time available to safely egress a building, we cannot assume that doubling the fire size (heat-release rate) will achieve this goal. Heat-release rate is not linearly related to time to critical temperature.

When an explicit factor of safety is applied, one may choose a value of 1.5, 2, or even higher. How much of a margin of safety is appropriate is as much a function of how much confidence we have in the predictive equations (i.e., are we using a factor of safety as a factor of uncertainty?) used in the calculations as it is of the stakeholders' risk tolerance. It should be noted, however, that increasing the margin of safety usually corresponds to an increase in cost of the project. When historical performance data are available, they can be used to set factors of safety. Otherwise, safety factors are usually set by expert judgment or mandated in policy. Safety factors are set to reflect confidence in the design equations as well as to reflect the stakeholders' acceptable risk tolerance. New specialized methods are being developed for deriving appropriate factors of safety.

Combining Safety Factors

First, it must be stated that there are no official rules for combining safety factors, i.e., none published and agreed on by the fire safety community at large. The following list of suggestions and potential pitfalls was compiled by the author. After a thorough review of the literature, specific numbers and justifications for safety factors were found lacking. To get good quantitative numbers for safety factors, historical data are needed.

Track the effect of each factor of safety: The effect of each factor of safety on the outcome criteria can be determined by changing the value of the safety factor and observing the net change in the outcome criteria relative to the net change in the safety factor. When the equations are not overly complicated, it may be possible to derive this relationship directly using partial derivatives. For conservative assumptions, the effect of the assumption should be tested by repeat calculations.

Watch for variance: If the normal variation in the population is sufficiently large, a factor of safety applied to the mean will not cover all or even most of the people who will be in the building. For example, if the baseline walking speed is estimated as the walking speed of a young, healthy individual and a safety factor of 2 is used, that would not cover the walking speed of an elderly person or person with physical disabilities if his or her speed was less than half the average.

Don't assume safety factors are additive: Factors of safety applied to two individual parameters in the analysis will not necessarily provide a total factor of safety equal to the sum of each individual safety factor. The total safety factor could be more or less than the sum of the two individual safety factors. As discussed earlier, analysis parameters are often not linearly related to outcome criteria. They are most likely in different units of measure, and analysis parameters are likely not linearly related to each other. For these reasons, safety factors cannot be assumed to be additive.

Account for both positive and negative effects on safety: An explicit factor of safety or design assumption may have either a positive or negative contribution toward safety. Careful thought, engineering judgment, and testing using the calculation procedure must be used to test for the effects of each factor of safety and/or design assumption made. For example,

doubling the heat of combustion may be conservative in predicting upper-layer temperature, whereas doubling the radiative fraction will have the opposite effect.

Evaluate for multiple performance criteria: Since most fire safety engineering designs are judged on multiple performance criteria, what might constitute an implied factor of safety for one outcome criterion might constitute a reduction in safety for another parameter. For example, if a soot yield value is conservative for smoke detector activation, then it could not simultaneously be conservative for life safety [20].

Realize effects may change with time: The relative importance of individual input variables, and thus the factors of safety applied to them, may be a function of time. In particular, variables may be limiting factors in the analysis during the time period of preflashover, and in the post flashover time period they may have little or no effect. In fire protection engineering we often deal with two distinct phases of the fire represented by different physics and mathematics; consequently we must be careful to be aware of changes in the effects of a parameter in these very different phases of fire development.

Derivation of Safety Factors

Researchers at the University of Lund [21, 22] have been conducting research on the application of the FOSM (first-order second-moment) methodology for fire safety engineering design. They have applied the FOSM method to derive safety factors for use in fire safety engineering design calculations. The safety index is represented by β, the distance from the origin to a failure line (limit state). β is also referred to as a reliability index, where reliability is defined as the probabilistic measure of assurance of performance. β can also be thought of as the overall safety factor for the design.

The overall concept for conducting a design is to specify input data, choose a target reliability index β (researchers suggest 1.4, which is approximately equivalent to a probability of failure of 8 % on condition that a fire has started), and vary the design parameters to be determined until the chosen value of β has been obtained. In this type of analysis, design parameters include design door width and time to detection [21].

Researchers have also applied the FOSM methodology to derive the safety factor, β, for a design. In this case, design parameters such as door widths and time to detection are already known. An example is worked out for a shopping center [34]. There are some admitted shortcomings to applying this methodology to an actual design problem. First, the importance of the uncertainties in the input parameters needs to be investigated via a sensitivity analysis. A method of incorporating this uncertainty would then need to be standardized.

Linking Safety Factor and Failure Probability

The concept of safety factors can be addressed in the context of assessing failure probability for fire safety engineering. The complete elimination of risk is impossible, but the traditional engineering approach can be improved by involving a probabilistic methodology H. Yaping, in his paper "Linking Safety Factor and Failure Probability for Fire Safety Engineering," *Journal of Fire Protection Engineering*, 2010 [23], gave three levels of treating uncertainties in engineering designs include (1) using a single characteristic value for a particular uncertain parameter due to a lack of knowledge about the parameter, (2) describing parameters by a mean and standard deviation, and (3) describing parameters by full probability distributions.

So called "evaluation parameters," such as ASET (A) and RSET (R), are determined by "design parameters," such as fuel load or detection time. Risk is defined as the expected loss and is the product of an event's consequence and probability. The safety margin, in this case the difference between ASET and RSET (W), is referred to as the "performance parameter," as it is used to evaluate the system performance.

The use of a safety factor is considered only a partial or first-order measure of failure probability. A more detailed analysis of the properties of the probability distribution that describes a performance parameter will provide a higher-order measure. ASET and RSET can be considered random variables. Likewise, the safety margin is a random variable. If A and R are normally distributed, their difference, W, will be as well. μ_W and σ_W can be determined from A and R, and the ratio $\beta_W = \frac{\mu_W}{\sigma_W}$ is defined as the safety index. It is a measure of the distance of μ_W from $W = 0$, the failure point, in terms of σ_W. An analysis of β_W demonstrates that, for a given safety factor, the safety index may still be small. Therefore, even a large safety factor may not guarantee a low failure probability. A similar approach can be used for log-normal A and R. The α-percentile approach may be appropriate especially when distributions of design parameters are not known, or distributions of ASET and RSET are difficult to obtain. In such a situation, the performance of a "worst-case" scenario may be evaluated. In order to avoid ambiguity in the definition of "worst-case," the α-percentile approach assigns a percentile ranking (α) to a particular fire scenario. Determination of W for associated α's will allow the calculation of μ_W and σ_W, and thus an assessment of failure probability. The greatest difficulty in this type of analysis lies in determining the choice of a percentile, α, for a given scenario. This will rely largely on the use of expert solicitation.

Techniques for the Quantitative Treatment of Uncertainty

It is important not only to recognize the various types of uncertainty but also the different types of quantities for which the uncertainty exists, since they need to be treated in different ways. There is a standard procedure for quantifying uncertainty in empirical quantities. This procedure, sometimes referred to as classical uncertainty analysis, is based on the mathematics of probability and statistics. However, as shown by the taxonomy, in any fire safety engineering calculation or decision there are many non-empirical parameters and assumptions used in the calculations. It is not always appropriate, meaningful, or even possible to treat the uncertainty in these non-empirical parameters by these same probabilistic methods. It has been argued that "probability is an appropriate way to express some of these kinds of uncertainty but not others" [1]. The next sections present quantitative methods appropriate for the expression of uncertainty in various types of quantities.

Techniques for Quantifying Measurement Uncertainty

Many calculation and model inputs are empirical in nature. To be empirical, variables must be measurable and have a true value. Empirical quantities in the domain of fire protection engineering include the heat-release rate, the burning rate, and the radiative fraction of a given fuel. Classical uncertainty analysis refers to a statistical method of determining the random and systematic errors (and from them the total error) for a set of measurements. Random error and statistical variation result because no measurement of an empirical quantity can be absolutely exact. Imperfections in the measuring instruments and observational technique will inevitably give rise to variations from one observation to the next. The resulting uncertainty depends on the size of the variations between observations and the number of observations taken.

Classical statistical techniques such as standard deviation, confidence intervals, and others can be used to quantify this uncertainty. These statistical techniques are presented in Chap. 73. A full discussion on uncertainty in measurement is found in the U.S./ISO guide [2] and in the NIST guide [24]. The NIST guide describes two types of evaluations of uncertainty. A Type A evaluation of standard uncertainty may be based on any valid statistical method for treating data. Three examples are (1) calculating the standard deviation of the mean of a series of independent observations; (2) using the method of least

squares to fit a curve to data in order to estimate the parameters of the curve and their standard deviations; and (3) carrying out an analysis of variance (ANOVA) in order to identify and quantify random effects in certain kinds of measurements.

A Type B evaluation of standard uncertainty is usually based on scientific judgment using all the relevant information available, which may include previous measurement data, experience, manufacturer's specifications, and calibration reports. There is not always a simple correspondence between the classification of uncertainty components into categories A and B and the commonly used classification of uncertainty components as random and systematic.

The nature of an uncertainty component is conditioned by the use made of the corresponding quantity, that is, on how that quantity appears in the mathematical model that describes the measurement process. When the corresponding quantity is used in a different way, a random component may become a systematic component and vice versa. The NIST guide also differentiates between uncertainty and error. It is assumed that a correction is applied to compensate for each recognized systematic effect that significantly influences the measurement result. The relevant uncertainty to associate with each recognized systematic effect is then the uncertainty of the applied correction.

Techniques for Assessing Uncertainty in Analysis Parameters, Assumptions, and Value Parameters

Probabilistic techniques used to quantify measurement uncertainties are not applicable to uncertainties in establishing performance criteria or uncertainties regarding values such as the value of life. These uncertainties should be evaluated with techniques that make explicit the effect of the uncertainty on the value of all decision variables. Decision variables in fire protection engineering include elements such as level of acceptable fire safety and installation of fire protection devices. If a quantity is a decision variable, then by definition it has no absolute, true value. It is up to the decision maker who exercises direct control to decide its value. Morgan and Henrion state that, "The question of whether a specific quantity is a decision variable, an empirical quantity, or some other type of quantity depends on the context and intent of the model, *and particularly who the decision maker is*" (emphasis added) [1]. For example, in performance-based design, the minimum, permissible escape time during a fire may be a decision variable for the regulatory body, but it may be an empirical quantity from the viewpoint of the fire protection engineer.

Value parameters represent preferences of individuals. One controversial value parameter is the value of premature death avoided, often referred to as the value of life. Another is risk tolerance or risk preference, a parameter used to specify a degree of risk aversion when comparing uncertain outcomes. The effect on the outcome of an analysis caused by differences in value parameters should be demonstrated explicitly. This is done by repeating the analysis for a range of possible inputs of the value parameter (s) to determine if a change in the outcome occurs that someone would care about. Several techniques that aid in the evaluation of uncertainty in these types of quantities are presented below. For all these techniques, the effect of various values of analysis parameters, assumptions, and value parameters is made explicit.

Bounding: Bounding is the evaluation of the extremes of the range of possible values of an uncertain quantity. If the extreme values at both ends are acceptable, a more complex and costly analytical uncertainty analysis may be avoided. For example, suppose we bound the ambient room temperature between a low and a high value. If we are trying to predict carbon monoxide buildup in a room, we may find that the results are either not sensitive to ambient temperature, or the range of predicted values of carbon monoxide, based on the range of ambient temperatures, is completely acceptable. We may either eliminate ambient temperature as a variable or set it to our best-guess estimate.

We do not need to quantify the uncertainty in the ambient temperature any further.

Sensitivity and sensitivity analysis: The sensitivity of a design to modest variability and uncertainty must be explicitly understood. Sensitivity analysis is useful in assessing the consequences of uncertainty in data and in assumptions. By testing the responsiveness of calculation results to variations in values assigned to different parameters, sensitivity analysis enables the identification of those parameters that are most important to the outcome criteria. It does not tell the decision maker the value that should be used, but it can show the impact of using different values.

Parametric analysis: A parametric analysis is a particular type of sensitivity analysis. In parametric analysis, detailed information is obtained about the effect of a particular input on the value of the outcome criterion. This is done by evaluating and plotting the outcome criterion for a sequence of different values for each input, holding the others constant.

Importance and importance analysis: An importance analysis is a particular type of sensitivity analysis that determines which of the uncertain input variables contributes most to the uncertainty in the outcome variable. The results are used to focus on getting more precise estimates or building a more detailed model for the one or two, or small group, of the most important inputs. Importance here is defined as the rank-order correlation between the output value and each uncertain input. Each variable's importance is calculated on a relative scale from 0 to 1. An importance value of 0 indicates that the uncertain input variable has no effect on the uncertainty in the output.

Comparative analysis: Comparative analysis is a technique used to evaluate risks, and the costs to mitigate them, by means of comparison with other similar risks. This technique is useful in evaluating perceptions of risk tolerance. Researchers [25] conducted a comparative analysis of the cost of mandating residential fire sprinklers with the cost of mandating other methods of reducing residential deaths, such as radon remediation and ground fault interrupters.

Expert elicitation: When hard data do not exist and are not possible to create experimentally, an expert elicitation is often conducted in order to obtain expert judgment of an uncertain quantity. An excellent discussion of the techniques for conducting an expert elicitation is provided in Chapter 6 of *Uncertainty* [1].

Switchover: Variations in analysis parameters, assumptions, or model inputs will cause output criteria to change. Switchover occurs when outcome criteria change enough so as to cause a change in the design decision (e.g., the acceptability of a final design).

Techniques for Assessing Uncertainty and Sensitivity in Complex Models

Several of the scientific uncertainties discussed in the taxonomy presented above can be evaluated only by examining the structure of the fire model. These include theory and model uncertainties, calculation limitations, and level of detail of the model. Uncertainties arise when physical processes (1) are modeled based on empirically derived correlations and/or (2) simplifying assumptions are made. Other physical processes are not modeled due to lack of knowledge of how to include them. As stated earlier, most compartment fire models are zone models, which make the simplifying assumption that each room can be divided into two volumes or layers, each of which is assumed to be internally uniform. Current fire models do not contain a combustion model to predict fire growth, and many compartment fire models use an empirical correlation to determine the amount of mass moving between the layers [26]. These modeling approximations introduce uncertainties.

Fire-Model Validation Because fire models have been relied on as a means of verifying that a fire safety engineering design meets a set of performance objectives, fire-model validation has become a much-discussed topic. Work is

being done to characterize the additional output uncertainty due to modeling approximations. Part of this work focuses on aiding the user in selecting a model, or set of models, appropriate to the type of prediction(s) needed. Some researchers have suggested a Bayesian framework, where each available model is treated as a source of information that can be used in a prediction [27, 28]. In addition, work is ongoing to evaluate computer fire models by comparing model predictions to predictions of other models or with experimental data. These comparisons are helpful to the user in determining the level of uncertainty likely from a model prediction for a similar set of conditions. However, these comparisons are difficult, since they involve comparing two time-series curves, the experimental measurements, and the predicted values. Historically these comparisons have been largely qualitative. The use of a branch of mathematics called functional analysis, to make comparisons of these time-series curves, is being investigated. This analysis enables lengths, angles, and distances between two arbitrary curves to be defined and quantified [29]. Further validation issues that must be addressed were discussed among various groups of fire safety professionals at the Conference on Fire Safety Design in the Twenty-First Century [30]. Jones discusses issues that must be addressed in *Progress Report on Fire Model Validation* [31]. Once a model is selected, it is useful to know the sensitivity of that model's output predictions to the values selected for the inputs.

Quantifying Model Bias and Standard Deviation Experimentally Independent of the errors associated with input parameters, numerical calculations also involve errors that are specific to the model itself. Sources include theoretical and numerical assumptions, numerical techniques, and user error. As the work of Lundin points out, most studies of model error with respect to fire safety design are qualitative in nature. However, a quantitative understanding of model error allows even models with significant error to be useful tools. Lundin's work [32, 33] utilizes a comparison between model outputs of the CFAST 2.0 two-zone model for smoke transport and experimental measurements. Lundin develops a systematic method for evaluating model error and applying this evaluation to future simulations to improve output values. For a model such as CFAST, model error varies both within a given fire scenario and between different scenarios. In order to generate a straightforward method for output adjustment, the different scenarios represent changes in parameters, such as room height within a limited range, such that the error predictions in each case are of the same magnitude. The method is applied to a particular set of scenarios, referred to as a scenario configuration.

This method uses a regression technique to evaluate both the systematic error (the curve of how error develops in a given scenario, such as error in upper layer temperature with the value of upper layer temperature) and the random error (variations about that curve). This is done for both the error in a particular scenario as well as the error between scenarios. The method is designed to create a prediction interval, the upper or lower bound of which can be used as the adjustment curve to create a more conservative estimate. The application of this method allows for a quantitative treatment of model error and subsequent adjustments in model outputs. However, the experimental scenarios used must have limited uncertainties in order to decouple model errors from those generated by poor input values.

Similar to Lundin, McGratten and Toman [34] have developed a method for quantifying model uncertainty. This approach relies only on model predictions and experimental measurements and can be easily understood by persons with limited modeling or uncertainty experience. Unlike Lundin, this method considers only the error at a single event in a fire scenario. The peak value of a particular parameter, such as upper layer temperature, is compared for a series of paired experiment and model simulations for similar scenarios. The similarity of particular fire scenarios, and hence their applicability to this method, must be determined by comparison of key non-dimensional parameters. McGratten and Toman show that, given a particular model

prediction, a normal distribution can be generated to represent the "true" value. This is given by the equation

$$\theta' \left| M' \sim N\left(\frac{M'}{\hat{\delta}}, \left(\frac{M'}{\hat{\delta}}\right)^2 \left(\frac{\hat{\omega}_M}{\hat{\delta}}\right)^2\right)\right.$$

where θ' is the true value, M' is the model prediction, and $\hat{\delta}$ and $\hat{\omega}_M$ are the model bias and relative uncertainty, which are derived using the relevant values from all of the scenarios considered and obtaining the relative experimental uncertainty ω_E. It should be noted that relative uncertainty refers to the uncertainty of a value with respect to that value. This method has the benefit of providing outputs as probability distributions without having to run a full Monte Carlo analysis. However, having a limited number of similar experimental and model comparisons has been shown to be problematic, particularly in determining the relative model uncertainty, where imaginary numbers may be obtained.

Sensitivity of Output Predictions to Input Values When selecting and using a fire model, it is important to know the sensitivity of the predicted outcome criteria to the model inputs. In order to facilitate this, several quantitative methods for determining the sensitivity of model predictions to model inputs are described below, along with a brief discussion of their positive and negative attributes and limitations of application. These methods are also discussed in ASTM 1355-92, *Standard Guide for Evaluating Predictive Capability of Computer Fire Models* [35].

A Differential/Direct Method For a system of time-dependent, ordinary differential equations, it is possible to solve directly for the partial derivative of the predicted values with respect to each input variable. This set of partial derivatives measures the sensitivity of the solution with respect to changes in the input parameters:

$$Y_I = f_I = (c_1, c_2, \ldots, y_1, y_2, \ldots, t)$$

where c_k are rate parameters.

We simultaneously solve for both y_I and a set of sensitivity functions, $\delta y_i/\delta c_k$, over all times t. These partial derivatives measure the sensitivity of the solution with respect to uncertainties in the parameters c_k and in initial conditions. Often these parameters are not accurately known. Dickson provides an example of a direct solution of a set of ordinary differential equations that composes a large computational model of atmospheric chemical kinetics [36].

Response Surface Replacement Multiple runs, n, of the computer model are made. The model output Y_i and inputs $X_{1i} \ldots, X_{ki}$, $I = 1, \ldots, n$ are used to estimate the parameters of a general linear model of the form:

$$Y = \beta_0 + \sum_i \beta_j X_j$$

The estimated model is known as a fitted response surface, and this response surface is used as a replacement for the computer model. All inferences with respect to uncertainty analysis and sensitivity analysis for the computer model are then derived from this fitted model [37]. Construction of a response surface without specification of the probability distributions for all input variables is discussed by Iman [38]. It is suggested, in fact, that when using certain sampling techniques to build a response surface, it may be desirable to ignore probability distributions and use only the ranges of the variables. Iman provides a good discussion of using a response surface method to conduct a sensitivity analysis and provide a ranking of input variables in a second paper [39]. Beller has discussed the use of response surfaces for modeling upper-layer temperature and layer height [40].

Monte Carlo Sampling In uncertainty analysis employing Monte Carlo sampling,[3] it is desired to estimate the distribution function and the

[3] There are many sampling techniques. Monte Carlo is a well-accepted sampling method that has certain statistical advantages but may not be the best choice in all cases.

variance for the particular output variables under consideration. The uncertainty surrounding each input is represented mathematically and often probabilistically by its individual distribution. When all probability distributions for all uncertain quantities are put together, a simulation model is built that is believed to capture the relevant aspects of the uncertainty in the problem. After running the simulation many times, an approximation of the probability distribution of the output variables is generated. The more simulations that are carried out, the more accurate the approximation becomes.

Comparison of Sampling-Based Uncertainty Analysis A model under consideration can be written as $\mathbf{x} = \mathbf{y}(\mathbf{x}) = \mathbf{f}(\mathbf{x})$ with $\mathbf{x} = [x_1, x_2, \ldots, x_{nX}]$ and $\mathbf{y} = [y_1, y_2, \ldots, y_{nY}]$. It is possible that the dimensions nX and nY are large, and the function $\mathbf{f}$ is complex. If model uncertainty is not considered, i.e., the "correct" value of $\mathbf{y}$ is generated from the appropriate value of $\mathbf{x}$, there are two aspects of the effect of uncertainty on $\mathbf{x}$ on $\mathbf{y(x)}$. The first aspect is the uncertainty in $\mathbf{y(x)}$ given the uncertainty in $\mathbf{x}$, and the second is the importance of the individual elements of $\mathbf{x}$ on the uncertainty in $\mathbf{y(x)}$. These are the uncertainty analysis and sensitivity analysis, respectively.

If the uncertainty of the individual elements of $\mathbf{x}$ is given by probability distributions, then a sample-based analysis is conducted by evaluating the pairs $[\mathbf{x}_k, \mathbf{y}(\mathbf{x}_k)], k = 1, 2, \ldots, nS$, where $\mathbf{x}_k = [x_{k1}, x_{k1}, \ldots, x_{knX}], k = 1, 2, \ldots nS$ represents nS samples from the distributions for each element of $\mathbf{x}$. Sampling from these distributions can be carried out by either a random method or another procedure, such as Latin-hypercube sampling. The work of Helton and Davis [41] demonstrates how correlation coefficients, partial-correlation coefficients, and standardized-regression coefficients can be used to assess the strength of a linear relationship between $\mathbf{x}_k$ and $\mathbf{y}(\mathbf{x}_k)$. Rank-correlation coefficients, standardized rank regression coefficients, and partial-rank correlation coefficients can be used to assess the strength of a monotonic relationship. Common means, common locations, common medians, and statistical independence can be used to assess nonlinear and nonmonotonic relationships. Methods for sampling based sensitivity analysis are tested for simple test problems and a more complex performance assessment of a radioactive waste disposal facility. Both parametric-regression procedures (linear regression, rank regression, and quadratic regression) and nonparametric procedures (locally weighted regression, additive models, projection-pursuit regression, and recursive-partitioning regression) are used. For correctly ordering the importance of inputs and the R^2 value, the recursive partitioning regression is found to the best of all those tested. However, it generally took longer to implement. The locally weighted and projection-pursuit methods used introduced some difficulties that might limit their usability.

Quantification of Margins of Uncertainty (QMU) Quantification of Margins and Uncertainties (QMU) is a broad methodology for obtaining critical information to be used in U.S. nuclear-weapon stockpile management [42]. QMU is a "decision-support methodology for complex technical decisions that are made under conditions of uncertainty and that center on performance thresholds and associated margins for engineered systems." Results may be expressed as a confidence ratio of margin to uncertainty (CR = M/U). However, this representation is of limited value, and a more rigorous study of uncertainty should be conducted. Three key elements of the performance characteristics are (1) identification and specification of performance thresholds, (2) identification and specification of associated performance margins, and (3) quantification of uncertainty in thresholds and margins. The underlying components of QMU are the scenario identification, the likelihood of scenarios, the consequence of scenarios, and the credibility of the evaluation of the first three components. Credibility is a driving factor when modeling and simulation are used in QMU. This can be assessed through verification and validation. Epistemic uncertainty is especially important and should be acknowledged and quantified separate from aleatory uncertainty.

Sensitivity analysis is also a vital aspect to QMU. Risk informed decision analysis (RIDA) utilizes the results of QMU along with considerations of other factors in order to make decisions. Schematically, this can be represented as $Decision = D\left[\frac{M_1}{U(M_1)}, \ldots, \frac{M_n}{U(M_n)};\ other\ factors\right]$. However, it is important to note that this representation is deceptively simplistic. The details of the uncertainty, the "other factors," and how other factors may also play into the ratios are all implicit in this form.

Helton offers a detailed overview of QMU, a form of risk-assessment that is applied to nuclear weapons stockpiles. He defines aleatory and epistemic uncertainty and presents examples of how to represent them mathematically. For analysis involving both types of uncertainty, final results should separate the effects of the two types. Additionally, documentation about the analysis should be highly detailed, and the presentation of results should be in a form that provides information about system behavior and the uncertainty involved in predicting that behavior.

Generalized Information Theory (GIT)

Oberhampf et al. offer a discussion of the differences between epistemic and aleatory uncertainty . They identify three different classes of information: (1) The classification strong *statistical information refers* to a large data set that can be used to derive or convincingly verify a particular statistical model. (2) *Sparse statistical information* refers to a small collection of data from which a statistical model must be indirectly inferred, and fitting will result in epistemic uncertainty. (3) *Intervals* refers to bounds or graded levels that typically form expert elicitation. Multiple sources may give conflicting data. The article gives essentially no information on what "general information theory," "possibility theory," "fuzzy set theory," or "evidence theory" are. It does provide "challenge problems" used in a workshop, as well as numerical inputs so that participants can compare.

Other investigators, such as Vasquez and Whiting [43], suggest that random errors on experimental measurements are often the only type considered, and that systematic errors (or bias) are often discounted. Systematic errors are often not reported, as there is a psychological perception that it diminishes the credibility of experimental results. However, such errors do exist and are not completely reducible. They offer a method utilizing Monte Carlo methods to separate and compare the effects of both random and systematic error on model outputs. Random errors are propagated by creating n pseudo-data sets, in which each particular datum is randomly sampled, according to the probability distribution with which it is associated, for each of the n sets. Systematic errors are propagated by creating n pseudo-data sets, in which the entire original set is randomly shifted within a defined bias range. This is often done by defining a uniform distribution for the mean value of each stochastic variable. However, bias adjustments may be dependent on the value of the variable (called a dynamic bias range), so proper probability distributions should be selected as appropriate. The effects of random and systematic errors can be assessed independently or simultaneously. By creating cumulative probability distributions of the outputs, comparisons can be made between the relative importance of random and systematic errors for a given model. In particular, the importance of systematic errors can be used to motivate more thoughtful experimentation, which attempts to quantify both error types adequately.

Advantages and Disadvantages of Each Technique

Iman and Helton state in their paper, *Investigation of Uncertainty and Sensitivity Analysis Techniques for Computer Models*, some of the characteristics of large and complex computer models [37]:

- There are many input and output variables.
- The model is time-consuming to run on the computer.
- Alterations to the model are difficult and time-consuming.
- It is difficult to reduce the model to a single system of equations.

- Discontinuities exist in the behavior of the model.
- Correlations exist among the input variables, and the associated marginal probability distributions are often nonnormal.
- Model predictions are nonlinear, multivariate, time-dependent functions of the input variables.
- The relative importance of the individual input variables is a function of time.

Fire models often possess many and sometimes all of these characteristics. Iman and Helton evaluated the above three techniques as applied to large, complex models having many of the listed characteristics. Their evaluation included ease of implementation, flexibility, estimate of the cumulative distribution function (CDF) of the output, and adaptability to different methods of sensitivity (analysis). Their findings clearly show that the technique that had the best overall performance was Monte Carlo sampling. They found that a differential analysis provides good local information about the inputs but does not extend well to a global interpretation. Also, a very real problem with differential analysis lies in the difficulty of implementation. Response surface replacements were not recommended because the underlying models are often too complex to be adequately represented by a simple function.

The following section describes a methodology for application of uncertainty analysis to fire safety engineering calculations. This methodology employs Monte Carlo sampling. It also incorporates many of the techniques described in previous sections for quantifying measurement uncertainty and assessing uncertainty in analysis parameters, assumptions, and value parameters.

Application of Uncertainty Analysis to Fire Safety Engineering Calculations

The fire safety community needs to begin to move forward from discussing a set of issues and concerns relating to uncertainty in fire protection engineering to agreeing as a community on practical steps to execute an uncertainty analysis. This section demonstrates a suggested methodology that quantitatively treats variability and uncertainty, and applies them to a complex fire protection engineering problem. The methodology suggested is a generic methodology that is applicable to a wide range of fire protection engineering calculations and fire safety design issues. For example, application of the methodology is appropriate for engineering calculations such as those that predict upper-layer temperatures and concentrations of products of combustion. The methodology may also be applied to calculations of time needed to egress. It ties together the issues discussed earlier regarding uncertainties in the design process and the problem of switchover. Here, a brief introduction to and overview of the methodology are presented. A full description of the methodology and a worked case study of an actual building can be found in Notarianni [44].

Overview of the Performance-Based Design Process with Uncertainty

The methodology is rigorous but comprehensible. It breaks up the process of conducting an engineering design calculation with uncertainty analysis into identifiable steps, each of which can be expanded or contracted to fit specific design problems. Table 76.1 shows the steps in conducting a performance-based fire protection engineering design. The column labeled Performance-Based Design Process lists the steps in the performance-based design process as detailed in the SFPE guide [13]. The right column lists the steps in the performance-based process with uncertainty. Steps or parts of steps in bold signify suggested modifications to the current design process. Steps 1–3 are modified by incorporating treatment of uncertainties noted in parentheses and detailed in the taxonomy presented earlier. The intent of each step does not change; however, the process is made explicit and standardized.

Table 76.1 Steps in the performance-based design process with and without uncertainty

Performance-based design process [13]		Performance-based design process with uncertainty [44]
Step 1	Define project scope	Define project scope **(uncertainties related to life-cycle use and safety of buildings)**
Step 2	Identify goals	Identify goals **(uncertainties related to equity and incorporation of societal values)**
Step 3	Define stakeholder and design objectives	Define stakeholder and design objectives **(uncertainties related to risk perception and values)**
Step 4	Develop performance criteria	Develop probabilistic statement of performance **(criteria, threshold, probability, time)**
Step 5	Develop design fire scenarios	**Develop a distribution of design fire scenarios**
		(a) **Select calculation procedure(s)**
		(b) **Identify uncertain input parameters**
		(c) **Generate a distribution of design fire curves**
		(d) **Define distributions of and model correlations among other input parameters**
		(e) **Select sampling method and determine number of scenarios**
Step 6	Develop candidate designs	Develop candidate designs
Step 7	Evaluate candidate designs	Evaluate candidate designs
		(a) **Calculate a set of values for each outcome criterion and create cumulative distribution functions**
		(b) **Determine sensitivity to elements of probabilistic statement of perfor**mance
		(c) **Evaluate base case (optional)**
		(d) **Determine effect of each candidate design on each of the scenarios**
		(e) **Evaluate uncertainty importance**
Step 8	Design meets performance criteria?	Design meets **all four elements of probabilistic statement of performance?**
Step 9	Select final design	Select final design
Step 10	Prepare design documentation	Prepare design documentation

The quantitative methodology for the application of uncertainty analysis is applied throughout Steps 4–8. In Step 4 a probabilistic statement of performance is developed. In Steps 5–7, candidate designs are developed, and a process for evaluating these designs through simulation with uncertainty analysis is described. Step 8 now includes a decision of acceptability that makes use of the results of the quantitative uncertainty analysis. Steps 9 and 10 remain the same. It should be noted that performance-based designs might require an iterative process. If, in Step 8, the candidate designs are deemed unacceptable, the process returns to Step 6 to develop new candidate designs. If no acceptable design is found to meet the goals and objectives, Steps 1–3 must be revisited.

Steps 1–3: Define Scope, Goals, and Objectives

Many of the types of uncertainties discussed in the taxonomy are important to consider during the process of setting the scope, goals, and objectives of a project. These three steps are described next; for each step, one example of a type of uncertainty to consider is provided.

The first step in the performance-based design process is to define the scope of the project. The project scope is an identification of the boundaries of the performance-based analysis or design. The SFPE guide suggests consideration of several aspects of scope, such as occupant and building characteristics, and intended use of the building. In the first section of this chapter, indeterminacy was discussed as well as

uncertainties related to the life-cycle use and safety of buildings. Indeterminacy affects the scope in that it is impossible to know what the occupancy and furnishings will be in a building at some point in the future. Therefore, when assumptions are made regarding occupant and building characteristics, some investigation of the sensitivity of the final design to changes in occupant and building characteristics should be made and documented. If switchover occurs for a particular value of one or a combination of analysis parameters, assumptions, or values, this switchover needs to be made explicit.

The second step in the design process is identifying and documenting fire safety goals of various stakeholders. These goals include levels of protection for people and property, and provide for continuity of operations, historical preservation, and environmental protection. For example, when identifying goals of various stakeholders, a mechanism needs to be provided to ensure equal outcomes for subgroups, including the building owner, design engineer, architect, code official, and the public (end users). Because it is difficult to assign worth in the usefulness or importance of something and apply it across all individual and societal issues, the key here is that decisions that change when a value, attitude, or risk perception varies must be made explicit in the design documentation.

The third step in the design process is the development of objectives, which are essentially the design goals that have been further refined into values quantifiable in engineering terms. Objectives might include mitigating the consequences of a fire expressed in terms of dollar values; loss of life; or maximum allowable conditions such as the extent of fire spread, temperature, or spread of combustion products. Uncertainties arise here in risk perceptions and values. There are both uncertainty and variability in the way people perceive and value risk.

Capturing differences people have in their perceptions and values related to risk is a necessary step in the design process. For example, it may be a goal of the stakeholders to protect historical features of the building or to protect against business interruption or loss of operating capability. Stakeholders with different values may see these needs differently. It is important to identify where value judgments enter into a performance-based calculation and to make any assumptions explicit regarding values and the impact of different values on the final design.

The following discussion focuses on incorporating uncertainty directly into Steps 4–8. Here we develop a probabilistic design statement, develop a distribution of statistically significant fire scenarios, calculate a set of values for critical outcome criteria, and evaluate each candidate design to determine whether the design meets the performance criteria within acceptable uncertainty bounds.

Step 4: Develop Probabilistic Statement of Performance

The fourth step in the design process is the development of a probabilistic statement(s) of performance, i.e., criteria by which to judge the acceptability of the design. These criteria are a further refinement of the design objectives and contain numerical values to which the expected performance of the candidate designs can be compared. Each probabilistic design statement contains a minimum of four elements: probability, time, performance criteria, and threshold value. For example, an objective may be to maintain tenable gas concentrations in the corridor. A corresponding probabilistic design statement for life safety might specify that the design must allow for a 0.9 probability of having 4 min or more before a temperature of 65 °C is reached in the corridor. Thus, all four elements are included: probability, time, performance criteria, and threshold value. A location is also specified.

There are many issues to be addressed when establishing probabilistic statements of performance. For example, which criterion should one evaluate? One could select, instead of or in addition to temperature, levels of carbon monoxide, heat flux, or obscuration. There is disagreement in the literature as to what values of each of these cause negative consequences. The negative consequences must be defined; i.e., should the threshold values represent incapacitation or lethality? Also, the probability element involves

determining the level of acceptable risk to the stakeholders, and establishing criteria for time to untenability involves understanding behavioral patterns of people in a fire as well as making value judgments as to which subpopulations to try to protect. The sensitivity of the design to each element of the probabilistic statement of performance is evaluated in Step 7b.

Based on this type of sensitivity analysis, a two-tiered probabilistic statement of performance may be developed based on any of the four elements as well as location. For example, the probabilistic statement of performance may say that the design must allow for a 0.9 probability of having 4 min or more before untenability based on a temperature of 65 °C is reached *and* a 0.9 probability of having 6 min or more before 100 °C is reached. The design statement may be specified in other ways, including the following:

- Include two probability levels, such as the design must have greater than or equal to a 0.95 probability of *X and* less than or equal to a 0.1 or more probability of *Y*.
- Provide a variation, such as the design must provide for a 0.9 probability of providing 4 min before untenability is reached and a 0.9 probability of having 8 min or more before untenable gas conditions are reached.

These are just a few of the possible specification options. Also, the location of evaluation matters. Untenability can be evaluated as a minimum anywhere in any room, including the room of origin, or it can be evaluated along the egress path. These two analyses may give different results in terms of acceptability.

Step 5: Develop a Distribution of Design Fire Scenarios

One of the most important pieces of the methodology is how to generate a set of realistic input scenarios. It is important that this set include a combination of scenarios that represents statistically both the types of fires and the frequency at which they occur in a given occupancy. The input scenario generator should integrate information about the uncertainty, variability, and correlational structure of the input parameters. Using an appropriate sampling method (e.g., Monte Carlo method), a set of any given number of fire scenarios may be constructed. This distribution of scenarios generated will contain the typical cases as well as the worst-case scenarios in the tails of the distribution. The steps involved in developing a distribution of design fire scenarios are (1) selecting a calculation procedure, (2) identifying the uncertain and crucial input parameters, (3) generating a distribution of design fire curves, (4) defining distributions of and modeling correlations among input parameters, and (5) selecting a sampling method and determining the number of scenarios.

Note: When selecting a design fire, a single choice is inadequate for PBD purposes. Monte Carlo is one possible simulation method for (1) propagating this uncertainty through a design calculation or fire model and (2) generating a cumulative distribution of outputs. However, for more complex fire models, conducting the necessary number of simulation iterations may be computationally prohibitive. An alternative method, using the Quadrature Method of Moments (QMOM), greatly reduces the number of simulations needed in order to create the CDF of an output variable. It should be noted that this approach is appropriate only when the uncertainty of only one input variable is being considered.

Upadhyay and Ezekoye [45] focus on a comparison of the QMOM method to the Monte Carlo method for both the ASET and CFAST models. The input value, heat release rate $\dot{S}$, is defined by a particular distribution $m(\dot{S})$. The output quantity of interest, the smoke layer height Z at some critical time t_{cr}, is described by a distribution $n(Z)$. The same analysis, however, can be carried out for any other input/output pair. The k^{th} moment of $n(Z)$ can be found by $M_k^{(Z)} \approx \sum_{n=1}^{N_0} Z(\dot{S}_n, t_{cr})^k W_n$ where $\dot{S}_n$ are the quadrature points and W_n are the quadrature weights obtained from the moments of $m(\dot{S})$. N_Q, the number of simulations needed, is typically 3 or 4, which greatly reduces the number of iterations from a Monte Carlo simulation. The moments of the output distribution, $n(Z)$, can be used to reconstruct a CDF.

Step 5a: Select a Calculation Procedure(s)

There is a range of calculation tools and models currently available from which to select the calculation procedure(s) to be used in the performance-based design. The *Fire Protection Handbook* provides a good overview of the various types of fire models [46]. Which model or type of model is selected depends on several factors, including the application of interest. Fire models can be used to predict a hazard, predict a risk, reconstruct a fire, interpolate between or extrapolate beyond test results, or evaluate a parametric variation. The application of fire models for each of these purposes is discussed by Nelson [47]. Each of these applications may have purpose at some stage of the performance-based design process.

Step 5b: Identify Uncertain Input Parameters

Once a calculation procedure is chosen and candidate designs have been selected, the input parameters necessary for the calculation are evaluated. Which input parameters will be treated as uncertain must be determined. Ideally, only parameters or combinations of parameters with uncertainty great enough to change decisions regarding the final design are treated as uncertain. These are referred to as the *crucial variables*. Unfortunately, we do not always know a priori which of the input parameters possess crucial uncertainty. Therefore, we must use a combination of judgment and results of previous analyses. The uncertainty importance of each of the uncertain input parameters is determined so that future analyses may be simplified. Eventually, only a few key parameters may be needed to capture the uncertainty in each calculation.

Step 5c: Generate a Distribution of Design Fire Curves

Design fire scenarios are made up of both possible fire events (heat release rate curves) and characteristics of the material burning, of the building, and other relevant information, such as weather conditions. A set of design fires is established to mimic the type and frequency of fires expected for that occupancy. These design fire curves are based on statistically collected data, judgments, and the goals of the design. Each design fire is assigned a likelihood of occurrence.

Step 5d: Define Distributions of and Model Correlations Among Other Input Parameters

The uncertainty and variability surrounding each variable must be captured in the mathematical description of that variable. Any and all available knowledge regarding the value of that parameter should be incorporated into the input scenario generator. This information includes empirically measured values, known variations, and statistically compiled data. For example, for a given occupancy type, the NFPA publishes statistical data on the percentage of fires that start in each potential room of fire origin. This information should be incorporated into the random scenario generator so that the generator mimics these statistics. Distributions can be constructed for variables such as temperature, wind, and relative humidity from regional data published by the National Weather Service. Methods for quantifying measurement uncertainty [2] are used to capture uncertainty and variability in empirically measured parameters, such as rates of production of products of combustion. In many cases, where hard data do not exist and are not possible to create, expert elicitation is needed to quantify the uncertainty.

When two or more variables are correlated, knowledge of the value of one variable tells something about the value of the other variable (s). Correlation among variables is modeled so that the input scenario generator will not generate unrealistic scenarios. For example, if the design incorporates a weather module, a month of the year would be randomly selected. For that given month, a value is sampled from an outdoor temperature distribution based on National Weather Service data for that region. Outdoor temperature is correlated to external pressure, wind, relative humidity, likelihood of windows/doors being open, indoor temperature and pressure, and initial fuel temperature. This information prevents the software from generating, for example, a scenario where there is a fire on a below-freezing

day in August in Southern California and all the windows are open.

Step 5e: Select a Sampling Method and Determine the Number of Scenarios

A sampling method, such as Monte Carlo, Latin Hypercube, or quasi-random, must be selected. By sampling a single value from each of the distributions in the input scenario generator and combining those numbers with the values of input parameters that are being treated as certain, any number of independent fire scenarios may be generated.

A large number of scenarios increases the statistical significance of the results. However, this relationship is dependent on the sampling method chosen and is not linear. Using 2000 runs may not provide any more insight than using 500. The number of scenarios chosen depends on (1) the number of uncertain input parameters, (2) the average calculation time per scenario for the calculation procedure chosen, and (3) the statistical significance needed. When conducting correlational analyses between inputs and outputs, one obtains importance or correlation coefficients, c, between 0 and 1. Hald provides a formula for determining the relationship between the number of runs, n, and the statistical significance (as measured by a t-test) of the correlation coefficient [48].

$$t = \frac{c}{\sqrt{1 - c^2}}\left(\sqrt{n - 2}\right)$$

The value for t is related to the confidence level, which is typically chosen as 95 %.

Step 6: Develop Candidate Designs

The candidate design is intended to meet the project requirements. A candidate design includes proposed fire protection systems, construction features, and operations that are provided in order to meet the performance criteria when evaluated using the design fire scenarios.

Step 7: Evaluate Candidate Designs

Each candidate design must be evaluated using each design fire scenario. The evaluations indicate whether the candidate design will meet the elements of the probabilistic statements of performance. Only candidate designs that meet the performance criteria may be considered as final design proposals. Without the quantitative treatment of uncertainties in the design, each calculation will provide a point estimate of only the important outcome criteria. For example, the performance criterion for a design may be a 100 °C maximum temperature reached in the upper layer. The time to an upper-layer temperature of 100 °C may be predicted as 175 s, and the time to activation of a sprinkler may be predicted as 171.2 s by a given computer model. Because the sprinkler is predicted to activate before the performance criteria is exceeded, this would be deemed an acceptable design. However, the uncertainty in the prediction of time to 100 °C may be ±20 s. This would mean that the temperature in the room may reach 100 °C at 155 s or before activation of the sprinkler. Also, the predicted time to activation of the sprinkler has an uncertainty surrounding it, as does the temperature at which untenability might actually occur.

The performance-based design process with uncertainty will aid in the calculation of a range of possible values for each key outcome criterion instead of a single point value. This methodology is useful for and may need to be applied to several parts of the design calculations. For example, it could be applied to the calculation of upper-layer temperatures, to the prediction of time to response of devices, and to the prediction of time needed to egress a building.

Step 7a: Calculate a Set of Values for Each Outcome Criterion

A single value will be determined for each outcome criterion calculated for each design fire scenario run. Much information can be obtained from observation of both the range of values for criteria of interest and from cumulative distribution functions generated from the set of all values.

If criteria are time-series values, each scenario will predict a different curve of the key outcome criteria versus time. For example, if upper-layer temperature is the criterion of interest, four

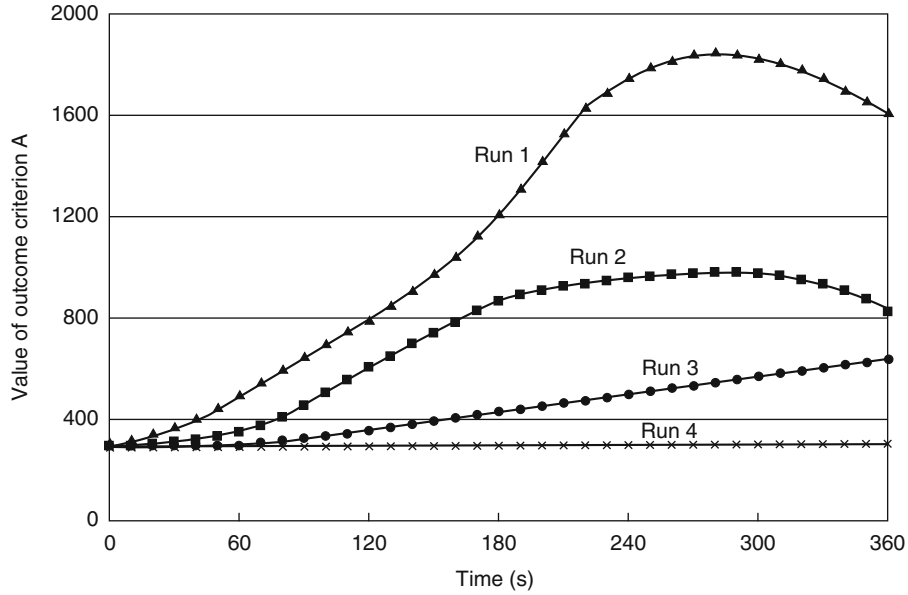

Fig. 76.2 Variation in prediction of time-series values of outcome criterion A

design fire scenarios would produce four curves of upper-layer temperature versus time. Figure 76.2 shows a representative graph of the value of outcome criterion A plotted against time from ignition (in seconds). For any given design, there will be as many curves as there are design fire scenarios calculated. One can see that the curves vary both in the magnitude of the peak value and in the time to the peak value.

The range of values predicted from the set of design fire scenarios represents the uncertainty in the value of the outcome criterion. From the set of predicted values of a single outcome criterion, a cumulative distribution function may be generated. This is done by graphing the value of the criterion against its rank order. For example, for n design fire scenarios, n values of a given criterion are generated. These values are then sorted in descending order. The largest value is graphed versus $1/n$, the second largest against $2/n$, . . ., and the smallest value against n/n or 1.

An example of a cumulative distribution function (CDF) is shown in Fig. 76.5. The time to reach a threshold value of 1 or more of the tenability criteria, that is, a value determined to cause injury or death, can be determined from the time-series predictions. The threshold value may be a particular temperature or carbon monoxide level or a parameter used to represent some synergistic effect of a combination of the tenability variables. One value of time to untenability is obtained for each scenario run. The set of all possible values provides a distribution of the outcome criteria.

Figure 76.3 shows that, for the distribution of design fire scenarios, there is almost a 1.0 probability that the time to a critical value of criterion A is 30 s or more. Likewise, there is a 0.75 probability that the time to this value is 120 s or more, a 0.50 probability that it is 180 s or more, and a 0.1 probability that it is 390 s or more.

Step 7b: Determine Sensitivity to Elements of the Probabilistic Statement of Performance

The sensitivity of key outcome criteria to each of the four elements of the probabilistic statement of performance on which a design is judged must be known before good policy and good design practice can be established. Elements such as criteria, threshold values, probabilities, and times are neither mandated nor agreed on by fire safety and health professionals or the public. Therefore, major conclusions of all designs

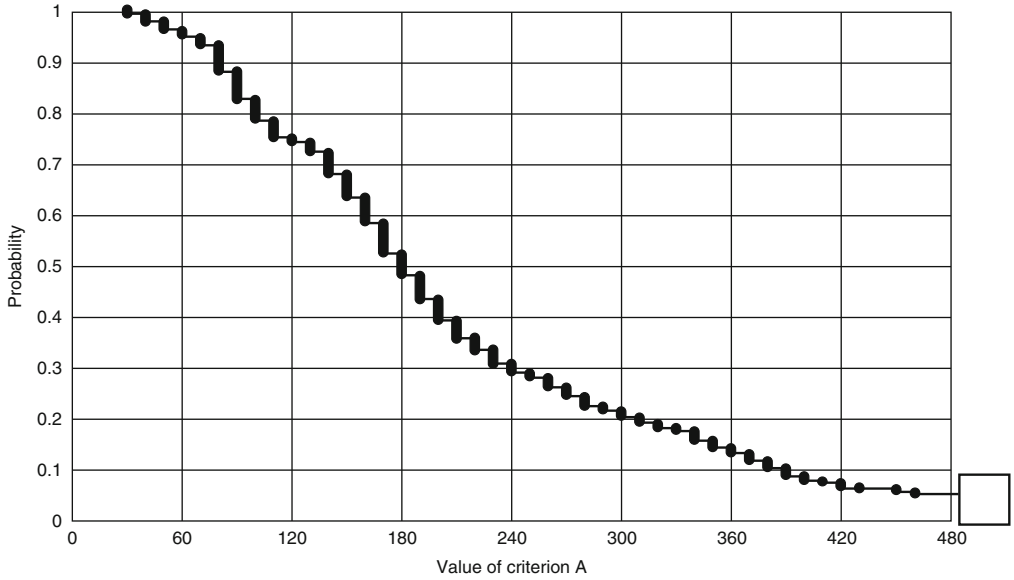

Fig. 76.3 Cumulative distribution function of time to the critical value of criterion A

should be checked in order to demonstrate the sensitivity to uncertainty in each of these elements. For example, checks should be made of times to untenable temperature, carbon monoxide, carbon dioxide, reduction in oxygen, and synergistic effects of the presence of these substances. It may also be appropriate to evaluate for heat flux and visibility.

The same design may be judged on two different performance criteria or by two different critical values of the same performance criterion. Figure 76.4 shows an example of time to untenability based on different values of upper-layer temperature. This type of presentation could also be used to determine the effect on time to untenability by selecting a group of tenability criteria or by including different sets of components in the specification of tenability criteria.

This type of evaluation is a good way to focus discussions among stakeholders on deciding which tenability criteria should be included, what effect the selection of different threshold values of tenability criteria has, what probability level is acceptable to the stakeholders, and how to select the final design. At the end of this step, final performance criteria must be selected for use in judging acceptability of designs and choosing a final design.

Step 7c: Evaluate the Base Case

Depending on the needs and the scope of the project, it is helpful to compare a candidate design to a base-case design. The base case can be the design that meets the prescriptive code, the design that includes the fire protection options currently in the building, or the design with no active fire-suppression systems. The purpose of having a base case is to benchmark the effects of fire on the building and on the building conditions against each of the designs.

In Fig. 76.5, the results of multiple scenario runs are used to show the probability of safe egress graphed against the time to untenable conditions for two different designs. Design 1 and Design 2 may represent two different performance designs or a performance design and a prescriptive design. Reiss discusses the need for this comparative approach [49]. The graph shows two design curves that exhibit crossover. Design 1 provides a higher probability of tenability out to 50 s. Design 2, however, provides a higher probability of tenability at longer times.

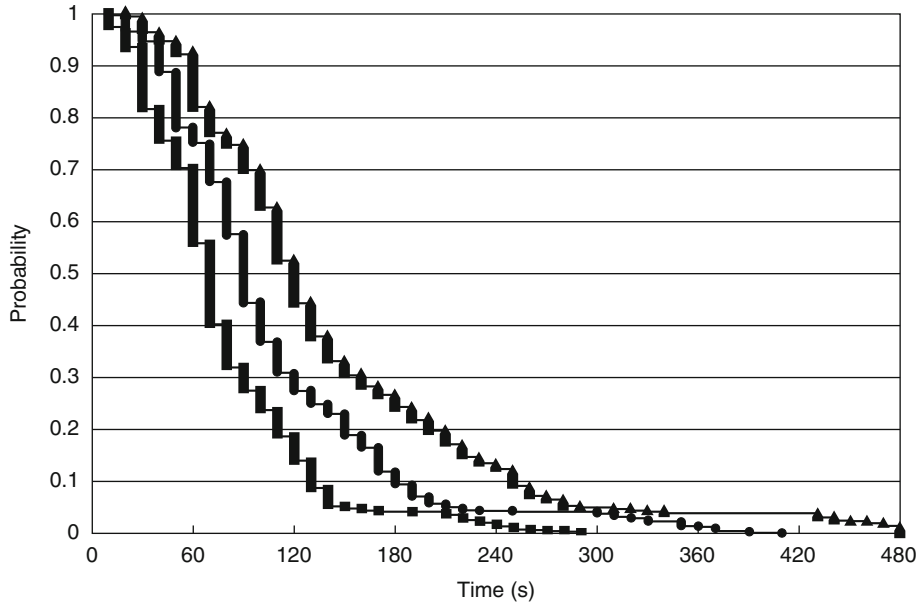

Fig. 76.4 Probability of having X seconds or more before untenable upper-layer temperatures are reached for three different values of untenable temperature

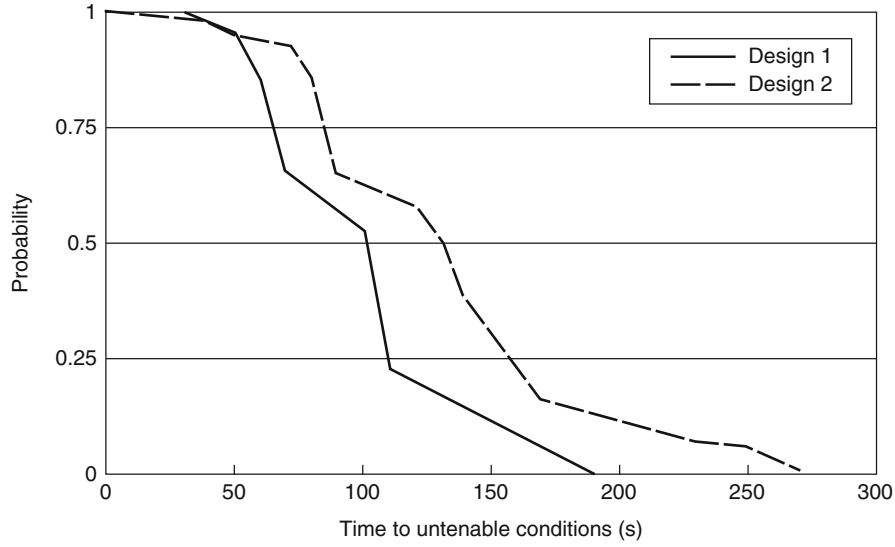

Fig. 76.5 Comparison of cumulative distribution functions of time to untenable conditions for two different designs

Another way that the acceptability of a design is judged is by comparing the level of safety provided with that provided by the corresponding prescriptive design. There is uncertainty associated with the prescriptive design also. The prescriptive code will mandate certain building materials and fire detection and suppression schemes. However, uncertainty and variability remain in the weather, ventilation conditions, human behavioral aspects, and where and how

the fire will start. Thus multiple scenarios can be constructed in a parallel manner to that shown above, holding as constants those factors required by the prescriptive code. Thus a CDF for the prescriptive code can be generated and compared with the CDF for the performance code.

Step 7d: Determine the Effect of Each Candidate Design on Each of the Scenarios

To compare two different candidate designs, we may want to look at the distribution of differences between the two designs based on the final selected performance criteria. One may consider differences between a design and the reference base case or differences in time to untenability provided by Design 1 versus Design 2. For example, Fig. 76.6 is a cumulative distribution function of the difference in time to untenability provided by Design 1 minus the time to untenability provided by Design 2.

Figure 76.6 shows that there is a 0.25 probability that Design 1 will provide a longer time-to-untenable conditions than will Design 2. Conversely, there is a 0.75 probability that Design 2 will provide a longer time to untenability than will Design 1 and a 0.25 probability that the difference will be 100 s or more. In selecting a final design, it may be helpful to investigate what factors might lead to Design 1 providing more time to untenability than Design 2, which could highlight ways to improve the design.

Step 7e: Evaluate Uncertainty Importance

An importance analysis is a particular type of sensitivity analysis that determines which of the uncertain input variables contributes most to the uncertainty in the outcome variable. The results are used to simplify future performance-based designs by identifying the one, two, or small group of most important inputs. Importance here is measured by the correlation between the output value and each uncertain input. Each variable's importance is calculated on a scale from 0 to 1 (or −1). A correlation of 0 indicates that uncertainty in the input variable has no effect on the uncertainty in the output parameter. The input parameters can be correlated to composite or derived outcomes (i.e., an outcome that is not directly an output of the model but one that is derived from the output data). Likewise, input variables can be combined (e.g., the volume of a room can be determined from the dimension).

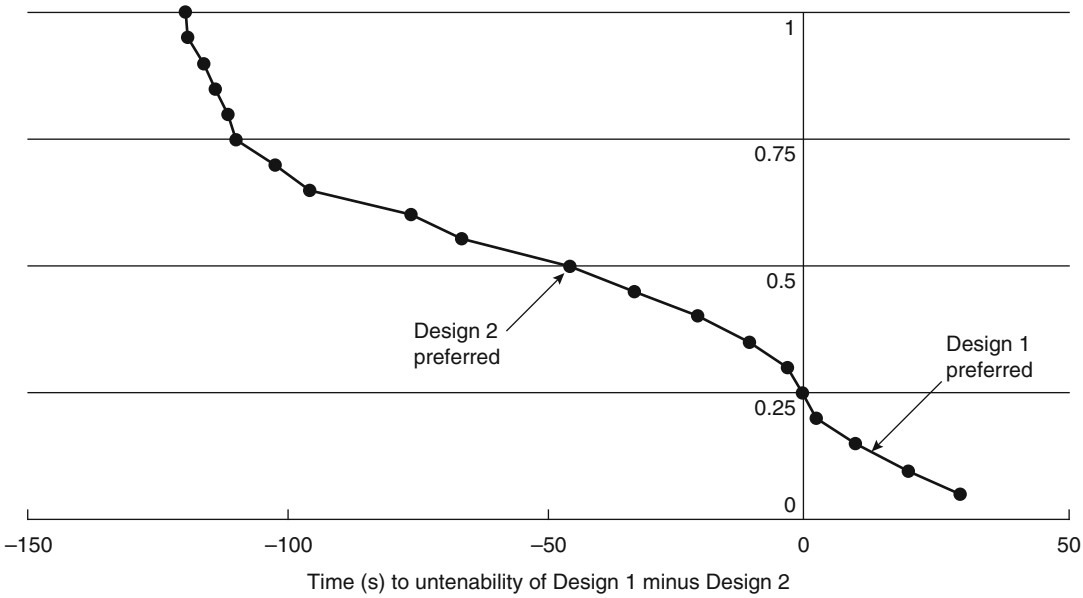

Fig. 76.6 Cumulative distribution function of time to untenability of Design 1—Design 2

Room volume may be correlated with key outcome criteria, for example, peak temperature or time to peak temperature.

Importance analysis can be used to simplify a future uncertainty analysis by determining the input uncertainties that are most crucial. This analysis can simplify the process for a class of buildings and can demonstrate where additional research would be effective in reducing uncertainty and ensuring a safer, more predictable building. It must be remembered, however, that correlation does not equal causation. Thus, any apparent, strong correlation that is counterintuitive should be investigated with good engineering judgment. Also, for each design, the value of the correlation coefficient that is statistically significant will depend on the number of scenarios run and the sampling method used.

Step 8: Judge a Design's Acceptability Based on All Four Elements of Probabilistic Statement of Performance

There are two ways to judge acceptability of a design. The first is based on the minimum time to untenability anywhere in the building, including the room of origin. The second is the time to untenability along the egress path. In general, for both cases, cumulative distribution functions are used to judge acceptability of a design. For example, Fig. 76.3 is a cumulative distribution function of the time to a specific value of criterion A in the room of origin. If the probabilistic statement of performance required a 0.9 probability of having 30 s or more before reaching this value, it can be determined from the CDF that this criterion is met. In fact, Fig. 76.3 shows that there is a 0.9 probability of having 80 s or more. However, if the probabilistic statement of performance requires a 1.0 probability of having 50 s or more, Fig. 76.3 shows that this criterion is not met because the CDF demonstrates a 1.0 probability of having only 30 s or more.

Another way of judging the acceptability of a performance-based design is with a time-to-egress analysis. The time needed to egress a building is often represented in the literature as the time to detect the fire, plus the time to react, plus the time to travel to a safe place. This analysis is represented mathematically as

$$\text{Time}_{\text{egress}} < \text{Time}_{\text{untenability}}$$

$$\text{Time}_{\text{egress}} = \text{Time}_{\text{detect}} + \text{Time}_{\text{react}} + \text{Time}_{\text{travel}}$$

One problem with this approach is that it is very difficult to predict human behavior in terms of reaction time and travel time during a fire. There are both variability due to age and health of the individual and uncertainty as to individual goals and concerns (e.g., will the person try to fight the fire, locate valuables, rescue pets, or notify other occupants about the fire?). The methodology described in this chapter may be applied to egress calculations. Because these are difficult to predict, however, it is suggested that perhaps these are best handled as societal and policy decisions. Regulatory decisions may be made as to the available, safe egress time. For example, more time may be mandated for a healthcare facility, where patients may be nonambulatory and/or asleep at the time of the fire, than in an office building, where occupants are generally awake and ambulatory.

Steps 9–10: Select a Final Design and Prepare Documentation

Candidate designs that satisfy the probabilistic design statement(s) may be considered for selection as the final design. When more than one candidate design meets all four elements of the probabilistic statement of performance, other factors, such as cost and preference, are considered. When considering multiple designs or designs with very different features, a multicriteria decision-analysis model may be developed to aid in selecting the final design.

Proper documentation of a performance design is critical and should be written so that all parties involved understand what is necessary for the design implementation, maintenance, and continuity of the fire protection design. The *SFPE Engineering Guide to Performance-Based Fire Protection* suggests that the documentation have four parts: the fire protection engineering design brief, the performance design

report, the detailed specifications and drawings, and the building operations and maintenance manual [13]. It is important that the performance-based design report convey the expected hazards, risks, and performance over the entire building life. It should include the project scope, goal, and objectives, the probabilistic design statements, a discussion of the design fires and design fire scenarios, and any critical design assumptions.

In conclusion, incorporating uncertainty in a fire safety engineering design calculation aids in ensuring performance. The methodology described in the foregoing section can be used in combination with standard performance-based design procedure. Each step in the methodology may be expanded or contracted to fit the needs of a given calculation. In the future, one may be able to construct libraries of models with families of input scenario generators and develop reusable models for classes of buildings. Ultimately, a fire safety engineering model should be developed that directly incorporates uncertainty.

Application of Uncertainty to Cost-Benefit Models, Improving Regulation, and Overall Decision Making

Decision Making Under Uncertainty

The importance of making good decisions under conditions of uncertainty is becoming better understood in many fields, including fire safety design. The recently released National Science Policy study, *Unlocking Our Future: Toward a New National Science Policy*, states, "Decision makers must recognize that uncertainty is a fundamental aspect of the scientific process." Good decisions can be made under uncertain conditions; however, one must capture the nature and magnitude of the uncertainty in order to make a good decision [50].

There is uncertainty involved in deciding among fire safety options, such as whether to install smoke detectors, sprinklers, or both. Another example is deciding whether the cost of redundant pumps or entire redundant systems is justified. These types of decisions are typically modeled using fire safety trees [51]. However, average or best-guess estimates typically are used for parameters in the decision model, and uncertainty and variability in these are rarely considered.

Decisions made by municipalities on whether to mandate fire safety systems, such as residential sprinklers, are likewise often made based on economic analyses using best-guess and national average values. Integration of uncertainty and variability into these types of cost-benefit studies would provide the decision maker more insights into the issues at hand. It would also highlight where engineering technology is able to reduce risks and where regulatory solutions might be more helpful.

This process is becoming more complex because implementation of any form of a performance-based standard will require more decisions to be made. These decisions will be more difficult, more complex, and more uncertain than under a prescriptive-based code. Robert Clemen discusses in his book, *Making Hard Decisions*, four reasons making decisions is so difficult [52].

- *First, decisions can be difficult simply because of their complexity*. In the case of decisions regarding fire protection features, one must consider the potential for property protection, life safety, injury mitigation, and business continuity. One must also consider the diverse impacts on people with special needs, such as the very young, the elderly, or persons with limited mobility.
- *Second, decisions can be difficult because the decision maker may be working toward multiple or competing objectives*. In fire protection analyses, typically competing objectives are low cost and high level of safety. Progress in one direction, such as installing automatic fire sprinklers for increased fire safety, may impede progress of a competing objective, such as designing an economical building.
- *Third, a problem may be difficult if different perspectives lead to different conclusions*. In a fire protection decision, the perspective of the

building owner, designer, and authority having jurisdiction may very well differ.

- *Finally, decisions can also be difficult because of the inherent uncertainty*. Uncertainties may arise in the model physics, the values of the inputs, the reliability of the devices, and the frequency of events. Yet a decision must be made without knowing for sure what these uncertain values will be. In fact, the most important decisions are often those that must be made under the greatest uncertainty, have the highest complexity, and involve multiple perspectives and goods.

The quantitative treatment of variability and uncertainty using the tools and techniques presented earlier in this chapter can help in identifying important sources of uncertainty and representing that uncertainty in a quantitative way.

The following section introduces an analytical approach that enables quantitative models and decision models to be built with the integrated treatment of uncertainty. The final section demonstrates how these tools were used in a cost-benefit model of the decision to mandate residential fire sprinklers from a municipal standpoint.

Available Software That Incorporates Uncertainty

Decision analysis applications often use generic modeling software, such as spreadsheets, statistics packages, and financial modeling languages. Specialized software is also available for modeling decision problems using decision trees, influence diagrams, belief networks, multiattribute utility functions, hierarchical value structures, Monte Carlo simulation, and multicriteria optimization.

Two of the many such pieces of software that allow for direct treatment of uncertainty are Analytica™ by Lumina and @RISK™ by Palisade. They are described here for informational purposes only, intended to provide the reader with an idea of the capabilities of currently available software. The reader is encouraged to evaluate the full range of available software before selecting a package.

@RISK is a risk-analysis and simulation add-in for Microsoft Excel or Lotus 1-2-3. @RISK adds the power of Monte Carlo simulation to spreadsheet models. It allows users to replace uncertain values in a spreadsheet with probability functions, which represent a range of possible values. @RISK can recalculate users' spreadsheets hundreds or even thousands of times, each time selecting random numbers from the functions entered. The result is distributions of possible outcomes and the probabilities of getting those results. This result identifies not only what could happen in a given situation but also how likely it is that it will happen.

Analytica is another program that allows for the direct treatment of uncertainty. A model built in Analytica uses a graphical interface that resembles an influence diagram. This diagram conveys the model structure. A complicated model can be easily organized into a hierarchy of comprehensible and simple modules. The influence diagram format easily distinguishes between decision variables (those you can control), chance variables (uncertain quantities that cannot be controlled), and objectives (criteria to maximize).

Other distinctive features of Analytica are what the company terms *intelligent arrays* and turnkey importance analysis. With intelligent arrays, data may be entered as an array indexed by several parameters. The software handles operations on these multidimensional values, such as adding, multiplying element by element, or summing over a dimension. Examples of intelligent arrays are presented in the following section.

In Analytica uncertainty can be treated explicitly with probabilities. The user can express uncertainty about any variable, selecting a probability distribution using a graphical browser; propagate uncertainties with the model using Monte Carlo sampling; and display uncertain results as standard statistics, probability bands, probability density functions, or cumulative probability functions. Analytica conducts rank-order and importance analyses. These tools help users decide which uncertainties make a

difference to help determine whether getting better data or expanding the model is worthwhile. Analytica also allows for parametric analysis by graphing model behavior as one or more inputs are varied.

Example of Cost-Benefit Model with Variability and Uncertainty

In the United States, approximately 3500 people die each year in residential fires. The number of residential fire deaths, however, varies with the type of housing, area of the country, and community size. The cost of installing residential fire sprinklers varies with areas of the country and house age. Thus, the true cost-benefit analysis will be different for each combination of the above parameters. However, cost-benefit models typically use average costs and probabilities and do not incorporate uncertainty.

A model was built using Analytica that incorporated variability and uncertainty to determine the societal benefits and costs of mandating residential sprinklers. A full description of the mathematical model and the results is beyond the scope of this chapter but can be found in "The Role of Uncertainty in Improving Fire Protection Regulation" [49]. A brief overview of that study is presented in order to demonstrate the techniques used in the treatment of variability and uncertainty and the implications for fire protection analyses.

Treatment of Variability and Uncertainty

Inter-year Variability in Fire Loss Statistics To conduct a cost-benefit study of residential fire sprinkler systems, many fire statistics (e.g., death rates, injury rates, and average direct dollar losses) are needed as inputs. National average values of these numbers are often used in these analyses. For example, the national average value for the residential death rate would be equal to the number of residential fire deaths nationally divided by the number of occupied residential units. The actual fire death rate will vary with a number of parameters.

The U.S. National Fire Protection Association publishes death rates discretized by three of four index variables: region of the country, community size, and house type [53]. The fourth index variable, house age, is accounted for in the cost functions, as it is more expensive to retrofit sprinklers than it is to install them during the construction phase. There are four regions of the country, eight community sizes, and three house types. Thus, the death rate used in these calculations is a $4 \times 8 \times 3$ matrix consisting of 96 values for death rate. Two examples would be the death rate in manufactured homes in a small community (2500 or less) in the South and the death rate in a one- or two-family dwelling in a community size of 25,000–50,000 in the West.

Yearly Variability in Fire Loss Statistics It is important to differentiate between variability and uncertainty. Variability in fire statistics from year to year arises because of the randomness of the occurrence of fires. For instance, in one particular year, several large-loss fires may occur followed by few or none the next year. In this study, since there is an interest in benefits and costs over the life of a fire sprinkler system, mean yearly values were chosen. Yearly variance in deaths, injuries, property loss, and indirect losses due to fires is thus accounted for by taking mean yearly values over a 5-year period. Mean values were calculated from the 1989–1993 data.

Uncertainty in the Fire Statistics Uncertainty in fire loss statistics exists due to the impossibility of a full and accurate accounting of all fires and all fire losses. Mathematical techniques are thus used to provide estimates [54]. Uncertainty in the fire data is represented as uncertainty about the mean values. An expert elicitation of the chief statistician of NFPA was conducted to set the uncertainty bands for the fire statistics [55].

Uncertainty in Other (Empirical) Model Inputs Uncertainty in the cost data and parameters, such as the sprinkler reduction factor, were determined by bounding. For example, uncertainty in the sprinkler reduction factor arises because of the small number of fires occurring in homes with automatic sprinklers installed. Data from other occupancies were used to bound the uncertainty.

Propagation of Uncertainty Once the uncertainties in the model inputs have been expressed, the question becomes how to propagate these uncertainties through the model to discover the uncertainty in the predicted consequences. In this analysis a Monte Carlo simulation was used. A value for each input is randomly selected from its actual probability distribution. From these values, a value for the outcome criteria is calculated. This process is repeated many times, resulting in a probability distribution for each outcome variable.

Value/Cost of Death Averted For any cost-benefit analysis regarding health and safety, one of the most highly contentious points is setting a value of life. Economists have come up with various ways of estimating the value of a life. These include willingness to pay for safety devices and income-based estimates [56]. All these methods are highly debated. For this study, the problem of establishing a value of life was avoided by means of careful selection of the outcome criteria. By selecting the outcome criteria to be dollars per premature death averted and dollars per life-year saved, no explicit value of life needs to be specified.

Results—National Average Calculation Versus Indexed Calculations When variability due to region, community size, house type, and house age is accounted for, the net cost of residential sprinklers varies tremendously. The net cost for installing residential sprinklers varies by greater than a factor of 35 times from a low of $1.4 million per premature death averted (for a new manufactured home in a small community in the South) to a high of $35.1 million (for a retrofit of a one- and two-family dwelling in a medium-size community in the Western U.S.). Based on a national average calculation, our model predicts that residential fire sprinklers have a median net cost of $7.3 million per premature death averted.

Comparison to Other Lifesaving Interventions An article in *Risk Analysis* identified over 500 lifesaving interventions, reporting their net cost in terms of dollars per life-year saved [57]. The accuracy of the results is limited by the accuracy of the data and assumptions in each original analysis, but the results are believable within an order of magnitude. In this study the cost per life-year saved for residential fire sprinklers was compared to the cost per life-year saved for chlorination of drinking water, banning urea-formaldehyde insulation in homes, installing oxygen depletion sensors for gas space heaters, conducting radon remediation, mandating child-resistant cigarette lighters, and installing ground fault interrupters. Figure 76.7 shows this comparison. The heights of the bars

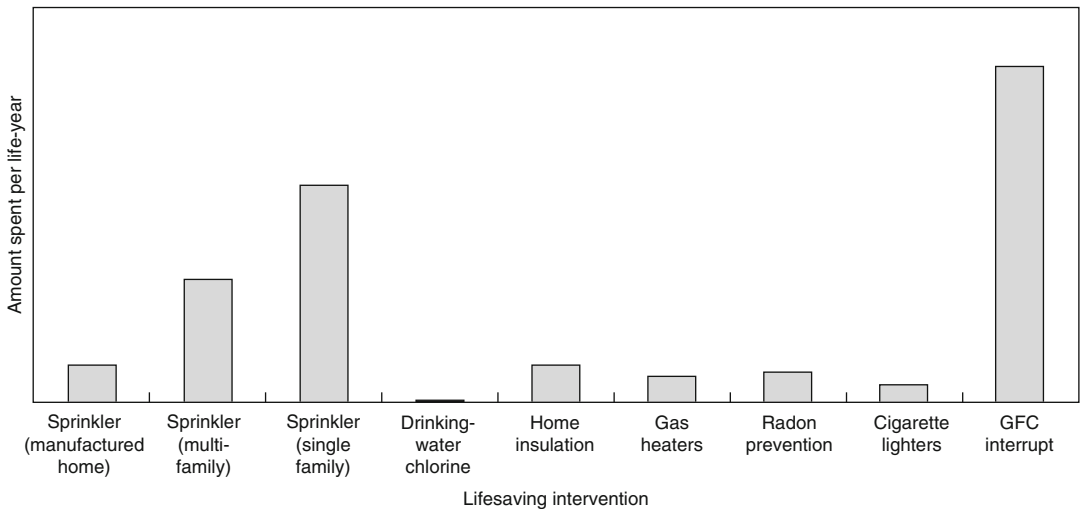

Fig. 76.7 Comparison of net cost of fire sprinklers in manufactured homes with other residential lifesaving interventions

represent the relative costs per life-year saved and have all been normalized to the cost of chlorination of drinking water.

Uncertainty in Cost-Benefit and Decision Analysis Models

This example demonstrates how uncertainty and variability may be treated in a cost-benefit or decision analysis model. It also shows that effectively treating variability and uncertainty and use of tools such as importance analysis and comparative analysis can lead to greater insights. The cost of mandating residential fire sprinklers in new manufactured homes is shown to be as low as five times less than the cost of mandating residential fire sprinklers using national average values for fire risk and costs. The cost of mandating residential fire sprinklers in existing single family homes is shown to be up to five times more than using national average numbers. The comparative analysis provides lawmakers with a frame of reference by comparing the cost of mandating residential fire sprinklers to the costs of mandating other residential safety options with lifesaving potential.

Uncertainty in Probabilistic Risk Assessment

Definition of the Problem

This example discusses an approach to a particular problem, namely decision making on the acceptability of changes to the licensing basis of a nuclear power plant using results from a probabilistic risk assessment (PRA), which includes contributions from accidents initiated by fires occurring within the plant. The licensing basis is a legal requirement that determines how the plant is built and operated. The elements of a PRA that can be used to investigate the risk from fires are discussed in Chap. 89 and in more detail in "EPRI/NRC-RES Fire PRA Methodology for Nuclear Power Facilities" [58].

Role of the PRA in the Decision

In order to use the results of any analysis, in this case a PRA, in decision making, the decision makers must first determine what role the analysis is to play in the decision and how it is going to fulfill that role. In this section, the approach taken by the U.S. Nuclear Regulatory Commission (NRC) for using results from PRAs in decision making is used as an example to illustrate this process [59]. The approach is described in detail in Regulatory Guide (RG) 1.174 [18]. Although RG 1.174 focuses on one type of application, namely changes to the licensing basis of an operating nuclear plant, the principles involved have been adopted in a more general way in the development of risk-informed regulatory decision making at the U.S. Nuclear Regulatory Commission.

In deciding how to use risk information in decision making, two approaches can be considered. The first, a *risk-based approach*, would use the risk results as the sole basis for the decision. The second, a *risk-informed approach*, would use risk information as one of the elements in making decisions. The recognition that the PRA, although a detailed model, is still a model, which is an approximation of reality, coupled with a recognition that there is an incompleteness of the collective state of knowledge about all the possible failure causes and mechanisms, led the NRC to adopt the use of risk-informed rather than risk-based decision making. To develop the concept further, it is necessary to define what other factors are to be taken into account in the decision. In RG 1.174, this effort led to the development of five principles of risk-informed decision making, all of which must be met for the proposed change to be accepted (Fig. 76.8). The incorporation of defense-in-depth and the use of safety margins have been an integral part of the design and operation of nuclear power plants and are significant defenses against unknown causes of failure. Similarly, the requirement to perform monitoring following a change is a response to

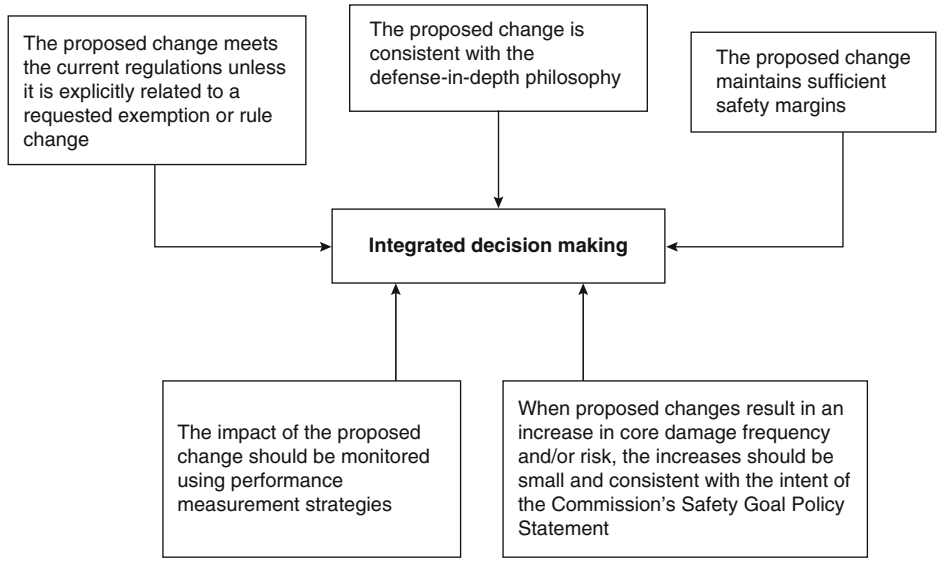

Fig. 76.8 Principles of risk-informed decision making

the potential for incompleteness in the analysis of the impact of the change.

In this example, the result of the engineering calculation, in this case the PRA, is one, but only one, input to the decision.

Acceptance Criteria Given that the role of risk information has been determined, it is necessary to develop criteria that can be used to determine when the results of the risk calculations are acceptable, which includes defining the following:

- Risk metrics to be used
- Decision criteria

In this particular application, the decision metrics were chosen to be the core damage frequency (CDF) and the large early-release frequency (LERF), both of which are results that can be obtained from PRA. The risk-acceptance criteria (one for each of CDF and LERF) were based on the impact on those metrics, measured as ΔCDF and ΔLERF, resulting from the proposed change. The acceptance criteria for CDF are included as Fig. 76.9.

When defining a decision criterion, it is crucial to define how uncertainty is accommodated by the choice of criterion, which to a large extent depends on how the uncertainties can be incorporated into the results of the analysis. This process will be discussed later, after the detailed discussion of the analysis of uncertainty.

Analysis of Uncertainty

The steps needed to perform an analysis of uncertainty in the results of the analysis are the following:

- Identifying the sources of uncertainty.
- Characterizing the uncertainty on the individual inputs to the model.
- Propagating these uncertainties to obtain a characterization of the uncertainty on the output of the model.
- Interpreting the results in light of the uncertainty.
- Presenting the results in a way that is meaningful to the user (e.g., decision maker).

Before discussing the steps in more detail, we present a discussion of the fire PRA model as it relates to uncertainty. Much of the discussion here can be generalized to other types of fire safety engineering calculations.

Uncertainty in the Context of Developing Fire Risk Models In general terms, a model can be

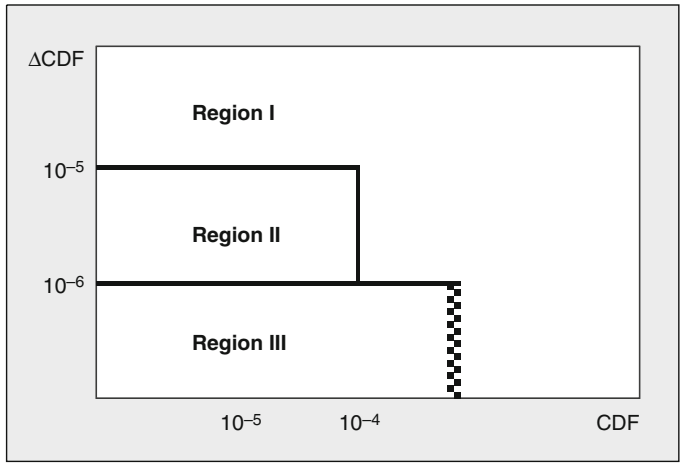

1. Region I
—No changes
2. Region II
—Small changes
—Track cumulative impacts

3. Region III
—Very small changes
—More flexibility with respect to baseline
—Track cumulative impacts

Fig. 76.9 Acceptance guidelines for core damage frequency

described as an analyst's attempt to represent a system (using the term *system* in a very general way) in a form that can be used as an explanatory and an exploratory tool. In almost all cases, it is impossible to capture all the subtleties of the system behavior. Therefore, any model is, at best, an approximation. A model in the physical sciences or engineering disciplines is usually a mathematical model, which is to say that it has a mathematical form, and can produce numerical results that represent some observable aspects of system behavior. Such a mathematical model will generally have several parameters. Since any model is an approximate representation, it follows that there must be some uncertainty associated with the formulation and predictions of the model. For some models, however, this uncertainty is so small that it can essentially be ignored. For example, the mathematical formulation of many of the models created by physicists to explain natural phenomena is sufficiently well supported or verified that the models are very precise in their predictions, as long as they are used within their region of applicability.

In addition, many of the parameters are so well known that they can be thought of as universal constants. An example of one such model is Newtonian mechanics and Newton's law of gravity, which is capable of making very accurate predictions of such things as planetary motion and can be used to define the trajectories of planets or space vehicles with great accuracy. Not only is the model rather simple, but also the parameter of the model, the gravitational constant, is known very accurately. Of course, it is well known that, under specific boundary conditions and for particular problems, Newtonian mechanics breaks down and must be replaced with the general theory of relativity. Newtonian mechanics is an example of a deterministic model. However, a model need not necessarily be deterministic to be precise. Quantum electrodynamics (QED) is a model that is capable of making very accurate predictions. However, because of the quantum mechanical nature of matter in the small scale, it does so only in a probabilistic sense, making predictions about the average behavior of a population of events rather than about the outcome of a particular event. It is, therefore, a probabilistic model of the world. The uncertainty associated with this lack of predictability for single occurrences of events is an example of aleatory uncertainty.

As described in Chap. 89, a fire-risk model or a fire PRA is typically constructed using logic structures, such as event trees and fault trees, to identify the different combinations of more elementary events, called basic events, that could lead to undesired system states. What these logic models represent is a discretization of the potentially unlimited range of scenarios into a manageable set that are supposed to be representative of and encompass the range of consequences of that larger set.

The types of basic events found in fire PRAs include events that (1) represent the occurrence of a fire scenario, defined as a fire with specified initial conditions, type (e.g., cable fire, pool fire), and size in a specific location; (2) delineate the different levels of severity of fire damage, taking into account the potential for fire growth and the potential for fire suppression; and (3) events that represent failures or states of unavailability of components or human failures that contribute to the failure of the systems designed to protect against the undesirable consequences should the plant be damaged by fire. The occurrence of the fire scenarios is modeled as a random process, and a frequency of occurrence is associated with each fire scenario. The basic events in the third group discussed above are typically events such as the failure of a pump to start, the failure of a pump to run for 24 h, and failure of an operator to take the appropriate actions to prevent system damage. For the most part these basic events are also regarded as resulting from random occurrences with respect to the demand created by the initiating event and are described by probabilistic models.

The events that delineate the different levels of damage caused by a fire are chosen on the basis of an analysis using models of fire growth and damage, and models for the detection and suppression of fires. Some of these models are deterministic in nature, whereas others are probabilistic. For example, the time of successful fire suppression is treated as a random process in that the time of successful suppression is treated as a distributed variable. Typically, fire growth and cable damage are treated deterministically by creating a time line for the development of damaging conditions within a fire area and by defining failure as occurring after exposure to a specified temperature for a specified time, respectively. This model is recognized as an approximation, since fire growth and fire damage are essentially stochastic processes; there would in reality be variability in factors such as the precise location of the origin of the fire, for example. However, it is typically convenient to model this infinite variability by a set of representative fires and model their growth in an average way.

Therefore, a fire PRA is a probabilistic model of aleatory uncertainty. Unlike the physics models discussed above, however, there are significant epistemic uncertainties that must be recognized. The reasons for these uncertainties include the following:

- For many of the basic events of the PRA model, the associated probability models adopted are simple with only one or two parameters. Examples include the simple constant failure rate reliability model, which assumes that the failures of a component, while it is in standby, occur at a constant rate; and the uniformly distributed (in time) likelihood of a fire scenario. The model for both these processes is the well-known Poisson model. The parameter(s) of such models can be estimated using appropriate data, which in the examples above comprise the number of failures observed in a population of like components in a given time and the number of occurrences of a fire scenario in a given time, respectively. However, most of the events that constitute the building blocks of the risk model (e.g., the fire initiation) and the non-fire-induced equipment failures are rare events. Because the occurrences are rare, there are statistical uncertainties in the estimates of the parameters of the model.
- Events exist for which there may be uncertainties associated with interpreting the data to be used for estimation. For example, when collecting data on fire scenarios, there can be uncertainty on what data to collect. For example, should all fires be counted, or should minor fires that were self-extinguishing

or those that were suppressed quickly be excluded? Should historical fires that were not damaging be included in the count if in a different location they might have been significant? These and other issues are discussed in NUREG/CR-6850 [17]. As another example, when counting failures based on the review of maintenance records, it is not always clear whether the failure would have prevented the component from performing the mission required of it to meet the success criteria assumed in the risk model.

- There can also be uncertainty about the form of the probability model. Although the Poisson and binomial models are typically adopted for the occurrence of initiating events and for equipment failures, it has to be recognized that these are assumptions and may not be appropriate for all situations.
- The fire PRA model is also dependent on models of fire growth and damage and on models of fire detection and suppression. The modeling of fire growth, taking into account the geometry of targets and intervening combustibles, the influence of hot gas layers, and so on, is extremely complicated, and the models at best are approximate. For a detailed discussion see NUREG/CR-6850 [17]. The simplifications that are necessary to develop a model can produce conservative or nonconservative biases.
- Given that the form of the model has been decided on, there is an additional source of uncertainty associated with the parameters of those models (e.g., the temperature at which damage is assumed to occur).
- The number of potential fire scenarios is very large, and it is necessary to choose a representative set to model the impact. This sample also introduces uncertainty in the form of a potential bias, which is usually intended to be somewhat conservative.

As mentioned previously, the uncertainty associated with the structure of and input to the fire risk model could be in the choice of mathematical form of the input models, it could be in the values of its parameters, or both. To the extent that changes in the parameter values are little more than subtle changes in the form of the model, it could be argued that there is really no precise distinction between model uncertainty and parameter uncertainty. However, as discussed below, parameter uncertainties and model uncertainties are dealt with differently.

Identifying the Sources of Uncertainty It is helpful to categorize uncertainty into parameter and model uncertainties. As will be seen below, this is primarily because the methods for the characterization and analysis of uncertainty are different for the two types. However, it is also necessary to identify a third type of uncertainty, namely uncertainty about the completeness of the model, which while it cannot be handled analytically, must be taken into account when making decisions using the results of a risk analysis.

Parameter Uncertainty Parameter uncertainty is the uncertainty in the values of the parameters of a model, conditional on an acceptance of the mathematical form of that model. The uncertainty arises in different ways depending on how the data on which the parameter values are estimated are obtained.

For continuous variables, such as heat of combustion, which can be measured directly, there is measurement uncertainty, which is typically not a major source of uncertainty for the types of parameters found in risk models. However, the uncertainty in some variables, such as the temperature at which damage occurs, can have a significant impact. Although in principle it might be considered that such a variable is directly measurable, doing so can be challenging.

Statistical uncertainty occurs in two of the following ways:

- When a parameter (such as the temperature at which damage occurs) that can be measured directly is obtained from a series of experiments, and the phenomena being tested are random in the sense that the experiments cannot be strictly reproduced except in some overall sense, such as establishing gross boundary conditions. The measured value

will be variable from experiment to experiment and, in the foregoing example, will depend on such variables as where and how the temperature is measured. This variability can, in principle, be captured statistically in a probability distribution. This type of uncertainty could be embedded into the aleatory structure of the risk model if the model were intended to explicitly model that variability. However, because of the need to limit the granularity in the model, it is likely instead to be treated as an uncertainty on the representative value of the parameter. This case is an example of a gray area in terms of separating aleatory and epistemic uncertainty. Analysts should be particularly careful in defining their approach so that their intent in modeling is clear.

- When a parameter value is inferred from event data using a statistical process, as is the case with failure rates of components, for example.
- In many cases, data are limited, or may be only indirectly relevant. In such cases, expert judgment has to be applied to determine the value of the data.

Model Uncertainty Because of the potential for a large number of scenarios, the analysis of which would be prohibitive, as discussed previously, it is common to choose a small set of scenarios to analyze that is representative and bound or encompass the effects of all potential fire scenarios. The smaller the set of scenarios, the more approximate will be the results. Depending on the purpose of the analysis, different degrees of discretization may be appropriate. In developing the set of representative scenarios, fire models may be used to screen out a number of scenarios. Typically, it would be expected that the models used for this step would be conservative and fairly simple. However, the use of screening models is another source of uncertainty.

These representative scenarios are analyzed using models of fire growth, fire damage, and fire detection and suppression. As discussed earlier, the models used for fire growth and for fire damage are essentially deterministic. Because of the complexity of the physical phenomena involved, they are of necessity approximate. The models have limitations, and these must be recognized when using them. Some models are largely empirical, whereas other models, such as zone models, models based on computational fluid dynamics, and fire dynamics models, are analytical, with a variation in their degree of sophistication. These different models have different capabilities and will give different results when used in the same context. Thus the sources of uncertainty are not restricted to uncertainties in the parameters (e.g., heat-release rate) of those models, though these may be the easiest to deal with analytically. Typically the model limitations will produce results that are biased, and the biases have to be understood.

Completeness Uncertainty Completeness uncertainty can be thought of also as a type of model uncertainty. However, it is discussed separately here because it represents a type of uncertainty that cannot be quantified, because it represents those aspects of the real world that, either knowingly or unknowingly, are not addressed in the model. Incompleteness in the model, therefore, can be thought of as arising in two different ways:

- Some contributors/effects may be knowingly left out of the model for a number of reasons. There may currently be no analytical model for the particular issue (e.g., the impact of safety culture). Resources may not be available to develop a complete model, leading to a decision not to model certain contributors to risk (e.g., seismically induced fires).
- Some phenomena or failure mechanisms may be omitted because their potential existence has not been recognized.

For some of the known sources of incompleteness, the limitations may be recognized and the formulation of the models may be designed to address the issues by, for example, providing somewhat conservative results. This possibility is addressed under the

model uncertainty category. Some issues, however, cannot be compensated for in that way. An example in the area of nuclear power plant PRAs is that many of the models do not address the seismically induced plant disturbances. It is clear that, if something is not modeled, it cannot be addressed quantitatively in the same manner as those issues that are modeled. The true unknowns in particular (i.e., those related to issues whose existence is not recognized) cannot be addressed analytically. However, in the interest of making defendable decisions, they still have to be addressed during the decision making, as will be discussed later.

Characterization of Input Uncertainty Current practices for characterizing the different types of uncertainty are discussed below.

Parameter Uncertainty In most recent PRAs, the representation of uncertainty in parameter values has been accomplished by adopting a Bayesian or subjectivist framework [60]. In this framework, the uncertainty is characterized by a continuous probability distribution function on the value of the parameter, which is interpreted as being an expression of the analyst's degree of belief in the corresponding value as bounding the true value of the parameter. The representation of the uncertainty in the form of a probability distribution lends itself to propagation, so that the uncertainties on the constituent elements can be combined in a meaningful way. Whereas classical statistical methods can be used to provide a maximum likelihood estimate and associated confidence intervals on parameter estimates, the mathematical propagation of confidence intervals is difficult to perform and interpret [61].

As discussed earlier, for many of the basic events of the PRA model, the associated probability models are simple, with only one or two parameters. These models include the Poisson model and the binomial model. The parameter (s) of such models can be estimated using appropriate data, which in the example above comprise the number of events observed in a population of like components in a given time or in a given number of trials, respectively. The estimation of parameter values of simple reliability models and the characterization of their associated uncertainties have been addressed in many places. The most recent and comprehensive treatment can be found in NUREG/CR-6823 [62].

There are other parameters, such as the temperatures at which cables fail or heat-release rates, that are not based on simple counting statistics, as is the case for failure rates and initiating events. The characterization of these uncertainties should be compatible with the way in which they are to be formally propagated through the analysis of the likelihood of specific damage states resulting from a fire scenario to evaluate the probability of damage. The parameters associated with the models for fire growth, damage, and suppression will be discussed in the context of the model uncertainty.

Uncertainty in the Data Used to Estimate Parameters In some cases, although the underlying model may be simple, there may be uncertainties associated with interpreting the data to be used for estimation. Examples include the following:

- When estimating fire frequencies for use in risk models, the question arises whether all fires should be included or whether those that are extinguished early should be excluded.
- When considering the completeness of the data records, it is necessary to determine if the facilities required to report occurrences, whether they be fires or failures, do so in a consistent manner.
- When evaluating equipment "failures" identified from maintenance records, it is necessary to assess whether the need for maintenance constitutes a failure in the context of the success criteria used in the risk model.

The uncertainties associated with interpretation of data to apply to a specific model are not typically amenable to an analytical closed form. However, some idea of the uncertainty in the parameter value can be obtained by performing sensitivity studies. The difficulty with constructing a probability distribution is

that one would have to give a degree of belief to each sensitivity study. This would typically be a discrete distribution.

Model Uncertainty The characterization of model uncertainty is very much dependent on the way in which the uncertainty is manifested. Many of the models used are approximate and have certain biases. The key to dealing with such uncertainties is to understand the nature of the approximations and to try to understand the degree of conservatism or nonconservatism in the use of the models. Doing so is clearly difficult with models of very complex phenomena, as there can be no direct comparison with experiments. Some sources of uncertainty may be explored by varying the parameters in the model. When model complexity makes it not feasible to represent the uncertainty in a closed analytical form, it is acceptable to provide a range of potential results that can be used later to perform sensitivity studies to explore the impact of uncertainty on the results.

As discussed earlier, there is a range of models that could be used. Typically, an analyst will adopt one model for a specific application. However, since all the models presumably have some validity, the differences in their predictions represent a source of uncertainty. The only way to address this uncertainty explicitly is to perform the analysis using more than one model and use the results of the different models to develop a range of results for the analysis. These could be combined to give a probability distribution on the results of the analysis by assigning a probability to each model to represent the level of confidence in the different models. However, as discussed later, the approach in RG 1.174 would be to look at each analysis separately. However it is done, if there are models that could potentially produce significantly different results, it is important that there be confidence in the results from the model of choice.

Completeness Uncertainty Relating to things that are not included in the model, completeness uncertainty cannot be characterized in the same manner as input uncertainties. However, this uncertainty is important and must be recognized when using the results of the risk assessment.

Propagation of Uncertainty Propagation of uncertainty refers to the process of analyzing the impact of the input uncertainties on the results of the model. Typically, in the PRA literature this term has been used in the context of generating a probability distribution on the numerical results of the risk analysis.

Parameter Uncertainty Methods are relatively well established for the propagation of the uncertainty on the basic event probabilities that are characterized by probability distributions, through the quantification process, to generate a characterization of uncertainty on the output of the PRA [63]. Because epistemic uncertainties on parameters are generally characterized as probability distributions, whether the distributions are continuous or discrete, the most common technique is Monte Carlo analysis or variants thereof, such as the Latin Hypercube Sampling [64].

Model Uncertainty To the extent that the uncertainty in the modeling of fire growth, fire damage, and detection and suppression can be expressed as a probability distribution on the probability of a specific fire damage state, it can be treated as a parameter uncertainty as discussed above.

When more than one model is in common usage for a specific issue, such as fire growth, it is possible to represent the uncertainty as a discrete distribution over the results of the models and propagate that discrete distribution through the analysis to produce a potentially multimodal distribution on the results. This is not typically done and, in the interest of identifying what factors are determining the results, such an uncertainty is perhaps addressed better using sensitivity studies as discussed later [65, 66].

Interpretation of the Results of a PRA Interpreting the significance of the results of a PRA in the light of the uncertainties is important if the PRA results are to be applied to making meaningful decisions about changes in design or operating practices or if they are to

be used for economic decisions. Probability distributions on the numerical results, such as the core-damage frequency, can be used to calibrate the confidence level at which a safety goal is being met, for example. However, although it may be important to characterize the overall uncertainty, it is equally important to understand which factors drive the uncertainty. If the results of alternate models are included in the final PRA results, it is essential to be able to distinguish between the results of the alternate models [65, 66].

Several methods are available for identifying the drivers of uncertainty. The two principal tools are importance analysis and sensitivity analysis.

Importance Analysis Several different importance measures are in common usage. These include the Fussell-Vesely, Birnbaum, Risk Achievement Worth, and Risk Reduction Worth [67]. When applied to the results of a risk analysis, they measure the significance of a basic event to the overall result. Once identified as significant, the uncertainty associated with the evaluation of that basic event is also significant to the results.

Sensitivity Analysis Sensitivity analysis is a powerful tool for investigating the impact of uncertainty on results. To be meaningful, however, the sensitivity analyses must be chosen carefully and must represent reasonable alternatives to the model of choice. Because uncertainties can have synergistic effects on the results, it may be necessary to perform sensitivity analyses on more than one of the uncertain issues simultaneously.

Presentation of Results of Uncertainty Analysis The most appropriate way to present the results of an uncertainty analysis is a function of how the results are going to be used. Options include the following and combinations thereof:

- Continuous probability distribution on numerical results. This is feasible only when there is an analytical means of propagating uncertainty.
- Discrete probability distribution representing the impact of different models or assumptions. This is practical only when the analysts are willing to weigh their beliefs in the different models or assumptions that may be used.
- Bounds or ranges of results that represent the results of the extreme assumptions.
- Discrete set of results that represents the results of making different assumptions or using different models, or that represents the impact of varying key parameters in the model that have significant uncertainty.

However the results are presented, the analyst has to understand and be able to communicate what is driving the uncertainty.

Comparison of PRA Results with the Acceptance Criteria

The acceptance guidelines used in RG 1.174 for one of the metrics, core damage frequency (or CDF), is shown in Fig. 76.9. In RG 1.174 the acceptance guidelines are not intended to be interpreted as being overly prescriptive. They are intended to provide an indication, in numerical terms, of what is considered acceptable. This is largely because the state-of-knowledge, or epistemic, uncertainties associated with PRA calculations preclude a definitive decision with respect to which region the application belongs, based purely on the numerical results. In the case of RG 1.174, the term *acceptance guidelines* was used rather than acceptance criteria, primarily to recognize that not all of the analysis uncertainty was captured in the uncertainty distribution.

In the context of RG 1.174, the intent of comparing the PRA results with the acceptance guidelines is to demonstrate with reasonable assurance that the principle that requires the risk change to be small is indeed being met. This decision must be based on a full understanding of the contributors to the PRA results and the impacts of the uncertainties, both those that are explicitly accounted for in the results and those that are not. This is a somewhat subjective process, and the reasoning behind the decisions must be well documented.

As mentioned earlier in this section, when defining a decision criterion, it is crucial to define how the choice of criterion accommodates

uncertainty. When defining the acceptance criteria of RG 1.174, the following alternatives were discussed: (1) the mean value of the distribution representing the epistemic uncertainty should be used for comparison; and (2) some specified percentile of the uncertainty distribution, corresponding to a specified confidence level, should be used. The guidelines were chosen such that the appropriate measure for comparison is the mean value of the corresponding uncertainty distribution. The reason was to some extent historical, since the guidelines were based on prior guidelines that were to be compared to mean values. However, in addition, there is a philosophical problem associated with determining what would be the appropriate confidence level to choose if that route were taken. More details of the reasoning behind the approach can be found in Caruso et al. [68].

Because parameter, model, and completeness uncertainties are represented differently, different approaches were used to take them into account as discussed below.

Parameter Uncertainty Because of the way the acceptance guidelines were developed, the appropriate numerical measures to use in the initial comparison of the PRA results to the acceptance guidelines are mean values. The mean values referred to are the means of the probability distributions that result from the propagation of the uncertainties on the input parameters and those model uncertainties explicitly represented in the model. A formal propagation of the uncertainty is the best way to correctly account for state-of-knowledge uncertainties that arise from the use of the same parameter values for several basic event probability models [69]. Under certain circumstances, however, a formal propagation of uncertainty may not be required if it can be demonstrated that the state-of-knowledge correlation is unimportant. This will involve, for example, a demonstration that the bulk of the contributing scenarios (cutsets or accident sequences) do not involve multiple events that rely on the same parameter for their quantification.

Model Uncertainty Although the analysis of parametric uncertainty is fairly mature and is addressed adequately through the use of mean values, the analysis of the model and completeness uncertainties cannot be handled in such a formal manner. To address model uncertainty it is necessary to demonstrate that the choice of reasonable alternative hypotheses, adjustment factors, or modeling approximations or methods to those adopted in the PRA model would not significantly change the assessment. This demonstration can take the form of well-formulated sensitivity studies or qualitative arguments. In this context, "reasonable" is interpreted as implying some precedent for the alternative, such as use by other analysts, and also that there is a physically reasonable basis for the alternative. It is not the intent that the search for alternatives should be exhaustive and arbitrary. The alternatives that would drive the result toward being unacceptable should be identified and sensitivity studies performed or reasons given as to why they are not appropriate for the particular application or for the particular plant. In general, the results of the sensitivity studies should confirm that the guidelines are still met even under the alternative assumptions (i.e., change generally remains in the appropriate region). Alternatively, this analysis can be used to identify candidates for compensatory actions or increased monitoring.

Completeness Uncertainty Completeness is not in itself an uncertainty but rather a reflection of a limitation in the scope of the model. The result is, however, an uncertainty about where the true risk lies. The problem with completeness uncertainty is that, because it reflects an unanalyzed contribution, it is difficult (if not impossible) to estimate its magnitude. Some contributions are unanalyzed, not because methods are not available, but because they have not been refined to the level of the analysis of what is included in the model. Examples are the analysis of errors of commission, and the low-power and shutdown modes of operation. There are issues, however, for which methods of analysis have not been developed, and they have to be accepted as

potential limitations of the technology. Thus, for example, the impact on actual plant risk from unanalyzed issues, such as the influences of organizational performance, cannot now be explicitly assessed.

The issue of completeness of scope of a PRA can be addressed for those scope items for which methods are in principle available and, therefore, some understanding of the contribution to risk exists in a number of ways. For example, the out-of-scope items can be addressed by supplementing the analysis with additional analysis to enlarge the scope, by providing arguments that, for the application of concern, the out-of-scope contributors are not significant, or by designing the proposed change such that the major sources of uncertainty will not have an impact on the decision-making process. For example, in region III of the acceptance guidelines, where small increases are allowed regardless of the value of the baseline CDF or LERF, the proposed change to the licensing basis could be designed such that the modes of operation or the initiating events that are missing from the analysis would not be affected by the change.

The degree to which supplementary arguments can be used to support the claim that the uncertainties do not impact the decision depends on the proximity to the guidelines. When the contributions from the modeled contributors are close to the guidelines, the argument that the contribution from the missing items is not significant must be convincing and in some cases may require additional PRA analyses. When the margin is significant, a qualitative argument may be sufficient.

Incompleteness that is the result of unknown phenomena can clearly not be addressed in this way. It is to address this source of uncertainty that the principles of safety margins and defense-in-depth play such an important role.

This section has described an example of an approach to addressing uncertainty in a decision-making context. Although the example is specific to regulatory decision making for nuclear power plants, it serves to illustrate the essential elements of the approach that can be generalized to other applications. The example discussed later on the performance-based design process follows much the same approach.

Uncertainties in Fire Modeling and Egress Modeling

The Fire Protection community, especially the fire model developers and researchers, have begun over the past 8–10 years, to look more seriously at uncertainty in fire and egress modeling. In 2005, the International FORUM of fire research directors published a position paper on verification and validation of numerical models [70] and in 2012, the Standard Guide for Evaluating the Predictive Capability of Fire Models, was updated by ASTM E1355 [71].

Fire Dynamics Simulator (FDS)

In an attempt to characterize the ability of FDS to predict the response of thermal detectors, *Hurley and Munguia* place a heptane burner in a room [72]. Temperature measurements from thermocouples is soldered to brass disks to represent thermal detectors with known RTIs. The ceiling height is adjusted across a range from 3.0 to 12.2 m. The heat release rate is estimated to follow a modified t^2 curve, which is adjusted to account for limitations of the heptane flow control in the early stages of the fire. Quantitative uncertainty in temperature measurements is accounted for from three sources. These are the measurement capabilities of the thermocouples, the measurement capabilities of the flow controls, and the repeatability. Other sources, such as exact location of the burner, potential drafts, and the quality of the values used for combustion efficiency and radiative fraction, is not quantified. FDS results showed a trend of over-prediction of temperatures within the plume. However, it is determined that grid-insensitive convergence is not established in this region, so these values are not used in the final analysis. Comparisons are made of

measurements and predicted values at a radial distance of 2.2 m. It is determined that, at worst, FDS predicted temperature rise values within a factor of 1.9 of the measurements. An example is offered that, for simulating a device with a given activation temperature, the temperature rise should be multiplied by 1.9 and 1/1.9 and added to the ambient temperature. The modeler should then also determine the predicted activation time of a device with these two bounding activation temperatures in order to account for the range of model error.

CFAST

In 2002, W. D. Davis published his study, "Comparison of Algorithms to Calculate Plume Centerline Temperature and Ceiling Jet Temperature with Experiments," Journal of Fire Protection Engineering, 12(1), pp. 9–29 which covered some basic calculations for plumes and ceiling jets [73] and in 2007, Peacock and Reneake published, Verification and Validation of Selected Fire Models for Nuclear Power Plant Applications. Volume 5. Consolidated Fire Growth and Smoke Transport Model (CFAST) [74]. This study conducted an evaluation of the sensitivity and predictive capability of the CFAST model for nuclear risk calculations.

Using the methodology previously developed by Lundin, a quantitative analysis of the model error in the two-zone model CFAST can be used to evaluate the model, measure improvements in the model, assess predictive capabilities for uncertainty analysis, and make adjustments of model predictions. Error in model predictions is assumed to contain bias (which varied with the magnitude of the predicted value) and uncertainty (which was independent of the predicted value). Uncertainty is assumed to vary between different scenarios.

Lundin uses previous experimental data for model comparison for several distinct scenario configurations [74]. A scenario configuration, as defined previously, consists of a number of similar scenarios where parameters, such as ceiling height, are adjusted over a limited range. Direct comparisons are made between model predictions of upper layer temperature and experimental data. A linear regression method is used to develop an adjustment formula for predicted temperature $T\_adj = \beta T\_p + U\_adj$. The value of U_adj depends on whether one adjusts the line to either bound of a 95 % prediction interval in order to make more conservative adjustments for a particular application. β and U_adj are shown to differ between scenario configurations, demonstrating that the use of a single adjustment factor for all configurations would not be appropriate. Difficulties with defining the limits of a particular scenario configuration are acknowledged, especially as it is not practical to have a very large number of adjustment formulas for very specific scenario configurations. However, introducing more variability into a scenario configuration adds to uncertainty in model error assessment.

ASET-B

An assessment of the predictive capabilities of the computer fire model ASET-B can be made by comparing data from two full-scale tests. SFPE formed a computer fire model evaluation task group that follows the methodology of ASTM E-1355. This standard gives three methods for analyzing model predictive capabilities: blind calculations, specified calculations, and open calculations. Blind calculations provide the modeler with a basic description of the scenario to be modeled. For specified calculations, the modeler is given a complete description of model inputs. For open calculations, the modeler is given a complete description of the scenario and must choose the model inputs.

This work employed open calculations using previously published research. Model predictions of smoke filling were compared to a test in a $6 \times 6 \times 6$ m enclosure and rectangular barracks building. Assumptions were required in translating the scenarios to model inputs, specifically for - heat-release rates and heat-loss fractions. ASET-B was found to provide "reasonably accurate"

predictions of smoke layer temperatures, though no real quantitative assessment was made [75].

Heat Detector Models

The uncertainty and sensitivity of a classical deterministic heat fire detector activation model, as presented by Schifiliti et al., uses a Monte Carlo approach with LHS to (1) quantify both how uncertainties in inputs propagate through the model—uncertainty analysis—and (2) identify which uncertain inputs have the most significant impact on the result—sensitivity analysis. The model uses a lumped-mass formulation, ignores radiation and convection, and assumes a flat, large ceiling and a symmetrical plume. The study focused on a hypothetical one-story building. Seven input parameters were identified: fire growth rate, convective fraction, radial distance to the detector, height above the fire, detector RTI, detector response temperature, and ambient temperature. Distributions were assigned to each variable. The uncertainty analysis yielded CDFs of activation time for the specific scenario, which could be used to assess confidence intervals for design purposes. The uncertainty analysis focused on CCs, SRCs, PCCs, RCCs, SRRCs, and PRCCs, and their respective statistical significance. Analysis revealed that detector position and fire-growth rate had the most significant impact. Limitations of this approach were acknowledged, such as the fact that model uncertainty was not considered, and that the distributions used as inputs were assigned somewhat arbitrarily [76].

DETACT

Uncertainty in fire detection is evaluated using the deterministic fire detection model, DETACT. The formulation is similar to that evaluated by Kong et al.; however, the conduction losses are considered. A Monte Carlo approach with random sampling is used to adjust the input parameters based on defined distributions. Distributions of activation time are generated with uncertainty considered only in geometry-type inputs, only in fire-type inputs, only in detector-type inputs, and finally with uncertainty considered in all inputs. The distribution of outputs is examined for the particular scenario considered. As in the study of Kong et al., model uncertainty is not addressed. It is suggested that, in order to avoid the limitations of the semi-empirical nature of the model, the range of its assumptions should be applied [77, 78].

Uncertainties in Egress Modeling

Computer egress modeling is becoming widely accepted in building design. However, the inherent difficulties associated with the unpredictable nature of human behavior, as well as a general lack of data needed to calculate evacuation times, means that there is significant uncertainty associated with these models. Uncertain variables include occupant loads, occupant-movement characteristics, and pre-movement times. The work of Lord et al., represents one particular effort to quantify the effect of uncertainty in these models [79]. The goals are to (1) understand the sources of uncertainty and variability in egress models, (2) apply a method of uncertainty analysis to egress models, (3) identify significant variables which may have a "cross-over" effect, and (4) provide guidance for building engineers in the appropriate implementation of egress models. The egress model STEPS was used to simulate egress in a six-story office building in London, Ontario, Canada, for which evacuation data existed. Monte Carlo analysis was used to generate CDFs that represented the effect of adjusting different input variables on evacuation time. Variables such as occupant load, pre-movement time, walking speed, door flow rate, etc. were studied. Occupant loads, pre-movement times, queuing coefficient, and lock-solver depth were found to be significant. Lock-solver depth dictates how circular locks in the simulation are resolved.

Continuing the work presented above, the STEPS egress model is used to simulate egress in a 14-story apartment building in Calgary, for

which evacuation data exists. Monte Carlo analysis is used to generate CDFs that represented the effect of adjusting different input variables on evacuation time. Additionally, correlation coefficients (CC) are evaluated for the variables in question in order to test for a linear relationship. The magnitude, sign, and statistical significance of the coefficients are considered. Initial findings, showing differences in the properties of the CCs for the two buildings, indicate that a single set of uncertain variables may not be important for all building designs [80].

Similar to the study conducted for STEPS, a Monte Carlo analysis is carried out in order to quantify the effect of uncertain parameters for the FDS+EVAC evacuation model. Because FDS+EVAC employs a stochastic evacuation model, multiple simulations with the same inputs will not produce identical results. The effect of this aleatory uncertainty is reduced by running each iteration of the Monte Carlo analysis ten times and taking an average time to represent the particular scenario. Pre-movement time, the percentage of adults, the occupant density, and effective width are all specified by distributions. It should be noted that the standard deviation of the pre-movement time is studied, not the pre-movement time itself, and it is also specified by a distribution. Correlation coefficients are examined to assess the linear influence of the inputs, and rank correlation coefficients are examined to assess the monotonic influence of the inputs. Both coefficients indicate that the standard deviation of pre-movement time has the strongest influence on the output, followed by the effective width. It is suggested that for sufficiently large distributions of these two variables—variations in occupant density and occupant type—have minimal effects and can be ignored. It is also demonstrated that simply using the most likely values for the input parameters and applying a safety factor should be approached with caution. Using a safety factor of 1.5 is found to fail the performance criteria (which is chosen as the time of upper bound of the 95 % confidence interval for the Monte Carlo analysis), while a safety factor of two passes [81].

Uncertainties in FPE Measurements and Test Standards

Individual Measurements (HRR, Temperature, Burn Patterns)

The work of Zhao and Dembsey focuses on measurement uncertainty analysis for calorimetry, specifically using a Cone Calorimeter [82]. A lack of standardized methodology for this type of uncertainty analysis makes comparisons between data from different laboratories difficult. Uncertainties intrinsic to the device components and their calibration are considered. Other sources, such as drift, data reduction, or personal operation, are not included in the context of this study. Type A and B uncertainty are evaluated. Using ISO guides (guide to the expression of uncertainty in measurement) and NIST (guidelines for evaluating and expressing the uncertainty of NIST measurement results), a detailed study of the uncertainties of direct measurements in the Cone, such as mass or O_2 concentration, is carried out. Using the Law of Propagation of Uncertainty, direct measurement uncertainty is then used to evaluate the uncertainty in indirect measurements (such as HRR). Monte Carlo simulation is used to verify the 95 % confidence intervals calculated for the indirectly measured quantities. The intent of the work is to demonstrate a detailed methodology that could be applied to better quantify measurement uncertainty and improve the quality and applicability of reported fire test data.

Given the importance of heat release measurements in fire safety, the quantitative quality of quantitative reporting of the measurements is critical. Measurements using a gas burner in a large open hood, capable of measuring heat release rates up to 3 MW, are evaluated. Uncertainty for the value of input-heat release, based on the gas flow, and measured heat release, are both considered [83]. Similar to the study of Zhao and Dembsey, the uncertainty associated with independent direct measurements is evaluated first. In this study, the drift of the gas analyzer is also included. The uncertainty propagation of the individual variables in the equation for heat release is

then carried out. The standard deviation of repeat measurements is combined with the values from the uncertainty propagation to create a combined uncertainty. This methodology can be applied to a full-scale test facility to obtain a quantitative evaluation of uncertainty in measured values.

In 2003, Pitts, W. M.; Braun, E.; Peacock, R. D.; Mitler, H. E.; Johnsson, E. L.; Reneke, P. A.; Blevins, L. of NIST studied temperature uncertainties for Bare-Bead and Aspirated Thermocouple Measurements in Fire Environments. Temperature measurements were made for natural-gas and heptane fires in a reduced-scale enclosure using a variety of bare-bead and aspirated thermocouples in order to characterize the uncertainties. The focus is the role of radiative heat transfer and the effects of finite time response on the measurements. The findings show that significant errors are possible for all thermocouples considered. Aspirated thermocouples reduce, but do not eliminate, such uncertainties. An alternate approach, use of several bare-bead thermocouples with extrapolation to zero diameter, is not easily implemented in the time-varying temperature environments characteristic of fires [84].

A study carried out at NIST investigated the role of uncertainty in fire measurements when conducting fire pattern repeatability experiments [85]. Gypsum board is exposed to a fire from a natural-gas burner, a gasoline-pan fire, or a polyurethane foam fire, with each fuel type being tested multiple times. Confidence intervals of 95 % for heat release, temperature, and flame height are obtained through statistical analysis of the individual test results for each fuel type. Dimensions of burn patterns based on fuel type are also measured, and uncertainties are obtained through the same type of statistical analysis. The repeatability of the gas-burner tests is highest, due to their well-controlled nature. Conversely, the polyurethane foam has the lowest repeatability due to the inconsistent nature of the flame spread on the solid fuel. Comparisons repeatability of flame heights to burn pattern heights has the highest agreement for the gas-burner fuel.

Uncertainty in Fire Test Standards

In 2012, ASTM published a collection of 11 papers on uncertainty related to fire test standards, J. R. Hall, and A. D. Library led off the discussion with their paper, "Uncertainty in fire standards and what to do about it" [86]. Many of the papers addressed how different parties, such as testing laboratories, enforcement authorities, manufacturers, and practicing engineers, incorporate uncertainty into their use of results from fire safety tests and calculations. It also examines the larger implications of different approaches and provides overviews of some of the newest methods and approaches for handling uncertainty.

A distinction is made between measurement uncertainty and variability in uncontrolled variables for fire tests. The measurement uncertainty, as discussed in ISO 17025 (general requirements for the competence of testing and calibration laboratories), and addressed in the previously mentioned studies of small and large scale calorimetry, is represented as a range for a specific confidence interval and is quantitative in nature. Uncontrolled variability is related to uncertainty parameters, such as the arrangement of test components, laboratory drafts, specimen ignitability, specimen uniformity, and so on. The effects of such variability are not quantifiable in the same manner as measurement uncertainty, and Trevino and Curkeet [87] propose that the overall contribution to test variability from these factors is much more significant than from measurement uncertainty. An example is given in which HRR curves for identical mattresses are compared. The variability is much greater than the measurement uncertainty of the calorimeter, and it is attributed largely to differences in flame spread between the tests. A "precision" analysis, in which the repeatability (within a lab) and reproducibility (among multiple labs) of fire tests, is suggested as one way to quantify test variability. If the reproducibility of a particular test is shown to be good, it is suggested that the repeatability will also be, as it is almost always

preferable. Due to the fact that a full repeatability and reproducibility study for multiple fire tests would be a significant undertaking, a cost/benefit analysis should be carried out first.

The Steiner Tunnel, ASTM E84 offers techniques for understanding, improving, and controlling measurement uncertainty in a fire test [88]. Variation of test parameters is quantified using Statistical Process Control (SPC). Parameters that have variations falling outside of control limits can be identified, and necessary improvements can be made to individual elements of the test. Additionally, a "Poke-yoke," or "Go" and "No Go" technique is used. This involves a system for operator notification if a parameter is out of control limits based on SPC. A repeatability and reproducibility study of the improved tunnel test demonstrates that the approach is successful in controlling variability. The variation between test results is largely due to changes in the test material, and not the specific user or the test method itself. Thus confidence in the test is improved.

A round-robin repeatability and reproducibility study was conducted for cone calorimeter and intermediate-scale calorimeter (ICAL). A set of four laboratories participated in each round-robin (not the same set for cone and ICAL). Sixteen materials are tested with the cone (at 75 kw/m^2), and four materials are tested with ICAL (at 40 and 25 kw/m^2). The cone shows better overall repeatability and reproducibility than ICAL, though there is less difference in reproducibility between the two. The conclusion of this work, however, is that more work needs to be put into this type of analysis. A number of limitations could be improved in future studies, including the fact that the involvement of more laboratories would improve the statistical analysis, as would more materials. Additionally, assurance must be made that all laboratories strictly comply with the test standards, pre-round-robin calibrations are made, and any problems are identified and rectified. More detailed instructions on test configuration and measurement should be provided to the laboratories to ensure consistency. Though it does not provide a full quantitative treatment of uncertainty, it does characterize the repeatability and reproducibility of individual measurements.

Use of Uncertainty to Determine Effectiveness

Uncertainty in Estimating Effectiveness of Sprinklers for Fire Control

The assessment of sprinkler system effectiveness is important, particularly when evaluating performance-based design criteria. A study of data from the New Zealand Fires Service [89] incident reports was conducted in an effort to quantify uncertainty in sprinkler system effectiveness, rather than providing only a single figure. Effectiveness is considered to consist of both reliability (whether the sprinkler operated when a sufficient fire was present) and efficiency (whether the sprinkler suppressed or controlled the fire as expected). The available data is used to inform the creation of probability distributions for the different events in a sprinkler-system effectiveness decision tree. Monte Carlo analysis is then used to create distributions for reliability, efficiency, and effectiveness. A mean effectiveness of 86 % is found, which is lower than previously reported values. Limitations of the analysis are acknowledged, including the uncertainty inherent in the accuracy of incident reports. Additionally, the definition of "effectiveness" is not well established, and assumptions are required when assessing this performance of sprinklers for specific events.

Decisions on Needed Water Demand

A proposed model for estimating the quantity of water required for fire suppression assumes a t-squared fire growth curve $\dot{Q} = \alpha t_{in}^2$, where α is a growth coefficient and t_{in} is the time from fire ignition to the start of fire service intervention.

The mass of water needed is given by $m_c = 3 \times 10^{-4} \alpha t_{in}{}^1 t_s$, where t_s is the suppression time. Data from 100 incidents in Taoyuan County, Taiwan, R.O.C., are used to determine the variables. Growth coefficients are selected based upon the occupancy type for a particular incident. Comparisons between the calculated mass of water needed and the actual water used, which was determined by the number and size of responding vehicles, show that a suppression time of 20 min gives the best agreement. Distributions are used to introduce estimated uncertainty in the department time-to-intervention and the growth coefficient. Monte Carlo analysis reveals a standard deviation of ±30 % for calculations of required water for a particular incident. It is suggested that this fast calculation method can be coupled with GIS data on a particular occupancy to provide an assessment of required resources at the time an incident is reported to the fire service. Limitations of the model originate from the limited amount of reported data available. The 100 incidents used do not describe whether all the water sent to a scene is used or if additional water sources are utilized. The time from fire ignition to the reporting of a fire also must be assumed. The inclusion of additional data would assist in refining choices of the model parameters [90].

Summary

An understanding and characterization of the impact of the uncertainties on the results of fire safety engineering calculations are essential to ensuring that the decisions made using those results are meaningful and defendable. Distributions of outcomes are a much richer description of what is possible than the typical point value answers. Though stakeholders and/or policy decisions must still determine how much risk to accept, with thorough uncertainty analyses, this decision will be informed and free of the uneasiness that typically surrounds acceptance of a deterministic performance calculation. The information provided in this chapter is intended to help the fire protection community understand the nature and sources of uncertainty, aid in the selection of a calculation procedure, apply a methodology for the treatment of uncertainty, and incorporate uncertainty into cost-benefit models and decisions.

References

1. G.M. Morgan and M. Henrion, *Uncertainty: A Guide to Dealing with Uncertainty in Quantitative Risk and Policy Analysis,* Cambridge University Press, New York (1990).
2. American National Standards Institute, *U.S. Guide to the Expression of Uncertainty in Measurement,* National Conference of Standards Laboratories, Boulder, CO (1997).
3. W.M. Pitts, E. Braun, R.D. Peacock, H.E. Mitler, E.L. Johnsson, P.A. Reneke, and L.G. Blevins, *Temperature Uncertainties for Bare-Bead and Aspirated Thermocouples Measurements in Fire Environments,* National Institute of Standards and Technology, Gaithersburg, MD (1998).
4. R.L.P. Custer and B.J. Meacham, *Introduction to Performance-Based Fire Safety,* Society of Fire Protection Engineers and National Fire Protection Association, Quincy, MA (1997).
5. J.C. Helton and D.E. Burmeister (eds.), "Treatment of Aleatory and Epistemic Uncertainty," special issue of *Reliability Engineering and System Safety,* 54, pp. 2–3 (1996).
6. G.A. Apostolakis, "A Commentary on Model Uncertainty," in *Proceedings of Workshop 1 in Advanced Topics in Risk and Reliability Analysis, Model Uncertainty: Its Characterization and Quantification,* NUREG/CP-0138 (1994).
7. S. Kaplan, "On the Use of Data and Judgement in Probabilistic Risk and Safety Analysis," *Nuclear Engineering and Design,* 93, pp. 123–134 (1986).
8. G.W. Parry, "The Characterization of Uncertainty in Probabilistic Risk Assessments of Complex Systems," *Reliability Engineering and Systems Safety,* special issue on aleatory and epistemic uncertainty, 54, pp. 119–126 (1996).
9. K.A. Notarianni and W.D. Davis, "The Use of Computer Fire Models to Predict Temperature and Smoke Movement in High-Bay Spaces," *NISTIR 5304,* National Institute of Standards and Technology, Gaithersburg, MD (1993).
10. V. Brannigan and C. Smidts, "Performance Based Fire Safety Regulation under Intentional Uncertainty," in *Human Behaviour in Fire: First International Symposium* (J. Shields, ed.), Fire Safety Engineering Research and Technology Centre, University of Ulster, Belfast, Northern Ireland, pp. 411–420 (1998).

11. T.J. Shields, "Human Behaviour in Fire," in *First International Symposium on Human Behaviour in Fire* (T.J. Shields, ed.), University of Ulster, Belfast, Northern Ireland (1998).
12. C. Starr, "Social Benefit vs. Technological Risk," *Science,* 165, pp. 1232–1238 (1969).
13. Society of Fire Protection Engineers, *SFPE Engineering Guide to Performance-Based Fire Protection,* 2nd ed., Society of Fire Protection Engineers and National Fire Protection Association, Quincy, MA (2007).
14. K.A. Notarianni and P.S. Fischbeck, "Dealing with Uncertainty to Improve the Regulatory System," in *Fire Safety Design in the Twenty-First Century* (D. Lucht, ed.), Worcester, MA (1999).
15. D.W. Stroup, "Using Performance-Based Design Techniques to Evaluate Fire Safety in Two Government Buildings," in *Second International Conference on Performance-Based Codes and Fire Safety Design Methods,* International Code Council and Society of Fire Protection Engineers, Maui, HI, pp. 429–438 (1998).
16. P.D. Sullivan, "Existing Building Performance-Based Fire Safety Design," in *Second International Conference on Performance-Based Codes and Fire Safety Design Methods,* International Code Council and the Society of Fire Protection Engineers, Maui, HI, pp. 49–60 (1998).
17. R.W. Portier, R.D. Peacock, and P.A. Reneke, *FASTLite: Engineering Tools for Estimation Fire Growth and Smoke Transport,* National Institute of Standards and Technology, Gaithersburg, MD (1996).
18. L. Benthorn and H. Frantzich, "Fire Alarm in a Public Building: How Do People Evaluate Information and Choose Evacuation Exit?" in *Human Behaviour in Fire* (J. Shields, ed.), Fire Safety Engineering Research and Technology Centre, University of Ulster, Belfast, Northern Ireland, pp. 213–222 (1998).
19. G. Proulx, "The Impact of Voice Communication Messages during a Residential Highrise Fire," in *Human Behaviour in Fire* (J. Shields, ed.), Fire Safety Engineering Research and Technology Centre, University of Ulster, Belfast, Northern Ireland, pp. 265–274 (1998).
20. J. Fleming, "A Code Official's View of Performance-Based Codes," in *Fire Risk and Hazard Assessment Symposium,* National Fire Protection Research Foundation, San Francisco, pp. 93–117 (1996).
21. H. Frantzich, S.E. Magnusson, B. Holmquist, and J. Ryden, "Derivation of Partial Safety Factors for Fire Safety Evaluation Using the Reliability Index Beta Method," in *Fifth International Symposium on Fire Safety Science,* International Association for Fire Safety Science, Boston, pp. 667–678 (1997).
22. S.E. Magnusson, H. Frantzich, B. Karlsson, and S. Sardqvist, "Determination of Safety Factors in Design Based on Performance," in *Fourth International Symposium on Fire Safety Science,* International Association for Fire Safety Science, Boston, pp. 937–948 (1994).
23. H. Yaping "Linking Safety Factor and Failure Probability for Fire Safety Engineering," *Journal of Fire Protection Engineering*, 20(3), pp. 199–217. doi: 10.1177/1042391510372726, (2010)
24. B. Taylor and C. Kuyatt, *Guidelines for Evaluating and Expressing the Uncertainty of NIST Measurement Results,* National Institute of Standards and Technology, Gaithersburg, MD (1994).
25. K.A. Notarianni and P. Fischbeck, "A Methodology for the Quantitative Treatment of Variability and Uncertainty in Performance-Based Engineering Analysis," in *Second International Conference on Performance-Based Codes and Fire Safety Design Methods,* International Code Council and Society of Fire Protection Engineers, Maui, HI, pp. 225–239 (1998).
26. W. Jones, G. Forney, R. Peacock, and P. Reneke, *A Technical Reference for CFAST: An Engineering Tool for Estimating Fire and Smoke Transport,* National Institute of Standards and Technology, Gaithersburg, MD (2000).
27. R. Lantz, "Model Validity Defined and Applied to the Problem of Making Legitimate Predictions from Fire Protection Engineering Models," in *Third International Conference on Performance-Based Codes and Fire Safety Design Methods,* Society of Fire Protection Engineers, Lund, Sweden (2000).
28. N. Siu, E. Droguett, and A. Mosleh, "Model Uncertainty in Fire Risk Assessment," in *SFPE Symposium on Risk, Reliability, and Uncertainty in Fire Protection Engineering,* Society of Fire Protection Engineers, Baltimore (1999).
29. R. Peacock, P. Reneke, W. Davis, and W. Jones, "Quantifying Fire Model Evaluation Using Functional Analysis," *Fire Safety Journal,* 33, pp. 167–184 (1999)
30. D. Lucht, *Strategies for Shaping the Future,* Worcester Polytechnic Institute, Worcester, MA (1991).
31. W. Jones, *Progress Report on Fire Modeling and Validation,* National Institute of Standards and Technology, Gaithersburg, MD (1996).
32. J. Lundin, "On quantification of error and uncertainty in two-zone models used in fire safety design," *Journal of Fire Sciences*, 23(4), pp. 329–354 (2005)
33. J. Lundin, "Quantifying Error and Uncertainty in CFAST 2.0 Temperature Predictions," *Journal of Fire Sciences*, 23(5), pp. 365–388 (2005)
34. K. McGratten & B. Toman, "Quantifying the predictive uncertainty of complex numerical models," *Metrologia*, 48(3), pp. 73. doi:10.1088/0026-1394/48/3/011 (2011)
35. ASTM, *Standard Guide for Evaluating the Predictive Capability of Fire Models,* American Society for Testing and Materials, Philadelphia (1992).
36. R. Dickson, "Sensitivity Analysis of Ordinary Differential Equation Systems—A Direct Method," *Journal of Computational Physics,* 21, pp. 123–143 (1976).
37. R. Iman and J. Helton, "An Investigation of Uncertainty and Sensitivity Analysis Techniques for Computer Models," *Risk Analysis,* 8(1), pp. 71–90 (1988).

38. R. Iman, "An Approach to Sensitivity Analysis of Computer Models: Part I—Introduction, Input Variable Selection and Preliminary Variable Assessment," *Journal of Quality Technology,* 13(3), pp. 174–183 (1981).
39. R. Iman, J. Helton, and J. Campbell, "An Approach to Sensitivity Analysis of Computer Models: Part II—Ranking of Input Variables, Response Surface Validation, Distribution Effect and Technique Synopsis," *Journal of Quality Technology,* 13(4), pp. 232–240 (1981).
40. D. Beller, "Computer Modeling Related to Fire and Decision Support Systems," in *Second International Conference on Performance-Based Codes and Fire Safety Design Methods,* International Code Council and Society of Fire Protection Engineers, Maui, HI (1998).
41. J. C. Helton & F. J. Davis, "Illustration of sampling-based methods for uncertainty and sensitivity analysis," *Risk Analysis,* Society for Risk Analysis, 22(3), pp. 591–622. (2002)
42. J. C. Helton, "Quantification of margins and uncertainties: Conceptual and computational basis," *Reliability Engineering and System Safety*, 96(9), pp. 976–1013. (2011)
43. V. R. Vasquez & W. B. Whiting, "Accounting for both random errors and systematic errors in uncertainty propagation analysis of computer models involving experimental measurements with Monte Carlo methods," Risk Analysis, Society for Risk Analysis, 25(6), pp. 1669–1681. doi: 10.1111/j.1539-6924.2005.00704.x (2005)
44. K.A. Notarianni, "The Role of Uncertainty in Improving Fire Protection Regulation," Ph.D. Dissertation, Carnegie Mellon University, Pittsburgh, PA (2000).
45. R. R. Upadhyay & O. A. Ezekoye, "Treatment of design fire uncertainty using Quadrature Method of Moments," *Fire Safety Journal*, 43(2), pp. 127–139. (2008)
46. C. Beyler, "Introduction to Fire Modeling," in *Fire Protection Handbook* (A. Cote, ed.), National Fire Protection Association, Quincy, MA, pp. 10-82–10-85 (1991).
47. H. Nelson, "Application of Fire Growth Models to Fire Protection Problems," in *Fire Protection Handbook* (A. Cote, ed.), National Fire Protection Association, Quincy, MA, pp. 10-109–10-112 (1991).
48. A. Hald, *Statistical Theory with Engineering Applications,* John Wiley and Sons, New York (1952).
49. M. Reiss, "Global Performance-Based Design: Is It the Solution?" in *Second International Conference on Performance-Based Codes and Fire Safety Design Methods,* International Code Council and Society of Fire Protection Engineers, Maui, HI, pp. 191–195 (1998).
50. House Committee on Science, *Unlocking Our Future: Toward a New National Science Policy,* U.S. Congress, Washington, DC (2007).
51. NFPA, 550, *Guide to the Fire Safety Concepts Tree,* National Fire Protection Association, Quincy, MA (2007).
52. R. T. Clemen, *Making Hard Decisions: An Introduction to Decision Analysis,* PWS-KENT Publishing Company, Belmont, CA (1990).
53. M. Karter, *U.S. Fire Experience by Region, 1989–1993,* National Fire Protection Association, Quincy, MA (1995).
54. J. Hall and B. Harwood, "The National Estimates Approach to U.S. Fire Statistics," *Fire Technology,* 26(2). pp. 99–113 (1989).
55. J. Hall, Personal Communication, Uncertainty Bands (Jan. 1996).
56. W.K. Viscusi, "A Survey of Values of Risk to Life and Health," in *Fatal Tradeoffs: Public and Private Responses to Risk,* Oxford University Press, New York, pp. 51–54 (1992).
57. T.O. Tengs et al., "Five-Hundred Life-Saving Interventions and Their Cost-Effectiveness," *Risk Analysis,* 15, 3 (1995).
58. "EPRI/NRC-RES Fire PRA Methodology for Nuclear Power Facilities," EPRI 1011989/NUREG/CR-6850 (Sept. 2005).
59. USNRC, "An Approach for Using Probabilistic Risk Assessment in Risk-Informed Decisions on Plant-Specific Changes to the Licensing Basis," Regulatory Guide 1.174, Revision 1, (2002).
60. G.A. Apostolakis, "Probability and Risk Assessment: The Subjectivist Viewpoint and Some Suggestions," *Nuclear Safety,* 19(3), pp. 305–315 (1978).
61. G.W. Parry and P.W. Winter, "Characterization and Evaluation of Uncertainty in Probabilistic Risk Analysis," *Nuclear Safety,* 22, p. 1 (1981).
62. USNRC, "Handbook of Parameter Estimation for Probabilistic Risk Assessment," NUREG/CR-6823 (2003).
63. M.P. Bohn, T.A. Wheeler, and G.W. Parry, "Approaches to Uncertainty Analysis in Probabilistic Risk Assessment," NUREG/CR-4826 (1988).
64. R.L. Iman and J.C. Helton, "An Investigation of Uncertainty and Sensitivity Analysis Techniques for Computer Models," *Risk Analysis,* 8(1), pp. 71–90 (1988).
65. G.W. Parry, "A Discussion on the Use of Judgment in Representing Uncertainty in PRAs," *Nuclear Engineering and Design,* 93, pp. 135–144 (1986).
66. M.E. Pate-Cornell, "Uncertainties in Risk Analyses: Six Levels of Treatment," *Reliability Engineering and System Safety,* 54, pp. 95–112 (1996).
67. M.C. Cheok, G.W. Parry, and R.R. Sherry, "Use of Importance Measures in Risk-Informed Regulatory Applications," *Reliability Engineering and System Safety,* 60, pp. 213–226 (1998).
68. M.A. Caruso, M.C. Cheok, M.A. Cunningham, G.M. Holahan, T.L. King, G.W. Parry, A.M. Ramey-Smith, M.P. Rubin, and A.C. Thadani, "An Approach for Using Risk Assessment in Risk-Informed

Decisions on Plant-specific Changes to the Licensing Basis," *Reliability Engineering and System Safety,* 63, pp. 231–242 (1999).
69. G. Apostolakis and S. Kaplan, "Pitfalls in Risk Calculations," *Reliability Engineering,* 2, 135–145 (1981).
70. L. A. Gritzo, P. E. Senseny, Y. Xin & R. Thomas, J. "The international FORUM of fire research directors: A position paper on verification and validation of numerical fire models," *Fire Safety Journal*, 40 (5), pp. 485–490. (2005)
71. A. S. f. T. Materials, *Standard Guide for Evaluating the Predictive Capability of Fire Models,* ASTM E1355. West Conshohocken, PA: ASTM International. (2012).
72. M. Hurley & A. Munguia, "Analysis of Prediction Capability of FDS for Response of Thermal Detectors," Journal of Fire Protection Engineering, 20(2). pp. 77–99 (2010).
73. W. D. Davis, "Comparison of Algorithms to Calculate Plume Centerline Temperature and Ceiling Jet Temperature with Experiments," *Journal of Fire Protection Engineering*, 12(1), pp. 9–29. (2002)
74. Verification and Validation of Selected Fire Models for Nuclear Power Plant Applications. Volume 5. Consolidated Fire Growth and Smoke Transport Model (CFAST). Peacock, R. D.; Reneke, P. A, NUREG-1824; EPRI 1011999; Volume 5; 206 p. May 2007.
75. M. Hurley, "ASET-B: Comparison of Model Predictions with Full-Scale Test Data," *Journal of Fire Protection Engineering*, 13(1), pp. 37–65. (2003)
76. Kong, et al., "Uncertainty and sensitivity analyses of heat fire detector model based on Monte Carlo simulation," *Journal of Fire Sciences*. (2011)
77. F. Joglar, F. Mowrer & M. Modarres, "A Probabilistic Model for Fire Detection with Applications," *Fire Technology*, 41(3), pp. 151–172. (2005)
78. "Evaluation of Smoke Detector Response Estimation Methods: Optical Density, Temperature Rise, and Velocity at Alarm," *Journal of Fire Protection Engineering*, 16(4), pp. 251–268. (2006)
79. Lord, et al, "Uncertainty in Egress Models and Data: Investigation of Dominant Parameters and Extent of Their Impact on Predicted Outcomes – Initial Findings," in *Guide for Evaluating the Predictive Capabilities of Computer Egress Models*, http://fire.nist.gov/bfrlpubs/fire05/PDF/f05156.pdf (2005)
80. B. J. Meacham, "Investigation of uncertainty in egress models and data," Paper presented at the Third International Symposium on Human Behavior in Fire, Belfast, United Kingdom (2004)
81. Xie et al., "The effect of uncertain parameters on evacuation time in commercial buildings," *Journal of Fire Sciences*, 30(1), pp. 55–67. (2012)
82. L. Zhao & N. A. Dembsey, "Measurement uncertainty analysis for calorimetry apparatuses," Fire and Materials, 32(1), pp. 1–26. doi: 10.1002/fam.947 (2008)
83. R. A. Bryant, & G.E. Mulholland, "A guide to characterizing heat release rate measurement uncertainty for full-scale fire tests," *Fire and Materials*, 32 (3), pp. 121–139. doi: 10.1002/fam.959 (2008)
84. M. W. Pitts, E. Braun, R. D. Peacock, H. E. Mitler, E. L. Johnson, P. A. Reneke & L. G. Blevins, *Temperature Incertainties for Bare-bead and Aspirated Thermocouple Measurements in Fire Environments*, ASTM Special Technical Publication, 1427, pp. 3–15 (2003)
85. D. Madrzykowski & C. Fleischmann, "Fire Pattern Repeatability: A Study in Uncertainty," *Journal of Testing and Evaluation,* 40(1) (2012)
86. J. R. Hall, & A. D. Library, "Uncertainty in fire standards and what to do about it" (Vol. STP1541). West Conshohocken, PA: ASTM International (2012)
87. J. O. Trevino & R. Curkeet, "Measurement Uncertainty in Fire Tests-A Fire Laboratory Point of View," *Journal of testing and Evaluation*, 39(6), pp. 1040–1048. (2011)
88. J. Resing et al., "Measurement Uncertainty and Statistical Process Control for the Steiner Tunnel," *Journal of Testing and Evaluation*, 39(6) (2011)
89. K. Frank, "Uncertainty in Estimating the Fire Control Effectiveness of Sprinklers from New Zealand Fire Incident Reports," *Fire Technology*, pp. 1–22 (2012)
90. C. Chang & H. Huang, "A Water Requirements Estimation Model for Fire Suppression: A Study Based on Integrated Uncertainty Analysis," *Fire Technology*, 41(1), pp. 5–24 (2005)

Kathy A. Notarianni is on the faculty of the Department of Fire Protection Engineering at Worcester Polytechnic Institute. She is an associate professor of fire protection engineering and an associate professor of both chemical and mechanical engineering. Her research has focused on topics such as smoke detection, water-based suppression, fire fighter safety and deployment of resources for the fire service, application of fire models, and uncertainty analysis.

Gareth W. Parry is a senior advisor on probabilistic risk assessment (PRA) in the Office of Nuclear Reactor Regulation at the United States Nuclear Regulatory Commission.

Decision Analysis

77

H.A. Donegan

Introduction

This chapter is devoted to some of the basic elements of decision analysis, a subject that has its roots firmly established in the area of management science, but now enjoys a much wider application. The present article, which is not intended as an exhaustive discussion paper, aims to introduce basic terminology and to illustrate some of the techniques that can be applied to situations in fire protection engineering, one of the many areas of application. The growth in application can be attributed to the significant developments that have taken place within information technology, particularly with regard to the ready availability of user-friendly decision support software. Practitioners interested in particular aspects of the subject and in software will find appropriate references listed in context. The reader should be aware at the outset that decision analysis is more general than risk analysis, which, in terms of fire protection, has its own extensive and highly specialized literature—see, for example, Castino and Harmathy [1], Gretener [2], Hall [3], Hirschler [4], Watts [5, 6].

The engineering of fire protection necessitates a high degree of decision making at all levels of application, and because of the capricious nature of unwanted fire, it involves a high degree of subjectivity and therefore uncertainty. In practically every aspect of fire protection, the practitioner is faced with choices when presented with options or alternative courses of action, each of which has one or more consequences. If a choice is subjective, then it can be made only when the following pieces of information are known to the decision maker:

1. An understanding of each possible consequence
2. The likelihood of occurrence of each consequence
3. The method for combining values and probabilities of consequences into a meaningful course of action

Sometimes the sheer number of options will limit the time that can be spent on evaluating each single option, as when one is faced with large product lists—for example, smoke alarms or fire-resistant doors. Or the possible consequences of a course of action are difficult to enumerate, as in the case of increasingly complex new technology. Often the value of a consequence can be estimated only on the basis of sample information, for example, studying a selection of literature. In other cases, the value of a consequence may depend on many dimensions, such as choosing where to live—taxes, transport, amenities, employment, and so on. Or there may be several possible consequences distributed over time, and it is difficult to predict which one of them will occur and at what time—typically when the fire brigade is attempting to suppress a raging fire.

H.A. Donegan (✉)
School of Computing and Mathematics at the University of Ulster, Northern Ireland

M.J. Hurley (ed.), *SFPE Handbook of Fire Protection Engineering*,
DOI 10.1007/978-1-4939-2565-0_77, © Society of Fire Protection Engineers 2016

In complex problems, decisions often have to be made when there are several sources of difficulty interacting or competing. For example, deciding whether or not to build a nuclear power plant instead of a conventional alternative in the face of increasing energy demands is perhaps typical. In this situation, the decision makers have to deal with short- and long-term multidimensional consequences; they know that despite extremely low outcome probabilities, a small number of uncertain events could lead to a catastrophe. With the benefit of hindsight, it is a chilling reality that Chernobyl is the epitome of the above scenario and therefore a timely reminder to those engaged in subjective decisions that impact on life safety.

Consequences are often a reflection of the mathematical modeling strategy that underpins many decisions and are therefore only as valid as the appropriateness of the chosen model or, inclusively, the reliability of its input data. Moreover, the fact that much of the data are subjective places the opinion experts at a key point in the chain of responsibility for good decision making (see Winkler and Murphy [7]). In what follows, it is assumed that methodologies under the various decision classifications are supported by the best efforts of practitioners and software designers.

Before proceeding to look at decision classifications, some key words that frequently appear in the literature of decision theory are now discussed. For example, in the above preamble, casual reference was made to the terms *subjectivity* and *uncertainty,* yet these are emotive words with a vast and formal literature—see, for example, Bunn [8], French [9, 10], Lindley [11], Raiffa [12], Viek and Wagenaar [13].

The concept of probability in decision theory embraces two distinct schools of probabilists—the frequentists and the subjectivists.

The *frequentists* believe that probability can only have meaning in the context of an infinitely repeatable experiment, in which the probability of an event A, namely $P(A)$, is taken to be its long-run relative frequency of occurrence in repeated trials of the experiment—termed *objective probability*. In the reality of risk assessment, approximations called actuarial estimates are used; the relative frequency of the number of times A has previously occurred in some finite experiment is taken as an indication of likely occurrences in the future. For example, if the statistics [14] of residential fire deaths in the sample period (finite experiment) 1983–1987 show that on average 47.8 % of the deaths are identified as occupants aged 65 years and over, then 0.478 is regarded as the probability that a fatal casualty in a residential fire is a person aged 65 or above. Approximations are common in production scenarios. For example, if A represents the event that a sprinkler head is defective, and during the inspection (finite experiment) of a random batch of 240 sprinkler heads 2 are found to be defective, then the chance of picking, at random, a faulty head from the batch is 2 in 240, yet $P(A)$ is stated in general as being 1/120 until revised in another finite experiment.

The *subjectivists* associate probability not with the system under observation, but with the observer of that system identifying probability as the degree or strength of belief that the system will adopt a certain state—termed *subjective probability*. For example, in the modeling of fire spread, the probability of flashover in the room of origin is a measure of opinion relating to the change of state from preflashover to postflashover. It would be decided by the modeler on the basis of experience regarding uncertainties associated with the fire variables in the room of origin. However, such decisions need considerable care; the article by Bunn [8] addresses some of the fundamental issues regarding the assessment of subjective probabilities. A highly pertinent article by Noonan and Fitzgerald [15] discusses the role of subjective probabilities in fire risk management studies.

Developments in artificial intelligence and in expert systems have shown that probability theory in itself is insufficient to cater to the advancement of theories relating to the management of uncertainty in knowledge-based systems. For example, lexical elasticity, which relates to the fuzziness of words in natural language, provides a clear example. A simple relation between X, Y, and Z expressed as

if X is small and Y is very large,
then Z is not very small

does not lend itself to a simple interpretation within the field of probability theory. This is by reason of the lexical elasticity of the predicates *large* and *small* [16]. Such developments have inspired the formation of a new school of practitioners focused on imprecision rather than uncertainty. The topics are rather specialized and outside the scope of the present article, but the interested reader will find appropriate background reading in Zadeh [17] and in Klir and Folger [18].

The term *uncertainty* is used prolifically in decision theory, and yet textbooks generally sidestep any attempt at a formal definition. This presentation will not dissent from that established pattern, but will nevertheless construct an interpretation from the axioms of probability. (The subject of probability is discussed elsewhere in this handbook). The axioms are restated here for convenience:

- Axiom 1: *Positiveness*—the probability of an event occurring must be nonnegative.
- Axiom 2: *Certainty*—the probability of an event that is certain to occur is 1.
- Axiom 3: *Addition*—if events A and B are mutually exclusive, then the probability

$$P(A \text{ or } B) = P(A) + P(B)$$

Axioms 1 and 2 imply that the probability of an event occurring must be at least 0 and no greater than 1. Hence uncertainty (for the purpose of this discussion) identifies with the probability of an event A such that $0 \leq P(A) < 1$. In a subjective environment, the location of $P(A)$ in the interval [0, 1] lies within a subneighborhood of uncertainty, which is clearly articulated by Bell et al. [19]. They point to the confrontation between abstract theory and realistic behavior, particularly when subjective assessments are required. Real people do not behave like the models say they should. For example,

- Many experts are willing to answer hypothetical questions about uncertain quantities.
- Lay people and indeed experts do not calibrate well. By and large, assessed probability distributions are too tight; people think they know more than they really know and are surprised far too often.
- Some assessment methods lead to less distortion than others.
- It is extremely difficult to assess small probabilities.
- Subjects can learn to calibrate better if they are given systematic feedback.

It is intended that these observations, which are highly pertinent in fire safety, will alert the reader to the realization that decision making is as much an art as it is a science.

Decision Classifications

Broadly speaking, decision classifications can be characterized by the qualitative knowledge spectrum shown in Fig. 77.1. Given that the spectrum ranges from ambiguous data to well-defined data, in

- Decision making under certainty—the data are known deterministically
- Decision making under risk—the data are described statistically
- Decision making under uncertainty—the data cannot be assigned relevant weights

Decision making under any condition involves alternatives whose payoffs (outcomes) depend on the states of nature, which may be random events. Specifically, the *payoff matrix* of a decision problem with m alternatives and n states of nature can be represented as in Fig. 77.2. The element a_i represents the alternative i, and the element s_j represents state of nature j. The payoff or outcome associated with a_i and sj is denoted by $v(a_i, s_j)$.

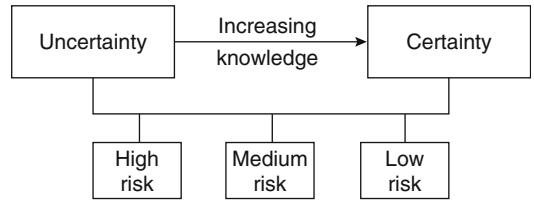

Fig. 77.1 Qualitative knowledge spectrum

Fig. 77.2 Payoff matrix

Alternatives a_i	States of nature s_j: s_1	s_2	s_n
a_1	$v(a_1, s_1)$	$v(a_1, s_2)$	$v(a_1, s_n)$
a_2	$v(a_2, s_1)$	$v(a_2, s_2)$	
a_m	$v(a_m, s_1)$		$v(a_m, s_n)$

Decision Making Under Certainty

Decision making under certainty means the decision maker knows with certainty the consequence of every alternative or decision choice. For example, a fire engineering consultant with resources to take on a single contract has the choice of two 1 year guaranteed contracts *A* and *B*, each with similar conditions and each capable of being carried out within the consultant's office environment. If the value of *A* exceeds that of *B* by $4000, then there is certainty that contract *A* will maximize the consultant's well-being. Of course, there is the classic and perhaps paradoxical phrase that accompanies any certainty, "all other things being equal." The payoff matrix would take the form shown in Fig. 77.3.

Alternatives	State of nature (event)	
	Contract *A*	$v(A) = v(B) + 4000$
	Contract *B*	$v(B)$

Fig. 77.3 Contract payoff matrix

Such matrices are clearly unnecessary for straightforward decision making. However, they offer decision makers a useful structure when the choice of alternative is compounded by more than one state of nature, as in decision making under risk or uncertainty.

Decision Making Under Risk

Decision making under risk assumes that the payoff (gain or cost) associated with each alternative, for a given state of nature, has an associated probability. The payoff is usually based on the expected value criterion, which seeks the maximization of expected (average) gain or the minimization of expected cost among the alternatives. The procedure stems from the concept of expectation, perhaps the most important concept in decision theory, which is discussed in elementary textbooks on probability.

Table 77.1 Probability distribution for a large, medium, or small fire

Probability of fire type	Large fire	Medium fire	Small fire
Pessimistic case	0.6	0.2	0.2
Optimistic case	0.4	0.4	0.2

Basically, *expectation* is a weighted average, and to compute its value, one takes the following steps:

1. List all possible alternatives a_i and states of nature (exclusive events) s_j together with the corresponding probabilities $P(s_j)$.
2. Relative to a given fixed state of nature, note the value of each alternative $v(a_i, s_j)$.
3. Calculate $P(s_j) \times v(a_i, s_j)$ as j ranges across all states for each fixed i.
4. Add and note the products for each alternative i.

Consider the situation where a building's lease has just been extended for a 10 year period, and although the building is fire-safety compliant, the management, in reviewing a number of factors, invite consultants to assess the fire risk with respect to stock. The results of their inquiry are summarized in Table 77.1, which reveals

Fig. 77.4 Payoff matrix showing various outcomes

		States of nature		
		Large fire	Medium fire	Small fire
		P(large fire)	*P(medium fire)*	*P(small fire)*
		0.5	0.3	0.2
Alternatives	UUS	24,000	16,000	8,000
	UWS	18,000	11,000	4,000
	REB	30,000	15,000	5,000

pessimistic and optimistic discrete probability distributions for large, medium, and small fires, conditional on there being a fire within the observed stock. The article by Noonan and Fitzgerald [15] discusses such a risk assessment for a warehouse.

The management, who have some understanding of decision theory, agree in the light of the consultant's report to examine the following alternatives:

- Upgrade using a sprinkler system (UUS).
- Upgrade without sprinklers (UWS).
- Retain the existing building (REB).

Increasing the degree of fire protection requires additional investment, and for simplicity it is assumed that a proportion of upgrade costs (dollars) are included in the potential loss values as estimated by management. Also, management, who are neither pessimistic nor optimistic, settle on the following mean probabilities of fire size risk: $P(\textit{large fire}) = 0.5$, $P(\textit{medium fire}) = 0.3$, and $P(\textit{small fire}) = 0.2$. The payoff matrix takes the form shown in Fig. 77.4.

Hence the expectation for each alternative is given by

$$\text{UUS} : 0.5 \times 24,000 + 0.3 \times 16,000 + 0.2 \times 8,000 = 18,400$$

$$\text{UWS} : 0.5 \times 18,000 + 0.3 \times 11,000 + 0.2 \times 4,000 = 13,100$$

$$\text{REB} : 0.5 \times 30,000 + 0.3 \times 15,000 + 0.2 \times 5,000 = 20,500$$

Based on this information, the management would opt for upgrading without sprinklers. The reader should note that the expected value for an alternative is the average cost to the company that would be expected if the decision were repeated a large number of times—it is not the value that would be returned every time. Clearly, if the decision is made only once, the loss could be any of the three values \$18,000, \$11,000, or \$4000.

Such problems can be represented using a decision tree, as shown in Fig. 77.5. Taha [20] recommends the following nodal notation—a square (□) to represent a decision point and a circle (○) to represent a chance event. Shields and Silcock [21] offer a tree structure in fire safety terminology. See also the *Guide to Fire Safety Concepts Tree,* NFPA 550 [22].

Decision Making Under Uncertainty

Decision making under uncertainty differs from decision making under risk in that in the probability distribution associated with the states of nature, s_j is either unknown or cannot be determined. To overcome this dearth of information, the following models have been developed:

- Laplace paradigm
- Wald (minimax/maximin) paradigm
- Savage paradigm
- Hurwicz paradigm

Each reflects the degree of conservation exhibited by the decision makers in the face of uncertainty.

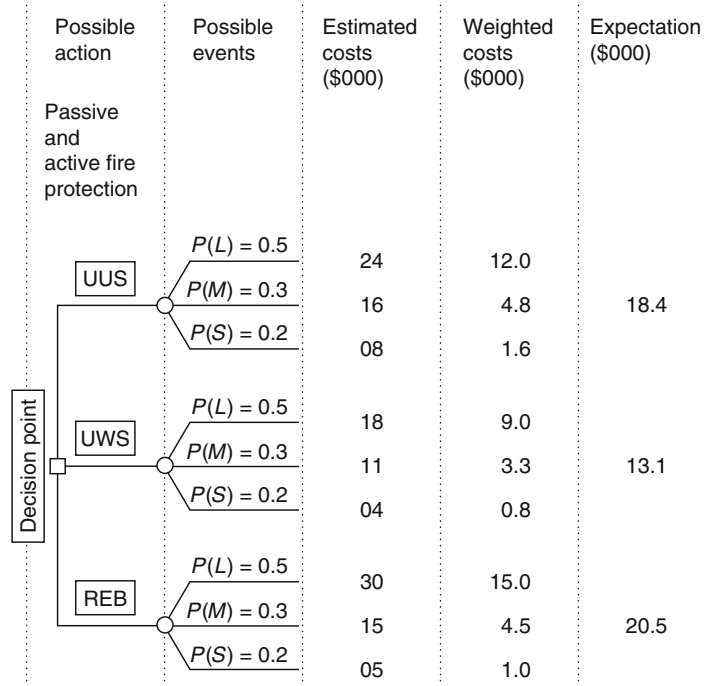

Fig. 77.5 Decision tree to illustrate decision making under risk

The Laplace Paradigm The Laplace paradigm [23] is based on the principle of insufficient reason [10]. This simply means that, because the probability distribution of the states of nature are not known, there is no reason to believe that they are different. Hence, the j alternatives are evaluated using the optimistic belief that $P(s_j) = 1/n$ where n is the number of states of nature. If the payoff $v(a_i, s_j)$ represents cost (as opposed to gain), then the best alternative is the one that yields

$$\min_{a_i}\left[\frac{1}{n}\sum_{j=1}^{n} v(a_i, s_j)\right]$$

with min changing to max in a gain situation.

The Wald (Minimax/Maximin) Paradigm The Wald paradigm [24] stems from the conservative attitude of caution—it is a pessimistic criterion of choice insofar as it assumes that the worst will happen. The paradigm aims to get the best out of the worst possible conditions. Given as before, that $v(a_i, s_j)$ is a cost, then the most appropriate alternative selected conforms to

$$\min_{a_i}\left\{\max_{s_j} v(a_i, s_j)\right\}$$

In a gain situation, the operators min and max are transposed.

The Savage Paradigm Often referred to as the Savage regret criterion, the Savage paradigm [25] aims at moderating the pessimistic outlook of Wald's paradigm. Here the payoff matrix $[v(a_i, s_j)]$ is replaced with a regret matrix $[r(a_i, s_j)]$, where the function r is defined as follows:

$$r(a_i, s_j) = \begin{cases} \max\limits_{a_k}\left[v(a_k, s_j)\right] - v(a_i, s_j) & \text{if } v \text{ is a gain} \\ v(a_i, s_j) - \max\limits_{a_k}\left[v(a_k, s_j)\right] & \text{if } v \text{ is a cost} \end{cases}$$

Regret is the difference between actual outcome and best possible outcome, as in the trivial example of a student who gets 85 % instead of 100 %; the student's regret is 15 %. Likewise, a home owner who pays $300 for house insurance, when a neighbor insures a similar house with a different company for $250, experiences a regret of $50.

The subtlety of moderation in the case of the Savage paradigm over the Wald criterion becomes clear in the following contrived situation. Consider a potential cost matrix where the choice is between a property with smoke alarms adjacent to the fire brigade (a_1) or one with smoke alarms but 50 miles from the fire brigade (a_2), and the states of nature are s_1 (alarm works) and s_2 (alarm fails) (see Fig. 77.6). It is clear from the minimax criterion that alternative a_2 with a definite loss of $20,000 is preferable. However, a_1 looks attractive if s_1 is realized with a chance loss of only $90. Clearly, the a_2 alternative is totally conservative.

Now, using Savage's paradigm, the regret matrix in Fig. 77.7 emerges. The minimax criterion applied to the regret matrix now selects a_1—the less pessimistic option.

The Hurwicz Paradigm The Hurwicz paradigm [26] reflects a range of attitudes from the most optimistic to the most conservative. Letting $v(a_i, s_j)$ represent a cost (or loss), and if t is an index of optimism such that $0 \leq t \leq 1$, then Hurwicz claims that the most appropriate alternative conforms to

$$\min_{a_i} \left\{ t \min_{s_j} v(a_i, s_j) + (1-t) \max_{s_j} v(a_i, s_j) \right\}$$

In a gain situation, the operators min and max are interchanged. If $t = 0$, the criterion reduces to the Wald condition, and when $t = 1$, the result is totally optimistic in selecting the best of the best. The decision maker has control over the choice of t, which, in the absence of strong feelings, is taken as 0.5.

	s_1	s_2	Row max	
a_1	90	21,000	$21,000	
a_2	20,000	20,000	$20,000	→ Minimax

Fig. 77.6 Potential cost matrix

	s_1	s_2	Row max	
a_1	0	1,000	$1,000	→ Minimax
a_2	20,910	0	$20,910	

Fig. 77.7 Regret matrix

Summary Example

The Faculty of Inferno Research Engineers (FIRE) is planning an international conference in Geneva, and FIRE estimates that there are 4 likely bands of attendance: 150, 200, 250, and 300 attendees. The cost of organization will be a minimum if FIRE can select a venue in Geneva that meets the demand exactly. Clearly, deviations above or below the demand levels incur additional costs resulting from unused seating capacity or lost income opportunities when some of the demand is not satisfied. At the proposed date set for the conference, the organizing committee of FIRE can select one of four appropriate venues that match the corresponding attendance bands. Letting a_1, a_2, a_3, and a_4 represent the alternative venues with respective seating capacities (150, 200, 250, and 300), and letting s_1 through s_4 represent the levels of attendance (150, 200, 250, or 300), the payoff matrix in Fig. 77.8 summarizes the relative seating and venue costs to FIRE in hundreds of dollars.

The organizing committee applies the above four methods with the results shown below.

- *Laplace paradigm.* If $E(a_i)$ denotes the expectation associated with a_i, then

$$E(a_1) = 1/4(4 + 9 + 17 + 24) = \$1350$$
$$E(a_2) = 1/4(7 + 6 + 11 + 22) = \$1150 \text{ (Optimum)}$$
$$E(a_3) = 1/4(20 + 17 + 11 + 20) = \$1700$$
$$E(a_4) = 1/4(28 + 22 + 18 + 14) = \$2050$$

		States of nature			
		s_1	s_2	s_3	s_4
Alternatives	a_1	4	9	17	24
	a_2	7	6	11	22
	a_3	20	17	11	20
	a_4	28	22	18	14

Fig. 77.8 Cost payoff matrix

Fig. 77.9 Matrix resulting from Wald's paradigm

	s_1	s_2	s_3	s_4	Row max	
a_1	4	9	17	24	$2400	
a_2	7	6	11	22	$2200	
a_3	20	17	11	20	**$2000**	(Optimum)
a_4	28	22	18	14	$2800	

Fig. 77.10 Regret matrix resulting from the Savage paradigm

	s_1	s_2	s_3	s_4	Row max	
a_1	0	3	6	10	$1000	
a_2	3	0	0	8	**$800**	(Optimum)
a_3	16	11	0	6	$1600	
a_4	24	16	7	0	$2400	

- *Wald paradigm*. See the matrix in Fig. 77.9.
- *Savage paradigm*. The regret matrix (Fig. 77.10) is determined by subtracting 4, 6, 11, and 14 from columns 1 through 4, respectively.
- *Hurwicz paradigm*. The data in Table 77.2 summarizes the picture for arbitrary t.

If you were chairman of FIRE, how would you interpret the above set of results and hence advise your committee on what decision to make?

Table 77.2 Outcome of the Hurwicz paradigm

Alternative	Row min	Row max	t(row min) + $(1-t)$(row max)
a_1	4	24	$24-20t$
a_2	6	22	$22-16t$
a_3	11	20	$20-9t$
a_4	24	28	$28-14t$

Multiobjective Decisions

The above classification examples have one property in common; they all belong to the class of problems where the desired alternative is chosen exclusively on the basis of a single objective—to either minimize cost or maximize gain. When a problem involves two or more objectives, the decision maker must decide on the relative importance of each before analyzing the merits of each alternative. Multiple objectives are often conflicting; for example, a fire authority, in citing a new fire station, might have to balance key objectives such as minimizing cost, minimizing risk, and minimizing travel distance. A problem of this kind never has a correct solution, but the nature of its analysis can offer the stakeholders considerable insight into the quality of any emerging decision.

Terminology

There is a profusion of terminology used in connection with such decision making. For instance, the formal literature uses the terms *multiattribute decision making*, *multiobjective decision making*, and *multicriteria decision making* (the terminology preferred by this author) almost interchangeably, and the inexperienced practitioner could well be forgiven for being confused. However, the following definitions should assist the reader who is trying to come to terms with multicriteria decision theory.

Objectives Objectives are task actions, such as

- To reduce the number of deaths due to unwanted fire

- To improve the level of fire safety in public assembly buildings
- To minimize the number of toxic hazards in the event of a fire
- To maximize the efficiency of fire modeling

French [10] claims that an objective has a dimension together with an indication of the "good" and "bad" ends of the dimension. Thus, to minimize toxic hazards is an objective that indicates that a reduced number of hazards is preferred. This concurs with Keeney and Raiffa [27], who described an objective as an indication of the preferred direction of change. The performance of a stated objective is measured by its attributes.

Attributes Synonymous with criteria, attributes are the dimensions of an objective along which alternatives are represented [10]. For example, if alternatives are to be judged against three attributes, picture these as the three axes X, Y, and Z. Then an alternative $\mathrm{a} = (a_1, a_2, a_3)$ is effectively a point in three-dimensional space such that a_1 is in the X dimension, a_2 is in the Y dimension, and a_3 is in the Z dimension. For example, Donegan et al. [28] list the attributes of domestic fire safety evaluation as Occupants, Doors, Communications, Internal Planning, Travel Distance, and Flues/Ducts. In mathematical terms, these represent a six-dimensional attribute space in which, for example, a domestic norm $\mathrm{n} = (n_1, n_2, n_3, n_4, n_5, n_6)$ can be used as a comparator against which to judge the m alternatives $\mathrm{a}^k = \left(a_1^k, a_2^k, a_3^k, a_4^k, a_5^k, a_6^k\right)$ where $1 \leq k \leq m$. It is not the intention of this article to dwell on mathematical formalism; the interested reader will find a full axiomatic treatment in French [10].

Value and Utility For each alternative facing a decision maker, it is conventional to measure the alternative's attractiveness by means of a numerical score aggregated from the attribute scores. If the decisions involve no element of risk or uncertainty, scores are described as *values* of the course of action; otherwise they are known as *utilities* of the course of action. This article, given its introductory status, will restrict its illustrations to the former. For an introduction to utility theory and an excellent account of its application in decision making, with special reference to insurance risk, see Ramachandran [29].

Weighting Although the decision maker has chosen, or agreed on, a set of attributes, it does not mean that each attribute has the same merit. Each attribute will rate a degree of importance, but the actual cardinal priority of the attributes is seldom obvious. Although a decision maker familiar with the task at hand might intuitively identify the ordinal priority, it is usually necessary to employ a formal process to arrive at credible weights. Such a process may be as informal as the Delphi method [30] or as formal as the eigenvector technique of the analytic hierarchy process [31]. More will be said of these processes later in this chapter. Figure 77.11 summarizes the problem environment.

Dominance An alternative X is dominated if another alternative Y is "better" in at least one attribute and performs equally with respect to the remaining attributes. This definition permits the initial screening of alternatives insofar as all dominated alternatives are discarded.

Satisficing The word *satisficing* is probably a contraction of *sufficient to satisfy* [32], although Watts [33] believes the term was coined by Simon [34] for identifying a solution that is good enough although not necessarily optimal. The method of satisficing, often referred to as the conjunctive method, is purely a screening technique. In order for an alternative to be acceptable, it must exceed stated performance thresholds for all attributes. This compares with the norm strategy used by Shields et al. [35] in their fire safety evaluation of public assembly buildings.

Disjunctive The term *disjunctive* also applies to screening. Disjunctiveness is the logical complement of satisficing in that an acceptable alternative must exceed a given performance threshold for at least one attribute.

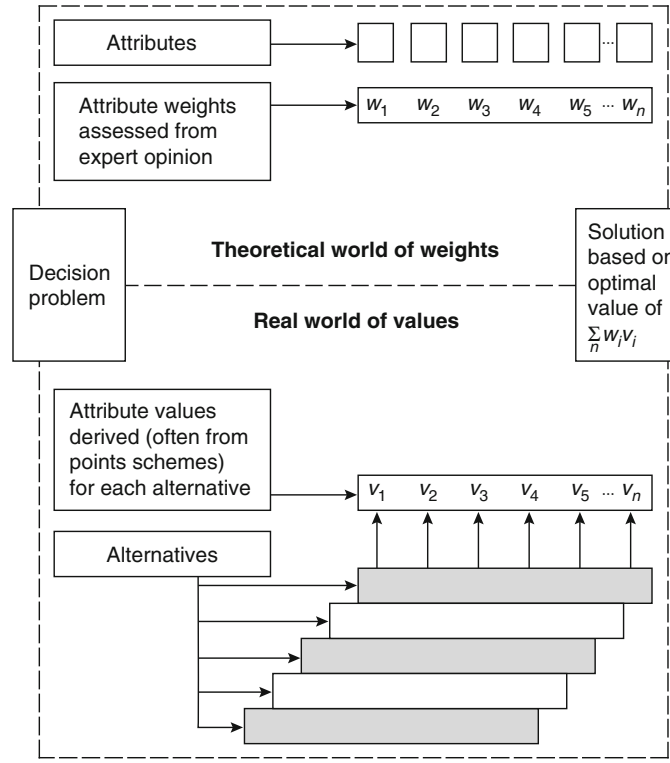

Fig. 77.11 Attributes, values, and weights

Additive Weighting The additive weighting method will be demonstrated later in this chapter. Basically, the score attached to an alternative is equal to the weighted sum of its attribute preference valuations (frequently, the generic term *utilities* is used, albeit in the absence of probability distributions). The weights are subjective percentages of importance given to each attribute label. The resulting weighted sums for each alternative can be used to rank, screen, or choose an alternative. It has been shown that, provided trade-offs among the attributes in any subset of the attributes do not depend on the levels of the remaining attributes, the additive weighting model can be applied without reservation. The trade-off proviso is described by Keeney and Raiffa [27] as preferential independence, which is neatly formalized in French [10].

Simple Multicriteria Illustration

Consider the situation where a new fire station is to be located in a large conurbation offering five potential sites—A, B, C, D, E. Deciding on the most appropriate site is a nontrivial matter, and as with any building project, there are costs and benefits to be considered. This illustration will focus only on the benefits of siting, with considerable simplification to ensure transparency of the methodology. The technique is based on the Simple Multi-Attribute Rating Technique (SMART) of Edwards [36], and the stages in the process are outlined as follows:

Nominate the Decision Maker(s) (DM) In this case, an architect is charged with this responsibility. Group decision making is possible (see Goodwin and Wright [37]).

Recognize the Alternatives The alternatives correspond to the siting locations A, B, C, D, E.

Identify the Attributes The attributes are usually finalized with the assistance of a value tree, such as Fig. 77.12. Here the architect identifies two main predesign attributes, called Site and Situation, and also specifies their

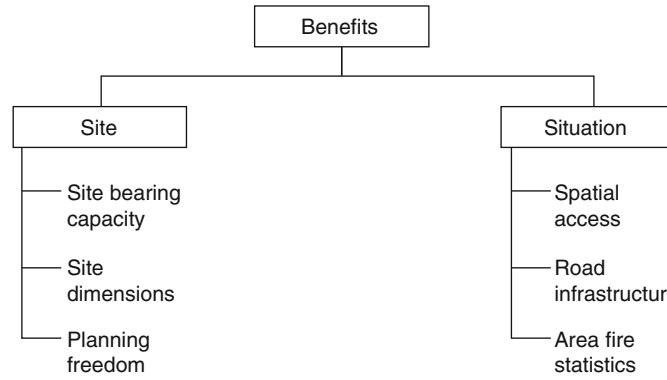

Fig. 77.12 Value tree for fire station location problem

Table 77.3 Architect's attribute-scale values

	A	B	C	D	E
Spatial access	70	75	65	45	55
Road infrastructure	95	15	75	65	35
Area statistics	25	95	05	25	55
Site dimensions	45	25	05	50	95
Bearing capacity	60	05	05	25	85
Planning freedom	75	25	95	85	65

subattributes, that is, criteria that can be readily assessed or valued with respect to each site—Spatial Access, Road Infrastructure, Area Fire Statistics, Site Dimensions, Site Bearing Capacity, and Planning Freedom.

Assess Each Alternative Using the six attribute labels, the architect assesses each site (alternative) and assigns to it a corresponding attribute value, v_i $(1 \leq i \leq 6)$. The valuation of site attributes can be carried out using direct measurement (if appropriate), a logical points scheme, or, as the architect chose to do in this case, a simple linear rating scale from 0, meaning horrible, to 100, meaning best possible. Attribute valuation using the linear rating scale approach is succinctly discussed in Edwards and Newman [38]. An interesting and instructive observation made by these authors is that a curved (nonlinear) value function almost never makes any difference to the decision. The architect's survey reveals the matrix of values shown in Fig. 77.13.

Determine a Weighting Factor $w_i(1 \leq i \leq 6)$ for Each Attribute The weighting factor could reflect the decision maker's point of view, or a consensus point of view derived from experts. In any event, there are a number of specialized techniques for obtaining such weights, and these will be discussed later in this article. Suffice for the present example that the architect has access to weights. Thus, Spatial Access (26 %), Road Infrastructure (34 %), Area Statistics (8 %), Site Dimensions (10 %), Bearing Capacity (19 %), Planning Freedom (3 %). Note that the weights are in percentages, which must sum to 100 %, or if stated in decimal format, they should sum to 1.

Take a Weighted Average of the Values Assigned to Each Site (Alternative) See Table 77.4. The weighted average will give the architect a measure of how well a particular site performs over all the attributes. The weighted average (aggregate benefit) is obtained from the sum $\sum_{i=1}^{6} w_i v_i$.

Table 77.4 Values and weights for each site

		Site				
Attribute	Weight	A	B	C	D	E
Road infrastructure	0.34	95	15	75	65	35
Spatial access	0.26	70	75	65	45	55
Bearing capacity	0.19	60	5	5	25	85
Site dimensions	0.10	45	25	5	50	95
Area statistics	0.08	25	95	5	25	55
Planning freedom	0.03	70	25	95	85	65
Aggregate benefits		70.50	36.4	47.10	48.10	58.20

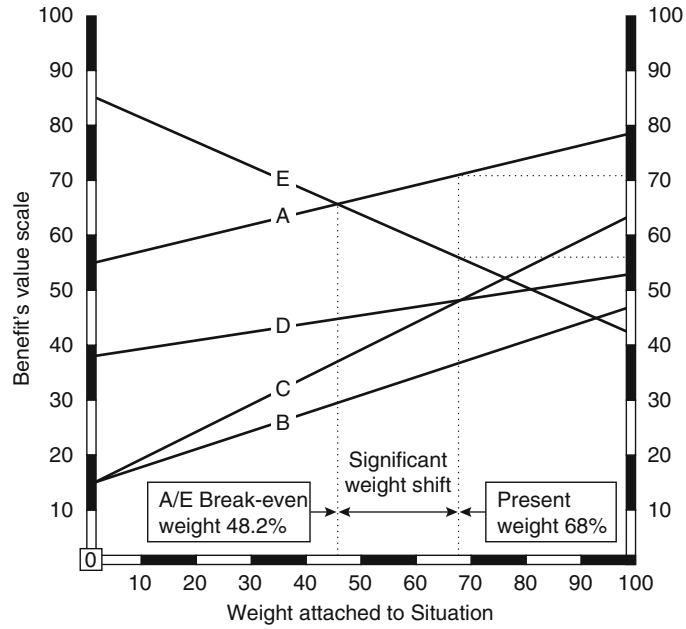

Fig. 77.13 Sensitivity analysis for weight attached to situation

Make a Provisional Decision The apparent answer is site A, but the architect must be reassured, and therefore must check the robustness of the results as follows.

Carry Out a Sensitivity Analysis to Test the Robustness of the Decision The sensitivity analysis is an important aspect of the analysis that is often overlooked in practice, yet it is perhaps the most revealing part of the process and can contribute significantly to the decision maker's understanding of the problem. It is imperative that the procedure not be haphazard. The following strategy is recommended in Goodwin and Wright [37].

The architect, upon reflecting on the above results, notices that the Situation attribute accounts for 34 % + 26 % + 8 % = 68 % of the benefit's weighting, whereas Site features account for the remaining 32 %. Accordingly, before giving a formal decision, the architect proceeds to investigate the consequences of varying the weight attached to Situation. Figure 77.13 summarizes how the value of benefits for the different sites varies with changes in the Situation weights. The graphical technique is based on the following proposition: If Situation, for example, had a weight of 0, this would imply that the three corresponding attributes (Spatial Access, Road Infrastructure, Area Statistics) would each

Table 77.5 Values and weights when situation is zero weighted

		Site				
Attribute	Weight	A	B	C	D	E
Road infrastructure	0.00	95	15	75	65	35
Spatial access	0.00	70	75	65	45	55
Bearing capacity	0.60	60	5	5	25	85
Site dimensions	0.31	45	25	5	50	95
Area statistics	0.00	25	95	5	25	55
Planning freedom	0.09	70	25	95	85	65
Aggregate benefits		56.25	13.00	13.10	38.20	86.30

have zero weights. Correspondingly, the weights of the six lowest attributes would be Spatial Access (0), Road Infrastructure (0), Area Statistics (0), Site Dimensions (10), Bearing Capacity (19), and Planning Freedom (3). When normalized and rounded, these amount to 0, 0, 0, 60, 31, and 9, respectively, as shown in Table 77.5. It is not difficult to draw the corresponding graphs for each site, as shown in Fig. 77.13.

It is evident from the graphs that a zero weighting on Situation would immediately elevate site E to priority status. This status would maintain so long as the weight attached to Situation is less than 48.2 %. However, this is clearly significantly lower than the professionally judged figure of 68 %. The tangibility of the attributes in this example provides little scope for opinion variance, particularly among experts, and therefore it is unlikely that the opinion swing required to put site E in the frontier of consideration is likely to happen. The architect would be justified in the recommendation of site A.

A similar approach could be taken with the lower-level weights. For example, the architect may be instructed to explore the effect of varying the weights attached to Road Infrastructure and Spatial Access while keeping the weight attached to Area Statistics constant. Such in-depth analyses are clearly worthwhile when large amounts of resources are being expended. The reader is reminded that this example dealt only with the multicriteria related to benefits; it did not address the issue of costs and the relationship between costs and benefits. A useful discussion on trade-off between costs and benefits, pitched at the level of this example, can be gleaned from Goodwin and Wright [37].

Fire Safety Attribute Weighting

Rational solutions for many of today's decision-making problems in fire safety evaluation are difficult to formulate. This is often due not only to the complexity of the problems themselves, but also to the vagueness (also referred to as "fuzziness") of certain concepts. Despite the increased accessibility of modern computing technology, the complexity factor can be handled only by the introduction of a multiattribute structure into the elements of a problem. Consistent judgments of weight and value must be made on individual fire safety attributes to enable an overall assessment, and it is important to distinguish the tasks involved (see Fig. 77.11). Finding attribute weights is a theoretical exercise that, for many evaluation problems, reduces to finding a cardinal ranking of criteria (see Watts [6]). On the other hand, finding the corresponding values for each alternative is a real-world exercise, which can involve complex points schemes and specialized economic functional analysis. The buoyant literature devoted to both tasks is conveniently reviewed by Watts [39]. Definitive articles are presented by Nelson and Schibe [40], Marchant [41, 42], Stollard [43], Shields et al. [44], and Dodd and Donegan [45, 46].

The generally accepted attribute levels—objectives, tactics, and components—are shown in Fig. 77.14, with nomenclature attributed to Marchant [41]. The levels conform to a

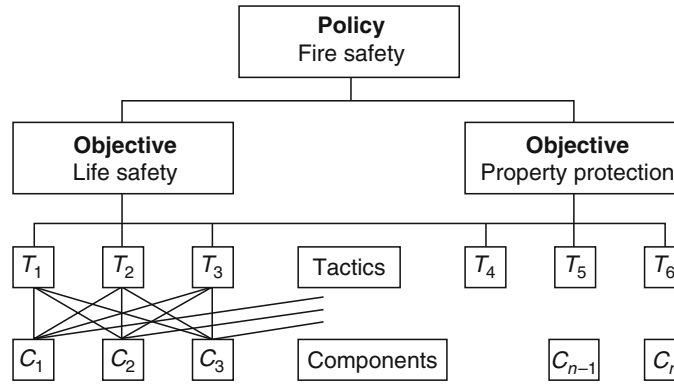

Fig. 77.14 Typical fire safety evaluation hierarchy

hierarchical structure with decreasing generality from the apex.

The Hierarchy Philosophy

The example in the preceding section, "Simple Multicriteria Illustration," did not discuss strategies for obtaining the weights of criteria or attributes. These strategies have a vast and specialized literature within the realm of decision theory, but the accepted nature of attribute decomposition within fire safety evaluation has enabled the following distillation of methods.

These all hinge on the structure of a fire safety evaluation hierarchy, shown in Fig. 77.14. Typically, if the key objective or policy is "fire safety," the next level of the hierarchy lists the secondary, or supporting, objectives—"to save lives" and "to protect property." Sometimes a third objective, "to prevent conflagration," is included, but this will be dictated by the environment of the problem. These objectives are very general, and their balance of importance can be crucial to the ranking outcome of a set of weights (see Dodd and Donegan [45]). The next reduced level of generality comprises the tactics that would be employed by a safety analyst in support of the objectives. For example, "to improve egress capability" or "to facilitate rescue" would be recognized tactics in support of "life safety." At the components level, usually the lowest level, the criteria are chosen to identify with the tactics, but at a much lower level of generality. Each component is seen as a pragmatic dimension to which an engineer can attach a value when surveying an alternative. Most components have long lists of subcomponents, which are useful when seeking an attribute value. The value emerges as a synthesis of scores or points attached in some logical manner to each subcomponent. A typical component could be "doors" and these would be valued on the basis of subcomponents such as "dimensions," "fire resistance," "glazing," or "intumescent stripping."

Effectiveness Matrices

Effectiveness matrices are opinion matrices. (The term *effectiveness matrix* is taken from Lai and Hopkins [47].) Already, it has been stated that attributes are dimensions along which alternatives can be represented. However, it is possible, as follows, to extrapolate this idea to cater for the cardinal ranking of fire safety components relative to the stated policy. Assume that there are m components, n tactics, and k objectives. A decision maker (DM) can represent each component as a vector of tactics, and, a fortiori, the set of components as an effectiveness matrix $[c_{ij}]_{m \times n}$ in which the rows represent components and the columns represent tactics. The element c_{ij} is the numerical equivalent of the DM's opinion as to the importance of the ith component relative to the jth tactic. Similarly, each tactic can be represented as a vector of

objectives, the set of tactics being represented by the effectiveness matrix $[t_{ij}]_{n \times k}$, where t_{ij} represents the importance of the *i*th tactic relative to the *j*th objective. Finally, DM declares the importance of each objective relative to the stated policy in the effectiveness matrix $[o_{ij}]_{k \times 1}$ (vector, since there is only a single policy). The product of the three effectiveness matrices,

$$\left[c_{ij}\right]_{m \times n} \times \left[t_{ij}\right]_{n \times k} \times \left[o_{ij}\right]_{k \times 1}$$

yields the components-to-policy vector, which, when linearly normalized gives the required attribute weightings.

The preceding numerical routine is the same for all weighting methods. Any differences in the routine relate to the determination of the effectiveness matrices. These are discussed in the next section using notation that has previously appeared in fire research literature.

Weighting Methods Used in Fire Safety Evaluation

The hierarchical model is amenable to either cross-impact analysis or analysis involving pairwise comparisons. These two analysis methods will be discussed in some depth. In either case, the aim is the attachment of subjective weights to all of the objectives, tactics, and components, so that in vector form, components are prioritized with respect to each tactic, tactics are prioritized with respect to each objective, and finally, objectives are prioritized with respect to policy. Ultimately, the decision weight vectors at each level are grouped in matrix format (effectiveness matrices) such that, if they are identified as

C/T—the components-to-tactics matrix
T/O—the tactics-to-objectives matrix
O/P—the objectives-to-policy matrix

then the matrix product **C/T** × **T/O** × **O/P** yields a components-to-policy vector that, when normalized, gives the desired prioritization weights.

Edinburgh Cross-Impact Analysis

The unformalized approach used in the Edinburgh model, attributed in the main to Marchant [41], is perhaps the most basic form of cross-impact analysis. The decision maker uses a pseudo Likert scale having values from 0 (least important) to 5 (most important). A Likert scale (named after its inventor) is used to measure a respondent's level of agreement on some issue. The values may be considered to be ordinal, ranging from least agreement to most agreement [48]. The decision maker uses the Likert scale to assess the importance of each element on a given hierarchical level relative to each element of the next-highest level, and produces a corresponding effectiveness matrix. When more than one decision maker is involved (as is usually the case), a consensus matrix that summarizes all the decisions can be calculated. The dimensions of all the resulting matrices for the complete hierarchy permit their consecutive multiplication, as shown in the previous section. It is noteworthy that Edwards et al. [49] have shown that judgments of magnitude, although amenable to semantic scaling (classical Likert), "are best when made numerically." This characterizes the pseudo Likert scale (see the discussion in the subsection titled "Interval Scale" later in this chapter).

The simplicity of the cross-impact approach has an obvious appeal because of its acquiescence with intuition. The input data are essentially bias-free, absolute values chosen from a Likert-type scale; there is no limit to the number of elements at a single level; and reasonable precision can be used in determining scores. The lack of uniformity among experts in their perceptions of component independence is accommodated by an *interaction percentage contribution matrix (IPCM)*. This is a component-to-component square matrix showing the degree to which the contribution of a component to fire safety is enhanced by the interaction of other components. The reader will find an example in Stollard [43].

Hierarchical Cross-Impact Analysis (HCIA) Methodology

Hierarchical cross-impact analysis (HCIA) is a multiattribute weighting strategy developed at the University of Ulster using a similar philosophy to the Edinburgh approach. The characterization of HCIA, fully developed by Donegan et al. [28], addresses the cross-impact approach at two levels—the fundamental level and the pragmatic level. In the *fundamental level*, a pseudo axiomatic approach is taken to

- Define a hierarchy in relation to fire safety
- Explain the meaning of interactive importance
- Propose the notion of a partial impact
- Define a total impact
- Introduce sequential perturbations

In the *pragmatic level,* a modeling approach is taken to

- Maintain the assessment interval through each stage of the quantification
- Stretch the component ranking intervals to enhance the important components and decrease the psychological significance of the less-important components
- Perturb consensus weightings with interaction noise

HCIA methodology formalizes many aspects of the Edinburgh approach. It uses a similar hierarchical cross-impact analysis over the different levels in the system, but allows for interactions between issues at the same level by the use of perturber matrices. Again, it can be used only for hierarchical networks.

Using the attribute terminology outlined above, the partial impact of tactic T_j on component C_i relative to the rth objective O_r is written and defined as

$$\partial I\left(C_i/T_j\right)_{O_r} = \left(C_i/Tj\right)\left(T_j/O_r\right)$$

The total impact of the collection of tactics on C_i relative to O_r is then defined as

$$\sum_{j=1}^{n} \partial I\left(C_i/T_j\right)_{O_r} = \sum_{j=1}^{n} t_{ij}\sigma_{jr}$$

which is clearly a matrix product. The elimination of the tactics collection of attributes is completed by defining the interaction

$$C_i/O_r = \sqrt{\frac{1}{n}\sum_{j=1}^{n} t_{ij}\sigma_{jr}}$$

thus giving a components-to-objectives interaction matrix. Similarly, the objectives collection of attributes is eliminated leaving a components-to-policy vector.

The pairwise comparison perturbation matrices, utilized at all the levels in the hierarchy to eliminate the problems of interdependence of issues, are symmetric and generally sparse. These adjust for "noise" in the system resulting from vagueness in the definitions of the attributes at each level.

While the forced stretching of the final vector as described in Donegan et al. [28] was purely subjective and appeared to have some significance at that time, it was recognized that such a strategy was contextually motivated and, unless unanimously adopted by the fire research community, could result in serious obfuscation. Research reported in Dodd and Donegan [45] points to indigenous stretching as a naturally occurring feature of some scales and therefore a factor in scale choice. Although research by Saaty and Vargas [50] illustrates how particular measurement techniques are more appropriate in certain situations, there is the concomitant psychological impact on scoring that results from the manner in which a question is posed—see, for example, the paper by Salo and Hämäläinen [51]. Insufficient contextual research to date leaves this psychological issue unresolved.

In spite of its formality, HCIA, just like its parent the Edinburgh model, suffers from one serious drawback—the absence of a consistency check. Even in the short time taken to score a set of issues, mood changes, tiredness, or lack of concentration can influence judgment. Short of an alternative to cross-impact analysis, no reliable quality measure has yet been devised to allay this shortcoming. It was this concern that

prompted Shields and Silcock [52] to consider using the analytic hierarchy process due to Saaty [31].

Analytic Hierarchy Process (AHP)

The analytic hierarchy process (AHP) is a procedure that has been widely recognized and used as a method of prioritizing the elemental issues in complex problems in a variety of applications (see, for example, Rahman and Frair [53], Liu and Xu [54], and Vachnadze and Markozashvili [55]). Unlike traditional multiattribute techniques, AHP permits the integration of alternatives into the hierarchy, a merging of the real and theoretical worlds depicted in Fig. 77.11, though this is not an essential requirement of the process. AHP can also be used as a means of weighting attributes, if desired; it is this latter option that is of concern here. The procedure entails the comparison of all the pairs of individual attributes at each level relative to each attribute in the superior level. The intrinsic complexity of the process prohibits a simple description.

The technique is based on the fact that for a square matrix, **C,** of nonnegative real numbers representing, for example, pairwise comparisons of the importance of component attributes of the hierarchy with respect to one element of the next-higher tactics level, there is a dominant eigenvalue, λ, and a corresponding right eigenvector, **x,** emerging from the characteristic equation $\mathbf{Cx} = \lambda\mathbf{x}$. Given that $\mathbf{C} = (c_{ij})$, where $c_{ij} > 0$ and $i, j = 1, 2, 3, \ldots, m$; and given that $c_{ij} = 1/c_{ij}$ and the consistency condition $c_{ik} = c_{ij} \times c_{jk}$: $i, j = 1, 2, 3, \ldots, m$ holds; then it is easily shown that $\lambda = m$ and, by virtue of the fact that **C** is of unit rank, the remaining m—1 eigenvalues are each zero. For such a matrix, any column is essentially the dominant right eigenvector of priorities (weights). In reality, it is unreasonable to expect decision makers to be perfectly consistent, although a fair degree of consistency is expected. Variations from perfect consistency in **C** perturb the eigenvalues such that l is greater than m [31], the proximity of the maximum eigenvalue to the order of **C** being an indication of the consistency.

The corresponding eigenvector is normalized and the procedure repeated for each tactic in the tactics collection. The set of dominant eigenvectors is considered as an effectiveness matrix of priorities (**C/T**) between components and tactics. Similarly, priority effectiveness matrices are established for tactics to objectives (**T/O**) and for objectives to policy (**O/P**). A combined matrix multiplication (**C/T**)(**T/O**)(**O/P**) yields a component-to-policy priority (weighting) vector. In the calculation of such priorities, the matrix entries are selected from a statistically optimized set of Saaty's weightings:

$$S = \left\{\frac{1}{9}, \frac{1}{8}, \frac{1}{7}, \frac{1}{6}, \frac{1}{5}, \frac{1}{4}, \frac{1}{3}, \frac{1}{2}, 1, 2, 3, 4, 5, 6, 7, 8, 9\right\}$$

AHP Example Consider, for example, the situation where five components, C_1–C_5, must be prioritized with respect to, say, tactic T_3. The decision maker indicates the relative importance of C_1 and C_2, C_1 and C_3, C_1 and C_4, and so on, on a scale of 1–9. A score of 1 on this scale implies that the two components being compared are "of equal importance," whereas a score of 9 signifies that one of the components is "of absolute importance" relative to the other. The intermediate scores indicate varying degrees of importance between the two extremes. Obviously, the importance of any component relative to itself is unity, and the law of reciprocity holds; that is, if C_1 rates a score of 3 against C_2, then C_2 rates a score of 1/3 against C_1, and so on. Thus, these pairwise criteria comparisons by the decision maker can be incorporated into a "positive reciprocal" (terminology used by Saaty [31]) decision matrix, as shown in Fig. 77.15.

Such a matrix is a typical response from a decision maker; if it were perfectly consistent, then the eigenspectrum would be {5,0,0,0}. However, a simple calculation shows the spectrum to have a right dominant eigenvalue, λ, of 6.7 and a corresponding normalized dominant right eigenvector of [0.25, 0.14, 0.19, 0.19,

	C_1	C_2	C_3	C_4	C_5
C_1	1	3	2	2	1
C_2	$\frac{1}{3}$	1	$\frac{1}{4}$	$\frac{1}{4}$	2
C_3	$\frac{1}{2}$	4	1	$\frac{1}{2}$	3
C_4	$\frac{1}{2}$	4	2	1	$\frac{1}{5}$
C_5	1	$\frac{1}{2}$	$\frac{1}{3}$	5	1

Fig. 77.15 Positive reciprocal decision matrix

0.24] in this case. Saaty [31] defines a consistency index,

$$CI = \frac{\lambda - k}{k - 1}$$

where k is the order of the matrix, and a corresponding consistency ratio

$$CR = \frac{CI}{\text{Random consistency number}}$$

Saaty [31] provides a list of random consistency numbers, which are reviewed and updated by Donegan and Dodd [56].

The consistency check is designed to provoke the decision maker into reconsidering the entries in the decision matrix should the consistency ratio be unacceptable—for example, greater than 10 %.

Difficulties with AHP The main user criticism that can be labeled against the procedure is the number of questions that must be posed to busy experts in the exhaustive completion of a questionnaire structured around a given hierarchy. This is particularly frustrating to a research manager who may experience attrition of experts on having to elicit expert opinions on a number of rounds in pursuit of consensus. The availability of convenient AHP analysis software such as Expert Choice (by Decision Support Software Inc., in Pittsburgh) does not reduce this particular inconvenience at present. Perhaps, with increasing World Wide Web facilities and new methods in survey computing, the problem will not be so manifest. Implicit in this main criticism is the problem associated with obtaining group consensus in AHP. The question of whether to obtain consensus among experts before inputting the data into AHP, or whether to seek vector consensus when each expert's weighting vector has been evaluated, is discussed with an illustration of both methods in Tung [57].

Criticisms of a theoretical nature continue to be debated in the technical literature stemming from the paper by Dyre [58], but these are really of academic interest only and should not inhibit the potential user. Perhaps the most abused criticism is that of *rank reversal,* which, among other things, refers to the possibility that ordinal changes can take place in a list of remaining attributes when one is removed from the analysis. The debate is far from being settled, but as AHP was developed by Saaty, it is not unreasonable to quote his view on the concept of rank reversal:

> An important question in decision making is whether adding new alternatives to a decision structure should or should not affect the rank of the old ones. It was once thought that irrelevant alternatives should not affect their rank. But experiments reported in the literature have shown that rank reversal can occur for many different reasons. The decision to preserve rank depends on whether the number of alternatives added, and how good they are, influences preference among the old ones. The AHP has a procedure to preserve rank, as in buying a best computer even if there are many like it, and another to allow rank to change, as in buying a beautiful tie if there are many like it. [59]

The different opinions and complex arguments are beyond the scope of this article, but users of proprietary AHP software will have a mode selection option that will facilitate either rank reversal possibilities or absolute rank preservation.

Measurement

Measurement is defined as the assignation of a number to the entity under consideration in accordance with a rule; this number then reflects the measured property of the entity [60]. In mathematical terminology, the measurement is the image under a *monotonic,* that is, order-preserving, mapping of the dimensional property into a real line.

Considerations

Measurement of the physical entities encountered in experimental work presents a large number of fundamental problems that must be recognized by researchers. For example, the precision of the result cannot exceed the precision of any of the data used in its calculation. Thus, a result to ten significant digits is pointless when even one item of the contributory data is approximated to two significant figures. This is why 10.000 is not the same as 10; the former indicates that the measuring equipment allowed for measurements of three decimal places, and the "correct" result is therefore between 9.9995 and 10.0005, whereas the latter shows much less precision—between 9.5 and 10.5.

Further allowance must be made for experimental error. Many external factors (e.g., heavy road traffic outside the laboratory) can introduce random elements into the measuring process. These factors, however small, must be taken into account in the result. Systematic errors, caused by a bias in the measurement process, assume an even greater significance with the introduction of opinions, which can compromise the work and should be eliminated. The opinion problem is present in most questionnaire design. These opinions, or psychological components, where linearity is less measurable, can jeopardize experimental results (see detailed discussion in Viek and Wagenaar [13]).

Scaling

The four types of scale most relevant to fire protection engineering are (1) nominal, (2) ordinal, (3) interval, and (4) ratio. Each scale, in order, represents progressively stronger properties [61].

Nominal Scale The values on a *nominal scale* classify or categorize the objects represented; in other words, no information on size is implied. For example, the number identifying food items on a menu or the room number in an office block might be regarded as nominal scales. The property common to such items is the *category property*. Many coding systems are nominal scales. For example, the computer system of a car dealer might store car type as a single digit: 01 for Ford, 02 for General Motors, 03 for Lincoln, 04 for Buick, and so on. Such a number does not reflect the size or power of the car; it merely indicates the manufacturer. Similarly, fire extinguishers might be classified by type: 1 for water, 2 for CO_2, 3 for halon, and so on. However, the numbers 1–3 have no implications with regard to quality.

Ordinal Scale The *ordinal scale* not only characterizes the entities represented, but also ranks or orders them. However, proportion is not necessarily maintained. This type of scale is exemplified by examination grades: in a descending scale, a grade 2 is better than a grade 3, but one cannot say by how much. Glenburg [61] offers the stripes on military personnel as an ordinal scale: a sergeant (three stripes) is "superior" to a corporal (two stripes), but it is nonsense to argue that the sergeant is one and a half times as authoritative. Ordinal scale examples abound in organizations; one example is the ranking of daily tasks in order of priority.

Interval Scale More mathematically tractable and, hence, of greater importance in quantitative assessments, the interval scale is a continuous scale between two points, for example, from 0 to 10, or 1–5. Relative difference is maintained; that is, equal intervals of the scale have the same meaning. For example, the effective difference between 1 and 2 is exactly the same as the effective difference between 4 and 5. An example of an interval scale is a ruler or similarly graduated device. Celsius and Fahrenheit temperature scales are interval, and the *equal intervals property,* or *relative difference property,* is essential when one scale is converted to the other. Arithmetic-based operations involving addition, subtraction, and multiplication by a scalar (a number with no units) can be used on numbers from an interval scale.

Not infrequently, the integer range from 0 to 5 has been used to assign relative values of importance to the attributes of a fire safety hierarchy. The adoption of this numerical range over a spectrum of attributes, described in the literature (e.g., Dunn Rankin [62] and Torgenson [63]) as a Likert-type scale, entails a consideration of its validity in terms of the measurement it achieves. Strictly speaking, the scale is ordinal since it cannot be taken for granted that the distances between attributes are equal. Kumar [64] states that a Likert scale is based on the assumption that each item (attribute) has a priori equal attitudinal value (importance or weight) in terms of reflecting an attitude (from 0 to 5) toward the issue in question, which in the context of fire safety attribute weighting is not the case. Nevertheless, the work of Schiebe et al. [30] has demonstrated that the error in assuming the equal interval property is not significant. Hence, the results obtained from such measurements can be used in combinatorial calculations.

Ratio Scale The *ratio scale* is an interval scale with the *absolute zero property;* in other words, one end is fixed so that the values on it are absolute rather than relative. For example, the Kelvin (K) scale relates temperature to absolute zero temperature, at which all motion ceases. This scale is fundamental to the operation of AHP (see the previous section titled "Analytic Hierarchy Process (AHP)"), and due consideration must be given to the entity of measurement. For example, a body having a temperature of 40 °C indicates twice the temperature of another body at 20 °C, but not twice the heat content, which must be referred to the absolute zero of temperature, −273 °C.

Panels of Experts

The development of expert systems and case-based reasoning tools implies an underlying assumption as to the meaning of expertness. Consequently the assessment of expert opinion using, for example, a Delphi process, may lead to conclusions that, without some formal insight, could on some occasions be considered ambiguous. A review of Delphi literature (Rowe and Wright [65]) will not solve this problem, since Delphi researchers fail to define the term *expert* as applied to their study. If, in simplistic terms, an expert is regarded as one practiced or skillful within the area of consideration, there is an intuitive extrapolation as to the notion of expertise, and the assessment of expert opinion relies to some extent on a global understanding of this extrapolation. In general, the expert response must conform to some form of measurement criterion in relation to consensus if any conclusion is to be reached on any issue that is the subject of expert opinion.

On the assumption that more heads are better than one in achieving a balanced view, many different forums for assessing group opinion have been utilized over the years (see Schiebe et al. [30]). Some of the most common means of assessing group opinion are discussed as follows.

Committee

The traditional method of forming group opinion is the committee. Under the guidance of a (impartial) chairperson, the issue is isolated (if necessary) and debated, with consensus determined by a majority vote. Besides the obvious discrepancy that a majority and consensus are not synonymous, the recognized difficulties with the method are the existence of one dominant member and group pressure upon an individual to conform (the herd instinct). Thus, the resultant group pronouncement may not be at all representative of the group.

Nominal Group

A committee is strictly a subgroup of a large organization from which its authority is derived. More relevant to a panel of experts, that is, the pooling of considered opinion, are nominal groups and variations thereof. In this situation,

the alternatives are created by the panel members when they are each outside the group context. The individual members' lists, circulated before meetings, are then pooled. Personality issues are reduced, the dominant member should be the member best prepared, authorship of ideas is on record and cannot be disputed, and preconsideration should reduce the herd instinct.

Delphi Panel

Of more rigorous delineation is the Delphi panel (Linstone and Turoff [66], Render and Stair [67], Rowe and Wright [65], Wheelwright and Makridakis [68]), devised as a method of obviating the practical difficulties inherent in the committee concept. In the Delphi panel, the group members never meet physically; all communication is through a group controller or coordinator who selects the members of the panel, presents the basic problem, and informs the individuals in the group of progress to date (feedback). When the atomic or elemental issues that constitute the main problem have been determined (the qualitative phase), consensus is sought on the quantitative value to be ascribed to each of these issues (statistical response).

A series of rounds of voting is held. After each round the group controller returns to each panel member his or her scores together with a measure of the group opinion on each issue. The panel members are then asked if they wish to revise their opinions. The process is repeated until group opinion has converged sufficiently to be described as consensus, or until it is recognized that a consensus is unattainable. Unanimity is less important in the method than the absence of group pressure.

The two essential characteristics in a Delphi panel are (1) the anonymity of panelists and (2) feedback (histograms, measures of central tendency, or analytic consensus). The former eliminates the problem of the dominant member and group pressure to conform. However, a new problem is introduced—a considerable time scale is involved in the sending and receiving of questions and answers. While this (at least) theoretically guarantees a considered opinion, a substantial attrition rate is almost inevitable. Members of the group lose interest, change jobs, or become otherwise indisposed. Also, the group controller has a role of far greater significance than a committee chairperson; only a high level of awareness on his or her part can prevent the unconscious bias that might be introduced. Other doubts about and difficulties with the method are summarized by Marchant [69], Shields et al. [70], Sackman [71], and Ayton et al. [72].

Computer Conferencing

Modern technology enables remote participation in group discussion. Participants input their views into a computer system, and their views are circulated to the other panelists for comment and reply. A suitable schedule allows either a quick result or a more leisurely, considered process. Anonymity is optional.

This concept can be combined with others, for example, the Delphi method, with a reduction of time scale and consequent diminishing of attrition (i.e., drop-outs). Further, if a computer system for analyzing these data exists, the results may be obtained almost instantaneously. Hence, the group may have access to the consequences of their polling before their views are forgotten. The almost universal availability of the Internet and ISDN developments in survey computing are already having a considerable impact on this type of conferencing.

DACAM Group

A DACAM group [73] is an alternative method of overcoming the problem with committees. Here, the group meets physically but is divided (usually systematically) into subgroups for discussion sessions. Between each session, representatives from the subgroups meet to compare progress and coordinate the agenda for the next session. In this way, the dominant member, being limited to one subgroup, is less influential on the group decision.

While this method guarantees a quick result (e.g., in a day), the facility to organize such a

group is dependent on at least substantial goodwill, if not considerable finance.

Consensus

The notion of consensus is very much an intuitive one. In politics, there is "consensus" on a policy that is acceptable to a majority. If no consensus exists, then it can often be achieved by broadening the policy. However, the concept is very largely negative in that the emphasis is on avoidance of what is intolerable to others.

The nature of consensus depends on the context or terms of reference of the problem. For example, the arrangement of a number of options in order of importance or preference (comparative consensus) is essentially different from assessing the importance of a single elemental issue within the problem (definitive consensus).

Definitive Consensus

Definitive consensus involves panel members who assign to each issue a score chosen from a Likert-type scale, that is, a range of values, such as (0,10) or (0,5). For example, one might say that a very definite consensus had been reached if a comfortable majority (say, 60 %) agreed on an exact value, or if a substantial majority (say, 75 %) agreed on a small range, or if all agreed to within a slightly larger range. Thus, there is a balance between the number conforming to the view and the range permitted.

The essential problem, however, is finding mechanisms for representing and assessing the opinions on each individual issue for the complete panel, in other words, mechanisms that provide the following for the set of scores for each issue:

- A profile of the scores
- A focal point of agreement (if any)
- A measure of the agreement at that point

Additional problems arise if the panel is divided into several groups, each of which is in internal accord. This is referred to as *split consensus,* or a *multimodal* situation. The interested reader will find a mathematical function (neighborhood consensus) that addresses these issues in Donegan and Dodd [74].

Traditionally, a histogram was generally used as a profile, and the presence or absence of consensus was determined by a statistical measure of dispersion. Chatterjee and Chatterjee [75] discuss mean- and median-based methods together with the compromises referred to as the trimmed and windsorized means. A *trimmed mean* excludes extreme values, and in a *windsorized mean,* the extreme values are replaced by the second-most extreme values. Some of the assumptions and drawbacks of these measures, for example, the nonrepresentativeness of the mean, the instability of the mode, and the inconsistency and precision-dependence of the median, are described in Dodd and Donegan [76].

It is worth pointing out here the difference between consensus and compromise. If on a scale of 0–5, one-half of a group selects 0 and the other half selects 5, then 2.5 is a compromise score. It would be inaccurate, however, to describe 2.5 as a consensus score, since this figure is not representative of any members of the group and, therefore, not a measure of the group itself. There is, in fact, no consensus among the group.

Alternative Stability Approach

A major problem with, for example, Delphi studies is that stability may set in before consensus has been achieved, and the latter might therefore never be reached. When seeking consensus on a large number of issues, this is highly likely for some of the issues and quite consistent with Delphi philosophy, which is more concerned with narrowing the spread of diverse opinions than enforcing an artificial consensus.

It is possible and perhaps simpler to use a definition of stability (based on a comparison of successful rounds) as the termination criterion for a Delphi panel. This would also allow item/individual/tactic/group stability to be considered. The definition of stability might be based on the

ratio of total scores for two rounds, for example, the average of the moduli of the differences between the rounds. Linstone and Turoff [66] suggest the quadratic mean as a refinement of this. Alternatively, if the data were normalized (i.e., translated and magnified to fit a uniform distribution), it might be simpler to use Pearson's correlation coefficient.

The principal advantage of the alternative stability approach is that stability is almost certain to be achieved, and fairly rapidly. It is generally recognized that stability is normally achieved within four polling rounds in most Delphi panels (see Render and Stair [67]).

Comparative Consensus

Comparative consensus involves a panel of individuals who must decide on an arrangement of *n* issues (or objects) in order of importance or merit. For the sake of simplicity, let the issue be a number from 1 to *n*. Each panel member decides on an arrangement that might be expected to differ from the arrangements of others. Two problems can arise—(1) establishing a universally acceptable arrangement, and (2) the amount of agreement among the panel. A typical example of this situation might be the selection of an agreed priority list from ten independent lists returned by experts whose task is to rank in order of importance the following safety features: fire extinguishers, smoke alarms, sprinklers, flashing lights, and direction signs.

Comparative consensus [77] also involves only the *ranking* of a number of issues (in contrast to the simpler notion of definitive consensus, as described above, in which the agreement of a panel on a single issue is assessed). The obvious question in the situation where several panelists judge several issues is whether (1) it is preferable to determine the agreement on each issue on the basis of scores and then determine rank on the basis of the consensus scores, or whether (2) each panel member should rank all the issues on the basis of his or her scores and subsequently look for consensus on the set of rankings. This has never been satisfactorily resolved.

Compound Consensus

Compound consensus arises when, for example, a panel is required to produce an agreed ranking (with weightings) for a set of issues. This type of consensus can occur when AHP is used by a relatively small panel to produce a set of rankings. The obvious question is whether it is better to (1) find (definitive) consensus among the panel on the issue and then rank the issue for the whole panel, or (2) let each panel member rank the issues and then seek (comparative) consensus on the rankings. Compound consensus allows a weighting of each of the issues to be taken into account.

References

1. G.T. Castino and T.Z. Harmathy, "Fire Risk Assessment," *ASTM (STP) 762,* ASTM, Philadelphia (1982).
2. M. Gretener, *Fire Risk Evaluation,* Association of Cantonal Institutions for Fire Insurance, Society of Engineers and Architects and Fire Prevention Services for Industry and Trade, Zurich, Switzerland (1980).
3. J.R. Hall, "Key Distinctions in and Essential Elements of Fire Risk Analysis," *Fire Safety Science—Proceedings of the 3rd International Symposium on Fire Safety Science,* Edinburgh, Scotland, pp. 467–474 (1991).
4. M.M. Hirschler, "Fire Hazard and Risk Assessment," *ASTM (STP) 1150,* ASTM, Philadelphia (1992).
5. J.M. Watts, "Dealing with Uncertainty: Some Applications in Fire Protection Engineering," *Fire Safety Journal,* 11, pp. 127–134 (1986).
6. J.M. Watts, "Criteria for Fire Risk Ranking," *Fire Safety Science—Proceedings of the 3rd International Symposium on Fire Safety Science,* Edinburgh, Scotland, pp. 457–466 (1991).
7. R.L. Winkler and A.H. Murphy, "Good Probability Assessors," *Journal of Applied Meteorology,* 7, pp. 751–758 (1968).
8. D.W. Bunn, *Applied Decision Analysis.* McGraw-Hill, New York (1984).
9. S. French, "On the Axiomatisation of Subjective Probabilities," *Theory and Decision,* 14, pp. 19–33 (1982).

10. S. French, *Decision Theory—An Introduction to the Mathematics of Rationality,* Ellis Horwood, Chichester, UK (1988).
11. D.V. Lindley, *Making Decisions,* Wiley, New York (1971).
12. H. Raiffa, *Decision Analysis,* Addison-Wesley, Glenview, IL (1968).
13. C. Viek and W.A. Wagenaar, *Judgment and Decision Under Uncertainty,* Institute for Experimental Psychology, University of Groningen, The Netherlands. (Reprinted from *Handbook of Psychonomics,* Vol. II., North-Holland Publishing Company, Amsterdam 1979.)
14. A. Sekizawa, *Statistical Analyses of Fatalities—Characteristics of Residential Fires,* ISFSS, Edinburgh, Scotland, pp. 475–484 (1991).
15. F. Noonan and R. Fitzgerald, "On the Role of Subjective Probabilities in Fire Risk Management Studies," *Fire Safety Science—Proceedings of the 3rd International Symposium on Fire Safety Science,* Edinburgh, Scotland, pp. 495–504 (1991).
16. D. Dubois and H. Prade, *Possibility Theory: An Approach to Computerized Processing of Uncertainty,* Plenum, New York (1988).
17. L.A. Zadeh, "The Role of Fuzzy Logic in the Management of Uncertainty in Expert Systems," *Fuzzy Sets and Systems,* 11, pp. 149–184 (1983).
18. G. Klir and T.A. Folger, *Fuzzy Sets, Uncertainty and Information,* Prentice Hall, Upper Saddle River, NJ (1988).
19. D.E. Bell, H. Raiffa, and A. Tversky, "Descriptive, Normative and Prescriptive Interactions in Decision Making," in *Decision Making*: *Descriptive, Normative and Prescriptive Interactions* (D.E. Bell, H. Raiffa, and A. Tversky, eds.), Cambridge University Press, Cambridge, UK, pp. 9–30 (1988).
20. H.A. Taha, *Operations Research,* Prentice Hall, Upper Saddle River, NJ (1997).
21. T.J. Shields and G.W. Silcock, *Buildings and Fire,* Longman Scientific and Technical, Harlow, UK (1987).
22. NFPA 550, *Guide to the Fire Safety Concepts Tree,* National Fire Protection Association, Quincy, MA (2007).
23. P.S. Laplace, *Essai Philosophique sur les Probabilities,* 5th ed., Paris. Translation by Dover, New York (1952).
24. A. Wald, *Statistical Decision Functions,* Wiley, New York (1950).
25. L.J. Savage, "The Theory of Statistical Decision," *Journal of the American Statistical Association,* 46, pp. 55–67 (1951).
26. L. Hurwicz, "Optimality Criteria for Decision Making Under Ignorance," *Discussion Paper No. 370,* Cowles Commission (1951).
27. R.L. Keeney and H. Raiffa, *Decisions with Multiple Objectives: Preferences and Value Trade-Offs,* Wiley, New York (1976).
28. H.A. Donegan, T.J. Shields, and G.W.H. Silcock, "A Mathematical Strategy to Relate Fire Safety Evaluation and Fire Safety Policy Formulation for Buildings," in *Proceedings of the 2nd International Symposium on Fire Safety Science,* Tokyo, Japan, pp. 433–441 (1988).
29. G. Ramachandran, *The Economics of Fire Protection,* E & FN Spon, London, UK (1995).
30. M. Schiebe, M. Scutsch, and J. Schofer, "Experiments in Delphi Methodology," in *The Delphi Method: Techniques and Applications* (H.A. Lindstone and M. Turoff, eds.), Addison-Wesley, Glenview, IL, pp. 262–282 (1975).
31. T.L. Saaty, *The Analytical Hierarchy Process,* McGraw-Hill, New York (1980).
32. N.P. Loomba, *Management—A Quantitative Perspective,* Collier Macmillan, Canada (1978).
33. J.M. Watts, personal communication (2000).
34. H.A. Simon, *Administrative Behaviour,* Macmillan, New York (1961).
35. T.J. Shields, G.W. Silcock, and H.A. Donegan, "Towards the Development of a Fire Safety Systems Evaluation for Public Assembly Buildings," *Construction Management and Economics,* 8, pp. 147–158 (1990).
36. W. Edwards, "Social Utilities," *Engineering Economist,* 6, pp. 119–129 (1971).
37. P. Goodwin and G. Wright, *Decision Analysis for Management Judgement,* Wiley, New York (1998).
38. W. Edwards and J.R. Newman, *Multiattribute Evaluation,* Paper No. 26, Sage Publications, London, UK (1982).
39. J.M. Watts, "Fire Risk Ranking," in *SFPE Handbook of Fire Protection Engineering,* 5th ed., National Fire Protection Association, Quincy, MA, pp. 5-12–5-26 (1995).
40. H.E. Nelson and A.J. Schibe, "A System for Fire Safety Evaluation of Health Care Facilities," *NBSIR 78-1555,* Center for Fire Research, National Bureau of Standards, Washington, DC (1980).
41. E.W. Marchant, *Fire Safety Evaluation (Points) Scheme for Patient Areas Within Hospitals: A Report on Its Origins and Development,* University of Edinburgh, Scotland (1982).
42. E.W. Marchant, "Fire Safety Engineering—A Quantified Analysis," *Fire Prevention,* 210, pp. 34–38 (1988).
43. P. Stollard, "The Development of a Points Scheme to Assess Fire Safety in Hospitals," *Fire Safety Journal,* 7, 2, pp. 145–153 (1984).
44. T.J. Shields, G.W. Silcock, and Y. Bell, "Fire Safety Evaluation of Dwellings," *Fire Safety Journal,* 10, 1, pp. 29–36 (1986).
45. F.J. Dodd and H.A. Donegan, "Prioritisation Methodologies in Fire Safety Evaluation," *Fire Technology,* 30, 2 (2nd Quarter), pp. 232–249 (1994).
46. F.J. Dodd and H.A. Donegan, "Some Considerations in the Combination and Use of Expert Opinions in

Fire Safety Evaluation," *Fire Safety Journal,* 22, 4, pp. 315–327 (1994).
47. S.-K. Lai and L.D. Hopkins, "The Meaning of Trade-Offs in Multiattribute Evaluation Methods: A Comparison," *Environment and Planning B*: *Planning and Design,* 16, pp. 155–170 (1989).
48. R.M. Sirkin, *Statistics for the Social Sciences,* Sage Publications, Thousand Oaks, CA (1995).
49. W. Edwards, M. Guttentag, and K. Snapper, "Effective Evaluation: A Decision Theoretic Approach," in *Evaluation and Experiment: Some Critical Issues in Assessing Social Programmes* (C.A. Bennett and A. Lumsdaine, eds.), Academic, New York (1975).
50. T.L. Saaty and L.G. Vargas, "Experiments on Rank Preservation and Reversal in Relative Measurement," *Mathematical and Computer Modelling,* 17, pp. 13–18 (1993).
51. A.A. Salo and R.P. Hämäläinen, "On the Measurement of Preferences in the Analytic Hierarchy Process," *Journal of Multi-Criteria Decision Analysis,* 6 (1998).
52. T.J. Shields and G.W. Silcock, "An Application of the Analytic Hierarchy Process to Fire Safety Evaluation," *Fire Safety Journal,* 11, 3, pp. 235–242 (1986).
53. S. Rahman and L.C. Frair, "A Hierarchical Approach to Utility Planning," *Energy Research,* 8, pp. 185–196 (1984).
54. B. Liu and S. Xu, "Development of the Theory and Methodology of the Analytic Hierarchy Process and Its Applications in China," *Mathematical Modelling,* 9, 3–5, pp. 179–184 (1987).
55. R.G. Vachnadze and N.I. Markozashvili, "Some Applications of the Analytic Hierarchy Process," *Mathematical Modelling,* 9, 3–5, pp. 185–191 (1987).
56. H.A. Donegan and F.J. Dodd, "A Note on Saaty's Random Indexes," *Mathematical and Computer Modelling,* 15, 10, pp. 135–137 (1991).
57. Y.A. Tung, "Time Complexity and Consistency Issues in Using the AHP for Making Group Decisions," *Journal of Multi-Criteria Decision Analysis,* 7, pp. 144–154 (1998).
58. J. Dyer, "Remarks on the Analytic Hierarchy Process," *Management Science,* 36, 3, pp. 249–258 (1990).
59. T.L. Saaty, *The Analytic Network Process,* RWS Publications, Pittsburgh, PA (1996).
60. N.C. Barford, *Experimental Measurements: Precision, Error, and Truth,* 2nd ed., John Wiley and Sons, New York (1987).
61. A.M. Glenburg, *Learning from Data: An Introduction to Statistical Reasoning,* Harcourt Brace Jovanovich, Orlando, FL (1980).
62. P. Dunn Rankin, *Scaling Methods,* Lawrence Erlbaum Associates, NJ (1983).
63. W.S. Torgenson, *Theory and Methods of Scaling,* Wiley, New York (1958).
64. R. Kumar, *Research Methodology,* Sage Publications, London, UK (1999).
65. G. Rowe and G. Wright, "The Delphi Technique as a Forecasting Tool: Issues and Analysis," *International Journal of Forecasting,* 15, pp. 353–375 (1999).
66. H.A. Linstone and M. Turoff, *The Delphi Method: Techniques and Applications,* Addison-Wesley, Glenview, IL (1975).
67. B. Render and R.M. Stair, *Quantitative Analysis for Management,* 2nd ed., Allyn and Bacon, Boston (1985).
68. S.C. Wheelwright and S. Makridakis, *Forecasting Methods for Management,* 4th ed., Wiley, New York (1985).
69. E.W. Marchant, "Problems Associated with the Delphi Technique," *Fire Technology,* 24, 1, pp. 59–62 (1989).
70. T.J. Shields, G.W. Silcock, H.A. Donegan, and Y. Bell, "Methodological Problems Associated with the Delphi Technique," *Fire Technology,* 23, 3, pp. 175–185 (1987).
71. H. Sackman, "Delphi Assessment: Expert Opinion, Forecasting and Group Progress," *Paper R-1283-PR,* Rand Corporation, Santa Monica, CA (1974).
72. P. Ayton, W.R. Ferrell, and T.R. Stewart, "Commentaries on 'The Delphi Technique as a Forecasting Tool: Issues and Analysis' by Rowe and Wright," *International Journal of Forecasting,* 15, pp. 377–381 (1999).
73. R.E. Norton, *The DACAM Handbook,* Leadership Series 67, National Center for Research in Vocational Education, Columbus, OH (1987).
74. H.A. Donegan and F.J. Dodd, "An Analytical Approach to Consensus," *Applied Mathematics Letters,* 4, 2, pp. 21–24 (1991).
75. S. Chatterjee and S. Chatterjee, "On Combining Expert Opinions," *American Journal of Mathematical and Management Science*, 7, 3 and 4, pp. 271–295 (1987).
76. F.J. Dodd and H.A. Donegan, "The Representation and Combination of Opinions," in *Proceedings of ILIAM,* 6 (H.A. Donegan, ed.), University of Ulster, Belfast, Northern Ireland, pp. 17–29 (1989).
77. F.J. Dodd and H.A. Donegan, "Comparative and Compound Consensus," *Applied Mathematics Letters,* 5, 3, pp. 31–33 (1992).

H.A. Donegan is Reader Emeritus in the School of Computing and Mathematics at the University of Ulster, Northern Ireland.

Data for Engineering Analysis

78

Marty Ahrens and John R. Hall Jr.

Introduction

This chapter addresses sources of input data required for deterministic (e.g., fire hazard) or probabilistic (e.g., fire risk) engineering analysis, such as performance-based design, code change analysis, product evaluation analysis, or major fire reconstruction. An overview of types of analysis engineers may perform, with a brief discussion of the kinds of engineering problems that should be addressed using those kinds of analysis, is given in the list below. Table 78.1 shows the fire-related phenomena that must be characterized and types of data required to model the phenomenon for each type of analysis listed.

Types of Analysis and Data Needs

- (General) fire risk analysis refers to a comprehensive analysis of fire risk associated with a range of situations, whether or not there is a particular focus for the analysis, and is set up in a classic risk analysis format, using scenarios and scenario clusters in a scenario structure, and requiring data on probabilities for each scenario cluster and consequences for each scenario.
- Fire hazard or risk analysis of a burnable product is needed for evaluation and possibly certification for acceptability (possibly for equivalence to a product regulation) of a product, material, assembly, component, and so on whose role in fire is as something that burns, either the first item ignited or a major fuel source during fire development.
- Fire hazard or risk analysis of a design for an occupiable space is needed for assessment and possibly approval of a design for an entire building (possibly under equivalence or relative to a performance-based code).
- Fire hazard or risk analysis is also appropriate for evaluation and possibly approval of products whose roles in fire are as heat sources that initiate fires.
- Engineering analysis can be appropriately applied to the performance of automatic detection/alarm or suppression systems or of other active fire protection systems.
- Engineering analysis can be appropriately applied to the performance of passive fire protection, such as walls, doors, and structural members.
- Engineering analysis can be appropriately applied to the performance of features designed to ensure safe evacuation of occupants from a building with a developing fire.

As Table 78.1 shows, regardless of the type of analysis required, the same generic types of data are typically needed, which may be organized into these few sources:

- Fire incident and field observation (i.e., nonincident event) data
  Probabilities of ignition or of reliability, given naturally occurring variation in conditions

M. Ahrens (✉) • J.R. Hall Jr.

M.J. Hurley (ed.), *SFPE Handbook of Fire Protection Engineering*,
DOI 10.1007/978-1-4939-2565-0_78, © Society of Fire Protection Engineers 2016

Table 78.1 Types of analysis and associated data needs

Type of analysis	Phenomena	Data needs
General fire risk analysis	Ignition—probability of fire, by scenario	Fire incident data, exposure data
	Consequence—measures of severity of fire, by scenario	Fire incident data, laboratory test results
Burnable product fire hazard or risk analysis	Ignition—probability of fire, by scenario, for different versions of the product	Laboratory test results (related to scenarios, including specific ignition sources), fire incident data, product usage data
	Burning characteristics of product once ignited—time curve for heat release rate, peak heat release rate, flame spread rate, effective heat of combustion, rate of production of smoke or toxic species	Laboratory test results
	Reliability of product—probability, mode or nature, and magnitude of "failure," defined as any deviation from nominal product performance	Field observations (e.g., probability of poor quality control in manufacture of product), usage data (e.g., age effects related to performance, degradation due to wear or vandalism)
	Contribution to harm to people—toxic species production by mass loss ratio or mass loss rate, toxic potency of species, time rate of production of vision-reducing products of combustion	Laboratory test results (of characteristics and effects of fire conditions produced when product burns)
	Contribution to harm to property—mass loss rate by combustion product, corrosivity or other chemical characteristics by combustion product	Laboratory test results (of characteristics and effects of fire conditions produced when product burns)
	Contribution to other harm—environmental impact, impact on heritage	
Design for occupiable space fire hazard or risk analysis	Ignition and burning characteristics	Laboratory test results (related to scenarios, including specific ignition sources), fire incident data, product usage data
	Transition to flashover	Design specifications (e.g., compartment dimensions, thermal properties of compartment surface linings, venting), laboratory test results, other measured or estimated conditions
	Burnout time	Field surveys (fuel load or fuel mass available, compartment geometry, ventilation), laboratory tests (mass burning rate, heat of combustion)
	Space to space fire spread—flame spread rate	Design specifications (e.g., measures of barrier integrity), laboratory test results, other measured or estimated conditions (e.g., paths of fire spread such as HVAC), fire duration (see burnout time)
	Structural performance—collapse or damage making use of building unsafe	Laboratory test results, field observations
	Contribution to harm to people	Same as for burnable product analysis
	Contribution to harm to property	Same as for burnable product analysis
	Contribution to other harm	Same as for burnable product analysis

(continued)

Table 78.1 (continued)

Type of analysis	Phenomena	Data needs
Heat source product fire hazard or risk analysis	Ignition—probability of fire, by scenario, for different versions of the product	Laboratory test results, fire incident data, product usage data
	Reliability of product—probability, nature, and magnitude of deviations from nominal product performance	Field observations (e.g., probability of poor quality control in manufacture of product, testing, and maintenance records), usage data (e.g., component failure due to age, degradation due to usage or vandalism)
Active fire protection performance	Time of activation	Laboratory test results (e.g., physical conditions leading to system activation), fire incident data
	System effect—measures of system output (e.g., sound, suppression agent)	Laboratory test results, fire incident data
	Reliability—probability, nature, and magnitude of deviations from nominal system performance	Field observations (e.g., probability of poor quality control in manufacture of product, testing, and maintenance records), usage data (e.g., component failure due to age, degradation due to usage or vandalism)
Passive fire protection performance	Time performing function (e.g., time blocking spread of fire, time providing structural integrity while subjected to fire conditions)	Laboratory test results (on passive fire protection element, reflecting materials, and type of design or construction), fire incident data, burnout time (see previous reference to burnout time as a phenomenon; it is a calculated time for fire duration exposing a passive fire protection element)
	Feature effect—degree to which function is performed (e.g., quantity of fire effects permitted to pass barrier)	Laboratory test results, fire incident data
	Reliability—probability, nature, and magnitude of deviations from nominal feature performance	Field observations (e.g., impairment prior to fire, such as poke- through holes in wall or doors blocked open, probability of poor quality control in manufacture of product), usage data (e.g., component failure due to age, degradation due to usage or vandalism), laboratory test results
Evacuation and other human behavior	Occupant characteristics	Field observations, laboratory test results, design specifications, and estimated conditions

Fire size and consequences, given specified values of certain conditions, factors, or characteristics of interest and naturally occurring variation in all others

Characteristics and behavior of people

- Usage or exposure data

  Denominators for probability calculations from event data (e.g., number of portable electric heaters versus wood stoves in use, to support estimates of fires per year per unit; number of gasoline service stations, to support estimates of probability of fire per service station per year; number of square feet of office space, to support estimates of probability of fire per square foot of office space per year)

- Laboratory test results

  Fire size (e.g., heat release rate) as a function of time, given planned variation in certain conditions (e.g., fuel load) and unplanned variation in those not recognized or measured (e.g., exact location of fuel items and their proximity to each other)

  Probabilities of ignition or of reliability, given planned variation in conditions (measured as numbers of ignitions or numbers of failures divided by numbers of trials, although fire and equipment failure tend to be such rare events that measurement of probabilities in the laboratory can be impractical)

Fire consequences, including specific effects on people (actually data for estimation of effects on people, for example, via animal tests or toxic effects models based on species concentrations and exposure times) or on property, as a function of time and of specified or measured conditions

Discussion of data types and sources will be organized, therefore, around incident data, field observation data, usage or exposure data, and laboratory test results. The last type will be addressed only briefly, as it is the type most familiar already to fire protection engineers and most thoroughly discussed in the other chapters of this handbook.

Incident Data

How often do certain items catch fire, or certain types of equipment start fires, or certain types of occupancies have fires? The first component in all these calculations is data on event frequencies per unit of time. Fire experience data will include a number of fires involving products, occupancies, or other subjects of analysis that are in widespread use and identified in a fire data collection system. These data can be combined with usage data to calculate event frequencies.

If the product, occupancy class, or circumstance is new or not identifiable in the data system, it will not be reflected in current fire experience data. Laboratory tests in a full range of relevant scenarios may be necessary to calibrate the likelihood of ignition for a new product against the likelihood of ignition for a typical established product or mix of products.

There are no standard test protocols for such a calibration. Because ignition is typically a rare event, it may be difficult and expensive to obtain test-based estimates of these relative likelihoods. Subjective estimation and interpretive judgment will likely be required and may in some instances be the only basis available for ignition probability estimates for new products. (For example, experts might agree that a new product will be roughly a third to a half less likely to be involved in fire ignitions than a typical product now in use.)

If fire experience history is relevant, it is important that estimates be drawn from suitable, statistically representative databases and procedures. In the United States, this means starting with national estimates derived from the detail in the U.S. Fire Administration's (USFA's) National Fire Incident Reporting System (NFIRS) and the estimated totals from the National Fire Protection Association's (NFPA) annual survey of fire departments for projection of NFIRS to national estimates [1–3].

National Fire Incident Reporting System

NFIRS Overview In the United States, local fire departments use NFIRS to document their responses. In the process, they function as data collectors for a system that enables analysis of local, state, and national fire problems. NFIRS captures data about the property use or occupancy where the fire occurred, the item first ignited and its composition, general type of equipment involved in ignition, heat source, factor contributing to ignition, number of stories, level of fire origin, and performance of automatic detection and suppression systems.

NFIRS is the largest and most detailed fire incident database in the world, capturing almost a million individual fire incidents a year in 2006–2010, or roughly two–thirds of the fires reported to local fire departments. In the 1980s and 1990s, NFIRS received data from some or all communities in roughly 40 of the 50 states, plus the District of Columbia, although not all participating communities or states were able to submit data every year. In 2010, the NFIRS database included at least some reports from all 50 states and the District of Columbia. Participation in NFIRS is voluntary at the federal level. Different states have different reporting requirements, ranging from mandatory reporting of all incidents or fires to mandatory reporting of just those fires resulting in a casualty or dollar loss of a certain size or to completely voluntary reporting. State resources can affect participation

even if local fire departments are completing the NFIRS reports. Participation rates in NFIRS and practices regarding the types and severity of incidents reported are not necessarily uniform across regions and sizes of community. Also, some incidents from participating departments are never submitted or have errors that prevent inclusion into the national database. Both region and community size, in turn, are correlated with frequency and severity of fires, which means NFIRS may be susceptible to systematic biases.

A 2005 NFPA survey of NFIRS participant communities versus nonparticipant communities found that participant communities tended to have statistically significant differences in annual rates of dwelling and other structure fires and in some other (but far from all) major measures of fire experience [4].

Version 5.0 of NFIRS Like most well-established data systems, NFIRS has had both major and minor revisions. The most extensive and last major revision was the introduction of Version 5.0, or NFIRS 5.0, in 1999. Due to the extensive changes in data elements, categories, and coding procedures, extreme caution must be used in comparing data from 1980 to 1998 with data from the later years. NFIRS 5.0 was adopted gradually, so the transition years of 1999–2002 are also volatile. More questions were added about automatic fire suppression and detection equipment, including presence, type, operation, effectiveness, and reasons for failure or ineffectiveness. Structure Status, which indicates if a property is normally occupied, idle, vacant, under construction, renovation or demolition, is another new data element. More choices were added for Equipment Involved in Ignition, which is no longer a required field. When equipment is involved, information on the power or fuel source is also requested. Other optional data elements collect information about On-Site Materials and Suppression Factors. NFIRS 5.0 dropped a few data elements, including Construction Type, Method of Alarm, and Method of Extinguishment, and greatly reduced the number of Property Use (occupancy) categories. Some fields, such as Factors Contributing to Ignition, On-Site Materials, Suppression Factors, and Actions Taken, allow multiple entries. A manual containing the NFIRS 5.0 data elements, code choices and coding rules is available online [5].

Some of the features of NFIRS 5.0 that make it easier for fire departments to document incidents can make data interpretation and analysis more challenging. Different analysts or organizations may choose to handle these features differently and consequently obtain different results.

The number of incident type choices has been greatly expanded. The structure fire incident types are shown Table 78.2. In NFPA's analyses, structure fires also include fires in mobile property used as a fixed structure, such as manufactured housing and portable buildings (incident types 120–123).

To ease the burden on the fire service, NFIRS now requires only minimal information on certain types of structure fires, collectively called "confined fires" (incident type 113–118), that did not spread beyond the object of origin, such as small cooking fires, chimney fires, confined fuel burner or boiler fires, and trash fires that did not spread to other contents or the structure itself. Note that these incident types may apply to fires that occur in mobile properties that are used as structures and would require less information to complete. Some jurisdictions and some fire officers do complete the entire report for these confined fires. This makes it possible to do some data analysis when the focus is on a large number of incidents. Because such data is not routinely provided, these estimates will be more volatile and more uncertain. Just as the operation of automatic detection or extinguishing equipment can mean that a fire that would have been reported to a fire department is handled by occupants and not reported, such equipment can also mean that a fire that would have grown and spread remains confined. In many confined fires, automatic detection equipment sounded an early warning. Some of these fires were quickly extinguished by one sprinkler. At the same time, a typical confined fire may be too small to activate an operational detector or an operational sprinkler.

Table 78.2 NFIRS 5.0 structure fire incident types

Structure fire
111. Building fire, excluding confined fires (113–118)
112. Fire in a structure other than a building, including fires on or in piers, quays, or pilings; tunnels or underground connecting structures,; bridges; trestles, or overhead elevated structures; transformers; power or utility vaults or equipment fences; and tents
113. Cooking fire involving the contents of a cooking vessel with fire extension beyond the vessel
114. Chimney or flue fire originating in and confined to a chimney or flue, excluding fires that extend beyond the chimney
115. Incinerator overload or malfunction with no flame damage outside the incinerator
116. Fuel burner or boiler fire or delayed ignition or malfunction where flames cause no damage outside the fire box
117. Commercial compactor fire that is confined to contents of compactor, excluding home trash compactors
118. Trash or rubbish fire in a structure with no flame damage to the structure or its contents
Fire in mobile property used as a fixed structure, including manufactured housing, mobile homes, motor homes and camping trailers
121. Fire in manufactured housing or mobile home used as a fixed residence, including units not in transit and used as a structure for residential purposes and manufactured homes built on a permanent chassis
122. Fire in a motor home, camper or recreational vehicle when used as a structure, including fires in motor homes when not in transit and used as a structure for residential purposes
123. Fire in a portable building when used at a fixed location, including portable buildings used for commerce industry or education and trailers used for commercial purposes
120. Fire in mobile property, used as a fixed structure, other

Any calculation of loss rates per fire or per 100 fires for purposes of assessing the impact of automatic fire protection equipment therefore should include confined fires that stayed small or were kept small.

When analyzing for other factors such as area of origin or equipment involved in ignition, some groupings are reasonable. NFPA groups incident type 114, confined chimney or flue fire, with fireplace or chimney fires, and confined fuel burner or boiler fire with central heating equipment fires. Confined cooking fires can be assumed to involve cooking equipment and to have usually occurred in a kitchen or cooking area.

The confined or contained trash fires pose the most problems because the scenario provides little information about cause or area of origin. Many such fires are intentional. They may be started by a discarded cigarette or fireplace ashes. A child could have been playing with fire. Omitting these fires could lead to underestimates of the problem. The downside to analyzing confined fires is that there is less usable data that is less representative.

Some analysts omit fires in structures other than buildings (incident type 112). However, many of the areas of origin entered for these fires appear to indicate that these "structures" are in fact parts of buildings, which would suggest they should be included in any analysis of building fires.

National Estimates from NFIRS and NFPA's Fire Department Experience Survey

Because of the differing reporting practices, NFIRS used alone does not provide accurate estimates of the size of the fire problem in general or of specific fire problems. The annual NFPA Department Experience Survey is a more traditional sample-based survey, allowing projections to be made. The NFPA survey is a stratified random-sample survey that captures roughly one-tenth of all U.S. fire departments, including most departments protecting a population of at least 50,000. This stratification preserves randomness, hence representativeness, in the sample while reducing total variance, for more precise answers with less sampling uncertainty. National estimates of the extent of the general fire problem are

projected from the survey results and published annually [6].

By dividing the projected totals from the NFPA survey by the reported totals in NFIRS, multipliers are obtained that can be applied to the NFIRS data to develop national estimates of specific fire problems, a method developed by analysts at the USFA, Consumer Product Safety Commission (CPSC), and NFPA [3].

This multiple calibration approach makes use of the annual NFPA survey where its statistical design advantages are strongest. There are separate projection formulas for four major property classes (residential structures, nonresidential structures, vehicles, and other) and for each measure of fire severity (fire incidents, civilian deaths, civilian injuries, and direct property damage).

For example, the scaling ratio for 2010 civilian deaths in residential structures is equal to the total number of 2010 civilian deaths in residential structure fires reported to fire departments according to the NFPA survey (2665) divided by the total number of 2010 civilian deaths in residential structure fires reported to NFIRS (1534). Therefore, the scaling ratio is $2665/1534 = 1.74$. However, note that the scaling ratios for fires, civilian deaths and injuries and direct property damage can differ markedly from each other. The scaling ratios for a particular loss measure also can differ markedly from one property class to another. The most stable scaling ratios will be the residential scaling ratios and the fire incident scaling ratios for any property class. The other scaling ratios will be more uncertain because they are based on smaller numbers and because the distorting effects of individual fires with high death tolls or large property loss are not smoothed out over a large number of total fires.

Most analyses of interest involve calculating not just the estimated total number of fires per year within a particular occupancy but more specifically the estimated number per year of a certain type of fire in the particular occupancy, most frequently those defined by some ignition-cause or property. The six cause-related characteristics most commonly used to describe fires are two characteristics related to the source of heat of ignition (Heat Source, Equipment Involved in Ignition), two characteristics related to the first fuel item ignited (Item or Type of Material First Ignited), the Factor(s) Contributing to Ignition by bringing the heat source and ignited material together, and Area of Origin. Other characteristics of interest involve fire protection, number of stories, and victim characteristics, such as ages of persons killed or injured in fire, victim location at ignition, and victim activity at time of injury.

In the next few sections of the chapter, nearly all the examples cited involve analyses of fire cause, which will tend to be of greatest value in analyses for public education or for evaluation of the fire performance of burnable products. Engineering analyses of candidate designs for whole buildings will depend more on analysis of other data elements, such as fire size and the performance of fire protection equipment. The points being made about good analysis practice transfer from the data elements used in the examples to all other NFIRS data elements.

Handling Unknown Data

Some fire incident reports may not include a particular characteristic of interest in NFIRS or may indicate that the information was undetermined or unknown. If the unknowns are not taken into account, then the propensity to report or not report a characteristic may influence the results far more than the actual patterns of that characteristic. For example, suppose the number of fires remained the same for several consecutive years, but the percentage of fires with cause unreported steadily declined over those years. If the unknown-cause fires were ignored, it would appear as if fires due to every specific cause increased over time while total fires remained unchanged. This, of course, does not make sense.

Consequently, most national estimates analyses allocate unknowns by using scaling ratios defined by NFPA survey estimates of totals divided by only those NFIRS fires for which the dimension in question was known and reported.

Inherent in this approach is the assumption that the fires with unreported characteristics, if known, would show the same proportions as the fires with known characteristics. For example, it assumes that the hotel fires with unknown Area of Origin codes contain the same relative shares of guest room fires, kitchen fires, laundry room fires, and so forth, as are found in the hotel fires for which the Area of Origin was reported.

There are more sophisticated statistical techniques for imputing missing values or for "raking" unknowns simultaneously in two or more dimensions, but these are rarely used in routine analysis.

Issues Regarding Unknown Data in NFIRS The confined-fire option with its very limited reporting requirements has also complicated the process of handling unknown or missing data. Analyses of heating equipment have historically been done by using data in the Equipment Involved in Ignition field. Code choices in this field include a range of codes corresponding to heating equipment, other ranges corresponding to other well-defined types of equipment, and some other codes indicating that the Equipment Involved in Ignition is completely or partially unclassified or unknown, or blank. The Equipment Involved in Ignition field is blank for most confined fires. For the few that are known, the heating equipment share will differ substantially by specific type of confined fire. When Equipment Involved is known, fires listed as confined to furnace or boiler will usually show some type of heating equipment with furnaces or central heating units dominating. Fires listed as confined to cooking vessel will occasionally show heating equipment. If confined and non-confined fires are analyzed together, the unknowns will be dominated by the confined-fire unknowns, which do not have the same equipment distribution as the non-confined-fire unknowns. If the analyst infers equipment from the dominant type for each type of confined fire, the pool of residual unknowns will be dominated by the non-confined-fire unknowns—the only ones remaining—and they will tend to be allocated based on the confined-fire shares of equipment. (Confined fires are dominated by confined cooking vessel fires, but non-confined fires are not so dominated by cooking equipment fires.) The best choices appear to be separate allocation of unknowns for confined and non-confined fires or allocation of unknowns for non-confined fires and inference for confined fires. But none of the choices are as clean or as logically appealing as the old simple rule of proportional allocation of all unknowns when the same fields were required for all incidents.

Version 5.0 also introduced new "skip patterns" so that certain data elements are required only when specific values are or are not entered into a different element. For example, information on the Type of Material First Ignited is no longer required for fires in which the Item First Ignited is blank, undetermined, or some type of "general material." General materials can include items as diverse as electrical wire or cable insulation; transformers or transformer fluids; conveyor, drive, or V-belts; tires; railroad ties; pyrotechnics; fences or poles; dust, fiber, or lint; books, magazines, or files; film residue; adhesive; rubbish; oily rags; and multiple items first ignited. One could reasonably assume that when the Item First Ignited was unknown or undetermined, then the Type of Material First Ignited was also. However, information about the Type of Material First Ignited could be inferred for many of the general items, so these are not always true unknowns. Because the Type of Material First Ignited is often supplied even when not required, any time the field is left blank NFPA now treats it as unknown.

NFIRS also has fields for the Item Contributing Most to Flame Spread and Type of Material Contributing Most to Flame Spread. Analysis of this field is complicated by a checkbox that is to be used to indicate any of the following conditions:

1. There was no flame spread;
2. The Item First Ignited was the same as Item Contributing Most to Flame Spread; or

3. The Item Contributing Most to Flame Spread was undetermined.

Sometimes the same item is entered despite the directions. "None" is a valid choice in several fields: Equipment Involved in Ignition, Fire Suppression Factors, and Factor Contributing to Ignition. For Factor Contributing to Ignition, it appears that "None" is greatly overused. NFPA treats "None" in this field as an unknown. For Equipment Involved in Ignition, a substantial share of incident reports indicate that no equipment was involved in ignition, but indicate that the Heat Source was some type of operating equipment. Some fire officials seem reluctant to list equipment involved when the equipment itself was operating correctly and user error was the greater issue. Electrical wiring is sometimes not perceived as equipment because it is not something that gets plugged in or turned on. When the Heat Source entry does not confirm that no equipment was involved in ignition, NFPA considers the Equipment Involved in Ignition to be unknown. If the Heat Source was entered as "Radiated or conducted heat from operating equipment," the Equipment Involved in Ignition would be considered unknown if entered as "none."

Errors and Uncertainty in NFIRS-Based National Estimates It may be useful at this point to summarize sources of error and uncertainty in NFIRS-based national estimates, both those that can be readily quantified and those that cannot:

- *Sample-size-based uncertainty*. Uncertainty due to sample size is negligible from NFIRS itself because of its enormous scope, unless the problem being examined accounts for hundreds of fires per year or less, and modest from the calibrating NFPA survey (about 10 % for deaths and much less for other measures of fire loss).
- *Sample-bias-based uncertainty*. The NFPA survey is designed to reduce sample bias; however, some may exist. For example, departments who submit all incidents to NFIRS may be better able to complete the survey, whereas other departments may report to the NFPA survey only what is required by their states' NFIRS programs. On the other hand, departments using NFIRS software from vendors who include the survey as an output report are more likely to respond to the survey. Some departments do not participate or may participate in some years but not others. NFIRS is not sample based, and it is hard to quantify the impact of reporting differences.

The completeness and quality of data also vary by jurisdiction.

- *Uncertainty due to missing data*. The percentage of NFIRS cases with blank or unknown data can be somewhat addressed, as noted above, by proportional allocation but can also be used to estimate the uncertainty, which, in the extreme, ranges from all the unknowns being relevant to none of the unknowns being relevant.
- *Uncertainty due to terminology or category choices*. Some of the choices in NFIRS do not use terms firefighters would know. When looking at home wiring fires, it might seem reasonable to look at fires involving either electrical branch circuit wiring and outlets or receptacles. However, many firefighters are not familiar with the term "branch circuit wiring". In 2006–2010, three times as many home fires involved "electrical wiring, other" as involved electrical branch circuits. Karyl Kinsey of the Austin Texas Fire Department found that almost one-third of Austin's fire reports that mentioned smoking as a fire cause and completed the Fire Module reported that the Heat Source was a hot ember or ash (43) rather than a cigarette or other form of smoking material (61–63) [7]. It is possible that the first entry that looks reasonable is chosen, even when it is not the most appropriate.
- *Uncertainty about what should be considered unknown*. When something is coded as "other" or "unclassified," particularly when used with a category, such as 'electrical distribution or lighting equipment, other," (Equipment Involved in Ignition 200) does it truly mean that the particular fire

circumstances do not fit into any of the choices? Is it more accurate to treat these as unknown or partially unknown? NFPA treats the "other" broad categories of equipment as partially unknown and distributes them across their respective categories. However, an absolute "other" is taken at face value. NFPA treats Heat Source 60 "Heat form open flame or smoking material, other" as a partial unknown and distributes these incidents proportionally across the other categories of smoking materials and open flames.

- *Uncertainty due to coding inconsistencies*. More difficult to address because few coding combinations are truly inconsistent (unusual fires are possible), coding inconsistency can be analyzed as with missing, blank, or unknown data by eliminating a range of suspect cases from consideration.
- *Uncertainty due to error in determining and recording the facts of the case*. If the initial investigation is flawed, resulting errors will be carried forward into the incident report. Data entry errors can also occur. Factual errors are unmeasureable in the absence of some indicator within the incident record (e.g., inconsistency in coding two or more data elements) or access to a more reliably accurate source of incident data; however, few incidents have a second source of data, and second sources of data are not necessarily more reliable.
- *The impact of inclusion or exclusion of unusually serious incidents on estimates*. The casualties and property damage from the events of September 11, 2001, were not included in NFIRS. NFPA made a conscious decision to exclude these deaths when calculating scaling ratios for national estimates. On a much smaller scale, NFPA is aware of some dormitory and fraternity fire deaths that were not reported to NFIRS. Trend tables show no deaths in these occupancies in those years. For most occupancies other than homes, fire deaths are very rare events, sometimes so rare that years may pass with no deaths reported to fire departments anywhere in the country. For such occupancies, single-year NFIRS-based national estimates are almost certain to miss the true values. If the only fatal fire that occurred was in the NFIRS sample, the estimating procedure will double or triple the number of deaths, producing an overly high estimate. If the only fatal fire was not in the NFIRS sample, the estimate will be zero, which is too low. In some years, NFPA is able to identify some fatal fires through news clips and confirm the deaths through fire departments even though those fire deaths are not part of the NFIRS sample, but this information cannot be used to adjust the NFIRS-based estimates because it is one-sided. Inserting events identified outside the sampling process undercuts the entire basis of sample-based statistical estimation. When the average number of deaths per year is this low, rolling multiyear averages are more appropriate. Even multi-year averages can give a misleading impression of confidence about patterns of fire death factors when the numbers are small and the portion with unknown data high. If one occupancy had six deaths in 5 years, based on projection from two deaths including in the NFIRS dataset, and the cause was known in only one death or both deaths occurred in the same fire, there would be a high degree of uncertainty if we followed our normal allocation of unknown data and conclude that all the deaths in this occupancy resulted from that one cause. At the same time, it would be misleading to treat all the deaths as having unknown cause, and it could be confusing to confine all the information on cause to a footnote.

Firefighters provide NFIRS data using a standardized coding system after a fire to complete an incident report. The strengths of the system are also limiting factors. By utilizing a standard classification system, with a limited number of standardized data elements and choices within each data element, to capture the circumstances at all types of fires, data can be captured easily and practically about a wide variety of events. The limited number of data

elements mean that the data will not be as detailed as many people would like. The fire service personnel collecting the data are generalists, not specialists. They can usually identify that a particular piece of equipment was the source of ignition, but they are unlikely to know which part of the equipment was involved. Information on brand, model, or component of equipment involved is not coded and is often not captured. Nor does NFIRS capture very specific types of equipment that are used in only a small number of industries. And even at the level of detail addressed by the database coding, there are many gray areas of interpretation.

If these weaknesses seem substantial, it may be useful to consider the much greater weaknesses of any other currently available statistical database. If one uses only data collected by experts and specialists, then the dataset will be small and is almost certain to be unrepresentative of the larger set of fires. If one uses data mining techniques to look for patterns in unstructured or narrative incident reports, then results can be distorted because many incident reports will not have included information on the characteristics selected for analysis by the data mining. If one withholds results unless certain standards of statistical significance have been met, then one will have no data-based estimates for many parameters necessary to engineering analysis.

It is possible to use Bayesian statistical analysis techniques to combine subjective estimates with limited or flawed datasets, but there are no well-known major examples of applying these techniques to NFIRS, let alone any solid guidance on how to set up engineering problems for this kind of analysis.

Going back to the limitations and complexities of NFIRS, consider this example of applying the data to a particular product, specifically, the steps required just to fully capture the detail available in NFIRS to estimate fires involving a particular type of carpet. Carpet is one of several products that falls within the NFIRS category of floor covering. The NFIRS Item Ignited code 14 for floor covering includes floor covering or surface rugs, carpets, or mats. The NFIRS database can be checked for number of fires coded as starting with floor covering. However, floor covering will also account for a proportional share of fires with Item First Ignited unknown. Floor covering may also account for a proportional share of fires under Item First Ignited code 10, which is other or unclassified structural component or finish. The standard references on developing national estimates provide guidance on these steps and the specific statistical methods needed to execute them.

To distinguish carpets from other floor coverings, consider the Type of Material First Ignited data. This data element has codes for several broad categories of fabrics and textiles, including code 71-fabric, fiber, cotton, blends, rayon, wood, or finished good, including yarn and canvas, but excluding fur and silk; code 74-fur, silk, or other fabric or finished goods excluding those included in code 71; code 77-plastic coated fabric, including plastic upholstery fabric and other vinyl fabrics; and code 70-unclassified fabric, textile, or fur. Carpets or rugs could be estimated by including only fires in which the Type of Material First Ignited was any one of the three codes for identifiable fabric-codes 71, 74, and 77. You might include all or a proportional share of fires coded as Type of Material First Ignited as code 70 (unclassified fabric, textile, or fur) as well as a proportional share of fires coded as totally unknown. This would properly separate carpet fires from hardwood or unfinished floors (Type of Material First Ignited codes in the 60–69 range, which is processed wood and paper) and from vinyl floor coverings (Type of Material First Ignited code 41-plastic; or perhaps code 81-linoleum; or code 80-unclassified materials compounded with oil). But what about fires classified as code code 51-rubber; code 54-hay or straw; code 50-unclassified natural product; code 76-human hair; or code 00-completely unclassified? If each of these possibilities corresponds to another real product—say, an exercise mat—then exclusion of these inappropriate codes makes sense. But any code that does not correspond to another real product is probably a miscoding and so is best

treated as another type of partial or complete unknown, to be proportionally allocated and so added to the estimated number of total carpet fires.

For example, gasoline (code 23) is in the top 15 most frequently reported Types of Material First Ignited for home floor covering fires. Gasoline clearly refers not to the floor covering but to a substance spilled or poured onto the floor covering. Should such fires be excluded because they clearly do not involve a true floor covering as the first item ignited? Or should they be included on the basis that the gasoline leads to accelerated early involvement of the real floor covering in fire, and so floor covering is the first true product involved in fire? Or should they be excluded on the basis that the burning properties of the floor covering are irrelevant to a fire started with gasoline? Or should they be included on the basis that the relative ability of different floor coverings to absorb gasoline could make a difference in fire development? No matter what the decision, it will not be a simple one.

The gasoline example illustrates another general point. It may be tempting, when constructing national estimates, to exclude certain types of fires as not being fair tests of the product or the building design. This practice is unsound, as all fires involving a product or occupancy are relevant to an overall description of the fire problem associated with it. Factors that make the fire challenge seem unfair can be properly addressed at the stage of analyzing how much fire probabilities can be reduced or interpreting whether a certain fire probability is acceptably low. But exclusions should occur at those points, not at the initial stages of analysis, or else the engineering analysis will be conducted against a misleadingly optimistic view of the size of the problem to be addressed.

The most detailed and appropriate estimate of the incident frequency derivable from NFIRS-based national estimates may have been obtained after these decisions have been made and steps completed. It is not possible to ascertain, for example, age, style, specific materials, or specific burning properties of carpet from NFIRS. In some cases, further refinement is possible based on differential patterns of usage and their implications for areas of origin or for exposure to certain heat sources. Further progress depends on inference from a combination of incident data, usage data, and laboratory test data. The inference rules will be discussed after those types of data have been reviewed and discussed individually.

For now, let us return to the earlier statement that valid analysis of incident rates requires the use of a statistically representative database, like NFIRS and the NFPA survey. Many other databases exist that are much more detailed than NFIRS but are either known to be statistically unrepresentative or at best not known to be representative. To see why it is imperative that analysts not sacrifice statistical validity for detail, it may be useful to review a number of half-truths and widely held myths surrounding databases.

Data Half-Truths and Myths

Someone Must Collect the Data I Need Why? Who would have that much interest? It takes time and resources to collect data. Any organization that collects data will have a reason to do so. And the data they collect will be the data *they* need. On the other hand, some databases were developed to serve diverse purposes and constituencies. In 1974, the National Fire Prevention and Control Act, Public Law 93-498, Section 9, established the National Fire Data Center to "provide an accurate, nationwide analysis of the fire problem, identify major problem areas, assist in setting priorities, determine possible solutions to problems, and monitor the effectiveness of programs to reduce fire losses." This act established the U.S. Fire Administration and the National Fire Incident Reporting System (NFIRS). As another example, the U.S. Consumer Product Safety Commission (CPSC) uses data from the sample-based National Electronic Injury Surveillance System (NEISS) [8], which CPSC created, to develop estimates of the

number of injuries associated with consumer products and treated at hospital emergency rooms. In 2000, NEISS was expanded to provide estimates of all injuries seen in emergency rooms, not just injuries associated with products.

NFIRS and NEISS are examples of event databases. Both were designed to help quantify a very wide variety of problems and were not designed to "prove" a particular point.

When considering the use of data from a particular source, it is wise to consider why the data collection effort was undertaken in the first place. Who paid for it? Would the sponsors have a vested interest in a particular outcome? In some cases, data may be collected to promote an agenda. Because leading questions or other methodological flaws may make the data virtually useless, it is often helpful to review the survey instrument or form.

Biases may be unintentional but still serious. Sometimes a data collection effort was designed to answer one specific question and the results would not be applicable in other settings. Rural and urban experiences may differ considerably from each other; a study of big-city fire problems could not be applied to rural settings without refinement or reconfirmation. Moreover, data collection budgets are typically small. Most databases are limited to data that are easy to obtain. Both the accuracy of the data and the representativeness of the incidents captured must be considered highly suspect in any so-called opportunity sample.

Even in a well-designed and adequately funded data collection system with no deliberate bias some biases arise because of the relative difficulty of obtaining reliable information and universal participation. For example, fires in fully sprinklered buildings or buildings with good detection/alarm systems are more likely to be discovered and controlled by on-site resources. No data collection system based in organizations like the fire service can expect to capture unreported fires. The national estimates of fire problems that are produced by combining NFIRS data and the results of the NFPA survey only reflect data reported to municipal fire departments and exclude those handled by private fire brigades, federal fire-fighting organizations, or the occupants themselves. Further increasing this bias is the fact that some occupancies, particularly high-hazard occupancies, are more likely to have fire brigades than others.

Data on heat release rates at key points during a fire could be quite useful. Unfortunately, no one has the technology to measure or estimate such data outside a laboratory. Suppose one asked for readily observable change points in the fire, such as spread to a new room or floor. No one can expect to be in position to observe such change points at most fires. Firefighters do not have the discretionary time during a fire to check specific times and record them. When seeking data, it is important to ask how the data collectors would be able to obtain the data and how reliable they would be.

Anecdotes Describe Typical Incidents This is often not true. *Anecdotes* are what statisticians call data points from a database that has not been designed to ensure statistical representativeness. The NFPA Fire Analysis and Research Division runs an anecdotal database called the Fire Incident Data Organization (FIDO). A clipping service identifies significant incidents (e.g., large loss, multiple deaths), and additional information is requested from the fire service and other sources. NFPA conducts follow-up surveys of state fire marshals to ensure that records of fire fighter fatalities and these very serious fires are complete. However, FIDO also captures well-documented fires on an opportunity basis, and for these fires, FIDO is only anecdotal.

From early in the twentieth century until the mid-1970s, NFPA collected information on sprinkler activations [5]. However, over time the easily available data sources became less and less reliable in capturing smaller fires. As FIDO's representativeness for smaller fires declined, so did its representativeness in capturing sprinkler successes. More and more such incidents were missed, and a disproportionate number of captured incidents therefore showed sprinkler problems.

Anecdotal information like that provided by FIDO, NFPA Fire Investigations, or CPSC's In-Depth Investigations file can indicate the range and diversity of fires that *can* happen. Anecdotes cannot be used to estimate incident rates or probabilities.

A Rose Is a Rose Is a Rose Anecdotes are relevant but may not be representative. It is also possible to have representative data that are not relevant, even though they appear to be, because of differing definitions for the same terms. For example, definitions of data elements may differ in different countries or even different data collection systems. In fire incident databases, *space heater* refers to a heater for a relatively small area. The U.S. Department of Energy's Energy Information Administration uses the term *space heater* to describe *all* heating systems, including furnaces and other central heating units, on the theory that all of them are heating space, as opposed to heating water or food [9]. However, the term *heating equipment* in fire incident databases includes not only equipment to heat spaces but also water heaters.

If Data Were Collected, They Must Be Available The analyst's life would be easier if this statement were true. Unfortunately, it's not. Some data, such as the detailed information collected by insurance companies, are proprietary and confidential. Corporations may maintain incident records when injuries or mishaps occur, but they are usually under no obligation to share that information with the general public. Information collected by the government *should* be available. The public can generally obtain copies of reports or files that already exist. However, data may not be kept indefinitely and older data may never have been entered into modern, electronically accessible media. Many computer systems have not been integrated so analyses that are theoretically quite easy may be impossible without major conversion efforts. However, these problems are usually not insurmountable. Some modifications may be needed and sources of uncertainty must be documented. Considerable data are available, as noted, which means estimates of sampling-based uncertainty can be readily constructed.

Field Observation Data

Switching now from fire incident data to other kinds of data based on observations in the field, Table 78.1 cites field observation data as relevant to reliability analysis, including instances of unavailability or failures to perform with full effectiveness when needed despite being available, and emergency evacuation analysis. The chapter on reliability (Chap. 74) elsewhere in this handbook provides an overview of issues in, data sources on, and mathematical methods for analyzing reliability. At present, data to support reliability analysis are very scarce. However, the five types of data sources listed below are also relevant to other aspects of engineering analysis:

- Judgments and opinions
- Inspection and testing
- Simulations and laboratory studies
- Incident and other field data on systems performance
- Product life tracking systems

Judgments and Opinions

In the absence of data from systematic field observations, one can use estimates from individuals whose work experience has provided them with a long period of nonsystematic field observations. Methods like Delphi panels try to eliminate bias from the group process of consolidating expert opinions into consensus estimates. (Modified Delphi panels have been used to specify many of the scoring parameters for NFPA 101A, *Guide on Alternative Approaches to Life Safety*, the alternative evaluation scheme to NFPA *101®*, *Life Safety Code®*.) But shared biases remain and are commonplace. In particular, the mix of observations that occur in the normal course of a job in fire suppression, fire reconstruction, design, and so forth, is subject to many biases that may not be recognized by the experts. (For example, new buildings are more likely to be designed for the affluent end of the general or business population, whereas fires are more likely to occur at the less affluent end,

but neither tendency is absolute.) In addition, there is a tendency for individuals to shade their recollections in favor of a pattern that is simpler than the often complex truth. Thus, a system or feature with relatively high reliability will have its reliability estimated even higher (sometimes called the *halo effect*), while a system or feature with relatively low reliability will have its reliability estimated even lower (sometimes called the *horns effect*).

Inspections and Testing

A program of routine inspection and testing can provide statistically representative data on failure frequencies and severities and is particularly useful for failures that are less than total or that otherwise may not draw attention to themselves when they occur. *Frequency* is how often failure occurs, and *severity* is how damaging failure is when it occurs, so frequency numbers are in fact relative to the failure severity level being tallied. However, inspection and testing-based databases are usually proprietary and so not available for routine engineering analysis. And even when available, they are subject to some critical gaps and biases.

First, the inspections that provide this kind of data tend to be part of a very advanced maintenance program, which provides the principal justification for the high cost of frequent inspection and testing. Frequent maintenance and inspection, in turn, are more likely to occur with a better-trained and more safety-conscious workforce, so human error reliability problems, which tend to dominate mechanical and electrical problems for most systems and features in practice, are likely to be sharply lower. The resulting reliability figures will therefore tend to be much better than those achieved for more typical properties that lack the maintenance to achieve high reliability and the inspections and testing to measure their reliability.

Second, this form of data collection can miss transitory failure conditions, such as blocking a door open, or vulnerability to extremely rare external events, such as earthquakes. In both cases, the sampling in time represented by the inspections and tests may not be sufficient to identify an important problem, in the former case because the sampling points are too far apart and in the latter case because the sampling does not (and perhaps could not) cover a sufficiently long period of time.

Finally, the process of inspection and testing is itself subject to error. If inspection is limited to observation only, without more active involvement as with testing, the probability of error in observation can be quite significant. Most databases derived from inspections or tests do not consider this type of error.

In 2012 NFPA's Fire Protection Research Foundation began a project to develop guidance on how to use risk and reliability data and modeling more frequently and more systematically in the specification of inspection, testing and maintenance programs. There may be additional resources available from this project.

Simulations and Laboratory Studies

Exit drills are a form of simulation or laboratory study that provides data on human reliability (and performance) with regard to a range of safety-related behaviors. They illustrate the larger point that simulations and related studies are particularly useful for studying human error reliability, a critical aspect that tends to be less well addressed by other controlled-study data sources.

However, simulations may be less than realistic as a result of simplifications done to make the experiment repeatable and manageable, as well as those made to avoid undue risks to participants. A bench-scale fire test cannot be readily scaled up to real-scale fire effects and will avoid the high flux levels of a fully developed fire, in part to avoid harm to operators and equipment, but in so doing may create a misleadingly mild picture of real fire conditions. Even a room-scale test is unlikely to be set up with accelerants, high wind-speed ventilation, conditions promoting backdrafts, or some other factors that can produce the most severe fire conditions.

An evacuation drill may avoid bad weather days to avoid injury to occupants, but this may paint an unrealistically optimistic picture of how slow and hazardous real evacuations may be.

The field of ergonomics provides design solutions to many of the people–equipment interaction problems that studies and data like these identify.

Incident and Other Field Data on Systems Performance

In theory, the most appropriate database on the reliability of a system or feature would capture every naturally occurring test of its availability and performance (i.e., unwanted fires) and every other activation of the system (e.g., unwanted alarms). In practice, this requires constant monitoring, which is almost always too expensive to be implemented. Attempts to approximate such a database using only fires reported to fire departments or, even worse, fires reported in the media, will miss most incidents and can give a misleadingly pessimistic picture of reliability.

NFIRS makes it possible to estimate the percentage of fires in a specific occupancy in which fire detection equipment operated. In homes that had smoke alarms and reported fires considered large enough to activate the alarms in 2005–2009, the smoke alarms operated 85 % of the time. When powered by batteries only, they operated only 77 % of the time, but when hardwired, they operated in 92 % of the fires. The leading reason they did not operate was a missing or disconnected power source [10]. It is generally *not* possible to tell from aggregated fire experience data the portion of fires occurring in properties that complied with a specific portion of any applicable codes. NFIRS collects more information on automatic detection type, power source and failure reason, but it does not indicate proximity to area of origin, type of sensor used, if smoke alarms were interconnected or if the detection system was monitored. Nor does it capture the performance of fire protection features triggered by fire detection systems.

NFIRS provides useful data on sprinkler reliability. After excluding confined fires, fires in properties under construction, and fires in which the reason for sprinkler failure to operate was "Not in area of fire," wet pipe sprinklers were found to have operated in 95 % of the 2006–2010 residential fires that were large enough to activate the system and in 91 % of such fires in all occupancies combined. The reason for 53 % of the residential failures and 60 % of overall failures was because the system had been shut off [11].

All the databases described here tend to focus on active systems and other fire protection equipment. Passive fire protection features, such as fire walls, are less likely to be captured, in part because their failures tend not to be time-specific events (e.g., when a smoke alarm has its battery removed or a sprinkler valve is shut off, both events occur at defined points of time) but rather partial deficiencies in performance (e.g., a door is normally left slightly ajar or a wall has a hole in it). A poke-through hole in a wall, for example, is not a total failure of the wall and does not appear as an event in the course of the fire. Although it may have played a role in extension of the fire, it is unlikely to be identified in a post-fire analysis. It also may not fit your definition of a reliability problem, but it is clearly a deviation from intended design that affects and degrades performance. No incident database routinely documents fire development and related factors in enough detail to capture this kind of problem.

Product Life Tracking Systems

Some buildings maintain comprehensive tracking systems for safety equipment or other equipment throughout their productive lives. There will be information on what was bought; when it was bought; when it was installed; when and how it was maintained; and often when, how, and why it failed. When such a system includes enough identical products—or is connected to a larger database, such as might cover all the buildings owned by a large corporation or government agency—it

can support the development of very detailed reliability statistical distributions.

Usage and Exposure Data

Engineering analyses require usage and exposure data at several points. First, if the analysis addresses fire risk, then usage or exposure data (e.g., number of units of product in use, number of establishments of a particular type, number of people using a product or occupying a building, number of square feet of space devoted to a type of occupancy) are needed to convert incident data to estimates of ignition probability or to convert failure event data to estimates of reliability. Many engineering analyses, however, frame problems in ways that do not require explicit, quantitative treatment of ignition or reliability. Even these analyses still need some usage and exposure data in order to define and specify transitory conditions, such as the numbers, locations, and capabilities of occupants, that affect the achievement of fire safety objectives and so the performance of a design. For risk calculation, the principal challenge is to find statistically representative numerator data with enough detail and data definitions that are consistent or compatible with the definitions used by the denominator incident or data.

Heating Example of Matching Coding Categories Between Databases

NFIRS Version 5.0 has the following codes for heating equipment

100 Unclassified heating, ventilation, or air conditioning equipment
112 Heat pump
120 Unclassified fireplace or chimney
121 Masonry fireplace
122 Factory-built fireplace
123 Fireplace insert/stove
124 Heating stove
125 Chimney or vent connector
126 Brick, stone, or masonry chimney
127 Metal chimney, stovepipe, or flue
131 Built-in furnace or local heating unit, including built-in humidifiers, but excluding process furnaces or kilns
132 Furnace or central heating unit, including built-in humidifiers, but excluding process furnaces or kilns
133 Boiler (power, process, or heating)
141 Heater, including floor furnaces, wall heaters, and baseboard heaters, but excluding catalytic heaters, oil-filled heaters, and hot water heaters
142 Catalytic heater
143 Oil-filled heater, excluding kerosene heaters
144 Heat lamp
145 Heat tape
151 Water heater, including sink-mounted hot water heaters and waterbed heaters
152 Steam line, heat pipe, or hot air duct, including radiators and hot water baseboard heaters

Some of these specific types of equipment are part of distribution and are not specifically linked to any particular devices. A chimney, chimney connector, vent pipe, steam line, or hot air duct could be associated with a variety of different types of heat-generating equipment. Code 100 covers equipment that is unclassified or unknown as to heating equipment versus air conditioning or venting equipment. Heat pumps appear to be positioned as air conditioning equipment, in that the codes numerically to either side of code 112 are for air conditioning equipment or fans, but heat pumps can be used for either heating or air conditioning.

These categories correspond reasonably well but not exactly with the categories used by the U.S. Department of Energy to organize information on household usage of heating equipment [9]:

- Heat pump
- Central furnace with ducts to individual rooms
- Steam/hot water system with radiators or convectors in each room or pipes in the floor
- Built-in electric units in each room installed in walls, ceilings, baseboard or floors
- Built-in floor/wall pipeless furnace

- Built-in room heater burning gas, oil, or kerosene
- Heating stove (burning wood, coal, or coke)
- Portable electric heaters
- Portable kerosene heaters
- Fireplace
- Some other equipment)

As noted earlier, the U.S. Department of Energy uses the term "Space Heating" to encompass equipment intended to heat the environment as opposed to cooking equipment or lighting which might also get hot.

Version 5.0 of NFIRS captures data on the equipment power source when equipment is involved in the ignition, as shown in the following list, which also shows the Department of Energy categories:

- Three categories of electric-powered equipment: electrical line voltage, including typical house current; batteries and low voltage (less than 50 V); and other electrical (compared to the single electricity category in the Department of Energy usage categories)
- Three categories of gas fuel: natural and other lighter-than-air gas; LP- or other heavier-than-air gas; and other gas fuels, (compared to natural gas vs. bottled LP or propane gas in the Department of Energy usage categories)
- Five categories of liquid-fueled equipment: gasoline; alcohol; kerosene, diesel fuel, or numbers 1 and 2 fuel oil including furnace and bunker oil; numbers 4, 5, and 6 fuel oils; and other liquid fuels (compared to fuel oil vs. kerosene in the Department of Energy usage categories)
- Four categories of solid-fueled equipment: wood or paper; coal or charcoal; chemical; and other solid fuels (compared to wood, the only solid fuel specifically identified in the Department of Energy usage categories)
- Eight other specific power sources may also be recorded: compressed air, steam, water, wind, solar, geothermal, nuclear, and fluid or hydraulic power source

This comparison will suffice to illustrate the point that even modestly detailed incident and usage databases can present a multitude of compatibility problems. Some problems can be solved by one-time special data collection efforts to devise assignment rules for estimation purposes Some problems can be solved by examination of the technology alternatives and by asking data collectors what rules they use to resolve questions in the field. Some problems can be addressed by expert judgment. And some problems create limits to the level of detail achievable in the data.

Occupancy Example of Matching Coding Categories Between Databases

Another example has to do with occupancies. *Occupancy* refers to the use made of a space, and "property use" is the NFIRS code that describes occupancy of a property, whether a building or part of a building (such as a restaurant in a mall or on the ground floor of a high-rise multiuse building). The North American Industry Classification System (NAICS) codes for establishments are designed to classify the primary activity or line of the business that owns or occupies the building. In pursuit of its primary activity, a business may require and oversee many types of occupancies, from manufacturing to sales to office to storage to public assembly. The codes for businesses also distinguish retail from wholesale sales, whereas the NFIRS codes for occupancies do not. Is a wholesale sales operation an office building or a mercantile occupancy? Or is it an office occupancy and a storage occupancy sharing a building? (Or the two parts might not be sharing a building).

There are far more storage occupancies than there are buildings housing businesses whose defining purpose is storage. This means that no matter how one groups fires in storage occupancies, it is not clear that the data will match the data on establishments. Some storage occupancy fires will be in storage businesses, but many, perhaps most, will involve storage buildings in complexes associated with stores,

factories, or even homes. Garages, sheds, fire stations, barns, docks and marinas are all considered storage properties in NFIRS.

Mixed use complexes, such as shopping malls and high-rise buildings may host retail establishments, restaurants, parking garages, and residential living space all in one structure. A fire that starts in one type of occupancy may impact other types within the same structure.

Even when major categorization mismatches are not an issue, minor ones can be. NAICS codes identify gasoline service stations as a type of retail business. Version 5.0 property use code 571 identifies public service stations, but that category also includes LP-gas stations with associated convenience stores. In NAICS, LP-gas (bottled gas) dealers are under a separate retail code for fuel dealers.

Storage Shed $\neq$ Warehouse

If all the matching issues are addressed, then one must still consider the measurement scales available. The business code categories are used to count establishments, which is probably the best measure of exposure but also mixes very large and very small buildings without distinction. A better measure for fire risk analysis would probably be square footage, but those data exist only for highly aggregated categories of buildings. Business-coded data also exist on numbers of employees and dollars of payroll, both already related to business size but not clearly relevant to exposure proportional to fire risk. NFIRS collects total square feet or dimensions for non-confined structure fires. Users of this data would need to establish ranges to make the number of choices manageable.

Occupant Characteristics

Occupant characteristics must also be considered. Engineering analysis is done using scenarios, whether in terms of fire hazard or full analysis of fire risk. Most fire safety objectives trace, directly or indirectly, to a goal of protecting people. Short of a highly conservative (and generally unachievable) objective of preventing any fire effects in any occupied area, engineering analysis will need to address the fates of occupants, explicitly and quantitatively. This, in turn, requires data on the occupants, effective when fire begins. How many are there, where are they, how will they act, and what are they capable of?

A wealth of information exists regarding household structures, which may be useful in defining *occupant sets*—alternative descriptions of occupants for analysis, analogous to fire scenarios—for homes. Information is much less detailed for occupants of any other occupancy, and these will tend to be the types of buildings where engineering analysis is sought. For those properties, one will need to seek data from industry sources and special surveys. Absent such data, it will be tempting, and possibly necessary, to use ad hoc, heuristic methods to shape subjective estimates. Certain cautions must be noted in so doing.

1. Occupants do not respond in an ideal or perfectly efficient manner. They do not react immediately to the first cues of fire, they do not evacuate on the basis of perfect knowledge of conditions throughout the building, and they may evacuate in accordance with their normal patterns of movement rather than along rarely used paths best designed for quick, safe evacuation. Occupants may try to defend in place when they should not or try to evacuate when it would be safer to defend in place. None of this is a matter of panic or of irrational behavior or choices. It is not even unusual conservatism. It is simply a realistic view of how people respond to fire. In her article about how people respond to fire alarms, Guylène Proulx wrote that fire alarms are intended to meet four objectives: (1) warning occupants, (2) getting them to respond immediately, (3) starting the evacuation process, and (4) providing enough time to escape. She found that, in practice, people who hear a fire alarm tend to seek the reason for the alarm rather than assuming that a fire is occurring. They seek other cues such as the smell of

smoke, the sound of sirens, etc. If they do recognize a fire, they may engage in other activities such as fighting the fire, calling the fire department before evacuating, collecting belongings, or warning others [12]. Some evacuation models incorporate best available data on typical behavior and the time it takes. Optimizing models do not.

2. The places that have the most fires differ, not in kind but to a significant degree, from the mix of places in general. States that have higher fire death rates tend to have larger percentages of the population who are poor and less educated. These factors can have implications for buildings whose design, maintenance, and operation may be less fire safe, reflecting the limitations of their occupants, managers, and owners [13]. If a larger percentage of the adult population smokes, that is also associated with higher death rates. In 2010, smoking materials caused 21 % of all home structure fire deaths [14].
3. There are little data on how best to reflect occupant characteristics, and some of them may be moot for an engineering analysis of a well-designed new building, but analysts are advised to shade their assumptions and parameters toward less capability for occupants than the norm and much less capability than engineers see in their own lives, since engineers, like all professionals, are more affluent and better educated than the national average.
4. There are far more people with limitations in the general population than ever before, if only because there are far more people in the older age groups. Buildings open to the general public will see more and more occupants with limitations of age. The Americans with Disabilities Act has facilitated access to workplaces and places of assembly for many more physically challenged individuals, and the deinstitutionalization of many people with chronic mental illness decades ago led to a larger share of occupants with mental or emotional limitations. The diversity of physical challenges is also increasingly recognized. Many people have some limitations (wear corrective eyeglasses or contact lenses, for example), and there may be less data with which to model the many moderately limited occupants than there is to model the much fewer severely limited occupants. Data on health status, hearing and vision impairment, and difficulties in physical function are captured by the Centers for Disease Control and Prevention's National Health Information Survey. In 2010, 9 % of noninstitutionalized U.S. residents 18 years and older found it very difficult or impossible to stoop, bend, or kneel. Among those at least 75 years old, the percentage increased to 26 % [15]. These individuals could find it difficult to get below a smoke layer in a fire situation. Similarly 5 % of the surveyed population could not climb at least 10 steps without resting; 20 % of those 75 or over could not do so. Data on going *down* stairs were not provided but would be unlikely to be much more favorable. Sixteen percent of those over 18 had hearing trouble if they were not using a hearing aid, and 9 % had vision trouble, even with glasses or contact lenses. For those 75 and over, these percentages increased to 45 % and 16 % respectively. These limitations have important implications for relaying emergency information.
5. Occupant profiles can often be specified by linkage to time of day. Fewer occupants are in homes during the day on weekdays, and a different mix of ages and roles is found among those home during the day than the mix of home occupants in the evening or at night. In the evening, people will tend to be awake, while at night, most will be asleep. The American Time Use Survey collects data about how Americans 15 or older spend their time and the times of day they are engaging in specific activities [16]. In office buildings, the number, location, and other characteristics of occupants are clearly different during normal working hours than outside them. In hotels, different times of day will find different mixes

of occupants in the guest rooms, the small meeting rooms, the large function rooms, and the recreational facilities.

6. Fire incidence and casualty data can and should be used as input to the process of setting occupant characteristics, but usually those data should not be used directly. Suppose you created a list of scenarios, each associated with a different family structure, and you assigned scenario probabilities so that every age group was weighted the same as its share of civilian fire deaths. In such a case, when scenario fires were run and analyzed, the high-risk age groups would receive additional weighting based on their higher rate of deaths per fire, and the net result would be an age distribution for deaths that would overstate the death rate for the high-risk groups and understate it for the low-risk groups. In essence, the higher risk for certain age groups would have been factored in twice. It is easier to fix this problem for ages, because data exist on the age distribution for the population. However, for many other factors of interest—such as the number of deaths or injuries in which physical disability or alcohol impairment played a role, both of which are captured in fire casualty records—there may be no general-population data available for specific occupancies.
7. It is dangerous to limit the challenge posed by occupant characteristics with an assumption of code compliance or compliance with the latest model codes. The most deadly fires in eating and drinking establishments have involved serious code violations, including severe overcrowding. Many deadly fires have occurred in facilities that were not designed, operated, or licensed to provide more than personal care services, but that nevertheless proved to have occupants with severe limitations when a fire occurred [17]. It is unreasonable to expect a building design to protect occupants from fire in the face of pervasive, serious code violations, but it is not unreasonable to conservatively plan for at least occasional, transitory, but possibly significant violations, such as overcrowding or deterioration of occupant capability below the minimum level that allowed them to be admitted for residency. Serious fires do not usually happen where everyone follows all the rules and best practices. A design should be robust enough to protect people even when challenged beyond the strict limits of what is supposed to be possible.

Laboratory Data

For laboratory data on physical properties of fire, products, buildings, and so on, you should start with the other chapters of this handbook, which identify the measures of interest, put them in context, and in many instances, provide or reference best available data. Also, read the Chap. 73 for general guidance on handling error and uncertainty in data. For guidance on error and uncertainty in data from particular test methods consult precision and bias statements in the standards for those test methods or consult ASTM E691, *Practice for Conducting an Interlaboratory Study to Determine the Precision of a Test Method*.

On a related point, read the other chapters closely for guidance, specific to each type of data, on what to do if your case does not exactly match the specifications for any available test data. For example, consider the following questions.

1. Is it best to choose the closest documented case, or is extrapolation or interpolation better? How do you determine what is the closest? How far outside tested values can you extrapolate with reasonable confidence?
2. What do you do if the tests do not align along any linear scale, making direct interpolation and extrapolation impossible? (For example, there may be one result for each of several materials). Are there scaled characteristics that can be used as a legitimate, if unproven, basis for interpolation or extrapolation?

3. Is linear interpolation or extrapolation appropriate, or would another functional form be more appropriate?
4. In addition to the characteristics of the object or space for which you need data, are the fire conditions you anticipate the same as those used in the available tests? If not, do the differences matter and can they be adjusted for?

When analyzing data, also keep the following points in mind:

1. Scale matters. Results from bench-scale fire tests cannot be assumed to reflect full-scale performance.
2. Interactions also matter. Fire performance of products that are composites or layered combinations of materials cannot be predicted from test data on their constituent materials.
3. Time and usage change things. Products may change chemically or be altered physically, up to and including vandalism. All such changes may affect the applicability of test data on new products. This is even more true if the laboratory tests were on prototypes—or even prototypes with simplified design features—rather than on actual products ready for use.

In addition to direct use of laboratory test data, such data can be combined with incident data to provide greater detail. Consider the use of laboratory test data to build on the ignition probability estimates developed earlier for a specific product in the carpet and rug class. Under the section headed "Incident Data," the discussion showed how to develop floor covering fire estimates and then fabric or textile floor covering fire estimates. Suppose this national estimates approach suffices to provide probabilities of ignition for a product class (e.g., carpet or rug) but not for any type, style, or brand of that product class.

First, the universe of products in use (not the universe of products currently offered for sale) must be divided into a small number of representative pieces such that every variation of product in use is represented by one of these reference pieces. Second, data must be developed on the share of current usage (not the current market share). Then, laboratory tests must be conducted to determine relative ignitability.

Let $i = 1,\ldots, n$ be designations for n different representative pieces. Let u_i be the collective share of total usage accounted for by the ith piece and all the pieces represented by the ith piece. Let p' be the probability of ignition, derived from fire incident national estimates for the product in all its variations. Let p_i be the proportion of laboratory trials of the ith piece in which ignition occurred. Then, with all variations of product represented and none double counted,

$$\sum_{i=1}^{n} u_i = 1$$

The usage-weighted average frequency of ignition for the tested pieces is proportional to the experience-derived overall ignition probability for the product class.

$$\sum_{i=1}^{n} u_i p_i \propto p'$$

Therefore, the best estimate of the ignition probability for a piece of type i is

$$\frac{p' u_i p_i}{\sum_{i=1}^{n} u_i p_i}$$

This formula uses the incident data to calibrate the laboratory test data, or it uses the laboratory data to subdivide the ignition probability for the product class into more product-specific ignition probabilities.

Data Sources

It is impossible to list all the data sources that may be useful for engineering analyses. However, a number of principal sources are listed below, and the organizations that provide those databases will often have leads to specialized databases for specific purposes.

Incident or Event Data

National (U.S.) estimates based on NFIRS and the NFPA survey of the frequency and severity of reported fires can be obtained from

One-Stop Data Shop
National Fire Protection Association
1 Batterymarch Park
Quincy, MA 02269-9101
Telephone: (617) 984-7451
Fax: (617) 984-7478
E-mail: osds@nfpa.org
Website: http://www.nfpa.org/research

The National Fire Incident Reporting System (NFIRS) itself is administered by the U.S. Fire Administration. The codes used by NFIRS may be downloaded from http://www.nfirs.fema.gov/documentation/reference. Specific questions about NFIRS and requests for raw data may be submitted online or addressed to
NFIRS Help Desk
U.S. Fire Administration
16825 South Seton Avenue
Emmitsburg, MD 21727
Telephone: (888) 382-3827
E-mail: FEMA-NFIRSHELP@fema.dhs.gov
Website: http://www.usfa.fema.gov/data/nfirs/support/

The U.S. Department of Labor's Bureau of Labor Statistics collects a wealth of data about industries, employees, occupational outlook, demographics, workplace injuries, illnesses and deaths, prices, wages, and time use. Data may be accessed at http://www.bls.gov/data/.

The Department of Labor's Occupational Safety & Health Administration (OSHA) has an online database of accident investigations that may be searched by keyword, the North American Industry Classification System (NAICS) code, or the older Standard Industry Classification (SIC) code. These reports may be useful in fleshing out scenarios. Associated inspection reports indicate the number of violations found. Data may be accessed at http://www.osha.gov/pls/imis/accidentsearch.html. Additional resources on the site let the user search by OSHA standard to determine which SIC groupings have the most violations of that standard or which OSHA standards had the most violations. Searches for specific establishments are also possible. See http://www.osha.gov/oshstats/index.html.

Four types of data can be ordered from the National Injury Information Clearinghouse, including

- Sample-based estimates of injuries treated at hospital emergency rooms, from the National Electronic Injury Surveillance System (NEISS)
- Summaries of death certificate data on product-related fatalities
- In-depth investigations of product-related injuries or incidents, from CPSC's special studies and ongoing program of investigations
- Summaries, indexed by product, of CPSC Hotline reports, product-related newspaper accounts, and medical examiner reports

The NEISS data and the death certificate data could be used for event data and can be obtained from

National Injury Information Clearinghouse
U.S. Consumer Product Safety Commission (CPSC)
Washington, DC 20207-0001
Telephone: (800) 638-2775
Fax: (301) 504-0025
E-mail: clearinghouse@cpsc.gov
Website: http://www.cpsc.gov/about/clrnghse.html

NEISS data may be queried and publications, investigations, and related materials may be found at http://www.cpsc.gov/en/research–Statistics/.
Australian injury data can be obtained from
The National Injury Surveillance and Prevention Project
Research Centre for Injury Studies
GPO Box 2100
Adelaide SA 5001
Australia
Telephone: +61 8 8201 7602
Fax: +61 8 8374 0702
E-mail: nisu@flinders.edu.au
Website: http://www.nisu.flinders.edu.au

Sources of Usage and Exposure Data

For every year through 2012, the Bureau of the Census has released an updated *Statistical Abstract of the United States*. This publication

contains close to 1400 tables on demographics and economic activity and is a compilation of data collected by the U.S. Census and other entities. Some of the data would help establish usage and exposure. The companion publications, *State and Metropolitan Area Data Book* and the *County and City Data Book* contain similar data on their respective jurisdictions. Due to limited funds, the Census Bureau has stopped collecting data for these publications. It is possible that a private company may do so. Table source notes will help users from the published editions can lead users to the original sources.

Tables and ordering information on these publications are available http://www.census.gov/compendia/statab

Sources for data in the *Statistical Abstract* are often worth checking for possible additional information that may or may not be published elsewhere. Much of the information was originally collected by the U.S. Census Bureau. The Census Bureau's Statistics of U.S. Businesses uses Business Register, the NAICS coding system, a file of business establishments maintained by the Bureau, with Company Organization Survey for multi-establishment businesses as well as records from other agencies [18]. The Economic Census, conducted every 5 years, measures business activity by establishment [19]. Data are available at http://www.census.gov/econ/.

The Bureau of the Census and the U.S. Department of Housing and Urban Development (HUD) together produce the *American Housing Survey*. Data on housing can be obtained from http://www.census.gov/programs-surveys/ahs/. Additional information may be obtained by e-mailing ahsn@census.gov or phoning 7-888-518-7365.

Demographic and economic (exposure and usage) data from countries in the European Union can be obtained from Eurostat at http://ec.europa.eu/eurostat.

The U.S. Department of Energy's Energy Information Administration (EIA) conducts energy consumption surveys of residential, commercial, and industrial users. These surveys provide valuable information on equipment and fuel usage. The EIA will also be conducting surveys on alternative-fueled vehicles. Information can be obtained by contacting the
Energy Information Administration
1000 Independence Avenue, SW
Washington, DC 20585
Telephone: (202) 586-8800
E-mail: InfoCtr@eia.gov
Website: http://www.eia.gov/consumption/

Data from roughly 100 U.S. agencies have been compiled and are accessible through FedStats. Many databases may be downloaded by the user at http://fedstats.sites.usa.gov/.

Laboratory Data

The National Institute of Standards and Technology's (NIST's) Building and Fire Research Laboratory (BFRL) maintains a number of databases with experimental data that may be useful for modeling. All can be accessed through http://fire.nist.gov/ by following the menu to the data listings. They include the following:

- Fire experiment results, emphasizing heat release rates, suitable for zone modeling
- Diffusion flame measurements
- Residential fire sprinkler tests done by BFRL
- Home smoke alarm tests conducted as part of the so-called Dunes II project
- Tests of rail vehicles and their interiors and contents
- Firefighting agents
- Tests of treated versus untreated vinyl siding in wildland/urban interface

References

1. M. Ahrens and S. Stewart, "Fire Data Collection and Databases," *NFPA Fire Protection Handbook, 20th edition,* (ed. A. Cote), pp. 3-43–3-60 (2008).
2. M. Ahrens, P. Frazier and G. Kelch, "Use of Fire Incident Data and Statistics," *NFPA Fire Protection Handbook, 20th edition,* (ed. A. Cote), pp. 3-61–3-92 (2008).
3. J.R. Hall, Jr., and B. Harwood, "The National Estimates Approach to U.S. Fire Statistics," *Fire Technology,* May, Volume 25, Issue 2, pp. 99–113 (1989).

4. National Fire Protection Association, *Final Report: Study of NFIRS Non-Response Bias Using NFPA Survey Data,* DHS Cooperative Agreement EME-2004-CA-0378 (Aug. 24, 2005).
5. U.S. Fire Administration. National Fire Incident Reporting System 5.0 Complete Reference Guide, 2012, accessed online at http://www.nfirs.fema.gov/documentation/reference on August 13, 2012.
6. M.J. Karter, Jr., *Fire Loss in the United States* series, Quincy, MA: National Fire Protection Association Fire Analysis & Research Division, annual reports (1980–2014).
7. K. Kinsey. E-mail correspondence "Austin smoking fire content codes" May 15, 2012.
8. U.S. Consumer Product Safety Commission, *NEISS—The National Electronic Injury Surveillance System—A Tool for Researchers, Division of Hazard and Data Systems,* Mar. 2000, online at http://www.cpsc.gov/neiss/2000d015.pdf.
9. Energy Information Administration, *Residential Energy Consumption Survey: Housing Characteristic Tables 2001,* Table HC6.1-2a, "Space Heating in U.S. Homes, by Housing Unit type, 2009," accessed Aug. 13, 2012, http://www.eia.gov/consumption/residential/data/2009/.
10. M.Ahrens. *Smoke Alarms in U.S. Home Fires,* National Fire Protection Association Fire Analysis & Research Division, Quincy, MA, (2011), pp. 6, 14
11. J.R. Hall, Jr., *U.S. Experience with Sprinklers,* National Fire Protection Association Fire Analysis & Research Division, Quincy, MA, pp. 20, 23 (2011).
12. G Proulx. Response to Fire Alarms," *Fire Protection Engineering,* Winter 2007, pp. 8–15.
13. J.R. Hall, Jr., *U.S. Unintentional Fire Death Rates by State,* National Fire Protection Association Fire Analysis & Research Division, Quincy, MA (2011).
14. J.R. Hall, Jr., *the Smoking Material Fire Problem,* National Fire Protection Association Fire Analysis & Research Division, Quincy, MA (2012).
15. J.S. Schiller, J.W. Lucas, B.W. Ward, and J.A. Peregoy, *Summary Health Statistics for U.S. Adults: National Health Interview Survey, 2010,* Vital Health Stat 10(225), 2005, Tables 12 and 19, National Center for Health Statistics, accessed Aug. 9, 2012, from http://www.cdc.gov/nchs/data/series/sr_10/sr10_252.pdf.
16. Bureau of Labor Statistics, American Time Use Survey, accessed at http://www.bls.gov/tus/ on August 13,2012
17. P.R. Jose, "Board and Care Facilities," *NFPA Fire Protection Handbook, 20th edition,* (ed. A. Cote), pp. 20-15–20-21 (2008).
18. U.S. Census Bureau Statistics of U.S. Businesses, accessed at http://www.census.gov/econ/susb/introduction.html on August 13, 2012.
19. U.S. Census Bureau. Economic Census, accessed at http://factfinder2.census.gov/faces/nav/jsf/pages/wc_econ.xhtml on August 13, 2012

Marty Ahrens is Senior Manager of Fire Analysis Services in the National Fire Protection Association's Fire Analysis and Research Division.

John R. Hall Jr. is retired from his former position of division director for the Fire Analysis and Research Division at the National Fire Protection Association.

Measuring Consequences in Economic Terms

79

G. Ramachandran and John R. Hall Jr.

Introduction

In any fire risk analysis or risk-based assessment, valid measurements of the severity of the fire hazard—the consequences of fire, if it occurs—are of paramount importance. Most analyses are limited to simple outcome measures, such as numbers of deaths or injuries or direct property damage, defined as direct harm to property requiring repair or replacement.

Consequences have to be expressed in monetary values if the purpose of the analysis is to permit a decision maker to express and compare all relevant costs and benefits of different choices in comparable terms that truly capture what is important to the decision maker or the group represented (such as the general public).

The rapidly growing use of performance-based fire protection design exemplifies the need for these advanced methods of consequence measurement at the level of an individual building or product, just as the growing number of countries demanding cost-benefit analysis of proposed new national regulations illustrates the need for these methods of measurement at the level of national policy.

This chapter describes some of the oft-neglected aspects of consequence measurement in support of economic decisions about fire protection engineering choices, specifically

- An overview of the total cost of fire and of efforts to prevent or mitigate fire
- A discussion of how the relevant costs and benefits for the same choices may vary, depending on whether they are analyzed from the point of view of an individual, an organization, or society as a whole
- An overview of how costs and benefits are treated for insurance purposes
- Methods for translating nonmonetary consequences—notably deaths and injuries—into monetary equivalents for purposes of analysis
- Methods for estimating indirect losses—mainly business interruption costs—caused particularly by large fires
- Utility theory and its role in capturing people's preferences for certainty in outcomes

Principles of life-cycle costing are relevant but are covered at length in Chap. 81. Chapter 81 also provides additional material relevant to many of the subjects covered in this section. A more extensive treatment of these topics, with a range of examples, can be found in *The Economics of Fire Protection* by G. Ramachandran [1].

Components of Total National Fire Cost

For more than two decades, the World Fire Statistics Centre (WFSC) has issued periodic

G. Ramachandran (✉)
Operations Research Section at the Fire Research Station of the United Kingdom

J.R. Hall Jr.
Retired from National Fire Protection Association

M.J. Hurley (ed.), *SFPE Handbook of Fire Protection Engineering*,
DOI 10.1007/978-1-4939-2565-0_79, © Society of Fire Protection Engineers 2016

studies with comparative statistics from 15 to 20 countries on the total cost of fire [2]. Their methods are the starting point for most national analyses, including more detailed analyses from the United States and Canada [3]. The WFSC methodology tracks deaths and injuries, which are not converted to monetary equivalents, but focuses on four core economic components:

- Damages due to fire, whether reported or unreported (for a fire service database), insured or uninsured (for an insurance database), direct or indirect (where indirect loss includes business interruption losses—also called consequential loss), temporary lodging, missed work, and other costs or lost income associated with recovery from a fire
- Costs of fire-fighting organizations, typically dominated by or limited to the costs of municipal career fire service organizations
- Incremental construction costs for buildings attributable to fire safety requirements or concerns
- Administrative costs of fire insurance, including profits

Table 79.1 shows these costs from 1980 to 2011 for the United States [4]. The reports of the World Fire Statistics Centre show comparable figures for many other countries, primarily in Europe but including Japan and Canada. Comparisons are made easier because all loss figures are also shown as percentages of national gross domestic product (GDP). The total U.S. percentage for these core components typically runs about 1 % of the GDP. The United States tends to have one of the lower percentages for fire damage and fire insurance administration (although the latter is especially hard to calculate and has proven quite volatile from year to year). The United States tends to have one of the higher percentages for costs of fire-fighting organizations and for fire-related costs of building construction (although the latter is a subjective estimate, based on some special studies).

Table 79.2 shows the relative importance of the four core components of total cost and how that relative importance has changed over the 32 years studied. The costs of fire-fighting organizations and building construction for fire protection—where the U.S. figures tend to represent one of the higher GDP percentages—are by far the two dominant components of the total cost core, and their dominance has been growing. Not shown in Tables 79.1 and 79.2 are two other important points. First, in nearly every country providing indirect loss figures, indirect losses tend to be less than 25 % of direct damages (notably excepting Switzerland at roughly 40 %). Second, the U.S. fire death rate, relative to national population, consistently ranks among the highest rates in the countries studied by the World Fire Statistics Centre.

Indirect Loss Estimation: NFPA Approach to U.S. Losses

NFPA did a special study to provide a better basis for calculating indirect loss for properties other than homes. It found that indirect loss varied considerably as a fraction of direct damage from one type of property to another. Based on analysis of 109 fires from 1989, indirect losses (principally business interruption costs) add the following amounts to direct loss, based on property class:

- 65 % for manufacturing and industrial properties
- 25 % for public assembly, educational, institutional, retail, and office properties
- 10 % for residential, storage, and special-structure properties
- 0 % for vehicle and outdoor fires

These percentages may appear low to anyone whose sense of indirect loss is based primarily on a few well-publicized incidents where indirect losses were much larger than direct damages. From a statistical standpoint, however, such incidents are more than offset by the far more numerous incidents where indirect loss is either small or nonexistent.

There remains the problem of quantifying indirect loss associated with properties that never reopen. Here again, the overall pattern is much more modest than some figures that have circulated. Each year, an estimated 2 % of reported nonresidential structure fires, excluding fires in storage facilities and special structures

Table 79.1 Estimated core total cost of fire in the United States (in billions of dollars)

Component of cost	1980	1985	1990	1991	1992	1993	1994	1995	1996
Economic losses	7.9	9.1	9.8	11.8	10.8	10.9	10.4	11.7	12.0
Reported	6.3	7.3	7.8	9.5	8.3	8.5	8.2	8.9	9.4
Unreported	0.3	0.4	0.6	0.8	0.7	0.9	0.8	0.9	1.0
Indirect	1.3	1.4	1.4	1.5	1.7	1.5	1.5	1.9	1.6
Career fire departments	5.7	8.5	13.2	13.8	14.4	15.4	16.1	17.1	17.7
Net fire insurance	4.1	4.5	4.9	3.1	4.5	4.8	6.7	6.0	3.8
Building construction for fire protection	10.6	16.9	24.0	18.0	17.6	21.1	23.0	24.7	27.4
Total	28.3	39.0	51.9	46.7	47.3	52.2	56.2	59.4	63.2
Total in 2011 dollars	77.3	81.3	89.3	77.0	75.8	81.2	85.2	87.7	87.3
Component of cost	1997	1998	1999	2000	2001	2002	2003	2004	2005
Economic losses	10.9	10.9	13.2	13.1	55.5	13.3	15.5	12.5	13.6
Reported	8.5	8.6	10.0	10.2	44.0	10.3	12.3	9.8	10.7
Unreported	0.9	1.0	1.2	1.2	1.3	1.3	1.6	1.3	1.5
Indirect	1.5	1.3	2.1	1.7	10.2	1.6	1.6	1.4	1.5
Career fire departments	19.4	20.3	21.3	23.1	25.0	26.0	27.9	28.3	31.4
Net fire insurance	3.6	4.2	2.9	6.8	7.8	12.0	14.8	16.1	15.7
Building construction for fire protection	31.4	34.3	35.8	38.8	38.5	35.4	37.3	42.0	44.5
Total	68.7	73.3	76.3	81.8	126.8	86.7	95.5	98.9	105.2
Total in 2011 dollars	91.4	96.2	98.7	106.7	161.0	108.3	116.7	117.8	121.0
Component of cost	2006	2007	2008	2009	2010	2011			
Economic losses	14.5	18.6	20.1	16.1	14.8	14.9			
Reported	11.3	14.6	15.5	12.5	11.6	11.7			
Unreported	1.5	2.0	2.1	1.7	1.6	1.6			
Indirect	1.7	1.9	2.5	1.9	1.7	1.7			
Career fire departments	34.2	36.8	39.7	40.3	42.6	42.3			
Net fire insurance	17.8	17.8	15.0	17.0	19.2	20.2			
Building construction for fire protection	48.5	48.5	50.8	41.6	31.7	31.0			
Total	115.0	121.7	125.6	115.1	108.4	108.4			
Total in 2011 dollars	128.1	131.9	131.0	120.5	111.8	108.4			

Sources: NFPA survey; *Statistical Abstract of the United States*, *Property/Casualty Insurance Facts*; websites related to data sources; formulas from special studies

Note: Sums may not equal totals because of rounding error. Figures are not adjusted for inflation except for total rows in 2011 dollars; other figures are as reported in those years. Some figures for earlier years have been changed from earlier total cost reports to reflect revisions shown in published sources. Net fire insurance includes the difference in economic losses between published insurance figures and the figures shown here. Economic losses in 2001 include the unique events of the 9/11 attacks

(e.g., vacant properties, properties under construction, structures that are not buildings), result in business closings. For NFPA's analysis of indirect losses in the United States, a closing is estimated to imply indirect losses equal to four times the reported direct loss in the fire.

These very rough calculations suffice to estimate indirect loss for purposes of a national analysis of total cost from society's point of view. They clearly are not sufficient to produce estimates suitable for insurance purposes or any other decision making at the level of an individual firm. Also, detailed estimates of consequential losses to the national economy should reflect several economic factors, including level of employment or unemployment, level of capacity utilization, volume of exports and imports, exchange rates, and performance of national and international competitors. Due to the interactions of these factors, a detailed evaluation of consequential losses to the national economy is a complex problem requiring the application of

Table 79.2 Changes in components of core of total cost of fire in the United States, 1980–2011

Component of cost	Percent change 1980–2011	1980 percent share	2011 percent share
Economic loss	+89	28	14
Career fire departments	+641	20	39
Net fire insurance	+392	14	19
Building construction for fire protection	+193	38	29
Total	+283	100	100
Consumer price index [a]	+173		

Sources: Table 79.1; consumer price index data from U.S. Bureau of the Census, Statistical Abstract of the United States, Washington, DC (1999–2013)

Note: Sums may not equal totals because of rounding error. The estimated core of total cost of fire has increased more from 1980 to 2011 (283 %) than the increase due to inflation for the same years (173 %)

[a]In other words, $1.00 in 1980 consumer goods would have cost $2.73 in 2011

econometric models, such as input-output analysis. These national factors do not apply to analysis at the level of an individual firm.

The effects of a fire on the earning capacity of a firm can be measured in terms of loss of profits during the period of interruption following the damage until the resumption of the activity in which the firm was engaged before the fire. Loss of profits is usually expressed as a percentage of loss of turnover. A cover against this loss can be obtained by purchasing a consequential loss insurance policy, the premium for which is a function of the period of indemnity. Loss of profits sustained by a supplier or customer of the firm that suffered the fire (called the "fire-hit firm" from here on) can be covered by a normal consequential loss policy based on reduction in turnover.

The form of insurance policy in more general use in the United States is known as business interruption insurance (BII). BII operates on lines similar to the U.K. contract of consequential loss insurance (CLI) with a turnover specification, though there are some differences. For private sector level insurance firms transacting BII or CLI, there are useful sources of data for estimating consequential losses due to fires in industrial and commercial premises. Organizations such as the Insurance Information Institute in the United States compile consequential loss data furnished by major insurance firms.

Indirect Loss Estimation: Unpublished U.K. Study

Returning to national- and society-level analyses of indirect or consequential loss, some now-old studies done in the United Kingdom illustrate how a more detailed analysis can be done. The U.K. government's Home Office carried out two research studies between 1970 and 1980 on consequential losses to the national economy. The first study adopted an input-output-type model in which all losses were considered output losses [5]. Losses were either (1) losses in the type of output actually hit by fire or (2) losses in some other output, because production factors (e.g., fixed assets, entrepreneurial effort, or labor) have been less effectively employed as a result of the fire. The effects of a fire were assumed to have the most impact on the fire-hit firm, the supplying firm, the purchasing firm, the parallel firm, and the rest of the economy. A fire-hit firm was defined as a compartment of production covering just that type of output hit by a fire and no other output. A parallel firm was defined as the compartment of a firm that produced in parallel to the fire-hit compartment (which might be in the same firm or in another firm). Any effects in a parallel firm or somewhere else in the rest of the economy were assumed to be included in the calculation of the effects in a fire-hit firm, in a supplying firm, or in a purchasing firm.

In this Home Office study, consequential losses were measured by the net present values of streams of annual outputs lost by the fire-hit firm, supplying firms, and purchasing firms. In regard to the fire-hit firm, it was necessary to determine a length of time over which fixed assets destroyed by fire were assumed not to be replaced by extra investment in the economy. This time choice had to depend on a view of the future course of the economy, which depended on unknown events and influences. Hence,

alternative calculations were produced based on the remaining lives of the assets and on a number of shorter periods. The net present values were corrected within the fire-hit firm, supplying firms, and purchasing firms for offsetting influences due to two factors. First, some production factors affected by fire might be used elsewhere in the economy. Second, production factors already employed elsewhere might be used more intensively. The extent of such offsetting influences would depend largely on the level of employment and the pressure of demand in the economy. Separate calculations were made for three alternative cases—slack, middle, and tight conditions in the economy. Results were given for each of 15 industries, including a factor by which a fixed assets valuation should be multiplied to give the sum of all the corrected output losses.

In order to verify the assumptions employed and results obtained in this study, the Home Office commissioned field research aimed at an in-depth investigation of a small sample of fires [6], which involved direct contact with fire-hit firms and concentrated on direct, consequential, and, hence, the total loss to the U.K. economy from industrial, distributive, and service sector fires. Consequential losses were considered to arise from loss of exports, extra imports, the diversion of resources from other productive activities, and reduction in the efficiency of resource use following the fire. The study assumed that there was full-capacity utilization of resources and that market values of the resources reflected their true worth. Insurance estimates of losses were used as measures of the assets destroyed in fires. Application of national capital output ratios translated these asset losses into losses of output from fire. Allowances were made for the secondary impact on suppliers and customers of fire-hit firms and for the impact of the level of capacity utilization. A correction factor was applied to account for the ability of the economy to "make good" the losses of the fire-hit firm by other firms.

The analysis produced estimates of the ratios of consequential to direct losses to the economy for "off-peak" and "peak" years and for each industry and service sector. The main conclusion was that most fires, except those in chemical and allied industries, produced no consequential losses to the national economy. Only in one sector (chemicals) was evidence found of a statistical link between consequential losses and direct losses. The study failed to estimate this link for other sectors and a number of other possible effects on consequential losses. Note the similarity of this conclusion to the results of the much smaller, rougher, and more recent NFPA study, leading to the indirect loss parameters still used in the United States.

Indirect Loss Estimation: Private Sector Level

A study by Hicks and Liebermann deals with costs and losses from the community and private perspective as they impact the fire victim [7]. The property class categories addressed in this study were commercial occupancies only, separated into four types: (1) mercantile, (2) nonmanufacturing, (3) manufacturing, and (4) warehouses. The authors considered first the following expression, based on a convenient formulation of the Cobb-Douglas production function [8]:

$$IL = ke^{rT}E^{a}X^{1-a} \tag{79.1}$$

where
IL = Indirect loss
K = Constant
r, a = Regression coefficients
E = Expenditure for fire protection (–)
X = Number of fires (+)
T = Time (surrogate for technological advance) (–)

The signs in parentheses relate to the expected values of the coefficients for the independent variables. The term ke^{rT} is a scalar factor in which r measures increases in fire department efficiency due to technological advances in suppression equipment, training, or facilities as well as altered building codes, smoke alarms, and the like. Equation 79.1 can be converted to a multiple-regression model by taking logarithms of terms on both sides.

In principle, the parameters r and a can be estimated but, in practice, sufficiently detailed statistics typically are not available. The authors therefore adopted the following, much more simplified, form:

$$IL = c(DL)^b \tag{79.2}$$

where DL is the direct loss and c and b are constants. Equation 79.2 is based on the assumption that very small fires typically generate small indirect losses while large fires produce larger indirect losses. If $b = 1$, this model reduces to the earlier-cited approach used by NFPA, wherein indirect losses are estimated as proportional to direct damages.

The results obtained by Hicks and Liebermann [7] are given in Table 79.3. Note that all values of the parameter b are near 1, which means the deviations from the even simpler model used by NFPA are modest. Statistical tests of significance showed that the regression model fitted well with the data in all the cases except warehouses. Since nationally aggregated data were utilized, it was recommended that the occupancy-specific models be used only at the national level and that any desired analysis of local impacts be accomplished using a local model. The value of parameter b has been estimated to be greater than unity for local and national levels and less than unity for the occupancy levels. For any increase in direct loss, the ratio of indirect to direct loss would increase if $b > 1$, and decrease if $b < 1$. The ratio would be a constant if $b = 1$. From the information given in the study, it was not possible to test whether the value of b was significantly different from unity for any of the six levels.

Table 79.3 Relationship between direct and indirect fire loss model parameters [7]

	Parameters (from Equation 79.2)	
Level	c	b
Local	0.203	1.146
National	0.015	1.245
Mercantile	0.109	0.889
Nonmanufacturing	0.069	0.874
Manufacturing	0.135	0.890
Warehouse	0.047	0.804

Indirect Loss: Illustrations from Some Major U.S. Fires

It is not difficult to identify large, well-publicized fires in which the cost of business interruption far exceeds direct property loss, such as a property that offers lodging or workspace and suffers so much damage that the slack capacity of the facility or even the community is not sufficient to absorb the displaced demand. An example is the MGM Grand Hotel fire, where the hotel claimed total direct damage and business interruption costs of $211 million, whereas NFPA's best information placed direct damage at $30–50 million [9].

Sometimes, though, it can be difficult to determine what the true net loss due to business interruption is—what constitutes an "interruption." Compare two large high-rise office building fires [10, 11]. Fire destroyed four floors of the 62-story First Interstate Bank building in Los Angeles in 1988 but also took the entire building out of service for 6 months—a true business interruption, because the property reopened after repairs.

By contrast, the 1991 One Meridian Plaza fire destroyed more floors in a shorter high-rise office building (38 stories) and the building never reopened. Dozens of firms, occupying nearly a million square feet of office space, had to seek new permanent homes, but the real estate community estimated, a year after the fire, that vacancy rates would still be 11–12 % *after* every displaced firm had been absorbed.

One Meridian Plaza represented an estimated 2.5 % of Philadelphia's office space, whereas the MGM Grand represented a larger share of Las Vegas area hotel rooms. These are all factors in determining how easily a market can compensate for interruption of capacity from one provider. Similar concerns arise for fires in any type of large multiunit residential or health care occupancy.

The most clear-cut examples of widespread vulnerability involve critical elements of the nation's infrastructure. Fears of great damage from a widely distributed computer virus have so far not materialized, and two major interruptions to the northeast electrical power

grid in the last third of the twentieth century were not due to fire. However, there have been two fires involving telephone exchanges, the more recent in Hinsdale, Illinois, in 1988 [12].

A total of 38,000 customers were served by the Hinsdale office. The majority were still without service 5 days after the fire, and some did not regain service until 9 days after the fire. An estimated 9000 businesses were affected, including a nationwide hotel chain's reservation service, a florist delivery service networked to 12,500 florists around the country, and communications between a Federal Aviation Administration control tower and both of Chicago's major commercial airports. The most conservative estimate of the costs of the associated delays and lost business would exceed the estimated $40–$60 million in direct damage.

Economic Costs Not Usually Calculated Within the Core

Several cost components have been estimated by Meade but cannot be readily estimated each year [3]. They totaled $27.8 billion in 1991 and consist of the following:

- Costs of meeting fire grade standards in the manufacture of equipment, particularly electrical systems equipment and "smart" equipment with its greater use of computer components ($18.0 billion)
- Costs of fire maintenance, defined to include system maintenance, industrial fire brigades, and training programs for occupational fire protection and fire safety ($6.5 billion)
- Costs of fire retardants and all product testing associated with design for fire safety ($2.5 billion)
- Costs of disaster recovery plans and backups ($0.6 billion)
- Costs of volunteer and paid activities involved in preparing and maintaining codes and standards ($0.2 billion)

The largest piece by far is the first one. Meade's study developed estimates, by industry, firm, or individual making the estimate, that ranged over two orders of magnitude, from 20 % to 2000 % add-on cost. He settled on 30 %, which seems conservative. However, out of the fraction of equipment that could be affected by these costs, his estimate of the share that is built to these more demanding standards is not conservative. His estimate raises the concern that the fire safety spending habits of industry's most fire-conscious companies have been treated as typical of all industry.

Based on the Consumer Price Index, the $27.8 billion estimated by Meade for 1991 would translate to $45.9 billion in 2011 in the United States. The NFPA now adds a figure for national and state fire agency costs, which was $3.0 billion in 2011.

Costs and Benefits Based on Level

The previous discussion noted that the calculation of indirect loss is done differently if the focus is on an individual firm or on the entire society. Any calculation of costs and benefits associated with fire, fire prevention, or mitigation activities and decisions will show differences based on level, because costs and benefits do not fall equally on all parties.

A fire that interrupts or destroys the ability of a single firm to offer its goods or services to the market results in devastating indirect loss to that firm. Society, however, may experience no discernable effect, provided that

1. The firm represents a small part of its industry, so that neither price nor availability of its products or services is affected by the removal of the firm.
2. The firm represents a small part of the employment opportunities in its community, so that its employees are able to find comparable work and income quickly and easily.

Conversely, a fire that results in little on-site damage but creates devastating environmental damage on the surrounding area, through air or water pollution, may represent a negligible cost to the firm, provided it is able to disown the off-site costs and pay minimal legal costs to do so. Meanwhile, the cost to society is enormous.

The second example cited above involves direct damage to property, and its central premise—that the firm could disavow off-site

damages if they were sufficiently difficult to measure and to trace to an event on the firm's site—is probably far-fetched in today's world. The first example cited above involves a major type of indirect loss, sometimes called business interruption loss or consequential loss, and that example is not at all unusual.

Analysis can be done at many different levels—the individual person, the individual firm, the individual community, the individual industry, the individual state or province, the individual industry plus all industries strongly dependent on it, the individual nation, the entire world—but for purposes of analyzing business interruption or consequential loss, it may be useful to focus on two major levels of economic activity: (1) private sector and community level and (2) national and societal level. The first level includes the fire-hit firm and the firms supplying to or purchasing from the fire-hit firm's materials, components, or services. Costs associated with moving, temporary accommodation, and lost profits are valid costs at the private sector level but not at the national level.

At the national level, the loss of a specific unit of productive capacity may be spread among the remaining capacity in the nation such that competitors may seize the opportunity to enter the market and maintain the national rate and volume of manufacture. In such cases, there may be little or no incremental loss to the national economy as a result of a fire in the premises of, for example, a manufacturing firm. Several studies by the now-defunct Insurance Technical Bureau (ITB) in the United Kingdom provide an indication of the various special factors one should consider in the evaluation of consequential losses due to fires and other hazards.

A small share of the total number of production lines in a plant manufacturing pharmaceutical products may generate a very large proportion of total gross profits [13]. Regulatory restrictions may limit possibilities for shifting manufacture to other plants or even to other lines in the same plant. Natural raw materials may be irreplaceable or out of season, creating another source of delay in recovery or another obstacle to meeting demand during the recovery process. Specialized plant equipment (e.g., tailor-made driers or centrifuges) may involve long delays for replacement. Loss of laboratory facilities may seriously interrupt testing and quality control programs.

The aerospace industry is another example where innovation driven by research creates a very short cycle time for the introduction of new products. In such cases there may be little redundancy in the supply of prototypes or other essential elements needed to keep the program on schedule [14]. Examples might include a new aircraft prototype assembly, untried or unproven research and development projects, or specimens for fatigue testing of aircraft structures. Loss of any of the above could result in a significant interruption to the program. In addition, the effect of delays in the development or supply of components or assemblies from specialist equipment manufacturers can be serious. The interactions of the many activities and firms involved in the manufacture of aerospace products makes for involved consequential loss considerations.

An example from the other end of the spectrum of industries would be resin, paint, and ink manufacture, which would not normally be expected to give rise to unduly high consequential loss [15]. Facilities are generally dispersed in small units throughout a given country, and there may be sufficient manufacturing capacity to absorb temporary loss at individual sites. Also few, if any, products are so special that they cannot be made elsewhere in the industry. Consequential loss, therefore, hinges primarily on the time for reinstatement of the plant and the ability of management to arrange for the supply of goods from other sources, pending a return to full production. Loss of raw materials or finished goods normally results in relatively short interruption periods. However, longer periods may be required for the replacement of tanks and pumps destroyed by fires, and for other hazards, such as explosion.

Due to high investment costs, specialized equipment (e.g., electronically or computer-controlled equipment) is generally used at full

capacity in some industrial processes. Continuous operation of these processes may reduce the chance of a fire spreading but provides no scope for making up for lost production following a fire. Specialized equipment damaged by fire cannot be replaced easily or quickly, especially if the assemblies or spare parts for them have to be imported. Industries using such equipment are liable to sustain high consequential losses.

Measurement Approaches in the Insurance Industry

Statistical (actuarial) techniques are well developed for calculating the insurance premium for loss of profits due to fire (e.g., see Benckert) [16].

The risk premium is a function of the period of indemnity and is generally expressed as the product of the loss frequency and the mean amount of loss. The loss frequency is assumed to be independent of the period of indemnity. The frequency function of the period of interruption following a fire has a log-normal distribution [16, 17].

An insurance company generally adds two types of loading to the risk premium to calculate the premium payable by a policyholder. First, a safety loading is added toward chance fluctuations of loss beyond the expected loss. Second, another loading is imposed to cover the insurer's operating costs, which include profits, taxes, and other administrative expenses. A number of texts have been published on different types of insurance and claims concerned with consequential losses (e.g., see Riley) [18].

Monetary Equivalents for Nonmonetary Costs and Consequences

Deaths and Injuries

Damage to life or health in terms of injuries and deaths is an important consequence in fire risk assessment and is usually the first priority consequence cited in national codes or regulations. Its importance is not in question. What is difficult is identifying a valid and acceptable method for estimating and comparing monetary equivalents of consequences of this type with costs and monetary equivalents of consequences of other types, such as property damage or indirect/consequential loss.

Insurance claims provide some data for the valuation of injury, though they are likely to be limited to costs mediated by the marketplace, such as treatment costs and the value of work time lost. Other costs, such as pain and suffering, are more difficult to evaluate.

The specification of a dollar equivalent for human losses, particularly for loss of life, remains an extremely controversial subject. It is important to emphasize that no one intends to suggest that there is an acceptable price for losing one's life. Rather, these figures are intended to reflect a social consensus on the value of changes in the risk of death by fire. For example, if most people say they would be willing to pay $1500 to reduce their lifetime risk of dying in a fire from, say, one chance in 500 to one chance in 1000, then a simple way of restating that is that people value a life saved at $1500 for 1/1000 of a life, or $1.5 million per life.

Four approaches to valuing human life have been identified. The first method is concerned with gross output based on goods and services that a person can produce if not deprived, by death, of the opportunity to do so. Sometimes gross productivity is reduced by an amount representing consumption (net output). Discounted values are generally taken to allow for the lag with which the production or consumption occurs. The output approach usually gives a small value for life, especially if discounted consumption is deducted from discounted production. This must be so since the community as a whole consumes most of what it produces. It is argued that when a person dies, although the community loses that person's future output, it also saves concurrent future consumption. The person's own consumption or the utility that would be derived if the person were alive is not counted as a loss. This approach received considerable emphasis, say, 30 years

ago, but not today. A variation of this approach is called the "livelihood approach" [19].

The second approach assumes that if an individual has a life insurance policy for $\$x$, then he or she implicitly values his or her life at $\$x$. Collection of necessary data from insurance companies is not a difficult task, and this is the major advantage in adopting the insurance method. There are, however, two drawbacks to this method. First, a decision whether or not to purchase insurance and the amount of insurance is not necessarily made in a manner consistent with one's best judgment of the value of his or her life. This decision depends largely on the premium the insured can bear from his or her income, taking into account family expenditures. Second, purchasing an insurance policy does not affect the mortality risk to an individual. This purchase is not intended to compensate fully for death or to reduce the risk of accidental death. Hence insuring life is not exactly a value tradeoff that is considered between mortality risks and costs.

The third method for assessing value of life involves court awards to heirs of a deceased person as restitution from a party felt to be responsible for the fatality. Here again, collection of necessary data is not a problem. Assessment of values of life could also be expected to be reasonably accurate since lawyers and judges have a massive professional expertise in the ex post analysis of accidents. The object of such an analysis is to discover whether the risk could have been reasonably foreseen and whether the risk was justified or unreasonable.

There are, however, a few problems in using court awards for valuing human life. The court should ideally be concerned with the assessment of suitable sums as compensation for an objective loss (e.g., loss of earnings of the deceased) as well as for a subjective loss (e.g., damages to spouse and children for their bereavement and grief). In some countries damages can include a subjective component for pain and suffering of survivors, but certain courts are generally against such compensation for subjective losses to persons who are not themselves physically injured, believing that bereavement and grief are not losses which deserve substantial compensation. It is also difficult to value the quality of a life that has been lost. People who themselves suffer severe personal injury, of course, qualify for substantial damages for subjective losses. Resource costs such as medical and hospital expenses are significantly higher for obvious reasons in serious injury cases than in fatal cases; hence, awards for subjective losses tend to be much larger and more important in serious nonfatal cases than in fatal cases. Some courts have also limited to very low levels the damages that may be awarded for reductions of life expectancy. Last, in court awards risks to individuals are considered relative to the plaintiff and costs to the defendant. However, value judgments are likely to vary according to whether the individuals making these judgments are associated with the plaintiff, the defendant, or the court.

The fourth approach is the one most widely adopted for valuing life. The willingness to pay is based on the money people are willing to spend to increase their safety or reduce a particular mortality risk [20, 21]. It is difficult to differentiate between the benefit from increasing people's feeling of safety and that from reducing the number of deaths. Anxiety is a disbenefit even if the risk is much smaller than believed. Likewise, a person who dies from something whose risk is not known to him or her still suffers a loss.

This approach to value of life rests on the principle that living is a generally enjoyable activity for which people would be willing to sacrifice other activities, such as consumption. The implied value of life revealed by a willingness-to-pay criterion would depend on a number of factors. The acceptable expenditure per life saved for involuntary risks is likely to be higher than the acceptable expenditure for voluntary risks, as people are generally less willing to accept involuntarily the same level of risk they will accept voluntarily. The sum people are prepared to pay to reduce a given risk will also depend on the total level of risk, the amount already being spent on safety, and the earnings of the individuals.

The theoretical superiority of the willingness-to-pay method begins with its connection to the

principle of consumer sovereignty, which says goods should be valued according to the value individuals put on them. Despite this individual-oriented underpinning, this approach can also be used to develop a general figure for a typical person, based on consensus patterns in the values individuals select. This, in turn, permits analysis of societal decisions using the willingness-to-pay principle.

Surveys have shown variability and inconsistencies in responses, because individuals have difficulty in answering questions involving very small changes in their mortality risks [22–24]. Due to insufficient knowledge about the risk, most people find it difficult to accurately quantify the magnitude of a risk. Also, the benefits are often intangible (e.g., enjoyment, peace of mind). It is difficult to put a monetary value on these factors.

Economists therefore use a variety of inferential methods to develop value of life and value of injury averted estimates for purposes of analysis. These include examination of patterns from the other three approaches—foregone future earnings, insurance policy amounts, and especially court judgments. It is also possible to develop an inferred value of life risk reduction from any action that has a cost and achieves such a reduction. Studies have been done of the implied value of life associated with hundreds of safety- and health-related regulatory actions. Studies could be done based on the price and demand curves for safety-oriented products, such as smoke alarms and child-resistant lighters.

It is useful to keep in mind the very wide variation in the estimates and valuations and the implied uncertainty as to what values are reasonable. For example, a landmark 1981 study cited sources for values of statistical life ranging from $50,000 to $8 million [25]. More recent valuations have been higher generally but still vary widely.

Economists at the U.S. Consumer Product Safety Commission (CPSC) have an ongoing program of studies of injury costs. Periodically, they review the literature, including their own studies, and select dollar values for use in policy analysis of fire safety and other product hazard analysis. The NFPA studies of the total cost of fire in the United States use values of $5 million per death and $166,000 per injury as 1993 values, then use the Consumer Price Index to calculate corresponding values for later years *for injuries only*, all in accordance with the practices of CPSC economists. Special studies have changed the NFPA methodology of estimating costs for injuries, adding a multiplier of 60% to civilian injuries, 30% to firefighter foreground injuries, and 10% to firefighter non-fireground injuries.

The total dollar equivalent for reported and unreported fire deaths and injuries in the United States, calculated in this way, was $31.7 billion in 2011 [4].

It is beyond the scope of this chapter or this handbook to review, even briefly, the many nuances, methods, and applications of value of life estimation. For those who wish to pursue the subject in more detail, several listed references are recommended [26–33].

Value of Donated Time

In the United States, the largest block of donated time for fire safety consists of that donated by the roughly 800,000 volunteer fire fighters who provide municipal fire protection to a sizeable fraction, mostly rural, of the U.S. population. One approach to valuing their donated time is to assume that costs are generated not so much by the workload of emergencies as by the need to provide coverage and readiness to respond for a certain area, that is, the ability to provide an effective response within a certain response time. If this approach is used, the primary factor in costs would not be workload, but geographical area. The low-density rural areas covered by volunteer fire departments would then require more personnel than would more compact areas of equal population covered by career fire departments.

Communities seeking to set such fire protection coverage at an appropriate level might begin with a response time objective. The part of response time that is most related to resource decisions is travel time, which may be treated

as proportional to travel distance. If one thinks of a typical response area as a circle with the fire station in the middle, one can see that travel distance is proportional to the square root of area. For example, if the distance from the fire station to the edge of the response area doubles, that is equivalent to doubling the radius of a circle, whose area then is quadrupled. This also means that if the same population is spread out over an area four times as large, it will need twice as many fire stations to provide equivalent travel times, which means the needed number of fire fighters may be treated as inversely proportional to the square root of the population density.

In 2000, the metropolitan statistical areas of the United States had 80.3 % of the U.S. population in 20.0 % of the area. If one assigns all the remaining area and population to volunteers (which is a rough approximation), then the metropolitan population density (proportional to 80.3 % divided by 20.0 %) exceeds the nonmetropolitan population density (proportional to 19.7 % divided by 80.0 %) by a factor of 16. The square root is 4.0, which is somewhat higher than the actual ratio in fire fighters (2.8:1 in 2002).

Using the 4:1 ratio for personnel needed, assuming their costs would be the same as in career fire departments, and again adjusting for nonpersonnel costs included in reported local fire expenditures, the result is $139.8 billion in 2011 for the value of time donated by volunteer fire fighters.

If this estimate of the value of donated time by volunteer fire fighters is combined with the earlier estimates of the core components of total cost of fire, the other economic components estimated from data that is not updated yearly, and the estimated monetary equivalent of deaths and injuries associated with fire, the resulting total is $329 billion for the United States in 2011. This is 2.1 % of the total U.S. gross domestic product, a figure that fully justifies appeals from the fire protection engineering community for more support of research seeking to reduce the total, either through improved safety or through sustained safety at reduced cost.

Utility Theory

Even after all costs and benefits (e.g., risk reduction) have been converted to monetary equivalents, an important aspect of people's preferences may be overlooked if expected-value techniques are used directly in a cost-benefit analysis of fire safety measures to include the certainty-equivalent of uncertain costs and benefits.

Suppose a person is offered a choice between $5 or a 50/50 coin toss wager between $10 and nothing. The expected values of the two choices are equal, assuming a fair coin. A person who prefers the sure thing is called *risk averse*. Most people are somewhat risk averse in some situations. Just how risk averse a person is can be measured by determining how low the sure-thing offer can be set before the person will choose the wager with the $5 expected value.

Fire loss is never a sure thing, and so people's risk preferences are always relevant to assessing their preferences for choices involving fire risk.

People differ not only in their degree of risk aversion but also as a function of the type of choice being offered. Some people may prefer to take risks in most situations. It also is not unusual to find that a person is a *risk preferer* for ventures involving small losses but a *risk avoider* for those involving large values.

Any pattern of risk preferences can be quantified by the use of *utility functions*. *Disutility*, the negative counterpart of utility, is the appropriate term in an analysis involving negative outcomes such as fire loss, cost of fire protection, and insurance premiums.

Consider a few more examples based on participation in a game of chance. Suppose a person is offered the following bet on the toss of a coin—to win $100 if the coin comes up heads or lose $75 if the coin comes up tails. If the coin is a fair coin, the $probability of heads or tails coming up is one-half. The expected payoff is

$$\frac{1}{2}(\$100) + \frac{1}{2}(-\$75) = \$12.5$$

if the person playing the game takes the bet and $0 if he or she does not take the bet. According to

the expected value criterion, the bet should be accepted because its expected value is greater than the expected value of not taking the bet.

Now suppose the amounts involved are $1,000,000 and $750,000 rather than $100 and $75. The expected payoff is now $125,000 if the bet is taken and $0 if the bet is not taken. Every value has been multiplied by 10,000. According to the expected value criterion, the bet should still be taken and is even more attractive. But would you take this bet? Probably not, unless you are wealthy enough that you could afford to lose $750,000. The possible gain of $1,000,000 is tempting, but losing could be devastating or even intolerable.

As another example, consider a choice between two bets. In the first bet, the person playing the game wins $2 million if a coin comes up heads and wins $1 million if the coin comes up tails. In the second bet $8 million can be won if the coin comes up heads, but nothing will be won if the coin comes up tails. The expected payoffs of the two bets are $1.5 and $4 million, respectively. The second bet has a much larger expected payoff than the first, and hence should be chosen on the basis of the expected value criterion. However, many would choose the first bet because they focus on the larger minimum gain—the closest thing to the "sure thing" in a choice between two bets. With the first bet, you are assured of at least $1 million. With the second bet, there is a 50 % chance of winning nothing.

Consider a third example, defined more directly in terms of fire safety. Suppose the owner of a home or other building faces a probability, p, of fire occurring in the coming year and a loss, L, in the event of a fire. (In this simplified example, only one kind and severity of fire is possible.) The expected annual loss due to fire in that building is pL, and it is a two-outcome bet, like a coin toss.

The sure-thing alternative, from the owner's point of view, can be achieved through insurance. The property owner has two options—to insure or not insure the building. The expected loss (cost) is equal to the insurance premium (call it I) if insured, and pL if not insured.

On the basis of the expected value principle, the owner should choose the insurance option only if I is less than pL. This condition will never be satisfied since an insurance firm would determine the premium, I, for a risk category by adding to the risk premium, pL, two loadings—a safety loading and another loading to cover the operating costs of the firm which include profits, taxes, and other administrative expenses. From the insurance company's point of view, it should offer the insurance only if I is greater than pL. How is it that insurance even exists under these conditions?

The risk aversion of most people provides the foundation for breaking this dilemma. Based on risk aversion, the building owner will accept a sure-thing loss of I even if I is greater than pL. The difference is typically large enough not only to make a mutually acceptable deal possible, but to allow I to be large enough to cover the two loadings mentioned above.

In practice, many different sizes and severities of fire are possible. For the smallest fires, the building owner's risk aversion will probably be much less pronounced, and insurance may seem unattractive. The creation of a deductible threshold solves that problem by allowing the insurance to be limited to losses large enough for the owner's risk aversion to be strong. If a very large fire occurs, the insurance company may be unable to cover the loss. This leads to reinsurance markets, particularly for properties with the potential for more than one very large loss in a short period of time. For smaller losses, the safety loadings on the risk premium would provide a safety margin for the insurance company, depending on its calculations of the probability distribution for the fire loss. There may also be an upper bound set on the maximum loss the insurance company can cover.

The preference for a small fixed loss over a risk of large loss originates primarily from an aversion to the psychological state of uncertainty. For the reasons mentioned previously, the expected monetary value is not a satisfactory criterion for decisions involving potential losses in ranges where risk aversion is an issue for many people. Note that the ranges of risk aversion can

depend on the size of the decision maker's resource base—how large a loss can be sustained at all, and how large a loss can be absorbed without serious inconvenience or harm—and on the number of "bets" undertaken. An insurance purchaser has one bet (at least one per year) going, so he or she is exposed to the full uncertainty of the risk. An insurance company with many customers has many bets going, so the company's annual loss experience will fit a much narrower range around the expected value, except in certain circumstances. If many customers are exposed to a common risk, such as will happen if many customers live in the same hurricane-prone region, the range of probable outcomes for the insurance company will be much wider. If the insurance company's evaluation of the probabilities and consequences is seriously deficient or simply outdated, then its exposure may be quite different than it believes.

Utility and Disutility

For positive outcomes (gains), *utility* means a measurement scale for desirability [34]. It is a number measuring the attractiveness of a consequence—the higher the utility, the more desirable the consequence. A utility function translates monetary consequences into a scale for which expected-value calculations accurately reflect the preferences of an individual, a firm, or a decision maker. For negative outcomes (losses and costs), *disutility* is a measurement scale for undesirability—the higher the disutility, the less desirable the consequence.

The examples given earlier illustrate the fact that, for a specific person, firm, or decision-making entity, the value of gaining x dollars (or consequence of losing x dollars) is not necessarily x multiplied by the value of gaining a single dollar (or consequence of losing a single dollar). Issues of certainty and of the ability to accept loss can cause substantial deviations from the simple multiplicative relationship.

If it were possible to measure the true relative values to the decision maker of the various possible payoffs in a problem of decision making under uncertainty, expected values could be calculated in terms of these true values instead of the monetary values. The theory of utility seeks to develop such values, permitting choices to be analyzed using the decision-making rule—the maximization of expected utility or minimization of expected disutility. Utility theory provides a means of encoding risk preferences in such a way that the risky venture with the highest expected utility or lowest expected disutility is preferred. Symbolically, if the monetary value of the ith outcome is X_i the utility corresponding to a gain X_i is $U(X_i)$ the disutility corresponding to a loss X_i may be denoted by $D(X_i)$.

Utility Functions

The mathematical structure of the function $U(X)$ is central to the application of utility theory. Figure 79.1 graphically shows three typical utility functions that are usually encountered in this analysis [35]. The utility function represented by the straight line A is appropriate for a decision maker operating on an expected monetary value (EMV) basis. This line satisfies the equation $U(X) = X$ and represents risk neutrality. The concave curve B corresponds to a risk-averse (or risk-avoiding) decision maker, and the convex curve C to a risk-prone (or risk-taking) decision maker. For a decision maker who is more risk prone than the EMV individual or who prefers a risk, the utility of a fair game exceeds the utility of not gambling and hence a fair game will always be played. On the other hand a decision maker who is more risk averse than the EMV person does not like or cannot afford risks and is a risk avoider.

Some individuals could have a sigmoid form of utility function as illustrated by Fig. 79.2. Such a person is a risk preferer for small values of X but a risk avoider for larger values.

Consider now a game with a 50 % chance of winning \$100 and a 50 % chance of winning nothing, which has the expected value \$50. The expected value line A in Fig. 79.1 connects the points [0, $u(0)$] and [100, $u(100)$]. To find the utility of the game for the risk avoider (curve B),

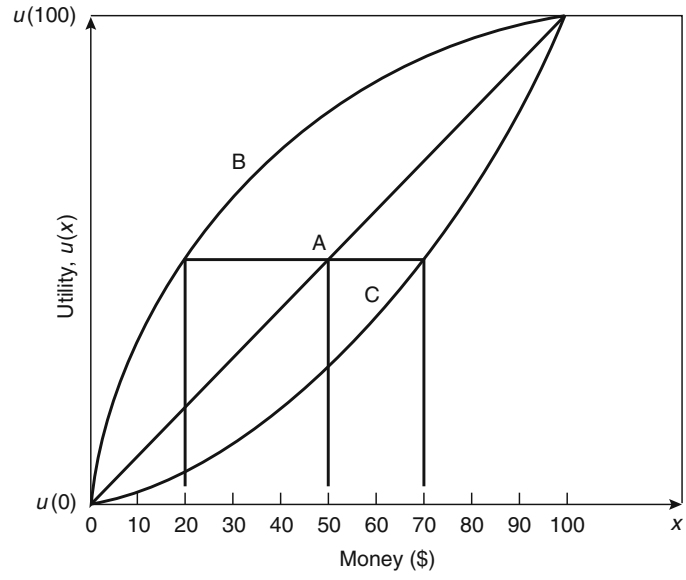

Fig. 79.1 Typical utility functions

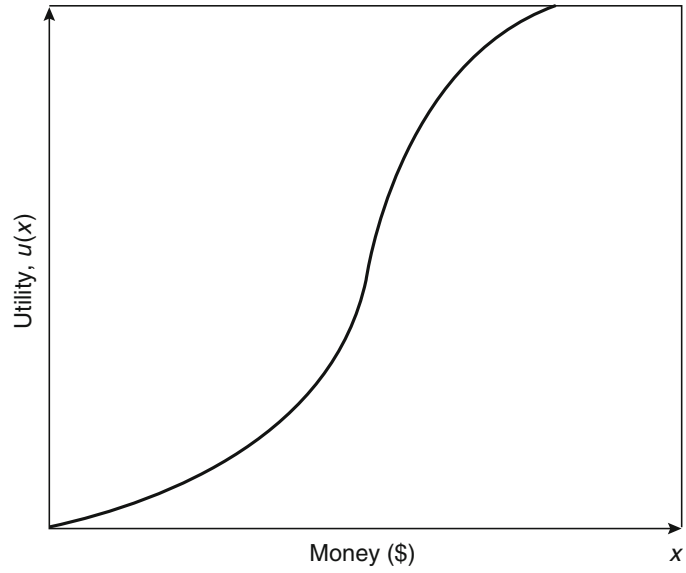

Fig. 79.2 Sigmoid utility function

find the utility value corresponding to the point on the straight line above the expected \$50 value of the game. By reading to the left, cutting curve *B*, this value is equal to *U*(\$20) so that the decision maker's cash equivalent (CE) for the game is \$20. He or she would be willing to pay up to \$20 to be able to participate in the game. This is still below the EMV of \$50 since the utility function *B* is that of a risk avoider.

The difference between the EMV and CE is the *risk premium*, which is \$30 in this example. The decision maker would be willing to pay \$30 to avoid the risk involved in participating in the game.

In the case of the risk taker denoted by curve *C*, the utility of the game is equal to *U*(\$70), so \$70 is the cash equivalent for the game. Although the expected value is only \$50, the risk taker is

willing to pay up to $70 to be able to participate in the game. Hence the risk premium is –$20. It is negative because the decision maker, instead of being willing to pay a premium to avoid the risk in the game, is willing to pay a premium (above and beyond the expected value) to be able to participate in the game.

The risk premium, RP, discussed above is the amount that a decision maker, on the basis of his or her utility function, is willing to pay to avoid or participate in a risky activity. For increasing utility functions such as those shown in Fig. 79.1, the risk premium for any risky venture is defined as

$$\mathrm{RP} = \mathrm{EMV} - \mathrm{CE}\,dx \tag{79.3}$$

where EMV is the expected monetary value and CE the cash equivalent. The parameter CE is also referred to as *certainty monetary equivalent*, CME, in the literature on utility theory [36].

For a risk avoider whose increasing utility function is concave, the risk premium RP given by Equation 79.3, for any situation in which the outcome is uncertain, is positive (EMV is greater than CE). For a risk taker whose increasing utility function is convex, RP is negative. For a risk neutral person whose utility function is linear, RP is always zero (EMV = CE).

The CE is defined mathematically as

$$U(CE) = E[U(x)] = \overline{U} \tag{79.4}$$

where the right-hand side is the expected value of the utility over the range of values taken by x. If $x_1, x_2, \ldots, x_n$ are the values (consequences) with probabilities $p_1, p_2, \ldots, p_n$

$$\overline{U} = E[U(x)] = \sum_{i=1}^{n} p_i U(x_1) \tag{79.5}$$

If x is a continuous variable with probability density function $h(x)$, the expected utility is given by

$$\overline{U} = \int_x U(x)h(x)dx \tag{79.6}$$

The CE or CME of a risky venture, V, is an amount, $\hat{x}$, such that the decision maker is indifferent between the risky venture, V, and the certain amount, $\hat{x}$. Put another way, $\hat{x}$ is the value for which $U(\hat{x})$, the utility function on $\hat{x}$, is equal to the expected value of the utility function on the full range of possible outcomes.

The expected value of a random variable, x, is given by

$$\overline{x} = E(x_i) = \sum_{i=1}^{n} p_i x_i \tag{79.7}$$

or by

$$\overline{x} = \int_x xh(x)dx \tag{79.8}$$

in the continuous case.

To illustrate the procedure for calculating a CE or CME, consider, as an example, the specific utility function

$$U(x) = -\mathrm{e}^{-cx} \tag{79.9}$$

Suppose the decision maker is faced with a venture with two possible outcomes: x_1 with probability ½ and x_2 with probability ½. The expected value of the venture is

$$\overline{x} = \frac{x_1 + x_2}{2}$$

The certainty equivalent (CE) is therefore the solution to this equation:

$$\begin{aligned} U(\hat{x}) &= \mathrm{e}^{-c\hat{x}} \\ &= -\frac{\mathrm{e}^{-cx_1} + \mathrm{e}^{-cx_2}}{2} \end{aligned}$$

It may be verified that for $c = 1$, $x_1 = 10$, and $x_2 = 20$, the certainty equivalent is

$$\hat{x} = 10.69$$

The expected value is

$$\frac{(10 + 20)}{2} = 15$$

Consider a second example in which the risky venture has a continuous range of outcomes, ranging from 0 to 20, with an exponential probability density function

$$f(x) = \mathrm{e}^{-x}$$

The expected value is

$$\overline{x} = \int_0^{20} x e^{-x} dx = 1$$

Suppose we further assume a utility function as

$$U(x) = -\mathrm{e}^{-2x}$$

The certainty equivalent is given by $\hat{x}$ such that

$$-\mathrm{e}^{-2\hat{x}} = -\int_0^{20} \mathrm{e}^{-2x}\mathrm{e}^{-x} dx$$
$$= -\int_0^{20} \mathrm{e}^{-3x} dx = -\frac{1}{3} \quad \hat{x} - 0.55$$

Specific Probability Distributions for Utility Analysis of Fire Safety Choices

Based on the formulations just discussed, a utility analysis requires a probability distribution function for the outcomes of a risky choice and a utility function on those same outcomes. For a risky choice where fire loss is the source of risk, the key variable in differentiating the outcomes is the size of the fire loss (in monetary terms). Let that be defined as x.

Consider a property owner with an asset value of W. If a loss of x is incurred in a fire, the asset value would be reduced to

$$X = W - x \tag{79.10}$$

The property owner's utility function will be defined in terms of the reduced asset value, rather than the fire loss, because the reduced asset value reflects the owner's wealth and ability to absorb a loss. An appropriate utility function in terms of positive X would be

$$U(X) = -\mathrm{e}^{-\theta X}, \quad \theta > 0 \tag{79.11}$$

which is an increasing risk averse utility function [36].

Although the extent of risk aversion quantified by θ is constant for all X, this exponential utility function is widely used in view of its computational simplicity.

Next, in order to match the form of the utility function to the form of a distribution on probabilities of fire loss size, Equation 79.11 should be rewritten as

$$U(x) = -\mathrm{W}'\mathrm{e}^{\theta x} \tag{79.12}$$

where $W' = e^{-\theta W}$ and is a constant. As discussed earlier, the certainty equivalent $\hat{x}$ is given by solving the following equation for $\hat{x}$:

$$-W'\,\mathrm{e}^{\theta x} = -W' \int_x \mathrm{e}^{\theta x} v(x) dx \tag{79.13}$$

where $v(x)$ is the probability density function of fire loss, x.

As x increases from zero, $U(x)$ decreases from a value of $-W'$ A larger loss means a lower adjusted asset value and hence lower utility.

According to statistical studies carried out by Ramachandran [37–39], Shpilberg [40], and other authors, loss in a fire has a skewed (nonnormal) probability distribution. Ramachandran has concluded that a good fit is obtained from an exponential-type distribution applied to the logarithm, z, of fire loss size, x (i.e., $z = \log x$ follows an exponential distribution). Among distributions of this type, a normal distribution for z or a log-normal distribution for x is commonly used. An exponential distribution for z or a Pareto distribution for x has also been considered by some actuaries.

If the probability distribution function for fire loss is expressed in terms of z (= log x) instead of x, it will be computationally necessary to have a utility function expressed in terms of z as well. Ramachandran [41] has argued that z (= log x) may be used in Equation 79.12 instead of x so that the utility function is

$$U(z) = -\mathrm{e}^{\theta z} \tag{79.14}$$

which is equivalent to

$$U(x) = -x^{\theta} \tag{79.15}$$

The utility function in Equation 79.15 is a decreasing function with $\theta = 1$ representing risk neutrality. The value of θ should be greater than unity to express a risk averse attitude. The degree of risk aversion increases with θ.

Consider a property worth total financial value V belonging to a risk category with fire loss x having a log-normal distribution. If μ and σ are the mean and standard deviation of z ($= \log x$), following the method described by Ramachandran [1], the certainty equivalent for the range $(0, V)$ is given by

$$\hat{x}^{\theta} = \frac{1}{G(k)} \frac{1}{\sqrt{2\Pi}\sigma} \int_{-\infty}^{\log V} \exp\left[-\frac{1}{2}\left(\frac{z-\mu}{\sigma}\right)^2\right] e^{\theta z} = \frac{G(k-\sigma\theta)}{G(k)} \exp\left(\mu\theta + \frac{\sigma^2\theta^2}{2}\right) \tag{79.16}$$

where

$$k = (\log_e V - \mu)/\sigma$$

$$G(k) = \frac{1}{\sqrt{2\pi}} \int_{\infty}^{k} \exp\left(-\frac{t^2}{2}\right)$$

$$G(k-\sigma\theta) = \frac{1}{\sqrt{2\pi}} \int_{-\infty}^{k-\sigma\theta} \exp\left(-\frac{t^2}{2}\right)$$

and $G(t)$ is the standard normal distribution. The expected monetary value of the loss is given by $\theta = 1$ in Equation 79.16, because risk neutrality means utility is linearly related to loss. For a decreasing utility function (or increasing disutility function) such as Equation 79.15, the certainty equivalent, CE, is greater than the EMV.

For a property with a given level of fire protection, the CE corresponding to a given degree (θ) of risk averse attitude of the owner is the maximum insurance premium the owner will be willing to pay to meet the uncertain consequences of a fire. The CE will increase with θ; an owner more risk averse than another will be prepared to spend more money on insurance.

Both EMV and CE will decrease with increasing levels of fire protection. Hence, by adopting efficient fire protection measures, a property owner with a given degree of risk aversion can reduce the cost of the insurance premium. He or she can also obtain a further reduction in the premium by taking self-insurance for small losses.

References

1. G. Ramachandran, *The Economics of Fire Protection,* E & FN Spon, London (1998).
2. R.T.D. Wilmot (ed.), *World Fire Statistics Centre Bulletin,* Geneva Association, Geneva, Switzerland (1995).
3. W.P. Meade, "A First Pass at Computing the Cost of Fire Safety in a Modern Society," *NIST-GCR-91-592,* National Institute of Standards and Technology, Building and Fire Research Laboratory, Gaithersburg, MD (1991).
4. J.R. Hall, Jr., *The Total Cost of Fire in the United States,* NFPA Fire Analysis & Research Division, Quincy, MA (2014).
5. "The Economic Cost of Fire," Economist Intelligence Unit Ltd., unpublished report, London (1971).
6. "Investigation of Consequential Losses to the Economy from Fires," PA Management Consultants Ltd., unpublished report, London (1977).
7. H.L. Hicks and R.R. Liebermann, "A Study of Indirect Fire Losses in Non-Residential Properties," *Foubrand,* 1, pp. 8–15 (1979).
8. J.M. Henderson and R.E. Quandt, *Microeconomic Theory,* Chapter 3, McGraw-Hill, New York (1971).
9. "MGM Fire Litigation," *Business Insurance,* p. 10 (January 2, 1984); and "Fire at the MGM Grand," *Fire Journal,* pp. 19 f. (January 1982).
10. T.J. Klem, "Los Angeles High-Rise Bank Fire," *Fire Journal,* p. 85 (May/June 1989).
11. D.M. Halbfiner, "Incalculable Cost of One Meridian Fire," *Philadelphia Business Journal,* February 24, 1992, pp. 1, 30.
12. M.S. Isner, "Telephone Central Office, Hinsdale, Illinois, May 8, 1988," NFPA Fire Investigation Report, Quincy, MA (1989).
13. *Fire and Explosion Hazards in the UK Pharmaceutical Industry,* The Insurance Technical Bureau, London (1977).
14. *Fire and Explosion Hazards in the UK Aerospace Industry,* The Insurance Technical Bureau, London (1976).
15. *Fire and Explosion Hazards in the UK Paint and Ink Manufacturing Industries,* The Insurance Technical Bureau, London (1978).
16. L.-G. Benckert, "The Premium for Insurance Against Loss of Profit Due to Fire as a Function of the Period of Indemnity," in *Transactions of the 15th International Congress of Actuaries,* New York, pp. 297–305 (1957).
17. D. Flach, J. Schlunz, and J. Straub, "An Analysis of German Fire Loss of Profits Statistics," *Blatter der*

Deutschen Gesellschaft fur Vesicherungsmathematik, Vol. X, Part 2 (1971).
18. D. Riley, *Consequential Loss Insurance and Claims,* Sweet and Maxwell Ltd., London (1967).
19. R.F.F. Dawson, "Current Costs of Road Accidents in Great Britain," *Report No. RRLLR 396,* Road Research Laboratory, Crowthorne, UK (1971).
20. J. Linnerooth, "The Evaluation of Life Saving," *Research Report RR-75-21,* International Institute of Applied Systems Analysis, Laxenbury, Austria (1975).
21. S.J. Melinek, "A Method of Evaluating Human Life for Economic Purposes," *Accident Analysis and Prevention,* 6, p. 103 (1974).
22. J.P. Acton, "Measuring the Social Impact of Heart and Circulatory Disease Programs: Preliminary Framework and Estimates," *Rand R-1697/NHLI,* Rand Corporation, Santa Monica, CA (1975).
23. G.W. Fischer and J.W. Vaupel, "A Lifespan Utility Model; Assessing Preferences for Consumption and Longevity," working paper, Durham, NC (1976).
24. E. Keeler, "Models of Disease Costs and Their Use in Medical Research Resource Allocations," *P-4537,* Rand Corporation, Santa Monica, CA (1970).
25. J.D. Graham and J.W. Vaupel, "Value of a Life: What Difference Does It Make?" *Risk Analysis,* 1, p. 89 (1981).
26. M.W. Jones-Lee (ed.), *The Value of Life and Safety,* Elsevier, North Holland, New York (1982).
27. G. Blomquist, *Estimating the Value of Life and Safety: Recent Developments in the Value of Life and Safety,* Elsevier, North Holland, New York (1982).
28. T.C. Schelling, "The Life You Save May Be Your Own," in *Problems in Public Expenditure Analysis,* Brookings Institution, Washington, DC (1968).
29. G. Maycock, "Accident Modelling and Economic Evaluation," *Accident Analysis and Prevention,* 18, p. 169 (1986).
30. S.G. Helzer, B. Buchbinder, and F.L. Offensend, "Decision Analysis of Strategies for Reducing Upholstered Furniture Fire Losses," *Technical Note 1101,* National Bureau of Standards, Washington, DC (1979).
31. S.E. Chandler and R. Baldwin, "Furniture and Furnishings in the Home—Some Fire Statistics," *Fire and Materials,* 7, p. 76 (1976).
32. I.C. Appleton, "A Cost-Benefit Analysis Applied to Foamed Plastics Ceilings," *Current Paper CP 50/77,* Fire Research Station, Borehamwood, UK (1977).
33. M.W. Jones-Lee, *The Value of Life: An Economic Analysis,* Martin Robertson, London (1976).
34. J. von Neumann and O. Morgenstern, *Theory of Games and Economic Behavior,* Princeton University Press, Princeton (1947).
35. P.G. Moore, *Risk in Business Decision,* Longman Group, London (1972).
36. R.L. Keeney and H. Raiffa, *Decisions with Multiple Objectives: Preferences and Value Trade-Offs,* John Wiley and Sons, New York (1976).
37. G. Ramachandran, "Extreme Value Theory and Fire Losses—Further Results," *Fire Research Note No. 910,* Fire Research Station, Borehamwood, UK (1972).
38. G. Ramachandran, "Extreme Value Theory and Large Fire Losses," *ASTIN Bulletin,* 7, p. 293 (1974).
39. G. Ramachandran, "Extreme Order Statistics in Large Samples from Exponential Type Distributions and Their Application to Fire Loss," in *Statistical Distributions in Scientific Work,* 355, D. Reidel, Dordrecht, Netherlands (1975).
40. D.C. Shpilberg, "Risk Insurance and Fire Protection; A Systems Approach. Part 1: Modelling the Probability Distribution of Fire Loss Amount," *Technical Report No. 22431,* Factory Mutual Research Corp., Norwood, MA (1974).
41. G. Ramachandran, *The Interaction Between Fire Protection and Insurance,* Seminar, Zurich, Switzerland (1984).

G. Ramachandran retired in November 1988 as head of the Operations Research Section at the Fire Research Station of the United Kingdom. Since then he has been practicing as a consultant in risk evaluation and insurance. He is a visiting professor at the universities of Manchester and Leeds. His research has focused on statistical and economic problems in fire protection and actuarial techniques in fire insurance.

John R. Hall Jr. is retired from the division director for fire analysis and research of the National Fire Protection Association. He has been involved in studies of fire experience patterns and trends, models of fire risk, and studies of fire department management experiences since 1974 at NFPA, the National Bureau of Standards, the U.S. Fire Administration, and the Urban Institute.

Computer Simulation for Fire Risk Analysis

80

William G.B. Phillips and Rita F. Fahy
Revised by Douglas K. Beller

Introduction

Fire protection engineers are required to deal with complex fire scenarios that include human reactions and behavior, in addition to the physical and chemical fire processes. Operations research (OR) pioneered the application of the scientific method to the management of organized systems in which human behavior is a key element. Fire protection engineering could be defined as the application of operations research to the fire system.

Systems involving human beings are difficult to study because realistic experiments may be impossible and neither past experience nor the available data provide sufficient insight to any given fire situation. Operations research overcomes these difficulties by the use of simulation models. Simulation models are widely used in science, engineering, and mathematics to study problems that involve ordinary and partial differential equations (either overtly or implicitly). In fire science, for example, simulation models have been used to handle phenomena such as smoke movement and absorption of toxic substances. Both computational fluid dynamics (CFD) models and zone models are solved by similar techniques. These matters are dealt with elsewhere in this handbook. This chapter concentrates on the variety of procedural simulation models that may be applied to interdisciplinary systems, specifically those involving human agents and objectives.

Simulation models describe the system under study in terms of individual events of the individual components of the system [1]. In a gross sense, the simulation model of interest to fire protection practitioners can be divided into human (i.e., evacuation or egress) and physics (i.e., fire effects) components. The simulation model then combines these parts in their natural order and allows the computer to present the effect of their interaction on each other [1]. After the model is constructed, it is provided with data and run to simulate the actual operation of the system. Advances in computer software and hardware have greatly reduced the cost and simplified the use of simulation models. Recent developments in virtual reality are expected to facilitate more realistic interaction between the model and its user.

Uncertainty can be handled by introducing stochastic elements into the model. Estimates of risk can be derived from simulation models by the use of Monte Carlo techniques. Regression analysis can be applied to obtain compact expressions that can be used to measure the sensitivity of the output variables to variations in the inputs.

Types of Models

A model can represent a system as a unified and precisely definable whole, all of whose aspects are simultaneously and unambiguously accessible

W.G.B. Phillips (✉) • R.F. Fahy
Research Engineer, WPI Fire Science Lab, Worcester Polytechnic Institute, Worcester, MA, USA

M.J. Hurley (ed.), *SFPE Handbook of Fire Protection Engineering*,
DOI 10.1007/978-1-4939-2565-0_80, © Society of Fire Protection Engineers 2016

for assessment. Models include pictures, diagrams, and "scale models," as well as mathematical structures.

Models can be classified as descriptive, physical, and symbolic [2]. The *descriptive model* is expressed in ordinary language and is the most common tool for decision making in science, engineering, and everyday life. Descriptive models function like metaphors. For example, the flow of smoke through a vent might be compared to the flow of water in a channel, implying that buoyancy and gravity play a similar role, albeit with a reversal of sign.

Physical models include scale models, and examples can range from basic hydraulic models of harbors and estuaries to transparent plastic models to demonstrate the flow of smoke in buildings. They make it possible to try out alternative arrangements in the search for an optimum design or strategy. Analogue models are a special type of physical model that exploits the isomorphisms that exist between different physical processes. The behavior of voltages, currents, resistance, capacitance, and inductance in an electrical circuit has many analogies with processes in heat and fluid flow and acoustic, electromagnetic, and mechanical systems.

Science and engineering depend heavily on *symbolic models* in which algebraic symbols represent the values of variables and the relationships between them. Once a model has been cast in symbolic form, the whole mathematical apparatus can be deployed to deduce additional relationships and solve equations to find optimal solutions. Symbolic models may be static or dynamic; in the latter case they specifically include a variable representing time. A very important type of dynamic model is formulated in terms of ordinary or partial differential equations. Many problems in fire science lead to models that can be expressed in the form of one or more simultaneous differential equations. Some of these have simple analytic solutions, but many interesting cases do not; for example, the partial differential equations that arise in fluid dynamics (Navier-Stokes equations). Such equations are normally solved on computers by standard numerical methods.

A *simulation model* treats the dynamic relationships that are assumed to exist in the real situation as a series of elementary operations on the appropriate variables. A simulation model is made to predict outcomes by actually executing the procedural steps with appropriate initial data and parameters. All of the components comprising a simulation model need not be contained in a single piece of software. Furthermore, as long as each procedural step is represented in the model, the model need not be entirely computer-based. This is to say that, the procedural steps associated with some components of the model may be determined using simple hand calculations. The model user then ensures that the components are constructed in the proper manner to provide the intended output. Running the model creates the prediction. The variables in a simulation may change continuously in value or take on only certain discrete values. These changes may take place at any time or only at certain times, or both. For example, a simulation of a fire incident might handle the flow of hot gases by a differential equation expressed in continuous terms, while the people would be treated as discrete individuals moving at prescribed moments in time. However, because such a model would almost certainly be implemented on a computer, the differential equations would be approximated by a difference equation for the purposes of numerical integration (a computer cannot handle "real" numbers). Therefore, the distinction between continuous simulation models and the dynamic symbolic models discussed in the previous paragraph tends to blur.

Simulation Models

A procedural simulation model is a representation of a dynamic system in which the processes or interactions bear a close resemblance or relationship to those of the specific system being simulated or studied. These models are concrete rather than abstract and may contain approximations and subjective elements. They are amenable to manipulations that would be

impossible, too expensive, or impractical to perform on the entity portrayed. The operation of the model can be studied, and properties concerning the behavior of the actual system or its subsystems can be inferred. Manipulation of a procedural model requires the acceptance of inputs and the generation of outputs that are similar or analogous to those of the system represented.

Procedural simulation is essentially a technique that involves setting up a model of a real situation and then performing experiments on the model. The idea that a computer model might partly replace experimentation is both dangerous and attractive. It is, therefore, appropriate to remember a warning given by Ackoff and Beer: [3]

> Often when an operations researcher does not understand a phenomenon which he can nevertheless describe well, he can simulate it on a computer and thus conduct experiments. These are experiments on the model on which the simulation is based, not on the system involved. The fact that a simulation may reproduce history with some accuracy does not by itself establish a correspondence of structure between the model and reality. This is true for the same reason that a straight line may have been generated by a sine function, not one that is linear.

Procedural simulation modeling has been widely applied; examples are Link (aircraft pilot) trainers, military war games, business management games, space exploration, physical models of river basins and estuaries, econometric models, electrical analogue devices, and wind-tunnel tests for aircraft. It has proved particularly useful in situations involving human intervention of one kind or another. There are great opportunities for improving the interface between the model and operator, making use of virtual reality techniques. In this way, "realistic experience" of rare events can be acquired without danger and at low cost.

Types of Simulation Models

Simulation models can be classified as either discrete or continuous. In the real world there is no such distinction, yet it is possible to model some real-world systems either discretely or continuously. In both types of simulation what is of concern are the changes in the state of the model. Continuous simulations are analogous to a stream of fluid passing through a pipe. The volume may increase or decrease, but the flow is continuous. Using the pipe analogy for discrete event simulation, the pipe could either be empty or have something traveling through it. Whether anything came out of the pipe would depend on some event occurring at the other end.

Both types of simulation can be applied to fire. As time progresses the state of a building changes continuously as the once small fire becomes larger, overwhelms the building, and eventually dies out as it runs out of fuel. The chemical processes in the fire and the physical processes that mediate the flow of heat and hot gases naturally lend themselves to the continuous type of model. On the other hand, discrete simulations are more appropriate to the strategies used to fight the fire and evacuate the building. For example, the fire is ignited and detected, fire fighters and equipment arrive, hoses are deployed, water is applied, more equipment may be called in, and so on. Similarly the occupants respond to the alarm, collect their belongings, locate their household members, and go toward the exits in a sequence of clear-cut stages.

In continuous models, changes in the variables are directly based on changes in time. The values of the variables reflect the state of the model at any particular time, and simulated time advances from one step to the next, usually in equal increments. In discrete event models, events occur as items move through the simulation. The state of the model changes only when those events occur. Simulated time advances from one event to the next (generally in unequal increments) and the mere passing of time has no direct effect.

Discrete Event Simulation Models

Discrete event simulation models are built up from several different elements. These are given

different names in different programming languages. A terminology based on *blocks, items,* and *events* will be used in this discussion. *Items* are characterized by *attributes, priorities,* and *values.*

A *block* is used to represent an action, operation, resource, or process. It is like a block in a block diagram. These blocks are connected in an activity or data flow diagram that represents the system. Information comes into the block and is processed by the program that is in the block. The block then transmits information out of the block to the next block in the simulation. Some blocks may simply represent a source of information that is passed on to other blocks. Other blocks may modify information as it passes through them. Output blocks take information from the simulation and present it to the user in graphic form.

The basic unit passed between the blocks is called an *item.* An item is a data set that carries information about the item's attributes, priorities, and values. In a manufacturing model, an item might be a part on an assembly line; in a network model, an item would be a packet of information; in an evacuation model, an item would be an occupant. Items are generated by special blocks, either according to a fixed schedule or a random distribution.

The model moves items from block to block only when an *event* occurs. Events occur only when specific blocks specify that they should. For example:

1. Blocks that depend on time cause events to happen at an appropriate time. For example, a block representing an activity, say the journey from the fire station to the fire location, might introduce a delay of t min into the system representing the duration of the journey. If the alarm was received by the fire station at T min, the block would post an event in the event queue at $T + t$ min.
2. Blocks that have an accumulated demand for inputs cause an event immediately after they receive items. For example, a block representing a parent searching for a child, following a fire alarm, would cause an event when the child is located.
3. Blocks that do not generate events allow the blocks after them to pull items during a single event. Thus, an item can pass through many blocks after a single event if those blocks do not stop it.

Note that every event has the potential to cause every block in a model to move items. Thus, one event may cause many unrelated items to progress in the simulation.

In order to provide true discrete event simulation, the time clock that controls the simulation must move to the exact time of each event. The most common way of doing this is to have an event queue. Each block places the time of its next event in a slot in the event queue. In each cycle the event queue is checked to find the next closest time point; the current time is set to that value, and a "simulate" message is sent to every block. Most blocks ignore these messages unless the message occurs at the event time that was previously posted by the block, or there are items waiting in the block's inputs that can be pulled in. For example, a block representing a queue should pull in an available item whenever it gets a "simulate" message, no matter which block posted the event.

Attributes are an important aspect of discrete event simulation. Attributes are characteristic properties of an item that stay with it as it moves through the simulation. For example, an occupant making an escape from a building might have attributes representing mobility and the amount of carbon monoxide absorbed. *Priorities* specify the relative importance of an item. *Values* allow the model to deal with items that represent groups of identical entities.

Continuous Simulation Models

There is a close similarity between continuous simulation models and the solution of ordinary differential equations by numerical methods. Almost any phenomenon that can be represented by differential equations may be modeled by continuous simulation. This classification includes virtually the whole of classical physics,

and the method can easily be extended to chemistry and biology, and more speculatively to economics, ecology, and human behavior. The fundamental principle is that the rate of change of certain variables can be expressed as a function of a set of variables (the state variables) that describe the state of the system at a given time. Therefore,

$$\frac{dx_i}{dt} = f(x_1 \ldots x_i \ldots x_n), i = 1 \ldots n$$

The solution to this set of equations is found by integration and yields a function that depends on time, which characterizes the dynamic behavior of the system. For example, suppose the rate at which a chemical reagent is consumed is proportional to the concentration of the reagent. This relationship could be expressed in the form of a differential equation, with the following solution:

$$\frac{dx}{dt} = -kx$$

and, therefore,

$$x = Ae^{-kt}$$

This result can be interpreted to mean that the concentration declines exponentially and tends toward zero as the reaction proceeds. Note that the result is a function of time and not concentration. This example leads to a first-order linear differential equation that has an analytic solution. Many systems of interest, however, give rise to higher order nonlinear differential equations, which, in general, do not have analytic solutions or have solutions only if drastic simplifications are imposed. Their solution is normally carried out on computers using one of the standard numerical methods (e.g., Euler, Runge-Kutta). Higher order differential equations can lead to very complex dynamic behavior, for example, various types of oscillation. (It is useful to note that differential equations of an order above the first can always be replaced by one or more first-order simultaneous differential equations).

For a computer to handle a differential equation expressed in continuous terms, the equation has to be replaced by an equivalent difference equation. Consider the following differential equation that shows that the rate of change in volume is equal to flow.

$$\frac{d(\text{volume})}{dt} = \text{flow}$$

This equation has an analytic solution that can be found by integration; that is,

$$\text{volume} = \int_{t=\text{start}}^{t=\text{stop}} \text{flow} \cdot dt$$

The original differential equation can be written as a difference equation:

$$\frac{\text{volume}_t - \text{volume}_{t-\Delta t}}{\Delta t} = \text{flow}$$

which can be rearranged to show that

$$\text{volume}_t = \text{volume}_{t-\Delta} + \Delta t \cdot \text{flow}$$

This equation implies that the value of volume at time t is simply the sum of the value of volume at time $t - \Delta t$ plus the time interval Δt multiplied by flow. This solution (which amounts to Euler's method) can be implemented directly on a computer. Note that the analytic integral solution and the finite difference method will give the same result only if flow is constant. If flow is changing rapidly, the finite difference method will require a large number of iterations (i.e., $\Delta t \to 0$) to converge to the analytic integral solution.

Continuous simulation models are particularly suited to the analysis of dynamic processes. Frequently, the system under examination will display a particular behavior pattern that may be interesting in itself or may be causing a problem. The objective of the model designer is then to construct a model based on differential equations that will reproduce this reference pattern. Decisions need to be made as to which state variables and rates of change are significant. If the model is being used to address some well-understood phenomena, it may be possible to use established relationships that have been tested by experiment. Otherwise, it may be necessary to introduce parameters into the model that lack theoretical backing but enable the model to exhibit the reference behavior either qualitatively or quantitatively.

The overall behavior of the model often depends not as much on the precise value of the parameters and the detailed algebra as on the structure of the model itself. Systems of simultaneous differential equations can usually be shown to be linked together in longer or shorter loops that can be of either positive or negative sign. Positive feedback loops tend to reinforce change and often give rise to exponential growth. Negative feedback loops tend to negate change and are usually associated with goal-seeking activity.

Model building can be thought of as passing through a sequence of iterations in which the model becomes more and more realistic. At each iteration the model designer makes observations, forms hypotheses, carries out tests, modifies the model, and tests the model again. The advantage of working within this framework is that simulation models can be objective and explicit rather than subjective and implicit. These characteristics make them particularly valuable for (1) communicating results and (2) acting as a workbench on which alternative solutions to problems can be tested.

Monte Carlo Procedures

Monte Carlo analysis is a simulation technique applicable to problems having a stochastic or probabilistic basis. Two different types of problems give rise to the use of this technique. Firstly, there are those problems that involve some kind of stochastic process. The rate of flame spread and fire growth and the response of individuals to fire alarms are examples of variables that may be considered to be stochastic in nature. In this case, the stochastic element may be introduced at any point in the model run so that the value of a variable at any time depends in some way on its previous value and a random component. Second, there are problems in which the process is treated as deterministic, but the starting conditions and model parameters are randomly selected from probability distributions.

The model may be used simply to estimate the value of the endogenous variables at a given location and time. The estimate will, of course, depend on the values of the parameters supplied to the model. However, the exact value of a parameter may not be known, but it might be possible to estimate its mean and variance and the form of its distribution. This information can be encoded as a probability density. A sequence of runs of the model can then be carried out using samples drawn from this distribution. Methods have been developed for generating values from most of the well-known probability distributions as well as any empirical distribution (For details see Appendix A of this chapter.). It is then possible to estimate probability densities representing, for example, the fire conditions or the number of casualties from the model output. If sensitivity analysis shows that the uncertainty in the input has little effect on the uncertainty in the output, it would not be necessary to go to great expense to refine the value of the input parameter.

Everything said so far about Monte Carlo methods has been on the assumption that there is only one input variable and one output variable. This assumption can now be relaxed so that all the uncertain input parameters can be treated as random samples from probability densities. The probability density of the output variables is now generated by the probability densities of all the input variables. This function is important because it allows analysis of synergistic effects in which certain combinations of symmetrically distributed input variables can give rise to strongly skewed distributions of the output variables. Distributions of this type are typical of multiplicative stochastic processes. Probability distributions of fire damage are frequently skewed and can often be described by a density of the log-normal variety with a pronounced right-hand tail [4]. This result may be due to the simultaneous occurrence of several adverse factors which tend to reinforce each other due to nonlinearities in the system.

The input parameters can be interpreted as exogenous variables and the model outputs as endogenous variables. This approach suggests that it would be possible to regress the outputs on the inputs using a standard multiple linear regression routine. This method is equivalent to

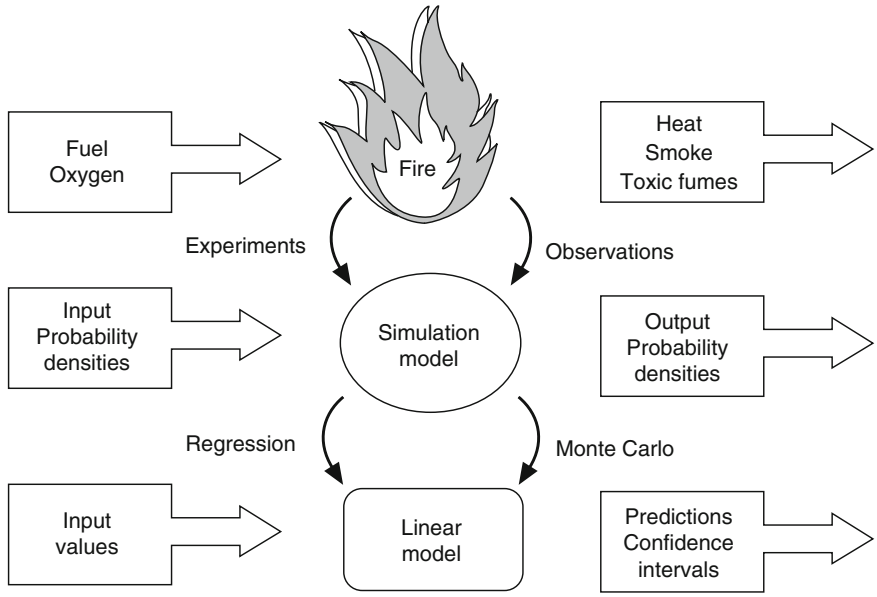

Fig. 80.1 Relationships between observations and models [5]

creating a linear model of the nonlinear simulation model. The relationships between the actual fire, the simulation model, and the linear approximation to the simulation model are shown in Fig. 80.1 [5].

It can be shown [6] that the resulting regression coefficients correspond to the partial differential coefficients (i.e., the rate of change of an endogenous variable, y, with respect to each of the exogenous variables, x).

Sensitivity Analysis

Sensitivity analysis can be used to draw useful conclusions to guide decisions on fire safety design and priorities for research. In its simplest form, sensitivity analysis is carried out by varying one of the input parameters in steps over a prescribed range and observing the effect on chosen output parameters, either at the end of the model run or at a set time after the run commences. (Advanced methods of sensitivity analysis are available that allow more than one variable to be varied at a time.) The results of this exercise can then be presented as a table or, more usefully, the output parameter can be regressed against the input parameters to give a simple linear or nonlinear expression that summarizes the results and permits interpolation and extrapolation.

The rate of change of the output parameter, with respect to the input parameter, is defined as the *sensitivity*. In fire safety terms, sensitivity might indicate how much the risk is reduced as fire protection measures are improved. If the cost of improved protection is also known, it is possible to estimate the cost of saving a life.

Figure 80.2 shows five runs of an evacuation model in which the delay in giving the fire alarm has been increased in steps of 1 min, from 6 to 10 min. The number of people trapped in a building at, for example, 18 min is represented by the distances between the curves and the horizontal axis. If the number of casualties is regressed against the delay, the results shown in Fig. 80.3 are obtained. The number of casualties that would occur if the alarm were delayed by t minutes can be calculated directly from the formula. Conversely, the formula can be used to predict the number of lives that might be saved if the delay were reduced by, for example, an improved alarm system. Note that in this case,

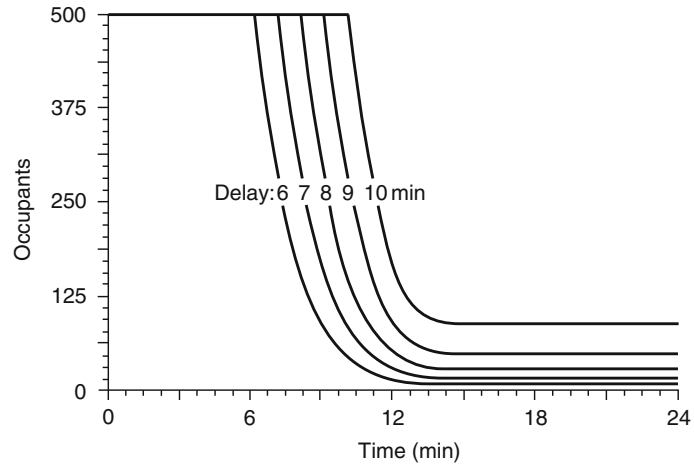

Fig. 80.2 Occupants remaining in a place of assembly if the alarm is delayed for the periods shown

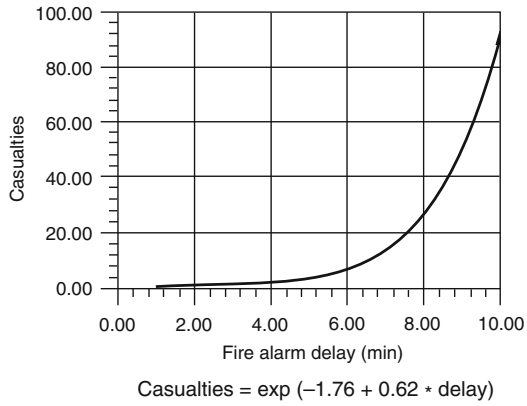

Fig. 80.3 The number of casualties rises exponentially as the delay in giving the signal to evacuate is increased

the sensitivity is not a constant, but an exponential function of time.

A similar exercise can be undertaken for fire effects models. Ideally, every input parameter that is based on an assumption should be the subject of a sensitivity analysis. After establishing a base case, the user should vary the "assumed" input parameter values by ± 10 % and observe what effect this change has on the output variable of interest. If the predicted output value varies by less than ± 10 %, then the output variable is insensitive to that input variable. Conversely, if the predicted output value varies by more than ± 10 %, then the output variable is sensitive to the input variable in question. The more sensitive input parameters may require further investigation depending on their degree of sensitivity.

The significance of calculations like these is that they enable designers to select those areas where expenditure on fire protection measures would earn the greatest return in terms of lives saved. It also makes it possible to identify those areas where additional expenditure might have little or no effect. This approach is also helpful for making decisions on research priorities. If preliminary calculations indicate that the fire risk can be substantially reduced by a small change in a parameter, it would make sense to put research effort into investigations designed to refine the measurement of that parameter and reduce the level of uncertainty associated with it.

Sensitivity analysis makes it possible to place the tools of fire protection engineering in the hands of designers and other users who might not have the time or the inclination to work directly with a simulation model. The results of the analysis could be published as tables or graphs in manuals for the guidance of draftspersons who would not need to know in detail how the figures were derived. It is vital to ensure that figures are not applied outside their range of application. This criterion implies that the work must be verified by a fully qualified professional who would check that the guidance was appropriate to the circumstances. Similar

problems of professional self-regulation have been successfully resolved in other disciplines.

Applications

There are not many fully developed applications of procedural simulation models to fire protection engineering. For example, CRISP II would certainly qualify, while FIRE STATION is not a complete system model because it ignores the interactions between the fire and the occupants. FIRE STATION might be better described as an OR simulation model. Suites or collections of applications are also available.

CRISP II (Computation of Risk Indices by Simulation Procedures) [7]

Simulation models can be used to compensate for lack of information about "real" fires and to work out the fire risk implications of new materials, building designs, and protection systems. A fire risk assessment model called CRISP II was developed at the Fire Research Station of the United Kingdom to decide priorities for remedial action and to test the validity of new guidelines for building control officers. CRISP II is a Monte Carlo simulation of an entire fire scenario. The model consists essentially of a two-zone model of smoke flow for multiple rooms and a detailed model of human behavior and movement, supervised by a Monte Carlo controller. Its component submodels, which include rooms, doors, windows, detectors and alarms, items of furniture, hot smoke layers, and people, run simultaneously so they can continually interact with each other. The model is capable of generating a rich variety of fully interactive behavior patterns. It calculates the fractional effective dose (FED) for occupants as they move through the building and are exposed to smoke. When an occupant's FED reaches 100 %, that person is considered dead. CRISP II expresses the fire risk of a building design in terms of the number of deaths predicted over a large number of simulations.

FIRE STATION [8], Optimum Fire Station Location for Minimum Loss of Life and Property

The FIRE STATION model determines the optimum location, among five alternate sites, for an urban fire station in a community of 25 wards. Optimization is the minimization of lives lost, building damage, and capital outlay. The model generates a sample population from an observed distribution by ward, structure value, and relative population density. The travel time from the station to the fire is also chosen from an observed distribution. The amount of damage and the number of lives lost is then calculated with reference to the delay in reaching the fire, which depends on the travel time.

Suites or Collections of Fire Protection Computer-Simulated Procedures

Computer models can also be packaged in an integrated set or suite of models that are linked but do not interact as directly as do the modules of CRISP II. Independent models can also be used sequentially, as will be described below. Two examples of integrated suites of computer models are HAZARD I [9] and FiRECAM [10].

HAZARD I is a fire hazard assessment method that is comprised of four distinct computer models: (1) FAST [11], a multicompartment energy and mass transport model; (2) DETACT [12], a detector/sprinkler activation model; (3) EXITT [13], a human decision/behavior evacuation model; and (4) TENAB [9], a tenability model that considers incapacitation and lethality from temperature and toxicity. Figure 80.4 illustrates how these, and other, software modules are organized. Figure 80.4 follows the progress of a hypothetical scenario entitled "CASE" and shows why HAZARD I is a semiautomatic simulation model.

HAZARD I can model up to 15 compartments on multiple floors of a building. Like all zone models, HAZARD I is applicable to spaces with the dimensions of normal-size rooms with conventional contents. The egress component,

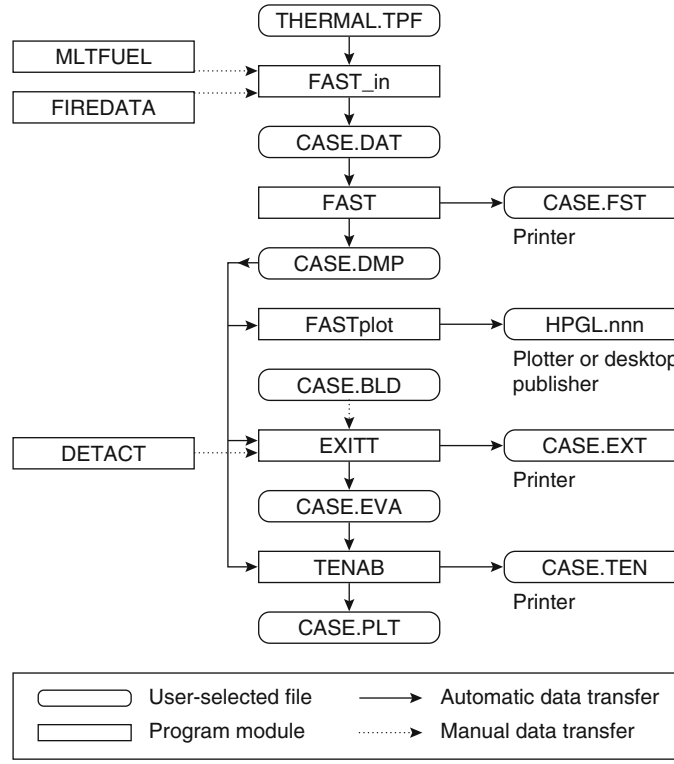

Fig. 80.4 HAZARD I software

however, is based on data from fires in one- and two-family dwellings, and the dynamics of family groups.

The method guides the user to identify the fire problems of concern and then to specify representative fire scenarios. The user then employs a computer software package to predict the outcome of each of the identified scenarios in considerable detail. The software predicts over time the temperature, smoke, and fire-gas concentrations in each room of the building; the behavior and movement of the building occupants as they interact with the fire, the building, and each other; and the impact of exposure of each occupant to the fire-generated environment. The occupant exposures are presented as a prediction of successful escape, physical incapacitation, or death along with time, location, and cause. By accounting for the interactions of a large array of factors on the result of a given fire scenario, the method enables the user to analyze the impact of changes in the fire performance of products, building design and arrangement, or of the inherent capabilities of occupants in the likely outcome of fires. With such information it should be possible to provide better, more cost-effective strategies for reducing fire losses. An overview of the process used by HAZARD I is shown in Fig. 80.5.

FiRECAM (Fire Risk Evaluation and Cost Assessment Model) consists of submodels that are run in sequence to assess the fire safety performance of a building design in terms of expected risk to life and expected cost of fire. These submodels include a building and risk evaluation model, a fire department response model, a boundary element failure model, an economic model, a design fire model, a fire growth model, a smoke movement model, an occupant response model, a fire department effectiveness model, an evacuation model, a smoke hazard model, a fire spread model, a life loss probability model, a property loss model, an expected number of deaths model, an expected risk to life model, and a fire cost expectation model. FiRECAM has been used to assess

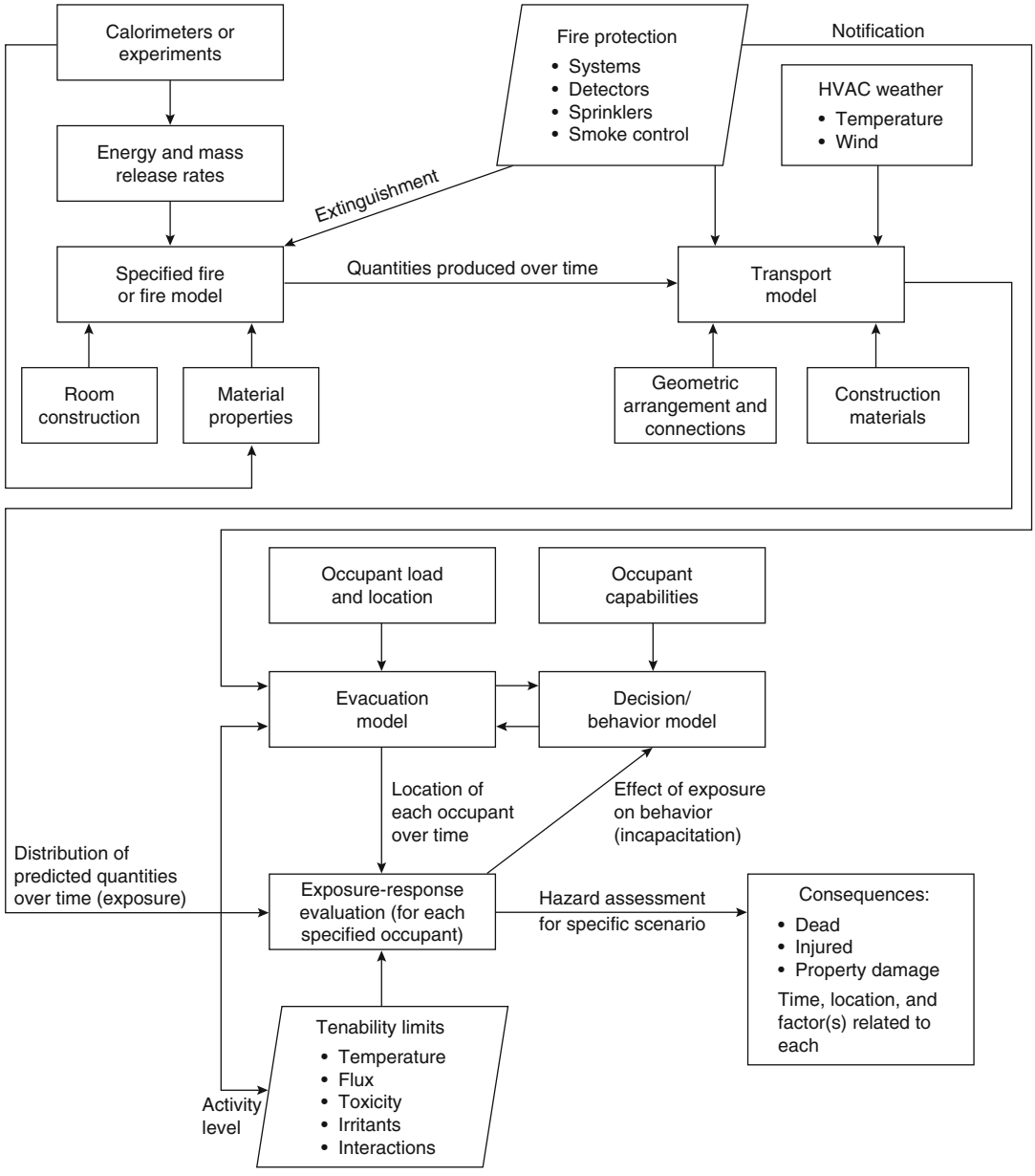

Fig. 80.5 Interrelationships of major components of a fire hazard model

whether a proposed design meets the requirements of a performance-based code and can determine whether the design is cost effective.

HAZARD I and FiRECAM are examples of methods that link a variety of computer models in such a way that the output from one model can be used directly as the input for the next. It is also possible for the fire protection engineer to use independent models in sequence. There are available collections of programs that cover different aspects of fire technology and science that are components of fire protection simulation models. For example, these collections contain individual programs that predict gas temperatures, heat fluxes on objects, activation of devices, and some aspects of human behavior or evacuation.

These collections do not tend to be comprehensive in nature in that the individual programs are independent of other programs in the collection. Therefore, these programs must be run sequentially and data manually transferred between programs. Although less sophisticated and more cumbersome than the integrated simulation models, these models have their uses and may be adequate in some cases. Two advantages of these collections of programs are that they offer the user a significant amount of control over the input to any given component, and they lend themselves to being run many times. This latter point is important when the user wishes to characterize a single component. By running the component program many times the user can adequately define the probabilistic nature of the component in question. Examples of these collections include FPEtool [14] and FireCalc [15].

The fire protection engineer can also evaluate a design by combining more specialized standalone models of the individual components of interest, for example, a human behavior or egress model with a fire effects model. This approach to simulation modeling, while more cumbersome (because it requires more user intervention), may also be more effective because it allows the user greater control over the process as well as the use of more sophisticated models.

In this approach, the fire effects model would be run independently of the human behavior or egress model. This approach would facilitate analyzing a number of fire scenarios and choosing the ones that most closely reflect the expected conditions. The human behavior or egress model could also be run for a number of conditions and assumptions. The user would then go through the exercise of comparing the predicted output from the two component models and arriving at the final answer.

A number of human behavior or egress models and fire effects models are available that can be used in tandem to perform fire protection simulation modeling. (Space does not permit an attempt to list all models known to the authors, but compendia have been developed [16, 17] and are updated regularly to reflect the state of the art. See http://www.firemodelsurvey.com). Given the predicted fire effects obtained from a fire model and the predicted locations of occupants from an evacuation model, the designer or engineer could then use a toxicity model, either a computer model or one of the available calculation methods, to predict the cumulative exposure of the occupants as they move through the modeled fire environment.

Model Validation

Simulation models can never be validated over the whole range of their behavior. However, confidence in the reliability of a model is enhanced if the relationships built into it are based on accepted scientific theory supported by experimental evidence. The model must also stand up to tests designed to show it behaves reasonably in response to exogenous disturbance. The calibrated model should also be able to simulate time-series data from instrumented experimental fires. Finally, the model should be able to mimic the sequence of events recorded by observers at real fires.

Like other models, the validity of simulation models depends on goodness of fit and predictive power. In the fire situation, deterministic predictions are not feasible except in very simple cases. In a typical case, a simulation model would be calibrated to produce an output distribution whose mean and variance were in agreement with an observed distribution. Changes in fire protection strategy would be reflected in the model, which would then be used to generate a new output distribution with a different mean and variance. Comparisons between the output distributions before and after implementing the strategy can be used to calculate confidence intervals for statements such as "if strategy B is preferred to A, casualties will be reduced in x percent of cases." Statistical predictions of this kind are quite sufficient for the purposes of fire protection engineering.

Models undergo limited validation; that is, they are applicable to the experimental results they are based on and/or the limited set of

scenarios to which the model developers compared the model's output. The Society of Fire Protection Engineers formed a task group to independently evaluate computer models. They have completed and published an evaluation of DETACT-QS. Guides exist for the validation and verification of computer models [18]. Until more models can be independently evaluated, the model user must rely on the available documentation and previous experience for guidance regarding the appropriate use of a given model. By choosing a specific model, the user is tacitly assuming that the model is valid for the scenario under consideration.

Summary

Overall, progress in fire protection engineering is handicapped by data limitations and the difficulty of conducting realistic experiments on complete fire systems involving human behavior; although efforts in the collection of the data on human behavior have intensified over the past several years, particularly in the areas of occupant characteristics and premovement delay times [19–30]. These problems may be overcome by applying a variety of procedural simulation models originally developed in operations research. These models make efficient use of the available data and can be used to test fire protection strategies. They can be complemented by Monte Carlo methods to take account of uncertainty in the data, measure the sensitivity of the casualty rate to fire protection measures, and estimate fire risk.

Appendix A: Handling Uncertainty

Generating Random Numbers

In order to introduce a stochastic element into simulation modeling, a source of random numbers is required. Virtually every computer is equipped with a subroutine that can generate a pseudo-random number in the interval [0, 1] on demand. These are not truly random numbers because they are generated by a deterministic algorithm that will repeat itself cyclically after an interval. The algorithm is designed to make this interval as long as possible given the capacity of the computer. A variety of methods, most of which are based on congruence relationships, are discussed by Naylor et al. [31]

Generating Probability Distributions for Monte Carlo Studies

The generation of simulated statistics is entirely of a numerical nature and is carried out by supplying pseudo-random numbers into the process or system under study and obtaining probability distributions from it as the result. As a rule, statistical simulation involves replacing an actual sample population by some assumed theoretical distribution and then sampling from this theoretical population by means of some type of random number generator. In some cases it may not be possible to find a standard theoretical distribution that describes a particular stochastic process. In these cases the process can be simulated by sampling from an empirical distribution rather than a theoretical one. Naylor et al. [31] provide specific techniques for generating variates from several of the widely used probability distributions as well as general methods for generating variates from empirical distributions.

Inverse Transformation Method This method depends on the relationship between the probability density function (pdf) and the cumulative distribution function (cdf). The pdf gives the probability that the variate x lies between x and $x + dx$. The cdf gives the probability that $x \leq x$. The cdf $F(x)$ is obtained from the pdf $f(x)$ by integrating $f(x)dx$ over the interval from—∞ to x.

To generate variates x_i from some particular statistical population whose pdf is given by $f(x)$, one must first obtain the cdf $F(x)$. Since $F(x)$ is defined over the range [0, 1], one can generate uniformly distributed random numbers and set $F(x) = r$. It is clear that x is uniquely determined by $r + F(x)$. It follows that for any particular value of r, say r_0, that is generated, it is possible

to find the value of x, in this case x_0 corresponding to r_0 by the inverse function, if it is known. That is,

$$x_0 = F^{-1}(r_0)$$

where $F^{-1}(r)$ is the inverse transformation or mapping of r on the unit interval into the domain of x.

Example 1 Generate variates x with pdf $f(x) + 2x$, $0 \leq x \leq 1$.

Solution

$$\begin{aligned} r = F(x) &= \int_{-\infty}^{x} f(t)dt \\ &= \int_{0}^{x} 2tdt \quad 0 \leq x \leq 1 \\ &= x^z \end{aligned}$$

Then taking the inverse transformation, $F^{-1}(r)$, that is, solving this equation for x, one obtains

$$x = F^{-1}(r) = \sqrt{r} \quad 0 \leq r \leq 1$$

Therefore, values of x with pdf $f(x) = 2x$ can be generated by taking the square root of random numbers r.

Example 2 Generate a variate x with density function

$$\begin{aligned} f(x) &= \frac{1}{4} \quad 0 \leq x < 1 \\ &= \frac{3}{4} \quad 1 \leq x < 2 \end{aligned}$$

Solution The pdf and cdf are illustrated graphically in Fig. 80.6. Using the previous results

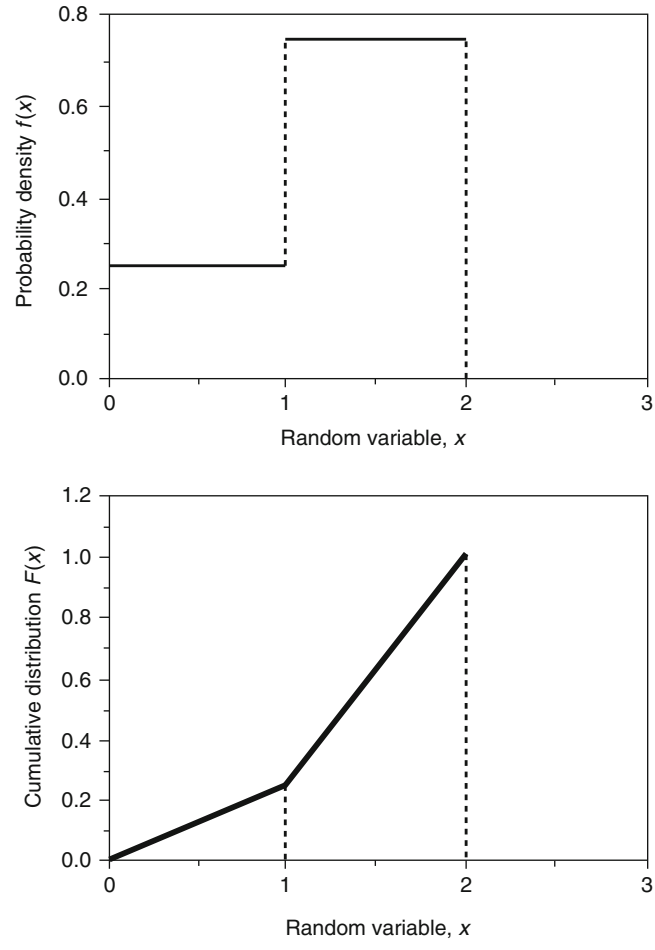

Fig. 80.6 Probability density function (*top*) and cumulative distribution (*bottom*) for empirical data

$$r = F(x) = \int_0^x \frac{1}{4}dt \quad 0 \le x < 1 = \frac{x}{4}$$

$$r = F(x) = \frac{1}{4} + \int_1^x \frac{3}{4}dt \quad 0 \le x \le 2$$

$$= \frac{3}{4}x - \frac{1}{2}$$

Taking the inverse transformation, that is, solving the above equations for x, one obtains

$$x = 4r \qquad 0 \le r < \frac{1}{4}$$

$$x = \frac{4}{3}r + \frac{2}{3} \quad \frac{1}{4} \le r \le 1$$

The Rejection Method In many cases it is either impossible or very difficult to express x in terms of the inverse transformation of the probability distribution, $F^{-1}(r)$. In these cases it is necessary to obtain a numerical approximation to the inverse function, F^{-1}, or make use of the rejection method. The application of the rejection method requires the following steps:

1. Normalize the range of f by a scale factor, c, such that

$$cf(x) \le 1 \quad a \le x \le b$$

2. Define x as a linear function of r

$$x = a + (b - a)r$$

3. Generate pairs of random numbers (r_1, r_2)
4. Whenever one encounters a pair of random numbers that satisfy the relationship

$$r_2 \le cf[a + (b - a)r_1]$$

then "accept" the pair and use $x + a + (b - a)r_1$ as the variate generated.

The theory behind this method is based on the realization that the probability of r being less than or equal to cf(x) is

$$P[\mathrm{r} \le cf(x)] = cf(x)$$

Consequently if x is chosen at random from the range $[a, b]$ according to Step 2 above and then rejected if $r >$ cf(x), the probability density function of accepted x will be exactly $f(x)$. It can be shown [32] that the expected number of trials before a successful pair is found is equal to $1/c$. This result implies that the method may be quite inefficient for certain probability density functions. The rejection method can also be used as a Monte Carlo technique to evaluate definite integrals. This application may be particularly useful for the evaluation of multivariate functions.

Example 3 Use the rejection method to generate variates x with density function $f(x) = 6(x - x^2)$, where $0 \le x \le 1$.

Solution Since x was defined over the unit interval, $x = r$. But $f(r) = 6(r - r^2)$ is defined over the interval $0 \le f(r) \le 1.5$. Scaling will transform $f(r)$ to the unit interval if $g(r) = 2/3f(r)$, in which case $g(r) = 4(r - r^2)$. The rejection method then consists of the following four steps:

1. Generate r_1 and calculate $g(r_1)$.
2. Generate r_2 and compare with $g(r_1)$.
3. If $r_2 \le g(r_1)$, accept r_1 as x from $f(x)$. If $r_2 > g(r_1)$, then reject r_1 and repeat Step 1.
4. Repeat this procedure until n values of x have been generated.

A comparison between the theoretical distribution and the distribution obtained by using the rejection method is shown in Fig. 80.7.

Example 4 Generate a variate with a normal distribution.

Solution If a random variable x has a pdf $f(x)$ given as

$$f(x) = \frac{1}{\sigma\sqrt{2\pi}} e^{-\frac{1}{2}\left(\frac{x-\mu}{\sigma}\right)^2}, \quad -\infty < x < \infty$$

it is said to have a normal or Gaussian distribution with parameters μ and σ.The graph of this function is the familiar bell-shaped curve. The cdf $F(x)$ does not exist in explicit form and, therefore, the inverse transformation method cannot be applied. There are several ways to avoid this difficulty, which are fully described in the literature. However, it is useful to include here a method for generating variates from a normal distribution, because data with this type of distribution is so widely encountered in practice.

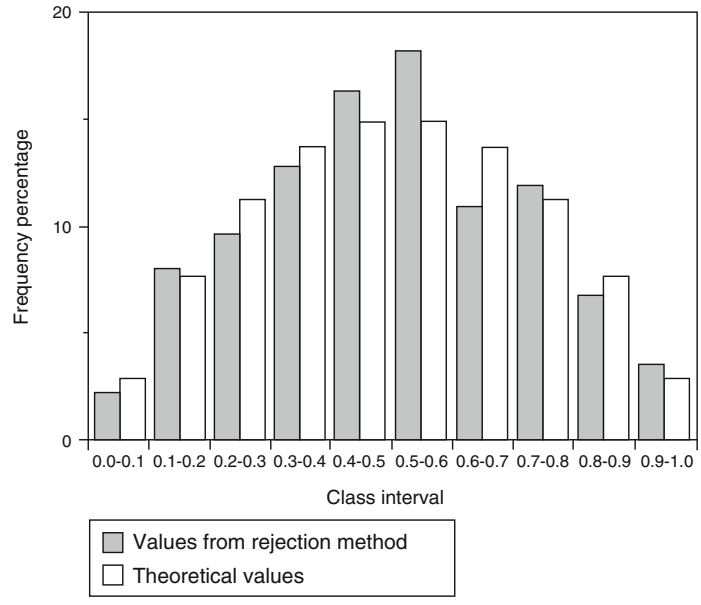

Fig. 80.7 Generating a sample from a quadratic pdf using the rejection method

Let r_1 and r_2 be two uniformly distributed random variables defined on the interval [0, 1]. Then

$$x_1 = (-2\log_e r_1)^{1/2} \cos 2\pi r_2$$

$$x_2 = (-2\log_e r_1)^{1/2} \sin 2\pi r_2$$

are two variates from a standard normal distribution. This method produces exact results and is quite fast, subject to the efficiency of the special function subroutines [33].

Appendix B: Analysis of Model Output

Local Linearization

Suppose that at a given time, *t,* the output variables are dependent on the input variables of the model, according to a set of functions:

$$y_i = f_i(x_1, x_2, \ldots, x_n); \quad \mathrm{i} = 1, \ \ldots, n$$

Then, in the neighborhood of x_1, x_2, . . ., x_n, one can make a local linear approximation to y_i by expanding $f_i(x_1 + \Delta x_1, x_2 + \Delta x_2, \ldots, x_n + \Delta x_n)$ as a Taylor series about $f_i(x_1, x_2, \ldots, x_n)$ and then truncating all terms after the second. The Taylor series expansion of the *i*th variable is

$$y_i = f_i(x_1 + \Delta x_1, x_2 + \Delta x_2, \ \ldots, \ x_n + \Delta x_n)$$

$$\therefore y_i = f_i(x_1, x_2, \ldots, x_n) + \sum_j \Delta x_j \frac{\partial y_i}{\partial x_j}$$

$$+ \frac{1}{2!}\left(\sum_j \Delta x_j^2 \frac{\partial^2 y_i}{\partial x_j^2} + 2 \sum_{j \neq k} \sum_k \Delta x_j \Delta x_k \frac{\partial^2 y_i}{\partial x_j \partial x_k} \right)$$

$$+ \ldots . \therefore \Delta y i \cong \sum_j \Delta x_j \frac{\partial y_i}{\partial x_j}; \quad i = 1, \ldots, n$$

provided that Δx_j is small. It is more convenient to express this in matrix notation:

$$\Delta y = A \Delta x$$

where A is the Jacobian for the *y*s, that is,

$$a_{ij} = \frac{\partial y_i}{\partial x_j}$$

Note that, if S is the variance-covariance matrix for the *x*s, then V is the variance-covariance matrix for the *y*s and is given by

$$\mathrm{V} = \mathrm{A}'\mathrm{SA}$$

Additivity of Variances

It can often be shown that a model is stable, with respect to variations in any one of its input variables taken one at a time. However, it is

possible that, if more than one variable were allowed to change simultaneously, the variance of the sum would be greater than the sum of the variances. This result would imply that the interaction or covariance term could not be ignored. However, if the regression procedure establishes that the linear hypothesis is valid, then the variance of the output is equal to the sum of the variances of the inputs weighted by the squares of the coefficients. Note, however, that the linear hypothesis will probably hold only over a limited range, and can be estimated by examining a plot of the residuals.

If it is established that the linear hypothesis holds over a certain range, that is,

$$y = a_0 + a_1x_1 + a_2x_2 + \cdots + a_nx_n$$

and if $x_1, \ldots, x_n$ are random variables, then

$$\operatorname{var}(a_0 + a_1x_1 + a_2x_2 + \cdots + a_nx_n) = \sum_i a_i^2 \operatorname{var}(x_i) + \sum_i \sum_j a_i a_j \operatorname{cov}(x_i, x_j)$$

The variables $x_1, \ldots, x_n$ have been generated so as to be independent, which implies that the covariance term vanishes, and, therefore,

$$\operatorname{var}(y) = \sum_i a_i^2 \operatorname{var}(x_i)$$

The regression model can, therefore, be used to predict the variance of a dependent variable on any assumptions that are chosen about the variances of the independent variables.

If it turned out that the contribution of one variable to the total variance were large, it would be desirable to undertake further studies to establish more exact values for this parameter. A smaller variance could then be assigned to this variable, and one could immediately deduce how much effect this would have on the uncertainty in the dependent variable, without having to carry out any further Monte Carlo runs. Within limits there is no need to be too particular about the variances ascribed to the independent variables in the preliminary studies, since these can be revised at a later date. It is necessary to make a distinction between (1) parameters that have a large variance due to measurement uncertainties (which can be improved), and (2) parameters drawn from populations having a large variance (where further measurement may reduce the uncertainty of the variance but not the variance itself).

Appendix C: Monte Carlo Simulation Example

Introduction

Because of the nature of a Monte Carlo simulation providing a real world, step by step example is prohibitive. Instead, an outline of the procedure is provided below. This procedure is meant to be universal and can be used with computer fire models other than the ones discussed in this example.

Monte Carlo simulation consists of the following steps:

1. Define a domain of possible inputs.
2. Generate inputs randomly from a probability distribution over the domain.
3. Perform a deterministic computation on the inputs.
4. Aggregate the results.

The first step identifies the random variables of interest in the given problem. The second step involves drawing a random sample from each of the previously identified random variables. The third step is where all of the calculations are performed and the results stored. Steps 2 and 3 are repeated a "large" number of times (i.e., n), typically anywhere from 1000 up to 10,000 times. In step 4, the results are analyzed using various tools: histograms, summary statistics, confidence intervals, etc.

The life safety of occupants is of paramount importance in fire scenarios. Typically, this "fire problem" can be viewed as a race between the time when the toxic effects of a fire may be experienced by a given occupant and the time required for that occupant to reach a point of safety; specifically, the available safe egress time (ASET) and the required safe egress time (RSET). Both of these variables have the units of time and are functions of other variables as

detailed in other sections of this handbook. ASET has three input variables whose values are not fixed by room geometry (heat loss fraction, fire radiation fraction, height of base of flames) and RSET has six input variables which may be considered randomly distributed (travel speed on level routes, vertical travel speed on stairs, flow rate through doors, flow rate on stairway, population, speed of slowest evacuee).

In this fire problem, the goal of a Monte Carlo simulation would be to determine the probability that occupants will safely evacuate a fire scenario, i.e., p(ASET $>$ RSET).

Setup

There are at least two possible ways to accomplish step 1 of a Monte Carlo simulation for determining whether occupants may safely evacuate a fire scenario. The domain of possible inputs could be either the values of variables that comprise ASET and RSET or the domain could be values of ASET and RSET. When considering the first possibility, each of the variables for ASET and RSET discussed above are assumed to be described by some kind of distribution. Using ASET as an example:

1. ASET may be simulated using the high, low, and most likely values of each variable; or,
2. A simulation could be generated by assuming each input variable has a uniform distribution.

Instead of defining or assuming a distribution for individual variables that constitute ASET, one may assume, a priori, that ASET has a known distribution, e.g., log-normal, based on available data or other calculations. One way of doing this calculation is to use "best guess" values of the input variables for ASET. The resulting value of ASET is then assumed to be the mean of a log normal distribution. A value for the standard deviation is then assumed.

The domain of possible RSET inputs would then be determined as described above; either define distributions for the RSET input variables or a distribution for RSET itself.

Analysis

If the input variables of ASET and RSET are defined as distributions, then these distributions are randomly sampled n times as indicated above. These input values are then used to deterministically compute n values for ASET (and RSET), which are stored for later analysis. The probability of safely evacuating from the fire of interest is found by adding the number of times ASET $>$ RSET and dividing this sum by n.

If distributions of ASET and RSET are assumed, a priori, or calculated as described above, then these distributions are sampled n times and the values stored for later analysis. This sampling is greatly facilitated by the use of a spreadsheet, e.g., EXCEL. EXCEL's = RAND() function will generate uniformly distributed random numbers between zero and one. These random values and EXCEL's = LOGINV() function can then be used to generate the n ASET and RSET values required for further analysis. Once again, the probability of safely evacuating from the fire of interest is found by adding the number of times ASET $>$ RSET and dividing this sum by n. When this method is used, a sensitivity analysis should also be performed on the standard deviations assumed for the log normal distributions of ASET and RSET.

References

1. F.S. Hillier and G.J. Lieberman, *Operations Research,* 2nd ed., Holden-Day, Inc., San Francisco (1974).
2. M. Black, *Models and Metaphors,* Cornell University Press, Ithaca, NY (1962).
3. R.L. Ackoff and Stafford Beer, "In Conclusion: Some Beginnings," *Progress in Operations Research (*J.S. Aronofsky, ed.), John Wiley and Sons, New York (1969).
4. G. Ramachandran, "Probabilistic Approach to Fire Risk Evaluation," *Fire Technology,* 24, 3, p. 149 (1988).
5. W.G.B. Phillips, "The Development of a Fire Risk Assessment Model," *BRE Information Paper IP 8/92,* Fire Research Establishment, Borehamwood, UK (1992).

6. W.G.B. Phillips, "Monte Carlo Tests of Conclusion Robustness," in *Proceedings of the Fifth International System Dynamics Conference,* Geilo, Norway, p. 19 (1976).
7. J.N. Fraser-Mitchell, "Risk Assessment of Factors Relating to Fire Protection in Dwellings," in *Fire Safety Science: Proceedings of the 5th International Symposium* (Y. Hasemi, ed.), International Association for Fire Safety Science, Melbourne, Australia (1997).
8. J. Oberstone, in *Management Science: Concepts and Applications,* West Publishing Company, St. Paul, MN (1990).
9. R.D. Peacock, W.W. Jones, G.P. Forney, R.W. Portier, P.A. Reneke, R.W. Bukowski, and J.H. Klote, "An Update Guide for HAZARD I Version 1.2," *NISTIR 5410*, National Institute of Standards and Technology, Gaithersburg, MD (1994).
10. D. Yung et al., "Modelling Concepts for the Risk-Cost Assessment Model FiRECAM™ and Its Application to a Canadian Government Office Building," in *Proceedings of the Fifth International Symposium on Fire Safety Science (*Y. Hasemi, ed.), International Association for Fire Safety Science, pp. 619–630 (1997).
11. R.D. Peacock, P.A. Reneke, W.W. Jones, R.W. Bukowski, and G.P. Forney, "A User's Guide for FAST: Engineering Tools for Estimating Fire Growth and Smoke Transport," *NIST Special Publication 921,* National Institute of Standards and Technology, Gaithersburg, MD (2000).
12. D.D. Evans and D.W. Stroup, "Methods to Calculate the Response Time of Heat and Smoke Detectors Installed Below Large Unobstructed Ceilings," *NBSIR 85-3167,* National Bureau of Standards, Gaithersburg, MD (1985).
13. B.M. Levin, "EXITT—A Simulation Model of Occupant Decisions and Actions in Residential Fires: User's Guide and Program Description," *NBSIR 87-3591,* National Bureau of Standards, Gaithersburg, MD (1987).
14. S. Deal, *Technical Reference Guide for FPEtool Version 3.2,* National Institute of Standards and Technology, Gaithersburg, MD (1995).
15. V.O. Shestopal and S.J. Grubits, "Computer Program for an Uninhibited Smoke Plume and Associated Computer Software," *Fire Technology,* 29, 3, pp. 246–267 (1993).
16. R. Freidman, *Survey of Computer Models for Fire and Smoke,* 2nd ed., Factory Mutual Research Corporation, Norwood, MA (1991).
17. S.M. Olenick and D.J. Carpenter, "An Updated International Survey of Computer Models for Fire and Smoke," *Journal of Fire Protection Engineering,* 13, May (2003).
18. ASTM, ASTM E1355, "Standard Guide for Evaluating Predictive Capability of Deterministic Fire Models," American Society for Testing and Materials, West Conshohoken, PA (2005).
19. R.F. Fahy and G. Proulx, "Toward Creating a Database on Delay Times to Start Evacuation and Walking Speeds for Use in Evacuation Modeling," in *Proceedings of the Second International Symposium on Human Behaviour in Fire 2001,* Interscience Communications Ltd., London (2001).
20. G. Proulx and R.F. Fahy, "The Time Delay to Start Evacuation: Review of Five Case Studies," in *Proceedings of the Fifth International Symposium on Fire Safety Science (*Y. Hasemi, ed.), International Association for Fire Safety Science, pp. 783–794 (1997).
21. K.E. Boyce, T.J. Shields, and G.W.H. Silcock, "Toward the Characterization of Building Occupancies for Fire Safety Engineering: Prevalence, Type, and Mobility of Disabled People," *Fire Technology,* 35, 1, pp. 35–50 (1999).
22. K.E. Boyce, T.J. Shields, and G.W.H. Silcock, "Toward the Characterization of Building Occupancies for Fire Safety Engineering: Capabilities of Disabled People Moving Horizontally and on an Incline," *Fire Technology,* 35, 1, pp. 51–67 (1999).
23. K.E. Boyce, T.J. Shields, and G.W.H. Silcock, "Toward the Characterization of Building Occupancies for Fire Safety Engineering: Capability of Disabled People to Negotiate Doors," *Fire Technology,* 35, 1, pp. 68–78 (1999).
24. K.E. Boyce, T.J. Shields, and G.W.H. Silcock, "Toward the Characterization of Building Occupancies for Fire Safety Engineering: Capability of People with Disabilities to Read and Locate Exit Signs," *Fire Technology,* 35, 1, pp. 79–86 (1999).
25. G. Proulx, J.C. Latour, J.W. McLaurin, J. Pineau, L.E. Hoffman, and C. Laroche, "Housing Evacuation of Mixed Abilities Occupants in Highrise Buildings," *Internal Report No. 706,* National Research Council of Canada, Ottawa (1995).
26. G. Proulx, "Evacuation Time and Movement in Apartment Buildings," *Fire Safety Journal,* 24, 3 (1995).
27. T.J. Shields, K.E. Boyce, and G.W.H. Silcock, *Unannounced Evacuation of Marks & Spencer Sprucefield Store,* University of Ulster Fire SERT, Carrickfergus, Northern Ireland, unpublished report (1997).
28. G. Proulx, A. Kaufman, and J. Pineau, "Evacuation Time and Movement in Office Buildings," *Internal Report No. 711,* National Research Council of Canada, Ottawa (1996).
29. G. Proulx, J. Latour, and J. MacLaurin, "Housing Evacuation of Mixed Abilities Occupants," *Internal Report No. 661,* National Research Council of Canada, Ottawa (1994).
30. S.M.V. Gwynne, R. Muhdi, and J. David, "Development and Validation of a Crawling Model in an Existing Computational Egress Tool," in *Proceedings of the Interflam 2007 Conference,* 1, Interscience Communications Ltd., London (2007).
31. T.H. Naylor, J.L. Balintfy, D.S. Burdick, and K. Chu, *Computer Simulation Techniques,* John Wiley and Sons, New York (1966).

32. K.D. Tocher, *The Art of Simulation,* Van Nostrand Co., New York (1963).
33. Mervin E. Muller, "A Comparison of Methods for Generating Normal Deviates on Digital Computers," *Journal of the Association for Computing Machinery,* 6, pp. 376–383 (1959).

Further Readings

J. Banks (ed.), *Handbook of Simulation: Principles, Methodology, Advances, Applications, and Practice,* John Wiley, New York (1998).
J. Banks, B. Nelson, and J. Carson, *Discrete-Event System Simulation,* 2nd ed., Prentice Hall, Upper Saddle River, NJ (1995).
P. Bratley, B.L. Fox, and L.E. Schrage, *A Guide to Simulation,* 2nd ed., Springer-Verlag, New York (1987).
J.R. Emshoff and R.L. Sisson, *Design and Use of Simulation Models,* Macmillan, New York (1970).
G.S. Fishman, *Principles of Discrete Event Simulation,* John Wiley, New York (1973).
J.M. Garrido, *Performance Modeling of Operating Systems Using Object-Oriented Simulation: A Practical Introduction,* Plenum Press, New York (2000).
S. Hostikka, O. Keski Rahkonen, and T. Korhonen, *Probabilistic Fire Simulator, Theory and User's Manual for Version 1.2*, VTT Publication 503, VTT Technical Research Centre of Finland, 2003.
S.V. Hoover and R.F. Perry, *Simulation: A Problem Solving Approach,* Addison-Wesley, New York (1989).
A.M. Law, D.W. Kelton, W.D. Kelton, and D.M. Kelton, *Simulation Modeling and Analysis,* 3rd ed., McGraw-Hill, New York (1999).
A.S. Mavor and R.W. Pew (eds.), *Modeling Human and Organizational Behavior: Application to Military Simulations,* National Academy Press, Washington, DC (1999).
J.H. Mize and J. Cox, *Essentials of Simulation,* Prentice Hall, Englewood Cliffs, NJ (1968).
T.H. Naylor, J.L. Balintfy, D.S. Burdick, and K. Chu, *Computer Simulation Techniques,* John Wiley, New York (1966).
G. Santos and B.E. Aguirre, *A Critical review of Emergency Evacuation Simulation Methods*, Disaster Research Center, University of Delaware, NIST Workshop on Building Occupant Movement During Fire Emergencies, June 9–10, 2004.
R.E. Shannon, *Systems Simulation: The Art and Science,* Prentice Hall, Englewood Cliffs, NJ (1975).
R. Suleiman and K.G. Troitzsch (eds.), *Tools and Techniques for Social Science Simulation,* Physica Verlag, Heidelburg, Germany (2000).
Z. Xue, *A Particle Swarm Optimization Based Behavioral and Probabilistic Fire Evacuation Model Incorporating Fire Hazards and Human Behaviors*, Master's Thesis, Department of Mechanical and Aerospace Engineering, University of New York at Buffalo, 2006.
B.P. Zeigler, H. Praehofer, and T.G. Kim, *Theory of Modeling and Simulation: Integrating Discrete Event and Continuous Complex Dynamic Systems,* 2nd ed., Academic Press, New York (2000).
G.W. Zobrist and J.V. Leonard (eds.), *Simulation Systems,* Gordon and Breach, Amsterdam (2000).

William G.B. Phillips was a member of the Fire Risk Unit at the Fire Research Station of the Building Research Establishment at Borehamwood, Hertfordshire.

Rita F. Fahy is the manager of fire databases and systems at NFPA.

Engineering Economics

81

John M. Watts Jr. and Robert E. Chapman

Introduction

Engineering economics is the application of economic techniques to the evaluation of design and engineering alternatives [1]. The role of engineering economics is to assess the appropriateness of a given project, estimate its value, and justify it from an engineering standpoint.

This chapter discusses the time value of money and other cash-flow concepts, such as compound and continuous interest. It continues with economic practices and techniques used to evaluate and optimize decisions on selection of fire safety strategies. The principles of benefit-cost analysis are then introduced. The chapter concludes with a discussion of standards for evaluating economic performance and software tools for implementing those standards.

An in-depth treatment of the practices and techniques covered in this chapter is available in the ASTM compilation of standards on building economics [2]. The ASTM compilation also includes case illustrations showing how to apply the practices and techniques to investment decisions.

A broader perspective on the application of engineering economics to fire protection engineering can be found in *The Economics of Fire Protection* by Ramachandran [3]. This work is intended as a textbook for fire protection engineers and includes material and references that expand on several other chapters in the SFPE handbook.

Cash-Flow Concepts

Cash flow is the stream of monetary (dollar) values—costs (inputs) and benefits (outputs)—resulting from a project investment.

Time Value of Money

The following are reasons why $1000 today is "worth" more than $1000 1 year from today:

1. Inflation
2. Risk
3. Cost of money

Of these, the cost of money is the most predictable, and, hence, it is the essential component of economic analysis. Cost of money is represented by (1) money paid for the use of borrowed money, or (2) return on investment. Cost of money is determined by an interest rate.

Time value of money is defined as the time-dependent value of money stemming both from changes in the purchasing power of money (inflation or deflation) and from the real earning potential of alternative investments over time.

J.M. Watts Jr. (✉) • R.E. Chapman

M.J. Hurley (ed.), *SFPE Handbook of Fire Protection Engineering*,
DOI 10.1007/978-1-4939-2565-0_81, © Society of Fire Protection Engineers 2016

Cash-Flow Diagrams

It is difficult to solve a problem if you cannot see it. The easiest way to approach problems in economic analysis is to draw a picture. The picture should show three things:

1. A time interval divided into an appropriate number of equal periods
2. All cash outflows (deposits, expenditures, etc.) in each period
3. All cash inflows (withdrawals, income, etc.) for each period

Unless otherwise indicated, all such cash flows are considered to occur at the end of their respective periods.

Figure 81.1 is a cash-flow diagram showing an outflow or disbursement of $1000 at the beginning of year 1 and an inflow or return of $2000 at the end of year 5.

Notation

To simplify the subject of economic analysis, symbols are introduced to represent types of cash flows and interest factors. The symbols used in this chapter conform to ANSI Z94 [4]; however, not all practitioners follow this standard convention, and care must be taken to avoid confusion when reading the literature. The following symbols will be used here:

P = Present sum of money ($)
F = Future sum of money ($)
N = Number of interest periods
i = Interest rate per period (%)

A complete list of the ANSI Z94 symbols is given in Appendix 1 of this chapter.

Interest Calculations

Interest is the money paid for the use of borrowed money or the return on invested capital. The economic cost of construction, installation, ownership, or operation can be estimated correctly only by including a factor for the economic cost of money.

Simple Interest To illustrate the basic concepts of interest, an additional notation will be used:

$$F(N) = \text{Future sum of money after } N \text{ periods}$$

Then, for simple interest,

$$F(1) = P + (P)(i) = P(1 + i)$$

and

$$F(N) = P + (N)(P)(i) = P(1 + Ni)$$

For example: $100 at 10 % per year for 5 years yields

$$\begin{aligned} F(5) &= 100[1 + (5)(0.1)] \\ &= 100(1.5) \\ &= \$150 \end{aligned}$$

However, interest is almost universally compounded to include interest on the interest.

Compound interest:

$$F(1) = P + (P)(i) = P(1 + i)$$

is the same as simple interest,

$$F(2) = (F)(1) + F(1)(i)$$

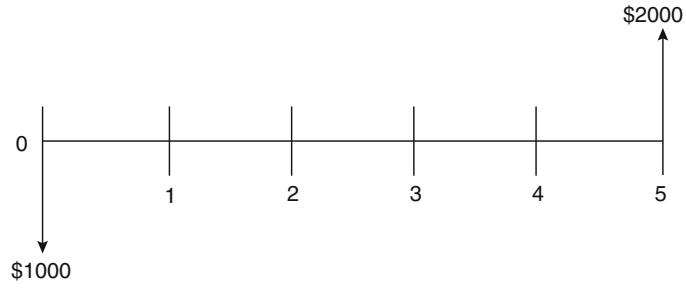

Fig. 81.1 Cash-flow diagram

Interest is applied to the new sum:

$$\begin{aligned} &= F(1)(1+i) = P(1+i)^2 \\ F(3) &= F(2)(1+i) = P(1+i)^3 \end{aligned}$$

and by mathematical induction,

$$F(N) = P(1+i)^N$$

Example \$100 at 10 % per year for 5 years yields

$$\begin{aligned} F(5) &= 100(1+0.1)^5 \\ &= 100(1.1)^5 \\ &= 100(1.61051) \\ &= \$161.05 \end{aligned}$$

which is over 7 % greater than with simple interest.

Example In 1626 Willem Verhulst bought Manhattan Island from the Canarsie Indians for 60 florins (\$24) worth of merchandise (a price of about 0.5 cents per hectare [0.2 cents per acre]). At an average interest rate of 6 %, what is the present value (2006) of the Canarsies' \$24?

$$\begin{aligned} F &= P(1+i)^N \\ &= \$24(1+0.06)^{380} \\ &= \$9.9 \times 10^{10} \end{aligned}$$

Ninety-nine billion dollars is a reasonable approximation of the present land value of the island of Manhattan.

Interest Factors

Interest factors are multiplicative numbers calculated from interest formulas for given interest rates and periods. They are used to convert cash flows occurring at different times to a common time. The functional formats used to represent these factors are taken from ANSI Z94 [4], and they are summarized in Appendix 2 of this chapter.

Compound Amount Factor

In the formula for finding the future value of a sum of money with compound interest, the mathematical expression $(1 + i)^N$ is referred to as the *compound amount factor*, represented by the functional format $(F/P, i, N)$. Thus,

$$F = P(F/P, i, N)$$

Interest tables: Values of the compound amount, present worth, and other factors that will be discussed shortly, are tabulated for a variety of interest rates and number of periods in most texts on engineering economy. Example tables are presented in Appendix 3 of this chapter. Although calculators and software tools have greatly reduced the need for such tables, they are often still useful for interpolations.

Present Worth

Present worth is the value found by discounting future cash flows to the present or base time.

Discounting The inverse of compounding is determining a present amount that will yield a specified future sum. This process is referred to as discounting. The equation for discounting is found readily by using the compounding equation to solve for P in terms of F:

$$P = F(1+i)^{-N}$$

Example What present sum will yield \$1000 in 5 years at 10 %?

$$\begin{aligned} P &= 1000(1.1)^{-5} \\ &= 1000(0.62092) \\ &= \$620.92 \end{aligned}$$

This result means that \$620.92 "deposited" today at 10 % compounded annually will yield \$1000 in 5 years.

Present Worth Factor In the discounting equation, the expression $(1 + i)^{-N}$ (is called the *present worth factor* and is represented by the symbol $(P/F, i, N)$. Thus, for the present worth of a future sum at i percent interest for N periods,

$$P = F(P/F, i, N)$$

Note that the present worth factor is the reciprocal of the compound amount factor. Also note that

$$(P/F, i, N) = \frac{1}{(F/P, i, N)}$$

Example What interest rate is required to triple \$1000 in 10 years?

$$P = \frac{F}{3} = (P/F, i, 10)$$

therefore,

$$(P/F, i, 10) = \frac{1}{3}$$

From Appendix 3,

$$(P/F, 10\ \%,\ 10) = 0.3855$$

and

$$(P/F,\ \ 12\ \%,\ \ 10) = 0.3220$$

By linear interpolation,

$$i = 11.6\ \%$$

Interest Periods

Normally, but not always, the interest period is taken as 1 year. There may be subperiods of quarters, months, weeks, and so forth.

Nominal versus effective interest: It is generally assumed that interest is compounded annually. However, interest may be compounded more frequently. When this occurs, there is a *nominal interest* or annual percentage rate and an *effective interest*, which is the figure used in calculations. For example, a savings bank may offer 5 % interest compounded quarterly, which is not the same as 5 % per year. A nominal rate of 5 % compounded quarterly is the same as 1.25 % every 3 months or an effective rate of 5.1 % per year. If

$$r = \text{Nominal interest rate}$$

and

$$M = \text{Number of subperiods per year}$$

then the effective interest rate is

$$i = \left(1 + \frac{r}{M}\right)^{M} - 1$$

Example Credit cards usually charge interest at a rate of 1.5 % per month. This amount is a nominal rate of 18 %. What is the effective rate?

$$\begin{aligned} i &= (1 + 0.015)^{12} - 1 \\ &= 1.1956 - 1 \\ &= 19.56\ \% \end{aligned}$$

Continuous Interest A special case of effective interest occurs when the number of periods per year is infinite. This represents a situation of *continuous interest*, also referred to as continuous compounding. Formulas for continuous interest can be derived by examining limits as M approaches infinity. Formulas for interest factors using continuous compounding are included in Appendix 2. Continuous interest is compared to monthly interest in Table 81.1.

Example Compare the future amounts obtained under various compounding periods at a nominal interest rate of 12 % for 5 years, if $P = \$10{,}000$ (Table 81.2).

Table 81.1 Continuous interest (%)

	Effective	
Nominal %	Monthly	Continuous
5	5.1	5.1
10	10.5	10.5
15	16.1	16.2
20	21.9	22.1

Table 81.2 Example of continuous interest $N = 5$ years, $r = 12\ \%$

Compounding	M	i	NM	F/P	F
Annual	1	12.000	5	1.76234	17,623.40
Semiannual	2	12.360	10	1.79085	17,908.50
Quarterly	4	12.551	20	1.80611	18,061.10
Monthly	12	12.683	60	1.81670	18,167.00
Weekly	52	12.734	260	1.820860	18,208.60
Daily	365	12.747	1,825	1.821938	18,219.38
Hourly	8,760	12.749	43,800	1.822061	18,220.61
Instantaneously	∞	12.750	∞	1.822119[a]	18,221.19

[a]F/P (instantaneous) $= e^{Ni} = e^{5(0.12)} = e^{0.6}$

Series Payments

Life would be simpler if all financial transactions were in single lump-sum payments, now or at some time in the future. However, most situations involve a series of regular payments, for example, car loans and mortgages.

Series Compound Amount Factor Given a series of regular payments, what will they be worth at some future time?

Let

$$A = \text{the amount of a regular end} - \text{of} - \text{period payment}$$

Then, note that each payment, A, is compounded for a different period of time. The first payment will be compounded for $N-1$ periods (yr):

$$F = A(1+i)^{N-1}$$

and the second payment for $N-2$ periods:

$$F = A(1+i)^{N-2}$$

and so forth. Thus, the total future value is

$$F = A(1+i)^{N-1} + A(1+i)^{N-2} + \cdots + A(1+i) + A$$

or

$$F = \frac{A\left[(1+i)^N - 1\right]}{i}$$

The interest expression in this equation is known as the *series compound amount factor*, $(F/A, i, N)$—thus

$$F = A(F/A, i, N)$$

Sinking fund factor: The process corresponding to the inverse of series compounding is referred to as a *sinking fund*; that is, what size regular series payments is necessary to acquire a given future amount?

Solving the series compound amount equation for A,

$$A = F\left\{\frac{i}{\left[(1+i)^N - 1\right]}\right\}$$

Or, using the symbol $(A/F, i, N)$ for the *sinking fund factor*

$$A = F(A/F, i, N)$$

Here, note that the sinking fund factor is the reciprocal of the series compound amount factor, that is, $(A/F, i, N) = 1/(F/A, i, N)$.

Capital recovery factor: It is also important to be able to relate regular periodic payments to their present worth; for example, what monthly installments will pay for a \$10,000 car in 3 years at 15 %?

Substituting the compounding equation $F = P(F/P, i, N)$ in the sinking fund equation, $A = F(A/F, i, N)$, yields

$$A = P(F/P, i, N)(A/F, i, N)$$

And, substituting the corresponding interest factors gives

$$A = P\frac{\left[i(1+i)^N\right]}{\left[(1+i)^N - 1\right]}$$

In this equation, the interest expression is known as the *capital recovery factor*, since the equation defines a regular income necessary to recover a capital investment. The symbolic equation is

$$A = P(A/P, i, N)$$

Series present worth factor: As with the other factors, there is a corresponding inverse to the capital recovery factor. The *series present worth* factor is found by solving the capital recovery equation for P.

$$P = A\frac{\left[(1+i)^N - 1\right]}{\left[i(1+i)^N\right]}$$

or, symbolically

$$P = A(P/A, i, N)$$

Other Interest Calculation Concepts

Additional concepts involved in interest calculations include continuous cash flow, capitalized costs, beginning of period payments, and gradients.

Continuous cash flow: Perhaps the most useful function of continuous interest is its application to situations where the flow of money is of a continuous nature. *Continuous cash flow* is representative of

1. A series of regular payments for which the interval between payments is very short
2. A disbursement at some unknown time (which is then considered to be spread out over the economic period)

Factors for calculating present or future worth of a series of annual amounts, representing the total of a continuous cash flow throughout the year, may be derived by integrating corresponding continuous interest factors over the number of years the flow is maintained.

Continuous cash flow is an appropriate way to handle economic evaluations of risk, for example, the present value of an annual expected loss.

Formulas for interest factors representing continuous, uniform cash flows are included in Appendix 2.

Capitalized Costs Certain undertakings such as some public works projects are considered to last indefinitely and thereby provide perpetual service. For example, how much should a community be willing to invest in a reservoir that will reduce fire insurance costs by some annual amount, A? Taking the limit of the series present worth factor as the number of periods goes to infinity gives the reciprocal of the interest rate. Thus, *capitalized costs* are just the annual amount divided by the interest rate. When expressed as an amount required to produce a fixed yield in perpetuity, it is sometimes referred to as an *annuity*.

Beginning-of-Period Payments Most returns on investment (cash inflows) occur at the end of the period during which they accrued. For example, a bank computes and pays interest at the end of the interest period. Accordingly, interest tables, such as those in Appendix 3, are computed for end-of-year payments. For example, the values of the capital recovery factor assume that the regular payments, A, occur at the end of each period.

On the other hand, most disbursements (cash outflows) occur at the beginning of the period (e.g., insurance premiums). When dealing with beginning-of-period payments, it is necessary to make adjustments. One method of adjustment for beginning-of-period payments is to calculate a separate set of factors. Another way is to logically interpret the effect of beginning-of-period payments for a particular problem, for example, treating the first payment as a present value. The important thing is to recognize that such variations can affect economic analysis.

Gradients It occasionally becomes necessary to treat the case of a cash flow that regularly increases or decreases at each period. Such patterned changes in cash flow are called *gradients*. They may be a constant amount (linear or arithmetic progression), or they may be a constant percentage (exponential or geometric progression). Various equations for dealing with gradient series may be found in Appendix 2.

Software Tools for Interest Calculations

Modern computer spreadsheet software typically includes a significant array of economic functions. Within these are the 18 standard factors for computation of compound interest found in Appendix 2. However, not all software follows the terminology or notation of ANSI Z94. For example, sometimes "present worth" is referred to as "present value." Thus, care must be taken in selecting spreadsheet functions for economic analysis.

Comparison of Alternatives

Most decisions are based on economic criteria. Investments are unattractive unless it seems likely they will be recovered with interest. Economic decisions can be divided into two classes:

1. Income expansion—that is, the objective of capitalism
2. Cost reduction—the basis of profitability

Fire protection engineering economic analysis is primarily concerned with cost-reduction decisions, finding the least expensive way to fulfill certain requirements, or minimizing the sum of expected fire losses plus investment in fire protection.

There are four common methods of comparing alternative investments: (1) present worth, (2) annual cost, (3) rate of return, and (4) benefit-cost analysis. Each of these is dependent on a selected interest rate or discount rate to adjust cash flows at different points in time.

Discount Rate

The term *discount rate* is often used for the interest rate when comparing alternative projects or strategies.

Selection of Discount Rate If costs and benefits accrue equally over the life of a project or strategy, the selection of discount rate will have little impact on the estimated benefit-cost ratios. However, most benefits and costs occur at different times over the project life cycle. Thus, costs of constructing a fire-resistive building will be incurred early in contrast to benefits, which will accrue over the life of the building. The discount rate then has a significant impact on measures such as benefit-cost ratios, since the higher the discount rate, the lower the present value of future benefits.

In view of the uncertainty concerning appropriate discount rate, analysts frequently use a range of discount rates. This procedure indicates the sensitivity of the analysis to variations in the discount rate. In some instances, project rankings based on present values may be affected by the discount rate as shown in Fig. 81.2. Project A is preferred to project B for discount rates below 15 %, whereas the converse is true for discount rates greater than 15 %. In this instance, the decision to adopt project A in preference to project B will reflect the belief that the appropriate discount rate is less than or equal to 15 %.

A comparison of benefits and costs may also be used to determine the payback period for a particular project or strategy. However, it is important to discount future costs or benefits in such analyses. For example, an analysis of the Beverly Hills Supper Club fire compared annual savings from a reduction in insurance premiums to the costs of sprinkler installation. Annual savings were estimated at $11,000, whereas costs of sprinkler installation ranged from $42,000 to $68,000. It was concluded that the installation would have been paid back in 4–7 years (depending on the cost of the sprinklers). However, this analysis did not discount future benefits, so that $11,000 received at the end of 4 years was deemed equivalent to $11,000 received in the first year. Once future benefits were discounted, the payback period ranged from 5 to 11 years with a discount rate of 10 %.

Inflation and the Discount Rate Provision for inflation may be made in two ways: (1) estimate all future costs and benefits in constant prices, and use a discount rate that represents the opportunity cost of capital in the absence of inflation;

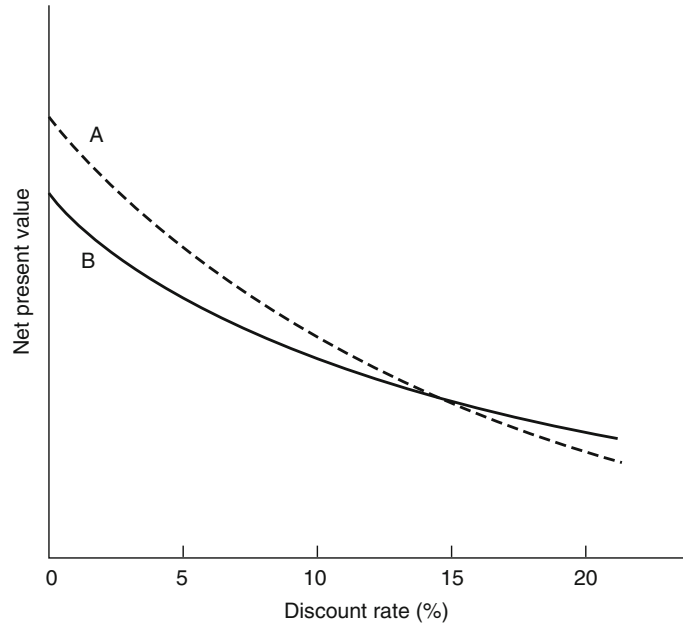

Fig. 81.2 Impact of discount rate on project selection

Table 81.3 Estimated cost data for two alternate plans for increasing water transmission capacity

	Plan A pipeline	Plan B pumping station
Construction cost	$1,000,000	$200,000
Life	40 years	40 years (structure)
		20 years (equipment)
Cost of replacing equipment at the end of 20 year	0	$75,000
	$1,000/year	$50,000/year
Operating costs		

or (2) estimate all future benefits and costs in current or inflated prices, and use a discount rate that includes an allowance for inflation. The discount rate in the first instance may be considered the real discount rate, whereas the discount rate in the second instance is the nominal discount rate. The use of current or inflated prices with the real discount rate, or constant prices with the nominal discount rate, will result in serious distortions in economic analysis.

Present Worth

In a *present worth* comparison of alternatives, the costs associated with each alternative investment are all converted to a present sum of money, and the least of these values represents the best alternative. Annual costs, future payments, and gradients must be brought to the present. Converting all cash flows to present worth is often referred to as *discounting*.

Example Two alternate plans are available for increasing the capacity of existing water transmission lines between an unlimited source and a reservoir. The unlimited source is at a higher elevation than the reservoir. Plan A calls for the construction of a parallel pipeline and for flow by gravity. Plan B specifies construction of a booster pumping station. Estimated cost data for the two plans are as shown in Table 81.3.

If money is worth 12 %, which plan is more economical? (Assume annual compounding, zero salvage value, and all other costs equal for both plans.)

$$\begin{aligned}\text{Present worth (Plan A)} &= P + A(P/A,\ 12\ \%,\ 40)\\ &= \$1,000,000 + \$1000(8.24378)\\ &= \$1,008,244\end{aligned}$$

$$\begin{aligned}\text{Present worth (Plan B)} &= P + A(P/A,\ 12\ \%,\ 40)\\ &\quad + F(P/F,\ 12\ \%,\ 20)\\ &= \$200,000 + \$50,000(8.24378)\\ &\quad + \$75,000(0.10367)\\ &= \$619,964\end{aligned}$$

Thus, plan B is the least-cost alternative.

A significant limitation of present worth analysis is that it cannot be used to compare alternatives with unequal economic lives. That is, a 10-year plan and a 20-year plan should not be compared by discounting their costs to a present worth. A better method of comparison is annual cost.

Annual Cost

To compare alternatives by annual cost, all cash flows are changed to a series of uniform payments. Current expenditures, future costs or receipts, and gradients must be converted to annual costs. If a lump-sum cash flow occurs at some time other than the beginning or end of the economic life, it must be converted in a two-step process: first moving it to the present and then spreading it uniformly over the life of the project.

Alternatives with unequal economic lives may be compared by assuming replacement in kind at the end of the shorter life, thus maintaining the same level of uniform payment (Table 81.4).

Example Compare the value of a partial or full sprinkler system purchased at 10 % interest.

$$\begin{aligned}\text{Annual cost (partial system)} &= A + P(A/P,\ 10\ \%,\ 15)\\ &= \$1000 + \$8000(0.13147)\\ &= \$2051.75\end{aligned}$$

$$\begin{aligned}\text{Annual cost (full system)} &= A + P(A/P,\ 10\ \%,\ 20)\\ &= \$250 + \$15,000(0.11746)\\ &= \$2011.90\end{aligned}$$

The full system is slightly more economically desirable. When costs are this comparable, it is especially important to consider other relevant decision criteria such as uninsured losses.

Rate of Return

Rate of return is, by definition, the interest rate at which the present worth of the net cash flow is zero. Computationally, this method is the most

Table 81.4 Comparison of alternatives by annual cost

	System cost	Insurance premium	Life (in years)
Partial system	$8000	$1000	15
Full system	$15,000	$250	20

complex method of comparison. If more than one interest factor is involved, the solution is by trial and error. Microcomputer programs are most useful with this method.

The calculated interest rate may be compared to a discount rate identified as the "minimum attractive rate of return" or to the interest rate yielded by alternatives. Rate-of-return analysis is useful when the selection of a number of projects is to be undertaken within a fixed or limited capital budget.

Example An industrial fire-fighting truck costs \$100,000. Savings in insurance premiums and uninsured losses from the acquisition and operation of this equipment are estimated at \$60,000 per year. Salvage value of the apparatus after 5 years is expected to be \$20,000. A part-time driver during operating hours will accrue an added cost of \$10,000 per year.

What would the rate of return be on this investment at 40 % present worth? At 50 % present worth?

By linear interpolation, the rate of return is 43 %.

$$\begin{aligned} 40\ \%\ \text{Present worth} &= P + F(P/F, 40\ \%, 5) + A(P/A, 40\ \%, 5) \\ &= -\$100,000 + \$20,000(0.18593) + (\$60,000 - \$10,000)(2.0352) \\ &= \$5,478.60 \end{aligned}$$

$$\begin{aligned} 50\ \%\ \text{Present worth} &= P + F(P/F,\ 50\ \%,\ 5) + A(P/A,\ 50\ \%,\ 5) \\ &= -\$100,000 + \$20,000(0.13169) + (\$60,000 - \$10,000)(1.7366) \\ &= -\$10,536.40 \end{aligned}$$

Benefit-Cost Analysis

Benefit-cost analysis, also referred to as cost-benefit analysis, is a method of comparison in which the consequences of an investment are evaluated in monetary terms and divided into the separate categories of benefits and costs. The amounts are then converted to annual equivalents or present worths for comparison.

The important steps of a benefit-cost analysis are

1. Identification of relevant benefits and costs
2. Measurement of these benefits and costs
3. Selection of best alternative
4. Treatment of uncertainty

Identification of Relevant Benefits and Costs

The identification of benefits and costs depends on the particular project under consideration. In the case of fire prevention or control activities, the benefits are based on prior fire losses, classified either as direct or indirect. Direct economic losses are property and content losses. Indirect losses include such things as the costs of injuries and deaths, costs incurred by business or industry due to business interruption, losses to the community from interruption of services, loss of payroll or taxes, loss of market share, and loss of reputation. Direct costs of fire protection activities include constructing fire-resistive buildings, installation of fire protection systems, and operating fire departments. Indirect costs are more difficult to measure. They include items such as the constraints on choice due to fire protection requirements by state and local agencies. In the measurement of benefits, it is appropriate to adjust for utility or disutility that may be associated with a fire loss.

A major factor in the identification of relevant benefits and costs pertains to the decision unit involved. Thus, if the decision maker is a property owner, relevant benefits from fire protection are likely to be reduced fire insurance premiums and less fire damage or business interruption losses not covered by insurance. For a

municipality, relevant benefits are the protection of members of the community, avoidance of tax and payroll losses, and reductions in costs associated with assisting fire victims. Potential benefits, in these instances, are considerably greater than those faced by a property owner. However, the community may ignore some external effects of fires. For example, the 1954 automobile transmission plant fire in Livonia, Michigan, affected the automobile industry in Detroit and various automobile dealers throughout the United States. However, there was little incentive for the community to consider potential losses to persons outside the community in their evaluation of fire strategies. It might be concluded, therefore, that the more comprehensive the decision unit, the more likely the inclusion of all relevant costs and benefits, in particular, social costs and benefits.

Measurement of Benefits and Costs

Direct losses are measured or estimated statistically or by a priori judgment. Actuarial fire loss data collected nationally or for a particular industry may be used, providing the information is adequately specific and the collection mechanism is reliable. More often, an experienced judgment of potential losses is made, sometimes referred to as the *maximum probable loss* (MPL).

Indirect losses, if considered, are much more difficult to appraise. A percentage or multiple of direct losses is sometimes used. However, when indirect loss is an important decision parameter, a great deal of research into monetary evaluation may be necessary. Procedures for valuing a human life and other indirect losses are discussed in Ramachandran [3].

Costs may be divided into two major categories: (1) costs of private fire protection services, and (2) costs of public fire protection services. In either case, cost estimates will reflect the opportunity cost of providing the service. For example, the cost of building a fire-resistive structure is the production that is foregone due to the diversion of labor and resources to make such a structure. Similarly, the cost of a fire department is the loss of other community services that might have been provided with the resources allocated to the fire department.

Selection of Best Alternative

Two considerations pertain to determining benefit-cost criteria: project acceptability and project selection.

Project acceptability may be based on benefit-cost difference using subtraction or benefit-cost ratio, in which the monetary equivalent benefits are divided by the monetary equivalent costs. The first criterion requires that the value of benefits less costs be greater than zero, whereas the second criterion requires a benefit-cost ratio greater than one.

The issue is more complicated in the case of project selection, since several alternatives are involved. It is no longer a question of determining the acceptability of a single project, but rather selecting from among alternative projects. Consideration should be given to changes in costs and benefits as various strategies are considered. Project selection decisions are illustrated in Fig. 81.3. The degree of fire protection is given on the horizontal axis; the marginal costs and benefits associated with various levels of fire safety are given on the vertical axis. As the diagram indicates, marginal costs are low initially and then increase. Less information is available concerning the marginal benefit curve, and it may, in fact, be horizontal. The economically optimum level of fire protection is given by the intersection of the marginal cost and marginal benefit curves. Beyond this point, benefits from increasing fire protection are exceeded by the costs of providing the additional safety.

The numerical example shown in Table 81.5 presents five possible strategies or programs. Strategy A represents the initial situation, with the remaining four strategies representing various fire loss reduction activities, each with various costs, arranged in ascending order of costs. Fire losses under each of the five strategies are given in the second row. The sum of fire losses and fire reduction costs for each strategy given in

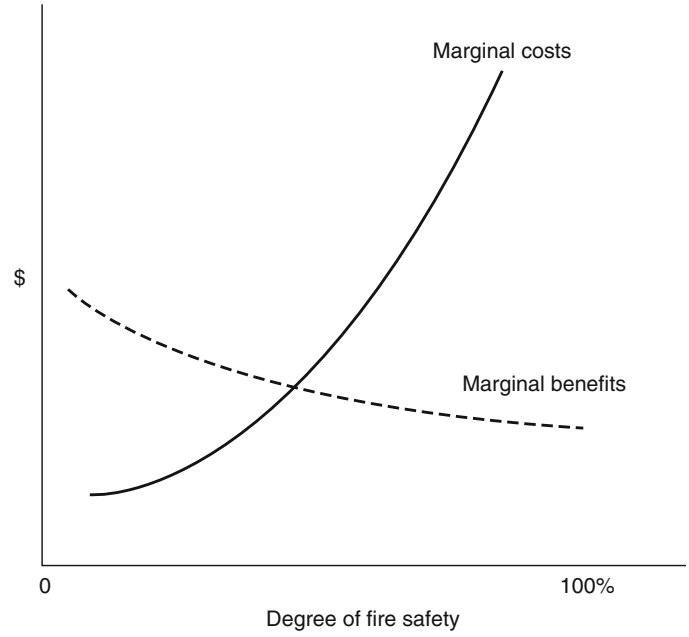

Fig. 81.3 Project selection

Table 81.5 Use of benefit-cost analyses in strategy selection

	Strategy				
Category	A	B	C	D	E
Fire reduction costs	0	10	25	45	70
Fire losses	100	70	50	40	35
Sum of fire reduction costs and fire losses	100	80	75	85	105
Marginal benefits	0	30	20	10	5
Marginal costs	0	10	15	20	25
Marginal benefits minus marginal cost	0	20	5	–10	–20
Marginal benefit-cost ratio	–	3.0	1.33	0.5	0.2

the third row is equivalent to the life-cycle cost of that strategy. Life-cycle cost analysis is an alternative to benefit-cost analysis when the goal of the investment decision is cost savings rather than benefits. Additional information on life-cycle cost analysis is found in Fuller and Petersen [5].

Data in the first two rows may then be used to determine the marginal costs or marginal benefits of replacing one strategy with another. Thus, strategy B has a fire loss of $70 compared to $100 for strategy A, so the marginal benefit is $30. Similarly, the marginal benefit from strategy C is the reduction in fire losses from B to C of $20. The associated marginal cost of strategy C is $15. Declining marginal benefits and rising marginal costs result in the selection of strategy C as the optimum strategy. At this point, the difference between marginal benefits and marginal costs is still positive.

Marginal benefit-cost ratios are given in the last row. It is worth noting that, while the highest marginal benefit-cost ratio is reached at activity level B (as is the highest marginal benefit-cost difference), project C is still optimum, since it yields an additional net benefit of $5. This finding is reinforced by examining changes in the sum of fire reduction costs and fire losses (i.e., life-cycle costs). Total cost plus loss first declines, reaching a minimum at point C, and

then increases. This pattern is not surprising, since as long as marginal benefits exceed marginal costs, total losses should decrease. Thus, the two criteria—equating marginal costs and benefits and minimizing the sum of fire losses and fire reduction costs—yield identical outcomes.

Treatment of Uncertainty

A final issue concerns the treatment of uncertainty. One method for explicitly introducing risk considerations is to treat benefits and costs as random variables that may be described by probability distributions. For example, an estimate of fire losses might consider the following events: no fire, minor fire, intermediate fire, and major fire. Each event has a probability of occurrence and an associated damage loss. The total expected loss (EL) is given by

$$\mathrm{EL} = \sum_{i=0}^{3} p_i D_i$$

where
p_0 = Probability of no fire
p_1 = Probability of a minor fire
p_2 = Probability of an intermediate fire
p_3 = Probability of a major fire
D_n = Associated damage loss, $n = 0, 1, 2, 3$

Expected losses may be computed for different fire protection strategies. Thus, a fire protection strategy that costs, C_3 and reduces damage losses of a major fire from D_3 to $D_3^{'}$ will result in an expected loss

$$\mathrm{EL} = p_0 D_0 + p_1 D_1 + p_2 D_2 + p_3 D_3^{'} + C_3$$

Similarly, a fire control strategy that costs C_3 and reduces the probability of an intermediate fire from p_2 to $p_2^{'}$ as an expected loss

$$\mathrm{EL} = p_0 D_0 + p_1 D_1 + p_2^{'} D_2 + p_3 D_3 + C_2$$

Comparing expected losses from alternative strategies may then be used to determine the optimal strategy. Use of expected value has the limitation of considering only the average value of the probability distribution. Discussion of other procedures for evaluating uncertain outcomes is given by Anderson and Settle [6].

Dealing with Extreme Events

Protecting buildings from extreme events—fires, floods, earthquakes, and other natural and man-made hazards—is a constant challenge for building owners and managers. Choosing among alternative protection strategies is complicated by the fact that such strategies frequently have significant up-front investment costs, result in operations and maintenance costs that are spread over many years, and impact key stakeholders in different ways. A methodology is needed to ensure that all relevant costs are captured and analyzed via well-defined metrics.

To address this need, the National Institute of Standards and Technology (NIST) is developing economic tools to aid building owners and managers in the selection of cost-effective strategies for responding to extreme events. Economic tools include evaluation methods for measuring economic performance, standards that support and guide the use of those methods, and software for implementing the evaluation methods.

An economic analysis integrates the economic tools and facilitates the identification and selection of cost-effective building protection strategies. Since an economic analysis is only as good as the data and assumptions on which it is based, NIST developed a three-step protocol that establishes a methodology for dealing with extreme events, documented in NISTIR 7073 [7].

Three-Step Protocol

The three-step protocol helps decision makers assess the risk to their facility of damages from extreme events; identify engineering, management, and financial strategies for abating damage risk; and use standardized economic evaluation methods to select the most cost-effective combination of risk mitigation strategies to protect their facility.

Step 1 is to assess the risk of uncertain and costly hazards, whether man-made or natural. Because limited resources do not allow full protection of all facilities against every possible hazard, economic efficiency dictates that investments for protection be a function of the likelihood of a disaster occurring, the expected value of damages, and the cost of protection. By assessing the risks facing a facility and the damages that might result from various disasters, decision makers can determine if a facility merits some degree of protection over and above that required by building codes and standards.

Step 2 is to identify engineering, management, and financial strategies to abate the risk of damages. Some strategies will lower the probability of a disaster occurring; others will lower the damages incurred once the disaster happens. Engineering strategies include structural upgrades, HVAC upgrades, and strengthening or tightening the building envelope. Management strategies include access controls, background checks, and emergency training and drills. Financial strategies include insurance, tax incentives, and cost-sharing arrangements. NISTIR 7073 stresses the need to employ a combination of risk mitigation strategies rather than focusing only on engineering-based approaches. Although engineering approaches are essential to protecting capital assets, management practices and financial mechanisms have the potential to both harden a particular asset and offer flexibility in responding to new challenges. Once engineering, management, and financial mitigation strategies have been identified, it is necessary to create a candidate set of alternatives, each of which combines mitigation strategies that address some or all of the hazards identified in the risk assessment. Each alternative has a set of costs based on the unique combination of mitigation strategies employed, varying according to both their timing and magnitude. In most cases, higher up-front costs result in lower future costs.

Step 3 uses economic analysis to select the most cost-effective alternative. The life-cycle cost method is the core component of the economic evaluation. It measures the sum of all relevant costs associated with owning or operating a constructed facility over a specified time period. Other standardized methods, such as present value net savings and the savings-to-investment ratio, can be derived directly from life-cycle cost calculations, so decision makers have multiple measures of economic performance on which to base their choice. By using these economic evaluation methods, building owners and managers can reduce the life-cycle costs associated with extreme events.

Developing a risk mitigation plan requires both guidance and data—guidance to help owners and managers assess the risks facing their facility and data about the frequency and consequences of natural and man-made hazards to measure the risks facing a particular facility. Cost estimates of protection are needed to ensure that the operational budget for safeguarding personnel and physical assets is kept in balance. Guidance on the use of economic evaluation methods helps ensure that the correct economic method, or combination of methods, is used. Despite the large amount of high-quality information available on risk assessment and management, natural and man-made hazards, and economic tools, there are few central sources of data and tools to which owners and managers of constructed facilities and other key decision makers can turn for help in developing a cost-effective risk mitigation plan. NISTIR 7390 [8] serves as such a central source.

Standards Development

A suite of standards and materials for a training course on how to apply the standards to produce a cost-effective risk mitigation plan has been developed by ASTM. The suite consists of three standards: (1) a revised and expanded version of the life-cycle cost standard practice, E917 [9]; (2) a revised and expanded version of the standard guide for summarizing economic impacts, E2204 [10]; and (3) a new standard guide on how to use the three-step protocol to produce a cost-effective risk mitigation plan, E2506 [11].

The life-cycle cost standard practice, E917, is the core standard of ASTM Subcommittee

E06.81 on Building Economics. The life-cycle cost standard occupies a unique position, since three other E06.81 standards can be derived from it and nine others reference it. Consequently, the focus was on a major rewrite of E917 to incorporate the treatment of extreme events into not only the life-cycle cost standard but also into the present value net savings (E1074) [12], the savings-to-investment ratio (E964) [13], and the adjusted internal rate of return (E1057) [14] standards as well.

The impact summary guide, E2204, provides a generic format for summarizing the economic impacts of building-related projects. The guide provides technical persons, analysts, and researchers a means for communicating project impacts in a condensed format to management and nontechnical persons. Effective communication of project impacts to senior management and other decision makers is a critical part of the economic analysis (Step 3 in the three-step protocol). Communicating the pros and cons of the alternative identified as the most cost-effective risk mitigation plan requires both concise statements and adequate back-up documentation. Consequently, the impact summary guide was substantially rewritten and a case study illustrating the treatment of extreme events was incorporated as an appendix.

Cost-Effectiveness Tool

The Cost-Effectiveness Tool for Capital Asset Protection is a user-friendly decision support system for choosing among alternative building protection strategies. It includes multiple evaluation methods, event-modeling features, a cost accounting framework, and a multitiered analysis strategy. All evaluation methods employed within the Cost-Effectiveness Tool are consistent with ASTM standard measures of economic merit. The event-modeling features are the means for assessing and managing the risks associated with natural and man-made hazards. The cost accounting framework classifies costs by who bears them, which budget category they fall into, and how they are distributed across building systems and across mitigation strategies. These different dimensions of cost provide important perspectives to the decision problem.

A key component informing the decision maker is the analysis strategy, which uses multiple levels of analysis to promote an increased understanding of the decision problem. The Cost-Effectiveness Tool addresses uncertainty and financial risk—the probability of investing in a project whose economic outcome is different from that desired or expected—in a structured, three-part manner.

First, best-guess estimates are used to establish a baseline analysis, which uses fixed parameter values to calculate economic measures of performance. The results of the baseline analysis allow the alternative combinations of risk mitigation strategies to be ranked according to their economic measures of performance. The ranking and the calculated measures of performance provide a frame of reference for the treatment of uncertainty and financial risk.

Second, a sensitivity analysis is performed in which selected inputs are varied about their baseline values. Despite being helpful in identifying shifts in the rank ordering of alternatives and addressing uncertainty in input values, the sensitivity analysis produces only a crude measure of financial risk.

Third, a Monte Carlo simulation is performed to obtain an explicit measure of financial risk associated with the competing alternatives. Monte Carlo simulation is especially useful in identifying shifts in the rank ordering of alternatives and documenting the factors and circumstances associated with those shifts.

Example The results of an economic analysis (Step 3 in the three-step protocol) for a case study building are presented in Fig. 81.4. The case study covers a renovation project for the data center of a major financial institution. The case study findings presented in Fig. 81.4 use the generic format specified in ASTM Standard Guide E2204. The generic format calls for a description of the significance of the project, the analysis strategy, a listing of data and

1.a Significance of the Project:

The data center undergoing renovation is a single-story structure located in a suburban community.The floor area of the data center is 3716 m^2 (40,000 ft^2). The replacement value of the data center is $20 million for the structure plus its contents. The data center contains financial records that are in constant use by the firm and its customers. Thus, any interruption of service will result in both lost revenues to the firm and potential financial hardship for the firm's customers.

The building owners employ two different renovation strategies. The first, referred to as the Base Case, employs upgrades that meet the minimum building performance and security requirements. The second, referred to as the Proposed Alternative, results in enhanced security as well as selected improvements in building performance. Both alternatives recognize that in the post-9/11 environment the data center faces heightened risks in two areas. These risks are associated with the vulnerability of information technology resources and the potential for damage to the facility and its contents from chemical, biological, radiological, and explosive (CBRE) hazards. Two scenarios—the potential for a cyber attack and the potential for a CBRE attack—are used to capture these risks.

1.b Key points:

1. The objective of the renovation project is to provide cost-effective operations and security protection for the data center.
2. The renovation is to upgrade the data center's HVAC, telecommunications and data processing systems, and several security-related functions.
3. Two upgrade alternatives are proposed:
   - Base Case (Basic Renovation) and
   - Proposed Alternative (Enhanced Renovation), which augments the Base Case by strengthening portions of the exterior envelope; limiting vehicle access to the data center site, significantly improving the building's HVAC, data processing, and telecommunications systems; and providing better linkage of security personnel to the telecommunications network.

2. Analysis Strategy: How Key Measures Are Estimated

The following economic measures are calculated as present-value (PV) amounts:

1. **Life-Cycle Costs** (LCC) for the Base Case (Basic Renovation) and for the Proposed Alternative (Enhanced Renovation), including all costs of acquiring and operating the data center over the length of the study period. The selection criterion is lowest LCC.
2. **Present Value Net Savings** (PVNS) that will result from selecting the lowest-LCC alternative, PVNS greater than zero indicates an economically worthwhile project.

Additional measures:

1. **Savings-to-Investment Ratio** (SIR), the ratio of savings from the lowest LCC to the extra investment required to implement it. A ration of SIR greater than one indicates an economically worthwhile project.
2. **Adjusted Internal Rate of Return** (AIRR), the annual return on investment over the study period. An AIRR greater than the discount or hurdle rate indicates an economically worthwhile project.

Data and Assumptions:

- The Base Date is 2006.
- The alternative with the lower first cost (Basic Renovation) is designated the Base Case.
- The study period is 25 years and ends in 2030.
- The discount or hurdle rate is 7.0 percent real.
- The minimum acceptabel rate or return is 7.0 percent real.
- Annual probabilities for the outcomes for each attack scenario are given along with outcome cost.
- Annual probabilities and outcome costs differ by renovation strategy.

(continued)

Fig. 81.4 Summary of data center case study

assumptions, and a presentation of key economic measures of project impact.

The building owners wish to employ the most cost-effective risk mitigation plan (i.e., the plan that results in the lowest life-cycle cost) that will meet their objectives. Two alternative combinations of mitigation strategies—Base Case and Proposed Alternative—are available to the building owners (see Section 1.b of Fig. 81.4). The case study covers a 25-year period beginning in 2006. Life-cycle costs are calculated using a 7 % real rate for the baseline analysis. A sensitivity analysis was used to identify five key cost drivers. These five input variables were analyzed in-depth via a Monte Carlo simulation, which produced 1000 observed values for each of the economic measures of performance.

The results of the baseline analysis and the Monte Carlo simulation indicate that the Proposed Alternative is the most cost-effective risk mitigation plan. These results are summarized in Sections 3.a and 3.b of Fig. 81.4. Reference to the

3.a Calculation of Savings, Costs, and Additional Measures

Savings and Cost in Thousands of Dollars ($K)

PV of Investment Costs	**Base Case**	**Proposed Alt.**
Capital Investment	$1150K	$1765K

PV of Increased Investment Costs for Proposed Alternative $615K

PV of Noninvestment Costs	**Base Case**	**Proposed Alt.**
O&M Costs	3000K	2369K
Other Costs	493K	224K
	$3493K	$2593K

PV of Noninvestment Savings for Proposed Alternative $900K

LCC	**Base Case**	**Proposed Alt.**
PV of Investment Costs	1150K	1765K
PV of Noninvestment Costs	393K	2593K
	$4643K	$4358K

PVNS from Proposed Alternative $285K

Savings-to-Investment Ratio (SIR)

PV of Noninvestment Savings $900K
Divided by PV of Incr. Investment $615K
SIR = 1.46

Adjusted Internal Rate of Return (AIRR)

$(1 + 0.07)\ 1.46^{1/25} - 1 = 0.086$
AIRR = 8.6 percent
which exceeds the minimum acceptable rate of return of 7.0 percent

3.b Key Results:

- **LCC**
  Base Case $4643K
  Proposed Alt. $4358K
- **PVNS from Alt.** $285K
- **SIR** 1.46
- **AIRR** 8.6%

3.c Traceability:

Life-cycle costs and supplementary measures were calculated according to ASTM standards E917, E964, E1057, and E1074.

Treatment of uncertainty and measures of project risk were calculated according to ASTM standard E1369.*

Results of Monte Cario Simulation

Economic Measure	**Computed Statistics**				
	Minimum	**Median**	**Maximum**	**Mean**	**Standard Deviation**
LCC_{BC}	$3614K	$4687K	$6171K	$4755K	$605K
LCC_{ALT}	$3549K	$4447K	$5600K	$4492K	$447K
PVNS	–$5K	$240K	$587K	$264K	$160K
SIR	0.99	1.36	2.77	1.41	0.28
AIRR	6.0%	8.4%	10.7%	8.5%	1.0%

Fig. 81.4 (continued)

table showing the results of the Monte Carlo simulation at the bottom of Section 3.a reveals that the minimum values for present value net savings (PVNS), savings-to-investment ratio (SIR), and adjusted internal rate of return (AIRR) indicate improved marginal performance of the Proposed Alternative vis-à-vis the Base Case (i.e., a rank reversal has occurred). An examination of the raw data, however, reveals that marginal performance is associated with a single observation. Readers wishing an in-depth discussion of the Data Center Case Study are referred to NISTIR 7349.

How to Obtain the Cost-Effectiveness Tool Released in September 2006, Version 2.0 of the Cost-Effectiveness Tool produces the types of analysis results that provide decision makers with the means for choosing among alternative combinations of the three risk mitigation strategies. NISTIR 7349 [15] serves as a users' manual for Version 2.0; it is available as a printed copy or in electronic format as part of the software's online "Help" feature. The Cost-Effectiveness Tool is available free of charge to users through NIST at http://www2.bfrl.nist.gov/software/CET.

Appendix 1: Symbols and Definitions of Economic Parameters

Symbol	Definition of parameter
A_j	Cash flow at end of period j
A	End-of-period cash flows (or equivalent end-of-period values) in a uniform series continuing for a specified number of periods
$\bar{A}$	Amount of money (or equivalent value) flowing continuously and uniformly during each period, continuing for a specified number of periods
F	Future sum of money—the letter F implies future (or equivalent future value)
G	Uniform period-by-period increase or decrease in cash flows (or equivalent values); the arithmetic gradient
M	Number of compounding periods per interest period[a]
N	Number of compounding periods
P	Present sum of money—the letter "P" implies present (or equivalent present value). Sometimes used to indicate initial capital investment
S	Salvage (residual) value of capital investment
f	Rate of price level increase or decrease per period; an "inflation" of "escalation" rate
g	Uniform *rate* of cash flow increase or decrease from period to period; the geometric gradient
i	Effective interest rate per interest period[a] (discount rate), expressed as a percent or decimal fraction
r	Nominal interest rate per interest period,[a] expressed as a percent or decimal fraction

[a]Normally, but not always, the interest period is taken as 1 year
Subperiods, then, would be quarters, months, weeks, and so forth

Appendix 2: Functional Forms of Compound Interest Factors[1]

Name of factor	Algebraic formulation	Functional format
Group A. All cash flows discrete: end-of-period compounding		
Compound amount (single payment)	$(1+i)^N$	$(F/P, i, N)$
Present worth (single payment)	$(1+i)^{-N}$	$(P/F, i, N)$
Sinking fund	$\frac{i}{(1+i)^N-1}$	$(A/F, i, N)$
Capital recovery	$\frac{i(1+i)^N}{(1+i)^N-1}$	$(A/P, i, N)$
Compound amount (uniform series)	$\frac{(1+i)^N-1}{i}$	$(F/A, i, N)$
Present worth (uniform series)	$\frac{(1+i)^N-1}{i(1+i)^N}$	$(P/A, i, N)$
Arithmetic gradient to uniform series	$\frac{(1+i)^N-iN-1}{i(1+i)^N-i}$	$(A/G, i, N)$
Arithmetic gradient to present worth	$\frac{(1+i)^N-iN-1}{i^2(1+i)^N}$	$(P/G, i, N)$
Group B. All cash flows discrete: continuous compounding at nominal rate r per period		
Continuous compounding compound amount (single payment)	e^{rN}	$(F/P, r, N)$
Continuous compounding present worth (single payment)	e^{-rN}	$(P/F, r, N)$
Continuous compounding present worth (single payment)	$\frac{e^{rN}-1}{e^{rN}(e^r-1)}$	$(P/A, r, N)$
Continuous compounding sinking fund	$\frac{e^r-1}{e^{rN}-1}$	$(A/F, r, N)$
Continuous compounding capital recovery	$\frac{e^{rN}(e^r-1)}{e^{rN}-1}$	$(A/P, r, N)$
Continuous compounding compound amount (uniform series)	$\frac{e^{rN}-1}{e^r-1}$	$(F/A, r, N)$
Group C. Continuous, uniform cash flows: continuous compounding		
Continuous compounding sinking fund (continuous, uniform payments)	$\frac{r}{e^{rN}-1}$	$\bar{A}/F, r, N$
Continuous compounding capital recovery (continuous, uniform payments)	$\frac{re^{rN}}{e^{rN}-1}$	$\bar{A}/P, r, N$
Continuous compounding compound amount (continuous, uniform payments)	$\frac{e^{rN}-1}{r}$	$(F/\bar{A}, r, N)$
Continuous compounding present worth (continuous, uniform payments)	$\frac{e^{rN}-1}{re^{rN}}$	$(P/\bar{A}, r, N)$

[1] See Appendix 1 for definitions of symbols used in this table.

Appendix 3: Interest Tables

Table 81.6 Present worth factor (changes F to P)

Year	2 %	4 %	6 %	8 %	10 %	12 %	15 %	20 %	25 %	30 %	40 %	50 %
1	0.9804	0.9615	0.9434	0.9259	0.9091	0.8929	0.8696	0.8333	0.8000	0.7692	0.7143	0.6667
2	0.9612	0.9246	0.8900	0.8573	0.8264	0.7972	0.7561	0.6944	0.6400	0.5917	0.5102	0.4444
3	0.9423	0.8890	0.8396	0.7938	0.7513	0.7118	0.6575	0.5787	0.5120	0.4552	0.3644	0.2963
4	0.9238	0.8548	0.7921	0.7350	0.6830	0.6355	0.5718	0.4823	0.4096	0.3501	0.2603	0.1975
5	0.9057	0.8219	0.7473	0.6806	0.6209	0.5674	0.4972	0.4019	0.3277	0.2693	0.1859	0.1317
6	0.8880	0.7903	0.7050	0.6302	0.5645	0.5066	0.4323	0.3349	0.2621	0.2072	0.1328	0.0878
7	0.8706	0.7599	0.6651	0.5835	0.5132	0.4523	0.3759	0.2791	0.2097	0.1594	0.0949	0.0585
8	0.8535	0.7307	0.6274	0.5403	0.4665	0.4039	0.3269	0.2326	0.1678	0.1226	0.0678	0.0390
9	0.8368	0.7026	0.5919	0.5002	0.4241	0.3606	0.2843	0.1938	0.1342	0.0943	0.0484	0.0260
10	0.8203	0.6756	0.5584	0.4632	0.3855	0.3220	0.2472	0.1615	0.1074	0.0725	0.0346	0.0173
11	0.8043	0.6496	0.5268	0.4289	0.3505	0.2875	0.2149	0.1346	0.0859	0.0558	0.0247	0.0116
12	0.7885	0.6246	0.4970	0.3971	0.3186	0.2567	0.1869	0.1122	0.0687	0.0429	0.0176	0.0077
13	0.7730	0.6006	0.4688	0.3677	0.2897	0.2292	0.1625	0.0935	0.0550	0.0330	0.0126	0.0051
14	0.7579	0.5775	0.4423	0.3405	0.2633	0.2046	0.1413	0.0779	0.0440	0.0254	0.0090	0.0034
15	0.7430	0.5553	0.4173	0.3152	0.2394	0.1827	0.1229	0.0649	0.0352	0.0195	0.0064	0.0023
16	0.7284	0.5339	0.3936	0.2919	0.2176	0.1631	0.1069	0.0541	0.0281	0.0150	0.0046	0.0015
17	0.7142	0.5134	0.3714	0.2703	0.1978	0.1456	0.0929	0.0451	0.0225	0.0116	0.0033	0.0010
18	0.7002	0.4936	0.3503	0.2502	0.1799	0.1300	0.0808	0.0376	0.0180	0.0089	0.0023	0.0007
19	0.6864	0.4746	0.3305	0.2317	0.1635	0.1161	0.0703	0.0313	0.0144	0.0068	0.0017	0.0005
20	0.6730	0.4564	0.3118	0.2145	0.1486	0.1037	0.0611	0.0261	0.0115	0.0053	0.0012	0.0003
21	0.6698	0.4388	0.2942	0.1987	0.1351	0.0926	0.0531	0.0217	0.0092	0.0040	0.0009	
22	0.6468	0.4220	0.2775	0.1839	0.1228	0.0826	0.0462	0.0181	0.0074	0.0031	0.0006	
23	0.6342	0.4057	0.2618	0.1703	0.1117	0.0738	0.0402	0.0151	0.0059	0.0024	0.0004	
24	0.6217	0.3901	0.2470	0.1577	0.1015	0.0659	0.0349	0.0126	0.0047	0.0018	0.0003	
25	0.6095	0.3751	0.2330	0.1460	0.0923	0.0588	0.0304	0.0105	0.0038	0.0014	0.0002	
30	0.5521	0.3083	0.1741	0.0994	0.0573	0.0334	0.0151	0.0042	0.0012			
35	0.5000	0.2534	0.1301	0.0676	0.0356	0.0189	0.0075	0.0017	0.0004			
40	0.4529	0.2083	0.0972	0.0460	0.0221	0.0107	0.0037	0.0007	0.0001			
45	0.4102	0.1712	0.0727	0.0313	0.0137	0.0061	0.0019	0.0003				
50	0.3715	0.1407	0.0543	0.0213	0.0085	0.0035	0.0009	0.0001			1	
60	0.3048	0.0951	0.0303	0.0099	0.0033	0.0011	0.0002				$(1 + i)^y$	
70	0.2500	0.0642	0.0169	0.0046	0.0013	0.0004						
80	0.2051	0.0434	0.0095	0.0021	0.0005							
90	0.1683	0.0293	0.0053	0.0010	0.0002							
100	0.1380	0.0198	0.0030	0.0005								

Table 81.7 Capital recovery factor (changes P to A)

Year	2 %	4 %	6 %	8 %	10 %	12 %	15 %	20 %	25 %	30 %	40 %	50 %
1	1.020	1.040	1.060	1.080	1.100	1.120	1.150	1.200	1.250	1.300	1.400	1.500
2	0.5150	0.5302	0.5454	0.5608	0.5762	0.5917	0.6151	0.6545	0.6944	0.7348	0.8167	0.9000
3	0.3468	0.3603	0.3741	0.3880	0.4021	0.4163	0.4380	0.4747	0.5123	0.5506	0.6294	0.7105
4	0.2626	0.2755	0.2886	0.3019	0.3155	0.3292	0.3503	0.3863	0.4234	0.4616	0.5408	0.6231
5	0.2122	0.2246	0.2374	0.2505	0.2638	0.2774	0.2983	0.3344	0.3719	0.4106	0.4914	0.5758
6	0.1785	0.1908	0.2034	0.2163	0.2296	0.2432	0.2642	0.3007	0.3388	0.3784	0.4613	0.5481
7	0.1545	0.1666	0.1791	0.1921	0.2054	0.2191	0.2404	0.2774	0.3163	0.3569	0.4419	0.5311
8	0.1365	0.1485	0.1610	0.1740	0.1874	0.2013	0.2229	0.2606	0.3004	0.3419	0.4291	0.5203
9	0.1225	0.1345	0.1470	0.1601	0.1736	0.1877	0.2096	0.2481	0.2888	0.3312	0.4203	0.5134
10	0.1113	0.1233	0.1359	0.1490	0.1627	0.1770	0.1993	0.2385	0.2801	0.3235	0.4143	0.5088
11	0.1022	0.1141	0.1268	0.1401	0.1540	0.1684	0.1911	0.2311	0.2735	0.3177	0.4101	0.5059
12	0.0946	0.1066	0.1193	0.1327	0.1468	0.1614	0.1845	0.2253	0.2685	0.3135	0.4072	0.5039
13	0.0881	0.1001	0.1130	0.1265	0.1408	0.1557	0.1791	0.2206	0.2645	0.3102	0.4051	0.5026
14	0.0826	0.0947	0.1076	0.1213	0.1357	0.1509	0.1747	0.2169	0.2615	0.3078	0.4036	0.5017
15	0.0778	0.0899	0.1030	0.1168	0.1315	0.1469	0.1710	0.2139	0.2591	0.3060	0.4026	0.5011
16	0.0737	0.0858	0.0990	0.1130	0.1278	0.1434	0.1679	0.2114	0.2572	0.3046	0.4019	0.5008
17	0.0700	0.0822	0.0954	0.1096	0.1247	0.1405	0.1654	0.2094	0.2558	0.3035	0.4013	0.5005
18	0.0667	0.0790	0.0924	0.1067	0.1219	0.1379	0.1632	0.2078	0.2546	0.3027	0.4009	0.5003
19	0.0638	0.0761	0.0896	0.1041	0.1195	0.1358	0.1613	0.2065	0.2537	0.3021	0.4007	0.5002
20	0.0611	0.0736	0.0872	0.1019	0.1175	0.1339	0.1598	0.2054	0.2529	0.3016	0.4005	0.5002
21	0.0588	0.0713	0.0850	0.0998	0.1156	0.1322	0.1584	0.2044	0.2523	0.3012	0.4003	0.5000
22	0.0566	0.0692	0.0830	0.0980	0.1140	0.1308	0.1573	0.2037	0.2519	0.3009	0.4002	
23	0.0547	0.0673	0.0813	0.0964	0.1126	0.1296	0.1563	0.2031	0.2515	0.3007	0.4002	
24	0.0529	0.0656	0.0797	0.0950	0.1113	0.1285	0.1554	0.2025	0.2512	0.3006	0.4001	
25	0.0512	0.0640	0.0782	0.0937	0.1102	0.1275	0.1547	0.2021	0.2510	0.3004	0.4001	
30	0.0446	0.0578	0.0726	0.0888	0.1061	0.1241	0.1523	0.2008	0.2503	0.3001	0.4000	
35	0.0400	0.0536	0.0690	0.0858	0.1037	0.1223	0.1511	0.2003	0.2501			
40	0.0366	0.0505	0.0664	0.0839	0.1023	0.1213	0.1506	0.2001	0.2500			
45	0.0339	0.0483	0.0647	0.0826	0.1014	0.1207	0.1503	0.2001			$i(1+i)^y$	
50	0.0318	0.0466	0.0634	0.0817	0.1009	0.1204	0.1501	0.2000			$(1+i)^y-1$	
60	0.0288	0.0442	0.0619	0.0808	0.1003	0.1200	0.1500					
70	0.0267	0.0428	0.0610	0.0804	0.1001							
80	0.0252	0.0418	0.0606	0.0802	0.1000							
90	0.0241	0.0412	0.0603	0.0801								
100	0.0232	0.0408	0.0602	0.0800								

References

1. ASTM E833, *Definitions of Terms Relating to Building Economics,* American Society for Testing and Materials, West Conshohocken, PA (2006).
2. ASTM *Standards on Building Economics,* 6th ed., American Society for Testing and Materials, West Conshohocken, PA (2007).
3. G. Ramachandran, *The Economics of Fire Protection,* E & FN Spon, London (1998).
4. ANSI Z94.0-1989, "Industrial Engineering Terminology," Chapter 5, *Engineering Economy,* Engineering and Management Press, Atlanta, GA (2000).
5. S.K. Fuller and S.R. Petersen, "Life-Cycle Costing Manual for the Federal Energy Management Program," *NIST Handbook 135,* National Institute of Standards and Technology, Gaithersburg, MD (1996).
6. L.G. Anderson and R.E. Settle, *Benefit-Cost Analysis: A Practical Guide,* Lexington Books, Lexington, MA (1977).
7. R.E. Chapman and C.J. Leng, "Cost-Effective Responses to Terrorist Risks in Constructed

Facilities," *NISTIR 7073,* National Institute of Standards and Technology, Gaithersburg, MD (2004).
8. R.E. Chapman and D.S. Thomas, "A Guide to Printed and Electronic Resources for Developing a Cost-Effective Risk Mitigation Plan for New and Existing Constructed Facilities," *NISTIR 7390,* National Institute of Standards and Technology, Gaithersburg, MD (2007).
9. ASTM E917, *Standard Practice for Measuring Life-Cycle Costs of Buildings and Building Systems,* ASTM International, West Conshohocken, PA (2005).
10. ASTM E2204, *Standard Guide for Summarizing the Economic Impacts of Building Related Projects,* ASTM International, West Conshohocken, PA (2005).
11. ASTM E2506, *Standard Guide for Developing a Cost-Effective Risk Mitigation Plan for New and Existing Constructed Facilities,* ASTM International, West Conshohocken, PA (2006).
12. ASTM E1074, *Standard Practice for Measuring Net Benefits and Net Savings for Investments in Buildings and Building Systems,* ASTM International, West Conshohocken, PA (2006).
13. ASTM E964, *Standard Practice for Measuring Benefit-to-Cost and Savings-to-Investment Ratios for Investments in Buildings and Building Systems,* ASTM International, West Conshohocken, PA (2006).
14. ASTM E1057, *Standard Practice for Measuring Internal Rate of Return and Adjusted Internal Rate of Return for Investments in Buildings and Building Systems,* ASTM International, West Conshohocken, PA (2006).
15. R.E. Chapman and A.S. Rushing, "Users Manual for Version 2.0 of the Cost-Effectiveness Tool for Capital Asset Protection," *NISTIR 7349,* National Institute of Standards and Technology, Gaithersburg, MD (2006).

Dr. John M. Watts Jr. holds degrees in fire protection engineering, industrial engineering, and operations research. He is director of the Fire Safety Institute, a not-for-profit information, research, and educational corporation located in Middlebury, Vermont. Dr. Watts also serves as editor of NFPA's *Fire Technology.*

Robert E. Chapman is chief of the Office of Applied Economics, Building and Fire Research Laboratory, National Institute of Standards and Technology, Gaithersburg, Maryland.

Fire Risk Indexing

82

John M. Watts Jr.

Introduction

Fire risk indexing is a link between fire science and fire safety. As we learn more about the behavior of fire, it is important that we implement new knowledge to meet fire safety goals and objectives. One of the barriers to implementing new technology is the lack of structured fire safety decision making. Fire risk indexing is evolving as a method of evaluating fire safety that is valuable in assimilating research results. Fire safety decisions often have to be made under conditions where the data are sparse and uncertain. The technical attributes of fire risk are very complex and normally involve a network of interacting components. These interactions are generally nonlinear and multidimensional. However, complexity and sparseness of data do not preclude useful and valid approaches. Such circumstances are not unusual in decision making in business or other risk venues. (The space program illustrates how success can be achieved when there are few relevant data). However, detailed risk assessment can be an expensive and labor-intensive process, and there is considerable room for improving the presentation of results. Indexing can provide a cost-effective means of risk evaluation that is both useful and valid.

J.M. Watts Jr. (✉)

Fire risk indexing systems are heuristic models of fire safety. They constitute various processes of analyzing and scoring hazard and other system attributes to produce a rapid and simple estimate of relative fire risk. They are also known as rating schedules, point schemes, ranking, numerical grading, and scoring. Using professional judgment and past experience, fire risk indexing assigns values to selected variables representing both positive and negative fire safety features. The selected variables and assigned values are then operated on by some combination of arithmetic functions to arrive at a single value, which is then compared to other similar assessments or to a standard.

There are numerous approaches to fire safety evaluation that can be construed as risk indexing. A more general description of this area is presented in "Index Approach to Quantifying Risk," [1] whereas greater detail on the more rigorous application is given in "Fire Risk Assessment Using Multiattribute Evaluation" [2].

Fire Risk Indexing

Quantitative fire risk assessment originated with the insurance rating schedule. The approach has broadened to include a wide variety of applications [3, 4]. In general, fire risk rating schedules assign values to selected variables based on professional judgment and past experience. The selected variables represent both positive and negative fire safety features, and

M.J. Hurley (ed.), *SFPE Handbook of Fire Protection Engineering*,
DOI 10.1007/978-1-4939-2565-0_82, © Society of Fire Protection Engineers 2016

the assigned values are then operated on by some combination of arithmetic functions to arrive at a single value. This single value can be compared to other similar assessments or to a standard to rank the fire risk.

A risk index is defined as a single number measure of the risk associated with a facility [5]. Thus, insurance rates are fire risk indexes, as are the outputs of other similar schedules or scoring methods. Fire risk indexing, then, is the process of modeling and scoring hazard and exposure attributes to produce a rapid and simple estimate of relative risk. The concept has gained widespread acceptance as a cost-effective prioritization and screening tool for fire risk assessment programs. It is a useful and powerful approach that can provide valuable information on the risks associated with fire.

Figure 82.1 [6] provides a graphic view of the relative power and limitations of three broad levels of risk quantification. Curves A, B, and C do not represent actual data points but are demonstrative of a continuum of fire risk analysis possibilities.

Curve A is representative of a rigorous probabilistic risk analysis where hazard and exposure are analyzed through full quantitative analysis of the hazard and the statistics of exposure. It is clear that this analysis is the most accurate approach to defining risks, especially where the risk is low. However, it is also clear that a large resource investment is necessary to accomplish this task.

Curve C is a simple fire risk indexing that provides the ability to screen for high-risk catastrophic-type situations where the analysis can be consequence oriented. However, for small differences in risk, the ability of the more simplistic screening system to differentiate between two more subtle risks diminishes.

A more complex and accurate assessment model will provide greater differentiation between lesser risks and an improved overall accuracy. The trade-off for this approach is increased time and resources expended for model development, implementation, and data collection.

Applications

Choosing the depth of the risk analysis is a critical decision that depends on such factors as time, resource commitment, and the intended use of the results. Each approach may have certain advantages or trade-offs for specific tasks. A fire risk indexing approach may be appropriate in several situations:

1. Where greater sophistication is not required
2. Where risk screening will be cost effective
3. Where there is a need for risk communication

The level of accuracy demanded for a fire risk analysis is not typically the same as for other

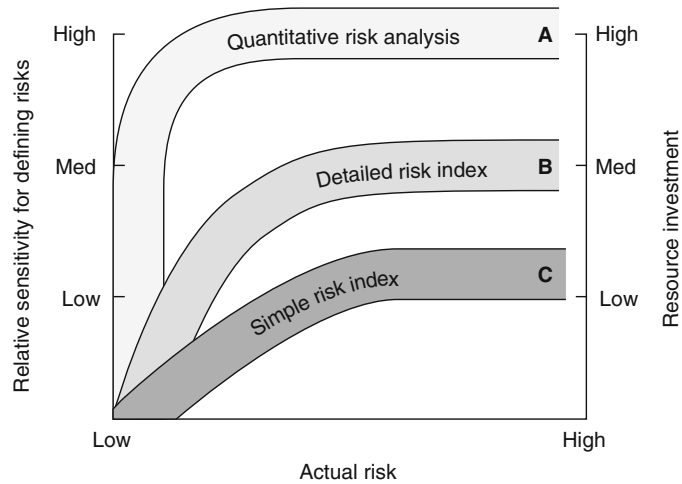

Fig. 82.1 Risk index systems and relative sensitivity for defining actual risk [6]

engineering purposes. Often, establishing an order of magnitude will suffice. Time and resource expenditure will increase as the depth of analysis is increased. Where resources are scarce and efficiency is prized, maximizing the utility of the fire risk indexing is clearly desirable.

The principles of fire risk indexing have been applied to a variety of hazard and risk assessment projects to set priorities and help manage resources. Risk assessment can be an expensive and labor-intensive process. Much time and money can be wasted if the products or facilities with the greatest potential for risk and associated liability are not identified and assessed first. Without a prioritization plan, it will not be known whether a risk was worth assessing until after the time and money have been spent.

Fire risk indexing also has appeal to staff charged with risk management decision-making responsibilities and those who may be unfamiliar with the details and mechanics of the risk assessment process. Because fire risk indexing simplifies basic fire risk assessment principles, it can be an effective way to acquire a global grasp of the issues.

Significance

The importance of fire risk indexing has been widely recognized. A working group of educators and researchers addressed the issue of fire risk indexing at the National Academy of Sciences 1987 "Workshop on Analytical Methods for Designing Buildings for Fire Safety" [7]. They concluded there is a need for a three-part system of fire safety comprised of (1) codes; (2) the methods of fire risk indexing, referred to as numerical grading systems; and (3) the means of supplying inputs to that system derived, as far as feasible, from basic principles of decision science. The working group went on to state the rationale for its conclusion:

> The advantage of keeping numerical grading systems in the trio is that they provide a coherent structure that still allows some qualitative analysis of fire safety. These systems also readily accept change associated with aspects of operations research, management science, risk analysis, and quantitative analytical solutions or models to the fire safety problem or parts of it [7].

The importance of scientific rigor in the development of fire risk indexing methods cannot be overemphasized and will be addressed in more detail in a later section of this chapter.

Examples of Approaches to Fire Risk Indexing

It is difficult to describe a typical fire risk indexing method. The practical necessity of trying to assess dozens or hundreds of risks with limited resources has led to the creation of an array of fire risk indexing systems. Approaches to fire risk indexing are virtually limitless in their possible variations. Representative examples of fire risk indexing were selected from the literature and are summarized in the following sections. They provide some idea of the types of variations involved with modeling and quantifying fire risk. Publicly available computer applications of these and other fire risk indexing methods are described in the final section of this chapter.

Insurance Rating

The purpose of risk analysis is to facilitate the process of risk management. One of the most fundamental tools of risk management is the transference of risk by insurance. To be acceptable to an insurer, the risk is rated by actuarial means, applying principles of mathematics to the particular pricing problems of the insurance industry.

Fire insurance rates are promulgated as *class* rates and *specific* rates. Class rates apply to all properties that fall within a given category or classification. The most common example of class rating is for dwellings or residences. When class rates do not apply, specific rates are determined by the application of a schedule or formula designed to measure the relative

quantity of fire hazard present. This process, known as *schedule rating*, is typically used for institutions, manufacturing properties, and business establishments.

The two most widely used schedules in the United States are known as the *mercantile schedule* and the *analytic system* [8]. At present, the analytic system is predominantly used throughout the country. It is more generally referred to as the Dean Schedule, named for A. F. Dean, author of the plan [9]. The schedules differ basically in their fundamental analysis of the factors affecting insurance rates, but they are alike in that they establish an arbitrary point from which to build up the rate, based on various physical hazards. A schedule of additions and reductions is computed, and the difference is applied to the arbitrary point of departure.

Schedule rating, then, is a plan by which fire hazards to any particular property are measured. A schedule has been defined as "an empirical standard for the measurement of relative quantity of fire hazard" [10]. Schedule rating takes into consideration the various factors contributing to the peril of fire, such as construction and occupancy, and helps determine which features either enhance or minimize the probability of loss. Credits and charges representing departures from standard conditions are incorporated in the schedules. Thus, the schedule rate is typically the sum of all charges less the sum of its credits and constitutes a standard for the measurement of the fire risk.

Specific Commercial Property Evaluation Schedule

The most commonly used insurance rating schedule in the United States is the Insurance Services Office's Specific Commercial Property Evaluation Schedule [11]. For each building, a percentage occupancy charge is determined from tabulated charges for classes of occupancy modified by factors such as the specific hazards of a particular occupancy. The basic building grade is a function of the resistance to fire of structural walls and floor and roof assemblies. The building fire insurance rate is the product of occupancy charges and building grade modified by factors such as the exposure to fire in nearby buildings and protection provided by portable extinguishers, fire alarm systems, and so forth.

An important concept of insurance rating is the use of loss experience. In general, tabulated values and conversion factors are based on actuarial analysis of fire losses paid by insurers and reported to the insurance industry.

Gretener Method

In 1960, Max Gretener of the Swiss Fire Protection Association began to study the possibility of an arithmetical evaluation of fire risk in buildings. His premise was that determining fire risk by statistical methods based on loss experience was no longer adequate for the following reasons [12]:

1. Lack of exchange of loss experience
2. Inadequate analysis with respect to causes and factors determining the size of loss, resulting in distortion of statistical data
3. Rapid technological change altering the credibility of previous experience
4. Different criteria, according to country and company, for data collection and evaluation

As a result of this new approach to schedule rating, the Gretener method has developed into a widely used fire risk index in Switzerland [13] and other European countries [14, 15]. The basic idea of the process consists of expressing, in relative, empirically derived numerical values, factors for fire initiation and spread and factors for fire protection. The product of the hazard factors is a value for potential hazard, whereas the product of the fire protection factors expresses a value for protective measures. The ratio of these products is taken as the measure of expected fire severity.

Of immediate appeal is that the approach begins with the explicit concept of risk as the expectation of loss given by the product of hazard probability and hazard severity:

$$R = A \times B$$

where

R = Fire risk
A = Probability that a fire will start
B = Fire hazard, degree of danger, or probable severity

Thus, the Gretener method is based on these two probabilities and combines them in accordance with probability theory.

A further departure from U.S. schedule rating is the calculation of fire hazard as a ratio rather than a sum:

$$\text{Fire hazard} = \frac{\text{Potential hazard}}{\text{Protective measures}}$$

that is,

$$B = \frac{\mathrm{P}}{N \times S \times F}$$

where
B = Fire hazard
P = Potential hazard
N = Standard fire safety measures
S = Special measures
F = Fire resistance of the building

Potential hazard, P, is the product of hazard elements whose magnitudes are influenced on the one hand by the building contents, that is, materials and merchandise present, and on the other hand by the building itself.

As with most other schedule approaches, the values for these individual factors are not based on statistics but are empirical figures resulting from a comparison of analyses of fire risks for which fire protection measures are either common or required by law.

Dow's Fire and Explosion Index

A need for systematic identification of areas with significant loss potential motivated Dow Chemical Company to develop the Fire and Explosion Index and risk guide [16]. The original edition issued in 1964 was a modified version of the Chemical Occupancy Classification rating system developed by Factory Mutual prior to 1957. It has been subsequently improved, enhanced, and simplified, and is now in its seventh edition [17].

Today there are many risk assessment methods available that can examine a chemical plant in great detail. The Fire and Explosion Index (FEI) remains a valuable screening tool that serves to quantify the expected damage from potential fire, explosion, and reactivity incidents and to identify equipment that could likely contribute to the creation or escalation of an incident [18]. Risks associated with operations where a flammable, combustible, or reactive material is stored, handled, or processed can be evaluated with this system. The guide is intended to provide a direct and logical approach for determining the probable "risk exposure" of a process plant and to suggest approaches to fire protection and loss prevention design. An important application of the FEI is to help decide when a more detailed quantitative risk analysis is warranted, as well as the appropriate depth of such a study [19]. This section will provide an overview of the method. The source document [17] should be consulted for specific application.

The concept of the Fire and Explosion Index (FEI) is to divide a process plant into separate operations or units and consider each of these individually. The key aspect of the method is the identification and assessment of thermodynamic properties of the dominant combustible material in the unit being studied. This basic material factor is then built up with a series of individual features concerning operation of the unit. These potential hazards are based on experience and information from incident records. They are intended to cover the majority of likely abnormal situations leading to fires, explosions, and material releases. Features considered are those on which all hazard and reliability analyses are based. However, the FEI does not purport to be as comprehensive as a detailed hazard and reliability study. The approach identifies most of the potentially hazardous features of a unit. Quantitative measurements used in the analysis are based on historic loss data, the energy potential of the key material, and the extent to which loss prevention practices are applied.

Index Calculation

The basic procedure for calculation of the Fire and Explosion Index is shown in Fig. 82.2. The first step is to identify those process units considered pertinent to the process and having the greatest potential impact in the event of loss by fire or explosion. A *unit* is considered to be a part of the plant that can be readily and logically characterized as a separate entity. Generally a unit consists of a segment of the process, such as reactors, blenders, furnaces, storage tanks, and so forth. In some instances, units may be portions of a plant separated from the remainder by distance, fire walls, or other barriers. In other cases, the unit may be an area where a particular hazard exists.

The next step is the determination of the material factor for the dominant combustible component of the process unit. The *material factor* is a measure of intensity of energy release from a chemical compound, mixture of compounds, or substance. It is determined by considering the flammability and reactivity of a material as described in NFPA 704, *Standard System for the Identification of the Fire Hazards of Materials*, 1990 edition [20]; NFPA 49, *Hazardous Chemicals Data*, 1991 edition [21]; and NFPA 325, *Guide to Fire Hazard Properties of Flammable Liquids, Gases, and Volatile Solids*, 1991 edition [22]. Based on these values the material factor is denoted by a number from 1 to 40. This arrangement is an arbitrary ordinal ranking.

Subsequent to selecting the appropriate material factor, penalties for contributing hazards are assessed as indicated by the schedule shown in Fig. 82.3. Items listed in the schedule are considered contributing factors to an incident that may result in fire or explosion. Not every hazard is applicable to a given process unit; however, all applicable items should be evaluated and an appropriate penalty applied. The list is divided into two parts, "General Process Hazards" and "Special Process Hazards." General process hazards relate to a type of process and represent conditions that may increase the magnitude or severity of an incident. Special process hazards are items that increase the probability of a fire or explosion.

Penalties are summed separately for each class of process hazard. These sums are then multiplied (severity × probability) to yield a process unit hazards factor. This factor has

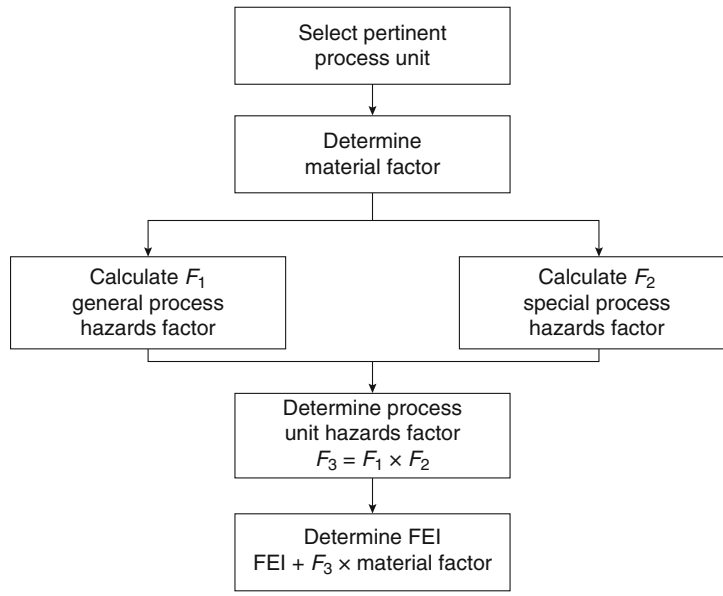

Fig. 82.2 Dow procedure for calculating the fire and explosion index

FIRE & EXPLOSION INDEX

AREA/COUNTY	DIVISION	LOCATION	DATE
SITE	MANUFACTURING UNIT	PROCESS UNIT	
PREPARED BY:	APPROVED BY: (Superintendent)	BUILDING	
REVIEWED BY: (Management)	REVIEWED BY: (Technology Center)	REVIEWED BY: (Safety & Loss Prevention)	
MATERIALS IN PROCESS UNIT			
STATE OF OPERATION _____ DESIGN _____ START UP _____ NORMAL OPERATION _____ SHUTDOWN		BASIC MATERIAL(S) FOR MATERIAL FACTOR	
MATERIAL FACTOR (see Table 1 or Appendices A or B). Note requirements when unit temperature over 140°F (60°C)			

1. GENERAL PROCESS HAZARDS	**Penalty Factor Range**	**Penalty Factor Used** (1)
Base Factor	1.00	1.00
A. Exothermic Chemical Reactions	0.30 to 1.25	
B. Endothermic Processes	0.20 to 0.40	
C. Material Handling and Transfer	0.25 to 1.05	
D. Enclosed or Indoor Process Units	0.25 to 0.90	
E. Access	0.20 to 0.35	
F. Drainage and Spill Control _____ gal or cu.m.	0.25 to 0.50	
General Process Hazards Factor (F_1)		
2. SPECIAL PROCESS HAZARDS		
Base Factor	1.00	1.00
A. Toxic Materials	0.20 to 0.80	
B. Sub-Atmospheric Pressure (<500 mmHg)	0.50	
C. Operation In or Near Flammable Range _____ Inerted _____ Not Inerted		
1. Tank Farms Storage Flammable Liquids	0.50	
2. Process Upset or Purge Failure	0.30	
3. Always in Flammable Range	0.80	
D. Dust Explosion (see Table 3)	0.25 to 2.00	
E. Pressure (see Figure 2) Operating Pressure _____ psig or kPa gauge Relief Setting _____ psig or kPa gauge		
F. Low Temperature	0.20 to 0.30	
G. Quantity of Flammable/Unstable Material: Quantity _____ lb or kg H_c = _____ BTU/lb or kcal/kg		
1. Liquids or Gases in Process (see Figure 3)		
2. Liquids or Gases in Storage (see Figure 4)		
3. Combustible Solids in Storage, Dust in Process (see Figure 5)		
H. Corrosion and Erosion	0.10 to 0.75	
I. Leakage—Joints and Packing	0.10 to 1.50	
J. Use of Fired Equipment (see Figure 6)		
K. Hot Oil Heat Exchange System (see Table 5)	0.15 to 1.15	
L. Rotating Equipment	0.50	
Special Process Hazards Factor (F_2)		
Process Unit Hazards Factor ($F_1 \times F_2$) = F_3		
Fire and Explosion Index ($F_3 \times MF$ = F&EI)		

Fig. 82.3 Dow fire and explosion index schedule

a numerical range from 1 to 8 and is considered a measure of the probable relative damage exposure magnitude. The Fire and Explosion Index (FEI) is the product of the material factor and the process unit hazards factor.

Risk Analysis

The process unit hazards factor and the material factor are also used to derive a damage factor. The damage factor represents the overall effect of fire, plus blast damage resulting from a fire or reactive energy release, caused by the various contributing factors associated with the process unit. It is estimated graphically. A radius of exposure in feet is estimated as 84 % of the FEI. The dollar value exposed is the estimated value of all equipment within the circle prescribed by the exposure radius. That is, the defined circular area of exposure indicates those assets that may be exposed to a fire or explosion generated by the process unit being evaluated. The replacement value of equipment in this area multiplied by the damage factor provides the base maximum probable property damage (MPPD), that is, the value at risk times the relative damage potential.

Three categories of loss control features have been assigned credits that can potentially reduce the base MPPD to an actual MPPD: (1) process control, (2) material isolation, and (3) fire protection. Twenty-two potential credit factors are shown in Table 82.1. The base MPPD reduced by the loss control credit factor gives the actual MPPD. This value represents the probable resulting loss from an incident of a reasonable magnitude given the proper functioning of protective equipment. Failure of the protective equipment could revert the probable loss to the base MPPD. Final steps include determination of the maximum probable days outage and the business interruption cost. The risk analysis procedure is summarized in Fig. 82.4.

The most important goal of the FEI analysis is to make the engineer aware of the loss potential of each process area and to help identify ways to lessen the severity and resultant loss of potential incidents. The Dow Chemical Company requires an FEI analysis for existing plants [18]. The requirement for use of the FEI has been adopted into law in the Netherlands [23]. The FEI has been found to be a valuable screening tool that can be used in conjunction with other analyses to help determine the relative risk of process units and to provide valuable guidance to both engineering and management staffs.

Mond Fire, Explosion, and Toxicity Index

The Mond division of Imperial Chemical Industries (ICI), Ltd., identified that the Dow Fire and Explosion Index method had considerable scope for the evaluation of plant hazard potential at the earliest design stages. Following trials with the published Dow method, it was clear that there was a need to extend the method in a number of directions to develop its potential for new project design. The resulting Mond Fire, Explosion, and Toxicity Index [24, 25] was developed and has been applied to a range of new projects within ICI.

The main contribution of the Mond method is the inclusion of *offsetting features*, which allow the effect of good design concepts, good management attitudes, and other preventative measures to reduce the overall hazard. An important outcome of using the technique is to raise questions concerning hazard potential at an early enough stage in planning to allow for adequate investigations to be made before the process is in operation. Achieving some measure of hazard early in the planning process provides information that can be used to select appropriate protection features as the planning proceeds. Early assessment of hazards has value in dealing with possible problems in obtaining approval for proposals and in predicting possible delays and problems that are likely to be encountered.

Table 82.1 Dow loss control credit factors

1. Process Control Credit Factor (C_1)

Feature	Credit Factor Range	Credit Factor Used (2)	Feature	Credit Factor Range	Credit Factor Used (2)
a. Emergency power	0.98		f. Inert gas	0.94–0.96	
b. Cooling	0.97–0.99		g. Operating instructions/procedures	0.91–0.99	
c. Explosion control	0.84–0.98		h. Reactive chemical review	0.91–0.98	
d. Emergency shutdown	0.96–0.99		i. Other process hazard analysis	0.91–0.98	
e. Computer control	0.93–0.99				

C_1 Value (3) ____

2. Material Isolation Credit Factor (C_2)

Feature	Credit Factor Range	Credit Factor Used (2)	Feature	Credit Factor Range	Credit Factor Used (2)
a. Remote control valves	0.96–0.98		c. Drainage	0.91–0.97	
b. Dump/blowdown	0.96–0.98		d. Interlock	0.98	

C_2 Value (3) ____

3. Fire Protection Credit Factor (C_3)

Feature	Credit Factor Range	Credit Factor Used (2)	Feature	Credit Factor Range	Credit Factor Used (2)
a. Leak detection	0.94–0.98		f. Water curtains	0.97–0.98	
b. Structural steel	0.95–0.98		g. Foam	0.92–0.97	
c. Fire water supply	0.94–0.97		h. Hand extinguishers/monitors	0.93–0.98	
d. Special systems	0.91		i. Cable protection	0.94–0.98	
e. Sprinkler systems	0.74–0.97				

C_3 Value (3) ____

Loss Control Credit Factor = $C_1 \times C_2 \times C_3$ (3) = ____

Fire Safety Evaluation System

The Fire Safety Evaluation System (FSES) [26, 27] is a risk indexing approach to determining equivalencies to the NFPA *101®*, *Life Safety Code®*, 2000 edition [28], for certain institutional occupancies. The technique was developed at the Center for Fire Research, National Bureau of Standards in cooperation with the U.S. Department of Health and Human Services (formerly Health, Education, and Welfare) in the late 1970s. It was adapted to new editions of the *Life Safety Code* and is presently published in NFPA 101A, *Guide on Alternative Approaches to Life Safety*, 2001 edition [29]. (The tables in this section are taken from the worksheets for health care occupancies in Chapter 4 of NFPA 101A.)

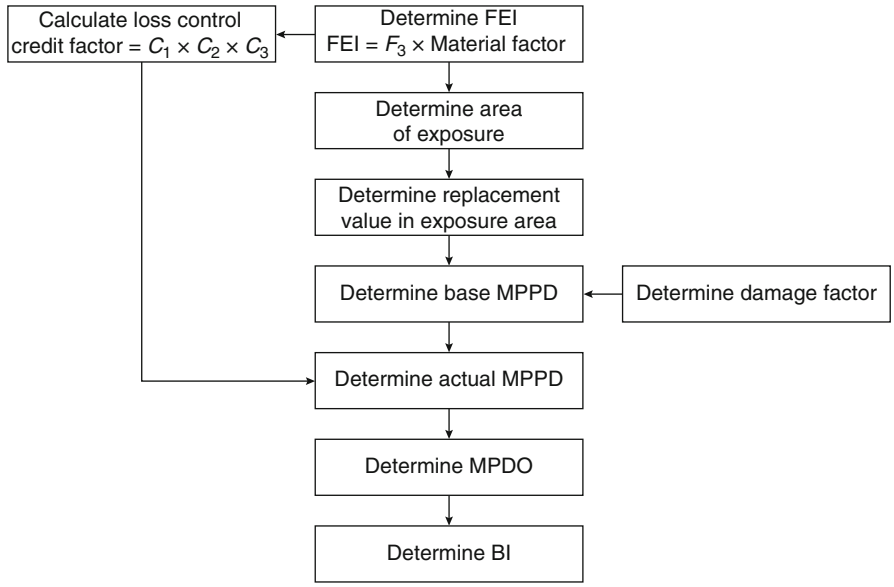

Fig. 82.4 Dow procedure for calculating other risk analysis information

Equivalency Concept

In an effort to promote economical upgrading of fire safety, U.S. codes include an equivalency option. This provision allows alternative designs to satisfy regulations if they provide a level of fire safety equivalent to that called for by the regulations. The difficult decision as to what constitutes equivalency has been left to local jurisdictions. Local interpretations lead to a lack of uniformity across the country in terms of what may be waived and what constitutes an adequate alternative to provide the required level of safety. The FSES was developed to provide a uniform method of evaluating health care facilities to determine what fire safety measures would provide a level of fire safety equivalent to that provided by the *Life Safety Code*. The objective was to compile an evaluation system that would be easily workable, presenting useful information for the amount of effort expended.

Fire Zone Concept

Unlike the Life *Safety Code*, the FSES subdivides a building into fire zones for evaluation. A fire zone is defined as a space separated from other parts of the building by floors, fire barriers, or smoke barriers. When fire or smoke barriers do not partition a floor, the entire floor is the fire zone. In application, every zone in the facility should be evaluated. Repetitive arrangements may be evaluated by selection of a typical zone.

Risk

Also unlike the *Life Safety Code*, the FSES begins with a determination of relative risk deriving from characteristics of a health care occupancy. Five occupancy risk parameters are used: (1) patient mobility, (2) patient density, (3) fire zone location, (4) ratio of patients to attendants, and (5) average patient age. Variations of these parameters have been assigned relative weights, as indicated in Table 82.2. These values were determined from the experienced judgment of a group of fire safety professionals and represent the opinions of that panel of experts. There is no documented process for validating or revising these values.

Occupancy risk factor for a zone is calculated as the product of the assigned values for the five risk parameters. Multiplication implicitly

Table 82.2 FSES occupancy risk parameter factors

Risk parameters	Risk factor values					
1. Patient mobility (M)	Mobility status	Mobile	Limited mobility	Not mobile	Not movable	
	Risk factor	1.0	1.6	3.2	4.5	
2. Patient density (D)	No. patients	1–5	6–10	11–30	>30	
	Risk factor	1.0	1.2	1.5	2.0	
3. Zone location (L)	Floor	1st	2nd or 3rd	4th to 6th	7th and above	Basements
	Risk factor	1.1	1.2	1.4	1.6	1.6
4. Ratio of patients to attendants (T)	Patients / Attendant	1 – 2 / 1	3 – 5 / 1	6 – 10 / 1	> 10 / 1	One or more[a] / None
	Risk factor	1.0	1.1	1.2	1.5	4.0
5. Patient average age (A)	Age	Under 65 years and over 1 year		65 years and over, 1 year and younger		
	Risk factor	1.0		1.2		

[a]Risk factor of 4.0 is charged to any zone that houses patients without any staff in immediate attendance

suggests these factors are interdependent. A hardship adjustment for existing buildings is applied to the occupancy risk factor. This adjustment modifies the risk in existing buildings to 60 % of that for an equivalent new building.

Fire Safety Parameters

Safety features must offset the calculated occupancy risk. Thirteen fire safety parameters were selected. These parameters and their respective ranges of values (shown in Table 82.2) were also developed by the same panel of experts. Table 82.2 is designed to be used as a survey instrument whereby appropriate values for each safety parameter can be selected by inspection of the fire zone. There is no attempt made to directly correlate these fire safety parameters to the previously defined risk parameters.

Fire Safety Redundancies

An important concept of the FSES is redundancy through simultaneous use of alternative safety strategies. The purpose is to ensure that failure of a single protection device or system will not result in a major fire loss. Three fire safety strategies are identified: (1) containment, (2) extinguishment, and (3) people movement. Table 82.3 indicates the expert panel's opinion of which fire safety parameters apply to each fire safety strategy. Values from Table 82.2 are entered in the appropriate places on Table 82.3 and summed for each column. The implication of addition is that there is no interaction among the fire safety parameters. The limited value of automatic sprinklers for people movement safety is adjusted for by using one-half of the parameter value in this column. The resulting sums are considered to be the available level of each fire safety strategy.

Equivalency Evaluations

The FSES determines whether the fire zone in question possesses a level of fire safety equivalent to that of the *Life Safety Code*. This conclusion is made by comparing the calculated level for each fire safety strategy to stated minimum values. These values for existing buildings range from 100 % down to 12 % of those for new buildings. For the column of Table 82.4 labeled "General Safety," the sum of all available safety parameter values is compared to the occupancy risk factor calculated from the parameters in Table 82.3.

Supplemental Requirements

Because the 13 selected fire safety parameters were found not to cover all requirements of the

Table 82.3 FSES safety parameter values

Parameters	Parameter values						
1. Construction	Combustible types III, IV, and V				Noncombustible types I and II		
Floor or zone	000 (U)	111	200 (U)	211 + 2HH	000 (U)	111	222, 322, 433
First	−2	0	−2	0	0	2	2
Second	−7	−2	−4	−2	−2	2	4
Third	−9	−7	−9	−7	−7	2	4
Fourth and above	−13	−7	−13	−7	−9	−7	4
2. Interior finish (corridors and exits)	Class C		Class B		Class A		
	–5 (0)[a]		0 (3)[a]		3		
3. Interior finish (rooms)	Class C		Class B		Class A		
	–3 (1)[a]		1 (3)[a]		3		
4. Corridor partitions/walls	None or incomplete		<1/3 h		≥1/3 < 1 h		≥1 h
	−10 (0)[b]		0		1 (0)[b]		2 (0)[b]
5. Doors to corridor	No door		<20 min fpr		≥20 min fpr		≥20 min fpr and auto clos
	−10		0		1 (0)[c]		2 (0)[c]
6. Zone dimensions	Dead end				No dead ends >30′ and zone length is:		
	>100′	>50′–100′	30′–50′		>150′	100′–150′	<100′
	−6 (0)[d]	−4 (0)[d]	−2 (0)[d]		−2	0	1
7. Vertical openings	Open 4 or more floors		Open 2 or 3 floors		Enclosed with indicated fire resist		
	−14		−10		<1 h	≥1 h < 2 h	≥2 h
					0	2 (0)[e]	3 (0)[e]
8. Hazardous areas	Double deficiency		Single deficiency		No deficiencies		
	In zone	Outside zone	In zone	In adjacent zone			
	−11	−5	−6	−2	0		

(continued)

Table 82.3 (continued)

Parameters	Parameter values					
9. Smoke control	No control		Smoke barrier serves zone		Mech. assisted systems by zone	
	−5 (0)[f]		0		3	
10. Emergency movement routes	<2 routes		Multiple routes			
	−8		Deficient	w/o horizontal exit(s)	Horizontal exit(s)	Direct exit(s)
			−2	0	1	5
11. Manual fire alarm	No manual fire alarm			Manual fire alarm		
	−4			w/o F.D. Conn.		w/F.D. Conn.
				1		2
12. Smoke detection and alarm	None	Corridor only	Rooms only	Corridor and habit. space		Total space in zone
	0 (3)[g]	2 (3)[g]	3 (3)[g]	4		5
13. Automatic sprinklers	None	Corridor and habit. space	Entire building			
	0	8	10			

[a]Use ( ) if the area of Class B or C interior finish in the corridor and exit or room is protected by automatic sprinklers and Parameter 13 is 0
[b]Use (0) when Parameter 5 is −10
[c]Use (0) when Parameter 4 is −10
[d]Use (0) when Parameter 10 is −8
[e]Use (0) when Parameter 1 is based on first floor zone or on an unprotected type of construction (columns marked "U")
[f]Use (0) on floor with less than 31 patients (existing buildings only)
[g]Use this value in addition to Parameter 13, Automatic Sprinklers value, if the entire zone is protected with quick-response automatic sprinklers
Conversion: 1 ft 0.3048 = m

Table 82.4 FSES worksheet for evaluating fire safety strategies

Safety Parameters	Containment Safety (S_1)	Extinguishment Safety (S_2)	People Movement Safety (S_3)	General Safety (S_4)
1. Construction				
2. Interior Finish (Corr. & Exit)				
3. Interior Finish (Rooms)				
4. Corridor Partitions/Walls				
5. Doors to Corridor				
6. Zone Dimensions				
7. Vertical Openings				
8. Hazardous Areas				
9. Smoke Control				
10. Emergency Movement Routes				
11. Manual Fire Alarm				
12. Smoke Detection & Alarm				
13. Automatic Sprinklers			2	
Total Value	S_1	S_2	S_3	S_4

Life Safety Code, an addendum to the FSES was created. The addendum consists of 12 additional parameters that may be required by the *Life Safety Code*. It should not be implied that these parameters are extraneous to the risk and safety factors of Tables 82.2 and 82.3 or to the identified fire safety strategies.

Optimization

A distinct advantage of index approaches to fire risk assessment is that they lend themselves to optimization techniques. This characteristic has been exploited for the FSES through incorporation of a linear programming

optimization algorithm [30–35]. Linear programming refers to a mathematical model for allocating limited resources among competing activities subject to a set of constraints. The procedure finds the distribution of values that optimizes an objective function.

For a fire risk index, the objective is to minimize cost of fire protection that will meet a prescribed acceptable level. In the FSES, the acceptable levels are given and the variables are the safety parameters that can take on the values indicated in Table 82.2. By assigning a cost to each value in Table 82.2, an economic optimum can be calculated. A personal computer version of this model is described in the last section of this chapter.

Derivative Applications

NFPA 101A now includes FSESs for health care occupancies, correctional facilities, board and care homes, and business occupancies. One of the most widely used of these is Chap. 8. NFPA 101A classifies the transaction of business other than mercantile, the keeping of accounts and records, and similar purposes as a business occupancy. Typical examples are professional, financial, and governmental offices. The FSES for business occupancies was derived from a project to appraise the relative level of life safety from fire in existing office buildings and combination office-laboratory buildings of a U.S. government agency [36]. It was based on the approach developed for health care occupancies and was subsequently incorporated into NFPA 101A. An analysis of the FSES for business occupancies, using the attribute value spread as a measure of importance to rank the fire safety attributes, found a difference between criteria for new and existing buildings of 6–10 % [37]. A PC-based computer program, Enhanced Fire Safety Evaluation System for Business Occupancies (EFSES), is described later in this chapter.

Also derived from the original FSES is Section 3408, "Compliance Alternatives," of the BOCA *National Building Code*® [38], an indexing system for fire safety in existing buildings. As stated in paragraph 3408.1, the purpose of this section is to maintain or increase safety in existing buildings without full compliance of other chapters of the code. This system allows for older designs to be judged on their performance capabilities rather than forcing the buildings to comply with modern standards for new construction. Originally adopted in the 1985 code, significant changes were effected between the 1993 and 1996 editions. Section 3408 is applicable to all occupancy use groups. For each use group there are separate point values for each safety attribute and separate mandatory values to be considered as criteria for equivalency. This procedure for compliance alternatives has also been adopted as an appendix to Chapter 34 in the *International Building Code* [39]. A detailed comparison of both qualitative and quantitative aspects of Section 3408 of the BOCA *National Building Code* and Chapter 8 of NFPA 101A shows some significant differences [40].

Chapter ILHR 70 of the *Wisconsin Administrative Code* is a building code for historic structures [41]. Its purpose is to provide alternative building standards for preserving or restoring buildings or structures designated as historic. Subchapter IV of the code is a risk indexing system, called the Building Evaluation Method. It assesses life safety for a qualified historic building by comparing 17 building safety attributes with the requirements of the prevailing code. If a historic building has less of a safety attribute than is required by the prevailing code, a negative number is assigned. If a historic building has more of a safety attribute than is required by the prevailing code, a positive number is assigned. Thus, evaluation is directly related to the prevailing code. If the sum of all the attributes is greater than or equal to zero, the building is compliant. The same trade-offs previously would have been allowed under the variance petition process but are now codified. This system adds a degree of certainty of approval that did not previously exist, often impeding development of historic buildings. Unlike the FSES and BOCA Chapter 34, the Building Evaluation Method has no mandatory scores. If the total

safety score is equal to or greater than zero, the building is considered code compliant. Also unlike the FSES and BOCA, Wisconsin Subchapter IV does not vary by occupancy. A table for each attribute gives a set of numerical values, one of which is selected for each evaluation. Criteria for these values refer directly to the prevailing code. The same set of values applies for all nonexcluded building uses and occupancies. This code can be accessed through the State of Wisconsin, Department of Commerce website (http://www.commerce.state.wi.us).

Hierarchical Approach

Development of a hierarchical approach to fire risk ranking was initially undertaken at the University of Edinburgh, sponsored by the U.K. Department of Health and Social Services [42–44]. The objective of this study was to improve the evaluation of fire safety in U.K. hospitals through a systematic method of appraisal. This approach was further developed at the University of Ulster for application to dwelling occupancies [45, 46]. It has been refined and implemented for the assessment of fire risk in telecommunications facilities [47, 48].

Defining fire safety is difficult and often results in a listing of factors that together comprise the intent. These factors tend to be of different sorts. For example, fire safety may be defined in terms of goals and aims, such as fire prevention, fire control, occupant protection, and so forth. These broad concepts are usually found in the introductory section of building codes and other fire safety legislation. Or, fire safety may be defined in terms of more specific hardware items, such as combustibility of materials, heat sources, detectors, sprinklers, and so forth. These topics are more akin to items listed in the table of contents of building codes. A meaningful exercise is to construct a matrix of fire safety goals versus more specific fire safety features. This matrix helps to identify the roles of these two concepts in theory and in practice.

Decision-Making Levels

As a logical extension of a single fire safety matrix, consider that there are more than two categories of fire safety factors. This idea suggests a hierarchy of decision-making levels, or lists denoting things that comprise fire safety. A hierarchy of fire safety decision-making levels is presented in Table 82.5.

These represent common levels of fire safety decision making, but there may be more or fewer in a particular application. For example, an even lower level dealing with individual physical items could be added or intermediate levels could be used to better define certain relationships.

This hierarchy of levels of detail of fire safety suggests that a series of matrices is appropriate to model the relationships among various fire safety factors; that is, a matrix of policy versus objectives would define a fire safety policy by identifying the specific objectives that are held most desirable. In turn, a matrix of objectives versus strategies would identify the relationship of these factors, and a matrix of strategies versus attributes would suggest where to use what. Thus, a matrix may be constructed to examine the association of any two adjacent levels in a hierarchy of fire safety factors.

An even more appealing aspect of this approach is that two or more matrices may be

Table 82.5 Hierarchy of fire safety decision-making levels

Level	Name	Description
1	Policy	Course or general plan of action adopted by an organization to achieve security against fire and its effects
2	Objectives	Specific fire safety goals to be achieved
3	Strategies	Independent fire safety alternatives, each of which contributes wholly or partly to the fulfillment of fire safety objectives
4	Attributes	Components of fire risk that are determinable by direct or indirect measure or estimate
5	Survey	Measurable feature that serves as items a constituent part of a fire safety attribute

combined (multiplied) to produce information on the importance of specific detail of building elements to an overall fire safety policy—information not previously available. This approach is the only such grading of fire safety with an explicitly defined relationship to fire safety goals and objectives.

Generalized Procedure

A generalized procedure for ranking fire safety attributes to determine their relative importance is summarized in the following five steps:

1. Identify hierarchical levels of fire safety specification.
2. Specify items comprising each level.
3. Construct and assign values to matrices of each sequential pair of levels.
4. Combine (multiply) matrices to yield importance ranking of items.
5. Verify the results.

Table 82.4 represents an example of Step 1. Step 2 requires that lists of objectives, strategies, attributes, and survey items be developed. A list of fire safety objectives might include statements about life safety, property protection, continuity of operations, environmental protection, and heritage preservation.

No significant work has been done to identify just what it is that fire safety is trying to achieve (i.e., allocation of resources for fire safety is not generally directly associated with a specific corporate objective), so these objectives are a very subjective list. (One benefit of the hierarchical approach is facilitating the incorporation of fire safety into more global organizational objectives).

In most applications a Delphi process is used to define fire safety policy in terms of the specified list of objectives. That is, a group of experts is asked to rank fire safety objectives with respect to their importance to policy. Each member of the Delphi group receives feedback in the form of response averages, and the process repeats until an acceptable level of consensus is reached. The Delphi exercise yields a vector representing the relative importance of each objective to organizational policy. In some work the more formal analytic hierarchy process (AHP) is used [49, 50]. However, this process is unstable when there are more than six or seven factors to be ranked [2].

The next decision-making level involves fire safety strategies. A list of strategies can be derived by taking a cutset of the NFPA Fire Safety Concepts Tree [51]. Example fire safety strategies are ignition prevention, limitation of combustibles, compartmentation, fire detection and alarm, fire suppression, and protection of exposed people or things.

Now, a matrix of objectives versus strategies can be constructed. Values of the cells are again supplied by Delphi or some other subjective decision-making process. In this case the question to be answered is, how important is each strategy to the achievement of each objective?

In order to facilitate mathematical manipulation, the values of the matrices can be normalized. Then, multiplying the objectives/strategies matrix by the policy vector yields a new vector that shows the relative contribution of each strategy to overall fire safety policy. Although this vector is not essential to the fire safety evaluation, it illustrates the matrix manipulation process that is the essence of the hierarchical approach.

Continuing this procedure, the next level of fire safety attributes is considered. The following is a typical list of these attributes:

Construction	Equipment	Fixed suppression
Height	Special hazards	Fire department
Compartmentation	Detection	Egress system
Building services	Alarm	Personnel
Furnishings	Smoke control	Management

A matrix of strategies versus fire safety attributes is then constructed and evaluated. Multiplying this matrix by the previously derived vector yields a new vector that weighs each fire safety attribute according to its relative contribution to organizational fire safety policy. The significance of this vector is that it is the only such weighing of fire safety factors that has an explicit link to fire safety goals and objectives. The matrix manipulation process is summarized in Fig. 82.5.

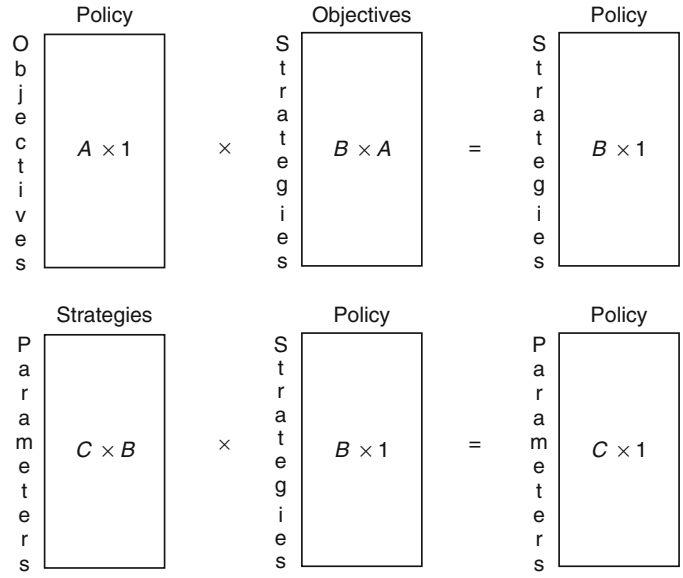

Fig. 82.5 Schematic summary of hierarchical approach

Attribute Weighting

Not all fire safety attributes are equally important. The role of weight serves to express the importance of each attribute compared with the others. Hence the assignment of weights is a key component of fire risk indexing. Formal methods of analysis generally require information regarding the relative importance of each attribute, which is usually supplied by a cardinal scale. Weights can be directly supplied or developed by specific methods. In some simple cases the weights default to equality as in a checklist. There are many weight assessment techniques used in multiattribute evaluation that are reviewed in the literature [52, 53].

Generally, hierarchical methods have been found effective in fire safety evaluation. For example, importance weighting of fire safety attributes can be developed using pairwise comparisons and the analytic hierarchy process (AHP). AHP has been widely reviewed and applied in the literature and its use is supported by several commercially available user-friendly software packages. The best known and most supported by commercial software is the eigenvalue prioritization method [54, 55]. However, there are limitations to the use of AHP in a fire risk index. The analytic hierarchy process is not as intuitive or transparent as simpler approaches, and it significantly restricts the number of attributes that can be considered. Also, under certain unusual circumstances AHP can be subject to distortion and rank reversal.

Evaluating Attributes

In order to use the resulting vector of attribute weights to develop a fire risk ranking of a building or facility space, the extent to which each attribute is present must be evaluated. That is, a level of functional value of each fire safety attribute must be assessed. These attribute grades may be directly observable or, more often, they are derived from various functions of a lower level of features that includes specific hardware components, for example, fire safety survey items.

Attributes are defined as components of fire risk that are quantitatively determinable by direct or indirect measurement or estimation. They are intended to represent factors that account for an acceptably large portion of the total fire risk. In most cases they are not directly measurable. This case is especially true for existing buildings for which only limited information is readily available.

Each attribute has a specific relative importance that is universal for all facilities within the scope of the assessment method. Individual buildings will vary in the degree to which attributes exist or occur in a space. Attribute grades are a measure of the intensity level or degree of danger or security afforded by the attribute. Partitioning them into measurable constituent parts facilitates grading of attributes. Usually these parts are directly assessable survey items, the next lower level in the decision hierarchy. The determination of attribute grades is dependent on those features of a space identified as survey items.

A survey item is a measurable feature of a space that serves as a constituent part of one or more attributes. In developing means to grade attributes in a given building, each attribute is associated with one or more survey items. These specific features evolve from analysis of the attributes. Items are chosen for contributing significantly to the effectiveness of the irrespective attributes and for being directly measurable. It is, therefore, necessary that survey items be defined in sufficient detail to support these traits. Detailed descriptions of the survey items are required to frame questions that provide input into the decision logic that produces the attribute grades.

In one application, grades were established for each fire risk attribute by associating readily measurable survey items, using logic described by decision tables [56]. Input to these tables included fire test results, fire hazard modeling, field experience from previous fire events, logic diagrams, and professional judgment. The scalar product of the resulting attribute weights and grades yields a relative measure of fire risk. The result may be used to rank facilities, or it can be compared to a standard value.

Areas of Application

As indicated in the beginning of this section, the hierarchical approach has evolved from applications in the areas of health care facilities, dwellings, and telecommunications central office facilities. Recent applications of this approach to fire risk indexing have developed in many forms and for many uses. In the United States, a Historic Fire Risk Index has been developed that includes an assessment of the cultural significance as a parameter of fire risk [57, 58]. In Hong Kong, aspects of fuzzy systems theory have been incorporated into a fire risk indexing technique to evaluate existing high-rise buildings [59]. Also in Hong Kong, a derived fire risk index has been tested on 122 existing high-rise buildings [60].

Whereas most fire risk indexing methods focus on life safety issues, FireSEPC (fire safety evaluation procedure for the property of parish churches) is insurance motivated and deals with building worth [61]. Using the hierarchical framework, the procedure rates the contribution of 18 fire safety components and compares the score to a "collated norm" developed from guidance documents.

In Sweden there is a significant program for the development and verification of a fire risk index method for timber-frame, multistory apartment buildings [62, 63]. This work is of particular importance due to its comprehensive documentation and validation procedures.

Criteria for Development and Evaluation of Fire Risk Ranking

The fire protection engineering community appears to be largely unconcerned with the proliferation of fire risk ranking and how it is being used. The available literature deals only with development and application of a specific method or general descriptions of several selected approaches. Like any analytical technique, risk-ranking methods have their limitations and should not be used uncritically.

The purpose of fire risk ranking is to provide a useful aid to decision making. It must be easy to apply but sophisticated enough to provide a minimum of technical validity. Credibility can also be improved through consistency and transparency. The approach should be systematic, and it should be clear to all interested parties that the

relevant technical issues have been appropriately covered. Based on the review of numerous fire risk ranking systems, ten criteria have been proposed to aid in the development and evaluation of other such systems [64].

Criterion 1 *Development and implementation of the method should be thoroughly documented according to standard procedures*. One of the hallmarks of professionalism is that, as a study proceeds, a record is made of assumptions, data, attribute estimates and why they were chosen, model structure and details, steps in the analysis, relevant constraints, results, sensitivity tests, validation, and so on. Little of this information is available for most fire risk ranking methods.

In addition to facilitating review, there are three other practical reasons not to slight the documentation: (1) if external validation is to be conducted, adequate documentation will be a prerequisite; (2) during the life cycle of a fire risk ranking system the inescapable changes and adjustments will require appropriate documentation; and (3) clear and complete documentation enhances confidence in the method, whereas its absence inevitably carries with it the opposite effect.

The value of the documentation will be improved if it follows established guidelines. Standard formats for documentation are primarily directed at large-scale computer models [65, 66] but can be readily adapted in principle to more general applications.

Criterion 2 *Partition the universe rather than select from it*. One of the least well-established procedures in fire risk ranking is the choice of attributes. In following a systemic approach it is best to be comprehensive. Using an exhaustive model of fire safety, such as the NFPA Fire Safety Concepts Tree [51], is helpful in being inclusive. This logic tree branches out from the holistic concept of fire safety objectives. A cut set on the tree will then identify a group of attributes that encompasses all possible fire safety features.

Criterion 3 *Attributes should represent the most frequent fire scenarios*. In determining the level of detail of the attributes, it is necessary to look at those factors that are most significant, statistically or by experienced judgment. This criterion may also be used as an alternative to Criterion 2, providing the need for systemic comprehensiveness is satisfied.

Criterion 4 *Provide operational definitions of attributes*. If the methodology is to be used by more than a single individual, it is necessary to ensure precise communication of the intent of key terms. Many fire risk attributes are ambiguous concepts that have a wide variety of interpretation even within the fire community.

Criterion 5 *Elicit subjective values systematically*. Most fire risk ranking methods rely heavily on experienced judgment. The use of formalized, documented procedures, such as the multiattribute utility theory, analytic hierarchy process, and Delphi process, significantly increases credibility of the system. Similarly, use of recognizable scaling techniques will enhance credibility.

Criterion 6 *Attribute values should be maintainable*. One variable that is not explicitly included in fire risk ranking, but which is very important, is time. It influences the fire risk both internally (e.g., deterioration) and externally (e.g., technological developments). In order for a method to have a reasonable, useful lifetime, it must be amenable to updating. This requirement implies that the procedure for generating attribute values must be repeatable. Changes over time and new information dictate that the system facilitate revisions.

Criterion 7 *Treat attribute interaction consistently*. In the majority of cases, treating attribute interaction consistently will consist of an explicitly stated assumption of no interaction among attributes. Where interactions are considered, it is important that they be dealt with systematically to avoid bias.

Criterion 8 *State the linearity assumption*. Although the linearity assumption is universal

in fire risk ranking, it is also well known that fire risk variables do not necessarily behave in a linear fashion. It is important to the acceptance of ranking methods and their limitations that such assumptions are understood.

Criterion 9 *Describe fire risk by a single indicator*. The objective of most fire risk ranking methods is to sacrifice details and individual features for the sake of making the assessment easier. Information should be reduced to a single score, even in the most complex applications. The results should be presented in a manner that makes their significance clear in a simple and unambiguous way. Unless all those involved can understand and discuss the meaning of the ranking, there will not be general confidence in its adequacy.

Criterion 10 *Evaluate predictive capability*. Some attempt should be made to verify that the method does in fact differentiate between lesser and greater fire risks with sufficient precision. It is not feasible to validate a model per se, but some testing should be documented. The American Society for Testing and Materials [67] gives some guidance on this subject. The level of accuracy demanded here is not the same as for other engineering purposes, and establishing an order of magnitude will generally suffice.

Computer Models for Fire Risk Indexing

In most cases, a fire risk index can be readily implemented on a typical computer spreadsheet. However, several software packages or programs have been developed to facilitate optimization, file management, and extensions of fire risk indexing methods. The following programs are presented as illustrative examples and do not constitute an exhaustive list.

ALARM 1.0 (Alternative Life Safety Analysis for Retrofit Cost Minimization) is a PC software tool that helps decision makers in health care facilities to achieve cost-effective compliance with the *Life Safety Code* [68, 69]. The program is based on earlier work by Chapman and Hall [30–35]. It uses a mathematical optimization algorithm called linear programming to quickly evaluate all possible code compliance solutions and identify the least-cost means of achieving compliance. ALARM 1.0 generates a set of options from which the most appropriate code compliance strategy based on cost and design considerations can be selected. Also listed—for both individual zones and the entire building—are up to 20 alternative, low-cost compliance plans and the prescriptive solution for benchmarking purposes. The software includes the integrated code compliance optimizer, full-screen data editor, and file manager.

ALARM 2.0 is a follow-up to ALARM 1.0 that is specific to life safety analysis of detention and correctional occupancies corresponding to Chapter 5 of NFPA 101A [70]. It allows users to enter data about the physical dimensions of a prison facility through an interface that mirrors the main worksheet of NFPA 101A. The program then applies its cost algorithms and unit cost data to estimate the cost of each safety improvement to be considered. The cost estimates automatically vary by facility location using the built-in geographic area cost factors of the nearest major city. Finally, the software quickly finds the most cost-effective construction plan for achieving compliance with the *Life Safety Code*.

COFRA (Central Office Fire Risk Assessment) is a proprietary computer program that assesses risk in telephone central office facilities [71]. Two incidents in the last decade have shown the potential severity of a fire that causes interruption of a telecommunications network. Conformance with fire safety code requirements does not adequately address the susceptibility of critical equipment or service continuity. Initial evaluation of this issue revealed that significant conflicts existed among demands for technical accuracy, ease of use, and implementation cost. This evaluation led to the development of a fire risk indexing method for the assessment of telecommunications network integrity. The approach uses a multiattribute evaluation model to determine the potential contributions to fire risk from individual fire safety attributes of a

facility space [47, 48]. Weights for the identified attributes were developed systematically from fire safety policy, objectives, and strategies. Methods were constructed to grade the attributes from onsite survey information. Principles of the Delphi process, decision tables, analytic hierarchy process (AHP), and other techniques of decision analysis were used in the development of attribute weights and grading methods. The scalar product of the attribute weights and grades produces a relative measure of the fire risk to integrity of a communications network. This program is presently an unsupported product of Telcordia Technologies.

EFSES (Enhanced Fire Safety Evaluation System for Business Occupancies) [72, 73] is a PC-based computer implementation of Chapter 8 in NFPA 101A and has been adopted as Chapter 9 of NFPA 101A. The PC-based software automates the calculation process and forms generation. Also, it provides the user with guidance and online help in making the decisions involved in completing the FSES. The help screens provide background information and reference material to assist the user in choosing attribute values. Another enhancement allows the user to interpolate between attribute values in the worksheet table. The program also allows "refinement calculations" that consider attributes in more depth. For example, the construction refinement calculation uses Law's fire severity calculation to estimate the fire duration in the worst-case space in the building. If this result is less than the fire resistance of the building's structural elements, then the attribute value can be increased. The program is distributed through NFPA and can be downloaded and installed from ftp://209.21.183.33/efsesinstall.exe, where the EFSES user manual is online in PDF format.

FREM (Fire Risk Evaluation Model) is Windows-based software that calculates a simplified assessment of fire risk associated with a given building [74, 75]. FREM follows the general approach of the Gretener method [13]. Developed by National Risk Control Services in Australia, the program was sold to Gallagher Basset Services, Inc., in Itasca, Illinois, in 1996.

RiskPro is another model based on the Gretener method [13] that was also developed in Australia [76]. It incorporates a database of input values for more than 400 typical occupancies.

The software tool Dow Indices [77] uses the Dow Fire and Explosion Index [17] in an interactive, computer-based environment to identify hazards associated with the storage and use of flammable and explosive materials in a chemical plant. The program includes a library of chemicals, online help, and a variety of visual tools to determine the dominant contributors to the overall hazard. The Dow Indices tool can be linked to existing chemical process simulators through the Visual Basic programming platform. In addition, the software can be coupled with economic evaluators, such as a cash flow analysis, using the maximum probable property damage and business interruptions loss predicted by the index. The American Institute of Chemical Engineers (AIChE) is currently reviewing the program for marketing opportunities.

Summary

Fire risk indexing systems have become common because of their high utility and relative ease of application. Fire safety evaluation involves a large number of ill-defined factors that are hard to assess in a uniform and consistent way. Analysis of such a complex system is difficult but not impossible, as evidenced by activities in the fields of nuclear safety and environmental protection. More detailed risk assessment can be an expensive and labor-intensive process that is sometimes not transparent. A fire risk index can provide a cost-effective means of fire safety evaluation that is sufficient in both utility and validity. Additional information can be found in Chapter 13 of Rasbash et al. [78].

References

1. J.M. Watts, Jr., "Index Approach to Quantifying Risk," in *Proceedings—SFPE Symposium on Risk, Uncertainty, and Reliability in Fire Protection Engineering,* Society of Fire Protection Engineers, Bethesda, MD (1999).
2. J.M. Watts, Jr., "Fire Risk Assessment Using Multiattribute Evaluation," in *Fire Safety Science—Proceedings of the 5th International Symposium,* International Association for Fire Safety Science (1997).
3. H.E. Nelson, "Overview—Numerical Grading Systems," *Report from the 1987 Workshop on Analytical Methods for Designing Buildings for Fire Safety,* Building Research Board, National Academy Press, Washington, DC (1988).
4. J.M. Watts, Jr., "Fire Risk Rating Schedules," in *ASTM STP1150, Fire Hazard and Fire Risk Assessment* (M.M. Hirschler, ed.), American Society for Testing and Materials, Philadelphia, pp. 24–34 (1992).
5. *Tools for Making Acute Risk Decisions with Chemical Process Safety Applications,* American Institute of Chemical Engineers, New York, p. 35 (1994).
6. G.R. Rosenblum and S.A. Lapp, "The Use of Risk Index Systems to Evaluate Risk," in *Risk Analysis: Setting National Priorities, Proceedings of the Society for Risk Analysis,* Society for Risk Analysis, McLean, VA (1987).
7. *Report from the 1987 Workshop on Analytical Methods for Designing Buildings for Fire Safety,* Building Research Board, National Academy Press, Washington, DC (1988).
8. J.H. Magee and D.L. Bickelhaupt, *General Insurance,* Richard D. Irwin, Homewood, IL, p. 153 (1964).
9. A.F. Dean, *Analytic System for the Measurement of Relative Fire Hazard,* Western Actuarial Bureau, Chicago (1902).
10. J.S. Glidden, *Analytic System for the Measurement of Relative Fire Hazard, an Explanation,* Western Actuarial Bureau, Chicago, p. 17 (1916).
11. *Specific Commercial Property Evaluation Schedule,* Insurance Services Office, New York (1990).
12. BVD, *Evaluation of Fire Hazard and Determining Protective Measures,* Association of Cantonal Institutions for Fire Insurance (VKF) and Fire Prevention Service for Industry and Trade (BVD), Zurich, Switzerland (1973).
13. M. Fontana, "Swiss Rapid Risk Assessment Method, Institute of Structural Engineering," *SIA 81,* ETH, Zurich, Switzerland (1984).
14. J. Kaiser, "Experiences of the Gretener Method," *Fire Safety Journal,* 2, pp. 213–222 (1980).
15. J.C. Valente, "The Evaluation of the Fire Safety Level in a Historic Centre in Lisbon," in *Proceedings, International Conference on Fire Protection of Cultural Heritage* (K.K. Papaioannou, ed.), Aristotle University of Thessaloniki, Greece, pp. 225–234 (2000).
16. Dow Chemical Company, "Process Safety Manual," *Chemical Engineering Progress,* 62, 6 (1966).
17. Dow Chemical Company, *Dow's Fire and Explosion Index Hazard Classification Guide,* 7th ed., American Institute of Chemical Engineers, New York (1994).
18. N.E. Scheffler, "Improved Fire and Explosion Index Hazard Classification," *AICHE Spring National Meeting* (1994).
19. Center for Chemical Process Safety, *Guidelines for Chemical Process Quantitative Risk Analysis,* American Institute of Chemical Engineers, New York, p. 32 (1989).
20. NFPA 704, *Standard System for the Identification of the Hazards of Materials for Emergency Response,* National Fire Protection Association, Quincy, MA, 2007 edition.
21. NFPA 49, *Hazardous Chemicals Data,* National Fire Protection Association, Quincy, MA, 1994 edition.
22. NFPA 325, *Fire Hazard Properties of Flammable Liquids, Gases, and Volatile Solids,* National Fire Protection Association, Quincy, MA, 1994 edition.
23. P172-2E, *Occupational Safety Report Guideline for Compilation,* Directorate-General of Labour of the Ministry of Social Affairs and Employment, Voorburg, The Netherlands (1990).
24. J. Lewis, "The Mond Fire Explosion, and Toxicity Index—A Development of the Dow Index," paper presented at the AIChE Loss Prevention Symposium, Houston, TX, April 1–5, 1979.
25. *The Mond Index,* 2nd ed., Imperial Chemical Industries (ICI) PLC, Explosion Hazards Section, Technical Department, Winnington, UK (1985).
26. I.A. Benjamin, "A Firesafety Evaluation System for Health Care Facilities," *Fire Journal,* 73, 2 (1979).
27. H.E. Nelson and A.J. Shibe, "A System for Fire Safety Evaluation of Health Care Facilities," *NBSIR 78-1555,* Center for Fire Research, National Bureau of Standards, Washington, DC (1980).
28. NFPA *101®*, *Life Safety Code®*, National Fire Protection Association, Quincy, MA, 2000 edition.
29. NFPA 101A, *Guide on Alternative Approaches to Life Safety,* National Fire Protection Association, Quincy, MA (2001).
30. R.E. Chapman, "Cost-Effective Methods for Achieving Compliance to Firesafety Codes," *Fire Journal,* 73, pp. 30–39, 123 (1979).
31. R.E. Chapman, W.G. Hall, and P.T. Chen, "Economic Aspects of Fire Safety in Health Care Facilities: Guidelines for Cost-Effective Retrofits," *NBSIR 79-1902,* National Bureau of Standards, Washington, DC (1979).
32. R.E. Chapman, W.G. Hall, and P.T. Chen, "A Computerized Approach for Identifying Cost-Effective Fire Safety Retrofits in Health Care Facilities," *NBSIR 79-1929,* National Bureau of Standards, Washington, DC (1980).

33. R.E. Chapman and W.G. Hall, "Code Compliance at Lower Costs: A Mathematical Programming Approach," *Fire Technology,* 18, 1, pp. 77–89 (1982).
34. R.E. Chapman and W.G. Hall, "User's Manual for the Fire Safety Evaluation System Cost Minimizer Computer Program," *NBSIR 83-2796,* National Bureau of Standards, Washington, DC (1983).
35. R.E. Chapman and W.G. Hall, "Programmer's Manual for the Fire Safety Evaluation System Cost Minimizer Computer Program," *NBSIR 83-2749,* National Bureau of Standards, Washington, DC (1983).
36. H.E. Nelson, "Fire Safety Evaluation System for NASA Office/Laboratory Buildings," *NBSIR 86-3404,* National Bureau of Standards, Gaithersburg, MD (1986).
37. J.M. Watts, Jr., "Analysis of the NFPA Fire Safety Evaluation System for Business Occupancies," *Fire Technology,* 33, 3, pp. 276–282 (1997).
38. *The BOCA National Building Code,* Building Officials and Code Administrators International, Country Club Hills, IL (1996).
39. *International Building Code,* International Code Council, Whittier, CA (2000).
40. J.M. Watts, Jr., "Fire Risk Evaluation in the Codes: A Comparative Analysis," in *Proceedings—Second International Conference on Fire Research and Engineering,* Society of Fire Protection Engineers, Bethesda, MD, pp. 226–237 (1998).
41. "Chapter ILHR 70, Historic Buildings," in *Wisconsin Administrative Code,* Department of Industry, Labor, and Human Relations, Madison, WI (1995).
42. *Fire Safety Evaluation (Points) Scheme for Patient Areas Within Hospitals,* Department of Fire Safety Engineering, University of Edinburgh, Scotland (1982).
43. P. Stollard, "The Development of a Points Scheme to Assess Fire Safety in Hospitals," *Fire Safety Journal,* 7, 2, pp. 145–153 (1984).
44. E. Marchant, "Fire Safety Engineering—A Quantified Analysis," *Fire Prevention,* 210, pp. 34–38 (1988).
45. T.J. Shields and G.W. Silcock, "An Application of the Hierarchical Approach to Fire Safety," *Fire Safety Journal,* 11, 3, pp. 235–242 (1986).
46. H.A. Donegan, T.J. Shields, and G.W. Silcock, "A Mathematical Strategy to Relate Fire Safety Evaluation and Fire Safety Policy Formulation for Buildings," in *Fire Safety Science—Proceedings of the 2nd International Symposium (*Takao Wakamatsu et al., eds.), Hemisphere, New York, pp. 433–441 (1989).
47. L.L. Parks, B.D. Kushler, M.J. Serapiglia, L.A. McKenna, Jr., E.K. Budnick, and J.M. Watts, Jr., "Fire Risk Assessment for Telecommunications Central Offices," *Fire Technology,* 34, 2, pp. 156–176 (1998).
48. E.K. Budnick, L.A. McKenna, Jr., and J.M. Watts, Jr., "Quantifying Fire Risk for Telecommunications Network Integrity," in *Fire Safety Science—Proceedings of the 5th International Symposium,* International Association for Fire Safety Science, London, UK, pp. 691–700 (1997).
49. T.J. Shields, G.W. Silcock, and Y. Bell, "Fire Safety Evaluation of Dwellings," *Fire Safety Journal,* 10, 1, pp. 29–36 (1986).
50. F.J. Dodd and H.A. Donegan, "Prioritization Methodologies in Fire Safety Evaluation," *Fire Technology,* 30, 2, pp. 232–249 (1994).
51. NFPA 550, *Guide to the Fire Safety Concepts Tree,* National Fire Protection Association, Quincy, MA, 2002 edition.
52. R.T. Eckenrode, "Weighting Multiple Criteria," *Management Science,* 12, pp. 180–192 (1965).
53. C.L. Hwang and K. Yoon, *Multiple Attribute Decision Making: Methods and Applications,* Springer-Verlag, New York (1981).
54. T.L. Saaty, *The Analytic Hierarchy Process,* John Wiley, New York (1980).
55. T.L. Saaty, *Multicriteria Decision Making: The Analytic Hierarchy Process,* RWS Publications, Pittsburgh (1990).
56. J.M. Watts, Jr., E.K. Budnick, and B.D. Kushler, "Using Decision Tables to Quantify Fire Risk Parameters," in *Proceedings, International Conference on Fire Research and Engineering* (D.P. Lund, ed.), Society of Fire Protection Engineers, Boston, pp. 241–246 (1995).
57. J.M. Watts, Jr., and M.E. Kaplan, "Fire Risk Index for Historic Buildings," *Fire Technology,* 37, 1 (2001).
58. M.E. Kaplan and J.M. Watts, Jr., "A Prototypical Fire Risk Index to Evaluate Fire Safety in Historic Buildings," *APT Bulletin,* 30, 2–3, pp. 49–55 (1999).
59. S.M. Lo, "A Fire Safety Assessment System for Existing Buildings," *Fire Technology,* 35, 2, pp. 131–152 (1999).
60. L.T. Wong and S.W. Lau, "A Fire Safety Evaluation System for Prioritizing Fire Improvements in Old High-Rise Buildings in Hong Kong," *Fire Technology*, 43, 3 pp. 233–249 (2007).
61. A.G. Copping, "Fire Safety Evaluation Procedure for the Property Protection of English Parish Churches: A Tool to Aid Decision Making," in *Proceedings, International Conference on Fire Protection of Cultural Heritage,* Aristotle University of Thessaloniki, Greece, pp. 255–268 (2000).
62. S.E. Magnusson and T. Rantatalo, "Risk Assessment of Timberframe Multistorey Apartment Buildings: Proposal for a Comprehensive Fire Safety Evaluation Procedure," *IR 7004,* Department of Fire Safety Engineering, Lund University, Sweden (1998).
63. H. Hultquist and B. Karlsson, "Evaluation of a Fire Risk Index Method for Timber-Frame, Multi-Storey Apartment Buildings," *Report 31XX,* Department of Fire Safety Engineering, Lund University, Sweden (2000).
64. J.M. Watts, Jr., "Criteria for Fire Risk Ranking," in *Fire Safety Science—Proceedings of the 3rd International Symposium* (G. Cox and B. Langford, eds.), Elsevier, London, pp. 457–466 (1991).

65. S.I. Gass, "Documenting a Computer Based Model," *Interfaces,* 14, 3, pp. 84–93 (1984).
66. ASTM, *ASTM* E1472, *Documenting Computer Software for Fire Models,* American Society for Testing and Materials, Philadelphia (1998).
67. ASTM, *ASTM* E1355, *Evaluating the Predictive Capability of Deterministic Fire Models,* American Society for Testing and Materials, Philadelphia (1992).
68. S.F. Weber and B.C. Lippiatt, "Cost-Effective Compliance with Life Safety Codes," *Fire Technology,* 32, 4, pp. 291–296 (1996).
69. S.F. Weber and B.C. Lippiatt, "ALARM 1.0, Decision Support Software for Cost-Effective Compliance with Fire Safety Codes," *NISTIR 5554,* National Institute of Standards and Technology, Gaithersburg, MD (1994).
70. S.F. Weber and L.I. Schultz, "ALARM 2.0 Users Manual: Minimizing Compliance Costs of the Life Safety Code for Prisons," *NISTIR 6807*, National Institute for Standards and Technology, Gaithersburg, MD (2001).
71. L.L. Parks, "COFRA-2: A Tool to Aid in Telecommunications Central Office Fire Risk Assessment," in *Proceedings, Fire Risk and Hazard Assessment Symposium,* National Fire Protection Research Foundation, Quincy, MA, pp. 523–540 (1996).
72. Hughes Associates, Inc., "Fire Safety Evaluation System (FSES) for Business Occupancies Software (Version 1.0 for Windows) User's Manual," *NIST-GCR-96-692,* National Institute of Standards and Technology, Gaithersburg, MD (1996).
73. Hughes Associates, Inc., *Enhanced Fire Safety Evaluation System for Business Occupancies Software,* Version 1.2, Hughes Associates, Inc., Baltimore (1999).
74. *FREM for Windows, User's Manual,* National Risk Control Services Pty. Ltd., Bayswater, Victoria, Australia (1995).
75. J.M. Watts, Jr., "Fire Risk Evaluation Model" (review), *Fire Technology,* 31, 4, pp. 369–371 (1995).
76. *RiskPro,* SimCo Consulting, Wantirna South, Victoria, Australia (2000).
77. P.B. Parikh and D.A. Crowl, "Implementation and Application of the Dow Hazard Evaluation Indices in a Computer-Based Environment," in *Proceedings: International Conference and Workshop on Reliability and Risk Management, San Antonio, TX,* American Institute of Chemical Engineers, New York, pp. 65–83 (1998).
78. D.J. Rasbash, G. Ramachandran, B. Kandola, J.M. Watts, Jr., and M. Law, *Evaluation of Fire Safety,* John Wiley, London (2004).

John M. Watts Jr. is retired from his position as director of the Fire Safety Institute, which he founded and which closed upon his retirement. He remains active in several fields of fire safety research.

Risk-Informed Industrial Fire Protection Engineering

83

Thomas F. Barry

Introduction

Risk-informed fire protection evaluation is a risk-based decision support tool that evaluates fire and explosion consequence likelihood and includes an analysis of fire protection system (s) performance reliability [1].

The type of risk-based evaluation and level of detail should be dependent on the complexity of the risk and the needs of the decision maker. Table 83.1 lists three general levels of decisions to help decision makers choose an appropriate basis for their decisions [2, 3].

Based on the decision class, risk management goals, and risk-informed project objectives, the most efficient risk assessment and risk communication methods should be applied. The results must provide the information needed to make informed fire protection decisions based on risk tolerance and cost-effectiveness.

The risk-informed evaluation framework, presented in Fig. 83.1, includes the following:

- Hazard evaluation
- Consequence analysis
- Fire risk evaluation method selection
- Risk-reduction decision making
- Risk monitoring

The purpose of this chapter is to provide an overview of fire risk-informed evaluation methods. References are included to allow the reader to pursue further detail. Emphasis is given to the fire risk evaluation method called fire protection system–layer of protection analysis (FPS-LOPA), which is becoming a popular approach for evaluating industrial process fire and explosion risks. An example FPS-LOPA is included in the chapter.

Hazard Evaluation

All fire risk-informed methods start with hazard evaluation and consequence analysis. Risk-informed approaches supplement these evaluations but do not replace them.

The purpose of a hazard evaluation is to identify and analyze the hazards, identify initiating events and scenarios, and provide appropriate documentation. A hazard evaluation can be conducted in any stage of design, operation, or decommissioning. In industrial applications, there are generally the following three types of hazard evaluations:

1. Process hazard analysis (PHA) using techniques such as the following:
   - Hazard and operability analysis (HAZOP)
   - What-if analysis
   - What-if checklists [2]
2. Fire hazard analysis (FHA)
3. Special analysis
   - Failure modes and effects analysis (FMEA)
   - Human reliability analysis (HRA)

T.F. Barry (✉)
Risk and Reliability Services for HSB Global Standards

M.J. Hurley (ed.), *SFPE Handbook of Fire Protection Engineering*,
DOI 10.1007/978-1-4939-2565-0_83, © Society of Fire Protection Engineers 2016

Table 83.1 Decision class and fire risk assessment approach

Decision class	Decision context	Fire risk assessment approach	Remarks
Class A	Nothing new or unusual	Codes and standards	Easiest to apply, generally uses qualitative risk analysis
	Well-understood risk	Good practice	
	Established risk	Engineering judgment	
Class B	Life cycle implications	Fire protection system–layer of protection analysis (FPS-LOPA), which provides order-of-magnitude risk estimates based on specific cause-consequence scenarios	Simplified quantitative risk-informed evaluation methods are gaining popularity in the industry
	Some risk trade-offs		
	Some uncertainty or deviation from standard or best practice		
	Economic implications		
Class C	Very novel or challenging	Quantitative risk assessment (QRA), which provides additional detail regarding event, contributing factors, risk reduction options, and cost-benefit analysis	Most demanding on resources and skill sets but delivers most detailed understanding and best decision basis if major expenditures are involved
	Significant risk trade-offs		
	Large uncertainties		
	Strong stakeholder views or perceptions		

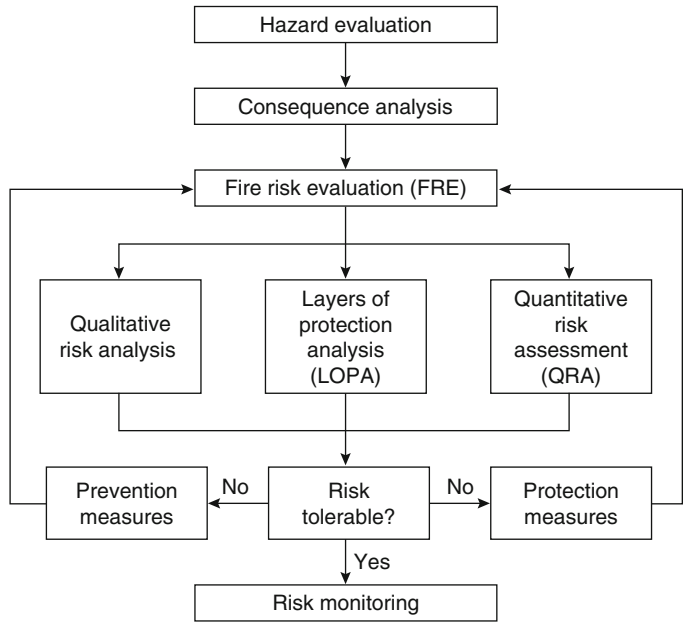

Fig. 83.1 Risk-informed evaluation framework

The most common hazard analysis and documentation techniques employed for industrial processes are what-if analysis and HAZOP. What-if analysis provides an adequate evaluation method for processes that are not highly complex and for processes that require a fair degree of operator monitoring and intervention. In general, for more complex processes, hazard and operability analysis (HAZOP) is typically used. For specific equipment failure mode analysis, failure mode and effect analysis (FMEA) is often used in combination with HAZOP or what-if analysis. Human reliability analysis is applied when operator actions are a critical component in the hazard evaluation. These methods are described in detail in *Guidelines for the Hazard Evaluation Procedures with Examples*, [4] Lees, [5] and Sutton [6].

Fire hazard analysis (FHA) specifically focuses on fire and explosion hazards, protection

features, scenarios, life safety, and property exposures, with fire protection recommendations. Numerous chapters in the *SFPE Fire Protection Engineering Handbook* and NFPA *Fire Protection Handbook*®, [7] Schroll, [8] and Zalosh [9] provide further information on industrial fire and explosion hazards.

Consequence Analysis

Consequence analysis is the process of determining the impact of initiating event scenarios to a defined target or targets independent of frequency and probability. Consequence analysis approaches range from the use of loss experience and historical data (e.g., plant or companywide loss experience, industry incident data, applicable generic accident data) to the application of deterministic fire and explosion models. Depending on consequence analysis complexity, models can range from the use of spreadsheet fire dynamics equations to zone models to computational fluid dynamics (CFD) models. In many cases consequence analysis involves a hybrid approach using available historical incident data, modeling tools, and engineering judgment to derive a consequence category.

Fire and explosion consequence analysis generally involves the evaluation of the following two segments:

- The rate of development of a hazardous environment (intensity, distance, time) within the boundaries of the predicted hazardous event, sometimes called the hazard footprint, hazard or consequence envelope, or consequence boundary. This is generally known as a physical effects severity measure. Physical effects can include thermal, combustion products, and/or overpressure effects.
- The susceptibility or vulnerability of people to harm; physical damage to equipment, stock, or structures; production downtime or business interruption; environmental damage; or other indirect losses such as loss of customers, regulator penalties or fines, or an overall financial impact estimate. This is generally known as a vulnerability measure. Overall vulnerability may be affected by variables such as the potential number of people present, evacuation capabilities, contingency plans to minimize business interruption, and so on.

When estimating consequence vulnerabilities levels for understanding by management decision makers, simplicity and consistency are key aspects. Whether it is a qualitative consequence analysis provided by a fire protection engineer or explosion expert or a deterministic first- or second-order modeling effort, the use of consequence categories provides a consistent approach and is a good risk management communication tool.

Life safety exposure and consequence levels can be broken down into categories related to injury or fatality potential to operators, employees, on-site contractors, and off-site exposure to the public. Table 83.2 presents a general example of establishing life safety exposure and consequence levels [1].

Property damage impact levels can also be broken down into categories as shown in Table 83.3 [1].

Consequence categories can also be set up for production downtime, environmental damage potential, and other various direct and indirect financial impacts, regulatory penalties or fines, media reaction, and/or loss of customers, financial (economic) impact, and so on [1].

Target threshold damage limits are generally used to provide the link between physical effects (thermal effects, products of combustion,

Table 83.2 Example life safety exposure categories

Life safety exposure	General definition	Remarks
1—Low	First aid (minor injury associated with fighting fires or evacuation)	
2—Moderate	Single-person injury requiring hospital treatment	
3—Heavy	Multiple-person injuries requiring hospital treatment	
4—High	Life-threatening injury or death on-site	
5—Major	Life-threatening injury or death off-site	

Table 83.3 Example property damage impact categories

Property damage levels	Damage factor range (%)	General definition	Remarks
1—Slight	0–1	Limited localized minor damage, not requiring repair	
2—Light	1–10	Significant localized damage of some components, generally not requiring major repair	
3—Moderate	10–25	Significant localized damage of many components warranting repair	
4—Heavy	25–60	Extensive process equipment damage requiring major repairs	
5—Major	60–100	Major widespread damage including major structural damage	

explosion overpressure, domino effects such as chemical or radiological releases, etc.), which are usually derived from fire and explosion modeling and potential end consequences (life safety injuries or fatalities, property damage, production downtime, environmental impacts, etc.). Fire and explosion modeling techniques are discussed in many chapters of the *SFPE Fire Protection Engineering Handbook*, as well as elsewhere [1, 5, 10–12].

Fire Risk Evaluation Method Selection

Risk is the product of the expected frequency (events/year) and consequences (effects/event) of a single accident or group of accidents. The equation is generally shown as

$$\text{Risk}_{\text{accident scenario}} = \text{Event frequency} \times \text{Expected consequences}(s)$$

For a group of accident scenarios, which could affect a defined target area, the equation can be expressed as

$$\text{Risk} = \sum_{\text{scenarios}} \text{Event frequency} \times \text{Expected consequences(s)}$$

In fire risk-informed evaluations we are concerned with how the performance of fire protection systems mitigates an existing risk level. Mitigated risk requires the evaluation of the following three components:

- Frequency or likelihood of the initiating event
- Probability of the failure of fire protection system performance
- Expected consequence(s)

The risk associated with the potential realization of an undesirable consequence level, taking the performance of fire protection systems into account, can be shown as

$$\text{Risk}_{\text{accident scenario}} = \text{Initiating event frequency} \times \text{Probability of FPS performance failure} \times \text{Expected consequence(s)}$$

The three primary risk methods or risk assessment techniques that are addressed in this chapter include the following:

- Qualitative risk analysis (for Class A decisions)
- Fire protection system–layer of protection analysis (for Class B decisions)
- Quantitative risk assessment (for Class C decisions)

Class A Decisions: Qualitative Risk Analysis

Qualitative risk analysis is an extension of the hazard evaluation and consequence analysis, and is primarily conducted for risk screening, risk ranking, and recommendation prioritization activities. Basis can be unmitigated risk,

Table 83.4 Example event likelihood categories

Likelihood	General definition
1—Very low	Very remote possibility of occurrence (e.g., 1/300 to 1/1000 years)
2—Low	Possibility of occurrence once over two to three times the useful life of the process (e.g., 1/100 years)
3—Moderate	Possibility of occurrence once over the lifetime of the process (e.g., 1/30 years)
4—High	Possibility of occurrence once per average process life cycle (e.g., 1/15 years)
5—Very high	Occasional possibility of occurrence (e.g., 1/5 years)

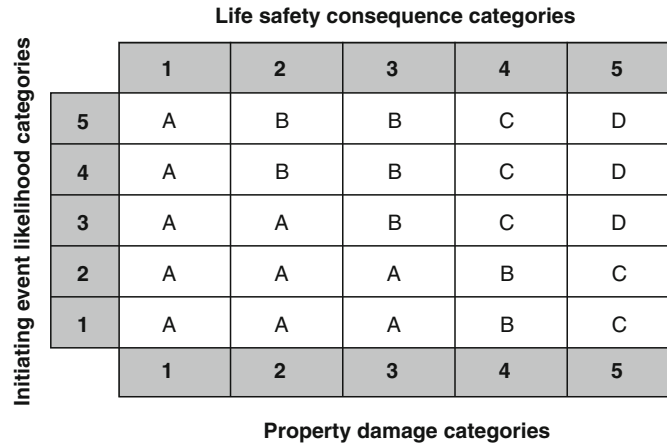

Fig. 83.2 Risk classification screening matrix

Table 83.5 Risk classification actions

Risk class	General description	Actions
A	Low-risk events	Require no further risk reduction actions
B	Low- to moderate-risk events	Require minor risk reduction improvements; generally addressed by codes, standards, industry practices, and engineering judgment
C	Moderate- to high-risk events	Require further analysis to determine an optimal risk reduction strategy or analysis of the performance and reliability of risk controls
D	High-risk events	Require immediate risk reduction analysis

mitigated risk, or both to show the relative change in risk with mitigation measures.

This method normally employs the following:

- Consequence category tables (refer to example Tables 83.2 and 83.3)
- Event likelihood category tables (refer to example Table 83.4)
- Risk classification matrix (refer to Fig. 83.2)
- Associated risk class action matrix (refer to Table 83.5)

Table 83.4 provides an example of likelihood categories [1].

Figure 83.2 presents an example of a risk classification table. In this particular example, life safety consequences and property damage categories are labeled on the same matrix for illustration purposes.

Table 83.5 presents an example of a risk class action table. This table lists action items associated with the risk classifications presented in Fig. 83.2.

Qualitative risk methods usually employ consequence categories, event likelihood ranges with qualitative descriptors, and simplified risk matrix–action item tables.

Team members' experience with similar events will have a major impact on their judgment. It is sometimes difficult to visualize and judge the risk of events that have not occurred at the plant. Uncertainty in risk judgments seems to

increase for more complex scenarios and moderate to high consequences in terms of how much credit should be given to risk mitigation measures (i.e., fire protection systems). Because of this uncertainty, many scenarios fall into a risk classification action (such as Risk Class C in Table 83.5), which recommends further detailed risk analysis (i.e., may lead to a resource-intensive QRA). Therefore, it was clear to the chemical process industry that an intermediate risk analysis method was needed, one that provided additional information on the performance of independent risk reduction measures as related to specific scenarios. This spurred the development of layer of protection analysis (LOPA), which is discussed next.

Class B Decisions: FPS-LOPA

FPS-LOPA Basics

Fire protection system–layer of protection analysis (FPS-LOPA) goes beyond the typical use of a qualitative risk matrix but is less detailed than quantitative risk analysis (QRA). FPS-LOPA provides an order-of-magnitude risk analysis tool. It addresses the fire risk mitigation equation by separating the question of "how likely is it?" into the following two components [13]:

- Likelihood (frequency) of the initiating fire event
- Probability of failure on demand (P_{fod}) of independent fire protection layers (IFPLs)

This method has proven to be an effective tool to determine whether there are enough protection layers and sufficient risk reduction to meet the risk tolerance criteria for scenarios developed from process hazard analysis (PHA) and fire hazard analysis (FHA) information. The method uses event tree logic in a table or spreadsheet format to assess moderate to high fire or explosion consequences in terms of the likelihood of occurrence. The initiating event likelihood and the probability of success of fire protection systems are evaluated quantitatively and compared to risk tolerance criteria to determine if additional fire protection layers are needed.

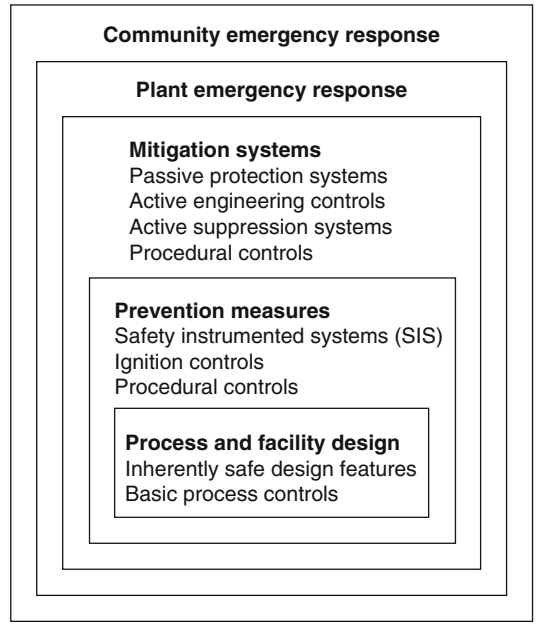

Fig. 83.3 Typical risk reduction layers at industrial facilities

Figure 83.3 illustrates typical risk reduction layers at industrial facilities.

Prevention measures can be defined as the act of causing an event not to happen and can include elimination of hazards, ignition source controls, and procedural methods such as combustible control measures.

Mitigation systems are related to measures that cause a consequence to be less severe and generally include passive protection systems, detection systems and active engineering controls, active suppression systems, and procedural systems.

- *Passive protection systems*. Systems that reduce consequences without the active functioning of any device, such as dikes, blast walls, fire barrier walls, and so on
- *Detection systems and active engineering controls*. Detection and alarms, controls, safety interlocks, and emergency shutdown systems designed to detect potentially hazardous process deviations, conditions, or equipment malfunctions and to take corrective action, including pressure relief devices; gas, smoke, and fire detection and alarm systems;

emergency shutdown systems; smoke exhaust/control systems, and so on
- *Active suppression systems*. Active suppression systems may include both automatic and manual systems: automatic systems may include sprinkler and water spray deluge systems, foam systems, gas extinguishing systems, and so on; manual suppression may include responses from operators, plant fire brigade, and public fire department
- *Procedural systems*. Operating procedures, administrative checks, plant site emergency responses, and other management approaches to minimize the severity of an incident

Discussions regarding the amount or layers of fire protection needed can result in heated debates when approached on a purely qualitative basis. Underprotection (too few layers) can potentially lead to loss of life, excessive property damage, and unexpected business interruption. Overprotection (too many layers) can lead to increased and unwarranted costs. Industrial plant risk management decision makers have to live within the constraints of available time, money, and resources. A common question is whether the company's money should be invested in prevention, mitigation, or emergency response. For example, if a system is designed to prevent a fire and provide passive mitigation features, then why are active mitigation features or additional plant fire brigade improvements necessary? Or if there is an active mitigation system, such as a sprinkler system, why are any additional fire protection features needed?

From a fire or explosion risk analyst's viewpoint, the degree of reason (need for mitigation layering) is based on the potential consequence levels, likelihood of realizing the consequences (risk level), confidence in the performance of fire protection measures (effectiveness, reliability), degree of human element involved in the scenario, and degree of risk tolerance. Inherently safe design and prevention measures should receive first attention and should be evaluated and documented through the process hazard analysis and fire hazard analysis to verify that the design features minimize the potential occurrence of a fire or explosion event.

Mitigation systems usually receive attention next and are evaluated in terms of independent fire protection layers (IFPLs): how much passive protection, how many active engineering controls, what type and how many active suppression systems, and how much procedural action will be needed. Emergency response from internally funded plant fire brigades generally receives next consideration along with public fire department response.

Several reasons not to rely on one type of fire protection, especially when dealing with uncertain fire or explosion risks, include the following:

1. No one independent fire protection system is perfect, meaning that 100 % performance, 100 % of the time is not possible.
2. Fire protection systems are subject to human error (e.g., fire door blocked open, etc.).
3. Arson or security breaches can compromise a fire protection system.
4. Inspection, maintenance, and testing deficiencies can reduce the performance reliability of a fire protection system.
5. Explosion overpressures can render a fire protection system inoperative.

These items should especially be kept in mind when developing a performance-based fire protection system design for moderate-high fire or explosion risks. This not only applies to industrial facilities but also should apply to high-rise buildings, health care facilities, airports, large assembly areas, and so on where the life safety consequences of a fire are high.

LOPA Definition and Steps

Layer of protection analysis (LOPA) defines risk as the likelihood of a specific consequence resulting from a postulated hazardous incident scenario. LOPA involves identifying initiating events, assessing existing or proposed layers of safety-related controls, and establishing tolerable frequency targets for people, property, or business interruption exposure. *Layers of Protection Analysis* [14] and Dowell [15] provide information on LOPA methods.

LOPA is a useful tool for prioritizing hazard scenarios and supporting risk-based decisions regarding the most cost-effective measures to meet risk tolerance criteria. LOPA is becoming a popular and widely used tool in the chemical, oil, gas, nuclear, and various high-tech industries. In the nuclear fuels processing industry a similar approach called risk indexing is required by the Nuclear Regulatory Agency as part of integrated safety assessments.

The Center for Chemical Process Safety (CCPS) book, *Layer of Protection Analysis, Simplified Process Risk Assessment*, states "The techniques of LOPA can be extended to most any type of risk reduction decision" [14]. LOPA methodology, whose most common application has been in the evaluation of the release of hazardous chemicals, is being applied more and more to postignition fire scenarios, pre- and postexplosion scenarios, and evaluation of emergency action plans following fire or explosion incidents. LOPA methods are also being applied to the evaluation of security failure scenarios, which could lead to terrorist-caused toxic material, fire, or explosion exposures. This type of evaluation is known as rings of protection analysis, the security equivalent of LOPA [16].

Fire protection system–layer of protection analysis (FPS-LOPA) is used in this chapter to focus on the evaluation of fire protection systems. FPS-LOPA provides a rational, objective, and simplified risk-based approach for decision making on the fire protection layers needed for specific scenarios to meet established risk tolerance criteria.

The steps involved in conducting an FPS-LOPA evaluation include the following:

1. Develop accident scenarios
2. Determine initiating fire event likelihood (events/year)
3. Quantify the performance of independent fire protection layers (IFPLs)
4. Evaluate target vulnerability
5. Estimate scenario risk
6. Conduct risk tolerance comparison
7. Make decisions on risk reduction
8. Monitor the risk

Step 1: Develop Accident Scenarios

Once a scenario has been identified and screened as a candidate for fire or explosion risk evaluation, it must be further developed and documented to a level where an understanding of the initiating events, enabling events, and independent fire protection layers (IFPLs) is achieved.

The primary components of FPS-LOPA scenario development are the following:

- Initiating event
- Enabling event(s)
- Independent fire protection system layer(s) (IFPLs)

FPS-LOPA follows an event tree calculation approach toward quantifying the likelihood of a specific cause-consequence scenario with a primary focus on the performance reliability (or probability of performance failure) of independent fire protection layers. Figure 83.4

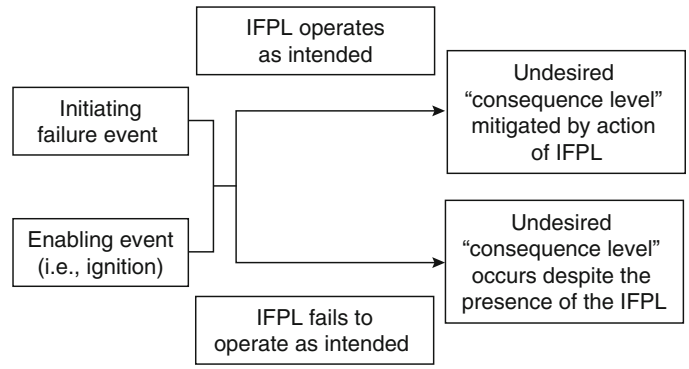

Fig. 83.4 Effect of IFPL failing to operate as intended

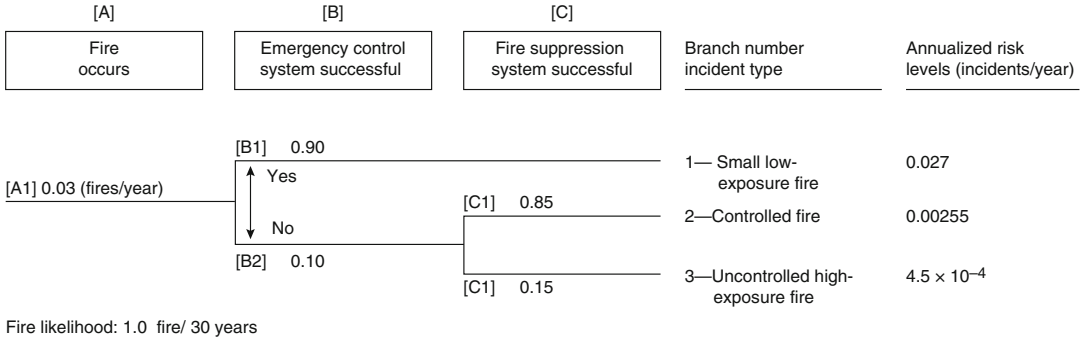

Fig. 83.5 Example of a simple fire event tree

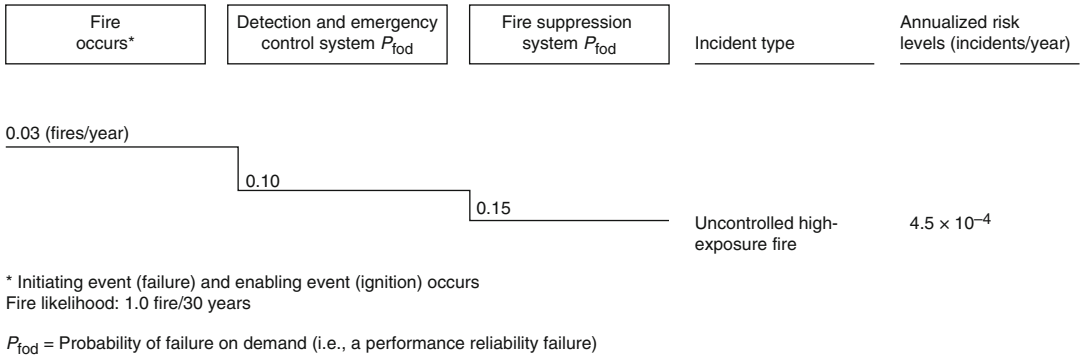

Fig. 83.6 Example of the correlation between a simple fire event tree and FPS-LOPA

illustrates an event tree showing the effect of IFPL success or failure.

As indicated, FPS-LOPA estimates the likelihood of an undesirable consequence occurring by applying a similar approach and calculation methods used in typical fire event tree analysis. As shown in Fig. 83.5, branch 3 logic indicates occurrence of an undesirable consequence in terms of an uncontrolled high-exposure fire. For this example, the likelihood of this event scenario occurring is predicated on failure of two independent protection layers: failure of (B) emergency control system, and failure of (C) fire suppression system.

The math in Fig. 83.5 for the uncontrolled high-exposure fire is as follows:

$$\begin{aligned}\text{Likelihood}_{\text{uncontrolled high-exposure fire}} &= (\text{A1}) \times (\text{B2}) \times (\text{C2}) = 0.03\,\text{fires/yr} \\ &\times 0.10 \times 0.15 = 4.5 \times 10^{-4}\,\text{events/yr}\end{aligned}$$

FPS-LOPA specifically focuses on the cause-consequence scenario pathway that leads to the high-exposure or high-consequence event, as shown in Fig. 83.6. In most cases it evaluates the likelihood of reaching that upper-bound credible or worst-case credible consequence.

Information extracted from hazard evaluations, including what-if analysis, HAZOP, fire hazard analysis, or insurance probable maximum loss reports, can form the basis for the FPS-LOPA cause-consequence scenario selection and development [1, 17].

Step 2: Determine Initiating Fire Event Likelihood

$$\begin{aligned}\text{Fire}_{\text{likelihood}} = {} & \text{Initiating event failure frequency} \\ & (\text{i.e., component failure, human error}) \times \\ & \text{Ignition probability (i.e., enabling event)}\end{aligned}$$

In most cases, when evaluating industrial processes, the primary component failure is viewed as the initiating event and ignition is the enabling event leading to a fire scenario. They are usually evaluated separately in terms of initiating event frequency and enabling event probability. In rare cases, applicable confident fire statistics may be available and can be input directly into the FPS-LOPA evaluation as the initiating fire event frequency.

For industrial FPS-LOPA evaluations, initiating events of concern are generally related to equipment component failures or human errors that cause the release or availability of flammable or highly combustible materials, which could lead to major fire or explosion incidents. These incidents usually present bounding-type scenarios in terms of people and property damage exposure.

Equipment component failure rates and human error data are extracted from plant-specific records, industry failure data, and/or generic failure databases. Table 83.6 presents an example of some equipment component failure rate ranges [14].

It is preferable to extract equipment component failure rate data from plant-specific data sources. The best sources of data are obtainable from operational and maintenance logs, other records, and interviews conducted with experienced plant personnel. Engineering judgments concerning the use and adjustment of these data can be based on plant surveys, available data, interviews, and experience. Some published failure rate data are provided in Barry, [1] *Guidelines for Process Equipment Reliability Data*, [18] *Guide to the Collection and Presentation of Electrical*, *Electronic*, *Sensing Component*, [19] and *Offshore Reliability Data Handbook* [20].

Human Error Human error probabilities are generally estimated from actual operating experience, task simulation, or expert opinion. Data derived from actual operating experience are best, but sufficient data may not be available. Expert opinion is acceptable and useful if a consistent methodology is applied within a team consensus framework. Based on review of numerous human error and human reliability references, Fig. 83.7 presents an example of human failure probability ranges for the following three cases [1]:

1. Unplanned emergencies (i.e., postfire or explosion)
2. Routine oversight (normal operations)
3. Error in operator judgment

Within each case (i.e., probability range) there is a midpoint range and upper and lower bounds that relate knowledge, experience, and training factors. How often an operation is performed, stress factors, and other relevant performance-shaping factors should also be considered. The important part in human error probability estimation is to recognize the contributing factors and to apply a credible and consistent evaluation method.

Enabling Event: Probability of Ignition Characterizing the probability of ignition following an equipment failure or human error scenario starts with the identification and understanding

Table 83.6 Example of some initiating event frequency ranges

Initiating event	Frequency range from literature (events/year)
Piping leak (10 % section)—100 m	10^{-3}–10^{-4}
Atmospheric tank failure	10^{-3}–0^{-5}
Gasket/packing blowout	10^{-2}–10^{-6}
Turbine/diesel engine overspeed with casing breach	10^{-3}–10^{-4}
Safety valve opening spuriously	10^{-2}–10^{-4}
Pump seal failure	10^{-1}–10^{-2}
Unloading/loading hose failure	1–10^{-2}
Basic process control system (BPCS) instrument loop failure	1–10^{-2}
Regulator failure	1–10^{-1}

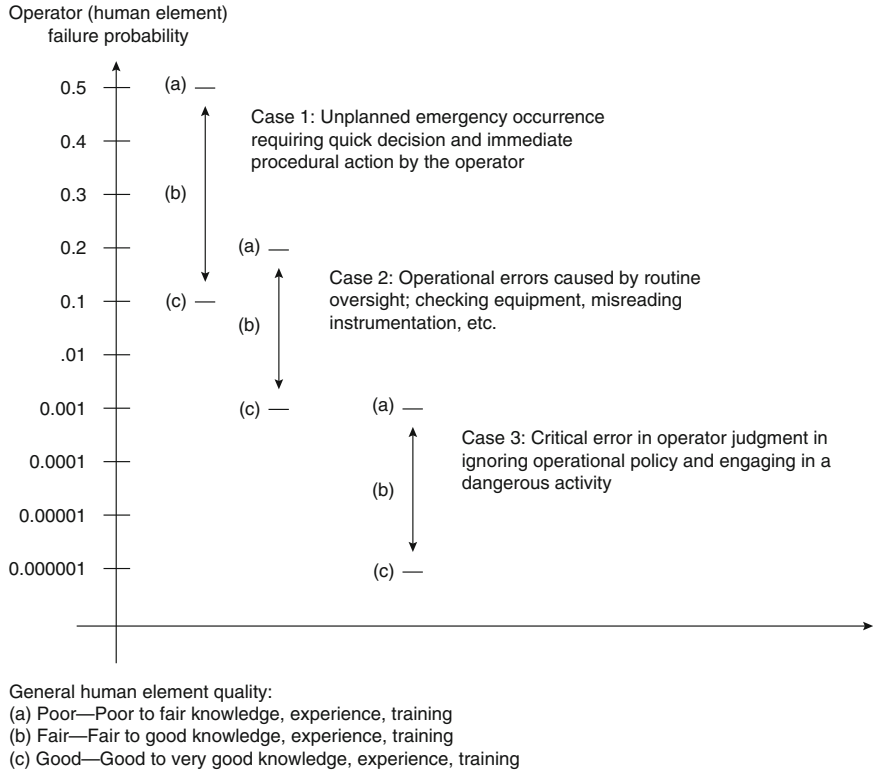

Fig. 83.7 Example of human failure probability ranges

of relevant ignition sources within the FPS-LOPA evaluation boundaries. This approach includes the following:

- Identifying ignition sources (fixed, mobile, variable) within defined exposure boundaries
- Evaluating ignition source strength (temperature, energy) in relation to the fuel's ignition sensitivity
- Estimating the frequency of time the ignition source is present

In addition to reviewing available historical fire incident data that may describe ignition factors for similar scenarios, a plant survey of the area under FPS-LOPA evaluation should be conducted to identify and evaluate specific ignition source potentials. Based on engineering review and evaluation, identified ignition sources can then be categorized in terms of availability, source strength, and ignition probability. Table 83.7 provides an example of ranking ignition source strengths in categories and relating ignition probability ranges [1].

Table 83.7 Example ignition source strength vs. ignition probability range

Ignition source strength ranking	Ignition probability ranges
Strong (S)	0.25–1.0
Medium (M)	0.05–0.24
Weak (W)	0.01–0.049

Support sources for ignition identification and availability (i.e., frequency that ignition source is present) include the following:

- Identification of plant specific ignition sources
  Plant survey
  Plant records
  Plant interviews
- Review of available industry or generic historical incident ignition data sources similar to the hazard/ignition potentials being evaluated
  Identification of major ignition contributing factors
  Ignition flame spread propagation potentials

Various sections in the *SFPE Fire Protection Engineering Handbook*, Lees, [5] and the NFPA *Fire Protection Handbook*, [7] provide information on ignition sources. *Ignition Handbook* [21] provides a comprehensive examination of ignition dynamics. Barry [1] provides information on characterizing potential ignition likelihood.

Step 3: Quantify the Performance of Independent Fire Protection Layers (IFPLs)

An independent fire protection layer (IFPL) is a device, system, or action that is capable of preventing a scenario from proceeding to the undesired consequence level regardless of the initiating event frequency or the action of any other fire protection layer associated with the scenario. In addition, the effectiveness and independence of an IFPL must be auditable. The audit process confirms that the IFPL design, installation, and functional testing and maintenance systems are in place to achieve the specified performance reliability for the IFPL [14].

In a standard LOPA evaluation, usually conducted for chemical process hazards, the focus is on measures to prevent a consequence, such as a toxic chemical release or explosion, via instrumentation, emergency isolation valves, pressure relief valves, and so on. A major assumption is that the protection safeguard is designed to perform its intended function in an effective manner and, therefore, only the operational reliability parameter is estimated [22].

Operational reliability is a measure of the probability that a protection system will operate as intended when needed. Performance reliability is a measure of the adequacy of the system to successfully perform its intended function under specific fire scenario conditions. Performance reliability, or the probability of success of a fire protection system to perform its functional performance objectives, includes both operational reliability and design effectiveness parameters.

The probability of failure of a fire protection system (P_{fod}) is the failure of the protection measure to perform its designed functional performance requirement to mitigate a scenario consequence. Fire protection systems are usually evaluated in terms of their probability of performance success (i.e., they performed their functional performance requirement as intended). The correlation here is

$$\text{Probability of success} = 1.0 - \text{Probability of failure}$$

For example, if the probability of failure due to design ineffectiveness, response time, unavailability, or operational reliability is estimated at 0.10, meaning that it may fail to perform its full functional requirements 1 out of 10 times, then the probability of success is estimated at 0.90, meaning that 9 out of 10 times it should perform successfully in meeting its functional performance requirements.

As fire protection systems (FPS) are mitigation systems, they must be viewed in terms of a performance-based reliability, which incorporates design effectiveness and operational reliability. In FPS-LOPA we are interested in the probability of success of an FPS meeting its functional performance objectives and are thus concerned with estimating the performance reliability. This is generally approached in the following ways:

1. Using historical operational reliability data (statistical data from plant records, industry data, generic databases, published equipment or component failure rate data tables) along with an analysis of the design effectiveness to meet the functional performance objectives for the specific FPS-LOPA scenario
2. Using an engineering assessment model to evaluate a performance integrity level (PIL) that is used to select performance reliability from within a range of failure probability categories, which are established from Item 1 type sources and engineering judgment
3. Using qualitative fault tree analysis (FTA) to identify contributing factors to the success or failure of the IFPL, and then using Item 1 and Item 2 sources and methods toward quantitative estimation

Operational Reliability Data and Engineering Design Assessment Statistical data on the performance of fire protection systems under exact or comparable scenario conditions are generally hard to find. Bukowski et al. [23] and British Standard 7974 [24] are often cited when first-order estimates are applied in fire risk assessments. Both references are based on compilation of available statistics from worldwide sources and expert opinion surveys. Both references use many of the same sources and, therefore, the data are fairly comparable. Bukowski et al. [23] provides a definition and distinction between operational reliability (operates as intended) and performance reliability (meets a performance requirement) and indicates data are based on operational reliability statistics. Table 83.8 provides a range of operational reliability data from published estimates [23].

It should be noted that the majority of data were compiled from residential, commercial, and institutional occupancies. The data do, however, provide an insight into an operational reliability range or bandwidth for the selected fire protection systems.

When using such data in an FPS-LOPA evaluation, selection of either an upper or lower bound for the operational reliability is generally done by conducting a survey of the installation quality and evaluating the inspection, testing, and maintenance (IMT) program. The design effectiveness is based on an engineering design evaluation and may incorporate deterministic modeling to evaluate the protection system response to the specific scenario. Uncertainty in the design effectiveness may be expressed probabilistically based on engineering evaluation and judgment. The combination of the design effectiveness (P_{de}) and operational reliability (P_{or}) probabilities can be expressed as

$$\text{Fire protection system (FPS) performance reliability} = P_{de} \times P_{or}$$

For example, if the FPS design effectiveness was evaluated by an engineer who graded the P_{de} at 0.99 and selected P_{or} at 0.95 for the specific scenario, the FPS performance reliability would be estimated as

$$\begin{aligned}\text{FPS performance reliability} &= 0.99 \times 0.95 \\ &= 0.94\end{aligned}$$

This result would indicate that the FPS should meet the functional performance objectives for the specific scenario 94 out of 100 times.

Developing an Engineering Assessment Model to Evaluate a Performance Integrity Level An engineering assessment approach that incorporates a performance-integrity basis can be applied in an FPS-LOPA evaluation. To develop a relationship between performance integrity levels (PILs) and performance reliability, the following actions are recommended:

- Conduct a code and practices compliance review
- Evaluate performance integrity measures (PIMs), based on a site-specific survey
- Assess the quality of the inspection, maintenance, and testing (IMT) program

Current codes such as mechanical, plumbing, or electrical codes, along with specific National Fire Protection Association (NFPA) standards, provide various levels of FPS design criteria. In addition, some industry associations and property insurance companies provide interpretive guides to certain NFPA standards and "good

Table 83.8 Some operational reliability ranges

Fire protection system	Operational reliability probability of success (%)	General criteria
Automatic sprinkler systems	95–97	Sprinklers operate
Masonry construction	70–95	Limit flame spread, maintain structural integrity
Gypsum partitions	69–95	Limit flame spread, compartmentation
Heat detection systems	89–95	Notify occupants and fire service
Smoke detection systems	70–90	Notify occupants and fire service

practice" design supplements based on lessons learned from fire and explosion losses.

In general, design criteria developed by these sources focus on equipment, components and materials of construction, installation requirements, and acceptance testing. Normally, very little information is provided on FPS performance factors such as the following:

- System response time design guidance and quantification methods
- Online availability issues such as design factors, which could minimize downtime
- Failure rate data references for systems, equipment, components
- Common cause failure effects (i.e., corrosion, freezing, etc.)
- Relationship of system reliability versus various design enhancement options
- Effect of inspection, maintenance, and testing on FPS reliability

What FPS design codes and standards do provide, however, is design guidance based on past failure experience; therefore, in a qualitative sense, they provide a level of reliability. In addition, FPS equipment and components must be listed or approved by nationally recognized testing laboratories.

Some primary performance integrity measures (PIMs) for FPS evaluation might also include the following:

- Design suitability, capacity, and duration for the specific hazard being evaluated
- Installation: certified installers, quality control, full acceptance test
- Response time: meets functional response time objectives
- Management of change (MOC) program: a written procedure in place for hazard review versus FPS performance
- Online availability: not subject to excessive IMT downtime, false-trip downtime, physical damage unscheduled downtime, external common cause exposure downtime, such as freezing weather, and so on
- Life cycle: age of components, repair-replacement program
- Operating environment: subject to abnormal temperatures, dust, corrosion, vibration, and so on
- Continuous online diagnostics (i.e., continuous electronic fault detection, supervision)
- Redundancy features (redundant components, secondary power supply, etc.)

Operational reliability is impacted by the frequency of proof testing as well as by the failure rate of FPS components. For fire protection systems, documenting the required test interval and test procedure associated with a required reliability and performance level is critical. The test procedure must prove the correct functioning of all parts of the FPS (i.e., input devices, control unit, and output functions). Proof testing is particularly important for detecting hidden failures that may not be revealed during normal operations.

An Engineering-Based Performance Reliability Model Barry [1] discusses the use of engineering evaluation scoring models, using grading and importance weighting measures to relate PIM quality scores for adjusting and selecting FPS failure rates (or performance success probability) from a range of generic data or statistical data bandwidths.

Using an engineering evaluation model, based on site-specific assessment, to select an FPS performance success probability may in many cases be a better choice at an industrial facility than trying to rely on some generic operational reliability statistics.

Table 83.9 presents a generic example of relating performance measures to a performance success probability range (This table is shown solely for example purposes.). The last column provides performance reliability ranges in terms of performance success probability. Again, performance reliability is based on meeting functional performance objectives or requirements based on a specific scenario.

Fault Tree Analysis Qualitative fault tree analysis (FTA) is a good tool for breaking down the contributing component failures that could lead to failure of a fire protection system. FTA can assist in the understanding of the components and factors that affect performance reliability parameters such as design effectiveness, online availability, and operational reliability. This

Table 83.9 Relating performance measures to performance success probability (solely for example purposes)

Performance measures	Performance integrity level (PIL) rating	Performance failure on demand (P_{fod}) range	Performance success probability range
Design standards, minor to major deviations	PIL-1	>0.20	<0.80
Low–medium PIM quality score			
Below average IMT program			
Design standards, no major deviations, only minor	PIL-2	0.10–0.20	0.80–0.89
Medium PIM quality score			
Average IMT program			
Design standards, compliance met	PIL-3	0.10–0.05	0.90–0.95
High PIM quality score			
Above average IMT program			
Design standards, exceed compliance requirements	PIL-4	0.05–0.01	0.96–0.99
Very high PIM quality score			
Excellent quality IMT program			

analysis provides supplemental information for assessing FPS operational reliability. FTA quantification is not usually done in an FPS-LOPA but can be used to supplement an evaluation of a complex FPS if warranted.

Use of Engineering Judgment and Subjective Probabilities In most cases a hybrid approach must be taken to estimate FPS performance reliability. A hybrid approach generally uses available frequency or probability data, engineering-based assessments and models, and engineering judgment to estimate FPS performance reliability as related to a specific scenario. Subjective engineering judgment, when used in a structured and consistent manner, has great value in understanding FPS performance under specified scenario conditions and for documenting the reliability selection rationale. In cases of industrial facilities with unique design features, unique process hazards, or new technology, supplementing the evaluation with subjective probabilities by engineers and knowledge experts may be the best approach for judging performance reliability. Vick [25] provides detailed discussion on the use of subjective engineering judgment.

Step 4: Evaluate Target Vulnerability

FPS-LOPA can be used to evaluate multiple targets including people, property, and production downtime (business interruption). The primary target in most FPS-LOPA evaluations is the potential exposure vulnerability to people in terms of the probability of serious injury or fatality from the postulated FPS-LOPA scenario. This evaluation mainly relates to emergency response actions. For example, for a given fire scenario that presents a life safety risk, the probability of occupant vulnerability is based on the population affected (i.e., people present at the time of the potential incident), evacuation or life safety egress capability beyond the fire scenario exposure boundaries, egress response time, sheltering capabilities, and so on.

Vulnerability assessment requires an understanding of the manner in which the physically described quantities and types of fire effects (e.g., thermal exposure, combustion products, and overpressure) combine with characteristics of the target (e.g., exposed people, exposed property) to produce a particular level of impact. Unusual vulnerabilities of occupants (e.g., operators must shut down equipment before

exiting), high number or density of occupants, unusual vulnerability of property (e.g., clean rooms), vulnerability to escalation (e.g., chemical releases, radiological release, collapse of structure, etc.) must also be considered [17].

The probability of fatal injury to a person, within the boundaries of the exposure zone, is evaluated as an enabling event within the cause-consequence scenario. The base equation is the product of the frequency (F) of people present and the probability (P) that the people are vulnerable (i.e., susceptible to the effects of the fire or explosion). The vulnerability component may have multiple subfactors such as the notification system reliability, effectiveness of evacuation routes, sheltering facilities, time-related human response reliability, and so on.

$$\text{Likelihood}_{\text{fatal injury}} = F_{\text{people present}} \times P_{\text{vulnerability}}$$

The presence of humans in the exposure zone raises the level of risk. If people are present 100 % of the time, then the risk will be much higher than if people are present in the area 1 % of the time. The frequency of people present can "normally" be derived from plant records and interviews with operations and maintenance managers. However, many incidents occur under nonnormal situations such as when maintenance workers or contractors are working in an area performing nonroutine maintenance, testing, or emergency repairs.

The objective of planned evasive action is to reduce the potential consequences to people from fire or explosion incidents and, thus, is a mitigation factor. Evasive actions can include sheltering-in-place, blast-resistant control rooms, escape to a designated safe shelter, or evacuation from a building, a process area, or the plant area. For assessing evacuation time effectiveness from a building, there are numerous factors to consider, such as the nature of the incident and its intensity level, the type of building, building construction, ventilation systems, fire or blast resistance integrity, type of occupants, populations, efficiency of egress routes, and frequency and quality of occupant training. For an existing facility, based on specific initiating event scenarios, these factors can be evaluated and evacuation drills can be conducted and timed. For proposed facility design for new construction or renovation projects, evacuation time effectiveness may have to be modeled. Building evacuation models are commonly termed *egress models* and are based on studies of peoples' movement within buildings.

Human performance reliability or actions in fires versus emergency response and evacuation time can be a complex evaluation. Other chapters in this handbook and *Guidelines for Evaluating Process Plant Buildings* [26] and *Engineering Guide* [27] provide further information on this subject area.

Step 5: Estimate Scenario Risk

The likelihood of realizing a specific cause-consequence scenario is calculated using the general equation format

$$\begin{aligned}\text{Likelihood}_{\text{cosequence}} = {} & \text{Frequency (initiating failure event)} \\ & \times \text{Probability of Ignition (enabling event)} \\ & \times \Pi\ \text{IFPL}\ P_{\text{fod}}\ \text{(probability of failure on demand of IFPLs)} \\ & \times \text{Probability of target vulnerability (enabling event)}\end{aligned}$$

Each of these items has been addressed in previous sections of this chapter. The enabling events in this general equation include ignition and target vulnerability. Additional enabling events may be needed to realize the consequences associated with a specifically defined scenario.

Having a consistent format in which to perform FPS-LOPA risk calculations and providing

the appropriate level of documentation are very important parts of the evaluation. The general process is illustrated in the FPS-LOPA example included in this chapter.

Step 6: Conduct Risk Tolerance Comparison

In this step, the calculated risk is compared to the risk tolerance criteria established by the plant and/or company. For FPS-LOPA evaluations at industrial facilities, the term *risk tolerance criteria* is normally used instead of acceptable risk limits. *Risk tolerance* infers an internal guideline that establishes risk threshold guidelines on fire and explosion incidents in terms of affecting life safety, company stability, and profitability. Risk criteria establish the types of risks and risk levels a company will tolerate for existing, new, or proposed processes, facilities, and plant operations.

Sources used to assist in the development of risk tolerance criteria include both human-caused and natural hazard accident statistics. The elements of acceptable risk, risk tolerance, risk perception, and so on are beyond the scope of this chapter. Barry [1] and Barry and Johnson [28] provide additional information on this subject.

For a project that involved the processing of combustible liquids, company management authorized a risk-based evaluation and established life safety and property risk tolerance criteria. Examples of the established fire risk tolerance criteria are presented in Tables 83.10 and 83.11 (for example purposes only). Table 83.10 presents an example of risk tolerance limits for life safety exposure levels. Table 83.11 presents an example of risk tolerance limits for property damage impacts from fire.

Step 7: Make Decisions on Risk Reduction

FPS-LOPA can provide the following information for a scenario on a consistent basis [13]:

- Worst-case unmitigated risk (assuming all fire protection layers fail)
- As-is mitigated risk (with existing or proposed fire protection layers in place)
- Fire protection layer improvements necessary to reach a tolerable risk threshold

Table 83.10 Life safety exposure categories for ABC complex

Life safety exposure	General definition	Likelihood tolerance limits (events/year)
1—Low	First aid (minor injury associated with firefighting or evacuation)	0.100
2—Moderate	Single-person injury requiring hospital treatment	0.010
3—Heavy	Multiple-person injuries requiring hospital treatment	0.001
4—High	Life-threatening injury or death on-site	1×10^{-5}
5—Major	Life-threatening injury/rad exposure or death off-site	1×10^{-6}

Table 83.11 Property damage impact categories for ABC complex

Property damage levels	Damage factor range (%)	General definition	Likelihood tolerance limits (events/year)
1—Slight	0–1	Limited localized minor damage not requiring repair	0.1
2—Light	1–10	Significant localized damage of some components generally not requiring major repair	1×10^{-3}
3—Moderate	10–25	Significant localized damage of many components warranting repair	1×10^{-4}
4—Heavy	25–60	Extensive process equipment damage requiring major repairs	1×10^{-5}
5—Major	60–100	Major widespread damage that may result in major structural damage	1×10^{-6}

If risk tolerance criteria are not met, the following can be further evaluated:

1. Existing (or proposed) IFPLs need improvement (e.g., increased performance reliability)
2. More independent fire protection layers are needed
3. A combination of both may be needed

The foregoing three items are usually evaluated by the risk assessment team by listing fire protection system options and examining each alternative in terms of independence, effectiveness (to meet risk tolerance criteria), initial and annual costs, and the ability to audit the measure. The FPS-LOPA example included in this chapter illustrates the general process.

Step 8: Monitor the Risk

The effectiveness and independence of an IFPL must be auditable. The audit process confirms that the IFPL design, installation, and functional testing and maintenance systems are in place to achieve the specified performance reliability for the IFPL [14].

The plant must adopt a zero tolerance toward IFPL inspection, maintenance, and testing (IMT) deviations and enforcement of administrative IFPLs. Any deviation without prior approval should be considered a serious deficiency on internal audits, as it can significantly modify the risk.

A management of change (MOC) program must also be implemented to address changes in occupancy, process operations, facility modifications, and so on, as these changes may substantially affect the performance reliability of IFPLs and, thus, affect the risk level. An impairment program must be in place to address the level of contingency (temporary protection equivalent to the IFPL being taken out of service) needed for an impaired IFPL. If an IFPL is taken out of service for a planned or emergency impairment, the risk level will be affected. A continuous, high-quality, risk monitoring program is crucial for performance-based and risk-based fire protection design approaches.

Simple Example to Illustrate FPS-LOPA Steps

For the purpose of illustrating the steps involved in FPS-LOPA, a simple example related to a chemical process facility will be used. Plant X, utility area ABC, contains chemical pipe racks, cable trays, solvent pumps, and steam and cooling water lines for supplying process facilities A, B, and C. A fire in this area could expose operators and maintenance staff to fire and toxic chemicals and could potentially shut down production in all three process areas.

As discussed at the beginning of this chapter, the type of risk-informed evaluation and level of detail should depend on the complexity of the risk and the needs of the decision maker. Plant management realizes the importance of the utility area in the operation of process areas A, B, and C and the potential exposure it could present to workers.

Due to the uncertainty involving the potential likelihood of a major fire event, concerns about the performance reliability of the existing fire protection in this area, and various past opinions regarding fire protection improvements, plant management has identified this as a Class B decision (see Table 83.1) and has requested an FPS-LOPA evaluation. The following summarizes the steps conducted by the FPS-LOPA team, which consists of representatives from engineering, operations, maintenance, safety, environmental, and fire protection.

Step 1: Develop Accident Scenarios

Table 83.12 provides a summary of FPS-LOPA components related to the specific scenario involving a combustible solvent pool fire, exposing overhead chemical lines and operations and maintenance personnel. It was assumed that, based on hazard evaluation, consequence analysis, and risk screening, this scenario provides an upper-bound credible scenario in terms of people exposure. In addition, it provides a primary

Table 83.12 Example of FPS-LOPA scenario components

Fire hazard	Initating event(s)[a]	Enabling event(s)[b]	Expected consequence(s)[c]	Prevention controls[d]	Mitigation measures[d]
Combustible solvent	Mechanical failure—pump seal failure releases solvent into utility area	1. Ignition of the solvent creates a pool fire	Potential for major fire, which exposes chemical lines and could expose operators or maintenance staff in the area to fire and toxic chemicals	Pump design—double mechanical seals	Dike around pump
		2. Operators and maintenance staff are present in the area for instrumentation checks, sampling, safety checks, equipment maintenance, and testing		Pump mechanical integrity program	Ceiling-level sprinkler system
				Combustible control program to keep combustibles away from equipment	Trained plant fire brigade

[a]Extracted from hazard evaluation, what-if analysis
[b]Based on site-specific survey, ignition source identification and mapping, and interviews with operators and maintenance staff
[c]Fire modeling was conducted as part of consequence analysis
[d]Existing controls and measures

Table 83.13 Continuing example, FPS-LOPA initiating fire event likelihood

Scenario number	Initiating event	Enabling event—ignition	Initiating failure event frequency	Enabling event—ignition event probability[a]	Initiating fire likelihood (fires/year)
SN-01	Mechanical failure—pump seal failure releases solvent into utility area ABC	Ignition of solvent creates a pool fire scenario	0.03 failures/year	0.60	0.018 fires/year
			Note: There are three solvent pumps	Engineering judgment[a]	
			Reference Table 83.6 for pump seal failure, lists a lower-bound failure frequency of 0.01 failures/pump-year		

[a]Enabling event—ignition event probability; engineering judgment based on hazard evaluation, site-specific inspection, interviews with plant operators and maintenance staff. Ignition sources in area identified in terms of availability, ignition source locations mapped, and ignition source strengths evaluated in relationship to the initiating event scenario(s)

design-basis scenario for evaluating the performance reliability of existing fire protection systems in this area.

Step 2: Determine Initiating Fire Event Likelihood

Table 83.13 provides a summary of FPS-LOPA initiating fire event likelihood. The lower-bound failure rate for pump seal failures from Table 83.6, "Example of Some Initiating Event Frequency Ranges," was used in this example based on the engineering evaluation of the prevention features.

Information on prevention controls is generally used in an FPS-LOPA analysis to choose between an upper or lower bound for initiating event failure frequency. In this example pump design includes a double mechanical seal making it less prone to leakage. The pump is used in a relatively low-pressure, low-flow-rate application. The pump is part of the plant's mechanical integrity program so it receives scheduled IMT (inspection, maintenance, and testing). The plant has a combustible control program, which

involves monthly self-inspections and quarterly audits, and includes limiting and maintaining transient combustibles in the utility area so a transient combustible fire will not cause failure in utility area equipment such as the solvent pump system.

The solvent pool fire bounds an electrical fire, transient combustible fire, electric forklift fire in terms of the risk of exposure to the chemical pipe rack and to people in the area at the time of a potential incident. Therefore, it represents a credible design-basis fire scenario in which to evaluate the performance reliability of fire protection mitigation measures in meeting the established risk tolerance criteria.

Step 3: Assess Performance Reliability of Independent Fire Protection Layers (IFPLs)

Fire protection evaluation boundaries are the utility area, which is cut off from the adjacent process areas A, B, and C by 2.0-h fire-rated walls and 1.5-h fire-rated doors. Since the fire scenario being evaluated is exposure within the utility area to operators, maintenance staff, and chemical pipes, the performance of the fire walls is not directly evaluated within this example FPS-LOPA. However, because of the fire barrier importance in confining the fire to the utility area, it could be further reviewed in a supplemental fire wall performance reliability analysis to validate the selection of the fire evaluation boundaries.

The following provides a brief description of the fire protection mitigation measures listed in Table 83.12 in terms of their functional performance expectations or requirements.

Dike Around Solvent Pump The existing dike is 4.0 in. (10.16 cm) high and was initially designed to contain small solvent spills. At the existing solvent flow rate, a seal failure or failure at a flanged inlet or outlet connection to the pump could result in a solvent release rate that could overflow the existing solvent dike within 2–3 min. The dike has not been credited as an IFPL.

Ceiling-Level Sprinkler System This system is an automatic active mitigation measure. The original design intent was to provide for fire control and suppression of fires in the utility area. This design allowed the pipe rack, which contains a variety of process chemicals (some of which are highly corrosive and highly toxic), to be protected from excessive temperatures that could cause pipe failure and release of these materials. The existing system is designed for 0.40 gpm per ft^2 (16.3 L/min·m^2) over the most remote 2500 ft^2 (232 m^2).

Operation of the sprinkler system sounds an outside water motor gong alarm and transmits a water flow signal to a constantly attended control room, from which the plant's fire brigade is notified. There are obstructions to water spray distribution over the solvent pump equipment due to sprinklers being obstructed by overhead pipe runs and ventilation ducts. Some sprinkler heads are corroded; some IMT records are missing information and are not consistent.

For this example, we will assume the use of an engineering evaluation model approach (see Table 83.9) to assess the potential performance success of the existing sprinkler system. Based on identified minor design compliance deficiencies, medium PIM (performance integrity measure) score, and average IMT (inspection, maintenance, testing), a PIL-2 (performance integrity level) lower bound was selected, which is equivalent to a 0.20 P_{fod} (probability of failure on demand).

Plant Fire Brigade Response The plant fire brigade response performance can provide a minimum of five responders to this fire area in full turnout gear within 10–12 min. Based on evaluation of alarm notification time, resource availability analysis, and timed response drills, this capability can be provided 80 % of the time. The public fire department response time is approximately 20–25 min.

Based on fire modeling, an uncontrolled solvent pool fire could initiate failure of chemical pipe lines and a severe people exposure within 5–10 min. Based on the response time constraints for this specific scenario neither the plant fire

Table 83.14 Example FPS-LOPA—IPL probability of failure on demand

Independent fire protection layers—IFPLs	Engineering-based performance integrity level (PIL)	Probability of FPS performance success based on functional Requirements	P_{fod} of IFPL (probability of failure on demand)	Remarks
Dike around solvent pump				Not being credited as an IFPL
Ceiling-level sprinkler system	PIL-2 Lower bound	0.80	0.20	Can be credited as an automatic IFPL; refer to Table 83.9
Plant fire brigade response				Not being credited as an IFPL
Fire barrier wall between utility area and process areas A, B, and C				Not directly relevant to the solvent pool fire scenario affecting chemical lines in the utility area or operators/maintenance staff present in the utility area

brigade nor the public fire department is credited as an IFPL.

Table 83.14 provides a summary of FPS-LOPA independent fire protection layers (IFPLs). Based on the specific solvent pool fire scenario and the time frame for target vulnerability, the only existing credible IFPL is ceiling-level automatic sprinkler protection.

Step 4: Evaluate Target Vulnerability

Vulnerability evaluation involves solvent fire exposure to overhead chemical pipes, which contain corrosive and toxic chemicals, and exposure to operators and maintenance staff from fire and released toxic chemicals.

Based on fire modeling, an uncontrolled solvent pool fire could initiate failure of chemical pipe lines and a severe people exposure within 5–10 min. The factor that enables the life safety exposure likelihood is the probability of having operators or maintenance staff present in the utility area at the time of a potential solvent pool fire incident and the probability of severe or fatal injury vulnerability.

$$\text{Likelihood}_{\text{fatal injury}} = \text{Probability}_{\text{people present}} \times \text{Probability}_{\text{life safety vulnerability}}$$

The probability of having people in this area can generally be estimated from interviews with department supervisors. The probability of severe or fatal injury requires evaluation of the expected fire growth profile, smoke generation, and the domino effect from heated toxic chemicals being released into the area versus the time the fire is detected by the people in the area (either by sensing the situation or by alarm notification) and the time to exit the area.

Table 83.15 provides a summary of the life safety exposure likelihood evaluation for the solvent pool fire scenario.

Step 5: Estimate Scenario Risk

The general FPS-LOPA equation for estimating the likelihood for a specific cause-consequence scenario, such as the solvent pool fire scenario in this example, can be shown as

Table 83.15 Example FPS-LOPA—life safety exposure likelihood

Scenario	Consequences	Frequency of people in area	Probability of fatal injury	Life safety exposure likelihood
SN-01	Major fire that exposes chemical lines and could expose operators or maintenance staff in area to fire and toxic chemicals	Operators and maintenance staff are in the utility area approximately 4100 h per year	This is the probability of fatal injury if a person is in area at the time of an uncontrolled solvent fire incident	People availability (frequency) × Probability of fatal injury = 0.57 people present/year × 0.60 fatal injury potential = 0.34
		4100 h/8760 h-year = 0.47 1–3 people are in the utility area approximately 47 % of the time. To be conservative, estimate people availability at 57 % of time	Based on deterministic modeling and engineering judgment of the rate of fire growth and toxic gas development versus evaluation of the time for personnel sensing of the fire or alarm notification and time to exit the area, a probability of 0.60 has been assigned	To be conservative, round up to 0.40 as life safety exposure likelihood

$$\begin{aligned}\text{Likelihood}_{\text{consequence}} = {} & \text{Frequency (initiating failure event)} \\ & \times \text{Probability of ignition (enabling event)} \\ & \times \Pi \text{ IFPL } P_{\text{fod}} (\text{probability of failure on demand of IFPLs}) \\ & \times \text{Probability of target vulnerability (enabling event)}\end{aligned}$$

Substituting the results from the example (from Tables 83.12, 83.13, 83.14, and 83.15)

$$\begin{aligned}\text{Likelihood}_{\text{consequence}} = {} & 0.03 \text{ pump seal failures/year} \\ & \times 0.60 \text{ ignition} \times 0.020 \ P_{\text{fod}} \text{ sprinkler system} \\ & \times 0.40 \text{ life safety exposure} \\ = {} & 1.44 \times 10^{-3} \text{events/year}\end{aligned}$$

Normally a form or spreadsheet is used to document an FPS-LOPA scenario evaluation. Table 83.16 provides an example of a documentation format.

Step 6: Conduct Risk Tolerance Comparison

Based on Step 5, the existing risk is estimated at 1.44×10^{-3} events/year. The plant's risk tolerance criterion is 1.0×10^{-5} events/year (assumes a risk tolerance based on Table 83.10, "Example Life Safety Exposure Categories," for life-threatening injury or death on-site, established at 1.0×10^{-5} events/year). For this example, the estimated existing risk level exceeds the established risk tolerance level; therefore, additional IFPLs are needed (i.e., to reduce the existing risk level approximately two orders of magnitude).

Step 7: Make Decisions on Risk Reduction

The general approach for this step involves conducting an FPS-LOPA team brainstorming

Table 83.16 Example FPS-LOPA—documentation table

FPS-LoPA no: **Sn-01**		**Date**:	
Plant X: **ABC utility area**		**Evaluation by**:	
Location: **Bldg. 601- utility corridor**		**Review by**:	
Process: utility area ABC contains chemical pipe racks, cable trays, solvent pump, steam and cooling water lines for supplying process facilities A, B, C. A fire in this area would expose operators and maintenance staff to fire and toxic chemicals and could shut down production in all three process areas		**Area/process** ⊠ Existing Design ❍ New Design ❍ Proposed Design Modifications	
Scenario source: process hazard analysis (PHA) Item ABC-01; pump seal failure resulting in a solvent pool fire		**P&ID nos. or equipment IDs**: 601-A, 602-B, 603-C **risk tolerance**:	
Scenario: mechanical failure of pump seal failure releases combustible solvent into utility area; ignition of the solvent creates a pool fire		**Maximum target Likelihood**: 1.0×10^{-5} events/year	
Operators and maintenance staff are in area approximately 4100 h per year, generally 1–3 people. Major fire would fail chemical lines and could expose operators or maintenance staff in area to fire and toxic chemicals		**Reference**: plant risk assessment guideline RA02	
Item	Description	Probability	Frequency
Initiating event likelihood: solvent pump seal failure	Pump seal failure releases solvent into the utility area		0.03 events/year
	Note: there are three solvent pumps. Reference Table 83.6 for pump seal failure, lists a lower-bound failure frequency of 0.01 failures/pump-year		
Enabling event likelihood: ignition occurs	Ignition event probability; engineering judgment based on hazard evaluation, site-specific inspection, and interviews with plant operators and maintenance staff. Ignition sources in area were identified in terms of availability and ignition source strengths in relationship to the initiating event scenario	0.6	
Likelihood of an initiating fire		P_{fod}	0.018 fires/year
IFPL fire protection layers	Ceiling-level sprinkler system activates, suppresses fire, and prevents failure of chemical lines with corrosive and toxic chemicals	0.20	
P_{fod}—probability of performance failure on demand	Based on engineering evaluation used a PIL-2 (performance integrity level) lower bound from Table 83.9		
Other safeguards not directly credited as independent protection layers	Dike around solvent pump		
	Plant fire brigade (response time to this scenario not adequate)		
Likelihood of an unmitigated fire (uncontrolled fire)			3.6×10^{-3} uncontrolled fire events/year
Target vulnerability: life safety exposure to operators/ maintenance people	Enabling event: life safety exposure likelihood to operators/maintenance people	0.40	
	Probability of fatal injury (see Table 83.15)		
Likelihood of consequence being realized			1.44×10^{-3} events/year
Fire risk tolerance established by plant	**1×10^{-5} events per year**; **maximum tolerable risk of a** major fire that could cause extensive equipment damage; maximum tolerable risk of a fatal injury		Comment: fire risk tolerance criteria are not met with existing IFPLs

session, where various fire protection options and alternatives are discussed in terms of the risk reduction potential, feasibility, initial and annual costs, installation issues, process downtime during installation, and so on. For this example, it is assumed that relocating solvent pumps outside, rerouting chemical pipes, and constructing a fire-rated compartment around the solvent pumps are not feasible alternatives. It is further assumed that based on review of several different alternatives, the following fire protection measures are selected for further FPS-LOPA evaluation.

Install Heat Detection System and Interlocks to Minimize the Size of a Solvent Release Install a localized heat (fire) detection system for the three solvent pumps. Operation of the heat detection system would be interlocked to automatically close a safety shutoff valve on the solvent line outside the building and send an alarm to the control room. This detection and mitigation measure would reduce the potential size, intensity, and burning duration of a solvent fire and reduce the likelihood of overhead chemical line failure. This system would be designed for a minimum 0.95 performance reliability.

Make Improvements to the Existing Automatic Sprinkler System Install radiant heat flame shields at the underside of the chemical pipe rack. Install sprinkler protection under flame shields and under the ventilation air-supply duct, which is over 4.0 ft (1.22 m) in width. This will provide improved water spray coverage in this area, especially over the solvent pump equipment. Interlock the activation of the sprinkler systems to automatically close isolation valves on the bulk chemical tanks and the solvent safety shutoff valve and activate local alarms. Replace the corroded sprinkler heads and inspect the rest. Improve the sprinkler system inspection, maintenance, and testing program.

For this example, we will again assume the use of an engineering evaluation model approach (see Table 83.9) to assess the potential performance success of the proposed sprinkler system improvements. Based on engineering evaluation and judgment, improvements would increase the PIL (performance integrity level) to an upper bound PIL-3 level, which is equivalent to a 0.05 P_{fod} (probability of failure on demand) or a 0.95 performance reliability.

Reduce Life Safety Vulnerability by Early-Response Fire Alarm Notification Install two beam-type smoke detectors at the ceiling level. Operation of any one detector activates local alarms in the utility area, including strobe lights, as this area has moderate noise levels. Manual fire alarm pull boxes will be installed at both exterior exit doors and will be interlocked to automatically close isolation valves on the bulk chemical tanks and the solvent safety shut off valve. Operation of one detector, a manual fire alarm pull box, or sprinkler system will transmit a signal to a constantly attended control room and the plant fire brigade will be immediately dispatched.

Plant management realizes the importance of the utility area in the operation of process areas A, B, and C. The installation of beam smoke detectors also provides the capability for detection of potential electrical cable fires and faster response of the plant's fire brigade. The provision of automatic interlocks reduces the potential for a large solvent or toxic chemical release inside the utility area.

Table 83.17 illustrates spreadsheet-type documentation of the proposed risk reduction strategy. The proposed risk reduction measures reduce the solvent pool fire life safety exposure likelihood to 9.0×10^{-6} events/year, which meets the plant's established risk tolerance criteria.

Step 8: Monitor the Risk

As previously stated, the effectiveness and independence of an IFPL must be auditable. The audit process must confirm that the risk reduction system IFPL design, installation, and functional testing and maintenance systems are in place to achieve the specified performance reliability for the IFPL based on the FPS-LOPA risk reduction decision analysis.

Table 83.17 Example FPS-LOPA risk reduction evaluation spreadsheet

Design Phase	*A* Initiating failure event	*B* Enabling event 1: ignition	*C* FPS-IPL 1 P_{fod}	*D* FPS-IPL-2 P_{fod}	*E* Enabling event 2: target vulnerability	Likelihood Fire scenario incident likelihood
Existing design	0.03	0.60	0.20		0.40	1.44×10^{-3} events/year
	Pump seal failure	Ignition of solvent release	Ceiling-level sprinkler protection		Life safety exposure 1–3 people	
Proposed risk reduction design strategy	0.03	0.60	0.05	0.05	0.20	9.0×10^{-6} events/year
	Pump seal failure	Ignition of solvent release	Install an independent heat detection system interlocked to shut down bulk chemical isolation valves and solvent safety shut off valve	Make improvements to the sprinkler system	Life safety exposure reduced 50 % based on installation of beam smoke detectors and local alarms	
			Design for a minimum 0.95 performance reliability	Design for a minimum 0.95 performance reliability	Engineering evaluation and judgment	

Auditing, management of change (MOC), and impairment procedures will be established for the independent solvent heat detection system and interlocks, the ceiling-level automatic sprinkler protection system protecting the utility area, and the beam early-warning smoke detection system and alarms for improved independent people notification and evacuation time response (i.e., independent from the sprinkler system water flow local alarm). It is critical that these risk-monitoring measures are implemented to continuously maintain the risk tolerance criteria established by plant management.

Class C Decisions: Quantitative Risk Assessment (QRA)

FPS-LOPA goes beyond the typical use of a qualitative risk matrix but is less detailed than quantitative risk analysis (e.g., QRA used for Class C decisions).

FPS-QRA methods provide a higher degree of detail and accuracy than FPS-LOPA. For example, in FPS-QRA, fault tree analysis is normally applied to assess the primary contributing factors associated with initiating fire events and fire protection system performance. Having a detailed breakdown of contributing risk factors and quantification of these factors allows more insight into options and alternatives to reduce the risk to a tolerable level in a cost-effective manner. Event tree analysis of multiple scenarios, use of input sensitivity analysis, use of probability distribution, and use of uncertainty analysis methods provide additional information on which more intelligent risk-based decisions can be made [1, 12].

Figure 83.8 [1] presents an example of the steps to take in an FPS-QRA risk-informed, performance-based fire protection evaluation, which can be used to address Class C decisions when additional levels of analysis and detail are warranted. Risk-informed, performance-based assessments involve the quantification of initiating fire event likelihoods, development of exposure and consequence profiles (life safety, property, business interruption) using fire and explosion modeling and event tree analysis, evaluation of the performance success probability (i.e., performance reliability) of existing or proposed fire protection systems, comparison of risk results with risk tolerance criteria, and cost-benefit analysis of risk reduction alternatives if risk tolerance limits are exceeded.

Table 83.18 provides a brief comparison between FPS-LOPA and FPS-QRA methods.

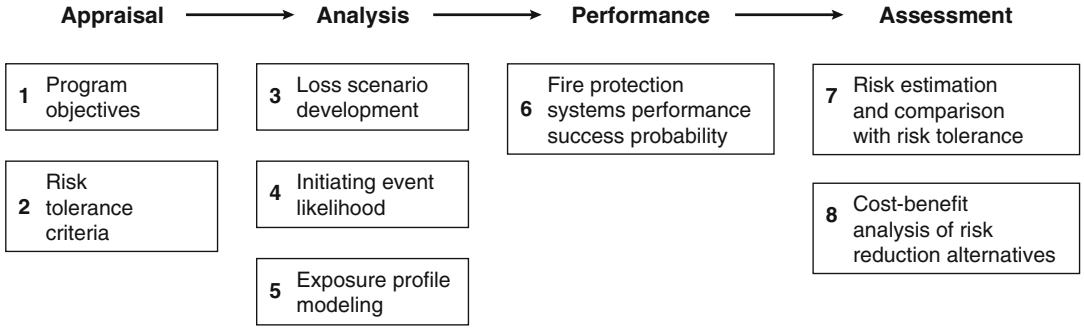

Fig. 83.8 Risk-informed performance-based fire protection steps [1]

Table 83.18 Brief comparison between FPS-LOPA and FPS-QRA methods

Item	FPS-LOPA	FPS-QRA
Decision level (note: refer to Table 83.1)	Class B decisions	Class C decisions
Accident scenario development	Evaluates a defined (normally bounding) cause-consequence pairing (typically identified during a qualitative hazard evaluation)	Can accommodate multiple cause-consequence scenarios using event tree analysis (ETA)
Initiating event frequency	Generally evaluates single component failure or single human error with a probability estimate for ignition	Can assess multiple failures and contributing factors leading to a fire or explosion event, using fault tree analysis (FTA)
	Single point frequency estimate	Probability distributions can be applied within the ETA
Performance of independent fire protection system layers (IFPLs)	Generally applies an engineering judgment-based performance reliability estimate	Usually applies a performance success tree, which allows a more detailed evaluation of performance reliability in terms of
Probability of performance failure		• Design effectiveness
		• Availability
		• Operational reliability
Scenario risk estimation	Proves an order-of-magnitude estimate of the likelihood of realizing a specific cause-consequence scenario	Provides higher-accuracy risk estimates through application of FTA and ETA
		Can accommodate sensitivity and uncertainty analysis to improve confidence
Risk reduction analysis and decision analysis	FPS-LOPA takes a specific cause-consequence scenario, determines how many protection layers are provided by existing and/or recommended independent fire protection layers (IFPLS), and evaluates whether the number and performance reliability of IFPLs provide adequate risk mitigation to meet risk tolerance criteria	Goes beyond FPS-LOPA in terms of evaluating contributing risk factors through FTA and ETA, thus allowing better decisions to be made regarding risk reduction strategies
		Provides necessary information to conduct a credible cost-benefit economic analysis

Summary

The use of an integrated or layered fire safety design approach (fire prevention, detection, passive and active protection levels, and emergency response) within a risk-informed framework provides both a balanced and quantitative method for addressing complex fire and explosion issues. It delivers supplemental decision-support information and alternatives, which allow engineers, risk managers, and regulators

the capability to make cost-effective decisions based on the unique risk factors associated with a specific building, facility, or process.

The authority having jurisdiction (AHJ) is responsible for ensuring that the layers of independent fire protection needed are relative to the risk level and imposed risk tolerance criteria. However, it may be difficult to do without risk-based information that supports the level of fire safety achieved with the fire protection design strategy under review.

The use of risk-based computations, including quantification of the performance reliability of independent fire protection layers for scenarios with uncertainty factors or potentially moderate to high consequence levels, needs to be incorporated into performance-based fire protection design submittals if this supplemental information is requested by the AHJ.

The risk-informed evaluation approaches discussed in this chapter have been performed for numerous types of industrial processes, facilities, and operations. The techniques present many crossover application capabilities to examine design-based fire scenarios and risk levels at commercial buildings, high-rise buildings, hospitals and health care facilities, large assembly areas, and so on.

A robust performance-based fire safety design code cannot be achieved without practical guidelines for delivering supplemental risk-informed information either as a supplement to performance-based design submittals on a voluntary basis or as requested by the building code official or regulator.

Nomenclature

AHJ	Authority having jurisdiction
ETA	Event tree analysis
F	Frequency
FHA	Fire hazard analysis
FMEA	Failure modes and effects analysis
FPS	Fire protection system
FPS-LOPA	Fire protection system-layer of protection analysis
FPS-QRA	Fire protection system-quantitative risk assessment
FRE	Fire risk evaluation
FTA	Fault tree analysis
HAZOP	Hazard and operability analysis
HRA	Human reliability analysis
IFPL	Independent fire protection layer
IMT	Inspection, maintenance, testing
IPL	Independent protection layer
LOPA	Layer of protection analysis
MOC	Management of change
NFPA	National fire protection analysis
P	Probability
P_{de}	Probability of design effectiveness
P_{fod}	Probability of failure on demand
PHA	Process hazard analysis
PIL	Performance integrity level
PIMs	Performance integrity measures
PML	Probable maximum loss
P_{or}	Probability of operational reliability

References

1. T.F. Barry, *Risk-Informed, Performance-Based Industrial Fire Protection, An Alternative to Prescriptive Codes,* TFBarry Publications and Tennessee Valley Publishing, Knoxville, TN (2002). Available from http://www.fireriskforum.com.
2. Marine Risk Assessment, prepared by Det Norske Veritas for the Health and Safety Executive, London Technical Consultancy, London, UK (2002).
3. UKOOA, *A Framework for Risk Related Decision Support,* UK Offshore Operators Association, London (1999).
4. Center for Chemical Process Safety (CCPS), *Guidelines for Hazard Evaluation Procedures with Examples,* 2nd ed., American Institute of Chemical Engineers (AIChE), New York (1992).
5. F.P. Lees, *Lee's Loss Prevention in the Process Industry, Hazard Identification, Assessment, and Control,* 2nd ed., Butterworth-Heineman, Oxford, UK (1996).
6. I.S. Sutton, *Process Hazards Analysis,* SW Books, Houston, TX (2001).
7. NFPA, *Fire Protection Handbook,* 20th ed., National Fire Protection Association, Quincy, MA (2008).
8. C.R. Schroll, *Industrial Fire Protection Handbook,* 2nd ed., CRC Press, Boca Raton, FL (2002).
9. R.G. Zalosh, *Industrial Fire Protection Engineering,* John Wiley & Sons, Hoboken, NJ (2003).
10. Center for Chemical Process Safety, *Guidance for Consequence Analysis of Chemical Releases,*

American Institute of Chemical Engineers, New York (1999).
11. Center for Chemical Process Safety, *Guidelines for Evaluating the Characteristics of Vapor Cloud Explosions, Flash Fires, and BLEVEs,* American Institute of Chemical Engineering, New York (1994).
12. Center for Chemical Process Safety (CCPS), *Guidelines for Chemical Process Quantitative Risk Analysis,* American Institute of Chemical Engineers (AIChE), New York (1999).
13. A.M. Dowell III and T. Williams, "Layer of Protection Analysis: Generating Scenarios Automatically from HAZOP Data," *Process Safety Progress,* 24, 1 (Mar. 2005).
14. Center for Chemical Process Safety (CCPS), *Layers of Protection Analysis: Simplified Process Risk Assessment,* American Institute of Chemical Engineers, New York (2001).
15. A.M. Dowell, *Layer of Protection Analysis, A New PHA Tool After Hazop, Before Fault Tree Analysis,* CCPS/AIChE International Conference and Workshop on Risk Analysis in Process Safety, Center for Chemical Process Safety, American Institute for Chemical Engineers, New York (1997).
16. P. Baybutt, "Cyber Security Risk Analysis for Process Control Systems Using Rings of Protection Analysis, ROPA," *Process Safety Progress,* 23, 4 (Dec. 2004).
17. Society of Fire Protection Engineers, *Engineering Guide: Fire Risk Assessment,* Society of Fire Protection Engineers, Bethesda, MD (2006).
18. Center for Chemical Process Safety (CCPS), *Guidelines for Process Equipment Reliability Data, with Data Tables,* American Institute of Chemical Engineers (AIChE), New York (1989).
19. IEEE Std 500–1991, *Guide to the Collection and Presentation of Electrical, Electronic, Sensing Component, and Mechanical Equipment Reliability Data for Nuclear Power Generating Stations,* Institute of Electrical and Electronic Engineers, New York (1991).
20. OREDA, *Offshore Reliability Data Handbook,* 4th ed., OREDA, Stavanger, Norway (2002).
21. V. Babrauskas, *Ignition Handbook,* Fire Science Publishers, Issaquah, WA (2003).
22. ISA-S84.01, *Application of Safety Instrumented Systems to the Process Industries,* Instrument Society of America (ISA), Research Triangle Park, NC (1996).
23. R.W. Bukowski, E.K. Budnick, and C.F. Schemel, *Estimates of the Operational Reliability of Fire Protection Systems,* NIST, Gaithersburg, MD (2002).
24. British Standard 7974, *Application of Fire Safety Engineering Principles to the Design of Buildings,* British Standards Institute, London, UK (2001). (supersedes DD 240-1-1997)
25. S.G. Vick, *Degrees of Belief, Subjective Probability and Engineering Judgment,* American Society of Civil Engineers, Reston, VA (2002).
26. Center for Chemical Process Safety (CCPS), *Guidelines for Evaluating Process Plant Buildings for External Explosions and Fire,* American Institute of Chemical Engineers, New York (1996).
27. Society of Fire Protection Engineers, *Engineering Guide, Human Behavior in Fire,* Society of Fire Protection Engineers, Bethesda, MD (2003).
28. T. Barry and P. Johnson, "Establishing Quantitative Fire Risk Tolerance Benchmarks," Paper presented at 5th International SFPE Conference on Performance-Based Codes and Fire Safety Design Methods, Luxembourg (Oct. 2004).

Further Readings

Center for Chemical Process Safety (CCPS), *Guidelines for Preventing Human Error in Process Safety,* American Institute of Chemical Engineers (AIChE), New York (1994).

Center for Chemical Process Safety (CCPS), *Tools for Making Acute Risk Decisions with Chemical Process Safety Applications,* American Institute of Chemical Engineers, New York (1995).

F. Noonan and R. Fitzgerald, "On the Role of Subjective Probabilities in Fire Risk Management Studies, Fire Safety Science," *Proceedings for the 3rd International Symposium,* July 8–12, 1991, Edinburgh, Scotland, pp. 495–504 (1991).

D.J. Rasbash, G. Ramachandran, B. Kandola, J.M. Watts, and M. Law, *Evaluation of Fire Safety,* John Wiley & Sons, Ltd., London (2004).

I.S. Sutton, *Process Reliability and Risk Management,* Van Nostrand Reinhold, New York (1992).

D. Vose, *Quantitative Risk Analysis: A Guide to Monte Carlo Simulation Modelling*. John Wiley & Sons, Chichester, UK (1997).

Thomas F. Barry is principal engineer and director of Risk and Reliability Services for HSB Global Standards and director of http://FireRiskForum.com, an independent website that provides fire and explosion risk-based educational and training materials. Thomas, who is a member of NFPA, SFPE, and AIChE, has over 28 years of experience as an industrial fire protection engineer and fire and explosion risk analyst in the chemical, oil, gas, power, and nuclear industries. He has written many articles on fire and explosion risk assessment; has conducted seminars on fire dynamics, fire modeling, and fire risk assessment; and is the author of the book *Risk-Informed, Performance-Based Industrial Fire Protection*.

Product Fire Risk Analysis

84

John R. Hall Jr.

Introduction

Since the late 1990s, there has been an explosion of fire risk assessment guidance documents, both in the United States and around the world. Some address the whole subject of fire risk assessment, whereas others are focused on major component tasks, such as the selection of scenarios. But nearly all of these documents are intended for assessments at the level of whole buildings or similar-sized construction projects. Almost none are intended to support design and purchase decisions at the level of products.

Most risk applications conducted by fire protection engineers will be of the whole-building type. Even for product decisions, most applications will probably be in the context of a larger design for a new building.

This chapter discusses fire risk assessment as applied to product choices. These techniques may be of use to fire protection engineers responsible for changing over the contents and furnishings of an existing building or, better still, a collection of buildings of similar type and design. However, these techniques are more likely to be used by manufacturers and industry groups—and fire protection engineers working for such employers—as part of design decisions for products to be offered to all buildings of a certain type. Someone deciding on the design of the next generation of chairs for a general office environment or carpeting for use in the lodging industry will have enough money riding on the decision to justify the nontrivial cost of analysis. Those deciding on which currently available chairs to buy for an office renovation or which carpeting to buy for use in a hotel remodeling probably will not be able to justify the cost of analysis by the value of the information to their decision. Another application of product fire risk assessment would be in the evaluation of candidate new regulations—will the risk reduction benefits exceed the costs?—and in manufacturers' product design decisions aimed at providing performance-based equivalent proof of satisfying existing regulations.

In the big picture of fire safety, there are only two ways to make changes—change things or change behavior. Every *thing* you can change could be seen as a product, in that it is a physical object that people buy, for example, from the raw materials that are used to make furniture to the finished furniture, from the components of fire detection and suppression systems to the complete systems, from wood and steel and concrete to whole buildings. That definition of product is too broad for one chapter.

For purposes of this chapter, a product will be a finished product, not raw materials or components in an assembly, but objects in an end-use form. And a product will be something that starts or feeds a fire as either a heat source or

J.R. Hall Jr. (✉)
Director for Fire Analysis and Research of the National Fire Protection Association,

M.J. Hurley (ed.), *SFPE Handbook of Fire Protection Engineering*,
DOI 10.1007/978-1-4939-2565-0_84, © Society of Fire Protection Engineers 2016

a fuel source. Computationally, fuel-source products involve much more elaborate calculations and effects, because the risk of heat-source products is measured solely in terms of whether or not ignition occurs. The treatment in this chapter will reflect that.

The fire risk of a product captures the range of severities of fires associated with the product and the probabilities that fires will occur having those severities. Fire risk is usually measured as expected loss, that is, the sum over all fires of probability times severity, or as the probability of having a fire more severe than a stated threshold. Either way, fire risk analysis relies heavily on fire scenarios, which are used to set up calculations of both probabilities and severities. This is *not* the same as choosing a handful of specific fires and calculating their severities and probabilities. A valid calculation must demonstrate that each specific fire analyzed is representative of a larger class of fires, that probabilities are calculated for the larger classes of fires rather than the specific fires, and that collectively the larger classes include every type of fire there can be.

For additional guidance, examine the sections on fire risk analysis in the two Society of Fire Protection Engineers references on performance-based design [1, 2] and the SFPE guide on fire risk assessment [3].

Steps in a Product Fire Risk Analysis

Of the many fire protection engineering guides and standards now available on fire risk assessment, only the guide from the American Society for Testing and Materials (ASTM) is designed for application to products rather than whole buildings. ASTM E1776 [4] is actually written as a guide to writing more product-specific fire risk assessment standards within ASTM rather than as a full guide to conducting product fire risk assessments, and ASTM E1776 relies for much of its content on ASTM E1546 [5], a counterpart document on fire hazard assessments. Therefore, the steps and substeps briefly described in this chapter reflect not only the ASTM E1776 structure but also the other documents that elaborate on fire risk assessment for application to buildings.

Here is a brief overview of the steps in a product fire hazard assessment:

1. *Define the scope of products*. In nearly all cases, one will calculate the risk reduction benefit associated with a product as a percentage reduction in the baseline risk associated with the product group or class that best fits the product of interest. A new design for upholstered furniture will be assessed against the baseline of risk in fires due to the involvement of upholstered furniture. A new design for carpeting will be assessed against the baseline of risk in fires due to the involvement of floor coverings. The product group or class contains all and only the products for which the new product of interest is a suitable substitute.
2. *Specify the class of properties in which the product will be used*. The class of properties will help to specify not only the context or environment in which the product will be used but may also specify ranges of product characteristics.
3. *Specify goals*, *objectives*, *and measures*. Are you interested in risks of death, injury, property damage, or environmental impact? Do you intend to measure those risks in those terms or are you going to use functional statements to define proxy measures in engineering terms?
4. *Set assumptions*. The assumptions referred to here are all those characteristics that will influence the ignition or development of the fire and the achievement of the goals and objectives but that are not addressed in the product or building design. For example, what are the burnable items that will make it easy or difficult for a fire begun on the product to grow to a larger fire? Or, for buildings, what are the contents and furnishings brought in by occupants but not specified in the building design that will make it easy or difficult for a fire to begin and grow rapidly?
5. *Identify and specify scenarios and scenario clusters*. For a heat-source product, this involves dividing up all the fires started by

such a product into scenario clusters based primarily on the types of burnable items the product ignites. For a burnable product, this involves dividing up the fires where the product is the first item ignited by different types of heat sources and also addressing the fires where the product is the primary fuel package though not the first fuel package.

6. *Identify test methods*, *models*, *and other data sources and calculation procedures*. The centerpiece of the necessary elements for risk calculation will be a suitably assembled and structured database on baseline fire experience.

Here are the six steps with more detail on what the steps involve. Later sections expand on techniques to be used in executing these steps.

1. *Define the scope of products to be analyzed*, *including context of use*.
   (a) Define the product or, more typically, the product class to be evaluated. Assuming you wish to match the product class specifications to a fire incident data base, the product class will likely be defined first by the product's function (e.g., for heat-source products, heating vs. cooking vs. lighting vs. power distribution; for burnable items, floor covering vs. upholstered furniture vs. cooking material). For burnable items, the product class may also be defined by the material composition of the product (e.g., fabric vs. wood vs. metal vs. plastic).
   (b) Specify where and how the product is used. For example, the product class of floor coverings would not include all uses of carpeting, because carpeting is sometimes used as a wall covering. The specification of application will not only limit the range of product characteristics, but also specify or limit the input parameters used to identify fire scenarios in which the product may play a role.
2. *Specify the class of properties in which the product will be used*. Part of identifying the scope is categorizing and specifying the property in which the product is used. The end-use or principal activity in a property defines it as an *occupancy*, which will imply a variety of characteristics and conditions in the environment of the product. For example, a risk analysis of upholstered furniture in homes will be different from a risk analysis of upholstered furniture in offices, and both will be different from a risk analysis of upholstered furniture in hotels. The types of pieces used are different, the applicable standards are different, the mix of fires they could be exposed to are different, and the mix of people likely to be present (and their capabilities) are different.
3. *Specify goals*, *objectives*, *and measures*.
   (a) Specify goals in terms of acceptable target outcomes, usually in terms of types of harm to be prevented, minimized, or otherwise reduced. Life safety, defined in terms of fatal injury or other health effects, is usually the principal goal. Property protection, avoidance of indirect loss, and protection of heritage and the environment are other typical goals.
   (b) Specify objectives, which are more specific means to the end, that is, the goals. If objectives are restated in terms of the systems and features that engineers design, they may be called *functional statements*, but for calculation purposes, they are used in the same way as objectives, as a source of quantitative performance criteria defining a threshold of acceptable fire safety or at least a scale dividing better from worse. Alternatively, objectives may be stated in terms of events (e.g., flashover) or other physical conditions of fire.
   (c) Specify or quantify goals and objectives in the form of performance criteria or other measures of loss or harm. Some measures, called *end* measures, are meaningful in and of themselves but are very difficult to predict in models or measure in tests (e.g., monetary damages, injuries). Some measures are easily predicted in models or measured in tests, but are not meaningful in

themselves (e.g., temperature or toxic gas concentrations or obscuration for particular areas or volumes). Typically, models must be used to convert readily measurable quantities to end measures of loss.

4. *Set assumptions*. Set assumptions covering all aspects of the building, occupant, system, feature, fuel load, modeling, or other elements affecting the outcomes that are not defined either by the product specifications (for the product being assessed) or by the scenarios, which address factors that vary. Set assumptions in terms of *average* conditions (or, if necessary, *typical* conditions), in order to predict overall risk-severity weighted by probability.
5. *Identify and specify the relevant scenarios and scenario clusters*. A scenario is a description of fire conditions from ignition to extinguishment. For calculation purposes, a scenario is usually defined by a set of initial conditions that can be used as input conditions to a test method or fire model. A scenario cluster is a set of scenarios, suitable for calculation of probability or likelihood. (a) To describe the baseline, it is necessary to sort and group all the fires in the baseline into non-overlapping scenario clusters that collectively include all fires. For risk analysis of a heat-source product, the clusters can most usefully be defined by groups of items that will react to the heat of the product in similar ways, for example, by smoldering or by transitioning immediately from pyrolysis to flaming. For risk analysis of a burnable-item product, the clusters can most usefully be defined by groups of heat sources that will ignite the product in similar ways, such as (i) ignitions by a smoldering heat source, typically a cigarette, (ii) ignitions by close exposure to an open flame heat source, (iii) ignition by radiative and/or convective heat at a distance or by other heat transfer from a hot object in contact with the burnable item, and (iv) ignition as a secondary item ignited by an existing unwanted fire. (b) To capture fires where the product is the main fuel package but not the initial fuel package, one begins by identifying the baseline fires where items from the product's product class played that role of main fuel package. Then those fires will need to be divided into clusters based on type of item first ignited, the size of initial fire that will tend to be produced by such items, and the proximity of such items to the product. Each cluster describes a fire challenge to the product, typically described by a heat flux at a defined range of distances. If the product is made more resistant to such ignitions or the product is changed to produce slower fire growth or lower peak intensities, then this can be modeled as a change from the baseline consequences associated with that group of fires. The baseline may provide information on the presence and performance of fire protection systems and on other nearby combustibles that may become more important to fire growth if the product is made less susceptible to ignition or rapid fire growth. In that case, test methods and engineering models can be used to provide a better estimate of the expected fire consequences if baseline fires were to begin in the same way but grow without the baseline product characteristics to feed or spread the fire.
6. *Identify test methods*, *models*, *and other data sources and calculation procedures*. The models needed will depend, in part, on the scenarios to be addressed. Each model has implications for data needs, including fire tests and statistical databases.

These are commonly available models that may be useful when estimating the likely change in consequences in a type of baseline fire that became large and consequential because of the baseline product's role as a secondary item ignited:

(a) Fire growth model
    (i) Model of rate of growth in terms of heat release rate, for example, as a function of fuel load and distances between items
    (ii) Horizontal flame spread model
    (iii) Barrier failure (e.g., door, ceiling, window)

(iv) Exterior vertical flame spread model
(v) Flame spread model in concealed spaces
(vi) Building-to-building flame spread

(b) Smoke spread model
(i) Model of room filling
(ii) Model of spread between rooms
(iii) Flashover models, including timing of flashover and postflashover smoke spread
(iv) Model of spread via heating, ventilation, or air conditioning system

(c) Occupant behavior model
(i) Model of automatic detection equipment performance
(ii) Model of how fire is discovered in the absence of automatic detection
(iii) Model of decision-making activities leading to decisions to egress or attempt rescue
(iv) Model of egress and rescue activities

(d) Intervention models
(i) Automatic suppression models, including timing of activation and effects on fire growth
(ii) Model of other suppression or extinguishment efforts and their effects (e.g., whether fire extinguishers will be used and to what effect)
(iii) Fire fighter response models

These are models that may be useful to convert outputs of calculation from engineering terms, such as physical measures of fire size, into outcomes valued for themselves, such as deaths or property damage.

(a) Fire effects or outcome models
(i) Predicted deaths and injuries due to fire effects in affected areas as a function of time
(ii) Structural damage or failure models
(iii) Predicted extent or monetary value of property damage

These are models that may be useful in estimating from test results the expected reduction in likelihood of fires based on product changes designed to prevent ignitions:

(a) Ignition probability models
(i) Fault tree, success tree, or event tree
(ii) Bayesian analysis of test results, historic fire probabilities, and other data

Defining the Scope of Products to Be Analyzed

The scope definition should define a class of interchangeable items having a common function or application in a specified occupancy and with a range of allowable choices for composition. Specification of the product should be done in a way that facilitates use of existing data, from fire incident data to product test data.

For heat-source products and fuel-source products, this means that initial specification of the product by function and construction should begin with the categories used in the National Fire Incident Reporting System (NFIRS) (see Chap. 78).

Further specification of the product by function may be needed (e.g., selecting bookcases from the cabinetry group). In such cases, the nationally representative fire incident databases will not be sufficient to estimate probabilities. Other, special fire incident databases and expert judgment will be needed.

When calculating probabilities, be sure to include appropriate shares of fires involving products that were partially or wholly undefined (e.g., upholstered furniture fires should include shares of fires involving unknown-type furniture or unknown-type form of material first ignited, and might include shares of fires involving unclassified furniture or unclassified form of material first ignited).

The range of items defined as examples of the product—which may be referred to as members of the product class—must, for analysis purposes, be reduced to a manageable number of subgroups. Each subgroup will be *defined* by a range of characteristics (e.g., all cellulosic versions of the product) but will be *represented* by one specific set of product fire characteristics.

Ordinarily, these product fire characteristics will be identified from review of results of actual fire tests on one or more representatives of the product class.

Specifying the Class of Properties

For reasons similar to those already cited for product scope definitions, property classes (i.e., occupancies) should have their primary definitions stated in terms of the categories used in NFIRS. Whenever occupancy scenarios can be defined using nationally representative, valid fire incident data, the analyst will have the strongest possible basis for estimating probabilities. The principal weakness of this data source involves the level of detail of readily available fire incident data, which often falls well short of the detail needed to run the fire hazard analysis portion of the method.

Specifying Goals, Objectives, and Measures

Overall goals for fire safety tend to fall into one of the following categories:

- Prevent adverse health effects, particularly fatal injury, to people exposed to fire. Emergency responders are normally addressed separately and may be excluded from consideration.
- Prevent monetary losses due to direct property damage.
- Prevent indirect losses due to fire, such as business interruption, missed work, and temporary housing. The types of indirect losses will differ for residential versus nonresidential occupancies, as will the relative importance of direct damage versus indirect loss.
- Prevent environmental damage. This may be damage due to fire, damage incidental to firefighting or other suppression activities, or damage associated with fire prevention or protection strategies. The negative impact of some fire retardants on recyclability of plastics could be addressed under the latter type of goal.
- Prevent harm to cultural heritage. This refers to historic buildings and similar structures for which fire damage may be more expensive or impossible to repair if historical authenticity is an objective.

A fire risk assessment of products can be conducted using the overall goals and objectives. It is also possible to use the overall goals and objectives to set functional statements for the product class.

For fire risk assessment, both severity and likelihood are important measures. Two common summary measures are expected loss (i.e., a sum over all scenarios of scenario probability times predicted scenario hazard) and probability of loss exceeding a certain threshold. Both measures can be calculated for a baseline directly from nationally representative fire incident databases, provided that the product class and property use specifications match the categories used in those databases. For example, a fire risk analysis comparison of the major types of home heating equipment is possible, because each can be identified within the fire incident databases. However, a comparison of different designs for, say, portable electric heaters could not be done using national statistics alone, because different designs are not distinguished in the national database.

Even if the national data suffices to set the baseline, a product fire risk analysis will usually require test methods and models to develop likelihood estimates and possibly revised consequence estimates for the new product. In such cases, estimation of consequence can often be simplified by focusing on flashover, and specifically on whether flashover occurs, and if so, how quickly:

1. Likelihood of flashover and/or of flame spread beyond the room of origin
2. Likelihood that time to flashover exceeds x minutes (where x could be chosen to reflect

the expected arrival of suppression and rescue forces or the time required for occupants to safely exit the building)

One approach that should usually be avoided is to try to measure loss in terms of the product's share of responsibility for overall fire severity. Such measures tend to be far too subjective and require answers to inherently unanswerable questions. For example, suppose a small trash can fire leads to a large couch fire. If *either* factor in the initial trash ignition or the burning properties of the couch is changed, no large fire would have resulted. How much loss should be assigned to the couch? There is no good answer to that question.

Instead, fire risk analysis should proceed through calculations of differences, that is, fire risk with the product of interest versus fire risk with something else substituted for the product of interest.

From this perspective, one can see how fire risk analyses can be constructed as extensions of past successful applications of fire modeling. For example, one of the earliest practical applications of the Harvard code was to the reconstruction of the 1980 MGM Grand Hotel fire. As suggested above, flashover was used as a well-defined event to focus the analysis, after it was shown that most of the fatal fire victims would have survived if flashover had been prevented. Professor Howard Emmons then used the model to rerun the fire with changes, considered individually, in the room of origin's ceiling covering; its benches and chairs; and the area's heating, ventilating, and air-conditioning (HVAC) arrangements.

If one wished to do a fire risk analysis on, say, benches and chairs for dining areas of hotels, one could define a range of possible fire scenarios, do a similar fire development analysis of each, weight the consequences by the scenario likelihoods, and thereby calculate an overall likelihood of flashover with two different choices of benches and chairs. The difference between the two likelihoods would be a valid product fire risk measure.

Setting Assumptions

Fire risk assessment requires the analyst to make assumptions. Some of the assumptions are embedded in elements of the analysis, such as a zone model's assumption that fire conditions in a room can be reasonably approximated by dividing the room into an upper and a lower layer. Some assumptions set boundaries to the analysis, such as an assumption that an effective local public fire department will respond within 5 min, which permits the designer to track fire development and effects for a limited period of time.

Many assumptions address the building, occupant, fuel load, or system characteristics that do not vary from one scenario to another. These assumptions may be treated as scenario characteristics in one assessment and as assumptions in the next assessment. Therefore, the more detailed discussion of elements of scenarios, in the next section, also applies to most of the candidate assumptions.

There is a critical difference in the handling of assumptions in fire risk assessment versus fire hazard assessment. In fire risk assessment, the purpose of the calculation is to predict what *will* happen. Challenging, high-severity scenarios must be addressed but given only as much or as little weight as the probabilities of those scenarios would justify. In fire hazard assessment, the purpose of the calculation is to predict what *might* happen for which the designer is responsible. This is where concepts like *probable worst-case scenario* become relevant. Fire hazard assessment needs to address only challenging, high-severity scenarios, and does not discount the scenarios it addresses by their probabilities. But some high-severity scenarios will be declared too challenging for a fire hazard assessment. Thus, fire hazard assessment takes an all-or-nothing approach to scenarios.

Fire risk assessment, for these reasons, will assign more variables to scenarios and fewer to assumptions than will hazard assessment. Fire risk assessment needs to address all possible scenarios. But fire risk assessment will tend to

set assumptions in terms of reproducing conditions that are typical or average *for the particular scenario or scenario cluster*.

Put another way, fire hazard assessment—a typical engineering analysis—addresses the potential for high-challenge, very severe fires by deciding which of those fires need to be addressed to satisfy the acceptable safety thresholds and constructing and conducting the analysis accordingly. Fire risk assessment addresses the potential for high-challenge, very severe fires by creating scenarios clusters of such fires so that they will receive the appropriate weight in terms of their likelihood and their severe consequences will not be lost amid a much larger number of less severe fires in the same scenario cluster.

Specifying Fire Scenarios: Using Fire Size to Shape Calculation of Change in Consequences

The baseline fires should be marked not only as to loss but also as to fire size. The fire size scale used in NFIRS has the following categories: A critical element in this approach is data on final extent of flame damage, which are captured in the major fire incident databases, as follows:

- Confined to certain specific objects—cooking vessel, chimney, flue, boiler, fuel burner, compactor, incinerator, or trash
- Confined to object of origin
- Confined to room of origin
- Confined to floor of origin
- Confined to building of origin
- Extended beyond building of origin

It may be easier to estimate how a product change will alter the mix of fire sizes, then use estimates of loss per fire as a function of fire size, than to develop a more sophisticated and precise estimation of fire size and then cope with the absence of comparably detailed data tying detailed fire size to estimated loss per fire. Also this scale directly identifies two key events in fire development—spread beyond the first fuel package and spread beyond the room of origin (which is the best proxy for flashover available in the national fire incident database).

One can assume that a fire confined to object of origin involved only the first item ignited and that a fire extending beyond the room of origin reached flashover in the room of origin.

When fire spread beyond the first item ignited and especially when fire spread beyond the room of origin, it is possible to isolate the fires for which the product class provided the item contributing most to fire spread or flame spread and to limit that group to fires in which the same product class did not provide the item first ignited. With this calculation available for calibration purposes, the risk analyst can construct and weight representative scenarios—specifying burnable items near the first item ignited and near the product, as well as room dimensions and linings—so that the models used to estimate consequences will reproduce the baseline statistics, showing the baseline's historic likelihoods of fire spread beyond the room of origin and of product involvement as the item contributing most to fire spread.

Specifying Fire Scenarios: Characterizing the Environment the Fire Is Growing Into

The previous section indicated the need to specify scenarios and then calibrate that the specifications and weights will reproduce the baseline characteristics of historic fire experience as closely as possible.

This section provides an overview of the characteristics of the environment around the product and the initial fire that will likely need to be included in those specifications.

1. *Nearby combustibles*. Characteristics of the fuel load of the room of origin whose burning properties and proximity to the initial fire and the product may play a significant role in fire development.
2. *Room linings*. Thermal properties of rooms that may bear on burning at and after flashover.

3. *Building dimensions and geometry*. Dimensions of rooms and other areas in which fire may grow or smoke may spread.
4. *Openings*. Dimensions of openings between rooms and areas relating to paths of flame or smoke spread and sources of air to feed the fire.

Nearby Combustibles One can use surveys of typical fuel loads, room configurations, and the like. Then, one can run a fire growth model with these specifications. Such survey data are very scarce, but when they exist, they may not be in the form needed. What you would like ideally would be a large database on the probability distribution of distances between possible first ignited items and the product, and a second large database on the heat flux profile for burning objects from each of the categories of possible first ignited items. The latter may be available, but the former generally is not. The surveys that are available may provide detail on too many specific combustibles, most of which will not be major contributors to the fire, or too little detail, specifying only mass per square meter normalized to some heat of combustion figure. There are few if any published examples of developing scenarios in this way, which means the risk analyst will need to experiment until he or she finds an approach that provides credible, useable results.

As in so many other areas, the temptation will be to reshape the analysis to bypass elements that cannot now be modeled with confidence. However, the analysis must somehow provide a valid basis for combining different product burning properties, and the phenomenon of secondary ignition is central to any evaluation of the product's relative ignitability. Each of the questions needs to be answered through a crosswalk between the physical parameters measured in tests and used in models and the parameters recorded in fire incident databases, because the latter is always needed to calibrate probability estimation.

Room Linings Linings of rooms and other areas need to be addressed in terms of the thermal properties required for calculations of time to flashover, speed of vertical flame spread, and the like.

Room and area linings for most occupancies are tightly regulated by codes. However, some of the most important occupancies (e.g., dwellings) are not so covered, and even for those that are, one must allow for a significant probability that the codes will not have been in force when fire occurs. Unfortunately, there is little or no data on the probabilities of different combinations of fuels in particular occupancies; and there is only very limited, dated information on typical or average fuel loads and only for some occupancies.

Building Dimensions and Geometry The overall building size and geometry can be structured into a series of questions on which data must be sought and decisions made. The first is the range of variation in the number of floors. After determining this point, the user must specify a number of floors for each occupancy scenario and assign a probability to each.

The second is a room layout for each floor. Room heights and the sizes of openings connecting rooms tend to be standardized by common industry practices, so there may be no need to consider variations. For other factors, (e.g., the number and sizes of rooms) there usually is too much variation in practice and too little data on the relative likelihood of these variations to do much more than (1) estimate one or two values for the number of rooms or the total square feet per floor, and (2) use expert panels to develop detailed layouts for the purposes of modeling and analysis of the rooms or spaces specified in (1).

However, panels of people who are experts on buildings of a certain type are likely to think in terms of the characteristics of the particular buildings they know best. They may therefore give estimates biased toward characteristics of new construction or characteristics of the buildings they live in or frequent. Fires are more likely to occur in smaller, less prestigious units in any property class. The expert panel needs to be continually reminded to adjust their perspective to think in terms of those kinds of buildings.

Openings There usually will be some information on the sizes of doors and windows, because construction practices are highly standardized even beyond code requirements. However, in a fire, the openings will depend critically on whether and how much key doors and windows are open. There are little or no data on this point for any occupancy. It may be possible to ignore windows, because there are studies indicating that windows affect most fires only after the point in time where fire severity has been determined. (However, the few exceptions will tend to be very large fires, so the reasonableness of an assumption excluding windows will need to be rechecked for any analysis.) How does one set the assumptions for doors, short of large-scale property surveys or special fire data collection projects?

For most fire protection engineering studies, the answer would be to make conservative assumptions, that is, those that present the greatest fire challenge. It is important to understand that this is usually not the right answer for fire risk analysis. If conservative assumptions lead to an overestimate of fire risk, then they may also lead to a gross overestimate or underestimate of the fire risk consequences of particular product choices. There is no substitute for a best estimate, without conservatism, in fire risk analysis.

However, an assumption that might be made in fire hazard analysis because it is conservative may also turn out to be a reasonable best estimate for fire risk analysis, if it reflects a pattern in actual fire experience. If a certain arrangement *could* produce more serious fires, it qualifies as a conservative assumption for fire hazard analysis. If that same arrangement *is producing* more serious fires, then it is more likely that that arrangement is present when a reported fire occurs than that it is present in buildings in general, and one could be justified in assuming that that arrangement is likely, in a fire risk analysis.

However, this line of reasoning has limits. Suppose that open doors is the conservative assumption, but that we know that doors tend to be open only 5 % of the time. In that case, the fire risk analysis could reasonably assume that doors are open 10–20 % of the time, reflecting the likelihood that open doors will be more likely in reported fires than in buildings, in general. But the typical situation would still be closed doors.

The analysis would need to have scenarios with open doors and scenarios with closed doors, because neither condition is dominant enough to justify omitting the other condition for a variable (i.e., whether doors are open) that is so influential on final fire size. Or, it might be possible to use one condition, consisting of doors open slightly, trying to seek a single physical condition that will reproduce the appropriate average between fully open and fully closed. Either way, considerable judgment would be needed.

Remember that, if an *average* value is used, the analyst is implicitly assuming that the fire severity associated with that average value is equal to the average of the fire severities associated with all the individual values that occur. In mathematics, this is sometimes called assuming that the average of the function equals the function of the average, and it is not usually the case. The analyst has to make the case that the assumption is reasonable in the situation being analyzed.

Specifying Fire Scenarios: Exposure of People or Property

The baseline will provide the analyst with the basics of loss per fire—life, health or damage—for different groups of fires. However, if the calculation indicates changes in fire development for particular groups of fires, then it will be necessary to match modeled predictions of changes in fire effects as a function of time and location with modeled predictions of target presence and vulnerability, also as a function of time and location. One must address (1) the locations of people or property as a function of time; and (2) the damage or loss consequences to people or property of the different possible physical characteristics of fire, for example, temperature,

quantities of toxic gases by type, corrosive properties, and quantities of smoke. The methods for doing this are not extensively developed, except for deaths. Therefore, this section will focus on that outcome.

Occupant exposure depends on (1) initial locations of the occupants relative to the fire, and (2) their escape behavior. A complete specification of the number of occupants with their initial locations and other characteristics is called an *occupant set*. The user must first define a group of occupant sets that can validly represent all possible combinations of people and their characteristics and locations, and then must estimate probabilities for each. These must then be joined to a model of occupant behavior. (See Custer and Meacham [2] for a list of evacuation models.)

Occupant behavior models consist of a set of rules for calculating the locations of occupants at a time, *t*, as a function of their locations, other occupant characteristics, and fire characteristics at the time stage just prior to *t*. Some such models track occupants individually; others give only the number of people at each location. Some, but not all, models include interactions among occupants, such as congestion or queuing effects or behavioral rules based on relationships between occupants (e.g., parents who seek to rescue babies). The more comprehensive the model may be in capturing potentially important phenomena, the more computationally demanding it will be and the more data it will demand, possibly including data that are not readily available. As in all other aspects of fire risk analysis, tradeoffs must be made in the modeling.

A brief summary of the steps required is as follows:

- Develop a probability distribution for the number of people present in the building.
- Expand the basic distribution to address relevant characteristics, including ages and relationships of occupants, time of day, and occupant conditions.
- Develop probability distributions for occupant activity as a function of time of day and of occupant characteristics, specified in the previous step.
- Develop probability distributions for occupant location given occupant activity and other occupant characteristics. (If every activity implies a unique location, this will reduce to a crosswalk.)
- Combine all probability distributions to produce a probability distribution for all occupant sets. Merge very similar occupant sets, if needed, for computational simplicity.

Specifying Fire Scenarios: Fire Protection Systems and Features

Here again, this modeling is only necessary if the analyst has shifted into the use of physical models to estimate changes in consequences. The baseline will usually indicate whether fire protection systems were present and whether they were operational, and so the calculations here will need to focus on performance under different fire conditions. Here again, there are few if any published examples of fire risk analysis using these approaches—most product fire risk assessments limit their scope to prevention—but there is increasing interest in product fire performance during the fire's growth phase.

It will be necessary to specify rules for how the system or feature will affect the fire development, the evacuation, or other conditions being tracked. Often, this will be fairly simple. One could assume that a fully operational sprinkler system will activate once a specified set of fire conditions are reached and, once activated, will totally and immediately stop the fire, except for certain specified fire scenarios (e.g., fire origin in concealed spaces), when its effect will be only to block fire entry into sprinklered areas. One could assume that a full-coverage automatic detection system will activate once a specified set of smoke or heat conditions is reached and, once activated, will alert everyone in the building to the fire, leading anyone not already in motion in the occupant evacuation model to begin evacuating. In fact, both these examples are oversimplified and possibly dangerously so. A sprinkler's full effect on fire and a detection/alarm system's full effect on occupant behavior will not be

instantaneous. The delay may be critical to outcomes and needs to be addressed in the analysis, if only to make explicit what simplifying assumptions have been made.

Identifying Test Methods and Models

Analyzing Ignition Probability While historic fire data may suffice to estimate ignition probabilities for the mix of existing products, they may not suffice to estimate ignition probabilities for specific existing products, and they will not suffice for new products. The basic approach involves converting laboratory test results to ignition probabilities.

Probabilities of ignition must be estimated from frequencies of ignition in laboratory tests of existing and new products. In essence, it is assumed that, if the new product produces more or fewer ignitions in laboratory tests than the existing products did, then the new product will have a higher or lower probability of ignition, increased or decreased by the same proportion as the ratio of the laboratory ignition frequencies. This key assumption is rarely literally true, because the test conditions are rarely weighted so as to provide a valid representation of the variety of real fire initiating conditions. Sensitivity analysis is especially important.

For fuel-source products, this estimation should be done separately for each of the major classes of heat sources (e.g., flaming versus smoldering), because product ignitability may vary across different heat sources. For heat-source products, it should be done for suitably chosen classes of initial fuel sources.

To prepare a set of laboratory test data for use in these calculations on a fuel-source product, organize the data according to the following terminology:

- Distinguish different versions of the product ($i = 1, 2, \ldots$).
- Distinguish different heat sources ($j = 1, 2, \ldots$).
- Estimate the share of all the product now in use that is version i; call this q, where $\Sigma_i\ q_i = 1$.
- Let N_{ij} be the number of times that version i of the product has been tested in the laboratory against heat source j; let n_n be the number of times that ignition occurred; and let $f_{ij} = n_{ij}/N_{ij}$.
- Let p_j be the probability of ignition of the mix of existing product by heat source j, calculated from fire experience data on the occupancy being studied.

Then assume that p_j (the product's overall probability of ignition) is proportional to $\Sigma_i\ q_i f_{ij}$ (the weighted frequency of laboratory ignitions). For a more sophisticated approach, one may wish to use Bayesian analysis, which requires estimating prior probability distributions to which one can apply the lab tests.

- Let f_{Ij} be corresponding values summarizing laboratory tests on new product I against heat source j. Note that every heat source must have its own body of test results.
- Let p_{Ij} refer to the quantities to be estimated, which are the probabilities of ignition of product I by each heat source j. Estimate as follows:

$$P_{Ij} = P_j \left[\frac{f_{ij}}{\left(\sum_i q_i f_{ij} \right)} \right]$$

In general, the p values will be much smaller than the f values, which is assumed to reflect the fact that the p values incorporate all the probabilities involved in bringing the heat source and the product in contact with one another. This estimation procedure is not so reliable if the f values are equal to, or very near, 0 or 1. Bayesian analysis is definitely required in such cases.

Calibration, Sensitivity, and Uncertainty Analysis Any fire risk analysis will involve complex calculations, with many unavoidable assumptions. While you should not use a more complex method than necessary, you also should not use a less complex method than is valid. A fire risk analysis model without a long list of stated assumptions is bound to be a model with many hidden assumptions, which are almost certain to be less well-founded, if examined, than a list of shaky but explicit assumptions.

For these reasons, running the calculations in a product fire risk analysis is easier to do well than the blend of science and art required to set up the analysis correctly (e.g., appropriate models, reasonable assumptions, best data) and to interpret the results, which includes calibration and sensitivity analysis.

Every step, starting with framing the problem and choosing the models, tests, and data, is subject to error and uncertainty, and that uncertainty must be examined in any interpretation or evaluation of the analytical conclusions. A design analyzed as having an acceptably low risk may also have enough uncertainty in the analysis to create a significant probability of unacceptably high risk.

The principal rule to remember is that the model is calibrated by assessing how well it reproduces recent fire experience from data on recent product use patterns and other practices. If the model captures the principal aspects of fire risk, then it will predict rates of loss that are very close to those actually experienced in the properties being analyzed. Results should be close not only from an overall perspective, but also for major groups of scenarios. Use the specifics of the scenarios that need better calibration as guides to which assumptions need to be modified. For example, if predictions are poor for fires with long smoldering periods, but good for all other fires, then one might want to adjust the assumptions on length of smoldering period or on fire profiles (e.g., rate of heat release curve) during smoldering periods.

Some options involve changes not just to the parameter values, but to the model structure. Examples include changes that would further multiply scenarios by allowing for multiple values (and associated probabilities) of walking speeds, evacuation decision rules, rules for waking people without detectors, and so forth.

Another approach to calibration is to use the model not to directly predict losses, but to predict percentage changes in losses due to product choices, by major scenario group. The advantage of this approach is that it allows the analyst to use the fire experience statistics to do a great deal of automatic recalibration. The disadvantage is that it does not directly address, or correct, the flawed assumptions and estimates that are preventing the model from producing accurate results without such recalibration.

Most analysts will need to both (1) adjust the structure of the analysis, and (2) use fire statistics to recalibrate.

Identify Data Sources

Product and Property Survey Data There are many good sources of national data on the characteristics of occupancies or products in general. For occupancies, this kind of data may be obtained from ongoing federal government data collection activities (typified by publications of the U.S. Census Bureau; the General Services Administration, e.g., fuel load per room, by type of room; and the U.S. Departments of Defense and Energy), from major one-time studies, or from industry association surveys (e.g., Building Owners and Managers Association, American Hotel and Motel Association, and American Restaurant Association).

For products, there may exist market surveys on patterns of composition or use. The U.S. Census Bureau and, for certain types of products, the U.S. Departments of Commerce, Energy, Housing and Urban Development, and Health and Human Services are all likely sources of information. Much of the data gathered by the U.S. government can be found in summary form in the *Statistical Abstract of the United States* or in the primary sources cited by the *Statistical Abstract*, now that the *Statistical Abstract* as a publication has been discontinued by the U.S. government. Another source of information is the U.S. Consumer Product Safety Commission, which carries out some field surveys of product performance and usage.

Chapter 78, gives specific references for these data sources if they are readily accessible. Industry association data are available through the association's periodicals or by special request to the association.

For products, however, often the only source of such information is trade associations of

manufacturers and sellers of the product. It is important to recall, however, that some products have a lifetime longer than that of a trade association, which means the association's knowledge of current industry practice, however accurate, may not describe use patterns as a whole. Upholstered furniture, for example, is typically cushioned today with synthetics, with previously used natural materials, such as cotton batting and horsehair, now a rarity. Nevertheless, the lifetime of a piece of furniture can be 30 years or more, during which time it may be re-covered several times and pass through several owners, often of continually diminishing economic station. Therefore, it is reasonable to expect that a substantial fraction of the current furniture inventory retains the burning characteristics of products of a bygone era.

In general, people knowledgeable of today's product will tend to have statistics on, and think in terms of, what is currently being *sold*, not what is currently being *used*. Translating sales data into usage statistics is far from straightforward. Moreover, one might suspect that such products would be found disproportionately where fires are likely to be more common, that is, among people and places at the lower end of the economic spectrum.

For the method to operate, all of these qualitative observations must take a quantitative form, and it is the analyst who must decide how this is to be accomplished.

Always remember that, although data on national practices are more representative of the nation than fire incident data, they are less desirable for that very reason for fire risk analysis, because they do not provide probabilities implicitly weighted by the likelihood of having a fire. For example, if you walked into a randomly selected U.S. home in 1989, the chances were better than 85 % that you would find a smoke detector present; but if you focused on homes that had fires, the chances would drop below 50 %. It is the latter probability that is more relevant in determining how risk will develop in home fires. Therefore, when data on national practices are used, it is necessary to review the data for any adjustments that may be needed to better estimate probabilities relevant to fires.

Code Requirements Many relevant building characteristics are covered by provisions of building and fire codes. Some product fire characteristics also are covered by regulations. In the absence of direct data from the field, one may assume that all buildings and products have the characteristics implied by compliance with these codes and regulations. This assumption bypasses the need for probability estimation and usually provides enough detail to permit calculation of the input needs of the fire hazard analysis method.

When this approach is followed, the analyst needs to check a number of points that may undercut the central assumption of the approach, namely, that all buildings and products are as the codes and regulations would have them. In practice, many code provisions are of fairly recent vintage so that they were not in place when many or even most of the buildings and products now in use were put into place. Some jurisdictions do not follow national consensus codes, and many more lack the enforcement apparatus to ensure a high rate of compliance. Buildings and products can be altered or may deteriorate after being built, manufactured, or sold. And some building and product features may be better than code requirements because of marketplace demands.

Putting all this together, it is important that the user verify, through the expertise of people with broad familiarity with the state of old and new buildings and products around the country, that the particular characteristics of interest are ones where the code provisions are good indicators of actual practice in nearly all buildings and products in recent use.

Expert Judgment When all else fails and numbers are needed, there is no alternative but to make the best estimates possible. In some cases, it will be a judgment made by the user alone, but especially in areas where the user is least experienced, one or more true experts should be sought. For example, if the user is a maker or seller of the product, it would be wise to make use of fire scientists for assistance in assigning values to the product's fire properties.

One of the persistent potential pitfalls in the method is the danger that the typical product in use is not the typical product involved in fires. There is no foolproof way to avoid this situation, but one way to address it is to include fire service personnel in drawing up the profile of product characteristics. Firefighters and fire marshals see the products involved in fires, whether or not they make up a substantial fraction of the statistical profile of the product.

Another pitfall is that, no matter what the expert's area of expertise, he or she may tend to underestimate the (typically) enormous variation in every characteristic of interest. Manufacturers may focus on a few best-selling versions of the product; surveys may focus on a few most widely used versions; and fire officials may focus on a few of the worst, most obsolete versions, seen in the worst (but not necessarily the most) fires. This illustrates the value of (1) a panel of experts, where biases can be balanced; and (2) a facilitator sensitive to the variation in practice, who can steer the group away from premature or overly narrow consensus.

It also suggests that, even when data are available, expert judgment is needed to interpret the data and apply them correctly. Knowledge of common versus uncommon practices, relevant codes and standards, and the length of time they have been in place, are among the kinds of information essential to spot areas of likely bias or critical uncertainty.

For all these reasons, the user can expect to make extensive use of expert judgment and should make sure that the expertise available to the project is both broad and deep.

References

1. Society of Fire Protection Engineers, *SFPE Engineering Guide to Performance-Based Fire Protection: Analysis and Design of Buildings,* National Fire Protection Association, Quincy, MA, and Society of Fire Protection Engineers, Bethesda, MD (2000).
2. R.L.P. Custer and B.J. Meacham, *Introduction to Performance-Based Fire Safety,* Society of Fire Protection Engineers, Bethesda, MD, and National Fire Protection Association, Quincy, MA (1997).
3. Society of Fire Protection Engineers, *SFPE Engineering Guide to Fire Risk Assessment,* Society of Fire Protection Engineers, Bethesda, MD (2006).
4. ASTM E1776, *Standard Guide for Development of Fire-Risk-Assessment Standards,* ASTM, West Conshohocken, PA (2012).
5. ASTM E1546, *Standard Guide for Development of Fire-Hazard-Assessment Standards,* ASTM, West Conshohocken, PA (2012).

John R. Hall Jr. is retired from the division director for Fire Analysis and Research of the National Fire Protection Association. He has been involved in studies of fire experience patterns and trends, models of fire risk, and fire department management experiences since 1974 at NFPA, the National Bureau of Standards, the U.S. Fire Administration, and the Urban Institute.

Health Care Application of Quantitative Fire Risk Analysis

85

Håkan Frantzich

Introduction

Quantitative risk analysis (QRA) is a very powerful tool with which the fire protection engineer systematically can analyze fire safety problems. Risk analysis methods have during the last decades become more common for analyzing fire safety problems. This is partly because of the development of fire simulation tools enabling a quantitative estimation of the consequences. The increased use of risk analysis methods can also be traced back to the development of performance-based regulations and standards [1–4]. In such regulations and standards the requirement is to verify that the proposed design solution meets the fire safety objectives but they do not necessarily state how this shall be performed. The engineer, therefore, needs some tools by which he or she can structure the relevant problems and transform them to engineering problems that can be solved. Risk analysis is such a structured method.

Other chapters in this handbook provide the overall framework for performing a fire risk analysis. As evident the term *risk analysis* has no clear definition. It is, therefore, important to give a clear description of the meaning of risk analysis for every single case. It is important to state if the analysis is deterministic or probabilistic (i.e., implicitly how uncertainties are handled). This chapter deals with a quantitative and probabilistic approach to a fire safety problem.

To illustrate the methodology a sample case will be analyzed. The risk analysis covers patient safety on a fictive hospital ward. Although many of the assumptions can be traced back to Swedish building traditions, the methodology is universal. It must be noted that the calculations made are purely for the demonstration of the methodology and some of the assumptions may not be so well-founded. The sample calculations are complemented with discussions, many of which represent the personal opinion of the author. It is assumed that the reader is familiar with quantitative risk analysis procedures.

The risk measures will be derived using a standard procedure for a QRA. An extended procedure of a QRA will also be presented at the end of the chapter. The extended risk analysis can be used if one, for example, will answer the question: *How certain are we on the calculated risk measure*?

In the analysis the endpoints define when escape no longer is possible. This state will be derived using the kind of untenable conditions that are not considered lethal as is customary in fire safety engineering. It should, however, be pointed out that in using QRA for other engineering disciplines, lethal levels of untenable conditions are frequently used. There is no problem in using different definitions of untenable conditions as long as the tolerable risk levels are defined in the same manner. In performing

H. Frantzich (✉)
Department of Fire Safety Engineering,
University of Lund, Sweden

M.J. Hurley (ed.), *SFPE Handbook of Fire Protection Engineering*,
DOI 10.1007/978-1-4939-2565-0_85, © Society of Fire Protection Engineers 2016

comparative analyses, the choice of untenable levels becomes even less important. The level chosen to define untenable conditions is given by conditions commonly used for design purposes in Sweden.

For the extended QRA procedure at the end of the chapter, however, some slightly more severe conditions are used in the calculations. The reason for changing endpoint conditions is to observe the effect of the change.

Hospital Ward System Limits

General Assumptions and Limitations

The first step in this sample risk analysis is to define the engineering problem. This step is the most important as decisions made here affect the rest of the analysis. The problem is structured according to the event tree methodology. To limit the size of the event tree some limitations are introduced. First, the analysis is restricted to only one ward in the hospital. Second, only one fire source is used for the illustration. Third, the only targets specified in this analysis are the patients on the ward. A more complete analysis, not shown here, should cover all possible fire locations, sources, and targets including the staff members.

More fire sources and fire locations may not necessarily increase the reliability of the risk measures. The chosen fire source and location are assumed representative of all sources and locations on the ward. Separation of the chosen fire location into more locations could be performed within the analysis (Fig. 85.1).

When further subdivisions in the event tree are made, the result will only affect the resolution of the societal risk profile. It is then assumed that the initial part of the event tree is unaffected.

The current analysis, using only one representative fire source, will result only in a slightly less detailed risk profile.

Multiple fire sources are implicitly considered in the extended QRA as the development of the fire is subject to uncertainty. In this standard QRA procedure, a representative value is used for all fires chosen according to principles for this type of analysis.

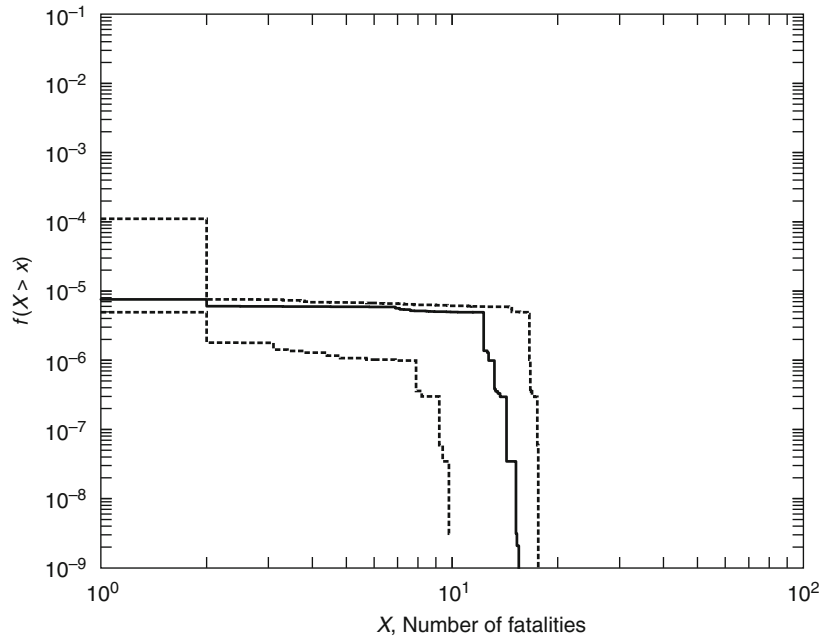

Fig. 85.1 Multiple fire scenario analysis

The magnitude of the societal risk is dependent only on the risk analysis perspective (i.e., whether the analysis covers one ward or the whole hospital). Therefore, the physical boundaries of the analysis must be made appropriately.

The risk analysis could be extended to consider, for example, the whole hospital. If a larger part of the hospital is considered in the analysis, the fire frequency will also be higher because of the higher number of possible fire locations. If this more global analysis is chosen, the event tree and initial frequency must be chosen accordingly, which can be illustrated as shown in Fig. 85.2.

The probability of the fire starting in any of the wards in the hospital will not differ due to the more global analysis perspective, but the total frequency of fire occurring will be higher for the whole hospital. This result displaces the risk profile higher up in the diagram, indicating a higher risk than when only considering a single ward.

If identical situations are assumed for the four wards in Fig. 85.2 and the likelihood of fire occurrence is the same for all the wards, the societal risk profile for the whole hospital is increased by a factor of four compared with the single-ward risk profile. The consequences are not changed, if the fires are independent events and fire spread between wards is neglected, but the probabilities are increased. In the real situation it might not be appropriate to assume similar likelihood of fire in the wards. Different activities on the wards and differences in types of installations may affect the likelihood of fire breaking out.

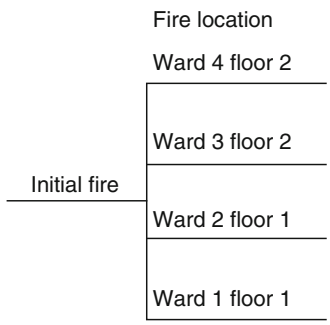

Fig. 85.2 Example of initial part of a complete event tree for risk analysis of a smaller hospital

The true risk level for the hospital is, of course, dependent on the actual situation on each floor, but the fire probability at a specific location is not changed by changes in the analysis perspective. Therefore, the risk measures will depend on the limitations set out for the analysis. If tolerable risk measures are available, it might be possible to determine the maximum allowed size of, for example, a building, as the risk increases with building size.

It is also necessary to be aware of how "the society" is defined. From a societal point of view it may be different, with respect to fire hazards, whether we have one hospital with four wards or four hospitals with one ward each. The risk to society is the same but the societal risk for each facility is different. This is based on the assumption that the fire does not spread from one ward to another in the four-ward hospital.

The purpose of this example is merely to demonstrate the methodology. It is assumed that the quantitative risk analysis has been preceded by qualitative screening methods to determine the quantitative scenario. The members of staff are excluded from the risk measure and are only considered as an aid to patient evacuation.

Hospital Ward Conditions

The calculations are performed on a hospital ward with fixed dimensions. It is always assumed that the fire is located in a room close to one exit preventing it from being used. Figure 85.3 shows the assumed ward with 11 patient rooms, a TV room, and a staff room. The exit to the right leads to a protected lobby, which, in the other direction, is connected to a second ward. The patients and the staff are considered to be safe when they have reached the protected lobby.

All rooms in the ward are $5 \times 6 \times 3.2\ m^3$ and the corridor is $35 \times 3 \times 3\ m^3$. All patient rooms are equipped with one window to the outside and a door leading to the corridor. The window is $0.9 \times 0.9\ m^2$ and the windowsill is located 1.2 m

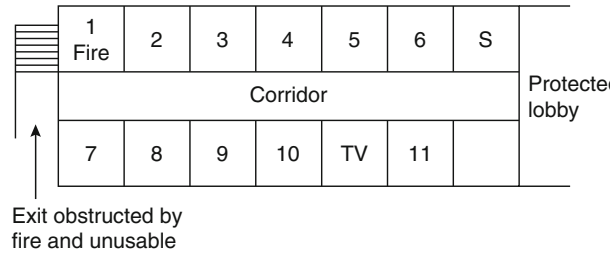

Fig. 85.3 Ward layout, with *TV* indicating a TV room and *S* indicating the staff room

above floor level. It is assumed that the window is initially closed in the fire room and breaks when the fire in the room reaches a certain temperature. The door between the patient room and the corridor is 1.2×2.1 m^2. It may be open or closed according to the scenario definition.

The door between the corridor and the protected lobby is open only during evacuation. Otherwise it is closed, as it is equipped with a closing device. The door has a height of 2.1 m. The patient rooms are not separate fire compartments, but it is assumed that no smoke can leak directly from one patient room to another. The walls between the patient rooms and the corridor prevent smoke from leaking into the corridor.

The ceiling and walls are covered with gypsum plasterboard and the floor is concrete. These conditions are common for the whole ward.

The ward is equipped with a sprinkler system designed to extinguish a fire. The sprinkler system is designed according to the current regulation. The sprinkler heads activate at a temperature of 68 °C and are of quick-response type (*RTI* value $35\sqrt{m \cdot s}$). The coverage area of each sprinkler head is 20 m^2, which means two sprinkler heads per patient room.

The likelihood that a sprinkler system will work and be able to extinguish a fire is assumed to correspond to a probability of operation of 0.96. This value is chosen based on judgement combined with information in Bukowski [5]. This value will be used without any uncertainty.

An automatic fire alarm system is installed in the building. The alarm system is equipped with smoke detectors in every patient room and in common areas. The alarm system does not only indicate the presence of a fire but also gives an alarm to the staff and patients in the ward. The sounding of the alarm informs the staff that there is a fire in the ward.

Table 85.1 Proportions of patients in various groups according to need for help in evacuation

Need for help	Day Sleeping	Day Awake	Night Sleeping	Night Awake
Much help needed	0.70	0.10	0.75	0.10
Little help needed	0.20	0.20	0.15	0.15
No help needed	0.10	0.70	0.10	0.75
Total	1.00	1.00	1.00	1.00

The likelihood that the automatic fire detection system will work and be able to detect a fire is assumed to correspond to a probability of operation of 0.94. This value is chosen based on judgment combined with information in Bukowski [5]. The reliability of this system is considered less well defined than that of the sprinkler system. It has, therefore, been subjected to uncertainty in some of the extended QRA calculations. The probability of operation will then follow a uniform distribution (0.9, 0.98). The mean probability value will be the same with and without the uncertainty consideration.

Patients and Members of Staff

There are 22 patients on the ward, two in each patient room. The physical conditions of the patients may vary according to the scenario. Three different physical conditions are used to determine their need for help and their mobility. The number of patients in each of the three categories depends on whether day or night is considered (Table 85.1). These proportions, used as branch probabilities in the event

Table 85.2 Duration of t_{care} and t_{patM} for the standard QRA

Awake or asleep	Need for help	t_{care}	t_{patM}
Awake	None	10	25
Awake	Little	15	40
Awake	Much	20	50
Asleep	None	13	25
Asleep	Little	25	50
Asleep	Much	40	60

Note: Values are in seconds

Table 85.3 Duration of t_{care} and t_{patM} for the extended QRA

Awake or asleep	Need for help	t_{care}	t_{patM}
Awake	None	(5, 5)	(20, 5)
Awake	Little	(10, 5)	(30, 30)
Awake	Much	(15, 5)	(40, 40)
Asleep	None	(10, 3)	(20, 5)
Asleep	Little	(20, 5)	(40, 30)
Asleep	Much	(30, 10)	(50, 30)

Note: Values are the mean and standard deviation in seconds

tree, are arbitrarily chosen and may vary between wards.

Help is needed to make the patient aware of the situation and to prepare the patient for evacuation. Different patient categories require different amounts of time. The time period, t_{care}, is defined as the time spent by the staff in preparing a patient for movement and the physical movement time to the corridor. The values of t_{care} for the six different patient categories are given in Tables 85.2 and 85.3.

Rather low values have been chosen for t_{care}. This implies that patients requiring a great deal of help in preparation and movement have been excluded from this investigation. The movement time along the corridor to the safe lobby is determined by t_{patM} and includes the time required by the staff to reach the next patient. In the extended QRA, both t_{care} and t_{patM} are normally distributed.

The number of staff members on the ward depends on whether it is daytime or nighttime. During the day, four nurses are on the ward and during the night two nurses are on duty.

After the fire has been detected by either the automatic fire alarm or manually, the staff spend some time reacting and interpreting the situation. As they are trained to respond to various kinds of signals, the response time, $t_{\text{resp}}^{\text{staff}}$, is rather short. The staff response time is assumed to be normally distributed (10, 3) seconds in the extended QRA. In the standard QRA, the value is assumed to be 10 s.

Table 85.4 Untenable conditions

Type	Tolerable	Severe
Radiation at floor level	2.5 kW/m^2	2.5 kW/m^2
Smoke layer height (z)	1.5 m if $T_g > 80$ °C	1.0 m if $T_g > 100$ °C
Temperature in layer (T_g)	80 °C if $z < 1.5$ m	100 °C if $z < 1.0$ m
Toxicity	FED = 0.5	FED = 1.0

If a fire occurs, the staff members will most likely be able to put it out. Therefore, situations in which the ward must be evacuated have the following characteristics: the staff members are not able to extinguish the fire and it does not self-extinguish. This event is very infrequent and its probability has been estimated on the basis of statistics and discussions with other fire professionals. The probability of successful extinguishment by the staff or self-extinguishment has been set to 0.95.

If the staff members do not tackle the fire, they will move toward the patients. This movement time, t_{staffM}, is assumed to follow a normal distribution (15, 5) seconds. In the standard QRA the value used is 20 s.

The evacuation of the ward must be completed before untenable conditions arise. The limits used to define untenable conditions are given in Table 85.4. The tolerable conditions are used in the standard QRA calculations. In the extended QRA the severe conditions are, however, used for illustration purposes.

Toxicity is measured in terms of the fractional effective dose (FED), which considers the effect of a number of toxic gases [6].

Fire Frequency

In defining the risk to which patients in a hospital ward are exposed, it is necessary to know the fire

occurrence rate (i.e., the frequency that a fire will start). The statistics in this area are, unfortunately, rather limited. It is usually possible to predict the number of fires occurring in a town or country each year. Some information is given in Rutstein [7] that relates the frequency of fires occurring to the floor area of the building. According to this reference, the frequency of having a fire in a hospital ward per year can be calculated as

$$f_{\text{fire}} = 0.0007 \cdot A^{0.75} \qquad (85.1)$$

This relationship has been derived from reports from fire departments in the United Kingdom. The expression gives an average value of the fire frequency and the deviation can be large. As the number of fires in hospitals is low, the reliability of the expression can be questioned. The value of the exponent has been arbitrarily assumed to be 0.75 due to low incident rate. It is, however, generally assumed that the frequency increases with increasing building area.

Using this expression for the hospital ward studied in this research gives a frequency of a fire event of 0.077 fires per year. The floor area used for this calculation was 35×15 m^2.

Some preliminary Swedish data concerning fire occurrence rates are available from fire departments in the country. The data have been collected from the rescue reports following an emergency operation handled by the fire departments (Table 85.5). Almost all Swedish health care facilities (including hospitals) are equipped with smoke detectors that are connected to the local fire department, which means that if a fire occurs in a hospital, it is very likely that the fire department will be notified. The fire department rescue reports are, therefore, a good estimate of the number of actual fires in a hospital. The total number of fires reported was 59 per year.

Table 85.5 Fire frequencies in hospital wards per year in three towns in Sweden [8]

Town	Fire frequency per year
Town 1	0.038
Town 2	0.078
Town 3	0.068

The fire frequency, f_{fire}, has been set at 0.07 fires per year. The value for the wards in town 1 is half that of the others but still of the same order of magnitude. This difference will be examined in the extended QRA, where f_{fire} is treated as a random variable. The variable f_{fire} will then be assumed to follow a uniform distribution (0.04, 0.1) fires per year. On the basis of the statistics from the fire departments, it is assumed that the frequency of a fire occurring at night is 0.33 and, during the day, the frequency is 0.67.

The condition leading to evacuation of the ward is that a fire is initiated and will continue to grow, which means that a smoldering fire will not lead to evacuation unless it develops into a flaming fire. It is assumed that a smoldering fire is harmless, at least on the time scale considered here. Calculations of the conditions in a room in which there is a smoldering fire have been performed using input parameters from Quintiere et al. [9].

Fire Growth

The energy release rate from the fire is simply assumed to follow an $\alpha_f t^2$ relationship. It is assumed that the fire always arises in a patient room and does not spread to a neighboring room or corridor during the time of interest. The time available for escape depends on how fast the fire grows (i.e., the growth rate of the fire, α_f).

It is reasonable to assume a low value for the growth rate. Tests on the fire behavior of hospital beds indicate a growth rate of approximately 0.01 kW/s^2 [10]. The bed used for that test was a standard bed used in hospitals until a couple of years ago. Newer beds are especially designed to be difficult to ignite and fires in such beds are reported to have a substantially slower growth rate in initial fire development.

After the fire in the Hillhaven Nursing Home in Norfolk, Virginia, in 1989, it was determined that the fire in the bed ignited and had a growth

rate of approximately 0.01 kW/s^2 [11]. In simulations of patient room fires growth rates in the region of 0.0001–0.00025 kW/s^2 have been used, which are very low [12].

After examining similar fires, it was decided to use a fire growth rate following a log-normal distribution (0.01, 0.005) kW/s^2. This will result in untenable conditions in the fire room within a few minutes, which is in good agreement with experiments and postfire investigations. The value used for the standard QRA was chosen to be 0.007 kW/s^2 to include the very slow growing fires reported.

The Event Tree

The event tree for the sample calculation is defined by the scenarios illustrated in Figs. 85.4 and 85.5. Figure 85.4 shows the initial part of the event tree leading to the two final parts, A and B. Part A defines scenarios 1–48 and is shown in Fig. 85.5. Part B, defining scenarios 49–96, has the same general appearance but differs in terms of when the fire starts. In the initial part of the event tree, four scenarios are identified, which do not result in any unwanted consequences. In these scenarios, the fire may have been suppressed by the staff or will not grow. If these scenarios occur, no evacuation will be necessary.

Each scenario is defined by an individual expression that, considering the variables, reflects the current condition. How the consequences for the scenarios are calculated will be shown in the following paragraph.

Model Description

Available Escape Time

The unwanted consequences are derived by comparing the available time and the escape time. For situations where the difference (i.e., the escape time margin) is negative, some people will not be able to evacuate in time. The unwanted consequences are expressed in the number of patients not being able to escape safely. The safety factor is expressed by the time expression for each location of interest. In this case, two locations will be studied: the fire room and the corridor. The choice of the fire room is obvious, but the choice of the corridor may need some explanation. As all patients are moved out from their rooms, they all must pass along the corridor. The conditions in the corridor will then determine the time available for evacuation of the ward. Untenable conditions will only occur in the corridor if the door to the fire room is left open. Otherwise, untenable conditions will not arise at that location.

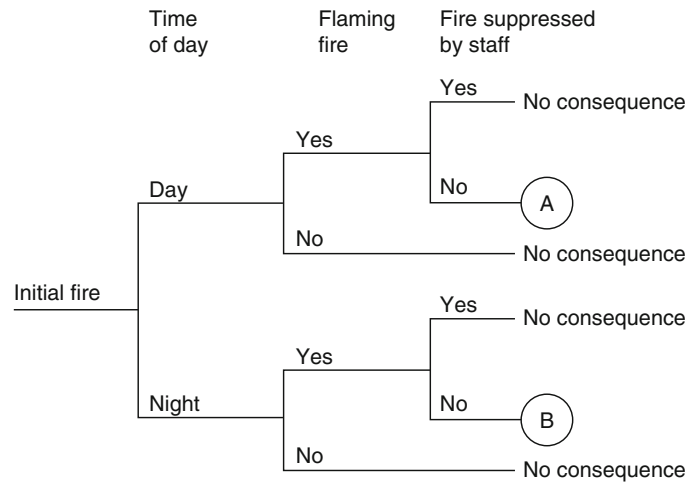

Fig. 85.4 Initial part of the event tree for fire on the hospital ward

Fig. 85.5 Continuation of the event tree for daytime conditions

The program CFAST [13] has been used to derive a response surface, an equation describing the time taken to reach untenable conditions as a function of the growth rate of the fire, α_f. The purpose of using the response surface methodology is mainly for the extended QRA. Using only a standard QRA technique one can more efficiently use the CFAST results directly

(if CFAST is the chosen software). But as the response surface equations are available in this sample analysis they are also used in the standard QRA. All response surface equations in this sample risk analysis will have the same general appearance as follows

$$t_u = \exp(\lambda + \delta \ln \alpha_f) \qquad (85.2)$$

where λ and δ are the regression coefficients (Tables 85.6, 85.7, and 85.8). A more detailed model like a CFD model can be used instead of the simple zone model CFAST. But as many scenarios are to be analyzed, a fast model is preferred.

The event tree results in a number of different fire situations, each with a new response surface equation describing the time available for evacuation. New expressions must be derived describing whether the door to the patients' room is open or closed after passage and whether the sprinkler system operates or not.

Door Open/Closed After patients have been removed, the door between the corridor and the patients' room can either be left open or it can be closed. If the door is closed after passage of both patients, the conditions in the corridor will never reach untenable levels. If the door is left open after the patients have been removed, untenable conditions will eventually arise in the corridor. Untenable conditions will always occur in the patient room in which the fire started, independent of whether the door is open or closed. For the CFAST calculations it is assumed that the door is opened after 90 s to let the patients escape. If it is closed after passage, it is assumed that the door will be completely closed after 150 s; otherwise, it will be kept open.

Equations have been derived for scenarios both with and without the sprinkler system. The sprinkler activation times in the patient room are, for all scenarios, much longer than the time taken to reach untenable conditions. The sprinkler operation will, therefore, not affect the time available for escape from the fire room. The sprinklers will, however, affect the conditions in the corridor if the door to the patient room is left open, thus increasing the overall safety. When sprinklers activate, they will for many situations result in an infinite available escape time (i.e., the conditions will never reach untenable levels).

The available escape time in the corridor is also dependent on when or whether the window breaks in the patient room. There are few data for window breakage and how much glass falls out. It is assumed here that the windows are 60 % open when the fire gas temperature in the room reaches 250 °C.

Table 85.6 Regression coefficients for time taken to reach tolerable conditions, mean and standard deviation

Condition	λ	δ	R^2
Fire room Open door	(2.77, 0.03)	(−0.42, 0.01)	1.00
Fire room Closed door	(2.71, 0.06)	(−0.43, 0.01)	0.99
Corridor Sprinklers work	(4.60, 0.10)	(−0.13, 0.04)	0.90[a]
Corridor Sprinklers fail	(4.10, 0.11)	(−0.35, 0.02)	0.96

[a]Untenable conditions only for fire growth rate $\alpha_f > 0.05$ kW/s^2

Table 85.7 Regression coefficients for time taken to reach severe conditions, mean and standard deviation

Condition	λ	δ	R^2
Fire room Open door	(2.95, 0.09)	(−0.48, 0.02)	0.99
Fire room Closed door	(3.21, 0.05)	(−0.37, 0.01)	0.99
Corridor Sprinklers work	–[a]	–	–
Corridor Sprinklers fail	(4.28, 0.10)	(−0.34, 0.02)	0.97

Note: This information is only used in the extended QRA
[a]The severe conditions did not arise in corridor

Table 85.8 Regression coefficients for smoke detector detection time

Condition	λ	δ	R^2
All conditions	(3.02, 0.04)	(−0.31, 0.01)	0.99

Detection Time

The model Detact-t2 is used to calculate detection times for smoke detectors for different fire growth rates [14]. The Detact-t2 model calculates the activation time for a given fire and detector configuration. The smoke detectors are assumed to behave like heat detectors but with a much faster response. The detectors have the following characteristics: $RTI = 0.5\sqrt{m \cdot s}$, activation temperature = 25 °C (i.e., 5 °C above ambient temperature). A response surface equation is created for the detection time. The equation has the same format as Equation 85.2 but using t_{det} instead of t_u. The parameters are presented in Table 85.8.

If the smoke detectors fail to operate, someone on the ward must observe the fire and alert the staff. The manual detection time, t_{det}, is assumed to be a random variable, normally distributed with the parameters (90, 45) seconds for daytime and (120, 60) seconds for nighttime. These two distributions are chosen purely based on judgment. The nighttime distribution results in longer detection times as there are fewer staff members present than during the day. In the standard QRA, the mean values plus one standard deviation were chosen to represent the conditions.

Model Uncertainty

There is no computer model that predicts reality without any error. Limitations and simplifications in the models inevitably result in deviations between the predicted values and those measured in a test or a real fire. A correction factor must be used to compensate for some of the differences between experimental results and predictions.

Two computer models are used in this study. CFAST is used for the prediction of the time available for evacuation or the time taken to reach untenable conditions. Detact-t2 is used to calculate the activation times for detectors and sprinkler heads. Based on the results of a few experiments, the difference in available escape time may be treated as a random variable, M_S, normally distributed (1.35, 0.1) [15]. The model CFAST underestimates the time available for evacuation by a factor of 1.35 on average.

The uncertainty in the Detact-t2 model is assumed to be unknown. The activation time in reality is highly dependent on the ceiling configuration and other obstructions in the upper part of the room. The variation in detection time may be significant.

Movement Time

Movement will take place from two locations: from the patient room to the corridor and from the corridor to a safe place outside the ward. First, after the staff members have responded to the alarm, they move toward the patients during the time period t_{staffM}. Then they start to prepare the patients for movement. The time required to move the patients from their room to the corridor can be derived using the following equation:

$$t_{\text{move}}^{\text{room}} = t_{\text{care}} \cdot (PatInRm/StaffInRm) \qquad (85.3)$$

The variables *PatInRm* and *StaffInRm* indicate the number of patients and staff members in the patient room during evacuation (i.e., two patients and two nurses).

After the patients have been evacuated from the room in which the fire started, the rest of the patients may also need to be evacuated. This will be the situation if the door between the corridor and the patient room is left open. If it is closed, there is no acute need to evacuate the other patients.

The expression for the evacuation time for the whole corridor is

$$t_{\text{move}}^{\text{corr}} = \left(t_{\text{care}} + t_{\text{patM}}\right) \cdot (NoPat/NoStaff) \qquad (85.4)$$

The time required to evacuate each patient is now the sum of the preparation time, t_{care}, and the movement time to the safe place, t_{patM}. *NoPat* and *NoStaff* are equal to the total number of patients and staff members on the ward.

Calculation of the Consequences

The problem can now be formulated in terms of the number of people who might not be able to be evacuated before untenable conditions arise. The governing equation is based on the escape time margin, which expresses the time difference between the available time and the required escape time. The appearance of the equation depends on whether the door to the patient room where the fire starts is open or not. The closed door scenario means that only the patient room containing the fire must be evacuated. Differences in variable values will result in different consequence values, defined by the variable c_i indicating the consequences for scenario i.

The maximum number of patients who may be trapped in the scenarios in which the door is being closed is two, as this is the maximum number of patients in a room. If the door is left open, the number is increased to 22 as the other patients also have to be evacuated and might be subjected to the hazard. The two governing equations can be formulated as escape time margins for the fire room and the corridor as

$$\text{Room margin} = t_u^{\text{room}} M_S - t_{\text{det}} - t_{\text{resp}}^{\text{staff}} - t_{\text{staffM}} - t_{\text{move}}^{\text{room}} \quad (85.5)$$

$$\text{Corridor margin} = t_u^{\text{corr}} M_S - t_{\text{det}} - t_{\text{resp}}^{\text{staff}} - t_{\text{staffM}} - t_{\text{move}}^{\text{corr}} \quad (85.6)$$

These can be expressed, for each scenario i, in terms of the number of patients as follows:

- When the door is closed
  $RoomCons = 2$, if Room margin <0
  $c_i = RoomCons$
- When the door is left open
  $CorrCons = (Corridor\ margin\ t_{\text{move}}^{\text{corr}})\ NoPat$ if Corridor margin <0
  $c_i = RoomCons + CorrCons$

If the escape time margin is positive, all patients have been evacuated before untenable conditions occur. A short summary of the values used in the risk analysis is presented in Tables 85.9 and 85.10.

Table 85.9 Values of variable used in the risk analysis

Variable	Standard QRA	Extended QRA
α_f	0.007 kW/s^2	LN(0.01, 0.005) kW/s^2
M_S	1.35	N(1.35, 0.1)
t_{det} (day)	135 s	N(90, 45) s
t_{det} (night)	180 s	N(120, 60) s
$t_{\text{resp}}^{\text{staff}}$	10 s	N(10,3) s
t_{staffM}	20 s	N(15,5) s
t_{care}	See Table 85.2	See Table 85.3
t_{patM}	See Table 85.2	See Table 85.3
PatInRm	2	2
StaffInRm	2	2
NoPat	22	22
NoStaff (day)	4	4
NoStaff (night)	2	2

Table 85.10 Variables used in the risk analysis

Variable	Standard QRA	Extended QRA
f_{fire}	0.07	Unif(0.04, 0.1)
p_{day}	0.67	0.67
p_{flaming}	0.50	0.50
$p_{\text{suppressed}}$	0.95	0.95
$p_{\text{sprinkler}}$	0.96	0.96
$p_{\text{detection}}$	0.94	Unif(0.9, 0.98)
p_{door}	0.90	0.90
p_{sleeping} (day)	0.05	0.05
p_{sleeping} (night)	0.95	0.95
p_{help}	See Table 85.1	See Table 85.1

Presenting the Risk

Societal Risk

Based on the preceding information, the risk to the hospital ward can be analyzed. The QRA results in 100 scenarios. The first 96 scenarios represent the final outcomes of the event tree; 48 for daytime conditions and 48 for nighttime conditions. The last four scenarios can be found in the initial part of the event tree (Fig. 85.4) but do not result in any unwanted consequences as the fire is either extinguished or will not continue to grow.

The scenario frequency (f_i) and consequences (c_i) are derived and collected in two vectors.

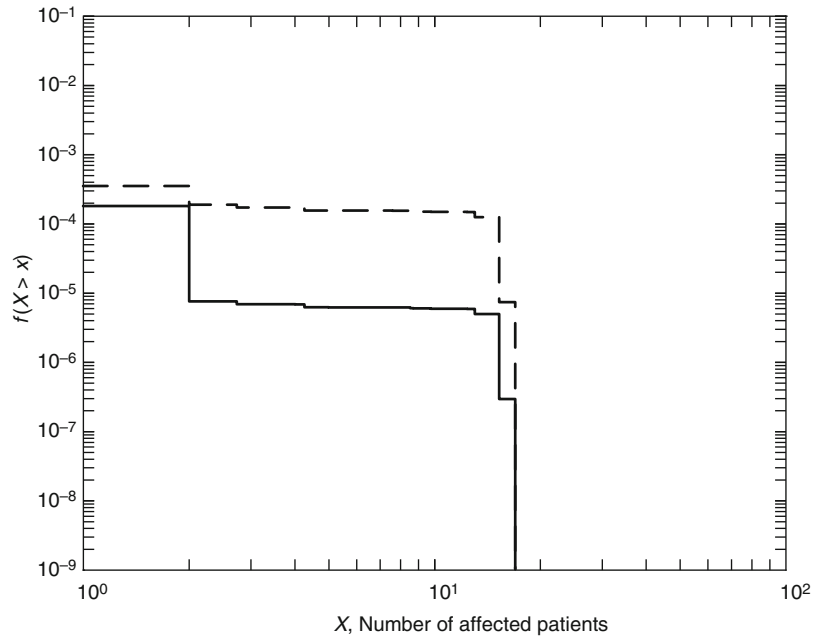

Fig. 85.6 Risk profile for the standard quantitative risk analysis using critical untenable conditions. *Dashed line* represents risk profile for design alternative without sprinkler system

The consequences are expressed in terms of the number of patients not being able to escape within the available time. The vectors are sorted by increasing consequences and the resulting cumulative risk profile (see Chap. 83 in this handbook) is shown in Fig. 85.6 as the solid line.

An alternative design strategy, with no sprinkler system on the ward, was also examined using this method. The dashed line shows this design risk profile. This risk profile indicates a higher risk, which is rational and understandable as sprinkler systems are assumed to decrease the hazard of fires.

The profiles in Fig. 85.6 were derived using the critical conditions for untenable environment.

Based on the results, the average societal risk can also be obtained. The products of the frequency and the consequences for each scenario are summed to give the average societal risk. For this scenario the average risk using tolerable conditions is $4.4 \cdot 10^{-4}$ persons per year per ward.

The alternative design solution without the sprinkler system has also been analyzed in terms of the average societal risk. The corresponding values for the average societal risk are $2.7 \cdot 10^{-3}$ patients per year per ward. There is, thus, an approximate difference in risk of six times between the scenarios with and without sprinklers.

This comparison between a ward with and without sprinklers was presented to illustrate the capability of the method. Similar results can be obtained by comparing situations with and without an automatic fire detection device, and so on. The risk profiles and average risk measures will be different, but it is possible to illustrate the benefit of devices that increase safety in a quantitative manner.

The question is whether the ward without the sprinkler system is acceptable or not. The sprinkler-equipped ward may result in an "oversafe" and too expensive situation. On the other hand, with a sprinkler system, a higher number of patients could be housed on the ward with the same risk level as the ward without the sprinkler system.

Individual Risk

The individual risk has also been derived for the two levels of untenable conditions. The individual risk is defined here as the frequency per year of the escape routes being blocked by the fire.

In the sprinklered case, the individual risk was equal to $1.8 \cdot 10^{-4}$ per year using the endpoint criteria corresponding to tolerable levels. If the more severe conditions are applied, the individual risk measure is $1.0 \cdot 10^{-4}$ per year. The measure of risk is the sum of the scenario outcome frequencies leading to the unwanted event (i.e., that the escape routes are blocked).

Extended Quantitative Risk Analysis Procedure

The standard QRA is performed without explicitly considering the uncertainty that is inevitably present in each variable. Instead, the variables are assigned values that, for example, are the most likely values.

The results from such an analysis are usually presented as a single risk profile as in Fig. 85.6, but such profiles do not contain any information on the uncertainty of the profiles themselves. If one wishes to know how certain the calculated risk profiles are the uncertainties in the variables involved must also be considered. To obtain this information, risk analysis, according to the standard QRA method, should be combined with uncertainty analysis. Formalizing this methodology results in the extended QRA.

Basically, the procedure for performing an extended QRA is similar to that for the standard QRA. As the variables not are constant but are expressed in terms of frequency distributions, the propagation of uncertainty must be modeled for all scenarios simultaneously. Simply, the process can be seen as a standard QRA that is repeated a large number of times. For each new iteration, the variables are assigned new values according to the frequency distribution. Figure 85.7 shows the process schematically.

This analysis results in a new risk profile for each iteration, providing a family of risk profiles (Fig. 85.8). The family of risk profiles can be used to describe the uncertainty inherent in the resulting risk measure. The figure shows the uncertainty in the risk profiles for the sample calculation on the hospital ward using data presented for the extended QRA in the previous paragraph, which means that the variables are represented in terms of a distribution instead of a single value.

It is clear that the information is very extensive. Therefore, alternative presentation methods may have to be used in order to be able to interpret the information, which is why it is better to present the societal risk profiles in terms of the median or mean risk profile and to complement these with relevant confidence bounds. The confidence interval can, for example, be the 80 % interval. The extended QRA can be used to express the degree of credibility in the resulting median risk profile by complementing the profile with confidence bounds (Fig. 85.9).

The technique can be used to see when the standard QRA analysis and the extended analysis coincide. Which percentile in the extended QRA is represented by the standard analysis? To answer this question the results of the standard QRA and the percentiles obtained from the extended QRA using severe conditions can be plotted in the same diagram. It is then possible to get information on how safe a design solution using conservative estimates of the variables actually is.

The method can also, as for the standard QRA, be used to evaluate the benefits of different design strategies in efforts to obtain an optimal solution. As the variation in risk profiles originates from the uncertainty in the actual scenario if it occurs, it can be used to determine if additional safety measures afford any measurable increase in safety. If the new design risk profile falls between the accepted confidence limits, there is no statistically significant change in safety, on the specified confidence level, due to the additional safety measures. The risk profile resulting from a new design might not be different from the inherent uncertainty of the scenario.

In the same manner as for the standard QRA, the average risk can be calculated. But as the variables are subject to uncertainty, the average risk will also be subject to uncertainty and will consequently be presented as an empirical distribution. Each iteration will generate one sample of the average risk. These average risk values will form the distribution of the average risk.

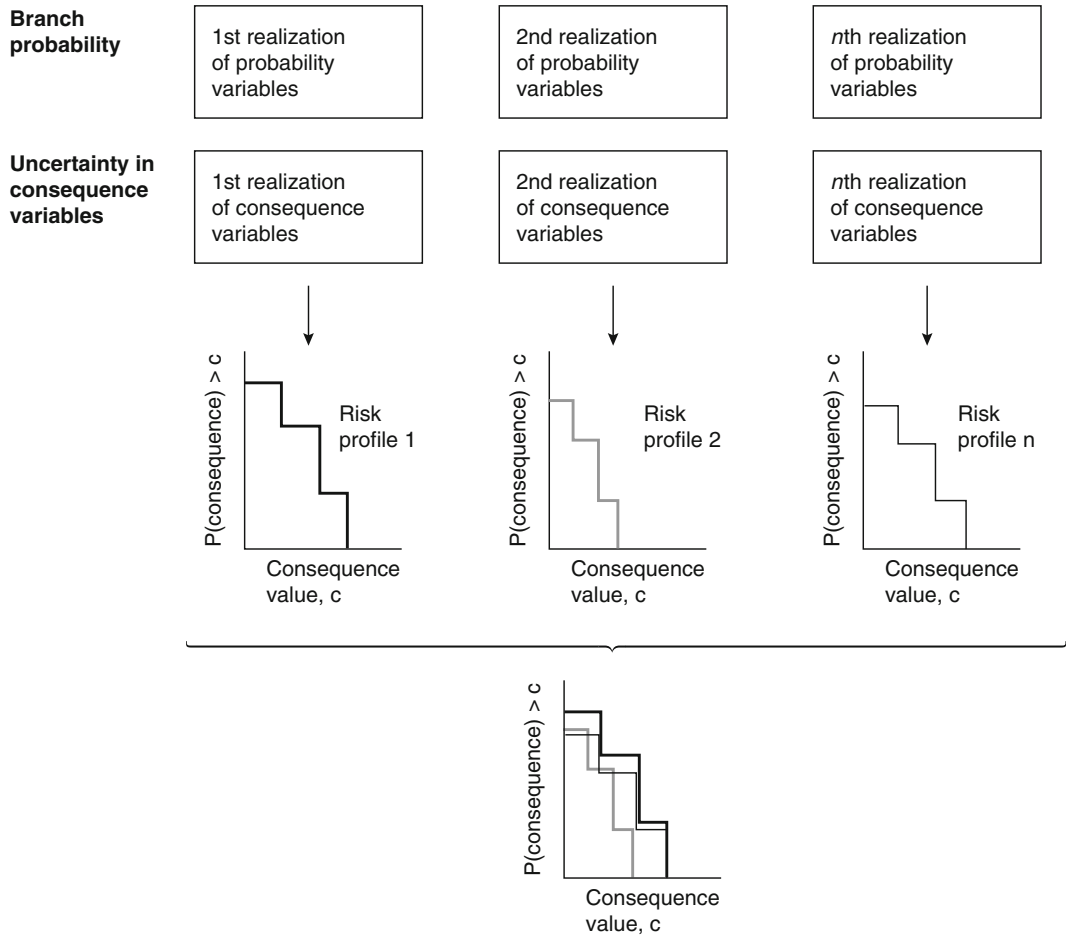

Fig. 85.7 Uncertainty analysis of a QRA

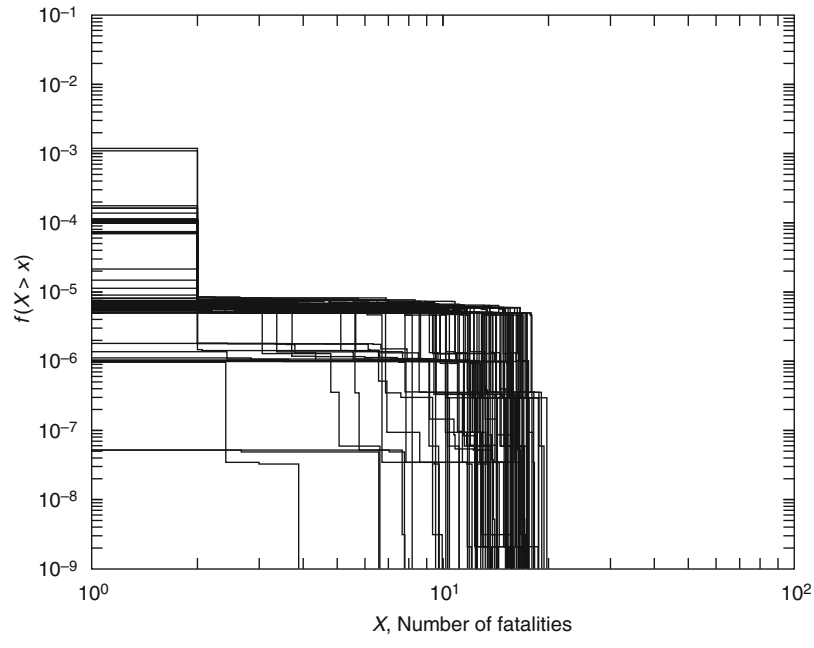

Fig. 85.8 Family of risk profiles for the extended quantitative risk analysis using severe untenable conditions

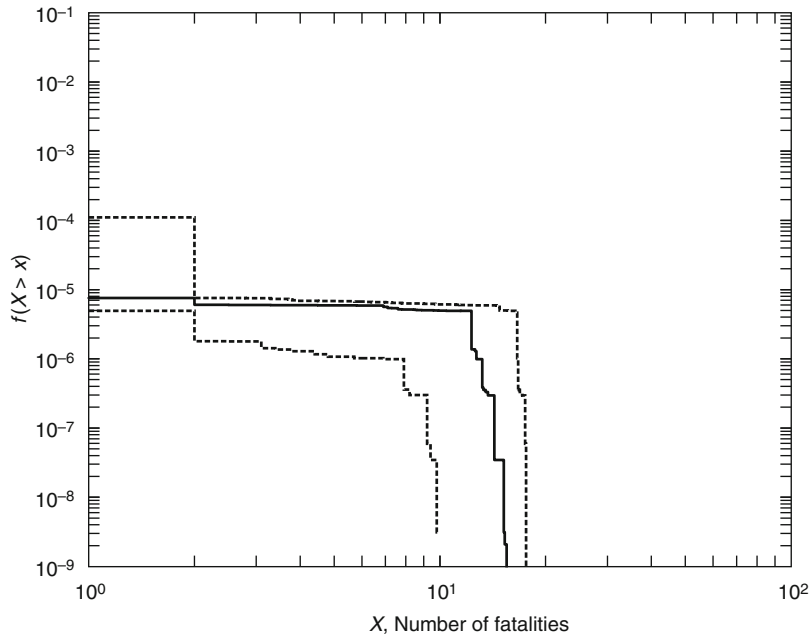

Fig. 85.9 Percentiles from the extended quantitative risk analysis using the severe untenable conditions in which *lines* represent the 10th, 90th, and 50th (or median) percentiles

Also the individual risk measure can be derived from the extended QRA. Some combinations of the variables used to derive the consequence in a scenario will lead to conditions resulting in fatalities or blocked escape routes. Similarly, due to randomness, some scenarios will not always contribute to the individual risk measure. Therefore, there will be a degree of uncertainty in the individual risk originating from variable uncertainty.

The extended QRA is performed as a numerical procedure that involves Monte Carlo sampling techniques. Today, no commercial software exists that can handle both scenario variable uncertainty and branch probabilities. The calculated data can, however, be treated with Matlab or similar software.

Summary

The chapter has used a methodology for performing a quantitative fire risk analysis and various ways to consider parameter uncertainty. Using these methods, it is possible to derive risk measures both with and without explicitly considering the inherent uncertainty in the system. These risk measures can be used either to compare different design solutions or to compare a solution with tolerable risk levels. The former use is the most likely as tolerable risk levels have not been fully defined for most architectural work. Only in very special cases have tolerable risk levels been used in the design process (e.g., in large infrastructures). The risk analysis methods can be used for comparison with traditionally accepted design solutions.

References

1. Society of Fire Protection Engineers, *SFPE Engineering Guide to Performance-Based Fire Protection: Analysis and Design of Buildings,* National Fire Protection Association, Quincy, MA, and Society of Fire Protection Engineers, Bethesda, MD (2000).
2. ISO/TS 16732, Fire Safety Engineering—Guidance on Fire Risk Assessment, International Organization for Standardization, Geneva (2005).
3. BS 7974:2001, *Application of Fire Safety Engineering Principles to the Design of Buildings—Code of Practice,* British Standards Institution, London (2001).
4. PD 7974-7:2003, *Application of Fire Safety Engineering Principles to the Design of Buildings—Part 7:*

Probabilistic Risk Assessment, British Standards Institution, London (2003).
5. R.W. Bukowski, "Engineering Evaluation of Building Fire Safety Performance," CIB W14 TG1 (1997).
6. R.W. Bukowski, R.D. Peacock, W.W. Jones, and C.L. Forney, "Technical Reference Guide for the HAZARD I Fire Hazard Assessment Method," *NIST Handbook 146,* Vol. II, National Institute of Standards and Technology, Gaithersburg, MD (1989).
7. R. Rutstein, "The Estimation of the Fire Hazard in Different Occupancies," *Fire Surveyor,* 8, 2, pp. 21–25 (1979).
8. H. Frantzich, "Fire Safety Risk Analysis of a Health Care Facility," Report 3085, Department of Fire Safety Engineering, Lund University, Lund (1996).
9. J.G. Quintiere, M. Birky, F. McDonald, and G. Smith, "An Analysis of Smouldering Fires in Closed Compartments and Their Hazard Due to Carbon Monoxide," NBSIR 82-2556, National Bureau of Standards, Washington, DC (1982).
10. G. Holmstedt and I. Kaiser, Brand i vårdbäddar. SP-RAPP 1983:04 Statens Provningsanstalt, Borås (1983). (In Swedish)
11. H.E. Nelson and K.M. Tu, "Engineering Analysis of the Fire Development in the Hillhaven Nursing Home Fire, October 5, 1989," NISTIR 4665, National Institute of Standards and Technology, Gaithersburg, MD (1991).
12. K.A. Notarianni, "Measurement of Room Conditions and Response of Sprinklers and Smoke Detectors During a Simulated Two-Bed Hospital Patient Room Fire," NISTIR 5240, National Institute of Standards and Technology, Gaithersburg, MD (1993).
13. R.D. Peacock, W.W. Jones, G.C. Forney, R.W. Portier, P.A. Reneke, R.W. Bukowski, and J.H. Klote, "An Update Guide for HAZARD I Version 1.2," NISTIR 5410, National Institute of Standards and Technology, Gaithersburg, MD (1994).
14. D.D. Evans and D.W. Stroup, "Methods of Calculating the Response Time of Heat and Smoke Detectors Installed Below Large Unobstructed Ceilings," NBSIR 85-3167, National Bureau of Standards, Gaithersburg, MD (1985).
15. S.E. Magnusson, H. Frantzich, and K. Harada, "Fire Safety Design Based on Calculations: Uncertainty Analysis and Safety Verification," Report 3078, Department of Fire Safety Engineering, Lund University, Lund (1995).

Håkan Frantzich is assistant professor at the department of Fire Safety Engineering and Systems Safety at Lund University, Sweden. He has been involved in research projects related to performance-based fire safety design and evacuation and human behavior during fires.

The Building Envelope: Fire Spread, Construction Features and Loss Examples

86

Daniel J. O'Connor

General Mechanisms of Exterior Fire Spread

Exterior building fire spread occurs in three basic ways. One scenario considers fire spread from one building to an adjoining building separated by a wall or barrier. In this case, the fire spread occurs when fire exposure to the wall or barrier and any protected openings has sufficient duration and intensity to negate the integrity of the fire wall/barrier or any protected openings. Additionally, flame extension (often exacerbated by wind) above the roof or around the edges the fire barrier/wall can cause the fire to spread to the adjoining building by radiation, direct flame contact or possibly burning brands.

Fire Spread Between Buildings Separated by Distance

A second scenario considers fire spread from one building to another building located some distance away. Here, the risk of fire spreading from a burning building to an adjacent structure is related to the intensity of heat radiation transferred to combustible materials on the exterior of the distant building or radiation through windows to combustible contents within the structure. Additionally, if flying brands alight on surfaces heated by radiation, the potential for ignition is increased. Various guides and procedures have been developed to evaluate the separation distances between adjacent buildings or properties and the potential effects of the radiation emitted from a burning building. A generalized engineering approach for assessing separation distances between adjacent properties/buildings has been outlined [1] and restated in an edited form in Table 86.1. This approach relies on the basic principles of radiation transfer from a flame front (radiator) across some distance to an exposed building as generalized in Figs. 86.1 and 86.2.

For complex scenarios (e.g., varied windows, angled exposure, varying fuel loads) NFPA 80A, *Recommended Practice for Protection of Buildings From Exterior Fire Exposures* and the BRE Fire Research Station's document titled *External Fire Spread*: *Building Separation and Fire Distances* (BR 187) [2] provide discussions on methods for assessing potential radiation transfer and associated considerations and assumptions important to addressing fire spread between adjacent properties. One key assumption in both guides is that the fire service will respond in the 10–20 min range. During this period, maximum radiation levels are not expected to be obtained (NFPA 80A and BR 187) and it is anticipated ignition time requires roughly 10 min of preheating before ignition occurs (BR 187.)

NFPA 80A and BR 187 consider that radiation can cause fire spread when there is direct line-of-sight from the radiating building to an

D.J. O'Connor (✉)
Aon Fire Protection Engineering Corporation

M.J. Hurley (ed.), *SFPE Handbook of Fire Protection Engineering*,
DOI 10.1007/978-1-4939-2565-0_86, © Society of Fire Protection Engineers 2016

Table 86.1 Zalosh's nine step approach for assessing safe separation distances (as edited)

Step order	Engineering procedure
1	Postulate a credible worst-case exposure fire scenario in terms of the extent of the materials or structures that are burning
2	Determine the heat release rate and the effective flame ration temperature and emissivity
3	Calculate the flame emissive power for relevant fuel
4	Calculate the flame height
5	Determine the flame-target configuration factor
6	Calculate the radiant heat flux impinging on the target
7	Compare the calculated impinging heat flux to the critical heat flux for ignition or structural damage of the exposed structure property
8	Repeat the calculations accounting for wind effects on flame height, configuration factor for a wind tilted flame and a downwind target
9	If the calculated radiant heat flux is > the ignition/damage threshold and the distance cannot be increased, then evaluate the feasibility of the exposed structure with a more fire resistant material or using outside sprinkler/water spray protection

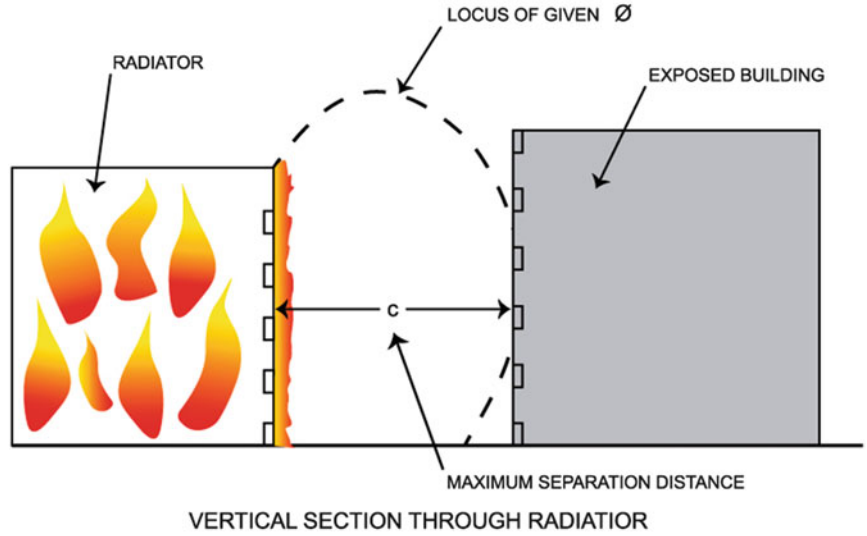

Fig. 86.1 Generalized concept of radiation transfer between buildings (vertical section)

exposed building. For buildings with combustible wall surfaces, the entire wall can act as the radiator. When windows are located in a wall of noncombustible construction (e.g. brick), then the windows and emitted flames only act as the source of radiant heat. The collective area of the windows (those that are radiating) and the distance from adjacent buildings directly impact the risk of fire spread since the size and distance determine the configuration factor, which influences the level of incident radiation on the exposed building. The configuration factor effectively is a measure of how much an exposed building sees the radiation from the burning building. The configuration, or view factor is used to determine the heat flux to the exposed building based on the following general relationship for incident radiation, I_R (kW/m^2).

$$I_R = K_1\, \theta\, \varepsilon\sigma(273 + T_e)^4$$

θ—*configuration factor*
ε—*emissivity of the emitter (generally assumed ~ 1)*

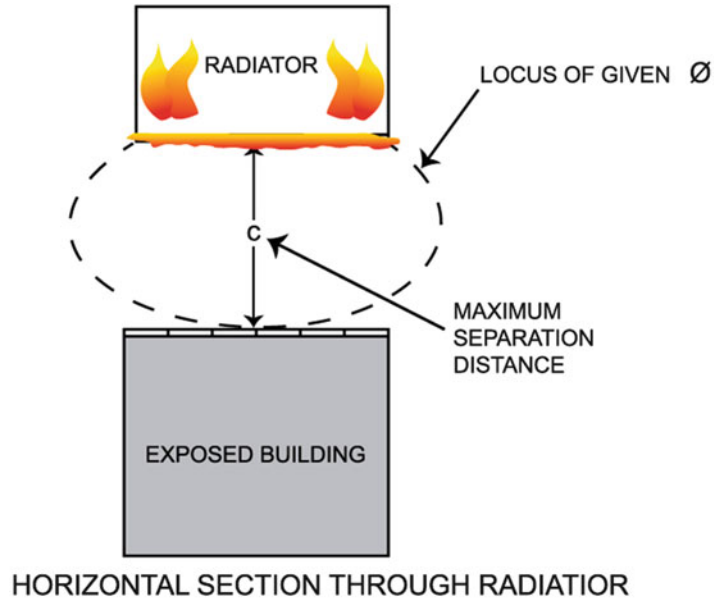

Fig. 86.2 Generalized concept of radiation transfer between buildings (plan view)

σ —*Stefan-Boltzmann constant*, 56.7×10^{-12} (kW/m^2K^4)

T_e—*temperature of the emitting surface*, °C

K_1—*radiation reduction factor for glazing of exposed building when wall cladding is noncombustible*

The irradiance levels needed to cause ignition of a distant exposed building were originally related to that needed to ignite wood materials. For spontaneous ignition the value is 33.5 kW/m^2 and for piloted ignition, as may occur with an exposure to burning brands, is 12.5 kW/m^2. The two guides noted above err on the side of conservatism recommending the use of the pilot ignition irradiance threshold for wood or cellulosic materials in their described methodologies. NFPA 80A notes, however, that newer building materials available today may have greater or lesser ability to resist ignition. Therefore, materials with greater propensity to ignite need greater separation distances and those with higher ignition resistance could be separated by smaller distances.

Example 1 A simple example that illustrates the application of the configuration factor and radiation calculations considers the case of two wood clad buildings with one the wall (red oak) of one building fully in flames [1]. In this situation the two wood frame buildings face each other with a separation of 6.1 m. A 3.7 m high by 7.6 m wide wall facing the adjacent building, is ignited and the flaming façade exposes the adjacent building as illustrated in Fig. 86.3. The question of concern, "Is the 6.1 m separation adequate to prevent flame propagation to the adjacent building?"

The heat release rate for a 3.7 m high wood wall fire is about 1040 kw/m per 0.3 m of width. The corresponding flame height calculated using Delichatsios correlation for rectangular wall flames [3] is 5.1 m. The emissive power is the radiant heat release rate per unit flame surface, which for a radiant heat release fraction (red oak) of 0.26 is,

$$0.26(1040)/5.1 = 53 \text{ kW/m}^2$$

This value is significantly lower than would be calculated using know flame temperatures and an emissivity of unity. The lowest expected flame temperature of 1100 K would produce an emissive power as follows

$$\sigma(273 + T_e)^4 = 56.7 \times 10^{-12} \left(kW/m^2K^4\right) 1100^4 \left(K^4\right) = 83 \text{ kW/m}^2$$

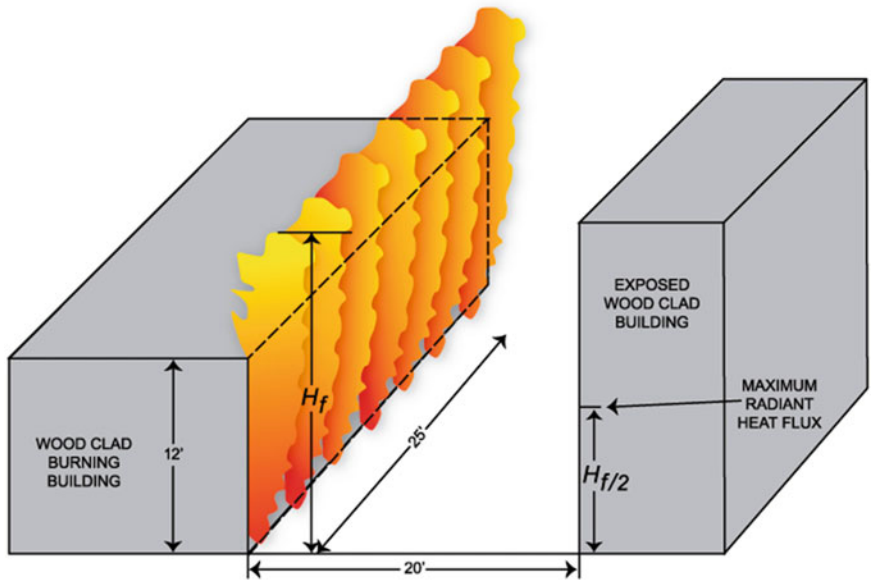

Fig. 86.3 Fire involved building with 17 ft high flame front radiative exposure

Since this radiative heat flux is higher than the 53 kW/m^2 calculated using the heat release rate, it will be used in the interest of estimating a conservative safe separation distance. The configuration factor needed to complete the analysis can be found from Fig. 86.4, which provides the view or configuration factors for a parallel rectangular radiator. It is about 0.6 for a target at mid-flame height and the given combination of flame height, wall width, and separation distance.

Assuming an atmospheric transmissivity of unity, the incident radiation is therefore,

$$I_R = (0.6)(83) = 49.8\ \text{kW/m}^2$$

This value is higher than the threshold for pilot ignition of many woods (12 kW/m^2), and more importantly exceeds the critical threshold for spontaneous ignition of 33.5 kW/m^2. Flame spread would be expected even without exposure to burning brands. Zalosh notes wind effects would not be expected to affect this conclusion given that the wind would be expected to produce some flame leaning above the wall and slightly increase the already high heat flux on the exposed building [1].

Vertical Building Fire Spread

A third scenario considers the fire spread from floor-to-floor in a single structure rather than fire spread between buildings separated by some distance. From a fire dynamics perspective, flames emitting from an exterior window can extend higher than 5 m above the top of the window [5]. One test of Yokoi's was a test room with plywood walls/ceilings and a fire load of 40 kg/m^2, which is characteristic of residential occupancies and at the lower end of the fire load scale. The hot gases from the fire room window measured 400–600 °C at 1.750 m above the top edge of the fire room window. The glass broke out under this exposure.

Analysis of 400 fire compartment experiments [6] helped to more fully explain the physical phenomena of ventilation controlled fires. Ventilation-controlled fires represent the scenario where a fire burning in a building breaks the window glazing, permitting hot gases to flow out the top portion of the opening. A portion of the hot gases are unable to burn inside the room due to limited air (ventilation

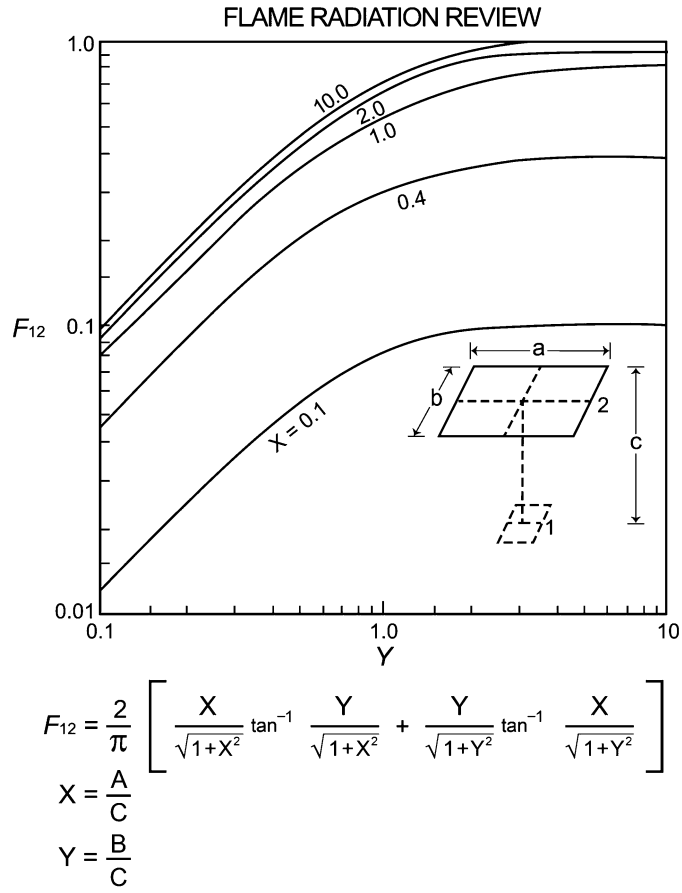

Fig. 86.4 View or configuration factors for a parallel rectangular radiator (Based on Blackshear [4])

controlled) but, upon movement to the exterior, encounter sufficient air entrainment, allowing the hot fuel gases to burn outside the building. The result is a flame projecting out and upward from the window. From a visual perspective, flame extension is estimated at the point that flame temperature drops below 540 °C, which corresponds to the flame no longer appearing luminous.

Taking the data of various researchers, Ove Arup and Partners developed a number of correlations to estimate flame projections and flame temperatures under natural or forced draft conditions [7]. This work showed that the fire flame projection and temperature profile will be a factor of window area and height, room geometry, fuel contents and burning rate, and wind velocity.

Figure 86.5 illustrates several of the common conditions and notational flame structure that is used to predict flame position and extension. All these factors have been combined in into a guide for evaluating the temperatures from exposed exterior structural steel members when subjected to flames emitting from the windows or vents of exterior walls. However, this methodology can be useful in evaluating the temperature and heat flux exposure to other elements on the exterior side of the wall such as widow glazing or wall cladding. This methodology can be found in the American Iron and Steel Institute's *Fire Safe Structural Steel*: *Design guide* [8].

Figure 86.6 illustrates the potential temperature and heat flux characteristics of a fully developed, unsprinklered compartment fire.

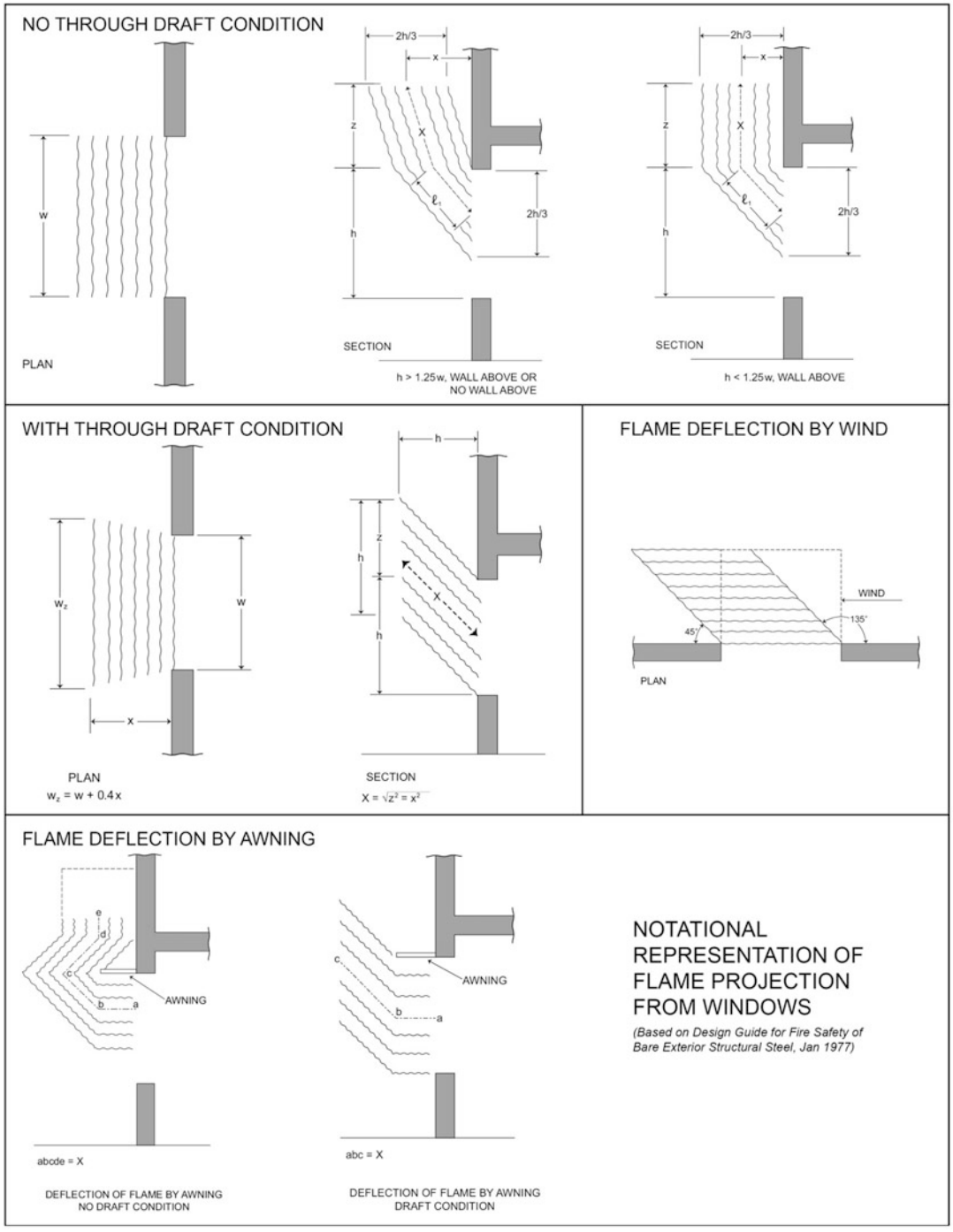

Fig. 86.5 Notational representation of flame projection from windows

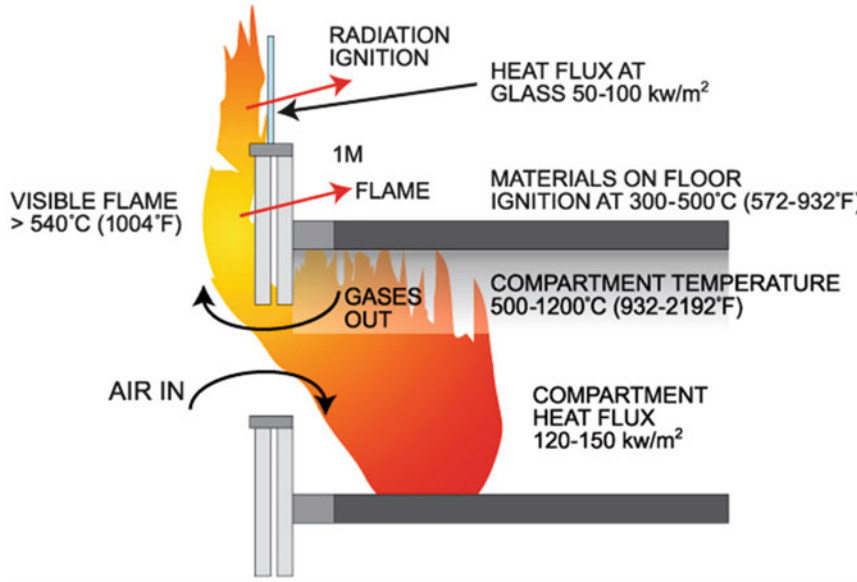

Fig. 86.6 Exterior wall and floor fire exposure mechanisms [9] (Courtesy of CTBUH)

The three principal floor-to-floor flame spread mechanisms at work in Fig. 86.6 are as follows:

- Inside—Flames and fire gases in the building attack the interior surfaces and details of the wall assembly and associated perimeter fire barrier materials.
- Outside—Flames and hot gases projecting from fire-broken glazing or other openings directly impinge on the wall exterior face (convection). Wall designs using exterior combustible cover or claddings (e.g. insulated metal panels, metal composite material panels) may be subject to further fire development posed by the combustible components of the exterior cover/cladding.
- Outside—Flames projecting from broken glazing or other openings radiate heat to and through glazed surfaces or through other openings to building contents and furnishings.

Building Exterior Wall and Enclosure Systems

Exterior wall types commonly associated with above-grade, modern building design can generally be classified as follows: as a cavity wall, a barrier wall, or a mass wall, or cladding systems which include curtain walls. In addition to these four basic wall types, there is a mixed or hybrid type of enclosure system known as "double skin façades" which are described later in this Chapter.

There are numerous sources for descriptions and detailed explanations regarding the construction of exterior walls. Several documents [10–12], address building envelop wall system design and curtain wall design concepts. These sources are relied upon for their descriptive information which is included in the following narrative that summarizes key characteristics of the basic four building enclosure methods. Additional specific details related to construction of walls can be found in *Construction—Principles, Materials, and Methods* [13].

Cavity Wall

Cavity walls are also referred to as "screen" or "drained" wall systems and in Europe as "cold façades". These cavity walls or cold façades are identifiable by the presence of a cavity, ventilated internally, between the outer layer

which offers weather protection and an internal insulation layer. This allows the insulating layer to dry if water penetrates in to the façade.

Often this is a preferred method of construction in climatic and rainfall zones. The term "cavity wall" is most often used to describe clay brick and/or concrete masonry wall systems installed over a largely open, unobstructed air space or drainage cavity. This term is now generally used to define any wall system or assembly that relies upon a partially or fully concealed air space and drainage plane to resist bulk rainwater penetration and which is also used to improve the thermal performance at the building enclosure. Drained cavity walls typically include the following characteristics [11] as depicted in Fig. 86.7:

- An exterior cladding element that is intended to either shed or absorb the majority of bulk rainwater penetration before it enters the concealed spaces of the wall assembly.
- A drainage cavity or air space, that is intended to collect and control rainwater that passes through the exterior cladding element and re-direct that water to the building exterior. The cavity may be ventilated for pressure equalization, either mechanically or passively, to facilitate this process by preventing negative pressure that may draw rainwater across the cavity into the "dry" sections of the wall assembly via anchors, wall ties, and similar penetrations).
- An internal drainage plane that is intended to function as the primary line of defense against uncontrolled rainwater penetration. This layer serves functionally as the dividing line between the "wet" and "dry" sections, or "zones," of the exterior wall assembly.

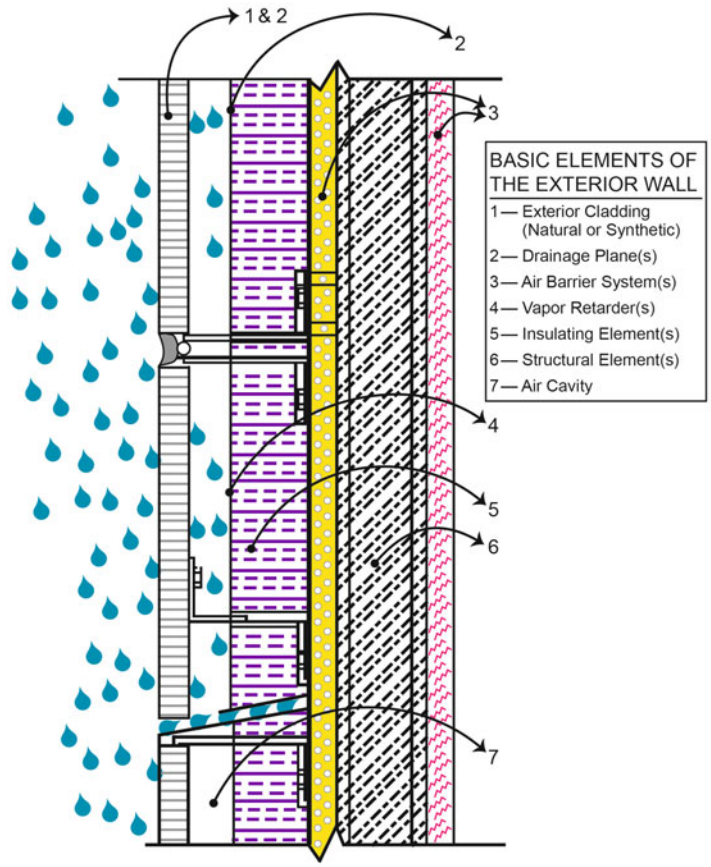

Fig. 86.7 Cavity wall diagram showing rainwater penetration into air cavity bounded by insulation layer (Based on Lemieux and Totten [11])

This layer can be created using a variety of both dry sheet-goods or wet, trowel-applied products depending upon the climate in which the building is to be located and the desired level of vapor permeability necessary to prevent condensation and potential mold growth on the dry side of the exterior wall assembly.

- An insulating layer, which can be located either inboard or outboard of the internal drainage plane depending upon the geographic region and climate in which the building or structure is to be located. In colder climates, the insulation is also placed outboard of the innermost (primary) drainage plane in this type of wall assembly, inside the wet zone (drainage cavity) of the wall. The combination of a combustible insulation layer adjoining the air cavity poses a risk of fire spread via the cavity if fire breaches into this zone.

Barrier Wall

A barrier wall or "warm façade" (European nomenclature) is commonly used to describe any exterior wall system of assembly that relies principally upon the weather-tight integrity of the outermost exterior wall surfaces and construction joints to resist bulk rainwater penetration and/or moisture penetration as shown in Fig. 86.8. Barrier walls have a thermal insulation layer applied directly to the surface of the building. If the insulation is on the exterior side, it must be water resistant to maintain the insulating properties. If the insulating layer is on the inside, the ability of the solid wall to store heat and contribute to the interior environment will be negated. This type of wall system is commonly associated with precast concrete spandrel panels, certain types of composite and solid metal plate exterior cladding systems, and exterior insulation and finish systems (EIFS). Although a cost-effective solution, barrier walls are cause for concern since they are difficult to implement correctly and can require substantial maintenance.

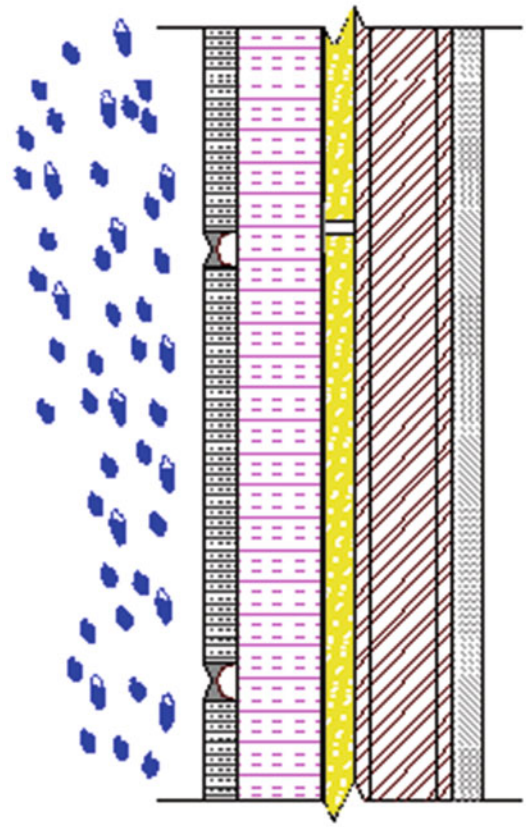

Fig. 86.8 Barrier wall section showing outermost layer resisting water penetration (Lemieux and Totten [11])

Mass Wall or Solid Wall

Unlike a cavity wall system, where the wall is constructed with a wall cavity and through-wall flashing to collect and redirect bulk rainwater to the building exterior, mass or solid walls rely principally upon a combination of wall thickness, moisture storage capacity, and (in masonry construction) bonding between masonry units and mortar to effectively resist bulk rainwater penetration (See Fig. 86.9).

For economic reasons, mass walls are less common in design and construction today. However, when constructing an addition, or incorporating a portion of an existing building into a new building or structure, the design and behavior of mass walls relative to storage

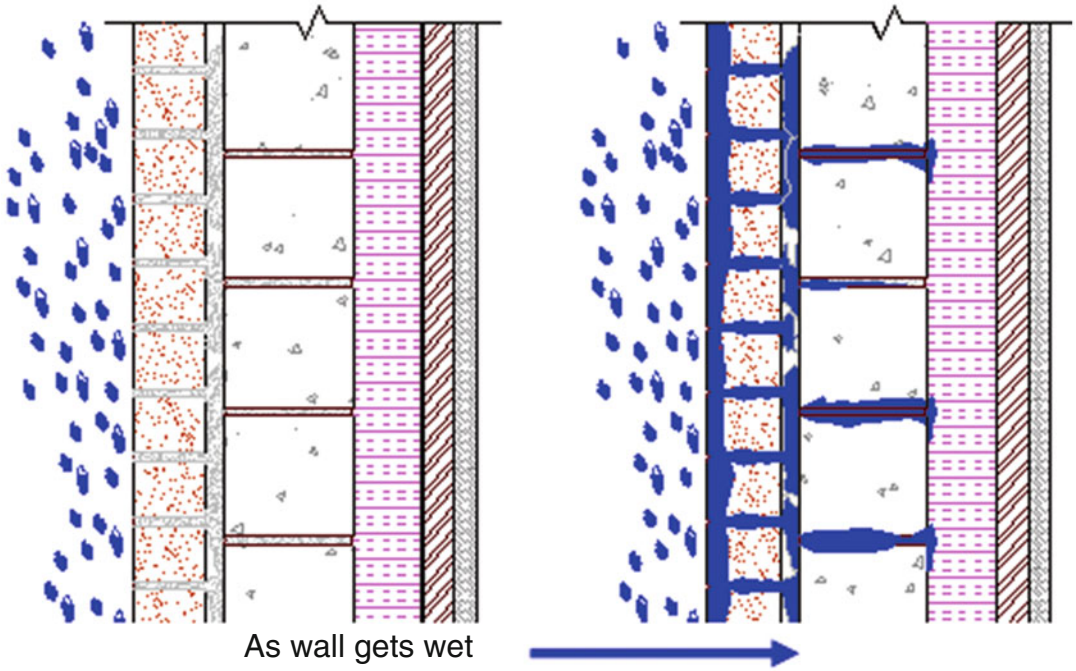

Fig. 86.9 Mass wall section showing reliance on masonry and mortar to resist rainwater penetration (Lemieux and Totten [11])

capacity and both heat and moisture transfer must be considered by the designer.

In addition to bulk rainwater penetration and moisture ingress that is often difficult to track (and therefore effectively isolate and repair) in this type of wall construction, the potentially negative effects of drying must also be considered when designing around or otherwise restoring this type of wall system. Evaporative drying across this type of wall assembly, either to the interior or exterior, can contribute to efflorescence (soluble salts deposited at or near the wall surface, with visible discoloration, sometimes spalling), deterioration of interior cement plaster finishes (common finish in early twentieth century), and organic/microbial growth on either the interior or exterior exposed wall surfaces.

Curtain Wall Construction

A curtain wall is relatively thin, lightweight type of wall assembly used to provide a weather resistant building envelope. A curtain wall is usually an aluminum-framed wall, containing in-fills of glass, metal panels, or thin stone. Curtain wall framing components are attached to the building structure and are not designed to carry any structural floor loading or roof loads of the building. Imposed wind loads and gravity loads of the curtain wall components are transferred to the building structure, typically supported at the floor line. The loads are primarily positive and negative wind loads but might also include a snow load applied to large horizontal areas, seismic loads, maintenance loads and others.

Curtain walls can be classified by their method of fabrication and installation as stick systems and unitized/modular systems. With stick systems (See Fig. 86.10), the curtain wall frame (mullions) and glass or opaque panels are installed and connected together piece by piece, such that all installation and glazing is typically performed at the construction site.

In the building of unitized or modular type system, the curtain wall is composed of large units that are assembled and glazed in the

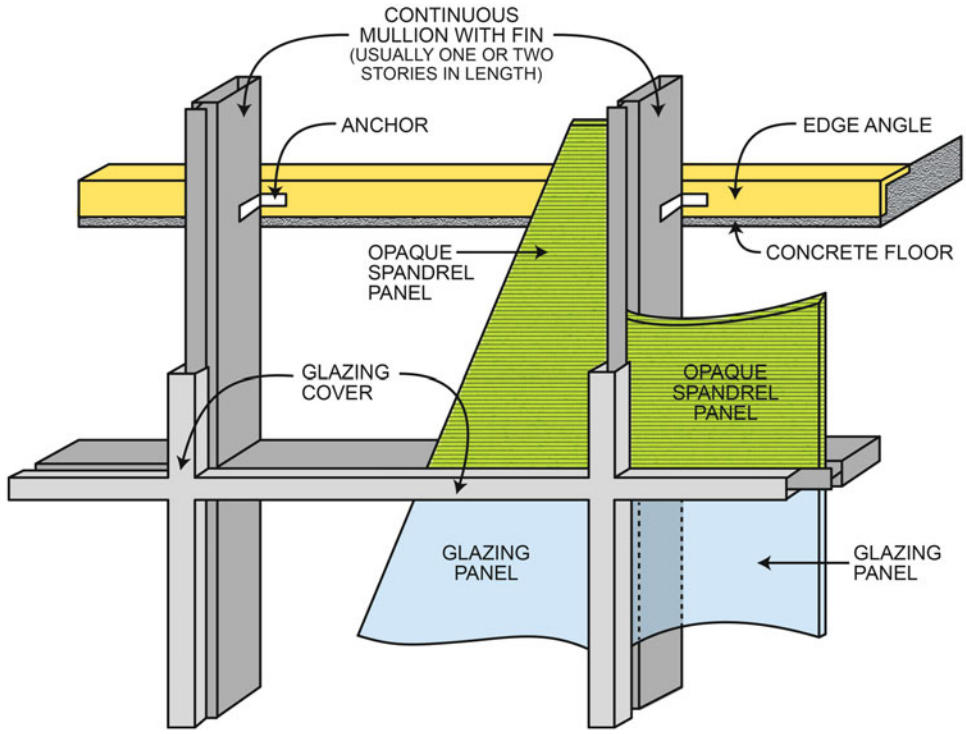

Fig. 86.10 Basic details of a stick type curtain wall

factory, shipped to the site and hung on the building to form the building enclosure. Vertical and horizontal mullions of the modules fit together with the adjoining modules. Modules are generally constructed one story tall and one module wide (typically 1.5–2 m) but may incorporate multiple modules. There are variations on these themes of stick systems and unitized/modular systems as shown in Fig. 86.11 [14].

There are several components that make up a curtain wall assembly. Typical opaque panels include spandrel glass, metal panels, thin stone, and other materials, such as terra cotta or FRP (fiber-reinforced plastic). Vision glass is predominantly insulating glass and may have one or both lites laminated, usually fixed, but sometimes glazed into operable window frames that are incorporated into the curtain wall framing. Spandrel glass can be monolithic, laminated, or insulating glass. The spandrel glass can be made opaque through the use of film/paint or ceramic frit treatment applied on an unexposed surface or through "shadow box" detailing.

Shadow box construction creates a perception of depth behind the spandrel glass by providing an enclosed space behind clear spandrel glass. Metal panels can take various forms, including aluminum plate, stainless steel or other non-corrosive metal, thin composite panels consisting of two thin aluminum sheets sandwiching a thin plastic interlayer, or panels consisting of metal sheets bonded to rigid insulation, with or without an inner metal sheet to create a sandwich panel. Thin stone panels are typically 75–100 mm thick and of granite, marble, travertine or limestone. White marble is not recommended due to its susceptibility to deformation. In cases where the weight of the stone is to be reduced, such stone may be attached to an aluminum honeycomb backing, which also increases the strength of the panel.

Back pans are metal sheets, usually aluminum or galvanized steel that are attached and sealed to the curtain wall framing around the perimeter behind opaque areas of a curtain wall. In cold climates insulation is typically installed between

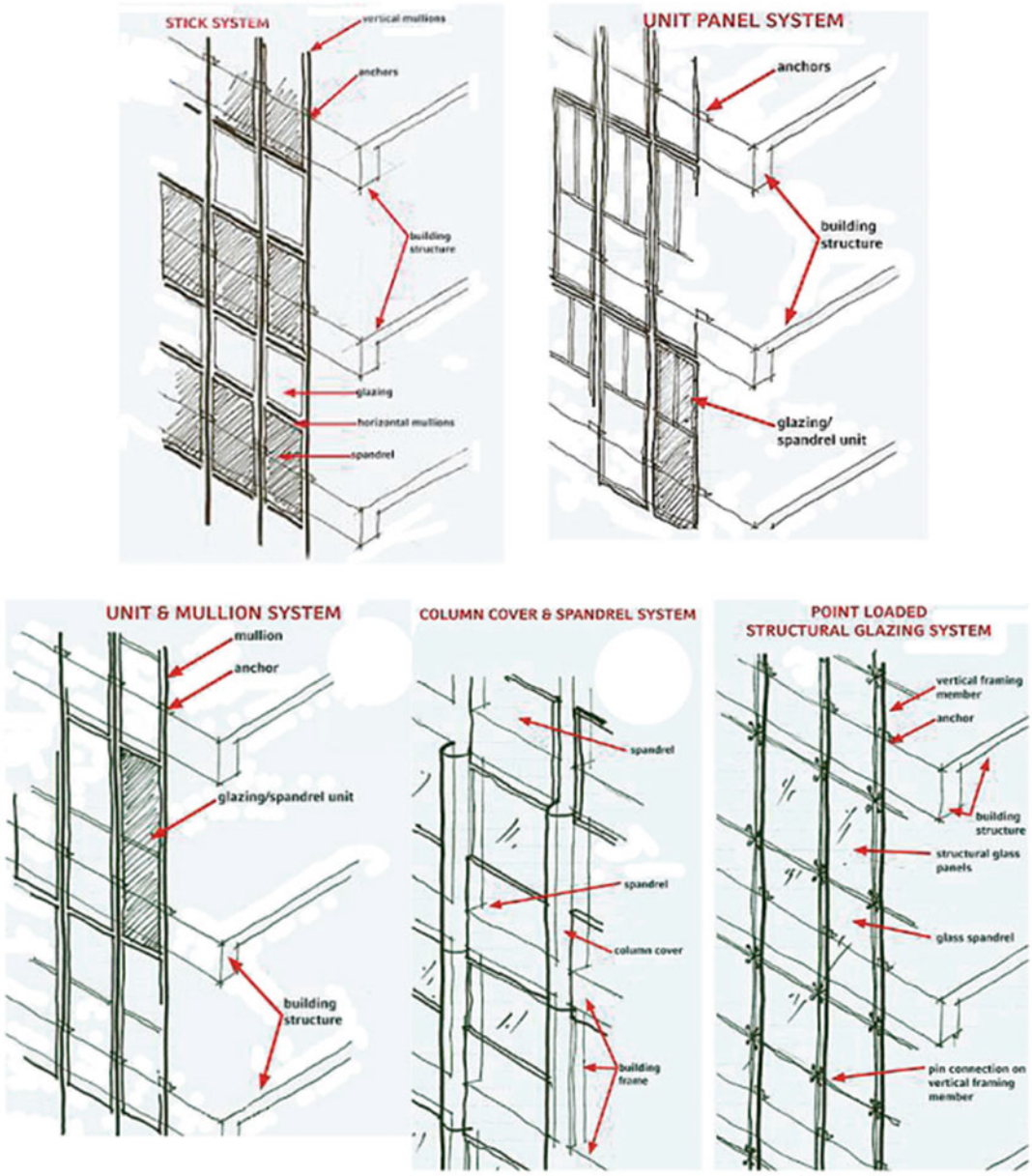

Fig. 86.11 Variations of curtain wall systems [14]

the back pan and the exterior cladding in order to maintain the dew point outboard of the back pan so that the back pan acts as an air and vapor barrier. Back pans provide a second line of defense against water infiltration for areas of the curtain wall that are not visible from the interior and are difficult to access.

Because the aluminum framing components of a curtain wall have a high thermal conductivity, it is common practice to incorporate thermal breaks of low conductivity materials and reduce the temperature transmission via the aluminum components. PVC, Neoprene rubber, polyurethane and polyester-reinforced nylon are

materials used to create the thermal break for improved thermal performance.

In 1986, South West Research Institute performed full scale fire tests of aluminum curtain walls. This testing identified problems of fire spread through voids that appear between the aluminum curtain wall and the edge of the floor slab. The voids were created when tested panels became distorted or when sufficient distortion occurred that allowed fire stopping to fall out of place [15].

The ability of curtain wall systems to remain intact for only short periods of time under fire exposure, uncontrolled by sprinklers, was shown in tests sponsored by the Loss Prevention Council (UK) using an aluminum stick curtain wall assembly. In those tests, failure of the glazed window and spandrel panel units occurred after 13 min, failure of the aluminum façade frames after 24 min and failure of aluminum attachment brackets after 28 min [16]. The Loss Prevention Council tests show the relative short duration of integrity afforded by a stick panel curtain wall, however, there are available passive design techniques where the integrity of the curtain wall components can be designed to provide longer duration resistance (based on specific test criteria) to fire exposure [16, 17].

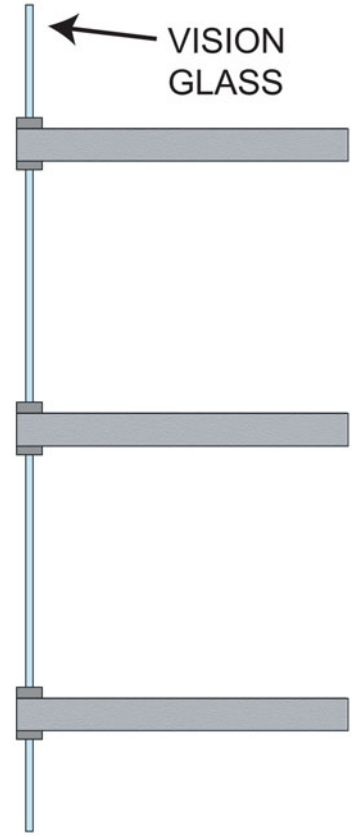

Fig. 86.12 Curtain wall supported on slab edge [9]

Curtain Walls and the Building Edge Condition

Today's codes, such as the *International Building Code* [18] and the National Fire Protection Association's *Building Construction and Safety Code* (NFPA 5000), recognize that with a properly designed and operational sprinkler system, the threat of fire spread along the exterior of the curtain wall is effectively mitigated. This is a critical assumption that deserves further consideration in the context of super high-rise buildings and is discussed in detail later.

From a fire containment perspective, there are two basic ways to provide a code complying curtain wall design in fully sprinklered buildings. The most basic approach is for the curtain wall to be supported directly on the structural floor slab edge, which precludes any gap or joint condition, given that the floor slab is continuous to or extends past the building envelope. This type of installation would permit floor-to-floor glazed curtain wall assemblies in fully sprinklered buildings as shown in Fig. 86.12. This approach is sometimes observed in high-rise building design, but it is not the most common approach for the installation and support of curtain walls. The second approach is applicable when the curtain wall assembly is positioned just outside the edge of a fire rated floor system, such that a void space results between the floor system and the curtain wall assembly as shown in Fig. 86.13.

The noted codes require that the void space at the slab edge in Fig. 86.13 be sealed with an approved material or system to prevent the interior spread of fire (IBC, NFPA 5000). This

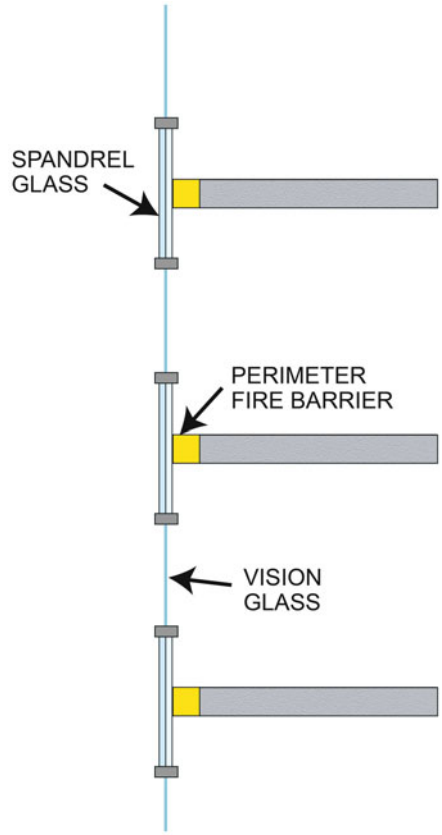

Fig. 86.13 Curtain wall hung-off Slab edge [9]

requires some form of a joint system or what are called "perimeter fire barrier systems." The basic performance criterion for these perimeter fire barrier systems is either one of the following:

1. Such material or systems shall be securely installed and capable of preventing the passage of flame and hot gases sufficient to ignite cotton waste, where subject to ASTM E119 time-temp fire conditions for a time period equal to the fire resistance of the floor assembly, or
2. Such material or systems are to be tested in accordance with ASTM E2307, "*Standard Test Method for Determining Fire Resistance of Perimeter Fire Barrier Systems Using Intermediate-Scale Multi-Story Test Apparatus*".

The methodology for compliance with either the criteria of item 1 above or item 2 is essentially the same, the former being the original performance intent statement which evolved into the more recent and formally defined ASTM Standard. Although a defined ASTM Standard does exist, there is confusion in the building industry resulting from differences in the rating criteria imposed by various testing laboratories. Underwriters Laboratories (UL) certifies perimeter fire barrier systems under the product category "Perimeter Fire Barrier Containment Systems" [17]. The systems certified by UL use the same two-story large scale fire test apparatus as are described in the ASTM E2307 Standard. However, the systems certified by UL are measured in four aspects—an F-Rating, a T-Rating, an Integrity Rating and an Insulation Rating. The ASTM E2307 Standard requires the reporting of an F-Rating and a T-Rating. This is in contrast to the F-rating which is the only requirement stipulated by the IBC and NFPA 5000. It is important to understand these ratings and the purpose behind each rating.

F-Rating An F-rating evaluates the most fundamental function of a perimeter fire barrier system. The F-rating is given if the vertical passage of flame and hot gases sufficient to ignite a cotton pad is prevented by the perimeter fire barrier system. This tests the ability of the perimeter fire barrier system to maintain fire resistance in the void space between the interior surface of the curtain wall assembly and the floor slab edge. The F-rating is expressed in hours (e.g. 2 h) for comparison to the fire resistance rating of an associated floor assembly.

T-Rating A T-rating evaluates the extent of temperature increase on the non-fire side of the perimeter fire barrier system. The temperature measurements are taken at a point 25.4 mm (or less above the fill materials perimeter fire barrier system. A T-rating is expressed in hours for perimeter fire barrier systems that do not show a temperature rise of 181 °C for any individual thermocouple, or a temperature rise of 139 °C for averaged thermocouple points (required for wide voids). T-ratings are typically on the order of 0, 0.25 and 0.50 h.

Insulation Rating This rating provided under the UL certification process is similar to the T-Rating per the ASTM E2307 procedure; however, UL additionally evaluates the temperature rise on the unexposed interior surface of the curtain wall assembly above the fill materials. This is intended to determine if fire can spread to a floor above through the curtain wall construction and not just the fill material of the perimeter fire barrier system. Insulation ratings are typically on the order of 0, 0.25 and 0.50 h.

Integrity Rating This rating provided under the UL certification process is similar to the F-Rating per the ASTM E2307 procedure; however, UL additionally evaluates if there is any flame passage or surface flaming on the interior surface of the curtain wall assembly above the fill materials. In addition, the glazing above the fire exposed floor is monitored to determine when the glazing breaks. The intent of monitoring the glazing integrity is to identify how long in hours the curtain wall glazing will survive, resisting the fire leapfrog that has been observed to occur in multi-story buildings.

The F-Rating and Integrity Rating are sometimes interrelated in that a perimeter fire barrier system will not be capable of achieving an F-Rating if the curtain wall does not maintain integrity and allows the perimeter fire barrier system to become dislocated or displaced during the fire test. This is generally the case for fully glazed curtain wall systems that incorporate glazed insulated spandrel panels. The failure mode for such assemblies occurs if the spandrel glazing and framing members are not sufficiently insulated. Under these conditions, the perimeter fire barrier system fill materials will fall out of place when the glazing panel and associated insulation fail to maintain a compression fit with the fill materials of the perimeter fire barrier system.

Given that the IBC and NFPA 5000 codes only require the void at the intersection of the curtain wall and the floor assembly be protected with fire barrier fill materials, there is often confusion. There are no formally published tested perimeter fire barrier systems that allow for floor-to-floor height vision glazing. This is mostly an artifact of the nature of compression-fit type fire barrier methods and their integration with fully glazed curtain walls. If a tested perimeter fire barrier system could be shown to stay in-place in the void after the glazing failed, then code compliance would be achieved. However, the extent of the failed glazing may raise concerns for flames readily entering adjacent spaces above. This lack of such capable perimeter fire barrier systems poses a challenge to curtain wall designers/architects who wish to create façades using expansive vision glass panels.

The issue of performance expectations of non-fire rated curtain walls and the associated perimeter fire barrier assembly has been a significant item of discussion in the United States. As a result of recent code changes, it is reported [19] that the code intent is to recognize that if the curtain wall assembly does not have the same fire resistive capability of the floor slab, then the system protecting the void space need not perform after curtain wall integrity is lost.

Curtain Wall Components: Performance Factors

Curtain walls are a relatively complex combination of components that include aluminum frames; vision glass; spandrel panels of glass, metal or stone; metal back pans; insulation; gaskets; sealants; and anchors or connectors of steel or aluminum. Given a fully-developed fire exposure in a room or space (i.e. sprinkler system out of service or failure scenario) bordered by a building's curtain wall system, it can be expected that vision glass failure will occur within minutes. Once the failure occurs and flames extend to the exterior, the various curtain wall components and any perimeter fire barrier system are then subject to thermal forces and degradation that can result in fire spread to the floor above.

The possible complexity of a curtain wall is illustrated in Fig. 86.14. In this hypothetical case, a number of components are used to build,

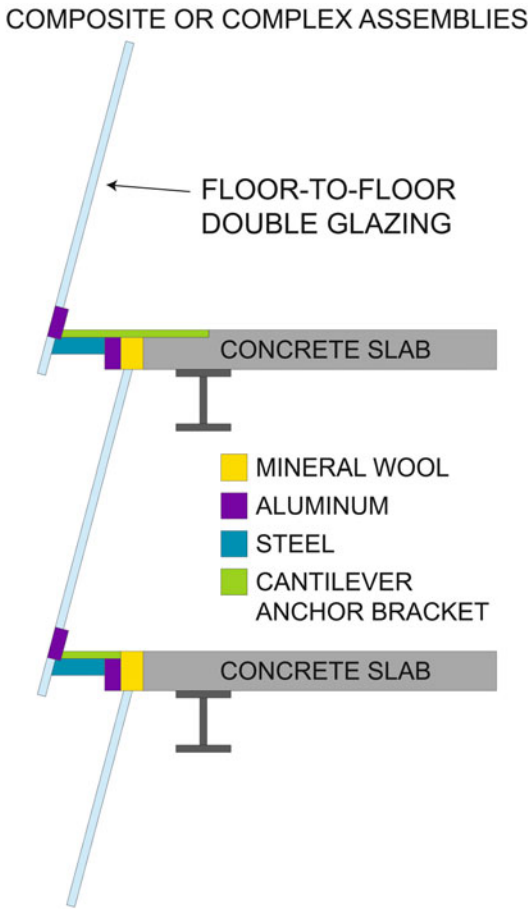

Fig. 86.14 Hypothetical illustration of a complex constructed curtain wall assembly using an inclined glazing surface with slight bottom extension of the glazing to create a shingle effect [9]

support and anchor the curtain wall system to the structure. Additional materials such as mineral wool are used to provide perimeter fire barrier protection. Although it can be straightforward to design and size the components to readily fit together and form an appropriate weather enclosure, it is difficult to know how the components and attachment methods will survive a high temperature fire exposure and the resulting thermal expansion, particularly, when unlike materials are interconnected. Aluminum loses roughly 50 % of its strength at 200 °C and will melt in the range of 550–600 °C. The steel component is not expected to melt, but will expand, inducing stress in other elements of the composite assembly. In Fig. 86.14, potential flame exposure to the curtain wall components is likely exacerbated by the geometry of the inclined overlapping shingle design.

The nature of the curtain wall design will dictate the relative capability to resist floor-to-floor fire spread. Key factors that impact the curtain wall's resistance to vertical fire spread are as follows:

- Full height or partial height (e.g. spandrel panel design) vision glass systems
- Nature of the glass used to construct glazing system
- Nature of the curtain wall components (e.g. framing, spandrel panels)
- Height of spandrel panels
- Vertical or horizontal projections on exterior that may deflect or enhance flame behavior
- Building geometry at curtain wall—twister, staggered, sloped, etc.
- Operable windows/openings—size, vertical or horizontal orientation
- Ability of perimeter fire barrier system to remain in void during fire exposure

When full height vision glass systems are used, flame extension and heat fluxes to the window areas above can be expected to be greater than that expected for curtain walls using a spandrel panel design. A spandrel panel design will limit the flame extension and reduce heat flux to the areas above by providing an opaque surface to block the heat transfer. To prevent the leapfrog effect using a spandrel design requires a vertical spandrel dimension of approximately 4 and 5 ft in order to match the performance, respectively, of 1 and 2 h fire rated floors [20]. The construction of the spandrel can be an important factor to the performance of the perimeter fire barrier system. Typical aluminum framed curtain walls using spandrel glass require that the glass be appropriately insulated using mineral wool rather than fiberglass-based insulations that will melt. Additionally, the aluminum mullions require insulation protection; otherwise the aluminum frame will melt and no longer support the wall system. These measures will help keep the glass spandrel panel and any associated fire barrier

system intact. Precast panels offer the advantage of high resistance to heat exposure and offer a solid rigid surface for securely positioning or compression fitting a perimeter fire barrier system into the void between the precast panel and the floor slab edge. Metal curtain wall panels or metal back pans that, when subjected to the fire heat, may warp or distort allowing gaps to develop at the perimeter fire barrier system, and specific measures may be needed to stiffen the metal pans.

Glass used in curtain wall assemblies may be one of several types—float glass which may be heat strengthened or tempered glass, and laminated or wired glass. Vision glass can be single, double or triple glazed, and are typically assembled into an insulating glass unit (IGU). Vision glass may also be tinted to provide a heat absorbing quality, or coated to provide a heat reflective capability. All of these features can impact the performance of glass under fire exposure, however, very little is currently known about the fire performance of the wide variety of IGUs that are possible. What we do know about glass performance is limited to standard single glazed assemblies and, recently, some information on double glazed units has been presented (see glass discussion in later sections of this Chapter). More testing to determine the performance of large IGUs is needed to better understand these fire-related performance metrics. It may be that actual IGUs may show fire performance benefits not yet understood, however, full installations with framing elements, sealants and gaskets may play a key role—positive or negative. Such full scale installations are not known to have been tested to any degree that allows for reasonable conclusions about installed performance.

Building geometry and exterior projections of the curtain wall or building structural elements can have a beneficial or negative effect on flame length extension and heat flux exposure to curtain wall elements above the fire compartment. This can be particularly important if operable windows or ventilation openings are used. Of course, any such opening can allow the unrestricted passage of flames and hot gases from a fire on a floor below into the floor above. The position of the window or ventilation opening relative to the expected flame extension is a factor in assessment of the risk of upward flame spread.

Today many unique wall designs veer from the more traditional continuous vertical façade surfaces of the past, often using curved surfaces and rotated floor plates that complicate the façade connections and hidden details of fire barrier assemblies. Such new designs can result in an orientation that allows for either more direct flame exposure (Fig. 86.15) or diminishes the threat of direct flame contact (Fig. 86.16). It is important to note that regardless of the façade

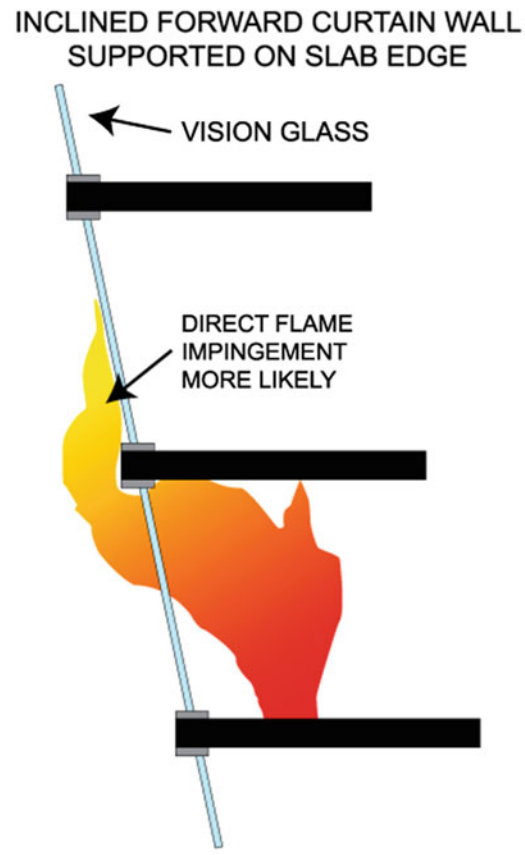

Fig. 86.15 An inclined forward curtain wall condition can allow for more direct flame impingement and higher exposure temperatures on curtain wall components [9]

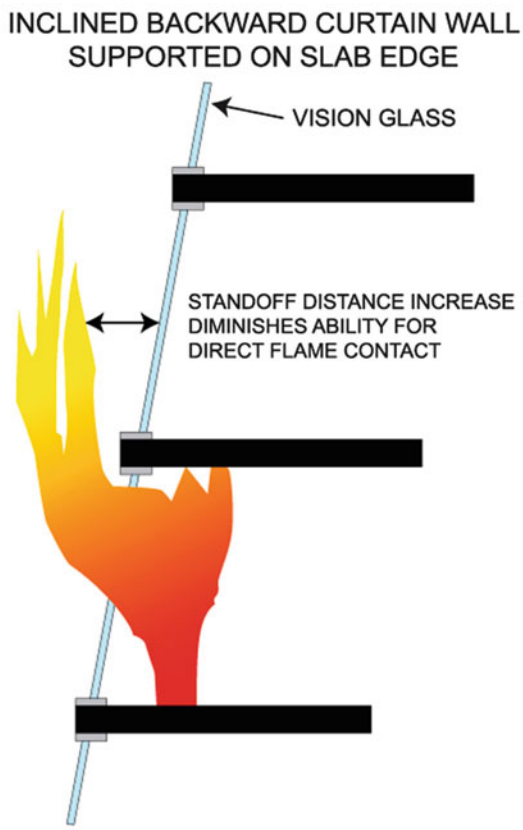

Fig. 86.16 An inclined backward curtain wall condition can diminish the ability of flames to contact the curtain wall components [9]

orientation that wind conditions are a significant factor which may reduce or exacerbate the flame and temperature exposure.

Double Skin Façades

The idea of double skin façades dates back to 1849 with first implementation noted to be in 1903 at the Steiff Factory in Gienge/Brenz, Germany [21]. In recent years, the green building/sustainability movement has resulted in the deployment of new concepts in façade or curtain wall design that intended to enhance the energy efficiency of building façades.

Double-skin façades are a key development in this area that offers solutions to heating, cooling, sound control and lighting efficiency for buildings. The basic components of a double skin façade system often involve the use of an outer glazed curtain wall, usually with ventilation openings, a cavity (usually ventilated) with dimensions of centimeters to meters in depth, and a second inner curtain wall with insulated glazed units.

There are wide variations possible for the design of these double skin façades. Design variables include the ventilation scheme (passive or active), use of louvers, motor operated openings or fans, shading devices, horizontal or vertical partitions within the cavity and operable windows on the inner skin of the double façade. Depending on local climate, the double façade concept may be used in different ways.

For example, in winter climates, the air cavity is closed and the system is used as a triple glazed system with the air in the cavity acting as a transparent insulator. The temperature of the internal glazing is effectively raised, reducing heating costs and increasing occupant comfort at vicinities close to the glazing. In hot climates, air inlets and outlets may be opened to develop a stack effect (hot air rises) allowing hot air to be released at the top of the cavity and replaced by fresh air from the lower regions of the cavity. Within the air cavity, sun shades can be used to absorb and reflect solar heat energy which can promote an even higher temperature differential for the stack effect to take place within the cavity. As a result, cooling costs for inhabited areas are reduced and occupant comfort increased.

Building enclosure designs using ventilated double skin façades should not be confused with windows made of sealed, double or multiple glazed assemblies. A concise but comprehensive definition/explanation (edited) of double skin façades is provided by the Belgian Building Research Institute (BBRI) [22] as follows:

> A ventilated double façade can be defined as a traditional single façade doubled inside or outside by a second, essentially glazed façade. Each of these façades is commonly called a skin. A ventilated cavity—having a width which can range from several centimeters at the narrowest to several meters for the widest accessible cavities—is located between these two skins.

There exist façade concepts where the ventilation of the cavity is controllable, by fans and/or openings, and other façade concepts where this ventilation is not controllable. The indoor and outdoor skins are not necessarily airtight (e.g. louver type façades). Automated equipment, such as shading devices, motorized openings or fans, are most often integrated into the design.

Ventilated double skin façades offer advantages in terms of reducing peak wind pressure on building elements, noise control and improving the overall energy efficiency of buildings. Such energy benefits can accrue from one or a combination of the following mechanisms.

- Natural ventilation enhancement (using stack effect principles)
- Solar heat gain reduction (summer season)
- Thermal heat loss reduction (winter season)
- Passive solar heat gain (winter season)

The BBRI offers a classification system for double skin façades [22]. The classification method considers (1) the type of ventilation scheme, (2) how the façade is partitioned to create vertical and horizontal cavities or spaces for airflows (one example is shown in Fig. 86.17), and (3) the modes of ventilation (see Fig. 86.18). Table 86.2 summarizes the variety of basic features that may be found in the design of double skin façades.

There are a number of issues for the fire engineer to consider when a double skin façade is used. The double-skin façade concept poses conditions that impact fire spread that are not encountered with single skin or more common curtain wall designs. The risk of fire spread through such double-skinned façades introduces concerns arising from the fact that should flame break through the inner façade it would then be confined within a long tall shaft-like space as shown in Fig. 86.19.

The dynamics of the flame and radiant heat exposure for this case are potentially more severe than a flame freely flowing to the open atmosphere. Other types of double-skinned façades may reduce the risk of fire spread, particularly those using a partitioning scheme within the cavity of the double-skinned façade. The cavity can act as shaft for fire and smoke spread, but depending on the cavity design and ventilation scheme, the result may be either an increase or decrease in flame extension and risk of fire spread.

In addition, a naturally ventilated building can challenge the operational aspects of mechanical smoke control systems and pressurized stair systems that generally rely on tightly closed façades in order to develop the pressure differentials and appropriate air flow patterns necessary to manage or resist the movement of smoke and fire with in a tall building. Although no credible research exists on the subject, it is plausible that the presence of a ventilated double skin façade could be used to the advantage of fire department or fire brigade for smoke management during a fire emergency.

There are many sources of case studies and design considerations for double skin façades [21–23]. One well described case study [23] that illustrates the implementation of

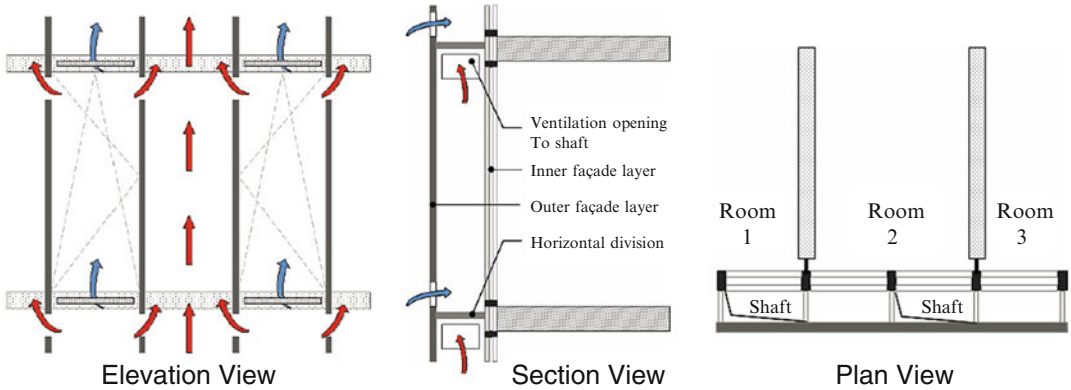

Fig. 86.17 Elevation, section and plan view of "shaft-box" VDF (Ventilated Doubles Façades—classification and illustration of façade concepts, Belgian Building Research Institute (BBRI))

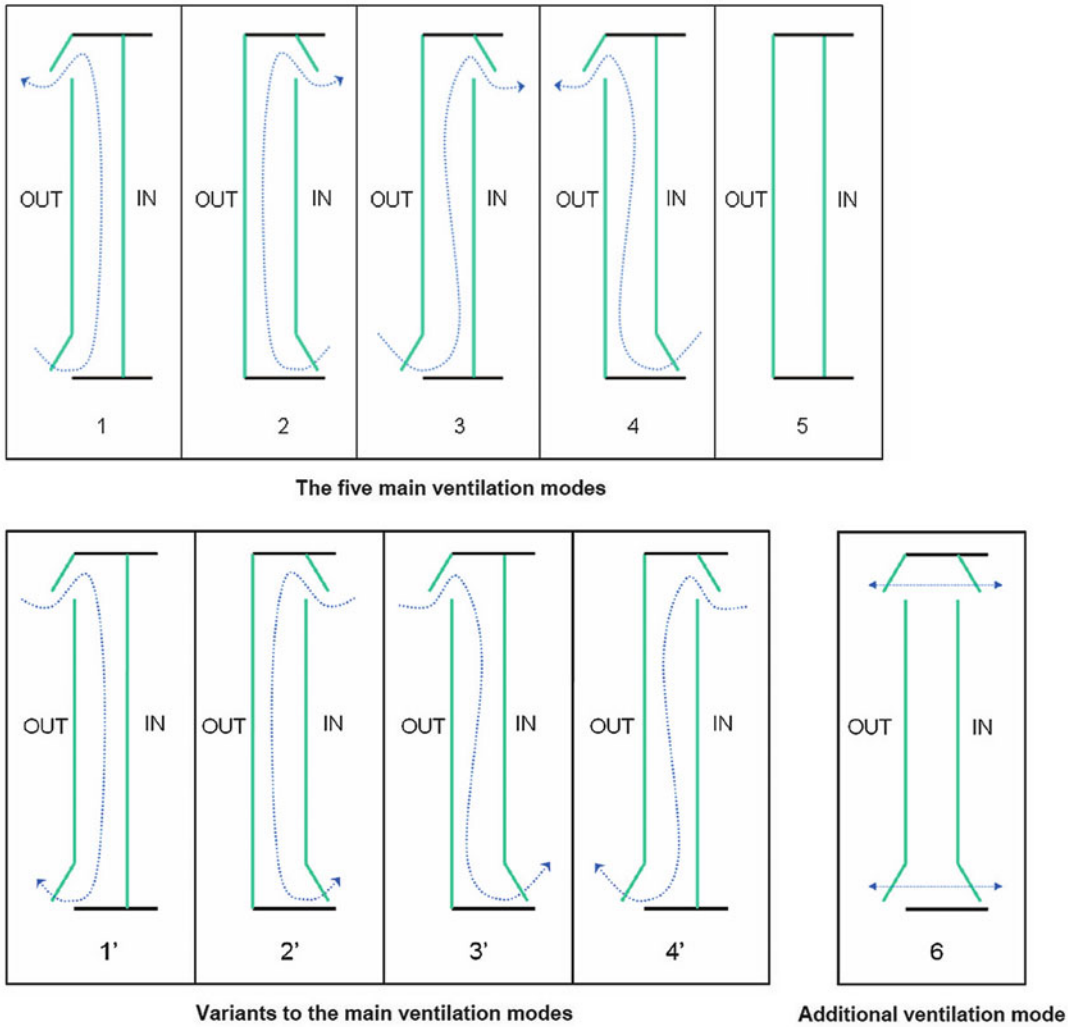

Fig. 86.18 Basic and variant ventilation modes for VDFs (ventilated doubles façades—classification and illustration of façade concepts, Belgian Building Research Institute (BBRI))

ventilation schemes throughout a building including the use of atrium spaces in support of the ventilation scheme is the Commerzbank in Frankfurt, Germany. The BBRI definition recognizes that atrium spaces can be regarded as a ventilated double façade with a very large cavity [22].

The Commerzbank, built in 1997, uses a double skin façade with a cavity of 200 mm. the exterior cladding modules measure 1.5 m horizontally and 2.4 m vertically. The building uses a hybrid scheme and the natural ventilation mode relies on both cross ventilation and stack effect air movement.

Perimeter offices use a outdoor air curtain ventilation mode and offices facing atrium spaces are ventilated by air moving from windward sky gardens across central atrium spaces to leeward sky gardens. Figure 86.20 [23] illustrates the natural ventilation flow patterns in plan and section views of the building, which is utilized approximately 80 % of the year, resulting in a 63 % annual energy savings compared to measurements of a fully air conditioned office buildings in Germany.

With regard to fire protection, the case study reviewers offer a few fire-related observations of the Commerzbank design [23].

Table 86.2 Features of ventilated double façades (Based on [22])

Ventilation type
• Natural ventilation (passive)—ventilation that relies on the differences in pressure created by stack effect and wind
• Mechanical ventilation (active)—ventilation aided by powered air moving components (e.g. fans)
• Hybrid ventilation—both natural and mechanical modes used, with mechanical systems triggering when natural ventilation is inadequate to assure performance
Partitioning of the cavity
• Ventilated double window (box window)—characterized by a window doubled inside or outside by a single glazing or by a second window. From the partitioning perspective, it is thus a window which functions as a filling element in a wall
• Ventilated double façade partitioned by story—the façade module has a height limited to one story. The cavity dimensions are generally consistent with the horizontal and vertical dimensions of the modules
• Corridor-type ventilated double façade partitioned by story—characterized by a large cavity in which it is generally possible to walk. While the cavity is physically partitioned at the level of each story (the cavities of each story are independent of one another), it is not limited vertically, and generally extends across several structural bays or even an entire floor
• 'Shaft-box' ventilated double façade—composed of an alternation of juxtaposed façade modules partitioned by story and vertical ventilation ducts set up in the cavity which extends over several floors. Each façade module is connected to one of these vertical ducts, which encourages the stack effect, thus supplying air via the façade modules. This air is naturally drawn into the ventilation duct and evacuated via the outlet located several floors above which represents a schematic view of the partitioning of this type of façade
• Multi-story ventilated double façade—characterized by a cavity which is not partitioned either horizontally or vertically, the space between the two glazed façades therefore forming one large volume. The cavity is wide enough to permit access and floors which can be walked on are installed at the level of each story in order to make it possible to access the cavity, primarily for reasons of cleaning and maintenance
• Multi-story louver naturally ventilated double façade—cavity is not partitioned either horizontally or vertically and therefore forms one large volume. The outdoor façade is composed exclusively of pivoting louvers rather than a traditional monolithic façade equipped (or not) with openings. The outside façade is not airtight, even when the louvers have all been put in closed position
Ventilation/non-ventilation modes
• Outdoor air curtain—in this ventilation mode, the air introduced into the cavity comes from the outside and is immediately rejected towards the outside. The ventilation of the cavity therefore forms an air curtain enveloping the outside façade
• Indoor air curtain—the air comes from the inside of the room and is returned to the inside of the room or via the ventilation system. The ventilation of the cavity therefore forms an air curtain enveloping the indoor façade
• Air supply—the ventilation of the façade is created with outdoor air. This air is then brought to the inside of the room or into the ventilation system. The ventilation of the façade thus makes it possible to supply the building with air
• Air exhaust—the air comes from the inside of the room and is evacuated towards the outside. The ventilation of the façade thus makes it possible to evacuate the air from the building
• Buffer zone—this ventilation mode is distinctive inasmuch as each of the skins of the double façade is made airtight. The cavity thus forms a buffer zone between the inside and the outside, with no ventilation of the cavity being possible

- The vertical segmentation of the atrium into 12 story-high segments through the use of glass and steel diaphragms prevents the development of extreme stack flows and drafts due to large pressure differentials between the top and bottom of the atrium.
- The segmentation of the atrium also provides fire separation and ventilation zones.
- Though the atrium is compartmentalized into 12-story sections for smoke spread, there is still the potential for significant smoke/fire spread within the villages due to the amount of open atrium space.

The Commerzbank is illustrative of the degree to which double skin façades can influence the air movement in a building. Other building designs have similarly relied on using the stack effect to move air through atriums, or multi-story escalator wells as in the example of the 23-story Liberty Tower of Meiji University in Tokyo, shown in Fig. 86.21.

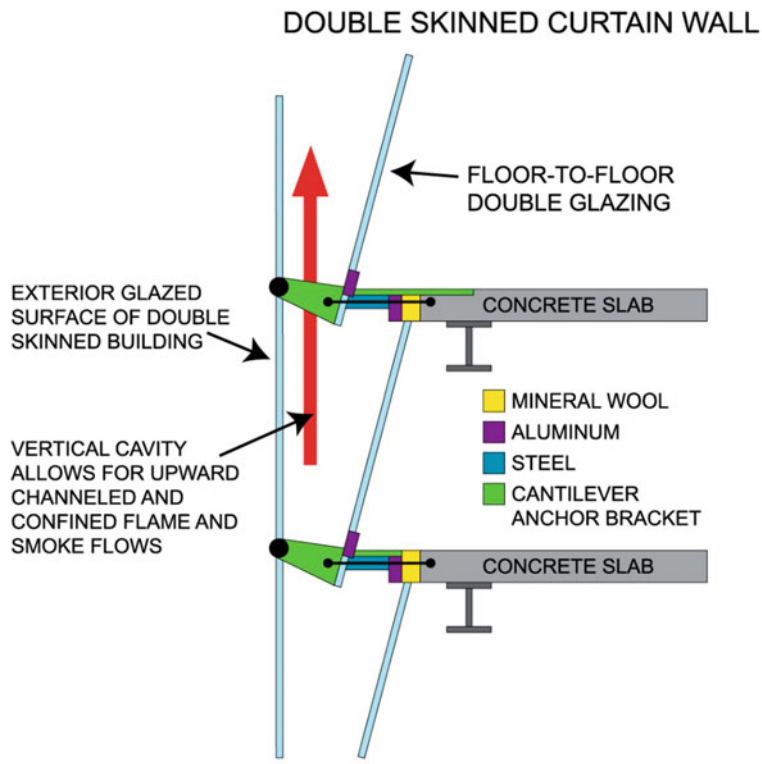

Fig. 86.19 Vertical cavity and potential fire spread route

In this case the fire protection concern is the intentional movement of smoke through the multi-story escalator well. Fire/smoke shutters are arranged to be lowered at the 18th floor atrium openings, presumably to suspend the stack effect created by the "wind floor" concept.

Another concern may be the window ventilation opening detail that poses a risk for exterior floor-to-floor fire spread. If a sufficiently developed fire breaks the exterior glazing, then there may be flame exposure upward and through the vent. Of course, a fire resistive damper may exist in the vent design; however, the case study [23] does not indicate such a protective device being installed in the vent opening.

Exterior Cladding Materials for Wall Construction

There are a variety of materials that may be used to create the outer most, directly weather-exposed surface of a building enclosure wall commonly known as the "cladding". Exterior wall claddings may be noncombustible or combustible materials. Primary categories are as follows:

- Noncombustible Cladding materials
  - Brick
  - Masonry
  - Stone
  - Terracotta
  - Concrete
  - Stucco (Cementitious)
  - Fiber Cement boards/panels
  - Metal siding
  - Glass/metal/concrete curtain wall panels
- Combustible Cladding Materials
  - Wood
  - Vinyl siding
  - Aluminum siding
  - Exterior Insulation and Finish Systems (EIFS)
  - Metal/Aluminum composite Materials (ACM, MCM)
  - Fiberglass Reinforced Plastics (FRP)
  - High Pressure Laminates (HPL)

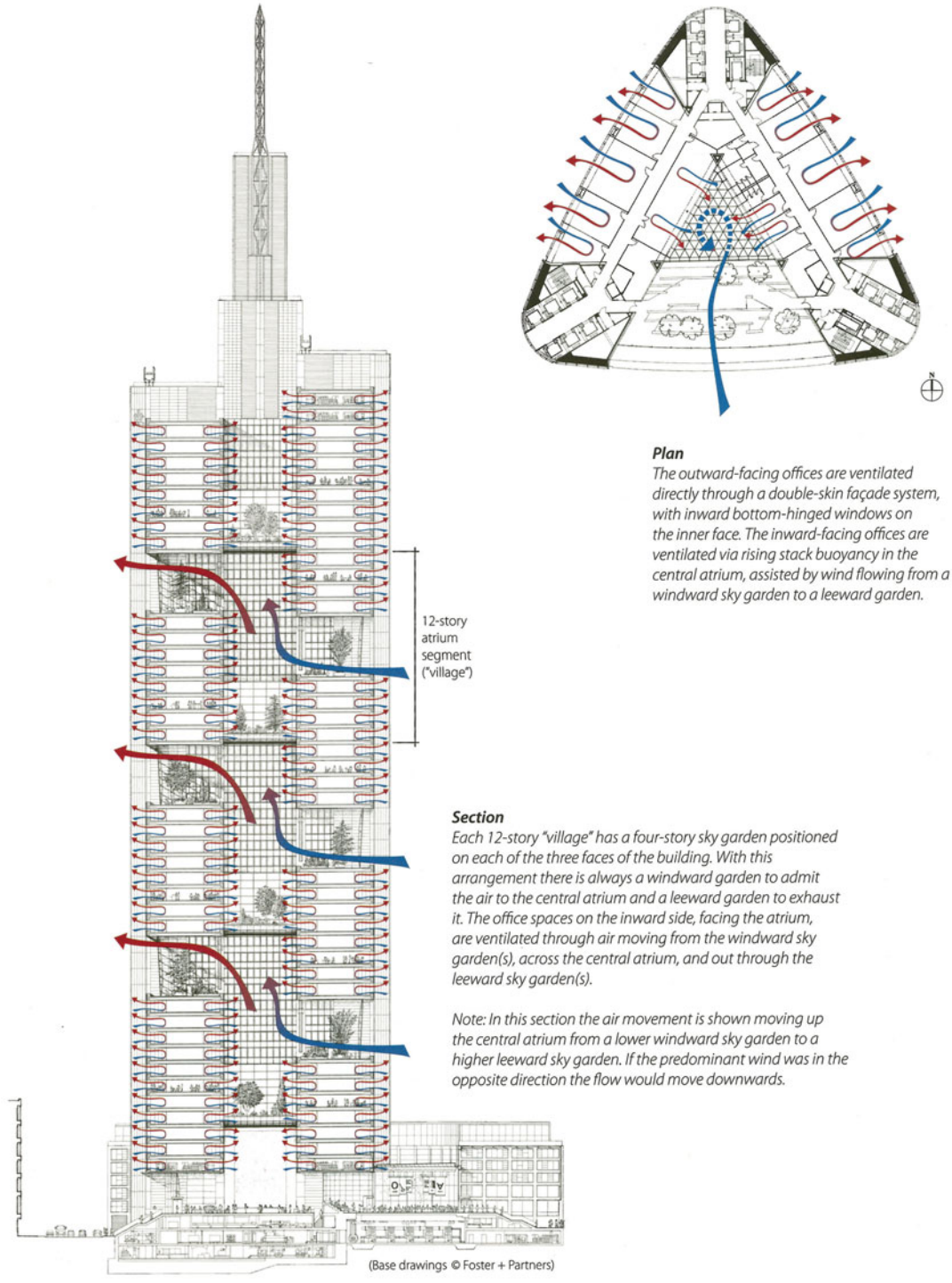

Fig. 86.20 Ventilated façade concept at Commerzbank [23] (Courtesy of CTBUH)

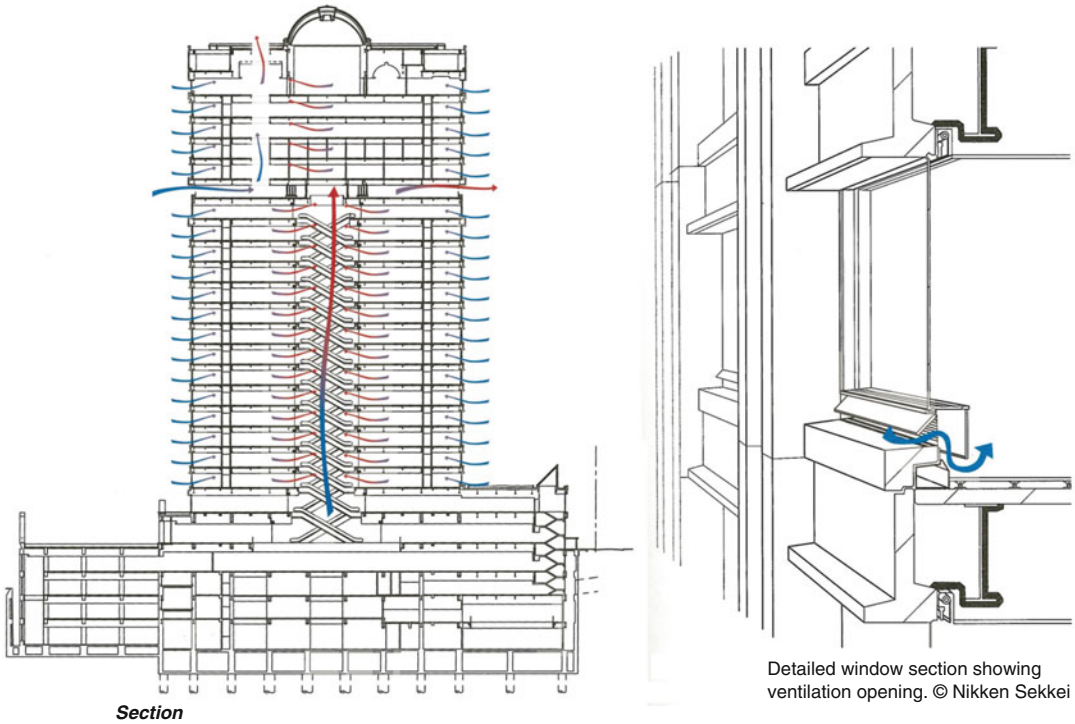

Section

The stack effect in the central escalator void (the "Wind Core") pulls air from the classrooms at each floor. Fresh air enters the classrooms through openings at the base of each window. The eighteenth floor, "Wind Floor" has openings on four sides. As wind passes through the Wind Floor it creates suction, pulling warm air from the escalator void. A similar effect is achieved through an atrium in the upper section of the building, between floors 19–23.

Detailed window section showing ventilation opening. © Nikken Sekkei

Fig. 86.21 Ventilation concept utilizing escalator well at the Liberty Tower of Meiji University [23] (Courtesy of CTBUH)

– Insulated foam core sandwich panels

Model building codes in the United States traditionally have required exterior walls to be constructed of noncombustible materials in buildings of Type I, II, III or IV construction. This requirement is intended to serve multiple objectives, including:

- Resistance to ignition from external exposure fires
- Resistance to ignition from interior fires propagating through wall openings
- Prevention of vertical fire spread on building façades
- Prevention of building-to-building fire spread by means of exterior wall ignition
- Assurance of fire resistive capability of the wall (when structural fire resistance required)

From the 1980s forward, the requirements for noncombustible exterior walls have been revised to allow for the use of combustible materials in exterior walls, including metal composite materials (MCM), exterior insulation and finish systems (EIFS, See Fig. 86.22) and foam plastic insulation (FPI), and most recently high-pressure decorative exterior grade compact laminates (HPL). Generally, assemblies incorporating these materials can be used provided that such assemblies constructed with combustible materials can demonstrate through large-scale fire testing that they can meet these objectives.

A number of well-publicized fires involving foam plastic insulation or MCM assemblies in high-rise buildings have demonstrated potential fire safety issues associated with these products,

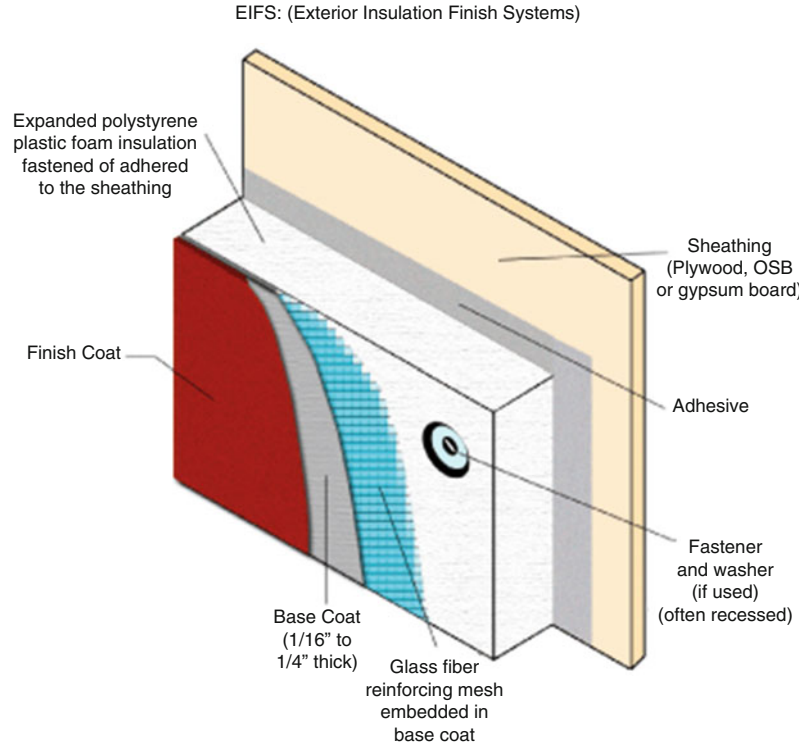

Fig. 86.22 Cutaway view showing typical EIFS assembly components (Courtesy of Pro Stucco http://pro-stucco.com/images/efis-instalation.gif.png)

as well as difficulties associated with fighting fires involving these products in high-rise buildings. These fires include the Borgata Water Club fire in Atlantic City [24] and the Monte Carlo Hotel fire in Las Vegas [25].

In 2007 the Atlantic City Fire Department responded to a fire at the 41 story Water Club Tower finding MCM panels composed of 3 mm aluminum sheets bonded to a 6 mm polyethylene core in flames. The back sides of the panels were covered with 18 mm polystyrene insulation.

The panels were used as a decorative finish on a structural frame set approximately 2 m distant from a concrete sheer wall that prevented major fire extension into the building. This fire resulted in large pieces of aluminum flying off of the MCM support structure and upward flame spread from the third to 38th floor (Fig. 86.23). Fire department personnel indicated that the fire was of relatively short duration having subsided 10–15 min after fire service crews began their engagement at the building [24].

This installation of the MCM panels was not a standard installation where the panels would be mounted closely against an exterior wall assembly. In this case, the panels were simply attached to a structural frame open on all sides to the exterior environment. The Water Club Tower fire is an example of building designers using MCM panels and polystyrene insulation in a creative, but nonstandard way that did not fully consider the fire risk implications.

In the case of the 32-story Monte Carlo Hotel & Casino in Las Vegas, Nevada, exterior wall cladding features were the fuel source for a fire reportedly started by work activities on the roof. The exterior cladding consisted of an EIFS used to clad flat areas of the building from the 29th to 32nd floor.

EIFS assemblies generally consist of a layer of 50–100 mm thickness of expanded polystyrene (EPS) foam insulation adhered to or mechanically fastened over a substrate such as gypsum sheeting. A multi-layer covering or lamina is then provided over the EPS consisting of a polymer/cement adhesive, fiberglass mesh and a final outer coating of a colorized weather-resistant, polymer/cement mixture.

Fig. 86.23 Fire at the water club tower (Courtesy of J. Foley, Atlantic City Fire Department)

Non-EIFS material was also installed to add decorative cornices between the 28th and 29th levels and at the top of the 32nd floor. Although EIFS was involved in the fire, the investigation report [25] cites the decorative elements consisting of expanded polystyrene (EPS) with a polyurethane resin as the primary reason for fire progression. Also, although the EIFS was found to have a non-compliant thickness of lamina, it was observed to burn only in the area of fire exposure [25]. In summary, the decorative EPS features lacked an EIFS covering and were formed into components of relatively large thickness (200–900 mm) which provided the primary fuel for this fire incident, while the EIFS contribution to this incident was limited.

The Water Club Tower and the Monte Carlo Hotel & Casino are two U.S. examples that illustrate the negative consequences of using combustible materials as part of the exterior wall cladding or decorative exterior features. Others [26, 27] cite other international incidents of fires and fire spread where EIFS, insulated sandwich panels, FRP and MCM panels have been involved.

Combustible Components in the Wall Cavity

From a fire perspective, there are a wide variety of combustible components that contribute to the thermal insulating performance and weather resistive performance of exterior walls and enclosure systems. Insulation in walls may be noncombustible material such as fiberglass or mineral wool, but often combustible foam plastic materials with high insulating capabilities; such as extruded polystyrene, expanded polystyrene, spray foam polyurethane insulation and polyisocyanurate insulation; are common insulation choices.

Also, to control air, water and vapor penetration from the exterior to interior spaces, various types of thin membrane or sheet materials of combustible nature are used. Air barriers are used to resist airflow, water-resistive barriers (WRBs) provide resistance to bulk-water penetration and vapor barriers serve to retard or resist moisture vapor diffusion.

Modern day energy codes are driving the design and multi-layered configuration of

exterior wall systems with significant emphasis on achieving a layer of continuous insulation and WRBs. The relative location of these insulating and weather barrier materials in three example steel framed wall configurations is shown in Fig. 86.24. This Figure shows the main types of steel framed wall construction (similar design options and compliance criteria apply to wood stud construction) and their compliance with prescriptive U.S. energy code requirements [28]. Spinu explains the three designs as follows:

Traditional Wall Design (with insulation inside the stud cavity) will no longer meet the prescriptive energy code criteria in most or all climate zones because of continuous insulation requirements.

Hybrid Wall Design (or split insulation design, with insulation within the stud cavity and exterior continuous insulation) is becoming the most common design for framed wall construction which meets energy code requirements.

Exterior Insulated Wall Design (or EXULTATION) with entire insulation placed outside the framed structure, is unlikely to meet the prescriptive code requirements with current insulation materials, especially in cold climates.

As the demand for improved energy performance of building envelopes has increased, new technologies such as continuous insulation shown in Fig. 86.24 have been developed to meet this demand. But it is important that improvements in energy efficiency are achieved without undue compromise of fire safety.

It has been common for architects and building constructors to select individual components of insulation, WRBs, air barriers, brick, masonry, panels and combine then to create an insulated and water resistant wall system. The combination of these materials in to a wall system may not have considered the fire performance of the composite assembly.

One prominent example of was the fire at the 44-story Mandarin Oriental Hotel in 2009. This fire was the result of an illegal fireworks display that ignited building materials at the top of the structure, which then spread downward through the air cavity between the exterior metal cladding and the building insulation and weather resistant barrier layers.

This fire was remarkable in that it demonstrated on a large scale the potential for a downward conflagration along the skin of a high-rise building. Such rapid downward fire spread has not been noted on such a scale in recent

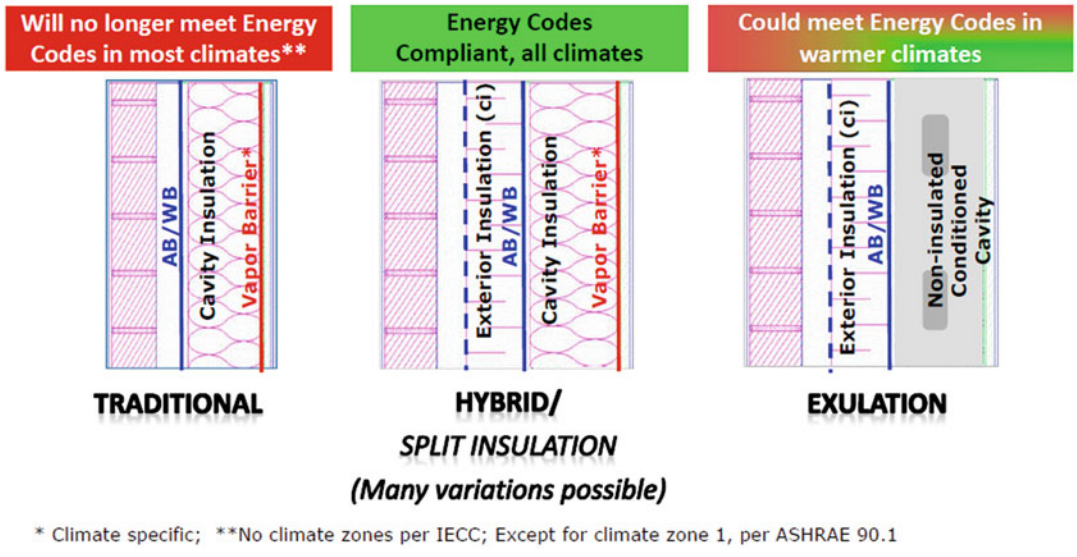

Fig. 86.24 Wall sections showing locations of insulating layers and weather resistant membranes [28]

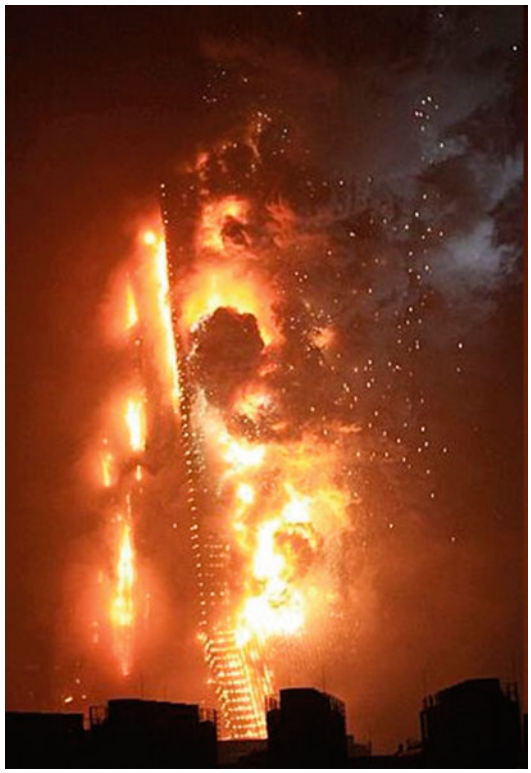

Fig. 86.25 Mandarin Oriental Hotel on fire (Source: Twitter user @Green67)

Fig. 86.26 Exterior condition of building after fire (By BeiBar (panoramio) [CC-BY-SA-3.0 (http://creativecommons.org/licenses/by-sa/3.0)], via Wikimedia Commons

times. Most all large scale high rise fire spread incidents have occurred in the upward direction (Figs. 86.25 and 86.26).

Fire Performance Tests for Exterior Cladding

The need to quantify the performance of combustible claddings and exterior walls using combustible components (insulation, WRBs, etc.) has been recognized for decades. Various full scale and intermediate scale tests have been developed. Reviews and summaries of these various test methods listed in below can be found in the literature [26, 27, 29]:

- NRC Canadian Full Scale Façade Test (CAN/ULC 5-134)
- Modified ASTM E108 Test Method
- UBC 26-9 or NFPA 285—Intermediate-Scale Multi-story Apparatus
- British Standard Cladding System Test
- ISO/DIS Intermediate Scale Façade Tests (ISO 13785-1)
- ISO/DIS Full Scale Façade Tests (ISO 13785-2)
- ISO/DIS Intermediate Scale Sandwich Panel Tests (ISO 13784-1)
- ISO/DIS Full Scale Sandwich Panel Tests (ISO 13784-2)
- Factory Mutual 25-ft and 50-ft Corner Tests
- Loss Prevention Council Test Method (LPS 1181)
- Swedish Full Scale Façade Test (SP105)
- Vertical Channel Test Apparatus

An important aspect of these tests is the variation in heat flux exposure scenarios. Figure 86.27 [29] shows a comparison of total heat flux profiles for seven test methods. The variation among the test methods is significant.

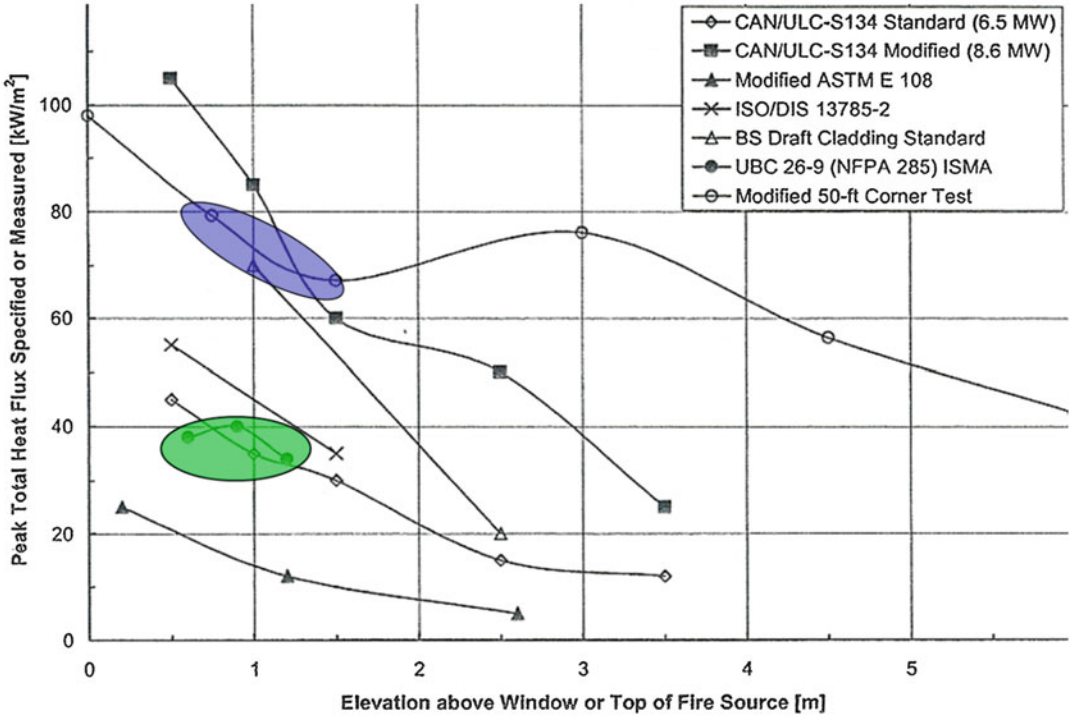

Fig. 86.27 Comparison of heat flux exposures. Colored/shaded areas compare UBC 26-9/NFPA 285 versus the modified 50-ft corner test [29]

The reasons for variation are attributable to the nature of the type of exposure used in the tests, the performance metrics being judged by each test method and the heat flux imposed by the assumed fire source. For example, the modified 50-ft (15 m) Corner Test protocol (Fig. 86.27) may be most relevant for combustible cladding materials subject to an exterior fire source juxtaposed to two walls forming a 90° angle. However, for exposure flames from interior fires onto a flat wall cladding, the UBC 26-9/NFPA 285 test may be appropriate. UBC 26-9/NFPA 285 assumes flames project out a window from an interior post-flashover fire, while the modified 50-ft Corner Test addresses an exterior combustible fuel package set near (0.15 m) a 90° corner façade geometry and the associated re-radiation effects. These two scenarios pose significantly different heat flux exposures on the exterior cladding or exterior walls having combustible components.

Glass and Glass Performance

Glass in a window or curtain wall system can present a route for flames to spread should the glass break and fall from its containment or framing system. Today's windows and curtain wall systems use a wide variety of glass types and framing methods (vinyl, wood, aluminum). Glass can be of a variety of colors, opacity, area, varying sheet thickness and with or without multilayer construction (e.g. single, double, or triple glazed). Glass panels may be annealed or float glass, heat strengthened, tempered/toughened, reflective, laminated, or wired as further described in Table 86.3. The complexity of glass installations from building to building can vary significantly and the current state-of-the art available to predict glass breakage is limited with high degrees of uncertainty given the possible

Table 86.3 Basic glass types and characteristics [30]

Annealed/float glass	Manufacturing process: glass is cooled gradually from a high temperature to minimize residual stress
	Characteristics: can be cut by scoring and snapping. Weakest type of glass; when forced to break tends to form sharp edged pointed shards. Differential Temperatures of 33 °C in the sheet of glass will cause thermal shock stresses and cracking
Tempered/toughened glass	Manufacturing process: glass is heat treated to a uniform temperature of approximately 650 °C and rapidly cooled to induce compressive stresses on the surfaces and edges
	Characteristics: extremely strong glass, but if subject to deep scratch or impact the glass will break into small relatively blunt glass fragments. Used in safety glazing applications
Heat strengthened glass	Manufacturing process: a type of tempered glass strengthened thermally by inducing surface compression that is twice that of annealed glass through only half that of fully tempered glass
	Characteristics: retains the normal properties of annealed glass but provides resistance to thermal stress associated with high performance glazing (tinted, reflective glass). Suitable for spandrel and vision panels and for laminated glass panels for safety
Reflective glass	Manufacturing process: metallic coating is applied to one side of the glass to increase significantly the amount of reflection by both visible and infra-red (heat and light) radiation
	Characteristics: mirror like appearance, reduces heat gain and glare from exterior yet allows optimum visible light transmission
Laminated glass	Manufacturing process: uses normal or tempered glass in two or more layers with one or more layers of a transparent/pigmented specially treated plastic Polyvinyl Butyral (PVB) sandwiched between the glass layers
	Characteristics: if glass is broken, it does not shatter like normal glass, but rather absorbs impact, resisting penetration with broken fragments tending to adhere to the PVB interlayer

configurations and variations in window and curtain wall construction.

Additionally, the age of the installation and associated seals/edge supports as well as environmental stress factors such as temperature and wind loads can impact the performance at the time of a fire exposure. Several reviews of glass breakage research due to fires and heat exposure [31, 32] provide data that is largely limited to single-glazed assemblies. Table 86.4 presents the data of several studies reviewed by Heron et al.; however, the authors' summary comment regarding glass breakage data is that "A number of studies have been conducted on the breakage of glazing under heat stress but no conclusive results have been recorded".

Table 86.4 Summary of glass breakage studies [32]

Glass type	Temperature/ heat flux	Condition
Toughened	43 kW/m^2	Falls out
3 mm float	4–5 kW/m^2	Cracks
3 mm float	16 kW/m^2	Doesn't fall out
Normal float	150–200 °C	Cracks
6 mm toughened	300 °C	Falls out
Plain	150–175 °C	Breaks
6 mm plain	110 °C or 3 kW/m^2	Cracks
6 mm plain	35 kW/m^2	Falls out
3 mm plain	9 kW/m^2	8–24 % falls out
6 mm plate	23 kW/m^2	Breaks and falls out

Small scale tests have shown that plain float glass exposed to radiation at 10 kW/m^2 and 40 kW/m^2 in glass broke at temperatures of 150–175 °C within 8 min and 1 min respectively. In these same tests, heat strengthened and tempered glass survived 43 kW/m^2 for 20 min without breaking while reaching temperatures of 350 °C. Additional small scale tests [33] showed that single glazed windows failed in the range of 40–50 kW/m^2, noting that 33 kW/m^2 appeared to be a level below which failure did not occur.

Of course, fire spread via windows or glass curtain walls is dependent on the potential for the ignition of materials on the unexposed side of a glazed surface. It is known that glass is effectively opaque in the infra-red wavelengths associated with natural fires, and as a result

the heat flux transmission is typically reduced by approximately 50 % for single glazed systems.

For double glazed windows, the radiation transmitted through the first pane is transmitted only in a spectrum where the second pane shows no heat absorption [31]. It is important to know what quantity of radiation will be transmitted through a glass layer to combustible materials on the unexposed side, given that 10–40 kW/m^2 can ignite materials in the range of lightweight fabric materials to common cellulosics [34]. Again, the results of small scale tests have shown that a double glazed assembly will absorb approximately 90 % of the thermal flux and is capable of reducing heat flux from 100 to 8 kW/m^2 (unsprinklered conditions.) This is significant only if the glass does not break and maintains its integrity as a solid barrier. Another study [57] indicated that double glazed systems exposed to heat fluxes as high as 25–170 kW/m^2 provided better integrity than single glazed systems. Tests using fire resistant glass products [35], known as SAFTI Superlite II XL and Superlite I, showed that single pane glass would fall from the frame at temperatures of 400–500 °C with nearby heat fluxes measured at 50–70 kW/m^2.

Fire Behavior at Exterior Wall Openings

Exterior building detailing or articulations incorporated as elements of the façade or, which perhaps, are due to the structural floor plate changes, can impact the flame projection and associated heat exposure to the façade. Work done at the National Research Council of Canada [36, 37] showed the extent to which a horizontal projection located above flames issuing from a window can be effective at reducing the flame exposure. This work also showed that vertical exterior elements could have a negative impact by increasing the vertical projection of flames along a façade. Figure 86.28 illustrates the change in fire flame position and extension due to a horizontal projection above a window and vertical panels located at each side of a window.

In terms of hazard reduction or increase, Fig. 86.29 illustrates how the deflection of the flame by a horizontal projection reduces the heat transferred to the wall above the burning compartment. Conversely, the vertical projections increase the heat transfer to the wall. The increase in heat flux with vertical projections installed is due to the restriction of lateral air entrainment, which forces a lengthening of the gas plume as it seeks to entrain more air for combustion.

Oleszkiewicz conducted propane fueled experiments in a three-story high facility using a window of 2.6 m width and 1.37 m high and fires on the order of 6 MW. Horizontal projections of 0.3, 0.6 and 1.0 m were compared to the case of flames issued from the window along a vertical wall with no projections. Heat flux (connective + radiative) measurements taken at 1, 2, and 3 m above the top of the window showed a significant decrease in heat flux with horizontal flame deflectors in place.

For example, at the 1 m height above the window opening, heat flux ranged from approximately 50 to 100 kW/m^2. However, as indicated in Fig. 86.30, at the 1 m height, total heat flux was reduced by approximately 55 %, 60 % and 85 % respectively for projections of 0.3, 0.6 and 1.0 m. These reductions show the relative effectiveness of a horizontal projection. By comparison, Oleszkiewicz noted that a vertical spandrel wall was not found to be a practical means of protection against flames issuing from an opening. Achieving a 50 % decrease in heat flux exposure via a vertical spandrel panel in this same test would require a 2.5 m high spandrel. It is noted that the same performance in heat flux reduction was achieved with the 0.3 m horizontal projection at 1 m above the opening.

Based on Oleszkiewicz's data, Bong has observed trends and variations of total heat flux density in relation to compartment heat release rates and window parameters [26]. Bong notes the variation of heat flux with height above the window for a 2.6 m wide by 2 m high window at

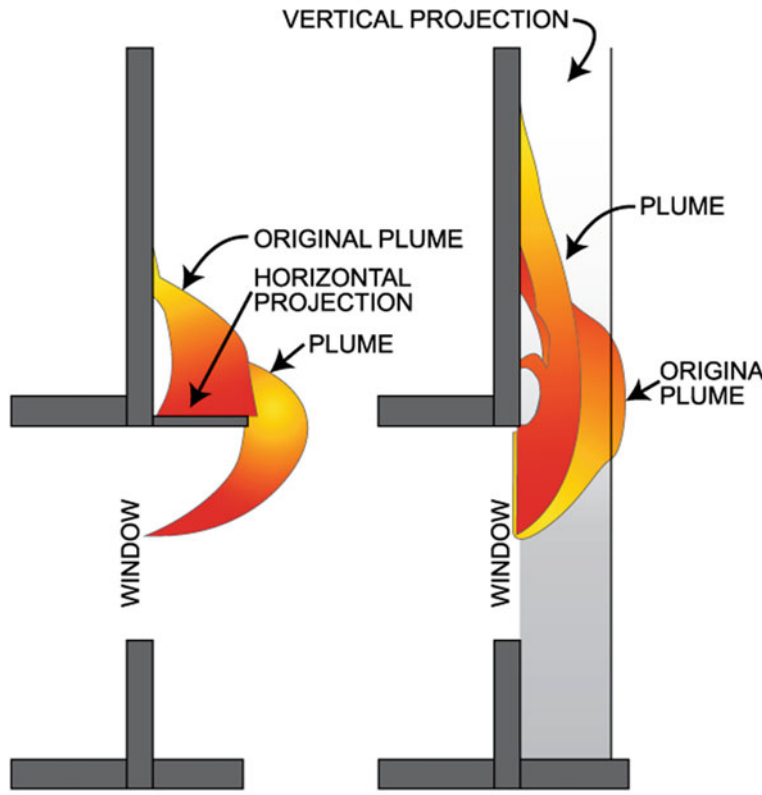

Fig. 86.28 Impact of horizontal and vertical projections on window plume (Based on Oleszkiewicz [36])

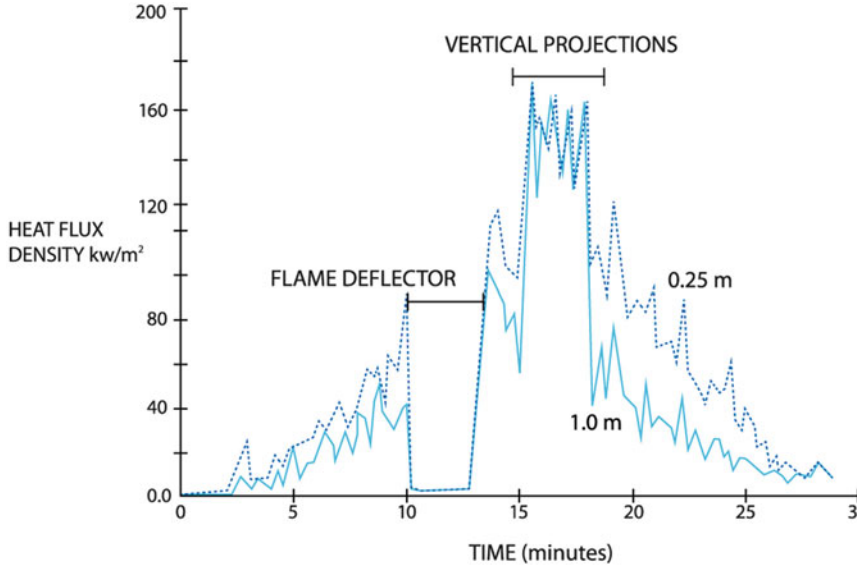

Fig. 86.29 Decrease and increase of heat transfer for horizontal and vertical projections on window plume [9] (Based on Oleszkiewicz [36])

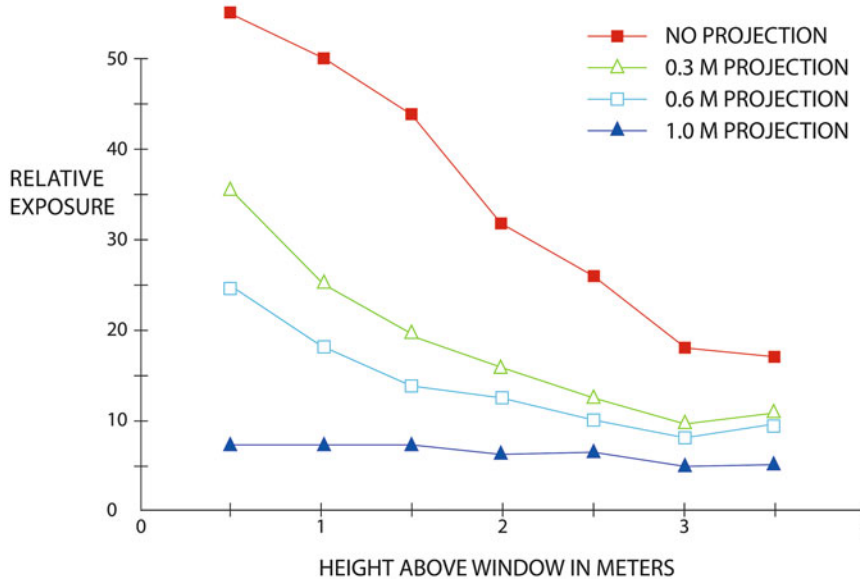

Fig. 86.30 Heat transfer comparison of exposures for 0.3, 0.6 and 1.0 m horizontal flame deflectors. The data is normalized to readings taken at 1 m above the opening with no horizontal deflector (Based on Oleszkiewicz [37])

various compartment heat release rates achieved with a propane gas burner. The total heat flux density (radiation + convection) received from the windows varies with the heat release rate and the position along the height of the wall above the window as indicated by Fig. 86.31. The heat flux measurement increases with increasing compartment heat release rates, yet decreases as the height above the window increases.

With respect to window dimensions, the relationship of heat release rate verses heat flux measured at 0.5 m above the top of the window is indicated in Fig. 86.32. The heat flux increases with increasing compartment heat release rate and decreasing window size. The smallest window (Window 1) has shown a higher heat flux on the exterior wall compared to most other windows (Window 3 is the exception). Total heat flux drops from 43.9 to 6.5 kW/m^2 at 0.5 m above the window with an window area increase from 1.88 m^2 (Window 1) to 7.02 m^2 (Window 5).

The imposed heat flux is shown to increase more rapidly with decreasing window area than increasing compartment heat release rate. This is attributed to the increasing portion of fuel burning outside the fire compartment when the compartment burning regime is ventilation controlled.

Building Codes have often recognized the benefit of providing a horizontal projection or a fire resistive spandrel panel to limit floor-to-floor fire spread, particularly in the case of nonsprinklered buildings [38]. However, such requirements in buildings codes do not preclude the potential for floor-to-floor fire spread along the exterior wall.

The findings of various researchers [27] as found in Table 86.5 point to the limited benefits of horizontal projections and spandrels. In several cases, researchers note the impossibility of preventing floor to floor fire spread (from fully developed fires) via the exterior except by omitting all windows or vents through which flames could project. To impose such restrictions for the purpose of preventing exterior flame spread via windows and openings would radically change the character of buildings and be contrary to current sustainability objectives (e.g. ventilation, natural lighting) in building design.

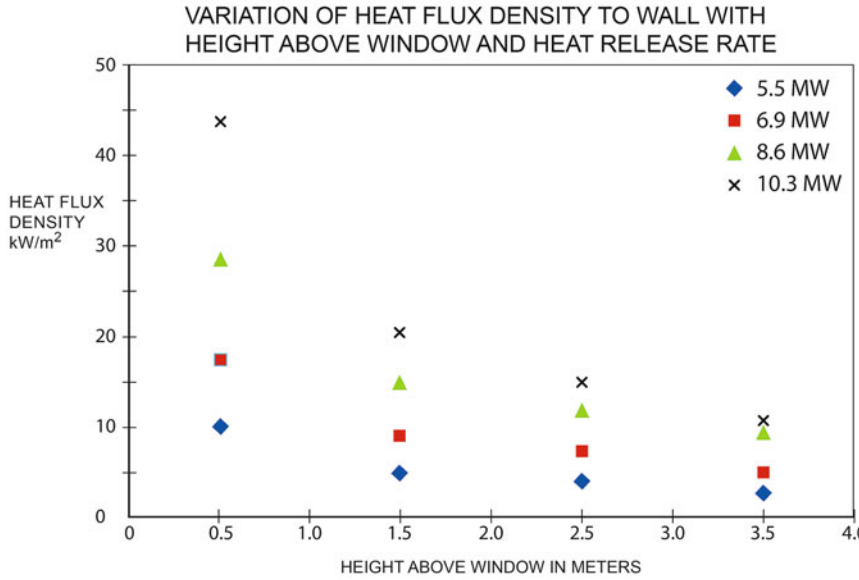

Fig. 86.31 For a Window of 2.6 m width and 2 m height the graph shows total heat flux density varying with compartment HRR and height above the window (Based on Bong [26])

Fig. 86.32 For windows of varying size the graph shows total heat flux density measured 0.5 m above the windows varying with compartment HRR (Based on Bong [26])

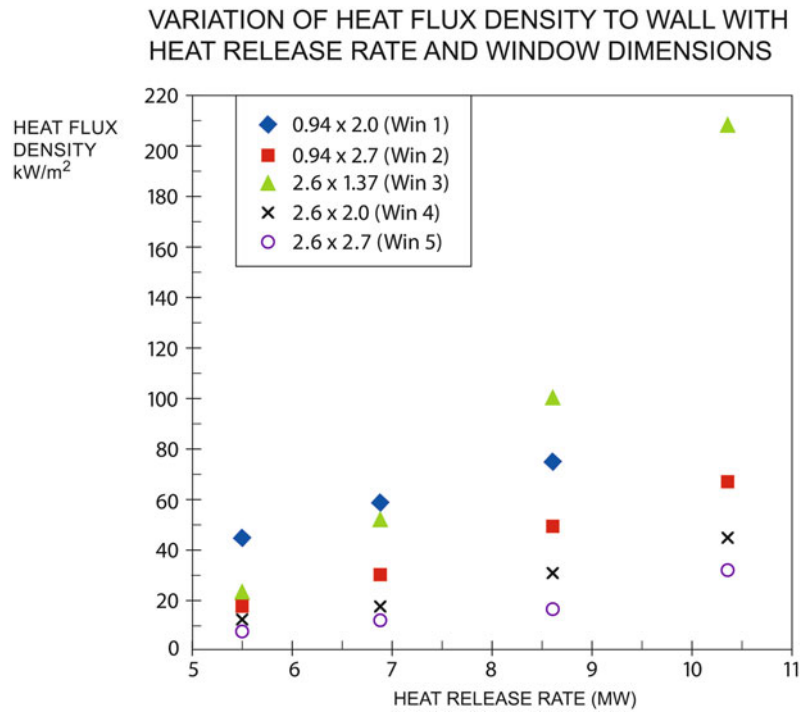

Table 86.5 Summary of research/viewpoints regarding apron (horizontal projection) and spandrels as method to prevent vertical fire spread [27]

Yokoi [5] Full scale experimental fires	0.74 m deep horizontal projection protected panes of ordinary glass from breaking despite the fact that the panes were install only 0.3 m above the top of the opening
[39] Large scale experiments of fire spread using a 4-story building	Vertical separation of 900 mm or a horizontal separation of 600 mm was inadequate to prevent entry of external flame from a fire in a lower story; the research did not determine what separation would be needed
Langdon-Thomas and Law [40]	To provide adequate protection, it would be necessary virtually to omit all windows from the story immediately above the one with window openings in it
NRCC [41]	A spandrel wall was found not be to a practical means of protection against flames issuing from an opening. In order to achieve a 50 % decrease in exposure to the wall above the opening, a 2.5 m high spandrel would be required
Moulen [42] Used one-tenth scale models to investigate various combinations of vertical and horizontal separating construction between story	Concluded that spandrel wall construction above and below the floor slab could not necessarily be considered to have equal effect. He also found that a horizontal projection of 650 mm would allow flames to curl back onto the face of the building when there was no vertical wall construction directly below the floor slab. However, a 900 mm vertical separation below the floor slab in combination with a 650 mm horizontal projection was sufficient to cause flames to be projected away from the façade
National Research Council of Canada [36, 43]	Significant drop in heat transfer from a window fire plume to a building façade above it when a horizontal panel was deployed immediately above the window opening
Oleszkiewicz [37] Using a three-story high burn facility with a window opening of 2.6 m wide by 1.37 m high and with compartment fire sizes of 5.75 MW and 6.9 MW, showed horizontal projections installed above the window offered substantial protection as follows.	A 300 mm horizontal projection reduced the exposure (at 1 m distance above the opening) by approximately 50 % A 600 mm horizontal projection reduced the exposure (at 1 m distance above the opening) by approximately 60 % A 1000 mm horizontal projection reduced the exposure (at 1 m distance above the opening) by approximately 85 %

Loss History: Vertical Fire Spread at the Exterior Façade

The threat of floor-to-floor fire spread at the exterior façade of any building is confirmed via actual unsprinklered high-rise building fires. A number of incidents have been identified in the literature [20, 44–50]). The extent of fire spread in ten well known incidents has been reviewed in order to report some key observations of past incidents which are graphically represented in Fig. 86.33.

John Hancock Center, Chicago, Illinois, USA, 100 Stories [47] In 1972, this fire started on the 96th story in an unsprinklered two-level cocktail lounge, and caused damage to the 95th through 97th stories. The fire burned for about an hour and 20 min. The floors throughout were of poured concrete; outer skin was of glass set in aluminum mullions with a 6 mm-thick aluminum skin over the steel beams and columns on the exterior of the building.

Plate glass windows that were 12 mm thick in aluminum mullions extended from the floor to the ceiling. At the firefighters' arrival, the fire had broken windows on the 96th floor, and burning fire gases were pushing out of the openings. Because the sides of the building tapered toward the top and because there was very little wind

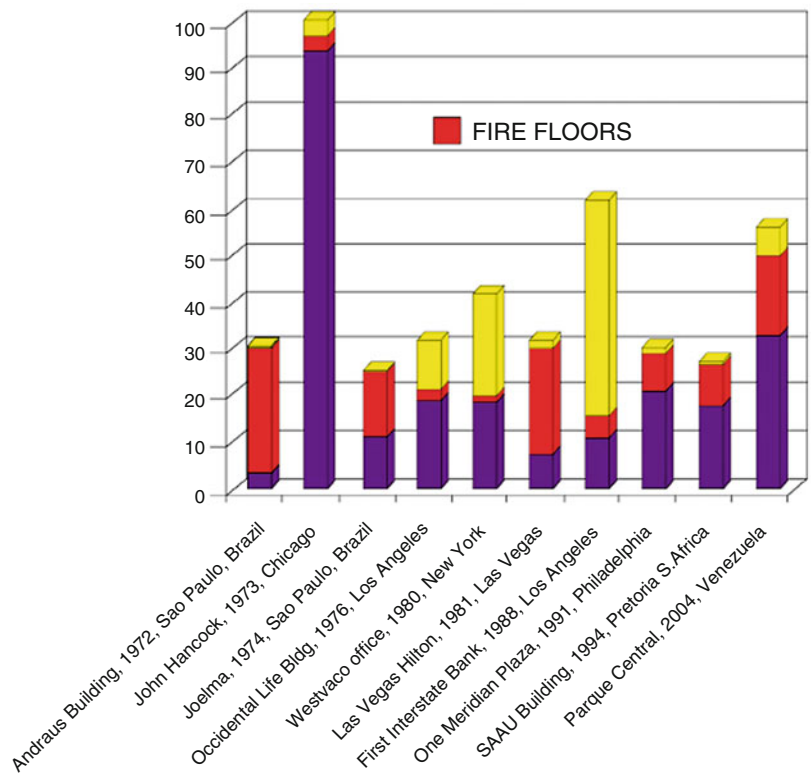

Fig. 86.33 Fire involved floors of ten past high-rise fire incidents (O'Connor [9])

that morning, breaking glass slid down the side of the building instead of falling freely. Windows along approximately 60 ft of the 96th story were cracked or broken, some exterior aluminum skin near them melted, as did some of the mullions.

Fire entered the 97th story through the window, but was confined to some combustibles on a test bench. Very little combustible material in the 97th story was a major reason the damage from this fire was not much greater. Investigators noted that had there been a different occupancy on the 97th floor, with more combustible materials near the windows, a serious fire probably would have developed.

Andraus Building, Sao Paulo, Brazil, 31 Stories [51] This building was a department store occupying the basement and seven stories above grade. The 8th–31st floors were office use. In 1972 this fire occurred on the fourth floor of the department store. The fire developed on the 4 floors of the department store and then spread externally up the side of the building, involving another 24 floors.

The fire gutted most areas of the building. A total of 16 fatalities resulted. The building façade had extensive floor-to-ceiling areas of 6 mm plate glass set in steel frames supported on a 360 mm high concrete spandrel that was integral with the concrete floor slab. Every other section of windows was operable.

From the fourth and fifth floors, the fire spread up the open stairs to involve the sixth and seventh floors. As heat broke window glass, flames broke out the north side on all four floors, forming a flame front that exposed three or four floors above the department store. The heat from exposing flames ignited combustible ceiling tiles and wood partitions on each floor.

The estimated time for full involvement of the façade after flame had emerged from the department store floors was 15 min. Approximately 300 people fled to the roof top heliport and

were eventually rescued by helicopters. Fire department response involved 28 pumpers, numerous tank trucks, and 4 aerial ladders.

Occidental Center Tower, Los Angeles, CA, USA, 32 Stories [46] In 1976 this fire was of incendiary origin on the 20th floor of a non-sprinklered building. A flammable liquid was used, and the fire was large from the very beginning.

The exterior curtain wall consisted of glazed terrazzo tile extending 1.3 m below the floor line, and 0.83 m above it. The window openings were approximately 1.8 m high. The windows were of tempered glass. Both horizontal and vertical aluminum sun screens were attached to the exterior of the building.

Fire damaged approximately 60 % of the floor of fire origin, and then spread externally to the 21st floor, destroying approximately 10 % of that floor. Broken glass falling from the building was reported to have hit the ground at distances up to 20 m from the building. The fire was knocked down approximately 1 h and 30 min after the initial alarm. A total firefighting force of approximately 300 men were utilized in suppressing the fire.

The Las Vegas Hilton, Las Vegas, NV, USA, 30 Stories [45] In 1981, this fire occurred on the eighth floor in the vicinity of the east tower elevator lobby. Fire spread from the 8th floor to the 30th floor vertically. The fire caused 8 fatalities and approximately 350 injuries.

On the exterior wall of the elevator lobbies, three 0.9 m-by 1.8 m windows of double-strength plate glass created a large glass area 1.8 m by 2.7 m set on the concrete slab. The glass was recessed 450 mm and was separated vertically by a 1 m spandrel. The spandrel was prefabricated assembly of masonry, plaster, and gypsum wallboard on steel studs, with no apparent evidence of combustible material.

The fire progressed vertically up the exterior of the building, floor by floor. After the eighth floor become involved, it is estimated that the vertical exterior spread took 20–25 min to reach the top of the 30-story building. Occupants evacuated the building by way of the stairway, were trapped in their rooms by the fire, or waited out the fire in their rooms. Many people encountered smoke in the stairway, especially in the east tower east interior stairway. Some people in the stairway were able to get to the roof and were rescued by helicopters. A total of 23 engines, 6 ladders, 2 snorkels, 9 rescue units, 2 air cascade units, and 12 helicopters were utilized during the firefighting and rescue operations.

First Interstate Bank Building, Los Angeles, CA, USA, 62-Story Office Building [52] In 1988, this fire started on an office floor, and by the time the fire department arrived, a significant portion of the floor was involved. Fire extended to four floors before being contained after 3–0.5 h.

The building was being retrofitted with sprinklers, but the system was not operational at the time of the fire. A 76 mm void between the floor slab and the exterior aluminum and glass curtain wall was filled with thermal insulating material extending approximately 450 mm above and below the floor slab. Gypsum board enclosed the safing material above the floor slab. The insulation below the floor deck was open to a ceiling return air plenum.

About 40 persons were in the building at the time of the fire. The fire department rescued two from the 37th floor and one from the 50th. The fire department with 64 fire companies and 383 fire fighters made a stand on the not-yet-involved 16th floor and was able to stop further spread.

One Meridian Plaza, Philadelphia, PA, USA, 30 Stories [53] In 1991, this fire started on the 22nd floor in a vacant office in a pile of linseed-soaked rags. It burned for more than 19 h, completely consuming eight floors. There were 3 firefighter fatalities, and 24 were injured.

The exterior of the building was covered by granite curtain wall panels with glass windows attached to the perimeter floor girders and spandrels. Exterior vertical fire spread occurred as a result of exterior window breakage, and this was the primary means of fire spread. There were no sprinklers in the building up to the 30th floor,

where ten sprinklers supplied by fire department pumpers stopped fire spread. Only building staff were in the building at the time of the fire. Fire attack was hampered by heavy smoke, complete failure of the building's electrical system, and inadequate water pressure. Firefighting was abandoned after 11 h due to risk of structural collapse.

Parque Central, East Tower, Caracas, Venezuela, 56-Story Office Building In 2004, this fire started on the 34th floor and eventually extended to the top of the 56-story building. There were no functioning sprinkler systems. Pumps and standpipe systems were not in service.

Photographs show evidence of fire spread along the exterior façade. The building was unoccupied, but 3 employees and up to about 25 firefighters were injured. Firefighters backed by helicopters and troops battled the blaze for 12 h before abandoning the effort due to fear of structural collapse.

Several observations are apparent upon review of the ten reviewed incidents, which point to fire risk assessment considerations.

1. Large fire department personnel and apparatus response was observed in eight of the ten incidents. In two cases, One Merdian Plaza and Parque Central, the fire departments abandoned their efforts due to fears of structural collapse.
2. In several incidents, occupants fled to the roof of the building to be rescued by helicopters. In contrast, many of today's super high-rise buildings will not have an accessible roof to facilitate occupant rescue operations. The fact that many tall buildings may not have an accessible roof should not be cause for requiring such. Roof top operations pose significant challenges and hazards.
3. Fire spread was attributable to broken windows and flame extension along the exterior façades. The number of floors involved was as few as two stories in a 32 story building, but ranged up to as many as 23 stories in three of the ten incidents reviewed.
4. The value of sprinklers was observed in the One Meridian Plaza incident where ten sprinklers supplied by fire department pumpers stopped fire spread. It is reported [53] that the sprinklers activated as a result of heat transmission via broken windows and through the void space that existed between the floor slab and exterior granite façade, as well as heat conduction through the floor slab. As combustibles ignited at multiple locations, the sprinklers operated and extinguished the fires.

Risk Assessment Factors

Several factors to consider in a risk assessment of upward fire spread at the building façade include, but may not be limited to, the following:

- Automatic sprinkler systems' reliability
- Fire department/brigade response capabilities
- Building height
- Building occupancy considerations—e.g., office, residential, hospitals, mercantile
- Building compartmentation features
- Building evacuation strategies
- Fire hazard—fuel loads, continuity of combustibles, compartment sizes
- Security threat assessment scenarios

Sprinklered high-rise buildings have a very successful record of life safety and property protection performance. For this reason, the IBC and NFPA 5000 do not require fire resistance rated spandrels or flame deflectors at the building façade in fully sprinklered buildings. Significant reliance on sprinkler systems becomes exceedingly more critical for super high-rises. As the height of buildings increase, so does the complexity of sprinkler systems with an integrated network of piping zones, valves, pumps, power supplies, and water supply tanks. Many components are required to be operational and operated properly for the sprinkler system's success.

Sprinkler system maintenance can be a major maintenance activity for today's super high-rise buildings and is key to successful performance. A recent analysis [54] of data from the National Fire Incident Reporting System (U.S. data) indicates that for all building types, sprinklers failed to operate in 7 % of structure fires. The identified reasons for these failures were 65 % of the systems

were shut off, 16 % were defeated by manual intervention, 11 % were due to lack of maintenance, 5 % of the systems were the wrong type, and 3 % were due to damaged system components. These failure rates may or may not be applicable to new super high-rise buildings, but it is important to note that human error is the primary factor. Consequently, it is important for buildings with complex sprinkler system design to have features and redundancies that can overt issues of human error and maximize sprinkler system reliability.

Sprinkler system designs can be enhanced to improve their reliability. Gravity feed systems that do not rely solely on electric pumps and emergency power supplies can assure that pressure is available to supply sprinklers. Also, piping schemes that use riser cross connections or feeds from alternate floors can provide additional assurances that a single closed valve does not negate sprinkler water flow. Electrical supervision of valves and other sprinkler components has long been recognized to be a most important feature to monitor sprinkler operational status. The value of sprinklers was observed in the One Meridian Plaza incident where ten sprinklers supplied by fire department pumpers are reported to have stopped fire spread after burning for 19 h. If buildings' sprinkler systems can be designed so that successive floors cannot be turned off with a single valve, then a significant level of redundancy to protect against vertical exterior fire spread can be maintained.

Fire department response capabilities should be factored into the vertical exterior fire spread analysis for super high-rise buildings. Prior incidents in unsprinklered buildings demonstrate the difficulty that large, capable fire departments may have for buildings 60 stories or less in height. Many of the new class of high-rise buildings will double or triple this height. An important question in this regard is, "Does the local fire department have the response capabilities and response plan to handle an unsprinklered fire in a super high-rise building?" If the answer is "no," then, again, great reliance is shifted to the automatic sprinkler system.

Several basic building features and occupancy considerations that may impact the assessment of vertical exterior fire spread risk are:

- Assembly occupancies—have large and potentially dense populations of occupants. Often these occupancies are found at the very top levels of super high-rise buildings.
- High-rise residential—have sleeping occupants in buildings that generally have a high degree of fire resistive construction and floor-to-floor compartmentation (except for the façade). The defend-in-place concept has been used in apartment buildings of fire-resistive construction, where it can be safer to remain in the apartment than to attempt evacuation. If the defend-in-place concept is to be viable for the wide variety of possible fire scenarios, then the vertical exterior fire spread issue needs to be addressed. Human behavior has been, on several occasions, cited as playing a major role in the fatalities and injuries in high-rise residential buildings [55, 56]. Both authors' works have seriously questioned the appropriateness of evacuation of high-rise residential buildings, including hotels. Frequently, occupants who stayed in their apartments or hotel rooms were safe and uninjured, while those who evacuated became casualties. In an unsprinklered super high-rise fire scenario, maintaining safe floor areas (safe from vertical exterior fire spread) for residential occupancies could be a critical need.
- Hospital facilities—these are facilities in which occupants can be expected to require assistance from staff and are physically not capable of relocating down stairs or to the building exterior. This may be the most critical situation that deserves consideration of the vertical exterior fire spread risk. Horizontal exits, where a floor is subdivided into two fire areas, are often used in hospital facilities and can be a mitigating factor in the risk assessment for hospitals or other occupancy groups.
- Super tall buildings—buildings with large occupant loads and long total evacuation times (e.g., >1 h). In an unsprinklered, super high-rise fire scenario, fire spread by vertical means, whether exterior or interior, may unnecessarily subject large numbers occupants to adverse conditions from a single fire event.

The relative fire hazard of various occupancies can present varying levels of concern in assessment of vertical exterior fire spread risk. Residential occupancies are generally well compartmented units. In the event of a sprinkler failure and fire spread to a residential unit on the floor above, it should be recognized that the fire would not propagate readily due to the fire-resistive enclosure walls of apartment units. This generally assumes vertical stacking of units. Conversely, in retail or office occupancy, there is far less subdivision to provide passive fire containment, increasing the risk of fire spread.

Security threat assessment scenarios should consider the impact of any damage scenarios on the performance of the buildings fire protection features and, specifically, the sprinkler systems. The survivability of sprinkler system features and water supplies may be critical to prevent a major fire spread event that results from a security threat scenario.

References

1. Zalosh RG (2003) Industrial fire protection engineering. Center for Fire Safety Studies, Worcester Polytechnic Institute. Wiley, West Sussex, England.
2. Read REH (1991) External fire spread: Building separation and boundary distances. Fire Research Station, Building Research Establishment Report BR187
3. Delichatsios M (1984) Modeling of Aircraft Cabin Fires, Factory Mutual Research Corporation J.I. OH5N5.BU, prepared for Federal Aviation Administration.
4. Blackshear, P. (1974) Heat Transfer in Fires, Scripta Book Co., Washington, D.C.
5. Yokoi, S. (1960) Study on the Prevention of Fire-Spread Caused by Hot Upward Current. Japanese Building Research Institute, Report No. 34, Tokyo, 1960.
6. Heselden A, Thomas P (1972). Fully Developed Fires in Single Compartments CIB Report No. 20, Fire Research Note 923. Joint Fire Research Organisation, Borehamwood, 1972.
7. OVE ARUP AND PARTNERS, London, England (January 1977). Design Guide for Fire Safety of Bare Exterior Structural Steel, Technical Reports: 1. Theory & Validation, 2. State of the Art. American Iron & Steel Institute, Washington, D.C.
8. American Iron and Steel Institute (1979) Fire Safe Structural Steel: Design Guide, AISI, Washington, D.C
9. O'Connor DJ (2008) Building façade or fire safety façade. CTBUH Journal: 2008 Issue II, Council on Tall Buildings and Urban Habitat
10. Knaack U, Klien T, Bilow M, Auer T (2007) Facades-principles of construction. Birkhauser Verlag AG, Basil, Switzerland
11. Lemieux DJ, Totten PE (2010) Whole Building Design Guide: Building envelope design guide—walls systems. National Institute of Building Sciences. http://www.wbdg.org/design/env_wall.php
12. Vigener N, Brown MA, Keleher R, Kistler R (2012) Whole Building Design Guide: Building envelope design guide—curtain walls. National Institute of Building Sciences. http://www.wbdg.org/design/env_fenestration_cw.php
13. Simmons HL, Olin NB (2001) Construction: principles, materials, methods 7th edition. Wiley, Canada
14. Kientz H, (2008). Shedding light on curtain wall systems. http://www.hixson-inc.com/_images/SheddingLight_Curtainwall_article0308.pdf, 2008.
15. Belles, D. W.; Beitel, J. J. (1988). Between the cracks . . . how fire spreads from floor to floor in a building with aluminium curtain walls. Fire Journal Vol. 82 No. 3, 76–84, 1998.
16. Glockling, J. (1999). A study of external fire spread on multi-storey buildings and some prevention techniques. Submission to NFPA World Safety Congress and Exposition, Baltimore, May 1999.
17. Underwriters Laboratories Inc. (2007). *Fire Resistance Directory Volume 2A*. 2007 Underwriters Laboratories Inc., Northbrook, IL.
18. International Code Council ***(2003–2012).*** International Building Code, Falls Church, VA, 2003.
19. Koffel W, Memari A, Rittenhouse T, Dawson H, and Ettouney M. (2005). Structural Practices – Curtainwalls in Modern Buildings. STRUCTURE magazine, January 2005.
20. Shriver, J.C.; Building perimeter fire protection (no date), Thermafiber, Inc.
21. Streicher W., Editor (2005) Best Practice for Double Skin Façades EIE/04/135/S07.38652, WP 1 Report "State of the Art" Institut of Thermal Engeneering, Graz University of Tecnology
22. Loncour, X.; Deneyer A.; Blasco, M.; Flamant, G.; Wouters, P. (2004). Ventilated Double Facades – Classification & Illustration of Façade Concepts. Department of Building Physics, Indoor Climate & Building Service, Belgian Building Research Institute, October 2004.
23. Wood A, Salib R (2012) Natural Ventilation in High-Rise Office Buildings: An output of the CTBUH Sustainability Working Group. Council on Tall Buildings and Urban Habitat: Chicago.
24. Foley J.M. (2010). Modern Building Materials Are Factors in Atlantic City Fires. Fire Engineering, http://www.fireengineering.com/articles/2010/05/modern-building-materials-are-factors-in-atlantic-city-fires.html, 2010.
25. Beitel, Jesse J; Fay, Terry S.; Parker, Arthur J. (2008). Report Concerning the Exterior Wall Claddings Involved in the Monte Carlo Hotel Fire. Hughes Associates Inc., Project No. 1JJB05264.006, 2008.
26. Bong FNP (2000) Fire spread on exterior walls—Fire Engineering Research Report. University of Canterbury

27. Wade, C. A.; Clampett, J. C. (2000). Fire Performance of Exterior Claddings. Study Report No xx. Building Research Association of New Zealand.
28. Spinu M (2012). Vapour permeable or impermeable building materials, does it matter? Dupont Building Innovations –White Paper. 2012.
29. Alpert RL, Davis RJ (2002). Evaluation of Exterior insulation and finish system fire hazard for commercial applications. Journal of Fire Protection Engineering, Vol. 12, November 2002.
30. Gunasekaran U, E P, Malina A (2010) Facades of tall buildings –state of the art. Modern Applied Science Volume 4, No. 12, December
31. Babrauskas V (2006) Glass breakage in fires. Fire Science and Technology Inc., http://www.doctorfire.com/GlassBreak.pdf
32. Heron D, Cousins J, Lukovic B (2003) Modelling fire-spread in and around urban centres. Institute of Geological & Nuclear Sciences Limited
33. MOWRER, F. (June 1998). NIST-GCR-98-751 Window Breakage Induced by Exterior Fires. U.S. Department of Commerce, National Institute of Standards and Technology, Gaithersburg, MD.
34. DEAL, S. (April 1995). *NISTIR 5486-1 Technical Reference Guide for FPEtool Version 3.2*. National Institute of Standards and Technology, Gaithersburg, MD.
35. Manzello, S. L.; Gann, R. G.; Kukuck, S. R.; Prasad, K. R.; Jones, W.W. (2007). Experimental Determination of a Real Fire Performance of a Non-Load Bearing Glass Wall Assembly. Fire Technology, Vol 43, No. 1, 77–89, March 2007.
36. Oleszkiewicz, I (1990). Fire Exposure to Exterior Walls and Flame Spread on Combustible Cladding. Fire Technology Nov 1990, 357–375, 1990.
37. Oleszkiewicz I (1991) Vertical Separation of Windows Using Spandrel Walls and Horizontal Projections. Fire Technology, Vol. 25(4), pp. 334–340
38. NFPA 5000 (2012) Building Construction and Safety Code. National Fire Protection Association, Quincy, MA.
39. Ashton, L. A.; Malhotra, H. L. (1960). External Walls of Building – Part I the Protection of Openings against Spread of Fire From Storey to Storey. FR Note No. 436 Department of Scientific and Industrial Research and Fire Offices' Committee, Joint Fire Research Organization. 1960.
40. Langdon-Thomas, G. J.; Law, M. (1996). Fire and the External Wall. Fire Note No. 8. Ministry of Technology and Fire Offices' Committee Joint Fire Research Organization. 1996.
41. Harmathy, T. Z. (1974). Flame Deflectors. Building Research Note No. 96, Division of Building Research, National Research Council of Canada. 1974.
42. Moulen, A. W. (1974). A Model Study of the External Likely Spread of Fire From Storey to Storey of a Building. Technical Record TR 44/153/416, Experimental Building Station, Australia, 1974.
43. Oleszkiewicz, I. (1989). Heat Transfer from a Window Plume to a Building Façade. Proceedings of the Winter Annual Metting of the American Society of Mechanical Engineers, San Francisco, HOT-Vol 123, 163–170, 1989
44. Belles, D (1986). External Walls of Building-Preservation of Fire Spread from Story to Story. Building Standards, May/June 1986, International Conference of Building Officials.
45. Dewers D (1982) *"Investigation Report on the Last Vegas Hilton Hotel Fire"*. FIRE JOURNAL, Volume 76, No. 1 (January 1982), p. 52.
46. LATHROP, J. (1977). "Building Design, 300 Firefighters Save Los Angeles High-Rise Office Building. FIRE JOURNAL, Volume 71, No. 5 (September 1977), p. 34.
47. PETERSON, C. (1973). "John Hancock Center Fire, Chicago, Illinois". FIRE JOURNAL, Volume 67, No. 2 (March 1973), p. 9.
48. BEST, R. (1975). *"High-Rise Apartment Fire in Chicago Leaves One Dead"*. FIRE JOURNAL, Volume 69, No. 5 (September 1975), p. 38.
49. BELL, J. (1981). *"137 Injured in New York City High-Rise Building Fire"*. FIRE JOURNAL, Volume 75, No. 2 (March 1981), p. 38.
50. Dewers D (1983) *"Twelve Die in Fire at Westchase Hilton Hotel"*. FIRE JOURNAL, Volume 77, No. 1 (January 1983), p. 10.
51. Willey E. (1972) "High-Rise Building Fire, Sao Paulo, Brazil". FIRE JOURNAL, National Fire Protection Association, July 1972.
52. KLEM, T. (1988). "First Interstate Bank Building Fire, Los Angeles, CA, May 4, 1988". NFPA Fire Investigation Report, Quincy, MA.
53. KLEM, T. (1991) "One Meridian Plaza, Philadelphia, PA, Three Fire Fighter Casualties, February 23, 1991". NFPA Fire Investigation Report, Quincy, MA.
54. Hall, J. (2001). "High-Rise Building Fires". September 2001, NFPA, Quincy, MA. 2001.
55. Macdonald, J. "Non-evacuation in compartmented Fire-Resistive Buildings can save lives and it makes sense, Travelers Insurance Co., Harford, CT, 1985.
56. Proulx, G., "Highrise Evacuation; A Questionable Concept," Fire Risk Management Program, Institute for Research in Construction, National Research Council, Canada.
57. Shields, T. J.; Silcock, G. W. H.; Hassani S. K. S. (1997-1998). The Behavior of Double Glazing in an Enclosure Fire, J. Applied Fire Science 7, 267-286, 1997-1998.

Daniel J. O'Connor is Aon Fire Protection Engineering's Chief Technical Officer and a Senior Vice President. A member of the firm since 1980, O'Connor provides technical guidance and direction to Aon FPE's engineering staff on all types of project design and code compliance issues. He also mentors and encourages participation in professional associations - to help them advance in their careers as authors, speakers and leaders in industry associations.

Wildland Fires

87

Albert Simeoni

Introduction

Wildland fires have a big impact on the environment, human life, and property and have posed significant economic losses as demonstrated by devastating wildfires that occurred over the last few years. In August 2012, the total of 1470 km^2 (3.64 million acres) burned by wildfires in the United States ranked as the highest for any August since 2000. Moreover, nearly half the entire acreage burned since January 2012 occurred within the single month of August and brought the total acreage burned in a year to the highest on record, exceeding 3100 km^2 (7.72 million acres) [1]. The ignition and corresponding spread of these fires were predominantly influenced by extreme drought and high winds. At the global scale, the impact of wildfires is expected to increase dramatically in the future because of the combined effects of the spreading of the Wildland Urban Interface (WUI) and climate changes [2, 3].

The WUI problem is particularly relevant to fire protection engineering because it impacts people's safety and activities, as well as property and structures. In the future, this problem will shape the way of life of a large part of the population as the WUI is growing faster than any other populated areas [4]. The main differences between building fires and WUI fires are the scale of the phenomenon—with a large number of structures being impacted at the same time (an example is the Waldo Canyon fire in Colorado in June 2012 [5])—and the fact that the structures have to be protected from a fire coming from the outside.

Several issues linked to WUI fires can benefit from further developing fire protection engineering solutions, such as improving structure design to make them more fire resistant, creating new protection systems for houses and other structures, improving evacuation schemes, or supporting communities to develop their wildfire protection plans [6]. The scientific community has developed many tools through research in wildland fire spread, prevention, and suppression that are helpful to mitigate wildland and WUI fire problems. However, fire behavior is still a young and immature topic, particularly compared to other fields of science relevant to wildland fires, such as forestry, ecology and geoscience. It would benefit greatly from the application of approaches developed in fire science as some of the already developed tools could be adapted and applied to wildland and WUI fires.

This chapter presents some basic knowledge about fire behavior and the basic tools that are available in literature to help dealing with wildland and WUI fire problems. The next section presents the wildland fire context both in terms of the general problem and the related scientific

A. Simeoni (✉)
BRE Centre for Fire Safety Engineering, Institute for Infrastructure & Environment, The University of Edinburgh, The King's Buildings, Edinburgh EH9 3JL, UK

M.J. Hurley (ed.), *SFPE Handbook of Fire Protection Engineering*,
DOI 10.1007/978-1-4939-2565-0_87, © Society of Fire Protection Engineers 2016

issues. Then, the fundamental mechanisms that drive fire behavior are detailed in the following section and different kinds of extreme fire behavior are reviewed as they become more common every day. Two additional sections present the different kinds of models that allow predicting fire spread and the fire danger estimation systems that are available and currently used around the world. Finally, the last section presents some ways to estimate fire impact on people and structures.

The Wildland Fire Context

Beyond the fact that they already represent a global problem, wildland fires are emerging as an increasing threat on humans and ecosystems. The dire consequences of these fires include loss of life and injuries, health impact through smoke exposure, property and infrastructure loss, business interruption, ecosystem degradation, and soil erosion, all of this despite huge firefighting costs. In addition to the 2012 fires cited in the previous section, the fires in Southern California in October 2007 and the Black Saturday fires in Australia in February 2009 are perfect examples of the increasing impact that wildland fires have on people, property and the environment. These fires had a large impact on the WUI. The state of emergency was declared in California in 2007 and over 1600 houses were burnt for losses estimated over $1.8 billion [7].

Wildland fires are likely to occur more frequently and to be more intense because of global warming. For instance, the number of uncontrolled fires is expected by USDA to increase by around 50 % in the region of San Francisco and by more than 100 % in Northern California [8]. Their impact will also increase because the Wildland Urban Interface (WUI) is spreading quickly. As an example, during the 1990s, WUI area in the three States of the U.S. West Coast increased by 11 % to nearly 53,000 km^2 and the number of housing units at the WUI was around 6.9 million units in 2000, increasing by more than 15 % every 10 years [2]. This combination of factors is not specific to the US and is relevant to many other regions of the world [9, 10].

The occurrence of massive fires at a growing WUI overwhelms fire fighting and induces huge losses. This growing problem is fully described in the final report of the 2009 Victorian Bushfires Royal Commission [11], which documents Australia's highest loss of life ever induced by bushfires. Among the 173 fatalities, 113 people died inside their houses. The cost of the disaster is estimated to be more than $4 billion. Similar events could potentially happen in other locations, such as California or the South of Europe [11]. The report is very extensive and includes a lot of recommendations about safety policy, emergency management, fire fighting, fuel management and research among others, which are based on the statement that these kind of fires are likely to occur more frequently.

In this context, it is of primary importance to develop the auto-resistance of structures at the WUI and to make them more defendable. It would reduce the economic loss and provide shelter to the population. All protagonists are concerned with this global threat, from private owners, who have to clean vegetation around their houses to central governments, which create regulations and national policies. Some of the players lack the technical skills required to understand fire behavior and evaluate its impact and they would benefit greatly from the development of fire protection engineering solutions.

The fires in developed countries are given extensive media coverage because their impact on human lives, human activities and infrastructures is huge. However, greater surfaces are burned in Asia and South-America for agricultural reasons. Every year, Amazonian and South-Asian forests burn because of the development of cropping, grazing and plantations [12] or because of extreme weather events, of which the intense fires caused by El Niño in 1997 in Kalimantan and Borneo, Indonesia are examples [13]. These fires have dramatic effects on the ecosystem and produce emissions that have a global impact. In addition to these regions, Africa is named the 'Fire Continent' and experiences large savannah

fires on a yearly basis. It is also subjected to changing fire regimes in damp forests and excessive logging.

Wildland fire can be mitigated through fire fighting and prevention. In many countries, fire fighting absorbs the great majority of the financial and human resources devoted to wildfires [14]. In the US, the total (federal, state and local) government firefighting cost grew from $1.3 billon/year in the 1990s to $3.3 billion/year in the 2000s [15]. Despite the huge resources used in firefighting, there is always a threshold when firefighting is overwhelmed by the size and intensity of the fire. Then, the fighting means can only be devoted to protect infrastructure and people at the WUI or to prepare future actions to fight the fire under more favorable conditions. In the US, 97 % of all fires are contained to 40,000 m^2 (10 acres) or less, and the remaining 3 % of large fires have a strong impact on the WUI [15]. It is estimated that the majority of the suppression costs are devoted to protect private homes [16].

On the other hand, prevention is necessary to decrease fire intensity over the long term and make fire fighting more efficient. This objective becomes of primary importance in the frame of global climate and socioeconomic changes (such as urban sprawling), leading to the emergence of new and more intense fire regimes. The most developed prevention approach is fuel treatment (or fuel reduction) in forests or at the WUI to increase the auto-resistance of vegetation.

In the US, congress devoted $500 M/year in the 2000s to support this activity [17]. Fuel treatment is done by cleaning the understory and/or thinning trees in order to avoid crowning and fires that consume the whole vegetation layer. Mechanical or chemical fuel reduction techniques can be used, but prescribed burning remains the main tool because it allows covering large areas with low resources and it can be applied in difficult topographies. Prescribed burning consists in conducting low to medium intensity fires out of the peak fire season to "clean" vegetation, mainly the fuel laying on the ground and the shrub layer but also sometimes the tree branches. The aim is to remove the dry and live fuel that may sustain fire.

The technique used in the specific location will depend on the local context and none is better than the others. At the WUI, cleaning around infrastructures can be drastic in order to break the fire dynamics and decrease infrastructure exposure. Several best practice programs exist to support fuel treatment around infrastructures, such as FireWise (USA), FireSmart (Canada) and FireSafe (California). Fire resistant structures can also be developed, and several standards exist as displayed in Table 87.1, which includes the standards applicable to the WUI.

These programs, codes and standards provide some guidance to develop fire protection solutions at the WUI (NFPA), to provide guidance for building construction at the WUI (ICC) or to develop test methods for materials exposed to fires at the WUI (ASTM). While they represent very valuable tools to help protecting the WUI, a lot remains to be done. For instance, the exposure techniques used in the different codes and standards need to be better linked to the actual exposure conditions happening during WUI fires. Recent field studies show the tendency of firebrands to ignite many houses during WUI fires, even the ones protected by fuel treatment, and the ability of a burning house to create a large amount of firebrands that may propagate a fire in a community, even when the wildland fire no longer impacts it [18]. These topics are the object of research [19].

Over the last 60 years, the scientific community has become more involved in the modeling of forest fires, and a number of physical approaches have emerged. The understanding of the physical mechanisms that control wildfire ignition and spreading constitutes the keystone of the development of fire protection engineering tools useful to management and fire fighting. Wildfire is a complex phenomenon in which the levels of description cover a huge range, from the details of the kinetics of gaseous combustion and thermal degradation of fuels, up to the chemical and physical characterization of the flame and the vegetation cover as a fuel. Figure 87.1 represents an overview of the different space and time scales involved in wildfires and the related difficulties for modeling.

Table 87.1 Existing code and standards related to the WUI

National Fire Protection Association (NFPA)	
1141	Standard for Fire Protection Infrastructure for Land Development in Suburban and Rural Areas
1142	Standard for Water Supplies for Suburban and Rural Fire Fighting
1143	Standard for Wildland Fire Management
1144	Standard for Reducing Structure Ignition Hazards from Wildland Fires
1145	Guide for Use of Class A Foams in Manual Structural Fire Fighting
International Code Council (ICC)	
2012 (year)	International Wildland-Urban Interface Code
ASTM International (E05.14 Subcommittee on External Fire Exposure)	
E108—11	Standard Test Methods for Fire Tests of Roof Coverings
E2632/E2632M—13e1	Standard Test Method for Evaluating the Under-Deck Fire Test Response of Deck Materials
E2707—09	Standard Test Method for Determining Fire Penetration of Exterior Wall Assemblies Using a Direct Flame Impingement Exposure
E2726/E2726M—12a	Standard Test Method for Evaluating the Fire-Test-Response of Deck Structures to Burning Brands

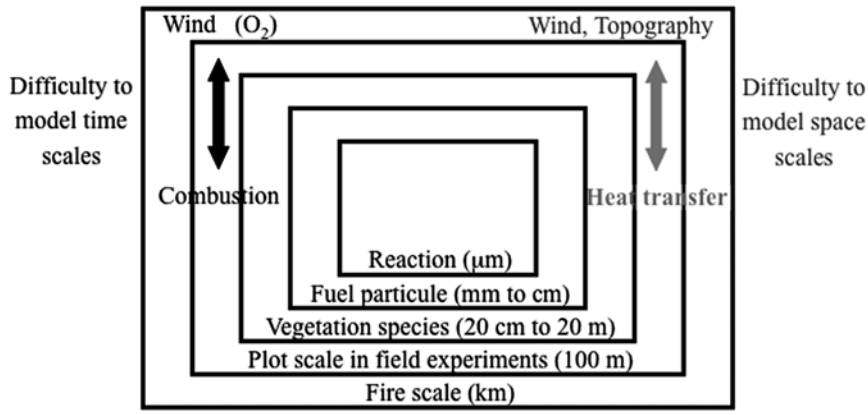

Fig. 87.1 Different space and time scales involved in wildfires

Even if the physical laws are known and GIS and weather models can provide the environmental data, modeling fire spread is really challenging. The difficulties rely in the high variability of the environmental parameters, in the large range of scales, and also in the huge number of phenomena involved in the process, such as drying and degradation of vegetation, flaming and smoldering combustion, flow inside and above the fuel bed, turbulence, and radiative transfer. These phenomena are all coupled and their respective importance in driving fire spread is difficult to assess and varies with the fuel and external condition. The next section describes the basics of wildfire spread in general terms, as well as different kinds of extreme fire behavior.

Fire Behavior

Mechanisms of Fire Spread

Basic Mechanisms

An unburned piece of vegetation (Fig. 87.2a) can be approximated as being a fuel particle. This particle is submitted to a heat insult when the fire front is getting closer.

The heat transfer influence on fire spread is essentially through two modes: radiation and

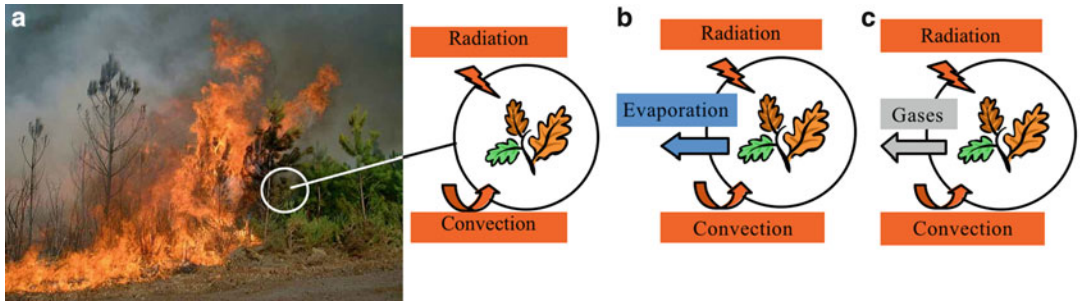

Fig. 87.2 Fire spread mechanisms—(**a**) fuel particle and thermal transfer, (**b**) drying, (**c**) pyrolysis

convection. Radiative heat transfer acts at a larger range than convective heat transfer ahead of the fire front. Radiant sources are the flame front and the smoldering vegetation. Heating by convective heat transfer needs some flow to come from the burning area and to be in contact with unburned vegetation (otherwise, vegetation is only cooling by convection).

When a vegetation particle is submitted to thermal transfer from the fire front, it heats. When its temperature is high enough (usually around 100 °C), it starts to dehydrate (see Fig. 87.2b). The water content in vegetation, called fuel moisture content (FMC), plays an important role in fire spread because it acts as a heat sink, which can delay or even prevent fuel ignition.

Once the vegetation particle has dried, it starts to pyrolyze. The proximity of flames makes the flammable mixture ignite and the fire spread. First, combustion occurs in the gas phase. Then, embers appear when the particle has finished emitting gases and is fully converted into char. The combustion appears at the surface of the char and the particle glows. The embers emit a large amount of radiation and burn slowly. When the embers are fully consumed, the particle turns into ash.

A fire spreads in the presence of three simultaneous factors: flammable gases, oxygen (in air) and a heat source strong enough to ignite the flammable mixture.

Parameters

The most obvious parameters driving fire behavior are the properties of vegetation, wind and topography. They are diverse kinds of vegetation properties: particle and bulk properties, fuel moisture content (FMC), and the spatial distribution of vegetation [20]:

- The particle properties represent vegetation as a fuel. They include the physical and chemical properties. The physical properties are the thermal properties—such as the heat capacity, heat conductivity, absorptivity and emissivity of radiation—the density, and the surface-to-volume ratio. The surface-to-volume ratio is an important parameter regarding heat transfer that will condition radiative and convective transfer between vegetation and the flame. The chemical properties are the chemical composition of vegetation (cellulose, hemicellulose, lignin, extractives, and minerals) that conditions the nature and quantity of the degradation gases, the latent heats of drying and pyrolysis, the heats of combustion of the pyrolysis gases and of the char. Some vegetal species are more flammable than others, such as sapwood compared to hardwood.
- The bulk properties represent vegetation as a fuel layer. They include bulk density, permeability (or drag forces) and attenuation of radiation [21]. All of these bulk quantities are a mix of particle properties and porosity. For instance, permeability depends on many fuel properties, including the surface-to-volume ratio, the roughness of the particle's surface and the fuel bed porosity. Wildland fuels are different from the usual fuels encountered in the built environment. Among all fuels present in a vegetation layer, it is commonly

accepted that only the thinner particles (diameter lower than 6 mm) are involved in fire spread [20], i.e. the leaves or needles, burn faster than branches or trunks and are the main contributors to fire spread. However, larger particles can burn later and participate in a structure's or soil's life exposure to heat. They can also create hot spots that have the potential of igniting new fires after the initial fire has gone. Vegetation is porous, with porosities ranging from 0.05 for pine needle litters to 0.002 for tree canopies [22, 23]. The bulk density represents the quantity of fuel mass (usually only considering thin particles) per unit volume. The permeability represent the interaction between vegetation and flow, either meteorological wind or wind induced by the fire itself. The attenuation of radiation represents how radiation coming from the fire front is absorbed by unburned vegetation. Many other properties can be represented as bulk properties. For instance, convective and conductive transfer will be conditioned by porosity and empirical laws including porosity can be derived [24]. Combustion in the fuel layer will depend on the availability of oxygen and hence be a function of porosity and drag forces.

- FMC is one of the most critical parameters. It is the main energy sink that can slow down ignition and decrease the fire heat release rate. Its value will condition the ability of a fire to spread and its rate of spread. The factors influencing FMC are as diverse as the air humidity, the air temperature, the sunlight exposure, the soil moisture, and plant physiological factors [25]. FMC varies in time and space, depending on local conditions and can create heterogeneous burn patterns [26]. The dynamics of FMC variations is very different for dead and dry fuels. Dry fuels are very sensitive to short term variations of weather conditions whereas moist fuels are more sensitive to long term variations. Dry fuels are mainly located on—or close to—the ground (litter/grass) and live fuel can be located at the surface (grass, shrubs) or at the top of higher vegetation (chaparral and tree canopies). The dry fuel is classified as 1 h, 10 h, 100 h, and 1000 h fuel, depending on the time it takes to adjust to changes in the external conditions. The time-lag classification is directly related to the size of the particles, 1 h fuels being particles no greater than 6 mm in diameter and 1000 h fuels being larger than 7.5 cm in diameter [20]. Fine dead FMC determines the rate of fire spread in surface fires. Live fuels are less sensitive to weather conditions in the short term but exhibit seasonal FMC variations due to plant physiology. This pattern is important to estimate the risk of crown fires. The worst-case scenario is the combination of drought and low seasonal FMC that can lower canopy FMC and even add dead fuel from otherwise live plants. In some ecosystems, this combination happens in winter or spring.
- The spatial distribution of the fuel can influence fire spread. There are two types of spatial distributions: vertical and horizontal. Vertical distribution is related to fuel layers. Fuel layers are usually defined as ground layer (duff or peat), surface layer (litter, herbaceous vegetation, and low shrubs), and crown layer (large shrubs and tree canopy). If these layers get very close to each other or overlap, a 'fuel ladder' exists that may create intense fires involving all vegetation at once. Horizontal distribution represents the fuel layer density, as for instance open or close canopies, as well as larger heterogeneities such as non-flammable areas (for instance rocks, rivers, and roads). The horizontal heterogeneities have a strong influence on fire spread. They also condition the occurrence of crown fires and can create heterogeneous fire patterns [26].

Wind has the effect of tilting flames. It also brings fresh air and thus fresh oxygen to enhance combustion and make flames longer. The flames being longer and tilted, the thermal transfer towards the unburned fuel will be increased greatly (see Fig. 87.3a and compare to Fig. 87.2a): the radiative source is larger and

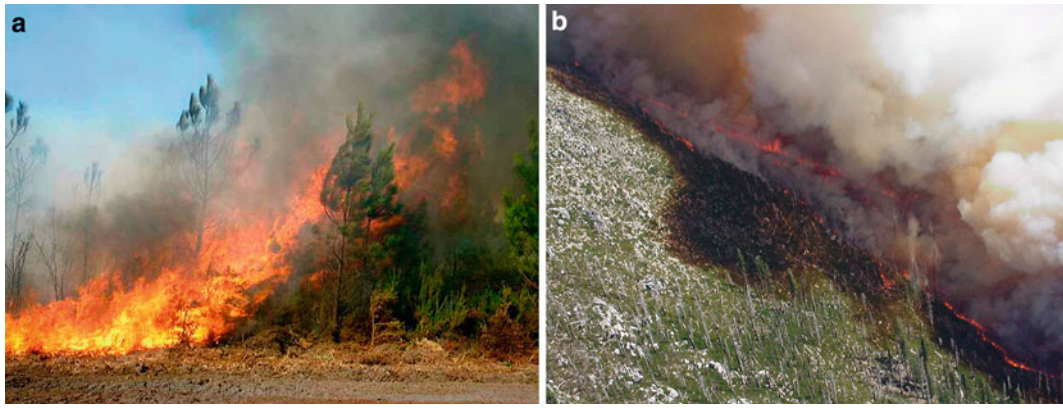

Fig. 87.3 External parameters for fire spread—(**a**) wind effects, (**b**) slope effects

closer and sometimes flames will engulf unburned vegetation and increase convective transfer. This change in behavior can induce steep accelerations of the fire front. Another wind effect is to make the fire front deeper by increasing the fire rate of spread. More vegetation is ignited ahead of the fire while vegetation is still burning at the back of the fire. Such fires are usually intense and difficult to fight. However, the impact on the ecosystem can sometimes be less dramatic because wind also cools the fuel after the fire, and the heat insult on vegetation and on the soil can be shorter.

The last effect is the effect of topography and more specifically of slope. The flame front is closer to vegetation in the slope direction, so a particle located ahead of the fire in the direction of slope will be heated more by radiation than another particle located on the flanks of the fire (because of the radiative view factor between the fire font and the particles). The fire head will then spread faster than the flanks and it will accelerate. This effect creates the specific pointed heads that are encountered for upslope fire spread as seen in Fig. 87.3b. For fires spreading under windy conditions, the flames are tilted in the wind direction and this effect of pointed head does not appear.

Except for the pointed head, the effects of wind and slope are similar for low winds and low slopes. For instance, when a fire spreads upslope, the vegetation facing the slope will be closer to the flames and the radiative transfer will be enhanced. Air is entrained more into the fire front from downslope than upslope. In confined conditions, such as canyons, this effect can increase the fire rate of spread as described in the next section for eruptive fires.

Obviously, this representation of the basics of fire spread is simplified, and all the phenomena are coupled, making predictions difficult. The coupling between the fire and the atmosphere will be mentioned later.

Extreme Fire Behavior

The previous section described the basics of fire behavior, but under specific conditions, fire can shift to extreme behavior that, when unexpected, can have catastrophic consequences. Several types of extreme fire behavior exist. Fire eruptions or blowups, crown fires, spot fires, fire whirls, and peat fires will be presented in this section.

Eruptive Fires

Eruptive fires imply a sharp acceleration of the fire in confined topography. Under specific slope, wind, and vegetation conditions, a fire that spreads in a usual way can ‘erupt’ and multiply its rate of spread by 5–10 [27]. This induces the creation of a large area simultaneously on fire.

An example of such a fire can be seen in Fig. 87.4a for a fire that happened in Corsica, France in 2000 [29]. The picture is extracted from a movie taken by a tourist and is the only

Fig. 87.4 (**a**) Video capture of a fire eruption [28]. (**b**) Eruption laboratory experiment at ADAI laboratory, Portugal

known video recording of such an event. The area simultaneously on fire was estimated to be around 6 ha and the fire rate of spread during the eruption was estimated to be around 20 km/h. When firefighters are caught in such a phenomenon, they usually die or are severely injured, even when sheltering in their vehicles. Europe has a long record of death by such events, numbering more than 200 fatalities over a 30 years period [29].

The factors leading to eruptions are only partially understood. Several physical and chemical phenomena could cause them: wind, topography, vegetation distillation, and smoke accumulation are found as potential explanations in literature. Experimental studies conducted in Portugal [28] allowed reproducing eruptions at the laboratory scale and demonstrate a strong coupling effect between a canyon—in the case of the experiments, a bi-panel tilted bench (see Fig. 87.4b)—and the fire that increases heat transfer at the fire head. This explanation is similar to the trench effect demonstrated for the King's Cross station fire in London [30]. However, laboratory studies and feedback studies from past accidents do not allow separating all the potential causes of fire eruptions, and a general theory is still to be developed. More research is necessary to understand the phenomena involved in fire eruptions and the mechanisms that trigger them. This research will have the potential to improve fire fighter safety, particularly in canyon configurations.

This behavior in canyons is called 'blowup' in the US, and the difficulty of conducting feedback studies for such complex and extremely rapid phenomena led to the definition of an alignment of factors. The difficulty lays in identifying which of these factors really triggers blowups. However, the specific meteorological phenomenon of 'Cold front' seems to be one of them and was apparently involved in several accidents [31].

Crown Fires

Crown fires can produce intense wildfires and are overwhelming for anyone who observes them. Van Wagner [32] defined three classes of crown fires:

- Passive crown fire: When the crown cannot sustain fire spread and needs the energy from the surface fire to get a flame in the crown layer. In this case, the rate of spread of the surface fire controls the crown fire.
- Active crown fire: When the crown cannot sustain fire spread but can develop a substantial flame that creates a heat feedback to the surface fire. Then, the crown fire and the surface fire spread together at a rate that is greater than the rate of spread of the surface fire, would it be alone.
- Independent crown fire: When the crown can sustain fire spread and does not need to receive additional heat from the surface fire. Then, the crown fire will spread on its own, faster than the surface fire.

The latter class is the most dangerous with the highest rates of spread and heat release rates and is most likely to occur under strong winds. However, the optimal conditions to get independent spread are so difficult to reach that long-lasting independent crown fires are rare events.

Another way to classify crown fires is between wind-driven and plume-dominated fires [33]. For wind-driven fires, the plume is tilted in the direction of wind, and for plume-dominated fires the plume is vertical. Under wind conditions, the power of wind and the power of the buoyancy-induced fire plume compete to create one or the other kind of plume, depending on the size and intensity of the fire. The wind-driven fires are more likely to lead to independent crown fires and to send a large quantity of firebrands in front of the fire. However, the turbulence created by the plume-dominated fires can create a recirculation of hot gases in front of the fire and induce sudden and unexpected accelerations of the fire front [20].

Spot Fires

Spot fires are created by firebrands that land on unburned vegetation. Firebrand generation is the process through which fuels such as shrubs and trees are heated and broken into smaller burning pieces during a fire [34]. Subsequently, they may be transported far away from the fire through the plume [35]. If firebrands are still burning when landing and if the recipient vegetation on the ground is dry and dense enough, they may create spot fires.

Firebrand effects can be split in long-range and short-range effects. Long-range firebrands are lifted by the fire plume at high altitude and are transported horizontally by wind over a long distance. If these firebrands start a new fire, it will be independent from the source fire, at least during its growth. The very short-range firebrands don't really influence fire spread because the fires they may start are absorbed by the main fire front before having time to develop. However, they can sometimes allow a fire to cross small natural or man-made obstacles. Short-range firebrands that land at a longer distance from the fire front can accelerate the fire spread by creating a spot fire that had enough time to develop and that is drawn into to the main front when getting closer to it, hence accelerating the fire spread. This phenomenon is dangerous for firefighters if they get caught in the middle, before they realized that a fire has ignited behind them [20].

The analysis of spot fires is complex because they are made of several distinct stages that are still poorly described [35]:

- Firebrand production that depends on the fuel type, the fire plume intensity, and the local burning dynamics of vegetation.
- Travel distance that is a function of the size and shape of firebrands, the plume intensity, and the wind velocity.
- Landing conditions that depend on the burning state of the firebrand (smoldering or flaming), the fuel type at the landing spot, the FMC and even the type of contact to transfer enough heat to ignite the ground fuel.

For more than 40 years, studies have focused on understanding how far firebrands can fly [36, 37], whereas more recent studies evaluated the production and ignition processes [19, 38].

Fire Whirls

Fire whirls are due to the combination of the strong buoyancy created by the fire front and any phenomenon that creates air rotation. They can pose an issue for prescribed burning or for fire fighting safety [20]. In wildland fires, this rotation usually happens on flat ground, at the leeside of obstructions, or at mountain ridges [20]. The combustion rate is multiplied inside the fire whirl, increasing the heat release rate and the fuel consumption [20]. Some fire whirls can propagate the fire front by moving towards unburned vegetation or by producing a large amount of firebrands that land close to the fire. The resulting firebrands can be larger than usual because of the strength of the vertical winds inside the fire whirl that can lift large burning particles. The created spot fires can suddenly enlarge the fire front and make it much more intense than the supporting fire [20].

Fire tornadoes can be created when large pyro-cumulonmibi develop over massive fires.

Fire tornadoes occurred during the 2003 Camberra fires that were estimated to be at least of F2 intensity on the Fujita scale [39].

Fire whirl mechanisms are not different from those encountered in other fires in the open like urban conflagrations and they can be described in the same way [40].

Peat Fires

Peat fires are not labeled as extreme because of their rate of spread or their intensity but because of their magnitude and the fact that they happen during extreme weather conditions, such as the fires that circled Moscow in June 2010.

Peat fires are smoldering flameless fires that spread slowly in the soil layer [41]. They occur relatively frequently in Northern boreal ecosystems and can also happen in humid tropical forests like during the Indonesia fires of 1997 [13]. Usually, peat fires are ignited by surface wildfires that migrate into the peat layer, which thickness ranges from 0.5 to 12 m. The fires can be totally underground because of the low intensity of smoldering combustion that does not require much oxygen. Once ignited, they are particularly difficult to extinguish despite extensive rains or fire-fighting attempts and can linger for long periods of time (weeks and up to years) [13] and spread over very extensive areas of forest and deep into the soil. The oxygen is supplied through cracks in the ground, and the heat loss is low in the insulating soil layer, which can sustain fire for months. Very often, they allow flaming combustion to re-establish during wildfires at unexpected locations (e.g. across a fire break) and at unexpected times (e.g. long after burnout of the flame front). This feature is also shared with duff fires, and to a lesser extent, with hummus fires. The usual way to fight these fires is to create trenches by digging to the mineral soil and creating a fuel break or trying to soak them with water. These techniques are challenging to use when the underground fire is not accurately located and the area to cover is large [41].

Peat fires can cover wide areas and consume large quantities of carbon. It has been reported that smoldering of surface fuels can consume around 50 % or more of the total burned biomass in temperate and boreal fires, as well as in Amazonian tropical-woodland fires [42]. Smoldering of forest fuels is also responsible for a significant fraction of the total pollutants emitted into the atmosphere during a wildfire [13]. Peat fires play a major role in the global emission to the atmosphere, the destruction of carbon storage in the soil and the damage to the natural environment. In addition, large peat fires can create health issues for the exposed population and economic losses, such as those induced by airport closure or the loss of activity for industries sensitive to smoke pollution.

Small-scale laboratory experiments have studied the ignition and spread of peat fires [43]. The governing factors are heat transfer, oxygen availability and FMC [44].

Models and Simulators

Several reviews have been published about fire-spread modeling [45–49]. Based on the classification proposed by Weber [45], three types of models can be identified. The first type includes statistical models that do not consider any physical information at all. The second type of models incorporates semi-empirical models. They are based on the principle of energy conservation without distinction between the different mechanisms of heat transfer. Finally, physical models describe the various mechanisms of heat transfer and production. Among those, the detailed approach takes the finest physical and chemical mechanisms into account and is the most detailed modeling that has been developed so far [24]. Contrarily, simplified physical models only consider the main mechanisms involved in fire spread [47].

Empirical Models

Empirical models are based on simple equations that do not include any physical information but that relate the fire head rate of spread to a set of statistically significant parameters. The data is

collected in experimental fires or in well documented prescribed or wildland fires. Some of these models are part of simulators that are efficient for places with homogeneous vegetation and external parameters, such as Australian grasslands or Canadian boreal forest.

The Australian fire behavior meters provide the rate of spread of the fire head as a function of environmental parameters, FMC, and fuel availability for fire spread in grasslands [50] or Eucalyptus forests [51]. Fire predictions are given by fire danger meters, which are disks for which the alignment of the parameter values will give the fire head rate of spread. These meters are used on a day-to-day basis by foresters and firefighters in the field. Noble et al. [52] have expressed the meters as equations. For instance, the MK4 meter for grasslands predictions provides the rate of spread as [53]:

$$F = 2\exp\left(-23.6 + 5.01\,C_d + 0.0281\,T_a - 0.226\,H_r^{1/2} + 0.663\,U_{10}^{1/2}\right) \tag{87.1}$$

where C_d is the degree of curing, T_a is the ambient temperature in Celsius, H_r is the air humidity in percentage and U_{10} is he wind velocity at 10 m in m/s. F is the fire index and the rate of spread is given by:

$$V = 0.036\,F \tag{87.2}$$

The Canadian Fire Behavior Prediction System is not directly used as a prediction system for the fire rate of spread by itself, but it is integrated in the fire weather index (FWI) that provides a daily estimation of the fire risk in Canada [54]. The following equation provides the fire rate of spread:

$$RSI = a\,[1 - \exp(-b\,ISI)]^c \tag{87.3}$$

where ISI is the Initial Spread Index and a, b, and c are fuel-dependent factors that are divided in eight classes representative of Canadian ecosystems [54]. ISI is expressed as:

$$ISI = 0.208\exp(0.0504\,U_{10})\,91.9\exp(-0.138\,FMC)\left(1 + \frac{FMC^{5.31}}{4.93}10^7\right) \tag{87.4}$$

These models are statistically derived to provide the rates of spread for a given range of fuel and weather conditions, and they must be used with care when the conditions differ from the ones used to derive the model. The Canadian FWI has been extended and adapted with success to other regions of the world for the local ecosystems [55].

Semi-empirical Models

Semi-empirical models are based on the principle of energy conservation but do not discriminate the different types of heat transfer and the different combustion processes. The energy conservation principle means that the energy produced by the fire is either transferred to the unburned fuel to maintain the fire, or lost to the ambient. The formulation of the energy balance takes the following general form:

$$Q = \rho\,h_i\,R \tag{87.5}$$

where Q is the net energy going through the ignition surface per unit of surface area, ρ is the fuel density, h_i is the enthalpy per unit mass that is required to ignite the fuel and R is the rate of fire spread. These models are steady-state—in the sense that one set of conditions gives one rate of spread—and one-dimensional.

Q is expressed by using heat transfer laws but its different components are estimated

empirically by conducting a large number of laboratory fire spread experiments under varied experimental conditions.

The most famous of these models that is still extensively used is Rothermel's model [56], which is based on Frandsen's model of fire spread [57]. The equation for the rate of spread of the fire head is expressed as:

$$R = \frac{(I_p)_0 (1 + \varphi_W + \varphi_S)}{\rho_b \varepsilon Q_{ig}} \tag{87.6}$$

where R is the rate of spread (m/s), $(I_p)_0$ is the heat flux from the fire front that reaches the unburned fuel ahead of it for a fire spreading on a flat surface and without wind (kW/m^2), ρ_b is the fuel bulk density (kg/m^3), ε is an effective number that defines the amount of fuel which is available to sustain fire spread (-), Q_{ig} is the heat which is necessary to bring the fuel to ignition (kJ/kg), and φ_w and φ_s are correction factors for wind and slope, respectively (-).

The different parameters are either obtained from the physic-chemical properties of the fuel or empirically derived. The huge number of experiments conducted along time in the most diverse configurations allows the model to provide a good estimation of the fire rate of spread for a large range of conditions. As for the Canadian system [54], several fuel classes have been developed that are characteristic of American ecosystems [58, 59]. The model—and in general terms, the semi-empirical approach—is more general than the empirical approach and provides acceptable results in diverse configurations. However, the parameters still remain in a relatively narrow range, and the model is challenged when applied to areas with a large variability of parameters, like the Mediterranean basin.

The main simulation tools currently used by foresters and firefighters in the field are based on Rothermel's model [56]. For instance, Behave Plus [60] provides a quick estimation of the fire head rate of spread through nomograms and Farsite [61] is a whole GIS-based simulation suite that extends Rothermel's model to two-dimensions along the ground by applying Huggens' ellipse principle. Farsite also includes other models as detailed later. Even if they are widely used, these tools are more of strategic value, as they give an indication of the long term tendencies of a fire, than of tactical value to base any immediate decision on their short term predictions. These predictions can be biased because of the simplified nature of the models.

Physical Models

Simplified Physical Models

These models are conceptually more general than empirical and semi-empirical models. They can provide the fire shape and rate of spread, as well as an estimation of heat transfer and energy release with simulation times that can be close or even under real time, if some optimization techniques are used for computation. However, they have not been used extensively until now due to the fact that it is difficult to ensure that the chosen simplifications are relevant to diverse sets of conditions. Contrarily, empirical and semi-empirical models have the benefit of being statistically relevant to given conditions.

Simplified models do not calculate the flow as it is too computationally expensive but usually provide the fire rate of spread and the fire shape on the ground. The general formulation is around a single thermal balance with the addition of sub-models to take into account phenomena such as combustion or wind [62, 63]. The fuel is assumed as being a medium equivalent to the gas and the solid phases that coexist inside the fuel layer, and thermal equilibrium is assumed between phases. The flame has to be modeled as it cannot be computed in the absence of flow. It is often described as a radiant panel with a given height and emissivity.

As an example, the following thermal balance can be written, taking into account heat transfer mechanisms (radiation and convection) and heat production [64]:

$$\frac{\partial T}{\partial t} + k\vec{V}_g \cdot \vec{\nabla} T = -h(T - T_a) + K\Delta T + R - q\frac{\partial \sigma}{\partial t} \tag{87.7}$$

where k is the advection coefficient, K is the diffusion coefficient, h represents the loss to the ambient, q is the heat of combustion of the fuel and σ is the fuel load (mass per unit area). The model is closed by using sub-models: a simplified flow model to obtain the horizontal flow velocity in the fuel layer $\vec{V}_g$, a radiant panel approximation to describe the radiative transfer from the flame R, and a simplified mass loss law to describe the variation of σ due to the combustion reaction.

Several other variations exist that complicate more or less the formulation to describe better some aspects of the fire [65, 66].

A recent simplified model has been tested with a large set of available experimental data at laboratory scale for fire spread under diverse conditions [67]. The model has demonstrated good predictive capabilities that demonstrate the potential of simplified physical models to provide a general frame for improved predictions compared to the existing tool based on semi-empirical models. The predictive ability of the model at field scale has been improved by coupling it with an atmospheric model [68].

Detailed Physical Models

The multiphase approach is described as an example of detailed physical models as it is the most detailed available formulation. The full details of the model presented below can be found in [69]. This approach represents the fire spread medium as being multiphase, reactive and radiative [24]. The medium is defined by the fluid phase and N solid phases. Each solid phase consists of a set of particles that possess the same geometry and thermochemical properties (see Fig. 87.5). An elementary multiphase volume is defined that allows describing the fire phenomena at the relevant scale. A volume averaging procedure is applied to the volume to obtain averaged properties for both the gaseous and solid phases.

The system of averaged equations includes balances of mass, species, momentum and energy for each species, as well as a radiative transfer equation. The strong coupling between the solid and gas phases is represented by interface relationships. For clarity, no volume averaging symbol is added and only the mass equations are presented:

$$\text{Gas phase}: \quad \frac{\partial}{\partial t}\left(\alpha_g \rho_g\right) + \vec{\nabla}\left(\alpha_g \rho_g \vec{V}_g\right) = \sum_{k=1}^{N} \left[\dot{M}\right]_{gk} \tag{87.8}$$

$$\text{Solid phase } (N \text{ equations}): \frac{\partial}{\partial t}\left(\alpha_k \rho_k\right) = -\left[\dot{M}\right]_k^{surf} - \left[\dot{M}\right]_k^{pyr} \tag{87.9}$$

$$\text{Interface equations}(N \text{ equations}): \left[\dot{M}\right]_{gk} = \left[\dot{M}\right]_k^{surf} + \left[\dot{M}\right]_k^{pyr} \tag{87.10}$$

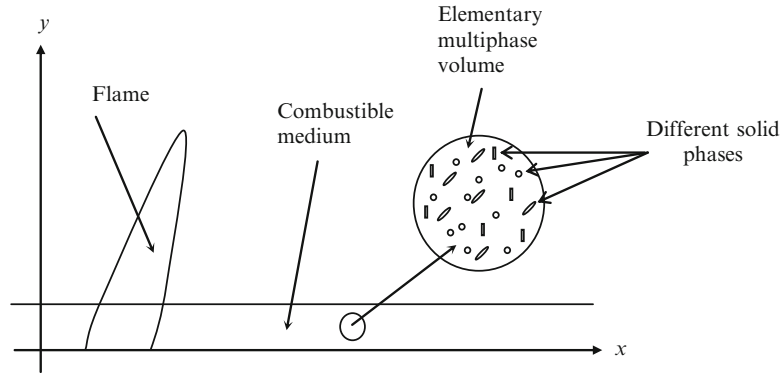

Fig. 87.5 Schematic representation of the problem for the multiphase approach

where α is the volume fraction of the considered phase (percentage of the volume occupied by the phase), ρ is the density and $[\dot{M}]$ is the mass flux. The subscripts g, k and gk denote the gas phase, the k^{th} solid phase and the flux from the k^{th} solid phase into the gas phase, respectively. The superscript *surf* denotes the surface reaction of oxidation (smoldering) and *pyr* denotes the gasification of the solid phase (pyrolysis gases fuelling the flames).

From this method, different terms appear on the right side of the balance equations that need to be determined via sub-models. For the mass equations, they consist mainly in Arrhenius type laws for drying, pyrolysis and charring of vegetation. One of the key issues of applying the model is to design proper experiments to evaluate the sub-models under actual fire conditions, which can be very difficult, if not impossible to achieve for some of the sub-models.

The model—as other CFD models—provides fields for all variables, such as temperature and velocity, but also species mass fractions and turbulent kinetic energy. However, it is difficult to design experiments to validate its results. Usually, the rate of spread and the flame geometry are compared to experiments [70], but it does not represent a proper validation as these experimental parameters are not directly related to the variables of the model.

Simulators

Table 87.2 presents the main simulators that are available to describe fire spread and provide at least the fire rate of spread and the fire shape. Other tools exist that provide nomograms, statistical fire behavior or spatial analysis, such as Behave plus [60], Nexus [70], and FlamMap [73].

Farsite [61] provides the fire shape and rate of spread as a function of vegetation and external parameters. Several other outputs are available, such as the fire-line intensity [74] (defined as the mean heat release rate per meter of fire front), crown fire initiation [32] and spread [33], as well as the basic effects of fire-fighting on fire spread. The predictions for crown fire spread underestimate actual fire spread because the crown fire models have been developed based on a very limited set of experiments and have not been fully validated [75]. Additionally, the surface and crown fire models are of different nature, making their coupling very difficult to achieve [75]. This statement extends to the other simulation tools based on empirical and semi-empirical surface fire models that are not described in this section. Simple wind modeling that represents the variability of wind with topography can be coupled to Farsite and allows substantially improving its predictions [76].

NCAR [25] is dedicated to the understanding and description of the direct atmosphere/fire interaction, as well as fire emissions. As it uses Rothermel's model [56], the description of the fire is submitted to the same limitations described for the semi-empirical approach. However, the atmospheric aspect allows describing the large scale effects that happen due to the fire/atmosphere coupling and that can influence fire spread, particularly for massive fires.

WFDS [71] is a full simulation suite that is based on the multiphase approach detailed above. It is dedicated to describe Wildand urban interface fires. It resolves flow, heat transfer and combustion at the scale of vegetation.

Table 87.2 Simulation tools available in literature

Simulator	Type of fire model	Fire/atmosphere interaction
Farsite [61]	Semi-empirical	Constant or topographical wind effect on fire
NCAR [25]	Semi-empirical	Atmospheric coupling (MM5)
WFDS [71]	Detailed physical	Detailed physic-based (no atmospheric coupling)
Firetec [72]	Detailed physical	Atmospheric coupling (HighGrad)
Forefire [68]	Simplified physical	Atmospheric coupling (Meso-Nh)

The simplifications in the model based on the Fire Dynamics Simulator [77] allow the model to describe the fire at the fire front scale with the use of heavy parallel computational power.

Firetec [72] couples fire spread modeling in a simpler way than the multiphase approach to atmospheric modeling. It is very efficient to describe fire spread in relation with the local flow around the fire. However, the computational needs imply the use of supercomputing capacities to be able to simulate the scale of a small wildland fire.

Forefire [68] couples simplified physical fire-spread modeling to atmospheric modeling to study fire spread and emissions. The fire plume and the fire/atmosphere interaction are described at a scale much larger than the fire.

WFDS [71] and Firetec [72] are still research tools but they represent the future of fire-spread simulation that will allow going beyond the current limitations of available simulators. They will not be used as operational simulation tools for a long time, and their applicability is not even assured because of their complexity and the large number of parameters and inputs they require. However, they will allow developing simpler models that will include the relevant phenomena that actually drive fire behavior. This is something that the semi-empirical models are not able to achieve. Forefire [68] is already a step in this direction.

Another approach, which could improve the predictive capability of fire spread models, is data assimilation. This approach was initially developed in meteorology. It consists in informing the fire spread model with real-time measurements from the fire it aims to predict. The data is used to correct the model's predictions through a reevaluation of its parameters [78], hence avoiding the increasing gap between model predictions and actual fire behavior that systematically happen along time. This divergence is due to many factors, such as the variation of conditions, the inaccuracy of parameters, or the approximate nature of the fire spread model. The application to Rothermel's model showed that this approach has the potential to improve predictions [79].

Fire Danger

Operational fire danger rating systems have mainly been developed in Australia [80] Canada [54] and the US [58]. The Canadian system has particularly been adopted by several countries and adapted to local conditions [55]. The main variables taken into account in the systems are live and dead fuel FMC, as well as meteorological variables, such as wind, air temperature and air humidity [81].

The most empirical approach is used in Australia because of the fairly constant external conditions that exist in many parts of the country and the large amount of empirical data that was collected allow obtaining good results with the empirical models for fire spread in grassland [50] and eucalyptus forests [51]. The meteorological parameters are wind velocity and ambient air conditions, as well as rain history. For grasslands, the percentage of dead material (curing) is an important parameter because it drives fire behavior for such very fine fuels constituting a single vegetation layer.

The Canadian Forest Fire Danger Rating System [59] is more detailed than the Australian one and aggregates different types of fuel ecosystems from grassland to forest through its fuel models. It combines the effect of weather conditions and FMC on fire behavior. The moisture of the soil fuel layer is finely described as it represents the potential of a fire to ignite. The danger is expressed as the expected fire-line intensity [74], which is a combination of the initial rate of spread (given in the previous section) and the fuel load:

$$I = HWR \tag{87.11}$$

where H is the heat of combustion of the fuel (kJ/kg), W is the fuel mass consumed per unit area (kg/m^2), and R is the rate of fire spread (m/s).

The National Fire Danger Rating System is used in the US [82] and is similar in nature to the Canadian system. The main difference is that it includes semi-empirical modeling that is more detailed than the modeling used in the Canadian

System. For instance, the fire rate of spread is determined with Rothermel's model [56] and the soil moisture is determined by a semi-empirical approach that balances precipitation and evapotranspiration [82].

All these models have proven to be efficient and are used routinely for the daily assessment of fire danger all around the world. However, they have shown their limitation in the context of the occurrence of extreme conditions when the values of the parameters are well out of range and the empirical and semi-empirical models cannot provide good predictions anymore. Despite this, there is no physical approach available yet and the models are extrapolated to try to anticipate higher levels of risk that become more and more common due to socio-economic and climate changes.

Fire Impact

Fire impact under the fire safety viewpoint refers mainly to the impact on people and structures. The main mechanism that supports the impact on people is heat transfer, i.e. radiative and convective transfer from the fire front. The main factor that influence structural ignition at the WUI is also heat transfer from approaching flames but firebrands deposit has to be added. Firebrands can ignite a structure by two ways: they can accumulate on the outer surface of a structure and ignite it, or they can find a way through the structure to reach easy-to-ignite fuels.

Other forms of impact, such as ecological impact or health impact are not developed here.

Heat Transfer

Heat transfer can impact people or structures. The impact on structures is mainly related to the WUI problem. It is difficult to ignite wood panels or vinyl siding only by radiation, and flame contact is often necessary [83]. Fuel treatment programs, such are FireWise are based on this observation and recommend fuel removal up to a certain distance around houses.

The people who are close enough to be impacted by fire and can sustain exposure to relatively high heat fluxes are fire-fighters wearing personal protective equipment. Thus, the main concern for people exposure is fire-fighters safety, and a better evaluation of safety distances would improve it greatly. The safety distance is related to three aspects: the intensity of the fire, the mode of heat transfer, and the resistance of the target to the heat insult. The exposure time is also an important parameter. In this context, the knowledge of fire behavior and the good representation of the heat transfer are of primary importance.

The current models used to evaluate safety distances are only based on radiative transfer. They use the solid flame assumption (flame equivalent to a radiant panel) with constant values of flame height and flame temperature [84, 85] and express the fire radiative impact as a function of the flame height. A latter model [86] takes into account finite fire front width, which is more realistic, and express the safety distance as a function of the fire front width/flame height ratio. The problem of these models is that they assume that the flames have constant properties, whereas flame radiation is defined by the turbulent nature of flames with changing geometry and distribution temperature. Furthermore, radiation has a relatively short range effect [87] and at a short distance, convective transfer is likely to have a strong role [88]. The models will need to take this transfer into account to provide better estimations of the safety distance. The solid flame models do not describe the flow, and adding convection could be difficult. CFD models could potentially yield much better results, but they are not mature enough to be used in this context. They are also very sensitive to radiation as a slight variation in flame properties (emissivity, temperature distribution, and volume) can have a large effect on radiative transfer.

Firebrands

If the research has focused for quite a long time on radiative and convective impact on structures, recent field studies have highlighted that structural ignition from embers is a main cause of structure loss at the WUI [18, 89].

The structure ignition can come from a single ember that found its way to the weak points in a structure, like going through vents or depositing under the roof. However, the main impact happens during exposure to the short-range firebrand shower that induces exposure to a large quantity of burning (smoldering and flaming) firebrands, creating accumulations in wedges, corners, and cracks [18, 90]. In this case, several parts of a structure are likely to ignite, such as roofs, decks, siding, and even surrounding elements, such as fences and any pile of combustible materials (as wood stored for winter) that would spread a fire to the structure when ignited.

NIST has a research program to characterize ember production, as well as vegetation and structure ignition when submitted to an ember shower [19]. In the case of a firebrand landing on vegetation, it is more likely that vegetation will ignite when the firebrand is still flaming [91]. In the case of an accumulation of firebrands, the structures are very weak and ignite quickly by the roof, sides and decks [90].

For fires spreading at the WUI, it is common to experience structural loss even at locations inside communities that were not touched by the fire front, highlighting the issue of structural ignition by firebrands [89]. When a structure is ignited, the fire can spread from structure to structure by two mechanisms: heat transfer from the burning structure to the next one if the structures are close enough. This is similar to the issue of building-to-building spread in urban settings [92]. The second mechanism is again by firebrands generated by the burning structure that have the potential to ignite neighboring structures, at distances greater than the zone of influence of the flames. It has been found that firebrands generated from structures are larger and broader than those generated by burning vegetation [93].

Summary

Societies face great challenges due to wildland and WUI fires, and they will benefit greatly from a more systematic approach of fire safety engineering.

Wildland fires represent an intricate problem that adds the complexity of vegetation, large scale effects and open boundaries to usual fire problems, rendering any quantitative estimation of fire spread and fire impact difficult.

If it is already difficult to predict fire behavior under usual conditions, extreme fires pose additional challenges and more research is needed to understand them and predict their occurrence.

Wildland fire science is still a young science that was able to deliver some operational tools at the empirical and semi-empirical levels. The physical approach is promising and may produce the tools of the future, but it will necessitate a long investment in the fundamentals and in validation.

Acknowledgements The author is grateful to A. Maranghides and D. Morvan for their discussions and the information they provided. It helped developing some critical aspects of this chapter.

References

1. Center, N. N. C. D. 2012. State of the climate: Wildfires for August 2012. http://www.ncdc.noaa.gov/sotc/fire/2012/8.
2. Hammer, R.B., Radeloff, V.C., Fried, J.S., Stewart, S.I. 2007. Wildland-urban interface housing growth during the 1990s in California, Oregon, and Washington. International Journal of Wildland Fire, 16(3), pp. 255–265.
3. Mortsch, L.D. 2006. Impact of climate change on agriculture, forestry and wetlands. *In*: Bhatti, J., Lal, R., Apps, M. & Price, M., eds. *Climate change and managed ecosystems,* pp. 45–67. Boca Raton, FL, USA: Taylor & Francis, CRC Press.
4. Radeloff, V.C., Hammer, R.B., Stewart, S.I., Fried, J. S., Holcomb, S.S., McKeefry, J.F. 2005. The Wildland–Urban Interface in the United States. Ecological Applications, 18(3), pp. 799–805.
5. http://waldofire.org/waldocanyonfire2012/
6. http://jfsp.fortlewis.edu
7. Karter M.J. Jr., US Fire Loss for 2007, NFPA Reports, NFPA.

8. Fried J.S., Torn M.S., Mills E. The Impact of Climate Change on Wildfire Severity: a Regional Forecast for Northern California. Climatic Change, 64, 169–191, 2004.
9. Williams J., Albright D., Hoffmann A.A., Eritsov A., Moore P.F., Mendes De Morais J.C., Leonard M., San Miguel-Ayanz J., Xanthopoulos X., van Lierop P. Findings and Implications from a Coarse-Scale Global Assessment of Recent Selected Mega-Fires. FAO, 2012.
10. Flannigan M.D., Stocks B.J., Wotton B.M. Climate change and forest fires. The Science of the Total Environment, 262(3), 221–229, 2000.
11. Teague B., Mcleod R., Pascoe S. Final Report. 2009 Victorian Bushfires Royal Commission – Summary and Volume 1: The Fires and the Fire-Related Deaths. Parliament of Victoria, State of Victoria, Australia, July 2010.
12. Global Forest Resources Assessment 2010, FAO.
13. Page S.E., Siegert F., Rieley J.O., Boehm H.D.V., Jaya A., Limin S. The amount of carbon released from peat and forest fires in Indonesia during 1997. Nature, 420, 61–65 (2002).
14. Rigolot E., Fernandes P., Rego F. Managing Wildfire Risk: Prevention, Suppression' in *Living with Wildfires: What Science Can Tell Us*, Yves Birot (Ed.), European Forest Institute, 2009.
15. The Blue Ribbon Panel on Wildland/Urban Interface Fire, International Code Council, 2008.
16. Forest Service – Large Fire Suppression Costs. Office of Inspector General, Western Region, USDA, Audit Report, 2006.
17. Wildland Fire Management – Better Information and a Systematic Process Could Improve Agencies' Approach to Allocating Fuel Reduction Funds and Selecting Projects. United States Government Accountability Office, Report GAO-07-1168, 2007.
18. Maranghides A., Mell W. Framework for Addressing the National Wildland Urban Interface Fire Problem – Determining Fire and Ember Exposure Zones using a WUI Hazard Scale. NIST Technical Note 1748, National Institute of Standard and Technology, Department of Commerce, USA (2012).
19. Manzello S.L., Suzuki, S. Hayashi Y. Enabling the study of structure vulnerabilities to ignition from wind driven firebrand showers: A summary of experimental results, Fire Safety Journal, 54, 181–196 (2012).
20. Pyne, S.J., Andrews, P.L., Laven, R. D. 1996. *Introduction to Wildland Fire*, Second Edition, New York: John Wiley & Sons, Inc., 168 p.
21. Bartoli P., Simeoni A., Torero J.L., Santoni P.A. Determination of the main parameters influencing forest fuel combustion dynamics, Fire Safety Journal, 46(1–2), 27–33 (2011).
22. Pereira J.M.C., Sequeira N.M.S., Carreiras J.M.B. Structural Properties and Dimensional Relations of Some Mediterranean Shrub Fuels. International Journal of Wildland Fire, 5(1), 35–42 (1995).
23. Catchpole E.A., Catchpole W.R., Viney N.R., McCaw W.L., Marsden-Smedley J.B. Estimating fuel response time and predicting fuel moisture content from field data. International Journal of Wildland Fire, 10, 215–222 (2001).
24. Grishin A.M. 1997. *Mathematical modeling of forest fires and new methods of fighting them*. Publishing House of the Tomsk State University, Albini (ed.), Russia.
25. Johnson E. A., Miayanishi K. (Eds) 2001. *Forest Fires: Behavior and Ecological Effects*. Academic Press, San Diego, USA.
26. Simeoni A., Salinesi P., Morandini F. Physical Modelling of Forest Fire Spreading through Heterogeneous Fuel Beds. International Journal of Wildland Fire, 20(5), 625–632 (2011).
27. Viegas D.X., Simeoni A. Eruptive Behaviour of Forest Fires. Fire Technology, 47(2), 303–320 (2011).
28. Viegas D.X. Parametric Study of an Eruptive Fire Behaviour Model, International Journal of Wildland Fire, 15, 169–177 (2006).
29. Viegas D.X. (Ed.) 2009. *Recent Forest Fire Accidents in Europe*. JRC-IES, European Commission, Ispra, Italy.
30. Drysdale D.D., Macmillan A.J.R., Shilitto D. The King's Cross fire: Experimental verification of the 'Trench effect'. Fire Safety Journal, 18(1), 75–82, (1992).
31. Butler B.W., Bartlette R.A., Bradshaw L.S., Cohen J. D., Andrews P.L., Putnam T., Mangan R.J. Fire Behavior Associated with the 1994 South Canyon Fire on Storm King Mountain, Colorado. USDA Research Paper RMRS-RP-9 (1998).
32. Van Wagner, C.E. Conditions for the start and spread of crown fire. Canadian Journal of Forest Research, 7, 23–34 (1977).
33. Rothermel, R.C. Predicting behavior and size of crown fires in the Northern Rocky Mountains. General Technical Report INT-438. USDA Forest Service, Ogden, UT (1991).
34. Manzello S.L., Maranghides A., Mell W.E. Firebrand generation from burning vegetation. International Journal of Wildland Fire, 16, 458–462 (2007).
35. Koo E., Pagni P., Weise D., Woicheese J. Firebrands and spotting ignition in large-scale fires. International Journal of Wildland Fire 19, 818–843 (2010).
36. Tarifa C.S., Notario P.P., Moreno F.G. On the flight paths and lifetimes of burning particles of wood. Proceedings of the 10th Combustion Institute, 1021–1037 (1965).
37. Albini, F.A. Spot fire distance from burning trees – a predictive model. General Technical Report INT-56, USDA Forest Service, Ogden, UT (1979).
38. Hadden R.M., Scott S., Lautenberger C., Fernandez-Pello C. Ignition of Combustible Fuel Beds by Hot Particles: An Experimental and Theoretical Study. Fire Technology, 47, 341–355 (2011).
39. McRae R.H.D., Sharples J.J., Wilkes S.R., Walker A. An Australian Pyro-Tornadogenesis Event. Journal

of Natural Hazards, Volume 65(3), 1801–1811 (2013).
40. Kuwana K., Sekimoto K., Saito K., Williams F.A. Scaling fire whirls. Fire Safety Journal, 43(4), 252–257, 2008.
41. Rein G. Smouldering Combustion Phenomena in Science and Technology. International Review of Chemical Engineering, 1, 3–18 (2009).
42. Bertschi I., Yokelson R.J., Ward D.E., Babbitt R.E., Susott R.A., Goode J.G. Hao, W.M. Trace gas and particle emissions from fires in large diameter and belowground biomass fuels. Journal of Geophysical Research 108(D13), 8472 (2003).
43. Frandsen, W.H. Ignition probability of organic soils. Canadian Journal of Forest Research, 27, 1471–1477 (1997).
44. Rein G., Cleaver N., Ashton C., Pironi P., Torero J.L. The severity of smouldering peat fires and damage to the forest soil. Catena, 74, 304–309 (2008).
45. Weber R.O. Modelling fire spread through fuel beds. Progress in Energy and Combustion Science, 17, 67–82 (1991).
46. Pastor E., Zarate L., Planas E., Arnaldos J. Mathematical models and calculations systems for the study of wildland fire behavior. Progress in Energy and Combustion Science, 29, 139–153 (2003).
47. Sullivan A.L. Wildland surface fire spread modelling, 1990–2007. 1: Physical and quasi-physical models. International Journal of Wildland Fire, 18, 349–368 (2009).
48. Sullivan A.L. Wildland surface fire spread modelling, 1990–2007. 2: Empirical and quasi-empirical models. International Journal of Wildland Fire, 18, 369–386 (2009).
49. Sullivan A.L. Wildland surface fire spread modelling, 1990–2007. 3: Simulation and mathematical analogue models. International Journal of Wildland Fire, 18, 387–403 (2009).
50. McArthur, A.G. Weather and Grassland Fire Behaviour. Department of National Development, Canberra, 23 p. (1966).
51. McArthur, A.G. Fire Behaviour in Eucalypt Forest. Department of National Development, Canberra, 36 p. (1967).
52. Noble I.R., Bary G.A.V., Gill A.M. McArthur's fire danger meters expressed as equations. Australian Journal of Ecology. 5, 201–203 (1980).
53. McRae R.H.D. Re-engineering fire danger index. Australian Capital Territory, Emergency Service Bureau, Technical Note TN031, 7p. (2002).
54. Stocks B.J., Lawson B.D., Alexander M.E., Van Wagner C.E., McAlpine R.S., Lynham T.J., Dubé D.E. The Canadian system of forest fire danger rating. Proceedings of a conference on bushfire modelling and fire danger rating systems, Canberra, Australia. CSIRO Division of Forestry, Yarralumla, Australia, 9–18 (1991).
55. Fiorucci P., Gaetani F., Minciardi R. Development and application of a system for dynamic wildfire risk assessment in Italy. Environmental Modelling and Software. 23(6), 690–702 (2008).
56. Rothermel R.C., A mathematical model for predicting fire spread in wildland fuels, USDA, Forest Service Research, paper INT-115, 40 p. (1972).
57. Frandsen W.H. Fire spread through porous fuels through the conservation of energy. Combustion and Flame. 16, 9–16 (1971).
58. Deeming J.E., Lancaster J.W., Fosberg M.A., Furman W.R., Shroeder M.J. The National Fire-Danger Rating System. United States Department of Agriculture, Forest Service, Research Paper RM 84, 1972, 165 p., revised (1974).
59. Burgan, R.E. 1988 revisions to the 1978 National Fire-Danger Rating System. United States Department of Agriculture, Forest Service, Research Paper SE-273, 39 p. (1988).
60. Andrews P.L.; Chase C.H. BEHAVE: Fire behavior prediction and fuel modeling system-BURN subsystem, Part 2. United States Department of Agriculture, Forest Service, General Technical Report INT-260, 93 p. (1989).
61. Finney M.A. FARSITE: A fire area simulator for fire managers, The Biswell Symposium, Walnut Creek, California, February 15–17 (1994).
62. Albini F.A. A model for fire spread in wildland fuels by radiation. Combustion Science and Technology. 42, 229–258 (1985).
63. Albini, F.A. Wildland fire spread by radiation – a model including fuel cooling by natural convection. Combustion Science and Technology. 45, 101–113 (1986).
64. Morandini F., Simeoni A., Santoni P.A., Balbi J.H. A model for the spread of fire across a fuel bed incorporating the effects of wind and slope. Combustion Science and Technology. 177, 1381–418 (2005).
65. Pagni P.J., Peterson T.G. Flame Spread through porous fuels. Proceedings of the Fourteenth Symposium (International) on Combustion. 14(1), 1099–1107 (1973).
66. Weber R.O. Toward a Comprehensive Wildfire Spread Model. International Journal of Wildland Fire. 1(4), 245–248 (1991).
67. Balbi J.H., Morandini F., Silvani X., Filippi J.B., Rinieri F. A Physical Model for Wildland Fires. Combustion and Flame. 156(12), 2217–2230 (2009).
68. Filippi J.B., Bosseur F., Mari C., Lac C., Le Moigne P., Cuenot B., Veynante D., Cariolle D., Balbi J.H. Coupled Atmosphere-Wildland Fire Modelling. Journal of Advances in Modeling Earth Systems. 1 (4) (2009).
69. Larini M., Giroud F., Porterie B., Loraud, J.C. A multiphase formulation for fire propagation in heterogeneous combustible media. International Journal of Heat and Mass Transfer. 41, 881–897 (1998).
70. Scott J.H. Nexus: a system for assessing crown fire hazard. Fire management Notes. 59(2), 20–24 (1999).
71. Mell W., Jenkins M.A., Gould J., Cheney P. A physics-based approach to modelling grassland fires.

International Journal of Wildland Fire. 16, 1–22, (2007).
72. Linn R.R., A transport model for prediction of wildfire behavior, Ph.D. thesis, New Mexico State University, Los Alamos National Laboratory (1997).
73. Stratton R.D. Guidance on Spatial Wildland Fire Analysis: Models, Tools and Techniques. General Technical Report, RMRS-GTR-183, Fort Collins, Colorado, USDA-Forest Service, 17 p. (2006).
74. Byram, G.M. Combustion of forest fuels. In Davis K.P. (ed.) *Forest Fire: Control and Use*. McGraw-Hill, New York, 90–123 (1959).
75. Cruz M.G., Alexander M.E. Assessing crown fire potential in coniferous forests of western North America: a critique of current approaches and recent simulation studies. International Journal of Wildland Fire. 19, 377–398 (2010).
76. Butler B.W., Finney M., Bradshaw L., Forthofer J., McHugh C., Stratton R., Jimenez D. WindWizard: a new tool for fire management decision support. RMRS-P-41, Fort Collins, Colorado, USDA-Forest Service, 787–796 (2006).
77. McGrattan K.B., Hostikka S. Floyd J.E. Fire Dynamics Simulator (Version 5), User's Guide. NIST Special Publication 1019-5, National Institute of Standards and Technology, Gaithersburg, Maryland (2007).
78. Mandel J., Bennethum L.S., Beezley J.D., Coen J.L., Douglas C.C., Kim M., Vodacek A. A wildland fire model with data assimilation, Mathematics and Computers in Simulation. 79(3), 584–606 (2008).
79. Rochoux M.C., Delmotte B., Cuenot B., Ricci S., Trouvé A. Regional-scale simulations of wildland fire spread informed by real-time flame front observations. Proceedings of the Combustion Institute. 34(2), 2641–2647 (2013).
80. Luke R.H,. McArthur A.G. Bushfires in Australia. Australian Government Publishing Service. 359 p. (1978).
81. Planas E., Pastor E. 2013. Wildfire Behaviour and Danger Ratings, *in: Fire Phenomena and the Earth System: An Interdisciplinary Guide to Fire Science*, Claire M. Belcher (Ed.), Wiley-Blackwell, 350 p.
82. Schlobohm P., Brain J. Gaining an Understanding of the National Fire Danger Rating System. National Wildfire Coordinating Group, PMS-932, Boise, Idaho. 82 p. 2002.
83. Cohen J.D. Relating flame radiation to home ignition using modeling and experimental crown fires. Canadian Journal of Forest Research. 34, 1616–1626 (2004).
84. Butler B.W., Cohen J.D. Firefighter Safety Zones: A Theoretical Model Based on Radiative Heating. International Journal of Wildland Fire. 8(2), 73–77 (1998).
85. Zàrate L., Arnaldos J., Casal J. Establishing safety distances for wildland fires. Fire Safety Journal. 43, 565–575 (2008).
86. Rossi J.L., Simeoni A., Moretti B., Leroy-Cancellieri V. An analytical model based on radiative heating for the determination of safety distances for wildland fires. Fire Safety Journal. 46, 520–527 (2011).
87. Santoni P., Simeoni A., Rossi J.L., Bosseur F., Morandini F., Silvani X.,. Balbi J.H, Cancellieri D., Rossi L. Instrumentation of wildland fire: characterisation of a fire spreading through a Mediterranean shrub. Fire Safety Journal. 41(3), 171–184 (2006).
88. Frankman D., Webb B.W., Butler B.W., Jimenez D., Forthofer J.M., Sopko P., Shannon K.S., Hiers J.K., Ottmar R.D. Measurements of convective and radiative heating in wildland fires. International Journal of Wildland Fire. 22, 157–167 (2013).
89. Mell W.E., Manzello S.L., Maranghides A., Butry D., Rehm R.G. The wildland–urban interface fire problem – current approaches and research needs. International Journal of Wildland Fire. 19, 238–251 (2010).
90. Manzello S.L., Park S.H., Cleary T.G. Investigation on the ability of glowing firebrands deposited within crevices to ignite common building materials. Fire Safety Journal. 44, 894–900 (2009).
91. Manzello S.L., Cleary T.G., Shields J.R., Yang J.C. Ignition of mulch and grasses by firebrands in wildland–urban interface fires. International Journal of Wildland Fire. 15, 427–431 (2006).
92. Drysdale D.D. *An Introduction to Fire Dynamics*, 3rd Edition, John Wiley & Sons: West Sussex, 2011.
93. Suzuki S., Manzello S.L., Hayashi Y. The size and mass distribution of firebrands collected from ignited building components exposed to wind. Proceedings of the Combustion Institute. 34(2), 2479–2485 (2013).

Professor Albert Simeoni is the BRE Research chair of Fire Safety Engineering and the director of the BRE Centre for Fire Safety Engineering at the University of Edinburgh.

Fires in Vehicle Tunnels

88

Ricky Carvel and Haukur Ingason

Introduction

The scenario of a large vehicle fire remains one of the most troublesome issues for designers of tunnels and underground facilities. Two of the main questions which continue to be raised and debated at tunnel safety symposia are:

- What should be used as 'design fires' for road, rail and subway tunnel design?
- What fire protection and prevention measures are effective against fires in tunnels?

Most of the major experimental research projects investigating vehicle fires in tunnels carried out in the past two decades, including the EUREKA EU499 project [1], the Runehamar fire tests [2, 3] and the METRO project [4, 5], have shown that real vehicle fires in tunnels may be more severe than the scenarios which have historically been used as 'design fires' for vehicle tunnels, subway stations, etc. The reason is twofold;

- The knowledge on fire development and sizes is limited due to limited number of tests leading to "expert views" on reasonable worst case fire sizes. These views tend to lower the values used in design as they usually are a product of a consensus between the experts.
- The tests performed sometimes may exaggerate the real conditions. For example in the Runehamar tests, the fuel load was fully exposed to the wind conditions whereas in reality the load may be blocked by the truck or the front wall of the trailer resulting in a lower fire growth rate.

This chapter provides a review of the published data produced as part of these studies and identifies the characteristics common to most of these fire experiments. If design fires used for vehicle tunnels are to be in any way realistic, these characteristics must be taken into account. The chapter then looks at the question of fire protection for vehicle tunnels and discusses the current state-of-the-art.

Full Scale Fire Experiments in Tunnels

This section considers only very large vehicle (and solid fuel) fire tests carried out in full-scale tunnels, it is not intended to be a comprehensive review of all tunnel fire tests. In particular, the Memorial Tunnel Fire Ventilation Test Program (MTFVTP) results are not considered here as these tests involved fuel pools, not vehicles or realistic vehicle cargoes [6]. Similarly, smaller fire tests carried out as part of other test series will not be discussed. For a reasonably comprehensive summary of fire experiments at full and reduced scale, see Carvel and Marlair [7] or chap. 3 in Ingason et al [8]. As most design fires are specified in terms of the heat release rate (HRR) of the fire, and as this is a good

R. Carvel (✉)
BRE Centre for Fire Safety Engineering, University of Edinburgh, Edinburgh EH9 3JL, UK

H. Ingason
SP Technical Research Institute of Sweden, Boras, Sweden

M.J. Hurley (ed.), *SFPE Handbook of Fire Protection Engineering*,
DOI 10.1007/978-1-4939-2565-0_88, © Society of Fire Protection Engineers 2016

measure of the severity of such fires, this review will focus on HRR data from the experiments considered. A summary with focus on HRR data from each vehicle type is given in Ingason and Lönnermark [9].

The EUREKA EU499 Fire Tests (1992)

The EUREKA EU499 'Fires in Transport Tunnels' project involved researchers from nine European countries and the main data were gathered from a series of 21 fire tests which were carried out in a disused tunnel in Repparfjord in the north of Norway, near Hammerfest [1]. The tunnel has a rough-rock, irregular surface and varies between 4.8 and 6.0 m high and 5.3–7.0 m wide; the average cross-sectional area is about 34 m^2; the tunnel is 2.3 km long and has a 1 % uphill gradient towards the 'downstream' end of the tunnel, which terminates in a shaft, open to the air. The large vehicles fire tested in this series (for which HRR data were estimated) were a subway carriage, two full railway carriages, one 'joined' railway carriage, one bus, and a heavy goods vehicle (HGV); a large 'mixed load' was also tested, which may be considered analogous to a vehicle cargo. In each case, the fire load was positioned approximately 295 m from the 'upstream' (downhill) end of the tunnel.

The bus fire test (B11) involved a single decker, Volvo school bus built in the early 1960s [10]. It was 12 m long and had 40 seats. During the fire test the luggage compartment door and the front door of the bus were both open, and the partition between the luggage compartment and the passenger compartment had been removed. 310 pine sticks, 800 × 40 × 40 mm, were distributed throughout the bus to represent luggage. The bus fire test was carried out without forced longitudinal ventilation. During the test, smoke from the fire travelled in the 'upstream' direction with a velocity of about 0.3 ms^{-1}, while the smoke velocity in the 'downstream' direction was not recorded. Estimates of the HRR were made using oxygen and CO/CO_2 concentration measurements taken on both sides of the fire location [11]. The fire reached a peak HRR of 29 MW within 8 min of ignition. By 18 min after ignition, the HRR had diminished to less than 13 MW, after which the fire gradually burned out over a period of more than an hour. Figure 88.1 shows a simplified representation of the measured HRR data [11].

The mixed fire load test (LF1) involved a load of 2850 kg, three-fourth of which was wood, one-eight of which was tyres, and one-eight of which was other plastic materials. This was distributed in a stack approximately 2.4 m long, 2.2 m high and 2.4 m wide. No forced ventilation was used during the test and the smoke travelled

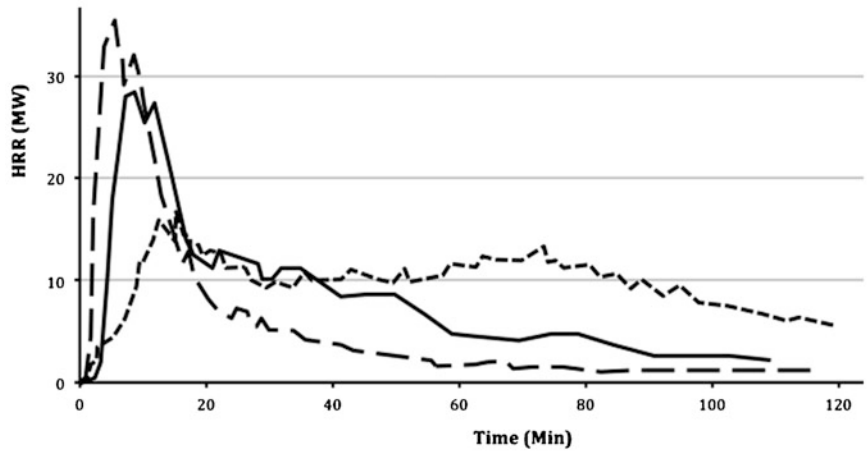

Fig. 88.1 Approximate HRR data from EUREKA EU499 bus fire test B11 (*solid line*), mixed load test LF1 (*short dash*) and subway carriage fire test F42 (*long dash*) (Adapted from [10])

in the 'upstream' direction until it reached about 115 m upstream of the fire, where the smoke front stopped. The smoke transport in the downstream direction was not recorded. The fire grew rapidly to a peak HRR of about 17 MW in about 15 min; the HRR data [11] are shown in Fig. 88.1.

The HGV fire test (HF1) is described in several places in the literature including [12, 13]. The fuel load in this instance consisted of a tractor unit (built by Leyland DAF in 1988) and a double axle trailer unit loaded with about 2 tonnes of wooden framed furniture. The trailer was 12.5 m long, 2.4 m wide and 2.5 m high. During the test, the HGV was positioned with the tractor unit facing upstream. A blockage of two shipping containers was positioned in the tunnel 29 m upstream of the HGV. The ventilation in the tunnel was forced longitudinally and was varied during the test. In the initial stages of the test the ventilation flow was about 6 ms^{-1}, after the fire spread from the cab to the trailer the fan was switched off for 2 min, then restated at 2.9 ms^{-1} (the velocity corresponding to the intended emergency ventilation flow rate in the Channel Tunnel, which the test was designed to partially replicate). All smoke from the fire was blown downstream of the fire, except during the period that the fan was switched off. The ventilation system was switched off after about 15 min into the test while the fire was still growing, so it is not known how large the fire would have grown with a flow of 6 ms^{-1}. Once the fans were established again at 2.9 ms^{-1} (after about 2 min), the fire reached a peak of 128 MW. The most reliable HRR data from this test were obtained by Grant and Drysdale and are shown in adapted form in Fig. 88.2 [12].

A fire test was carried out using two joined half railway carriages as a fuel load. The half-carriage designated F2Al was an aluminium bodied carriage, while the half designated F7 was steel bodied. The carriages were joined by a corrugated bellows, similar to those common on railway carriages. The tunnel was initially longitudinally ventilated at about 6–8 ms^{-1}. The first and second ignitions of the fuel load were rapidly

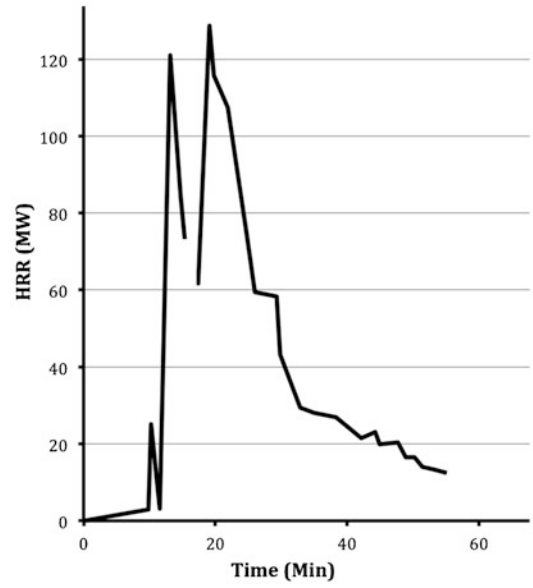

Fig. 88.2 Approximate representation of HRR data from Hammerfest HGV fire test HF1 (Adapted from [11]). The HRR during the period when the fan was shut down could not be estimated, so is not presented

extinguished following instrument failures. The third ignition of the fuel was carried out after adding about 360 wooden sticks to the carriages. The fire was ignited in the upstream aluminium carriage. After 32 min, the ventilation was stopped and restarted at a lower flow rate 4 min later. At approximately 48 min after ignition, the fire appears to have spread to the steel half carriage, and 'the whole car seems to ignite immediately' [1]. Shortly after this, the HRR peaked at about 43 MW, as shown in Fig. 88.3. The atypical fire behaviour during this test was due to the unusual test setup, ignition location and ventilation changes during the test.

Two fire tests were carried out with full railway carriages. The first test, designated FS1, involved an old steel bodied railway carriage which was refurbished with a 'modern' interior, similar to that used on a German 'Inter City Express' train. Tunnel ventilation was set on 'low' with the longitudinal airflow before the test being less than 0.4 ms^{-1}. The first ignition of this fuel load burned out without growing

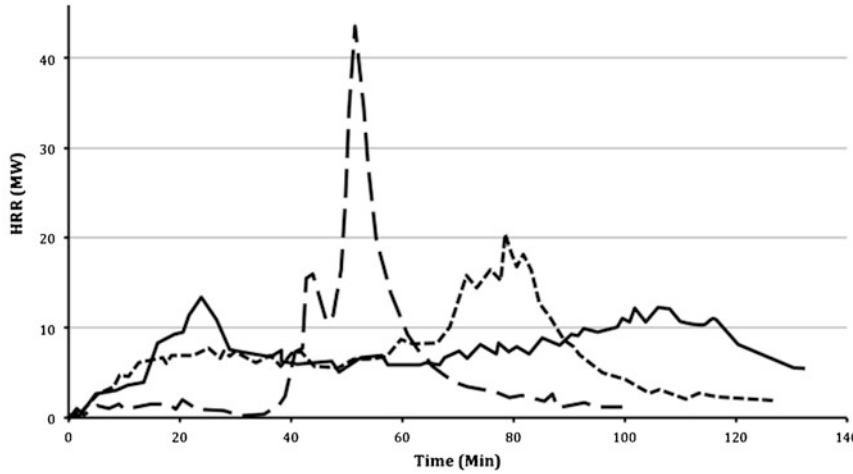

Fig. 88.3 Approximate HRR data from Hammerfest IC train test F11 (*solid line*) [10], ICE train carriage test FS2 (*short dash*) and joined half-carriage test FA3 (*long dash*) (Adapted from [13])

significantly after 18 min. Following this, 170 wood sticks were added to the carriage, in the vicinity of the ignition location, and some of the windows were opened. The fire was reignited, designated Test FS2. The fire grew and consumed all combustibles in the vehicle, reaching a peak HRR of 19 MW after 80 min, as shown in Fig. 88.3.

The second rail carriage test also featured a steel bodied inter-city vehicle, but with an older style interior to that tested in FS2. This test was designated F11. Once again, the ventilation was set to 'low'. The fire reached a peak of about 13 MW after about 25 min, which quickly diminished by about 50 % and then grew again to a second peak of about 12 MW after 90 min. A simplified representation of the HRR data from this test is given in Fig. 88.3.

The subway carriage tested was aluminium bodied and the seats in it were replaced with seats corresponding to the contemporary standards at the time of testing. Two ventilation panels and one of the carriage doors were left open for the test. Ventilation was set to 'low' as with other tests. The first ignition of the load (Test F41) used 0.7 kg of isopropanol in two fuel pans as an initial fuel, but this burned out before spreading to involve the rest of the carriage. The second ignition (Test F42) involved 6.2 kg of isopropanol in two larger fuel pans. This resulted in a very rapid fire growth and witnesses report the entire carriage was involved in the fire within 2 min. The peak HRR was about 35 MW after about 5 min, as shown in Fig. 88.1.

Large Fire Test in the 2nd Benelux Tunnel (2001)

A number of fire tests were carried out in the 2nd Benelux Tunnel, Rotterdam, the Netherlands, shortly before the tunnel was opened to the public [15]. The tunnel is rectangular in section and is approximately 5.1 m high by 9.8 m wide. While several of these fire tests involved vehicles and vehicle mock-ups, only one of the tests (Test 14) had a very large fire load using 72 wood pallets using a longitudinal velocity of 1–2 ms^{-1}. In three tests, designated tests 8–10, half this fuel load was used (36 pallets) but the velocity was varied from test to test.

In Test 14, eight stacks, each containing nine wooden 'Euro pallets', were arranged in a 2 × 4 configuration to represent a HGV cargo. Six car tyres were added to the load and two small bowls of petrol were ignited at the centre of the load to start the fire. The ventilation used was longitudinal at about 1–2 ms^{-1}. The primary aim of Test 14 was to investigate the capabilities of a sprinkler system in protecting a fuel tanker, which was

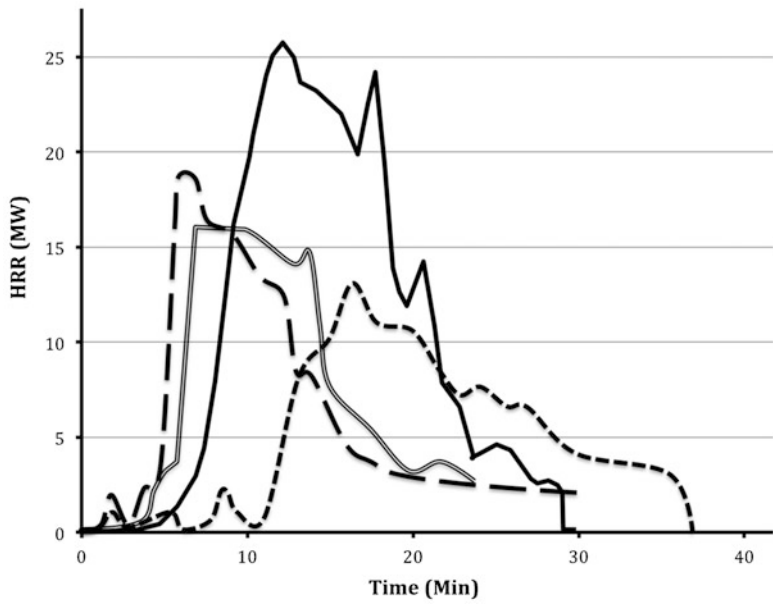

Fig. 88.4 Approximate representation of HRR data from [15]. Test 14 (*solid line*, 72 pallets, 1–2 m/s), Test 8 (*short dash*, 36 pallets, natural ventilation), Test 9 (*double line*, 36 pallets, 4–6 m/s) and Test 10 (*long dash*, 36 pallets, 6 m/s) of the Benelux tunnel fire tests

positioned downstream of the fire. The sprinklers above the tanker were activated after 21 min into the test. The sprinklers cooled the tanker, but were not directed toward the fire source until after 31 min into the tests when they were manually activated, meaning it burned freely most of the test time. In Tests 8–10, the fuel load consisted of four stacks with nine pallets in each without any interaction of the sprinkler system or any cover. In Fig. 88.4 the adapted data from Lemair and Kenyon [16] is given.

When observing Fig. 88.4 two important observations can be made. The maximum heat release rate is affected by both the ventilation rate and the number of wood pallets (tilt the flames), (i.e. the amount of fuel). Higher ventilation rates tend to spread the flames faster inside the pallets, and thereby increase the fire growth rate considerably (the growth rate of the fires varies considerably depending on ventilation rate). Consequently the maximum heat release rate is increased as the tilted flames spread faster through the entire fuel surface.

The Runehamar Tunnel Fire Tests (2003)

A series of four fire tests was carried out in a disused two-lane road tunnel in Norway in September 2003 [2, 3]. The tunnel is 1.6 km long and has a rough rock cross-sectional area of about 47–50 m^2. At the location of the fire experiments (approximately 1 km into the tunnel), a 75 m length of the tunnel was lined with fire-protective panels, and this reduced the cross-sectional area of the tunnel to 32 m^2 in the vicinity of the fire.

Each of the tests comprised a fire load of equivalent size and shape to a standard HGV trailer (10.45 m long, 2.9 m wide, 4.5 m high). In test 1, the fire load consisted of 11.0 tonnes of wooden pallets and mattresses. There was no plastic material except the tarpaulin, but that was the case in all the tests and a 'target' object positioned 15 m downstream of the fire. In test 2, the fire load consisted of 6.9 tonnes of wooden pallets and mattresses. In test 3, the fire load consisted of 7.8 tonnes of furniture on wooden pallets, and ten tyres (800 kg) were positioned around the frame at the locations where they would be on a real HGV trailer. In test 4, the fire load consisted of 2.85 tonnes of plastic cups in cardboard boxes on wooden pallets. In each test the amount of plastic materials was estimated to be about 18–19 % (by weight). Similar tarpaulin coverings were used in all four tests. In each test, two mobile fans positioned near the tunnel portal were used to generate a longitudinal

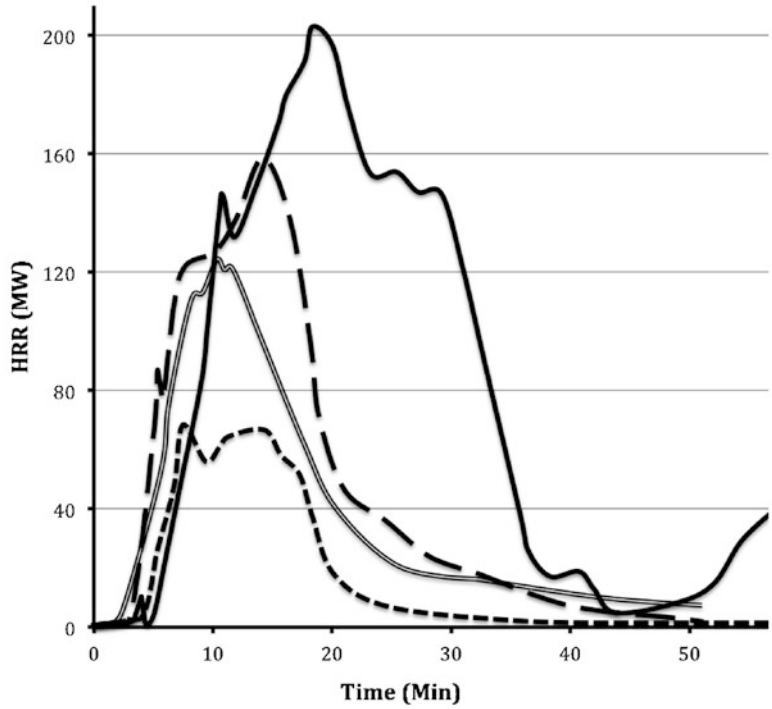

Fig. 88.5 HRR data from the Runehamar fire tests [2, 3] with Test 1 (*solid line*), Test 2 (*long dash*), Test 3 (*double line*) and Test 4 (*short dash*)

airflow, this was about 3 ms^{-1} at the start of each test, but reduced to about 2–2.5 ms^{-1} once the fires became fully active. The peak heat-release rates of the fires in tests one to four were 202, 157, 119 and 67 MW, respectively. The HRR data are shown in Fig. 88.5.

Fire Tests at Carleton University (2011)

Two full scale fire tests were carried out in a 10 m wide, 5.5 m high by 37.5 m long 'tunnel' facility at Carleton University in Canada [17]. The facility is open to the outside through a reduced height opening at the 'upstream' end and is blocked at the 'downstream' end, with an opening in the ceiling leading to smoke/air extraction ducts. The ventilation in the facility is generated by extraction fans, with a maximum capacity of 132 m^3/s. One of the tests involved an intercity style railway carriage, 23 m long, 3 m wide and 3.7 m high, while the other test involved a subway car which was 19.7 m long, 3.15 m wide and 3.45 m high. The estimated fire load of the railway car was 50 GJ and the estimated fire load of the subway car was about half of that. In both tests the extraction system was initially set to 50 % capacity, but was increased to maximum capacity after 3 min into the subway car test and 6 min into the intercity car test. The longitudinal flow during the experiments is not reported in the paper, but is assumed to decrease as the fires grew, due to greater volumes of smoke generated, yet a constant extraction rate. The HRR data, estimated by oxygen consumption, are shown in Fig. 88.6.

Subway Car Tests During Project METRO (2011)

Two fire tests involving fires inside subway cars were carried out as part of the METRO project in Sweden in 2011 [4, 5]. The fire tests were carried out in the 276 m long abandoned 'Old Brunsberg Tunnel' in Western Sweden. The tunnel is an irregular horseshoe in shape and varies from 6.7 to 7.3 m high and from 5.9 to 6.8 m wide. One

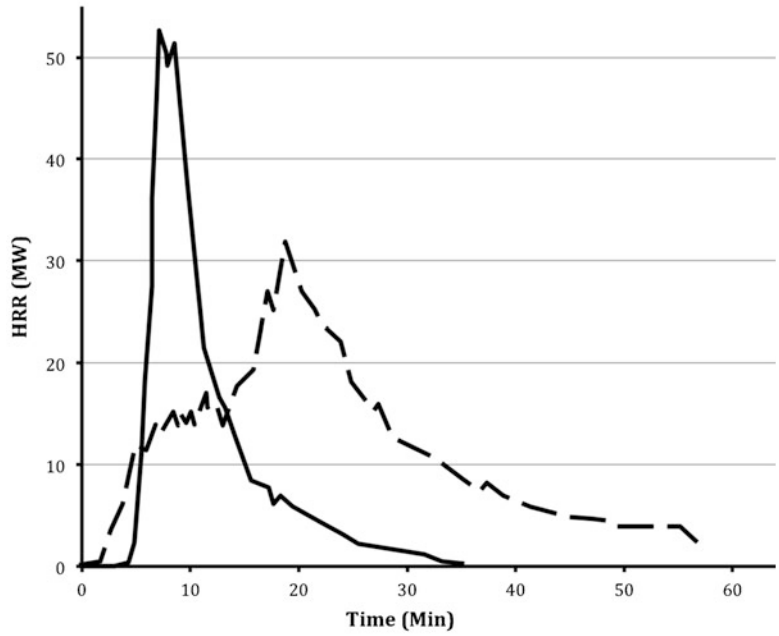

Fig. 88.6 Approximate representation of HRR data from the Carleton University fire tests. The rail car is indicated by the *broken line* and the subway car by the *continuous line* (Adapted from [16])

subway carriage was used as supplied, with older style seats and furnishings, the other was refurbished inside to resemble a modern 'C20' train carriage. This was obtained by cover the combustible wall and ceiling linings with 1.5 mm thick aluminium sheets. A realistic selection of luggage types were placed in the subway carriages as fire load. Longitudinal flow in the tunnel was generated by a mobile fan, positioned upstream of the fire location. This generated a flow of between 2 and 2.5 ms^{-1}, before the fire was ignited. At peak burning, the fires both resisted the airflow, effectively reducing the flow velocity (see the discussion of the 'throttling effect' in section "Using Ventilation Systems for Fire Safety in Tunnels," below). The fire tests were intended to simulate an arson fire on a subway carriage, so both fire tests were initiated with a small quantity of gasoline/petrol on one of the seats. In the test involving the old style carriage, the fire rapidly took hold and grew to flashover-like conditions within the carriage in a few minutes. In the test involving the refurbished carriage, the fire remained small and localised for over 100 min. However, this test also eventually reached flashover-like conditions and from there rapidly transitioned to a fully involved fire, much like the earlier fire test had done at about 12 min after ignition. This was due to the 'melted' aluminium sheets. Following this rapid fire growth, both tests exhibited very similar fire behaviour, as shown in Fig. 88.7, both reached a peak of about 77 MW, both burned at this level of intensity for about 12 min, before rapidly decreasing in intensity to below 20 MW, then slowly burning out over the next 30 min.

Observed Tunnel Fire Characteristics

In the design of fire safety systems in tunnels there is often a need for a "design fire". This fire may be obtained from tabulated data or it may be based on engineering methods calculating the actual fire growth and maximum HRR. The tabulated data is often based on consensus of technical committees such as NFPA or PIARC. A round table discussion using the latest test results such as those presented above informs proposals about the highest value for different vehicle types. This gives guidance to engineers that need the information for design of ventilation systems, the tunnel structure or evacuation

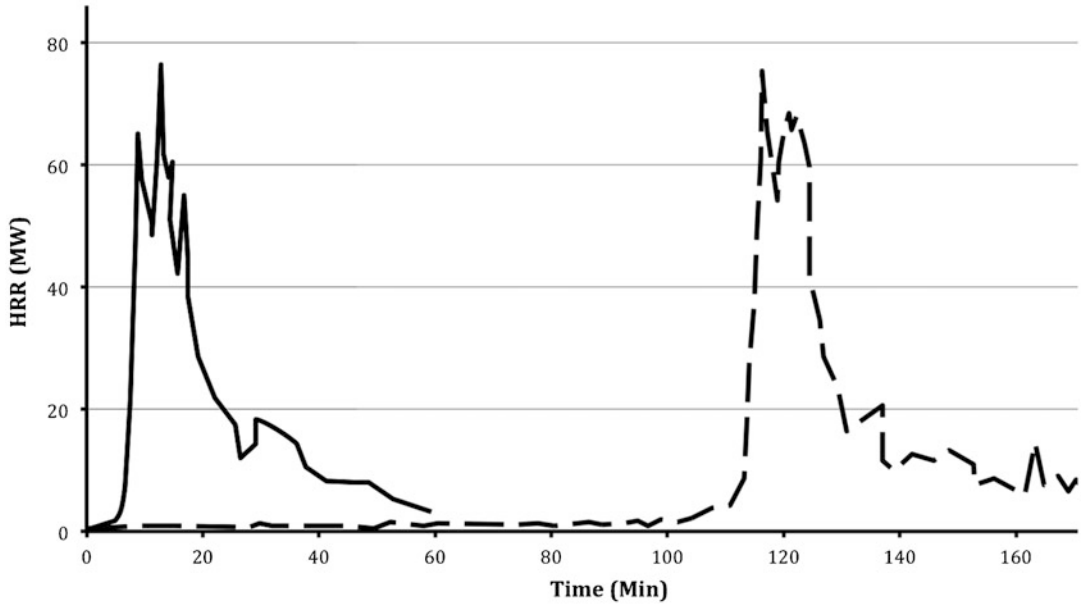

Fig. 88.7 Approximate representation of HRR data from the METRO project fire tests [4, 5]. Test 2 is indicated by a *solid line* and Test 3 with a *double line*

procedures. Traditionally it has been the design of the ventilation capacity that has been the primary focus of designers, although structural considerations have become more important in recent years. As advanced calculation models have been created and developed, the need for realistic design fires has increased.

Most fire protection engineers are familiar with the general picture of a compartment fire which grows in a 't^2' manner from ignition to flashover, burns at a more or less constant, ventilation controlled, peak heat release rate for a significant period of time, before beginning to burn out and entering a decay phase. Because of this familiarity, fire protection engineers have frequently tried to apply the same concepts and assumptions to tunnel fires. However, the above survey through the published tunnel fire heat release rate data should be sufficient to demonstrate that vehicle fires in tunnels do not conform to this common assumption.

It is clear from the above presented data that tunnel fires, particularly when influenced by longitudinal ventilation, do not grow in anything like a t^2 manner. Instead the growth of a tunnel fire may more readily be characterised by a two step linear growth model [18]. The first step in this process, which is generally characterised by slow fire growth is variously described in the literature as the 'incipient', 'incubation' or 'delay' phase, may last for a very long time, as demonstrated by the METRO results (see Fig. 88.7), but may be as short as a few minutes. It is currently unclear exactly what factors govern how long the incipient phase lasts, although it has been suggested that variations in ventilation velocity may reduce or extend the duration of this phase [18]. The second step in this process is a very rapid growth phase which, in tunnels with significant ventilation flow, generally appears to reach peak fire size in just a few minutes. As is clear from Fig. 88.4, above, the rate of growth in this phase varies with longitudinal ventilation velocity [18]. Other models of fire growth are available, including the exponential model presented by Ingason [19] which has the benefit that the entire fire growth, peak and decay process can be described with a single mathematical expression.

Another way in which vehicle fires in tunnels differ from the common compartment fire model is in the duration of peak burning. By peak burning we mean the period where most of the fuel is fully involved in an intensive burning. In the majority of cases described above, the period of peak burning was relatively short, mostly less than 10 min and almost always shorter than 20 min, and was generally followed by a decay which was almost as fast as the rapid growth phase.

Another interesting aspect of vehicle fires is the observation that the HRR per square meter of exposed fuel is generally found to be in a very narrow range. This was first observed through analysis of the several tunnel fire tests [20] and it has been shown that the recent large scale tests in the METRO project confirm this trend. For most vehicles the maximum HRR per square meter of exposed burning fuel surface between 0.27 MW/m^2 and 0.4 MW/m^2, even for fully involved 'post flashover' railway carriages. The METRO tests were equivalent to 0.31 MW/m^2 at maximum HRR. This information can be used to estimate the potential maximum HRR for different types of vehicles. In HGV cargo this value may vary from 0.1 to 0.5 MW/m^2, where the cellulosic materials will tend to have values at the lower end of the range, whereas plastics will tend to have higher values.

It is proposed that these features, common to all large fire experiments in longitudinally ventilated tunnels, be considered when defining 'design fires' for tunnels. This will be discussed in more detail below.

Multiple-Vehicle Fires and Fire Spread

All tunnel fire incidents which have been characterised under the heading of 'catastrophic tunnel fires' have involved fire spread from the initial vehicles involved in the incident, to other vehicles in the vicinity. Table 88.1 lists some of the most significant multiple vehicle fires of recent years. For a more comprehensive list, with details of these and many other incidents, see Carvel and Marlair [21].

In order to understand the fire spread in many large tunnel fires with multiple vehicles involved it is necessary to recognise how these fires progress and spread. Fires in road tunnels may start in one vehicle or in two vehicles due to a collision and then spread to the adjacent vehicles largely by radiation from the flames and the hot smoky gases. In rail vehicles at least one carriage needs to become fully involved in order to obtain fire spread between different carriages. It is not only the nature of the vehicles themselves that is required for a fire spread, but also the geometry of the tunnel, especially the tunnel height, and the ventilation conditions. The main mechanism of fire spread is through heat transfer by convection, radiation and conduction from the volume

Table 88.1 Significant recent multiple vehicle fires [20]

Tunnel	Initial cause	Vehicles involved	Country	Year
Eiksund tunnel	Collision	Lorry and van	Norway	2009
Channel Tunnel	Possible electrical fire	25 HGV and 2 vans, train locomotive and carriages	UK/France	2008
Newhall pass tunnel	Collision	33 HGV	USA	2007
Burnley tunnel	Collision	3 HGV and 4 cars	Australia	2007
Viamala tunnel	Collision	Bus and 2 cars	Switzerland	2006
Fréjus tunnel	Overheating	4 HGV	France/Italy	2005
Baregg tunnel	Collision	3 HGV and car	Switzerland	2004
Daegu subway	Arson	2 subway trains	South Korea	2003
St Gotthard tunnel	Collision	23 vehicles, mostly HGV	Switzerland	2001
Tauern tunnel	Collision	16 HGV and 24 cars	Austria	1999
Mont Blanc tunnel	Overheating	34 vehicles, mostly HGV	France/Italy	1999
Channel tunnel	Possible overheating	10 HGV, train locomotive and carriages	UK/France	1996

of flames and hot gases. The difference in the temperatures between the cooler solids and the hot gases drives this heat transfer.

Among the more spectacular fires that have occurred in tunnels are the large fires in the Channel Tunnel with HGVs on open train wagons in 1996 and 2008 [22]. Rew and Deaves [23] postulated five mechanisms for fire spread in tunnels in their analysis of the 1996 incident. These mechanisms are discussed in detail by Carvel [24] or chapter 11 in Ingason et al. [8]. The first mechanism of fire spread in large fires is **flame impingement**. In low ventilation conditions, the flames are deflected by the presence of the ceiling, mainly in the direction of the ventilation flow. The flames appear to 'crawl' along the ceiling above the vehicles, see Fig. 88.8. Rew and Deaves [23] presented a flame length model for tunnels, which included the heat release rate of the initial fire and the longitudinal flow velocity but not the tunnel width or height. Much of their work is based on the investigation of the Channel Tunnel fire in 1996, with test data from the HGV-EUREKA 499 fire test [1] and the Memorial Tests [6]. They defined the horizontal flame length, L_f, as the distance of the 600 °C contour from the centre of the HGV or the pool, or from the rear of the HGV, see Fig. 88.8.

The other mechanisms of fire spread in tunnels are **surface spread**, that is to say flame spread across the surface of the fire load, **remote ignition** (or spontaneous ignition); the conditions at vehicles that are not very close to the initial fire are raised to the point of spontaneous ignition due to the high temperatures produced by the fire. Another is **fuel transfer**, since burning flammable liquids can spread from fuel tanks in the downhill direction, or flaming debris may blow downwind of the fire. The last mechanism postulated was **explosion** i.e. explosion of fuel tanks may spread burning fuel to adjacent vehicles. None of these other postulated mechanisms fully explain the fire spread between multiple vehicles which has occurred in large tunnel fires. The first mechanism postulated, i.e. **flame impingement**, in combination with spontaneous ignition when the flames virtually crawl over the target vehicle, as shown in Fig. 88.8, is generally the most plausible option. This has been confirmed through numerous full scale and model scale tests performed by SP, the Technical Research Institute of Sweden (SP) [3, 25–28]. Other works on fire spread in tunnels can be found in the work by Beard et al. [29–32].

The possibility of ignition of the target vehicle can be obtained by investigating whether or not the exposed surfaces of the vehicle would attain a critical ignition temperature, T_{cr}. There are two types of ignition, piloted ignition or spontaneous ignition. The possibility of ignition of the target vehicle can be obtained by evaluation of whether or not the exposed surface would attain a critical ignition temperature. The critical temperature, T_{cr}, varies with the nature of the target material, but is generally estimated as follows: 600 °C for radiant exposure or 500 °C for pure convective exposure in the case of spontaneous ignition; or, 300–410 °C for radiant exposure or 450 °C for pure convective exposure in the case of piloted ignition. Note that these values are mostly deduced from experiments on small vertical specimens [33]. Newman and Tewarson [34] argued that, at ignition, $T_{cr} \approx T_{avg}$ (the average gas temperature over the cross-section at a

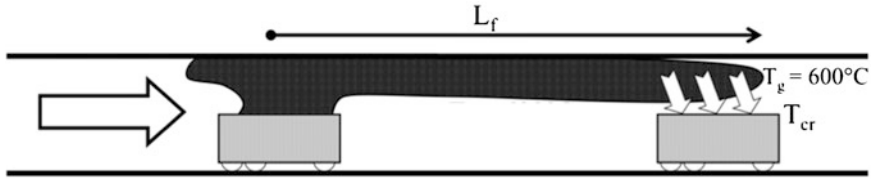

Fig. 88.8 The flame impingement mechanism in tunnels with longitudinal flow. The target vehicle is about to ignite and L_f is the flame length [24]

certain position) for a duct flow, i.e. when the T_{avg} has obtained a critical ignition temperature, the material at that location will ignite. This would comply with the flame impingement mode discussed earlier and complies well with the experimental observations obtained by SP.

There is a strong correlation between the ignition and the ceiling gas temperature in a ventilated tunnel fire [3]. The critical ceiling gas temperature, i.e. the minimum ceiling gas temperature required to ignite the material, has been analyzed for full and model scale tests. In the vicinity of the flame volume, radiation dominates the heat transfer. Since the tunnel ceiling is enclosed by the flame and hot gases, the view factor can be regarded as being unity. Thus the incident heat flux at the ceiling can be simply expressed as [3]:

$$\dot{q}''_{inc} = \varepsilon_g \sigma \left(T_g^4 - T_s^4 \right) \qquad (88.1)$$

where ε_g is the gas emissivity, σ Stefan-Boltzmann constant (kW/m^2·K^4), T_g is the gas temperature in degrees Kelvin and T_s is the solid surface temperature, also expressed in Kelvin. According to Ingason and Li [35], a gas temperature of 600 °C should be obtained for wood before its spontaneous ignition in model tunnels, see Fig. 88.9.

In a recent work by Ingason et al. [3] analyzing the Runehamar fire test data, it was concluded that the critical ceiling gas temperature is about 700 °C for fire spread to a wooden object *at the floor level* and about 600 °C for fire spread to a wooden object with *surface close to the ceiling* in a tunnel fire. The location of vehicle target surface relative to the smoke layer height plays therefore an important role in fire spread. Therefore, the authors argue that fire spread to subsequent vehicles is very difficult to occur if the vehicle height is small compared to the tunnel height, perhaps below about half the tunnel height [3].

When the fire starts to spread to the second vehicle the fire development is difficult to stop if there are more vehicles in the vicinity of the first two vehicles. Figure 88.10 gives a schematic description of a large tunnel fire with relatively high forced longitudinal ventilation rate and multiple vehicles. The burning process can be viewed as stationary and the fire-spread progress can be divided into different key zones [25, 36]:

Provided there are sufficient vehicles in the vicinity of the initial fire, these different zones move forward in a dynamic manner. The 'burnt out zone' involves vehicles that have been completely consumed in the fire and where the fire gases are now cool. The 'glowing ember

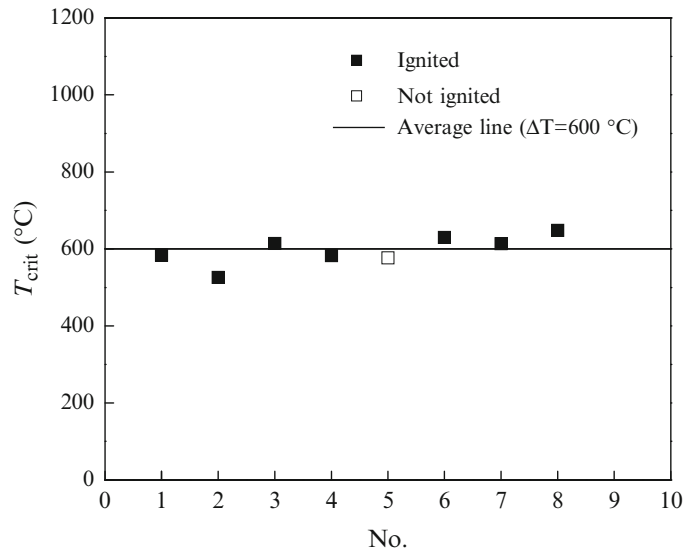

Fig. 88.9 The critical gas temperature beneath ceiling when a second wood crib ignites [26]. The number on the *horizontal axis* refers to test number in the test series

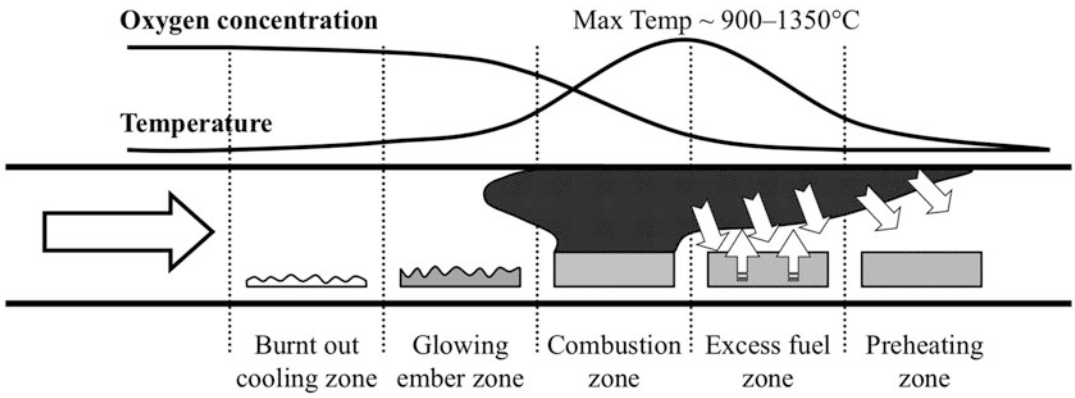

Fig. 88.10 Schematic presentation of a flame impingement fire spread process in a tunnel with multiple vehicles/coaches [24, 35]. Note: there may be multiple vehicles in each designated zone, and the zones are only shown as having the same length as each other for convenience

zone' contains vehicles at a very late stage of the decay phase (predominantly a pile of glowing embers). The 'combustion zone', contains the violently burning vehicles (fully developed fire) where sufficient fuel is vaporising to support gas phase combustion. Flaming combustion is observed throughout this zone. The gas phase temperature in this zone increases rapidly. Simultaneously the oxygen is rapidly depleted and the temperature reaches a maximum just beyond the 'combustion zone'. This gas temperature can vary between 900 and 1365 °C.

If all the oxygen is consumed within the combustion zone, an 'excess fuel zone' starts behind this. In the case where all the oxygen has been depleted we have a **ventilation-controlled** fire. In the case where useful oxygen is still available (due to flammability limits, oxygen concentrations below about 8–10 % may not be 'useful' unless the gas phase temperature is high enough to sustain combustion) we have a **fuel-controlled** fire and no excess fuel (no more vehicles in place to sustain the progress). In the case of ventilation-controlled fire, the fuel continues to vaporise from the vehicles throughout this zone up to a point along the tunnel where the gas stream has cooled to the fuel vaporisation (pyrolysis) temperature ($T_{vap} \geq 300$ °C for the majority of solid materials). Beyond this point, no vaporisation of the vehicle materials occur but the gas flows into a 'preheating zone' and loses its heat to the tunnel walls and preheats the vehicle material within this zone.

de Ris [36] showed that the combustion and excess fuel zone lengths are proportional to the forced ventilation rate when the fire becomes ventilation-controlled and Comitis et al. that the fire will propagate at a constant speed [37] (when ventilation-controlled) provided that there is enough combustible material available. Delichatsios [38] concluded that active burning in a fibreglass-reinforced plastic duct will take place up to a maximum length corresponding to $L_c/D_h = 10$ where D_h is the hydraulic diameter of the duct (m) and L_c is the combustion length (m). Assuming that this number is reasonable for tunnels the combustion zone, for a ventilation-controlled fire with forced ventilation, would not exceed 50–100 m for most common road and rail tunnels (assuming high vehicle density) where D_h is ranging between 5 and 10 m.

Considerations for Design Fires for Vehicle Tunnels

Tunnel designers, ventilation engineers, suppression system manufacturers and others commonly need to define the characteristics of the fire which they are designing their facilities or systems to be able to manage. Thus, specification of *realistic*

design fires is of great importance, if tunnel facilities and systems are to be made robustly.

A design fire need not be the most severe fire imaginable for a given situation, but should be at the upper bound of fire scenarios deemed credible, or likely to happen within a specified timescale. In other words, it need not be necessary to design a system to be able to manage a 'once in 10,000 years' incredible event, but consideration should be given to the more likely, though still improbable, 'once in 1000 years' type event.

Design fires should also be tailored to the system being designed. For example, a design fire for structural protection or structural resistance calculations should be radically different to the design fire used for the detection and alarm system.

There are a number of guidance documents which discuss design fires for tunnels, which go into the subject in far greater detail than can be devoted here, including [39–41]. These brief comments are intended to enable the designer to consider realistic fire features in design fires.

Design fires for tunnel structures, fire protection system design and smoke management should be based on the realistic maximum peak fire size. Such design fires need not consider the incipient stage of the fire, and assuming the growth phase to be of only a few minutes in duration, this can be neglected too. The design fire here should therefore be characterised by a maximum HRR plateau, from the outset, the duration of which should be prescribed on the basis of the maximum number of vehicles deemed likely to be involved in a fire. The duration of peak burning is limited by the availability of fuel and the availability of oxygen, and therefore this period of peak burning can be extended if additional fuel becomes available by means of the fire spreading to an adjacent vehicle or vehicles.

For property protection purposes it is also important to consider the cooling/decay phase of the fire, as it is well known that some structures which have endured throughout a fire or a furnace test at high temperature have failed as they cool, however this is rarely commented upon in the literature.

In situations like the experiments described above, where the fire load was large, relative to the tunnel, the peak HRR may be defined and limited by the available oxygen in the airflow. The maximum theoretical (ventilation-controlled) HRR may be estimated using the well known correlation between HRR and the mass of oxygen consumed in a longitudinal ventilation flow:

$$\dot{Q} = \left(0.21 - \eta_{O_2}\right) V \rho \Delta H_{c,ox} \qquad (88.2)$$

where η_{o2} is the depleted oxygen level on the downstream side, V is the volumetric airflow, ρ is density of the inflowing airflow (approx. 1.2 kg/m^3) and $\Delta H_{c,ox}$ is the heat of combustion for oxygen, generally taken to be 13 kJg^{-1} [42].

Thus, for example, in a tunnel with a 40 m^2 cross section and a 2 ms^{-1} longitudinal flow, we might expect the theoretical maximum ventilation controlled HRR to be about:

$$\dot{Q} = (0.21 - 0.0) \times 2 \times 40 \times 1.2 \times 13.02 = 262\ MW$$

It should be noted that in most circumstances with one or two collided vehicles involved in a fire, it is not likely that all the oxygen in the airflow will be usable by the fire as much of it may bypass the combustion zone. In the case when another vehicle is standing downstream a fire, the environment may not be combustible due to flammability limits (relation between the oxygen concentration and gas phase temperature).

It is important to note here that, provided sufficient fuel is available (for example, in multiple vehicle fire scenarios), it is the tunnel airflow which defines the theoretical peak fire size, and hence should define the design fire for structural purposes. A similar design fire should be used also for dimensioning the ventilation system. If fuel is limited, for example by considering only a single vehicle fire, then the fire may remain fuel controlled and the peak size may be estimated based on the fuel area, as described above [20].

However, this idea goes against the notion, so prevalent in the tunnel fire and design literature, that a ventilation system designer should first

identify a 'design fire' size and then dimension the ventilation system in order to generate adequate smoke control. In the case of a multiple vehicle fire, the fire size does not define the required airflow, rather the airflow entirely defines the maximum possible fire size.

This relationship, where the theoretical maximum fire size is defined entirely on the basis of ventilation flow, will hold in general terms in situations like most of those described above, where the vehicle on fire is large, relative to the cross-section of the tunnel; that is to say, in single lane tunnels, which are generally subway and railway tunnels. The relationship is not likely to be as simple as this in two or more lane tunnels, such as are common for road transport. In larger tunnels, it is expected that a greater proportion of the longitudinal airflow will bypass, not directly feed the fire, so the resulting HRR could be significantly lower.

For single lane tunnels where multiple vehicle fires are possible, however, it is proposed that the peak HRR of a 'design fire' for structural and ventilation considerations, should be based entirely on the anticipated longitudinal airflow in the tunnel.

As noted above, the factors governing the duration of the incipient phase are not well understood at the present time, therefore, without further tests to demonstrate the performance of a particular system, it should be assumed—for design purposes of all tunnel systems—that the incipient stage will remain short, perhaps only of the order of a few minutes. Assuming an extended incipient phase as part of a design fire cannot be justified from the above data.

Design fires for detection systems and water spray systems need to consider the growth phase of the fire. Such systems are intended to detect the fire while it is as small as possible, and to suppress or control the fire, that is to say, prevent the fire from reaching its unsuppressed potential. The important characteristics of a fire for design of a water spray system are therefore those relating to fire growth [18]. Important parameters to consider here are the ventilation rate in m/s and the ceiling height. These parameters govern, together with the HRR at each time interval, the gas temperature at the tunnel ceiling. The location of the maximum gas temperature varies along the ceiling depending on these parameters. For further information see Li and Ingason [43].

Using Ventilation Systems for Fire Safety in Tunnels

The systems which we commonly consider to be safety systems for tunnels were not, in most instances, initially installed in tunnels as safety devices. The most common safety system in tunnels is the ventilation system, yet it must be recalled that the original and primary function of ventilation systems is not smoke management in the event of a rare event like a fire, but rather is pollution and environmental control in everyday usage.

The first ventilation system installed in a railway tunnel was in Liverpool's Edge Hill tunnel in the UK, in 1870, although mechanical ventilation had been commonplace in mine tunnel networks for at least three centuries before this [44]. This was an exhaust fan for the removal of smoke from steam engines. In 1927, the Holland Tunnel in the USA became the first road tunnel equipped with a (fully) transverse ventilation system, that is, a system of ducts and openings provided fresh air into the tunnel at periodic locations along its length, while a second system of openings and ducts extracted polluted air from the tunnel at periodic locations. The first tunnel to have longitudinal ventilation with jet fans was the Bargagli-Ferriere tunnel in Italy in 1971. While all these systems were originally conceived as means of replacing polluted air with fresh air, these systems began to be understood as a means of controlling smoke in the event of a fire in a tunnel. The addition of jet fans to transversely ventilated tunnels in the 1980s (for example, the Dartford tunnel in the UK) reflects this change in mindset. In 1994, the Channel Tunnel opened with the world's first ventilation system intended 'from the drawing board' as a smoke control system as well as a pollution control system [45].

Because almost all tunnels of significant length have ventilation systems, it is easy to understand why these systems became adapted to be emergency response devices. For the past two decades, perhaps longer, the tunnel safety industry appears to have been fixated on questions associated with using ventilation for smoke control in the event of a tunnel fire. The question of appropriate design for ventilation systems has therefore been generally reduced to the question of extract capacity, for transversely ventilated tunnels, or of identifying the 'critical ventilation velocity' (CVV) for tunnels with longitudinal ventilation.

The CVV is generally defined as the minimum longitudinal ventilation velocity required to blow all the smoke produced by a fire in a tunnel to one side of the fire location, that is, to prevent any smoke propagating upstream of the fire location, against the prevailing airflow. CVV varies with tunnel geometry and with fire size, up to a certain limit. A number of studies, including that of Oka and Atkinson [46], have identified that there is generally a 'super critical ventilation velocity' which is sufficient to control the smoke from all sizes of fire, for a given tunnel geometry. A review of tunnel CVV studies is presented by Ingason [47] and need not be repeated here.

The critical flow conditions are generally expressed in the literature in terms of a single ventilation velocity, which is commonly taken to be the average flow across the tunnel cross-sectional area, however, it may be better in some instances to speak in terms of a critical volumetric flow rather than a velocity. The focus on ventilation velocity also masks the throttling effect of tunnel fires, identified in the 1970s by Lee et al. [48]. In a given tunnel it may well be the case that, say, a 3 ms^{-1} airflow may be sufficient to control smoke in the event of either a 50 MW fire or a 100 MW fire, but expressing the situation in these terms hides the fact that more ventilation devices will be required in the case of a 100 MW fire to generate the 3 ms^{-1} airflow than would be required to generate the same magnitude flow in the case of a 50 MW fire. A computational example of this, derived from Vaitkevicius et al. [49], expanding on the work of Colella et al. [50], is shown in Fig. 88.11. Here, there is no increase in CVV beyond 31 MW, yet the number of fans required to generate the CVV continues to increase with fire size.

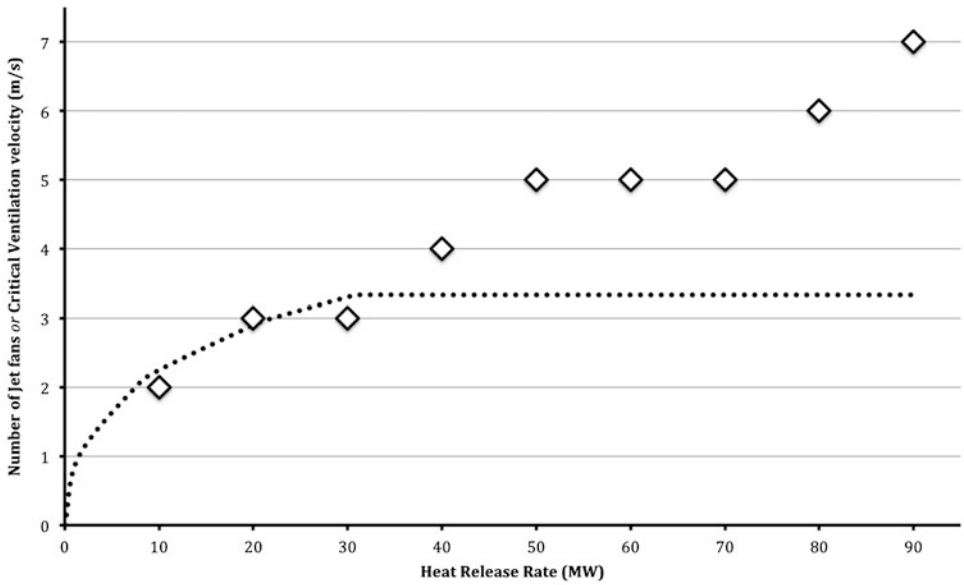

Fig. 88.11 Critical Ventilation Velocity (CVV; *dotted line*) and the number of jet fans required to generate CVV (*diamonds*) vs. fire heat release rate, for a modelled rectangular tunnel (Adapted from Vaitkevicius et al. [49, 50])

While our understanding of longitudinal ventilation for smoke control is reasonably advanced [51], our understanding of the influence of ventilation on fire behavior is considerably less mature. Various studies in the past decade have shown that peak fire size is influenced by longitudinal ventilation velocity [52] and by the geometry of the tunnel [53], other studies have shown that longitudinal ventilation also has a significant influence on fire growth rates [18, 27]. Each of these factors must be considered when designing ventilation systems for use in emergency situations.

As observed above, in tunnel fire experiments the fire tends to grow in two reasonably distinct stages. For the first few minutes after ignition there is an incipient phase, followed by a period of much more rapid fire growth. From observation of the experimental tunnel fire data, there appears to be a weak relationship between the length of the incubation phase and the longitudinal ventilation velocity [18]. Such limited data as are available suggest that the incipient phase is generally shorter at longitudinal velocities of about 2–3 ms^{-1} than it is at lower (0–1 ms^{-1}) and higher (circa 6 m/s) velocities. This suggests that ventilation flows of about 2–3 ms^{-1} should be avoided in the initial stages of a fire. Unfortunately, 3 ms^{-1} is close to the CVV for design fires in many tunnels, so has commonly been used as an emergency ventilation flow. However, it should be noted that many different (and apparently contradictory) emergency ventilation strategies are used in tunnels worldwide, some opting to increase the flow greatly when a fire is detected, in order to dilute the smoke, while others opt to reduce the flow below about 1.5 ms^{-1}, in order to maintain smoke stratification.

There are also issues associated with reversing ventilation direction [54]. It appears, from an analysis of the Channel Tunnel fire incidents, that changes in the direction of the airflow, after a fire is fully developed, can lead to very rapid fire spread between vehicles and very fast fire growth rates, but further work is required to confirm these observations.

Passive Fire Protection: Tunnel Lining Systems

As with ventilation systems, the original intent of the tunnel lining system was not as a fire protection system, and many older tunnel lining systems which are still in use today serve only a cosmetic function and provide no fire protection. Tunnel lining systems were primarily installed to act as drip shields, to provide a visual aesthetic and, in some instances, for acoustic reasons.

Today, while the above reasons remain valid, the main design consideration for tunnel lining systems is how much thermal protection they can provide for the primary tunnel structure. Modern tunnels are generally made of concrete, although many older tunnels constructed out of cast iron segments or masonry are still in use. Concrete has excellent structural properties at ambient temperatures, but may fail when subjected to high temperatures and rapid heating, under fire conditions.

According to the guidance of NFPA 502 [55], the primary concrete structure in tunnels with cast in situ concrete provided with structural fire protection material temperatures shall not exceed 380 °C at the concrete surface and 250 °C at any of the rebar, when subjected to a time-temperature curve deemed equivalent to a tunnel fire. These requirements are mirrored in other standards [56]. Temperatures up to these limits will not significantly reduce the load carrying capacity of concrete.

One major concern with concrete structures is the still inadequately understood phenomenon of spalling [57]. Spalling is an explosive failure which commonly occurs when concrete is rapidly heated and steep temperature gradients are formed in the bulk material, leading to thermal stresses and high pore pressures in the material. Spalling has also been observed during rapid cooling, such as during fire-fighting activities [58]. Spalling has even been observed to occur at relatively low temperatures [59], so the function of a fire protection system is not merely to protect the structure from exposure to high

temperatures, but also to protect the structure from rapid heating. As well as having excellent thermal barrier properties, it is vitally important that passive fire protection systems not be prone to spalling themselves.

Passive protection systems for tunnels are generally either a bolted on panel system or a sprayed on mortar system. Other options, such as intumescent coatings which are common in the building industry, do not seem to have been considered for tunnel applications. Research is on-going into the performance in fire of concrete containing various forms of fibres, some of which have been demonstrated to resist spalling and, thus, improve the fire resisting properties of concrete [60]. However, neither a spalling proof concrete mixture, nor a method for accurately predicting spalling behaviour has yet been developed. If suitable concrete mixes can be developed, this may have a considerable impact on the way that future concrete tunnel structures are made.

Finally, there is an increasing tendency in the tunnel protection industry to consider fire suppression systems as structural protection systems, and a number of recent papers have discussed 'trade-offs', that is, reducing or removing the requirement for a passive thermal barrier system if a suppression system is being installed [61, 62]. This will be discussed further in the next section.

Water Spray Systems

It is the opinion of one of the authors that the terminology used to describe water based fire protection systems these days is somewhat misleading [63]. The way the word 'suppression' is used by fire protection engineers strays considerably from the dictionary definitions of the word 'suppression' used by the rest of the world. Describing water spray systems as 'suppression' systems implies that these technologies have the ability to halt the growth of, or reduce the size of fires in tunnels. According to the definition given by NFPA 502, "Fire suppression systems are designed to arrest the rate of fire growth and significantly reduce the energy output of the fire shortly after operation". In order to do that the system has to be able to deliver certain amount of water onto the burning fuel surface and actively cool it. Simultaneously it has to have the ability to hinder fire spread to adjacent fuel surfaces. As will be discussed below, neither of these abilities is guaranteed or even commonly observed with many 'suppression' systems promoted for use in tunnels. Such systems do not fulfill the basic requirements implied in the word 'suppression'.

Similarly, the terminology which seems to be in vogue at present, 'fixed fire fighting systems' (FFFS), implies that the systems so described are actually able to 'fight' fires. Once again, this is not always guaranteed. There is a need for clear definitions that should be accepted by all involved partners. The term "deluge system" relates to systems with open nozzles operated on zone-to-zone basis creating water droplets in order of 1 mm, whereas "water mist system (WMS)" is a high-pressure deluge system creating very small droplets, in order of 50–250 μm. The blanket term FFFS is used to include all these system, together with foam based systems (high expansion, CAFS), which we do not consider in the short discussion here. The terms 'suppression' and 'fire fighting' both imply performance criteria which not all systems described as such can achieve. Thus, the term water spray system will be use here to include both deluge systems (even with foam additives) and water mist systems.

Although the benefits of fire sprinkler systems in buildings have been recognized widely for many years, the use of water spray systems in tunnels has generally been discouraged until comparatively recently. However, this generalisation is not universal. Deluge systems have been routinely used in Japanese tunnels since the 1960s, and in Australian tunnels since the early 1990s. There were hardly any European or North American tunnels with water spray systems until the last decade. In 1999, the World Road Association, PIARC reported that no road tunnels in Belgium, Denmark, France, Italy, the Netherlands, the UK or the USA were equipped with water spray systems, while Sweden had only one and Norway had two [64].

Deluge systems have been routinely installed in Japanese tunnels since 1963, when the first system was installed in the Tennozan Tunnel. Eighteen experimental test series were carried out in Japan between 1960 and 1985, the majority of these being carried out using fuel pans, although fire tests using cars, a small van, trucks and a bus were also carried out [65]. In general, these tests demonstrated the effectiveness of the deluge system in reducing temperatures in the tunnel and hindering fire spread. However it was observed that "the fire tends to expand less in vertical and more in horizontal direction" and that while fires of "wood or other open load" could be extinguished, fires inside or underneath vehicles "could not be extinguished at all".

In practice, the Japanese experience is also good. Between 1963 and 1990 there were 90 fire incidents in tunnels operated by the Japan Highway Public Corporation. The vast majority of these fires (80 %) did not require the application of the (manually operated) water spray systems. In the 16 instances when the deluge system was used, the results were found to be "fairly satisfactory" [65]. No incident escalated to disastrous proportions. Australia has a shorter length of experience of deluge systems—the first system was installed in the Sydney Harbour Tunnel in 1992—but their experience is also positive [66]. The deluge systems have proven to be effective in vehicle fire exercises and during fire incidents, the highest profile of which was the fire in the Burnley Tunnel in March 2007 [67]. In general, testing and experience has demonstrated that water spray systems are reasonably able to contain vehicle fires and prevent fire spread in tunnels, allowing safe evacuation of people, effective fire fighting by the fire brigade and a rapid return to normal operation of the tunnel.

However, elsewhere in the world, the negative attitude to water spray systems in tunnels extends back to the 1960s and 1970s, but was enshrined in international recommendations up until the late 1990s and early 2000s, as exemplified by this quote from the 1999 PIARC report "Fire and Smoke Control in Road Tunnels" [64]:

> *. . .the use of sprinklers raises a number of problems which are summarised in the following points*:
> - *water can cause explosion in petrol and other chemical substances if not combined with appropriate additives*,
> - *there is a risk that the fire is extinguished but flammable gases are still produced and may cause an explosion*,
> - *vaporised steam can hurt people*,
> - *the efficiency is low for fires inside vehicles*,
> - *the smoke layer is cooled and de-stratified, so that it will cover the whole tunnel*,
> - *maintenance can be costly*,
> - *sprinklers are difficult to handle manually*,
> - *visibility is reduced.*
>
> *As a consequence, sprinklers must not be started before all people have evacuated.*
>
> *Based on these facts, sprinklers cannot be considered as an equipment useful to save lives. They can only be used to protect the tunnel once evacuation is completed. Taking into account this exclusively economic aim (protection of property and not life safety) sprinklers are generally not considered as cost-effective and are not recommended in usual road tunnels.*

The spate of catastrophic tunnel fires in road tunnels which occurred almost immediately following the publication of this report forced the transport tunnel industry to reconsider the importance of property protection and continuity of business, particularly on the trans-European road network, and the industry very quickly realised that water spray systems were a viable and economic option for improving life safety levels and ensuring business continuity.

A number of large, government funded, research projects were carried out in the 2000s to address the issues of tunnel safety, security and sustainability, including the UPTUN project [68], the SAFE-T project and the SOLIT project [69]. Integral to each of these projects was a fresh consideration of suppression technologies for tunnel applications, and as the focus of much of the research was on 'novel' technologies, deluge systems were generally overlooked in favour of water mist systems (WMS).

Detailed reviews of the findings of these projects are published and summarised elsewhere [e.g. 70] and do not need repeated here. To date, no WMS has been deployed during a

real fire incident in a tunnel, so there is no information on their capabilities in practice.

Some testing of WMS for tunnels has been presented in the public literature. Almost all of these tests have involved either open pans of liquid fuel or stacks of wooden (occasionally plastic) pallets. In general, it is claimed that water mist systems have been demonstrated to: reduce the temperature in the vicinity of the fire, reduce visibility in the locality of the fire, improve visibility at locations distant from the fire, slow or halt the fire growth rate, reduce the 'peak' fire size, prevent fire spread and protect the tunnel structure.

However, in some instances (in the public literature, presumably also in some of the many unpublished tests), the WMS have not performed as expected [71]. For example, in one of the fire tests carried out in the Hagerbach tunnel complex in Switzerland for the Paris A86 project [72] the fire (initially involving three cars in a 'collision' configuration) spread to two adjacent cars while the WMS was operational. From the presented data, WMS seem unable to halt fire growth on solid cargo loads, but fire growth rate is, in general, observed to slow or, at least to be interrupted for a period of time upon WMS activation. Under certain circumstances (cargoes covered by tarpaulin, mixed load of wood and plastics) fires have been observed to grow considerably, over a period of minutes, during WMS operation. In one instance the WMS was switched on when the (covered, mixed load) fire was only about 10 MW in size, and the fire continued to grow to over 60 MW [73]. In another similar instance, the WMS was switched on when the (covered, wooden cribs) fire was about 10 MW in size and the fire grew to about 55 MW during system operation [74].

Thus, it appears that for all but the simplest, uncovered, fire loads, fire control cannot be guaranteed using a water mist system. However, such systems do appear to perform very well in terms of temperature control (hence structural protection) and, to some extent, for smoke control.

WMS (and other water spray systems) effectively cool the hot smoke layer in tunnel fire scenarios. This tends to destroy stratification, but also to reduce the momentum of the smoke. Thus, if water spray systems are operated in tunnels, considerably smaller ventilation velocities should be required to control smoke. This has yet to be studied in any detail. There may also be an optimum ventilation airflow for promoting the suppressing effects of water spray systems. This also has yet to be studied in any detail.

It should be stressed that the emphasis of this discussion is on the influence of the various systems on the fire itself. Even though the behavior of the fire itself may not be greatly impacted by the activation of certain types of FFFS, in some situations, such systems may have a large effect by mitigating the consequences of the fire on the structure and on persons and objects distant from the fire. Water sprays have excellent thermal radiation blocking properties, which serve to protect the structure, to allow the fire brigade to approach the fire to fight it and also to prevent fire spread to other vehicles, in conditions where there is no direct flame impingement [63].

At a workshop presenting the results of the SOLIT^2 project in Gijon, Spain, in 2011 [75], one of the delegates, having heard the project results and having witnessed a very large fire (comprised of wooden pallets, approximately 20–25 MW at peak HRR) in a tunnel with an active water mist system, commented that the action of the WMS effectively made the magnitude of the fire (expressed as a heat release rate) an irrelevant concept for specifying the design fire for structural design of tunnels. While the WMS may not be able to suppress or reduce the absolute HRR of a vehicle fire in a tunnel, it has been demonstrated able to considerably mitigate the effects of such a fire, such that the thermal attack on the structure due to, say, a 25 MW fire in water mist may be less than that due to a 4 or 5 MW fire without water mist.

Observations such as these suggest that fixed water spray systems in tunnels should really be considered as 'protection' systems rather than 'suppression' systems. The ability to suppress a fire is not guaranteed, the ability to protect a

structure, on the other hand, has been more than adequately demonstrated [76].

Of course, if we were to re-classify water spray systems as protection systems, then the question of 'trade-offs' mentioned above becomes less controversial. It is no longer a question of reducing passive structural protection if a suppression system is installed, the question resolves to which system is better in the instance considered—a passive thermal barrier, or an active water spray thermal management system? There is no 'one size fits all' solution for all tunnel environments, but in every instance it is a matter of engineering judgment and calculation.

Concluding Comments

Tunnel fire safety is a complex problem with no clear solution at this moment in time. Even in tunnels with cross passages to another tube or a safety gallery, egress distances can be several hundreds of metres. Vehicles carrying 'non-hazardous' cargoes can result in rapidly growing fires with peak heat release rates of over a hundred megawatts. Yet systems exist which can mitigate the effects of large fires in tunnels and provide adequate protection for escaping tunnel users and thermal protection for the tunnel structure. Few countries have prescriptive standards for tunnel fire safety, so defining how such systems are to be installed and used in the event of a fire inevitably involves a 'performance based' analysis of each tunnel on a case by case basis. The data and discussions presented here are provided in order that such analyses are based on realistic 'design fires' and realistic assessments of the performance of protection systems under consideration. In many rural and urban parts of the world, tunnels provide essential, efficient and sustainable transportation links. We can make them safer.

Nomenclature

CAFS	Compressed Air Foam System
CVV	Critical Ventilation Velocity
FFFS	Fixed Fire Fighting System
HGV	Heavy Goods Vehicle
HRR	Heat Release Rate
MTFVTP	Memorial Tunnel Fire Ventilation Test Program
NFPA	National Fire Protection Association
UPTUN	Upgrading of Existing Tunnels Project
PIARC	World Road Association
SAFE-T	Safe Tunnels Project
SOLIT	Safety Of Life In Tunnels Project
WMS	Water Mist System
D_h	Hydraulic diameter of the tunnel (m)
$\Delta H_{c,ox}$	Heat of combustion for oxygen (13.02 kJ/g)
L_c	Combustion zone length (m)
L_f	Flame length (m)
Q	Heat release rate (kW or MW)
q_{inc}	Incident heat flux (kW/m^2)
T_{avg}	Average gas temperature across a tunnel cross-section (K or °C)
T_{cr}	Critical ignition temperature (K or °C)
T_g	Gas temperature (K or °C)
T_s	Solid (surface) temperature (K or °C)
T_{vap}	Vaporization/ pyrolysis temperature (K or °C)
V	Volumetric airflow (m^3/s)
ε_g	Gas emissivity (between 0 and 1)
η_{O2}	Depleted oxygen level (less than 0.21)
ρ	Density of air (1.2 kg/m^3)
σ	Stefan-Boltzmann constant (5.67×10^{-8} W/m^2·K^4)

References

1. "Fires in Transport Tunnels: Report on Full-Scale Tests", edited by Studiensgesellschaft Stahlanwendung e. V., EUREKA-Project EU499: FIRETUN, Düsseldorf, Germany, 1995.
2. Ingason, H., and Lönnermark, A., "Heat Release Rates from Heavy Goods Vehicle Trailers in Tunnels", *Fire Safety Journal,* **40,** 646–668, 2005.

3. Ingason, H., Lönnermark, A., and Li, Y. Z., "Runehamar Tunnel Fire Tests", SP Technical Research Institute, SP Report 2011:55, 2011.
4. Lönnermark, A., Lindström, J., Li, Y. Z., Ingason, H., and Kumm, M., "Large-scale Commuter Train Tests—Results from the METRO Project", Proceedings from the Fifth International Symposium on Tunnel Safety and Security (ISTSS 2012), pp. 447–456, New York, USA, 14–16 March, 2012.
5. Lönnermark, A., Lindström, J., Li, Y. Z., Claesson, A., Kumm, M., and Ingason, H., "Full-scale fire tests with a commuter train in a tunnel", SP Technical Research Institute of Sweden, SP Report 2012:05, Borås, Sweden, 2012.
6. "Memorial Tunnel Fire Ventilation Test Program—Test Report", Massachusetts Highway Department and Federal Highway Administration, 1995.
7. Carvel, R. & Marlair, G. "A history of experimental tunnel fires" Chapter 12 in Handbook of Tunnel Fire Safety 2nd Edition, Ed Beard & Carvel, ICE Publishing, 2011, ISBN 978-0-7277-4153-0. pp 239-271. Doi: 10.1680/htfs.41530.239.
8. Ingason, H., Li, Y. Z., and Lönnermark, A., The Handbook of Tunnel Fire Dynamics, Springer, 2015 Edition.
9. Ingason, H., and Lönnermark, A., "Heat Release Rates in Tunnel Fires : A Summary" Chapter 14 in Handbook of Tunnel Fire Safety 2nd Edition, Ed Beard & Carvel, ICE Publishing, 2011, ISBN 978-0-7277-4153-0. pp 309–327. Doi: 10.1680/htfs.41530.309.
10. Ingason, H., "Heat Release Rate Measurements in Tunnel Fires", International Conference on Fires in Tunnels, 86–103, Borås, Sweden, October 10–11, 1994, 1994.
11. Ingason, H., Gustavsson, S., and Dahlberg, M., "Heat Release Rate Measurements in Tunnel Fires", SP Swedish National Testing and Research Institute, SP Report 1994:08, Borås, Sweden, 1994.
12. Grant, G. B., and Drysdale, D., "Estimating Heat Release Rates from Large-scale Tunnel Fires", Fire Safety Science—Proceedings of the Fifth International Symposium, 1213–1224, Melbourne, 1995.
13. Malhotra, H.L. "Goods Vehicle Fire Test in a Tunnel" 2nd Int. Conf. on Safety in Road and Rail Tunnels, Granada, Spain, 1995, pp. 237–244.
14. Steinert, C., "Smoke and Heat Production in Tunnel Fires", The International Conference on Fires in Tunnels, 123–137, Borås, Sweden, 10–11 October, 1994.
15. "Project 'Safety Test' – Report on Fire Tests" Directorate-General for Public Works and Water Management, Civil Engineering Division, Utrecht, The Netherlands, August 2002
16. Lemaire, T., and Kenyon, Y., "Large Scale Fire Tests in the Second Benelux Tunnel", *Fire Technology,* **42,** 329–350, 2006.
17. G. Hadjisophocleous, D.H. Lee & W.H. Park "Full scale experiments for heat release rate measurements of railcar fires" Proceedings from the Fifth International Symposium on Tunnel Safety and Security (ISTSS 2012), pp. 457–466, New York, USA, 14–16 March, 2012.
18. Carvel, R.O. (2008) Design fires for tunnel water mist suppression systems. Proc. 3rd Int Symp. on Tunnel Safety and Security, Stockholm, Sweden, March 12–14 2008. ISBN 978-91-85829-25-5. pp. 141–148.
19. Ingason, H., "Design fire curves in tunnels", *Fire Safety Journal,* **44,** 2, 259–265, 2009.
20. Ingason, H., "Fire Testing in Road and Railway Tunnels". In *Flammability testing of materials used in construction, transport and mining* (V. Apted, Ed.), Woodhead Publishing, 231–274, 2006.
21. Carvel, R. & Marlair, G. "A history of fire incidents in tunnels" Chapter 1 in Handbook of Tunnel Fire Safety 2nd Edition, Ed Beard & Carvel, ICE Publishing, 2011, ISBN 978-0-7277-4153-0. pp 3–24. Doi: 10.1680/htfs.41530.003.
22. Beard, A. & R. Carvel (2011) "The Handbook of Tunnel Fire Safety' Second Edition ICE Publishing, 2011, ISBN 978-0-7277-4153-0. (1st edition, published by Thomas Telford, 2005. ISBN 0-7277-3168-8).
23. Rew, C., and Deaves, D., "Fire spread and flame length in ventilated tunnels—a model used in Channel tunnel assessments", Proceedings of the International Conference on Tunnel Fires and Escape from Tunnels, 397–406, Lyon, France, 5–7 May, 1999.
24. Carvel, R. "Mechanisms of fire spread between vehicle fires in tunnels" Proc. Int. Conf. on Fire Safety in Terrestrial Passenger Transportation, Santander, Spain, 20th October 2005, ISBN 84-8102-978-5, pp. 27–37.
25. Ingason, H., "Fire Development in Large Tunnel Fires", 8th International Symposium on Fire Safety Science, 1497–1508, Beijing, China, 18–23 September, 2005.
26. Lönnermark, A., and Ingason, H., "Fire Spread and Flame Length in Large-Scale Tunnel Fires", *Fire Technology,* **42,** 4, 283–302, 2006.
27. Ingason, H., and Li, Y. Z., "Model scale tunnel fire tests with longitudinal ventilation", *Fire Safety Journal,* **45,** 371–384, 2010.
28. Ingason, H., and Li, Y. Z., "Model Scale Tunnel Fire Tests with Point Extraction Ventilation", *Journal of Fire Protection Engineering,* **21,** 1, 5–36, 2010.
29. Carvel, R. O., Beard, A. N., and Jowitt, P. W., "Fire Spread Between Vehicles in Tunnels: Effects of Tunnel Size, Longitudinal Ventilation and Vehicle Spacing", *Fire Technology,* **41,** 271–304, 2005.
30. Beard, A. N., "Major Fire Spread in a Tunnel, Assuming Flame Impingement: Effect of Separation and Ventilation Velocity", Fifth International Conference on Tunnel Fires, 317–326, London, UK, 25–27 October, 2004.
31. Beard, A. N., "Major Fire Spread in a Tunnel: A Non-linear Model with Flame Impingement", Proceedings of the 5th International Conference on Safety in Road and Rail Tunnels, 511–521, Marseille, France, 6–10 October, 2003.

32. Carvel, R. O., Beard, A. N., and Jowitt, P. W., "CERBERUS: A New Model to Estimate Size and Spread for Fires in Tunnels with Longitudinal Ventilation", Proc. Int. Conf. on Tunnel Safety & Ventilation, New Developments in Tunnel Safety, 69–76, Graz, Austria, 8–10 April, 2002.
33. Kanury, A. M., "Flaming Ignition of Solid Fuels". In *SFPE Handbook of Fire Protection Engineering* (P. J. DiNenno, Ed.), National Fire Protection Association, Quincy, Massachusetts, USA, 2002.
34. Newman, J. S., and Tewarson, A., "Flame Propagation in Ducts", *Combustion and Flame,* **51,** 347–355, 1983.
35. Ingason, H., and Y.Z., Li., "Model scale tunnel fire tests with point extraction ventilation", *Journal of Fire Protection Engineering,* **21,** 1, 5–36, 2011.
36. de Ris, J., "Duct Fires", *Combustion and Science Technology,* **2,** 239–258, 1970.
37. Comitis, S. C., Glasser, D., and Young B. D., "An experimental and Modeling Study of Fires in Ventilated Ducts, Part II: PMMA and Stratification", *Combustion and Flame* **104,** 138–156, 1996.
38. M.A. Delichatsios, "Fire protection of fibreglass-reinforced plastic stacks in ducts", Factory Mutual Systems, Report RC75-T-51, File, Serial No. 22493, 1975.
39. "Design Fires in Road Tunnels" National Cooperative Highway Research Program (NCHRP) Synthesis 415, Transportation Research Board, Washington D.C., 199 pp., 2011. ISBN 978-0-309-14330-1.
40. Forthcoming PIARC design fires guidance. See Tarada, F. "Fires in Tunnels – Can the risks be designed out?" Eurotransport, Volume 9, Issue 4, 2011, pp. 46–49.
41. Cheong, M.K., Spearpoint, M.J. and Fleischmann, C.M. "Design fires for vehicles in road tunnels" Proc. 7th Int. Conf. on Performance-Based Codes and Fire Safety Design Methods, Auckland, New Zealand, pp. 229–240, 2008.
42. Drysdale, D. "An Introduction to Fire Dynamics" 3rd Edition, Wiley, 2011. ISBN 978-0-470-31903-1.
43. Li, Y.Z. & Ingason, H. "The maximum ceiling gas temperature in a large tunnel fire" Fire Safety Journal, Volume 48, 2012, pp. 38–48.
44. McPherson, M.J. (1993) Subsurface Ventilation and Environmental Engineering. Springer, 1993. ISBN 978-0412353000.
45. S.E. French, "Fire safety in the Channel Tunnel, an Overview", Proc. Int. Conf. on Fires In Tunnels, Borås, Sweden, 1994, pp. 253–275.
46. Oka, Y., and Atkinson, G. T., (1995) "Control of Smoke Flow in Tunnel Fires", Fire Safety Journal, 25, 305–322.
47. Ingason, H. (2008) "State of the art of tunnel fire research" Proc. 9th Int Symp on Fire Safety Science, Karlsruhe, Germany, 2008, pp 33–48.
48. Lee C.K., Chaiken R.F., Singer J.M. (1979) Interaction between duct fires and ventilation flow: an experimental study. Combustion Science & Technology 1979; 20 (1–2):59–72.
49. Vaitkevicius, A., Colella, F. & Carvel, R. "Rediscovering the throttling effect" Proc. 6th Int. Symp. On Tunnel Safety and Security (ISTSS), Mar-seilles, France, March 2014 pp. 373–380
50. Colella, F., G. Rein, R. Borchiellini and J.L. Torero (2011) "A Novel Multiscale Methodology for Simulating Tunnel Ventilation Flows During Fires" Fire Technology, Volume 47, Issue 1, pp. 221–253.
51. Grant, G & Jagger, S "The use of tunnel ventilation for fire safety" Chapter 10 in Handbook of Tunnel Fire Safety 2nd Edition, Ed Beard & Carvel, ICE Publishing, 2011, ISBN 978-0-7277-4153-0. pp 177–216. Doi: 10.1680/htfs.41530.177.
52. Carvel, R.O., Beard, A.N. & Jowitt, P.W "The influence of longitudinal ventilation systems on fires in tunnels" Tunnelling & Underground Space Technology, Volume 16 (2001) pp. 3–21.
53. Carvel, R.O., Beard, A.N., Jowitt, P.W. & Drysdale, D.D. (2004) The influence of tunnel geometry and ventilation on the heat release rate of a fire. Fire Technology, Volume 40, pp. 5–26.
54. Carvel, R.O. (2010) Fire Dynamics during the Channel Tunnel Fires, Proc 4th Int Symp on Tunnel Safety & Security (ed. A Lonnermark & H. Ingason), Frankfurt am Main, Germany, March 17-19, 2010, ISBN 978-91-86319-44-1, pp. 463–470.
55. NFPA 502: Standard for Road Tunnels, Bridges and other Limited Access Highways. 2014.
56. Carvel, R. & Both, K. "Passive fire protection in concrete tunnels" Chapter 7 in Handbook of Tunnel Fire Safety 2nd Edition, Ed Beard & Carvel, ICE Publishing, 2011, ISBN 978-0-7277-4153-0. pp 109–125. Doi: 10.1680/htfs.41530.109.
57. C. Bailey & G. Khoury "Performance of Concrete Structures in Fire" MPA – The Concrete Centre, February 2011, ISBN 978-1-904818-83-0.
58. "Concrete and Fire" (in Swedish) Swedish Tariff Association, Stockholm, Sweden, 1959.
59. Connolly, R.J. "The spalling of concrete in fires" PhD Thesis, Ashton University, UK, 1995.
60. Jansson, R. "Fire Spalling of Concrete" PhD Thesis, KTH Royal Institute of Technology, Stockholm, Sweden, 2013.
61. Jönsson, J. & P. Johnson (2010) "Suppression systems – trade-offs and benefits" Proc 4th Int Symp on Tunnel Safety & Security (ed. A Lonnermark& H. Ingason), Frankfurt am Main, Germany, March 17–19, 2010, pp. 271–282.
62. Melvin, B. & W. Connell "Cost benefits in tunnel ventilation and other systems resulting from installation of fixed fire fighting systems in road tunnels" Proc. 14th Int. Symp. on Aerodynamics and

Ventilation of Tunnels, Ed. Kate Hunt, Dundee, Scotland, 11–13 May 2011. ISBN 978 1 85598 123 2. pp. 333–345.
63. R. Carvel "Mitigation of tunnel fires" Proc. 5th Int. Symp. on Tunnel Safety and Security, New York, USA, 14–16 March 2012, edited by Lönnermark& Ingason, Published by SP, Sweden, Report 2012:10. pp 27–39.
64. PIARC (1999) Technical Report on "Fire and Smoke Control in Road Tunnels" 1999. Report 05.05.B. ISBN: 2-84060-064-1.
65. Stroeks, R. (2001) Sprinklers in Japanese Road Tunnels, Report produced by Chiyoda Engineering Consultants Co. Ltd, prepared for BouwdienstRijkswaterstaat, The Netherlands, December 2001.
66. MacDonald, C. & Messenger, S. (2003) Life Safety Facilities in Road Tunnels: An Australian Perspective, Proc 5th Int. Conf. on Safety in Road and Rail Tunnels, Marseille, France, 6–10 October 2003, pp. 573–582.
67. Dix, A. (2010) Tunnel fire safety in Australasia, 4th Int Symp on Tunnel Safety and Security, Frankfurt, Germany, March 2010. pp. 69–79
68. Both, K. "The UPTUN project: a brief summary" Chapter 31 in Handbook of Tunnel Fire Safety 2nd Edition, Ed Beard & Carvel, ICE Publishing, 2011, ISBN 978-0-7277-4153-0. pp 651–662. Doi: 10.1680/htfs.41530.651
69. www.solit.info
70. Carvel, R. & Wu, Y. "Water-based fire-suppression systems for tunnels" Chapter 8 in Handbook of Tunnel Fire Safety 2nd Edition, Ed Beard & Carvel, ICE Publishing, 2011, ISBN 978-0-7277-4153-0. pp 127–151. Doi: 10.1680/htfs.41530.127
71. Carvel, R.O. (2011) Water Mist Systems in Tunnels: Some Unanswered Questions, Proc Tunnel Safety Forum 2011, Nice, France, 4–6 April, pp. 11–20.
72. Guigas, X., Weatherill, A., Bouteloup, C. & Wetzig, V. (2005) Water Mist Tests for the A86 East Tunnel, International Congress on Safety Innovation Criteria Inside Tunnels, Gijón, Spain, June 29th – July 1, 2005, pp. 163–173
73. Tuomisaari, M. (2008) Full scale fire testing for road tunnel applications – evaluation of acceptable fire protection performance, Proc. 3rd Int. Symp on Tunnel Safety & Security, Stockholm, Sweden, March 12–14, 2008. pp. 181–193
74. Kratzmeir, S. & M. Lakkonen. Road Tunnel Protection by Water Mist Systems – Implementation of full scale fire test results into a real project. Proc. 3rd Int. Symp on Tunnel Safety & Security, Stockholm, Sweden, March 12–14, 2008. pp. 195–203
75. SOLIT^2 Workshop, 22–23 June 2011, Gijon, Spain. Presentation materials distributed to delegates, but not published otherwise.
76. SOLIT^2 "Engineering Guidance for a Comprehensive Evaluation of Tunnels With Fixed Fire Fighting Systems" Scientific Final Report of the SOLIT^2 Project. 2012

Dr Ricky Carvel is Lecturer in Combustion & Fire Dynamics in the BRE Centre for Fire Safety Engineering at the University of Edinburgh, Scotland. Originally from Edinburgh he studied Chemistry and Physics as an undergraduate at The University of St Andrews, and stayed there to do a Masters degree in Chemistry. Since then he has worked for the University of Wales, Aberystwyth, Heriot-Watt University, International Fire Investigators and Consultants and the University of Edinburgh. In 2004 he was awarded a PhD from Heriot-Watt University (Edinburgh, Scotland) for his thesis "Fire Size in Tunnels".

Dr Haukur Ingason is a senior research scientist at SP Fire Research since 1988 and adjunct professor since 2007. At the present he is adjunct professor at the Department of Fire Safety Engineering at Lund University where he is supervising and giving classes for students on fire dynamics in tunnels, foam systems and rack storage fires. He has nearly twenty five years of international experience in fire safety research and engineering and published nearly 50 peer review journal papers.

Fire Risk Analysis for Nuclear Power Plants

89

Nathan O. Siu, Nicholas Melly, Steven P. Nowlen, and Mardy Kazarians

Introduction

Fire risk analysis for nuclear power plants, as currently performed in the U.S. and abroad, is focused on assessing the likelihood of a particular industrial accident: the loss of cooling to the reactor core and subsequent core damage.[1] This is one main area nuclear power plant fire protection differs from many industrial facilities. The main focus on nuclear fire protection is to mitigate reactor core damage events which can be caused by fires within the plant. Nuclear power plants have numerous safety systems intended to prevent or mitigate such accidents, thus the fire risk analysis concentrates on assessing the potential effects of fires on these systems' equipment (components and cables). The effects of fire on building occupants (the plant operators in this case) or the building itself, are factors in the analysis, but are addressed only to the extent that these effects can contribute to the accident.

The nuclear power industry uses a general risk analysis method, known as Probabilistic Risk Assessment (PRA), to estimate the risk associated with all recognized threats to the plant. These threats include equipment failures, human errors, extreme weather conditions, seismic events, and fires within the plant. This chapter addresses fire PRA, i.e., PRA conducted specifically for internal fires.

As discussed by Kaplan and Garrick [1] and in Chap. 72 risk analysis is the process of:

1. Identifying potentially important accident scenarios ("what can go wrong"),
2. Determining their consequences ("what can happen when something goes wrong"), and

[1] From a public health and risk standpoint, the integrity of the nuclear fuel is the main safety concern at nuclear power plants. Absent sufficient cooling, the heat generated from radionuclide decay can lead to fuel melting and the potential release of radioactivity into the environment. Past studies have shown that accidents involving the loss of cooling to the reactor core (see Figs. 89.1 and 89.2) are the dominant contributors to risk, and these accidents continue to be the focus of current risk studies. Recent analytical studies, as well as the March 11, 2011 accident at the Fukushima nuclear power plant in Japan, have indicated that accidents involving used ("spent") nuclear fuel outside of the core may be more risk significant than previously thought. Studies to re-assess the potential importance of these accidents are ongoing.

This paper was prepared, in part, by employees of the United States Nuclear Regulatory Commission. It presents information that does not represent an official staff position. The NRC has neither approved nor disapproved its technical content. The views and conclusions in this chapter are those of the authors and should not be interpreted as necessarily representing the views or official policies, either expressly or implied, of the U.S. Nuclear Regulatory Commission.

N.O. Siu (✉) • N. Melly
U.S. Nuclear Regulatory Commission Office of Nuclear Regulatory Research, Washington, DC 20555-0001, USA

S.P. Nowlen (retired)

M. Kazarians
Kazarians and Associates, 221 East Glenoaks Boulevard, Suite 101 Glendale, CA 91207-2123, USA

M.J. Hurley (ed.), *SFPE Handbook of Fire Protection Engineering*,
DOI 10.1007/978-1-4939-2565-0_89, © Society of Fire Protection Engineers 2016

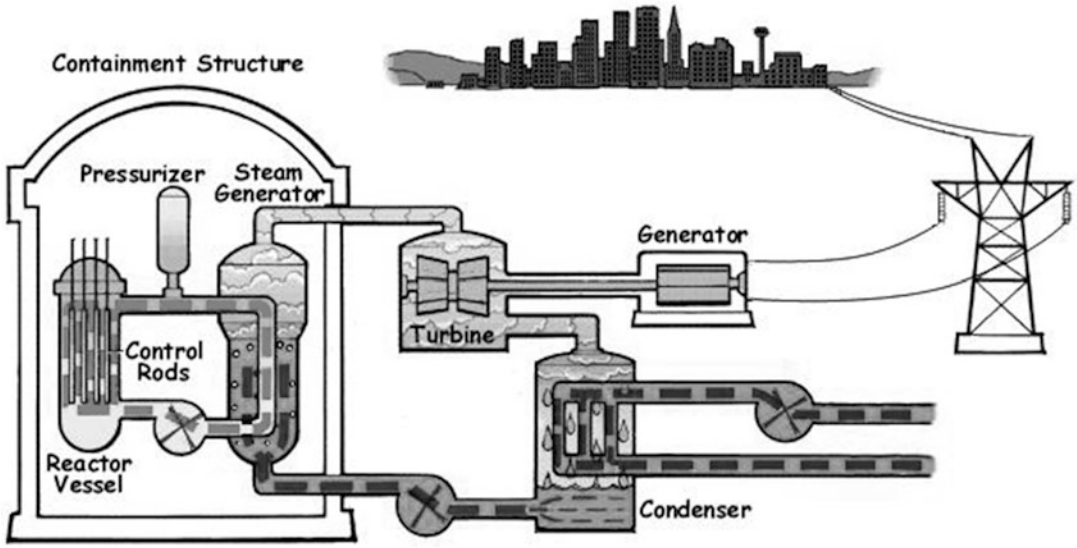

Fig. 89.1 Pressurized Water Reactor (PWR) nuclear power plant schematic overview

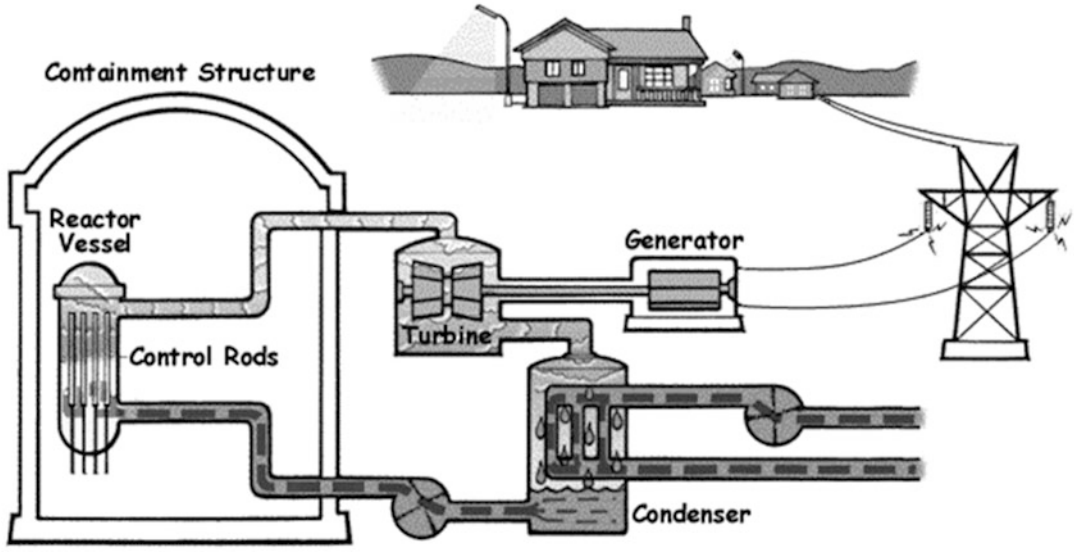

Fig. 89.2 Boiling Water Reactor (BWR) nuclear power plant schematic overview

3. Assessing their likelihood ("how likely is it that something will go wrong")

PRA is a form of risk analysis in which both the consequences and likelihood are expressed in quantitative terms. In particular, the likelihood is expressed in terms of mathematically defined probabilities.

PRA has been used in all U.S. plants and most international plants to evaluate the risk associated with electric power generation from nuclear power plants since the landmark "Reactor Safety Study" (*WASH-1400*) published in 1975 [2]. PRA, sometimes called "probabilistic safety assessment" (PSA) in international reports,

provides a systematic, multidisciplinary approach for using a wide range of information sources including model predictions, experimental results, and plant operational experience, including reported event data, to assess plant behavior under a variety of conditions, sensitivities, and areas of uncertainty and importance.

Numerous fire PRA studies have shown that fire can be a significant or even dominant contributor to the overall risk for a given nuclear power plant. Past estimates for fire-induced Core Damage Frequency (CDF) range from 4E-8 to 2E-4 per reactor year, with the majority of estimates lying between 1E-6 and 1E-4 per reactor year. Fire events are not formally designated as design basis accidents for the nuclear industry, yet their contribution to risk can equal or exceed contributions from other causes (including equipment failures). Lessons learned from a number of serious events, including Browns Ferry (United States, 1975), [3] Armenia (Armenia, 1982), [4] Vandellos (Spain, 1989), [5] and Narora (India, 1993), [6] further emphasize fire's potential importance. NUREG/CR-6738, "Risk Methods Insights Gained from Fire Incidents," provides a useful, PRA-oriented review of these and other notable nuclear power plant fires [7].[2]

Whether fire is an important risk contributor at a particular plant is determined by, not only the reactor design, but also such plant-specific differences as locations for redundant, diverse safety equipment, routing of key electrical cables (e.g., the separation and orientation of the respective cable trays and conduit), fire protection schemes for particular rooms, and the procedures employed by plant operators in response to a fire. Fire PRA evaluates these details and shows how they relate to risk. It provides a systematic framework for examining the complex phenomenology underlying a fire using a wide variety of information sources (e.g., experimental results, model predictions and reported event data), and furnishes a useful context for discussions of areas with significant controversies and uncertainties.

Fire PRA (and PRA in general) is performed to support decision making. The decision problems can be faced by the plant owner (e.g., how to rationally allocate safety resources) or by the regulator (e.g., whether to accept a proposed plant change). The increasing, more direct use of fire PRA in regulatory applications, which is consistent with the NRC's PRA Policy Statement, [8][3] implies a need for a high level of fidelity. It is important that the fire PRA be sufficiently realistic to appropriately address the decision problem at hand. Both excessive optimism and excessive conservatism need to be avoided, as biased analyses could lead to suboptimal or even inappropriate decisions. The problems associated with an overly optimistic analysis are clear. On the other hand, conservatism has traditionally been viewed as, in effect, the price paid for imperfect knowledge. Common engineering practice is to apply realistic assumptions wherever possible, but when in doubt, conservative assumptions generally prevail. However, excessive or uneven levels of conservatism might lead to inappropriate conclusions. For example, an excess of conservatism in the analysis of one particular set of fire sources may cause the fire risk for those sources to be sharply over-estimated. This might, in turn, mask the importance of another risk contributor where more realism and less conservatism have been applied.

Numerous papers and reports have been written on fire PRA. The objective of this chapter is to provide a general review of the subject as it applies to nuclear power plants. The chapter presents some key characteristics of fire PRA, discusses the fire PRA methodology employed by most current domestic studies, summarizes results of a number of analyses, and then briefly outlines current activities and anticipated future developments. Detailed guidance needed to perform a fire PRA can be found in cited references,

[2] The U.S. Nuclear Regulatory Commission (NRC) designates its staff-prepared reports using the nomenclature "NUREG." NUREG/CR contractor reports are reports prepared by NRC contractors.

[3] Among other things, this statement indicates that the NRC intends to increase its use of PRA technology "in all regulatory matters to the extent supported by the state-of-the-art in PRA methods and data. . .".

notably NUREG/CR-6850/EPRI TR-1011989, [9][4] a fire PRA methodology report jointly developed by the Electric Power Research Institute (EPRI) and the U.S. Nuclear Regulatory Commission (NRC) Office of Nuclear Regulatory Research (RES). Recognizing that fire PRA is a multidisciplinary enterprise, this chapter touches on all elements of the fire PRA but the emphasis is placed on topics of direct interest to fire protection engineers. Details on those aspects of fire PRA requiring input from other disciplines, including electrical engineering, human factors, and nuclear power plant systems analysis can be found in NUREG/CR-6850 and other guidance documents cited in this chapter.

Nuclear Power Plant PRA and Fire PRA

Before discussing some of the details of fire PRA, it is useful to note some of its key characteristics and history.

First, in most applications of interest, the risks of eventual concern involve the health of the general public. Thus, the focus of the analysis is on accidents that can have significant health effects offsite. Fire PRA methods can be applied to plant worker safety and economic issues, but have not been to date.

Second, rather than directly estimating the likelihood of offsite health effects, fire PRA studies typically are aimed at assessing a surrogate measure of risk, the plant "core damage frequency" (CDF). This measure characterizes the likelihood that the plant will suffer an accident that damages nuclear fuel contained in the reactor core.[5] As discussed previously, the attention on core damage is due to the results of past studies (e.g., WASH-1400) that have shown that core damage accidents are the dominant contributors to overall plant risk. It is important to recognize that nuclear power plant fires, by themselves, will not lead to core damage; that is, plant fires do not directly threaten core integrity. In order to cause core damage, a fire-initiated scenario must involve a plant upset condition (i.e., an accident scenario "initiating event") and the compromise of plant safety systems. Damage to plant systems may occur either directly (e.g., fire-induced damage to a pump) or indirectly (e.g., fire-induced damage to supporting equipment such as electrical cables or power distribution busses).

Third, fire PRAs usually focus on accident scenarios involving fire-induced failure of critical electrical cables and cabinets. The notion of "critical" arises from the degree of redundancy and defense-in-depth built into nuclear power plant designs. In practice, a risk significant fire must actually damage most or all of the safety systems provided to handle the initiating event. Multiple, independent safety system failures due to random causes (i.e., non-fire causes), while possible, tend to be far less likely and therefore less important to overall risk. Risk significant fires typically involve multiple system failures caused by fire-induced damage to collocated electrical cables (including instrument and control cables) that support these systems. In fact, one of the most predominant fire safety strategies in nuclear power plant applications is ensuring physical separation (or passive fire protection) for important electrical cables.

Fourth, fire PRA is normally performed following, or in concert with, the performance of a PRA addressing accident scenarios initiated by hardware failures or operator errors. Such a PRA, which is called an "internal events" PRA for historical reasons, includes detailed event tree and fault tree models that identify potential responses of the nuclear power plant and operators to postulated initiating events (Figs. 89.3 and 89.4 provide abbreviated examples.) In the fire PRA, these internal event models are modified to address those events and conditions introduced by potential fires. It is important to recognize that the set of modified models, called the "plant response model" later in this chapter, needs to include the effects of both fire- and non-fire caused equipment failures and human errors.

Fifth, those fire PRA studies that quantitatively treat uncertainties do so within the methodological framework employed by the overall plant PRAs. Consistent with Chap. 76 and as

[4] NUREG/CR-6850/EPRI TR-1011989 will be referred to as NUREG-6850 for simplicity.

[5] Technically, the CDF is the expected (in a statistical sense) number of core damage events per unit time.

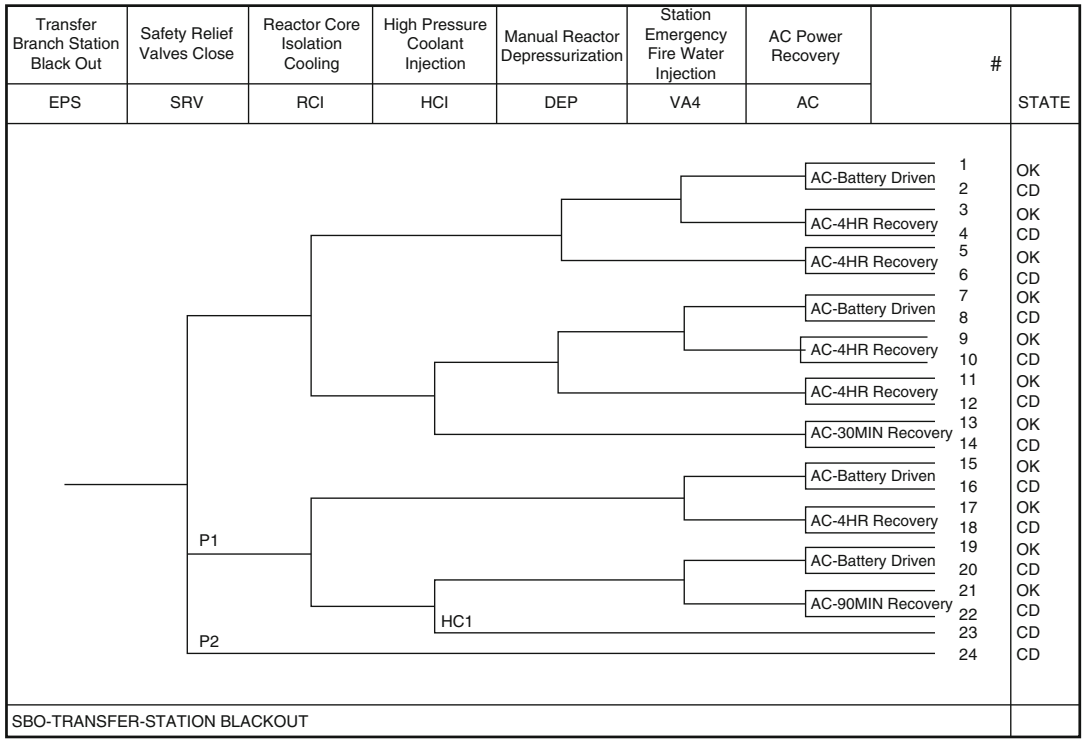

Fig. 89.3 Example event tree for internal events analysis

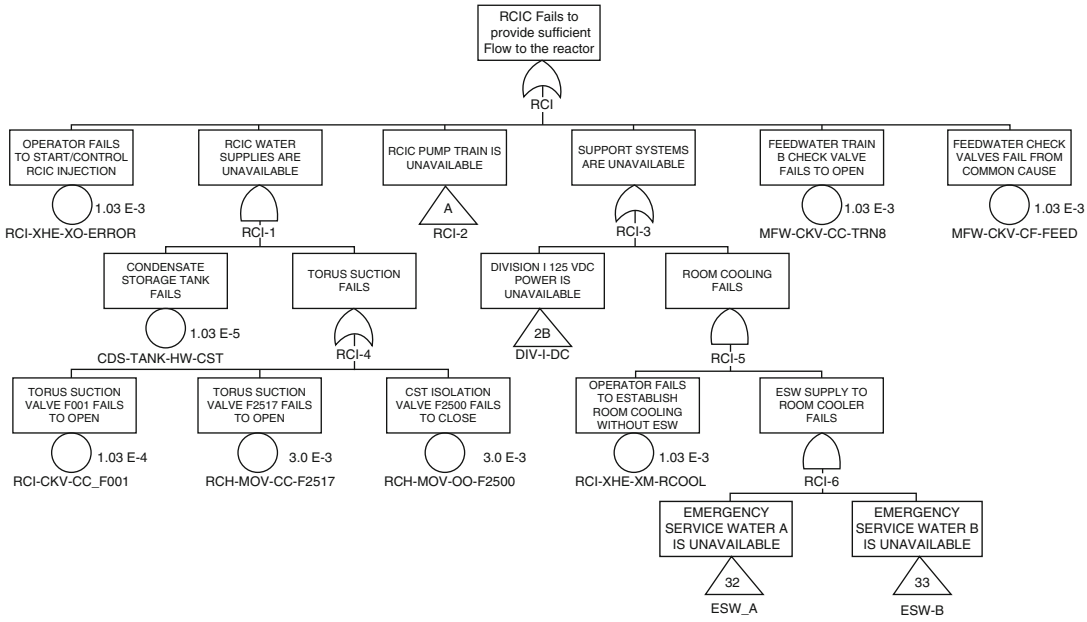

Fig. 89.4 Example portion of a fault tree for internal events analysis (model used depicts a Boiling Water Reactor BWR)

discussed later in this chapter, this framework distinguishes between aleatory (also called random or stochastic) uncertainties and epistemic (also called state of knowledge) uncertainties [10]. The distinction between aleatory and epistemic uncertainties is useful for decision making because it helps identify appropriate risk management options. For example, aleatory uncertainty in the occurrence of core damage events can be reduced by making design changes to reduce CDF, whereas epistemic uncertainty can be reduced through research on key phenomenology (e.g., electrical circuit behavior when cable bundles are exposed to fires). NUREG-1855 [11] describes the treatment of uncertainty in a decision support context.

Sixth, because fire PRAs often need to consider the risk contributions of an enormous number of scenarios, these analyses are almost always performed in an iterative fashion. Starting with a fairly coarse analysis using conservative modeling assumptions, the analysis team develops an understanding as to what scenarios are likely to be important contributors to overall risk. Focusing attention on important scenarios, the team progressively adds detail and more realistic modeling approaches until the analysis is sufficiently accurate to support the decision problem being addressed by the fire PRA. This approach does not guarantee an accurate assessment of absolute CDF (or risk). A conservative assessment that is adequate for one decision problem (e.g., whether additional regulatory action is needed to address fire vulnerabilities in the nuclear fleet) may be overly conservative with respect to a different decision problem (e.g., selecting between different plant-specific risk management solutions).

We note that certain situations that have received little or no coverage from general PRA studies also receive little or no coverage in the fire PRA. These situations include the scenarios associated with acts of sabotage and scenarios when the plant is not operating at steady-state, full power conditions. Sabotage is usually excluded from the scope of general PRA studies. Regarding scenarios during low power or plant shutdown operating conditions, fire PRAs have been performed [12, 13], but such assessments are not yet routine. Draft NUREG/CR-7114 [14] provides a framework for performing fire PRA for these conditions.

History of Fire PRA

The earliest fire risk assessment for a nuclear power plant was performed in 1975 as a supplement to WASH-1400 (the Reactor Safety Study) [2]. The assessment was aimed at providing a quick estimate of the risk implications of the Browns Ferry cable fire in 1975. The analysis indicated that the CDF associated with that fire was around 10^{-5} per year, or about 20 % of the total plant CDF associated with the accidents addressed in the main body of the study. It also noted the usefulness of developing a more detailed fire PRA methodology (including improved models and data). Another early fire PRA was performed in 1979 as part of a PRA for a proposed high-temperature gas-cooled reactor design. The analysis focused on the risk contribution of cable spreading room fires, and it concluded that the core heat-up frequency due to such fires was also around 10^{-5} per year, or about 25 % of the total core heat-up frequency due to all causes.

The first comprehensive, detailed fire PRAs for commercial nuclear power plants were performed in 1981 and 1982 as part of the commercially-sponsored Zion [15] and Indian Point [16] PRA studies, respectively. A key question addressed by both PRA efforts was if additional accident mitigation systems (e.g., filtered, vented containments) were needed for the two plants. The study results indicated that the fire risk for Zion Units 1 and 2 was relatively small (the mean CDF was about 5×10^{-6} per year for each unit, about 10 % of the total mean CDF) and that the fire risk at the Indian Point plants was relatively large (the mean fire-induced CDF for Unit 2 was about 2×10^{-4} per year, about 40 % of the total mean CDF). Because the Zion and Indian Point fire PRA studies were performed by the same analysis team using the same analysis methodology and tools, these studies demonstrated how plant-specific features could greatly affect fire risk. More important, the studies also identified

plant design changes for reducing risk (e.g., fire barriers, a self-contained charging pump, provisions for an alternate power source in the event of damaging fires) that were assessed to be more cost-effective than the proposed accident mitigation systems prompting the studies.

In the years following the Zion and Indian Point studies, a number of additional fire PRA studies were performed. The results of these analyses confirmed that fire could be a significant and even dominant contributor to the overall risk for a given plant. Many of these studies resulted in estimates of mean fire-induced CDFs of 10^{-4} per year or greater, predicted contributions to total CDF of 20 % or greater, or both. In the late 1980s through very early 1990s, the NRC sponsored a Risk Methods Integration and Evaluation Program (RMIEP) [17] addressing the LaSalle Unit 2 nuclear power plant and the NUREG-1150 [18, 19] PRA studies, each of which included assessments of fire risk. The RMIEP study involved an analysis of the LaSalle nuclear power plant and the goal of the study was to extend and demonstrate state of the art analysis methods for PRA in general. The NUREG-1150 studies focused on the application of existing methods, rather than the development of new methods, to a set of five reactors representing a range of U.S. designs. From the standpoint of fire PRA, both studies used similar frameworks and (for the most part) methods. Insights from both of these programs paralleled other PRA studies of the era and again found that fires were potentially significant contributors to overall plant risk. Both studies also confirmed that plant-specific details can substantially impact both the magnitude and source of fire risk.

In 1991, recognizing the value of systematic assessments of fire (and other so-called "external events"), the NRC requested that licensees perform Individual Plant Examination of External Events (IPEEE) studies for their plants [20]. The primary goal of the fire risk portion of the IPEEE program was for plant licensees to identify plant-specific vulnerabilities to fire-induced severe accidents that could be fixed with low-cost improvements. Four supporting objectives with respect to external events were for licensees to (1) develop an appreciation of severe accident behavior, (2) understand the most likely severe accident sequences that could occur under full-power conditions, (3) gain a qualitative understanding of the overall likelihood of core damage and fission product releases, and (4) reduce, if necessary, the overall likelihood of core damage and radioactive material releases by appropriately modifying hardware and procedures to prevent or mitigate severe accidents. Guidance on the performance of an IPEEE analysis was provided by Chen et al. [21].

The results of the NRC's review of the IPEEE submittals are presented in NUREG-1742 [22]. The review showed that fire was a significant contributor to overall risk at a number of plants. In addition, it also showed that over half of the IPEEE submittals identified cost-effective improvements. Finally, as discussed earlier in the section on fire modeling, the review process also identified a number of technical issues associated with then-current guidance.

In the early 2000s, as the IPEEE review process was coming to a close, EPRI and the NRC's Office of Nuclear Regulatory Research initiated a joint effort to update available fire PRA methods and guidance. This effort was intended to consolidate lessons learned from the IPEEEs and from ongoing fire PRA research and development activities, and was aimed at supporting anticipated regulatory applications of fire PRA (discussed in the following section). This joint effort resulted in the guidance document NUREG/CR-6850, cited extensively in this chapter.

Currently, a number of U.S. plants are using NUREG/CR-6850 and more recent guidance [23] to update their fire PRAs. These efforts have resulted in a number of lessons learned, including the following.

- As in previous fire PRAs, the fire risk profile is often dominated by the contribution from a relatively small number (on the order of ten) scenarios. These scenarios often involve situations identified in past studies (e.g., electrical cabinets, control rooms, locations with large concentrations of cables) with major consideration given to targets vulnerable to fire-induced spurious operations. These targets can have a pronounced impact on the fire scenarios selected.

- Overall, current estimates of fire CDF (with mean values on the order of 10^{-5} to 10^{-4} per year) are consistent with the results of past studies. Note that some of these estimates reflect the assumption that planned modifications are in place and operational [24].
- NUREG/CR-6850 provides guidance on performing screening-level (intentionally conservative) analysis as well as guidance for detailed (realistic) analysis. Fire PRAs that do not employ the latter guidance can produce unrealistically conservative fire CDF estimates.
- Although the fire CDF tends to be dominated by the contribution from a few scenarios, the total fire CDF is also a function of the contributions from other scenarios. A realistic fire PRA can require the quantitative analysis of large number (on the order of a few thousand) scenarios. Such a study requires considerable resources to trace cables as well as perform analyses [24].
- Fire PRA is a useful tool for identifying plant modifications that will improve plant safety with respect to non-fire as well as fire-initiated accidents.

The recent updating efforts have also identified areas where additional improvements are needed to increase the realism of results and to reduce the effort needed to perform a realistic fire PRA. These areas are the subject of current fire PRA research and development activities. The results of these activities are aimed at supporting the continued use of fire PRA in ensuring and, as needed, improving the fire safety of U.S. nuclear power plants.

Although this chapter is centered on U.S. plants and practices, we note that fire PRA is also widespread internationally. In particular, the Organization for Economic Cooperation and Development's (OECD) Nuclear Energy Agency (NEA) has published the results of a member country survey on their PRA activities. This report and its more recent update indicate that fire PRAs have been performed for a large number of nuclear power plants abroad [13, 26]. The OECD/NEA has also published a state-of-the-art report [25] and supports a number of activities aimed facilitating the exchange of fire-PRA relevant information among member countries. Guidance on the performance of fire PRA is also available from the International Atomic Energy Agency [27]. In general, current international guidance and practices are generally consistent with those in the U.S., and the results of international studies are also qualitatively consistent regarding the relative importance of fire (as compared with other hazards) and the plant areas that are important contributors to risk.

Fire PRA Guidance and Standards

Fire protection for the U.S. commercial nuclear power industry is governed by several NRC-issued documents. The primary regulations are published in Title 10, Section 50.48 of the Code of Federal Regulations (10CFR50.48) [28]. These primary regulations are supported by a number of subsidiary regulatory guidance documents. Of particular interest to fire PRA are Regulatory Guides (RG) 1.205, "Risk-Informed, Performance-Based Fire Protection for Existing Light-Water Nuclear Power Plants" [29] and 1.200, "An Approach For Determining The Technical Adequacy Of Probabilistic Risk Assessment Results For Risk-Informed Activities" [30]. These documents, respectively, provide one acceptable method to develop and maintain risk-informed, performance-based fire protection programs; and on quality expectations for the use of general PRA (including fire PRA) in regulatory decision making. Also of interest are RGs 1.174, "An Approach for Using Probabilistic Risk Assessment in Risk-Informed Decisions on Plant-Specific Changes to the Licensing Basis," [31] and 1.189, "Fire Protection for Nuclear Power Plants" [32]. The former provides a framework for the application of PRA information in the regulatory context, and the latter addresses specific fire protection issues. Links to current fire protection regulation, guidance, and other regulatory documents

can be found on the NRC's fire protection website.[6]

The current guidance for performing a fire PRA is provided in NUREG/CR-6850 and a series of companion documents covering various methods refinements, clarifications, and expansions developed since that publication was released [23].[7] NUREG/CR-6850 is built on lessons learned from the performance and review of past fire PRAs, including the NRC sponsored NUREG-1150 studies [18] and the industry methods and corresponding studies performed as part of the NRC's Individual Plant Examinations of External Events (IPEEE) program [21, 22, 33, 34]. The document also reflects the results of research and development activities (e.g., regarding the treatment of fire-induced failure of cables and circuits) that led to improvements in the treatment of specific fire PRA issues, as well as lessons learned from the application of a draft form of the document in a number of field tests. Similarly, fire PRA guidance developed after NUREG/CR-6850 have benefitted from industry applications of that report. Fire PRA will continue to evolve, and it is often through applications that refinement needs are identified. Research is also ongoing. As research results are developed, these are factored into the fire PRA methods and guidance as appropriate. Methods development and related research activities are discussed later in this chapter.

A joint American Society of Mechanical Engineers (ASME)/American Nuclear Society (ANS) consensus standard providing requirements for nuclear power plant PRAs quality and scope, including fire PRAs, is also available [35]. This standard delineates the requirements (i.e., the "whats") for a quality fire PRA, but does not prescribe particular methods (i.e., the "hows") for achieving these requirements. The discussion of methods is left to guidance documents, such as those discussed above. A second national consensus standard, National Fire Protection Association (NFPA) 805, "Performance-Based Standard for Fire Protection for Light Water Reactor Electric Generating Plants," provides requirements for developing and maintaining a risk-informed, performance-based fire protection program [36]. The 2001 edition of NFPA 805 has been endorsed by the NRC (10 CFR 50.48(c)) as an optional alternative to the deterministic regulatory requirements in place since 1980.

As noted above, PRAs have historically focused on at-power plant conditions (i.e., with the plant up and running at full power). This is reflected in the cited methodology documents and implementation standards. For example, NFPA 805 focuses on the use of fire PRA as a tool supporting fire protection decision making under at-power plant conditions. This standard does require consideration of low-power and shutdown (LPSD) risk, but current decision making relies mainly on qualitative, defense-in-depth methods. Defense in depth is an approach to designing and operating nuclear facilities that prevents and mitigates accidents that release radiation or hazardous materials. The key is creating multiple independent and redundant layers of defense to compensate for potential human and mechanical failures so that no single layer, no matter how robust, is exclusively relied upon. Defense-in-depth includes the use of access controls, physical barriers, redundant and diverse key safety functions, and emergency response measures. It is envisioned that LPSD applications may evolve to be more quantitative. Standard approaches for performing LPSD PRAs are in the developmental stage. NUREG/CR-7114 [14] presents a PRA method framework for quantitatively analyzing fire risk in commercial nuclear power plants during LPSD conditions.

[6] http://www.nrc.gov/reactors/operating/ops-experience/fire-protection.html

[7] Guidance documents on a number of specific fire PRA issues can be found on the NRC public web site. Agency documents are maintained on its Agencywide Documents Access and Management System (ADAMS) at http://www.nrc.gov/reading-rm/adams.html#web-based-adams. A number of fire PRA methodology enhancements and clarifications have been developed as a part of industry and NRC efforts to implement risk-informed performance-based fire protection based on the NFPA-805 standard. These can be found using the search term "NFPA 805 FAQ".

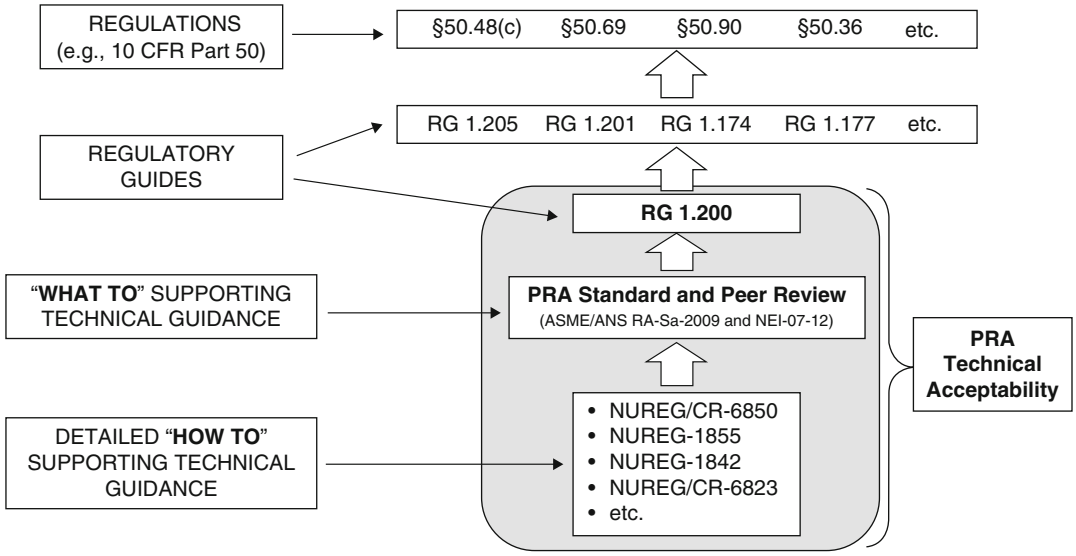

Fig. 89.5 Document hierarchy associated with nuclear power plant fire risk regulatory applications

Figure 89.5 illustrates the relationship between various classes of documents and specific documents that govern the application of risk information to nuclear power plant applications. The top tier represents the actual regulations that govern plant operations as published in the U.S. Code of Federal Regulations (CFR). For example, NRC's endorsement of the NFPA 805 standard is found in 10CFR50.48(c). The second tier represents various regulatory guides (RG) which are documents prepared by the NRC staff that generally describe one acceptable method (non-exclusive) for meeting the regulatory requirements. (Four relevant RGs were cited above.) Also represented in the fourth tier is a Nuclear Energy Institute (NEI) guidance document (NEI 07-12 [37]) which provides specific guidance on implementing the ASME/ANS standard. Finally, the fifth tier represents specific methodology guidance documents that express how to perform various aspects of a risk study and includes NUREG/CR-6850 which is heavily cited in this chapter. Tiers 3-5 are all associated with PRA quality expectations: that is, these tiers together define quality expectations for analyses that are to be used in the regulatory decision making process.

Fire PRA Overview

The fundamental structure of current fire PRAs is little changed from that used in the Zion [15] and Indian Point [16] PRA studies of the early 1980s and described by Apostolakis et al. [38, 39] a structure that is also called out in the 1983 PRA Procedures Guide [40]. In this structure, the CDF arising due to fire-initiated accidents is the sum of the CDF contributions from individual fire-initiated scenarios contributing to this total CDF. The CDF contribution due to a single fire scenario (where, in this discussion, a fire scenario is defined by the location and burning characteristics of the initiating fire), in turn, can be divided into three principal components:

1. Frequency of the fire scenario
2. Conditional probability of fire-induced damage to critical equipment given the fire
3. Conditional probability of core damage given the specified equipment damage

Mathematically,

$$CDF_i = \lambda_i \times p_{ed,\,j|i} \times p_{CD,k|i,j} \qquad (89.1)$$

Where:

λ_i = Frequency of fire scenario i

$p_{ed,j|i}$ = Conditional probability of damage to critical equipment set ("target set")[8] *j* given the occurrence of fire scenario *i*

$p_{CD,k|i,j}$ = Conditional probability of core damage due to plant response scenario *k* given fire scenario i *and* damage to target set *j*

The first term accounts for the likelihood that a fire of specified characteristics will occur in a given location within the plant. The second term addresses the likelihood that the fire will not be suppressed prior to component damage (this term may include a measure for the severity of the fire). Analysis of this term requires treatment of the issues of fire growth, detection, suppression, and component damageability. The third term, often referred to as the Conditional Probability of Core Damage (CCDP), addresses the ability of the plant to achieve safe shutdown given the loss of equipment damaged by the fire. Analysis of this term also requires treatment of the unavailability or random failure of equipment unaffected by the fire and the treatment of potential errors by plant operators.

The total fire CDF is obtained by summing Equation 89.1 over all possible fire scenarios (index i), target sets (index j), and plant responses (index k):

$$CDF = \sum_{i} \lambda_i \left[\sum_{j} p_{ed,\,j|i} \left(\sum_{k} p_{CD,k|i,\,j} \right) \right] \tag{89.2}$$

The three-term breakdown used in these equations provides a useful discussion framework because it aligns with the objectives of fire protection defense-in-depth for nuclear power plants, as discussed in RG 1.189. Three objectives of defense in depth are: first to prevent fires from starting; if that fails, then to detect rapidly, control, and extinguish those fires that do occur; and if that fails to provide protection for structures, systems, and components important to safety so that a fire not promptly extinguished by fire suppression activities will not prevent safe shutdown of the plant. Further, the breakdown aligns with the modeling approaches used in different parts of a fire PRA. In particular, the fire frequencies are generally estimated using simple statistical models for fire occurrences, the likelihood of fire damage is estimated using combinations of deterministic and probabilistic models for the physical processes involved, and the likelihood of core damage is estimated using PRA event tree and fault tree models (modified appropriately to address the needs of fire PRA). The current approach for addressing each of these technical elements is more fully discussed later in this chapter.

Fire PRA Process

Figure 89.6 provides a schematic of the overall process for performing a fire PRA. This figure is based on the technical elements set forth in Section 4 of the ASME/ANS PRA Standard, which closely parallels the process defined in NUREG/CR-6850.[9]

As discussed in greater detail in the remainder of this section, the fire PRA process identifies and characterizes, for each plant area, potentially important fire scenarios, installed fire protection systems and features, physical and geometric characteristics required to support fire modeling, and potentially important equipment, components and cables (i.e., nuclear-safety relevant items potentially susceptible to fire damage). The Plant Familiarization elements shown in Fig. 89.6 establish the boundaries of the analysis and define the key characteristics of the plant in both physical and systems modeling contexts. Qualitative screening is then done to identify locations and

[8] "Targets" in this context are PRA components and cables near the fire location and "target sets" are simply collections of individual targets that may be threatened by a given fire.

[9] As one minor difference, NUREG/CR-6850 defines two stages of physical fire analysis; namely, a preliminary fire source screening task called "scoping fire modeling" and a follow-up task called "detailed fire modeling". In the ASME/ANS standard, these two tasks have been incorporated into one technical element called "fire scenario selection and analysis".

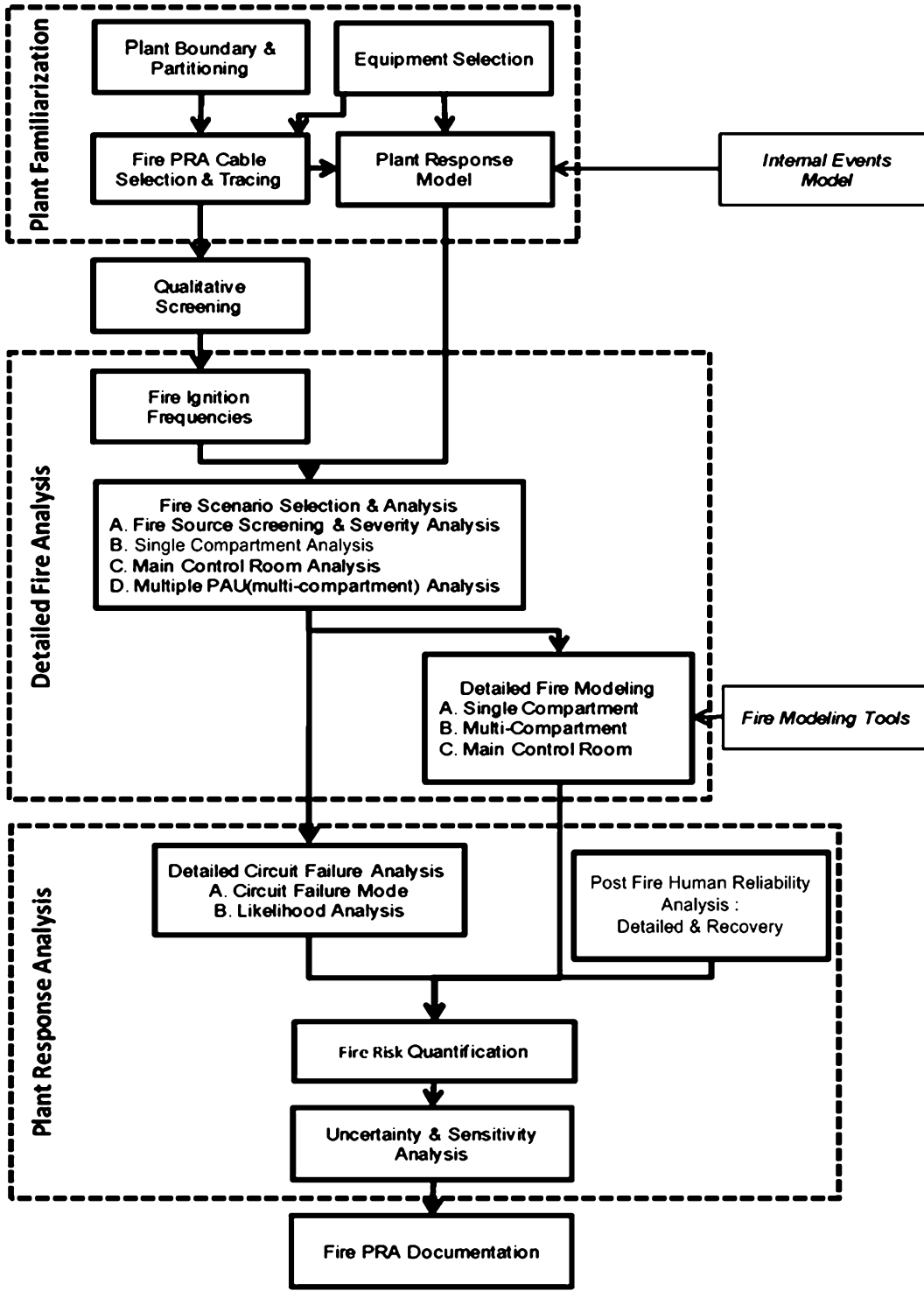

Fig. 89.6 Fire PRA elements

scenarios that need not be quantitatively analyzed because they are not expected to contribute to the fire CDF. This first screening step typically eliminates plant areas that meet the following criteria: (1) the area houses no potentially important equipment, components, or cables and (2) a fire in the area would not be able to initiate a plant upset condition (i.e., an accident scenario "initiating event").

Following qualitative screening, the fire PRA continues with Detailed Fire Analysis and Plant Response Analysis elements. These elements involve a series of progressively more detailed quantitative assessments for unscreened plant areas. Conservative quantitative analyses are usually performed in initial evaluations of CDF to identify additional plant areas and scenarios that can be screened from detailed analysis (based on their contribution to total fire CDF). Progressively more accurate models are then employed for unscreened locations. The objective of this iterative approach is to focus analysis resources on those locations that contribute most to CDF. For example, in many screening analyses, suppression efforts are initially assumed to fail to prevent fire-induced component damage. This conservative assumption is relaxed only for those locations where a detailed analysis is needed.

When documenting the fire PRA, the results of the analysis are typically presented on a location by location basis, and the key or dominant fire scenarios associated with each plant area are typically described in some detail. This detail usually includes some discussion of plant-specific characteristics driving those scenarios, often including relevant design and operational practices, in addition to key fire protection features credited in the analysis. The importance of providing qualitative as well as quantitative results cannot be overstated. Such information ("what can go wrong") is part of the triplet definition of "risk" provided at the beginning of this chapter and is needed when efficiently managing fire risk.

For the purpose of clarity, Fig. 89.6 provides a simplified, once-through picture of the process. In actual practice, the analysis can involve multiple iterations. (In some situations, even early elements might need to be revisited should the results of detailed analysis indicate that additional information is needed.) Note also that that the figure does not emphasize the location-by-location nature of a fire PRA; many of the elements are exercised for each plant area.

Fire PRA Elements

In this section, we discuss each of the technical elements identified in Fig. 89.6.[10] The discussion provides an overview of current analysis approaches, addresses important sources of uncertainty and ongoing development, and identifies references for further reading.

Plant Definition and Partitioning

The purpose of the plant definition and partitioning element is to: (a) prescribe the analysis boundaries separating what's included in the analysis (i.e., that portion of the plant addressed in the fire PRA) from what's not included in the analysis, and (b) define how the analyzed plant is to be separated into smaller, non-overlapping spatial units of analysis (spatial partitions). In the language of the ASME/ANS Standard, the first step is referred to as defining the "global analysis boundary" and the second step is referred to as "plant partitioning." The term used in this chapter to identify fire PRA spatial

[10] The ASME/ANS Standard includes a requirement to address Seismic-Fire Interactions that is not shown in Fig. 89.6. Current methods for analyzing these interactions are mainly qualitative and have no direct impact on the fire PRA process or results. Furthermore, since a seismic event is the actual initiating cause, the consequential fire scenarios should, following typical PRA conventions, be included in the seismic portion of the PRA rather than the fire portion. (Of course, care should be taken to ensure the issue does not fall through any gaps.) With recent events in Japan, including seismically-induced fires at the Kashiwazaki and Onagawa plants in Japan, the NRC and the nuclear power industry are considering developments to address the risk of such events quantitatively.

partitions is "plant areas".[11] Regardless of terminology, the key point is that the fire PRA is typically managed and organized based on where a postulated fire occurs. The intent of the plant partitioning element is to define a set of plant areas, each with specific boundaries (physical or not), that collectively account for all locations within the plant while also ensuring that no location is encompassed within more than one plant area.

Plant areas are ideally bounded by non-combustible barriers, such as fire-rated, or non-fire-rated, barriers. However, plant areas may also be defined on other bases including active features, such as water curtains, and in some cases spatial separation (i.e., extended distances between fire sources or concentrations of in-situ fuels). These distinct plant areas are where heat and products of combustion from a fire will be substantially confined. For example, in typical practice, the main control room will generally be treated as a single distinct plant area whereas areas within the auxiliary building may be segregated into many different plant areas. Note that the potential failure of a credited partitioning feature is addressed in the multi-compartment fire scenario analysis element described later in this section.

The analysis team has considerable flexibility in defining plant areas. For example, it can group several rooms together and treat them as a single plant area, as long as this grouping does not substantially affect the realism of the analysis results. Such grouping can reduce the amount of analysis required for risk-insignificant scenarios. In general, the fire PRA process is designed to minimize the level of effort spent on low-risk scenarios and focus analysis attention on risk-significant scenarios. Since the analysis results are not known beforehand, analyst judgment and some iteration are necessary.

From the above discussion, it can be seen that plant partitioning relies heavily upon fire protection engineering expertise, as this is needed to determine the extent to which provided fire protection features will substantially confine heat and products of combustion from potential fires associated with the fire hazards in a given area. Plant partitioning also requires substantial input from other disciplines, as it requires knowledge of the general location and PRA-model relevance of plant systems and equipment (including cables). For example, returning to the above discussion on grouping plant areas, if detailed information for the routing of key cables is unavailable, then a detailed partitioning of a plant area containing those cables may provide little benefit to the analysis.

It is important to recognize that, as in other parts of the fire PRA, plant definition and partitioning is not just a paper exercise. Confirmatory walkdowns are essential to confirm the existence and integrity of the fire protection features and elements credited in defining each plant area.

Equipment Selection

The equipment selection element defines those pieces of plant equipment and components (other than electrical cables) that will be included in the "plant response model"; that is, the PRA systems model used to perform the plant response analysis. (The development of the plant response model will be discussed later in this chapter.) The selected equipment and components are often referred to as *PRA* or *fire PRA components*.

[11] The terminology surrounding the naming of fire PRA spatial partitions has a somewhat checkered history. Various terms used in fire protection engineering have definitions that were not developed for fire PRA. For example, in fire protection engineering "fire zone" is often defined in the context of coverage areas for a fire detection or suppression system. Similarly, "fire area" has a very specific meaning in the context of the NRC fire protection regulations (see Regulatory Guide 1.189 for related discussions). NUREG/CR-6850 avoids the use of these and other preexisting terms and instead refers the spatial units as "fire compartments," although the fire PRA spatial partitions may or may not be enclosed spaces. The more accurate, albeit fairly technical phrase used in the ASME/ANS Standard is "physical analysis units" or PAUs. Fire PRA spatial units may correspond to a fire zone, a fire area, a compartment, a subset of any of these, or indeed a superset of smaller compartments. For the sake of simplicity, this chapter uses the very generic term "plant area."

This element does not start from a blank sheet of paper; rather, the selection of plant equipment for the fire PRA usually begins with the equipment already included in the internal events PRA plant response model. It is common that most, if not all, of the equipment credited for safe shutdown in the internal events PRA is also credited in the fire PRA. The ultimate goal of the fire PRA equipment selection element is to refine the list of credited equipment. The analyst adds new equipment with unique fire induced failure modes such as spurious operation,[12] not considered in the internal events PRA.

The equipment selection element is performed in close coordination with the development of the fire PRA plant response model. Indeed, it is often the case that choices made in development of the plant response model are what ultimately drive equipment selection decisions. In some cases, these two elements are performed as, in effect, one larger element encompassing the goals of both as described here.

The analysis team performing this element should have collective knowledge of plant systems operation, potential component failure modes, and potential operator responses to different component and instrumentation behaviors. Fire protection engineering inputs include the above-mentioned fire response procedures and the supporting technical basis for those procedures (including the plant's safe shutdown analysis, developed to ensure compliance with fire protection regulations).

The output of the Equipment Selection Element is a list of equipment (with associated characteristics) to be considered when developing the plant response model, and to be used in identifying key electrical cables, as discussed in the next section.

[12] Spurious operations are defined as a circuit-fault mode wherein an operational mode of the circuit is initiated (in full or in part) due to failure(s) in one or more components (including the cables) of the circuit; examples are a pump spuriously starting, or the spurious repositioning of a valve.

Cable Selection and Tracing

The purpose of the cable selection and tracing element is to identify the power, control, and instrumentation cables associated with the components identified in the equipment selection task, plus any other cables whose failure might adversely affect the plant response. Once identified, it is also necessary to determine their physical routing through the plant. This element is usually performed by electrical engineers with extensive plant personnel support.

For reasons previously discussed, risk-significant fire scenarios typically involve damage to electrical cables. The ability of a fire to damage cables decreases rapidly with distance; hence, the more detailed the cable routing information the more realistic the results will be. However, the development of detailed information can be an extremely resource intensive activity depending on the extent and quality of pre-existing information. Clearly, plants that have up-to-date cable routing databases are much better placed to support detailed analyses. Ideally, cables are traced not just to plant areas, but down to the tray/conduit level. This effort has proven to be one of the most costly elements of a fire PRA.

The output of the Cable Selection and Tracing element is not simply a list of cables. This element also establishes, for each cable, a link to the associated plant response model components, to specific component failure modes (e.g., loss of function and/or spurious operation), and to the cable's routing and location. These relationships provide the basis for identifying potential component functional failures at a plant area or raceway level. Inaccurate selection of cables will ripple through the entire PRA and can result in erroneous CDF estimates. It should be noted that many analysts perform this task in conjunction with a detailed circuit analysis (discussed later) in order to avoid unnecessary effort. For example, plant records may "associate" cables with a component whose failure would not, in fact, impact component function (so-called "off-scheme" cables). Identifying such cables early may avoid time consuming cable tracing efforts.

Qualitative Screening

The qualitative screening element is the first pass made at identifying plant areas that are of such low risk importance that quantitative analysis is not needed. It is not intended to develop CDF estimates for particular plant areas at this stage. It is intended, however, to identify those plant areas where, according to pre-determined criteria (already described above), the fire risk is expected to be very low or nonexistent both compared to other plant areas and in absolute terms. This step can be performed by both system engineers and fire protection engineers once the plant partitioning, equipment selection and cable tracing tasks are completed.

As PRA is an iterative process, if the analyst chooses to modify the list of credited equipment or the cable list at a later stage of analysis, the qualitative screening analysis should also be reviewed to ensure that plant areas initially screened out still satisfy the screening criteria. Plant areas qualitatively screened in this element will be reexamined in a later step for fires that may cause potentially risk-significant damage to equipment located in adjacent plant areas (see the later discussion on multi-compartment fire scenarios).

Plant Response Model

The plant response model characterizes how combinations of equipment failures and operator errors can lead to core damage. Equipment failure can occur either from causes internal to the component itself (also known as random failures) or from sources external to the component (e.g., fire, earthquake and flooding). As noted above, the plant response model is typically developed by modifying an existing internal events model. This internal events model is typically expressed using event trees and fault trees, as discussed in the PRA Procedures Guide [40].

As in the case of the internal events model, the fire PRA plant response model supports the analysis of initiating events and ensuing chains of events. Initiating events are conditions that may occur randomly or, in the case of the fire PRA, due to fire-induced component and cable damage. These conditions perturb the balance of plant operation requiring response from automatically or manually activated systems to prevent unsafe conditions. Two examples of initiating events are a loss of offsite power (LOOP) and loss of coolant accident (LOCA). The chains of events ensuing from each initiating event can be represented at different levels of detail. At a high level, as typically represented using event trees (see Fig. 89.3), the events often represent system or functional failures. At a more detailed level, as typically represented using fault trees (see Fig. 89.4), the events can represent failures of specific equipment or operator actions that can contribute to the higher level system or functional failures. These are generally defined in terms of equipment status (failed positions) and erroneous operator actions.

Event trees and fault trees help the analyst to break down potential event progressions into their elemental parts and also to identify a wide range of event sequences. The plant response model specifies many of the important conditions affecting the probability of equipment failures and operator errors, and also provides a mathematical mechanism to estimate CDF based on the equipment failure and operator error probabilities. The event tree and fault tree models can be very complicated, containing thousands of scenarios and a total number of event sequences that easily number in the millions. Dedicated computer programs (e.g., SAPHIRE [41] and CAFTA [42]) have been developed to support the development, execution, review, and documentation of these models.

Since the fire PRA typically starts with an internal events model, the primary concern of the fire PRA analyst is to ensure that the internal events PRA plant response model is appropriately modified to address the special conditions imposed by the fire scenarios analyzed. These conditions include: (1) the failure of plant equipment directly caused by the fire; (2) spurious actuation of equipment due to control circuit failures; (3) new accident sequences that may have been dismissed in the internal events

model as very unlikely to occur given only random failures; (4) new accident sequences due to implementation of plant procedures specific to fire conditions (e.g., alternate shutdown in the event of a main control room fire); (5) instrumentation failures not included in the internal events model; and (6) new or modified plant operator performance related events. (These topics are discussed in some detail later in this chapter.) The information management demands arising during the development and execution of the plant response model can be considerable. Specialized computer programs (e.g., FRANX [43]) have been developed to aid the analysts.

Fire Frequency Analysis

The fire frequency analysis involves two primary goals. The first is to define representative fire scenarios for the area of interest; that is, to define those fire ignition sources that might lead to risk-relevant fire scenarios. The second is to estimate the frequency of fires (typically events per year) involving each identified ignition source. Depending on the particular objectives of the fire PRA and the potential risk significance of the plant area, the scenarios can be defined in a broad or detailed manner. For example, for plant areas where a conservative analysis is sufficient to demonstrate low risk, the representative fire scenario can be defined as a fire anywhere in the area. For plant areas where a more detailed analysis is needed, multiple fire scenarios defined in terms of the precise location and initial magnitude may need to be specified. The estimation process generally involves the statistical analysis of historical data and the application of engineering judgment.

In many past PRAs, the statistical analysis has been done on an area/location basis [38, 40]. However, under current guidance, the analysis is typically done on an ignition source basis. The first approach involves estimating fire frequencies for common plant area types (e.g., main control room, cable spreading room, switchgear room, auxiliary building, turbine building, etc.). The second approach involves estimating fire frequencies for common component types (e.g., pumps, electrical panels, transformers) and objects of particular interest to fire analysis (e.g., collections of transient combustibles). Currently, the component-based approach is preferred because it enables the analyst to account for plant-specific differences in the location of ignition sources. NUREG/CR-6850 identifies roughly 40 unique fire ignition source groupings (bins) that reflect both component and source types and, in some cases, the specific fire type to be postulated for a given component type. (For example, pumps may be involved in either oil fires or electrical motor fires, and higher energy electrical switching equipment may be involved in either slower developing "thermal" fires or rapid high energy arcing fault fires).

The fire frequency for a specified component group (or plant area type) is estimated using conventional statistical modeling methods[13] [44, 45]. (See also Chap. 74.) These methods include direct approaches that assume that all of the industry data for a particular fire type come from the same population and can be pooled, and more sophisticated approaches that assume that there is plant-to-plant variability in fire occurrence rates even for a specified fire type. In the first class of approaches, generic industry

[13] Consistent with typical PRA modeling practices for many hazards it is generally assumed that fire frequencies are constant over time. One uncertainty regarding fire frequencies is whether or not this is a good assumption. The U.S. nuclear industry has documented fire event data going back to 1965, but the appropriateness of using of older events in a current analysis has been questioned. Prior analyses of fire frequency trends have reached divergent conclusions. One review of fire event data published in 2001 [44] showed that the frequencies of reported fires in key U.S. nuclear power plant compartments had not changed dramatically when comparing the periods 1965–1985 and 1986–1994, and thereby supported the use of the Poisson model for U.S. nuclear power plant fire occurrences. However, a more recent analysis demonstrated an apparent shift towards lower fire occurrence rates around 1990. The fire PRA community has not reached consensus on the subject, and as discussed in the "Current Activities and Future Directions" section below, an ongoing effort to gather additional fire event data is being performed, in part, to resolve the question.

frequencies are generated using observations of the form n occurrences (events) in time t, grouped by the component types defined in the fire PRA. In a Bayesian approach, the generic industry data are used to develop a prior distribution for the fire frequency. This prior distribution is then updated using plant-specific data. Regarding the second class of approaches, a two-stage Bayes method, described by Kazarians and Apostolakis [46], has been used in developing the frequencies provided in NUREG/CR-6850.

Regarding the data used in the statistical estimation process, reports of fire events at U.S. nuclear power plants beyond those that require reporting to the NRC are provided to Nuclear Electric Insurance Limited (NEIL) by the plant licensees on a voluntary basis. For fire PRA, the event reports are screened to exclude construction fires and other plant fires not relevant to fire CDF (e.g., office building or warehouse fires). The remaining reports were used by EPRI to establish a proprietary fire event database used to develop the fire frequencies reported in NUREG/CR-6850. Limited fire event information from the EPRI database, modified to ensure plant anonymity, is provided in NUREG/CR-6850. The proprietary database has many shortcomings, one of which being its completeness (since the reporting of many fire events is voluntary). A plant-to-plant variability analysis has been performed to address the impact of apparent differences in reporting. The result was a moderate increase in fire frequencies for all fire ignition sources, but the question of potential underreporting remains an area of uncertainty relative to fire event frequencies. As discussed further below, efforts are currently underway to gather a more complete, comprehensive and consistent set of event data from the entire U.S. commercial nuclear fleet. This work is being performed as a collaborative activity between the NRC and EPRI.

Despite the large uncertainties typically resulting from any of these approaches (due to the small amount of data available for each fire type), it is common practice to use simple point estimates of fire frequencies. The mean values of the uncertainty distributions provided in NUREG/CR-6850 are generally used for this purpose. In recent fire PRAs, these uncertainty distributions are propagated through the risk model only for dominant contributors to estimate the uncertainties in the total fire CDF.

The above discussion focuses on estimating the occurrence rate of fires (regardless of fire magnitude). We note that the severity of a fire event is also an important element of fire PRA. In many early studies, "severity fractions" or "severity factors" were used to address the relative likelihood of "challenging fires," fires that have the potential to cause significant damage in a relatively short amount of time, as a fraction of all the fires included in the fire frequency calculation. One complication of this approach was that, in general, the applied severity factors implicitly took some credit for early fire suppression activities and fire suppression that was then independently credited later in the analysis. Care must be taken when analyzing fire detection and suppression (as discussed in the following section) to avoid double-counting their effectiveness. Under current approaches, the event data are pre-screened to eliminate fire events that would not have led to risk-relevant challenges under any foreseeable circumstances. While severity factors remain a part of the current analysis methods, their role in the analysis has changed. Severity factors are now used to reflect aleatory uncertainty regarding the severity of fires that do occur; that is, even for a given fire ignition source, no two fires will develop exactly the same and this is reflected using a severity factor approach. This topic is discussed in the following section.

The component-based frequency approach has not yet reached full maturation. Current practice begins with the generic plant-wide frequency values and then partitions those values within the plant based on the locally calculated population of specific fire ignition source types (e.g., pumps, motors, electrical cabinets, etc.). Hence, it represents something of a hybrid between the earlier location-based approaches (where in this case the location is in effect the entire plant) and a true component-based frequency where a given pump would have a specific frequency value and

the plant-wide pump fire frequency would then be based on the number of pumps present at the plant. There are challenges to implementing such an approach and a true component based frequency approach remains a challenge for the future. This is discussed further in the Current Activities and Future Directions section.

Fire Scenario Selection and Analysis

General Approach The goal of the fire scenario selection and analysis element is to perform a detailed analysis of the fire growth, propagation and possibility of fire suppression before damage to a specific target set for each applicable fire scenario per plant area. Plant areas that have been previously screened out because the plant area of fire origin does not contain important equipment are reexamined for the potential that fire damage might spread to adjacent, important plant areas. The analysis is based on the evaluation of fire scenarios which are defined based on the general characteristics of the fire being postulated, the potential extent of fire-induced damage, and fire mitigation measures that will be credited for preventing damage.

As discussed by Apostolakis et al. [38, 39], the assessment models the occurrence of fire damage as the outcome of a "race" between two parallel processes: (1) fire growth and damage, and (2) fire detection and suppression. To determine the outcome for a particular fire scenario, the analyst needs to address two key questions: "how quickly (if at all) will this fire cause damage if it is allowed to burn without intervention?" and "how quickly will the fire be suppressed?" Since the fire growth and suppression processes are both subject to random variability, this race is a probabilistic process and the probability of equipment damage, the $p_{ed,j|i}$ term in Equation 89.1, can be conceptually represented by the following equation:

$$p_{ed,\,j|i} = P\left(t_{ed,\,j|i} < t_{s|i}\right) \tag{89.3}$$

where:

$t_{ed,j|i}$ = the damage time for target set *j* given fire scenario *i*; *and*

$t_{s|i}$ = the suppression time for fire scenario *i*.

In practice, the probability of equipment damage is decomposed into two parts as given by:

$$p_{ed,\,j|i} = SF_i \times P_{ns,\,j|i} \tag{89.4}$$

Where

SF_i = severity factor for fire source i; and

$P_{ns,j|i}$ = probability of non-suppression prior to damage to target set j given ignition source i.

The severity factor reflects the fraction of fires involving the fire source that are potentially damaging and the non-suppression factor reflects the probabilistic outcome of the fire damage versus fire suppression race given a potentially damaging fire. Both of these terms are discussed further below.

From a process standpoint, the assessment generally requires:

1. The identification of specific combinations of fire sources and target sets,
2. An analysis of the fire-induced environmental conditions,
3. An assessment of the response of each target set to these conditions, and
4. An assessment of the effectiveness and timeliness of fire mitigation features including detection, suppression and fire barriers.

The fire barrier assessment needs to address barrier effectiveness in preventing fire propagation to adjacent plant areas, as well as in preventing fire damage to protected equipment in the room of fire origin.

In practice, the fire PRA must, at some level, consider any fire that might occur anywhere within the plant. Hence, the analysis may initially consider several hundred to a few thousand potential fire scenarios. The fire scenario selection and analysis element is structured to allow progressive scenario screening to optimize analysis resources by identifying and focusing on those fire scenarios that are the most important CDF contributors. Less important scenarios are analyzed in limited detail and then set aside (screened out) once the conclusion of low CDF importance has been reached. Other fire

scenarios are carried forward through the analysis and ultimately quantified[14] as substantive contributors to fire CDF. The decision as to which scenarios to screen out and which to carry forward is typically based on a quantitative screening criteria designed to ensure that the vast majority of the fire-induced CDF is captured by detailed analysis. This process follows the same iterative approach that is commonplace in most fire PRAs. In the end, a typical fire PRA may quantify well over 100 fire scenarios in considerable detail. The next four subsections provide an overview of this analysis process.

Preliminary Fire Source Screening and Severity Factor Analysis Fire Source Screening is the first task in the Fire PRA framework where fire modeling tools are used to identify and analyze ignition sources that may impact the fire-induced CDF. Screening some of the ignition sources in a plant area may, in effect, reduce the compartment fire frequency previously calculated. This task also introduces the previously discussed severity factor (SF_i). The two main objectives of this task are to screen out fixed ignition sources that do not pose a threat, and to assign severity factors to unscreened fixed ignition sources. This task is performed by fire protection engineers using various fire modeling tools (discussed later) in coordination with methods described in this section with the following material readily available;

- List of components in plant areas,
- Equipment layout drawings, and
- Elevation drawings of rooms and equipment.

The fire protection engineer will also have to establish the characteristics of a credible fire associated with a specific ignition source. The exact nature of the information will depend on the characteristics of the ignition source. The following are examples of such information:

- Quantity of the oil maintained inside rotating machinery,
- Power and voltage of a motor,
- Power of electrical cabinets, and
- Quantity and nature of combustible and flammable materials maintained in an enclosure.

This task is commonly based on plant walkdowns and zone of influence (ZOI) considerations. Regarding the latter, the fire protection engineer specifies a ZOI for the ignition sources in a specific plant area. Each ZOI reflects the potential for an ignition source to cause some level of damage beyond the ignition source itself. Those sources that cannot, by themselves, damage target sets of interest or cause the spread of fire to secondary combustibles are screened out from further analysis.

The analysis should consider the following potential targets:

- The closest component (including cabinets and cables) to the fixed ignition source if no specific knowledge about PRA target locations in the area is currently available;
- Known fire PRA components (targets of interest to the analysis) in the area, if the specific target locations are known; or
- Another intervening combustible material.

These targets can be affected through the following exposure situations:

1. Engulfed in flames,
2. Within fire plume,
3. Within the ceiling jet,
4. Within the smoke layer, or
5. Within the flame irradiation zone.

The type of exposure will depend on the location of the target with respect to the fire. The fire ZOI is defined using fire models to determine the regions where fire conditions will cause target damage or ignition. Conservative fire modeling calculations are then performed to predict the fire conditions near a target to assess if target damage or ignition is possible. The analyst can then be confident that an ignition source can be screened out if no relevant targets receive thermal damage or are ignited. Ignition sources that are part of the fire PRA component list cannot be screened because the loss of the ignition source itself represents loss of at least one PRA target.

[14] In the context of a PRA study, scenarios are "quantified" by estimating their frequencies of occurrence. Ideally, the estimates are expressed in terms of probability distributions for these frequencies.

However, it is rare for scenarios limited to loss of the ignition source to be found risk-significant. Exceptions typically involve electrical cabinets and, in some cases, cable raceways. (It should also be recognized that the internal events PRA model includes the independent component failures, regardless of the failure cause.) For ignition sources that do not screen out, the severity level of the fire needed to cause damage can be established and the corresponding severity factor is estimated.

Fire source burning behavior is commonly characterized by a distribution on peak heat release rate (HRR) reflecting the aleatory uncertainty associated with fire development. Once the peak HRR distribution is developed, higher percentiles of the distribution can be used to estimate the severity factor. For example, if the minimum HRR needed to cause target damage (or ignition, in the case of intervening combustibles) corresponds to the 98th percentile of the distribution, the severity factor for that case is 0.02. This is illustrated in Fig. 89.7, which involves the case of a target within the range of damaging flame radiation. After determining the probability distribution for the peak HRR, the lowest HRR required for damage, $\dot{Q}_{dam}$, is computed. The percentile corresponding to $\dot{Q}_{dam}$ is determined from the probability distribution. The complement of this percentile is the fraction of fires whose peak HRR exceeds the minimum required for damage.

At this point, the analyst should have a list of unscreened ignition sources with the respective distance to the nearest target and fire condition affecting it (ignition or damage) as well as the corresponding severity factor.

Analysis of Fires Impacting Single Plant Areas The next step in the Fire Scenario Selection and Analysis element is to perform a more complete analysis of unscreened plant areas as individual contributors to fire CDF. This task, which is performed by fire protection engineers, involves a detailed analysis of fire scenarios involving unscreened ignition sources in each unscreened plant area that damage target sets located within the same plant area. The majority of fire scenarios analyzed in the fire PRA generally fall into this category.

In early stages of the iterative fire PRA process, the analysis is based on conservative assumptions regarding fire growth and damage. In particular, the fire ignition frequency, plant response (as characterized by the CCDP), and all other relevant parameters are based on the simplifying assumption that any fire in an area would damage all important target sets in that area. In this step, the focus is shifted towards specific damaging fire scenarios impacting a single plant area, and the objective is to estimate their frequencies of occurrence; that is, the frequency of fires leading to the loss of specific target sets within a plant area.

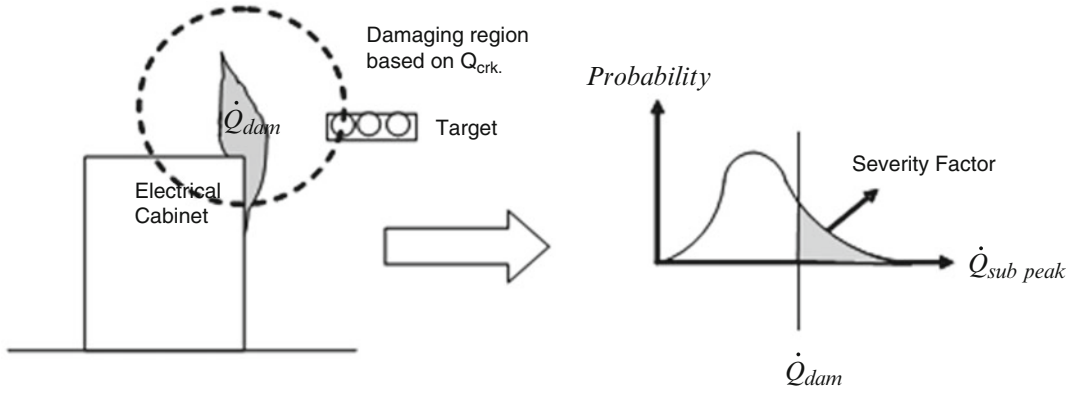

Fig. 89.7 Determination of severity factor using fire models

The analysis includes both fixed ignition sources (e.g., fixed plant equipment) and transients. Transients, in turn, include both transient fuel packages such as trash or temporary storage items, and transient activity related ignition sources such as welding and cutting operations.

The initial steps performed in this analysis characterize the plant area and, in practice, are often performed during execution of the Plant Partitioning element. These steps involve:

- Identifying and characterizing the plant area,
- Identifying and characterizing fire detection and suppression features and systems,
- Characterizing fire ignition sources,
- Identifying secondary combustibles, and
- Identifying and characterizing target sets.

Most of this information will be identified during plant walkdowns as well as various equipment selection and cable tracing tasks.

The next steps in this process will largely dictate the resources and time needed to complete the fire PRA. These are:

- Defining the fire scenarios to be analyzed,
- Conducting fire growth and propagation analysis, and
- Conducting fire detection and suppression analysis

In order to define a scenario, the analyst starts with an ignition source, postulates potential growth and propagation to other combustibles, and identifies the target set (or target sets) that may be exposed to the specific fire. The process commonly includes the consideration of an expanding ZOI over time for a single fire ignition source. That is, the ZOI is expanded over time until all relevant targets are included. Another ignition source is then selected and the process repeated until all target set and ignition source combinations are considered. This process should yield all potential fire scenarios that may damage the various target sets identified in the preceding steps. Note that this process represents a "one-to-many" mapping of ignition sources to potential risk scenarios because each target set that is defined has unique implications relative to plant safe shutdown. That is, each unique target set implies that a unique CCDP value ($p_{CD,klj,i}$) will be calculated using the plant response model.

The typical analysis approach for detection and suppression is relatively simple. Fixed fire protection systems are credited provided they actuate in time to prevent target damage (based on fire modeling) and are deemed effective against the postulated fire source (based on engineering judgment). Manual fire suppression is typically credited based on historical event data. These topics are discussed in greater detail in the section entitled "Fire Detection and Suppression Analysis".

Depending on the characteristics of the plant area, the analysis may need to treat the potential for dynamic fire growth. Such growth can, over time, cause damage to more and more equipment. This implies more serious plant response challenges and higher CCDP values. On the other hand, the equipment is often spatially separated, and more distance implies longer damage times. Longer damage times, in turn, imply a greater chance that the fire will be put out prior to damage (i.e., a lower non-suppression probability; $P_{ns,jli}$—value). A multi-stage approach to assess damage allows for a proper balancing of these two competing effects.

A typical example is illustrated in Fig. 89.8 which shows a stack of cable trays above the fire with fire PRA targets in the first and fourth trays (T1 and T2). A third target tray (T3) is also present but will only be damaged given formation of a damaging hot gas layer.

The conservative approach to this case is to assume all targets are damaged at the same time but this approach requires that damage be assumed for *all* targets as soon as the *first* target fails (in order to avoid an optimistic result). In this case, all trays would be assumed to fail when the first tray fails. The more complex but also more realistic multi-stage alternative is to represent the scenario as a progression of discrete steps accounting for the success or failure of fire suppression efforts within each relevant time frame. Figure 89.8 illustrates the multi-stage damage state model as applied to the 3-tray example.

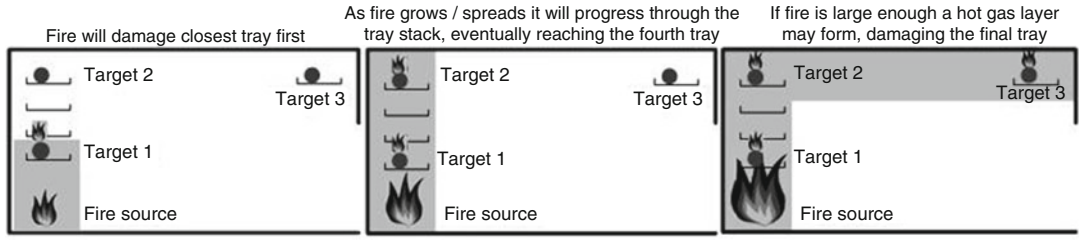

Fig. 89.8 Example case with three PRA targets present that have some degree of spatial separation

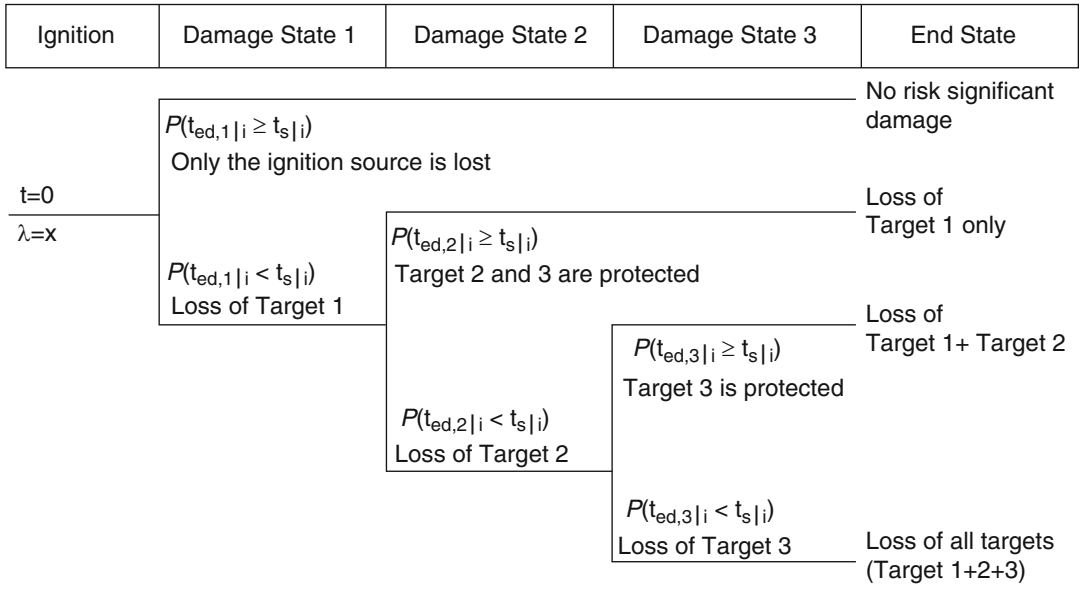

Fig. 89.9 Conceptual event tree representing a scenario progression

It is important that the various damage states be properly balanced in terms of scenario frequency because all arise from the same fire source. One common approach to modeling this type of scenario is through the use of a fire event tree as illustrated in Fig. 89.9. The events in the tree begin with ignition of a damaging fire, and progress through a series of three suppression success/failure events ultimately leading to one of four possible outcomes: namely; no damage to PRA targets; loss of Tray 1 only; loss of Trays 1 and 2; and loss of all PRA targets (Trays 1, 2 and 3). The branch point conditional probability values based on factors that include, as appropriate, the reliability of automatic detection and suppression systems, timing of each fire damage state, and the performance of manual firefighting. Inherent in the event structure is the condition that the success of an event implies a timely response; that is, the fire must be mitigated before a given damage state is reached. Chapter 38 provides additional discussion regarding event trees as used in fire protection engineering applications.

A wide range of tools is available for the analyst to conduct fire growth and spread analysis and most of those tools have been described in other Chapters of this Handbook. The tools range from simple empirical equations to computerized, numerical, three-dimensional models. Later in this Chapter, we discuss some of the more common tools used in fire PRA applications.

Analysis of Fires Impacting the Main Control Room The Main Control Room (MCR) has a unique role in nuclear power plant operations and fire risk, and is typically treated separately from other general plant areas due to its unique fire risk aspects. In MCRs the control and instrumentation circuits of all redundant trains for almost all plant safety systems are present. Furthermore, redundant train controls may be installed within a short distance of one another (e.g., on the main control boards). Therefore, even small fires within control panels may be risk-significant. Additional scrutiny is placed on the MCR also because plant safety depends on the performance of control room operators. A fire adversely affecting the operators' ability to perform needed functions may have severe safety implications. In extreme situations, fire-generated conditions (loss of control functions, high temperature and heat flux, toxic gases, and reduced visibility) could force control room abandonment. All U.S. plants have an alternate shutdown capability, that is, a critical set of independent controls and instrumentation outside the MCR, to deal with control room abandonment scenarios. Part of the MCR analysis is to analyze the reliability of this capability. On the risk-reducing side, another unique feature of the MCR is that it is continuously occupied with trained operators. This increases the probability that a fire will be promptly detected and addressed.

The MCR analysis task covers all fires that occur within the MCR. This task also covers scenarios involving fires in plant areas other than the MCR that may force MCR abandonment, for example, due to fire-induced loss of a critical set of plant controls and instrumentation. Within the MCR, the target sets consist, for the most part, of control- and instrumentation-related components and wiring within one, adjacent, or nearby electrical control panels and cabinets. As opposed to other plant areas, where targets are usually cables throughout the area, control room targets are cabinets controlling safe shutdown related functions. Cabinets in some MCRs are equipped with smoke detectors, which can reduce the fire detection time and indicate which specific cabinet is on fire. Although MCRs are equipped with smoke detector systems, due to potential risk of spurious activation no fixed suppression is available. Manual suppression is typically the extinguishing method used. Each of these characteristics will impact the risk analysis by influencing the non-suppression or abandonment probabilities.

As compared with the analysis of other plant areas, the unique aspects of the MCR analysis include the consideration of much smaller fire damage footprints (due to the expectation of prompt detection and suppression). For example, a typical scenario in the MCR will assume that damage is limited to a small portion of the main control board rather than assuming loss of an entire electrical cabinet plus external targets. The MCR analysis also considers the impact of fire on operators whereas the analysis of most plant areas considers only equipment and cables. The MCR analysis also involves unique human performance considerations including the decision-making process associated with abandonment. Another unique aspect of the analysis is that, unlike other plant areas, most MCRs are equipped with some form of a smoke purge system. Such systems provide the ability to ramp-up exhaust flow and switch to full fresh-air makeup at a minimum. A well-designed smoke purge capability can delay, or even prevent, forced abandonment. The analysis of such systems calls for more sophisticated models than are typically needed for fire scenarios in general plant areas.

Analysis of Fires Impacting More Than One Plant Area The analysis of multi-compartment fire scenarios covers all fire scenarios involving fire spread from one plant area to another and, therefore, damage in multiple plant areas. Adjacent plant areas are considered systematically and generally in pairs only. That is, based on the occupancy of most nuclear power plant fire areas and the existence of robust fire protection measures, fire spread beyond to a third plant area is generally not considered likely.

Commercial nuclear power plants have numerous interconnected compartments that may be aligned horizontally or vertically. Connections between plant areas include fire doors, stairways, sealed cable and piping penetrations, openings, and gratings. Depending on how plant areas were defined during plant partitioning, plant area interfaces may also include open space (free of combustibles), active fire protection features (such as water curtains or a normally open fire door) and non-rated fire barrier elements. Considering the numerous interconnected compartments and the amount of analysis needed to evaluate fire-generated conditions in multi-compartment scenarios, a detailed multi-compartment analysis can be resource intensive. Practical analysis, therefore, emphasizes screening multi-compartment combinations before identifying fire scenarios that need to undergo detailed fire modeling.

The analysis often involves combining plant areas of interest into a single area and assessing the potential for fires leading to formation of a damaging hot gas layer in the combined area. This analysis uses standard fire modeling tools, described elsewhere in this Handbook. The analysis also considers paths for direct spread of fire across a barrier element, including the potential that a fire barrier element (e.g., a penetration seal) may randomly fail (e.g., it may have a hole through it due to improperly completed maintenance activities at the time of the fire). The analysis also considers that multi-compartment scenarios will only have a unique risk contribution if new target sets are threatened given fire spread to a second plant area (i.e., as compared to those already threatened in the area of fire origin and encompassed by the single compartment scenarios).

The methods of analysis for multi-compartment scenarios remain relatively unsophisticated, and some areas of uncertainty remain. For example, the random failure probability for a rated fire barrier element is not well characterized. Current practice is to define the plant areas during the plant partitioning task such that risk-significant multi-compartment fire scenarios are unlikely. In theory, regardless of how partitioning decisions are made, the analysis should reach the same conclusions.

Circuit Analysis

Circuit Failure Mode Analysis

Circuit analysis has become an increasingly complex and important aspect of fire PRAs in recent years. All past fire PRA studies have addressed fire-induced circuit failures that lead to a loss of function and many have included the possibility of fire-induced spurious operation of plant equipment (although the treatment was limited by current standards). The latter failure mode has become an increasingly important analysis topic over time based on the results of tests and analysis indicating the likelihood of spurious operations, and especially multiple spurious operations, is higher than previously thought [47–50]. Spurious operations can be caused by hot shorts (i.e., electrical faults between cable conductors without a loss of circuit power). Depending on the specifics of the circuit, they can also be caused by other fire-induced cable faults (e.g., single ground shorts or a ground equivalent hot short on an ungrounded power source like station batteries) [47, 49]. The likelihood of fire-induced spurious operations and the associated contribution to fire CDF appears to be influenced by a number of plant-specific factors. Although the precise values are uncertain, under any circumstances a modern analysis of these failures is a resource-intensive effort.

Circuit failure mode analysis is performed by electrical engineers. The analysis involves the deterministic failure analysis of important circuits. The purpose of the analysis is to identify those circuits and cables that can adversely affect the credited functionality of essential equipment/components, and to document the equipment responses to the possible cable failure modes induced by fire damage. As noted above, this element is often conducted in close coordination with the Cable Selection and Tracing element, which is aimed at identifying cables. This

element determines the functional impact of potential failures of these cables.

Although this element is performed by electrical engineers, it is useful for fire protection engineers to recognize: (a) the importance of this element to the overall fire PRA results, (b) the potential need to model scenarios involving damage to multiple cables (since multiple cable faults may be needed to induce a spurious operation, and also since multiple spurious operation scenarios might be important to fire CDF), and (c) the particular fire-induced cable faults (shorts to conductors within a single cable, shorts to conductors in another cable, shorts to ground) that may need to be modeled in the analysis.

Circuit Failure Mode Likelihood Analysis

The circuit failure mode likelihood analysis is the probabilistic complement to the deterministic circuit failure mode analysis. That is, this step assigns conditional probability values to specific component failure modes given fire-induced cable failures. Should a fire damage a target cable or set of cables, the likelihood of the above-mentioned cable faults and the durations of these faults are complex functions of many factors, including raceway fill, thermal exposure conditions, fuse size, circuit type, cable construction, and raceway routing. Experiments have been performed to evaluate cable electrical performance for a number of different configurations [51]. The results of these experiments have directly supported deterministically-oriented analyses of fire-induced circuit damage phenomena. In addition, although the tests were not designed to generate a representative random sample, their results provide valuable input to expert elicitation panels tasked with developing estimates for the conditional probability of spurious operations (given fire-induced cable damage) and the duration of these spurious operations. The panels include fire protection engineers (to bring in knowledge regarding both the test conditions and fire modeling approaches for nuclear power plant scenarios), as well as electrical engineers and PRA experts.

The results of an expert panel elicitation for estimating the likelihood of fire-induced spurious operations involving alternating current circuits (AC) are provided in EPRI TR-1006961 [52]. An analogous effort aimed at addressing direct current (DC) circuits is ongoing. This latter effort, building on lessons learned from past elicitations, is using guidance on conducting structured expert elicitations originally developed for seismic PRA applications but applicable to other areas as well [53, 54].

Human Reliability Analysis

In the context of nuclear power plant PRA, Human Reliability Analysis (HRA) is the process used to identify, characterize, and estimate the likelihood of potentially important human errors. These errors can occur prior to the occurrence of an accident (e.g., failure to properly re-align equipment after maintenance), trigger an accident (e.g., inadvertently initiate a reactor shutdown), or during the course of the accident (e.g., fail to appropriately execute a step in plant procedures). HRA has both qualitative and quantitative analysis elements. A general overview is provided in Chap. 74.

In the context of fire PRA, the focus of the HRA element is on errors that may occur as plant operators (including but not limited to the crew of operators in the MCR) respond to fire-initiated scenarios. Human errors causing fires (e.g., inadequately controlled hot work) are built into the fire event data used to estimate fire frequencies, as described earlier in this chapter. Human errors in detecting and suppressing fires are addressed as part of the detailed fire analysis effort. (Such errors affect the time to suppress a fire, denoted by t_{sli} in Equation 89.3. Additional discussion on analyzing this term is provided later in this Chapter).

The specific errors of interest in the HRA element involve operator manual actions taken, in accordance with the operators' procedures and training, to perform needed safety functions (e.g., initiate emergency cooling). These manual actions are typically represented in the plant

response model as human failure events (HFEs). HFEs can be provided in event trees (as illustrated by "Manual Reactor Depressurization" branch in Fig. 89.3) or in fault trees (as illustrated by the basic event "Operator Fails to Start/Control RCIC Injection" in Fig. 89.4). They can be errors that are already included in the internal events model (albeit with potentially different probabilities) or they can be introduced into the plant response model due to unique conditions created by the fire scenario (e.g., an inability to complete a desired action due to the fire's location). These conditions are extremely important to the estimation of the HFE probabilities (commonly referred to as Human Error Probabilities or "HEPs"), since human error probabilities depend strongly on the context for the actions being taken. In the case of fire PRA, the analysis team needs to consider such factors as the potential effects of the fire on needed equipment (including such plant support systems as lighting) as well as such physical hazards as heat and toxic gases.

NUREG-1921/EPRI 1023001 [55] provides detailed guidance for performing fire HRA. As indicated in this guidance, fire HRA is a multidisciplinary effort. The analysis requires input regarding a wide range of information, including plant procedures,[15] associated operator training, potential fire-induced environmental effects, fundamental psychological and social mechanisms leading to human error, and the "Performance Shaping Factors" (PSFs) affecting these mechanisms. The general steps involve:

1. HFE identification and definition,
2. Qualitative analysis of each HFE and,
3. Quantitative analysis of each HFE.

The first step identifies those operator actions and associated instrumentation necessary for the successful mitigation of fire scenarios and defines associated HFEs at a level of detail appropriate to support qualitative analysis and quantification.

In the second step, the HRA team develops an understanding as to how each HFE interacts with the overall plant PRA. This understanding should reflect the "as-built, as-operated" response of the operators and plant. Key characteristics include:

- Potential fire-induced initiating events,
- Potential accident sequences (particularly functional failures and successes, including preceding operator errors and successes),
- Event timing information,
- Accident-specific procedural guidance,
- Availability of cues and other associated indications that may be needed to identify necessary actions, as well as those that might subsequently enable the operators to detect the need for a correct action that has been omitted or performed incorrectly,
- Preceding operator errors or successes in sequence,
- Criteria defining operator action success, and
- Physical environment information.

The team translates this information into a form useful for the estimation of HEPs. A sound qualitative analysis also allows the HRA to provide feedback to the plant on the factors contributing to the success of an operator action and those contributing to the failure of an operator action.

In the third step, the HRA team develops estimates for the HEPs. This quantification process can be carried out at varying levels of detail, depending on the significance of the HFE. Screening-level analyses using conservative HEP estimates are commonly used for unimportant HFEs, thereby enabling the team to focus attention on those HFEs important to the overall fire CDF.

As with the rest of fire PRA, fire HRA is typically performed in an iterative fashion. Initially simple, conservative analyses are upgraded with more detailed analyses as the team gains a more accurate understanding of the fire CDF and its principal contributors.

Fire Risk Quantification

Risk quantification is where the results of the various elements of fire PRA are assembled to produce the desired risk estimates. This chapter

[15] These procedures include Emergency Operating Procedures (EOPs), Annunciator/Alarm Response Procedures (ARPs), and Abnormal Operating Procedures (AOPs), as well as specific fire response procedures.

has focused on the fire CDF. Estimates of another risk metric of interest, the large early release frequency (LERF), is developed in a similar fashion to CDF. As its name implies, the LERF metric represents the likelihood of a large, relatively quick release of radionuclides into the environment after a core damage event. A LERF analysis builds on a CDF analysis, but adds models to address the possibility of a breach in the containment structure (see Figs. 89.1 and 89.2) following a core damage accident.

Conceptually, risk quantification is performed by summing the contributions of individual fire scenarios, as shown in Equation 89.2. In practice, the large number of fire scenarios considered in a typical fire PRA, compounded by the multiplicity of potential plant responses to each fire scenario, calls for the use of specialized PRA software tools to ensure correct treatment of model complexities (e.g., dependencies between different parts of the model) and avoidance of inappropriate conservatism or non-conservatism in the final results. The previously mentioned SAPHIRE [41], CAFTA [42] and FRANX [43] are examples of software packages used in current studies. These programs support the construction and documentation of models, the development of results, and the analysis of results. The last activity includes the identification of key scenarios, the use of diagnostic ("importance") measures to better understand the contributors to these scenarios, and the performance of sensitivity studies to better understand the impact of different modeling assumptions.

Uncertainty Analysis

Uncertainty analysis is that element where the key state-of-knowledge uncertainties (often called "epistemic uncertainties") associated with the fire PRA are identified and treated.[16] Various approaches to uncertainty analysis can be used, depending on the needs of the decision problem addressed by the fire PRA as well as the technical nature of the uncertainties themselves.

In general, the epistemic uncertainties in fire PRA model parameters (e.g., fire frequencies, fire model parameters such as the heat release rate for a specified fire) and in the fire PRA models themselves (e.g., physical models for fire-induced component damage, event tree models for plant safety impacts of fire) are handled as described in this Chap. 76. Assuming the decision problem (including potential future decision problems) and the role of the fire PRA in addressing this decision problem have already been defined, the uncertainty analysis involves:

- Identifying the sources of uncertainty in all aspects of the fire PRA model (including such non-fire protection engineering aspects as the plant response model);
- Characterizing the uncertainty in the fire PRA model (both inputs and model structure);
- Characterizing the uncertainty in the fire PRA model output; and
- Interpreting the results of the uncertainty analysis and presenting this information in a form suitable for use by decision maker(s)

The notion of "characterizing" (as opposed to "quantifying") uncertainties is used to include situations for which a rigorous analysis may not be needed. From a decision support perspective,

[16] As with nuclear power plant PRA in general, fire PRA addresses two types of uncertainty: aleatory and epistemic uncertainty [10]. Aleatory uncertainty, also called "random uncertainty" or "stochastic uncertainty," is that associated with inherent, potentially observable variability in the events and behaviors being modeled. Epistemic uncertainty is associated with limitations in the PRA analyst's state of knowledge, and can involve such things as uncertainties in the true value of an input parameter for a fire model or in the appropriateness of the model itself. Unlike aleatory uncertainty, epistemic uncertainty can be reduced through the collection of additional information (e.g., via experiments).

The fundamental structure of fire PRA is aimed at assessing aleatory uncertainty, as the fire-induced CDF is a measure of aleatory uncertainty (it addresses the likelihood of a random event—the occurrence of a core damage accident due to fire). The uncertainty analysis element discussed in this section deals with the epistemic uncertainty in the fire PRA inputs, models, results, and insights.

the key point is not whether the uncertainty analysis results in a mathematically-derived probability distribution for a fire PRA output metric (e.g., the fire-induced CDF), but whether the output uncertainty and its drivers are sufficiently understood to enable selection of the best decision option.

NUREG/CR-6850 provides a number of different possible strategies for treating uncertainties. These strategies, some of which can be used in combination, include:

- Explicitly quantifying epistemic uncertainties in model parameters using probability distributions, and propagating these probability distributions through the fire PRA model using such techniques as Monte Carlo sampling or Latin hypercube sampling;
- Developing multiple models for an issue (e.g., the rate of fire growth for a particular fire), assigning a probability that each model best represents the situation based on engineering judgment, and propagating these probabilities through the fire PRA model;
- Identifying a base case as the best estimate model with best estimate data values, performing sensitivity analyses where the models or parameters of interest are varied within a reasonably expected range, and documenting the quantitative effect on the overall results;
- Identifying sources of uncertainty that can be (or should be) treated in a single group;
- Addressing the uncertainty in only qualitative terms (e.g., describing which scenarios would be affected and providing a qualitative judgment as to the effects); and
- Using a quality review process to ensure sufficient accuracy and a reasonable level of completeness (such as a review of the identified cables in a plant area to be sure none have been missed in the PRA model).

The choice of which strategy (or set of strategies) to use may include consideration of the perceived importance of the uncertainty on the overall results of the Fire PRA; the possible effects on future applications or other decision-making activities; and the resources needed and available, including schedule constraints, to execute the strategy.

NUREG/CR-6850 also points out that, given finite analysis resources, not all sources of uncertainties can be treated. The analysis team therefore needs to:

- Identify those uncertainties that will not be addressed because they are expected to be unimportant (e.g., they are associated with screened out scenarios) or they cannot be addressed (with reasons noted); and
- Identify the strategy (or strategies) to be used to address remaining uncertainties (including which issues that will be treated using sensitivity analysis).

Fire PRA Documentation

As with any engineering analysis, it is important to document the fire PRA to a level sufficient to enable review of the study by external parties and its use in decision support applications. Specific documentation requirements are provided in the ASME/ANS PRA Standard. These requirements cover such things as the need to document, as appropriate, the methods, data, key factors, modeling assumptions, and results of each of the fire PRA elements discussed earlier in this section.

Somewhat unique to PRA (and therefore fire PRA), it is important to recall that the triplet definition of risk mentioned at the beginning of this chapter includes qualitative as well as quantitative elements. Thus, in general, the results of a PRA need to include descriptions of the scenarios contributing significantly to the overall risk, as well as estimates of the total quantitative risk. These descriptions can be organized along many themes, including the general hazard triggering the scenarios (e.g., fires, floods, hardware failures), the particular initiating event demanding a response from plant safety systems (e.g., unplanned reactor trip, loss of electrical power, loss of coolant), the types of safety functions or systems involved (e.g., low pressure versus high pressure coolant injection systems), or even specific contributing elements (e.g., operator errors).

In the case of fire PRA, a common approach is to present aggregated results for specific plant areas (e.g., the estimated CDF associated with fires in a particular switchgear room, and the uncertainties in the estimated CDF). Depending on the needs of the decision problem addressed by the fire PRA, these area-level results can be further broken down into results for specific scenarios within an area or for specific target sets (e.g., if strategies to protect cable trays from fire damage are being considered).

Another useful presentation of results involves the CCDP for all analyzed plant areas. A given plant area may have many scenarios each with a corresponding CCDP value. However, one value typically generated is the CCDP given loss of all PRA targets in the area. This term, which quantifies the likelihood of core damage assuming that a severe damaging fire occurs, provides a sense of how serious a damaging fire could be. Recognizing that the independent failure probability of typical safety systems can be on the order of 10^{-2} to 10^{-3}, a CCDP in that range indicates that, in addition to the fire damage, an independent failure of an additional safety system would be needed before core damage could occur. This would be an indication that redundancy in safety functions remains even given loss of the entire area. Conversely, a CCDP closer to 1.0 would indicate that a severely damaging fire would be likely to cause core damage by itself. An area with a high CCDP value but a low CDF contribution is also of interest because this indicates that some factor, or factors, have been given substantial risk-reduction credit. Credited factors might typically include assumed fire characteristics, physical separation of PRA targets from fire sources, or fire protections systems and features. Understanding the importance of such factors can be important to decision making.

Armed with these results, decision makers have the information to understand not only the "bottom line" results, but also the reason for the bottom line. This detailed information has proven useful in the development and assessment of potentially effective risk management alternatives.

The Use of Fire Modeling Tools in Fire PRA

The preceding section has discussed all of the elements of fire PRA. Most of these elements require at least some input from the fire protection engineer. The two elements requiring the most substantial fire protection engineering involvement lie at the middle of Fig. 89.6: "Fire Scenario Selection and Analysis" and "Detailed Fire Modeling." Both of these elements require the use of fire modeling tools. These tools are further discussed in this section.

Fire Environment Analysis

Predicting the time to fire-induced failure of PRA targets requires two types of calculations. The first estimates the time-dependent environmental conditions created by the postulated fire in the proximity of the equipment and cables of interest (i.e., the targets). The second addresses the response of the damage target to that environment. This section discusses modeling of the exposure environment; target response modeling is discussed in the following section.

The environmental conditions that a fire model is asked to predict correspond to the target's damage mechanisms. Most commonly, the assessment focuses on temperature and/or heat flux leading to thermal damage. However, other environmental conditions such as heavy smoke may also be of interest, depending on the vulnerability of the target to these conditions. The estimation of environmental conditions requires the treatment of a variety of phenomena as the fire grows in size and severity, including: the spread of fire over (or within) the initiating component (or fuel), the characteristics of the fire plume and ceiling jet, the spread of the fire to noncontiguous components, the development of a hot gas layer, and the propagation of the hot gas layer or fire to adjacent compartments.

The modeling tools used to analyze nuclear power plant fire scenarios are much the same as those described elsewhere in this handbook.

Common empirical correlations are employed for the aforementioned phenomena, including initial estimates of hot gas layer development. The commonly available compartment fire models including both zone models and computational fluid dynamics (CFD) models are also used.

Nuclear plant fire scenarios have a number of characteristics that may not be directly addressed by fire models not explicitly designed to model these scenarios. These characteristics include: a variety of source fire types unique to industrial facilities such as cable trays, electrical cabinets, and pressurized gases; the possibility of propagation through complex fuel arrays such as cable tray stacks; the lack of openings to the external environment; generally complex and often highly congested geometries; the elevated location of many important fire sources and fuels (note that many plume correlations have been based on experiments where the fire is at ground level); local obstructions such as ventilation ducts, piping, and structural members; and a range of localized fire barriers including raceway fire wraps. By and large, the ability to model such features in detail is limited and often either a conservative approach or an empirical approach are employed in lieu of detailed fire modeling.

Another special aspect of fire risk assessment for nuclear power plants is that fire PRA studies often require that fire modeling be done for many fire scenarios. Within a given plant area, many fire scenarios can be defined depending on the number of fixed and transient combustible sources, the number of unique target sets, the success or failure of fire barriers, and the variety of ventilation conditions, including possible changes (e.g., the opening of a fire door to allow fire-fighting access or the shutdown of a forced ventilation system due to closing of fire dampers). Even a single fire source may be modeled using different assumptions regarding, in particular, peak fire intensity. Given that multiple plant areas may need to be analyzed, and given the potential need to perform calculations to support a quantitative uncertainty analysis, the number of scenarios to be modeled can be quite large.

A variety of fire-modeling tools, or tool packages, have been developed to address these needs. In U.S. fire PRA studies, including Individual Plant Examinations of External Events (IPEEEs) [21, 22, 33, 34], the most commonly used tools were the package of closed-form empirical correlations drawn from handbooks and provided by the FIVE methodology [33], the compartment fire zone model COMPBRN IIIe [56], and the methods described in the FPRAIG [34]. More recent tools include the Fire Dynamics Tools (FDTs) [57], another collection of handbook correlations provided in spreadsheet form and developed to support NRC's risk-informed fire protection-related inspection activities, and the zone models MAGIC and CFAST [58, 59]. Other general purpose fire models that have been used in fire PRAs include the field model Fire Dynamics Simulator (FDS) [60].

Empirical correlations such as those assembled in FIVE and FDTs are generally used in quick scoping analyses and during ignition source screening analyses. As such, it is preferable that such tools provide conservative estimates but in particular, optimistic results are to be avoided. The zone and field models are typically used to support more detailed analyses where more realistic values are desired.

Information relevant to fire modeling for fire PRA, including data on cable properties (e.g., ignition thresholds, mass burning rates, heat release rates), is contained in several reports [61–66]. Other required parameters (e.g., for cable thermal conductivity, specific heat, density) are typically estimated using data for generic materials. Most zone models follow one of two approaches to modeling the fire source. One approach is to translate all fire sources into an equivalent liquid fuel pool fire (e.g., based on pool size, fuel properties, and fuel quantity). The second approach is to directly specify the fire in terms of a predefined heat release rate versus time. Discussions on appropriate heat release rates for a range of fire sources (e.g., for electrical cabinet fires, based on experimental data reported by Chavez [67] and Chavez and Nowlen [68]) are provided in NUREG/CR-6850 and in a

more recent "Nuclear Power Plant Fire Modeling Application Guide" [69]. This later report consolidates previously available information and details modeling approaches as they apply to nuclear power plant fire PRA needs.

As discussed earlier in this chapter and Chap. 76 it is important to treat uncertainties. The predictions of fire models are, of course, subject to significant uncertainties. Applications of fire models that neglect these uncertainties (e.g., applications that neglect the possibility of damage to critical cables because they are a few centimeters above the damage height predicted by a given model, or, conversely, those that neglect the possibility of cable survival when the predicted damage height is just above the cable location) can lead to unrealistic assessments of fire risk. The treatment of uncertainty is needed not only to indicate the degree of confidence in analysis predictions, but can also indicate whether improvements in fire modeling sophistication are likely to change the risk insights for a given scenario. Uncertainty is also an important factor in the assessment of safety margin as called for in the NFPA-805 Standard.

The uncertainties in the predictions of the fire models arise from: (a) "model uncertainties," those uncertainties arising from inherent limitations of current understanding of governing phenomena as well as from model simplifications arising when applying fire models to a specific situation, and (b) from a lack of knowledge concerning the actual values of key model parameters.

Regarding uncertainties in fire models, many of the same issues discussed elsewhere in this handbook apply to the analysis of fires in nuclear power plants. For the purposes of this chapter, it is useful to observe that, as discussed earlier in this section, fire PRAs can involve unique concerns and associated complexities (e.g., the spread of a fire over complex fuel beds such as partially filled cable trays, the propagation of fire to secondary combustibles separated from the initial fire source, and the behavior of fires initiated by explosive electrical faults). Available empirical data, for example, those from the 20 ft (6.1 m) separation tests documented by Cline et al. [70] the German Heissdampfreaktor (HDR) tests (see Nicolette and Yang) [71] the Baseline Validation Tests (see Nowlen [72]), and the recent tests performed as part of the International Collaborative Fire Modeling Project [73], address only some of these complexities, and do so in a limited fashion. Thus, it is not surprising that there can be considerable uncertainties in the predictions of fire models (including state-of-the-art fire models) when applied in fire PRAs.

Model simplifications, such as assumptions made by software code developers or the code user, are not necessarily from lack of knowledge but rather are routinely made to enable assessments within time and resource constraints. These simplifications can introduce both conservative and non-conservative biases. As examples of conservative simplifications, analyses often ignore (1) the effect of intervening obstacles when calculating heat transfer to a specified target, (2) the heat sink effect of room equipment and the impact of local oxygen starvation on heat release rates, (3) the limiting effect of forced ventilation, and (4) the time required for the fire to reach the "initial" size used to start the fire model simulation. Examples of non-conservative simplifications include the neglect of radiation feedback to the burning fuel in some models and the common assumption that fires in closed metal cabinets will stay confined within these cabinets.

Engineering methods for quantifying fire model uncertainty using integral test data have been developed and applied in a small number of studies [74, 75]. A systematic framework for treating model uncertainties, including applications to fire modeling, is provided by Droguett and Mosleh [76]. However, as mentioned in this Handbook's discussions on model uncertainty and in NUREG-1855 [11], a quantitative treatment of model uncertainty may not be needed. For example, appropriate efforts to characterize model uncertainty (e.g., through the performance of sensitivity studies to assess the effect of different modeling assumptions) may be sufficient to meet the needs of the fire PRA.

The uncertainty in model parameter values is due to the sparseness of experimental data for some of the parameters (e.g., piloted and non-piloted ignition temperatures for cables) and the uncertainty as to the applicability of the existing data to the situation in the field (i.e., the particular fire scenario being analyzed). Distributions for a number of parameters have been developed (e.g., see Brandyberry and Apostolakis) [77] and used in a number of fire PRA studies. The propagation of these uncertainties through the fire model can be done using readily available tools and methods (e.g., Monte-Carlo or Latin hypercube sampling), as discussed in Chap. 76.

Equipment Response Analysis

Given a predicted fire environment for a PRA target, the fire PRA needs to assess the target's response to that environment and determine the timing of equipment failure. Grouped electrical cables present a common cause failure mechanism for multiple plant systems; hence, a key fire PRA concern is the response of electrical cables. However, the responses of other potentially vulnerable equipment (e.g., electromechanical and electronic components in electrical cabinets) are also of interest. Information relevant to the estimation of thermal fragilities of key equipment is provided in a number of reports [62–64, 78–80]. Information on the effects of smoke on sensitive equipment is more limited [81, 82]. Smoke effects on sensitive equipment are not yet explicitly addressed in detailed fire PRA analyses. (The effects of smoke and fire suppressants on sensitive equipment are implicitly addressed in those screening analyses that assume that any fire within a plant area will damage all equipment within that area).

Current fire PRA treatments of equipment failure due to heat typically involve very simple thermal models. In the early stages of analysis, it is generally assumed that damage will occur if a representative temperature (e.g., the air temperature surrounding a cable) exceeds a threshold value. Similarly, component damage may also be assumed if the incident heat flux exceeds a critical value. These both represent conservative approaches and a relaxation of this conservatism typically involves the use of simple heat transfer models such as lumped capacitance models or one-dimensional transient heat conduction models. One model recently developed specifically for the analysis of cables is called THIEF [83]. This model is a relatively simple one-dimensional heat transfer model than can take a predicted environmental temperature and estimate the thermal response of cables either in open air or in a conduit. THIEF was calibrated based on an extensive series of small-scale cable exposure tests and validated based on large-scale cable fires. This model incorporates some conservatism because it does not account for the thermal mass effects of grouped cables which will tend to slow down cable heat-up. Instead, the model treats cable bundles as a single target cable. However, the use of even simple thermal response models such as THIEF can substantially reduce analysis conservatism because they account for damage time delays associated with target heating. The longer the predicted time to damage, the more credit can be taken for fire suppression prior to damage.

Fire Detection and Suppression Analysis

Equation 89.3 shows that within the context of a fire PRA, the objective of a detection and suppression analysis is to determine the likelihood that a fire will be detected and suppressed before the fire can damage critical equipment. This objective requires an assessment of both the performance of automatic systems and the effectiveness of manual fire-fighting efforts.

Most fire PRA studies performed to date have used a simple detection/suppression model in which automatic systems, if they actuate, are assumed to be immediately effective so long as the fire suppression system is appropriately designed and installed to be effective against the postulated fire. The effectiveness assessment is commonly based on expert judgment and on traditional fire protection design and installations

practices (see the guidance provided in the EPRI FPRAIG) [34]. The results of calculations for equipment damage times are sometimes compared with the results of simple fire modeling calculations for fire detector and sprinkler actuation times to determine if automatic systems can be credited. Random failure of the system is also considered. If automatic suppression is unsuccessful (i.e., automatic suppression is not available or, if available, it either fails or is not timely), the likelihood that manual suppression efforts will be effective before equipment damage is then determined. The event data clearly indicate the importance of manual fire fighting because the vast majority of reported fires are suppressed manually rather than by fixed suppression systems.

A weakness with many fire PRA studies that model both automatic and manual suppression is the failure to treat a number of potentially important dependencies between automatic and manual suppression activities. Although the fire water supply system is generally designed such that a single failure of a valve, pump, or piping should not compromise both the primary and backup suppression systems, common cause failure (e.g., due to fire water pumps) cannot be excluded. Most current fire PRA studies do not include a systematic search for such common cause failures. As a second example, if an automatic suppression system were to fail on demand, some delay in manual fire-fighting efforts might occur while personnel attempt to recover the failed automatic system. This dependency has been acknowledged in various methods [9, 34] but the actual means for treating this dependency is not well defined and left to the discretion of the analyst. These deficiencies can lead to non-conservative results. Another weakness is that analyses typically neglect delays in fire suppression following fixed-system actuation. However, because the fire growth models used in fire PRA studies do not account for the retarding effects of suppression activities, the risk impact of this neglect is not clear.

Ultimately, manual fire fighting is the final line of defense relative to fire suppression. All U.S. nuclear power plants maintain a fire brigade or fire department. The most common approach to incorporate the fire brigade response in the fire PRA is based on non-suppression curves that are derived from event data. These curves express the probability that a fire will remain unsuppressed as a function of time. An example of such a curve, taken from NUREG/CR-6850, is shown in Fig. 89.10. This particular curve is based on data from all fire events in the EPRI fire events database [44]. NUREG/CR-6850 also provides curves for various specific fire types (e.g., electrical fires, oil fires, etc.) and for certain unique plant areas (e.g., the MCR).

The following process is followed to use the non-suppression curves in deriving a probability of non-suppression due to manual means.

1. Using fire models, predict both the time to fire damage and the time to fire detection.
2. Compute the time available for manual fire suppression as the difference between the time to damage and the time to detection.

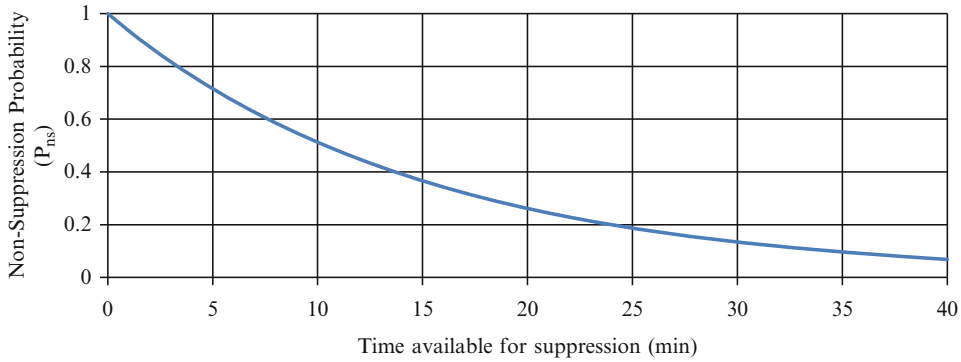

Fig. 89.10 Non-suppression probability curve

3. If the computed damage time is less than the computed detection time, set the probability of non-suppression to 1.0 (no suppression credit).
4. Otherwise, use the computed time available on the x-axis of the non-suppression curve to determine the appropriate point on the non-suppression curve and read the corresponding probability of non-suppression from the y-axis.

Note that this simple approach includes an assumption that manual suppression activities begin once the fire has been detected.

This simple approach to modeling manual suppression has some weaknesses. In particular, the non-suppression curves provided in NUREG/CR-6850 neglect scenario and location-specific effects on initial brigade response time. Different plant locations imply different response times for fire fighters to arrive on scene. However, the NUREG/CR-6850 curves are based on generic, industry-wide statistics partly because, for most events, it is not possible to discern the response times. Also, the currently available event records do not provide sufficient information to address plant- and scenario-specific factors such as fire brigade staffing, training, procedures, and equipment available. As a result, the impact of plant-to-plant differences on the fire suppression response cannot currently be reflected in the analysis.

Siu and Apostolakis [84] describe a state-transition methodology that provides a more detailed probabilistic treatment of the detection and suppression process intended to address weaknesses in current practice. This methodology identifies multiple detection/suppression scenarios involving different possible pathways to eventual fire suppression, based on available fire protection equipment for the area of interest. The methodology identifies and treats possible sources of dependencies between elements in these scenarios. Model parameters characterizing key event times (e.g., the time to suppression) are quantified in a Bayesian framework [10] using generic fire protection system reliability estimates and detection/suppression time data obtained from nuclear power plant fire events. The Bayesian framework provides a direct means for updating model parameters to reflect plant-specific information. (A condensed and somewhat simplified version of this methodology employing data from operational experience has also been developed [85].) The methodology has been used in a few fire PRA studies (e.g., see Musicki et al. [12]). An alternate methodology was used in a study of the LaSalle plant, [17] but that method (1) does not explicitly identify different detection and suppression scenarios, (2) uses physical models included in FPETOOL [86] to estimate detector and sprinkler actuation times, and (3) uses expert judgment to estimate other characteristic delay times in the fire detection/suppression process.

In NUREG/CR-6850, the state-transition model of Siu and Apostolakis has been restructured in the form of an event tree model, and fire event data have been used to support quantification of the model. As the availability of fire event data has expanded, the data available to support statistical assessments of fire brigade response and suppression times has also expanded. For example, NUREG/CR-6850 provides fire brigade non-suppression curves appropriate for various categories of fires. However, the analysis weaknesses cited above remain. Related activities are described in the "Current Activities and Future Directions" section.

Fire Barrier Analysis

As part of determining the immediate environment of equipment potentially affected by a fire, the fire PRA needs to consider the effectiveness of fire barriers. Two general types of fire barriers appear in the analysis. First there are the primary physical structures and features (walls, floors, ceiling and associated penetration seals, doors, hatchways, etc.). Second there are also localized fire barrier systems used to protect plant equipment and cables. The most common localized systems are Electrical Raceway Fire Barrier

Systems (ERFBS) including, for example, thermal insulating wraps used to protect cable trays, conduits, or groups of raceways.

The primary fire barriers come into the PRA through the multi-compartment analysis described earlier in this chapter. In the U.S., the most extensive investigation of multi-compartment fires and the effect of inter-compartment barriers was performed by the Risk Methods Integration and Evaluation Program (RMIEP) study [17]. In that study, which was intended to extend the PRA state-of-the-art in a number of areas, the possibility of fire propagation across rated fire barriers between up to three fire areas was treated explicitly. Screening analyses using barrier failure probabilities and assuming the loss of all equipment in all affected fire areas were employed to eliminate unimportant combinations of fire areas. More refined analyses, which distinguished between active barriers (e.g., doors, dampers) and passive barriers (e.g., penetration seals) and employed less conservative barrier failure probabilities (but still assumed the failure of all equipment in all affected areas), were then performed for the remaining combinations of fire areas. The study determined that no combinations passed its CDF screening criterion of 10^{-8} per year, and so multi-area fires were determined to be insignificant contributors to fire risk at the LaSalle plant. One factor in that conclusion is that the plant partitioning analysis was based on physical barriers rather than spatial separation. Hence, in all cases, the inter-compartment barriers were all substantial physical barriers. If an analyst chooses to credit less robust boundaries (e.g., spatial separation) in defining the PRA plant areas, then multi-area scenarios may prove to be more important.

Regarding the treatment of local fire barriers, these barriers are usually either assumed to be completely reliable for up to their rated fire endurance or are conservatively neglected. It is common, for example, to neglect features such as radiant energy shield and partial height walls. Even when physical models for barrier performance are employed (e.g., COMPBRN IIIe provides a one-dimensional steady-state heat conduction model) [56], these models do not address such behaviors as gross distortion and mechanical failure of the barrier system. Fire tests have shown that such behaviors are strongly affected by installation practices (e.g., the method of sealing joints) [87]. Furthermore, the physical properties of the barriers needed to address such complex issues are not readily available.

In typical practice, a fire barrier that is monitored as a part of the plant maintenance program, and that has been demonstrated by testing to provide a specific fire endurance, is credited for providing equipment protection consistent with the fire endurance rating. Again, the most common form of such barriers is raceway wraps. Such wraps can sharply impact the estimated risk. For example, the presence of a 1-hour rated raceway barrier systems reduces the likelihood of fire-induced damage to the protected cables substantially. In a typical fire scenario such a barrier can reduce risk estimate by approximately two orders of magnitude (based on manual fire suppression credit given for a fire lasting greater than 1 h).

Current Activities and Future Directions

Fire PRA currently supports a wide range of activities in the nuclear industry. The most visible activities involve licensee actions to risk-inform their fire protection programs. However, fire PRA support of other activities, both licensee- and regulator-driven, are also important. This section provides a brief overview of both sets of activities, as well as of current research activities aimed at improving the technical basis and performance of fire PRA.

It is important to note that the fire PRA study results (and, more generally, PRA study results) are typically not used as the sole basis for decision making. Other sources of information, including other engineering analyses, are also used to support the decision. In other words, the decision making process is risk informed, rather than risk based. Under this risk-informed approach, the decision maker can make use of

information from imperfect or even flawed PRA models, as long as the use of the PRA results and insights improves the decision-making approach for the problem of interest. Siu and Cunningham [88] provide a discussion of challenges of using risk information in fire protection applications and identify a number of lessons from NRC's experience that may be useful to the general fire protection community.

Risk-Informing Plant Fire Protection Programs

In 2004, the NRC amended Section 48 to Part 50 of Title 10 of the Code of Federal Regulations (10 CFR 50.48) [28], which governs fire protection programs for operating U.S. nuclear power plants. The amendment added a risk-informed, performance-based option to what had been a completely deterministic rule. In particular, the amended rule allows (with some exceptions specified in the rule) licensees to maintain a fire protection program that complies with NFPA 805 2001 Edition, the National Fire Protection Association standard for a risk-informed, performance-based fire protection program mentioned earlier in this chapter. The purpose of this amendment, as discussed in NRC staff paper SECY-00-0009, "Rulemaking Plan, Reactor Fire Protection Risk-Informed, Performance-Based Rulemaking," [89] was to, among other things, establish a more reactor-safety-oriented fire protection rule, add appropriate flexibility in some aspects of a licensee's fire protection program, and facilitate the use of alternate approaches that may reduce the need for NRC-approved exemptions from deterministic requirements. The implementation of this rule relies on the licensee's use of a plant-specific fire PRA.

As of mid-2012, as discussed by Harrison et al. [90], two licensees have received NRC approval for their requests to transition their previously deterministic fire protection programs to the risk-informed, performance-based approach allowed by the amended rule. As part of the approval process, the licensees, the broader regulated industry, and the NRC have learned a number of important lessons, some of which apply to the methods, models, and tools of fire PRA. A number of these fire PRA technology issues were addressed during the approval process and documented in a supplement [23] to NUREG/CR-6850 and other publicly available documents (e.g., the NRC's response to a "frequently asked question" on changes to fire frequencies over time [91]). Other issues are being addressed by EPRI and the NRC's Office of Nuclear Regulatory Research. It is expected that the results of this work will support future updates of NUREG/CR-6850, and thereby the development, review, and approval of the three dozen license amendment requests received or anticipated in the next few years.

Other Uses of Fire PRA

Fire PRA methods, tools, data, results, and insights have become integral to the treatment of many fire protection and fire-related issues. For example, the results of work on fire-induced cable failures and circuit faults has been used to rank (by risk significance) potentially important factors governing the likelihood of spurious actuations [90]. This risk ranking has allowed the categorization of these factors into sets governing how they will be treated during fire protection inspections or future research. As another example, NRC is using fire PRA results to focus plant fire inspections on the most important fire protection systems and uses a fire PRA—based tool in its Reactor Oversight Program (ROP) to assess the significance of findings from inspections. Using the results of the Significance Determination Process (SDP), the NRC can employ a number of regulatory responses (e.g., fines, heightened levels of regulatory oversight) [93].

More generally, because the risk from fires is a component of total risk, fire PRA can also play an important role in broader risk-informed activities, even those that are not focused on fire. For example, fire PRA is being used in support of analyses supporting the management

of changing plant configuration (e.g., to inform decisions as to how long a plant may continue to operate when certain equipment is taken out of service for maintenance). As another example, the NRC's guidance on the use of risk information in proposing plant changes indicates under what conditions a small increase in total CDF could be allowed [31]. If fire is an important contributor to either the baseline (pre-change) total CDF or to the change in total CDF, fire PRA can provide important input to decisions regarding the acceptability of the proposed plant change.

Uncertainty in Fire PRA and Current Research

As mentioned earlier, the NRC's 1995 PRA policy statement [8] states that:

> The use of PRA technology should be increased in all regulatory matters to the extent supported by the state-of-the-art in PRA methods and data . . .

The statement's concern with the limitations of PRA remains important in the case of fire PRA, where research is ongoing to address the still-significant uncertainties in results. (Variations in key analytical assumptions can lead to orders of magnitude variations in estimates of fire-induced CDF and qualitatively different risk insights).

The uncertainties in fire PRA results are not due to the general analytical approach described at the beginning of this chapter. All current nuclear power plant fire PRAs use this approach or some slight variant on it. Rather, a good deal of the uncertainty is due to weaknesses and gaps in the current treatment of a number of application details and to the assumptions used by analysts when addressing these weaknesses and gaps. Significant uncertainties can arise in the estimation of the likelihood of important fire scenarios (e.g., when addressing the frequency of large, transient-fueled fires or of self-ignited cable fires), identifying initial conditions leading to fire growth (e.g. size of an oil pool fire upon pump system failure), the modeling of fire growth and suppression (challenges include fire propagation through a stack of cable trays and the incorporation of plant-specific factors as fire brigade training and staffing in the treatment of manual fire fighting), the prediction of fire-induced loss of systems (e.g., when quantifying the likelihood of spurious actuations, when addressing the effect of smoke on equipment), and the analysis of plant and operator responses to the fire (e.g., when modeling operator actions during a severe control room fire). Uncertainties also extend to the mode of operation, as no standard approach has been developed to address fire risk at low power and shutdown operations. Research to reduce (or at least better understand) uncertainties in a number of these areas is continuing. Much of this research is being performed as a collaboration between EPRI and the NRC's Office of Nuclear Regulatory Research. The research activities include:

- The development of a comprehensive U.S. fire events database (FEDB)
- The collection of statistics characterizing potential fire sources in U.S. nuclear power plants
- The performance of experimental studies to examine fire effects and behaviors relevant to fire PRA
- The verification and validation (V&V) of currently available fire models
- The development of improved fire PRA models

Regarding the FEDB, current fire PRAs rely heavily on an EPRI database based largely on voluntary reports [44]. Concerns with the completeness of the reported data have been a limiting factor in the application of event data to fire PRA. The current activity to develop a new, comprehensive FEDB has been planned jointly by EPRI and RES with the actual data gathering activities being led by EPRI. The goal of the effort is to compile a complete list of all fire events at every operating U.S. reactor site occurring between 2000 and 2009. The effort is based on a direct search of plant records. To date, hundreds of thousands of reports have been searched and filtered to identify a few hundred

potentially risk-relevant fire events. This effort is nearing completion as of the fall of 2012 with somewhat more than 80 % of all reactor sites expected to be represented in the initial database release.

Once the new FEDB is complete, EPRI and the NRC are planning to use the data to support new estimates of fire event frequencies and of the manual fire suppression curves. The updated fire frequencies are expected to generally follow the fire frequency bins defined in NUREG/CR-6850, although some refinements may be pursued as feasible (e.g., electrical cabinets may be segregated into voltage or functional classes). The effort is also expected to re-examine the question as to whether fire frequencies are changing over time and to address the treatment of historical events in the fire frequency estimation process.

The update of the manual fire suppression curves will be performed to ensure consistency with the fire frequency analysis. If, for example, the fire frequency estimates include many fires of very short duration, then the suppression curves, which are conditioned on the occurrence of a fire, will be quite aggressive (indicating a high likelihood of successful suppression in a short amount of time). If instead very short duration fires are uniformly screened from the fire frequency analysis, then the estimated fire frequencies will be lower but the matching suppression curves would reflect a higher likelihood of longer duration fires.

Regarding plant fire source population statistics, the estimation of component-based fire frequencies requires data characterizing the potential sites for fires (e.g., electrical cabinets, pumps), as well as data for actual fire event occurrences. Many U.S. plants are currently performing fire PRAs and are counting their ignition source populations. EPRI is working with these plants to compile this information.[17]

Regarding experimental studies, work is continuing on a number of projects. These include the Cable Heat Release, Ignition, and Spread in Tray Installations During Fire (CHRISTIFIRE) project [92], whose data is intended to support the development of improved cable tray fire growth models; the Direct Current Electrical Shorting in Response to Exposure Fire (DESIREE-Fire) project [50], whose data will be used in an expert-elicitation based effort to estimate the likelihood and duration of fire-induced spurious operations in direct current circuits; and an international collaboration with OECD member countries addressing the behavior of high energy arc fault (HEAF) fires associated with electrical switchgear faults. The NRC is also sponsoring research investigating the effectiveness of fire retardant cable coatings to delay fire spread and fire-induced damage, and is planning further research on the behavior of electrical cabinet fires.

Regarding fire model V&V, EPRI and the NRC have jointly addressed a set of fire modeling tools used in current fire PRAs: FIVE-Rev 1 [94], the Fire Dynamics Tools (FDTs) [57], MAGIC [58], CFAST [59], and FDS [52]. The V&V effort, which was performed according to ASTM E1355 ("Evaluating the Predictive Capability of Deterministic Fire Models"), selected appropriate fire scenarios for testing the models, established the theoretical basis and assumptions for the models and their implementation, and validated the models over the range of conditions covered by available fire tests. NUREG-1824/EPRI 1911999 [95] and NUREG-1934/EPRI TR-1023259 [69] provide qualitative and quantitative comparisons of the model predictions versus measurements. Currently the NRC, in conjunction with the National Institute of Standards and Technology (NIST), is in the process of updating the V&V effort to include additional data. This effort is intended to expand the validation ranges of the models for

[17] In addition to data collection, the development of a component-based fire frequency approach that goes beyond that provided in NUREG/CR-6850 will require further analysis. This analysis is needed to characterize the relationship between the number of ignition sources and fire frequency, since this relationship may not be linear. (For example, a plant with 50 pumps may not have twice as many pump fires as a plant with just 25 pumps.)

some application and to refine current understanding of biases. The results of these efforts are documented during routine updates of the FDS technical reference guide [96].

Finally, regarding fire PRA models, a range of analytical methods development activities are underway by NRC and various industry groups. These activities are addressing a variety of topics, including manual fire suppression modeling, fixed fire suppression system reliability, multi-compartment analysis, fire barrier analysis, multiple spurious operation likelihood analysis, and the characterization and analysis of transient fires. NRC and industry are working on suitable processes to develop, review, endorse, and promulgate new or revised analysis methods. The vetting process continues to evolve but has already yielded a number of methods improvements and clarifications.

Additional summary-level information can be found in NUREG-1925 [97], which provides an overview of NRC's research efforts in a wide variety of areas (including but not limited to fire safety).

Summary

Fire probabilistic risk assessment (PRA) is a systematic quantitative tool for dealing with the complex issues that arise when assessing fire safety at a nuclear power plant. Nuclear power plant fire PRA development efforts date back to the late 1970s. While the supporting methods, tools and data used in the analysis process have been refined substantially, the fundamental analysis framework remains essentially unchanged. The most significant change that has occurred over this time is the manner in which fire risk information is being used. In particular, the NRC's development of a risk-informed option to its previously deterministic fire protection regulations, as part of NRC's broader push to increase its use of PRA and risk in all of its regulatory activities, has increased the attention of industry and regulators on fire PRA.

The increased use of fire PRA in regulatory applications implies a need for higher levels of completeness, realism, accuracy, consistency across the analysis and overall quality. Consistency and realism across the multiple analysis elements are goals that continue to challenge fire PRA methods development activities. A particularly important current challenge involves the treatment of fire-induced spurious equipment operation. This analysis, which involves substantial effort to identify key electrical circuits and analyze the potential effects of fire, holds the potential to significantly alter the insights and quantitative results of a fire PRA. A range of efforts are being undertaken by both the NRC and industry to support the evolutionary process of fire PRA maturation in this and other areas. Development needs and priorities are currently being driven in large part by the desire to increase realism. The overarching goal is to increase analysis fidelity and thereby increase decision makers' confidence in the risk insights gained.

Acknowledgements The authors gratefully acknowledge the thoughtful comments of Mark Salley and David Gennardo.

References

1. S. Kaplan and B.J. Garrick, "On the Quantitative Definition of Risk," *Risk Analysis,* 1, pp. 11–27 (1981).
2. "Reactor Safety Study: An Assessment of Accident Risks in U.S. Commercial Nuclear Power Plants," *WASH-1400 (NUREG-75/014),* U.S. Nuclear Regulatory Commission, Washington, DC (1975).
3. "Recommendations Related to Browns Ferry Fire," *NUREG-0050*, U.S. Nuclear Regulatory Commission, Washington, DC (1976).
4. H. Aulamo, J. Martilla, and H. Reponen, "The Full Stories on Armenia and Beloyarsk," *Nuclear Engineering International*, 40, 492, pp. 32–33 (1995).
5. E. Pla, "Fire at Vandellos 1: Causes, Consequences and Problems Identified," in *Proceedings of Fire Protection and Safety at Nuclear Facilities Conference,* Nuclear Engineering International, Barcelona, Spain (1994).
6. S.A. Bohra, "The Narora Fire and Its Continuing Consequences: Backfitting the Indian PHWRs," in *Proceedings of Fire and Safety 1997: Fire Protection and Prevention in Nuclear Facilities,* London, pp. 219–234 (1997).

7. S.P. Nowlen, M. Kazarians, and F. Wyant, "Risk Methods Insights Gained from Fire Incidents," *NUREG/CR-6738,* U.S. Nuclear Regulatory Commission, Washington, DC (2001).
8. "Use of Probabilistic Risk Assessment Methods in Nuclear Activities: Final Policy Statement," U.S. Nuclear Regulatory Commission, *Federal Register,* 60, p. 42622 (60 FR 42622) (1995).
9. S. Nowlen, et al., "EPRI/NRC-RES Fire PRA Methodology for Nuclear Power Facilities," *EPRI TR-1011989* and *NUREG/CR-6850,* Electric Power Research Institute (EPRI), Palo Alto, CA, U.S. Nuclear Regulatory Commission, Washington, DC (2005).
10. G. Apostolakis, "The Concept of Probability in Safety Assessments of Technological Systems," *Science,* 250, pp. 1359–1364 (1990).
11. "Guidance on the Treatment of Uncertainties Associated with PRAs in Risk-Informed Decision Making," *NUREG-1855*, U.S. Nuclear Regulatory Commission, Washington, DC (2009).
12. Z. Musicki et al., "Evaluation of Potential Severe Accidents During Low Power and Shutdown Operations at Surry, Unit 1: Analysis of Core Damage Frequency from Internal Fires During Mid-Loop Operations," *NUREG/CR-6144,* Vol. 3, U.S. Nuclear Regulatory Commission (1994).
13. "Use and Development of Probabilistic Safety Assessment: A CSNI WGRISK Report on the International Situation," *NEA/CSNI/R(2007)12*, Nuclear Energy Agency (2007).
14. S. Nowlen and T. Olivier, "Methodology for Low Power/Shutdown Fire PRA," *NUREG/CR-7114,* draft report for comment, U.S. Nuclear Regulatory Commission (2011).
15. "A Review and Evaluation of the Zion Probabilistic Safety Study," *NUREG/CR-3300*, U.S. Nuclear Regulatory Commission, Washington, DC, (1984).
16. "A Review and Evaluation of the Indian Point Probabilistic Safety Study," *NUREG/CR-2934*, U.S. Nuclear Regulatory Commission, Washington, DC(1982).
17. J.A. Lambright, D.A. Brosseau, A.C. Payne, Jr., and S.L. Daniel, "Analysis of the LaSalle Unit 2 Nuclear Power Plant: Risk Methods Integration and Evaluation Program (RMIEP), Internal Fire Analysis," *NUREG/CR-4832,* Vol. 9, U.S. Nuclear Regulatory Commission, Washington, DC (1993).
18. "Severe Accident Risks: An Assessment for Five U.S. Nuclear Power Plants," *NUREG-1150*, U.S. Nuclear Regulatory Commission, Washington, DC (1990).
19. M.P. Bohn and J. A. Lambright, "Procedures for the External Event Core Damage Frequency Analysis for NUREG-1150," *NUREG/CR-4840,* U.S. Nuclear Regulatory Commission, Washington, DC (1990).
20. "Individual Plant Examination of External Events (IPEEE) for Severe Accident Vulnerabilities, 10 CFR 50.54(f)," *Generic Letter 88–20,* Supplement 4, U.S. Nuclear Regulatory Commission, Washington, DC (June 28, 1991).
21. "Procedural and Submittal Guidance for the Individual Plant Examination of External Events (IPEEE) for Severe Accident Vulnerabilities, Final Report," *NUREG-1407,* U.S. Nuclear Regulatory Commission, Washington, DC (1991).
22. "Perspectives Gained from the Individual Plant Examination of External Events (IPEEE) Program," *NUREG-1742,* U.S. Nuclear Regulatory Commission, Washington, DC (2002).
23. K. Canavan and J.S. Hyslop, "Fire Probabilistic Risk Assessment Methods Enhancements," *EPRI TR-1019259 and NUREG/CR-6850 Supplement 1*, Electric Power Research Institute (EPRI), Palo Alto, CA, U.S. Nuclear Regulatory Commission, Washington, DC (2010).
24. J. Lai "Transcript of ACRS Reliability and PRA Subcommittee Meeting July 26, 2012 [Open], Pages 1-292" ACRS Subcommittee Meeting, Agency Documents Access and Management System (ADAMS) ML122260813, U.S. Nuclear Regulatory Commission, Washington, DC (2012).
25. "Fire Risk Analysis, Fire Simulation, Fire Spreading and Impact of Smoke and Heat on Instrumentation Electronics," *NEA/CSNI/R(99)27*, Nuclear Energy Agency, Paris, France (2000).
26. "Use and Development of Probabilistic Safety Assessment: An Overview of the Situation at the End of 2010," *NEA/CSNI/R(2012)11*, Nuclear Energy Agency (2012).
27. "Development and Application of Level 1 Probabilistic Safety Assessment for Nuclear Power Plants," *IAEA Specific Safety Guide No. SSG-3*, International Atomic Energy Agency, Vienna, Austria (2010).
28. U.S. Code of Federal Regulations, "Fire Protection," *10 CFR 50.48*, August 28, 2007.
29. "Risk-Informed, Performance-Based Fire Protection for Existing Light-Water Nuclear Power Plants," *RG 1.205, Rev. 1*, U.S. Nuclear Regulatory Commission, Washington, DC, (2009).
30. "An Approach For Determining The Technical Adequacy Of Probabilistic Risk Assessment Results For Risk-Informed Activities," *RG 1.200, Rev. 2*, U.S. Nuclear Regulatory Commission, Washington, DC, (2009).
31. "An Approach for Using Probabilistic Risk Assessment in Risk-Informed Decisions on Plant-Specific Changes to the Licensing Basis," *Regulatory Guide 1.174 Rev. 2,* U.S. Nuclear Regulatory Commission, Washington, DC (2011).
32. "Fire Protection for Nuclear Power Plants," *RG 1.189, Rev. 2*, U.S. Nuclear Regulatory Commission, Washington, DC, (2009).
33. Professional Loss Control, Inc., "Fire-Induced Vulnerability Evaluation (FIVE)," *EPRI TR-100370,* Electric Power Research Institute, Palo Alto, CA (1992).

34. W.J. Parkinson et al., "Fire PRA Implementation Guide," *EPRI TR-105928,* Electric Power Research Institute, Palo Alto, CA (1995).
35. "Standard for Level 1/Large Early Release Frequency Probabilistic Risk Assessment for Nuclear Power Plant Applications," *ASME/ANS RA-Sa-2009, Addendum A to RA-S-2008*, ASME, New York, NY, American Nuclear Society, La Grange Park, Illinois (2009).
36. "Performance-Based Standard for Fire Protection for Light Water Reactor Electric Generating Plants, National Fire Protection Association," *NFPA 805*, National Fire Protection Association, Quincy, MA (2001).
37. "Fire Probabilistic Risk Assessment (FPRA) Peer Review Process Guidelines," Draft Version H, Revision 0, *NEI 07-12*, Nuclear Energy Institute, Washington, DC, (2008).
38. G. Apostolakis, M. Kazarians, and D. C. Bley, "Methodology for Assessing the Risk from Cable Fires," *Nuclear Safety,* 23, pp. 391–407 (1982).
39. M. Kazarians, N. Siu, and G. Apostolakis, "Fire Risk Analysis for Nuclear Power Plants: Methodological Developments and Applications," *Risk Analysis,* 5, pp. 33–51 (1985).
40. American Nuclear Society and the Institute of Electrical and Electronics Engineers, "PRA Procedures Guide: A Guide to the Performance of Probabilistic Risk Assessment for Nuclear Power Plants," *NUREG/CR-2300,* U.S. Nuclear Regulatory Commission, Washington, DC (1983).
41. C.L. Smith and S.T. Wood, "Systems Analysis Programs for Hands-on Integrated Reliability Evaluations (SAPHIRE) Version 8," *NUREG/CR-7039,* U.S. Nuclear Regulatory Commission, Washington, DC (2011).
42. F. Rahn, "Computer Aided Fault Tree Analysis System, Version 5.4", *EPRI 1018460*, Electric Power Research Institute, Palo Alto, California (2009).
43. F. Rahn, "FRANX, Version 4.1", *EPRI 1021231*, Electric Power Research Institute, Palo Alto, California (2010).
44. "Fire Events Database and Generic Ignition Frequency Model for U.S. Nuclear Power Plants", *EPRI 1003111*, Electric Power Research Institute, Palo Alto, California (2001).
45. C.L. Atwood, et al., "Handbook of Parameter Estimation for Probabilistic Risk Assessment," NUREG/CR-6823, U.S. Nuclear Regulatory Commission, Washington, DC (2002).
46. M. Kazarians and G. Apostolakis, "Modeling Rare Events: The Frequencies of Fires in Nuclear Power Plants," in *Proceedings of Workshop on Low Probability/High Consequence Risk Analysis, Society for Risk Analysis,* Arlington, VA (1982).
47. D. Funk and E. Davis, "Characterization of Fire-Induced Circuit Faults," *TR-1003326,* Electric Power Research Institute, Palo Alto, CA (2002).
48. F.J. Wyant and S.P. Nowlen, "Cable Insulation Resistance Measurements Made During Cable Fire Tests," *NUREG/CR-6776,* U.S. Nuclear Regulatory Commission, Washington, DC (2002).
49. J.L. LaChance, S.P. Nowlen, F.J. Wyant, and V.J. Dandini, "Circuit Analysis—Failure Mode and Likelihood Analysis," *NUREG/CR-6834,* U.S. Nuclear Regulatory Commission, Washington, DC (2003).
50. S.P. Nowlen, J.W. Brown, T.J. Olivier, and F.J. Wyant, "Direct Current Electrical Shorting in Response to Exposure Fire (DESIREE-Fire): Test Results," *NUREG/CR-7100*, U.S. Nuclear Regulatory Commission, Washington, DC (2012).
51. G. Taylor, et al., "Electrical Cable Test Results and Analysis During Fire Exposure (ELECTRA-FIRE): A Consolidation of Three Major Fire-Induced Circuit and Cable Failure Experiments Performed Between 2001 and 2011," *NUREG-2128*, draft report for comment, U.S. Nuclear Regulatory Commission, Washington, DC (2012).
52. R.J. Budnitz "Spurious Operation of Electrical Circuits Due to Cable Fires: Results of an Expert Elicitation," *TR-1006961,* Electric Power Research Institute, Palo Alto, CA (2002).
53. R.J. Budnitz, et al., "Recommendations for Probabilistic Seismic Hazard Analysis: Guidance on Uncertainty and Use of Experts," *NUREG/CR-6372*, U.S. Nuclear Regulatory Commission, Washington, DC, 1997.
54. A.M. Kammerer and J.P. Ake, "Practical Implementation Guidelines for SSHAC Level 3 and 4 Hazard Studies," NUREG-2117, U.S. Nuclear Regulatory Commission, Washington, DC (2012).
55. S. Cooper and S. Lewis, "EPRI/NRC-RES Fire Human Reliability Analysis Guidelines," *EPRI 1023001*, Electric Power Research Institute, Palo Alto, CA, *NUREG-1921*, U.S. Nuclear Regulatory Commission, Washington, DC (2012).
56. V. Ho, S. Chien, and G. Apostolakis, "COMPBRN IIIe: An Interactive Computer Code for Fire Risk Analysis," *EPRI NP-7282,* Electric Power Research Institute, Palo Alto, CA (1991).
57. N. Iqbal and M. Salley, "Fire Dynamics Tools (FDTs): Quantitative Fire Hazard Analysis Methods for the U.S. Nuclear Regulatory Commission Fire Protection Inspection Program," *NUREG-1805,* U.S. Nuclear Regulatory Commission, Washington, DC (2004).
58. B. Gautier and C.H. Le Maitre, "User's Guide for the Softward MAGIC: Version 3.4.2," HT-31/99/007/A, Electricité de France, Paris, France (1998).
59. R. Peacock, W. Jones, P. Reneke, and G. Forney, "User's Guide for CFAST: An Engineering Tool for Estimating Fire and Smoke Transport," *NIST Special Publication 929,* National Institute for Standards and Technology, Gaithersburg, MD (2000).
60. K. McGrattan et al., "Fire Dynamics Simulator, Technical Reference Guide," *NISTIR-6467,* National Institute for Standards and Technology, Gaithersburg, MD (2002).

61. A. Tewarson, J.L. Lee, and R.F. Pion, "Categorization of Cable Flammability, Part 1: Laboratory Evaluation of Cable Flammability Parameters," *EPRI NP-1200,* Part 1, Electric Power Research Institute, Palo Alto, CA (1979).
62. J.L. Lee, "A Study of Damageability of Electrical Cables in Simulated Fire Environments," *EPRI NP-1767,* Electric Power Research Institute, Palo Alto, CA (1981).
63. L.L. Lukins, "Nuclear Power Plant Electrical Cable Damageability Experiments," *NUREG/CR-2927,* U.S. Nuclear Regulatory Commission, Washington, DC (1982).
64. W.T. Wheelis, "Transient Fire Environment Cable Damageability Test Results: Phase I," *NUREG/CR-4638,* U.S. Nuclear Regulatory Commission, Washington, DC (1986).
65. S.P. Nowlen, "The Impact of Thermal Aging on the Flammability of Electric Cables," *NUREG/CR-5619,* U.S. Nuclear Regulatory Commission, Washington, DC (1991).
66. S.P. Nowlen, "The Impact of Thermal Aging on the Fire Damageability of Electric Cables," *NUREG/CR-5546,* U.S. Nuclear Regulatory Commission, Washington, DC (1991).
67. J.M. Chavez, "An Experimental Investigation of Internally Ignited Fires in Nuclear Power Plant Control Cabinets: Part 1: Cabinet Effects Tests," *NUREG/CR-4527,* Vol. 1, U.S. Nuclear Regulatory Commission, Washington, DC (1987).
68. J.M. Chavez and S.P. Nowlen, "An Experimental Investigation of Internally Ignited Fires in Nuclear Power Plant Control Cabinets: Part II: Cabinet Effects Tests," *NUREG/CR-4527,* Vol. 2, U.S. Nuclear Regulatory Commission, Washington, DC (1988).
69. "Nuclear Power Plant Fire Modeling Application Guide (NPP FIRE MAG)—Draft Report for Comment," *EPRI TR-1023259,* Electric Power Research Institute (EPRI), Palo Alto, CA, *NUREG-1934,* U.S. Nuclear Regulatory Commission, Washington, DC U.S. (2012).
70. D. Cline, W. A. von Riesemann, and J. M. Chavez, "Investigation of Twenty Foot Separation Distance as a Fire Protection Method as Specified in 10CFR50, Appendix R," *NUREG/CR-3192,* U.S. Nuclear Regulatory Commission, Washington, DC (1983).
71. V.F. Nicolette and K.T. Yang, "Fire Modeling of the Heiss Dampf Reaktor Containment," *NUREG/CR-6017,* U.S. Nuclear Regulatory Commission, Washington, DC (1995).
72. S.P. Nowlen, "Enclosure Environment Characterization Testing for the Base Line Validation of Computer Fire Simulation Codes," *NUREG/CR-4681,* U.S. Nuclear Regulatory Commission, Washington, DC (1987).
73. "International Collaborative Project to Evaluate Fire Models for Nuclear Power Plant Applications: Proceedings of 5th Meeting held at National Institute of Standards and Technology, Gaithersburg, MD on May 2–3, 2002," *NUREG/CP-0181,* U.S. Nuclear Regulatory Commission, Washington DC (2002).
74. N. Siu and G. Apostolakis, "Probabilistic Models for Cable Tray Fires," *Reliability Engineering,* 3, pp. 213–227 (1982).
75. N. Siu, D. Karydas, and J. Temple, "Bayesian Assessment of Modeling Uncertainty: Application to Fire Risk Assessment," in *Analysis and Management of Uncertainty: Theory and Application* (B.M. Ayyub, M.M. Gupta, and L.N. Kanal, eds.), North-Holland, New York, pp. 351–361 (1992).
76. E. Droguett and A. Mosleh, "Bayesian Methodology for Model Uncertainty Using Model Performance Data," *Risk Analysis*, *28*, No. 5, pp. 1457–1476 (2008).
77. M. Brandyberry and G. Apostolakis, "Response Surface Approximation of a Fire Risk Analysis Computer Code," in *Proceedings of International Topical Meeting on Probabilistic Reliability and Safety Assessment* (PSA '89), American Nuclear Society, LaGrange Park, IL (1989).
78. J. Wanless, "Investigation of Potential Fire-Related Damage to Safety-Related Equipment in Nuclear Power Plants," *NUREG/CR-4310,* U.S. Nuclear Regulatory Commission, Washington, DC (1985).
79. M.J. Jacobus, "Screening Tests of Representative Nuclear Power Plant Components Exposed to Secondary Fire Environments," *NUREG/CR-4596,* U.S. Nuclear Regulatory Commission, Washington, DC (1986).
80. R.A. Vigil and S.P. Nowlen, "An Assessment of Fire Vulnerability for Aged Electrical Relays," *NUREG/CR-6220,* U.S. Nuclear Regulatory Commission, Washington, DC (1995).
81. T. Tanaka, S.P. Nowlen, and D.J. Anderson, "Circuit Bridging of Components by Smoke," *NUREG/CR-6476,* U.S. Nuclear Regulatory Commission, Washington, DC (1996).
82. R.D. Peacock, T.G. Cleary, P.A. Reneke, and D.-C. Murphy, "A Literature Review of the Effects of Smoke from a Fire on Electrical Equipment," *NUREG/CR-7123*, U.S. Nuclear Regulatory Commission, Washington, DC, (2012).
83. K. McGrattan, "Cable Response to Live Fire (CAROLFIRE) Volume 3: Thermally-Induced Electrical Failure (THIEF) Model," NUREG/CR-6931, Vol. 3, U.S. Nuclear Regulatory Commission, Washington, DC (2008).
84. N. Siu and G. Apostolakis, "A Methodology for Analyzing the Detection and Suppression of Fires in Nuclear Power Plants," *Nuclear Science and Engineering,* 94, pp. 213–226 (1986).
85. N. Siu and G. Apostolakis, "Modeling the Detection and Suppression of Fires in Nuclear Power Plants," in *Proceedings of the International ANS/ENS Topical Meeting on Probabilistic Safety Methods and Applications,* San Francisco, pp. 56-1–56-8 (1985).

86. "FPETOOL 3.0," U.S. Department of Commerce, Washington, DC, and National Institute of Standards and Technology, Gaithersburg, MD (1992).
87. G. Taylor and M.H. Salley, "Electric Raceway Fire Barrier Systems in U.S. Nuclear Power Plants," *NUREG-1924*, U.S. Nuclear Regulatory Commission, Washington, DC (2010).
88. N. Siu and M. Cunningham, "Using Risk Information: Lessons Learned from One Agency's Approach," Proceedings of United Engineering Foundation Conference on the Technical Basis for Performance-Based Fire Regulations, San Diego, CA, January 7–11, 2001, pp. 130–140.
89. "Rulemaking Plan, Reactor Fire Protection Risk-Informed, Performance-Based Rulemaking," SECY-00-0009, U.S. Nuclear Regulatory Commission, Washington, DC (2000).
90. D. Harrison, A. Klein, H. Barrett, and P. Lain, "Lessons Learned from Risk-Informed, Performance-Based Fire Protection (NFPA 805) Regulatory Reviews," *Proceedings of International Conference on Probabilistic Safety Assessment and Management (PSAM 11/ESREL 2012),* Helsinki, Finland (2012).
91. A.R. Klein, "Closure Of National Fire Protection Association 805 Frequently Asked Question 08-0048 Revised Fire Ignition Frequencies," Staff memorandum, Agency Documents Access and Management System (ADAMS) ML092190457, U.S. Nuclear Regulatory Commission, Washington, DC (2009).
92. K. McGrattan, et al., "Cable Heat Release, Ignition, and Spread in Tray Installations During Fire (CHRISTIFIRE)," draft report for comment, *NUREG/CR-7010*, U.S. Nuclear Regulatory Commission, Washington, DC (2010).
93. "Fire Protection Significance Determination Process," *Inspection Manual,* Chapter 0609, Appendix F, U.S. Nuclear Regulatory Commission, Washington, DC (2005).
94. B. Najafi and F. Joglar-Billoch, "Fire Modeling Guide for Nuclear Power Plant Applications," *TR-1002981,* Electric Power Research Institute (2002).
95. M.H. Salley and R.P. Kassawara,"Verification and Validation of Selected Fire Models for Nuclear Power Plant Applications," *EPRI 1011999*, Electric Power Research Institute, Palo Alto, CA, *NUREG-1824*, U.S. Nuclear Regulatory Commission, Washington, DC (2007).
96. K. McGrattan, S. Hostikka, J. Floyd, and R. McDermott, "Fire Dynamics Simulator (Version 5) Technical Reference Guide," NIST Special Publication 1018-5, National Institute for Standards and Technology, Gaithersburg, MD (2010).
97. "Research Activities 2009," *NUREG-1925*, U.S. Nuclear Regulatory Commission, Washington, DC (2009).

Nathan O. Siu is a senior technical adviser for PRA analysis in the Office of Nuclear Regulatory Research of the U.S. Nuclear Regulatory Commission. His major activities involve the development of improved methods for probabilistic risk assessment, including fire risk assessment.

Nicholas Melly is a fire protection engineer in the Office of Nuclear Regulatory Research. His major activities involve development of improved methods for fire risk assessment.

Steven P. Nowlen is now retired, but was distinguished member of the technical staff at Sandia National Laboratories. His major activities involve fire protection research for nuclear power plants including experimental investigations and the development and application of fire PRA methods, tools, and data.

Mardy Kazarians is a consultant who has conducted several fire PRAs in the U.S. and abroad. He was a major contributor in the development of the fire PRA methods used in early fire PRAs and still in use today.

Fire Risk in Mass Transportation

90

Armin Wolski and Jarrod Alston

Introduction

For many, the concept of fire risk elicits thoughts of the built environment. Yet occupants in the built environment are also passengers on airplanes, in trains, and on ships. According to the U.S. Department of Transportation, the number of passengers boarding scheduled commercial airlines exceeded 700 million in 2014. Rail rapid transit systems throughout the United States (U.S.) carry almost two billion passengers annually. APTA reports that ferryboats account for more than 400 million passenger miles per year nationally [1]. In 2010, motor coaches (or buses) topped 76.1 billion passenger miles in the U.S. and Canada [2]. Every mode of transportation carries with it unique risks; the risks are dependent on a myriad of factors, including design, construction, maintenance, and operation. Understanding or comparing the risks associated with and between the various methods of transport is not always direct. It is complicated by various metrics that can be used for example, risk per distance, risk per trip, risk per passenger exposure hour. For example per mile traveled, the fatality risk in air transport is less than that for bus transport, however, per trip, the risk in air transport is on the order of 100 times greater than that of bus transport [3].

The fire risk problem in most passenger transportation systems is unlike the fire risk problem in the built environment. In comparison to small fires in buildings, the small fires in many modes of transportation could have a significant impact on life and business continuity. From the regulatory perspective, the fire risk problem in transportation systems is undoubtedly affected by risk perceptions. Passengers may perceive risk, including fire risk, in airplanes different from fire risk in buildings. And from an engineering perspective, standard fire risk management solutions for buildings may not be appropriate for transportation systems. For example, options such as compartmentation or automatic fire sprinkler systems may not be available to some transportation systems.

This chapter discusses some of the unique fire risks posed by transportation systems, the current regulatory framework for various systems, and how risk assessment can be or has been used by regulators, operators, or owners to their benefit. Since the three transit systems share common risk factors, decision makers and risk managers face similar risk problems and might be served well by similar risk assessment methods. The methods can be applied either at the regulatory level in order to optimize safety regulations or at the project level, where decision analysis is a means to choose between design options.

A. Wolski (✉) • J. Alston
Armin is based in the San Francisco Bay Area

M.J. Hurley (ed.), *SFPE Handbook of Fire Protection Engineering*,
DOI 10.1007/978-1-4939-2565-0_90, © Society of Fire Protection Engineers 2016

Fire Risk in Transportation Systems

Distinguishing characteristics in transportation systems amplify the risk factors compared to building fire safety. A (small) 40 kW fire in the middle of a five story atrium poses little threat to the building or its occupants, whereas the same fire in a subway carriage is a major and possibly imminent life safety threat with additional and significant financial impacts. Or, compared to building occupants, passengers 25,000 ft (7620 m) above ground, or 25 ft (7.62 m) underground, or 25 mi (40.2 km) out to sea may not have the option of "leaving" the scene of the fire at their discretion. Furthermore, in contrast to buildings, egress from a train or a vessel may be impaired, due to an accident-induced fire. In extreme cases, a train may be overturned [4] or a boat may be listing, affecting egress.

Solving the risk problem in transportation systems is further complicated by the sensitivity to operational issues. Vessel, vehicle, or aircraft operation is highly dependent on human factors. Improper operation of a vessel or vehicle has higher consequences, many relating to fire safety. As dynamic systems, fire safety systems in transportation systems rely more on proper operations and maintenance than do static structures.

Aviation Fire Safety

Over the course of 100 years, air transport has developed into an international and transcontinental business. For some, it is the only option for long-range travel, and for many, it is a mode of mass transit. A complicated set of international agreements is required to ensure safe design and operation of aircraft between countries. Most countries have their own airworthiness codes and regulations to some degree. However, many countries accept sections of other countries' codes, particularly Federal Aviation Regulations of the United States, British Civil Airworthiness Requirements (BCARs) of the United Kingdom, [5] and Joint Airworthiness Regulations (JARs) from the Joint Aviation Authorities of Europe.

The overall general risk to aircraft and air passengers has been reduced over the decades with improvements in warning systems (both ground proximity and transponders), de-icing operations, runway overrun design, aircraft controls, and improvements in material/structural testing. Still, aircraft risk, including aircraft fire risk, remains a high-risk problem characterized by low-frequency, high-consequence potential. The overall accident rate of aircraft on a per-mile basis is roughly 1000 times safer than that of rail or ferry; however, the likelihood of fatality is significantly higher per occurrence [6].

Efforts have been ongoing to address the aviation fire risk problem among passenger aircraft. Key improvements include the following:

1. *Electrical systems*. The aging of electrical systems and improper maintenance of damaged or worn systems are areas of vulnerability. Advancements in wiring insulation technology and maintenance operation are reported to have reduced the number of accidents attributed to electrical systems.
2. *Combustible furnishings*. Combustible furnishings in the main cabin present a significant fire load. Ongoing research and development is expected to improve the performance of furnishings and finishes, particularly composite materials.
3. *Lavatories*. As a result of numerous in-flight fires, the Federal Aviation Administration (FAA) amended regulations to require a smoke detector in each lavatory and an automatic fire extinguisher in each lavatory trash receptacle [7]. Small fires in lavatories have been responsible for several fatal accidents [1].

More recent areas of concern include the following [8]:

1. *Cargo holds*. Cargo holds can harbor dangerous goods that pose either a significant ignition threat or fuel load. Cargo hold fires have been one of the most significant sources of fires in major fire incidences in modern passenger jet transportation [9]. Further research and development has been intent on improving test methods, suppression system effectiveness, and fire resistive integrity [7].
2. *Fuel tanks*. Fuel tanks present an explosion and rupture hazard. Developments in gaseous

inerting systems are expected to decrease the incidences of fuel tank fires in the future. In addition, efforts are under way in reducing the fire impact due to fuel tank rupture.

3. *Hidden materials fires*. Insulation within the hull cavity is under investigation for possible improvements [10].
4. *Postcrash survivability*. When the crash involves high-impact forces, passenger and crew survivability is unlikely; however, risk reduction has focused on what is referred to as "impact survivable, postcrash fire" scenario. Under this scenario, increased attention has been placed on improving egress [11].

Improvements in these areas are making in-flight fires on new commercial airplanes extremely rare and the trend of fire fatalities has been falling [12, 13] (Figs. 90.1, 90.2, and 90.3).

Simply the scale and geometry of an aircraft creates a fire environment wherein the occupants are much vulnerable to fires. A small fire, which would ordinarily pose little or no threat in a

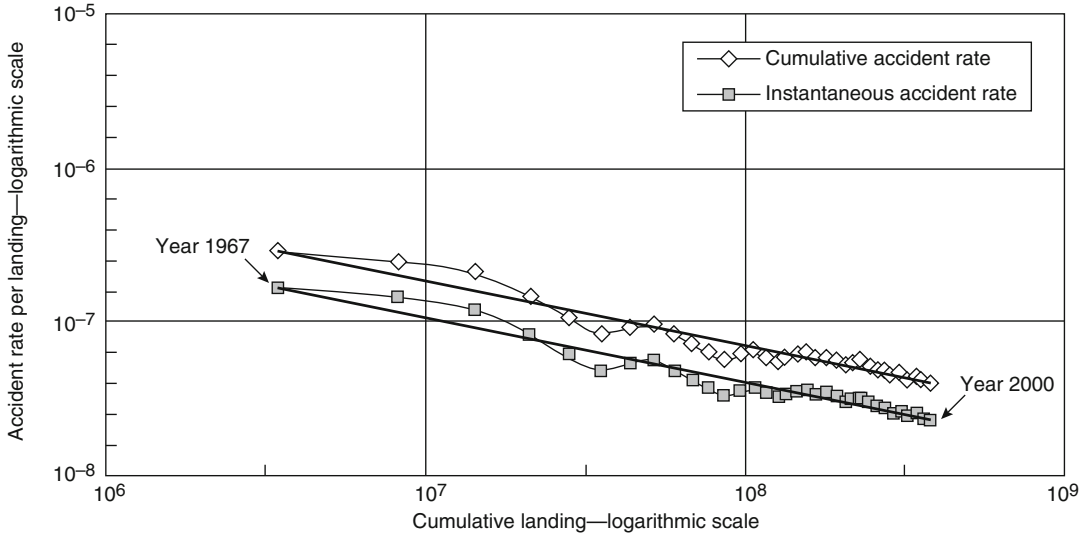

Fig. 90.1 Rate of fire-caused accidents

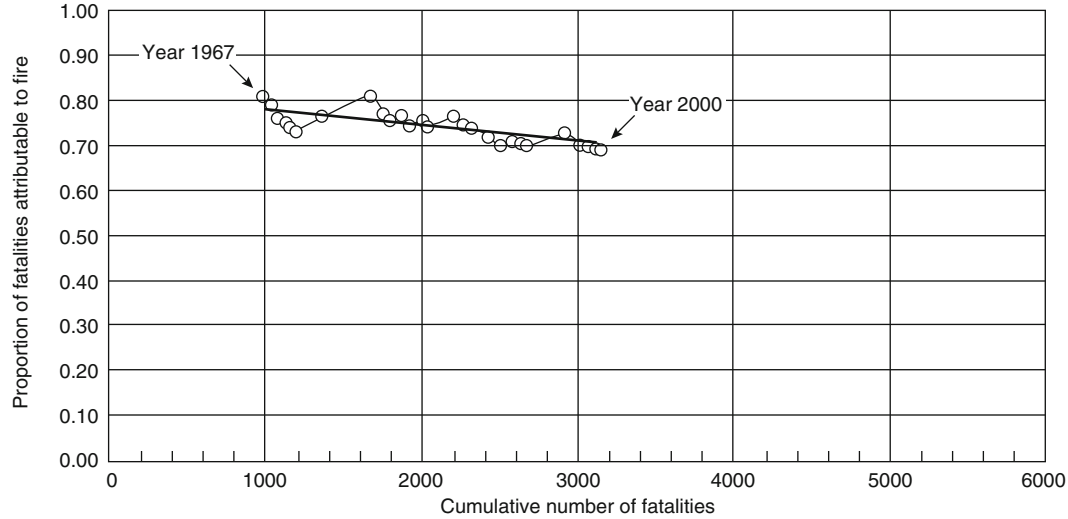

Fig. 90.2 Proportion of fatalities attributed to fire

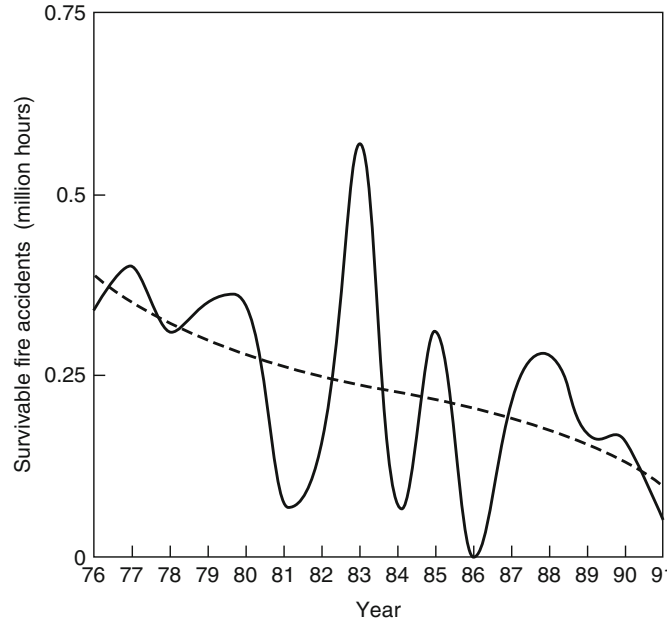

Fig. 90.3 Survivable fire incidents per million flight hours (larger jet/turboprop)

building, could be catastrophic in an aircraft. The cabin space of even the largest airplanes could rapidly fill with smoke endangering the lives of passengers.

Unlike occupants of a building, passengers do not have the option of escape during an in-flight fire occurrence. Obviously, passengers and crew must await landing the plane before any reasonable egress can begin. In the 1980s research conducted by the FAA on commercial aircraft exposed to an external fuel fire indicated that the time available for passenger egress before flashover occurred in the cabin was approximately 90 s. This 90-s emergency evacuation performance, through half the number of exits, is demonstrated in every commercial aircraft in order for an aircraft to be certified. The demonstration is based on a configuration with a full load of passengers having a distribution of gender and age approximating that of the flying public. Evacuation modeling has been shown to be a useful tool in initial assessments [14].

Rail Fire Safety

Similar to the aircraft risk problem, a small fire in a rail carriage, which would ordinarily pose no threat in a building, could pose a serious emergency issue in a rail vehicle. Like an aircraft cabin, a rail carriage could rapidly fill with smoke endangering the lives of passengers, have immediate impact on sensitive and expensive equipment, and affect schedules and operations for hours. And, although rail passengers may, like in aircraft, be more vulnerable to smaller fires, rail passengers often have better means and more options to remove themselves from the imminent hazard by escaping to other rail compartments, into a station, or into a tunnel.

One source of U.S. rail accident statistics is the Federal Railroad Administration (FRA). Taking the time period from 2002 to 2006 as an example, the FRA reports that most fires are electrical in origin. For the reported time period, fire caused more than $20 million in damage [15]. Another source of fires is collisions with vehicles at grade crossings or with other trains, which lead the list of all accidents. Similar to an aircraft liquid fuel fire, a fuel fire spilled from the collided vehicle or a (diesel-electric) train is a common fire exposure. An example of such an accident occurred near Bourbonnais, Illinois, in 1999 [16] when a train struck a truck at a grade crossing. Leaking fuel from one of the locomotives ignited and engulfed a sleeping car

where 11 deaths occurred. Interior fires in moving rail vehicles are uncommon with most such incidents involving small quantities of smoke from malfunctioning or overheating equipment. A fatality involving an Amtrak bilevel sleeping car (cigarette on a mattress) occurred in 1982 in Gibson, California [17].

Vandalism is another source of fires in subways and commuter rail systems. Scenarios may involve newspapers and small amounts of flammable liquids used to ignite seats that may be slashed to expose interior padding. Flammable liquids were the ignition source in a catastrophic fire in the 2003 Daegu subway fire in Korea, which resulted in 193 fatalities and 146 injuries. The fire started while the car was still in the station. Many of the fatalities were passengers who arrived in a later incoming train on adjacent tracks. The passengers on the second train, delayed in evacuation, were exposed to heavy smoke as they moved through the station to their nearest exits. Operational errors are alleged to have led to the delays and significant life losses [18].

Tunnels and bridges represent further complications for rail fire safety. Fires in tunnels pose an additional threat because the fire effluent is contained around the train where it can expose passengers both inside and outside the carriages. Although emergency procedures usually require trains to continue to travel to a point outside a tunnel, fires can be coincident with breakdowns and accidents in these sensitive areas. Exiting is then often difficult and often severely restricted. Furthermore, a fire may affect the tunnel's structural integrity necessitating the interruption in service for an indeterminate period for inspection and repair. Bridges or other elevated track sections also restrict the ability of people to move to a safe location away from the train.

The 1996 English Channel tunnel fire involved a fire originating in a carrier wagon at the rear of the train [19]. Normally, the standard emergency procedure under such conditions was to continue travel to the end of the tunnel; however, a warning light on the train's control panel indicated an abnormality that necessitated stopping the train. When the chef de train (conductor) investigated the fire, heavy smoke entered the occupied club car affecting more than 30 passengers. The passengers needed to be evacuated into the tunnel through a cross passage and onto a train in the adjacent tunnel. The fire burned for more than 8 h and resulted in significant spalling of the tunnel's concrete liner. These issues need to be addressed where trains operate in long tunnels or have extended elevated sections.

In the United States, although all serious passenger rail accidents are investigated by the National Transportation Safety Board (NTSB), public pressure for safety regulation of rail transportation has not always been strong [20]. However, following the 1996 Silver Spring accident where a Marc commuter train collided with an Amtrak passenger train, resulting in 11 deaths, there was increased interest by the Federal Railroad Administration (FRA) to replace 1984 Federal Transit Administration safety guidelines with regulations. These regulations, updated with information from National Institute of Standards and Technology (NIST) research, were promulgated in 1999 [21] and the associated performance criteria can be found in NFPA 130 [22]. The focus is on providing a high level of fire performance for combustible materials found in vehicles. Like aircraft materials, many are designed to be difficult to ignite, and generate less smoke.

There are other fire databases that can be examined, such as the National Fire Incident Reporting System (NFIRS). A recent search of NFIRS for passenger rail fire incidents for the 10 year period from 1988 to 1997 identified 71 fires resulting in 2 civilian deaths and 4 injuries. Federal regulations (49CFR, Part 225) require that incidents that result in a fatality or injury or result in damage to property exceeding a threshold ($6700 for 2004) be reported. A recent search of this database identified 156 fire incidents of interest in United States for the 14 year period from 1985 to 1998.

Fire Safety in Motor Coaches and Buses

According to the Federal Transit Administration, bus fires are considered a serious problem: they cause safety, financial, and service problems for transit agencies [23]. Not unlike a fire in a rail vehicle, a small fire in a bus could pose a serious emergency issue. Should a fire occur within the passenger compartment of a bus, the compartment can rapidly fill with smoke and generate a dangerous environment for passengers. Similarly, if a fire originates in the engine compartment or the wheel housing and is able to develop and penetrate into the passenger compartment, a dangerous environment can rapidly develop. The majority of fires originate in the engine compartment, often due to damaged wiring near fuel and oil lines, mechanical problems, and electrical deficiencies [24]. Some fires are caused by humans, discarded smoking materials and/or arson. However, buses typically operate as surface vehicles in open environments which would allow the operator to rapidly bring the vehicle to a stop upon detection of the fire and initiate evacuation. Additionally, the passengers would be evacuating to a relatively safe environment unless operating in a shared or dedicated tunnel.

The United States Federal Transit Administration collects statistics of transit accidents, casualties, and crimes under the National Transit Database (NTD) reporting system. The statistics are collected for multiple modes of transportation including heavy rail, light rail, busses, and vanpools, among others. The data (available online at http://transit-safety.volpe.dot.gov/Data/SAMIS.aspx) are compiled into *Transit Safety & Security Statistics & Analysis Annual Report* [25, 26]. Data from 1997 to 2007 relating to busses are provided in Table 90.1.

The focus of the statistics is the occurrence of incidents that result in property losses, injury, or fatalities. The data also include operating statistics useful in risk analyses such as numbers of vehicles in operation, vehicle miles travelled, numbers of passengers, and numbers of passenger miles travelled. Information regarding the fire area of origin cause is not available in the NTD. Focusing on the period after 2002, as this is the point at which the NTD's thresholds for reporting were changed, an average of 207 bus fires occurred annually in which medical treatment was necessary or resulted in damage in excess of $7500. In that period, an average of 23 injuries were reported and no fatalities.

In 2006, in response to a September 2005 Texas motorcoach fire that results in 23 fatalities, the National Fire Protection Association published *Vehicle Fires Involving Buses and School Buses* [27]. The data in the report was drawn from the National Fire Incident Reporting System (NFIRS) and is indicative of the number of incidents to which fire departments in the United States responded. As such, it was not subject to the NTD threshold levels and is more extensive than the NTD database as it extends beyond those agencies or operators that are required by law to submit to the NTD. The statistics were later updated in *U.S. Vehicle Fire Trends and Patterns* [28] and indicated that on average of 2350 bus or school bus fires were reported annually or more than six (6) per day, during the 5-year period of 2003–2007. From these 2350 fires were annual averages of seven (7) civilian deaths, 27 civilian injuries, and $26 million in direct property damage which equate to 1 % of vehicle fires, 2 % of vehicle fire deaths, 2 % of vehicle fire injuries, and 2 % of vehicle fire property damage. Further examination of the statistics reveals an increased risk of bus fires in relation to other highway vehicles. The rate of bus vehicle fires on a miles travelled basis is almost four (4) times that of all other highway vehicles. The increase in risk is further exaggerated when considering the rate of fatalities (7×) or injuries (9×) from bus fires relative to that from all other highway vehicles.

With respect to the vehicle fire causes, the majority (59 %) of bus and school bus fires were attributed to a mechanical failure or malfunction. An additional 25 % were the result of electrical failures or malfunctions. Collisions or overturns only accounted for 10 (<1 %) bus or school bus fires per year. Exposure fires were attributed as the cause of up to 90 (1 %) fires

Table 90.1 Bus incidents from 1997 to 2007 resulting in losses and/or casualties broken down by incident type (Source: National Transit Database [25])

	1997	1998	1999	2000	2001	2002	2003	2004	2005	2006	2007
Total incidents	40,524	41,616	41,094	41,677	40,321	19,892	11,053	11,787	11,940	13,112	12,419
Collisions	22,919	22,220	21,370	22,069	21,769	12,767	6677	6802	6916	7645	7186
Running of road	76	57	37	58	30	54	43	35	66	93	47
Fires	240	325	282	296	384	194	161	168	172	247	297
Not otherwise classified	17,285	19,011	19,403	19,252	18,137	6,831	4141	4755	4754	5071	4835
Property damage (× $1,000,000)	34.2	41.3	41.0	41.3	41.0	25.7	28.7	20.5	16.6	22.1	21.5
Total fatalities	109	109	102	90	95	78	87	77	66	94	90
Fatalities from collisions	100	90	90	81	89	64	73	61	49	76	76
Fatalities from running off road	0	0	1	1	0	0	0	0	0	0	0
Fatalities from fires	0	0	0	0	0	0	0	0	0	0	0
Fatalities from not otherwise Classified	8	17	10	7	5	13	14	14	17	14	9
Total injuries	39,181	41,035	41,221	40,925	38,840	11,995	11,493	11,898	11,560	11,812	12,859
Injuries from collisions	20,032	20,043	20,243	20,276	19,511	7172	7126	7133	7113	7074	7710
Injuries from running off road	113	93	48	53	21	39	54	32	74	112	65
Injuries from fires	42	52	36	47	105	32	17	9	15	45	22
Injuries from not otherwise classified	18,992	20,844	20,888	20,548	19,203	4746	4292	4713	4357	4572	5057
vehicles	40,909	42,621	43,743	44,024	45,011	45,325	53,680	52,984	53,091	54,139	74,192
Vehicle miles (× 1,000,000)	1719	1779	1835	1868	1911	1919	1876	1891	1853	1849	1872
Passengers (× 1,000,000)	4554	4712	4926	4959	5065	5078	4810	4732	4815	4822	4804
Passenger miles (× 1,000,000)	16,696	17,113	17,743	17,763	18,369	18,120	17,241	16,855	17,207	17,655	17,635

The drop in the incidents, injuries, collisions, and not otherwise classifieds (personal casualties) starting in 2002 is due to the change of the incident thresholds. The injury definition was changed in 2002 to only incidents involving immediate medical treatment away from the scene; previously, any reported incident/injury was reported. The property damage reportable threshold was also changed in 2002 to total property damage exceeding $7500; previously, the threshold for property damage incidents was $1000 in transit property damage only

Table 90.2 U.S. bus and school bus fires by cause, 1999–2003 averages (Source: Vehicle Fires Involving Buses and School Buses [27])

Cause	Fires		Civilian deaths		Civilian injuries		Direct property damage (in millions)	
Failure of equipment or heat source	1320	(60 %)	1	(39 %)	22	(74 %)	$14.0	(58 %)
Unintentional	660	(30 %)	1	(34 %)	6	(19 %)	$7.8	(32 %)
Unclassified cause	130	(6 %)	1	(27 %)	0	(0 %)	$1.3	(5 %)
Intentional	100	(4 %)	0	(0 %)	0	(0 %)	$1.1	(5 %)
Act of nature	10	(0 %)	0	(0 %)	2	(7 %)	$0.0	(0 %)
Total	2210	(100 %)	3	(100 %)	30	(100 %)	$24.2	(100 %)

per year. Roughly 4 % of bus and school bus fires were designated as intentional in nature. Based on the previous statistics, it would be expected that the majority (69 %) of fires originate in the bus "engineering" areas (engine area, running gear, wheel area) [27, 28] (Table 90.2).

Outside of the U.S., the problem of bus fires has garnered special attention. The SP Technical Research Institute of Sweden undertook a project on bus fire safety with the objective of decreasing the number and consequence of bus fires [29]. Of particular focus in the project was the adequacy or inadequacy of current test methods in screening materials used in bus construction. A key part of the SP project, was a statistical survey of fires in Norway and Sweden focusing on fire causes and consequences. The survey results showed that an annual average of 49 and 122 bus fires were reported in Norway and Sweden, respectively [30]. The number of incidents implies that roughly 1.0–1.4 % of buses in service in Norway and Sweden are involved in a fire incident each year. The study identified several principle causes of fires in buses: arson, heat, vibration, material fatigue/malfunction, and inadequate maintenance. Measures to reduce the impact of a fire event on a bus include good engineering, detection systems, manual and automatic suppression/extinguishment systems, and inherently ignition resistant interior finish materials.

Fire Safety at Sea

The regulation of commercial vessels that operate internationally, including ferries and cruise ships, is primarily conducted under international law. The International Maritime Organization (IMO), headquartered in London, is an agency of the United Nations and is the repository of all treaties dealing with commercial vessel safety. The IMO promulgates regulations established by the International Convention for the Safety of Life at Sea (SOLAS) treaty. SOLAS includes both design requirements and test methods for fire resistance and flame spread on interior materials. The U.S. Coast Guard (USCG) enforces these and some other safety and sanitation requirements for foreign flag vessels that operate in U.S. waters. Fire protection of marine vessels in the United States (operated as U.S. flag vessels) is regulated by a collection of Code of Federal Regulations promulgated by the USCG. Vessels and their associated levels of regulations are divided into classes depending on their size and capacity.

Table 90.3 Passenger casualty rates, 1963–1997

Mode	Fatalities	Fatalities or seriously injured
Air	0.13	0.20
Rail	0.73	3.19
Water	6.69	44.28

In order to frame the maritime risk problem, comparative passenger accident and casualty rates are illustrative. Passenger casualty rates for different modes of transport for the 15 year period from 1963 to 1997 are given on a per billion passenger kilometers as shown in Table 90.3 [31].

Peachey [31] asserts that the casualty rates for water transport are dominated by two large-scale accident events, the *Herald of Free Enterprise* in

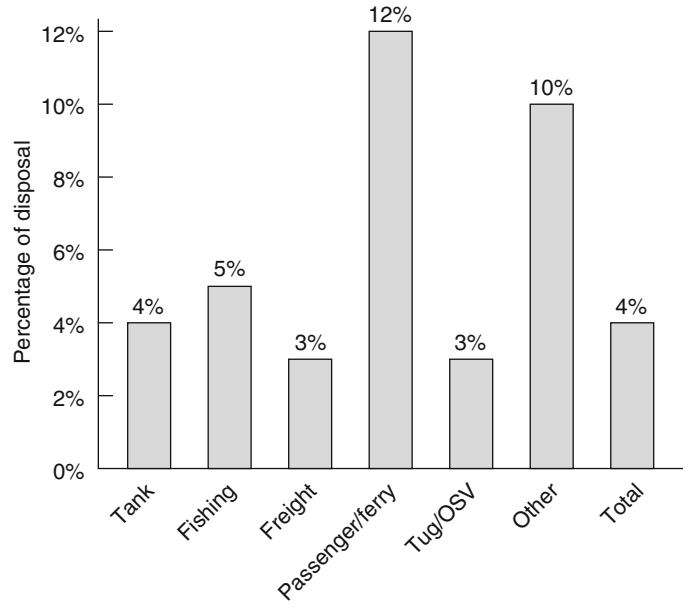

Fig. 90.4 Percentage of world fleet's vessel disposals caused by fire or explosion, from Lloyd's database by vessel type in 1997

1987 and the *Marchioness* in 1989, which, if excluded, would result in an underlying fatality rate of about 0.5 per billion passenger kilometers.

Providing further context, the major risks in cruise ships for the same period are collisions and fires. Between 1963 and 1997, fatalities were roughly divided between the two with 436 collisions and 411 fires, whereas grounding only led to one fatality [32].

The statistical distribution of fire risk based on vessel type can be found in Lloyds Casualty System database and the Marine Safety Information System [33]. Notably, the number of "disposals," or vessels "written off," in sample year 1997 found passenger ships to be of the highest percentage type of vessel in the fleet (Fig. 90.4).

In Washington State the rate of ferry accidents in the state ferry system was estimated at 1.8 per million miles (1.1 per million kilometers) whereas the rate of fire was 0.59 per million miles (0.37 per million kilometers). The accident rate for ferry passengers is roughly half that of aircraft [6].

Cruise ships are often larger than most buildings. Cruise ships in particular, once built as floating hotels, are now built as floating resorts. In some cases, cruise ships carry great population loads, and can have more passengers than some cities have residents. There are, in addition, unique aspects to such large passenger vessels that make the fire safety risk problem in ships a greater fire safety design challenge than in buildings. Unique fire safety design factors of passenger vessels include geometry, construction materials and design, and fire-extinguishing systems [34].

The basic geometry of a passenger ship creates challenges not often found in building fire safety. Multistory passenger ships are commonplace; however, unlike most multistory buildings, which have similar footprints on each floor, passenger ships' floor-by-floor geometry can vary both in size and in use. The typical rectilinear floorplate arrangements found in buildings simplify fire safety design challenges such as fire barrier locations and egress strategies. With some exceptions, as in convention centers, factories, and casinos, most buildings have grown vertically versus horizontally. In order to maintain fire compartmentation, additional subdivisions are necessary, and atypical floorplates creates greater challenges.

Similar to air and rail systems, exiting is more complex in a ship than in a building. Although it may be "easier" to evacuate a ship than an

airplane, it is more difficult than evacuating a train. Take, for example, the geometry of a cruise ship: the larger size, the variation in decks, the need to (counterintuitively) ascend stairs in order to evacuate, and the fact that passengers may be asleep further complicates evacuation. Furthermore, exiting in a ship entails the movement to a safe place of assembly in order to await further instruction. Only if the ship is in peril does exiting lead to shipboard evacuation into survival craft.

The installation and use of combustible materials in ship design is a significant concern. Although significant advances have been made in the areas of composites and use of aluminum in shipbuilding, particularly for high-speed craft, most modern ships (as opposed to boats) are constructed of steel and other noncombustible materials. Although this construction provides a certain increased reliability in ship integrity under fire conditions, it does not solve the fire risk problem associated with combustible interior finish and furnishings. Because of these hazards, SOLAS requires areawide sprinkler protection and smoke detector coverage of all accommodation areas.

Not unexpected, vehicle holds and engine rooms are common sources of fire origins. In fact, engine spaces account for more than half of the reported fire incidents [35]. For this reason they are given additional attention. Some suggested protection measures for such spaces include the following [36]:

- Fire separations of engine rooms and redundant machinery spaces
- Mist or gaseous suppression systems
- Fire/flame detection and video monitoring
- Rigorous training in emergency procedures

A number of accidents in the 1980s provided evidence that fires were a serious and growing concern. In 1991 the IMO adopted amendments to SOLAS, which became effective in January 1994 [37]. These included additional requirements for exiting, sprinkler systems, and smoke control. After a 1993 special report on passenger vessels by the National Transportation Safety Board, the U.S. Coast Guard obtained international agreement to require various fire safety improvements on all passenger ships, including existing ships. The focus of the improvements—automatic sprinklers, fire detection and alarm systems, and emergency lighting—are compulsory on all ships able to carry 36 or more passengers that were delivered after October 1994 [1].

As a result of U.S. regulatory reform, the USCG initiated and chaired an NFPA technical committee to develop consensus standards as an alternative to the current fire regulations. Various NFPA 301, *Code for Safety to Life from Fire on Merchant Vessels*, requirements are described for vessels carrying more than 12 passengers [38]. Material requirements are similar to the USCG regulations with some exceptions. The passenger capacity, type of service (day or overnight), and whether or not the space is protected with automatic sprinklers determine flame spread limits. NFPA 301 means-of-egress provisions are adapted maritime equivalents of NFPA *101*®, *Life Safety Code*®, [39] egress provisions. Among the requirements, many depend on the number of passengers and whether or not overnight accommodations are provided.

Fire Risk-Informed Decision Making in Air, Rail, and Sea Transportation

Risk-Based Decision Making Defined

In risk-based decision making, an orderly structure is applied to a situation in which one or more options are available and one or more unwanted outcomes, or losses, in varying severity may result. These losses can include such things as harmful effects on occupants or passengers, property, or business continuity. The risks for an engineered system or activity are determined by the types of possible losses, the frequency at which they are expected to occur, and the effects they might have. Risk-based decision making is not only hazard assessment, although it may be included. One difference between hazard assessment and risk-based decision making is that hazard assessments might include likelihood and frequency or the recognition of relative risk,

whereas risk-based decision making explicitly considers issues of likelihood and frequency or relative risk.

Risk-based fire safety analysis and decision making is a concept gaining momentum in the fire safety community. Publications including the *SFPE Engineering Guide to Fire Risk Assessment*, the *National Fire Protection Research Foundation Guidance Document for Incorporating Risk Concepts into NFPA Codes and Standards*, and NFPA 551, *Guide for Evaluation of Fire Risk Assessments*, are resources for decision makers, regulators, analysts, and designers. The concepts can be used for the development of air, rail, or maritime regulations or for the benefit of the vehicle or vessel designers and operators. The key to applying the concepts is to identify the appropriate assessment tool or tools, completing each step in the most simple, practical way to provide the information the decision maker needs, and recognition of its limitations as a tool for the decision maker. There are many issues that might seem overwhelmingly complex; however, they can often be investigated with simpler risk assessment tools.

Although many of the fire risk characteristics of the three transit systems are similar, such as the confined spaces, the lack of readily available exits, and the potential for catastrophic consequences, the approaches to manage those risks and their solutions can vary. Solutions that may be acceptable to one mass transit system may not be acceptable to another transit system. In some cases, this may be obvious, like the installation of a fire sprinkler system, which may be acceptable for ships, yet unacceptable for airplanes.

The primary objective of safety regulations for transportation is to minimize loss of life and injuries in accidents. Preserving property or avoiding business interruption is a secondary regulatory effect; however, it might be of significant interest to transit operators. Thus, regulations that focus on design, material selection, and emergency procedures may prove to be an adequate approach to managing the passenger safety risk problem, but may not be far-reaching enough for an owner or operator.

Fire Safety Objectives

The following fire safety objectives, suggested for rail, [40] have been adapted here to show the wide application they could have in the three transit options:

1. Preservation of the personal safety of passengers and staff capable of reacting readily to a fire situation
2. Preservation of the personal safety of passengers and staff who through illness, age, or disability cannot respond readily to a hazard situation
3. Preservation of the structure of vehicle/vessel involved in the fire
4. Preservation of the operating function of the vehicle/vessel
5. Reasonable preservation of the contents of the vehicle/vessel
6. Protection of the traveling and non-traveling community from the effects of fire

The risk managers intent on improving fire safety in the air, on rails, in buses, or at sea face a decision problem as they consider managing their fire risk problem. In the aviation industry, safeguarding the public might have priority to maintaining a viable business; however, cost-benefit analyses play a major role in determining viable risk management approaches. The direct cost of just one significant commercial aviation fire can total hundreds of millions of dollars. Small fires, such as those that are fuel limited or those that are extinguished by staff, can have great business consequences. Larger uncontrolled fires can have disastrous effects. Investment in risk reduction can save on overall costs. Because of inherent characteristics associated with the physics of air travel, the aviation industry has limitations when resolving the fire risk problem.

In the rail industry, a transit agency might accept the risk of a small fuel-controlled fire, as such fires are unlikely to cause injury or significant business interruption. However, because it is land based, during the risk management process, the rail industry may have a larger palette of safety options from which to decide. Automatic fire sprinklers, on-board alternative suppression

systems, smoke and flame detection systems, and materials (fuel) restrictions are all reasonable options for trains and/or stations.

Marine transit risk management has a combination of issues. Similar to air travel, normal exiting is not readily available or is at least significantly delayed. However, size and weight issues are less of a concern, and water-based fire suppression including sprinklers is a viable option. One unique aspect of some marine transit vessels is size. Significantly more passengers can be put at risk in the event of a large fire. Another is fire fighting; external fire-fighting efforts from a fireboat or from dock side must be enacted with caution. If too much water is applied, the ship can be in jeopardy of sinking.

Risk-Based Decision-Making Methods

As we have noted, fire risk in mass transit, whether in the United States, Europe, or on the seas, is addressed by various regulatory organizations. Historically the approach has been either one of bootstrapping, addressing specific concerns as they arise with new prescriptive regulations, or the ALARP method (i.e., "as low as reasonably practical"). Data gathering and statistical evidence for aircraft accidents, rail accidents, and marine accidents are part of the regulatory structure.

Many systematic risk assessment methods used to assist the decision-making process can be broken down into two generalized families, as suggested by Modarres: [41] the economic method and the noneconomic method. Examples of economic methods include cost-benefit, cost-effectiveness, and risk-effectiveness methods. Examples of noneconomic methods include exceedence analysis, value analysis, decision trees, and the analytical hierarchy process (AHP). Hazard assessments, including what-if and hazard and operability (HAZOP) analyses, although not necessarily strict risk analyses, may include frequency or likelihood assessments and, therefore, can also be considered examples of noneconomic methods.

Depending on the transport mode, the mass transit risk manager may need to consider applying a combination of two or more of the economic and noneconomic methods. The following sections describe various risk assessment methodologies or risk issues in light of the fire risk problem in the three systems.

Fire Risk Decision Making in Air Transportation

FAA System Safety Process

From a regulatory process, the FAA is a leading authority in developing safety systems for the flying public. Over its history, the concept of risk, reliability, redundancies, and analysis of statistics for the improvement of safety has been recognized and implemented. Fire risk is a large part of the risk problem in aircraft. It is estimated that one-fifth of passengers who die in air crashes are killed by fire. Recently, the FAA has published a forward-looking approach to risk management, known as the System Safety Process [42]. Although the experience of the past has great value in addressing risk issues today, the System Safety Process is intended to be a forward-looking document, a proactive means to incorporate risk assessment. Figure 90.5 describes the method.

Through the systematic review and risk assessment process, the *System Safety Process Handbook* is intended to achieve numerous objectives. Among the most important are the following:

1. Implementation of cost-effective, timely safety measures
2. Identification of hazards throughout a system
3. Recognition of residual risk
4. Support of best engineering and management practices
5. Use of statistical and historical data
6. Recognition of risk reduction through best available technology
7. Appropriate and timely retrofit actions
8. Consideration of the life cycle
9. Development of a lessons learned data bank

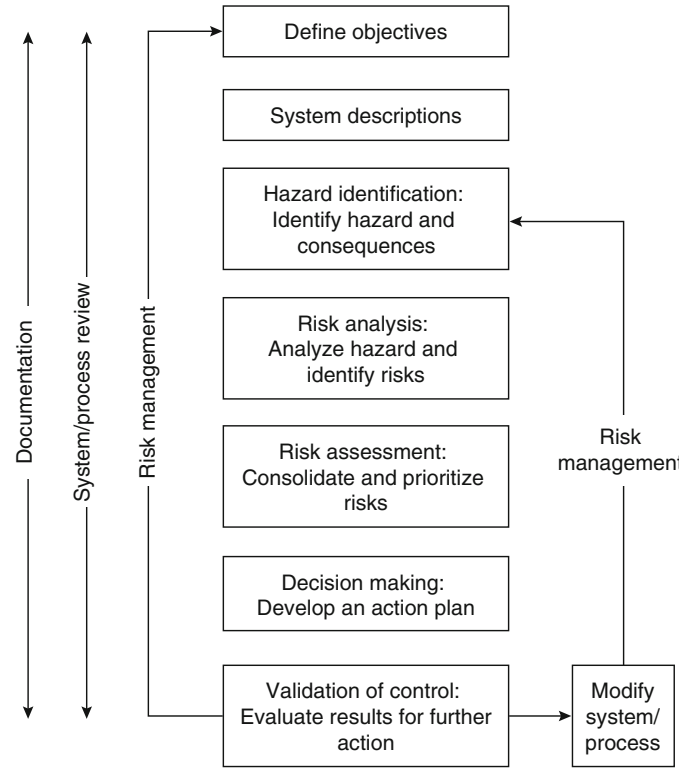

Fig. 90.5 FAA system safety process

Many of the preceding points can be addressed by formal risk assessment methods, including but not limited to cost-benefit analyses, ALARP analyses, and risk effectiveness.

Cost-Benefit Analyses

Optimizing the cost-benefit relationship is a particularly significant part of the fire risk management challenge in aircraft. In building fire safety, the installation of an automatic suppression system throughout most new buildings comes at a small cost relative to the cost of the building. In aviation fire safety, the introduction of a fire suppression system comes at a relatively significant cost due to the weight of the suppression agent, as increased weight has a relatively great impact on the airplane's fuel consumption and operating costs. In fact, any automatic active fire safety system, including fire detection and suppression systems, can have cost impacts not normally associated with buildings. Besides the issue of weight, a false alarm by cargo area smoke detection in aircraft can be costly if it means that the aircraft is required to enact emergency landing procedures in the event of detector activation.

In contrast to buildings, aircraft fire safety design and regulatory structure have the luxury of tightly controlling the fire hazard of aircraft interior furnishings. As part of the risk and decision-making process, a great deal of focus has been placed on this issue recently. In 2006, in a relatively minor "crash" incident, an Airbus A340 could not stop on landing and headed into a ravine with an ensuing fire, but everyone was able to escape. The successful evacuation was in large part attributed to the use of fire-retardant materials [43].

It has been estimated that a 73 % risk reduction results in approximately $620 million annual savings to the industry [44]. Nevertheless, cost-benefit analyses can be deceptive and difficult to quantify. Both benefits and the costs of implementing a strategy can have direct and

indirect components that should be considered. Whereas *direct* benefits and costs may seem clear, *indirect* benefits and costs may be difficult to quantify. A direct benefit of implementing a cabin mist suppression system may be uninterrupted business operations, whereas an indirect benefit may be a higher marketable safety reputation. And whereas direct costs may be attributed to the potential loss of the aircraft, indirect costs may be related to the fees associated with litigation and increased insurance costs.

The cost-benefit ratio (R_{b-c}) is defined as

$$R_{b-c} = B/C$$

where B represents the benefit and C represents costs, typically in monetary units.

Cost-benefit analysis in aviation fire safety has been performed for [45]:

1. Nitrogen inerting of aircraft fuel tanks
2. Cabin water spray systems and enhanced fuselage burn-through protection
3. Analysis for enhanced protection from fires in hidden areas on transport aircraft
4. Installation of automatic hatches

At the current time, cabin-based suppression systems, although shown to provide potential benefits, have been disputed to be too costly to install and maintain, in part due to the additional fuel costs related to weight. The systems are estimated to cost $20 to 30 million per life saved [46] in comparison to $0.4 million per life saved for aircraft seat cushion flammability standards [47]. Furthermore, a cabin suppression system may not be effective for all fire scenarios, particularly the postcrash survivable scenario in which the system may be damaged. Still, the debate is not without merit. As aircraft become more fuel efficient, as the fire safety issues change, such as with two-story commercial passenger aircraft, as suppression technology changes, or as risk tolerances decrease, new analyses may be warranted.

In general, cost-benefit analyses need to be considered with some level of caution. Some argue [48] that there may be situations in which the benefits of a new safety system may not exceed the costs. And there is always the difficulty of applying the value of human lives to the analysis. Even in the comparison of two options, holding the value of human life constant in the analysis could lead to different outcomes, particularly if one option would result in more life safety protection while the other results in more property protection.

Without compelling cost-benefit data for active cabin fire suppression equipment, fire risk management in aviation fire safety has historically focused on passive systems: fuselage integrity, seat cushion materials, lighting, and evacuation effectiveness. In the past decade a shift has occurred to address hidden in-flight fires and fuel tank explosions.

ALARP Analyses

Another risk-based decision-making tool, which may be complementary to the cost-benefit analyses, is the "**a**s **l**ow **a**s **r**easonably **p**ractical" (ALARP) principle. With ALARP, risk reductions are implemented into a system until risks are as low as reasonably practical, or as low as reasonably cost-effective. Often this is combined with and compared to the concept of best available technology. Figure 90.6 conceptually represents the idea of an ALARP curve for passenger aircraft cabin fire safety, using in-cabin automatic fire suppression as an example of a currently considered cost-prohibitive, but possibly very effective, fire risk management solution for managing passenger fire risk.

Risk Effectiveness

Risk effectiveness is a measure of the cost of a risk reduction or control per unit of risk reduction. The solution is an excellent comparative method for introduction of a discrete technology, regulation, or operation [41].

$$RE = \frac{S}{\sum_{i=1}^{n} F_i C_i - \sum_{i=1}^{n} F_i' C_i'}$$

where S is the annualized cost of the risk reduction, F is the frequency of scenario I without

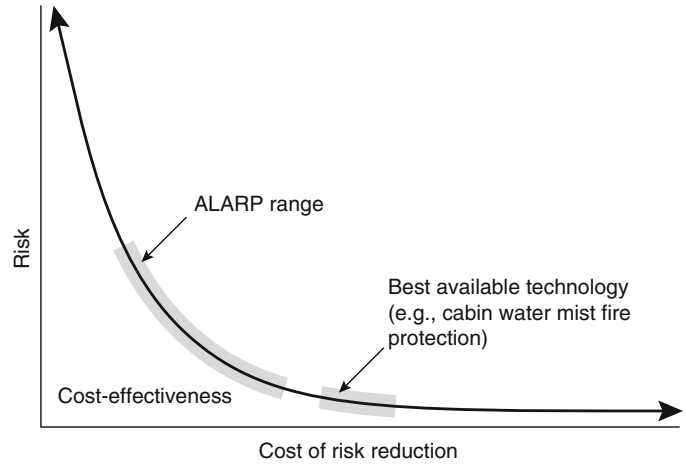

Fig. 90.6 ALARP curve for accidental passenger aircraft cabin fire safety (Source: Adapted from Modarres [41])

implementation of the risk reduction, C is the consequence of scenario I, and F' and C' are the frequency and consequence after implementation of the risk solution.

As part of a risk assessment, some level of deterministic modeling can be anticipated, particularly when there is a need to evaluate the benefits associated with lives saved. Several models have been developed for building fire safety and a limited few have been developed for aircraft [14, 49]. The challenge with such predictive accident analysis tools is in dealing with the quantity diversity and detailed amount of information both available and unavailable.

Fire Risk Decision Making in Rail Transportation

Rail transport fire risk managers face a variation of the aircraft fire risk problem. Business interruption issues due to fire are not as acute. The loss of a carriage is not typically as significant as the loss of an aircraft. Fire safety options are broader and, due in part to risk perceptions, a higher level of risk is tolerated.

Regulation of Combustible Materials

The primary method to manage fire risk in rail transport involves the regulation of combustible materials. Combustible materials may be used on seats, seat shrouds, interior liners, insulation, floors, and ceilings. In contrast to commercial passenger aircraft, many rail operators are less inclined, from a business perspective, to provide comfortable, cushioned seating. Operators have the option of limiting or restricting the amount of combustible, cushioned materials used for seating or insulation, thereby reducing the fire risk significantly. However, other rail operators may seek the benefits (increased ridership) provided by more comfortable carriages while acknowledging some increased potential risks associated with padded (combustible) seating or increased costs associated with new fire-resistant cushions. Another option, particularly for those rail systems that are more luxurious, is the consideration of on-board fire suppression systems. Compared to aircraft cabins, on-board fire suppression or carriage mist systems are significantly less expensive in trains as they minimally affect running costs.

Decision Tree as Decision-Making Tool

With more options, the risk management tools may need to consider more than just cost-benefit analyses. As options increase, decision trees can help form a balanced picture of risks and benefits associated with each course of action. As a simple example, consider two types of subway carriages. Subway transit operators are considering two types of new carriages and are very

concerned about fire safety in their system. They have experienced many fires and estimate that there is a 5 % probability of fire in a given carriage per year. The first option of carriages is the Spartan option. It is outfitted with basic furnishings resulting in minimal combustible loading, but equipped with surveillance cameras with the intent of reducing probability of vandalism related fires (to 1 %) and assist in early detection. The second type of subway carriage is the luxury option. It is outfitted with cushioned seating and well-insulated, acoustically treated walls that may be lined with fire retardant but with combustible seats and panels. The second type is equipped with on-board mist systems but no surveillance cameras. Although the first type of carriage may be much more economical to build and maintain, the second may produce more revenue as it attracts more riders.

For the purposes of this example, we assume that the annualized costs of the two types of carriages are $100,000 and $200,000 respectively. Based on expert opinion, and the expected ignition source used, the probability of fire causing a flashover in carriage option 1 is estimated at 60 %. The probability of the mist system working effectively to prevent flashover in carriage option 2 is estimated at 95 %. If flashover occurs, the carriages are considered complete losses; if flashover does not occur, the carriages are expected to suffer some damage.

All other things being equal, a simple decision tree can be drawn as shown in Fig. 90.7.

Rolling back the tree, the decision analyst calculates the expected annual cost for carriage option 1 as

$$[(0.40 \times \$20{,}000) + (0.60 \times \$100{,}000)] \times 0.01 = \$680$$

The analyst calculates the expected annual cost for carriage option 2 as

$$[(0.95 \times \$10{,}000) + (0.05 \times \$200{,}000)] \times 0.05 = \$975$$

For this example, the decision maker may wish to consider carriage option 1, the more Spartan carriage of the two. However, as discussed previously, these values are only meant for assisting the decision maker in an overall cost-benefit decision-making process. There may be indirect benefits or costs associated with choosing the more Spartan carriage. A Spartan carriage may attract fewer riders, leading to less revenue; however, a Luxury carriage may carry higher maintenance costs. These indirect costs need to be considered carefully through a full risk characterization and sensitivity analysis.

NFPA 130, Standard for Fixed Guideway Transit and Passenger Rail Systems

NFPA 130, *Standard for Fixed Guideway Transit and Passenger Rail Systems*, is an internationally recognized standard on fire life safety throughout

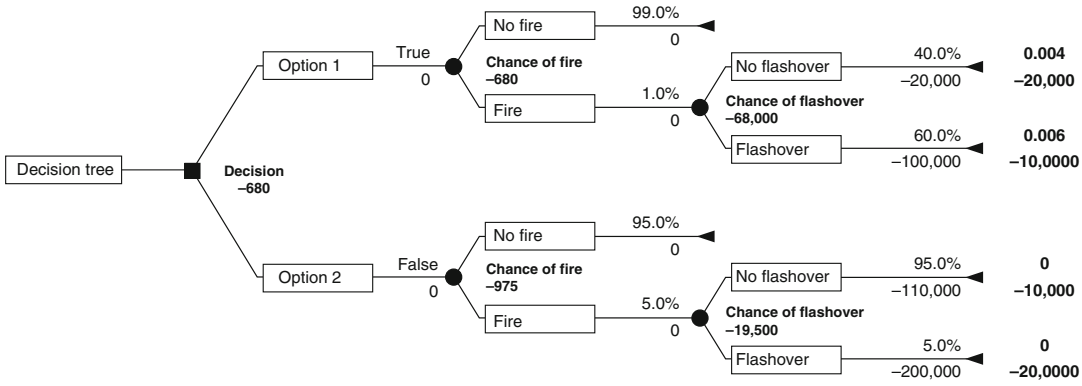

Fig. 90.7 Simple decision tree

passenger rail systems including carriages, tunnels, and stations [22]. The purpose of the standard is to establish minimum requirements that will provide a reasonable degree of safety from fire for passengers throughout such systems. The standard is used throughout the United States and as a reference in many countries, including Hong Kong, Australia, and the United Kingdom.

NFPA 130, primarily a prescriptive set of regulations for rail systems, permits the use of an engineering hazard analysis or performance-based approach for the design of carriages and station egress systems. The required fire hazard analysis is outlined in Annex E of NFPA 130. For performance-based egress design, Annex E refers to the *SFPE Guide to Performance-Based Fire Protection Engineering* and NFPA *101*®, *Life Safety Code*®. In turn, Annex E gives directions for performing a fire hazard analysis for vehicles. It suggests the following four-step evaluation process:

1. Define vehicle performance objectives and design.
2. Calculate vehicle fire performance.
3. Evaluate specific vehicle fire scenario.
4. Evaluate vehicle car design suitability.

The two concepts, performance-based engineering analysis of egress systems and the hazard analyses of carriages, are intertwined and dependent on issues of risk. To some extent, the prescriptive structure of NFPA 130 addresses some issues of risk such as the likelihood that an escalator will be nonfunctioning, the likelihood of one missed headway (resulting in more people at risk), and specifies safety electrical and mechanical equipment of a reliability that is higher than in standard building applications. However, in the event that a true performance-based approach for rail safety is pursued, the designer and risk manager should consider further risk issues such as the following:

1. *Passenger loads*. What is the likelihood of passenger loads on platforms and trains exceeding the code prescribed loads? What is the resulting impact?
2. *Reliability of station or tunnel safety systems*. What is the likelihood of equipment failure?
3. *Ignition source*. What is the ignition source and would it have an effect on the peak heat release rate? Is it acceptable to utilize an accidental ignition source or does arson need to be evaluated? In the evaluation of vehicle fire performance through material testing, has the testing been performed assuming the appropriate ignition source strength?
4. *Fire scenario*. The fire may have a different impact depending on when it starts along the rail line. For example, what is the likelihood/impact of a fire when the train is in the middle of a long tunnel or in the middle of a long elevated track?
5. *Coincident problems*. What is the likelihood of a fire while a train is disabled in a tunnel or on a bridge?
6. *Fire location*. Given a fire on a train, what is the likelihood that the fire will be at the front, the middle, or the end carriage? Can this lead to different consequences on the train passengers or in the station?

Each of the preceding risk issues is representative of a short list of questions that should be either implicitly or explicitly considered or discussed during the course of an engineered performance-based hazard assessment in rail fire safety design. How the issues are resolved is, in part, a value decision that should be considered by the transit agency. Not surprisingly, resolution of these issues can be assisted by a decision analysis framework in the determination of appropriate policy.

Fire Risk Decision Making in Motor Coaches or Buses

A fundamental goal of transit systems is to provide passengers and employees the highest level of safety that is practical and consistent with the mission of the system. To do so, a transit agency or bus operator needs to develop a safety program that addresses the hazards and risks associated with the operation of the system in order to: (1) prevent the occurrence of accidents, (2) respond to and recover from accidents, and (3) learn from accidents that have occurred [24].

While the occurrence of a bus fire is a relatively rare event in terms of vehicle miles or passenger miles, the risk of fire is present and attention must be paid to fire hazards and mitigating measures put in place to identify them, reduce their probability, and limit their consequence.

Bus Characteristics

The term bus covers a wide category of vehicles that vary significantly along a number of characteristics. The choice and selection of bus type are often dictated by their intended operational use. However, each type poses varying hazards based on their characteristics, some of which include:

- Chassis (rigid, articulated);
- Levels (single-decker, double-decker, open-air double-decker);
- Size/capacity (large, medium, midi, mini-buses);
- Propulsion type/fuel (gasoline, diesel, CNG, LPG, hybrid, electric);
- Engine location (front, rear);
- Floor height (high-floor, low-floor, kneeling);
- Use (long-distance, transit, student transport, tourism, private charter);
- Ownership (public, private);
- Service life (light-, medium-, heavy-duty).
- Operating environment (guided, fixed/dedicated lanes, shared roads/tunnels, dedicated tunnels).

Each bus, depending on its characteristics, will be subject to certain hazards. For example, electric buses will have different ignition hazards owing to the necessary electric equipment than those associated with a diesel engine. Buses intended for long-distance travel will likely have cushioned upholstered seating for comfort, which might increase the interior combustible load. Alternatively, mass transit buses, meant for intra urban travel, would more likely have seating made of hard surfaces which are easy-to-clean. A bus fire risk assessment would begin with characterization of the hazards, from the combustible materials, notably the interior finish and furnishings, to the operating systems, the propulsion, air conditioning and the braking system.

Regulation of Combustible Materials

Materials used in bus construction can possibly increase the severity of a fire incident depending on their susceptibility to ignition or propensity to support flame spread. Different materials can be expected to produce varying level of toxic combustion products. The impact of accidents involving fire and smoke development may be minimized through the selection of proper vehicle materials. For automobiles and school buses, passenger compartment materials (exposed to the air) must meet the flame spread test in FMVSS (Federal Motor Vehicle Safety Standard) 302, as regulated by the National Highway Traffic Safety Administration (NHTSA) [50]. In addition to FMVSS 302, many commercial bus operators use a set of voluntary guidelines based primarily on a flame spread test (ASTM E162 [51]) and a smoke test (ASTM E662 [52]).

FMVSS 302 (ISO 3795) [53] specifies burn resistance requirements for materials used in the occupant compartments of motor vehicles. Its purpose is to reduce deaths and injuries to motor vehicle occupants caused by vehicle fires, especially those originating in the interior of the vehicle from sources such as matches or cigarettes. The test exposes a sample of material in a horizontal orientation to a Bunsen burner flame at one end; the horizontal flame spread rate away from the burner is measured and compared to a limiting acceptable rate of 102 mm/min (4 in./min) [54, 55]. However, recent studies have highlighted limitations of the test protocol as the sole regulatory tool as is (1) applies only to passenger compartment materials, (2) does not consider the potential for fires originating outside of and penetrating the passenger compartment [29, 30, 56, 57]. Further, the horizontal orientation of the test does not correlate well to the potential burning in the vertical configuration. The aforementioned SP study reviewed the fire performance of a number of materials typically used in bus interiors. All materials were tested in accordance with FMVSS 302 and several alternative fire test methods used for other applications such as trains, ships and buildings. The study demonstrated that FMVSS 302 does not provide a sufficiently high level of fire safety

insomuch that products fulfilling the horizontal test for buses would not even meet the lowest performance requirements for buildings [30].

Other Risk Reduction Measures

In gasoline- or diesel-powered buses, additional safety considerations are given to the engine compartment. Fires occur when flammable materials come in contact with an ignition source in the presence of oxygen. Within an engine compartment fires can occur when fuel or hydraulic fluid leaks and comes in contact with a hot surface (ignition source) such as the engine manifold. Fuel and hydraulic lines should be routed and placed such that leaking fluids are not likely to come in contact with a hot surface [24]. Additional safety measures often incorporated in buses that can reduce the potential and/or magnitude of fire events include: master shut-off switch to cut all current from the battery, engine-shut-down switch, fuel tank protection, engine compartment overheat detection, and engine compartment fire suppression [24].

Bus Fire Hazard Analysis

Transit systems and bus operator often must utilize scarce funds for costs associated with liability claims; property and equipment damage; the replacement of service, equipment and employees; and insurance premiums. Risk analysis and risk management is essential in identifying fire hazards and means for limiting and controlling those hazards as part of a comprehensive system safety program. The objectives of such a program is the reduction of accidents, specifically fires, in order to costs associated with claims, vehicle, repair, and insurance while also reducing employee and passenger injuries [24].

The FTA Office of Safety and Security has published guidelines for the hazard analyses of all transit projects including buses and bus systems [58]. The proposed approach is general in nature encompassing all systems and sub-systems and all associated hazards, not just fire.

The FTA process involves three separate analyses: a Preliminary Hazard Analysis (PHA) to provide an early assessment of hazards; a Failure Modes and Effects Analysis (FMEA) to determine the effects of system and sub-system failures; and an Operating Hazard Analysis (OHA) to identify and analyze hazards during operations, maintenance, and emergencies. The objective of each analysis is to identify risks and hazards early and to provide preventive or corrective measures to eliminate the hazard or to minimize the risk.

Hazards in bus systems will likely include one or more of the following types of hazards [24]:

- Design Deficiencies (inadequate or inappropriate wiring, fuel lines vulnerable to damage or heat, etc.)
- Inherent Hazards (mechanical wear/failure, presence of flammable liquids/fuel)
- Malfunctions (mechanical and/or electrical failures)
- Maintenance Hazards (improper connections, damage)
- Environmental Hazards (extreme weather, lightning)
- Human Factors (errors, improper connections, intentional acts)

While a number of hazards are inherent in the operation of a bus transit system, for which there may be no means of preventing or controlling (such as acts of nature). There are, however, a number of control methods that may be employed upon identification of a hazard. These may include [24]:

- Improved or changed design (fail-safe design, increased margins, redundancy, fire-resistant materials)
- Safety devices (interlocks, temperature sensors, pressure release valves)
- Warning devices (visible and audible)
- Procedures and training (use of safe procedures, emergency procedures, training, protective equipment)
- Preventive maintenance (scheduled maintenance, upgrades and replacement).

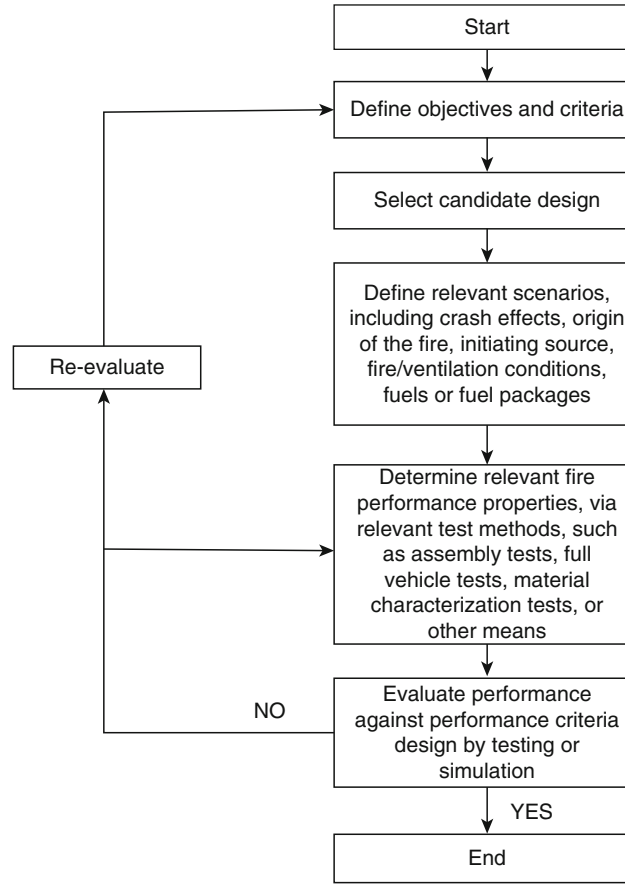

Fig. 90.8 Flow chart for the performance-based approach recommended by NFPA 556 for evaluation of vehicle designs

Additional guidance on fire risk assessments that can be applied to bus systems can be found in the *Guide on Fire Safety Risk Assessment: Transport Premises and Facilities* [59].

Fire Hazard in Passenger Road Vehicles

The development of NFPA 556, Guide on Methods for Evaluating Fire Hazard to Occupants of Passenger Road Vehicles [60] was prompted by vehicle fire statistics documented by the National Highway Traffic Safety Administration and the understood limitations of FMVSS 302. The guide identifies major fire safety concerns associated with passenger road vehicles, particularly material selections, and provides guidance on (1) alternative testing and evaluation methods, (2) tools for decreasing fire hazard or fire risk in passenger road vehicles, and (3) a hazard-based assessment for fires involving passenger road vehicles.

The guide proposes a performance-based approach to analyzing candidate vehicle designs with the objectives of reducing expected loss of life and the likelihood of injuries due to fires in passenger vehicles [61]. The process, illustrated in Fig. 90.9, allows for the objectives to be satisfied in a number of ways whether by increasing resistance to ignition, reducing flame spread and/or heat release rate, or reducing the rate of production of smoke and other combustion products.

NFPA 556 addresses issues associated with the development of hazardous conditions from fire involving passenger road vehicles and the time available for safe egress or rescue. The guide identifies fire scenarios for consideration

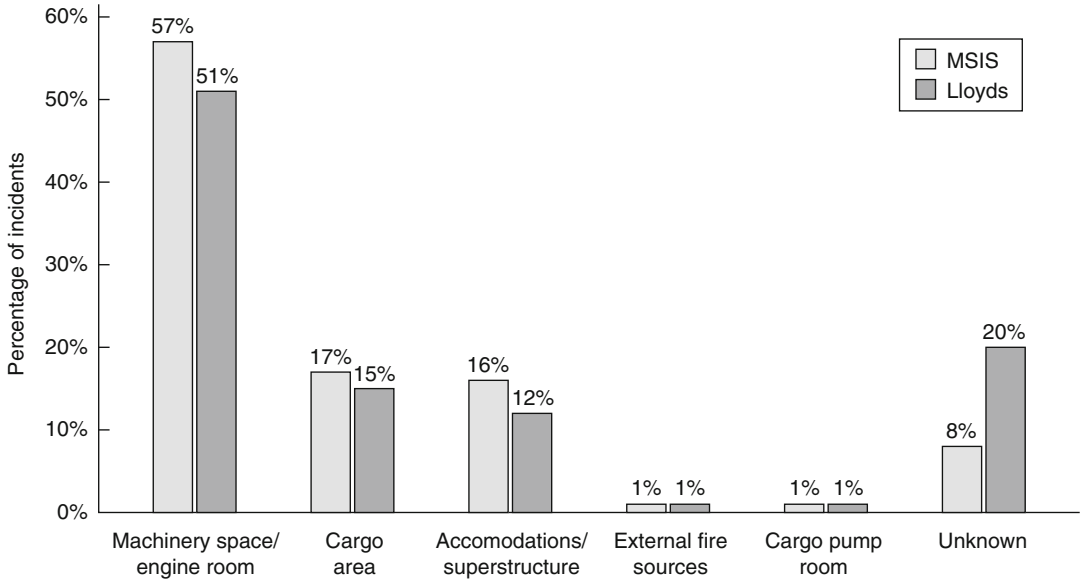

Fig. 90.9 1993–1998 cumulative percentages for MSIS and Lloyds databases by location of origin

that start: (1) inside the passenger compartment, (2) in the engine compartment, (3) in the trunk or load carrying area, (4) from pool fires resulting from fuel tank failure and burning under the vehicle, and (5) from other external heat sources. The key issue in each case, as it pertains to fire risk, is the impact of a fire in the passenger compartment.

Factors to be considered in the analysis are:

- Fuel type (lining materials, upholstery, insulation, flammable liquids),
- Status of vehicle including motion (engine on or off, collision. overturn),
- Ignition sources (mechanical sparks, electrical arcing, hot surfaces (manifold), pool fire),
- Area of fire origin (passenger compartment, engine compartment, exterior), and
- Means for penetrating the passenger compartment (ductwork, bulkheads, windshield).

While allowing for multiple approaches to mitigate the consequences of a vehicle (bus) fire, such as vehicle/engine compartment fire separation, the underlying premise of the guide is the reduction of risk and hazard through appropriate, engineering informed material selection to reduce the potential heat release rate and minimize the hazard presented by the products of combustion.

Fire Risk Decision Making at Sea

U.S. Coast Guard Safety Alert

The 2006 fire on the *Star Princess*, which started on a balcony of a sprinkler-protected cruise ship, led to 1 fatality and 13 hospitalizations, spread to 5 decks with a loss of 79 cabins, and resulted in a safety alert published by the United States Coast Guard (USCG). The alert included recommendations to institute risk assessments for shipboard fire safety [62]. The recommendations outlined the following steps:

1. Identify apparent fire hazards.
2. Assess severity of potential fires that could occur involving the hazards.
3. Identify safeguards for reducing risks associated with the hazards.
4. Identify actions to reduce the risk such that, should a fire occur, it will not spread and will be readily extinguished.

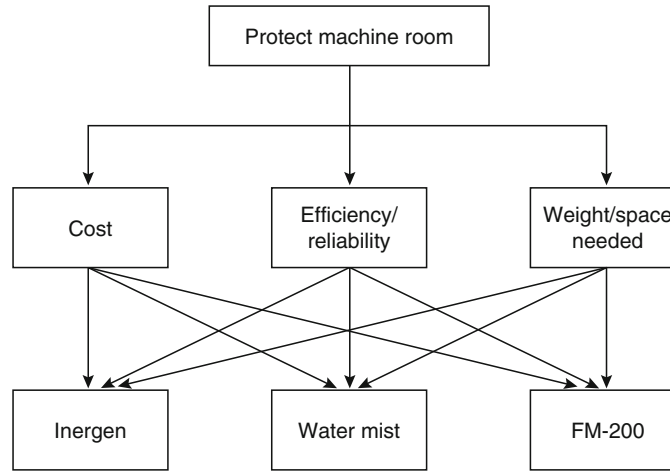

Fig. 90.10 Example of analytical hierarchy process setup

Although these steps may appear more like a hazard assessment rather than a risk assessment, each of the steps involves consideration of a separate risk subproblem in the overall hazard assessment context. In turn, this assists the decision maker in understanding the most appropriate action.

In determining the most appropriate fire safety solutions for any industry or system, one needs to analyze the risk problem in order to understand where the risks lie. Bayesian analysis and the use of conditional probability have also been used in analyzing both ferry safety issues as well as the overall fire safety problem [63]. Hanson reduced World Fleet data regarding ship fires of all types on a ship-type basis, location, and ignition source for the period of 1993–1998 [33]. Data were analyzed from Lloyds and Coast Guard Marine Safety Information System (MSIS) and an AHP analysis was performed. Figure 90.10 and Tables 90.4, 90.5, and 90.6 highlight key fire statistics.

Hanson used the MSIS data to develop probabilities of a fire occurring on a given vessel type, location, and ignition source. Due to the lack of total vessel population data, the probabilities are based on the condition that a fire occurs in the population of vessels. Nevertheless, the results are noteworthy, as shown in Table 90.2.

Almost 15 % of all fires reported occurred on passenger ships. Table 90.6 shows a breakdown of the ignition sources/origin points.

Table 90.4 Conditional probabilities by vessel type

Vessel type	Total incidents	Average number of incidents/year	Conditional probability
Fishing	420	70.0	0.3336
Tug	274	45.7	0.219
Tanker	87	14.5	0.070
Passenger	182	30.3	0.146
Other	71	11.8	0.057
Freight	118	19.7	0.95
Recreational	98	16.3	0.078
Totals	1250	208.3	1.00

Table 90.5 Conditional probabilities for locations of origin

Fire location	Number of incidents	Conditional probability
Machinery spaces	715	0.5720
Cargo areas	217	0.1736
Accommodations	201	0.1608
External fire sources	12	0.0096
Cargo pump rooms	8	0.0064
Unknown	97	0.0776
Totals	1250	1.0000

Understanding the statistical data and their limitations is the first step in risk management. Once the risk is understood, appropriate risk management tools are applied in order to assist in implementing the appropriate solution. Risk tools for maritime fire safety decision analysis

Table 90.6 Conditional probabilities of ignition sources in machinery spaces

Fire location	Number of incidents	Conditional probability
Heat/hot surfaces	324	0.4538
Electrical	198	0.2773
Internal to machinery	28	0.0392
Welding/hotwork	17	0.0238
Unknown	147	0.2059
Totals	714	1.0000

have included the ship fire safety engineering method and computer program SAFE used by the U.S. Coast Guard [64]. Other risk and decision analysis tools can also be employed. For example, when faced with options with multiple objectives, multicriteria decision-making approaches such as SMART [65], or the analytical hierarchy processes (AHP) [33] can also be applied to analyze appropriate risk reduction options.

Analytical Hierarchy Processes (AHP)

For example, an AHP process could be used discretely for a ship design to assist in the decision of the desired fire protection system for a ship or it could be used to assist the decision making for policy makers. AHP is a decision-making tool that is based on weighting and expert subjective assessment [41]. For example, assume that the risk manager has performed a risk assessment of a fleet of cruise ships to analyze where the most significant fire risks lie and has found that the ship's engine room presents the greatest fire risk. In the next stage the risk manager may wish to explore various options to protect an engine room. Several extinguishing options may be considered, including Inergen, water mist, and FM-200. The attributes to be explored could be cost, effectiveness, and space requirements. The AHP would be set up as shown in Fig. 90.11.

In this case, only one set of three attributes is established: cost, efficiency/reliability, and weight/space needed. The merits of each attribute are subjectively assessed against each other and assigned a value between 1 and 9. Typically, the values assigned are simply either 1, 3, 5, 7, or 9. The three fire protection system choices are assessed on a 9 point scale in terms of each attribute as well. A 3×3 matrix is established for each choice attribute combination. The normalized principal eigenvector of each matrix is calculated and is called the priority vector. The three priority vectors associated with the three choices are weighted by the priority vector associated with the attributes to provide a solution. As this process can be relatively tedious, Expert Choice™ software is one tool that can be used to solve such problems. A benefit to using the AHP versus other multicriteria approaches is that it can check for consistency in the expert judgment.

Hanson [33] listed a set of alternative maritime safety and regulatory priorities to be examined through the AHP process, as analyzed by experts. Eighteen fire safety alternatives with 19 associated attributes were analyzed by eight fire maritime safety experts. Examples of the alternatives included smoke control, hazard review of regulations, investigation into use of alternates to welding, egress of passengers and crews, international fire protection system standards, fire-fighting doctrine review, review of electrical fire safety standards, and so on. The process resulted in top two alternatives: egress of passengers and crew and hazard analysis review of regulations.

Notably, hazard analysis review of regulations was an alternative that was described as a systematic review of the fire safety regulations from a holistic performance-based perspective. Such systems approach reviews often benefit from an understanding of the underlying risks.

NFPA 301, Code for Safety to Life from Fire on Merchant Vessels

NFPA 301 includes an appendix intended to allow the vessel designer and operator to comply with the code while accommodating new or unique vessel uses or incorporating new or transfer technology. The appendix provides a standardized hazard analysis and risk assessment

methodology to use in demonstrating equivalent safety. The methodology includes a description of several analysis techniques including systems hazard, fault tree, event tree analysis, HAZOP, what-if, and criticality analysis. As part of these analyses, deterministic assessments may be necessary [66].

The U.S. Coast Guard has developed guidelines in risk-based decision making for both assessment of risks of its fleet and systems and of its regulations that affect U.S. flagged maritime vehicles over certain minimum sizes. The guidelines include detailed explanations and examples of various methods. A number of risk assessment studies have been undertaken by the Coast Guard in recent years from what-if scenarios to checklists to event trees [67]. Comprehensive risk assessment studies have also been carried out and published by others for passenger ferries in various locations including Washington State and the San Francisco Bay Area [68, 69].

Summary

The fire safety challenge in modern air, rail, and maritime transit systems differs from building fire safety risk challenges. The environments are more sensitive, populations are more vulnerable, and the business impact is potentially greater. Although there has been a significant improvement, which has resulted in an excellent record in all of the systems, as stakeholders in the transit systems look to improve matters, they are faced with a more complicated risk problem. Transit systems change—bigger planes, bigger ships, and faster trains are creating new challenges. The traditional prescriptive approach to fire safety is shifting as these industries are recognizing that they have a problem of risk management with a need for proactive risk-informed solutions. At a minimum, the FAA, the IMO, the Coast Guard, the FRA, and the NFPA have either acknowledged or recognized the use of risk and hazard assessments in order to improve safety.

It is important to recognize that most risk assessment and decision-making tools are universal and can be applied across many industries at many different levels. Independent of their perspectives, the stakeholders—regulators, owners, and operators—who may have different reasons and perspectives on the fire risk challenges, can benefit from their application. This chapter includes only a sampling of the challenges faced across these industries as well as basic examples of how and where the tools could be applied. Further insight and more detailed instruction can be found in either the references or in other chapters of this handbook.

References

1. *We Are All Safer, NTSB-Inspired Improvements in Transportation Safety,* National Transportation Safety Board, Washington, DC (1998).
2. Motorcoach Census 2011, American Bus Association Foundation, June 18, 2012.
3. Fire Safety Assessment of Bus Transportation, Proceedings of the Institution of Mechanical Engineers, Bus'92, The Expanding Role of Buses Towards the Twenty First Century, Charters, D.A., 1992PP 91–100.
4. E.R. Galea and S. Gwynne, "Evacuating an Overturned Smoke Filled Rail Carriage," in *Proceedings of the 2nd International Symposium Human Behaviour in Fire,* Boston, pp. 135–146 (2001).
5. *Aircraft Materials Fire Test Handbook,* Federal Aviation Administration, Department of Transportation, Washington, DC, Appendix D (last updated May 18, 2006).
6. J. Harrald, M. Grabowski, J.R.W. Merrick, and J.R. Van Dorp, *The Washington State Ferries Risk Assessment: Final Report,* George Washington University, Washington, DC, Rensselaer Polytechnic Institute, Troy, NY, and Virginia Commonwealth University, Richmond, VA (1999).
7. C.P. Sarkos, "Development of Improved Fire Safety Standards Adopted by the FAA," in *Proceedings No. 467,* Advisory Group for Aerospace Research and Development Conference, Neuilly, France (1989).
8. R. Hill and C. Sarkos, "FAA Fire Safety R&D Program: Past, Present and Future," *Proceedings of the Fourth Triennial International Fire and Safety Cabin Research Conference,* Cabin Safety Research Technical Group and National Technical Information Service, Springfield, VA (2004).

9. R. Hill, "Investigation and Characteristics of Major Fire Related Accidents in Civil Air Transports over the Past Ten Years," in *Proceedings No. 467,* Advisory Group for Aerospace Research and Development Conference, Neuilly, France (1989).
10. F. Jia, M. Patel, E. Galea, A. Grandison, and J. Ewer, "CFD Fire Simulation of the Swissair Flight 111 In-Flight Fire—Part 2: Fire Spread Analysis," *The Aeronautical Journal,* 110, 1107, pp. 303–314 (2006).
11. E.R. Galea, K.M. Finney, A.J.P. Dixon, A. Siddiqui, and D.P. Cooney, "Aircraft Accident Statistics and Knowledge Database: Analyzing Passenger Behaviour in Aviation Accidents," *AIAA Journal of Aircraft,* 43, 5, pp. 1272–1281 (2006).
12. R.W. Cherry, *Reduction in Rate of Fire Caused Accidents and Deaths,* The Fourth Triennial International Fire and Safety Cabin Research Conference, Lisbon (2004).
13. M. Khouzam, *Fire and Cabin Safety Research: A Perspective,* The Fourth Triennial International Fire and Safety Cabin Research Conference, Lisbon (2004).
14. E.R. Galea, "Proposed Methodology for Use of Computer Simulation to Enhance Aircraft Evacuation Certification," *Journal of Aircraft,* 43, 5 (Sept.–Oct. 2006).
15. Railroad Safety Statistics, 2004 Annual Report, U.S. DOT, Federal Railroad Administration, Washington, DC (Nov. 30, 2005).
16. National Transportation Safety Board, "Railroad Accident Report: Collision of National Railroad Passenger Corporation (AMTRAK) Train 59 with a Loaded Truck-Semitrailer Combination at a Highway/Rail Grade Crossing in Bourbonnais, Illinois, March 15, 1999," National Transportation Safety Board, Washington, DC (2002).
17. NTSB, "Railroad Accident Report—Fire Onboard Amtrak Passenger Train No. 11, the Coast Starlight, Gibson, California, June 23, 1982, Adopted: April 19, 1983," Report No. NTSB/RAR-83/03, Washington, DC (1983).
18. *2002 Korean Fire Data,* Risk Management Department, Korean Fire Protection Association, Seoul, Republic of Korea (Mar. 2003).
19. G. Colonna, *Fire Protection Handbook,* 19th ed. (A.E. Cote et al., eds.), National Fire Protection Association, Quincy, MA, p. 14–1 (2003).
20. R. Bukowski, "Fire Hazard Assessment for Transportation Vehicles," *The SFPE Handbook of Fire Protection Engineering,* 3rd ed., Society of Fire Protection Engineers, Bethesda, MA, 5-227–5-233 (2002).
21. FRA 49 CFR, Transportation, Parts 216, 223, 229, 231, 232, and 238, "Passenger Equipment Safety Standards, Final Rule," *Federal Register,* 64, 91 (May 12, 1999).
22. NFPA 130, *Standard for Fixed Guideway Transit and Passenger Rail Systems,* National Fire Protection Association, Quincy, MA (2007).
23. National Transit Database Safety & Security Newsletter, Spring 2005, Volume 3, Issue 1, U.-S. Department of Transportation – Federal Transit Administration.
24. FTA-MA-26-0010-94-1/DOT-VNTSC-FTA-94-2, *Bus and Passenger Accident Prevention*, U.S. Department of Transportation Research and Special Programs Administration, John A. Volpe National Transportation Systems Center, Cambridge, MA, 1994.
25. National Transit Database (NTD) FTA Safety and Security – Transit Safety – Safety and Security Statistics, http://transit-safety.volpe.dot.gov/data/samis.aspx.
26. FTA-MA-26-0053-05-1/ DOT-VNTSC-FTA-07-02 Transit Safety & Security Statistics & Analysis 2003 Annual Report, U.S. Department of Transportation – John A. Volpe National Transportation Systems Center, Cambridge, MA, 2003.
27. Ahrens, M. *Vehicle Fires Involving Buses and School Buses,* National Fire Protection Association – Fire Analysis and Research Division, Quincy, MA, 2006.
28. Ahrens, M. *U.S. Vehicle Fire Trends and Patterns,* National Fire Protection Association – Fire Analysis and Research Division, Quincy, MA, 2010.
29. Forsth, M. "Bus Fires – Presentation of a Large Nordic Research Project" in Proceedings of the 1st International Conference on FIVE – Fires in Vehicles, Gothenburg, Sweden, 2010.
30. Hammarstrom, R., J. Axelsson, M. Forsth, P. Johansson, B. Sundstrom, *Bus Fire Safety*, SP Report 2008:41, SP Technical Research Institute of Sweden, Borås 2008
31. J. Peachey, "Passenger Safety Ensuring Acceptable Risk," in *Conference Proceedings, Safety of Large Passenger Ships,* Institute of Marine Engineers and the Maritime and Coastguard Agency, London, UK (2000).
32. R.P. Skjong, M.L. Adamcik, S. Eknes, J. Gran, and J. Spouge, "Formal Safety Assessment of Helicopter Landing Areas on Passenger Ships as a Safety Measure," *DNV Report 97-2053* (available as IMO/COMSAR 3/2), Det Norske Veritas (DNV), Oslo, Norway (1997).
33. R. Hanson, "Risk Based Fire Research Decision Methodology," Master's Thesis, Worcester Polytechnic Institute, Worcester, MA (1999).
34. R. Eberly and G. Colonna, "Marine Vessels," *Fire Protection Handbook,* 19th ed., National Fire Protection Association, Quincy, MA, pp. 14-91–14-123 (2003).
35. *DNV Report 98-0552*, Det Norski Veritas (DNV), Oslo, Norway.
36. T. Staalstgrom and A. Eknes, "Complexity of Safety Considerations with Large Passenger Vessels," in *Conference Proceedings, Safety of Large Passenger Ships,* Institute of Marine Engineers and the Maritime and Coastguard Agency, London, UK (2000).
37. W.A. O'Neil, "Opening Address," in *Conference Proceedings Fire Safety on Ships Developments into*

the 21st Century, Institute of Marine Engineers, London, UK (1994).
38. NFPA 301, *Code for Safety to Life from Fire on Merchant Vessels,* National Fire Protection Association, Quincy, MA (2001).
39. NFPA *101®, Life Safety Code®,* National Fire Protection Association, Quincy, MA (2006).
40. P.J. Allender, "Fire Safety Analysis for Public Mass Transit Trains," *Fire and Materials,* 3, 2 (1979).
41. M. Modarres, *Risk Analysis in Engineering,* CRC Press, Boca Raton, FL (2006).
42. *Federal Aviation Administration System Safety Handbook,* Federal Aviation Administration, Department of Transportation, Washington DC *(*Dec. 2000).
43. "No Air Crash Miracle, Just Safer Design," *New Scientist Magazine* (13 Aug. 2005).
44. D. Downey, "Commercial Aviation Safety Team," in *Proceedings of the Fourth Triennial International Fire and Safety Cabin Research Conference,* Lisbon, Portugal (2004).
45. R. W. Cherry, *The Accident Database of the CSRTG,* The Fourth Triennial International Fire and Safety Cabin Research Conference, Lisbon (2004).
46. T. Marker, C. Sarkos, and R. Hill, *"*Water Spray System Development and Evaluation for Enhanced Postcrash Fire Survivability and In-Flight Protection in Cargo Compartments," *Advisory Group for Aerospace Research and Development Conference Proceedings No. 587,* Neuilly Sur Seine, France (1997).
47. T.O. Tengs, *"*Five Hundred Life Saving Interventions and Their Cost Effectiveness," *Risk Analysis,* 15 (3), 369 (1995)
48. S. Kelman, *"*Cost-Benefit Analysis: An Ethical Critique," *AEI Journal on Government and Society regulations,* 5 (1) (1981).
49. P. Macey and M. Hayes, "Computer Based Simulation and Risk Assessment Model for Investigation of Airliner Fire Safety," *Advisory Group for Aerospace Research and Development Conference Proceedings No. 587,* Neuilly Sur Seine, France (1996).
50. 49 CFR Part 571.302 Federal Motor Vehicle Safety Standards Standard No. 302; Flammability of interior materials.
51. ASTM E 162, *Standard Test Method for Surface Flammability of Materials Using a Radiant Heat Energy Source*, 2008b.
52. ASTM E 662, *Standard Test Method for Specific Optical Density of Smoke Generated by Solid Materials*, 2009.
53. ISO 3795, *Road Vehicles, and Tractors and Machinery for Agriculture and Forestry — Determination of Burning Behaviour of Interior Materials*, 1989.
54. TP-302-03, U.S. Department of Transportation – National Highway Traffic Safety Administration, *Laboratory Test Procedure for FMVSS 302 – Flammability of Interior Materials,* 1991.
55. Directive 95/28/EC of the European Parliament and of the Council of 24 October 1995 relating to the burning behaviour of materials used in the interior construction of certain categories of motor vehicle.
56. Sundstrom, B., "Comparison of Product Evaluation Systems in Europe for Road and Rail Vehicles, in Proceedings of the 1st International Conference on FIVE – Fires in Vehicles, Gothenburg, Sweden, 2010.
57. Hirschler, M., "New NFPA Guide on Fire Hazard in Road Vehicles", in Proceedings of the 1st International Conference on FIVE – Fires in Vehicles, Gothenburg, Sweden, 2010.
58. DOT-FTA-MA- 26-5005-00-01/DOT-VNTSC-FTA-00-01, *Hazard Analysis Guidelines for Transit Projects,* U.S. Department of Transportation – Research and Special Programs Administration, John A. Volpe National Transportation Systems Center, Cambridge, MA, January 2000.
59. *Guide for Fire Safety Risk Assessment – Transport Premises and Facilities,* Department for Communities and Local Government Publications, 2007.
60. NFPA 556, *Guide on Methods for Evaluating Fire Hazard to Occupants of Passenger Road Vehicles*, National Fire Protection Association, Quincy, MA (2011).
61. *SFPE Engineering Guide to Performance-Based Fire Protection: Analysis and Design of Buildings*, 2000 edition.
62. *Coast Guard Safety Alert, Star Princess Cruise Ship Fire,* U.S. Coast Guard, Department of Homeland Security (Apr. 27, 2006).
63. J.R. Merrick and R. Van Dorp, "Speaking the Truth in Maritime Risk Assessment," *Risk Analysis,* 26, 1 (2006).
64. C. Sprague, D. White, and B. Dolph, *Fire Safety Analysis of the USCGC Dependable,* United States Department of Transportation, United States Coast Guard, Portsmouth, VA (Jan. 1999).
65. P. Goodwin and G. Wright, *Decision Analysis for Management Judgment,* 3rd ed., John Wiley and Sons (2004).
66. E. Galea, A. Grandison, L. Filippidis, S. Gwynne, J. Ewer, and P. Lawrence, "The Simulation of Fire and Evacuation at Sea," in *Proceedings of the 10th International Interflam Conference,* Edinburgh, pp. 755–760 (2004).
67. B. Macesker, B. Dolph, J. Myers, D.A. Walker, and S.G. Schoolcraft, *Building a Toolbox for Risk Based Decision Making Within Your Organization,* U.S. Coast Guard, Washington, DC (2003).
68. J.R. Van Dorp, J.R.W. Merrick, J.R. Harold, T.A. Mazzuchi, and M. Grabowski, "A Risk Management Procedure for the Washington State Ferries," *Risk Analysis,* 21 (1), pp. 127–142 (2001).
69. J.R.W. Merrick, J.R. van Dorp, J.P. Blackford, G.L. Shaw, J. Harrald, and T.A. Mazzuchi, "Traffic Density Analysis of Proposed Ferry Service Expansion in San Francisco Bay Using a Maritime Simulation Model," *Reliability Engineering and System Safety,* 81 (2), p. 119 (2003).

Armin Wolski, P.E. holds a B.Sc. in civil engineering from U.C. Berkeley and a M.Sc. in fire protection engineering from Worcester Polytechnic Institute. He is two-time Fulbright Specialist Grantee having taught in Spain and South Korea. He has published extensively on the subject of acceptable risk in fire safety regulation. Armin is based in the San Francisco Bay Area.

Jarrod Alston, P.E. holds a B.Sc. from Worcester Polytechnic Institue. He is the secretary of the NFPA 130 Technical Committee on Fixed Guideway Tranist and Passenger Rail Systems and is a member of the NFPA 502 Technical Committee on Road Tunnels, Bridges and Limited Access Highways. Jarrod is Associate Principal in Arup, currently based in Australia.

Appendix

Appendix 1: Conversion Factors

The names of multiples and submultiples of SI units can be formed by application of the prefixes in Table A.3. The International Organization for Standardization (ISO) recommends the following rules for the use of SI prefixes:

1. Prefix symbols are printed in roman (upright) type without spacing between the prefix symbol and the unit symbol.
2. An exponent affixed to a symbol containing a prefix indicates that the multiple or submultiple of the unit is raised to the power expressed by the exponent.
   Example: $1\ \mathrm{cm}^3 = 10^{-6}\ \mathrm{m}^3$
   $1\ \mathrm{cm}^{-1} = 10^2\ \mathrm{m}^{-1}$
3. Compound prefixes, formed by the juxtaposition of two or more SI prefixes, are not to be used.
   Example: 1 nm *but not:* 1 mmm

ISO has issued additional recommendations with the aim of securing uniformity in the use of units. According to these recommendations,

1. The product of two or more units is preferably indicated by a dot. The dot may be dispensed with when there is no risk of confusion with another unit symbol.
   Example: $\mathrm{N \cdot m}$ or Nm *but not:* mN
2. A solidus (oblique stroke, /), a horizontal line, or negative powers may be used to express a derived unit formed from two others by division.
   Example: m/s, $\frac{\mathrm{m}}{\mathrm{s}}$, or $\mathrm{m \cdot s^{-1}}$
3. The solidus must not be repeated on the same line unless ambiguity is avoided by parentheses. In complicated cases negative powers or parentheses should be used.
   Example: $\mathrm{m/s^2}$ or $\mathrm{m \cdot s^{-2}}$ *but not:* m/s/s
   $\mathrm{m \cdot kg/(s^3 \cdot A)}$ or $\mathrm{m \cdot kg \cdot s^{-3} \cdot A^{-1}}$
   but not: $\mathrm{m \cdot kg/s^3/A}$

Table A.4 lists physical constants from the work of B. N. Taylor, W. H. Parker, and D. N. Langenberg [2]. Their least-squares adjustment of values of the constants depends strongly on a highly accurate (2.4 ppm) determination of *e/h* from the ac Josephson effect in superconductors and is believed to be more accurate than the 1963 adjustment, which appears to suffer from the use of an incorrect value of the fine structure constant as an input datum. See also *NBS Special Publication 344,* issued March 1971.

The following tables express the definitions of miscellaneous units of measure as exact numerical multiples of coherent SI units, and provide multiplying factors for converting numbers and miscellaneous units to corresponding new numbers and SI units.

The first two digits of each numerical entry represents a power of 10. An asterisk following a number expresses an exact definition. For example, the entry −02 2.54* expresses the fact that 1 in. $= 2.54 \times 10^{-2}$ m, exactly, by definition. Most of the definitions are extracted from National Bureau of Standards (NBS) documents. Numbers not followed by an asterisk are only approximate representations of definitions, or are the results of physical measurements.

The conversion factors are listed alphabetically in Table A.5 and by physical quantity in

M.J. Hurley (ed.), *SFPE Handbook of Fire Protection Engineering*,
DOI 10.1007/978-1-4939-2565-0, © Society of Fire Protection Engineers 2016

Table A.1 Names and symbols of SI units [1]

Quantity	Name of unit	Symbol	
SI base units			
Length	Meter	m	
Mass	Kilogram	kg	
Time	Second	s	
Electric current	Ampere	A	
Thermodynamic temperature	Kelvin	K	
Luminous intensity	Candela	cd	
Amount of substance	Mole	mol	
SI-derived units			
Area	Square meter	m^2	
Volume	Cubic meter	m^3	
Frequency	Hertz	Hz	s^{-1}
Mass density (density)	Kilogram per cubic meter	kg/m^3	
Speed, velocity	Meter per second	m/s	
Angular velocity	Radian per second	rad/s	
Acceleration	Meter per second squared	m/s^2	
Angular acceleration	Radian per second squared	rad/s^2	
Force	Newton	N	$kg \cdot m/s^2$
Pressure (mechanical stress)	Pascal	Pa	N/m^2
Kinematic viscosity	Square meter per second	m^2/s	
Dynamic viscosity	Newton-second per square meter	$N \cdot s/m^2$	
Work, energy, quantity of heat	Joule	J	$N \cdot m$
Power	Watt	W	J/s
Quantity of electricity	Coulomb	C	$A \cdot s$
Potential difference, electromotive force	Volt	V	W/A
Electric field strength	Volt per meter	V/m	
Electric resistance	Ohm	Ω	V/A
Capacitance	Farad	F	$A \cdot s/V$
Magnetic flux	Weber	Wb	$V \cdot s$
Inductance	Henry	H	$V \cdot s/A$
Magnetic flux density	Tesla	T	Wb/m^2
Magnetic field strength	Ampere per meter	A/m	
Magnetomotive force	Ampere	A	
Luminous flux	Lumen	lm	$cd \cdot sr$
Luminance	Candela per square meter	cd/m^2	
Illuminance	Lux	lx	lm/m^2
Wave number	1 per meter	m^{-1}	
Entropy	Joule per kelvin	J/K	
Specific heat capacity	Joule per kilogram kelvin	$J/(kg \cdot K)$	
Thermal conductivity	Watt per meter kelvin	$W/(m \cdot K)$	
Radiant intensity	Watt per steradian	W/sr	
Activity (of a radioactive source)	1 per second	s^{-1}	
SI supplementary units			
Plane angle	radian	rad	
Solid angle	Steradian	sr	

Table A.2 Definitions of SI units [1]

Meter (m)	The *meter* is the length equal to 1 650 763.73 wavelengths in vacuum of the radiation corresponding to the transition between the levels 2 p_{10} and 5 d_s of the krypton-86 atom	Volt (V)	The *volt* is the difference of electric potential between two points of a conducting wire carrying a constant current of 1 ampere, when the power dissipated between these points is equal to 1 watt
Kilogram (kg)	The *kilogram* is the unit of mass; it is equal to the mass of the international prototype of the kilogram. (The international prototype of the kilogram is a particular cylinder of platinum-iridium alloy that is preserved in a vault at Sèvres, France, by the International Bureau of Weights and Measures)	Ohm (Ω)	The *ohm* is the electric resistance between two points of a conductor when a constant difference of potential of 1 volt, applied between these two points, produces in this conductor a current of 1 ampere, this conductor not being the source of any electromotive force
Second (s)	The *second* is the duration of 9 192 631 770 periods of the radiation corresponding to the transition between the two hyperfine levels of the ground state of the cesium-133 atom	Coulomb (C)	The *coulomb* is the quantity of electricity transported in 1 second by a current of 1 ampere
Ampere (A)	The *ampere* is that constant current, which, if maintained in two straight parallel conductors of infinite length, of negligible circular cross section, and placed 1 meter apart in a vacuum, would produce between these conductors a force equal to 2×10^{-7} newton per meter of length	Farad (F)	The *farad* is the capacitance of a capacitor between the plates of which there appears a difference of potential of 1 volt when it is charged by a quantity of electricity equal to 1 coulomb
Kelvin (K)	The *kelvin*, unit of thermodynamic temperature, is the fraction 1/273.16 of the thermodynamic temperature of the triple point of water	Henry (H)	The *henry* is the inductance of a closed circuit in which an electromotive force of 1 volt is produced when the electric current in the circuit varies uniformly at a rate of 1 ampere per second
Candela (cd)	The *candela* is the luminous intensity, in the perpendicular direction, of a surface of 1/600 000 square meter of a blackbody at the temperature of freezing platinum under a pressure of 101 325 newtons per square meter	Weber (Wb)	The *weber* is the magnetic flux that, linking a circuit of one turn, produces in it an electromotive force of 1 volt as it is reduced to zero at a uniform rate in 1 second
Mole (mol)	The *mole* is the amount of substance of a system that contains as many elementary entities as there are carbon atoms in 0.012 kg of carbon 12. The elementary entities must be specified and may be atoms, molecules, ions, electrons, other particles, or specified groups of such particles	Lumen (lm)	The *lumen* is the luminous flux emitted in a solid angle of 1 steradian by a uniform point source having an intensity of 1 candela
Newton (N)	The *newton* is that force that gives to a mass of 1 kilogram an acceleration of 1 meter per second per second	Radian (rad)	The *radian* is the plane angle between two radii of a circle that cut off on the circumference an arc equal in length to the radius
Joule (J)	The *joule* is the work done when the point of application of 1 newton is displaced a distance of 1 meter in the direction of the force	Steradian (sr)	The *steradian* is the solid angle that, having its vertex in the center of a sphere, cuts off an area of the surface of the sphere equal to that of a square with sides of length equal to the radius of the sphere
Watt (W)	The *watt* is the power that gives rise to the production of energy at the rate of 1 joule per second		

Table A.3 SI prefixes [1]

Factor by which unit is multiplied	Prefix	Symbol
10^{12}	Tera	T
10^{9}	Giga	G
10^{6}	Mega	M
10^{3}	Kilo	k
10^{2}	Hecto	h
10	Deka	da
10^{-1}	Deci	d
10^{-2}	Centi	c
10^{-3}	Milli	m
10^{-6}	Micro	μ
10^{-9}	Nano	n
10^{-12}	Pico	p
10^{-15}	Femto	f
10^{-18}	Atto	a

Table A.6. The listing by physical quantity (Table A.6) includes only relationships that are frequently encountered, and deliberately omits the great multiplicity of combinations of units that are used for more specialized purposes. Conversion factors for combinations of units are easily generated from numbers given in the alphabetical listing (Table A.5) by the technique of direct substitution or by other well-known rules for manipulating units. These rules are adequately discussed in many science and engineering textbooks and are not repeated here.

Table A.4 Physical constants [2]

Quantity	Symbol	Value	Error (ppm)	Prefix	Unit
Speed of light in vacuum	c	2. 997 925 0	0.33	$\times 10^{8}$	$m \cdot s^{-1}$
Gravitational constant	G	6. 673 2	460	10^{-11}	$N \cdot m^{2} \cdot kg^{-2}$
Avogadro constant	N_A	6. 022 169	6.6	10^{26}	$kmol^{-1}$
Boltzmann constant	k	1. 380 622	43	10^{-23}	$J \cdot K^{-1}$
Gas constant	R	8. 314 34	42	10^{3}	$J \cdot kmol^{-1} \cdot K^{-1}$
Volume of ideal gas, standard conditions	V_0	2. 241 36	–	10^{1}	$m^{3} \cdot kmol^{-1}$
Faraday constant	F	9. 648 670	5.5	10^{7}	$C \cdot kmol^{-1}$
Unified atomic mass unit	u	1. 660 531	6.6	10^{-27}	kg
Planck constant	h	6. 626 196	7.6	10^{-34}	$J \cdot s$
	h/2π	1. 054 591 9	7.6	10^{-34}	$J \cdot s$
Electron charge	e	1. 602 191 7	4.4	10^{-19}	C
Electron rest mass	m_e	9. 109 558	6.0	10^{-31}	kg
		5. 485 930	6.2	10^{-4}	u
Proton rest mass	m_p	1. 672 614	6.6	10^{-27}	kg
		1. 007 276 61	0.08	–	u
Neutron rest mass	m_n	1. 674 920	6.6	10^{-27}	kg
		1. 008 665 20	0.10	–	u
Electron charge to mass ratio	e/m_e	1. 758 802 8	3.1	10^{11}	$C \cdot kg^{-1}$
Stefan-Boltzmann constant	σ	5. 669 61	170	10^{-8}	$W \cdot m^{-2} \cdot K^{-4}$
First radiation constant	$2\pi hc^2$	3. 741 844	7.6	10^{-16}	$W \cdot m^{2}$
Second radiation constant	hc/k	1. 438 833	43	10^{-2}	$m \cdot K$
Rydberg constant	R_∞	1. 097 373 12	0.10	10^{7}	m^{-1}
Fine structure constant	α	7. 297 351	1.5	10^{-3}	
	α^{-1}	1. 370 360 2	1.5	10^{2}	
Bohr radius	α_0	5. 291 771 5	1.5	10^{-11}	m
Classical electron radius	r_e	2. 817 939	4.6	10^{-15}	m
Compton wavelength of electron	λ_C	2. 426 309 6	3.1	10^{-12}	m
	$\lambda_C/2\pi$	3. 861 592	3.1	10^{-13}	m
Compton wavelength of proton	$\lambda_{C,p}$	1. 321 440 9	6.8	10^{-15}	m
	$\lambda_{C,p}/2\pi$	2. 103 139	6.8	10^{-16}	m

(continued)

Table A.4 (continued)

Quantity	Symbol	Value	Error (ppm)	Prefix	Unit
Compton wavelength of neutron	$\lambda_{C,n}$	1. 319 621 7	6.8	10^{-15}	m
	$\lambda_{C,n}/2\pi$	2. 100 243	6.8	10^{-16}	m
Electron magnetic moment	μ_e	9. 284 851	7.0	10^{-24}	$J \cdot T^{-1}$
Proton magnetic moment	μ_p	1. 410 620 3	7.0	10^{-26}	$J \cdot T^{-1}$
Bohr magneton	μ_B	9. 274 096	7.0	10^{-24}	$J \cdot T^{-1}$
Nuclear magneton	μ_n	5. 050 951	10	10^{-27}	$J \cdot T^{-1}$
Gyromagnetic ratio of protons in H_2O	γ'_p	2. 675 127 0	3.1	10^{8}	$rad \cdot s^{-1}\ T^{-1}$
	$\gamma'_p/2\pi$	4. 257 597	3.1	10^{7}	$Hz \cdot T^{-1}$
Gyromagnetic ratio of protons in H_2O	γ'_p	2. 675 196 5	3.1	10^{8}	$rad \cdot s^{-1}\ T^{-1}$
Corrected for diamagnetism of H_2O	$\gamma'_p/2\pi$	4. 257 707	3.1	10^{7}	$Hz \cdot T^{-1}$
Magnetic flux quantum	Φ_0	2. 067 853 8	3.3	10^{-15}	Wb
Quantum of circulation	$h/2m_e$	3. 636 947	3.1	10^{-4}	$J \cdot s \cdot kg^{-1}$
	h/m_e	7. 273 894	3.1	10^{-4}	$J \cdot s \cdot kg^{-1}$

Unitless	Numerical ratios	Value	Error (ppm)	Prefix
(c^2)	kg/eV	5. 609 538	4.4	10^{35}
(c^2)	u/eV	9. 314 812	5.5	10^{8}
	u/kg	1. 660 531	6.6	10^{-27}
(c^2)	m_c/eV	5. 110 041	3.1	10^{5}
(c^2)	m_p/eV	9. 382 592	5.5	10^{8}
(c^2)	m_n/eV	9. 395 527	5.5	10^{8}
	eV/J	1. 602 191 7	4.4	10^{-19}
(h^{-1})	eV/Hz	2. 417 965 9	3.3	10^{14}
(hc^{-1})	eVm	8. 065 465	3.3	10^{5}
(k^{-1})	eV/K	1. 160 485	42	10^{4}
(hc)	$(eVm)^{-1}$	1. 239 854 1	3.3	10^{-6}
(hc)	R_∞/J	2. 179 914	7.6	10^{-18}
(hc)	R_∞/eV	1. 360 582 6	3.3	10^{1}
(c)	R_∞/Hz	3. 289 842 3	0.35	10^{15}
(hc/k)	R_∞/K	1. 578 936	43	10^{5}
	m_p/m_e	1. 836 109	6.2	10^{3}
	μ_e/μ_B	1. 001 159 638 9	0.0031	
	μ'_p/μ_B	1. 520 993 12	0.066	10^{-3}
	μ_p/μ_B	1. 521 032 64	0.30	10^{-3}
	μ'_p/μ_n	2. 792 709	6.2	
	μ_p/μ_n	2. 792 782	6.2	

Other important constants
π = 3.141 592 653 589
e = 2.718 281 828 459
μ_0 = $4\pi \times 10^{-7}$ H/m (exact), permeability of free space
=1.256 637 061 $\times 10^{-6}$ H/m
$\varepsilon_0 = \mu_0^{-1}c^{-2}$ F/m, permittivity of free space
= 8.854 185 $\times 10^{-12}$ F/m

Table A.5 Alphabetical listing of conversion factors [1]

To convert from	to	Multiply by
Abampere	Ampere	10^1 (exact)
Abcoulomb	Coulomb	10^1 (exact)
Abfarad	Farad	10^9 (exact)
Abhenry	Henry	10^{-9} (exact)
Abmho	Siemens	10^9 (exact)
Abohm	Ohm	10^{-9} (exact)
Abvolt	Volt	10^{-8} (exact)
Acre	Meter^2	$4.046\,856\,422\,4 \times 10^3$ (exact)
Angstrom	Meter	10^{-10} (exact)
Are	Meter^2	10^2 (exact)
Astronomical unit (IAU)	Meter	$1.496\,00 \times 10^{11}$
Astronomical unit (radio)	Meter	$1.495\,978\,9 \times 10^{11}$
Atmosphere	Newton/meter^2	$1.013\,25 \times 10^{-5}$ (exact)
Bar	Newton/meter^2	10^5 (exact)
Barn	Meter^2	10^{-28} (exact)
Barrel (petroleum, 42 gallons)	Meter^3	$1.589\,873 \times 10^{-1}$
Barye	Newton/meter^2	10^{-1} (exact)
Board foot ($1' \times 1' \times 1''$)	Meter^3	$2.359\,737\,216 \times 10^{-3}$ (exact)
British thermal unit		
IST before 1956	Joule	$1.055\,04 \times 10^3$
IST after 1956	Joule	$1.055\,056 \times 10^3$
British thermal unit (mean)	Joule	$1.055\,87 \times 10^3$
British thermal unit (thermochemical)	Joule	$1.054\,350 \times 10^3$
British thermal unit (39 °F)	Joule	$1.059\,67 \times 10^3$
British thermal unit (60 °F)	Joule	$1.054\,68 \times 10^3$
Bushel (U.S.)	Meter^3	$3.523\,907\,016\,688 \times 10^{-2}$ (exact)
Cable	Meter	$2.194\,56 \times 10^2$ (exact)
Caliber	Meter	2.54×10^{-4} (exact)
Calorie (international steam table)	Joule	4.1868
Calorie (mean)	Joule	4.190 02
Calorie (thermochemical)	Joule	4.184 (exact)
Calorie (15 °C)	Joule	4.185 80
Calorie (20 °C)	Joule	4.181 90
Calorie (kilogram, international steam table)	Joule	4.1868
Calorie (kilogram, mean)	Joule	$4.190\,02 \times 10^3$
Calorie (kilogram, thermochemical)	Joule	4.184×10^3 (exact)
Carat (metric)	Kilogram	2.00×10^{-4} (exact)
Celsius (temperature)	Kelvin	$t_K = t_c + 273.15$
Centimeter of mercury (0 °C)	Newton/meter^2	$1.333\,22 \times 10^3$
Centimeter of water (4 °C)	Newton/meter^2	$9.806\,38 \times 10^1$
Chain (engineer or ramden)	Meter	3.048×10^1 (exact)
Chain (surveyor or gunter)	Meter	$2.011\,68 \times 10^1$ (exact)
Circular mil	Meter^2	$5.067\,074\,8 \times 10^{-10}$
Cord	Meter^3	3.624 556 3
Cubit	Meter	4.572×10^{-1} (exact)
Cup	Meter^3	$2.365\,882\,365 \times 10^{-4}$ (exact)
Curie	Disintegration/second	3.70×10^{10} (exact)
Day (mean solar)	Second (mean solar)	8.64×10^4 (exact)

(continued)

Table A.5 (continued)

To convert from	to	Multiply by
Day (sidereal)	Second (mean solar)	$8.616\,409\,0 \times 10^{4}$
Degree (angle)	Radian	$1.745\,329\,251\,994\,3 \times 10^{-2}$
Denier (international)	Kilogram/meter	10^{-7} (exact)
Dram (avoirdupois)	Kilogram	$1.771\,845\,195\,312\,5 \times 10^{-3}$ (exact)
Dram (troy or apothecary)	Kilogram	$3.887\,934\,6 \times 10^{-3}$ (exact)
Dram (U.S. fluid)	Meter^3	$3.696\,691\,195\,312\,5 \times 10^{-3}$ (exact)
Dyne	Newton	10^{-5} (exact)
Electron volt	Joule	$1.602\,191\,7 \times 10^{-19}$
Erg	Joule	1.00×10^{-7} (exact)
Fahrenheit (temperature)	Kelvin	$t_K = (5/9)(t_F + 459.67)$
Fahrenheit (temperature)	Celsius	$t_c = (5/9)(t_F - 32)$
Faraday (based on carbon 12)	Coulomb	$9.68\,70 \times 10^{4}$
Faraday (chemical)	Coulomb	$9.649\,57 \times 10^{4}$
Faraday (physical)	Coulomb	$9.652\,19 \times 10^{4}$
Fathom	Meter	1.828 8 (exact)
Fermi (femtometer)	Meter	10^{15} (exact)
Fluid ounce (U.S.)	Meter^3	$2.957\,352\,967\,25 \times 10^{-5}$ (exact)
Foot	Meter	3.048×10^{-1} (exact)
Foot (U.S. survey)	Meter	$3.048\,006\,096 \times 10^{-1}$ (1,200/3,937)
Foot of water (39.2 °F)	Newton/meter^2	$2.988\,98 \times 10^{3}$
$\text{Foot}^{1/2}/\text{second}^{1/2}$	$\text{Meter}^{1/2}/\text{second}^{1/2}$	$5.520\,869\,5 \times 10^{-1}$
Percent per foot (light obscuration)	Percent per meter	$\%/\text{m} = (1-(1-[\%/\text{ft}])/100)^{3.28} \times 100$
Footcandle	Lumen/meter^2	$1.076\,391\,0 \times 10^{1}$
Footlambert	Candela/meter^2	3.426 259
Free fall, standard	Meter/second^2	9.806 65
Furlong	Meter	$2.011\,68 \times 10^{3}$ (exact)
Gal (galileo)	Meter/second^2	10^{-2} (exact)
Gallon (U.K. liquid)	Meter^3	$4.546\,087 \times 10^{-3}$
Gallon (U.S. dry)	Meter^3	$4.404\,883\,770\,86 \times 10^{-3}$ (exact)
Gallon (U.S. liquid)	Meter^3	$3.785\,411\,784 \times 10^{-3}$ (exact)
Gallons per minute per square foot	mm/min	$4.074\,583\,33 \times 10^{-1}$
Gamma	Tesla	10^{-9} (exact)
Gauss	Tesla	10^{-4} (exact)
Gilbert	Ampere turn	$7.957\,747\,2 \times 10^{-1}$
Gill (U.K.)	Meter^3	$1.420\,652 \times 10^{-4}$
Gill (U.S.)	Meter^3	$1.182\,941\,2 \times 10^{-4}$
Grad	Degree (angular)	9.000×10^{-1} (exact)
Grad	Radian	$1.570\,796\,3 \times 10^{-2}$
Grain	Kilogram	$6.479\,891 \times 10^{-5}$ (exact)
Gram	Kilogram	10^{-3} (exact)
Hand	Meter	1.016×10^{-1} (exact)
Hectare	Meter^2	10^{4} (exact)
Hogshead (U.S.)	Meter^3	$2.384\,809\,423\,92 \times 10^{-1}$ (exact)
Horsepower (550 ft · lbf/second)	Watt	$7.456\,998\,7 \times 10^{2}$
Horsepower (boiler)	Watt	$9.809\,50 \times 10^{3}$
Horsepower (electric)	Watt	7.46×10^{2} (exact)
Horsepower (metric)	Watt	$7.354\,99 \times 10^{2}$
Horsepower (U.K.)	Watt	7.457×10^{2}

(continued)

Table A.5 (continued)

To convert from	to	Multiply by
Horsepower (water)	Watt	$7.460\,73 \times 10^{2}$
Hour (mean solar)	Second (mean solar)	3.60×10^{3} (exact)
Hour (sidereal)	Second (mean solar)	$3.590\,170\,4 \times 10^{3}$
Hundredweight (long)	Kilogram	$5.080\,234\,544 \times 10^{1}$ (exact)
Hundredweight (short)	Kilogram	$4.535\,923\,7 \times 10^{1}$ (exact)
Inch	Meter	2.54×10^{-2} (exact)
Inch of mercury (32 °F)	Newton/meter^2 (Pa)	$3.386\,389 \times 10^{3}$
Inch of mercury (60 °F)	Newton/meter^2 (Pa)	$3.375\,85 \times 10^{3}$
Inch of water (39.2 °F)	Newton/meter^2 (Pa)	$2.490\,82 \times 10^{2}$
Inch of water (60 °F)	Newton/meter^2 (Pa)	2.4884×10^{2}
Kayser	1/meter	10^{2} (exact)
Kilocalorie (International Steam Table)	Joule	$4.186\,8 \times 10^{3}$
Kilocalorie (mean)	Joule	$4.190\,02 \times 10^{3}$
Kilocalorie (thermochemical)	Joule	4.184×10^{3} (exact)
Kilogram force (kgf)	Newton	9.806 65 (exact)
Kilopound force	Newton	9.806 65 (exact)
Kip	Newton	$4.448\,221\,615\,260\,5 \times 10^{3}$ (exact)
Knot (international)	Meter/second	$5.144\,444\,444 \times 10^{-1}$
Lambert	Candela/meter^2	$3.183\,098\,86 \times 10^{3}$ ($1/\pi \times 10^{4}$)
Langley	Joule/meter^2	4.184×10^{4}
Lbf (pound force, avoirdupois)	Newton	4.448 221 615 260 5 (exact)
Lbm (pound mass, avoirdupois)	Kilogram	$4.535\,923\,7 \times 10^{-1}$ (exact)
League (U.K. nautical)	Meter	$5.559\,552 \times 10^{3}$ (exact)
League (international nautical)	Meter	5.556×10^{3}
League (statute)	Meter	$4.828\,032 \times 10^{3}$ (exact)
Light-year	Meter	$9.460\,55 \times 10^{15}$
Link (engineer or ramden)	Meter	3.048×10^{-1} (exact)
Link (surveyor or gunter)	Meter	$2.011\,68 \times 10^{-1}$ (exact)
Liter	Meter^3	10^{-3} (exact)
Lux	Lumen/meter^2	1.00 (exact)
Maxwell	Weber	10^{-8} (exact)
Meter	Wavelengths Kr 86	$1.650\,763\,73 \times 10^{6}$ (exact)
Micron	Meter	10^{-6} (exact)
Mil	Meter	2.54×10^{-5} (exact)
Mile (U.S. statute)	Meter	$1.609\,344 \times 10^{3}$ (exact)
Mile (U.K. nautical)	Meter	$1.853\,184 \times 10^{3}$ (exact)
Mile (international nautical)	Meter	1.852×10^{3} (exact)
Mile (U.S. nautical)	Meter	1.852×10^{3} (exact)
Millibar	Newton/meter^2	10^{2} (exact)
Millimeter of mercury (0 °C)	Newton/meter^2	$1.333\,224 \times 10^{2}$
Minute (angle)	Radian	$2.908\,882\,086\,66 \times 10^{-4}$
Minute (mean solar)	Second (mean solar)	6.00×10^{1} (exact)
Minute (sidereal)	Second (mean solar)	$5.983\,617\,4 \times 10^{1}$
Month (mean calendar)	Second (mean solar)	2.628×10^{6} (exact)
Nautical mile (international)	Meter	1.852×10^{3} (exact)
Nautical mile (U.S.)	Meter	1.852×10^{3} (exact)
Nautical mile (U.K.)	Meter	$1.853\,184 \times 10^{3}$ (exact)
Oersted	Ampere/meter	$7.957\,747\,2 \times 10^{1}$

(continued)

Table A.5 (continued)

To convert from	to	Multiply by
Ounce force (avoirdupois)	Newton	$2.780\ 138\ 5 \times 10^{-1}$
Ounce mass (avoirdupois)	Kilogram	$2.834\ 952\ 312\ 5 \times 10^{-2}$ (exact)
Ounce mass (troy or apothecary)	Kilogram	$3.110\ 347\ 68 \times 10^{-2}$ (exact)
Ounce (U.S. fluid)	$Meter^3$	$2.957\ 352\ 956\ 25 \times 10^{-2}$ (exact)
Pace	Meter	7.62×10^{1} (exact)
Parsec (IAU)	Meter	$3.085\ 7 \times 10^{16}$
Pascal	$Newton/meter^2$	1.00 (exact)
Peck (U.S.)	$Meter^3$	$8.809\ 767\ 541\ 72 \times 10^{-3}$ (exact)
Pennyweight	Kilogram	$1.555\ 173\ 84 \times 10^{-3}$ (exact)
Perch	Meter	5.0292 (exact)
Phot	$Lumen/meter^3$	10^4 (exact)
Pica (printers)	Meter	$4.217\ 517\ 6 \times 10^{-3}$ (exact)
Pint (U.S. dry)	$Meter^3$	$5.506\ 104\ 713\ 575 \times 10^{-4}$ (exact)
Pint (U.S. liquid)	$Meter^3$	$-04\ 4.731\ 764\ 73 \times 10^{-4}$ (exact)
Point (printers)	Meter	$-04\ 3.514\ 598 \times 10^{-4}$ (exact)
Poise	$Newton\ second/meter^2$	10^{-1} (exact)
Pole	Meter	5.0292 (exact)
Pound force (lbf avoirdupois)	Newton	4.448 221 615 260 5 (exact)
Pound mass (lbm avoirdupois)	Kilogram	$4.535\ 923\ 7 \times 10^{-1}$ (exact)
Pound mass (troy or apothecary)	Kilogram	$3.732\ 417\ 216 \times 10^{-1}$ (exact)
Poundal	Newton	$1.382\ 549\ 543\ 76 \times 10^{-1}$ (exact)
Quart (U.S. dry)	$Meter^3$	$1.101\ 220\ 942\ 715 \times 10^{-3}$ (exact)
Quart (U.S. liquid)	$Meter^3$	$9.463\ 592\ 5 \times 10^{-4}$
Rad (radiation dose absorbed)	Joule/kilogram	10^{-2} (exact)
Rankine (temperature)	Kelvin	$t_K = (5/9)t_R$
Rayleigh (rate of photon emission)	$1/second\ meter^2$	10^{10} (exact)
Rhe	$Meter^2/newton\ second$	10^{1} (exact)
Rod	Meter	5.0292 (exact)
Roentgen	Coulomb/kilogram	$2.579\ 76 \times 10^{-4}$ (exact)
Rutherford	Disintegration/second	10^6 (exact)
Second (angle)	Radian	$4.848\ 136\ 811 \times 10^{-6}$
Second (ephemeris)	Second	1.00 (exact)
Second (sidereal)	Second (mean solar)	$9.972\ 695\ 7 \times 10^{-1}$
Section	$Meter^2$	$2.589\ 988\ 110\ 336 \times 10^6$ (exact)
Scruple (apothecary)	Kilogram	$1.295\ 978\ 2 \times 10^{-3}$ (exact)
Shake	Second	10^{-8}
Skein	Meter	$1.097\ 28 \times 10^{2}$ (exact)
Slug	Kilogram	$1.459\ 390\ 29 \times 10^{1}$
Span	Meter	2.286×10^{-1} (exact)
Statampere	Ampere	$3.335\ 640 \times 10^{-10}$
Statcoulomb	Coulomb	$3.335\ 640 \times 10^{-10}$
Statfarad	Farad	$1.112\ 650 \times 10^{-12}$
Stathenry	Henry	$8.987\ 554 \times 10^{11}$
Statohm	Ohm	$8.987\ 554 \times 10^{11}$
Statute mile (U.S.)	Meter	$1.609\ 344 \times 10^3$ (exact)
Statvolt	Volt	$2.997\ 925 \times 10^2$
Stere	$Meter^3$	1.00 (exact)
Stilb	$Candela/meter^2$	10^4

(continued)

Table A.5 (continued)

To convert from	to	Multiply by
Stoke	$Meter^2$/second	10^{-4} (exact)
Tablespoon	$Meter^3$	$1.478\ 676\ 478\ 125 \times 10^{-5}$ (exact)
Teaspoon	$Meter^3$	$-4.928\ 921\ 593\ 75 \times 10^{-6}$ (exact)
Ton (assay)	Kilogram	$2.196\ 666\ 6 \times 10^{-2}$
Ton (long)	Kilogram	$1.016\ 046\ 908\ 8 \times 10^{3}$ (exact)
Ton (metric)	Kilogram	10^{3} (exact)
Ton (nuclear equivalent of TNT)	Joule	4.20×10^{9}
Ton (register)	$Meter^3$	2.831 684 659 2 (exact)
Ton (short, 2,000 pound)	Kilogram	$9.071\ 847\ 4 \times 10^{2}$ (exact)
Tonne	Kilogram	10^{3} (exact)
Torr (0 °C)	Newton/$meter^2$	$1.333\ 22 \times 10^{2}$
Township	$Meter^2$	$9.323\ 957\ 2 \times 10^{7}$
Unit pole	Weber	$1.256\ 637 \times 10^{-7}$
Yard	Meter	9.144×10^{-1} (exact)
Year (calendar)	Second (mean solar)	3.1536×10^{7} (exact)
Year (sidereal)	Second (mean solar)	$3.155\ 815\ 0 \times 10^{7}$
Year (tropical)	Second (mean solar)	$3.155\ 692\ 6 \times 10^{7}$
Year 1900, tropical, Jan., day 0, hour 12	Second (ephemeris)	$3.155\ 692\ 597\ 47 \times 10^{7}$ (exact)
Year 1900, tropical, Jan., day 0, hour 12	Second	$3.155\ 692\ 597\ 47 \times 10^{7}$ (exact)

Table A.6 Listing conversion factors by physical quantity [1]

To convert from	to	Multiply by
Acceleration		
Foot/$second^2$	Meter/$second^2$	3.048×10^{-1} (exact)
Free fall, standard	Meter/$second^2$	9.806 65 (exact)
Gal (galileo)	Meter/$second^2$	10^{-2} (exact)
Inch/$second^2$	Meter/$second^2$	2.54×10^{-2} (exact)
Area		
Acre	$Meter^2$	$4.046\ 856\ 422\ 4 \times 10^{3}$ (exact)
Are	$Meter^2$	10^{2} (exact)
Barn	$Meter^2$	10^{-28} (exact)
Circular mil	$Meter^2$	$5.067\ 074\ 8 \times 10^{-10}$
$Foot^2$	$Meter^2$	$9.290\ 304 \times 10^{-2}$ (exact)
Hectare	$Meter^2$	10^{4} (exact)
$Inch^2$	$Meter^2$	6.4516×10^{-4} (exact)
$Mile^2$ (U.S. statute)	$Meter^2$	$2.589\ 988\ 110\ 336 \times 10^{6}$ (exact)
Section	$Meter^2$	$2.589\ 988\ 110\ 336 \times 10^{6}$ (exact)
Township	$Meter^2$	$9.323\ 957\ 2 \times 10^{7}$
$Yard^2$	$Meter^2$	$8.361\ 273\ 6 \times 10^{-1}$ (exact)
Density		
Gram/$centimeter^3$	Kilogram/$meter^3$	10^{-3} (exact)
Lbm/$inch^3$	Kilogram/$meter^3$	$2.767\ 990\ 5 \times 10^{4}$
Lbm/$foot^3$	Kilogram/$meter^3$	$1.601\ 846\ 3 \times 10^{1}$
Slug/$foot^3$	Kilogram/$meter^3$	$5.153\ 79 \times 10^{-2}$

(continued)

Table A.6 (continued)

To convert from	to	Multiply by
Energy		
British thermal unit		
IST before 1956	Joule	$1.055\ 04 \times 10^3$
IST after 1956	Joule	$1.055\ 056 \times 10^3$
British thermal unit (mean)	Joule	$1.055\ 87 \times 10^3$
British thermal unit (thermochemical)	Joule	$1.054\ 350 \times 10^3$
British thermal unit (39 °F)	Joule	$1.059\ 67 \times 10^3$
British thermal unit (60 °F)	Joule	$1.054\ 68 \times 10^3$
Calorie (international steam table)	Joule	4.1868
Calorie (mean)	Joule	4.190 02
Calorie (thermochemical)	Joule	4.184 (exact)
Calorie (15 °C)	Joule	4.185 80
Calorie (20 °C)	Joule	4.181 90
Calorie (kilogram, international steam table)	Joule	4.1868×10^3
Calorie (kilogram, mean)	Joule	$4.190\ 02 \times 10^3$
Calorie (kilogram, thermochemical)	Joule	4.184×10^3 (exact)
Electron volt	Joule	$1.602\ 191\ 7 \times 10^{-19}$
Erg	Joule	10^{-7} (exact)
Foot lbf	Joule	$1.355\ 817\ 9 \times 10^3$
Foot poundal	Joule	$4.214\ 011\ 0 \times 10^{-2}$
Joule (international of 1948)	Joule	1.000 165
Kilocalorie (international steam table)	Joule	4.1868×10^3
Kilocalorie (mean)	Joule	$4.190\ 02 \times 10^3$
Kilocalorie (thermochemical)	Joule	4.184×10^3 (exact)
Kilowatt hour	Joule	3.60×10^6 (exact)
Kilowatt hour (international of 1948)	Joule	$3.600\ 59 \times 10^6$
Ton (nuclear equivalent of TNT)	Joule	4.20×10^9
Watt hour	Joule	3.60×10^3 (exact)
Energy/area time		
Btu (thermochemical)/foot^2 second	Watt/meter^2	$1.134\ 893\ 1 \times 10^4$
Btu (thermochemical)/foot^2 minute	Watt/meter^2	$1.891\ 488\ 5 \times 10^2$
Btu (thermochemical)/foot^2 hour	Watt/meter^2	3.152 480 8
Btu (thermochemical)/inch^2 second	Watt/meter^2	$1.634\ 246\ 2 \times 10^6$
Calorie (thermochemical)/cm^2 minute	Watt/meter^2	$6.973\ 333\ 3 \times 10^2$
Erg/centimeter^2 second	Watt/meter^2	10^3 (exact)
Watt/centimeter^2	Watt/meter^2	10^{-4} (exact)
Force		
Dyne	Newton	10^{-5} (exact)
Kilogram force (kgf)	Newton	9.806 65 (exact)
Kilopound force	Newton	9.806 65 (exact)
Kip	Newton	$4.448\ 221\ 615\ 260\ 5 \times 10^3$ (exact)
Lbf (pound force, avoirdupois)	Newton	4.448 221 615 260 5 (exact)
Ounce force (avoirdupois)	Newton	$2.780\ 138\ 5 \times 10^1$
Pound force, lbf (avoirdupois)	Newton	4.448 221 615 260 5 (exact)
Poundal	Newton	$1.382\ 549\ 543\ 76 \times 10^{-1}$ (exact)
Length		
Angstrom	Meter	10^{-10} (exact)
Astronomical unit (IAU)	Meter	$1.496\ 00 \times 10^{11}$

(continued)

Table A.6 (continued)

To convert from	to	Multiply by
Astronomical unit (radio)	Meter	$1.495\ 978\ 9 \times 10^{11}$
Cable	Meter	$2.194\ 56 \times 10^{2}$ (exact)
Caliber	Meter	2.54×10^{-4} (exact)
Chain (surveyor or gunter)	Meter	$2.011\ 68 \times 10^{1}$ (exact)
Chain (engineer or ramden)	Meter	3.048×10^{1} (exact)
Cubit	Meter	4.572×10^{-1} (exact)
Fathom	Meter	1.8288 (exact)
Fermi (femtometer)	Meter	10^{-15} (exact)
Foot	Meter	3.048×10^{-1} (exact)
Foot (U.S. survey)	Meter	$3.048\ 006\ 096\ 10^{-1}$ (1,200/3,937)
Furlong	Meter	$2.011\ 68 \times 10^{2}$ (exact)
Hand	Meter	1.016×10^{-1} (exact)
Inch	Meter	2.54×10^{-2} (exact)
League (U.K. nautical)	Meter	$5.559\ 552 \times 10^{3}$ (exact)
League (international nautical)	Meter	5.556×10^{3} (exact)
League (statute)	Meter	$4.828\ 032 \times 10^{3}$ (exact)
Light-year	Meter	$9.460\ 55 \times 10^{15}$
Link (engineer or ramden)	Meter	3.048×10^{-1} (exact)
Link (surveyor or gunter)	Meter	$2.011\ 68 \times 10^{-1}$ (exact)
Meter	Wavelengths Kr 86	$1.650\ 763\ 73 \times 10^{6}$ (exact)
Micron	Meter	10^{-6} (exact)
Mil	Meter	$-05\ 2.54 \times 10^{-5}$ (exact)
Mile (U.S. statute)	Meter	$1.609\ 344 \times 10^{3}$ (exact)
Mile (U.K. nautical)	Meter	$1.853\ 184 \times 10^{3}$ (exact)
Mile (international nautical)	Meter	1.852×10^{3} (exact)
Mile (U.S. nautical)	Meter	1.852×10^{3} (exact)
Nautical mile (U.K.)	Meter	$1.853\ 184 \times 10^{3}$ (exact)
Nautical mile (international)	Meter	1.852×10^{3} (exact)
Nautical mile (U.S.)	Meter	1.852×10^{3} (exact)
Pace	Meter	7.62×10^{-1} (exact)
Parsec (IAU)	Meter	$3.085\ 7 \times 10^{16}$
Perch	Meter	5.0292 (exact)
Pica (printers)	Meter	$4.217\ 517\ 6 \times 10^{-3}$ (exact)
Point (printers)	Meter	$3.514\ 598 \times 10^{-4}$ (exact)
Pole	Meter	5.0292 (exact)
Rod	Meter	5.0292 (exact)
Skein	Meter	$1.097\ 28 \times 10^{2}$ (exact)
Span	Meter	2.286×10^{-1} (exact)
Statute mile (U.S.)	Meter	$1.609\ 344 \times 10^{3}$ (exact)
Yard	Meter	9.144×10^{-1} (exact)
Mass		
Carat (metric)	Kilogram	2.00×10^{-4} (exact)
Gram (avoirdupois)	Kilogram	$1.771\ 845\ 195\ 312\ 5 \times 10^{-3}$ (exact)
Gram (troy or apothecary)	Kilogram	$3.887\ 934\ 6 \times 10^{-3}$ (exact)
Grain	Kilogram	$6.479\ 891 \times 10^{-5}$ (exact)
Gram	Kilogram	10^{-3} (exact)
Hundredweight (long)	Kilogram	$5.080\ 234\ 544 \times 10^{1}$ (exact)
Hundredweight (short)	Kilogram	$4.535\ 923\ 7 \times 10^{1}$ (exact)

(continued)

Table A.6 (continued)

To convert from	to	Multiply by
Kgf second^2 meter (mass)	Kilogram	9.806 65 (exact)
Kilogram mass	Kilogram	1.00 (exact)
Lbm (pound mass, avoirdupois)	Kilogram	$4.535\ 923\ 7 \times 10^{-1}$ (exact)
Ounce mass (avoirdupois)	Kilogram	$2.834\ 952\ 312\ 5 \times 10^{-2}$ (exact)
Ounce mass (troy or apothecary)	Kilogram	$3.110\ 347\ 68 \times 10^{-2}$ (exact)
Pennyweight	Kilogram	$1.555\ 173\ 84 \times 10^{-3}$ (exact)
Pound mass, lbm (avoirdupois)	Kilogram	$4.535\ 923\ 7 \times 10^{-1}$ (exact)
Pound mass (troy or apothecary)	Kilogram	$3.732\ 417\ 216 \times 10^{-1}$ (exact)
Scruple (apothecary)	Kilogram	$1.295\ 978\ 2 \times 10^{-3}$ (exact)
Slug	Kilogram	$1.459\ 390\ 29 \times 10^{1}$
Ton (assay)	Kilogram	$2.196\ 666\ 6 \times 10^{-2}$
Ton (long)	Kilogram	$1.016\ 046\ 908\ 8 \times 10^{3}$ (exact)
Ton (metric)	Kilogram	10^3 (exact)
Ton (short, 2,000 pound)	Kilogram	$9.071\ 847\ 4 \times 10^{2}$ (exact)
Tonne	Kilogram	10^3 (exact)
Power		
Btu (thermochemical)/second	Watt	$1.054\ 350\ 264\ 488 \times 10^{3}$
Btu (thermochemical)/minute	Watt	$1.757\ 250\ 4 \times 10^{1}$
Calorie (thermochemical)/second	Watt	4.184 (exact)
Calorie (thermochemical)/minute	Watt	$6.973\ 333\ 3 \times 10^{-2}$
Foot lbf/hour	Watt	$3.766\ 161\ 0 \times 10^{-4}$
Foot lbf/minute	Watt	$2.259\ 696\ 6 \times 10^{-2}$
Foot lbf/second	Watt	1.355 817 9
Horsepower (550 ft.lbf/second)	Watt	$7.456\ 998\ 7 \times 10^{2}$
Horsepower (boiler)	Watt	$9.809\ 50 \times 10^{3}$
Horsepower (electric)	Watt	7.46×10^{2} (exact)
Horsepower (metric)	Watt	$7.354\ 99 \times 10^{2}$
Horsepower (U.K.)	Watt	7.457×10^{2}
Horsepower (water)	Watt	$7.460\ 43 \times 10^{2}$
Kilocalorie (thermochemical)/minute	Watt	$6.973\ 333\ 3 \times 10^{1}$
Kilocalorie (thermochemical)/second	Watt	4.184×10^{3} (exact)
Watt (international of 1948)	Watt	1.000 165
Pressure		
Atmosphere	Newton/meter^2	$1.013\ 25 \times 10^{5}$ (exact)
Bar	Newton/meter^2	10^5 (exact)
Barye	Newton/meter^2	10^{-1} (exact)
Centimeter of mercury (0 °C)	Newton/meter^2	$1.333\ 22 \times 10^{3}$
Centimeter of water (4 °C)	Newton/meter^2	$9.806\ 38 \times 10^{1}$
Dyne/centimeter^2	Newton/meter^2	1.00×10^{-1} (exact)
Foot of water (39.2 °F)	Newton/meter^2	$2.988\ 988 \times 10^{3}$
Inch of mercury (32 °F)	Newton/meter^2	$3.386\ 389 \times 10^{3}$
Inch of mercury (60 °F)	Newton/meter^2	$3.376\ 85 \times 10^{3}$
Inch of water (39.2 °F)	Newton/meter^2	$2.480\ 82 \times 10^{2}$
Inch of water (60 °F)	Newton/meter^2	2.4884×10^{2}
Kgf/centimeter^2	Newton/meter^2	$9.806\ 65 \times 10^{4}$ (exact)
Kgf/meter^2	Newton/meter^2	9.806 65 (exact)
Lbf/foot^2	Newton/meter^2	$4.788\ 025\ 8 \times 10^{1}$
Lbf/inch^2 (psi)	Newton/meter^2	$6.894\ 757\ 2 \times 10^{3}$

(continued)

Table A.6 (continued)

To convert from	to	Multiply by
Millibar	Newton/meter^2	10^2 (exact)
Millimeter of mercury (0 °C)	Newton/meter^2	$1.333\ 224 \times 10^2$
Pascal	Newton/meter^2	1.00 (exact)
Psi (lbf/inch^2)	Newton/meter^2	$6.894\ 757\ 2 \times 10^3$
Torr (0 °C)	Newton/meter^2	$1.333\ 22 \times 10^2$
Speed		
Foot/hour	Meter/second	$8.466\ 666\ 6 \times 10^{-5}$
Foot/minute	Meter/second	5.08×10^{-3} (exact)
Foot/second	Meter/second	3.048×10^{-1} (exact)
Inch/second	Meter/second	2.54×10^{-2} (exact)
Kilometer/hour	Meter/second	$2.777\ 777\ 8 \times 10^{-1}$
Knot (international)	Meter/second	$5.144\ 444\ 444 \times 10^{-1}$
Mile/hour (U.S. statute)	Meter/second	4.4704×10^{-1} (exact)
Mile/minute (U.S. statute)	Meter/second	$2.682\ 24 \times 10^{-1}$ (exact)
Mile/second (U.S. statute)	Meter/second	$1.609\ 344 \times 10^3$ (exact)
Temperature		
Celsius	Kelvin	$t_K = t_C + 273.15$
Fahrenheit	Kelvin	$t_K = (5/9)(t_F + 459.67)$
Fahrenheit	Celsius	$t_C = (5/9)(t_F - 32)$
Rankine	Kelvin	$t_K = (5/9)t_R$
Time		
Day (mean solar)	Second (mean solar)	8.64×10^4 (exact)
Day (sidereal)	Second (mean solar)	$8.616\ 409\ 0 \times 10^4$
Hour (mean solar)	Second (mean solar)	3.60×10^3 (exact)
Hour (sidereal)	Second (mean solar)	$3.590\ 170\ 4 \times 10^3$
Minute (mean solar)	Second (mean solar)	6.00×10^1 (exact)
Minute (sidereal)	Second (mean solar)	$5.983\ 617\ 4 \times 10^1$
Month (mean calendar)	Second (mean solar)	2.628×10^6 (exact)
Second (sidereal)	Second (mean solar)	$9.972\ 695\ 7 \times 10^{-1}$
Year (calendar)	Second (mean solar)	3.1536×10^7 (exact)
Year (sidereal)	Second (mean solar)	$3.155\ 815\ 0 \times 10^7$
Year (tropical)	Second (mean solar)	$3.155\ 692\ 6 \times 10^7$
Year 1900, tropical, Jan., day 0, hour 12	Second (ephemeris)	$3.155\ 692\ 597\ 47 \times 10^7$ (exact)
Year 1900, tropical, Jan., day 0, hour 12	Second	$3.155\ 692\ 597\ 47 \times 10^7$
Viscosity		
Centistoke	Meter^2/second	10^{-6} (exact)
Stoke	Meter^2/second	10^{-4} (exact)
Foot^2/second	Meter^2/second	$9.290\ 304 \times 10^{-2}$ (exact)
Centipoise	Newton second/meter^2	10^{-3} (exact)
Lbm/foot second	Newton second/meter^2	1.488 163 9
Lbf.second/foot^2	Newton second/meter^2	$4.788\ 025\ 8 \times 10^1$
Poise	Newton second/meter^2	10^{-1} (exact)
Poundal second/foot^2	Newton second/meter^2	1.488 163 9
Slug/foot second	Newton second/meter^2	$4.788\ 025\ 8 \times 10^1$
Rhe	Meter^2/newton second	10^1 (exact)
Volume		
Acre foot	Meter^3	$1.233\ 481\ 837\ 547\ 52 \times 10^3$ (exact)
Barrel (petroleum, 42 gallons)	Meter^3	$1.589\ 873 \times 10^{-1}$

(continued)

Table A.6 (continued)

To convert from	to	Multiply by
Board foot	$Meter^3$	$2.359\ 737\ 216 \times 10^{-3}$ (exact)
Bushel (U.S.)	$Meter^3$	$3.523\ 907\ 016\ 688 \times 10^{-2}$ (exact)
Cord	$Meter^3$	3.624 556 3
Cup	$Meter^3$	$2.365\ 882\ 365 \times 10^{-4}$ (exact)
Dram (U.S. fluid)	$Meter^3$	$3.696\ 691\ 195\ 312\ 5 \times 10^{-6}$ (exact)
Fluid ounce (U.S.)	$Meter^3$	$2.957\ 352\ 946\ 25 \times 10^{-5}$ (exact)
$Foot^3$	$Meter^3$	$2.831\ 684\ 659\ 2 \times 10^{-2}$ (exact)
Gallon (U.K. liquid)	$Meter^3$	$4.546\ 087 \times 10^{-3}$
Gallon (U.S. dry)	$Meter^3$	$4.404\ 883\ 770\ 86 \times 10^{-3}$ (exact)
Gallon (U.S. liquid)	$Meter^3$	$3.785\ 411\ 784 \times 10^{-3}$ (exact)
Gill (U.K.)	$Meter^3$	$1.420\ 652 \times 10^{-4}$
Gill (U.S.)	$Meter^3$	$1.182\ 941\ 2 \times 10^{-4}$
Hogshead (U.S.)	$Meter^3$	$2.384\ 809\ 423\ 92 \times 10^{-1}$ (exact)
$Inch^3$	$Meter^3$	$1.638\ 706\ 4 \times 10^{-5}$ (exact)
Liter	$Meter^3$	10^{-3} (exact)
Ounce (U.S. fluid)	$Meter^3$	$2.957\ 352\ 956\ 25 \times 10^{-5}$ (exact)
Peck (U.S.)	$Meter^3$	$8.809\ 767\ 541\ 72 \times 10^{-3}$ (exact)
Pint (U.S. dry)	$Meter^3$	$5.506\ 104\ 713\ 575 \times 10^{-4}$ (exact)
Pint (U.S. liquid)	$Meter^3$	$4.731\ 764\ 73 \times 10^{-4}$ (exact)
Quart (U.S. dry)	$Meter^3$	$1.101\ 220\ 942\ 715 \times 10^{-3}$ (exact)
Quart (U.S. liquid)	$Meter^3$	$9.463\ 592\ 5 \times 10^{-4}$
Stere	$Meter^3$	1.00 (exact)
Tablespoon	$Meter^3$	$1.478\ 676\ 478\ 125 \times 10^{-5}$ (exact)
Teaspoon	$Meter^3$	$4.928\ 921\ 593\ 75 \times 10^{-6}$ (exact)
Ton (register)	$Meter^3$	2.831 684 659 2 (exact)
$Yard^3$	$Meter^3$	$7.645\ 548\ 579\ 84 \times 10^{-1}$ (exact)

Conversion Factor Tables [3]

Table A.7 Length (L)

Multiply number of → by → to obtain ↓	Centimeters	Feet	Inches	Kilometers	Nautical miles	Meters	Mils	Miles	Millimeters	Yards
Centimeters	1	30.48	2.540	10^5	1.853×10^5	100	2.540×10^{-3}	1.609×10^5	0.1	91.44
Feet	3.281×10^{-2}	1	8.333×10^{-2}	3,281	6,080.27	3.281	8.333×10^{-5}	5,280	3.281×10^{-3}	3
Inches	0.3937	12	1	3.937×10^4	7.296×10^4	39.37	0.001	6.336×10^4	3.937×10^{-2}	36
Kilometers	10^{-5}	3.048×10^{-4}	2.540×10^{-5}	1	1.853	0.001	2.540×10^{-8}	1.609	10^{-6}	9.144×10^{-4}
Nautical miles		1.645×10^{-4}		0.5396	1	5.396×10^{-4}		0.8684		4.934×10^{-4}
Meters	0.01	0.3048	2.540×10^{-2}	1,000	1,853	1		1,609	0.001	0.9144
Mils	393.7	1.2×10^4	1,000	3.937×10^7		3.937×10^4	1		39.37	3.6×10^4
Miles	6.214×10^{-6}	1.894×10^{-4}	1.578×10^{-5}	0.6214	1.1516	6.214×10^{-4}		1	6.214×10^{-7}	5.682×10^{-4}
Millimeters	10	304.8	25.40	10^6		1,000	2.540×10^{-2}		1	914.4
Yards	1.094×10^{-2}	0.3333	2.778×10^{-2}	1,094	2,027	1.094	2.778×10^{-5}	1,760	1.094×10^{-3}	1

Table A.8 Area (L^2)

Multiply number of → by → to obtain ↓	Acres	Circular mils	Square centimeters	Square feet	Square inches	Square kilometers	Square meters	Square miles	Square millimeters	Square yards
Acres	1			2.296×10^{-5}		247.1	2.471×10^{-4}	640		2.066×10^{-4}
Circular mils		1	1.973×10^{5}	1.833×10^{8}	1.273×10^{6}		1.973×10^{9}		1,973	
Square centimeters		5.067×10^{-6}	1	929.0	6.452	10^{10}	10^{4}	2.590×10^{10}	0.01	8,361
Square feet	4.356×10^{4}		1.076×10^{-3}	1	6.944×10^{-3}	1.076×10^{7}	10.76	2.788×10^{7}	1.076×10^{-5}	9
Square inches	6,272,640	7.854×10^{-7}	0.1550	144	1	1.550×10^{9}	1,550	4.015×10^{9}	1.550×10^{-3}	1,296
Square kilometers	4.047×10^{-3}		10^{-10}	9.290×10^{-8}	6.452×10^{-10}	1	10^{-6}	2.590	10^{-12}	8.361×10^{-7}
Square meters	4,047		0.0001	9.290×10^{-2}	6.452×10^{-4}	10^{6}	1	2.590×10^{6}	10^{-6}	0.8361
Square miles	1.562×10^{-3}		3.861×10^{-11}	3.587×10^{-8}		0.3861	3.861×10^{-7}	1	3.861×10^{-13}	3.228×10^{-7}
Square millimeters		5.067×10^{-4}	100	9.290×10^{4}	645.2	10^{12}	10^{6}		1	8.361×10^{5}
Square yards	4,840		1.196×10^{-4}	0.1111	7.716×10^{-4}	1.196×10^{6}	1.196	3.098×10^{6}	1.196×10^{-6}	1

Table A.9 Volume (L^3)

Multiply number of → by → to obtain ↓	Bushels (dry)	Cubic centimeters	Cubic feet	Cubic inches	Cubic meters	Cubic yards	Gallons (liquid)	Liters	Pints (liquid)	Quarts (liquid)
Bushels (dry)	1		0.8036	4.651×10^{-4}	28.38			2.838×10^{-2}		
Cubic centimeters	3.524×10^{4}	1	2.832×10^{4}	16.39	10^{6}	7.646×10^{5}	3,785	1,000	473.2	946.4
Cubic feet	1.2445	3.531×10^{-5}	1	5.787×10^{-4}	35.31	27	0.1337	3.531×10^{-2}	1.671×10^{-2}	3.342×10^{-2}
Cubic inches	2,150.4	6.102×10^{-2}	1,728	1	6.102×10^{4}	46,656	231	61.02	28.87	57.75
Cubic meters	3.524×10^{-2}	10^{-6}	2.832×10^{-2}	1.639×10^{-5}	1	0.7646	3.785×10^{-3}	0.001	4.732×10^{-4}	9.464×10^{-4}
Cubic yards		1.308×10^{-6}	3.704×10^{-2}	2.143×10^{-5}	1.308	1	4.951×10^{-3}	1.308×10^{-3}	6.189×10^{-4}	1.238×10^{-3}
Gallons (liquid)		2.642×10^{-4}	7.481	4.329×10^{-3}	264.2	202.0	1	0.2642	0.125	0.25
Liters	35.24	0.001	28.32	1.639×10^{-2}	1,000	764.6	3.785	1	0.4732	0.9464
Pints (liquid)		2.113×10^{-3}	59.84	3.463×10^{-2}	2,113	1,616	8	2.113	1	2
Quarts (liquid)		1.057×10^{-3}	29.92	1.732×10^{-2}	1,057	807.9	4	1.057	0.5	1

Table A.10 Plane angle (no dimensions)

Multiply number of → by → to obtain ↓	Degrees	Minutes	Quadrants	Radians	Revolutions (exact) (circumferences)	Seconds
Degrees	1	1.667×10^{-2}	90	57.30	360	2.778×10^{-4}
Minutes	60	1	5,400	3,438	2.16×10^{4}	1.667×10^{-2}
Quadrants	1.111×10^{-2}	1.852×10^{-4}	1	0.6366	4	3.087×10^{-6}
Radians[a]	1.745×10^{-2}	2.909×10^{-4}	1.571	1	6.283	4.848×10^{-6}
Revolutions[a] (circumferences)	2.788×10^{-3}	4.630×10^{-5}	0.25	0.1591	1	7.716×10^{-7}
Seconds	3,600	60	3.24×10^{5}	2.063×10^{5}	1.296×10^{6}	1

[a]2π rad = 1 circumference = 360° by definition

Table A.11 Linear velocity (LT^{-1})

Multiply number of → by → to obtain ↓	Centimeters per second	Feet per minute	Feet per second	Kilometers per hour	Kilometers per minute	Knots (exact)	Meters per minute	Meters per second	Miles per hour	Miles per minute
Centimeters per second	1	0.5080	30.48	27.78	1,667	51.48	1.667	100	44.70	2,682
Feet per minute	1.969	1	60	54.68	3,281	101.3	3.281	196.8	88	5,280
Feet per second	3.281×10^{-2}	1.667×10^{-2}	1	0.9113	54.68	1.689	5.468×10^{-2}	3.281	1.467	88
Kilometers per hour	0.036	1.829×10^{-2}	1.097	1	60	1.853	0.06	3.6	1.609	96.54
Kilometers per minute	0.0006	3.048×10^{-4}	1.829×10^{-2}	1.667×10^{-2}	1	3.088×10^{-2}	0.001	0.06	2.682×10^{-2}	1.609
Knots[a]	1.943×10^{-2}	9.868×10^{-3}	0.5921	0.5396	32.38	1	3.238×10^{-2}	1.943	0.8684	52.10
Meters per minute	0.6	0.3048	18.29	16.67	1,000	30.88	1	60	26.82	1,609
Meters per second	0.01	5.080×10^{-3}	0.3048	0.2778	16.67	0.5148	1.667×10^{-2}	1	0.4470	26.82
Miles per hour	2.237×10^{-2}	1.136×10^{-2}	0.6818	0.6214	37.28	1.152	3.728×10^{-2}	2.237	1	60
Miles per minute	3.728×10^{-4}	1.892×10^{-4}	1.136×10^{-2}	1.036×10^{-2}	0.6214	1.919×10^{-2}	6.214×10^{-4}	3.728×10^{-2}	1.667×10^{-2}	1

[a]Nautical miles per hour

Table A.12 Linear acceleration (LT^{-2})

Multiply number of → by → to obtain ↓	Centimeters per second per second	Feet per second per second	Kilometers per hour per second	Meters per second per second	Miles per hour per second
Centimeters per second per second	1	30.48	27.78	100	44.70
Feet per second per second	3.281×10^{-2}	1	0.9113	3.281	1.467
Kilometers per hour per second	0.036	1.097	1	3.6	1.609
Meters per second per second	0.01	0.3048	0.2778	1	0.4470
Miles per hour per second	2.237×10^{-2}	0.6818	0.6214	2.237	1

Note: The (standard) acceleration due to gravity (g_0) = 9.087 m/s^2 = 32.17 ft/s^2 = 35.30 km/h · s = 21.94 mph/s

Table A.13 Mass (M) and weight

Multiply number of → by → to obtain ↓	Grains	Grams	Kilograms	Milligrams	Ounces[a]	Pounds[a]	Tons (long)	Tons (metric)	Tons (short)
Grains	1	15.43	1.543×10^{4}	1.543×10^{-2}	437.5	7,000			
Grams	6.481×10^{-2}	1	1,000	0.001	28.35	453.6	1.016×10^{6}	$\times 10^{6}$	9.072×10^{5}
Kilograms	6.481×10^{-5}	0.001	1	10^{-6}	2.835×10^{-2}	0.4536	1,016	1,000	907.2
Milligrams	64.81	1,000	10^{6}	1	2.835×10^{4}	4.536×10^{5}	1.016×10^{9}	10^{9}	9.072×10^{8}
Ounces	2.286×10^{-3}	3.527×10^{-2}	35.27	3.527×10^{-5}	1	16	3.584×10^{4}	3.527×10^{4}	3.2×10^{4}
Pounds	1.429×10^{-4}	2.205×10^{-3}	2.205	2.205×10^{-6}	6.250×10^{-2}	1	2,240	2,205	2,000
Tons (long)		9.842×10^{-7}	9.842×10^{-4}	9.842×10^{-10}	2.790×10^{-5}	4.464×10^{-4}	1	0.9842	0.8929
Tons (metric)		10^{-6}	0.001	10^{-9}	2.835×10^{-5}	4.536×10^{-4}	1.016	1	0.9072
Tons (short)		1.102×10^{-6}	1.102×10^{-3}	1.102×10^{-9}	3.125×10^{-5}	0.0005	1.120	1.102	1

Note: These conversion factors apply to the gravitational units of force having the corresponding names
[a]Avoirdupois pounds and ounces

Table A.14 Density or mass per unit volume (ML^{-3})

Multiply number of → by → to obtain ↓	Grams per cubic centimeter	Kilograms per cubic meter	Pounds per cubic foot	Pounds per cubic inch
Grams per cubic centimeter	1	0.001	1.602×10^{-2}	27.68
Kilograms per cubic meter	1,000	1	16.02	2.768×10^{4}
Pounds per cubic foot	62.43	6.243×10^{-2}	1	1,728
Pounds per cubic inch	3.613×10^{-2}	3.613×10^{-5}	5.787×10^{-4}	1
Pounds per mil foot[a]	3.405×10^{-7}	3.405×10^{-10}	5.456×10^{-9}	9.425×10^{-6}

[a]Unit of volume is a volume one foot long and one circular mil in cross-section area

Table A.15 Force (MLT^{-2}) or (F)

Multiply number of → by → to obtain ↓	Dynes	Grams	Joules per centimeter	Newtons or joules per meter	Kilograms	Pounds	Poundals
Dynes	1	980.7	10^{7}	10^{5}	9.807×10^{5}	4.448×10^{5}	1.383×10^{4}
Grams	1.020×10^{-3}	1	1.020×10^{4}	102.0	1,000	453.6	14.10
Joules per centimeter	10^{-7}	9.807×10^{-5}	1	0.01	9.807×10^{-2}	4.448×10^{-2}	1.383×10^{-3}
Newtons or joules per meter	10^{-5}	9.807×10^{-3}	100	1	9.807	4.448	0.1383
Kilograms	1.020×10^{-6}	0.001	10.20	0.1020	1	0.4536	1.410×10^{-2}
Pounds	2.248×10^{-6}	2.205×10^{-3}	22.48	0.2248	2.205	1	3.108×10^{-2}
Poundals	7.233×10^{-5}	7.093×10^{-2}	723.3	7.233	70.93	32.17	1

Note: Conversion factors between absolute and gravitational units apply only under standard acceleration due to gravity conditions

Table A.16 Pressure or force per unit area ($ML^{-1}T^{-2}$) or (FL^{-2})

Multiply number of → by → to obtain ↓	Atmospheres[a]	Baryes or dynes per square centimeter	Centimeters of mercury at 0°C[b]	Inches of mercury at 0°C[b]	Inches of water at 4°C	Kilograms per square meter[c]	Pounds per square foot	Pounds per square inch	Tons (short) per square foot	Pascal
Atmospheres[a]	1	9.869×10^{-7}	1.316×10^{-2}	3.342×10^{-2}	2.458×10^{-3}	9.678×10^{-5}	4.725×10^{-4}	6.804×10^{-2}	0.9450	9.689×10^{-6}
Baryes or dynes per square centimeter	1.013×10^{6}	1	1.333×10^{4}	3.386×10^{4}	2.491×10^{-3}	98.07	478.8	6.895×10^{4}	9.576×10^{5}	10
Centimeters of mercury at 0°C[b]	76.00	7.501×10^{-5}	1	2.540	0.1868	7.356×10^{-3}	3.591×10^{-2}	5.171	71.83	7.501×10^{-4}
Inches of mercury at 0°C[b]	29.92	2.953×10^{-5}	0.3937	1	7.355×10^{-2}	2.896×10^{-3}	1.414×10^{-2}	2.036	28.28	2.953×10^{-4}
Inches of water at 4°C	406.8	4.015×10^{-4}	5.354	13.60	1	3.937×10^{-2}	0.1922	27.68	384.5	4.015×10^{-3}
Kilograms per square meter[c]	1.033×10^{4}	1.020×10^{-2}	136.0	345.3	25.40	1	4.882	703.1	9,765	0.1020
Pounds per square foot	2,117	2.089×10^{-3}	27.85	70.73	5.204	0.2048	1	144	2,000	2.089×10^{-2}
Pounds per square inch	14.70	1.450×10^{-5}	0.1934	0.4912	3.613×10^{-2}	1.422×10^{-3}	6.944×10^{-3}	1	13.89	1.450×10^{-4}
Tons (short) per square foot	1.058	1.044×10^{-6}	1.392×10^{-2}	3.536×10^{-2}	2.601×10^{-3}	1.024×10^{-4}	0.0005	0.072	1	1.044×10^{-5}
Pascal	1.013×10^{5}	10^{-1}	1.333×10^{3}	3.386×10^{3}	2.49×10^{2}	9.807	47.88	6.895×10^{3}	9.576×10^{4}	1

[a]Definition: One atmosphere (standard) = 76 cm of mercury at 0°C

[b]To convert height h of a column of mercury at t degrees centigrade to the equivalent height h_0 at 0°C, use $h_0 = h[1 - (m - l)t/(1 + mt)]$ where $m = 0.0001818$ and $I = 18.4 \times 10^{-6}$ if the scale is engraved on brass; $I = 8.5 \times 10^{-6}$ if on glass. This assumes the scale is correct at 0°C; for other cases (any liquid) see *International Critical Tables*, Vol. 1 (1968)

[c]$1\ g/cm^2 = 10\ kg/m^2$

Table A.17 Energy, work, and heat (ML^2T^{-2}) or (FL)

Multiply number of → by → to obtain ↓	British thermal units[a]	Centimeter grams	Ergs or centimeter dynes	Foot pounds	Horsepower hours	Joules[b] or watt seconds	Kilogram calories[a]	Kilowatt hours	Meter kilograms	Watt hours
British thermal units[a]	1	9.297×10^{-8}	9.480×10^{-11}	1.285×10^{-3}	2,545	9.480×10^{-4}	3.969	3,413	9.297×10^{-3}	3.413
Centimeter grams	1.076×10^{7}	1	1.020×10^{-3}	1.383×10^{4}	2.737×10^{10}	1.020×10^{4}	4.269×10^{7}	3.671×10^{10}	10^{5}	3.671×10^{7}
Ergs or centimeter dynes	1.055×10^{10}	980.7	1	1.356×10^{7}	2.684×10^{12}	10^{7}	4.186×10^{10}	3.6×10^{13}	9.807×10^{7}	3.6×10^{10}
Foot pounds	778.0	7.233×10^{-5}	7.367×10^{-8}	1	1.98×10^{6}	0.7376	3,087	2.655×10^{6}	7.233	2,655
Horsepower hours	3.929×10^{-4}	3.654×10^{-11}	3.722×10^{-14}	5.050×10^{-7}	1	3.722×10^{-7}	1.559×10^{-3}	1.341	3.653×10^{-6}	1.341×10^{-3}
Joules[b] or watt seconds	1,054.8	9.807×10^{-5}	10^{-7}	1.356	2.684×10^{6}	1	4,186	3.6×10^{6}	9.807	3,600
Kilogram calories[a]	0.2520	2.343×10^{-8}	2.389×10^{-11}	3.239×10^{-4}	641.3	2.389×10^{-4}	1	860.0	2.343×10^{-3}	0.8600
Kilowatt hours	2.930×10^{-4}	2.724×10^{-11}	2.778×10^{-14}	3.766×10^{-7}	0.7457	2.788×10^{-7}	1.163×10^{-3}	1	2.724×10^{-6}	0.001
Meter kilograms	107.6	10^{-5}	1.020×10^{-8}	0.1383	2.737×10^{5}	0.1020	426.9	3.671×10^{5}	1	367.1
Watt hours	0.2930	2.724×10^{-8}	2.778×10^{-11}	3.766×10^{-4}	745.7	2.778×10^{-4}	1.163	1,000	2.724×10^{-3}	1

Note: The *horsepower* used in Tables A.17 and A.18 is equal to 550 foot pounds per second by definition. Other definitions are one horsepower equals 746 watts (U.S. and Great Britain) and one horsepower equals 736 watts (continental Europe). Neither of these latter definitions is equivalent to the first; the *horsepowers* defined in these latter definitions are widely used in the rating of electrical machinery

[a]Mean calorie and Btu used throughout. One gram-calorie = 0.001 kilogram-calorie; one Ostwald calorie = 0.1 kilogram-calorie. The IT cal, 1,000 international steam table calories, has been defined as the 1/860th part of the international kilowatt-hour (see *Mechanical Engineering*, Nov., 1935, p. 710). Its value is very nearly equal to the mean kilogram-calorie, 1 IT cal-1.00037 kilogram-calories (mean). 1 Btu = 251.996 IT cal

[b]Absolute joule, defined as 10^7 ergs. The international joule, based on the international ohm and ampere, equals 1.0003 absolute joules

Table A.18 Power or rate of doing work (ML^2T^{-3}) or (FLT^{-1})

Multiply number of → by → to obtain ↓	British thermal units per minute	Ergs per second	Foot pounds per minute	Foot pounds per second	Horsepower	Kilogram calories per minute	Kilowatts	Metric horsepower	Watts
British thermal units per minute	1	5.689×10^{-9}	1.285×10^{-3}	7.712×10^{-2}	42.41	3.969	56.89	41.83	5.689×10^{-2}
Ergs per second	1.758×10^{8}	1	2.259×10^{5}	1.356×10^{7}	7.457×10^{9}	6.977×10^{8}	10^{10}	7.355×10^{9}	10^{7}
Foot pounds per minute	778.0	4.426×10^{-6}	1	60	3.3×10^{4}	3,087	4.426×10^{4}	3.255×10^{4}	44.26
Foot pounds per second	12.97	7.376×10^{-8}	1.667×10^{-2}	1	550	51.44	737.6	542.5	0.7376
Horsepower	2.357×10^{-2}	1.341×10^{-10}	3.030×10^{-5}	1.818×10^{-3}	1	9.355×10^{-2}	1.341	0.9863	1.341×10^{-3}
Kilogram calories per minute	0.2520	1.433×10^{-9}	3.239×10^{-4}	1.943×10^{-2}	10.69	1	14.33	10.54	1.433×10^{-2}
Kilowatts	0.01758	10^{-10}	2.260×10^{-5}	1.356×10^{-3}	0.7457	0.06977×10^{-2}	1	0.7355	0.001
Metric horsepower	2.390×10^{-2}	1.360×10^{-10}	3.072×10^{-5}	1.843×10^{-3}	1.014	9.485×10^{-2}	1.360	1	1.360×10^{-3}
Watts	17.58	10^{-7}	2.260×10^{-2}	1.356	745.7	69.77	1,000	735.5	1

See general note to Table A.17

1 Cheval vapeur = 75 kilogram meters per second

1 Poncelet = 100 kilogram meters per second

Table A.19 Heat flux (power/area)

From → multiply by → to obtain ↓	Btu/(min.ft^2)	Btu/(s.ft^2)	kW/m^2	W/m^2	W/cm^2
Btu/(min.ft^2)	1	1.6×10^{-2}	5.28	5.2×10^{-3}	5.2×10^{-1}
Btu/(s.ft^2)	60	1	6.81×10^{-2}	8.8×10^{-5}	8.8×10^{-3}
kW/m^2	0.18923	11.3565	1	10^{-3}	10^{-1}
W/m^2	189.273	1.1356×10^{4}	10^{3}	1	10^{4}
W/cm^2	1.89273	1.1356×10^{2}	10	10^{-4}	1
kg-cal/s · m^2	6.135×10^{-6}	1.02×10^{-7}	8.60400×10^{5}	8.6×10^{2}	8.604×10^{4}
kg-cal/s · m^2	3.681×10^{-4}	6.07×10^{-6}	1.434×10^{4}	1.4341×10^{1}	1.434×10^{3}

Table A.20 Specific heat ($L^2T^{-2}\,t^{-1}$, t = temperature) (To change specific heat in gram calories per gram per degree centigrade to the units given in any line of the following table, multiply by the factor in the last column)

Unit of heat or energy	Unit of mass	Temperature scale (exact)	Factor
Gram calories	Gram	Centigrade	1
Kilogram calories	Kilogram	Centigrade	1
British thermal units	Pound	Centigrade	1.800
British thermal units	Pound	Fahrenheit	1.000
Joules	Gram	Centigrade	4.186
Joules	Pound	Fahrenheit	1,055
Joules	Kilogram	Kelvin	4.187×10^{3}
Kilowatt hours	Kilogram	Centigrade	1.163×10^{-3}
Kilowatt hours	Pound	Fahrenheit	2.930×10^{-4}

(exact)Temperature conversion formulae:
t_C = temperature in centigrade degrees
t_f = temperature in Fahrenheit degrees
t_K = temperature in kelvin degrees
$1^\circ\text{F} = \frac{5^\circ}{9}\text{C}$
1 K = 1°C
$t_C = \frac{5}{9}(t_f - 32)$
$t_f = \frac{9}{5}t_C + 32$
$t_K = t_C + 273$

Table A.21 Thermal conductivity ($LMT^{-3}\,t^{-1}$)

From → multiply by → to obtain ↓	Btu · ft per h · ft^2 · °F	Btu · in. per h · ft^2 · °F	Btu · in. per s · ft^2 · °F	Joules per m · s · °C	Kcal per m · h · °C	Erg per cm · s · °C	Kcal per m · s · °C	Cal per cm · s · °C	W per ft · °C	W per m · K
Btu · ft per h · ft^{2}·°F	1	8.333×10^{-2}	3.0×10^{2}	5.778×10^{-1}	6.720×10^{-1}	5.778×10^{-6}	2.419×10^{3}	2.419×10^{2}	1.895	5.778×10^{-1}
Btu · in. per h · ft^{2}·°F	12	1	3.6×10^{3}	6.933	8.064	6.933×10^{-5}	2.903×10^{4}	2.903×10^{3}	2.275×10^{1}	6.933
Btu · in. per s · ft^{2}·°F	3.333×10^{-3}	2.778×10^{-4}	1	1.926×10^{-3}	2.240×10^{-3}	1.926×10^{-8}	8.064	8.064×10^{-1}	6.319×10^{-3}	1.926×10^{-3}
Joules per m · s · °C	1.731	1.442×10^{-1}	5.192×10^{2}	1	1.163	1.000×10^{-5}	4.187×10^{3}	4.187×10^{2}	3.281	1.0
Kcal per m · h · °C	1.483	1.240×10^{-1}	4.465×10^{2}	8.599×10^{-1}	1	8.599×10^{-6}	3.6×10^{3}	3.6×10^{2}	2.821	8.599×10^{-1}
Erg per cm · s · °C	1.731×10^{5}	1.442×10^{4}	5.192×10^{7}	1.0×10^{5}	1.163×10^{5}	1	4.187×10^{8}	4.187×10^{7}	3.281×10^{5}	1.0×10^{5}
Kcal per m · s · °C	4.134×10^{-4}	3.445×10^{-5}	1.240×10^{-1}	2.388×10^{-4}	2.778×10^{-4}	2.388×10^{-9}	1	1.0×10^{-1}	7.835×10^{-4}	2.388×10^{-4}
Cal per cm · s · °C	4.134×10^{-3}	3.445×10^{-4}	1.240	2.388×10^{-3}	2.778×10^{-3}	2.388×10^{-8}	10	1	7.835×10^{-3}	2.388×10^{-3}
W per ft · °C	5.276×10^{-1}	4.395×10^{-2}	1.582×10^{2}	3.048×10^{-1}	3.545×10^{-1}	3.048×10^{-6}	1.276×10^{3}	1.276×10^{2}	1	3.048×10^{-1}
W per m · K	1.731	1.442×10^{-1}	5.192×10^{2}	1.0	1.163	1.00×10^{-5}	4.187×10^{3}	4.187×10^{2}	3.281	1

Note: International table Btu $= 1.055056 \times 10^{3}$ joules; and International table cal $= 4.1868$ joules are used throughout

Appendix 2: Thermophysical Property Data

Table A.22 Approximate properties of common gases [3]

	Engineering gas constant, R (J/kg · K)	Universal gas constant, $\Re = mR$ (J/kg · K)	Adiabatic exponent, k	Specific heat at constant pressure, c_p (J/kg · K)	Dynamic viscosity at 20°C, (Pa · s)
Carbon dioxide	187.8	8,264	1.28	858.2	1.47×10^{-5}
Oxygen	259.9	8,318	1.40	909.2	2.01×10^{-5}
Air	286.8	8,313	1.40	1,003	1.81×10^{-5}
Nitrogen	296.5	8,302	1.40	1,038	1.76×10^{-5}
Methane	518.1	8,302	1.31	2,190	1.34×10^{-5}
Helium	2,076.8	8,307	1.66	5,223	1.97×10^{-5}
Hydrogen	4,126.6	8,318	1.40	14,446	0.90×10^{-5}

M.J. Hurley (ed.), *SFPE Handbook of Fire Protection Engineering*,
DOI 10.1007/978-1-4939-2565-0, © Society of Fire Protection Engineers 2016

Table A.23 Thermophysical property values for gases at standard atmospheric pressure [4]

T (K)	ρ (kg/m^3)	c_p (Ws/kg · K)	μ (kg/ms)	ν (m^2/s)	k (W/m · K)	α (m^2/s)	Pr
Air							
100	3.6010	1.0266×10^3	0.6924×10^{-5}	1.923×10^{-6}	0.009246	0.0250×10^{-4}	0.768
150	2.3675	1.0099	1.0283	4.343	0.013735	0.0574	0.756
200	1.7684	1.0061	1.3289	7.514	0.01809	0.1016	0.739
250	1.4128	1.0053	1.488	10.53	0.02227	0.1568	0.722
300	1.1774	1.0057	1.983	16.84	0.02624	0.2216	0.708
350	0.9980	1.0090	2.075	20.76	0.03003	0.2983	0.697
400	0.8826	1.0140	2.286	25.90	0.03365	0.3760	0.689
450	0.7833	1.0207	2.484	31.71	0.03707	0.4636	0.683
500	0.7048	1.0295	2.671	37.90	0.04038	0.5564	0.680
550	0.6423	1.0392	2.848	44.27	0.04360	0.6532	0.680
600	0.5879	1.0551	3.018	51.34	0.04659	0.7512	0.682
650	0.5430	1.0635	3.177	58.51	0.04953	0.8578	0.682
700	0.5030	1.0752	3.332	66.25	0.05230	0.9672	0.684
750	0.4709	1.0856	3.481	73.91	0.05509	1.0774	0.686
800	0.4405	1.0978	3.625	82.29	0.05779	1.1951	0.689
850	0.4149	1.1095	3.765	90.75	0.06028	1.3097	0.692
900	0.3925	1.1212	3.899	99.3	0.06279	1.4271	0.696
950	0.3716	1.1321	4.023	108.2	0.06525	1.5510	0.699
1,000	0.3524	1.1417	4.152	117.8	0.06752	1.6779	0.702
1,100	0.3204	1.160	4.44	138.6	0.0732	1.969	0.704
1,200	0.2947	1.179	4.69	159.1	0.0782	2.251	0.707
1,300	0.2707	1.197	4.93	182.1	0.0837	2.583	0.705
1,400	0.2515	1.214	5.17	205.5	0.0891	2.920	0.705
1,500	0.2355	1.230	5.40	229.1	0.0946	3.266	0.705
1,600	0.2211	1.248	5.63	254.5	0.100	3.624	0.705
1,700	0.2082	1.267	5.85	280.9	0.105	3.977	0.705
1,800	0.1970	1.287	6.07	308.1	0.111	4.379	0.704
1,900	0.1858	1.309	6.29	338.5	0.117	4.811	0.704
2,000	0.1762	1.338	6.50	369.0	0.124	5.260	0.702
2,100	0.1682	1.372	6.72	399.6	0.131	5.680	0.703
2,200	0.1602	1.419	6.93	432.6	0.139	6.115	0.707
2,300	0.1538	1.482	7.14	464.0	0.149	6.537	0.710
2,400	0.1458	1.574	7.35	504.0	0.161	7.016	0.718
2,500	0.1394	1.688	7.57	543.0	0.175	7.437	0.730
Helium							
144	0.3379	5.200	125.5×10^{-7}	37.11×10^{-6}	0.0928	0.5275×10^{-4}	0.70
200	0.2435	5.200	156.6	64.38	0.1177	0.9288	0.694
255	0.1906	5.200	181.7	95.50	0.1357	1.3675	0.70
366	0.13280	5.200	230.5	173.6	0.1691	2.449	0.71
477	0.10204	5.200	275.0	269.3	0.197	3.716	0.72
589	0.08282	5.200	311.3	375.8	0.225	5.215	0.72
700	0.07032	5.200	347.5	494.2	0.251	6.661	0.72
800	0.06023	5.200	381.7	634.1	0.275	8.774	0.72
Hydrogen							
150	0.16371	12.602	5.595×10^{-6}	34.18×10^{-5}	0.0981	0.475×10^{-4}	0.718
200	0.12270	13.540	6.813	55.53	0.1282	0.772	0.719
250	0.09819	14.059	7.919	80.64	0.1561	1.130	0.713

(continued)

Table A.23 (continued)

T (K)	ρ (kg/m^3)	c_p (Ws/kg · K)	μ (kg/ms)	ν (m^2/s)	k (W/m · K)	α (m^2/s)	Pr
300	0.08185	14.314	8.963	109.5	0.182	1.554	0.706
350	0.07016	14.436	9.954	141.9	0.206	2.031	0.697
400	0.06135	14.491	10.864	177.1	0.228	2.568	0.690
450	0.05462	14.499	11.779	215.6	0.251	3.164	0.682
500	0.04918	14.507	12.636	257.0	0.272	3.817	0.675
550	0.04469	14.532	13.475	301.6	0.292	4.516	0.668
600	0.04085	14.537	14.285	349.7	0.315	5.306	0.664
700	0.03492	14.574	15.89	455.1	0.351	6.903	0.659
800	0.03060	14.675	17.40	569	0.384	8.563	0.664
900	0.02723	14.821	18.78	690	0.412	10.217	0.676
Oxygen							
150	2.6190	0.9178	11.490×10^{-6}	4.387×10^{-6}	0.01367	0.05688×10^{-4}	0.773
200	1.9559	0.9131	14.850	7.593	0.01824	0.10214	0.745
250	1.5618	0.9157	17.87	11.45	0.02259	0.15794	0.725
300	1.3007	0.9203	20.63	15.86	0.02676	0.22353	0.709
350	1.1133	0.9291	23.16	20.80	0.03070	0.2968	0.702
400	0.9755	0.9420	25.54	26.18	0.03461	0.3768	0.695
450	0.8682	0.9567	27.77	31.99	0.03828	0.4609	0.694
500	0.7801	0.9722	29.91	38.34	0.04173	0.5502	0.697
550	0.7096	0.9881	31.97	45.05	0.04517	0.6441	0.700
Nitrogen							
200	1.7108	1.0429	12.947×10^{-6}	7.568×10^{-6}	0.01824	0.10224×10^{-4}	0.747
300	1.1421	1.0408	17.84	15.63	0.02620	0.22044	0.713
400	0.8538	1.0459	21.98	25.74	0.03335	0.3734	0.691
500	0.6824	1.0555	25.70	37.66	0.03984	0.5530	0.684
600	0.5687	1.0756	29.11	51.19	0.04580	0.7486	0.686
700	0.4934	1.0969	32.13	65.13	0.05123	0.9466	0.691
800	0.4277	1.1225	34.84	81.46	0.05609	1.1685	0.700
900	0.3796	1.1464	37.49	91.06	0.06070	1.3946	0.711
1,000	0.3412	1.1677	40.00	117.2	0.06475	1.6250	0.724
1,100	0.3108	1.1857	42.28	136.0	0.06850	1.8591	0.736
1,200	0.2851	1.2037	44.50	156.1	0.07184	2.0932	0.748
Carbon dioxide							
220	2.4733	0.783	11.105×10^{-6}	4.490×10^{-6}	0.010805	0.05920×10^{-4}	0.818
250	2.1657	0.804	12.590	5.813	0.012884	0.07401	0.793
300	1.7973	0.871	14.958	8.321	0.016572	0.10588	0.770
350	1.5362	0.900	17.205	11.19	0.02047	0.14808	0.755
400	1.3424	0.942	19.32	14.39	0.02461	0.19463	0.738
450	1.1918	0.980	21.34	17.90	0.02897	0.24813	0.721
500	1.0732	1.013	23.26	21.67	0.03352	0.3084	0.702
550	0.9739	1.047	25.08	25.74	0.03821	0.3750	0.685
600	0.8938	1.076	26.83	30.02	0.04311	0.4483	0.668
Ammonia, NH_3							
273	0.7929	2.177	9.353×10^{-6}	1.18×10^{-5}	0.0220	0.1308×10^{-4}	0.90
323	0.6487	2.177	11.035	1.70	0.0270	0.1920	0.88
373	0.5590	2.236	12.886	2.30	0.0327	0.2619	0.87
423	0.4934	2.315	14.672	2.97	0.0391	0.3432	0.87
473	0.4405	2.395	16.49	3.74	0.0467	0.4421	0.84

(continued)

Table A.23 (continued)

T (K)	ρ (kg/m^3)	c_p (Ws/kg · K)	μ (kg/ms)	ν (m^2/s)	k (W/m · K)	α (m^2/s)	Pr
Water vapor							
380	0.5863	2.060	12.71×10^{-6}	2.16×10^{-5}	0.0246	0.2036×10^{-4}	1.060
400	0.5542	2.014	13.44	2.42	0.0261	0.2338	1.040
450	0.4902	1.980	15.25	3.11	0.0299	0.307	1.010
500	0.4405	1.985	17.04	3.86	0.0339	0.387	0.996
550	0.4005	1.997	18.84	4.70	0.0379	0.475	0.991
600	0.3652	2.026	20.67	5.66	0.0422	0.573	0.986
650	0.3380	2.056	22.47	6.64	0.0464	0.666	0.995
700	0.3140	2.085	24.26	7.72	0.0505	0.772	1.000
750	0.2931	2.119	26.04	8.88	0.0549	0.883	1.005
800	0.2739	2.152	27.86	10.20	0.0592	1.004	1.010
850	0.2579	2.186	29.69	11.52	0.0637	1.130	1.019

Table A.24 Approximate properties of common liquids at standard atmospheric pressure [3]

	Temperature, T (°C)	Density, ρ (kg/m^3)	Specific gravity	Modulus of elasticity, K (kPa)	Dynamic viscosity, μ (Pa · s)	Surface tension, σ (N/m)	Vapor pressure, ρ_ν (kPa)
Benzene	20	876.2	0.88	1,034,250	6.56×10^{-4}	0.029	10.0
Carbon tetrachloride	20	1,587.4	1.59	1,103,200	9.74×10^{-4}	0.026	13.1
Crude oil	20	855.6	0.86	–	71.8×10^{-4}	0.03	–
Ethyl alcohol	20	788.6	0.79	1,206,625	12.0×10^{-4}	0.022	5.86
Freon-12	15.6	1,345.2	1.35	–	14.8×10^{-4}	–	–
	−34.4	1,499.8	–	–	18.3×10^{-4}	–	–
Gasoline	20	680.3	0.68	–	2.9×10^{-4}	–	55.2
Glycerin	20	1,257.6	1.26	4,343,850	14.939×10^{-1}	0.063	0.000014
Hydrogen	−257.2	73.7	–	–	0.21×10^{-4}	0.0029	21.4
Jet fuel (JP-4)	15.6	773.1	0.77	–	8.7×10^{-4}	0.029	8.96
Mercury	15.6	13,555	13.57	26,201,000	15.6×10^{-4}	0.51	0.00017
	315.6	12,833	12.8	–	9.0×10^{-4}	–	47.2
Oxygen	−195.6	1,206.0	–	–	2.78×10^{-4}	0.015	21.4
Sodium	315.6	876.2	–	–	3.30×10^{-4}	–	–
	537.8	824.6	–	–	2.26×10^{-4}	–	–
Water	20	998.2	1.00	2,170,500	10.0×10^{-4}	0.073	2.34

Table A.25 Properties of water [5]

T (°F)	T (°C)	c_p (kJ/kg · °C)	ρ (kg/m^3)	μ (kg/m · s)	k (W/m · °C)	Pr	$\frac{g\beta\rho^2 C_p}{\mu k}$(1/m^3 · °C)
32	0	4.225	999.8	1.79×10^{-3}	0.566	13.25	1.91×10^{9}
40	4.44	4.208	999.8	1.55	0.575	11.35	6.34×10^{9}
50	10	4.195	999.2	1.31	0.585	9.40	1.08×10^{10}
60	15.56	4.186	998.6	1.12	0.595	7.88	1.46×10^{10}
70	21.11	4.179	997.4	9.8×10^{-4}	0.604	6.78	1.91×10^{10}
80	26.67	4.179	995.8	8.6	0.614	5.85	2.48×10^{10}
90	32.22	4.174	994.9	7.65	0.623	5.12	3.3×10^{10}
100	37.78	4.174	993.0	6.82	0.630	4.53	4.19×10^{10}
110	43.33	4.174	990.6	6.16	0.637	4.04	4.89×10^{10}
120	48.89	4.174	988.8	5.62	0.644	3.64	5.66×10^{10}
130	54.44	4.179	985.7	5.13	0.649	3.30	6.48×10^{10}
140	60	4.179	983.3	4.71	0.654	3.01	7.62×10^{10}
150	65.55	4.183	980.3	4.3	0.659	2.73	8.84×10^{10}
160	71.11	4.186	977.3	4.01	0.665	2.53	9.85×10^{10}
170	76.67	4.191	973.7	3.72	0.668	2.33	1.09×10^{11}
180	82.22	4.195	970.2	3.47	0.673	2.16	
190	87.78	4.199	966.7	3.27	0.675	2.03	
200	93.33	4.204	963.2	3.06	0.678	1.90	
220	104.4	4.216	955.1	2.67	0.684	1.66	
240	115.6	4.229	946.7	2.44	0.685	1.51	
260	126.7	4.250	937.2	2.19	0.685	1.36	
280	137.8	4.271	928.1	1.98	0.685	1.24	
300	148.9	4.296	918.0	1.86	0.684	1.17	
350	176.7	4.371	890.4	1.57	0.677	1.02	
400	204.4	4.467	859.4	1.36	0.665	1.00	
450	232.2	4.585	825.7	1.20	0.646	0.85	
500	260	4.731	785.2	1.07	0.616	0.83	
550	287.7	5.024	735.5	9.51×10^{-5}			
600	315.6	5.703	678.7	8.68			

$\mathrm{Gr_x Pr}\left(\frac{g\beta\rho^2 \mathrm{C_p}}{\mu \mathrm{k}}\right)\Delta \mathrm{T}$

Table A.26 Properties of saturated liquids [4]

t (°C)	ρ (kg/m^3)	c_p (kJ/kg · °C)	ν (m^2/s)	k (W/m · °C)	α (m^2/s)	Pr	β (K^{-1})
Ammonia, NH_3							
−50	703.69	4.463	0.435×10^{-6}	0.547	1.742×10^{-7}	2.60	
−40	691.68	4.467	0.406	0.547	1.775	2.28	
−30	679.34	4.476	0.387	0.549	1.801	2.15	
−20	666.69	4.509	0.381	0.547	1.819	2.09	
−10	653.55	4.564	0.378	0.543	1.825	2.07	
0	640.10	4.635	0.373	0.540	1.819	2.05	
10	626.16	4.714	0.368	0.531	1.801	2.04	
20	611.75	4.798	0.359	0.521	1.775	2.02	2.45×10^{-3}
30	596.37	4.890	0.349	0.507	1.742	2.01	
40	580.99	4.999	0.340	0.493	1.701	2.00	
50	564.33	5.116	0.330	0.476	1.654	1.99	
Carbon dioxide, CO_2							
−50	1,156.34	1.84	0.119×10^{-6}	0.0855	0.4021×10^{-7}	2.96	
−40	1,117.77	1.88	0.118	0.1011	0.4810	2.46	
−30	1,076.76	1.97	0.117	0.1116	0.5272	2.22	
−20	1,032.39	2.05	0.115	0.1151	0.5445	2.12	
−10	983.38	2.18	0.113	0.1099	0.5133	2.20	
0	926.99	2.47	0.108	0.1045	0.4578	2.38	
10	860.03	3.14	0.101	0.0971	0.3608	2.80	
20	772.57	5.0	0.091	0.0872	0.2219	4.10	14.00×10^{-3}
30	597.81	36.4	0.080	0.0703	0.279	28.7	
Sulfur dioxide, SO_2							
−50	1,560.84	1.3595	0.484×10^{-6}	0.242	1.141×10^{-7}	4.24	
−40	1,536.81	1.3607	0.424	0.235	1.130	3.74	
−30	1,520.64	1.3616	0.371	0.230	1.117	3.31	
−20	1,488.60	1.3624	0.324	0.225	1.107	2.93	
−10	1,463.61	1.3628	0.288	0.218	1.097	2.62	
0	1,438.46	1.3636	0.257	0.211	1.081	2.38	
10	1,412.51	1.3645	0.232	0.204	1.066	2.18	
20	1,386.40	1.3653	0.210	0.199	1.050	2.00	1.94×10^{-3}
30	1,359.33	1.3662	0.190	0.192	1.035	1.83	
40	1,329.22	1.3674	0.173	0.185	1.019	1.70	
50	1,299.10	1.3683	0.162	0.177	0.999	1.61	
Dichlorodifluoromethane (freon), CCl_2F_2							
−50	1,546.75	0.8750	0.310×10^{-6}	0.067	0.501×10^{-7}	6.2	2.63×10^{-3}
−40	1,518.71	0.8847	0.279	0.069	0.514	5.4	
−30	1,489.56	0.8956	0.253	0.069	0.526	4.8	
−20	1,460.57	0.9073	0.235	0.071	0.539	4.4	
−10	1,429.49	0.9203	0.221	0.073	0.550	4.0	
0	1,397.45	0.9345	0.214	0.073	0.557	3.8	
10	1,364.30	0.9496	0.203	0.073	0.560	3.6	
20	1,330.18	0.9659	0.198	0.073	0.560	3.5	
30	1,295.10	0.9835	0.194	0.071	0.560	3.5	
40	1,257.13	1.0019	0.191	0.069	0.555	3.5	
50	1,215.96	1.0216	0.190	0.067	0.545	3.5	
Glycerin, $C_3H_5(OH)_3$							
0	1,276.03	2.261	0.00831	0.282	0.983×10^{-7}	84.7×10^3	

(continued)

Table A.26 (continued)

t (°C)	ρ (kg/m^3)	c_p (kJ/kg · °C)	ν (m^2/s)	k (W/m · °C)	α (m^2/s)	Pr	β (K^{-1})
10	1,270.11	2.319	0.00300	0.284	0.965	31.0	
20	1,264.02	2.386	0.00118	0.286	0.947	12.5	0.50×10^{-3}
30	1,258.09	2.445	0.00050	0.286	0.929	5.38	
40	1,252.01	2.512	0.00022	0.286	0.914	2.45	
50	1,244.96	2.583	0.00015	0.287	0.893	1.63	
Ethylene glycol, $C_2H_4(OH)_2$							
0	1,130.75	2.294	57.53×10^{-6}	0.242	0.934×10^{-7}	615	
20	1,116.65	2.382	19.18	0.249	0.939	204	0.65×10^{-3}
40	1,101.43	2.474	8.69	0.256	0.939	93	
60	1,087.66	2.562	4.75	0.260	0.932	51	
80	1,077.56	2.650	2.98	0.261	0.921	32.4	
100	1,058.50	2.742	2.03	0.263	0.908	22.4	
Engine oil (unused)							
0	899.12	1.796	0.00428	0.147	0.911×10^{-7}	47,100	
20	888.23	1.880	0.00090	0.145	0.872	10,400	0.70×10^{-3}
40	876.05	1.964	0.00024	0.144	0.834	2,870	
60	864.04	2.047	0.839×10^{-4}	0.140	0.800	1,050	
80	852.02	2.131	0.375	0.138	0.769	490	
100	840.01	2.219	0.203	0.137	0.738	276	
120	828.96	2.307	0.124	0.135	0.710	175	
140	816.94	2.395	0.080	0.133	0.686	116	
160	805.89	2.483	0.056	0.132	0.663	84	
Mercury, Hg							
0	13,628.22	0.1403	0.124×10^{-6}	8.20	42.99×10^{-7}	0.0288	
20	13,579.04	0.1394	0.114	8.69	46.06	0.0249	1.82×10^{-4}
50	13,505.84	0.1386	0.104	9.40	50.22	0.0207	
100	13,384.58	0.1373	0.0928	10.51	57.16	0.0162	
150	13,264.28	0.1365	0.0853	11.49	63.54	0.0134	
200	13,144.94	0.1570	0.0802	12.34	69.08	0.0116	
250	13,025.60	0.1357	0.0765	13.07	74.06	0.0103	
315.5	12,847	0.134	0.0673	14.02	81.5	0.0083	
Water, H_2O							
0	1,002.28	4.2178×10^3	1.788×10^{-6}	0.552	1.308×10^{-7}	13.6	0.18×10^{-3}
20	1,000.52	4.1818	1.006	0.597	1.430	7.02	
40	994.59	4.1784	0.658	0.628	1.512	4.34	
60	985.46	4.1843	0.478	0.651	1.554	3.02	
80	974.08	4.1964	0.364	0.668	1.636	2.22	
100	960.63	4.2161	0.294	0.680	1.680	1.74	
120	945.25	4.250	0.247	0.685	1.708	1.446	
140	928.27	4.283	0.214	0.684	1.724	1.241	
160	909.69	4.342	0.190	0.680	1.729	1.099	
180	889.03	4.417	0.173	0.675	1.724	1.004	
200	866.76	4.505	0.160	0.665	1.706	0.937	
220	842.41	4.610	0.150	0.652	1.680	0.891	
240	815.66	4.756	0.143	0.635	1.639	0.871	
260	785.87	4.949	0.137	0.611	1.577	0.874	
280.6	752.55	5.208	0.135	0.580	1.481	0.910	
300	714.26	5.728	0.135	0.540	1.324	1.019	

Table A.27 Properties of metals [4]

	Properties at 20 °C				Thermal conductivity k (W/m · °C)									
Metal	ρ (kg/m^3)	c_p (kJ/kg · °C)	k (W/m · °C)	α (m^2/s × 105)	−100 °C	0 °C	100 °C	200 °C	300 °C	400 °C	600 °C	800 °C	1,000 °C	1,200 °C
Aluminum														
Pure	2,707	0.896	204	8.418	215	202	206	215	228	249				
Al-Cu (Duralumin) 94–96 % al, 3–5 % CU, trace Mg	2,787	0.883	164	6.676	126	159	182	194						
Al-Si (Silumin, copper bearing) 86.5 % Al, 1 % Cu	2,659	0.867	137	5.933	119	137	144	152	161					
Al-Si (Alusil) 78–80 % Al, 20–22 % Si	2,627	0.854	161	7.172	144	157	168	175	178					
Al-Mg-Si 97 % Al, 1 % Mg, 1 % Si, 1 % Mn	2,707	0.892	177	7.311		175	189	204						
Lead	11,373	0.130	35	2.343	36.9	35.1	33.4	31.5	29.8					
Iron														
Pure	7,897	0.452	73	2.034	87	73	67	62	55	48	40	36	35	36
Wrought iron 0.5 % C	7,849	0.46	59	1.626		59	57	52	48	45	36	33	33	33
Steel (C max ≈ 1.5 %):														
Carbon steel														
C ≈ 0.5 %	7,833	0.465	54	1.474		55	52	48	45	42	35	31	29	31
1.0 %	7,801	0.473	43	1.172		43	43	42	40	36	33	29	28	29
1.5 %	7,753	0.486	36	0.970		36	36	36	35	33	31	28	28	29
Nickel steel														
Ni ≈ 0 %	7,897	0.452	73	2.026										
20 %	7,933	0.46	19	0.526										

40 %	8,169	0.46	10	0.279										
80 %	8,618	0.46	35	0.872										
Invar 36 % Ni	8,137	0.46	10.7	0.286										
Chrome steel														
Cr = 0 %	7,897	0.452	73	2.026	87	73	67	62	55	48	40	36	35	36
1 %	7,865	0.46	61	1.665		62	55	52	47	42	36	33	33	
5 %	7,833	0.46	40	1.110		40	38	36	36	33	29	29	29	
20 %	7,689	0.46	22	0.635		22	22	22	22	24	24	26	29	
Cr-Ni, chrome- nickel 15 % Cr, 10 % Ni	7,865	0.46	19	0.526										
18 % Cr, 8 % Ni (V2A)	7,817	0.46	16.3	0.444		16.3	17	17	19	19	22	26	31	
20 % Cr, 15 % Ni	7,833	0.46	15.1	0.415										
25 % Cr, 20 % Ni	7,865	0.46	12.8	0.361										
Tungsten steel														
W = 0 %	7,897	0.452	73	2.026										
1 %	7,913	0.448	66	1.858										
5 %	8,073	0.435	54	1.525										
10 %	8,314	0.419	48	1.391										
Copper														
Pure	8,954	0.3831	386	11.234	407	386	379	374	369	363	353			
Aluminum														
bronze 95 % Cu, 5 % Al	8,666	0.410	83	2.330										
Bronze 75 % Cu, 25 % Sn	8,666	0.343	26	0.859										
Red brass 85 % Cu, 9 % Sn, 6 % Zn	8,714	0.385	61	1.804		59	71							
Brass 70 % Cu, 30 % Zn	8,522	0.385	111	3.412	88		128	144	147	147				
German silver														
62 % Cu, 15 % Ni, 22 % Zn	8,618	0.394	24.9	0.733	19.2		31	40	45	48				
Constantan														
60 % Cu, 40 % Ni	8,922	0.410	22.7	0.612	21		22.2	26						
Magnesium														
Pure	1,746	1.013	171	9.708	178	171	168	163	157					

(continued)

Table A.27 (continued)

Metal	Properties at 20 °C				Thermal conductivity k (W/m · °C)									
	ρ (kg/m^3)	c_p (kJ/kg · °C)	k (W/m · °C)	α (m^2/s × 105)	−100 °C	0 °C	100 °C	200 °C	300 °C	400 °C	600 °C	800 °C	1,000 °C	1,200 °C
Mg-Al														
(electrolytic) 6–8 % Al, 1–2 % Zn	1,810	1.00	66	3.605	138	52	62	74	83					
Molybdenum	10,220	0.251	123	4.790		125	118	114	111	109	106	102	99	92
Nickel														
Pure (99.9 %)	8,906	0.4459	90	2.266	104	93	83	73	64	59				
Ni-Cr 90 % Ni, 10 % Cr	8,666	0.444	17	0.444		17.1	18.9	20.9	22.8	24.6				
80 % Ni, 20 % Cr	8,314	0.444	12.6	0.343		12.3	13.8	15.6	17.1	18.0	22.5			
Silver														
Purest	10,524	0.2340	419	17.004	419	417	415	412						
Pure (99.9 %)	10,524	0.2340	407	16.563	419	410	415	374	362	360				
Tin, pure	7,304	0.2265	64	3.884	74	65.9	59	57						
Tungsten	19,350	0.1344	163	6.271		166	151	142	133	126	112	76		
Zinc, pure	7,144	0.3843	112.2	4.106	114	112	109	106	100	93				

Table A.28 Properties of nonmetals [5]

Substance	Temperature (°C)	k (W/m · °C)	ρ (kg/m^3)	C (kJ/kg · °C)	α (m^2/s)
Insulating material					
Asbestos					
Loosely packed	−45	0.149	470–570	0.816	3.3–4 × 10^{-7}
	0	0.154			
	100	0.161			
Asbestos-cement boards	20	0.74			
Sheets	51	0.166			
Felt, 40 laminations/in.	38	0.057			
	150	0.069			
	260	0.083			
20 laminations/in.	38	0.078			
	150	0.095			
	260	0.112			
Corrugated, 4 plies/in.	38	0.087			
	93	0.100			
	150	0.119			
Asbestos cement	–	2.08			
Balsam wool, 35 kg/m^3	32	0.04	35		
Cardboard, corrugated	–	0.064			
Celotex	32	0.048			
Corkboard, 160 kg/m^3	30	0.043	160		
Cork, regranulated	32	0.045	45–120	1.88	2–5.3 × 10^{-7}
Ground	32	0.043	150		
Diatomaceous earth (Sil-o-cel)	0	0.061	320		
Felt, hair	30	0.036	130–200		
Wool	30	0.052	330		
Fiber, insulating board	20	0.048	240		
Glass wool, 24 kg/m^3	23	0.038	24	0.7	22.6 × 10^{-7}
Insulex, dry	32	0.064 0.144			
Kapok	30	0.035			
Magnesia, 85 %	38	0.067	270		
	93	0.071			
	150	0.074			
	204	0.080			
Rock wool, 160 kg/m^3	32	0.040	160		
Loosely packed	150	0.067	64		
	260	0.087			
Sawdust	23	0.059			
Silica aerogel	32	0.024	140		
Wood shavings	23	0.059			
Structural and heat-resistant materials					
Asphalt	20–55	0.74–0.76			
Brick					
Building brick, common	20	0.69	1,600	0.84	5.2 × 10^{-7}
Face		1.32	2,000		
Carborundum brick	600	18.5			
	1,400	11.1			

(continued)

Table A.28 (continued)

Substance	Temperature (°C)	k (W/m · °C)	ρ (kg/m^3)	C (kJ/kg · °C)	α (m^2/s)
Chrome brick	200	2.32	3,000	0.84	9.2×10^{-7}
	550	2.47			9.8×10^{-7}
	900	1.99			7.9×10^{-7}
Diatomaceous earth, molded and fired	200	0.24			
	870	0.31			
Fireclay brick, burnt 1,330 °C	500	1.04	2,000	0.96	5.4×10^{-7}
	800	1.07			
	1,100	1.09			
Fireclay brick, burnt 1,450 °C	500	1.28	2,300	0.96	5.8×10^{-7}
	800	1.37			
	1,100	1.40			
Missouri	200	1.00	2,600	0.96	4.0×10^{-7}
	600	1.47			
	1,400	1.77			
Magnesite	200	3.81		1.13	
	650	2.77			
	1,200	1.90			
Cement, portland		0.29	1,500		
Mortar	23	1.16			
Concrete, cinder	23	0.76			
Stone 1-2-4 mix	20	1.37	1,900–2,300	0.88	$8.2–6.8 \times 10^{-7}$
Glass, window	20	0.78 (avg)	2,700	0.84	3.4×10^{-7}
Corosilicate	30–75	1.09	2,200		
Plaster, gypsum	20	0.48	1,440	0.84	4.0×10^{-7}
Metal lath	20	0.47			
Wood lath	20	0.28			
Stone					
Granite		1.73–3.98	2,640	0.82	$8–18 \times 10^{-7}$
Limestone	100–300	1.26–1.33	2,500	0.90	$5.6–5.9 \times 10^{-7}$
Marble		2.07–2.94	2,500–2,700	0.80	$10–13.6 \times 10^{-7}$
Sandstone	40	1.83	2,160–2,300	0.71	$11.2–11.9 \times 10^{-7}$
Wood (across the grain)					
Balsa 140 kg/m^3	30	0.055	140		
Cypress	30	0.097	460		
Fir	23	0.11	420	2.72	0.96×10^{-7}
Maple or oak	30	0.166	540	2.4	1.28×10^{-7}
Yellow pine	23	0.147	640	2.8	0.82×10^{-7}
White pine	30	0.112	430		

M.J. Hurley (ed.), *SFPE Handbook of Fire Protection Engineering*,
DOI 10.1007/978-1-4939-2565-0, © Society of Fire Protection Engineers 2016

Appendix 3: Fuel Properties and Combustion Data

Table A.29 Physical and combustion properties of selected fuels in Air [6]

						Stoichiometry		Flammability limits (% stoichio.)						Ign. energy		Quenching dist.	
Fuel	Mol. wt.	Spec. grav.	T_{Boil} (°C)	Heat of vap. (kJ/kg)	Heat of comb. (MJ/kg)	% Vol.	f[a]	Lean	Rich	Spont. Ign. temp. (°C)[b]	Fuel for max. flame speed (% stoichio.)	Max. flame speed (cm/s)	Flame temp. at max. Fl. speed (K)	Stoich.	Min.	Stoich.	Min.
														(10^{-5} cal.)		(mm)	
Acetaldehyde	44.1	0.783	−56.7	569.4	–	0.0772	0.1280	–	–	–	–	–	–	8.99	–	2.29	–
Acetone	58.1	0.792	56.7	523.0	30.8	0.0497	0.1054	59	233	561.1	131	50.18	2,121	27.48	–	3.81	–
Acetylene	26.0	0.621	−83.9	–	48.2	0.0772	0.0755	31	–	305.0	133	155.25	–	0.72	–	0.76	–
Acrolein	56.1	0.841	52.8	–	–	0.0564	0.1163	48	752	277.8	100	61.75	–	4.18	–	1.52	–
Acrylonitrile	53.1	0.797	78.3	–	–	0.0528	0.1028	87	–	481.1	105	46.75	2,461	8.60	3.82	2.29	1.52
Ammonia	17.0	0.817	−33.3	1,373.6	–	0.2181	0.1645	–	–	651.1	–	–	2,600	–	–	–	–
Aniline	93.1	1.022	184.4	432.6	–	0.0263	0.0872	–	–	593.3	–	–	–	–	–	–	–
Benzene	78.1	0.885	80.0	431.8	39.9	0.0277	0.0755	43	336	591.7	108	44.60	2,365	13.15	5.38	2.79	1.78
Benzyl alcohol	108.1	1.050	205.0	–	–	0.0240	0.0923	–	–	427.8	–	–	–	–	–	–	–
1,2-butadiene (methylallene)	54.1	0.658	11.1	–	45.5	0.0366	0.0714	–	–	–	117	63.90	2,419	5.60	–	1.30	–
n-butane	58.1	0.584	−0.5	385.8	45.7	0.0312	0.0649	54	330	430.6	113	41.60	2,256	18.16	6.21	3.05	1.78
Butanone (methylethyl ketone)	72.1	0.805	79.4	–	–	0.0366	0.0951	–	–	–	100	39.45	–	12.67	6.69	2.54	2.03
1-butene	56.1	0.601	−6.1	443.9	45.3	0.0377	0.0678	53	353	443.3	116	47.60	2,319	–	–	–	–
d-camphor	152.2	0.990	203.4	–	–	0.0153	0.0818	–	–	466.1	–	–	–	–	–	–	–
Carbon disulfide	76.1	1.263	46.1	351.0	–	0.0652	0.1841	18	1,120	120.0	102	54.46	–	0.36	–	0.51	–

(continued)

Table A.29 (continued)

						Stoichiometry		Flammability limits (% stoichio.)						Ign. energy		Quenching dist.	
Fuel	Mol. wt.	Spec. grav.	T_{Boil} (°C)	Heat of vap. (kJ/kg)	Heat of comb. (MJ/kg)	% Vol.	f^a	Lean	Rich	Spont. Ign. temp. (°C)[b]	Fuel for max. flame speed (% stoichio.)	Max. flame speed (cm/s)	Flame temp. at max. Fl. speed (K)	Stoich.	Min.	Stoich.	Min.
Carbon monoxide	28.0	–	−190.0	211.7	–	0.2950	0.4064	34	676	608.9	170	42.88	–	–	–	–	–
Cyclobutane	56.1	0.703	12.8	–	–	0.0377	0.0678	–	–	–	115	62.18	2,308	–	–	–	–
Cyclohexane	84.2	0.783	80.6	258.1	43.8	0.0227	0.0678	48	401	270.0	117	42.46	2,250	32.98	5.33	4.06	1.78
Cyclohexene	82.1	0.810	82.8	–	–	0.0240	0.0701	–	–	–	–	44.17	–	20.55	–	3.30	–
Cyclopentane	70.1	0.751	49.4	388.3	44.2	0.0271	0.0678	–	–	385.0	117	41.17	2,264	19.84	–	3.30	–
Cyclopropane	42.1	0.720	−34.4	–	–	0.0444	0.0678	58	276	497.8	113	52.32	2,328	5.74	5.50	1.78	1.78
trans-decalin	138.2	0.874	187.2	–	–	0.0142	0.0692	–	–	271.7	109	33.88	2,222	–	–	–	–
n-decane	142.3	0.734	174.0	359.8	44.2	0.0133	0.0666	45	356	231.7	105	40.31	2,286	–	–	2.06	–
Diethyl ether	74.1	0.714	34.4	351.6	–	0.0337	0.0896	55	2,640	185.6	115	43.74	2,253	11.71	6.69	2.54	2.03
Ethane	30.1	–	−88.9	488.3	47.4	0.0564	0.0624	50	272	472.2	112	44.17	2,244	10.04	5.74	2.29	1.78
Ethyl acetate	88.1	0.901	77.2	–	–	0.0402	0.1279	61	236	486.1	100	35.59	–	33.94	11.47	4.32	2.54
Ethanol	46.1	0.789	78.5	836.8	26.8	0.0652	0.1115	–	–	392.2	–	–	–	–	–	–	–
Ethylamine	45.1	0.706	16.7	611.3	–	0.0528	0.0873	–	–	–	–	–	–	57.36	–	5.33	–
Ethylene oxide	44.1	1.965	10.6	581.1	–	0.0772	0.1280	–	–	428.9	125	11.35	2,411	2.51	1.48	1.27	1.02
Furan	68.1	0.936	32.2	400.0	–	0.0444	0.1098	–	–	–	–	–	–	5.40	–	1.78	–
n-heptane	100.2	0.688	98.5	364.9	44.4	0.0187	0.0661	53	450	247.2	122	42.46	2,214	27.49	5.74	3.81	1.78
n-hexane	86.2	0.664	68.0	364.9	44.7	0.0216	0.0659	51	400	260.6	117	42.46	2,239	22.71	5.50	3.56	1.78
Hydrogen	2.0	–	−252.7	451.0	119.9	0.2950	0.0290	–	–	571.1	170	291.19	2,380	0.36	0.36	0.51	0.51
iso-propanol	60.1	0.785	82.2	664.8	–	0.0444	0.0969	–	–	455.6	100	38.16	–	15.54	–	2.79	–
Kerosene	154.0	0.825	250.0	290.8	43.1	–	–	–	–	–	–	–	–	–	–	–	–
Methane	16.0	–	−161.7	509.2	50.0	0.0947	0.0581	46	164	632.2	106	37.31	2,236	7.89	6.93	2.54	2.03
Methanol	32.0	0.793	64.5	1,100.9	19.8	0.1224	0.1548	48	408	470.0	101	52.32	–	5.14	3.35	1.78	1.52

Methyl formate	60.1	0.975	31.7	472.0	–	0.0947	0.2181	–	–	–	–	–	–	14.82	–	2.79	–
n-nonane	128.3	0.772	150.6	288.3	44.6	0.0147	0.0665	47	434	238.9	–	–	–	–	–	–	–
n-octane	114.2	0.707	125.6	300.0	44.8	0.0165	0.0633	51	425	240.0	–	–	2,251	–	–	–	–
n-pentane	72.1	0.631	36.0	364.4	45.3	0.0255	0.0654	54	359	284.4	115	42.46	2,250	19.60	5.26	3.30	1.78
1-pentene	70.1	0.646	30.0	–	45.0	0.0271	0.0678	47	370	298.3	114	46.75	2,314	–	–	–	–
Propane	44.1	0.508	−42.2	425.5	46.3	0.0402	0.0640	51	283	504.4	114	42.89	2,250	7.29	–	2.03	1.78
Propene	42.1	0.522	−47.7	437.2	45.8	0.0444	0.0678	48	272	557.8	114	48.03	2,339	6.74	–	2.03	–
n-propanol	60.1	0.804	97.2	685.8	–	0.0444	0.0969	–	–	433.3	–	–	–	–	–	–	–
Toluene	92.1	0.872	110.6	362.8	40.9	0.0227	0.0743	43	322	567.8	105	38.60	2,344	–	–	–	–
Triethylamine	101.2	0.723	89.4	–	–	0.0210	0.0753	–	–	–	–	–	–	27.48	–	3.81	–
Turpentine	–	–	–	–	–	–	–	–	–	252.2	–	–	–	–	–	–	–
Xylene	106.0	0.870	130.0	334.7	43.1	–	–	–	–	–	–	–	–	–	–	–	–
Gasoline 73 octane	120.0	0.720	155.0	338.9	44.1	–	–	–	–	298.9	–	–	–	–	–	–	–
Gasoline 100 octane	–	–	–	–	–	–	–	–	–	468.3	106	37.74	–	–	–	–	–
Jet fuel JP1	150.0	0.810	–	–	43.0	0.0130	0.0680	–	–	248.9	107	36.88	–	–	–	–	–
JP3	112.0	0.760	–	–	43.5	0.0170	0.0680	–	–	–	–	–	–	–	–	–	–
JP4	126.0	0.780	–	–	43.5	0.0150	0.0680	–	–	261.1	107	38.17	–	–	–	–	–
JP5	170.0	0.830	–	–	43.0	0.0110	0.0690	–	–	242.2	–	–	–	–	–	–	–

[a] f is the stoichiometric air/fuel ratio; i.e., $f = {}^{1}/_{r}$
[b] For additional information, see Table A.33 and Chap. 18, "Ignition of Liquids"

Table A.30 Heats of combustion and related properties of pure substances [7]

Material	Composition	Molecular Weight, W	Gross, $\Delta h_c{}^u$ (MJ/kg)	Net, $\Delta h_c{}^l$ (MJ/kg)	$\Delta h_c{}^l / r_o$ (MJ/kg O_2)	Oxygen fuel mass ratio, r_o	Boiling temp., T_b (°C)	Latent heat of vaporization, Δh_v (kJ/kg)	Liquid heat capacity, C_{pl} (kJ/kg · °C)	Vapor heat capacity, C_{pv} (kJ/kg · °C)
Acetaldehyde	C_2H_4O	44.05	27.07	25.07	13.81	1.816	20.8	–	1.94	1.24
Acetic acid	$C_2H_4O_2$	60.05	14.56	13.09	12.28	1.066	118.1	395		1.11
Acetone	C_3H_6O	58.08	30.83	28.56	12.96	2.204	56.5	501	2.12	1.29
Acetylene	C_2H_2	26.04	49.91	48.22	15.70	3.072	−84.0	–	–	1.69
Acrolein	C_3H_4O	56.06	29.08	27.51	13.77	1.998	52.5	505	–	1.17
Acrylonitrile	C_3H_3N	53.06	33.16	31.92	14.11	2.262	77.3	615	2.10	1.20
(Allene) → propadiene										
Ammonium perchlorate[a]	NH_4ClO_4	117.49	2.35	2.16	3.97	0.545	–	–	–	
iso-amyl alcohol	$C_5H_{12}O$	88.15	37.48	34.49	12.67	2.723	132.0	501	2.90	1.50
Aniline	C_6H_7N	93.12	36.44	34.79	13.06	2.663	184.4	478	2.08	1.16
Benzaldehyde	C_7H_6O	106.12	33.25	32.01	13.27	2.412	179.2	385	1.61	
Benzene	C_6H_6	78.11	41.83	40.14	13.06	3.073	80.1	389	1.72	1.05
Benzoic acid[a]	$C_7H_6O_2$	122.12	26.43	25.35	12.90	1.965	250.8	415	–	0.85
Benzyl alcohol	C_7H_8O	108.13	34.56	32.93	13.09	2.515	205.7	467	2.00	1.19
Bicyclohexyl	$C_{12}H_{22}$	166.30	45.35	42.44	12.61	3.367	236.0	263		
1,2-butadiene	C_4H_6	54.09	47.95	45.51	13.99	3.254	10.8	–	–	1.48
1,3-butadiene	C_4H_6	54.09	46.99	44.55	13.69	3.254	−4.4	–	–	1.47
(1,3-butadiyne) → diacetylene										
n-butane	C_4H_{10}	58.12	49.50	45.72	12.77	3.579	−0.5	–	2.30	1.68
iso-butane	C_4H_{10}	58.12	48.95	45.17	12.62	3.579	−11.8	–	–	1.67
1-butene	C_4H_8	56.10	48.44	45.31	13.24	3.422	−6.2	–	–	1.53
n-butylamine	$C_4H_{11}N$	73.14	41.75	38.45	12.84	2.994	77.8	372	2.57	1.62
d-camphor[a]	$C_{10}H_{16}O$	152.23	38.75	36.44	12.84	2.838	203.4	–	–	0.82
Carbon[a]	C	12.01	32.80	32.80	12.31	2.664	4,200.0	–	–	0.71
Carbon disulfide	CS_2	76.13	6.34	6.34	5.03	1.261	46.5	351	1.00	0.60
Carbon monoxide	CO	28.01	10.10	10.10	17.69	0.571	−191.3	–	–	1.04
Cellulose[a]	$C_6H_{10}O_5$	162.14	17.47	16.12	13.61	1.184	–	–	1.16	–
(Chloroethylene) → vinyl chloride										
(Chloroform) → trichloromethane										

Chlorotrifluoroethylene	C_2F_3Cl	116.47	2.00	2.00	3.64	0.549	−28.3	188	1.34	0.72
m-cresol	C_7H_8O	108.13	34.26	32.64	12.98	2.515	202.2	399	2.00	1.13
Cumene	C_9H_{12}	120.19	43.40	41.20	12.90	3.195	152.3	312	1.77	1.26
Cyanogen	C_2N_2	52.04	21.06	21.06	17.12	1.230	−21.2	–	–	1.12
Cyclobutane	C_4H_8	56.10	48.91	45.77	13.38	3.422	12.9	–	–	1.29
Cyclohexane	C_6H_{12}	84.16	46.58	43.45	12.70	3.422	80.7	357	1.84	1.26
Cyclohexene	C_6H_{10}	82.14	45.67	42.99	12.99	3.311	82.8	371	1.80	1.28
Cyclohexylamine	$C_6H_{13}N$	99.18	41.05	38.17	12.79	2.984	134.5			
Cyclopentane	C_5H_{10}	70.13	46.93	43.80	12.80	3.422	49.3	389	2.23	1.18
Cyclopropane	C_3H_6	42.08	49.70	46.57	13.61	3.422	−32.9	–	1.92	1.33
(Decahydronaphthalene) → cis-decalin										
cis-decalin	$C_{10}H_{18}$	138.24	45.49	42.63	12.70	3.356	195.8	309	1.67	1.21
n-decane	$C_{10}H_{22}$	142.28	47.64	44.24	12.69	3.486	174.1	276	2.19	1.85
Diacetylene	C_4H_2	50.06	46.60	45.72	15.89	2.877	10.3	–	–	1.47
(Diamine) hydrazine										
Diborane	H_6B_2	27.69	79.80	79.80	23.02	3.467	−92.5	–	–	1.75
Dichloromethane	CH_2Cl_2	84.94	6.54	6.02	10.65	0.565	39.7	330	1.18	0.80
Diethyl cyclohexane	$C_{10}H_{20}$	140.26	46.30	43.17	12.58	3.422	174.0		1.87	
Diethyl ether	$C_4H_{10}O$	74.12	36.75	33.79	13.04	2.590	34.6	360	2.34	1.52
(2,4 diisocyanotoulene) → toluene diisocyanate										
(Diisopropyl ether) → *iso*-propyl ether										
Dimethylamine	C_2H_7N	45.08	38.66	35.25	13.24	2.662	6.9	–	–	1.80
(Dimethyl aniline) → xylidene										
Dimethyldecalin	$C_{12}H_{22}$	166.30	45.70	42.79	13.15	3.254	220.0	260		
(Dimethyl ether) → methyl ether										
1,1-dimethylhydrazine (UDMH)	$C_2H_8N_2$	60.10	32.95	30.03	14.10	2.130	25.0	578	2.73	
Dimethyl sulfoxide	C_2H_6SO	78.13	29.88	28.19	15.30	1.843	189.0	677	1.89	1.14
1,3 dioxane	$C_4H_8O_2$	88.10	26.57	24.58	9.66	2.543	105.0	404		
1,4 dioxane	$C_4H_8O_2$	88.10	26.83	24.84	9.77	2.543	101.1	406	1.74	1.07
Ethane	C_2H_6	30.07	51.87	47.49	12.75	3.725	−88.6	–	–	1.75
Ethanol	C_2H_6O	46.07	29.67	26.81	12.87	2.084	78.5	837	2.43	1.42
(Ethene) → ethylene										
Ethyl acetate	$C_4H_8O_2$	88.10	25.41	23.41	12.89	1.816	77.2	367	1.94	1.29

(continued)

Table A.30 (continued)

Material	Composition	Molecular Weight, W	Gross, Δh_c^u (MJ/kg)	Net, Δh_c^l (MJ/kg)	$\Delta h_c^l / r_o$ (MJ/kg O_2)	Oxygen fuel mass ratio, r_o	Boiling temp., T_b (°C)	Latent heat of vaporization, Δh_v (kJ/kg)	Liquid heat capacity, C_{pl} (kJ/kg · °C)	Vapor heat capacity, C_{pv} (kJ/kg · °C)
Ethyl acrylate	$C_5H_8O_2$	100.12	27.44	25.69	13.39	1.918	100.0	290		1.14
Ethylamine	C_2H_7N	45.08	38.63	35.22	13.23	2.662	16.5	–	2.89	1.61
Ethyl benzene	C_8H_{10}	106.16	43.00	40.93	12.93	3.165	136.1	339	1.75	1.21
Ethylene	C_2H_4	28.05	50.30	47.17	13.78	3.422	−103.9	–	2.38	1.56
Ethylene glycol	$C_2H_6O_2$	62.07	19.17	17.05	13.22	1.289	197.5	800	2.43	1.56
Ethylene oxide	C_2H_4O	44.05	29.65	27.65	15.23	1.816	10.7	–	1.97	1.10
(Ethylene trichloride) → trichloroethylene										
(Ethyl ether) → diethyl ether										
Formaldehyde	CH_2O	30.03	18.76	17.30	16.23	1.066	−19.3	–	–	1.18
Formic acid	CH_2O_2	46.03	5.53	4.58	13.15	0.348	100.5	476	2.15	0.98
Furan	C_4H_4O	68.07	30.61	29.32	13.86	2.115	31.4	398	1.69	0.96
a-D-glucose[a]	$C_6H_{12}O_6$	180.16	15.55	14.08	13.21	1.066	–	–	–	–
(Glycerine) → glycerol										
Glycerol	$C_3H_8O_3$	92.10	17.95	16.04	13.19	1.216	290.0	800	2.42	1.25
(Glycerol trinitrate) → nitroglycerin										
n-heptane	C_7H_{16}	100.20	48.07	44.56	12.68	3.513	98.4	316	2.20	1.66
n-heptene	C_7H_{14}	98.18	47.44	44.31	12.95	3.422	93.6	317	2.17	1.58
Hexadecane	$C_{16}H_{34}$	226.43	47.25	43.95	12.70	3.462	286.7	226	2.22	1.64
Hexamethyldisiloxane	$C_6H_{18}Si_2O$	162.38	38.30	35.80	15.16	2.364	100.1	192	2.01	–
(Hexamethylenetetramine) → methenamine										
n-hexane	C_6H_{14}	86.17	48.31	44.74	12.68	3.528	68.7	335	2.24	1.66
n-hexene	C_6H_{12}	84.16	47.57	44.44	12.99	3.422	63.5	333	2.18	1.57
Hydrazine	H_4N_2	32.05	52.08	49.34	49.40	0.998	113.5	1,180	3.08	1.65
Hydrazoic acid	HN_3	43.02	15.28	14.77	79.40	0.186	35.7	690	–	1.02
Hydrogen	H_2	2.00	141.79	130.80	16.35	8.000	−252.7	–	–	14.42
(Hydrogen azide) → hydrazoic acid										–
Hydrogen cyanide	HCN	27.03	13.86	13.05	8.82	1.480	25.7	933	2.61	1.33
Hydrogen sulfide	H_2S	34.08	48.54	47.25	16.77	2.817	−60.3	548	–	1.00
Maleic anhydride[a]	$C_4H_2O_3$	74.04	18.77	18.17	14.01	1.297	202.0	–	–	–

Melamine[a]	$C_3H_6N_6$	126.13	15.58	14.54	12.73	1.142	–	–	–	–
Methane	CH_4	16.04	55.50	50.03	12.51	4.000	−161.5	–	–	2.23
Methanol	CH_4O	32.04	22.68	19.94	13.29	1.500	64.8	1,101	2.37	1.37
Methenamine[a]	$C_6H_{12}N_4$	140.19	29.97	28.08	13.67	2.054	–	–	–	–
2-methoxyethanol	$C_3H_8O_2$	76.09	24.23	21.92	13.03	1.682	124.4	583	2.23	–
Methylamine	CH_5N	31.06	34.16	30.62	13.21	2.318	−6.3	–	–	1.61
(2-methyl 1-butanol) → iso-amyl alcohol										
(Methyl chloride) → dichloromethane										
Methyl ether	C_2H_6O	46.07	31.70	28.84	13.84	2.084	−24.9	–	–	1.43
Methyl ethyl ketone	C_4H_8O	72.10	33.90	31.46	12.89	2.441	79.6	434	2.30	1.43
1-methylnaphthalene	$C_{11}H_{10}$	142.19	40.88	39.33	12.95	3.038	244.7	323	1.58	1.12
Methyl methacrylate	$C_5H_8O_2$	100.11	27.37	25.61	12.33	2.078	101.0	360	1.91	–
Methyl nitrate	CH_3NO_3	77.04	8.67	7.81	75.10	0.104	64.6	409	2.04	0.99
(2-methyl propane) → iso-butane										
Naphthalene[a]	$C_{10}H_8$	128.16	40.21	38.84	12.96	2.996	217.9	–	1.18	1.03
Nitrobenzene	$C_6H_5NO_2$	123.11	25.11	24.22	14.90	1.625	210.7	330	1.52	–
Nitroglycerin	$C_3H_5N_3O_9$	227.09	6.82	6.34	–	–	Unstable	462	1.49	–
Nitromethane	CH_3NO_2	61.04	11.62	10.54	15.08	0.699	101.1	567	1.74	0.94
n-nonane	C_9H_{20}	128.25	47.76	44.33	12.69	3.493	150.6	295	2.10	1.65
Octamethyl-cyclotetrasiloxane	$C_8H_{24}Si_4O_4$	296.62	26.90	25.10	14.56	1.725	175.0	127	1.88	–
n-octane	C_8H_{18}	114.22	47.90	44.44	12.69	3.502	125.6	301	2.20	1.65
iso-octane	C_8H_{18}	114.22	47.77	44.31	12.65	3.502	117.7	272	2.15	1.65
1-octene	C_8H_{10}	112.21	47.33	44.20	12.92	3.422	121.3	301	2.19	1.59
(1-octylene) → 1-octene										
1,2-pentadiene	C_5H_8	68.11	47.31	44.71	13.60	3.288	44.9	405	2.21	1.55
n-pentane	C_5H_{12}	72.15	48.64	44.98	12.68	3.548	36.0	357	2.33	1.67
1-pentene	C_5H_{10}	70.13	47.77	44.64	13.04	3.422	30.0	359	2.16	1.56
Phenol[a]	C_6H_6O	94.11	32.45	31.05	13.05	2.380	181.8	433	1.43	1.10
Phosgene	$COCl_2$	98.92	1.74	1.74	10.74	0.162	8.3	247	1.02	0.58
Propadiene	C_3H_4	40.06	48.54	46.35	14.51	3.195	−34.6	–	–	1.44
Propane	C_3H_8	44.09	50.35	46.36	12.78	3.629	−42.2	–	2.23	1.67
n-propanol	C_3H_8O	60.09	33.61	30.68	12.81	2.396	97.2	686	2.50	1.45
iso-propanol	C_3H_8O	60.09	33.38	30.45	12.71	2.396	80.3	663	2.42	1.48

(continued)

Table A.30 (continued)

Material	Composition	Molecular Weight, W	Gross, Δh_c^u (MJ/kg)	Net, Δh_c^l (MJ/kg)	$\Delta h_c^l / r_o$ (MJ/kg O_2)	Oxygen fuel mass ratio, r_o	Boiling temp., T_b (°C)	Latent heat of vaporization, Δh_v (kJ/kg)	Liquid heat capacity, C_{pl} (kJ/kg · °C)	Vapor heat capacity, C_{pv} (kJ/kg · °C)
Propene	C_3H_6	42.08	48.92	45.79	13.38	3.422	−47.7	–	–	1.52
(iso-propylbenzene) → cumene										
(Propylene) → propene										
iso-propyl ether	$C_6H_{14}O$	102.17	39.26	36.25	12.86	2.819	67.8	286	2.14	1.55
Propyne	C_3H_4	40.06	48.36	46.17	14.45	3.195	−23.3	–	–	1.51
Styrene	C_8H_8	104.14	42.21	40.52	13.19	3.073	145.2	356	1.76	1.17
Sucrose[a]	$C_{12}H_{22}O_{11}$	342.30	16.49	15.08	13.44	1.122	–	–	1.24	–
(1,2,3,4-tetrahydronaphthalene) → tetralin										
Tetralin	$C_{10}H_{12}$	132.20	42.60	40.60	12.90	3.147	207.0	425	1.64	1.19
Tetranitromethane	CN_4O_8	196.04	2.20	2.20	–	–	125.7	196	–	–
Toluene	C_7H_8	92.13	42.43	40.52	12.97	3.126	110.4	360	1.67	1.12
Toluene diisocyanate	$C_9H_6N_2O_2$	174.16	24.32	23.56	13.50	1.746	120.0	–	1.65	–
Triethanolamine	$C_6H_{15}NO_3$	149.19	29.29	27.08	15.30	1.770	360.0	–	–	–
Triethylamine	$C_6H_{15}N$	101.19	43.19	39.93	12.95	3.083	89.5	303	2.22	1.59
1,1,2-trichloroethane	$C_2H_3Cl_3$	133.42	7.77	7.28	11.02	0.660	114.0	260	1.11	0.67
Trichloroethylene	C_2HCl_3	131.40	6.77	6.60	12.05	0.548	86.9	245	1.07	0.61
Trichloromethane	$CHCl_3$	119.39	3.39	3.21	9.60	0.335	61.7	249	0.97	0.55
Trinitromethane	CHN_3O_6	151.04	3.41	3.25	–	–	Unstable	–	–	–
Trinitrotoluene[a]	$C_7H_5N_3O_6$	227.13	15.12	14.64	19.80	0.740	240.0	322	1.40	–
Trioxane	$C_3H_6O_3$	90.08	16.57	15.11	14.17	1.066	114.5	450	–	–
Urea[a]	CH_4ON_2	60.06	10.52	9.06	11.34	0.799	–	–	–	1.55
Vinyl acetate	$C_4H_6O_2$	86.09	24.18	22.65	13.54	1.673	72.5	167	2.00	1.05
Vinyl acetylene	C_4H_4	52.07	47.05	45.36	14.76	3.073	5.1	–	–	1.41
Vinyl bromide	C_2H_3Br	106.96	12.10	11.48	13.95	0.823	15.6	–	2.42	0.53
Vinyl chloride	C_2H_3Cl	62.50	20.02	16.86	11.97	1.408	−13.8	–	–	0.86
(Vinyl trichloride) → 1,1,2-trichlorolthane										
Xylenes	C_8H_{10}	106.16	42.89	40.82	12.90	3.165	138–144	343	1.72	1.21
Xylidene	$C_8H_{11}N$	121.22	38.28	36.29	12.79	2.838	192.7	366	1.77	–

[a]Denotes substance in crystalline solid form; otherwise, liquid if $T_b > 25$ °C, gaseous if $T_b > 25$ °C

Table A.31 Heats of combustion and related properties of plastics [7]

Material	Unit composition	Molecular weight, W	Gross, Δh_c^u (MJ/kg)	Net, Δh_c^l (MJ/kg)	$\Delta h_c^l / r_o$ (MJ/kg O_2)	Oxygen fuel mass ratio, r_o	Heat capacity solid, C_{ps} (kJ/kg · °C)
Acrylonitrile-butadiene styrene copolymer	–	–	35.25	33.75			1.41–1.59
Bisphenol A epoxy	$C_{11.85}H_{20.37}O_{2.83}$ $N_{0.3}$	212.10	33.53	31.42	13.41	2.343	
Butadiene-acrylonitrile 37 % copolymer	–	–	39.94				
Butadiene/styrene 8.58 % copolymer	$C_{4.18}H_{6.09}$	56.30	44.84	42.49	13.11	3.241	1.94
Butadiene/styrene 25.5 % copolymer	$C_{4.60}H_{6.29}$	61.55	44.19	41.95	13.07	3.209	1.82
Cellulose acetate (triacetate)	$C_{12}H_{16}O_8$	288.14	18.88	17.66	13.25	1.333	1.34
Cellulose acetate-butyrate	$C_{12}H_{18}O_7$	274.27	23.70	22.30	14.67	1.517	1.70
Epoxy, unhardened	$C_{31}H_{36}O_{5.5}$	496.63	32.92	31.32	13.05	2.400	
Epoxy, hardened	$C_{39}H_{40}O_{8.5}$	644.74	30.27	28.90	13.01	2.221	
Melamine formaldehyde (Formica™)	$C_6H_6N_6$	162.08	19.33	18.52	12.51	1.481	1.46
Nylon 6	$C_6H_{11}NO$	113.08	30.1–31.7	28.0–29.6	12.30	2.335	1.52
Nylon 6,6	$C_{12}H_{22}N_2O_2$	226.16	31.6–31.7	29.5–29.6	12.30	2.405	1.70
Nylon 11 (Rilsan)	$C_{11}H_{21}NO$	183.14	36.99	34.47	12.33	2.796	1.70–2.30
Phenol formaldehyde	$C_{15}H_{12}O_2$	224.17	27.9–31.6	26.7–30.4	11.80	2.427	1.70
Foam			21.6–27.4	20.2–26.2			
Polyacenaphthalene	$C_{12}H_8$	152.14	39.23	38.14	12.95	2.945	
Polyacrylonitrile	C_3H_3N	53.04	32.22	30.98	13.70	2.262	1.50
Polyallylphthalate	$C_{14}H_{14}O$	198.17	27.74	26.19	9.54	2.745	
(Polyamides) → nylon							
Poly-1,4-butadiene	C_4H_6	54.05	45.19	42.75	13.13	3.256	
Poly-1-butene	C_4H_8	56.05	46.48	43.35	12.65	3.426	1.88
Polycarbonate	$C_{16}H_{14}O_3$	254.19	30.99	29.78	13.14	2.266	1.26
Polycarbon suboxide	C_3O_2	68.03	13.78	13.78	14.64	0.941	
Polychlorotrifluorethylene	C_2F_3Cl	116.47	1.12	1.12	2.04	0.549	0.92
Polydiphenylbutadiene	$C_{16}H_{10}$	202.18	39.30	38.20	13.05	2.928	

(continued)

Table A.31 (continued)

Material	Unit composition	Molecular weight, W	Gross, Δh_c^u (MJ/kg)	Net, Δh_c^l (MJ/kg)	$\Delta h_c^l / r_o$ (MJ/kg O_2)	Oxygen fuel mass ratio, r_o	Heat capacity solid, C_{ps} (kJ/kg · °C)
Polyester, unsaturated	$C_{5.77}H_{6.25}O_{1.63}$	101.60	21.6–29.8	20.3–28.5	11.90	2.053	1.20–2.30
Polyether, chlorinated	$C_5H_8OCl_2$	154.97	17.84	16.71	12.45	1.342	
Polyethylene	C_2H_4	28.03	46.2–46.5	43.1–43.4	12.63	3.425	1.83–2.30
Polyethylene oxide	C_2H_4O	44.02	26.65	24.66	13.57	1.817	
Polyethylene terephthalate	$C_{10}H_8O_4$	192.11	22.18	21.27	12.77	1.666	1.00
Polyformaldehyde	CH_2O	30.01	16.93	15.86	14.88	1.066	1.46
Poly-1-hexene sulfone	$C_6H_{12}SO_2$	148.13	29.78	28.00	14.40	1.944	
Polyhydrocyanic acid	HCN	27.02	23.26	22.45	15.17	1.480	
(Polyisobutylene) → poly-1-butene							
Polyisocyanurate foam	–		26.30	22.2–26.2			
Polyisoprene	C_5H_8	68.06	44.90	42.30	12.90	3.291	
Poly-3-methyl-1-butene	C_5H_{10}	70.06	46.55	43.42	12.67	3.426	
Polymethyl methacrylate	$C_5H_8O_2$	100.06	26.64	24.88	12.97	1.919	1.44
Poly-4-methyl-1-pentene	C_6H_{12}	84.08	46.52	43.39	12.67	3.425	2.18
Poly-α-methylstyrene	C_9H_{10}	118.11	42.31	40.45	13.00	3.116	
Polynitroethylene	$C_2H_3O_2N$	73.03	15.96	15.06	19.64	0.767	
Polyoxymethylene	CH_2O	30.01	16.93	15.65	14.68	1.066	
Polyoxytrimethylene	C_3H_6O	58.04	31.52	29.25	13.27	2.205	
Poly-1-pentene	C_5H_{10}	70.06	45.58	42.45	12.39	3.426	
Polyphenylacetylene	C_8H_6	102.09	40.00	38.70	13.00	2.978	
Polyphenylene oxide	C_8H_8O	120.09	34.59	33.13	13.09	2.531	1.34
Polypropene sulfone	$C_3H_6SO_2$	106.10	23.82	22.58	16.64	1.357	
Poly-β-propiolactone	$C_3H_4O_2$	72.14	19.35	18.13	13.62	1.331	
Polypropylene	C_3H_6	42.04	46.37	43.23	12.62	3.824	2.10
Polypropylene oxide	C_3H_6O	58.04	31.17	28.90	13.11	2.205	
Polystyrene	C_8H_8	104.10	41.4–42.5	39.7–39.8	12.93	3.074	1.40
Polystyrene-foam	–		39.70	35.6–40.8			
Polystyrene-foam, FR	–		41.2–42.9				
Polysulfones, butene	$C_4H_8SO_2$	120.11	24.04–26.47	22.25–25.01	14.79	1.598	1.30

Polysulfur	S	32.06	9.72	9.72	9.74	0.998	
Polytetrafluoroethylene	C_2F_4	100.02	5.00	5.00	7.81	0.640	1.02
Polytetrahydrofuran	C_4H_8O	72.05	34.39	31.85	13.04	2.443	
Polyurea	$C_{15}H_{18}O_4N_4$	318.20	24.91	23.67	13.45	1.760	
Polyurethane	$C_{6.3}H_{7.1}NO_{2.1}$	130.30	23.90	22.70	13.16	1.725	1.75–1.84
Polyurethane-foam	–		26.1–31.6	23.2–28.0			
Polyurethane-foam, FR	–		24.0–25.0				
Polyvinyl acetate	$C_4H_6O_2$	86.05	23.04	21.51	12.86	1.673	
Polyvinyl alcohol	C_2H_4	44.03	25.00	23.01	12.66	1.817	1.70
Polyvinyl butyral	$C_8H_{14}O_2$	142.10	32.90	30.70	13.00	2.365	
Polyvinyl chloride	C_2H_3Cl	62.48	17.95	16.90	12.00	1.408	0.90–1.20
Polyvinyl-foam	–		22.83				1.30–2.10
Polyvinyl fluoride	C_2H_3F	46.02	21.70	20.27	10.60	1.912	
Polyvinylidene chloride	$C_2H_2Cl_2$	96.93	10.52	10.07	12.21	0.825	1.34
Polyvinylidene fluoride	$C_2H_2F_2$	64.02	14.77	14.08	11.26	1.250	1.38
Urea formaldehyde	$C_3H_6O_2N_2$	102.05	15.90	14.61	13.31	1.098	1.60–2.10
Urea formaldehyde-foam	–	–	14.80				

Table A.32 Heats of combustion of miscellaneous materials [7]

Material	Gross, $\Delta h_c{}^u$ (MJ/kg)	Net, $\Delta h_c{}^l$ (MJ/kg)
Acetate (see cellulose acetate)		
Acrylic fiber	30.6–30.8	
Blasting powder	2.1–2.4	
Butter	38.5	
Celluloid (cellulose nitrate and camphor)	17.5–20.6	16.4–19.2
Cellulose acetate fiber, $C_8H_{12}O_6$	17.8–18.4	16.4–17.0
Cellulose diacetate fiber, $C_{10}H_{14}O_7$	18.7	
Cellulose nitrate, $C_6H_9N_1O_7/C_6H_8N_2O_9/C_6H_7N_3O_{11}$	9.11–13.48	
Cellulose triacet ate fiber, $C_{12}H_{16}O_8$	18.8	17.6
Charcoal	33.7–34.7	33.2–34.2
Coal—anthracite	30.9–34.6	30.5–34.2
—bituminous	24.7–36.3	
Coke	28.0–31.0	23.6–35.2
Cork	26.1	28.0–31.0
Cotton	16.5–20.4	
Dynamite	5.4	
Epoxy, $C_{11.9}H_{20.4}O_{2.8}N_{0.3}/C_{6.064}H_{7.550}O_{1.222}$	32.8–33.5	31.1–31.4
Fat, animal	39.8	
Flint powder	3.0–3.1	
Fuel oil—No. 1	46.1	
—No. 6	42.5	
Gasketing—chlorosulfonated polyethylene (Hypalon)	28.5	
—vinylidene fluoride/hexafluoropropylene (Fluorel, Viton A)	14.0–15.1	
Gasoline	46.8	43.7
Jet fuel—JP1		43.0
—JP3		43.5
—JP4	46.6	43.5
—JP5	45.9	43.0
Kerosene (jet fuel A)	46.4	43.3
Lanolin (wool fat)	40.8	
Lard	40.1	
Leather	18.2–19.8	
Lignin, $C_{2.6}H_3O$	24.7–26.4	23.4–25.1
Lignite	22.4–33.3	
Modacrylic fiber	24.7	
Naphtha	43.0–47.1	40.9–43.9
Neoprene, C_5H_5Cl—gum	24.3	
—foam	9.7–26.8	
Nomex™ (polymethaphenylene isophthalamide) fiber, $C_{14}H_{10}O_2N_2$	27.0–28.7	
Oil—castor	37.1	
—linseed	39.2–39.4	
—mineral	45.8–46.0	
—olive	39.6	
—solar	41.8	
Paper—brown	16.3–17.9	
—magazine	12.7	
—newsprint	19.7	
—wax	21.5	

(continued)

Table A.32 (continued)

Material	Gross, $\Delta h_c{}^u$ (MJ/kg)	Net, $\Delta h_c{}^l$ (MJ/kg)
Paraffin wax	46.2	43.1
Peat	16.7–21.6	
Petroleum jelly ($C_{7.118}H_{12.957}O_{0.091}$)	45.9	
Rayon fiber	13.6–19.5	
Rubber—buna N	34.7–35.6	
—butyl	45.8	
—isoprene (natural) C_5H_8	44.9	42.3
—latex foam	33.9–40.6	
—GRS	44.2	
—tire, auto	32.6	
Silicone rubber (SiC_2H_6O)	15.5–16.8	
—foam	14.0–19.5	
Sisal	15.9	
Spandex fiber	31.4	
Starch	17.6	16.2
Straw	15.6	
Sulfur—rhombic		9.28
—monoclinic		9.29
Tobacco	15.8	
Wheat	15.0	
Wood—beech	20.0	18.7
—birch	20.0	18.7
—douglas fir	21.0	19.6
—maple	19.1	17.8
—red oak	20.2	18.7
—spruce	21.8	20.4
—white pine	19.2	17.8
—hardboard	19.9	
Woodflour	19.8	
Wool	20.7–26.6	

Table A.33 Heats of combustion of selected metals and nonmetallic elements [8]

Element symbol	Element name	Oxide formed	Δh_c (MJ/kg)
Al	Aluminum	Al_2O_3	31.06
B	Boron	B_2O_3	58.83
Ba	Barium	BaO	4.03
Beq	Beryllium	BeO	67.48
Ca	Calcium	CaO	15.58
Cd	Cadmium	CdO	2.30
Ce	Cerium	CeO_2	7.77
Cr	Chromium	Cr_2O_3	10.78
Cu	Copper	CuO	2.48
Fe	Iron	FeO	4.87
Hf	Hafnium	HfO_2	6.42
Li	Lithium	Li_2O	43.08

(continued)

Table A.33 (continued)

Element symbol	Element name	Oxide formed	Δh_c (MJ/kg)
Mg	Magnesium	MgO	24.73
Na	Sodium	Na_2O	9.00
Sr	Strontium	SrO	6.76
Th	Thorium	ThO_2	5.29
Ti	Titanium	ThO_2	19.6
U	Uranium	UO_2	4.56
W	Tungsten	WO_3	4.59
Zn	Zinc	ZnO	5.37
Zr	Zirconium	ZrO_2	12.03

Table A.34 Autoignition temperatures for liquids [9]

Fuel	Autoignition temperature (°C)
Acetaldehyde	185.0
Acetone	537.8
Acetylene	305.0
Acrolein	233.9
Acrylonitrile (564)	481.1
Ammonia	651.1
Aniline	617.2
Benzene	562.2
Benzyl alcohol	436.1
1,2-butadiene	428.9
Butanone (methyl ethyl ketone)	515.6
1-butene	383.9
n-butene	405.0
d-camphor	466.1
Carbon disulfide	90.0
Carbon monoxide	608.9
Cyclobutane	426.7
Cyclohexane	260.0
Cyclohexene	265.0
Cyclopentane	361.1
Cyclopropane	497.8
n-decane	207.8
Diethyl ether	180.0
Ethane	515.0
Ethanol	422.8
Ethyl acetate	426.7
Ethylamine	383.9
Ethylene oxide	428.9
n-heptane	222.8
n-hexane	408.9
Hydrogen	400.0
iso-propanol	398.9

(continued)

Table A.34 (continued)

Fuel	Autoignition temperature (°C)
Methane	600.0
Methanol	463.9
Methyl formate	456.1
n-nonane	206.1
n-octane	220.0
n-pentane	260.0
1-pentene	217.2
Propane	450.0
n-propanol	371.1
Propene	455.0
Toluene	536.1
m-xylene	527.8
o-xylene	463.9
p-xylene	528.9

For more information, see Table A.29 and Chap. 18, "Ignition of Liquids"

Table A.35 Critical heat flux and thermal response parameter of materials [10–14]

	CHF (kW/m^2)		TRP ($kW \cdot s^{1/2}/m^2$)	
Material	ASTM E2058 FPA	ASTM E1354 Cone	ASTM E2058 FPA	ASTM E1354 Cone
Natural				
Flour	10	–	218	–
Sugar	10	–	255	–
Tissue paper	10	–	95	–
Newspaper	10	–	108	–
Wood (red oak)	10	–	134	–
Wood (douglas fir)	10	–	138	–
Wood (douglas fir)/fire retarded (FR)	10	–	251	–
Wood (hemlock)	–	–	–	175
Corrugated paper (light)	10	–	152	–
Corrugated paper (heavy)	–	–	–	–
No coating	10	–	189	–
Coating (10 % by weight)	15	–	435	–
Coating (15 % by weight)	15	–	526	–
Coating (20 % by weight)	15	–	714	–
Wool 100 %	–	–	–	252
Synthetic (ordinary polymers)				
Acrylic fiber 100 %	–	–	–	180
Acrylic (modified)/FR	–	–	–	526
Acrylonitrile-butadiene- styrene (ABS)	–	9–15	–	317–365
ABS-FR	–	13	–	330
Butyl rubber (BR, polyisobutylene)	–	19	–	211
Epoxy (EP)	13	20	162	–
Isophthalic polyester	–	–	–	296

(continued)

Table A.35 (continued)

Material	CHF (kW/m^2)		TRP (kW·s$^{1/2}$/m^2)	
	ASTM E2058 FPA	ASTM E1354 Cone	ASTM E2058 FPA	ASTM E1354 Cone
Nitrile-butadiene (buna-N, NBR)	–	26	–	308
Polyamide (PA, nylon) 6	15	15–20	154–270	379–461
PA66	–	15–21	–	352
PA 11	–	15–21	–	352
PPO-PS	–	–	–	455
Polyethylenephthalate (PEN)	–	24	–	545
Polyethyleneterephthalate (PET)	10	–	174	–
Polyethylene (PE) high density (HD)	15	15	321–454	343
PE (cross-linked)	15	–	224–301	442
PE (cross-linked)/nonhalogenated FR	15	–	652–700	581
Polyisoprene (natural rubber, NR)	10	17	174	294
Polymethylmethacrylate (PMMA)	10	6–23	274	274
Polymethylpentene (PMP)	–	–	–	–
Polyoxymethylene (POM)	13	–	250–269	–
Polypropylene (PP)	10–15	15	277–333	193–336
PP/FR panel	15	–	315	–
Polyphenyleneether (PPE)	–	–	–	323
Polystyrene (PS)	13	–	162	–
PS-FR	–	–	221–667	–
Polyvinyl ester	–	–	–	263
Polyvinyl ester panels	13–15	–	440–700	–
Styrene-butadiene rubber (SBR)	–	10–15	–	198
Unsaturated polyester (UPT)	–	–	343	–
Vinyl ester (VE)	–	–	–	285
Vinyl thermoplastic elastomer	–	–	294	–
Foams (wall, ceiling insulation materials, etc.)				
Polyurethanes	13–40	–	55–221	–
Polystyrenes	10–15	–	111–317	–
Latex	16	–	113–172	–
Phenolic	20	–	610	–
Synthetic high-temperature engineered polymers				
Melamine formaldehyde (MF)	–	25	–	324
Phenol formaldehyde (PF)	–	15–26	–	537
Polyamideimide (PAI, Torlon®)	–	40–50	–	378
Polybenzimidazole (PBI)	–	~60	–	–
Polybenzoylphenylene (PX)	–	–	–	626
Polycarbonate (PC)	15	15–20	357–455	455
PC panel	16	–	420	–
PC/ABS (70/30)	–	–	–	344
PC/ABS-FR	–	–	–	391
Polydimethylphenyleneoxide (PPO)	–	19	–	342
Polyethylenephthalate (PEN)	–	–	545	–
Polyethersulfone (PESU, Radel-A®)	–	19–30	–	360
Polyether ether ketone (PEEK)	30	30–40	550	623
Polyetherimide (PEI)	25	25–40	435	435

(continued)

Table A.35 (continued)

Material	CHF (kW/m^2)		TRP (kW·s$^{1/2}$/m^2)	
	ASTM E2058 FPA	ASTM E1354 Cone	ASTM E2058 FPA	ASTM E1354 Cone
Polyphenyleneether (PPE)	–	–	–	323
Polyphenylenesulfide (PPS)	–	35–38	–	395
Polyphenylsulfone				
(Radel-R® PPSU)	–	32–35	512	512
Polyphenyleneether (PPE)	–	–	–	323
Polysulfone (PSU)	30	26	469	424
Polydimethylsiloxane (SIR)	–	34	–	429
Halogenated				
Polychloroprene				
(neoprene, CR)	–	20–37	–	245
Polytetrafluoroethylene-perfluoroether (PFA)	–	–	–	787
Polytetrafluoroethylene (PTFE)	50	–	680	–
Polytrifluoroethylene (P3FE)	–	–	–	504
Polyvinylidenefluoride (PVDF)	–	–	609	–
Polyvinylfluoride (PVF)	–	–	–	303
Polychlorotrifluoroethylene (CTFE)	–	30	–	460
Polyethylene-tetrafluoroethyl-ene (ETFE, Tefzel®)	25	17–27	481	478
Polyethylenechlorotrifluoro-ethylene (ECTFE)	38	38–74	450	410
Fluorinated ethylene propylene (FEP, Teflon®)	38–50	–	680	–
FEP fabric	50	–	299	–
FEP coated on metal	20	–	488	–
Polytrifluoroethylene (P3FE)	–	–	–	504
Polyvinylchloride (PVC, flexible)	10	21	215–263	194
PVC flexible (LOI = 0.20)	–	–	–	285
PVC flexible (LOI = 0.25)	–	–	–	401
PVC flexible, FR (alkyl aryl phosphate, LOI = 0.28)	–	–	–	401
PVC flexible, FR (Sb2O3, LOI = 0.30)	–	–	–	397
PVC flexible, FR (tertiary phosphate, LOI = 0.34)	–	–	–	345
PVC flexible, FR	–	–	–	222–263
PVC, rigid	15	15–28	357	357–418
PVC, rigid (LOI = 0.50)	–	–	–	388
PVC sheets	15	–	446–590	–
PVC panel	17	–	321	–
PVC fabric	26	–	217	–
Chlorinated PVC (CPVC)	40	40	435	590–1,111
Polyvinylfluoride (PVF)	–	–	–	303
Composite and fiber reinforced (glass—Gl and graphite—Gr)				
Acrylic/Gl	–	–	–	180
Bismaleimide (BMI)/Gr	–	–	–	513–608
Cyanate ester/Gl	–	–	–	302
Epoxy (EP)/Gl (thin sheet)	10	–	156	198
EP/Gl	10–15	–	388–540	288–665
EP/Gr	15	–	395–481	395–554
EP/Gr/intumescent coating (IC)	–	–	962	–
EP/Gr/ceramic coating (CC)	–	–	2,273	–

(continued)

Table A.35 (continued)

Material	CHF (kW/m^2)		TRP (kW·s$^{1/2}$/m^2)	
	ASTM E2058 FPA	ASTM E1354 Cone	ASTM E2058 FPA	ASTM E1354 Cone
EP/Gr/CC/IC	–	–	1,786	–
EP/Kevlar (thin sheet)	–	–	–	120
Graphite composite	40	–	400	–
Isophthalic polyester/Gl (77 %)	–	–	–	426
Polyarylsulfone/Gr	–	–	–	360
Polyamide (PA6)/Gl (10 %)	–	–	–	303
PA6/Gl (20 %)	–	–	–	315
PA6/Gl (30 %)	–	–	–	318
PA6/Gl (50 %)	–	–	–	359–371
Polybutyleneterephthalate (PBT)/Gl (10 %)	–	–	–	317
PBT/Gl (20 %)	–	–	–	308
PBT/Gl (30 %)	–	–	–	325
PBT/Gl (50 %)	–	–	–	381
Polycarbonate (PC)/Gl (10 %)	–	–	–	383
PC/Gl (20 %)	–	–	–	362
PC/Gl (30 %)	–	–	–	373
PC/Gl (50 %)	–	–	–	402
Polyether ether ketone (PEEK)/Gl (30 %)	–	–	–	301
PEEK/Gr	–	–	–	514
Polyester (PEST)/Gl	10–15	–	275–406	–
Polyether ketoneketone (PEKK)/Gl	–	–	–	710
Polyethersulfone (PESU)/Gl (30 %)	–	–	–	256
Polyethersulfone (PESU)/Gr	–	–	–	352
Polyimide/Gl	–	–	844	–
Phenol formaldehyde (PF)/Gl	20	–	–	610
Phenol/Gl (thin sheet)	33	–	105	172
Phenol/Gl (thick sheet)	20	–	610	–
Phenolic/Gl	–	–	–	382–998
Phenolic/Gl (45 %)	–	–	–	683
Phenolic/Gr	20	–	333	398–982
Phenolic/PE fibers	–	–	–	267
Phenolic/aramid fibers	–	–	–	287
Phenolic/Kevlar (thin sheet)	20	–	185	258
Phenolic/Kevlar (thick sheet)	15	–	403	–
Phenolic/Gr/ceramic coating	–	–	807	–
Phenolic/Gr/intumescent coating	–	–	1,563	–
Phenolic laminate/Gl (45 %)	–	–	–	683
Polypropylene (PP)/Gl panel	–	–	–	315–377
Polyvinylester/Gl	–	–	281	312–429
Polyvinylester/Gl (69 %)	–	–	–	444
Polyvinylester/Gl/ceramic coating (CC)	–	–	676	–
Polyvinylester/Gl/intumescent coating (IC)	–	–	1,471	–
Polyvinylester/Gl/IC/CC	–	–	1,923	–
Polyphenylenesulfide (PPS)/ Gl	–	–	–	588–623
PPS/Gr	–	–	–	330–510

(continued)

Table A.35 (continued)

Material	CHF (kW/m^2)		TRP (kW·s$^{1/2}$/m^2)	
	ASTM E2058 FPA	ASTM E1354 Cone	ASTM E2058 FPA	ASTM E1354 Cone
Materials with fiberweb, netlike, and multiplex structures				
Polypropylenes	8–15	–	108–417	–
Polyester-polypropylene	10	–	139	–
Wood pulp-polypropylene	8	–	90	–
Polyester	8–18	–	94–383	–
Rayon	14–17	–	161–227	–
Polyester-rayon	13–17	–	119–286	–
Wool-nylon	15	–	293	–
Nylon	13–16	–	149–217	–
Cellulose	15	–	264	–
Cellulose-polyester	13	–	159	–
Electrical cables—power				
PVC/PVC	13–25	–	156–341	–
PE/PVC	15	–	221–244	–
PVC/PE	15	–	263	–
Silicone (Si)/PVC	19	–	212	–
Si/cross-linked polyolefin (XLPO)	25–30	–	435–457	–
Ethylene-propylene rubber (EPR)/EPR	20–23	–	467–567	–
Cross-linked PE (XLPE)/XLPE	20–25	–	273–386	–
XLPE/ethyl-vinyl acetate (EVA)	12–22	–	442–503	–
XLPE/neoprene	15	–	291	–
XLPO/XLPO	16–25	–	461–535	–
XLPO/polyvinylidine fluoride (PVF)/XLPO	14–17	–	413–639	–
EPR/chlorosulfonated PE	14–19	–	283–416	–
EPR, FR	14–28	–	289–448	–
Electrical cables—communications				
PVC/PVC	15	–	131	–
PE/PVC	20	–	183	–
XLPE/XLPO	20	–	461–535	–
Si/XLPO	20	–	457	–
EPR-FR	19	–	295	–
Chlorinated PE	12	–	217	–
Polyethylene-tetrafluoroethylene (ETFE)/EVA	22	–	454	–
PVC/PVF	30	–	264	
Fluorinated ethylene propylene(FEP)/FEP	36	–	638–652	–
Conveyor belts				
Styrene-butadiene rubber (SBR)	10–15	–	336–429	–
Chloroprene rubber (CR)	20	–	760	–
CR/SBR	15	–	400	–
PVC	15–20	–	343–640	–

Table A.36 Thermal properties and thermal response parameter values of polymers [15]

Material	T_{ig} (°C)	ρ (10^{-3} kg/m^3)	c_P (kJ/kg · K)	k (10^3 kW/m · K)	TRP (kW·s$^{1/2}$/m^2) Measured	Calculated
Synthetic (ordinary polymers)						
Acrylonitrile-butadiene-styrene (ABS)	394	1.05	1.50	0.26	317–365	212
Polybutadiene (BDR)	378	0.97	1.96	0.22	–	205
Butyl rubber (BR, polyisobutylene)	330	0.92	1.96	0.13	211	133
Cellulose acetate (CA)	348	1.25	1.67	0.25	–	210
Cellulose acetate butyrate (CAB)	–	1.20	1.46	0.25	–	–
Cellulose acetate propionate (CAP)	–	1.21	1.46	0.25	–	–
Cyanate ester (typical) (CE)	468	1.23	1.11	0.19	–	202
Cellulose nitrate (CN)	–	1.38	1.46	0.23	–	–
Cellulose propionate (CP)	–	1.30	1.46	0.20	–	–
Diallylphthalate (DAP)	–	1.35	1.32	0.21	–	–
DAP/glass fibers	–	1.80	1.69	0.42	–	–
Ethylene-acrylic acid salt (EAA ionomer)	–	0.95	1.62	0.26	–	–
Epoxy (EP)	427	1.20	1.70	0.19	162	225
EP/Gl	–	1.80	1.60	0.42	–	–
Epoxy novolac (EPN)	–	1.21	1.26	0.19	–	–
Ethylene-propylene diene (EPDM)	–	0.93	2.00	0.20	–	–
Ethylene vinyl acetate (EVA)	–	0.93	1.37	0.34	–	–
Nitrile-butadiene (Buna-N, NBR)	–	1.35	1.33	0.25	308	–
Polyamide (PA, nylon) 6	432–497	1.13–1.20	1.55–2.19	0.24	154–461	236–336
PA6/glass fibers	390	1.38	1.34	0.22	–	–
PA 66	456	1.14	1.57	0.23	352	248
PA 11	–	1.12	1.74	0.28	352	–
PA 11/glass fibers	–	1.35	1.76	0.37	–	–
PA 12	–	1.04–1.01	1.69–1.79	0.18–0.25	–	–
PA 610	–	1.10	1.51	0.23	–	–
PA 612	–	1.08	1.59	0.22	–	–
Polyacrylonitrile (PAN)	460	1.15	1.30	0.26	–	243
Polyarylate (PAR)	–	1.21	1.20	0.18	–	–
Polyamideimide (PAI)	526	1.42	1.00	0.24	–	262
Polybutene (PB)	–	0.92	2.09	0.22	–	–
Polybutyleneterephthalate (PBT)	382	1.35	1.61	0.22	–	222
Polyimide (PI)	–	1.40	1.10	0.11	–	–
Polyethyleneterephthalate (PET)	407	1.35	1.15	0.20	174	191
PET/glass fibers	–	1.70	1.20	0.29	–	–
Polyethylene (PE) high density (HD)	380–443	0.94–0.96	2.00–2.15	0.42–0.43	321–454	283–353
PE low density	377	0.93	1.55	0.30–0.38	–	208–234
PE medium density	–	0.93	1.70	0.40	–	–
Polyethyleneoxide (PEO)	–	1.13	2.01	0.21	–	–
Polyisoprene (natural rubber, NR)	297	0.92	1.55	0.14	174–294	110
Polyethylmethacrylate (PEMA)	–	1.13	1.47	0.18	–	–
Polymethylmethacrylate (PMMA)	378–383	1.19	2.09	0.27	274	264
Polymethylpentene (PMP)	–	0.83	1.73	0.17	–	–
Polymethyl styrene (PMS)	–	1.02	1.28	0.20	–	–
Polyoxymethylene (POM)	374	1.42	1.92	0.27	250–269	269

(continued)

Table A.36 (continued)

Material	T_{ig} (°C)	ρ (10^{-3} kg/m^3)	c_P (kJ/kg · K)	k (10^3 kW/m · K)	TRP (kW·s$^{1/2}$/m^2) Measured	Calculated
Polypropylene (PP)	443	0.96	2.16	0.20	193–336	242
Polystyrene (PS)	356	1.05	1.25	0.14	162	128
PS/glass fibers	–	1.29	1.05	0.13	–	–
Polyisocyanurate (PU) rigid	378	1.27	1.67	0.21	–	–
Polyurethane rubber (PUR)	356	1.10	1.76	0.19	–	181
Polyurethane thermoplastic (TPU)	271	1.27	1.67	0.21	–	149
Polyvinyl acetate (PVAC)	–	1.19	1.33	0.16	–	–
Polyvinylalcohol (PVOH)	–	1.35	1.55	0.20	–	–
Styrene-butadiene rubber (SBR)	–	1.10	1.88	0.17	198	–
Styrene-acrylonitrile (SAN)	368	1.07	1.38	0.15	–	145
Unsaturated polyester (UPT)	380	1.23	1.30	0.17	343	166
UPT/glass fibers	–	1.65	1.05	0.42	–	–
Vinyl ester (VE)	–	1.11	1.30	0.25	285	–
Synthetic high-temperature engineered polymers						
Melamine formaldehyde (MF)	350	1.25	1.67	0.25	324	211
MF/glass fibers	–	1.75	1.67	0.44	–	–
Phenol formaldehyde (PF)	429	1.30	1.42	0.25	537	246
PF/glass fibers	580	1.85	1.26	0.40	610	479
Polyamideimide (PAI, Torlon®)	526	1.42	1.00	0.24	378	262
Polybenzimidazole (PBI)	–	1.30	0.93	0.41	–	–
Polybenzoylphenylene (PX)	–	1.22	1.30	0.32	626	–
Polycarbonate (PC)	500–580	1.20	1.20–1.22	0.20–0.21	357–455	228–296
PC/glass fibers	–	1.43	1.10	0.21	402	–
Polyethersulfone (PESU, Radel-A®)	502	1.40	1.12	0.18	360	227
Polyaryl ether ketone (PAEK)	–	1.30	1.02	0.30	–	–
Polyether ether ketone (PEEK)	570–580	1.31–1.32	1.70–1.80	0.20–0.25	550	325–383
Polyetherketoneketone (PEKK)	–	1.28	1.00	0.22	–	–
Polyetherimide (PEI)	528–540	1.27	1.22–1.40	0.22–0.23	435	262–295
Polyphthalamide (PPA)	–	1.17	1.40	0.15	–	–
Polyphenyleneether (PPE)	426	1.10	1.19	0.23	323	198
Polydimethyleneoxide (PPO)	418	1.11	1.25	0.16	342	166
PPO/glass fibers	–	1.32	1.31	0.17	–	–
Polyphenylenesulfide (PPS)	575	1.30	1.02	0.29	395	305
Polyphenylsulfone (Radel-R® PPSU)	575	1.32	1.01	0.18	512	241
Polyphenyleneether (PPE)	426	1.10	1.19	0.23	323	–
Polysulfone (PSU)	510–580	1.24	1.11–1.30	0.26–0.28	424–469	259–334
Polydimethylsiloxane (SI)	–	1.24	1.30	0.28	–	–
Silicone/glass fibers (Si/G)	–	1.90	1.17	0.30	–	–
Silicone rubber (SIR)	407	0.97	1.59	0.23	429	204
Urea formaldehyde (UF)	–	1.25	1.55	0.25	–	–
Halogenated polymers						
Polychloroprene (neoprene, CR)	406	1.42	1.12	0.19	245	188
Polytetrafluoroethylene-perfluoroether (PFA)	–	2.15	1.00	0.25	787	–
PFA/glass fibers	–	1.85	1.26	0.40	–	–
Polytetrafluoroethylene (PTFE)	630–700	2.15–2.18	1.00–1.05	0.25	680	396–456
Polytrifluoroethylene (P3FE)	–	1.83	1.08	0.31	504	–

(continued)

Table A.36 (continued)

Material	T_{ig} (°C)	ρ (10^{-3} kg/m^3)	c_P (kJ/kg · K)	k (10^3 kW/m · K)	TRP (kW·s$^{1/2}$/m^2) Measured	Calculated
Polyvinylidenefluoride (PVDF)	643	1.76	1.30	0.13	609	301
Polyvinylfluoride (PVF)	476	1.48	1.30	0.13	303	202
Polychlorotrifluoroethylene (CTFE)	580	1.67–2.11	0.90–0.92	0.22–0.23	460	285–332
Polyethylene-tetrafluoroethylene (ETFE, Tefzel®)	540	1.70	0.90–1.00	0.23–0.24	478–481	273–294
Polyethylenechlorotrifluoroethylene (ECTFE)	613	1.69	1.00–1.17	0.15–0.16	410–450	264–296
Fluorinated ethylene propylene (FEP, Teflon®)	630–700	2.15	1.17–1.20	0.25	680	428–484
Polyvinylchloride (PVC, flexible)	318–374	1.26–1.95	1.14–1.38	0.17–0.26	194–263	130–263
PVC, rigid 395		1.42	0.98	0.19	357–418	171
Chlorinated PVC (CPVC)	643	1.50	0.78	0.22	435	280
Polyvinylidenechloride (PVDC)	468	1.70	1.07	0.13	–	193

Table A.37 Thermal properties and thermal response parameter values for plastic parts of a minivan [10, 11]

Part	Material	T_{ig} (°C)	ρ (10^{-3} kg/m^3)	c_P (kJ/Kg · K)	k (10^3 kW/m · K)	TRP (kW·s$^{1/2}$/m^2) Experimental	Calculated
Head liner							
Backing top layer	Polyethyleneterephthalate (PET)	–	0.69	1.56	0.04	–	–
Fabric, exposed	Nylon 6	497	0.12	2.19	0.24	154	120
Instrument Panel							
Foam	Polyether urethane (PEU)	–	0.11	1.77	0.04	–	–
Cover	Polyvinylchloride (PVC)	357	1.20	1.37	0.14	263	162
Structure	Polycarbonate (PC)	–	1.12	1.68	0.18	–	–
Shelf, main panel	PC	497	1.18	1.51	0.27	357	331
Shelf, foam—small seals	PEU	–	0.09	1.56	0.06	–	–
Resonator							
Structure	Polypropylene (PP)	374	1.06	2.08	0.23	277	252
Intake tube	Ethylene-propylene-diene monomer (EPDM)	–	1.15	1.75	0.30	–	–
Effluent tube	EPDM	–	1.16	1.39	0.36	–	–
Kick panel insulation							
Foam	PEU	–	0.02	1.65	0.02	–	–
Backing	PVC	374	1.95	1.14	0.25	215	264
Air ducts							
Small ducts	Polyethylene (PE)	–	0.95	2.03	0.31	–	–
Large ducts	PP	443	1.04	1.93	0.31	333	334
Brake fluid reservoir, wire harness tube, and windshield wiper tray structure							
Reservoir	PP	–	0.90	2.25	0.19	–	–
Cap	PP	–	0.90	2.48	0.21	–	–
Tube	PE	–	0.95	2.12	0.37	–	–
Structure	Sheet molding compound (SMC)	497	1.64	1.14	0.37	483	397

(continued)

Table A.37 (continued)

Part	Material	T_{ig} (°C)	ρ (10^{-3} kg/m^3)	c_P (kJ/Kg · K)	k (10^3 kW/m · K)	TRP (kW·s$^{1/2}$/m^2)	
						Experimental	Calculated
Sound reduction fender insulation and fuel tank shield							
Low-density foam	Polystyrene (PS)	–	0.90	1.70	0.17	–	–
High-density foam	PS	497	0.13	1.62	0.10	146	69
Face	PET	374	0.66	1.32	0.09	174	97
Fuel tank shield	PP	443	0.93	2.20	0.20	288	271
HVAC unit door							
Seal	PP/EPDM	–	0.93	1.96	0.20	–	–
Structure	Nylon 66	–	1.50	1.69	0.58	–	–
Seal	Thermoplastic polyolefin (TPO)	–	0.97	1.87	0.13	–	–
HVAC unit							
Cover	PP	–	1.19	1.90	0.39	–	–
Seal, foam	Acrylonitrile-butadiene-styrene (ABS)-PVC	487	0.10	1.35	0.02	73	22
Top main housing	PP	–	NM	NM	–	310	–
Fan bottom cover	PP	–	1.21	1.76	0.39	–	–
Actuator casing	PP	–	1.11	1.95	0.34	–	–
Seals	ABS-PVC	–	0.07	2.02	0.15	–	–
Defogger tube	PP/EPDM	–	0.97	1.87	0.33	–	–
Fuel tank							
Tank	PE	443	0.94	2.15	0.30	454	329
Hoses	Nylon 12	–	1.04	1.79	0.18	–	–
Headlight							
Lens	PC	–	1.19	2.06	0.20	–	–
Backing	PC	497	1.20	2.18	0.22	434	362
Retainer	Polyoxymethylene (POM)	–	1.41	1.92	0.27	–	–
Leveling mechanism	PC	–	1.18	1.10	0.19	–	–
Battery casing							
Top	PE-PP	–	0.91	1.98	0.17	–	–
Sides and bottom	PE-PP	–	0.88	2.15	0.21	–	–
cover	PP	443	0.90	2.22	0.23	323	286
Hood to cowl weather stripping							
Foam	EPDM	–	0.44	2.30	0.07	–	–
Rubber base	EPDM	–	0.41	1.51	0.21	–	–
Insides	PVC-glass	–	1.00	1.05	0.23	–	–
Bulkhead insulation (engine side)							
Support structure	PVC-hydrocarbon elastomer (HE)	–	1.60	1.24	0.10	–	–
Grommet, wire harness cap	High-density polyethylene (HDPE)	–	1.21	1.48	0.45	–	–

NM not measured

Table A.38 Net Heats of Complete Combustion per Unit Mass of Fuel and Oxygen Consumed and Carbon Dioxide and Carbon Monoxide Generated[15,a]

Fuel[d]	Formula[b]	ΔH_T (kJ/g)	$\Delta H_O{}^*$ (kJ/g)	ΔH_{CO_2} ΔH_{CO_2} (kJ/g)	$\Delta H_{CO}{}^*$ (kJ/g)
Normal alkanes					
Methane	CH_4	50.1	12.5	-18.2	-18.6
Ethane	C_2H_6	47.1	12.7	16.2	15.4
Propane	C_3H_8	46	12.9	15.3	14
Butane	C_4H_{10}	45.4	12.7	15.1	13.7
Pentane	C_5H_{12}	45	12.6	14.7	13.2
Hexane	C_6H_{14}	44.8	12.7	14.6	12.9
Heptane	C_7H_{16}	44.6	12.7	14.5	12.8
Octane	C_8H_{18}	44.5	12.6	14.4	12.7
Nonane	C_9H_{20}	44.3	12.7	14.3	12.5
Decane	$C_{10}H_{22}$	44.4	12.7	14.3	12.4
Undecane	$C_{11}H_{24}$	44.3	12.7	14.3	12.4
Dodecane	$C_{12}H_{26}$	44.2	12.7	14.2	12.3
Tridecane	$C_{13}H_{28}$	44.2	12.7	14.2	12.3
Kerosene	$C_{14}H_{30}$	44.1	12.7	14.1	12.2
Hexadecane	$C_{16}H_{34}$	44.1	12.7	14.2	12.3
		Average	**12.7**	**14.6**	**12.9**
Substituted alkanes					
Methylbutane	C_5H_{12}	45	12.6	14.7	13.1
Dimethylbutane	C_6H_{14}	44.8	12.7	14.6	13
Methylpentane	C_6H_{14}	44.8	12.7	14.6	12.9
Dimethylpentane	C_7H_{16}	44.6	12.7	14.5	12.9
Methylhexane	C_7H_{16}	44.6	12.6	14.4	12.7
Isooctane	C_8H_{18}	44.5	12.6	14.4	12.7
Methylethylpentane	C_8H_{18}	44.5	12.6	14.4	12.7
Ethylhexane	C_8H_{18}	44.5	12.6	14.4	12.7
Dimethylhexane	C_8H_{18}	44.5	12.7	14.5	12.8
Methylheptane	C_8H_{18}	44.5	12.6	14.4	12.7
		Average	**12.6**	**14.6**	**12.8**
Cyclic alkanes					
Cyclopentane	C_5H_{10}	44.3	12.8	13.9	11.9
Methylcyclopentane	C_6H_{12}	43.8	12.7	13.9	11.9
Cyclohexane	C_6H_{12}	43.8	12.7	13.8	11.7
Methylcyclohexane	C_7H_{14}	43.4	12.7	13.8	11.7
Ethylcyclohexane	C_8H_{16}	43.2	12.7	13.8	11.7
Dimethylcyclohexane	C_8H_{16}	43.2	12.7	13.8	11.7
Cyclooctane	C_8H_{16}	43.2	12.7	13.9	11.9
Decalin	$C_{10}H_{18}$	42.8	12.7	13.4	11
Bicyclohexyl	$C_{12}H_{22}$	42.6	12.6	13.3	11
		Average	**12.7**	**13.8**	**11.6**
Normal alkenes					
Ethylene	C_2H_4	48	13.8	15	13.6
Propylene	C_3H_6	46.4	13.4	14.6	12.9
Butylene	C_4H_8	45.6	14.3	14.3	12.5

(continued)

Table A.38 (continued)

Fuel[d]	Formula[b]	ΔH_T (kJ/g)	$\Delta H_O{}^*$(kJ/g)	ΔH_{CO_2} ΔH_{CO_2} (kJ/g)	$\Delta H_{CO}{}^*$(kJ/g)
Pentene	C_5H_{10}	45.2	14.3	14.3	12.5
Hexene	C_6H_{12}	44.9	12.9	14.1	12.2
Heptene	C_7H_{14}	44.6	12.9	14.1	12.2
Octene	C_8H_{16}	44.5	12.9	14.1	12.1
Nonene	C_9H_{18}	44.3	12.9	14.1	12.1
Decene	$C_{10}H_{20}$	44.2	12.9	14.1	12.2
Dodecene	$C_{12}H_{24}$	44.1	12.9	14.1	12.2
Tridecene	$C_{13}H_{26}$	44	12.9	14.1	12.2
Tetradecene	$C^{14}H^{28}$	44	12.9	14.1	12.2
Hexadecene	$C^{16}H^{32}$	43.9	12.9	14.1	12.1
Octadecene	$C^{18}H^{36}$	43.8	12.9	14.1	12.1
		Average	**13.2**	**14.2**	**12.4**
Cyclic alkenes					
Cyclohexene	C_6H_{10}	43	13	13.4	11
Methylcyclohexene	$C7H_{12}$	43.1	12.9	13.4	11.1
		Average	**13**	**13.4**	**11.1**
Dienes					
1,3-Butadiene	C_4H_6	44.6	13.7	13.7	11.5
Cyclooctadiene	C_8H_{12}	43.2	13.3	13.3	10.9
		Average	**13.5**	**13.5**	**11.2**
Normal alkynes					
Acetylene	C_2H_2	47.8	-15.6	14.3	12.4
Heptyne	C_7H_{12}	44.8	13.4	13.9	11.8
Octyne	C_8H_{14}	44.7	13.3	14	11.9
Decyne	$C_{10}H_{18}$	44.5	13.2	13.9	11.9
Dodecyne	$C_{12}H_{22}$	44.3	13.2	14	12
		Average	**13.3**	**14**	**12.0**
Arenes					
Benzene	C_6H_6	40.1	13	11.9	8.7
Toluene	C_7H_8	39.7	12.9	12.1	9
Styrene	C_8H_8	39.4	13.1	12	8.8
Ethylbenzene	C_8H_{10}	39.4	12.9	12.3	9.4
Xylene	C_8H_{10}	39.4	13	12.4	9.5
Propylbenzene	C_9H_{12}	39.4	12.9	12.5	9.6
Trimethylbenzene	C_9H_{12}	39.2	12.9	12.5	9.7
Cumene	C_9H_{12}	39.2	12.9	12.9	9.6
Naphthalene	$C_{10}H_8$	39	12.9	11.3	7.7
Tetralin	$C_{10}H_{12}$	39	12.9	12.2	9.2
Butylbenzene	$C_{10}H_{14}$	39	12.9	12.7	9.9
Diethylbenzene	$C_{10}H_{14}$	39	13.7	13.5	11.1
p-Cymene	$C_{10}H_{14}$	39	13	12.5	9.6
Methylnaphthalene	$C_{11}H_{10}$	38.9	12.9	11.5	8.1
Pentylbenzene	$C_{11}H_{16}$	38.8	13	12.8	10.2
Triethylbenzene	$C_{12}H_{18}$	38.7	12.7	12.7	10
		Average	**13**	**12.4**	**9.4**

(continued)

Table A.38 (continued)

Fuel[d]	Formula[b]	ΔH_T (kJ/g)	$\Delta H_O{}^*$(kJ/g)	ΔH_{CO_2} ΔH_{CO_2} (kJ/g)	$\Delta H_{CO}{}^*$(kJ/g)
Alcohols					
Methyl alcohol	CH_4O	20	13.4	14.5	12.9
Ethyl alcohol	C_2H_6O	27.7	13.2	14.5	12.7
n-Propyl alcohol	C_3H_8O	31.8	13.3	14.5	12.7
Isopropyl alcohol	C_3H_8O	31.8	13.3	14.5	12.7
Allyl alcohol	C_3H_6O	31.4	14.2	13.8	11.7
n-Butyl alcohol	$C_4H_{10}O$	34.4	13.3	14.5	12.8
Isobutyl alcohol	$C_4H_{10}O$	34.4	13.3	14.5	12.8
Sec-butyl alcohol	$C_4H_{10}O$	34.4	13.3	14.5	12.8
Ter-butyl alcohol	$C_4H_{10}O$	34.4	13.3	14.5	12.8
n-Amyl alcohol	$C_5H_{12}O$	36.2	13.3	14.5	12.8
Isobutyl carbinol	$C_5H_{12}O$	36.2	13.3	14.5	12.8
Sec-butyl carbinol	$C_5H_{12}O$	36.2	13.3	14.5	12.8
Methylpropylcarbinol	$C_5H_{12}O$	36.2	13.3	14.5	12.8
Dimethylethylcarbinol	$C_5H_{12}O$	36.2	13.3	14.5	12.8
n-Hexyl alcohol	$C_6H_{14}O$	37.4	13.3	14.5	12.7
Dimethylbutylalcohol	$C_6H_{14}O$	37.4	13.3	14.5	12.7
Ethylbutyl alcohol	$C_6H_{14}O$	37.4	13.3	14.5	12.7
Cyclohexanol	$C_6H_{12}O$	37.3	13.7	14.1	12.2
Benzyl alcohol	C_7H_8O	32.4	13	11.4	8
n-Heptyl alcohol	$C_7H_{16}O$	39.8	13.7	15	13.6
n-Octyl alcohol	$C_8H_{18}O$	40.6	13.7	15	13.6
n-Nonyl alcohol	$C_9H_{20}O$	40.3	13.4	14.7	13
		Average	**13.3**	**14.5**	**12.8**
Aldehydes					
Formaldehyde	CH_2O	18.7	-17.5	12.7	10.1
Acetaldehyde	C_2H_4O	25.1	13.8	12.6	9.7
Butyraldehyde	C_4H_8O	33.8	13.9	13.9	11.7
Crotonaldehyde	C_4H_6O	34.8	15.2	13.8	11.8
Benzaldehyde	C_7H_6O	32.4	13.4	11.2	7.5
Ethyl hexaldehyde	$C_8H_{16}O$	39.4	13.7	12.7	9.9
		Average	**14.2**	**13.3**	**10.6**
Ketones					
Acetone	C_3H_6O	29.7	13.4	13.1	10.5
Methylethyl ketone	C_4H_8O	32.7	13.4	13.4	11
Diethyl ketone	$C_5H_{10}O$	33.7	12.9	13.2	10.7
Cyclohexanone	$C_6H_{10}O$	35.9	13.8	13.3	11
Methyl butyl ketone	$C_6H_{12}O$	35.2	12.9	13.3	11
Di-acetone alcohol	$C_6H_{12}O_2$	37.3	-16.9	-16.4	-15.7
Dipropyl ketone	$C_7H_{14}O$	38.6	13.8	14.3	12.5
Phenylbutyl ketone	$C_{11}H_{14}O$	34.8	12.6	11.6	-8.4
		Average	**13.2**	**13.2**	**11.1**
Acids					
Formic acid	CH_2O_2	5.7	16.4	5.96	0
Acetic acid	$C_2H_4O_2$	14.6	13.7	9.95	5.65
Benzoic acid	$C_7H_6O_2$	24.4	12.4	9.66	5.18
Cresylic acid	$C_8H_80_2$	34	-16	13.1	10.6

(continued)

Table A.38 (continued)

Fuel[d]	Formula[b]	ΔH_T (kJ/g)	$\Delta H_O{}^*$(kJ/g)	ΔH_{CO_2} ΔH_{CO_2} (kJ/g)	$\Delta H_{CO}{}^*$(kJ/g)
Esters					
Ethyl formate	$C_2H_6O_2$	20.2	13.3	11.3	7.8
n-Propyl formate	$C_4H_8O_2$	23.9	13.2	12	8.8
n-Butyl formate	$C_5H_{10}O_2$	26.6	13	12.3	9.4
Methyl acetate	$C_3H_6O_2$	20.2	13.3	11.3	7.8
Ethyl acetate	$C_4H_8O_2$	23.9	13.2	12	8.8
n-Propyl acetate	$C_5H_{10}O_2$	26.6	13	12.3	9.4
n-Butyl acetate	$C_6H_{12}O_2$	28.7	13	12.6	9.8
Isobutyl acetate	$C_6H_{12}O_2$	28.7	13	12.6	9.8
Amyl acetate	$C_7H_{14}O_2$	30.3	13	12.8	10.1
Cyclohexyl acetate	$C_8H_{14}O_2$	31.5	13.3	12.7	10
Octyl acetate	$C_{10}H_{20}O_2$	33.6	12.9	13.1	10.6
Ethylacetoacetate	$C_6H_{10}O_3$	30.3	(17.6)	(14.9)	(13.5)
Methyl propionate	$C_4H_8O_2$	23.9	13.2	12	7.4
Ethyl propionate	$C_5H_{10}O_2$	26.6	13	12.3	9.4
n-Butyl propionate	$C_7H_{14}O_2$	30.3	13	12.8	10.1
Isobutyl propionate	$C_7H_{14}O_2$	30.3	13	12.8	10.1
Amyl propionate	$C_8H_{18}O_2$	31.6	12.9	12.9	10.3
Methyl butyrate	$C_5H_{10}O_2$	26.6	13	12.3	9.4
Ethyl butyrate	$C_6H_{12}O_2$	28.7	13	12.6	9.8
Propyl butyrate	$C_7H_{14}O_2$	30.3	13	12.8	10.1
n-Butyl butyrate	$C_8H_{16}O_2$	31.6	12.9	12.9	10.3
Isobutyl butyrate	$C_8H_{16}O_2$	31.6	12.9	12.9	10.3
Ethyl laurate	$C_{14}H_{28}O_2$	37.2	13.3	13.8	11.6
Ethyl lactate	$C_5H_{10}O_3$	30.8	(18.9)	(16.5)	(16)
Butyl lactate	$C_7H_{14}O_3$	33.3	(16.8)	(15.8)	(14.8)
Amyl lactate	$C_8H_{16}O_3$	34.3	(16.4)	(15.6)	(14.5)
Ethyl benzoate	$C_9H_{10}O_2$	34.5	(15.4)	13.1	10.5
Ethyl carbonate	$C_5H_{10}O_3$	30.8	(18.9)	(16.5)	(16)
Ethyl oxalate	$C_6H_{10}O_4$	28.7	(20.2)	(16.6)	(20.2)
Ethyl malonate	$C_5H_8O_4$	32.2	(17.9)	(19.3)	(20.4)
		Average	**13**	**12.5**	**9.7**
Others					
Camphor	$C_{10}H_{16}O$	38.8	13.7	13.4	11.1
Cresol	C_7H_8O	34.6	13.7	12.1	9.1
Resorcinol	$C_6H_6O_2$	26	13.7	10.8	5.9
Acrolein	C_3H_4O	29.1	14.6	12.3	9.4
C-H-N fuels					
Acrylonitrile	C_3H_3N	24.5	8.5	9.8	5.4
Diethylamine	$C_4H_{11}N$	38	11.2	15.8	14.8
n-Butylamine	$C_4H_{11}N$	38	11.2	15.8	14.8
sec-Butylamine	$C_4H_{11}N$	38	11.2	15.8	14.8
Pyridine	C_5H_9N	32.2	11	11.6	8.2
Aniline	C_6H_7N	33.8	11.2	11.9	8.7
Picoline	C_6H_7N	33.8	11.2	11.9	8.7
Triethylamine	$C_6H_{15}N$	39.6	11.6	15.2	13.8
Toluidine	C_7H_9N	34.9	11.3	12.1	9.1
Dimethylaniline	$C_8H_{11}N$	35.7	11.5	12.3	9.3

(continued)

Table A.38 (continued)

Fuel[d]	Formula[b]	ΔH_T (kJ/g)	$\Delta H_O{}^*$(kJ/g)	ΔH_{CO_2} ΔH_{CO_2} (kJ/g)	$\Delta H_{CO}{}^*$(kJ/g)
Di-*n*-butylamine	$C_8H_{19}N$	40.6	11.9	14.9	13.4
Quinoline	C_9H_7N	36.1	12.4	11.8	8.5
Quinaldine	$C_{10}H_9N$	36.7	12.4	11.9	8.7
Butylaniline	$C_{10}H_{15}N$	37	11.7	12.5	9.7
Tri-n-butylamine	$C_{12}H_{27}N$	41.6	12.1	14.6	12.9
		Average	**11.5**	**15.4**	**14.1**
C-H-S fuels					
Carbon disulfide	CS_2	13.6	10.8	-23.5	-27
Thiophene	C_4H_4S	31.9	14	15.2	14
Methylthiophene	C_5H_6S	33.2	13.6	14.8	13.2
Thiophenol	C_6H_6S	34.1	13.8	14.2	12.3
Hexyl mercaptan	$C_6H_{14}S$	33	11.6	14.8	13.2
Thiocresol	C_7H_8S	34.9	13.5	14.1	12.1
Heptyl mercaptan	$C_7H_{16}S$	33.7	11.6	14.4	12.7
Cresolmethylsulfide	$C_8H_{11}S$	36.2	13.4	15.9	15
Decylmercaptan	$C_{10}H_{22}S$	34.9	11.5	13.8	11.7
Dodecyl mercaptan	$C_{12}H_{26}S$	35.5	11.5	13.6	11.4
Hexyl sulfide	$C_{12}H_{26}S$	35.5	11.5	13.6	11.4
Heptyl sulfide	$C_{14}H_{30}S$	35.9	11.5	13.4	11.1
Octyl sulfide	$C_{16}H_{34}S$	36.3	11.5	13.3	10.9
Decyl sulfide	$C_{20}H_{42}S$	36.8	11.4	13.1	10.7
		Average	**11.3**	**13.1**	**11.5**
Carbon-hydrogen atoms in the structure					
Polyethylene	CH_2	43.6	12.8	13.9	11.8
Polypropylene	CH	43.4	12.7	13.8	11.7
Polyisobutylene	CH_2	43.7	12.7	13.9	11.9
Polybutadiene	$CH_{1.5}$	42.8	13.1	13.1	10.7
Polystyrene	CH	39.2	12.7	12.2	9.2
Expanded polystyrene					
GM47	$CH_{1.1}$	38.1	12.4	11.3	7.7
GM49	$CH_{1.1}$	38.1	12.4	11.3	7.7
GM51	CH	35.6	11.6	10.8	7
GM53	$CH_{1.1}$	37.6	12.4	11.3	7.7
		Average	**12.5**	**12.4**	**9.5**
Carbon-hydrogen-oxygen-nitrogen atoms in the structure					
Polyoxy-methylene	CH_2O	15.4[c]	14.4	10.5	6.6
Polymethyl-methacrylate	$CH_{1.6}O_{0.4}$	25.2[c]	13.1	11.5	8
Polyester	$CH_{1.4}O_{0.22}$	32.5[c]	13.9	12.5	9.6
Epoxy	$CH_{1.3}O_{0.20}$	28.8[c]	12.1	10.8	6.9
Polycarbonate	$CH_{0.88}O_{0.19}$	29.7[c]	13.1	10.7	6.9
Cellulose triacetate	$CH_{1.3}O_{0.67}$	17.6[c]	13.3	9.6	5.1
Polyethylene-terephthalate	$CH_{0.80}O_{0.40}$	22[c]	13.2	9.6	5.1
Rigid phenolic foam	$CH_{1.1}O_{0.24}$	36.4[c]	(16.8)	(14)	(12)
Polyacrylonitrile (PAN)	$CHN_{0.33}$	30.8[c]	10.7	12.3	9.4
Red oak	$CH_{1.7}O_{0.72}N_{0.001}$	17.1[c]	13.2	10.2	6
Douglas fir	$CH_{1.7}O_{0.74}N_{0.002}$	16.4[c]	12.4	9.5	5
Nylon	$CH_{1.8}O_{0.17}N_{0.17}$	30.8[c]	11.9	13.3	10.8

(continued)

Table A.38 (continued)

Fuel[d]	Formula[b]	ΔH_T (kJ/g)	$\Delta H_O{}^*$(kJ/g)	ΔH_{CO_2} ΔH_{CO_2} (kJ/g)	$\Delta H_{CO}{}^*$(kJ/g)
Flexible polyurethane foams					
GM21	$CH_{1.8}O_{0.30}N_{0.05}$	26.2[c]	12.1	11.5	8
GM23	$CH_{1.8}O_{0.35}N_{0.06}$	27.2[c]	13.7	12.5	9.7
GM25	$CH_{1.7}O_{0.32}N_{0.07}$	24.6[c]	12	11.1	7.5
GM27	$CH_{1.7}O_{0.03}N_{0.08}$	23.2[c]	11.2	10.4	6.2
Rigid polyurethane foams					
GM29	$CH_{1.1}0_{0.23}N_{0.10}$	26[c]	12.6	10.7	6.8
GM31	$CH_{1.2}0_{0.22}N_{0.10}$	25[c]	11.9	10.2	6.1
GM37	$CH_{1.2}0_{0.20}N_{0.08}$	28[c]	12.7	11.2	7.5
Rigid polyisocyanurate foams					
GM41	$CH_{1.0}O_{0.19}N_{0.11}$	26.2[c]	12.5	10.4	6.4
GM43	$CH_{0.93}O_{0.20}N_{0.11}$	22.2[c]	10.8	8.9	-4
		Average	**12.5**		**7.2**
Carbon-hydrogen-chlorine atoms in the structure					
Polyethylene with					
25% chlorine	$CH_{1.9}CI_{0.13}$	31.6[c]	12.7	13.4	10.8
36% chlorine	$CH_{1.8}CI_{0.22}$	26.3[c]	12.8	12.9	10.2
48% chlorine	$CH_{1.7}CI_{0.36}$	20.6[c]	12.8	12.3	9.4
Polychloroprene	$CH_{1.3}CI_{0.30}$	25.3[c]	13.3	12.7	9.5
Polyvinylchloride	$CH_{1.5}CI_{0.50}$	16.4[c]	11.7	11.7	8.2
Polyvinyl-idenechloride	CHCI	9[c]	13.5	9.8	-5.5
		Average	**12.8**	12.1	**9.6**
Carbon-hydrogen-fluorine atoms in the structured					
Teflon TFE	CF_2	6.2[c]	9.7	(7.1)	(1.1)
Teflon FEP	$CF_{1.8}$	4.8[c]	(6.9)	(5)	(0)
Tefzel ETFE	CHF	12.6[c]	12.6	9.2	-4.4
Teflon PFA	$CF_{1.7}O_{0.01}$	5[c]	(8)	(5.3)	(0)
Kel-F (CTFE)	$CF_{1.5}CI_{0.50}$	6.5[c]	11.8	8.6	(3.5)
Halar (E-CTFE)	$CHF_{0.75}CI_{0.25}$	12[c]	9.8	9.8	(5.4)
Kynar (PVF_2)	CHF	13.3[c]	12.4	9.1	(4.2)
Tedlar (PVF)	$CH_{1.5}F_{0.50}$	13.5[c]	(6.5)	(7.1)	(1.1)
Carbon-hydrogen-oxygen-silicone atoms in the structure					
Silicone-1	$CH_{1.3}O_{0.25}Si_{0.18}$	21.7[c]	12.6	11	7.4
Silicone-2	$CH_{1.5}O_{0.30}Si_{0.26}$	21.3[c]	13.9	12.4	9.4
Silicone-3	$CH_3O_{0.50}Si_{0.50}$	25.1[c]	14.5	21	23

Note: Numbers in parentheses not used for averaging

[a]From the data measured in the FM Global Research Flammability Laboratory

[b]From the data for the elemental composition of the polymeric materials measured in the FM Global Research Flammability Laboratory

[c]From the data measured by the FM Global Research Flammability Laboratory in the oxygen bomb calorimeter and corrected for water as a gas and for the residue

[d]Trade names from Harper CA (ed) (1975) Handbook of Plastics and Elastomers. McGraw-Hill Book Company, New York

Table A.39 Yields of fire products and chemical, convective, and radiative heats of combustion for well-ventilated fires[a] [15]

Material	ΔH_T (kJ/g)	y_{CO_2} (g/g)	y_{CO} (g/g)	y_{ch} (g/g)	y_S (g/g)	ΔH_{ch} (kJ/g)	ΔH_{con} (kJ/g)	ΔH_{rad} (kJ/g)
Common gases								
Methane	50.1	2.72	–	–	–	49.6	42.6	7.0
Ethane	47.1	2.85	0.001	0.001	0.013	45.7	34.1	11.6
Propane	46.0	2.85	0.005	0.001	0.024	43.7	31.2	12.5
Butane	45.4	2.85	0.007	0.003	0.029	42.6	29.6	13.0
Ethylene	48.0	2.72	0.013	0.005	0.043	41.5	27.3	14.2
Propylene	46.4	2.74	0.017	0.006	0.095	40.5	25.6	14.9
1,3-butadiene	44.6	2.46	0.048	0.014	0.125	33.6	15.4	18.2
Acetylene	47.8	2.60	0.042	0.013	0.096	36.7	18.7	18.0
Common liquids								
Methyl alcohol	20.0	1.31	0.001	–	–	19.1	16.1	3.0
Ethyl alcohol	27.7	1.77	0.001	0.001	0.008	25.6	19.0	6.5
Isopropyl alcohol	31.8	2.01	0.003	0.001	0.015	29.0	20.6	8.5
Acetone	29.7	2.14	0.003	0.001	0.014	27.9	20.3	7.6
Methylethyl ketone	32.7	2.29	0.004	0.001	0.018	30.6	22.1	8.6
Heptane	44.6	2.85	0.010	0.004	0.037	41.2	27.6	13.6
Octane	44.5	2.84	0.011	0.004	0.038	41.0	27.3	13.7
Kerosene	44.1	2.83	0.012	0.004	0.042	40.3	26.2	14.1
Benzene	40.1	2.33	0.067	0.018	0.181	27.6	11.0	16.5
Toluene	39.7	2.34	0.066	0.018	0.178	27.7	11.2	16.5
Styrene	39.4	2.35	0.065	0.019	0.177	27.8	11.2	16.6
Hydrocarbon	43.9	2.64	0.019	0.007	0.059	36.9	24.5	12.4
Mineral oil	41.5	2.37	0.041	0.012	0.097	31.7	–	–
Polydimethyl siloxane	25.1	0.93	0.004	0.032	0.232	19.6	–	–
Silicone	25.1	0.72	0.006	0.008	–	15.2	12.7	2.5
Chemicals and solvents								
Tetrahydrofuran (C_4H_8O)	32.2	2.29	0.021	–	–	30.3	–	–
Phenol (C_6H_6O)	31.0	2.63	0.057	–	0.099	27.6	13.3	14.3
Acetonitrile (C_2H_3N)	29.6	2.04	0.025	–	0.026	29.0	23.0	6.0
Ethylisonicotate ($C_8H_9O_2N$)	26.3	2.37	0.029	–	0.142	24.3	12.8	11.5
Adiponitrile ($C_6H_8N_2$)	33.1	2.35	0.045	–	0.045	31.1	22.1	9.0
Hexamethylenediamine ($C_6H_{16}N_2$)	35.3	2.28	0.029	–	0.045	32.6	15.7	16.9
Toluenediisocyanate ($C_9H_6O_2N_2$)	23.6	1.77	0.052	–	0.141	19.3	11.1	8.2
Diphenylmethanediisocyanate MDI ($C_{15}H_{10}O_2N_2$)	27.1	0.95	0.042	–	0.154	19.6	13.7	5.9
Polymeric MDI ($C_{23}H_{19}O_3N_3$)	29.6	1.22	0.032	–	0.165	23.3	15.0	8.3
Isoproturon ($C_{12}H_{18}ON_2$)	32.8	1.70	0.056	–	0.115	23.9	14.0	9.9
3-chloropropene (C_3H_5Cl)	23.0	0.75	0.076	–	0.179	10.8	6.9	3.9
Monochlorobenzene (C_6H_5Cl)	26.4	0.86	0.083	–	0.232	11.2	–	–
Dichloromethane (CH_2Cl_2)	6.0	0.11	0.088	–	0.081	2.0	–	–
1,3-dichloropropene ($C_3H_4Cl_2$)	14.2	0.35	0.090	–	0.169	5.6	–	–
Ethylmonochloroacetate ($C_4H_7O_2Cl$)	15.7	1.24	0.019	–	0.138	14.1	10.1	4.0
Chloronitrobenzoic acid ($C_7H_4O_4NCl$)	15.9	0.39	0.057	–	–	4.4	–	–
Aclonifen ($C_{12}H_9O_3N_2Cl$)	19.7	0.68	0.063	–	0.186	7.0	–	–

(continued)

Table A.39 (continued)

Material	ΔH_T (kJ/g)	y_{CO_2} (g/g)	y_{CO} (g/g)	y_{ch} (g/g)	y_S (g/g)	ΔH_{ch} (kJ/g)	ΔH_{con} (kJ/g)	ΔH_{rad} (kJ/g)
2,6-dichlorobenzonitrile (dichlobenil) ($C_7H_3NCl_2$)	17.8	0.39	0.068	–	–	4.3	–	–
Diuron ($C_9H_{10}ON_2Cl_2$)	20.3	0.76	0.080	–	0.159	10.2	7.7	2.5
Trifluoromethylbenzene ($C_6H_5CF_3$)	18.7	1.19	0.069	–	0.185	10.8	5.1	5.7
Metatrifluoromethylphenylacetonitrile ($C_9H_6NF_3$)	16.0	0.89	0.058	–	0.168	7.3	4.0	3.3
Tetramethylthiurammonosulfide ($C_6H_{12}N_2S_3$)	22.6	1.06	0.041	–	–	19.6	–	–
Methylthiopropionylaldehyde (C_4H_8OS)	25.0	1.62	0.001	–	0.005	23.8	18.8	5.0
Pesticides								
2,4-D acid (herbicide, $C_8H_6O_3Cl_2$)	11.5	0.50	0.074	–	0.163	4.5	3.0	1.5
Mancozeb ($C_4H_6N_2S_4Mn)_iZn_{0,4}$)	14.0	0.50	–	–	–	9.5	–	–
Folpel ($C_9H_4O_2NSCl_3$)	9.1	0.37	0.072	–	0.205	3.6	–	–
Chlorfenvinphos ($C_{12}H_{24}O_4Cl_3P$)	18.0	0.43	0.011	–	0.288	7.7	–	–
Chlormephos ($C_5H_{12}O_2S_2ClP$)	19.1	0.51	0.075	–	0.055	13.9	–	–
Natural materials								
Tissue paper	–	–	–	–	–	11.4	6.7	4.7
Newspaper	–	–	–	–	–	14.4	–	–
Wood (red oak)	17.1	1.27	0.004	0.001	0.015	12.4	7.8	4.6
Wood (Douglas fir)	16.4	1.31	0.004	0.001	–	13.0	8.1	4.9
Wood (pine)	17.9	1.33	0.005	0.001	–	12.4	8.7	3.7
Corrugated paper	–	–	–	–	–	13.2	–	–
Wood (hemlock)[b]	–	–	–	–	0.015	13.3	–	–
Wool 100%[b]	–	–	–	–	0.008	19.5	–	–
Synthetic materials–solids (abbreviations/names in the nomenclature)								
ABS[b]	–	–	–	–	0.105	30.0	–	–
POM	15.4	1.40	0.001	0.001	–	14.4	11.2	3.2
PMMA	25.2	2.12	0.010	0.001	0.022	24.2	16.6	7.6
PE	43.6	2.76	0.024	0.007	0.060	38.4	21.8	16.6
PP	43.4	2.79	0.024	0.006	0.059	38.6	22.6	0
PS	39.2	2.33	0.060	0.014	0.164	27.0	11.0	16.0
Silicone	21.7	0.96	0.021	0.006	0.065	10.6	7.3	3.3
Polyester-1	32.5	1.65	0.070	0.020	0.091	20.6	10.8	9.8
Polyester-2	32.5	1.56	0.080	0.029	0.089	19.5	–	–
Epoxy-1	28.8	1.59	0.080	0.030	–	17.1	8.5	8.6
Epoxy-2	28.8	1.16	0.086	0.026	0.098	12.3	–	–
Nylon	30.8	2.06	0.038	0.016	0.075	27.1	16.3	10.8
Polyamide-6[b]	–	–	–	–	0.011	28.8	–	–
IPST[b]	–	–	–	–	0.080	23.3	–	–
PVEST[b]	–	–	–	–	0.076	22.0	–	–
Silicone rubber	21.7	0.96	0.021	0.005	0.078	10.9	–	–
Polyether ether ketone (PEEK-$CH_{0.63}O_{0.16}$)	31.3	1.6	0.029	–	0.008	17.5	–	–
Polysulfone (PSO-$CH_{0.81}O_{0.15}S_{0.04}$)	29.0	1.8	0.034	–	0.020	24.3	–	–
Polyethersulfone (PES-$CH_{0.67}O_{0.21}S_{0.08}$)	25.2	1.5	0.040	–	0.021	20.4	–	–
Polyetherimide (PEI-$CH_{0.68}$ $N_{0.05}O_{0.14}$)	30.1	2.0	0.026	–	0.014	27.2	–	–
Polycarbonate (PC-$CH_{0.88}O_{0.13}$)	31.6	1.5	0.054	–	0.112	18.4	–	–

(continued)

Table A.39 (continued)

Material	ΔH_T (kJ/g)	y_{CO_2} (g/g)	y_{CO} (g/g)	y_{ch} (g/g)	y_S (g/g)	ΔH_{ch} (kJ/g)	ΔH_{con} (kJ/g)	ΔH_{rad} (kJ/g)
Polyurethane (flexible) foams								
GM21	26.2	1.55	0.010	0.002	0.131	17.8	8.6	9.2
GM23	27.2	1.51	0.031	0.005	0.227	19.0	10.3	8.7
GM25	24.6	1.50	0.028	0.005	0.194	17.0	7.2	9.8
GM27	23.2	1.57	0.042	0.004	0.198	16.4	7.6	8.8
Polyurethane (rigid) foams								
GM29	26.0	1.52	0.031	0.003	0.130	16.4	6.8	9.6
GM31	25.0	1.53	0.038	0.002	0.125	15.8	7.1	8.8
GM35	28.0	1.58	0.025	0.001	0.104	17.6	7.8	9.8
GM37	28.0	1.63	0.024	0.001	0.113	17.9	8.7	9.2
GM41	26.2	1.18	0.046	0.004	–	15.7	5.7	10.0
GM43	22.2	1.11	0.051	0.004	–	14.8	6.4	8.4
Polystyrene foams								
GM47	38.1	2.30	0.060	0.014	0.180	25.9	11.4	14.5
GM49	38.2	2.30	0.065	0.016	0.210	25.6	9.9	15.7
GM51	35.6	2.34	0.058	0.013	0.185	24.6	10.4	14.2
GM53	37.6	2.34	0.060	0.015	0.200	25.9	11.2	14.7
Polyethylene foams								
1	41.2	2.62	0.020	0.004	0.056	34.4	20.2	14.2
2	40.8	2.78	0.026	0.008	0.102	36.1	20.6	15.5
3	40.8	2.60	0.020	0.004	0.076	33.8	18.2	15.6
4	40.8	2.51	0.015	0.005	0.071	32.6	19.1	13.5
Phenolic foams								
1[b]	–	–	–	–	0.002	10.0	–	–
2[b]	–	–	–	–	–	10.0	–	–
Halogenated materials (abbreviations/names in the nomenclature)								
Polyethylene with								
25 % chlorine	31.6	1.71	0.042	0.016	0.115	22.6	10.0	12.6
36 % chlorine	26.3	0.83	0.051	0.017	0.139	10.6	6.4	4.2
48 % chlorine	20.6	0.59	0.049	0.015	0.134	7.2	3.9	3.3
PVC	16.4	0.46	0.063	0.023	0.172	5.7	3.1	2.6
PVC-1[b] (LOI = 0.50)	–	–	–	–	0.098	7.7	–	–
PVC-2[b] (LOI = 0.50)	–	–	–	–	0.076	8.3	–	–
PVC[b] (LOI = 0.20)	–	–	–	–	9.099	11.3	–	–
PVC[b] (LOI = 0.25)	–	–	–	–	0.078	9.8	–	–
PVC[b] (LOI = 0.30)	–	–	–	–	0.098	10.3	–	–
PVC (LOI = 0.35)	–	–	–	–	0.088	10.8	–	–
PVC panel	–	–	–	–	–	7.3	–	–
CPVC ($CH_{1.3}Cl_{0.70}$)	12.8	0.48	0.052	–	0.043	4.4	–	–
PVDF (CHF)	13.3	0.53	0.055	–	0.037	3.8	–	–
ECTFE ($CHF_{0.75}Cl_{0.25}$)	12.0	0.41	0.095	–	0.038	4.6	–	–
ETFE (Tefzel, CHF)	12.6	0.78	0.035	–	0.028	7.3	–	–
PFA (Teflon, $CF_{1.6}O_{0.01}$)	5.0	0.42	0.099	–	0.002	2.2	–	–

(continued)

Table A.39 (continued)

Material	ΔH_T (kJ/g)	y_{CO_2} (g/g)	y_{CO} (g/g)	y_{ch} (g/g)	y_S (g/g)	ΔH_{ch} (kJ/g)	ΔH_{con} (kJ/g)	ΔH_{rad} (kJ/g)
FEP (Teflon, $CF_{1.8}$)	4.8	0.25	0.116	–	0.003	1.3	–	–
TFE (Teflon, $CF_{1.8}$)	6.2	0.38	0.092	–	0.003	2.0	–	–
Building products[c]								
Particleboard (PB)	–	1.2	0.004	–	–	14.0	–	–
Fiberboard (FB)	–	1.4	0.015	–	–	14.0	–	–
Medium-density FB	–	1.2	0.002	–	–	14.0	–	–
Wood panel	–	1.2	0.002	–	–	15.0	–	–
Melamine-faced PB	–	0.8	0.025	–	–	10.7	–	–
Gypsumboard (GB)	–	0.3	0.027	–	–	4.3	–	–
Paper on GB	–	0.4	0.028	–	–	5.6	–	–
Plastic on GB	–	0.4	0.028	–	–	14.3	–	–
Textile on GB	–	0.4	0.025	–	–	13.0	–	–
Textile on rock wool	–	1.8	0.091	–	–	25.0	–	–
Paper on PB	–	1.2	0.003	–	–	12.5	–	–
Rigid PU	–	1.1	0.200	–	–	13.0	–	–
EPS	–	1.9	0.054	–	–	28.0	–	–
Composite and fiberglass-reinforced materials (FGR) (abbreviations/names in the nomenclature)								
PEEK/FGR[b]	–	–	–	–	0.042	20.5	–	–
IPST/FGR[b]	–	–	–	–	0.032	27.0	–	–
PES/FGR[b]	–	–	–	–	0.049	27.5	–	–
PEST1/FGR[b]	–	–	–	–	–	16.0	–	–
PEST2/FGR[b]	–	–	–	–	–	12.9	–	–
PEST1/FGR	–	–	–	–	–	19.0	–	–
PEST2/FGR	–	–	–	–	–	13.9	–	–
PEST3/FGR	–	1.47	0.055	0.007	0.070	17.9	10.7	7.2
PEST4/FGR	–	1.24	0.039	0.004	0.054	16.0	9.9	6.1
PEST5/FGR	–	0.71	0.102	0.019	0.068	9.3	6.5	2.8
Epoxy/FG[b]	–	–	–	–	0.056	27.5	–	–
PVEST/FGR	–	–	–	–	0.079	26.0	–	–
Kevlar/phenolic	–	1.27	0.025	0.002	0.041	14.8	11.1	3.7
Phenolic-1/FGR	–	0.98	0.066	0.003	0.023	11.9	8.9	3.0
Phenolic-2/FGR[b]	–	–	–	–	0.016	22.0	–	–
Aircraft panel materials								
Epoxy/FGR/paint	–	0.828	0.114	0.016	0.166	11.3	6.2	5.1
Epoxy/Kevlar/paint	–	0.873	0.091	0.016	0.126	11.4	6.3	5.1
Phenolic/FGR/paint	–	1.49	0.027	0.002	0.059	22.9	11.5	11.4
Phenolic/Kevlar/paint	–	1.23	0.088	0.011	0.094	18.6	8.9	9.7
Phenolic/graphite/paint	–	1.67	0.026	0.003	0.062	24.6	14.0	10.6
Polycarbonate	–	–	–	–	–	20.5	–	–
Electric cables (abbreviations/names in the nomenclature) *polyethylene/polyvinylchloride*								
1	–	2.08	0.100	0.021	0.076	31.3	11.6	19.7
2	–	1.75	0.050	0.013	0.115	25.1	11.1	14.0
3	–	1.67	0.048	0.012	–	24.0	13.0	11.0

(continued)

Table A.39 (continued)

Material	ΔH_T (kJ/g)	y_{CO_2} (g/g)	y_{CO} (g/g)	y_{ch} (g/g)	y_S (g/g)	ΔH_{ch} (kJ/g)	ΔH_{con} (kJ/g)	ΔH_{rad} (kJ/g)
4	–	1.39	0.166	0.038	–	22.0	14.0	8.1
5	–	1.29	0.147	0.042	0.136	20.9	10.7	10.2
EPR/Hypalon								
1	–	1.95	0.072	0.014	–	29.6	15.8	13.9
2	–	1.74	0.076	0.022	–	26.8	17.0	9.8
3	–	1.21	0.072	0.014	–	19.0	12.3	6.7
4	–	0.99	0.090	0.085	0.082	17.4	6.6	10.8
5	–	0.95	0.122	0.024	–	17.3	7.5	9.8
6	–	0.89	0.121	0.022	0.164	13.9	9.2	4.7
Silicone								
1	–	1.65	0.011	0.001	–	25.0	17.5	7.3
2	–	1.47	0.029	0.001	–	24.0	20.0	4.0
XLPE/XLPE								
1	–	1.78	0.114	0.029	0.120	28.3	12.3	16.0
2	–	0.83	0.110	0.024	0.120	12.5	7.5	5.0
XLPE/neoprene								
1	–	0.68	0.122	0.031	–	12.6	5.9	6.7
2	–	0.63	0.082	0.014	0.175	10.3	4.9	5.5
Silicone/PVC								
1	16.4	0.76	0.110	0.015	0.111	10.0	–	–
2	16.4	1.19	0.065	0.005	0.119	15.6	–	–
PVC/nylon/PVC-nylon								
1	–	0.63	0.084	0.024	–	10.2	5.0	5.2
2	–	0.49	0.082	0.032	0.115	9.2	4.8	4.4
PTFE								
1	–	0.180	0.091	0.012	0.011	3.2	2.7	0.4
2	6.2	0.383	0.103	–	0.005	5.7	–	–
Materials with fiberweb, netlike, and multiplex structure (abbreviations/names in the nomenclature)								
Olefin	–	1.49	0.006	–	–	16.5	13.3	3.2
PP-1	–	1.25	0.0029	–	–	14.0	10.8	3.2
PP-2	–	1.56	0.0048	–	–	17.2	10.5	6.7
Polyester-1	–	2.21	0.015	–	–	24.6	8.9	15.7
Polyester-2	–	1.51	0.0079	–	–	16.8	9.1	7.7
Polyester-3	–	2.55	0.020	–	–	28.5	22.6	5.9
Polyester-4	–	1.92	0.014	–	–	21.4	12.4	9.0
Rayon-1	–	1.80	0.043	–	–	20.3	14.1	6.2
Rayon-2	–	1.91	0.043	0.002	–	21.5	13.3	8.2
Rayon-3	–	1.18	0.047	–	–	13.5	8.3	5.2
Polyester-rayon	–	1.52	0.005	–	–	16.8	9.1	7.7
Polyester-polyamide	–	1.82	0.008	–	–	20.2	10.4	9.8
Two to eight 100-mm × 100-mm × 100-mm corrugated paper boxes with and without the polymers with three-dimensional arrangement (abbreviations/names in the nomenclature)[d]								
Empty	–	1.53	0.023	0.001	–	14.2	10.7	3.5
With PVC (62 %-thick)	–	1.01	0.073	0.007	0.119	10.7	9.5	1.2

(continued)

Table A.39 (continued)

Material	ΔH_T (kJ/g)	y_{CO_2} (g/g)	y_{CO} (g/g)	y_{ch} (g/g)	y_S (g/g)	ΔH_{ch} (kJ/g)	ΔH_{con} (kJ/g)	ΔH_{rad} (kJ/g)
With PC (59 %-thick)	–	1.73	0.047	0.002	0.061	18.4	13.5	4.9
With PS (58 %-thick)	–	1.40	0.138	0.026	0.285	16.2	12.5	3.7
With PS (60 %-thin)	–	1.88	0.068	0.020	0.140	19.4	10.1	9.3
With PS (40 %-thin)	–	1.74	0.042	0.005	0.167	18.0	11.7	6.7
With ABS (59 %-thick)	–	1.53	0.089	0.006	0.143	16.1	12.7	3.4
With PET (41 %-thin)	–	1.87	0.050	0.006	0.053	19.9	11.8	8.1
With PU (40 %-foam)	–	1.56	0.024	–	–	14.4	8.6	5.8
High-pressure liquid spray combustion[e]								
Hydraulic fluids								
Organic polyol esters								
1	36.6	–	–	–	–	35.5	–	–
2	35.7	–	–	–	–	35.1	–	–
3	40.3	–	–	–	–	37.2	–	–
4	37.0	–	–	–	–	35.7	–	–
Phosphate esters								
1	31.8	–	–	–	–	29.3	–	–
2	32.0	–	–	–	–	29.6	–	–
Water-in-oil emulsions								
1	27.6	–	–	–	–	2.5	–	–
Polyglycol-in-water								
1	11.0	–	–	–	–	10.4	–	–
2	11.9	–	–	–	–	11.1	–	–
3	14.7	–	–	–	–	12.2	–	–
4	12.1	–	–	–	–	10.6	–	–
Liquid fuels								
Mineral oil	46.0	–	–	–	–	44.3	–	–
Methanol	20.0	–	–	–	–	19.8	–	–
Ethanol	27.7	–	–	–	–	26.2	–	–
Heptane	44.4	–	–	–	–	40.3	–	–

Note: Dashes = either not measured or are less than 0.001

[a]Data measured in the ASTM E2058 fire propagation apparatus. Data measured in the cone calorimeter are identified by superscripts [b] and [c]. Some of the data are corrected to reflect well-ventilated fire conditions. All the data are reported for turbulent fires, that is, materials exposed to higher external heat flux values

[b]Calculated from the data measured in the cone calorimeter as reported in [16,17]

[c]Calculated from the data measured in the cone calorimeter as reported in [18]

[d]100-mm × 100-mm × 100-mm corrugated paper boxes with and without the 99-mm × 99-mm × 99-mm polymer boxes or pieces on corrugated paper compartments. The boxes are arranged in one and two layers, about 12 mm apart, with one to four boxes in each layer, separated by about 12 mm. All the boxes are placed on a very light metal frame made of rods with screen base. Measurements made in the ASTM E2058 fire propagation apparatus; numbers in parentheses are the weight percents

[e]Data from [19] measured in high-pressure liquid spray combustion in the fire products collector (5,000-kW scale apparatus)

Table A.40 Combustion properties of fuels [15] (shaded cells show measurements by Tewarson [112])

Fuel	Formula	L_{sp} (m)	M (g/mol)	S	Heat of Combustion (kJ/g)				Yield (g/g)	
					ΔH_T	ΔH_{ch}	ΔH_{con}	ΔH_{rad}	CO	Smoke
Normal alkanes										
Ethane	C_2H_6	0.243	30	16.0	47.1	47.0	37.4	9.6	<0.001	0.002
n-Propane	C_3H_8	0.162	44	15.6	46.0	44.1	31.6	12.5	0.005	0.019
n-Butane	C_4H_{10}	0.160	58	15.4	45.4	43.5	31.0	12.4	0.005	0.020
n-Pentane	C_5H_{12}	0.155	72	15.3	45.0	42.3	29.3	13.1	0.006	0.022
n-Hexane	C_6H_{14}	0.125	86	15.2	44.8	41.7	28.2	13.4	0.009	0.031
n-Heptane	C_7H_{16}	0.110	100	15.1	44.6	41.2	27.6	13.6	0.012	0.042
n-Octane	C_8H_{18}	0.118	114	15.1	44.5	41.3	27.5	13.8	0.010	0.034
n-Nonane	C_9H_{20}	0.110	128	15.0	44.4	40.9	26.9	14.1	0.012	0.037
n-Decane	$C_{10}H_{22}$	0.110	142	15.0	44.3	40.9	26.8	14.0	0.012	0.037
n-Undecane	$C_{11}H_{24}$	0.110	156	15.0	44.3	40.9	26.8	14.0	0.012	0.037
n-Dodecane	$C_{12}H_{26}$	0.108	170	14.9	44.2	40.7	26.6	14.1	0.012	0.038
n-Tridecane	$C_{13}H_{28}$	0.106	184	14.9	44.2	40.6	26.5	14.1	0.012	0.039
n-Tetradecane	$C_{14}H_{30}$	0.109	198	14.9	44.1	40.6	26.6	14.0	0.012	0.037
Hexadecane	$C_{16}H_{34}$	0.118	226	14.9	44.1	41.0	27.3	13.7	0.010	0.034
Branched alkanes										
Methylbutane	C_5H_{12}	0.113	72	15.3	45.0	41.6	27.5	14.1	0.011	0.035
Dimethylbutane	C_6H_{14}	0.089	86	15.2	44.8	40.4	25.5	15.0	0.015	0.046
Methylpentane	C_6H_{14}	0.094	86	15.2	44.8	40.7	25.9	14.8	0.014	0.043
Dimethylpentane	C_7H_{16}	0.096	100	15.1	44.6	40.6	25.9	14.6	0.014	0.043
Methylhexane	C_7H_{16}	0.109	100	15.1	44.6	41.1	26.9	14.2	0.012	0.037
Isooctane (trimethylpentane)	C_8H_{18}	0.080	114	15.1	44.5	40.5	26.7	13.8	0.016	0.051
Methylethylpentane	C_8H_{18}	0.082	114	15.1	44.5	39.9	24.7	15.1	0.016	0.049
Ethylhexane	C_8H_{18}	0.093	114	15.1	44.5	40.4	25.6	14.7	0.014	0.044
Dimethylhexane	C_8H_{18}	0.089	114	15.1	44.5	40.2	25.3	14.9	0.015	0.046
Methylheptane	C_8H_{18}	0.101	114	15.1	44.5	40.7	26.3	14.4	0.013	0.040
Cyclic alkanes										
Cyclo-pentane	C_5H_{10}	0.067	70	14.7	44.3	38.9	23.2	15.6	0.020	0.059
Methylcyclopentane	C_6H_{12}	0.052	84	14.7	43.8	37.5	21.5	16.0	0.025	0.070
Cyclohexane	C_6H_{12}	0.085	84	14.7	43.8	39.9	24.5	15.3	0.016	0.049
Methylcyclohexane	C_7H_{14}	0.075	98	14.7	43.4	38.5	23.5	15.0	0.018	0.054
Ethylcyclohexane	C_8H_{16}	0.082	112	14.7	43.2	38.7	24.0	14.7	0.017	0.050
Dimethylcyclohexane	C_8H_{16}	0.057	112	14.7	43.2	37.3	21.7	15.6	0.023	0.066
Cyclooctane	C_8H_{16}	0.085	112	14.7	43.2	38.8	24.2	14.6	0.016	0.049
Decalin	$C_{10}H_{18}$	—	138	14.4	42.8	34.2	17.9	16.3	0.015	0.097
Bicyclohexyl	$C_{12}H_{22}$	—	166	14.5	42.6	36.2	20.9	15.3	0.010	0.071
Alkenes										
Ethylene	C_2H_4	0.106	28	14.7	48.0	44.2	29.8	14.4	0.013	0.045
Propylene	C_3H_6	0.029	42	14.7	46.4	37.6	19.0	18.6	0.036	0.103
Butylene	C_4H_8	0.019	56	14.7	45.6	35.3	17.3	18.0	0.042	0.115
Pentene	C_5H_{10}	0.053	70	14.7	45.2	38.7	22.3	16.5	0.024	0.070
Hexene	C_6H_{12}	0.063	84	14.7	44.9	39.2	23.2	16.0	0.021	0.062
Heptene	C_7H_{14}	0.073	98	14.7	44.6	39.5	24.0	15.5	0.019	0.055
Octene	C_8H_{16}	0.080	112	14.7	44.5	39.8	24.5	15.2	0.017	0.051
Nonene	C_9H_{18}	0.084	126	14.7	44.3	39.8	24.8	15.0	0.016	0.049
Decene	$C_{10}H_{20}$	0.079	140	14.7	44.2	39.4	24.3	15.2	0.017	0.052
Dodecene	$C_{12}H_{24}$	0.080	168	14.7	44.1	39.4	24.3	15.1	0.017	0.051
Tridecene	$C_{13}H_{26}$	0.084	182	14.7	44.0	39.5	24.6	14.9	0.016	0.049
Tetradecene	$C_{14}H_{28}$	0.079	196	14.7	44.0	39.3	24.2	15.1	0.017	0.052
Hexadecene	$C_{16}H_{32}$	0.080	224	14.7	43.9	39.2	24.2	15.0	0.017	0.051
Octadecene	$C_{18}H_{36}$	0.075	252	14.7	43.8	38.9	23.7	15.2	0.018	0.054
Polyethylene	$(C_2H_4)_n$	0.045	601	14.7	43.6	37.9	21.8	16.1	0.024	0.060
Polypropylene	$(C_3H_6)_n$	0.050	720	14.7	43.4	37.0	21.1	15.9	0.024	0.058

Cyclic alkenes										
Cyclohexene	C_6H_{10}	0.044	82	14.2	43.0	36.2	20.2	16.0	0.028	0.080
Methylcyclohexene	C_7H_{12}	0.043	96	14.3	43.1	36.2	20.1	16.1	0.028	0.080
Pinene	$C_{10}H_{16}$	0.024	136	14.1	36.0	28.5	14.5	14.0	0.039	0.108
Alkynes and Butadiene										
Acetylene	C_2H_2	0.019	26	13.2	47.8	37.0	18.2	18.8	0.045	0.124
Heptyne	C_7H_{12}	0.035	96	14.3	44.8	36.8	19.8	17.0	0.032	0.090
Octyne	C_8H_{14}	0.030	110	14.4	44.7	36.2	19.0	17.2	0.035	0.096
Decyne	$C_{10}H_{18}$	0.043	138	14.4	44.5	37.4	20.7	16.6	0.028	0.080
Dodecyne	$C_{12}H_{22}$	0.030	166	14.5	44.3	35.9	18.8	17.0	0.034	0.096
1,3-Butadiene	C_4H_6	0.015	54	14.0	44.6	33.7	16.0	17.7	0.048	0.130
Arenes										
Benzene	C_6H_6	0.007	78	13.2	40.1	28.1	11.9	16.2	0.064	0.171
Toluene	C_7H_8	0.005	92	13.4	39.7	27.0	11.1	15.9	0.064	0.173
Styrene	C_8H_8	0.006	104	13.2	39.4	27.2	11.2	16.0	0.066	0.178
Ethylbenzene	C_8H_{10}	0.005	106	13.6	39.4	26.7	10.7	16.0	0.069	0.184
Xylene	C_8H_{10}	0.006	106	13.6	39.4	27.2	11.2	16.0	0.065	0.175
Indene	C_9H_8	0.008	116	13.0	39.2	27.8	12.0	15.8	0.062	0.166
Propylbenzene	C_9H_{12}	0.009	120	13.7	39.2	28.1	12.4	15.8	0.057	0.155
Trimethylbenzene	C_9H_{12}	0.006	120	13.7	39.2	27.0	11.2	15.9	0.065	0.174
Cumene	C_9H_{12}	0.006	120	13.7	39.2	27.0	11.2	15.9	0.065	0.174
Naphthalene	$C_{10}H_8$	0.005	128	12.9	39.0	26.4	10.6	15.8	0.071	0.190
Tetralin	$C_{10}H_{12}$	0.006	132	13.5	39.0	26.9	11.1	15.8	0.065	0.176
Butylbenzene	$C_{10}H_{14}$	0.007	134	13.8	39.0	27.3	11.5	15.8	0.062	0.166
Diethylbenzene	$C_{10}H_{14}$	0.007	134	13.8	39.0	27.3	11.5	15.8	0.062	0.166
p-Cymene	$C_{10}H_{14}$	0.007	134	13.8	39.0	27.3	11.5	15.8	0.062	0.166
Methylnaphthalene	$C_{11}H_{10}$	0.006	142	13.0	38.9	26.8	11.1	15.8	0.067	0.180
Pentylbenzene	$C_{11}H_{16}$	0.009	148	13.9	38.8	27.9	12.2	15.6	0.057	0.154
Dimethylnaphthalene	$C_{12}H_{12}$	0.006	156	13.2	38.8	26.8	11.0	15.7	0.066	0.178
Cyclohexylbenzene	$C_{12}H_{16}$	0.007	160	13.7	38.7	27.1	11.5	15.6	0.062	0.167
Diisopropylbenzene	$C_{12}H_{18}$	0.007	162	14.0	38.7	27.1	11.5	15.6	0.061	0.165
Triethylbenzene	$C_{12}H_{18}$	0.006	162	14.0	38.7	26.7	11.0	15.7	0.064	0.172
Triamylbenzene	$C_{21}H_{36}$	0.007	288	14.3	38.1	26.7	11.3	15.4	0.060	0.162
Polystyrene	$(C_8H_8)_n$	0.015	200	13.2	39.2	27.0	11.0	16.1	0.060	0.166

Fuel	Formula	L_{sp} (m)	M (g/mol)	S	Heat of Combustion (kJ/g) ΔH_T	ΔH_{ch}	ΔH_{con}	ΔH_{rad}	Yield (g/g) CO	Smoke
Aliphatic esters										
Ethyl formate	$C_3H_6O_2$	0.137	74	6.5	20.2	19.0	13.1	5.9	0.005	0.016
n-Propyl formate	$C_4H_8O_2$	0.114	88	7.8	23.9	22.1	14.6	7.5	0.007	0.023
n-Butyl formate	$C_5H_{10}O_2$	0.099	102	8.8	26.6	24.3	15.6	8.7	0.009	0.029
Methyl acetate	$C_3H_6O_2$	0.137	74	6.5	20.2	19.0	13.1	5.9	0.005	0.016
Ethyl acetate	$C_4H_8O_2$	0.114	88	7.8	23.9	22.1	14.6	7.5	0.007	0.023
n-Propyl acetate	$C_5H_{10}O_2$	0.099	102	8.8	26.6	24.3	15.6	8.7	0.009	0.029
n-Butyl acetate	$C_6H_{12}O_2$	0.093	116	9.5	28.7	26.0	16.5	9.5	0.011	0.032
Isobutyl acetate	$C_6H_{12}O_2$	0.093	116	9.5	28.7	26.0	16.5	9.5	0.011	0.032
Amyl acetate	$C_7H_{14}O_2$	0.086	130	10.0	30.3	27.3	17.1	10.2	0.012	0.036
Cyclohexyl acetate	$C_8H_{14}O_2$	0.083	142	10.2	31.5	28.2	17.6	10.7	0.013	0.039
Octyl acetate	$C_{10}H_{20}O$	0.077	172	11.2	33.6	29.9	18.3	11.6	0.015	0.043
Ethyl acetoacetate	$C_6H_{10}O_3$	0.086	130	7.4	30.3	27.3	17.1	10.2	0.010	0.031
Methyl propionate	$C_4H_8O_2$	0.114	88	7.8	23.9	22.1	14.6	7.5	0.007	0.023
Ethyl propionate	$C_5H_{10}O_2$	0.099	102	8.8	26.6	24.3	15.6	8.7	0.009	0.029
n-Butyl propionate	$C_7H_{14}O_2$	0.086	130	10.0	30.3	27.3	17.1	10.2	0.012	0.036
Isobutyl propionate	$C_7H_{14}O_2$	0.086	130	10.0	30.3	27.3	17.1	10.2	0.012	0.042
Amyl propionate	$C_8H_{16}O_2$	0.082	144	10.5	31.6	28.3	17.5	10.8	0.013	0.024
Methyl butyrate	$C_5H_{10}O_2$	0.099	102	8.8	26.6	24.3	15.6	8.7	0.009	0.035
Ethyl butyrate	$C_6H_{12}O_2$	0.093	116	9.5	28.7	26.0	16.5	9.5	0.011	0.038
Propyl butyrate	$C_7H_{14}O_2$	0.086	130	10.0	30.3	27.3	17.1	10.2	0.012	0.042
n-Butyl butyrate	$C_8H_{16}O_2$	0.082	144	10.5	31.6	28.3	17.5	10.8	0.013	0.039
Isobutyl butyrate	$C_8H_{16}O_2$	0.082	144	10.5	31.6	28.3	17.5	10.8	0.013	0.069
Ethyl laurate	$C_{14}H_{28}O_2$	0.196	228	12.0	37.2	36.3	27.3	9.1	0.002	0.004
Ethyl oxalate	$C_6H_{10}O_4$	0.224	146	6.1	28.7	33.0	25.7	7.3	<0.001	0.003
Ethyl malonate	$C_5H_8O_4$	0.210	132	7.7	32.2	31.7	24.2	7.5	<0.001	0.005
Ethyl lactate	$C_5H_{10}O_3$	0.214	118	7.0	30.8	30.4	23.3	7.0	<0.001	0.005
Butyl lactate	$C_7H_{14}O_3$	0.206	146	8.5	33.3	32.7	24.9	7.8	0.001	0.007
Amyl lactate	$C_8H_{16}O_3$	0.203	160	9.0	34.3	33.6	25.5	8.1	0.001	0.007
Ethyl carbonate	$C_5H_{10}O_3$	0.214	118	7.0	30.8	30.4	23.3	7.0	<0.001	0.005
Aliphatic alcohols										
Methyl alcohol	CH_4O	0.305	32	6.4	20.0	19.4	16.6	2.8	0.001	<0.001
Ethyl alcohol	C_2H_6O	0.225	46	9.0	27.7	26.9	20.5	6.4	0.001	0.008
n-Propyl alcohol	C_3H_8O	0.155	60	10.3	31.8	30.3	21.5	8.8	0.004	0.016
Isopropyl alcohol	C_3H_8O	0.148	60	10.3	31.8	29.9	20.7	9.2	0.003	0.017
n-Butyl alcohol	$C_4H_{10}O$	0.141	74	11.1	34.4	32.5	22.5	10.0	0.006	0.020
Isobutyl alcohol	$C_4H_{10}O$	0.141	74	11.1	34.4	32.5	22.5	10.0	0.006	0.020
Sec butyl alcohol	$C_4H_{10}O$	0.141	74	11.1	34.4	32.5	22.5	10.0	0.006	0.020
Ter butyl alcohol	$C_4H_{10}O$	0.141	74	11.1	34.4	32.5	22.5	10.0	0.006	0.020
n-Amyl alcohol	$C_5H_{12}O$	0.131	88	11.7	36.2	34.0	23.2	10.8	0.007	0.024
Isobutyl carbinol	$C_5H_{12}O$	0.131	88	11.7	36.2	34.0	23.2	10.8	0.007	0.024
Sec butyl carbinol	$C_5H_{12}O$	0.131	88	11.7	36.2	34.0	23.2	10.8	0.007	0.024
Methylpropyl carbinol	$C_5H_{12}O$	0.131	88	11.7	36.2	34.0	23.2	10.8	0.007	0.024
Dimethylethyl carbinol	$C_5H_{12}O$	0.131	88	11.7	36.2	34.0	23.2	10.8	0.007	0.024
n-Hexyl alcohol	$C_6H_{14}O$	0.125	102	12.1	37.4	34.9	23.6	11.4	0.008	0.026
Dimethylbutyl alcohol	$C_6H_{14}O$	0.125	102	12.1	37.4	34.9	23.6	11.4	0.008	0.026
Ethylbutyl alcohol	$C_6H_{14}O$	0.125	102	12.1	37.4	34.9	23.6	11.4	0.008	0.026
Allyl alcohol	C_3H_6O	0.159	58	9.5	31.4	30.0	21.4	8.6	0.004	0.015
Cyclohexanol	$C_6H_{12}O$	0.124	100	11.7	37.3	34.8	23.5	11.4	0.008	0.027
Aliphatic ketones										
Acetone	C_3H_6O	0.205	58	9.5	29.7	28.5	21.7	6.8	0.001	0.009
Methyl ethyl ketone	C_4H_8O	0.169	72	10.5	32.7	31.5	22.8	8.7	0.003	0.014
Cyclohexanone	$C_6H_{10}O$	0.164	98	11.2	35.9	34.5	24.7	9.7	0.004	0.017
Di-acetone alcohol	$C_6H_{12}O_2$	0.161	116	9.5	37.3	35.7	25.5	10.2	0.004	0.015
Other aliphatic fuels										
Monoethyl ether	$C_4H_{10}O_2$	0.232	90	8.4	26.7	26.5	20.8	5.7	<0.001	0.003
Monoethylether acetate	$C_6H_{12}O_3$	0.204	132	7.8	32.2	31.6	24.0	7.6	0.001	0.006
Monoethylether diacetate	$C_6H_{10}O_4$	0.208	146	6.1	33.3	32.7	25.0	7.8	<0.001	0.005
Glycerol triacetate	$C_9H_{14}O_6$	0.195	218	6.0	36.9	36.0	27.0	9.0	0.001	0.007
Other aromatic fuels										
Benzaldehyde	C_7H_6O	0.010	106	10.4	32.4	23.5	10.5	13.0	0.049	0.132
Benzyl alcohol	C_7H_8O	0.010	108	10.8	32.6	23.7	10.6	13.1	0.048	0.130
Cresylic acid	C_8H_8O	0.015	136	9.1	34.0	25.7	12.2	13.5	0.038	0.103
Ethyl benzoate	$C_9H_{10}O_2$	0.029	150	9.6	34.5	27.8	14.6	13.3	0.029	0.081

Fuel	Formula	L_{sp} (m)	M (g/mol)	S	Heat of Combustion (kJ/g) ΔH_T	ΔH_{ch}	ΔH_{con}	ΔH_{rad}	Yield (g/g) CO	Smoke
Aliphatic fuels with carbon, hydrogen, and nitrogen										
Diethylamine	$C_4H_{11}N$	0.089	73	14.6	38.0	34.3	21.6	12.7	0.012	0.036
n-Butylamine	$C_4H_{11}N$	0.089	73	14.6	38.0	34.3	21.6	12.7	0.012	0.036
Sec-Butylamine	$C_4H_{11}N$	0.089	73	14.6	38.0	34.3	21.6	12.7	0.012	0.036
Triethylamine	$C_6H_{15}N$	0.085	101	14.6	39.6	35.6	22.2	13.4	0.013	0.041
Di-*n*-butylamine	$C_8H_{19}N$	0.083	129	14.6	40.6	36.4	22.6	13.8	0.014	0.043
Tri-*n*-butylamine	$C_{12}H_{27}N$	0.082	185	14.7	41.6	37.3	23.1	14.2	0.015	0.046
Aromatic fuels with carbon, hydrogen, and nitrogen										
Pyridine	C_5H_5N	0.022	79	12.6	32.2	25.3	12.7	12.6	0.035	0.096
Aniline	C_6H_7N	0.018	93	12.9	33.8	26.0	12.7	13.3	0.039	0.106
Picoline	C_6H_7N	0.018	93	12.9	33.8	26.0	12.7	13.3	0.039	0.106
Toluidine	C_7H_9N	0.014	107	13.2	34.9	26.2	12.3	13.9	0.043	0.118
Dimethylaniline	$C_8H_{11}N$	0.013	121	13.3	35.7	26.6	12.4	14.2	0.045	0.122
Quinoline	C_9H_7N	0.012	129	12.5	36.1	26.7	12.2	14.4	0.049	0.132
Quinaldine	$C_{10}H_9N$	0.011	143	12.7	36.7	26.9	12.2	14.7	0.050	0.136
Butylaniline	$C_{10}H_{15}N$	0.009	149	13.6	37.0	26.6	11.7	14.9	0.051	0.139
Aliphatic fuels with carbon, hydrogen, and sulfur										
Hexyl mercaptan	$C_6H_{14}S$	0.062	118	12.2	33.0	28.7	16.9	11.8	0.015	0.045
Heptyl mercaptan	$C_7H_{16}S$	0.063	132	12.5	33.7	29.4	17.4	12.0	0.016	0.046
Decyl mercaptan	$C_{10}H_{22}S$	0.062	174	13.0	34.9	30.4	17.9	12.5	0.017	0.050
Dodecyl mercaptan	$C_{12}H_{26}S$	0.063	202	13.3	35.5	31.0	18.3	12.7	0.018	0.052
Hexyl sulfide	$C_{12}H_{26}S$	0.063	202	13.3	35.5	31.0	18.3	12.7	0.018	0.052
Heptyl sulfide	$C_{14}H_{30}S$	0.061	230	13.4	35.9	31.2	18.4	12.9	0.019	0.054
Octyl sulfide	$C_{16}H_{34}S$	0.061	258	13.6	36.3	31.6	18.6	13.0	0.019	0.055
Decyl sulfide	$C_{20}H_{42}S$	0.062	314	13.8	36.8	32.0	18.9	13.1	0.019	0.056
Aromatic fuels with carbon, hydrogen, and sulfur										
Thiophene	C_4H_4S	0.016	84	9.8	31.9	24.3	11.6	12.6	0.030	0.082
Methylthiophene	C_5H_6S	0.014	98	10.5	33.2	24.9	11.7	13.2	0.034	0.092
Thiophenol	C_6H_6S	0.013	110	10.6	34.1	25.4	11.8	13.6	0.037	0.101
Thiocresol	C_7H_8S	0.011	124	11.1	34.9	25.6	11.6	14.0	0.041	0.110
Cresolmethyl sulfide	$C_8H_{11}S$	0.011	155	11.6	36.2	26.5	12.0	14.5	0.041	0.112

Appendix 4: Configuration Factors

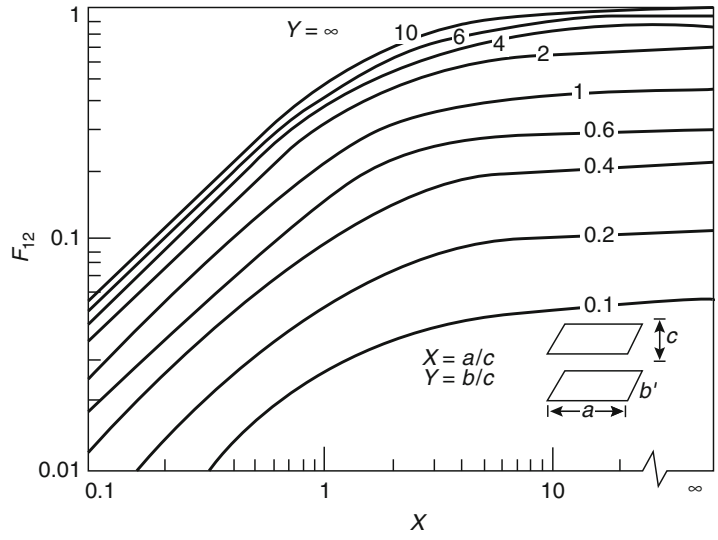

Fig. A.1 View factor for parallel, rectangular plates [21]

$$F_{1-2} = \frac{2}{\pi XY}\left\{ \begin{array}{l} \ln\left[\frac{(1+X^2)(1+Y^2)}{1+X^2+Y^2}\right]^{1/2} + X\sqrt{1+Y^2}\tan^{-1}\frac{X}{\sqrt{1+Y^2}} \\ +Y\sqrt{1+X^2}\tan^{-1}\frac{Y}{\sqrt{1+X^2}} - X\tan^{-1}X - Y\tan^{-1}Y \end{array} \right\}$$

M.J. Hurley (ed.), *SFPE Handbook of Fire Protection Engineering*,
DOI 10.1007/978-1-4939-2565-0, © Society of Fire Protection Engineers 2016

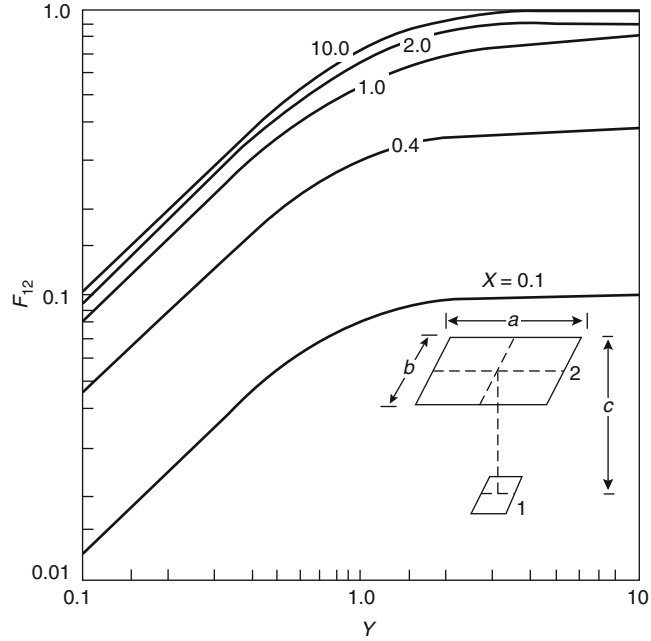

Fig. A.2 View factor for parallel, rectangular radiator [21]

$$F_{12} = \frac{2}{\pi}\left[\frac{X}{\sqrt{1+X^2}}\tan^{-1}\frac{Y}{\sqrt{1+X^2}} + \frac{Y}{\sqrt{1+Y^2}}\tan^{-1}\frac{X}{\sqrt{1+Y^2}}\right]$$

$$X = \frac{a}{2c}$$

$$Y = \frac{b}{2c}$$

$$F_{1-2} = \frac{1}{2\pi}\left\{\begin{array}{l}\tan^{-1}\dfrac{1}{L} + V(N\cos\phi - L)\tan^{-1}V \\ + \dfrac{\cos\phi}{W}\left[\tan^{-1}\left(\dfrac{N - L\cos\phi}{W}\right) + \tan^{-1}\left(\dfrac{L\cos\phi}{W}\right)\right]\end{array}\right\}$$

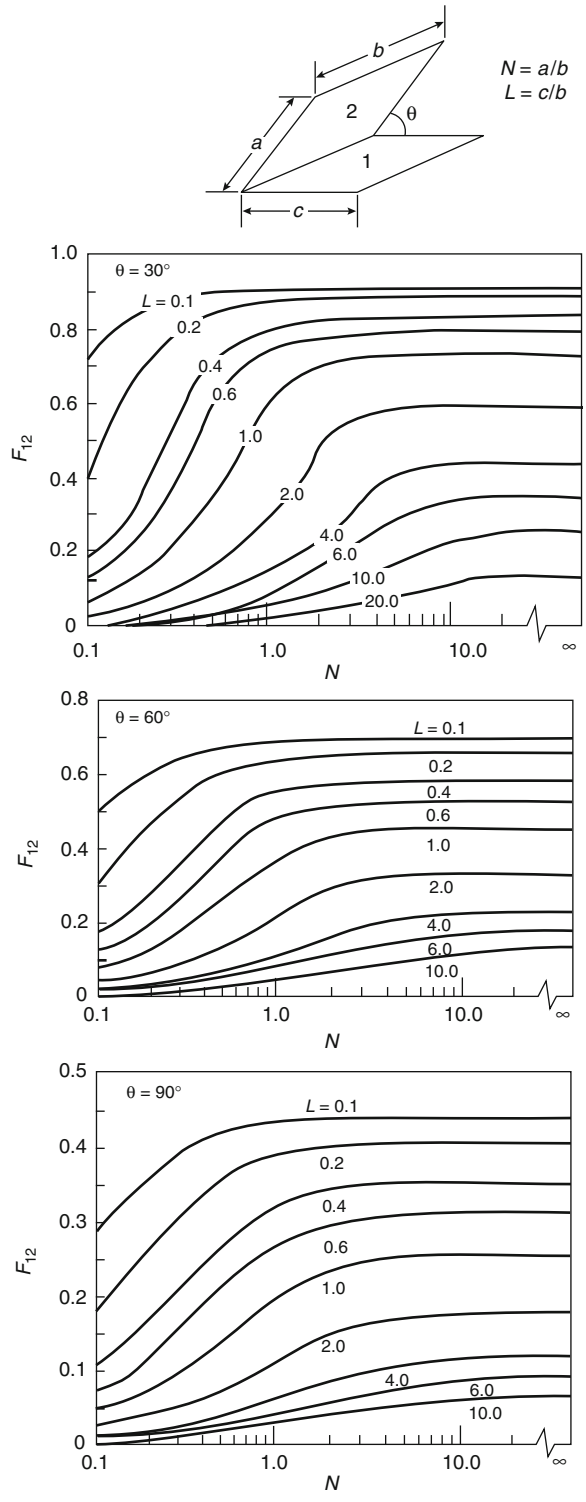

Fig. A.3 View factor for rectangular plates at various angles [21]

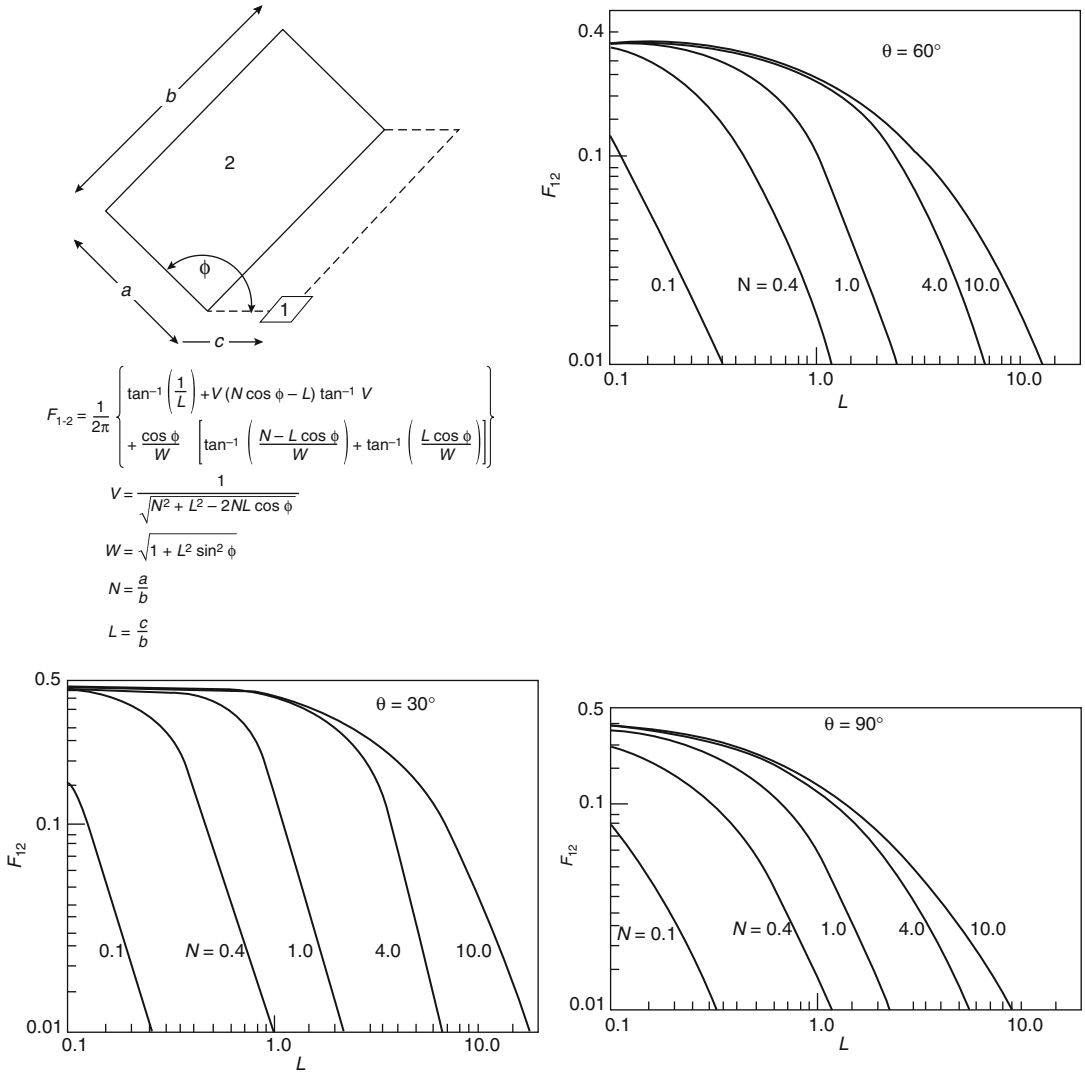

$$F_{1\text{-}2} = \frac{1}{2\pi}\left\{\begin{array}{l}\tan^{-1}\left(\frac{1}{L}\right) + V\,(N\cos\phi - L)\tan^{-1} V \\ + \frac{\cos\phi}{W}\left[\tan^{-1}\left(\frac{N - L\cos\phi}{W}\right) + \tan^{-1}\left(\frac{L\cos\phi}{W}\right)\right]\end{array}\right\}$$

$$V = \frac{1}{\sqrt{N^2 + L^2 - 2NL\cos\phi}}$$

$$W = \sqrt{1 + L^2\sin^2\phi}$$

$$N = \frac{a}{b}$$

$$L = \frac{c}{b}$$

Fig. A.4 View factor for rectangular radiator to differential area at various angles [21]

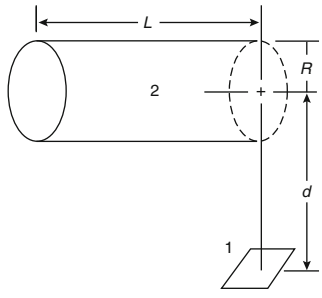

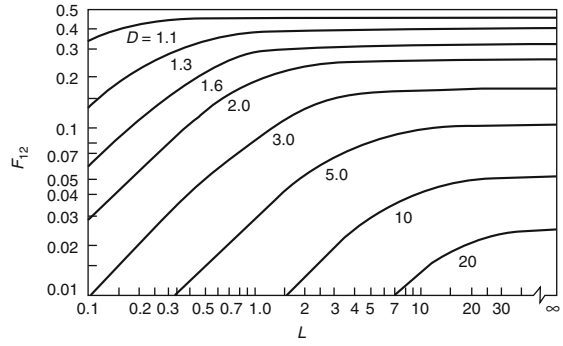

$$F_{12} = \frac{1}{\pi D}\tan^{-1}\left(\frac{L}{\sqrt{D^2-1}}\right) + \frac{L}{\pi}\left[\frac{A-2D}{D\sqrt{AB}}\tan^{-1}\sqrt{\frac{A(D-1)}{B(D+1)}} - \frac{1}{D}\tan^{-1}\sqrt{\frac{D-1}{D+1}}\right]$$

$$D = \frac{d}{R} \qquad L = \frac{L}{R}$$

$$A = (D+1)^2 + L^2 \qquad B = (D-1)^2 + L^2$$

Fig. A.5 Cylindrical radiator to parallel receiver [21]

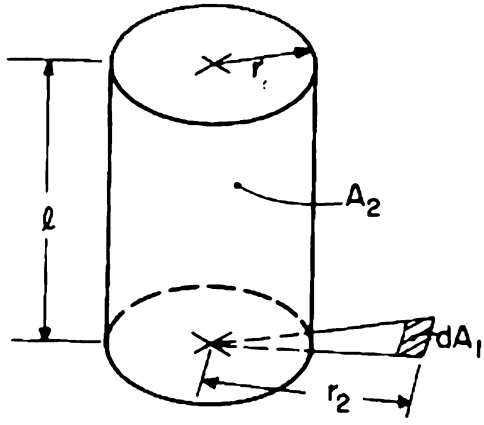

$$R = \frac{r_1}{r_2}$$

$$L = \frac{h}{r_2}$$

$$X = \sqrt{\left(1 + L^2 + R^2\right)^2 4R^2}$$

$$F_{d1-2} = \frac{1}{2\pi}\cos^{-1}R + \frac{1}{\pi}\left\{\tan^{-1}\left[\frac{R}{\left(1-R^2\right)^{1/2}}\right] - \frac{\left(1+L^2-R^2\right)}{X}\tan^{-1}\left[\frac{X\tan\left(0.5\cos^{-1}R\right)}{1+L^2+R^2-2R}\right]\right\}$$

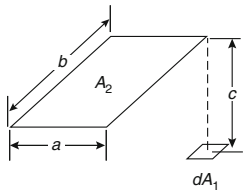

Plane element dA_1 to plane parallel rectangle; normal to element passes through corner of rectangle

$$X = \frac{a}{c} \qquad Y = \frac{b}{c}$$

$$F_{d1-2} = \frac{1}{2\pi}\left(\frac{X}{\sqrt{1+X^2}}\tan^{-1}\frac{Y}{\sqrt{1+X^2}} + \frac{X}{\sqrt{1+Y^2}}\tan^{-1}\frac{X}{\sqrt{1+Y^2}}\right)$$

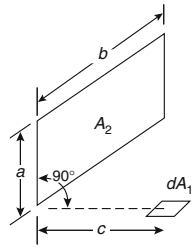

Plane element dA_1 to rectangle in plane 90° to plane of element

$$X = \frac{a}{b} \qquad Y = \frac{c}{b}$$

$$F_{d1-2} = \frac{1}{2\pi}\left(\tan^{-1}\frac{1}{Y} - \frac{Y}{\sqrt{X^2+Y^2}}\tan^{-1}\frac{1}{\sqrt{X^2+Y^2}}\right)$$

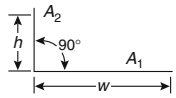

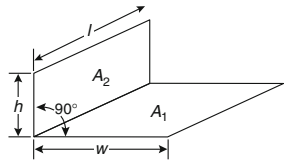

$$F_{1-2} = \frac{1}{\pi W}\left(\begin{array}{l} W\tan^{-1}\frac{1}{W} + H\tan^{-1}\frac{1}{H} - \sqrt{H^2+W^2}\tan^{-1}\frac{1}{\sqrt{H^2+W^2}} \\ + \frac{1}{4}\ln\left\{\frac{(1+W^2)(1+H^2)}{1-W^2+H^2}\left[\frac{W^2(1+W^2+H^2)}{(1+W^2)(W^2+H^2)}\right]^{W^2}\left[\frac{H^2(1+H^2+W^2)}{(1+H^2)(H^2+W^2)}\right]^{H^2}\right\} \end{array}\right)$$

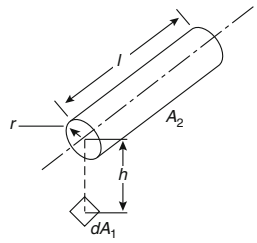

Plane element dA_1 to right circular cylinder of finite length l and radius r; normal to element passes through one end of cylinder and is perpendicular to cylinder axis

$$L = \frac{l}{r} \qquad H = \frac{h}{r}$$

$$X = (1+H)^2 + L^2$$
$$Y = (1-H)^2 + L^2$$

$$F_{d1-2} = \frac{1}{\pi H}\tan^{-1}\frac{L}{\sqrt{H^2-1}} + \frac{L}{\pi}$$

$$\left[\frac{X-2H}{H\sqrt{XY}}\tan^{-1}\sqrt{\frac{X(H-1)}{Y(H+1)}} - \frac{1}{H}\tan^{-1}\sqrt{\frac{(H-1)}{(H+1)}}\right]$$

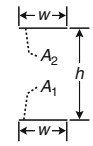

Two infinitely long, directly opposed parallel plates of the same finite width

$$H = \frac{h}{w}$$

$$F_{1-2} = F_{2-1} = \sqrt{1+H^2} - H$$

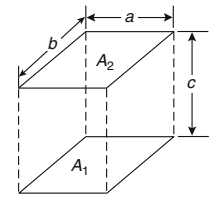

Identical, parallel, directly opposed rectangles

$$X = \frac{a}{c} \qquad Y = \frac{b}{c}$$

$$F_{1-2} = \frac{2}{\pi XY}\left\{\begin{array}{l} \ln\left[\frac{(1+X^2)(1+Y^2)}{1+X^2+Y^2}\right]^{1/2} + X\sqrt{1+Y^2}\tan^{-1}\frac{X}{\sqrt{1+Y^2}} \\ + Y\sqrt{1+X^2}\tan^{-1}\frac{Y}{\sqrt{1+X^2}} - X\tan^{-1}X - Y\tan^{-1}Y \end{array}\right\}$$

Two infinitely long plates of unequal widths h and w, having one common edge and having an angle of 90° to each other

$$H = \frac{h}{w}$$

$$F_{1-2} = \frac{1}{2}\left(1 + H - \sqrt{1+H^2}\right)$$

Two finite rectangles of same length, having one common edge and having an angle of 90° to each other

$$H = \frac{h}{l} \qquad H = \frac{w}{l}$$

Fig. A.6 View factor equations for various geometries [22]

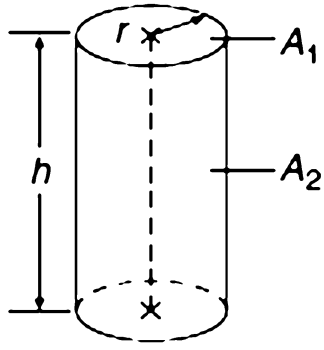

$H = h/2r$

$F_{1-2} = 2H\left[\left(1 + H^2\right)^{1/2} - H\right]$

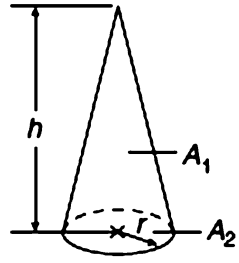

$H = h/2r$

$F_{1-2} = \frac{1}{\left(1+H^2\right)^{1/2}}$

M.J. Hurley (ed.), *SFPE Handbook of Fire Protection Engineering*,
DOI 10.1007/978-1-4939-2565-0, © Society of Fire Protection Engineers 2016

Appendix 5: Piping Properties

Table A.41 Properties of steel pipe [23]

Nominal pipe size (in.)	Outside diam. (in.)	Schedule no.	Wall thickness (in.)	Inside diam. (in.)	Cross-sectional area		Circumference (ft) or surface (ft^2/ft of length)		Capacity at velocity (1 ft/s)		Weight of plain-end pipe (lb/ft)
					Metal ($in.^2$)	Flow (ft^2)	Outside	Inside	U.S. gal/min	Water (lb/h)	
1/8	0.405	10S	0.049	0.307	0.055	0.00051	0.106	0.0804	0.231	115.5	0.19
		40St, 40S	0.068	0.269	0.072	0.00040	0.106	0.0705	0.179	89.5	0.24
		80XS, 80S	0.095	0.215	0.093	0.00025	0.106	0.0563	0.113	56.5	0.31
1/4	0.540	10S	0.065	0.410	0.097	0.00092	0.141	0.107	0.412	206.5	0.33
		40St, 40S	0.088	0.364	0.125	0.00072	0.141	0.095	0.323	161.5	0.42
		80XS, 80S	0.119	0.302	0.157	0.00050	0.141	0.079	0.224	112.0	0.54
3/8	0.675	10S	0.065	0.545	0.125	0.00162	0.177	0.143	0.727	363.5	0.42
		40St, 40S	0.091	0.493	0.167	0.00133	0.177	0.129	0.596	298.0	0.57
		80XS, 80S	0.126	0.423	0.217	0.00098	0.177	0.111	0.440	220.0	0.74
1/2	0.840	5S	0.065	0.710	0.158	0.00275	0.220	0.186	1.234	617.0	0.54
		10S	0.083	0.674	0.197	0.00248	0.220	0.176	1.112	556.0	0.67
		40St, 40S	0.109	0.622	0.250	0.00211	0.220	0.163	0.945	472.0	0.85
		80XS, 80S	0.147	0.546	0.320	0.00163	0.220	0.143	0.730	365.0	1.09
		160	0.188	0.464	0.385	0.00117	0.220	0.122	0.527	263.5	1.31
		XX	0.294	0.252	0.504	0.00035	0.220	0.066	0.155	77.5	1.71
3/4	1.050	5S	0.065	0.920	0.201	0.00461	0.275	0.241	2.072	1,036.0	0.69
		10S	0.083	0.884	0.252	0.00426	0.275	0.231	1.903	951.5	0.86
		40St, 40S	0.113	0.824	0.333	0.00371	0.275	0.216	1.665	832.5	1.13
		80XS, 80S	0.154	0.742	0.433	0.00300	0.275	0.194	1.345	672.5	1.47
		160	0.219	0.612	0.572	0.00204	0.275	0.160	0.917	458.5	1.94
		XX	0.308	0.434	0.718	0.00103	0.275	0.114	0.461	230.5	2.44
1	1.315	5S	0.065	1.185	0.255	0.00768	0.344	0.310	3.449	1,725	0.87
		10S	0.109	1.097	0.413	0.00656	0.344	0.287	2.946	1,473	1.40
		40St, 40S	0.133	1.049	0.494	0.00600	0.344	0.275	2.690	1,345	1.68

(continued)

Table A.41 (continued)

Nominal pipe size (in.)	Outside diam. (in.)	Schedule no.	Wall thickness (in.)	Inside diam. (in.)	Cross-sectional area		Circumference (ft) or surface (ft^2/ft of length)		Capacity at velocity (1 ft/s)		Weight of plain-end pipe (lb/ft)
					Metal ($in.^2$)	Flow (ft^2)	Outside	Inside	U.S. gal/min	Water (lb/h)	
		80XS, 80S	0.179	0.957	0.639	0.00499	0.344	0.250	2.240	1,120	2.17
		160	0.250	0.815	0.836	0.00362	0.344	0.213	1.625	812.5	2.84
		XX	0.358	0.599	1.076	0.00196	0.344	0.157	0.878	439.0	3.66
$1^1/_4$	1.660	5S	0.065	1.530	0.326	0.01277	0.435	0.401	5.73	2,865	1.11
		10S	0.109	1.442	0.531	0.01134	0.435	0.378	5.09	2,545	1.81
		40St, 40S	0.140	1.380	0.668	0.01040	0.435	0.361	4.57	2,285	2.27
		80XS, 80S	0.191	1.278	0.881	0.00891	0.435	0.335	3.99	1,995	3.00
		160	0.250	1.160	1.107	0.00734	0.435	0.304	3.29	1,645	3.76
		XX	0.382	0.896	1.534	0.00438	0.435	0.235	1.97	985	5.21
$1^1/_2$	1.900	5S	0.065	1.770	0.375	0.01709	0.497	0.463	7.67	3,835	1.28
		10S	0.109	1.682	0.614	0.01543	0.497	0.440	6.94	3,465	2.09
		40St, 40S	0.145	1.610	0.800	0.01414	0.497	0.421	6.34	3,170	2.72
		80XS, 80S	0.200	1.500	1.069	0.01225	0.497	0.393	5.49	2,745	3.63
		160	0.281	1.338	1.429	0.00976	0.497	0.350	4.38	2,190	4.86
		XX	0.400	1.100	1.885	0.00660	0.497	0.288	2.96	1,480	6.41
2	2.375	5S	0.065	2.245	0.472	0.02749	0.622	0.588	12.34	6,170	1.61
		10S	0.109	2.157	0.776	0.02538	0.622	0.565	11.39	5,695	2.64
		40St, 40S	0.154	2.067	1.075	0.02330	0.622	0.541	10.45	5,225	3.65
		80St, 80S	0.218	1.939	1.477	0.02050	0.622	0.508	9.20	4,600	5.02
		160	0.344	1.687	2.195	0.01552	0.622	0.436	6.97	3,485	7.46
		XX	0.436	1.503	2.656	0.01232	0.622	0.393	5.53	2,765	9.03
$2^1/_2$	2.875	5S	0.083	2.709	0.728	0.04003	0.753	0.709	17.97	8,985	2.48
		10S	0.120	2.635	1.039	0.03787	0.753	0.690	17.00	8,500	3.53
		40St, 40S	0.203	2.469	1.704	0.03322	0.753	0.647	14.92	7,460	5.79
		80XS, 80S	0.276	2.323	2.254	0.02942	0.753	0.608	13.20	6,600	7.66
		160	0.375	2.125	2.945	0.02463	0.753	0.556	11.07	5,535	10.01
		XX	0.552	1.771	4.028	0.01711	0.753	0.464	7.68	3,840	13.70

3	3.500	5S	0.083	3.334	0.891	0.06063	0.916	0.873	27.21	13,605	3.03
		10S	0.120	3.260	1.274	0.05796	0.916	0.853	26.02	13,010	4.33
		40St, 40S	0.216	3.068	2.228	0.05130	0.916	0.803	23.00	11,500	7.58
		80XS, 80S	0.300	2.900	3.016	0.04587	0.916	0.759	20.55	10,275	10.25
		160	0.438	2.624	4.213	0.03755	0.916	0.687	16.86	8,430	14.31
		XX	0.600	2.300	5.466	0.02885	0.916	0.602	12.95	6,475	18.58
$3^1/_2$	4.0	5S	0.083	3.834	1.021	0.08017	1.047	1.004	35.98	17,990	3.48
		10S	0.120	3.760	1.463	0.07711	1.047	0.984	34.61	17,305	4.97
		40St, 40S	0.226	3.548	2.680	0.06870	1.047	0.929	30.80	15,400	9.11
		80XS, 80S	0.318	3.364	3.678	0.06170	1.047	0.881	27.70	13,850	12.51
4	4.5	5S	0.083	4.334	1.152	0.10245	1.178	1.135	46.0	23,000	3.92
		10S	0.120	4.260	1.651	0.09898	1.178	1.115	44.4	22,200	5.61
		40St, 40S	0.237	4.026	3.17	0.08840	1.178	1.054	39.6	19,800	10.79
		80XS, 80S	0.337	3.826	4.41	0.07986	1.178	1.002	35.8	17,900	14.98
		120	0.438	3.624	5.58	0.07170	1.178	0.949	32.2	16,100	18.98
		160	0.531	3.438	6.62	0.06647	1.178	0.900	28.9	14,450	22.52
		XX	0.674	3.152	8.10	0.05419	1.178	0.825	24.3	12,150	27.54
5	5.563	5S	0.109	5.345	1.87	0.1558	1.456	1.399	69.9	34,950	6.36
		10S	0.134	5.295	2.29	0.1529	1.456	1.386	68.6	34,300	7.77
		40St, 40S	0.258	5.047	4.30	0.1390	1.456	1.321	62.3	31,150	14.62
		80XS, 80S	0.375	4.813	6.11	0.1263	1.456	1.260	57.7	28,850	20.78
		120	0.500	4.563	7.95	0.1136	1.456	1.195	51.0	25,500	27.04
		160	0.625	4.313	9.70	0.1015	1.456	1.129	45.5	22,750	32.96
		XX	0.750	4.063	11.34	0.0900	1.456	1.064	40.4	20,200	38.55
6	6.625	5S	0.109	6.407	2.23	0.2239	1.734	1.677	100.5	50,250	7.60
		10S	0.134	6.357	2.73	0.2204	1.734	1.664	98.9	49,450	9.29
		40St, 40S	0.280	6.065	5.58	0.2006	1.734	1.588	90.0	45,000	18.97
		80XS, 80S	0.432	5.761	8.40	0.1810	1.734	1.508	81.1	40,550	28.57
		120	0.562	5.501	10.70	0.1650	1.734	1.440	73.9	36,950	36.42
		160	0.719	5.187	13.34	0.1467	1.734	1.358	65.9	32,950	45.34
		XX	0.864	4.897	15.64	0.1308	1.734	1.282	58.7	29,350	53.16

(continued)

Table A.41 (continued)

Nominal pipe size (in.)	Outside diam. (in.)	Schedule no.	Wall thickness (in.)	Inside diam. (in.)	Cross-sectional area		Circumference (ft) or surface (ft^2/ft of length)		Capacity at velocity (1 ft/s)		Weight of plain-end pipe (lb/ft)
					Metal ($in.^2$)	Flow (ft^2)	Outside	Inside	U.S. gal/min	Water (lb/h)	
8	8.625	5S	0.109	8.407	2.915	0.3855	2.258	2.201	173.0	86,500	9.93
		10S	0.148	8.329	3.941	0.3784	2.258	2.180	169.8	84,900	13.40
		20	0.250	8.125	6.578	0.3601	2.258	2.127	161.5	80,750	22.36
		30	0.277	8.071	7.265	0.3553	2.258	2.113	159.4	79,700	24.70
		40St, 40S	0.322	7.981	8.399	0.3474	2.258	2.089	155.7	77,850	28.55
		60	0.406	7.813	10.48	0.3329	2.258	2.045	149.4	74,700	35.66
		80XS, 80S	0.500	7.625	12.76	0.3171	2.258	1.996	142.3	71,150	43.39
		100	0.594	7.437	14.99	0.3017	2.258	1.947	135.4	67,700	50.93
		120	0.719	7.187	17.86	0.2817	2.258	1.882	126.4	63,200	60.69
		140	0.812	7.001	19.93	0.2673	2.258	1.833	120.0	60,000	67.79
		XX	0.875	6.875	21.30	0.2578	2.258	1.800	115.7	57,850	72.42
		160	0.906	6.813	21.97	0.2532	2.258	1.784	113.5	56,750	74.71
10	10.75	5S	0.134	10.842	4.47	0.5993	2.814	2.744	269.0	134,500	15.19
		10S	0.165	10.420	5.49	0.5922	2.814	2.728	265.8	132,900	18.65
		20	0.250	10.250	8.25	0.5731	2.814	2.685	257.0	128,500	28.04
		30	0.307	10.136	10.07	0.5603	2.814	2.655	252.0	126,000	34.24
		40St, 40S	0.365	10.020	11.91	0.5475	2.814	2.620	246.0	123,000	40.48
		80S, 60XS	0.500	9.750	16.10	0.5185	2.814	2.550	233.0	116,500	54.74
		80	0.594	9.562	18.95	0.4987	2.814	2.503	233.4	111,700	64.40
		100	0.719	9.312	22.66	0.4729	2.814	2.438	212.3	106,150	77.00
		120	0.844	9.062	26.27	0.4479	2.814	2.372	201.0	100,500	89.27
		140, XX	1.000	8.750	30.63	0.4176	2.814	2.291	188.0	94,000	104.13
		160	1.125	8.500	34.02	0.3941	2.814	2.225	177.0	88,500	115.65
12	12.75	5S	0.156	12.438	6.17	0.8438	3.338	3.26	378.7	189,350	20.98
		10S	0.180	12.390	7.11	0.8373	3.338	3.24	275.8	187,900	24.17
		20	0.250	12.250	9.82	0.8185	3.338	3.21	367.0	183,500	33.38
		30	0.330	12.090	12.88	0.7972	3.338	3.17	358.0	179,000	43.77
		St, 40S	0.375	12.000	14.58	0.7854	3.338	3.14	352.5	176,250	49.56

		40	0.406	11.938	15.74	0.7773	3.338	3.13	349.0	174,500	54.56
		XS, 80S	0.500	11.750	19.24	0.7530	3.338	3.08	338.0	169,000	65.42
		60	0.562	11.626	21.52	0.7372	3.338	3.04	331.0	165,500	73.72
		80	0.688	11.374	26.07	0.7056	3.338	2.98	316.7	158,350	88.57
		100	0.844	11.062	31.57	0.6674	3.338	2.90	299.6	149,800	107.29
		120, XX	1.000	10.750	36.91	0.6303	3.338	2.81	283.0	141,500	125.49
		140	1.125	10.500	41.09	0.6013	3.338	2.75	270.0	135,000	139.68
		160	1.312	10.126	47.14	0.5592	3.338	2.65	251.0	125,500	160.33
14	14	5S	0.156	13.688	6.78	1.0219	3.665	3.58	459	229,500	23.07
		10S	0.188	13.624	8.16	1.0125	3.665	3.57	454	227,000	27.73
		10	0.250	13.500	10.80	0.9940	3.665	3.53	446	223,000	36.71
		20	0.312	13.376	13.42	0.9750	3.665	3.50	438	219,000	45.68
		30, St	0.375	13.250	16.05	0.9575	3.665	3.47	430	215,000	54.57
		40	0.438	13.124	18.66	0.9397	3.665	3.44	422	211,000	63.37
		XS	0.500	13.000	21.21	0.9218	3.665	3.40	414	207,000	72.09
		60	0.594	12.812	25.02	0.8957	3.665	3.35	402	201,000	85.01
		80	0.750	12.500	31.22	0.8522	3.665	3.27	382	191,000	106.13
		100	0.938	12.124	38.49	0.8017	3.665	3.17	360	180,000	130.79
		120	1.094	11.812	44.36	0.7610	3.665	3.09	342	171,000	150.76
		140	1.250	11.500	50.07	0.7213	3.665	3.01	324	162,000	170.22
		160	1.406	11.188	55.63	0.6827	3.665	2.93	306	153,000	189.15
16	16	5S	0.165	15.670	8.21	1.3393	4.189	4.10	601	300,500	27.90
		10S	0.188	15.624	9.34	1.3314	4.189	4.09	598	299,000	31.75
		10	0.250	15.500	12.37	1.3104	4.189	4.06	587	293,500	42.05
		20	0.312	15.376	15.38	1.2985	4.189	4.03	578	289,000	52.36
		30, St	0.375	15.250	18.41	1.2680	4.189	3.99	568	284,000	62.58
		40, XS	0.500	15.000	24.35	1.2272	4.189	3.93	550	275,000	82.77
		60	0.656	14.688	31.62	1.1766	4.189	3.85	528	264,000	107.54
		80	0.844	14.312	40.19	1.1171	4.189	3.75	501	250,500	136.58
		100	1.031	13.938	48.48	1.0596	4.189	3.65	474	237,000	164.86
		120	1.219	13.562	56.61	1.0032	4.189	3.55	450	225,000	192.40
		140	1.438	13.124	65.79	0.9394	4.189	3.44	422	211,000	223.57
		160	1.594	12.812	72.14	0.8953	4.189	3.35	402	201,000	245.22

(continued)

Table A.41 (continued)

Nominal pipe size (in.)	Outside diam. (in.)	Schedule no.	Wall thickness (in.)	Inside diam. (in.)	Cross-sectional area		Circumference (ft) or surface (ft^2/ft of length)		Capacity at velocity (1 ft/s)		Weight of plain-end pipe (lb/ft)
					Metal ($in.^2$)	Flow (ft^2)	Outside	Inside	U.S. gal/min	Water (lb/h)	
18	18	5S	0.165	17.670	9.25	1.7029	4.712	4.63	764	382,000	31.43
		10S	0.188	17.624	10.52	1.6941	4.712	4.61	760	379,400	35.76
		10	0.250	17.500	13.94	1.6703	4.712	4.58	750	375,000	47.39
		20	0.312	17.376	17.34	1.6468	4.712	4.55	739	369,500	59.03
		St	0.375	17.250	20.76	1.6230	4.712	4.52	728	364,000	70.59
		30	0.438	17.124	24.16	1.5993	4.712	4.48	718	359,000	82.06
		XS	0.500	17.000	27.49	1.5763	4.712	4.45	707	353,500	93.45
		40	0.562	16.876	30.79	1.5533	4.712	4.42	697	348,500	104.76
		60	0.750	16.500	40.64	1.4849	4.712	4.32	666	333,000	138.17
		80	0.938	16.124	50.28	1.4180	4.712	4.22	636	318,000	170.84
		100	1.156	15.688	61.17	1.3423	4.712	4.11	602	301,000	208.00
		120	1.375	15.250	71.82	1.2684	4.712	3.99	569	284,500	244.14
		140	1.562	14.876	80.66	1.2070	4.712	3.89	540	270,000	274.30
		160	1.781	14.438	90.75	1.1370	4.712	3.78	510	255,000	308.55
20	20	5S	0.188	19.624	11.70	2.1004	5.236	5.14	943	471,500	39.78
		10S	0.218	19.564	13.55	2.0878	5.236	5.12	937	467,500	46.06
		10	0.250	19.500	15.51	2.0740	5.236	5.11	930	465,500	52.73
		20, St	0.375	19.250	23.12	2.0211	5.236	5.04	902	451,000	78.60
		30, XS	0.500	19.000	30.63	1.9689	5.236	4.97	883	441,500	104.13
		40	0.594	18.812	36.21	1.9302	5.236	4.92	866	433,000	123.06
		60	0.812	18.376	48.95	1.8417	5.236	4.81	826	413,000	166.50
		80	1.031	17.938	61.44	1.7550	5.236	4.70	787	393,500	208.92
		100	1.281	17.438	75.33	1.6585	5.236	4.57	744	372,000	256.15
		120	1.500	17.000	87.18	1.5763	5.236	4.45	707	353,500	296.37
		140	1.750	16.500	100.3	1.4849	5.236	4.32	665	332,500	341.10
		160	1.969	16.062	111.5	1.4071	5.236	4.21	632	316,000	379.14
24	24	5S	0.218	23.564	16.29	3.0285	6.283	6.17	1,359	679,500	55.37
		10, 10S	0.250	23.500	18.65	3.012	6.283	6.15	1,350	675,000	63.41
		20, St	0.375	23.250	27.83	2.948	6.283	6.09	1,325	662,500	94.62

		XS	0.500	23.000	36.90	2.885	6.283	6.02	1,295	642,500	125.49
		30	0.562	22.876	41.39	2.854	6.283	5.99	1,281	640,500	140.80
		40	0.688	22.624	50.39	2.792	6.283	5.92	1,253	626,500	171.17
		60	0.969	22.062	70.11	2.655	6.283	5.78	1,192	596,000	238.29
		80	1.219	21.562	87.24	2.536	6.283	5.64	1,138	569,000	296.53
		100	1.531	20.938	108.1	2.391	6.283	5.48	1,073	536,500	367.45
		120	1.812	20.376	126.3	2.264	6.283	5.33	1,016	508,000	429.50
		140	2.062	19.876	142.1	2.155	6.283	5.20	965	482,500	483.24
		160	2.344	19.312	159.5	2.034	6.283	5.06	913	456,500	542.09
30	30	5S	0.250	29.500	23.37	4.746	7.854	7.72	2,130	1,065,000	79.43
		10, 10S	0.312	29.376	29.10	4.707	7.854	7.69	2,110	1,055,000	98.93
		St	0.375	29.250	34.90	4.666	7.854	7.66	2,094	1,048,000	118.65
		20, XS	0.500	29.000	46.34	4.587	7.854	7.59	2,055	1,027,500	157.53
		30	0.625	28.750	57.68	4.508	7.854	7.53	2,020	1,010,000	196.08

Table A.42 Properties of copper water tube, types K, L, M

Nominal Size	Actual outside diam. (in.)	Mean outside diam. tolerances (in.)		Wall thickness (in.)						Theoretical weight (lb/ft)		
				Type K		Type L		Type M				
		Soft annealed	Hard drawn	Nominal	Tolerance	Nominal	Tolerance	Nominal	Tolerance	Type K	Type L	Type M
1/4	0.375	0.002	0.001	0.035	0.004	0.030	0.0035	–	–	0.145	0.126	
3/8	0.500	0.0025	0.001	0.049	0.004	0.035	0.0035	0.025	0.0025	0.269	0.198	0.145
1/2	0.625	0.0025	0.001	0.049	0.004	0.040	0.0035	0.028	0.0025	0.344	0.285	0.204
5/8	0.750	0.0025	0.001	0.049	0.004	0.042	0.0035	–	–	0.418	0.362	
3/4	0.875	0.003	0.001	0.065	0.0045	0.045	0.004	0.032	0.003	0.641	0.455	0.328
1	1.125	0.0035	0.0015	0.065	0.0045	0.050	0.004	0.035	0.0035	0.839	0.655	0.465
1 1/4	1.375	0.004	0.0015	0.065	0.0045	0.055	0.0045	0.042	0.0035	1.04	0.884	0.682
1 1/2	1.625	0.0045	0.002	0.072	0.005	0.060	0.0045	0.049	0.004	1.36	1.14	0.940
2	2.125	0.005	0.002	0.083	0.007	0.070	0.006	0.058	0.006	2.06	1.75	1.46
2 1/2	2.625	0.005	0.002	0.095	0.007	0.080	0.006	0.065	0.006	2.93	2.48	2.03
3	3.125	0.005	0.002	0.109	0.007	0.090	0.007	0.072	0.006	4.00	3.33	2.68
3 1/2	3.625	0.005	0.002	0.120	0.008	0.100	0.007	0.083	0.007	5.12	4.29	3.58
4	4.125	0.005	0.002	0.134	0.010	0.110	0.009	0.095	0.009	6.51	5.36	4.66
5	5.125	0.005	0.002	0.160	0.010	0.125	0.010	0.109	0.009	9.67	7.61	6.66
6	6.125	0.005	0.002	0.192	0.012	0.140	0.011	0.122	0.010	13.9	10.2	8.92
8	8.125	0.006	0.002 0.004	0.271	0.016	0.200	0.014	0.170	0.014	25.9	19.3	16.5

Table A.43 Properties of copper and red brass pipe

Nominal pipe size (in.)	Nominal dimensions (in.)			Cross-sectional area of bore ($in.^2$)	lb/ft		Nominal pipe size (in.)	Nominal dimensions (in.)			Cross-Sectional area of bore ($in.^2$)	lb/ft	
	Outside diam.	Inside diam.	Wall thickness		Red brass	Copper		Outside diam.	Inside diam.	Wall thickness		Red brass	Copper
A. dimensions and weights of regular pipe													
1/8	0.405	0.281	0.062	0.062	0.253	0.259	2 1/2	2.875	2.501	0.187	4.91	5.99	6.12
1/4	0.540	0.376	0.082	0.110	0.447	0.457	3	3.500	3.062	0.219	7.37	8.56	8.75
3/8	0.675	0.495	0.090	0.192	0.627	0.641	3 1/2	4.000	3.500	0.250	9.62	11.2	11.4
1/2	0.840	0.626	0.107	0.307	0.934	0.955	4	4.500	4.000	0.250	12.6	12.7	12.9
3/4	1.050	0.822	0.114	0.531	1.27	1.30	5	5.562	5.062	0.250	20.1	15.8	16.2
1	1.315	1.063	0.126	0.887	1.78	1.82	6	6.625	6.125	0.250	29.5	19.0	19.4
1 1/4	1.660	1.368	0.146	1.47	2.63	2.69	8	8.625	8.001	0.312	50.3	30.9	31.6
1 1/2	1.900	1.600	0.150	2.01	3.13	3.20	10	10.750	10.020	0.365	78.8	45.2	46.2
2	2.375	2.063	0.156	3.34	4.12	4.22	12	12.750	12.000	0.375	113.0	55.3	56.5
B. Dimensions and weights of extra-strong pipe													
1/8	0.405	0.205	0.100	0.033	0.363	0.371	2 1/2	2.875	2.315	0.280	4.21	8.66	8.85
1/4	0.540	0.294	0.123	0.068	0.611	0.625	3	3.500	2.892	0.304	6.57	11.6	11.8
3/8	0.675	0.421	0.127	0.139	0.829	0.847	3 1/2	4.000	3.358	0.321	8.86	14.1	14.4
1/2	0.840	0.542	0.149	0.231	1.23	1.25	4	4.500	3.818	0.341	11.5	16.9	17.3
3/4	1.050	0.736	0.157	0.425	1.67	1.71	5	5.562	4.812	0.375	18.2	23.2	23.7
1	1.315	0.951	0.182	0.710	2.46	2.51	6	6.625	5.751	0.437	26.0	32.2	32.9
1 1/4	1.660	1.272	0.194	1.27	3.39	3.46	8	8.625	7.625	0.500	45.7	48.4	49.5
1 1/2	1.900	1.494	0.203	1.75	4.10	4.19	10	10.750	9.750	0.500	74.7	61.1	62.4
2	2.375	1.933	0.221	2.94	5.67	5.80							

Table A.44 SI (metric) conversions for pipe sizes [24]

Nominal pipe size (NPS) (inches)	Masterspec dimension nominal (mm)
1/8	6
3/16	8
1/4	10
3/8	12
1/2	15
5/8	18
3/4	20
1	25
1-1/4	32
1-1/2	40
2	50
2-1/2	65
3	80
3-1/2	90
4	100
4-1/2	115
5	125
6	150
8	200
10	250
12	300
14	350
16	400
18	450
20	500
24	600

References

1. E.A. Mechtly, "The International System of Units, Physical Constants and Conversion Factors," 2nd revision, National Aeronautics and Space Administration, Washington, DC (1973).
2. B.N. Taylor, W.H. Parker, and D.N. Langenberg, "Determination of $^{e}/^{h}$, QED, and the Fundamental Constants," Reviews of Modern Physics, 41 (1969).
3. B.D. Tapley and T.R. Poston (eds.), *Eshbach's Handbook of Engineering Fundamentals,* 4th ed., John Wiley and Sons, New York (1990).
4. E.R.G. Eckert and R.M. Drake, *Analysis of Heat and Mass Transfer,* McGraw-Hill, New York (1972).
5. J.P. Holman, *Heat Transfer,* McGraw-Hill, New York (1986).
6. A.M. Kanury, *Introduction to Combustion Phenomena,* Gordon and Breach Science Publishers, New York (1975).
7. V. Babrauskas, "Tables and Charts," *Fire Protection Handbook,* 17th ed. (A.E. Cote and J. Linville, eds.), National Fire Protection Association, Quincy, MA (1991).
8. V. Babrauskas, *Ignition Handbook*, Fire Science Publishers, Issaquah, WA, 2003.
9. C.L. Yaws, *Chemical Properties Handbook: Physical, Thermodynamic, Environmental, Transport Safety and Health Related Properties for Organic and Inorganic Chemicals,* McGraw-Hill, New York (1999).
10. Tewarson A (2003) Flammability of Polymers. In: Andrady AL (ed) Plastics and Environment. John Wiley & Sons, Inc., Hoboken, NJ, pp. 403–489.
11. Tewarson A (2005) Thermophysical and Fire Properties of Automobile Plastic Parts and Engine Compartment Fluids. Technical Report #0003018009, Volume III, Motor Vehicle Fire Research Institute, Charlottesville, VA.
12. Babrauskas V (1992) The Cone Calorimeter, In: Babrauskas V, Grayson SJ (eds) Heat Release in Fires, Elsevier Publishing Company, London, UK, pp. 61–92.
13. Tewarson A, Chin W, Shuford R (2004) Materials Specifications, Standards, and Testing. In: Harper CA (ed) Handbook of Building Materials for Fire Protection. McGraw-Hill, New York, pp. 2.1–2.54.
14. Lyon RE (2004) Plastics and Rubber. In: Harper CA (ed) Handbook of Building Materials for Fire Protection. McGraw-Hill, New York, pp. 3.1–3.51.
15. See Chapter 36, "Combustion Characteristics of Materials and Generation of Fire Products."
16. Scudamore MJ, Briggs PJ, Prager FH (1991) Cone Calorimetry – A Review of Tests Carried Out on Plastics for the Association of Plastics Manufacturers in Europe. Fire Mater 15:65–84. doi:10.1002/fam.810150205
17. Hirschler MM (1987) Fire Hazard and Toxic Potency of the Smoke from Burning Materials. J Fire Sci 5:289–307. doi:10.1177/073490418700500501
18. Tsantarides L, Ostman B (1989) Smoke, Gas, and Heat Release Data for Building Products in the Cone Calorimeter. Technical Report I 8903013, Swedish Institute for Wood Technology Research, Stockholm, Sweden.
19. Khan MM (1992) Characterization of Liquid Fuel Spray Fires. In: Cho P, Quintiere J (eds) Heat and Mass Transfer in Fire and Combustion Systems, American Society of Mechanical Engineers, New York, NY.
20. Tewarson A (1986) Prediction of Fire Properties of Materials Part 1: Aliphatic and Aromatic Hydrocarbons and Related Polymers. Technical Report NBS-GCR-86-521, National Institute of Standards and Technology, Gaithersburg, MD.
21. P. Blackshear (ed.), *Heat Transfer in Fires,* Scripta Book Company, Washington, DC (1974).
22. R. Siegel and J.R. Howell, *Thermal Radiation Heat Transfer,* 3rd ed., Taylor & Francis, Washington, DC (1992).
23. R.H. Perry and C.H. Chilton (eds.), *Chemical Engineers Handbook,* McGraw-Hill, New York (1973).
24. Basic Mechanical Materials and Methods – Metric Appendix, Masterspec, American Institute of Architects, Washington, DC, 1992.

DOI 10.1007/978-1-4939-2565-0, © Society of Fire Protection Engineers 2016